The conversion of 7-acetoxyroyleanone to 14-methoxytaxodione

ANNE-MARIE FAUCHER AND ROBERT H. BURNELL[1]
Département de chimie, Université Laval, Québec (Qué.), Canada G1K 7P4

Received July 6, 1988

ANNE-MARIE FAUCHER and ROBERT H. BURNELL. Can. J. Chem. **67**, 1 (1989).

7-Acetoxyroyleanone (**1***a*) has been converted in five steps to the methoxy-*p*-quinone **9**. Since the latter was the penultimate intermediate in Eugster's partial synthesis of 14-methoxytaxodione (**2**), the transformation reported represents a formal synthesis of the latter.

Key words: 7-acetoxyroyleanone, 14-methoxytaxodione, synthesis.

ANNE-MARIE FAUCHER et ROBERT H. BURNELL. Can. J. Chem. **67**, 1 (1989).

L'acétoxy-7 royléanone (**1***a*) fut transformée en cinq étapes en méthoxy-*p*-quinone **9**. Ceci complèta la synthèse formelle de la méthoxy-14 taxodione (**2**) parce que cette *p*-quinone a déjà servi comme pénultième intermédiaire dans une synthèse partielle décrite par Eugster.

Mots clés : acétoxy-7 royléanone, méthoxy-14 taxodione, synthèse.

[Traduit par la revue]

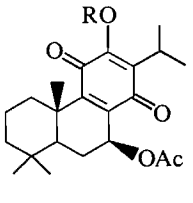
Can. J. Chem. Downloaded from www.nrcresearchpress.com by 122.72.124.2 on 09/07/12
For personal use only.

The similarity of the royleanones, such as the 7-acetoxy derivative **1***a*(1), to the often synthesized taxodione chromophore (2) as found for example in 14-methoxytaxodione **2**(3), suggests that the transformation of the former to the latter should be easy. In practice, however, we found it to be far from trivial. In essence it involves only the transposition of the oxygen function at C7 to C6 and suitable adjustment of the oxidation level. We were amazed at the fragile nature of the compounds when subjected to even the simplest of reactions and for this reason we chose to experiment first with the relatively stable 12-*O*-methyl derivative **1***b*.

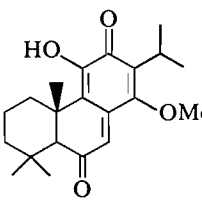
Sodium dithionite in acetone reduced **1***b* to the hydroquinone **3***a* but, despite many variations of procedure, some elimination occurred, affording also **4***a*, and often the latter was the major product (typically 1:3). In practice we found it advantageous to subject the crude reaction mixture to methylation (using potassium carbonate and dimethyl sulfate) because, after this, only the methylated elimination product **4***c* was isolated (82% from **1***b*).

To introduce the necessary oxygen function at C6 we used the *N*-methylmorpholine *N*-oxide mediated *cis*-hydroxylation with osmium tetroxide (4), which allowed us to isolate, with difficulty, the 6α,7α-diol **5***a*. Acid catalysed dehydration of the latter (*p*-TsOH, benzene) gave the 6-ketone **6***a*. For both greater simplicity and higher yield, we found the best route to this ketone was by epoxidation of the double bond in **4***c* (*m*-CPBA in CH_2Cl_2) and subjecting the crude product to rearrangement, which raised the yield to a respectable 92% (from **4***c*). We considered that this relatively stable ketone **6***a* would be a key intermediate since we felt that any derivative with a phenolic hydroxyl at C12, such as **6***c*, which could conceivably arise by partial demethylation, should be readily oxidized, and the extended quinone chromophore of the taxodiones was a likely oxidative end product.

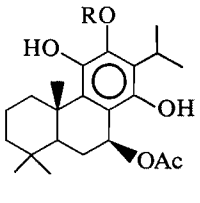
Of the many demethylation conditions to which the ketone **6***a* was subjected, none afforded a meaningful result. The reaction with boron trichloride (5) did afford recognisable products in the form of two coleon U derivatives **7***a* and **7***b* (13% and 7% respectively), confirming our suspicion that the methylene at C7, which is activated by the aromatic ring on one side and the C6 ketone on the other, is extremely susceptible to oxidation. Our *O*-methyl model had reached the end of its usefulness.



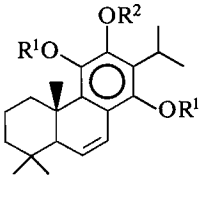
1*a* R = H
1*b* R = Me
1*c* R = Ac



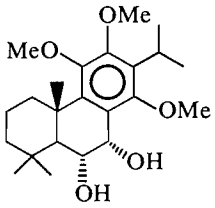
2



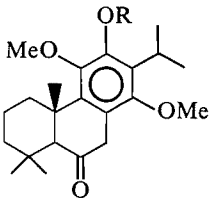
3*a* R = Me
3*b* R = Ac



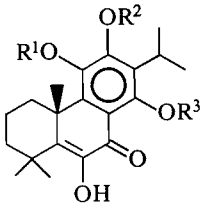
4*a* R^1 = H, R^2 = Me
4*b* R^1 = H, R^2 = Ac
4*c* R^1 = R^2 = Me
4*d* R^1 = Me, R^2 = Ac



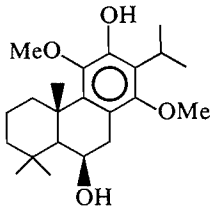
5



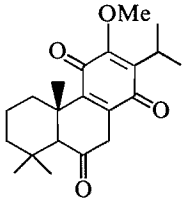
6*a* R = Me
6*b* R = Ac
6*c* R = H



7*a* R^1 = R^3 = H, R^2 = Me
7*b* R^1 = R^2 = Me, R^3 = H
7*c* R^1 = R^3 = Me, R^2 = H
7*d* R^1 = Me, R^2 = R^3 = H



8



9

We prepared the 12-*O*-acetyl derivative **1***c* and subjected it to the dithionite reduction/methylation for a 71% yield of **4***d* and the latter was epoxidized and rearranged to afford the analogous C6 ketone **6***b* (in 68% yield from **4***d*). The *O*-acetyl residue was, of course, easily removed by hydrolysis but, again, the only products identified from the very colored mixture were two more coleon U ethers **7***c* and **7***d* (32% and 11% respectively). Since we did not detect these in the initial crude reaction mixture (tlc) we assumed that oxidation takes place on the silica gel used for purification (**6***a*,*b*). The C6 ketone was an obvious embar-

[1]Author to whom correspondence may be addressed.

TABLE 1. ^{13}C nuclear magnetic resonance data[a]

	Compound									
Carbon	**1***a*	**1***b*	**1***c*	**9**	**4***c*	**4***d*	**4***a*[b]	**6***a*	**6***b*	**8**
1	36.07	36.15	35.53	36.20	36.65	35.84	36.40	38.04	37.47	36.49
2	18.95	18.88	18.63	18.48	19.50	19.30	19.26	19.25	19.03	19.59
3	41.27	41.34	40.87	40.44	40.89	40.46	40.91	41.73	41.26	38.86
4	33.07	33.07	32.83	32.53	33.31	33.16	33.16	32.80	32.76	34.36
5	46.32	46.46	45.91	42.06	51.06	50.46	51.30	42.31	41.95	42.64
6	24.80	25.02	25.07	206.35	122.13	122.04	119.73	210.23	209.17	65.09
7	64.76	64.61	64.21	62.85	128.46	128.88	129.68	62.78	62.28	54.34
8	139.83	137.49	138.83	138.32	132.43	132.68	124.08	133.15	133.50	130.86
9	125.05	136.17	137.65	135.15	123.20	124.06	118.78	122.08	123.24	122.95
10	39.29	39.29	39.11	43.71	41.49	41.17	41.57	45.15	44.26	42.64
11	185.63	186.51	185.05	186.32	150.31	150.09	143.49	150.51	150.65	144.32
12	151.02	156.95	152.73	156.62	154.47	152.93	144.72	152.29	153.33	149.92
13	150.22	152.85	149.05	148.98	139.12	138.12	130.81	139.59	138.83	132.94
14	184.10	184.02	179.92	182.72	147.78	138.17	140.12	148.74	138.96	143.92
15	33.07	33.07	32.83	32.63	33.07	32.87	32.98	32.98	32.85	34.18
16	19.83	20.27	20.14	20.45	22.23	22.38	21.25	22.01	22.10	22.34
17	19.83	20.63	20.14	20.79	22.54	22.41	22.47	22.01	22.45	22.63
18	24.37	24.73	24.61	24.45	25.65	25.76	25.76	25.94	25.94	25.96
19	18.66	18.88	18.48	20.27	18.97	18.46	17.50	22.21	22.83	21.34
20	21.00	20.92	20.92	21.68	22.17	22.12	21.10	22.56	22.03	24.05
Others	169.46	60.51	169.12	60.61	60.14	61.38	61.98	59.85	61.32	61.78
	21.73	169.39	167.86		62.30	61.36		60.85	60.90	60.90
		21.73	21.50		59.85	169.12		59.67	168.68	
			20.27			21.23				21.25

[a]In ppm from TMS.
[b]These values were abstracted from the spectrum of a 3:1 mixture of **4***a* and **3***a*.

rassment so we removed the C12 *O*-acetyl residue with lithium aluminium hydride, which also reduced the ketone, affording the hydroxy compound **8** (in 77% yield).

Our first cautious oxidation of **8** was with Jones reagent for 30 s and this gave mostly the phenolic ketone **6***c* (40%) accompanied by the methoxy *p*-quinone **9** (28%), but by extending the period of oxidation to 30 min we raised the yield of the latter to 70%. During the oxidation there is a methyl group migration from the methoxyl at C11 in the starting material to form that at C12 in the product. Due to its limited stability at room temperature we could not analyse **9** in the usual manner, but its nmr spectrum is identical with that described by Rüedi and Eugster (7). Thus, our preparation represents a formal synthesis of 14-methoxytaxodione (**2**) since Rüedi and Eugster also reported the transformation of **9** to the natural product.

Experimental

Unless otherwise stated, the conditions and instruments used to characterize the products were as follows: melting points, Electrothermal, uncorrected; ultraviolet spectra, ethanol solutions (ε in parentheses), Hewlett Packard 8450 A; infrared spectra, carbon tetrachloride solutions, Beckman 4250 and Perkin Elmer 457; 200-MHz proton and 50-MHz carbon-13 magnetic resonance spectra, deuteriochloroform solutions, TMS internal standard (where relevant — multiplicity, integrated peak areas, coupling constants and assignments in parentheses), "dis. D_2O" signifies that the peaks in question disappeared on shaking the solution with a small volume of D_2O, Varian XL-200; mass spectra, Hewlett Packard 5992. Elemental analyses were by Galbraith Laboratories, Knoxville, TN. The high resolution mass spectra were recorded at the Centre régional de spectrométrie de masse, Université de Montréal. Unless otherwise stated, dry column chromatography implies the use of Merck Kieselgel 60F (70–230 mesh) and elution with hexane–ethyl acetate (proportions determined by prior thin-layer chromatography using Baker-flex Silica gel 1B2-F precoated plastic sheets).

*7-Acetoxy-12-*O*-methylroyleanone* **1***b*

Diazomethane generated from Diazald (4 g) was introduced to a suspension of 7-acetoxyroyleanone **1***a* (1.19 g) in ether (80 mL) and the mixture was stirred until the reaction was complete (tlc). The solvent was removed, affording a quantitative yield (1.234 g) of the *O*-methyl derivative **1***b*, mp 178–180°C (yellow needles from methanol); uv: 269(11 840) and 393(620) nm; ir: 1730, 1635, 1660, and 1600 cm^{-1}; ^1H nmr δ: 0.88 and 0.89 (2s, Me at C4), 1.16 and 1.21 (2d, J = 7 Hz, Me at C15), 1.29 (2, Me at C10), 2.02 (s, Me-CO), 2.62 (m, 1H, H-C1), 3.17 (sept, J = 7 Hz, H-C15), 3.88 (s, Me-O), 5.91 (dd, J = 4 and 2 Hz, H-C7); ^{13}C nmr, see Table 1. *Anal.* calcd. for $C_{23}H_{32}O_5$: C 71.10, H 8.30; found: C 70.94, H 8.20.

*7-Acetoxy-*O*-acetylroyleanone* **1***c*

Acetic anhydride (13 mL) was added to a solution of 7-acetoxyroyleanone **1***a* (355 mg) in pyridine (25 mL). The color changed almost immediately from orange brown to bright yellow. After stirring for 15 min the product was isolated by diluting with ether, washing with dilute aqueous HCl, and then with saturated aqueous $NaHCO_3$ solution. Removal of the solvent afforded a yellow oil (373 mg; quant), which crystallized slowly on standing, mp 99–100°C (from ethanol–water); uv: 222(2850) and 262(14 970) nm; ir: 1780, 1745, 1665, 1655(sh), and 1610 cm^{-1}; ^1H nmr δ: 0.88 (s, 6H, *gem*-diMe), 1.18 and 1.20 (2d, J = 7 Hz, Me at C15), 1.26 (s, Me at C10), 2.03 and 2.34 (Me in acetoxy at C7 and C12 resp), 3.10 (sept, J = 7 Hz, H-C15), 5.93 (dd, J = 4 and 1.7 Hz, H-C7); ^{13}C nmr, see Table 1; ms m/z: 416 (1.6, M^+), 374 (13), and 356 (20). *Exact Mass* calcd. for $C_{22}H_{28}O_4$ ($M - CH_3COOH$): 356.1988; found (hrms): 356.2057 (no molecular ion was detected).

*Dithionite reduction of 7-acetoxy-*O*-methylroyleanone* **1***b*

7-Acetoxy-*O*-methylroyleanone (2.50 g) was dissolved in acetone (100 mL) and sodium dithionite (3.0 g) was added. With vigorous

Can. J. Chem. Downloaded from www.nrcresearchpress.com by 122.72.124.2 on 09/07/12
For personal use only.

Can. J. Chem. Downloaded from www.nrcresearchpress.com by 122.72.124.2 on 09/07/12
For personal use only.

stirring, water (100 mL) was introduced in one portion and the solution became colorless in just a few minutes. Most of the acetone was evaporated and the aqueous solution then saturated with NaCl before extracting with ether. After washing and drying, the product (2.48 g) was unstable so the slightly orange oil was used without further purification for the next step.

From the ^{1}H nmr spectrum, the product was a 1:3 mixture of the two compounds **3***a* and **4***a*. After arduous and costly purification, they were identified as the following: *7-acetoxy-12-methoxy-11,14-dihydroxy-abieta-8,11,13-triene* **3***a*, ^{1}H nmr δ: 0.96 and 1.02 (2s, *gem*-diMe), 1.10, s, Me at C10, 1.35 (d, 6H, Me at C15), 2.16 (s, Me-CO), 3.33 (sept, J = 7 Hz, H-C15), 3.74 (s, Me-O-Ar), 6.09 (m, Ac-O-C*H*), and 7.27 (s, 2H, dis. D_2O, HO at C11 and C14). For ^{13}C nmr, see Table 1. *12-Methoxy-11,14-dihydroxy-abieta-6,8,11-13-tetraene* **4***a*, ^{1}H nmr δ: 0.96 and 1.03 (2s, Me at C4), 1.10 (s, Me at C10), 1.36 and 1.40 (2d, J = 7 Hz, Me at C15), 2.16 (t, 1H, H-C5), 3.34 (sept, J = 7 Hz, H-C15), 3.73 (s, Me-O-Ar), 6.01 (dd, J = 9.6 and 3 Hz, H-C6), 6.62 (dd, J = 9.6 and 3 Hz, H-C7) and 7.26 (s, 2H, dis. D_2O, HO at C11 and C14).

Methylation of mixture containing **3***a and* **4**a

The mixture from the preceding reaction (2.48 g, **3***a* and **4***a*) was dissolved in acetone (100 mL), solid potassium carbonate (15.6 g) was added, and the mixture was heated at reflux while dimethyl sulfate (15 mL) was slowly introduced. Refluxing was continued until the starting material was no longer detected by tlc (24–48 h). The mixture was then filtered and evaporated to give an oil, which was chromatographed over silica gel (petroleum ether/EtOAc 99:1). Only one product was isolated as a colorless oil (**4***c*, 1.924 g; 82% from **1***b*), which eventually crystallized, mp 92–93°C (from MeOH), *11,12-14-trimethoxy-abieta-6,8,11,13-tetraene*; uv: 220(20 325), 271(8980), 295(2920, sh), and 307(1960) nm; ir (film): 3040, 1735, 1625, and 1565 cm^{-1}; ^{1}H nmr δ: 0.97 and 1.04 (2s, Me at C4), 1.11 (s, Me at C10), 1.33 (d, 6H, J = 7 Hz, Me at C15), 2.15 (t, J = 3.2 Hz, H-C5), 3.39 (sept, J = 7 Hz, H-C15), 3.66, 3.75, and 3.80 (3s, Me-O-Ar at C14, C11, and C12 resp.), 5.95 (dd, J = 10 and 3.2 Hz, H-C6), and 6.70 (dd, J = 10 and 3.2 Hz, H-C7); ms m/z: 358(100, M$^+$), 359(29, M$^+$ + 1), 360(10, M$^+$ + 2), 343(13), 315(13), 301(21), and 276(85). *Exact Mass* calcd. for $C_{23}H_{34}O_3$: 358.2508; found (hrms): 358.2502. For ^{13}C nmr, see Table 1.

*Reduction and methylation of 7-acetoxy-*O*-acetylroyleanone* **1**c

Following exactly the same procedure as described for the reduction of **1***b* and the methylation of the product mixture (**3***a* and **4***a*), the *O*-acetyl derivative **1***c* afforded the analogous **4***d*, *12-acetoxy-11,14-dimethoxy-abieta-6,8,11,14-tetraene* in 71% yield, mp 134–135°C (from hexanes); uv: 220 (24 280), 269(11 570), and 305(1650, sh) nm; ir (CCl_4): 3040, 1765, 1650, 1620, 1570, and 1540 cm^{-1}; ^{1}H nmr δ: 0.96 and 1.02 (2s, Me at C4), 1.08 (s, Me at C10), 1.32 and 1.33 (2d, J = 7 Hz, Me at C15), 2.19 (t, J = 3.2 Hz, H-C5), 2.31 (s, Me-CO), 3.38 (sept, J = 7 Hz, H-C15), 3.70 and 3.71 (2s, Me-O-Ar), 6.00 (dd, J = 9.8 and 3.2 Hz, H-C6) and 6.71 (dd, J = 9.8 and 3.2 Hz, H-C7); ms m/z: 386(39, M$^+$), 344(68), and 262(100). *Exact Mass* calcd. for $C_{24}H_{34}O_4$: 386.2457; found (hrms): 386.2489. *Anal.* calcd. for $C_{24}H_{34}O_4$: C 74.56, H 8.87; found: C 74.06, H 8.71.

cis-*Dihydroxylation of* **4**c

To a solution of *N*-methylmorpholine-*N*-oxide (81 mg) in water (2 mL), acetone (1 mL), and *tert*-butanol (1 mL) was added a solution of osmium tetroxide (5 mg) in CCl_4 (2 mL). The olefin **4***c* (170 mg) in CCl_4 (2 mL) was then introduced and the mixture stirred at room temperature for 162 h. The crude product was obtained by diluting the reaction mixture with water and ether extraction, and chromatography over silica gel (CCl_4:EtOAc 98.2) afforded the *6α,7α-dihydroxy-11,12,14-trimethoxy-abieta-8,11,13-triene* **5** (62 mg; 35%), mp 200°C (sublimes, from hexanes); ir: 3460–3580, 1685, 1455, and 1240 cm^{-1}; ^{1}H nmr δ: 1.03 (s, Me at C4), 1.31 (s, Me at C10), 1.30 and 1.36 (2d, J = 7 Hz, Me at C15), 1.73 (s, Me at C4), 2.74 (s, 1H, dis. D_2O), 3.30 (sept, J = 7 Hz, H-C15), 3.77, 3.78, and 3.79 (3s, Me-O-Ar), 4.49 (d, 1H, J = 2.7 Hz, H-C6), 4.76 (d, J = 2.7 Hz, H-C7), 5.28 (s, 1H, dis. D_2O); ms m/z: 392 (M$^+$, 47), 289 (10), and 247 (15). For ^{13}C nmr, see Table 1. *Anal.* calcd. for $C_{23}H_{36}O_5$: C 73.81, H 9.81; found: C 73.81, 9.78.

Heating this diol in refluxing benzene containing a catalytic amount of *p*-toluenesulfonic acid gave the ketone **6***a* in quantitative yield. For the characterization of **6***a* see below.

Epoxidation of **4**c *and rearrangement to the ketone* **6**a

To the cooled (0–5°C) solution of olefin **4***c* (250 mg) in chloroform (15 mL) was added *m*-chloroperbenzoic acid (152 mg, 80%), also dissolved in chloroform (12 mL). The mixture was stirred at room temperature until no starting material was detected by tlc (20 h). The excess per-acid and benzoic acid were removed by extraction, but on evaporating the solvent it was clear that several products were present. Thin-layer chromatography, mass spectroscopy, and nmr pointed to the epoxide, the C6 ketone (**6***a*), C6, C7-diols, and the *m*-chlorobenzoate of the latter. All of these could afford the ketone **6***a* so the crude mixture was taken up in benzene and refluxed with *p*-TsOH (25 mg) until only one product was detectable (tlc). The cooled solution was diluted with ether, washed, and dried and evaporation gave an oil that crystallized on standing, *6-oxo-11,12,14-trimethoxy-abieta-8,11,13-triene* **6***a* (237 mg, from methanol), mp 99–101°C; ir (film): 1710 and 1615 cm^{-1}: ^{1}H nmr ($CDCl_3$) δ: 0.95 (s, Me at C4), 1.19 (s, Me at C4), 1.25 and 1.27 (2s, Me at C15), 1.29 (s, Me at C10), 2.53 (d, J = 1.5 Hz, H-C5), 3.22 (dd, J = 21 and 1.5 Hz, Hβ-C7), 3.27 (sept, J = 7 Hz, H-C15), 3.58 (s, Me-O-C11), 3.60 (d, J = 21 Hz, Hα-C7), 3.71 (s, Me-O-C14), and 3.74 (s, Me-O-C12); ^{1}H nmr (benzene-d_6) δ: 1.15 (Me at C4), 1.35 (Me at C10), and 1.45 and 1.49 (2d, J = 7 Hz, Me at C15), 1.60 (Me at C4), 2.38 (d, J = 1 Hz, H-C5), 3.25 (s, Me-O-C11), 3.47 (dd, J = 21 and 1 Hz, Hβ-C7), 3.55 (sept, H-C15), 3.56 (s, Me-O-C14), 3.68 (s, Me-O-C12), and 3.68 (d, J = 21 Hz, Hα-C7); ms m/z: 374 (M$^+$, 100), 359(9), and 331(18). *Anal.* calcd. for $C_{23}H_{34}O_4$: C 73.76, H 9.16; found: C 73.81, H 9.26. For ^{13}C nmr, see Table 1.

Epoxidation of **4**d *and rearrangement of the product to ketone* **6**b

Following exactly the same procedure as described above, the olefin **4***d* afforded the ketone **6***b* (68% yield) as a colorless oil that crystallized very slowly on standing, mp 146–147°C (from petroleum ether); ir (CCl_4): 1775, 1720, 1590, and 1560 cm^{-1}; ^{1}H nmr δ: 1.03 (s, Me at C4), 1.21 (s, Me at C10), 1.32 (d, J = 7 Hz, Me at C15), 1.34 (s, Me at C4), 2.34 (s, Me-CO), 2.59 (br s, H-C5), 3.35 (d, 1H, J = 20 Hz, Hβ-C7), 3.37 (sept, J = 7 Hz, H-C15), 3.70 and 3.75 (2s, Me-O at C14 and C11), and 3.71 (d, 1H, J = 20 Hz, Hα-C7); ms m/z: 402 (M$^+$, 8), 362 (8), 361 (50), 360 (100). *Exact Mass* calcd. for $C_{23}H_{34}O_5$: 402.2406; found (hrms): 402.2364. *Anal.* calcd. for $C_{23}H_{34}O_5$: C 71.60, H 8.87; found: C 71.84, H 8.40.

Attempted preparations of ketone **6**c

(a) By demethylation of **6**a *with boron trichloride–methyl sulfide*

The ketone (200 mg) was dissolved in dichloromethane (10 L) and, after cooling the mixture to 0°C, boron trichloride–methyl sulfide (10 mL of 0.1 M in CH_2Cl_2) was added, diluted with more CH_2Cl_2 (10 mL). All solvents were rigorously dried and the experiment was conducted under dried nitrogen. The mixture was refluxed for 24 h and, after the usual work-up, chromatography gave some starting material (71 mg; 27%) and two diosphenols **7***a* and **7***b*.

7-Oxo-12-methoxy-6,11,14-trihydroxy-abieta-5,8,11-13-tetraene (**7***a*, 33 mg; 13%): ir (CCl_4): 3500, 3380, 1720, 1610, and 1590 cm^{-1}; uv: 266(4130), 282(3050), 328(1960), and 402(2200) nm; ^{1}H nmr δ: 1.40 and 1.42 (2d, J = 7 Hz, Me at C15), 1.44 (s, 6H, Me at C4 and at C10), 1.65 (s, Me at C4), 3.36 (sept, J = 7 Hz, H-C15), 3.81 (s, 3H, Me-O-C12), 5.76 and 6.94 (2s, dis. D_2O, Ar-OH); ms m/z: 360(M$^+$, 47) and 345(100).

7-Oxo-11,12-dimethoxy-6,14-dihydroxy-abieta-5,8,11,13-tetraene (**7***b*, 19 mg; 7%): ^{1}H nmr δ: 1.34 and 1.35 (2d, J = 7 Hz, Me at C15), 1.44 (s, 6H, Me at C4 and C10), 1.45 (br s, dis. D_2O, HO-C6), 1.62 (s, Me at C4), 3.51 (sept, J = 7 Hz, H-C15), 3.82 and 3.83 (Me-O at C11 and C12), 6.93 (s, dis. D_2O, HO-C14).

(b) By hydrolysis of the acetyl derivative **6**b

To the acetyl compound **6***b* (85 mg) in methanol (15 mL) was added

aqueous sodium hydroxide (1 N, 5 mL) and the mixture was stirred at room temperature for 20 h. More water was then added, most of the methanol removed under vacuum, and the product obtained by ether extraction was chromatographed, affording two diosphenols (**7***c* and **7***d*) and a larger unidentified acid fraction (61 mg).

7-Oxo-11,14-dimethoxy-6,12-dihydroxy-abieta-5,8,11-13-tetraene(**7***c*, 25 mg; 32%), mp 207–209°C (pale yellow powder, from ether); ^{1}H nmr δ: 1.38 and 1.39 (2d, J = 7 Hz, Me at C15), 1.45 and 1.46 (2s, Me at C4 and C10), 1.67 (s, Me at C4), 3.41 (sept, J = 7 Hz, H-C15), 3.77 and 3.81 (Me-O at C14 and C11), 5.97 and 7.44 (2s, dis. D_2O, HO at C6 and C12); ms m/z: 374 (M^+, 58), 359(27), 331(39), 306(20), and 305(100). *Exact Mass* calcd. for $C_{22}H_{30}O_5$: 374.2093; found: 374.2064.

7-Oxo-11-methoxy-6,12-14-trihydroxy-abieta-5,8,11-13-tetraene (**7***d*, 8 mg; 11%), ^{1}H nmr δ: 1.40 and 1.42 (2d, J = 7 Hz, Me at C15), 1.44 (s, 6H, Me at C4 and C10), 1.65 (s, Me at C4), 3.35 (sept, J = 7 Hz, H-C15), 3.81 (s, Me-O-C11), and 5.75 and 6.93 (2s, dis. D_2O).

Hydride reduction of **6**b *(formation of alcohol 8)*

The acetyl derivative **6***b* (174 mg) in anhydrous ether was treated with lithium aluminium hydride (61 mg, added in small portions) and stirring continued at room temperature for 3 h. The excess hydride was decomposed by the cautious addition of water (20 mL) and the product recovered by ether extraction was crystallized from hexane affording the *11,14-dimethoxy-6*β*, 12-dihydroxy-abieta-8,11,13-triene* **8** (121 mg; 77%), mp 169–170°C (from hexane); ir ($CHCl_3$): 3600, 3520, 1600, and 2460 cm^{-1}; ^{1}H nmr δ: 1.05, 1.27 and 1.71 (3s, Me at C4 and C10 resp.), 1.35 (d, 6H, J = 7 Hz, Me at C15), 2.83 (dd, J = 17.6 and 4.3 Hz, Hα-C7), 3.08 (dt, J = 17.6 and 2 Hz, Hβ-C7), 3.35 (sept, J = 7 Hz, Hα-C15), 3.67 and 3.75 (2s, Me-O at C14 and C11), 4.69 (m, H-C6) and 5.76 (s, dis. D_2O, HO-C12); ms m/z: 362 (M^+, 100), 347(9), 330(17), and 329(79). *Exact Mass* calcd. for $C_{22}H_{34}O_4$: 362.2457; found(hrms): 362.2451. For ^{13}C nmr, see Table 1.

Jones oxidation of alcohol 8

(a) Formation of 6-oxoroyleanone methyl ether **9**

The alcohol **8** (33 mg) was dissolved in acetone (2 mL) and the solution cooled to 0°C. Freshly prepared Jones reagent (8 drops), also cooled to 0°C, was added and the mixture stirred for 30 min at 0°C and then diluted with saturated brine (20 mL). Ether extraction and chromatography afforded an orange oil, *6-oxoroyleanone methyl ether* **9** (22 mg; 70%); ir ($CHCl_3$): 1725, 1660, 1645, and 1600 cm^{-1}; ^{1}H nmr δ: 1.01 (s, Me at C4), 1.18 and 1.21 (2d, J = 7 Hz, Me at C15), 1.26 (s, Me at C4), 1.31 (s, Me at C10), 2.41 (br s, width at half height 3.4 Hz, H-C5), 3.07 (dd, J = 22 and 1.3 Hz, Hα-C7), 3.19 (sept, J = 7 Hz, H-C15), 3.36 (d, J = 22 Hz, Hβ-C7), and 3.92 (s, Me-O-C12). For ^{13}C nmr, see Table 1. This product was unstable at room temperature.

(b) Shorter oxidation time, formation of ketone **6**c

The alcohol (33 mg) was oxidized by exactly the same procedure (above) but the product was isolated after 30 s at 0°C. Chromatography gave some 6-oxoroyleanone methyl ether **9** (9 mg; 28%) and *6-oxo-11,14-dimethoxy-12-hydroxy-abieta-8,11,13-triene* **6***c* (13 mg; 40%), mp 175–178°C (from petroleum ether); uv: 287 (1390) nm; ir: 3500, 1590, and 1435 cm^{-1}; ^{1}H nmr δ: 1.03 and 1.27 (2s, Me at C4), 1.36 (s, Me at C10), 1.35 (d, 6H, J = 7 Hz, Me at C15). 2.64 (br. s, H-C5), 3.33 (dd, J = 20.5 and 1.46 Hz, Hα-C7), 3.34 (sept, J = 7 Hz, H-C15), 3.66 (d, J = 20.5 Hz, Hβ-C7), 3.68 and 3.77 (2s, Me-O and C14 and C11), and 5.73 (s, dis. D_2O, HO-C12); ms m/z: 360(M^+, 100), 345(11), and 317(22). *Exact Mass* calcd. for $C_{22}H_{32}O_4$: 360.2301; found (hrms): 360.2334.

Acknowledgments

We thank the Natural Sciences and Engineering Research Council of Canada and the Ministère de l'éducation du Québec (F.C.A.R.) for operating and equipment grants. A graduate bursary from the Fonds J. A. Vincent (Université Laval) is also warmly acknowledged. The gift of the acetoxyroyleanone by Dr. O. E. Edwards was much appreciated.

1. O. E. Edwards, G. Feniak, and M. Los. Can. J. Chem. **40**, 1540 (1962).
2. R. H. Burnell, M. Jean, and D. Poirier. Can. J. Chem. **65**, 775 (1987), and references cited therein.
3. F. Marletti, F. Dell Monoche, G. B. Marini-Bettolo, M. Do Carmo, M. De Aranzo, M. De Salete, B. Cavalconit, I. L. D'Alburquerque, and O. Gonzalves de Lima. Gazz, Chim. Ital. **106**, 119 (1976).
4. F. M. Hauser and S. Prasanna. Synthesis, 621 (1980).
5. P. G. Williard and B. F. Craig. Tetrahedron Lett. **21**, 3731 (1980).
6. *(a)* S. Marceau, M. Jean, and R. H. Burnell. Can. J. Chem. **66**, 227 (1988); *(b)* G. M. Strunz, Chao-Mei Yu, and A. Salonius. Submitted for publication.
7. P. Rüedi and C. H. Eugster. Helv. Chim. Acta, **64**, 2219 (1981).

Can. J. Chem. Downloaded from www.nrcresearchpress.com by 122.72.124.2 on 09/07/12
For personal use only.

Protium–deuterium exchange of substituted pyridines in neutral D_2O at elevated temperatures

NICK HENRY WERSTIUK[1] AND CHEN JU[2]

Department of Chemistry, McMaster University, Hamilton, Ont., Canada L8S 4M1

Received May 14, 1988

NICK HENRY WERSTIUK and CHEN JU. Can. J. Chem. **67**, 5 (1989).

H–D exchange of a series of pyridines **1**–**15**, 10*H*-pyridino[3,2-*b*][1,4]benzothiazine (**16**), phenothiazine (**17**), and aniline has been carried out in neutral D_2O at elevated temperatures. The substrates undergo selective exchange and are generally isolated in good yield. Cyanopyridines **4**, **5**, and **6** hydrolyze readily in D_2O at elevated temperatures, and the resultant carboxylic acids decarboxylate. This reaction provides a convenient one-step route to selectively labelled pyridines. Possible mechanisms of exchange are presented.

Key words: protium–deuterium exchange, substituted pyridines, temperature effect

NICK HENRY WERSTIUK et CHEN JU. Can. J. Chem. **67**, 5 (1989).

Opérant dans du D_2O, à des températures élevées, on a réalisé l'échange H–D sur une série de pyridines (**1**–**15**), sur la 10*H*-pyridino[3,2-*b*][1,4]benzothiazine (**16**), sur la phénothiazine (**17**) ainsi que sur l'aniline. Les substrats subissent un échange sélectif et ils sont généralement isolés avec de bons rendements. Dans ces conditions, les cyanopyridines **4**, **5** et **6** s'hydrolysent facilement et les acides carboxyliques qui en résultent se décarboxylent. Cette réaction fournit une route en une étape conduisant à des pyridines marquées d'une façon sélective. On présente des mécanismes possibles pour ces échanges.

Mots clés : échange protium–deutérium, pyridines substituées, effet de température

[Traduit par la revue]

Introduction

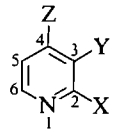
There have been many studies of acid- and base-catalyzed hydrogen isotope exchange of heteroaromatics in the past decade (1–3). However, it is apparent that no studies designed to detail the scope and limitations of exchange of aromatic compounds in neutral D_2O at elevated temperatures have been undertaken although some papers on this subject have been published (4–7).

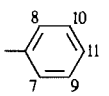
As an extension of our research on hydrogen-isotope exchange of heteroaromatic compounds in neutral D_2O at elevated temperatures (8), we undertook a study of the H–D exchange of an extensive series of pyridine derivatives **1**–**16**, phenothiazine (**17**), and aniline to begin to detail the scope and limitations of this potentially useful labelling method; the results are documented in this publication. While **1**–**3** and **8**–**17** undergo selective H–D exchange and generally can be isolated in good yield, cyanopyridines **4**, **5**, and **6** undergo hydrolysis in D_2O even at 170°C and the resultant carboxylic acids decarboxylate; this provides a useful one-step route to hydrogen-isotope-labelled pyridines. Pyridineacetonitrile (**7**) also undergoes hydrolysis and the acid decarboxylates, but can be labelled at the methylene group under mild conditions, as can 2-pyridinemethanol (**8**). Possible mechanisms of H–D exchange of the substrates are presented.

Results and discussion

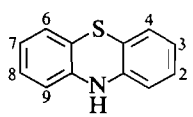
H–D exchange of phenylpyridines

As shown in Table 1, phenylpyridines **1**, **2**, and **3** can be selectively labelled by heating the compounds in D_2O at elevated temperatures. While the pK_as of 2-, 3-, and 4-phenylpyridine are 4.55, 4.85, and 5.83, respectively (9), the basicities do not significantly affect the rate of H–D exchange,

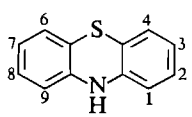




1 X = Ph; Y = H; Z = H
2 X = H; Y = Ph; Z = H
3 X = H; Y = H; Z = Ph
4 X = CN; Y = H; Z = H
5 X = H; Y = CN; Z = H
6 X = H; Y = H; Z = CN
7 X = CH_2CN; Y = H; Z = H
8 X = CH_2OH; Y = H; Z = H
9 X = H; Y = Ch_2OH; Z = H
10 X = OH; Y = H; Z = H
11 X = SH; Y = H; Z = H
12 X = $NHCH_3$; Y = H; Z = H
13 X = SH; Y = OH; Z = H
14 X = NH_2; Y = OH; Z = H
15 X = H; Y = H; Z = pyrrodilinyl



16



17

[1]Author to whom correspondence may be addressed.
[2]Visiting Scholar, Xian Modern Chemistry Research Institute, People's Republic of China.

Can. J. Chem. Downloaded from www.nrcresearchpress.com by 122.72.124.2 on 09/07/12
For personal use only.

TABLE 1. Hydrogen–deuterium exchange of pyridines

Entry	Substrate[a]	Conditions	Medium	Percent exchange C2	C3	C4	C5	C6	Other sites	D atoms incorporated[c]
1	2-Phenylpyridine	250°C, 48 h	D_2O		4	3	3	95	[b]	1.14
2		300°C, 62 h	D_2O		64	64	74	95	7,8(4) 9,10(1)	3.18
3	3-Phenylpyridine	250°C, 48 h	D_2O	95		10	6	95	[b]	2.02
4		300°C, 62 h	D_2O	95		95	95	95	7,8(4) 9,10(4)	3.95
5	4-Phenylpyridine	250°C, 48 h	D_2O	95	10		10	95	[b]	2.27
6		300°C, 62 h	D_2O	95	95		95	95	7,8(1) 9,10,11(4)	3.93
7		250°C, 24 h	1% w/v DCl–D_2O	42				42	[b]	0.85
8		300°C, 24 h	DCl–D_2O	95	[d]		[d]	95	7,8(28) 3,5,9,10(17) 11(24)	3.46
9		250°C, 24 h	2% w/v DCl–D_2O	5	1		1	5	7,8(14) 9,10(3)11(19)	0.63
10	Pyridine	300°C, 62 h	D_2O	95	95	95	95	95		4.94

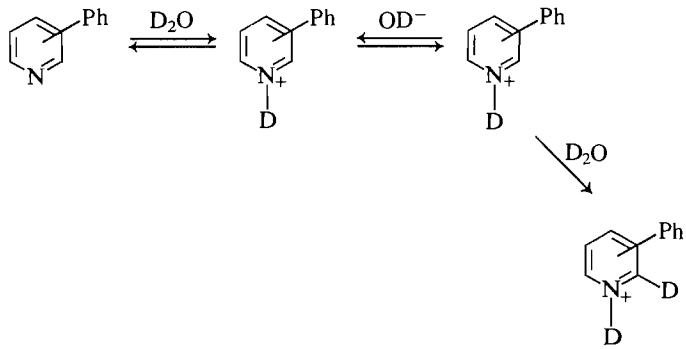
[a]The recovered yields of the deuterated substrates were over 80%.
[b]Exchange at C7, C8, C9, C10, and C11 is <1%.
[c]In excess of natural abundance.
[d]The signals due to the deuterons at C3, C5, C9, C10, and C11 overlap.

as shown by the data in Table 1 (entries 1–6). The mechanism of H–D exchange involves deprotonation of the pyridinium ion by deuteroxide ion to give an ylide, which is deuterated as shown in Scheme 1 (4, 5). The relative rates of exchange at C2(6), C3, and C4 are in accord with the relative stabilities of the 1,2-, 1,3-, and 1,4-ylides (6, 7). In 2% DCl–D_2O solution, the pyridinium ion is the predominant species but the OD^- concentration is low. Consequently, exchange of the pyridine ring is very slow (entry 9 of Table 1). Under these conditions H–D exchange of the phenyl rings occurs by electrophilic substitution with the expected *ortho* and *para* selectivity. In 1% acid at 250°C, only exchange α to nitrogen is observed although at 300°C exchange of the phenyl ring occurs as well (entries 7 and 8, Table 1). Back exchange in H_2O will provide a route to other specifically deuterium-labelled derivatives of **1**, **2**, and **3**. It is interesting to note also that pyridine can be prelabelled in D_2I at 300°C (entry 10).

The H–D exchange studies in D_2O establish that it will be possible to tritiate phenylpyridines by using tritiated water of the appropriate activity; at low levels of incorporation, the location of the tritium can be inferred from the distribution of deuterium obtained in D_2O.

H–D exchange of cyanopyridines

H–D exchange of cyanopyridines **4**, **5**, and **6** in D_2O is more complicated due to hydrolysis of the cyano group, which occurs readily even at 170°C and which yields the corresponding pyridine carboxylic acid amides and acids; pyridine is produced by decarboxylation of the pyridine carboxylic acids (10). Since the basicities of the 2-, 3-, and 4-cyanopyridines are lower than the basicity of pyridine,[3] hydrolysis competes with exchange. Furthermore, picolinic acid obtained from 2-cyanopyridine decarboxylates before exchange of the pyridine ring occurs to a significant extent. Therefore, direct deuterium labelling of cyanopyridines and picolinic acid is not possible in neutral D_2O. However, hydrolysis of **4**, **5**, and **6** in D_2O followed by decarboxylation of the acid provides a useful one-step route to labelled pyridines (Table 2). When the corresponding acids are used as the substrates, several washings with D_2O are required to exchange the hydroxyl hydrogen (13). Figure 1 shows the 90-MHz ^1H nmr spectra of the deuterium-labelled pyridines obtained from **4** (entry 2, Table 2), **5** (entry 4), **6** (entry 7), and from exchange of pyridine at 260°C (entry 10, Table 2). The values in parentheses indicate the degree of exchange determined by a combination of the mass spectrometry and electronic integration of the nmr signals. We estimate the error to be ±5%. Since nicotinic acid undergoes decarboxylation more slowly than picolinic acid and isonicotinic acid, exchange of 3-cyanopyridine in D_2O (or THO) (entry 4, Table 2) is a useful route to nicotinic acid deuterated (tritiated) at C4 and C5 as well as at C2 and C6.



SCHEME 1

The facile hydrolysis of **4** and **6** — it is interesting to note that **5** is much less reactive than **4** and **6** — is most likely due to the fact that protonation of the pyridine at nitrogen activates the nitrile to nucleophilic attack by H_2O.

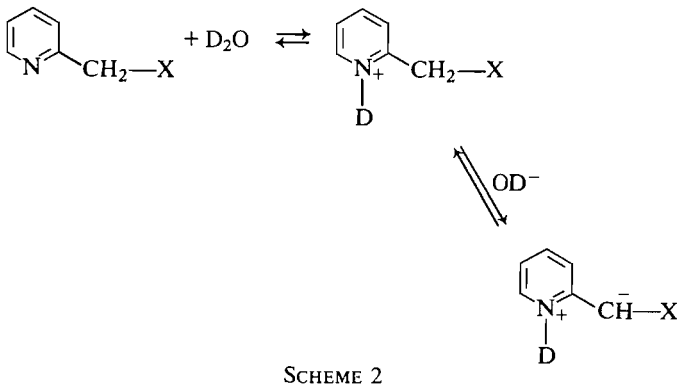
[3]The pK_as of pertinent pyridine derivatives are as follows: picolinic acid, 5.37; pyridine, 5.25; isonicotinic acid, 4.89; nicotinic acid, 4.73; 2-cyanopyridine, −0.26 (11). The order of basicity of other pyridine derivatives is 4Ph > H > 3Ph > 4CN > 3CN > 2Ph > 2CN (12).

Can. J. Chem. Downloaded from www.nrcresearchpress.com by 122.72.124.2 on 09/07/12
For personal use only.

TABLE 2. H–D exchange of cyanopyridines and hydrolysis products in D_2O

Entry	Substrate	Conditions	Yield of products (%)			Percent exchange					D atoms incorporated
			Cyanopyridine	Pyridine[a]	Amide/acid	C2	C3	C4	C5	C6	
1	2-Cyanopyridine	170°C, 48 h	8				3		4	4	0.11
					73[c]						0.08[d]
2		260°C, 25 h		98		95	10	7	10	95	2.27
					4[b,c]						
3	3-Cyanopyridine	170°C, 48 h	73	trace		89		24	19	34	1.66
					46						0.58[d]
4		260°C, 25 h		28		95	91[f]	15	16	95	3.15
					86[b]	95		24	13	95	2.45
5		285°C, 48 h		85		95	95[f]	44	47	95	3.87
					6[e]						2.71[d]
6	4-Cyanopyridine	170°C, 48 h	9			41	27		27	41	1.37
					94[b]						1.10[d]
7		260°C, 48 h		26		95	21	92	21	95	3.32
					98[b]	95	18		18	95	2.35[d]
8		285°C, 48 h		62		95	62	95	62	95	4.01
					15[g]						4.62[d]
9	Pyridine	200°C, 24 h		75		15				15	0.30
10	Pyridine	260°C, 48 h		75		95	13	14	13	95	2.38

[a]The yield of pyridine was determined by analytical gc by using an internal standard.
[b]The yield was over 100% because the acid and amide contained water of hydration.
[c]The yield was estimated from the ^1H nmr.
[d]Determined for a mixture of acid and amide.
[e]The nmr spectra not obtained.
[f]In calculating the degree of deuteration at C3 from the ^1H nmr, we assumed that 2-, 3-, 6- and 2-, 3-, 4-, 6-sites were equilibrated with the deuterium pool (95% exchange).
[g]The product was intractable.



SCHEME 2

H–D exchange of 2-pyridineacetonitrile and pyridinemethanol

The methylene hydrogens of 2-pyridineacetonitrile (**7**) are easily exchanged in D_2O at 100°C (entry 1, Table 3). At 180°C, hydrolysis yields the amide and the acid, which decarboxylates to picoline. At 150°C after 24 h, **7** gives 28% picoline, 28% amide/acid, and 25% deuterated 2-pyridineacetonitrile; at 200°C after 24 h, the main product is picoline. While we find that **7** is decyanated readily in water even at 150°C, Van der Plas and Jongejan (14), in reporting on their studies on the decyanation of cyanomethyl derivatives of aza-aromatic compounds with hydrazine, stated that **7** yields only a trace of picoline at 210°C after 5 h in aqueous alkaline solution. The authors concluded that this demonstrated that decyanation of the nitriles studied did not proceed via hydrolysis to the acid followed by decarboxylation. Obviously, in their case hydrolysis occurs, but decarboxylation of the carboxylate anion is slow. This is so because at high pH the equilibrium concentration of the pyridinium ion required for ylide formation and facile decarboxylation is very low.

Like **7**, 2-pyridinemethanol (**8**) undergoes H–D exchange at the methylene group, albeit more slowly than **7** (entry 2, Table 3). Exchange at C6 occurs at a comparable rate to exchange of the methylene, in keeping with the results of our study on picolines (8). Exchange of **7** and **8** most likely proceeds via a 1,3-ylide as shown in Scheme 2. In the case of 3-pyridinemethanol (**9**), where neutralization of charge is not possible upon deprotonation, a higher temperature is required to exchange the hydrogens of the methylene group (entry 4, Table 3); at 200°C polymerization occurs. This provides support for the proposed mechanism of exchange of **7** and **8**.

H–D exchange of 2-hydroxy-, 2-mercapto-, 2-N-methylamino-pyridine, and 4-pyrrolidinopyridine

As shown in entries 5–7 and 8–10 of Table 3, 2-hydroxypyridine (**10**) and 2-mercaptopyridine (**11**) undergo exchange selectively at C3, C5, and C6. It has been reported that **10** exists predominantly in the lactam form in aqueous solution, and as the lactim in cyclohexane (Scheme 3). Analysis of the ^1H nmr spectrum of **10** in D_2O established that only the lactam form is present, in keeping with the results of the previous study (15). The sulfur analogue **11** also exists in one form in D_2O, according to its 500-MHz ^1H nmr spectrum. To account for the selectivity (C3, C5, and C6), we propose that exchange at C6 occurs via an ylide involving the lactim form as shown in Scheme 1, and exchange at C3 and C5 occurs via the pyridinolate and thiopyridinolate ions although the lactam[4] and lactim forms can undergo H–D exchange directly by electrophilic substitution. In the case of 2-*N*-methylaminopyridine

[4]A referee has suggested that **10** and **11** undergo exchange at C3 and C5 via the lactam forms by deuteration–deprotonation of the enamine subunits.

Can. J. Chem. Downloaded from www.nrcresearchpress.com by 122.72.124.2 on 09/07/12
For personal use only.

Can. J. Chem. Downloaded from www.nrcresearchpress.com by 122.72.124.2 on 09/07/12
For personal use only.

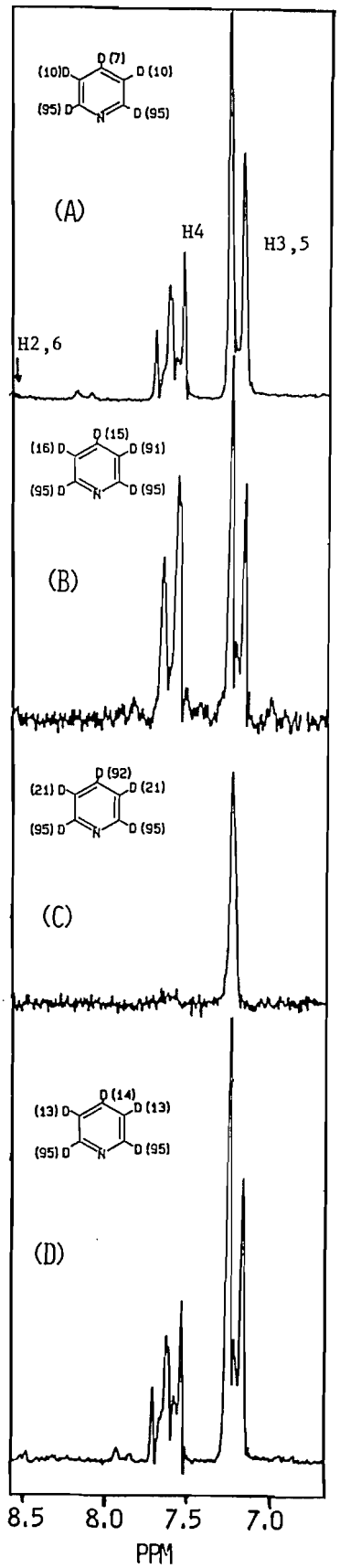


FIG. 1. The 90-MHz ^{1}H nmr spectra of (A) deuterated pyridine obtained from 2-cyanopyridine at 260°C (entry 2, Table 2); (B) pyridine obtained from 3-cyanopyridine at 260°C (entry 4, Table 2); (C) pyridine obtained from 4-cyanopyridine at 260°C (entry 7, Table 2); (D) deuterated pyridine obtained from exchange at 260°C (entry 10, Table 2).

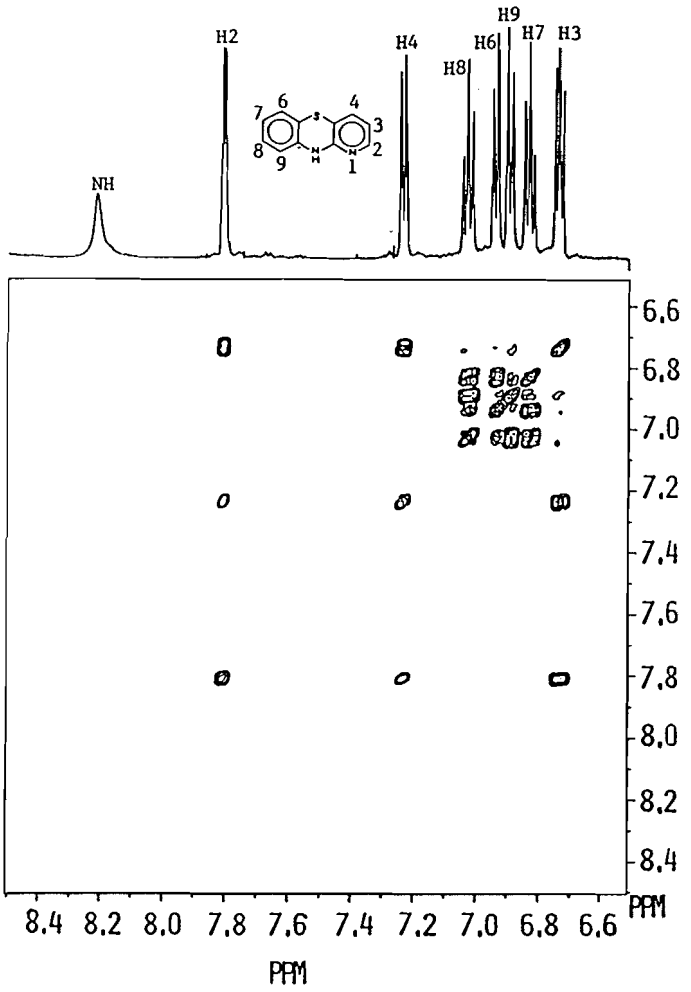
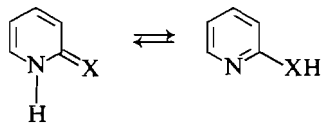


FIG. 2. 2D nuclear proton correlation (COSY) spectrum of **16**.

(**12**), exchange occurs much more slowly at C3 and C5 (entries 11–13, Table 3) than at C3 and C5 of **10** and **11**. This is due to the much lower acidity of the -$NHCH_3$ group and is in keeping with our proposal that **10** and **11** exchange at C3 and C5 via deuteration of the oxy and thio anions, respectively. It is interesting to note that H–D exchange of 2-mercapto- and 2-amino-3-hydroxypyridine (**13** and **14**) *ortho* and *para* to the hydroxy group occurs faster than exchange *para* to the mercapto (or amino) group.

It is noteworthy that hydrogens at C3 and C5 of the pyridine ring of 4-pyrrolidinopyridine (**15**) exchange faster (entries 17 and 18, Table 3) than the corresponding hydrogens of pyridine (entries 23 and 26, Table 3). When the data in entries 17 and 24 of Table 3 are compared, it also appears that exchange occurs more readily at C2 and C6 of **15** than in pyridine. When pyridine is heated with an equimolar amount of pyrrolidine, there is no enhancement of exchange (entry 24, Table 3). Consequently, the pyrrolidine group at C4 of **15** can accelerate exchange at C2, C3, C5, and C6 by increasing the basicity of the pyridine; this results in an increase of the concentration of the pyridinium ion. It is also possible that H3 and H5 are exchanged by electro-



SCHEME 3

TABLE 3. H–D exchange of pyridines and aniline in D_2O

Entry	Substrate[a]	Conditions	Percent exchange C2	C3	C4	C5	C6	Other sites	D atoms incorporated[b]
1	7	100°C, 24 h					5	CH_2(93)	1.91
2	8	175°C, 24 h			7		7	CH_2(41)	0.97
3		200°C, 48 h					64	CH_2(86)	2.35
4	9	200°C, 48 h	72	6			72	CH_2(9)	1.68
5	10	200°C, 24 h		6		6	18		0.30
6		240°C, 24 h		27		40	80		1.47
7		260°C, 24 h		96	11	96	96		2.99
8	11	220°C, 24 h		25		49			0.7[c]
9		240°C, 24 h		38		54	5		1.0[c]
10		260°C, 24 h		93		95	32		2.2[c]
11	12	200°C, 24 h					36		0.36
12		220°C, 24 h				2	72		0.74
13		240°C, 24 h		5		7	92		1.04
14	13	220°C, 24 h			95	2	45		1.60
15		260°C, 24 h			95	36	95		2.43
16	14	195°C, 24 h			82	15	80		1.77
17	15	200°C, 24 h	85	13		13	85		1.96
18		260°C, 24 h	95	95		95	95		3.87
19	16	240°C, 24 h	16	27				C7(33), C9(30)[d]	1.06
20		260°C, 24 h	62	54	6		12	C7(62), C9(56)	2.52
21		285°C, 24 h	99	82	14		5	C7(93), C8(4), C9(87)	3.84
22	17	285°C, 24 h	9	28	9		9	C1, C7, C9(28), C8(9)	1.50
23	Pyridine	200°C, 24 h	15				15		0.30
24		200°C, 24 h	13				13		0.26[e]
25		220°C, 24 h	84				84		1.69
26		240°C, 24 h	>95	17	22	17	95		2.58
27	Aniline	260°C, 25 h	47	3	64	3	47		1.66

[a]The recovered yields were over 80% except in the case of the pyridine.
[b]Determined mass spectrometrically at low ionizing voltage.
[c]Estimated from ^1H and ^2H nmr spectra.
[d]Peaks of D6 and D9 overlap.
[e]Equimolar in pyrrolidine.

Can. J. Chem. Downloaded from www.nrcresearchpress.com by 122.72.124.2 on 09/07/12
For personal use only.

philic substitution — the pyrrolidine ring is strongly electron donating. That exchange can occur by electrophilic substitution in D_2O at elevated temperatures is established by the fact that aniline (entry 27 of Table 3) undergoes facile exchange at 260°C *ortho* and *para* to the amino group.

*H–D exchange of 10*H*-pyridino[3,2-*b*][1,4]benzothiazine and phenothiazine*

It is remarkable that 10*H*-pyrido[3,2-*b*][1,4]benzothiazine (**16**) undergoes selective H–D exchange in neutral D_2O (entries 19, 20, and 21, Table 3) at C2, C3, C4, C6, C7, C8, and C9. The degree of exchange at each site was determined by mass spectrometry and by ^1H and ^2H nmr spectroscopy. Assignment of the resonances of **16** (Table 4) is based on four parts: (*a*) the coupling constants $J(2,3)$ and $J(3,4)$ of the pyridine ring are different; (*b*) the proton α to the nitrogen of pyridine is downfield of the other resonances; (*c*) while a proton *ortho* to an amino nitrogen is shielded relative to the other protons, a mercapto group causes a downfield shift of this resonance; (*d*) a COSY experiment (Fig. 2) confirmed the coupling relation. The ^1H and ^2H nmr spectra of deuterated **16** (entry 21, Table 3), including the deuterium distribution, are given in Fig. 3. Exchange at C9 and C7, *ortho* and *para* to the amino group, occurs by electrophilic substitution. The ease of substitution at these sites in D_2O is remarkable. That **16** undergoes exchange at C3, which is *para* to N10, faster than pyridine undergoes exchange at C3 indicates that H3 is also exchanged by electrophilic substitution. This selectivity is enhanced in the case of benzothiazine (**17**), which also undergoes H–D exchange (entry 22, Table 3). That **16** undergoes exchange faster than **17** may be simply due to the fact that **16** is more soluble in D_2O than is **17**.

TABLE 4. Chemical shifts and coupling constants of protons of 10*H*-pyrido[3,2-*b*][1,4]benzothiazine

Chemical shifts[a] (ppm)	Coupling constants (Hz)
H2 7.82; H3 6.74; H4 7.24; H6 6.94; H7 6.83; H7 7.03; H9 6.89	$J(2,3)$ 4.93; $J(2,4)$ 1.50; $J(3,4)$ 7.53; $J(6,7)$ 7.59; $J(6,8)$ 1.37; $J(7,8)$ 7.29; $J(7,9)$ 1.24; $J(8,9)$ 8.00

[a]Solvent acetone-d_6, reference TMS.

Conclusions

This study established that a variety of substituted pyridines can be selectively labelled simply by heating the compounds in neutral D_2O at elevated temperatures. While the pyridines exchange via formation of ylides, it is also clear that activated aromatics readily undergo H–D exchange by electrophilic substitution in neutral D_2O at temperatures between 200 and 300°C. It should be possible to prepare the analogous tritiated compounds simply by using tritiated water of the appropriate activity.

Can. J. Chem. Downloaded from www.nrcresearchpress.com by 122.72.124.2 on 09/07/12
For personal use only.

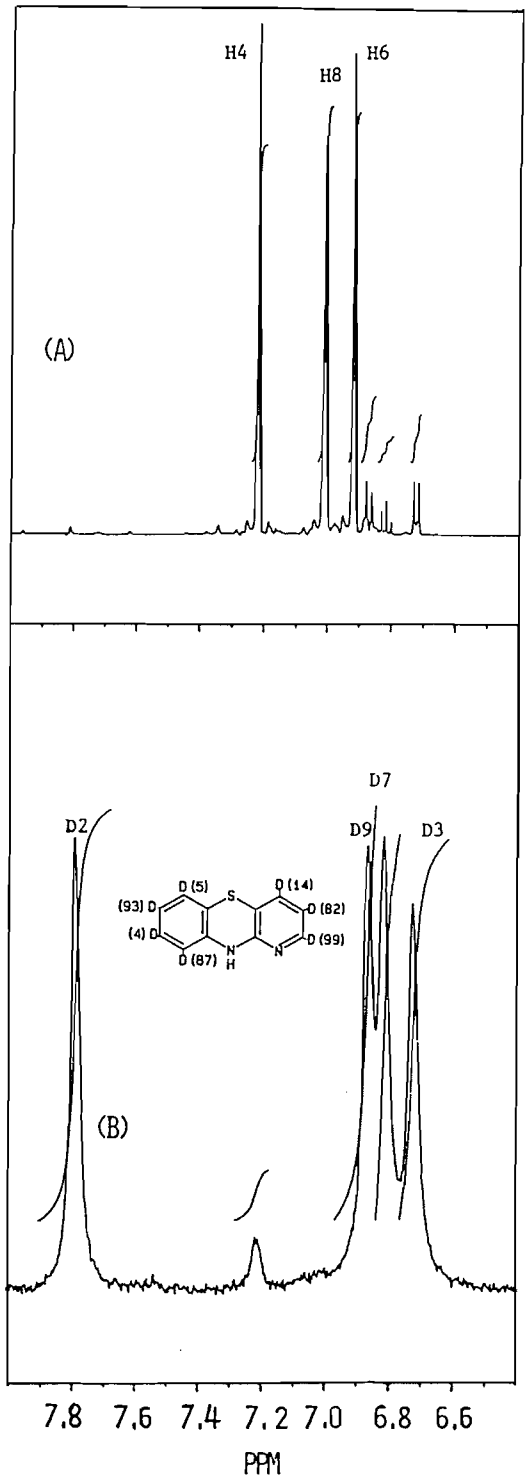


FIG. 3. (A) The 500-MHz ^1H nmr spectrum of deuterated **16** (entry 21, Table 3); (B) 76.8-MHz ^2H nmr spectrum of deuterated **16** (entry 21, Table 3).

Experimental

The reagents (95–98% purity) were obtained from Aldrich Chemical Co. and were used without further purification.

Proton and deuterium magnetic resonance spectra were recorded on Bruker AM 500 (^1H, 500 MHz; ^2H, 76.8 MHz), WM 250 (^1H, 250 MHz; ^2H, 38.4 MHz), and Varian EM 390 spectrometers. CCl_4 was used as nmr solvent for **1**, **2**, **4**, **5**, **6**, **7**, **11**, **12**, **13**, **14**, aniline, and pyridine; CCl_4 and trifluoroacetic acid were used for **3**; D_2O and H_2O were used for pyridinecarboxylic acid and **10**; acetone was used for **14**, **16**, and **17**. Deuterium assay analyses were performed on a VG Micromass 7070 mass spectrometer at low ionization voltage (12–15 eV) and expressed as atoms of deuterium per molecule in excess of natural abundance deuterium. All samples containing OH, SH, or NH were back-exchanged before mass determination.

Analytical gc analyses were performed on a Tracor 560 dual column analytical gas chromatograph equipped with flame ionization. Helium was the carrier gas with a 3% OV-17 column. Deuterated pyridine was isolated by preparative gc using a Varian Associates Aerograph model 700 chromatograph equipped with a 2 m × 6 mm o.d. 20% SE-30 on Chromasorb W column.

In a typical exchange reaction, substrate (0.20 g) was added to D_2O (5 mL) in a 15-mm o.d. medium-walled glass tube. The mixture was degassed via three freeze–pump–thaw cycles and sealed under vacuum. The tube was placed in a 600-mL Parr pressure vessel, which contained water to equalize pressure, and heated at the desired temperature for an appropriate period.

The data in Table 2 were obtained using the following procedure. After the reaction was complete, the substrate was extracted with ether. For reactions carried out at 260°C and 285°C (entries 2, 4, 5, 7, and 8, Table 2), the ether extract was concentrated by distillation and the percent of pyridine was determined by analytical gc using *tert*-butanol as a standard. Pyridine was separated by preparative gc and the deuterium content was determined by mass spectrometry. For reactions at 170°C (entries 1, 3, and 6, Table 2), the ether extract was evaporated to obtain a white solid, which was a mixture of cyanopyridine and pyridinecarboxylic acid and (or) amide. The cyanopyridines were isolated by preparative tlc (silica gel, 2 mm; developing solvent: ether). The D_2O layer that remained after ether extraction was evaporated in a stream of nitrogen with heating. The deuterium content of the acid/amide mixture was determined by mass spectrometry.

Acknowledgement

We thank the Natural Sciences and Engineering Research Council of Canada for financial support.

1. J. ELVIDGE, J. R. JONES, C. O'BRIEN, E. A. EVANS, and H. C. SHEPPARD. Adv. Heterocycl. Chem. **16**, 1 (1974).
2. G. E. CALF and J. L. GARNETT. Adv. Heterocycl. Chem. **15**, 137 (1973).
3. I. F. TUPITSYN, N. N. ZATSEPINA, A. V. KIROVA, YU, L. KAMINSKII, and A. G. IVANENKO. Reakts. Sposobn. Org. Soedin. **10**, 143 (1973).
4. J. A. ZOLTEWICZ and C. L. SMITH. J. Am. Chem. Soc. **89**, 3358 (1967).
5. J. A. ZOLTEWICZ and L. S. HELMICK. J. Am. Chem. Soc. **92**, 7547 (1970).
6. J. A. ZOLTEWICZ, G. M. KAUFFMAN, and C. L. SMITH. J. Am. Chem. Soc. **90**, 5940 (1968).
7. J. A. ZOLTEWICZ and P. E. KANDETZKI. J. Am. Chem. Soc. **93**, 6562 (1971).
8. N. H. WERSTIUK and G. TIMMINS. Can. J. Chem. **59**, 1022 (1981).
9. B. BOUWHUIS and M. J. JANSSAN. Tetrahedron Lett. **3**, 233 (1972).
10. S. B. BOKISOSA and V. A. SORAZEFARINOVA. Akad. Nauk Kaz. SSR Izv. Ser. Khim. **4**, 76 (1985).
11. N. FURUKAWA, K. IIDA, T. KAWAI, S. OGAWA, and S. OAE. Phosphorus Sulfur, **19**, 239 (1984).
12. M. BERTHLOT, J. GAL, C. LAURENCE, and P. MANA. J. Chim. Phys. **81**, 319 (1984).
13. J. A. ZOLTEWICZ, C. L. SMITH, and J. D. MEYER. Tetrahedron, **24**, 2269 (1968).
14. H. C. VAN DER PLAS and H. JONGEJAN. Recl. Trav. Chim. Pays-Bas, **91**, 133 (1972).
15. P. BEAK. Acc. Chem. Res. **10**, 186 (1977).

Investigation of stereoelectronic bond–antibond orbital interactions in 3-halogenated-1-benzoxepins

P. DIONNE AND M. ST-JACQUES[1]

Département de chimie, Université de Montréal, C.P. 6128, Succursale A, Montréal (Qué.), Canada H3C 3J7

Received May 31, 1988

P. DIONNE and M. ST-JACQUES. Can. J. Chem. **67**, 11 (1989).

The conformational properties of the 3-halogenated-1-benzoxepins (compounds **6–9**) have been studied by ^1H and ^{13}C dynamic nuclear magnetic resonance. The results show that for the heavier halogen derivatives (Cl, Br, and I), only two chair forms (C_a and C_e) are observed while for the F substituent, three forms (C_a, C_e, and *TB*) are detected. This is in contrast with the 3-halogenated-1,5-benzodioxepins (**2–5**), which were shown to exist as a mixture of three forms for the heavier halogens (Cl, Br, and I) and show only two forms (C_a and *TB*) for the F substituent. The results for these two systems characterize the conformational effects produced by one and two O—C—C—X vicinal interactions between polar bonds, which shed light on the nature of the intramolecular stereoelectronic σ–σ^* orbital interactions operative in both families of molecules.

Key words: 3-halogenated-1-benzoxepins, conformational properties, nuclear magnetic resonance, stereoelectronic orbital interactions

P. DIONNE et M. ST-JACQUES. Can. J. Chem. **67**, 11 (1989).

Faisant appel à la résonance magnétique nucléaire dynamique du ^1H et du ^{13}C, on a étudié les propriétés conformationnelles des halogéno-3 benzoxépines-1, **6–9**. Les résultats démontrent que, avec les dérivés halogénés de masse élevée (Cl, Br et I), on n'observe que deux formes chaises (C_a et C_e); par ailleurs, avec le fluor comme substituant, on peut détecter les trois formes (C_a, C_e et *BC*). Ce résultat est en opposition avec ceux obtenus avec les halogéno-3 benzodioxépines-1,5 (**2–5**) pour lesquels on a pu mettre en évidence l'existence d'un mélange des trois formes avec les halogènes de masse élevée (Cl, Br et I) et uniquement deux formes (C_a et *BC*) avec le fluor comme substituant. Les résultats obtenus avec ces deux systèmes caractérisent les effets conformationnels qui sont provoqués par une et deux interactions O—C—C—X vicinales entre des liaisons polaires et nous éclairent aussi sur la nature des interactions stéréoélectroniques intramoléculaires des orbitales σ–σ^* qui sont en opération dans ces deux familles de molécules.

Mots clés : halogéno-3 benzoxépines-1, propriétés conformationnelles, résonance magnétique nucléaire, interactions stéréoélectroniques des orbitales

[Traduit par la revue]

Can. J. Chem. Downloaded from www.nrcresearchpress.com by 122.72.124.2 on 09/07/12
For personal use only.

Introduction

In previous publications (1–3), we have shown that conformational analysis of 3-substituted-2,3-dihydro-1,5-benzodioxepins (**1–5**) provides insight into the mechanism of the *gauche* conformational effect (4) between two polar bonds. Whereas studies of this phenomenon in 5-substituted-1,3-dioxanes (5–7) involved only the chair conformation, the twist-boat conformation (*TB*) of the 1,5-benzodioxepin system, being significantly stabilized, was observed for **1–5** together with the equatorial and axial chair forms (C_e and C_a). The variation in the amounts of the three conformers as a function of substituent electronegativity was used advantageously to define the contributing factors to the "*gauche* effect". Thus it has become apparent that the greater flexibility of the seven-membered ring provides a most convenient probe for the experimental investigation of certain aspects of stereoelectronic interactions.

The present work reports the conformational analysis of 3-halogenated-1-benzoxepins (**6–9**). It was designed to investigate the consequence of removing one oxygen atom from the seven-membered ring for which only a single O—C—C—X vicinal interaction between polar bonds remained.

The fact that the parent compound of series **6–10** exists as a single chair (8) form while that of the series **1–5** exists (3) as a mixture of *C* and *TB* suggested different behavior for the two series, so that predictions from one series to the other are not possible. But a comparison of both series should help define the extent to which stereoelectronic stabilization is a factor controlling conformational populations.

Results and spectral analysis

The high-field ^1H and ^{13}C nmr spectra for compounds **6–9** were recorded between 0 and −125°C. For ^1H and ^{13}C spectra, CHF_2Cl was used as polar solvent with some CD_2Cl_2 as locking agent. Less polar solvents used were CF_2Cl_2 with acetone-d_6 for ^1H and CH_3OCH_3 with CD_2Cl_2 for ^{13}C spectra.

The ^1H and ^{13}C nmr spectral analyses of compound **7** (X = Cl) at room temperature were carried out at 300 MHz using a 2D COSY experiment (9) together with a ^{13}C and ^1H nmr Heteronuclear Shift Correlation (HSC) experiment (10).

Figure 1 shows the 2D COSY contour spectrum of **7** in $CDCl_3$. The correlations between coupled protons appear off the diagonal line and the chemical shifts of these protons are obtained from the diagonal line. From recent work by Lachapelle and St-Jacques (8) on 1-benzoxepins, the two most shielded signals at 1.88 and 2.37 ppm can be unambiguously assigned to the H-4 protons. The diagonal peaks 1 and 6 (corresponding to the H-4 protons) each show four correlations. The 2 and 2′ correlation peaks arise from the coupling of the two H-4 protons. Knowing that these protons couple with H-5 and H-3 protons, it is reasonable to say that the most deshielded signal at ~4.32 ppm (correlations 5 and 5′) corresponds to H-3 because of the deshielding effect of the chlorine atom. Thus correlation peaks 3, 3′, 4, and 4′ suggest that the signals at 2.94 and 2.79 ppm correspond to the H-5 protons. Because the H-5 protons couple only with H-4 protons, additional evidence for this last assignment is given by the correlations 9, 9′, 10, and 10′ on the same horizontal line as the 7 and 8 diagonal peaks. Finally, the two last H-2 protons are situated at 3.75 and ~4.32 ppm.

To assign the aliphatic ^{13}C signals of compound **7**, an HSC experiment (10) was carried out at room temperature in $CDCl_3$. Figure 2 shows the ^{13}C and ^1H nmr HSC contour spectrum. For each proton signal there corresponds a correlation peak that ties it to a ^{13}C signal. Thus, the two H-4 signals each show one

[1]Author to whom correspondence may be addressed.

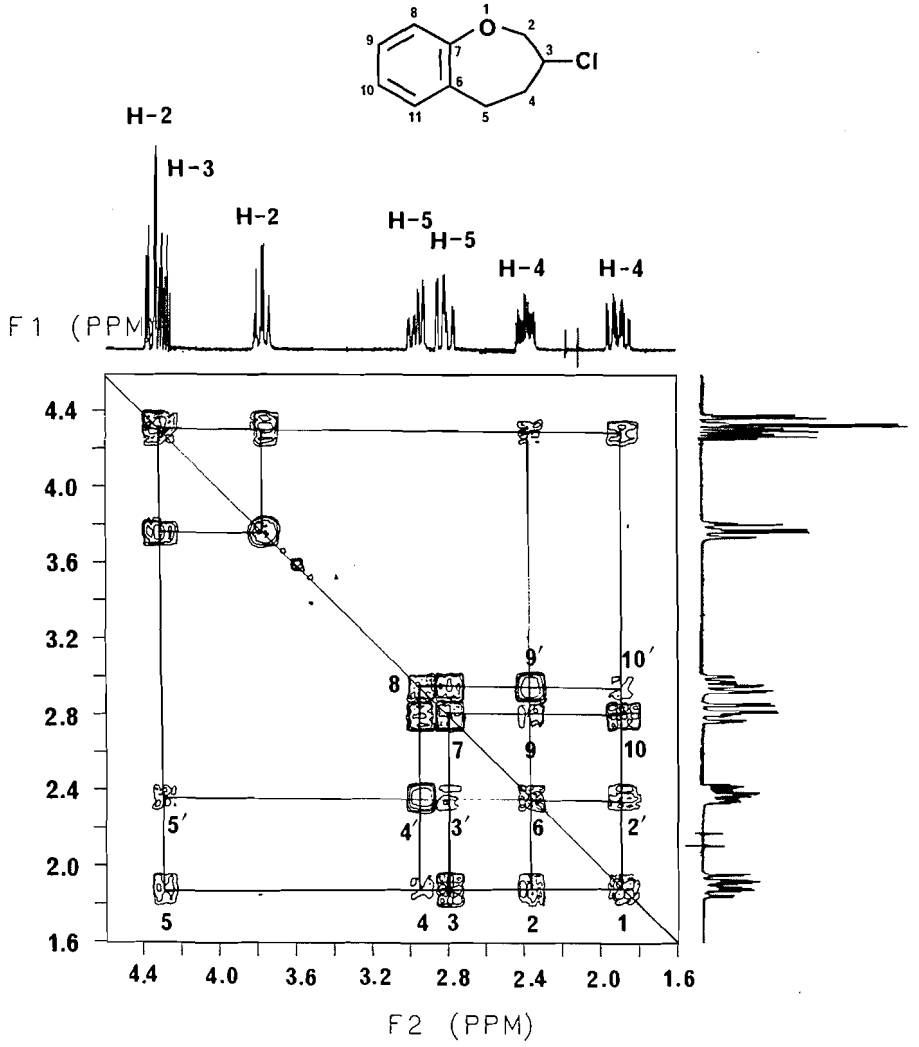


FIG. 1. The 300-MHz two-dimensional ^1H nmr (COSY) spectrum of **7** in $CDCl_3$ at room temperature.

correlation, namely 1 and 2, indicating that the C-4 signal is situated at 35.46 ppm. All carbon signals have been assigned by this procedure and their positions are indicated on Fig. 2.

Figure 3 illustrates the 100.62-MHz ^{13}C nmr spectral modifications observed for **7** (X = Cl) in CHF_2Cl on reducing the temperature. At 0°C, each carbon signal can readily be assigned using the results obtained from the HSC experiment and the aromatic chemical shifts of parent molecules (8). The results are summarized in Table 1.

At low temperature (−120°C), each carbon signal has split into two lines of unequal intensity. The identification of the ring conformation (*C* vs. *TB*) can be made, using the C-6 signals as a probe. For example, at −125°C in CHF_2Cl, the C-6 signals of compound **10** at lower field (137.93 and 137.04 ppm) are characteristic (8) of the C_a and C_e forms respectively, while the upfield signal at 130.54 ppm corresponds to the *TB* conformation. For compound **7** at −120°C, the two C-6 signals at 137.58 and 136.20 ppm are therefore associated with the C_a and C_e forms respectively. These assignments are supported by the analysis of the ^1H spectrum at −120°C described next and by the fact that there is no upfield *TB* signal detected for C-6. Because of the unequal intensity of the C_e and C_a signals, each peak can readily be assigned and the chemical shifts are reported in Table 1. Integration of the C-3 signals indicates that the ratio of the two chair forms is C_a:C_e = 42:58.

In the less polar CH_3OCH_3 solvent, the ^{13}C spectral analysis of compound **7** gave a C_a:C_e ratio of 25:75 at −120°C, as summarized in Table 1.

Figure 4 shows the 400.13-MHz ^1H nmr spectral changes observed for **7** (X = Cl) in CHF_2Cl. At 0°C, the assignment of all signals was readily made using the ^1H 2D COSY spectrum of **7** in $CDCl_3$ and the parameters are reported in Table 2.

Lowering the temperature to −120°C causes spectral modifications and it has been possible to assign the majority of the signals by homonuclear decoupling and integration. From studies on 1-benzoxepin derivatives (8) and 3-halotetrahydropyrans (11), the most shielded quartet at 1.69 ppm corresponds to the 4a-C_e proton (symbol 4a-C_e refers to the axial proton at the 4-position of the C_e conformation, etc...) and the triplet at 1.95 ppm should be due to the 4a-C_a signal. Selective irradiation of the 4a-C_e quartet transforms the triplet at 2.91 ppm to a doublet and changes the appearance of the signals at 4.28 and ~2.53 ppm, indicating that the multiplet at 4.28 ppm corresponds to the 3a-C_e proton. Furthermore, we can assign the signal at 2.91 ppm to the 5a-C_e proton because of its multiplicity (triplet) and the size of the coupling constants

Can. J. Chem. Downloaded from www.nrcresearchpress.com by 122.72.124.2 on 09/07/12
For personal use only.

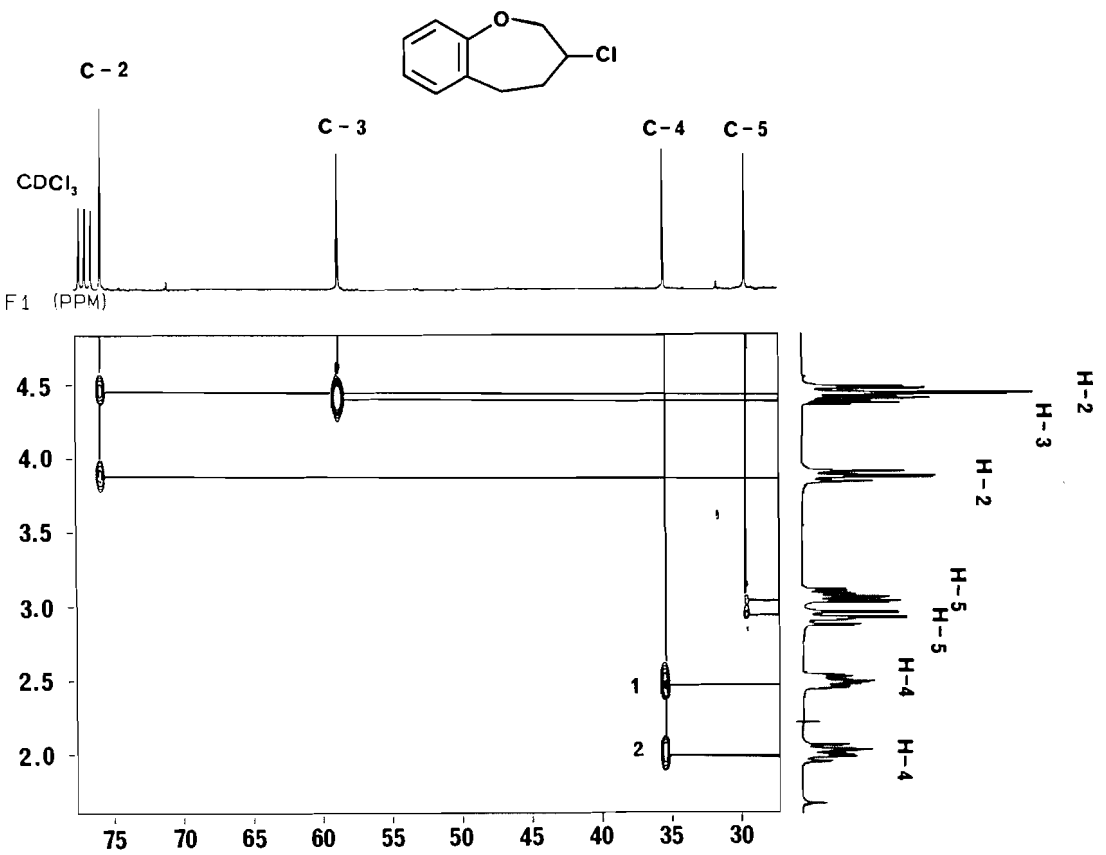


FIG. 2. 2D proton–carbon heteronuclear chemical shift correlation (HSC) spectrum of **7** in $CDCl_3$ at room temperature at 75.431 MHz for ^{13}C with F_1 = 300 MHz in the second dimension.

involved ($^2J_{HH}$ and $^3J_{HH} \approx 13.5$ Hz). Thus, the broadened signal at ~2.53 ppm represents the 4e-C_e proton. A second irradiation of the 5a-C_e proton changes the appearance of the split doublet at 2.77 ppm that corresponds to the 5e-C_e proton. Subsequent irradiations allowed assignment of all signals and the results are summarized in Table 2. Finally, integration of 4a-C_e and 4a-C_a signals indicates that the relative populations are 41:59 for C_a and C_e respectively.

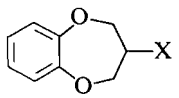
The ^1H nmr spectral analysis of compound **7** (X = Cl) at low temperature in CF_2Cl_2 was carried out to give a C_a:C_e ratio of 23:77.

The ^1H and ^{13}C nmr spectral analyses of compounds **6** (X = F), **8** (X = Br), and **9** (X = I) were carried out similarly. On lowering the temperature two forms (C_a and C_e) were observed for compounds **8** and **9** while for compound **6**, three forms (C_a, C_e, and *TB*) were detected. Furthermore, the spectrum of compound **6** presents additional coupling with the fluorine atom. All pertinent data are reported in Tables 1 and 2.

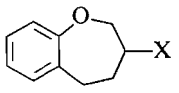
Discussion

The geometry of the TB *form of* **6**

In the previous section, it was shown that two conformations (C_a and C_e) are observed for compounds **7**, **8**, and **9** while a third one (*TB*) is detected for compound **6** (X = F). Two *TB* conformations are possible depending on the orientation of the fluorine atom relative to oxygen, as illustrated by **11** (TB_g), in which the C—F and C—O bonds are *gauche*, and by **12** (TB_a), in which these bonds are *anti*. From the ^{13}C nmr spectrum of **6** at low temperature, only one set of *TB* resonances is detected,



1 X = OCH_3
2 X = F
3 X = Cl
4 X = Br
5 X = I



6 X = F
7 X = Cl
8 X = Br
9 X = I
10 X = OCH_3

indicating either a predominance of one *TB* form or a rapid equilibrium between these two forms. The multiplicity of the *TB* ^1H signals cannot be used to identify one of these forms because they are overlapping with the C_a signals or are too small to be resolved clearly. The ^{13}C chemical shifts of the *TB* carbon signals of compound **6** can be compared with those of compound **10** from which the predominance of the TB_g form has already been suggested (8). It is observed that the difference between the position of each aromatic carbon signal of compounds **6** and **10** is no more than 1 ppm. Furthermore, changing from the polar CHF_2Cl solvent to a less polar CH_3OCH_3 for compound **10** reduces the *TB* (10% to 6%) and C_a (70% to 44%) populations, indicating similar dipole moments for C_a and TB_g in accord with the predominance of the TB_g over the TB_a. For compound **6**, the same trend is observed, suggesting that TB_g also prevails.

Because the amount of this *TB* conformer is small for both **6** and **10**, it does not constitute as useful a probe for stereoelectronic interactions as do the C_a and C_e forms discussed next.

Can. J. Chem. Downloaded from www.nrcresearchpress.com by 122.72.124.2 on 09/07/12
For personal use only.

Can. J. Chem. Downloaded from www.nrcresearchpress.com by 122.72.124.2 on 09/07/12
For personal use only.

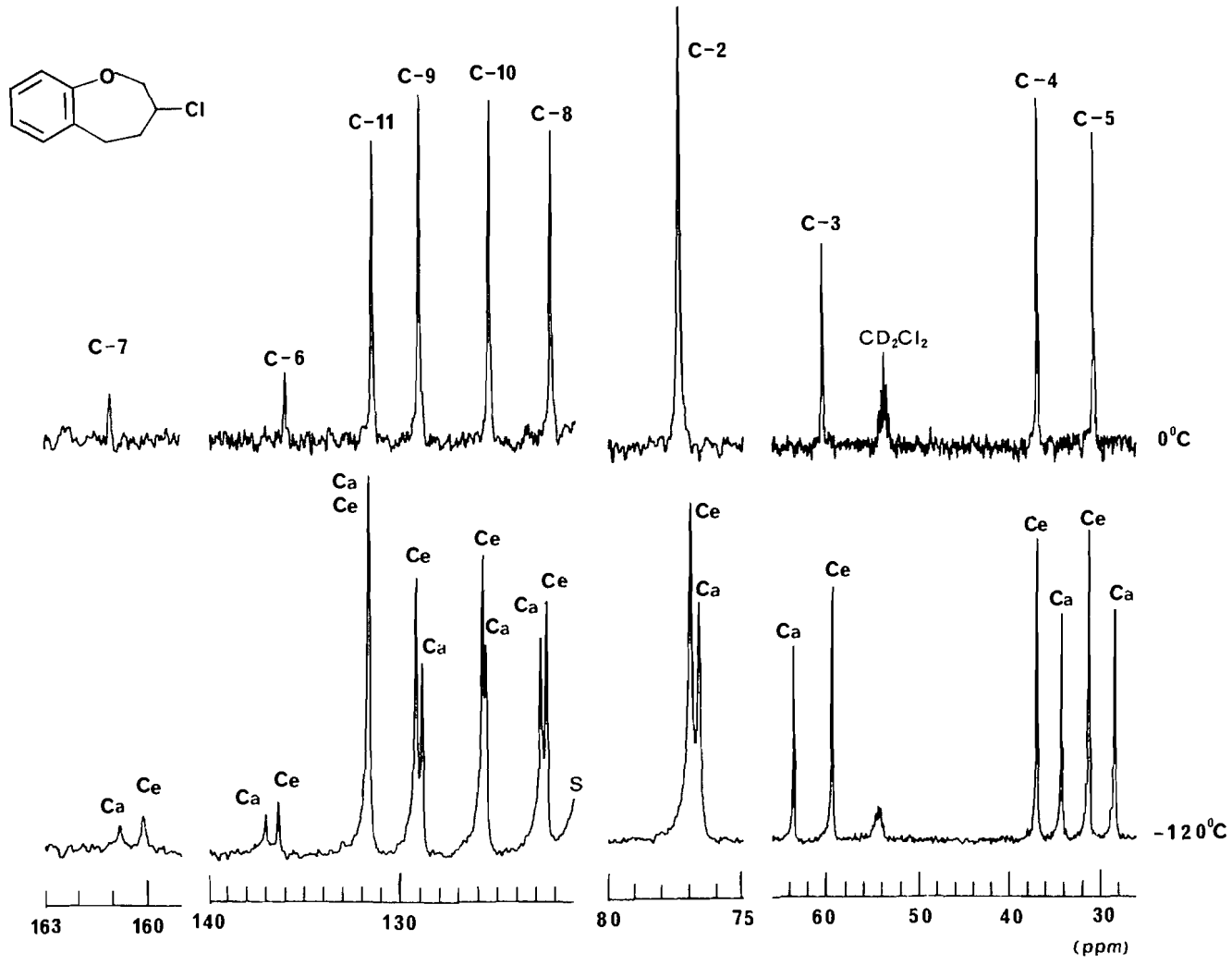
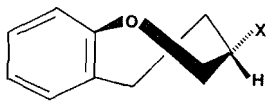
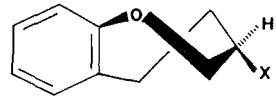


FIG. 3. The 100.62-MHz ^{13}C spectra of **7** in CHF_2Cl at 0°C and −120°C (C_e, equatorial chair; C_a, axial chair).



11

TBg



12

TBa

Stereoelectronic effects

Previous results (3) suggest that the factors expected to be prominent in the conformational analysis of 1-benzoxepins are electrostatic interactions, orbital interactions between vicinal polar bonds, and solvation. Whereas the solvation and electrostatic interactions have been amply described over the years and can easily be visualized (12), the bond–antibond orbital interactions are much more difficult to define. It is therefore useful to review briefly the rules that govern orbital interactions between two vicinal bonds.

From molecular orbital theory (13, 14) stabilization occurs when an occupied and an unoccupied orbital overlap. In fragments such as X—C—C—Y or H—C—C—X, bond–antibond interactions are important when C—H, C—X, and C—Y bonds are antiperiplanar. Furthermore, stabilization between a bonding orbital σ and an antibonding orbital σ^* is proportional to $S^2/\Delta E$ where S is the orbital overlap and ΔE represents the energy difference between the σ and σ^* orbitals (15). Thus the combination of a decreasing ΔE and an increasing S leads to better stabilization.

The dependence of the overlap contribution on electronegativity is specific to the nature of the orbital of the C—X bond, σ_{C-X} or σ^*_{C-X}. Indeed, increasing the electronegativity of X leads to an increase of electronic density (16) near C in a σ^*_{C-X} orbital while for σ_{C-X}, the charge density is displaced away from C toward X. This statement is valid for a series of X in the same row of the periodic table (13) as well as for the halogen substituents (17–19). Consequently, better overlap occurs in a σ_{C-Y}–σ^*_{C-X} interaction as the electronegativity of X increases for Y constant. The effect of substituent on ΔE is discussed later.

Figure 5 illustrates the effects of the substituent change on the populations of the C_e and C_a forms, which have been plotted against the electronegativity (20) of each substituent for the series of compounds **6–10**. Data for the OCH_3 substituent (8) are included in this figure and the points are joined to the others by a broken line. Thus, the lines drawn for C_e in both polar and nonpolar solvents show a gradual decrease from I to F, whereas

Can. J. Chem. Downloaded from www.nrcresearchpress.com by 122.72.124.2 on 09/07/12
For personal use only.

TABLE 1. Carbon-13 chemical shifts for compounds **6–9** at high and low temperatures

Compound	Solvent and temperature (°C)		Conformation (%)		C-2	C-3	C-4	C-5	C-6	C-7	C-8	C-9	C-10	C-11
6	CHF_2Cl	−15			74.77 (^2J = 23.09)	92.41 (^1J = 170.75)	32.33 (^2J = 21.23)	27.76	136.44	160.99	122.32	128.94	125.37	131.41
(X = F)		−125	88	C_a	74.41 (^2J = 18.11)	92.42 (^1J = 169.03)	31.35 (^2J = 22.14)	27.27	137.58	160.59	122.62	128.94	125.69	131.34
			8	C_e	[a]	92.42 (^1J = 169.03)	32.84 (^2J = 19.11)	[a]	136.20	160.02	122.62	129.24	126.10	131.83
			4	*TB*	[a]	94.76 (^1J = 172.05)	29.54 (^2J = 22.14)	[a]	129.96	159.46	[b]	128.36	123.52	133.00
	CH_3OCH_3	−20			74.36 (^2J = 24.02)	91.71 (^1J = 172.29)	32.32 (^2J = 21.01)	27.61	135.80	160.89	121.97	128.51	124.74	130.99
		−120	87	C_a	73.90 (^2J = 19.40)	91.37 (^1J = 171.27)	31.41 (^2J = 21.69)	27.06	137.07	160.73	122.15	128.49	125.00	130.66
			10	C_e	[a]	91.64 (^1J = 169.03)	32.97 (^2J = 19.19)	[a]	135.53	160.10	122.32	128.87	125.19	131.29
			3	*TB*	[a]	93.83 (^1J = 174.06)	29.74 (^2J = 22.14)	[a]	129.43	159.83	120.49	128.68	125.52	132.33
7	CHF_2Cl	0			77.43	60.36	36.95	30.80	136.07	161.07	122.33	129.10	125.49	131.54
(X = Cl)		−120	42	C_a	76.63	63.50	34.20	28.42	137.01	160.82	122.45	129.15	125.72	131.60
			58	C_e	76.95	59.36	36.91	31.25	136.36	160.12	122.74	128.84	125.54	131.60
	CH_3OCH_3	0			76.98	59.98	36.93	30.69	135.54	160.91	122.00	128.70	124.96	131.11
		−120	25	C_a	76.05	63.27	34.21	28.20	136.51	160.95	122.26	128.48	124.94	131.04
			75	C_e	76.41	59.22	36.95	30.96	135.77	160.25	122.03	128.79	125.20	131.04
8	CHF_2Cl	0			77.56	52.33	37.65	32.43	135.98	161.01	122.29	129.07	125.47	131.47
(X = Br)		−120	30	C_a	76.96	58.04	34.70	29.88	136.79	160.82	122.82	128.84	125.72	131.73
			70	C_e	76.96	51.51	37.44	32.85	136.37	160.14	122.43	129.14	125.53	131.53
	CH_3OCH_3	0			77.16	52.17	37.66	32.33	135.54	160.92	121.99	128.72	124.99	131.07
		−120	15	C_a	76.37	58.10	34.69	29.62	136.29	[a]	122.32	128.48	124.94	131.14
			85	C_e	76.37	51.63	37.43	32.50	135.80	160.28	121.99	128.77	125.18	130.97
9	CHF_2Cl	0			79.18	31.89	39.56	35.18	136.10	161.14	122.23	129.02	125.44	131.41
(X = I)		−125	22	C_a	78.21	40.33	35.80	32.86	136.43	160.91	122.90	128.78	125.41	131.90
			78	C_e	78.48	31.42	39.20	35.50	136.58	160.31	122.34	129.04	125.64	131.41
	CH_3OCH_3	0			78.72	31.85	39.50	35.00	135.60	160.99	121.88	128.61	124.91	130.96
		−125	10	C_a	77.56	40.02	35.76	32.56	135.83	161.01	122.36	128.39	124.81	131.31
			90	C_e	77.92	31.12	39.12	35.18	135.96	160.42	121.86	128.62	125.05	130.83

[a]These signals were not identified, either because they are overlapping with the C_a or C_e signals or are too small to be resolved clearly.
[b]This signal is not observed clearly because of the solvent (CHF_2Cl) overlapping peak.

TABLE 2. ^{1}H spectral parameters for

Compound	Temperature (°C)		Conformation (%)		H-2a	H-2e	H-3a
6	CHF_2Cl	0			3.93dd (J = −13.4, 29.8)	4.24 br	—
(X = F)		−125		C_a	3.71dd (J = −14.0, 41.62)	4.60t ($J \approx$ 13–14)	—
				C_e	[b]	[b]	[b]
				TB	[b]	[b]	—
	CF_2Cl_2	0			3.96dd (J = 12.9, 2.0, 25.6)	4.05 br	—
		−120		C_a	3.63dd (J = 13.8, 40.32)	4.45t ($J \approx$ 12–13)	—
				C_e	[b]	[b]	[b]
				TB	[b]	[b]	—
7	CHF_2Cl	0			3.76t ($J \approx$ 10)	4.28 overlap	—
(X = Cl)		−120	41	C_a	3.86d (J = −13.4)	4.49d (J = −13.5)	—
			59	C_e	3.47t (J = 11.5)	4.53 (J = −11.6)	4.28 m
	CF_2Cl_2	0			3.60t ($J \approx$ 10–11)	4.31dd (J = −12.1, 2.6)	4.21 m
		−120	23	C_a	3.81d (J = −13.5)	4.33d (J = −13.7)	—
			77	C_e	3.36t (J = 11.4)	4.48dd (J = −10.8, 2.1)	4.19tt (J = 11.4, 11.4, 3.3, 3.3)
8	CHF_2Cl	0			3.78 br	4.38 br	4.38 br
(X = Br)		−120	30	C_a	3.87d (J = −13.7)	4.52d (J = −13.1)	—
			70	C_e	3.56t ($J \approx$ 11–12)	4.60dd (J = −12.4, 3.6)	4.37tt ($J \approx$ 12, 4.0)
	CF_2Cl_2	0			3.63t ($J \approx$ 10–11)	4.41dd (J = −12.4, 3.1)	4.29tt (J = −10.1, 10.1, 3.9, 3.9)
		−120	11	C_a	3.82d (J = −13.9)	4.41d (J = −14.2)	—
			89	C_e	3.46t ($J \approx$ 11–12)	4.48dd (J = −12.1, 2.3)	4.27tt (J = 11.6, 4.0)
9	CHF_2Cl	0			3.81t ($J \approx$ 10–11)	4.44d (J = −10.7)	4.53tt (J = −10.0, 10.0, 3.7)
(X = I)		−125	19	C_a	3.7 overlap	4.5 overlap	—
			81	C_e	3.65t (J = 11.9)	4.68dd (J = −12.0, 3.0)	4.49 m
	CF_2Cl_2	0			3.70t ($J \approx$ 11)	4.49 br	4.49 br
		−120	9	C_a	3.5 overlap	[b]	—
			91	C_e	3.56t (J = 11.8)	4.56d (J = −11.1)	4.44 br

[a]The aromatic signals are not reported because of solvent (CHF_2Cl) overlapping peaks. All aromatic signals for compounds **6–9** appear between 6.8 and 7.1 ppm
[b]These signals were not identified, either because they are overlapping with the C_a and C_e signals or are too small to be resolved clearly.

the amount of C_a increases from I to F. Furthermore, inversion of the relative stabilities of the C_a and C_e forms occurs between Cl and O in each of the two solvents.

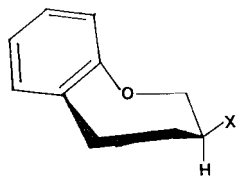
Because small amounts of the *TB* form are observed only for **6** and **10**, it is preferable to consider the conformational results in terms of two subgroups: the first part will bear on compounds **7**, **8**, and **9**, which show only two conformations (C_a and C_e), while the second part will consider compounds **6** and **10**.

From studies on 3-halogenated-1,5-benzodioxepins (3), it has been shown that for the I, Br, and Cl substituents, steric and electrostatic interactions are not dominant factors responsible for the population differences. Also, from studies on 3-halotetrahydropyrans (11), it has been suggested that some effect other than dipolar forces is responsible for the conformational behavior. Then, in this work, the same arguments lead to the conclusion that the trends noted for the three heavier halogen substituents in Fig. 5 cannot be due to steric and dipolar interactions.

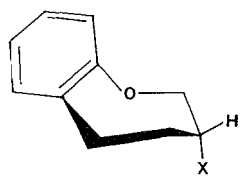
Furthermore, changing solvent from CH_3OCH_3 to CHF_2Cl increases the C_a populations for all derivatives, as seen in Fig. 5, thus indicating that solvation is not a determining factor. Therefore, as for compounds **3**, **4**, and **5**, these observations point to the stereoelectronic bond–antibond orbital interactions (21, 22).

The relative energy levels of the σ^*_{C-X} orbitals given by CNDO/2 calculations (21) follow the order $\sigma^*_{C-H} > \sigma^*_{C-O} > \sigma^*_{C-F} > \sigma^*_{C-Cl} > \sigma^*_{C-Br} > \sigma^*_{C-I}$, while the order of the σ orbitals is $\sigma_{C-I} > \sigma_{C-Br} > \sigma_{C-Cl} > \sigma_{C-H} > \sigma_{C-O} > \sigma_{C-F}$, as revealed by CNDO/2 and *ab initio* calculations (21) and an analysis of ionization potentials of CH_3X molecules (19, 23). Figure 6 shows a qualitative assessment of the relative energy differences (ΔE) for σ–σ^* interactions from these trends (3). Normally donor σ and acceptor σ^* orbitals are assigned so as to minimize ΔE (21).

Important orbital interactions for the C_a and C_e forms are shown below structures **13** and **14**, where it is seen that the



13



14

C_e X = Cl, Br I X = F, O C_a

$\sigma_{C-X} - \sigma^*_{C-O}$ $\sigma_{C-H} - \sigma^*_{C-X} + \sigma_{C-H} - \sigma^*_{C-O}$

$\sigma_{C-O} - \sigma^*_{C-X}$ $\sigma_{C-H} - \sigma^*_{C-X} + \sigma_{C-H} - \sigma^*_{C-O}$

Can. J. Chem. Downloaded from www.nrcresearchpress.com by 122.72.124.2 on 09/07/12
For personal use only.

compounds **6–9** at high and low temperatures[a]

H-3e	H-4a	H-4e	H-5a	H-5e
4.80d (J = 44.7)	1.94dt ($J \approx$ 12–14, 31.9)	2.16 br	3.17t ($J \approx$ 12–13)	2.60ddd (J = −14.8, 8.2, 1.8)
4.92d (J = 43.4)	1.72dt (J = −14.4, 14.3, 47.26)	2.38 br	3.35t (J = 13.7)	2.55dd (J = −14.1, 4.1)
—	[b]	[b]	[b]	[b]
[b]	[b]	[b]	[b]	[b]
4.74d (J = 44.93)	2.06–1.91 br	2.06–1.91 br	3.11 br	2.58 br
4.81d (J = 43.89)	1.67dt (J = −14.1, 14.1, 45.4)	2.26 br	3.28t (J = 13.6)	2.43dd (J = −13.9, 4.5)
—	[b]	[b]	[b]	[b]
[b]	[b]	[b]	[b]	[b]
4.28 overlap	1.88q ($J \approx$ 10–12)	2.35t ($J \approx$ 10–11)	2.97 br	2.80t ($J \approx$ 11–13)
	1.95t ($J \approx$ 13–14)	2.30d (J = 13.6)	3.55 overlap	2.60dd (J = 14.2, 5.8)
—	1.69q (J = 12.3, 12.3, 12.1)	2.53 br	2.91t ($J \approx$ 13–14)	2.77dd (J = −14.1, 6.1)
—	1.79q ($J \approx$ 10–13)	2.38 br	2.85 br	2.85 br
4.53 s	1.94t ($J \approx$ 13–14)	2.20d (J = −14.2)	3.40t overlap	2.47 overlap
—	1.62q ($J \approx$ 12–13)	2.47 br	2.87t ($J \approx$ 13–14)	2.70dd (J = −14.1, 5.9)
—	1.96q ($J \approx$ 10–13)	2.46 br	2.89 br	2.89 br
4.70 s	1.96t (J = 13.3)	2.36d (J = 13.4)	3.47t (J = 13.4)	[b]
—	1.82q (J = 12.6)	2.63 br	2.92t ($J \approx$ 13–14)	2.75dd (J = −14.4, 5.8)
—	1.89qd ($J \approx$ 10–12, 3–4)	2.51 br	2.82 br	2.82 br
3.66 s	1.95t ($J \approx$ 14)	2.27d (J = −14.4)	3.4 overlap	[b]
—	1.77q ($J \approx$ 12.5)	2.56 br	2.89t ($J \approx$ 13–14)	2.67dd (J = −14.4, 5.9)
—	2.04qd ($J \approx$ 11–13, 2–3)	2.50 br	2.85t ($J \approx$ 11–13)	2.74 br
4.89 s	1.67t ($J \approx$ 13–14)	2.33d (J = −14.6)	3.35t ($J \approx$ 14)	[b]
—	1.97q (J = 12.7)	2.73 br	2.92t ($J \approx$ 13–14)	2.62dd (J = 14.2, 6.0)
—	1.98qd ($J \approx$ 12)	2.55 br	2.85t ($J \approx$ 12–13)	2.68dd (J = −14.3, 6.8)
4.92 s	1.71t ($J \approx$ 12–13)	2.26d (J = −12.7)	3.30 overlap	[b]
—	1.91q (J = 12.0, 12.5, 12.5)	2.67 br	2.89t ($J \approx$ 13–14)	2.57dd (J = 13.6, 5.4)

in the CF_2Cl_2 solvent.

C_a (**14**) form could have two orbital interactions, namely $\sigma_{C—H}$–$\sigma^*_{C—X}$ and $\sigma_{C—H}$–$\sigma^*_{C—O}$. The $\sigma_{C—H}$–$\sigma^*_{C—O}$ interaction cannot explain the population changes because it is independent of X. Thus, $\sigma_{C—H}$–$\sigma^*_{C—X}$ must be the dominant interaction. In this case, ΔE stabilizes this interaction increasingly from Cl to I whereas the S term increases stabilization in the opposite sense. This divergence is useful to estimate the relative importance of the two terms using the experimental trends observed in Fig. 5. Thus, if ΔE were more important, stabilization of C_a would increase in the order Cl to I, whereas if S were predominant, then stabilization would increase from I to Cl. Figure 5 shows that the latter prediction corresponds to the observed C_a population change, thus indicating that the S term is the more important one.

For the C_e form (**13**), the dominant interaction is most difficult to determine in the absence of quantitative ΔE values. We must choose between $\sigma_{C—O}$–$\sigma^*_{C—X}$ and $\sigma_{C—X}$–$\sigma^*_{C—O}$. From a qualitative point of view, these interactions appear to have similar ΔE values and both may be operative with one being more stabilizing than the other. If the S term were more important than ΔE, because the oxygen atom is more electronegative than the halogen atoms, then the $\sigma_{C—X}$–$\sigma^*_{C—O}$ orbital interaction should be dominant and it would increase in the order Cl to I for both ΔE and S terms. Otherwise, if the $\sigma_{C—O}$–$\sigma^*_{C—X}$ orbital interaction were the dominant one, stabilization from ΔE would increase from Cl to I, whereas the S contribution would increase in the opposite sense. Figure 5 shows that the dominant interaction must be in line with an increasing stabilization from Cl to I, indicating that the $\sigma_{C—X}$–$\sigma^*_{C—O}$ orbital interaction ought to be more important because it is stabilized by both ΔE and S terms, in agreement with the earlier analysis for C_a, which suggested that the S term is more important than ΔE.

The results noted for the second subgroup with more electronegative substituents, compounds **6** (X = F) and **10** (X = OCH_3), show that a third conformation (*TB*) is present. Furthermore, contrary to the group of compounds **7–9** for which the C_e form is favored, the C_a form predominates for compounds **6** and **10**. Because the oxygen atom is not in the same family (i.e., in the same column of the periodic table) as the halogens, the OCH_3 points in Fig. 5 are joined to the others by broken lines. As well, it is likely that the electrostatic interactions are modified for OCH_3 because the dipole orientation of the methoxy group bisects the C—O—C angle of the most stable rotamer (8), whereas that of the halogen substituents is located along the C—X bond. Because dipolar interactions are expected to be repulsive for C_a and weakly attractive for C_e, the *TB* form provides an alternative to the C_a form for which the same orbital interactions can be maximized. Consequently, lowering the solvent polarity from CHF_2Cl to CH_3OCH_3 reduces significantly the populations of the most polar C_a form, as seen in Fig. 5.

Can. J. Chem. Downloaded from www.nrcresearchpress.com by 122.72.124.2 on 09/07/12
For personal use only.

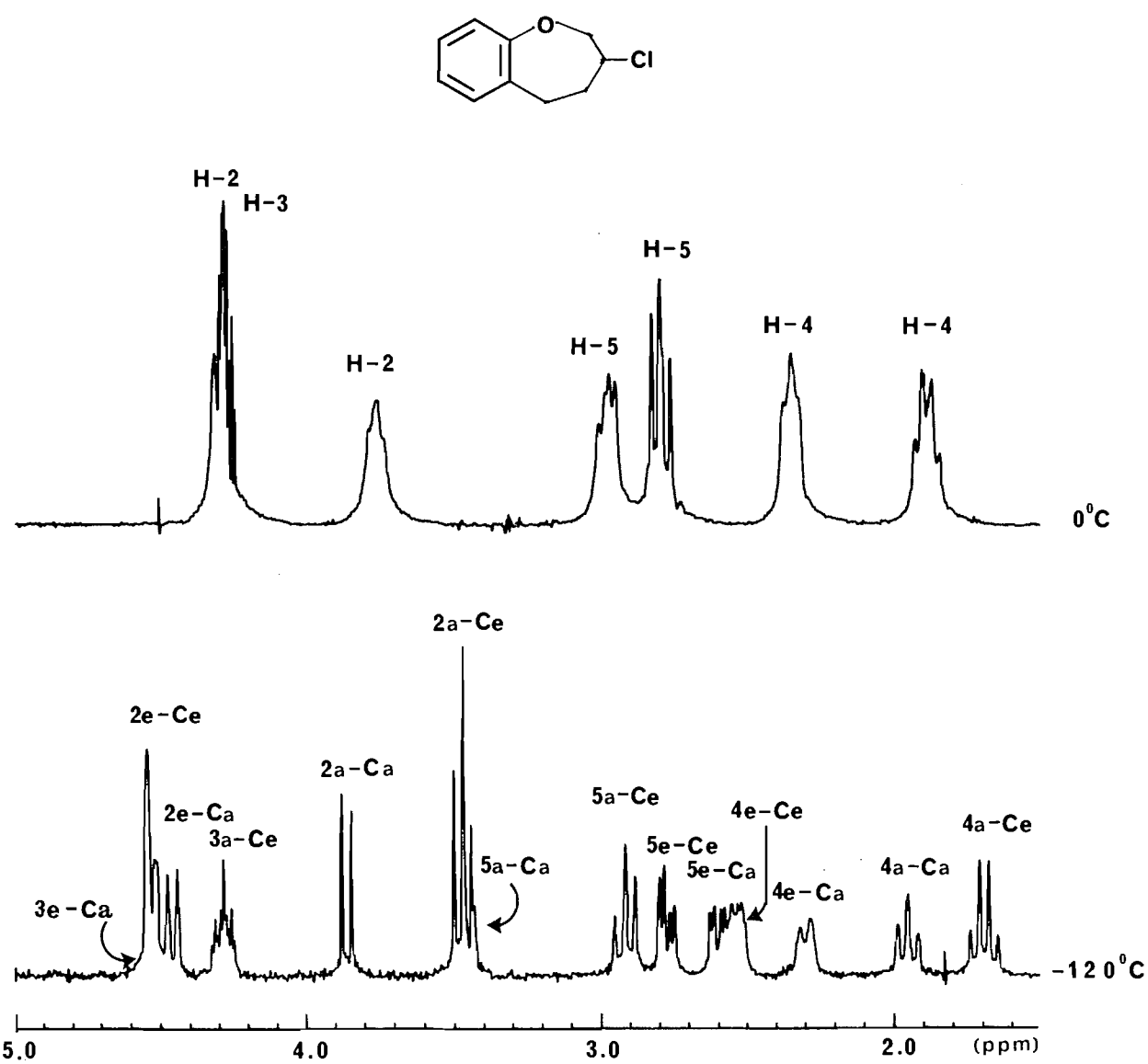


FIG. 4. The 400.13-MHz ^{1}H nmr spectra of the aliphatic protons of **7** in CHF_2Cl at 0°C and −120°C. The abbreviations refer to proton environments described in the text.

The dominant interaction for compounds **6** and **10** (X = F, O) in the C_e (**13**) form, is $\sigma_{C—O}$–$\sigma^*_{C—X}$. From a consideration of the ΔE and S contributions for X = F and OCH_3, this interaction should be more stabilizing for X = F because ΔE is larger and overlap is poorer for OCH_3. Similarly, in the C_a (**14**) form, the $\sigma_{C—H}$–$\sigma^*_{C—X}$ orbital interaction should be more stabilizing for X = F. The trends observed in Fig. 5 for both F and OCH_3 are in agreement with the fact that the $\sigma_{C—H}$–$\sigma^*_{C—X}$ interaction is more stabilizing than $\sigma_{C—O}$–$\sigma^*_{C—X}$, thus favoring the C_a form for both substituents. Finally, the population differences for X = F and OCH_3 indicate that the $\sigma_{C—H}$–$\sigma^*_{C—X}$ interaction is also more stable for X = F, in accord with predictions from the above theoretical framework.

In conclusion, conformational analysis of the 3-halogenated 1,5-benzodioxepins (**1**–**5**) and 1-benzoxepins (**6**–**10**) has revealed that intramolecular orbital interactions constitute an important force complementing electrostatic interactions and solvation. For the heavier halogens (I, Br, and Cl), the bond–antibond orbital interactions alone can explain the observed conformational trends, whereas for the most electronegative substituents, F and OCH_3, these interactions are in competition with dipolar interactions. In addition, the same orbital interactions lead to different overall conformational observations for each series of compounds, due to the fact that the *TB* form is more stabilized and accessible in the benzodioxepin system. Finally, the two systems, having two and one O—C—C—X vicinal interactions between polar bonds respectively, show that the effect of orbital interactions on conformations is not predictable using straightforward additivity schemes.

Experimental

Routine ^{1}H nmr spectra were recorded on a Bruker WH-90 spectrometer as solutions in $CDCl_3$ (10% w/v) containing Me_4Si as reference.

The two-dimensional spectra were recorded on a Varian VXR-300 instrument. The 2D COSY experiment was made using the following pulse sequence: RD–90°–t_1–90°–t_2 (FID) (9). A spectral width of 1080 Hz and quadrature detection were used to collect a 128 × 512 data matrix. Digital resolution was 2.1 Hz/point.

Can. J. Chem. Downloaded from www.nrcresearchpress.com by 122.72.124.2 on 09/07/12
For personal use only.

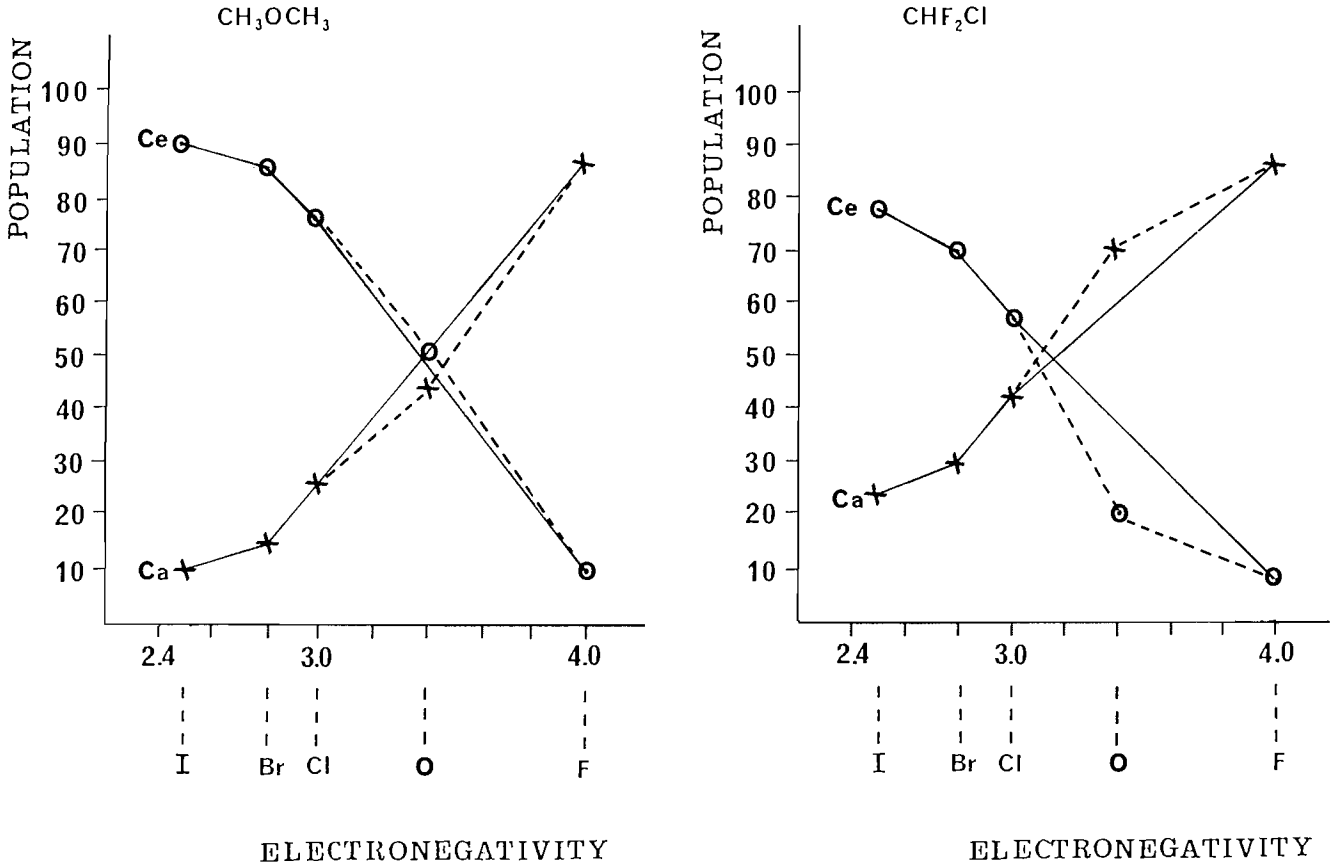


FIG. 5. Plots of the population of the C_e form (○) and C_a form (×) versus the electronegativity of I, Br, Cl, and F in CH_3OCH_3 and CHF_2Cl solutions. Data for OCH_3 are joined to the other plots by broken lines.

Can. J. Chem. Downloaded from www.nrcresearchpress.com by 122.72.124.2 on 09/07/12
For personal use only.

The 2D proton–carbon heteronuclear chemical shift correlation (HSC) was obtained using the standard pulse sequence (10). The experiment was performed on a VXR-300 spectrometer operating at 75.431 MHz for ^{13}C with F_2 = 299.949 MHz in the second dimension. The spectrum was acquired with 256 × 1K data points.

The low temperature ^1H nmr spectra at 400.13 MHz and ^{13}C nmr spectra at 100.62 MHz were obtained by using a Bruker WH-400 spectrometer equipped with a B-VT-1000 variable temperature unit. Calibration using a thermocouple inside a solvent-containing nmr tube indicates that the low temperatures reported are accurate within 3°C. For all ^{13}C nmr spectra, the following parameters are typical: flip angle = 20°–60°; SW (scan width) = 20 000 Hz; data size = 8–16K; AQ (acquisition time) = 0.43 s; RD (relaxation delay) = 0.6 s. For proton spectra, the typical instrumental parameters used are as follows: flip angle = 10°–70°; SW = 5000 Hz; data size = 8 and 16K; AQ = 0.8–1.0 s; RD = 0.01 s.

The ^{13}C samples were studied as solutions in CHF_2Cl or CH_3OCH_3 (100–150 mg in 2.2 mL of solution) containing Me_4Si and about 15–20% of CD_2Cl_2 as locking agent in standard 10-mm tubes that had been degassed and sealed. Integrations were carried out by using Bruker software and are precise within 2%.

Proton samples in standard 5-mm tubes (degassed and sealed) were recorded as solutions in CHF_2Cl or CF_2Cl_2 (10–20 mg in 0.55 mL of solution) containing Me_4Si and about 15–20% of CD_2Cl_2 or CD_3COCD_3 for locking purpose.

The high resolution mass spectra were taken using a modified MS-9 spectrometer at 70 eV.

2,3,4,5-Tetrahydro-3-fluoro-1-benzoxepin (6)

A solution of 1.0 g (0.006 mol) of 2,3,4,5-tetrahydro-1-benzoxepin-3-ol (8) in 100 mL of dry dichloromethane was cooled to 0°C and 2.3 mL (0.018 mol) of diethylaminosulfur trifluoride was added dropwise. The mixture was stirred at room temperature for 48 h, then cooled to −25°C, and 40 mL of methanol was added very slowly. Extraction was carried out with 2 × 100 mL of saturated $NaHCO_3$ solution, 2 × 100 mL of HCl 5%, and 2 × 50 mL of brine. The organic fraction was dried with $MgSO_4$, filtered, and the solvent was evaporated. The product was purified by flash chromatography with 10% dichloromethane and 90% hexane as eluant, giving 352 mg (51%) of a yellow liquid; ^1H nmr δ ($CDCl_3$): 4.82 (1H, m, H-3), 4.20 (1H, m, H-2), 4.07 (1H, dd, H-2), 3.12 (1H, t, H-5), 2.62 (1H, dd, H-5), 1.9–2.3 (2H, br, H-4), 7.0–7.2 (4H, m, Ar). *Exact Mass* calcd. for $C_{10}H_{11}OF$: 166.0794; found (70 eV): 166.0094.

2,3,4,5-Tetrahydro-3-mesylate-1-benzoxepin

A solution of 1.0 g (0.006 mol) of 2,3,4,5-tetrahydro-1-benzoxepin-3-ol in 100 mL of dry dichloromethane was cooled to 0°C and 1.3 mL of triethylamine was added dropwise followed by 0.72 mL (0.007 mol) of methanesulfonyl chloride. The mixture was stirred at room temperature for 16 h. The solution was then washed with 2 × 50 mL of cold water, 2 × 50 mL of cold HCl 10%, 2 × 50 mL of cold saturated $NaHCO_3$ solution, and 2 × 50 mL of cold brine. The organic phase was dried over $MgSO_4$, filtered, the solvent was evaporated, and 1.45 g (98%) of a yellow solid was obtained; ^1H nmr δ ($CDCl_3$): 2.14 (2H, m, H-4), 2.2–3.0 (2H, m, H-5), 3.10 (3H, s, CH_3), 4.15 (2H, br, H-2), 5.03 (1H, m, H-3), 7.0–7.2 (4H, m, Ar).

2,3,4,5-Tetrahydro-3-chloro-1-benzoxepin (7)

A solution of 1.5 g (0.006 mol) of the above mesylate, 6.93 g (0.025 mol) of benzyltriethylammonium chloride, and 15 mL of dry dimethyl sulfoxide was heated at 80°C for 16 h. The solution was cooled to room temperature and 150 mL of ether was added. The

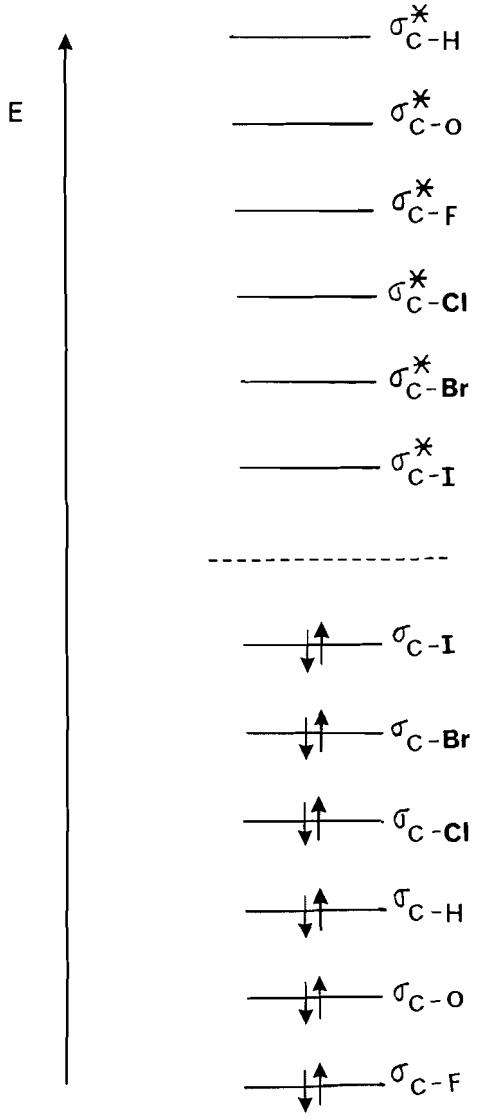


FIG. 6. Order of bond and antibond orbital energies of the C—X bond in various X—CH_2—CH_2—Y and CH_3X molecules.

mixture was washed with 3 × 100 mL of brine. The organic fraction was dried over $MgSO_4$, filtered, and evaporated to give 0.921 g of yellow liquid. Purification by flash chromatography with CCl_4 as eluant gave 0.706 g (62%) of a colorless liquid. Further purification was made by gas chromatography using an SE-30, 30% column; ^{1}H nmr δ ($CDCl_3$): 4.2–4.3 (2H, m, H-3 + H-2), 3.75 (1H, dd, H-2), 2.7–3.0 (2H, m, H-5), 2.37 (1H, m, H-4), 1.88 (1H, m, H-4), 7.0–7.2 (4H, m, Ar). *Exact Mass* calcd. for $C_{10}H_{11}OCl$: 182.0498; found (70 eV): 182.0508.

2,3,4,5-Tetrahydro-3-bromo-1-benzoxepin (8)

A mixture of 0.807 g (0.003 mol) of 2,3,4,5-tetrahydro-3-mesylate-1-benzoxepin, 4.33 g (0.013 mol) of tetrabutylammonium bromide, and 15 mL of dimethyl sulfoxide was stirred at 80°C for 16 h. After cooling the solution to room temperature, 150 mL of ether was added and this mixture was washed with 3 × 100 mL of brine. The organic fraction was dried over $MgSO_4$, filtered, and evaporated to give 0.738 g (97%) of a yellow liquid. Purification was made by distillation under reduced pressure; ^{1}H nmr δ ($CDCl_3$): 1.9–2.1 (1H, m, H-4), 2.4–2.6 (1H, m, H-4), 2.7–2.9 (2H, m, H-5), 3.80 (1H, dd, H-2), 4.41 (2H, m, H-2 and H-3), 7.0–7.2 (4H, m, Ar). *Exact Mass* calcd. for $C_{10}H_{11}OBr$: 225.9993 (50.54%), 227.9973 (49.46%); found (70 eV): 227.9971 and 225.9998.

2,3,4,5-Tetrahydro-3-iodo-1-benzoxepin (9)

A solution of 0.900 g (0.004 mol) of 2,3,4,5-tetrahydro-3-mesylate-1-benzoxepin, 2.80 g (0.019 mol) of NaI, and 50 mL methyl isobutyl ketone was refluxed for 16 h. After cooling the mixture to room temperature, the mixture was filtered and the solvent was evaporated under reduced pressure. The product was purified by flash chromatography on silica gel to give 0.706 g (69%) of brown liquid. Further purification by distillation under reduced pressure gave a pink liquid; ^{1}H nmr δ ($CDCl_3$): 2.0–2.2 (1H, m, H-4), 2.55 (1H, br, H-4), 2.7–2.9 (2H, m, H-5), 3.83 (1H, dd, H-2), 4.5–4.6 (2H, m, H-2 + H-3), 7.0–7.2 (4H, m, Ar). *Exact Mass* calcd. for $C_{10}H_{11}OI$: 273.9814; found (70 eV): 273.9838.

Acknowledgments

We acknowledge the assistance of Dr. Phan Viet Minh Tan, manager of the "Laboratoire régional de RMN à haut champ" in Montréal. We thank the Natural Sciences and Engineering Research Council of Canada for financial assistance.

1. D. MÉNARD and M. ST-JACQUES. Can. J. Chem. **59**, 1160 (1981).
2. D. MÉNARD and M. ST-JACQUES. J. Am. Chem. Soc. **106**, 2055 (1984).
3. P. DIONNE and M. ST-JACQUES. J. Am. Chem. Soc. **109**, 2606 (1987).
4. S. WOLFE. Acc. Chem. Res. **5**, 102 (1972).
5. L. CAZAUX, G. CHASSAING, J.-P. GORRICHON, P. MARONI, and I. PREJZNER. Bull. Soc. Chim. 563 (1976).
6. R. J. ABRAHAM, H. D. BANKS, E. L. ELIEL, O. HOFER, and M. K. KALOUSTIAN. J. Am. Chem. Soc. **94**, 1913 (1972).
7. N. J. KOTITE, M. HARRIS, and M. K. KALOUSTIAN. J. Chem. Soc. Chem. Commun. 911 (1977).
8. A. LACHAPELLE and M. ST-JACQUES. Can. J. Chem. **65**, 2575 (1987).
9. A. BAX and R. FREEMAN. J. Magn. Reson. **44**, 542 (1981).
10. (*a*) G. BODENHAUSEN and R. FREEMAN. J. Magn. Reson. **28**, 471 (1977); (*b*) A. BAX and G. A. MORRIS. J. Magn. Reson. **42**, 501 (1981).
11. C. B. ANDERSON and M. P. GEIS. Tetrahedron, **31**, 1149 (1975).
12. M. K. KALOUSTIAN. J. Chem. Educ. **51**, 777 (1974).
13. T. K. BRUNCK and F. WEINHOLD. J. Am. Chem. Soc. **101**, 1700 (1979).
14. A. J. KIRBY. *In* The anomeric effect and related stereoelectronic effect at oxygen. Springer Verlag, Berlin, Heidelberg, New York. 1983.
15. T. A. ALBRIGHT, J. K. BURDEH, and M. WHANGHO. *In* Orbital interactions in chemistry. John Wiley and Sons, New York. 1985.
16. V. MINKIVE, B. SIMKINE, and R. MIHIAEV. *In* Théorie de la structure moléculaire (couches électroniques). French translation: Mir, Moscow. 1982. pp. 132, 249, 250.
17. R. F. HUDSON. Angew. Chem. Int. Ed. Engl. **12**, 36 (1973).
18. Y. KARTON and A. PROSS. Tetrahedron Lett. 3827 (1978).
19. K. KIMURA, S. KESUMATA, Y. ACHIBA, T. Y. AMAZAKI, and S. IWAKA. Handbook of the HeI photoelectron spectra of fundamental organic molecules. Japan Scientific Societies Press, Tokyo; Halsted Press, New York. 1981.
20. L. PAULING. *In* The chemical bond. Cornell University Press, Ithaca, NY. 1967.
21. N. D. EPIOTIS, W. R. CHERRY, S. SHALK, R. L. YATES, and F. BERNARDI. Top. Curr. Chem. 70 (1977).
22. N. D. EPIOTIS, L. R. YATES, J. R. LARSON, C. R. KIRMAIER, and F. BERNARDI. J. Am. Chem. Soc. **99**, 8379 (1977).
23. R. C. BINGHAM. J. Am. Chem. Soc. **97**, 6743 (1975).

Can. J. Chem. Downloaded from www.nrcresearchpress.com by 122.72.124.2 on 09/07/12
For personal use only.

Isotope effects in nucleophilic substitution reactions. VII. The effect of ion pairing on the substituent effects on S_N2 transition state structure

ZHU-GEN LAI AND KENNETH CHARLES WESTAWAY[1]
Chemistry Department, Laurentian University, Sudbury, Ont., Canada P3E 2C6
Received October 6, 1987[2]

ZHU-GEN LAI and KENNETH CHARLES WESTAWAY. Can. J. Chem. **67**, 21 (1989).

The secondary α-deuterium kinetic isotope effects and substituent effect found in the S_N2 reactions between a series of *para*-substituted sodium thiophenoxides and benzyldimethylphenylammonium ion are significantly larger when the reacting nucleophile is a free ion than when it is a solvent-separated ion pair complex. Tighter transition states are found when a poorer nucleophile is used in both the free ion and ion pair reactions. Also, the transition states for all but one substituent are tighter for the reactions with the solvent-separated ion pair complex than with the free ion. Hammett ρ values found by changing the substituent on the nucleophile do not appear to be useful for determining the length of the sulfur–α-carbon bond in the ion pair and free ion transition states.

Key words: Isotope effects, ion pairing, nucleophilic substitution, S_N2 reactions, transition states.

ZHU-GEN LAI et KENNETH CHARLES WESTAWAY. Can. J. Chem. **67**, 21 (1989).

On a trouvé que, lorsque le nucléophile est un ion libre, les effets isotopiques cinétiques secondaires des atomes deutérium en α ainsi que l'effet de substituant qui ont été observés lors de réactions S_N2 d'une série de thiophénolates de sodium substitués en *para* avec l'ion benzyldiméthylphénylammonium sont beaucoup plus importants que lorsque ce nucléophile est une paire d'ions complexe séparée par le solvant. On a trouvé que les états de transition sont beaucoup plus compacts lorsqu'on utilise un mauvais nucléophile tant dans des réactions d'ions libres que dans des réactions de paires d'ions. Par comparaison avec les réactions se produisant avec l'ion libre, les états de transition de tous les substituants, à l'exception d'un, sont plus compacts pour les réactions avec la paire d'ions complexe séparée par le solvant. Il ne semble pas que les valeurs ρ de Hammett que l'on trouve en faisant varier la nature du substituant attaché au nucléophile soient utiles pour déterminer la longueur de la liaison entre le soufre et le carbone en α, tant dans la paire d'ions que dans les états de transition de l'ion libre.

Mots clés : Effets isotopiques, couplage ionique, substitution nucléophile, réactions S_N2, états de transition.

[Traduit par la revue]

Introduction

Recent work by Westaway and Lai (1) has shown that the form of the reacting anion has a significant effect on the magnitude of the secondary α-deuterium kinetic isotope effect and transition state structure of an S_N2 reaction. For example, changing the form of the reacting anion from a solvent-separated ion pair complex (ref. 1, *vide infra*) to a free ion in the S_N2 reaction between *n*-butyl chloride and sodium thiophenoxide in DMSO at 20°C, eq. [1], changes the secondary α-deuterium kinetic isotope effect from 1.034 ± 0.003 to 1.118 ± 0.009 (1). In fact, this change in the form of the reacting nucleophile seems to be a general phenomenon because the secondary α-deuterium kinetic isotope effect changes in at least three other S_N2 reactions when the form of the nucleophile is altered (1).[3] These results clearly demonstrate that the magnitude of the secondary α-deuterium kinetic isotope effect and transition state structure can be strongly dependent on the form of the reacting anion in an S_N2 reaction. Our interest in the substituent effects on the structure of S_N2 transitions states (3–5) and the many cases where the substituent effects found experimentally do not show a consistent pattern (6) made it important to determine how the form of the reacting anion in an S_N2 reaction affects the substituent effects on transition state structure.

[1] $(Na^+)\ ^-SC_6H_5 + CH_3CH_2CH_2CL_2Cl$

$CH_3CH_2CH_2CL_2SC_6H_5 + Cl^-$ L = H, D

Results and discussion

The effect of ion pairing (the form of the reacting anion) on the substituent effect on transition state structure has been assessed by measuring the secondary α-deuterium kinetic isotope effects for the S_N2 reactions of a series of *para*-substituted sodium thiophenoxides and benzyldimethylphenylammonium ion in methanol at 20°C, eq. [2].

[2] $(Na^+)\ ^-S$–C$_6$H$_4$–$Z + C_6H_5CL_2\overset{+}{N}(CH_3)_2C_6H_5\ NO_3^- \rightarrow$

$C_6H_5CL_2$—S–C$_6$H$_4$–$Z + (CH_3)_2NC_6H_5 + NaNO_3$

L = H, D Z = CH_3O, CH_3, H, and Cl

Obviously, the first requirement for this study of the effect of ion pairing on substituent effects was to demonstrate that the form of the reacting thiophenoxide ion could be changed from a free ion to a solvent-separated ion pair complex under the reaction conditions. Several results indicate that sodium thiophenoxide exists as ion pairs in methanol at high concentrations (1). First, the slope of the conductance versus concentration plot decreases sharply at a sodium thiophenoxide concentration of approximately 2×10^{-4} M. In addition, there is a rapid change in the uv spectrum when the sodium thiophenoxide concentration is 1×10^{-4} M. Finally, the addition of 15-crown-5 ether causes the same changes as dilution in the uv spectrum of sodium thiophenoxide solutions.

The cation independent λ_{max} of the uv spectra of lithium, sodium, and cesium thiophenoxide solutions, at concentrations where the salts exist as ion pairs in methanol, indicates that the nucleophilic reactant is a solvent-separated ion pair (7). Finally, the extremely sharp change in the uv spectrum and in the

[1]Author to whom correspondence may be addressed.
[2]Revision received September 2, 1988.
[3]Also, K. C. Westaway and Z.-g. Lai. Unpublished results.

Can. J. Chem. Downloaded from www.nrcresearchpress.com by 122.72.124.2 on 09/07/12
For personal use only.

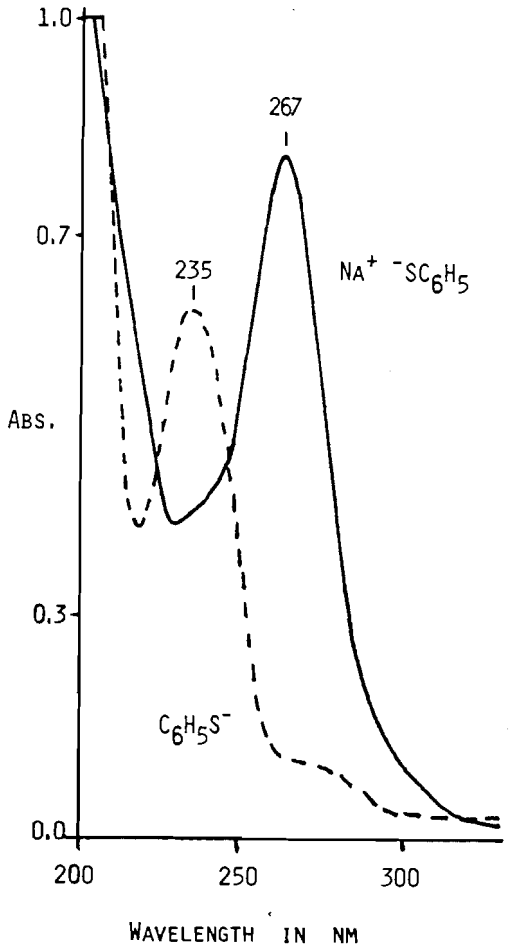


FIG. 1. The ultraviolet spectrum of a 1.54×10^{-3} M solution of the solvent-separated sodium thiophenoxide ion pair complex (—) and the free thiophenoxide ion (---) in methanol at 20°C. The free thiophenoxide ion was generated by adding 15-crown-5 ether.

secondary α-deuterium kinetic isotope effects with concentration (1) indicate that the solvent-separated ion pair must exist as a complex consisting of several solvent-separated sodium thiophenoxide ion pairs, eq. [3].

[3] $m\,Na^+ + m\,SC_6H_5^- \rightleftarrows (Na^+(solvent)_n(SC_6H_5^-))_m$

All of the experimental findings are consistent with such an equilibrium. First, the form of the reacting anion would only change rapidly with concentration if this equilibrium existed. As a result, this equilibrium will produce the rapid changes in the uv spectra and in the secondary α-deuterium kinetic isotope effects with concentration that are observed. The conductivity data are also consistent with the formation of the ion pair complex because the conductance of the ion pair complex is lower than that of the free ions (8). Finally, when 15-crown-5 ether is present, the secondary α-deuterium kinetic isotope effect for the S_N2 reaction between *n*-butyl chloride and sodium thiophenoxide at concentrations where the salt exists as a solvent-separated ion pair complex is identical to those found in the free ion reactions. This occurs because the 15-crown-5 ether complexes the sodium ions (9), preventing the formation of the ion pair complex.

The above experiments indicate that the sodium thiophenoxide exists as a solvent-separated ion pair complex at concentrations greater than 1×10^{-4} M in methanol at 20°C. However,

TABLE 1. The rate constants and secondary α-deuterium kinetic isotope effects for the S_N2 reaction between benzyldimethylphenylammonium ion and a series of *para*-substituted thiophenoxide ions in methanol at 20°C

para Substituent	$k_H \times 10^3$ (L mol^{-1} s^{-1})	$k_D \times 10^3$ (L mol^{-1} s^{-1})	$(k_H/k_D)_\alpha$
CH_3O	10.33 ± 0.088[a]	8.127 ± 0.048[a]	1.271 ± 0.013[b]
CH_3	6.874 ± 0.021	5.557 ± 0.034	1.237 ± 0.008
H	5.141 ± 0.034	4.210 ± 0.033	1.222 ± 0.013
Cl	3.663 ± 0.027	3.267 ± 0.034	1.121 ± 0.014

[a]The errors are the standard deviation from at least three different kinetic runs.
[b]The error is $1/k_D[(\Delta k_H)^2 + (k_H/k_D)^2 \times (\Delta k_D)^2]^{1/2}$ where Δk_H and Δk_D are the standard deviations for the rate constants for the undeuterated and deuterated substrates, respectively (4).

TABLE 2. The rate constants and secondary α-deuterium kinetic isotope effects for the S_N2 reaction between benzyldimethylphenylammonium ion and a series of solvent-separated *para*-substituted sodium thiophenoxide ion pair complexes in methanol at 20°C

para Substituent	$k_H \times 10^3$ (L mol^{-1} s^{-1})	$k_D \times 10^3$ (L mol^{-1} s^{-1})	$(k_H/k_D)_\alpha$
CH_3O	10.09 ± 0.10[a]	8.299 ± 0.011[a]	1.216 ± 0.012[b]
CH_3	7.058 ± 0.049	5.818 ± 0.045	1.213 ± 0.013
H	5.176 ± 0.033	4.288 ± 0.017	1.207 ± 0.008
Cl	3.692 ± 0.026	3.209 ± 0.012	1.150 ± 0.009

[a]The errors are the standard deviation from at least three different kinetic runs.
[b]The error is $1/k_D[(\Delta k_H)^2 + (k_H/k_D)^2 \times (\Delta k_D)^2]^{1/2}$ where Δk_H and Δk_D are the standard deviations for the rate constants for the undeuterated and deuterated substrates, respectively (4).

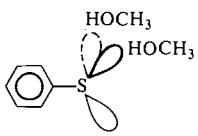
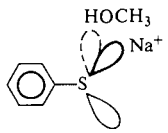
the uv spectra in Fig. 1 show that the addition of 15-crown-5 ether clearly changes the form of the thiophenoxide ion. When the sodium thiophenoxide concentration is 3×10^{-3} M, the concentration used throughout this study, the uv spectrum shows a strong maximum at 267 nm, where the solvent-separated sodium thiophenoxide ion pair complex absorbs (1). When 15-crown-5 ether is added, the absorption at 267 nm almost completely disappears and a new absorption at 235 nm, where the free thiophenoxide anion absorbs, is found (1). Thus, the form of the reacting thiophenoxide ion can be changed from the solvent-separated ion pair complex to the free anion by adding 15-crown-5 ether, and a study of the effect of ion pairing on the substituent effects in S_N2 reactions is feasible.[4]

The secondary α-deuterium kinetic isotope effects found for the S_N2 reactions between benzyldimethylphenylammonium ion and a series of *para*-substituted free thiophenoxide ions and solvent-separated sodium thiophenoxide ion pair complexes, Tables 1 and 2, differ in several ways. First, the substituent effects on the secondary α-deuterium kinetic isotope effects cover a much larger range in the free ion reactions, i.e., the isotope effects range from 1.271 to 1.121 when the nucleophile is a free ion but only from 1.216 to 1.150 when the solvent-separated sodium thiophenoxide ion-pair complex is the reacting species. This observation is important because it illustrates

[4]Neither adding benzyldimethylphenylammonium nitrate nor changing the *para* substituent on the thiophenoxide ion affects the concentration at which the solvent-separated ion pair complexes begin to form in methanol.

Can. J. Chem. Downloaded from www.nrcresearchpress.com by 122.72.124.2 on 09/07/12
For personal use only.

TABLE 3. The CNDO/2 calculated charge densities on the sulfur atom of the partially solvated thiophenoxide ion and sodium thiophenoxide ion pair in methanol

para Substituent	Charge density on the sulfur atom of 	Charge density on the sulfur atom of 
CH_3O	−0.5166	−0.3088
CH_3	−0.5112	−0.3071
H	−0.5080	−0.2998
Cl	−0.4958	−0.2917
Change in the charge density on sulfur	0.0208	0.0171
Change in the $(k_H/k_D)_\alpha$	0.150	0.076

that the substituent effect on S_N2 transition state structure is strongly dependent on the form of the ionic nucleophile.

One possible explanation for the different secondary α-deuterium kinetic isotope effects in the free ion and ion pair complex reactions is that the sodium ion alters the reduced mass of the nucleophile sufficiently to affect the isotope effect. This explanation seems unlikely for several reasons. First, the ion pair is a solvent-separated ion pair so the change in mass does not occur near the nucleophilic atom, i.e., the sodium is replacing a methanol molecule in the second or perhaps third solvent shell around the free ion and should have little or no effect on the reduced mass of the nucleophile. In any case, the mass of the methanol molecule and a sodium ion are similar. Also, theoretical calculations (10) indicate that the secondary α-deuterium kinetic isotope effect in the S_N2 reaction between benzyl chloride and an alkoxide ion only changes by 0.0002 when the developing chloride ion is solvated with three hydrogen-bonding solvent molecules. Since this change in the reduced mass of the chloride ion is much larger than that associated with changing a solvent molecule (methanol) to a sodium ion, it is unlikely that the mass of the sodium ion is responsible for the difference in the isotope effect.

A more plausible explanation for the change in the secondary α-deuterium kinetic isotope effect is that the sodium ion of the solvent-separated ion pair complex reduces the charge on the sulfur atom of the thiophenoxide ion. If the charge on the sulfur of the solvent-separated ion pair complex were indeed smaller than that on the sulfur of the free ion, one would expect that the nucleophile would have to approach closer to the α carbon to distort the α-carbon–chlorine bond and cause reaction. This would result in a tighter transition state and the smaller secondary α-deuterium kinetic isotope effect that is observed for all but one of the ion pair complex reactions (*vide infra*).

The sodium ion could also reduce the magnitude of the substituent effect resulting from a change in the *para* substituent on the nucleophile, by reducing the charge on the sulfur atom of the thiophenoxide ion. If the charge on the sulfur of the solvent-separated ion pair complex were smaller than that on the sulfur of the free ion, a change in the *para* substituent might have a smaller effect on the charge on the sulfur atom of the sodium thiophenoxide ion pair. If this occurred, the nucleophilicity of the thiophenoxide ion would not be altered as much by a change in substituent, and the change in transition state structure with *para* substituent (secondary α-deuterium kinetic isotope effect (substituent effect)) should also be smaller in the ion pair complex reactions.

This rationalization is supported by the results from CNDO/2 calculations of the charge on the sulfur atom of the partially solvated free thiophenoxide ion and the contact sodium thiophenoxide ion pair, Table 3. The CNDO/2 calculations were carried out on the thiophenoxide ion solvated by two methanol molecules and on the contact ion pair[5] solvated by only one methanol molecule because one of the lone pairs of electrons on the sulfur is involved in bond formation in the S_N2 transition state and cannot be solvated. As expected, the calculations indicate that the negative charge on the sulfur atom of the nucleophile is much smaller when the positive sodium ion is present. Although the substituent changes the amount of negative charge on the sulfur atom by the same relative amount, i.e., changing a hydrogen to a *para*-chloro substituent reduces the charge on the sulfur atom by the same percentage in both the free ion and the ion pair, it is important to note that the absolute change in charge on the sulfur ion with substituent is greater for the free ion. Since the substituent effect on the charge on the nucleophile is greater for the free ion than for the ion pair complex, the change in the nucleophilicity should be greater in the free ion reactions. As a result, one would expect the substituent effect on the secondary α-deuterium kinetic isotope effect (transition state structure) to be greater for the free ion than for the ion pair complex reactions. This is, in fact, what is observed.

Although CNDO/2 calculations predict charges in molecules very well (11), the calculated charges on the sulfur atom of the free ion and ion pair complex transition states are only representative of the changes in charge that occur in the actual reactions. However, the same trends in the charge on the sulfur ion with substituent were found for both the unsolvated and fully solvated ion pairs and free ions in methanol.[3] Moreover, the same trends were also found when the position of the sodium ion in the ion pair was varied. Since the same trends in the charge

[5]The calculations were not done on the solvent-separated ion pair complex because neither the structure nor the number of solvent molecules between the sodium and sulfur ions is known.

Can. J. Chem. Downloaded from www.nrcresearchpress.com by 122.72.124.2 on 09/07/12
For personal use only.

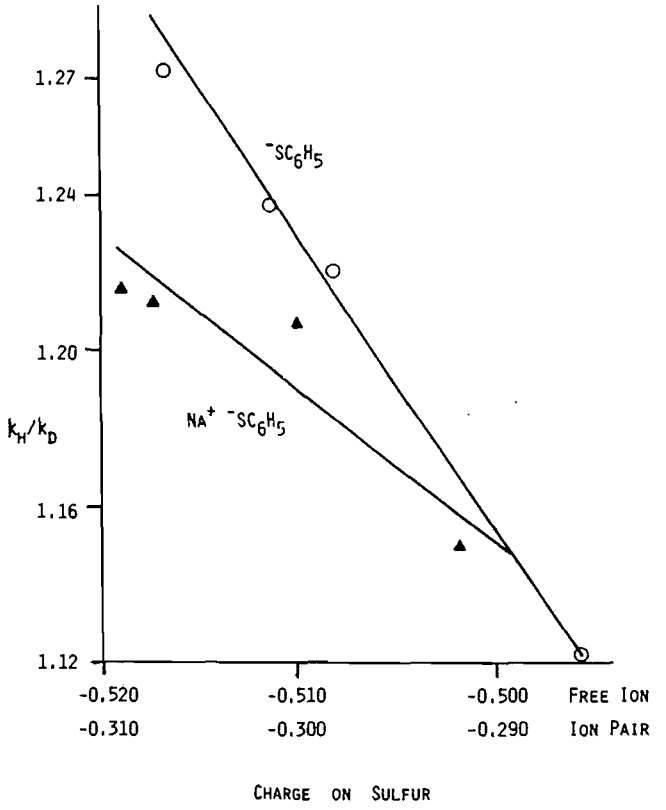


FIG. 2. The secondary α-deuterium kinetic isotope effect versus the charge on the sulfur atom of the free thiophenoxide ion (open circles) and the solvent-separated sodium thiophenoxide ion pair complex (solid triangles).

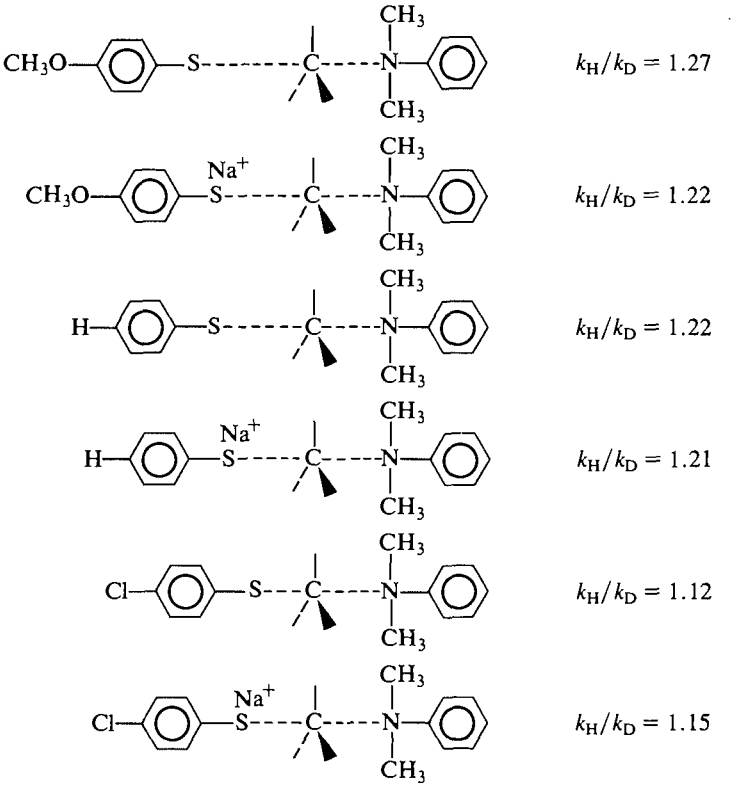


FIG. 3. The relative transition state structures for the S_N2 reactions between benzyldimethylphenylammonium ion and the free ion and solvent-separated ion pair complex forms of a series of *para*-substituted sodium thiophenoxides.

on the sulfur of the free ion and ion pair were observed regardless of the position of the sodium ion and the solvation of the contact ion pair and free ion, it is reasonable to assume that the sodium ion would also reduce the substituent effect on the charge on the sulfur anion of the solvent-separated ion pair complex. Thus, it is not surprising that the substituent effect on the nucleophilicity and, therefore, on transition state structure (the secondary α-deuterium kinetic isotope effect) is smaller for the solvent-separated ion pair complex than for the free ion S_N2 reactions.

The secondary α-deuterium kinetic isotope effects for the S_N2 reactions with the free ion and with the solvent-separated ion pair complex, Tables 1 and 2, both decrease when a poorer nucleophile is used. Since the C_α–H(D) bending vibrations are the same in the initial state of all of the free ion and ion pair reactions, the differences in the isotope effects must reflect differences in transition state structure. This suggests that the transition states are tighter, with shorter α-carbon–nucleophile and (or) α-carbon – leaving group bonds, when a poorer nucleophile is used in both the free ion and ion pair reactions. In fact, a plot of the secondary α-deuterium kinetic isotope effect (the tightness of the transition state) versus the negative charge on the sulfur atom for the free thiophenoxide ion reactions has a correlation coefficient of 0.996, Fig. 2. Thus, the structure of the free ion transition state depends directly on the charge on the sulfur atom (the nucleophilicity) of the reacting nucleophile. The smaller secondary α-deuterium kinetic isotope effect and tighter transition state found when a more electron-withdrawing substituent is in the free ion is expected. A poorer nucleophile should have to come closer to the α carbon to distort the α-carbon – leaving group bond and cause reaction (14).

Both the slope and correlation coefficient for the plot of the secondary α-deuterium kinetic isotope effect versus the charge on the sulfur ion in the solvent-separated ion pair complex reactions, Fig. 2, are smaller than the corresponding values found in the free ion reactions, i.e., the slope is only 3.86 rather than the 7.21 found for the free ion reactions and the correlation coefficient of 0.92 is significantly smaller than the 0.996 found for the free ion reactions. Thus, although the transition state structures for the ion pair reactions seem to depend on the nucleophilicity of the nucleophile, the relationship is not as strong as for the free ion reactions and it appears that some factor(s) other than the charge on the sulfur ion must be important in determining the transition state structures of the solvent-separated ion pair complex reactions.

The magnitude of these secondary α-deuterium kinetic isotope effects can also be used to compare the transition state structures for the solvent-separated ion pair complex and free ion reactions. When the *para* substituent on the nucleophile is methoxy, methyl, and hydrogen, the secondary α-deuterium kinetic isotope effects for the free ion reaction are larger than those found for the corresponding ion pair reactions. This suggests that the free ion transition states are looser (have longer nucleophile–α-carbon and (or) α-carbon – leaving group bonds) than the ion pair transition states, Fig. 3.[6] This is reasonable because the higher charge on the free ion nucleophile

[6]The length of the α-carbon – leaving group bonds has not been changed in these transition states when the substituent on the nucleophile is changed because other work in our laboratory has suggested that the length of the stronger transition state bond does not change significantly when a substituent is changed in the substrate, the nucleophile, or the leaving group of an S_N2 reaction (3, 4).[3]

Can. J. Chem. Downloaded from www.nrcresearchpress.com by 122.72.124.2 on 09/07/12
For personal use only.

TABLE 4. The rate constants and Hammett ρ values for the free ion and the solvent-separated ion pair complex S_N2 reactions between benzyldimethylphenylammonium ion and a series of *para*-substituted sodium thiophenoxides in methanol at 20°C

para-Substituent on the nucleophile	$k_{free\ ion} \times 10^3$ (L mol^{-1} s^{-1})	$k_{ion\ pair} \times 10^3$ (L mol^{-1} s^{-1})
CH_3O	10.33 ± 0.11	10.09 ± 0.10
CH_3	6.87 ± 0.02	7.06 ± 0.05
H	5.14 ± 0.03	5.18 ± 0.03
Cl	3.66 ± 0.03	3.69 ± 0.03
ρ	−0.85 ± 0.14	−0.84 ± 0.11
Correlation coefficient	0.98	0.98

would distort the α-carbon – leaving group bond and cause reaction at a greater distance from the α carbon (14).

Unfortunately, not all of the free ion transition states are looser than the ion pair transition states. The secondary α-deuterium kinetic isotope effect for the reaction with the *para*-chlorothiophenoxide ion pair complex is greater[7] (1.150 ± 0.009 versus 1.121 ± 0.014) than the isotope effect for the corresponding free ion reaction. Although other factors, such as a change in the amount of conjugation to the phenyl ring on the α carbon (10, 15), changes in the reaction coordinate motion (16, 17), tunneling (16, 17), and changes in the product composition (18), can affect the magnitude of secondary α-deuterium kinetic isotope effects, the simplest explanation is that the free ion transition state is tighter than the ion pair transition state when the nucleophile is *para*-chlorothiophenoxide ion, Fig. 3, and that some factor(s) other than the charge on the sulfur of the nucleophile is important in determining transition state structure.

The unexpected changes in the secondary α-deuterium kinetic isotope effect found when the *para*-chlorothiophenoxide ion is the nucleophile are not caused by changes in product composition (18) for two reasons. First, quantitative yields of the S_N2 products, benzyl phenyl sulfide and *N,N*-dimethylaniline, are found in these reactions. Secondly, the isotope effects in the side reaction would be very similar to that in the major reaction. Thus, even if a small amount of the side reaction occurred, the effect on the observed secondary α-deuterium kinetic isotope effect would be very small. Thus product composition cannot be responsible for the unexpected changes in the isotope effect.

Conjugation between the α carbon and the phenyl ring, which reduces the magnitude of secondary α-deuterium kinetic isotope effects, only appears to be important when strongly electron-donating groups are on the benzene ring on the α carbon (15). Thus, changes in conjugation would not seem to be the cause of the unexpected isotope effects.

Finally, the secondary α-deuterium kinetic isotope effects found in this study are less than or equal to those found in the S_N2 reactions of other quaternary ammonium salts (5, 19, 20). Since large secondary α-deuterium kinetic isotope effects, significantly greater than the equilibrium isotope effect, are found when changes in the reaction coordinate motion and (or) tunneling are important in determining the magnitude of secondary α-deuterium isotope effects (16, 17), it seems unlikely that this factor is important in affecting the magnitude of these isotope effects. As a result, it would appear that the more likely explanation is the simple one, i.e., that the magnitude of the isotope effects is related to the structure of the transition state. In any case, it would seem unlikely that changing a *para*-hydrogen to a *para*-chloro substituent, which only changes the rate constant by 40%, would change the reaction coordinate motion and (or) tunneling enough to cause the different behaviour of the isotope effect.

The Hammett ρ values, obtained by changing the *para* substituent on the nucleophile, were determined for both the solvent-separated ion pair complex and the free ion reactions, Table 4, in an effort to learn more about the relative S_N2 transition state structures for these reactions. The identical Hammett ρ values for the two types of reactions show that this technique is not useful in distinguishing between the lengths of the α-carbon–sulfur bonds in the free ion and solvent-separated ion pair complex transition states (1).

Finally, the difference between the secondary α-deuterium kinetic isotope effects for the free ion and the ion pair complex reactions is large when the nucleophile is *para*-methoxythiophenoxide ion but becomes smaller when a more electron-withdrawing substituent is on the thiophenoxide ion. In fact, the difference in the isotope effects is almost zero when the nucleophile is thiophenoxide ion and is inverse when the reactant is the *para*-chlorothiophenoxide ion. Although we do not understand these observations, these results are interesting because they suggest that the effect of ion pairing is largest when strongly electron-donating and electron-withdrawing substituents are present.

It is interesting that the difference between the rate constants for the free ion and solvent-separated ion pair complex reactions is very small. Although we do not understand why this is so, similar differences in rate have been found in several other S_N2 reactions we have studied (1).[3]

Conclusion

This work has shown that the secondary α-deuterium kinetic isotope effect (transition state structure) is altered significantly when the form of the reacting ionic nucleophile is altered from a free ion to a solvent-separated ion pair complex in the S_N2 reactions between benzyldimethylphenylammonium ion and a series of *para*-substituted sodium thiophenoxides in methanol. Also, the magnitude of the substituent effect found by changing a *para* substituent on the ionic nucleophile is significantly larger when the nucleophile is a free ion rather than a solvent-separated ion pair complex. The transition states are tighter when a poorer nucleophile is used in both the free ion and ion pair reactions. Also, with one exception, the S_N2 reaction between *para*-chlorothiophenoxide ion and benzyldimethylphenylammonium ion, the ion pair transition states are tighter than the free ion transition states. Finally, the Hammett ρ values found by changing the substituent on the nucleophile do not appear to be useful in determining the relative lengths of the α-carbon–sulfur bonds in the ion pair complex and free ion transition states.

Experimental

Preparation of reagents

The preparation of the benzyldimethylphenylammonium nitrate and the *para*-substituted sodium thiophenoxides is described elsewhere (2, 19). The purification of the solvent is described in ref. 1. The 15-crown-5 ether was purchased from Parrish Chemical Co.

Product analysis

Approximately 0.12 g of benzyldimethylphenylammonium nitrate was reacted with 0.12 g sodium thiophenoxide in 85 mL of purified

[7]Two different statistical tests, the Wilcoxin test and the Student's T test (12, 13) indicate that the secondary α-deuterium kinetic isotope effects for the ion pair and free ion reactions with *para*-chlorothiophenoxide ion are significantly different at the 99% confidence level.

Can. J. Chem. Downloaded from www.nrcresearchpress.com by 122.72.124.2 on 09/07/12
For personal use only.

methanol for 5500 min (approximately 14 half-lives) at 20°C. Then, the reaction mixture was poured into 1400 mL of pH 12 water and the products were extracted once with 200 mL, twice with 150 mL, and twice with 100 mL of ether. The combined ether layers wre extracted twice with 40 mL, and once with 30 mL of a 10% sulfuric acid solution. Evaporation of the ether layer under reduced pressure left a solid whose nmr spectrum was consistent with that of the expected S_N2 product, benzyl phenyl sulfide. No peaks associated with the other possible product, methyl phenyl sulfide, were apparent even at a high spectrum amplitude.

Most of the water was removed from the combined 10% sulfuric acid solutions on a rotary evaporator. A Kjeldahl analysis (2) of the concentrate was consistent with a 98% yield of *N,N*-dimethylaniline (the expected S_N2 product). If even a small amount of the other possible product, *N*-benzyl-*N*-methylaniline, had been present, a much lower yield of *N,N*-dimethylaniline would have been obtained.

An identical experiment, except that 2 mL of 15-crown-5 ether was present in the reaction mixture, gave the same results. The only substitution product visible in the nmr spectrum was benzyl phenyl sulfide, and the Kjeldahl analysis indicated the yield of *N,N*-dimethylaniline was 99%.

Kinetic method

After all of the apparatus had been cleaned and dried at 140°C, it was sealed while hot or cooled in a desiccator. Six 125-mL Erlenmeyer flasks with ground glass stoppers were filled with extra dry nitrogen and weighed accurately. Then, these flasks, samples of the appropriate *para*-substituted sodium thiophenoxide and benzyldimethylphenylammonium nitrate, a crude balance, and some spatulas were placed in an IR^2 glove bag that was sealed, filled, evacuated, and refilled with extra-dry nitrogen. About 520 mg (3.9×10^{-3} mol) of the *para*-substituted sodium thiophenoxide was placed in three of the Erlenmeyer flasks and approximately 59 mg (2.2×10^{-4} mol) of benzyldimethylphenylammonium nitrate was placed in the other Erlenmeyer flasks. These flasks were removed from the glove bag and the amount of each salt determined by weighing them accurately.

The Erlenmeyers containing the *para*-substituted sodium thiophenoxide, the Erlenmeyers containing the quaternary ammonium salt, adaptors fitted with a serum cap, a bottle of purified methanol (*vide supra*), a graduated cylinder, three glass-stoppered 50-mL Erlenmeyer flasks for each *para*-substituted sodium thiophenoxide sample, three 1-mL and one 75-mL pipettes, and a rubber pipetting bulb, were placed in the glove bag under a nitrogen atmosphere (*vide supra*). Approximately 40 mL of methanol was added to each Erlenmeyer containing the *para*-substituted sodium thiophenoxide and 75 mL of methanol was pipetted into the Erlenmeyers containing the quaternary ammonium salt. Finally, three 1-mL samples of each sodium thiophenoxide solution were transferred to the three 50-mL Erlenmeyers.

The reaction flasks containing the quaternary ammonium salt and the sodium thiophenoxide solutions were temperature equilibrated at 20.00 ± 0.02°C for at least 45 min. The purity of the thiophenoxide salt was determined by titrating the samples in the 50-mL Erlenmeyers with standard mercury II nitrate (2). Finally, the kinetic run was begun by injecting 5 mL of the *para*-substituted sodium thiophenoxide solution into the reaction vessel with a 5-mL Hamilton air-tight syringe.

The kinetic data were obtained by withdrawing 5-mL aliquots of the reaction mixture with a 5-mL Hamilton gas-tight syringe fitted with a 6-in. needle. Each sample was quenched by adding it to 15 mL of a solution prepared by diluting 2.3 mL of a 25% solution of nitric acid to 1 L with methanol. The unreacted thiophenoxide ion was determined in a titration using a standard mercury II nitrate (2). The rate constants were calculated using standard methods (3).

Acknowledgement

The authors gratefully acknowledge the financial support provided by the Natural Sciences and Engineering Research Council of Canada.

1. K. C. WESTAWAY and Z.-G. LAI. Can. J. Chem. **66**, 1263 (1988).
2. K. C. WESTAWAY and R. A. POIRIER. Can. J. Chem. **53**, 3216, (1975).
3. K. C. WESTAWAY and S. F. ALI. Can. J. Chem. **57**, 1354 (1979).
4. K. C. WESTAWAY and Z. WASZCZYLO. Can. J. Chem. **60**, 2500 (1982).
5. H. A. JOLY and K. C. WESTAWAY. Can. J. Chem. **64**, 1206 (1986).
6. K. C. WESTAWAY. *In* Isotopes in organic chemistry. Vol. 7. *Edited by* E. Buncel and C. C. Lee. Elsevier, New York, NY. 1987. p. 275.
7. E. BUNCEL, B. C. MENON, and J. P. COLPA. Can. J. Chem. **57**, 999 (1979).
8. R. J. WILLIAMS, J. N. PHILLIPS, and K. J. MYSELS. Trans. Faraday Soc. **51**, 728 (1955).
9. J. J. CHRISTENSEN, D. J. EATOUGH, and R. M. IZATT. Chem. Rev. **74**, 351 (1974).
10. D. M. BRUBAKER. Ph. D. dissertation. University of Arkansas, Fayetteville, AR. 1978.
11. J. A. POPLE and D. L. BEVERIDGE. Approximate molecular orbital theory. McGraw–Hill, New York, NY. 1970.
12. R. D. G. STEEL and J. H. TORRIE. Principles and procedures of statistics with special reference to biological sciences. McGraw–Hill, Toronto, Ont. 1960. pp. 404 and 470.
13. C. WHITE. Biometrics, **8**, 33 (1950).
14. J. E. GORDON. The organic chemistry of electrolyte solutions. J. Wiley and Sons, Toronto, Ont. 1975. p. 372.
15. Z. WASZCZYLO and K. C. WESTAWAY. Tetrahedron Lett. **23**, 143 (1982).
16. W. P. HUSKEY and R. L. SCHOWEN. J. Am. Chem. Soc. **105**, 5704 (1983).
17. W. H. SAUNDERS, JR. J. Am. Chem. Soc. **106**, 2223 (1984).
18. D. J. MCLENNAN and P. M. W. GILL. Isr. J. Chem. **26**, 378 (1985).
19. K. C. WESTAWAY and S. F. ALI. Can. J. Chem. **57**, 1089 (1979).
20. E. C. F. KO and K. T. LEFFEK. Can. J. Chem. **49**, 129 (1971).

Can. J. Chem. Downloaded from www.nrcresearchpress.com by 122.72.124.2 on 09/07/12
For personal use only.

Mobility of thermal cations in liquids of *n*-alkanes, *n*-pentane to *n*-tetradecane: effect of viscosity and comparison to neutral molecule diffusion

NORMAN GEE AND GORDON R. FREEMAN

Chemistry Department, University of Alberta, Edmonton, Alta., Canada T6G 2G2

Received July 5, 1988

NORMAN GEE and GORDON R. FREEMAN. Can. J. Chem. **67**, 27 (1989).

The cation mobility μ_+ was measured in *n*-pentane at 295 K and in *n*-C_6 to C_{11} and *n*-C_{14} alkanes from ~295 K to their normal boiling points. The dependence on viscosity $\mu_+ \propto \eta^{-p}$ was reexamined and the best fit occurred with $p = 1.0$. The ratio of diffusion coefficients of neutral molecules to analogous cations was ~3 because of the stronger interaction of ions with the fluid molecules (electrostriction). The dependence of μ_+ on free volume is illustrated.

Key words: thermal cation mobility, *n*-alkane solvents, viscosity effects

NORMAN GEE et GORDON R. FREEMAN. Can. J. Chem. **67**, 27 (1989).

Opérant dans le pentane à 295 K de même que dans les alcanes *n*-C_6 à C_{11} et *n*-C_{14} de 295 K jusqu'à leurs points d'ébullition normaux, on a mesuré les mobilité cationiques μ_+. On a réévalué la relation qui existe entre μ_+ et η^{-p} et on a déterminé que la meilleure corrélation se produit lorsque $p = 1{,}0$. Le rapport des coefficients de diffusion des molécules neutres et ceux des cations analogues est d'environ 3; ce fait est le résultat de l'interaction plus forte des ions avec les molécules de fluide (électrostriction). On donne une illustration de la relation qui existe entre μ_+ est le volume libre.

Mots clés : mobilité cationique thermique, solvants des alcanes-*n*, effets de viscosité

[Traduit par la revue]

Can. J. Chem. Downloaded from www.nrcresearchpress.com by 122.72.124.2 on 09/07/12
For personal use only.

Introduction

On the basis of Stokes' Law (1) and Walden's Rule (2) the mobility of cations μ_+ in liquids is often compared to the fluid viscosity η using

[1] $\mu_+ \propto \eta^{-p}$

While the rules suggest $p = 1$, experimentally a range of p from 0 to 1.5 has been reported (3–9). Indeed if a liquid is heated from below its normal boiling point T_b towards its critical fluid region the value of p varies in a complicated fashion with changing η/η_c (subscript c denotes critical fluid property) (9, 10).

In the *n*-alkane liquids *n*-pentane to *n*-hexadecane $p = 1.5$ has been reported (3–5), although examination of each liquid separately ($281 \leq T/K \leq 324$) showed that p varied from 1.0 to 1.7 (Table 1 of ref. 4). This contrasted with our findings in small *n*-alkanes methane to *n*-hexane (10, 11) where in the dense liquids $p \approx 1.0$. Recently we obtained sufficiently purified samples of *n*-pentane to *n*-tetradecane that electrons generated in them decayed with half lifes of 5 to 240 μs (12, 13). In this study μ_+ was measured in the purified liquids at temperatures from (295 ± 1) K to near T_b. The application of eq. [1] to the large *n*-alkanes is re-examined and the transport of the cations is compared to that of the neutral molecules in the liquids.

Experimental

A. Materials and sample preparation

The *n*-alkanes were (supplier, mol% purity): *n*-pentane (Aldrich HPLC, 99.5), *n*-hexane (Phillips Research Grade, >99.99), *n*-heptane (Aldrich HPLC, 99.9), *n*-octane (Phillips Research Grade, >99.88), *n*-nonane (Aldrich, 99), *n*-decane (Phillips Research Grade, >99.85), *n*-undecane (Aldrich, 99), *n*-tetradecane (Terochem Labs., >99). Each hydrocarbon was further purified by the procedure of ref. 12: 125 mL of liquid was (*a*) stirred with concentrated H_2SO_4 to remove unsaturated impurities and water; (*b*) decanted onto and held on Molecular Sieves 4A to remove trace acid; (*c*) vigorously bubbled with argon (Liquid Carbonic UHP, >99.999 mol%) and isolated under argon to exclude air; (*d*) transferred without further contact with atmosphere into a grease-free glass vacuum line and degassed to remove argon; (*e*) transferred into a glass bulb connected by a Hoke Inc. (model 4251N6Y) valve to the vacuum line. The bulb contained a 50/50 sodium/potassium alloy. After transfer, the valve was closed and the liquid gently stirred for >3 weeks on the alloy.

To get high purity samples, in which electron half lives of 10–100 μs could be obtained, two steps were needed: (*a*) the transfer distance from the bulb containing sample and alloy to the conductance cell was <30 cm; (*b*) the transfer time to the cell was <10 min.

After the sample was transferred onto alloy and stirred >3 weeks the sideline was isolated and the glass cut above the Hoke valve of the alloy bulb. The bulb was then repositioned and attached to the sideline above a second valve leading to the conductance cell such that when both valves were opened, the liquid would flow under the pull of gravity from the storage bulb into the reservoir bulb of the cell. The sideline was then repaired and evacuated. Before the cell was filled, it was evacuated to $<10^{-4}$ Pa and heated at >530 K while pumping for >1 week, then cooled back to room temperature (295 ± 1 K). After ~50 mL of liquid was flowed into the cell the material was frozen to liquid N_2 temperature, and the cell was sealed using a flame.

B. Apparatus and other techniques

The conductance cell was like that shown in ref. 14 with the electrode geometry shown in ref. 15*a* (plate separation $l = 4.76$ mm, collector area = 7.92 cm^2). The heating apparatus (15*a*), temperature control (15*a*) and measurement (11), voltage sources (15*b*), and data collection system (15*b*) have been described.

The cations were produced by ionizing the liquid in the cell with 0.3 or 1.0 μs pulses of X-rays, 1.3 or 4.0 (10^{11} eV/g), from a Van de Graaf accelerator. The free ion yield was less than 0.7 ion-pairs/(100 eV absorbed dose) at all (E,T) of this work (13), so that [ions]/[molecules] $< 10^{-12}$. The mobility was obtained from

[2] $\mu_+ = l^2/t_d V$

where V is the applied voltage. The time of flight t_d was taken to equal the time required for the radiation-induced ion current to return to the baseline (15*b*) or for the integrated charge to reach its maximum value (10*b*). The first method was used for *n*-heptane, *n*-octane, *n*-nonane, and *n*-undecane, and the second for the other liquids. These methods give the mobility of the slowest ion in the liquid, which is the cation rather than the anion (4, 8).

C. Physical properties

Values of the viscosity were from ref. 16 for *n*-decane and *n*-tetradecane, and from refs. 17 and 18 for the other liquids. Densities d were from ref. 18, but the tetradecane density at 293.2 K is 762.7 kg/m^3 not 772.7.

Results and discussion

The cation mobilities were independent of electric field strength at $2.1 \leq E\,(10^5\ V/m) \leq 21$. The value of μ_+ cited at

TABLE 1. Summary of results in n-C_xH_{2x+2} liquids

x^a	T (K)	η^b (10^{-3} Pa s)	d^c (kg m^{-3})	μ_+ (10^{-8} m^2 V^{-1} s^{-1})	$D_{mol}{}^d$ (10^{-9} m^2 s^{-1})
5	295	0.233	624	7.0	5.1
6	296	0.302	657	5.3	4.0
	319	0.241	635	6.4	5.2
	338	0.208	617	7.4	6.4
	343	0.201	612	8.0	6.7
7	296	0.400	681	4.3	2.9
	319	0.320	662	5.1	3.9
	329	0.294	653	5.6	4.3
	338	0.272	645	6.1	4.7
	359	0.229	626	7.1	5.9
	366	0.217	619	7.5	6.3
	372	0.205	613	7.9	6.7
8	295	0.535	701	2.9	2.1
	332	0.361	670	3.8	3.4
	356	0.293	650	4.9	4.4
	380	0.239	629	5.9	5.7
	400	0.201	610	7.8	7.1
9	296	0.690	715	2.4	1.70
	313	0.557	702	3.0	2.2
	341	0.411	679	3.7	3.2
	373	0.308	652	4.8	4.5
	402	0.247	627	6.6	6.0
	423	0.213	609	7.7	7.4
10	295	0.898	728	1.58	1.28
	310	0.725	717	1.85	1.61
	323	0.615	707	2.2	1.95
	337	0.523	695	2.6	2.4
	370	0.374	669	3.9	3.4
	423		625	5.7	6.1
11	295	1.15	739	1.45	
	352	0.543	697	3.0	
	401	0.342	658	5.0	
	452	0.236	614	7.2	
	473	0.205	595	8.3	
14	296	2.19	761	0.68	
	319	1.43	744	1.10	
	348	0.932	724	1.72	
	373	0.690	706	2.6	
	397	0.541	688	3.2	
	426		666	4.4	
	455		644	5.4	
	486		619	6.9	
	506		601	8.1	

[a]No. of carbon atoms in alkane molecule.
[b]Dynamic fluid viscosity, refs. 16–18, 10^{-3} Pa s = 10^{-2} Poise.
[c]Reference 18.
[d]Neutral–neutral self diffusion coefficient, refs. 24–26.

each temperature of this work was obtained by averaging ~10 measurements, half using positive and half using negative applied voltage. The average deviation of the measurements from the mean was ~3%. The present results are summarized in Table 1.

A. Effect of viscosity

The cation mobilities are plotted against viscosity in Fig. 1. The η/η_c values are for n-pentane to n-octane in which $\eta_c = (2.68 \pm 0.04) \times 10^{-5}$ Pa s (18); this connects the present work to previous studies that related p (eq. [1]) to η/η_c (9, 10). At higher η the best fit of the present μ_+ was to

$$[3] \quad \mu_+ = A\eta^{-1.0}$$

with μ_+ (m^2/V s), η (Pa s), and $A = 1.6 \times 10^{-11}$ C/m. The mean deviation between the present experimental values and eq. [3] is 6%.

To show the lack of fit if $p = 1.5$, the dot–dashed line in Fig. 1 has the equation

$$[4] \quad \mu_+ = B\eta^{-1.5}$$

where $B = 4.0 \times 10^{-13}$ (C/m) (Pa s)$^{1/2}$.

Can. J. Chem. Downloaded from www.nrcresearchpress.com by 122.72.124.2 on 09/07/12
For personal use only.

Can. J. Chem. Downloaded from www.nrcresearchpress.com by 122.72.124.2 on 09/07/12
For personal use only.

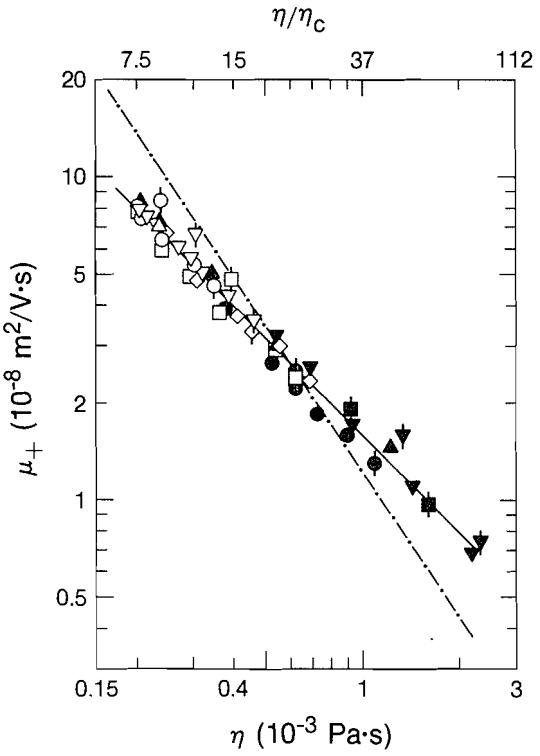


FIG. 1. Plot of cation mobility against fluid viscosity. The η/η_c scale is for *n*-pentane to *n*-octane ($\eta_c = (2.68 \pm 0.04) \times 10^{-5}$ Pa s (18)). Symbols are as follows: *n*-pentane (△,△), *n*-hexane (○,○), *n*-heptane (▽,▽), *n*-octane (□,□), *n*-nonane (◇,◇), *n*-decane (●,●), *n*-undecane (▲), *n*-dodecane (■), and *n*-tetradecane (▼,▼). The symbols with vertical bars are refs. 4 and 5; others are present work. —, eq. [3] with $A = 1.6 \times 10^{-11}$ C/m, ···, eq. [4] with $B = 4.0 \times 10^{-13}$ (C/m) (Pa s)$^{1/2}$.

Cation mobilities from Table 1 of ref. 4 are included in Fig. 1. The pioneering measurements of Adamczewski (3*a*, 4), which introduced the use of eq. [4], were excluded. Those measurements gave two cation mobilities, the values of which bracket the single values reported in later work (4, 5). For example in *n*-hexane at 294 ± 2 K Adamczewski reported 2.8×10^{-8} and 8.4×10^{-8} m^2/V s compared with 5.8×10^{-8} m^2/V s (5). The more recent values given in ref. 4 are in general agreement with the present work (Fig. 1) and are fitted by eq. [3] within the experimental uncertainty.

B. Comparison to molecular diffusion

Although positive hole (electron hopping) mobilities have been observed in two cyclic hydrocarbons (cyclohexane and transdecalin) (19, 20), the motion of cations in *n*-hydrocarbons is like that of the neutral molecules. Each diffusive displacement is small compared to a molecular diameter. The diffusion coefficient for the cations D_+ is related to the mobility μ_+ by the Nernst–Einstein or Nernst–Townsend equation

$$[5] \quad D_+ = \mu_+ k_B T/\xi$$

where k_B is Boltzmann's constant and ξ the protonic charge (21). Diffusion coefficients in turn are related to fluid properties by the Stokes–Einstein relation

$$[6] \quad D = k_B T/S\pi r\eta$$

where r is the radius of the diffusing particle and $S = 4$ in the slipping boundary limit or 6 in the sticking boundary limit

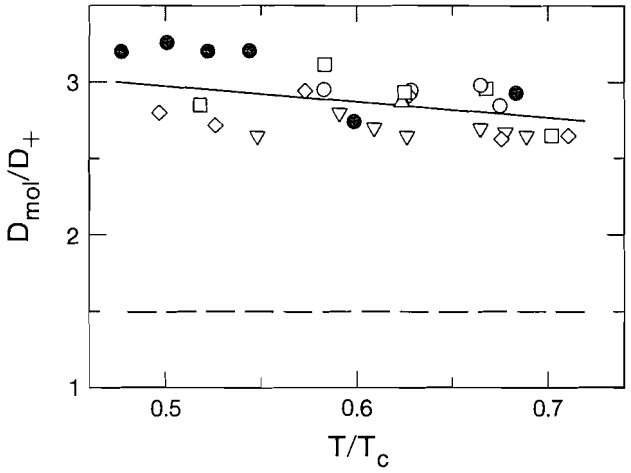


FIG. 2. Ratio of neutral molecule diffusion coefficient to cation diffusion coefficient (eq. [5]) against reduced temperature. T_c are from ref. 18. The dashed line indicates the value expected from the difference in eq. [6] between slip and stick boundary conditions. Symbols as Fig. 1.

(22, 23). For hydrocarbon liquids the neutral molecule self diffusion coefficient D_{mol} correlated with eq. [6] with $S \approx 4$. Available D_{mol} values for the present liquids are given in Table 1 (24–26). Using eq. [6] with $S = 4$ gave a radius r_{mol} that was constant in each liquid within a typical average deviation of ~2%. These radii were intermediate in value to radii estimated from polarizability α (27) using

$$[7] \quad r_\alpha = (\alpha/4\pi\epsilon_0)^{1/3}$$

where ϵ_0 is the permittivity of vacuum and α is in C m^2 V^{-1} (28), and radii estimated from neutral–neutral molecule Lennard–Jones collision diameters σ_{LJ} (29) using $r_{LJ} = \sigma_{LJ}/2$ (Table 2).

Because of their charge, ions interact more strongly with fluid molecules than do neutral molecules, so $S = 6$ in eq. [6] might apply (stick condition). Then if the cation radius r_+ is similar to r_{mol}, $D_{mol}/D_+ \sim 6/4 = 1.5$ would result (dashed line in Fig. 2). Experimentally $D_{mol}/D_+ \approx 3$. This larger ratio is largely due to electrostriction about the cations (30). In dense liquids of the less polarizable molecules xenon and argon, values of D_{mol}/D_+ were ~2.5 and ~1.7 respectively (30). Electrostriction (relative compaction of molecules about the ion) increased as the critical fluid was approached, so the values in Fig. 2 are shown against reduced temperature (critical point temperatures T_c are from ref. 18). By analogy with the Ar and Xe results (30), D_{mol}/D_+ in the present hydrocarbon liquids should increase as $T/T_c \rightarrow 1$.

Liquid phase diffusion coefficients (2, 25*a*, 26) and ion mobilities (5, 8, 9) are often presented as Arrhenius plots and discussed in terms of the associated activation energies. An alternate view describes transport in terms of temperature and density (or molar volume $v = M/d$ where M = molecular weight) without reference to energy barriers (31–34). Instead of plotting ln D against T^{-1}, straight or slightly curved lines are obtained by plotting D against molar volume v at constant T (35, 36), or for the saturated liquid (37), by plotting D against $T^{1/2}$ $(v - v_0)/v_0$ in which v_0 is the molar volume at which the liquid molecules are too crowded for diffusion to occur (32, 33). From eq. [5] it might be expected that

$$[8] \quad \mu_+ \propto (v - v_0)/v_0 T^{1/2}$$

This relation is examined for the present mobilities in Fig. 3

TABLE 2. Physical properties of n-C_xH_{2x+2} liquids

x	T_c[a] (K)	$\frac{\alpha}{4\pi\epsilon_0}$[b] ($10^{-30}$ m^3)	r_{mol}[c] (10^{-10} m)	r_α[d] (10^{-10} m)	r_{LJ}[e] (10^{-10} m)	v_0[f] (10^{-30} m^3/molecule)
5	470	10.0	2.7	2.2	3.1	156
6	508	11.8	2.8	2.3	3.0	184
7	540	13.6	2.9	2.4		214
8	569	15.5	3.0	2.5	3.7	243
9	595	17.3	2.9	2.6	4.2	274
10	619	19.1	3.0	2.7		304
11	640	20.9		2.8		334
14	695	26.4		3.0		420

[a]Critical point temperature, ref. 18.
[b]Molecular volume from polarizability, ref. 27.
[c]From D_{mol} and eq. [6] with $S = 4$.
[d]Equation 7.
[e]From neutral–neutral Lennard–Jones diameter, ref. 29.
[f]Reference 32.

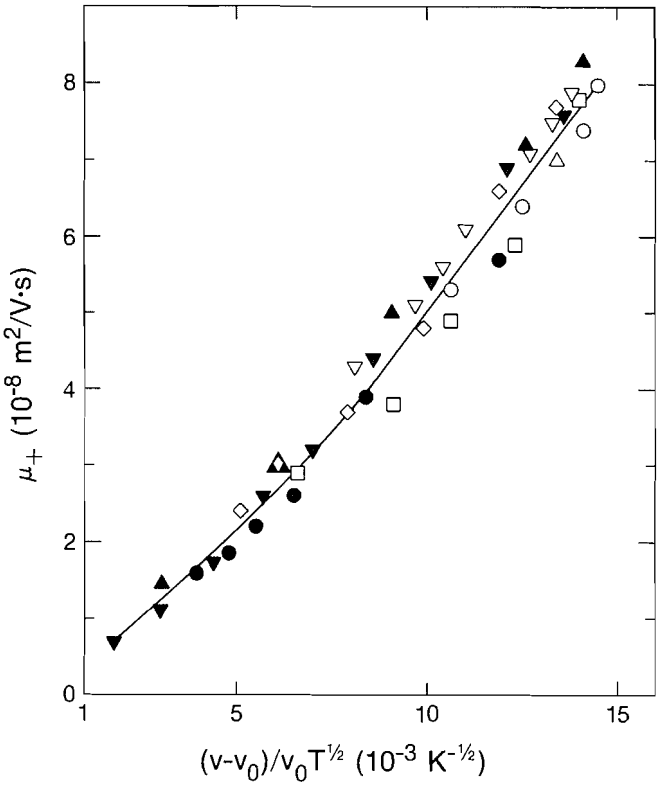


FIG. 3. Cation mobility against $(v - v_0)/v_0T^{1/2}$ (eq. [8]). Values of v_0 from Table 2. Symbols as in Fig. 1.

using v_0 values from Table 2. A slightly curved dependence results, with most deviation occurring at smaller free volumes $(v - v_0)$. All the present values seem to fall near the same curve. This illustrates the dominant effect of free volume on μ_+. The viscosity effect (Section III-A) is then indirect and reflects the fact that η is also determined by free volume (32).

Acknowledgement

We thank the Radiation Research Centre for providing the experimental equipment and facilities.

1. M. BORN. Z. Phys. **1**, 221 (1920).
2. P. WALDEN and H. ULICH. Z. Phys. Chem. **107**, 219 (1923).
3. I. ADAMCZEWSKI. (*a*) Ann. de Phys. **8**, 309 (1937); (*b*) IEEE EI-20, 481 (1985).
4. I. ADAMCZEWSKI and B. JACHYM. Acta Phys. Polon. **30**, 767 (1966).
5. O. GZOWSKI. (*a*) Nature **192**, 173 (1962); (*b*) Z. Phys. Chem. Leipzig, **221**, 288 (1962).
6. N. TSUCHIDA and M. UEDA. J. Phys. D**13**, 1681 (1980).
7. J. CASANOVAS, A. CHEMIN, J. P. GUELFUCCI, R. GROB, and J. P. CRINE. Revue Phys. Appl. **22**, 1037 (1987).
8. J.-P. DODELET and G. R. FREEMAN. Can. J. Chem. **53**, 1263 (1975); **55**, 2264 (1977).
9. S. S.-S. HUANG and G. R. FREEMAN. J. Chem. Phys. **70**, 1538 (1979); **72**, 1989 (1980).
10. N. GEE and G. R. FREEMAN. Can. J. Chem. (*a*) **58**, 1490 (1980); (*b*) **59**, 2988 (1981).
11. M. A. FLORIANO, N. GEE, and G. R. FREEMAN. Can. J. Chem. **66**, 1872 (1988).
12. N. GEE and G. R. FREEMAN. J. Chem. Phys. (*a*) **86**, 5716 (1987); (*b*) **87**, 5052 (1987).
13. N. GEE, P. C. SENANAYAKE, and G. R. FREEMAN. J. Chem. Phys. **89**, 3710 (1988).
14. J.-P. DODELET, K. SHINSAKA, U. KORTSCH, and G. R. FREEMAN. J. Chem. Phys. **59**, 2376 (1973).
15. N. GEE, M. A. FLORIANO, and G. R. FREEMAN. (*a*) J. Chem. Phys. **84**, 6799 (1986); (*b*) Z. Naturforsch. **39a**, 1225 (1984).
16. D. DUCOULOMBIER, H. ZHOU, C. BONED, J. PEYRELASSE, H. SAINT-GUIRONS, and P. XANS. J. Phys. Chem. **90**, 1692 (1986).
17. A. K. DOOLITTLE. J. Appl. Phys. **22**, 1032 (1951).
18. N. B. VARGAFTIK. Tables on the thermophysical properties of liquids and gases. 2nd ed. J. Wiley and Sons, Halsted Press, New York. 1975.
19. M. P. DE HAAS, A. HUMMEL, P. P. INFELTA, and J. M. WARMAN. J. Chem. Phys. **65**, 5019 (1976).
20. M. C. SAUER JR., K. H. SCHMIDT, and A. LIU. J. Phys. Chem. **91**, 4836 (1987).
21. E. W. MCDANIELS. Collision phenomena in ionized gases. J. Wiley and Sons, New York. 1964. p. 491.
22. J. JONAS and J. A. AKAI. J. Chem. Phys. **66**, 4946 (1977).
23. J. JONAS, D. HASHA, and S. G. HUANG. J. Phys. Chem. **84**, 109 (1980).
24. D. C. DOUGLASS and D. W. MCCALL. J. Phys. Chem. **62**, 1102 (1958).

Can. J. Chem. Downloaded from www.nrcresearchpress.com by 122.72.124.2 on 09/07/12
For personal use only.

25. G. M. PANCHENKOV, N. N. BORISENKO, and V. V. ERCHENKOV. Russ. J. Phys. Chem. (*a*) **43**, 1328 (1969); (*b*) **44**, 1633 (1970).
26. F. BACHL and H.-D. LÜDEMANN. Z. Naturforsch **41**a, 963 (1986).
27. H. STUART. *In* Landolt–Börnstein zahlenwerte und funktionen, I. Band, 3. Teil, Sect. 14207. *Edited by* A. Eucken and K. H. Hellwege. Springer-Verlag, Berlin. 1951. pp. 512, 513.
28. J. R. REITZ, F. J. MILFORD, and R. W. CHRISTY. Foundations of electromagnetic theory. 3rd ed. Addison-Wesley, Reading MA. 1979. p. 105.
29. E. A. MASON. *In* Molecular theory of gases and liquids. *Edited by* J. O. Hirschfelder, C. F. Curtiss, and R. B. Bird. J. Wiley and Sons, New York. Corrected printing, 1964. pp. 1213, 1214.
30. N. GEE, S. S.-S. HUANG, T. WADA, and G. R. FREEMAN. J. Chem. Phys. **77**, 1411 (1983).
31. J. H. DYMOND and B. J. ALDER. J. Chem. Phys. **45**, 2061 (1966).
32. J. H. HILDEBRAND and R. H. LAMOREAUX. Proc. Natl. Acad. USA **69**, 3428 (1972).
33. B. J. ALDER and J. H. HILDEBRAND. Ind. Eng. Chem. Fundam. **12**, 387 (1973).
34. D. CHANDLER. J. Chem. Phys. **62**, 1358 (1975).
35. R. L. HURLE and L. A. WOOLF. J. Chem. Soc. Faraday Trans. 1, **78**, 2233 (1982).
36. S. MECKL and M. D. ZEIDLER. Molec. Phys. **63**, 85 (1988).
37. I. GYÖRGY, N. GEE, and G. R. FREEMAN. Can. J. Chem. **63**, 1105 (1985).

Can. J. Chem. Downloaded from www.nrcresearchpress.com by 122.72.124.2 on 09/07/12
For personal use only.

Complexes of 18-crown-6 with oxonium ions derived from transition metal chlorides and hydrochloric acid: 18-crown-6.H_3O^+.$FeCl_4^-$, 18-crown-6.H_3O^+.$InCl_4^-$, (18-crown-6.H_3O^+)$_2$.$Pd_2Cl_6^{2-}$

ROBERT CHÊNEVERT[1] AND DANIEL CHAMBERLAND
Département de Chimie, Faculté des Sciences et de Génie, Université Laval, Québec (Qué.), Canada G1K 7P4

AND

MICHEL SIMARD AND FRANÇOIS BRISSE
Département de Chimie, Université de Montréal, C.P. 6128, Succ. A, Montréal (Qué.), Canada H3C 3J7

Received June 28, 1988

ROBERT CHÊNEVERT, DANIEL CHAMBERLAND, MICHEL SIMARD and FRANÇOIS BRISSE. Can. J. Chem. **67**, 32 (1989).

The macrocyclic polyether 18-crown-6 forms complexes with hydrates of strong acids derived from transition metal chlorides and hydrochloric acid. The following charged-component complexes have been isolated and characterized: 18-crown-6.H_3O^+.$FeCl_4^-$, 18-crown-6.H_3O^+.$InCl_4^-$, and (18-crown-6.H_3O^+)$_2$.$Pd_2Cl_6^{2-}$. X-ray diffraction study of the palladium complex is reported. The oxonium ion is located at the center of the macrocyclic ether cavity and the symmetry of the ring is close to D_{3d}.

Key words: 18-crown-6 complexes, oxonium ions, X-ray diffraction, crystal structure

ROBERT CHÊNEVERT, DANIEL CHAMBERLAND, MICHEL SIMARD et FRANÇOIS BRISSE. Can. J. Chem. **67**, 32 (1989).

L'éther macrocyclique 18-couronne-6 forme des complexes avec les hydrates des acides forts dérivés des chlorures des métaux de transition et de l'acide chlorhydrique. Nous avons isolé et caractérisé les complexes suivants : 18-couronne-6.H_3O^+.$FeCl_4^-$; 18-couronne-6.H_3O^+.$InCl_4^-$; (18-couronne-6.H_3O^+)$_2$.$Pd_2Cl_6^{2-}$. La structure du complexe de palladium a été déterminée par diffraction des rayons X. L'ion oxonium se trouve au centre de la couronne dont la conformation est voisine de la symétrie D_{3d}.

Mots clés : complexes 18-couronne-6, ions d'oxonium, diffraction des rayons-X, structure cristalline

Can. J. Chem. Downloaded from www.nrcresearchpress.com by 122.72.124.2 on 09/07/12
For personal use only.

Introduction

The macrocyclic polyether 18-crown-6 readily forms complexes with hydrates of strong acids (pK_a of the acid < pK_a of H_3O^+ at −1.7) which exist as hydronium salts. This type of complexation was first observed for the *cis-syn-cis*-dicyclohexano-18-crown-6 with $H_3O^+ClO_4^-$ or $H_3O^+PF_6^-$ (1). In recent years, it has been shown that 18-crown-6 is a good complexing agent for the hydronium ion, and complexes have been obtained with several strong acids (2–7). In these studies, it was generally assumed that the H_3O^+ ion in the adduct is located at the center of the macrocyclic ether cavity, as this would maximize the electrostatic interactions between the two units. This was also expected on the basis of the strong hydrogen bonds revealed by infrared spectroscopy (4), as these bonds presumably involve the H_3O^+ ion and the oxygen atoms lining the interior of the ether cavity. This hypothesis has been confirmed by X-ray diffraction studies (5–7).

With weak acids (pK_a of the acid > pK_a of H_3O^+ at −1.7) such as carboxylic acids and weak inorganic acids, neutral component complexes have been obtained (8, 9). These usually have a 1:1:1 or 2:2:1 (acid:water:crown) stoichiometry, although some anhydrous complexes have been reported (8, 10). The adduct formed with cyanoacetic acid (11) and later characterized by X-ray diffraction (12), provides a good structural model for these aqua complexes, in which the water molecule presumably serves as a linker between the acid and the ether.

In the present study, we report the preparation and characterization of complexes of 18-crown-6 with the hydronium ions derived from transition metal chlorides and hydrochloric acid.

Experimental

Preparation of the complexes (general procedure)

The transition metal chloride (2 mmol) is dissolved in tetrahydrofuran (25 mL) and concentrated hydrochloric acid (2 mL). This solution is added to a solution of 18-crown-6 (2 mmol) in tetrahydrofuran (15 mL). The complex crystallizes immediately at room temperature. The solid complex is filtered and dried under vacuum. The complex is recrystallized in tetrahydrofuran and dried under vacuum until constant melting points are obtained.

Physical data pertaining to the individual complexes are given below:

H_3O^+.18-crown-6.$FeCl_4^-$, **1**. Yield: 89%; mp 155–156°C (yellow). *Anal.* calcd. for $C_{12}H_{27}O_7FeCl_4$: C 29.96, H 5.66, Fe 11.61, Cl 29.48; found: C 30.34, H 5.79, Fe 11.51, Cl 29.69.

H_3O^+.18-crown-6.$InCl_4^-$, **2**. Yield: 83%; mp 129–130°C (colorless). *Anal.* calcd. for $C_{12}H_{27}O_7InCl_4$: C 26.69, H 5.04, Cl 26.26; found: C 26.46, H 5.49, Cl 26.63.

(H_3O^+.18-crown-6)$_2$.$Pd_2Cl_6^{2-}$, **3**. Yield: 80%; mp 159–160°C (reddish-brown). *Anal.* calcd. for $C_{24}H_{54}O_{14}Pd_2Cl_6$: C 29.05, H 5.49, Cl 21.44; found: C 29.47, H 5.52, Cl 21.40.

The NMR spectra were taken on a Varian XL-200 multinuclear spectrometer. The infrared spectra, obtained from Nujol mulls contained between Irtran-2 (ZnS) windows, were recorded on a Beckman-4250 spectrometer. The Raman spectra were recorded on a microcomputer controlled Spex Model 1400 spectrometer using the 514.5 nm exciting line from a Spectra Physics Model 165 argon ion laser. The spectra were obtained from the solids contained in sealed glass capillary cells. Ultraviolet–visible spectra were taken on a Hewlett-Packard-8450 spectrometer. The microanalyses were peformed by Dr. C. Daessle, Organic Microanalysis, Montreal, or by ourselves on a Carlo Erba Strumentazione-1106 elemental analyses instrument.

Crystallographic work for the (18-C-6.H_3O^+)$_2$.($Pd_2Cl_6^{2-}$) complex

The compound was very stable at room temperature which permitted an initial precession camera work to be done before mounting the crystal on a Nonius CAD-4 diffractometer. From the camera work, the symmetry of the unit cell is found to be monoclinic.

The automatic centering procedure of 25 reflections initially yielded a triclinic reduced cell. However, the Niggli matrix revealed that this cell could be transformed to a monoclinic C-centered cell, this symmetry being consistent with the earlier camera work. No systematic absences beside those due to the C-centering were found upon verification by a rapid precollection technique. Thus the three possible

[1]To whom correspondence should be addressed.

TABLE 1. Crystal data for the palladium complex (**3**) $(C_{12}H_{24}O_6.H_3O)_2.(Pd_2Cl_6)$

Formula weight	992.24
a (Å)	13.198(2)
b (Å)	18.439(4)
c (Å)	8.404(2)
β (deg)	101.95(2)
V (Å^3)	2000.8
d_c (g cm^{-3})	1.647
μ (CuKα) (cm^{-1})	117.13
λ (CuKᾱ) (Å)	1.54178
T (°C)	22
Crystal size (mm)	$0.12(010, 0\bar{1}0) \times 0.14(001, 00\bar{1}) \times 0.43(20\bar{1}, \bar{2}01)$

space groups $C2$, Cm, and $C2/m$ should be examined. The final unit cell was obtained after accurately centering higher angle reflections ($20° \leq \theta \leq 25°$). The final parameters are presented in Table 1.

As the absorption coefficient is relatively high, the intensity diffraction data were collected over the complete Laue diffraction sphere at higher scan speed (4°/s). This technique gives better intensity data after averaging of the symmetry related reflections once the absorption correction has been applied. The transmission factor has values between 0.11 and 0.36. Seven reference reflections were monitorized for the orientation and stability of the crystal. They showed less than ±1.6% variation of their intensities. Also, no reorientation of the crystal was necessary during the collection, the direction of the scattering vectors of the standard reflections being always less than 0.18° from the direction computed from the orientation matrix. Of the 7437 measured reflections, 6893 of them were declared observed based on the $I \geq 3\sigma(I)$ criteria. From this, 1975 unique reflections remained after averaging ($R_{av} = 0.039$) and were used in the structure resolution and refinement.

The structure was solved in the $C2/m$ space group by direct method and refined by full-matrix least-squares using the SHELX programs.[2] The palladium and two chlorine atoms were located first and were used as an initial phasing model. All the non-hydrogen emerged from the first difference Fourier synthesis, and upon isotropic refinement, the R ratio $\Sigma\Delta F/\Sigma F_o$, reached 0.116. Anisotropic refinement of the non-H atoms and the refinement of the H-atom coordinates and their isotropic temperature factors lowered the R-factor to 0.028. The introduction of a weighting scheme based on the counting statistics, $w = 1/(\sigma^2(F) + 0.00005(F)^2$, gave the following values at convergence: $R = 0.025$, $R_w = (\Sigma w\Delta F^2/\Sigma wF_o^2)^{1/2} = 0.034$ and the goodness-of-fit $S = [\Sigma w\Delta F^2/(m - n)]^{1/2} = 2.08$. The final difference Fourier synthesis showed only a background of less than 0.25 e/Å^3 with two residual peaks of 0.46 and 0.36 e/Å^3 at about 0.88 Å from the chlorine atoms. In all the above calculations the anomalous dispersion of Pd and Cl were included.

Results and discussion

Oxonium ion – crown ether complexes are prepared in 80–90% yield by mixing the transition metal chloride, aqueous hydrochloric acid, and 18-crown-6 in tetrahydrofuran. The complexes are stable solids with sharp melting points. The stoichiometry of the compounds were determined by elemental analysis (hydrogen, carbon, chlorine) and by atomic absorption analyses in the case of the iron complex. The analyses are in agreement with the stoichiometries defined by reactions [1] and [2] and with that observed in the X-ray determination for the palladium complex.

[2]The programs used here are modified versions of NRC-2, data reduction, NRC-10, bond distances and angles and NRC-22, mean planes; SHELX, program for structure determination and refinement and ORTEP, stereodrawings (13–15).

[1] 18-crown-6 + H_2O + HCl + $MCl_3 \rightarrow$ 18-crown-6.H_3O^+.MCl_4^-

M = Fe, **1**

M = In, **2**

[2] 2(18-crown-6) + 2H_2O + 2HCl + 2MCl_2 $\rightarrow$ (18-crown-6.H_3O^+)$_2$.$M_2Cl_6^{2-}$

M = Pd, **3**

Spectroscopy

The infrared spectra are clearly indicative of the presence of the H_3O^+ ion in each complex. The bands are readily assigned by comparison to literature (16, 17) values for hydronium salts: 2780–3250 cm^{-1} (ν_1, symmetric stretching), 2500–3100 cm^{-1} (ν_3, asymmetric stretching), 1480–1705 cm^{-1} (ν_4, asymmetric bending), and 1050–1180 cm^{-1} (ν_2, symmetric bending). The stretching modes of H_3O^+ (ν_1, ν_3) are responsible for the strong and broad band at ~2950 cm^{-1} which overlaps with the sharper maximum arising from the C—H stretching of the crown in the 2925 cm^{-1} region (Table 2). The exact position of the ν_2 mode is difficult to determine as it occurs in a region of strong absorption by the C—O stretching of the crown ether. However, the first harmonic of ν_2 is always present at ~2190 cm^{-1}. The asymmetric bending mode (ν_4) gives a characteristic band at ~1650 cm^{-1}. Infrared spectra also indicate some departure from the D_{3d} symmetry for the crown. Infrared spectra of symmetric complexes such as M^+.18-C-6.Br^- contain two singlets in the 800–1000 cm^{-1} region: CH_2 rocking at 960 cm^{-1} and C—C stretching at 835 cm^{-1} (18, 19). The crown is distorted to a lower symmetry and two doublets are observed at ~805, 830 and ~930, 960 cm^{-1} in the spectra of oxonium complexes **1**–**3**. This distortion of the ring is confirmed by the X-ray diffraction study of the palladium adduct.

Compared with those of 18-crown-6, the ^{1}H NMR signals of the crown ether protons in the complexes are shifted downfield and new signals characteristic of the oxonium ion protons appear in the region 7–11 ppm (Table 2). The chemical shift for the oxonium ion protons is concentration-dependent. A significant paramagnetic shift of the crown proton resonance is observed in the iron compound whereas the shifts in other two complexes are small. The integrations further confirm the 1:1 stoichiometry of the complexes. In ^{13}C NMR, the chemical shift of the crown carbons in the indium and palladium adducts are close to the shift of the free crown carbons in the same solvent. Again, a larger shift (to higher field) can be observed with the iron adduct. Nuclear magnetic resonance signals of the indium and palladium adducts are relatively sharp whereas line broadening occurs for the iron compound as expected from the paramagnetic properties of iron.

Can. J. Chem. Downloaded from www.nrcresearchpress.com by 122.72.124.2 on 09/07/12
For personal use only.

TABLE 2. Spectroscopic data of the complexes **1–3**

Compound	NMR (CD_2Cl_2)[a] (δ, ppm) ^1H	^{13}C	IR (Nujol) cm^{-1}	UV–VIS $\nu_{max}(\epsilon)$ (nm)
1	4.4 (24H, crown) 7.3 (3H, H_3O^+)	62.43	2950, 2160, 1680, 1345, 1285, 1245, 1135, 1080, 965, 935, 830, 805, 370[b]	242 (1.04×10^4) 316 (6.03×10^3) 364 (6.28×10^3) 534 (1.31) 620 (0.35) 688 (0.57) 730 (0.40)
2	3.74 (24H, crown) 9.9 (3H, H_3O^+)	70.30	2950, 2190, 1640, 1350, 1290, 1250, 1140, 1095, 950, 920, 835, 805, 320[b]	—
3	3.84 (24H, crown) 11.14 (3H, H_3O^+)	70.45	2950, 2190, 1650, 1350, 1285, 1245, 1135, 1095, 965, 940, 835, 810	251 (2.82×10^4)

[a]NMR data of the free crown in CD_2Cl_2: ^1H NMR: 3.60 ppm; ^{13}C NMR: 70.67 ppm.
[b]Irtran-2 cells are opaque below 700 cm^{-1} and the KBr pressed-pellet method was used for these bands.

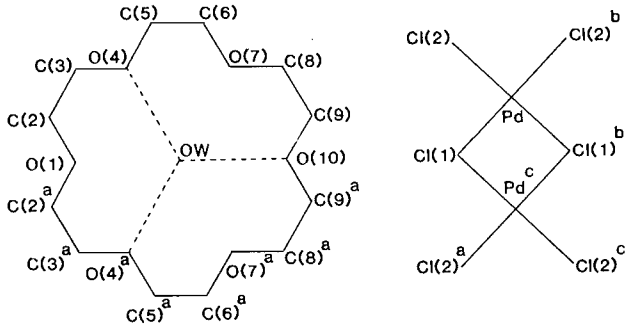


FIG. 1. Numbering scheme adopted for the $(18\text{-C-6}.H_3O)_2.(Pd_2Cl_6)$ complex, (*a*: $x, -y, z$; *b*: $-x, y, 1-z$; *c*: $-x, -y, 1-z$).

The tetrachloroferrate ion in compound **1** and the tetrachloroindate ion in compound **2** are characterized by very strong infrared absorptions at 370 and 320 cm^{-1}, respectively. These bands are attributable to the asymmetric stretching (ν_3) mode of the tetrahedral anions (20, 21). The Raman spectra of compounds **1** and **2** in the crystalline state show strong peaks at 332 and 322 cm^{-1} attributed to the symmetric stretching (ν_1) of regular tetrahedral $FeCl_4^-$ and $InCl_4^-$ ions (21). The electronic spectrum (Table 2) of the iron compound (**1**) is closely similar to those found for genuine organic salts of the tetrahedral $FeCl_4^-$ ion (20, 22). The palladium complex (**3**) shows an absorption at 251 nm while the indium complex has no significant absorption in the region studied.

Structural results

To gain further insight in the structures, X-ray analyses were undertaken; we report here the structure of $(18\text{-crown-6}.H_3O^+)_2.Pd_2Cl_6^{2-}$. It has been so far impossible to grow crystals of other compounds suitable for X-ray analysis. The X-ray structures of three complexes of H_3O^+ coordinated to macrocycles have been reported. The structure $[H_3O^+.18\text{-crown-6(COOH)}_4]Cl^-$ has been reported by Behr *et al.* (5). More recently the X-ray diffraction studies of $(18\text{-crown-6}.H_3O^+)_2.Mo_6O_{19}^{2-}$ and $(18\text{-crown-6}.H_3O^+).HCl_2^-$ have also been published (6, 7).

The unit-cell dimensions and other crystal data of interest determined from X-ray diffraction study of compound **3** are given in Table 1. The atomic numbering is given in Fig. 1. The bond distances and angles, calculated from the final atomic coordinates (see Table 3) are given in Tables 4 and 5.[3]

TABLE 3. Fractional atomic coordinates and their esd's ($\times 10^5$ for Pd and Cl, $\times 10^4$ for O and C), and U_{eq} ($\times 10^3$) for the $(18\text{-C-6}.H_3O)_2.(Pd_2Cl_6)$ complex

Atom	*X*	*Y*	*Z*	U_{eq}
Pd	0	9234(1)	50000	46
Cl(1)	10904(7)	0	44890(15)	65
Cl(2)	11797(7)	17741(4)	46679(12)	79
O(W)	3758(3)	0	1511(6)	117
O(1)	5910(2)	0	2843(4)	70
O(4)	4694(2)	1231(1)	2532(3)	68
O(7)	2726(2)	1362(1)	648(3)	78
O(10)	1791(3)	0	−3(4)	85
C(2)	6254(3)	636(2)	3710(5)	81
C(3)	5806(3)	1269(2)	2764(5)	80
C(5)	4225(3)	1913(2)	2109(4)	73
C(6)	3095(3)	1846(2)	1937(4)	78
C(8)	1636(3)	1255(2)	368(6)	96
C(9)	1377(3)	648(3)	−795(5)	94

The crown ether

Since there are only two formulas, $(18\text{-C-6}.H_3O^+)_2.Pd_2Cl_6^{2-}$, per unit cell and the space group is $C2/m$ the 18-crown-6 ether has a mirror plane of symmetry passing through O(1) and O(10). The average C—O distance is 1.419 Å. The average C—C distance is 1.473 Å showing the characteristic shortening observed in all crystal structure analysis of the crown ethers so far published (accepted distance for a C—C bond is 1.535 Å). O—C—C angles (average value 108.6°) are smaller than tetrahedral (109.5°) while the average C—O—C angle is 113.1°. The detailed conformation of 18-crown-6 is best

[3]Tables of H-atom coordinates, anisotropic temperature factors, and the list of observed and calculated structure amplitudes have been deposited. Copies may be purchased from the Depository of Unpublished Data, CISTI, National Research Council of Canada, Ottawa, Ont., Canada K1A 0S2.

Can. J. Chem. Downloaded from www.nrcresearchpress.com by 122.72.124.2 on 09/07/12
For personal use only.

TABLE 4. Bond distances (Å) and angles (deg) for the $(18\text{-C-6}.H_3O)_2.(Pd_2Cl_6)$ complex

Bond	Distances (esd's)	Bonds	Angles (esd's)
18-Crown-6			
O(1)—C(2)	1.406(4)	C(2)[a]—O(1)—C(2)	113.1(3)
C(2)—C(3)	1.466(5)	O(1)—C(2)—C(3)	109.4(3)
C(3)—O(4)	1.442(4)	C(2)—C(3)—O(4)	108.6(3)
O(4)—C(5)	1.414(4)	C(3)—O(4)—C(5)	111.8(2)
C(5)—C(6)	1.474(5)	O(4)—C(5)—C(6)	109.4(3)
C(6)—O(7)	1.410(4)	C(5)—C(6)—O(7)	108.1(3)
O(7)—C(8)	1.422(5)	C(6)—O(7)—C(8)	113.0(3)
C(8)—C(9)	1.479(6)	O(7)—C(8)—C(9)	107.6(3)
C(9)—O(10)	1.421(5)	C(8)—C(9)—O(10)	108.2(3)
		C(9)—O(10)—C(9)[a]	114.5(3)
$Pd_2Cl_6^{2-}$			
Pd—Cl(1)	2.3260(7)	Cl(1)—Pd—Cl(2)	90.96(3)
Pd—Cl(2)	2.6677(9)	Cl(1)—Pd—Cl(1)[b]	85.89(3)
		Cl(1)—Pd—Cl(2)[b]	174.78(3)
		Cl(2)—Pd—Cl(2)[b]	92.47(3)
		Pd—Cl(1)—Pd[c]	94.11(3)

[a] $x, -y, z$.
[b] $-x, y, 1-z$.
[c] $-x, -y, 1-z$.

TABLE 5. Bond distances (Å) and angles (deg) related to the hydrogen bonding in the $(18\text{-C-6}.H_3O)_2.(Pd_2Cl_6)$ complex

Bond	Distances (esd's)	Bonds	Angles (esd's)
O(W)—O(4)	2.641(3)	O(4)—O(W)—O(10)	120.2(2)
O(W)—O(10)	2.644(6)	O(4)—O(W)—O(4)[a]	118.5(2)
		O(W)—O(4)—C(3)	118.7(2)
		O(W)—O(4)—C(5)	122.1(2)
		O(W)—O(10)—C(9)	118.0(2)
O(W)—H(W1)	0.88(3)	H(W1)—O(W)—H(W2)	119(2)
O(W)—H(W2)	0.78(3)	H(W2)—O(W)—H(W2)[a]	117(2)
O(4)—H(W2)	1.86(3)	O(W)—H(W2)—O(4)	175(2)
O(10)—H(W1)	1.77(3)	O(W)—H(W1)—O(10)	177(2)

[a] $x, -y, z$.

described in terms of the torsion angles about the ring bonds (Table 6). All torsion angles about C—C bonds are close to *gauche* (average value is 64.2°) and those about C—O bonds are close *trans* (average value is 171.6°). The oxonium ion appears to be too small to fill the annular space within the ligand cavity and there is some departure from the crown conformation with D_{3d} symmetry. This distorsion is not as severe as in the $[H_3O^+.18\text{-crown-6(COOH)}_4]Cl^-$ complex reported by Behr *et al.* (5) where there is a highly disordered and pseudo-eclipsed O—C—C—O fragment.

The oxonium ion

The oxonium ion is also in the mirror plane of symmetry near the center of the crown (Fig. 2). It is 0.161(5) Å above the plane defined by O(4), O(10), O(4)[a] to which it is H-bonded and at −0.124(5) Å from the plane of the remaining ether oxygens, O(1), O(7), and O(7)[a]. Three strong hydrogen bonds hold the oxonium to the crown. The O(oxonium)...O(crown) separations are 2.641(3) and 2.644(6) Å. These distances are smaller than O(oxonium)...O(crown) distances found in other complexes (2.672–2.737 Å) so far reported (5–7). There has been some controversy about the geometry (pyramidal versus planar) of the oxonium cation (23). The X-ray study reported by Behr *et al.* (5) lends support for a pyramidal ion while in other studies (6, 7) the hydrogen atoms of the oxonium group could not be unequivocally located. In the present work, the H_3O^+

TABLE 6. Torsion angles (deg) in the 18-crown-6 moiety of the $(18\text{-C-6}.H_3O)_2.(Pd_2Cl_6)$ complex

Bonds	Angles (esd's)
C(2)[a]—O(1)—C(2)—C(3)	−176.3(3)
O(1)—C(2)—C(3)—O(4)	61.4(4)
C(2)—C(3)—O(4)—C(5)	161.0(3)
C(3)—O(4)—C(5)—C(6)	−178.3(3)
O(4)—C(5)—C(6)—O(7)	−62.9(3)
C(5)—C(6)—O(7)—C(8)	−180.0(3)
C(6)—O(7)—C(8)—C(9)	−170.2(3)
O(7)—C(8)—C(9)—O(10)	68.4(4)
C(8)—C(9)—O(10)—C(9)[a]	163.9(3)

[a] $x, -y, z$.

Can. J. Chem. Downloaded from www.nrcresearchpress.com by 122.72.124.2 on 09/07/12
For personal use only.

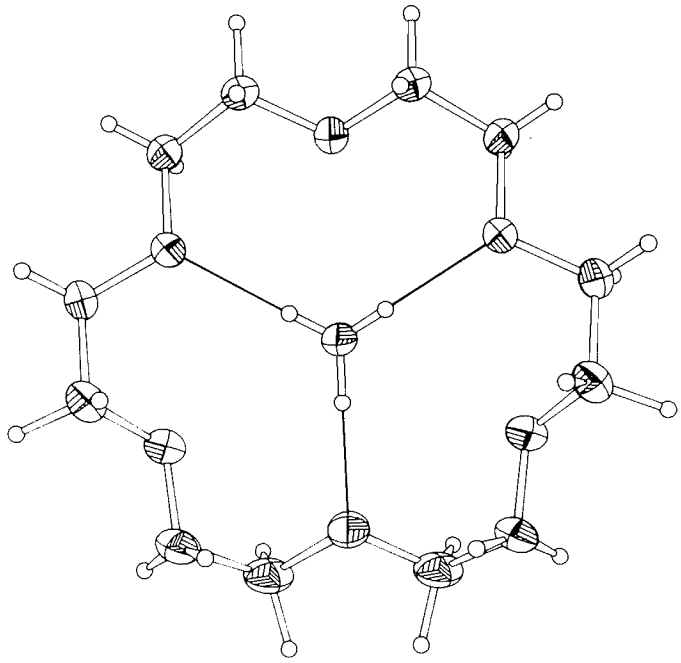


FIG. 2. View of the [18-6-C.H_3O^+] cation with the mirror plane of symmetry placed horizontally. The hydrogen atoms are represented by spheres of arbitrary size while the thermal ellipsoids of C and O atoms are drawn at the 50% probability level.

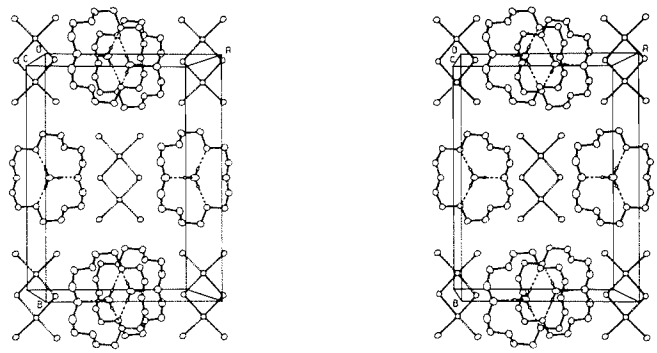


FIG. 3. Stereoview of the unit cell. The crown hydrogen atoms are omitted for clarity. Hydrogen bonds are represented as broken lines.

cation is *pyramidal*, the H—O—H angles are smaller (117° and 119°) than 120° and the oxygen atom is 0.091(5) Å above the plane of the H atoms.

The hexachlorodipalladate(II) anion

The anion is derived from the association of two square planar $PdCl_4^{2-}$ moieties by sharing two bridging chlorine atoms. The distances of 2.3260(7) and 2.6677(9) Å for the Pd—Cl bridge and Pd—Cl term are normal (24, 25). The bond angles around the metal centers, 85.89(3)–92.47(3)°, reflect the fact that the geometry is distorted from the planar shape due to the close arrangement of the Pd atoms. The Pd—Pd distance is 3.4053(3) Å. The two bridging chlorine atoms deviate the most, by ±0.116(1) Å, from the $Pd_2Cl_6^{2-}$ least-squares plane.

Acknowledgements

We acknowledge the financial support of this work from the Natural Sciences and Engineering Research Council of Canada and the Ministère de l'Éducation du Québec.

1. R. M. IZATT, B. L. HAYMORE, and J. J. CHRISTENSEN. J. Chem. Soc. Chem. Commun. 1308 (1972).
2. R. CHÊNEVERT, A. RODRIGUE, M. PIGEON-GOSSELIN, and R. SAVOIE. Can. J. Chem. **60**, 853 (1982).
3. G. S. HEO and R. A. BARTSCH. J. Org. Chem. **47**, 3557 (1982).
4. R. CHÊNEVERT, A. RODRIGUE, P. BEAUCHESNE, and R. SAVOIE. Can. J. Chem. **62**, 2293 (1984).
5. J. P. BEHR, P. DUMAS, and D. MORAS. J. Am. Chem. Soc. **104**, 4540 (1982).
6. C. B. SHOEMAKER, L. V. MCAFEE, D. P. SHOEMAKER, and C. W. DEKOCK. Acta Crystallogr. C, **42**, 1310 (1986).
7. J. L. ATWOOD, S. G. BOTT, A. W. COLEMAN, K. D. ROBINSON, S. B. WHETSTONE, and C. M. MEANS. J. Am. Chem. Soc. **109**, 8100 (1987).
8. R. SAVOIE, A. RODRIGUE, M. PIGEON-GOSSELIN, and R. CHÊNEVERT. Can. J. Chem. **63**, 1457 (1985).
9. R. CHÊNEVERT, A. RODRIGUE, D. CHAMBERLAND, J. OUELLET, and R. SAVOIE. J. Mol. Struct. **131**, 187 (1985).
10. S. DEGUIRE, F. BRISSE, J. OUELLET, and R. SAVOIE. Can. J. Chem. **64**, 142 (1986).
11. A. ELBASYOUNY, J. KLIMES, A. KNOCHEL, J. OEHLER, and G. Z. RUDOLPH. Naturforsch. Teil B, **31**, 1192 (1976).
12. A. ELBASYOUNY, H. J. BRUGGE, K. VON DEUTEN, M. DICKER, A. KNOCHEL, K. V. KOCH, J. KOPF, D. MELZER, and G. RODOLPH. J. Am. Chem. Soc. **105**, 6568 (1983).
13. F. R. AHMED, S. R. HALL, M. E. PIPPY, and C. P. HUBER. The NRC system of crystallographic computer programs for the IBM/360. Accession Nos. 133–147 in J. Appl. Crystallogr. **6**, 309 (1973).
14. G. M. SHELDRICK. SHELX, Programs for structure determination and refinement, University of Cambridge, England. 1976.
15. C. K. JOHNSON. ORTEP, Report ORNL-3794, Oak Ridge National Laboratory, TN.
16. R. D. GILLARD and G. WILKINSON. J. Chem. Soc. 1640 (1964).
17. R. SAVOIE and P. A. GIGUÈRE. J. Chem. Phys. **41**, 2698 (1964).
18. M. FOUASSIER and J. C. LASSEGUES. J. Chem. Phys. **75**, 865 (1978).
19. J. DALE and P. O. KRISTIANSEN. Acta Chem. Scand. **26**, 1471 (1972).
20. R. J. H. CLARK, B. CROCIANI, and A. WASSERMANN. J. Chem. Soc. 2458 (1970).
21. L. A. WOODWARD and M. J. TAYLOR. J. Chem. Soc. 4473 (1960).
22. N. S. GILL. J. Chem. Soc. 3512 (1961).
23. W. R. RODWELL and L. RADOM. J. Am. Chem. Soc. **103**, 2865 (1981).
24. E. A. KELLY, P. M. BAILEY, and P. M. MAITLIS. J. Chem. Soc. Chem. Commun. 289 (1977).
25. L. G. KUZ'MINA and YU. T. STRUCHKOV. Kodid. Khum. **9**, 705 (1983).

Can. J. Chem. Downloaded from www.nrcresearchpress.com by 122.72.124.2 on 09/07/12
For personal use only.

Some 6,6-disubstituted 2,4-cyclohexadien-1-ones and the facial selectivity in their Diels–Alder reactions with dimethyl acetylenedicarboxylate

PETER YATES, ANABELA GOMES, D. JEAN BURNELL,[1] DONG DAO CONG,[2] AND JEFFERY F. SAWYER
Lash Miller Chemical Laboratories, University of Toronto, Toronto, Ont., Canada M5S 1A1

Received June 30, 1988

PETER YATES, ANABELA GOMES, D. JEAN BURNELL, DONG DAO CONG, and JEFFERY F. SAWYER. Can. J. Chem. **67**, 37 (1989).

6,6-Disubstituted 2,4-cyclohexadien-1-ones can be prepared by dibromination–bisdehydrobromination of the corresponding 6,6-disubstituted 2,2-dibromocyclohexanones. Such dienes undergo Diels–Alder reactions with dimethyl acetylenedicarboxylate to give 3,3-disubstituted 5,6-di(methoxycarbonyl)bicyclo[2.2.2]octa-5,7-dien-2-ones; when the substituents at C-6 in the dienones are different, two diastereomers of the adducts are formed in a ratio dependent on the "facial selectivity" in the Diels–Alder reactions. For the cases where one of the 6-substituents is methyl and the other is methoxycarbonyl, acetoxymethyl, dibromomethyl, or dichloromethyl it has been established via X-ray crystallography and chemical correlation that the *endo*-3-methyl/*exo*-3-methyl product ratio is 3.0, 0.9, 8, and 6, respectively. The origin of these differences is discussed briefly and a spectroscopic method for the assignment of structures to the individual diastereomers is proposed.

Key words: Diels–Alder reactions, substituted 2,4-cyclohexadien-1-ones, facial selectivity, dimethyl acetylenedicarboxylate.

PETER YATES, ANABELA GOMES, D. JEAN BURNELL, DONG DAO CONG et JEFFERY F. SAWYER. Can. J. Chem. **67**, 37 (1989).

On peut préparer les cyclohexadiène-2,4 ones-1 disubstituées en 6,6 en procédant à la dibromation, suivie d'une bisdéhydrobromation, des dibromo-2,2 cyclohexanones disubstitués en 6,6. De tels dièmes peuvent être soumis à des réactions de Diels–Alder avec l'acétylènedicarboxylate de diméthyle et ces réactions conduisent à des di(méthoxycarbonyl)-5,6 bicyclo[2.2.2]octadiène-5,7 ones-2 disubstituées en 3,3; lorsque les deux substituants en position 6 sont différents, il y a formation des deux diastéréoisomères des adduits et leur rapport dépend de la «sélectivité faciale» des réactions de Diels–Alder. Dans les cas où l'un des substituants est un méthyle alors que l'autre est un méthoxycarbonyle, un acétoxyméthyle, un dibrométhyle ou un dichlorométhyle, on a déterminé, par diffraction des rayons-X ainsi que par corrélation chimique, que les rapports des méthyl-3-*endo*/méthyl-3-*exo* sont respectivement 3,0, 0,9, 8 et 6. On discute brièvement de l'origine de ces différences et on propose une méthode spectroscopique permettant d'attribuer les structures des diastéréoisomères individuels.

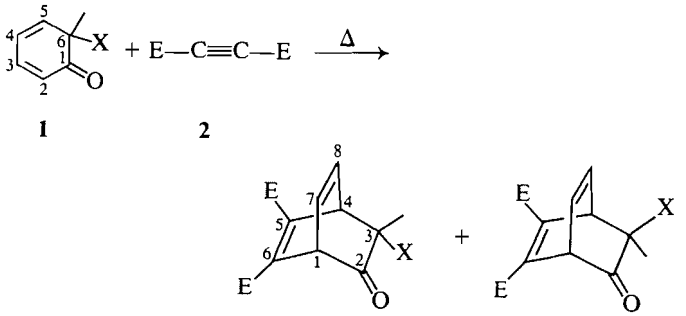
Mots clés : réactions de Diels–Alder, cyclohexadiène-2,4 ones-1 substituées, sélectivité faciale, acétylènedicarboxylate de diméthyle.

[Traduit par la revue]

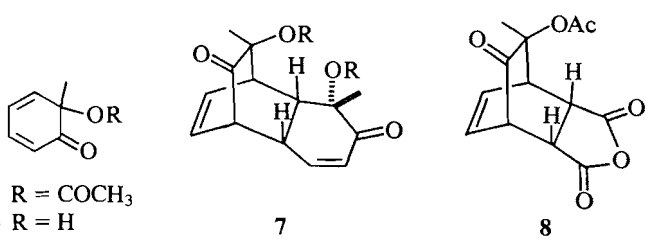
Introduction

In work in these Laboratories on the synthesis of cedranoid sesquiterpenes (1), the "facial selectivity" in the Diels–Alder reaction between 2,4-cyclohexadien-1-ones of type **1** and dimethyl acetylenedicarboxylate (DMAD; **2**) (Scheme 1) is of importance in the exercise of stereochemical control. Two diastereomeric bicyclo[2.2.2]octadiene derivatives, **3** and **4**, can be formed in such reactions by attack of the dienophile on one or the other face of the diene. Although the *endo–exo* terminology is strictly applicable only to bicyclo[2.2.1]heptane derivatives and other bridged bicyclic systems with at least one bridge of different length than the others, we have found it convenient to extend it in the present cases in the sense shown in Scheme 1, where the *unsubstituted* bridge corresponds to the one-carbon bridge of the bicyclo[2.2.1]heptane system. Thus **3** is designated as the *exo*-3-methyl-*endo*-3-X isomer and **4** as the *endo*-3-methyl-*exo*-3-X isomer.[3]

Surprisingly, until relatively recently there has been little systematic work on facial selectivity in Diels–Alder reactions in general.[4] Many of the investigations pertaining to 2,4-cyclohexadien-1-ones have concerned compounds of types **5** and **6** formed via Wessely oxidation of phenols. These give Diels–Alder dimers that, when formed under kinetic control, have the stereochemistry shown in **7**, i.e., attack in both the diene and dienophile partner occurs selectively on the face bearing the OR group. They show this same selectivity when they react with dienophiles other than themselves, e.g., in **8** (2).



SCHEME 1



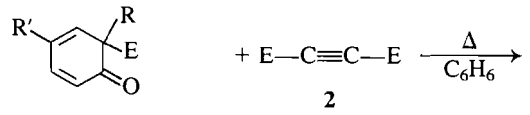
[1]Present address: Department of Chemistry, Memorial University of Newfoundland, St. John's, Nfld., Canada A1B 3X7.

[2]Present address: Uniroyal Research Laboratories, Guelph, Ont., Canada N1H 6N3.

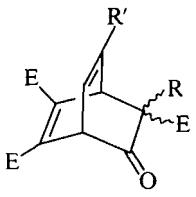
[3]It should be noted that the ring numbering for **3** and **4** and other bicyclo[2.2.2]octane derivatives in the Discussion is based on that for bicyclo[2.2.2]octan-2-one, to facilitate comparison among these compounds. For similar reasons the ring numbering for the dienones is based on 2,4-cyclohexadien-1-one. The IUPAC names for the compounds are used in the experimental section.

[4]Some early observations are summarized in ref. 2.

Can. J. Chem. Downloaded from www.nrcresearchpress.com by 122.72.124.2 on 09/07/12
For personal use only.



9 R = CH_3, R′ = H
10 R = $CH_2C_6H_5$, R′ = H
11 R = R′ = CH_3

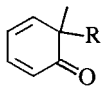


		Ratio
12*a,b*	R = CH_3, R′ = H	3:1
13*a,b*	R = $CH_2C_6H_5$, R′ = H	2:1
14*a,b*	R = R′ = CH_3	9:1

SCHEME 2

During the course of the present work Schultz *et al.* (3) reported the synthesis of the three 2,4-cyclohexadien-1-ones **9–11** and the Diels–Alder reaction of these with DMAD in boiling benzene to give diastereomeric mixtures of adducts **12***a,b*–**14***a,b*, respectively, in the ratios shown in Scheme 2. Because of the mild conditions of the reactions, it is probable that these product ratios are kinetically determined. However, configurational assignments were not made for the individual diastereomers.

There has been a great deal of recent work, both experimental and theoretical, on the facial selectivity of other dienes. Important contributions (4–8) have been made by Gleiter, Paquette, Vogel, Houk, Hehre, Valenta, and Fallis *inter al.*[5] This work has shown that the facial selectivity can be affected by a number of factors, although not all are necessarily important in a particular case. These include (*i*) steric effects, (*ii*) secondary orbital overlap, (*iii*) orbital tilting, (*iv*) torsional effects, (*v*) electrostatic interactions, (*vi*) polarizability, and (*vii*) coordination of the diene and dienophile. Although much has been learned about the dependence of facial selectivity on some of these factors, their number often makes it difficult to predict the facial selectivity in specific terms. Thus these results must be supplemented with additional empirical data. In the case of the reactions of 2,4-cyclohexadien-1-ones (**1**) with DMAD (**2**) we have sought to do this by determining the product ratios and the individual diastereomeric structures of the adducts of DMAD with compounds **9** and **15–17**. The syntheses of the dienones are first described, since some aspects of these are of intrinsic interest.



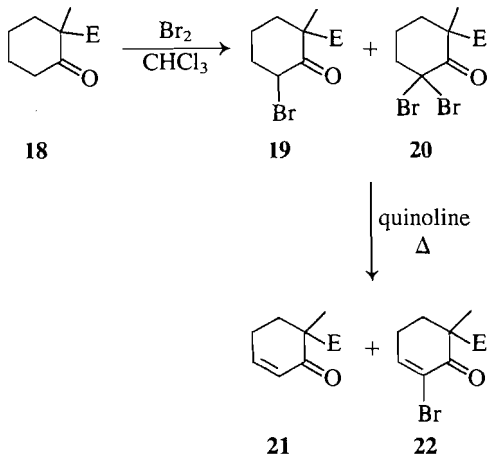
9 R = E
15 R = CH_2OCOCH_3
16 R = $CHBr_2$
17 R = $CHCl_2$

Results

Preparation of 2,4-cyclohexadien-1-ones

The method we used for the preparation of 6-methoxycarbonyl-6-methyl-2,4-cyclohexadiene-1-one (**9**) involved introduction of two ethylenic bonds into the saturated keto ester **18**, and was initially based on an earlier synthesis of the analogous

[5]For summaries of some of these contributions, see ref. 9.



SCHEME 3

ethyl ester (10). Bromination of **18** with slightly more than one molar equivalent of bromine gave the monobromo product **19** contaminated with 30% of the dibromo compound **20** (Scheme 3). The ^{1}H nmr spectrum of the crude reaction product suggested that a single diastereomer of **19** was formed, but its configuration was not determined. Dehydrobromination of the crude bromination product in boiling quinoline gave methyl 1-methyl-2-oxo-3-cyclohexenecarboxylate (**21**) accompanied by a small amount of its 3-bromo derivative **22**. The latter must arise by dehydrobromination of the dibromo compound **20**. The yields obtained in the dehydrobromination were low (~25%).

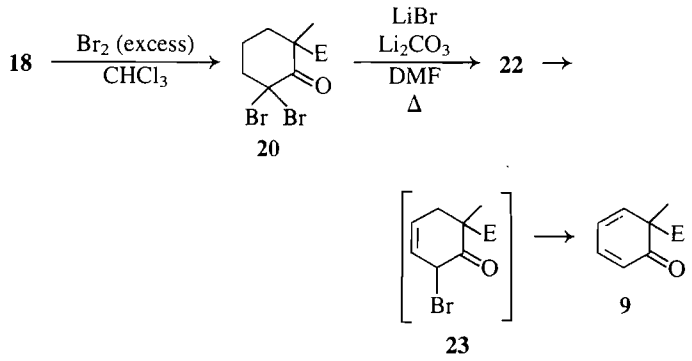
We had originally planned to synthesize **9** by allylic bromination of **21** followed by dehydrobromination (10). However, it was observed that dehydrobromination of the dibromo compound **20** with boiling quinoline also gave **9**, albeit in poor yield. We therefore decided to prepare the dibromo compound **20** deliberately and to carry out its bisdehydrobromination. We also took the opportunity to use different dehydrobromination conditions, viz., treatment with lithium bromide and lithium carbonate in hot *N*,*N*-dimethylformamide (DMF) (11). Under these conditions the diene **9** was obtained, but still in low yield. Monitoring of the progress of the reaction by ^{1}H nmr spectroscopy showed that, as expected, the monodehydrobromination product **22** was first formed and then underwent slower conversion to **9**. The intermediacy of **22** under these conditions was also demonstrated by its dehydrobromination to **9** under the same conditions. This conversion is considered to proceed via base-catalyzed isomerization of **22** to the 3-cyclohexen-1-one **23** followed by 1,4-dehydrobromination (Scheme 4).

Because of the occurrence of competing reactions (*vide infra*) it was necessary to terminate the dehydrobromination before the reaction was complete, resulting in the isolation of a mixture of **9** and **22**. These could not be separated by chromatography, but the mixture could be used for the Diels–Alder reaction of **9**.

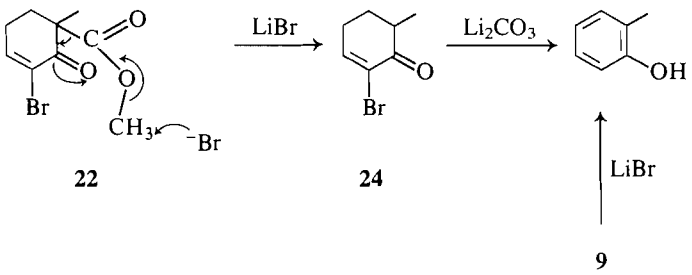
Although the yield via this route is very low (~15%), the method is preferable to that via **19** in that, in the latter, two separate dehydrobromination steps are required, while the former involves only a "one-pot" procedure for the dehydrobromination steps.

To obtain some insight into the cause of the low yields in the dehydrobromination reactions we treated compound **22** with lithium carbonate and lithium bromide in DMF for 3 h. Chromatography of the crude reaction product gave two major fractions; one was shown by ^{1}H nmr spectroscopy to be a

Can. J. Chem. Downloaded from www.nrcresearchpress.com by 122.72.124.2 on 09/07/12
For personal use only.



SCHEME 4



SCHEME 5

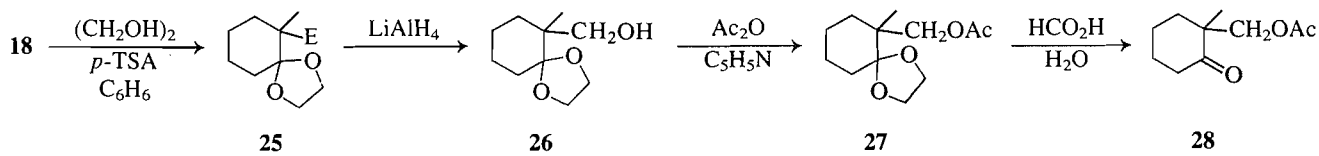
mixture of **22** and **9**, while the spectrum of the other showed that it was a mixture of two components, neither of which contained a methoxycarbonyl group. The ir and ^1H and ^{13}C nmr spectra of the latter mixture indicated strongly that the two components were 2-bromo-6-methyl-2-cyclohexen-1-one (**24**) and *o*-cresol. The formation of these products is readily accounted for as shown in Scheme 5. It has previously been shown (12) that esters undergo dealkoxycarbonylation on being heated with lithium bromide. Dehydrobromination of **24** would give *o*-cresol. Thus the low yield in the preparation of **9** by this route is attributable, at least in part, to the loss of the methoxycarbonyl group under the reaction conditions. In the case of 6-alkyl-6-alkoxycarbonyl-2,4-cyclohexadien-1-ones of type **9**, the route designed by Schultz *et al.*, involving Birch reduction — alkylation of *o*-hydroxybenzoic acid derivatives (3), is certainly preferable to the route that we have used. However, in the case of other 6,6-disubstituted 2,4-cyclohexadien-1-ones the dibromination–bisdehydrobromination route is practicable (*vide infra*) and the Birch reduction route may not be applicable.

Compound **15**, 6-(acetoxymethyl)-6-methyl-2,4-cyclohexadien-1-one, was synthesized from **25**, the ethylene ketal of **18**, by a route similar to that used in the case of **9**. Compound **28** was obtained by the route shown in Scheme 6. As in the case of **9**, conversion of **28** to **15** was first attempted via monobromination to **29** followed in this instance by dehydrobromination with 1,8-diazabicyclo[5.4.0]undec-7-ene (DBU) (cf. ref. 3) to **30**; however, allylic bromination of this with *N*-bromosuccinimide proved to be unsuccessful. Compound **28** was therefore dibrominated to give **31**, the analogue of **20**. Bisdehydrobromination of this with DBU was unsuccessful, but treatment with lithium bromide and lithium carbonate in DMF for 16.5 h gave an excellent yield of the diene **15** (Scheme 7).

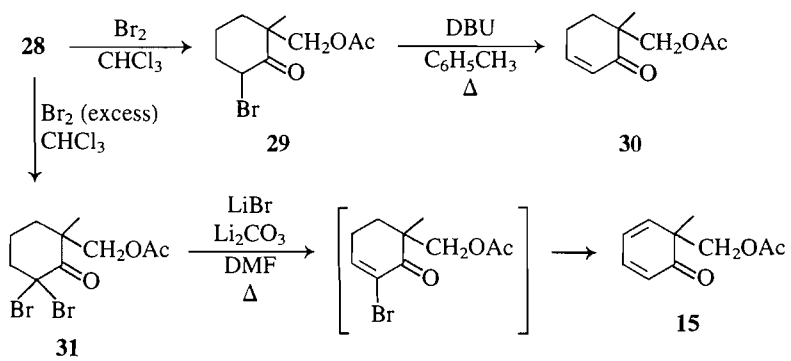
The remaining 2,4-cyclohexadienones, **16** and **17**, were prepared as described previously via "abnormal Reimer–Tiemann" reactions of *o*-cresol (13) (Scheme 8). Because complex mixtures of products are formed, the yields of **16** and **17** are low; however, the starting materials are in abundant supply.

Diels–Alder reactions of 2,4-cyclohexadien-1-ones

Reaction of **9** with DMAD in boiling benzene for 2 days gave a 3:1 mixture of the diastereomeric Diels–Alder adducts, **12***a* and **12***b* (Scheme 9), as determined by ^1H nmr spectroscopy. The isomers were separated chromatographically. The most egregious differences in their spectra are the chemical shift difference ($\Delta\delta$ 0.05) between the highest field methoxyl proton signals and the difference in splitting patterns of the C-5 and C-8 vinyl proton signals. These differences must involve the 3-methoxycarbonyl group, which is situated at the seat of the difference in the relative configurations of the isomers. In the ^{13}C nmr spectra the signals of the corresponding C-7 and C-8 ($\Delta\delta$ 1.2, 1.6) carbon atoms and the signals of the C-2 ketonic carbonyl carbons ($\Delta\delta$ 3.5) adjacent to C-3 show the significant

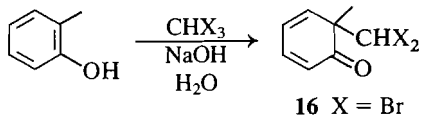


SCHEME 6



SCHEME 7

Can. J. Chem. Downloaded from www.nrcresearchpress.com by 122.72.124.2 on 09/07/12
For personal use only.



16 X = Br
17 X = Cl

SCHEME 8

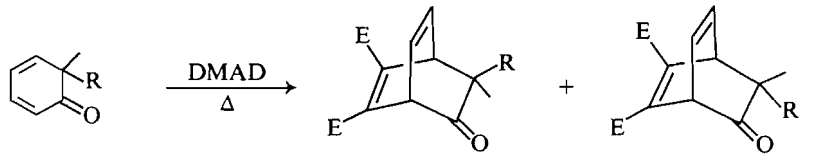
differences. Although these differences are small they are sufficient to distinguish the isomers; however, they provide no conclusive basis for the assignment of individual structures to these isomers. For this we had resort to an X-ray crystallographic determination of the structure of the major isomer, which was thus found to have structure **12***a* (14).

Reaction of **15** with DMAD in boiling benzene for 2 days gave a 0.9:1 mixture of the adducts **32***a* and **32***b* (Scheme 9). These stereoisomers were separated by repeated chromatography; their R_f values were very similar and the recovery of the pure compounds was low. Their gross structures and ratio in the reaction mixture were determined spectroscopically. In the ^{1}H nmr spectrum of the major isomer the vinyl proton assignments (H-7 and H-8) were established by double irradiation experiments with irradiations at the frequencies of the bridgehead proton signals, H-1 and H-4. In its ^{13}C nmr spectrum the assignments were verified by the use of ^{1}H–^{13}C 2-D chemical shift correlation via long-range coupling.

The minor isomer has similar spectra, which are distinct enough to allow the isomers to be differentiated, but not sufficiently so to permit unambiguous individual stereochemical assignments. An indication that the major isomer has structure **32***b* was obtained from an nOe experiment: irradiation at the frequency of the C-methyl signal at δ 1.11 resulted in an 8% enhancement of the C-4 bridgehead signal at δ 4.10 and a 5% enhancement of the C-8 vinyl proton signal at δ 6.60. However, the relatively low values of these enhancements were insufficient to establish the stereochemistry firmly, and the individual structural assignments in Scheme 9 were later confirmed by correlation with other Diels–Alder adducts (*vide infra*).

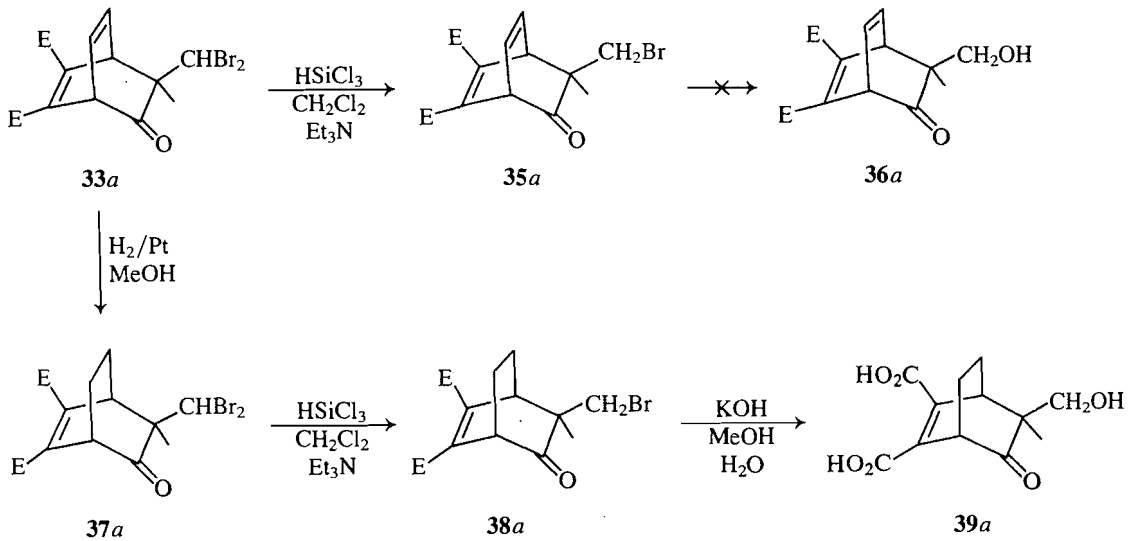
Reaction of the dienone **16** with DMAD was very much slower than that of **9** or **15**, and was carried out neat at 105–160°C for 2 days. It gave an 8:1 mixture of the adducts **33***a* and **33***b*, of which the first was isolated by crystallization and the other was obtained as an oil by chromatography of the mother liquor. As in the previous cases the spectra of the diastereomeric products could be distinguished but could not be used for individual stereochemical assignments. This was carried out by an X-ray crystallographic determination of the structure of the major isomer, which showed it to be the *endo*-methyl *exo*-(dibromomethyl) isomer **33***a* (Scheme 9) (15).

It was hoped originally that the structure of **33***a* could be established by correlation with that of **12***a* (Scheme 10). To this end **33***a* was reduced with trichlorosilane and triethylamine (16) to the monobromomethyl compound **35***a*, but this could not be converted to the corresponding hydroxymethyl compound **36***a* by basic treatment under a variety of conditions. Since this failure could result from cleavage reactions facilitated by the



			a:*b*
9 R = E	**12***a* R = E	**12***b* R = E	3:1
15 R = CH_2OAc	**32***a* R = CH_2OAc	**32***b* R = CH_2OAc	0.9:1
16 R = $CHBr_2$	**33***a* R = $CHBr_2$	**33***b* R = $CHBr_2$	8:1
17 R = $CHCl_2$	**34***a* R = $CHCl_2$	**34***b* R = $CHCl_2$	6:1

SCHEME 9

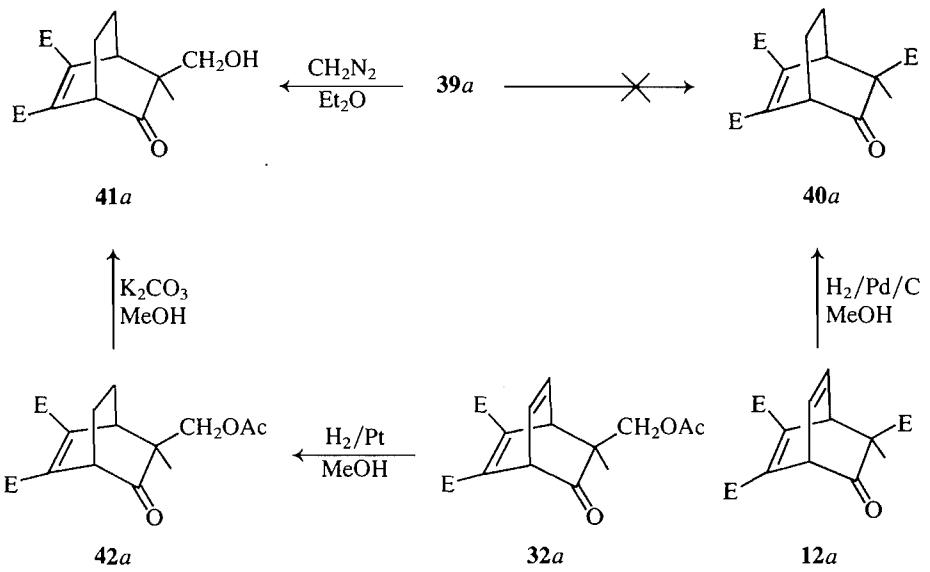


33*a* **35***a* **36***a*

37*a* **38***a* **39***a*

SCHEME 10

Can. J. Chem. Downloaded from www.nrcresearchpress.com by 122.72.124.2 on 09/07/12
For personal use only.



SCHEME 11

C-7—C-8 double bond, the dibromomethyl compound was converted to its dihydro derivative **37***a* by hydrogenation and this was reduced with trichlorosilane to give **38***a*, which on treatment with aqueous base gave the hydroxymethyl dicarboxylic acid **39***a*. This could not be converted to the triester **40***a*, which would have been correlatable with the dihydro derivative of **12***a*.

However, **39***a* served the purpose of correlation of the major dibromomethyl isomer **33***a* with the minor acetoxymethyl isomer **32***a* (Scheme 11). Esterification of **39***a* with diazomethane gave the hydroxymethyl diester **41***a*, which was shown to be spectroscopically identical with the hydroxymethyl diester formed by hydrolysis of the dihydro derivative **42***a* of the isomer **32***a*. The major isomer **32***b* was converted by the same route to **41***b* via the dihydro compound **42***b*. The spectra of this were found to be readily distinguishable from those of its isomer **41***a*. These observations confirmed the tentative assignments for **32***a* and **32***b* based on the nOe experiment discussed earlier.

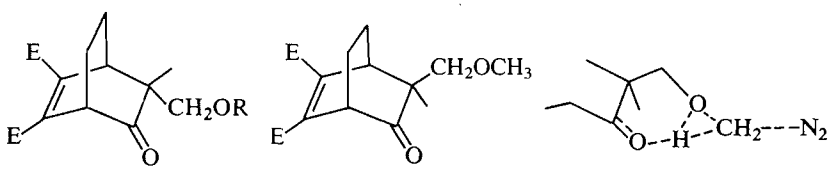
Methylation of **39***a* with diazomethane gave a minor product in addition to **41***a*; this is assigned structure **43***a* on the basis of the similarity of its ir spectrum to that of **41***a*, except for the absence of a hydroxyl-stretching band, and its molecular formula as determined by high resolution mass spectrometry. The methylation of an alcoholic hydroxyl group under these conditions is unusual, and may be ascribable to the formation of a transition state of type **44**.

The dichloromethyl analogue **17** of the dibromomethyl dienone **16** gives, with DMAD, a mixture of adducts, **34***a* and **34***b*, which in this case are formed in a 6:1 ratio. Only the major isomer was isolated in pure form and fully characterized spectroscopically. However, comparison of the ^{13}C nmr spectra of this isomer and a mixture of isomers enriched in the minor isomer **34***b* permitted the identification and assignment of the signals of the latter. The individual structures assigned to the major and minor isomers are based on analogy with the case of the dibromomethyl compounds.

Discussion

Facial selectivity

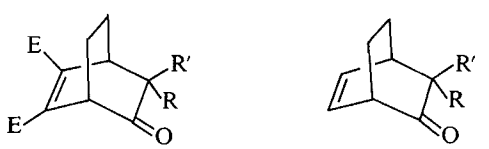
Valenta and co-workers have noted (7) that the major product in the Diels–Alder reaction of a planar non-symmetric diene results in most cases from addition to the less hindered face, although in some cases facial selectivity is determined by "what might loosely be called 'electronic' effects." We propose that for the 6-(dihalomethyl)-6-methyl-2,4-cyclohexadien-1-ones **16** and **17** the steric effect predominates, and that the bulky



41*b* R = H
42*b* R = Ac

43*a*

44



45*a* R = CH_3, R′ = $CHCl_2$
46 R = R′ = CH_3

47*a* R = CH_3, R′ = H
47*b* R = H, R′ = CH_3
48 R = R′ = CH_3

Can. J. Chem. Downloaded from www.nrcresearchpress.com by 122.72.124.2 on 09/07/12
For personal use only.

Can. J. Chem. Downloaded from www.nrcresearchpress.com by 122.72.124.2 on 09/07/12
For personal use only.

dihalomethyl groups hinder attack by DMAD, resulting in a strong preference for attack on the methyl face of the dienones and the formation of the *endo*-3-methyl *exo*-3-(dihalomethyl) isomers **33***a* and **34***a* as the major products.

It seems unlikely that for the 6-(acetoxymethyl)-6-methyl and 6-(methoxycarbonyl)-6-methyl dienones **15** and **9**, steric effects will be predominant with the *acetylenic* dienophile DMAD, whose steric demand is small. In conformity with this view **15** gives closely similar amounts of the adducts **32***a* and **32***b*, with a slight preference for the latter. Steric control, if operative, would be expected to favor formation of the former, since it is expected that the van der Waals radius of an acetoxymethyl group would be slightly greater than that of a methyl group. It is possible that the slight preference for attack on the acetoxymethyl face results from favorable secondary orbital interactions analogous to those postulated by Anh to occur in the Diels–Alder reaction of 5-acetoxycyclopentadiene with ethylene (17), where preferential attack also occurs on the more hindered, acetoxy face of the diene.

In the case of the 6-(methoxycarbonyl)-6-methyl dienone **9**, it is more difficult to assess which is the sterically more favorable pathway. The methyl face is expected to be more hindered than the methoxycarbonyl face, based on the conformational free energy differences of the appropriately substituted cyclohexanes (18). However, this criterion must be used with caution (19), and all that can be concluded is that there is a small steric factor favoring attack on the methoxycarbonyl face. The observed 3:1 preference for attack on the methyl face indicates that there is an unfavorable electronic interaction between the methoxycarbonyl group and DMAD. This could involve destabilizing interaction of the filled π-orbital of the acetylenic system that is perpendicular to the π-orbital directly involved in the cycloaddition. An unfavorable dipole–dipole interaction between the ester groups in the diene and dienophile could also contribute to disfavoring of attack on the methoxycarbonyl face of the former.

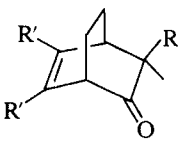
A further point of interest concerns our qualitative observation that reaction of DMAD with the dihalomethyl cyclohexadienones is significantly slower than with **9** and **15**. This indicates that additional unfavorable interactions occur in the transition states involving bulky substituents at C-6 arising either from increased steric interaction between these substituents and the methyl group at C-6 or from steric interaction between the bulky substituents and the diene on the face opposite to that on which addition occurs. The reference to transition states here draws attention to the fact that all the interpretations above are based on kinetic rather than thermodynamic control. This is considered to be a reasonable assumption based on general experience with non-aromatic-type dienes (7) and on the relatively mild conditions under which the present reactions occurred. Thus it has been found that in the Diels–Alder dimerization of 2,4-cyclohexadien-1-ones of type **5** the reaction is under kinetic control at 120°C and only comes under thermodynamic control at 160–190°C (20).

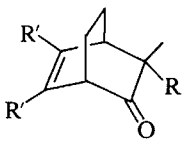
Configurational assignments

In discussing the assignments of configurations to individual adducts we have emphasized that the ^{1}H and ^{13}C nmr spectra of pairs of epimers are sufficiently different to permit their distinction, but insufficiently so to allow unambiguous individual structural assignments. The latter were made by X-ray crystallographic studies and by chemical correlation. It would be, of course, more convenient and expeditious if these assignments could be made spectroscopically. We propose that this is possible by comparison of the ^{13}C nmr spectra of the *dihydro derivatives* of the adducts. As shown in Table 1 the chemical shifts of the 3-methyl protons in pairs of C-3 epimers are consistently greater for the *endo*-3-methyl *exo*-3-X diastereomers than for the *exo*-3-methyl *endo*-3-X diastereomers ($\Delta\delta$ 2.2–3.2). In the cases of geminal methyl substitution at C-3, analogous chemical shift differences are observed.

Our suggestion that stereochemical assignments can be made on this basis is fortified by the fact that a rationale for their chemical shift differences can be discerned. The upfield shift of the *exo*-3-methyl signal relative to the *endo*-3-methyl signal is attributable to the γ-effect of C-8. Although a γ-effect of C-5 could be operative on the *endo*-3-methyl signal, it is expected that such an effect would be greater in the case of the sp^3 carbon atom at C-8. This interpretation provides an explanation for the difficulties encountered in making assignments for the adducts themselves, where both C-5 and C-8 are sp^2 carbon atoms.

TABLE 1. Chemical shifts of 3-CH_3 carbons in ^{13}C nmr spectra of 3-methylbicyclo[2.2.2]oct-5-en-2-ones





		δ^a		
		a	*b*	$\Delta\delta^b$
37	R = $CHBr_2$, R′ = E	22.9	20.1	2.8
40	R = R′ = E	22.0	19.8	2.2
42	R = CH_2OAc, R′ = E	21.9	19.6	2.3
46[c]	R = CH_3, R′ = E	26.4	23.8	2.6
47[d]	R = R′ = H	17.5	14.4	3.1
48[d]	R = CH_3, R′ = H	27.6	24.4	3.2

[a]In $CDCl_3$.
[b]$\delta_a - \delta_b$.
[c]Reference 1*a*.
[d]Reference 21.

Experimental[6]

Melting points were taken on a Fisher–Johns melting point apparatus and are uncorrected. Infrared (ir) spectra were taken neat or in chloroform with a Perkin Elmer 137 or 337 spectrophotometer. Proton nuclear magnetic resonance (^{1}H nmr) spectra were taken in deuteriochloroform at 60 MHz with a Varian T-60 spectrometer, unless otherwise specified. The ^{1}H nmr spectra were recorded at 200 and 400 MHz on Varian XL-200 and XL-400 spectrometers, respectively. Carbon-13 nuclear magnetic resonance (^{13}C nmr) spectra were taken in deuteriochloroform on a Varian CFT-20, XL-200, or XL-400 spectrometer. Mass spectra were recorded at 70 eV with a Dupont 21-490 single focussing mass spectrometer. Accurate mass measurements were made with an AEI MS 3074 double focussing mass spectrometer with a DS 50 data system.

Solutions were concentrated on a Buchi "Rotavapor ⟨*R*⟩" rotary evaporator under water aspirator pressure and the concentrates were then placed under the vacuum provided by a Welch "Duo Seal" two-stage vacuum pump.

Column chromatography was carried out on silica (Merck, grade 60, 230–400 mesh, 60 Å mean pore diameter). A slurry of silica gel in the solvent to be used for elution was prepared and added to the column.

[6]For further details of general experimental conditions, see ref. 9.

Can. J. Chem. Downloaded from www.nrcresearchpress.com by 122.72.124.2 on 09/07/12
For personal use only.

Thin-layer chromatography was carried out on aluminum-backed plates precoated with a 0.20 mm thickness of silica gel (Merck).

*Methyl 1-methyl-2-oxocyclohexanecarboxylate (**18**)*

Methyl iodide (80.0 mL, 182.4 g, 1.29 mol), methyl 2-oxocyclohexanecarboxylate (22) (93.48 g, 0.60 mol), and dry methanol (250 mL) were added to a 1-L 3-necked round-bottomed flask under nitrogen atmosphere. A solution of sodium methoxide (16.0 g) in methanol (375 mL) was added dropwise over 2.5 h, at room temperature, and stirring was continued for an additional 19 h (cf. ref. 23). The mixture was treated with water (400 mL) and extracted with ethyl acetate (3 × 100 mL) and the combined organic layers were washed with brine (3 × 100 mL) and water (2 × 100 mL). The organic layer was dried over anhydrous $MgSO_4$ and concentrated to yield a yellow oil. This was distilled to give **18** as a colorless oil (175.1 g, 1.03 mol; 80%); ir λ_{max}: 5.73 (sh), 5.82 (s) μm; ^{1}H nmr δ: 1.30 (s, 3H), 1.5–2.7 (m, 8H), 3.42 (s, 3H) ppm; ^{13}C nmr (100 MHz) δ: 20.5 (q), 21.95 (t), 26.8 (t), 37.5 (t), 39.85 (t), 51.6 (q), 56.35 (s), 172.7 (s), 206.9 (s) ppm.

*Methyl 3-bromo-1-methyl-2-oxocyclohexanecarboxylate (**19**)*

Chloroform (100 mL) and compound **18** (5.0 g, 29 mmol) were added to a 200-mL round-bottomed flask and cooled in an ice–salt bath. A solution of bromine (1 mL, 3.10 g, 398 mmol) in chloroform (30 mL) was added dropwise from a pressure-equalized dropping funnel over a 3-h period. The reaction mixture was allowed to warm up to room temperature, and saturated aqueous sodium metabisulfite was added until the solution became colorless. Extraction with chloroform (2 × 70 mL) followed and the organic layer was washed with saturated aqueous sodium metabisulfite (1 × 25 mL), saturated aqueous sodium bicarbonate (3 × 25 mL), and brine (2 × 25 mL). The organic layer was dried over anhydrous $MgSO_4$, concentrated, and chromatographed on silica gel with hexanes/ethyl acetate (3:1 v/v) as the eluent to yield **19** as a yellow oil (R_f 0.36; 2.83 g, 11.4 mmol; 39%); ^{1}H nmr δ: 1.40 (s, 3H), 1.55–2.7 (m, 7H), 3.78 (s, 3H), 4.50–5.05 (m, 1H) ppm.

Other chromatographic fractions, on treatment with hexanes, gave the dibromination product **20** (*vide infra*) as crystals (1.86 g, 19%).

*Methyl 1-methyl-2-oxo-3-cyclohexenecarboxylate (**21**)*

Freshly distilled quinoline (20 mL) and compound **19** (2.03 g, 8.16 mmol) containing some **20** were added to a 50-mL round-bottomed flask. The air was displaced with nitrogen, and the flask was heated in an oil bath at 113–123°C for 7 h. The reaction mixture was allowed to cool to room temperature and washed with 20% hydrochloric acid (~10 mL) until the aqueous layer was slightly acidic. Extraction with ethyl acetate (4 × 25 mL) followed and the combined organic layers were washed with 10% hydrochloric acid (4 × 10 mL) and water (3 × 10 mL), dried over anhydrous Na_2SO_4, and concentrated. The residual oil was chromatographed on silica gel with hexanes/ethyl acetate (3:1 v/v) as the eluent to yield a mixture of **21** (R_f 0.23; 0.35 g, 2.1 mmol; 25%) and **22** (*vide infra*), which was not separated. For **21**, ^{1}H nmr δ: 1.30 (s, 3H), 1.6–2.7 (m, 4H), 3.67 (s, 3H), 5.8–6.4 (m, 1H), 6.75–7.1 (m, 1H) ppm.

*Methyl 3,3-dibromo-1-methyl-2-oxocyclohexanecarboxylate (**20**)*

Chloroform (250 mL) and compound **18** (9.0 g, 53 mmol) were added to a 500-mL round-bottomed flask and cooled in an ice–salt bath. A solution of bromine (16.0 mL, 49.90 g, 0.312 mol) in chloroform (70 mL) was added dropwise from a pressure-equalized dropping funnel, over a 2.25-h period. The reaction mixture was allowed to warm to room temperature and saturated aqueous sodium metabisulfite was added until the solution became colorless. The mixture was extracted with chloroform (2 × 70 mL) and the combined organic layers were washed with saturated aqueous sodium metabisulfite (1 × 50 mL), saturated aqueous sodium bicarbonate (3 × 50 mL), and brine (2 × 50 mL). The organic layer was dried over anhydrous $MgSO_4$ and concentrated. The crude material was recrystallized from hexanes to yield **20** (14.45 g, 44 mmol; 83%) as white needles, mp 103–104°C; ir λ_{max}: 5.76 (sh), 5.71 (s) μm; ^{1}H nmr δ: 1.48 (s, 3H), 1.6–2.6 (m, 4H), 2.6–3.05 (m, 2H), 3.2 (s, 3H) ppm; ^{13}C nmr (50 MHz) δ: 21.2 (t), 24.7 (q), 35.6 (t), 50.2 (t), 52.7 (q), 54.6 (s), 67.95 (s), 171.6 (s), 192.6 (s) ppm; ms *m/z*: 330 (2.5), 328 (5), 326 (2.5). *Exact Mass* calcd. for $C_9H_{12}O_3Br_2$: 329.9111, 327.9130, 325.9149; found: 329.9113, 327.9143, 325.9174. *Anal.* calcd. for $C_9H_{12}O_3Br_2$: C 32.94, H 3.96, Br 48.74; found: C 32.76, H 3.65, Br 49.11.

*Methyl 1-methyl-6-oxo-2,4-cyclohexadienecarboxylate (**9**) and methyl 3-bromo-1-methyl-2-oxo-3-cyclohexenecarboxylate (**22**)*

Compound **20** (5.18 g, 16 mmol), lithium bromide (2.52 g, 29 mmol), lithium carbonate (3.47 g, 47 mmol), and dry, freshly distilled *N*,*N*-dimethylformamide (65 mL) were added to a 250-mL round-bottomed flask and the mixture was heated under a nitrogen atmosphere. The temperature of the oil bath ranged from 104 to 126°C in the 6.75-h period. The reaction mixture was allowed to cool and the excess lithium carbonate was destroyed by the careful addition of dilute sulfuric acid (100 mL). Extraction with dichloromethane (4 × 75 mL) followed and the organic layer was washed with water (5 × 50 mL) and dried over anhydrous $MgSO_4$. Concentration yielded a mixture of **9** and **22** as an oil. This was chromatographed on silica gel with hexanes/ethyl acetate (3:1 v/v) as the eluent to yield a mixture of **9** (R_f 0.27; 0.416 g, 2.5 mmol; 16%) and **22** (R_f 0.27; 0.674 g, 2.8 mmol; 18%), which could not be separated. This mixture was used for the preparation of the adduct of **9** with dimethyl acetylenedicarboxylate (*vide infra*). Compound **22** was not consumed and could be isolated free of **9** from the reaction mixture.

For **22**, ir λ_{max}: 3.55 (s), 5.76 (s), 5.95 (s), 6.21 (s) μm; ^{1}H nmr δ: 1.47 (s, 3H), 2.2–2.8 (m, 4H), 3.73 (s, 3H), 7.23–7.43 (distorted t, 1H) ppm; ^{13}C nmr (100 MHz) δ: 20.5 (s), 25.6 (t), 32.8 (t), 52.4 (q), 53.9 (s), 122.1 (s), 150.0 (d), 171.9 (s), 189.0 (s) ppm; ms *m/z*: 248 (18%), 246 (18%). *Exact Mass* calcd. for $C_9H_{11}O_3Br$: 247.9871, 245.9892; found: 247.9864, 245.9908.

For **9**, ^{1}H nmr δ: 1.50 (s, 3H), 3.67 (s, 3H), 6.0–6.35 (m, 3H), 6.8–7.4 (m, 1H) ppm.

*2-Bromo-6-methyl-2-cyclohexen-1-one (**24**)*

Compound **20** (3.34 g, 10.3 mmol), lithium bromide (1.78 g, 20.4 mmol), lithium carbonate (2.49 g, 34.3 mmol), and dry, freshly distilled *N*,*N*-dimethylformamide (45 mL) were heated at 120–125°C for 3.0 h. The reaction mixture was worked up as above and chromatographed to yield a mixture of **9** and **22** and a mixture of *o*-cresol and **24** (R_f 0.33; 0.40 g), whose spectra showed the following features in addition to those of *o*-cresol: λ_{max}: 5.95 (sh), 6.10 (s) μm; ^{1}H nmr δ: 1.10 (d, J = 6 Hz, 3H), 1.9–2.8 (m, 5H), 7.2–7.4 (m, 1H) ppm; ^{13}C nmr δ: 194.0 (s), 150.4 (s), 123.25 (s), 42.2 (d), 30.3 (t), 27.45 (t), 15.3 (q) ppm.

*Methyl 2,2-(ethylenedioxy)-1-methylcyclohexanecarboxylate (**25**)*

Compound **18** (2.48 g, 14.6 mmol), dry benzene (80 mL), ethylene glycol (2 mL, 2.224 g, 35.8 mmol), and a spatula-tip of *p*-toluenesulfonic acid were added to a 250-mL round-bottomed flask equipped with a Dean–Stark apparatus and a condenser. The system was placed under nitrogen and allowed to reflux for 23 h. After the mixture cooled, the benzene was evaporated and the residue was dissolved in ethyl acetate (200 mL). The solution was washed with brine (3 × 50 mL), dried over anhydrous Na_2SO_4, concentrated, and distilled (bp 180–181°C at 760 Torr; 1 Torr = 133.3 Pa) to yield **25** (2.44 g, 11.4 mmol; 78%) as a colorless oil; ir λ_{max}: 5.78 (s) μm; ^{1}H nmr δ: 1.23 (s, 3H), 1.4–2.1 (m, 8H), 3.67 (s, 3H), 3.93 (s, 4H) ppm; ^{13}C nmr (50 MHz) δ: 18.95 (q), 21.4 (t), 23.3 (t), 31.7 (t), 34.55 (t), 51.05 (s), 51.6 (q), 64.5 (t), 65.2 (t), 110.45 (s), 175.2 (s) ppm; ms *m/z*: 214 (47%). *Exact Mass* calcd. for $C_{11}H_{18}O_4$: 214.1205; found: 214.1202.

*2,2-(Ethylenedioxy)-1-(hydroxymethyl)-1-methylcyclohexane (**26**)*

Compound **25** (0.209 g, 0.168 mmol), lithium aluminum hydride (0.221 g, 5.83 mmol), and freshly distilled, dry tetrahydrofuran (15 mL) were added to a 50-mL round-bottomed flask, equipped with a condenser (cf. ref. 24). The reaction mixture was allowed to reflux under nitrogen for 24 h. After the mixture cooled, the excess lithium aluminum hydride was destroyed with ethyl acetate followed by ethanol and water. A gel was obtained; it was filtered from the solution

Can. J. Chem. Downloaded from www.nrcresearchpress.com by 122.72.124.2 on 09/07/12
For personal use only.

and the aqueous layer was extracted with ethyl acetate (3 × 50 mL). The combined organic layers were washed with brine (2 × 25 mL), dried over anhydrous Na_2SO_4, and evaporated. The residual product was chromatographed on silica gel with hexanes/ethyl acetate (3:1 v/v) as the eluent to yield **26** as a colorless oil (R_f 0.09; 0.125 g, 0.674 mmol; 69%); ir λ_{max}: 3.13 (br), 3.68 (s) μm; ^{1}H nmr δ: 1.00 (s, 3H), 1.3–2.4 (m, 8H), 3.03 (br s, 1H), 3.53 (br s, 2H), 3.97 (s, 4H) ppm; ^{13}C nmr (50 MHz) δ: 18.7 (q), 20.4 (t), 23.5 (t), 30.4 (t), 33.2 (t), 41.8 (s), 64.3 (t), 64.5 (t), 68.8 (t), 113.8 (s) ppm; ms *m/z*: 186 (9%). *Exact Mass* calcd. for $C_{10}H_{18}O_3$: 186.1256; found: 186.1250.

1-(Acetoxymethyl)-2,2-(ethylenedioxy)-1-methylcyclohexane (27)

Compound **26** (1.39 g, 7.47 mmol), acetic anhydride (20 mL, 21.64 g, 0.212 mol), and pyridine (15 mL) were added to a 100-mL round-bottomed flask equipped with a drying tube. The mixture was stirred at room temperature for 20 h; water (100 mL) was added to destroy the excess acetic anhydride and this mixture was extracted with ether (3 × 50 mL). The ethereal layers were combined and washed with water (3 × 25 mL), brine (3 × 25 mL), 3% aqueous hydrochloric acid (3 × 20 mL), and dried over anhydrous $MgSO_4$. The ethereal layer was concentrated and distilled (bp 93.0–93.5°C at ~0.5 Torr) to yield **27** (1.26 g, 5.52 mmol; 74%) as a colorless oil; ir λ_{max}: 5.74 (s) μm; ^{1}H nmr δ: 0.96 (s, 3H), 1.3–1.7 (br s, 8H), 2.07 (s, 3H), 3.92 (s, 4H), 4.03 (d, J = 10 Hz, 1H), 4.14 (d, J = 10 Hz, 1H) ppm; ^{13}C nmr (50 MHz) δ: 17.6 (q), 20.3 (t), 20.8 (q), 23.2 (t), 30.55 (t), 32.45 (t), 41.9 (s), 64.4 (t), 64.7 (t), 67.9 (t), 111.2 (s), 171.1 (s) ppm; ms *m/z*: 228 (14%). *Exact Mass* calcd. for $C_{12}H_{20}O_4$: 228.1362; found: 228.1353.

2-(Acetoxymethyl)-2-methylcyclohexanone (28)

Compound **27** (39.41 g, 0.173 mol), 95% formic acid (350 mL), and water (13 mL) were added to a 500-mL round-bottomed flask and the mixture was stirred, at room temperature, for 4 h. Water (300 mL) was added slowly and the aqueous layer was extracted with dichloromethane (3 × 100 mL). The organic layer was washed with brine (5 × 75 mL) and saturated aqueous sodium bicarbonate (3 × 50 mL) and dried over anhydrous Na_2SO_4, concentrated, and distilled (bp 80.5–82.0°C at 0.5 Torr) to yield **28** (28.55 g, 0.155 mol; 90%); ir λ_{max}: 5.75 (s), 5.84 (s) μm; ^{1}H nmr δ: 1.17 (s, 3H), 1.6–1.9 (m, 6H), 2.07 (s, 3H), 2.3–2.6 (m, 2H), 4.15 (s, 2H) ppm; ^{13}C nmr (50 MHz) δ: 20.4 (q), 20.6 (q), 20.7 (t), 26.85 (t), 35.9 (t), 38.5 (t), 48.3 (t), 68.4 (t), 170.7 (s), 212.7 (s) ppm; ms *m/z*: 184 (7%). *Exact Mass* calcd. for $C_{10}H_{16}O_3$: 184.1100; found: 184.1105.

6-(Acetoxymethyl)-2-bromo-6-methylcyclohexanone (29)

Compound **29** was prepared from **28** in 82% yield as described previously for **19**; the crude reaction mixture was passed through a silica gel plug with hexanes/ethyl acetate (1:1 v/v) as the eluent to yield the product as a mixture of diastereomers; ^{1}H nmr δ: 1.27 (d, 3H), 1.7–2.2 (m, 6H), 2.07 (s, 3H), 3.93 (d, J = 10 Hz, 1H), 4.41 (d, J = 10 Hz, 1H), 4.8–5.2 (m, 1H) ppm.

6-(Acetoxymethyl)-6-methylcyclohex-2-enone (30)

Compound **29** (0.20 g, 0.76 mmol), toluene (30 mL), and 1,8-diazabicyclo[5.4.0]undec-7-ene (0.2 mL, 0.20 g, 1.34 mmol) were added to an 100-mL round-bottomed flask, set under nitrogen, and allowed to reflux for 11.25 h. Once cooled, dilute aqueous hydrochloric acid was added until the solution was neutral, and the mixture was extracted with ethyl acetate (4 × 30 mL) and dried over anhydrous Na_2SO_4. The residue obtained by concentrating the organic layer was chromatographed on silica gel with hexanes/ethyl acetate (1:1 v/v) as the eluent to yield **30** (0.069 g, 3.79 mmol; 50%) as an oil; ^{1}H nmr δ: 1.13 (s, 3H), 1.7–1.9 (m, 2H), 2.05 (s, 3H), 2.3–2.6 (m, 2H), 4.02 (d, J = 10 Hz, 1H), 4.32 (d, J = 10 Hz, 1H), 5.8–6.1 (dt, J = 10, 2 Hz, 1H), 6.7–7.1 (m, 1H) ppm.

2-(Acetoxymethyl)-6,6-dibromo-2-methylcyclohexanone (31)

Compound **28** (5.01 g, 27.2 mmol) and chloroform (125 mL) were added to a 250-mL round-bottomed flask and cooled in an ice–salt bath. A solution of bromine (4.0 mL, 12.48 g, 78.1 mmol) in chloroform (66 mL) was added dropwise over a 1.3-h period after which the solution was stirred in an ice–water bath for an additional 2.25 h. The excess bromine was destroyed with saturated aqueous sodium metabisulfite and the mixture was extracted with chloroform (3 × 50 mL). The organic layer was washed with saturated aqueous sodium bicarbonate (3 × 75 mL) and dried over anhydrous $MgSO_4$. Concentration of the organic layer yielded **31** (6.90 g, 20.3 mmol; 74.5%) as a pale yellow oil; ir λ_{max}: 5.75 (s), 5.80 (sh) μm; ^{1}H nmr δ: 1.47 (s, 3H), 1.8–2.2 (m, 4H), 2.10 (s, 3H), 2.8–3.3 (m, 2H), 4.02 (d, J = 10 Hz, 1H), 4.28 (d, J = 10 Hz, 1H) ppm; ^{13}C nmr (50 MHz) δ: 19.75 (t), 20.7 (q), 25.2 (q), 33.5 (t), 48.55 (s), 49.6 (t), 66.8 (s), 69.75 (t), 170.4 (s), 197.5 (s) ppm; ms *m/z*: 346 (6%), 342 (9%), 340 (6%).

6-(Acetoxymethyl)-6-methyl-2,4-cyclohexadien-1-one (15)

Compound **31** (4.53 g, 13.2 mmol), lithium bromide (7.53 g, 87.0 mmol), lithium carbonate (14.52 g, 0.197 mol), and freshly distilled and dried *N*,*N*-dimethylformamide (60 mL) were added to a 500-mL round-bottomed flask, equipped with a condenser on a nitrogen gas inlet. The reaction mixture was heated on an oil bath, at 102–110°C, and stirred for 15.5 h. After cooling, the excess lithium carbonate was destroyed by the careful addition of 10% aqueous hydrochloric acid (300 mL); extraction with chloroform (3 × 100 mL) followed and the organic layer was washed with water (3 × 50 mL) and dried over anhydrous Na_2SO_4. Concentration of the organic layer followed by chromatography on silica gel with chloroform/ethyl acetate (90:10 v/v) as the eluent yielded the dienone **15** (R_f 0.40; 2.136 g, 11.8 mmol; 90%) as a yellow oil; ir λ_{max}: 5.73 (sh), 5.78 (s), 6.03 (s), 6.14 (s), 6.90 (s) μm; ^{1}H nmr δ: 1.20 (s, 3H), 1.95 (s, 3H), 4.25 (s, 2H), 5.9–6.1 (d, J = 10 Hz, 1H), 6.2–6.3 (distorted d, J = 4 Hz, 2H), 6.8–7.2 (m, 1H) ppm; ^{13}C nmr (100 MHz) δ: 20.65 (q), 21.3 (q), 68.0 (s), 69.3 (t), 121.7 (d), 125.8 (d), 141.6 (d), 144.7 (d), 170.6 (s), 203.0 (s) ppm; ms *m/z*: 180 (3%). *Exact Mass* calcd. for $C_{10}H_{12}O_3$: 180.07865; found: 180.0787.

Trimethyl 5-methyl-6-oxobicyclo[2.2.2]octa-2,7-diene-2,3,5-tricarboxylates (12)

A mixture of compound **9** (1.26 g, 7.60 mmol) and compound **22**, dimethyl acetylenedicarboxylate (9 mL, 10.40 g, 73.2 mmol), two spatula-tips of hydroquinone, and dry benzene (200 mL) were added to a 500-mL round-bottomed flask. The mixture was refluxed under nitrogen for 46 h. The mixture was cooled, the hydroquinone filtered off, and the benzene was evaporated; the residue was chromatographed on silica gel with hexanes/ethyl acetate (55:45 v/v) as the eluent, yielding a 3:1 mixture of isomers (2.11 g, 6.85 mmol; 90%). Repeated chromatography with the same eluent yielded the major isomer **12***a* (R_f 0.33), which was recrystallized from water, mp 97–98°C, and the minor isomer **12***b*, also recrystallized from water, mp 103–104°C. Major isomer **12***a*, ir λ_{max}: 5.73 (br), 6.07 (sh) μm; ^{1}H nmr δ: 1.46 (s, 3H), 3.70 (s, 3H), 3.83 (s, 3H), 3.86 (s, 3H), 4.3–4.6 (dt, J = 6, 2 Hz, 2H), 6.4–6.9 (m, 2H) ppm; ^{13}C nmr δ: 23.9 (q), 48.4 (d), 49.4 (s), 52.5 (q), 56.8 (d), 128.7 (d), 135.7 (d), 137.4 (s), 141.8 (s), 163.9 (s), 165.4 (s), 170.8 (s), 197.9 (s) ppm. *Anal.* calcd. for $C_{15}H_{16}O_7$: C 58.44, H 5.23; found: C 58.35, H 5.31.

Minor isomer **12***b*, ir λ_{max}: 5.70 (sh), 5.80 (s) μm; ^{1}H nmr δ: 1.43 (s, 3H), 3.65 (s, 3H), 3.85 (s, 6H), 4.28–4.65 (m, 2H), 6.53–6.75 (m, 2H) ppm; ^{13}C nmr δ: 24.1 (q), 48.5 (d), 48.7 (s), 51.9 (q), 52.2 (q), 52.4 (q), 57.0 (d), 130.3 (d), 134.5 (d), 136.5 (s), 141.5 (s), 164.3 (s), 164.9 (s), 170.3 (s), 194.4 (s) ppm.

Dimethyl 6-(acetoxymethyl)-6-methyl-5-oxobicyclo[2.2.2]octa-2,7-diene-2,3-dicarboxylates (32)

2-(Acetoxymethyl)-2-methylcyclohexa-2,4-dien-1-one (2.00 g, 11.0 mmol), dimethyl acetylenedicarboxylate (11 mL, 12.716 g, 89.5 mmol), two spatula-tips of hydroquinone, and benzene (200 mL) were added to a 250-mL round-bottomed flask and placed under nitrogen. The reaction mixture was refluxed for 45.5 h. After cooling, the benzene was evaporated and the residue was chromatographed on silica gel with hexanes/ethyl acetate (55:45 v/v) as the eluent. Two isomers were obtained in a ratio of 1.1:1 in nearly quantitative yield; repeated chromatography of the crude oil on silica gel with the same

Can. J. Chem. Downloaded from www.nrcresearchpress.com by 122.72.124.2 on 09/07/12
For personal use only.

eluent yielded the major isomer **15***b* (R_f 0.28; 1.475 g, 4.58 mmol) and the minor isomer **15***a* (R_f 0.32; 0.9203 g, 28.6 mmol) as pale, yellow oils. Major isomer **15***b*, ir λ_{max}: 5.78 (sh), 5.82 (s), 5.87 (s), 6.15 (s), 6.30 (s) μm; ^{1}H nmr (400 MHz) δ: 1.11 (s, 3H), 1.96 (s, 3H), 3.71 (s, 3H), 3.72 (s, 3H), 3.86 (s, 2H), 4.11–4.13 (dd, J = 6, 2 Hz, 1H), 4.42–4.44 (dd, J = 6, 1.5 Hz, 1H), 6.49–6.52 (ddd, J = 7, 6, 2 Hz, 1H), 6.57–6.61 (ddd, J = 7, 6, 1.5 Hz, 1H) ppm; ^{13}C nmr (100 MHz) δ: 20.4 (q), 23.8 (q), 42.6 (s), 47.8 (d), 52.35 (q), 52.4 (q), 57.6 (d), 68.9 (t), 129.2 (d), 135.9 (d), 136.1 (s), 142.25 (s), 164.3 (s), 165.3 (s), 170.2 (s), 202.6 (s) ppm; ms m/z $(M + 1)^+$: 323 (8%). *Exact Mass* calcd. for $C_{16}H_{19}O_7$ (M + 1): 323.1125; found: 323.1123. *Anal.* calcd. for $C_{16}H_{18}O_7$: C 59.61, H 5.61; found: C 59.42, H 5.76.

Minor isomer **15***a*, ir λ_{max}: 5.80 (s), 5.85 (s), 5.95 (sh), 6.15 (s), 6.34 (s) μm; ^{1}H nmr (400 MHz) δ: 1.15 (s, 3H), 2.07 (s, 3H), 3.76 (s, 3H), 3.79 (s, 3H), 3.90 (s, 2H), 4.09–4.11 (dd, J = 6, 2 Hz, 1H), 4.47–4.49 (dd, J = 6, 1.5 Hz, 1H), 6.49–6.53 (ddd, J = 7, 6, 2 Hz, 1H), 6.60–6.64 (ddd, J = 7, 6, 1.5 Hz, 1H) ppm; ^{13}C (100 MHz) nmr δ: 20.8 (q), 22.15 (q), 43.2 (s), 47.7 (d), 52.6 (q), 57.3 (d), 69.9 (t), 128.6 (d), 135.85 (d), 136.2 (s), 143.1 (s), 164.3 (s), 165.9 (s), 170.5 (s), 202.4 (s) ppm; ms m/z $(M - 70)^+$: 252 (5%). *Exact Mass* calcd. for $C_{12}H_{12}O_6$ $(M - 70)^+$: 252.0634; found: 252.0616.

*Dimethyl 6-(dibromomethyl)-6-methyl-5-oxobicyclo[2.2.2]octa-2,7-diene-2,3-dicarboxylates (**33**)*

6-(Dibromomethyl)-6-methyl-2,4-cyclohexadien-1-one (**16**) was prepared according to the procedure of Wenkert *et al.* (13*a*).

Compound **16** (3.43 g, 12.6 mmol) and dimethyl acetylenedicarboxylate (1.60 mL, 1.85 g, 13.0 mmol) were heated in a steel pressure bottle at 120°C for 24 h. An orange oil was obtained, containing an 8:1 mixture of two isomeric adducts (4.82 g, 0.115 mol; 93%). The major isomer **33***a* was recrystallized from diethyl ether as colorless crystals, mp 152–153°C; the minor isomer **33***b* was chromatographed on silica gel with hexanes/ether (3:1 v/v) as the eluent, yielding a yellow, dense oil. Major isomer **33***a*, ir (KBr) λ_{max}: 5.81 (s), 6.09 (s), 6.27 (m) μm; ^{1}H nmr δ: 1.47 (s, 3H), 3.77 (s, 3H), 3.80 (s, 3H), 4.3–4.6 (m, 2H), 5.53 (s, 1H), 6.5–6.8 (m, 2H) ppm; ^{13}C nmr δ: 21.6 (q), 46.8 (s), 50.5 (d), 51.9 (d), 52.7 (q), 58.3 (d), 130.2 (d), 133.6 (d), 137.8 (s), 142.5 (s), 163.8 (s), 165.2 (s), 197.6 (s) ppm; ms m/z: 343 (0.4%), 341 (0.4%). *Anal.* calcd. for $C_{14}H_{14}Br_2O_5$: C 39.84, H 3.34, Br 37.86; found: C 40.01, H 3.44, Br 38.50.

Minor isomer **33***b*, ir λ_{max}: 5.80 (s), 6.06 (s), 6.21 (s) μm; ^{1}H nmr δ: 1.46 (s, 3H), 3.82 (s, 3H), 3.86 (s, 3H), 4.42 (dd, J = 5, 3 Hz, 1H), 4.60 (dd, J = 5, 3 Hz, 1H), 5.67 (s, 1H), 6.5–6.7 (m, 2H) ppm; ^{13}C nmr δ: 23.4 (q), 47.0 (s), 50.7 (d), 50.8 (d), 52.7 (q), 57.9 (d), 131.2 (d), 135.6 (s), 142.4 (s), 163.9 (s), 165.4 (s), 197.1 (s) ppm; ms m/z: 343 (0.4%), 341 (0.4%).

Dimethyl exo-*6-bromomethyl*-endo-*6-methyl-5-oxobicyclo[2.2.2]octa-2,7-diene-2,3-dicarboxylate (**35**a)*

Compound **33***a* (0.247 g, 0.589 mmol), dichloromethane (2 mL), and trichlorosilane (0.2 mL, 0.269 g, 1.99 mmol) were added to a 50-mL round-bottomed flask placed in an ice bath. A solution of triethylamine (0.2 mL, 0.152 g, 1.51 mmol) and dichloromethane (1 mL) was added. The ice bath was removed and the reaction mixture was stirred at room temperature for 4 h. Diethyl ether (20 mL) was added and the reaction mixture was filtered to remove the solid formed. The ethereal solution was concentrated and the oil was chromatographed on silica gel with hexanes/ethyl acetate (3:1 v/v) as the eluent to yield **35***a* (R_f 0.25; 0.146 g, 0.427 mmol; 72.5%); ir λ_{max}: 5.78 (s), 6.09 (m), 6.25 (w) μm; ^{1}H nmr (200 MHz) δ: 1.26 (s, 3H), 3.21 (d, J = 10.5 Hz, 1H), 3.39 (d, J = 10.5 Hz, 1H), 3.81 (s, 3H), 3.85 (s, 3H), 4.40 (dd, J = 6, 2 Hz, 1H), 4.71 (dd, J = 6, 2 Hz, 1H), 6.55–6.6 (ddd, J = 7, 6, 2 Hz, 1H), 6.7–6.8 (ddd, J = 7, 6, 1.5 Hz, 1H) ppm; ms m/z: 344 (2%), 342 (2%).

Dimethyl exo-*6-(dibromomethyl)*-endo-*6-methyl-5-oxobicyclo[2.2.2]-oct-2-ene-2,3-dicarboxylate (**37**a)*

Compound **33***a* (0.1977 g, 0.471 mmol), dry methanol (10 mL), and a spatula-tip of platinum dioxide were placed in a 50-mL round-bottomed flask and stirred under hydrogen for 10 min. The platinum was filtered through a Celite plug and the solution was concentrated. Crystallization from diethyl ether gave **37***a* (0.172 g, 0.408 mmol; 87%) as colorless crystals, mp 148–149°C; ir λ_{max}(KBr): 5.83 (s), 6.12 (m) μm; ^{1}H nmr δ: 1.36 (s, 3H), 1.5–2.5 (m, 4H), 3.53 (m, 1H), 3.70 (m, 1H), 3.77 (s, 3H), 3.83 (s, 3H), 5.75 (s, 1H) ppm; ^{13}C nmr δ: 19.6 (t), 20.6 (t), 22.9 (q), 45.0 (d), 48.8 (d), 49.7 (d), 51.0 (s), 52.6 (q), 133.6 (s), 144.7 (s), 164.0 (s), 165.8 (s), 204.7 (s) ppm; ms m/z: 426 (2%), 424 (5%), 422 (2%), 165 (100%). *Anal.* calcd. for $C_{14}H_{16}Br_2O_5$: C 39.65, H 3.80, Br 37.68; found; C 39.85, H 3.89, Br 38.01.

Dimethyl endo-*6-(dibromomethyl)*-exo-*6-methyl-5-oxobicyclo[2.2.2]-oct-2-ene-2,3-dicarboxylate (**37**b)*

Compound **37***b* was prepared by hydrogenation of **33***b* under the same conditions as those used for the preparation of **37***a* from **33***a* (*vide supra*). It was obtained in 70% yield as colorless crystals, mp 89–90.5°C; ir λ_{max}(KBr): 5.80 (s), 6.10 (m) μm; ^{1}H nmr δ: 1.44 (s, 3H), 1.7–2.3 (m, 4H), 3.56 (m, 1H), 3.66 (m, 1H), 3.80 (s, 3H), 3.85 (s, 3H), 5.73 (s, 1H) ppm; ^{13}C nmr δ: 20.1 (q), 20.8 (t), 24.2 (t), 44.6 (d), 50.0 (d), 50.2 (d), 52.1 (s), 52.6 (q), 132.5 (s), 142.9 (s), 164.3 (s), 165.6 (s), 205.2 (s) ppm; ms m/z: 426 (2%), 424 (4%), 422 (2%), 165 (100%). *Anal.* calcd. for $C_{14}H_{16}Br_2O_5$: C 39.65, H 3.80, Br 37.68; found: C 39.85, H 3.85, Br 37.73.

Dimethyl exo-*6-(bromomethyl)*-endo-*6-methyl-5-oxobicyclo[2.2.2]-oct-2-ene-2,3-dicarboxylate (**38**a)*

Compound **37***a* (0.171 g, 0.408 mmol), dichloromethane (2 mL), and trichlorosilane (0.2 mL, 0.269 g, 1.99 mmol) were added to a 50-mL round-bottomed flask placed in an ice bath. The mixture was cooled and a solution of triethylamine (0.2 mL, 0.152 g, 1.51 mmol) and dichloromethane (1 mL) was added. The ice bath was removed and the reaction mixture was stirred at room temperature for 3.5 h. Diethyl ether (20 mL) was added and the reaction mixture was filtered to remove the solid formed. The ethereal solution was concentrated and the oil was put through a short column of silica gel with dichloromethane as the eluent to yield **38***a* (0.133 g, 0.378 mmol; 95%) as a colorless oil; ir λ_{max}: 5.81 (s), 6.12 (s) μm; ^{1}H nmr δ: 1.22 (s, 3H), 1.6–2.3 (m, 4H), 3.3–3.6 (m, 2H), 3.6–3.8 (m, 2H), 3.82 (s, 3H), 3.87 (s, 3H) ppm; ^{13}C nmr δ: 19.8 (t), 22.1 (t), 22.6 (q), 39.3 (t), 43.4 (d), 46.9 (s), 49.3 (d), 52.5 (q), 132.4 (s), 145.1 (s), 164.2 (s), 166.3 (s), 209.8 (s) ppm; ms m/z: 346 (2.5%), 344 (2.5%). *Exact Mass* calcd. for $C_{14}H_{17}O_5Br$: 346.0238, 344.0259; found: 346.0259, 344.0252.

exo-*6-(Hydroxymethyl)*-endo-*6-methyl-5-oxobicyclo[2.2.2]oct-2-ene-2,3-dicarboxylic acid (**39**a)*

Compound **38***a* (1.30 g, 3.78 mmol), potassium hydroxide (2.0 g, 35.6 mmol), methanol (10 mL), and water (10 mL) were placed in a 50-mL round-bottomed flask and the mixture was stirred at room temperature for 24 h. The mixture was neutralized with 10% hydrochloric acid and extracted with ethyl acetate (3 × 50 mL) and dried over anhydrous Na_2SO_4. The crude solid was recrystallized from diethyl ether/pentanes to give **39***a* (0.60 g, 2.36 mmol; 62.5%) as a colorless solid, mp 189–191°C; ir λ_{max}(KBr): 3.92 (br), 5.81 (s), 5.84 (s), 6.29 (s) μm; ms m/z $(M - 17)^+$: 237 (8%). *Anal.* calcd. for $C_{12}H_{14}O_6$: C 56.69, H 5.55; found: C 56.47, H 5.70.

Trimethyl endo-*5-methyl-6-oxobicyclo[2.2.2]oct-2-ene-2,3,* exo-*5-tricarboxylate (**40**a)*

Compound **12***a* (0.085 g, 0.262 mmol), dry methanol (10 mL), and a spatula-tip of 10% palladium on carbon were placed in a 50-mL round-bottomed flask and stirred under hydrogen for 10 min. The mixture was filtered through a Celite plug and the solution was concentrated. The residue was chromatographed on silica with hexanes/ethyl acetate (1:1 v/v) as the eluent to yield **40***a* (R_f 0.06; 0.081 g, 0.249 mmol; 95%) as a colorless oil (lit. (3) mp 46–47°C); ir λ_{max}: 5.76 (s), 6.13 (m) μm; ^{1}H nmr δ: 1.40 (s, 3H), 1.5–2.1 (m, 4H), 3.3–3.6 (m, 2H), 3.80 (s, 3H), 3.85 (s, 3H), 3.90 (s, 3H) ppm; ^{13}C nmr δ: 20.5 (t), 22.0 (q + t), 44.4 (d), 49.1 (d), 52.5 (q), 53.7 (s), 133.6 (s), 143.0 (s), 164.3 (s), 171.7 (s), 205.1 (s) ppm.

Trimethyl exo-*5-methyl-6-oxobicyclo[2.2.2]oct-2-ene-2,3,* endo-*5-tricarboxylate (**40** b)*

Compound **40***b* was prepared by hydrogenation of **12***b* under the same conditions as those used for the preparation of **40***a* from **12***a* (*vide supra*). It was obtained as a colorless oil; ir λ_{max}: 5.82 (s), 6.08 (w) μm; ^{1}H nmr δ: 1.47 (s, 3H), 1.6–2.1 (m, 4H), 3.3–3.6 (m, 2H), 3.67 (s, 3H), 3.82 (s, 3H), 3.85 (s, 3H) ppm; ^{13}C nmr δ: 19.0 (t), 19.8 (q), 23.7 (t), 43.8 (d), 49.0 (d), 52.3 (q), 53.8 (s), 133.4 (s), 142.9 (s), 164.3 (s), 165.6 (s), 170.7 (s) ppm (ketonic C=O signal not detectable above noise level).

Dimethyl exo-*6-(acetoxymethyl)*-endo-*6-methyl-5-oxobicyclo[2.2.2]-oct-2-ene-2,3-dicarboxylate (**42** a)*

Compound **32***a* (0.109 g, 0.338 mmol), dry methanol (15 mL), and platinum dioxide (2 spatula-tips) were added to a 50-mL round-bottomed flask. The mixture was stirred under hydrogen for 10 min; the mixture was filtered through a Celite plug and the solution was concentrated. The crude product was chromatographed on silica gel with hexanes/ethyl acetate (55:45 v/v) as the eluent to yield **42***a* (R_f 0.11) in quantitative yield as a colorless oil; ir λ_{max}: 5.70 (sh), 5.75 (s), 5.81 (sh), 6.10 (s) μm; ^{1}H nmr (400 MHz) δ: 1.15 (s, 3H), 1.5–1.6 (m, 2H), 1.7–1.85 (m, 1H), 1.85–2.0 (m, 1H), 2.08 (s, 3H), 3.19–3.20 (t, J = 3 Hz, 1H), 3.63–3.65 (dd, J = 4, 2 Hz, 1H), 3.77 (s, 3H), 3.82 (s, 3H), 4.01–4.04 (d, J = 11 Hz, 1H), 4.05–4.08 (d, J = 11 Hz, 1H) ppm; ^{13}C nmr (100 MHz) δ: 20.5 (t), 20.8 (q), 21.9 (q), 22.2 (t), 43.0 (d), 46.5 (s), 49.1 (d), 52.5 (q), 52.55 (q), 66.85 (t), 132.3 (s), 145.05 (s), 164.4 (s), 166.5 (s), 170.5 (s), 210.25 (s) ppm; ms m/z: 324 (4%).

Dimethyl endo-*6-(acetoxymethyl)*-exo-*6-methyl-5-oxobicyclo[2.2.2]-oct-2-ene-2,3-dicarboxylate (**42** b)*

Compound **42***b* was prepared from **32***b* in 80% yield as described for the minor isomer. Purification by chromatography on silica gel with hexanes/ethyl acetate (55:45 v/v) as the eluent gave the product (R_f 0.26) as a colorless oil; ir λ_{max}: 5.76 (sh), 5.80 (s), 5.85 (s), 5.90 (sh), 6.18 (s) μm; ^{1}H nmr (400 MHz) δ: 1.13 (s, 3H), 1.46–1.54 (m, 1H), 1.70–1.78 (m, 1H), 1.85–2.08 (m, 2H), 1.94 (s, 3H), 3.17–3.19 (t, J = 3 Hz, 1H), 3.56–3.58 (q, J = 4, 2 Hz, 1H), 3.72 (s, 3H), 3.73 (s, 3H), 3.83–3.86 (d, J = 11 Hz, 1H), 3.90–3.93 (d, J = 11 Hz, 1H) ppm; ^{13}C (100 MHz) nmr δ: 19.6 (q), 20.3 (t), 20.4 (q), 21.9 (t), 42.1 (d), 45.9 (s), 49.5 (d), 52.25 (q), 52.3 (q), 68.4 (t), 132.2 (s), 143.7 (s), 164.7 (s), 165.6 (s), 170.2 (s), 209.4 (s) ppm; ms m/z: 324 (4.5%).

Dimethyl exo-*6-(hydroxymethyl)*-endo-*6-methyl-5-oxobicyclo[2.2.2]-oct-2-ene-2,3-dicarboxylate (**41** a)*

*(i) From compound **42** a*

Compound **42***a* (0.109 g, 0.338 mmol), potassium carbonate (0.0637 g, 0.461 mmol), and dry methanol (15 mL) were added to a 50-mL round-bottomed flask, placed under argon, and stirred at room temperature for 3.3 h. The alcoholic solution was filtered, the methanol was evaporated and the concentrate was extracted with ethyl acetate. The extract was dried over anhydrous Na_2SO_4 and concentrated and the residue was chromatographed on silica gel with hexanes/ethyl acetate (1:3 v/v) as the eluent to yield **41***a* (R_f 0.40; 0.0568 g, 0.201 mmol; 60%) as a colorless oil; ir λ_{max}: 3.06 (br), 5.80 (s), 5.85 (s), 5.90 (sh), 6.10 (s) μm; ^{1}H nmr δ: 1.17 (s, 3H), 1.7–2.1 (m, 4H), 2.3–2.5 (br m, 1H, D_2O exchangeable), 3.1–3.3 (m, 1H), 3.3–3.5 (m, 1H), 3.5–3.8 (br s, 2H), 3.82 (s, 3H), 3.87 (s, 3H) (s, 3H) ppm; ^{13}C nmr (100 MHz) δ: 20.4 (t), 21.4 (q), 22.7 (t), 43.7 (d), 45.25 (s), 49.5 (d), 52.5 (q), 66.9 (t), 132.1 (s), 145.7 (s), 164.6 (s), 166.7 (s), 213.1 (s), ppm; ms m/z: 282 (5%). *Exact Mass* calcd. for $C_{14}H_{18}O_6$: 282.1103; found: 282.1105. *Anal.* calcd. for $C_{14}H_{18}O_6$: C 59.57, H 6.42; found: C 59.41, H 6.64.

*(ii) From compound **39** a*

Compound **39***a* (0.60 g, 2.36 mmol) was added to an ethereal solution of diazomethane (2.44 g, 5.78 mmol) and allowed to stand overnight. The concentrate was chromatographed on a preparative plate of silica gel with diethyl ether as the solvent, which yielded **41***a* (R_f 0.28; 0.61 g, 2.16 mmol; 91%) as a colorless oil, whose spectra were identical with those of the sample of **41***a* prepared from **42***a*.

Compound **43** a (R_f 0.46; 0.025 g; 3%) was also isolated from the preparative plate as a colorless oil; ir λ_{max}: 5.80 (s), 6.10 (s) μm; ms m/z: 296 (7), 165 (100). *Exact Mass* calcd. for $C_{15}H_{20}O_6$: 296.1260; found: 296.1272.

Dimethyl endo-*6-(hydroxymethyl)*-exo-*6-methyl-5-oxobicyclo[2.2.2]-oct-2-ene-2,3-dicarboxylate (**41** b)*

Compound **41***b* was prepared in 27% yield by adding compound **42***b* (0.094 g, 0.29 mmol), anhydrous potassium carbonate (0.099 g, 0.71 mmol), and methanol (15 mL) to a 50-mL round-bottomed flask and repeating the procedure described for the minor isomer; ^{1}H nmr: 1.23 (s, 3H), 1.3–2.2 (br s, 4H), 2.2–2.5 (br s, 1H), 2.5–2.9 (br s, 1H), 3.3–3.5 (br s, 1H), 3.67 (s, 6H), 3.90 (s, 2H) ppm.

*Dimethyl 6-(dichloromethyl)-6-methyl-5-oxobicyclo[2.2.2]octa-2,7-diene-2,3-dicarboxylates (**34**)*

6-(Dichloromethyl)-6-methyl-2,4-cyclohexadien-1-one (**17**) was prepared according to the procedure of Auwers and Keil (13*b*).

Compound **17** was treated with dimethyl acetylenedicarboxylate under the conditions used in the case of compound **16** (*vide supra*). The crude product consisted of a 6:1 mixture of the adducts **34***a* and **34***b*. The major isomer **34***a* crystallized from diethyl ether, as cubic crystals, mp 129–130°C; ir λ_{max}(KBr): 5.81 (s), 6.08 (s), 6.27 (s) μm; ^{1}H nmr δ: 1.40 (s, 3H), 3.81 (s, 3H), 4.3–4.7 (m, 2H), 5.60 (s, 1H), 6.5–6.8 (m, 2H) ppm; ^{13}C nmr δ: 19.5 (q), 47.8 (s), 49.3 (d), 52.7 (q), 58.0 (d), 78.0 (d), 130.2 (d), 133.8 (d), 137.9 (s), 142.3 (s), 163.9 (s), 165.3 (d), 197.9 (s); ms m/z: 297 (0.6; M − Cl), 221 (1.4), 195 (11), 163 (100). *Anal.* calcd. for $C_{14}H_{14}Cl_2O_5$: C 50.47, H 4.24, Cl 21.28; found: C 50.20, H 4.27, Cl 21.25.

The minor isomer **34***b* was not isolated; its presence was evident from the ^{13}C nmr spectrum of the crude product, δ: 21.2 (q), 47.9 (s), 49.4 (s), 52.8 (q), 57.9 (d), 77.2 (d), 131.1 (d), 135.2 (d), 138.2 (s), 142.1 (s), 164.0 (s), 165.3 (s), 197.7 (s).

Dimethyl exo-*6-(dichloromethyl-*endo-*6-methyl-5-oxobicyclo[2.2.2]-oct-2-ene-2,3-dicarboxylate (**45** a)*

Compound **34***a* was hydrogenated under the conditions used in the case of compound **33***a* (*vide supra*). Crystallization from diethyl ether gave **45***a* as colorless crystals, mp 112–114°C; ir λ_{max}(KBr): 5.78 (s), 6.10 (s) μm; ^{1}H nmr δ: 1.34 (s, 3H), 1.5–1.8 (m, 4H), 3.53 (m, 1H), 3.66 (m, 1H), 3.80 (s, 3H), 3.83 (s, 3H), 5.80 (s, 1H); ms m/z: 338 (1), 336 (77), 334 (11), 299 (7), 269 (3), 239 (7), 201 (8), 196 (7), 165 (100). *Anal.* calcd. for $C_{14}H_{16}Cl_2O_5$: C 50.16, H 4.81, Cl 21.15; found: C 50.17, H 4.84, Cl 21.21.

Acknowledgment

We thank the Natural Sciences and Engineering Research Council of Canada for support of this work.

1. (*a*) P. YATES and K. E. STEVENS. Tetrahedron, **37**, 4401 (1981); (*b*) P. YATES and K. E. STEVENS. Can. J. Chem. **60**, 825 (1982); P. YATES, D. J. BURNELL, V. J. FREER, and J. F. SAWYER. Can. J. Chem. **65**, 69 (1987); P. YATES, R. S. GREWAL, P. C. HAYES, and J. F. SAWYER. Can. J. Chem. **66**, 2805 (1988).
2. H. AUKSI and P. YATES. Can. J. Chem. **59**, 2510 (1981).
3. A. G. SCHULTZ, J. P. DITTAMI, F. P. LAVIERI, C. SALOWEY, P. SUNDARARAMAN, and M. B. SZYMULA. J. Org. Chem. **49**, 4429 (1984).
4. R. GLEITER and L. A. PAQUETTE. Acc. Chem. Res. **16**, 328 (1983).
5. M. AVENATI and P. VOGEL. Helv. Chim. Acta, **65**, 204 (1982); Helv. Chim. Acta, **66**, 1279 (1983).
6. F. K. BROWN and K. N. HOUK. J. Am. Chem. Soc. **107**, 1971 (1985); F. K. BROWN, K. N. HOUK, D. J. BURNELL, and Z. VALENTA. J. Org. Chem. **52**, 3050 (1987); S. D. KAHN and W. J. HEHRE. J. Am. Chem. Soc. **109**, 663 (1987).

Can. J. Chem. Downloaded from www.nrcresearchpress.com by 122.72.124.2 on 09/07/12
For personal use only.

7. D. J. BURNELL, H. B. GOODBRAND, S. M. KAISER, and Z. VALENTA. Can. J. Chem. **65**, 154 (1987).
8. J. B. MACAULAY and A. G. FALLIS. J. Am. Chem. Soc. **110**, 4074 (1988).
9. A. L.-N. GOMES. M.Sc. thesis, University of Toronto (1986).
10. J. S. MOFFATT. J. Chem. Soc. 3045 (1960).
11. E. J. COREY and A. G. HARTMAN. J. Am. Chem. Soc. **87**, 5736 (1965).
12. P. D. GEAN. J. Chem. Soc. 6656 (1965).
13. (*a*) E. WENKERT, P. BAKUZIS, R. J. BAUMGARTEN, D. DODDRELL, P. W. JEFFS, C. L. LEICHT, R. A. MUELLER, and A. YOSHIKOSHI. J. Am. Chem. Soc. **92**, 1617 (1970); E. WENKERT and P. M. WOVKULICH. J. Org. Chem. **42**, 1105 (1977); (*b*) K. AUWERS and G. KEIL. Chem. Ber. **35**, 4207 (1902).
14. J. F. SAWYER, A. GOMES, and P. YATES. Acta Crystallogr. Sect. C: Cryst. Struct. Commun. **C42**, 708 (1985).
15. A. GOMES, J. F. SAWYER, D. DAO CONG, and P. YATES. Acta Crystallogr. Sect. C: Cryst. Struct. Commun. **C43**, 713 (1986).
16. R. A. BENKESER. Acc. Chem. Res. **4**, 94 (1971).
17. N. T. ANH. Tetrahedron, **29**, 3227 (1973).
18. E. L. ELIEL. Stereochemistry of carbon compounds. McGraw–Hill, New York. 1962. p. 236.
19. R. J. OUELETTE, J. D. RAWN, and S. N. JREISSATY. J. Am. Chem. Soc. **93**, 7117 (1971).
20. K. HOLMBERG. Acta Chem. Scand. Ser. B: **B28**, 857 (1974).
21. K. R. STEVENS, J. B. STOTHERS, and C. T. TAN. *In* Mass spectrometry and NMR spectroscopy in pesticide chemistry. *Edited by* R. Hague and F. J. Biros. Plenum Press, New York. 1974. pp. 179–196.
22. L. RUEST, G. BLOUIN, and P. DESLONGCHAMPS. Synth. Commun. **6**, 169 (1976).
23. W. E. BACHMANN and A. S. DREIDING. J. Org. Chem. **13**, 317 (1948).
24. E. R. CLARK and P. F. EPSTEIN. J. Chem. Soc. 2042 (1955).

Can. J. Chem. Downloaded from www.nrcresearchpress.com by 122.72.124.2 on 09/07/12
For personal use only.

Reactions of "cyclen-" and "cyclam-phosphorane" with $[Pt_2Cl_4(PEt_3)_2]$. Monodentate and bidentate complexes and the crystal and molecular structure of $[PtCl(PEt_3)(cyclamPH)]Cl.CH_2Cl_2$

DAVID ERIC BERRY, JANE BROWNING, GORDON WILLIAM BUSHNELL, KEITH ROGER DIXON,[1] AND ALAN PIDCOCK
Department of Chemistry, University of Victoria, Victoria, B.C., Canada V8W 2Y2

Received February 22, 1988

DAVID ERIC BERRY, JANE BROWNING, GORDON WILLIAM BUSHNELL, KEITH ROGER DIXON, and ALAN PIDCOCK. Can. J. Chem. **67**, 48 (1989).

Reaction of "cyclamphosphorane" (cyclamPH) with $[Pt_2Cl_4(PEt_3)_2]$ yields $[PtCl(PEt_3)(cyclamPH)]Cl$. The complex crystallizes as a dichloromethane solvate in the monoclinic space group $P2_1/n$, with a = 13.877(3), b = 23.231(7), c = 8.295(2) Å, β = 91.86(4)°, and an X-ray diffraction study shows square planar platinum coordination in which the labile proton of cyclamPH has transferred from phosphorus to nitrogen and the ligand is attached via simple P(III)---N(III) chelation. The phosphorus is *trans* to chlorine in the platinum coordination plane.

The corresponding product, *trans*-$[PtCl_2(PEt_3)(cyclenPH_2)]Cl$, derived from reaction of "cyclenphosphorane" (cyclenPH) with $[Pt_2Cl_4(PEt_3)_2]$, is shown by NMR studies to have a quite different structure in which the ligand is protonated at two nitrogen sites but not at phosphorus. The phosphorus is pentacoordinate with four attachments to nitrogen atoms and one to platinum. The two chlorine atoms are mutually *trans* in the platinum coordination plane.

Key words: crystal structure, cyclenphosphorane reaction, cyclamphosphorane reaction, X-ray diffraction.

DAVID ERIC BERRY, JANE BROWNING, GORDON WILLIAM BUSHNELL, KEITH ROGER DIXON et ALAN PIDCOCK. Can. J. Chem. **67**, 48 (1989).

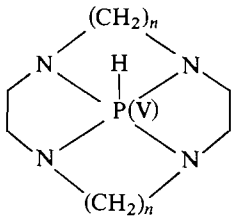
La réaction du «cyclamphosphorane» (cyclamPH) avec le $[Pt_2Cl_4(PEt_3)_2]$ conduit au $[PtCl(PEt_3)(cyclamPH)]Cl$. Les cristaux du complexe, qui cristallise avec une molécule de dichlorométhane, sont monocliniques, groupe d'espace $P2_1/n$, avec a = 13,877(3), b = 23,231(7) et c = 8,295(2) Å et β = 91,86(4)°; une étude par diffraction des rayons-X montre que la coordination du platine est plan carré, que le proton labile du cyclamPH a été transféré du phosphore à l'azote et que le ligand est attaché par le biais d'une simple chélation P(III)---N(III). Le phosphore est *trans* par rapport au chlore dans le plan de coordination du platine.

En se basant sur des études de rmn, on a démontré que la structure du produit correspondant, $[PtCl_2(PEt_3)(cyclenPH_2)]Cl$-*trans*, qui provient de la réaction du «cycloenphosphorane» (cyclenPH) avec le $[Pt_2Cl_4(PEt_3)_2]$, est très différente; le ligand est protoné à deux sites azotés, mais pas au phosphore. Le phosphore est pentacoordonné avec quatre azotes et un platine. Les deux atomes de chlore sont mutuellement *trans* dans le plan de coordination du platine.

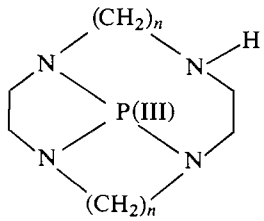
Mots clés : structure cristalline, réaction du «cycloenphosphorane», réaction du «cyclamphosphorane», diffraction des rayons-X.

[Traduit par la revue]

Introduction



Ia



Ib

The coordination chemistry of "cyclenphosphorane", **I** (n = 2, and "cyclamphosphorane", **I** (n = 3), has attracted recent attention for several reasons (1, 2). Most novel are complexes in which a P—N bond of the deprotonated P^V form is η^2-coordinated to a metal to form a three-membered ring (1–3). However, the relatively subtle effects of ring size on the distribution of *a* and *b* forms are also interesting. In the free ligands cyclenPH[2] exists entirely as the *a* form whereas cyclamPH is about 18% in the *b* form (4). These differences seem to be exaggerated in metal complexes. Thus reactions of cyclenPH with $[Co_2(CO)_8]$ and $[Mo(CO)_3(\eta^5\text{-}C_5H_5)]_2$ yield respectively $[Co(CO)_3(cyclenP)]$ and $[Mo(CO)_2(\eta^5\text{-}C_5H_5)$-(cyclenP)] as the initial products, both complexes having η^2-coordinated P—N bonds (1). In contrast, in the reaction of cyclamPH with $[MoCl(CO)_3(\eta^5\text{-}C_5H_5)]$ the first product is $[Mo(CO)_2(\eta^5\text{-}C_5H_5)(cyclamPH)]Cl$, a simple P(III)---N(III) chelate compound derived from form *b* of the ligand (2, 3). A strong base, methyl lithium, is required to convert this initial product to $[Mo(CO)_2(\eta^5\text{-}C_5H_5)(cyclamP)]$, with an η^2-coordinated P—N bond (2, 3). The rhodium complex, [RhCl(CO)(cyclamPH)], also contains a P(III)---N(III) chelated ligand (2).

A recent report (5) of the reaction of cyclenPH with *cis*-$[PtCl_2(PPh_3)_2]$, leading to an η^2-(P—N) bond in $[PtCl(PPh_3)$-(cyclenP)], prompts us to report our own results on platinum complexes. These results confirm the differences between cyclenPH and cyclamPH and also provide the first structural characterisation of one of these ligands coordinated in the simple chelate, P(III)---N(III) form, **I***b* (n = 3).

Results

(a) [PtCl(PEt$_3$)(cyclamPH)]Cl

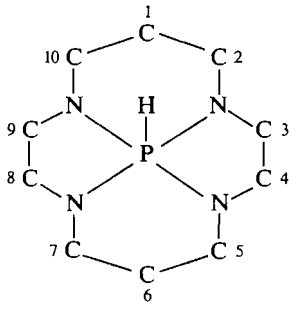
The chlorobridged platinum dimer, $[Pt_2Cl_4(PEt_3)_2]$, reacts with cyclamPH under mild conditions to give a white, crystalline product in high yield. After recrystallization of the product from a dichloromethane/diethyl ether solvent mixture, microanalysis is consistent with the formulation, $[PtCl(PEt_3)$-(cyclamPH)]$Cl.CH_2Cl_2$. ^1H NMR confirms the presence of CH_2Cl_2 and a proton decoupled ^{31}P spectrum shows two

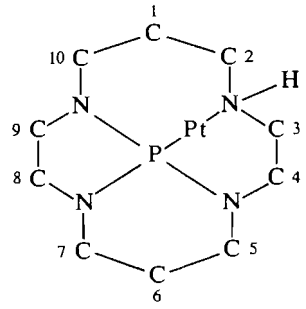
[1]To whom all correspondence should be addressed.

[2]In the present paper we use the abbreviations "cyclenPH" and "cyclamPH" to represent respectively the ligands "cyclenphosphorane", **I** (n = 2), and "cyclamphosphorane", **I** (n = 3).

Can. J. Chem. Downloaded from www.nrcresearchpress.com by 122.72.124.2 on 09/07/12
For personal use only.

TABLE 1. Carbon-13 NMR assignments for cyclamPH and $[PtCl(PEt_3)(cyclamPH)]^+$





Carbon number	cyclamPH (ppm)	J(P—C) (Hz)	Pt complex (ppm)	J(P—C) (Hz)	J(Pt—C) (Hz)
1	26.67		25.9		ca. 14
2	44.84		45.76		ca. 22
3	47.52	9.7	53.84	11.7	41.9
4, 8, 9	47.52	9.7	48.27	9.7	
			48.66	3.8	
			49.73	8.8	
5, 7	44.84		41.92		
			44.75		
6	26.67		21.91	4.3	
10	44.84		54.81		

resonances, each with ^{195}Pt sidebands, δ(PN) +69.16 ppm, J(Pt—P) 4649 Hz, δ(PEt_3) +12.65 ppm, J(Pt—P) 3294 Hz. The small phosphorus–phosphorus coupling of 19.3 Hz indicates *cis* geometry at the metal centre (6). As expected the ^{195}Pt spectrum at Ξ 21.400375 MHz (δ +17.52 ppm) is a doublet of doublets confirming the Pt—P couplings. The very normality of the phosphorus data suggests that the complex is a simple P(III)---N(III) chelate rather than any more exotic structure. For example, the parameters for *cis*-$[PtCl(PEt_3)_2(pyridine)]^+$, δ +3.6 and +7.9 ppm, J(Pt—P) 3057 and 3454 Hz, J(P—P) 20 Hz, are closely comparable (7) except that electron withdrawal by nitrogen increases the magnitude of the Pt—PN_4 coupling in the present complex.

A proton NMR resonance at 5.66 ppm has ^{195}Pt sidebands with J(Pt—H) 68 Hz, and may be assigned to a proton on nitrogen, whereas a proton coupled ^{31}P spectrum shows no evidence for a direct P—H bond. The ^{13}C spectrum is discussed in detail below and shows a complete loss of symmetry for the cyclamPH ligand, with all ten carbon sites separately identifiable. All of these data indicate a complex cation, $[PtCl(PEt_3)(cyclamPH)]^+$ in which the cyclamPH proton has been transferred from phosphorus to nitrogen and the ligand coordinated in form **I***b* (n = 3) with the cyclam phosphorus *trans* to chlorine and the cyclam nitrogen *trans* to PEt_3, a structure which was ultimately confirmed by the X-ray diffraction study discussed below.

(b) Carbon-13 nuclear magnetic resonance

The fully symmetrical ligand, cyclenPH, shows a doublet ^{13}C resonance at 44.96 ppm, J(P—C) 9.0 Hz. By comparison, the three resonances of cyclamPH, which occur at 26.67, 44.84, and 47.52 ppm, in a 1:2:2 intensity ratio, are easily assigned to carbons 1, 2, and 3, respectively, as shown in Table 1. Only the 47.52 ppm resonance is doubled by coupling to phosphorus (9.7 Hz). The absence of coupling from phosphorus to C(2) is somewhat puzzling but may be explained by the multiple coupling paths available. Thus C(3), which shows significant coupling, is coupled to phosphorus via two bond and three bond paths whereas C(2) is coupled via two bond and four bond paths.

In the ^{13}C NMR of $[PtCl(PEt_3)(cyclamPH)]^+$, the expected resonances for triethylphosphine, δ(CH_3) 8.15, J(P—C) 2.5 Hz, J(Pt—C) 28.2 Hz, and δ(CH_2) 15.43, J(P—C) 39.2 Hz, J(Pt—C) 36.9 Hz, are accompanied by ten clearly resolved resonances of closely equal intensity for the cyclam ring. The assignment of these resonances cannot be unambiguous but the observed couplings to phosphorus and platinum, combined with the comparison with free ligand parameters, suggest the assignments shown in Table 1 as the most likely.

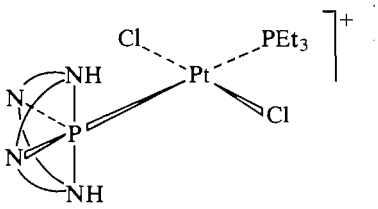
(c) $[PtCl_2(PEt_3)(cyclenPH_2)]Cl$

The reaction of cyclenPH with $[Pt_2Cl_4(PEt_3)_2]$ is superficially similar to that of cyclamPH. After recrystallization of the product from a dichloromethane/diethyl ether solvent mixture, microanalysis is consistent with the formulations, $[PtCl_2(PEt_3)(cyclenPH_2)]Cl.\frac{1}{2}CH_2Cl_2$ or $[PtCl_2(PEt_3)(cyclenPH)].CH_2Cl_2$. The presence of dichloromethane solvent is confirmed by ^1H NMR and it proved difficult to remove completely. The correctness of the diprotonated ionic formulation rather than the monoprotonated covalent structure is shown by conductance measurement and by a further reaction with potassium hexafluorophosphate which yields a PF_6^- salt with essentially the same NMR parameters as the chloride. In the ^1H spectra, broad resonances at 6.41 ppm (integral 1.6) for the chloride and 6.25 ppm (integral 1.9) for the hexafluorophosphate are assigned to protons on nitrogen. These protons exchange with D_2O and the precise extent of protonation in solution may vary with the conditions.

A proton decoupled ^{31}P NMR spectrum of $[PtCl_2(PEt_3)(cyclenPH_2)]Cl$ shows an AB pattern with ^{195}Pt sidebands, δ(PN) −6.33 ppm, J(Pt—P) 3659 Hz, δ(PEt_3) +9.51 ppm, J(Pt—P) 2234 Hz. A large P—P coupling of 793 Hz indicates mutually *trans* positions at the metal centre (6). The ^{195}Pt resonance at Ξ 21.416884 MHz (δ + 788.96 ppm) appears superficially simple as the expected doublet of doublets due

Can. J. Chem. Downloaded from www.nrcresearchpress.com by 122.72.124.2 on 09/07/12
For personal use only.

to coupling to phosphorus but interestingly requires analysis as the X region of an ABX pattern in order to match the J(Pt—P) values obtained from the phosphorus spectrum. In the ^{13}C NMR, the expected resonances for triethylphosphine, $\delta(CH_3)$ 7.78 ppm, J(P—C) < 3 Hz, J(Pt—C) ca. 30 Hz, and $\delta(CH_2)$ 13.13 ppm, J(P—C) 5.3 and 29.5 Hz, J(Pt—P) ca. 30 Hz, are accompanied by only two resonances, 42.11 (d 5.3 Hz) and 44.00 (s) ppm, for the cyclen ring, indicating a very symmetrical structure. This symmetrical ^{13}C spectrum is unchanged at −60°C. An X-ray diffraction study of the complex was attempted but ultimately failed to refine fully due to uncertainties in locating solvent of crystallization. However, as detailed in the experimental section, the space group symmetry requires that the molecule possess either a mirror plane or a two-fold axis of symmetry. There appears to be no reasonable structure which would have a two-fold axis, and the platinum coordination plane must therefore be a mirror plane with two nitrogens of the cyclenP ligand in this plane, and the other pair of nitrogens symmetrically above and below the plane, as illustrated in structure **II**. The protonated nitrogens could lie in the coordination plane or perpendicular to it. Coordination of the cyclenP ligand is via form **I***a* (n = 2) with the metal replacing the proton on phosphorus, in contrast to the chelate **I***b* (n = 3) form described above for the cyclamPH complex.



II

A similar structure has been proposed recently by Lattman and co-workers (5) for one of the products from reaction of cyclenPH with *cis*-[$PtCl_2(PPh_3)_2$], except that in that case the product had *cis* stereochemistry at the metal centre.

(d) Structure of [PtCl(PEt$_3$)(cyclamPH)]Cl.CH$_2$Cl$_2$

The atomic labelling scheme and the structure of a single cation of [$PtCl(PEt_3)$(cyclamPH)]Cl.CH_2Cl_2 are shown in Fig. 1. Fractional atomic coordinates and isotropic temperature parameters, bond lengths, and bond angles are collected in Tables 2–4, and further Tables of structure factors, anisotropic temperature factors, selected intermolecular distances, and fractional atomic coordinates, isotropic temperature parameters, and bond angles for the hydrogen atoms have been deposited as supplementary material.[3]

The structure of [$PtCl(PEt_3)$(cyclamPH)]$^+$ shows a platinum atom coordinated by chlorine, triethylphosphine, and by one nitrogen and the phosphorus of the cyclamPH ligand. The platinum and all four coordinating atoms lie within 0.05 Å of the least squares coordination plane, and the angles around Pt sum to exactly 360°. As predicted from the ^{31}P NMR data, the two phosphorus atoms are in mutually *cis* positions.

The bond lengths and angles in the coordination plane are summarized in Table 5. The Pt—Cl, Pt—N, and Pt—PEt_3 lengths fall within the normal ranges for these bonds when due allowance is made for the *trans* ligands. Thus previous results suggest 2.33–2.37 Å for Pt—Cl *trans* to phosphorus (8), 2.08–2.15 Å for Pt—N *trans* to phosphorus (8), and 2.24–2.31 Å for Pt—P *trans* to nitrogen (8). The Pt—PN_4 length, 2.136(11) Å, is relatively short for a bond *trans* to chlorine (more normal is 2.24–2.27 Å (8)), but not sufficiently so to suggest any unusual bonding. The most interesting comparison is to the coordination geometry of [$PtCl(PPh_3)$(cyclenP)] as summarized in Table 5. This complex was obtained by Lattman and co-workers from

[3]Copies of these tables may be purchased from the Depository of Unpublished Data, CISTI, National Research Council of Canada, Ottawa, Ont., Canada K1A 0S2.

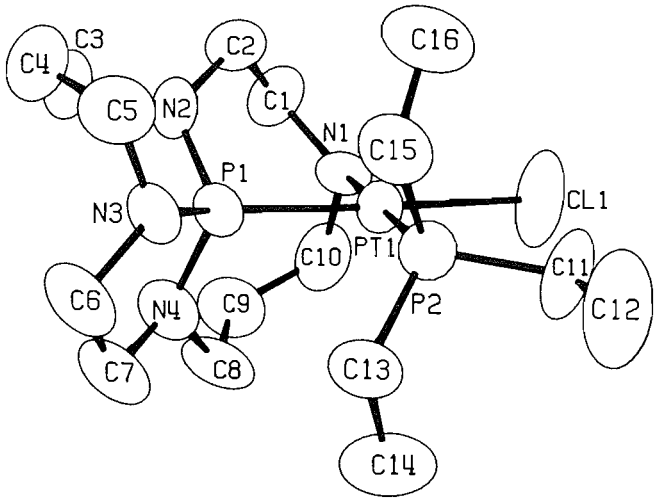


FIG. 1. ORTEP Plot of a single cation of [$PtCl(PEt_3)$(cyclamPH)]-Cl.CH_2Cl_2.

TABLE 2. Fractional atomic coordinates and temperature parameters for [$PtCl(PEt_3)${cyclamPH}]Cl.CH_2Cl_2[a]

Atom	x/a	y/b	z/c	U_{eq}
Pt(1)	45612(4)	19180(2)	23655(7)	462(2)
Cl(1)	5691(4)	2309(2)	619(8)	105(2)
Cl(2)	1801(3)	4177(2)	4197(5)	66(1)
Cl(3)	8691(7)	−585(5)	741(12)	175(5)
Cl(4)	8932(8)	397(5)	2804(16)	221(7)
P(1)	3649(3)	1422(2)	3968(5)	50(1)
P(2)	3777(3)	2759(2)	2674(5)	56(1)
N(1)	5361(8)	1141(5)	2072(14)	51(4)
N(2)	3357(9)	818(5)	3000(15)	60(5)
N(3)	2590(9)	1625(6)	4674(14)	59(5)
N(4)	4168(10)	1314(7)	5743(16)	70(5)
C(1)	4846(12)	586(6)	1651(23)	66(6)
C(2)	3772(12)	662(8)	1484(20)	68(7)
C(3)	2634(12)	440(7)	3726(22)	70(7)
C(4)	1666(12)	735(8)	3819(26)	84(8)
C(5)	1745(11)	1399(8)	3744(23)	78(7)
C(6)	2583(14)	1585(11)	6435(21)	93(9)
C(7)	3625(15)	1555(11)	7061(22)	96(9)
C(8)	5243(12)	1323(8)	5975(19)	77(7)
C(9)	5748(13)	883(8)	5054(22)	77(7)
C(10)	6111(12)	1044(8)	3395(25)	76(7)
C(11)	4362(13)	3360(7)	1722(29)	83(8)
C(12)	3918(16)	3944(9)	1855(34)	124(12)
C(13)	3628(13)	2981(7)	4749(21)	71(7)
C(14)	4603(18)	3061(10)	5714(31)	115(11)
C(15)	2532(11)	2751(8)	1847(21)	72(7)
C(16)	2434(15)	2513(9)	158(24)	96(9)
C(17)	8570(31)	125(19)	901(47)	218(24)

[a]Estimated standard deviations are given in parentheses; coordinates $\times 10^n$ where n = 5 for Pt, and 4 otherwise; temperature parameters $\times 10^n$ where n = 4 for Pt and 3 otherwise; U_{eq} = the equivalent isotropic temperature parameter; $U_{eq} = (1/3)\Sigma_i\Sigma_j U_{ij} a_i^* a_j^* (a_i . a_j)$.

Can. J. Chem. Downloaded from www.nrcresearchpress.com by 122.72.124.2 on 09/07/12
For personal use only.

TABLE 3. Interatomic distances (Å) for [PtCl(PEt$_3$){cyclamPH}]-Cl.CH$_2$Cl$_2$[a]

Atoms	Distance	Atoms	Distance
Cl(1)—Pt(1)	2.352(4)	C(3)—N(2)	1.48(2)
P(1)—Pt(1)	2.192(4)	C(5)—N(3)	1.48(2)
P(2)—Pt(1)	2.254(4)	C(6)—N(3)	1.46(2)
N(1)—Pt(1)	2.136(11)	C(7)—N(4)	1.46(2)
C(17)—Cl(3)	1.67(4)	C(8)—N(4)	1.50(2)
C(17)—Cl(4)	1.76(4)	C(2)—C(1)	1.50(2)
N(2)—P(1)	1.660(13)	C(4)—C(3)	1.51(2)
N(3)—P(1)	1.668(11)	C(5)—C(4)	1.55(2)
N(4)—P(1)	1.636(14)	C(7)—C(6)	1.52(3)
C(11)—P(2)	1.81(2)	C(9)—C(8)	1.47(2)
C(13)—P(2)	1.82(2)	C(10)—C(9)	1.53(3)
C(15)—P(2)	1.84(2)	C(12)—C(11)	1.50(2)
C(1)—N(1)	1.51(2)	C(14)—C(13)	1.56(3)
C(10)—N(1)	1.51(2)	C(16)—C(15)	1.51(3)
C(2)—N(2)	1.45(2)		

[a]Estimated standard deviations are given in parentheses.

the reaction of cyclenPH with *cis*-[PtCl$_2$(PPh$_3$)$_2$] (5). During the reaction, cyclenPH loses its proton and becomes attached to platinum by η^2-coordination of a P—N bond. This is reflected in the structure by the very short N(1)—P(1) distance, 1.872(11) Å and the narrow N(1)—Pt—P(1) angle, 51.0(3)°. As is illustrated by Table 5, the present complex is quite different with a normal square planar angle (86.4(3)°) at N(1)—Pt—P(1) and a long N(1)—P(1) distance, 2.96(1) Å. The other P—N lengths are similar in the two complexes, ranging from 1.64–1.70 Å. In the present structure the final difference map gave evidence of additional electron density adjacent to N(1), indicating the presence of a proton on this atom. It is therefore clear that cyclamPH coordinates to platinum as a simple P(III)---N(III) chelate in which the proton has been transferred from phosphorus to nitrogen, rather than the deprotonation and η^2-(P—N) attachment adopted by cyclenPH.

Experimental

(a) Synthesis and spectroscopic studies

Data relating to the characterization of the complexes are given in the tables, the Results section, and in the preparative descriptions below. Microanalysis was by the Canadian Microanalytical Service, Vancouver, B.C., Canada.

^{1}H, ^{31}P, ^{13}C, and ^{195}Pt NMR spectra were recorded in $CDCl_3$ solution at 250.1, 101.3, 62.9, and 53.5 MHz, respectively, using a Bruker WM250 Fourier transform spectrometer locked to the solvent deuterium resonance. For ^{31}P, ^{13}C, and ^{195}Pt spectra, protons were decoupled by broad band ("noise") irradiation at appropriate frequencies. ^{1}H and ^{13}C chemical shifts were measured relative to external $Si(CH_3)_4$. ^{31}P chemical shifts were measured relative to external $P(OMe)_3$ and are reported in parts per million relative to 85% H_3PO_4 using a conversion factor of +141 ppm. ^{195}Pt chemical shifts are reported in ppm relative to $\Xi(^{195}Pt) = 21.4$ MHz (9). For all nuclei, positive chemical shifts are downfield of the appropriate reference. Simulated NMR spectra were calculated on an IBM 3083 computer and plotted on a Tektronix 4013 graphics screen for preliminary work or a Calcomp 1039 plotter for final data. The programs used were a locally constructed package based on UEAITR (10) and NMRPLOT (11).

All operations were carried out under an atmosphere of dry nitrogen using standard Schlenk tube techniques. Solvents were dried by appropriate methods and distilled under nitrogen prior to use. [$Pt_2Cl_4(PEt_3)_2$] (12) and cyclamPH (4) were prepared as previously described, the latter using the reaction of $P(NMe_2)_3$ (13) with 1,4,8,11-tetraazacyclotetradecane (cyclam) purchased from Strem Chemicals Inc.

(1) Reaction of [$Pt_2Cl_4(PEt_3)_2$] with cyclamPH

A solution of cyclamPH (0.37 g, 1.6 mmol) in tetrahydrofuran (4 mL) was added dropwise to a stirred solution of [$Pt_2Cl_4(PEt_3)_2$] (0.57 g, 0.74 mmol) in tetrahydrofuran (20 mL). The mixture was stirred for 90 min, during which time a white precipitate formed. The precipitate was collected by filtration, dissolved in dichloromethane

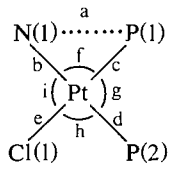
TABLE 4. Bond angles (deg) for [PtCl(PEt$_3$){cyclamPH}]Cl.CH$_2$Cl$_2$[a]

Atoms	Angle	Atoms	Angle
P(1)—Pt(1)—Cl(1)	170.5(2)	C(3)—N(2)—P(1)	117.6(11)
P(2)—Pt(1)—Cl(1)	94.0(2)	C(3)—N(2)—C(2)	120.1(13)
P(2)—Pt(1)—P(1)	95.5(1)	C(5)—N(3)—P(1)	114.2(10)
N(1)—Pt(1)—Cl(1)	84.1(3)	C(6)—N(3)—P(1)	111.5(12)
N(1)—Pt(1)—P(1)	86.4(3)	C(6)—N(3)—C(5)	117.9(14)
N(1)—Pt(1)—P(2)	177.6(3)	C(7)—N(4)—P(1)	113.2(12)
N(2)—P(1)—Pt(1)	106.7(4)	C(8)—N(4)—P(1)	121.3(11)
N(3)—P(1)—Pt(1)	126.7(5)	C(8)—N(4)—C(7)	115.8(14)
N(3)—P(1)—N(2)	101.8(7)	C(2)—C(1)—N(1)	112.3(12)
N(4)—P(1)—Pt(1)	112.4(5)	C(1)—C(2)—N(2)	111.8(14)
N(4)—P(1)—N(2)	113.5(7)	C(4)—C(3)—N(2)	111.6(14)
N(4)—P(1)—N(3)	95.4(7)	C(5)—C(4)—C(3)	112.6(14)
C(11)—P(2)—Pt(1)	113.2(6)	C(4)—C(5)—N(3)	112.9(15)
C(13)—P(2)—Pt(1)	115.1(6)	C(7)—C(6)—N(3)	107.8(14)
C(13)—P(2)—C(11)	105.1(10)	C(6)—C(7)—N(4)	106(2)
C(15)—P(2)—Pt(1)	113.6(6)	C(9)—C(8)—N(4)	114.5(15)
C(15)—P(2)—C(11)	105.9(9)	C(10)—C(9)—C(8)	119(2)
C(15)—P(2)—C(13)	102.8(8)	C(9)—C(10)—N(1)	116.9(13)
C(1)—N(1)—Pt(1)	120.3(9)	C(12)—C(11)—P(2)	118.4(13)
C(10)—N(1)—Pt(1)	113.1(9)	C(14)—C(13)—P(2)	113.4(14)
C(10)—N(1)—C(1)	110.6(12)	C(16)—C(15)—P(2)	113.9(12)
C(2)—N(2)—P(1)	122.3(10)	Cl(4)—C(17)—Cl(3)	114(2)

[a]Estimated standard deviations are given in parentheses.

Can. J. Chem. Downloaded from www.nrcresearchpress.com by 122.72.124.2 on 09/07/12
For personal use only.

TABLE 5. Comparison of coordination geometries in $[PtCl(PEt_3)(cyclamPH)]^+$ and $[PtCl_2(PPh_3)$-(cyclenP)] (data for the latter compound are from ref. 5)



Compound	a	b	c	d	e
$[PtCl(PEt_3)(cyclamPH)]^+$	2.96(1)	2.136(11)	2.192(4)	2.254(4)	2.352(4)
$[PtCl(PPh_3)(cyclenP)]$	1.872(11)	2.120(10)	2.223(3)	2.214(3)	2.440(3)

Compound	f	g	f	i
$[PtCl(PEt_3)(cyclamPH)]^+$	86.4(3)	95.5(1)	94.0(2)	84.1(3)
$[PtCl(PPh_3)(cyclenP)]$	51.0(3)	110.3(1)	100.7(1)	97.6(3)

and crystallized by careful addition of diethyl ether followed by cooling to −18°C to yield $[PtCl(PEt_3)(cyclamPH)]Cl.CH_2Cl_2$ as colourless crystals (0.53 g, 0.76 mmol). *Anal.* calcd. for $C_{17}H_{38}Cl_4N_4P_2Pt$: C 29.3, H 5.49, Cl 20.3, N 8.03; found: C 29.1, H 5.55, Cl 18.1, N 8.06. ^{1}H NMR: PEt_3, δ(CH_3) 1.00 ppm (d, 17.9 Hz, of t, 7.7 Hz), δ(CH_2) 1.86 ppm (multiplet); cyclam, series of multiplets, 2.8–3.8 ppm; NH 5.66 ppm (1:4:1 t, J(Pt—H) 68 Hz). Other spectroscopic data are given in the Results section.

(2) Reaction of $[Pt_2Cl_4(PEt_3)_2]$ with cyclenPH

(i) Preparation of cyclenPH

Cyclen.4HCl was purchased from Geneva Chemical Co. but we were not successful in synthesising the required cyclenPH by direct reaction of cyclen.4HCl with $P(NMe_2)_3$. Previous workers used reaction of the free base with $P(NMe_2)_3$ (14). Accordingly, a Rexyn 201 OH^- column was prewashed with water until the washings were pH 7 and an aqueous solution of cyclen.4HCl was then passed through the column. The initial solution was acidic but the eluant was basic. After removal of the solvent water under reduced pressure the eluted material analyzed approximately as cyclen.$2H_2O$ and showed no appreciable chloride content by either addition of $AgNO_3$ or by potentiometric titration. *Anal.* calcd. for $C_8H_{24}N_4O_2$: C 46.1, H 11.61; found: C 46.2, H 10.19. This product was then reacted with $P(NMe_3)_3$ to prepare cyclenPH as previously described (14). ^{13}C and ^{31}P NMR spectra of the product were consistent with those reported previously. *Anal.* calcd. for $C_8H_{17}N_4P$: C 48.0, H 8.56; found: C 47.6, H 8.61.

(ii) Reaction with $[Pt_2Cl_4(PEt_3)_2]$

A solution of cyclenPH (0.11 g, 0.53 mmol) in dichloromethane (15 mL) was added dropwise to a stirred solution of $[Pt_2Cl_4(PEt_3)_2]$ (0.20 g, 0.26 mmol) in dichloromethane (15 mL). The mixture was stirred for 1 h before removal of the solvent *in vacuo*. The residue was washed with hexane (20 mL), dissolved in dichloromethane and crystallized by careful addition of diethyl ether followed by cooling to −18°C to yield $[PtCl_2(PEt_3)(cyclenPH_2)]Cl.\frac{1}{2}CH_2Cl_2$ as colourless crystals (0.16 g, 0.24 mmol). *Anal.* calcd. for $C_{14.5}H_{34}Cl_4N_4P_2Pt$: C 26.3, H 5.17, Cl 21.4, N 8.45; found: C 26.3, H 5.27, Cl 22.0, N 8.54. ^{1}H NMR: PEt_3, δ(CH_3) 1.14 ppm (d, 15.8 Hz, of t, 7.4 Hz), δ(CH_2) 1.78 ppm (multiplet); cyclen, complex multiplets, 3.40 and 3.59 ppm; NH 6.41 ppm. Other spectroscopic data are given in the Results section. Conductance in CH_3CN: 141 S cm^2 mol^{-1}.

A crystal of the complex was orthorhombic with a = 9.166(2), b = 20.063(3), and c = 14.283(3) Å, and the systematic absences in its X-ray diffraction pattern were consistent with space groups $Cmc2_1$ (No. 36), $Ama2$ (No. 40), or $Cmcm$ (No. 63). The density (1.66 g cm^{-3}) indicates four molecules per unit cell (calculated for $[PtCl_2(PEt_3)(cyclenPH_2)]Cl.\frac{1}{2}CH_2Cl_2$ is 1.68) which in space group No. 63 would lead to an impossibly high symmetry for the molecule. With four molecules per unit cell, space group No. 40 requires either that the molecule possess a plane of symmetry or a two-fold axis, and No. 36 requires a plane of symmetry.

(iii) Conversion to PF_6^- salt

A solution of $[PtCl_2(PEt_3)(cyclenPH_2)]Cl.\frac{1}{2}CH_2Cl_2$ (0.1 mmol) in dichloromethane (5 mL) was stirred with finely powdered KPF_6 (1 mmol) for 2 h. The supernatant was separated, diethyl ether added, and the solution cooled to −18°C to yield $[PtCl_2(PEt_3)(cyclenPH_2)]PF_6$ as pale yellow crystals. *Anal.* calcd. for $C_{14}H_{33}Cl_2F_6N_4P_3Pt$: C 23.0, H 4.55, N 7.67; found: C 23.0, H 4.48, N 7.65. ^{31}P NMR: δ(PN_4) −6.77 ppm (^1J(Pt—P) 3648 Hz); δ(PEt_3) 10.39 ppm (^1J(Pt—P) 2216 Hz); ^2J(P—P) 787 Hz; δ(PF_6) −143.87 ppm, ^1J(P—F) 713 Hz.

(b) X-Ray data collection

Crystals of $[PtCl(PEt_3)\{cyclamPH\}]Cl.CH_2Cl_2$ suitable for study by X-ray diffraction were grown by cooling (to −18°C) a solution of the complex in a mixture of diethyl ether and dichloromethane. Preliminary photographic work was carried out with Weissenberg and precession cameras using Cu K_α radiation. After establishment of the symmetry and an approximate unit cell the crystal was transferred to a Picker 4-circle diffractometer automated with a PDP11/10 computer and utilising Zr filtered Mo K_α radiation (λ = 0.71069 Å). The unit cell was refined by least-squares methods employing 22 pairs of centering measurements at ±2θ in the range $|2\theta|$ = 11–34°. The crystal was mounted approximately along the c axis. The crystal data at approximately 24°C were as follows:

$C_{17}H_{38}Cl_4N_4P_2Pt$ M_r = 697.37

Monoclinic, space group $P2_1/n$; a = 13.877(3), b = 23.231(7), c = 8.295(2) Å; β = 91.86(4)°; V(cell) = 2673(1) Å^3; Z = 4.

The asymmetric unit consisted of one molecule of the complex together with one molecule of dichloromethane. Intensity measurements were collected for two reciprocal space octants (h unrestricted, $k \geq 0$, $l \geq 0$) up to 2θ = 45°. A θ/2θ step scan was used with 160 steps of 0.01° in 2θ, counting for 0.25 s per step. Background measurements were for 20 s at each end of the scan. Each batch of 50 reflections was preceded by the measurement of three standard reflections (0,0,2; 0,8,0; and 2,0,0). The Lorentz and polarization factors were applied and each batch was scaled to maintain the sum of the standards constant. There was evidence of about 37% sample decomposition, possibly due to loss of CH_2Cl_2 during the data collection. Absorption corrections were applied with a numerical integration procedure utilizing a Gaussian grid (6 × 6 × 24). The crystal shape was defined by perpendicular distances to crystal faces from a central origin as follows: ±{100}, 0.1144 mm; ±{010}, 0.1234 mm; ±{001}, 0.4049 mm. The absorption coefficient was 60.50 cm^{-1}, and the

Can. J. Chem. Downloaded from www.nrcresearchpress.com by 122.72.124.2 on 09/07/12
For personal use only.

range of transmission factors was 0.22–0.30. Symmetry equivalent data were averaged and the final file contained 3481 independent reflections.

(c) Structure solution and refinement

The structure was found and refined using the SHELX-76 program package (15) and illustrations were drawn using ORTEP (16). The atomic scattering factors used were for neutral atoms, with corrections for anomalous dispersion (17). The structure was solved by direct methods, completed by standard Fourier synthesis procedures using difference maps, and refined by the method of least squares minimising $\Sigma w\Delta^2$ where $\Delta = ||F_o| - |F_c||$. The weights were obtained from counting statistics using $w = 1/(\sigma^2(F) + 0.001F^2)$. Hydrogen atoms were not located but, except for that on the coordinated nitrogen atom and those in the CH_2Cl_2 solvent, their positions were calculated and included in the refinement. They were allowed to ride at 1.080 Å from their respective carbon atoms and temperature factors were calculated for the CH_n groups. All non-hydrogen atoms were treated anisotropically. There were 256 variable parameters to be determined from 3481 independent observations. Convergence was obtained with a maximum shift/esd ratio of 0.11. The residuals were $R = 0.0872$ and $R_w = (\Sigma w\Delta^2/\Sigma wF_o^2)^{1/2} = 0.0795$. The final difference map had a maximum of +3.5 e Å^{-3} close to the platinum atom and a minimum of −3.1 e Å^{-3}, but gave no indication that any material had been overlooked. A peak of 0.68 e Å^{-3} at 1.16 Å from the coordinated nitrogen atom was evidence for a hydrogen at this location.

Acknowledgements

We thank the Natural Sciences and Engineering Research Council of Canada and the University of Victoria for research grants, and Mrs. C. Greenwood for recording NMR spectra.

1. M. LATTMAN, S. K. CHOPRA, A. H. COWLEY, and A. M. ARIF. Organometallics, **5**, 677 (1986), and references therein.
2. J. M. DUPART, A. GRAND, and J. G. RIESS. J. Am. Chem. Soc. **108**, 1167 (1986), and references therein.
3. J. M. DUPART, A. GRAND, S. PACE, and J. G. RIESS. J. Am. Chem. Soc. **104**, 2316 (1982).
4. T. J. ATKINS and J. E. RICHMAN. Tetrahedron Lett. **19**, 5149 (1978).
5. M. LATTMAN, E. G. BURNS, S. K. CHOPRA, A. H. COWLEY, and A. M. ARIF. Inorg. Chem. **26**, 1926 (1987).
6. K. R. DIXON. *In* Multinuclear NMR. *Edited by* J. Mason. Plenum Press, New York. 1987. pp. 369–402.
7. K. R. DIXON. Inorg. Chem. **16**, 2618 (1977).
8. G. W. BUSHNELL, R. J. DENSMORE, K. R. DIXON, and A. C. RALFS. Can. J. Chem. **61**, 1132 (1983), and references therein.
9. R. G. KIDD and R. J. GOODFELLOW. *In* NMR and the Periodic Table. *Edited by* R. K. Harris and B. E. Mann. Academic Press, London. 1978. p. 249.
10. R. B. JOHANNSEN, J. A. FERRETI, and R. K. HARRIS. J. Magn. Reson. **3**, 84 (1970).
11. J. D. SWALEN. *In* Computer programmes for chemistry. Vol. I. *Edited by* D. F. Detar. W. A. Benjamin, New York. 1968.
12. R. J. GOODFELLOW and L. M. VENANZI. J. Chem. Soc. 7533 (1965).
13. V. MARK. Org. Synth. **46**, 42 (1966).
14. J. E. RICHMAN and T. J. ATKINS. Tetrahedron Lett. **19**, 4333 (1978).
15. G. M. SHELDRICK. SHELX-76. A computer program for crystal structure determination. University of Cambridge, Cambridge, England. 1976.
16. C. K. JOHNSON. ORTEP: A Fortran thermal ellipsoid plot program for crystal structure illustrations. ORNL-3794, Oak Ridge National Laboratory, Oak Ridge, U.S.A. 1965.
17. D. T. CROMER and J. T. WABER. *In* International tables for X-ray crystallography. Vol. IV. *Edited by* J. A. Ibers and W. C. Hamilton. Kynoch Press, Birmingham, England. 1974. pp. 99, 148.

Can. J. Chem. Downloaded from www.nrcresearchpress.com by 122.72.124.2 on 09/07/12
For personal use only.

The orientational behaviour of dichlorobenzenes in nematic liquid crystal solvents

C. T. YIM
Department of Chemistry, Dawson College, 350 Selby St., Westmount, P.Q., Canada H3Z 1W7

AND

D. F. R. GILSON
Department of Chemistry, McGill University, 801 Sherbrooke St. W., Montreal, P.Q., Canada H3A 2K6

Received July 6, 1988

C. T. YIM and D. F. R. GILSON. Can. J. Chem. **67**, 54 (1989).

The orientational order parameters of *ortho*-, *meta*-, and *para*-dichlorobenzene, dissolved in the nematic solvents EBBA and 1132, have been measured as functions of temperature and concentration, and used to determine the values of the potential energy parameters for each solute–solvent pair. These potentials have been interpreted in terms of a short-range contribution, which depends upon the shape and size of the solute molecule, plus a long-range term due to the interaction between the average electric field gradient from the solvent and the molecular quadrupole moment of the solute.

Key words: dichlorobenzenes, nematic solvents, liquid crystals, orientation, potential energy parameters.

C. T. YIM et D. F. R. GILSON. Can. J. Chem. **67**, 54 (1989).

Les paramètres d'ordre d'orientation des *ortho*-, *meta*- et *para*-dichlorobenzènes dissous dans les solvants nématiques EBBA et 1132 ont été mesurés en fonction de la température et de la concentration et ils ont été utilisés pour déterminer les paramètres d'énergie potentielle de chacune des paires de soluté–solvant. On a interprété ces potentiels en fonction d'une contribution à courte distance, qui dépend de la forme et de la grosseur de la molécule soluté, et d'une contribution à longue distance qui dépend de l'interaction entre le gradient du champ électrique moyen provenant du solvant et la moment quadripolaire moléculaire du soluté.

Mots clés : dichlorobenzènes, solvants nématiques, cristaux liquides, orientation, paramètres d'énergie potentielle.

[Traduit par la revue]

Can. J. Chem. Downloaded from www.nrcresearchpress.com by 122.72.124.2 on 09/07/12
For personal use only.

Introduction

The factors that determine the orientation of a solute molecule dissolved in a liquid crystal solvent are of interest in view of the technological applications of guest–host liquid crystal display devices, and also as probes of intermolecular forces in anisotropic media. The aim of the present studies is to derive parameters that link the terms in an orientational potential function with molecular properties of the solute. Early attempts by Saupe and Nehring (1, 2) to derive such expressions used a bond additive model for various fluoro- and chloro-benzene derivatives, which gave approximate agreement with the experimental results, but, due to the lack of experimental data at that time, this approach did not examine the effects of temperature, concentration, and solvent. Subsequent studies (3–18) have shown that the behaviour is more complicated, and the mean field approach, with a dependence on dispersion forces alone, is probably an oversimplification.

Burnell and co-workers (19–23) have proposed that the interaction between the solute molecular quadrupole moment and the solvent electric field gradient makes an important contribution to the ordering potential, particularly for small molecules. In recent studies of the orientation behaviour of monochlorobenzene (17), dissolved in two nematic liquid crystal solvents of different properties, EBBA and 1132, it was shown that the ring moiety played an important role in determining the difference in the solute orientational order in these two solvents. Since the field gradients in these two solvents are of opposite sign, it now seems probable that the observed differences in the orientation of chlorobenzene arise from the interaction with the quadrupole moment. The present study extends this to examine the effect of additional chlorine substitution.

The order parameters can be conveniently determined from an analysis of the proton magnetic resonance of the partially aligned solute molecules (24). Since all three solute molecules possess two perpendicular planes of symmetry, the orientation can be described by the elements of the Saupe order matrix S_{33} and $(S_{11} - S_{22})$. For the dichlorobenzenes, the 3-axis is taken to be the long molecular axis, and the 2-axis to be perpendicular to the benzene ring (Fig. 1). Thus S_{33} describes the tendency of the long molecular axis to align parallel to the director, and $(S_{11} - S_{22})$ describes the difference in alignment of the two perpendicular axes.

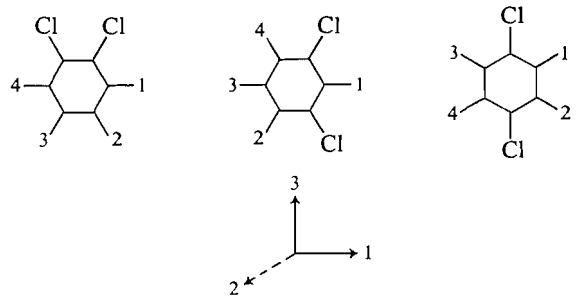


FIG. 1. Coordinate system and atomic labelling for dichlorobenzenes.

The calculated order parameters are obtained via the integrations of eqs. [1] and [2]:

$$[1] \quad S_{33} = (3/2Z)\int\int(\cos^2\theta \exp\{-U(\theta,\phi)/kT\}\sin\theta d\theta d\phi) - (1/2)$$

$$[2] \quad S_{11} - S_{22} = (3/2Z) \times \int\int(\sin^2\theta \cos 2\phi \exp\{-U(\theta,\phi)/kT\}\sin\theta d\theta d\phi)$$

where

$$Z = \int\int \exp\{-U(\theta,\phi)/kT\}\sin\theta d\theta d\phi$$

The intermolecular interaction potential $U(\theta,\phi)$, in this

Can. J. Chem. Downloaded from www.nrcresearchpress.com by 122.72.124.2 on 09/07/12
For personal use only.

study, is written as

$$[3] \quad U(\theta,\phi) = -AS_1(\cos^2\theta + B\sin^2\theta\cos 2\phi)$$

where S_1 is the solvent order parameter, and

$$[4] \quad A = a[3] - (1/2)(a[1] + a[2])$$

and

$$[5] \quad B = (a[1] - a[2])/(2a[3] - a[1] - a[2])$$

The constants $a[i]$ characterize the interaction energy along the corresponding axis. The parameter A corresponds to a potential energy difference between two solute orientations with axis 3 parallel and perpendicular to the liquid crystal director, and AB is the difference between orientations with axis 1 and axis 2 parallel to the director. The parameter A will include both solute and solvent terms, but B should depend only upon the solute properties.

Experimental

The two liquid crystal solvents used were 1132, a mixture of cyanophenylcyclohexanes and cyanobiphenylcyclohexanes, which was supplied by BDH Chemicals Ltd., and EBBA (*N*-(*p*-ethoxybenzylidine)-*p'*-*n*-butylaniline), which was synthesized and purified by literature methods (25). The dichlorobenzenes were purchased from commercial sources and used without further purification. Samples of various concentrations were prepared by weighing appropriate amounts of solute and solvent into NMR tubes and then sealing under vacuum. The concentrations and nematic to isotropic transition temperatures of the samples studied are listed in Table 1.

The proton NMR spectra were recorded on either a Varian XL-200 or a Varian XL-300 spectrometer. Since spectra obtained with or without the use of the deuterium lock did not show any difference, most spectra were recorded without the lock. The temperatures were calibrated against the proton chemical shift difference in an ethylene glycol sample.

The spectral analyses were performed with a modified LAOCN 3 program using either an Olivetti M-24 or IBM PC microcomputer. For *p*-dichlorobenzene, the geometry published by Burnell *et al.* (26) was used to determine the order parameters. For the other dichlorobenzenes the geometry was varied until reasonable fits (rms error less than 1.0 Hz) to the experimental room temperature spectra were achieved, and the same geometry was used for analyzing the spectra recorded at other temperatures.

Results and discussion

The relative interproton distances of *ortho*- and *meta*-dichlorobenzene, Table 2 (for atomic labelling see Fig. 1), are in reasonable agreement with those reported by Diehl *et al.* (27–30) but, since the early results were obtained in azoxy-type liquid crystal solvents, exact agreement is not expected. Vibrational averaging effects have been ignored in the present work as the effect upon the calculated order parameters is small, and can be neglected in studying the orientation behaviour and its variation with temperature (12).

The A and B terms in the potential function were calculated by computing fits to eqs. [1] and [2] for each experimental value of the orientation parameter. The solvent order parameter values were obtained from the literature (32, 33).[1] The order parameter values cited for 1132 were derived from refractive index measurements (33), which depend upon the method used in their interpretation; those derived according to Neugebauer's approach (34) have been used. The order parameter of the solvent is a function of reduced temperature and is, therefore, independent of the solute and its concentration (35). The parameter A is expected to be dependent on temperature since it includes the distance dependence of the intermolecular forces. However, including this dependence by using the molar volume did not lead to significant improvement in the fit (17) and, in view of the uncertainty in the values of solvent order, the volume dependence of A was neglected in our analyses.

The variation of $S_{11} - S_{22}$ with S_{33} is a convenient way of

[1]Also D. F. R. Gilson, unpublished results.

TABLE 1. Sample concentration, transition temperatures, and energy parameters A and B

Solute/solvent, concn. (mol%)	Transition temperature (N→I) (K)	Average B value	Average A value (10^{-20} J molecule^{-1})
para/1132			
1.4	343.5	0.458	1.57
3.1	340.9	0.464	1.57
6.0	336.6	0.453	1.53
9.5	331.2	0.444	1.49
ortho/1132			
1.0	343.5	0.806	1.10
2.7	341.0	0.803	1.08
5.5	335.7	0.798	1.04
10.5	327.7	0.790	0.98
meta/1132			
1.2	342.6	0.696	1.18
2.8	340.2	0.693	1.16
5.5	336.7	0.685	1.11
10.6	327.7	0.687	1.04
para/EBBA			
1.9	349.5	0.114	1.56
3.9	346.9	0.111	1.55
9.6	337.2	0.107	1.46
ortho/EBBA			
1.9	348.8	0.549	0.68
4.1	344.2	0.545	0.63
6.3	339.6	0.543	0.61
10.1	330.6	0.533	0.57
meta/EBBA			
2.2	347.1	0.342	0.90
3.5	345.7	0.340	0.87
6.9	339.2	0.335	0.82
9.7	331.8	0.329	0.76

TABLE 2. Interproton distance ratios in (*a*) *ortho*- and (*b*) *meta*-dichlorobenzenes

(*a*) *ortho*-Dichlorobenzene:

	ZLI 1132	EBBA	Ref. 27	Ref. 29
r_{12}/r_{23}	1.006	1.000	1.017	0.9977
r_{13}/r_{23}	1.727	1.732	1.742	1.733
r_{14}/r_{23}	1.970	1.998	2.002	2.007

(*b*) *meta*-Dichlorobenzene:

	ZLI 1132	EBBA	Ref. 28	Ref. 30*a*
r_{12}/r_{23}	1.731	1.732	—	1.725
r_{13}/r_{23}	2.002	2.000	—	1.990
r_{24}/r_{23}	1.729	1.732	1.732	1.734

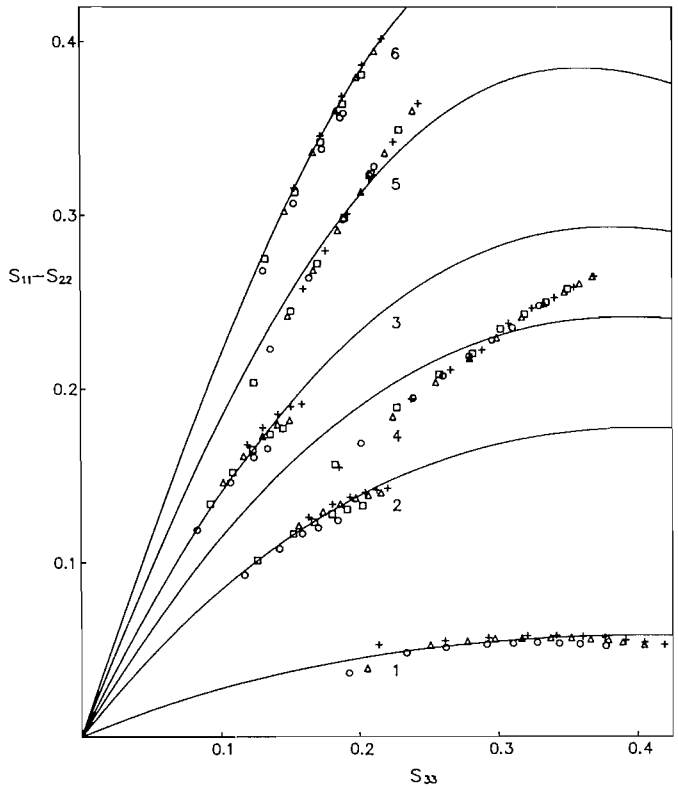


FIG. 2. Variation of $(S_{11} - S_{22})$ with S_{33} of dichlorobenzenes. 1, *p*-dichlorobenzene in EBBA, concentrations (in mol%) are: ○, 9.6; △, 3.9; +, 1.9; 2, *m*-dichlorobenzene in EBBA, concentrations are ○, 9.7; □, 6.9; △, 3.5; +, 2.2; 3, *o*-dichlorobenzene in EBBA, concentrations are ○, 10.1; □, 6.3; △, 4.1; +, 1.9; 4, *p*-dichlorobenzene in 1132, concentrations are ○, 9.5; □, 6.0; △, 3.1; +, 1.4; 5, *m*-dichlorobenzene in 1132, concentrations are ○, 10.6; □, 5.5; △, 2.8; +, 1.2; 6, *o*-dichlorobenzene in 1132, concentrations are ○, 10.5; □, 5.5; △, 2.7; +, 1.0. The solid lines are the calculated dependences of $(S_{11} - S_{22})$ on S_{33}, based on the average value of B for the most dilute solution (see Table 1).

illustrating the solute orientation parameter dependence upon the value of the parameter B. Plots of $S_{11} - S_{22}$ vs. S_{33} are shown in Fig. 2, together with calculated curves for different B values. The derivation of eq. [3] requires that B should be independent of solvent and of temperature, but, as was observed in the case of chlorobenzene (17) and for a number of other aromatic solutes (12, 15, 18), there is a strong solvent dependence of the parameter B (or its equivalent). Figure 2 also shows that there is a smaller variation with temperature and concentration, where the experimental value of B increases with increasing temperature in EBBA, but decreases in 1132. Emsley *et al.* (15, 16) have suggested that, for rigid molecules, the temperature dependence of B can be attributed to the neglect of higher rank terms in the assumed orientation potential, or to the biaxiality of the solvent molecules. Except for the case of *p*-dichlorobenzene in 1132, a reasonable fit of the order parameters can be obtained for a given value of B, and, rather than introduce additional terms in the potential, we choose to consider the averaged values of the energy parameters for each concentration, and to compare these with those derived for various molecular properties. The average values of A and B are listed in Table 1 for each of the systems studied. Both parameters A and AB were found to decrease with increasing solute concentration and have been fitted as linear functions of concentration to give A_0 or A_0B_0, the infinite dilution values, as the intercepts. For each solute, both A and AB are less dependent on concentration for 1132 than for EBBA. Similarly, the nematic to isotropic transition temperatures show a smaller depression in 1132, indicating a greater compatibility between solute and solvent (36). This indicates that these aromatic solutes are more capable of correlating their molecular orientations with the solvent 1132 than with EBBA, and hence are less effective in disordering 1132. Gas–liquid chromatographic studies (37) have shown that aromatic solutes prefer nematic solvents of the cyanobiphenyl type to Schiff-base type solvents (in this case MBBA). These conclusions are consistent with the present results and confirm that aromatic solutes are more highly oriented in 1132 than in EBBA.

If the $a[i]$ terms in eqs. [4] and [5] are replaced by the components of the polarizability tensor (38), or by molecular dimensions (based on van der Waals radii (39) and length model (18)), then the parameters B[pol] and B[vdW], given also in Table 3, can be derived and compared with the experimental values. There is no agreement for either solvent, but if the experimental values of B_0 are plotted against the calculated values, as in Fig. 3, there is a nearly linear dependence of B_0 on these parameters for the mono, *meta*, and *para* derivatives. Furthermore, the lines for each solvent are nearly parallel, with slopes close to unity. The point for *ortho*-dichlorobenzene lies above the line in the case of polarizability, but below in the case of molecular shape. This difference arises because the polarizability tensor for *ortho* and *meta* derivatives should be the same, but there is a difference in the dimensional or shape parameter.

The experimental values of A_0 are plotted in Fig. 4 against the values of A_0[vdW] calculated using eq. [4] with the appropriate molecular dimensions and van der Waals radii. The earlier results on benzene, trichlorobenzene, and tribromobenzene (18) are included. A reasonable correlation exists and the behaviour resembles that shown in Fig. 3 in that parallel lines are obtained. This result for both potential terms A_0 and B_0 for the two solvents suggests that there is a contribution to the ordering potential that leads to an enhancement of the solute orientation in 1132 and a diminution in EBBA. In their recent study of the orientation of small molecules with C_3 or higher symmetry, Burnell and co-workers (19, 23, 40) have demonstrated the importance of an interaction between the electric field gradient of the solvent and the molecular quadrupole moment of the solute. To include this contribution to the potential, each $a[i]$ is assumed to consist of a long-range interaction due to the field gradient – molecular quadrupole moment interaction, plus a size–shape dependent short-range interaction. Then $A_0 = A_{0LR} + A_{0SR}$, and $A_0B_0 = (A_0B_0)_{LR} + (A_0B_0)_{SR}$.

The short-range interactions are given by eqs. [4] and [5] with the $a[i]$ terms replaced by the van der Waals dimensions, and the long-range terms, A_{0LR} and $(A_0B_0)_{LR}$, by

$$[6] \quad A_{0LR} = (1/2)(Q_{33} - (Q_{11} + Q_{22})/2)F_{zz}/S_1$$

$$[7] \quad (A_0B_0)_{LR} = (1/4)(Q_{11} - Q_{22})F_{zz}/S_1$$

where Q_{ii} are the components of the molecular quadrupole moment tensor, and F_{zz} is the average electric field gradient along the liquid crystal director, the z-axis. The electric field gradient is temperature dependent, and it seems reasonable to assume that it is proportional to the solvent order parameter,

Can. J. Chem. Downloaded from www.nrcresearchpress.com by 122.72.124.2 on 09/07/12
For personal use only.

TABLE 3. Experimental and calculated potential energy parameters. Units are $\times 10^{-20}$ J molecule^{-1} for A_0, A_{0LR}, $(A_0B_0)_{LR}$, A_{0SR}, and $(A_0B_0)_{SR}$, and $\times 10^{-10}$ m for A[vdW]

Solvent	Solute	A_0	B_0	A_{0LR}	$(A_0B_0)_{LR}$	A_{0SR}	$(A_0B_0)_{SR}$	B_{0SR}	A[vdW]	B[vdW]	B[pol]
1132	*p*-Dichloro	1.60	0.462	−0.089	0.239	1.684	0.498	0.296	4.60	0.343	0.343
	o-Dichloro	1.11	0.808	0.152	0.211	0.956	0.684	0.716	2.33	0.818	0.565
	m-Dichloro	1.19	0.699	0.063	0.211	1.130	0.623	0.551	3.44	0.556	0.565
	Mono-[a]	1.21	0.610	0.106	0.215	1.104	0.523	0.474	3.42	0.461	0.486
EBBA	*p*-Dichloro	1.59	0.115	0.096	−0.260	1.497	0.443	0.296	4.60	0.343	0.343
	o-Dichloro	0.684	0.554	−0.166	−0.229	0.850	0.608	0.716	2.33	0.818	0.565
	m-Dichloro	0.936	0.346	−0.069	−0.230	1.005	0.554	0.551	3.44	0.556	0.565
	Mono-[a]	0.866	0.267	−0.115	−0.234	0.981	0.465	0.474	3.42	0.461	0.486

[a]From ref. 17.

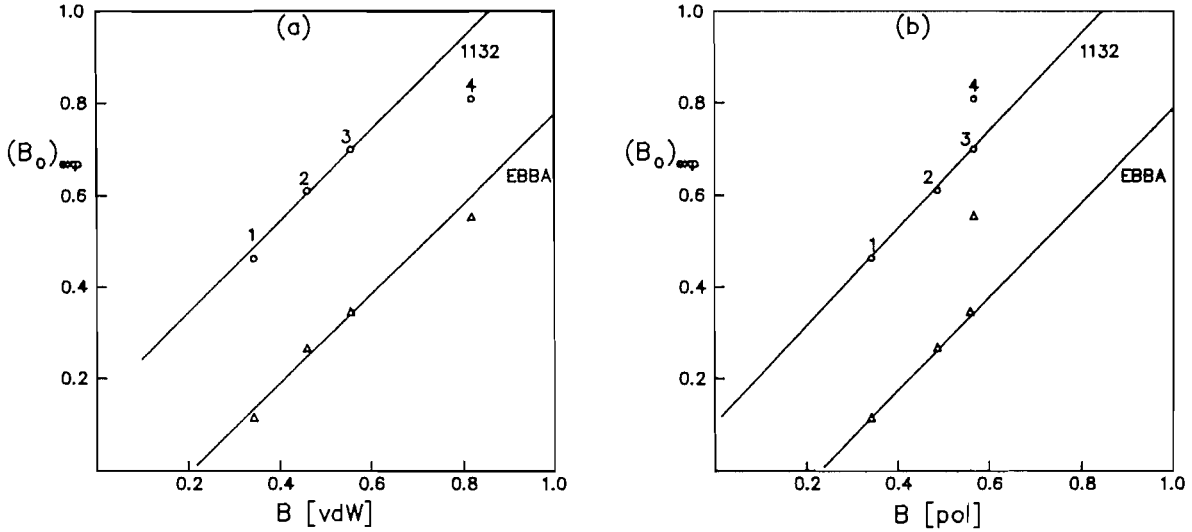


FIG. 3. Experimental vs. calculated energy parameters B_0; (a) vs. B[vdW] calculated based on molecular dimensions; and (b) vs. B[pol] calculated based on polarizability tensors. 1, *p*-dichloro; 2, monochloro; 3, *m*-dichloro; and 4, *o*-dichloro.

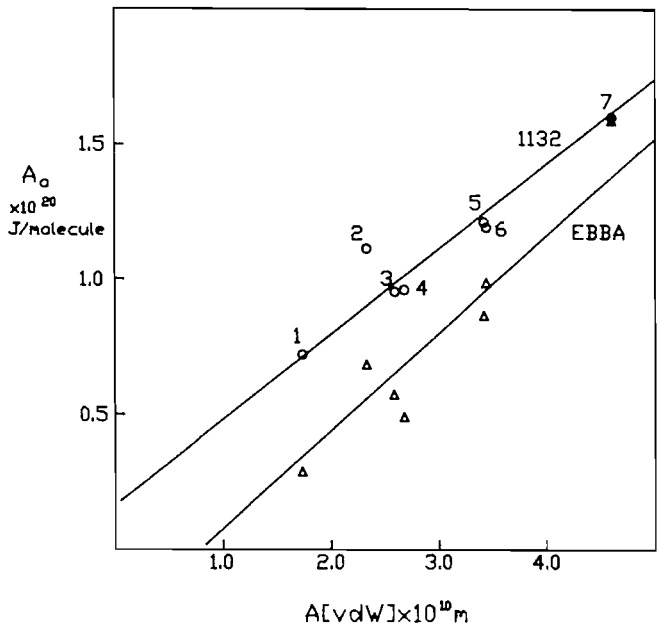


FIG. 4. Experimental A_0 vs. A[vdW]. 1, benzene; 2, *o*-dichloro; 3, trichloro; 4, tribromo; 5, monochloro; 6, *m*-dichloro; and 7, *p*-dichloro.

S_1, so that $F_{zz} = F_{zz}^0 \cdot S_1$ and where F_{zz}^0 should be a constant for a given solvent.[2]

Using the average of the data reported (21) for the two solvents at 298 and 320 K, the F_{zz}^0 values were found to be 2.41×10^{18} and -2.62×10^{18} V m^{-2} for 1132 and EBBA, respectively. Thus, if the molecular quadrupole moments are known, the long-range contributions can be calculated, but, unfortunately, the available data on the quadrupole moments of chloro-substituted benzenes are extremely sparse and do not permit any direct calculation of A_{0LR} and $(A_0B_0)_{LR}$, using eqs. [6] and [7]. The required data have been reported, however, for benzene and the trichloro and tribromo derivatives (41–44) and the two terms $(Q_{33} - (Q_{11} + Q_{22})/2)$ and $(Q_{11} - Q_{22})$ are both positive quantities in all cases. The results shown in Figs. 3 and 4 are thus explained by the opposite signs of the electric field gradients since the long-range interactions make a positive contribution to the total orientational potential in 1132 but a negative contribution in EBBA.

[2]The assumption that the electric field gradients are proportional to the solvent order parameter can be avoided if the data are compared at the same reduced temperatures used by Burnell and co-workers (21) since the order parameter is a universal function of reduced temperature. This limits the fit to only two temperatures in each case. The results are unchanged.

Can. J. Chem. Downloaded from www.nrcresearchpress.com by 122.72.124.2 on 09/07/12
For personal use only.

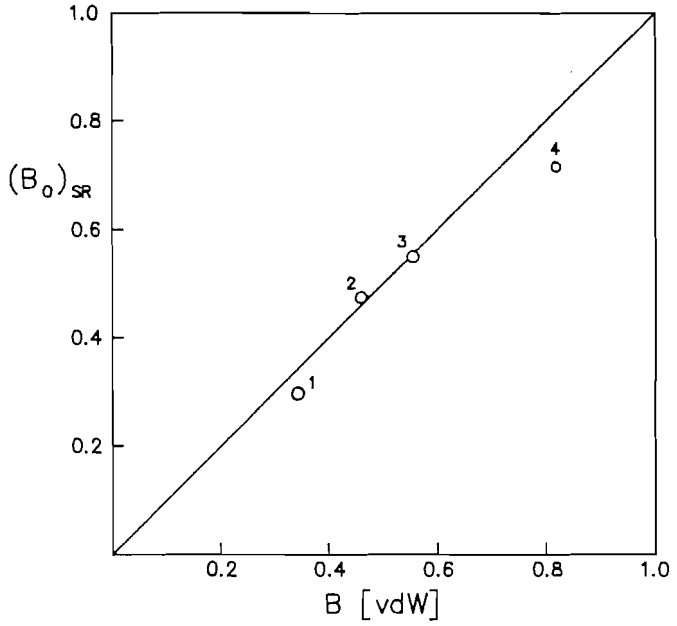


FIG. 5. Short-range interaction parameters B_{0SR} vs. B[vdW]. 1, *p*-dichloro; 2, monochloro; 3, *m*-dichloro; and 4, *o*-dichloro.

In the absence of molecular quadrupole moment data on chlorobenzene and the dichloro derivatives, it is necessary to eliminate some of the unknown parameters and to assume that, for a given solute, the ratios of the functions ${A_{0SR}}^{1132}/{A_{0SR}}^{EBBA}$ and $(A_0B_0)_{SR}{}^{1132}/(A_0B_0)_{SR}{}^{EBBA}$ should be equal. The short-range interaction can be written, eq. [8],

$$[8] \quad {A_{0SR}}^{1132} = w({A_0}^{EBBA} - x.{A_0}^{1132})/(1 - w.x)$$

where $w = {A_{0SR}}^{1132}/{A_{0SR}}^{EBBA}$, and x is the ratio of the two electric field gradients, $(F_{zz}^0)^{EBBA}/(F_{zz}^0)^{1132}$. Similar equations can be derived for ${A_{0SR}}^{EBBA}$ and for the $(A_0B_0)_{SR}$ terms. B_{0SR} is solvent independent and can be expressed as, eq. [9],

$$[9] \quad B_{0SR} = ((A_0B_0)^{EBBA} - x.(A_0B_0)^{1132})/({A_0}^{EBBA} - x.{A_0}^{1132})$$

so that it is independent of the ratio w. Using the F_{zz}^0 values given previously, the B_{0SR} values have been calculated and are given in Table 3 and plotted versus B_0[vdW] in Fig. 5. It can be seen that there is now good agreement for both solvents. This confirms the hypothesis that the short-range forces are proportional to a molecular shape or dimension function.

The values of $(F_{zz}^0)^{1132}$ and $(F_{zz}^0)^{EBBA}$ were calculated from the field gradient data of Burnell and co-workers (21) from their studies on the orientation of HD and D_2, and the extension to the molecules studied in the present work assumes that benzene and the chlorobenzenes experience the same average electric field gradient as the much smaller molecules. However, since the *ratio* of the field gradients is used, the calculated values of B_{0SR} are not likely to be strongly affected by this assumption.

Equation [8] can be used to derive individual values of the short- and long-range contributions, if a value for w is known. For example, if w is assumed to be independent of the solute, then w can be obtained in those cases where the molecular quadrupole moments are known. From the results obtained in earlier studies (18) on benzene, trichloro-, and tribromobenzene, the values of w are 0.90, 1.24, and 1.24, respectively. However, these ratios are subject to the rather large uncertainties involved in the experimental molecular quadrupole moments; for benzene the values reported for the principal component of the quadrupole tensor range from -10 to -42×10^{-40} C m^2 (31, 41–43). Using the average of the values given above for w, the calculated short- and long-range A_0 and A_0B_0 quantities are given in Table 3, and Table 4 lists the molecular quadrupole moments calculated from the long-range interactions. These values are reasonable but, in view of the errors involved, it is not suggested that they have any claim to accuracy.

TABLE 4. Molecular quadrupole moments, $\times 10^{-40}$ C m^2

	Q_{11}	Q_{22}	Q_{33}	Q_{22}(exp)
para-	22.3	−17.4	−4.9	
ortho-	13.3	−21.7	8.4	
meta-	15.8	−19.3	3.5	
Mono-	14.9	−20.8	5.9	
Benzene		−19.9		−10.4 – −33.3[a]
Trichloro-		−15.2		−10.8[b]
Tribromo-		−20.2		−16.0[c]

[a]References 31, 41–43.
[b]Reference 44.
[c]Reference 44.

Both the short- and the long-range interactions are assumed to have the same dependence on the solvent order parameter. We also assume that the local environment in the host solvent seen by different solute molecules is unchanged, in particular that the solvent order parameter and the electric field gradient are invariant over all the local environments that a solute molecule might prefer.

Since there are two different mechanisms responsible for the solute orientation, and since molecular quadrupole moments are not additive properties, bond additive models are not suitable for describing the orientation of solute molecules in liquid crystal solvents.

Acknowledgements

This work was supported by grants from F.C.A.R. (Quebec) (C.T.Y.) and from N.S.E.R.C. (D.F.R.G.). We are grateful to Professor E. E. Burnell for communicating results prior to publication.

1. A. SAUPE. Mol. Cryst. **1**, 527 (1966).
2. J. NEHRING and A. SAUPE. Mol. Cryst. Liq. Cryst. **8**, 403 (1969).
3. J. C. ROBERTSON, C. T. YIM, and D. F. R. GILSON. Can. J. Chem. **49**, 2345 (1971).
4. E. SACKMANN, P. KREBS, H. U. REGA, J. VOSS, and H. MOHWALD. Mol. Cryst. Liq. Cryst. **24**, 283 (1973).
5. K. G. ORRELL and V. SIK. J. Chem. Soc. Faraday Trans. 2, **71**, 1360 (1975).
6. D. F. HILLENBRAND and H. YU. J. Chem. Phys. **67**, 957 (1977).
7. Y. P. LEE and D. F. R. GILSON. J. Chem. Phys. **70**, 2042 (1979).
8. J. JOKISAARI, T. VAANANEN, and J. LOUNILA. Mol. Phys. **54**, 141 (1982).
9. T. VAANANEN, J. JOKISAARI, and J. LOUNILA. J. Magn. Reson. **49**, 7 (1982).
10. T. VAANANEN, J. JOKISAARI, and J. LOUNILA. J. Magn. Reson. **54**, 436 (1983).
11. D. CATALANO, C. FORTE, C. A. VERACINO, and C. ZANNONI. Isr. J. Chem. **23**, 283 (1983).
12. J. W. EMSLEY, R. HASHIM, G. R. LUCKHURST, G. N. RUMBLES, and F. R. VILORIA. Mol. Phys. **49**, 1321 (1983).
13. D. F. R. GILSON. Mol. Cryst. Liq. Cryst. **104**, 173 (1984).

Can. J. Chem. Downloaded from www.nrcresearchpress.com by 122.72.124.2 on 09/07/12
For personal use only.

14. R. HASHIM, G. R. LUCKHURST, and S. ROMANO. Mol. Phys. **56**, 1217 (1985).
15. J. W. EMSLEY, R. HASHIM, G. R. LUCKHURST, and G. N. SHILSTONE. Liq. Cryst. **1**, 437 (1986).
16. J. W. EMSLEY, G. R. LUCKHURST, G. N. SHILSTONE, and I. SAGE. J. Chem. Soc. Faraday Trans. 2, **83**, 371 (1987).
17. C. T. YIM and D. F. R. GILSON. Can. J. Chem. **65**, 2513 (1987).
18. C. T. YIM and D. F. R. GILSON. Can. J. Chem. **66**, 1749 (1988).
19. E. E. BURNELL, A. J. VAN DER EST, G. N. PATEY, C. A. DE LANGE, and J. G. SNIJDERS. Bull. Magn. Reson. **9**, 4 (1987).
20. C. A. DE LANGE, J. G. SNIJDERS, and E. E. BURNELL. *In* Nuclear magnetic resonance of liquid crystals. *Edited by* J. W. Emsley. Reidel Publishing Co., Dordrecht. 1985. Chap. 8.
21. G. N. PATEY, E. E. BURNELL, J. G. SNIJDERS, and C. A. DE LANGE. Chem. Phys. Lett. **99**, 271 (1983).
22. P. B. BARKER, A. J. VAN DER EST, E. E. BURNELL, G. N. PATEY, C. A. DE LANGE, and J. G. SNIJDERS. Chem. Phys. Lett. **107**, 426 (1984).
23. A. J. VAN DER EST, M. Y. KOK, and E. E. BURNELL. Mol. Phys. **60**, 397 (1987).
24. J. W. EMSLEY and J. C. LINDON. NMR spectroscopy using liquid crystal solvents. Pergamon Press, Oxford. 1975.
25. H. KELKE and B. SCHUERLE. Angew. Chem. Int. Ed. Engl. **8**, 884 (1969).
26. E. E. BURNELL, P. DIEHL, and W. NIEDERBERGER. Can. J. Chem. **52**, 15 (1974).
27. P. DIEHL and C. L. KHETRAPAL. Mol. Phys. **15**, 201 (1968).
28. P. DIEHL and C. L. KHETRAPAL. Mol. Phys. **15**, 633 (1968).
29. P. DIEHL and H. BOSIGER. J. Mol. Struct. **42**, 103 (1977).
30. P. DIEHL and H. BOSIGER. Org. Magn. Reson. **9**, 98 (1977).
31. A. CHABLO, D. W. J. CRUICKSHANK, A. HINCHCLIFFE, and R. W. MUNN. Chem. Phys. Lett. **78**, 424 (1981).
32. B. BAHADUR and S. CHANDRA. J. Phys. C: Solid State Phys. **9**, 5 (1976).
33. B. BAHADUR, R. K. SARNA, and V. G. BHIDE. Mol. Cryst. Liq. Cryst. **72**, 139 (1982); Mol. Cryst. Liq. Cryst. **82**, 183 (1982).
34. H. E. J. NEUGEBAUER. Can. J. Phys. **32**, 1 (1954).
35. B. KRONBERG, D. F. R. GILSON, and D. D. PATTERSON. J. Chem. Soc. Faraday Trans. 2, **72**, 1673 (1976).
36. D. E. MARTIRE. *In* The molecular physics of liquid crystals. *Edited by* G. R. Luckhurst and G. W. Gray. Academic Press, London. 1979. Chap. 10.
37. G. A. OWEIMREEN, G. C. LIN, and D. E. MARTIRE. J. Phys. Chem. **63**, 2111 (1979).
38. O. EXNER. Dipole moments in organic chemistry. George Thieme, Stuttgart. 1975.
39. A. BONDI. J. Phys. Chem. **68**, 441 (1964).
40. A. J. VAN DER EST. Ph.D. thesis, University of British Columbia (1987).
41. R. L. SHOEMAKER and W. H. FLYGARE. J. Chem. Phys. **51**, 2988 (1969).
42. J. VRBANCICH and G. L. D. RITCHIE. J. Chem. Soc. Faraday Trans. 2, **76**, 648 (1980).
43. M. R. BATTAGLIA, A. D. BUCKINGHAM, and J. H. WILLIAMS. Chem. Phys. Lett. **78**, 421 (1981).
44. G. D. L. RITCHIE. Chem. Phys. Lett. **93**, 410 (1982).

Can. J. Chem. Downloaded from www.nrcresearchpress.com by 122.72.124.2 on 09/07/12
For personal use only.

Preparation and absolute stereochemistry of (−)-acenaphthenol

YULIN HU AND HERMAN ZIFFER
Laboratory of Chemical Physics, NIDDK, National Institutes of Health, Bethesda, MD 20892, U.S.A.

AND

J. V. SILVERTON
Laboratory of Chemistry, NHLBI, National Institutes of Health, Bethesda, MD 20892, U.S.A.

Received April 11, 1988

YULIN HU, HERMAN ZIFFER, and J. V. SILVERTON. Can. J. Chem. **67**, 60 (1989).

1-Acenaphthenol was resolved by fractional crystallization of its camphanate ester followed by hydrolysis. The absolute stereochemistry of the (+)-camphanate and (−)-alcohol, derived therefrom, was established as (*R*) by X-ray crystallography.

Key words: (−)-acenaphthenol, stereochemistry, synthesis, X-ray crystallography.

YULIN HU, HERMAN ZIFFER et J. V. SILVERTON. Can. J. Chem. **67**, 60 (1989).

On a résolu l'acénaphténol-1 par le biais de la cristallisation fractionnée de son ester camphanique qui a été suivie par la suite hydrolysé. Faisant appel à la diffraction des rayons-X on a établi que la stéréochimie absolue du (+)-camphanate ainsi que du (−)-alcool qui en dérive est (*R*).

Mots clés : acénaphténol-1, stéréochimie, synthèse, diffraction des rayons-X.

[Traduit par la revue]

Can. J. Chem. Downloaded from www.nrcresearchpress.com by 122.72.124.2 on 09/07/12
For personal use only.

Introduction

1-Acenaphthenol has been shown, by Schocken and Gibson (1), to form as an early metabolite in the bacterial oxidation of acenaphthene and acenaphthylene. The metabolism of acenaphthylene and acenaphthalene in mammalian systems was first examined by Young and co-workers, who established that these were metabolized to mixtures of *cis*- and *trans*-1,2-diols, acenaphthenequinone, and 1,8-naphthalic acid (2). Later studies by Simmons *et al.* (3) showed that a possible metabolite 1-acenaphthen-1-ol was oxidized to the ketone, which was further oxidized to 1,8-naphthalic acid. In an effort to learn more about the stereochemical preferences of some of the enzymes involved in these oxidations, we first established the configuration of *trans*-1,2-dihydroxyacenaphthene (4) and now turn our attention to the configuration of 1-acenaphthenol. Although this alcohol has been shown to be a substrate for several dehydrogenases (5–7), we were unable to find any reports describing the preparation of chiral material. We describe here a procedure for resolving the alcohol via its camphanate ester and the results of an X-ray structure determination of the (+)-camphanate ester of the (−)-alcohol, which establishes its configuration.

Discussion

The crystal conformation is depicted in Fig. 1 as an ORTEP (8) drawing and a packing diagram is given as Fig. 2. Molecular dimensions are given in Table 1 and a short table of C and O parameters as Table 2. Full refinement parameters, including anisotropic thermal parameters and hydrogen parameters, are available as supplemental material.[1] Since the observed absolute configurations at C1′ and C4′, *S* and *R* as depicted in Fig. 1, agree with the known configuration of (−)-camphanic acid as unambiguously determined by its synthesis from (+)-camphor following Gerlach (9), the absolute configuration at C1 is *R* as depicted. The chiral angles, which Ito, Kasai, and Silverton (10) have designated χ, are −69.9(1), +56.1(2), and +64(2)° for C1′, C4′, and C1, respectively. The molecular packing, as shown in Fig. 2, is reasonably efficient and contacts are of the order of van der Waals distances.

As mentioned in the introduction, 1-acenaphthenol has been employed as a substrate in assaying an indanol dehydrogenase found in rabbit liver (6) and in a dehydrogenase found in a *Beijerinckia sp.* strain B8/36 (1). While the optical purities of 1-acenaphthenol obtained by fractional crystallization of the camphanate were adequate for the crystallographic study, higher purities are required for studies of the relative rates of oxidation of the different enantiomers. We have found that the diastereomeric camphanates can be completely separated by preparative hplc on a silica column employing either methylene chloride (α = 1.13) or a 4:1 mixture of cyclohexane:ether (α = 1.23).

There have been previous crystallographic investigations of the racemates of acenaphthenol (11), acenaphthendiol (12), and acenaphthenquinone (13). These are early studies involving photographic, visually estimated intensity data but in all cases the molecular skeleton is reported to be flat and to possess symmetry consonant with the chemical formula. In the alcohols, but not in the quinone, the C1—C2 bond is longer than the usual value for a single bond and this observation also applies to the present structure where the length of the C1—C2 bond is 1.561(6) Å. The acenaphthenol skeleton in this structure exhibits small but significant deviations from planarity, with the greatest deviations at C2, which is 0.024 and 0.043 Å from the planes of the five-membered ring and the acenaphthene skeletons, respectively (Table 3). The fused naphthalene and cyclopentane rings are close to coplanarity and the individual ring dihedral angles do not exceed 1.5°. There are small differences in bond lengths that would not be predicted from the chemical formula, C7—C8:C3—C4, C2a—C3:C8a—C8, and C2a—C8b:C8a—C8b having differences of 0.044, 0.014, and 0.023 Å, respectively, but only the first difference is significant.

Experimental

Preparation of (+) 1-acenaphthenyl camphanate

To a cold (0°C) solution of 1.70 g of racemic 1-acenaphthenol and 1.34 g of 4-dimethylaminopyridine in 50 mL of methylene chloride

[1]These data may be purchased from the Depository of Unpublished Data, CISTI, National Research Council of Canada, Ottawa, Ont., Canada K1A 0S2.

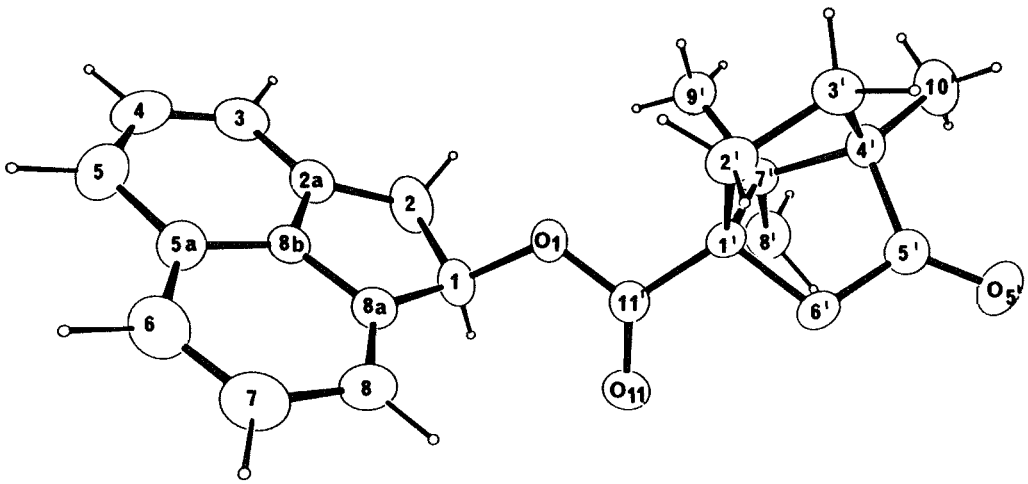


FIG. 1. ORTEP drawing showing the crystal conformation.

TABLE 1. Molecular dimensions in Å or degrees as appropriate

Atoms	Length (Å)	Atoms	Length (Å)
C1—O1	1.471(4)	C8a—C8b	1.387(4)
C1—C2	1.561(6)	C1′—C2′	1.522(4)
C1—C8a	1.501(4)	C1′—O6′	1.460(3)
O1—C11′	1.339(3)	C1′—C7′	1.551(4)
C2—C2a	1.506(6)	C1′—C11′	1.500(4)
C2a—C3	1.369(5)	C2′—C3′	1.535(5)
C2a—C8b	1.406(4)	C3′—C4′	1.556(4)
C3—C4	1.395(6)	C4′—C5′	1.514(4)
C4—C5	1.368(6)	C4′—C7′	1.542(4)
C5—C5a	1.406(4)	C4′—C10′	1.508(5)
C5a—C6	1.407(5)	C5′—O5′	1.195(4)
C5a—C8b	1.403(4)	C5′—O6′	1.368(3)
C6–C7	1.363(6)	C7′—C8′	1.523(5)
C7—C8	1.439(5)	C7′—C9′	1.527(4)
C8—C8a	1.355(4)	C11′—O11′	1.195(3)

Atoms	Angle (deg)	Atoms	Angle (deg)
O1—C1—C2	107.2(3)	C2′—C1′—C11′	117.9(2)
O1—C1—C8a	110.5(2)	O6′—C1′—C7′	102.3(1)
C2—C1—C8a	104.7(3)	O6′—C1′—C11′	108.1(2)
C1—O1—C11′	118.1(2)	C7′—C1′—C11′	117.3(2)
C1—C2—C2a	105.0(3)	C1′—C2′—C3′	101.5(2)
C2—C2a—C3	132.9(3)	C2′—C3′—C4′	104.2(2)
C2—C2a—C8b	108.1(3)	C3′—C4′—C5′	101.7(2)
C3—C2a—C8b	119.0(3)	C3′—C4′—C7′	102.2(2)
C2a—C3—C4	118.3(4)	C3′—C4′—C10′	116.6(3)
C3—C4—C5	123.5(3)	C5′—C4′—C7′	99.7(2)
C4—C5—C5a	119.5(3)	C5′—C4′—C10′	115.3(3)
C5—C5a—C6	127.6(3)	C7′—C4′—C10′	118.6(3)
C5—C5a—C8b	116.7(3)	C4′—C5′—O5′	130.6(2)
C6—C5a—C8b	115.7(3)	C4′—C5′—O6′	107.4(2)
C5a—C6—C7	120.7(3)	O5′—C5′—O6′	122.0(2)
C6—C7—C8	122.1(3)	C1′—O6′—C5′	105.8(2)
C7—C8—C8a	117.6(3)	C1′—C7′—C4′	91.7(2)
C1—C8a—C8	131.1(3)	C1′—C7′—C8′	112.5(2)
C1—C8a—C8b	109.0(2)	C1′—C7′—C9′	114.7(2)
C8—C8a—C8b	119.9(3)	C4′—C7′—C8′	114.1(2)
C2a—C8b—C5a	122.9(2)	C4′—C7′—C9′	113.5(2)
C2a—C8b—C8a	113.1(2)	C8′—C7′—C9′	109.5(2)
C5a—C8b—C8a	124.0(2)	O1—C11′—C1′	108.4(2)
C2′—C1′—O6′	105.1(2)	O1—C11′—O11′	125.0(2)
C2′—C1′—C7′	104.4(2)	C1′—C11′—O11′	126.6(2)

TABLE 2. Parameters for C and O atoms*

Atom	*x*	*y*	*z*	*U* (equiv.)
C1	1941(4)	−437(3)	5569(2)	63(1)
O1	1295(3)	261(2)	4919(1)	61(1)
C2	2689(5)	−1483(5)	5143(3)	83(2)
C2a	1984(4)	−2581(3)	5438(2)	61(1)
C3	2161(5)	−3759(4)	5278(3)	74(2)
C4	1347(5)	−4571(4)	5686(3)	75(2)
C5	400(4)	−4255(3)	6251(3)	70(1)
C5a	182(4)	−3051(3)	6421(2)	58(1)
C6	−765(4)	−2560(4)	6962(3)	71(2)
C7	−866(4)	−1366(4)	7056(3)	77(2)
C8	−13(4)	−556(4)	6620(2)	64(1)
C8a	906(4)	−1021(3)	6099(2)	54(1)
C8b	994(3)	−2237(3)	6004(2)	45(1)
C1′	625(3)	1964(2)	4261(2)	42(1)
C2′	−657(4)	1455(3)	3901(2)	55(1)
C3′	−694(4)	2054(3)	3057(2)	61(1)
C4′	606(3)	2814(3)	3034(2)	53(1)
C5′	304(4)	3749(3)	3672(2)	59(1)
O5′	67(4)	4779(2)	3599(2)	77(1)
O6′	324(2)	3207(2)	4422(1)	51(1)
C7′	1599(3)	2043(2)	3522(2)	45(1)
C8′	2905(4)	2667(4)	3738(3)	69(2)
C9′	1909(4)	860(4)	3112(3)	60(1)
C10′	1031(7)	3279(5)	2208(3)	81(2)
C11′	1151(3)	1426(3)	5037(2)	51(1)
O11′	1437(3)	1939(2)	5654(1)	67(1)

*Positional parameters are multiplied by 10 000 and equivalent *U* values by 1000. The equivalent *U* values are the geometric means of the diagonal terms of the vibration tensors.

was added 2.38 g of (−)-camphanic acid chloride. The reaction mixture was stirred overnight and allowed to warm to room temperature. The methylene chloride solution was first washed with water, then with saturated $NaHCO_3$, and dried over Na_2SO_4. The organic solution was concentrated and the residue crystallized 4 times from hexane. The resolution was monitored by gc on a HP 5890A gas chromatograph at 230°C using a 25-m SE-30 capillary column.[2] The ee of the crystalline material was 91%, mp 139–140°C; $[\alpha]_D$ +75.0° (*c* 2.25, $CHCl_3$).

[2]Y. Hu and H. Ziffer. Manuscript in preparation on the use of a capillary SE-30 gc column for determining enantiomeric excess of alcohols.

Can. J. Chem. Downloaded from www.nrcresearchpress.com by 122.72.124.2 on 09/07/12
For personal use only.

TABLE 3. Least-squares planes

Plane	Defining atoms, deviations (Å × 1000), and the coefficients in the equation of the plane, $AX + BY + CZ = D$, defined with respect to the crystal axes										
1	C2a	C3	C4	C5	C5a	C8b					
	+5	+0	−11	+11	−2	−3					
	6.74(1)		−0.58(2)		12.01(2)		8.01(1)				
2	C5a	C6	C7	C8	C8a	C8b					
	−5	+3	−3	+0	+2	−1					
	6.66(1)		−0.45(2)		12.13(2)		8.05(1)				
3	C1	C2	C2a	C8b	C8a						
	−6	+24	−15	+8	−3						
	6.57(2)		−0.57(2)		12.26(2)		8.13(1)				
4	C1	C2	C3	C4	C5	C6	C7	C8	C2a	C5a	C8a
	+4	+43	−20	−20	+16	+12	−7	−14	−8	+11	−9
	6.65(1)		−0.55(1)		12.14(1)		8.07(1)				

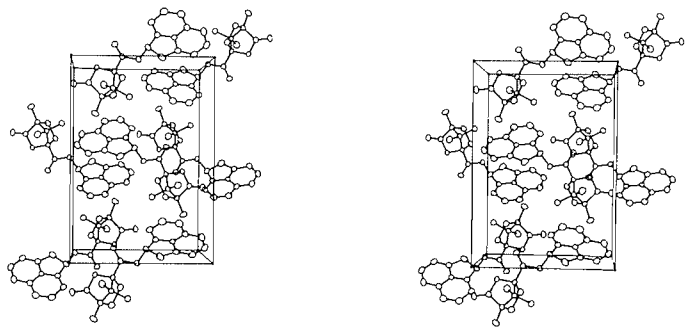


FIG. 2. Packing diagram. The direction of projection is *a*.

A sample strongly enriched in the (−)-camphanate was prepared by removing the higher melting, more crystalline (+)-enantiomer.

Preparation of (−)-1-acenaphthenol

To a solution of 100 mg (0.28 mmol) of (+)-1(*R*)-acenaphthenyl camphanate, $[\alpha]_D$ +75.0° (*c* 2.25, $CHCl_3$), was added 1.7 mL of 0.2 N NaOH and the solution refluxed for 3 h. The solution was concentrated and the residue extracted with ethyl acetate. The extract was washed with saturated $NaHCO_3$, water, dried, and concentrated. The crude alcohol was purified by flash chromatography on silica gel to yield (−)-1(*R*)-acenaphthenol (41 mg; 83%), $[\alpha]_D$ −1.46° (*c* 1.23, $CHCl_3$); mp 127–127.5°C.

Preparation of (+)-1-acenaphthenol

Hydrolysis of the (−)-camphanate, ee 88% as determined by gc,[2] yielded a sample of the (+)-alcohol, mp 125°C; $[\alpha]_D$ +1.34° (*c* 1.16, $CHCl_3$).

Crystallography: (+)-1-Acenaphthenyl camphanate

$C_{22}H_{22}O_4$ M_r 350.41

Orthorhombic, $P2_12_12_1$, a = 9.982(1), b = 11.306(1), c = 16.316(2) Å, V = 1841.37 Å^3, Z = 4, D_x = 1.263 g cm^{-3}, λ(Cu Kα) = 1.5418 Å, μ = 6.59 cm^{-1}, $F(000)$ = 744, T = 23°C, final R = 0.038 for 1504 observed reflections. Diffractometer and data collection method: Enraf–Nonius CAD4, graphite monochromator, CuKα (λ = 1.5418 Å), θ/2θ scan; maximum θ: 74°. Variation of intensity standards: 3%, measured every 3 h. Phase problem solution: MITHRIL (14); refinement: full-matrix least squares: H atoms isotropic, other atoms anisotropic; anisotropic parameters: exp $(-2\Pi^2\Sigma_i\Sigma_j U_{ij}h_ih_ja^*_ia^*_j)$. Function minimized: $\Sigma w(|F_o| - |F_c|)^2$; weights ($w$): $1/\sigma(F_o)$; $\sigma(F_o)$: statistical following Peterson and Levy (15). Refinement program: XTAL (16); atomic scattering factors: from XTAL, derived from Cromer and Mann (17). Crystal habit: flat orthorhombic prisms with pinacoid faces developed at ends. Crystal size: 0.40 × 0.15 × 0.15 mm; Friedel symmetry: 2/*m* 2/*m* 2/*m*. Conditions limiting reflections: *hkl*: all; *h*00: $h = 2n$; *k*00: $k = 2n$; 00*l*: $l = 2n$; counter aperture: 1.3 mm; scan width (θ): 1.2 + 0.35 tan θ. Reflections used for lattice parameters: 13 (22° < θ < 27°); maximum (sin θ/λ): 0.6230 Å^{-1}; range of h,k,l: 0:12, 0:14, 0:20. Reflections measured: 2136 (1504 with $I > \sigma(I)$); intensity standards: 3 3 6, 2 2 8, 0 2 8; R and Rw: 0.038, 0.038; S: 1.86; (Δ/σ)max: 0.04; extrema of density, at C, O positions in final difference map: −0.18, +0.13 e Å^{-3}.

1. M. J. SCHOCKEN and D. T. GIBSON. Appl. Environ. Microbiol. **48**, 10 (1984).
2. R. P. HOPKINS, C. J. W. BROOKS, and L. YOUNG. Biochem. J. **82**, 457 (1962).
3. C. J. SIMMONS, R. P. HOPKINS, and P. CALLAGHAN. Xenobiotica, **3**, 633 (1973).
4. M. IMUTA, M. KASAI, and H. ZIFFER. Bioorg. Chem. **13**, 131 (1985).
5. (*a*) H. R. GLATT, K. VOGEL, P. BENTLEY, and F. OESCH. Nature (London), **277**, 319 (1979); (*b*) H. R. GLATT, C. S. COOPER, P. L. GROVER, P. SIMS, P. BENTLEY, M. MERDES, F. WAECHTER, K. VOGEL, T. M. GUENTHNER, and F. OESCH. Science, **215**, 1507 (1982); (*c*) H. R. GLATT, K. VOGEL, P. BENTLEY, P. SIMS, and F. OESCH. Carcinogenesis, **2**, 813 (1981).
6. A. HARA, K. KARIYA, M. NAKAMURA, T. NAKAYAMA, and H. SAWADA. Arch. Biochem. Biophys. **249**, 225 (1986).
7. E. C. DRUMMOND, P. CALLAGHAN, and R. P. HOPKINS. Xenobiotica, **2**, 529 (1972).
8. C. K. JOHNSON. ORTEP, Technical Report, OR-3794, Oak Ridge National Laboratory, Oak Ridge, TN. 1965.
9. H. GERLACH. Helv. Chim. Acta, **51**, 1587 (1968).
10. S. ITO, M. KASAI, H. ZIFFER, and J. V. SILVERTON. Can. J. Chem. **65**, 574 (1987).
11. M. P. GUPTA and T. N. P. GUPTA. Acta Crystallogr. Sect. B: Struct. Crystallogr. Cryst. Chem. **31**, 7 (1975).
12. J. TROTTER and T. C. W. MAK. Acta Crystallogr. **16**, 1032 (1963).
13. T. C. W. MAK and J. TROTTER. Acta Crystallogr. **16**, 811 (1963).
14. C. J. GILMORE. MITHRIL, a computer program for the automatic solution of crystal structures from X-ray data. Chemistry Department, The University, Glasgow, Scotland. 1983.
15. S. W. PETERSON and H. A. LEVY. Acta Crystallogr. **10**, 70 (1957).
16. J. M. STEWART, S. R. HALL, R. A. ALDEN, R. OLTHOF-HAZECAMP, and R. M. DOHERTY. The XTAL system of crystallographic programs. 2nd ed. Report TR-1364.1, University of Maryland, College Park, MD. March 1985.
17. D. T. CROMER and J. B. MANN. Acta Crystallogr. Sect. A: Cryst. Phys. Diffr. Theor. Gen. Crystallogr. **24**, 321 (1968).

Can. J. Chem. Downloaded from www.nrcresearchpress.com by 122.72.124.2 on 09/07/12
For personal use only.

Pentacoordination and ionic character: crystal structure of Ph_4SbBr

OSVALD KNOP,[1] BEVERLY R. VINCENT, AND T. STANLEY CAMERON
Department of Chemistry, Dalhousie University, Halifax, N.S., Canada B3H 4J3

Received March 29, 1988

OSVALD KNOP, BEVERLY R. VINCENT, and T. STANLEY CAMERON. Can. J. Chem. **67**, 63 (1989).

Ph_4SbBr ($P2_1/n$, a = 12.282(2) Å, b = 10.656(1) Å, c = 16.156(1) Å, β = 104.92(7)°, Z = 4) crystallizes with the same space group as Ph_4SbCl, but the two compounds are not isostructural. The structure of Ph_4SbBr consists of layers of Ph_4SbBr molecules with the Br atoms almost exactly in the 10$\bar{1}$ planes. The coordination figure of the Sb atom is a trigonal bipyramid (TBP) with Br in an axial position. The Sb—Br distance, 2.950(1) Å, is the longest reported for Sb(V) to date. The Sb(V)—Hal bond lengths and the Ph_4SbBr and Ph_4SbCl structures are compared in detail. Analysis of a large sample of Ph_4EX (E = P, As) structures and of all the available R_4EX (E = Sb, Bi; R = Ph, Me) structures shows that the former are always ionic, $R_4E^+X^-$, whereas in the latter the observed coordination figures represent R_4EX trigonal bipyramids with various degrees of axial distortion. The inverse variation of the axial bond lengths (the *trans* effect) in the TBP Sb compounds can be quantified as $Sb—C_{ax} \sim 2.4(Sb—X)^{-1/9}$ to a very high degree of correlation. This and other geometric relationships show that there exists a limiting E—X bond length (~3.3 Å for E = Sb and ~3.5 Å for E = Bi when X is oxygen) at which the TBP coordination becomes unstable and changes over to a tetrahedral R_4E. This change is accompanied by a rearrangement of the structure to an ionic $R_4E^+X^-$ solid (of high symmetry where permitted by the size and shape of the anion) with E···X separations no smaller than ~4 Å when E = Sb or Bi and X = O. The distribution of the CEC angles in the Ph_4EX (E = P, As) sample is analyzed; the mean (uncorrected) P—C and As—C bond lengths in Ph_4E^+ are found to be 1.789(11) and 1.902(12) Å, respectively.

Key words: crystal structure, organoantimony compounds, Ph_4SbBr, pentacoordination, tetraphenylantimony bromide.

OSVALD KNOP, BEVERLY R. VINCENT et T. STANLEY CAMERON. Can. J. Chem. **67**, 63 (1989).

Le Ph_4SbBr ($P2_1/n$, a = 12,282(2), b = 10,656(1) et c = 16,156(1) Å, β = 104,92(7)° et Z = 4) cristallise dans le même groupe d'espace que le Ph_4SbCl; toutefois, les deux composés ne sont pas isostructuraux. La structure du Ph_4SbBr est formée de couches de molécules Ph_4SbBr comportant des atomes de Br qui sont pratiquement dans les plans 10$\bar{1}$. La coordinence autour de l'atome de Sb est du type trigonal bipyramidal (TBP) avec un Br dans la position axiale. La distance Sb—Br, 2,950(1) Å, est la plus longue rapportée à date pour un Sb(V). On a effectué une comparaison détaillée des longueurs des liaisons Sb—Hal ainsi que des structures des Ph_4SbBr et Ph_4SbCl. Un examen d'un grand échantillon de structures de Ph_4EX (E = P, As) ainsi que de toutes les structures disponibles de R_4EX (E = Sb, Bi; R = Ph, Me) montre que les premières sont toujours ioniques, $R_4E^+X^-$, alors que dans les dernières les coordinences observées pour les composés R_4EX sont du type trigonal bipyramidal avec divers degrés de déformation. L'équation $Sb—C_{ax} \approx 2{,}4(Sb—X)^{-1/9}$ permet de quantifier avec un très haut degré de corrélation la variation inverse des longueurs des liaisons axiales (l'effet *trans*) des composés TBP du Sb. Cette relation ainsi que d'autres relations géométriques montrent qu'il existe une longueur limite de la liaison E—X (≈3, 3 Å pour E = Sb et ≈3,5 Å pour E = Bi lorsque X est un oxygène) au-delà de laquelle la coordinence TBP devient instable et se transforme en un tétraèdre R_4E. Ce changement est accompagné par une transposition de la structure en un solide ionique $R_4E^+X^-$ (de haute symétrie lorsque la grosseur ainsi que la forme de l'anion le permettent) dans lequel les séparations E···X ne sont pas plus faibles que ≈4 Å lorsque E = Sb ou Bi et X = O. On a analysé la distribution des angles CEC dans l'échantillon de composés Ph_4EX (E = P, As); on a trouvé que les longueurs moyennes des liaisons (non corrigées) P—C et As—C des composés Ph_4E^+ sont respectivement de 1,789(11) et 1,902(12) Å.

Mots clés : structure cristalline, composés organo-antimoniés, Ph_4SbBr, pentacoordination, bromure de tetraphenylantimoine.

[Traduit par la revue]

Crystalline compounds of the compositions $(Ph_4E)_mX_n$ (E = P, As, Sb, Bi) may be salts of the cations Ph_4E^+ or they may contain E with covalent bonds additional to the four C—C bonds. With E = P and As the E atom is, to the authors' knowledge, always four-coordinated, forming tetrahedral Ph_4E^+ cations.[2] The large size of these ions makes them very suitable as counter ions in the stabilization and characterization of large anions. Since this in fact is the main reason for the appearance of the very numerous tetraphenylphosphonium and -arsonium salts in the literature, it is not surprising that the interest in the properties of these cations *per se* has been secondary and that in only a fraction of the known salts has the cation received attention for its own sake.

Table 1 lists Ph_4P^+ and Ph_4As^+ salts of monatomic and other small anions the structures of which may be regarded as being dominated essentially by the Ph_4E^+ geometry.[3] The features of the cations in these compounds may be summarized as follows. The CEC angles range from ~103° to ~116° and have a distribution shown in Fig. 1, with statistics as in Table 2. The weakly bimodal character of the total CEC distribution appears to arise from the fairly large proportion of Ph_4E^+ ions of symmetry S_4 or $C_2 \sim S_4$ in the sample: the CEC angle 2α bisected by the C_2 axis is in these cases smaller than the CEC angle 2α′ between C atoms not related by C_2.[4] For ions of S_4 symmetry, $\tan\alpha' = [1 + 2(\tan^2\alpha)^{-1}]^{1/2}$; the distribution of these angles is also shown in Fig. 1. A more comprehensive sample would be needed to determine whether the separate distributions for E = P and E = As are significantly different. The mean of the (uncorrected) E—C bond lengths in these compounds is 1.789(11) Å for P and 1.902(12) Å for As (Table 2), the total ranges being 1.768–1.812 Å for P and 1.878–1.918 Å for As. The deviations of the internal CCC angles in the phenyl rings from 120° are not statistically significant even for the CCC angle adjacent to the E atom.

[1]To whom correspondence may be addressed.

[2]For a classification of structure types and packing arrangements see ref. 1.

[3]Although *geometrically* Ph_4E^+ could attain the D_{2d} symmetry, the highest observed symmetry in these ions is S_4.

[4]The exception appears to be $Ph_4As[HCl_2]$ (9), in which the C_2 symmetry of the cation does not approximate S_4 closely. In ref. 16 the angles 2α and 2α′ in $Ph_4As[FeCl_4]$ should be reversed.

Can. J. Chem. Downloaded from www.nrcresearchpress.com by 122.72.124.2 on 09/07/12
For personal use only.

TABLE 1. Structural character of E in crystalline $(Ph_4E)_mX_n$ compounds with small X[a]

X	E = P	As	Sb	Bi
		$m = n = 1$		
F			TBP[b]	Unstable
Cl			**TBP** $P2_1/n$ (5)	Unstable
Br	**TC**[c]		**TBP** (this work)	
I	**TC** $I\bar{4}$ (6)	**TC** $I\bar{4}$ (7, 8)		
HCl_2		**TC** $B2/b$ (9)		
N_3			Covalent	
Br_3	**TC** $P2/c$ (10)	**TC** *I*, $P2_1/c$ (11)		
		TC *II*, $P2/c$ (12)		
Br_2I, I_3	**TC** $P2/n$ (13)	**TC** $P2/n$ (14)		
NCS			TBP	Covalent
$SnCl_3$, $SnBr_3$	**TC** $P\bar{1}$ (15)			
BF_4			TC	TC
MCl_4		**TC**[d] $I\bar{4}$		
$AuCl_4$		**TC** $P4/n$ (18)		
PF_6				TC
$NbBr_6$		**TC** $B2/b$ (19)		
WCl_6		**TC** $P4/n$ (20)		
NO_3		[e]	TBP	
ClO_4		**TC** $I\bar{4}$ (22)	TC	**TC** $I\bar{4}$ (23)
$MoOBr_4(H_2O)$		**TC** $P4/n$ (24)		
OH			**TBP** $P\bar{1}$ (25)	
OMe			**TBP** *Pbca* (26)	
OCH(O)			**TBP** $P2_1/c$ (27)	
ON=C(NO)Me			**TBP** $P2_1/c$ (28)	
$O_3SC_6H_4Me$-1,4				**TBP** $C2/c$ (29)
O_3SPh[f]			**TBP** $P2_1/c$ (30)	
$BiPh_2(CF_3COO)_2$				**TBP** $P2_1/c$ (29)
Ph	**TBP** *Cc* (31)	**TBP** *Cc* (31)	**SP**[g] $P\bar{1}$ (33)	
		$m > 1$		
$CuCl_4$	**TC**[h]			
Cu_2Cl_6	**TC** $P2_1/c$ (35)	**TC** $P2_1/c$ (35, 36)	TC	
$PtCl_6$		**TC**[i] $P\bar{1}$ (37)		
$TcCl_6$		**TC**[i] $P\bar{1}$ (38)		
$In(NCS)_6$		**TC** $C2/c$ (39)		
CO_3			**TBP** + **DO** $P\bar{1}$ (40)	
SO_4		TC ?		
CrO_4		TBP		

[a]TC, tetrahedral Ph_4E^+ cation; TBP, trigonal bipyramid; SP, square pyramid; DO, distorted octahedron. Boldface indicates that crystal structure has been determined; ordinary type refers to evidence from vibrational spectra, Mössbauer spectra, conductometry etc. For method and particulars see refs. 2 and 3.
[b]In Ph_3MeSbF ($P2_1/c$) the axial positions of the TBP are occupied by Ph and F (4).
[c]In $Ph_4PBr \cdot H_2O$ and $Ph_4PBr \cdot 2H_2O$ (54).
[d]Fe (16), Ga (8), In (8, 16), Tl (17).
[e]$Ph_4AsNO_3 \cdot HNO_3$ ($C2/c$) (21).
[f]Monohydrate.
[g]TBP in $Ph_5Sb \cdot \frac{1}{2}C_6H_{12}$ ($P\bar{1}$) (32).
[h]$(Ph_4P)_2CuCl_4 \cdot H_2O$ ($P2_1/n$) (34).
[i]Distorted *anti*-CdI_2-type structure.

For E = Sb and Bi the situation is less simple. Here the only Ph_4EX crystal to date shown to be ionic on crystallographic evidence is Ph_4BiClO_4, although other evidence (vibrational and Mössbauer spectra, conductometry etc.; cf. refs. 2 and 3) points to the salt-like character of Ph_4SbClO_4, Ph_4EBF_4, and a number of other crystals containing composite anions (Table 1).[5] In all the other known structures Sb and Bi are five-coordinated, with trigonal-bipyramidal (TBP) coordination geometry (for Ph_5Sb see below) and with X in an axial position.

[5]The differences in the character of solid Ph_4EX compounds are reflected in their melting points. The trends observed in the Ph_4EHal, Ph_4EBF_4, and Ph_4EBPh_4 series are shown in Fig. 2.

The criteria of existence of the onion salts *vis-à-vis* the TBP species do not seem to have been formulated, and since pentacoordination presents interesting problems of its own, we have attempted, in the following, to analyze the existing structural evidence with this in mind. To increase the size of the small Ph_4EX (E = Sb, Bi) sample, we have determined the crystal structure of Ph_4SbBr and included in our considerations Me_4EX (41, 42, 53) and Ph_3MeSbF (4). Particulars of the main geometric features are assembled in Table 3.

Coordination geometry of Ph_4EX (E = Sb, Bi) species

The existence of the deviations of the $C_{ax}EX$ (E = Sb, Bi) angles from 180° (Table 3) might be thought to be indicative of

Can. J. Chem. Downloaded from www.nrcresearchpress.com by 122.72.124.2 on 09/07/12
For personal use only.

Can. J. Chem. Downloaded from www.nrcresearchpress.com by 122.72.124.2 on 09/07/12
For personal use only.

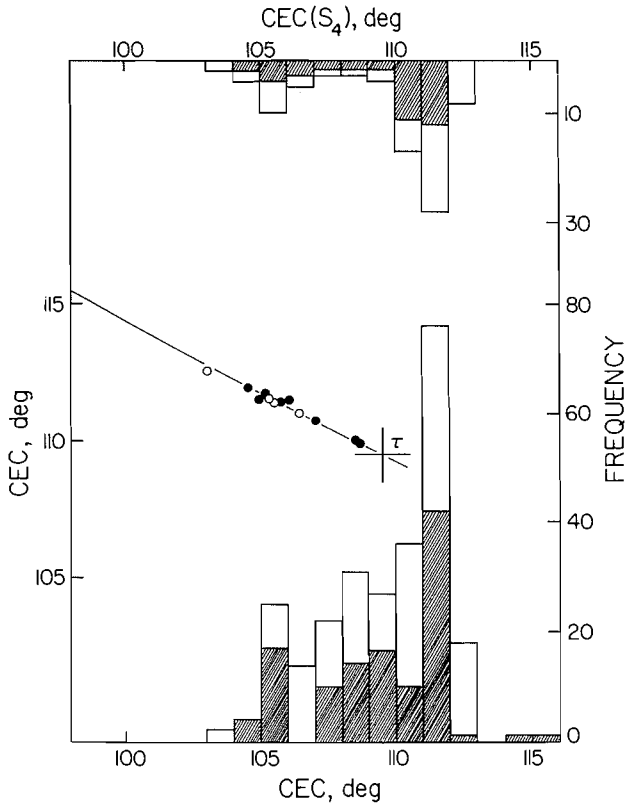


FIG. 1. CEC angles in Ph_4E^+ cations: open circles and columns, E = P; full circles and shaded columns, E = As. (*Bottom*) Distribution of CEC angles in the sample of Table 2 (frequency vs. CEC). (*Top*) Distribution of the CEC angles in cations of symmetry S_4 or C_2 close to S_4 (frequency vs. CEC(S_4)). (*Line plot*) Observed values, in cations of symmetry S_4 or C_2 close to S_4, of CEC angles not related by C_2 vs. CEC angles bisected by C_2 (CEC vs. CEC(S_4)). Solid line, theoretical relationship for S_4 (see text); τ, tetrahedral angle.

TABLE 2. CEC angles and E—C bond lengths in $Ph_4E^+X^-$ compounds (E = P, As) of Table 1

	Angles			Bond lengths[a]	
	P	As	P + As	P	As
n	72	60	132	44	39
⟨CEC⟩, deg	109.5	109.4	109.5	—	—
⟨E—C⟩, Å	—	—	—	1.789	1.902
σ, deg or Å	2.3	2.6	2.5	0.011	0.012
γ_1[b]	−0.65	−0.34	−0.50	−0.19	−0.60
γ_2[c]	2.52	2.39	2.47	2.33	2.30

[a]Uncorrected for thermal motion.
[b]Moment coefficient of skewness.
[c]Moment coefficient of kurtosis.

an incipient tendency of the TBP coordination geometry at the pentacoordinate E atom to undergo a distortion toward a square-pyramidal (SP) geometry, i.e. of a frustrated intramolecular ligand-exchange process via a pseudorotation mechanism. In that case the $C_{ax}EX$ angle and one of the geometric indices of the extent of the TBP → SP transition, the dihedral angle δ_{24} (= the $C_{ax}C_{eq}C_{eq}'/C_{eq}C_{eq}'X$ angle at the $C_{eq}C_{eq}'$ edge enclosed in the $C_{ax}EX < 180°$ angle), would be expected to follow a Berry coordinate, i.e. show a linear association (cf. for example ref. 43). However, the scatter in a plot of $C_{ax}EX$ vs. δ_{24} for the

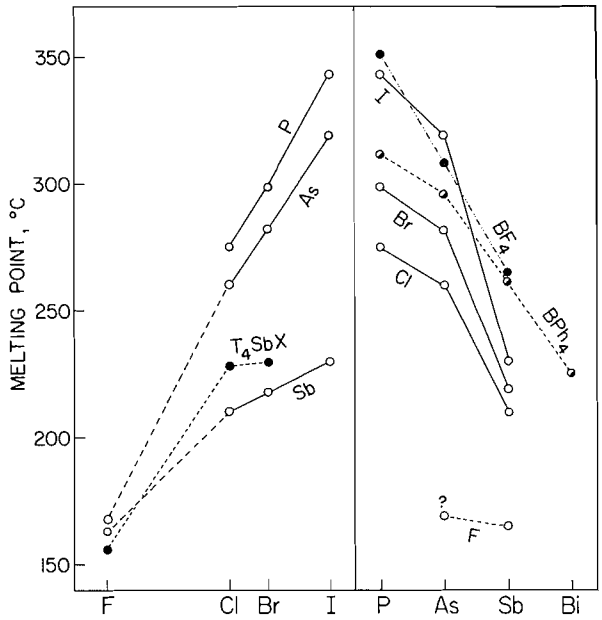


FIG. 2. Variation of the melting points of Ph_4EX with the effective radius of Hal^- (*left*) and with E (*right*; reliable effective radii of E(V) not available). The melting points shown are the highest found in the literature. The differences in trends between the ionic $Ph_4E^+X^-$ and the molecular Ph_4EX are consistent and clearly visible. T_4SbX = $(4\text{-}C_6H_4Me)_4SbX$ (cf. ref. 2).

compounds of Table 3 was such ($r^2 = 0.10$) that the notion of such a relationship could not be entertained, especially in view of the small range of $C_{ax}EX$ (less than 10°) and the sensitivity of this angle to uncertainties in the underlying interatomic distances when the angle is close to 180°. Since the only SP Ph_4EX species on record is Ph_5Sb (33), and that only in the pure Ph_5Sb crystal,[6] the tendency of the Ph_4EX species to assume SP configurations must be very weak. It is thus unlikely that the non-collinearity of the C_{ax}—E—X groupings finds its explanation in incipient pseudorotation, and other reasons must be looked for.

Examination of Table 3 reveals that the (uncorrected) Sb—C_{ax} bond length decreases with increasing Sb—X (the *trans* effect) both in the tetraphenyl and the tetramethyl species. A power-function regression of the ratio (Sb—C_{ax})/(Sb—X) on Sb—X for **1**–**14** results in a very high degree of correlation:

$$[1] \quad (Sb—C_{ax})/(Sb—X) = 2.3798(Sb—X)^{-1.1112}$$

$r^2 = 0.998$, $\sigma = 0.007 \sim 1.6\%$ of the ratio range (Fig. 3). For Bi the corresponding bond lengths are available for only two compounds, **16** and **17**, and then only with low accuracy, but the positions of the two points in Fig. 3 suggest that a similar correlation is to be expected also for the Ph_4BiX species.

Equation [1] shows that Sb—C_{ax} varies only slowly and within narrow limits with the strength of the Sb—X bond (as measured by its length), $Sb—C_{ax} \sim 2.4(Sb—X)^{-1/9}$. Equally importantly, the existence of the correlation over a wide Sb—X range and the relative smallness of the deviations of the $C_{ax}SbX$ angles from 180° demonstrate that the coordination at the Sb atom is properly described as TBP even at long Sb—X distances.

[6]In $Ph_5Sb \cdot \frac{1}{2}C_6H_{12}$ (32) the Sb coordination is TBP, as it also is in $(4\text{-}MeC_6H_4)_5Sb$ (43), and there are reasons to believe that the SP geometry in the Ph_5Sb crystal has its origin in packing factors (32, 44–46).

Can. J. Chem. Downloaded from www.nrcresearchpress.com by 122.72.124.2 on 09/07/12
For personal use only.

TABLE 3. Coordination of the E atom in crystalline R_4EX and related compounds[a]

No.	X	E—X	E—C_{ax}	⟨E—C_{eq}⟩	⟨$C_{ax}EC_{eq}$⟩	$C_{ax}EX$
			Ph_4SbX			
1	Cl	2.740(6)	2.15(2)	2.11(4)	95.8(14)	173.6(4)
2	Br (this work)	2.950(1)	2.131(8)	2.114(23)	96.0(14)	175.7(2)
3	OH	2.048	2.218(5)	2.131(19)	93.4(3)	175.4(2)
4	OMe	2.061(7)	2.199(14)	2.119(24)	92.8(7)	178.1(5)
5	OCHO	2.223	2.176	2.108	95.9	
6	OCO_2—$SbPh_4$, Sb(1)	2.257(7)	2.153(12)	2.120(11)	95.2(5)	176.2(4)
7	ON=C(NO)Me, Sb(1)	2.266	2.173	2.133(43)	96.1	171.3
8	ON=C(NO)Me, Sb(2)	2.235	2.176	2.145(10)	96.5	176.8
9	O_3SPh[b]	2.506(4)	2.131(5)	2.108(9)	98.5(2)	176.0(2)
			Ph_3MeSbX			
10	F (4)	2.067(3)	2.183(5)	2.120(13)	96.9(27)	175.5(1)
			Me_4SbX			
11	$O_2CC_6H_3(OH)(OEt)$[c]	2.890	2.099(12)	2.078(29)	105.9(8)	176
12	OP(S)Me_2 (42), Sb(1)	2.532(4)	2.150(6)	2.109(14)	101.2(3)	~180
13	OP(S)Me_2 (42), Sb(2)	2.749(4)	2.144(6)	2.107(12)	103.6(3)	177.7
14	$O_2C(COOH)C_6H_4$[d]	3.204(16)	2.074(15)	2.068(30)	107.9(30)	172.1
			Ph_4BiX			
15	ClO_4	>5.1	2.18(2)			
16	$O_3SC_6H_4Me$-1,4	2.77(3)	2.22(3)	2.20(6)	101(3)	177
17	$(O_2CCF_3)_2BiPh_2$	3.11(2)	2.22(2)	2.21(4)	104(4)	177

[a]Interatomic distances in Å, bond angles in deg. For references see Table 1.
[b]Monohydrate.
[c]1,2,4-C_6H_3(COO)(OH)(OEt) (41).
[d]1,2-C_6H_4(COO)(COOH) (41); X = O(2), C_{ax} = C(3′) (mirror image of C(3)), Sb···O(1) = 4.016(11) Å.

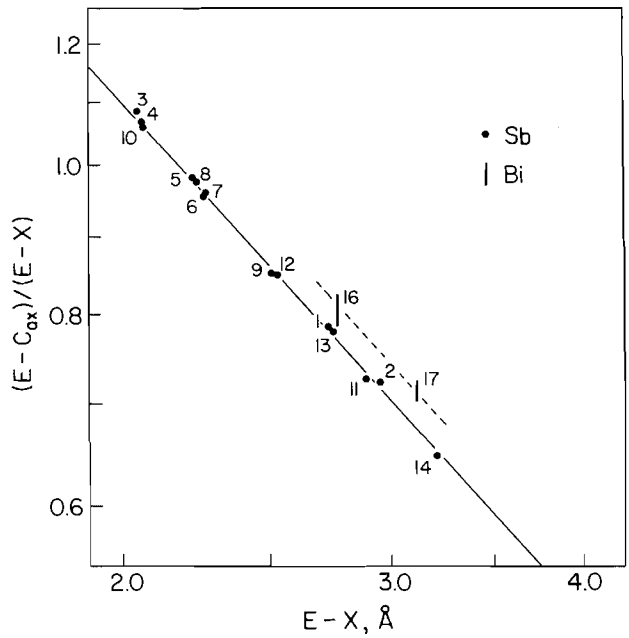


FIG. 3. Variation of log [(Sb—C_{ax})/(Sb—X)] with log (Sb—X) in R_4SbX species. The line through the Ph_4BiX points **16** and **17** is the best line parallel to the fitted Sb—X line (see text).

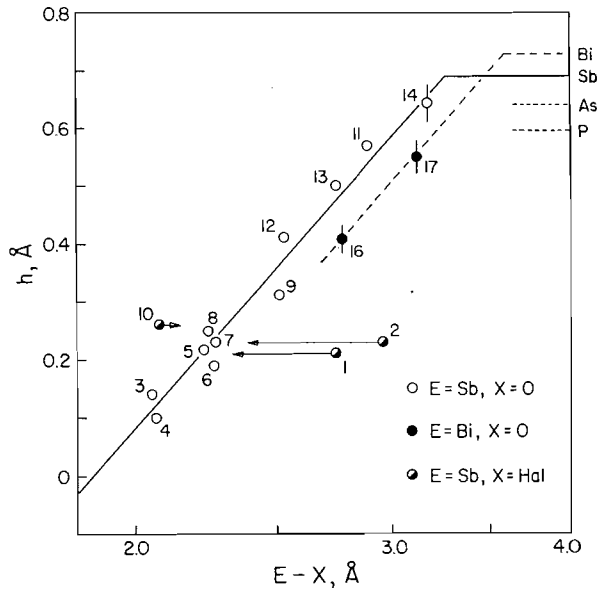


FIG. 4. Height h of atom E above the $C_{eq}C_{eq}'C_{eq}''$ plane toward C_{ax} vs. log (E—X). Estimated limiting h values for C_4E (E = P, As, Sb, Bi) tetrahedra (T_d) are indicated. The positions of the arrows indicate the E—Hal distances in **1**, **2**, and **10** on adjustment to the E—O scale.

The limits to the progressive axial distortion of the coordination TBP may be established from Fig. 4, where the height h of the E atom above the $C_{eq}C_{eq}'C_{eq}''$ triangle (toward C_{ax}) is plotted against E—X. At $h = 0$ the E atom is coplanar with the C_{eq} atoms, but with increasing h the coordination eventually becomes tetrahedral. The value of h at which this happens will depend on the (E—C_{ax})/⟨E—C_{eq}⟩ ratio, but as this ratio appears to converge toward unity as E—X increases, the tetrahedral limit may be estimated as $h \sim 0.69$ for Sb and ~0.73 for Bi. Since for the E—oxygen species of Table 3 h can be very satisfactorily represented by $h = -0.777 + 1.24$ ln (E—O) ($r^2 = 0.97$, $\sigma = 0.03$ Å), one can estimate the E···O distance beyond which C_4E coordination tetrahedra will be encountered

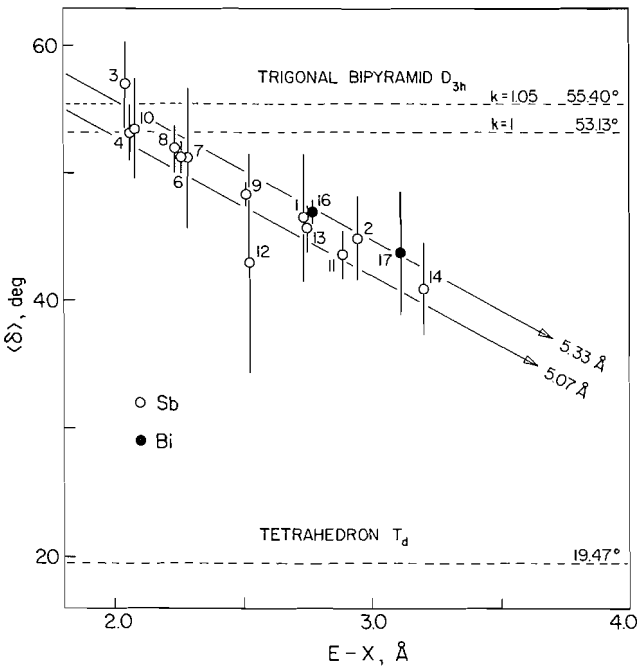


FIG. 5. Variation of the mean dihedral angle ⟨δ⟩ in trigonal-bipyramidal R_4EX (E = Sb, Bi) with the length of the E—X bond. Width of band, 2σ; $k = a/e = (E—C_{ax})/(E—C_{eq})$.

as ~3.3 Å for Sb and ~3.5 Å for Bi. In the Sb—oxygen species this distance would correspond to a limiting Sb—C bond length of 2.05(15) Å.

The extent of the departure from TBP(C_{3v}) coordination geometry can also be described by the mean dihedral angle $\langle\delta\rangle = \langle C_{ax}C_{eq}C_{eq}'\rangle/\langle C_{eq}C_{eq}'X\rangle$. This index is more general than h, since it is purely geometric and thus independent of the chemical nature of X, and is calculated directly from the positional coordinates, i.e. without any assumptions or simplifications. For a TBP of symmetry C_{3v},

$$[2]\quad \delta(C_{3v}) = \arctan\{2(x+a)(e^2-h^2)^{1/2}/[4(a+h)(x-h) - (e^2-h^2)]\}$$

where x = E—X, a = E—C_{ax}, e = E—C_{eq}. For the limiting situations this simplifies to

$$\delta[C_{3v}, x \rightarrow \infty, a = e] = \arctan[(e-h)/4(e+h)]^{1/2}$$

$$\delta(T_d) = \arctan 8^{-1/2} = 19.47°$$

and

$$\delta(D_{3h}) = \arctan[(a/e) - (e/4a)]^{-1}$$

$$\delta[D_{3h}, a = e] = \arctan \tfrac{4}{3} = 53.13°.$$

The general expression [2] for $\delta(C_{3v})$ cannot be represented graphically as a model function in a plot of δ against E—X because of the involvement of a, e, and h. However, when the actual ⟨δ⟩ values are plotted against E—X (Fig. 5), a linear regression turns out to be sufficient to yield a high degree of correlation: $\langle\delta\rangle = 76.22 - 10.92(E—X)$, $r^2 = 0.91$, $\sigma = 1.4° \sim 9\%$ of the ⟨δ⟩ range. Furthermore, when extrapolated the regression line intersects the $\delta(T_d) = 19.47°$ line at E—X = 5.20(13) Å, i.e. at a distance which matches the E···O distances observed in $Ph_4As^+ClO_4^-$ and $Ph_4Bi^+ClO_4^-$.

Transition from TBP R_4EX to $R_4E^+X^-$

As shown above, the increasing axial distortion of the coordination TBP corresponds to a continuous, progressive dissociative process which ultimately leads to tetrahedral R_4E^+ cations. The only genuinely ionic $R_4Sb^+X^-$ structure that appears to have been determined so far, $Me_4Sb^+[Al(OSiMe_3)_4]^-$ (*Pmmn*) (53), is untypical because of the size and geometry of the anion[7] and therefore perhaps not quite suitable as an example of the end result of the TBP → ionic transition. However, in $Ph_4As^+ClO_4^-$ (22) and $Ph_4Bi^+ClO_4^-$ (23) the shortest E···O separations cannot be smaller than ~5.1 Å, the orientational disorder of the ClO_4^- ion notwithstanding, and since it is highly probable that Ph_4SbClO_4 is ionic (cf. ref. 2 and the Ph_4EBF_4 series in Fig. 2) and isostructural with the As and Bi salts, we shall take these E···O distances as typical of the process discussed below.

The mean $C_{ax}SbX$ angle in **1–4** and **6–14** is 176(3)°.[8] In the oxy-ligand subset (**3–9**, **11–14**), $\langle C_{ax}SbC_{eq}\rangle$ increases with Sb—O from 93(1)° to 108(3)°, and from the increase in h with increasing Sb—O we have estimated that the C_4Sb portion of the TBP R_4SbO— will become a regular tetrahedron at Sb—O ~ 3.3 Å (~3.5 Å for Bi; for X ≠ O the E—X distance can be adjusted to the E—O scale, cf. Fig. 4). At this tetrahedral limit the R_4EX unit will be effectively an $R_4E^+ + X^-$ pair, with the C_4E tetrahedron still correctly oriented with respect to X, i.e. with C_{ax}—Sb—X more or less collinear, and that in spite of the effects of crystal packing. The dihedral angle ⟨δ⟩ becomes $\delta(T_d)$ at E···X ~ 5.2 Å (Fig. 5), but at this distance X is no longer in any particular geometric relationship to the C—Sb bonds and the C—Sb—X collinearity is lost. As a consequence the ions initially in the TBP oriented $R_4E^+ + X^-$ pairs will now redistribute themselves and the R_4E^+ cations will assume orientations in the structure such as to minimize the Coulombic energy of the crystal consistent with maximizing the packing density. With small regular anions this requirement is likely to result in arrangements of highly symmetry, as here the reorganization of the structure can proceed with a minimum of steric hindrance. This is indeed observed in $Ph_4As^+ClO_4^-$ and $Ph_4Bi^+ClO_4^-$, both of $I\bar{4}$ symmetry and in which E···O > 5.1 Å.

In these circumstances it is probable that the energy difference corresponding to Coulombic interactions at 3.5 Å and at 5.2 Å in individual $R_4Sb^+ + X^-$ pairs will not be a dominant factor compared to the collective Coulombic interactions in the crystal as a whole. Consequently the tetrahedral C_4Sb geometry will be indifferent to the length of the Sb···O distance between these limits. Thus while in the perchorates E···O > 5.1 Å, in $[Me_4Sb]^+[Al(OSiMe_3)_4]^-$ (in which the anion shares two mirror planes with the neighbouring cations[7]) the shortest Sb···O separations are ~3.9 and ~4.5 Å.

Of the Sb compounds in Table 3, **14** is the closest to the tetrahedral limit and has indeed been described (41) as purely ionic. However, Table 3 shows that the Sb coordination geometry in this crystal still qualifies as TBP. The reason why the TBP → $Me_4Sb^+X^-$ transition in **14** has not proceeded to completion is to be looked for in the particulars of its

[7]In the structure determination the Me_4Sb group was assumed to be a regular tetrahedron, Sb—C = 2.20 Å. The site symmetry at Sb is C_{2v}; the nearest oxygen atoms are two O(1) at ~3.9 Å and two O(2) at ~4.5 Å. If these oxygens are considered as completing the coordination figure of the Sb atom to form four individual distorted TBPs, the $C_{ax}SbO$ angles will be in the vicinity of 145°. Using $(Sb—O)_{eff} = (Sb—O)\cos(180 - 145)$ in eq. [1] yields Sb—C ~ 2.09 and 2.06 Å from O(1) and O(2), respectively, in agreement with the expected limiting Sb—C value of 2.05(15) Å.

[8]At $C_{ax}EX = 135.27°$ the E···X line will bisect an edge of a regular C_4E tetrahedron and there will be *two* symmetry-equivalent C_{ax} atoms. The TBP coordination geometry may be regarded as reaching its limit at this angle.

Can. J. Chem. Downloaded from www.nrcresearchpress.com by 122.72.124.2 on 09/07/12
For personal use only.

Can. J. Chem. Downloaded from www.nrcresearchpress.com by 122.72.124.2 on 09/07/12
For personal use only.

TABLE 4. Ph_4SbBr: positional parameters ($\times 10^4$) and isotropic temperature factors ($\times 10^3$) of nonhydrogen atoms

Atom	x	y	z	U_{iso}
Sb	2287.2(3)	1776.5(4)	−0094.6(3)	42(1)
C(11)	2915(5)	1556(5)	−1197(4)	49(1)
C(12)	2842(5)	2576(6)	−1759(4)	60(2)
C(13)	3270(6)	2458(8)	−2454(4)	79(2)
C(14)	3721(6)	1355(8)	−2633(5)	72(2)
C(15)	3769(5)	0349(7)	−2116(5)	71(2)
C(16)	3371(5)	0419(6)	−1385(4)	59(2)
C(21)	0803(5)	2676(7)	−0761(4)	49(2)
C(22)	0023(7)	2057(9)	−1342(6)	99(3)
C(23)	−0899(7)	2694(10)	−1845(6)	111(3)
C(24)	−1008(6)	3945(10)	−1745(4)	78(3)
C(25)	−0245(6)	4578(8)	−1164(5)	83(2)
C(26)	0682(5)	3961(7)	−0657(5)	68(2)
C(31)	2361(5)	−0136(5)	0242(4)	49(2)
C(32)	1620(5)	−0997(7)	−0204(4)	65(2)
C(33)	1773(7)	−2244(7)	−0032(5)	78(2)
C(34)	2692(7)	−2657(8)	0568(6)	88(3)
C(35)	3448(7)	−1817(7)	1013(6)	84(3)
C(36)	3307(5)	−0552(7)	0866(5)	69(2)
C(41)	3606(5)	2929(5)	0622(4)	49(2)
C(42)	4634(5)	2732(8)	0500(5)	69(2)
C(43)	5545(7)	3451(8)	0954(6)	89(3)
C(44)	5376(7)	4356(8)	1507(5)	91(2)
C(45)	4331(6)	4567(7)	1608(5)	74(2)
C(46)	3429(6)	3845(6)	1178(4)	59(2)
Br	1295.3(6)	1930.0(8)	1378.5(5)	60(3)

chemistry,[9] which prevent a more uniform redistribution of the pro-ion positions in space given the size and shape of the acid phthalate ion and the magnitude and distribution of its charge. The observed structure is a compromise between a tendency to complete ionization and the impossibility of attaining an ion packing arrangement of high symmetry (like that in $Ph_4As^+ClO_4^-$) owing to the one-sided concentration of charge in the anion. Similar considerations appear to apply to **17**, where the pro-anion is very asymmetric both because of the ligand geometries and the presence of a stereochemically active lone pair on the Bi atom.

The foregoing analysis of the available evidence provides a useful phenomenological rationale and norm for an understanding of the variability of the TBP coordination geometry in crystalline R_4EX (E = Sb, Bi) species. It also leads to the conclusion that the observed deviations of the $C_{ax}EX$ angles from 180° are due to accidents of crystal packing. The question of why covalency in these crystals takes precedence over ionization even in cases where on chemical grounds the latter might be expected to prevail is much more difficult to answer in general terms, considering the extensive dissociation into R_4E^+ and X^- which occurs in solution. For example, ionic (cf. Fig. 2) $Ph_4Sb^+BPh_4^-$ readily precipitates from aqueous or alcoholic solutions of Ph_4SbBr with $NaBPh_4$, and similar behaviour is well documented from solution studies of numerous R_4SbX and R_4BiX compounds containing pentacoordinated E in the solid state (cf. refs. 2 and 3).

[9]In **14** both the pro-cation and the pro-anion are on (020) mirror planes. The mirror bisecting the pro-anion 1,2-C_6H_4[CO(1)O(2)][C′O(1′)O(2′)]H contains the H atom which bridges O(1) and O(1′). An Me_4Sb tetrahedron is flanked symmetrically on the left by an O(2) and on the right by an O(2′) atom, each from a different pro-anion. The O(2) atom completes the coordination figure of Sb to a TBP on the left, while O(2′) completes it to a TBP on the right. The result is thus a superposition of two reflection-related TBPs, but the Sb atom is six-coordinated only in a formal sense, the two Sb—O distances being so long, and may as well be regarded as a limiting case of TBP coordination on one side at a time. The structure of **14** may thus be viewed as consisting of zig-zag···C_4Sb···O(2)—[ ]—O(2′)···C_4Sb··· chains ∥*b*.

TABLE 7. Ph_4SbBr: interatomic distances and bond angles

Bond	Distance (Å)	Bonds	Angle (deg)
Sb—C(11)	2.131(8)	C(11)—Sb—Br	175.7(2)
Sb—C(21)	2.106(6)	C(21)—Sb—Br	84.1(2)
Sb—C(31)	2.105(6)	C(31)—Sb—Br	81.1(2)
Sb—C(41)	2.131(6)	C(41)—Sb—Br	87.2(2)
Sb—Br	2.950(1)	C(11)—Sb—C(21)	94.6(3)
		C(11)—Sb—C(31)	96.2(3)
		C(11)—Sb—C(41)	97.1(3)
		C(21)—Sb—C(31)	123.1(3)
		C(21)—Sb—C(41)	117.5(3)
		C(31)—Sb—C(41)	116.2(3)
		Sb—C(11)—C(12)	118.6(5)
		Sb—C(11)—C(16)	122.0(5)
		Sb—C(21)—C(22)	120.9(6)
		Sb—C(21)—C(26)	119.5(4)
		Sb—C(31)—C(32)	122.4(5)
		Sb—C(31)—C(36)	117.6(5)
		Sb—C(41)—C(42)	116.7(5)
		Sb—C(41)—C(46)	122.2(5)

Crystal structure of Ph_4SbBr

The positional parameters and anisotropic temperature factors of the non-hydrogen atoms are listed in Tables 4 and 5; the hydrogen atoms are detailed in Table 6, and bond lengths and angles in Tables 7 and 8.[10]

A conspicuous feature of the structure is the arrangement of the Br atoms (Fig. 6). They are situated almost exactly in the $10\bar{1}$ planes, the perpendicular distance of a Br atom from the nearest $10\bar{1}$ plane being only 0.09 Å. The Ph_4Sb units are thus completely contained within the parallel slabs into which the structure is divided by the $10\bar{1}$ planes. The structure may therefore be regarded as a layer structure and as such it would be more suitably described on a unit cell which reflects the layer character, e.g. $P'(-\mathbf{a}, \mathbf{b}, \mathbf{a}+\mathbf{c})$ or $B(\mathbf{a}+\mathbf{c}, \mathbf{b}, \mathbf{a}-\mathbf{c})$, except that P' is more oblique than $P(\mathbf{a}, \mathbf{b}, \mathbf{c})$, $\beta(P') = 117.5°$. Cell B is only marginally more oblique than P, $\beta(B) = 106.0°$, but it is twice the size of P.

The Sb—Br bonds are practically parallel (~3°) to the 010 plane. The Sb atom is coplanar with the phenyl rings 1 and 4, and about 0.25 Å out of the best planes of rings 2 and 3. The rings are planar to $\sigma = 0.011$ Å or better (Table 9).[10] The planes of rings 2 and 3 are only 14° from parallel; the axial ring 1 is approximately perpendicular to the mean plane of rings 2 and 3, and ring 4 is roughly at 90° to ring 1. The internal CCC angles in the rings are all 120° within 2 esd's. The Sb—C(11) and Sb—C(41) bonds are coplanar with their respective phenyl rings, while Sb—C(21) and Sb—C(31) are tilted by ~7°.

The means of the uncorrected bond lengths and angles are listed in Table 3. Additionally, $\langle C_{eq}SbBr\rangle = 84.1(27)°$ and $\langle SbCC\rangle = 120.0(26)°$, the latter with a range of 5.7(8)°.

[10]Copies of Tables 5, 6, and 8–10 can be purchased from the Depository of Unpublished Data, CISTI, National Research Council of Canada, Ottawa, Ont., Canada K1A 0S2.

Can. J. Chem. Downloaded from www.nrcresearchpress.com by 122.72.124.2 on 09/07/12
For personal use only.

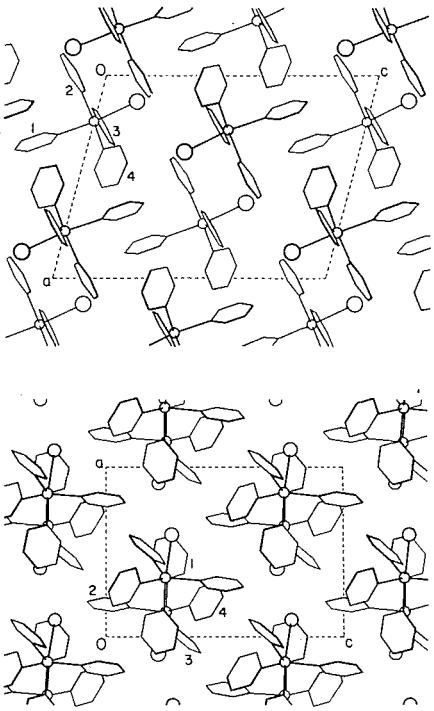


FIG. 6. (*Top*) Ph_4SbBr: projection on (010) (H atoms omitted for clarity). (*Bottom*) Ph_4SbCl (after ref. 5): projection on (010). The coordinates of ref. 5 have been transformed and the rings renumbered ($I \rightarrow 2$, $II \rightarrow 4$, $III \rightarrow 3$, $IV \rightarrow 1$) to match our description of the Ph_4SbBr structure. The two projections are on the same scale.

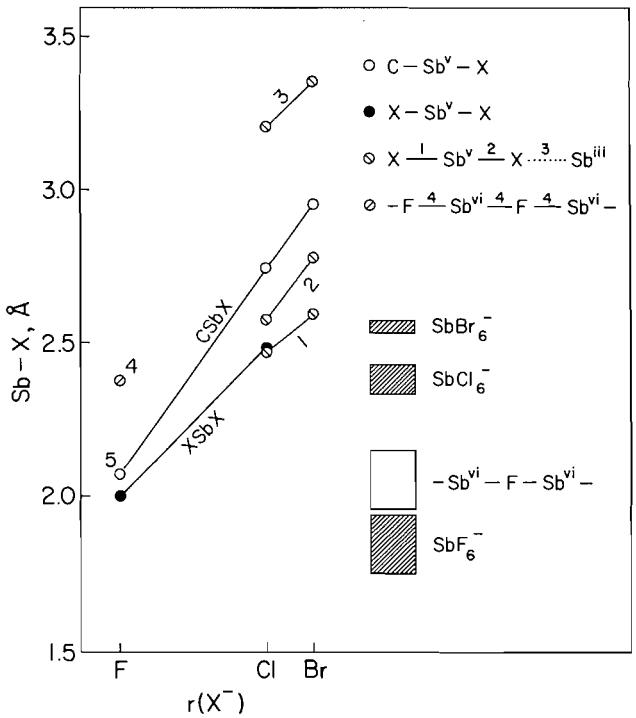


FIG. 7. Sb—X distances involving pentavalent Sb: CSbX (axial) in Ph_4SbX; XSbX (axial) in R_3SbX_2 (R = Ph, Me); XSbX···Sb(III) (axial) in $Me_3SbX_2 \cdot SbX_3$; —FSbFSb— in Me_4SbF (cf. ref. 2). (*Right*) Ranges of Sb(V)—X bond lengths reported in $Sb_mF_n^{k-}$ (terminal and bridging), $SbCl_6^-$ and $SbBr_6^-$ ions and some other compounds (48); the bond lengths in $SbBr_6^-$ have been corrected for thermal motion (49). *4*, Me_4SbF; *5*, Ph_3MeSbF. Sb^{iv}, Sb^v, and Sb^{vi} indicate four-, five-, and six-coordinated Sb atoms, respectively.

The Sb—Br bond of 2.95 Å appears to be the longest Sb(V)—Br bond reported to date (Fig. 7). Comparison of the Sb(V)—Hal bond lengths observed in Ph_4SbHal with those in R_3SbHal_2 (R = Ph, Me), $Me_3SbHal_2 \cdot SbHal_3$ and a variety of $Sb_mHal_n^{k-}$ ions as well as in a few other compounds shows that the bonds in Ph_4SbCl and Ph_4SbBr are considerably (about 15%) longer than the rest of the corresponding bonds. The Sb—F bond in Ph_3MeSbF also is about 15% longer than the terminal bonds in $Sb_mF_n^{k-}$ but in the range of the *bridging* Sb—F—Sb bonds in such ions; in Me_4SbF, however, the Sb—F bonds are longer than even the latter.

Compared with the purely inorganic Sb(V) halogen species, the Sb—Hal bonds in R_4SbHal are thus always longer, and that even in spite of the anionic, size-expanding charge on $SbHal_6^-$ and the higher coordination number of the Sb atom in these ions. That these bonds are abnormally long is seen from a comparison with Sb—Hal in the TBP R_3SbHal_2, in which the two *trans* Sb—Hal bonds are balanced, and with Sb(V)—Hal in the adducts $Me_3SbHal_2 \cdot SbHal_3$, where one of the two *trans* bonds is weakened by a Hal···Sb(III) interaction (Fig. 7). These bond lengths thus furnish evidence that even in *absolute* terms (as distinct from the correlation of Fig. 3) Ph_4SbCl and Ph_4SbBr represent Ph_4SbX species well *en route* from molecular to ionic, onium solids.

Comparison with Ph_4SbCl

The two compoudns crystallize with the same space group, $P2_1/n$, but they are not isostructural.[11] However, there are similarities as well as differences in their structural features. The two structures are compared in Fig. 6.

The Cl atoms again are close to the 101 planes but less so than the Br atoms in Ph_4SbBr; the shortest perpendicular distance is 0.97 Å. The Ph_4Sb skeletons here, too, are contained within the parallel slabs bounded by the 101 planes. However, the dominant feature of the chloride structure is the columns of Ph_4SbCl molecules parallel to *b*. In each column the molecules are related by a 2_1 axis, and the columns are arranged in a pseudohexagonal array.[12] The Sb—Cl bonds form an angle of ~19° with (010) as against ~3° in the bromide, which accounts for the increase in the $2b/(a + c)$ ratio relative to Ph_4SbBr, 1.21 compared to 0.75; $b(Cl)/b(Br) = 1.37$.

The differences between the structures of Ph_4SbCl and Ph_4SbBr are difficult to account for from the size disparity (~8% on radius) of the halogen atoms alone. Hydrogen–hydrogen repulsions clearly are involved, but as the actual structures are the result of a fine balance of a number of factors, assigning any *one* of them as the main or sole cause of the differences would seem mere speculation. The *similarities* of the gross features of the two structures are discussed in a larger context in ref. 54.

Experimental

Commercial Ph_4SbBr (Alfa) was recrystallized from $MeNO_2$, MeCN, and EtOH. The compound is very soluble in $MeNO_2$ and MeCN, and recrystallization therefore occurred from very concentrated solutions. Crystals from $MeNO_2$ were quite large, clear, and colourless; they melted at 203–212°C (dec.) to a golden-yellow melt (ref. 50, 210–218°C). Crystals from MeCN were similar but much smaller. In both cases ir spectra showed that the crystals were

[11]For Ph_4SbCl, $a = 10.141(4)$ Å, $b = 14.590(6)$ Å, $c = 14.027(6)$ Å, $\beta = 90.03(4)°$ (5).

[12]The c/a axial ratio, 1.38, differs by ~25% from $\sqrt{3}$ required for an orthohexagonal cell; $\beta \sim 90°$.

anhydrous Ph_4SbBr. Evaporation of EtOH solutions always resulted in gradual precipitation of a white powder (not characterized). For structure analysis a crystal was selected from the $MeNO_2$ crop.

Crystal data

$BrC_{24}H_{20}Sb$ fw = 510.08

Monoclinic, $P2_1/n$ (no. 14) (systematic absences: $0k0$, k odd; $h0l$, $h + l$ odd); $a = 12.282(2)$ Å, $b = 10.656(1)$ Å, $c = 16.156(1)$ Å, $\beta = 104.92(7)°$, $V = 2060(1)$ Å^3, $Z = 4$, $\rho_c = 1.645(1)$ g/cm^3; $\mu_{Mo} = 34.2$ cm^{-1}, $F000) = 1000$ e. Crystal, $0.28 \times 0.48 \times 0.75$ mm^3; CAD-4 four circle diffractometer; Mo $K\alpha_1$, $\lambda = 0.70926$ Å (graphite monochromator); θ range, 2–23°. Reflections: 3280 measured, 2877 unique, 2349 ($I > 2\sigma(I)$) unique used. Lorentz, polarization, and absorption corrections applied; $R_{merg} = 8.8\%$ before, 4.8% after absorption corrections. Scattering factors for neutral atoms and corrections for anomalous scattering from ref. 51.

Structure determination

The structure was solved using the SHELX 76 system (52). After the nonhydrogen atoms had been located, full-matrix least-squares ($w\Delta F^2$ = minimum) refinement was carried out with isotropic temperature factors until R was reduced to a reasonably low value. Although the hydrogen atoms were observable, at this stage they were placed, and the refinement was continued with anisotropic factors on the nonhydrogen atoms and isotropic factors on the hydrogens. The anisotropic temperature factor is defined as $T = \exp[-2\pi^2(U_{11}h^2a^{*2} + U_{22}k^2b^{*2} + U_{33}l^2c^{*2} + 2U_{23}klb^*c^* + 2U_{13}hla^*c^* + 2U_{12}hka^*b^*)]$. The least-squares weights were $w = 1.204(\sigma^2|F| + 0.001F^2)^{-1}$. The 002, 751, and 961 reflections suffered from extinction and were omitted from the final refinement. The highest peak in the final difference map was 1.3 e/Å^3 followed by six smaller peaks, all seven located within 1.2 Å of the Sb or Br positions; after these the next highest peak was 0.66 e/Å^3. Final $R = 5.46\%$, $R_w = 5.66\%$. The structure factors are listed in Table 10.[10]

Acknowledgments

We wish to thank Miss K. N. Robertson for the preparative work and Dr. A. Linden for assistance with the preparation of the manuscript. This investigation was supported by grants from the Natural Sciences and Engineering Research Council of Canada to O.K. and T.S.C.

1. U. Müller. Acta Crystallogr. B, **36**, 1075 (1980).
2. M. Wieber. Gmelin Handbuch der anorganischen Chemie. 8th ed. Organoantimony compounds, pts. 3 and 4. Springer, Berlin. 1982 and 1986.
3. M. Wieber. Gmelin Handbuch der anorganischen Chemie. 8th ed. New suppl. ser. vol. 47: Bismuth-organische Verbindungen. Springer, Berlin, 1977.
4. J. Bordner, B. C. Andrews, and G. G. Long. Cryst. Struct. Commun. **5**, 801 (1976).
5. V. A. Lebedev, R. I. Bochkova, E. A. Kuz'min, V. V. Sharutin, and N. V. Belov. Dokl. Akad. Nauk SSSR, **260**, 1124 (1981).
6. T. L. Khotsyanova and Yu. T. Struchkov. Kristallogr. **1**, 669 (1956).
7. R. C. L. Mooney. J. Am. Chem. Soc. **62**, 2955 (1940).
8. R. C. Gearhart, Jr., J. D. Beck, and R. H. Wood. Inorg. Chem. **14**, 2413 (1975).
9. U. Müller and H.-D. Dörner. Z. Naturforsch. **37b**, 198 (1982).
10. M. P. Bogaard and A. D. Rae. Cryst. Struct. Commun. **11**, 175 (1982).
11. J. Ollis, V. J. James, D. Ollis, and M. P. Bogaard. Cryst. Struct. Commun. **5**, 39 (1976).
12. M. P. Bogaard, J. Peterson, and A. D. Rae. Cryst. Struct. Commun. **8**, 347 (1979).
13. U. Müller. Z. Naturforsch. **34b**, 1064 (1979).
14. J. Runsink, S. Swen-Walstra, and T. Migchelsen. Acta Crystallogr. B, **28**, 1331 (1972).
15. U. Müller, N. Mronga, C. Schumacher, and K. Dehnicke. Z. Naturforsch. **37b**, 1122 (1982).
16. F. A. Cotton and C. A. Murillo. Inorg. Chem. **14**, 2467 (1975).
17. F. A. Cotton, B. F. G. Johnson, and R. M. Wing. Inorg. Chem. **4**, 502 (1965).
18. P. G. Jones, J. J. Guy, and G. M. Sheldrick. Acta Crystallogr. B, **31**, 2687 (1975).
19. U. Müller, R. Dübgen, and K. Dehnicke. Z. Anorg. Allg. Chem. **473**, 115 (1981).
20. G. Uhl, E. Hey, G. Becker, F. Weller, and K. Dehnicke. Z. Anorg. Allg. Chem. **497**, 213 (1983).
21. B. D. Faithful and S. C. Wallwork. J. Chem. Soc. Commun. 1211 (1967).
22. M. C. Couldwell. Cryst. Struct. Commun. **8**, 469 (1979).
23. J. Bordner and L. D. Freedman. Phosphorus, **3**, 33 (1973).
24. J. G. Scane. Acta Crystallogr. **23**, 85 (1967).
25. A. L. Beauchamp, M. J. Bennett, and F. A. Cotton. J. Am. Chem. Soc. **91**, 297 (1969).
26. K. W. Shen, W. E. McEwen, S. J. La Placa, W. C. Hamilton, and A. P. Wolf. J. Am. Chem. Soc. **90**, 1718 (1968).
27. S. P. Bone and D. B. Sowerby. J. Chem. Res. S, 82 (1979).
28. J. Kopf, G. Vetter, and G. Klar. Z. Anorg. Allg. Chem. **409**, 285 (1974).
29. D. H. R. Barton, B. Charpiot, E. Tran Huu Dau, W. B. Motherwell, C. Pascard, and C. Pichon. Helv. Chim. Acta, **67**, 586 (1984).
30. R. Rüther, F. Huber, and H. Preut. J. Organomet. Chem. **295**, 21 (1985).
31. P. J. Wheatley. J. Chem. Soc. 2206 (1964).
32. C. Brabant, B. Blanck, and A. L. Beauchamp. J. Organomet. Chem. **82**, 231 (1974).
33. A. L. Beauchamp, M. J. Bennett, and F. A. Cotton. J. Am. Chem. Soc. **90**, 6675 (1968).
34. R. L. Harlow and S. H. Simonsen. Cryst. Struct. Commun. **5**, 265 (1976).
35. M. Textor, E. Dubler, and H. R. Oswald. Inorg. Chem. **13**, 1361 (1974).
36. R. D. Willett and C. Chow. Acta Crystallogr. B, **30**, 207 (1974).
37. B. Viossat, A. Hourfar, and N. Rodier. Bull. Soc. Chim. Fr. I 454 (1981).
38. J. Baldas, J. Bonnyman, D. L. Samuels, and G. A. Williams. Acta Crystallogr. C, **40**, 1343 (1984).
39. F. W. B. Einstein, M. M. Gilbert, D. G. Tuck, and P. L. Vogel. Acta Crystallogr. B, **32**, 2234 (1976).
40. G. Ferguson and D. M. Hawley. Acta Crystallogr. B, **30**, 103 (1974).
41. B. Milewski-Mahrla and H. Schmidbaur. Z. Naturforsch. **37b**, 1393 (1982).
42. W. Schwarz and H. D. Hausen. Z. Anorg. Allg. Chem. **441**, 175 (1978).
43. R. R. Holmes. J. Am. Chem. Soc. **106**, 3745 (1984).
44. C. Brabant, J. Hubert, and A. L. Beauchamp. Can. J. Chem. **51**, 2951 (1973).
45. C. P. Brock and J. A. Ibers. Acta Crystallogr. A, **31**, 38 (1975).
46. C. P. Brock. Acta Crystallogr. A, **33**, 193 (1977).
47. C. P. Brock. Acta Crystallogr. A, **33**, 898 (1977).
48. A. F. Wells. Structural inorganic chemistry. 5th ed. Clarendon Press, Oxford. 1984.
49. S. L. Lawton, R. A. Jacobson, and R. S. Frye. Inorg. Chem. **10**, 701 (1971).
50. J. Chatt and F. G. Mann. J. Chem. Soc. 1192 (1940).
51. International tables for X-ray crystallography. Vol. IV. The Kynoch Press, Birmingham, Eng. 1974.
52. G. M. Sheldrick. SHELX system report. University Chemical Laboratories, Lensfield Road, Cambridge, Eng. 1976.
53. P. J. Wheatley. J. Chem. Soc. 3200 (1963).
54. B. R. Vincent, O. Knop, K. N. Robertson, and T. S. Cameron. Can. J. Chem. In press.

Can. J. Chem. Downloaded from www.nrcresearchpress.com by 122.72.124.2 on 09/07/12
For personal use only.

Isomerization, fluorine exchange, and stereoselective synthesis of *cis*- and *trans*-F_2TePh_3Cl: application of the coordination model of reaction mechanisms

ALEXANDER F. JANZEN AND MEEHAE JANG

Department of Chemistry, University of Manitoba, Winnipeg, Man., Canada R3T 2N2

Received May 16, 1988

ALEXANDER F. JANZEN and MEEHAE JANG. Can. J. Chem. **67**, 71 (1989).

The stereoselective synthesis of *cis*- and *trans*-F_2TePh_3Cl (phenyl substituents adopt a *mer* arrangement) via 5-coordinate cations Ph_3TeFCl^+ and $Ph_3TeF_2^+$ is described. *trans*-F_2TePh_3Cl isomerizes to the thermodynamically more stable *cis* isomer, and *cis*-F_2TePh_3Cl has non-equivalent fluorines which undergo stereoselective fluorine exchange, as confirmed by ^{19}F and ^{125}Te nmr spectroscopy. These results are consistent with an intermolecular mechanism of isomerization and fluorine exchange involving Te—F bond cleavage.

The coordination model of reaction mechanisms provides a unified description of stereochemical rearrangements, ligand exchange processes, and chemical reactions in these, and related, octahedral and trigonal bipyramidal compounds.

Key words: synthesis of *cis*- and *trans*-F_2TePh_3Cl, isomerization of octahedral Te compounds, fluorine exchange in *cis*-F_2TePh_3Cl, synthesis of Ph_3TeF, coordination model of reaction mechanisms.

ALEXANDER F. JANZEN et MEEHAE JANG. Can. J. Chem. **67**, 71 (1989).

On décrit la synthèse stéréosélective des F_2TePh_3Cl-*cis* et -*trans* (les substituants adoptent une arrangement *mer*) réalisée par le biais des cations penta-coordonnés Ph_3TeFCl^+ et $Ph_3TeF_2^+$. Le F_2TePh_3Cl-*trans* se transforme en isomère *cis* qui est thermodynamiquement plus stable; le F_2TePh_3Cl-*cis* possède deux atomes de fluor qui ne sont pas équivalents et qui subissent un échange stéréosélectif de fluor qui est confirmé par la spectroscopie rmn du ^{19}F et du ^{125}Te. Ces résultats sont en accord avec un mécanisme d'isomérisation intermoléculaire et un échange de fluor impliquant un clivage de la liaison Te—F.

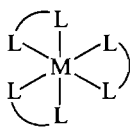
Le modèle de coordination des mécanismes de réaction fournit une description unifiée des transpositions stéréochimiques, des processus d'échange de ligand et des réactions chimiques dans ces composés ainsi que dans les composés apparentés octaédriques ainsi que trigonaux bipyramidaux.

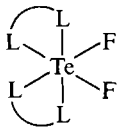
Mots clés : synthèse des F_2TePh_3Cl-*cis* et -*trans*, isomérisation de composés Te octaédriques, échange de fluor dans F_2TePh_3Cl-*cis*, synthèse de Ph_3TeF, modèle de coordination des mécanismes de réaction.

[Traduit par la revue]

Introduction

The mechanisms of stereochemical rearrangements of octahedral metal complexes may be placed into two categories: those which involve changes in coordination number of the metal, and those which do not. Isomerizations and racemizations of tris(bidentate) complexes are generally placed into the former category (1), as originally suggested by Werner (2), while isomerization of other octahedral complexes (3, 4), including tellurium fluorides (5), have been placed into the latter category.

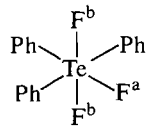




Our nmr studies of ligand exchange in 4-, 5, and 6-coordinate silicon (6), phosphorus (7), sulfur (8), and tellurium (9, 10) fluorides are all consistent with the view that rapid coordination changes of metal and ligand are responsible for the lowest energy pathway of ligand exchange and chemical reaction. Stereochemical changes, including axial-equatorial scrambling of ligands in trigonal bipyramidal molecules, may accompany the formation of octahedral intermediates such as $SiF_5(base)^-$ (6), $PF_5(base)$ (7), $Me_2PF_3(solvent)$ (11), or $AsF_5(FCH_3)$ (12), while racemization and base-catalyzed hydrolysis of silanes may involve octahedral intermediates such as $R_3SiCl(solvent)_2$ (13) and $Me_3SiF(NHEt_2)(H_2O)$ (14), furthermore, many chemical reactions of pentacoordinated compounds probably require the formation of octahedral intermediates (15) as the first step along a reaction pathway. Since these mechanistic views are at variance with the postulate of low energy polytopal rearrangements, we decided to investigate the isomerization of some octahedral phenyltellurium(VI) fluorides which have been prepared by the oxidative-fluorination with XeF_2 (16). The problem of stereoselective fluorine exchange in Ph_3TeF_3 and Ph_3TeF_2OH has recently been studied by ^{19}F and ^{125}Te nmr and the structures of these molecules have been determined by X-ray crystallography (9, 10).

Results and discussion

Ph_3TeF was prepared from Ph_3TeCl and carbonyl fluoride (17) and converted to *mer*-Ph_3TeF_3, **1**, by addition of XeF_2 (9, 16).

[1] $Ph_3TeCl \xrightarrow{COF_2} Ph_3TeF \xrightarrow{XeF_2}$ 

mer-**1**

mer-**1** was then used in the synthesis of *cis*- and *trans*-F_2TePh_3Cl (phenyl substituents retain their *mer* arrangement) and our evidence for intermolecular mechanisms of isomerization and exchange involving Te—F bond cleavage is based on the following experiments: (*A*) stereoselective synthesis of *cis*- and *trans*-F_2TePh_3Cl, (*B*) stereoselective Te—F bond cleavage in *cis*-F_2TePh_3Cl, and (*C*) catalysis of isomerization and fluorine exchange by Lewis acids but inhibition by fluoride or chloride ions.

Preliminary experiments showed that *trans*-F_2TePh_3Cl, **3**, was the kinetically favoured isomer while *cis*-F_2TePh_3Cl, **5**, was the thermodynamically favoured isomer. *trans*-**3** was prepared in two-stages: treatment of *mer*-**1** with PF_5 removed either F^a or F^b and gave the cation $Ph_3TeF_2^+$, **2**, and addition of chloride then gave *trans*-**3**. The stereochemical outcome of each step in reaction [2] is presumably determined by the preference of three phenyl substituents for a planar arrangement in *mer*-**1**, cation **2**, and *trans*-**3**.

^{19}F and ^{125}Te nmr data for cation **2** and *trans*-**3** are given in

Can. J. Chem. Downloaded from www.nrcresearchpress.com by 122.72.124.2 on 09/07/12
For personal use only.

TABLE 1. ^{19}F and ^{125}Te nmr data of some phenyltellurium(VI) fluorides*

Compound	Spin system	F^a	F^b	Te	$J(F^aF^b)$	$J(TeF^a)$	$J(TeF^b)$	Reference
mer-Ph_3TeF_3, **1**	ab_2	−3	−98	+786	40	2860	2081	9
trans-F_2TePh_3Cl, **3**	b_2		−99	+783			1800	†
cis-F_2TePh_3Cl, **5**	ab	+3.1	−86.2	+776	50	2565	1892	16
$Ph_3TeF_2^+PF_6^-$, **2**	b_2		−122	+896			1600	9
$Ph_3TeFCl^+PF_6^-$, **4**	b		−90	+886			1425	†

*Chemical shifts in ppm and coupling constants in Hz. Solvent is CD_2Cl_2. The ^{19}F and ^{125}Te chemical shifts were measured relative to internal C_6F_6 (−162.9 ppm with respect to $CFCl_3$) and external Ph_2Te (692 ppm with respect to Me_2Te).
†This work.

[2] *mer*-**1** $\xrightarrow{PF_5}$ **2** $\xrightarrow{Et_4NCl}$ *trans*-**3**

Table 1 and the chemical shifts and coupling constants of F^b in *trans*-**3** are very similar to those of the corresponding *trans* fluorines in *mer*-**1**.

Treatment of *trans*-**3** with PF_5 removed F^b and gave the cation Ph_3TeFCl^+, **4**, and addition of fluoride then gave *cis*-F_2TePh_3Cl, **5**, as confirmed by ^{19}F and ^{125}Te nmr (Table 1). *cis*-**5** was characterized previously by nmr, elemental analysis, and mass spectrometry (16).

[3] *trans*-**3** $\xrightarrow{PF_5}$ **4** $\underset{PF_5}{\overset{NaF}{\rightleftharpoons}}$ *cis*-**5**

A trigonal bipyramidal geometry for cations **2** and **4** is consistent with the equivalence of fluorines in **2** and the equivalence of phenyl rings in **2** and **4**, as judged by carbon-13 nmr.[1] As seen in Table 1, the formation of cations **2** and **4** from octahedral *mer*-**1**, *trans*-**3** or *cis*-**5** results in an upfield shift of 100 to 120 ppm in the ^{125}Te nmr, and a decrease of 200–656 Hz in the Te—F^b coupling. Cation **4** was also prepared by the addition of PF_5 to *cis*-**5** and the loss, presumably, of either F^a or F^b.

In view of the report that octahedral *trans*-$F_2Te(C_6H_4CMe_2O)_2$ is converted to the *cis*-isomer after 3 days at 60°C by a *nondissociative* mechanism (5), we decided to estimate how quickly the step-by-step isomerization of *trans*-**3** to *cis*-**5** could be carried out according to eq. [3], with verification by nmr at each stage. It required a total of 1 h to add PF_5 to *trans*-**3**, remove excess PF_5, record the nmr of cation **4**, add NaF, filter off solid NaF, and record the nmr of *cis*-**5**. As far as we could tell, the chemical reactions during this time occurred more or less instantaneously and we conclude that the lowest energy pathway of *trans*-to-*cis* isomerization in octahedral Te(VI) fluorides occurs by an intermolecular route involving Te—F bond cleavage. This conclusion is supported by the report that *trans*-to-*cis* isomerization in $F_2Te(C_6H_4CMe_2O)_2$ and $F_2S(C_6H_4C(CF_3)_2O)_2$ is catalyzed by Lewis acids such as SbF_5 and SO_3 (5, 18).

The previous finding that intermolecular fluorine exchange in *mer*-Ph_3TeF_3 is initiated by impurities but stopped by NaF or R_4NCl (9), suggests that impurities might also initiate exchange and isomerization in *cis*- and *trans*-F_2TePh_3Cl. This was found to be the case, as confirmed by monitoring a sample containing 100% *trans*-F_2TePh_3Cl, **3**, prepared according to eq. [2]. After 24 h in dichloromethane solution, only 64% *trans*-**3** remained, and the rest was mainly *cis*-F_2TePh_3Cl, **5**, along with smaller amounts of *mer*-Ph_3TeF_3, **1**. The formation of *mer*-**1** implies the presence of fluoride impurities, and nmr examination at this stage confirmed the presence of small amounts of $P(O)F_2OH$, $P(O)F(OH)_2$, and BF_4^- which may originate from the reaction of PF_5 and HF with moisture and glass nmr tubes. We therefore assume that Lewis acid impurities can generate cations **2** or **4** which in turn catalyze fluorine exchange and isomerization in octahedral Te(VI) fluorides. After one month in solution, all *trans*-**3** had disappeared and only *cis*-**5** and *mer*-**1** remained.

The fact that reactions of XeF_2 with Ph_3TeCl give the thermodynamically stable *cis*-**5** product (16) can probably be attributed to the slowness of the XeF_2 reactions, which take 8 h or more for completion. During this time XeF_2 is known to react with organic solvents (19), and an impurity-catalyzed isomerization, eq. [4], is then likely.

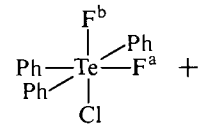
[4] *trans*-**3** $\xrightarrow[\text{e.g. HF, } BF_3]{\text{Lewis acid}}$ *cis*-**5**

cis-F_2TePh_3Cl, **5**, has non-equivalent fluorines, F^a and F^b, and it was possible to carry out stereoselective Te—F^a bond cleavage by adding small amounts of cation **4** to *cis*-**5**. The ^{19}F and ^{125}Te nmr spectra were very similar to those observed in the Ph_3TeF_3—$Ph_3TeF_2^+$ (9) and Ph_3TeF_2OH—Ph_3TeFOH^+ (10) systems and showed that F^a—F^b and Te—F^a couplings are lost, but Te—F^b coupling is retained in the *cis*-F_2TePh_3Cl–Ph_3TeFCl^+ system, consistent with a mechanism involving a fluorine-bridged intermediate in which F^a occupies the bridging position, eq. [5].

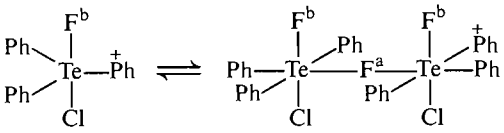
Occasionally, during reactions of PF_5 with *cis*-**5**, some *mer*-**1** was present and consequently both cations **2** and **4** were formed in solution, but the nmr spectra showed that there was no intermolecular fluorine exchange between cations **2** and **4**.

[1] A. F. Janzen and M. Jang. Unpublished result.

Can. J. Chem. Downloaded from www.nrcresearchpress.com by 122.72.124.2 on 09/07/12
For personal use only.

[5] 

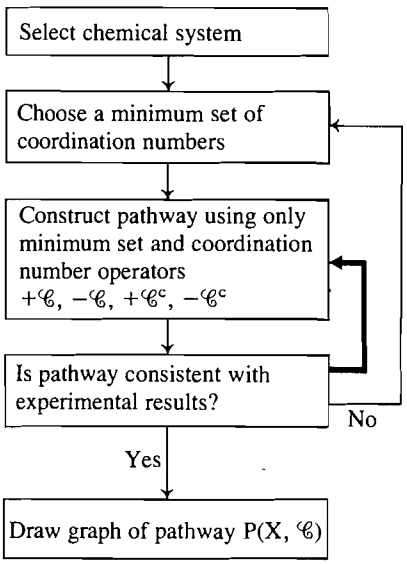
cis-**5**



4

The coordination model of reaction mechanisms and the stereodynamics and reactivity of 4-, 5-, and 6-coordinate compounds

The coordination model of reaction mechanisms (20)[2] describes the connectivity of atoms and the discrete changes in coordination number that occur during a chemical process. A summary of this model is given below:



Changes in coordination numbers are described by coordination number operators, $\mathscr{C}$: $+\mathscr{C}_{M(m)N(n)}$, abbreviated as $+\mathscr{C}$, increases the coordination number of elements M and N by 1, from m to $m + 1$ and n to $n + 1$; $-\mathscr{C}_{M(m)N(n)}$ decreases the coordination numbers by 1, from $m + 1$ to m and $n + 1$ to n; operators $+\mathscr{C}^{n\text{-center}}_{M(m)N(n)}$, abbreviated as $+\mathscr{C}^c$, and $-\mathscr{C}^{n\text{-center}}_{M(m)N(n)}$ define coordination changes which occur via cyclic n-center steps and these are particularly favoured for 3- to 6-center steps.

Each operation $\mathscr{C}$ generates a single step along a pathway P, and these multistep pathways are represented by a directed graph P(X,$\mathscr{C}$), in which the vertex set X consists of reactants, intermediates, and products, and the edge set $\mathscr{C}$ consists of the coordination number operators $+\mathscr{C}$, $-\mathscr{C}$, $+\mathscr{C}^c$, and $-\mathscr{C}^c$. Operators $+\mathscr{C}$ and $-\mathscr{C}$, representing intermolecular steps, are drawn above dashed lines, while $+\mathscr{C}^c$ and $-\mathscr{C}^c$, representing intramolecular steps, are drawn above solid lines; $\mathscr{C}$ is drawn below the lines for the reverse reaction. These pathways P(X,$\mathscr{C}$) may be labelled according to the number of vertices and steps ("edges") in the graph e.g. P(3,1) or P(4,2) or by the sequence of steps P{$\mathscr{C}_n$} in an n-step pathway. Such a graph (topological) description can serve as the basis of a unified analysis of stereochemical rearrangements, ligand exchange processes, and reaction mechanisms.

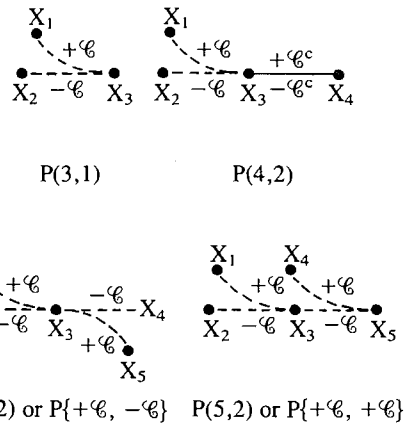
Table 2 illustrates the application of this model to phenyltellurium(VI) fluorides and a variety of other 4-, 5-, and 6-coordinate compounds. For the Ph_3TeF_2Cl–PF_5–Ph_3TeFCl^+–PF_6^- system we choose the minimum set of coordination numbers,

Te(5) Te(6)

P(5) P(6)

F(1) F(2)

and the coordination numbers of the other elements are specified in Table 2. Using only these coordination numbers it is possible to construct four pathways which can account for the exchange and chemical behaviour of all the examples listed in Table 2.



A rapid equilibrium between trigonal bipyramidal molecules X_1, donor solvents or bases X_2, and octahedral intermediates X_3, may be described by pathway P(3,1) which must, necessarily, be accompanied by axial–equatorial and apical–basal scrambling of ligands. If solvent interactions are indeed mechanistically significant, as suggested previously (7, 11) and confirmed by low temperature nmr identification of $SiF_5(base)^-$, $PF_5(base)$, $AsF_5(FCH_3)$, and numerous other donor adducts $MX_5(base)$, then pathway P(3,1) represents a lower energy pathway than alternative polytopal processes such as Berry pseudorotation or turnstile rotation (21).

All four pathways have P(3,1) as the first step. Adding a 5-center step gives pathway P(4,2) which is illustrated in Table 2 by the reaction of SiF_4 with 2,2′-bipyridine. Such a 5-center step is very common in inorganic systems ("chelate effect") or in phosphate hydrolysis ("five-membered ring effect") (22).

Fluorine transfer reactions of Si, Ge, P, As, or Te fluorides can be accommodated by pathway P(5,2) or P{+𝒞, −𝒞}, while racemization and base-catalyzed hydrolysis of R_3SiX appears to follow pathway P(5,2) or P{+𝒞, +𝒞}, as illustrated in Table 2.

In summary, the above analysis provides a unified description of the stereodynamics and chemical reactivity of tellurium(VI) fluorides, as well as numerous other 4-, 5-, and 6-coordinate compounds, all of which participate in rapid equilibria involving coordination changes of the metal and ligand.

[2]An earlier paper entitled "The coordination model and its application to reaction mechanisms, particularly hydrolysis of some P, Si, and C compounds" was presented at a departmental seminar, University of Manitoba, October 1, 1974.

Can. J. Chem. Downloaded from www.nrcresearchpress.com by 122.72.124.2 on 09/07/12
For personal use only.

Can. J. Chem. Downloaded from www.nrcresearchpress.com by 122.72.124.2 on 09/07/12
For personal use only.

TABLE 2. Stereochemical rearrangements, ligand exchange processes, and chemical reactions of some 4-, 5-, and 6-coordinate compounds*

Reactants		Coordination number operator	Intermediate or product				
X_1	X_2	$\mathscr{C}$	X_3	$\mathscr{C}$	X_4	X_5	Reference
Pathway P(3,1) or P{+$\mathscr{C}$}							
SiF_5^-	NH_3	$+\mathscr{C}_{Si(5)N(3)}$	$F_5Si—NH_3^-$				6
SiF_5^-	$NHEt_2$	$+\mathscr{C}_{Si(5)N(3)}$	$F_5Si—NHEt_2^-$				6
PF_5	OEt_2	$+\mathscr{C}_{P(5)O(2)}$	$F_5P—OEt_2$				7
SiF_5^-	SiF_5^-	$+\mathscr{C}_{Si(5)F(1)}$	$F_4SiF—SiF_5^{2-}$				6
AsF_5	CH_3F	$+\mathscr{C}_{As(5)F(1)}$	$F_5As—FCH_3$				12
AsF_5	PF_3	$+\mathscr{C}_{As(5)P(3)}$	$F_5As—PF_3$				23
Pathway P(4,2) or P{+$\mathscr{C}$, +$\mathscr{C}^c$}							
SiF_4	bpy	$+\mathscr{C}_{Si(4)N(2)}$	$F_4Si—bpy$	$+\mathscr{C}^{5\text{-center}}_{Si(5)N(2)}$	$F_4Si(bpy)$		24
Pathway P(5,2) or P{+$\mathscr{C}$, −$\mathscr{C}$}							
SiF_5^-	SiF_6^{2-}	$+\mathscr{C}_{Si(5)F(1)}$	$F_5Si—F—SiF_5^{3-}$	$-\mathscr{C}_{Si(5)F(1)}$	SiF_6^{2-}	SiF_5^-	6
PF_5	PF_6^-	$+\mathscr{C}_{P(5)F(1)}$	$F_5P—F—PF_5^-$	$-\mathscr{C}_{P(5)F(1)}$	PF_6^-	PF_5	25
AsF_5	AsF_6^-	$+\mathscr{C}_{As(5)F(1)}$	$F_5As—F—AsF_5^-$	$-\mathscr{C}_{As(5)F(1)}$	AsF_6^-	AsF_5	26
$PhPF_4$	$PhPF_5^-$	$+\mathscr{C}_{P(5)F(1)}$	$PhF_4P—F—PPhF_4^-$	$-\mathscr{C}_{P(5)F(1)}$	$PhPF_5^-$	$PhPF_4$	7, 27
Me_2PF_3	AsF_5	$+\mathscr{C}_{As(5)F(1)}$	$Me_2F_2P—F—AsF_5$	$-\mathscr{C}_{P(4)F(1)}$	$Me_2PF_2^+$	AsF_6^-	28
H_2PF_3	AsF_5	$+\mathscr{C}_{As(5)F(1)}$	$H_2F_2P—F—AsF_5$	$-\mathscr{C}_{P(4)F(1)}$	$H_2PF_2^+$	AsF_6^-	29
$MeSiF_3$	SiF_6^{2-}	$+\mathscr{C}_{Si(4)F(1)}$	$MeF_3Si—F—SiF_5^{2-}$	$-\mathscr{C}_{Si(5)F(1)}$	$MeSiF_4^-$	SiF_5^-	6
GeF_4	GeF_6^{2-}	$+\mathscr{C}_{Ge(4)F(1)}$	$F_4Ge—F—GeF_5^{2-}$	$-\mathscr{C}_{Ge(5)F(1)}$	GeF_5^-	GeF_5^-	30
Ph_3TeF_3	PF_5	$+\mathscr{C}_{P(5)F(1)}$	$Ph_3F_2Te—F—PF_5$	$-\mathscr{C}_{Te(5)F(1)}$	$Ph_3TeF_2^+$	PF_6^-	9
Ph_3TeF_2Cl	PF_5	$+\mathscr{C}_{P(5)F(1)}$	$Ph_3FClTe—F—PF_5$	$-\mathscr{C}_{Te(5)F(1)}$	Ph_3TeFCl^+	PF_6^-	This work
Ph_3TeF_3	$Ph_3TeF_2^+$	$+\mathscr{C}_{Te(5)F(1)}$	$Ph_3F_2Te—F—TeF_2Ph_3^+$	$-\mathscr{C}_{Te(5)F(1)}$	$Ph_3TeF_2^+$	Ph_3TeF_3	9
Ph_3TeF_2Cl	Ph_3TeFCl^+	$+\mathscr{C}_{Te(5)F(1)}$	$Ph_3FClTe—F—TeFClPh_3^+$	$-\mathscr{C}_{Te(5)F(1)}$	Ph_3TeFCl^+	Ph_3TeF_2Cl	This work
Ph_3TeF_2OH	Ph_3TeFOH^+	$+\mathscr{C}_{Te(5)F(1)}$	$Ph_3FOHTe—F—TeFOHPh_3^+$	$-\mathscr{C}_{Te(5)F(1)}$	Ph_3TeFOH^+	Ph_3TeF_2OH	10
Pathway P(5,2) or P{+$\mathscr{C}$, +$\mathscr{C}$}							
R_3SiCl	DMSO	$+\mathscr{C}_{Si(4)O(1)}$	$R_3SiCl—DMSO$	$+\mathscr{C}_{Si(5)O(1)}$	DMSO	$R_3SiCl(DMSO)_2$	13
Me_3SiF	$NHEt_2$	$+\mathscr{C}_{Si(4)N(3)}$	$Me_3SiF—NHEt_2$	$+\mathscr{C}_{Si(5)O(2)}$	H_2O	$Me_3SiF(NHEt_2)(H_2O)$	14

*Pathway P(X,$\mathscr{C}$) is defined in the text.

Can. J. Chem. Downloaded from www.nrcresearchpress.com by 122.72.124.2 on 09/07/12
For personal use only.

Experimental

^{19}F nmr spectra were recorded on a Bruker WH90 spectrometer at 84.66 MHz. The chemical shifts were measured relative to internal C_6F_6 (−162.9 ppm with respect to $CFCl_3$). ^{125}Te nmr spectra were recorded on a Bruker AM300 spectrometer at 94.76 MHz. The chemical shifts were measured relative to external Ph_2Te (692 ppm with respect to Me_2Te). XeF_2, PF_5, COF_2 (PCR/SCM Specialty Chemicals), and Ph_3TeCl (K & K Laboratories) were used as supplied. Tetraethylammonium chloride was dried over P_2O_5 in a vacuum desiccator. All gases were handled in a standard vacuum line and reactions were carried out in Teflon inserts in glass reaction vessels. All Teflon apparatus was dried at 110°C for several days.

Triphenyltellurium(IV) fluoride, Ph_3TeF, and mer-*Ph_3TeF_3 (1)*

Excess carbonyl fluoride was condensed into a Teflon tube containing triphenyltellurium chloride (0.073 g, 0.19 mmol) in CH_2Cl_2 (4 mL) at −196°C, in a method similar to that reported by Shreeve and Gupta (17). After 8 h at 22°C all volatile materials were removed under vacuum to give a white solid which was identified as Ph_3TeF (90%) by ^{19}F nmr.

Addition of XeF_2 to Ph_3TeF in a 1:1 molar ratio (9) gave *mer*-Ph_3TeF_3, **1** (95%), which was recrystallized from a mixture (2:7) of dichloromethane and hexane, washed twice with acetonitrile, and identified by ^{19}F and ^{125}Te nmr (Table 1).

Preparation of trans-*F_2TePh_3Cl, 3*

Addition of excess PF_5 into a Teflon tube at −196°C containing a purified sample of *mer*-Ph_3TeF_3, **1** (0.48 mmol), in CH_2Cl_2 (4 mL), and keeping the sample at 22°C for 30 min gave $Ph_3TeF_2^+PF_6^-$, **2**, in quantitative yield (9). Solid Et_4NCl (0.087 g, 0.52 mmol) was then added to a solution of **2** in CH_2Cl_2 with continuous shaking until a clear solution containing *trans*-F_2TePh_3Cl, **3**, was formed, as confirmed by ^{19}F and ^{125}Te nmr (Table 1). After 24 h in dichloromethane solution, 36% of *trans*-F_2TePh_3Cl, **3**, had rearranged to *cis*-F_2TePh_3Cl, **5**, as well as small amounts of *mer*-Ph_3TeF_3, **1**. After 6 days, 77% of *trans*-**3** had isomerized, and after one month all *trans*-**3** had disappeared and only *cis*-**5** and *mer*-**1** remained.

Preparation of cis-*F_2TePh_3Cl, 5*

Solid XeF_2 (0.029 g, 0.17 mmol) was added to triphenyltellurium(IV) chloride (0.067 g, 0.17 mmol) in CH_3CN (3 mL) in a Teflon bottle. The reaction mixture was stirred at 0°C for 8 h until a slightly yellow solution formed. The crude product contained *cis*-F_2TePh_3Cl, **5**, as well as *mer*-Ph_3TeF_3, **1**, in a 4:6 molar ratio. *mer*-**1** was removed by recrystallization from a mixture (2:7) of CH_2Cl_2 and hexane and washed with acetonitrile. *cis*-F_2TePh_3Cl, **5**, is soluble in CH_2Cl_2 and CH_3CN.

Preparation of $Ph_3TeFCl^+PF_6^-$, 4

Condensation of PF_5 into a solution of either *cis*- or *trans*-F_2TePh_3Cl (0.073 g, 0.17 mmol) in CH_2Cl_2 (4 mL) gave $Ph_3TeFCl^+PF_6^-$ **4** (95%), as confirmed by ^{19}F and ^{125}Te nmr (Table 1). A small amount of $Ph_3TeF_2^+PF_6^-$, **2**, was also formed due to the presence of *mer*-Ph_3TeF_3. The two cations **2** and **4** were stable in CH_2Cl_2 for at least 1 day and no intermolecular fluorine exchange was observed between cations **2** and **4**.

$Ph_3TeFCl^+PF_6^-$, 4, and cis-*F_2TePh_3Cl, 5*

The cation Ph_3TeFCl^+, **4**, was also characterized by its chemical reaction with NaF. An excess of NaF was added to a solution of cation Ph_3TeFCl^+, **4**, in CH_2Cl_2. After 1 day, excess NaF was filtered off and ^{19}F nmr of the solution showed the formation of *cis*-F_2TePh_3Cl, **5**.

Acknowledgements

The financial assistance of the Natural Sciences and Engineering Research Council of Canada is gratefully acknowledged. The purchase of the AM300 spectrometer was made possible by grants from NSERC and the Manitoba Health Research Council.

1. N. Serpone and D. G. Bickley. Prog. Inorg. Chem. **17**, 391 (1972); W. B. Farnham and J. F. Whitney. J. Am. Chem. Soc. **106**, 3992 (1984).
2. A. Werner. Ber. **45**, 3061 (1912).
3. W. R. Robinson, D. E. Wigley, and R. A. Walton. Inorg. Chem. **24**, 918 (1985); J. J. H. M. Font Freide and S. Trippett. J. Chem. Soc. Chem. Commun. 934 (1980).
4. E. L. Muetterties. Acc. Chem. Res. **3**, 266 (1970).
5. R. S. Michalak, S. R. Wilson, and J. C. Martin. J. Am. Chem. Soc. **106**, 7529 (1984).
6. R. K. Marat and A. F. Janzen. Can. J. Chem. **55**, 3845 (1977).
7. R. K. Marat and A. F. Janzen. Inorg. Chem. **19**, 798 (1980); J. A. Gibson, D. G. Ibbott, and A. F. Janzen. Can. J. Chem. **51**, 3203 (1973); C. Wang and A. F. Janzen. Can. J. Chem. **62**, 1563 (1984).
8. D. G. Ibbott and A. F. Janzen. Can. J. Chem. **50**, 2428 (1972).
9. A. S. Secco, K. Alam, B. J. Blackburn, and A. F. Janzen. Inorg. Chem. **25**, 2125 (1986).
10. A. F. Janzen, K. Alam, M. Jang, B. J. Blackburn, and A. S. Secco. Can. J. Chem. **66**, 1308 (1988).
11. H. Dreeskamp and K. Hildenbrand. Z. Naturforsch. **26**b, 269 (1971).
12. J.-Y. Calves and R. J. Gillespie. J. Am. Chem. Soc. **99**, 1788 (1977).
13. R. J. P. Corriu and M. Henner. J. Organomet. Chem. **74**, 1 (1974).
14. J. A. Gibson and A. F. Janzen. Can. J. Chem. **50**, 3087 (1972); R. E. Wasylishen, G. S. Birdi, and A. F. Janzen. Inorg. Chem. **15**, 3054 (1976).
15. R. Schmutzler. *In* Halogen chemistry. Vol. 2. *Edited by* V. Gutmann. Academic Press, London. 1967. p. 31; D. Hellwinkel. *In* Organic phosphorus compounds. Vol. 3. *Edited by* G. M. Kosolapoff and L. Maier. Wiley-Interscience, New York. 1972. Chapt. 5B; S. N. Tandura, M. G. Voronkov, and N. V. Alekseev. Top. Curr. Chem. **131**, 99 (1986).
16. K. Alam and A. F. Janzen. J. Fluor. Chem. **27**, 467 (1985).
17. O. D. Gupta and J. M. Shreeve. J. Chem. Soc. Chem. Commun. 416 (1984).
18. R. S. Michalak and J. C. Martin. J. Am. Chem. Soc. **104**, 1683 (1982).
19. J. A. Gibson and A. F. Janzen. Can. J. Chem. **49**, 2168 (1971).
20. A. F. Janzen. Abstracts of 70th Canadian Chemical Conference and Exhibition, Quebec, Canada, June 7–11, 1987.
21. R. Luckenbach. Dynamic stereochemistry of pentacoordinated phosphorus and related elements. Georg Thieme, Stuttgart, 1973; R. R. Holmes. Pentacoordinated phosphorus. ACS monograph 176. Washington, D.C. 1980, and references therein.
22. A. F. Janzen, A. E. Lemire, R. K. Marat, and A. Queen. Can. J. Chem. **61**, 2264 (1983).
23. G. S. H. Chen and J. Passmore. J. Chem. Soc. Dalton, 1251 (1979).
24. A. D. Adley, P. H. Bird, A. R. Fraser, and M. Onyszchuk. Inorg. Chem. **11**, 1402 (1972).
25. S. Brownstein and J. Bornais. Can. J. Chem. **46**, 225 (1968).
26. P. A. W. Dean, R. J. Gillespie, R. Hulme, and D. A. Humphreys. J. Chem. Soc. A, 341 (1971).
27. R. Appel, I. Ruppert, and F. Knoll. Chem. Ber. **105**, 2492 (1972).
28. M. Brownstein and R. Schmutzler. J. Chem. Soc. Chem. Commun. 278 (1975).
29. H. W. Roesky, K.-L. Weber, and J. Schimkowiak. Angew. Chem. Int. Ed. **20**, 973 (1981).
30. K. O. Christe, C. J. Schack, and R. D. Wilson. Inorg. Chem. **15**, 1275 (1976).

Stability relationships between solid cesium aluminosilicates in aqueous solutions at 200°C[1]

PETER TAYLOR,[2] SHEILA D. DEVAAL, and DERREK G. OWEN
Research Chemistry Branch, Atomic Energy of Canada Limited, Whiteshell Nuclear Research Establishment, Pinawa, Man., Canada R0E 1L0
Received April 20, 1988

PETER TAYLOR, SHEILA D. DEVAAL, and DERREK G. OWEN. Can. J. Chem. **67**, 76 (1989).

Interconversion reactions among the solids SiO_2 (quartz and fused), γ-AlOOH (boehmite), $CsAlSiO_4$, $CsAlSi_2O_6$ (pollucite), and $CsAlSi_5O_{12}$, in contact with aqueous solutions at 200°C, have been investigated. Results support earlier suggestions that $CsAlSi_5O_{12}$ is not stable with respect to $CsAlSi_2O_6 + SiO_2$. $CsAlSiO_4$ is only stable, if at all, when the activity product of dissolved Cs^+ and OH^-, with respect to unit molality standard states, exceeds about 10^{-2}. $CsAlSi_2O_6$ is stable with respect to boehmite and quartz when the cesium hydroxide activity product exceeds $10^{-7.8\pm1.5}$. The significance of these results to the possible immobilization of radioactive cesium as a solid aluminosilicate is discussed. Based on a comparison with published estimates of enthalpies of formation, the following revised values are suggested:

$$\Delta_f H^0(CsAlSi_2O_6, s, 298\ K) = -3070 \pm 20\ kJ\ mol^{-1}$$

$$\Delta_f H^0(CsAlSiO_4, s, 298\ K) = -2133 \pm 20\ kJ\ mol^{-1}$$

Key words: cesium aluminosilicates, enthalpy of formation, hydrothermal reactions, pollucite, thermodynamic stability.

PETER TAYLOR, SHEILA D. DEVAAL et DERREK G. OWEN. Can. J. Chem. **67**, 76 (1989).

On a étudié les réactions d'interconversion entre les SiO_2 (quartz et quartz fondu), γ-AlOOH (boehmite), $CsAlSiO_4$, $CsAlSi_2O_6$ (pollucite) et $CsAlSi_5O_{12}$ solides, en contact avec des solutions aqueuses, à 200°C. Les résultats obtenus supportent les suggestions faites antérieurement à l'effet que le $CsAlSi_5O_{12}$ n'est pas stable par rapport au système $CsAlSi_2O_6 + SiO_2$. Le $CsAlSiO_4$ n'est stable, s'il l'est, que lorsque, par rapport à des états standard d'unité molaire, le produit d'activité des ions Cs^+ et OH^- dissous est supérieur à 10^{-2}. Lorsque le produit d'activité de l'hydroxyde de césium est supérieur à $10^{-7.8\pm1.5}$, le $CsAlSi_2O_6$ est stable par rapport à la boehmite et au quartz. On discute de l'importance de ces résultats sur la possibilité d'immobiliser du césium radioactif sous la forme d'aluminosilicate solide. En se bazant sur une comparaison d'évaluations publiées pour les enthalpies de formation, on suggère les valeurs révisées suivantes:

$$\Delta_f H^0(CsAlSi_2O_6, s, 298\ K) = -3070 \pm 20\ kJ\ mol^{-1}$$

$$\Delta_f H^0(CsAlSiO_4, s, 298\ K) = -2133 \pm 20\ kJ\ mol^{-1}$$

Mots clés : aluminosilicates de cesium, enthalpie de formation, réactions hydrothermales, pollucite, stabilité thermodynamique.

[Traduit par la revue]

1. Introduction

Solid cesium aluminosilicates, especially pollucite, have attracted attention as possible host phases for the immobilization of radioactive cesium (1–19), and as possible alteration products arising from the interaction of cesium-containing waste, groundwater, and aluminosilicate minerals (20–29). Synthetic pollucite has a composition close to the stoichiometric formula $CsAlSi_2O_6$, but in nature, it invariably occurs in solid solution with analcime, $NaAlSi_2O_6 \cdot H_2O$ (9–11). It is the only mineral containing cesium as a principal component. According to Cerny (10, 11), typical natural pollucites contain between 68 and 82 mol% $CsAlSi_2O_6$. There is some systematic deviation from the ideal solid-solution stoichiometry (10), so that the compositions of natural pollucites are close to the general formula, $(Cs_xNa_y)(Al_{x+y}Si_{3-x-y})O_6 \cdot (1-x)H_2O$, where $x + y \simeq 0.90$, and $y \simeq 0.15$. As well as $CsAlSi_2O_6$, two other synthetic cesium aluminosilicates, $CsAlSiO_4$ and $CsAlSi_5O_{12}$, have been investigated as possible waste forms for radioactive cesium (6, 7, 12–15).

The preparation of these three cesium aluminosilicates, by high-temperature dry syntheses from a variety of cesium salts and aluminosilicate precursors, has been investigated by several groups (1, 6, 7, 9, 14–17). Leaching and hydrothermal alteration of these materials have also been reported in some detail (7, 8, 11, 12, 14, 15, 18, 19). In addition, pollucite has been observed as a product of hydrothermal reactions between cesium-containing solutions and a variety of natural and synthetic aluminosilicate materials (12, 20–29). In contrast, there are few reports of $CsAlSiO_4$, and none of $CsAlSi_5O_{12}$, being produced hydrothermally (6, 22, 23). Some cesium-containing zeolites have also been prepared by hydrothermal reactions (21, 24, 30, 31).

Leaching and alteration studies indicate that $CsAlSiO_4$ is the least stable of the three cesium aluminosilicates in aqueous solutions at 100–300°C (12). Komarneni and Roy (14) concluded that $CsAlSi_2O_6$ is the best of these three candidates for Cs-137 immobilization. They presented indirect evidence that $CsAlSi_5O_{12}$ is not stable with respect to pollucite and quartz:

[1] $$CsAlSi_5O_{12}(s) \rightarrow CsAlSi_2O_6(s) + 3SiO_2(s)$$

Nonetheless, $CsAlSi_5O_{12}$ is more resistant than $CsAlSi_2O_6$ to acid leaching because of its higher Si/Al ratio (7, 14, 15).

Although the preparation and hydrothermal reactions of the cesium aluminosilicates have thus been studied quite extensively, there is little information on equilibrium phase relationships involving these solids. The only thermodynamic data for their formation appear to be some estimates by Lindemer *et al.* (32) and Grossman (33), the latter work being restricted to high temperatures (800–2000 K). Therefore, we have tried to obtain some experimental information on phase equilibria in the aqueous cesium aluminosilicate system.

2. Experimental procedure

The following reagent-grade starting materials were used: CsOH, Cs_2CO_3, Cs_2SO_4, $Al(NO_3)_3 \cdot 9H_2O$, SiO_2 (crystalline quartz and fused

[1]AECL No. 9664.
[2]Author to whom correspondence should be addressed.

Can. J. Chem. Downloaded from www.nrcresearchpress.com by 122.72.124.2 on 09/07/12
For personal use only.

Can. J. Chem. Downloaded from www.nrcresearchpress.com by 122.72.124.2 on 09/07/12
For personal use only.

silica powders, and 30 wt% colloidal aqueous suspension), and H_3PO_4. Solutions were prepared with freshly deionized, distilled water. Solids were identified by X-ray powder diffraction (XRD), sometimes supplemented by Fourier-transform infrared spectroscopy (FTIR).

Boehmite, γ-AlOOH, was chosen as a source of aluminum in these experiments because it was easily prepared as a pure phase, and it was sufficiently reactive to form pollucite under our experimental conditions, but was not converted to other aluminum oxyhydroxides or aluminosilicates other than pollucite. To prepare boehmite, we first converted aluminum nitrate to Al_2O_3, using a Bunsen burner until visible evolution of NO_2 ceased, then heating to 600°C in an electric furnace to complete decomposition. The resulting alumina powder was converted to boehmite by heating in stirred water in a Teflon-lined stainless steel autoclave at 200°C for 2 days. Its identity was confirmed by XRD and FTIR (34–36).

To prepare cesium aluminosilicates in 5–10 g quantities, we first made precursor powders, $Al_2O_3 \cdot zSiO_2$, with the appropriate value of z, by dehydration and thermal decomposition of solutions containing aluminum nitrate and colloidal silica. In this way, the Al and Si were sufficiently well mixed that phase-pure cesium aluminosilicates could be obtained, with the exception of $CsAlSi_5O_{12}$ (see below). $CsAlSiO_4$ was made by firing an $Al_2O_3 \cdot 2SiO_2$ powder with a 50% excess of Cs_2CO_3 over that required for reaction [2], for 0.5 h at 1000°C, then for 1 h at 1200°C:

[2] $Cs_2CO_3(s) + Al_2O_3(s) + 2SiO_2(s) \rightarrow 2CsAlSiO_4(s) + CO_2(g)$

The excess Cs_2CO_3 was necessary to sustain a high Cs_2O activity during crystallization, and thus prevent the formation of $CsAlSi_2O_6$ as a by-product from the competing reaction [3]; this excess sublimed from the sample during firing.

[3] $Cs_2CO_3(s) + Al_2O_3(s) + 4SiO_2(s) \rightarrow 2CsAlSi_2O_6(s) + CO_2(g)$

The XRD pattern of the product was in good agreement with data reported by Gallagher *et al.* (6).

Gallagher and McCarthy (9) reported difficulty in preparing phase-pure $CsAlSi_2O_6$ by high-temperature dry synthesis. We found that it was more conveniently prepared by hydrothermal reaction of an $Al_2O_3 \cdot 4SiO_2$ powder with a small excess of CsOH or Cs_2CO_3 over that required for reaction [4]:

[4] $2Cs^+(aq) + 2OH^-(aq) + Al_2O_3(s) + 4SiO_2(s) \rightarrow 2CsAlSi_2O_6(s) + H_2O(1)$

The XRD pattern of the product, formed during 2 days in an autoclave at 200°C, agreed well with published data (9).

$CsAlSi_5O_{12}$ is the most difficult of these three compounds to prepare in a pure state (7, 14, 15), and we never obtained it completely free of $CsAlSi_2O_6$ or other aluminosilicate impurities. It was obtained as the major product, with $CsAlSi_2O_6$ impurity, when an $Al_2O_3 \cdot 10SiO_2$ powder was fired at 1200°C for 16 h with the appropriate quantity of Cs_2CO_3 for reaction [5]:

[5] $Cs_2CO_3(s) + Al_2O_3(s) + 10SiO_2(s) \rightarrow 2CsAlSi_5O_{12}(s) + CO_2(g)$

The major features in the XRD pattern were in good agreement with ref. 34.

Two types of autoclave were used in experiments to determine stability limits of these cesium aluminosilicates. All of the experiments with $CsAlSiO_4$ and $CsAlSi_5O_{12}$, and some with $CsAlSi_2O_6$, were run with individually heated, 0.5-L capacity, stirred, Teflon-lined stainless-steel vessels, containing 175 mL of solution when loaded at room temperature. The remaining experiments with $CsAlSi_2O_6$ were run with 10 mL of solution in 20-mL capacity unstirred vessels, also constructed of stainless steel with Teflon liners, heated in an oven. All autoclave experiments were carried out at 200°C; this temperature was chosen because it was the lowest at which formation or depletion of the solids could be detected on a convenient time scale. Usually 2 to 4 days were sufficient to determine the direction of reaction. Longer runs (up to 26 days) were required for some more sluggish reactions and a few equilibration experiments. In selected experiments, dissolved cesium analyses were performed on both starting and final solutions, by atomic absorption spectrophotometry. Measurements of pH in cooled solutions were calibrated against standard buffer solutions at ambient temperatures.

3. Experimental strategy

We have tried to avoid some of the complexities of this multicomponent system by attempting to measure equilibria involving two or three solids, chosen to reduce the number of degrees of freedom of the equilibrium solution composition. The conceptual equilibria we have considered are shown in eqs. [6] to [11]; {X} represents the product of the activity coefficient and the molal concentration of species X in aqueous solution.

[6] $2CsAlSiO_4(s) + H_2O(l) \rightleftharpoons Cs^+(aq) + OH^-(aq) + CsAlSi_2O_6(s) + AlOOH(s)$
$k_6 = \{Cs^+\}\{OH^-\}$

[7] $CsAlSiO_4(s) + H_2O(l) \rightleftharpoons Cs^+(aq) + OH^-(aq) + AlOOH(s) + SiO_2(s)$
$k_7 = \{Cs^+\}\{OH^-\}$

[8] $CsAlSi_2O_6(s) + 2H_2O(l) \rightleftharpoons CsAlSiO_4(s) + H_4SiO_4(aq)$
$k_8 = \{H_4SiO_4\}$

[9] $CsAlSi_2O_6(s) + H_2O(l) \rightleftharpoons Cs^+(aq) + OH^-(aq) + AlOOH(s) + 2SiO_2(s)$
$k_9 = \{Cs^+\}\{OH^-\}$

[10] $(1/3)CsAlSi_5O_{12}(s) + 2H_2O(l) \rightleftharpoons (1/3)CsAlSi_2O_6(s) + H_4SiO_4(aq)$
$k_{10} = \{H_4SiO_4\}$

[11] $CsAlSi_5O_{12}(s) + H_2O(l) \rightleftharpoons Cs^+(aq) + OH^-(aq) + AlOOH(s) + 5SiO_2(s)$
$k_{11} = \{Cs^+\}\{OH^-\}$

According to the phase rule, not all of these equations can represent stable equilibria. For example, only one of the three cesium aluminosilicates can coexist with a solution saturated with quartz and boehmite, so two out of equilibria [7], [9], and [11] must be metastable with respect to the third, whichever has the lowest equilibrium ionic product, $\{Cs^+\}\{OH^-\}$. Furthermore, available Gibbs energy data for aluminosilicates (37) indicate that even this would be a metastable equilibrium with respect to kaolinite $(Al_2Si_2O_5)OH)_4)$, or some other clay mineral, although no such products were detected with XRD in these experiments. We therefore believe that the following is a valid account of stability relationships at 200°C between the three cesium aluminosilicates, boehmite, and silica.

4. Results and discussion

4.1 Experiments involving $CsAlSiO_4$

There are few reports of the formation of $CsAlSiO_4$ is hydrothermal reactions, all of them involving concentrated CsOH solutions (6, 22, 23). In dilute solutions, $CsAlSiO_4$ is rather easily altered to $CsAlSi_2O_6$ (12). Therefore, it appeared likely that K_6 and K_7 would be relatively high and K_8 low. The constants K_6 and K_8 both define the relative stability of $CsAlSiO_4$ and $CsAlSi_2O_6$. Given the difficulty of controlling and measuring low dissolved silica activities, we attempted to measure K_6 rather than K_8. Using experimental values for K_6 and K_9, we could then calculate K_7 and K_8 (see Section 5, below).

In preliminary experiments with $CsAlSiO_4$ alone, 1.0 g samples were extensively converted to $CsAlSi_2O_6$ when contacted with water, 0.01 mol kg^{-1} Cs_2CO_3, or 0.01 mol kg^{-1}

CsOH, for 2 days at 200°C. Boehmite was also formed in the reaction with water, but was not detected in the products from the more alkaline solutions, in which Al is more soluble.

When a mixture of $CsAlSiO_4$, $CsAlSi_2O_6$, and γ-AlOOH (0.5 g each) was contacted with 0.01 mol kg^{-1} CsOH for 2 days at 200°C, the $CsAlSiO_4$ was almost entirely consumed. The final pH, measured at rom temperature, was still close to 12, and the analysed cesium concentration was 0.013 mol kg^{-1}. We can thus set a lower limit for K_6 of 10^{-4} mol^2 kg^{-2}. In similar experiments with higher CsOH concentrations (0.1 or 0.3 mol kg^{-1}), both the $CsAlSiO_4$ and $CsAlSi_2O_6$ persisted, in approximately equal amounts, but the AlOOH was dissolved completely. Since the solution was thus undersaturated with respect to AlOOH, equilibrium [6] no longer holds for interpreting these runs.

When either $CsAlSiO_4$ or $CsAlSi_2O_6$ was contacted with 0.1 or 0.3 mol kg^{-1} CsOH, together with AlOOH, each cesium aluminosilicate persisted unchanged, even after 7 days at 200°C, suggesting that the solutions in each case were not far from equilibrium, i.e., $K_6 \simeq 10^{-2}$ mol^2 kg^{-2}. We were unable, however, to determine equilibrium [6] reversibly, i.e., we never observed the hydrothermal formation of $CsAlSiO_4$, even at high CsOH concentrations, so this conclusion is tentative. We did not go to CsOH concentrations above 0.3 mol kg^{-1}, because the extremely high solubility of boehmite under such conditions make K_6 inaccessible. We therefore estimate that $\log_{10} K_6 = -2 \pm 2$.

4.2. Experiments involving $CsAlSi_5O_{12}$

If, as Komarneni and Roy have suggested, $CsAlSi_5O_{12}$ is not stable with respect to pollucite and quartz (reaction [1]), then K_{10} must exceed the solubility of quartz (14). We have attempted to verify this, by examining conditions under which $CsAlSi_5O_{12}$ is converted to $CsAlSi_2O_6$, and by trying to prepare $CsAlSi_5O_{12}$ hydrothermally.

When 0.5 g each of $CsAlSi_2O_6$ and silica (either crystalline quartz or fused SiO_2) were contacted with 175 g of water at 200°C for 2 days, or with 10^{-3} mol kg^{-1} CsOH for 7 days, no $CsAlSi_5O_{12}$ could be detected in the products. Reaction of an $Al_2O_3 \cdot 10SiO_2$ powder with either CsOH or Cs_2CO_3 solutions also failed to produce $CsAlSi_5O_{12}$; $CsAlSi_2O_6$ and γ-AlOOH were the only detectable crystalline products.

When $CsAlSi_5O_{12}$ (1.0 g), containing $CsAlSi_2O_6$ impurity, was contacted with 175 g of water at 200°C for 3 days, XRD revealed an increase in the relative intensities of $CsAlSi_2O_6$ diffraction peaks. This occurred even when quartz saturation was assured by adding 4×10^{-3} mol kg^{-1} of colloidal silica; the result was reproduced in a duplicate experiment. These results support the conclusion in ref. 14 that $CsAlSi_5O_{12}$ is unstable with respect to reaction [1] at 200°C, although the reaction is slow, with only about 10% conversion of powdered starting material in 3 days. In another experiment, the $CsAlSi_5O_{12}$ was completely consumed, and $CsAlSi_2O_6$ was the sole crystalline product, after contacting with 0.1 mol kg^{-1} CsOH for 2 days at 200°C, but in this case, the solution was not presaturated with silica.

Given that $CsAlSi_5O_{12}$ is unstable with respect to reaction [1], it follows that K_{11} must be greater than K_9, even though $CsAlSi_2O_6$ is the more cesium-rich phase.

4.3. Experiments on the stability limits of $CsAlSi_2O_6$

The preceding sections describe stability relationships of $CsAlSi_2O_6$ with $CsAlSiO_4$ and $CsAlSi_5O_{12}$. To complete this survey of the stability of $CsAlSi_2O_6$ in the system Cs_2O–Al_2O_3–SiO_2–H_2O–[pH] at 200°C, we have investigated equilibrium [9]. This sets a lower limit to the range of cesium hydroxide activity products over which pollucite can occur.

TABLE 1. Cesium analyses and room-temperature pH of solutions after contact with quartz + boehmite + pollucite powders at 200°C

Starting solution	Time (days)	Final pH (room temperature)	Final [Cs] (mmol kg^{-1})
H_2O	2	7.5	0.29[a]
H_2O	7	6.8	0.33[a]
H_2O	26	6.5	0.28[b]
3×10^{-4} mol kg^{-1} CsOH	7	7.2	0.36[a]
10^{-3} mol kg^{-1} CsOH	7	7.9	0.46[a]
10^{-3} mol kg^{-1} CsOH	10	8.0	0.26[a]
5×10^{-4} mol kg^{-1} $Cs_2B_4O_7$ (CsOH + H_3BO_3)	10	7.5	0.25[a]
5×10^{-4} mol kg^{-1} Cs_2CO_3	26	6.6	0.28[b]
5×10^{-4} mol kg^{-1} Cs_2SO_4	15	5.9	1.05[a]
5×10^{-4} mol kg^{-1} Cs_2SO_4	26	6.1	0.99[b]
5×10^{-4} mol kg^{-1} Cs_2SO_4 + 10^{-3} mol kg^{-1} H_2SO_4	15	6.6	1.66[a]

[a] ±10%
[b] ±5%

We first determined conditions under which $CsAlSi_2O_6$ can be formed hydrothermally from γ-AlOOH and SiO_2 powders and Cs-containing solutions. It was produced when these powders were contacted with solutions of CsOH down to 10^{-3} mol kg^{-1}, and Cs_2CO_3 down to 5×10^{-4} mol kg^{-1}, for 2 days at 200°C. At cesium concentrations of 10^{-4} mol kg^{-1} or less, insufficient cesium would be present to form enough $CsAlSi_2O_6$ to detect by XRD. We can thus estimate an upper limit of 5×10^{-7} mol^2 kg^{-2} for K_9 at 200°C (dilute solutions of CO_3^{2-} are almost completely hydrolyzed to $HCO_3^- + OH^-$ at this temperature (38)), i.e., $\log_{10} K_9 \leq -6.3$. For reasons given below, we cannot use the final pH of these runs to define an upper limit of K_9.

To define K_9 more narrowly, we investigated the equilibration of mixtures of SiO_2, γ-AlOOH, and $CsAlSi_2O_6$ with aqueous solutions having different initial cesium activities and pH. Resulting pH (measured at ambient temperature, ~22°C) and cesium concentrations from eleven such experiments are presented in Table 1.

For experiments starting with alkaline cesium solutions or pure water, results are clustered around pH 6.5–8.0, with cesium concentrations in the range 0.25–0.46 mmol kg^{-1}. Since initial conditions in these runs were above and below the equilibrium activity product, K_9 (cesium solutions and pure water, respectively), the convergence of composition to these narrow ranges of pH and [Cs] suggests approach to equilibrium. We cannot rule out overshooting or undershooting, however, which could arise from slow dissolution of one or more of the solids. The increase in both pH and [Cs] in the run with acidified Cs_2SO_4 is also consistent with the equilibrium pH being close to neutral at cesium concentrations near 10^{-3} mol kg^{-1}.

If the mass balance, as well as the equilibrium solution compositions, was determined by eq. [9], then changes in $[Cs^+]$ and $[OH^-]$ in the course of reaction should be equal. This was not the case; final $[Cs^+]$ values always exceeded $[OH^-]$, even when initial values were equal. Consumption of OH^- to form hydrolyzed species such as $Al(OH)_4^-$ and $OSi(OH)_3^-$ could not completely account for this discrepancy (39, 40); rather,

Can. J. Chem. Downloaded from www.nrcresearchpress.com by 122.72.124.2 on 09/07/12
For personal use only.

Can. J. Chem. Downloaded from www.nrcresearchpress.com by 122.72.124.2 on 09/07/12
For personal use only.

reaction of dilute hydroxide solutions with the Teflon liners of the autoclave appears to be at least partly responsible.

In our experience, it is difficult to control pH in the slightly alkaline region (10^{-4} mol kg^{-1} OH^- or less) in Teflon-lined vessels at or above 200°C, apparently because of reaction with the Teflon itself. Such control of pH is necessary for an accurate determination of K_9. In blank experiments with 10^{-4} or 10^{-3} mol dm^{-3} NaOH, and no solid reagents, pH fell towards neutral, and solution analyses revealed fluoride concentrations up to 10^{-5} mol dm^{-3} after 6–10 days at 200°C. This confirms the occurrence of some reaction with the Teflon, although mass balance considerations show that simple hydrolysis does not account entirely for the pH change. Other, more complex possibilities include the presence of perfluorocarboxylic acid groups in the Teflon, or the solution, or both. Since the Teflon liner was an integral part of the seal in the small pressure vessels, we did not have a convenient method to duplicate experiments in the absence of Teflon. These vessels also had a rather high ratio of Teflon surface area to solution volume ($\sim 2\ cm^{-1}$), which likely compounded the problem.

Experiments to control the pH with phosphate-buffered solutions were inconclusive, probably because of reaction between the boehmite and phosphate. Borax (41) and bicarbonate/carbonate (38) buffers are too alkaline for our purposes at 200°C. We can only conclude, therefore, that the combination of neutral pH and a cesium concentration of 3×10^{-4} mol kg^{-1} represents a lower limit for K_9 at 200°C. The value of pK_w at 200°C is 11.30 (42), whence neutral pOH = pH = 5.65, and $\log_{10} K_9 \leq 9.2$. Combining this with the upper limit of −6.3, determined above, we estimate that $\log_{10} K_9 = -7.8 \pm 1.5$ at 200°C. This uncertainty represents the span of the upper and lower limits; for calculation purposes, it is treated below as a 95% confidence limit.

Since the assemblage quartz + boehmite + water is not thermodynamically stable with respect to kaolinite formation, the limiting ionic products for coexisting pollucite + quartz + kaolinite, or pollucite + boehmite + kaolinite (eqs. [12] and [13]) will be somewhat higher than K_9.

[12] $CsAlSi_2O_6(s) + (3/2)H_2O(l) \rightleftharpoons (1/2)Al_2Si_2O_5(OH)_4(s) + SiO_2(s) + Cs^+(aq) + OH^-(aq)$ Kaolinite

$k_{12} = \{Cs^+\}\{OH^-\}$

[13] $CsAlSi_2O_6(s) + AlOOH(s) + 2H_2O(l) \rightleftharpoons Al_2Si_2O_5(OH)_4(s) + Cs^+(aq) + OH^-(aq)$

$k_{13} = \{Cs^+\}\{OH^-\}$

Also, K_9 for well-crystallized quartz and boehmite is likely to be somewhat higher than our experimental value. Our boehmite showed some XRD line-broadening typical of material prepared at 200°C (35), and we made no attempt to remove the amorphous-silica-like layer that is believed to exist on powdered quartz (43, 44).

In more complex solutions, such as groundwaters, which contain other silicate-forming cations (especially Ca^{2+} and Mg^{2+}), the stability field of pollucite will be encroached upon, or even obliterated, by those of other solids (12, 14).

5. Calculated equilibria

Having obtained values for the equilibrium constants K_6 and K_9, we can derive K_7 and K_8. Simple algebraic operations on equilibria [6] and [9] yield relationships [14] to [16].

[14] $[7] = \{[6] + [9]\}/2$

whence

$$\log_{10} K_7 = 0.5\,(\log_{10} K_6 + \log_{10} K_9) = -4.9 \pm 1.8 \text{ at } 200°C$$

[15] $[16] = \{[6] + [9]\}/2$

[16] $CsAlSiO_4(s) + SiO_2(s) \rightleftharpoons CsAlSi_2O_6(s)$

The equilibrium constant K_{16} can be expressed as a silica activity ($a(SiO_2)$) with reference to a quartz standard state:

$$\log_{10} K_{16} = 0.5\,(\log_{10} K_6 - \log_{10} K_9) = -2.9 \pm 1.8 \text{ at } 200°C$$

Rimstidt and Barnes (44) reported relationships between the silica-water equilibrium constant, K_{17}, and absolute temperature.

[17] $SiO_2(s) + 2H_2O(l) \rightleftharpoons H_4SiO_4(aq)$

$$K_{17} = \log \{H_4SiO_4\} = \text{(for quartz) } 1.881 - 2.028 \times 10^{-3}T - 1560/T = -2.38 \text{ at } 200°C$$

whence

$$\log_{10} K_8 = \log_{10} K_{16} + \log_{10} K_{17} = -5.3 \pm 1.8$$

6. Comparisons with estimated thermodynamic values

It is desirable to compare our results with the thermodynamic quantities estimated by Lindemer *et al.* (32) for the solid cesium aluminosilicates. These quantities are shown in Table 2, together with ancillary data from other sources. The estimated uncertainties in the enthalpies of formation of $CsAlSiO_4$ and $CsAlSi_2O_6$ in ref. 32 are 10–20 kJ mol^{-1}.

Similar uncertainties in Gibbs energies of reaction arise from the 200°C equilibrium constants. These uncertainties dominate in the following calculations, and limit the extent to which comparison is possible.

Comparisons are most straightforward with the all-solid reactions, [16] and [18].

[16] $CsAlSiO_4(s) + SiO_2(s) \rightleftharpoons CsAlSi_2O_6(s)$

[18] $(1/3)CsAlSi_2O_6(s) + SiO_2(s) \rightleftharpoons (1/3)CsAlSi_5O_{12}(s)$

Although literature values vary considerably, reactions of this general type [19] most commonly have small positive entropies (based on data in refs. 37, 45, and 46).

[19] $A(s) + SiO_2(s) \rightleftharpoons B(s)$

where A and B are both aluminosilicates.

The literature data in Table 2 give $\Delta_r G^0 = -11$ kJ mol^{-1} for reaction [16] at 25°C. From $\log K_{16} = -2.9 \pm 1.8$ (see above) we obtain $\Delta_r G^0 = -26 \pm 16$ kJ mol^{-1} at 200°C. Since $\Delta_r S^0$ and, presumably, $\Delta_r C_p^0$ for reaction [16] are small, $\Delta_r G^0$ varies only slightly with temperature (~0.6 kJ mol^{-1} difference between 25 and 200°C, according to entropy values in Table 2; up to about 3 kJ mol^{-1} can be reasonably expected based on the preceding paragraph). There is thus a strong indication that the data from ref. 32 underestimate the stability of $CsAlSi_2O_6$ relative to $CsAlSiO_4$ in reaction [16]. In other words, if the data in ref. 32 were exactly correct, then K_6 and K_9 would lie near the upper and lower limits, respectively, of our experimental estimates. Such a narrow stability range seems unlikely, given the widespread occurrence of $CsAlSi_2O_6$, and the rarity of $CsAlSiO_4$, as hydrothermal reaction products.

The published Gibbs energy data in Table 2 give $\Delta_r G^0 = -30$ kJ mol^{-1} for reaction [18] at 25°C, whereas our results set a lower limit of zero at 200°C. As with reaction [16], the Gibbs

TABLE 2. Thermodynamic quantities for solid cesium aluminosilicates, and ancillary data, $T = 25°C$, $P = 0.1$ MPa

Species	$\Delta_f H^0$ kJ mol^{-1}	S^0 J mol^{-1} K^{-1}	$\Delta_f G^0$ kJ mol^{-1}	Reference
$CsAlSiO_4$(s)	−2121	159.4	−2007[a]	32
	−2133	—	−2019	This work
$CsAlSi_2O_6$(s)	−3045	197.9	−2875[a]	32
	−3070	—	−2900	This work
$CsAlSi_5O_{12}$(s)	−5805	330.8[b]	−5475	32
Cs(s)	0	85.23	0	45
Al(s)	0	28.33	0	45
Si(s)	0	18.83	0	45
O_2(g)	0	205.14	0	45
α-Al_2O_3(s)	−1675.7	50.92	−1582.3	45
γ-AlOOH(s)	−990.35	48.43	−915.85	45
SiO_2(s, quartz)	−910.94	41.84	−856.64	45
H_2O(l)	−285.83	69.91	−237.13	45
Cs^+(aq)	−258.28	133.05	−292.02	45
OH^-(aq)	−229.99	−10.75	−157.24	45
H^+(aq)	0	0	0	45
H_4SiO_4(aq)	−1460.0	180.0	−1308.0	37[c]

[a]Calculated from enthalpy and entropy data within this table.
[b]T. B. Lindemer (personal communication). There is a typographical error in the value given in ref. 32.
[c]Data for H_4SiO_4 in ref. 45 are inconsistent with quartz solubility, as discussed by Sadiq and Lindsay (47).

energy of this reaction is not expected to be so temperature-sensitive. Therefore, we would not expect $\Delta_r G^0$ to be less than about −5 kJ mol^{-1} at 25°C. The thermodynamic data for SiO_2 are well established, and the entropy of reaction [18] is small; therefore, it appears that the enthalpy difference between $CsAlSi_2O_6$ and $CsAlSi_5O_{12}$ is overestimated in ref. 32.

Finally, we compare our experimental values of K_6 and K_9 at 200°C with calculated 25°C values. For this purpose, it is useful to express reactions [16] and [9] in the alternative forms [20] and [21], respectively, since the heat capacities of reactants and products should then be more closely matched.

[20] $2CsAlSiO_4(s) + H^+(aq) \rightleftharpoons Cs^+(aq) + CsAlSi_2O_6(s) + AlOOH(s)$

$K_{20} = \{Cs^+\}/\{H^+\}$

$\log_{10} K_{20} = \log_{10} K_6 + pK_w = 9.3 \pm 2$ at 200°C

whence

$\Delta_r G^0 = -84 \pm 18$ kJ mol^{-1} at 200°C

$\Delta_r S^0 = +60.6$ J mol^{-1} K^{-1} at 25°C (from Table 2)

whence

$\Delta_r G^0 = -73 \pm 20$ kJ mol^{-1} at 25°C

[21] $CsAlSi_2O_6(s) + H^+(aq) \rightleftharpoons Cs^+(aq) + 2SiO_2(s) + AlOOH(s)$

$K_{21} = \{Cs^+\}/\{H^+\}$

$\log_{10} K_{21} = \log_{10} K_9 + pK_w = 3.5 \pm 1.5$ at 200°C

whence

$\Delta_r G^0 = -32 \pm 14$ kJ mol^{-1} at 200°C

$\Delta_r S^0 = +67.3$ J mol^{-1} K^{-1} at 25°C (from Table 2)

whence

$\Delta_r G^0 = -20 \pm 16$ kJ mol^{-1} at 25°C

Corresponding values of $\Delta_r G^0$ at 25°C, again calculated from Table 2, are −69 kJ mol^{-1} for reaction [20] and −46 kJ mol^{-1} for reaction [21]. The large difference in values for reaction [21] indicates that the chief discrepancy lies in the data for $CsAlSi_2O_6$.

At first sight, there appears to be an inconsistency between the good agreement on $\Delta_r G^0$ for reaction [20] and the poor agreement for reaction [16], since both concern the relative stability of $CsAlSi_2O_6$ and $CsAlSiO_4$. The molar ratios of the two solids in the two reactions are different, however, and the good agreement for reaction [20] can be attributed to a fortuitous balancing of errors.

All of the discrepancies discussed above are greatly reduced if $\Delta_f G^0$ for $CsAlSi_2O_6$ is 20–30 kJ mol^{-1} lower than the value derived from ref. 32, and that for $CsAlSiO_4$ is lowered by half that amount. We can not separate enthalpic and entropic contributions to these changes, but the former likely predominate. We therefore suggest the following enthalpy values:

$\Delta_f H^0(CsAlSi_2O_6, 298\ K) = -3070 \pm 20$ kJ mol^{-1}

$\Delta_f H^0(CsAlSiO_4, 298\ K) = -2133 \pm 20$ kJ mol^{-1}

The enthalpy of formation of $CsAlSi_5O_{12}$ given in ref. 32, −5805 kJ mol^{-1}, represents a reasonable lower limit on the basis of our results and the discussion of reaction [18], above. It is unlikely that $CsAlSi_5O_{12}$ is more than marginally unstable at 200°C, so we suggest no change in this enthalpy value.

Given the roughness of these thermochemical estimates, caution is required in any discussion of ambient-temperature phase relationships. The following equilibrium constants outline the stability limits of pollucite at 25°C, with uncertainties of at least three log units: $\log_{10} K_6 = -1.8$; $\log_{10} K_8 = -8.3$; $\log_{10} K_9 = -10.3$; $\log_{10} K_{10} = -4.3$. The low value of $\log_{10} K_9$ (cf. -7.8 ± 1.5 at 200°C) points to a somewhat larger stability field for pollucite at the lower temperature, in alkaline solutions. In acidic solutions, however, this difference is offset by the change in K_w with temperature.

7. Conclusions

Experiments with $CsAlSiO_4$, $CsAlSi_2O_6$, and $CsAlSi_5O_{12}$ have confirmed that $CsAlSi_2O_6$ is the most stable of these solids in aqueous solutions at 200°C. It is stable with respect to quartz + boehmite at $\{Cs^+\}\{OH^-\}$ ionic activity products above about 10^{-8} mol^2 kg^{-2}. It is stable with respect to $CsAlSiO_4$ at $\{Cs^+\}\{OH^-\}$ products up to at least 10^{-4}, and probably 10^{-2} mol^2 kg^{-2}. It is stable with respect to $CsAlSi_5O_{12}$ in quartz-saturated solutions.

The relatively high equilibrium cesium concentrations (i.e., 10^{-3} to 10^{-4} mol dm^{-3} in neutral solution) associated with pollucite equilibria, even in simple systems, indicate that it would be difficult to justify pollucite as a waste-form material on thermodynamic grounds. Its stability range is likely to be even narrower in groundwaters containing high concentrations of other cations, especially Ca^{2+} and Mg^{2+}. Pollucite or $CsAlSi_5O_{12}$ may still be justifiable waste-form choices, however, on kinetic grounds, i.e., slow dissolution and alteration at moderate temperatures. It also appears unlikely that pollucite crystallization could retard migration of cesium from a waste vault, except with extremely high cesium release rates from the waste form, or if the pH is high. We note that analcime–pollucite solid solutions are likely to be somewhat more stable than pure $CsAlSi_2O_6$ in alkali-rich groundwaters. Partitioning of cesium into silicate phases (either pre-existing minerals or alteration products), such as zeolites or micas, also remains a plausible mechanism for retardation. Some aspects of the special affinity

Can. J. Chem. Downloaded from www.nrcresearchpress.com by 122.72.124.2 on 09/07/12
For personal use only.

of cesium for the mica structure have been discussed recently by Komarneni and Roy (48).

These results help to determine appropriate conditions for the hydrothermal synthesis of pollucite, or conversely, for the extraction of cesium from natural pollucite. They are consistent with most of the reports of pollucite formation and stability in hydrothermal experiments, cited in the Introduction, and may also throw some light on the conditions under which pollucite occurs in nature. They have led to experimental values, admittedly rough, for the enthalpies of formation of $CsAlSiO_4$ and $CsAlSi_2O_6$, and a lower limit for $CsAlSi_5O_{12}$.

Acknowledgements

We are grateful to A. M. Duclos and J. M. Snider for the X-ray diffraction measurements, E. Rochon for the dissolved cesium analyses, and C. Musick for the fluoride analyses. E. R. Vance, R. J. Lemire, and D. W. Shoesmith made helpful comments on the manuscript.

1. D. M. Strachan and W. W. Schulz. Am. Ceram. Soc. Bull. **58**, 865 (1979).
2. K. Yanagisawa, S. Kanahara, M. Nishioka, and N. Yamasaki. J. Nucl. Sci. Tech. **21**, 558 (1984).
3. K. Hilpert, R. Odoj, and H. W. Nurnberg. Nucl. Tech. **61**, 71 (1983).
4. S. A. Gallagher, G. J. McCarthy, and D. E. Pfoertsch. Am. Ceram. Soc. Bull. **55**, 461 (1976).
5. G. J. McCarthy. Nucl. Tech. **32**, 92 (1977).
6. S. A. Gallagher, G. J. McCarthy, and D. K. Smith. Mater. Res. Bull. **12**, 1183 (1977).
7. T. Adl and E. R. Vance. J. Mater. Sci. **17**, 849 (1982).
8. S. Komarneni, G. J. McCarthy, and S. A. Gallagher. Inorg. Nucl. Chem. Lett. **14**, 173 (1978).
9. S. A. Gallagher and G. J. McCarthy. J. Inorg. Nucl. Chem. **43**, 1773 (1981).
10. P. Cerny. Can. Miner. **12**, 334 (1974).
11. P. Cerny. *In* Scientific basis for nuclear waste management. Vol. 1. *Edited by* G. J. McCarthy. Plenum Press, New York. 1979. p. 231.
12. S. Komarneni and W. B. White. Nucl. Chem. Waste Manage. **3**, 169 (1982).
13. S. A. Gallagher and G. J. McCarthy. Mater. Res. Bull. **17**, 89 (1982).
14. S. Komarneni and R. Roy. J. Am. Ceram. Soc. **66**, 471 (1983).
15. E. R. Vance and F. J. Ahmad. Nucl. Chem. Waste Manage. **4**, 171 (1983).
16. J. Mukerji and P. B. Kayal. J. Am. Ceram. Soc. **57**, 229 (1974).
17. J. Mukerji and P. B. Kayal. Mater. Res. Bull. **10**, 1067 (1975).
18. S. Komarneni and W. B. White. *In* Scientific basis for nuclear waste management, Vol. 3. *Edited by* J. G. Moore. Plenum Press, New York. 1981. p. 387.
19. N. A. Karazhanov, R. S. Darev, and U. T. Isenzhulova. Izv. Akad. Nauk Kaz. SSR, Ser. Khim. **1**, 27 (1983).
20. D. L. Brown, R. I. Haines, D. G. Owen, F. W. Stanchell, and D. G. Watson. Am. Chem. Soc. Symp. Ser. 246, 217 (1984).
21. R. M. Barrer and N. McCallum. J. Chem. Soc. 4029 (1953).
22. S. Komarneni and B. E. Scheetz. J. Inorg. Nucl. Chem. **43**, 1967 (1981).
23. S. Komarneni and W. B. White. Clays Clay Miner. **29**, 299 (1981).
24. R. M. Barrer, J. F. Cole, and H. Sticher. J. Chem. Soc. (A) 2475 (1968).
25. N. Sasaki, S. Komarneni, and R. Roy. Am. Ceram. Soc. Bull. **61**, 649 (1982).
26. G. J. McCarthy, W. B. White, R. Roy, B. E. Scheetz, S. Komarneni, D. K. Smith, and D. M. Roy. Nature, **273**, 216 (1978).
27. W. P. Freeborn, M. Zolensky, B. E. Scheetz, S. Komarneni, G. J. McCarthy, and W. B. White. *In* Scientific basis for nuclear waste management Vol. 2. *Edited by* C. J. M. Northrup, Jr. Plenum Press, New York. 1980. p. 499.
28. V. Dubanska, M. Strohalmova, and D. Kolousek. Acta Mont. **64**, 21 (1983).
29. J. R. Holloway, D. M. Jenkins, J. F. Kacoyannakis, and M. J. Apted. Rockwell Report RHO-BWI-C-105 (1981).
30. T. B. Vance, Jr. and K. Seff. J. Phys. Chem. **79**, 2163 (1975).
31. O. A. Mulina, N. F. Meged', N. N. Krupina, and I. V. Baranova. Russ. J. Phys. Chem. **60**, 1384 (1986) (Zh. Fiz. Khim. **60**, 2308 (1986)).
32. T. B. Lindemer, T. M. Besmann, and C. E. Johnson. J. Nucl. Mater. **100**, 178 (1981).
33. L. N. Grossman. Rev. int. hautes Temper. Refract. Fr. **16**, 255 (1979).
34. H. E. Swanson, R. K. Fuyat, and G. M. Ugrinic. Circ. 539, Vol. III. U.S. Natl. Bur. Stds. 1953. p. 38.
35. R. Tettenhorst and D. A. Hofmann. Clays Clay Miner. **28**, 373 (1980).
36. A. B. Kiss, G. Keresztury, and L. Farkas. Spectrochim. Acta, **36A**, 653 (1980).
37. R. A. Robie, B. S. Hemingway, and J. R. Fisher. U.S. Geol. Surv. Bull. 1452 (reprinted with corrections, 1979).
38. H. C. Helgeson. J. Phys. Chem. **71**, 3121 (1967).
39. N. S. Kuyunko, S. D. Malinin, and I. L. Khodakovskiy. Geochim. Int. **20**, 76 (1983) (Geokhimiya, **3**, 419 (1983)).
40. R. H. Busey and R. E. Mesmer. Inorg. Chem. **16**, 2444 (1977).
41. R. E. Mesmer, C. F. Baes, Jr., and F. H. Sweeton. Inorg. Chem. **11**, 537 (1972).
42. F. H. Sweeton, R. E. Mesmer, and C. F. Baes, Jr. J. Solution Chem. **3**, 191 (1974).
43. R. S. Beckwith and R. Reeve. Geochim. Cosmochim. Acta, **33**, 745 (1969).
44. J. D. Rimstidt and H. L. Barnes. Geochim. Cosmochim. Acta, **44**, 1683 (1980).
45. D. D. Wagman, W. H. Evans, V. B. Parker, R. H. Schumm, I. Halow, S. M. Bailey, K. L. Churney, and R. L. Nuttall. J. Phys. Chem. Ref. Data, **11**, Suppl. 2 (1982).
46. T. L. Woods and R. M. Garrels. Thermodynamic values at low temperature for natural inorganic materials: an uncritical summary. Oxford University Press, New York. 1987.
47. M. Sadiq and W. L. Lindsay. Colorado State Univ. Exptl. Sta. Tech. Bull. **134**, 1013 (1979).
48. S. Kormaneni and R. Roy. Science, **239**, 1286 (1988).

Can. J. Chem. Downloaded from www.nrcresearchpress.com by 122.72.124.2 on 09/07/12
For personal use only.

The photochemistry of 5-cyano-2,3-benzobicyclo[4.2.0]octa-2,4,7-triene

CHRISTOPHER OWEN BENDER[1] AND DOUGLAS DOLMAN
Department of Chemistry, University of Lethbridge, Lethbridge, Alta., Canada T1K 3M4
Received June 13, 1988

CHRISTOPHER OWEN BENDER and DOUGLAS DOLMAN. Can. J. Chem. **67**, 82 (1989).

The direct irradiation of 5-cyano-2,3-benzobicyclo[4.2.0]octa-2,4,7-triene (**18**) led to 6-cyanobenzocyclooctatetraene (**17**; $\Phi = 0.00075$), 6-cyanobenzosemibullvalene (**14**; $\Phi = 0.0003$), and 2-cyanonaphthalene ($\Phi = 0.00015$). The triplet excited state of **18**, generated by sensitization with a variety of ketone sensitizers (e.g., Michler's ketone and acetophenone), showed no unimolecular reactivity. Compound **18** does not participate in Zimmerman di-π-methane rearrangement; the potential product from such a transformation, 8-cyanobenzosemibullvalene (**19**), was, however, isolated from direct (Corex filter; $\Phi = 0{,}0010$) irradiation of the semibullvalene **14**. Deuterium labelling experiments suggest that **14** derives from a mechanism involving initial C4—C8 bonding of **18**, and that cyclooctatetraene **17** is probably formed by simple electrocyclic opening of the cyclobutene ring of **18**.

Key words: photochemistry, rearrangement mechanism, di-π-methane, semibullvalenes.

CHRISTOPHER OWEN BENDER et DOUGLAS DOLMAN. Can. J. Chem. **67**, 82 (1989).

La photolyse directe du cyano-5 benzo-2,3 bicyclo[4.2.0]octatriène-2,4,7 (**18**) conduit au cyano-6 benzocyclooctatetraène (**17**; $\Phi = 0{,}00075$), au cyano-6 benzo semi-bullvalène (**14**; $\Phi = 0{,}0003$), et au cyano-2 naphtalène ($\Phi = 0{,}00015$). L'état excité triplet de **18**, qui se produit par des irradiations sensibilisées par l'acétophénone ou par le cétone de Michler, ne manifeste pas d'activité unimoleculaire. Le composé **18** ne subissait pas de transposition di-π-méthane de Zimmerman; le cyano-8 benzo semi-bullvalène (**19**), le produit potentiel d'une telle transposition, a été obtenu par irradiation directe (filtre de Corex; $\Phi = 0{,}0010$) du semi-bullvalène **14**. Des études de marquages au deuterium suggèrent que le semi-bullvalène **14** dérive d'un mécanisme qui comporte la formation d'une liaison initiale entre C4 et C8 de **18**, et que le cyclooctatetraène **17** se produit probablement par un mécanisme qui comporte la simple ouverture électrocyclique de l'anneau du cyclobutène de **18**.

Mots clés : photochimie, mécanisme de transposition, di-π-méthane, semi-bullvalènes.

Can. J. Chem. Downloaded from www.nrcresearchpress.com by 122.72.124.2 on 09/07/12
For personal use only.

Introduction

In recent publications we reported that upon irradiation with ultraviolet light 2,3-benzobicyclo[4.2.0]octa-2,4,7-trienes (e.g., **1** (1), **2** (2), **3** and **4** (3)) furnish, *inter alia*, semibullvalenes (SB's). Details of the reaction mechanisms were elaborated by the use of deuterium labelling and in all cases the SB formation could be accounted for in terms of a Zimmerman di-π-methane (DPM) rearrangement (4) of the starting diene (see Scheme 1); contending "1,3-vinyl,vinyl-bridging" and "1,2-vinyl-migration" versions of the rearrangements[2,3] are shown in Scheme 1. We now report on the photochemistry of 5-cyano-2,3-benzobicyclo[4.2.0]octa-2,4,7-triene (**18**) and provide evidence for the first diene-to-SB conversion that does not involve a DPM rearrangement.

Results

Diene **18** was isolated, as previously described (2), as the minor product from the photolysis of 6-cyanobenzocyclooctatetraene (6-CN-BCOT, **17**; Scheme 2). The diene is thermally labile (as are the dienes **2** (2), **3**, and **4** (3)) and ring-opens to COT **17**. The isomerization is detectable on the gc at column temperatures > 125°C, and is essentially quantitative on heating at ca. 150°C for 4 h. On direct irradiation with 313-nm light, **18** undergoes rearrangement to SB **14** and COT **17**, and fragmentation to 2-cyanonaphthalene; the chemical (analytical) yields and quantum yields (Φ's) are given in Scheme 2. The photoproducts were identified by comparison (nmr, gc, and tlc) with authentic samples. Gas chromatographic monitoring during the progress of the photolyses established that 8-CN-SB (**19**), the potential DPM rearrangement product from diene **18**, was absent; **19** was independently prepared from SB **14** (*vide infra*) and used for gc comparisons.

In contrast to the direct irradiation of diene **18**, sensitized runs did not lead to observable unimolecular processes. Thus with Michler's ketone, *p*-dimethylaminobenzophenone, thioxanthone, or acetophenone as sensitizers, only polymeric or other high molecular weight materials were formed, and products isomeric with the starting diene were not detected by gc analysis.

Control experiments with the diene photoproducts SB **14** and COT **17**, and the potential DPM rearrangement product SB **19**, were carried out to examine for possible interconversions. Under the conditions used for the direct photolysis of diene **18**, i.e., irradiation with 313-nm light, solutions of SB's **14** and **19** were stable since neither absorbs light appreciably at this wavelength. However, with Corex-filtered light ($\lambda > 280$ nm) SB **14** yielded SB **19** ($\Phi = 0.001$), whereas the latter compound gave only polymeric material. Attempts to sensitize the photolysis of **14** and **19** with acetone as sensitizer led to the slow disappearance of the SB's without isomer formation.

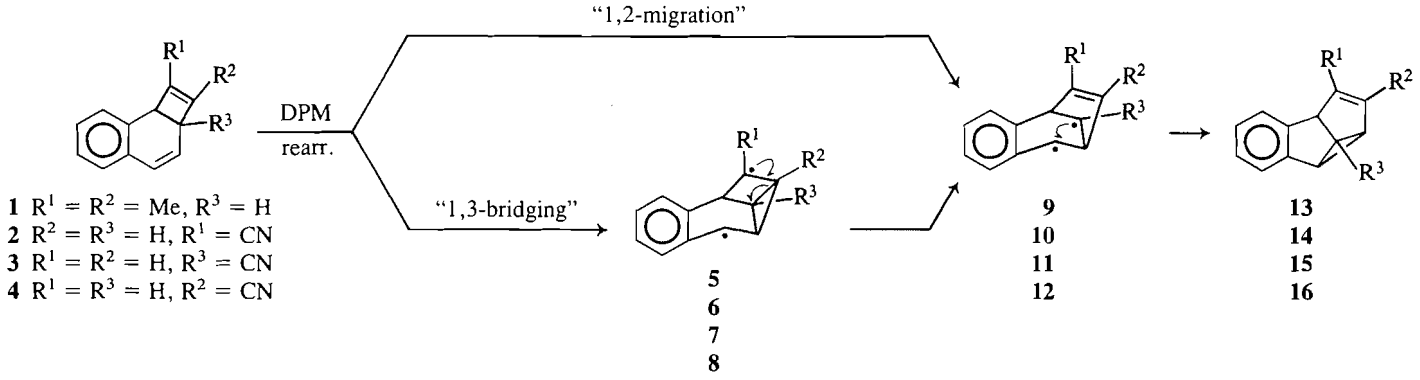
The physical characterization of **19** proved troublesome since, like SB's **14** (2) and **16** (3), it undergoes facile polymerization upon solvent removal. The structural proof is therefore limited, and relies on spectroscopic data and reduction results.

The mass spectrum (via gc/ms) established the molecular weight as 179, and the ^{1}H nmr spectrum displayed chemical shifts and coupling constants diagnostic of the rigid SB system. The nmr data for **19** are compared with those of **15** (6) and parent benzosemibullvalene (**21**) (7) in Table 1. Further support for

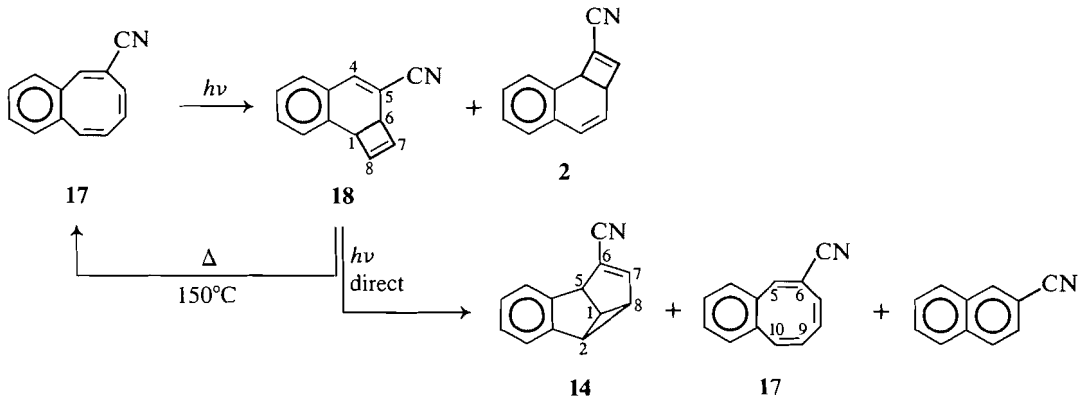
[1]Author to whom correspondence may be addressed.

[2]The topic of the position of the energy minimum in DPM rearrangements is controversial. For leading publications on this issue note refs. 4 and 5, and those contained therein.

[3]Zimmerman (4*c*) has carefully pointed that structures such as **5**–**8** (Scheme 1) are "... conveniences in organic chemical notation without implication whether these are intermediates or just points on an excited-state hypersurface."



SCHEME 1

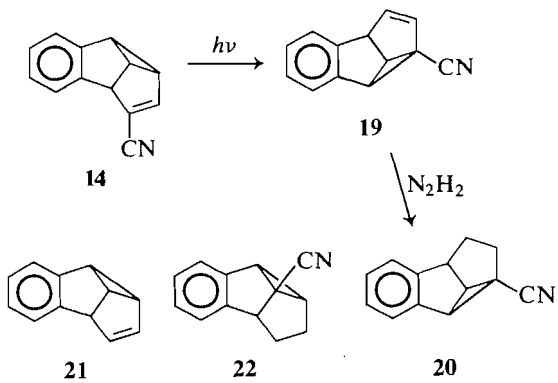


SCHEME 2

TABLE 1. The ^{1}H nmr of semibullvalenes **15**, **19**, and **21**

	Description and signal positions, $\delta^{a,b}$		
Assignment	**19**	**15**	**21**
Aromatics	7.09–7.47 m	7.00–7.44 m	6.80–7.33 m
H-1	3.78 t	—	3.14 q
H-2	3.74 d	3.66 d	2.86 t
H-5	4.09 dd	4.22 d	3.81 dd
H-6	5.72 dd	5.70 dd	5.47 dd
H-7	5.17 d	5.20 dd	5.08 dd
H-8	—	3.33 dd	2.60 dt

[a]Run in $CDCl_3$ (**15** and **19**) or CCl_4 (**21**) solvent with TMS as internal standard.
[b]Coupling constants for **19** are $J_{1,2} = J_{1,5} = 6$, $J_{5,6} = 2.5$, and $J_{6,7} = 5$ Hz; corresponding coupling constants for **15** and **21** are within 0.5 Hz.



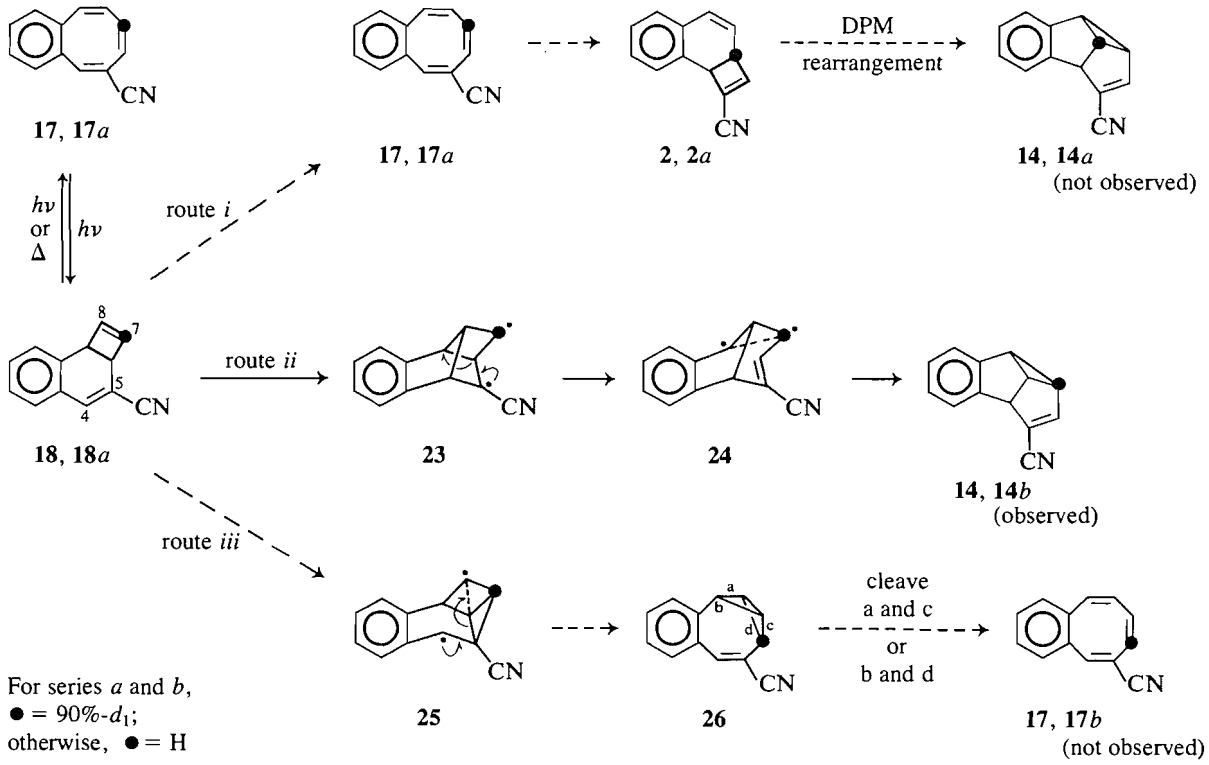
SCHEME 3

structure **19** derives from its treatment with diimide whereupon 8-cyano-3,4-benzotricyclo[3.3.0.0.^{2,8}]oct-3-ene (**20**), a stable crystalline dihydro derivative of **19**, was obtained as the unique product (Scheme 3). The identification of **20** is based on comparison of its ^{1}H nmr spectrum with that of the closely related dihydro semibullvalene **22** (8). Details of the spectra are given in Table 2. Here we note that in common with other 6,7-dihydro SB's, **20** shows the characteristic "*W*" coupling constant of 1.5 Hz between H-5 and H-7 (2).

In the case of interconversions of **17**, the sensitized photolysis with *p*-dimethylaminobenzophenone as sensitizer proved the COT to be remarkably stable, and product formation was not observed even on extended irradiations. For the direct photolysis, the dienes **2** and **18** were initially formed, as shown in Scheme 2, and further irradiation eventually produced SB **14**. Since **14** is known to be the major product from the photolysis of diene **2** (2), it is tempting to speculate that the SB **14** found in the direct irradiation of diene **18** derives from the subsequent photochemistry of COT **17**, i.e., via the three-photon sequence: diene **18** → COT **17** → diene **2** → SB **14** (route *i*, Scheme 4). However, the failure to detect diene **2** in photolysates of **18** mitigates against this proposal, as do results from experiments with the deuterium labelled diene **18***a*.

Compound **18***a*, with deuterium attached to C-7, was

Can. J. Chem. Downloaded from www.nrcresearchpress.com by 122.72.124.2 on 09/07/12
For personal use only.



SCHEME 4

TABLE 2. The ^{1}H nmr data of the ring-attached protons of the dihydrosemibullvalenes **20** and **22**

Assignment	Description and signal positions, δ[a,b]	
	20	**22**[c]
Aromatics	7.00–7.33 m	7.02–7.20 m
H-1	3.36 dd	—
H-2	3.09 dd	3.15 dd
H-5	3.76 br t	3.87 br t
H-6	2.45 m	2.45 m
H-6′	1.68 br dd	1.76 br dd
H-7	2.10 ddd	2.01 m
H-7′	1.38 ddd	1.20 m
H-8	—	2.60 ddd

[a]Run in $CDCl_3$ solvent with TMS as internal standard.

[b]Coupling constants for **20** are $J_{1,2} = J_{6',7'} = 6.5$, $J_{1,5} = J_{5,6} = 5.0$, $J_{2,6'} = 1$, $J_{5,7} = 1.5$, $J_{5,6'} = J_{6',7} = 0$, $J_{6,7} = 8.5$, $J_{6,7'} = 11.5$, $J_{7,7'} = 13.5$; corresponding coupling constants for **22** are within 1.0 Hz.

[c]The original assignments reported for H-7 and H-7′ were in error and have been reversed here (8).

obtained from the photolysis of the known (6) deuterated COT **17***a* (ca. 90%-d_1 at C-8). The direct irradiation of **18***a* led to SB product **14***b*, with the deuterium located exclusively at C-8, as determined by ^{1}H nmr analysis (the integration results for **14***b* and all other labelled compounds are given in the Experimental). Thus the mechanism depicted as route *i* (Scheme 4), which requires the formation of SB **14***a* with deuterium located at C-1, is clearly ruled out by the labelling results. A plausible rationale that does account for the label distribution of **14***b* is shown as route *ii* in Scheme 4. It is a one-photon process that commences with initial C4—C8 bridging of the diene.[4]

[4]Structures **23–25** should be interpreted as in footnote 3.

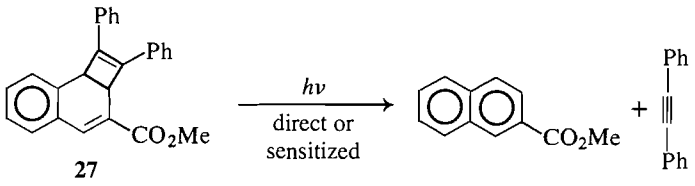
Also of mechanistic significance are the observations that the COT material obtained from the thermolysis and photolysis of **18***a* possessed the same label distribution as the original COT (**17***a*). Here we note that whereas the ground-state reaction cannot provide **17** by a single allowed electrocyclic process, the excited-state reaction can, by disrotatory opening of the cyclobutene ring. Interestingly, a previous study of the related diene **2** revealed that the deuterium distribution in the COT product resulting from thermolysis differed from that generated by direct irradiation, and involvement of an octavalene intermediate was proposed for the photochemical pathway (2). In the present case with diene **18**, an analogous mechanism (route *iii*, Scheme 4) cannot operate since this would engender the symmetric octavalene **26** and hence the formation of COT **17***b* rather than the observed COT **17***a*.[4]

Discussion

The singlet and triplet excited states of diene **18** show strikingly divergent behaviour. Thus whereas S_1 gives rise to both isomerization (to SB **14** and COT **17**) and fragmentation (to 2-cyanonaphthalene) processes, T_1 displays no unimolecular photochemistry. A pertinent point here is that regardless of the excited state multiplicity, the diene does not undergo DPM rearrangement (i.e., **18** does not give SB **19**). This observation is attributed to the known reluctance of DPM systems to rearrange via initial 1,3-bridging or 1,2-migration to the α-carbon of an acrylonitrile moiety. Note, for example, the avoidance of such a liaison in the sensitized rearrangements of 2-cyanobenzobarrelene (6), 5,6-dihydro-2-cyanobenzobarrelene (8), and 2-cyanobenzonorbornadiene (9). A similar rationale was used to account for the meager production (ca. 2% yield) of the DPM product SB **16** from diene **4** (3).

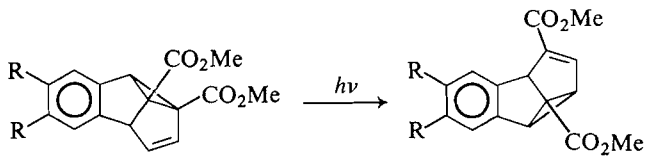
The most surprising finding in the present work is the formation of a semibullvalene product (SB **14**) from diene **18**, via a non-DPM pathway (route *ii*, Scheme 4). This result is unprecedented for a 2,3-benzobicyclo[4.2.0]octa-2,4,7-triene

Can. J. Chem. Downloaded from www.nrcresearchpress.com by 122.72.124.2 on 09/07/12
For personal use only.



27

SCHEME 5



28 R = H
29 R = OMe

30
31

SCHEME 6

and contrasts sharply with the photochemistry of diene **27** (10), the closest literature analogue to **18**, since it too is substituted with a strong electron-withdrawing group at C-5. Sasse and co-workers (10) found that on direct or sensitized irradiation **27** undergoes only cleavage to methyl 2-naphthoate and diphenylacetylene (Scheme 5).

A final unexpected result was the photoisomerization of SB **14** to SB **19**. The transformation is formally equivalent to a vinylcyclopropane rearrangement and can be viewed as an allowed Hückel 4-electron excited-state process (11), i.e., a $2\pi s + 2\sigma s$ sigmatropic [1,3] shift (12). Although the most common photoreaction of aro-fused SB's is isomerization to COT product (6, 13), there are at lest two literature examples of their participation in vinylcyclopropane interconversions. Both involve derivatives substituted at C-1 and C-8 with carbomethoxy groups, viz. **28** (→**30** (13); Scheme 6) and **29** (→**31** (14)), and the driving force for the conversions was suggested to be relief of the diester steric strain energy. Operation of the rearrangement in the case of SB **14**, which is devoid of such substituent strain, underscores the need for photochemical studies of other SB derivatives before further speculations on the product-controlling features of the reaction are warranted.

Experimental

The nmr spectra were recorded on a Bruker 400-MHz or a Varian 60-MHz instrument, with TMS as internal standard. The chemical shifts are in δ units and the coupling constants (*J*) in Hz. The abbreviations br, s, d, t, q, and m refer to broad, singlet, doublet, triplet, quartet, and multiplet, respectively. Melting points are uncorrected. Elemental analyses were performed by the Analytical Services Lab, Department of Chemistry, the University of Alberta. Column chromatography was carried out on Silica Gel 60 (Merck; 230–400 mesh) mixed with Sylvania 2282 phosphor and slurry packed into quartz columns permitting monitoring by a hand uv lamp. The gc analyses were made on a Varian 3700 instrument (FID), coupled to a Varian CDS 111 computing integrator, and fitted with an SE-30 fused silica capillary column 30 m × 0.32 mm; column temperatures of 125°C, or less, were used to minimize the thermal conversion of diene **18** to COT **17**. The gc/ms was recorded on an HP 5985 B instrument fitted with an SPB-1 fused silica capillary column, 30 m × 0.32 mm. Cyclohexane solvent for photolyses was prepared by scrubbing with 20% fuming sulfuric acid, followed by washing with 10% aqueous sodium hydroxide, drying ($MgSO_4$), and finally distilling from calcium hydride. Sensitizers were distilled or recrystallized (after sublimation) prior to use.

General procedures for preparative photolyses

The apparatus consisted of a 450-W Hanovia medium pressure mercury arc surrounded by a water-cooled quartz immersion well. The light was filtered through either cylindrical Corex or Pyrex sleeves, or an aqueous potassium chromate solution (300 mg K_2CrO_4 and 2.0 g of sodium carbonate in 1.6 L water; transmittance at 313 nm was 55%), or an aqueous lead nitrate solution (8 g $Pb(NO_3)_2$ and 750 g NaBr per 1 L of water; transmittance was 0% below 340 nm), or an aqueous copper sulfate solution (250 g $CuSO_4$ in 1 L of water; transmittance was 0% below 310 nm) contained in a concentric filter jacket (10-mm path length). Three types of sample cell were used. Cell A (250-mL sample volume) consisted of a cylindrical vessel (Pyrex), which surrounded the immersion well. Cell B (200-mL sample volume) consisted of a cylindrical collar (Pyrex), which surrounded the aqueous filter jacket. Both Cell A and Cell B were fitted with gas inlet and exit ports, and sample solutions were purged with argon prior to, and during, irradiations. Cell C (35-mL sample volume) was a test-tube-like vessel (quartz), and sample solutions contained therein were deoxygenated by flushing with argon and sealed under a positive pressure; the solutions were magnetically stirred throughout the course of the irradiations.

*Direct irradiation of diene **18***

A solution of 67.9 mg (0.38 mmol) of **18** (2) and 10.3 mg of tetradecane (gc standard) in 200 mL of cyclohexane was photolyzed at 313 nm for 4 h in Cell B (26% conversion by gc). The photolysate composition analysed (gc) for 0.6 mg (<1%) 2-cyanonaphthalene, 5.2 mg (8%) COT **17**, 50.0 mg (74%) diene **18**, and 1.8 mg (3%) SB **14**. The photolysate was concentrated and the residue chromatographed on Silica Gel 60 (2 cm × 45 cm; 2% ether–cyclohexane). The first band eluted was 4.6 mg (7%) of COT **17**, mp 72–74°C (from hexane; lit. (6) mp 73–74°C), identified by gc and nmr comparison with an authentic sample (6). The second band gave 48.4 mg (71%) of recovered diene **18**, and the third band contained a trace of 2-cyanonaphthalene (identified by gc, tlc, and nmr). The last band contained SB **14** of gc purity >98% (note: SB **14** polymerizes when solvent free), identified by gc and nmr comparison with an authentic sample (2).

*Sensitized irradiation of diene **18***

A solution of 33.0 mg (0.18 mmol) of diene **18**, 5.9 mg (0.026 mmol) of thioxanthone, and 13.8 mg of nonadecane (gc standard) in 35 mL of cyclohexane was irradiated at >340 nm (lead nitrate filter) for 2 h in Cell C. The photolysate composition analysed (gc) for 18.4 mg (56%) of diene **18** and 5.6 mg (95% recovery) of thioxanthone; no other products were detected. The photolysate was concentrated and the residue chromatographed on silica Gel 60 (2 cm × 45 cm; 2% ether–cyclohexane). The first band gave 17.3 mg (52%) of recovered diene **18**; the second band gave 5.1 mg (86%) of recovered sensitizer.

Under the same set-up, similar results were observed when Michler's ketone (at 0.57×10^{-3} M), *p*-dimethylaminobenzophenone (at 3.1×10^{-3} M), or acetophenone (at 1.4×10^{-1} M) were used as sensitizers.

*Thermolysis of diene **18***

A solution of 6.2 mg (0.035 mmol) of diene **18** and 2.3 mg of tetradecane (gc standard) in 2 mL of *n*-nonane was refluxed (ca. 150°C) during 5 h, under an argon atmosphere. The thermolysis product analysed (gc) for 6.0 mg (97%) COT **17**. Chromatography on Silica Gel 60 (1 cm × 10 cm; 2% ether–cyclohexane) gave 5.3 mg (85%) of COT **17**, mp 72–74°C (from hexane).

*Direct irradiation of SB **14***

A solution of ca. 28.5 mg (0.16 mmol) of SB **14** and 5.2 mg of tetradecane (gc standard) in 250 mL of cyclohexane was photolyzed for 50 min with Corex filtered light (66% conversion by gc) in Cell A. The photolysate composition analysed (gc) for 10.4 mg (36%) SB **19** and 9.8 mg (34%) SB **14**. The photolysate was concentrated to a small volume (ca. 5 mL; both SB's **14** and **19** polymerize when solvent free) and chromatographed on Silica Gel 60 (2.5 cm × 45 cm; 3% ether–cyclohexane). The first band contained SB **19** of gc purity >98%; details of the nmr data are given in Table 1; spin decoupling experiments: irradiation of H-6 collapsed H-7 to an s and H-5 to a d ($J_{1,5}$ = 6.0); irradiation of H-7 collapsed H-6 to a d ($J_{5,6}$ = 2.5); irradiation of H-5 collapsed H-6 to a d ($J_{6,7}$ = 5.0) and H-1 to a d ($J_{1,2}$ = 6.0); gc/ms showed molecular ion at m/e = 179 (65%), 178 (base peak). The second band contained recovered SB **14**.

Can. J. Chem. Downloaded from www.nrcresearchpress.com by 122.72.124.2 on 09/07/12
For personal use only.

Can. J. Chem. Downloaded from www.nrcresearchpress.com by 122.72.124.2 on 09/07/12
For personal use only.

*Diimide reduction of SB **19***

To a stirred mixture of ca. 25 mg (0.14 mmol) of **19** and 1.0 g (5.2 mmol) of potassium azodicarboxylate in 25 mL of dioxane at room temperature a 0.5-mL quantity of acetic acid was added in one portion. The mixture was stirred during 2.5 h, then added to 100 mL of toluene and washed with 10% sodium carbonate solution (100 mL), followed by water (2 × 75 mL). The toluene extract was dried ($MgSO_4$), concentrated, and the residue chromatographed on Silica Gel 60 (0.9 cm × 10 cm; 5% ether–cyclohexane). Sublimation (70°C/0.1 Torr; 1 Torr = 133.3 Pa) followed by crystallization of the main band from hexane gave 20.4 mg (81%) of colourless **20**, mp 58–60°C; ir (KBr): 2250 cm^{-1}, C≡N; uv (hexane): 258 sh (ε 370), 264 (600), 269 sh (820), 270 (910), and 278 nm (1 050); nmr (400 MHz; $CDCl_3$), see Table 2; spin decoupling experiments: irradiation of H-5 collapsed H-1 to a d ($J_{1,2}$ = 6.5), H-6 to a dt ($J_{6,6'} = J_{6,7'}$ = 11.5 and $J_{6,7}$ = 8.5), and H-7 to a dd ($J_{7,6}$ = 8.5 and $J_{7,7'}$ = 13.5); irradiation of H-1 collapsed H-5 to a br d ($J_{5,6}$ = 5) and H-2 to a br s; irradiation of H-2 collapsed H-1 to a d ($J_{1,5}$ = 5); irradiation of H-6 collapsed H-5 to a dd ($J_{5,1}$ = 5, $J_{5,7}$ = 1.5) and modified H-7, H-6′, and H-7′; irradiation of H-7 collapsed H-5 to a sharp t ($J_{5,1} = J_{5,6}$ = 5) and modified H-6 and H-7′; irradiation of H-6′ collapsed H-2 to a d ($J_{2,1}$ = 6.5) and modified H-6 and H-7′; irradiation of H-7′ collapsed H-6′ to a br d ($J_{6',6}$ = 11) and modified H-6 and H-7. Mass spectrum showed molecular ion at m/e = 181.0891 (68%), 128 (base peak); $C_{13}H_{11}N$ requires 181.0892. *Anal.* calcd. for $C_{13}H_{11}N$: C 86.15, H 6.12, N 7.73; found: C 86.26, H 6.04, N 7.71.

*Sensitized irradiation of SB **14***

A solution of ca. 32 mg (0.18 mmol) of SB **14** and 14.5 mg of tetradecane (gc standard) in 35 mL of acetone was irradiated for 7.5 h in Cell C with Pyrex-filtered light. The photolysate composition analysed (gc) for 15.8 mg (49%) of SB **14**; no other products were detected. The photolysate was concentrated and chromatographed on Silica Gel 60 (1 cm × 15 cm; 2% ether–cyclohexane). The nmr spectrum of the main band confirmed it to be recovered SB **14**.

*Labelled COT **17**a*

Deuterated COT **17***a* (90%-d_1 at C-8) was prepared as previously described (6); nmr (400 MHz; $CDCl_3$): 7.22–7.28 (m, 3.51H, H-5 + 2 aromatics + residual $CHCl_3$), 6.95–7.00 (m, 2.00H, 2 aromatics), 6.55 (d, 1.02H, H-10, $J_{10,9}$ = 11.5), 6.08 (dd, 0.07H, H-8, $J_{8,7}$ = 11, $J_{8,9}$ = 4), 6.04 (d, 1.00H, H-9, $J_{9,10}$ = 11.5), and 5.76 (br s, 0.97H, H-7). Integrations for **17***a* and all subsequent deuterium labelled compounds were normalized by assigning integer values to one or more aromatic proton signals, unless otherwise indicated; integration errors due to baseline undulations are estimated to be within ca. ±0.05H.

*Labelled diene **18**a from COT **17**a*

A solution of 238.9 mg (1.33 mmol) of COT **17***a* in 200 mL of cyclohexane was photolysed directly at >310 nm for 21 h in Cell B. The photolysate was concentrated and the residue crystallized from 5 mL of hexane to give 160.2 mg (67%) of recovered COT **17***a*. The mother liquors were column chromatographed on Silica Gel 60 (2 cm × 45 cm; 2.5% ethyl acetate – cyclohexane) into two bands. The second band gave 33.3 mg (14%) of diene **2***a* (2). The first band, containing diene **18***a* and COT **17***a*, was rechromatographed three times on Silica Gel 60 (2 cm × 45 cm; 2% ether–cyclohexane); COT **17***a* was eluted first, followed by diene **18***a*. This procedure led to the isolation of a further 26.4 mg (11%) of recovered COT **17***a*, and 12.6 mg (5%) of diene **18***a*; nmr (400 MHz; $CDCl_3$): 7.28–7.35 (m, 1.00H, 1 aromatic), 7.15–7.23 (m, 3.01H, 3 aromatics), 6.97 (br s, 1.00H, H-4), 6.22 (d, 0.09H, H-7, $J_{7,8}$ = 2.8), 6.10 (d, 0.97H, H-8, $J_{8,1}$ = 1), 4.27 (d, 1.00H, H-1, $J_{1,6}$ = 4.5), and 3.82 (d, 0.97H, H-6, $J_{6,1}$ = 4.5).

*Thermolysis of diene **18**a*

A solution of 5.3 mg (0.030 mmol) of diene **18***a* in 2 mL of *n*-nonane was refluxed (ca. 150°C) during 5 h, under an argon atmosphere. The thermolysis product was worked up as in the case of the nondeuterated diene to give 4.3 mg (81%) COT **17***a*; nmr (400 MHz; $CDCl_3$): 7.22–7.28 (m, 3.82H, H-5 + 2 aromatics + residual $CHCl_3$), 6.95–7.00 (m, 2.00H, 2 aromatics), 6.55 (d, 1.03H, H-10, $J_{10,9}$ = 11.5), 6.08 (dd, 0.10H, H-8, $J_{8,7}$ = 11, $J_{8,9}$ = 4), 6.04 (d, 0.98H, H-9, $J_{9,10}$ = 11.5), and 5.76 (br s, 0.97H, H-7).

*Direct irradiation of diene **18**a*

A solution of 29.5 mg (0.16 mmol) of **18***a* in 200 mL of cyclohexane was photolyzed at 313 nm for 4 h in Cell B. The photolysate, when worked up as in the case of the direct irradiation of unlabelled **18**, gave 2.8 mg (9%) COT **17***a*; nmr (400 MHz; $CDCl_3$): 7.22–7.28 (m, 3.35H, H-5 + aromatics + residual $CHCl_3$), 6.95–7.00 (m, 2.00H, 2 aromatics), 6.55 (d, 0.97H, H-10, $J_{10,9}$ = 11.5), 6.08 (dd, 0.10H, H-8, $J_{8,7}$ = 11, $J_{8,9}$ = 4), 6.04 (d, 1.00H, H-9, $J_{9,10}$ = 11.5), and 5.76 (br s, 0.96H, H-7); 18.2 mg (62%) of recovered diene **18***a*; nmr (400 MHz; $CDCl_3$): 7.28–7.35 (m, 1.00H, 1 aromatic), 7.15–7.23 (m, 2.90H, 3 aromatics), 6.97 (br s, 0.99H, H-4), 6.22 (d, 0.10H, H-7, $J_{7,8}$ = 2.8), 6.10 (d, 0.97H, H-8, $J_{8,1}$ = 1), 4.27 (d, 0.98H, H-1, $J_{1,6}$ = 4.5), and 3.82 (d, 0.98H, H-6, $J_{6,1}$ = 4.5); and ca. 1.0 mg (3%, estimated by gc) of SB **14***b*; nmr (400 MHz; $CDCl_3$): 7.33 (m, 1.00H, 1 aromatic) 7.18–7.28 (m, 3 aromatics + residual $CHCl_3$), 6.01 (s, 0.95H, H-7), 4.06 (d, 1.00H, H-5, $J_{5,1}$ = 6), 3.49 (t, 1.04H, H-1, $J_{1,2} = J_{1,5}$ = 6), 3.29 (d, 1.00H, H-2, $J_{2,1}$ = 6), and 2.79 (m, 0.08H, H-8).

Quantum yield determinations

Quantum yields were performed on an apparatus previously described (13), which includes an optical bench arranged for beam splitting into a ferrioxalate actinometer (15). Cyclohexane solutions (3 mL) of reactants (ca. (5–6.5) × 10^{-3} M) were deoxygenated prior to irradiation by flushing with argon. A positive pressure of argon was maintained over the stirred solutions throughout the course of the irradiations. The quantum yields (Φ's) were obtained from several runs extrapolated to zero conversion. Product analyses were determined by gc (internal tetradecane standard). For the direct irradiation of diene **18**, light of wavelength 313 nm was used; appearance Φ's were 0.00075 for COT **17**, 0.0003 for SB **14**, and 0.00015 for 2-cyanonaphthalene. For the direct irradiation of SB **14**, light of wavelength 280 nm was used; the appearance Φ for SB **19** was 0.0010.

Acknowledgements

The authors thank the Spectroscopic Services Laboratory of the University of Alberta and the Agriculture Canada Research Station at Lethbridge for the 400-MHz nmr and mass spectra. Financial support from the Natural Sciences and Engineering Research Council of Canada is gratefully acknowledged.

1. C. O. Bender, I. M. Cassis, D. Dolman, L. D. Heerze, and F. L. Schultz. Can. J. Chem. **62**, 2769 (1984).
2. C. O. Bender, D. Dolman, and G. K. Murphy. Can. J. Chem. **66**, 1656 (1988).
3. C. O. Bender, D. L. Bengtson, D. Dolman, and S. F. O'Shea. Can. J. Chem. **64**, 237 (1986).
4. (*a*) S. S. Hixson, P. S. Mariano, and H. E. Zimmerman. Chem. Rev. **73**, 531 (1973); (*b*) H. E. Zimmerman. Rearrangement in ground and excited states. Vol. 3. *Edited by* P. de Mayo. Academic Press, New York. 1980. pp. 131–166; (*c*) H. E. Zimmerman and A. P. Kamath. J. Am. Chem. Soc. **110**, 900 (1988).
5. (*a*) L. A. Paquette and E. J. Bay. J. Org. Chem. **47**, 4597 (1982); (*b*) J. Am. Chem. Soc. **106**, 6693 (1984); (*c*) L. A. Paquette, M. J. Coghlan, C. H. Cottrell, T. Irie, and H. Tanida. J. Org. Chem. **51**, 696 (1986); (*d*) L. A. Paquette, A. Varadarajan, and L. D. Burke. J. Am. Chem. Soc. **108**, 8032 (1986); (*e*) L. A. Paquette and L. D. Burke. J. Org. Chem. **52**, 2674 (1987); (*f*) L. A. Paquette, L. D. Burke, T. Irie, and H. Tanida. J. Org. Chem. **52**, 3246 (1987); (*g*) W. Adam, M. Dörr, J. Kron, and R. J. Rosenthal. J. Am. Chem. Soc. **109**, 7074 (1987).
6. C. O. Bender, D. W. Brooks, W. Cheng, D. Dolman, S. F. O'Shea, and S. S. Shugarman. Can. J. Chem. **56**, 3027 (1978).
7. H. E. Zimmerman, R. S. Givens, and R. M. Pagni. J. Am. Chem. Soc. **90**, 6096 (1968).

8. C. O. BENDER and S. F. O'SHEA. Can. J. Chem. **57**, 2804 (1979).
9. L. A. PAQUETTE, A. Y. KU, C. SANTIAGO, M. D. ROZENBOOM, and K. N. HOUK. J. Am. Chem. Soc. **101**, 5972 (1979).
10. G. SUGOWDZ, P. J. COLLIN, and W. H. F. SASSE. Aust. J. Chem. **26**, 147 (1973).
11. H. E. ZIMMERMAN. J. Am. Chem. Soc. **88**, 1565 (1966); **88**, 1566 (1966); Acc. Chem. Res. **4**, 272 (1972).
12. R. B. WOODWARD and R. HOFFMANN. The conservation of orbital symmetry. Verlag Chemie, Weinheim, and Academic Press, New York. 1970.
13. C. O. BENDER, D. L. BENGTSON, D. DOLMAN, C. E. L. HERLE, and S. F. O'SHEA. Can. J. Chem. **60**, 1942 (1982).
14. C. O. BENDER and J. WILSON. Helv. Chim. Acta, **53**, 1469 (1976).
15. (*a*) C. G. HATCHARD and C. A. PARKER. Proc. R. Soc. London, Ser. A, **235**, 518 (1956); (*b*) W. D. BOWMAN and J. N. DEMAS. J. Phys. Chem. **80**, 2434 (1976).

Can. J. Chem. Downloaded from www.nrcresearchpress.com by 122.72.124.2 on 09/07/12
For personal use only.

A method for evaluation of Hamiltonian and line shape parameters from electron paramagnetic resonance powder spectra

MINGDA SHE[1] AND XIANRONG CHEN
Department of Physics, Xiamen University, Xiamen, Fujian, China

AND

XIN-SHENG YU
Analysis and Test Center, Xiamen University, Xiamen, Fujian, China

Received December 17, 1987[2]

This paper is dedicated to Professor Charles A. McDowell on the occasion of his 70th birthday

MINGDA SHE, XIANRONG CHEN, and XIN-SHENG YU. Can. J. Chem. **67**, 88 (1989).

A least-square fitting method is given for exact evaluation of spin-Hamiltonian and line shape parameters from EPR powder spectra. The method is applicable to cases where the resonance fields can be analytically expressed or can only be obtained by diagonalization of Hamiltonian. It is also suitable for different line shapes and spin-Hamiltonians. The fitted spectra and corresponding refined parameters were obtained on FACOM-M340S computer with a Fortran 77 program.

Key words: spin-Hamiltonian, line shape parameters, electron paramagnetic resonance, calculated spectra, least squares fitting.

MINGDA SHE, XIANRONG CHEN et XIN-SHENG YU. Can. J. Chem. **67**, 88 (1989).

On présente une méthode d'ajustement par la méthode des moindres carrés pour évaluer d'une façon exacte l'Hamiltonien de spin et les paramètres de la forme des raies de spectres rpe de poudres. On peut appliquer la méthode à des cas où les champs de résonance peuvent soit être exprimés d'une façon analytique ou ne peuvent être obtenus que par une diagonalisation de l'Hamiltonien. Elle est aussi appropriée pour des formes de raies ou des Hamiltoniens de spin qui sont différents. On a obtenu les spectres ajustés ainsi que les paramètres affinés correspondants à l'aide d'un ordinateur FACOM-M340S opérant avec un programme Fortran 77.

Mots clés : Hamiltonien de spin, paramètres de la forme, résonance paramagnétique électronique, spectres calculés, ajustement par la méthode de moindres carrés.

[Traduit par la revue]

Can. J. Chem. Downloaded from www.nrcresearchpress.com by 122.72.124.2 on 09/07/12
For personal use only.

1. Introduction

To obtain information on interactions between unpaired electrons and ligands, one needs to know the Hamiltonian and line shape parameters of EPR spectra, such as the **g** factor, the fine or hyperfine tensors **D** and **A**, line widths, and so on. It is difficult to determine these parameters from powder spectra when the paramagnetic centers are strongly anisotropic or when the line is broad. The spectrum from powder samples is a superposition of a large number of lines from randomly oriented microcrystallites, resulting in parts of fine or hyperfine splittings being smeared out by the overlapping of spectra.

The analyses of powder spectra are usually carried out by computer. When the spin-Hamiltonian is known and a reasonable simulated spectrum is obtained, it is desirable to refine the EPR parameters as much as possible. Most such refinements are done by manual or brute-force fitting. Such fittings lack mathematical criteria and are time consuming. But because of their simplicity in programming, these methods are widely used. Hauser and Renaud (1) and McGavin and Tennant (2) fitted the powder spectra by these methods and obtained the fitted values of the Hamiltonian parameters. Other authors (3–5), who analyzed EPR powder spectra by simulation or fitting, seldom reported how to get the final values but just gave the simulated spectra.

It seems possible to minimize computer time and get refined spectroscopic parameters more quickly by using the optimization theory. A difficulty here is that the expression of a powder spectrum in most cases only can be written as an integral function instead of an analytical one. When the off-diagonal elements of the Hamiltonian are large compared with the diagonal ones, the resonance fields can only be calculated numerically. Even if the resonance fields can be expressed analytically, the integrations of powder spectra can be worked out only in a few cases. This hampers the direct application of optimization theory to EPR powder spectrum parameter refinement. In some cases, where certain approximations are made, analytical expressions are available. Ibers and Swalen (6), Lardon and Günthard (7), and Siderer and Luz (8) derived several expressions, which were only applicable to certain line shapes under some assumptions. For example, the expressions in refs. 6 and 7 were based on Lorentzian shape. Formulae in ref. 8 omitted the influence of the anisotropic transition probability factors. A general procedure for powder spectrum fitting is desirable.

In this paper we present a method for extracting parameters from an EPR powder spectrum by least-square fitting. It is applicable to cases where the resonance fields can be analytically expressed or can only be obtained by the diagonalization of Hamiltonian. It is also applicable to different spin-Hamiltonians and different line shapes. The method was used to fit the powder spectra of blue copper protein and $CuSO_4 \cdot 7H_2O$. The refined parameters as well as the fitted spectra were obtained and the line shapes were determined.

2. Calculation of powder spectrum

Since the EPR powder spectrum is a superposition of the spectra from a large number of randomly oriented paramagnetic centers, the expression for the powder spectrum is an integral

[1]Present address: Department of Scientific Instrumentation, Xiamen University, Xiamen, Fujian, China.

[2]Revision received September 26, 1988.

Printed in Canada / Imprimé au Canada

function (9)

$$[2.1]\quad I(H) = \int_0^{2\pi}\int_0^{\pi} \sin\theta\, d\theta\, d\varphi \sum_m P_m(\theta,\varphi)\left|\frac{\partial H_m(\theta,\varphi)}{\partial h\nu}\right| f_m\left(\frac{H - H_m(\theta,\varphi)}{\Delta H_m(\theta,\varphi)}\right)$$

where $I(H)$ is the microwave absorption, θ and φ are the orientation of applied field H with respect to principal axes of the **g** tensor, H_m, ΔH_m, $f_m((H - H_m)/\Delta H_m)$ and $P_m(\theta,\varphi)$ are the resonance field, line width, line shape function, and transition probability of the mth transition, respectively, and ν is the microwave frequency. In EPR spectra f_m is usually taken to be Gaussian or Lorentzian. Assuming the spin-Hamiltonian of the observed system to be $\mathcal{H}(H)$, H being the external applied field, we have

$$[2.2]\quad h\nu = E_j(H_m) - E_i(H_m)$$

where E_i is the eigenvalue of $\mathcal{H}$,

$$[2.3]\quad \mathcal{H}|i\rangle = E_i|i\rangle$$

The transition probability $P_m(\theta,\varphi)$ can be written as (9)

$$[2.4]\quad P_m(\theta,\varphi) = \left(\frac{\pi}{2}\right)\beta^2 H_1^2[|\langle i|g_x\cos\theta\cos\varphi\,\hat{S}_x + g_y\cos\theta\sin\varphi\,\hat{S}_y - g_z\sin\theta\,\hat{S}_z|j\rangle|^2 + |\langle i|g_x\sin\varphi\,\hat{S}_x - g_y\cos\varphi\,\hat{S}_y|j\rangle|^2]$$

where the $\hat{S}_i$ $(i = x, y, z)$ stand for electron spin operators, β is the Bhor's magneton, and H_1 is the magnetic field amplitude of the microwave radiation. $|\partial H_m/\partial h\nu|$ can be calculated from (13)

$$[2.5]\quad \left|\frac{\partial H_m}{\partial h\nu}\right| = \left|\frac{\partial \Delta E}{\partial H}\right|^{-1} = \left|\frac{\partial E_j}{\partial H} - \frac{\partial E_i}{\partial H}\right|^{-1}$$

Usually the complete powder spectrum [2.1] is calculated numerically. The major work involved is the evaluation of resonance fields. When perturbation theory can not be used, the brute-force (or consecutive) method is usually used so the computation time is long.

We find that the computation time can be greatly reduced by using the least-square fitting procedure given by Misra and Vasilopoulos (10) to find the angular variations of fields. In this method, first we calculate $H_m(\theta,\varphi)$ $(m = 1, 2, \ldots)$, at a certain orientation of the magnetic field by either the perturbation approach or by the brute-force method (9). Then using $H(\theta,\varphi)$ as the initial value of $H(\theta + \Delta\theta, \varphi + \Delta\varphi)$, we minimize the deviation

$$[2.6]\quad S = (|E_j - E_i| - h\nu)^2 = (|\Delta E| - h\nu)^2$$

until convergence is achieved by iteration

$$[2.7]\quad H_{k+1} = H_k + \lambda_k p_k$$

where

$$[2.8]\quad p_k = -\left(\frac{\partial S}{\partial H}\right)_{H_k}\left(\frac{\partial^2 S}{\partial H^2}\right)_{H_k}$$

Computing $\partial S/\partial H$ and $\partial^2 S/\partial H^2$ follows the method of Misra and Vasilopoulos (10):

$$[2.9]\quad \partial S/\partial H = 2(E_j - E_i)(|\Delta E| - h\nu)\left(\frac{\partial E_j}{\partial H} - \frac{\partial E_i}{\partial H}\right)\Big/ |\Delta E|$$

$$[2.10]\quad \partial^2 S/\partial H^2 = 2\left(\frac{\partial E_j}{\partial H} - \frac{\partial E_i}{\partial H}\right)^2 + (|\Delta E| - h\nu)(E_j - E_i)\left(\frac{\partial^2 E_j}{\partial H^2} - \frac{\partial^2 E_i}{\partial H^2}\right)\Big/ |\Delta E|$$

where

$$[2.11]\quad \partial E_i/\partial H = \mathrm{Tr}\left[\frac{\partial \mathcal{H}}{\partial H}|i\rangle\otimes\langle i|\right]$$

$$[2.12]\quad \partial^2 E_i/\partial H^2 = \sum_n{}' \mathrm{Tr}\left[\frac{\partial \mathcal{H}}{\partial H}(|i\rangle\otimes\langle i|)\frac{\partial \mathcal{H}}{\partial H}(|n\rangle\otimes\langle n|)\right]\Big/(E_i - E_n) + \text{c.c.}$$

In [2.12], c.c. stands for the complex conjugate of the first term, Tr stands for the trace, and

$$[2.13]\quad (|i\rangle\otimes\langle i|)_{pq} = |i\rangle_p|i\rangle_q^*$$

To find the angular variations of resonance fields we suggest that the number of fitting points of resonance fields be small. The values between two adjacent points can be found by interpolation.

3. The procedure for least-square fitting of powder spectrum

The general form of expression for a powder spectrum can be written

$$[3.1]\quad Q(H,\boldsymbol{a}) = \int_0^{2\pi}\int_0^{\pi} F(H,\boldsymbol{a},\theta,\varphi)\,d\theta\,d\varphi$$

from eqs. [2.1] and [3.1] we know

$$[3.2]\quad F(H,\boldsymbol{a},\theta,\varphi) = \sum_m \left|\frac{\partial H_m}{\partial h\nu}\right| P_m(\theta,\varphi) f_m\left(\frac{H - H_m}{\Delta H_m}\right)\sin\theta$$

F is an analytical function only when the resonance fields can be analytically expressed. When the line shape functions f_m are Gaussian or Lorentzian, Q represents the intensity of microwave absorption. When f_m are taken as the first derivatives of the functions, Q represents the derivative of the absorption spectrum; $\boldsymbol{a}$ is a vector the components of which are the parameters of both Hamiltonian and line shape. It can be written as

$$\boldsymbol{a} = (a_1, a_2, \ldots, a_N)$$

where N is the number of parameters.

From discrete sampling of the recorded spectrum (usually in the form of derivatives of absorption intensities), we can get a set of discrete data $e(H_i)$ $(i = 1, 2, \ldots, n_d)$, n_d being the number of sampling points. Using the DFP method (11) to fit the spectrum, we have to calculate the first derivatives of χ^2 with respect to $\boldsymbol{a}$. χ^2, the deviation of simulated and recorded spectrum, is given by

$$[3.3]\quad \chi^2 = \sum_{i=1}^{n_d}[Q(H_i,\boldsymbol{a}) - e(H_i)]^2$$

In [3.3], when $e(H_i)$ is the first derivative of the absorption, the shape functions f_m should also take the form of derivatives

Can. J. Chem. Downloaded from www.nrcresearchpress.com by 122.72.124.2 on 09/07/12
For personal use only.

Can. J. Chem. Downloaded from www.nrcresearchpress.com by 122.72.124.2 on 09/07/12
For personal use only.

so that Q represents the derivative of absorption. For calculation we can assume a theoretical model for the powder spectrum by giving the form of the spin-Hamiltonian and the line-shape function. After initial values of the parameters are guessed, the calculated spectrum $Q(H,\boldsymbol{a})$ can be obtained numerically.

In the DFP method, $\boldsymbol{a}_{k+1}$, the parameters in the $(k+1)$th iteration which leads to a smaller χ^2, can be obtained from $\boldsymbol{a}_k$:

$$[3.4] \quad \boldsymbol{a}_{k+1} = \boldsymbol{a}_k + \lambda_k \boldsymbol{p}_k$$

where λ_k is the search step length, $\boldsymbol{p}_k$ is the product of the DFP update matrix h and the gradient of χ^2 with respect to $\boldsymbol{a}$,

$$\boldsymbol{p}_k = -h_k . \boldsymbol{g}_k$$

$$\boldsymbol{g}_k = \left(\frac{\partial\chi^2}{\partial a_1}, \frac{\partial\chi^2}{\partial a_2}, \ldots, \frac{\partial\chi^2}{\partial a_N}\right)_k$$

$$[3.5] \quad h_k = h_{k-1} + \frac{s.s^{\mathrm{T}}}{s^{\mathrm{T}}.y} - \frac{h_{k-1}.y.y^{\mathrm{T}}.h_{k-1}}{y^{\mathrm{T}}.h_{k-1}.y}$$

$$s = \boldsymbol{a}_k - \boldsymbol{a}_{k-1}$$

$$y = \boldsymbol{g}_k - \boldsymbol{g}_{k-1}$$

where s^{T}, y^{T} are the column matrices of vectors s and y. Before iteration, the update matrix is set to unity. In constructing h, the derivatives of χ^2 in the kth iteration are only needed up to first order. When the integrand F in [3.1] is analytical, these derivatives can be obtained readily. Otherwise, F and its derivatives only can be found numerically.

For the calculation of

$$[3.6] \quad \frac{\partial\chi^2}{\partial a_l} = 2\sum_{i=1}^{n_d}[Q(H_i,\boldsymbol{a}_k) - e(H_i)]\frac{\partial Q(H_i,\boldsymbol{a}_k)}{\partial a_l} \qquad (l = 1, 2, \ldots, N)$$

we have to know $\partial F/\partial a_l$, which can be expressed as

$$[3.7] \quad \frac{\partial F}{\partial a_l} = \sum_m \left[D_h P_m f_m + \left|\frac{\partial H_m}{\partial h\nu}\right| D_p f_m + \left|\frac{\partial H_m}{\partial h\nu}\right| P_m D_f \right]$$

where

$$[3.8] \quad D_h = \frac{\partial}{\partial a_l}\left|\frac{\partial H_m}{\partial h\nu}\right|$$

$$[3.9] \quad D_p = \partial P_m/\partial a_l$$

$$[3.10] \quad D_f = \partial f_m/\partial a_l$$

From eq. [2.5] and [2.4] we get

$$[3.11] \quad D_h = -\left|\frac{\partial H_m}{\partial h\nu}\right| \left(\frac{\partial^2 E_j}{\partial H \partial a_l} - \frac{\partial^2 E_i}{\partial H \partial a_l}\right) \Big/ \left(\frac{\partial E_j}{\partial H} - \frac{\partial E_i}{\partial H}\right)$$

$$[3.12] \quad D_p = (\pi/2)\beta^2 H_1^2\{(\langle i|g_x \cos\theta \cos\varphi\, \hat{S}_x + g_y \cos\theta \sin\varphi\, \hat{S}_y - g_z \sin\theta\, \hat{S}_z|j\rangle)^*(\cos\theta\cos\varphi\langle g_x\hat{S}_x\rangle_{ij,l} + \cos\theta\sin\varphi\langle g_y\hat{S}_y\rangle_{ij,l} - \sin\theta\langle g_z\hat{S}_z\rangle_{ij,l}) + (\langle i|g_x \sin\varphi\, \hat{S}_x - g_y \cos\varphi\, \hat{S}_y|j\rangle)^*(\sin\varphi\langle g_x\hat{S}_x\rangle_{ij,l} - \cos\varphi\langle g_y\hat{S}_y\rangle_{ij,l})\} + \text{c.c.}$$

$$[3.13] \quad D_f = \frac{\partial f_m}{\partial a_l}\bigg|_{H_m} + \frac{\partial f_m}{\partial H_m}\cdot\frac{\partial H_m}{\partial a_l}$$

In eq. [3.12]

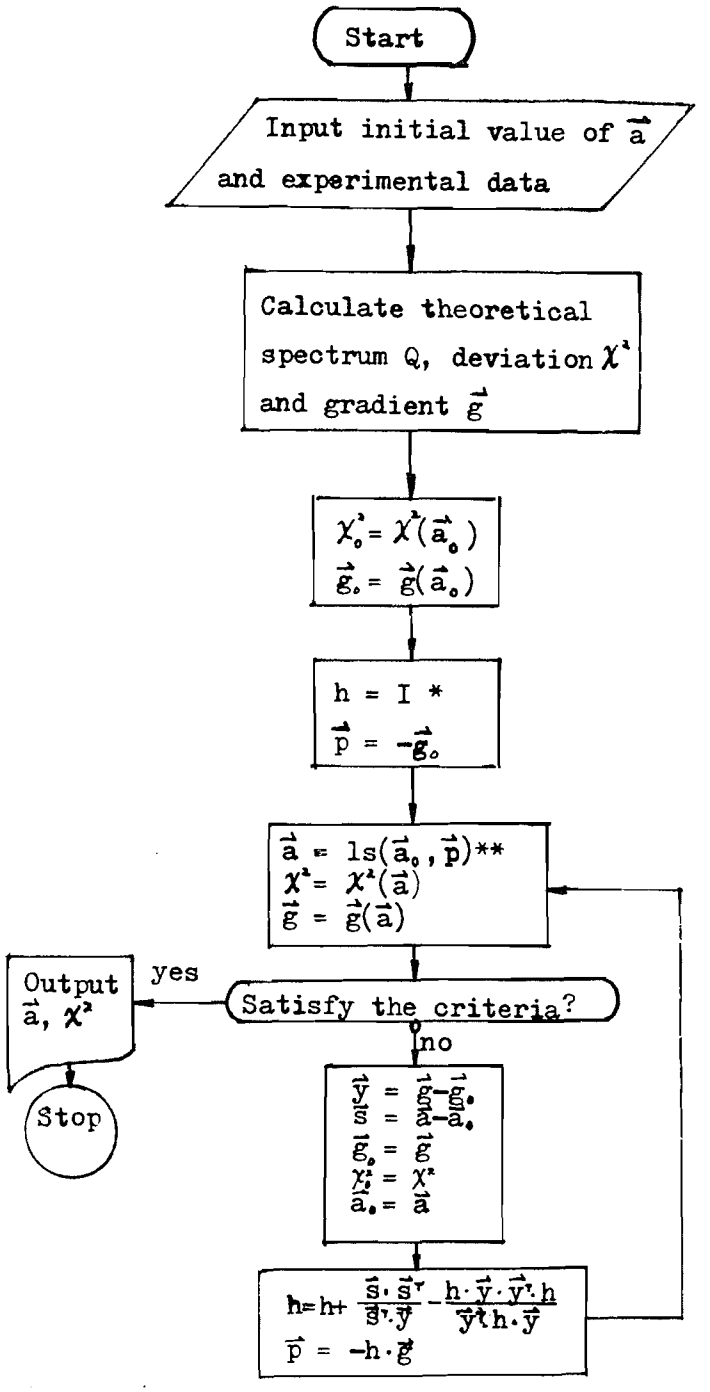


FIG. 1. The flow diagram of DFP subroutine (* I is a unit matrix. ** ls($\boldsymbol{a}_0$,$\boldsymbol{p}$) means the linear search of $\boldsymbol{a}$ which minimizes χ^2 following the search direction $\boldsymbol{p}$ and starting from $\boldsymbol{a}_0$ according to eq. [3.4]).

$$[3.14] \quad \langle g_k\hat{S}_k\rangle_{ij,l} = \frac{\partial g_k}{\partial a_l}\langle i|\hat{S}_k|j\rangle + g_k\Sigma_n{}'\,\mathrm{Tr}\left(\frac{\partial\mathcal{H}}{\partial a_l}|n\rangle\otimes\langle n|\hat{S}_k|j\rangle\otimes\langle i|\right)\Big/(E_i - E_n) + (\text{c.c. of second term with } i,j \text{ exchanged}) \qquad (k = x, y, z)$$

In eq. [3.13] the derivative of H_m is given by Van Veen (9)

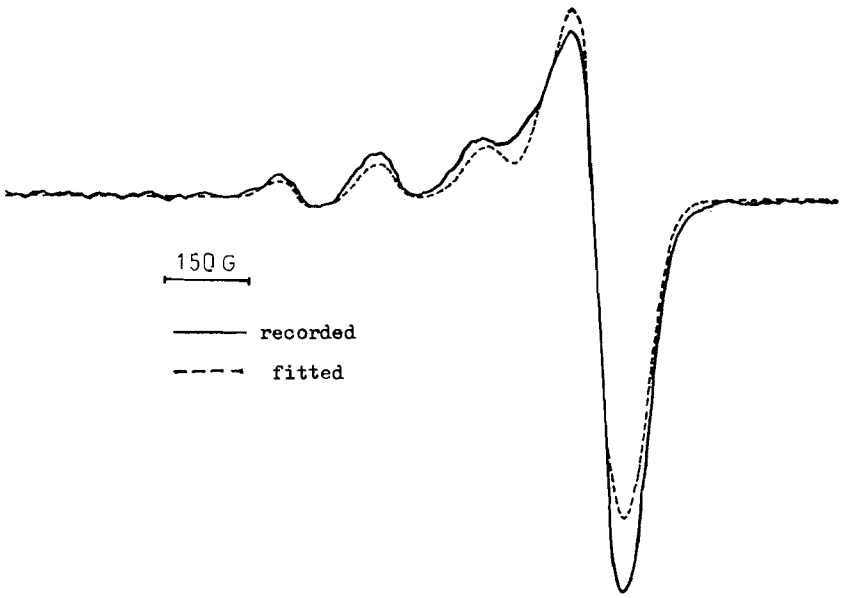


FIG. 2. Comparison of experimental and fitted spectrum of blue copper protein under Gaussian shape.

$$[3.15]\quad \frac{\partial H_m}{\partial a_l} = -\left(\frac{\partial E_j}{\partial a_l} - \frac{\partial E_i}{\partial a_l}\right) \Big/ \left(\frac{\partial E_j}{\partial H} - \frac{\partial E_i}{\partial H}\right)$$

In eqs. [3.11]–[3.15] only the first and second derivatives of energy E_i with respect to the parameters $\boldsymbol{a}$ and magnetic field H are needed. The way to calculate these derivatives numerically was given by Misra (10, 12).

4. Computer program for refining parameters by least-square fitting and illustrative examples

Using the method described above, we wrote a Fortran 77 program for powder spectrum fittings. The user must define the matrix elements of the Hamiltonian by writing a subroutine DEFHM. The initial parameters and experimental data are read first and then the DFP subroutine is called to fit the parameters. The flow diagram of DFP is shown in Fig. 1. The calculation of the gradients of χ^2 in DFP subroutine is performed by another subroutine GRD. In calculating the theoretical spectrum, the integration of [3.1] is performed and the values of resonance fields are obtained by least-square fitting as described in section 2. The values of $\Delta\theta$ and $\Delta\varphi$ are taken as 1 or 2 deg. As examples, we describe the fittings of room-temperature X-band EPR spectra of blue copper protein and $CuSO_4 \cdot 7H_2O$.

The number of fitting points N_d in both cases is taken as 45. Because the recorded spectra are the first derivatives of absorptions, the shape functions of individual lines which make up the powder spectra must take the form of first derivatives of Gaussian or Lorentzian functions,

$$[4.1]\quad f_G = y'_G\left(\frac{H - H_0}{\frac{1}{2}\Delta H_{pp}}\right) \exp\left[-\frac{1}{2}\left(\frac{H - H_0}{\frac{1}{2}\Delta H_{pp}}\right)^2\right]$$

$$[4.2]\quad f_L = y'_L\left(\frac{H - H_0}{\frac{1}{2}\Delta H_{pp}}\right)\left[1 + \frac{4}{3}\left(\frac{H - H_0}{\frac{1}{2}\Delta H_{pp}}\right)^2\right]^{-2}$$

where H_0 is the resonance field and ΔH_{pp} is the peak-to-peak line width of first derivative line shape and y'_G, y'_L are the normalization factors.

The spin Hamiltonian of blue copper protein can be written as

TABLE 1. Initial and fitted parameters of blue copper protein X-band EPR powder spectrum at room temperature

Parameter	Value	
	Initial	Final
$g_\parallel$	2.254	2.255
$g_\perp$	2.058	2.053
$A_\parallel$ (G)	167.8	162.8
$A_\perp$ (G)	7.8	7.1
ΔH_{pp} (G)	60.0	67.6

$$[4.3]\quad \mathcal{H} = \beta \boldsymbol{H}.\mathbf{g}.\boldsymbol{S} + \boldsymbol{I}.\mathbf{A}.\boldsymbol{S}$$

where $\mathbf{g}$ and $\mathbf{A}$ are axial symmetric. The initial values of the parameters listed in Table 1 are estimated from the experimental spectrum. In fitting, both Lorentzian and Gaussian line shapes are taken into consideration. The latter yields better result. When the fitting is completed, the reduction of χ^2 is 57% after 5 iterations and the CPU time taken in FACOM-M340S computer is 23 min. The fitted spectrum is given in Fig. 2.

In the spectrum fitting of $CuSO_4 \cdot 7H_2O$, the spin-Hamiltonian is taken as

$$[4.4]\quad \mathcal{H} = \beta \boldsymbol{H}.\mathbf{g}.\boldsymbol{S}$$

where $\mathbf{g}$ is asymmetric and the hyperfine splittings of Cu are neglected. The single crystal line width is assumed to be anisotropic due to the contribution of the unresolved hyperfine splittings (3),

$$[4.5]\quad \Delta H_{pp}^2 = \Delta H_1^2 \sin^2\theta\cos^2\varphi + \Delta H_2^2 \sin^2\theta \sin^2\varphi + \Delta H_3^2 \cos^2\theta$$

Like the case in ref. 1, the simulated spectrum using the initial guessed values, as extracted from the record spectrum, does not fit the experimental spectrum well and χ^2 is large. After 6 iterations χ^2 is reduced to 20% of the initial value. The

Can. J. Chem. Downloaded from www.nrcresearchpress.com by 122.72.124.2 on 09/07/12
For personal use only.

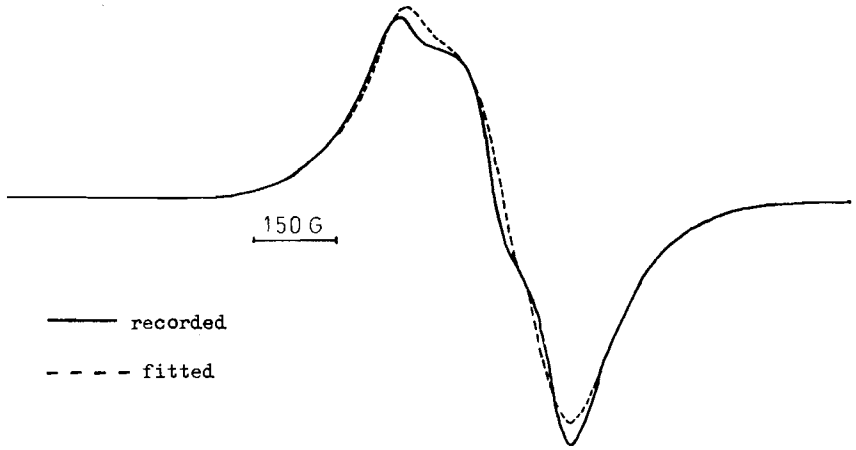


FIG. 3. Comparison of experimental and fitted spectrum of $CuSO_4 \cdot 7H_2O$ under Lorentzian shape.

TABLE 2. Initial and fitted parameters of $CuSO_4 \cdot 7H_2O$ X-band EPR powder spectrum at room temperature

	Value	
Parameter	Initial	Final
g_1	2.320	2.328
g_2	2.190	2.187
g_3	2.090	2.099
ΔH_1 (G)	160.0	149.5
ΔH_2 (G)	160.0	187.0
ΔH_3 (G)	160.0	162.0

computation time is 33 min. The initial and final parameters are listed in Table 2. Figure 3 shows the fitted spectrum.

5. Concluding remarks

The method presented in this paper is suitable for the quick refinement of EPR parameters after a reasonable simulated spectrum is obtained. It can be used to get the best fit of experimental data with certain theoretical models. In our program, the method of Misra is used to fit the angular variations of resonance fields. This method is much faster compared with the brute-force (or consecutive) method in finding the angular variations of resonance fields. It may happen that two or more resonance fields converge to the same value of the field at a particular orientation of θ or φ (10). In this case the calculation of the resonance fields needs manual intervention. But after that, the relationship between the resonance fields and corresponding levels is determined completely and further fitting of the fields can be performed automatically.

1. C. HAUSER and B. RENAUD. Phys. State Sol. (a), **10**, 161 (1972).
2. D. G. MCGAVIN and W. C. TENNANT. J. Magn. Reson. **62**, 357 (1985).
3. J. R. PILBROW and M. E. WINDFIELD. Mol. Phys. **25**, 1073 (1973).
4. A. M. MAURICE *et al.* J. Am. Chem. Soc. **105**, 3799 (1983).
5. YVES SERVANT *et al.* J. Magn. Reson. **24**, 335 (1976).
6. J. A. IBERS and J. D. SWALEN. Phys. Rev. **127**, 1914 (1962).
7. M. LARDON and Hs. H. GÜNTHARD. J. Chem. Phys. **44**, 2010 (1966).
8. Y. SIDERER and Z. LUZ. J. Magn. Reson. **37**, 449 (1980).
9. G. VAN VEEN. J. Magn. Reson. **30**, 91 (1978).
10. S. K. MISRA and P. VASILOPOULOS. J. Phys. C, **13**, 1083 (1980).
11. P. E. GILL, W. MURRAY, and M. H. WRIGHT. Practical optimization. Academic Press. 1981.
12. S. K. MISRA. J. Magn. Reson. **23**, 403 (1976).
13. R. S. DE BIASI and J. A. M. MANDONCA. Comp. Phys. Commun. **28**, 69 (1982).

Can. J. Chem. Downloaded from www.nrcresearchpress.com by 122.72.124.2 on 09/07/12
For personal use only.

Synthesis, characterization, and exchange of complexes of (*R*)-*N*,*N*-dimethylaminoethylferrocene with SO_2 and BF_3[1]

SYDNEY BROWNSTEIN, NAM FONG HAN, ERIC GABE, and FLORENCE LEE
Division of Chemistry, National Research Council of Canada, Ottawa, Canada K1A 0R9

Received May 11, 1988

SYDNEY BROWNSTEIN, NAM FONG HAN, ERIC GABE, and FLORENCE LEE. Can. J. Chem. **67**, 93 (1989).

Sulfur dioxide and (*R*)-*N*,*N*-dimethylaminoethylferrocene (**I**) react with an enthalpy of formation of 21.5 ± 1 kcal mol^{-1} to give a complex with sulfur bonded to nitrogen. The SO_2 exchanges between adduct molecules by a dissociation mechanism. BF_3 reacts with the above amine to give an adduct and its partly hydrolyzed product, $[(\eta^5\text{-}C_5H_5)Fe(\eta^5\text{-}C_5H_4\text{—}CH(CH_3)N(CH_3)_2\cdot BF(OH)_2]$ (**II**). **II** crystallizes in the orthorhombic space group $P2_12_12_1$ with a = 9.882(3), b = 10.625(5), and c = 13.988(13) Å and z = 4. R_f = 0.102 and R_w = 0.104.

Keywords: *N*,*N*-dimethylaminoethylferrocene complexes, X-ray structure, NMR exchange.

SYDNEY BROWNSTEIN, NAM FONG HAN, ERIC GABE et FLORENCE LEE. Can. J. Chem. **67**, 93 (1989).

Le dioxyde de soufre et le (*R*)-*N*,*N*-diméthylaminoéthylferrocène (**I**) réagissent avec une enthalpie de formation de 21.5 ± 1 kcal mol^{-1} pour donner un complexe dans lequel le soufre est lié à l'azote. Le SO_2 s'échange entre les molécules d'adduit par un mécanisme de dissociation. Le BF_3 réagit avec l'amine mentionnée plus haut; on obtient un adduit ainsi qu'un produit partiellement hydrolysé, $[(\eta^5\text{-}C_5H_5)Fe(\eta^5\text{-}C_5H_4\text{—}CH(CH_3)N(CH_3)_2\cdot BF(OH)_2]$ (**II**). Le produit **II** cristallise dans le groupe d'espace orthorhombique $P2_12_12_1$, avec a = 9,882(3), b = 10,625(5) et c = 13,988(13) Å et z = 4. R_f = 0.102 et R_w = 0,104.

Mots clés : complexes de *N*,*N*-diméthylaminoéthylferrocène, structure par rayons-X, échange RMN.

[Traduit par la revue]

Introduction

Reactions of aminoferrocenes with metal halides have been reported in the literature (1–3). Under certain reaction conditions 1:2 adducts of aminoferrocene – metal halides can be synthesized (3); but in most cases 1:1 adducts are the only products. *N*,*N*-Dimethylaminoethylferrocene, **I**, which can be easily resolved via its tartrate salt (4), is an important precursor for the synthesis of chiral ferrocenylphosphine ligands (5–10), but the donor ability of the amine itself seems to have not been studied with any common Lewis acid.

Complexes of sulfur dioxide and tertiary amines are well known, and the structure (11), and enthalpy of formation (12) of the simplest member $(CH_3)_3N\text{—}SO_2$, have been established. Boron trifluoride–amine complexes have been studied and the enthalpy of formation (13) and mechanism of exchange (14) determined for the triethylamine adduct.

As part of our continuing studies on the reactions of Lewis acids with tertiary aromatic amines (15), the reactions of **I** with SO_2 and BF_3 are presented here. The crystal structure of **II**, a partially hydrolyzed BF_3 adduct of **I**, is also described. There has been considerable study of the non-equivalence of groups in hindered tertiary amines arising either because of hindered rotation about the carbon–nitrogen bond (16), or because of slow inversion about pyramidal nitrogen (17). As far as we know, the present study is the first where the rate-determining step for averaging of magnetic non-equivalence of groups on a tertiary amine arises because of reversible quatenary complex formation.

Experimental

Chemicals

Boron trifluoride, from the suppliers cylinder, was stored over phosphorus pentoxide in a bulb on the vacuum line. Sulfur dioxide and methylene chloride were purified and stored as previously described (18). Chloroform was purified by a literature procedure (19). The amine **I** was prepared (20), and resolved (4) according to published procedures.

[1]NRCC No. 29696.

General procedures

*Reaction of **I** with SO_2*

The amine **I** was accurately weighed into an nmr tube equipped with a "Teflon" colinear "J. Young" valve so that the sequential addition of reactants could be done by vacuum transfer and each step of the reaction could be studied by nmr spectroscopy. A known quantity of $CHCl_3$ was condensed into the nmr tube and the nmr spectra of **I** were recorded. An appropriate amount of SO_2 (Table 1) was then transferred into the same tube and the nmr spectra at different temperatures were studied (Tables 1 and 2).

*Reaction of **I** with BF_3*

The reaction was carried out in essentially the same manner as for SO_2, using CH_2Cl_2 or $CHCl_3$ as solvent, and equimolar amounts of ***I*** (0.164 g) and BF_3 (0.043 g). After about 3 days at room temperature, the tube was opened and the solution was diluted with 5 mL of solvent followed by addition of 15 mL of hexane with stirring. A dark brown–green oily solid (*vide infra*) precipitated from the solution. The clear yellow–orange filtrate was kept at 4°C and orange crystals of **II** were obtained (ca. 40% isolated yield) and characterized by an X-ray crystal structure.

Magnetic resonance spectra were obtained on a "Bruker AM400" spectrometer at a magnetic field strength corresponding to 400 MHz for protons. Carbon and proton chemical shifts are reported with respect to tetramethylsilane, although the solvent was used as an internal reference and the appropriate correction applied. Fluorine resonance shifts are reported with respect to external $CFCl_3$.

X-ray diffraction intensities of an approximately 0.15 × 0.2 × 0.2 mm crystal of **II**, sealed in a glass capillary, were collected on a "Picker" diffractometer in the octants $+h$, $+k$, $+l$ to $2\theta_{max}$ = 45° with graphite monochromatized MoK_α radiation using the 2θ scan technique with profile analysis (21). A total of 1134 unique reflections were collected, of which 487 reflections were considered significant with $I_{net} \geq 2.5\sigma(I_{net})$. The absorption corrections were not made (μ = 1.0 mm^{-1}). The crystal decayed gradually and the intensities of the standard reflections at the end of the data collection were approximately 2/3 of the intensities at the start. The cell parameters were obtained by least-squares refinement of the setting angles of six reflections with two in the range of 28–32° (MoK_{α_1} = 0.70932 Å).

The structure was solved by direct methods and refined by full matrix least-squares techniques using the NRCVAX (22) program system. The final residuals are R_f = 0.103 and R_w = 0.104 for the significant

Can. J. Chem. Downloaded from www.nrcresearchpress.com by 122.72.124.2 on 09/07/12
For personal use only.

TABLE 1. Temperature dependance of the proton resonance spectra of **I** and SO_2 in $CHCl_3$ solutions

Mole fraction				
I	SO_2	T (K)	Line width (Hz)	Lifetime(s)
0.0763	0.0931	240	5.6, 6.1	0.2
0.0763	0.0931	247	14.6, 15.0	0.037
0.0763	0.0931	258	35.4	0.0045
0.0763	0.0931	272	9.17	0.0012
0.0382	0.1550	273	1.55[a]	0.0132
0.0382	0.1550	283	20.7	0.0031
0.0277	0.3885	272	18.3, 19.0	0.022

[a]The separate lines are not adequately separated so the peak/trough intensity ratio is listed.

data with unit weights. All atoms were refined isotropically except the Fe atom. H-atoms were placed at calculated positions on the ferrocene rings. The final atomic positional parameters and the equivalent isotropic temperature factors are listed in Table 3. The final structure factors are included as supplementary material as are the bond lengths and angles.[2]

The high R value is a consequence of the low crystal quality. Data were also collected for a second crystal and although the same structure was found, the final R values were even higher than reported here.

Results and discussion

Proton resonance spectra of chloroform solutions of **I** and SO_2 show, at room temperature, a single line for the hydrogens of the *N,N*-dimethyl group. As the temperature is lowered this line broadens, splits, and, at sufficiently low temperature, gives two sharp lines. These results are listed in Table 1. Since **I** contains a chiral carbon atom there will be magnetic non-equivalence for the two CH_2 groups bonded to nitrogen provided that it is co-ordinated to another ligand and therefore has a tetrahedral arrangement (23). The exchange which averages the two CH_3 signals in this system could arise either by dissociation of the SO_2 complex and recombination or by displacement of the complexed SO_2 by another SO_2 molecule in the solution, followed in each case by rapid inversion of pyramidal nitrogen. In the former case, the extent of dissociation, and therefore the rate of exchange, would be reduced by an excess of SO_2. In the latter case, the rate of displacement, and therefore the rate of exchange, would be increased by an excess of SO_2. The lifetimes towards exchange were determined by comparison of the experimental spectra with theoretical ones calculated for exchange via a stochastic procedure (24). These results, along with the concentrations, are listed in Table 1. It is obvious that the lifetime towards exchange increases with increasing SO_2 concentration, indicating that the exchange occurs by a dissociation mechanism.

The enthalpy of activation for exchange by a dissociation mechanism necessarily equals the enthalpy of formation of the SO_2 complex. From the temperature dependance of the lifetime for two of the samples of Table 1 activation enthalpies of 20.7 and 22.4 kcal mol^{-1} were calculated from the slope of the line fitted by a least-squares procedure. Therefore the heat of formation of the complex between **I** and SO_2 is 21.5 ± 1 kcal mol^{-1}. This is probably the first example of exchange averaging of two magnetically non-equivalent groups on a tertiary amine via dissociation of the quatenary adduct as the rate-determining step.

Additional weak peaks attributed to the H_2SO_3 adduct of **I** were observed at low temperature. At the temperatures used for the exchange studies there was no evidence for exchange on the nmr time scale between the SO_2 and H_2SO_3 adducts, although it did occur at room temperature. Although the SO_2 employed in these studies was dried over P_2O_5 traces of H_2SO_3 adducts, arising from H_2O in SO_2, or adsorbed on the glass of the vacuum system, were characterized in other amine systems (15). Chemical shifts of the assignable signals for these adducts are listed in Table 2.

The proton resonance spectra of $CHCl_3$ or CH_2Cl_2 solutions of **I** and BF_3 clearly indicate the presence of two different adducts which do not exchange at room temperature on the nmr time scale. As described in the experimental section, it is possible to isolate one of these species as orange crystals, **II** which are in the orthorhombic space group $P2_12_12_1$ with $a = 9.882(3)$, $b = 10.625(5)$, $c = 13.988(13)$ Å, $z = 4$, and $D_{calc} = 1.397$ Mg m^{-3}. A diagram of the structure is shown in Fig. 1 and bond distances and angles are listed in a supplementary table.[2] The iron atom is sandwiched between two cyclopentadienyl rings which are very close to planar and nearly parallel. The deviation from parallelism is 4.4°, and the rings are separated by an average of 3.30 Å. The atoms of one of the cyclopentadienyl rings are rotated by an angle of approximately 14° from the eclipsed position with the atoms of the other ring.

The crystal structure for **II** was solved in an effort to understand the magnetic resonance spectra of $CHCl_3$ or CH_2Cl_2 solutions of **I** and BF_3. Although the final refinement of the crystal structure of **II** is of poor quality, it is possible to unambiguously report that it is a partly hydrolyzed adduct of **I** and BF_3. Two equivalent atoms X, bonded to boron, have bond lengths of 1.48(7) and 1.59(9) Å. The third atom, Y, bonded to boron has a bond length of 1.18(9) Å. We assign the atoms X as oxygen, which will have a hydrogen bonded to it, and the atom Y as fluorine on the basis of the relative bond lengths and the ease of dissociation of the adduct (*vide supra*). A refinement of the crystal reflections with the X atoms as fluorine and Y as the OH fits the data equally well ($R_f = 0.102$ and $R_w = 0.104$). Unfortunately boron, oxygen, and fluorine are mutally interfering elements in the methods of elemental microanalysis. Boron–fluorine spin-coupling constants are frequently small and were not observable for this compound. Therefore, it is not possible to state with any confidence its exact identity. The primary purpose of showing that it is a partly hydrolyzed BF_3 adduct of **I** has been satisfied. The arrangement of the groups about the chiral carbon atom in **II** shows that it has retained its R configuration. The overall handedness of the crystal could not be determined with certainty.

Unlike the other amine adducts in this study, the proton resonance spectrum of the 1:1 adduct whose crystal structure was determined, **II** has only a single proton resonance signal for both methyl groups attached to nitrogen down to −60°C. The chemical shifts for **II** are listed in Table 2. Since $BF(OH)_2$ would be a weaker Lewis acid than BF_3, it is quite possible that exchange averaging of the two potential methyl resonances may be occurring by dissociation and recombination of the nitrogen–boron bond.

The proton, carbon, and fluorine magnetic resonance spectra of the other adduct, **III**, are listed in Table 2. These correspond in every way with what one would expect for a normal BF_3

[2]Supplementary material mentioned in the text may be purchased from the Depository of Unpublished Data, CISTI, National Research Council of Canada, Ottawa, Ont., Canada, K1A 0S2.

Can. J. Chem. Downloaded from www.nrcresearchpress.com by 122.72.124.2 on 09/07/12
For personal use only.

TABLE 2. Chemical shifts of **I** and its SO_2, H_2SO_3, and BF_3 complexes[a]

Nuclear species	Chemical shift					
	I	**I**·SO_2	**I**·H_2SO_3	**II**	**III**	**I**·$H^+BH_4^-$[b]
C—CH_3[c]	1.41	1.51	1.67	1.78	1.67	1.69
C—CH_3	16.1	15.4	15.0	15.5	16.7	14.7
C—*H*	3.56	3.81	4.38	4.46	4.11	4.32
C—H	58.4	58.9	62.6	62.6	61.5	63.8
N—CH_3	2.05	1.82,1.97[d]	2.38,2.55[d]	2.59	2.20,2.38	2.54,2.59
N—CH_3	40.6	37.7	37.1,40.6	39.4	37.1,44.8	38.5,39.9
Fe—C_5H_5	4.08	4.05	4.18	4.21	4.17	4.24
Fe—C_5H_5	68.4	68.8	69.1	69.4	69.1	69.5
Fe—C_5H_4[e]	4.10	4.12	4.12	4.33	4.20	4.39
Fe—C_5H_4	66.6,67.0	66.9,68.0	67.8,68.2	67.4,69.5	68.2,68.8	67.4,69.8
	67.2,69.1	68.1,70.0	68.6,71.2	69.7,70.5	68.9,71.6	70.0,70.3
	87.0	83.7	79.6	79.4	81.3	78.6
F	—	—	—	−151.8	−151.1	−151.9

[a]Unless otherwise quoted, all spectra were recorded in $CHCl_3$ or $CDCl_3$ solution and at room tempertaure.
[b]Spectra recorded in CH_2Cl_2.
[c]For all complexes $J_{H—CH3} = 6.8$ Hz.
[d]Spectra recorded at −58°C.
[e]These chemical shifts are the mean values for a group of unresolved multiplets.

TALBE 3. Atomic parameters *x*, *y*, *z* and B_{iso} for **II**

Atom	*x*	*y*	*z*	B_{iso}[a]
Fe	0.9101(5)	0.2469(8)	0.1867(3)	5.0(3)
O1	0.323(3)	0.1365(24)	0.2886(18)	3.4(6)
O2	0.2971(22)	0.2118(25)	0.4237(16)	5.4(7)
F	0.330(5)	0.342(4)	0.271(3)	13.6(16)
N	0.5197(25)	0.264(5)	0.3518(17)	4.9(7)
C1	1.028(4)	0.326(4)	0.080(3)	4.0(9)
C2	1.068(5)	0.202(4)	0.099(3)	6.9(14)
C3	0.954(4)	0.123(4)	0.079(3)	4.9(10)
C4	0.846(5)	0.215(7)	0.048(4)	9.8(20)
C5	0.882(4)	0.331(4)	0.0544(25)	2.9(8)
C6	0.840(4)	0.161(4)	0.302(3)	3.3(10)
C7	0.975(4)	0.210(4)	0.317(3)	4.6(10)
C8	0.960(3)	0.340(3)	0.310(3)	2.6(7)
C9	0.827(5)	0.377(4)	0.282(3)	4.5(11)
C10	0.750(3)	0.259(5)	0.2834(18)	3.3(6)
C11	0.604(3)	0.225(3)	0.2621(20)	3.7(7)
C12	0.564(4)	0.176(4)	0.191(3)	6.3(10)
C13	0.544(7)	0.136(5)	0.406(4)	7.1(16)
C14	0.558(6)	0.366(4)	0.420(3)	4.3(11)
B	0.347(5)	0.271(9)	0.335(4)	7.3(15)
H1	1.094	0.407	0.081	4.7
H2	1.166	0.171	0.125	7.4
H3	0.946	0.022	0.086	5.7
H4	0.751	0.185	0.021	10.5
H5	0.819	0.413	0.045	3.7
H6	0.814	0.062	0.306	4.2
H7	1.068	0.159	0.329	5.6
H8	1.039	0.406	0.325	3.0
H9	0.791	0.470	0.265	4.6

[a]B_{iso} is the mean of the principal axes of the thermal ellispoid.

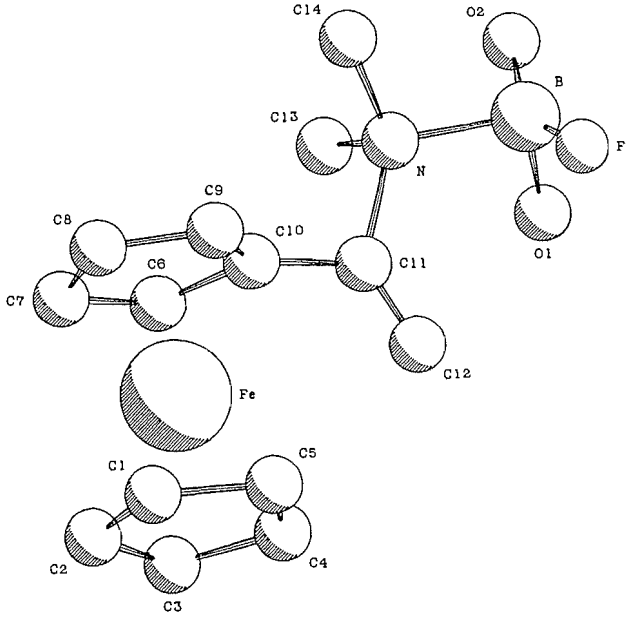


FIG. 1. The structure of $(\eta^5\text{-}C_5H_5)Fe(\eta^5\text{-}C_5H_4—CH(CH_3)N(CH_3)_2 \cdot BF(OH)_2$ (**II**), a partially hydrolyzed 1:1 adduct of **I** and BF_3.

adduct. The quadruplet of doublets assigned to the C—CH_3 group are assigned to a long range coupling ($J = 1.2$ Hz) with the three equivalent fluorines of the complexed BF_3. When the reaction mixture is diluted with *n*-hexane, a dark brown–green oily solid is precipitated. Its magnetic resonance spectral parameters, also listed in Table 2, are consistent with its assignment as the fluoborate salt of **I**. The most compelling evidence is the doubling of the signals for each N—CH_3 grouping by spin coupling with the H^+ bonded to nitrogen ($J = 4.9$ Hz). There is no magnetic resonance spectral evidence for a ring substituted species therefore the salt is thought to be produced from acid generated by hydrolysis of BF_3 by traces of water introduced in a similar fashion to that with SO_2, or in the workup of **II**.

We may conclude that addition of Lewis acids and the proton to **I** is solely on nitrogen in preference to iron. From the evidence for magnetic averaging of the two *N*-methyl groups we may conclude that the stability of the complexes to dissociation is $BF_3 \approx H^+ > SO_2 \approx H_2SO_3 > BF(OH)_2$.

Can. J. Chem. Downloaded from www.nrcresearchpress.com by 122.72.124.2 on 09/07/12
For personal use only.

1. S. C. JAIN and R. RIVEST. J. Inorg. Nucl. Chem. **32**, 1579 (1970).
2. B. BAJPAI and K. K. BAJPAI. J. Inorg. Nucl. Chem. **43**, 1938 (1981).
3. P. P. SINGH, R. CHAND, and R. RIVEST. J. Inorg. Nucl. Chem. **37**, 45 (1975).
4. G. W. GOKEL and I. K. UGI. J. Chem. Educ. **49**, 294 (1972).
5. W. R. CULLEN, S. V. EVANS, N. F. HAN, and J. TROTTER. Inorg. Chem. **26**, 514 (1987).
6. T. HAYASHI, T. MISE, M. FUKUSHIMA, M. KAGOTANI, N. NAGASHIMA, Y. HAMADA, A. MATSUMOTO, S. KAWAKAMI, M. KONISHI, K. YAMAMOTO, and M. KUMADA. Bull. Chem. Soc. Jpn. **53**, 1138 (1980).
7. I. R. BUTLER, W. R. CULLEN, and T. J. KIM. Synth. React. Inorg. Met. Org. Chem. **15**, 109 (1985).
8. W. R. CULLEN, F. W. B. EINSTEIN, C. H. HUANG, A. C. WILLIS, and E. S. YEH. J. Am. Chem. Soc. **102**, 988 (1980).
9. T. D. APPLETON, W. R. CULLEN, S. V. EVANS, T. J. KIM, and J. TROTTER. J. Organomet. Chem. **279**, 5 (1985).
10. W. R. CULLEN and N. F. HAN. Appl. Organomet. Chem. **1**, 1 (1987).
11. D. VAN DER HELM, J. D. CHILDS, and S. D. CHRISTIAN. J. Chem. Soc. Chem. Commun. 887 (1969).
12. J. GRUNDNESS and S. D. CHRISTIAN. J. Am. Chem. Soc. **90**, 2239 (1968).
13. H. C. BROWN, P. F. STEHLE, and P. A. TIERNEY. J. Am. Chem. Soc. **79**, 2020 (1957).
14. S. BROWNSTEIN, A. M. EASTHAM, and G. A. LATREMOUILLE. J. Phys. Chem. **67**, 1028 (1963).
15. S. BROWNSTEIN, E. GABE, F. LEE, and B. LOUIE. J. Org. Chem. **53**, 951 (1988).
16. S. BROWNSTEIN, E. C. HORSWILL, and K. U. INGOLD. J. Am. Chem. Soc. **92**, 7217 (1970).
17. C. H. BUSHWELLER, W. G. ANDERSON, P. E. STEVENSON, and J. W. O'NEILL. J. Am. Chem. Soc. **97**, 4338 (1975).
18. L. K. TAN and S. BROWNSTEIN. J. Org. Chem. **48**, 302 (1983).
19. A. I. VOGEL. Textbook of practical organic chemistry. Longman, London. Vol. 4. 1978. p. 267.
20. C. R. HAUSER and J. K. LINDSAY. J. Org. Chem. **22**, 906 (1957).
21. D. F. GRANT and E. J. GABE. J. Appl. Crystallogr. **11**, 114 (1978).
22. E. J. GABE, F. L. LEE, and Y. LEPAGE. Crystallographic computing 3: data collection, structure determination, proteins and databases. *Edited by* G. M. Sheldrick, C. Kruger, and R. Goddard. Clarendon Press, Oxford. 1985. p. 167.
23. P. M. NAIR and J. D. ROBERTS. J. Am. Chem. Soc. **79**, 4565 (1957).
24. S. BROWNSTEIN and J. BORNAIS. Can. J. Chem. **46**, 225 (1968).

Can. J. Chem. Downloaded from www.nrcresearchpress.com by 122.72.124.2 on 09/07/12
For personal use only.

Réactions ion/molécule de l'ion $C_2H_3Cl^+$ dans le mélange gazeux : chlorure de vinyle – chlorure d'éthyle

JAN A. HERMAN,[1] RODICA NEAGU-PLESU ET LESZEK WÓJCIK[2]

Département de chimie et Centre de recherches en atomes et molécules, Université Laval, Québec (Qué.), Canada G1K 7P4

Reçu le 13 juin 1988

JAN A. HERMAN, RODICA NEAGU-PLESU et LESZEK WÓJCIK. Can. J. Chem. **67**, 97 (1989).

Les réactions ion/molécule de $C_2H_3Cl^+$ ont été étudiées dans le mélange de chlorure de vinyle avec du chlorure d'éthyle. Les processus ioniques ont été suivis sur deux spectromètres de masse : le premier à résonance cyclotronique ionique (RCI), le deuxième à photoionisation et à haute pression. Les résultats obtenus sur ces deux instruments sont partiellement complémentaires. Il ressort que l'ion $C_2H_3Cl^+$ ne réagit pas directement avec le chlorure d'éthyle. Cependant, les ions $C_4H_3Cl^+$ et $C_4H_6Cl^+$, formés à la suite de la décomposition de l'ion-dimère excité du chlorure de vinyle, réagissent avec le chlorure d'éthyle dans une séquence de réactions de condensation avec élimination dans chaque étape du HCl ou Cl. Dans le mélange des deux chlorures les ions les plus abondants sont $C_8H_{13}^+$ et $C_8H_{14}^+$ dont l'intensité totale à 1 Torr de pression compte pour environ 50%.

Mots clés : réactions ion/molécule de $C_2H_3Cl^+$, mélange de chlorure de vinyle avec du chlorure d'éthyle, spectrométrie de masse.

JAN A. HERMAN, RODICA NEAGU-PLESU, and LESZEK WÓJCIK. Can. J. Chem. **67**, 97 (1989).

Ion/molecule reactions of $C_2H_3Cl^+$ have been studied in a mixture of vinyl and ethyl chlorides. The ionic processes have been followed using two mass spectrometers; one is based on the ionic cyclotronic resonance (ICR) while the other is based on photo-ionization at high pressure. The results obtained on these two instruments are complementary and they indicate that the ion $C_2H_3Cl^+$ does not react directly with ethyl chloride. However, the ions $C_4H_3Cl^+$ and $C_4H_6Cl^+$, which are formed following the decomposition of the excited ion-dimer of vinyl chloride, do react with ethyl chloride in a series of condensation reactions involving in each step an elimination of HCl or of Cl. In a mixture of the two chlorides, the most important ions are the $C_8H_{13}^+$ and $C_8H_{14}^+$; at a pressure of 1 Torr, their total intensity is equal to 50%.

Key words: ion/molecule reactions of $C_2H_3Cl^+$, vinyl and ethyl chloride mixtures, mass spectrometry.

[Journal translation]

Can. J. Chem. Downloaded from www.nrcresearchpress.com by 122.72.124.2 on 09/07/12
For personal use only.

Introduction

Les réactions ion/molécule de l'ion $C_2H_3Cl^+$ dans le chlorure de vinyle gazeux d'une part, et de l'ion $C_2H_5Cl^+$ avec le chlorure d'éthyle sont bien documentées (1–9).

Dans une étude des réactions ion/molécule par spectrométrie de masse RCI (Résonance Cyclotronique Ionique) du chlorure d'éthyle Beauchamp *et al.* ont remarqué que l'ion $C_2H_3Cl^+$, formé par décomposition de l'ion parent $C_2H_5Cl^+$, ne semble pas réagir avec le chlorure d'éthyle neutre (7). Il était intéressant de vérifier cette observation dans des conditions similaires à celles des expériences de Beauchamp *et al.* (ionisation par impact électronique à 15 eV) d'une part, et d'autre part dans les conditions d'un spectromètre de masse à haute pression où l'ion $C_2H_3Cl^+$ est formé à partir du chlorure de vinyle par photoionisation à 10,64 eV, ce qui est en dessous du seuil du potentiel d'ionisation du chlorure d'éthyle (PI = 10,97 eV) (10). Nous espérions que l'ion $C_2H_3Cl^+$, formé à partir de précurseurs C_2H_3Cl et C_2H_5Cl dans des conditions différentes, pourrait éventuellement réagir dans des processus ioniques distincts révélant leurs origines.

Partie expérimentale

Les mesures ont été exécutées sur deux spectromètres de masse : (*a*) à haute pression et à photoionisation, déjà décrit (11, 12), et (*b*) à résonance cyclotronique ionique dont voici une description succincte.

Ce spectromètre de masse, construit au laboratoire, est inspiré de celui décrit par McIver (13). L'électro-aimant avec son alimentation provient d'un spectromètre de masse cycloïdale M-66 de Varian Inc. Dans l'entrefer de 40 mm est logée la cellule cubique de 25 mm de côté qui sert à la détection des ions caractérisés par leur fréquence cyclotronique naturelle (14). Cette cellule est constituée de six plaques en molybdène isolées les unes des autres. Les deux plaques perpendiculaires aux lignes de force du champ magnétique, appelées plaques de piégeage, sont à un potentiel de +1 V. Les quatre autres plaques parallèles aux lignes de force du champ magnétique sont groupées par paire et servent à l'excitation et à la détection des ions. Les deux paires sont à un potentiel de −0,5 V. À une des paires de ces électrodes, dites d'excitation, est superposé un signal radiofréquence de 50–500 kHz de 0,5 V d'amplitude maximum. L'autre paire, appelée électrodes de détection, capte les signaux RF induits par le mouvement circulaire des ions en résonance cyclotronique avec le champ électrique alternatif de radiofréquence.

Le circuit électronique de détection est un pont capacitif décrit par McIver *et al.* (15), mais ayant le préamplificateur dans l'enceinte à vide le plus près possible de la cellule de mesure.[3] Un circuit d'impulsion dont la séquence est montrée à la figure 1 permet de varier le temps de réaction entre 2 et 1000 ms. Les périodes d'excitation et de détection sont respectivement de 2 et 4 ms.

L'enceinte principale contenant la cellule cubique de détection est évacuée au moyen d'une pompe de diffusion fonctionnant sur l'huile Santovac 5 et munie d'un piège à azote liquide. Le degré du vide est mesuré par une jauge à ionisation, modèle 844, de Varian Inc. et en absence d'échantillon gazeux il se situe à 10^{-7} Torr ($1,3 \times 10^{-4}$ N m^{-2}). Un système de robinets de haut vide à débit contrôlé, permet lors des mesures, de maintenir la pression de l'échantillon gazeux à une valeur fixe prédéterminée au voisinage de 10^{-5} Torr ($1,3 \times 10^{-2}$ N m^{-2}).

Les ions sont formés par impact d'électrons de 70 V dans une impulsion dont la durée est de 1,5 ms.

Le chlorure de vinyle et le chlorure d'éthyle de Matheson sont tous deux de pureté supérieure à 99,7% et sont utilisés tels quels. Leurs mélanges en proportions contrôlées sont préparés dans un système à vide conventionnel. Le chlorure de vinyle perdeutéré, 99,5%, provient de Merck, Sharp & Dohme.

1. Auteur à qui adresser toute correspondance.

2. Adresse actuelle : Institut de Physique, Université Marie Curie-Sklodowska, Lublin, Pologne.

3. J. Bartmess, communication privée.

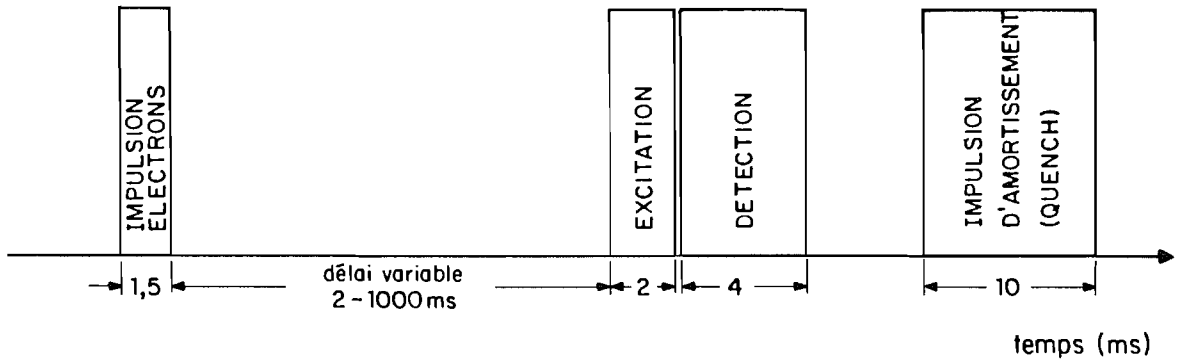


FIG. 1. Séquence d'impulsion du spectromètre de masse RCI.

Résultats et discussion

(a) Étude par spectrométrie de masse RCI

L'évolution des intensités fractionnaires des principaux ions des composés purs et de leurs mélanges est présentée à la figure 2. Le tableau 1 complète cette information en indiquant les intensités fractionnaires des autres ions présents dans la cellule de réaction après 20, 50 et 100 ms.

Les valeurs des intensités fractionnaires (figure 2 et tableau 1) pour le chlorure de vinyle pur peuvent être comparées à celles publiées par Baldeschwieler et coll. (1) et par Anicich et Bowers (4) obtenues par spectrométrie de masse RCI. Dans leurs cas la distribution des principaux ions formés dans les processus bimoléculaires est $C_3H_4Cl^+ : C_4H_5Cl^+ : C_4H_6Cl^+ = 0{,}29 : 0{,}57 : 0{,}14$, où les valeurs numériques sont les moyennes de leurs résultats. Dans le cas présent pour le temps le plus court de détection (2 ms), ce rapport devient : $C_3H_4Cl^+ : C_4H_5Cl^+ : C_4H_6Cl^+ = 0{,}19 : 0{,}57 : 0{,}24$. La différence entre les valeurs de ces rapports est probablement due aux différentes conditions expérimentales. L'utilisation d'une cellule à entraînement (anglais : drift cell), où le temps de séjour des ions est de l'ordre de 500 μs (1, 4), n'est pas comparable à nos conditions d'une cellule cubique où la présence des ions est beaucoup plus longue avant leur détection. D'autre part, il est reconnu que les constantes de vitesse absolues et relatives des réactions de condensation de l'ion $C_2H_3Cl^+$ sont très sensibles à des différences en énergie cinétique et interne, surtout entre 0 et 2 eV (4). Il n'est donc pas exclus que les résultats présents comparés à ceux d'Anicich et de Baldeschwieler ne soient le reflet que d'une différence en énergie interne des ions $C_2H_3Cl^+$.

Ces résultats confirment nos connaissances des processus ion/molécule dans le chlorure de vinyle et le chlorure d'éthyle purs (1, 4, 7–9). En effet, dans le chlorure de vinyle pur les réactions ion/molécule sont les suivantes :

[1] $C_2H_3Cl^+ + C_2H_3Cl \rightarrow (C_2H_3Cl)_2{}^+* \rightarrow C_4H_5Cl^+ + HCl$

[2] $\rightarrow C_4H_6Cl^+ + Cl^\cdot$

[3] $\rightarrow C_3H_4Cl^+ + CHCl^\cdot$

[4] $C_2H_3{}^+ + C_2H_3Cl \rightarrow C_2H_4Cl^+ + C_2H_2$

La réaction [4] apparaît dans le chlorure de vinyle ionisé par impact électronique, où l'énergie est suffisante pour dissocier l'ion parent en $C_2H_3{}^+$ (2). L'ion $C_4H_5{}^+$ (m/z = 53), qui apparaît dans le chlorure de vinyle pur, provient selon toute vraisemblance de la décomposition des ions $C_4H_5Cl^+$ et $C_4H_6Cl^+$ avec perte de chlore atomique ou de chlorure d'hydrogène. Remarquons que l'ion $C_4H_5{}^+$ ne semble plus

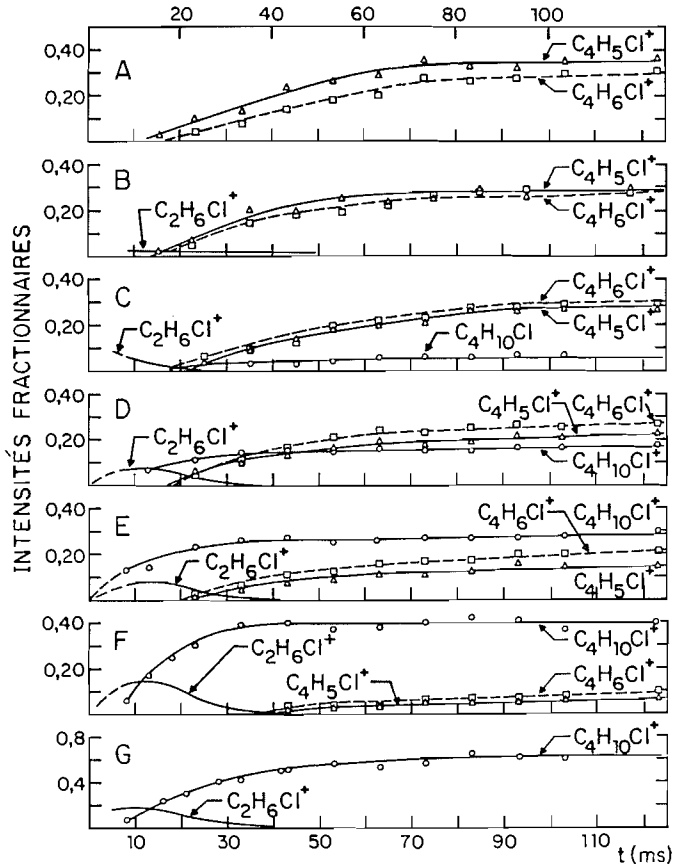


FIG. 2. Intensités fractionnaires des principaux ions dans les chlorure de vinyle et le chlorure d'éthyle purs et en mélange en spectrométrie RCI. (A) C_2H_3Cl (100%); (B) C_2H_3Cl (80%) + C_2H_5Cl (20%); (C) C_2H_3Cl (60%) + C_2H_5Cl (40%); (D) C_2H_3Cl (40%) + C_2H_5Cl (60%); (E) C_2H_3Cl (20%) + C_2H_5Cl (80%); (F) C_2H_3Cl (10%) + C_2H_5Cl (90%); (G) C_2H_5Cl (100%).

réagir avec les neutres, puisque son intensité fractionnaire augmente avec son temps de séjour dans la cellule de réaction (tableau 1).

L'ion moléculaire du chlorure d'éthyle pur réagit principalement dans un processus de formation de l'ion diéthylchloronium (7, 9) :

[5] $C_2H_5Cl^+ + C_2H_5Cl \rightarrow C_2H_6Cl^+ + C_2H_4Cl^\cdot$

[6] $C_2H_6Cl^+ + C_2H_5Cl \rightarrow (C_2H_5)_2Cl^+ + HCl$

et de plus il peut provenir de

Can. J. Chem. Downloaded from www.nrcresearchpress.com by 122.72.124.2 on 09/07/12
For personal use only.

TABLEAU 1. Intensités fractionnaires (%) des ions en spectrometrie de masse RCI

Système	Ion	Temps (ms) 20	50	100
C_2H_3Cl pur	$C_4H_5^+$ (m/z = 53)	10	10	12
	$C_2H_3Cl^+$ (m/z = 62, 64)	43	19	0
	$C_2H_4Cl^+$ (m/z = 63, 65)	23	18	0
	$C_3H_4Cl^+$ (m/z = 75, 77)	3	5	6
C_2H_3Cl (80%) + C_2H_5Cl (20%)	$C_4H_5^+$	6	5	5
	$C_4H_7^+$ (m/z = 55)	6	6	10
	$C_2H_3Cl^+$	40	20	3
	$C_2H_4Cl^+$	20	15	3
	$C_2H_6Cl^+$ (m/z = 65, 67)	2	0	0
	$C_3H_4Cl^+$	2	5	6
C_2H_3Cl (60%) + C_2H_5Cl (40%)	$C_4H_5^+$	2	3	1
	$C_4H_7^+$	8	10	10
	$C_2H_3Cl^+$	40	22	4
	$C_2H_4Cl^+$	27	15	3
	$C_2H_6Cl^+$	2	0	0
	$C_3H_4Cl^+$	1	4	6
	$C_6H_7^+$ (m/z = 79)	0	1	6
C_2H_3Cl (40%) + C_2H_5Cl (60%)	$C_4H_5^+$	1	1	0
	$C_4H_7^+$	11	10	10
	$C_4H_8^+$ (m/z = 56)	<0,5	Trace	
	$C_4H_9^+$ (m/z = 57)	1	1	1
	$C_2H_3Cl^+$	33	16	4
	$C_2H_4Cl^+$	21	10	1
	$C_2H_6Cl^+$	3	0	0
	$C_3H_4Cl^+$	1	3	4
	$C_6H_7^+$	0	2	9
C_2H_3Cl (20%) + C_2H_5Cl (80%)	$C_4H_5^+$	<0,5	0	0
	$C_4H_7^+$	8	8	8
	$C_4H_8^+$	2	3	3
	$C_4H_9^+$	3	3	3
	$C_2H_3Cl^+$	29	20	9
	$C_2H_4Cl^+$	23	14	5
	$C_2H_6Cl^+$	4	0	0
	$C_3H_4Cl^+$	1	2	3
	$C_6H_7^+$	0	1	5
C_2H_3Cl (10%) + C_2H_5Cl (90%)	$C_4H_7^+$	4	5	5
	$C_4H_8^+$	3	4	4
	$C_4H_9^+$	5	6	6
	$C_2H_3Cl^+$	23	20	16
	$C_2H_4Cl^+$	19	20	12
	$C_2H_6Cl^+$	7	<0,5	0
	$C_3H_4Cl^+$	0	<1	1
	$C_6H_7^+$	<0,5	1	1
C_2H_5Cl pur	$C_4H_8^+$	4	4	4
	$C_4H_9^+$	5	7	6
	$C_2H_3Cl^+$	13	15	14
	$C_2H_4Cl^+$	15	16	14
	$C_2H_6Cl^+$	9	0	0

[7] $C_2H_5^+ + C_2H_5Cl \rightarrow (C_2H_5)_2Cl^+$

L'ion $C_4H_{10}Cl^+$ ne réagit plus avec le chlorure d'éthyle neutre. Pareillement, les ions $C_2H_3Cl^+$ et $C_2H_4Cl^+$, formés par dissociation de l'ion parent $C_2H_5Cl^+$, semblent ne pas réagir avec le chlorure d'éthyle neutre puisque leurs intensités fractionnaires ne changent plus avec le temps (tableau 1). Les deux ions $C_4H_8^+$ et $C_4H_9^+$ proviennent probablement de la dissociation du $(C_2H_5)_2Cl^+$ excité, car ces ions apparaissent uniquement quand la proportion de l'ion diéthylchloronium est relativement importante dans le système.

En ce qui concerne les mélanges de C_2H_3Cl avec C_2H_5Cl, on note une absence totale des ions $C_4H_7Cl^+$ et $C_4H_8Cl^+$ qui pourraient être formés dans des réactions similaires aux processus [1] et [2]. On doit donc conclure que ni le $C_2H_3Cl^+$, ni l'ion $C_2H_5Cl^+$ ne réagissent respectivement avec le chlorure d'éthyle

Can. J. Chem. Downloaded from www.nrcresearchpress.com by 122.72.124.2 on 09/07/12
For personal use only.

Can. J. Chem. Downloaded from www.nrcresearchpress.com by 122.72.124.2 on 09/07/12
For personal use only.

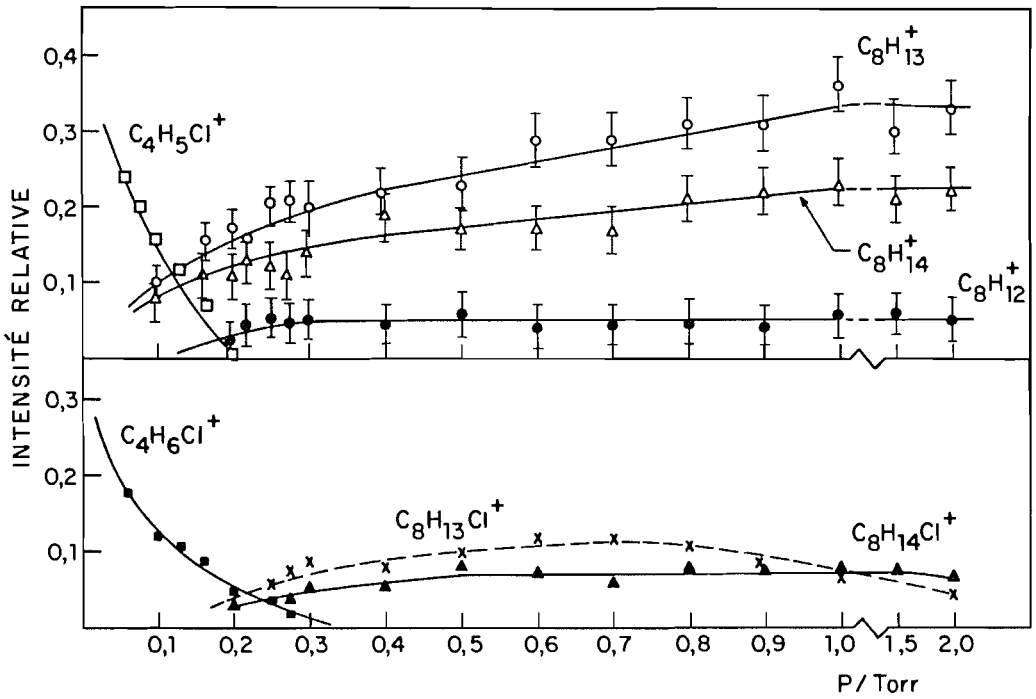


FIG. 3. Intensités fractionnaires en fonction de la pression totale des principaux ions dans le mélange C_2H_3Cl (10%) + C_2H_5Cl (90%) photoionisé.

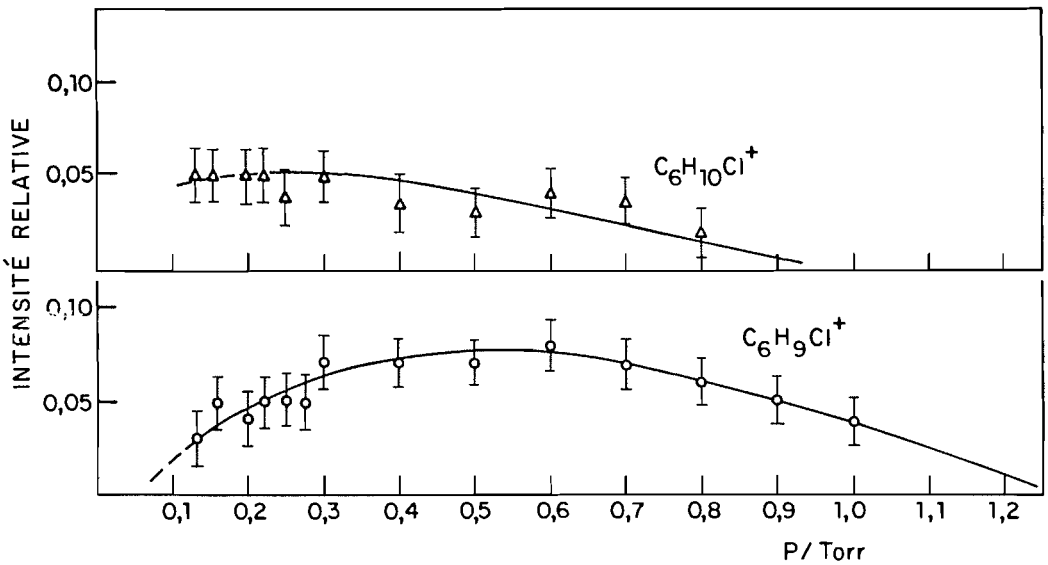


FIG. 4. Intensités fractionnaires en fonction de la pression totale des ions en C_6 dans le mélange C_2H_3Cl (10%) + C_2H_5Cl (90%) photoionisé.

neutre et le chlorure de vinyle neutre. Ceci est une indication que le complexe collisionnel excité $(C_2H_3Cl \cdot C_2H_5Cl)^+*$, formé dans le processus [8], a une vie trop courte pour un réarrangement de liaisons avant de se dissocier en réactifs initiaux.

$$[8] \quad C_2H_3Cl^+ + C_2H_5Cl \rightleftarrows (C_2H_3Cl^+ \cdot C_2H_5Cl)^* \longrightarrow\!\!\!\!\!\!\times\; C_4H_7{}^*Cl^+ + HCl \longrightarrow\!\!\!\!\!\!\times\; C_4H_8Cl^+ + Cl^\cdot$$

Cela confirme l'information de Beauchamp *et al.* (7), Łuczynski et Wincel (8) et Lampe (9), et en même temps, suggère que l'ion $C_2H_3Cl^+$ formé par dissociation du $C_2H_5Cl^+*$ garde (ou s'isomérise très rapidement en) la structure de l'ion moléculaire du chlorure de vinyle. Le seul ion qui semble provenir d'une interaction entre les ions issus des deux systèmes est le $C_4H_7{}^+$. Cet ion n'apparaît que dans les mélanges (tableau 1) et est absent pour les composés purs. Il est probable que cet ion soit formé dans les processus suivants où interviennent les ions fragmentaires des ions moléculaires :

$$[9] \quad C_2H_3{}^+ + C_2H_5Cl \rightarrow C_4H_7{}^+ + HCl$$

$$[10] \quad C_2H_5{}^+ + C_2H_3Cl \rightarrow C_4H_7{}^+ + HCl$$

Étude dans le spectromètre de masse à photoionisation

Les expériences faites avec le spectromètre de masse à photoionisation sont exécutées sur un mélange chlorure de

Can. J. Chem. Downloaded from www.nrcresearchpress.com by 122.72.124.2 on 09/07/12
For personal use only.

TABLEAU 2. Intensités fractionnaires (%) de quelques ions dans le mélange C_2H_3Cl (10%) + C_2H_5Cl (90%) photoionisé à 10,64 eV

	Pression (mTorr)		
Ion	40	100	200
$C_2H_3Cl^+$	9	11	2
$C_3H_4Cl^+$	8	3	1
$C_4H_5Cl^+$	20	16	2
$C_4H_6Cl^+$	32	12	6
$C_4H_7Cl^+$	5	3	1
$C_4H_8Cl^+$	2	1	—

vinyle – chlorure d'éthyle à une seule concentration, soit 10% de C_2H_3Cl dans 90% de C_2H_5Cl. Le choix de cette valeur de la concentration est motivé par le désir de favoriser le nombre de rencontres entre l'ion $C_2H_3Cl^+$ et le chlorure d'éthyle neutre avant qu'il ne réagisse avec le chlorure de vinyle.

Comme source de photoionisation nous avons utilisé les raies de résonance du krypton, λ = 123,6 nm (10,03 eV) et λ = 116,5 nm (10,64 eV). À ces énergies le chlorure de vinyle est ionisé (PI = 9,995 eV), tandis que le chlorure d'éthyle ne l'est pas (PI = 10,97 eV) (10). Des expériences de ce laboratoire indiquent qu'environ 80% des ions $C_2H_3Cl^+$ sont formés par absorption de l'énergie provenant de la raie de résonance plus énergétique du krypton (10,64 eV) (16). En ce qui concerne le chlorure d'éthyle, l'absorption de ce rayonnement est très intense et conduit à une fragmentation en de nombreux radicaux et molécules neutres insaturées (17, 18). Il en résulte alors un spectre de masse très riche en de nombreux pics de faible intensité (<1%) parmi lesquels on peut identifier quelques groupes d'ions d'intensité fractionnaire nettement supérieure à 2%. L'intensité relative de l'ensemble de ces petits pics que nous négligeons est estimée de 15–25%. Remarquons aussi, qu'en raison de la forte absorption du rayonnement par le chlorure d'éthyle les ions ne commencent à paraître avec une intensité raisonnable dans le spectre qu'à partir d'une pression relativement élevée du mélange, soit environ 60 mTorr.

Les intensités fractionnaires des ions les plus proéminents en fonction de la pression totale du système sont présentées dans les figures 3 et 4. Dans le tableau 2 sont décrits celles d'autres ions aperçus surtout à basse pression et qui, pour alléger les figures, ne sont pas présentées sur les graphiques.

Le point saillant de ces résultats est la formation de deux espèces ioniques non-halogénées (m/z = 109 et 110) dont l'abondance est nettement supérieure aux intensités des autres ions. À pression élevée (>1 Torr) l'intensité fractionnaire de ces deux espèces contribue pour environ 50% du spectre entier. Il faut aussi remarquer que ces deux espèces ioniques auxquelles nous attribuons les formules $C_8H_{13}^+$ et $C_8H_{14}^+$ apparaissent très tôt dans le spectre, puisqu'on les voit même aux basses pressions (>60 mTorr). Ces espèces ioniques ne sont pas observées dans les spectres de masse ni du chlorure de vinyle pur, ni de celui du chlorure d'éthyle pur. Parmi les autres ions notons la présence d'éventuels précurseurs aux ions m/z = 109 et 110 : $C_6H_9Cl^+$, $C_6H_{10}Cl^+$ (figure 4) accompagnés de $C_6H_{11}Cl^+$ en faible quantité et de $C_8H_{13}Cl^+$, $C_8H_{14}Cl^+$ (figure 3) avec un pic peu intense de $C_8H_{15}Cl^+$. On distingue aussi l'ion m/z = 108 de faible intensité (figure 3) qui est partiellement caché dans le pied du pic intense m/z = 109.

Contrairement au spectre de masse RCI du mélange chlorure

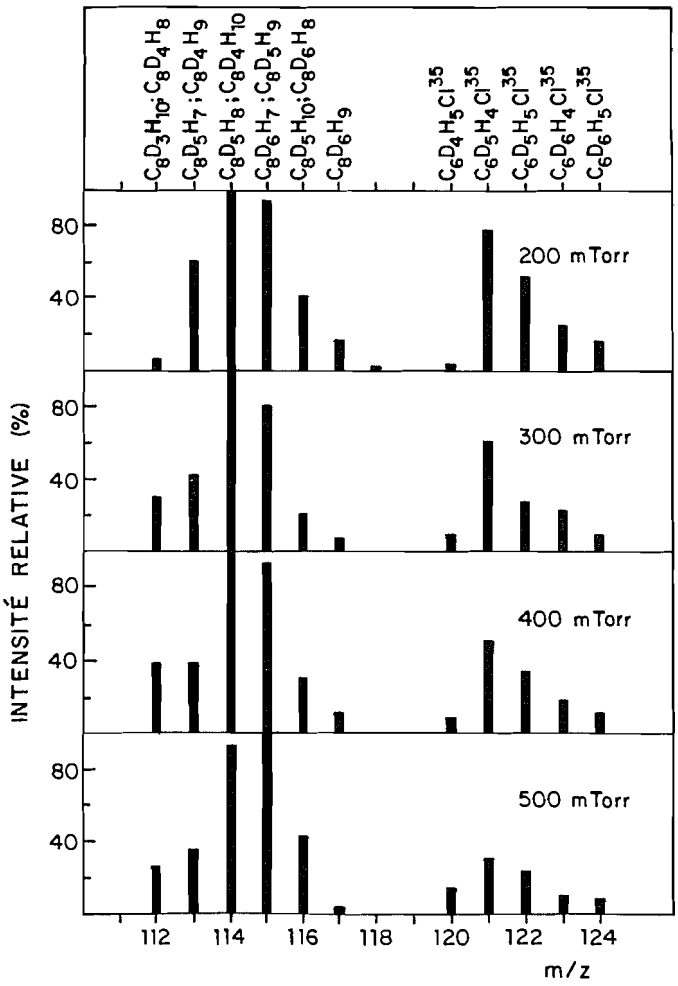


FIG. 5. Intensités relatives du groupe d'ions déshalogénés en C_8 et des ions chlorés en C_6 pour le mélange C_2D_3Cl (10%) + C_2H_5Cl (90%).

de vinyle – chlorure d'éthyle, où l'absence des espèces $C_4H_7Cl^+$ et $C_4H_8Cl^+$ était significative (voir la section précédente), on retrouve ces ions en faible intensité dans le spectre de masse du mélange photoionisé. Ces ions sont formés, selon toute vraisemblance, dans une séquence de réactions ayant pour origine le transfert du proton ou de l'atome d'hydrogène, puisqu'on les retrouve systématiquement dans les mélanges du chlorure de vinyle avec les alcanes :[4]

[11] $C_2H_3Cl^+ + C_2H_5Cl \rightarrow C_2H_4Cl^+ + C_2H_4Cl^{\cdot}$

[12] $C_2H_4Cl^+ + C_2H_5Cl \rightarrow [C_2H_4Cl\ C_2H_5Cl]^* \rightarrow C_4H_7Cl^+ + HCl$
$\rightarrow C_4H_8Cl^+ + Cl^{\cdot}$

Dans le cas présent ce processus reste marginale (tableau 2). Cependant, les ions ainsi formés participent aussi à des réactions de condensation, ce qui ne facilite pas le dépouillement du spectre de masse.

Le bilan en hydrogène des ions $C_8H_{13}^+$ et $C_8H_{14}^+$ suggère que ces espèces ioniques sont formées à partir des ions $C_4H_5Cl^+$ et $C_4H_6Cl^+$ qui réagissent successivement avec deux molécules de chlorure d'éthyle en éliminant du HCl et (ou) Cl. L'incorporation de deux squelettes carbonés du chlorure d'éthyle dans le complexe collisionnel est le résultat de la concentration élevée en C_2H_5Cl dans le mélange. Il est probable qu'une

4. J. A. Herman et R. Neagu-Plesu, résultats de ce laboratoire.

Can. J. Chem. Downloaded from www.nrcresearchpress.com by 122.72.124.2 on 09/07/12
For personal use only.

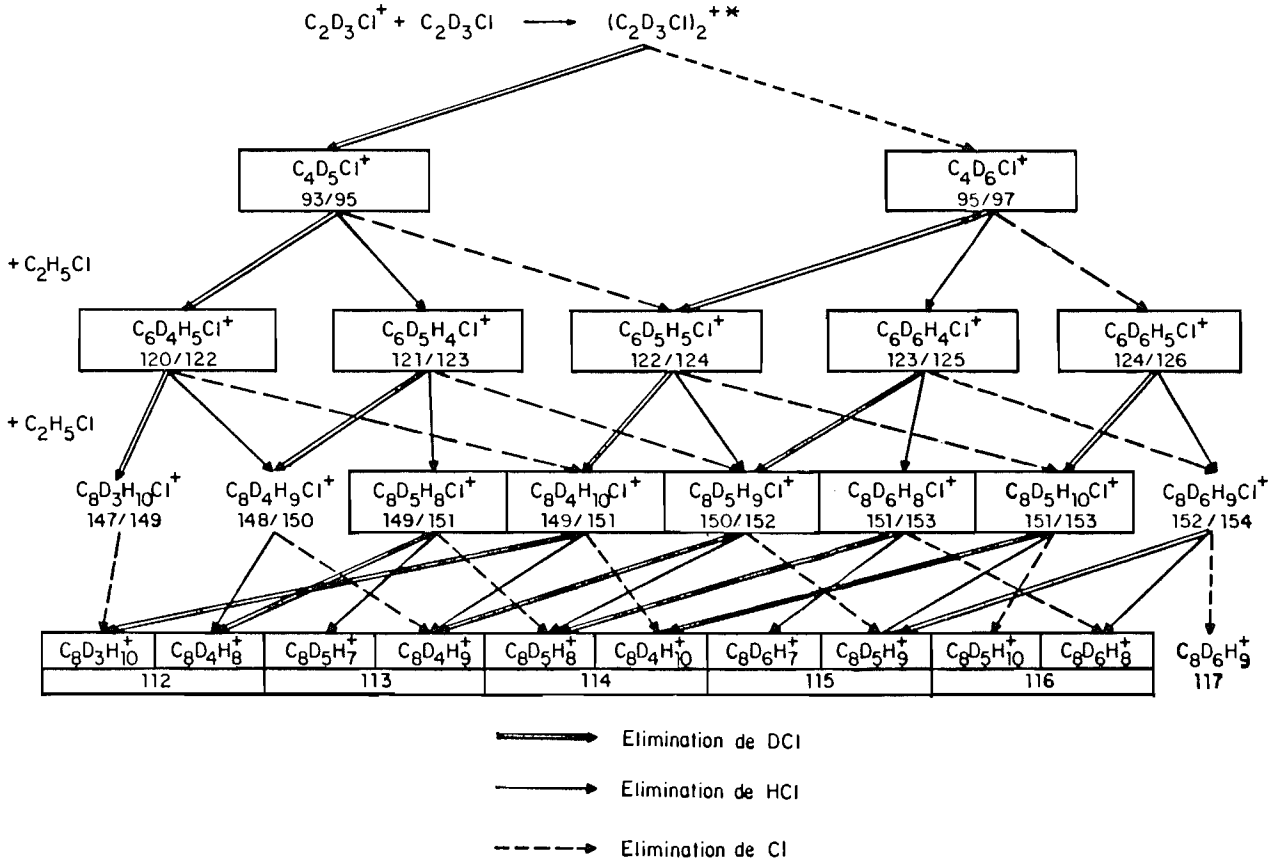


FIG. 6. Schéma des réactions ion–molécule conduisant à la formation des ions chlorés en C_6 dans le mélange C_2D_3Cl (10%) + C_2H_5Cl (90%). Les ions observés dans le spectre sont encadrés.

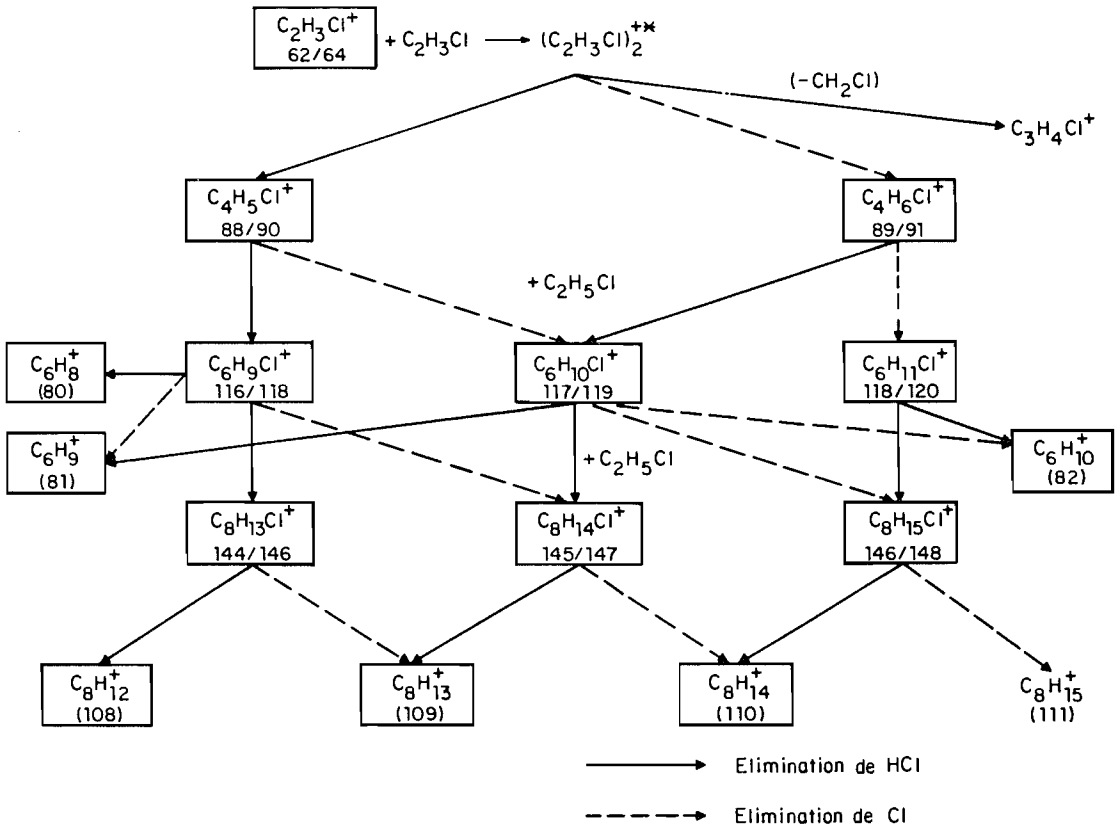


FIG. 7. Schéma des réactions ion–molécule pour la formation des principaux ions dans le mélange C_2H_3Cl + C_2H_5Cl. Les ions observés dans le spectre sont encadrés.

concentration plus forte en C_2H_3Cl dans le mélange aurait conduit à la formation d'espèces ioniques deshalogénées de formules brutes $C_8H_{11}^+$ et $C_8H_{12}^+$, impliquant des rencontres successives de trois chlorure de vinyle et d'un chlorure d'éthyle. En effet, on remarque qu'à pression élevée dans le chlorure de vinyle pur il y a formation de l'ion complètement déshalogéné, $C_8H_9^+$, qui proviendrait des processus suivants :[4]

$$[14]\quad C_2H_3Cl^+ \xrightarrow{V} C_4H_5Cl^+ \xrightarrow{V} C_6H_7Cl^+ \xrightarrow{V} C_8H_9$$
$$\xrightarrow{V} C_4H_6Cl^+ \xrightarrow{V} C_6H_8Cl^+ \longrightarrow ?$$

où le symbole V indique le chlorure de vinyle neutre.

Pour vérifier que les espèces $C_8H_{13}^+$ et $C_8H_{14}^+$ proviennent bien des processus impliquant deux molécules de chlorures d'éthyle neutres, nous avons refait le même genre d'expérience dans un mélange de C_2D_3Cl (10%) avec du C_2H_5Cl (90%). Si effectivement les ions m/z 109 et 110 ont comme précurseurs les espèces $C_4H_5Cl^+$ et $C_4H_6Cl^+$ formées dans les réactions [1] et [2], alors nous devrions trouver des ions ayant des formules $C_8D_5H_8$ et $C_8D_6H_8$ (m/z = 114 et 116) où nous négligeons les éventuels échanges entre les atomes d'hydrogène. La figure 5 montre les spectres de masse du groupe d'ions de m/z 112–124 à quatre pressions différentes.

En admettant que les complexes collisionnels dans lesquels survient l'élimination du chlorure d'hydrogène sont suffisamment fermes pour qu'il y ait mélange d'atomes d'hydrogène, alors il se peut que le fragment dissocié neutre soit du HCl ou du DCl. Puisqu'il y a deux étapes successives de rencontre avec le chlorure d'éthyle avec élimination chaque fois de chlorure d'hydrogène ou du chlore atomique, on assistera alors à l'apparition d'un groupe d'au moins six espèces ioniques : $C_8D_{3+n}H^+{}_{10-n}$ et $C_8D_{4+n}H^+{}_{10-n}$ où $n = 0$–2. Nous résumons l'ensemble des résultats à la figure 6, où les ions encadrés sont ceux observés expérimentalement.

En transposant ce mécanisme au mélange des espèces protonées : $C_2H_3Cl + C_2H_5Cl$, on aboutit à un schéma cinétique représenté à la figure 7. Cela semble bien correspondre aux observations.

Néanmoins, des questions restent sans réponses et méritent des études plus poussées. Entre autres, quelle est la configuration des espèces ioniques déshalogénées en C_8 plus stable que leur contre-partie contenant un atome de chlore? On peut aussi se demander si la formation des espèces $C_8H_{13}^+$ et $C_8H_{14}^+$ procède à partir des ions $C_6H_8^+$ et $C_6H_9^+$ qu'on observe en petite quantité dans le système, ou bien si la déshalogénation des ions $C_8H_{13}Cl^+$ et $C_8H_{14}Cl^+$ en est véritablement responsable, comme cela est indiqué à la figure 7.

Conclusions

Les ions $C_2H_3Cl^+$* excités ne réagissent pas par voie directe avec le chlorure d'éthyle. Cependant, cet ion à faible énergie interne peut former l'ion $C_2H_4Cl^+$ par transfert de proton ou d'atome d'hydrogène avec le chlorure d'éthyle. Néanmoins, ce processus semble être marginale.

Les principaux ions formés à pression élevée dans le mélange photoionisé à 10,64 eV sont les espèces $C_8H_{13}^+$ et $C_8H_{14}^+$. Ces ions sont probablement formés dans une séquence de processus de condensation à partir des espèces $C_4H_5Cl^+$ et $C_4H_6Cl^+$ avec le chlorure d'éthyle, et avec élimination concomitante de HCl ou Cl$^\bullet$.

Remerciements

Nous remercions MM. Bernard Boulé, André Bouffard, Réjean Drolet et Jocelyn Tremblay pour l'aide apportée à la construction du spectromètre de masse RCI. Nos remerciements vont aussi aux Dr. John E. Bartmess et Thomas Buckley pour les précieux conseils lors de la construction de cet instrument.

Finalement nous remercions le Conseil de recherche en sciences naturelles et en génie pour l'aide financière qui a permis la réalisation de cette étude.

1. J. L. Beauchamp, L. R. Anders et J. D. Baldeschwieler. J. Am. Chem. Soc. **89**, 4569 (1967).
2. J. A. Herman, J. J. Myher et A. G. Harrison. Can. J. Chem. **47**, 647 (1969).
3. B. M. Hughes, T. O. Tiernan et J. H. Futrell. J. Phys. Chem. **73**, 829 (1969).
4. V. G. Anicich et M. T. Bowers. Int. J. Mass Spectrom. Ion Phys. **12**, 231 (1973).
5. L. W. Sieck, R. Gorden, Jr., S. G. Lias et P. Ausloos. Int. J. Mass Spectrom. Ion Phys. **15**, 181 (1974).
6. V. G. Anicich et J. H. Futrell. Int. J. Mass Spectrom. Ion Phys. **21**, 383 (1976).
7. J. L. Beauchamp, D. Holtz, S. D. Woodgate et S. L. Patt. J. Am. Chem. Soc. **94**, 2798 (1972).
8. Z. Łuczynski et H. Wincel. (*a*) Int. J. Mass Spectrom. Ion Phys. **14**, 29 (1974); (*b*) Int. J. Radiat. Phys. Chem. **7**, 705 (1975); **7**, 713 (1975).
9. H. S. Tan, M. J. Pabst et J. L. Franklin. Int. J. Mass Spectrom. Ion Phys. **21**, 297 (1976).
10. K. Watanabe, T. Nakayama et J. Mottl. J. Quant. Spectrosc. Radiat. Transfer, **2**, 369 (1962).
11. H. Wincel et J. A. Herman. J. Chem. Soc. Faraday Trans. 1, **69**, 1797 (1973).
12. Z. Łuczynski et J. A. Herman. Int. J. Mass Spectrom. Ion Phys. **31**, 237 (1979).
13. R. T. McIver, Jr. Rev. Sci. Instrum. **41**, 555 (1970); **49**, 111 (1978).
14. M. B. Comisarow. Int. J. Mass Spectrom. Ion Phys. **37**, 251 (1981).
15. R. T. McIver, Jr., R. L. Hunter, E. B. Ledford, M. J. Locke et T. L. Francl. Int. J. Mass Spectrom. Ion Phys. **39**, 65 (1981).
16. R. Neagu-Plesu et J. A. Herman. Rapid Commun. Mass Spectrom. **1**, 65 (1987).
17. L. Crémieux et J. A. Herman. Can. J. Chem. **52**, 3098 (1974).
18. T. Ichimura, A. W. Kirk, G. Kramer et E. Tschuikow-Roux. J. Photochem. **6**, 77 (1976–77).

Can. J. Chem. Downloaded from www.nrcresearchpress.com by 122.72.124.2 on 09/07/12
For personal use only.

Influence de la complexation sur la réactivité de nitrates d'halogènes

DIDIER GAUDE, GISÈLE GELLON, RAYMOND LE GOALLER ET JEAN-LOUIS PIERRE[1]

Laboratoire d'études dynamiques et structurales de la sélectivité, Université scientifique, technologique et médicale de Grenoble, B.P. 68, 38402, Saint Martin d'Heres CEDEX, France

Reçu le 18 janvier 1988[2]

DIDIER GAUDE, GISÈLE GELLON, RAYMOND LE GOALLER et JEAN-LOUIS PIERRE. Can. J. Chem. **67**, 104 (1989).

La réaction du nitrate d'iode ou du nitrate de brome dans l'acétonitrile ou le chloroforme avec divers phénols conduit à des mélanges de produits halogénés et nitrés. En présence de complexants forts des ions halonium, aucune réaction n'est observée. En présence de pyridine ou de triéthylamine, seuls sont obtenus des produits halogénés avec un effet *ortho*-directeur marqué de la fonction phénol.

Mots clés : phénols, nitrate d'iode, nitrate de brome, halogénation, nitration.

DIDIER GAUDE, GISÈLE GELLON, RAYMOND LE GOALLER, and JEAN-LOUIS PIERRE. Can. J. Chem. **67**, 104 (1989).

Iodine nitrate or bromine nitrate in acetonitrile or in chloroform react with a variety of phenolic substrates to form both halogenated and nitrated products. In the presence of strong complexing agents of halonium ions, no reaction occurs, while in the presence of pyridine or triethylamine, only halogenated phenols exhibiting a strong *ortho*-directing effect of the phenolic function are produced.

Key words: phenols, iodine nitrate, bromine nitrate, halogenation, nitration.

Can. J. Chem. Downloaded from www.nrcresearchpress.com by 122.72.124.2 on 09/07/12
For personal use only.

Introduction

À la suite de nos travaux sur la complexation des ions iodoniums et bromoniums (1), il nous a semblé intéressant d'étudier l'influence de cette complexation sur la réactivité des nitrates d'halogènes. Le nitrate d'iode, obtenu «*in situ*» par réaction de l'iode sur le nitrate d'argent en milieu organique, peut être complexé par deux molécules de pyridine et, ainsi isolé, conservé à l'abri de l'air. La réactivité de ce complexe sur les composés éthyléniques a été étudiée par Diner *et al.* (2–4). La réaction d'addition fournit les nitrates d'iodoalkyles attendus, accompagnés de nitrates d'iodoalcanes pyridinium. Les alcools primaires et secondaires sont oxydés en dérivés carbonylés (5). Les systèmes conjugués conduisent à la formation de sels de pyridinium (6). Les phénols conduisent à des dérivés polyiodés; s'ils sont substitués par une chaîne insaturée, ils donnent d'abord la réaction d'addition, suivie de la substitution électrophile sur le noyau (6).

À notre connaissance, la réactivité des nitrates d'iode et de brome, vis-à-vis des phénols, n'a jamais été étudiée en l'absence de pyridine. Les composés du type hypohalogénites semblent pourtant de bons candidats pour les réactions d'halogénation du noyau aromatique, comme en témoignent les travaux récents sur la fluoration par réaction de l'hypofluorite d'acétyle (7–9), du fluoroxytrifluorométhane ou du bis(fluoroxy) difluorométhane (10), sur la chloration par l'hypochlorite de tetrtiobutyle déposé sur argile (11) ou sur zéolithe (12) ou encore les travaux plus anciens sur l'iodation par le trifluorométhane sulfonate d'iode (13).

Dans ce travail, nous présentons les résultats obtenus par réaction du nitrate d'iode ou de brome sur divers phénols, en présence ou non de différents complexants. Ce travail s'inscrit également comme la suite d'une étude sur la nitration des phénols (14).

Résultats

Réactions en l'absence de complexant

En l'absence de complexant, l'obtention du nitrate d'iode par addition d'une quantité stoechiométrique d'iode à du nitrate d'argent dans l'acétonitrile ou le chloroforme n'est pas quantitative. L'addition d'une solution contenant 5 mmoles d'iode à 5 mmoles de $AgNO_3$ conduit à la formation de 2,5 mmoles de AgI que l'on élimine par filtration.

L'addition de 5 mmoles de phénol à cette solution se traduit par la formation de dérivés iodonitrés et nitrés du phénol, en même temps qu'apparaît un précipité correspondant à 2,5 mmoles de AgI, indiquant la formation *in situ* du nitrate d'iode.[3]

Le nitrate de brome donne lieu aux mêmes observations. De plus, et contrairement à INO_3, il réagit sur les hydrocarbures benzéniques (entrées 9 tableau 1).

Le tableau 1 rassemble les résultats obtenus avec plusieurs dérivés du phénol et avec le toluène.

Réactions en présence de complexant

Dans les mêmes solvants, l'addition d'une solution d'iode (5 mmoles) à une solution de nitrate d'argent (5 mmoles) contenant 10 mmoles de pyridine (Π) donne lieu à la précipitation de 5 mmoles d'AgI, ce qui traduit la formation quantitative du complexe INO_3,2Π. Le tableau 2 montre que l'on obtient uniquement des produits iodés, ce qui confirme les travaux de Lown et Joshua (6).

Si on remplace la pyridine par de la triéthylamine, on observe une réactivité identique. Les résultats obtenus avec le nitrate de brome sont également rapportés dans le tableau 2.

En présence de cryptand [2.2.2], de Kryptofix 5 (1,13-bis(quinolyl-8) pentaoxa-1,4,7,10,13-tridécane), ou de diamines linéaires telles que le *N*,*N*,*N'*,*N'*-tétraméthyldiamino-1,6 hexane, utilisés à la place de la pyridine, la réaction est totalement inhibée et le phénol intégralement récupéré.

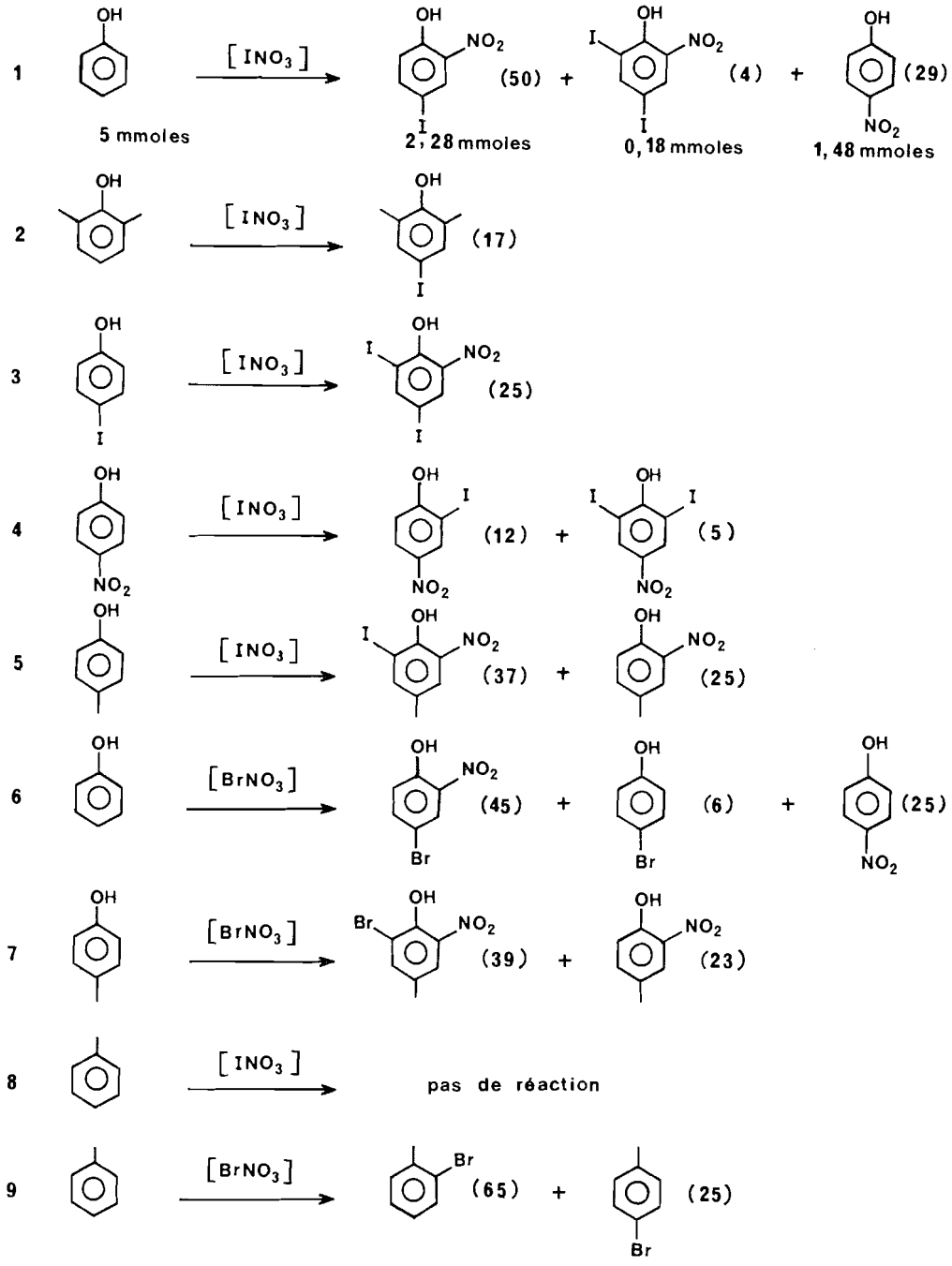
Discussion

En l'absence de complexant, INO_3 (ou $BrNO_3$) se comporte à la fois comme agent halogénant et nitrant. Les résultats quantitatifs (tableau 1, première ligne) montrent que 5 mmoles de INO_3 fournissent au minimum, compte-tenu des polymères, 6,6 mmoles d'électrophiles. Ils impliquent qu'une molécule de X—O—NO_2 soit donneur de deux électrophiles distincts

1. Auteur à qui adresser toute correspondence.
2. Revision reçue le 2 août 1988.
3. Nous ne pouvons expliquer ce fait expérimental surprenant.

Printed in Canada / Imprimé au Canada

TABLEAU 1. Réactions de INO_3 et $BrNO_3$ sans complexants (% isolé par rapport au substrat)



et que le mécanisme soit autre qu'une substitution électrophile classique mettant en jeu X^+ et NO_2^+.

Nous avons montré antérieurement (1) que le cryptand [2.2.2] en présence de nitrate d'iode forme un cryptate d'halonium ($K = 3{,}2 \times 10^6$). Un complexe encore plus stable ($K = 3{,}5 \times 10^7$) est également formé avec Br^+. Au contraire, la triéthylamine et la pyridine forment des complexes beaucoup moins stables. Ainsi, le complexe iodé avec la triéthylamine implique un échange rapide devant l'échelle de temps RMN entre espèces libres et complexées, même à −90°C dans $CHFCl_2$ (15) alors que dans le cas des cryptands l'échange est lent à température ordinaire.

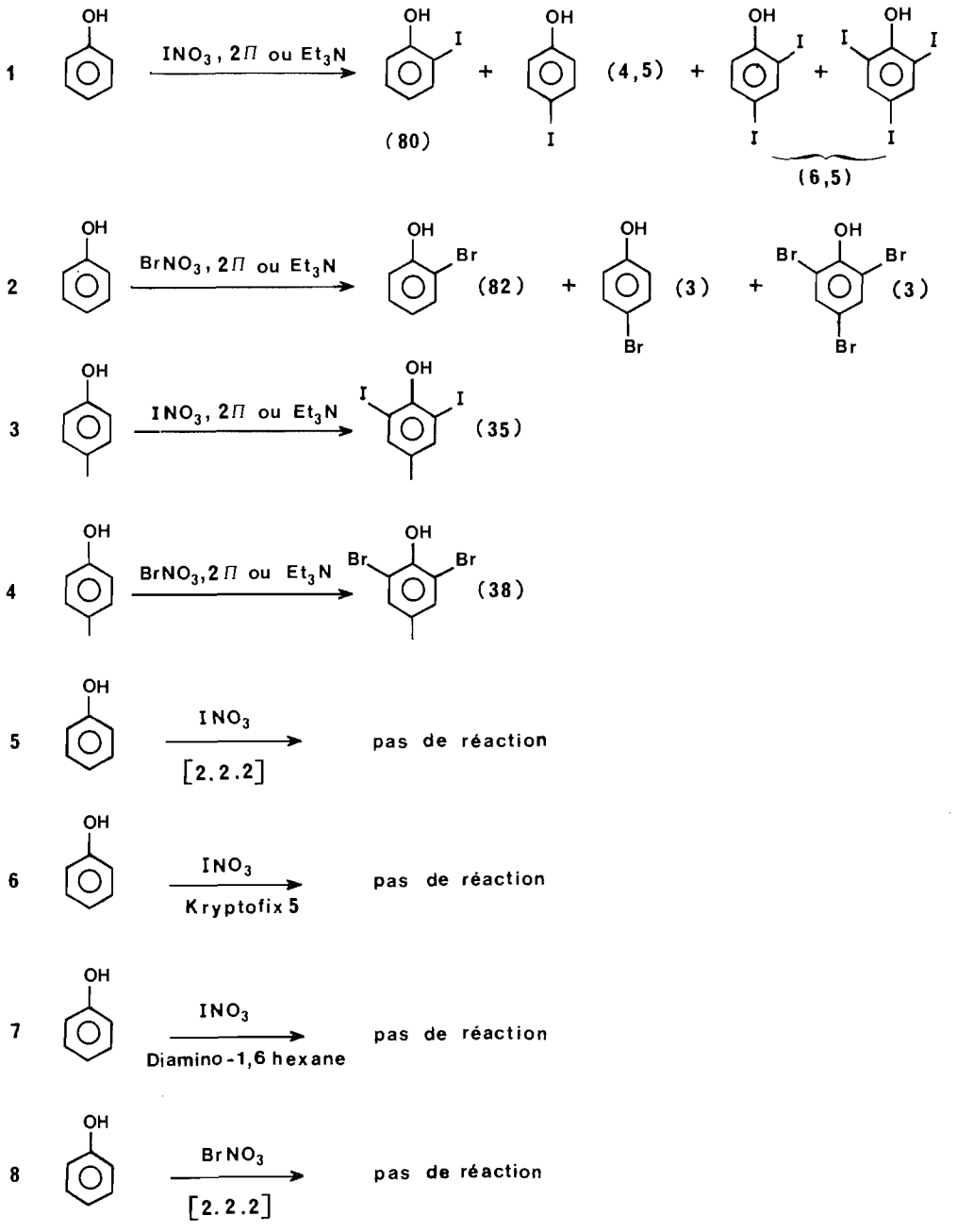
L'inhibition de réaction induite par le cryptand [2.2.2] que nous observons, implique sans nul doute la complexation de l'espèce X^+ : compte-tenu de la valeur de la constante d'équilibre on peut considérer qu'il n'y a pas de X^+ libre et que le X^+ complexé est soustrait au milieu par cryptation.

Bien qu'il n'ait pas été fait d'étude fondamentale correspondante, nos résultats montrent qu'il doit en être de même lorsque l'on utilise le Kryptofix 5 ou le diamino-1,6 hexane.

Lorsque X^+ est soustrait au milieu par un complexant fort, on n'observe pas non plus de nitration. Ce résultat suggère fortement que *l'halogénation précède la nitration et lui est nécessaire*.

Can. J. Chem. Downloaded from www.nrcresearchpress.com by 122.72.124.2 on 09/07/12
For personal use only.

TABLEAU 2. Réactions de INO_3 et $BrNO_3$ en présence de complexants (% isolé par rapport au substrat)



En présence de pyridine ou de triéthylamine, l'halogénation n'est pas inhibée, mais la nitration n'est pas observée. Le complexant doit donc interdire cette dernière réaction.

Il faut enfin noter la valeur du rapport de substitution *ortho/para*, supérieur à 1,8, dans le cas du phénol. Ce rapport reste constant lorsque les réactions sont effectuées dans une gamme de température allant de $-40°C$ à $+80°C$.

Ces observations nous amènent à proposer les mécanismes réactionnels suivants :

1. En l'absence de complexant, on peut envisager un schéma réactionnel en plusieurs étapes, dont la première est une substitution électrophile suivant :

[*a*] $ArH + XNO_3 \rightarrow [ArHX^+ \quad NO_3^-] \rightarrow ArX + HNO_3$

Pour ce qui concerne les étapes suivantes, il est possible d'envisager plusieurs processus expliquant la nitration et l'iodation ultérieure éventuelle :

[b_1] $HNO_3 + XNO_3 \rightarrow HOX + NO_2^+ + NO_3^-$

suivi d'une substitution électrophile mettant en jeu les espèces NO_2^+ ou X^+.

Ce processus peut être exclu car après la première étape il ne reste que 50% des molécules de XNO_3, or les exemples 1, 5, 6 et 7 du tableau 1 montrent qu'il s'est formé des produits nitrés qui nécessitent de 60 à 80% des molécules de XNO_3 mises en réaction.

De plus, les tentatives faites pour mettre en évidence

Can. J. Chem. Downloaded from www.nrcresearchpress.com by 122.72.124.2 on 09/07/12
For personal use only.

Can. J. Chem. Downloaded from www.nrcresearchpress.com by 122.72.124.2 on 09/07/12
For personal use only.

l'éventuelle formation de NO_2^+ se sont révélées négatives. Cette espèce est susceptible de réagir sur les amines (16). Des expériences menées en présence d'un excès de triéthylamine ou de pyridine n'ont pas permis de détecter les adduits attendus.

$$[b_2] \quad ArH + HNO_3 \xrightarrow{H^+} ArNO_2 + H_2O$$

$$H_2O + XNO_3 \rightarrow HOX + HNO_3$$

Ce processus autocatalytique nous semble très peu probable. En effet, dans nos conditions opératoires, les protons ne peuvent provenir que de la réaction de la première étape. De ce fait le milieu n'est probablement pas assez acide pour que l'équilibre d'autoprotolyse de l'acide nitrique soit déplacé dans le sens de la protonation.

Nous n'observons d'ailleurs pas de nitration du toluène ni du *para*-nitrophénol qui devraient réagir avec une telle espèce.

Les processus $[b_1]$ et $[b_2]$ ne nous semblant pas expliquer correctement nos résultats, nous avons été amenés à envisager un mécanisme faisant intervenir un transfert monoélectronique s'effectuant suivant l'une ou l'autre de ces équations :

$$[b_3] \quad ArH + H_2NO_3^+ \rightarrow [ArH^{\ddagger} \dot{N}O_2] + H_2O \rightarrow ArNO_2 + H_3O^+$$

$$[b_4] \quad ArH + HNO_3 \rightarrow [ArH^{\ddagger}, \dot{N}O_2] + OH^- \rightarrow ArNO_2 + H_2O$$

Dans les deux cas la nitration peut se faire sur ArH ou ArX présent dans le mélange réactionnel.

Bien que l'acide nitrique protoné devrait être un meilleur accepteur d'électron, nous pensons que le processus $[b_4]$ est plus vraisemblable pour les raisons invoquées précédemment (milieu trop faiblement acide).

Perrin (17) a été le premier à proposer, pour des réactions de nitration, un mécanisme faisant intervenir un transfert d'électron entre le noyau benzénique et NO_2^+ conduisant à la paire «radical cation du noyau aromatique – radical NO_2».

Laszlo et coll. (18) ont invoqué une interaction du même type entre phénol et ions métalliques pour expliquer la nitration de phénols par des nitrates métalliques déposés sur argile.

De la même façon, nous pensons qu'il est possible d'envisager que HNO_3 moléculaire, même à faible concentration, est assez oxydant pour accepter un électron du phénol et conduire à une paire de radicaux suivant le processus $[b_4]$. Ce mécanisme permet également d'expliquer que le toluène (tableau 1, lignes 8 et 9) et le *p*-nitrophénol (tableau 1, ligne 4), moins oxydables que les autres phénols, ne soient pas nitrés dans nos conditions réactionnelles. Nous avions déjà avancé une telle hypothèse pour expliquer la nitration de phénols en milieu biphasique (14).

En résumé, le mécanisme qui nous semble le plus probable comporte les deux étapes $[a]$ et $[b_4]$.

Cette interprétation justifie bien les faits observés : (*i*) une mole de XNO_3 peut fournir plus d'une mole d'électrophile; (*ii*) on observe toujours la formation d'au moins un produit halogéné, la nitration ultérieure pouvant se faire sur le phénol ou sur l'halogénophénol déjà formé (tableau 1, lignes 5 et 6).

2. En présence de complexants, les résultats dépendent de l'interaction XNO_3–complexant :

Une forte complexation de X^+ inhibe l'halogénation et la nitration ne peut avoir lieu (tableau 2, lignes 5–8).

Dans le cas d'une faible complexation par la triéthylamine ou la pyridine, l'ion X^+ n'est pas masqué et l'halogénation peut avoir lieu, mais le proton libéré est capté par l'amine et la nitration ne peut plus avoir lieu (tableau 2, lignes 1–4).

Conclusion

Nos résultats montrent qu'il est possible d'obtenir des nitrates d'halogènes *in situ* en l'absence de pyridine. Dans ce cas ils se comportent vis-à-vis des phénols comme des agents halogénonitrants. En présence d'amines telles que la pyridine ou la triéthylamine, on obtient uniquement des halogénophénols, et en présence de complexants plus forts tels que les cryptands, la réaction est totalement inhibée par cryptation de l'ion halonium. À notre connaissance, contrairement au nitrate d'iode, le nitrate de brome n'avait pas été utilisé à de telles fins. En l'absence de complexants, il s'est révélé plus réactif que le premier, et permet l'halogénation des hydrocarbures aromatiques.

Partie expérimentale

L'iode commercial bisublimé et le nitrate d'argent ont été utilisés tels quels. L'acétonitrile séché sur $CaSO_4$ est distillé deux fois et conservé sous azote. Les produits de réactions sont séparés sur colonne de silice (Merck Kieselgel 60, 230–400 mesh; éluant : hexane/acétate d'éthyle). Les rendements indiqués dans les tableaux 1 et 2 correspondent aux quantités de produits séparés. Ces produits ont été identifiés par comparaison de leurs spectres en infra-rouge (appareil Perkin–Elmer 397) et en résonance magnétique nucléaire du proton (appareil Bruker WP80 SY) avec ceux d'échantillons authentiques, commerciaux ou obtenus par synthèse. Leurs masses molaires ont été déterminées par spectrométrie de masse (70 eV) sur un appareil MS30 Kratos-AEI.

Réaction de INO_3 en l'absence de complexant

On dissout 5 mmol de $AgNO_3$ dans 15 mL d'acétonitrile auxquels on ajoute goutte à goutte une solution contenant 5 mmol d'iode dans de l'acétonitrile, en maintenant le ballon à 0°C. On filtre l'iodure d'argent obtenu (2,5 mmol) et on ajoute ensuite au filtrat 5 mmol de substrat dissout dans 10 mL d'acétonitrile. On poursuit l'agitation à température ambiante pendant 2 h. L'iodure d'argent qui précipite (2,5 mmol) est filtré. On évapore le solvant et on sépare les produits sur colonne.

Réaction de INO_3 en présence de complexant

On dissout 5 mmol de nitrate d'argent dans 15 mL d'acétonitrile contenant 2 mL du complexant (pyridine ou triéthylamine). On ajoute 5 mmol d'iode en solution dans l'acétonitrile, en maintenant le bain à 0°C. L'iodure d'argent (5 mmol) est ensuite filtré, et on ajoute au filtrat 5 mmol de substrat en solution dans l'acétonitrile. La réaction est terminée en 2 h à la température ambiante. Les produits sont isolés comme précédemment.

Dans les manipulations effectuées avec le cryptand [2.2.2], le Kryptofix 5 ou le diamino-1,6 hexane, le complexant est ajouté en quantité stoechiométrique.

Les réactions utilisant le nitrate de brome ont été effectuées suivant les mêmes modes opératoires.

Exemple type : réaction de INO_3 sur le phénol

(a) En présence de pyridine

La réaction, menée sur 5 mmol de phénol, conduit à un mélange dont les constituants sont élués sur colonne de silice par un mélange hexane – acétate d'éthyle (4:1). Les produits isolés sont

(*i*) *ortho*-Iodophénol (80%), identifié par comparaison de ses spectres avec ceux d'un échantillon authentique obtenu selon la référence 19. RMN ($CDCl_3$) δ (ppm) : 5,62 (1H, s) et 6,81–8,01 (4H, m).

(*ii*) *para*-Iodophénol (4,5%) dont les spectres sont identiques à ceux d'un échantillon commercial. RMN ($CDCl_3$) δ (ppm) : 6,62–7,50 (spectre AB, J = 8,8 Hz, 4H). Spectre de masse (intensité relative) : 220 (100), 93 (24, 4) 65 (29, 6).

On isole un mélange de deux produits (6,5%) qui ne peuvent être séparés. Ces produits sont le triiodo-2,4,6 phénol. RMN ($CDCl_3$) δ (ppm) : 7,91 (s); et le diiodo-2,4 phénol. RMN ($CDCl_3$) δ (ppm) : 6,75 (d, 1H), 7,55 (dd, 1H), 7,95 (d, 1H). Dans le spectre de masse

du mélange on trouve les masses molaires de ces deux produits : 346 (100%) et 472 (56%).

(b) En l'absence de pyridine

La réaction, effectuée sur 5 mmol de phénol, fournit, après les traitements décrits précédemment, les composés suivants :

Iodo-4 nitro-2 phénol (50%). RMN ($CDCl_3$) δ (ppm) : 6,95 (d, 1H), 7,75 (dd, 1H), 8,45 (d, 1H). Spectre de masse : 265 (100), 219 (8, 17), 92 (44, 92).

Diiodo-4,6 nitro-2 phénol (4%). RMN ($CDCl_3$) δ (ppm) : 8,34–8,39 (spectre AB). Spectre de masse : 391 (100), 345 (2, 6), 218 (15, 15), 189 (13, 34), 91 (16, 6).

para-Nitrophénol (29%) : spectres identiques à ceux d'un échantillon commercial.

1. R. Le Goaller, H. Handel, P. Labbe et J. L. Pierre. J. Am. Chem. Soc. **106**, 1694 (1984).
2. U. E. Diner et J. W. Lown. J. Chem. Soc. Chem. Commun. 333 (1970).
3. U. E. Diner et J. W. Lown. Can. J. Chem. **49**, 403 (1971).
4. U. E. Diner, M. Worsley et J. W. Lown. J. Chem. Soc. (C), 3131 (1971).
5. U. E. Diner. J. Chem. Soc. (C), 676 (1970).
6. J. W. Lown et A. V. Joshua. Can. J. Chem. **55**, 122 (1977).
7. S. Rosen et M. Brand. Synthesis, 665 (1985).
8. O. Lerman, Y. Tor, D. Hebel et S. Rozen. J. Org. Chem. **49**, 806 (1984).
9. O. Lerman, Y. Tor et S. Rozen. J. Org. Chem. **46**, 4629 (1981).
10. M. J. Fifolt, R. T. Olczak et R. F. Mundkenke. J. Org. Chem. **50**, 4576 (1985).
11. K. Smith, M. Butters et W. E. Paget. Synthesis, 1155 (1985).
12. K. Smith, M. Butters et B. Nay. Synthesis, 1157 (1985).
13. Y. Kobayashi, I. Kumadaki et T. Yoshida. J. Chem. Res. (S), 215 (1977).
14. D. Gaude, R. Le Goaller et J. L. Pierre. Synth. Commun. **16**, 63 (1986).
15. H. Handel, P. Labbe, R. Le Goaller et J. L. Pierre. J. Chim. Phys. **78**, 421 (1981).
16. G. A. Olah. Aldrichimica Acta, **12**, 43 (1979).
17. C. L. Perrin. J. Am. Chem. Soc. **99**, 5516 (1977).
18. A. Cornelis, P. Laszlo et P. Pennetreau. Bull. Soc. Chim. Belg. **93**, 961 (1984).
19. F. C. Whitmore et E. R. Hanson. Org. Synth. 326 (1948).

Can. J. Chem. Downloaded from www.nrcresearchpress.com by 122.72.124.2 on 09/07/12
For personal use only.

An NMR study of dinucleoside monophosphates with an O4-ethylated thymine. d(e^{4}TpT) and d(Tpe^{4}T)[1]

GARRY W. BUCHKO, FRANK E. HRUSKA,[2] AND KRISHAN L. SADANA
Department of Chemistry, The University of Manitoba, Winnipeg, Man., Canada R3T 2N2

Received June 3, 1988

GARRY W. BUCHKO, FRANK E. HRUSKA, and KRISHAN L. SADANA. Can. J. Chem. **67**, 109 (1989).

Syntheses are described for d(e^{4}TpT) (**1**) and d(Tpe^{4}T) (**2**), the O4-ethylated analogues of d(TpT) (**3**), and mass spectrometric (FAB), ^{1}H nuclear magnetic resonance (300 MHz), and circular dichroic data are provided for the three molecules. The $[M - H]^-$ ions as well as the aggregates $[2M - H]^-$ and, in the case of **1**, $[3M - H]^-$, are easily detected by FAB mass spectrometry operating in the negative ion mode. In contrast with the modified nucleoside, e^{4}dT, the two methylene protons of the O4-ethyl groups of **1** and **2** are nonequivalent in the NMR spectra, and their chemical shift difference decreases with increasing temperature. This chemical shift difference can be related to intramolecular base stacking. The vicinal coupling constants of the sugar rings reveal an unusual shift at low temperature towards the 3′-*endo* conformation of the e^{4}Tp unit of **1**, but this shift is not noted for the pe^{4}T unit of **2**. O4-Alkylation of either unit of **3** effects a large reduction in the amplitude of the negative CD peak at 252 nm. The CD spectra of **1** and **2** are qualitatively similar to those of d(CpT) and d(TpC), respectively, and suggest that in some respects an O4-alkylated thymine base is "cytosine-like". The amplitudes of the positive CD peaks of **1** and **3** are reduced by 40% as the temperature is increased from 10 to 65°C, indicating the presence of some base stacking at low temperatures. However, the CD spectrum of **2** shows a much smaller reduction (<10%).

Key words: O-alkylation, oligonucleotides, stereochemistry, NMR, mass spectrometry.

GARRY W. BUCHKO, FRANK E. HRUSKA, et KRISHAN L. SADANA. Can. J. Chem. **67**, 109 (1989).

On décrit des synthèses des produits d(e^{4}TpT) (**1**) et d(Tpe^{4}T) (**2**), les analogues O4-éthylés du d(TpT) (**3**), et on rapporte les données relatives aux spectres de masse (FAB), aux spectres en résonance magnétique nucléaire du ^{1}H et au dichroïsme circulaire de ces trois molécules. Dans les spectres de masse FAB obtenus dans le mode des ions négatifs, on peut facilement détecter les ions $[M - H]^-$ et les agrégats $[2M - H]^-$ et, dans le cas du composé **1**, on peut aussi détecter l'agrégat $[3M - H]^-$. Par opposition avec ce qui est observé dans le spectre RMN du nucléoside modifié, e^{4}dT, les deux protons méthyléniques des groupements O4-éthyles des composés **1** et **2** ne sont pas équivalents et les différences dans leurs déplacements chimiques diminuent avec une augmentation de la température. On peut attribuer cette différence dans les déplacements chimiques à un empilement intramoléculaire des bases. Les constantes de couplage vicinal des cycles de sucre révèlent un déplacement inhabituel, à basse température, vers la conformation *endo-3′* de l'unité e^{4}Tp du composé **1**; toutefois, on n'observe pas ce déplacement pour l'unité pe^{4}T du composé **2**. La O4-alkylation de l'une ou l'autre des unités du composé **3** provoque une réduction importante de l'amplitude du pic négatif observé à 252 nm, dans le spectre de DC. Les spectres de DC des composés **1** et **2** sont respectivement similaires, d'un point de vue qualitatif, à ceux des composés d(CpT) et d(TpC) et ces résultats suggèrent que, sous certains aspects, une thymine alkylée en position 4 devient semblable à une cytosine. Lorsqu'on augmente la température de 10 à 65°C, les amplitudes des pics positifs de DC des composés **1** et **2** sont réduits de 40%; ces résultats indiquent que, à basse température, il se produit un empilement des bases. Toutefois, le spectre de DC du composé **2** montre que la réduction est beaucoup plus faible (<10%).

Mots clés : O-alkylation, oligonucléotides, stéréochimie, RMN, spectrométrie de masse.

[Traduit par la revue]

Introduction

The mutagenic and carcinogenic consequences of O-alkylation of nucleic acid bases have been the focus of many studies. Research was initially centered on O6-alkylated guanine (r^{6}G), but considerable interest shifted to the O2- and O4-alkylated thymines following their identification in DNA treated with the potent carcinogen ethylnitrosourea (1). O-Alkylation of guanine and thymine effects an alteration in their hydrogen bonding capacity that forms the basis for interpretation of the misincorporations observed during transcription and replication (2–4). Information about the electronic and geometrical changes resulting from O-alkylation has been provided by the X-ray crystallographic studies of O4-methyluridine (m^{4}U) (5), O4-methylthymidine (m^{4}dT) (6), O4-ethylthymidine (e4dT) (7), and O2-isopropylthymidine (i^{2}dT) (8), as well as for several O6-alkylated purine nucleosides and analogues (9–11). ^{1}H and ^{13}C NMR data have been reported for a large number of O-alkylated nucleosides (8, 12–14). More relevant data about the changes produced in DNA structure are now being provided by NMR investigations of oligodeoxynucleotides, but these are limited to a few recent studies (15, 16). In the present work we describe the synthesis of d(e^{4}TpT) (**1**) and d(Tpe^{4}T) (**2**), the O4-ethylated analogs of d(TpT) (**3**), in which the modified thymine is at the 5′ end and 3′ end of the molecule, respectively (Fig. 1). These syntheses require considerable care since the O-alkyl groups are labile in acid or basic media (4, 13). The molecular ions of the three dimers are readily observed by FAB (fast atom bombardment) mass spectrometry (negative ion mode). ^{1}H NMR data as well as circular dichroic (CD) data are provided for the three dimers and are discussed in conformational terms. Of particular interest is the chemical shift nonequivalence of the methylene protons of the O-ethyl groups, which can be rationalized in terms of intramolecular base stacking, and could be a means of monitoring structural changes in the vicinity of the O-alkyl lesion. A preliminary report of this work has appeared (17).

[1]Presented at the 5th Conversation in Biomolecular Stereodynamics, Albany, NY, June 2–6, 1987 and the 70th Canadian Chemical Conference, Québec, P.Q., June 7–11, 1987.

[2]Author to whom correspondence may be addressed.

Can. J. Chem. Downloaded from www.nrcresearchpress.com by 122.72.124.2 on 09/07/12
For personal use only.

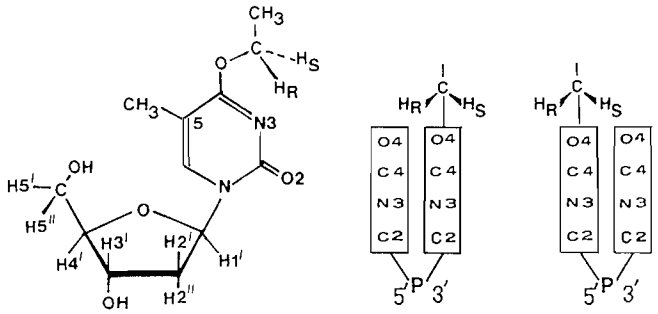


FIG. 1. Left, structure and numbering scheme for e^4dT (O4-ethylthymidine), the modified component of d(e^4TpT) (**1**) and d(Tpe^4T) (**2**). C7 and C8 refer respectively to the methylene and methyl carbons of the O4-ethyl group. H_R and H_S refer respectively to the *pro-R* and *pro-S* methylene protons of the O-ethyl group. Centre, sketch of **1** in a right-hand base-stacked conformation, which presents a view in the plane of the bases in the N3-to-C5 direction. The base are *anti* about the N-glycosyl bond and the O-ethyl group is oriented as in the crystal state (ref. 7). The sketch shows H_R projecting towards the thymine of the 3′-linked unit. Right, an analogous sketch of **2**, which shows H_S projecting towards the thymine of the 5′-linked unit.

Experimental

Materials and methods

Materials

All solvents used for synthesis, including absolute ethanol, were dried by standard procedures. Thymidine (Sigma Chemical Co.) was used without prior drying. 4-Chlorophenyl phosphodichloridate and 4-chlorophenyl phosphate were prepared as described earlier (18), as was tetra-*n*-butylammonium fluoride (0.6 M in tetrahydrofuran (THF)) (19). The oximate reagent for deprotection (0.3 M in 1:1 acetonitrile–dioxane) was prepared from *ortho*-nitrobenzaldoxime and 1,1,3,3-tetramethylguanidine (1.0 : 0.9 molar ratio). Chromatographic solvents were purchased from Fisher Scientific; all other reagents were purchased from Aldrich or Sigma Chemical Co. Kieselgel 60 (Merck) was used for dry-column flash chromatography (DCFC). Thin-layer chromatography (TLC) was carried out on Kieselgel 60 F_{254} plates from Merck. For paper chromatography, Whatman paper (No. 3001 917) was used.

Synthetic methods

The synthesized nucleoside derivatives were purified by DCFC, a modified flash chromatography (using suction instead of positive pressure (20)) that simplifies column loading and solvent elution. Deprotected nucleotides were purified initially by paper chromatography using solvent B′ (*n*-butanol:ethanol:water 4:1:5 v / v, organic phase). The dinucleoside monophosphates were purified by HPLC (Perkin Elmer Series 4 liquid chromatograph) using a semipreparative ODS-Hypersil column and a gradient of methanol and 0.1 M aqueous ammonium acetate (pH 6.0). The strategy used for the synthesis of **1** and **2** is shown in Scheme 1.

5′-O-tert-Butyldimethylsilylthymidine (**5**) was synthesized according to Ogilvie (19) with a slight modification to his purification procedure. Thymidine (**4**) (2.42 g, 10 mmol), *tert*-butyldimethylsilyl chloride (1.66 g, 11 mmol), imidazole (1.50 g, 22 mmol), and dimethylformamide (10 mL) were stirred (2.5 h) at room temperature and poured into water (1 L) to precipitate the crude product. (The product could also be isolated by extraction with chloroform or methylene chloride.) The product was separated from 3′, 5′-*tert*-butyldimethylsilylthymidine by DCFC using ethyl acetate as the eluting solvent (65% average yield) (λ_{max} = 267 nm in EtOH).

5′-O-tert-Butyldimethylsilyl-3′-acetylthymidine (**6**): Compound **5** (3.55 g, 10 mmol), pyridine (12.5 mL), and acetic anhydride (2.0 mL, 20 mmol) were stirred overnight. Methanol (10 mL) was added and the solvents were removed by codistillation with toluene, leaving a product that was sufficiently pure and dry for further synthesis.

5′-O-tert-Butyldimethylsilyl-3′-acetyl-4-(1,2,4-triazol-1-yl)-thymidine (**7**): The synthesis of **7** was based on the procedure of Divakar and Reese (21). The reaction was easily monitored by TLC (ethyl acetate) due to the appearance of a characteristic blue fluorescence, and was complete in an overnight reaction. The product was worked up as recommended (21) (λ_{max} = 251 nm in EtOH).

5′-O-tert-Butyldimethylsilyl-O4-ethylthymidine (**8**): Compound **7** (4.5 g, 10 mmol) was dried, and reacted with 60 mmol of sodium ethoxide (0.3 M in ethanol) for 30 min at room temperature. The mixture was neutralized with glacial acetic acid, the solvents were removed under vacuum, and the material was purified by DCFC with ethyl acetate (λ_{max} = 281 nm in EtOH).

3′-Acetyl-4-(1,2,4-triazol-1-yl)-thymidine (**9**): Compound **7** (4.5 g, 10 mmol) was dissolved in THF and stirred for 10 min with tetra-*n*-butylammonium fluoride (16.7 mL, 10 mmol). (*Cautionary note*: longer treatment leads to a gradual degradation of **9**.) Dowex-50 (Na^+-form) was added, stirred for 15 min, and then filtered out. The solvents were removed under vacuum and the product was purified by DCFC with ethyl acetate.

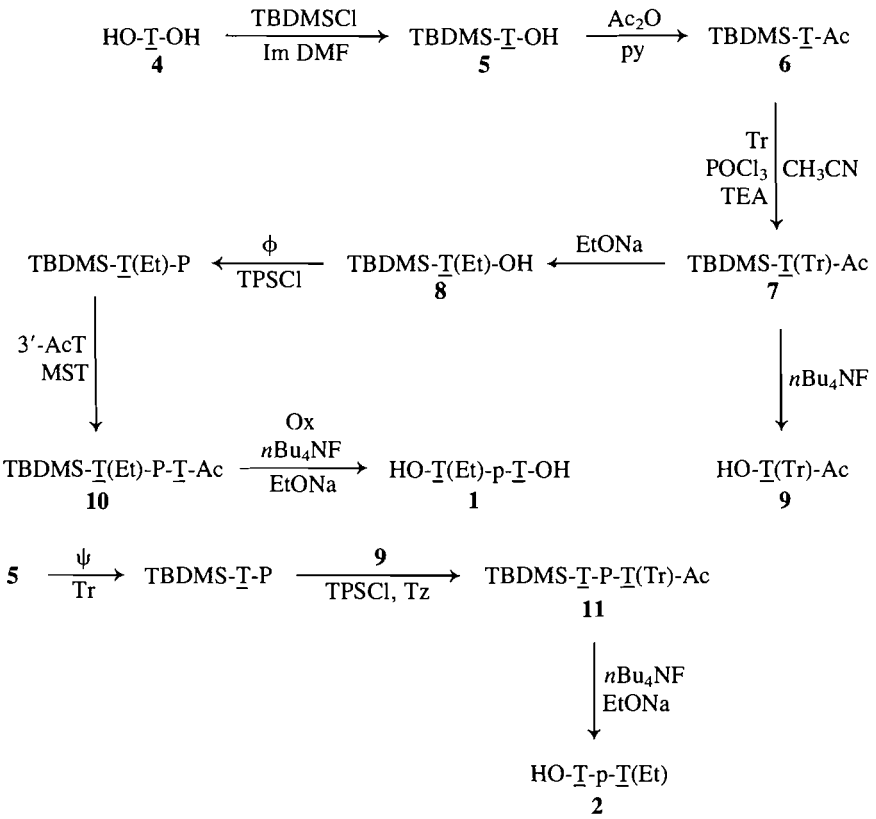
d(e^4TpT) (**1**): Pyridine-dried **8** (0.43 g, 1.1 mmol) was phosphorylated by stirring overnight with *p*-chlorophenyl phosphate (0.39 g, 1.3 mmol) and 2,4,6-triisopropylbenzenesulfonyl chloride (TPSCl) (0.83 g, cf. 2.8 mmol). 3′-Acetylthymidine (0.62 g, 2.2 mmol) and 1-(2-mesitylenesulfonyl)-tetrazole (0.83 g, 3.3 mmol) were added and the mixture was stirred overnight. The mixture was cooled in an ice bath and 1 mL H_2O was added. After 30 min most of the pyridine was removed by vacuum distillation and 40 mL H_2O was added. Extraction with methylene chloride followed and the organic solvent was dried over Na_2SO_4 and decanted. The fully-blocked dimer (**10**) was purified by DCFC (methylene chloride and methanol gradient). **10** (30 mg, 0.036 mmol) was treated overnight with oximate reagent (1 mL, 0.3 mmol). The mixture was poured over a silica gel column (40 mm length; 25 mm diameter) and the excess reagent was eluted with ether. The product was eluted with methanol, and the solvent was removed to obtain a dry material that was then treated overnight with tetra-*n*-butylammonium fluoride (0.23 mL, 0.14 mmol). Dowex-50 (Na^+-form) was added, followed by stirring for 15 min. The solid was filtered out; the filtrate was completely dried and then treated for 1 h with 0.3 M ethanolic sodium ethoxide (0.7 mL, 0.22 mmol). Excess reagent was neutralized with glacial acetic acid, and the solvents were removed. The material was redissolved in a few drops of water, streaked on Whatman No. 1 chromatographic papers, and developed in solvent B′. The material in the bands was eluted with H_2O and lyophilized. The appropriate band was selected on the basis of UV and 300-MHz ^{1}H NMR spectra and the desired product **1** was further purified by HPLC (λ_{max} = 273 nm; λ_{min} = 239 nm in H_2O).

d(Tpe^4T) (**2**): The phosphorylating agent was prepared from *p*-chlorophenyl phosphodichloridate (0.091 mL, 0.55 mmol) and triazole (0.14 g, 2.0 mmol) in 2–3 mL of pyridine, and was added to **5** (0.19 g, 0.5 mmol). After 15 min, the reaction was checked by TLC to ensure completion. **9** (0.26 g, 0.78 mmol), TPSCl (0.71 g, 2.34 mmol), and tetrazole (0.49 g, 7.02 mmol) were added; the condensation was complete in 1 h. The work-up and purification of the fully-blocked dimer (**11**) were carried out as for **10**. **11** (30 mg, 0.035 mmol) was treated for 1 min with 1 mL of the tetra-*n*-butylammonium fluoride solution. Dowex-50 (Na^+-form) was added and stirred for 10 min. The solids were filtered out and the solvents removed to dryness. The material was treated with 0.7 mL of sodium ethoxide (0.3 M in ethanol). After 1 h the solution was neutralized with glacial acetic acid and the product **2** was purified by chromatography and HPLC as described for **1** (λ_{max} = 272 nm; λ_{min} = 240 nm in H_2O).

Mass spectrometric experiments

Positive- and negative-ion FAB mass spectra (glycerol matrix, 8-keV xenon atoms) were obtained on a VG 7070E-HF spectrometer. The negative ion spectra proved more diagnostic and are reported here as follows: *m/z* (relative intensity, [ionic species]). *d(e^4TpT)*: 573(100, $[M - H]^-$); 1147(3.4, $[2M - H]^-$); 1721(0.05, [3M –

Can. J. Chem. Downloaded from www.nrcresearchpress.com by 122.72.124.2 on 09/07/12
For personal use only.



Abbreviations: T, thymidine; TBDMSCl, *tert*-butyldimethylsilyl chloride; Im, imidazole; DMF, dimethylformamide; Ac_2O, acetic anhydride; py, pyridine; Ac, acetyl; Tr, triazole; (Tr), 4-(1,2,4-triazol-1-yl); TEA, triethylamine; EtONa, ethanolic sodium ethoxide; (Et), O4-ethyl; ϕ, *p*-chlorophenyl phosphate; TPSCl, 2,4,6-triisopropylbenzenesulfonyl chloride; P, 3′-phosphate protected by *p*-chlorophenyl; 3′-AcT, 3′-acetylthymidine; MST, 1-(2-mesitylenesulfonyl)-tetrazole; Ox, oximate reagent; *n*-Bu_4NF, *n*-tetrabutylammonium fluoride; p, unprotected, diesterified phosphate; ψ, *p*-chlorophenyl phosphodichloridate; Tz, tetrazole.

SCHEME 1. Strategy for the synthesis of d(TpT) with an O4-alkylated thymine base.

H]$^-$); 125(27, [thymine − H]$^-$); 153(25, [O4-ethylthymine − H]$^-$); 321(17, 5′dTMP − H]$^-$); 349(23, [3′e^4dTMP − H]$^-$). *d(Tpe⁴T)*: 573(100, [M − H]$^-$); 1147(2.3, [2M − H]$^-$); 125(154, [thymine − H]$^-$); 153(14, [O4-ethylthymine − H]$^-$); 321(19, [3′dTMP − H]$^-$); 349(30, [5′e^4dTMP − H]$^-$). *d(TpT)*: 545(100, [M − H]$^-$); 125(61, [thymine − H]$^-$); 321(32, ([3′dTMP − H]$^-$) + [5′dTMP − H]$^-$); 419(6, [M − thymine − H]$^-$).

^{1}H nuclear magnetic resonance experiments

The ^{1}H NMR spectra were obtained at 300.13 MHz (Bruker AM300 spectrometer). All samples were examined in 5 mm (o.d.) tubes at the following concentrations in D_2O: **1**, 0.0070 M; **2**, 0.0017 M; **3**, 0.018 M. The concentrations were determined by UV absorbance measurements, assuming a molar extinction coefficient (ϵ) of 18 400 for **3** (22) and 16 300 for **1** and **2**. (The latter was calculated from the ϵ of the monomer units (22, 23) without correction for hypochromicity, which is not expected to be large for pyrimidine dimers (22)). At these concentrations intermolecular association should not be important. The solutions contained 0.01 M sodium phosphate buffer (pH = 6.9), EDTA (0.001 M) to chelate paramagnetic species, 0.1 M NaCl to maintain a constant ionic strength, and, for an NMR reference, a trace of *tert*-butanol, which is assigned a chemical shift of 1.231 ppm on the DSS scale. The samples were lyophilized twice from 99.8% D_2O and taken up in 99.9% D_2O. Spectra of the monomers (0.002 M) were obtained under the same conditions. Standard one-dimensional (1D) spectra were obtained at 10°C intervals from 10 to 70°C in 16K of computer memory (zero-filled to 32K). The HDO resonance was suppressed by presaturation (Bruker PRESAT. AU microprogram). Conventional homonuclear decoupling and two-dimensional (COSY-45°) (24) experiments were carried out for spectral assignments. The spectra were analyzed at 20 and 70°C (NUMARIT) (25) and computer-generated spectra confirmed the data. Using these data as guides, some chemical shift data were extracted from spectra at other temperatures (see Fig. 5) by assuming a first-order relationship between the protons, or an AB relationship in the case of H2′ and H2″.

Circular dichroism experiments

CD spectra were obtained on a Jasco J-500A spectropolarimeter using cells equipped for temperature control with a water bath. Each dimer at $(1.1–1.3) \times 10^{-4}$ M (calculated from UV absorption methods; see previous section) was dissolved in the phosphate buffer solution (pH 6.9) used for the NMR experiments.

Results and discussion

^{1}H nuclear magnetic resonance spectra, data, and assignments

The 1D NMR spectra of **1**, **2**, and **3** are shown in Figs. 2 and 3. Tables 1 and 2 provide chemical shift (δ) and coupling constant (*J*) data at 20 and 70°C obtained by computer analyses. Figures 4–6 show the temperature dependence of certain δ and *J* data in the 10–70°C range. The H6 and 5-CH_3 protons were assigned on the basis of the observed deshielding effect (0.22 ppm and 0.10 ppm, respectively) due to O4-alkylation at the monomer lever (7, 8, 12, 13). Also useful for assignments is the

Can. J. Chem. Downloaded from www.nrcresearchpress.com by 122.72.124.2 on 09/07/12
For personal use only.

Can. J. Chem. Downloaded from www.nrcresearchpress.com by 122.72.124.2 on 09/07/12
For personal use only.

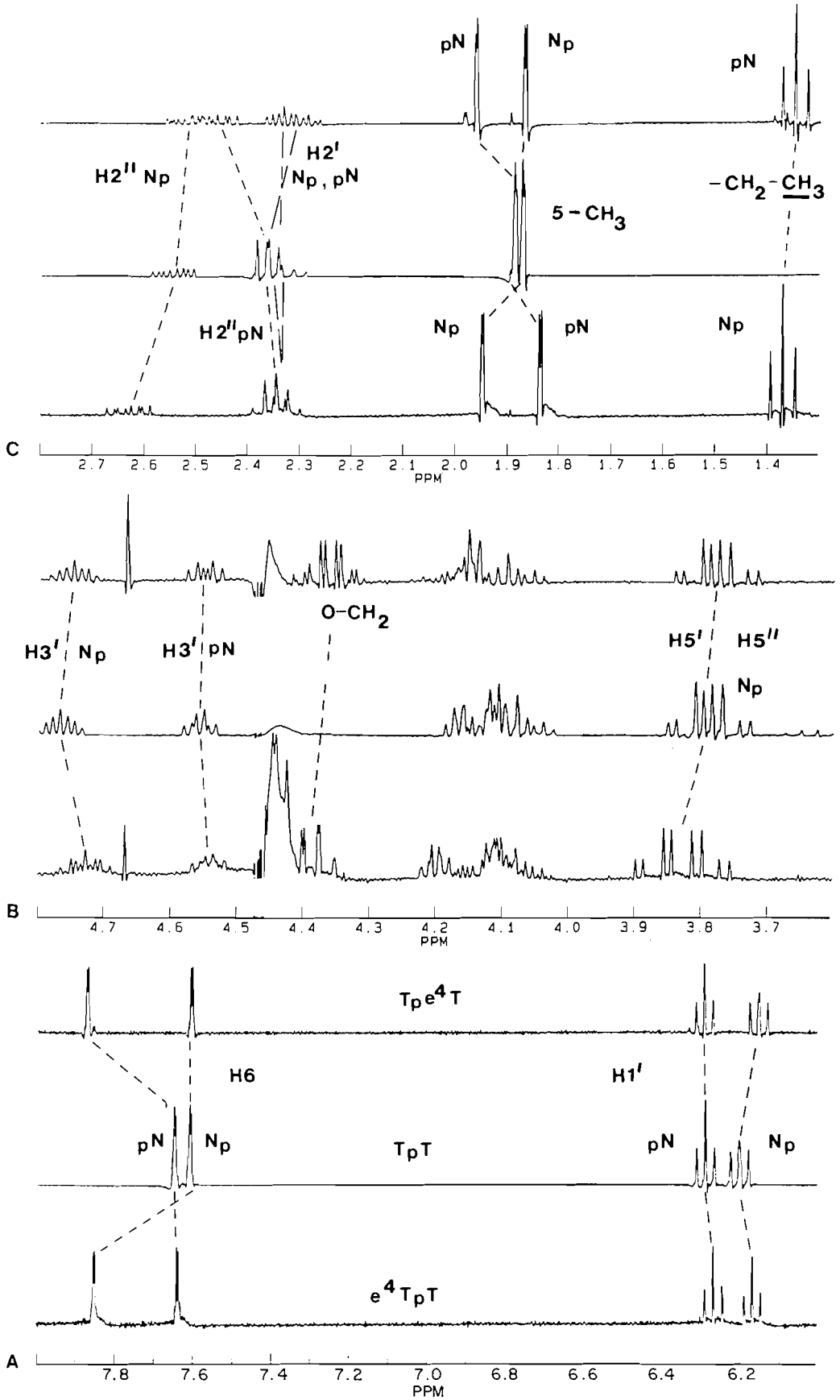


FIG. 2. Low-field (A), mid-field (B), and high-field (C) 300-MHz spectra (50°C) of d(Tpe^{4}T) (**2**) (upper panel of A, B, and C), d(TpT) (**3**) (middle panels), and d(e^{4}TpT) (**1**) (lowest panels). Np and pN represent the 3′- and 5′-linked nucleotidyl units, respectively. The 4.0 – 4.2 ppm bands in B comprise the H4′, H5′, H5″ of pN and H4′ of Np. The residual solvent-suppressed HDO signal appears at 4.45 ppm in B. An unidentified impurity is at 4.67 ppm in the spectra of **1** and **2**.

Can. J. Chem. Downloaded from www.nrcresearchpress.com by 122.72.124.2 on 09/07/12
For personal use only.

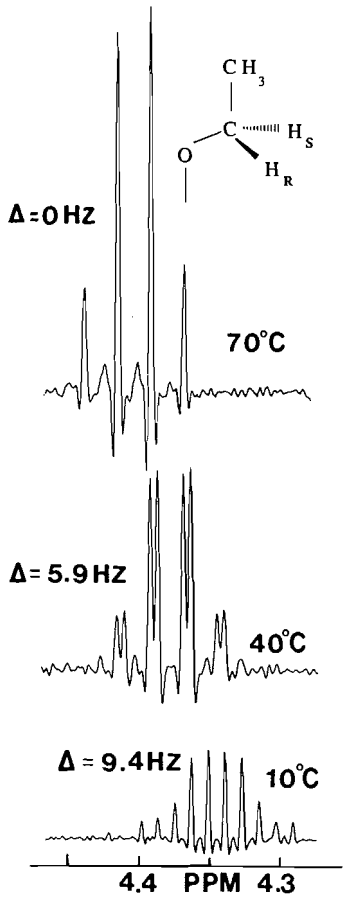


FIG. 3. Effect of temperature on the ^{1}H NMR band of the methylene H_R and H_S protons of the O4-ethyl group of d(e^{4}TpT). H_R and H_S refer to the *pro-R* and *pro-S* hydrogens (Fig. 1) and represent the AB part of an ABX_3 spin system (X_3 = 8-methyl protons). Δ is the chemical shift between H_R and H_S, with H_R assumed to be the more shielded. The decreasing value of Δ with increasing temperature is attributed to destacking of the bases. A similar phenomenon is noted for the methylene protons of d(Tpe^{4}T) (Δ = 10.7 Hz (10°C); 8.0 Hz (40°C); 4.7 Hz (80°C)), with H_S assumed to be the more shielded.

observation that the ^4J coupling between H6 and 5-CH_3 is consistently smaller by 0.1–0.2 Hz in the O4-alkylated thymine relative to the parent base (Table 2, Fig. 2).

Since the H3′ band of an Np fragment is easily distinguished from the corresponding band of the pN fragment, homonuclear decoupling can locate the connected H2′, H2″ bands and then the corresponding H1′ bands. The H2′ and H2″ protons of a particular residue are distinguished on the basis of (*a*) the larger deshielding effect of 3′-phosphorylation at H2″, (*b*) the deshielding effect of O4-alkylation at H2″ (0.09 ppm) and comparable shielding effect at H2′ (0.07 ppm) observed at the nucleoside level, and (*c*) coupling constant trends (26, 27). The H5′ and H5″ protons were assigned according to the literature (28). COSY-45° spectra were consistent with the assignments.

The O-alkyl group

Due to the presence of the chiral centres in the sugar, the C7 methylene protons of the O-ethyl groups of **1** and **2** are diastereotopic; the *pro-R* and *pro-S* protons are designated H_R and H_S in Fig. 1 and in Tables 1 and 2. At the nucleoside level (e^{4}dT), the ethyl group displays an A_2X_3 pattern in the ^{1}H NMR spectrum (methylene quartet, methyl triplet) (7), which indicates that the sugar is too distant to induce any observable differential shielding of H_R and H_S. However, in **1** and **2** these protons are not equally shielded, as is evident in the temperature-dependent ABX_3 patterns of their ethyl groups (Figs. 2, 3). At 20°C, for example, the relative H_R–H_S chemical shift (Δ) is 8.2 and 9.8 Hz in **1** and **2**, respectively (Table 1, Fig. 3). Δ decreases monotonically with increasing temperature (Table 1, Figs. 3, 5); at 70°C the quartet pattern for the methylene protons of **1** is restored (Fig. 3) but some residual splitting in the corresponding band of **2** remains even at 80°C.

Since Δ is not observed in e^{4}dT, it would seem to be a manifestation of intramolecular base stacking in **1** and **2**. Figure 1 provides a sketch of a right-handed base stack with the bases oriented in the *anti* conformation and the ethyl groups oriented as in crystalline e^{4}dT (7). In this conformation the shielding of H_R in **1** and of H_S in **2** should be more affected by the neighbouring thymine base. Disruption of the stack at elevated temperature would remove the differential shielding. Note (Fig. 4) that, in **1** and **2**, *both* methylene protons move downfield with increasing temperature, and tend toward the chemical shift of the methylene protons in e^{4}dT. This indicates that the neighbouring base shields each of the methylene protons, but it would seem that the proton inside the stack is more affected. With this reasoning we shall tentatively assign the high-field (more strongly temperature dependent) proton to H_R in **1** and to H_S in **2**. (We cannot discount some contribution from the conformation about the O4 — C7 bond that places H_S of **1** and H_R of **2** inside the stack; however, this conformation is deemed less likely since in it, unlike in the crystal conformation of e^{4}dT, the bulky 8-methyl group crowds the base.) No nuclear Overhauser enhancements between the bases were noted that could be used to distinguish the two protons. Temperature variation of the CD peaks confirms the presence of some structural ordering in **1** and **3** at low temperature (11°C), but little such variation is noted for **2** (see below).

In an ABX_3 system, the geminal (AB) as well as the vicinal (AX) coupling constants can be obtained. The geminal coupling between the *pro-R* and *pro-S* hydrogens ($J(RS)$ = −10.6 Hz) and the vicinal couplings between C7 and C8 hydrogens ($J(78)$ = 7.1 Hz) are identical in **1** and **2** (Table 2), and do not depend on temperature.

Sugar conformation

The sugar pucker can be evaluated from vicinal proton coupling constants (Table 2), or from certain sums of coupling constants (29). Figure 6 provides the temperature dependence of one such sum, $\Sigma 1' = J(1'2') + J(1'2'')$, which is easily obtained from the separation of the outer peaks of the H1′ region. The vertical axis also provides the *%S* (2′-*endo*) conformation as calculated in Rinkel and Altona (29). At the high temperature limit (70°C), the sugars of the unmodified units, including the monomer dT, have $\Sigma 1'$ in the narrow range 13.5 ± 0.2 Hz, which corresponds to *%S* ≅ 65%. The O-alkylated units, e^{4}Tp, pe^{4}T, and e^{4}dT, show $\Sigma 1'$ of 13.1 ± 0.2 Hz (55% *S*). Decreasing the temperature to 10°C effects a large decrease (1.4 Hz) in $\Sigma 1'$ of e^{4}Tp, and the 3′-*endo* (*N*) conformation now dominates (70% *N*); this proposed shift towards 3′-*endo* is consistent with the unusually large $J(3'4')$ (5.3 Hz) at 20°C (Table 2). Decreasing the temperature also reduces $\Sigma 1'$ in pT(**1**) and in each segment of **2**, but the changes here are much less (0.5 Hz). The two segments of **3** and the monomers are not influenced by temperature. Since no temperature effect is noted for the monomers, and since the pe^{4}T unit is much less affected, the shift towards 3′-*endo* in e^{4}Tp would seem to be a

TABLE 1. Chemical shifts δ (ppm from DSS) of d(e⁴TpT) (**1**), d(Tpe⁴T) (**2**), and d(TpT) (**3**)[a,b]

	d(e⁴TpT)				d(Tpe⁴T)				d(TpT)			
	e⁴Tp		pT		Tp		pe⁴T		Tp		pT	
	20°C	70°C	20°C	70°C	20°C	70°C	20°C	70°C	20°C	70°C	20°C	70°C
H1′	6.104	6.189	6.270	6.259	6.127	6.157	6.293	6.285	6.189	6.198	6.301	6.273
2′	2.409	2.329	2.336[c]	2.339	2.346	2.318	2.323	2.304	2.333	2.344	2.368	2.369[c]
2″	2.631	2.627	2.335[c]	2.362	2.519	2.513	2.443	2.466	2.544	2.541	2.346	2.362[c]
3′	4.688	4.744	4.552	4.533	4.733	4.755	4.569	4.538	4.752	4.773	4.578	4.543
4′	4.191	4.200	4.098	4.118	4.144	4.140	4.150	4.154	4.167	4.162	4.108	4.115
5′	3.887	3.858	4.148	4.120	3.811	3.806	4.174	4.148	3.811	3.818	4.136	4.116
5″	3.806	3.784	4.063	4.064	3.760	3.748	4.079	4.077	3.764	3.760	4.063	4.063
6	7.927	7.822	7.667	7.622	7.662	7.580	7.902	7.861	7.629	7.584	7.671	7.650
5M	1.939	1.951	1.800	1.852	1.861	1.869	1.948	1.965	1.890	1.874	1.870	1.859
7R	4.342	4.403	—	—	—	—	4.347	4.367	—	—	—	—
7S	4.370	4.403	—	—	—	—	4.314	4.386	—	—	—	—
Δ[d]	8.2	<3	—	—	—	—	9.8	5.7	—	—	—	—
8	1.375	1.368	—	—	—	—	1.351	1.349	—	—	—	—

[a]Temperature in °C.
[b]Proton labelling (Fig. 1); 5M: 5-methyl; 7R and 7S: diastereotopic *R* and *S* methylene protons of the O-alkyl group; 8: methyl protons of the O-alkyl group.
[c]Estimated since δ2′ ≃ δ2″.
[d]Δ: chemical shift in Hz at 300 MHz between 7R and 7S.

TABLE 2. Coupling constants (*J*, Hz) of d(e⁴TpT) (**1**), d(Tpe⁴T) (**2**), and d(TpT) (**3**)[a,b]

	d(e⁴TpT)				d(Tpe⁴T)				d(TpT)			
	e⁴Tp		pT		Tp		pe⁴T		Tp		pT	
	20°C	70°C	20°C	70°C	20°C	70°C	20°C	70°C	20°C	70°C	20°C	70°C
1′2′	5.9	6.5	6.4]	6.9	6.9	6.7	6.5	6.6	7.4	7.0	6.8	6.8
1′2″	5.9	6.4	6.4]	6.7	6.2	6.6	6.6	6.6	6.2	6.4	6.8	6.8]
2′2″	−13.9	−14.2	−14.0[c]	−14.2	−14.1	−14.2	−14.1	−14.1	−14.1	−14.1	−14.3	−14.2[c]
2′3′	6.1	6.7	5.9]	6.7	6.6	6.6	6.7	6.7	6.4	6.8	6.7	5.5
2″3′	6.1	4.3	5.9]	4.2	3.9	3.8	4.8	4.3	3.5	3.4	4.2	5.5]
3′4′	5.3	4.2	4.5	3.7	3.8	3.7	4.5	4.4	3.5	3.5	3.9	4.1
4′5′	2.9	3.4	2.5	2.9	3.3	3.5	2.5	2.8	3.4	3.5	2.3	2.6
4′5″	4.1	4.8	3.0	4.2	4.5	5.0	3.3	4.5	4.6	4.9	3.3	4.5
5′5″	−12.8	−12.6	−11.5	−11.7	−12.7	−12.6	−11.7	−11.9	−12.6	−12.4	−11.5	−11.8
56	1.2	1.2	1.3	1.3	1.3	1.3	1.1	1.2	1.3	1.3	1.3	1.3
7R, 7S	−10.6	—	—	—	—	—	−10.6	—	—	—	—	—
78	7.1	7.1	—	—	—	—	7.1	7.1	—	—	—	—
3′P	6.4	6.7	—	—	6.6	6.5	—	—	6.5	6.7	—	—
5′P	—	—	3.9	4.7	—	—	4.5	4.8	—	—	4.4	4.5
5″P[d]	—	—	3.6	5.0	—	—	4.1	4.5	—	—	4.2	5.1

[a]Temperature in °C.
[b]Proton labelling (Fig. 1). 5: 5-methyl; 7R, 7S: diastereotopic *R* and *S* methylene protons of the O-ethyl; 8: methyl protons of the O-ethyl.
[c]When δ(2′) ≃ δ(2″), $J_{(2'2'')}$ is arbitrary and only the sum of connected couplings (]) is significant.
[d]A ^4J(P–H4′) coupling of 2.0–2.5 Hz was observed in some of the spectra.

sequence-dependent, base-stacking related phenomenon. As noted above, the effect of temperature on Δ suggests the presence of some base stacking at low temperature. This shift towards the *N* pucker in e⁴Tp is unusual since *S* is favored in small 2′-deoxyoligonucleotides in aqueous solution (26, 27, 29). Note, however, that e⁴dT is 3′-*endo* in the crystal state (7).

Table 3 provides populations for the *gauche*$^+$ (g^+), *trans* (t), and *gauche*$^-$ (g^-) conformers about the C4′ — C5′ bond, calculated from the J(4′5′) and J(4′5″) data (Table 2) via Haasnoot *et al.* (30). At 20°C the Np and pN fragments of the three dimers show preferences for g^+ in the narrow range 61 ± 5 and 79 ± 2%, respectively. A preference for g^+ is generally observed in oligomers (27, 29, 30). Increasing the temperature to 70°C reduces this preference in Np to 52 ± 2%, and in pN to 64 ± 2%. The g^- conformer is always the least populated with t of intermediate importance. Thus, O4-alkylation of **3** does not have a large effect on the C4′—C5′ bond of either nucleotidyl unit.

The population of the favored t conformer about the C5′—O5′ (β) bond of the pN units can be estimated from Σ′ (J(5′P) + J(5″P) (Table 2). Assuming the parameters of ref. 27, we find that %t varies only slightly for **1**, **2**, **3**, and lies in the narrow

Can. J. Chem. Downloaded from www.nrcresearchpress.com by 122.72.124.2 on 09/07/12
For personal use only.

Can. J. Chem. Downloaded from www.nrcresearchpress.com by 122.72.124.2 on 09/07/12
For personal use only.

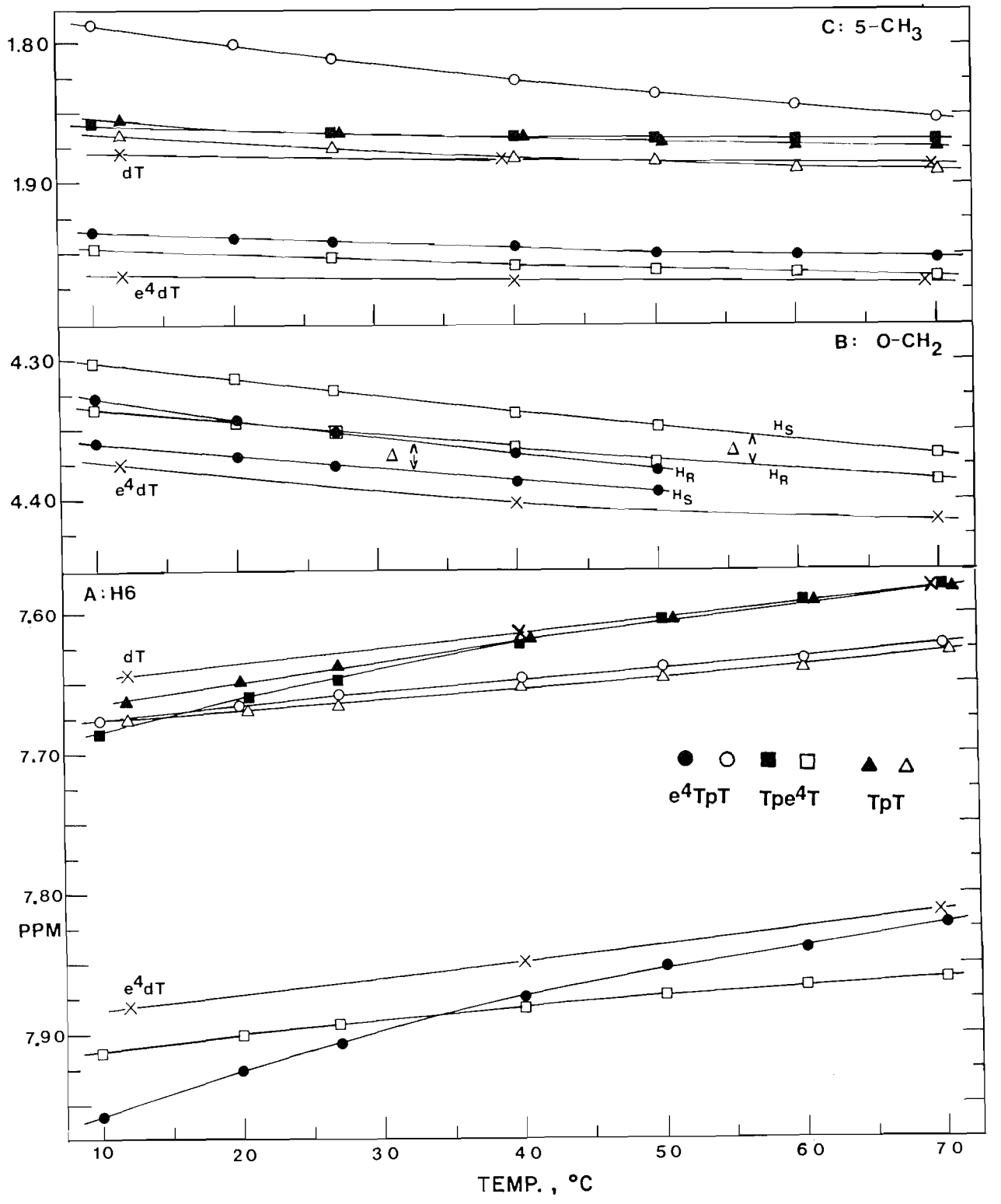


FIG. 4. Temperature profiles of the base proton chemical shifts of d(e^{4}TpT), d(Tpe^{4}T), d(TpT), and the nucleosides dT and e^{4}dT in ppm relative to internal DSS: H6 (panel A), methylene protons of the O—CH_2—CH_3 groups (panel B), and 5-CH_3 (panel C). The symbols are given in panel A; X refers to the nucleoside data. See captions of Figs. 1 and 3 for H_R, H_S, and Δ.

ranges 81 ± 3% at 20°C and 75 ± 1% at 70°C. The *J*(3′P) coupling constants that depend on the C3′—O3′ orientation of the Np units show little variation for **1**, **2**, and **3** (Table 2); preliminary unpublished $^{13}C - {}^{31}P$ coupling constant data indicate a preference for the *trans* conformation at the C5′—O5′ and C3′—O3′ bonds.

^1H chemical shifts

The effects of O4-alkylation and of temperature change on the proton shifts are shown in Figs. 4 and 5. Several trends are noteworthy.

1. *At high temperature* O4-alkylation of a thymine induces a downfield shift of about 0.25 and 0.10 ppm in its H6 and

Can. J. Chem. Downloaded from www.nrcresearchpress.com by 122.72.124.2 on 09/07/12
For personal use only.

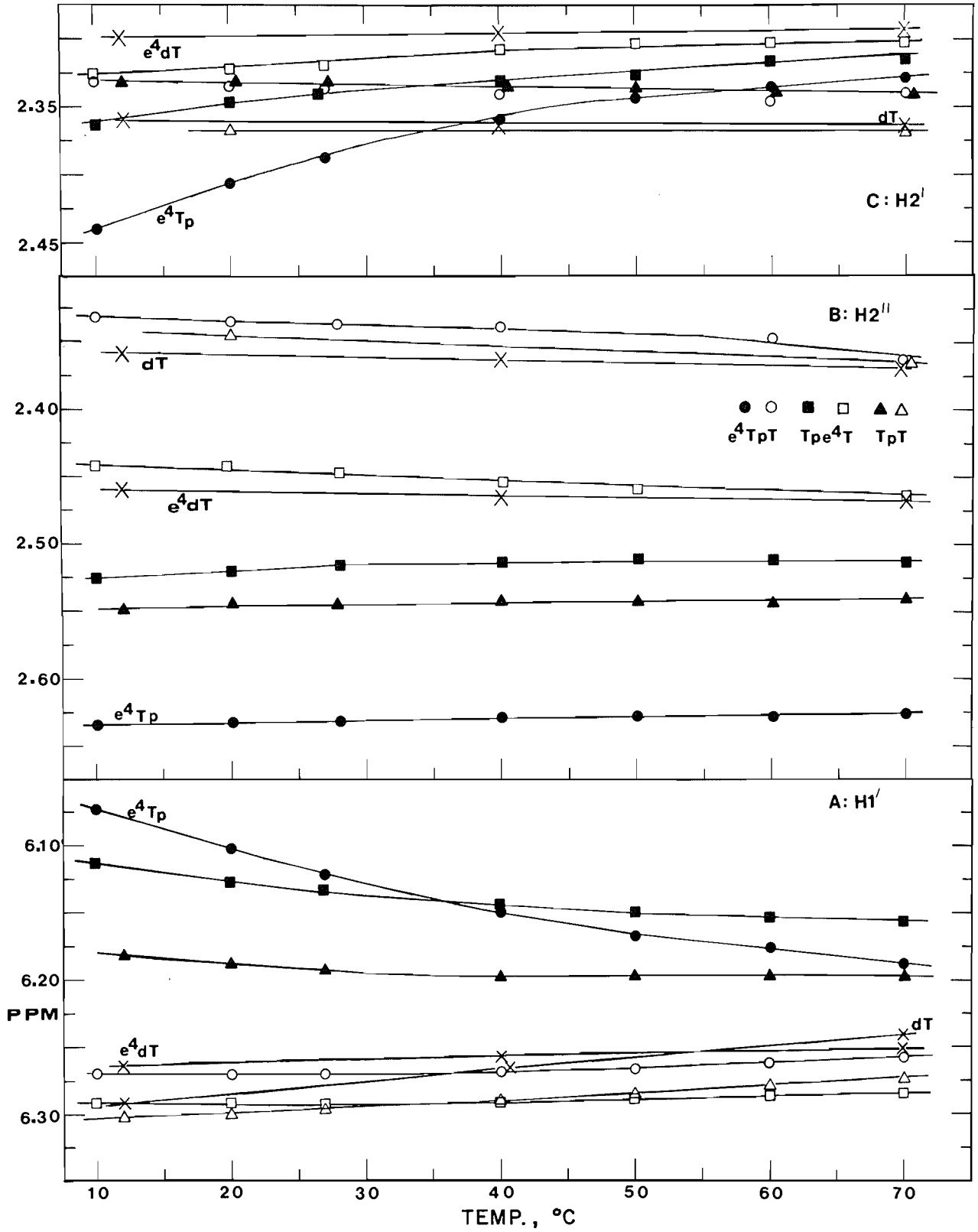


FIG. 5. Temperature profiles of the chemical shifts of the sugar protons of **1**, **2**, and **3**, and the nucleosides dT and e^4dT, in ppm relative to internal DSS: H1′(panel A), H2″(panel B), and H2′(panel C). The symbols are given in panel B; X refers to the nucleoside data. The data at 20 and 70°C are taken from Table 1; the other data were extracted from the spectra assuming a first-order relationship between the protons or an AB relationship in the case of H2′ and H2″.

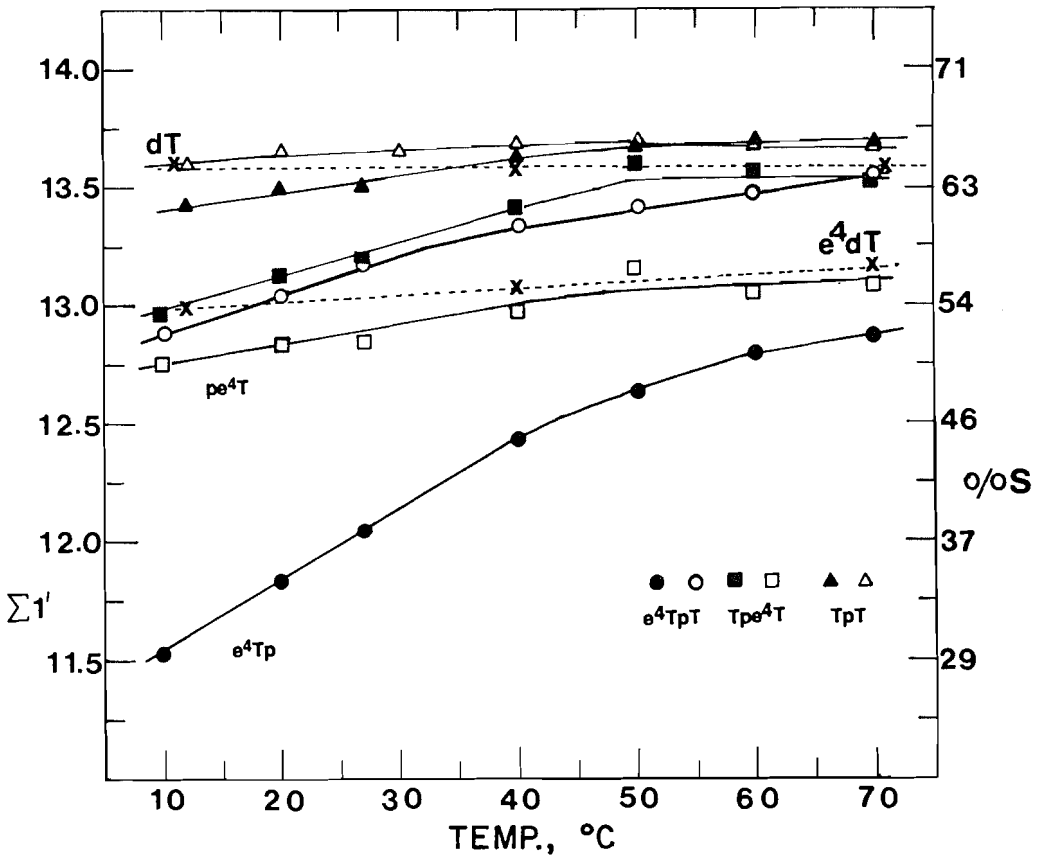


FIG. 6. Temperature profiles of $\Sigma 1' = J(1'2') + J(1'2'')$ in Hz for **1**, **2**, **3**, dT, and e⁴dT. The data at 20 and 70°C are from Table 2; the width of the H1′ band provides the values of $\Sigma 1'$ at the other temperatures. The vertical scale at the right provides the *%S* (2′-*endo*) conformation of the sugar ring calculated according to Rinkel and Altona (29). The symbols are defined in the diagram; X refers to the monomers.

TABLE 3. Calculated % populations[a] of the g^+, t, g^- rotamers about the C4′–C5′ bond for d(e⁴TpT) (**1**), d(Tpe⁴T) (**2**), and d(TpT) (**3**)

Dimer	Np	Temp (°C)	g^+	t	g^-	pN	Temp (°C)	g^+	t	g^-
1	e⁴Tp	20	66	29	5	pT	20	81	18	1
		70	54	35	11		70	65	30	5
2	Tp	20	58	32	10	pe⁴T	20	78	22	1
		70	51	37	13		70	62	34	4
3	Tp	20	56	33	11	pT	20	80	22	−2
		70	52	36	13		70	64	34	2

[a]Calculated according to ref. 30.

5-methyl protons, respectively (Fig. 4). The sugar protons are, in general, not much affected by the base modification except for H2″, which shifts downfield by 0.08–0.10 ppm (Fig. 5B); this reinforces the comparable deshielding of H2″ due to the 3′-phosphoryl group, and thus the H2″ (e⁴Tp) is the most deshielded of the six H2″ protons of the dimers. The relative chemical shifts of the H2″ protons can be understood in terms of this additivity of the deshielding influence of O-alkylation and 3′-phosphorylation.

2. For the most part, the various δ values show only slight variations as the temperature is increased from 10 to 70°C, with corresponding protons of the three dimers showing changes in the same direction. The largest changes are noted for **1**: the H6, H1′, and H2′ of the e⁴Tp unit and the 5-CH_3 of the pT unit. Since these protons are located on the base or near the N-glycosyl bond, we are inclined to suggest that the changes are, like the temperature variation of Δ, a reflection of some small degree of structural ordering of the dimers at low temperature. More precise structural details cannot be provided since the changes are small, presumably due to the low tendency for stacking at the dimer level and to the small ring currents associated with pyrimidine rings (31). Particularly interesting is the 0.10-ppm upfield shift of the H2′ proton of the e⁴Tp unit of **1**, which contrasts with the temperature independence of δ(H2″) of this unit. These trends can be rationalized on the basis of a right-hand base stack with a 3′-*endo* e⁴Tp unit since in this conformation the H2′ (but not H2″) of an Np unit is placed near to the base and O4′ atoms of the pN unit. Cheng and Sarma (32) have noted that the elevation of temperature (20 to 80°C) causes shielding of *both* the H2′ and H2″ protons of the Cp unit of

Can. J. Chem. Downloaded from www.nrcresearchpress.com by 122.72.124.2 on 09/07/12
For personal use only.

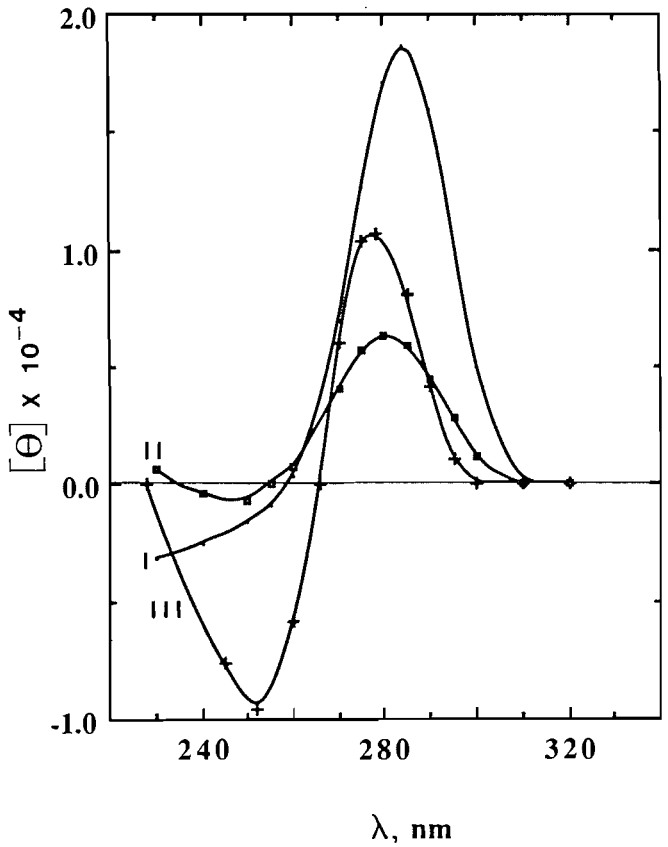


FIG. 7. Circular dichroism (CD) spectra (11–12°C) of **1**, **2**, and **3** at (1.1–1.3) × 10^{-4} M in aqueous solution. The vertical axis gives [θ] in deg M^{-1} cm^{-1}, the molar ellipticity per residue calculated following Cantor and Schimmel (35).

d(CpT). However, these authors observed that both sugars retain a preference for the 2′-*endo* pucker over the entire temperature range. Molecular models of a stacked dimer with a 2′-*endo* Np unit reveal that H2′ and H2″ of this unit make contacts with the pN unit, and hence the simultaneous variation of their δ values is not unexpected.

3. An interesting trend (Fig. 4A) is the downfield shift of all H6 resonances as the temperature is decreased from 70°C to 10°C. This shift is larger in the Np than in the pN and monomer units; the largest effect is seen in the e^4Tp unit (0.13 ppm relative to the DSS reference and 0.08 ppm relative to the H6 resonance of the corresponding monomer, e^4dT). The downfield shifts in the dimers indicate that some factor other than the ring current effect of the neighbouring base must be dominant. Comparable temperature effects have been noted earlier in dipyrimidine dimers, but were not easily explained (26, 33). The temperature dependence of the H6 resonances of the monomers indicates that simple solvent effects are relatively important. Indeed, evidence has been presented (34) that such effects can mask the upfield effects of ring currents even for stacked purine bases.

Circular dichroism

The CD spectra of **1**, **2**, and **3** at 11–12°C are shown in Fig. 7. The spectrum of **3** shows nearly equal positive and negative peaks at 278 and 252 nm, respectively, in good agreement with the observations at 26°C by Cantor *et al.* (36). The molar ellipticities per residue ([θ]) at the extrema of **3** are about 30% larger than those observed earlier (36), though their ratios are the same (278 nm : 252 nm = 1.2). The larger amplitudes observed in this work are due in part to the lower temperature of the experiment (see below). The two alkylated dimers are characterized by the dramatic reduction in the negative CD peak, and by the larger intensity of the positive peak in **1** relative to **2**. In view of the "cytosine-like" nature of the O4-ethyl base suggested by crystal structures (5–7), it is interesting to note that these features also characterize the CD spectra of d(CpT) and d(TpC) reported by Cantor *et al.* (36).

Increasing the temperature to 63–65°C leads to a 40% reduction in the amplitudes of the positive and negative peaks of **3**, and of the positive peak of **1**, which tend towards the values of [θ] measured for the constituent nucleosides (dT: λ_{max} = 276 nm, $[\theta]_{max}$ = 3800; e^4dT: λ_{max} = 279 nm; $[\theta]_{max}$ = 8560; measured here under the conditions used for the dimers and found to be independent of temperature in the 10–65°C range). The reduction in [θ] with increasing temperature is in line with the formation of some structural order in **1** and **3** at low temperature, and is consistent with the temperature variation of Δ noted above for **1**. However, **2** also shows a temperature-dependent Δ, yet we find that the amplitude of its positive band decreases by much less (10%) when the temperature is increased to 65°C. This could mean that variations in Δ and [θ] are reflecting different aspects of the ordered structure. Perhaps this interesting point would be better understood by the examination of longer oligonucleotides, which should be more extensively ordered, particularly if they contain purine bases.

Mass spectrometric experiments

Confirmation of the presence of the O-alkylated base in our dimers is provided by their FAB mass spectra, particularly when obtained in the negative ion mode. Prominent peaks in the spectra of **1** and **2** are observed at *m/z* 573 (and at *m/z* 545 in **3**), which can be assigned to the $[M - H]^-$ ion. Peaks at *m/z* 125 and *m/z* 153 are found in the spectra of **1** and **2**, and are assigned, respectively, to the base fragments $[thymine - H]^-$ and $[O4-ethylthymine - H]^-$ liberated by scission of the N-glycosyl bonds. The former (but not the latter) peak is observed in the spectrum of **3**. The peak at *m/z* 349 in **1** is assigned to $[3'e^4dTMP - H]^-$, the 3′-nucleotidyl fragment formed by scission of the O—C5′ bond to the nucleoside at the 3′ end. An *m/z* 349 peak is also observed in **2** and is assigned to the 5′-nucleotidyl unit $[5'e^4dTMP - H]^-$. Also of diagnostic value is the presence of the peaks at *m/z* 1147 in **1** and **2** (with intensities of 2–3% of the $[M - H]^-$ ion), which can be assigned to the molecular aggregates $[2M - H]^-$. In **1**, an assembly of three molecules, $[3M - H]^-$, is also apparent at *m/z* 1721, though at very low intensity (0.05% of $[M - H]^-$). Such aggregates were not detected in the spectrum of **3**. These observations demonstrate clearly the usefulness of the FAB technique for characterizing O-alkylated oligonucleotides.

Acknowledgements

We acknowledge the support of the following: NSERC (for operating grants to F.E.H. (A1549) and K.L.S. (A6434), and equipment grants for our NMR and mass spectrometric facilities); The University of Manitoba (research funds for F.E.H. and K.L.S., and a Manitoba Fellowship for G.W.B.); Mr. W. Buchanon (for acquiring and interpreting the FAB mass spectra); Mr. K. Marat (for help with acquiring the NMR spectra); Drs. B. Singer and J. B. Westmore (for discussions); Donna Hruska and Cheryl Armstrong (for help with manuscript preparation).

Can. J. Chem. Downloaded from www.nrcresearchpress.com by 122.72.124.2 on 09/07/12
For personal use only.

1. B. SINGER. Nature (London), **264**, 333(1976).
2. R. SAFFHILL, G. P. MARGISON, and P. J. O'CONNOR. Biochim. Biophys. Acta, **823**, 111(1985).
3. A. POROHILLE and G. H. LOEW. Biophys. Chem. **22**, 37(1985).
4. B. SINGER. Cancer Res. **46**, 4879(1986).
5. R. G. BRENNAN, G. G. PRIVE, W. J. P. BLONSKI, F. E. HRUSKA, and M. SUNDARALINGAM. J. Am. Chem. Soc. **105**, 7737(1983).
6. R. G. BRENNAN, D. PYZALSKA, W. J. P. BLONSKI, F. E. HRUSKA, and M. SUNDARALINGAM. Biochemistry, **25**, 1181(1986).
7. G. I. BIRNBAUM, K. L. SADANA, W. J. P. BLONSKI, and F. E. HRUSKA. J. Am. Chem. Soc. **108**, 1671 (1986).
8. G. I. BIRNBAUM, K. L. SADANA, M. T. RAZI, T. LEE, R. SEBASTIAN, G. W. BUCHKO, and F. E. HRUSKA. Can. J. Chem. **66**, 1628(1988).
9. W. J. COOK, G. L. GARTLAND, and C. E. BUGG. Acta Crystallogr. Sect. B: Struct. Crystallogr. Cryst. Chem. **36**, 2467(1980).
10. R. PARTHASARATHY and S. M. FRIDEY. Carcinogenesis, **7**, 221(1986).
11. T. SRIKRISHNAN, R. PARTHASARATHY, N. C. DE, and G. B. CHHEDA. Acta Crystallogr. Sect. C: Cryst. Struct. Commun. **C39**, 1441(1983).
12. F. E. HRUSKA and W. J. P. BLONSKI. Can. J. Chem. **60**, 3026(1982).
13. B. D. ALLORE, A. QUEEN, W. J. P. BLONSKI, and F. E. HRUSKA. Can. J. Chem. **61**, 2397(1983).
14. C.-J. CHANG, D. J. ASHWORTH, L.-J. CHERN, J. DASILVA GOMES, C.-G. LEE, P. W. MOU, and R. NARAYAN. Org. Magn. Reson. **22**, 671(1984).
15. B. F. L. LI, C. B. REESE, and P. F. SWANN. Biochemistry, **26**, 1086(1987).
16. M. W. KALNIK, M. KOUCHAKDJIAN, B. F. L. LI, P. F. SWANN, and D. J. PATEL. Biochemistry, **27**, 108(1988).
17. G. W. BUCHKO, F. E. HRUSKA, M. T. RAZI, and K. L. SADANA. Proceedings of the 5th Conversation in Biomolecular Stereodynamics, Albany, NY. 2–6 June, 1987. Adenine Press, Guilderland, NY. p. 83.
18. K. L. SADANA, F. E. HRUSKA, and P. C. LOEWEN. Tetrahedron Lett. **22**, 3367(1981).
19. K. K. OGILVIE. Can. J. Chem. **51**, 3799(1973).
20. L. M. HARWOOD. Aldrichchimica Acta, **18**, 25(1985).
21. K. J. DIVAKAR and C. B. REESE. J. Chem. Soc. Perkin Trans. **1**, 1171(1982).
22. P. S. MILLER, K. N. FANG, N. S. KONDO, and P. O. P. TS'O. J. Am. Chem. Soc. **93**, 6657(1971).
23. B. SINGER, J. SAGI, and J. T. KUSMIEREK. Proc. Natl. Acad. Sci. U.S.A. **80**, 4884(1983).
24. W. P. AUE, E. BARTHOLDI, and R. R. ERNST. J. Chem. Phys. **64**, 2229(1976).
25. A. R. QUIRT and J. S. MARTIN. J. Magn. Reson. **5**, 318(1971).
26. D. J. WOOD, F. E. HRUSKA, and K. K. OGILVIE. Can. J. Chem. **52**, 335(1974).
27. D. M. CHENG, M. M. DHINGRA, and R. H. SARMA. Nucleic Acids Res. **5**, 4399(1978).
28. M. REMIN and D. S. SHUGAR. Biochem. Biophys. Res. Commun. **48**, 636(1972).
29. L. J. RINKEL and C. ALTONA. J. Biomol. Struct. Dyn. **4**, 621(1987).
30. C. A. G. HAASNOOT, F. A. A. M. DE LEEUW, H. P. M. DE LEEUW, and C. ALTONA. Recl. Trav. Chim. Pays – Bas, **98**, 576(1979).
31. C. GIESSNER-PRETTRE and B. PULLMAN. J. Theor. Biol. **27**, 87(1970).
32. D. M. CHENG and R. H. SARMA. J. Am. Chem. Soc. **99**, 7333(1977).
33. C.-H. LEE, F. S. EZRA, N. S. KONDO, R. H. SARMA, and S. S. DANYLUK. Biochemistry, **15**, 3627(1976).
34. F. E. HRUSKA, C. L. BELL, T. A. VICTOR, and S. S. DANYLUK. Biochemistry, **7**, 3721(1968).
35. C. R. CANTOR and P. R. SCHIMMEL. Biophysical chemistry. Part II. Freeman, San Francisco, CA. 1980. p. 413.
36. C. R. CANTOR, M. W. WARSHAW, and H. SHAPIRO. Biopolymers. **1**, 1059(1970).

Can. J. Chem. Downloaded from www.nrcresearchpress.com by 122.72.124.2 on 09/07/12
For personal use only.

Comparison of muonium and positronium with hydrogen atoms in their reactions towards solutes containing amide and peptide linkages in water and micelle solutions

MARY V. BARNABAS, KRISHNAN VENKATESWARAN, AND DAVID C. WALKER
Department of Chemistry of TRIUMF, University of British Columbia, Vancouver, B.C., Canada V6T IY6

Received May 25, 1988

MARY V. BARNABAS, KRISHNAN VENKATESWARAN, and DAVID C. WALKER. Can. J. Chem. **67**, 120 (1989).

Rate constants have been sought for the reaction of muonium (Mu) and *o*-positronium (Ps) with solutions of thirteen solutes containing the CO—N< (or —CS—N<) groups. Values of k range from $<10^5\ M^{-1}\ s^{-1}$ to $3 \times 10^{10}\ M^{-1}\ s^{-1}$ and show a variety of trends. For instance, Mu adds across the carbonyl group much faster than does H, but abstracts from an adjacent methyl group more slowly. Mu adds exceptionally efficiently to the thiocarbonyl group. Abstraction reactions are identified by large enhancements in reaction rates when localized in micelles. Ps behaves quite differently to the others in neither abstracting nor adding to these compounds, consistent with it not being a pseudo-isotope of hydrogen.

Key words: muonium, positronium, hydrogen, hydrated electrons, micelles.

MARY V. BARNABAS, KRISHNAN VENKATESWARAN, et DAVID C. WALKER. Can. J. Chem. **67**, 120 (1989).

On a cherché à évaluer les constantes de vitesse pour les réactions du muonium (Mu) ainsi que de l'ortho-positronium (Ps) avec des solutions de treize solutés contenant les groupements —CO—N< (ou —CS—N<). Les valeurs de k s'étalent de $<10^5\ M^{-1}\ s^{-1}$ à $3 \times 10^{10}\ M^{-1}\ s^{-1}$ et elles présentent les tendances les plus diverses. Par exemple, le Mu s'additionne beaucoup plus rapidement au groupement carbonyle que le H; toutefois, il procède beaucoup plus lentement à un enlèvement sur un méthyle adjacent. Le Mu s'additionne d'une façon exceptionnellement efficace sur le groupement thiocarbonyle. Lorsque les réactions d'abstraction sont localisées dans des micelles, elles sont identifiées par des augmentations importantes dans les vitesses de réactions. Le Ps se comporte d'une façon bien différente; il ne conduit pas à des réactions d'abstraction ou des additions sur ces composés et ces résultats sont en accord avec le fait qu'il n'est pas un pseudo-isotope de l'hydrogène.

Mots clés : muonium, positronium, hydrogène, électrons hydratés, micelles.

[Traduit par la revue]

Introduction

Muonium (μ^+e^-, chemical symbol Mu) is the neutral atom having a short-lived (2.2 μs) positive muon as nucleus and an electron in a 1*s* orbital almost identical to that of H. For this reason Mu is expected to behave as a light isotope of H, with just one ninth the mass of protium. The study of Mu atom reactions in solution with different solutes yields fresh information about kinetic isotope effects when compared with H (1). Studies with micelles have revealed enhancements for certain types of reactions (2) and shifts in the reaction channel when alternative paths are available, as in reaction with acetone (3). Ordinary hydrogen atoms cannot be so readily studied with micelles because they react too rapidly with the surfactant molecules themselves. A further advantage of Mu is the directness with which identity, yield, and reactivity can be observed, given a source of muons and the μSR techniques.

Positronium (e^+e^-, chemical symbol Ps) can also be envisaged as an exotic atom with some analogies to hydrogen. But Ps differs from H and Mu by having no "nucleus" (because of the equal masses of the electron and positron) and this leads to considerable differences in size, polarizability, and binding energy. Its rate of diffusion in water is comparable to that of Mu and H (4), however, and its chemical reactivity is worth contrasting with Mu. Some ionic solutes have recently been compared in this regard (5).

Comparisons with solvated electrons as the lightest of the quartet H/Mu/Ps/e^-_{aq} are also of interest, because the mass and mean thermal velocity of Ps are much closer to e^- than H. In studies of all four species the rate of disappearance is observed and only very rarely is a product of reaction identified. Contrasts and inter-comparisons therefore have to be used to infer the mechanism and type of reaction involved.

In the present paper organic molecules have been selected as solutes which contain amido-linkages and are of some biological interest. Mu and Ps might be expected to attack them through abstraction or addition reactions. Furthermore, some related compounds have recently been seen to produce muonated free radicals when studied by μSR (3, 6–8).

Experimental

1. μSR technique

Muonium atoms form at the end of some muon tracks when energetic positive muons (from pion decays) are injected into water. They are observed in transverse magnetic fields by the muon spin rotation technique (μSR) (9, 10). The muons were provided on the M20 and M13 beamlines of TRIUMF. Chemical reaction rate constants of Mu were evaluated from spin precession signals as the relaxation constant (λ) of the "triplet" muonium signal (parallel muon and electron spins) oscillating at its Larmor frequency (ω_M) of 1.39 MHz G^{-1}. A MINUIT χ^2-minimization fit of the muon lifetime histogram (as in Fig. 1*a*) to eq. [1],

$$[1]\quad N_t = N_0 \exp(-t/\tau)[1 + A_M \exp(-\lambda t)\cos(\omega_M t + \phi_M) + A_D \cos(\omega_D t + \phi_D)] + B$$

gives λ as one of the fitted parameters. (In eq. [1], N_t is the number of counts in the histogram corresponding to time t; N_0 a normalization factor; τ the mean muon lifetime; A_M and A_D, ω_M and ω_D, and ϕ_M and ϕ_D are the asymmetries, frequencies, and initial phases of the "muonium atoms" and "diamagnetic muon components", respectively; and B is the time-independent background signal). λ is related to a bimolecular chemical rate constant of Mu (k_M) through eq. [2],

$$[2]\quad k_M = (\lambda - \lambda_0)/[S] = \Delta\lambda/[S]$$

where λ is the observed value with solute present at concentration [S] and λ_0 the background value in the same medium, including micelle, but with [S] = 0. A narrow observational time-window of ~0.3 to ~4 μs is imposed by the μSR technique, because it is a nuclear physics technique based on the intrinsic decay of the muon (τ = 2.2 μs). Therefore, all solutions to be studied must have their muonium chemical-lifetimes carefully selected so that λ falls in the limited range of 3×10^6 to $2.5 \times 10^5\ s^{-1}$. This precludes the possibility of

Can. J. Chem. Downloaded from www.nrcresearchpress.com by 122.72.124.2 on 09/07/12
For personal use only.

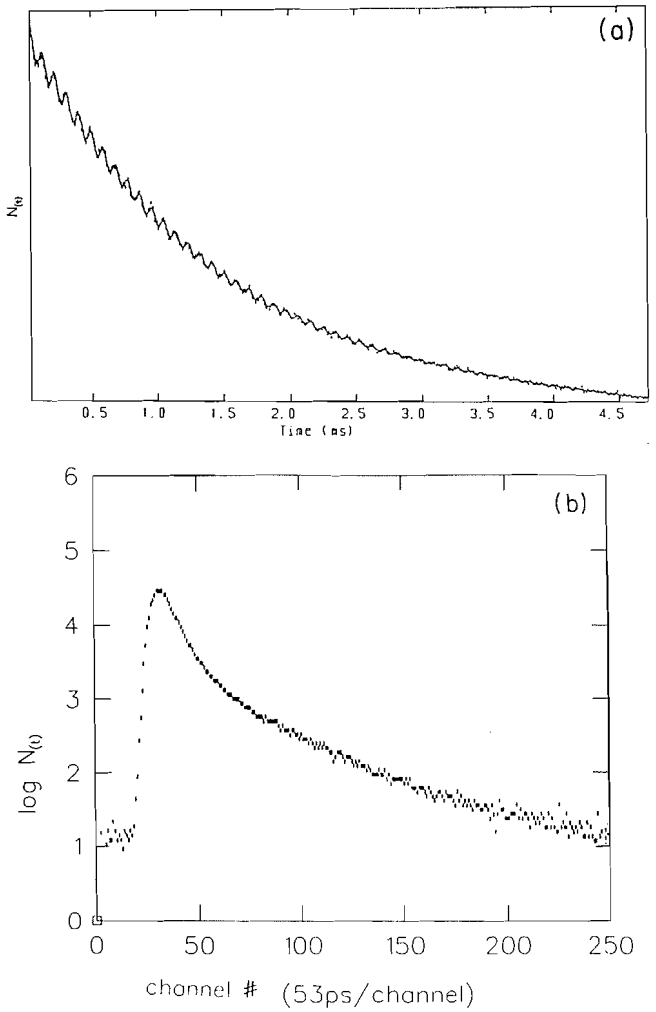


FIG. 1. Representative μSR and PAL "spectra" (counts vs. lifetime). (*a*) μSR lifetime histogram of water in a transverse field of 8 G. The line is the computer's fit to eq. [1]. (*b*) log(counts) vs. channel (lifetime) in pure water.

studying broad concentration-dependencies as one would normally like to undertake in a kinetic analysis. Furthermore, the micelle concentrations are restricted to $\leq 10^{-2}$ *M* because, with 50–80 surfactant molecules per micelles, the rate of reaction of muonium with surfactant, or its inseparable impurities, forces the "background" relaxation rate (λ_0) too close to λ for reasonable accuracy.

2. Positron annihilation lifetime (PAL) measurements

A positron source consisting of ~4 μCi of ^{22}Na sandwiched between two thin mylar sheets was used for positron lifetime measurements. About 2 mL of the appropriate solution under study was placed in a tube with the positron source centered in the liquid sample. The solution was deoxygenated by bubbling with N_2 gas using a hypodermic needle through a septum. All measurements were made at ~20°C. Positron lifetimes were measured by observing the time elapsed between the emission of a positron into the sample and its subsequent annihilation. A high energy (1.28 MeV) γ-photon is emitted simultaneously with the positron, and this is used as the trigger. The positron lifetime is determined as the time difference between the detection of the 1.28 MeV photon and detection of one of the 0.51 MeV annihilation photons, using the conventional delayed coincidence method (11). The resolution of this system was determined to be less than 350 ps by measuring the coincident photons from a ^{60}Co source.

Positrons emitted from the nuclear decay are thermalized in condensed matter (water in this case) within picoseconds, when some of them pick up electrons from the track to form Ps atoms. Annihilation occurs from all positron states. Some annihilate directly with electrons of the medium or after the formation of weak positron or positronium associations, others form *p*-Ps (too short-lived to study) and the relatively long-lived *ortho*-positronium atoms (parallel e^+ and e^- spins). Each of the annihilation processes contributes an exponential decay with a mean lifetime, τ_i, to the "spectrum". The lifetime spectrum is analysed (11) as a sum of exponentials, as in eq. [3],

$$[3] \quad N_t = \sum_{i=1}^{n} A_i \exp(-t/\tau_i)$$

where n corresponds to the number of components, $1/\tau_i$ is the annihilation rate constant of each component, and A_i is its amplitude.

The spectra obtained (as in Fig. 1*b*) were resolved into a multi-exponential function by a χ^2-minimization computer program POSITRONFIT EXTENDED (12). The results reported here are from three component fittings, with χ^2-values ~1. The resolved three different lifetimes $\tau_1 \sim 0.125$ ns, $\tau_2 \sim 0.50$ ns, and $\tau_3 \sim 1.5$ ns correspond to different positron and positronium states. The longest lived component τ_3 is due to the annihilation of free *o*-Ps atoms, which gives information about the chemical reactivity between Ps and molecules in the system. An intrinsic τ_3 decay in pure water of 1.8 ns restricts the time range that can be used to study Ps to about 10^{-9} s, and therefore to concentrations of solutes $> 10^{-2}$ *M*. The relationship between the concentration of solute molecules [S], the measured *o*-Ps lifetime τ_3, and the chemical reaction rate k_P is written as

$$[4] \quad k_P = \left(\frac{1}{\tau_3} - \frac{1}{\tau_3^0}\right) \Big/ [S]$$

where τ_3 and τ_3^0 are, respectively, the measured *o*-Ps lifetimes in aqueous (or aqueous micelle) solution with and without the solute present.

3. Solutions

The solutes used were reagent grade chemicals, their formulae and structures being given in Fig. 2. Aqueous solutions were prepared using triply distilled water. The surfactant used for μSR studies was CTAB (cetyltrimethylammonium bromide) and for *o*-Ps lifetime measurements was SHS (sodium hexylsulphate): the reason for this difference is that *o*-Ps studies require three orders of magnitude higher concentrations than those required for μSR studies. Figures 3*a* and *b* give the plots of λ_0 and $1/\tau_3$ versus concentration of $[CTAB]_{mic}$ and $[SHS]_{mic}$, respectively, from the μSR and PAL data. All the micellar solutions contained concentrations of the surfactant which are well above the critical micelle concentration (CMC), so the concentration is given by eq. [5]

$$[5] \quad [mic] = \frac{[surf] - CMC}{A}$$

where A is the mean aggregation number.

Results

Representative data from solute studied by μSR and PAL are given in Figs. 4 and 5. Figure 4*a* is the plot of λ against concentration of guanidine in water, and Fig. 4*b* is the plot of $\Delta\lambda$ against concentration of tetramethylthiourea in water and in dilute micelle solutions. The average number of solutes per micelle was fixed throughout these μSR studies at three to avoid a significant number of "empty" micelles (2). Figure 5 shows the plot of $1/\tau_3$ vs. concentration of benzoquinone in aqueous and in dilute micelle solutions.

Table 1 gives the thirteen solutes studied by μSR in aqueous solutions and in dilute CTAB micelle solutions, their maximum concentrations used, and the calculated rate constants of Mu using eq. [2]. Acetone is also listed for comparison with these solutes. Table 2 records the data from the PAL studies for the

Can. J. Chem. Downloaded from www.nrcresearchpress.com by 122.72.124.2 on 09/07/12
For personal use only.

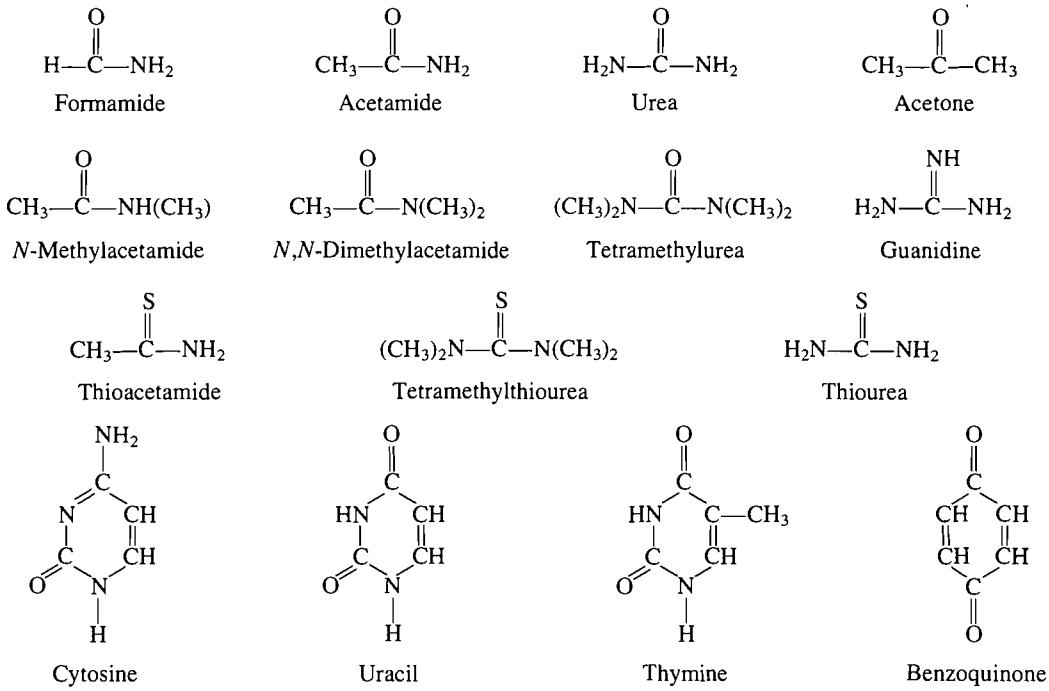


FIG. 2. Structures of the solutes used.

TABLE 1. Reactivity of muonium in water towards the compounds shown in Fig. 2, with and without added micelles

Solute	Max. conc. used in H_2O/mM	$k_M/M^{-1}\,s^{-1}$	Conc. used with mic./mM[a]	$k_{M(mic)}$[b]$/M^{-1}\,s^{-1}$
Formamide	2000	$<10^5$	0.180	1×10^9
Acetamide	1750	$<10^5$	0.180	1×10^9
N-Methylacetamide	1500	$<10^5$	0.180	$\sim10^9$
N,*N*-Dimethylacetamide	1000	$<10^5$	0.180	$\sim10^9$
Guanidine	1000	3×10^5	0.180	$\leq10^9$
Urea	1000	$<10^5$	0.180	$\leq10^9$
Tetramethylurea	1000	4×10^5	0.180	2×10^9
Thiourea	100	5×10^7	0.180	$\leq10^9$
Tetramethylthiourea	0.075	4×10^{10}	0.180	2×10^{10}
Thioacetamide	0.100	3×10^{10}	0.180	3×10^{10}
Uracil	0.40	6×10^9	0.075	$\leq2\times10^9$
Thymine	0.60	3×10^9	—	—
Cytosine	1.0	3×10^9	—	—
Acetone	50	8.7×10^7	0.180	2.5×10^{10}

[a]Micelle concentration always (1/3)[solute]. With 3 solutes per micelle on average there are few unoccupied micelles (Poisson statistical distribution).

[b]Calculated as $\Delta\lambda/[S]$ where [S] is overall number of moles of solute per litre of solution. If the concentration of occupied micelles were used the k values would all be 3× larger.

same solutes, the rate constants of Ps being calculated using eq. [4]. Since the solutes of interest show only upper limits, benzoquinone is included in Table 2 for comparison purposes. In most cases only an upper limit to k_p and $k_{p(mic)}$ were obtained (invariably limited by the natural τ_3 in pure water for the various concentrations accessible).

Discussion

1. Muonium

Muonium has been shown previously to react with different solutes in a variety of ways, by addition across double or triple bonds, by abstraction of H, by reductive electron transfer, and by electron spin exchange (4). Rate constants ranging from $10^5\,M^{-1}\,s^{-1}$ to $2\times10^{10}\,M^{-1}\,s^{-1}$ have been observed where the latter seems to be the diffusion-controlled limit. Furthermore, kinetic isotope effects, relative to protium, have been found from 10^2 to 10^{-2}. Yet there was no indication hitherto how Mu would attack the amido-group, where it could add to the carbonyl, as with acetone, or abstract H from the —NH— group or from a methyl, or be unreactive.

Evidently, Mu reacts very slowly, if at all, with the simple amide linkage. The rate constant k_M for these solutes is less than $10^5\,M^{-1}\,s^{-1}$, except for tetramethylurea which shows k_M to be close to (4×10^5) this limit of measurement. Substituents on the

Can. J. Chem. Downloaded from www.nrcresearchpress.com by 122.72.124.2 on 09/07/12
For personal use only.

Can. J. Chem. Downloaded from www.nrcresearchpress.com by 122.72.124.2 on 09/07/12
For personal use only.

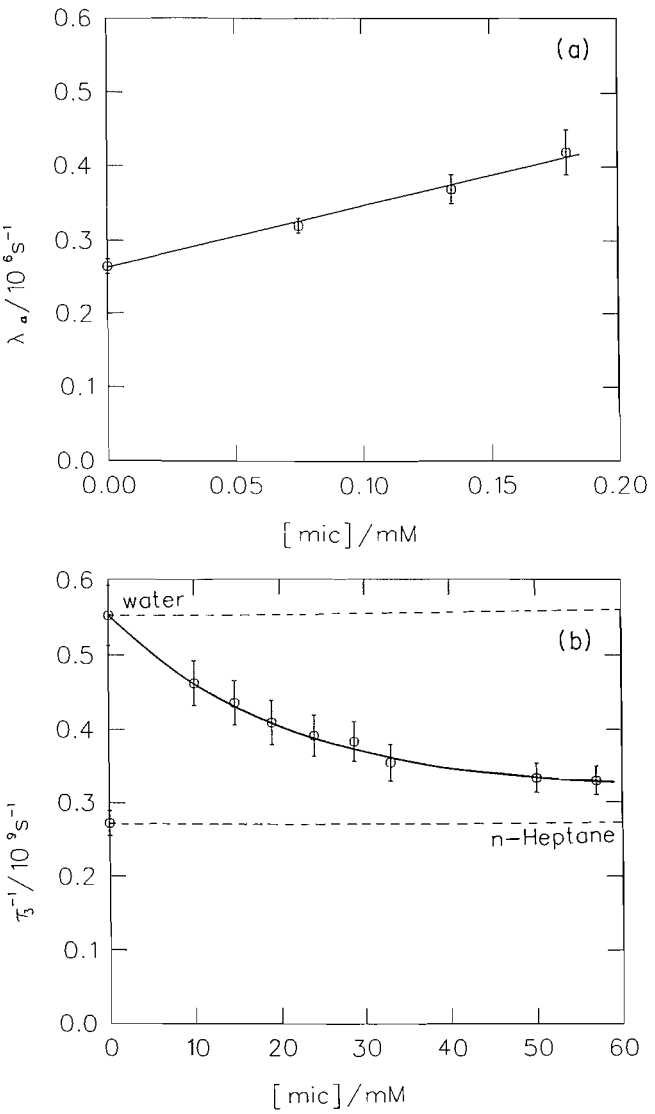


FIG. 3. (*a*) Plot of λ vs. [mic] for CTAB from μSR. (*b*) Plot of $1/\tau_3$ vs. [mic] for SHS from PAL. Positronium seen to localize in the micelle where the lifetime approaches that found in a pure hydrocarbon like *n*-heptane.

α-position and/or on the $—NH_2$ group do not change the rate very much. Use of higher concentrations could give a better limit for the rate constants, but impurities become too important at high concentrations since they can contribute to λ.

Addition of micelles to aqueous solutions of solutes containing just the simple amido-linkage increases the rate of reaction considerably. For tetramethylurea it is seen to increase by the factor 2×10^4 and for some of the others it is seen to increase by at least 10^4-fold. In two cases (*N*-methylacetamide and *N*,*N*-dimethylacetamide) the observed rate is very close to the limit of observation, and for guanidine and urea it was below that limit; but the indications are that $k_{M(mic)}$ is about 10^9 for these solutes. Again, higher concentrations can not be used, this time because of the background reactions (λ_0) of the surfactant molecules themselves. These 10^4-times enhancements are characteristic of abstraction reactions (2). Our conclusion therefore, is that Mu reacts very slowly but that there is an abstraction of H from methyl substituted amides.

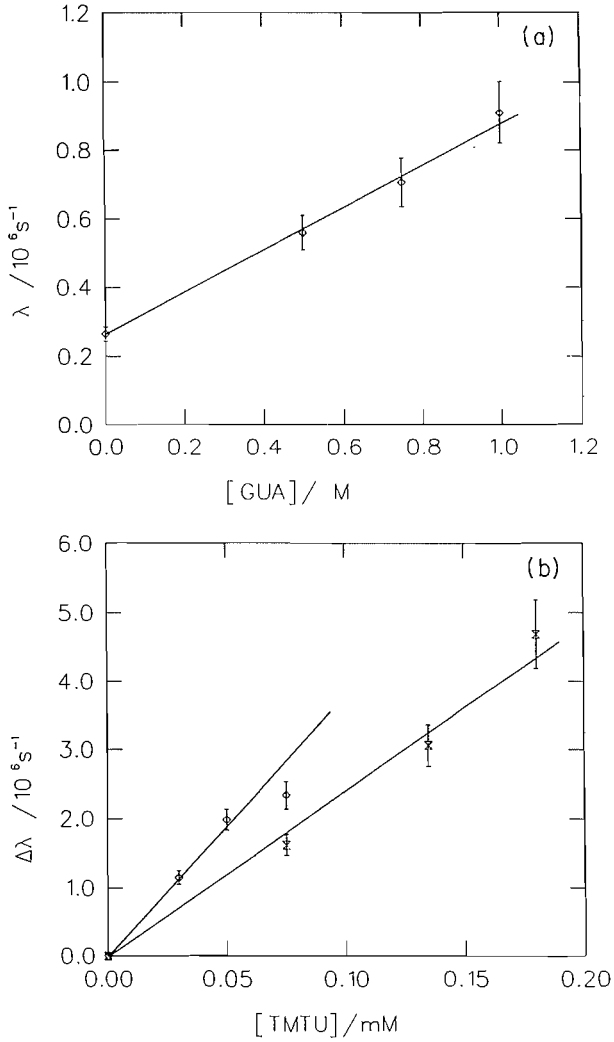


FIG. 4. (*a*) Plot of λ vs. [guanidine] in water. (*b*) Plot of Δλ vs. [tetramethylthiourea] in water (◇) and in CTAB micelle solutions (⧖).

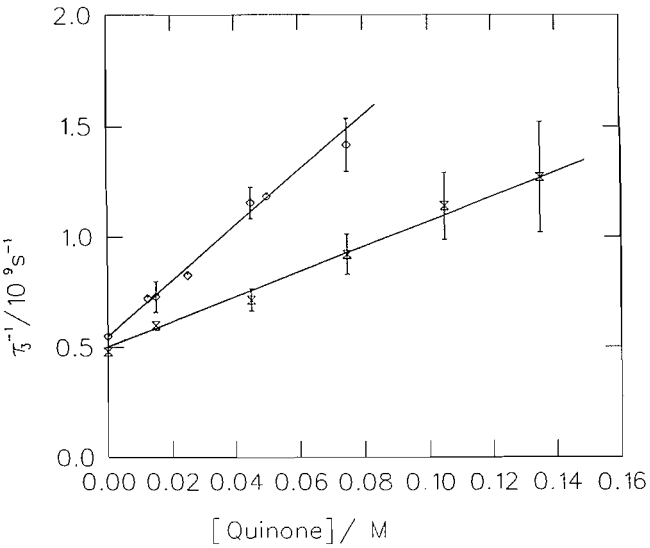


FIG. 5. Inverse lifetime vs. [benzoquinone] in water (◇) and in SHS micelle solutions (⧖).

TABLE 2. Upper limits to the positronium rate constants[a] for the compounds of Fig. 2

Solute	Conc. range/M	$k_P/M^{-1}s^{-1}$	Conc. used[b] with mic./M	$k_{P(mic)}/M^{-1}s^{-1}$
Formamide	2	$<10^8$	0.1	$<10^9$
Acetamide	3	$<10^8$	0.1	$<10^9$
N-Methylacetamide	2	$<10^8$	0.1	$<10^9$
N,*N*-Dimethylacetamide	2	$<10^8$	0.1	$\leq 5\times10^8$
Guanidine	2	$<10^8$	0.1	$<10^9$
Urea	4	$\leq 10^8$	0.1	$\leq 3\times10^8$
Tetramethylurea	1	$<10^8$	0.1	$<10^9$
Thiourea	2	$<10^8$	0.1	$<10^9$
Tetramethylthiourea	0.25	$<10^9$	0.1	$<10^9$
Thioacetamide	1	$<10^8$	0.1	$<10^9$
Thymine	0.01	$<10^9$	0.05	1×10^9
Uracil	0.02	$<10^9$	0.05	1×10^9
Cytosine	0.01	$<10^9$	0.05	1×10^9
Benzoquinone	0.075	3.5×10^{10}	0.045	1.5×10^{10}[c]

[a]The absence of a detectable decrease in *o*-Ps lifetime gives a measure of the upper limit to k_P and $k_{P(mic)}$.
[b]Always three solutes per micelle, on average.
[c]If the concentration of occupied micelle were used then $k'_{P(mic)} = 4.5\times10^{10}$.

TABLE 3. Rate constants for the reaction of Mu compared with that of H, e^-_{aq}, and *o*-Ps

Solute	$k_M/M^{-1}s^{-1}$	$k_H/M^{-1}s^{-1}$[a]	$k_{e^-_{aq}}/M^{-1}s^{-1}$[a]	$k_P/M^{-1}s^{-1}$
Formamide	$<10^5$	NA	1.8×10^7	$<10^8$
Acetamide	$<10^5$	1.5×10^5	4.5×10^7	$<10^8$
N-Methylacetamide	$<10^5$	NA	2.3×10^6	$<10^8$
N,*N*-Dimethylacetamide	$<10^5$	NA	9.0×10^6	$<10^8$
Guanidine	3×10^5	1.2×10^6	1.6×10^8	$<10^8$
Urea	$<10^5$	3×10^4	3×10^5	$\leq 10^8$
Tetramethylurea	4×10^5	NA	NA	$<10^8$
Thiourea	4×10^7	6×10^9	2.9×10^9	$<10^8$
Tetramethylthiourea	4×10^{10}	NA	NA	$<10^9$
Thioacetamide	3×10^{10}	6×10^9	NA	$<10^8$
Acetone	8.7×10^7	2.6×10^6	6.5×10^9	$<10^8$
Benzoquinone	2.5×10^{10}	8.3×10^9	3.5×10^{10}	2.3×10^{10}
Cytosine	3×10^9	9.2×10^7	1.3×10^{10}	$<10^9$
Uracil	6×10^9	3.8×10^8	1.5×10^{10}	$<10^9$
Thymine	3×10^9	5.7×10^8	1.8×10^{10}	$<10^9$

[a]From ref. 16.

For thioamides the situation is completely different. Muonium reacts with thioacetamide and tetramethylthiourea with $k_M > 10^{10}\ M^{-1}\ s^{-1}$, which means they react on nearly every encounter. Addition of micelles has almost no effect on this observed rate. (In the case of tetramethylthiourea there is a two-fold decrease, but it must be recalled there are three solutes per micelle and $k_{M(mic)}$ is calculated on the mean bulk concentration.) The absence of a large effect on adding micelles has been found previously for reactions which have no activation barrier (2). The fact that the reaction is not seriously inhibited shows that muonium penetrates the micelle boundary and reacts in a highly efficient reaction regardless of whether the microenvironment is water or hydrocarbon.

Rhodes *et al.* (7) have recently reported the formation of a muonated thioacetamide radical in the μSR of pure thioacetamide. This suggests that the reaction with muonium atoms in dilute solution is also addition across the C=S bond, with Mu attached to the C, as in eq. [6]

[6] $Mu + CH_3C(=S)NH_2 \rightarrow CH_3C(-\dot{S})(Mu)NH_2$

Such an addition is discussed by Rhodes *et al.* in terms of hyperconjugation. It is also interesting to contrast it with acetone where k_M is only $8.7\times10^7\ M^{-1}\ s^{-1}$ and where the product is known by level-crossing resonance (2, 13) as well as transverse-field μSR (14) to have Mu bonded to O, as in eq. [7]

[7] $Mu + (CH_3)_2CO \rightarrow (CH_3)_2\dot{C}OMu$

Evidence for this assignment comes from both the hyperfine coupling constant when compared to other radicals seen by ESR, and the effect of solvents on the hydrogen-bonding (muonium-bonding here) (2, 14*e*).

Thiourea seems to be different from the other two thiocarbonyls. Its value of k_M resembles that of acetone. Perhaps addition still occurs, but at much lower rate with Mu bonded

Can. J. Chem. Downloaded from www.nrcresearchpress.com by 122.72.124.2 on 09/07/12
For personal use only.

Can. J. Chem. Downloaded from www.nrcresearchpress.com by 122.72.124.2 on 09/07/12
For personal use only.

to S. There is no evidence that the Mu reaction with thiourea is enhanced by addition of micelles, as with urea itself, probably because these solutes are very weakly localized, if at all, at micelles.

The compounds of biological interest studied here which have amide linkages are uracil, thymine, and cytosine. These compounds have a ring structure and Mu is fairly reactive ($\sim 10^9\ M^{-1}\ s^{-1}$) towards these solutes. Since there is no enhancement with micelles it is concluded that addition is more likely than abstraction. These additions, however, are slower than that with thiocarbonyl groups in thioacetamide or tetramethylthiourea but faster than acetone or thiourea. Mu probably adds across the C=C group in the rings.

2. Positronium

Positronium reacts rapidly with benzoquinone. The rate observed ($k_P = 3.5 \times 10^{10}$) is probably at the diffusion-controlled limit, signifying reaction on every encounter between Ps and benzoquinone. A similar upper limit of 2 to $3 \times 10^{10}\ M^{-1}\ s^{-1}$ has been found to the second-order rate constants for reactive solutes in water reacting with Mu, H, and hydrated electrons. The diffusion of these small reactive species is evidently controlled by the solvent (4).

Addition of micelles to a benzoquinone solution barely affects the rate at which Ps reacts. The 2.3-fold decrease actually observed (Table 2) probably combines two effects: first the solutes have been bunched into packets of three, on average, as far as the diffusion time of a wandering Ps atom is concerned; but second, an occupied-micelle presents a larger encounter radius than a benzoquinone molecule in water. The relative importance of these two opposite effects depends on the relative diffusion coefficients in water compared to micelle cores. Most importantly, however, localization of benzoquinone did not significantly impede the reactivity of Ps, so it clearly penetrates the lipid phase with a diffusion coefficient comparable to that in water.

Ps reactions are often described simply as "pick-off" or "spin-exchange" interactions which convert *o*-Ps to *p*-Ps following the formation of a reaction complex (5, 11). In the case of benzoquinone, Ps may attack the carbonyls or the ring C=C groups to form such complexes. Both types of group appear in the range of solutes studied here, so that some fast positronium reactions were anticipated. However, as Table 2 shows, no reactions were found in water with rate constants greater than $10^8\ M^{-1}\ s^{-1}$, and none with observable micelle-enhancements. Ps differs strikingly from Mu in two areas then: first it does not respond to the C=S group as Mu does; and second, it does not undergo the slow abstraction reactions which are now characterized in muonium chemistry by micelle enhancements close to the diffusion-controlled limit (2).

3. Comparison with H and e^-_{aq}

Table 3 lists the published values of rate constants of H and e^-_{aq} for these solutes, when available, to compare with our values of k_M and k_P (first and fourth columns, from Tables 1 and 2). In the case of k_H, most data were obtained from e^-_{aq} in acidified water and the "not-available" blanks in some cases may mean the rate was too small to determine (but, unfortunately, an upper limit was not given). For the H reaction with acetamide, Neta *et al.* (15) have concluded that this very slow reaction is one of abstraction to form H_2.

For three of the first seven solutes (all those that can be compared) H reacts faster than Mu, and this is normal for abstraction reactions. However, there is only a factor of four favouring the heavier isotope with guanidine (which is the only case without limits) whereas for several alcohols, or formate ions, abstraction usually favours H by a factor of 10^2 or so (4). Hydrated electrons react with these solutes at intermediate rates, 10^6–$10^8\ M^{-1}\ s^{-1}$, probably by electron attachment to the amido group. Urea seems to be particularly unreactive towards all four species.

Substituting O by the more polarizable S causes k_H and $k_{e^-_{aq}}$ to increase by several orders of magnitude, as it does for Mu. There are too few S compounds studied so far with all four species for general trends to emerge; but addition of Mu to C in some C=S compounds look as if it is not mimicked by H.

For the solutes of biological interest (last three listed) Mu falls directly between H and e^-_{aq} in its absolute reactivity. As suggested above, these are probably ring addition reactions for Mu. It is pertinent to note that the Mu data were obtained in solutions of these compounds at neutral pH, where they have biological significance. Data for H, on the other hand, refer to strongly acid solutions (pH ~ 1), because of the need to produce H by conversion of e^-_{aq} in radiolysis. Whereas that limitation on H atom data may not be serious for many simple solutes, it presents a real problem for studies of proteins, peptides and many other naturally occurring compounds. Consequently, once the full range of kinetic-isotope effects are understood, this means that muonium studies may generally be preferred as the means of elucidating hydrogen atom chemistry.

Acknowledgements

The assistance of Dr. J. M. Stadlbauer, Dr. B. W. Ng, Zhennan Wu, and the staff of the μSR group at TRIUMF is very much appreciated for the Mu studies. Dr. Yasuhiro Miyake's contributions in assembling and initiating the PAL apparatus is warmly acknowledged. Funds for these experiments came from NSERC of Canada.

1. K. J. Laidler. Chemical kinetics. 3rd ed. Harper and Row. 1987. pp. 129, 200, 442–444.
2. K. Venkateswaran, M. V. Barnabas, Z. Wu, J. M. Stadlbauer, B. W. Ng, and D. C. Walker. Chem. Phys. Lett. **143**, 313 (1988).
3. K. Venkateswaran, R. F. Kiefl, M. V. Barnabas, J. M. Stadlbauer, B. W. Ng, Z. Wu, and D. C. Walker. Chem. Phys. Lett. **145**, 289 (1988).
4. D. C. Walker. Muon and muonium chemistry. Cambridge University Press, Cambridge. 1983.
5. A. L. F. Lazzarini and E. Lazzarini. J. Phys. B: At. Mol. Opt. Phys. **21**, 367 (1988).
6. P. W. F. Louwrier, G. A. Brinkman, C. N. M. Bakker, and E. Roduner. Hyperfine Interactions, **32**, 753 (1986).
7. C. J. Rhodes, M. C. R. Symons, and E. Roduner. J. Chem. Soc. Chem. Commun. **3**, 3 (1988).
8. S. F. J. Cox, D. A. Geeson, C. J. Rhodes, E. Roduner, C. A. Scott, and M. C. R. Symons. Hyperfine Interactions, **32**, 763 (1986).
9. J. H. Brewer and K. M. Crowe. Ann. Rev. Nucl. Part. Sci. **28**, 239 (1978).
10. A. Schenck. Muon spin rotation spectroscopy. Adam Hilger, Bristol and Boston. 1985.
11. H. J. Ache. Adv. Chem. Ser. **175**, 1 (1979).
12. P. Kirkegaard and M. Eldrup. Compt. Phys. Commun. **7**, 401 (1974).
13. M. Heming, E. Roduner, B. D. Patterson, W. Odermatt, J. Schneider, Hp. Baumeler, H. Keller, and I. M. Savic. Chem. Phys. Lett. **128**, 100 (1986).

14. (*a*) E. RODUNER, P. W. PERCIVAL, D. G. FLEMING, J. HOCHMANN, and H. FISCHER. Chem. Phys. Lett. **57**, 37 (1978); (*b*) A. HILL, G. ALLEN, G. STIRLING, and M. C. R. SYMONS. J. Chem. Soc. Faraday Trans. I, **78**, 2959 (1982); (*c*) E. RODUNER. Radiat. Phys. Chem. **28**, 75 (1986); (*d*) A. HILL, M. C. R. SYMONS, S. F. J. COX, R. DE RENZI, C. A. SCOTT, C. BUCCI, and A. VECLI. J. Chem. Soc. Faraday Trans. I, **81**, 433 (1985); (*e*) S. F. J. COX and M. C. R. SYMONS. Radiat. Phys. Chem. **27**, 53 (1985).

15. P. NETA, G. R. HOLDREN, and R. H. SCHULER. J. Phys. Chem. **75**, 449 (1971).

16. G. V. BUXTON, C. L. GREENSTOCK, W. P. HELMA, and A. B. ROSS. *In* Critical review of rate constants for reactions of hydrated electrons, hydrogen atoms, and hydroxyl radicals in aqueous solutions. NSRDS-NBS. 1988.

Can. J. Chem. Downloaded from www.nrcresearchpress.com by 122.72.124.2 on 09/07/12
For personal use only.

The direct electrochemical synthesis of phenylselenolato complexes of some main group and late transition elements

RAJESH KUMAR AND DENNIS G. TUCK

Department of Chemistry and Biochemistry, University of Windsor, Windsor, Ont., Canada N9B 3P4

Received August 18, 1988

RAJESH KUMAR and DENNIS G. TUCK. Can. J. Chem. **67**, 127 (1989).

The electrochemical oxidation of anodes of selected Main Group or late transition metals (M) in non-aqueous solutions of diphenyl diselenide gives the corresponding $M(SePh)_n$ compounds in high yields (M = Zn, Cd, $n = 2$; M = Cu, Ag, Tl, $n = 1$; M = Sn, $n = 4$). The addition of either 1,10-phenanthroline or triphenylphosphine to the electrochemical cell yields adducts in the case of cadmium and copper. The ^{77}Se nmr spectra have been recorded.

Key words: electrochemistry, synthesis, phenylselenates, ^{77}Se nmr spectra.

RAJESH KUMAR et DENNIS G. TUCK. Can. J. Chem. **67**, 127 (1989).

Lorsqu'on effectue l'oxydation électrochimique d'anodes formées de métaux du groupe principal ou de la fin des métaux de transition (M) dans des solutions non-aqueuses de disélénure de diphényle, il y a formation des composés $M(SePh)_n$ correspondants avec des rendements élevés (M = Zn, Cd et $n = 2$; M = Cu, Ag, Tl et $n = 1$; M = Sn et $n = 4$). Avec le cadmium et le cuivre, il y a formation d'adduits lorsqu'on ajoute de la phénanthroline-1,10 ou de la triphénylphosphine à la cellule électrochimique. On a déterminé les spectres rmn du ^{77}Se.

Mots clés : electrochimie, synthèse, phénylséléniates, ^{77}Se spectres en rmn.

[Traduit par la revue]

Can. J. Chem. Downloaded from www.nrcresearchpress.com by 122.72.124.2 on 09/07/12
For personal use only.

Introduction

Compounds in which a metal atom is bonded to sulphur or selenium donor ligands are presently of considerable interest because of their importance in biological systems, such as metallo-proteins, and in a different sense because they are possible precursors for binary compounds for the microelectronics industry. A number of papers from this laboratory have described the synthesis of $M(SR)_n$ compounds by the electrochemical oxidation of a sacrificial anode in a non-aqueous solution of either a thiol or a disulphide (1–6). The present paper shows that these techniques can be extended to the one-step high yield synthesis of phenylselenolato complexes $M(SePh)_n$, and in some cases, their adducts with neutral donor ligands.

Experimental

Materials

The metals zinc, cadmium, copper, silver, indium, thallium, and tin were used as rods, 3–6 mm diameter; gold was as a foil, approximately 1 cm^2 in area. Metals were obtained from Alfa Products, and were of 99.9% purity or higher. The surface of these metals was cleaned by washing successively with concentrated nitric acid and then distilled water; after being dried, the surface was abraded with fine sandpaper and polished with tissue paper. Solvents (acetonitrile, toluene) were distilled from calcium hydride and stored over molecular sieves. Diphenyl diselenide, 1,10-phenanthroline (phen), and triphenylphosphine (Aldrich) were used as supplied.

Metal analysis of products was by atomic absorption spectrophotometry, using an IL-250 instrument. Microanalysis was by Guelph Chemical Laboratories Ltd.

Infrared spectra of KBr discs were obtained with a Nicolet 5DX instrument. Proton nmr spectra were recorded on a Varian EM-360 spectrometer, and ^{77}Se spectra on a Bruker 200.

Electrochemical procedures

The general method was derived from that described in papers on the synthesis of thiolates (1–6), using a cell of the general form $Pt_{(-)}/CH_3CN/toluene + Ph_2Se_2/M_{(+)}$. The details of solution composition and electrochemical conditions are given in Table 1. To prepare the solution phase, diphenyl diselenide was dissolved in toluene, with stirring, under nitrogen, and the appropriate volume of acetonitrile containing a small quantity of Et_4NClO_4 added; the stirring was continued for a few minutes to ensure homogeneity. This solution was then placed in a 100-mL tall-form beaker, and the platinum wire cathode, and the anode suspended on a second platinum lead, were introduced through a tightly fitting rubber bung. Dry nitrogen purged the cell throughout the electrolysis. Electrical energy was supplied by a Coutant LQ 50/50 D.C. power supply.

As the electrolysis proceeded, solid products precipitated in the case of M = Cd, Cu, Ag, and Tl. At the end of the experiment the solid was collected, washed with cold acetonitrile (10–15 mL) and then cold *n*-pentane (10–15 mL) and finally dried *in vacuo*. With anodes of zinc or tin, the initial product dissolved in the electrolyte phase; subsequent slow evaporation *in vacuo* gave a solid deposit, which was collected, washed, and dried as described above. In each of these experiments, the yield was essentially quantitative, based on the quantity of metal dissolved from the anode.

In a few experiments with Cd or Cu, the neutral ligands 1,10-phenanthroline or triphenylphosphine were introduced into the solution phase before electrolysis (see Table 1). No precipitation occurred during the electrolysis, but when the volume was reduced by slowly bubbling nitrogen through the solution for periods between 5 and 20 h, crystals were formed; these were collected, washed with acetonitrile and then diethyl ether, and dried *in vacuo*. The product yields were better than 80%.

When a gold anode was used in such a cell, only a small quantity of metal dissolved (see Table 1), and the solution phase became cloudy and dark coloured. No product could be isolated from this solution.

In the case of indium, the anode was rapidly covered with an adherent deposit which caused the current to drop to almost zero. Again, no product could be obtained under these circumstances. We note a possible hazard with this metal, in that any substantial increase in applied voltage may cause this anode deposit to break off from the anode with an accompanying spark discharge, which on one occasion was sufficient to break the reaction vessel. In order to include an indium-phenyl selenolate in our ^{77}Se nmr studies, a sample of $In(SePh)_3$ was prepared by refluxing indium metal with diphenyl diselenide in toluene (7).

The electrochemical synthesis of TlSePh by the anodic oxidation of thallium in a non-aqueous solution of diphenyl diselenide has also been described previously (7); the present system differs only slightly in the solution composition.

Results and discussion

Preparative

The electrochemical oxidation of Main Group and late transi-

TABLE 1. Experimental conditions for the electrochemical synthesis of phenylselenolato derivatives

Metal	Solvent composition[a]	Mass Ph_2Se_2 (g)	Mass Ligand[b] (g)	Applied voltage[c] (V)	Time of electrolysis (h)	Mass metal dissolved (mg)	E_F (mol F^{-1})	Product[d]
Zn	3:1	3	—	10	3	282	0.75	ZnL_2
Cd	3:1	2	—	10	1.5	154	0.49	CdL_2
Cd	3:1	2	phen, 1	5	3	197	0.52	CdL_2.2phen
Cu	5:1	2	—	15	1.5	177	1.00	CuL
Cu	5:1	2	phen, 1	10	2.25	164	1.02	CuL.phen
Cu	5:1	2	Ph_3P, 1	10	2.25	269	1.01	CuL.1.5Ph_3P
Ag	5:1	1	—	15	1	204	1.01	AgL
Au	5:1	1	—	20	1	13	See text	—
In	5:1	2	—	15	1	See text	—	—
Tl	10:1	2	—	15	1	214	1.00	TlL
Sn	5:1	3	—	10	3	365	0.55	SnL_4

[a]Mixtures of acetonitrile + toluene; v/v composition. Total volume 60 mL; ca. 100 mg Et_4NClO_4 added.
[b]phen = 1,10-phenanthroline.
[c]To produce an initial current of 50 mA.
[d]L = SeC_6H_5.

TABLE 2. Analytical and nmr spectroscopic results for phenylselenolato derivatives

Compound	Colour	%M Found	%M Calcd	^1H nmr chemical shift[a]	^{77}Se nmr chemical shift[b]
$Zn(SePh)_2$[c]	Cream	17.7	17.3	8.0–7.05	−19.3
$Cd(SePh)_2$	Cream	26.1	26.5	8.0–7.05	−19.0
$Cd(SePh)_2$.2phen[d]	Yellow	14.0	14.3	8.3–6.4	41.6[h]
CuSePh[e]	Yellow	29.3	29.0	Insoluble	Insoluble
CuSePh.phen	Red	15.5	15.9	9.1–6.9	273.5
CuSePh.1.5Ph_3P[f]	Yellow	10.4	10.4	7.4–6.6	235.0
AgSePh[g]	Yellow	40.8	40.9	Insoluble	Insoluble
$In(SePh)_3$	Yellow	See text		7.7–6.0	38.8
TlSePh	Orange	56.2	56.7	Insoluble	Insoluble
$Sn(SePh)_4$	Yellow	15.7	16.0	7.6–7.2	193.1[i]

[a]In C_5D_5N solution. Values in ppm relative to internal Me_4Si = 0. All spectra are multiplets.
[b]In C_5D_5N solution. Values in ppm relative to external Me_2Se = 0.
[c]Found: C 37.6, H 2.40; calcd.: C 38.2, H 2.65.
[d]Found: C 55.6, H 3.43, N 6.92; calcd.: C 55.1, H 3.31, N 7.14.
[e]Found: C 32.9, H 2.24; calcd.: C 32.8, H 2.28.
[f]Found: C 65.1, H 4.81; calcd.: C 64.6, H 4.52.
[g]Found: C 26.9, H 1.71; calcd.: C 27.3, H 1.89.
[h]In $CDCl_3/d_6$-dmso solution.
[i]In d_6-dmso.

tion metals in non-aqueous solutions of diphenyl diselenide is clearly an efficient one-step route to the appropriate $M(SePh)_n$ compounds, and a slight modification serves to provide adducts in the few cases investigated. The method is no doubt applicable to other metals. The directness of this synthetic route offers several advantages over previously reported procedures to organoselenolato complexes, involving either metathesis between RSeH and a salt of the metal, or oxidative insertion into the Se—Se bond of R_2S_2.

The products, which involve the metals concerned in conventional oxidation states, were characterised by elemental analysis, and by infrared and ^1H nmr spectroscopy. The simple $M(SePh)_n$ compounds (or their alkyl analogues) are known compounds, but the adducts noted in Table 1 do not appear to have been reported previously. The spectroscopic results confirm the presence of the SePh ligand; Table 2 shows the standard broad multiple resonances of the phenyl ring, and the infrared spectra also demonstrated the typical absorption bands of the phenyl group. In addition, the characteristic modes of the —SePh ligand were observed at 665 and 1070 cm^{-1}.

Electrochemical

Following the standard procedure in this laboratory, we have measured the electrochemical efficiency, E_F, defined as moles of metal dissolved from the anode per Faraday of electricity, for each system. For copper, silver, and thallium, the value of 1.0 mol F^{-1} (see Table 1) corresponds to the sequence

[1] cathode: $(1/2)Ph_2Se_2 + e \rightarrow PhSe^-$

[2] anode: $PhSe^- + M \rightarrow MSePh + e$

and in keeping with this, the products are indeed the appropriate MSePh compounds. The value of 1.0 mol F^{-1} also holds for copper when neutral ligands are present, showing that complex formation is subsequent to the anode reaction [2] above. For

Can. J. Chem. Downloaded from www.nrcresearchpress.com by 122.72.124.2 on 09/07/12
For personal use only.

cadmium, $E_F = 0.5$ mol F^{-1}, corresponding to the overall anode reaction

[3] $2PhSe^- + Cd \rightarrow Cd(SePh)_2 + 2e$

One might have expected a similar value for the oxidation of zinc, but the reproducible value of 0.75 ± 0.05 mol F^{-1} implies a competing process occurring at the anode, causing dissolution of the metal by a non-electrochemical process, e.g.

[4] $Zn + Ph_2Se_2 \rightarrow Zn(SePh)_2$

For the oxidation of tin, we find $E_F = 0.5$ mol F^{-1}, although the final product is $Sn(SePh)_4$, as it is when tin metal reacts with Ph_2Se_2 in refluxing toluene (7). We conclude that the formation of $Sn(SePh)_2$ at the anode is followed by an oxidative addition reaction in solution

[5] $Sn(SePh)_2 + Ph_2Se_2 \rightarrow Sn(SePh)_4$

a process which is compatible with the known chemistry of tin(II) species. For indium, the E_F value of unity indicates the formation of In^ISePh as the primary product, in keeping with the behaviour of this metal in cells containing non-aqueous solutions of RSH, when the product is InSR (R = alkyl or aryl) (8). In this latter work, it was found that the aryl derivatives were readily oxidised or decomposed, and the present results suggest that InSePh is also very unstable.

Spectroscopic studies

As noted above, the infrared and ^1H nmr spectra confirmed the presence of the SePh ligand, and of the appropriate neutral donor ligands, in the compounds listed in Table 2. These results do not call for any detailed discussion. Table 2 also lists the ^{77}Se nmr chemical shifts for those products which are soluble in d_5-pyridine. Given that such resonance frequencies are influenced *inter alia* by coordination number, coordination geometry, and the properties of other ligands present (9, 10), it is not surprising that the results cover a range of values. The chemical shifts for $Zn(SePh)_2$ and $Cd(SePh)_2$ are very similar, implying the presence of isostructural species in solution, presumably $M(SePh)_2py_n$, resulting from the breakdown of the M ← Se cross-linked solid state homopolymer (c.f. ref. 1 for a discussion of analogous effects in $M(SPh)_n$ complexes). Replacement of pyridine in the coordination kernel by 1,10-phenanthroline causes a significant change in the resonance frequency.

The values for the copper(I) species are presumably also for pyridine solvates, but in view of the wide variety of structures which are known for the thiolato derivatives of copper(I), and their adducts, we cannot assign any structures from these results, although the closeness of the values implies similar copper-selenium environments. The value for $Sn(SePh)_4$ is close to that reported for this compound in CH_2Cl_2 (183.4 ppm) (11).

Acknowledgement

This work was supported in part by Operating Grants (to D.G.T.) from the Natural Sciences and Engineering Research Council of Canada.

1. F. F. Said and D. G. Tuck. Inorg. Chim. Acta, **59**, 1 (1982).
2. J. L. Hencher, M. A. Khan, F. F. Said, and D. G. Tuck. Polyhedron, **4**, 1263 (1985).
3. J. L. Hencher, M. A. Khan, F. F. Said, R. Sieler, and D. G. Tuck. Inorg. Chem. **21**, 2787 (1982).
4. R. K. Chadha, R. Kumar, and D. G. Tuck. Can. J. Chem. **65**, 1336 (1987).
5. M. A. Khan, R. Kumar, and D. G. Tuck. Polyhedron, **7**, 49 (1988).
6. R. K. Chadha, R. Kumar, J. R. Lopez-Grado, and D. G. Tuck. Can. J. Chem. **66**, 2151 (1988).
7. H. E. Mabrouk, R. Kumar, and D. G. Tuck. J. Chem. Soc. Dalton Trans. 1045 (1988).
8. J. H. Green, R. Kumar, N. Seudeal, and D. G. Tuck. Inorg. Chem. In press.
9. C. Rodger, N. Sheppard, H. C. E. McFarlane, and W. McFarlane. NMR and the Periodic Table. *Edited by* R. K. Harris and B. E. Mann. Academic Press, New York. 1978. Chap. 12B.
10. H. C. E. McFarlane and W. McFarlane. NMR of newly accessible nuclei. Vol. 2. *Edited by* P. Laszlo. Academic Press, New York. 1983. Chap. 10.
11. P. A. W. Dean and R. S. Srivastava. Inorg. Chem. Acta, **105**, 1 (1985).

Can. J. Chem. Downloaded from www.nrcresearchpress.com by 122.72.124.2 on 09/07/12
For personal use only.

Effect of temperature on cyclic voltammograms during the electrodeposition of lead

MAGDY GIRGIS
Department of Chemistry, Carleton University, Ottawa, Ont., Canada K1S 5B6

AND

EDWARD GHALI
Department of Mining and Metallurgy, Laval University, Québec, P.Q., Canada G1K 7P4

Received November 9, 1987[1]

MAGDY GIRGIS and EDWARD GHALI. Can. J. Chem. **67**, 130 (1989).

The electrochemical behavior of lead deposition process in a temperature range between 25 and 75°C was studied in a medium of lead chloride and ammonium acetate by linear and cyclic sweep perturbation. The study was undertaken on four substrates: Pb, Cu, Ag, and C. An increase in temperature resulted in accelerating the deposition process and promoted dendrite formation. Moreover, different kinetic parameters such as adsorption isotherms, Tafel slopes, and diffusion coefficient were affected as a function of temperature elevation. Surface analytical study performed by Auger electron spectroscopy revealed an increase in peak intensities of Cl and Pb as the temperature increased.

Key words: electrodeposition, cyclic voltammetry, potentiostatic transients, underpotential deposition, temperature effect.

MAGDY GIRGIS et EDWARD GHALI. Can. J. Chem. **67**, 130 (1989).

Faisant appel à des perturbations de balayages linéaire et cyclique et opérant à des températures allant de 25 à 75°C, dans un milieu de chlorure de plomb et d'acétate d'ammonium, on a étudié le comportement électrochimique du processus de déposition du plomb. On a entrepris l'étude sur quatre substrats: Pb, Cu, Ag et C. Des augmentations de température provoquent des augmentations du processus de déposition et favorisent la formation de dendrite. De plus, une augmentation de la température affecte des paramètres cinétiques comme les isothermes d'adsorption, les pentes de Tafel ainsi que le coefficient de diffusion. L'étude analytique de la surface, réalisée à l'aide de la spectroscopie électronique d'Auger, a permis de mettre en évidence qu'une augmentation de la température provoque une augmentation des intensités des pics du Cl ainsi que du Pb.

Mots clés: électrodéposition, voltamétrie cyclique, «fugacités» potentiostatiques, déposition de sous-potentiel, effet de température.

[Traduit par la revue]

Introduction

The use of stationary electrode voltammetry in qualitative and quantitative investigations of electrolysis mechanisms has been extensive (1–3), particularly in the field of electrocrystallization (4, 5). Considerable difficulties arise in the electrochemical studies of metal deposition due to the complex structure of the underlying metal (6) which lead to poor reproducibility, particularly in the appearance and structure of the deposits (7). There have been several studies of electrodeposition of lead (8–11).

The choice of the acidified ammonium acetate bath was based on previous studies carried out in our laboratory (12–14) to investigate the dissolution of galena in different media. The results showed that the anodic passivation caused mainly by lead chloride formation is reduced in acetate medium due to the strong activity of ammonium acetate in dissolving $PbCl_2$.

In the frame work of this approach, other studies (15, 16) have been undertaken to study lead deposition process from these media in order to find the optimum conditions necessary to obtain the metal directly from the sulphide ore. The investigation of this system at ambient temperature was carried out using different electrochemical techniques (17). To obtain more information about the cathodic process we tried to study the effect of elevated temperature on the system. To our knowledge, the effect of temperature on the behaviour of lead ions during the deposition process has not been reported in literature.

This paper, therefore, has been intended to shed some light on the reaction mechanism during the deposition process in acetate medium as a function of temperature by employing the techniques of linear and cyclic sweep polarization. Surface analyses were performed by Auger electron spectroscopy (AES) and the morphology of the deposit was determined by scanning electron microscopy (SEM). Further studies are currently under investigation to obtain more insightful information about the deposition process. The study will include the effect of temperature on the process of electrocrystallization and the nature of nucleation and growth.

Experimental

Four polycrystalline substrates of high purity (99.99%) were used: Pb and Cu (Cominco Ltd), Ag (Fisher spectrographically pure), and C (Union Carbide spectrographic grade graphite) were used as working electrodes. Graphite and saturated calomel electrodes served as auxiliary and reference electrodes, respectively. The preparation of electrodes and the electrochemical set up are described in previous studies (15, 17).

The bath under study was made up of B.D.H. Analar reagents of 2.5 *M* CH_3COONH_4, 2.4 *M* CH_3COOH, and 0.11 *M* $PbCl_2$. Oxygen was purged from the solution by bubbling a highly pure nitrogen in the electrolyte for at least 45 min before conducting the experiment. Slight pressure of nitrogen gas was kept during the experiments.

The analysis by Auger Electron Spectroscopy (AES) was available in a multifunction apparatus, model ESCLAB-500, V. G. Scientific Ltd. The electrode was mounted in the UHV-chamber of the spectrometry, till the evacuation (the base pressure of the system was 10^{-8} Torr). The operating conditions were as follows: 10 keV electron gun voltage and current density was 40 $\mu A/cm^2$. The morphological structure of the deposit was determined by scanning electron microscopy (SEM) Model JEOL-2553.

The temperature of the bath was controlled to within 1°C with a thermoregulator, type Thermomix 1480, B. Braun Melsungen AG. The experiments were conducted at temperatures between 25 and 75°C.

[1]Revision received September 19, 1988.

Can. J. Chem. Downloaded from www.nrcresearchpress.com by 122.72.124.2 on 09/07/12
For personal use only.

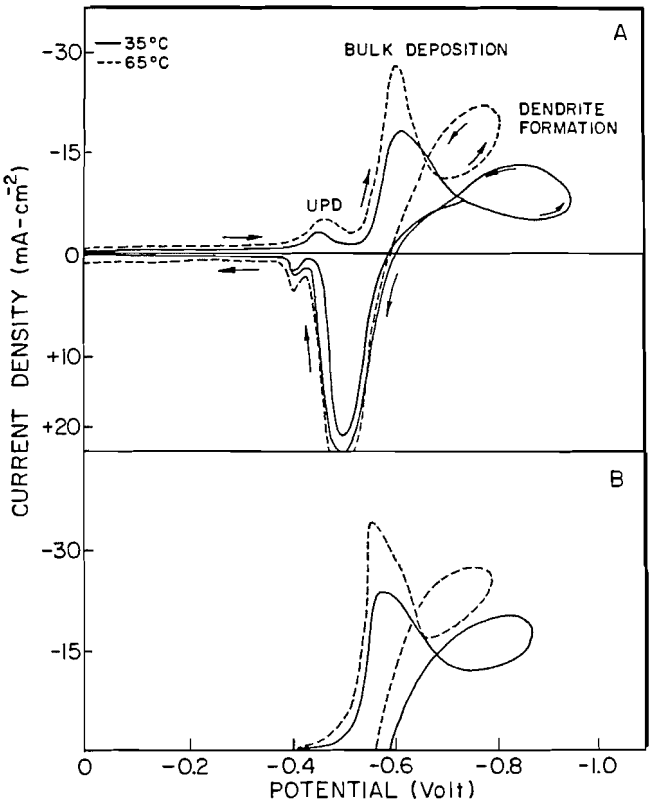


FIG. 1. General voltammogram for the deposition of lead from the acetate bath on (*A*) Ag electrode from the acetate bath, (*B*) Pb electrode at 35 and 65°C at scan rate 50 mV s^{-1}.

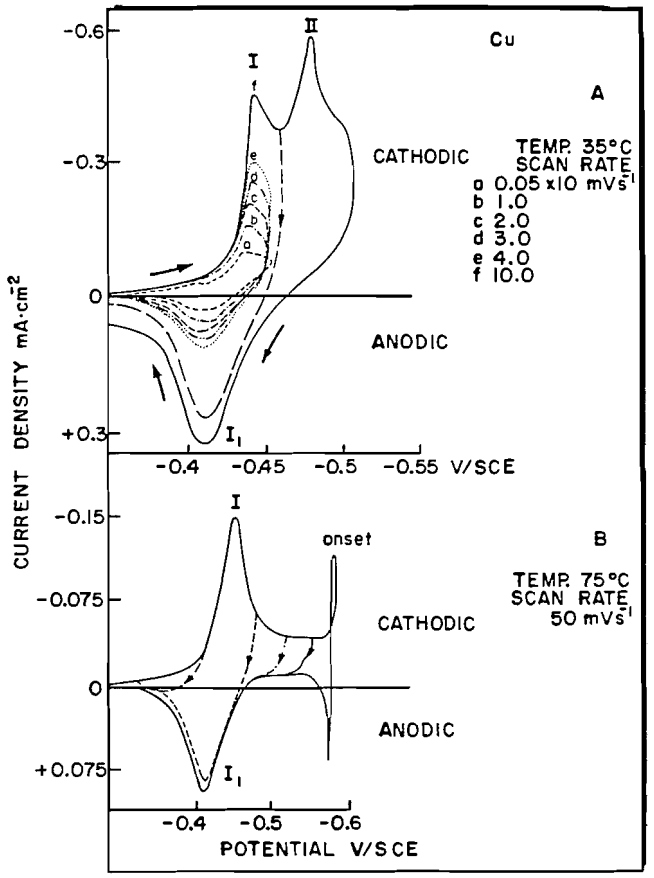


FIG. 2. Effect of temperature on the cyclic voltammograms in the UPD region for the deposition of Pb on the Ag electrode at (*A*) 35°C and (*B*) 75°C.

Results and discussion

As previously reported (17), various stages of lead deposition on different polycrystalline substrates were found to characterize the cyclic voltammograms, mainly and in the order: underpotential deposition (UPD), onset of the bulk deposition, bulk deposition, and dendrite formation. The lead UPD peaks appeared only on the Cu and Ag substrates. The voltammograms in the case of Pb electrode showed no anodic peak when the scan was driven in the anodic direction, indicating the irreversible nature of the deposition process. The general features of the voltammograms did not change as temperature increased from 25 to 75°C, i.e., the voltammograms were still characterized by the four regions as mentioned above. Figure 1 represents the general *C–P* profile of lead deposition on both Ag and Pb electrodes.

1. Effect of temperature on the voltammograms in the UPD Region

The voltammograms were characterized by a single UPD peak for both Cu electrode (at −0.47 V) and Ag electrode (at −0.44 V). Figures 2 and 3 depict a typical voltammograms for the underpotential peaks of lead on the Ag and Cu electrodes, respectively.

The increase in temperature from 35 to 75°C resulted in an anodic shift for the cathodic peak potentials for both electrodes; Cu (12 mV) and Ag (20 mV), while cathodic shift of 55 mV was observed for the anodic peak for the copper electrode and about 10 mV for the Ag electrode. To relate the anodic peaks with those appeared in the cathodic region, the negative limits to the potential range were changed. As shown in Fig. 2*B*, an anodic peak I was stripped when the cathodic scan was reversed at a potential beyond the region of peak I. Sweeping to further negative potential resulted in a further increase in the anodic current and was characterized by the formation of a cathodic current loop upon scan reversal (Fig. 2*B*). The current loop associated with the sudden increase in cathodic current is an indication of nucleation and multilayer growth of lead deposits.

The depolarization phenomenon observed at high temperature for both Cu and Ag electrodes may be discussed as follows.

In the presence of such large quantities of CH_3COONH_4 and CH_3COOH, one may expect that $PbCl_2$ will dissolve and the dominant species are likely to be $Pb(CH_3COO)_2$. In previous studies (15, 16), evidence for the formation of $Pb(CH_3COO)_2$ at room temperature was obtained from some surface analyses conducted by X-ray diffraction and Auger electron spectroscopy techniques.

The detection of such species formed on the electrode surface may imply that they exist in the solution. As temperature increases another kind of species, mainly lead chloride complexes $PbCl_1^+$, $PbCl_2^0$, $PbCl_3^-$, and $PbCl_4^{2-}$, start to form (18) and compete with lead acetate species. This interference of lead chloride complexes in the deposition process is probably the reason for the observed anodic shift of the cathodic peak potentials since lead chloride complexes are known to be reduced at potentials anodic to that of the lead acetate complexes (19). This hypothesis is strengthened by the fact that lead forms stable complexes with chloride ions at elevated temperatures. Also chloride ions have an effect on Ag and Au electrodes as competitive adsorbant (19) and form stable $CuCl^+$-type complexes with Cu (20).

Can. J. Chem. Downloaded from www.nrcresearchpress.com by 122.72.124.2 on 09/07/12
For personal use only.

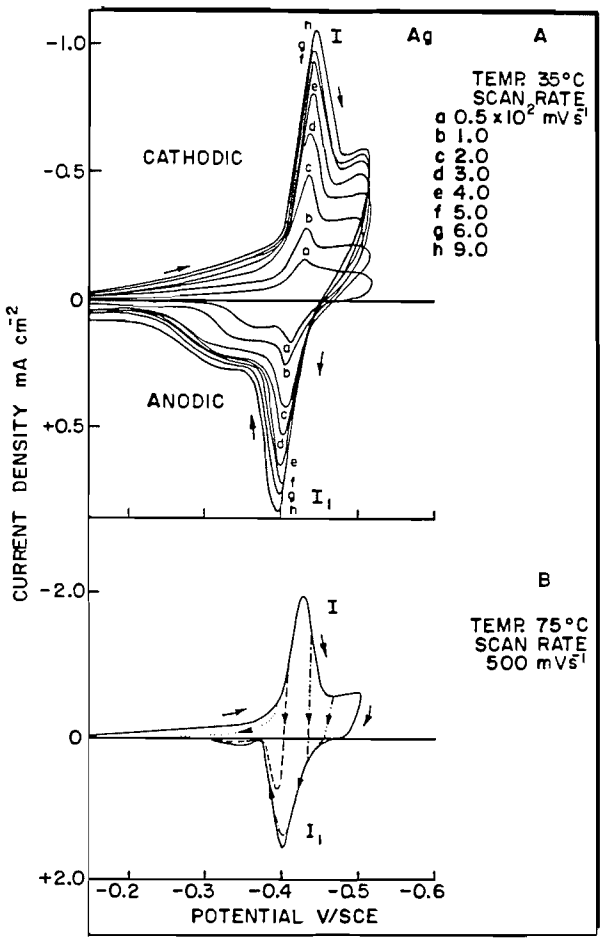


FIG. 3. Effect of temperature on the cyclic voltammograms in the UPD region for the deposition of Pb on the Cu electrode at (*A*) 35°C and (*B*) 75°C.

The analyses by Auger electron spectroscopy were performed after holding the substrate for about 20 min at potentials corresponding to the peak potentials in the UPD region. Figure 4 reveals the surface analysis for the lead deposit on Ag. The spectrum shows that the peak intensities of both Cl and Pb Auger signals increased as temperature was elevated from 25 to 50°C. This increase in peak intensity could be attributed to either strong adsorption of Cl^- ions (via the formation of lead chloride complexes) and/or to the entrapment of Cl^- ions in lead crystals which become porous at high temperatures. A change in the morphological structure was also observed from the scanning electron micrographs taken for lead deposits at −0.8 V (Fig. 5), where the deposit becomes more dendritic. Thus one may assume that the adsorption of chloride ions is favoured at high temperatures since the presence of chloride ion is known to promote the dendritic formation (15, 17).

The adsorption isotherm was determined by the integration of the cathodic peak corresponding to the adsorption of Pb after establishing adsorption equilibrium at defined underpotentials, $E_e - E_{Pb^{2+}}/Pb > 0$. The theoretical values calculated for a close packed lead monolayers (Q_s) with Pb^{2+} = 1.75 Å and for electrodes of surface areas of 1.1 (Cu) and 0.129 (Ag) cm^2 are 288 and 34 μC, respectively. Table 1 illustrates the experimental values (Q) and the degree of coverage θ. As shown in Table 1, the lead coverage on the Cu electrode is lower than that observed for Ag electrode under all conditions. This finding is in agreement with our previous observation (17) where SEM photomicrographs showed less formed nuclei on the surface of the copper electrode. This low coverage could be attributed to the specific anion adsorption, i.e., Cl^- and Ac^- ions on the surface of Cu electrode and this may hinder the formation of a complete monolayer of lead nuclei.

Lorenz (2) quoted from Staikov *et al.* (22) and Bewick *et al.* (23) that the 2D nucleation-like behavior in the systems $(Cu(111)/Pb^{2+}$ and $Ag(111)/Pb^{2+}$ in acetate media is probably caused by a pitting process within a pre-adsorbed anion layer consisting of specifically adsorbed acetate or oxygen, respectively. As also shown from the data in Table 1, more than one monolayer is formed on the Ag electrode. If the adsorption of Cl and/or acetate ions is the most influential factor on the surface of the substrate, it means that the effect of both ions on the Cu electrode is opposite to that on the Ag electrode. Further investigations using modern surface analyses are currently undertaken to clarify this point.

In the present study the effect of anions on the substrates manifested itself in a noticeable change in the underpotential shift ΔE_p, i.e. on the potential difference between the bulk and monolayer peaks as shown in Table 1. The data demonstrate lower values for the Cu electrode. The decrease in the underpotential shift is equivalent to a reduction in bond strength between the metal atom and the substrate surface (19). This confirms the above hypothesis that interaction of the anions with the Cu substrate is hindering the formation of lead monolayers, while promoting this process for the Ag electrode.

The behavior when the cathodic scan was reversed at the deposition potential was similar for all the foreign substrates used and at all temperatures. The voltammograms were characterized by a sharp increase in the cathodic current followed by an inductive current loop in the cathodic and anodic regions (Fig. 6). The current loop was inversely proportional to the scan rate, moreover the ratio of the cathodic/anodic peak currents approaches unity in all cases. The peak potentials in the cathodic and anodic regions were independent of the sweep rate. These observations, in addition to the symmetry of the *C–P* profiles, reflect that the reaction proceeds via a reversible mechanism and the process is related to nucleation in this particular region. The faster the sweep rate, the smaller the chance for the nuclei to form at a given degree of supersaturation. As a result, the current becomes smaller than in the same situation at a lower sweep rate.

It can also be assumed that the nuclei of the solid phase are separated by a distance greater than the diffusion layer, then a surface area greater than the geometric area is offered to the flux. This implies that the surface area is increasing with time (24). Pulsing the system to two cathodic limits (E_0, E_f) (see Fig. 6) which represent the beginning of the onset and the crossing potential upon scan reversal, respectively, resulted in a transient of the form shown in Fig. 8*B*. Pulsing to −0.55 (E_0) resulted in a transient which exhibits a falling current. This may represent the tailing current in the UPD region. The peak that is developed at −0.56 (E_f) is due probably to the formation of lead nuclei in the multilayer region followed by a subsequent overlap of the growing nuclei.

2. The behaviour in the bulk deposition region

The general profiles of the voltammograms showed no change from one substrate to another, characterized mainly by a cathodic peak that has the morphology of a diffusion-controlled process, followed by a large anodic peak (e.g. Fig. 1*A*) except for the Pb voltammograms where the absence of the anodic peak is evident (Fig. 1*B*).

Can. J. Chem. Downloaded from www.nrcresearchpress.com by 122.72.124.2 on 09/07/12
For personal use only.

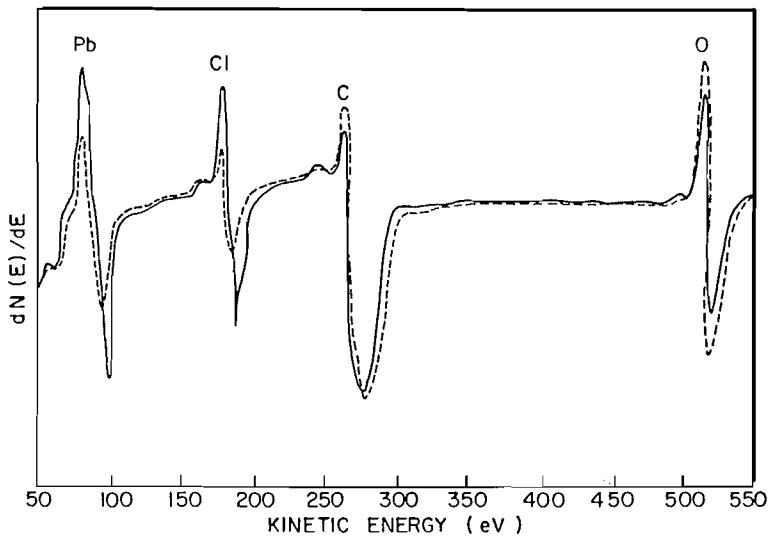


FIG. 4. Auger spectroscopy of lead deposit on the Ag electrode at 25°C (---) and 75°C (—).

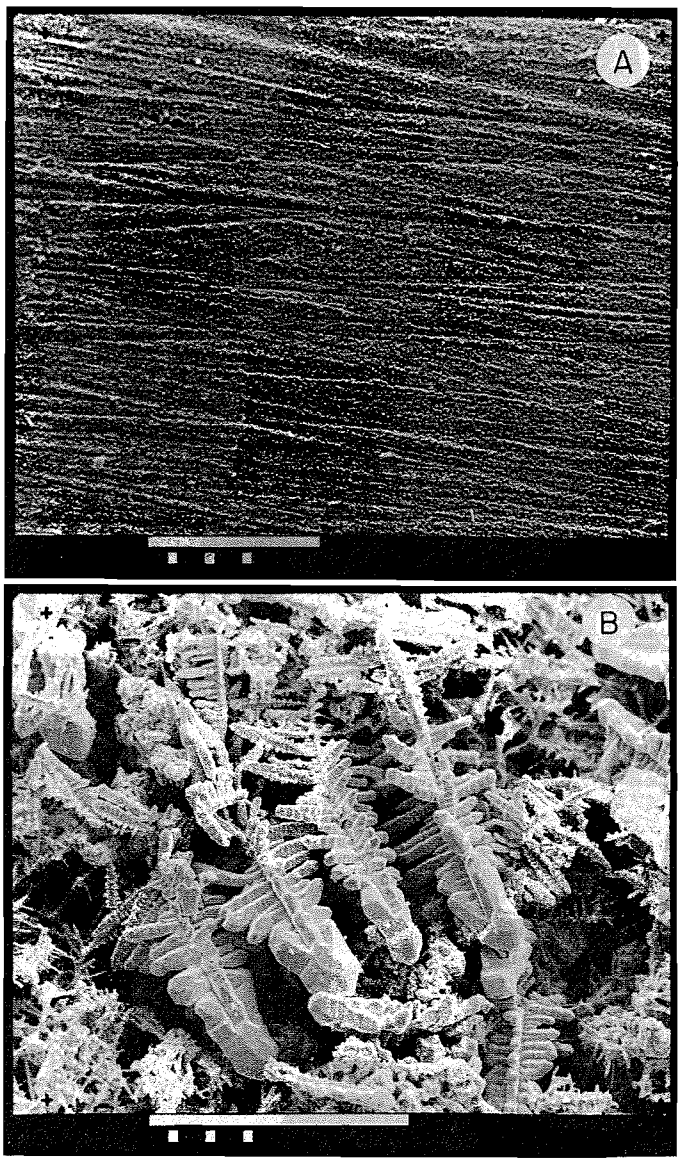


FIG. 5. Scanning electron micrographs of the Pb deposits after the potential was scanned to −0.8 V (at 50 mV s^{-1}) at (*A*) 25°C and (*B*) 75°C.

TABLE 1. Calculated values of charge Q, degree of coverage θ, and the underpotential shift ΔE_p*

	Cu		Ag	
	25°C	75°C	25°C	75°C
$Q_{cathode}$	140	193	105	154
θ	0.44	0.67	3.08	4.53
Q_{anode}	56	86	58	77
θ	0.19	0.29	1.7	2.26
ΔE_p	79	97	87	130

Q, experimental charge (in μC); θ, coverage Q/Q_s, Q_s is the theoretical value for a close packed lead monolayer; ΔE_p, underpotential shift (in mV).

The deposition potential varied slightly from substrate to another (maximum difference is 10 mV), as temperature increased the deposition potential shifted to less negative potentials which is similar to the behaviour in the UPD region. The anodic shift was 18 mV for Ag, 20 mV for Cu, 30 mV for C, and 29 mV for Pb. The anodic peaks were shifted cathodically by 7, 30, and 30 mV for Ag, C, and Cu electrodes, respectively. The depolarization process observed at high temperature indicates that Cl ions exert a strong effect on the UPD and on the bulk deposition peaks due to the formation of chloride complexes at high temperatures. The calculated Tafel slopes were higher at the ambient temperatures than at elevated temperatures, e.g. for the Pb electrode, it was 185 mV at 25°C, while at 75°C, the value became 120 mV (Fig. 7). X-ray analyses revealed the presence of peaks related to acetate compounds at temperatures lower than 55°C most likely arise from lead acetate compound (15). From the behaviour of Tafel slopes as a function of of temperature and from the XRD analyses, one may infer that acetate anion adsorption on lead deposit decreases as temperature increases.

The kinetic studies for each system will now be discussed separately:

(a) Pb/Pb^{2+} system

The irreversible reaction of the Pb^{2+}/Pb system is evident as no current response was recorded when the scan was reversed in

Can. J. Chem. Downloaded from www.nrcresearchpress.com by 122.72.124.2 on 09/07/12
For personal use only.

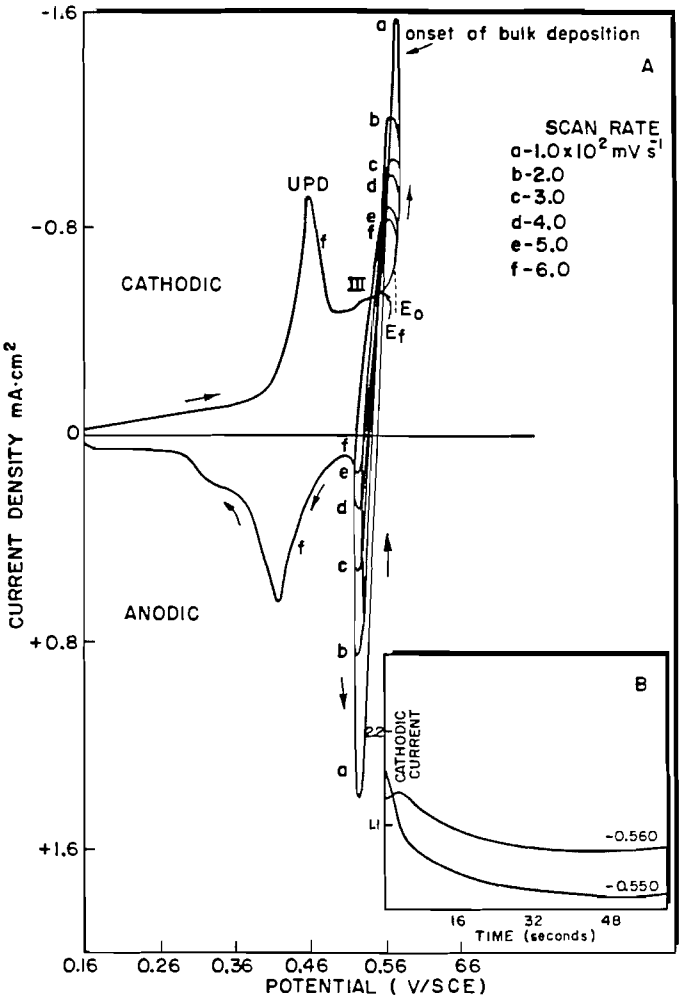


FIG. 6. (*A*) Cyclic voltammogram for lead deposition on Ag electrode in the region of onset at the bulk deposition at 35°C; (*B*) potentiostatic *i*–*t* curve for the Ag electrode at different imposed potentials at 35°C.

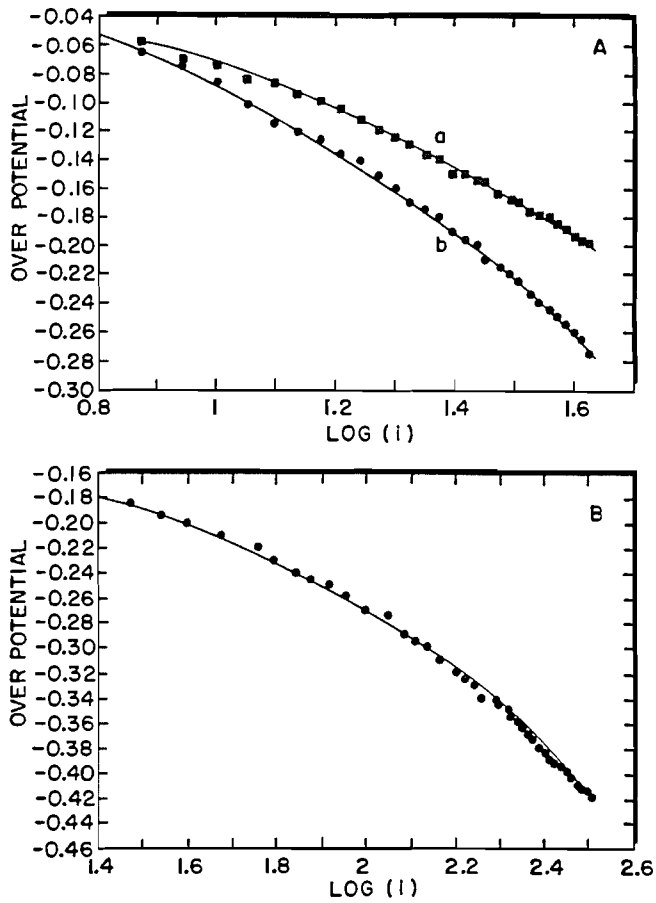


FIG. 7. (*A*) Calculated Tafel slops for the Pb electrode at (*a*) 35°C and (*b*) 55°C under unstirred conditions; (*B*) same as A except at 75°C.

the anodic direction. To evaluate the kinetic parameter αn_α, log i_p (peak current) was plotted against the potential E_p at different scan rates, according to eq. [1], which characterizes the irreversible system (25):

$$[1] \quad i_p = 0.227\, nFAC_0,K_s \exp\left[-\frac{\alpha nF}{RT}E_p - E^0)\right]$$

where C_0 is the concentration of lead ions (mol/cm^3) and α is the charge transfer constant. The slopes calculated at 25, 55, and 75°C gave the corresponding αn_α: 0.28, 0.3, and 0.32, respectively. The rate constant (K_s) calculated from the intercepts changed slightly as a function of temperature, e.g. it was about 1.1×10^{-4} cm/s at 25°C, while at 75°C it was 1.6×10^{-4} cm/s. This may strengthen the interpretation that the decrease of Tafel slopes as a function of temperature elevation is a result of the effect of anion adsorption.

Under diffusion-control process, the slope of $i_p - \nu^{1/2}$ plot at 25°C obeys the equation (26):

$$[2] \quad i_p/\nu^{1/2} = 2.69 \times 10^5\, n^{3/2}\, DC_0$$

where $i_p/\nu^{1/2}$ is the slope (A cm^{-2} $\nu^{-1/2}$ S$^{-1/2}$), n is the number of electrons, D is the diffusion coefficient (cm^2 s^{-1}), and C_0 is the concentration of the electroactive species (mol cm^{-3}).

The i_p was found to vary linearly with the square toot of scan rate ν as shown in Fig. 8. The extrapolation to the origin deviated only at temperatures higher than 45°C and the curves cut the current axis. This is probably due to the depolarization phenomenon exerted by the anions at higher temperature. In fact, if we substitute the following values in eq. [2], i.e. $C_{Pb^{2+}} = 0.11 \times 10^{-3}$ mol cm^{-3}, and the slopes obtained from Fig. 8 (e.g. 0.3 and 6.6 A cm^{-2}/$\nu^{1/2}$ s$^{-1/2}$) at 25 and 75°C, respectively, and $n = 2$, the diffusion coefficient of lead ions ($D_{Pb^{2+}}$) will have the value of 1.3×10^{-5} cm^2 s^{-1} (at 25°C) which is in perfect agreement with the D value reported in literature (27), while at 75°C the calculated D value was found to be 6.2×10^{-3} cm^2 s^{-1}.

b. Deposition on foreign substrates

The separation of the cathodic–anodic peak potentials was high for the C electrode (e.g. 120 and 183 mV at 25 and 75°C) and relatively low for the other electrodes (e.g. Ag 80 and 95 mV at 25 and 75°C, respectively). These data imply that the reaction may proceed via a quasi reversible mechanism and not through a complete reversible process, since E_p is dependent on scan rate and the potential shift increase with ν (28).

The plot of E_p vs. log ν gave two linear sections. The point of intersection gives the critical sweep rate, which may mark the transition from a quasi reversible to an irreversible behavior (it was $\geq$ 50 mV s^{-1} for the substrates used). The irreversible behaviour at high sweep rates ($>$ 50 mV s^{-1}) was evident from the increase in separation between the cathodic and anodic peak potentials, in addition, the decrease in magnitude of the anodic peak current is a function of the increase in sweep rate. Slopes

Can. J. Chem. Downloaded from www.nrcresearchpress.com by 122.72.124.2 on 09/07/12
For personal use only.

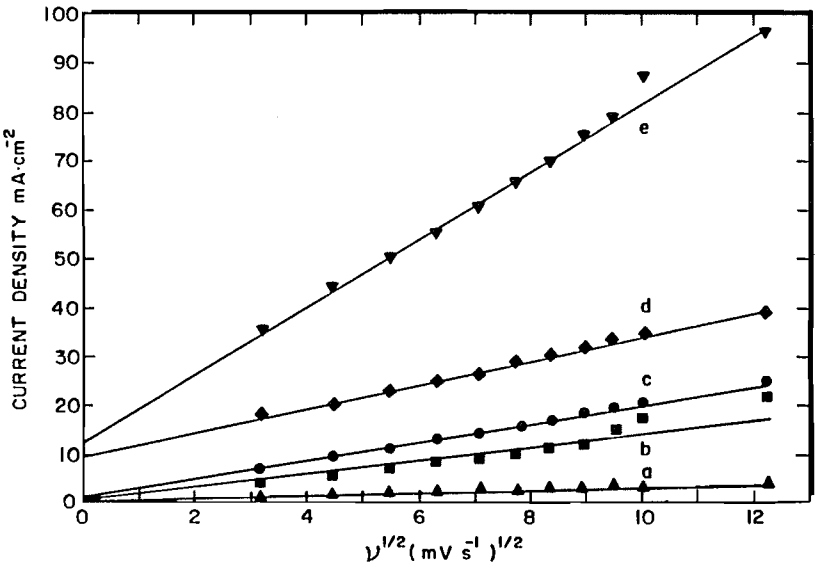


FIG. 8. The i_p–$\nu^{1/2}$ plot for Pb deposition on the Pb electrode at (*a*) 25°C, (*b*) 35°C, (*c*) 45°C, (*d*) 55°C, and (*e*) 75°C.

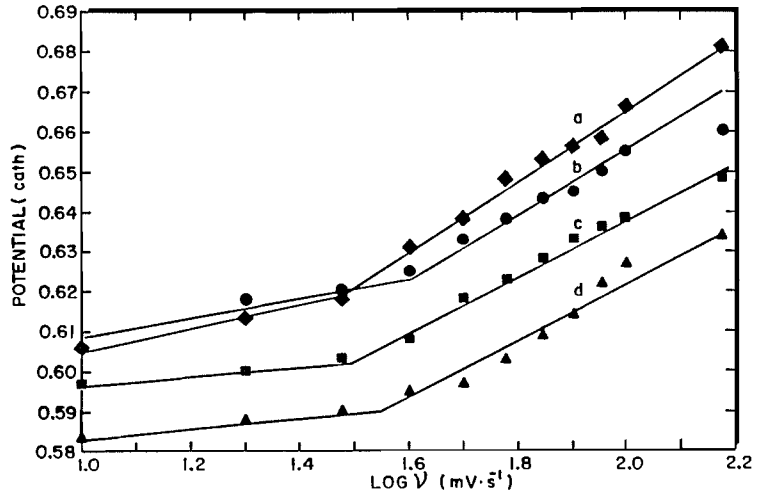


FIG. 9. The E_p – log ν plot for lead deposition on the Cu electrode at (*a*) 35°C, (*b*) 45°C, (*c*) 65°C, and (*d*) 75°C.

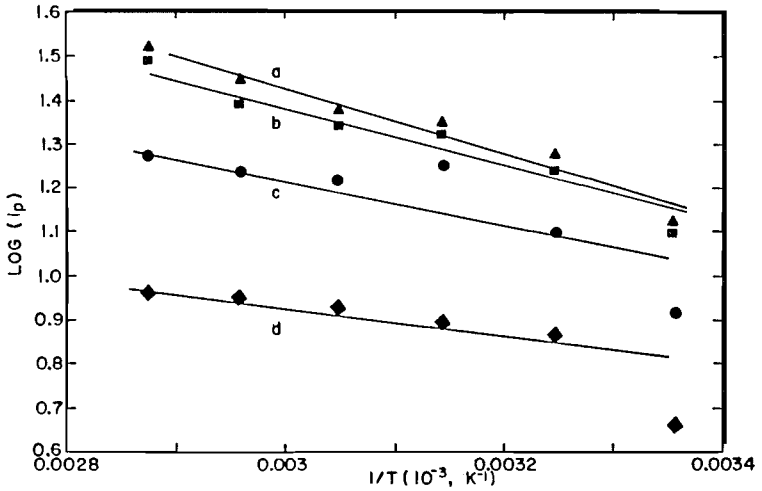


FIG. 10. Dependence of current peak (i_p) on the temperature for the deposition of lead on the carbon electrode at different scan rates, (*a*) 10, (*b*) 50, (*c*) 100, and (*d*) 150 mV s^{-1}.

Can. J. Chem. Downloaded from www.nrcresearchpress.com by 122.72.124.2 on 09/07/12
For personal use only.

TABLE 2. Calculated values of ΔH‡ (in kcal/mol) for different substrates in temperature range 25–75°C

Scan rate ($mV\ s^{-1}$)	$\Delta H‡$				
	Pb	Cu	Ag	Au	C
10	8.6	4.8	5.5	5.7	2.5
50	7.8	4.0	3.8	4.8	3.0
100	6.5	4.4	4.1	4.1	3.3
150	6.1	4.7	3.9	4.0	3.4

with corresponding number of electrons equal to or approaching 1 (e.g. Cu Fig. 9) were obtained in the irreversible section. These values were confirmed for all substrates used.

The 10-fold increase in scan rate resulted in a cathodic shift of 85, 75, and 64 mV in peak potential at 25, 55, and 75°C, respectively, with corresponding αn equal to 0.35, 0.4, and 0.46, respectively. Assuming that $n = 2$, this will give values of α equal to 0.175, 0.2, and 0.23 at 25, 55, and 75°C, respectively. These data will give Tefel slopes $2.3RT/\alpha nF$ of values greater than 120 mV. These values compare favorably with those obtained by the linear sweep polarization method (130 mV at 25°C and 120 mV at 75°C).

When the cathodic scan was swept to more negative values, i.e., beyond the region of the bulk deposition another current loop was formed (Fig. 1). The second loop formation is due eventually to further growth of the Pb nuclei in the form of dendrites. The cathodic potential at which this loop starts to form was different from one substrate to another and was in the order Cu, C, Ag, respectively. The effect of temperature elevation resulted in faster loop formation than that observed at low temperature, indicating that high temperature favors the formation of dendrites. The investigation of the nucleation and growth mechanism by potentiostatic pulses will be discussed in another communication.

3. Heat of activation of the Pb/substrate system

The values of the heat of activation $\Delta H‡$ were calculated by plotting log i_p against T^{-1} (e.g. C, Fig. 10). The slopes of these curves ($d \log i/d T^{-1}$) give the corresponding $\Delta H‡$ values according to the equation (29).

$$[3] \quad i = K \exp[-\Delta H†/RT]$$

The plots give excellent linear relations over the wide range of temperatures. As shown from the values given in Table 2, higher $\Delta H‡$ were obtained for Ph electrode.

Summary

The study has shown that the formation of lead chloride complexes at high temperatures resulted in a noticeable depolarization effect on the cathodic process as the deposition potential shifted to more anodic values. The SEM studies showed a marked growth of lead deposit in the form of dendrities at high temperatures. Auger electron spectroscopy revealed the strong influence of the Cl ion on the Cu electrode which resulted in a lower coverage of lead monolayers, while the opposite effect was observed for the Ag electrode.

Acknowledgement

The authors thank the National Sciences and Engineering Research Council of Canada (NSERC) for financial support. The facilities offered by the laboratories GRAPS, Laval University, and the participation of Dr A. Adnot are acknowledged.

1. R. S. NICHOLSON and I. SHAIN. J. Anal. Chem. **36**, 706 (1964).
2. R. S. NICHOLSON and I. SHAIN. J. Anal. Chem. **37**, 178 (1965).
3. R. S. NICHOLSON and I. SHAIN. J. Anal. Chem. **37**, 190 (1965).
4. D. D. MACDONALD. J. Electrochem. Soc. **11**, 651 (1974).
5. A. CAPRON and R. PARSON. J. Electroanal. Chem. **39**, 275 (1972).
6. D. J. ASTLEY, J. A. HARRISON, and H. R. THIRSK. J. Electroanal. Chem. **19**, 325 (1968).
7. A. R. DESPIC. *In* Proceedings of the Symposium on Electrocrystallization. Vol. 81–6. *Edited by* R. Weil and R. G. Barradas. 1981. p. 101.
8. HRABANKOVA, J. DOLEZAL, and P. BERON. J. Electroanal. Chem. **22**, 203 (1969).
9. A. BEWICK and B. THOMAS. J. Electroanal. Chem. **84**, 127 (1977).
10. W. J. LORENZ, E. SHMEDIT, G. STAIKOV, and H. BOST. Faraday Symp. Chem. Soc. **12**, 14 (1978).
11. J. A. HARRISON, R. P. J. HILL, and J. THOMPSON. J. Electroanal. Chem. **44**, 445 (1973).
12. E. GHALI and B. DANDAPANI. J. Appl. Electrochem. **10**, 335 (1980).
13. E. GHALI and B. DANDAPANI. J. Electrochem. Soc. **129**, 27 (1982).
14. E. GHALI and B. DANDAPANI. Metall. Trans. **15B**, 605 (1984).
15. E. GHALI and M. GIRGIS. Metall. Trans. **16B**, 489 (1985).
16. M. GIRGIS and E. GHALI. Unpublished data.
17. M. GIRGIS, E. GHALI, and A. WIECKOWSKI. Electrochem. Acta, **31**, 681 (1986).
18. H. C. HELGSON. Complexing and hydrothermal ore deposition. McMillan & Co., New York. 1964.
19. D. M. KOLB. Advances in electrochemistry and electrochemical engineering. Vol. II. *Edited by* H. Greischer and C. W. Tobias. John Wiley. 1978. p. 125.
20. J. C. WESTALL, F. MOREL, and D. N. HUME. J. Anal. Chem. **51**, 1972 (1979).
21. W. J. LORENZ. *In* Proceedings of the Symposium on Electrocrystallization. Vol. 81–6. *Edited by* R. Weil and R.G. Barradas, 1981. p. 81.
22. G. STAIKOV, K. JÜTTNER, W. G. LORENZ, and E. SCHMIDT. Electrochem. Acta, **23**, 305 (1978).
23. A. BEWICK, J. JOVICVIC, and B. THOMAS. Faraday Symp. Chem. Soc. **12**, 4 (1977).
24. G. ARCHDALE and J. A. HARRISON. J. Electroanal. Chem. **43**, 321 (1973).
25. H. R. THIRSK and J. A. HARRISON. J. Electroanal. Chem. **43**, 321 (1973).
26. A. J. BARD and L. R. FAULKNER. Electrochemical methods, fundamentals and applications. John Wiley, New York. 1980. p. 218.
27. T. BERZIN and P. DELHAY. J. Anal. Chem. **75**, 555 (1953).
28. A. WEISSBERGER and B. ROSSITER. *In* Physical methods of chemistry. Part IIA. Electrochemical methods. Vol. 1. Wiley and Sons, New York. 1971. Chap. VI.
29. B. E. CONWAY and D. J. MACKINNON. J. Electrochem. Soc. **116**, 1665 (1969).

Can. J. Chem. Downloaded from www.nrcresearchpress.com by 122.72.124.2 on 09/07/12
For personal use only.

Nucleophilic addition and substitution reactions between the cyanide ion and cyclopentadienyliron complexes of chlorobenzenes. Syntheses of benzonitriles and phthalonitriles

RONALD G. SUTHERLAND, CHUN-HAO ZHANG, ADAM PIÓRKO, and CHOI CHUCK LEE
Department of Chemistry, University of Saskatchewan, Saskatoon, Sask., Canada S7N 0W0

Received June 27, 1988

RONALD G. SUTHERLAND, CHUN-HAO ZHANG, ADAM PIÓRKO, and CHOI CHUCK LEE. Can. J. Chem. **67**, 137 (1989).

Reaction of cyclopentadienyliron (CpFe) complexes of chlorobenzenes with NaCN in DMF could give rise to products resulting from the addition of the cyanide ion or from substitution and addition reactions with the cyanide ion. Demetallation–oxidation of such products by treatment with DDQ would lead to the synthesis of benzonitriles and phthalonitriles. With the CpFe complex of chlorobenzene, reaction with NaCN in DMF for 3 min, 30 min, or 3 h gave rise to an approximately 90:10 mixture of (1–5-η^5-1-chloro-*exo*-6-cyanocyclohexadienyl)(η^5-cyclopentadienyl)iron (**9**) and (1–5-η^5-1,*exo*-6-dicyanocyclohexadienyl)(η^5-cyclopentadienyl)iron (**10**), a 40:60 mixture of **9** and **10** or pure **10**, respectively. When the 3-h reaction was worked up in the presence of an added aqueous solution of NH_4PF_6, only the substitution product, the (η^6-benzonitrile)(η^5-cyclopentadienyl)iron cation (**11**), was obtained as its hexafluorophosphate. Apparently, under the acidic conditions of the added aqueous NH_4PF_6, **10** could readily revert to **11** which then gave rise to its hexafluorophosphate. DDQ treatment of the 3-min or 3-h reaction product gave, respectively, *o*-chlorobenzonitrile or phthalonitrile. Similarly reaction of CpFe complexes of *o*-substituted chlorobenzenes could give rise to CpFe-complexed cyclohexadienyl systems with two cyano groups at the 1- and 6-positions and the original *o*-substituent at the 2-position. DDQ treatment of such products would lead to the formation of 3-substituted phthalonitriles, and in the present work, 3-methyl, 3-methoxy-, and 3-phenoxyphthalonitriles were prepared in this way. In another set of reactions, depending on the experimental conditions employed, the CpFe complex of 2,6-dichlorotoluene (**20**) could give products from cyanide addition only, the DDQ treatment of which led to the formation of 2,4-dichloro-3-methylbenzonitrile, or products from substitution and addition and subsequent DDQ treatment of which gave rise to 4-chloro-3-methylphthalonitrile.

Key words: η^6-chlorobenzene-η^5-cyclopentadienyliron cation, complexed chlorobenzenes, nucleophilic addition of cyanide ion, nucleophilic substitution with cyanide ion, synthesis of benzonitriles and phthalonitriles.

RONALD G. SUTHERLAND, CHUN-HAO ZHANG, ADAM PIÓRKO et CHOI CHUCK LEE. Can. J. Chem. **67**, 137 (1989).

La réaction des complexes des chlorobenzènes et du cyclopentadiénylfer (CpFe) avec la NaCN dans le DMF pourrait donner naissance à des produits provenant soit d'une addition de l'ion cyanure soit de réactions de substitution et d'addition avec l'ion cyanure. La réaction de tels produits avec de la DDQ provoque successivement une démétallation et une oxydation et devrait conduire à la synthèse de benzo- et de phtalo-nitriles. Avec le complexe du CpFe du chlorobenzène, des réactions de 3 min, 30 min ou 3 h avec du NaCN dans du DMF conduisent respectivement à un mélange environ 90:10 (η^5-chloro-1 cyano-6-*exo* cyclohexadiène-1–5 yl) (η^5-cyclopendiényl) (**9**) et de (η^5-dicyano-1,6-*exo* cyclohexadiène-1–5 yl) (η^5-cyclopentadiényl) (**10**), à un mélange environ 40:60 des composés **9** et **10** et au produit **10** pur. Lorsque les produits de la réaction de 3 h sont extraits en présence d'une solution aqueuse additionnée de NH_4PF_6, on n'obtient que le produit de substitution, le cation (η^6-benzonitrile) (η^5-cyclopentadiényl)fer (**11**) sous la forme d'hexafluorophosphate. Il semble que, dans les conditions acides obtenues par l'addition de NH_4PF_6 aqueux, le produit **10** se retransforme facilement en composé **11** qui conduit alors à son hexafluorophosphate. Lorsque les produits obtenus après des reactions de 3 min ou 3 h sont traités par de la DDQ, on obtient respectivement de l'*o*-chlorobenzonitrile et du phtalonitrile. De la même manière, la réaction des complexes des chlorobenzènes *o*-substitués et du CpFe pourrait donner lieu à la formation de CpFe complexés à des systèmes cyclohexadiényles portant des groupements cyano dans les positions 1 et 6 et le substituant ortho original dans la position 2. Le traitement de tels porudits par de la DDQ conduirait à la formation de phtalonitriles substitués en position 3; dans le présent travail, on a ainsi préparé les méthyl-3, méthoxy-3 et phénoxy-3 phtalonitriles. Dans un autre ensemble de réactions et suivant les conditions expérimentales, le complexe du CpFe et du dichloro-2,6 toluène (**20**) pourrait conduire soit au produit provenant exclusivement de l'addition du cyanure soit au produit provenant d'une substitution et d'une addition du cyanure; leur traitement subséquent par la DDQ conduirait DDQ conduirait respectivement soit à la formation de dichloro-2,4 méthyl-3 benzonitrile soit à la formation de chloro-4 méthyl-3 phtalonitrile.

Mots clés : cation η^6-chlorobenzène-η^5-cyclopentadiénylfer, chlorobenzènes complexés, addition nucléophile de l'ion cyanure, synthèse de benzonitriles et phtalonitriles.

[Traduit par la revue]

Introduction

Recently, we have reported (1) that reactions of the hexafluorophosphate salts of cyclopentadienyliron (CpFe) complexes of arenes containing an electron-withdrawing substituent with NaCN in dimethylformamide (DMF) resulted in a regiospecific *exo*-addition of the cyanide ion at a position *ortho* to the substituent, giving rise to CpFe complexes of cyclohexadienyl systems. It has also been found that DDQ (2,3-dichloro-5,6-dicyano-1,4-benzoquinone) is an effective reagent for the demetallation–oxidation of such complexed cyclohexadienyl systems, thereby providing a method for the synthesis of the liberated substituted arenes (2). Among the cyanide additions studied, for example, were the reactions with $C_6H_5(X)FeCp^+PF_6^-$, with X = NO_2 or COC_6H_5, and subsequent treatment of the adduct with DDQ gave *o*-$C_6H_4(NO_2)CN$ or *o*-$C_6H_4(COC_6H_5)CN$, in yields of 75% or 82%, respectively (2). As another illustration of such an introduction of a cyano group *ortho* to an electron-withdrawing substituent in a benzene ring, in the present work, the known CpFe complex of *p*-tolylsulfonylbenzene (**1**) (3) was treated with NaCN in DMF

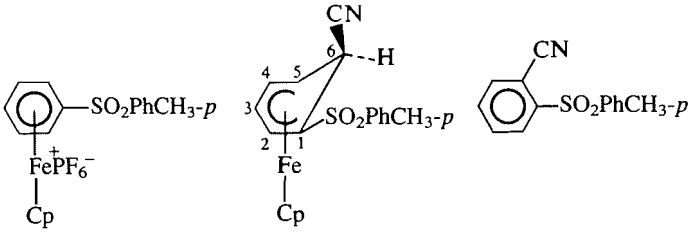
Can. J. Chem. Downloaded from www.nrcresearchpress.com by 122.72.124.2 on 09/07/12
For personal use only.

TABLE 1. ^{1}H nmr data for cyclohexadienyl complexes

Complex	δ($CDCl_3$), ppm from TMS[a]						
	Cp	H2	H3	H4	H5	H6	Others
2	4.72	5.31	6.30	4.82	3.04	3.75	2.35(3H,s,CH_3)
	J(2—3)=5.4, J(2—4)=1.1; J(3—2)=J(3—4)=5.4, J(3—5)=1.1;						7.27(2H,d,J=8.3,Ph)
	J(4—3)=J(4—5)=5.4, J(4—6)=0.4; J(5—6)=6.8, J(5—4)=5.4,						7.67(2H,d,J=8.3,Ph)
	J(5—3)=1.1, J(5—2)=0.4; J(6—5)=6.8, J(6—2)=0.7, J(6—4)=0.4						
9	4.46	4.79	6.09	4.48[b]	2.88	3.85	—
	J(2—3)=5.2, J(2—4)=J(2—6)=1.0; J(3—2)=J(3—4)=5.2, J(3—5)=1.3;						
	J(5—6)=6.8, J(5—4)=5.4, J(5—3)=1.3; J(6—5)=6.8, J(6—2)=1.0						
10	4.57	5.12	6.41	4.85	3.02	3.56	—
	J(2—3)=5.3; J(3—2)=J(3—4)=5.3, J(3—5)=1.0; J(4—3)=J(4—5)=5.3;						
	J(5—6)=6.7, J(5—4)=5.3, J(5—3)=1.0; J(6—5)=6.7						
15	4.51	—	6.27	4.83	2.93	3.60	3.91(3H,s,CH_3O)
	J(3—4)=5.8, J(3—5)=0.6; J(4—3)=J(4—5)=5.8, J(4—6)=0.6;						
	J(5—6)=6.5, J(5—4)=5.8, J(5—3)=0.6; J(6—5)=6.5, J(6—4)=0.6						
16	4.63	—	6.48	4.86	2.96	3.67	7.14–7.39(5H,m,Ph)
	J(3—4)=5.6; J(4—3)=J(4—5)=5.6; J(5—4)=5.6; J(5—6)=6.5;						
	J(6—5)=6.5						
21	4.39	—	—	4.92	3.49	3.78	2.32(3H,s,CH_3)
	J(4—5)=5.7; J(5—4)=5.7, J(5—6)=6.7; J(6—5)=6.7						
22	4.52	4.83	6.03	4.83	—	—	2.08(3H,s,CH_3)
	J(2—3)=5.4; J(3—2)=J(3—4)=5.4; J(4—3)=5.4						
25	4.51	—	—	5.26	2.95	3.50	2.41(3H,s,CH_3)
	J(4—5)=6.5; J(5—4)=J(5—6)=6.5; J(6—5)=6.5						
26	4.63	5.11	6.33	5.17	—	—	2.07(3H,s,CH_3)
	J(2—3)=5.4; J(3—2)=J(3—4)=5.4; J(4—3)=5.4						

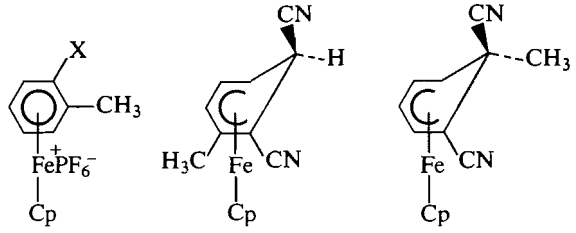
[a]All Cp absorptions are 5H singlets; H2 to H6 are the protons on cyclohexadienyl carbons 2 to 6, respectively. The J values are in Hz and J_{a-b} is the coupling constant for Ha and Hb.
[b]Overlapping with Cp.

to give adduct **2**, (1–5-η^5-*p*-tolysulfonyl-*exo*-6-cyanocyclohexadienyl)(η^5-cyclopentadienyl)iron. The spectral data in support of the assigned structure for **2** and for other cyclohexadienyl complexes are summarized in Tables 1 and 2. Upon treatment of **2** with DDQ, *o*-*p*-tolylsulfonylbenzonitrile (**3**), a compound that has not been prepared previously, was obtained.



1 **2** **3**

Nesmeyanov and co-workers (4) were the first investigators to report that a nucleophilic substitution reaction took place when the CpFe complex of chlorobenzene was treated with a number of nucleophiles, and such a reaction between the CpFe complex of *p*-chlorotoluene and the cyanide ion resulted in the replacement of the chloro group by the cyano group (5). In a recent study on possible steric hindrance effects in nucleophilic additions to CpFe complexed substituted benzenes (6), it was found, for example, that the reaction of the cyanide ion with the CpFe complex of *o*-chlorotoluene (**4**) or *o*-cyanotoluene (**5**) gave the same products, a 96:4 mixture of cyclohexadienyl complexes **6** and **7**. With **4** therefore, both cyanide addition and the substitution of the chloro group by the cyano group have taken place. The present work involved further studies on such addition–substitution reactions and their possible applications for the synthesis of benzonitriles and phthalonitriles.



4; X = Cl
5; X = CN
6 **7**

When the (η^6-chlorobenzene)(η^5-cyclopentadienyl)iron cation (**8**), as its hexafluorophosphate, was treated at room temperature with an excess of NaCN in DMF and the filtered reaction mixture was directly dissolved in ether and worked up to give the products, the nature of such products was found to be dependent on reaction time. With a short reaction time of 3 min, an approximately 90:10 mixture of cyclohexadienyl complexes **9** and **10** was obtained, **9** being derived from the cyanide addition to the chlorobenzene complex **8**, while **10** resulted from both substitution and addition. When the reaction time was extended to 30 min, the product ratio of **9**:**10** became 40:60, and for a reaction time of 3 h, pure **10** was obtained as the only product. Complex **10** was also prepared directly from the reac-

Can. J. Chem. Downloaded from www.nrcresearchpress.com by 122.72.124.2 on 09/07/12
For personal use only.

TABLE 2. ^{13}C nmr data for cyclohexdienyl complexes

Complex	δ($CDCl_3$), ppm from TMS[a]						
	Cp	Cl	C2,3,4	C5[b]	C6[b]	CN[c]	Others
2	76.4	43.1*	77.6,80.6,82.7	24.8	25.7	116.0	21.5(CH_3);127.2(2C),129.9(2C), 136.9*,144.0*(Ph)
9	76.4	53.6*	77.1,79.7,87.7	26.2	36.4	116.7	—
10	76.9	5.7*	80.1,81.2,83.6	24.1	28.0	116.8,123.1	—
15	76.1	2.4*	65.8,75.9,131.0*	23.5	29.5	116.7,121.4	56.3(CH_3O)
16	78.0	4.3*	75.6,77.1,127.4*	23.7	30.2	116.5,120.6	117.3(2C),123.8,129.9(2C), 157.5*(Ph)
21	79.1	53.4*	88.5,104.6*,107.4*	21.3	28.7	116.4	17.4(CH_3)
22	79.2	65.0*	77.9(2C),81.8	65.0*	46.4*	117.8	23.7(CH_3)
25	79.2	5.8*	81.7,92.7*,106.7*	21.2	28.7	116.5,122.1	18.4(CH_3)
26	79.5	39.3*	80.3,81.0,82.0	62.3*	19.2*	117.7,120.9	23.7(CH_3)

[a]Cl to C6 are the cyclohexadienyl carbons; asterisks denote quaternary carbons.

[b]Assignments of C5 and C6 based on C5 as aromatic carbons with J(C—H) values of 174.4, 174.6, 174.4, 176.1, and 176.0 Hz for **2**, **10**, **15**, **16**, **21**, and **25**, respectively, and C6 as aliphatic carbons with J(C—H) values of 147.5, 147.0, 152.4, 147.6, 152.0, and 147.3 Hz, respectively, for **2**, **10**, **15**, **16**, **21**, and **25**. No J(C—H) was obtained for **9** because of decomposition during gated decoupling experiments and the assignmet for C5 and C6 for **9** could be reversed.

[c]The absorptions at the 116–117 ppm region were due to the CN on C6 which showed J(CN—H6) values of 6–7 Hz, while the absorptions at the 120–123 ppm region were due to the CN on C1 (or C5 of **26**) which showed J(CN—H6) values of 3–4 Hz.

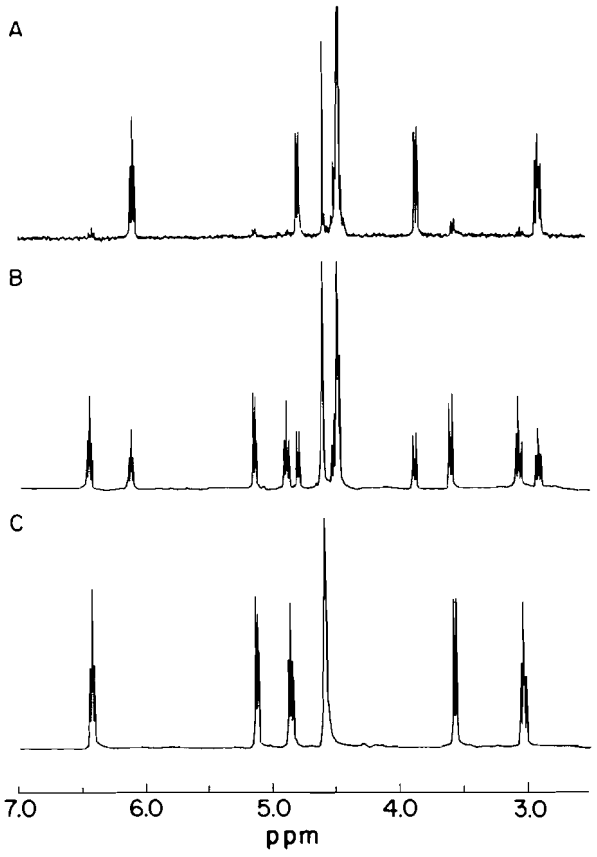
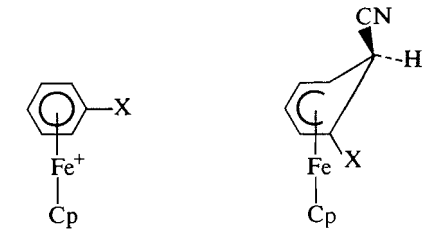


FIG. 1. A, B, and C are the ^1H nmr spectra of the products from the reaction of (η^6-chlorobenzene)(η^5-cyclopentadienyl)iron cation (**8**) with NaCN in DMF for 3 min, 30 min, and 3 h, respectively; A is an approximately 90:10 mixture of (1–5-η^5-1-chloro-*exo*-6-cvanocyclohexadienyl)(η^5-cyclopentadienyl)iron (**9**) and (1–5-η^5-1,*exo*-6-dicyanocyclohexadienyl)(η^5-cyclopentadienyl)iron (**10**), B is a mixture of about 40:60 of **9** and **10**, and C is pure **10**, which is also the product from the reaction of (η^6-benzonitrile)(η^5-cyclopentadienyl)iron cation (**11**) with NaCN in DMF.

7.27(2H,d,J=8.3,Ph)



8; X = Cl
11; X = CN

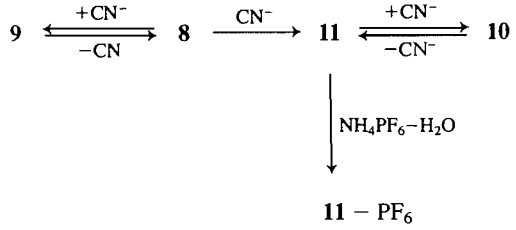
9; X = Cl
10; X = CN

tion of the (η^6-benzonitrile)(η^5-cyclopentadienyl)iron cation (**11**) with NaCN in DMF. Shown in Fig. 1 are the ^1H nmr spectra of these products obtained under the various reaction conditions.

When **8** was treated with NaCN in DMF for 3 h and then an aqueous solution of NH_4PF_6 was added and the mixture extracted with CH_2Cl_2–CH_3NO_2, the only product recovered was **11**, resulting from the substitution of the chloro group by the cyano group. Since cyanide adduct **10** was the sole product in the 3-h reaction when the reaction mixture was worked up without treatment with aqueous NH_4PF_6, **10** must have reverted back to **11** in the presence of aqueous NH_4PF_6. In our laboratory, we have found that CpFe complexes of cyclohexadienyl systems derived from nucleophilic additons could be readily reverted back to the complexed arenes under acidic conditions, and we have utilized the addition of the acetonyl anion to a complexed sulfone followed by acidification to regenerate the sulfone complex as a means for its purification (3). In the present reactions with chlorobenzene complex **8** to give substitution product **11**, the aqueous NH_4PF_6 solution added likely was sufficiently acidic to cause a ready reversal of adduct **10** to cationic complex **11**, which then gave rise to its hexaflurophosphate.

The present findings for the reactions of **8** with NaCN in DMF may, therefore, be summarized by Scheme 1. Initially, cationic complex **8** would undergo rapid and reversible cyanide addition to give **9**. Competing with the addition reaction would be a slower substitution reaction to give **11** and this substitution

Can. J. Chem. Downloaded from www.nrcresearchpress.com by 122.72.124.2 on 09/07/12
For personal use only.



SCHEME 1

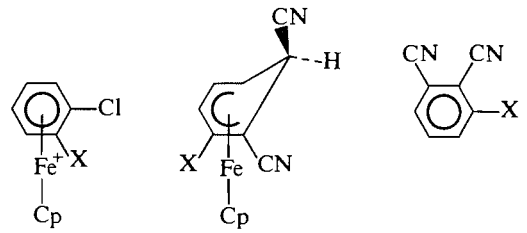
reaction would not be readily reversible. Complex **11**, once formed, would also undergo rapid and reversible cyanide addition to give **10**. Thus for a short reaction time of 3 min, the major product was **9**. As the reaction time was increased, more and more **10** would be formed. After a reaction time of 3 h, only **10** was obtained, except that if aqueous NH_4PF_6 was added, reversal of **10** and **11** would take place and **11** would then give rise to its hexafluorophosphate.

It is of interest to note from Scheme 1 that the reversal of cyanide adduct **9** to cationic complex **8**, which took place during the initial stages of these transformations, the reaction conditions were not acidic, while for the similar reversal of **10** to **11** the conditions were acidic. A factor that likely would enhance the ease of the conversion of **9** to **8** could be the competing irreversible reaction of **8** to give **11**, thus providing a driving force for the formation of **8** from **9**, while reversal of **10** to **11** did not result in a further reaction of **11** except for the formation of its hexafluorophosphate. Moreover, it is known that Meisenheimer-type of adducts of arenes are more stable and more readily formed for arenes containing more electron-withdrawing substituents (7). Possibly, adduct **10** derived from a complexed arene with a more electron-withdrawing cyano substituent would be more stable than adduct **9** derived from a complexed arene with a chloro substituent, and **10** would thus require more acidic conditions for its reversal to **11** than the reversal of **9** to **8**.

When the product mixture from the 3-min reaction, consisting of about 90% **9** and 10% **10**, was treated with DDQ, *o*-chlorobenzonitrile, derived from demetallation–oxidation of **9**, could be obtained. Similarly, DDQ treatment of pure **10** from the 3-h reaction between **8** and NaCN in DMF or from the direct cyanide addition to **11**, readily gave rise to phthalonitrile. Phthalonitrile is an important compound as it is utilized for the preparation of metal complexes known as phthalocyanines which have many commercial applications including their use as pigments and in dyestuffs (8). Phthalocyanines prepared from phthalonitriles with a substituent at the 3- or 4-position have been studied in order to ascertain the extent of changes in the properties of such substituted phthalocyanines, and it was concluded that a 3-substituted phthalonitrile would have a greater influence than a 4-substituted phthalonitrile on such properties as solubility, electronic absorption spectrum, and reactivity of the resulting phthalocyanine (9, 10). In the present work, a number of 3-substituted phthalonitriles have been prepared from the DDQ treatment of cyanide additon–substitution products.

It has already been stated that *o*-chlorotoluene complex **4** or *o*-cyanotoluene complex **5**, on reaction with NaCN in DMF, gave the same products consisting of a 96:4 mixture of cyclohexadienyl complexes **6** and **7** (6). DDQ treatment of this mixture of products gave rise to 3-methylphthalonitrile (**12**), a compound that has previously been prepared by Siegl and coworkers (11). It may be pointed out that the DDQ treatment gave only the arene derived from complex **6**, and no arene could be liberated from the minor product **7**, a cyclohexadienyl complex with two substituents at the 6-position.

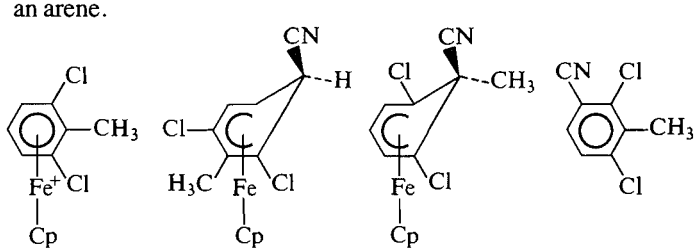
When the CpFe complex of *o*-methoxychlorobenzene (**13**) or *o*-phenoxychlorobenzene (**14**) (12) was treated with NaCN in DMF for 5 h and the reaction mixture worked up without any addition of aqueous NH_4PF_6, cyclohexadienyl complex **15** or **16**, respectively, was obtained, and these products were derived from both substitution and addition reactions with the cyanide ion. Upon treatment with DDQ, **15** or **16** readily gave rise to 3-methyoxyphthalonitrile (**17**) (10) or 3-phenoxyphthalonitrile (**18**) (9), respectively. Although **12**, **17**, and **18** have all been prepared previously (9–11), the present method provides an alternative approach to the synthesis of such 3-substituted phthalonitriles.



13; X = OCH_3 **15**; X = OCH_3 **12**; X = CH_3
14; X = OC_6H_5 **16**; X = OC_6H_5 **17**; X = OCH_3
19; X = Cl **18**; X = OC_6H_5

It is of interest to note that complexes of *o*-substituted chlorobenzenes, such as **13** and **14**, were prepared from the nucleophilic substitution of one of the two chloro groups of the CpFe complex of *o*-dichlorobenzene (**19**), and a variety of such mono-substitution products from **19** have been reported (12). Presumably, besides using **13** and **14**, if one were to start from the other *o*-substituted chlorobenzene complexes (12) and utilizing the substitution and addition reactions with the cyanide ion followed by demetallation–oxidation with DDQ, a general method for the synthesis of a variety of 3-substituted phthalonitriles may be feasible.

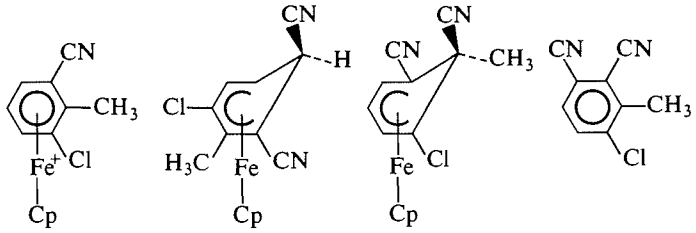
As another illustration of the addition and substitution reactions with the cyanide ion, when the (η^6-2,6-dichlorotoluene)(η^5-cyclopentadienyl)iron cation (**20**) was treated with NaCN in DMF for 15 min, a 66:33 mixture of adducts **21** and **22** were obtained. DDQ treatment of this product mixture gave a new compound, 2,4-dichloro-3-methylbenzonitrile (**23**), derived from demetallation–oxidation of **21**, while **22**, with two substituents at the 6-position, did not result in any liberation of an arene.



20 **21** **22** **23**

When **20** was treated with NaCN in DMF for 48 h and the reaction mixture worked up after the addition of an aqueous NH_4PF_6 solution, substitution product **24** was obtained and a subsequent reaction of **24** with NaCN in DMF gave a 55:45 mixture of adducts **25** and **26**. DDQ treatment of this mixture of products gave 4-chloro-3-methylphthalonitrile (**27**), a compound that has not been reported previously. Again it is seen that

Can. J. Chem. Downloaded from www.nrcresearchpress.com by 122.72.124.2 on 09/07/12
For personal use only.



24 25 26 27

no arene was liberated from **26**, a cyclohexadienyl complex with two substituents at the 6-position.

The above results from the reaction with **20** are entirely consistent with expectation. A short reaction time resulted in the addition of a cyanide ion *ortho* to a chloro group, giving rise to **21** and **22**. A longer reaction time with work-up in the presence of added aqueous NH_4PF_6 gave substitution product **24**, which in turn could undergo cyanide addition to give adducts **25** and **26**. It is of interest to note that even with an excess of the cyanide ion and a reaction time of 48 h, only one of the two chloro groups of **20** was replaced by a cyano group to give **24**. A possible explanation for the occurrence of only mono-substitution may be suggested by analogy to the processes given in Scheme 1 for the reactions with chlorobenzene complex **8**. In the reaction of **20** with the cyanide ion, before aqueous NH_4PF_6 was added in the work-up of the reaction mixture, formation of substitution product **24** would be followed by a rapid and irreversible addition of the cyanide ion to give **25** and **26**, and these adducts would not give rise to a further nucleophilic substitution reaction since these complexed cyclohexadienyl systems would be richer in electron density than the complexed cation **24**. In the presence of added aqueous NH_4PF_6, adducts **25** and **26** would readily revert back to **24**, resulting in the recovery of the mono-substituted product **24** as its hexafluorophosphate.

Experimental

*(1-5-η^5-1-*p*-Tolylsulfonyl-*exo*-6-cyanocyclohexadienyl)(η^5-cyclopentadienyl)iron (2)*

A mixture of 498 mg (1.0 mmol) of (η^6-*p*-tolylsulfonylbenzene)(η^5-cyclopentadienyl)iron hexafluorophosphate (**1**) (3) and 500 mg (10.2 mmol) of powdered NaCN in 5.0 mL of DMF was stirred at room temperature for 30 min. The reaction mixture was then filtered through a sintered glass filter and the filtrate added to 200 mL of ether. The resulting ether solution was thoroughly washed with H_2O (5 × 100 mL) to remove the DMF. After drying over $MgSO_4$, the ether was removed by a rotary evaporator. The residue was redissolved in ether, filtered, and the ether removed to give 276 mg (75%) of **2** as a red solid. Its ^1H and ^{13}C nmr data are given in Tables 1 and 2; ir ν_{CN}, 2215 cm^{-1}. For this and other compounds described in subsequent sections, the nmr and ir data, respectively, were obtained using a Bruker AM300 nmr spectrometer and a Perkin Elmer model 781 IR spectrometer. *Anal.* calcd. for $C_{19}H_{17}O_2NSFe$: C 60.16, H 4.49, N 3.69; found: C 60.05, H 4.64, N 3.49.

o-*p*-*Tolylsulfonylbenzonitrile (3)*

To a solution of 379 mg (1.0 mmol) of **2** in 10 mL of CH_3CN, 227 mg (1.0 mmol) of DDQ was added and the mixture was stirred at room temperature for 30 min. The resulting material was filtered through a sintered glass filter and the filtrate evaporated to dryness. The residue was redissolved in 5.0 mL of CH_2Cl_2 and the solution passed through a short (about 20 cm) alumina column with elution by CH_2Cl_2. Removal of the solvent from the eluate gave 154 mg (60%) of **3** as a colorless solid, mp 107–108°C; ^1H nmr ($CDCl_3$) δ: 2.42(3H, s, CH_3), 7.35(2H, d, J=8.3 Hz), 7.96(2H, d, J=8.3 Hz)(*p*-substituted Ph), 7.68–8.33 (4H, m, *o*-substituted Ph); ^{13}C nmr ($CDCl_3$) δ: 21.6(CH_3), 115.6(CN), 111.0)(quat-CN), 128.5(2C), 129.5, 129.6(2C), 133.1, 133.2, 136.4, 136.5(quat), 143.8(quat), 145.3(quat) (Ar); ir ν_{CN}, 2235 cm^{-1}. *Anal.* calcd. for $C_{14}H_{11}O_2NS$: C 65.37, H 4.28, N 5.45; found: C 65.57, H 4.20, N 5.52.

Reactions with the (η^6-chlorobenzene)(η^5-cyclopentadienyl)iron cation (8)

A mixture of 378 mg (1.0 mmol) of **8**, as its hexafluorophosphate, and 500 mg of powdered NaCN in 5.0 mL of DMF was stirred at room temperature for 3 min, 30 min, or 3 h and then worked up as described in the preparation of **2**. From the 3-min reaction, the yield of products was 40%, and the ^1H nmr spectrum showed these products to be an approximately 90:10 mixture of (1–5-η^5-1-chloro-*exo*-6-cyanocyclohexadienyl)(η^5-cyclopentadienyl)iron (**9**) and (1–5-η^5-1,*exo*-6-dicyanocyclohexadienyl)(η^5-cyclopentadienyl)iron (**10**). From the 30-min reaction, the yield of products was 48% and these products were also **9** and **10** in a ratio of about 40:60, while from the 3-h reaction, a 54% yield of pure **10** was obtained. The ^1H and ^{13}C nmr data for these products are given in Tables 1 and 2; ir ν_{CN}, 2208 and 2205 cm^{-1}, respectively, for **9** and **10**. *Anal.* calcd. for $C_{13}H_{10}N_2Fe$ (**10**): C 62.40, H 4.00, N 11.20; found: C 62.75, H 4.20, N 11.08.

In another experiment, 756 mg (2.0 mmol) of **8**, as its hexafluorophosphate, and 1.0 g of powdered NaCN in 10 mL of DMF was stirred at room temperature for 3 h. A solution of 1.0 g of NH_4PF_6 in 20 mL of H_2O was then added and the resulting material extracted with a 1:1 mixture of CH_2Cl_2–CH_3NO_2 (4 × 100 mL). The combined extract was washed with H_2O and dried over $MgSO_4$. After removal of the solvent, the residue was crystallized from acetone–ether to give 479 mg (65%) of the hexafluorophosphate salt of the (η^6-benzonitrile)(η^5-cyclopentadienyl)iron cation (**11**). Cation **11** has been prepared previously by Nesmeyanov and co-workers (13) from a ligand exchange reaction.

o-*Chlorobenzonitrile*

Treatment of 260 mg of the 90:10 mixture of **9** and **10** from the above 3-min reaction with DDQ as described in the preparation of **3** gave 60 mg (43%) of demetallation product which, after crystallization from ethanol–water, gave *o*-chlorobenzonitrile melting at 44–45°C (lit. (14), mp 45–46°C); ^1H nmr ($CDCl_3$) δ: 7.39–7.68(4H, m, Ar); ^{13}C nmr ($CDCl_3$) δ: 115.9(CN), 113.2(quat-CN), 127.1, 130.0, 133.8, 133.9, 136.7(quat) (Ar); ir ν_{CN}, 2218 cm^{-1}.

Phthalonitrile

The treatment of 1.0 mmol of **10** with DDQ as described in the preparation of **3** gave a 61% yield of phthalonitrile, mp 140–141°C (lit. (15), mp 141°C); ^1H nmr ($CDCl_3$) δ: 775–7.86(4H, m, Ar); ^{13}C nmr ($CDCl_3$) δ: 115.6(2C, CN), 115.3(2C, quat-CN), 133.2(2C), 133.5(2C) (Ar); ir ν_{CN}, 2230 cm^{-1}.

3-Methylphthalonitrile (12)

The DDQ treatment of the product mixture from the reaction of *o*-chlorotoluene complex **4** (6), a 96:4 mixture of (1–5-η-1,*exo*-6-dicyano-2-methylcyclohexadienyl)(η^5-cyclopentadienyl)iron (**6**) and (1–5-η^5-1,*exo*-6-dicyano-*endo*-6-methylcyclohexadienyl)(η^5-cyclopentadienyl)iron (**7**), gave a 69% yield of **12**, mp 142–143°C (lit. (11), mp 143°C); ^1H nmr ($CDCl_3$) δ: 2.64(3H, s, CH_3), 7.60–7.66(3H, m, Ar); ^{13}C nmr ($CDCl_3$) δ: 20.7(CH_3), 115.7, 115.9(CN), 114.6(quat-CN), 115.7(quat-CN), 130.9, 132.7, 134.5, 144.1(quat) (Ar); ir ν_{CN}, 2225 cm^{-1} (broad).

3-Methoxyphthalonitrile (17) and 3-phenoxyphthalonitrile (18)

A mixture of 204 mg (0.5 mmol) of the hexafluorophosphate of the (η^6-*o*-methoxylchlorobenzene)(η^5-cyclopentadienyl)iron cation (**13**) (12), or 235 mg (0.5 mmol) of the hexaflurophosphate of the (η^6-*o*-phenoxychlorobenzene)(η^5-cyclopentadienyl)iron cation (**14**) (12) and 500 mg of powdered NaCN in 5.0 mL of DMF was stirred at room temperature for 5 h and then worked up as described in the preparation of **2** to give a 55% yield of (1–5-η^5-1,*exo*-6-dicyano-2-methoxycyclohexadienyl)(η^5-cyclopentadienyl)iron (**15**) from **13** or a 50% yield of (1–5-η^5-1,*exo*-6-dicyano-2-phenoxycyclohexadienyl)(η^5-cyclopentadienyl)iron (**16**) from **14**. The ^1H and ^{13}C nmr data for these adducts are given in Tables 1 and 2.

Can. J. Chem. Downloaded from www.nrcresearchpress.com by 122.72.124.2 on 09/07/12
For personal use only.

Direct treatment of **15** from the above reaction with DDQ gave a 74% yield of 3-methoxyphthalonitrole (**17**), mp 182–183°C (lit. (10), mp 183–184°C; ^{1}H nmr ($CDCl_3$) δ: 4.00(3H, s, CH_3O), 7.25–7.66(3H, m, Ar); ^{13}C nmr ($CDCl_3$) δ: 56.7(CH_3O), 115.3, 117.0(CN), 106.0(quat-CN), 113.0(quat-CN), 115.9, 125.1, 134.6, 161.8(quat) (Ar); ir ν_{CN}, 2235 cm^{-1} (broad).

Similarly, a direct DDQ treatment of adduct **16** from the reaction with **14** gave a 68% yield of 3-phenoxyphthalonitrile (**18**), mp 110–111°C (lit. (9), mp 110–112°C); ^{1}H nmr ($CDCl_3$) δ: 7.05–7.60(8H, m, Ar); ^{13}C nmr ($CDCl_3$) δ: 115.1, 117.2(CN), 106.0(quat-CN), 112.7(quat-CN), 110.4, 120.4(2C), 126.2, 126.9, 130.5(2C), 134.4, 153.7(quat), 160.9(quat) (Ar); ir ν_{CN}, 2232 cm^{-1} (broad).

*(η^6-2,6-Dichlorotoluene)(η^5-cyclopentadienyl)iron cation (**20**)*

A ligand exchange reaction between ferrocene and 2,6-dichlorotoluene, carried out as described in a similar ligand exchange between ferrocene and *o*-chlorotoluene (16), gave a 35% yield of cation **20**, isolated as its hexafluorophosphate; ^{1}H nmr (acetone-d_6) δ: 2.89(3H, s, CH_3), 5.35(5H, s, Cp), 6.61(1H, t, J=6.2 Hz, H4), 6.84(2H, d, J=6.2 Hz, H3, 5); ^{13}C nmr (acetone-d_6) δ: 17.8(CH_3), 82.1(Cp), 87.2, 88.8(2C), 102.5(quat), 108.7(2C, quat) (Ar).

*(1-5-η^5-1,3-Dichloro-6-*exo*-cyano-2-methylcyclohexadienyl)(η^5-cyclopentadienyl)iron (**21**) and (1-5-η^5-1,5-dichloro-6-*exo*-cyano-6-*endo*-methylcyclohexadienyl)(η^5-cyclopentadienyl)iron (**22**)*

A mixture of 426 mg (1.0 mmol) of **20**, as its hexafluorophosphate, and 500 mg of powdered NaCN in 5.0 mL of DMF was stirred at room temperature for 15 min and then worked up as described in the preparation of **2** to give 217 mg (70%) of a 66:33 mixture of **21** and **22**. The ^{1}H and ^{13}C nmr data for these adducts are given in Tables 1 and 2. For this isomeric mixture, *anal.* calcd. for $C_{13}H_{11}NCl_2Fe$: C 50.81, H 3.58, N 4.56; found: C 50.51, H 3.78, N 4.62.

*2,4-Dichloro-3-methylbenzonitrile (**23**)*

DDQ treatment of the above mixture of **21** and **22** gave a 55% yield of **23**, mp 75–76°C; ^{1}H nmr ($CDCl_3$) δ: 2.53(3H, s, CH_3), 7.40(1H, d, J=8.4 Hz), 7.46(1H, d, J=8.4 Hz) (Ar); ^{13}C nmr, ($CDCl_3$) δ: 17.8(CH_3), 115.9(CN), 112.3(quat-CN), 128.2, 131.3, 136.6(quat), 137.8(quat), 140.5(quat) (Ar). *Anal.* calcd. for $C_8H_5NCl_2$: C 51.90, H 2.70, N 7.57; found: C 52.13, H 2.85, N 7.57.

*(η^6-3-Chloro-2-methylbenzonitrile)(η^5-cyclopentadienyl)iron cation (**24**)*

A solution of 856 mg (2.0 mmol) of **20**, as its hexafluorophosphate, in 10 mL of DMF was deaerated by bubbling N_2 through it for 20 min and then 1.0 g of powdered NaCN was added. The mixture was stirred at room temperature under N_2 for 48 h. A solution of 1.0 g of NH_4PF_6 in 20 mL of H_2O was then added and the resulting material was extracted with CH_3NO_2 (5 × 100 mL). The combined extract was washed with H_2O and dried over $MgSO_4$. After removal of the solvent by a rotary evaporator, the dark brown residue was treated again with 1.0 g of NH_4PF_6 in 20 mL of H_2O. The grayish yellow solid that resulted was collected by filtration, redissolved in CH_3NO_2, and dried over $MgSO_4$. After removal of the solvent, the product was recrystallized from acetone – methylene chloride – ether to give 460 mg (54%) of the hexafluorophosphate salt of **24** as a yellow powder; ^{1}H nmr (acetone-d_6) δ: 2.97(3H, s, CH_3), 5.56(5H, s, Cp), 6.88(1H, t, J=6.4 Hz), 7.02(1H, d, J=6.4 Hz), 7.16(1H, d, J=6.4 Hz) (Ar); ^{13}C nmr (acetone-d_6) δ: 18.8(CH_3), 82.8(Cp), 75.8(quat-CN), 88.5, 90.3, 91.3, 104.8(quat), 109.2(quat) (Ar), 115.9(CN). *Anal.* calcd. for $C_{13}H_{11}NClFePF_6$: C 37.41, H 2.64, N 3.46; found C 37.29, H 2.53, N 3.46.

*(1-5-η^5-3-Chloro-1,6-*exo*-dicyano-2-methylcyclohexadienyl)(η^5-cyclopentadienyl)iron (**25**) and (1-5-η^5-1-chloro-5,6-*exo*-dicyano-6-*endo*-methylcyclohexadienyl)(η^5-cyclopentadienyl)iron (**26**)*

A mixture of 417 mg (1.0 mmol) of the hexafluorophosphate of **24** and 500 mg of powdered NaCN in 5.0 mL of DMF was stirred at room temperature for 30 min and then worked up the usual way to give 238 mg (80%) of a 55:45 mixture of **25** and **26** as a red solid. The ^{1}H and ^{13}C nmr data for **25** and **26** are summarized in Tables 1 and 2. For this isomeric mixture, *anal.* calcd. for $C_{14}H_{11}N_2ClFe$: C 56.38, H 3.70, N 9.39; found: C 56.04, H 3.95, N 9.12.

*4-Chloro-3-methylphthalonitrile (**27**)*

DDQ treatment of the above mixture of **25** and **26** gave a 39% yield of **27**, mp 119–120°C; ^{1}H nmr ($CDCl_3$) δ: 2.68(3H, s, CH_3), 7.60(1H, d, J=8.3 Hz), 7.72(1H, d, J=8.3 Hz) (Ar); ^{13}C nmr ($CDCl_3$) δ: 19.1(CH_3), 115.1, 117.6(CN), 114.1(quat-CN), 114.5(quat-CN), 131.6, 133.7, 140.6(quat), 142.3(quat) (Ar); ir ν_{CN}, 2230 cm^{-1} (broad). *Anal.* calcd. for $C_9H_5N_2Cl$: C 61.36, H 2.84, N 15.90; found: C 61.53, H 2.84, N 15.97.

Acknowledgement

The financial support given by the Natural Sciences and Engineering Research Council of Canada is sincerely acknowledged.

1. R. G. SUTHERLAND, R. L. CHOWDHURY, A. PIÓRKO, and C. C. LEE. J. Organomet. Chem. **319**, 379 (1987).
2. R. G. SUTHERLAND, R. L. CHOWDHURY, A. PIÓRKO, and C. C. LEE. J. Org. Chem. **52**, 4618 (1987).
3. C. C. LEE, R. L. CHOWDHURY, A. PIÓRKO, and R. G. SUTHERLAND. J. Organomet. Chem. **310**, 391 (1986).
4. A. N. NESMEYANOV, N. A. VOL'KENAU, and I. N. BOLESOVA. Dokl. Akad. Nauk SSSR, **175**, 606 (1967).
5. E. I. SIROTKINA, A. N. NESMEYANOV, and N. A. VOL'KENAU. Izv. Akad. Nauk, SSSR, Ser. Khim. 1524 (1969).
6. C. H. ZHANG, R. L. CHOWDHURY, A. PIÓRKO, C. C. LEE, and R. G. SUTHERLAND. J. Organomet. Chem. **346**, 67 (1988).
7. P. BUCK. Angew. Chem. Internat. Edit. **8**, 120 (1969).
8. F. H. MOSER and W. H. RHODES. *In* Kirk–Othmer encyclopedia of chemical technology. Vol. 17. 3rd ed. John Wiley and Sons, New York. 1982. pp. 777–787.
9. V. M. DERKACHEVA and E. A. LUK'YANETS. Zh. Obsh. Khim. **50**, 2313 (1980).
10. V. M. DERKACHEVA, S. S. IODKO, O. L. KALIYA, and E. A. LUK'YANETS. Zh. Obsh. Khim. **51**, 2319 (1981).
11. W. O. SIEGL, F. C. FERRIS, and P. A. MUCCI. J. Org. Chem. **42**, 3442 (1977).
12. C. C. LEE, A. S. ABD-EL-AZIZ, R. L. CHOWDHURY, U. S. GILL, A. PIÓRKO, and R. G. SUTHERLAND. J. Organomet. Chem. **315**, 79 (1986).
13. A. N. NESMEYANOV, N. A. VOL'KENAU, and L. S. SHILOVTSEVA. Dokl. Akad. Nauk SSSR. **160**, 1327 (1965).
14. A. SAEDNYA. Synthesis, 184 (1985).
15. Dictionary of organic compounds. Vol. 1. 5th ed. Chapman and Hall, London. 1982. p. 532.
16. I. U. KHAND, P. L. PAUSON, and W. E. WATTS. J. Chem. Soc. (C), 2261 (1968).

Can. J. Chem. Downloaded from www.nrcresearchpress.com by 122.72.124.2 on 09/07/12
For personal use only.

The preparation and crystal structure of tetrakis(phenylmethoxy)methane

DARIN R. LATIMER, JOHN A. WEIL, AND J. WILSON QUAIL
Department of Chemistry, University of Saskatchewan, Saskatoon, Sask., Canada S7N 0W0

AND

WARD T. ROBINSON
Department of Chemistry, University of Canterbury, Christchurch, New Zealand

Received May 17, 1988

DARIN R. LATIMER, JOHN A. WEIL, J. WILSON QUAIL, and WARD T. ROBINSON. Can. J. Chem. **67**, 143 (1989).

The new compound tetrakis(phenylmethoxy)methane (also known as benzyl orthocarbonate) has been produced by the action of the sodium salt of benzyl alcohol on trichloronitromethane (chloropicrin), resulting in a white crystalline solid with a melting range of 68–70°C. The crystal structure has been determined at 153(5) K: triclinic, $P\bar{1}$, a = 10.161(4) Å, b = 12.664(4) Å, c = 20.472(5) Å, α = 71.78(2)°, β = 82.30(3)°, γ = 71.92(2)°. The results show the symmetry at each central carbon to be approximately S_4, with average C—O bond lengths of 1.397(4) Å, O—C—O angles ranging between 113–114° and 107–108°, and C—O—C angles of 115(1)°. Additional evidence for this structure is given by nuclear magnetic resonance, infrared and mass spectra.

Key words: benzyl orthocarbonate, orthocarbonate, tetrakis(phenylmethoxy)methane.

DARIN R. LATIMER, JOHN A. WEIL, J. WILSON QUAIL et WARD T. ROBINSON. Can. J. Chem. **67**, 143 (1989).

En faisant réagir le sel de sodium de l'alcool benzylique sur le trichloronitrométhane, on a obtenu le tétrakis(phénylméthoxy)méthane qui est aussi connu sous le nom d'orthocarbonate de benzyle); ce nouveau produit se présente sous la forme d'une poudre cristalline blanche, de point de fusion 68–70°C. On a déterminé sa structure cristalline à 153(5) K : les cristaux sont tricliniques, $P\bar{1}$, a = 10,161(4), b = 12,664(4) et c = 20,472 Å, α = 71,78(2), β = 82,30(3) et γ = 71,92(2)°. Les résultats montrent que la symétrie de chacun des atomes centraux est approximativement S_4, avec des longueurs de liaisons C—O de 1,397(4) Å, des angles O—C—O allant de 113–114° à 107–108° et des angles C—O—C de 115(1)°. On a obtenu des données additionnelles relatives à cette structure en faisant appel à la rmn et aux spectroscopies ir et de masse.

Mots clés : orthocarbonate de benzyle, orthocarbonate, tétrakis(phénylméthoxy)méthane.

[Traduit par la revue]

Introduction

Several aliphatic orthocarbonates have been produced, via various methods (1–3), since the synthesis of the first such compound reported by Bassett in 1864 (4). The method employed here for the production of tetrakis(phenylmethoxy)methane, **I** (also known as benzyl orthocarbonate), is analogous to that used by Bassett, and later extended by Tieckelmann and Post (3), to produce several low-molar-mass aliphatic orthocarbonates.

The new compound was produced in the hope that the central carbon atom might be close to tetrahedrally bonded to four oxygen atoms (as indeed is the case) so that the molecule could be used to model the site in which (hypothetically) a carbon atom might occur substitutionally for silicon in minerals, such as the α-quartz structure.

Most of the known aliphatic orthocarbonates are not solid at room temperature and thus are not suitable for the determination of bond lengths and angles by X-ray diffraction. It was deemed necessary to synthesize an orthocarbonate with substituents sufficiently massive for the compound to be a solid at room temperature. In fact, several known aryl orthocarbonates are solids at room temperature (5–8), but are not desirable for our purposes. Compound **I** was selected because the benzyl substituent was deemed sufficiently large for the compound to be a solid at room temperature. A recent publication (9) has predicted, via Hartree–Fock SCF-MO calculations, that the local symmetry of the central carbon in orthocarbonate molecules should be S_4, which is now found by X-ray analysis to be approximately true for **I** in the condensed phase.

Experimental

Benzyl alkoxide was prepared by reacting freshly-cut sodium metal with benzyl alcohol (BDH reagent grade, distilled and dried over calcium hydride) until the yellow mixture of benzyl alcohol and benzyl alkoxide became so viscous that it could no longer be stirred by a magnetic stirrer. Compound **I** was then produced by heating the mixture to approximately 40°C and very carefully adding trichloronitromethane (chloropicrin), commercially available from Pfaltz and Bauer, while maintaining the temperature in the 40–60°C range. Tieckelmann and Post (3), for the aliphatic orthocarbonates which they were synthesizing, report that temperatures any lower than this allow the accumulation of chloropicrin with an explosive reaction following eventually, while higher temperatures cause the yield to be lowered. Indeed, in our work, rapid addition of the chloropicrin to the benzyl alkoxide reaction mixture caused the temperature to increase drastically.

Compound **I** was extracted into the carbon tetrachloride layer from water/carbon tetrachloride and allowed to crystallize. The crystals of **I** formed in an unknown viscous yellow oil. They were physically separated from the oil, and then recrystallized twice from 95% ethanol. The resulting white crystals were dried under vacuum over phosphorus pentoxide for a day and when removed had a melting range of 68–70°C.

In an attempt to prevent formation of the yellow oil in the reaction mixture, a different technique to isolate the orthocarbonate was tried. Here, after the reaction of the alkoxide with chloropicrin was complete, the reaction mixture was steam-distilled, with a white substance coming over. The orthocarbonate was again extracted from the contents of the reaction flask, however with decreased yield. Again the yellow oil was present, although in a lesser amount. Thus the value of the modified procedure is questionable.

Compound **I** is very soluble in carbon tetrachloride, less soluble in ethanol, diethyl ether, chloroform, and methanol, and insoluble in water.

Crystals of **I** for X-ray analysis were grown by slow evaporation of solvent from a solution in methanol and diethyl ether. The crystals were found to deteriorate within hours in an X-ray beam at room temperature. At 153 K, no measurable deterioration was observed.

Can. J. Chem. Downloaded from www.nrcresearchpress.com by 122.72.124.2 on 09/07/12
For personal use only.

Can. J. Chem. Downloaded from www.nrcresearchpress.com by 122.72.124.2 on 09/07/12
For personal use only.

TABLE 1. Fractional coordinates and average thermal parameters for molecules A and B of **I** (estimated standard deviation of the last digit is given in parentheses; U_{eq} = (Trace U)/3 where matrix **U** is expressed in the Cartesian crystal basis

Atom	x/a	y/b	z/c	$10^3\ U_{eq}$
C(A)	0.5217(3)	0.9419(2)	0.2619(1)	28
O(1)	0.6102(2)	0.8305(1)	0.2856(1)	24
C(1)	0.7480(3)	0.8252(2)	0.2994(1)	30
C(11)	0.8056(3)	0.6227(2)	0.2892(1)	28
C(12)	0.8878(3)	0.5085(2)	0.3050(1)	34
C(13)	0.9987(3)	0.4717(3)	0.3476(2)	35
C(14)	1.0283(3)	0.5489(3)	0.3739(2)	37
C(15)	0.9454(3)	0.6632(3)	0.3586(1)	34
C(16)	0.8329(3)	0.7006(2)	0.3164(1)	25
O(2)	0.3968(2)	0.9316(2)	0.2472(1)	26
C(2)	0.4097(3)	0.8704(2)	0.1964(1)	31
C(21)	0.1817(3)	0.9877(2)	0.1438(1)	33
C(22)	0.0486(3)	0.9982(3)	0.1282(2)	39
C(23)	−0.0009(3)	0.9016(3)	0.1483(2)	44
C(24)	0.0827(3)	0.7961(3)	0.1846(1)	40
C(25)	0.2159(3)	0.7855(2)	0.2001(1)	31
C(26)	0.2661(3)	0.8810(2)	0.1799(1)	28
O(3)	0.5877(2)	1.0017(1)	0.2048(1)	24
C(3)	0.5081(3)	1.1182(2)	0.1703(1)	30
C(31)	0.6644(3)	1.0989(2)	0.0656(1)	34
C(32)	0.7481(3)	1.1403(3)	0.0106(1)	38
C(33)	0.7692(3)	1.2458(3)	0.0003(1)	43
C(34)	0.7066(4)	1.3102(3)	0.0449(2)	68
C(35)	0.6210(4)	1.2685(3)	0.1002(2)	55
C(36)	0.5995(3)	1.1626(2)	0.1104(1)	25
O(4)	0.4923(2)	1.0033(1)	0.3105(1)	27
C(4)	0.4403(3)	0.9450(2)	0.3763(1)	29
C(41)	0.3275(3)	0.9920(2)	0.4835(1)	36
C(42)	0.2642(3)	1.0687(3)	0.5214(1)	48
C(43)	0.2491(3)	1.1859(3)	0.4932(2)	44
C(44)	0.2948(3)	1.2267(2)	0.4254(2)	36
C(45)	0.3547(3)	1.1497(2)	0.3866(1)	28
C(46)	0.3733(3)	1.0315(2)	0.4154(1)	26
C(B)	0.5106(3)	0.4463(2)	0.2519(1)	31
O(5)	0.4319(2)	0.3984(2)	0.2241(1)	27
C(5)	0.2905(3)	0.4684(3)	0.2107(2)	40
C(51)	0.1562(3)	0.3307(3)	0.2134(1)	35
C(52)	0.0890(3)	0.2835(3)	0.1801(2)	47
C(53)	0.0915(3)	0.3141(3)	0.1092(2)	51
C(54)	0.1612(4)	0.3909(3)	0.0720(2)	54
C(55)	0.2283(3)	0.4398(3)	0.1044(2)	45
C(56)	0.2247(3)	0.4103(2)	0.1760(1)	29
O(6)	0.6401(2)	0.3658(2)	0.2663(1)	29
C(6)	0.6361(3)	0.2513(3)	0.3101(2)	38
C(61)	0.8592(3)	0.1927(3)	0.3690(2)	46
C(62)	0.9935(4)	0.1242(3)	0.3810(2)	61
C(63)	1.0505(3)	0.0392(3)	0.3481(2)	54
C(64)	0.9754(3)	0.0229(3)	0.3038(2)	46
C(65)	0.8409(3)	0.0929(3)	0.2906(1)	38
C(66)	0.7817(3)	0.1784(2)	0.3230(1)	29
O(7)	0.4356(2)	0.4738(2)	0.3094(1)	31
C(7)	0.5050(3)	0.5199(3)	0.3472(2)	44
C(71)	0.3263(3)	0.6691(3)	0.3924(1)	45
C(72)	0.2268(4)	0.7030(3)	0.4414(2)	58
C(73)	0.2044(4)	0.6209(3)	0.5006(2)	58
C(74)	0.2795(3)	0.5060(3)	0.5116(1)	49
C(75)	0.3784(3)	0.4731(3)	0.4625(2)	40
C(76)	0.4019(3)	0.5543(3)	0.4019(1)	35
O(8)	0.5332(2)	0.5477(2)	0.2063(1)	30
C(8)	0.5970(3)	0.5337(3)	0.1404(1)	46
C(81)	0.8060(3)	0.6049(3)	0.1204(1)	38
C(82)	0.8731(3)	0.6885(3)	0.0898(2)	54
C(83)	0.8058(4)	0.7924(3)	0.0464(2)	62
C(84)	0.6690(4)	0.8144(3)	0.0328(2)	50
C(85)	0.5992(3)	0.7306(3)	0.0642(2)	39
C(86)	0.6688(3)	0.6258(2)	0.1081(1)	30

The crystal data and X-ray diffraction conditions are as follows: $C_{29}H_{28}O_4$ molar mass = 440.57 g mol^{-1} Triclinic, $P\bar{1}$, a = 10.161(4) Å, b = 12.664(4) Å, c = 20.472(5) Å, α = 71.78(2)°, β = 82.30(3)°, γ = 71.92(2)°, V = 2376.7 Å^3, Z = 4, ρ_0 = 1.18 g cm^{-3} (298 K), ρ_c = 1.231 g cm^{-3} (153 K), $F(000)$ = 936 e, Mo K_α radiation (λ = 0.71069 Å), μ = 0.85 cm^{-1}, $(\sin\theta/\lambda)_{max}$ = 0.6278 Å^{-1}, crystal dimensions 0.34 × 0.50 × 0.52 (mm), no decay correction, temperature = 153(5) K.

Quantitative data collection was carried out with a single crystal on a Nicolet $R3m$ four-circle diffractometer using graphite-monochromated Mo K_α radiation; cell dimensions derived by least-squares calculations from angular settings of 25 reflections measured at $5 < 2\theta < 35°$; $\omega/2\theta$ scan mode. A total of 9911 reflections were collected to 2θ = 53°. A total of 7523 unique reflections (out of 9911) yielded values of the intensity $I > 2\sigma(I)$. Lorentz and polarization corrections were applied. Intensities of three standard reflections were monitored after every 97 reflections throughout the data collection. The average deviation of each standard reflection was less than 1%. Low temperature system: Nicolet LT-1 modified locally. No absorption correction was applied. Observed weights for the reflections were taken to be $[\sigma(F)]^{-2}$.

X-ray diffraction data collected on the orthocarbonate crystal were processed and the structure solved, in space group $P\bar{1}$, assuming two molecules per asymmetric unit, using a MSDOS version of SHELXS-86 (10). The structure was refined using the XTAL System (11) of Crystallographic Programs on a DEC Vax 8650 computer.

The positions of 65 of the 66 non-hydrogen atoms were determined from a calculated E map. The remaining non-hydrogen atom was found by use of a difference Fourier map. Least-squares isotropic refinement gave an R value of 0.078, using rigid C_6H_5 units with hydrogens at calculated positions. Anisotropic least-squares refinement of the non-hydrogens H atoms placed at fixed distance (1.00 Å) from C atoms; their isotropic temperature factors were assigned the final equivalent temperature factors of the attached carbons. Final R was 0.084, $R = (\Sigma||F_o| - |F_c||)/\Sigma|F_o|$. The R_w value was 0.053, $R_w = (\Sigma w\Delta F^2/\Sigma wF_o^2)^{1/2}$. The quantity minimized in refinement was $\Sigma w\Delta F^2$. The number of parameters refined was 596. The largest and average shift/error ratios were 0.336 and 0.012, respectively, in the final cycle. The value of the goodness-of-fit was 2.406. The largest residual peaks and holes on a difference Fourier synthesis were 0.51 and −0.62 e Å^{-3}, respectively. The peaks on the difference Fourier synthesis could be matched to most of the atoms of slightly disordered molecules of **I**. A stereo ORTEP (12) representation of an asymmetric unit of the orthocarbonate is shown in Fig. 1 and all final atomic coordinates[1] are given in Table 1.

Nuclear magnetic resonance (^{1}H and ^{13}C) spectra of **I** were run on a Bruker AM300 spectrometer at 25°C, with the orthocarbonate dissolved in deuterated chloroform containing approximately 1% TMS (Silanor C). All chemical shifts reported are with respect to TMS.

In the ^{1}H spectrum, the aromatic protons resonate in the region 7.33–7.35 ppm, and the aliphatic protons exhibit a single peak at

[1]Tables of observed and calculated structure factors and anisotropic thermal parameters are available as supplementary material. Complete sets of data may be purchased from the Depository of Unpublished Data, CISTI, National Research Council of Canada, Ottawa, Ont., Canada K1A 0S2.

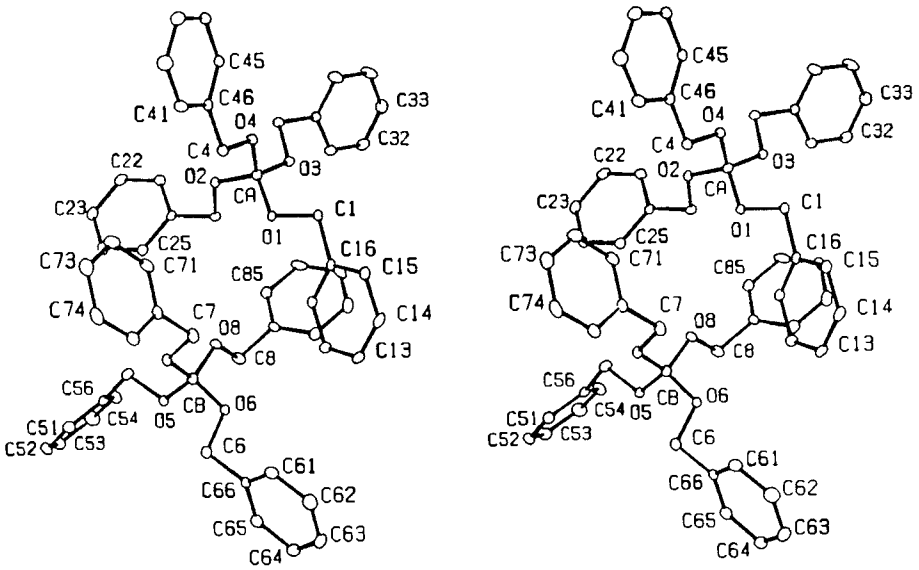


FIG. 1. Stereo ORTEP representation of an asymmetric unit of tetrakis(phenylmethoxy)methane. The plane of the figure is very close to being normal to the S_4 axis of the upper molecule (A).

TABLE 2. Selected bond angles for molecule A of **I** (degrees; estimated standard deviation of the last digit is given in parentheses)

Bond system	Angle	Bond system	Angle
O(1)—C(A)—O(3)	107.4(2)	C(2)—C(26)—C(21)	120.1(2)
O(1)—C(A)—O(2)	107.7(2)	C(2)—C(26)—C(25)	120.7(2)
O(1)—C(A)—O(3)	107.5(1)	C(21)—C(26)—C(25)	119.2(2)
O(1)—C(A)—O(4)	112.9(2)	C(A)—O(3)—C(3)	115.8(1)
O(2)—C(A)—O(3)	113.5(2)	O(3)—C(3)—C(36)	105.5(2)
O(2)—C(A)—O(4)	107.6(2)	C(32)—C(31)—C(36)	121.4(3)
O(3)—C(A)—O(4)	107.8(2)	C(31)—C(32)—C(33)	120.0(2)
C(A)—O(1)—C(1)	115.0(2)	C(32)—C(33)—C(34)	119.4(2)
O(1)—C(1)—C(16)	107.8(2)	C(33)—C(34)—C(35)	120.4(3)
C(12)—C(11)—C(16)	120.0(2)	C(34)—C(35)—C(36)	120.2(3)
C(11)—C(12)—C(13)	120.5(3)	C(3)—C(36)—C(31)	121.7(2)
C(12)—C(13)—C(14)	120.0(2)	C(3)—C(36)—C(35)	119.8(2)
C(13)—C(14)—C(15)	119.7(2)	C(31)—C(36)—C(35)	118.5(2)
C(14)—C(15)—C(16)	120.7(3)	C(A)—O(4)—C(4)	114.7(2)
C(1)—C(16)—C(11)	121.5(2)	O(4)—C(4)—C(46)	109.1(2)
C(1)—C(16)—C(15)	119.3(3)	C(42)—C(41)—C(46)	120.9(2)
C(11)—C(16)—C(15)	119.1(2)	C(41)—C(42)—C(43)	120.4(2)
C(A)—O(2)—C(2)	114.4(2)	C(42)—C(43)—C(44)	119.4(3)
O(2)—C(2)—C(26)	107.4(2)	C(43)—C(44)—C(45)	120.0(2)
C(22)—C(21)—C(26)	120.4(3)	C(44)—C(45)—C(46)	120.7(2)
C(21)—C(22)—C(23)	120.1(2)	C(4)—C(46)—C(41)	118.9(2)
C(22)—C(23)—C(24)	119.3(3)	C(4)—C(46)—C(45)	122.7(2)
C(23)—C(24)—C(25)	120.7(3)	C(41)—C(46)—C(45)	118.5(2)
C(24)—C(25)—C(26)	120.3(2)		

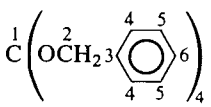


FIG. 2. Numbering scheme for ^{13}C NMR assignments.

4.80 ppm. A peak corresponding to the proton of chloroform is found at 7.25 ppm; this caused the ratio of the integral of aromatic protons to that of aliphatic protons to be 5.14:2 rather than the expected ratio of 5:2.

The peaks in the ^{13}C spectrum are assigned by comparison to an analogous compound, ethyl phenylacetate (13). Considering the numbering scheme in Fig. 2, the observed resonances in ppm, relative to TMS, of **I** carbon nuclei are: *1*, 120.29; *2*, 65.75; *3*, 137.85; *4*, 128.32; *5*, 127.59; *6*, 127.49.

Infrared spectra of **I** (in carbon tetrachloride) and of benzyl alcohol were run in the 4000–600 cm^{-1} region. No OH stretch peak of the alcohol was present in the orthocarbonate spectrum. The absorption in the 1150–1020 cm^{-1} region of the orthocarbonate spectrum, attributed to the C—O— stretches, becomes much more intense for the orthocarbonate than for the alcohol. This is consistent with the presence of C—O—C bonds (two unresolved C—O— stretches) replacing the C—O— stretch of the corresponding alcohol, resulting in a higher intensity due to the greater number of absorbers.

Mass spectra of **I** were obtained and both the 70 eV electron impact

Can. J. Chem. Downloaded from www.nrcresearchpress.com by 122.72.124.2 on 09/07/12
For personal use only.

TABLE 3. Selected bond angles for molecule B of **I** (degrees; estimated standard deviation of the last digit is given in parentheses)

Bond system	Angle	Bond system	Angle
O(5)—C(B)—O(6)	108.0(2)	C(6)—C(66)—C(61)	120.8(2)
O(5)—C(B)—O(7)	106.9(2)	C(6)—C(66)—C(65)	120.2(3)
O(5)—C(B)—O(8)	112.9(2)	C(61)—C(66)—C(65)	118.9(2)
O(6)—C(B)—O(7)	114.1(2)	C(B)—O(7)—C(7)	114.7(2)
O(6)—C(B)—O(8)	107.0(2)	O(7)—C(7)—C(76)	105.8(2)
O(7)—C(B)—O(8)	108.0(2)	C(72)—C(71)—C(76)	121.3(2)
C(B)—O(5)—C(5)	114.8(2)	C(71)—C(72)—C(73)	119.3(2)
O(5)—C(5)—C(56)	108.1(2)	C(72)—C(73)—C(74)	120.5(2)
C(52)—C(51)—C(56)	120.3(2)	C(73)—C(74)—C(75)	119.8(2)
C(51)—C(52)—C(53)	120.5(3)	C(74)—C(75)—C(76)	120.8(2)
C(52)—C(53)—C(54)	119.4(3)	C(7)—C(76)—C(71)	120.1(2)
C(53)—C(54)—C(55)	120.9(3)	C(7)—C(76)—C(75)	121.6(2)
C(54)—C(55)—C(56)	119.9(3)	C(71)—C(76)—C(75)	118.3(2)
C(5)—C(56)—C(51)	121.3(2)	C(B)—O(8)—C(8)	113.6(2)
C(5)—C(56)—C(55)	119.8(2)	O(8)—C(8)—C(86)	108.9(2)
C(51)—C(56)—C(55)	118.9(3)	C(82)—C(81)—C(86)	120.3(2)
C(B)—O(6)—C(6)	114.6(2)	C(81)—C(82)—C(83)	120.7(3)
O(6)—C(6)—C(66)	107.6(2)	C(82)—C(83)—C(84)	119.9(3)
C(62)—C(61)—C(66)	120.4(3)	C(83)—C(84)—C(85)	119.9(2)
C(61)—C(62)—C(63)	119.7(3)	C(84)—C(85)—C(86)	119.5(3)
C(62)—C(63)—C(64)	120.6(2)	C(8)—C(86)—C(81)	120.0(2)
C(63)—C(64)—C(65)	120.0(3)	C(8)—C(86)—C(85)	120.2(2)
C(64)—C(65)—C(66)	120.4(3)	C(81)—C(86)—C(85)	119.7(2)

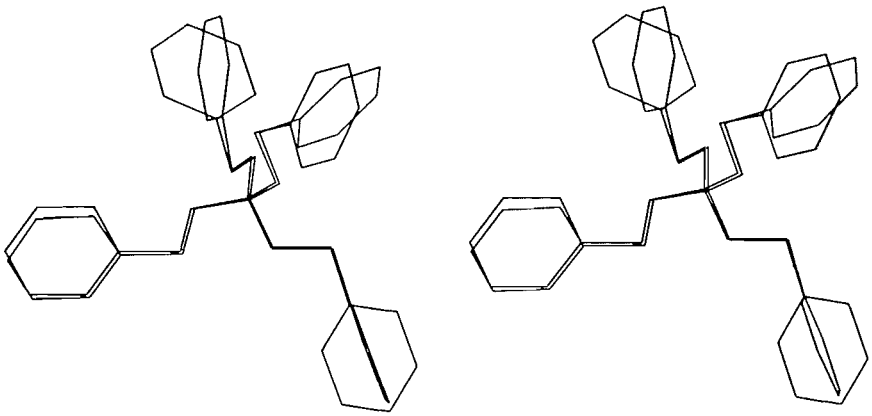


FIG. 3. Stereo view of the mapping of molecule A onto molecule B.

and the isobutane chemical ionization spectrum show the largest mass-to-charge ratio to be at $m/z = 333$. This ratio likely corresponds to the [tris(phenylmethoxy)methane]$^+$ cation; the parent ion could not be observed.

Chemical analysis for carbon and hydrogen found C 79.08%, H 6.37%, O 14.55% (by difference) which agreed very well with those expected: C 79.07%, H 6.40%, O 14.53%.

Results and discussion

Turning to the crystal structure, we note that the two molecules, A and B, of **I** in the asymmetric unit are not related by any element of symmetry. The bond angles around the central carbon atoms (Tables 2 and 3) show that there is appreciable distortion from tetrahedral symmetry at the central carbon atom in A and in B. Using an IRIS 3030 Graphics System and the program MMS (14), it was possible to superimpose molecule B onto molecule A (Fig. 3). To construct Fig. 3 the top molecule in Fig. 1 (molecule A) was held rigid. Atom C(B) was superimposed on C(A) and various orientations of molecule B were tested. In the superposition, O5 maps to O1, O2 to O6, O7 to O3, and O8 maps to O4. The configurations of the two molecules match remarkably closely. Only the rotations of the phenyl rings around their *para* axes are different. The symmetry at each central carbon is very close to S_4, with a compression along the S_4 axis, giving two O—C—O bond angles of 113–114° and the remaining four bond angles at 107–108°. This geometry is remarkably similar to the S_4 geometry predicted by *ab initio* calculations for tetramethoxymethane (9), including the actual values (112.4 and 108.0°, respectively) of the bond angles. The observed bond lengths, (1.40 Å) shown in Table 4, of the central carbon–oxygen bonds are very similar to the values (1.396 Å) found by electron diffraction reported by Mijlhoff *et al.* (15) in tetramethoxymethane, but the oxygen–carbon (peripheral) bonds are somewhat longer (0.02 Å).

We can compare the central skeleton of **I** with the silicon site

Can. J. Chem. Downloaded from www.nrcresearchpress.com by 122.72.124.2 on 09/07/12
For personal use only.

TABLE 4. Selected bond distances for molecules A and B of **I** (Å; estimated standard deviation of the last digit is given in parentheses)

Bond	Distance	Bond	Distance
C(A)—O(1)	1.392(2)	C(B)—O(5)	1.403(4)
C(A)—O(2)	1.396(3)	C(B)—O(6)	1.394(3)
C(A)—O(3)	1.394(3)	C(B)—O(7)	1.393(3)
C(A)—O(4)	1.393(3)	C(B)—O(8)	1.396(3)
O(1)—C(1)	1.442(3)	O(5)—C(5)	1.445(3)
C(1)—C(16)	1.499(3)	C(5)—C(56)	1.501(5)
C(11)—C(12)	1.388(3)	C(51)—C(52)	1.387(5)
C(11)—C(16)	1.386(5)	C(51)—C(56)	1.377(4)
C(12)—C(13)	1.389(4)	C(52)—C(53)	1.378(4)
C(13)—C(14)	1.375(5)	C(53)—C(54)	1.358(5)
C(14)—C(15)	1.391(3)	C(54)—C(55)	1.389(6)
C(15)—C(16)	1.395(4)	C(55)—C(56)	1.393(4)
O(2)—C(2)	1.451(4)	O(6)—C(6)	1.457(3)
C(2)—C(26)	1.497(4)	C(6)—C(66)	1.488(3)
C(21)—C(22)	1.387(4)	C(61)—C(62)	1.378(4)
C(21)—C(26)	1.391(3)	C(61)—C(66)	1.391(5)
C(22)—C(23)	1.389(5)	C(62)—C(63)	1.381(5)
C(23)—C(24)	1.379(3)	C(63)—C(64)	1.361(5)
C(24)—C(25)	1.388(4)	C(64)—C(65)	1.387(4)
C(25)—C(26)	1.381(4)	C(65)—C(66)	1.383(4)
O(3)—C(3)	1.446(2)	O(7)—C(7)	1.456(4)
C(3)—C(36)	1.505(3)	C(7)—C(76)	1.500(4)
C(31)—C(32)	1.384(4)	C(71)—C(72)	1.393(4)
C(31)—C(36)	1.378(4)	C(71)—C(76)	1.382(4)
C(32)—C(33)	1.366(5)	C(72)—C(73)	1.374(4)
C(33)—C(34)	1.376(5)	C(73)—C(74)	1.379(4)
C(34)—C(35)	1.401(4)	C(74)—C(75)	1.388(4)
C(35)—C(36)	1.372(5)	C(75)—C(76)	1.389(3)
O(4)—C(4)	1.439(3)	O(8)—C(8)	1.455(3)
C(4)—C(46)	1.497(4)	C(8)—C(86)	1.499(4)
C(41)—C(42)	1.382(4)	C(81)—C(82)	1.378(5)
C(41)—C(46)	1.395(3)	C(81)—C(86)	1.378(4)
C(42)—C(43)	1.380(4)	C(82)—C(83)	1.365(4)
C(43)—C(44)	1.391(4)	C(83)—C(84)	1.378(5)
C(44)—C(45)	1.392(4)	C(84)—C(85)	1.401(5)
C(45)—C(46)	1.388(3)	C(85)—C(86)	1.382(3)

in crystalline quartz, which has four oxygen nearest neighbors in a quasi-tetrahedral configuration, with only C_2 symmetry. The central C—O bond length in the orthocarbonate is 1.40 Å, as compared to 1.61 Å for Si—O in α-quartz. (The C—O—CH_2 angles are 115°, as compared to 143° for Si—O—Si in α-quartz.) When considering a large number of silicates, relatively constant Si—O bond lengths (1.62 ± 0.04 Å) but various Si—O—Si angles (145 ± 35°) are found; it is likely that Si...Si interactions are of importance in the silicates (16). Our results suggest that the carbon atom is too small to fit substitutionally into the silicate structure. This is consistent with the absence in the literature of reports of occurrence of carbon at silicon sites in minerals (17).

Acknowledgement

This work was sponsored in part by the Natural Sciences and Engineering Research Council of Canada.

1. S. SAKAI, Y. KOBAYASHI, and Y. ISHII. J. Org. Chem. **36**, 1176 (1971).
2. S. SAKAI, Y. KURODA, and Y. ISHII. J. Org. Chem. **37**, 4198 (1972).
3. H. TIECKELMANN and H. W. POST. J. Org. Chem. **13**, 265 (1948).
4. H. BASSETT. Ann. Chem. Liebig's, **132**, 54 (1864).
5. N. NARASIMHAMURTHY and A. G. SAMUELSON. Tetrahedron Lett. **27**, 991 (1986).
6. T. H. CHAN, J. F. HARROD, and P. VAN GHELUWE. Tetrahedron Lett. **49–50**, 4409 (1974).
7. J. F. HARROD and P. VAN GHELUWE. Proc. Int. Conf. Coord. Chem. 16th, R85 (1974).
8. J. F. HARROD and P. VAN GHELUWE. Can. J. Chem. **57**, 890 (1979).
9. R. J. MCEACHERN, J. A. WEIL, and P. G. MEZEY. Can. J. Chem. **66**, 2041 (1988).
10. G. M. SHELDRICK. SHELXS-86. Cyrstallographic Computing **3**, Oxford University Press. 1985. pp. 175–189.
11. S. R. HALL and J. M. STEWART (*Editors*). XTAL2.4 User's Manual. Universities of Western Australia and Maryland. 1988.
12. C. K. JOHNSON. ORTEP. II. Report ORNL-5138. Oak Ridge National Laboratory, TN. USA. 1976.
13. D. L. PAVIA, G. M. LAMPMAN, and G. S. KRIZ, JR. Introduction to spectroscopy. Saunders, Philadelphia, PA, USA. 1979.
14. S. DEMPSEY. MMS: The UCSD molecular modelling system. Department of Chemistry, University of California, San Diego, CA, USA. 1986.
15. F. C. MIJLHOFF, H. J. GEISE, and E. V. M. VAN SCHAICK. J. Mol. Struct. **20**, 393 (1973).
16. M. O'KEEFE and B. G. HYDE. Acta Crystallogr. B**34**, 27 (1978).
17. P. S. RAO and J. A. WEIL. Can. Miner. To be published.

Can. J. Chem. Downloaded from www.nrcresearchpress.com by 122.72.124.2 on 09/07/12
For personal use only.

Organic reactions in liquid crystalline solvents. 8. Deuterium NMR studies of the solubilization of some aromatic ketones in the liquid crystalline phases of 4′-butylbicyclohexyl-4-carbonitrile

BRIAN J. FAHIE, D. SCOTT MITCHELL, AND WILLIAM J. LEIGH[1]
Department of Chemistry, McMaster University, Hamilton, Ont., Canada L8S 4M1

Received April 6, 1988

BRIAN J. FAHIE, D. SCOTT MITCHELL, and WILLIAM J. LEIGH. Can. J. Chem. **67**, 148 (1989).

The nature of the solubilization of β-phenyl-4-methoxypropiophenone (**1**) in the nematic and crystal-B liquid crystalline phases of *trans*,*trans*-4′-butyl-(1,1′-bicyclohexyl)-4-carbonitrile (CCH-4) has been investigated by deuterium nmr spectroscopy. This has been carried out using deuterium quadrupolar splitting ($\Delta\nu_Q$) and T_1 measurements on 1–15 mol% solutions of two selectively deuterated derivatives of the ketone in CCH-4 over the 25–110°C temperature range. The nmr studies have been supplemented with differential scanning calorimetry (DSC) and thermal microscopic investigations of variously proportioned mixtures of the parent ketone with CCH-4, over a similar temperature range. For comparison, ^{2}H nmr measurements have also been carried out for solutions of 4-methoxyacetophenone-α,α,α-d_3, benzene-d_6, and β-(4-cyclohexylphenyl)-4-methoxypropiophenone-α,α-d_2 in the same liquid crystal as a function of temperature. Our results indicate that the limit of solubility of **1** in the smectic phase of CCH-4 is less than 0.5 mol%. At temperatures above 35°C, excess ketone is solubilized in a ketone-rich nematic phase that coexists with the bulk smectic phase, and the composition of the ketone-rich phase varies continuously with temperature throughout this range. At around 35°C, the ketone-rich phase transforms into a metastable, non-birefringent phase which is characterized by isotropic nmr behaviour. Prolonged storage at room temperature causes crystallization of this phase, forming a stable binary mixture of ca. 9:1 CCH-4/**1** that undergoes a K–Sm transition at 27–28°C, a Sm–N transition at 43.5–44°C, and a broad N–I transition at 58–63°C. This stable modification can also be prepared by rapid cooling of a 10 mol% **1**/CCH-4 mixure from the nematic phase. The ^{2}H nmr studies of 4-methoxyacetophenone-α,α,α-d_3 and benzene-d_6 in CCH-4 indicate that these solutes have somewhat higher solubility in the crystal-B phase of this mesogen. The data necessitate a re-interpretation of our previously reported studies of the excited triplet state behaviour of **1** in the liquid crystalline phases of this material, and may be broadly applicable to numerous other studies of photochemical reactivity in this mesogen that have been reported.

Key words: liquid crystal, smectic, ^{2}H nmr, photochemistry, aromatic ketone, bicyclohexyl-4-carbonitrile,4′-butyl.

BRIAN J. FAHIE, D. SCOTT MITCHELL et WILLIAM J. LEIGH. Can. J. Chem. **67**, 148 (1989).

Faisant appel à la rmn du deutérium, on a étudié la nature de la solubilisation de la β-phényl méthoxy-4 propiophénone (**1**) dans les phases nématique et cristalline du cristal liquide-B du butyl-4′ (bicyclohexyl-1,1′) carbonitrile-4-*trans*, *trans* (CCH-4). On a réalisé cette étude en effectuant des mesures de T_1 et de couplages quadripolaires du deutérium ($\Delta\nu_Q$) sur des solutions contenant de 1 à 15 mol% de deux dérivés sélectivement deutérés de la cétone **1** dissoutes dans le CCH-4, à des températures allant de 25 à 110°C. En plus des études rmn, on a aussi fait appel à la calorimétrie à balayage différentiel (CBD) et à la microscopie thermique qui ont été utilisés aux mêmes températures sur divers mélanges de la cétone **1** dans le CCH-4. Pour fins de comparaison, des études de rmn du ^{2}H ont aussi été effectuées sur des solutions de méthoxy-4 acétophénone-α,α,α-d_3 et de benzène-d_6, dans le même cristal liquide et dans les mêmes limites de température. Nos résultats indiquent que la limite de solubilité du composé **1** dans la phase smétique du CCH-4 est inférieure à 0,5 mol%. À des températures supérieures à 35°C, la phase riche en cétone se transforme en une phase métastable, qui n'est pas biréfringente et qui est caractérisée par une comportement rmn isotrope. Un entreposage prolongé de cette phase à la température ambiante provoque sa cristallisation et la formation d'un mélange binaire stable formé de CCH-4 et de **1** dans un rapport d'environ 9:1 et qui subit une transition K–Sm à 27–28°C, une transition Sm–N à 43,5–44°C et un large transition N–I entre 58 et 63°C. On peut aussi préparer cette modification stable en refroidissant rapidement un mélange contenant 10 mol% du composé **1** dans le CCH-4, à partir de la phase nématique. Les études par rmn du ^{2}H effectuées sur la méthoxy-4 acétophénone-α,α,α-d_3 et sur le benzène-d_6 dans le CCH-4 indiquent que ces solutés sont légèrement plus solubles dans la phase cristal-B de ce mésogène. Ces données nous obligent à réinterpréter nos études antérieures sur le comportement de l'état excité triplet du composé **1** dans les phases cristallines liquides de ce produit et elles peuvent s'appliquer d'une façon générale à de nombreuses autres études qui ont été effectuées antérieurement sur la réactivité photochimique de ce mésogène.

Mots clés : cristal liquide, smectique, rmn ^{2}H, photochimie, cétone aromatique, bicyclohexyl carbonitrile-4, butyl-4′.

[Traduit par la revue]

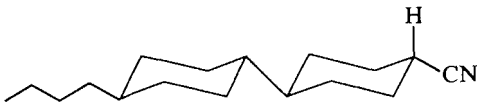
Introduction

There is considerable current interest in the potential effects of liquid crystalline order on the molecular mobility and associated chemical reactivity of dissolved solutes. A number of techniques have been used to study solute behaviour of this type in liquid crystals, including nanosecond laser flash photolysis (1–3), fluorescence (4, 5) and uv absorption (6) spectroscopy, electron spin (7) and nuclear magnetic (8) resonance, and product analysis methods (2, 3*b*, 9–14).

4′-Butylbicyclohexyl-4-carbonitrile (CCH-4; a.k.a. BCCN) has found particularly frequent use as a liquid crystalline solvent in the photochemical/photophysical investigations that have been reported to date (1–3, 4*c*, 14*d*). This mesogen has several advantages in studies of this type; it is commercially available in spectroscopic grade purity, is optically transparent at wavelengths above ca. 210 nm, and exhibits nematic and smectic liquid crystalline phases, as well as the isotropic phase, at convenient temperatures (K–Sm, 28°C; Sm–N, 54°C; N–I,

[1]Natural Sciences and Engineering Research Council (Canada) University Research Fellow (1983–1993). To whom all correspondence should be addressed.

Can. J. Chem. Downloaded from www.nrcresearchpress.com by 122.72.124.2 on 09/07/12
For personal use only.



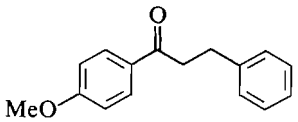
CCH-4

79°C (15)). The morphology of the smectic phase of this compound has recently been established by X-ray diffraction methods; it is classified as a bilayer crystal-B phase (16), similar to the high temperature smectic phase of the 4′-propyl homologue (CCH-3) that was characterized several years ago by Brownsey and Leadbetter (17). In this type of liquid crystal, the constituent molecules are arranged in correlated bilayers of thickness just slightly shorter than twice the molecular length. Within the bilayers, the molecules are hexagonally close-packed and oriented parallel to one another and perpendicular to the layer plane (refs. 16, 17; for comprehensive descriptions of the structure and properties of liquid crystals and leading references, see ref. 18). The feature of the morphology of the crystal-B phase that distinguishes it from the conventional smectic B phase is the presence of some degree of three-dimensional order (17). The 4′-butyl derivative forms an enantiotropic smectic phase, and is hence more useful as a reaction solvent than the 4′-propyl derivative, which forms monotropic smectic phases. However, a commercial material that contains CCH-3 as the ternary eutectic with the 4′-pentyl and -heptyl homologues is nematic at room temperature (15) and has found considerable use as a solvent for nmr studies (19) and uv absorption spectroscopy (6*c*, 20).

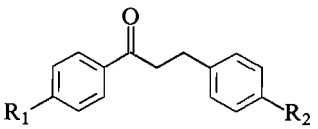
While the morphology of the liquid crystalline phases of pure CCH-4 is apparently well-established, the nature of its solubilization of guest molecules is unclear. Studies by us (1, 2) and others (3, 4*c*, 14*d*) have shown that solute conformational mobility can be substantially restricted in smectic CCH-4 compared to the corresponding behaviour in the nematic and isotropic phases, but the magnitude of the effect depends critically on the relationship between the structure of the solute and that of the liquid crystal, as well as the magnitude of the change in solute shape that accompanies the conformational motion. For example, the Arrhenius parameters for triplet decay of **1** (which depend directly on the energetics of C_α—C_β bond rotation in the ketone excited triplet state (21) are markedly phase-dependent in CCH-4; the Arrhenius plot shows a distinct change in slope at the bulk Sm–N phase transition temperature, corresponding to an increase in the activation energy and entropy for triplet decay (relative to their nematic phase values) of ca. 10 kcal/mol and 30 eu, respectively, at temperatures below 53°C (1*a*). On the other hand, when the length of the ketone is increased, for example as in **2**, phase-*independent* of phenylalkyl ketones (14*d*) in the smectic, nematic, and isotropic phases of CCH-4. All of these studies have more or less assumed homogeneous solubility of the probes in smectic CCH-4, although a recent report by Treanor and Weiss (22) has identified a solute-induced phase (previously assigned a plastic- or cubic-crystalline morphology on the basis of ^{13}C nmr results for solutions of benzene in CCH-4 (23)) that exists at temperatures less than *ca.* 35°C, and discussed the ramifications of the structure of this phase on the Norrish II reaction of alkylphenones. Recently, Sigaud and co-workers have reported that 1-aminopyrene and 1-aminofluorenone form stable, binary nematic and smectic A phases with CCH-4 (24).

Deuterium nmr spectroscopy is an extremely powerful technique for the investigation of the mobility and solubilization of solutes in liquid crystals, and several comprehensive reviews outline the theory and applications of the various techniques that have found widespread use (8*a*, 8*e*, 25). For a deuterated analog of a solute such as **1**, ^2H nmr spectroscopy can provide information on molecular motions that take place over considerably different time-scales than that probed in the laser flash photolysis technique. For example, the magnitude of the deuterium quadrupolar splitting ($\Delta\nu_Q$) that is observed of a deuterated molecule dissolved in an anisotropic solvent is dependent on the time-averaged motions of the molecule over a time scale of ca. 0.01–10 ms (25*b*), while the deuterium spin–lattice relaxation time (T_1) reflects molecular motions over the 0.01–10 ns time scale (25). Most importantly from our perspective, the pattern of response of these parameters to changes in temperature, solvent phase, and bulk solute concentration is capable of providing fairly detailed qualitative information on the variations in local solvation of the probe molecule with temperature and phase. Additional information on probe solubilization is available from differential scanning calorimetry (DSC) and thermal microscopy (TM) experiments, particularly when they are carried out with solute–liquid crystal mixtures over a wide range of concentrations.

We wish to report the results of ^2H nmr and deuterium T_1 measurements on two deuterated analogues of **1** (**3** and **4**) in the isotropic and liquid crystalline phases of CCH-4, as well as an investigation of the bulk phase behaviour of mixtures of **1** and CCH-4 by DSC and thermal microscopy. Our experiments have been carried out over a fairly wide range of sample composition, to permit more reliable identification of the type of solubilization experienced by **1** at the low (1 mol%) concentration employed in our previous (1) nanosecond laser flash photolysis experiments. For comparison, we also report ^2H nmr studies of CCH-4 mixtures with a few other representative solutes of substantially different structures compared to **1**; *viz.* 4-methoxyacetophenone-α,α,α-d_3 (**5**), β-(4-cyclohexylphenyl)-4-meth-

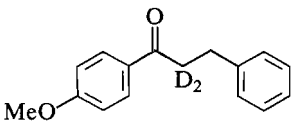


1

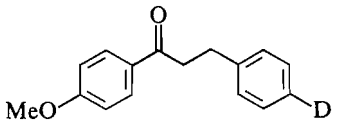


2

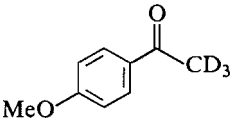
$R_1 = O(CH_2)_nH$; n = 5–8
R_2 = H; $^nC_6H_{14}$; $^cC_6H_{12}$



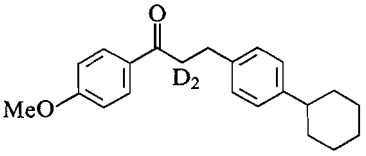
3



4



5



6

Arrhenius behaviour is observed for the triplet lifetime in CCH-4 (1*b*). Weiss and co-workers have reported similar dependencies of solute molecular mobility on molecular length in their studies of intramolecular excimer formation in bis-α,ω-pyrenylalkanes (4*c*), and the Norrish Type II reaction of a series

Can. J. Chem. Downloaded from www.nrcresearchpress.com by 122.72.124.2 on 09/07/12
For personal use only.

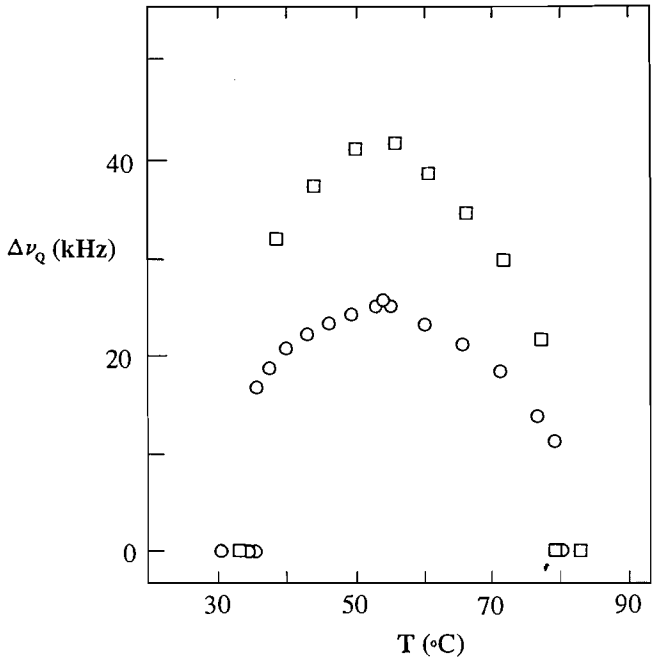


FIG. 1. Deuterium quadrupolar splitting ($\Delta\nu_Q$) versus temperature for 1 mol% mixtures of **3** (⊙) and **4** (□) in CCH-4.

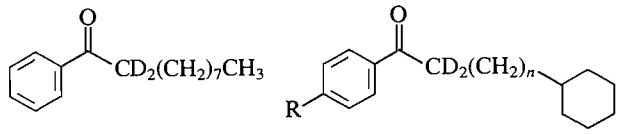
oxypropiophenone-α,α-d_2 (**6**), and deuteriobenzene (C_6D_6). These results allow a complete description of the solubilization of **1** in the liquid crystalline phases of CCH-4, and a detailed, more precise rationalization of the phase-dependent photochemical behaviour of **1** in this solvent than has been presented before (1). Furthermore, our results may be broadly applicable to the many other systems that have been investigated in this and related liquid crystalline solvents (2, 3, 4*c*, 14*d*, 22).

Results and discussion

β-Phenyl-4-methoxypropiophenone-α,α-d_2 (**3**) was synthesized from **1** by base-catalyzed deuterium exchange in NaOD/D_2O/dioxane. β-(4-Deuteriophenyl)-4-methoxypropiophenone (**4**) was synthesized from 4-deuteriobenzaldehyde by a similar procedure to that used previously for **1** (1*b*). 4-Methoxyacetophenone-α,α,α-d_3 (**5**) and β-(4-cyclohexylphenyl)-4-methoxypropiophenone-α,α-d_2 (**6**) were synthesized from their protio-analogues by a similar procedure to that used for **3**.

Deuterium nmr spectra of 1 mol% mixtures of **3** and **4** in CCH-4 were recorded at 76.8 MHz, at various temperatures between 20 and 80°C, using the quadrupolar echo pulse sequence (26). In the isotropic phase above 78°C, the spectra consist of single sharp singlets in both cases. As the sample temperature is lowered below this temperature, the singlet is replaced by a doublet of splitting $\Delta\nu_Q$, the appearance of which is characteristic of a uniformly-oriented sample (25*a*, *b*). The observed value of $\Delta\nu_Q$ for both samples varies with temperature, as is shown in Fig. 1. At *ca.* 35°C, the doublets in both spectra collapse to singlets. Careful control of the sample temperature within a 2° window of 35°C and a 1° window of 78°C allows the coincidental observation of both doublet and singlet patterns, whose relative intensities change monotonically as the phase transitions are traversed.

Treanor and Weiss have recently reported a (directly related) study correlating the ^2H nmr behaviour of a series of α-deuterated phenylalkyl ketones (**7**, **8**) in the various phases of CCH-4 (22)



7

8 *a*: $n = 0$; R = CH_2CH_3
b: $n = 2$; R = H
c: $n = 3$; R = H

with the Norrish II photoreactivity of their protio-analogues in the same liquid crystal (14*c*). These compounds exhibit ^2H nmr behaviour that is very similar to that described above for **3** and **4**. These workers emphasized the nature of the low temperature, solute-induced phase ("p-phase")[2] that exists below 20–35°C (the temperature depends on the solute), and the ramifications of the morphology of this phase on the nmr behaviour and photoreactivity of **7** and **8**. The isotropic solution-like mobility that characterizes ^2H nmr spectra of the "p-phase" (14*d*) is also manifested in the ^{13}C nmr spectra of the mixtures, which show well-resolved peaks for both solute and CCH-4 superimposed on a broad, structureless envelope corresponding to CCH-4 in the smectic phase. This behaviour was originally reported by Fung and Gangoda for solutions of benzene and dioxane in this liquid crystal (23), and we observe similar ^{13}C nmr behaviour for **3**/CCH-4 below 35°C. The p-phase has been assigned a cubic-or plastic-crystalline phase structure (23). In order to rationalize the substantial effects of the p-phase on the Norrish II reactivity of **7** and **8** with the ^2H nmr behaviour, Treanor and Weiss have proposed that the tumbling motions sampled in the nmr experiment correspond to coupled, isotropic tumbling of microscopic solute/solvent "clusters" which are individually ordered in such a way that the conformational mobility of the solute is still impeded to a similar extent as was the case in the higher temperature (smectic) phase (22). These authors reportedly did not observe p-phase formation by thermal microscopy, nor did they comment on the interesting behaviour of $\Delta\nu_Q$ above 35°C and below the "bulk" Sm→N transition temperature (22).

The variation in $\Delta\nu_Q$ with temperature between 30 and 80°C that is shown in Fig. 1 for the 1 mol% **3**/CCH-4 mixture is qualitatively very similar to those reported previously for **7** and **8** (22). The increase in $\Delta\nu_Q$ with decreasing temperature throughout the nematic phase is unexceptional, and indicates an increase in the order parameter of the solute as medium rigidity in the nematic phase increases (8, 25). The magnitude of $\Delta\nu_Q$ reaches a maximum at the *bulk* Sm–N transition temperature (53°C) and then decreases with temperature until at 35°C, the signal collapses to a narrow-line singlet due to "p-phase" formation. The main question that we wish to address in the following deals with the origin of the continuous decrease in $\Delta\nu_Q$ that accompanies decreasing temperature within the smectic phase of the bulk mixture.

The observation of a discontinuity in a plot of this type in the vicinity of a solvent phase transition is quite typical (8). The nature of the discontinuity depends on the difference between the microscopic structures of the two phases (i.e. the microscopic environment experienced by the C—D bond), rather than differences in macroscopic order that are reflected in the thermodynamics of the phase transition (8, 9, 25). Thus, a transition to a thermodynamically more-ordered phase may be

[2]The term "p-phase" is a short form for plastic (or cubic) phase (22). While we do not accept this morphological assignment (*vide infra*), we shall retain the terminology for the sake of convenience.

Can. J. Chem. Downloaded from www.nrcresearchpress.com by 122.72.124.2 on 09/07/12
For personal use only.

Can. J. Chem. Downloaded from www.nrcresearchpress.com by 122.72.124.2 on 09/07/12
For personal use only.

accompanied by an abrupt decrease in the magnitude of $\Delta\nu_Q$, an abrupt increase, or merely a change in the slope of the plot. The continuous decrease in the magnitude of $\Delta\nu_Q$ that accompanies reductions in temperature throughout the 35–53°C range in the present case indicates either that the order parameter of the solute decreases or that its favoured orientation (i.e. perpendicular or parallel to the applied field) changes with decreasing temperature in this region. Solute reorientation effects can be ruled out on the basis of our results for **4**. Since the orientation of the C—D bond in **4** with respect to the long molecular axis is roughly perpendicular to that in **3**, we would have expected $\Delta\nu_Q$ to respond differently to temperature in the two compounds, if an alteration in the favoured orientation of the solute were responsible for the decrease in $\Delta\nu_Q$ that accompanies decreasing temperature in the 35–53°C range. In fact, the similar behaviour exhibited by **3** and **4** probably indicates that the favoured orientation of the solute remains the same throughout the 53–78°C and 35–53°C temperature ranges. CCH-4 has negative diamagnetic anisotropy (19), and the sample will thus be aligned in a magnetic field such that the long molecular axes are oriented perpendicular to the field. Presumably, the difference in the magnitudes of $\Delta\nu_Q$ observed for **3** and **4** at a given temperature are predominantly the result of differences in the motionally-averaged orientations of the C—D bonds in the two molecules with respect to the applied field, and their relative magnitudes are consistent with the C—D bonds in **3** sampling a much larger range of angles than that in **4** (the difference between the quadrupolar coupling constants for aromatic and aliphatic deuterons is much too small to account for the factor of ca. 2 difference between $\Delta\nu_Q$ for **3** and **4**). This would be the case if rotation about the long molecular axis were the predominant motion that is sampled by the quadrupolar interaction.

It can thus be concluded that the observed behaviour of $\Delta\nu_Q$ below 53°C results from a decrease in the order parameter of the solute with decreasing temperature. Behaviour of this type is, in fact, not uncommon, and can be the result of any of a number of possible solvation phenomena. For example, if **1** is solubilized homogeneously in the smectic phase of CCH-4, then such behaviour could result if the probe's solubilization site within the smectic array *changes* from a relatively highly ordered region at the upper temperatures to a relatively disordered or more fluid one at the lower temperatures (27). A related possibility is that as the temperature is lowered within the smectic phase, the solvation shell about **1** adopts a cavity-like structure (28), and becomes less able to control solute orientation as the cavity becomes better defined with decreasing temperature. A third possibility is that the ketone resides in a continuously changing (composition-wise), *nematic* phase between 35 and 53°C, which could result if the limit of solubility of the ketone in the smectic phase is lower than the bulk solute concentration of the sample, and phase separation occurs at temperatures below 53°C. The Se possibilities have been investigated in detail by additional ^{2}H nmr experiments and DSC and TM techniques.

^{2}H nmr experiments were also carried out for 3, 5, and 10 mol% mixtures of **3** with CCH-4. The results for the 5 and 10 mol% mixtures are shown along with those for the 1 mol% mixture in Fig. 2. For the samples containing ≥5 mol% **3**, the solutions were allowed to equilibrate for 10–45 min at each temperature prior to obtaining the spectrum. In these cases, a change in temperature below that of the apex in the $\Delta\nu_Q$ vs. T plot is accompanied by a fairly slow transformation of the spectrum as

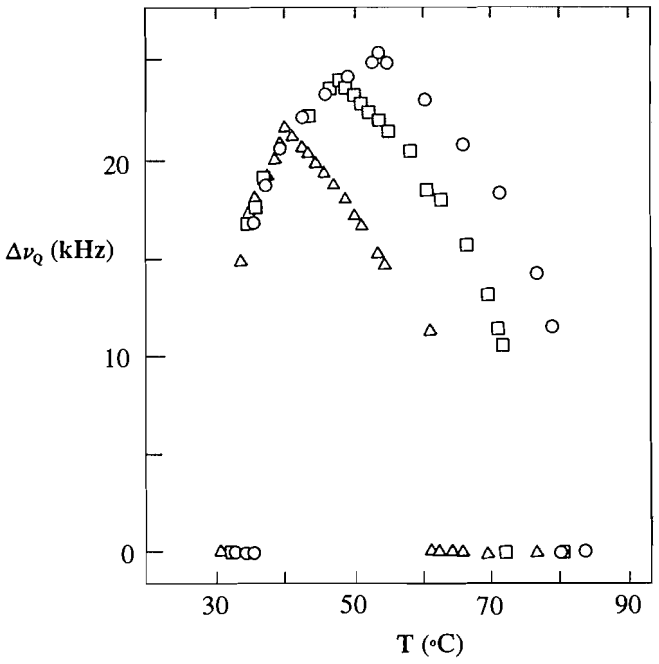


FIG. 2. Deuterium quadrupolar splitting ($\Delta\nu_Q$) versus temperature for 1.0 (⊙), 5.0 (□), and 10.0 (△) mol% mixtures of **3** in CCH-4.

the initial doublet gradually reduces in intensity and the final doublet grows in. For measurements at these temperatures, the samples were allowed to equilibrate for at least 2 h prior to recording the spectra. In the cases of the 5 and 10 mol% samples, we find that the apices in the $\Delta\nu_Q$ vs. T plots can be supercooled by up to *ca.* 5°C, if sufficient time is not permitted for sample equilibration. The phase transitions (N–I and the one at *ca.* 35°C) for the samples containing ≥5 mol% **1** are considerably broader than those for the samples of lower concentration, which results in the appearance of both the singlet and doublet patterns in the spectra of **3** over considerable temperature (approximately 3–7°) ranges.

The $\Delta\nu_Q$ vs. T plots in these nematic phases describe a series of approximately parallel curves that shift to lower temperature as the concentration of **1** in the solution is increased. This behaviour is exactly as expected for a series of homogeneous solutions of **1** in the bulk nematic phase, and a plot of the $\Delta\nu_Q$ values versus the reduced temperature ($T_{N-I} - T$) yields a single line that contains all the data for all concentrations. In each case, the data for temperatures below the apices fall on a single curve that is independent of the bulk sample composition. This is good evidence that at temperatures below the onset of the Sm–N transition, the ketone finds itself in a medium whose composition depends only on the temperature, and not on *bulk* solute concentration.

The ^{2}H nmr behaviour of the 3 mol% **3** sample described above is completely reversible, provided that the sample temperature is decreased slowly from above 50°C, and is not taken below 20°C for extended periods of time. Cooling the sample below 20°C, rapidly cooling it from above 50°C, or just allowing it to sit at room temperature for a few days causes apparent crystallization. The "crystallized" sample affords no deuterium signals under the same conditions as those used to record the above spectra until the sample temperature is raised above 43°C, at which point the characteristic doublet splitting of **3** in nematic CCH-4 is obtained.

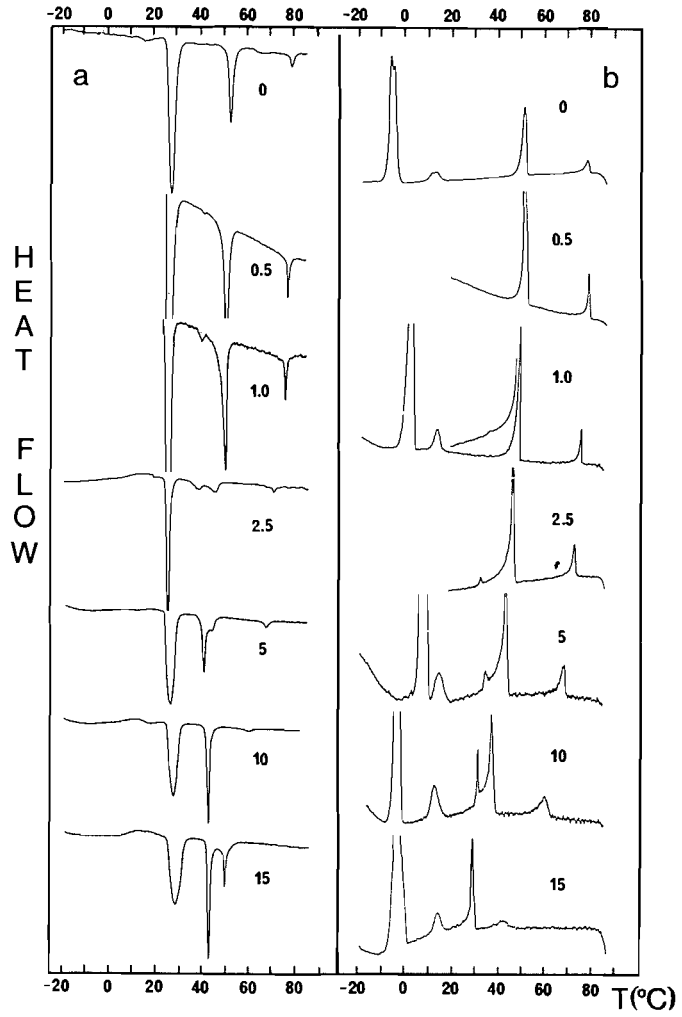


FIG. 3. Differential scanning calorimetry thermograms recorded for 0–15 mol% mixtures of **1** in CCH-4, measured with a 2°/min scanning rate. (*a*) Heating cycles; (*b*) cooling cycles. The mixtures of lower concentration in **1** were recorded at higher instrumental sensitivity.

DSC thermograms, recorded for several variously proportioned mixtures of **1** in CCH-4, are shown in Fig. 3. The addition of **1** to CCH-4 results in both a lowering and broadening of the N–I and Sm–N transitions, and the appearance of a new transition at 32–35°C. For the latter, the size of its corresponding peak in the DSC thermograms is proportional to the concentration of solute present, and it is reversible providing that the temperature of the sample is not taken below 5°C for extended periods of time. When the sample temperature is reduced to ca. −10°C (as was done routinely in the course of obtaining the DSC cooling cycles), the corresponding heating cycle does not mirror the cooling cycle; the transition at 32–35°C disappears and is replaced by a new one at 43–44°C. The DSC thermograms shown in Fig. 3 were recorded first as cooling cycles from 90°C to ca. −10°C (Fig. 3*a*), and then the corresponding heating cycles were obtained (Fig. 3*b*). Both sets of thermograms were obtained using a 2°/min temperature programme. For the mixtures containing <2.5 mol% **1**, the traces shown in Fig. 3 were recorded under conditions of higher instrumental sensitivity, to better resolve the weak transitions involving the solute-induced phases.

Thermal microscopic inspection of each of the above samples was carried out in order to ascertain the nature of the various phase transitions observed in the DSC experiments. These experiments are described in detail in the Experimental section, but can be summarized briefly as follows. In all samples of composition 0.5 ≤ **1** ≤ 15 mol%, slow cooling from the nematic phase results in phase separation (smectic + residual nematic) at temperatures below that at which the smectic phase initially appears, and at *ca.* 35°C the residual nematic phase transforms to an optically isotropic (non-birefringent) phase. This behaviour was missed in our earlier studies of the triplet state behaviour of **1** in CCH-4 (1); it is not readily obvious in the dilute mixtures without the benefit of the experience gained from examining mixtures of higher bulk concentration in **1**. We identify the optically isotropic phase as the "p-phase" that is responsible for the isotropic nmr behaviour of **3** and **4** below 35°C. In samples containing ≥5 mol% **1**, the p-phase can be discerned to have the character of a fairly viscous, isotropic *fluid*. The fluidity of this phase is more difficult to estimate in samples of lower bulk solute concentration, but in these cases, the relatively higher proportion of smectic phase is probably more effective at controlling the overall rigidity of the sample. Storage of the samples containing <10 mol% **3** for short periods of time at room temperature causes contraction of the p-phase fraction to form what appear to be crystallites dispersed throughout the mosaic monodomains of the bulk smectic phase. Upon heating, the "crystallites" undergo a distinct phase transition at 43–44°C to a nematic phase. Samples containing ≤0.25 mol% **1** showed no discernible evidence of phase separation, p-phase formation, or the 43–44°C transition by DSC or thermal microscopic inspection.

Rapid cooling of the 10 mol% sample to 23°C affords a homogeneous, solid binary mixture with a small number of microcrystals dispersed within it. The sample is stable indefinitely. The bulk of the sample undergoes a K–Sm transition at 27–28°C, a sharp Sm–N transition at 43.7–44°C, and a broad N–I transition at 58.5–63°C. The microcrystals (of presumably almost pure ketone) dissolve fairly rapidly between 44–48°C.

As Fung and Gangoda concluded, the solute-induced p-phase is indeed metastable, but in this case (at least) it is probably best described as an amorphous glass or (more likely) an isotropic liquid phase. With **1** as solute, the phase crystallizes to form a stable binary modification of composition 8–10 mol% **1**. While the microscopic texture of the binary phase that exists between 27 and 43.5°C is consistent with a smectic phase (18*c*), its precise morphology awaits identification.

The DSC and TM cooling and heating experiments are summarized in Fig. 4 as the complete binary phase diagrams for the **1**/CCH-4 binary system. These experiments clearly indicate that the presence of **1** in concentrations as low as 0.5 mol% causes phase separation below the bulk N–Sm transition temperature. The main features of the two diagrams differ considerably because of supercooling effects; in slowly-cooled mixtures containing <20 mol% **1**, the binary phase forms only after considerable storage times at room temperature. In mixtures containing ≥20 mol% **1**, the binary phase often (but not always) forms directly from the nematic phase; the cooling behaviour of these samples tends to be irreproducible because of erratic crystallization.

Several control experiments were carried out on the 1 and 3 mol% **3**/CCH-4 samples to verify that no additional doublet splittings (that might be attributed to ketone solubilized in the smectic phase component of the two-phase system) are present in the spectra at temperatures below 50°C. Using the 76.8 MHz spectrometer and the 1 mol% samples, the experiments con-

Can. J. Chem. Downloaded from www.nrcresearchpress.com by 122.72.124.2 on 09/07/12
For personal use only.

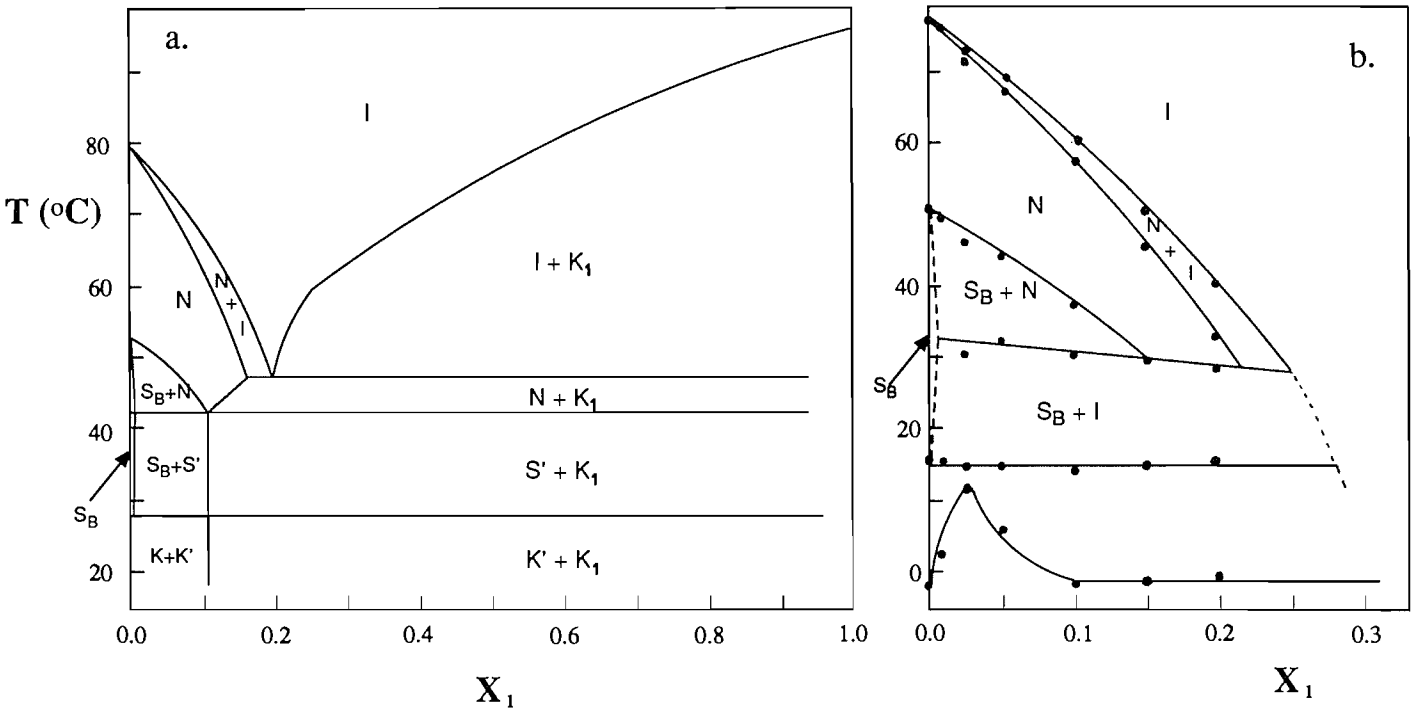


FIG. 4. Composition/temperature binary phase diagrams for **1**/CCH-4, constructed from DSC and thermal microscopy data. (*a*) Heating (idealized); (*b*) cooling (actual data), for 0–20 mol% **1**/CCH-4. (I, isotropic; N, nematic; S, smectic; K, solid. S′ and K′ represent the smectic and solid binary modification of composition *ca.* 10 mol% **1**).

sisted of varying the offset frequency in *ca.* 30 kHz steps up to 65 kHz from the carrier frequency, and scanning over a 165 kHz spectral window in each case; these failed to reveal any additional resonances within the limits of sensitivity of the instrument. With the largest variation in offset frequency, the spectrum suffered some distortion, but both components of the doublet were clearly observable. Spectra recorded with a 41.3 MHz spectrometer that is better equipped to carry out experiments on powder samples (see Experimental Section), similarly failed to reveal additional resonances within 100 kHz of centre-spectrum; in these cases, our limits of uncertainty can be taken to be much lower than those obtainable with the 76.8 MHz instrument.

Additional experiments were carried out with 0.2 and 0.5 mol% samples of **1** in CCH-4, in an attempt to define the limit of solubility of the ketone in the smectic phase. The 0.5 mol% sample exhibited behaviour similar to that of the 1.0 mol% sample, although the signal-to-noise ratio worsened dramatically as the temperature was lowered throughout the 52–35°C range. In the case of the 0.2 mol% sample, no deuterium signals could be observed at all between 10 and 50°C, but the isotropic singlet characteristic of p-phase formation could be clearly observed in spectra recorded below 8°C. We take the absence of spectral features below 50°C to indicate that the ketone is totally soluble in the crystal-B phase at these temperatures, and that the spectrum in this phase is either too broad or the components too widely separated to be observed with our spectrometer. These experiments afford upper and lower limits of 0.5 and 0.2 mol%, respectively, for the solubility limit of the ketone in the smectic phase of CCH-4. They also indicate that depending on bulk sample composition, p-phase formation can ensue from either smectic or nematic solutions of **1** in CCH-4.

The above results suggest that **1** is subject to rather more complicated solubilization in the smectic phase of CCH-4 under the conditions of our flash photolysis experiments than was previously thought (1*a*). Because sample (1 mol% in **1**) temperatures were routinely kept above 30°C (to keep them optically transparent (1)), the cooling phase diagram shown in Fig. 4*a* is the one that applies to the system under these conditions. Between ≈52–35°C, the sample consists of a biphasic system in which <50% of the ketone resides in a smectic phase of similar morphology to that of the pure mesogen and the remainder resides in a solute-enriched nematic phase. The relative proportions of the two phases present vary continuously with temperature, as do their compositions. Below 35°C, a second biphasic system is formed, that is comprised of a solute-depleted smectic phase (of a similar composition to that above 35°C) in equilibrium with a solute-enriched, isotropic liquid or glass phase.

For comparison purposes, ^{2}H nmr spectra of 3 mol% CCH-4 solutions of benzene-d_6, **5**, and **6** were recorded over the 20–85°C temperature range under similar conditions to those used above for **3** and **4**. The ^{2}H nmr behaviour of **6** is similar in all respects to that observed for **3**, except that $\Delta\nu_Q$ is somewhat larger in the former; the splitting varied between 12.9 and 27.7 kHz in the nematic phase and ultimately decreased to a value of 19.8 kHz as the temperature was lowered below 50°C, before collapsing to a singlet at *ca.* 30°C.

The ^{2}H nmr spectra of C_6D_6 and **5** show important differences at temperatures below 50°C compared to those of the other solutes investigated in this study, however. For these two compounds, cooling through the bulk N–Sm transition at ca. 50°C results in the appearance of a second doublet that coexists with that associated with the nematic phase.

Figure 5 summarizes the ^{2}H nmr behaviour of a 3 mol% sample of **5** in CCH-4 as a function of temperature, and representative spectra are included as inserts in the figure. Cooling the sample into the nematic phase affords a single

Can. J. Chem. Downloaded from www.nrcresearchpress.com by 122.72.124.2 on 09/07/12
For personal use only.

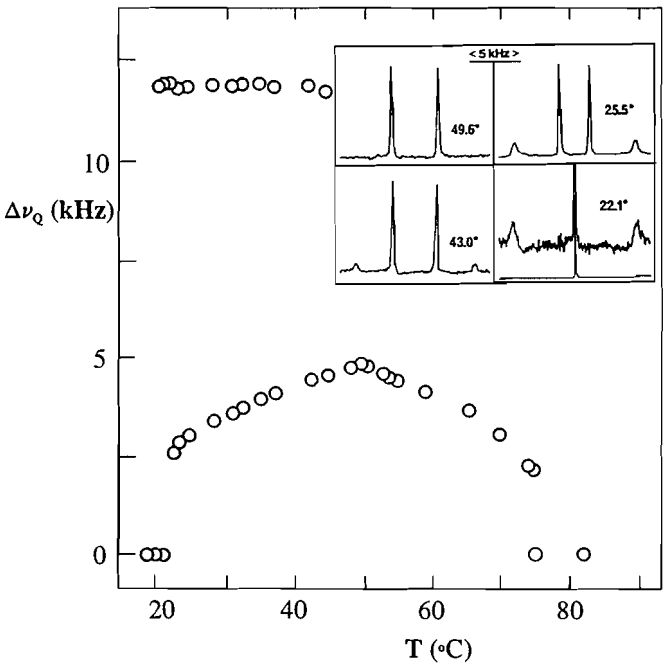


FIG. 5. Deuterium quadrupolar splitting ($\Delta\nu_Q$) versus temperature for a 3 mol% mixture of **5** in CCH-4. The insert shows some representative spectra measured at the various temperatures.

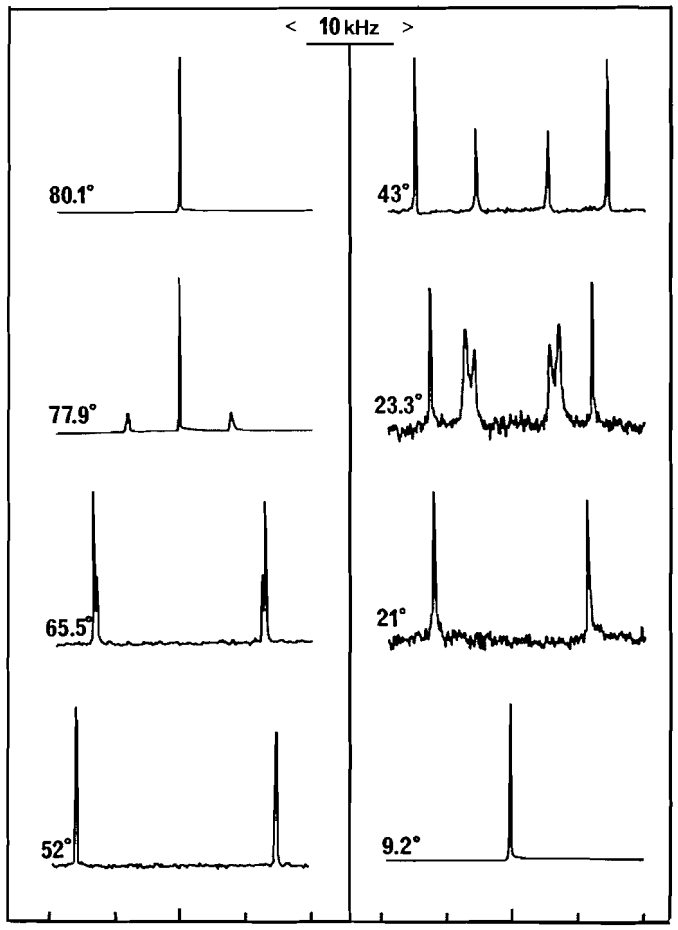


FIG. 6. Representative ^2H nmr spectra of a 3 mol% mixture of benzene-d_6 in CCH-4, at various temperatures between 9 and 80°C.

doublet of splitting 2.2 kHz at 75°C. Lowering the temperature below 50°C affords a second doublet signal, with splitting *ca.* three times that of the doublet associated with the nematic phase at this temperature, and which is assigned to **5** solubilized in the crystal-B phase of CCH-4. As expected for a biphasic system in which the solute is incorporated in *both* phases, further decreases in temperature results in an increase in the intensity of the outer (smectic) doublet compared to that of the inner doublet, presumably owing to progressive conversion of the nematic to smectic phase as the temperature is lowered. Interestingly, the magnitude of the outer doublet splitting remains constant at 11.8 ± 0.1 kHz with decreasing temperature in this range, indicating perhaps that the order parameter of the molecule does not vary significantly with temperature in the smectic phase. This may not be surprising, however, considering the very high degree of solvent order present in the crystal-B phase (18). As was found for the mixtures of **3** in the temperature region below 53°C, the doublet splitting associated with **5** in the nematic phase decreases in magnitude with decreasing temperature. At *ca.* 23–24°C, the spectrum collapses to a singlet (originating from the inner doublet) flanked by the outer doublet. This system thus also forms a p-phase at low temperatures, and it is clearly the binary nematic phase that is the precursor to the p-phase under these conditions. Further decreases in temperature result in the disappearance of the outer doublet at 19°C as the Sm phase crystallizes. Each of the above phase transitions appears to be completely reversible by ^2H nmr, although we have not cooled the sample to temperatures below 15°C to check the metastability of the p-phase.

A 1 mol% mixture of **5** in CCH-4 behaves similarly to the 3% sample, except that in the biphasic regions between 19 and 50°C, the intensity of the (outer) doublet assigned above to **5** in the crystal-B phase is considerably larger (compared to the residual nematic or p-phase signals) than is the case in the 3 mol% sample (32*b*).

The ^2H nmr behaviour of the C_6D_6/CCH-4 mixture is particularly interesting, and our results are summarized in Fig. 6. At temperatures between 52 and 71°C in the bulk nematic phase, each component of the original doublet is split into two signals, of intensity ratio *ca.* 1:2, within 250 Hz of each other. The origins of this splitting are not clear to us. By thermal microscopy, there is clearly only a single phase present at these temperatures, so the possibility of two solvation sites is unlikely. The size of the splitting and the relative intensities of the signals appear to be inconsistent with dipolar coupling (8*a–c*, 29), and previous ^2H nmr results for C_6D_6 in other nematic solvents (that revealed only a single quadrupolar doublet for the molecule (30)) render the possibility of restricted rotational motion about the short (D_{6h}) axis of the molecule unlikely.

As the temperature is lowered throughout the nematic phase, the doublet splittings increase in magnitude and the difference between the two decreases slightly. The two doublets finally coalesce to a singlet doublet ($\Delta\nu_Q$ = 15.5 Hz) at 51°C, and at 50°C a new doublet pattern ($\Delta\nu_Q$ = 5.4 Hz) appears in addition to that associated with the nematic phase. This inner doublet is attributed to C_6D_6 solubilized in the crystal-B phase of CCH-4. Continued cooling throughout the 50–33°C range causes the inner and outer doublet splittings to increase and decrease in magnitude, respectively. At 29°C, a third doublet splitting arises (of similar magnitude to the original inner doublet), and as the temperature is lowered to 23°C the relative intensity of the two inner doublets changes dramatically. At 21°C, the spectrum consists of a single doublet of splitting $\Delta\nu_Q$ = 11.9 kHz,

Can. J. Chem. Downloaded from www.nrcresearchpress.com by 122.72.124.2 on 09/07/12
For personal use only.

Can. J. Chem. Downloaded from www.nrcresearchpress.com by 122.72.124.2 on 09/07/12
For personal use only.

associated with C_6D_6 in the residual nematic phase. The appearance of the second inner doublet as the sample approaches 21°C may be associated with the formation of a second, monotropic smectic modification prior to crystallization to the solid phase; we have previously observed the formation of such a phase in pure CCH-4 in DSC cooling experiments (31). An alternate possibility that the spectral pattern is due to solubilization of the probe in two different environments within the crystal-B phase cannot be ruled out, however. The disappearance of the inner doublet splittings between 21–23°C is most reasonably due to the Sm–K transition, below which the polycrystalline nature of the sample precludes the observation of deuterium signals under the conditions used for these experiments. Continued cooling of the sample results in further decreases in the splitting of the remaining doublet until at *ca.* 10°C, it collapses to a singlet. This is close to the temperature reported by Fung and Gangoda for p-phase formation in 3.4 wt% solutions of benzene in CCH-4 (23). Again, it is clearly a solute-rich nematic phase that is the precursor to the p-phase.

The ^2H nmr results for the mixtures of **5** and C_6D_6 have considerable ramifications with respect to our interpretation of the various data presented above for solutions of **1**(**3**) in CCH-4. Most importantly, the relatively small solutes appear to be soluble in the crystal-B phase of CCH-4, but to a far more limited extent than might generally be appreciated. From our data for **3** and rough estimates of the relative intensities of the spectra associated with C_6D_6 and **5** in the nematic and smectic phases in the biphasic region (assuming the same proportionality between signal intensity and concentration in the two phases),[3] the solubility limits for C_6D_6, **5**, and **1** in smectic CCH-4 appear to be roughly 1–2, 0.5–0.8, and 0.2–0.4 mol%, respectively. There is an apparent trend to decreasing solubility with increasing solute size or substitution.

We have also carried out deuterium T_1 measurements on 3 mol% samples of **3** in CCH-4 and in 2:1 CCH-2/CCH-4 (EB: Sm–N, 25°C; N–I, 54°C (2, 31)) over temperature ranges of 23–110°C and 23–90°C, respectively, since it was hoped that this technique (which probes molecular motions occurring over much shorter time scales than $\Delta\nu_Q$ does — as short as 10 ps (25)) might provide information on the mobility of the ketone in CCH-4 that correlates more directly with our laser flash photolysis results for this compound. These experiments were carried out using a consecutive inversion-recovery/quadrupolar echo pulse sequence, and the results are plotted as $-\ln(T_1)$ vs. $1/T$ in Fig. 7. While there is a clear change in the slopes of both plots at the bulk N–I transition temperatures for the two liquid crystals, we are unable to identify any substantial changes in behaviour at either the bulk N–Sm or the "N–p" transition temperatures. T_1-values recorded for the **3**/CCH-4 sample at representative temperatures throughout the same range on a 33 MHz spectrometer were consistently slightly less than those measured at 76.8 MHz, but showed similar temperature dependence.

The deuterium spin–lattice relaxation time appears to be quite insensitive to changes in bulk solvent phase and composition, although our limits of uncertainty in the measurements below *ca.* 35°C are quite poor. While discontinuities at the temperatures corresponding to phase separation and p-phase formation may be revealed by more accurate T_1 determinations, it is clear that they will not be particularly pronounced. This

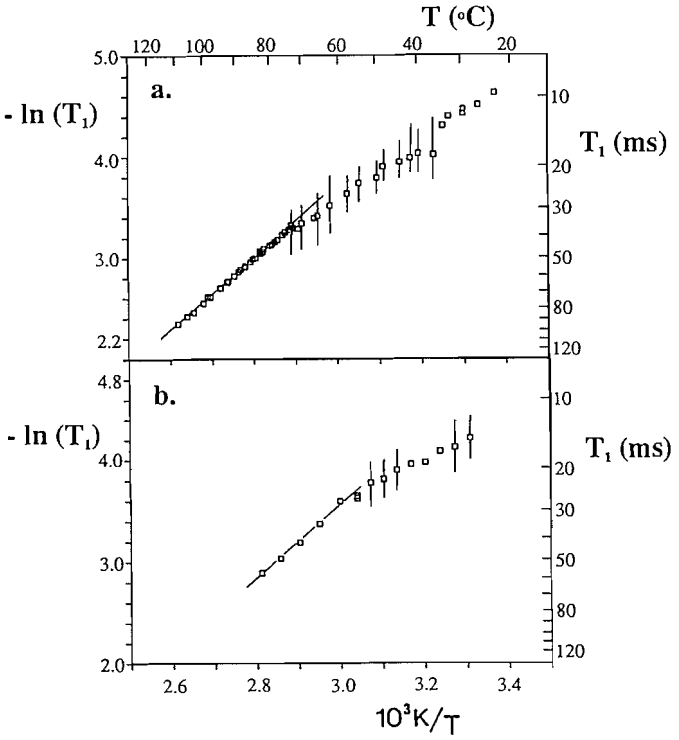


FIG. 7. Arrhenius plot showing the temperature dependence of T_1-values obtained for 3 mol% mixtures of **3** in (*a*) CCH-4 and (*b*) 2:1 CCH-2/CCH-4 (EB) between 25 and 120°C. Errors were calculated as twice the standard deviation for each point; error bars are shown only for those points with errors in excess of 10%.

behaviour is consistent with our assignment of the doublet splitting in the 35–53°C range as being due to solibilization in the nematic component of a two-phase system. Under these conditions, some difference in slope might be expected above and below 53°C, because the composition of the nematic phase is constant above this temperature and variant below it, but the difference should be small. Also, the very fast molecular reorientations that are reflected in T_1 are virtually unaffected by the transformation of the solute-rich nematic phase to the p-phase at 35°C.

The present study has very important ramifications to the interpretation of the triplet state behaviour of **1** in the liquid crystalline phases of CCH-4 (1*a*), and presumably, the behaviour of the considerable number of other solutes whose reactivity and/or normal behaviour has also been studied in this mesogen (1*b*, 2, 4*c*, 14*d*, 22, 27). It is interesting that **1** forms what appears to be a stable binary modification with CCH-4, and our experiments indicate that its composition is roughly 8–10 mol% in solute. Depending on conditions, the binary phase can be induced to form either with or without the intermediacy of the p-phase. While the morphology of the binary modification is unknown at present, it has a microscopic texture not unlike the classical mosaic texture of the Sm B phase (18*c*). We have been unable to observe ^2H nmr spectra of **3** in this phase on either the 76.8 or 41.3 MHz spectrometers, even with an 8 mol% sample. Interestingly, we have observed that the triplet lifetime of **1** in well-aged (at 20°C) samples in CCH-4 is considerably shorter than that observed when the sample is cooled slowly from the nematic phase (31). This would seem to indicate that the mobility of the probe with respect to C_α—C_β bond rotation is much higher in the binary modification than in the smectic or nematic phases. The propensity for aromatic

[3]This is not a good approximation, but it does serve to establish an upper limit for the solubility of the probe in the crystal-B phase.

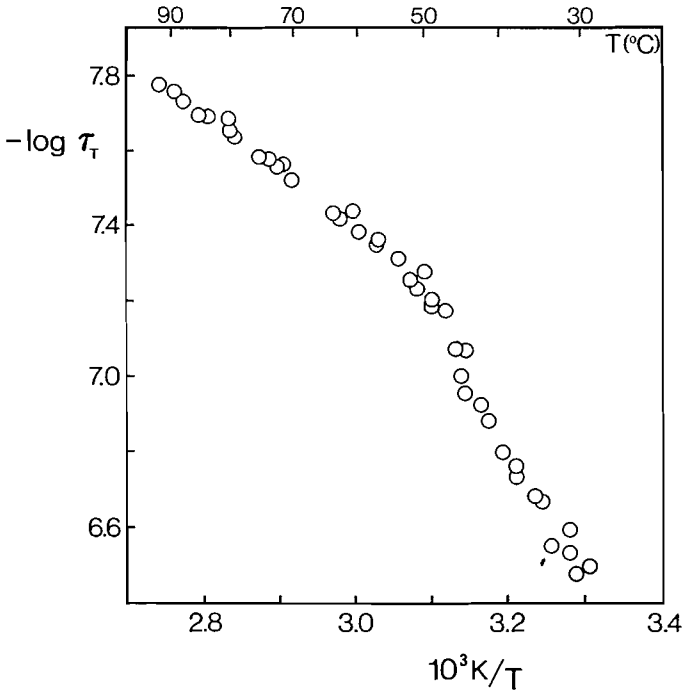


FIG. 8. Arrhenius plot showing the temperature dependence of the triplet lifetime of **1** as a 1 mol% mixture in CCH-4 (data from ref. 1*a*).

amines such as 1-aminopyrene and 1-aminofluorenone to form stable binary Sm A phases with CCH-4 (24) may provide an important clue to the identification of this binary phase.

The Arrhenius plot for the temperature dependence of the triplet lifetime of **1** as a 1 mol% mixture in CCH-4 is shown in Fig. 8 (1*a*). Clearly, the increase in the activation energy and entropy for triplet decay that is observed below the bulk N–Sm phase transition temperature *cannot* be attributed solely to the effects of solubilization of the ketone in the highly-ordered crystal-B phase of CCH-4, as was previously proposed (1). Rather, the lifetimes throughout the 53–30°C temperature range reflect a more complicated situation, since in a sample of this bulk composition, the nmr data indicate that *at least* 50% (perhaps as much as 80%) of the ketone *is excluded from the bulk crystal-B phase*. The excess solute is localized in a ketone-rich *nematic* phase whose composition varies with temperature between 35 and 53°C; below 35°C, the excess ketone is solubilized in a similarly enriched isotropic liquid or glass phase (the p-phase).

We have determined that the triplet lifetime of **1** in the nematic phase of CCH-4 is concentration-independent (between 1.0 and 10.0 mol% **1**) throughout the entire bulk nematic phase temperature range (32*a*). This rules out our initial suspicion that the increase in the Arrhenius parameters for triplet decay that occurs below the bulk Sm–N transition temperature might be due to a combination of temperature- and concentration effects on the lifetime of the ketone in the nematic phase component of the two-phase system. The ^2H nmr data shown in Fig. 2 illustrate that the continuously varying (composition-wise) nematic component of the two-phase system throughout the 53–35°C temperature range can be modelled fairly accurately by a series of bulk nematic solutions of the ketone in CCH-4. Thus, special effects on the mobility of the solute that might result in the 1 mol% sample from the intimate contact that would exist between the minor nematic component and the predominant, highly-ordered smectic component, can probably also be ruled out.

We suspect that the measured triplet lifetimes (between 30 and 53°C) in fact represent the averages of those due to ketone in the smectic phase and in the solute-rich nematic or p-phase at each temperature, in spite of the fact that at all temperatures, triplet decay appears to follow reasonably clean first-order kinetics.[4] The average would have to result from superposition of the first-order decay profiles due to ketone in the two phases in which it is solubilized; it is probably not a dynamic average caused by phase transfer equilibria, since this is expected to be much slower than the rate of triplet decay (given the very slow rate of diffusion that must characterize the highly ordered crystal-B phase (18)). Given the quality of the transient absorption data that is obtainable with such samples (1, 2), simple computer-modelling indicates that even an equally weighted sum of two independent first-order decay profiles would be difficult to distinguish from a single decay for differences of up to a factor of 3–4 in the decay rates of the two components. Extrapolation of the nematic phase portion of the plot to 35°C affords an estimate of *ca.* 90 ns for the triplet lifetime of **1** in the nematic phase at this temperature (in fact, a similar value has been measured at this temperature using EB as the nematic solvent (32*a*). Indeed, this is a factor of only *ca.* two shorter than the lifetime measured at the same temperature with the 1 mol% sample. To obtain a more accurate indication of the true effects of solubilization in the crystal-B phase on the conformational mobility of **1**, it will obviously be necessary to work with samples of much lower concentration (at or below the solubility limit) in the solute.

It is rather more difficult to estimate what is occurring below 35°C in the present case, where a *portion* of the ketone in the 1 mol% sample resides in the p-phase. Other workers have attributed solute behaviour in this temperature range to exclusive solubilization in this phase (22, 23, 27). This at least is probably not the case in the present instance, but it is impossible to distinguish whether the p-phase behaves as an isotropic or ordered phase with respect to its effects on the conformational motions that contribute to the triplet lifetime of **1**. If the p-phase is a viscous isotropic liquid, then because the Arrhenius behaviour of **1** in the nematic and isotropic phases are essentially indistinguishable (1), the Arrhenius plot below 35°C would be expected to simply continue without change from its character above this temperature. However, the same features will obtain if the p-phase affects the conformational mobility of the probe in a manner similar to the smectic phase, as Treanor and Weiss have proposed (22).

In a related study (23*b*), Gangoda and Fung ruled out the possibility that this phase could be an isotropic liquid, partly on the basis that there were no known examples of isotropic phases that exist at a *lower* temperature than the corresponding nematic phase. This is indeed a logical conclusion, provided that only two interconverting phases are involved in the transition. It is

[4]Correlation coefficients for data analysis by single-exponential, first-order decay were generally >0.99, and never less than 0.98. Nevertheless, reinspection of our data indicates that in the temperature range below 53°C, the first three or four points in the decays may deviate slightly from the least squares curve in some cases, although the deviation is not statistically significant. This may be indicative of the presence of a shorter-lived component. Occasionally, a small amount of longer-lived residual absorption occurred, but this was irreproducible and appeared to depend on sample quality (see ref. 1b).

Can. J. Chem. Downloaded from www.nrcresearchpress.com by 122.72.124.2 on 09/07/12
For personal use only.

Can. J. Chem. Downloaded from www.nrcresearchpress.com by 122.72.124.2 on 09/07/12
For personal use only.

possible though, that on cooling, a nematic phase could separate to give an isotropic liquid *and* a smectic or crystalline phase (i.e., N ⇄ Sm + I or N ⇄ K + I) (33). Our results are perfectly compatible with such behaviour, although it is difficult to obtain explicit experimental proof in the present case. Results with other systems offer a more clearcut indication that this is indeed the nature of the p-phase and the mechanism for its formation from either the nematic or smectic phases of solute/CCH-4 systems (32).

While some of the *details* or our interpretation of the temperature- and phase-dependent triplet state behaviour of **1** in the liquid crystalline phases of CCH-4 have now been defined more precisely, it is nevertheless clear that the major tenet of our original interpretation (1*a*) is correct. Solubilization in the crystal-B phase of CCH-4 *does indeed* impart dramatic inhibitory effects on the conformational mobility of **1**, compared to the situation in the more weakly ordered nematic phase or in the isotropic phase. However, the magnitude of the effect must be somewhat larger than is implied by the behaviour defined in Fig. 8 for a 1 mol% mixture. Furthermore, it seems likely that the phase-*independent* behaviour of other, differently substituted homologs of **1** in CCH-4 (and in CCH-2) (1) may result primarily from solubility factors.

Our experiments demonstrate that in mixtures of composition higher than the solubility limit of the solute in the smectic phase, the precursor to the p-phase is a solute-enriched nematic phase. In the case of **1**(**3**)/CCH-4 (and other solute/CCH-4 mixtures that we have studied (32*b*)), it is also formed in transitions involving the smectic phase, but at much lower temperatures. Furthermore, the **1**/CCH-4 p-phase is metastable, and transforms into a distinct binary smectic or solid modification. The latter can also be formed directly by rapid cooling from the nematic phase, without the intermediacy of the p-phase. This behaviour evidently does not extend to all solute/CCH-4 systems (*e.g.*, **5**/CCH-4 and benzene/CCH-4).

Given the close similarities between the ^{2}H nmr behaviour observed herein for **3** and that reported for **7** and **8** in the temperature range below 52–53°C, and the breadth of the N–Sm phase transition temperatures reported for mixtures of the latter compounds in CCH-4 (14*d*, 22), we speculate that the observed effects of this liquid crystal on the photochemistry of the latter compounds (as well as others that we have studied (2)) may in general be due to similar solubilization behaviour as that proposed above for **1**. In these cases, observed changes in ketone reactivity below 52–53°C is the result of some average between that of ketone in the smectic phase and that in a solute-enriched nematic or isotropic phase, with the relative weighting of the two contributions dependent on specific solubility limits.

Several questions remain to be answered with respect to the reactivity and conformational mobility of solutes in this liquid crystal and its homologs, and several new ones have arisen. The propensity of CCH-4 to form stable, solute-enriched binary smectic phases has now been demonstrated with three solutes (24) of very different structures, but the generality of these observations to other solute/CCH-4 systems remains to be determined. It is not clear how much information is available on the effects of these binary phases (or related ones) on the reactivity or conformational mobility of solutes relative to that in the nematic or smectic phase. Furthermore, we have yet to explain the reasons for the extraordinary substituent effects observed for the triplet state behaviour of **2** in this solvent (1); presumably, these effects are governed by similar solubilization phenomena to those observed with **1**. Experiments directed towards answering some of these questions are currently in progress.

Experimental

β-Phenyl-4-methoxypropriophenone (**1**) and β-(4-cyclohexylphenyl)-4-methoxypropriophenone were prepared in an earlier study (1) and had melting points of 96–97°C and 89–90°C, respectively. 4-Methoxyacetophenone (Aldrich Chemical Co.), benzene-d_6 (99.8% atom-*d*; MSD Isotopes), dichloromethane (Caledon HPLC), CCH-4, and CCH-2 (E. Merck) were all used as received from the suppliers.

β-Phenyl-4-methoxypropiophenone-α,α-d_2 (**3**), 4-methoxyacetophenone-α,α,α-d_3 (**5**), and β-(4-cyclohexylphenyl)-4-methoxypropiophenone-α,α-d_2 (**6**) were prepared from their protio-analogues by base-catalysed deuterium exchange. Typically, 1 g of the ketone was refluxed in a mixture of sodium hydroxide (1 g), dioxane (125 mL), and deuterium oxide (99.8% atom D; 5–10 mL) for 12–18 h. The resulting mixture was cooled to room temperature and extracted a few times with ether. After washing once with water, the combined ether extracts were dried over anhydrous sodium sulphate, filtered, and the solvent was evaporated on the rotary evaporator. The deuterated ketones were recrystallized two or three times from ethanol or ethanol/water and had melting points as follows: **3**, 95.5–97°C; **5**, 35.5–37.5°C; **6**, 89–90.5°C. Their ^{1}H nmr spectra (Varian EM390; chloroform-*d*) confirmed them to be >95% deuterated in the α-position in each case.

β-(4-Deuteriophenyl)-4-methoxypropiophenone (**4**) was prepared from 4-deuteriobenzaldehyde by the published route for **1** (21*e*). Benzaldehyde-4-*d* was prepared by D_2O/THF quenching of the aryllithium prepared from 4-bromo-(2-(1,3-dioxacyclopentyl)benzene and *n*-butyl lithium (in anhydrous tetrahydrofuran at −78°C), followed by hydrolysis of the acetal with 5% aqueous hydrochloric acid (30 mL) in THF (70 mL) under a nitrogen atmosphere. After isolation and three recrystallizations from ethanol/water, ketone **4** had a melting point of 96–97°C, and exhibited the following ^{1}H nmr spectrum (EM390; $CDCl_3$ *vs.* TMS): δ(ppm) = 3.14 (m, 4H), 3.83 (s, 3H), 6.90 (d, 2H), 7.30 (s, 4H), 7.93 (d, 2H). The high resolution ^{2}H nmr spectrum (76.8 MHz; in $CHCl_3$ with external $CDCl_3$ reference) for this compound showed a single resonance at 7.30 ppm.

Except where otherwise noted, ^{2}H nmr experiments were carried out at 76.78 MHz on a Bruker AM500 NMR spectrometer equipped with an Aspect 3000 computer, a Bruker BVT-100 Variable Temperature Unit, and a 10 mm VSP broadband probe. Temperatures were controllable to within ±1°, and were recorded with a copper–constantan thermocouple. Samples were prepared in 5 mm nmr tubes by adding the appropriate amounts of solute and liquid crystal and heating to the isotropic phase to ensure complete sample mixing. The sample and probe were allowed to equilibrate at each temperature for as long as was necessary to obtain reproducible spectra; this was generally 5–20 min for the samples containing ≤5 mol% solute, but extended to up to a few hours for those containing higher concentrations of **3**, particularly at temperatures below 45°C.

Deuterium nmr spectra were recorded on stationary samples using the quadrupolar echo pulse sequence (26), generally collecting 8–32K data points per scan over a 40–165 kHz sweep width. Typically, 96–512 such scans were collected and averaged (with a 0.2–0.8 s delay between scans, depending on sample temperature). The π/2 pulse width is *ca.* 27–30 μs on this instrument. The data were processed using 40–150 Hz line-broadening and exponential multiplication prior to obtaining the Fourier transform. At a given temperature, both the line-width and the observed splitting are approximately independent of the pulse sequence used (quadrupolar echo or single pulse) or whether the sample is spun or not.

A few experiments (mostly controls) were carried out at 41.3 MHz on a home-built spectrometer at the University of Guelph with assistance from Dr. K. H. Jeffrey. Samples were sealed under vacuum in 9 × 25 mm Pyrex tubes, and thereafter handled similarly to those

described above. The spectrometer has been described in detail elsewhere (34).

Deuterium T_1 measurements summarized in Fig. 7 for 3 mol% samples of **3** in CCH-4 and EB between 15–108°C were carried out on the Bruker AM500, and employed a $\pi-\tau-\pi/2$ or $\pi/2-\tau-\pi/2$ (for T_1 values less than 20 ms) non-selective inversion-recovery pulse sequence, followed by the quadrupolar echo. Typically, T_1 values were calculated from least squares analysis of data from 8–12 τ values. Errors were calculated as two standard deviations by a statistical method (35), and ranged from *ca.* 1–2% for values >50 ms to *ca.* 20% for those less than 15 ms. Error bars are included in the plot in Fig. 7 for those data with associated errors ≥ 10%.

T_1-values at a few representative temperatures in the 77–123°C range were measured on a Bruker AC200 NMR spectrometer equipped with a 10 mm broadband probe, with the assistance of Dr. C. Rodger (Bruker Canada). These values are not reported, but were consistently *ca.* 10% smaller than those measured on the AM500, and showed a similar variation with temperature.

DSC experiments employed a Setaram DSC-111 differential scanning calorimeter, interfaced to a Hewlett-Packard HP85 microcomputer. Samples (30–35 mg) of **1** in CCH-4 were prepared in aluminum crucibles after combining the appropriate amounts of CCH-4 and the ketone (as aliquots of a standard solution in dichloromethane), dissolving the mixture in *ca.* 5 mL dichloromethane, evaporating the solvent on the rotary evaporator, and finally pumping on the mixture under high vacuum (*ca.* 10^{-4} Torr) for 1–2 h. Heating and cooling scans (2°/min) were carried out at least twice for each sample between −10 and 90°C, in order to ensure reproducibility.

Thermal microscopy experiments were carried out with a Reichert Hot-Stage microscope fitted with polarizing filters and a glass thermometer. Transition temperatures are corrected. Samples were prepared in similar fashion to those for DSC experiments, and were contained on glass slides under a cover slip. Heating and cooling scans were carried out repetitively for each sample. Our observations are described in detail below.

Rapid cooling of samples containing 0.5 ≤ **1** ≤ 5 mol% to 23°C from the nematic phase yields a fairly uniform mosaic texture similar in appearance to that of the Sm phase of pure CCH-4 (18*c*). Heating the sample reveals a bulk K–Sm transition at 28–30°C, the development of fluid imperfections at 43–44°C, slow dissolution of the bulk smectic phase from 44–51°C, and finally a fairly abrupt transition of residual smectic phase to nematic at 51–53°C.

Compound **1** is uniformly soluble in the nematic phase of CCH-4 up to a concentration of ca. 20 mol%; in mixtures of higher concentration of **1**, the ketone crystallizes out of the nematic solution. For the mixtures containing ≤20 mol% **1**, the N–I transition is completely reversible (i.e. not "supercoolable"), but is lowered and broadened as [**1**] increases. The behaviour of the mixtures at lower temperatures (below the N–Sm transition of pure CCH-4), particularly the heating behaviour, depends strongly on the rate at which the sample is cooled to room temperature from the nematic phase, as well as the period of time for which the sample is allowed to equilibrate at room temperature. Slow (≤3°/min) cooling of *any* of the samples from the nematic phase results in the initial appearance of smectic monodomains interspersed in residual nematic phase. The appearance of the smectic phase is initially rapid (probably due to supercooling), but then slows down with further decreases in temperature. In the samples containing >2 mol% **1**, the smectic phase initially appears as serrated stars that gradually enlarge, leaving the nematic phase localized between the serrations. As sample cooling is continued, the proportion of smectic phase increases at the expense of the residual nematic phase. At 33–35°C, the latter transforms to an optically isotropic phase (the so-called "p-phase") which appears to be stable down to (at least) room temperature for short periods of time. Reheating these samples results in the reverse of their cooling behaviour. This initially rapid and then more gradual separation of smectic phase from nematic is readily discernible in the DSC traces shown in Fig. 2*a* as an incomplete return to baseline after the initial Sm–N endotherm. Complete formation of the smectic phase is, in all cases, arrested by transformation of residual nematic phase at 35°C to the "p-phase".

Allowing the samples to equilibrate at room temperature for extended periods of time (up to 2–3 days; the time is proportional to the bulk concentration of **1**) results in contraction of the isotropic fraction to yield (what appear to be) crystallites dispersed throughout the sample. This behaviour is observed for *all* compositions between 0.5 and 10 mol% **1**, but is especially pronounced in the samples containing >2 mol% **1**. Heating these samples results in a solid-smectic (K–Sm) transition involving the bulk monodomains at 28–30°C, a sharp transition at 43.5–44°C involving transformation of the "crystallites" to a nematic phase dispersed among the smectic monodomains, slow expansion of the nematic droplets as the temperature is increased further, and finally another relatively sharp transformation of the bulk residual smectic phase to nematic at 51–53.5°C.

Rapid cooling of the 10 mol% sample to 23°C affords a uniform, striated mosaic texture. The sample undergoes a K–K or K–Sm transition at 27–28°C, in which the striations disappear to leave a homogeneous, fine mosaic texture. Heating the sample further results in a single, sharp transition to an uniform nematic phase at 43.7–44°C, followed by a broad N–I transition at 58.5–63°C.

Samples containing 10 < [**1**] ≤ 15 mol% undergo phase separation and "p-phase" formation upon slow cooling as well, but the samples gradually reorganize to form a mixture of crystalline solid (presumably fairly pure **1**) and the binary mixture below 43°C. Samples containing > 15 mol% **1** undergo slow solidification without prior phase separation or p-phase formation, independent of cooling rate.

Acknowledgments

We are indebted to a number of people for lending their advice, expertise, and equipment for these studies, and making our introduction to nmr spectroscopy in ordered media a relatively painless one. We thank Dr. K. H. Jeffrey (University of Guelph) for graciously allowing us the use of his NMR spectrometer, giving generously of his time and expertise helping us operate it, and for enlightening discussions. We are especially grateful to Dr. A. D. Bain (McMaster University), who provided many helpful discussions and considerable assistance with the T_1 measurements. Dr. C. Rodger (Bruker Canada) is also gratefully acknowledged for making the Bruker AC200 spectrometer available to us and helping us with its operation. We also thank Dr. D. Hughes and Mr. B. Sayer (McMaster University) for technical assistance, and E. Merck (Darmstadt) for generous gifts of CCH-2 and CCH-4. Finally, the financial support of the Natural Sciences and Engineering Research Council of Canada is gratefully acknowledged.

1. (*a*) W. J. LEIGH. J. Am. Chem. Soc. **107**, 6114 (1985); (*b*) W. J. LEIGH. Can. J. Chem. **64**, 1130 (1986).
2. W. J. LEIGH and S. K. JAKOBS. Tetrahedron, **43**, 1393 (1987).
3. D. A. HROVAT, J. H. LIU, N. J. TURRO, and R. G. WEISS. J. Am. Chem. Soc. **106**, 7033 (1984).
4. (*a*) V. C. ANDERSON, B. B. CRAIG, and R. G. WEISS. J. Phys. Chem. **86**, 4642 (1982); (*b*) V. C. ANDERSON, B. B. CRAIG, and R. G. WEISS. Mol. Cryst. Liq. Cryst. **97**, 351 (1983); (*c*) V. C. ANDERSON and R. G. WEISS. J. Am. Chem. Soc. **106**, 6628 (1984); (*d*) V. C. ANDERSON, B. B. CRAIG, and R. G. WEISS. J. Am. Chem. Soc. **103**, 7169 (1981); **104**, 2972 (1982).
5. (*a*) E. SACKMANN and D. REHM. Chem. Phys. Lett. **4**, 537 (1970); (*b*) H. BEENS, H. MOHWALD, D. REHM, E. SACKMANN, and A. WELLER. Chem. Phys. Lett. **8**, 341 (1971); (*c*) G. BAUR, A. STIEB and G. MEIER. J. Appl. Phys. **44**, 1905 (1973); (*d*) E. D. CEHELNIK, R. B. CUNDALL, J. R. LOCKWOOD, and T. F. PALMER. J. Chem. Soc. Faraday Trans. 2, **70**, 244 (1974).
6. (*a*) E. SACKMANN, P. KREBS, H. U. REGA, J. VOSS, and H. MOHWALD. Mol. Cryst. Liq. Cryst. **24**, 283 (1973); (*b*) E.

Can. J. Chem. Downloaded from www.nrcresearchpress.com by 122.72.124.2 on 09/07/12
For personal use only.

Can. J. Chem. Downloaded from www.nrcresearchpress.com by 122.72.124.2 on 09/07/12
For personal use only.

SACKMANN and H. MOHWALD. Chem. Phys. Lett. **12**, 467 (1972); (*c*) B. O. MYRVOLD and P. KLAEBOE. Acta Chem. Scand. **A39**, 733 (1985); (*d*) G. SOLLADIE and G. GOTTARELLI. Tetrahedron, **43**, 1425 (1987) and references cited therein.

7. (*a*) K. V. S. RAO, C. F. POLNASZEK, and J. H. FREED. J. Phys. Chem. **81**, 449 (1977); (*b*) W. LIN and J. H. FREED. J. Phys. Chem. **83**, 379 (1979); (*c*) E. MEIROVITCH, D. IGNER, E. IGNER, G. MORO, and J. H. FREED. J. Chem. Phys. **77**, 3915 (1982); (*d*) M. S. BROIDO, I. BELSKY, and E. MEIROVITCH. J. Phys. Chem. **86**, 4197 (1982); (*e*) E. MEIROVITCH and M. S. BROIDO. J. Phys. Chem. **88**, 4316 (1984); (*f*) E. MEIROVITCH and J. H. FREED. J. Phys. Chem. **88**, 4995 (1984).
8. (*a*) Z. LUZ. *In* Nuclear magnetic resonance of liquid crystals. NATO ASI Series, Ser. C. Vol. 141. *Edited by* J. W. Emsley. D. Reidel Publishing Co., Dordrecht, 1985. Chapt. 13; (*b*) N. A. P. VAZ and J. W. DOANE. J. Chem. Phys. **79**, 2470 (1983); (*c*) A. G. AVENT, J. W. EMSLEY, S. NG, and S. M. VENABLES. J. Chem. Soc. Perkin Trans. II, 1855 (1984); (*d*) B. M. FUNG, R. V. SIGH, and M. M. ALCOCK. J. Am. Chem. Soc. **106**, 7301 (1984); (*e*) R. R. VOLD and R. L. VOLD. *In* Liquid crystals and ordered fluids. Vol. 4. *Edited by* A. C. Giffin and J. F. Johnson. Plenum Publishing Corp. 1984. p. 561; (*f*) R. BLINC, B. MARIN, J. PIRS, and J. W. DOANE. Phys. Rev. Lett. **54**, 438 (1985); (*g*) E. T. SAMULSKI. Polymer, **26**, 177 (1985).
9. (*a*) W. J. LEIGH, D. T. FRENDO, and P. J. KLAWUNN. Can. J. Chem. **63**, 2131 (1985); (*b*) W. J. LEIGH. Can. J. Chem. **63**, 2736 (1985); (*c*) W. J. LEIGH and D. S. MITCHELL. J. Am. Chem. Soc. **110**, 1311 (1988).
10. (*a*) W. E. BACON and G. H. BROWN. Mol. Cryst. Liq. Cryst. **12**, 229 (1971); (*b*) M. J. S. DEWAR and B. D. NAHLOVSKY. J. Am. Chem. Soc. **96**, 460 (1974).
11. (*a*) S. MELONE, V. MOSINI, R. NICOLETTI, B. SAMORI, and G. TORQUATI. Mol. Cryst. Liq. Cryst. **98**, 399 (1983); (*b*) B. SAMORI and L. FIOCCO. J. Am. Chem. Soc. **104**, 2634 (1982); (*c*) P. DE MARIA, A. LODI, B. SAMORI, F. RUSTICHELLI, and G. TORQUATI. J. Am. Chem. Soc. **106**, 653 (1984); (*d*) B. SAMORI, P. DE MARIA, P. MARIANI, F. RUSTICHELLI, and P. ZANI. Tetrahedron, **43**, 1409 (1987).
12. (*a*) C. ESKENAZI, J. F. NICOUD, and H. B. KAGAN. J.Org. Chem. **44**, 995 (1979); (*b*) P. SEURON and G. SOLLADIE. J. Org. Chem. **45**, 715 (1980); (*c*) Y. TANAKA, T. CHIYO, S. IIJIMA, T. SHIMIZU, and T. KUSANO. Mol. Cryst. Liq. Cryst. **99**, 255 (1983).
13. (*a*) E. G. CASSIS, JR. and R. G. WEISS. Photochem. Photobiol. **35**, 439 (1982); (*b*) J. P. OTRUBA III and R. G. WEISS. Mol. Cryst. Liq. Cryst. **80**, 165 (1982); (*c*) J. P. OTRUBA III and R. G. WEISS. J. Org. Chem. **48**, 3448 (1983).
14. (*a*) J. M. NERBONNE and R. G. WEISS. J. Am. Chem. Soc. **101**, 402 (1979); (*b*) J. M. NERBONNE and R. G. WEISS. Isr. J. Chem. **18**, 266 (1979); (*c*) D. A. HROVAT, J. H. LIU, N. J. TURRO, and R. G. WEISS. J. Am. Chem. Soc. **106**, 5291 (1984); (*d*) R. G. ZIMMERMANN, J. H. LIU, and R. G. WEISS. J. Am. Chem. Soc. **108**, 5264 (1986); (*e*) R. L. TREANOR and R. G. WEISS. J. Am. Chem. Soc. **108**, 3137 (1986); (*f*) R. L. TREANOR and R. G. WEISS. Tetrahedron, **43**, 1371 (1987).
15. Licristal Liquid Crystals. EM Chemicals, Hawthorne, N.Y. (1986).
16. E. RAHIMZADEH, T. TSANG, and L. YIN. Mol. Cryst. Liq. Cryst. **139**, 291 (1986).
17. G. J. BROWNSEY and A. J. LEADBETTER. J. Phys. Paris, **42**, L135 (1981).
18. (*a*) F. D. SAEVA. (*Editor*). Liquid Crystals. The fourth state of matter. Marcel Dekker, Inc. New York, 1979; (*b*) H. KELKER and R. HATZ. Handbook of liquid crystals. Verlag Chemie, Weinheim. 1980; (*c*) G. W. GRAY and J. W. GOODBY. Smectic liquid crystals. Textures and structures. Leonard Hill, Glasgow. 1984.
19. L. POHL and R. EIDENSCHINK. Anal. Chem. **50**, 1934 (1978).
20. (*a*) H. WEDEL and W. HAASE. Chem. Phys. Lett. **55**, 96 (1978); (*b*) F. JEDE, A. W. STRATMANN, and B. SCHRADER. Mol. Cryst. Liq. Cryst. **140**, 287 (1986).
21. (*a*) D. G. WHITTEN and W. E. PUNCH. Mol. Photochem. **2**, 77 (1970); (*b*) P. J. WAGNER, P. A. KELSO, A. E. KEMPPAINEN, A. HAUG, and D. R. GRABER. Mol. Photochem. **2**, 81 (1970); (*c*) J. C. SCAIANO, M. J. PERKINS, J. W. SHEPPARD, M. S. PLATZ, and R. L. BARCUS. J. Photochem. **21**, 137 (1983); (*d*) H. L. CASAL and J. C. SCAIANO. Can. J. Chem. **62**, 628 (1984); (*e*) J. C. NETTO-FERREIRA, W. J. LEIGH, and J. C. SCAIANO. J. Am. Chem. Soc. **107**, 2617 (1985); (*f*) W. J. LEIGH, J. C. SCAIANO, C. I. PARASKEVOPOULOS, G. M. CHARETTE, and S. E. SUGAMORI. Macromolecules, **18**, 2148 (1985).
22. R. L. TREANOR and R. G. WEISS. J. Phys. Chem. **91**, 5552 (1987).
23. (*a*) B. M. FUNG and M. GANGODA. J. Am. Chem. Soc. **107**, 3395 (1985); (*b*) M. GANGODA and B. M. FUNG. Chem. Phys. Lett. **120**, 527 (1985).
24. (*a*) G. SIGAUD, M. F. ARCHARD, F. HARDOUIN, and H. GASPAROUX. J. Phys. Lett. **46**, 321 (1985); (*b*) J. THOEN, H. BERINGHS, J. M. AUGUSTE, and G. SIGAUD. Liquid Crystals, **2**, 853 (1987).
25. (*a*) J. H. DAVIS. Biochim. Biophys. Acta, **737**, 117 (1983); (*b*) I. C. P. SMITH. *In* NMR of newly accessible nuclei. Academic Press, Inc. New York. 1983. Vol. 2, Chapt. 1; (*c*) R. L. VOLD and R. R. VOLD. Isr. J. Chem. **23**, 315 (1983); (*d*) J. W. DOANE. Isr. J. Chem. **23**, 323 (1983); (*e*) E. T. SAMULSKI. Isr. J. Chem. **23**, 329 (1983); (*f*) R. Y. DONG. Isr. J. Chem. **23**, 370 (1983); (*g*) J. W. EMSLEY, R. HASHIM, G. R. LUCKHURST, and G. N. SHILSTONE. Liquid Crystals, **1**, 437 (1986); (*h*) R. Y. DONG. Mol. Cryst. Liq. Cryst. **141**, 349 (1986); (*i*) R. Y. DONG. Bull. Magn. Res. **9**, 29 (1987).
26. (*a*) J. H. DAVIS, K. R. JEFFREY, M. BLOOM, M. I. VALIC, and T. P. HIGGS. Chem. Phys. Lett. **42**, 390 (1976); (*b*) M. BLOOM, J. H. DAVIS, and M. I. VALIC. Can. J. Phys. **58**, 1510 (1980).
27. H. FUJIWARA, J. HIRAI, Y. SASAKI, and K. TAKAHASHI. Mol. Cryst. Liq. Cryst. **150B**, 387 (1987).
28. J. S. HWANG, K. V. S. RAO, and J. H. FREED. J. Phys. Chem. **80**, 1490 (1976).
29. S. HSI, H. ZIMMERMANN, and Z. LUZ. J. Chem. Phys. **69**, 4126 (1978).
30. J. C. ROWELL, W. D. PHILLIPS, L. R. MELBY, and M. PANAR. J. Chem. Phys. **43**, 3442 (1965).
31. D. S. MITCHELL and W. J. LEIGH. Liquid Crystals. In press.
32. (*a*) M. WORKENTIN and W. J. LEIGH. To be published; (*b*) B. J. FAHIE, D. S. MITCHELL, M. S. WORKENTIN, and W. J. LEIGH. J. Am. Chem. Soc. In press.
33. H. A. J. OONK. Phase theory. The thermodynamics of heterogeneous equilibria. Elsevier, Amsterdam. 1981.
34. K. R. JEFFREY and R. E. WASYLISHEN. Can. J. Phys. **64**, 833 (1986).
35. G. E. P. BOX, W. G. HUNTER, and J. S. HUNTER. Statistics for experimenters. John Wiley and Sons, New York. 1978. p. 454.

Bifunctional reagents in organic synthesis. Total syntheses of the sesquiterpenoids (±)-pentalenene and (±)-9-*epi*-pentalenene

EDWARD PIERS AND VERANJA KARUNARATNE

Department of Chemistry, University of British Columbia, 2036 Main Mall, University Campus, Vancouver, B.C., Canada V6T 1Y6

Received July 28, 1988

EDWARD PIERS and VERANJA KARUNARATNE. Can. J. Chem. **67**, 160 (1989).

Transformation of the readily available keto acetal **14** into the enone **23** was accomplished via a seven-step sequence of reactions. Reaction of **23** with the bifunctional Grignard reagent **5** in the presence of copper(I) bromide – dimethyl sulfide, followed by intramolecular alkylation of the resultant chloro ketone **24**, gave the tetracyclic ketone **25**. Treatment of **25** with hydrogen in the presence of platinum afforded a mixture of the ketones **27** and **28** (42:58, respectively), which was transformed into a separable mixture of (±)-pentalenene (**1**) (32%) and (±)-9-*epi*-pentalenene (**30**) (33%).

Key words: ±-pentalenene synthesis, ±-9-*epi*-pentalenene synthesis, sesquiterpenoid synthesis, methylenecyclopentane annulation, bifunctional reagents, triquinane synthesis.

EDWARD PIERS et VERANJA KARUNARATNE. Can. J. Chem. **67**, 160 (1989).

Faisant appel à une série de sept réactions, on a réalisé la transformation du céto-acétal **14**, qui est facilement accessible, en énone **23**. La réaction du composé **23** avec le réactif de Grignard bifonctionnel **5** en présence de bromure de cuivre(I) – sulfure de diméthyle, suivie d'une alkylation intramoleculaire de la chloro-cétone **24** qui en résulte, conduit à la cétone tétracyclique **25**. Le traitement du composé **25** par de l'hydrogène en présence de platine fournit un mélange des cétones **27** et **28** (dans une proportion de 42:58) qui a été transformé en un mélange de (±)-pentalènène (**1**) (32%) et de (±)-*épi*-9 pentalènène (**30**) (33%) que l'on peut séparer.

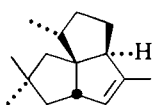
Mots clés: synthèse de ±-pentalènène, synthèse de ±-*epi*-9 pentalènène, synthèse sesquiterpénique, annelation de méthylènecyclopentane, réactifs bifonctionnels, synthèse de triquinane.

[Traduit par la revue]

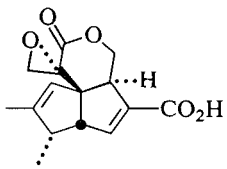
Can. J. Chem. Downloaded from www.nrcresearchpress.com by 122.72.124.2 on 09/07/12
For personal use only.

Introduction

The angularly fused triquinane (+)-pentalenene (**1**), isolated from *Streptomyces griseochromogenes* (1), is the parent hydrocarbon of the pentalenolactone family of sesquiterpenoid antibiotics. In fact, by carrying out appropriate feeding experiments with a culture of *Streptomyces* UC5319, Cane and Tillman (2) have shown that **1** is a biosynthetic precursor of (−)-pentalenolactone (**2**) and related substances. Since the absolute stereochemistry of (−)-**2** has been established (3), (+)-pentalenene is (1*S*,4*S*,8*R*,9*R*)-2,6,6,9-tetramethyltricyclo-[6.3.0.0^{4,8}]undec-2-ene (**1**).



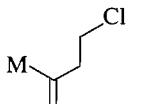
1



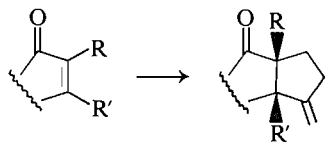
2

It is not particularly surprising that pentalenene (**1**) has attracted considerable attention within the community of synthetic organic chemists. Indeed, a considerable number of total syntheses of (±)-**1**, via notably diverse strategies, have been reported (4–11), while, recently, Hua described (12) an interesting enantioselective synthesis of (+)-**1**.

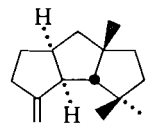
Recently, we reported that 4-chloro-2-trimethylstannyl-1-butene (**3**), upon transmetalation with methyllithium in tetrahydrofuran (THF) at −78°C, is transformed into the synthetically useful bifunctional reagent 4-chloro-2-lithio-1-butene (**4**) (13*a*,*d*). Furthermore, the latter species can readily be converted into the corresponding Grignard reagent **5** (13*c*,*d*) or the cuprates **6** and **7** (13*b*,*d*). Significantly, **5**–**7** serve as very useful conjunctive reagents for effecting methylenecyclopentane annulation sequences that can be represented in general terms by the conversion **8** → **9** (13*b*–*d*). Indeed, a total synthesis of the linearly fused triquinane sesquiterpenoid (±)-capnellene (**10**)



3 M = $SnMe_3$ **6** M = CuSPh(Li)
4 M = Li **7** M = CuCN(Li)
5 M = MgBr



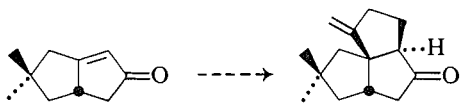
8 **9**



10

was achieved via a route in which both of the "outside" five-membered rings were added to the central ring by means of this type of transformation (13*c*,*d*).

An examination of the structure of pentalenene (**1**) readily reveals that a total synthesis of this substance might be accomplished via a route in which the above-mentioned annulation method would play a key role. Explicitly, methylenecyclopentane annulation of the bicyclic enone **11** would proceed in the desired stereochemical sense (13*b*,*d*) and, if successful, would provide the tricyclic ketone **12**. Presumably, the latter substance would serve as a suitable synthetic precursor of (±)-pentalenene



11 **12**

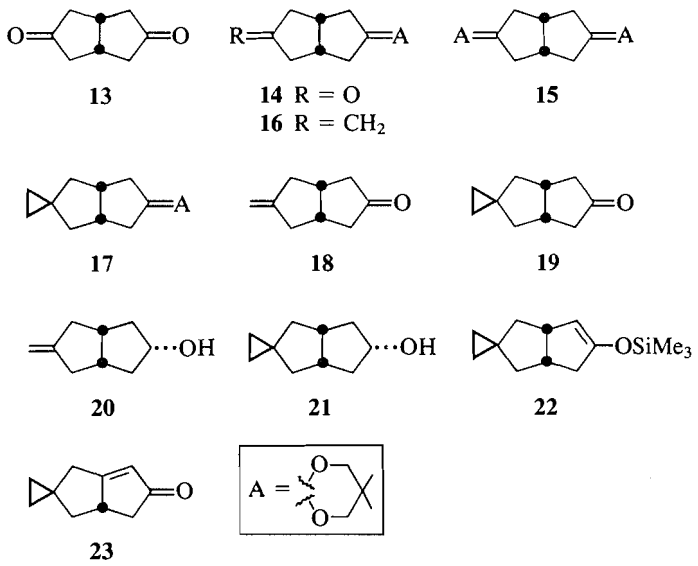


CHART 1

(**1**). We describe in this paper the details of a total synthesis of (±)-**1**, which is based on this synthetic plan.[1]

Results and discussion

(a) Preparation of the tricyclic enone 23

The starting material for our synthesis was the readily available *cis*-bicyclo[3.3.0]octane-3,7-dione (**13**) (15) (see Chart 1). Treatment of this substance with one equivalent of 2,2-dimethyl-1,3-propanediol in hot benzene containing *p*-toluenesulfonic acid provided an equilibrium mixture of the starting material **13**, the keto acetal **14**, and the bisacetal **15** (ratio 1:2:1, respectively). Fortunately, these compounds were readily separable by column chromatography. Furthermore, the dione **13** and the bisacetal **15** could be recycled and, after two such operations, the desired keto acetal **14** was obtained in 79% yield.

Treatment of **14** with methylenetriphenylphosphorane in THF provided the alkene **16** (84%). Attempted cyclopropanation of this material with diethylzinc–diiodomethane (16) gave a mixture of products from which the desired material **17** could be obtained in only poor yield (<25%). Although mild acid hydrolysis of **16** gave the keto alkene **18** in excellent yield, cyclopropanation (16) of the latter substance also proved to be problematic. At best, the tricyclic ketone **19** was produced in only 30% yield. Consequently, the ketone function in **18** was reduced ($LiAlH_4$) and the required cyclopropanation reaction (16) was carried out on the resultant alkene alcohol **20**. In this case, the carbenoid reaction proceeded smoothly and the tricyclic alcohol **21** was obtained in 76% yield from **18**. At this stage, it would undoubtedly have been possible to effect hydrogenolysis of the cyclopropyl ring. However, a future (envisaged) step of the synthetic sequence involved hydrogenation of a carbon–carbon double bond and, therefore, it was decided to retain the cyclopropane ring to that stage of the synthesis and then carry out the two reductive transformations in one operation.

Oxidation of the alcohol **21** with pyridinium chlorochromate (17) gave the ketone **19** in 87% yield. The method of Saegusa and co-workers (18) was employed to effect conversion of **19** into the corresponding enone **23**. Thus, reaction of **19** with freshly prepared iodotrimethylsilane (19) in cold (−78°C) dichloromethane containing triethylamine afforded the enol silyl ether **22**. The latter substance, upon treatment with palladium(II) acetate in acetonitrile (18), provided the required enone **23** (73% from **19**). The stage was thus set to carry out the key methylenecyclopentane annulation sequence.

(b) Conversion of the enone 23 into (±)-pentalenene (1) and (±)-9-epi-pentalenene (30)

Conjugate addition of the 2-(4-chloro-1-butenyl) group to the enone **23** was effected by reaction (THF, −78°C) of this material with the Grignard reagent **5** (13*c*,*d*) in the presence of copper(I) bromide – dimethyl sulfide complex (Scheme 1). The product **24**, upon treatment with potassium hydride in THF, cyclized smoothly to the tetracyclic annulation product **25** (66% from **23**).

Reaction of the intermediate **25** with hydrogen (3 atmospheres pressure; 1 atm = 101.3 kPa) in the presence of platinum in acetic acid resulted in hydrogenation of the alkene function and hydrogenolysis of the cyclopropane ring. Unfortunately, analysis (glc) of the product showed that it consisted of a mixture of the epimers **27** and **28**, in a ratio of 42:58, respectively. Attempts to increase the relative amount of the desired isomer **27** by use of other hydrogenation conditions proved to be fruitless. For example, hydrogenation of **25** in the presence of palladium-on-carbon in hexane effected only reduction of the alkene function. Subsequent hydrogenolysis (hydrogen, platinum) of the cyclopropane ring afforded **27** and **28** in a ratio of 22:78, respectively.

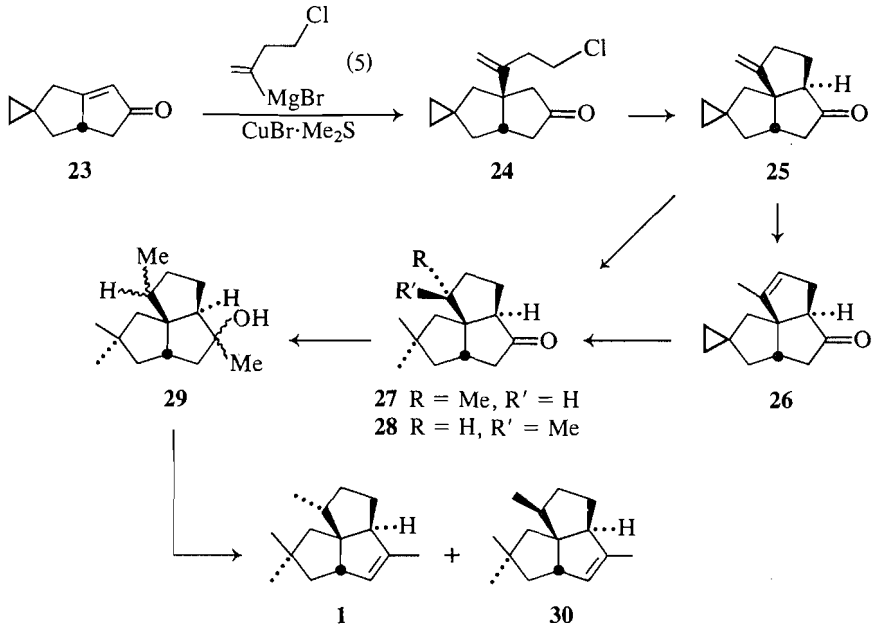
Upon treatment with *p*-toluenesulfonic acid in dichloromethane, compound **25** was converted cleanly into the endocyclic alkene **26**. Interestingly, however, hydrogenation–hydrogenolysis of the latter substance provided (80%) a 5:95 mixture of **27** and **28**, respectively.

In an earlier study (5) culminating in a synthesis of (±)-pentalenene (1), it was shown that conjugate addition of lithium dimethylcuprate to the enone **31** was completely stereoselective, providing the tricyclic ketone **33** in excellent yield. On the other hand, reaction of the enone **32** with triethylsilane – tris(triphenylphosphine)rhodium chloride afforded a mixture of the epimers **33** and **34** in a ratio of 2.24:1, respectively. Thus, interestingly, the cuprate delivers a methyl group exclusively to the concave (*endo*) face of the enone **31**, while, in the hydrosilylation reaction, the reagent transfers a proton primarily to the convex (*exo*) face of **32**. These findings, taken in conjunction with our hydrogenation results involving compounds **25** and **26**, demonstrate the difficulty associated with predicting the stereochemistry of (some) reactions of functionalized tricyclo[6.3.0.$0^{4,8}$]undecanes.

Since compounds **27** and **28** proved to be very difficult to separate by column chromatography, the 42:58 mixture of these substances was treated with methyllithium in THF. The product of this reaction consisted of a mixture of the starting materials (40%) and the desired alcohols **29** (60%). That the reaction had not proceeded to completion was undoubtedly due to the fact that proton transfer (enolate anion formation) was in competition with the desired nucleophilic addition reaction. Therefore, the product mixture was treated again with methyllithium and, after the recycling procedure had been carried out twice, the isolated material consisted of **27** and **28** (ratio 1:17, respectively) (18%) and the alcohols **29** (82%). Treatment of this mixture with *p*-toluenesulfonic acid in hot benzene, followed by chromatography of the resultant material on silver nitrate-

[1]For a preliminary account of this work, see ref. 14.

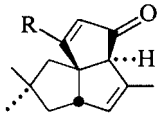
Can. J. Chem. Downloaded from www.nrcresearchpress.com by 122.72.124.2 on 09/07/12
For personal use only.



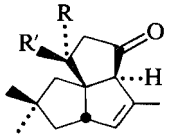
SCHEME 1

impregnated silica gel, afforded (±)-9-*epi*-pentalenene (**30**) (33%) and (±)-pentalenene (**1**) (32%). Our synthetic (±)-**1** exhibited spectra identical with those of the same material previously prepared by Paquette and Annis (5).[2]

When a 5:95 mixture of **27** and **28**, obtained by hydrogenation–hydrogenolysis of **26** (*vide supra*), was subjected to a sequence of operations identical with that described above, (±)-9-*epi*-pentalenene (**30**) was obtained in 68% yield.



31 R = H
32 R = Me



33 R = H, R' = Me
34 R = Me, R' = H

Experimental

General information

Melting points and distillation temperatures, which refer to short-path (Kugelrohr) distillations, are uncorrected. Infrared (ir) spectra were recorded on a Perkin–Elmer model 710B spectrophotometer and were calibrated using the 1601 cm^{-1} band of a polystyrene film. Proton (^1H) and carbon (^{13}C) nuclear magnetic resonance (nmr) spectra were recorded on $CDCl_3$ solutions. Signal positions are given in ppm (δ) relative to Me_4Si. High resolution mass spectra were recorded with Kratos/AEI MS 50 or MS 902 spectrometers. Gas–liquid chromatography (glc) was accomplished with a Hewlett–Packard model 5880 gas chromatograph equipped with a 25 m × 0.21 m fused silica column coated with cross-linked SE-54. Thin-layer chromatography (tlc) was carried out on commercial silica gel plates (Eastman Chromatogram Sheet, Type 13181 or E. Merck, Type 5554). Conventional and flash (20) column chromatography were done on 70–230 and 230–400 mesh silica gel (E. Merck), respectively. Reagents and solvents were purified and dried using standard methods. NOTE: All compounds for which high resolution mass measurements are given exhibited one spot on tlc analysis and, except for the mixture of **27** and **28**, essentially one peak on glc analysis.

Preparation of the keto acetal ***14***[3]

A stirred mixture of *cis*-bicyclo[3.3.0]octane-3,7-dione (**13**) (70 g, 0.51 mol), 2,2-dimethyl-1,3-propanediol (53 g, 0.51 mmol), *p*-toluenesulfonic acid (0.5 g), and benzene (500 mL) was refluxed for 2 h under a Dean–Stark water trap. The solution was cooled, diluted with diethyl ether (500 mL), washed successively with 10% aqueous sodium hydroxide, water, and brine, dried ($MgSO_4$), and concentrated. Analysis (glc) of the resultant white semisolid showed that it consisted of a 1:2:1 mixture of the diketone **13**, the keto acetal **14**, and the bisacetal **15**. A solution of this material in 140 mL of 3:2:1 petroleum ether – ethyl acetate – dichloromethane was added to a column of silica gel (300 g). Elution of the column with 2:1 petroleum ether – ethyl acetate removed a mixture of **14** and **15**, while elution with ethyl acetate provided 16.4 g of the dione **13**. The mixture of **14** and **15**, dissolved in 100 mL of 3:2:1 petroleum ether – ethyl acetate – dichloromethane, was added to a column of silica gel (1500 g) and the column was eluted with 3:1 petroleum ether – diethyl ether. Concentration of the appropriate fractions provided 53.4 g of the keto acetal **14** and 36.9 g of the bisacetal **15**, both as crystalline white solids.

A stirred solution of the dione **13** (16.4 g) and the bisacetal **15** (36.9 g), obtained from the above reaction, in 250 mL of dry benzene containing 250 mg of *p*-toluenesulfonic acid was refluxed for 1 h. Work-up and purification of the crude product as described above gave 7.6 g of the dione **13**, 24.7 g of the keto acetal **14**, and 17.1 g of the bisacetal **15**. The recovered **13** and **15** were equilibrated again and chromatographic separation provided **13** (3.5 g), **14** (11.3 g), and **15** (7.8 g). Thus, the total of the desired keto acetal **14** was 89.4 g (79%).

The keto acetal **14** exhibited mp 48°C (from heptane); ir ($CHCl_3$): 1730, 1110 cm^{-1}; ^1H nmr (400 MHz) δ: 0.97 (s, 6H), 1.82 (dd, 2H, J = 14, 5 Hz), 2.17 (dd, 2H, J = 19, 4.5 Hz), 2.29 (dd, 2H, J = 14, 9 Hz), 2.46 (dd, 2H, J = 19, 10 Hz), 2.28 (m, 2H), 3.44, 3.47 (s, s, 2H each). *Anal.* calcd. for $C_{13}H_{20}O_3$: C 69.61, H 8.99; found: C 69.55, H 8.85. *Exact Mass* calcd.: 224.1413; found: 224.1416.

The bisacetal **15** exhibited mp 140–142°C (from ethanol or methanol); ir ($CHCl_3$): 1210 cm^{-1}; ^1H nmr (400 MHz) δ: 0.95 (s, 12H), 1.72 (dd, 4H, J = 13, 6 Hz), 2.21 (dd, 4H, J = 13, 9 Hz), 2.55 (m, 2H), 3.45, 3.46 (s, s, 4H each). *Anal.* calcd. for $C_{18}H_{30}O_4$: C 69.64, H 9.74; found: C 69.94, H 9.70. *Exact Mass* calcd.: 310.2145; found: 310.2146.

[2]We are very grateful to Professor L. A. Paquette for his assistance in making this comparison possible.

[3]This experiment was carried out by Dr. Neil Moss. We are very grateful to Dr. Moss for providing us with a generous supply of the keto acetal **14**.

Can. J. Chem. Downloaded from www.nrcresearchpress.com by 122.72.124.2 on 09/07/12
For personal use only.

Can. J. Chem. Downloaded from www.nrcresearchpress.com by 122.72.124.2 on 09/07/12
For personal use only.

*Preparation of the alkene acetal **16***

To a cold (−78°C), stirred solution of methylenetriphenylphosphorane (11.6 mmol) in 10 mL of dry THF (argon atmosphere) was added a solution of the keto acetal **14** (2.0 g, 8.9 mmol) in 5 mL of dry THF. The solution was allowed to warm to room temperature and then was stirred for 3 h. Petroleum ether (40 mL) was added and the resultant suspension was filtered through a column of Florisil (20 g, elution with diethyl ether). Concentration of the eluate and distillation (105–110°C/10 Torr (1 Torr = 133.3 Pa)) of the residual oil afforded 1.66 g (84%) of the alkene **16** as a clear, colorless oil, which exhibited ir (neat): 3050, 1647, 1115, 895 cm^{-1}; ^1H nmr (400 MHz) δ: 0.96 (s, 6H), 1.50 (dd, 2H, J = 12, 6 Hz), 2.06 (br d, 2H, J = 14 Hz), 2.30 (dd, 2H, J = 12, 8 Hz), 2.42–2.60 (m, 4H), 3.44, 3.48 (s, s, 2H each), 4.81 (t, 2H, J = 2 Hz). *Exact Mass* calcd. for $C_{14}H_{22}O_2$: 222.1619; found: 222.1617.

*Preparation of the keto alkene **18***

A mixture of the alkene acetal **16** (1.8 g, 8.1 mmol), acetone (15 mL), and 0.1% aqueous sulfuric acid (15 mL) was stirred at room temperature under an argon atmosphere for 8 h. Saturated aqueous sodium bicarbonate (5 mL) and diethyl ether (25 mL) were added and the mixture was stirred vigorously for 5 min. The phases were separated and the aqueous layer was extracted twice with diethyl ether. The combined organic extracts were washed with brine, dried ($MgSO_4$), and concentrated. Column chromatography of the residue on silica gel (75 g, elution with 2:1 petroleum ether – diethyl ether) and distillation (75–80°C/10 Torr) of the oil thus obtained provided 0.94 g (82%) of the keto alkene **18**, a colorless oil that exhibited ir (neat): 3045, 1710, 1640, 1415, 1400, 1160, 1140 cm^{-1}; ^1H nmr (400 mHz) δ: 2.05 (dd, 2H, J = 19, 4 Hz), 2.14 (br dd, 2H, J = 16, 2 Hz), 2.40 (dd, 2H, J = 19, 8 Hz), 2.58–2.71 (m, 2H), 2.71–2.85 (m, 2H), 4.89 (t, 2H, J = 2 Hz); ^{13}C nmr (20 MHz) δ: 39.37, 39.52, 43.49, 107.59, 151.53, 221.16. *Exact Mass* calcd. for $C_9H_{12}O$: 136.0888; found: 136.0883.

*Preparation of the alkene alcohol **20***

To a cold (−78°C), stirred solution–suspension of lithium aluminum hydride (118 mg, 3.1 mmol) in 12 mL of dry diethyl ether was added a solution of the keto alkene **18** (0.85 g, 6.25 mmol) in 3 mL of dry diethyl ether and the mixture was stirred for 1.5 h. Saturated aqueous ammonium chloride (2 mL) and diethyl ether (15 mL) were added and the mixture was allowed to warm to room temperature. The white slurry was filtered through a column of Florisil (20 g, elution with diethyl ether). The eluate was dried ($MgSO_4$) and concentrated. Distillation (78–82°C/10 Torr) of the residual oil afforded 0.82 g (94%) of the alcohol **20**, a colorless oil that showed one peak on glc analysis and exhibited ir (neat): 3300, 3050, 1645, 1100, 895 cm^{-1}; ^1H nmr (80 MHz) δ: 1.02–1.45 (m, 3H), 1.90–2.70 (m, 8H), 4.12 (quintet, 1H, J = 6 Hz), 4.83 (br s, 2H). *Exact Mass* calcd. for $C_9H_{14}O$: 138.1045; found: 138.1042.

*Preparation of the tricyclic alcohol **21***

To a well-stirred, warm (55°C) solution of the alkene alcohol **20** (0.6 g, 4.3 mmol) in 2 mL of dry toluene was added successively 4.79 mL (5.85 mmol) of a solution of diethylzinc in toluene (15% w/v) and 0.488 mL (5.85 mmol) of diiodomethane. Dry air was slowly passed through the mixture for 1.5 h while the temperature was maintained at 55°C. The mixture was cooled, 5% hydrochloric acid (4 mL) was added, and the layers were separated. The aqueous phase was washed twice with diethyl ether (10 mL). The combined organic phases were washed twice with 5% hydrochloric acid (3 mL) and once with brine and then were dried ($MgSO_4$) and concentrated. The remaining oil was chromatographed on silica gel (45 g, elution with 3:2 petroleum ether – diethyl ether) and the oil thus obtained was distilled (80–84°C/10 Torr) to provide 0.535 g (81%) of the tricyclic alcohol **21**, a colorless oil that exhibited ir (neat):' 3300, 3050, 1084, 1100 cm^{-1}; ^1H nmr (100 MHz) δ: 0.18–0.64 (m, 4H), 1.14–2.65 (series of m, 11H), 4.15 (m, 1H). *Exact Mass* calcd. for $C_{10}H_{16}O$: 152.1201; found: 152.1193.

*Preparation of the tricyclic ketone **19***

To a stirred slurry of pyridinium chlorochromate (1.03 g, 4.8 mmol) and sodium acetate (65 mg, 0.8 mmol) in 10 mL of dry dichloromethane was added a solution of the alcohol **21** (0.5 g, 3.3 mmol) in 2 mL of dry dichloromethane. The mixture was stirred at room temperature for 2 h. Diethyl ether (15 mL) was added and the mixture was filtered through a column of Florisil (10 g, elution with diethyl ether). Concentration of the eluate and distillation (80–85°C/10 Torr) of the remaining oil gave 0.429 g (87%) of the tricyclic ketone **19**, a colorless oil that exhibited ir (neat): 3047, 1725, 1400, 1165, 1010 cm^{-1}; ^1H nmr (400 MHz) δ: 0.38–0.47, 0.47–0.55 (m, m, 2H each), 2.31 (dd, 2H, J = 14, 4 Hz), 1.92 (dd, 2H, J = 14, 8 Hz), 2.16 (dd, 2H, J = 19, 4 Hz), 2.48 (dd, 2H, J = 19, 8 Hz), 2.87 (m, 2H). *Exact Mass* calcd. for $C_{10}H_{14}O$: 150.1045; found: 150.1042.

*Preparation of the enone **23***

To a cold (−78°C), stirred solution of the ketone **19** (0.4 g, 2.6 mmol) and dry triethylamine (2.2 mL, 15.9 mmol) in 15 mL of dry dichloromethane (argon atmosphere) was added, dropwise, 2.92 mL (14.3 mmol) of freshly prepared iodotrimethylsilane. The resulting orange slurry was stirred at −78°C for 15 min. Saturated aqueous sodium bicarbonate (4 mL) was added and the mixture was allowed to warm to room temperature. The phases were separated and the aqueous layer was washed three times with diethyl ether (10 mL). The combined extracts were dried ($MgSO_4$) and concentrated to afford the enol silyl ether **22** as a yellow oil. This material was dissolved in 10 mL of dry acetonitrile (argon atmosphere), palladium(II) acetate (0.873 g, 3.9 mmol) was added, and the solution was stirred at room temperature for 3 h. The mixture was filtered through a short column of silica gel (10 g, thorough elution with diethyl ether). Concentration of the eluate provided a viscous brown oil, which was chromatographed on silica gel (45 g, elution with 3:2 diethyl ether – petroleum ether). Distillation (83–87°C/10 Torr) of the oil thus obtained gave 0.288 g (73%) of the tricyclic enone **23**, a colorless oil that exhibited ir (neat): 3025, 1690, 1620 cm^{-1}; ^1H nmr (400 MHz) δ: 0.55–0.69 (m, 4H), 1.55–1.68 (m, 2H), 2.19 (dd, 1H, J = 18, 4 Hz), 2.44, 2.74 (br d, br d, 1H each, J = 18 Hz in each case), 2.61 (dd, 1H, J = 18, 6 Hz), 3.29 (m, 1H), 6.17 (m, 1H). *Exact Mass* calcd. for $C_{10}H_{12}O$: 148.0888; found: 148.0893.

*Preparation of the chloro ketone **24***

To a cold (−78°C), stirred solution of 4-chloro-2-trimethylstannyl-1-butene (**3**) (0.48 g, 1.9 mmol) in 10 mL of dry THF (argon atmosphere) was added a solution of methyllithium (2.1 mmol) in diethyl ether and the solution was stirred at −78°C for 5 min. Anhydrous magnesium bromide (386 mg, 2.1 mmol) was added and the mixture was stirred at −78°C for 15 min. Copper(I) bromide – diethyl sulfide complex (110 mg, 0.54 mmol) and the tricyclic enone **23** (0.25 g, 1.6 mmol) were added successively and the deep yellow solution was stirred at −78°C for 1.5 h. Saturated aqueous ammonium chloride – ammonium hydroxide (pH 8) (5 mL) and diethyl ether (30 mL) were added and the vigorously stirred mixture was allowed to warm to room temperature. Stirring was maintained until the aqueous phase became deep blue. The organic layer was separated, washed with water and brine, dried ($MgSO_4$), and concentrated. Distillation (100–105°C/10 Torr) of the remaining oil gave 0.333 g (83%) of the chloro ketone **24**, a colorless oil that exhibited ir (neat); 3050, 1735, 1610, 1440, 1400, 1165, 900 cm^{-1}; ^1H nmr (80 MHz) δ: 0.52 (br signal, 4H), 1.31–3.12 (series of m, 11H), 3.67 (t, 2H, J = 7.5 Hz), 4.90 (t, 1H, J = 1.5 Hz), 5.02 (s, 1H). *Exact Mass* calcd. for $C_{14}H_{19}{}^{35}ClO$: 238.1124; found: 238.1129.

*Preparation of the tetracyclic keto alkene **25***

To a suspension of potassium hydride (116 mg, 2.9 mmol) in 6 mL of dry THF (argon atmosphere) was added a solution of the chloro ketone **24** (280 mg, 1.18 mmol) in 2 mL of dry THF and the mixture was stirred at room temperature for 3 h. Saturated aqueous ammonium chloride (5 mL) and diethyl ether (20 mL) were added and the mixture was stirred vigorously for 15 min. The phases were separated and the aqueous phase was extracted twice with diethyl ether (10 mL). The combined organic extracts were washed twice with brine (5 mL), dried ($MgSO_4$), and concentrated. Distillation (92–96°C/10 Torr) of the crude product afforded 190 mg (80%) of the ketone **25**, a colorless oil

Can. J. Chem. Downloaded from www.nrcresearchpress.com by 122.72.124.2 on 09/07/12
For personal use only.

that exhibited ir (neat): 3035, 1720, 1623, 895 cm^{-1}; ^1H nmr (400 MHz) δ: 0.46–0.55 (m, 4H), 1.20–1.36 (m, 2H), 1.61. 2.12 (d, d, 1H each, J = 13 Hz in each case), 1.81–1.99 (m, 2H), 2.15–2.67 (series of m, 6H), 4.96, 5.02 (t, t, 1H each, J = 1.5 Hz in each case). *Exact Mass* calcd. for $C_{14}H_{18}O$: 202.1357; found: 202.1357.

Preparation of the tetracyclic keto alkene **26**

To a solution of the exocyclic alkene **25** (80 mg, 0.39 mmol) in 3 mL of dry dichloromethane (argon atmosphere) was added 6 mg of *p*-toluenesulfonic acid and the solution was stirred at room temperature for 24 h. Diethyl ether (10 mL) was added and the solution was washed twice with saturated aqueous sodium bicarbonate (2 mL). The organic phase was dried ($MgSO_4$) and concentrated. Distillation (90–95°C/10 Torr) of the residual oil gave 70 mg (88%) of the endocyclic alkene **26**, a colorless oil that exhibited ir (neat): 3046, 1715 cm^{-1}; ^1H nmr (80 MHz) δ: 0.47 (br s, 4H), 1.10–1.52 (m, 2H), 1.70 (br d, 3H, J = 2 Hz), 1.82–2.80 (series of m, 8H), 5.25 (br s, 1H), *Exact Mass* calcd. for $C_{14}H_{18}O$: 202.1358; found: 202.1358.

Preparation of mixtures of the tricyclic ketones **27** *and* **28**

To a solution of the tetracyclic ketone **25** (65 mg, 0.32 mmol) in 2 mL of glacial acetic acid was added 14 mg (0.064 mmol) of platinum oxide. The resultant suspension was shaken mechanically under hydrogen (3 atmospheres) at room temperature for 8 h. The reaction mixture was filtered and saturated aqueous sodium bicarbonate was added to the filtrate until it was basic. The resultant mixture was extracted three times with diethyl ether (5 mL). The combined extracts were washed with brine, dried ($MgSO_4$), and concentrated. Distillation (90–95°C/10 Torr) of the remaining oil gave 63 mg (96%) of a clear, colorless oil. Although this material showed one spot on tlc analysis (5:1 petroleum ether – diethyl ether), analysis by glc showed that it consisted of a 42:58 mixture of the epimeric ketones **27** and **28**, respectively. This mixture exhibited ir (neat): 1718, 1445 cm^{-1}; ^1H nmr (400 MHz) δ: 0.98, 1.01 (d, d, 3H total, J = 6, 4 Hz, respectively), 1.03, 1.035 (s, s, 6H total), 1.17–2.70 (series of m, 13H). *Exact Mass* calcd. for $C_{14}H_{22}O$: 206.1670; found: 206.1667.

Subjection of the tetracyclic ketone **26** (45 mg, 0.22 mmol) to hydrogenation under conditions identical with those described above gave 41 mg (91%) of a mixture of **27** and **28**, in a ratio (glc analysis) of 5:95, respectively.

*Preparation of (±)-pentalenene (***1***) and (±)-9-*epi*-pentalenene (***30***)*

To a cold (−78°C), stirred solution of the tricyclic ketones **27** and **28** (ratio 42:58, respectively) (50 mg, 0.24 mmol) in 1.5 mL of dry diethyl ether (argon atmosphere) was added a solution of methyllithium (0.28 mmol) in diethyl ether and the mixture was stirred at −78°C for 1.5 h. Saturated aqueous ammonium chloride (1 mL) and diethyl ether (5 mL) were added and the mixture was allowed to warm to room temperature. The phases were separated and the aqueous phase was washed twice with diethyl ether (3 mL). The combined organic extracts were washed with brine (2 mL), dried ($MgSO_4$), and concentrated. Analysis of the remaining oil by glc indicated that it consisted of a mixture of the ketones **27** and **28** (40% of the mixture) and the alcohols **29** (60% of the mixture). This material was treated with excess methyllithium as described above and the product mixture thus obtained was again allowed to react with excess methyllithium. Analysis of the crude product by glc showed that it consisted of a mixture of the ketones **27** and **28** (ratio 1:17, respectively, 18% of the mixture) and the alcohols **29** (82% of the mixture). This material was dissolved in 5 mL of dry benzene containing *p*-toluenesulfonic acid (14 mg) and the solution was refluxed under a Dean–Stark water trap for 1.5 h. The solution was cooled, washed with saturated aqueous sodium bicarbonate (1 mL), dried ($MgSO_4$), and concentrated. The remaining oil was chromatographed on silica gel (15 g) impregnated with silver nitrate (21). The column was eluted with petroleum ether.

Distillation (76–80°C/10 Torr) of the first-eluted hydrocarbon gave 16 mg (33%) of (±)-9-*epi*-pentalenene (**30**) as a colorless oil that exhibited ir (neat): 3020, 1440, 1375, 1360 cm^{-1}; ^1H nmr (400 MHz) δ: 0.94 (d, 3H, J = 7 Hz), 0.97 (s, 6H), 1.24–1.69 (m, 9H), 1.60 (br s, 3H), 2.62 (br d, 1H, J = 9 Hz), 2.88 (m, 1H), 5.16 (br s, 1H); ^{13}C nmr (100 MHz) δ: 13.41, 15.22, 28.52, 29.13, 31.45, 32.96, 39.75, 45.01, 46.23, 50.52, 54.81, 63.44, 131.30, 140.58. *Exact Mass* calcd. for $C_{15}H_{24}$: 204.1878; found: 204.1880.

Distillation (75–80°C/10 Torr) of the second-eluted hydrocarbon provided 15 mg (32%) of (±)-pentalenene (**1**), a colorless oil that exhibited ir (neat): 3040, 1445, 1362, 1350 cm^{-1}; ^1H nmr (400 MHz) δ: 0.91 (d, 3H, J = 7 Hz), 0.990, 0.995 (s, s, 3H each), 1.14–1.88 (series of m, 9H), 1.63 (br s, 3H), 2.56 (br d, 1H, J = 9 Hz), 2.66 (m, 1H), 5.16 (br s, 1H); ^{13}C nmr (100 MHz) δ: 15.41, 16.94, 27.64, 29.13, 29.98, 33.59, 40.51, 44.61, 46.90, 48.98, 59.39, 62.14, 64.77, 129.53, 140.63. *Exact Mass* calcd. for $C_{15}H_{24}$: 204.1878; found: 204.1892.

When a 5:95 mixture of the ketones **27** and **28**, obtained by hydrogenation–hydrogenolysis of compound **26** (*vide supra*), was subjected to a sequence of treatments with methyllithium as described above and the resultant mixture of alcohols was dehydrated, (±)-9-*epi*-pentalenene (**30**) was obtained in 68% yield.

Acknowledgement

We are grateful to the Natural Sciences and Engineering Research Council of Canada for financial support.

1. H. Seto and H. Yonehara. J. Antibiot. **33**, 92 (1980).
2. D. E. Cane and A. M. Tillman. J. Am. Chem. Soc. **105**, 122 (1983).
3. D. G. Martin, G. Slomp, S. Mizsak, D. J. Duchamp, and C. G. Chidester. Tetrahedron Lett. 4901 (1970); D. J. Duchamp and C. G. Chidester. Acta Crystallogr. Sect. B: Struct. Crystallogr. Cryst. Chem. **28**, 173 (1972).
4. Y. Ohfune, H. Shirahama, and T. Matsumoto. Tetrahedron Lett. 2869 (1976); S. Misumi, T. Ohtsuka, Y. Ohfune, K. Sugita, H. Shirahama, and T. Matsumoto. Tetrahedron Lett. 31 (1979).
5. G. D. Annis and L. A. Paquette. J. Am. Chem. Soc. **104**, 4504 (1982); L. A. Paquette and G. D. Annis. J. Am. Chem. Soc. **105**, 7358 (1983).
6. G. Pattenden and S. J. Teague. Tetrahedron Lett. **25**, 3021 (1984); Tetrahedron, **43**, 5637 (1987).
7. G. Mehta and K. S. Rao. J. Chem. Soc. Chem. Commun. 1464 (1985); J. Am. Chem. Soc. **108**, 8015 (1986).
8. M. T. Crimmins and J. A. DeLoach. J. Am. Chem. Soc. **108**, 800 (1986).
9. T. Imanishi, F. Ninbari, M. Yamashita, and C. Iwata. Chem. Pharm. Bull. **34**, 2268 (1986).
10. T. Hudlicky, M. G. Natchus, and G. Sinai-Zingde. J. Org. Chem. **52**, 4641 (1987); T. Hudlicky, G. Sinai-Zingde, M. G. Natchus, B. C. Ranu, and P. Papadopolous. Tetrahedron, **43**, 5685 (1987).
11. N. E. Schore and E. G. Rowley. J. Am. Chem. Soc. **110**, 5224 (1988).
12. D. H. Hua. J. Am. Chem. Soc. **108**, 3835 (1986).
13. E. Piers and V. Karunaratne. (*a*) J. Org. Chem. **48**, 1774 (1983); (*b*) J. Chem. Soc. Chem. Commun. 935 (1983); (*c*) Can. J. Chem. **62**, 629 (1984); (*d*) Tetrahedron. In press.
14. E. Piers and V. Karunaratne. J. Chem. Soc. Chem. Commun. 959 (1984).
15. G. Kubiak, J. M. Cook, and U. Weiss. J. Org. Chem. **49**, 561 (1984).
16. J. Furukawa, N. Kawabata, and J. Nishimura. Tetrahedron, **24**, 53 (1968); S. Miyano and H. Hashimoto. Chem. Commun. 1418 (1971).
17. E. J. Corey and J. W. Suggs. Tetrahedron Lett. 2647 (1975).
18. Y. Ito, T. Hirao, and T. Saegusa. J. Org. Chem. **43**, 1011 (1978).
19. D. E. Seitz and L. Ferreira. Synth. Commun. **9**, 931 (1979).
20. W. C. Still, M. Kahn, and A. Mitra. J. Org. Chem. **43**, 2923 (1978).
21. L. F. Fieser and M. Fieser. Reagents for organic synthesis. Vol. 1. John Wiley and Sons, Inc., New York, NY. 1967. pp. 1009–1010.

High temperature–pressure aqueous oxidations. IV. A kinetic study of the oxidation and enolization of cyclohexanone in the presence of catalytic metal ions

JOHN W. THOMAS[1] AND JAY E. TAYLOR[2]

Department of Chemistry, Kent State University, Kent, OH 44242, U.S.A.

Received February 1, 1988

JOHN W. THOMAS and JAY E. TAYLOR. Can. J. Chem. **67**, 165 (1989).

The aqueous high pressure–temperature oxidation of cyclohexanone was found to be strongly catalyzed by silver, iron(III), and copper ions but not by aluminum, cobalt, manganese(II), or nickel ions. The reactivities of the catalytic ions were inhibited by the acidic oxidation products. Accordingly, initial reaction velocities were determined and used to correlate the kinetic data. A detailed kinetic study of copper ion catalysis has shown that in the presence of that ion the reaction was first order in cyclohexanone, one-half order in copper ion, and zero order in oxygen. The rate of enolization of cyclohexanone appeared to be unaffected by the presence of copper ion under conditions of constant acidity but was strongly catalyzed by both deuterium ion and acetate ion. Further, the rate of oxidation exceeded the rate of enolization at higher copper ion concentrations. These data contrast with the uncatalyzed oxidation, for which the kinetic reaction was first order in cyclohexanone, one-half order in oxygen, and the rate of oxidation was much less than the rate of enolization. The activation energies for the catalyzed and uncatalyzed oxidations were about the same, but the entropies of activation were quite different. From these data it is concluded that the enol is not a major intermediate for the catalyzed reaction. It is suggested that the copper ion may form an active peroxy complex with the oxygen molecule to serve as the reactive oxidant.

Key words: metal ion catalysis, kinetics, cyclohexanone, high temperature oxidation, high pressure oxidation.

JOHN W. THOMAS et JAY E. TAYLOR. Can. J. Chem. **67**, 165 (1989).

On a trouvé que l'oxydation de la cyclohexanone, en milieu aqueux et à des températures et des pressions élevées, est fortement catalysée par les ions de l'argent, du fer(III) et du cuivre, mais pas par les ions du aluminum, du cobalt, du manganèse(II) et du nickel. Le réactivité des ions catalytiques est inhibée par les produits acides de l'oxydation. On a donc déterminé les vitesses initiales des réactions et on les a utilisées pour établir une corrélation avec les données cinétiques. Une étude cinétique détaillée de la catalyse par l'ion du cuivre a montré que, en présence de cet ion, la réaction est du premier ordre en cyclohexanone, d'ordre un demi en ion du cuivre et d'ordre zéro en oxygène. Il semble que, à acidité constante, la vitesse d'énolisation de la cyclohexanone n'est pas affectée par la présence des ions du cuivre; toutefois, elle est fortement catalysée par l'ions deutérium et acétate. De plus, à des concentrations élevées d'ions du cuivre, la vitesse d'oxydation est plus élevée que la vitesse d'énolisation. Ces données sont en opposition avec ceux obtenus lors de l'oxydation non-catalysée de la cyclohexanone alors que la réaction cinétique était du premier ordre en cyclohexanone, d'ordre un demi en oxygène et que la vitesse d'oxydation était beaucoup plus faible que la vitesse d'énolisation. Les énergies d'activation pour les réactions catalysées et non-catalysées sont approximativement les mêmes, mais les entropies d'activation sont très différentes. Sur la base de ces données, on en conclut que l'énol n'est pas un intermédiaire important dans la réaction catalysée. On suggère que l'ion du cuivre et l'oxygène forment peut-être un complexe peroxy actif qui sert d'oxydant réactif.

Mots clés : catalyse par les ions du métal, cinétique, cyclohexanone, oxydation à pression élevée, oxydation à température élevée.

[Traduit par la revue]

Introduction

In previous studies of aqueous oxidations of low molecular weight ketones and alcohols (1–3) the reactions have been carried out under noncatalytic conditions. Catalysis of the oxidation of cyclohexanone was first indicated in preliminary work when difficulties in reproducing kinetic data were noted. Although glass or Teflon liners were used inside the stainless steel case, splashing or foaming over the liner occasionally permitted contact of the aqueous solution with the metal. The very corrosive combination of moisture, high pressure oxygen, and elevated temperatures effected formation of metal ions, which, upon reintroduction into the solution, caused seemingly irrational results. By avoiding overfilling and sudden pressure drops and using due care in stirring, this source of contamination was effectively eliminated, permitting the previously described studies.

The significance of metal ion catalysis was, however, indicated by these early results. This paper presents some quantitative studies that have been made on catalytic effects, particularly those of copper ion.

Very few studies of catalyzed aqueous oxidations of ketones have been made. Denisov *et al.* (4) studied the aqueous oxidation of 2-butanone in the presence of iron(III) ion and complexes of copper(II), iron(III), and manganese(II) ions at 50–60°C. Enolization followed by a series of complex radical reactions was proposed. There are, however, many references to metal ion catalyzed oxidations of aldehydes, ketones, hydrocarbons, etc. under nonaqueous conditions (5–7).

Experimental

The experimental procedures for the determination of the rates of oxidation and enolization and the purification of cyclohexanone have been previously described (1–3). Other chemicals were of reagent grade.

As will be further discussed, the rate constants for the catalyzed oxidations decreased with time, i.e., they were autoinhibited. To provide rate data that were interpretable, the initial rate constants were determined and evaluated. This was accomplished by dividing the initial reaction velocity (determined graphically as the initial slope) by the initial concentration of cyclohexanone. Some sacrifice in accuracy results from this procedure since variations in slope are more sensitive to experimental error at the outset of the reaction. An estimation of accuracy has been made from the data taken at 145°C. The average deviation was ±13%.

[1]Present address: Pfizer Inc., Terre Haute, IN 47808, U.S.A.

[2]Author to whom correspondence may be addressed.

Printed in Canada / Imprimé au Canada

Can. J. Chem. Downloaded from www.nrcresearchpress.com by 122.72.124.2 on 09/07/12
For personal use only.

TABLE 1. Effects of various metal ions on the rates of oxidation of cyclohexanone by elemental oxygen in aqueous solutions

Metal compound	M × 10^4	Medium	Temperature (°C)	$k \times 10^4$ (s^{-1})
—	—	H_2O	145	0.105
$Ag_2C_2H_3O_2$	53	H_2O	145	0.66[d]
—	—	H_2O	172	0.77
$Al_2(SO_4)_3$	12[a]	H_2O	172	0.63
$Co(C_2H_3O_2)_2$	29.5	[b]	172	0.64
$Cu(C_2H_3O_2)_2$	1.09	[b]	172	14.1[d]
$Fe_2(SO_4)_3$	1.29[a]	[c]	172	14.3[d]
$Fe_2(SO_4)_3$	100.[a]	[c]	172	120.[d]
$Mn(C_2H_3O_2)_2$	8.3	[b]	172	0.71
$Ni(C_2H_3O_2)_2$	200.	[c]	172	0.66

[a]M indicates molarity of Al^{3+} or Fe^{3+}.
[b]0.50 M sodium acetate with 0.25 M acetic acid.
[c]5.0×10^{-3} M sulfuric acid.
[d]Determined from the initial reaction velocity.

Results

A brief survey of the possible catalytic activity of the following ions: Ag^+, Al^{3+}, Co^{2+}, Cu^{2+}, Mn^{2+}, and Ni^{2+}, was made. Dilute solutions were tested so that only significant activity would be noted. Only Ag^+, Fe^{3+}, and Cu^{2+} were appreciably reactive. See Table 1.

Catalysis by silver ion

As with each of the three active catalytic ions, silver ion catalysis was autoinhibited. The decrease in rate constant with time appeared to correlate with the formation of a gray, silver-containing precipitate that formed as the reaction proceeded. The precipitate was soluble in ammonium hydroxide and was assumed to be either silver oxide or insoluble silver salts of the product acids, presumably the latter. The initial rate constant for the silver ion catalyzed reaction is compared with that of the uncatalyzed reaction in Table 1, and the rate curve is plotted in Fig. 1. The plot of log concentration with time is not a straight line, and the concentration–time graph shows an unduly large initial decrease in rate with time, indicating autoinhibition. No further studies were made with this ion.

Catalysis by iron(III) ion

Iron(III) ion was a potent catalyst, as seen in Table 1. The rate of oxidation of cyclohexanone increased initially as much as 150-fold upon the addition of 0.01 M iron(III) ion. The plot of the autoinhibited catalysis by iron(III) ion is shown in Fig. 2.

No further studies were made with this ion since strongly acidic solutions were required to hold iron(III) ion in solution. The combination of acid, high pressure oxygen, and elevated temperature was quite corrosive to the sampling valve mechanism.

Catalysis by copper ion

Copper(II) ion was also an excellent catalyst, as indicated in Table 1. This ion has the merit of retaining solubility under near neutral conditions, thereby permitting a more exhaustive survey. The remainder of this paper deals with the effects of this ion.

Mechanism of autoinhibition of copper ion catalysis

As with the two previously discussed ions, copper ion catalysis was autoinhibited. Dicarboxylic acids have been shown to be products of the aqueous oxidation of cyclohexanone (3). If it is assumed that the simple hydrated copper ion was the catalytic species, the formation of an inactivating salt

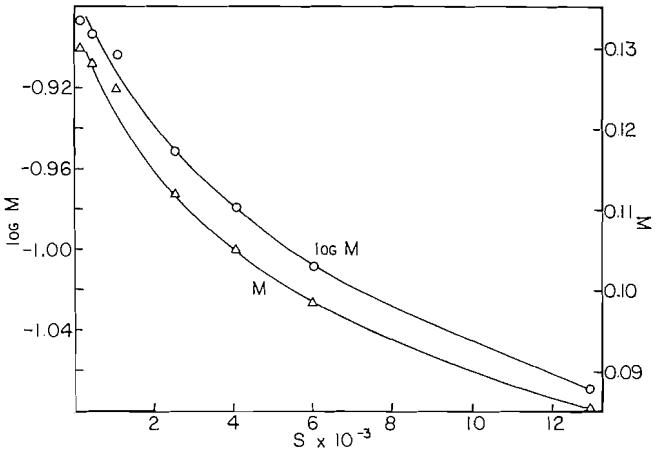


FIG. 1. The autoinhibited silver ion catalyzed oxidation of cyclohexanone. Dual plots show the variation of molarity and $\log_{10}$ molarity of cyclohexanone versus time in the presence of 0.0053 M silver acetate and 125 atm partial pressure of oxygen at 145°C.

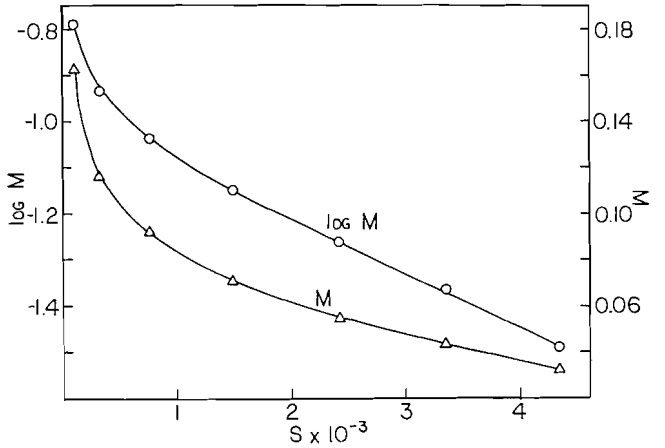


FIG. 2. The autoinhibited iron(III) catalyzed oxidation of cyclohexanone. Dual plots show the variation of molarity and $\log_{10}$ molarity of cyclohexanone versus time in the presence of 0.000129 M iron(III) sulfate, 0.005 M sulfuric acid, and 125 atm partial pressure of oxygen at 172°C.

(i.e., a salt with partial covalent bonding) between copper ion and the product acids should significantly decrease the catalytic activity of that ion. Further, the inhibitory effect should increase as the reaction proceeds and additional amounts of acids are formed.

To determine if such was the case, a copper ion catalyzed oxidation was carried out with 0.08 M butanedioic acid added, and was compared with a run not having this addition. The acid markedly inhibited the initial rate of oxidation (see Fig. 3). Another copper ion catalyzed mixture was allowed to oxidize to greater than 50% completion, and a fresh addition of cyclohexanone was made. Marked inhibition by the oxidation products was observed upon comparison with the initial rate of reaction (see Fig. 3).

It is therefore concluded that the decrease in rate was due to complexation of the catalytic copper ion by the product acids. The possibility of explaining the decreasing rates by assuming an involved mechanism seems unlikely since, as will be shown, the initial reaction rates may be readily correlated by well-defined kinetic relationships.

Can. J. Chem. Downloaded from www.nrcresearchpress.com by 122.72.124.2 on 09/07/12
For personal use only.

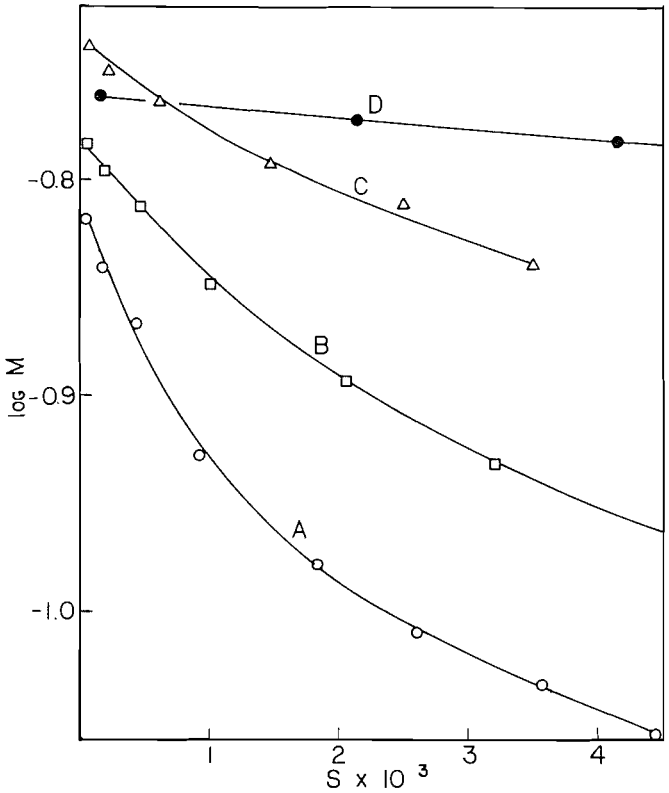


FIG. 3. The nature of autoinhibited copper(II) ion catalyzed oxidation of cyclohexanone. A, 0.00011 M copper(II) acetate, 0.50 M acetic acid, 0.25 M sodium acetate, and 125 atm partial pressure of oxygen at 145°C; B, same as A with the addition of 0.08 M butanedioic acid; C, after about 50% reaction with same conditions as A, fresh cyclohexanone was added to give these data; D, a corresponding uncatalyzed reaction at 145°C.

TABLE 2. Determination of the first-order rate constants for the 1.09×10^{-4} M copper ion catalyzed oxidation of cyclohexanone at 172°C in 0.50/0.25 M sodium acetate/acetic acid buffer at varying oxygen partial pressures

Partial pressure oxygen (atm)	$k \times 10^3$ (s^{-1})
125	1.4
128	1.5
59.9	1.3
27.6	1.3

The formation of these copper-carboxylic acid salts does not completely inhibit copper ion activity. Although the presence of reaction products greatly decreased the rate of the catalyzed oxidation, as seen in Fig. 3, the reaction was still appreciably more rapid (indicated by the greater slope) than under uncatalyzed conditions. The graph of the log rate constant versus time does, however, become a nearly straight line as compared to the initially catalyzed reaction. This suggests that a limiting inhibition of the catalysis may have been attained.

Kinetic order of oxygen

The partial pressure of oxygen was varied between 27.6 and 128 atm (1 atm = 101.3 kPa) with a constant copper ion concentration (see Table 2). The rate of oxidation was essentially

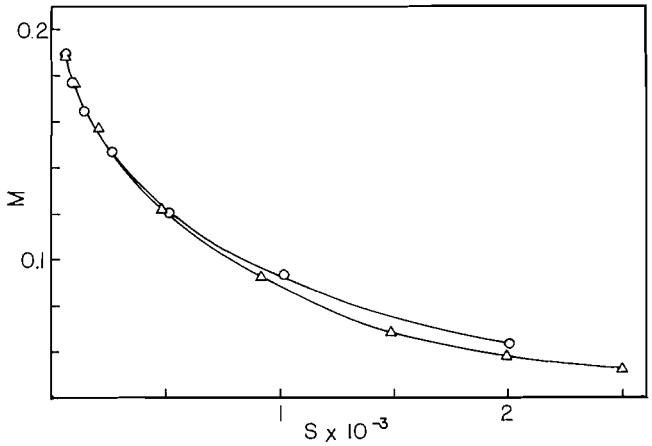


FIG. 4. Zero-order dependence on oxygen of the copper ion catalyzed oxidation of cyclohexanone. ○, 128 atm oxygen; △, 27.6 atm oxygen. Both reactions contained 0.000109 M copper acetate, 0.5 M acetic acid, 0.25 M sodium acetate, and were carried out at 172°C.

constant under widely varying oxygen pressures. The graphs of two extremes of oxygen partial pressures are shown in Fig. 4. Except for a small deviation the two graphs correlate quite closely over the range of the data. Since the lower pressure exhibits the slightly faster rate at the more advanced stages of oxidation, it is presumed that the difference is merely due to experimental error. The data conclusively demonstrate that the oxidation reaction was zero order with respect to elemental oxygen.

Kinetic order of cyclohexanone

A log–log plot of the initial rates of oxidation versus cyclohexanone concentrations is shown in Fig. 5. A slope of 1.04 indicates that, within experimental error, the order with respect to cyclohexanone was unity. The order of cyclohexanone under both catalytic and noncatalytic conditions was the same.

Kinetic order of copper ion

The plot of initial rate constants as they varied with copper ion concentrations at 145°C is seen in Fig. 6. The data are from Table 3. The slope and the indicated order with respect to copper ion are 0.5. As previously noted (3) the order with respect to oxygen in the absence of copper ion was 0.5. The addition of copper ion displaced oxygen in its kinetic order.

The integrity of the half-order relationship held over an extremely wide range of copper ion concentrations. This is particularly emphasized in both Fig. 6 and Table 3 where the copper ion concentration was varied from 1.5 to 1×10^{-4} M. Yet the three-halves-order rate constant held with excellent constancy.

Effect of copper ion on the rate of enolization

It has been shown that the rate of enolization of cyclohexanone was significantly faster than the rate of oxidation in the absence of catalytic ions (3). The concept that the enol served as an intermediate in the oxidation of ketones was definitely supported, but not proven.

The previously described technique for determining the rate of enolization (3) was applied in the presence of varying amounts of copper ion. That there was essentially no effect on the rate of enolization was demonstrated both in the presence of absence of buffers. Acetic acid-D_4 was added to give varying pD values at 116°C (see expts. 1–5, Table 4). Upon dividing the

Can. J. Chem. Downloaded from www.nrcresearchpress.com by 122.72.124.2 on 09/07/12
For personal use only.

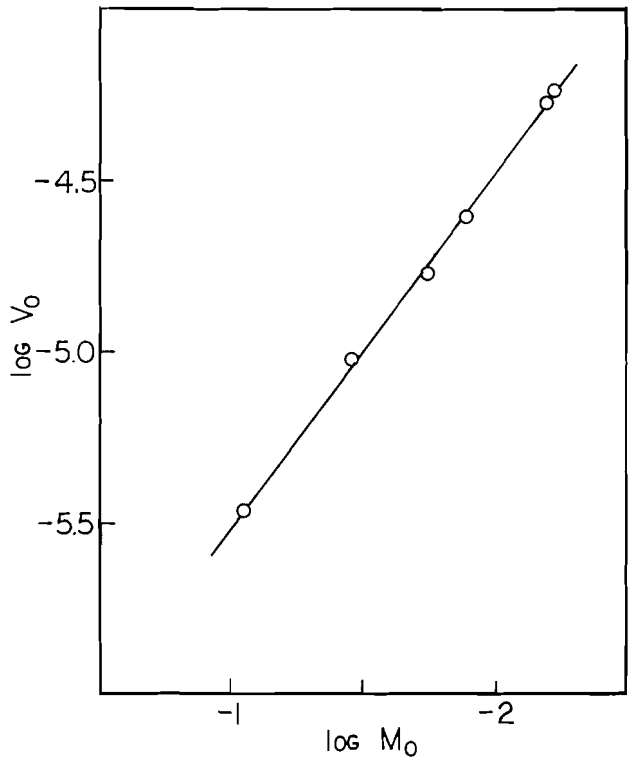


FIG. 5. The first-order dependence of cyclohexanone concentrations as indicated by a log–log plot of initial first-order rate constants versus initial cyclohexanone concentrations. The slope is 1.04. Conditions: 0.50/0.25 M acetate buffer or water, 0.00011 M copper acetate, 125 atm partial pressure oxygen, and 145°C.

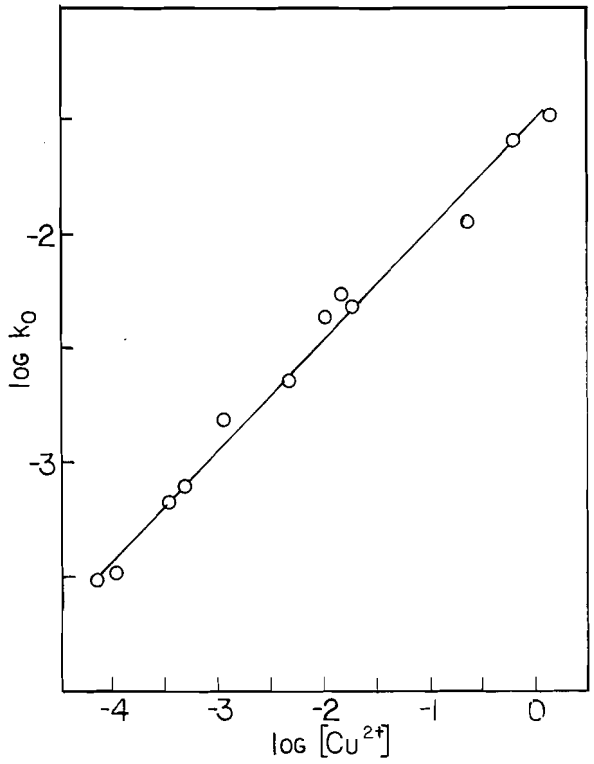


FIG. 6. Half-order dependence on copper ion concentrations at 145°C as indicated by a log–log plot of initial first-order rate constants versus added copper ion concentrations. The slope is 0.49.

TABLE 3. Rate constants for the oxidation of cyclohexanone at 125 atm partial pressure of oxygen in water except as indicated

Expt. no.	Temperature (°C)	$[Cu^{2+}]$ ($M \times 10^4$)	$k \times 10^{4a}$ (s^{-1})	$k \times 10^{2b}$ ($M^{-1/2}s^{-1}$)
1	116	5.19	0.56	0.246
2	116	15.2	0.87	0.224
3	116	180.	2.66	0.198
4	116	1360	7.4	0.201
5	116	4110	15.4	0.240
6	116	12600	20.0	0.178
7	145	0.71	3.05	3.62
8[c]	145	1.06	3.14[d]	3.06[d]
9	145	1.07	3.50	3.38
10	145	1.08	3.08	2.96
11[c]	145	1.09	3.42[e]	3.27[e]
12	145	3.36	6.72	3.67
13[c]	145	4.67	7.87	3.64
14[c]	145	11.3	15.3	4.55
15[c]	145	47.	23.2	3.37
16[c]	145	105.	43.6	4.25
17[c]	145	150.	55.	4.4
18	145	193.	46.5	3.35
19	145	2300	111.	2.31
20	145	6360	251.	3.15
21	145	14700	323.	2.66
22	172	1.09	14.5	14.5
23	172	4.6	45.	21.
24	172	8.9	70.	23.
25	172	74.9	170.	20.
26	172	104.	180.	18.

[a]First-order rate constants based on cyclohexanone concentrations.
[b]Three-halves-order rate constants based on cyclohexanone) × (square root of copper ion concentrations).
[c]0.5 M sodium acetate + 0.25 M acetic acid added.
[d]Average of three experiments.
[e]Average of two experiments.

k values for the enolizations by the deuterium ion concentrations a number was obtained that was constant over the range of pD and did not change with the presence or absence of copper ion.

Additional data were obtained at both 116 and 145°C in the presence of buffers. Upon altering the copper ion concentration by a factor of nearly 700 at 116°C and a constant pD, there was no significant impact upon the rate of enolization (see expts. 6 and 7, Table 4). Similarly, at 145°C the addition of copper ion had little effect upon the reaction rate at a constant pD (see expts. 8–11, Table 4). The rate was slightly faster in the absence of copper ion, but this appears to be merely an artifact. The lack of effect of copper ion is further emphasized in Fig. 7, where the similarity of the rate curves for the enolization of cyclohexanone with and without copper ion is clearly demonstrated. It may therefore be concluded that the addition of copper ion does not noticeably affect the rate of enolization.

Comparative rates of enolization and oxidation

Upon comparing the first-order oxidation rate constants of expts. 3–6, Table 3, with the first-order enolization rate constants of expts. 1–7, Table 4, it is seen that the oxidation rates equal or exceed the enolization rates at 116°C even under very favorable conditions for the latter, i.e., high buffer or acid conditions. Similarly, at 145°C the first-order copper catalyzed oxidation rate constants from expts. 13–21, Table 3, exceeded any of the first-order enolization rate constants from expts.

Can. J. Chem. Downloaded from www.nrcresearchpress.com by 122.72.124.2 on 09/07/12
For personal use only.

TABLE 4. Effect of copper ion on the exchange of α hydrogens by deuterium in cyclohexanone. Deuterium oxide solvent

Expt. no.	Temperature (°C)	Acetic acid-D_4 (M)	Sodium acetate-D_3 (M)	$[Cu^{2+}]$ ($M \times 10^2$)	pD[a]	$k \times 10^4$ (s^{-1})	k/D^+
1	116	0.257	—	2.05	2.85	2.27	0.161
2	116	0.108	—	9.0	2.92	1.74	0.144
3	116	0.057	—	7.8	3.12	1.15	0.151
4	116	0.108	—	—	3.20	0.78	0.124
5	116	0.057	—	—	3.68	0.30	0.146
6	116	0.25	0.50	7.2	5.2	2.67	
7	116	0.25	0.50	0.0113	5.49	2.52	
8	145	0.25	0.50	0.0113	5.40	6.77	
9	145	0.25	0.50	0.0113	5.42	6.39	
10	145	0.23	0.50	—	5.42	8.45	
11	145	0.23	0.49	—	5.42	7.66	

[a]Measured in a pH meter at room temperature (20°C).

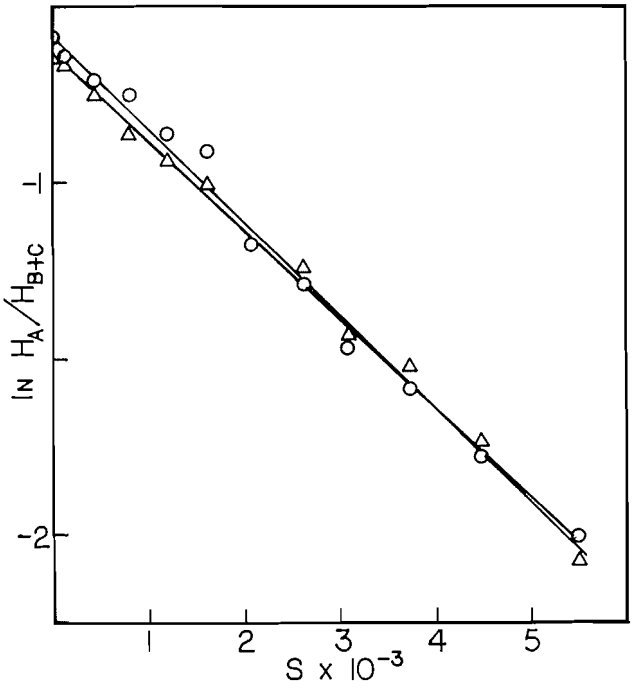


FIG. 7. The effect of copper ion on the rate of decay of the α-proton signal of cyclohexanone in D_2O with 0.50/0.25 M sodium acetate-D_3/acetic acid-D_4 buffer at 145°C. ○, no Cu^{2+}; △, with 1.13×10^{-4} M Cu^{2+}. H_A, H_B, and H_C represent the α, β, and γ protons of cyclohexanone, respectively.

8–11, Table 4. Again, at 172°C the first-order oxidation rate constants from expts. 23–26, Table 3, exceed any of the 172°C enolization rate constants of Table 1 from the preceding paper (3).

Accordingly, it may be concluded that the enol was not an intermediate for the copper ion catalyzed reaction. This obviously differs from the tentative conclusion made with the noncatalyzed oxidation suggesting that the enol is an intermediate. However, it may be necessary to reconsider the specific role of the enol for both the catalyzed and uncatalyzed reactions.

Buffer ion catalysis of the rate of enolization

The rates of enolization of cyclohexanone in D_2O were determined in the presence of acetic acid-D_4 or deuterated acetate buffers. With acetic acid-D_4 a constant number was obtained upon dividing the observed rate constant by the deuterium ion concentration, which was estimated at room temperature using a pH meter. See expts. 1–5, Table 4. The proportionality of the effect of deuterium ion on the rate of enolization is thereby indicated. Although the D^+ concentrations were undoubtedly higher at the elevated reaction temperatures than as measured, the actual high temperature D^+ concentrations were assumed to be proportional to the apparent values obtained from the room temperature pH measurements.

Upon introducing a deuterated acetate buffer, the D^+ proportionality no longer existed. Comparing expts. 5 and 7, Table 4, it is seen that at pD 3.68 (20°C) or $[D^+] = 2.1 \times 10^{-4}$, k was 0.30×10^{-4}, but at pD 5.40 (20°C) with 0.5 M sodium acetate-D_3 plus 0.25 M acetic acid-D_4, k was 2.52×10^{-4} or about eight times larger even though the $[D^+]$ had been reduced to 4.0×10^{-6}. Therefore, in addition to a deuterium ion promotion of the enolization reaction there is also a large buffer ion catalysis. The nature of this catalysis will not be further considered in this paper.

TABLE 5. Activation parameters for the oxidation of cyclohexanone

Reaction	E_a (kcal/mol)	$\Delta H^{\ddagger}$ (kcal/mol)	$\Delta S^{\ddagger}$ (eu)	log A
Uncatalyzed oxidation	23 ±2[a]	22	−27.	7.6
Catalyzed oxidation	26 ±3[a]	26	−5.	12.2
Enolization	12.7±0.2	11.9	−42.3	4.13

[a]Determined from the mean of the three-halves-order rate constants.

Activation parameters

The activation energies and entropies of log A values under both catalytic and noncatalytic conditions and for the enolization are tabulated in Table 5. The copper ion catalyzed oxidation has a slightly greater activation energy than the uncatalyzed oxidation, but this difference is within the range of experimental error. On the other hand the differences in the entropies of activation definitely reflect the large differences in reaction rates between the catalyzed and uncatalyzed oxidations.

Can. J. Chem. Downloaded from www.nrcresearchpress.com by 122.72.124.2 on 09/07/12
For personal use only.

Can. J. Chem. Downloaded from www.nrcresearchpress.com by 122.72.124.2 on 09/07/12
For personal use only.

Discussion

Although the specific acid content has not been determined for any of the metal ion catalyzed reactions as was done for the uncatalyzed oxidations, the products may be assumed to be a mixture of C_1 to C_6 acids of unspecified composition, carbon dioxide, and water. The difference between the heats of combustion of cyclohexanone and hexanedioic acid, for example, is 172 kcal/mol (8, 9). Yet even at 190°C the oxidation of cyclohexanone is relatively slow (3). A reaction with this large a potential for oxidation should be an ideal subject for catalysis, and this appears to be the case.

The characteristics of the catalyzed and uncatalyzed reactions differ markedly. The uncatalyzed reaction is first order in cyclohexanone, one-half order in oxygen, and appears to enolize before oxidation (though this is not conclusive). In contrast, the copper ion catalyzed oxidation is first order in cyclohexanone (the only similarity), zero order in oxygen, one-half order in copper ion, and the major reaction does not proceed via an enol intermediate.

Under conditions of copper ion catalysis the oxygen molecule serves as a secondary reactant; that is, it does not react directly with the cyclohexanone. On the other hand, the copper ion or a derivative of that ion is a direct reactant. The reservoir of oxygen, which is in constant supply (since it is kept at constant pressure), maintains the copper ion or its derivative in the reactive state.

The kinetic characteristics of the present work contrast sharply with those of earlier investigations. The study of the aqueous oxidation of 2-butanone (4) with iron(III) iron at 50–60°C showed that the rate of oxidation depended on pH, and the rate of oxygen dependence varied with ketone and iron(III) ion concentrations in a complex manner. Under nonaqueous conditions (5–7) cobalt, manganese(II), iron(III), and copper ions were indicated as catalysts for various substances, whereas only the latter two were shown to be highly reactive in this work.

Although numerous metal ion catalyses of lower temperature, nonaqueous, oxidations of aldehydes and ketones have been studied and characterized, there is neither reason nor evidence to conclude that higher temperature, aqueous, catalyzed reactions follow a similar mechanism. However, the data presented herein are insufficient to permit formulation of a detailed mechanism. Accordingly, two possibilities are presented.

1. Copper ion reacts directly with cyclohexanone to form a lower valence species, which is then reoxidized to the divalent ion by reaction with oxygen. This proposal implies a direct reaction of copper ion with the ketone, but, as such, does not explain the observed half order as noted for copper ion. Conceivably a radical chain process could be suggested, but again such a mechanism would be very difficult to correlate with the extremely wide range of concentrations over which the copper ion was seen to follow half-order kinetics.

2. An oxygen molecule forms a peroxy intermediate with copper ion, e.g., CuO_2^{2+}, and this in turn reacts with cyclohexanone. Since the oxygen was held at a specified pressure, an adequate supply of oxygen was present to maintain this intermediate during the course of the reaction.

This latter proposal appears to be the more reasonable since the peroxy copper ion could react in a manner similar to the mechanism suggested for the uncatalyzed reaction. The activation energy for the catalyzed reaction (Table 5) was about the same as for the uncatalyzed reaction; this indicates that the oxidation intermediate, whatever its nature, does not have a large heat of formation, either positive or negative. Therefore, the observed increase in rate correlates with the A or $\Delta S^{\ddagger}$ factor. With this mechanism an oxygen molecule becomes associated with the positive copper ion, and the resulting polarization creates a positive charge on an oxygen atom. Cyclohexanone is also a polar molecule. The presence of the keto group effects a negative polarity on the α carbons, presumably by partial enolization. The positive oxygen then is oriented to a negative carbon, effecting enhancement of the rate of reaction. This polar attraction should be manifested by an increase in the orientation factor, $\Delta S^{\ddagger}$ or $\log A$ with little effect on the activation energy, as observed in Table 5.

The possibility of enol intermediary was stressed in our previous paper (3), but with the clear reservation that it had not yet been proven. In keeping with the first mechanism from above, there is the possibility that the uncatalyzed oxidation proceeds by the previously suggested mechanism and the catalyzed reaction by a different mechanism.

There is then the possibility that the catalyzed and uncatalyzed oxidations may be quite similar in mechanism except for the initial interaction between the oxygen and ketone. With the uncatalyzed reaction the initial contact presumably is between the oxygen molecule and the enol or its equivalent, whereas with the catalyzed reaction the copper ion – oxygen adduct reacts as described in mechanism 2 above. Following these initial contacts, both reactions may be assumed to proceed in a similar manner, in keeping with the earlier proposed mechanism (3).

Further detailed research is planned to determine more accurately the mechanistic nature of this interesting reaction.

1. J. E. Taylor and J. C. Weygandt. Can. J. Chem. **52**, 1925 (1974).
2. J. W. Thomas and J. E. Taylor. Can. J. Chem. **64**, 2235 (1986).
3. J. W. Thomas and J. E. Taylor. Can. J. Chem. **66**, 294 (1988).
4. E. T. Denisov, V. D. Komissarov, and D. I. Metelitza. Discuss. Faraday Soc. **46**, 173 (1968).
5. N. M. Emanuel, E. T. Denisov, and Z. K. Maizus. Liquid-phase oxidation of hydrocarbons. *Translated by* B. J. Hazard. Plenum Press, New York. 1977. pp. 192–221.
6. E. T. Denisov, N. I. Mitskevich, and V. E. Agabekov. Liquid-phase oxidation of oxygen-containing compounds. *Translated by* D. A. Patterson. Consultants Bureau, New York. 1977. p. 98.
7. R. A. Sheldon and J. K. Kochi. Metal-catalyzed oxidations of organic compounds. Academic Press, New York. 1981. p. 140. See listed references.
8. E. W. Washburn. International critical tables. Vol. 5. McGraw–Hill, New York. 1929. p. 165.
9. D. R. Stull, E. F. Westrum, and G. C. Sinke. The chemical thermodynamics of organic compounds. Wiley, New York. 1969. p. 447.

Electron affinities and Marcus reorganization energies. A correlation between gas phase electron affinities and solution phase redox potentials

DENNIS D. TANNER, NATASHA DEONARIAN,[1] AND ABDELMAJID KHARRAT[2]
Department of Chemistry, University of Alberta, Edmonton, Alta., Canada T6G 2G2

Received August 4, 1988

DENNIS D. TANNER, NATASHA DEONARIAN, and ABDELMAJID KHARRAT. Can. J. Chem. **67**, 171 (1989).

Redox potentials determined by cyclic voltammetry were used in conjunction with published electron affinities to determine the solvation energies for series of three classes of compounds: substituted benzoquinones, substituted nitrobenzenes, and polynuclear aromatic hydrocarbons. Excellent linear correlations were obtained between the measured electron affinities and the E^0 of the substrates. The calculated electron affinities, EA(E^0), were computed using the average solvation energies for the three classes of compounds, and were found to be in excellent agreement with the measured values. The nitrobenzenes and quinones had one solvation energy, while the aromatic hydrocarbons were correlated with a significantly different value. The solvation energy of a variety of compounds could also be related to their Marcus reorganization energies, $\lambda(0)$, by a linear plot with a high correlation coefficient. From simple electrochemical measurements of similar compounds, either electron affinities or Marcus $\lambda(0)$ values can be estimated.

Key words: electron affinities, Marcus reorganization energies, cyclic voltammetry.

DENNIS D. TANNER, NATASHA DEONARIAN et ABDELMAJID KHARRAT. Can. J. Chem. **67**, 171 (1989).

On a utilisé des potentiels redox, déterminés par voltamétrie cyclique, de concert avec des valeurs publiées d'affinités électroniques pour déterminer les énergies de solvatation de séries de trois classes de composés : des benzoquinones substituées, des nitrobenzènes substitués et des hydrocarbures aromatiques polynucléaires. On a obtenu d'excellentes corrélations linéaires entre les affinités électroniques mesurées et les valeurs E^0 des substrats. On a calculé les affinités électroniques, EA(E^0), en utilisant les énergies moyennes de solvatation des trois classes de composés et on a trouvé qu'elles sont en excellent accord avec les valeurs mesurées. On n'a utilisé qu'une seule énergie de solvatation pour les nitrobenzènes et les quinones alors que l'on doit utiliser une valeur assez différente pour établir une corrélation avec les hydrocarbures aromatiques. On peut aussi établir une corrélation entre l'énergie de solvatation d'un grand nombre de composés et leurs énergies de réorganisation de Marcus, $\lambda(0)$; cette corrélation est linéaire avec un coefficient de corrélation élevé. En effectuant des mesures électrochimiques simples sur des composés semblables, on peut donc évaluer soit les affinités électroniques ou les valeurs $\lambda(0)$ de Marcus.

Mots clés : affinités électroniques, énergies de reorganisation de Marcus, voltamétrie cyclique.

[Traduit par la revue]

Introduction

The electron affinities of both organic and inorganic molecules are of interest in fundamental studies of both vapor phase (3) and condensed phase (4) reactions. Until relatively recently compilations of electron affinity data were conspicuously scarce. In the last several years EA data have become more readily available due to the rapid development of physical methods for their determination in the gas phase. These developments have been the subject of reviews by Chen and Wentworth (5), Brauman and co-workers (3), Lineberger and co-workers (6), and Kebarle *et al.* (7). In 1984 Brauman and co-workers listed a comprehensive compendium of EA's that had been determined by a variety of physical methods. In this review, only 24 neutral organic molecules were listed. Most recently Kebarle *et al.* (7), using pulsed electron high pressure mass spectrometry (HPMS), have extended this compilation six-fold.

The polarographic half-wave potential for a reversible redox couple has been related to the electron affinity of the molecule by eq. [1] (5, 8).

$$[1] \quad -E^0 = \mathrm{EA} - \Delta G_{\mathrm{sol}} - \mathrm{constant}$$

In the empirical equation [1], ΔG_{sol} equals the difference in solvation energy between the neutral substrate and its radical ion, $(\Delta G^0(\mathrm{S})_{\mathrm{sol}} - \Delta G^0(\mathrm{S}^{\cdot-})_{\mathrm{sol}})$, while the constant equals the difference between the work function of the electrode and the potential difference for reduction between the working electrode and the reference electrode at the half-wave potential. EA is assumed to be $\simeq\Delta G^0(\mathrm{S})$, the energy for electron attachment in solution. The differences in solvation energies between the anion and the neutral, ΔG_{sol}, is often assumed to be constant, even though the correlation of reduction potentials with absolute EA's for aromatic hydrocarbons is reported not to be constant, at least with the solvents dioxane and dimethoxyethanol (9). Although very few absolute EA's were available for comparison with the existing electrochemical data, the relationship appears to be potentially useful. Briegleb (10) has used the assumed value of 1.37 eV for the EA of chloranil to establish a half-wave reduction potential scale, and calculated a value of −3.66 eV for ΔG_{sol}. Farragher and Page (11) assumed eq. [1] to be valid and calculated an average value of −2.37 eV for (ΔG_{sol} + constant) for tetracyanoethylene (TCNE), tetracyano-1,4-benzoquinone (TCBQ), chloranil, tetracyanobenzene, and tetracyanobutadiene using the magnetron results for the absolute EA's ($\mathrm{EA}_{\mathrm{Mag}}$) of these compounds. Since the publication of the extensive studies by Kebarle has made available a large data base to establish very accurately the solvation correction factor it seemed possible to test whether redox couples having very different structures would utilize the same solvation correction which might depend only on the solvent and electrode used.

A closely related, and equally important parameter, the Marcus reorganization energy, $\lambda(0)$, should be related to ΔG_{sol}, since the reorganization energy is comprised of energy changes that are necessary to reach the transition state for electron transfer (eq. [2]), by bond and solvent reorganization.

$$[2] \quad \mathrm{A}^{\cdot-} + \mathrm{B} \rightarrow \mathrm{A} + \mathrm{B}^{\cdot-}$$

[1]NSERC undergraduate research fellow, 1987.
[2]Postdoctoral Fellow, University of Alberta, 1986–1988.

Can. J. Chem. Downloaded from www.nrcresearchpress.com by 122.72.124.2 on 09/07/12
For personal use only.

TABLE 1. Electron affinities, redox potentials and solvation energies (eV) for substituted nitrobenzenes, substituted benzoquinones and aromatic hydrocarbons

Compound	$(-E^0)^a$	$(EA_{exp})^b$	$(\Delta G^0_{sol} + const)^c$	$(EA(E^0)_{calc})^d$	$(EA(E^0)_{calc})^e$
Nitrobenzenes					
4-$C_7H_4N_2O_2$ (*p*-nitrobenzonitrile)	1.03	1.68	2.71	1.42	1.53
4-$C_6H_4ClNO_2$ (*p*-chloronitrobenzene)	1.23	1.22	2.45	1.22	1.33
$C_6H_5NO_2$ (nitrobenzene)	1.34	0.99	2.33	1.11	1.22
4-$C_7H_7NO_3$ (*p*-methoxynitrobenzene)	1.42	0.85	2.27	1.03	1.14
4-$C_7H_7NO_2$ (*p*-methylnitrobenzene)	1.37	0.92	2.29	1.08	1.19
3-$C_7H_4F_3NO_2$ (*m*-α,α,α-trifluoromethylnitrobenzene)	1.14	1.37	2.51	1.31	1.42
3-$C_7H_4N_2O_2$ (*m*-nitrobenzonitrile)	1.10	1.51	2.61	1.35	1.46
4-$C_6H_4FNO_2$ (*p*-fluoronitrobenzene)	1.31	1.09	2.40	1.15	1.26
			av: 2.45 ± 0.12		
Benzo- (BQ), naphtho- (NpA), and anthraquinones (AnQ)					
$C_{16}H_{12}O_2$ (2-Et-9,10-AnQ)	1.13	1.50	2.63	1.51	1.43
$C_{11}H_8O_2$ (2-Mc-1,4-NpQ)	0.93	1.67	2.60	1.71	1.63
$C_{10}H_{12}O_2$ (tetramethyl-*p*-BQ)	1.0	1.56	2.56	1.64	1.56
$C_6H_2Cl_2O_2$ (2,5-dichloro-*p*-BQ)	0.33	2.37	2.70	2.30	2.22
$C_{12}H_8O_2$ (2-phenyl-*p*-BQ)	0.65	1.96	2.61	1.98	1.90
$C_8H_8O_2$ (2,6-dimethyl-*p*-BQ)	0.83	1.70	2.53	1.80	1.72
$C_{14}H_8O_2$ (9,10-AnQ)	1.09	1.54	2.63	1.54	1.46
$C_{10}H_6O_2$ (1,4-NpQ)	0.85	1.74	2.60	1.78	1.70
$C_7H_6O_2$ (2-methyl-*p*-BQ)	0.75	1.78	2.53	1.88	1.80
$C_{10}H_4Cl_2O_2$ (2,3-dichloro-*p*-NpQ)	0.59	2.13	2.72	2.04	1.96
$C_{14}H_{20}O_2$ (2,6-di-*t*-Bu-*p*-BQ)	0.89	1.80	2.69	1.74	1.66
$C_6H_4O_2$ (*p*-BQ)	0.67	1.84	2.51	1.97	1.89
$C_6Cl_4O_2$ (tetrachloro-*p*-BQ)	0.12	2.71	2.83	2.51	2.43
$C_6H_2Cl_2O_2$ (2,6-dichloro-*p*-BQ)	0.32	2.42	2.74	2.31	2.23
			av: 2.63 ± 0.07		
Aromatic hydrocarbons					
Naphthalene	3.15	0.148	3.30	0.09	
Anthracene	2.59	0.556	3.15	0.65	
Phenanthrene	3.02	0.307	3.33	0.22	
Pyrene	2.64	0.591	3.23	0.60	
Dibenz(*a*,*h*)anthracene	2.57	0.595	3.17	0.67	
Benzo(*a*)pyrene	2.46	0.680	3.14	0.78	
Chrysene	2.90	0.397	3.30	0.34	
Triphenylene	3.04	0.285	3.33	0.20	
1,2-Benzanthracene	2.61	0.630	3.24	0.63	
			av: 3.24 ± 0.06		

[a]Obtained from cyclic voltammetry using a Au^0 electrode vs. $Ag/AgClO_4$ (0.001 *M*).
[b]Taken from ref. 7; for hydrocarbon the values were taken from ref. 5.
[c]Calculated using eq. [1].
[d]Calculated using the average value of $(\Delta G^0_{sol} + const)$ in the solution of eq. [1].
[e]Calculated from the combined nitrobenzenes and quinones using the average $(\Delta G^0_{sol} + const)$ values, 2.56, from eq. [1].

Can. J. Chem. Downloaded from www.nrcresearchpress.com by 122.72.124.2 on 09/07/12
For personal use only.

$$[3] \quad k_{obs} = 10^{11} \exp\left\{-\left[\frac{\lambda}{4}\left(1 + \frac{\Delta G^{0\prime}}{\lambda}\right)^2 \Big/ RT\right]\right\}$$

where

$$\lambda = (\lambda(0)_{ox} + \lambda(0)_{red})/2$$

When a change in charge occurs in an organic molecule, solvation stabilization is presumably the most important difference between its vapor and solution phase free energies. The λ(0) values for each reactant are usually determined from their self exchange reactions

$$A + A^{\cdot -} \rightleftharpoons [A A^{\cdot -} \leftrightarrow A^{\cdot -} A]^{\ddagger} \rightleftharpoons A^{\cdot -} + A$$

by such methods as isotopic exchange (12) and line broadening in NMR or ESR spectra (13). For this reason, it is profitable to determine whether a useful correlation between the thermodynamic ΔG_{sol} and the kinetic λ parameters exists. Although this relationship had been recognized prior to the present report, no correlation could be examined, since sufficient data were not previously available (14).

Results and discussion

The reduction potentials, E^0, for a series of ring-substituted nitrobenzenes (8), substituted 1,4-benzoquinones (14), and aromatic hydrocarbons (9) were determined using cyclic voltammetry (Au electrode vs. Ag/Ag^+, 0.001 *M* $AgClO_4$). All of the substrates were reduced in the same solvent, acetonitrile, with tetrabutylammonium perchlorate (0.1 *M*) as the supporting electrolyte, see Table 1. By using eq. [1] values of $\Delta G_{sol} + C$ were calculated with these electrochemical data and the data of

TABLE 2. Correlation(s) obtained for plots 1–4 of $EA(E^0)_{calc}$ vs. EA_{obs} for a series of several substrates, for plots 5–6 of E^0 vs. EA_{obs}, and for plot 7 of ΔG_{sol} vs. $\lambda(0)$

Plot	Substrates	(ΔG_{sol}), kcal mol^{-1}	Slope	Intercept	Correlation coefficient (r)
1	Nitroaromatics	2.45 ± 0.12	0.474	0.642	0.989
2	Quinones	2.63 ± 0.07	0.799	0.382	0.981
3	Hydrocarbons	3.24 ± 0.06	1.33	−0.0156	0.985
4	Quinones and nitroaromatics	2.56 ± 0.11	0.685	0.615	0.982
5	Quinones and nitroaromatics (Fig. 1)		−0.727	2.114	0.982
6	Hydrocarbons (Fig. 2)		−1.333	3.396	0.985
7	ΔG_{sol} vs. $\lambda(0)$ (Fig. 3)		−0.050	3.479	0.930

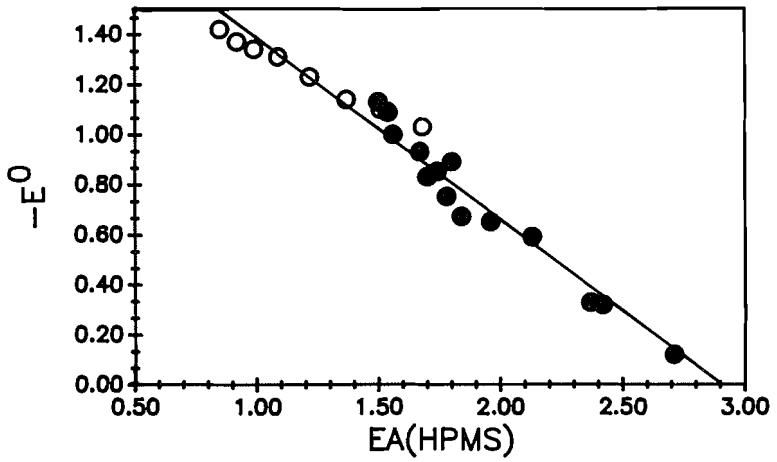


FIG. 1. Plot of $-E^0$ vs. EA(HPMS) for a series of substituted nitrobenzene, ○, and quinones, ●.

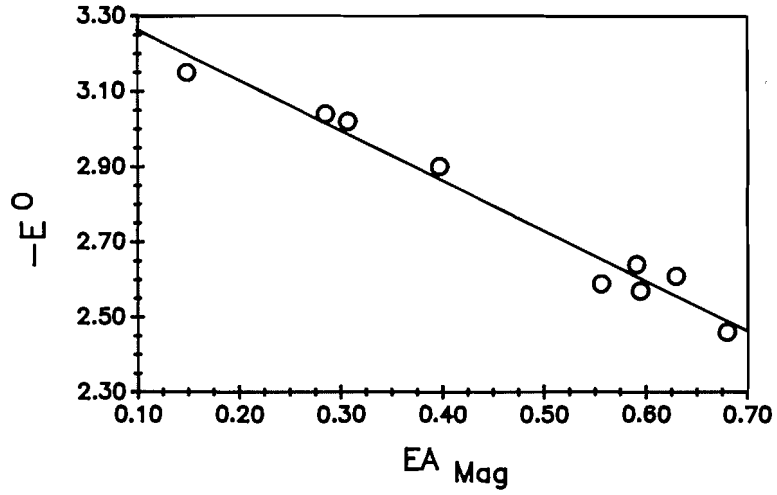


FIG. 2. Plot of $-E^0$ vs. EA_{Mag} (7) for a series of aromatic hydrocarbons.

Kebarle *et al.* (7) for the quinones and nitroaromatics, see Table 1. For the aromatic hydrocarbons the calculated values of $\Delta G_{sol} + C$ were based on our E^0 measurements and the EA's, EA_{Mag}, measurements by Chen and Wentworth (5) using the magnetron method (12). Average values of $EA + E^0$ were used to construct plots of the measured $(E^0 + \Delta G_{sol})$ vs. EA_{Mag}.

Excellent correlations were obtained for the plots of EA_{obs} vs. EA_{calc} for all three classes of compounds, see Table 2. The solvation energy, ΔG_{sol}, for all three classes of compounds measured, although somewhat different, seemed to be of two types: polar solvated substrates, quinones and nitrobenzenes, which are transformed into solvated delocalized radical anions, and nonpolar aromatic hydrocarbons which form ion-paired radical anions without resonance stabilization. A composite plot of E^0 vs. EA(HPMS) for the quinones and nitrobenzenes (Fig. 1), can be compared to one constructed for the hydrocarbons (Fig. 2). Since ΔG_{sol} (ave) for the quinones and for the nitrobenzenes are within experimental error (see Table 1), it was

Can. J. Chem. Downloaded from www.nrcresearchpress.com by 122.72.124.2 on 09/07/12
For personal use only.

TABLE 3. Marcus reorganization energies (kcal mol^{-1}), electron affinities, and redoxation potentials (eV) for a variety of organic substrates

Compound	$(\lambda(0))^a$	EA^b	$(-E^0)^c$	$EA + E^0$	$(\lambda(0)_{theory})^a$	$(\lambda(0)_{graph})$
p-Chloronitrobenzene	16.9	1.28	1.42	2.70	21.5	15.7
Nitrobenzene	19.2	0.99	1.49	2.48	22.1	20.1
p-Benzoquinone	13.1	1.84	0.86	2.70	22.9	15.9
Naphthalene	11.9	0.148	2.72	2.87	20.3	12.3
Anthracene	8.8	0.556	2.41	2.97	18.4	10.3
Tetracyanoethylene	8.2	3.17	−0.06	3.11	27.0	7.4
1,4-Naphthoquinone	12.8	1.75	1.07	2.82	20.1	13.3
m-Nitrobenzonitrile	15.1	1.56	1.25	2.81	21.5	13.5
m-Nitrobenzene	12.2	1.65	1.22	2.87	21.4	12.3
p-Dinitrobenzene	11.7	2.00	0.96	2.96	21.4	10.5
4-Cyanobenzonitrile	9.7	1.12	1.93	3.05	21.7	8.6

[a]Taken from ref. 14. Values determined in solvent DMF.
[b]Taken from ref. 7.
[c]Obtained by cyclic voltammetry vs. $Ag/AgClO_4$ (0.001 *M*).

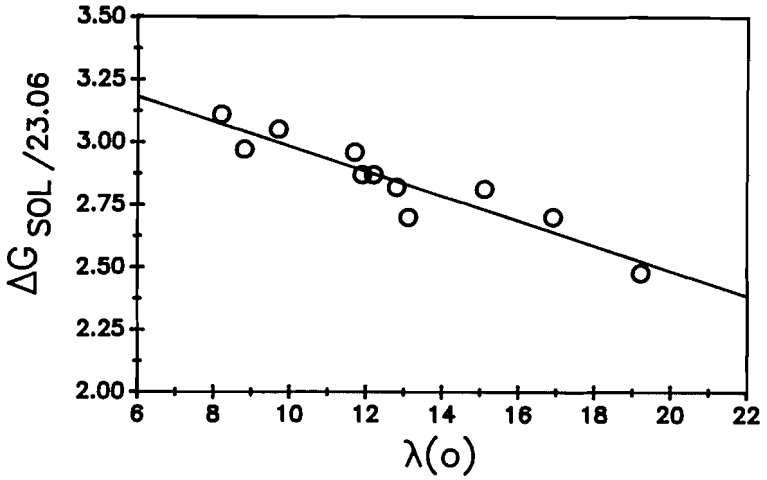


FIG. 3. Plot of ΔG_{sol} (kcal mol^{-1}) + *C* vs. Marcus reorganization energy $\lambda(0)$ (kcal mol^{-1}).

not surprising that a rather good correlation between $EA(E^0)_{calc}$ vs. EA(HPMS) exists for the composite plot using the average ΔG_{sol} for the two series of substrates, see Table 2. Although it is tempting to consider that changes in structure can cause an observable change in solvation energy (1, 7) in a series of substrates, in acetonitrile using our electrochemical data and Kebarles values for EA(HPMS) no dramatic changes in $EA(E^0)_{calc}$ from steric inhibition to solvation were apparent as a result of structural changes in the quinones studied.

The reorganization energies taken from the literature (Table 3) were used to construct a plot of $\Delta G_{sol} + C$ vs. $\lambda(0)$. The values of ΔG_{sol} determined for each substrate (i.e., E^0) were determined in the solvent (DMF) in which its $\lambda(0)$ value was determined. The results of this correlation are shown in Fig. 3. The plot, $\Delta G_{sol}/23.06 = -0.049\lambda(0) + 3.48$, showed a remarkably good straight line fit with $r = 0.930$, apart from its being of some theoretical interest (13), the correlation is of some practical use since the values of $\lambda(0)$ taken from the graph are in much better agreement with the experimentally determined values (i.e., ± 1.1 kcal mol^{-1}) than the theoretically calculated reorganization energies given in the literature (2), see Table 3.

Experimental

Materials

All the substrates were used as received. Tetrabutylammonium and silver perchlorate were dried over P_2O_5 under vacuum at 60°C before use. The solvents were purified by distillation over calcium hydride.

Cyclic voltammetry

Electrochemistry was performed using a Princeton Applied Research, EG and G Par Model 175 Universal Programmer wave form generator interfaced to an Amel model 551 potentiostat that provided feedback compensation for ohmic drop between the working and the reference electrodes. Cyclic voltammograms were recorded using a Princeton Applied Research Model RE0074 X-Y Recorder. Electrochemical measurements were carried out at room temperature in the appropriate solvent containing 0.001 *M* of the substrate and 0.1 *M* of tetrabutylammonium perchlorate as supporting electrolyte. The reference cell contains 0.001 *M* of the silver perchlorate and 0.1 *M* of tetrabutylammonium in the solvent.

Reversible waves were obtained at scan rates of between 20–500 mV/s.

1. F. M. PAGE and G. C. GOODE. Negative ions and the magnetron. Wiley Interscience, New York. 1969.
2. L. EBERSON. Advances in physical organic chemistry. Vol. 18. *Edited by* V. Gold and D. Bethell. Academic Press, London. 1982. p. 116.
3. P. S. DRZAIC, J. MARKOS, and J. I. BRAUMAN. *In* Gas phase ion chemistry. Vol. 3. *Edited by* M. T. Bowers. Academic Press, New York, NY. 1984.
4. (*a*) M. SZWARC. Prog. Phys. Org. Chem. **6**, 323 (1968); (*b*) G. BRIEGLEB. Angew. Chem. Int. Ed. Engl. **3**, 617 (1964).

Can. J. Chem. Downloaded from www.nrcresearchpress.com by 122.72.124.2 on 09/07/12
For personal use only.

5. E. C. M. CHEN and W. E. WENTWORTH. J. Chem. Phys. **63**, 3183 (1975).
6. R. D. MEAD, A. E. STEVENS, and W. C. LINEBERGER. *In* Gas phase ion chemistry. Vol. 3. *Edited by* M. T. Bowers. Academic Press, New York, NY. 1984.
7. P. KEBARLE and S. CHOWDHURY. Chem. Rev. **87**, 513 (1987).
8. T. HEINIS, S. CHOWDHURY, S. L. SCOTT, and P. KEBARLE. J. Am. Chem. Soc. **110**, 400 (1988).
9. R. S. BECKER and E. C. M. CHEN. J. Chem. Phys. **45**, 2403 (1966).
10. G. BRIEGLEB. Angew. Chem. Int. Ed. Engl. **3**, 617 (1964).
11. A. L. FARRAGHER and F. M. PAGE. Trans. Faraday Soc. **63**, 2369 (1967).
12. N. SUTIN. Ann. Rev. Nucl. Sci. **12**, 285 (1982).
13. (*a*) G. GRAMPP and W. JAENICKE. Ber. Bunsenges. Phys. Chem. **88**, 325 (1984); **88**, 335 (1984); (*b*) P. BERNHARD, L. HELM, A. LUDI, and A. E. MERBACH. J. Am. Chem. Soc. **107**, 312 (1985); (*c*) G. GRAMPP. Z. Physik. Chem. N.F. **148**, 53 (1986).
14. L. EBERSON. Electron transfer reactions in organic chemistry. Springer-Verlag, New York. 1987.

Can. J. Chem. Downloaded from www.nrcresearchpress.com by 122.72.124.2 on 09/07/12
For personal use only.

Alkyl versus hydrogen substitution: an *ab initio* study of the addition of hydroxide to formaldehyde and to acetone

C. I. BAYLY AND F. GREIN[1]

Department of Chemistry, University of New Brunswick, Fredericton, N.B., Canada E3B 6E2

Received April 22, 1988

C. I. BAYLY and F. GREIN. Can. J. Chem. **67**, 176 (1989).

The reaction profiles of the anionic nucleophilic addition of hydroxide to formaldehyde (system I) and to acetone (system II) were studied using theoretical *ab initio* methods. Calculations were carried out using the 4-31G basis set augmented with polarization and diffuse functions on some atoms. Electron correlation calculations were performed at the MP2 (frozen core), MP2, and MP4 levels for system I and at the MP2 (frozen core) level for system II. For both systems a local energy maximum was found at a C—OH distance of 2.5 Å. The barrier maximum was at lower energy than the separated reactants (−17.2 kcal/mol for system I and −5.6 kcal/mol for system II). This type of reaction profile is in accordance with a previous study on a prototype reaction. The energy difference between the barrier maximum and the secondary minimum (towards the reactants) was very small for system I (0.7 kcal/mol), but higher for system II (5.4 kcal/mol). The geometries of the two systems differed significantly in the region of the reaction coordinate containing the barrier and the secondary minimum.

Key words: quantum chemical study, addition of OH^- to H_2CO, addition of OH^- to $(CH_3)_2CO$, alkyl versus hydrogen substitution, potential energy curve.

C. I. BAYLY et F. GREIN. Can. J. Chem. **67**, 176 (1989).

Faisant appel à des méthodes théoriques *ab initio*, on a étudié les profils des réactions de l'addition nucléophile anionique de l'hydroxide sur le formaldéhyde (système I) et sur l'acétone (II). On a effectué les calculs à l'aide de l'ensemble 4-31G auquel on a ajouté des fonctions de polarisation et de diffusion sur quelques-uns des atomes. On a effectué des calculs de corrélation électronique aux niveaux MP2 (noyau solide). MP2 et MP4, pour le système I, et au niveaux MP2 (noyau solide),pour le système II. Dans chacun de ces systèmes, on a trouvé qu'il existe une énergie locale maximale à une distance C—OH de 2,5 Å. La barrière maximale se situe à une énergie plus faible que celle des réactifs séparés (−17,2 kcal/mol pour le système I et −15,6 kcal/mol pour le système II). Ce type de profil réactionnel est en accord avec une étude antérieure sur une réaction prototype. La différence d'énergie entre la barrière maximale et le minimum secondaire (par rapport aux réactifs) est très faible pour le système I (0,7 kcal/mol), mais plus élevée pour le systèmes II (5,4 kcal/mol). Les géométries des deux systèmes diffèrent beaucoup dans la région des coordonnées de la réaction contenant la barrière et le minimum secondaire.

Mots clés : étude de chimie quantique, addition de OH^- sur H_2CO, addition de OH^- sur $(CH_3)_2CO$, substitution alkyle versus hydrogène, courbe de l'énergie potentielle.

[Traduit par la revue]

Can. J. Chem. Downloaded from www.nrcresearchpress.com by 122.72.124.2 on 09/07/12
For personal use only.

Introduction

Chemical reactions involving alkyl substituted carbons are frequently examined by *ab initio* theoretical methods. In many cases, where the alkyl substituents do not participate directly in bond making or bond breaking processes, they are routinely replaced in the model system by hydrogens (ref. 1–7 for example). This gives a considerable reduction in the length of the computation, since a fragment of at least the size of a methyl, bringing four centers and nine electrons into the calculation, is instead represented by the single center and single electron of hydrogen. In addition, many systems undergo an increase in symmetry if alkyl groups are replaced by hydrogens, again reducing the computer time required for the calculation.

The reasoning behind the replacement of alkyl groups with hydrogen lies in the view that the major difference between these two substituents is steric in nature, while the difference in their electronic influence is considered to be minimal. Thus, when the study of interest is focussing on the electronic interactions occurring along a reaction pathway, in principle the substitution of a hydrogen for an alkyl group should not make a big difference.

Is this reasoning sound? To what extent does this replacement give rise to a significant change in the reaction pathway? In the present study, these questions are addressed through the comparison of the anionic nucleophilic attack of hydroxide on formaldehyde (system I) with the attack of the same nucleophile on acetone, the dimethyl substituted analogue of formaldehyde (system II).

These systems were chosen for study because they were considered to be representative examples of organic nucleophilic additions and because the calculations would be computationally feasible (examples of previous theoretical studies on these and similar reactions can be found in refs. 2–7). A recent *ab initio* study of a prototype reaction, the nucleophilic attack of hydride on formaldehyde (2) (paper I), found the gas-phase reaction profile to exhibit a double well potential, with only a small energy barrier in going from the secondary minimum to the global minimum. It was felt that an energy profile with such features would give clear and marked responses to changes in the substitution.

Also, as a result of testing several basis sets, a relatively small and efficient basis set for probing the reaction profile of this type of organic reaction was proposed in paper 1. Using this basis set to examine system I and system II, as extensions of the prototype reaction in paper I, made possible a valid RHF description of the reaction profile while keeping the inclusion of electron correlation within range computationally.

Calculations

Calculations were carried out at the RHF (restricted Hartree–Fock) and MP (Moeller–Plesset) levels using the GAUSSIAN 82 (8) computer program. The MP electron correlation calculations were performed on the SCF optimized geometries at the

[1]Author to whom all correspondence should be addressed.

TABLE 1. Optimized geometries for the $OH^- + H_2CO$ addition[a]

Distances				Angles				
C—OH	C=O	C—H	O—H	HO—C—X	O—C—X	O—C—O	H—C—X	H—O—C
1.4723	1.3068	1.1044	0.9494	113.0	224.9	111.9	53.2	101.1
2.0000	1.2283	1.0844	0.9500	87.8	201.8	114.0	56.9	100.4
2.2000	1.2129	1.0809	0.9507	76.1	193.6	117.5	57.7	106.3
2.3000	1.2079	1.0800	0.9506	68.5	189.8	121.3	57.8	115.3
2.3500	1.2061	1.0794	0.9505	63.6	188.0	124.4	57.9	122.5
2.4000	1.2045	1.0791	0.9501	59.0	186.4	127.4	57.9	129.7
2.5000	1.2031	1.0787	0.9502	44.0	182.7	138.7	57.8	151.7
2.7639	1.2019	1.0815	0.9502	00.0	180.0	180.0	57.0	180.0
3.0000	1.1992	1.0837	0.9504	00.0	180.0	180.0	57.0	180.0
∞	1.1848	1.0898	0.9530	00.0	180.0	180.0	58.1	180.0

[a]All distances are in Å and all angles are in degrees.

following levels: MP2 (frozen core) (henceforth referred to as MP2(FC)), MP2, and MP4 for system I, and MP2 (frozen core) for system II. In paper I, the prototype hydride–formaldehyde reaction intermediates were optimized at the MP2 level in addition to the RHF optimizations, but the RHF energy profiles remained very similar and the geometries varied little aside from some bond lengthening; hence it was felt that in this work geometry optimization beyond the SCF level was unnecessary. The 4-31G basis set was used, augmented with polarization d functions on the oxygens and the carbonyl carbon only (exponent 0.80), and with diffuse *s* and *p* functions on the oxygens (exponent 0.0680). This basis set was chosen in the light of basis set comparisons made in paper I.

The geometry was specified as follows: the Y—C—Y plane (Y = H for formaldehyde; Y = C for acetone) was chosen as the frame of reference, and a dummy atom X placed bisecting the Y—C—Y angle. The C—Y bond lengths, and bond angles Y—C—X were allowed to vary during optimization. The carbonyl oxygen and hydroxide were allowed movement only in the C_s plane, i.e. the plane perpendicular to the Y—C—Y plane and containing the line C—X, in accordance with generally accepted views (9, 10) on the optimum approach of these reactants. The hydroxide oxygen – carbonyl carbon distance *R*(C—OH) was used as the reaction coordinate. For the methyl groups of system II, the C—H bonds were fixed at 1.085 Å, and the H—C—C angles were fixed at 110° (the 4-31G optimized values for the product geometry).

For each fixed value of the reaction coordinate *R*(C—OH), all other geometry parameters were optimized at the SCF level with enforced C_s symmetry, using the GAUSSIAN 82 gradient-searching algorithms. For system II, methyl group rotation (maintaining C_s symmetry) was included in the optimization. All structures corresponding to RHF energy maxima and minima included *R*(C—OH) in the geometry optimization. The geometry-optimized SCF transition structure had a single negative eigenvalue in the Hessian matrix, showing it to be a true saddle point on the potential energy (PE) hypersurface.

Results and discussion

For system I, the RHF optimized geometries are given in Table 1 and the corresponding RHF energies in Table 2; the structures of several intermediates indicated in Table 2 are shown in Fig. 1. While the minimum energy reaction pathway (MERP) of system I has been thoroughly studied previously by Madura and Jorgensen (MJ) (3) at the RHF level, this pathway was re-investigated in this work because of the inclusion of electron correlation in this study and because a different basis set was used in order to compare the results with those of system II. A comparison will be made between our RHF results for system I and those of the previous study; the results from the better basis set (6-31+G*) used by those authors permit an evaluation of the adequacy of our basis set.

TABLE 2. $H_2CO + OH^-$: RHF, MP2(FC), MP2, and MP4 energies relative to separated reactants

R(C—OH) (Å)	Structure (Fig. 1)	*E*(rel)[a] (kcal/mol)			
		RHF	MP2(FC)	MP2	MP4
1.4723	d	−33.303	−32.738	−32.932	−32.597
2.0000		−19.160	−23.271	−23.364	−21.934
2.2000		−17.364	−19.600	−19.679	−18.854
2.3000		−17.075	−18.320	−18.386	−17.854
2.3500	c	−17.044	−17.855	−17.913	−17.507
2.4000		−17.082	−17.533	−17.584	−17.282
2.5000	b	−17.359	−17.247	−17.288	−17.174
2.7639	a	−18.475	−17.918	−17.948	−18.000
3.0000		−17.709	−16.964	−16.982	−17.055
∞		00.000	00.000	00.000	00.000

[a]The energy (in hartree) of the separated reactants is as follows: RHF, −189.07245; MP2(FC), −189.58936; MP2, −189.59949; MP4, −189.61423.

Both the geometries and the RHF relative energies obtained using our basis set were very close to those given by MJ; the RHF reaction profile of our results is compared with theirs in Fig. 2. The initial approach of the hydroxide is along the C_{2v} symmetry axis of formaldehyde towards the carbon. A shallow minimum (Fig. 1*a*) corresponding to a planar ion–dipole type complex then forms at a distance of 2.76 Å along the C_s reaction coordinate (still having C_{2v} symmetry). As in the MJ study this is not a real minimum but rather an extremely shallow maximum joining two identical planar species where the hydroxide is hydrogen bonding to a single formaldehyde hydrogen. The energy difference between this hydrogen bonding species and the C_s ion–dipole type complex was 0.01 kcal/mol (MJ: 0.1 kcal/mol), which is such a small energy difference that the C_s ion-dipole complex will henceforth be treated as a minimum in this work, as in the MJ study. The further approach of the hydroxide, now rising out of the plane H—C—H of formaldehyde, requires a very small energy barrier to be overcome (1.4

Can. J. Chem. Downloaded from www.nrcresearchpress.com by 122.72.124.2 on 09/07/12
For personal use only.

Can. J. Chem. Downloaded from www.nrcresearchpress.com by 122.72.124.2 on 09/07/12
For personal use only.

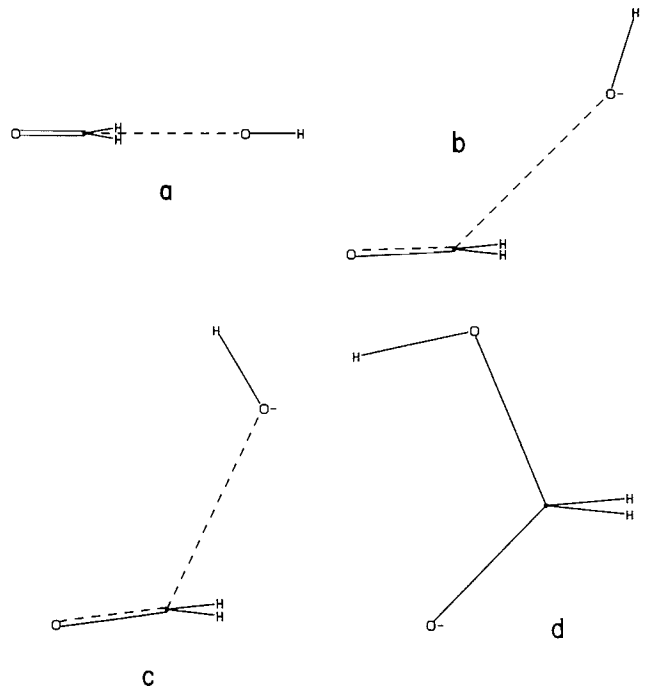


FIG. 1. The SCF optimized structures of several intermediates along the reaction pathway for system I (H_2CO + HO^-).

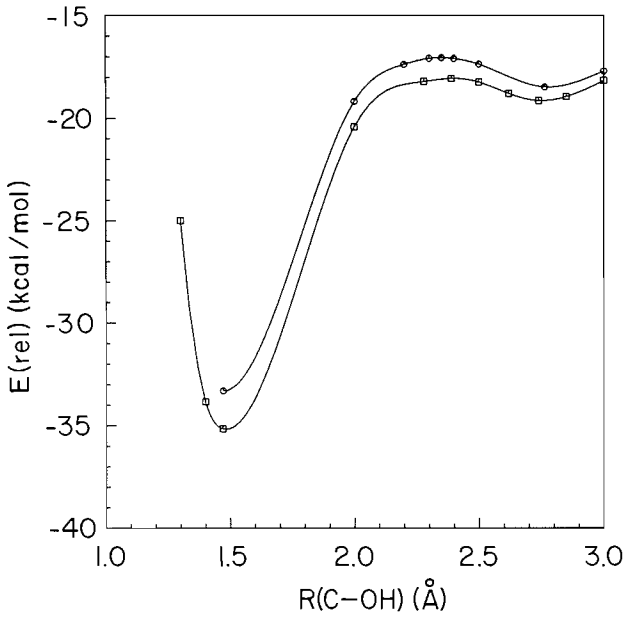


FIG. 2. RHF energy profiles for system I (H_2CO + HO^-); ○, this study; □, Madura and Jorgensen. Energies relative to separated reactants.

kcal/mol; MJ: 1.1 kcal/mol) whose energy maximum is lower than the energy of the separated reactants by −17.0 kcal/mol (MJ −18.0 kcal/mol). At the barrier maximum (Fig. 1*c*) the carbon–hydroxide distance is 2.35 Å (MJ 2.39 Å), the hydroxide is 63.6° above the H—C—H plane (MJ 59.3°), and the carbon is pyramidalizing, with the carbon-oxygen bond 8° below the H—C—H plane (MJ 6°) and lengthening. From here on the interaction is highly attractive, with the nuclei completing their trajectories to take up their equilibrium positions in the product (Fig. 1*d*) (energy relative to separated reactants E(rel) = −33.3 kcal/mol; MJ −35.1 kcal/mol). The similarities

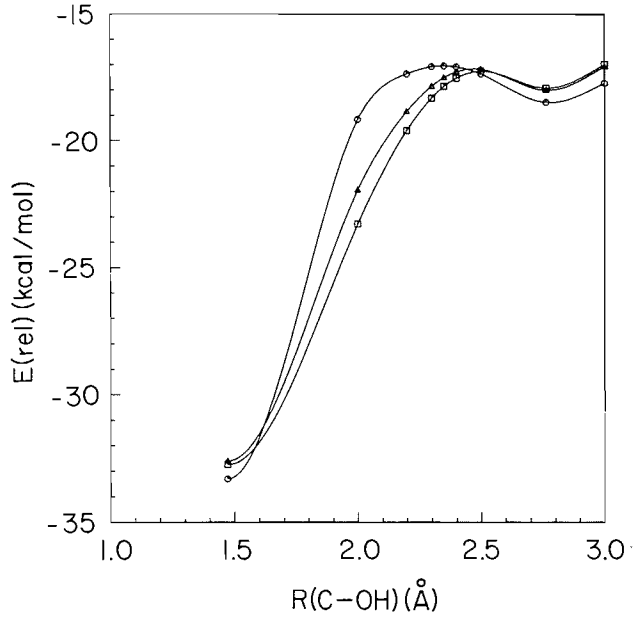


FIG. 3. Energy profiles for system I (H_2CO + HO^-) including eletron correlation; ○, RHF; □, MP2 (frozen core); △, MP4. Energies relative to separated reactants.

between our RHF results and those of Madura and Jorgensen, especially considering that small energy changes are preserved, shows that for this system our choice of basis set gives results comparable to those from the 6-31+G* basis set.

To show the effects of electron correlation, the energies of the intermediates along the MERP were calculated at several MP levels. The results are given in Table 2; in Fig. 3 are shown the MP2(FC) and MP4 energy profiles, along with the RHF results for comparison. From these it may be seen that while the introduction of electron correlation into the calculations does not qualitatively alter the PE profile of system I, some of the changes are quantitatively significant. The location of the transition state along R(C—OH) changes by about 0.15 Å, increasing from the RHF value of 2.35 Å to about 2.50 Å (structure Fig. 1*b*), although the position of the secondary minimum (the ion–dipole complex) does not move appreciably. The small energy difference between the PE maximum and the ion-dipole minimum decreases even further to less than 1 kcal/mol, but does not disappear completely. On the other side of the local PE barrier, however, the RHF relative energies are significantly higher than the corresponding MP energies.

Due to computational limitations the greater size of system II permitted only MP2(FC) as the highest level of calculation, so the comparison of systems I and II could not go beyond that level. It is important therefore to compare within system I the MP2(FC) results with the higher orders of MP calculations, to be confident that the major features of the electron correlation are manifest at the lower MP level. From Table 2 it can be seen that the MP2(FC) relative energies are almost identical to those from the MP2 calculations, and differ only slightly from the MP4 values. The greatest variation with the latter occurs in a region of the reaction coordinate between the local maximum and the global minimum (see Fig. 3), but in the vicinity of the local maximum and the secondary minimum the agreement is very good, differing by less than 0.2 kcal/mol. In paper I, a similar comparison showed that for the prototype reaction of hydride adding to formaldehyde, the MP2 and MP4 results were also very similar.

TABLE 3. Optimized geometries for the $(CH_3)_2CO + OH^-$ addition[a]

Distances				Angles					Torsion angles	
C—OH	C=O	C—C	O—H	HO—C—X	O—C—X	O—C—O	C—C—X	H—O—C	HCCX	HCCNu
1.4732	1.3115	1.5410	0.9485	115.7	225.9	110.2	54.8	100.8	57.1	−54.4
2.0000	1.2321	1.5152	0.9490	97.1	206.1	109.0	57.6	98.0	46.1	−49.9
2.2000	1.2162	1.5098	0.9499	90.2	199.2	109.0	58.3	100.2	43.0	−47.2
2.2934	1.2112	1.5080	0.9501	87.0	196.6	109.6	58.4	104.0	42.9	−44.5
2.5000	1.2045	1.5048	0.9501	79.6	191.7	112.1	58.5	121.0	48.4	−32.7
2.7500	1.2022	1.5002	0.9502	68.5	186.1	117.6	58.6	146.8	63.9	−7.5
3.0000	1.2033	1.4972	0.9504	55.6	182.6	127.0	58.6	158.5	62.6	−2.9
3.2500	1.2039	1.4973	0.9503	43.1	180.7	137.6	58.3	164.8	55.7	8.0
3.4895	1.2032	1.4999	0.9503	34.1	179.8	145.7	57.9	166.6	49.4	10.8
3.7500	1.2020	1.5033	0.9504	28.3	179.5	151.2	57.6	165.0	45.5	13.0
∞	1.1925	1.5086	0.9530	00.0	180.0	180.0	58.5	180.0	60.0	60.0

[a]All distances are in Å and all angles are in degrees.

TABLE 4. RHF and MP2(FC) energies relative to separated reactants

R(C—OH) (Å)	Structure (Fig. 4)	E(rel)[a] (kcal/mol) RHF	MP2(FC)
1.4732	d	−25.499	−30.383
2.0000		−12.182	−21.391
2.2000		−10.828	−17.968
2.2934	c	−10.727	−16.850
2.5000	b	−11.137	−15.583
2.7500		−13.096	−16.383
3.0000		−15.559	−18.571
3.2500		−17.433	−20.400
3.4895	a	−18.085	−21.015
3.7500		−17.416	−20.258
∞		00.000	00.000

[a]The energy (in hartree) of the separated reactants is RHF, −267.05910; MP2(FC), −267.75718.

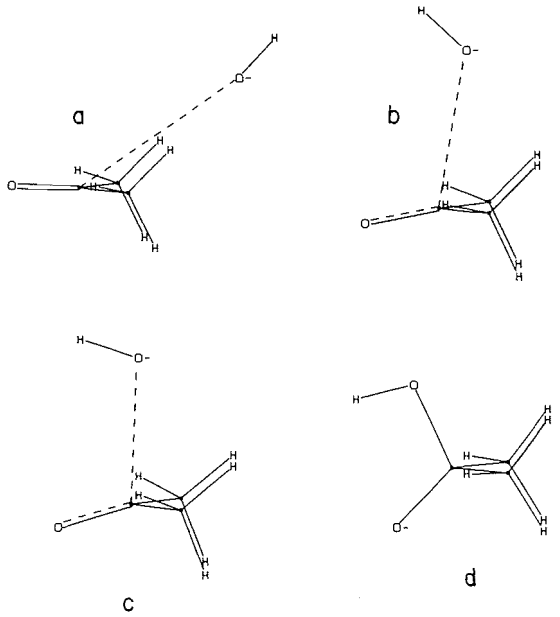


FIG. 4. The SCF optimized structures of several intermediates along the reaction pathway for system II ($(CH_3)_2CO + HO^-$).

For system II, the RHF optimized geometries are given in Table 3 and the corresponding RHF and MP2(FC) energies in Table 4; the structures of several intermediates indicated in Table 4 are shown in Fig. 4, and the reaction profile for both calculational levels is shown in Fig. 5. The same type of double-well reaction profile is present with this system as with system I: the PE decreases as the separated reactants are brought together, reaching a local minimum (Fig. 4*a*) analogous to the ion-dipole minimum of system I. As the reactants continue to approach, the PE increases to a local maximum (MP2(FC): Fig. 4*b*; RHF: Fig. 4*c*) which is lower than the energy of the separated reactants, and then it decreases quickly to form the tetrahedral adduct (Fig. 4*d*).

Some of the changes to the reaction profile upon the inclusion of electron correlation at the MP2(FC) level are qualitatively similar to the changes that took place in system I. The location of the PE local maximum moved farther out along *R*(C—OH) (by about 0.2 Å) while the location of the secondary minimum remained about the same, and the energy difference between the secondary minimum and the local maximum decreased. The energy difference between the local maximum and the global minimum remained about the same upon the addition of correlation. For system II, however, adding correlation caused the energy difference between the separated reactants and all the intermediates to increase, lowering the entire MP2(FC) curve in Fig. 5; this lowering was not found for system I (cf. Fig. 3).

Comparing the RHF reaction profiles of system I and system II at a more quantitative level, several major differences become apparent, as seen in Fig. 6 where the RHF profiles of both systems are shown together. The location of the secondary minimum is 0.75 Å further out along *R*(C—OH) in system II, which is easily explained in terms of an ordinary steric effect, as will be discussed later. The energy (relative to the separated reactants) at the secondary minimum is almost the same for both systems, suggesting that both systems achieve a similar amount of energetic stabilization up to this point in the reaction.

The energy change involved in proceeding from the secondary minimum to the local maximum, however, is significantly greater for system II than for system I. The 1.4 kcal/mol energy change for system I at the RHF level is very small, especially in the light of basis set inadequacy and the neglect of electron correlation, zero-point energy, and thermodynamic effects, even outside of considering possible solvent effects. The

Can. J. Chem. Downloaded from www.nrcresearchpress.com by 122.72.124.2 on 09/07/12
For personal use only.

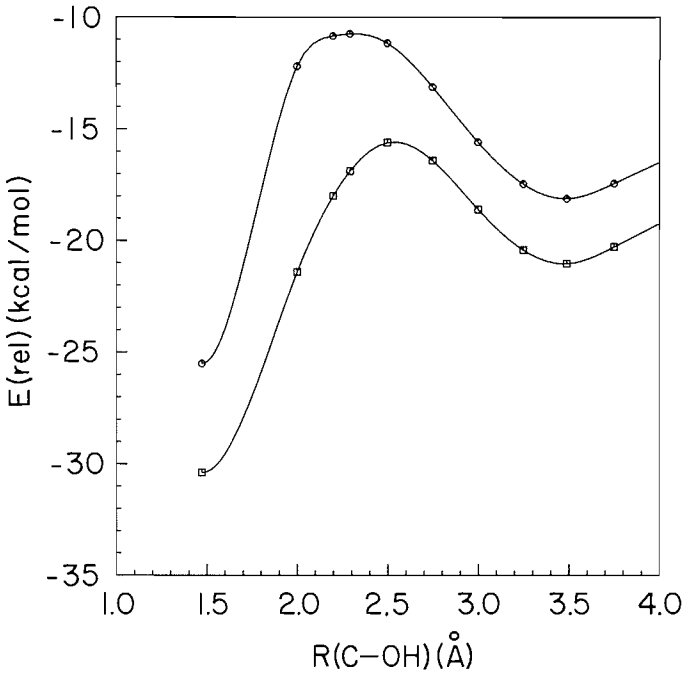


FIG. 5. Energy profiles for system II ($(CH_3)_2CO + HO^-$) including electron correlation; ○, RHF; □, MP2 (frozen core). Energies relative to separated reactants.

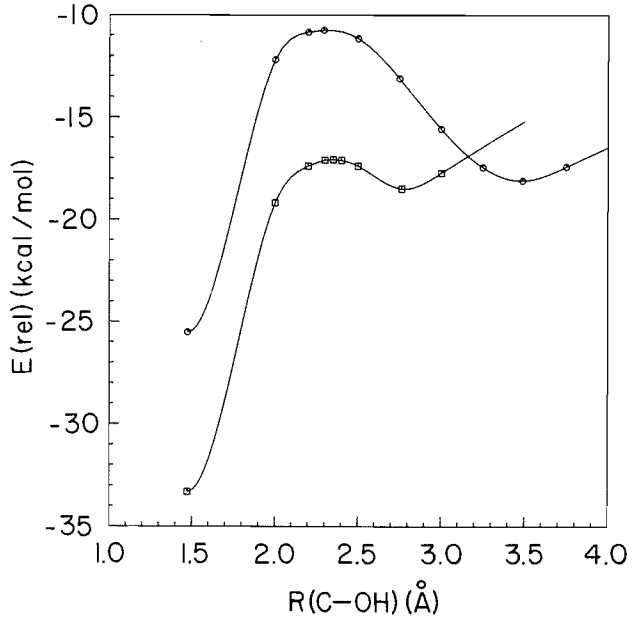


FIG. 6. RHF energy profiles for system I ($H_2CO + HO^-$) (□) and system II ($(CH_3)_2CO + HO^-$) (○). Energies relative to separated reactants.

increased size of the basis set used for system I in the MJ study (3), and the partial inclusion of electron correlation in our study (*vide infra*) both show a trend of decreasing this small energy difference. On the other hand, the energy difference of 7.4 kcal/mol for system II is large enough that correcting for the same factors mentioned above would probably still leave a barrier; after the inclusion of electron correlation at the MP2(FC) level, the barrier is still 5.4 kcal/mol (c.f. Table 4).

The comparison of the MP2(FC) results for systems I and II, shown together in Fig. 7, is similar to the RHF comparison, except for changes caused by the previously mentioned lowering of the system II MP profile. This now places the secondary minimum of system II several kcal/mol lower than that of system I, suggesting that a greater stabilization occurs for system II in going from reactants up to this stage. Otherwise, all the points mentioned above apply.

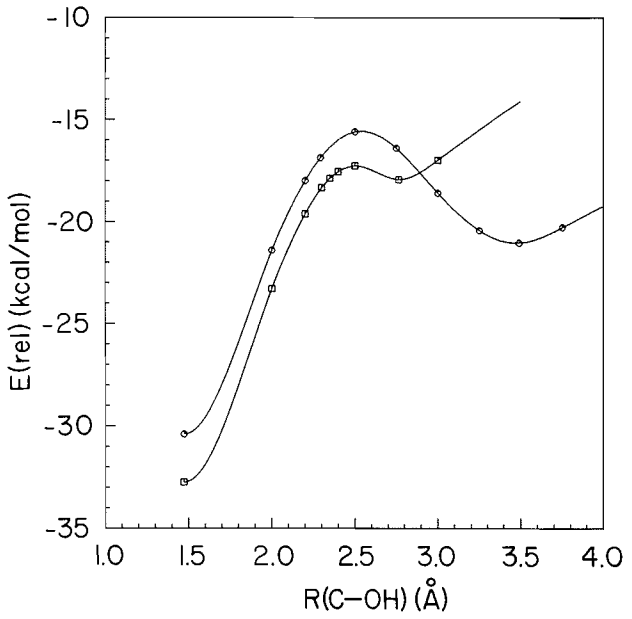


FIG. 7. MP2 (frozen core) energy profiles for system I ($H_2CO + HO^-$) (□) and system II ($(CH_3)_2CO + HO^-$) (○). Energies relative to separated reactants.

The geometry changes taking place over the course of the addition reaction are also an example of a qualitative similarity between these two systems having major differences at a quantitative level. Some of these dissimilarities can be attributed to the differences in steric effects between the two substituents, but others seem to be better explained in terms of an electronic effect.

During the initial stages of the reaction, before bonding interactions take place, the approach of the reactants is generally considered to be governed by charge dipole effects. That is, the negatively charged nucleophile (hydroxyl) will approach the substituted carbonyl dipole along the C_{2v} axis toward the carbonyl carbon, since this maximizes the electrostatic attractions. This leads to the formation of an ion–dipole type complex, giving rise to a PE minimum where the charge dipole attraction is countered by steric repulsion from the carbonyl substituents plus perhaps some other effects in addition. With system I, the ion–dipole complex (Fig. 1*a*) fits this description quite well, with the hydroxyl resting on the formaldehyde C_{2v} symmetry axis, 2.76 Å away from the carbonyl carbon and on the opposite side from the carbonyl oxygen. The analogous C_s species of system II (Fig. 4*a*), however, is quite different. The greater distance of the hydroxide from the carbonyl carbon in system II (3.49 Å) compared to system I is to be expected, reflecting the greater steric effects of the large methyl substituents compared to the small hydrogens of system I. What is interesting is that the nucleophile is significantly out of the molecular plane, with an angle HO—C—X of 34°, and the methyls rotated to direct one of their hydrogens towards the nucleophilic oxygen.

The out-of-plane position of the nucleophile can be explained in terms of a combination of hydrogen bonding to the methyl groups and steric interactions between the two methyls themselves. If the nucleophilic oxygen were to stay on the molecular

Can. J. Chem. Downloaded from www.nrcresearchpress.com by 122.72.124.2 on 09/07/12
For personal use only.

Can. J. Chem. Downloaded from www.nrcresearchpress.com by 122.72.124.2 on 09/07/12
For personal use only.

axis of acetone, maximizing the electrostatic attractions, then in principle the methyls could rotate, each bringing one of their hydrogens into the plane, directed towards the nucleophile to achieve the "best" hydrogen bonding situation. Under these circumstances, however, each methyl would have a hydrogen *syn* to the other methyl group, and these two hydrogens would be in close proximity to one another, giving bad steric interactions. In order to avoid these steric repulsions, the methyls in the structure of the secondary minimum have only partially rotated their hydrogen bonding hydrogens closer to the plane. The nucleophile, however, has maintained good hydrogen bonding in its position out of the plane, at the expense of some ion–dipole electrostatic interactions. This suggests that the secondary minimum for system II is significantly influenced by hydrogen bonding character, and hence is not strictly an ion dipole complex as the secondary minimum for system I appears to be.

The pattern of the methyl rotations of system II over the course of the reaction is interesting, reflecting the changes in hydrogen bonding to the nucleophile over the course of the reaction. The parameters HCCX and HCCNu in Table 3 can be used to follow methyl rotation and hydrogen bonding, respectively; the former expresses the torsion angle H—C—C—X between one of the methyl C—H bonds and the C—X reference line and the latter expresses the torsion angle H—C—C—OH between the hydrogen bonding methyl C—H bond and the developing C—OH bond. As the nucleophile moves out of the plane and over the methyl groups and carbonyl carbon, the methyls begin to rotate so as to keep a hydrogen directed towards the nucleophile for hydrogen bonding. This is the case over the region of the reaction coordinate from 3.75 Å up to about 2.75 Å, as indicated by HCCNu in this region showing an almost eclipsed H—C—C—OH torsion angle (~0°) while HCCX shows a continuous rotation to allow this near eclipsing. Between 2.75 Å and 2.50 Å there is a sudden change, with the HCCNu torsion angle now opening up again and the methyl rotation changing direction, as the methyls now begin to stagger their hydrogens between the two C—O bonds; this movement continues on to form the equilibrium structure of the tetrahedral adduct (Fig. 4*d*), with the HCCNu value of 54° showing that staggering is almost complete (60° would be "perfect" staggering). This shows that in terms of hydrogen bonding involving the methyl groups, the reaction of system II exhibits two stages, changing character around the position of the local energy barrier.

In proceeding along the reaction coordinate from the secondary minimum, the major difference between the geometries of system I and system II is seen in the angle HO—C—X, which expresses the amount the nucleophile has risen out of the reference plane Y—C—Y (*vide infra*). At a given point along *R*(C—OH) this angle is greater for system II than for system I (c.f. Tables 1 and 3). While the hydroxyl in system I remains in the plane until *R*(C—OH) has reached 2.76 Å (Fig. 1*a*), the hydroxyl at 2.75 Å in system II has risen 68.5° out of the plane, from its "head start" of 34° at the secondary minimum (Fig. 4*a*). From here the difference between the angle HO—C—X in system I and system II begins to decrease again, down to 2° at the tetrahedral adduct. Other geometrical parameters also reflect these differences, but to a lesser degree.

It is at the PE maximum that the dissimilarity between the geometry of system I and system II becomes most significant. Using the MP2(FC) results, which place the maximum at around 2.5 Å for both systems (structures Fig. 1*b* and Fig. 2*b*), the HO—C—X angles differ by 35°. For system I, the HO—C—X angle is 44°, an angle which, at that distance, would certainly create large steric interactions in system II. The larger angle of 80° in system II circumvents such large interactions, so in that sense this big geometry difference could be attributed to a steric effect. However, the two systems may also be at different stages electronically: the degree of pyramidalization of the carbonyl carbon is very small for system I (the CO bond has moved less than 3° below the H—C—H plane), whereas it is substantially larger for system II (the CO bond has moved almost 12° below the Me—C—Me plane). The Dunitz–Burgi attack angle (10), i.e. the HO—C—O angle, is 138.7° at the barrier maximum of system I, well outside the vicinity of 109° suggested by these authors. The corresponding angle for system II is 112.1°, in much better agreement. These comparisons suggest that system II has a better formed HO—C bond than system I at the barrier maximum. That different stages of bond formation between system I and system II are indicated does not necessarily mean that these electronic effects are a determining factor in the geometry differences. It could be other factors, such as the above-mentioned steric factor, which first dictates the larger HO—C—X angle for system II, with the bonding process adjusting *a posteriori* to accommodate the different approach.

These geometry differences for the maximum can become very important in terms of the alignment of reacting termini in an intramolecular reaction. For such reactions, extra energy is often required to distort the molecule into a geometry where the reacting termini can follow a trajectory leading to reaction. The amount of this "distortion energy" required is obviously strongly dependent on the actual geometries required by the reacting termini. Since the rate of reaction is determined by the height of the energy barrier, it is the geometry required by the reacting termini at the maximum that is of crucial importance. Given a reactant geometry having two available trajectories for the intramolecular reaction, each leading to a different product isomer, the preferred pathway will be the one with the lower energy maximum. In such a situation, the determining factor for which pathway is taken will be the difference in the distortion energy required for each pathway. For the reactions studied here, although the barrier maximum is of lower energy than the separated reactants, in an intramolecular situation the reactant geometry often falls within the range of the reaction coordinate containing the secondary minimum. In these circumstances, the local energy barrier would represent a real energy barrier to the reaction.

Conclusions

The comparison of the anionic nucleophilic addition of hydroxide to formaldehyde (system I) and to acetone (system II) is useful in examining the validity of replacing alkyl substituents with hydrogen in modeling organic reactions. For the reactions studied here, the replacement appears to be valid only at a qualitative level. The energy profiles of system I and system II exhibited the same number and relative ordering of maxima and minima, and the changes to the energy profile of a system in going from RHF to MP2(FC) levels of calculation were similar. Also, the general nature of the geometry changes taking place over the course of the reaction was the same for both systems. In particular, with the introduction of electron correlation, the position of the local energy maximum moved farther out along *R*(C—OH) by 0.15 to 0.2 Å.

There were several pronounced differences between the two systems at a quantitative level, however. At the RHF level, an insignificant-looking 1.4 kcal/mol energy difference in system I

between the secondary minimum and the local maximum becomes a definitely important 7.4 kcal/mol difference in system II. Upon the addition of electron correlation at the MP2(FC) level, this energy difference decreases to less than 1.0 kcal/mol in system I, and might disappear completely in the face of the neglect of other corrections. In system II, however, the barrier is still 5.4 kcal/mol. Also, the total energy change for the reaction (i.e. the energy difference between separated reactants and the tetrahedral adduct) increases significantly for system II in going from RHF to MP calculations, but for system I the change is again less than 1 kcal/mol.

The most important differences in geometry between system I and system II concern the angular movement of the nucleophilic oxygen out of the formaldehyde plane, described by the angle H—O—C—X. While the values for this angle differed very little between system I and system II for the product geometry (structures Fig. 1*d* and Fig. 4*d*), over most of the reaction pathway they differed substantially. Most significantly, at the MP2(FC) local energy maximum (structures Fig. 1*b* and Fig. 4*b*) they differed by 35°, with the nucleophile in system II positioned farther over the carbonyl group. Where this energy barrier could be rate-determining in an intramolecular reaction, the differing amounts of strain introduced into an intramolecular framework in requiring the reacting termini to adopt the geometry of system II versus system I could lead to quite different answers regarding the size of this barrier.

The results of this work suggest that the replacement of alkyl substituents by hydrogens in the modeling of organic reactions using theoretical *ab initio* methods does contain some pitfalls. Energy differences that appear to be small in the energy profile of the hydrogen substituted system may increase substantially with the introduction of alkyl groups. Also, while the reactants and products may exhibit very similar geometries, key intermediates along the pathway may have large and important differences in geometry. Such geometry differences may have particularly strong effects in intramolecular reactions.

Acknowledgements

We would like to thank NSERC Canada for an operating grant, and a postgraduate award to C.I.B. Generous financial support by the Leonard and Kathleen O'Brien Humanitarian Foundation to C.I.B. is much appreciated. Equipment grants by the University of New Brunswick Research Fund, as well as plentiful allocation of computer time by the University of New Brunswick are gratefully acknowledged.

1. K. N. Houk, M. N. Paddon-Row, N. G. Rondan, Y.-D. Wu, F. K. Brown, D. C. Spellmeyer, J. T. Metz, Y. Li, and R. J. Loncharich. Science, **231**, 1108 (1986).
2. C. I. Bayly and F. Grein. Can. J. Chem. **66**, 149 (1988).
3. J. D. Madura and W. L. Jorgensen. J. Am. Chem. Soc. **108**, 2517 (1986).
4. H. B. Burgi, J. M. Lehn, and G. Wipff. J. Am. Chem. Soc. **96**, 1956 (1974).
5. I. H. Williams, G. M. Maggiora, and R. L. Schowen. J. Am. Chem. Soc. **102**, 7831 (1980).
6. S. J. Weiner, U. C. Singh, and P. A. Kollman. J. Am. Chem. Soc. **107**, 2219 (1985).
7. Y. Li, M. N. Paddon-Row, and K. N. Houk. J. Am. Chem. Soc. 110, 3684 (1988).
8. J. S. Binkley, M. J. Frisch, D. J. De Frees, K. Raghavachari, R. A. Whiteside, H. B. Schlegel, E. M. Fluder, and J. A. Pople. GAUSSIAN 82 Release H. Carnegie-Mellon University, Pittsburgh. 1986.
9. F. M. Menger. Tetrahedron, **39**, 1013 (1983).
10. H. B. Burgi, J. D. Dunitz, J. M. Lehin and G. Wipff. Tetrahedron, **30**, 1563 (1974).

Can. J. Chem. Downloaded from www.nrcresearchpress.com by 122.72.124.2 on 09/07/12
For personal use only.

Reduction processes in the fast atom bombardment mass spectra of pyridinium salts. The effect of reduction potential and concentration

CLEMENT W. KAZAKOFF[1]

Department of Chemistry, University of Ottawa, 32 George Glinski, Ottawa, Ont., Canada K1N 6N5

AND

ROBIN T. B. RYE[1] AND OSWALD S. TEE

Department of Chemistry, Concordia University, 1455 de Maisonneuve Blvd. W., Montreal, P.Q., Canada H3G 1M8

Received July 12, 1988

CLEMENT W. KAZAKOFF, ROBIN T. B. RYE, and OSWALD S. TEE. Can. J. Chem. **67**, 183 (1989).

The enhancement of the $(C + 1)/C$ ratio in the fast atom bombardment mass spectra of seven pyridinium cations has been measured. No dependence of the enhancement on the cation reduction potential could be identified. The *N*-methyl pyridinium cation, which showed no enchancement under matrix-free conditions, exhibited an increase in the $(C + 1)/C$ ratio with decreasing concentration. This concentration dependence was eliminated when the bombardment energy was reduced from 9 to 5 keV. Possible mechanisms for the concentration dependence and the variation with bombardment energy are proposed.

Key words: fast atom bombardment, reduction, pyridinium salts.

CLEMENT W. KAZAKOFF, ROBIN T. B. RYE et OSWALD S. TEE. Can. J. Chem. **67**, 183 (1989).

On a déterminé l'augmentation du rapport $(C + 1)/C$ dans les spectres de masse, par bombardement avec des atomes rapides, de sept cations pyridinium. On n'a pas pu établir de corrélation entre l'augmentation de ce rapport et le potentiel de réduction du cation. La cation *N*-méthyl pyridinium ne présente pas d'augmentation dans des conditions où il n'y a pas de matrice; toutefois, on observe une augmentation du rapport $(C + 1)/C$ lorsqu'on diminue la concentration. On élimine cette relation avec la concentration lorsqu'on réduit l'énergie de bombardement de 9 à 5 keV. On propose des mécanismes qui pourraient expliquer la relation avec la concentration ainsi que la variation avec l'énergie de bombardement.

Mots clés : bombardement avec des atomes rapides, réduction, sels pyridinium.

[Traduit par le journal]

Can. J. Chem. Downloaded from www.nrcresearchpress.com by 122.72.124.2 on 09/07/12
For personal use only.

Introduction

It is well established that extensive chemical reaction may occur during the fast- atom bombardment (FAB) experiment. Adduct ion formation and dehalogenation reactions may result from reaction of the "analyte" with atomic or free radical species generated from the matrix by particle bombardment (1–3). Reduction reactions have been reported for organic and inorganic salts (4, 5), organometallics (6), nucleosides (7), and organic dyestuffs (5, 8). Mechanisms involving combinations of one- and two-electron reduction, hydrogen atom abstraction, and protonation have been proposed (5, 7, 9), and a correlation with the reduction potential of the analyte has been suggested (5, 8). Many of these analyate – solvent reactions can be minimized by an appropriate choice of matrix material. Nevertheless, glycerol is still the most commonly used solvent for FAB, and study of effects related to its use continues to be of interest. We have recently observed (10) enhancement of the $(C + 1)/C$ abundance ratios (C stands for cation) in the FAB spectra of N(1)-substituted pyrimidinium salts in glycerol, and noted that this enhancement showed a significant concentration dependence. To explore this effect further we have now examined the FAB spectra of selected ring-substituted N-alkyl pyridinium salts in a glycerol matrix. These compounds were chosen because the electrochemical and chemical reduction of 1-alkyl pyridinium cations has been extensively studied (11), and because a series of closely related compounds with a range of reduction potentials could be obtained.

Experimental

Fast atom bombardment spectra were taken on a VG-7070E instrument, with 9 keV xenon atoms as bombarding particles at a beam current of 1.5 mA. The accelerating voltage was 6 kV. Data were acquired using the VG DEC PDP8A data system; peak intensities used for calculation of enhancement ratios are based on an average of five scans. Samples for quantitative measurements were prepared by weight. Samples for matrix-free experiments were dissolved in methanol/water, applied to the probe tip, and air dried before insertion into the source. Compounds **1**, **2**, **5**, **9**, **10**, and **11** were obtained from commercial sources and used as received. Other pyridinium salts were prepared from the appropriately substituted pyridine by quaternization with methyl iodide.

[1]Authors to whom correspondence may be addressed.

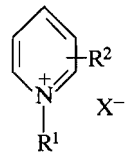
Results

Dependence on cation reduction potential

The seven pyridinium cations selected for study (see Table 1) have reduction potentials (vs. NHE, normal hydrogen electrode) ranging from −1.32 to −0.50 volts. Preliminary measurements showed that concentration effects (*vide infra*) were minor for the ca. 0.1 M solutions used. It is convenient to define an enhancement ratio, ER_n, as the ratio of the measured value of $(C + n)/C$ to the value expected on the basis of natural isotopic abundances. For compounds **1–4**, **6**, **8**, and **11** the values of ER_1 show little variation with cation reduction potential, with a mean value of 1.84 (Fig. 1). The ER_1 values for **5** and **7** are significantly higher (3.1 and 3.2, respectively), possibly reflecting the ease of protonation of the ring substituents, R^2, in these compounds. Substituted pyridinium cations with reduction potentials more positive than that of **8** were not available. The cationic dyes methyl violet, **9**, and methylene blue, **10**, with reduction potentials of −0.642 volts and −0.269 volts, respectively, gave results for ER_1 consistent with literature values (8). The results of Gale *et al.* (8) for **9**, **10**, and some other organic dyes (**12–16**) are also included in Fig. 1. A similar trend in the extent of reduction with E_{red} has been observed for inorganic cations. Thus, Fe(III) (E_{red} = 0.77 V) is strongly reduced, whereas Cr(III) (E_{red} = −0.41 V) is not (5). The facile reduction of Cu(II) to Cu(I) (E_{red} = 0.158 V) has also been

TABLE 1. Reduction potentials and $(C + 1)/C$ ratios

A. Pyridinium cations



Compound	R^1	R^2	X	E_{red} vs. NHE[a] (ref.)	$(C+1)/C$ ($C^+ = 100$) calcd.	obsd.
1	H	—	CL	−1.32[b] (16)	5.9	11.3
2	C_2H_5	—	Br	−1.07[c] (16)	8.2	11.8
3	CH_3	—	I	−1.05 (11)	7.1	12.4
4	CH_3	—	ClO_4	−1.05	7.1	14.3
5	CH_3	3-$CONH_2$	I	−0.86 (16)	8.6	26.6
6	CH_3	2-Cl	I	−0.67 (16)	7.1	13.3
7	CH_3	3-$COCH_3$	I	−0.64 (16)	9.3	29.9
8	CH_3	3-CN	I	−0.50 (16)	8.5	21

B. Other cations

Compound	Name	X	E_{red} vs. NHE (ref.)	$(C+1)/C$ ($C^+ = 100$) calcd-	obsd.
9	Crystal violet	Cl	−0.445 (8)	29	33.6
10	Methylene blue	Cl	−0.205 (8)	19	196
11	*N*-Ethylquinolinium	I	−0.59[a] (16)	12.7	18.2
12	Chrysoidin		−0.605 (8)	15	28[d]
13	Methyl red HCl		−0.385 (8)	18	30[d]
14	Safranin O		−0.535 (8)	24	44[d]
15	Basic blue 16		−0.335 (8)	35	160[d]
16	Janus green		−0.275 (8)	36	234[d]

[a]Converted to NHE using $E^0 = 0.245$ V for SCE.
[b]$E_{ref} = 0.00$ volts for mercury pool electrode vs. SCE (17).
[c]$E_{ref} = +0.09$ volts for normal silver ion electrode vs. SCE (17).
[d]Reference 8, magnetic sector instrument.

reported (6). It appears from these data that ER_1 is a function of reduction potential for cations with E_{red} more positive than −0.3 to −0.4 volts and, for the pyridinium cations, becomes essentially independent of E_{red} for values more negative than −0.4 volts.

The role of the solvent in the reduction processes observed in FAB has been the subject of a number of reports, and it is generally accepted that bombardment-induced matrix fragments can be involved in such reactions. Gale *et al.* noted that **10** did not undergo reduction using plasma desorption but such processes were significant in FAB (glycerol matrix). A recent study by Busch and co-workers (12) reports significant peaks due to reduction processes using a variety of solvent-free ionization methods, and it suggests several possible rationalizations of the earlier results. We have examined the solvent-free FAB spectra of **10** and three of the pyridinium salts available to us. For compounds **5** and **7** the measued ER_1 values (1.47 and 1.48, respectively) are lower than those measured for the 0.1 M solution, but are sufficiently large to confirm that reduction processes are occurring in the matrix-free system. For **3** and **10** the matrix-free FAB gave an ER_1 value of unity. The expected $(C + 2)/C$ ratios are very small for the pyridinium cations, typically in the 0.1–0.5 range, and in a glycerol matrix the signal-to-noise ratio was too low to permit reliable determinations of ER_2. For **1**, **3**, **5**, **7**, and **8** we estimate ER_2 values in the range 25–30, for 0.1 M solutions, with no obvious dependence on reduction potential. Values of ER_2 between 30 and 77 were reported (8) for the more easily reduced organic dyes.

Dependence on cation concentration

The effect of concentration as a variable in FAB has not received much attention. For the reduction processes considered here, where bombardment-generated fragments of both solvent and analyte may be involved, a complex variation of the extent of reduction with concentration would be expected. Such is clearly the case for **10**, with the relative abundances of the $(C + 1)$, $(C + 2)$, and $(C + 3)$ peaks showing a marked concentration dependence (Fig. 2). For **9** the effect of concentration is much less pronounced, and comparable to that observed for the pyridinium cations. Since reduction of **3** appears to be entirely solvent dependent, it was used to test for a concentration dependence of ER_1. Solutions of **3** in glycerol, at concentrations from 0.028 to 0.83 M, were run under experimental conditions such that the protonated glycerol peak at m/z 93 did not saturate the data system. The measured solute cation peak intensities at m/z 94 and m/z 95 were then corrected for isotope contributions from the solvent, before the ER_1 were calculated. The observed variation of ER_1 with concentration is shown in Fig. 3.

Can. J. Chem. Downloaded from www.nrcresearchpress.com by 122.72.124.2 on 09/07/12
For personal use only.

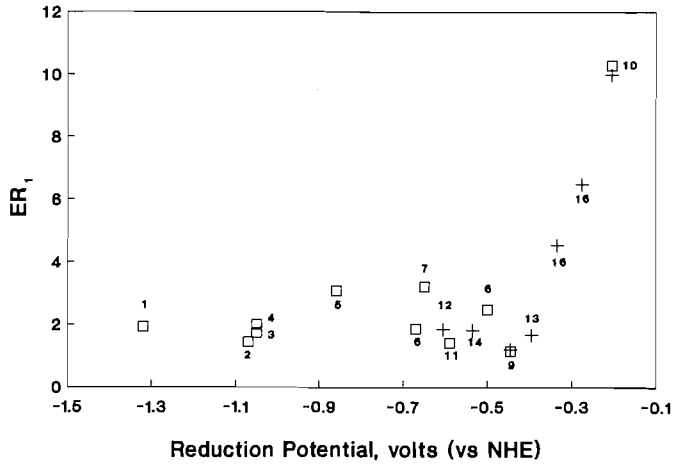


FIG. 1. Enhancement of the $(C + 1)/C$ ratio vs. cation reduction potential. Solute concentrations ca. 0.01 M. Squares, this work; crosses, data from ref. 8.

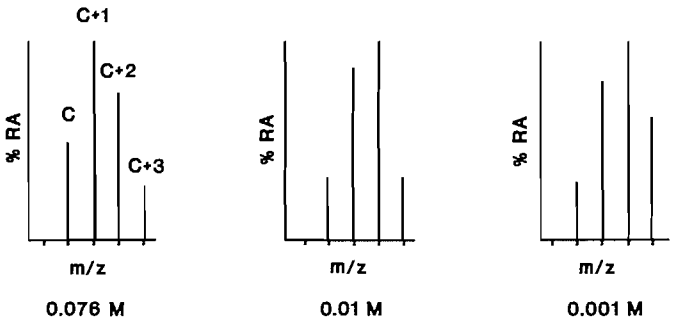


FIG. 2. Concentration dependence of the C^+ ion region of the FAB spectrum of methylene blue at 9 keV.

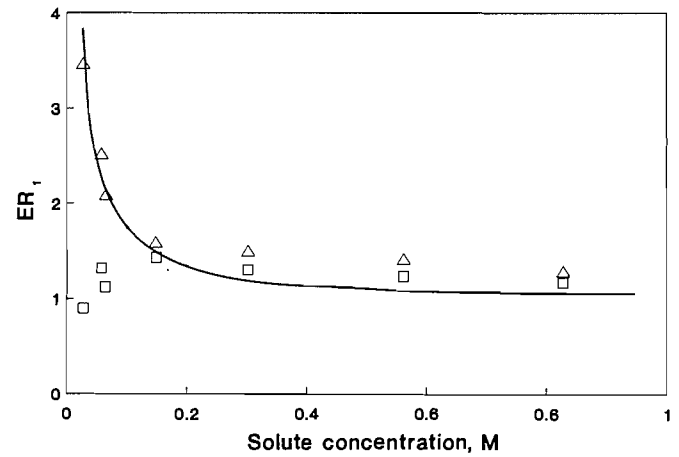


FIG. 3. Concentration dependence of the enhancement ratio ER_1 for *N*-methylpyridinium iodide (**3**): triangles, 9 keV; squares, 5 keV. The solid line was calculated from eq. [9] with $a = 0.005$ M.

The observed effect might possibly reflect changes in the solute concentration at the surface layer occurring when the bulk concentration is less than some critical value. However, if this were the case we would expect to see essentially the same effect in the experiments done at 5 keV (see below). From the absence of a significant concentration effect at the lower bombardment energy (Fig. 3) we conclude that an alternative explanation is required. It is well established (9) that particle bombardment produces electrons in the matrix via ionization, and that these electrons can then act as efficient reducing agents. Dissociation of the target molecule by loss of a hydrogen radical may also occur (13). At the concentrations employed in this work the most probable target molecule is the matrix, so that, as a first approximation, only ionization and dissociation of the glycerol needs to be considered:

[1] $G \rightarrow G^{+\cdot} + e$

[2] $G \rightarrow (G - H)^{\cdot} + H^{\cdot}$

Following these initial events, two pathways leading to $(C + H)^{+\cdot}$ are possible. Electron capture by the pyridinium cation, C^+, followed by protonation leads to the odd-electron ion:

[3] $C^+ + e \rightarrow C^{\cdot}$

[4] $C^{\cdot} + H^+ \rightarrow (C + H)^{+\cdot}$

Alternatively, hydrogen atom attack on C^+ generates the $(C + H)^{+\cdot}$ ion in one step:

[5] $C^+ + H^{\cdot} \rightarrow (C + H)^{+\cdot}$

Formation of the $(C + 2H)^+$ ion may then occur by competitive or consecutive reactions. The $(C + H)^{+\cdot}$ ion may abstract hydrogen from glycerol or it may be desorbed from the matrix. Hydrogen abstraction by $C^{\cdot}$ leads to the neutral species $(C + H)$ (eq. [7]), which may then be protonated.

[6] $(C + H)^{+\cdot} + G \rightarrow (C + 2H)^+ + (G - H)^{\cdot}$

[7] $C^{\cdot} + G \rightarrow (C + H) + (G - H)^{\cdot}$

Equations [2], [5], and [6], with application of the steady-state approximation to $[H^{\cdot}]$ and $[(C + H)^{+\cdot}]$, lead to the prediction that the concentration of $(C + H)^{+\cdot}$ is independent of $[C^+]$ and so

[8] $k'[(C + H)^{+\cdot}] = k_2[G]/((k_6/k')[G] + 1)$

where $k'[(C + H)^{+\cdot}]$ is the rate of loss of $(C + H)^{+\cdot}$ from the matrix. The alternative mechanism, using eqs. [1], [3], [4], and [7], also leads to a predicted independence of C^+ concentration. In the particular case where the rate of protonation of $C^{\cdot}$ (eq. [4]) is large compared to the rate of hydrogen abstraction (eq. [7]), an expression identical in form to [8] is obtained.

Although the individual rate constants are not known, the model can be tested in the following way. If x = concentration of solute in the prepared sample and a = steady-state concentration of $(C + H)^{+\cdot}$, then $(x - a)$ will be the concentration of solute cation sampled by the FAB experiment when the steady state has been established. The predicted $(C + 1)/C$ ratio is then $b + (a/x - a)$, and the calculated value of ER_1 is:

[9] $ER_1 = 1 + (a/(x - a))/b$

where b = the fraction of $C + 1$ from C^+ due to natural isotopic abundances. Equation [9] was fitted to the concentration vs. ER_1 data by trial and error. For a value of $a = 0.005$ M the agreement with experiment is reasonably good (Fig. 3). The question of whether ion formation in fast atom bombardment is a gas-phase or a solution-phase process has received considerable attention (14). Our proposed reaction scheme (eqs. [1]–[7]) would appear to be consistent with the gas collision model developed by Kebarle and co-workers (15), but we have not yet explored this possibility in detail.

A reduction of the bombardment energy from 9 to 5 keV reduced ER_1 values only slightly at the higher concentrations, but it essentially eliminated the concentration dependence

Can. J. Chem. Downloaded from www.nrcresearchpress.com by 122.72.124.2 on 09/07/12
For personal use only.

below 0.1 M (Fig. 3). The proposed mechanisms predict that a reduction in the rates of ionization or dissociation would result in a lower value of ER_1. Fast atom bombardment of glycerol has been shown (3) to generate predominantly carbon-centred radicals. The energy requirements for C—H bond breaking are significantly lower than for ionization; thus the latter process might be expected to show the greater dependence on bombardment energy. On these grounds, the electron capture – protonation mechanism would seem to be favoured, but the limited data presently available do not justify a more detailed analysis.

Acknowledgements

We thank Professor J. L. Holmes for access to the facilities of the Ottawa–Carleton Regional Mass Spectrometry Centre. O.S.T. acknowledges continuing support from the Natural Sciences and Engineering Research Council of Canada. We thank Mr. Bryan Takasaki for synthesizing a number of the pyridinium salts.

1. F. H. Field. J. Phys. Chem. **86**, 5115 (1982).
2. W. L. Ligon, Jr. Int. J. Mass Spectrom. Ion Phys. **52**, 189 (1983).
3. T. Keough, F. S. Ezra, A. F. Russel, and J. D. Pryne. Org. Mass Spectrom. **22**, 241 (1987).
4. D. N. Heller, J. Yergey, and R. J. Cotter. Anal. Chem. **55**, 1310 (1983).
5. G. Pelzer, E. DePauw, D. V. Dung, and J. Marien. J. Phys. Chem. **88**, 5065 (1984).
6. M. J. Connolly and R. G. Orth. Anal. Chem. **59**, 903 (1987).
7. R. L. Cerny and M. L. Gross. Anal. Chem. **57**, 1163 (1985).
8. P. J. Gale, B. L. Bentz, B. T. Chait, F. H. Field, and R. J. Cotter. Anal. Chem. **58**, 1070 (1986).
9. D. H. Williams, A. F. Findeis, S. Naylor and B. W. Gibson. J. Am. Chem. Soc. **109**, 1980 (1987).
10. C. W. Kazakoff, R. T. B. Rye, and O. S. Tee. Can. J. Chem. **65**, 718 (1987).
11. R. Raghaven and R. T. Iuamoto. J. Electroanal. Chem. **92**, 101 (1978).
12. D. J. Burinsky, R. J. Dilliplane, G. C. DiDonato, and K. L. Busch. Org. Mass Spectrom. **23**, 231 (1988).
13. E. Clayton and J. C. Wakefield. J. Chem. Soc. Chem. Commun. 969 (1984).
14. E. Schroder, H. Munster, and H. Budzikiewicz. Org. Mass Spectrom. **21**, 707 (1986), and references cited therein.
15. J. A. Sunner, R. Kulatunga, and P. Kebarle. Anal. Chem. **58**, 1312 (1986); Anal. Chem. **58**, 2009 (1986); J. Sunner, A. Morales, and P. Kebarle. Anal. Chem. **59**, 1378 (1987).
16. L. Meites and P. Zuman. CRC handbook series in organic electrochemistry. Vol. 1. CRC Press Inc., Cleveland, OH. 1977.
17. C. K. Mann and K. K. Barnes. Electrochemical reactions in non-aqueous systems. Marcel Dekker, Inc., New York. 1970.

Can. J. Chem. Downloaded from www.nrcresearchpress.com by 122.72.124.2 on 09/07/12
For personal use only.

^{13}C magnetic resonance studies. 138.[1] An examination of the [3.2.2.0] → [4.2.1.0] rearrangement via β-enolization and H/D exchange in tricyclic ketones

SRIYAWATHIE PEIRIS, J. B. STOTHERS, AND SHIRLEY E. THOMAS
Department of Chemistry, University of Western Ontario, London, Ont., Canada N6A 5B7

Received August 23, 1988

SRIYAWATHIE PEIRIS, J. B. STOTHERS, and SHIRLEY E. THOMAS. Can. J. Chem. **67**, 187 (1989).

The behavior of the *endo* and *exo* isomers of 7,7-dimethyltricyclo[3.2.2.$0^{2,4}$]nonan-6-one (**9**, **17**) under strongly basic conditions (*t*-BuO$^-$/*t*-BuOH/185°C) has been examined. In both cases rearrangement to the corresponding 8,8-dimethyltricyclo[4.2.1.$0^{2,4}$]nonan-7-one (**11**, **18**) was found, with the *exo* isomer reacting approximately 8 times faster. Experiments in *tert*-butyl alcohol-O-d_1 were carried out to determine the specific sites, the relative rates, and the stereochemistry of deuterium incorporation in the initial ketones. Although H/D exchange occurs most readily at the cyclopropyl methylene carbon in the *endo* isomer, none of the rearrangement product expected to arise via γ-enolate formation was observed. The results for these ketones are compared with our earlier observations in the related [2.2.2], [3.2.1.0], and [3.3.1.0] systems.

Key words: homoenolization, tricyclic ketones, H/D exchange.

SRIYAWATHIE PEIRIS, J. B. STOTHERS et SHIRLEY E. THOMAS. Can. J. Chem. **67**, 187 (1989).

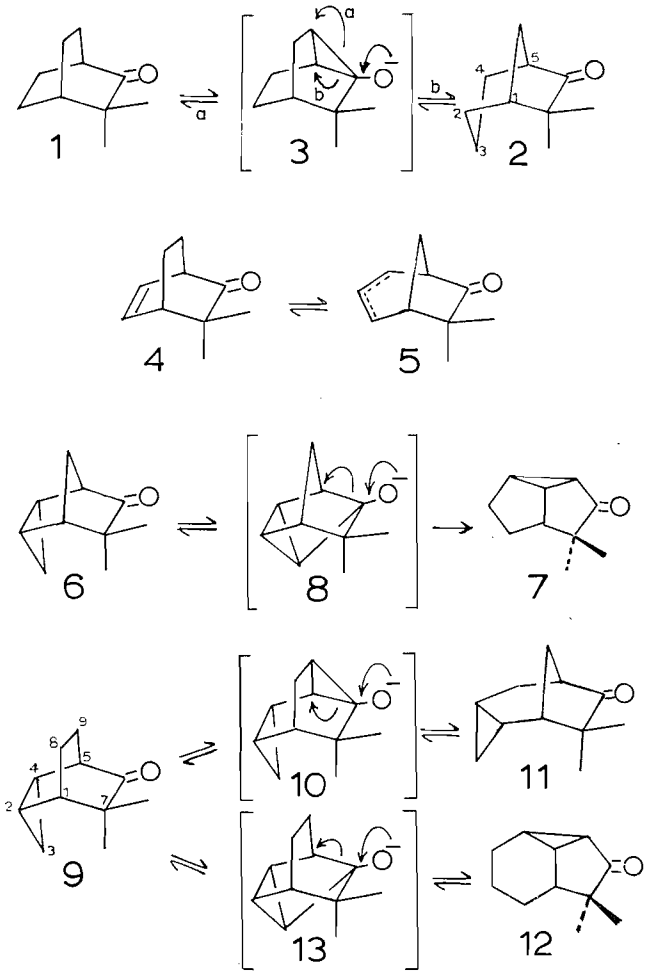
On a examiné le comportement des isomères *endo* et *exo* de la diméthyl-7,7 tricyclo[3.2.2.$0^{2,4}$]nonanone-6 (**9** et **17**) dans des conditions fortement basiques (*tert*-BuO$^-$/*tert*-BuOH/185°C). Dans chacun de ces cas, on a observé une transposition vers la diméthyl-8,8 tricyclo[4.2.1.$0^{2,4}$]nonanone-7 (**11** et **18**) correspondante; l'isomère *exo* réagit environ 8 fois plus rapidement. Afin d'identifier les sites spécifiques, les vitesses relatives et la stéréochimie de l'incorporation du deutérium dans les cétones initiales, on a effectué des expériences à l'aide d'alcool *tert*-butylique-O-d_1. Même si l'échange H/D se produit principalement au niveau du carbone méthylénique du cyclopropane de l'isomère *endo*, on n'observe pas la formation du produit de transposition que l'on pourrait attendre à la suite de la formation d'un énolate-γ. On compare les résultats auxquels ces cétones donnent lieu avec ceux observés antérieurement dans les systèmes [2.2.2], [3.2.1.0] et [3.3.1.0] apparentés.

Mots clés : homoénolisation, cétones tricycliques, échange H/D.

[Traduit par la revue]

Introduction

The activation of remote proton abstraction by a ketonic carbonyl group at centres two and three bonds removed has been recognized for many years and has been demonstrated in a variety of acyclic and cyclic monoketones (1). These systems, upon treatment with *t*-BuO$^-$/*t*-BuOH/≥185°C, the classical (2) homoenolization conditions, generally exhibit abstraction from β-carbons, or β-enolization, but there are a few examples of γ-enolization (3). The process leads, most simply, to deuterium exchange if carried out in a deuterated medium and, in many cases, to skeletal rearrangement. A few examples of the use of β-enolization for the generation of some naturally occurring carbon skeletons from more readily available systems have been described (4) but a much fuller understanding of the factors governing the regioselectivity and the relative reactivity of these proton abstractions should enhance the scope of potential synthetic applications. Our earlier examinations of bicyclooctanones under the usual conditions revealed that the [2.2.2] and [3.2.1] skeletons are interconvertible (5), e.g., **1** ⇌ **2** via β-enolate **3** or its equivalent, and the rate of isomerization is increased markedly, ca. 250-fold, in the unsaturated analogs **4** ⇌ **5** (6). Subsequently, it was found that 6,6-dimethyl-*endo*-tricyclo[3.2.1.$0^{2,4}$]octan-5-one (**6**) rearranges to 4,4-dimethyltricyclo[3.3.0.$0^{2,8}$]octan-3-one (**7**) at a rate comparable to that of **4** under the same conditions, presumably through γ-enolate **8** or its equivalent. From these observations, it seemed reasonable to investigate the behavior of **9** since this ketone has a skeleton in which intramolecular competition between β- and γ-enolization may occur; β-enolization at C-9 can lead to **10**, which may ketonize to form **11**, while γ-enolization at C-3 can lead to **12** via γ-enolate **13**. It may be noted that **14**, an earlier candidate



[1]For Part 137, see ref. 19.

Can. J. Chem. Downloaded from www.nrcresearchpress.com by 122.72.124.2 on 09/07/12
For personal use only.

Can. J. Chem. Downloaded from www.nrcresearchpress.com by 122.72.124.2 on 09/07/12
For personal use only.

for examination of competitive β- and γ-enolization, exhibited only H/D exchange while the *exo* isomer **15** rearranged smoothly, via β-enolization, to **16** (7). The failure of **14** to rearrange was attributed to the difference in orientation of the carbonyl group caused by the conformational change of the six-membered ring. Additional support for this conclusion was subsequently provided by the results for some closely related systems (8). For **9**, however, its relatively rigid skeleton would appear to render the orientation of the carbonyl group with respect to C-9, the expected β-enolization site, very similar to that in **1** and **4**, but the relationship of the carbonyl group and C-3, the potential γ-enolization site, will differ somewhat from that in **6**. In this report, we wish to describe the results of our examination of **9** and its *exo* isomer **17** upon treatment with *t*-BuO^-/*t*-BuOH/185°C for comparison with the earlier results for the related systems, including **1**, **4**, and **6**. The sites, rates, and stereoselectivity of proton abstraction from **9** and **17** were also established by the requisite H/D exchange experiments.

Results and discussion

Each of the parent ketones was prepared by the methods previously described in the literature (9, 10), and in each case methylation with MeI/$NaNH_2$/Et_2O gave the required dimethyl ketones in a single cycle.

Homoenolization experiments

The behavior of **9** under homoenolization conditions was examined initially following our usual procedures; **9** was dissolved in anhydrous *t*-BuO^-/*t*-BuOH and aliquots were transferred under nitrogen to predried glass tubes, which were then sealed and heated at 185°C for varying periods of time. The neutral product (>80% yields) was isolated by pentane extraction and analyzed by gas–liquid chromatography (glc) to reveal the smooth disappearance of the starting material **9** and the appearance of one new component (Table 1). Preparative glc provided samples of each and the ^{13}Cmr spectrum of recovered **9** showed the absence of any components with the same retention time. The new compound exhibited strong carbonyl absorption in the infrared (1736 cm^{-1}, liquid film), and a ^{13}C carbonyl signal at δ_C 225.8 indicated that the new ketone contained a cyclopentanone moiety; precise mass measurement confirmed that the new material is isomeric with **9**, having the molecular formula $C_{11}H_{16}O$. In addition to the carbonyl peak, the ^{13}C spectrum contained 10 signals (δ_C, $CDCl_3$): CH_3, 21.1, 26.7; CH_2, 13.7, 32.4_9, 32.5_3; CH, 5.3, 18.0, 40.8, 42.3, and a quaternary C, 48.4. The three signals at highest field (5.3, 13.7, 18.0) confirmed the presence of a 1,2-disubstituted cyclopropane ring, indicating that the product arose from β-enolization at C-9 to furnish **11** rather than through γ-enolization to yield **12**. This deduction was confirmed by the ^{1}Hmr spectrum having two methyl singlets (δ 0.955, 1.247), the cyclopropyl methylene multiplets centred at δ 0.04 and 0.66, with the corresponding methine absorptions at δ 0.70 and 1.26. In addition, the spectrum contained two bridgehead methine signals (2.22 and 2.38) and a doublet of doublets (δ 1.63, J = 1.3, 11.1 Hz, *anti*-H-9) coupled to a partially obscured one-proton multiplet at 2.10 (*syn*-H-9), which was flanked by the remaining methylene pattern at δ 2.00 and 2.15. The assignment of these methylene patterns was confirmed through a heteronuclear ^{13}C–^{1}H correlation spectrum and the specific ^{13}C signals for **11** are listed in Table 2.

The same treatment of **17** with *t*-BuO^-/*t*-BuOH/185°C also revealed the smooth conversion of the starting material to one new component and at a rate ca. 8-fold faster than that observed for **9** → **11** (Table 1). The new compound exhibited strong carbonyl absorption (1734 cm^{-1}, δ_C 226.7), again indicative of a cyclopentanone fragment, and precise mass measurement showed it to be isomeric with **17**, $C_{11}H_{16}O$. Its nmr data were consistent with structure **18**. The 10 sp^3 carbon signals (δ_C, $CDCl_3$) are as follows: CH_3, 20.0, 24.7; CH_2, 11.9, 25.0, 28.7; CH, 6.0, 15.6, 41.4, 43.7; and a quaternary C, 50.8. As in the case of **11**, the three signals at highest field (6.0, 11.9, 15.6) indicate the presence of a 1,2-disubstituted cyclopropane ring, as expected from β-enolization at C-9 in **17** followed by protonation at the original C-5 site to afford **18**. The proton spectrum contained two methyl singlets (δ 1.10 and 1.15), a cyclopropyl methylene pattern having δ_A 0.51 (ddd, J = 4.8, 4.8, 5.4 Hz) and δ_B 0.63 (ddd, J = 5.4, 8.6, 8.6 Hz), with two cyclopropyl methine multiplets δ 0.76 and 1.05. In addition, the spectrum contained two bridgehead patterns (2.06 and 2.27), a doublet of doublets (δ 1.46, J = 1.0, 12.8 Hz, *anti*-H-9), primarily coupled to a one-proton multiplet at 1.85 (*syn* H-9), with the remaining 5-methylene protons absorbing at δ 1.76

TABLE 1. Concentration[a] of the initial ketone in the neutral product after treatment with *t*-BuO^-/*t*-BuOH/185°C

Time (h)	9	17
3		96
12		84
24	96	74
48	93	54
72	88	
96	85	27
144	80	18

[a]Percentage by glc analysis, ±1%.

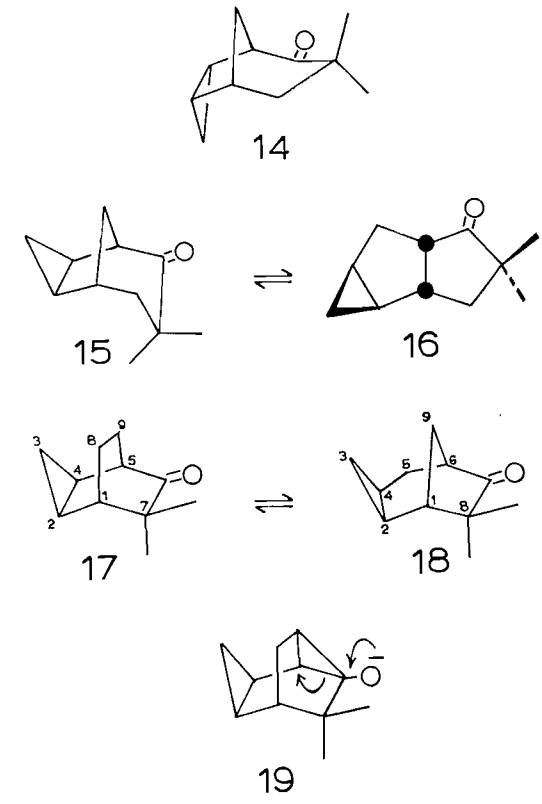


TABLE 2. ^{13}C shieldings[a] for ketones **9**, **11**, **17**, and **18**

Compound	C-1	C-2	C-3	C-4	C-5	C-6	C-7	C-8	C-9	Methyl
9	36.7	14.5	7.2	12.5	45.5	221.1	45.4	22.8	22.2	23.3 (*endo*) 26.6 (*exo*)
11	42.3	18.0	13.7	5.3	(32.4_9)	40.8	225.8	48.4	(32.5_3)	21.1 (*endo*) 26.7 (*exo*)
17	38.8	13.9	7.0	11.2	42.8	221.1	46.3	19.4	21.2	24.3 24.5
18	41.4	15.6	11.9	6.0	28.7	43.7	226.7	50.8	25.0	20.0 (*endo*) 24.7 (*exo*)

[a]In ppm from internal TMS for $CDCl_3$ solutions; values in parentheses may be interchanged.

(ddd, J = 1.3, 5.7, 14.0 Hz) and 2.02 (dddd, J = 2.0, 2.0, 8.6, 14.0 Hz). The ^{13}C–^{1}H heteronuclear correlation spectrum confirmed these assignments and the individual ^{13}C shieldings are listed in Table 2. Samples of **18**, isolated from the runs with **17**, were also heated with t-BuO^-/t-BuOH/185°C and found to give mixtures indicating the equilibrium concentrations to be 15% **17** and 85% **18**.

These and earlier experiments (5, 6) show that the reactivity toward proton abstraction at a β-methylene site in the ethano bridge of these [2.2.2] systems increases in the order **1** < **9** < **17** < **4** with rate constants for rearrangement of 1.0, 4.6, 37, and 240 × 10^{-7} s^{-1}, respectively. The significantly greater reactivity found for the unsaturated ketone **4** relative to its saturated analog **1** can be attributed to allylic stabilization of the incipient carbanion formed upon cleavage of the β-enolate leading to **5**. It could be anticipated that the cyclopropyl group in each of **9** and **17** may provide some stabilization of the developing carbanions on the route to the rearranged materials. Such an influence is clearly smaller for **9** than for **17**. Previously, the composition of the **1** ⇌ **2** equilibrium mixture was found to be 1:4, while for **4** ⇌ **5** the equilibrium composition is 8:92. To assess the equilibria for each of **9** and **17**, two tubes were heated at 200°C for >150 h after which it was found that the **17** ⇌ **18** ratio was 14:86, whereas **9** is favored by ca. 4:1 over **11**. Molecular mechanics (MM2) calculations (11) gave results that are in good agreement with the observations for the saturated systems. For the systems **1** ⇌ **2**, **9** ⇌ **11**, and **17** ⇌ **18**, the calculated equilibrium constants are 3.0, 0.24, and 6.4, respectively, compared with the observed values of 4.0, 0.25, and 6.1. Clearly, the *endo*-cyclopropyl ring in **11** destabilizes this ketone relative to **9** whereas, in the analogous *exo* system, **18** is more stable than **17**.

H/D exchange experiments

The rearrangements of **9** and **17** show that proton abstraction occurs at the β-methylene site of the ethano bridge in each; thus it was of interest to examine the stereoselectivity of this process and to find if other sites undergo exchange. For this purpose, samples of **9** were treated with t-BuO^-/t-BuOD at 185°C for 24, 72, 96, and 144 h.

After 144 h, the recovered **9**-d_x was found to contain 2.12 atoms ^{2}H/molecule by mass spectrometry and the ^{2}Hmr spectrum revealed eight sites of ^{2}H incorporation; the relative amounts at each site were determined by integration. These ^{2}Hmr signals and the ^{2}H content were found to be δ 0.14 (0.87), 0.52 (0.70), 0.98 (0.10), 1.04 (0.02), 1.18 (0.14), 1.70 (0.03), 1.84 (0.22), 2.61 (0.04). The ^{1}Hmr spectrum of **9** contained methyl singlets at δ 0.98 and 1.04, which correlate with the ^{13}C signals at δ_C 26.6 and 23.3, respectively, and can be assigned to the *exo*- and *endo*-methyl groups. Thus, **9** undergoes exchange at the methyl sites, with *exo*-methyl exchange favored, as expected by analogy with several related systems (1). The bridgehead protons H-1 and -5 gave rise to multiplets at δ 2.00 and 2.61, respectively, while the cyclopropyl methine protons H-2 and -4 exhibit multiplets at δ 1.06 and 1.18, as revealed by correlation with their corresponding ^{13}C signals at δ_C 14.5 and 12.5. The 3-methylene protons absorb at δ 0.14 and 0.52, J_{AB} = 7.2 Hz, with the higher field pattern containing additional couplings of 3.5 and 4.4 Hz and the lower field component having a coupling of 7.5 Hz to two other protons. The higher field absorption, δ 0.14, therefore was assigned to the *endo*-3 proton, since it is established that $J_{trans} < J_{cis}$ for vicinal coupling in cyclopropyl rings (12). The ^{13}C–^{1}H COSY spectrum gave the methylene correlations: δ_C 22.8 (δ_H 1.63, 1.80) and 22.2 (δ_H 1.70, 1.84), which were assigned to the 8- and 9-methylene groups, respectively, from the ^{2}H and ^{13}C spectra of the deuterated samples.

The ^{13}Cmr spectrum of the 144-h **9**-d_x sample revealed deuterium incorporation at the higher field 9-methylene site through the appearance of a characteristic triplet, J_{CD} = 20.4 Hz, centred 345 ppb upfield from the original δ_C 22.2 signal, while the absorption for the 8-methylene carbon contained an isotope-shifted component, $^{2}\Delta$ = 103 ppb, arising from ^{2}H at C-9. The ^{2}H spectra of the **9**-d_x samples showed that the less shielded of the two 9-protons, δ 1.84 and 1.70, exchanged more readily and is presumably the *exo*-9-H by analogy with the earlier results for **1**.

In the ^{13}C spectrum of the 24-h sample of **9**-d_x, two triplets centred upfield from the C-3 methylene signal were apparent, J_{CD} = 25.0 Hz for each, with one-bond ($^{1}\Delta$) isotope shifts of 296 and 323 ppb; the more intense triplet of this pair, $^{1}\Delta$ = 323 ppb, was readily attributed to *endo* exchange at C-3 since the intensity ratio of the δ 0.14 and 0.52 signals in the ^{2}H spectrum was found to be 5.0:3.5. The same intensity ratio was found for the two-bond, isotope-shifted components accompanying the signal for C-2 at δ_C 14.5 ($^{2}\Delta$ = 95, 124 ppb) and for C-4 at δ_C 12.5 ($^{2}\Delta$ = 98, 120 ppb); in each case, the more intense component exhibited the larger isotope shift. Each of these patterns also contained a third component indicative of dideuteration at C-3. A pair of isotope-shifted components, $^{3}\Delta$ = 40 and 65 ppb, in a 3.5:5.0 ratio, was also apparent for the C-5 absorption at δ_C 45.5, but the C-1 signal was only broadened without resolvable fine structure.

The ^{13}C spectrum of the 144-h sample revealed the appearance of deuterium at C-9 directly as noted above. Indirect evidence of ^{2}H was shown at C-5 through the presence of a $^{2}\Delta$ component of 105 ppb upfield from the δ_C 22.2 signal (C-9), and at C-4 by isotope-shifted components within the patterns for

Can. J. Chem. Downloaded from www.nrcresearchpress.com by 122.72.124.2 on 09/07/12
For personal use only.

Can. J. Chem. Downloaded from www.nrcresearchpress.com by 122.72.124.2 on 09/07/12
For personal use only.

C-2, $^2\Delta$ = 126 ppb, and C-3, $^2\Delta$ = 128 ppb. The incorporation level was too low at these and the methyl sites, however, to render the C—D triplets observable; also, the presence of additional isotope-shifted components in the absorptions for the bridgehead carbons was evident but the patterns were not resolved. Thus, deuterium incorporation occurred at C-3, -4, -5, and -9 as well as at both methyl groups. From the ^{2}Hmr spectra of the 24, 72, 96, and 144 h **9**-d_x samples the relative proportions of deuterium at the various sites of exchange were determined and these data permitted the extraction of approximate first-order rate constants, which are considered later.

To determine the regio- and stereochemistry of proton abstraction in **17**, a series of experiments in deuterated base was also carried out. Samples of **17**-d_x were isolated from the resulting mixtures with **18** by preparative glc after reaction times of 3, 12, and 20 h at 185°C in *t*-BuO$^-$/*t*-BuOD. The 20-h sample contained 1.04 atoms ^{2}H/molecule by mass spectrometry and its ^{2}Hmr spectrum revealed six sites of deuterium incorporation for which the relative amounts were measured by integration. These signals and the ^{2}H content were found at δ 0.63 (0.28), 1.05 (0.13), 1.08 (0.02), 1.50 (0.11), 1.65 (0.48), and 2.39 (0.02). The ^{1}Hmr spectrum of **17** exhibited methyl singlets at δ 1.08 and 1.23; thus, only one of the methyl groups exhibited slow exchange. The 3-methylene protons absorb at δ 0.63 and 1.03, J_{AB} = 6.0 Hz, and each is coupled to two vicinal protons with J = 7.8 and 3.7 Hz, respectively. Thus the higher field pattern arises from the *exo*-3 proton *cis* to H-2 and -4, since $J_{cis} > J_{trans}$ in cyclopropyl rings (12). The 2- and 4-protons absorb at δ 1.26 and 1.05, respectively, as shown by ^{13}C–^{1}H correlation, while H-1 and -5 appear at δ 1.93 and 2.39. The ^{13}C methylene signal at δ_C 19.4 correlated with proton multiplets near 1.4 and 1.6 ppm and that at δ_C 21.2 with multiplets near 1.5 and 1.65 ppm. Thus, the ^{2}H spectrum showed that deuterium exchange occurred at C-3, -4, -5, and -9 as well as at one of the methyls. Additional confirmation of the ^{1}H signal assignments was obtained by examination of the effect of added shift reagent, Eu(fod)$_3$, on the spectrum. In the presence of 0.2 equiv. of reagent, the bridgehead patterns initially at δ 1.93 and 2.39 shifted 0.36 and 1.03 ppm downfield, confirming the assignments for H-1 and -5, respectively, while the absorptions at δ 1.26 (H-2) and 1.05 (H-4) were shifted 0.35 and 0.50 ppm. The methylene multiplets near δ 1.5 and 1.65 moved 0.60 and 0.36 ppm, respectively, permitting their assignment to the *endo* and *exo* protons at C-9.

The ^{13}C spectrum of the 20-h sample gave direct evidence for deuterium at C-9 since the δ_C 21.2 signal was accompanied by a 1:1:1 triplet, J_{CD} = 20.3 Hz, $^1\Delta$ = 320 ppb, as was the C-3 signal (δ_C 7.0, J_{CD} = 24.2 Hz, $^1\Delta$ = 286 ppb). Deuterium at C-9 produced isotope-shifted components in the absorptions for C-8 ($^2\Delta$ = 112 ppb) and C-5 ($^2\Delta$ = 75 ppb) while that at C-3 was manifest in the patterns for C-2 ($^2\Delta$ = 90 ppb) and C-4 ($^2\Delta$ = 90 ppb). Indirect evidence for deuterium at C-4 was provided by the appearance of shifted components in the absorptions for C-2 ($^2\Delta$ = 120 ppb), C-3 ($^2\Delta$ = 120 ppb), and C-5 ($^2\Delta$ = 100 ppb). The incorporation levels at C-5 and the methyl site were too low to produce discernible signals in the absorptions for the neighbouring carbons but the ^{2}H spectrum clearly showed that slow exchange occurred at these positions and at both methylene protons on C-9, albeit at distinctly different rates with *exo* exchange favoured. The ^{2}H data for these samples permitted the extraction of approximate rate constants for the various exchange processes.

The samples of **18**-d_x resulting from the experiments with **17** in deuterated base were also examined by ^{2}Hmr to assess the stereoselectivity of deuterium incorporation at C-5 upon cleavage of β-enolate **19** leading to **18** from **17**. In the ^{2}H spectra of these **18**-d_x samples, two prominent signals, δ 1.75 and 2.05, together with three much weaker signals, δ 0.63, 0.76, and 1.10, were found. The individual assignments for these peaks followed readily from comparison with the ^{1}H spectrum of **18** in which the methyl singlets appeared at 1.10 and 1.15 and were correlated with the ^{13}C methyl signals at δ_C 24.7 and 20.0, respectively, arising from the *exo*- and *endo*-methyl carbons. The 3-methylene protons, δ 0.51 and 0.63, J_{AB} = 5.4 Hz, each of which is equally coupled to two other protons, J = 4.8 and 8.6 Hz, respectively, were readily assigned to the *endo*- and *exo*-3 protons, since the latter is expected to exhibit the larger vicinal couplings with the cyclopropyl methine protons. The multiplet arising from the 4-proton appeared at δ 0.76, correlating with the methine carbon signal at δ_C 6.0. The intense ^{2}H signal at δ 2.06 coincided with the bridgehead proton absorption in the ^{1}H spectrum and was, therefore, assigned to H-6, which was expected to undergo rapid exchange characteristic of bridgehead enolization in [3.2.1] bicyclic systems (13). The second prominent ^{2}H signal at δ 1.76 corresponds to an eight-line multiplet (ddd, J = 1.3, 5.7, 14.0 Hz) constituting the pattern for a methylene proton whose geminal partner absorbs at δ 2.02 (dddd, J = 2.0, 2.0, 8.6, 14.0 Hz), both of which correlate with a methylene carbon signal at δ_C 28.7. From the MM2 calculations noted earlier, the dihedral angles relating *exo* H-5 with H-4 and -6 are 98° and 50°, respectively, while the corresponding angles for *endo* H-5 are 17° and 65°. Thus, the absorption at δ 1.76 could be assigned to *exo* H-5 while *endo* H-5 gives rise to the δ 2.02 multiplet, which also contains a long-range coupling of 2.0 Hz to *syn* H-9. It was found that the δ 2.02 pattern is more than twice as sensitive to the addition of Eu(fod)$_3$ as its counterpart at δ 1.76, which is entirely consistent with the assignments.

Additional confirmation for the presence of deuterium at C-5 and -6 was provided by the ^{13}C spectra of the **18**-d_x samples. Characteristic 1:1:1 triplets were apparent in the patterns at δ_C 28.7 (J_{CD} = 20.1 Hz, $^1\Delta$ = 390 ppb, C-5) and 43.7 (J_{CD} = 20.5 Hz, $^1\Delta$ = 387 ppb, C-6). Deuterium at C-5 gave rise to isotope-shifted components in the absorptions for C-2 (δ_C 15.6, $^3\Delta$ = 50 ppb), C-3 (δ_C 11.9, $^3\Delta$ = 60 ppb), C-4 (δ_C 6.0, $^2\Delta$ = 110 ppb), and C-6 (δ_C 43.7, $^2\Delta$ = 82 ppb), while ^{2}H-6 produced such components in the patterns for C-4 (δ_C 6.0, $^3\Delta$ = 25 ppb), C-5 (δ_C 28.7, $^2\Delta$ = 112 ppb), and C-9 (δ_C 25.0, $^2\Delta$ = 107 ppb). From these results, deuterium exchange occurs primarily at the *exo*-5 and -6 positions with minor amounts at the *exo*-3, -4, and *exo*-methyl sites. It is particularly interesting that no deuterium signal at δ 2.02 was observed, showing that ketonization of β-enolate **19** proceeds to **18** exclusively by inversion of configuration at C-5.

The approximate first-order rate constants for exchange at the various sites in **9** and **17** extracted from the deuterium incorporation data are given in Fig. 1 together with earlier results for the parent [2.2.2] ketone **1** (5), the [3.2.1.0] analogs **6** and **20** (3), and the isomeric [3.3.1.0] ketones **14** and **15** (7). The stereoselectivity of deuteration at the β-methylene site in the ethano bridge of **9** and **17** is comparable to that found for

Can. J. Chem. Downloaded from www.nrcresearchpress.com by 122.72.124.2 on 09/07/12
For personal use only.

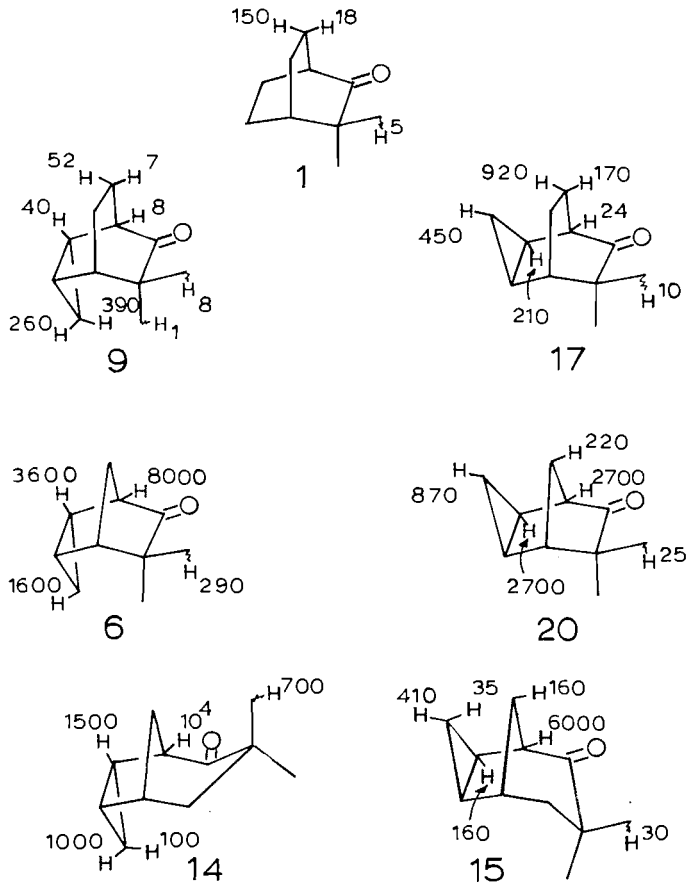


FIG. 1. Deuterium exchange rates ($k \times 10^8\ s^{-1}$) at the various sites in **1**, **6**, **9**, **14**, **15**, **17**, and **20** in *t*-BuO$^-$/*t*-BuOD at 185°C.

the parent ketone **1** with *exo* deuteration favored. Thus, one can conclude that the cleavage of the β-enolates formed by proton abstraction at this site, i.e., **3**, **10**, and **19**, proceeds preferentially with inversion of configuration to return to the initial ketone. This is consistent with the general tendency for β-enolate cleavage in many related systems (1). From these results for exchange at the β-methylene site, it could be anticipated that the alternative cleavage leading to the rearranged ketones, i.e., **3** → **2**, **10** → **11**, and **19** → **18**, would also favor inversion. In fact, it was found that, within the limits of detection, deuterium was only observed in the *exo* orientation at C-4 and C-5 in **2** and **18**, respectively. The enhanced rates at C-9 in **17** relative to the corresponding processes in **1** and **9** may implicate some interaction with the neighbouring cyclopropyl ring. There is also a significant increase in reactivity for exchange at the 5-bridgehead position in both **9** and **17** relative to **1**, for which it was not observed. This perhaps reflects an inductive effect of the cyclopropyl group, thereby increasing the acidity of the bridgehead proton in these tricyclic ketones. The bridgehead exchange rates in **9** and **17** are comparable to that found in the [2.2.1] system 3,3,6,6-tetramethylnorcamphor, $k = 30 \times 10^{-8}\ s^{-1}$ (14), which is markedly increased upon introduction of the cyclopropyl ring as in **6** and **20**.

By analogy with **6**, **14**, **15**, and **20**, exchange was expected to occur at C-3 and -4 in **9** and **17** but there are interesting quantitative differences between the three ring systems. Whereas the data for the *exo* ketones **15** and **17** are similar, although a higher stereoselectivity at C-3 in **17** is evident, the results for **9** differ strikingly from those for its *endo* analogs **6** and **14**. Exchange at these sites is distinctly slower in **9** and there is a marked difference in stereoselectivity at C-3, with *endo* exchange slightly favored in **9** contrasting sharply with the *exo* preference in **6** and **14**. It is conceivable that γ-enolate **13**, or its equivalent, is formed, which subsequently returns exclusively to **9** via cleavage with retention of configuration at C-3 with incorporation of *endo* deuterium. This has been found to be the favored mode of cleavage for other γ-enolates (1). As already noted, *exo*-methyl exchange occurred preferentially and at comparable rates in **9** and **17**. This contrasts sharply with the other tricyclic analogs, for which methyl exchange was found to be distinctly faster in the *endo*-cyclopropyl examples **6** and **14** relative to their *exo* counterparts **15** and **20**. Clearly, subtle factors must govern the reactivity of exchange in these systems and further data must be obtained before definitive interpretations can be put forward.

Experimental

Gas–liquid chromatography (glc) was carried out on Varian 920 and 3700 instruments using columns of 6% FFAP or 10% SE-30 on Chromosorb W as indicated. Flash chromatography columns were prepared as described in the literature (15). Diethyl ether was dried over Na/benzophenone and freshly distilled before use; methyl iodide was dried over 4 Å sieves.

Infrared spectra were recorded with a Bruker/IBM FTIR 32 instrument and mass spectra were obtained on a Finnigan MAT 8230 spectrometer at 70 eV (direct inlet). Routine ^1H spectra were recorded with a Varian EM-360 instrument while data for pure samples were collected with Varian XL-200 or -300 systems. The effect of Eu(fod)$_3$, as shift reagent, was utilized to increase the shift dispersion to permit unambiguous assignments, which were also confirmed by ^1H–^1H correlation (COSY) spectra; these gave definitive ^2H assignments since ^1H and ^2H shieldings are essentially identical. Integration of the ^2H spectra indicated the extent of ^2H incorporation at the sites undergoing exchange, while the total ^2H content was determined by mass spectrometry. The ^2H and ^{13}C nmr spectra were obtained at 46.1 and 75.4 MHz, respectively, on the Varian XL-300 system, and comparison of the fully decoupled ^{13}C spectra with those obtained with the APT sequence (16) identified the number of hydrogens directly bonded to each carbon. Correlation of the ^1H and ^{13}C spectra for **9**, **11**, **17**, and **18** was accomplished using the HETCOR sequence of the XL software with a 2048 × 128 data matrix, 3600-Hz spectral widths for ^{13}C, and 700–1000 Hz, as appropriate for ^1H, transforming 2048 and 512 points, respectively. ^1H–^1H COSY spectra were recorded for **11**, **17**, and **18** with the HOMCOR sequence of the XL software using a 1024 × 512 matrix, spectral widths of 600 (**11**), 700 (**17**), and 756 Hz (**18**), transforming 1024 points for both axes.

*7,7-Dimethyl-*endo*-tricyclo[3.2.2.0^{2,4}]nonan-6-one (**9**)*

A solution of *endo*-tricyclo[3.2.2.0^{2,4}]nonan-6-one (0.25 g, 1.8 mmol), prepared as described by Schueler and Rhodes (9), in anhydrous Et_2O (5 mL) was added to $NaNH_2$ (0.8 g) in Et_2O (5 mL) under a N_2 atmosphere and the mixture refluxed for 3 h. After cooling, methyl iodide (1.14 g, 8.0 mmol) was added and the mixture refluxed overnight. Methyl iodide (0.42 g, 3.0 mmol) was added and the mixture refluxed for 3 h before cooling to 0°C. Water (10 mL) was slowly added and the organic phase decanted. The aqueous phase was extracted with Et_2O (4 × 25 mL) and the combined extracts washed with water (3 × 30 mL) and twice with brine (20 mL) before drying over magnesium sulphate. After removal of solvent, the crude product was shown by glc (6% FFAP) to be essentially one component. This product was purified by flash chromatography (petroleum ether – Et_2O, 80:20) to provide **9** (0.23 g, 75%); ir (film): 1724 cm^{-1}; ^{13}Cmr: see Table 2; ^1Hmr ($CDCl_3$) δ: 2.61 (m, 1H), 2.00 (m, 1H), 1.50–1.95 (m, 4H), 1.00–1.25 (m, 2H), 1.04 (s, 3H), 0.98 (s, 3H), 0.52 (ddd,

J = 3.5, 4.4, 7.2 Hz, 1H), 0.14 (dt, J = 7.2, 7.5 Hz, 1H). *Exact Mass* calcd. for $C_{11}H_{16}O$: 164.1201; found: 164.1203.

*7,7-Dimethyl-*exo*-tricyclo[3.2.2.0^{2,4}]nonan-6-one (17)*

Following the method described by Freeman, Balls, and Brown (17), *exo*-tricyclo[3.2.2.0^{2,4}]non-6-en-8-one was prepared from cycloheptatriene and acrylonitrile. Hydrogenation according to the procedure reported by Wenzinger and Ors (10) furnished the saturated analog, which was methylated as described above such that 350 mg of *exo*-tricyclo[3.2.2.0^{2,4}]nonan-6-one gave a yellowish liquid found to be >95% pure by glc analysis (SE-30). This was purified by flash chromatography (petroleum ether – Et_2O, 95:5) to furnish 270 mg (64% yield) of **17**: ir ($CHCl_3$): 1724 cm^{-1}; ^{13}Cmr: see Table 2; ^{1}Hmr ($CDCl_3$) δ: 2.39 (m, 1H), 1.93 (m, 1H), 1.55–1.70 (m, 2H), 1.48 (m, 1H), 1.40 (m, 1H), 1.26 (m, 1H), 1.23 (s, 3H), 1.08 (s, 3H), 1.05 (m, 1H), 1.03 (dt, J = 3.7, 6.0 Hz, 1H), 0.63 (dt, J = 6.0, 7.8 Hz, 1H). *Exact Mass* calcd. for $C_{11}H_{16}O$: 164.1201; found: 164.1202.

Homoenolization experiments

Our standard procedures (18) for the rearrangement and exchange experiments were followed as illustrated for **9**. To a solution of t-BuO$^-$/t-BuOH (1.27 M, H_2O content <250 μg/mL) was added **9**, to give a solution that was 0.26 M in ketone. To a series of 5-mL predried, thick-walled glass tubes were transferred 0.35-mL aliquots of the reaction solution; the tubes were degassed and sealed before immersion in an oil bath at 185°C. Tubes were removed at intervals, cooled before opening, and the contents removed by washing with water (10 mL). The organic product was isolated by pentane extraction (3 × 15 mL). After drying the combined extracts over magnesium sulphate, removal of the solvent afforded a neutral organic product (>80% yields), which was analyzed by glc (FFAP) to reveal the presence of two barely resolved components, the major one of which was the initial ketone. The new component was ketonic (1736 cm^{-1}) and isomeric with the initial ketone. *Exact Mass* calcd. for $C_{11}H_{16}O$: 164.1201; found: C 164.1197. The new ketone was identified as **11** by ^{1}H and ^{13}Cmr as described in the text. In the same fashion, **17** was found to yield a mixture of two ketones upon heating at 185°C in t-BuO$^-$/t-BuOH for several hours. Separation by preparative glc (SE-30) furnished samples of the new ketone (1734 cm^{-1}), which was isomeric with **17**. *Exact Mass* calcd. for $C_{11}H_{16}O$: 164.1201; found: 164.1195. It was identified as **18** by ^{1}H and ^{13}Cmr as described in the text. A series of samples of **9** and **17** were also treated with t-BuO$^-$/t-BuOD (99% deuterated) to examine the exchange processes occurring under these reaction conditions; the results are described in the text.

Acknowledgements

We are grateful for the financial support provided by the Natural Sciences and Engineering Research Council of Canada.

1. N. H. Werstiuk. Tetrahedron, **39**, 205 (1983).
2. C. S. Shiner, A. H. Berks, and A. M. Fisher. J. Am. Chem. Soc. **110**, 957 (1988).
3. A. K. Cheng, A. K. Ghosh, and J. B. Stothers. Can. J. Chem. **62**, 1385 (1984), and references therein.
4. B. A. Dawson, A. K. Ghosh, J. L. Jurlina, A. J. Ragauskas, and J. B. Stothers. Can. J. Chem. **62**, 2521 (1984).
5. A. K. Cheng, J. B. Stothers, and C. T. Tan. Can. J. Chem. **55**, 447 (1977).
6. A. K. Cheng and J. B. Stothers. Can. J. Chem. **56**, 1342 (1978).
7. A. J. Ragauskas and J. B. Stothers. Can. J. Chem. **63**, 1250 (1985).
8. M. T. M. Clements, R. E. Klinck, S. Peiris, A. J. Ragauskas, and J. B. Stothers. Can. J. Chem. **66**, 454 (1988).
9. P. E. Schueler and Y. E. Rhodes. J. Org. Chem. **39**, 2063 (1974).
10. R. G. Wenzinger and J. A. Ors. J. Org. Chem. **39**, 2060 (1974).
11. N. L. Allinger. J. Am. Chem. Soc. **99**, 8127 (1977); N. L. Allinger and Y. Y. Yuh. QCPE, 423 (1985).
12. L. M. Jackman and S. Sternhell. Applications of nuclear magnetic resonance spectroscopy in organic chemistry. Pergamon Press Ltd., Oxford. 1969. p. 286.
13. K. W. Turnbull, S. J. Gould, and D. Arigoni. J. Chem. Soc. Chem. Commun. 597 (1972); D. H. Bowen and J. Macmillan. Tetrahedron Lett. 4111 (1972).
14. N. H. Werstiuk, S. Yeroushalmi, and G. Timmins. Can. J. Chem. **61**, 1945 (1983).
15. W. C. Still, M. Kahn, and A. Mitra. J. Org. Chem. **43**, 923 (1978).
16. S. L. Patt and J. N. Shoolery. J. Magn. Reson. **46**, 535 (1982).
17. P. K. Freeman, D. M. Balls, and D. J. Brown. J. Org. Chem. **33**, 2211 (1968).
18. A. L. Johnson, J. B. Stothers, and C. T. Tan. Can. J. Chem. **53**, 212 (1975).
19. J. B. Stothers and A. Stoessl. Can. J. Chem. **66**, 2816 (1988).

Can. J. Chem. Downloaded from www.nrcresearchpress.com by 122.72.124.2 on 09/07/12
For personal use only.

Cocatalysis by an internal carboxyl group and by α-cyclodextrin. The debromination of 4-bromo-4-methyl-2,5-cyclohexadienone-2-carboxylic acid

BRYAN K. TAKASAKI[1] AND OSWALD S. TEE[2]

Department of Chemistry, Sir George Williams Campus, Concordia University, Montréal, P.Q., Canada H3G 1M8

Received July 12, 1988

BRIAN K. TAKASAKI and OSWALD S. TEE. Can. J. Chem. **67**, 193 (1989).

Debromination of the title dienone (**1**), formed during the bromination of 5-methylsalicylic acid (**2**), is strongly catalyzed by α-cyclodextrin (CD). The bromination of **2** is also catalyzed by CD. The extent of the catalysis of the debromination of **1** is independent of pH in the range pH 3–5 and it tends to saturate at high [Br^-] and high [CD]. Analysis of the [Br^-] dependence data in the presence of 1 mM CD yields a value of 0.68 M for the dissociation constant of the CD·Br^- complex. Also, from the dependence of the rate of debromination on [CD], the anion of the dienone **1** (i.e., $\mathbf{1}^-$) forms a complex with CD with a K_d of 15 mM, which appears to react with Br^- at a rate 170 times faster than does free $\mathbf{1}^-$. However, the catalysis is more likely due to the reaction of free dienone, reacting as **1**, with the CD·Br^- complex, which is 3400 times more reactive than uncomplexed Br^-. The combined effect of the internal catalysis by the carboxyl group of **1** and the external catalysis by CD is an overall rate enhancement of 12 million.

Key words: catalysis, cocatalysis, cyclodextrin, debromination, intramolecular.

BRIAN K. TAKASAKI et OSWALD S. TEE. Can. J. Chem. **67**, 193 (1989).

La débromation de la diénone mentionnée dans le titre (**1**), qui se forme lors de la bromation de l'acide méthyl-5 salicylique (**2**), est fortement catalysée par l'α-cyclodextrine (CD). La bromation du composé **2** est aussi catalysée par la CD. Le degré de la catalyse de la débromation du composé **1** ne varie pas avec le pH (de 3 à 5) et il a tendance à atteindre une valeur limite à des concentrations élevées de Br^- ou de CD. Une analyse des données relatives à l'influence des ions [Br^-], en présence de 1 mM de CD, permet d'évaluer à 0,68 M la constante de dissociation du complexe CD·Br^-. De plus, en se basant sur la relation qui existe entre la vitesse de débromation et la [CD], on peut déduire que l'anion de la diénone **1** (soit $\mathbf{1}^-$) forme un complexe avec la CD et que la K_d est 15 mM; ce complexe semble réagir avec le Br^- avec une vitesse qui est 170 fois plus grande que celle du $\mathbf{1}^-$. Toutefois, il est plus probable que la catalyse soit due à la réaction de la diénone libre, réagissant sous la forme de **1**, avec le complexe CD·Br^-; en effet, celui-ci est 3400 fois plus réactif que le Br^- qui n'est pas complexe. Les effets combinés de la catalyse interne par le groupement carboxyle du composé **1** et de la catalyse externe par la CD conduisent à une augmentation de la vitesse qui est de l'ordre de 12 millions.

Mots clés : catalyse, cocatalyse, cyclodextrine, débromation, intramoléculaire.

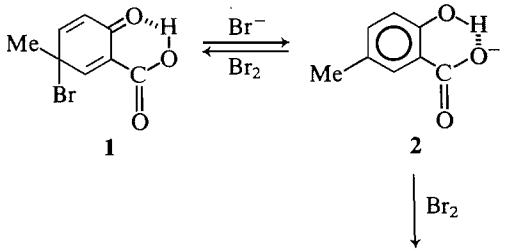
[Traduit par la revue]

Introduction

Cyclodextrins form inclusion complexes with many species, most notably with organic substrates (1, 2). As a consequence, they can have significant effects on the rates and products of organic reactions. Of particular note, they can function as catalysts in various kinds of reactions, although most attention has been paid to the cleavage of esters or amides and to various "model enzyme" reactions (1–4).

In this laboratory we have shown that α-cyclodextrin can function as a catalyst in the aqueous bromination of anisole (5), phenols and phenoxide ions (6), and in the debromination of "*ipso*-dienones" (7). These last derivatives are labile intermediates formed by *ipso* attack during the aqueous bromination of *p*-alkylphenols (8, 9). Under the reaction conditions they represent a "dead-end" and they decompose by a debromination that is bromide ion induced and general acid catalyzed (9). In the particular case of 4-bromo-4-methyl-2,5-cyclohexadienone-2-carboxylic acid (**1**), the debromination (**1** → **2**, eq. [1]) is catalyzed intramolecularly by the carboxyl group (9, 10).

The present paper reports a study of the catalysis of the debromination of the *ipso*-dienone **1** by α-cyclodextrin (CD). We hoped that the study would provide additional evidence for the mechanisms of CD-catalyzed bromination and debromination proposed earlier (6, 7), but the main object was to see how two very different forms of catalysis interact with one another. Independently, intramolecular catalysis by the carboxyl group

[1] 

ortho product

of **1** (9, 10) and the catalysis by CD of the debromination of other *ipso*-dienones (7) are both large; in combination they might afford very strong "cocatalysis", as long as they do not interfere with one another.

Enzymes achieve their remarkable efficiency by bringing together several catalytic effects in one process (4, 11). It is, therefore, of ongoing interest to find and understand chemical reactions in which more than one type of catalysis is operative.

Results

We have measured the rate of debromination of the dienone **I** as a function of [CD], pH, and bromide ion concentration. Also, we have measured the effect of added CD on the rate of bromination of 5-methylsalicylic acid (**2**).

At the high concentrations of bromide ion used in the present work, the formation of the weak CD·Br^- complex (12) results in an appreciable reduction in the amount of CD that is available for the complexation of other species, but this can be corrected for (5–7). Since [Br^-] >> [CD], the concentration of available

[1]Undergraduate participant.

[2]Author to whom correspondence may be addressed.

Can. J. Chem. Downloaded from www.nrcresearchpress.com by 122.72.124.2 on 09/07/12
For personal use only.

TABLE 1. Rate constants for the debromination of **1** as a function of the concentration of α-cyclodextrin[a]

$[CD]_T$ (mM)	k_{obs} (s^{-1})	k_{calc} (s^{-1})
0	0.111	0.111
1.0	1.01	1.02
2.0	1.86	1.84
3.0	2.62	2.60
4.0	3.23	3.29
6.0	4.54	4.51

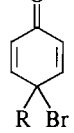
[a]At 25°C, $I = 0.11$ M (0.1 M KBr + 0.01 M buffer salt), at pH 4.5 (acetate buffer). The dienone **1** was generated *in situ* from [**2**] = 0.5 mM and $[Br_2] = 0.05$ mM. The values of k_{calc} were calculated from the values of K_d and k_c (see text), obtained by an Eadie–Hofstee analysis, and using corrected values of [CD] from eq. [2].

CD is given by:

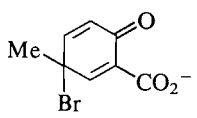
$$[2] \quad [CD] = [CD]_T K_I/(K_I + Br^-]); \qquad K_I = 0.286 \text{ M} \ (12)$$

where $[CD]_T$ is the total added CD and K_I is the dissociation constant of the CD·Br^- complex. The concentration of CD given by eq. [2] was used in all data analyses (5–7).

As with other *ipso*-dienones (**3**), generated by *ipso* bromine attack during the bromination of *p*-alkylphenols (7), we have found that the addition of CD leads to a considerable increase in the rate of debromination of the dienone **1** (see Table 1). The rate constants increase with [CD] in a curvilinear manner that conforms well to Michaelis–Menten behavior (1), and analysis by the Eadie–Hofstee approach yields a value of 14.7 mM for the dissociation constant (k_d) of the CD·dienone complex and 19.1 s^{-1} for the apparent rate constant (k_c) for the reaction of this complex, in 0.1 M KBr at pH 4.5. Thus, at saturation the rate increase is substantial: $k_c/k_u = 172$. Note also that the values of K_d and k_c must apply to the anion $\mathbf{1}^-$, since **1** ($pK_a = 3.06$ (10)) is largely ionized at the pH of 4.5.



3



$\mathbf{1}^-$

Figure 1 shows the pH dependence of rate constants for the debromination of **1** in the absence of CD and in the presence of 1 mM CD. The former results are in good agreement with those found earlier (10) and the dependence in the presence of 1 mM CD shows parallel behaviour,[3] the rate constants being about 7 times greater.

Figure 2 shows the dependence of the rate constant for debromination on [Br^-]: (a) without CD; (b) in the presence of 1 mM CD; (c) in the presence of 8 mM CD (Table 2). In the absence of CD the rate constant shows the expected first-order

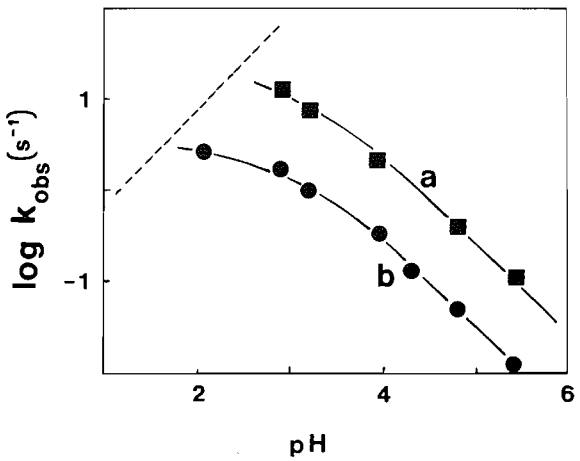


FIG. 1. The pH dependence of the rate of debromination of the dienone **1** in aqueous 0.1 M KBr + buffer ($I = 0.11$ M): (a) in the presence of 1 mM CD; (b) in the absence of CD. The latter results agree well with earlier work (10). The dashed line represents the pH dependence of the pseudo-first-order rate constant of the bromination of **2** under the same conditions (10).

dependence on [Br^-] (9), with a second-order rate constant of 0.950 M^{-1} s^{-1}, at pH 4.5. The larger rate enhancements due to increasing [Br^-] in the presence of CD (Fig. 2, b and c) confirm that both Br^- and CD are involved in the catalytic pathway. Moreover, the clear tendency to saturation-type behavior at high [Br^-] is further evidence of the formation of a weak CD·Br^- complex (12).

The dependence of the rate of bromination of **2** on [CD] has also been measured (Table 3). The apparent second-order rate constants (k_2^{app}) increase at low [CD] but then begin to decrease at high [CD], similar to the behaviour observed previously with simple phenols (6). The increase in k_2^{app} at low [CD] indicates that there is a significant contribution from a CD-catalyzed pathway for bromination while the decrease at high [CD] is due to the combined effects of the complexation of the substrate, Br_2, Br_3^-, and Br^- by CD (5, 6). If the bromination of **2** were not catalyzed by CD, the rate constants k_2^{app} would decrease substantially with increasing [CD] (see Fig. 1 of ref. 6).

Analysis of the variation with [CD] of k_2^{app} for the bromination of **2** is not as simple[4] as that for the phenols studied previously (6). This difference arises because the debromination of **1** is strongly catalyzed by the 2-carboxyl group such that this reaction is rapid enough to affect the overall rate of bromination of **2** (10). Thus, the value of k_2^{app} is dependent on the rate of debromination of **1**, as well as on the rate of bromine attack at the *ortho* and *para* positions of **2**. Furthermore, *all of these processes are catalyzed by CD*, which makes a rigorous analysis of the bromination data unmanageable.

Discussion

Bromide ion dependence

The curved dependence of the observed first-order rate constants for the debromination of **1** on the concentration of Br^- in the presence of CD, shown in Fig. 2b, can be analyzed using the following approach.

When a substrate reacts in the absence of CD (with rate con-

[3]Unfortunately, it was not possible to measure the rate of debromination of **1** in the presence of CD below pH 3 because there the rate of bromine attack on **2** is sufficiently slow as to interfere with the kinetics of debromination. However, in the pH region studied, the rate constant in the presence of CD shows the same pH dependence as in the absence of CD.

[4]In fact, the earlier analysis is not all that simple since several corrections must be made to account for the various equilibria involved (5, 6).

Can. J. Chem. Downloaded from www.nrcresearchpress.com by 122.72.124.2 on 09/07/12
For personal use only.

Can. J. Chem. Downloaded from www.nrcresearchpress.com by 122.72.124.2 on 09/07/12
For personal use only.

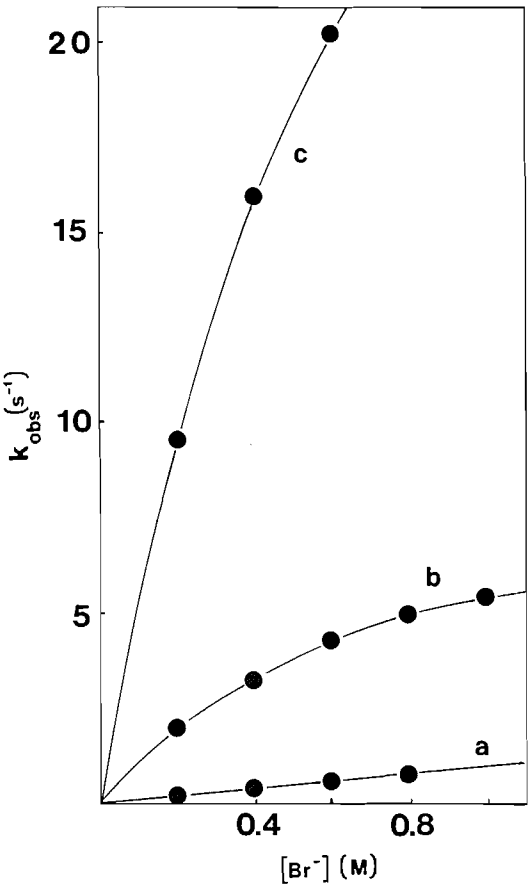


FIG. 2. The dependence of the rate of debromination of the dienone **1** on the concentration of bromide ion: (a) in the absence of CD; (b) in the presence of 1 mM CD; (c) in the presence of 8 mM CD. The ionic strength was maintained at 1.0 M (NaCl + KBr) and the pH at 4.5 with an acetate buffer (10 mM).

TABLE 2. Effect of $[Br^-]$ on the rate of debromination of **1** at different concentrations of α-cyclodextrin[a]

	k_{obs} (s^{-1})		
$[Br^-]$ (M)	$[CD]_T = 0$	1 mM	8 mM
0.2	0.216	1.97	9.54
0.4	0.408	3.27	15.97
0.6	0.601	4.28	20.34
0.8	0.785	4.99	[b]
1.0	—	5.51	[b]

[a]At 25°C, pH 4.5 (acetate buffer), I = 1.0 M (KBr + NaCl).
[b]Not measurable due to interference from the bromination step. At high $[Br^-]$ and [CD] the debromination is sufficiently fast as to be comparable in rate to the initial bromination (cf. Fig. 2).

stant k_u) and via a complex S·CD (with rate constant k_c) in the presence of CD, then:

[3*a*] $k_{obs} = (k_u K_d + k_c[CD])/(K_d + [CD])$

For the more complete set of data at [CD] = 1 mM (Fig. 2b) we can make use of the inequality K_d (= 15 mM) >> [CD], since [CD] < 1 mM due to the formation of the CD·Br^- complex. Then, eq. [3*a*] simplifies to

[3*b*] $k_{obs} = k_u + k_c[CD]/K_d$

TABLE 3. The effect of α-cyclodextrin on the rate of bromination of 5-methylsalicylic acid, **2**[a]

$[CD]_T$ (mM)	k_2^{app} ($M^{-1}\,s^{-1}$)
0	8 710
1.0	19 200
2.0	21 500
4.0	21 700
6.0	20 700
8.0	18 600

[a]At 25°C, pH 1.0 (0.1 M HCl), I = 0.2 M (KBr + HCl), [**2**] = 0.25 mM, $[Br_2]_0$ = 0.025 mM.

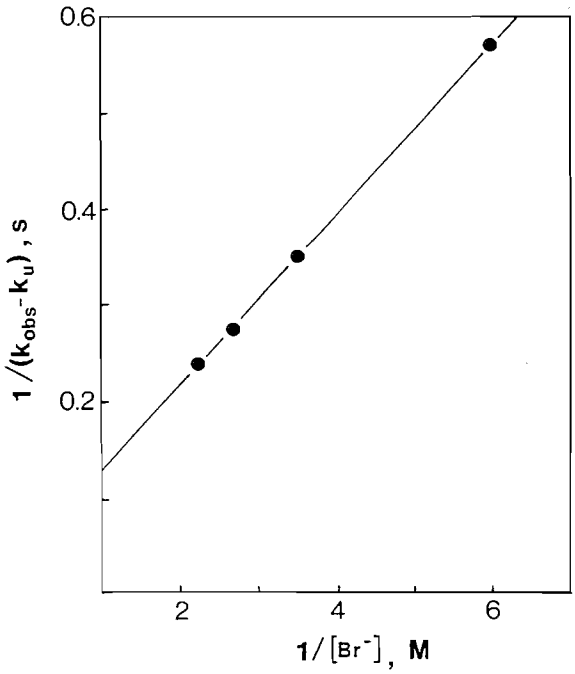


FIG. 3. Double-reciprocal plot of the $[Br^-]$ dependence data presented in Fig. 2b, based on eqs. [4] and [5] (see text).

To account for the overall dependence on $[Br^-]$ we must replace [CD] by the explicit expression given in eq. [2] and also include the dependence of k_c on $[Br^-]$ by expressing it as $k_2^c[Br^-]$. Hence:

$$[4] \quad (k_{obs} - k_u) = \frac{k_2^c[Br^-][CD]_T K_I}{(K_I + [Br^-])K_d}$$

Taking the reciprocal of both sides of this expression gives a Lineweaver–Burk type of equation,

[5] $1/(k_{obs} - k_u)$ = slope/$[Br^-]$ + intercept

where "slope" = $K_d/k_2^c[CD]_T$ and "intercept" = $K_d/k_2^c[CD]_T K_I$, and an estimate of K_I can be obtained from the slope/intercept.

For the data in Fig. 2b this treatment gives a good straight line, as shown in Fig. 3, and from the slope and intercept a value of K_I = 0.677 M is obtained. This value is only in fair agreement with the literature value of 0.286 M (12) and the reasons for the discrepancy between the two values are not immediately apparent. It may be due to the differences in ionic strength (I = 0.01–0.03 M (12) vs. I = 1.0 M, this work), the different assumptions involved in the two approachs, or it may

TABLE 4. Constants evaluated for the two models (eqs. [6*a*] and [6*b*]) for the CD-catalyzed debromination of 4-bromo-4-alkyl-2,5-cyclohexadienones, **3** and $\mathbf{1}^-$[a]

Dienone	K_d (mM)	k_c^a/k_u'	k_c^b/k_u'	k(1 mM CD)/k_u
3, R = Me	4.83	78	4600	5.7
Et	2.87	39	3900	8.7
i-Pr	2.43	23	2700	5.9
n-Pr	0.752	12	4600	6.4
t-Bu	2.32	28	3500	7.8
3,4-diMe	3.55	29	2400	5.9
$\mathbf{1}^-$ [b]	14.7	170	3400	7.1

[a]At 25°C. The data for **3** are taken from ref. 7 and are normalized to 0.1 M HCl in 0.1 M KBr. The constant k_u' is for the reaction of the dienone with Br^-, k_c^a is for the reaction of the CD·dienone complex with free Br^- (eq. [6*a*]), k_c^b is for the reaction of the CD·Br^- complex with free dienone (eq. [6*b*]).
[b]At pH 4.5 (acetate buffer), in 0.1 M KBr.

be a reflection of the difficulty of determining the dissociation constants of weakly bound complexes.

More importantly, the formation of a weak CD·Br^- complex is confirmed. In the present paper we retain the use of K_I = 0.286 M, for consistency with the earlier work (5–7).[5]

Dependence on [CD]

It is clear that the debromination of the *ipso*-dienones **3** (7), and now **1**, are catalyzed by bromide ion *and* by α-cyclodextrin. These processes may be characterized by third-order rate constants (k_3) but it is most likely that they arise from either of two, kinetically indistinguishable, second-order processes (7): the attack of *free* Br^- on the dienone·CD complex (eq.[6*a*]); or attack of the CD·Br^- complex on the *free* dienone, **3** (eq. [6*b*]).[6]

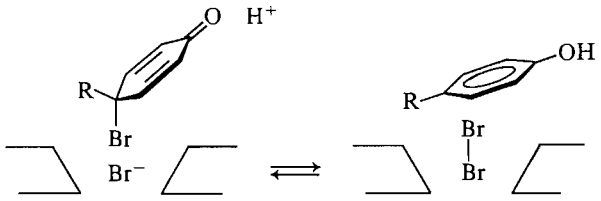
$$[6a]\quad \mathrm{CD} + \mathbf{3} + \mathrm{Br}^- \underset{K_d}{\rightleftharpoons} \mathrm{CD}\cdot\mathbf{3} + \mathrm{Br}^- \xrightarrow{k_c^a} \text{products}$$

$$[6b]\quad \mathrm{CD} + \mathrm{Br}^- + \mathbf{3} \underset{K_I}{\rightleftharpoons} \mathrm{CD}\cdot\mathrm{Br}^- + \mathbf{3} \xrightarrow{k_c^b} \text{products}$$

In the first case $k_3 = k_c^a/K_d$, while in the second $k_3 = k_c^b/K_I$ (7).

Analysis of the data in Table 1 according to eq. [6*a*] is straightforward (7) and it gives values of K_d = 14.7 mM and k_c^a = 191 $M^{-1}s^{-1}$ (cf. Results) for the reaction of the anion $\mathbf{1}^-$ at pH 4.5. As shown above, the values of k_c^a and k_c^b are related, through k_3, by the factor K_I/K_d; multiplication of k_c^a by this factor gives a value of 3720 $M^{-1}s^{-1}$ for k_c^b, for debromination of the anion $\mathbf{1}^-$ by pathway [6*b*].[6]

For reasons given earlier (7), it was concluded that the catalysis of the debromination of 4-alkyl-4-bromo-2,5-cyclohexadienones **3** by CD occurs via the pathway shown in eq. [6*b*]. This pathway is more compatible with the effects of different alkyl substituents (7) and with conclusions regarding the catalysis of the bromination of phenols (6, 7). Both of our earlier studies (6, 7) point to a transition state in which the organic moiety is basically outside the CD cavity, while the bromine atoms are largely inside (Scheme 1). We believe that the dienone **1** reacts in a similar manner.



SCHEME 1

The catalytic rate constants for the debromination of **1** vary with pH (Fig. 1) in a manner that makes direct comparison with the earlier work on **3**, which was carried out at a much lower pH (7), inappropriate. However, the ratios "k_c/k_u" are pH-independent measures of the extent of the catalysis by the cyclodextrin. Such "catalytic ratios", calculated for both reaction models (eqs. [6*a*] and [6*b*]), for the dienones studied previously (7) and for the dienone anion $\mathbf{1}^-$ are collected in Table 4. As seen there, the dienone $\mathbf{1}^-$ behaves quite similarly to the other dienones, particularly when viewed in terms of the mechanism [6*b*], the favoured pathway (Scheme 1). For this model, the catalytic ratios vary only from 2400 to 4600, with that for the anion $\mathbf{1}^-$ falling in the middle of the range, at 3400.

A similar conclusion may be arrived at by looking at the data in a manner that is independent of any mechanistic model. As shown in Fig. 1, the addition of 1 mM CD increases the rate of debromination of the dienone **1** by a factor of about 7, which is independent of pH. This increase in the rate falls in the middle of the range of values (5.7–8.7) found for other dienones, as shown in Table 4. Thus, even though the dienone **1** is much more reactive than the other dienones **3** previously studied (7, 9), the catalytic effect of CD on its debromination is much the same. It seems safe, therefore, to conclude that the CD-catalyzed debromination of **1** proceeds via the same type of pathway as the dienones **3** (eq. [6*b*] and Scheme 1).

Cocatalysis

The debromination of the *ipso*-dienones **3** by bromide ion is catalyzed by the proton (and by general acids) (9). For the methyl derivative **3** (R = Me) the observed rate constant is 1.01 s^{-1} in 1.0 M HCl containing 0.1 M KBr (9) and so the apparent third-order rate constant (k_3) for the reaction shown in eq. [7] is 10 $M^{-2}s^{-1}$.

$$[7]\quad \mathbf{3}\ (\mathrm{R} = \mathrm{Me}) + \mathrm{H}^+ + \mathrm{Br}^- \rightarrow \text{products};\ k_3 = 10\ M^{-2}s^{-1}$$

$$[8]\quad \mathbf{1}^- + \mathrm{H}^+ + \mathrm{Br}^- \rightarrow \text{products};\ k_3 = 3.5 \times 10^4\ M^{-2}s^{-1}$$

$$[9]\quad \mathbf{1}^- + \mathrm{H}^+ + \mathrm{CD}\cdot\mathrm{Br}^- \rightarrow \text{products};\ k_3 = 1.2 \times 10^8\ M^{-2}s^{-1}$$

The observed rate constant for debromination of the anion $\mathbf{1}^-$ in 0.1 M KBr at pH 4.5 is 0.111 s^{-1} (Table 1) and so $k_3 = 3.5 \times 10^4\ M^{-2}s^{-1}$ (eq. [8]). Thus, the dienone anion $\mathbf{1}^-$ appears to be 3500 times[7] more reactive than the related dienone **3** (R = Me), which lacks the carboxylate group (eqs. [7] and [8]). This large rate enhancement arises because the debromination actually occurs on the nonionized dienone **1** and the reaction is

[5]If the value of K_I = 0.286 M is too small many of the derived constants obtained in earlier work (5–7) would be in error. Sample analyses of phenol bromination data (6), using the higher value of K_I, show that the effect on the catalytic rate constants is small (0–30%) and largely self-compensatory, whereas with the debrominations (7) the effect is larger. In neither case, however, would the *conclusions* of the earlier studies (and the present one) be changed significantly since the rate constants for different substrates would all be affected in much the same way.

[6]Note that the rate constants k_c^a and k_c^b include the dependence on [H^+].

[7]The earlier estimate of 2300 times (10) was based on different rate constants for **3** (R = Me) and for the anion $\mathbf{1}^-$ (10).

Can. J. Chem. Downloaded from www.nrcresearchpress.com by 122.72.124.2 on 09/07/12
For personal use only.

catalyzed intramolecularly by the 2-carboxyl group (see eq. [1]) (9, 10).

For the reaction of the anion $\mathbf{1}^-$ with the CD complex of bromide ion, the rate constant $k_c^b = 3720\,M^{-1}s^{-1}$, at pH 4.5 (see previous section). Thus, for the reaction shown in eq. [9] the apparent value of k_3 is $1.2 \times 10^8\,M^{-2}s^{-1}$.

As argued above, the catalysis of the debromination of $\mathbf{1}^-$ by CD, actually reacting as **1**, is quantitively very similar to that of the dienones **3** (Table 4). This close similarity suggests that there is no significant cooperativity *or interference* between catalysis by the internal carboxyl group of **1** and that by α-cyclodextrin; the two catalytic effects are essentially independent of one another, and additive.

Nevertheless, as seen in eqs. [7]–[9], the combination of the two forms of catalysis is substantial: intramolecular catalysis increases the reactivity of the dienone anion $\mathbf{1}^-$, relative to **3** (R = Me), by a factor of 3500, and the apparent reactivity of the $CD \cdot Br^-$ complex towards $\mathbf{1}^-$ is 3400 times greater than that of free Br^-. Therefore, the combined result of internal catalysis by the carboxyl group of **1** and external catalysis by α-cyclodextrin is to enhance the reactivity by a factor of *12 million*!

Experimental

5-Methylsalicylic acid and α-cyclodextrin were obtained from Aldrich and they were used as received. All other reagents were of analytical grade.

Bromine solutions were made up by weight, as previously (5–7). Substrate solutions were prepared by diluting the appropriate amount of stock solution (0.25 M in hplc methanol) in the desired aqueous medium. The buffer solutions (I = 0.01 M) were prepared according to the recipes given by Perrin (13). The total ionic strength was generally maintained at 0.11 M (KBr + buffer), except for the experiments where $[Br^-]$ was varied, in which case the ionic strength was maintained at 1.01 M (KBr + NaCl + buffer). The effects of varying [CD] and $[Br^-]$ on the rate of debromination of **1** were measured at pH 4.5.

For the debromination experiments, the dienone **1** was generated *in situ* by the rapid mixing of equal volumes of 0.5 mM 5-methylsalicylic acid (**2**) and 0.2 mM bromine in the stopped-flow apparatus. The rate of bromination of **2** was measured using [**2**] = 0.25 mM and $[Br_2]$ = 0.025 mM. In both types of experiment one syringe contained **2** + CD in the desired medium, while the other contained bromine in the same medium. Thus, bromine was not brought into contact with CD until mixing in the stopped-flow apparatus (5–7).

The rate of debromination of the dienone **1** was measured as the decrease in absorbance at 250–255 nm (10). The rate of bromination of **2** was measured by monitoring the disappearance of bromine at 265 nm (Br_3^- band) (14). All rates were measurd at 25.0 ±0.1°C, using a stopped-flow apparatus interfaced to a microcomputer (15, 16). First-order rate constants were obtained by analysis of absorbance traces covering about 90% reaction, using an infinity reading taken after 10 half-lives (16).

Acknowledgements

One of us (O.S.T.) thanks the Natural Sciences and Engineering Research Council of Canada for an operating grant and Professors J.-M. Lehn and J. A. Osborn for their hospitality during a sabbatical leave spent at the Université Louis Pasteur, Strasbourg, France.

1. M. L. BENDER and M. KOMIYAMA. Cyclodextrin chemistry. Springer-Verlag, New York. 1978.
2. W. SAENGER. Angew. Chem. Int. Ed. Engl. **19**, 344 (1980); Isr. J. Chem. **25**, 43 (1985); J. L. ATWOOD, J. E. D. DAVIES, and D. D. MACNICOL. Inclusion compounds. Vols. 2 and 3. Academic Press, London. 1984.
3. I. TABUSHI. Acc. Chem. Res. **15**, 66 (1982); R. BRESLOW. Acc. Chem. Res. **13**, 170 (1980); Science, **218**, 532 (1982); C. SIRLIN. Bull. Soc. Chim. Fr. II-5 (1984); Y. MATSUI, T. NISHIOKA, and T. FUJITA. Top. Curr. Chem. **128**, 61 (1985); V. T. D'SOUZA and M. L. BENDER. Acc. Chem. Res. **20**, 146 (1987); V. RAMAMURTHY. Tetrahedron, **42**, 5753 (1986).
4. H. DUGAS and C. PENNEY. Bioorganic chemistry. Springer-Verlag, New York. 1981.
5. O. S. TEE and J. M. BENNETT. Can. J. Chem. **62**, 1585 (1984).
6. O. S. TEE and J. M. BENNETT. J. Am. Chem. Soc. **110**, 269 (1988).
7. O. S. TEE and J. M. BENNETT. J. Am. Chem. Soc. **110**, 3226 (1988).
8. O. S. TEE, N. R. IYENGAR, and M. PAVENTI. J. Org. Chem. **48**, 759 (1983).
9. O. S. TEE, N. R. IYENGAR, and J. M. BENNETT. J. Org. Chem. **51**, 2585 (1986).
10. O. S. TEE and N. R. IYENGAR. J. Org. Chem. **50**, 4468 (1985).
11. W. P. JENCKS. Catalysis in chemistry and enzymology. McGraw–Hill, New York. 1969; A. FERSHT. Enzyme structure and mechanism. 2nd ed. W. H. Freeman, New York. 1985.
12. J. F. WOJICK and F. M. ROHRBACH. J. Phys. Chem. **79**, 2251 (1975).
13. D. D. PERRIN. Aust. J. Chem. **16**, 572 (1963).
14. O. S. TEE and C. G. BERKS. J. Org. Chem. **45**, 830 (1980).
15. O. S. TEE, M. TRANI, R. A. MCCLELLAND, and N. E. SEAMAN. J. Am. Chem. Soc. **104**, 7219 (1982).
16. O. S. TEE and B. K. TAKASAKI. Can. J. Chem. **63**, 3540 (1985).

Can. J. Chem. Downloaded from www.nrcresearchpress.com by 122.72.124.2 on 09/07/12
For personal use only.

Crystal, molecular and electronic structure of 1-*H*-3-methyl-4-amine-5-thione-1,2,4-triazol[1]

J. L. ESCOBAR-VALDERRAMA, J. H. GARCÍA-TAPIA, J. RAMÍREZ-ORTÍZ, M. J. ROSALES, R. A. TOSCANO, AND J. VALDÉS-MARTÍNEZ[2]

Instituto de Química, Universidad Nacional Autónoma de México, Circuito Exterior, Ciudad Universitaria, Coyoacán 04510, México, D. F.

Received March 17, 1988

J. L. ESCOBAR-VALDERRAMA, J. H. GARCÍA-TAPIA, J. RAMÍREZ-ORTÍZ, M. J. ROSALES, R. A. TOSCANO, and J. VALDÉS-MARTÍNEZ. Can. J. Chem. **67**, 198 (1989).

The crystal and molecular structure of the title compound has been determined from three-dimensional X-ray intensity data. The crystals are orthorhombic with space group *Pbcm*, $a = 8.877(4)$, $b = 9.813(2)$, $c = 6.545(2)$ Å, $Z = 4$. The structure has been refined to $R = 0.029$ and $R_w = 0.035$. The molecules are present in the thione form as planar molecules with only intermolecular interactions. Bond lengths and angles suggest that the electron density is more localized in the N—N—C—S ring fragment. Theoretical calculations (MNDO method) were also carried out on the compound both in the thione and its thiol tautomeric forms. Some comparisons are made between several properties (formation enthalpies, proton affinities, molecular electrostatic potentials, atomic charges) of both tautomers. The results indicate some important differences in reactivity between both forms.

Key words: crystal structure, molecular structure, electronic structure, 1-*H*-3-methyl-4-amine-5-thione-1,2,4-triazol.

J. L. ESCOBAR-VALDERRAMA, J. H. GARCÍA-TAPIA, J. RAMÍREZ-ORTÍZ, M. J. ROSALES, R. A. TOSCANO et J. VALDÉS-MARTÍNEZ. Can. J. Chem. **67**, 198 (1989).

On a déterminé les structures cristalline et moléculaire du composé mentionné dans le titre en faisant appel à la diffraction des rayons-X en trois dimensions. Les cristaux sont orthorhombiques, groupe d'espace *Pbcm*, avec $a = 8,877(4)$, $b = 9,813(2)$ et $c = 6,545(2)$ Å et $Z = 4$. On a affiné la structure jusqu'à des valeurs de $R = 0,029$ et $R_w = 0,035$. Les molécules sont présentes sous la forme thione de molécules planes ne présentant que des interactions intermoléculaires. Les longueures ainsi que les angles des liaisons suggèrent que la densité électronique est plus délocalisée dans la portions des cycles N—N—C—S. On a aussi effectué des calculs d'orbitales moléculaires (méthode CNDO) sur le composé tant dans sa forme thione que dans sur son tautomère thiolique. On a fait quelques comparaisons entre plusieurs propriétés (enthalpies de formation, affinités protoniques, potentiels électrostatiques moléculaires et charges atomiques) de chacun des tautomères. Les résultats indiquent qu'il existe d'importantes différences de réactivité entre les deux formes.

Mots clés : structure cristalline, structure moléculaire, structure électronique, 1*H*-méthyl-3 amine-4 thione-5 triazole-1,2,3.

[Traduit par la revue]

Introduction

Mercapto derivatives of substituted 4-amino-1,2,4-triazoles are particularly interesting as complexing agents due to the presence of four potential donor atoms (three nitrogen and one sulphur), consequently many metal derivatives of ligands of this type have been prepared (1–5), and they have also been used as analytical reagents.

Mercapto triazoles have been proposed to exist as thione–thiol tautomers (Fig. 1), both in solution and in solid state. In coordination compounds, several coordination modes have been suggested, mostly based on infrared data. One result that has been considered of great importance is the absence of an S—H vibrational band (ca. 2500 cm^{-1}) in the spectra of all complexes and which has been taken as an indication of the ligand, considered to be in the thiol from when free, suffering deprotonation and coordinating through the sulphur atom (1–5).

In the course of a study of metal complexes derived from 1-*H*-3-methyl-4-amine-5-thione-1,2,4-triazol, **1**, we noticed that no band was present around 2500 cm^{-1} in the infrared spectrum of the uncomplexed ligand. Since this observation could nullify the importance assigned by Gadag *et al.* (1–5) to the absence of this band in metal complexes, an X-ray study of a single crystal of the ligand was undertaken to determine the structure of **1** in the solid state. Theoretical calculations of the molecular and electronic structure were also carried out to gain insight into the coordination properties of this ligand, and into the relative stability of both tautomers. The results of these studies are reported in this paper.

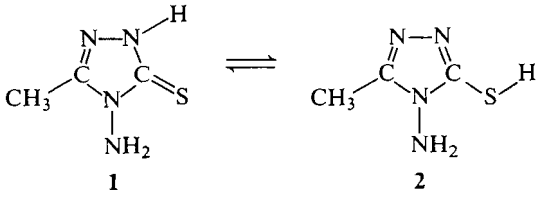


FIG. 1. Thione **1** and thiol **2** tautomers of 1-*H*-3-methyl-4-amine-5-thione-1,2,4-triazol.

Experimental

1 was prepared by the literature method (6), crystals were grown by slow evaporation of an ethanolic solution.

Crystals data are as follows:

$C_3H_6N_4S$ mw = 130.16

Cell dimension 0.1 × 0.4 × 0.36 mm, space group *Pbcm*, $a = 8.877(4)$, $b = 9.813(2)$, $c = 6.545(2)$ Å, orthorhombic, $V = 570.09$ Å^3, d(calc) 1.52 g cm^{-3}, $Z = 4$, μ(MoKα) 4.36 cm^{-1}, $F(000)$ 272.

Data collection, structure solution, and refinement

The data were collected on a Nicolet R3m four-circle diffractometer with monochromated MoK$\bar{\alpha}$ radiation (0.71069 Å) at 19.5°C. Of the 516 reflections measured up to $2\theta \leq 50°$, only 435 with $F > 3\sigma(F)$ were considered observed. No correction was made for absorption. The structure was solved by direct methods and Fourier difference techniques with SHELXTL (7). Full matrix least-squares refinement with anisotropic thermal parameters for all non-hydrogen atoms, reduced R to 0.0295 and R_w to 0.0348, $S = 1.119$, residual electron

[1]Contribution No. 928 of the Instituto de Química, UNAM.

[2]To whom correspondence should be addressed.

Can. J. Chem. Downloaded from www.nrcresearchpress.com by 122.72.124.2 on 09/07/12
For personal use only.

TABLE 1. Atom coordinates ($\times 10^4$) and temperature factors ($Å^2 \times 10^3$) of 1-*H*-3-methyl-4-amine-5-thione-1,2,4-triazol, **1**

Atom	*x*	*y*	*z*	U_{eq}*
S(1)	5817(1)	1140(1)	2500	34(1)
N(1)	3469(3)	2913(2)	2500	33(1)
N(2)	1915(3)	2991(3)	2500	37(1)
C(3)	1488(3)	1713(3)	2500	33(1)
N(4)	2718(3)	863(3)	2500	27(1)
C(5)	4001(3)	1646(3)	2500	27(1)
C(6)	−95(4)	1238(4)	2500	51(1)
N(3)	2621(3)	−558(3)	2500	37(1)

*Equivalent isotropic *U* defined as one third of the trace of the orthogonalised U_{ij} tensor.

TABLE 2. Bond lengths in **1** and the sodium salt of 4-amino-5-mercapto-1,2,4-triazol (15) **3**, and bond angles in **1**

Bond	Length (Å)	
	1	**3**
S(1)—C(5)	1.687(3)	1.724(4)
N(1)—C(5)	1.330(4)	1.315(4)
C(3)—N(4)	1.374(4)	1.364(4)
N(4)—C(5)	1.374(3)	1.391(4)
N(1)—N(2)	1.382(3)	1.412(4)
N(2)—C(3)	1.310(4)	1.301(4)
C(3)—C(6)	1.481(5)	
N(4)—N(3)	1.397(3)	1.414(4)

Bonds	Angle in **1** (deg)	Bonds	Angle in **1** (deg)
N(2)—N(1)—C(5)	114.2(2)	N(1)—N(2)—C(3)	103.6(2)
N(2)—C(3)—N(4)	110.6(2)	N(2)—C(3)—C(6)	125.1(3)
N(4)—C(3)—C(6)	124.3(3)	C(3)—N(4)—C(5)	108.6(2)
C(3)—N(4)—N(3)	123.8(2)	C(5)—N(4)—N(3)	127.5(2)
S(1)—C(5)—N(1)	127.9(2)	S(1)—C(5)—N(4)	128.9(2)
N(1)—C(5)—N(4)	103.2(2)		

± 0.25 e $Å^{-3}$. The hydrogen atoms bonded to the nitrogen atoms were located from a difference map and refined freely while the remaining hydrogen atoms were places in idealized positions. Atomic scattering factors are from ref. 8. All calculations were performed on a Nova 4S computer.

Final coordinates are given in Table 1, while bond distances and angles are listed in Table 2. Figure 2 shows a view of the molecule with the atomic numbering scheme.[3]

The semi-empirical method MNDO (9) was used to calculate the electronic structure of the ligand. Geometries of both tautomers was also optimized using MNDO.

Discussion

Structural results

The crystal consists of planar molecules in the thione form with intermolecular interactions involving the sulphur atoms and the hydrogen atoms bonded to N(1) and N(3) with N---S and H---S distances of 3.230(2) and 3.599(1) Å and 2.53(4) and 2.73(3) Å, respectively.

A characteristic of amine-1,2,4-triazoles that has been observed (10) is that the N—N distances in the triazol ring and in the side chain are similar. In this case the two bonds show a slight difference in bond length values with N(1)—N(2) and N(3)—N(4) distances of 1.382(3) and 1.397(3) Å, respectively. These values are larger than the corresponding one in 1,2,4-triazol (1.350 Å) (11), but smaller than the single bond value (1.470 Å).

The length for the C—S bond, 1.687(3) Å, is similar to that observed in 5-amino-2-thiol-1,3,4-thiadiazol (12) which was proposed to have substantial double bond character. Although it is shorter than a single S—C bond (1.801(5)–1.825(5) Å in some dithiacycloalkanes (13)), it is still longer than an S—C double bond distance (1.646(5) Å in (2-adipoyl)bis(1,3-thiazolidine-2-thione (14)).

The C—N bonds in **1** can be divided into two sets according to the bond distances observed. C(5)—N(1) and C(3)—N(2) have a mean value of 1.320 Å while C(5)—N(4) and C(3)—N(4) both show a distance of 1.374(3) Å. The C(5)—N(1) bond is 0.020 Å longer than C(3)—N(2); a difference that may be significant and which might suggest a larger double bond character in the second bond. The longer bonds observed in C(5)—N(4) and C(3)—N(4) suggest that the electron density is more localized among C(3)—N(2)—N(1)—C(5)—S(1). Taking into account all these observations, **1** can be assigned the thione tautomeric form, as shown in Fig. 1.

The crystal structure of the sodium salt of 4-amino-5-mercapto-1,2,4-triazol, **3**, has been described (15) and a comparison of bond lengths is given in Table 2. It can be observed that the distances between N(1) and N(2) and C(5) and S(1) are significantly longer in **3** than in **1**, indicating that the electron density in these bonds diminishes more than those in other bonds upon deprotonation of the ring.

Theoretical calculations

Structural data for tautomer **2** were calculated using MNDO and, to make the results of the theoretical calculations comparable, the geometries for both tautomers, the experimental and the calculated ones, were optimized with the same method. The geometry calculated for tautomer **1** agreed with the results experimentally obtained with a mean absolute error of 0.046 Å in bond length values. However, the MNDO method systematically assigns lower values to C=S distances (16) and this case was no exception, with a calculated bond length 0.113 Å shorter than the experimental value. If this distance is not considered, the mean absolute error is reduced to 0.037 Å.

In the calculated structure of tautomer **2**, as in the case of tautomer **1**, the ring is completely planar. Bond length values indicate an electronic delocalization, particularly along (C(3)---N(2)---N(1)---C(5). The C—S bond is longer in **2** than in **1** (1.668 Å against 1.574 Å). The hydrogen atom of the thiol group is coplanar to the triazol ring (ϕ: N(4)—C(5)—S(8)—H(9) = −179.6°).

The relative stability in the gas phase of tautomers **1** and **2** was evaluated by calculating their formation enthalpies by the MNDO method with the Dewar and McKee corrections (16). According to these results, the thione form, is more stable than the thiol form by 4.37 kcal/mol (50.91 and 55.28, respectively). Besides, it has been reported (17) than the MNDO method overestimates the stability of "hydroxy" tautomers by

[3]Tables of observed and calculated structure factor amplitudes, of temperature factors, of hydrogen coordinates and a list of non-bonded distances may be purchased from the Depository of Unpublished Data, CISTI, National Research Council of Canada, Ottawa, Ont., Canada K1A 0S2.

Can. J. Chem. Downloaded from www.nrcresearchpress.com by 122.72.124.2 on 09/07/12
For personal use only.

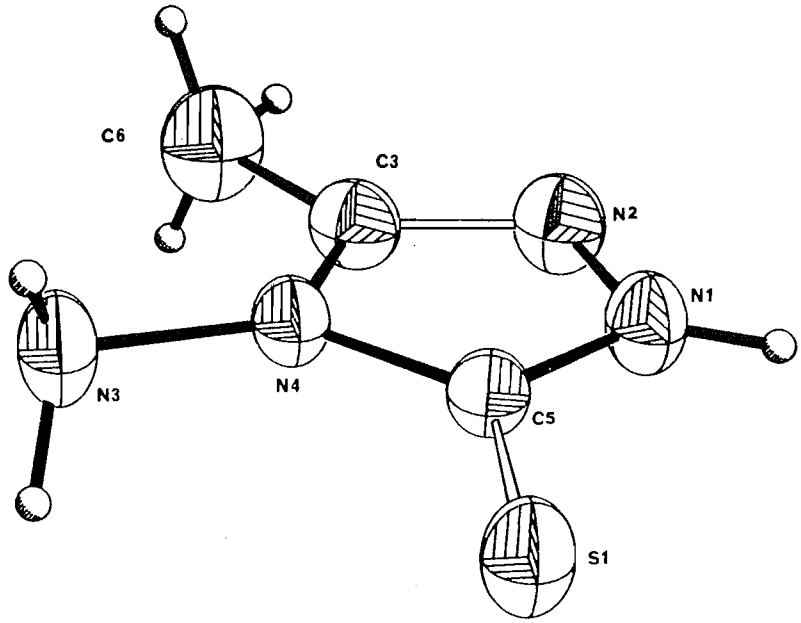


FIG. 2. ORTEP diagram of **1** showing the numbering scheme.

TABLE 3. Atomic charges and atomic contributions to the HOMO of the thione **1** and thiol **2** tautomers

	Atomic charges		Contributions to the HOMO	
Atom	**1**	**2**	**1**	**2**
N(1)	−0.227	−0.124	0.4020	0.3792
N(2)	−0.107	−0.125	−0.3090	−0.3627
C(3)	0.089	0.041	−0.2756	−0.4885
N(4)	−0.262	−0.191	0.3005	0.0401
C(5)	0.256	−0.071	−0.0250	0.4697
C(6)	0.101	0.110	−0.2756	0.0791
N(7)	−0.066	−0.072	−0.0223	−0.0022
S(8)	−0.356	0.057	−0.7502	−0.4838
H(1)	0.264			
H(6a)	0.026	0.026		
H(6b)	0.023	0.014		
H(6c)	0.024	0.014		
H(7a)	0.117	0.112		
H(7b)	0.117	0.112		
H(8)		0.097		

about 8.6 kcal/mol over the "keto" form. It is therefore reasonable to assume that in the gas phase, under normal conditions, only tautomer **1** will be present.

To obtain some information on the chemical reactivity of both tautomers, some parameters that could reflect this were calculated. One of these was the proton affinity which was calculated as the change of enthalpy (at 298 K) associated with the separation of a proton from the chemical species HX. The enthalpies used for this calculation were those calculated in this work and the experimental value for $\Delta H_f^\circ(H^+)$, 367.2 kcal/mol (18). The value calculated for the proton affinity of **1** and **2** were 316.2 and 311.9 kcal/mol, respectively, which compared to the value of 345.2 kcal/mol measured for $HCOO^-$ and other reported values, indicates that both tautomers can be considered as acidic species.

The atomic charges calculated for tautomers **1** and **2** are listed in Table 3. Some important differences observed are that in tautomer **1**, the sulphur atom is the one with the largest electron density in the molecule while in **2** the same atom is even slightly electron deficient. Consequently, the chemical behaviour of the system towards an electrophile would depend on the tautomeric form present in the reaction, assuming, of course, that the sulphur atom is involved in the reactive site.

The most acidic hydrogen atom was the one bonded to N(1) in tautomer **1** or S(8) in tautomer **2**, but the electronic deficiency was much lower in the second case. It would therefore seem easier to pull a proton from tautomer **1** than from **2** and that the hydrogen atom involved in such a process would be that bonded to N(1).

The highest occupied molecular orbital in both tautomers was basically formed by a combination of the P_z orbitals of each heavy atom. Table 3 lists the contribution of these atomic orbitals to the HOMO of the tautomers. In this figure, each P_z orbital is perpendicular to the plane that contains the ring of the molecule. In tautomer **1** the contribution of the sulphur atom S(8) to the HOMO is considerably larger than that of any other atom while in **2**, contributions are more uniform, this suggesting that when reacting with an electrophile, the molecule will orientate more selectively in the thione form than in thiol form.

From the calculated energy of the HOMO (−9.26 and −9.64 eV for **1** and **2**, respectively), the order of reactivity with an electrophile would be:

Tautomer **1** > Tautomer **2**

The molecular electrostatic potentials (MEP) generated by the electronic and nuclear distribution have been widely used as an index of chemical reactivity of the type of electrostatic interactions between molecules and ions or solvents (19, 20). In this work the MEP's were calculated with the VSS program (21) which uses the electronic distribution obtained with the CNDO program (22, 23). This type of MEP calculations give results which are qualitatively correct, specially when calculations are carried out at distances above the van der Waals surface of the molecule where results are similar to those obtained with more precise calculations (24–27). For this reason, in this work MEP's were evaluated on the plane and 2 Å above the molecular plane. The MEP's calculated for tautomer **1** shows that the

Can. J. Chem. Downloaded from www.nrcresearchpress.com by 122.72.124.2 on 09/07/12
For personal use only.

interaction of an electrophile with this molecule is directed towards the sulphur atom. However, in tautomer **2**, the attack is directed towards N(1) and N(2).

1. R. V. GADAG and M. R. GAJENDRAGAD. J. Indian Chem. Soc. **55**, 789 (1978).
2. R. V. GADAG and M. R. GAJENDRAGAD. Indian J. Chem. **19A**, 705 (1980).
3. R. V. GADAG and M. R. GAJENDRAGAD. J. Indian Chem. Soc. **57**, 270 (1980).
4. R. V. GADAG and M. R. GAJENDRAGAD. Rev. Roum. Chim: **23**, 745 (1980).
5. H. R. A. GADUJAR, R. V. GADAG, and M. R. GAJENDRAGAD. J. Indian Chem. Soc. **60**, 889 (1983).
6. K. S. DHAKA, J. MOHAN, V. K. CHADHA, and H. K. PUJARY. Indian J. Chem. **12**, 288 (1974).
7. G. M. SHELDRICK. SHEXTL Rev. 3. An integrated System for solving, refining, and displaying crystal structure from diffraction data. University of Gottingen. Federal Republic of Germany. 1981.
8. International tables of X-ray crystallography. Kynoch Press, Vol. IV. Birmingham, England. 1974. pp. 72–98.
9. M. J. S. DEWAR and W. THIEL. J. Am. Chem. Soc. **99**, 4899 (1977).
10. R. C. SECCOMBE and C. H. L. KENNARD. J. Chem. Soc. Perkin II, 1 (1973).
11. P. GOLDSTEIN, J. LADELOOL, and G. ABOWITZ. Acta Crystallogr. B**25**, 135 (1969).
12. T. C. DOWNIE, W. HARRISON, E. S. RAPER, and M. A. HEPMORTH. Acta Crysallogr. B**28**, 1584 (1972).
13. W. N. SETZER, G. S. WILSON, and R. S. GLASS. Tetrahedron, **37**, 2735 (1981).
14. E. FUYITA, Y. NAGAO, K. I. SENO, S. TAKAO, T. MIYASAKA, M. KIMURA, and W. H. WATSON. J. Chem. Soc. Perkin I, 914 (1981).
15. R. C. SECCOMBE, J. V. TILLACKI, and C. H. L. KENNARD. J. Chem. Soc. Perkin II, 6 (1973).
16. M. J. S. DEWAR nd M. L. MCKEE. J. Comp. Chem. **4**, 84 (1983).
17. J. MIREK and A. SYGULA. J. Mol. Struct. Theochem. **86**, 85 (1981).
18. D. R. STULL and J. PROPHET. JANAF thermochemical tables NSRDSNB937. 1971.
19. E. SOROCCO and J. TOMASSI. Adv. Quantum Chem. **2**, 115 (1978).
20. P. POLITZER and D. G. TRUHER (*Editors*). Chemical applications of atomic and molecular potentials. Plenum Press, New York. 1981.
21. C. GIESSNER-PRETTRE. QCPE Program No. 249, Indiana University. 1974.
22. J. A. POPLE, D. P. SANTRY, and G. A. SEGAL. J. Chem. Phys. **43**, 5129 (1965).
23. C. GIESSNER-PRETTRE and A. PULLMAN. Theoret. Chim. Acta, **25**, 83 (1972).
24. P. M. DEAN. Molecular foundation of drug-receptor interactions. Cambridge University Press, Cambridge. 1987. Chap. 3.
25. P. A. KOLLMAN and D. M. HAYES. J. Am. Chem. Soc. **103**, 2955 (1981).
26. S. BALDWIN, L. B. KIER, and D. SHILLADY. Mol. Pharm. **18**, 455 (1980).
27. M. L. MARTIN and J. A. HERNÁNDEZ. Afinidad, **35**, 187 (1978).

Can. J. Chem. Downloaded from www.nrcresearchpress.com by 122.72.124.2 on 09/07/12
For personal use only.

Differences between adsorption properties of two Rhodesian chrysotile samples. Relation with the DTA features introduced by leaching and grinding

HÉLÈNE SUQUET

Laboratoire de réactivité de surface et structure, Unité associée 1106 du Centre national de la recherche scientifique, Université Pierre et Marie Curie, 4 Place Jussieu, 75252 Paris CEDEX 05, France

Received May 9, 1988

HÉLÈNE SUQUET. Can. J. Chem. **67**, 202 (1989).

Substantial differences are founded between the absorption properties of two Rhodesian chrysotile samples (−1 and −2), which are, in most chemical and structural aspects, highly similar. The phenanthrene and CO_2 amounts adsorbed are much less important on chrysotile-2 than on chrysotile-1. This indicates that chrysotile-2 has fewer basic surface sites. DTA and XRD results show that dry grinding and leaching produce a breakdown of the chrysotile structure, yield amorphous silica, and lower the temperature of the dehydroxylation peak. The dehydroxylation peaks of chrysotile-1 and -2 are really doublets. As the low-temperature component of the dehydroxylation peak is greater in chrysotile-2 than in chrysotile-1, the chrysotile-2 contains more ground and (or) leached fibers than chrysotile-1 and consequently shows weaker absorption properties.

Key words: chrysotile, leaching, phenanthrene adsorption.

HÉLÈNE SUQUET. Can. J. Chem. **67**, 202 (1989).

On a observé des différences importantes dans les propriétés d'absorption de deux échantillons de chrysotile Rhodésiens (−1 et −2) qui sont, par leurs aspects chimiques et structuraux, très semblables. Les quantités de phénanthrène et de CO_2 qui sont adsorbées sur la chrysotile-2 sont beaucoup plus faibles que celles adsorbées sur la chrysotile-1. Ces données indiquent que la chrysotile-2 possède moins de sites basiques. Les résultats obtenus par ATD et par DRX montrent que le broyage à sec ainsi que la lixiviation provoquent un effondrement de la structure de la chrysotile qui conduit à de la silice amorphe et à un abaissement de la température du pic de déhydroxylation. Les pics de déhydroxylation des chrysotiles-1 et -2 sont en fait des doublets. Comme la composante basse température du pic de déhydroxylation est plus grande dans la chrysotile-2 que dans la chrysotile-1, on en conclut que la chrysotile-2 contient plus de fibres broyées et (ou) lixiviées que la chrysotile-1 et que, en conséquence, elle fait preuve de propriétés d'adsorption plus faibles.

Mots clés : chrysotile, lixiviation, adsorption de phénanthrène.

[Traduit par la revue]

Can. J. Chem. Downloaded from www.nrcresearchpress.com by 122.72.124.2 on 09/07/12
For personal use only.

Introduction

Epidemiological studies have clearly shown that for smokers exposed to asbestos, the risk of bronchopulmonary cancer is strongly raised (1, 2). Carcinogenic compounds, in particular certain polycyclic aromatic hydrocarbons (PAH), are present in cigarette smoke. These observations have led several authors to study the adsorption properties of asbestos towards PAH (3–5). Recently, an in-depth study has been carried out on the adsorption of PAH on several solids having an electron-donor character, especially a sample of Rhodesian chrysotile (chrysotile-1), provided by the Union Internationale Contre le Cancer (UICC) in 1980 (6–8). In chrysotile (Fig. 1), electron-donor sites derive from (*i*) OH groups in low coordination located at crystal edges, and (*ii*) external OH groups bearing a negative charge due to the existence of isomorphic substitutions or cationic vacancies.

In an attempt to reproduce the adsorption isotherm of one PAH, namely phenanthrene, on another sample of Rhodesian chrysotile (chrysotile-2), also provided by the UICC, we obtained much lower values for the adsorbed quantities than had been observed with chrysotile-1. Hence we looked for reasons to justify this weaker surface reactivity of chrysotile-2 as compared to chrysotile-1. We studied the adsorption properties of chrysotile-2, not only with respect to phenanthrene, but also in relation to CO_2, another molecule capable of fixing itself on the basic sites present on the surface of chrysotile. In addition, using DTA curves, we investigated the adsorption properties of the chrysotile samples in relation to fiber characteristics and to the modification of these charcteristics with surface treatments (grinding and leaching).

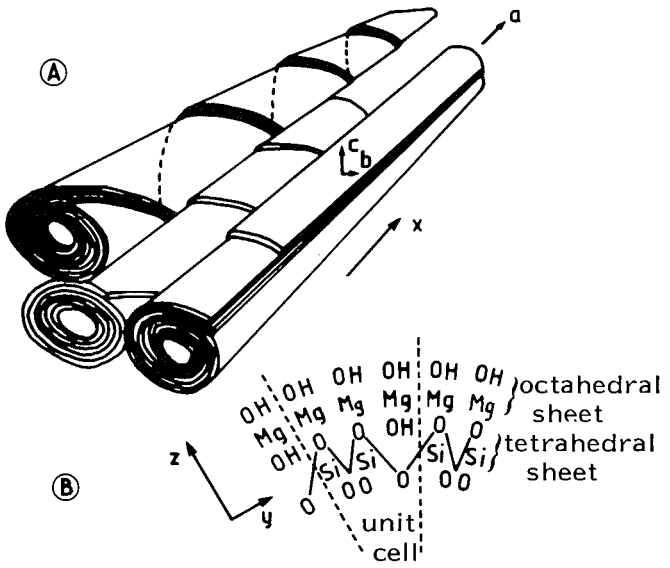


FIG. 1. Scheme of chrysotile structure.

Materials and methods

(a) Materials

The two samples of UICC chrysotile have a similar chemical composition, which is close to the theoretical composition (Table 1). Sample 1 contains about 30% more Al than sample 2 but its localization and its effect on the charge density are unknown. As there was not enough chrysotile-1 left, the charge was only determined in chrysotile-2: 1.7 electron/nm^2 (9). Moreover, Table 1 also indicates that there is a little more water in chrysotile-2 than in chrysotile-1. No

TABLE 1. Chemical composition of chrysotile samples

	SiO_2	Al_2O_3	FeO	Fe_2O_3	CaO	MgO	Na_2O	Weight loss (1030°C)
Chrysotile-1 (40% RH)	38.64	1.58	0.43	2.18	0.28	41.81	0.09	14.98
Chrysotile-2 (40% RH)	38.18	1.09	0.39	2.21	0.28	42.24	0.11	15.45
Theoretical values for $Mg_3Si_2O_5(OH)_4$	43.37					43.62		12.99
Values frequently observed	38–42	0–2	0–3	0–5	0–2	38–42	0–1	12–14

trace of nemalite, a fibrous brucite impurity of chrysotile, was found in the two chrysotile samples by IR, DTA, and X-ray diffraction (XRD). The two asbestos samples contain a black impurity, magnetite, which has been observed by XRD and by electron microscopy (SEM and TEM).

The chrysotile-1 and -2 have specific areas of 24 and 18 $m^2\ g^{-1}$ respectively.

Unlabeled phenanthrene, ^{14}C-marked phenanthrene, and xylene were supplied by Aldrich, Amersham, and Merck respectively.

(b) Methods

The adsorption properties were carried out on the bulk chrysotile-2.

Adsorption isotherm of phenanthrene

The chrysotile-2 was pre-washed twice with hot benzene to remove adsorbed organic impurities. Then it was dried under N_2 at 80°C and afterwards maintained under 40% relative humidity (RH).

The initial solution of PAH was obtained by mixing ordinary and radioactive phenanthrene in xylene to obtain a solute concentration varying between 2×10^{-3} and 30×10^{-3} mol L^{-1}. Twenty millilitres of the initial solution was brought into contact with 500 mg of chrysotile, the other 20 mL being kept as the standard solution. The slurry and the standard solution were shaken in a container maintained at 20°C for 18 h, to reach the adsorption equilibrium. The solutions were centrifuged for 10 min. Then, 1 mL of each solution (standard and supernatant) was mixed with 10 mL of scintillating liquid (Lumagel) and α-radioactivity was measured. Using the remainder method, the concentration at equilibrium (C_{eq}) and the absorbed quantity of phenanthrene (Q_a) were determined.

Three experiments were carried out for each initial concentration, and the precision is about 2% for C_{eq} and 5% for Q_a values in relation to the very weakly sorbed quantities.

Adsorption of CO_2

The adsorption of CO_2 was carried out using a Setaram microbalance model Mtb-10-8. For this test, the equilibrium states were always considered to have been achieved when the weight and the pressure were constant. The sample (100 mg) was desorbed under vacuum (10^{-4} Torr; 1 Torr = 133.3 Pa) to determine the anhydrous weight w_0. Then CO_2 (140 Torr) was introduced into the microbalance and the adsorption was achieved after 15 h. The sample was desorbed (10^{-4} Torr) until the equilibrium state (weight w) was reached. The amount of chemically sorbed CO_2 is given by $w - w_0$.

Grinding of chrysotile

Chrysotile-2 (200 mg) was severely hand ground for 15 min in an agate mortar. TEM examination indicated that chrysotile-2 had lost its silky appearance. The fibrils were very short (0.05–0.2 μm) and often agglomerated into an amorphous and shapeless material (10).

Leaching of chrysotile

The leaching was performed according to two operative methods. A partial leaching was obtained by treating the fibers at room temperature in non-stirred oxalic acid solution (0.05 mol L^{-1}) for 48 h (11). A total leaching was obtained by treating chrysotile at 50°C in 6 mol L^{-1} HCl–isopropanol solution, with stirring, for 56 h (12, 13). Thereafter the samples were thoroughly washed with hot water and dried at 80°C.

The amounts of magnesium and silicon remaining after leaching were determined by electron emission spectroscopy, and the rates of leaching (ratio of extracted Mg to initial Mg) were calculated as about 20% with oxalic acid and 100% with HCl.

Characterization of the two chrysotile samples

The X-ray diagrams (XRD) were obtained using a D500 Siemens diffractometer (Cu K_α radiation). The infrared spectra (IR) were recorded using a double beam Perkin–Elmer spectrometer 580B equipped with a data station. The KBr discs were prepared from a mixture of 150 mg KBr and 1 mg of chrysotile.

The surface areas of the fibers were determined from N_2 adsorption (BET method). The samples were initially heated at 40°C, under 10^{-4} Torr, for 16 h.

Thermogravimetric analyses (TGA) of chrysotile fibers (5 mg) were carried out under air and at a scanning rate of 5°C/min, using the Setaram Mtb-10-8 microbalance. Differential thermal analyses (DTA) were obtained with a micro-DTA M_4 Setaram at a scanning rate of 10°C/min in air, using 5 mg of fibers. The samples used for TGA and DTA were maintained under 40% RH.

Results and discussion

(A) Adsorption properties

Phenanthrene adsorption

The adsorption isotherm of phenanthrene on chrysotile-2 (Q_a vs. C_{eq}) is illustrated in Fig. 2a. This curve has an S shape, like the adsorption isotherm of phenanthrene on chrysotile-1 previously published (6), and reveals the presence of lateral interactions between adsorbed molecules (14). However, the quantities of phenanthrene adsorbed by chrysotile-2 are smaller, about 12 times less, than chrysotile-1 on the plateau (10 μmol g^{-1} vs. 118 μmol g^{-1}). As the phenanthrene molecules are adsorbed on the basic surface sites of the fibers, these curves show that there are fewer active surface sites in chrysotile-2 than in chrysotile-1.

The effect of water on the adsorption properties of chrysotile-2 is illustrated in Fig. 2: curves 2a and 2b correspond to fibers stored under 40% RH and 10% RH respectively and curve 2c relates to fibers dried in a stream of N_2 at 80°C and to xylene dried over zeolites. For this experiment the adsorption was carried out in a glove-box under an N_2 atmosphere. Comparison of the three curves of Fig. 2 shows that the amounts of adsorbed phenanthrene are greater when the samples contain less humidity. These results confirm the poisoning effect of water molecules for this PAH adsorption (6, 7). Besides, as the chrysotile-2 fixed only very small quantities of phenanthrene, it was necessary for precise analyses to increase the solid/liquid ratio from 5 (Fournier and Pezerat technique, refs. 6 and 7) to 25. In doing so, the precision is improved but water amounts introduced into the system are increased and, consequently, the competition of the adsorption between water and phenanthrene is enhanced.

CO_2 adsorption

The chrysotile-2 chemisorbs 0.52 mol CO_2 per nm^2 at a

Can. J. Chem. Downloaded from www.nrcresearchpress.com by 122.72.124.2 on 09/07/12
For personal use only.

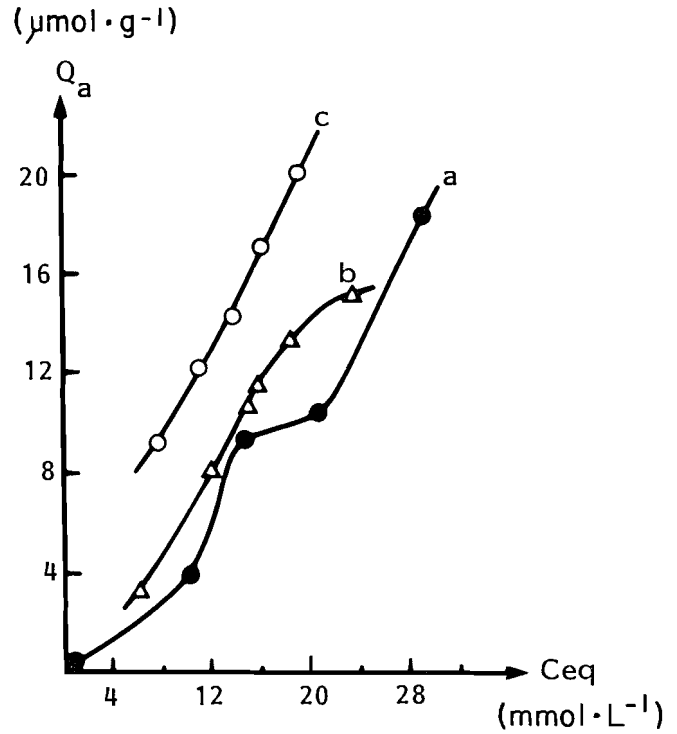


FIG. 2. Adsorption isotherm of phenanthrene on chrysotile-2: (a) chrysotile stored under 40% RH; (b) chrysotile stored under 10% RH; (c) chrysotile treated by a stream of N_2 at 80°C and xylene dried over zeolites.

pressure of 140 Torr. Under the same conditions, chrysotile-1 was observed to chemically adsorb 0.94 mol CO_2 per nm^2 (15). If a CO_2 molecule is supposed to be sorbed on a basic site (OH group acting as an electron-pair donor), the number of basic sites on the chrysotile-2 surface may be estimated to be about 45% lower than on the chrysotile-1. This result may partially explain the weaker affinity of chrysotile-2 for phenanthrene.

Water content

The fractional weight losses observed upon heating samples of chrysotile-1 and -2 in air are illustrated in Fig. 3, as a function of temperature (5°C/min). The TGA curves obtained are comparable to those reported by other authors (16–18). These curves exhibit three distinct portions corresponding to removal of residual water (up to about 370°C), dehydroxylation of fibers whose structure was modified by a surface treatment (up to about 600°C), and dehydroxylation of normal chrysotile fibers in the range 600–780°C. At 800–820°C well-crystallized forsterite, Mg_2SiO_4, and amorphous silica are produced. As the two initial samples do not contain nemalite or carbonate impurities, the second portion of the curves accounts for the loss due to water alone.

The TGA curves (Fig. 3) also show that, under 40% RH, chrysotile-2 contains more physisorbed water (about 36%) than chrysotile-1. As water is a poison for phenanthrene adsorption, chrysotile-2 adsorbs less phenanthrene than chrysotile-1, as previously observed.

(b) Characteristic properties of chrysotile-1 and -2

The preceding results show that two samples having the same origin (Rhodesia) but belonging to different lots exhibit adsorption properties that are *quantitatively* different. As the surface reactivity of minerals is strictly related to their surface state, further investigations were carried out to determine the characteristic properties of the two samples.

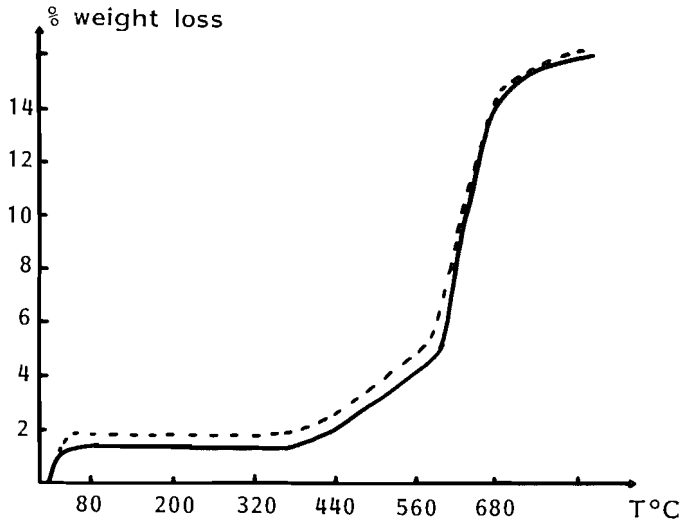


FIG. 3. Weight loss of the two samples of chrysotile fibers stored under 40% RH as a function of temperature in air heating (5°C/min): (—), chrysotile-1; (---), chrysotile-2.

IR absorption spectra

The IR absorption spectra of chrysotile-1 and -2 are similar and do not permit distinction between the surface states of the two lots. The frequencies of the vibrations agree with those reported previously (13, 16, 19–21). The intensities of some vibrations are similarly modified for the two samples, indicating that the fiber structure is slightly damaged (9).

Structure

The X-ray powder diagrams of chrysotile-1 and -2 are similar and indicate that the asbestos is mainly clinochrysotile. Furthermore, TEM examination shows that both chrysotiles have the same silky morphology and similar fiber lengths (10).

Differential thermal analysis

Typical DTA curves for chrysotile exhibit (*i*) a broad shallow endotherm below 150°C due to the removal of physisorbed water; (*ii*) a large endotherm peak at 650°C ± 20°C due to dehydroxylation; (*iii*) an exothermic reaction with a sharp peak at 810°C ± 10°C related to the crystallization of forsterite (17, 18, 22, 24).

The DTA curves of the Rhodesian chrysotiles show a significant difference: the 650°C dehydroxylation peak is really a doublet (Fig. 4). Chrysotile-1 shows a low-temperature component (660°C) that is less important than the high-temperature one (688°C) (Fig. 4A). In chrysotile-2, the two components (low and high temperature) are similar. This doublet phenomenon was first observed by Martinez (22) in a mixture of two samples of the same fiber that had been subjected to different degrees of intensive grinding in a ball mill.

We then tried to determine whether these observed doublet peaks correspond to two fiber morphologies (grinding) or to some other phenomenon such as leaching.

(i) Influence of dry grinding on DTA results. Chrysotile-2, strongly hand ground, becomes a dark grey powder because the size reduction results in a homogeneous distribution of the magnetite (the black impurity present in this sample). The XRD

Can. J. Chem. Downloaded from www.nrcresearchpress.com by 122.72.124.2 on 09/07/12
For personal use only.

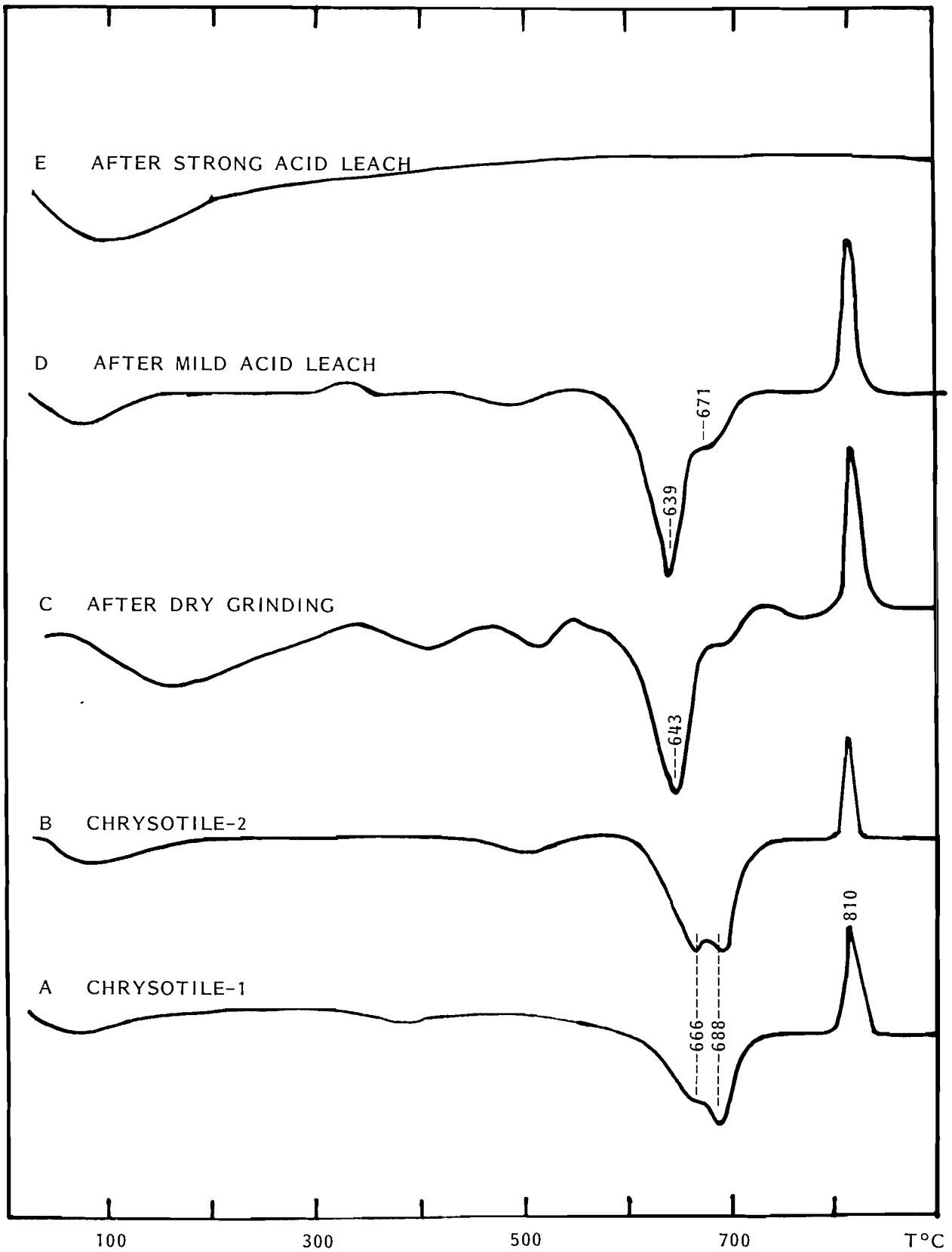


FIG. 4. DTA curves of the Rhodesian chrysotile samples (stored under 40% RH).

Can. J. Chem. Downloaded from www.nrcresearchpress.com by 122.72.124.2 on 09/07/12
For personal use only.

Can. J. Chem. Downloaded from www.nrcresearchpress.com by 122.72.124.2 on 09/07/12
For personal use only.

does not exhibit any of the characteristic reflections of the chrysotile structure. The crystalline network of the fibers is broken down and amorphous silico-magnesia compounds are formed upon severe dry grinding (25). We verified that chrysotile-2, heated at 600°C for 4 h in air, yields an amorphous material with the same appearance when viewed by XRD and IR. This suggests that the energy produced by intensive dry grinding is similar to increasing the fiber temperature.

The DTA curve of dry ground chrysotile-2 (Fig. 4C) confirms the presence of (*i*) a large amount of surface water (broad endotherm at approximately 150°C), (*ii*) magnetite (exotherm peak at 346°C), and (*iii*) carbonate species (endotherm peaks at about 410 and 520°C).

The exotherm due to the magnetite oxidation is not observable on the DTA curve of the initial samples (Fig. 4A,B) because the thermal effect is weak and the magnetite particles have large dimensions (0.5–0.7 μm). The presence of the carbonate species in the dry ground sample has been confirmed by IR study (large band at about 1410 cm^{-1}) (10). These carbonate species probably result from a fixation of atmospheric carbon dioxide during the grinding. Thus grinding chrysotile leads to a decrease of the particle size of magnetite and fibers and to a fixation of water and CO_2 present in the ambient atmosphere.

The major part of the sample dehydrates at 643°C, i.e., 23°C below the low-temperature component of the untreated chrysotile-2. The high-temperature component stays at the same temperature (688°C), but it appears considerably reduced. Thus the dehydration of asbestos has been facilitated by a severe dry grinding. As well, decreasing the particle size yields an increase of the rate of dehydration as well as in the peak height of the exotherm at 810°C. The particle size has already been illustrated and discussed (22, 26, 27). With a small-size particle, the water is easily expelled and the dehydroxylation occurs rapidly. An X-ray amorphous phase is created, making the formation of forsterite difficult. At about 810°C, forsterite crystallizes extremely quickly, producing the large exotherm, as illustrated in Fig. 4C. With coarse particles, the water is expelled with difficulty and forsterite formation and dehydroxylation occur more or less at the same time. At about 810°C, little material remains to crystallize into forsterite, so that the height of the exotherm peak is reduced for the initial chrysotile (Fig. 4B).

(ii) Influence of leaching on DTA results. A great deal of work has been done on acid attack on chrysotile (7, 11–13, 21, 23, 28, 29). According to these authors, strong acid attack leaves the fibrous morphology of the mineral intact and produces an amorphous silica gel. The hydrated silica residue is fragmented and partially transformed into microparticles, which explains the increase in the specific area of the leached asbestos fibers.

Chrysotile-2 treated with oxalic acid or HCl yields either a partially leached chrysotile (20%) or a totally leached chrysotile (100%).

The lattice of the 20% leached chrysotile has been partially degraded. On its X-ray diagram the characteristic reflections of the chrysotile are still observable but they are broad and diffuse. The general shape of the DTA curve is retained (Fig. 4D). However, the presence of amorphous hydrated silica is indicated by an increase in surface water (endotherm below 150°C). The shift towards lower temperatures of the dehydroxylation peaks, 639 and 671°C instead of 666 and 688°C for the initial chrysotile-2, indicates that acid attack (like dry grinding) damages the structure of the asbestos fibers, which then dehydroxylate more easily.

The 100% leached chrysotile is transformed into amorphous hydrated silica. Its DTA trace (Fig. 4E) shows, apart from a broad shallow endotherm below 150°C due to the removal of water, virtually no thermal effects at the sensitivity used. There is no crystallization of the silica.

Conclusion

The samples of Rhodesian chrysotile-1 and -2 provided by UICC exhibit quantitatively different adsorption properties. The adsorption of phenanthrene and CO_2 molecules is reduced in sample 2 as compared to sample 1. This illustrates that the chrysotile-2 has fewer basic sites on its surface, thus a weaker electrostatic surface field. Therefore any action damaging the surface active sites, such as dry grinding or leaching, may explain the difference between the two samples of chrysotile.

Dry grinding gives amorphous silico-magnesia compounds, which rapidly fix water and carbonate species, while acid attack yields hydrated amorphous silica. The two treatments decrease the particle size and, therefore, the dehydroxylation temperature. As the low-temperature component of the dehydroxylation peak is greater in chrysotile-2 than in chrysotile-1, it can be concluded that chrysotile-2 contains more damaged surface fibers than chrysotile-1.

As dry grinding and acid leaching reduce the particle size and increase specific area, adsorbed quantities of polycyclic aromatic hydrocarbons should be greater for the modified fibers of chrysotile than for the initial ones. This study, showing that the adsorbed amounts are smaller for chrysotile-2, which contains more damaged fibers, concludes that most of the active sites created by the surface treatments are immediately poisoned by molecules present in the atmosphere (water, CO_2...). Consequently a chrysotile with damaged fibers should possess smaller biological activity.

Acknowledgements

We wish to thank J. Fournier for helpful discussions and H. Pezerat for critically reviewing this manuscript.

1. I. J. Selikoff, E. C. Hammond, and J. Churg. J. Am. Med. Assoc. **204**, 106 (1968).
2. I. J. Selikoff, H. Seidman, and E. C. Hammon. J. Natl. Cancer Inst. **65**, 507 (1980).
3. J. S. Harington. Ann. N.Y. Acad. Sci. **132**, 31 (1965).
4. F. J. C. Roe, M. A. Walters, and J. S. Harington. Int. J. Cancer, **1**, 491 (1966).
5. J. Hilborn, R. S. Thomas, and R. C. Lao. Sci. Environ. **3**, 129 (1974).
6. J. Fournier and H. Pezerat. J. Chim. Phys. **79**, 589 (1982).
7. J. Fournier and H. Pezerat. Environ. Res. **41**, 276 (1986).
8. J. Fournier. Thèse de Doctorat, Univ. P. et M. Curie, Paris, France. 1987.
9. H. Suquet, C. Malard, J. Fournier, and H. Pezerat. Bull. Soc. Miner. **110**, 711 (1987).
10. H. Suquet. Clays Clay Miner. Submitted.
11. J. H. Thomassin, J. Goni, P. Baillif, J. C. Touray, and M. C. Jaurand. Phys. Chem. Miner. **1**, 385 (1977).
12. J. J. Fripiat and E. Mendelovici. Bull. Soc. Chim. Fr. **2**, 483 (1968).
13. F. Pacco, L. Van Gangh, and J. J. Fripiat. Bull. Soc. Chim. Fr. **7–8**, 1022 (1976).
14. C. H. Giles. Surf. Sci. **11**, 143 (1981).
15. L. Bonneau, H. Suquet, C. Malard, and H. Pezerat. Environ. Res. **41**, 251 (1986).
16. C. Jolicoeur and D. Duchesne. Can. J. Chem. **59**, 1521 (1981).

17. A. A. HODGSON. Asbestos. Vol. 1. John Wiley & Sons, New York. 1979. Chap. 3.
18. S. SPIEL and J. P. LEINEWEBER. Environ. Res. **2**, 166 (1969).
19. V. C. FARMER. The infrared spectra of minerals. Mineralogical Society, London. 1974.
20. S. YARIV and L. HELLER-KALLAI. Clays Clay Miner. **23**, 145 (1975).
21. M. J. LUYS, G. DE ROY, E. F. VANSANT, and F. ADAMS. J. Chem. Soc. Faraday Trans. 1, **78**, 3561 (1982).
22. E. MARTINEZ. Am. Mineral. **46**, 901 (1961).
23. C. BLEIMAN and J. P. MERCIER. Bull. Soc. Chim. Fr. **3–4**, 529 (1975).
24. A. W. NAUMANN and W. H. DRESHER. Am. Mineral. **51**, 1200 (1966).
25. E. PAPIRER and P. ROLAND. Clays Clay Miner. **29**, 161 (1981).
26. M. C. BALL and H. F. W. TAYLOR. Mineral. Mag. **33**, 467 (1963).
27. G. W. BRINDLEY and R. HAYAMI. Mineral. Magn. **35**, 189 (1965).
28. Z. JOHAN, J. GONI, C. SARCIA, G. BONNAUD, and J. BIGNON. Adv. Org. Geochem. Proc. 6th Int. Meeting, Paris, 883 (1973).
29. E. PAPIRER, G. DOVERGNE, and P. LEROY. Bull. Soc. Chim. Fr. **5–6**, 651 (1976).

Can. J. Chem. Downloaded from www.nrcresearchpress.com by 122.72.124.2 on 09/07/12
For personal use only.

Abietane diterpenes with antibiotic activity from the flowers of *Salvia canariensis*. Reaction of galdosol with diazomethane

ANTONIO G. GONZÁLEZ,[1] LUCIA S. ANDRÉS, JUAN R. HERRERA, JAVIER G. LUIS, AND ANGEL G. RAVELO

Centro de Productos Naturales Orgánicos Antonio González, C.S.I.C., Universidad de La Laguna, 38206 Tenerife, Canary Islands, Spain

Received July 13, 1988

ANTONIO G. GONZÁLEZ, LUCIA S. ANDRÉS, JUAN R. HERRERA, JAVIER G. LUIS, and ANGEL G. RAVELO. Can. J. Chem. **67**, 208 (1989).

The new diterpenes canariquinone (**9**), rosmaquinone (**10**), and 11-acetoxycarnosic acid (**6**), together with the already known 7-ethoxyrosmanol (**1**), 7-methoxyrosmanol (**2**), and rosmanol (**3**), were isolated from the flowers of *Salvia canariensis*. The structure of the new substances was established by a combination of chemical and spectroscopic means. Reaction of galdosol (**4**), isolated from the aerial part of the same plant, with diazomethane, unexpectedly gave the new homoditerpenes **15** and **16**, the structures of which were determined by spectroscopic methods. A mechanism accounting for the formation of these substances is suggested.

Key words: abietane diterpenes, *Salvia*, Labiatae, antibiotic activity, galdosol reactivity.

ANTONIO G. GONZÁLEZ, LUCIA S. ANDRÉS, JUAN R. HERRERA, JAVIER G. LUIS et ANGEL G. RAVELO. Can. J. Chem. **67**, 208 (1989).

Les nouveaux diterpénoïdes, la canariquinone (**9**), la rosmaquinone (**10**) et l'acide 11-acétoxycarnosique (**6**), avec le 7-éthoxyrosmanol (**1**), le 7-methoxyrosmanol **2** et le rosmanol (**3**), des composés connus antérieurement, ont été isolés des fleurs de la *Salvia canariensis*. On a établi les structures des nouvelles substances par des moyens chimiques et spectroscopiques. On a fait réagir le diazométhane avec le galdosol (**4**), isolé de la partie aérienne de la même plante, et on a obtenu les nouveaux homoditerpènes **15** et **16**, produits pas prévus, dont on a établi les structures par des méthodes spectroscopiques. On propose un mécanisme qui explique la formation de ces composés-ci.

Mots clés : diterpénoïdes abiétanes, *Salvia*, Labiatae, activité antibiotique, réactivité de galdosol.

Can. J. Chem. Downloaded from www.nrcresearchpress.com by 122.72.124.2 on 09/07/12
For personal use only.

Introduction

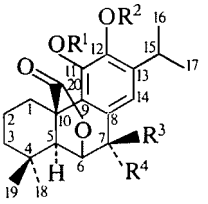
There are some 500 species of the genus *Salvia*, a member of the Labiatae family, extensively distributed throughout the world. Since ancient times, many species of this genus have aroused interest and have frequently been used for medicinal purposes. At present, they are used in the pharmaceuticals (1, 2), cosmetics, and preserving industries.

We have reported the isolation of the diterpenes galdosol (3) and arucatriol (4) from the aerial parts of *Salvia canariensis* L., a plant endemic to the Canary Islands; of deoxocarnosol-12-methyl ether, salvicanol, and 6α-hydroxydemethylcryptojaponol from the roots of the same plant; (5) and rosmanol, 11,12-dimethoxy-abieta-6,8,11,13-tetraen-20-oic acid methyl ester, rosmanoyl carnosate, 7-oxocarnosic acid, 6-oxo-7β-hydroxycarnosic acid, and 6-oxo-7α-hydroxycarnosic acid from its flowers (6, 7). All the latter compounds were isolated in acetate form from previously acetylated fractions of an acetone extract.

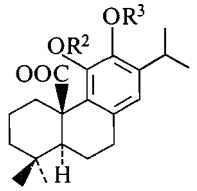
We here report the isolation of five diterpenes from less polar fractions of the untreated acetone extract of the flowers of *S. canariensis*, as well as the unexpected formation of two new homoditerpenes when galdosol was reacted with diazomethane.

Discussion

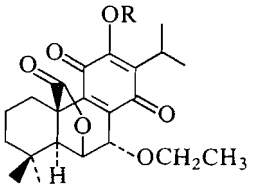
The least polar of the compounds was identified as 7-ethoxyrosmanol (**1**) from the following data. High resolution electron impact mass spectrometry (hreims) gives the molecular formula, $C_{22}H_{30}O_5$. The ir spectrum shows absorptions for lactone (1740, 1240 cm^{-1}), aromatic, ether, and phenol groups. In the ^1H nmr spectrum taken in $CDCl_3$ are signals typical of an aromatic isopropyl, two angular methyls, one aromatic proton, two broad singlets, interchangeable with D_2O, assigned to two phenolic protons, an AB system as two doublets of one proton



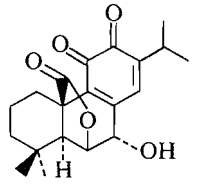
1 $R^1 = R^2 = R^3 = H$; $R^4 = OEt$
2 $R^1 = R^2 = R^3 = H$; $R^4 = OMe$
3 $R^1 = R^2 = R^3 = H$; $R^4 = OH$
4 $R^1 = R^2 = H$; $R^3, R^4 = O$
5 $R^1 = R^2 = Me$; $R^3 = H$; $R^4 = OMe$



6 $R^1 = R^3 = H$; $R^2 = Ac$
7 $R^1 = H$; $R^2 = R^3 = Ac$
8 $R^1 = Me$; $R^2 = R^3 = Ac$



9 R = H
9*a* R = Ac



10

each, attributable to H-7 and H-6, respectively, and a proton singlet corresponding to H-5. This spectrum is very similar to that of rosmanol (**3**) (6, 8), the main difference being that **1** has an extra quartet of two protons at δ 3.84 and a three-proton triplet at δ 1.33 assignable to a $-OCH_2CH_3$ group. Double resonance experiments showed them to be coupled. All the spectral data of this product are completely superimposable upon those given in the literature (9) for 7-ethoxyrosmanol (**1**).

For the second product eluted, **2**, hreims gives the molecular formula, $C_{21}H_{28}O_5$. The ir spectrum has bands for lactone, phenol, and aromatic groups. The ^1H nmr spectrum is very similar to that of rosmanol, differing in that it shows a methoxy group as three singlet protons at δ 3.66. When **2** was treated

[1]Author to whom correspondence may be addressed.

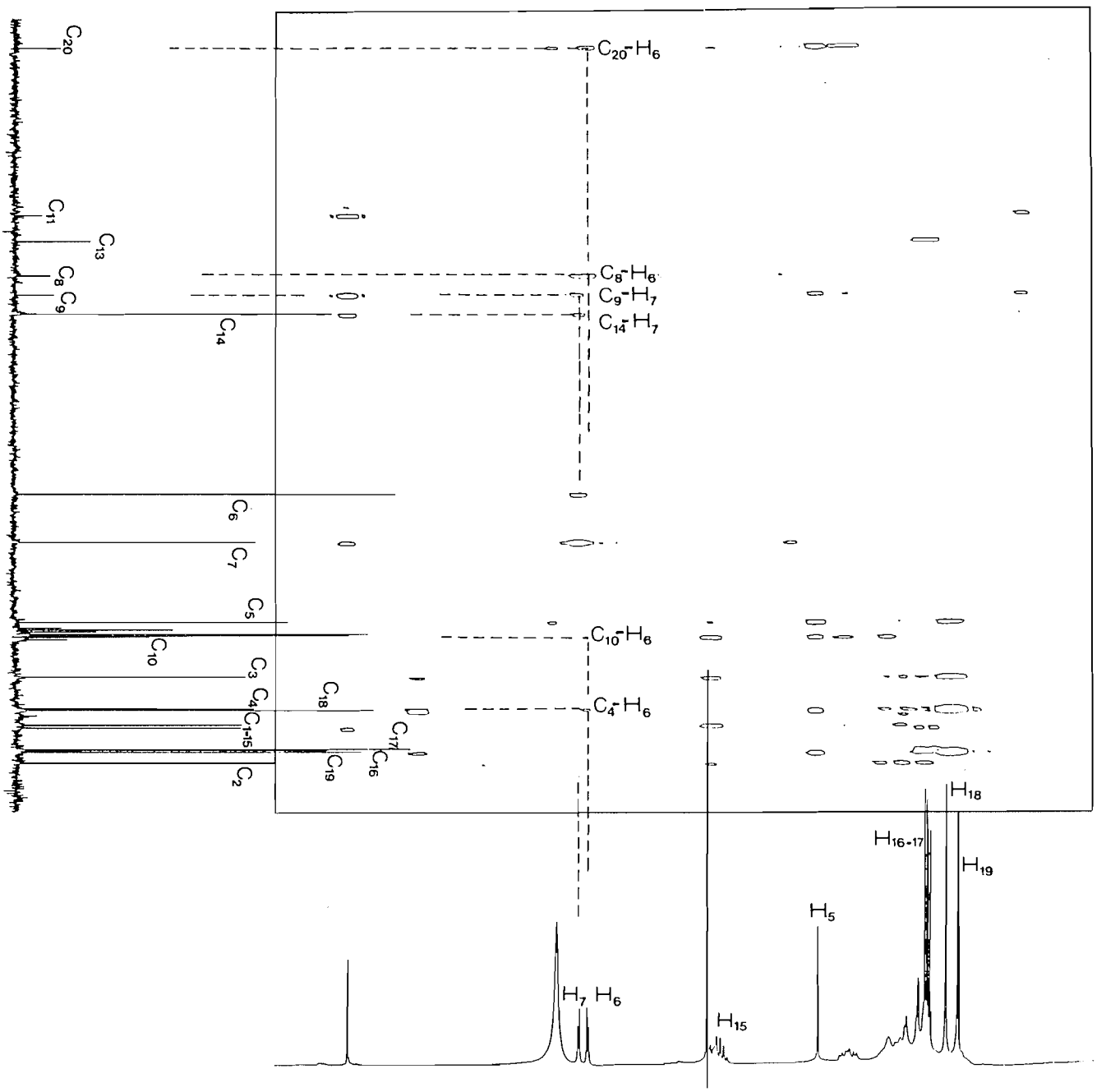


FIG. 1. Long-range $^{13}C-^{1}H$ correlation for rosmanol **3** in CD_3OD.

with methyl sulphate in acetone and potassium carbonate, a trimethoxy derivative was obtained, indicating that the free hydroxy groups in the original product are phenolic and that the methoxy group should, therefore, be situated on C-7. All the spectral data of this product are superimposable upon those given (9) for the 7-methoxy derivative of rosmanol.

The ^{1}H nmr spectrum of the trimethoxy derivative **5** is totally superimposable upon that given in the literature (10) for the 7β-methoxy isomer. The structure for this isomer should be corrected, since the absolute stereochemistry of rosmanol has been unequivocally determined by Nakatani and Inatani (11) and by ourselves (6) by means of X-ray diffraction studies, and the chemical shifts of H-6 and H-7 in **5** correspond to those of rosmanol and not to those of epirosmanol (11), in which H-6 and H-7 appear superimposed as a broad singlet at δ 4.72.

The benzylic H-7 should appear further downfield than the H-6 but, in the ^{1}H nmr of rosmanol (6, 8) and derivatives with different substituents on C-7, the proton that changes its chemical shift is at higher field and should thus be assigned to the H-7 while the chemical shift of the other proton is virtually unaltered (and should therefore be assigned to H-6). To clear up this apparent contradiction once and for all, $^{1}H-^{1}H$, ^{13}C and ^{1}H, and long-range $^{13}C-^{1}H$ COSY experiments were carried out. As seen in Fig. 1, long-range coupling is present between H-6 and C-4, C-8, C-10, and C-20, and also between H-7 and C-9 and C-14, determining the lower chemical shift as that of the H-7.

In an earlier paper (6), in order to correlate rosmanol (**3**) and galdosol (**4**), the latter was methylated with dimethyl sulphate to give the corresponding dimethyl derivative, **11**. In an attempt to obtain larger amounts of the same product, galdosol (**4**) was treated with excess diazomethane in ether but did not in fact

Can. J. Chem. Downloaded from www.nrcresearchpress.com by 122.72.124.2 on 09/07/12
For personal use only.

Can. J. Chem. Downloaded from www.nrcresearchpress.com by 122.72.124.2 on 09/07/12
For personal use only.

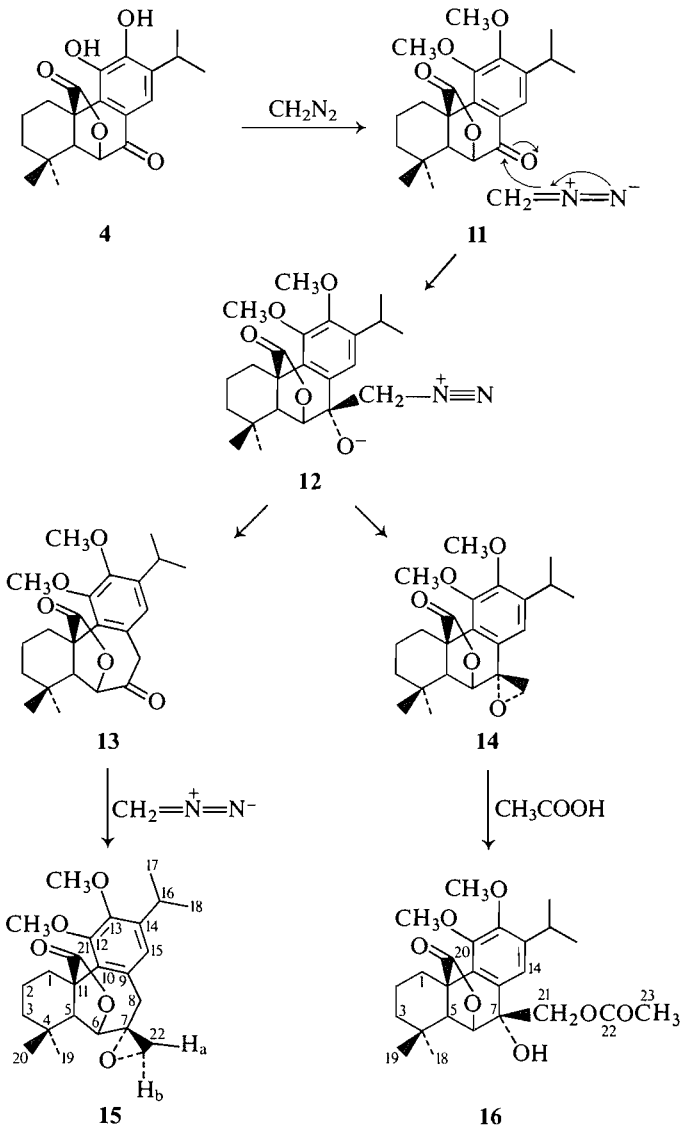
yield **11**, giving instead a mixture of products **15** and **16**, which was then subjected to column chromatography. Product **15** has the molecular formula $C_{24}H_{32}O_5$ under hrms. In its ir spectrum, absorptions for lactone and ether groups are seen. The most characteristic signals in the ^1H nmr spectrum are two one-proton singlets at δ 2.88 and 4.21 assigned to H-5 and H-6, respectively, indicating that the bridgehead proton and that of the lactone closure form a 90° angle (which is confirmed by a Dreiding stereo model); there is also an AB system assigned to the H-22 protons of the oxirane methylene, with the H-22a proton appearing as a doublet while the H-22b proton, also a doublet, shows long-range coupling. The H-8 protons appear as an AX system with H-8α as a doublet and H-8β as a doublet with long-range coupling. Irradiation of the H-8β proton makes its coupling with H-8α and its long-range coupling with H-22b disappear. All these data are completely in agreement with the structure proposed for **15** and with the α stereochemistry of the oxirane ring, where the low shift of the H-5 and H-8β protons is due to their being in front of the oxirane oxygen and lactone bridge, respectively. The ^{13}C nmr data are also in accordance with this structure.

Product **16** has the molecular formula $C_{25}H_{34}O_7$ (hrms). Its ir spectrum shows bands for hydroxy, lactone, ester, and ether groups. In its ^1H nmr spectrum, the most important signals are those corresponding to the H-5 and H-6 protons as two singlets, a proton interchangeable with D_2O for the hydroxy of a tertiary alcohol, and two protons of the methylene of an acetoxymethylene system as doublets with the methyl at δ 2.21. All these data are consistent with the structure proposed, **16**, and the stereochemistry assigned to C-7 accounts for H-14 being at δ 7.10 and for the H-5 being in front of the 7α OH at δ 2.25.

The formation of these products is accounted for by a well-documented process (12, 13) (Scheme 1). However, the diazomethane attack must take place on the less-hindered α face of the molecule (16). The attack on the β face could be due to anchimeric assistance of the lactone group ether bridge.

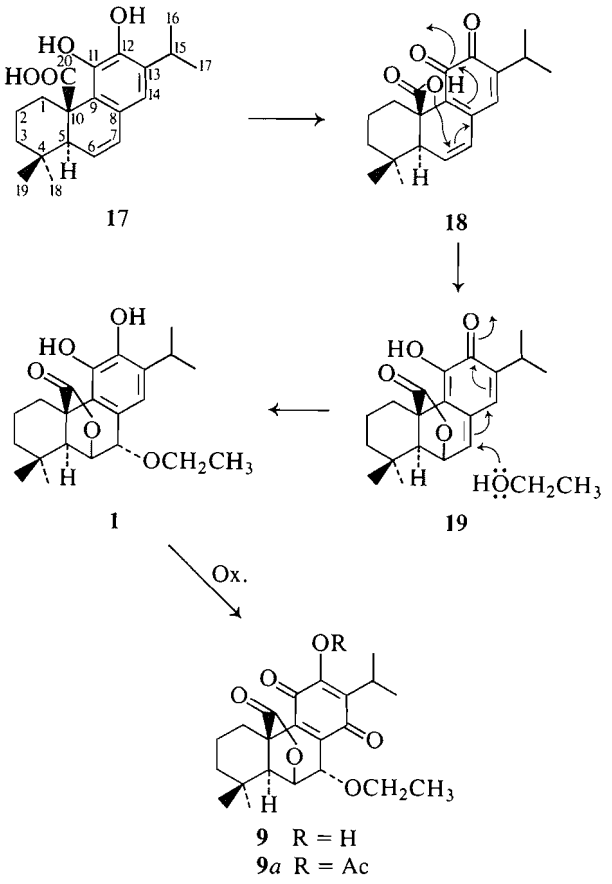
The following new products are described, in order of increasing polarity: **9** was isolated as an amorphous yellow solid. Its uv spectrum shows absorptions similar to those of royleanone (14), thus establishing the presence of an analogous chromophore. In ms, the greater mass fragment is observed at *m/z* 344, while hrms gives a formula of $C_{21}H_{28}O_4$ $[M - CO_2]^+$ with special importance being attached to the fragment at *m/z* 298, which corresponds to the loss of CH_3CH_2OH. In the ir spectrum, bands for the following are observed: hydroxy groups at 3380 cm^{-1}, lactone at 1770 cm^{-1}, quinone grouping at 1650 and 1635 cm^{-1}, and aromatic and ether groups. In the ^1H nmr spectrum, apart from signals corresponding to an isopropylic proton on an aromatic, only two angular methyls are observed, as singlets, with no methyl at C-10, which must, therefore, form part of the lactone ring. There are also signals corresponding to an ethoxy group. The H-5 proton appears as a singlet, indicating the existence of a single proton at C-6 forming a 90° angle with H-5, which puts the lactone closure at C-6. H-6 appears as a doublet coupled with another proton attributable to H-7, establishing the closure of the ethoxy group at C-7. The one-proton singlet at δ 7.06 is attributed to the phenolic hydrogen. **9** gives the aromatic monoacetate, **9***a*. All these data are in agreement with the quinone structure **9** for the product, which we have called canariquinone.

Since ethoxy compounds are very rare as natural products, it is just conceivable that diterpenoids **1** and **9** are artifacts arising from ethanol impurities in the organic solvent used in the extraction process (distilled cold acetone) and (or) in the chromatography (ethyl acetate). Other authors (15), however, have also isolated diterpene quinones with an ethoxy group on C-7 from *Salvia* species.



SCHEME 1

Diterpenoids **1** and **9** may be formed from 6,7-dehydrocarnosic acid (**17**) previously obtained in the form of its dimethyl ether from the same species (7) as shown in Scheme 2, whereby **17**, after oxidation, would give orthoquinone (**18**), which would later undergo an intramolecular nucleophile attack on C-6, on its β face, by the hydroxy group of the carboxyl acid to yield the methylene quinone **19**. This in turn, by nucleophile addition of ethanol at position 7α would give **1**, which would subsequently be oxidized to **9**. A similar sequence has been suggested by Wenkert *et al.* (16) for the formation of carnosol from carnosic acid. The stereochemistry of canariquinone at C-7 cannot be determined directly from the ^1H nmr since the dihedral angle between H-6 and H-7 is the same whether the ethoxy group is α or β, as can be seen from a Dreiding model. However, the chemical shifts of the H-6 and H-7 protons are similar to those of rosmanol, and the ethanol attack upon the methylene quinone diterpene lactone **19** should take place on the less-hindered α face of the molecule, as reported for this type of compound (16).



SCHEME 2

The structure of the next compound, **10**, was established from the following considerations: its ir spectrum shows the characteristic bands for alcohol, lactone (1770), and *o*-quinone (1660 cm^{-1}) groups, the *o*-quinone group being confirmed by the uv absorptions (270 and 402 nm). No phenol protons are visible in the ^1H nmr spectrum. This spectrum is very similar to that of rosmanol, with slight differences in the chemical shifts of the homologous signals. High resolution mass spectrometry gives the molecular formula $C_{20}H_{24}O_5$, with two hydrogen atoms less than rosmanol. All these data are in accordance with structure **10**, which was confirmed by chemical means, oxidation of rosmanol (**3**) with silver oxide (17) affording a substance with spectral constants totally superimposable upon those of **10**. We suggest the name rosmaquinone for this product.

The most polar product was established as 11-acetoxycarnosic acid (**6**) as follows: molecular formula, $C_{22}H_{30}O_5$ (hrms); ir with bands for acid (3720–2390 cm^{-1}), ester, and aromatic groups. The most characteristic signals in ^1H nmr are an isopropyl on an aromatic, an aromatic proton, an acetate methyl on an aromatic, and two angular methyls. The carboxyl group is situated on C-10 since there is no methyl on C-10 in this spectrum; in abietatriene diterpenes, the lowest-field methyl is always the C-10. All these data are consistent with structure **6** with the acetoxy group on C-11 or C-12. When **6** was treated with acetic anhydride in pyridine, the diacetate **7** was obtained with spectroscopic data superimposable on those of an authentic sample of carnosic acid diacetate. When **7** was treated with diazomethane, carnosic acid methyl ester diacetate (**8**) was obtained, also superimposable on an authentic sample.

The ^1H nmr spectra of **6** taken in py-d_5 and $CDCl_3$ show a difference of 0.20 ppm for the chemical shift of the isopropyl proton (18), H-15, and the acetoxy group was, therefore, placed at C-11.

11-Acetoxy-carnosic acid (**6**) and rosmaquinone (**10**) showed considerable antibiotic activity against the Gram (+) microorganisms, *Staphylococcus aureus* and *Bacillus subtilis* (19).

Experimental

General

High resolution elecronic impact mass spectra (hreims) were recorded on a V6-Micromass ZAB-2F spectrometer. Single scan infrared (ir) spectra were recorded on a Perkin–Elmer 681 spectrometer. Nuclear magnetic resonance (nmr) spectra were obtained on a Bruker WP-200 SY spectrometer. Tetramethylsilane was used as internal standard. Ultraviolet (uv) spectra were obtained on a Perkin–Elmer 550 SE. Melting points are uncorrected and were determined on a Kofler apparatus. Merck silica gel (0.063–0.2 mm) and Sephadex LH-20 were used for column chromatography. Analytical thin-layer chromatography (tlc) was carried out on precoated Schleicher and Schüll plates. Ultraviolet active materials were detected visually under uv lamp (254 or 350 nm). The plate was then sprayed with oleum and charred on a hot plate. *n*-Hexane, ethyl acetate, benzene, and mixtures of these were used as eluents for silica gel columns, as well as *n*-hexane/chloroform/methanol (2:1:1). Voucher plant specimens were lodged with the herbarium of the Department of Botany, Faculty of Biology, Universidad de La Laguna.

Plant extraction

The finely cut flowers of *S. canariensis* (4 kg) were extracted with distilled acetone (1 × 5 L) at room temperature. Filtering and evaporation of the solvent gave a reddish-brown extract (150 g). The extract was vacuum-chromatographed through dry column (24 × 10 cm) silica gel; 500-mL fractions were collected, using mixtures of *n*-hexane/ethyl acetate of increasing gradient. Only the fractions 2–4 were studied. The products were isolated by repetitive chromatography on silica gel and Sephadex columns.

Rosmanol (3): ^1H nmr (CD_3OD) δ: 0.87, 0.98 (each 3H, s, C-18 and C-19 Me), 1.15, 1.17 (each 3H, d, J = 7 Hz, $CH(CH_3)_2$ C-16 and C-17 Me), 2.22 (1H, s, H-5), 3.27 (1H, hept, J = 7 Hz, H-15), 3.28 (1H, bd, J = 10.48 Hz, H-1β), 4.48, 4.55 (each 1H, d, J = 3.24 Hz, H-6 and H-7), 6.80 (1H, s, H-14); ^{13}C nmr (CD_3OD) δ: 20.14 (C-2), 22.16 (C-17), 22.49 (C-19), 22.94 (C-16), 27.87 (C-15), 28.59 (C-1), 31.87 (C-18), 32.24 (C-4), 39.34 (C-3), 48.34 (C-10), 51.60 (C-5), 69.14 (C-7), 79.88 (C-6), 120.45 (C-14), 124.92 (C-9), 129.38 (C-8), 137.43 (C-13), 143.34 (C-12), 145.22 (C-11), 180.99 (C-20).

7-Ethoxyrosmanol (**1**) was isolated as a gum (8 mg) that did not crystallize: ir ($CHCl_3$): 3660, 3590, 3010, 2970, 2920, 1740, 1365, 1240, and 1040 cm^{-1}; uv (EtOH): 396, 327, and 286 nm; ^1H nmr ($CDCl_3$) δ: 0.92, 1.01 (each 3H, s, C-19 and C-18 Me), 1.22 (6H, d, J = 7 Hz, $CH(CH_3)_2$ C-16 and C-17 Me), 1.33 (3H, t, $-CH_2CH_3$), 1.99 (2H, ddd, H-2α,β), 2.28 (1H, s, H-5), 3.11 (1H, hept, J = 7 Hz, H-15), 3.84 (2H, q, CH_2CH_3), 4.36 (1H, d, J = 3.20 Hz, H-6), 4.66 (1H, d, J = 3.20 Hz, H-7), 5.59, 6.15 (each 1H, br s, 2 × Ar-O*H*), 6.79 (1H, s, H-14); hreims, m/z calcd. for $C_{22}H_{30}O_5$ (M^+): 374.2075; found: 374.2084 (100), 328 (87), 300 (29), 247 (17), 231 (24), 215 (68), 115 (24), 69 (40), 55 (51).

Methylation of 7-methoxyrosmanol (2)

Compound **2** (14.7 mg) dissolved in dry acetone was treated with anhydrous potassium carbonate (31.7 mg) and methyl sulphate (0.2 mL) and the reaction mixture stirred during 2 h, filtered, and evaporated *in vacuo*. Silica gel column chromatography gave **5** as a gum (12 mg); ir ($CHCl_3$): 3020, 2920, 2840, 1760, 1580, 1460, 1370, 1350, 1300, 1220, 1070, and 1040 cm^{-1}; hreims, m/z calcd. for $C_{23}H_{32}O_5$ (M^+): 388.2238; found: 388.2244 (100), 329 (74), 256 (32), 243 (39), 201 (31), 149 (63), 128 (20), 83 (37), 73 (31), 71 (31), 69 (70), 57 (71), 55 (90). The ^1H nmr was superimposable upon that given in the literature.

Can. J. Chem. Downloaded from www.nrcresearchpress.com by 122.72.124.2 on 09/07/12
For personal use only.

Can. J. Chem. Downloaded from www.nrcresearchpress.com by 122.72.124.2 on 09/07/12
For personal use only.

Methylation of galdosol (4) with diazomethane

Diazomethane in ether solution (15 mL) was added to 60 mg of galdosol (**4**) dissolved in ethyl ether (10 mL), and the mixture was left for 24 h at 0°C. Once the starting material had disappeared, the excess diazomethane was destroyed with acetic acid and the crude reaction product purified by chromatography, giving **15** (29.8 mg, 43.1%) and **16** (20.3 mg, 26.5%). **15** was a powder that could not be recrystallized; ir ($CHCl_3$): 3020, 2960, 1770, 1720, 1590, 1465, 1445, 1380, 1295, and 1170 cm^{-1}; ^1H nmr ($CDCl_3$) δ: 0.90 (3H, s), 1.07 (3H, s), 1.16 (3H, d, J = 7 Hz), 2.31, 4.11 (each 1H, d, J = 10 Hz, H-8α and H-8β), 2.82, 3.02 (each 1H, d, J = 4.5 Hz, H-22a and H-22b), 2.88 (1H, s), 3.24 (1H, m), 3.77 (3H, s), 3.78 (3H, s), 4.21 (1H, s), 6.54 (1H, s); ^{13}C nmr ($CDCl_3$) δ: 19.23 (t), 22.42 (q), 23.23 (q), 23.32 (q), 26.98 (d), 28.47 (t), 32.17 (q), 32.68 (s), 37.56 (t), 42.63 (t), 50.34 (d), 50.73 (s), 52.70 (t), 59.16 (s), 60.18 (q), 60.49 (q), 82.42 (d), 124.88 (d), 129.56 (s), 133.76 (s), 142.20 (s), 151.30 (s), 154.85 (s), 176.82 (s); hreims, m/z calcd. for $C_{24}H_{32}O_5$ (M^+): 400.2250; found: 400.2233 (100), 385 (2), 369 (3), 341 (5), 325 (5), 313 (6), 311 (4), 299 (3), 287 (6), 285 (4), 283 (5), 271 (6).

16 was isolated as a gum; ir ($CHCl_3$): 3020, 2960, 1770, 1740, 1600, 1465, 1450, 1390, 1380, 1325, 1285, 1215, 1170, 1110, and 1020 cm^{-1}; ^1H nmr ($CDCl_3$) δ: 0.96 (3H, s), 1.05 (3H, s), 1.20 (3H, d, J = 7 Hz), 1.33 (1H, m), 2.21 (3H, s, H-23), 2.25 (1H, s, H-5), 2.96 (1H, s, O*H*), 3.26 (1H, m), 3.27 (1H, d, J = 5.3 Hz), 3.77 (3H, s), 3.81 (3H, s), 4.07, 4.58 (each 1H, d, J = 4.90 Hz, 2 × H-21), 4.49 (1H, s, H-6), 7.10 (1H, s, H-14); hreims, m/z calcd. for $C_{25}H_{34}O_7$: 446.2303; found: 446.2342 (M^+) (3), 387 (2), 373 (100), 345 (6), 329 (6), 327 (9), 299 (6), 287 (5), 285 (6) and 259 (18).

Canariquinone (**9**) was isolated as an amorphous yellow solid (98.3 mg); ir ($CHCl_3$): 3380, 3020, 2960, 2920, 2860, 1770, 1710, 1650, 1635, 1630, 1590, 1465, 1390, 1370, 1330, 1290, 1245, 1170, 1155, 1085, 1030, 1000, 960, and 910 cm^{-1}; uv: (EtOH), 280 nm; (EtOH + MeONa), 283 nm; (EtOH + $AlCl_3$), 270, 300, and 303 nm; (EtOH + $AlCl_3$ + HCl), 277, 310, and 363 nm; ^1H nmr ($CDCl_3$) δ: 0.87, 1.00 (each 3H, s, 2 × Me), 1.18, 1.20 (each 3H, d, J = 7.0 Hz, $CH(CH_3)_2$ C-16 and C-17 Me), 1.23 (3H, t, -OCH_2CH_3), 2.23 (1H, s, H-5), 3.14 (1H, hept, J = 7 Hz, H-15), 3.80, 4.00 (each 1H, q, -OCH_2CH_3), 4.39, 4.56 (each 1H, d, J = 2.5 Hz, H-6 and H-7), 7.06 (1H, s, ArO*H*); hreims, m/z calcd. for $C_{22}H_{28}O_6$ ($M^+ - CO_2$): 344.1985; found: 344.1989 (9), 300 (42), 298 ($M^+ - CO_2 - CH_3CH_2OH$) (58), 283 (10), 275 (13), 265 (4), 258 (11), 249 (2), 231 (40), 230 (27), 229 (13), 182 (12), 149 (45), 128 (17).

Treatment of **9** with acetic anhydride in pyridine gave **9*a***; ir ($CHCl_3$): 3020, 2960, 2930, 2865, 1770, 1670, 1650, 1595, 1450, 1390, 1370, 1330, 1275, 1185, 1165, 1150, 1130, 1085, 1025, 1000, 960, 940, 910, 870, and 815 cm^{-1}; ^1H nmr ($CDCl_3$) δ: 0.89, 1.01 (each 3H, s, 2 × Me), 1.17, 1.21 (3H, d, J = 7.0 Hz, $CH(CH_3)_2$ C-16 and C-17 Me), 1.19 (3H, t, -OCH_2CH_3), 2.23 (1H, s, H-5), 2.32 (3H, s, ArOAc), 3.10 (1H, hept, J = 7 Hz, H-15), 3.20 (1H, bd, H-1β), 3.80, 4.01 (each 1H, q, -OCH_2CH_3), 4.36, 4.54 (each 1H, d, J = 2.5 Hz, H-6 and H-7); hreims, m/z calcd. for $C_{24}H_{30}O_7$: 388.1884; found: 388.1968 ($M^+ - C_2H_2O$) (3), 344 (388 − CO_2) (14), 342 (14), 340 (5), 300 (56), 298 (82), 296 (13), 283 (22), 242 (29), 231 (46), 229 (28).

Rosmaquinone (**10**) was isolated as a reddish-yellow amorphous solid (7 mg); ir ($CHCl_3$): 3590, 3440, 2960, 1770, 1660, 1460, 1390, 1170, and 1060 cm^{-1}; uv (EtOH): 402, 274, and 228 nm; ^1H nmr ($CDCl_3$) δ: 0.88, 1.02 (each 3H, s, C-19 and C-18 Me), 1.11, 1.12 (each 3H, d, J = 7 Hz, $CH(CH_3)_2$ C-16 and C-17 Me), 2.05 (1H, s, H-5), 2.93 (1H, hept, J = 7 Hz, H-15), 3.21 (1H, bd, J = 10.48 Hz, H-1β), 4.40, 4.52 (each 1H, d, J = 3.24 Hz, H-6 and H-7), 6.79 (1H, s, H-14); hreims, m/z calcd. for $C_{20}H_{24}O_5$: 344.1548; found: 344.1586 (M^+) (15), 316 (25), 285 (27), 257 (48), 238 (21), 231 (27), 230 (44), 229 (38), 215 (33), 211 (13), 203 (45), 201 (48), 187 (43), 173 (21), 161 (25), 159 (21), 141 (25), 131 (22), 128 (39), 115 (57), 105 (26), 91 (66), 55 (100).

Oxidation of rosmanol (3)

Rosmanol (46 mg) dissolved in dry ether was treated with freshly prepared excess Ag_2O and stirred at room temperature for 1 h. The solution was filtered and evaporated in a vacuum to give a product (45 mg) with ir and ^1H nmr superimposable upon that of **10**.

11-Acetoxy-carnosic acid (**6**) was obtained as a white crystalline solid; mp 123°C (*n*-hexane/ethyl acetate); ir ($CHCl_3$): 3720–2390, 1740, 1680, 1605, 1560, 1450, 1430, 1410, 1380, 1360, 1325, 1290, 1230, 1190, 1115, 1080, 1050, 1035, 1020, 985, 975, 955, 935, 915, 905, 890, 860, 815, and 640 cm^{-1}; uv (EtOH): 400, 330, and 284 nm; ^1H nmr ($CDCl_3$) δ: 0.89, 0.99 (each 3H, s, 19 and 18 Me), 1.15, 1.18 (each 3H, d, J = 7 Hz, $CH(CH_3)_2$ C-16 and C-17 Me), 2.28 (3H, s, ArOAc), 2.28 (1H, m, H-5), 2.86 (3H, m, H-15 and 2 × H-7), 3.33 (1H, d_b, J = 13.8 Hz, H-1β), 6.63 (1H, s, H-14); ^1H nmr (py-d_5) δ: 0.98, 1.21 (each 3H, s), 1.22 (6H, d, J = 7 Hz), 2.25 (3H, s), 3.06 (1H, hept, H-15), 6.73 (1H, s); hreims, m/z calcd. for $C_{22}H_{30}O_5$: 374.2101; found: 374.2097 (M^+) (2), 346 (1), 332 (2), 328 (9), 314 (1), 300 (2), 286 (100), 271 (11), 243 (19), 230 (48), 218 (20), 204 (21). Treatment of **6** with acetic anhydride gave a product with spectroscopic data superimposable on those of an authentic sample of carnosic acid diacetate (**7**). Treatment of **7** in its turn with ether solution of diazomethane gave **8**, identical to an authentic sample of carnosic acid diacetate methyl ester.

Acknowledgements

This study has been partly subsidized by the AIETI (Madrid) and GAICYT Grants Nos. PB85-0171 and 0694-84. J.R.H. is indebted to the Gobierno Autonomo and CajaCanarias for a research grant. We are obliged to Dr. E. Alvarez for carrying out the 2D nmr experiments.

1. K. Bergwein. Am. Cosmet. Perfum. **83**, 41 (1968).
2. G. Scott. Chem. Br. 648 (July) (1985).
3. A. G. González, B. M. Fraga, J. G. Luis, and A. G. Ravelo. Experientia, **29**, 1471 (1973).
4. A. G. González, B. M. Fraga, J. G. Luis, and A. G. Ravelo. An. Quim. **71**, 701 (1975).
5. A. G. González, B. M. Fraga, J. R. Herrera, J. G. Luis, and A. G. Ravelo. Phytochemistry, **25**, 269 (1986).
6. A. G. González, B. M. Fraga, J. R. Herrera, A. Perales, J. G. Luis, and A. G. Ravelo. Phytochemistry, **24**, 1853 (1985).
7. A. G. González, C. M. Rodríguez, and J. G. Luis. Phytochemistry, **26**, 1471 (1987).
8. R. Inakatani, N. Nakatani, and H. Fuwa. Agric. Biol. Chem. **47**, 353 (1983).
9. M. Arisawa, T. Hayashi, K. Ohmura, K. Nagagama, M. Shimizu, N. Morita, and L. Berganza. J. Nat. Prod. **50**, 1164 (1987).
10. C. H. Brieskorn and H. J. Dömling. Arch. Pharm. (Weinheim), **302**, 641 (1969).
11. N. Nakatani and R. Inatani. Agric. Biol. Chem. **45**, 2081 (1984).
12. C. D. Gutsche. Org. React. **8**, 364 (1954).
13. J. N. Bradley, G. W. Conwell, and A. Ledwith. J. Chem. Soc. 4334 (1964).
14. W. A. Dement, B. J. Tyson, and H. A. Mooney. Phytochemistry, **14**, 2555 (1975).
15. A. Michavila, F. Fernández-Gadea, and B. Rodríguez. Phytochemistry, **25**, 266 (1986).
16. E. Wenkert, A. Fuchs, and J. C. McChesney. J. Org. Chem. **30**, 2931 (1965).
17. A. Kelecom. Phytochemistry, **23**, 1677 (1984).
18. P. V. Demarco, E. Farcas, D. Doddrell, L. Banavara, and E. Wenkert. J. Am. Chem. Soc. **5**, 5480 (1968).
19. A. G. González, T. Abad, J. A. Jiménez, A. G. Ravelo, J. G. Luis, Z. Aguiar, L. S. Tejera, M. Plasencia, and J. R. Herrera. Biochem. Syst. Ecol. In press.

Photocyclization of aryl enaminones. An efficient route to indole alkaloid synthons

DANIEL GARDETTE, JEAN-CLAUDE GRAMAIN, MARIE-EVE LEPAGE, AND YVES TROIN
Chimie et biochimie des substances naturelles, Unité associée 485, Université de Clermont-II, B.P. 45, 63170 Aubière, France

Received October 28, 1987[1]

DANIEL GARDETTE, JEAN-CLAUDE GRAMAIN, MARIE-EVE LEPAGE, and YVES TROIN. Can. J. Chem. **67**, 213 (1989).

The photocyclization of enaminones was extended to aryl enaminones bearing a substituent on the aromatic moiety. This reaction was studied in order to achieve the synthesis of indole alkaloid synthons. Trials of regioselectivity control were made by using groups with enhanced steric hindrance. The reactivity of secondary enaminones was tested, and the ratio of C-alkylation to N-alkylation was shown to be dependent on the nature of the aromatic substituent. During this work, new hexahydrocarbazolones were synthesized, with substituents on the A ring or the modified C ring.

Key words: photocyclization, aryl enaminones, indole alkaloids, hexahydrocarbazolones-4, cyclopenta[*b*]indoles.

DANIEL GARDETTE, JEAN-CLAUDE GRAMAIN, MARIE-EVE LEPAGE et YVES TROIN. Can. J. Chem. **67**, 213 (1989).

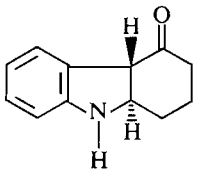
La photocyclisation d'énaminones a été généralisée aux aryl-énaminones substituées sur la partie aromatique. Cette réaction a été étudiée afin de synthétiser des précurseurs d'alcaloïdes indoliques. Des essais de contrôle de régiosélectivité ont été effectués en utilisant des groupements d'encombrement différent. La réactivité des énaminones secondaires a été testée et nous avons montré l'influence de la nature du substituant aromatique sur le rapport C-alkylation, N-alkylation. Au cours de ce travail, de nouvelles hexahydrocarbazolones ont été synthétisées avec des substituants sur le cycle A ou sur le cycle C-modifié.

Mots clés : photocyclisation, aryl-énaminones, alcaloidës indoliques, hexahydrocarbazolones-4, cyclopenta[*b*]indoles.

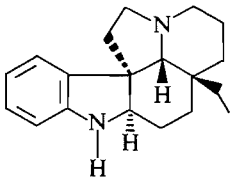
Can. J. Chem. Downloaded from www.nrcresearchpress.com by 122.72.124.2 on 09/07/12
For personal use only.

The hexahydrocarbazolone ring system **1** may be considered as a common structural element of a wide variety of indole alkaloids such as aspidospermidine **2**, vincadifformine **3**, and vindoline **4**. These alkaloids belong to a class of great interest due to their remarkable biological properties (1) and their importance in the preparation of active compounds like vincamine and vincaleucoblastine (2, 3).

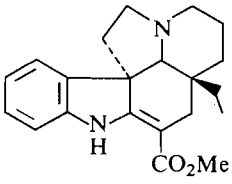
Hexahydro-4-carbazolones **5** (4) have been obtained in good yield by photocyclization of arylenaminones easily prepared from N-substituted anilines and 1,3-cyclohexanedione. This photocyclization reaction has recently received attention from



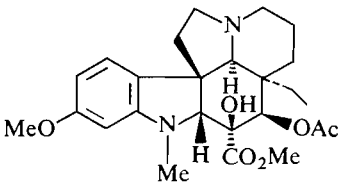
1



2



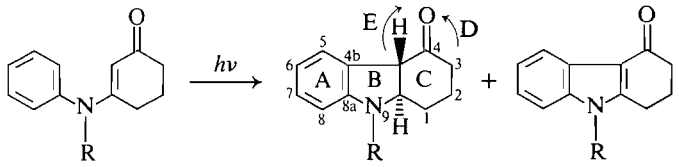
3



4

several laboratories (4–6) and leads to useful and original synthons for the building of such interesting heterocyclic compounds as the indole alkaloids. For instance, *N*(a)-benzyldeethyl aspidospermidine **6** (4, 5) can be obtained in a few steps with a 57% overall yield by a synthetic pathway based on this approach, and with a nearly perfect control of the crucial problem of the relative stereochemistry of rings C/D.

On the other hand, many natural alkaloids of *Aspidosperma* possess a substituent on ring A, usually methoxy groups on C-10, C-11, C-12 as in compound **7**, or sometimes hydroxy



5 **9**

groups on C-10 and C-11 as in compound **8** (alkaloid numbering (7)).

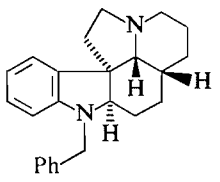
In the present paper we report, in Sect. 1, our investigations into the photocyclization of arylenaminones with a methoxy group on the aromatic moiety, a methoxy group which would be present on the final alkaloids. Because of the general synthetic interest of hexahydrocarbazole, we study and describe in Sect. 2 these tricyclic synthons with a modified C ring.

Results and discussion

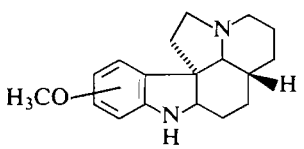
1. Preparation of hexahydrocarbazolone-4 with a substituent on the aromatic ring

(a) Synthesis of enaminones **11**a–c

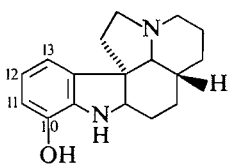
To test the regioselectivity of the photochemical process we studied the photocyclization of arylenaminones bearing a



6



7



8

[1]Revision received August 8, 1988.

TABLE 1. Alkylation of enaminones **11**

Starting products	Final products: N-alkylation	Final products: C-alkylation
11*a*	**12***a* 50%	**13***a* 27%
11*b*	**12***b* 39%	**13***b* 50%
11*c*	**12***c* 50%	**13***c* 10%

substituent on the aromatic ring, derived from *o*-, *p*-, and *m*-anilines.

Moreover, to simplify final product analysis, we started from 2-methyl-1,3-cyclohexanedione; indeed, using 1,3-cyclohexanedione may lead to oxidation product **9** (5) and would complicate the analysis of reaction mixtures.

Enaminones, useful for our study, must be prepared in two steps, according to standard procedures recently described (8, 9): condensation of 2-methyl-1,3-cyclohexanedione with substituted anilines followed by N-alkylation of the secondary enaminones thus obtained. Indeed, as we reported elsewhere (4), condensation between N-methylanilines and 2-methyl-1,3-cyclohexanedione failed, and secondary enaminones such as **10** are not photoreactive.

The enaminones **11***a–c* were prepared in good yields (74–87%) by condensation of *p*-, *o*-, or *m*-anisidine with 2-methyl-1,3-cyclohexanedione in toluene (10) (Dean–Stark apparatus).

The N-methylation of these secondary enaminones **11***a–c* was performed according to the procedure described by Greenhill *et al.* (9). But, beyond the expected N-methylation products **12***a–c*, C-alkylation compounds **13***a–c* were obtained as specified in Table 1. On the other hand the structure of products **13***a–c* was assigned on the basis of ir spectra, which exhibit absorptions at 1660 (C=N) and 1720 (C=O) cm^{-1}, and ^1H nmr spectra, which showed a *gem*-dimethyl group at 1.40 ppm. This structure was confirmed by chemical treatment: acidic hydrolysis of **13***a–c* leads to 2,2-dimethyl-1,3-cyclohexanedione in good yield (70%).

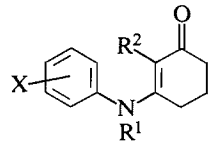
It will be noted that no C-alkylation product could be detected in the absence of a substituent on the aromatic ring (4). This C-alkylation is clearly linked to the donor effect of the methoxy group and is more important, as predicted, with *o*- and *p*-methoxy substituents (**11**). The *para*-methoxy group was changed to the *N,N*-dimethylamino group, a more powerful electron-donating group, to try to increase the yield of C-alkylation product. Thus we should obtain, after imine hydrolysis, an interesting method of preparation of 2-substituted 1,3-cyclohexanediones. Enaminone **14** was alkylated; the N-alkylation product **15** was obtained in 42% yield, and the C-alkylation product **16** in only 20% yield for unexplained reasons.

(b) Photocylization of enaminones **12**a–c

Enaminones **12***a–c* were irradiated under standard conditions (see experimental part).

Photocyclization of enaminone **12**a: Enaminone **12***a* was converted after 3 h of irradiation into *trans*-hexahydrocarbazolone **17***a* in 70% yield.

Photocyclization of enaminone **12**b: Photocyclization of enaminone **12***b* proceeded slowly to afford, after 22 h of irradiation, the expected *trans*-hexahydrocarbazolone **17***b* in moderate yield (30%). The low yield could be explained by the photocyclization of the alternate conformation, leading to an intermediate bearing the methoxy group on the C-4b position, followed by transformation, yielding products we were not able to isolate. Such complications have been described by Ninomiya *et al.* (12) in the case of photocylization of *o*-methoxy substituted enamides that lost one methoxy group.



Compound	R^1	R^2	X
10	H	H	H
11*a*	H	CH_3	*p*-OCH_3
11*b*	H	CH_3	*o*-OCH_3
11*c*	H	CH_3	*m*-OCH_3
12*a*	CH_3	CH_3	*p*-OCH_3
12*b*	CH_3	CH_3	*o*-OCH_3
12*c*	CH_3	CH_3	*m*-OCH_3
14	H	CH_3	*p*-NMe_2
15	CH_3	CH_3	*p*-NMe_2
18	H	CH_3	*m*-OH
19	H	CH_3	*m*-$OCPh_3$
20	CH_3	CH_3	*m*-$OCPh_3$
22	H	CH_3	*m*-OSitBu
23	CH_3	CH_3	*m*-OSitBu
26	CH_3	H	*m*-OTs

Photocyclization of enaminones **12**c: Of course, two regioisomers are expected in this case; treatment of enaminone **12***c* provided, in the same conditions as above, **17***c* and **17***d*, which were separated by fractional crystallization; they have the expected ir spectra (1720 cm^{-1}) and their structures were assigned on the basis of ^1H nmr spectra, by observing aromatic protons. For compound **17***c* the ^1H nmr spectrum indicated the presence of a methoxyl substituent on C-7 with H-5 at 7.55 ppm (d, J = 8.0 Hz), H-6 at 6.40 ppm (dd, J = 8.0 Hz and 2.2 Hz), and H-8 at 6.20 ppm (d, J = 2.2 Hz). For compound **17***d* H-7 appeared at 7.1 ppm (t, $J \simeq$ 8.0 Hz), H-6 at 6.40 ppm (d, J = 8 Hz), and H-8 at 6.15 ppm (d, J = 7.7 Hz). The two isomers are present in a 2:3 ratio, determined in ^{13}C nmr by time shared decoupling without nOe.

The results are summarized in Table 2 and, except in the case of enaminones **12***b*, support the great interest in this strategy for obtaining synthons that possess a methoxy group on the aromatic nucleus, the future ring A of *Aspidosperma* alkaloids.

Nevertheless, most of *Aspidosperma* alkaloids bear a methoxy group on the C-10 or C-11 position. Consideration of the molecular model showed that the regioselectivity of the photocyclization may be controlled by replacing the methoxy group by a bulky substituent whose interaction with CH_3 on C-4a would reduce the formation of C-5 substituted hexahydrocarbazolones. This bulky group has to be easy to introduce on a simple starting material such as aminophenol and easy to remove and replace by a methoxy group; it also must be photostable. Trityl and *tert*-butyldimethylsilyl groups for steric hindrance, and the tosyl group for steric hindrance and because of its electron-withdrawing effect, have been tried.

The enaminone **18**, prepared according to the usual proce-

Can. J. Chem. Downloaded from www.nrcresearchpress.com by 122.72.124.2 on 09/07/12
For personal use only.

TABLE 2. Photocyclization of tertiary enaminones

Enaminone	Irradiation time (h)	Product	Yield (%)
11*a*	3	**17***a*	70
11*b*	22	**17***b*	30
11*b*	1.5	**17***c* + **17***d*	70

dures from *m*-aminophenol and 2-methyl-1,3-cyclohexanedione, was treated with trityl chloride and triethylamine in the presence of 4-dimethylaminopyridine (13). The enaminone **19** thus obtained presented characteristic ir absorption (1640 cm^{-1}) and the assumed ^1H nmr data. The N-alkylation of **19** led to **20**.

The protected aminophenol **21** was prepared in 92% yield from aminophenol and *tert*-butyldimethylsilyl chloride (14) and was condensed with 2-methyl-1,3-cyclohexanedione to give enaminone **22**.

Alkylation of enaminone **22**, as described previously, gave enaminone **23** in 38% yield.

Enaminone **26** was prepared from the derivative **25** (obtained by reduction of the corresponding carbamate **24**) and 1,3-cyclohexanedione.

Irradiation of such enaminones, **20**, **23**, and **26**, led to complex mixtures: C-5, C-7 substituted *trans*-hexahydrocarbazolone deprotected products. The best results were obtained on irradiating enaminone **23**; **27***a* and **27***b* were prepared in 60% yield and in a 2:1 ratio, as determined by ^1H nmr. This result showed, in fact, the importance of steric hindrance: the major product **27***a* is the less hindered one. The structures of **27***a* and **27***b* were assigned, after chromatographic separation, on the basis of their ^1H nmr spectra. The multiplicity and the field of each aromatic proton (see experimental part) confirms the C-5 or C-7 position of the substituent.

In conclusion, these results proved the accuracy of the assumption that the regioselectivity of the photocyclization of substituted enaminones would be improved when bulky substituents were used. Nevertheless, this regioselectivity is not complete and the modest overall yield suffers from the number of the steps and the low yield of some of them. It will probably be better to separate the two isomers **17***c* and **17***d* bearing a methoxy group on the aromatic ring.

*2. Preparation of tricyclic compounds with modified C ring: dihydrocyclopenta[*b*]indole*

One of the first modifications tried was to replace 1,3-cyclohexanedione by 1,3-cyclopentanedione and 2-methyl-1,3-cyclopentanedione. Enaminones **28** and **29** were prepared.

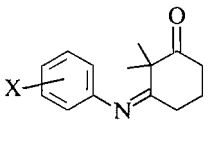
To our knowledge, photocyclization of such enaminones has not been studied. Kibayashi and co-workers (8) reported the cyclization of enaminone **30**, using palladium(II) acetate, leading to dihydrocyclopenta[*b*]indole **31** in modest yield (24%).

(a) Preparation of enaminones 28 and 29

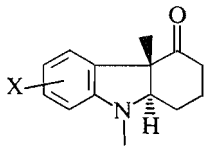
Enaminone **28** was obtained in almost quantitative yield by condensation of 1,3-cyclopentanedione and the corresponding aniline (toluene, *para*-toluenesulfonic acid, Dean–Stark apparatus).

Under the same conditions, treatment of 2-methyl-1,3-cyclopentanedione with *N*-methylaniline afforded enaminone **29** in good yield (88%).

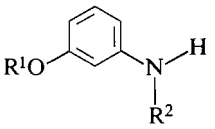
This result has to be compared with the same experiment between *N*-methylaniline and 2-methyl-1,3-cyclohexanedione, where the condensation was unsuccessful (4), and showed that the carbonyl group is less hindered in the case of 2-methyl-1,3-cyclopentanedione.



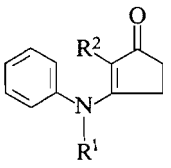
13*a* X = *p*-OCH_3
13*b* X = *o*-OCH_3
13*c* X = *m*-OCH_3
16 X = *p*-NMe_2



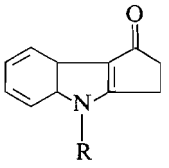
17*a* X = 6-OCH_3
17*b* X = 8-OCH_3
17*c* X = 7-OCH_3
17*d* X = 5-OCH_3
27*a* X = 7-$OSi(CH_3)_2{}^tBu$
27*b* X = 5-$OSi(CH_3)_2{}^tBu$



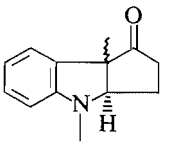
21 R^1 = $^tBu(CH_3)_2Si$, R^2 = H
24 R^1 = Tos, R^2 = CO_2Et
25 R^1 = Tos, R^2 = CH_2



28 R^1 = CH_3 R^2 = H
29 R^1 = R^2 = CH_3
30 R^1 = R^2 = H



31 R = H
32 R = CH_3



33

(b) Photocyclization of enaminones 28 and 29

Photocyclization of the enaminone **28** proceeded slowly to give the dihydrocyclopenta[*b*]indole **32**, after 4 days of irradiation, in 50% yield with only 25% conversion. Even when irradiation was accomplished in a perfectly deoxygenated solution, the nonoxidative photocyclization product was not isolated, in contrast with the results described in the 1,3-cyclohexanedione series (4). Consequently, the dihydro compound **32** acts as an internal filter with a large absorption at 313 nm and limits the conversion rate of **28**.

Photocyclization of enaminone **29** led to cyclopenta[*b*]indole **33** in almost quantitative yield based on consumed product **29**. The stereochemistry has not yet been assigned and would be difficult to predict, if we were to refer to analogous results reported in the literature (15, 16).

In conclusion, this work helps to illustrate the generality of photochemical ring closure of the 6π-electron system to afford tricyclic compounds. The good chemical yields and the availability of the starting materials make this an efficient method of great interest for obtaining useful synthons in new series and for the total synthesis of alkaloids.

Experimental

Melting points were determined on a Reichert micro hotstage apparatus and are uncorrected. Infrared spectra were obtained with a Perkin–Elmer 377 spectrophotometer and refer, unless otherwise stated, to carbon tetrachloride solutions. The ^1H nmr spectra were recorded on JEOL C60H and Bruker MSL 300H spectrometers and refer to deuteriochloroform solutions, tetramethylsilane serving as

Can. J. Chem. Downloaded from www.nrcresearchpress.com by 122.72.124.2 on 09/07/12
For personal use only.

Can. J. Chem. Downloaded from www.nrcresearchpress.com by 122.72.124.2 on 09/07/12
For personal use only.

internal standard. The ^{13}C nmr spectra were determined on a JEOL FX 60 (15.08 MHz) instrument. Mass spectra were run on a Varian CH5 spectrometer and uv spectra were recorded on a Beckman DU-8 spectrophotometer. Thin-layer chromatography was performed with Merck silica gel 60 F254 or with Merck aluminium oxide 60 F254.

Column chromatography was done with silica gel (Merck, 0.040–0.063 mm, 230–400 mesh ASTM) or with aluminium oxide (Merck, 0.063–0.200 mm, 70–230 mesh ASTM) in the specified solvent system. Microanalyses were performed in the Laboratoire central de microanalyses du CNRS in Lyon (France).

General procedure for condensation of aniline and 2-methyl-1,3-cyclohexanedione

To a solution of 2-methyl-1,3-cyclohexanedione (10 mmol) and aniline, freshly distilled (10 mmol), in toluene, was added *p*-toluenesulfonic acid monohydrate (50 mg). The solution was heated at reflux overnight in a Dean–Stark apparatus, then neutralised with K_2CO_3, filtered, and evaporated under reduced pressure to give, after chromatography (Al_2O_3, elution with AcOEt–hexane (5:5)), the desired enaminone.

2-Methyl-3-(4'-methoxyanilino)cyclohex-2-en-1-one **11***a*

The condensation of *p*-anisidine with 2-methyl-1,3-cyclohexanedione afforded the enaminone **11***a*, mp 155–157°C (AcOEt) in 87% yield; ν_{max} (CCl_4): 3430 (NH) and 1640 (C=O, enaminone) cm^{-1}; ^1H nmr ($CDCl_3$) δ: 6.8–7.4 (5H, m, aromatic H and N-H), 3.85 (3H, s, OCH_3), 2.2–2.6 (4H, m, H-4, H-6), 1.9 (3H, s, CH_3), 1.8–2.1 (2H, m, H-5); ^{13}C nmr ($CDCl_3$) δ: 8.1 (CH_3), 21.8 (C-5), 27.0 (C-4), 36.5 (C-6), 55.4 (OCH_3), 106.3 (C-2), 114.2 (C-5', C-3'), 127.3 (C-6', C-2'), 131.8 (C-1'), 157.6 (C-4'), 160.2 (C-3), 195.6 (C-1). Anal. calcd. for $C_{14}H_{17}NO_2$: C 72.40, H 7.41, N 6.06; found: C 72.05, H 7.46, N 5.91.

2-Methyl-3-(2'-methoxyanilino) cyclohex-2-en-1-one **11***b*

The condensation of *o*-anisidine with 2-methyl-1,3-cyclohexanedione afforded the enaminone **11***b*, mp 112–113°C (AcOEt) in 74% yield; ν_{max} (CCl_4): 3420 (NH) and 1640 (C=O, enaminone) cm^{-1}; ^1H nmr ($CDCl_3$) δ: 6.9–7.3 (4H, m, aromatic H), 6.4–6.5 (1H, NH), 3.9 (3H, s, OCH_3), 2.3–2.7 (4H, m, H-4, H-6), 1.9 (3H, s, CH_3), 1.8–2.1 (2H, m, H-5); ^{13}C nmr ($CDCl_3$), δ: 8.0 (CH_3), 21.9 (C-5), 26.9 (C-4), 36.6 (C-6), 55.6 (OCH_3), 107.8 (C-2), 111.0 (C-3'), 120.5 (C-5'), 124.2 (C-6'), 125.5 (C-4'), 128.2 (C-1'), 152.3 (C-2'), 158.8 (C-3), 195.6 (C-1). *Anal.* calcd. for $C_{14}H_{17}NO_2$: C 72.40, H 7.41, N 6.06; found: C 72.73, H 7.41, N 6.10.

2-Methyl-3-(3'-methoxyanilino)cyclohex-2-en-1-one **11***c*

The condensation of *m*-anisidine with 2-methyl-1,3-cyclohexanedione afforded the enaminone **11***c*, mp 136°C (AcOEt) in 78% yield; ν_{max} (CCl_4): 3425 (NH) and 1640 (C=O, enaminone) cm^{-1}; ^1H nmr ($CDCl_3$) δ: 7.0–7.4 (1H, m, H-2'), 6.55–6.9 (3H, m, H-4', H-5', H-6'), 6.3–6.5 (1H, NH), 3.8 (3H, s, OCH_3), 2.2–2.7 (4H, m, H-4, H-6), 1.8 (3H, s, CH_3), 1.8–2.1 (2H, m, H-5); ^{13}C nmr ($CDCl_3$) δ: 8.4 (CH_3), 22.0 (C-5), 27.4 (C-4), 36.6 (C-6), 55.3 (OCH_3), 107.9 (C-2), 110.5 (C-4', C-2'), 117.1 (C-6'), 129.8 (C-5'), 140.3 (C-1'), 158.8 (C-3), 160.2 (C-3'), 196.1 (C-1). *Anal.* calcd. for $C_{14}H_{17}NO_2$: C 72.4, H 7.41, N 6.06; found: C 72.69, H 7.52, N 6.05.

General procedure for alkylation of enaminones

To a suspension of sodium hydride (60% dispersion in mineral oil) (1.1 equivalent) in dry toluene, under nitrogen, was added, drop by drop, a solution of 1.0 equivalent of the enaminone dissolved in toluene. The mixture was refluxed while stirring for 1 hour, then allowed to cool to room temperature. Then 2.2 equivalents of methyl iodide were added and the mixture was refluxed for 2 hours. After quenching by addition of ice-water, the layers were separated. The aqueous layer was extracted with CH_2Cl_2 and the combined organic layers dried. After removal of the solvent, the residue was chromatographed (Al_2O_3, elution AcOEt–hexane 2:8).

*2-Methyl-3-(*N*-methyl-4'-methoxyanilino)cyclohex-2-en-1-one* **12***a*

The alkylation of **11***a* (4.5 g; 19.48 mmol) afforded 2.4 g of **12***a*, mp 100–101°C (acetone–hexane) in 50% yield; uv (EtOH) λ_{max}: 327 nm (17 700); ν_{max} (CCl_4): 1660 (C=O, enaminone) cm^{-1}; ^1H nmr ($CDCl_3$) δ: 6.85 (4H, s, aromatic H), 3.7 (3H, s, OCH_3), 3.2 (3H, s, NCH_3), 2.1–2.6 (4H, m, H-4, H-6), 1.4–2.0 (2H, m, H-5), 1.5 (3H, s, CH_3); ^{13}C nmr ($CDCl_3$) δ: 12.4 (CH_3), 21.1 (C-5), 29.4 (C-4), 37.2 (C-6), 41.1 (NCH_3), 55.4 (OCH_3), 114.4 (C-5', C-3'), 117.6 (C-2), 123.4 (C-6', C-2'), 140.9 (C-1'), 155.5 (C-3), 162.2 (C-4'), 198.6 (C-1). *Anal.* calcd. for $C_{15}H_{19}NO_2$: C 73.44, H 7.81, N 5.71, found: C 73.15, H 7.66, N 5.63.

*2-Methyl-3-(*N*-methyl-2'-methoxyanilino)cyclohex-2-en-1-one* **12**b

The alkylation of **11***b* (2.25 g; 9.74 mmol) afforded 0.9 g of **12***b*, mp 116–117°C (acetone–hexane) in 40% yield; uv (EtOH): λ_{max} 323.6 nm (20 800); ν_{max} (CCl_4): 1640 (C=O, enaminone) cm^{-1}; ^1H nmr ($CDCl_3$) δ: 6.7–7.3 (4H, m, aromatic H), 3.8 (3H, s, OCH_3); 3.2 (3H, s, NCH_3), 2.2–2.7 (4H, m, H-4, H-6), 1.6–2.1 (2H, m, H-5), 1.9 (3H, s, CH_3); ^{13}C nmr ($CDCl_3$) δ: 11.7 (CH_3), 20.4 (C-5), 28.9 (C-4), 36.6 (C-6), 41.1 (NCH_3), 55.2 (OCH_3), 111.7 (C-2, C-3'), 120.7 (C-5'), 126.7 (C-6'), 127.2 (C-4'), 136.6 (C-1'), 153.9 (C-2'), 163.3 (C-3), 197.3 (C-1). *Anal.* calcd. for $C_{15}H_{19}NO_2$: C 73.44, H 7.81, N 5.71; found: C 73.40, H 7.69, N 5.86.

*2-Methyl-3-(*N*-methyl-3'-methoxyanilino)cyclohex-2-en-1-one* **12**c

The alkylation of **11***c* (3.80 g; 16.45 mmol) afforded 2.01 g of **12***c* in 50% yield; uv (EtOH) λ_{max}: 334 nm (13 700); ν_{max} (CCl_4): 1660 (C=O, enaminone) cm^{-1}; ^1H nmr ($CDCl_3$) δ: 6.9–7.4 (1H, m, H-2'), 6.3–6.6 (3H, m, H-4', H-5', H-6'), 3.8 (3H, s, OCH_3), 3.2 (3H, s, NCH_3), 2.2–2.7 (4H, m, H-4, H-6), 1.7–2.1 (2H, m, H-5), 1.6 (3H, s, CH_3); ^{13}C nmr ($CDCl_3$) δ: 11.8 (CH_3), 21.4 (C-5), 28.7 (C-4), 37.6 (C-6), 38.7 (NCH_3), 55.2 (OCH_3), 104.3 (C-2), 105.5 (C-2'), 110.7 (C-4'), 125.5 (C-6'), 129.8 (C-5'), 147.9 (C-1'), 160.5 (C-3), 161.2 (C-3'), 199.6 (C-1); ms: 245 (M^+, 28), 228 (M^- OH, 100), 174 (97), 188 (76), 230 (55), 215 (14). *Mol. Wt.* (high resolution ms) calcd. for $C_{15}H_{19}NO_2$: 245.1416; found: 245.1409.

N-p-*Methoxybenzyl-3-imino-2,2-dimethylcyclohexanone* **13**a

The alkylation of **11***a* (4.5 g; 19.48 mmol) afforded 1.3 g of **13***a* in 27% yield; ν_{max} (CCl_4): 1720 (C=O, ketone) and 1650 (C=N, imine) cm^{-1}; ^1H nmr ($CDCl_3$) δ: 6.4–6.9 (4H, m, aromatic H), 3.7 (3H, s, OCH_3), 2.4–2.7 (4H, m, H-4, H-6), 1.7–2.1 (2H, m, H-5), 1.4 (6H, s, $(CH_3)_2$).

N-o-*Methoxybenzyl-3-imino-2,2-dimethylcyclohexanone* **13**b

The alkylation of **11***b* (2.25 g; 9.74 mmol) afforded 1.20 g of **13***b* in 50% yield; ν_{max} (CCl_4): 1720 (C=O, ketone) and 1660 (C=N, imine) cm^{-1}; ^1H nmr ($CDCl_3$) δ: 6.5–7.1 (4H, m, aromatic H), 3.7 (3H, s, OCH_3), 2.2–2.7 (4H, m, H-4, H-6), 1.4–1.8 (2H, m, H-5), 1.4 (6H, s, $(CH_3)_2$).

N-m-*Methoxybenzyl-3-imino-2,2-dimethylcyclohexanone* **13**c

The alkylation of **11***c* (3.80 g; 16.45 mmol) afforded 0.4 g of **13***c* in 10% yield; ν_{max} (CCl_4): 1720 (C=O, ketone) and 1650 (C=N, imine) cm^{-1}; ^1H nmr ($CDCl_3$) δ: 7.0–7.5 (1H, m, H-5'), 6.2–6.8 (3H, m, H-2', H-4', H-6'), 3.8 (3H, s, OCH_3), 2.2–2.7 (4H, m, H-4, H-6) 1.7–2.1 (2H, m, H-5), 1.4 (6H, s, $(CH_3)_2$).

*3-(*N,N-*Dimethyl-*p*-*phenylenediamino)-2-methylcyclohex-2-en-1-one* **14**

The condensation of *N,N*-dimethyl-*p*-phenylenediamine (1.49 g; 10.96 mmol) with 2-methyl-1,3-cyclohexanedione (1.39 g, 11.0 mmol) afforded **14**, mp 158–159°C (AcOEt) in 76% yield; ν_{max} (CCl_4): 3400 (NH) and 1620–1600 (C=O enaminone) cm^{-1}; ^1H nmr ($CDCl_3$) δ: 6.2–7.5 (5H, m, aromatic H and NH), 1.5–3.1 (6H, m, H-4, H-5, H-6), 2.9 (6H, s, $N(CH_3)_2$), 1.8 (3H, s, CH_3); ^{13}C nmr ($CDCl_3$) δ: 6.8 (CH_3), 19.9 (C-5), 25.3 (C-4), 34.7 (C-6), 38.9 ($N(CH_3)_2$), 103.1 (C-3), 110.6 (C-3' and C-5'), 125.5 (C-2' and C-6'), 126.63 (C-2), 146.7 (C-1'), 158.8 (C-4'), 191.3 (C-1); ms: 244 (100), 227 (10), 215 (10), 201 (20), 187 (5), 173 (13), 135 (11), 121 (41), 93 (3), 88 (4), 77 (3), 70 (10), 65 (3), 61 (10), 43 (52), 27 (10). *Mol. Wt.* (high resolution ms) calcd. for $C_{15}H_{20}N_2O$: 244.1419; found: 244.1468.

*3-(*N*-Methyl-(*N,N*-dimethyl-*p*-phenylenediamino)-2-methylcyclohex-2-en-1-one* **15**

The alkylation of **14** (1.0 g; 4.1 mmol) afforded **15** (42%); ν_{max} (CCl_4) 1640 (C=O, enaminone) cm^{-1}; ^1H nmr ($CDCl_3$) δ: 6.5–7.1 (4H, aromatic H), 3.3 (3H, s, NCH_3), 2.9 (6H, s, $N(CH_3)_2$), 1.5–2.6 (6H, m, H-4, H-5, H-6), 1.6 (3H, s, CH_3); ^{13}C nmr ($CDCl_3$) δ: 12.2

Can. J. Chem. Downloaded from www.nrcresearchpress.com by 122.72.124.2 on 09/07/12
For personal use only.

(CH_3), 20.6 (C-5), 29.4 (C-4), 36.6 (C-6), 40.4 ($N(CH_3)_2$), 41.8 (NCH_3), 122.7 (C-3′ and C-5′), 114.2 (C-2), 124.2 (C-2′ and C-6′), 137.2 (C-3), 147.0 (C-1′), 162.8 (C-4′), 197.9 (C-1); ms: 258 (26), 242 (6), 215 (4), 164 (14), 150 (86), 135 (100), 98 (38), 55 (74). *Mol. Wt.* (high resolution ms) calcd. for $C_{16}H_{22}N_2O$: 258.1732; found: 258.1728.

N-(N,N-*Dimethyl*-p-*phenylenediamino)-3-imino-2,2-dimethyl-cyclo-hexanone* ***16***

The alkylation of **14** (1.0 g; 4.1 mmol) afforded **16** (20%); ν_{max} (CCl_4): 1720 (C=O) and 1600 (C=N) cm^{-1}; ^1H nmr ($CDCl_3$) δ: 7.1–6.7 (4H, m, aromatic H), 2.9 (6H, s, $N(CH_3)_2$), 2.6–1.5 (6H, m, H-4, H-5, H-6), 1.4 (6H, s, $(CH_3)_2$).

General procedure for irradiation of enaminones

A solution of enaminone (3.5–6.4 mmol) in 200 mL of benzene was irradiated under nitrogen in a Pyrex reactor with a 400-W medium pressure uv lamp. After evaporating the resulting solution under reduced pressure, the residue was chromatographed (SiO_2).

trans-*4a,9-Dimethyl-6-methoxy-1,2,3,4,4a,9a-hexahydro-4-carbazolone* ***17***a

12*a* (1.58 g; 6.4 mmol) was irradiated in benzene under nitrogen during 3 h, affording **17***a* (1.1 g, 70%), mp 83–85°C; ν_{max} (CCl_4); 1725 (C=O, ketone) cm^{-1}; ^1H nmr ($CDCl_3$) δ: 7.2 (1H, d, J = 2.2 Hz, H-5), 6.7 (1H, dd, J = 8.5 Hz and 2.2 Hz, H-7), 6.55 (1H, d, J = 8.4 Hz, H-8), 3.7 (3H, s, OCH_3), 2.7 (3H, s, NCH_3), 2.3–2.6 (1H, m, C9a-H), 1.7–2.5 (6H, m, H-1, H-2, H-3), 1.2 (3H, s, CH_3); ^{13}C nmr ($CDCl_3$) δ: 19.2 (CH_3), 21.1 (C-2), 22.4 (C-1), 35.2 (NCH_3), 36.6 (C-3), 55.3 (C-4a), 55.6 (OCH_3), 74.7 (C-9a), 109.8 (C-5), 111.0 (C-8), 112.6 (C-7), 134.2 (C-4b), 145.8 (C-8a), 153.9 (C-6), 209.0 (C-4); ms: 245 (73), 230 (87), 228 (100), 202 (27), 188 (47), 174 (53). *Mol. Wt.* (high resolution ms) calcd. for $C_{15}H_{19}NO_2$: 245.1416; found: 245.1409.

trans-*4a,9-Dimethyl-8-methoxy-1,2,3,4,4a,9a-hexahydro-4-carbazolone* ***17***b

12*b* (0.87 g, 3.5 mmol) was irradiated in benzene under nitrogen during 22 h, affording **17***b* (0.11 g, 30%), mp 148–150°C; ν_{max} (CCl_4): 1720 (C=O, ketone) cm^{-1}; ^1H nmr ($CDCl_3$) δ: 7.3 (1H, d, J = 7.3 Hz, H-7), 6.9 (1H, t, J = 7.7 Hz, H-6), 6.8 (1H, d, J = 8.0 Hz, H-5), 3.7 (3H, s, OCH_3), 2.9 (3H, s, NCH_3), 2.6–2.8 (1H, m, C9a-H), 1.8–2.7 (6H, m, H-1, H-2, H-3), 1.1 (3H, s, CH_3); ^{13}C nmr ($CDCl_3$) δ: 19.8 (CH_3), 20.8 (C-2), 22.5 (C-1), 36.7 (NCH_3), 37.2 (C-3), 55.7 (OCH_3), 55.9 (C-4a), 74.9 (C-9a), 111.7 (C-7), 117.5 (C-6), 121.5 (C-5), 134.9 (C-4b), 139.5 (C-8), 147.4 (C-8a), 209.3 (C-4); ms: 245 (36), 228 (100), 230 (64), 202 (14), 188 (43), 174 (43). *Mol. Wt.* (high resolution ms) calcd. for $C_{15}H_{19}NO_2$: 245.1416; found: 245.1419.

trans-*4a,9-Dimethyl-7-methoxy-1,2,3,4,4a,9a-hexahydro-4-carbazolone* ***17***c *and* trans-*4a,9-dimethyl-5-methoxy-1,2,3,4,4a,9a-hexahydro-4-carbazolone* ***17***d

12*c* (1.0 g; 4.1 mmol) was irradiated in benzene under nitrogen during 1.5 h, affording 0.86 g of a mixture of **17***c* and **17***d* in 86% yield. These were separated by fractional recrystallization in ether.

17*c*: mp 115–116°C (ether); ν_{max} (CCl_4): 1720 (C=O, ketone) cm^{-1}; ^1H nmr ($CDCl_3$) δ: 7.55 (1H, d, J = 8.0 Hz, H-5), 6.4 (1H, dd, J = 8.0 Hz and 2.2 Hz, H-6), 6.2 (1H, d, J = 2.2 Hz, H-8), 3.75 (3H, s, NCH_3), 2.7 (3H, s, OCH_3), 2.3–2.45 (1H, m, C9a-H), 1.7–2.3 (6H, m, H-1, H-2, H-3), 1.2 (3H, s, CH_3); ^{13}C nmr ($CDCl_3$) δ: 19.6 (CH_3), 21.1 (C-2), 22.4 (C-1), 34.3 (NCH_3), 36.6 (C-3), 54.9 (C-4a), 55.4 (OCH_3), 74.3 (C-9a), 96.9 (C-8), 103.9 (C-6), 124.7 (C-4b), 125.7 (C-5), 153.3 (C-8a), 160.2 (C-7), 209.4 (C-4); ms: 245 (40), 230 (100), 217 (10), 202 (10), 188 (85), 174 (70), 160 (12), 145 (5), 128 (15). *Mol. Wt.* (high resolution ms) calcd. for $C_{15}H_{19}NO_2$: 245.1416; found: 245.1418.

17*d*: mp 143–145°C (Et_2O); ν_{max} (CCl_4): 1720 (C=O, ketone) cm^{-1}; ^1H nmr ($CDCl_3$) δ: 7.1 (1H, t, J = 8.2 Hz, H-7), 6.4 (1H, d, J = 8.0 Hz, H-6), 6.15 (1H, d, J = 7.7 Hz, H-8), 3.8 (3H, s, OCH_3), 2.6 (3H, s, NCH_3), 2.4–2.6 (1H, m, C9a-H), 1.5–2.5 (6H, m, H-1, H-2, H-3), 1.25 (3H, s, CH_3); ^{13}C nmr ($CDCl_3$) δ: 16.5 (CH_3), 21.6 (C-2), 23.6 (C-1), 34.6 (N-CH_3), 37.4 (C-3), 55.8 (OCH_3), 58.4 (C-4a), 75.2 (C-9a), 102.8 (C-8), 114.4 (C-6), 119.1 (C-4b), 129.4 (C-7), 153.6 (C-8a), 156.6 (C-5), 207.3 (C-4); ms: 245 (55), 230 (15), 217 (15), 202 (15), 188 (100), 174 (62), 160 (15). *Mol. Wt.* (high resolution ms) calcd. for $C_{15}H_{19}NO_2$: 245.1416; found: 245.1417.

3-(3′-Hydroxyanilino)cyclohex-2-en-1-one ***18***

This product was prepared, by condensation of aminophenol and 1,3-cyclohexanedione in quantitative yield, as a polar product insoluble in current solvents; ν_{max} (THF): 3560 (OH, phenol), 3300 (NH), and 1640 (C=O, enaminone) cm^{-1}; ^1H nmr (DMSO-d_6) δ: 7.8 (1H, s, OH), 6.1–7.4 (5H, m, aromatic H and NH), 5.35 (1H, s, H-2), 1.6–2.4 (6H, m, H-4, H-5, H-6); ^{13}C nmr ($CDCl_3$ + DMSO) δ: 21.9 (C-5), 29.1 (C-4), 36.7 (C-6), 98.6 (C-2′), 110.6 (C-2), 112.2 (C-4′), 113.6 (C-6′), 129.9 (C-5′), 140.3 (C-1′), 158.9 (C-3), 162.9 (C-3′), 196.9 (C-1); ms: 203 (3), 186 (32), 174 (42), 172 (50), 160 (10), 147 (40), 146 (75), 133 (10), 109 (25), 84 (20), 80 (15), 65 (40), 62 (12), 55 (35), 42 (100), 39 (90), 31 (30), 29 (32), 27 (10). *Mol. Wt.* (high resolution ms) calcd. for $C_{12}H_{13}NO_2$: 203.0946; found: 203.0935.

3-(3′-Triphenylmethyloxyanilino)cyclohex-2-en-1-one ***19***

To a solution of **18** (0.5 g; 2.46 mmol) in anhydrous CH_2Cl_2, under nitrogen, was added 3.0 equivalents of NEt_3 (1.03 mL, 7.38 mmol), 0.08 equivalent of DMAP (24.0 mg, 0.2 mmol), and 2.2 equivalents of trityl chloride (1.51 g, 5.41 mmol). The resulting solution was refluxed 12 h, then washed with H_2O and 5% $NaHCO_3$. After removal of the solvent under reduced pressure the residue was chromatographed (SiO_2 flash, elution AcOEt–hexane 9:1) to give 0.8 g of **19** in 73% yield; ν_{max} (CCl_4): 3430 (NH) and 1640 (C=O, enaminone) cm^{-1}; ^1H nmr ($CDCl_3$) δ: 6.3–7.6 (20H, m, aromatic H and NH), 5.35 (1H, s, H-2), 1.5–2.5 (6H, m, H-4, H-5, H-6); ^{13}C nmr ($CDCl_3$) δ: 21.6 (C-5), 29.0 (C-4), 36.3 (C-6), 90.6 ($OC(Ph)_3$), 99.2 (C-2), 116.6 (C-6′), 116.9 (C-4′), 117.9 (C-5′), 127.2 (C-10), 127.7 (C-9, C-9′), 128.7 (C-8, C-8′), 138.5 (C-1′), 143.7 (O—C(C)), 156.9 (C-3), 163.0 (C-3′), 198.0 (C-1); ms: 445 (5), 366 (51), 243 (96), 228 (10), 215 (2), 203 (10), 186 (4), 174 (17), 165 (100), 146 (19), 119 (78), 117 (73), 91 (22), 82 (12), 71 (12), 57 (20), 51 (12), 47 (12), 41 (12), 36 (32). *Mol. Wt.* (high resolution ms) calcd. for $C_{31}H_{27}NO_2$: 445.2124; found: 445.2042.

*3-(*N-*Methyl-3′-triphenylmethyloxyanilino)cyclohex-2-en-1-one* ***20***

This product was prepared by alkylation of **19** (1.0 g; 2.25 mmol) in 64% yield; uv (EtOH) λ_{max}: 300.3 nm (26 400); ν_{max} (CCl_4): 1635 (C=O, enaminone) cm^{-1}; ^1H nmr ($CDCl_3$) δ: 6.3–7.6 (19H, m, aromatic H), 5.2 (1H, s, H-2), 2.9 (3H, s, NCH_3), 1.6–2.5 (6H, m, H-4, H-5, H-6); ^{13}C nmr ($CDCl_3$) δ: 22.1 (C-5), 27.7 (C-4), 35.7 (C-6), 39.9 (NCH_3), 90.8 ($OC(C_6H_5)_3$), 99.7 (C-2), 119.8 (C-6′), 119.9 (C-5′), 120.1 (C-4′), 127.0 (C-10), 127.5 (C-9, C-9′), 128.5 (C-8, C-8′), 129.0 (C-2′), 143.5 (O—C—C), 144.9 (C-1′), 157.0 (C-3), 164.6 (C-3′), 197.1 (C-1); ms: 459 (5), 243 (80), 228 (10), 215 (10), 200 (10), 189 (10), 165 (62), 160 (15), 149 (10), 88 (10), 86 (40), 84 (65), 65 (10), 51 (30), 49 (100), 47 (17), 39 (10), 35 (10). *Mol. Wt.* (high resolution ms) calcd. for $C_{32}H_{29}NO_2$: 459.2198; found: 459.2190.

*3-*tert*-Butyldimethylsilyloxyaniline* ***21***

To a solution of *m*-aminophenol (1 g; 9.16 mmol) and *tert*-butyldimethylchlorosilane (1.66 g, 10.99 mmol) in *N*,*N*-dimethylformamide (8 mL), was added imidazole (1.56 g; 22.91 mmol). After 10 h under nitrogen, 40 mL of 5% $NaHCO_3$ was added and the resulting solution extracted three times with ether. The organic layers were washed with water and saturated NaCl. After evaporating under reduced pressure, the residue was flash chromatographed (SiO_2, elution AcOEt–hexane 75:25) to give 1.88 g of **21** in 92% yield; ν_{max} (CCl_4): 3500 (NH_2, as) and 3400 (NH_2, s) cm^{-1}; ^1H nmr ($CDCl_3$) δ: 6.8–7.2 (1H, m, H-2), 6.2–6.4 (3H, m, H-4, H-5, H-6), 3.55 (2H, s, NH_2), 0.98 (9H, s, *t*Bu), 0.2 (6H, s, OSi $(CH_3)_2$); ^{13}C nmr ($CDCl_3$) δ: 156.7 (C-3′), 147.6 (C-1′), 129.9 (C-5′), 110.4 (C-6′), 108.6 (C-4′), 107.1 (C-2′), 25.7 ($C(CH_3)_3$), 18.1 ($C(CH_3)_3$), 4.4 ($(CH_3)_2$).

*2-Methyl-3-(3′-dimethyl-*tert*-butylsilyloxyanilino)cyclohex-2-en-1-one* ***22***

The condensation of **21** (3.0 g; 13.44 mmol) with 2-methyl-1,3-cyclohexanedione (1.7 g; 13.44 mmol) afforded 1.98 g of **22** in 44.5% yield; ν_{max} (CCl_4): 3430 (NH) and 1640 (C=O, enaminone) cm^{-1}; ^1H

Can. J. Chem. Downloaded from www.nrcresearchpress.com by 122.72.124.2 on 09/07/12
For personal use only.

nmr ($CDCl_3$) δ: 6.55–6.8 (3H, m, H-4′, H-5′, H-6′), 6.9–7.3 (1H, m, H-2′), 6.4–6.5 (1H, NH), 2.2–2.6 (4H, m, H-4, H-6), 1.7–2.1 (2H, m, H-5), 1.83 (3H, s, CH_3), 0.98 (9H, s, *t*Bu), 0.2 (6H, s, $OSi(CH_3)_2$); ^{13}C nmr ($CDCl_3$) δ: 0.26 ($Si(CH_3)_2$), 8.1 (CH_3), 17.8 ($C(CH_3)_3$), 21.7 (C-5), 25.3 ($C(CH_3)_3$), 27.1 (C-4), 36.3 (C-6), 107.5 (C-2), 116.5 (C-4′, C-2′), 117.7 (C-6′), 129.3 (C-5′), 140.0 (C-1′), 155.8 (C-3), 158.92 (C-3), 195.8 (C-1).

*2-Methyl-3-(*N*-methyl-3′-dimethyl*-tert*-butylsilyloxyanilino)cyclohex-2-en-1-one* ***23***

This product was obtained in 38% yield from intermediate **22** (1.63 g, 4.92 mmol), as in the general procedure for alkylation of enaminones, as an orange oil; uv (EtOH) λ_{max}: 335.3 nm (10 000); ν_{max} (CCl_4): 1660 (C=O, enaminone) cm^{-1}; ^1H nmr ($CDCl_3$) δ: 6.2–6.6 (3H, m, H-2′, H-4′, H-6′), 6.9–7.4 (1H, m, H-5′), 3.2 (3H, s, NCH_3), 2.3–2.8 (4H, m, H-4, H-6), 1.8–2.2 (2H, m, H-5), 1.65 (3H, s, CH_3), 0.98 (9H, s, *t*Bu), 0.2 (6H, s, $OSi(CH_3)_2$); ^{13}C nmr ($CDCl_3$) δ: 0.0 ($Si(CH_3)_2$), 12.1 (CH_3), 18.4 ($C(CH_3)_2$), 21.5 (C-5), 25.9 ($C(CH_3)_3$), 28.9 (C-4), 37.7 (C-6), 39.4 (N-CH_3), 110.8 (C-2), 112.1 (C-2′), 113.2 (C-4′), 124.6 (C-6′), 129.9 (C-5′), 148.3 (C-1′), 156.8 (C-3), 161.9 (C-3′), 200.1 (C-1); ms: 345 (19), 328 (100), 314 (8), 288 (11), 274 (8), 272 (8), 214 (8). *Mol. Wt.* (high resolution ms) calcd. for $C_{20}H_{31}NO_2Si$: 345.2124; found: 345.2117.

N-*Methyl 3-(*p*-toluenesulfonyloxyphenyl) amine* ***25***

To a solution of 3-(*p*-toluenesulfonyloxyphenyl) amine (0.23 g, 0.87 mmol) in CH_2Cl_2 was added, under nitrogen at 0°C, 1.1 equivalents of NEt_3 (0.13 mL, 0.96 mmol), 0.04 equivalent of DMAP (5 mg, 0.03 mmol), and, drop by drop, a solution of ethyl chloroformate (0.09 mL, 0.96 mmol) in CH_2Cl_2 (1 mL). The resulting carbamate **24** (0.28 g, 0.84 mmol) in Et_2O (20 mL) was added to a suspension of $LiAlH_4$ (0.16 g, 4.18 mmol) in THF at 0°C under nitrogen. The solution was refluxed for 3 h; then isopropanol (0.54 mL) and water (0.54 mL) were added. The precipitate obtained was washed three times with Et_2O and the solvent removed under reduced pressure to give **26** (56%); ν_{max} (CCl_4): 3450 (NH) cm^{-1}; ^1H nmr ($CDCl_3$) δ: 8.0–6.0 (9H, m, aromatic H and NH), 2.65 (3H, s, NCH_3), 2.4 (3H, s, $-C_6H_4-CH_3$).

*3-(*N*-Methyl-3′-*p*-toluenesulfonyloxyanilino)cyclohex-2-en-1-one* ***26***

The condensation of **25** (0.277 g, 1.03 mmol) with 1,3-cyclohexanedione (0.22 g, 1.96 mmol) in benzene with *dl*-camphorsulfonic acid as catalyst gave **27** (63%); ν_{max} (CCl_4): 1640 (C=O, enaminone) cm^{-1}; ^1H nmr ($CDCl_3$) δ: 6.3–8.0 (8H, m, aromatic H), 5.3 (1H, s, H-2), 3.15 (3H, s, NCH_3), 2.45 (3H, s, $C_6H_4-CH_3$), 2.3–2.7 (4H, m, H-4, H-6), 1.8–2.1 (2H, m, H-5). *Anal.* calcd. for $C_{20}H_{21}NO_4S$: C 64.69, H 5.66, N 3.77; found: C 64.95, H 5.80, N 3.63.

Photocyclization of ***23***

A solution of enaminone **23** (0.15 g, 0.43 mmol) in 150 mL of benzene under nitrogen was irradiated during 30 min in a Pyrex reactor with a 400-W medium pressure uv lamp. After removal of the solvent under reduced pressure, the residue was chromatographed (SiO_2, elution AcOEt–hexane 5:95). Two products, **27***a* and **27***b*, were isolated.

trans-*4a,9-Dimethyl-7-dimethyl*-tert-*butylsilyloxy-1,2,3,4,4a,9a-hexahydro-4-carbazolone* **27**a

This product was obtained in 40% yield; ν_{max} (CCl_4): 1710 (C=O, ketone) cm^{-1}; ^1H nmr ($CDCl_3$) δ: 5.9–6.4 (2H, m, H-6, H-5), 6.7–7.0 (1H, d, H-8), 3.4 (1H, m, C9a-H), 2.7(3H, s, NCH_3), 2.2–2.5 (2H, m, H-2), 1.5–2.1 (4H, m, H-1, H-3), 1.4 (3H, s, CH_3), 0.98 (9H, s, *t*Bu), 0.2 (6H, s, $OSi(CH_3)_2$); ^{13}C nmr ($CDCl_3$) δ: 2.4, 18.1, 20.3, 20.9, 22.5, 24.7, 31.3, 36.4, 53.9, 66.3, 97.7, 107.4, 108.9, 122.8, 126.4, 154.3, 205.3; ms: 345 (30), 330 (6), 317 (45), 302 (9), 288 (100), 274 (15), 260 (11), 245 (3), 232 (5), 218 (8), 203 (3), 188 (3), 174 (3), 160 (3), 144 (4), 128 (3), 115 (8), 73 (12), 59 (3), 41 (43), 29 (2). *Mol. Wt.* (high resolution ms) calcd. for $C_{20}H_{31}SiNO_2$: 345.2124; found: 345.2172.

trans-*4a,9-Dimethyl-5-dimethyl*-tert-*butylsilyloxy-1,2,3,4,4a,9a-hexahydro-4-carbazolone* **27**b

This product was obtained in 20% yield; ν_{max} (CCl_4): 1715 (C=O, ketone) cm^{-1}; ^1H nmr ($CDCl_3$) δ: 6.8–7.1 (1H, m, H-7), 5.9–6.2 (2H, m, H-6, H-8), 3.32 (1H, m, C9a-H), 2.67 (3H, s, CH_3), 2.1–2.5 (2H, m, H-2), 1.6–2.0 (4H, m, H-1, H-3), 1.45 (3H, s, CH_3), 0.98 (9H, s, *t*Bu), 0.2 (6H, s, $OSi(CH_3)_2$); ^{13}C nmr ($CDCl_3$) δ: 1.8, 16.5, 18.7, 18.9, 22.3, 23.9, 30.9, 36.5, 55.1, 74.2, 98.6, 107.3, 118.6, 124.8, 127.5, 152.4, 210.2; ms: 345 (63), 317 (95), 302 (11), 288 (87), 274 (23), 260 (30), 245 (7), 232 (16), 218 (20), 202 (6), 188 (11), 174 (3), 160 (4), 144 (9), 128 (4), 115 (11), 100 (3), 73 (30), 59 (7), 51 (3), 41 (11), 29 (6). *Mol. Wt.* (high resolution ms) calcd. for $C_{20}H_{31}SiNO_2$: 345.2124; found: 345.2168.

*(*N*-Methyl anilino)-3-cyclopentene-2-one* ***28***

Prepared from 1,3-cyclopentanedione (0.5 g, 5 mmol) and *N*-methylaniline under the usual conditions and purified by flash chromatography (SiO_2, elution $CHCl_3$–MeOH, 95:5), yield: 99%; uv (EtOH) λ_{max}: 280 nm (28 800); ν_{max} (CCl_4): 1675 cm^{-1}; ^1H nmr ($CDCl_3$) δ: 7.7–7.1 (5H, m), 5.2 (1H, s), 3.4 (3H, s), 2.7–2.2 (4H, m); ^{13}C nmr ($CDCl_3$) δ: 277.7, 33.7, 40.6, 101.5, 125.5, 127.0, 129.1, 144.1, 176.9, 203.6. *Mol. Wt.* (high resolution ms) calcd. for $C_{12}H_{13}NO$: 187.0994; found: 187.1004.

*3-(*N*-Methyl anilino)-2-methyl 2-cyclopenten-1-one* ***29***

Prepared under standard conditions from 2-methyl-1,3-cyclopentanedione (1.10 g, 9.81 mmol) and *N*-methylaniline (2.14 g, 20 mmol) and purified by flash chromatography (SiO_2, elution AcOEt–hexane 70:30), yield: 88%; uv (EtOH) λ_{max}: 295 nm (35 700); ν_{max} (CCl_4): 1670 cm^{-1}; ^1H nmr ($CDCl_3$) δ: 7.7–7.2 (5H, m), 3.5 (3H, s), 2.9–2.2 (4H, m, H-4 and H-5), 1.2 (3H, s); ^{13}C nmr ($CDCl_3$) δ: 9.3, 27.9, 32.7, 41.6, 110.6, 126.6, 126.8, 129.2, 146.1, 171.6, 204.8. *Mol. Wt.* (high resolution ms) calcd. for $C_{13}H_{15}NO$: 201.1152; found: 201.1151.

*3-Oxo-8-methyl-1,2-dihydrocyclopenta[*b*]indole* ***32***

A solution of the enaminone **28** (0.78 g, 4 mmol) in benzene (150 mL) was irradiated, under nitrogen, for 4 days (Pyrex reactor, 400-W medium pressure uv lamp). After removal of the solvent and purification (SiO_2, elution AcOEt), **32** was isolated (0.190 g; 50% based on consumed product); ν_{max} (CCl_4): 1690 (C=O, ketone) cm^{-1}; ^1H nmr ($CDCl_3$) δ: 8–7.2 (4H, m, aromatic H), 3.8 (3H, s, N-CH_3), 2.8–2.4 (4H, m, H-1 and H-2); ^{13}C nmr ($CDCl_3$) δ: 20.4 (C-1), 30.4 (CH_3), 40.7 (C-2), 109.9 (C-3a), 120.7 (C-5), 119.0 (C-7), 121.3 (C-4), 122.6 (C-6), 123.3 (C-3b), 143.0 (C-8a), 168.3 (C-7a), 195.3 (C-3). *Mol. Wt.* (high resolution ms) calcd. for $C_{12}H_{11}NO$: 185.0841; found: 185.0845.

*3-Oxo-3a,8-dimethyl-1,2,3a,8a-tetrahydrocyclopenta[*b*]indole* ***33***

Irradiation of **29** under the usual conditions gave **33** (70%); ν_{max} (CCl_4): 1745 cm^{-1}; ^1H nmr ($CDCl_3$) δ: 7.4–6.4 (4H, m), 4–3.8 1H, m, H-8a), 2.85 (3H, s, *n*-CH_3), 2.7–1.7 (4H, m, H-1, H-2), 1.45 (3H, s); ^{13}C nmr ($CDCl_3$) δ: 20.4, 24.0, 33.5, 36.1, 57.4, 76.7, 106.7, 118.3, 123.3, 128.6, 130.0, 152.0, 218.4. *Mol. Wt.* (high resolution ms) calcd. for $C_{13}H_{15}NO$: 201.1154; found: 201.1155.

1. G. A. Cordell. *In* The alkaloids. Vol. XVII. *Edited by* R. H. F. Manske and R. Rodrigo. Academic Press, New York. 1979. Chap. 3.
2. J. D. Phillipson and M. H. Zenk. (*Editors*). Indole and biogenetically related alkaloids. Academic Press, New York. 1980.
3. D. J. Abraham. The catharantus alkaloids. Marcel Dekker, New York. 1975. Chaps. 7 and 8.
4. J. C. Gramain, H. P. Husson, and Y. Troin. Tetrahedron Lett. **26**, 2323 (1985).
5. J. C. Gramain, H. P. Husson, and Y. Troin. J. Org. Chem. **50**, 5517 (1985); J. Heterocycl. Chem. **25**, 201 (1988).
6. J. L. Berry, D. R. Dillin, and D. G. Wayson. Tetrahedron Lett. **26**, 143 (1985).
7. J. Le Men and W. I. Taylor. Experientia, **21**, 508. (1965).
8. H. Iida, Y. Yuasa, and C. Kibayashi. J. Org. Chem. **45**, 2938 (1980).
9. J. V. Greenhill and M. Ashraf Moten. Tetrahedron, **39**, 3405 (1983).
10. K. Yamada, T. Konakahara, and H. Iida. Bull. Chem. Soc. Jpn. **46**, 2504 (1973).

11. N. B. CHAPMAN and J. SHORTER. Correlation analysis in chemistry: recent advances. Plenum, New York. 1978. pp. 439–540.
12. I. NINOMIYA, T. KIGUCHI, O. YAMAMOTO, and T. NAITO. J. Chem. Soc. Perkin Trans. 1, 1723 (1979).
13. P. M. KENDALL, J. V. JOHNSON, and C. E. COOL. J. Org. Chem. **44**, 1421 (1979).
14. S. K. CHAUDHARY and O. HERNANDEZ. Tetrahedron Lett. 95 (1979).
15. A. G. SCHULTZ and M. B. DE TAR. J. Am. Chem. Soc. **98**, 3564 (1976).
16. O. L. CHAPMAN, G. L. ELIAN, A. BLOOM, and J. CLARDY. J. Am. Chem. Soc. **93**, 2978 (1971).

Can. J. Chem. Downloaded from www.nrcresearchpress.com by 122.72.124.2 on 09/07/12
For personal use only.

Nucleophilic photosubstitutions of *o*-methoxynitrobenzenes

NIGEL J. BUNCE AND KAREN LABONTE STEPHENSON

Guelph–Waterloo Centre for Graduate Work in Chemistry, Guelph Campus, University of Guelph, Guelph, Ont., Canada N1G 2W1

Received June 13, 1988

NIGEL J. BUNCE and KAREN LABONTE STEPHENSON. Can. J. Chem. **67**, 220 (1989).

We report a new synthesis of 3-nitroveratrole, based on the directed lithiation of veratrole, and photochemical substitutions of both 3-nitroveratrole and *o*-nitroanisole with several nucleophiles. Both aromatic substrates undergo photocyanation *meta* to the nitro group. With hydroxide ion, 3-nitroveratrole reacts *meta* to the nitro group, but 2-nitroanisole undergoes replacement of either substituent, the proportion of reaction at each site depending upon the OH^- concentration. 3-Nitroveratrole undergoes an inefficient reaction with butylamine at each methoxy group; this reaction is apparently second order in amine. The reaction between *o*-nitroanisole and diethylamine results only in photohydrolysis.

Key words: photosubstitution, nucleophilic, 3-nitroveratrole, *o*-nitroanisole.

NIGEL J. BUNCE et KAREN LABONTE STEPHENSON. Can. J. Chem. **67**, 220 (1989).

On a réalisé une nouvelle synthèse du nitro-3 vératrole qui est basée sur la lithiation directe du vératrole et on a examiné des réactions de substitutions photochimiques tant du nitro-3 vératrole que de l'*o*-nitroanisole avec plusieurs nucléophiles. Les deux substrats aromatiques subissent des photocyanurations en position *méta* du groupement nitro. Avec l'ion hydroxyde, le nitro-3 vératrole réagit en position *méta* du groupement nitro; toutefois, dans les mêmes conditions, le nitro-2 anisole subit un remplacement de l'un ou l'autre des substituants et la proportion des produits provenant des substitutions à chacun des sites dépend de la concentration en OH^-. Avec la buylamine, le nitro-3 vératrole subit une réaction inefficace au niveau de chacun des groupements méthoxy; il semble que cette réaction est du deuxième ordre en amine. La réaction de l'*o*-nitroanisole avec la diéthylamine ne fournit que le produit de photohydrolyse.

Mots clés : photosubstitution, nucléophilique, nitro-3 vératrole, *o*-nitroanisole.

[Traduit par la revue]

Can. J. Chem. Downloaded from www.nrcresearchpress.com by 122.72.124.2 on 09/07/12
For personal use only.

Introduction

Nucleophilic photochemical substitutions have been a subject of intense research activity since their first discovery in 1956. The scope of these reactions (1), empirical rules for product predictions (2), and possible mechanisms (3) have all been reviewed. Of considerable importance in developing our ideas about the scope and mechanisms of these photosubstitutions have been reactions carried out on methoxynitro compounds as substrates, notably with 3- and 4-nitroanisoles and 4-nitroveratrole. By contrast, the photochemical reactions of *o*-nitroanisole and of 3-nitroveratrole have been almost unexplored.

The whole area of methoxynitroaromatic compounds and their photochemistry has attracted new interest with the realization that nucleophilic photosubstitution reactions of these compounds can occur by two distinct pathways: a direct S_N2 Ar* photosubstitution and a route initiated by electron transfer from the "nucleophile" to the nitro compound (4, 5). Substitutions *meta* to the nitro group and those at the ipso position are S_N2 Ar* processes, and appear to be initiated by attraction of the incoming nucleophile to locations where the excited state HOMO electron density is low. Substitutions *para* to the nitro group are electron-transfer reactions in which the subsequent bond-forming step is a ground state process. For this type of substitution to occur, the nucleophile must be easily oxidizable (5).

Very little is known so far about the photochemistry of *o*-methoxynitrobenzenes. Letsinger and McCain (6) obtained the substitution products from the action of cyanide ion and de Vries[1] obtained those from the action of hydroxide ion with *o*-nitroanisole, but no mechanistic work was done. In the present work, we have devised a new route to the inaccessible 3-nitroveratrole, and have carried out preliminary investigations of the photosubstitution chemistry of both 3-nitroveratrole and *o*-nitroanisole.

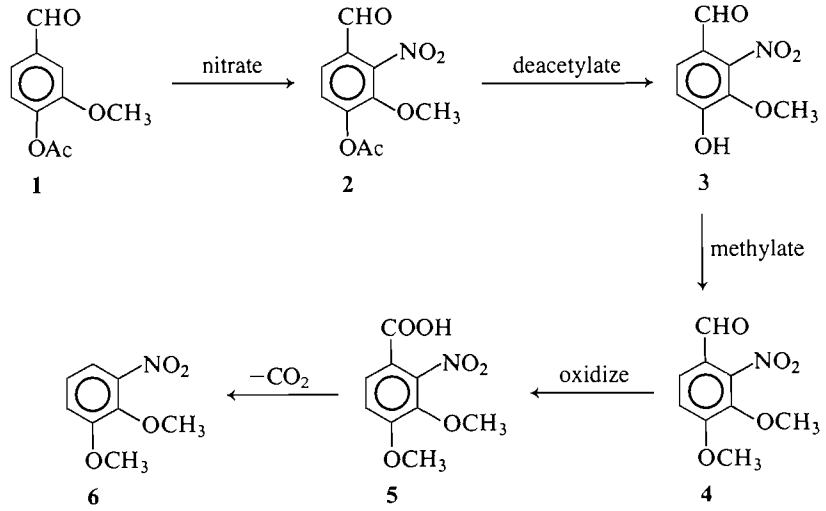
[1]S. de Vries, quoted in ref. 1.

Results and Discussion

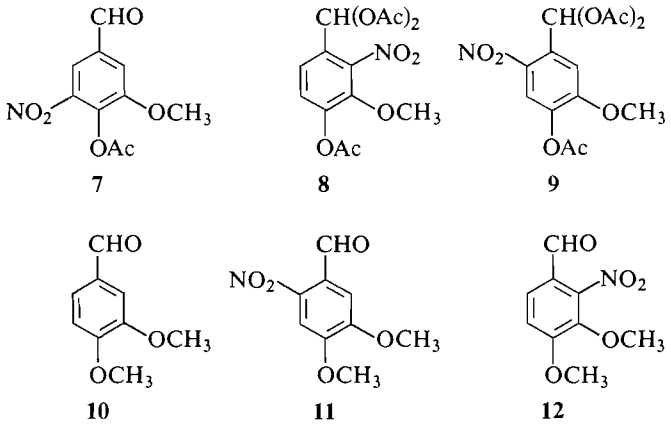
Synthesis of 3-nitroveratrole

We first attempted to reproduce an old synthesis (7, 8) of 3-nitroveratrole **6** from acetylvanillin **1** (Scheme 1). The critical step in this synthesis is the introduction of the nitro group at the 2-position of acetylvanillin to give the 1,2,3,4-tetrasubstituted benzene. According to the old literature (7) this is accomplished by dropping red fuming nitric acid onto dry, powdered acetylvanillin. In our hands, the major product of nitration by this route was **7**, with the two ring protons seen as narrow doublets ($J=2$ Hz), rather than the 8–10 Hz coupling that would be expected for protons *ortho* to each other, as in the desired compound **2**. Various nitrating conditions were tried, including HNO_3/H_2SO_4, HNO_3/Ac_2O, NO_2/Ac_2O, $HNO_3/NO_2/Ac_2O$, but in no case was the desired **2** more than a minor product. Concentrated, yellow fuming, and red fuming nitric acid were all tried. Under the milder conditions, the starting material was recovered; under forcing conditions the nitrotriacetates **8** (minor) and **9** were the major products. Nitration of vanillin methyl ether **10** was no more successful; the nitration product was **11** instead of the desired **12**.

We therefore abandoned a synthesis based on nitration in favour of a route based on the *ortho* lithiation of veratrole. Directed lithiations are particularly suited for the introduction of a new substituent *ortho* to one already present (9). The final synthesis is shown as Scheme 2. The lithiation of veratrole proceeded successfully as shown by the carbonation of the lithio derivative to the known 2,3-dimethoxybenzoic acid (10). The key to the synthesis of 3-nitroveratrole is the creation of the C—N bond. Unfortunately, few methods exist for this procedure. The direct introduction of an amino group occurs with methoxylamines (11) and reactions of aryllithiums with chloramine, nitrosyl chloride, and alkyl nitrates have all been reported, but the yields are poor. We attempted the direct introduction of the nitro group by the reaction of an aryllithium with



SCHEME 1. Planned synthesis of 3-nitroveratrole from acetylvanillin.



either N_2O_4 or $NO_2^+BF_4^-$, since NO_2^+ and CO_2 are isoelectronic. Unfortunately, electron transfer occurred, and the major organic product isolated was biphenyl (from phenyllithium as the lithio derivative).

We therefore employed the reaction between the aryllithium and *p*-toluenesulfonyl azide (12). The product was reduced to the amine by the use of sodium borohydride in a heterogeneous system with the aid of tetrabutylammonium hydrogen sulfate as a phase-transfer catalyst (13). Unfortunately, even under these conditions, the yield of the amine was relatively poor, and this meant that the overall synthesis of 3-nitroveratrole was not convenient for scaling up.

Oxidation of the amine to the nitro compound was achieved in two steps. The use of sodium tungstate/hydrogen peroxide (14) afforded comparable amounts of the nitroso compound and the corresponding azoxy compound, which was not wanted. This was circumvented by the modification of Agrawal and Bhattacharya (15) in which Mn(II) salts are used catalytically with sodium tungstate/H_2O_2, and the nitroso compound precipitates from the aqueous solution as it is formed. Finally, the nitroso to nitro conversion was effected by means of $Na_2Cr_2O_7/H_2SO_4$.

Photosubstitutions

In this preliminary survey, *o*-nitroanisole and 3-nitroveratrole were each reacted with three nucleophiles: OH^-, CN^-, and an amine. The solvent was 65:35 CH_3CN:H_2O by volume, and the reactions were carried out without deoxygenation. Control reactions showed that all of the reactions reported were true photochemical processes, and that no reaction occurred in the dark. Table 1 provides a summary of the study.

Photocyanation was the most straightforward reaction to interpret, with an exclusive *meta*-to-nitro orientation being observed. Thus 3-nitroveratrole afforded 2-methoxy-3-nitrobenzonitrile **13** in high yield, and with quantum yield (ϕ) close to 0.1, while *o*-nitroanisole yielded 4-methoxy-3-nitrobenzonitrile **14**, formal substitution of H^- having occurred. This behaviour is similar to that previously observed for the photoreaction of *p*-nitroanisole with this nucleophile (16). The selection of the position *meta* to the nitro group of *o*-nitroanisole is strongly influenced by solvent; in 65:35 CH_3CN:H_2O, **14** was the only product observed (HPLC), while in methanol we found that the alternative cyanation product **13** predominated. Previously, Letsinger and McCain (6) had found equal amounts of both products by the use of aqueous tertiary butyl alcohol as solvent.

Stern–Volmer plots of ϕ^{-1} vs. $[CN^-]^{-1}$ were linear for both substrates. For an S_N2 Ar* process, we would assume the mechanism of Scheme 3.

From Scheme 3, we obtain eq. [1] by the application of steady state kinetics.

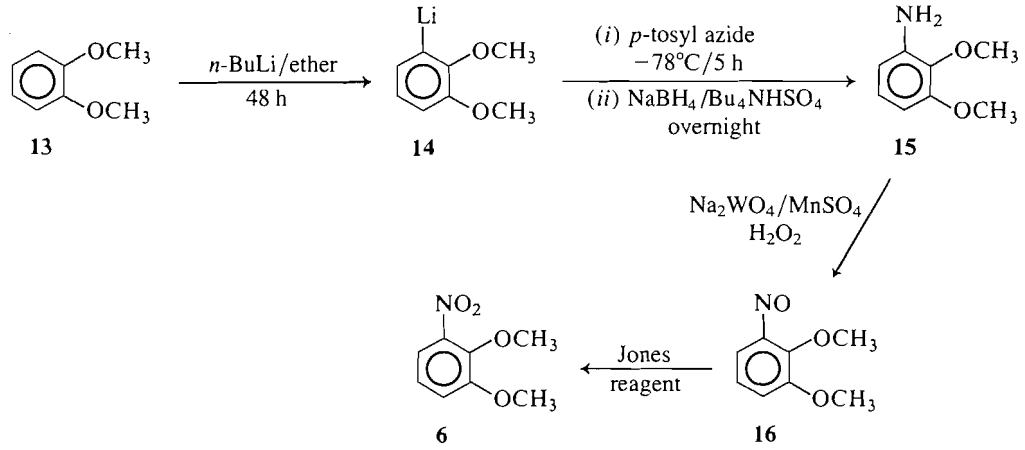
$$[1] \quad \phi^{-1} = \left(1 + \frac{k_3}{k_4}\right)\left(1 + \frac{k_1}{k_2[Nu^-]}\right)$$

As a generalization, the intercept of the double reciprocal plot gives the proportion of intermediates that return to starting material rather than proceed to product, while the ratio intercept/slope is the Stern–Volmer quenching constant K_{SV}, which is the product of the rate constant for quenching (k_2) and the unquenched excited state lifetime ($1/k_1$).

In the case of photocyanations involving the formal replacement of (H^-), the mechanism frequently occurs by way of radical ions and, in addition, the final step of Scheme 3 is complicated by the need for oxidation of the radical intermediate (ArHCN) (17). With these provisos, the K_{SV} and intercept can still be interpreted in terms of the efficiency of the original interaction between ArX* and CN^-, and the inefficiency of the steps following.

We see that photocyanation of *o*-nitroanisole proceeds with lower quantum yield than that of 3-nitroveratrole, as a result of the inefficiency of the later steps of the reaction. This is consistent with the need for oxidation of the intermediate. Most

Can. J. Chem. Downloaded from www.nrcresearchpress.com by 122.72.124.2 on 09/07/12
For personal use only.



SCHEME 2. Reaction sequence for the synthesis of 3-nitroveratrole.



probably, this photoreaction could be made much more efficient if it were to be assisted by an electron-accepting agent such as persulfate ion[2] or a polycyanoarene (19), but this was outside the scope of the present study.

The reactions with OH^- bore some resemblance to those with CN^-. 3-Nitroveratrole again reacted cleanly, and fairly efficiently (upper limit of $\phi = 0.1$) with replacement of the *meta* methoxy group. *o*-Nitroanisole reacted with lower quantum efficiency. This time no reaction occurred *meta* to nitro; instead, at $[OH^-] = 0.1$ M, replacement of the methoxy group (*ortho* to nitro, which is unusual) predominated over replacement of the nitro group (ipso, and also *ortho* to methoxy, which is more conventional). The behaviour of *o*-nitroanisole resembles that of the *para* isomer, which also undergoes replacement of both substituents upon photohydrolysis in aqueous *tert*-butyl alcohol (20).

In our study, *o*-nitroanisole afforded *o*-nitrophenol and *o*-methoxyphenol in the ratio ca. 3.6:1. This contrasts with an earlier study[1] in which a 10:1 ratio was observed. From our study of the effect of $[OH^-]$ upon ϕ, we see that, at least in aqueous CH_3CN, the product ratio is quite sensitive to the OH^- concentration. High hydroxide concentrations favour *o*-nitrophenol formation, and we predict that at sufficiently low concentrations ($[OH^-] < 5 \times 10^{-3}$ M) *o*-methoxyphenol should predominate.

Photosubstitutions involving amines are frequently complicated by electron-transfer processes, and either photoreduction at the nitro group (21) or substitution *para* (or *ortho* ?) to nitro may be anticipated. This was indeed observed in the reaction of 3-nitroveratrole with butylamine, where at $[BuNH_2] = 0.1$ M, *N*-butyl-2-methoxy-6-nitroanailine **15** and *N*-butyl-2-methoxy-3-nitroaniline **16** were formed with similar efficiency. However, the chemical yield and the quantum yield were both low. At lower concentrations of butylamine the replacement of the *meta* methoxy group predominated but, as shown by the double reciprocal plots (Fig. 1a), even this is not a conventional S_N2

[2]J. den Heijer, J. Cornelisse, and E. Havinga, quoted in ref. 1.

$$\begin{aligned}
ArX &\xrightarrow{h\nu} ArX^* \\
ArX^* &\xrightarrow{k_1} ArX \\
ArX^* + Nu^- &\xrightarrow{k_2} [ArXNu]^- \\
[ArXNu]^- &\xrightarrow{k_3} ArX + Nu^- \\
[ArXNu]^- &\xrightarrow{k_4} ArNu + X^-
\end{aligned}$$

SCHEME 3

Ar* reaction. When ϕ for formation of these two products was studied as a function of the butylamine concentration, the double reciprocal plots were curved. Empirically, it was discovered that a linear relationship existed between ϕ^{-1} and $[BuNH_2]^{-2}$ (Fig. 1b).

The photoreaction between *o*-nitroanisole and diethylamine, again in aqueous CH_3CN, yielded *o*-methoxyphenol as the only isolable product (yield 61%). The reaction has two notable features: first, the diethylamine does not become incorporated into the product; second, the quantum yield for formation of *o*-methoxyphenol is independent of $[Et_2NH]$ over the wide concentration range $4 \times 10^{-3} < [Et_2NH] < 0.1$ M (Fig. 2).

We were led to consider the possibility that the role of diethylamine in this reaction is simply to form a low concentration of hydroxide ion, through equilibrium [2].

$$[2] \quad Et_2NH + H_2O \rightleftharpoons Et_2NH_2^+ + OH^-$$

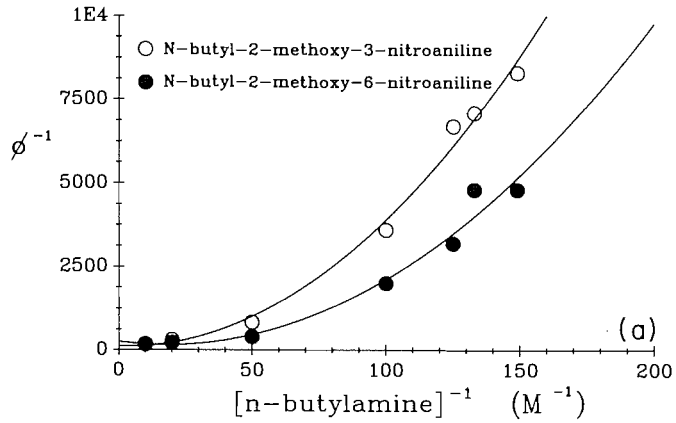
Aliphatic amines have $pK_b \sim 4$ in water, and hence in the partly aqueous solvent we can expect $K_b = 10^{-4}$ mol L^{-1} to be an upper limit. Over the concentration range $4 \times 10^{-3} < [Et_2NH] < 0.1$ M, the calculated maximum concentration of OH^- is $6 \times 10^{-4} < [OH^-] < 3 \times 10^{-3}$ M for $K_b = 10^{-4}$ mol L^{-1}. This is the concentration range for OH^- in which *o*-methoxyphenol is the predominant photosubstitution product. Since the Stern–Volmer plot for methoxyphenol production is rather flat (slope = 6 M, intercept = 2600), it is easily possible for the production of methoxyphenol to show no apparent dependence on $[Et_2NH]$. Nevertheless, it is still very unexpected that the only participation of diethylamine in the reaction is to be a source of OH^-; most methoxynitro compounds undergo reactions characteristic of electron transfer upon photoexcitation in the presence of secondary amines. To our knowledge, the only exception to this

Can. J. Chem. Downloaded from www.nrcresearchpress.com by 122.72.124.2 on 09/07/12
For personal use only.

TABLE 1. Photosubstitutions of *o*-nitroanisole and 3-nitroveratrole

Reactants[a]	Semipreparative, $Nu^- = 0.1$ M: Product	Yield	ϕ	Kinetic[b]: Slope	Intercept	K_{SV}
NA/CN^-	**14**	30	0.002	50±9	100±800	2
NA/OH^-	*o*-Nitrophenol	76	0.002	15±12	730±540	50
	o-Methoxyphenol	21	0.0006	5.8±6.5	2600±300	450
NA/Et_2NH	*o*-Methoxyphenol	61	0.002	0	580	—
NV/CN^-	**13**	79	0.095	0.52±0.02	5.2±1.0	10
NV/OH^-	2-Methoxy-3-nitrophenol	71	0.087	0.50±0.11	7.4±5.9	15
NV/$BuNH_2$	**16**	13	0.006	(39)[c]	—	—
	15	13	0.006	(22)[c]	—	—

[a]NA = *o*-nitroanisole; NV = 3-nitroveratrole.
[b]Slope: units M; K_{SV}: units M^{-1} from plot of ϕ^{-1} vs. $[Nu^-]^{-1}$.
[c]From plot of ϕ^{-1} vs. $[BuNH_2]^{-2}$.



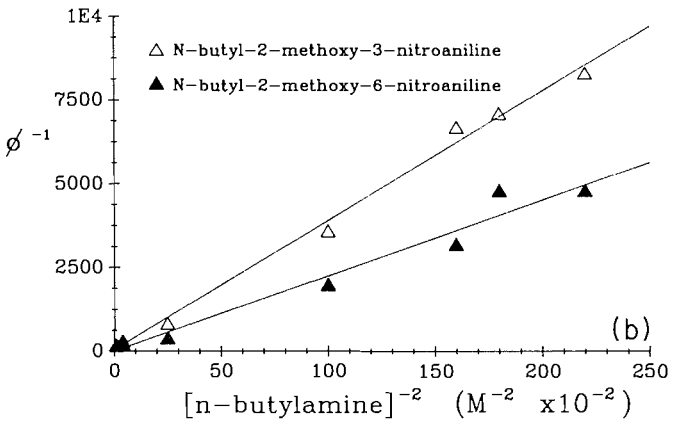


FIG. 1. Irradiation of 4.99×10^{-3} M 3-nitroveratrole and *n*-butylamine. (a) ϕ^{-1} versus $[nucleophile]^{-1}$; (b) ϕ^{-1} versus $[nucleophile]^{-2}$.

behaviour previously recorded is *m*-nitroanisole, which is unreactive towards diethylamine in aqueous CH_3CN solution (22).

Conclusions

o-Methoxynitro compounds display a range of behaviour upon photolysis in the presence of nucleophiles. Photocyanation is the most "conventional" process we have observed. Towards hydroxide ion, 3-nitroveratrole behaves similarly to 4-nitroveratrole,[3] with exclusive replacement of the *meta* methoxy group taking place. Likewise, *o*-nitroanisole undergoes photohydrolysis analogous to *p*-nitroanisole, with competing replacement of both substituents. Unexpected chemistry is seen with amines: 3-nitroveratrole reacts with butylamine in a reaction that appears to be second order in amine, while *o*-nitroanisole undergoes only photohydrolysis in the presence of diethylamine. Future work will be directed towards a more detailed study of the behaviour of these methoxynitro compounds with a range of amines, and towards time-resolved studies in order to elucidate reaction mechanisms in detail.

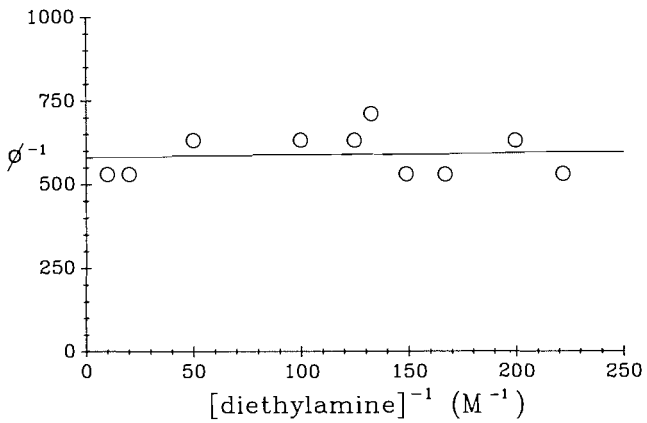


FIG. 2. Irradiation of 5.22×10^{-3} M *o*-nitroanisole and diethylamine; ϕ^{-1} versus $[nucleophile]^{-1}$.

Experimental

Materials and methods

Yellow fuming nitric acid was obtained from Fisher. Nitrogen dioxide was supplied by Matheson Gas Products.

Thin-layer chromatography (TLC) was performed using Eastman 13181 silica gel and 13252 alumina with fluorescent indicators. Column chromatography was performed on Davison Chemical silica gel 28–200 mesh, BDH silica gel 60–120 mesh, or Fisher neutral alumina. Small samples (≤1 g) were separated on Waters SEP-PAK silica or neutral alumina cartridges. Solvent compositions are given as volume ratios. Petroleum ether was the fraction of bp 30–60°C. Melting points were determined on a Mel-Temp apparatus and are uncorrected.

[3]J. L. Stratenus, quoted in ref. 1.

Can. J. Chem. Downloaded from www.nrcresearchpress.com by 122.72.124.2 on 09/07/12
For personal use only.

Can. J. Chem. Downloaded from www.nrcresearchpress.com by 122.72.124.2 on 09/07/12
For personal use only.

Nuclear magnetic resonance (NMR) spectra were obtained at 60 MHz in $CDCl_3$, using a Varian EM 360L NMR spectrometer, or at 400 MHz on a Bruker WH-400 NMR spectrometer.

Mass spectra of pure compounds were obtained using a VG Analytical 7070F mass spectrometer. Combined gas chromatography/mass spectrometry (gc/ms) was carried out on a VG MM 12000 analytical mass spectrometer interfaced to a Hewlett–Packard 5790 gas chromatograph equipped with a 30-m or 60-m quartz capillary column containing J & W DB-5 fused silica. Fourier transform – IR were processed using a Nicolet 20SX/C FTIR. UV/visible spectra were obtained using a Perkin–Elmer Lambda 3 UV/visible spectrometer.

HPLC analyses were performed on a Waters system: Waters 501 HPLC pump, U6K injector, and model 440 absorbance detector operated at 254 nm and recorded using a Hewlett–Packard 3390A integrator. Analytical separations were performed using a Waters NOVAPAK C_{18} 5 μ 3.9 mm × 7.5 cm column. Semi-preparative separations (≤ 1 g) were performed on a Whatman Magnum 9 Partisil ODS-3 C_{18} 9.4 mm × 25 cm column. All solvents used were HPLC grade and were filtered and degassed before use. Solvent compositions are given as volume ratios.

Preparation of red fuming nitric acid (ref. 24)

A distillation apparatus was set up, substituting a dropping funnel in place of a thermometer. The receiving flask was placed in ice. To the boiling flask was added 100 g KNO_3 and 3.5 g starch. Concentrated sulfuric acid (100 mL) was added slowly dropwise from the dropping funnel. The reaction, which proceeds virtually without the application of heat, was heated gently with a heating mantle only when necessary.

*Synthesis of 3,4-dimethoxy-6-nitrobenzaldehyde, **11** (ref. 7)*

A sample of 3,4-dimethoxybenzaldehyde (1.00 g) was cooled in an ice bath. Yellow fuming nitric acid was added slowly with stirring so that the temperature of the reaction did not exceed 6°C. The acid was added until all the 3,4-dimethoxybenzaldehyde had dissolved. The reaction mixture was poured into ice water. The nitro compound separated as an oil that solidified on standing. The solid was filtered, washed with 5% $NaHCO_3$, and then with water. TLC showed only one component to be present. The yellow solid was recrystallized from methanol/water. The resulting fluffy yellow precipitate of **11** (0.70 g) was filtered and dried. Yield 55%; mp 129–131°C (lit. (25) mp 129–131°C); NMR (60 MHz) δ: 4.00 (s, 6H), 7.36 (s, 1H), 7.58 (s, 1H), 10.5 (s, 1H) ppm.

Nitration of acetylvanillin

Several different nitration procedures were attempted. They are shown in Table 2.

Lithiation of veratrole (ref. 10)

All glassware was rinsed with acetone, followed by drying overnight at a temperature of ~110°C. The glassware was then flushed with nitrogen while still hot, to maintain a dry inert atmosphere. A solution of veratrole (3.45 g) in ether (50 mL) was dried over 3Å molecular sieves and added under a nitrogen atmosphere. To this was added with stirring 2.5 M *n*-butyllithium in hexanes (20 mL). The solution was stirred at room temperature for 48 h. The identity of the lithio derivative was confirmed in one experiment by pouring the reaction mixture onto Dry Ice. After the Dry Ice had sublimed, the organic residue was acidified with HCl. The aqueous mixture was then extracted into ether, followed by extraction with base. The base extract was acidified to yield a brown residue, which was recrystallized from water to yield the acid as a pale yellow solid; mp 120–121.5°C (lit. (10) mp 120–122°C); NMR (60 MHz) δ: 4.06 (s, 3H), 4.20 (s, 3H), 7.27 (d, J=8 Hz, 2H), 7.78 (t, J=8 Hz, 1H), 10.02 (br, 1H) ppm.

The attempted nitration of phenyllithium by $NO_2(g)$

In a well-dried round-bottom flask under positive pressure of nitrogen was placed 2.0 M phenyllithium in 70:30 cyclohexane/ether (20 mL). Nitrogen dioxide gas was bubbled through the solution for several minutes. The gas was then turned off and the reaction quenched using wet ether and then water. The organic and aqueous layers were separated, the aqueous layer being extracted twice with ether. The organic extracts were combined and dried over $MgSO_4$. The solvent was removed under reduced pressure, yielding a dark brown liquid that then solidified on standing. The solid, biphenyl, was purified on a Waters alumina SEP-PAK cartridge, eluting with 10% toluene/petroleum ether. It was further purified by recrystallization from 95% ethanol; mp 69–71°C (lit. (26) mp 71°C); NMR (60 MHz) δ: ~7.5 ppm (complex multiplet); MS m/e: 154(M^+, 100), 155(M+1, 13), 39(25).

The attempted nitration of phenyllithium by NO_2BF_4

To a 100-mL 3-necked round-bottom flask equipped with a dropping funnel was added by syringe 2.0 M phenyllithium in 70:30 cyclohexane/ether (5 mL). The solution was stirred at 0°C under positive pressure of nitrogen while 0.5 M NO_2BF_4 in sulfolane (20 mL) was added slowly dropwise. After ~10 min the reaction was quenched by adding sulfolane/water, followed by water. The reaction mixture separated into a brown lower layer and a thin yellow upper layer (believed to consist of cyclohexane and ether). The layers were separated, the brown layer being saved for determination of nitrite. The yellow layer smelled strongly of nitrobenzene. TLC on silica gel, eluting with 40% toluene/petroleum ether, showed two spots whose R_f values corresponded to nitrobenzene and biphenyl respectively. The two components were separated on Waters silica SEP-PAK cartridges using petroleum ether, affording biphenyl (78%) and nitrobenzene (3%).

Synthesis of p-*-toluenesulfonyl azide (ref. 27)*

The azide was prepared by adding, with swirling, sodium azide (14 g) in water (20 mL) to *p*-toluenesulfonyl chloride (34 g) in 95% ethanol (200 mL). After 1 h, the mixture was poured into water (400 mL). The sulfonyl azide (17 g) separated as an oily layer, which was collected, quickly washed three times with water, and dried over sodium sulfate. Yield 48%; IR: 2115 (N_3) cm^{-1}. It was dissolved in anhydrous ether and dried over 3Å molecular sieves. The solution was then refrigerated.

Formation of the amine (ref. 12)

A lithiated sample of veratrole was cooled in a Dry Ice/acetone bath while still under nitrogen. A solution of *p*-toluenesulfonyl azide (6 g) in ether (40 mL) was added dropwise. When the addition was complete, the resulting mixture was stirred for 5 h, maintaining the temperature at −78°C. It was then warmed to room temperature and tetrabutylammonium hydrogen sulfate (8.5 g) was added. Over a 30-min interval, sodium borohydride (2.9 g) in water (9 mL) was added dropwise, keeping the temperature below 30°C. After allowing the mixture to stir overnight, the ether layer was decanted. The aqueous layer was extracted with ether. The combined organic layers were dried over magnesium sulfate and the solvent evaporated, yielding 2,3-dimethoxyaniline as an amber liquid (0.99 g). Yield 26%; IR: ~3400, ~3500 (NH_2) cm^{-1}.

Oxidation of the amine to the nitroso compound (refs. 14, 15)

A solution of $MnSO_4 \cdot 7H_2O$ (1.9 g), $Na_2WO_4 \cdot 2H_2O$ (2.2 g), and water (50 mL) was prepared in a 125-mL Erlenmeyer flask. To this was added the 2,3-dimethoxyaniline (0.5 g). The mixture was stirred, producing a suspension of the amine, while 30% hydrogen peroxide (3 g) was added slowly dropwise. After several minutes a brown precipitate formed and rose to the top of the aqueous layer. The mixture was filtered by suction and the precipitate of 3-nitrosoveratrole was collected (0.39 g). Yield 72%; IR: 1596 (NO) cm^{-1}.

Oxidation to 3-nitroveratrole (ref. 28)

Jones reagent was prepared by dissolving chromium trioxide (26.72 g) in concentrated sulfuric acid (23 mL), which had been diluted to a volume of 100 mL with water. The crude 3-nitrosoveratrole (0.20 g) was dissolved in acetone (20 mL). The solution was cooled in a water bath, while maintaining a temperature of 15–20°C. To the solution was added dropwise with stirring 10 mL of Jones reagent, while maintaining the temperature below 20°C. The solution was stirred for 48 h, after which it was filtered by suction. The filtrate was then evaporated under reduced pressure. The residue was dissolved in ether and washed with water. The organic layer was dried over $MgSO_4$. The solvent was evaporated, yielding a yellow residue. The compound was purified on a

Can. J. Chem. Downloaded from www.nrcresearchpress.com by 122.72.124.2 on 09/07/12
For personal use only.

TABLE 2. Attempted nitrations of acetylvanillin

Procedure	Results
1. 90% HNO_3, cooled and added dropwise to acetylvanillin	Acetylvanillin; NMR δ: 2.30 (s, 3H), 3.84 (s, 3H), 7.27 (m, 3H), 9.91 (s, 1H) ppm
2. Red fuming HNO_3, cooled and added in excess to solid acetylvanillin	Major product: acetylvanillin; minor product: *o*-nitroacetylvanillin; NMR δ 2.36 (s, 3H), 3.92 (s, 3H), 7.56 (dd, J = 9 Hz, 2H), 9.94 (s, 1H) ppm
3. Red fuming HNO_3 at room temperature, added in excess	Acetylvanillin with minor nitro compound, identified by NMR
4. (*i*) Red fuming HNO_3 added; (*ii*) solution brought to room temperature	Oil; could not be precipitated
5. (*i*) Warm red fuming HNO_3; (*ii*) cooled in ice ~1 H	TLC indicated acetylvanillin
6. (*i*) Red fuming HNO_3; (*ii*) cool, 1 h; (*iii*) add more HNO_3	NMR: acetylvanillin and minor component of nitro compound
7. 3:1 H_2SO_4/HNO_3	No product isolated
8. 2:1 acetic anhydride/red fuming HNO_3	Oil; NMR: nitroacetylvanillin
9. 20% (m/v) acetylvanillin in acetic anhydride, red fuming HNO_3	Oil; TLC indicated nitro compound
10. 20% (m/v) acetylvanillin in acetic anhydride, saturated with NO_2 gas A. bubble NO_2 gas B. (*i*) red fuming NHO_3 (*ii*) bubble NO_2 gas	NMR: acetylvanillin Compound **9**: NMR δ: 2.10 (s, 6H), 2.33 (s, 3H), 3.95 (s, 3H), 6.26 (s, 1H), 7.90 (s, 1H), 8.30 (s, 1H) ppm; MS m/e: 299(15), 282(9), 253(23), 211(2), 198(60). Compound **8**: NMR δ: 2.13 (s, 6H), 2.38 (s, 3H), 3.92 (s, 3H), 7.30[a] (s, 2H), 7.68 (s, 1H) ppm; MS m/e: 299(15), 282(9), 239(23), 197(100), 196(13), 145(36), 103(52)

[a]Lanthanide shift experiments showed the splitting of this peak into two separate doublets.

Waters SEP-PAK silica cartridge using 10% petroleum ether/toluene. This procedure yielded a pale yellow solid, 3-nitroveratrole (0.16 g). Yield 74%; mp 62–64°C (lit. (ref. 25, p. 4266) mp 64–65°C; IR: 1550, 1340 cm^{-1}; NMR (400 MHz) δ: 4.93 (s, 3H), 4.99 (s, 3H), 7.11 (d, J=8 Hz, 2H), 7.33 (dd, J=8 Hz, J=3 Hz, 1H) ppm; MS m/e: 183(M^+, 50), 136(32), 122(30), 107(58), 92(33), 77(100), 65(18).

Preparative irradiation procedures

Preparative scale irradiations were performed in a 350-mL quartz immersion well equipped with a Hanovia 450-W medium pressure mercury lamp. The solutions were stirred using a magnetic stirrer. Alternatively, irradiations were performed in ~20-mL quartz ampoules, in a Rayonet model RPR photoreactor equipped with 16 mercury lamps. Three types of lamps were available, having maximum transmission at wavelengths of 254, 300, or 350 nm.

Determination of chemical yields

Standards for quantitation were prepared from products isolated or authentic samples where available: Solutions of 8.03×10^{-3} M *o*-nitroanisole in acetonitrile and aqueous 0.3 M nucleophile (NaOH, KCN, diethylamine) were prepared. In an 8 mm o.d. quartz ampoule the *o*-nitroanisole (1.3 mL) and nucleophile (0.7 mL) were combined to a final composition of 5.22×10^{-3} M *o*-nitroanisole and 0.1 M nucleophile in 65:35 acetonitrile/water. The samples were then irradiated for a specified period of time, after which they were analyzed for substrate and product by HPLC using the external standard method. A constant volume of external standard was added to each sample after irradiation. The height ratios of the product/external standard were calibrated against a prepared calibration standard. All samples were analyzed in triplicate. The values obtained are precise to within 5%.

Chemical yields for 3-nitroveratrole were determined in the same way with a solution of 7.67×10^{-3} M 3-nitroveratrole in acetonitrile. Also, *n*-butylamine was used as the aliphatic amine, rather than diethylamine as in the case of *o*-nitroanisole.

o-*Nitroanisole/OH^-*

A solution of $\sim 5 \times 10^{-3}$ M *o*-nitroanisole (0.23 g) and 0.1 M NaOH (1.2 g) in 1:1 tetrahydrofuran/water (300 mL) was irradiated for 6 h. After irradiation, the nonaqueous solvent was evaporated under reduced pressure. The remaining aqueous solution was extracted with dichloromethane. The aqueous solution was then neutralized and reextracted with dichloromethane. The two separated organic extracts were dried over $MgSO_4$ and the solvent removed under reduced pressure. The former extract yielded *o*-nitroanisole. The latter extract showed two spots on TLC. The two were separated on alumina with 10% petroleum ether/toluene. The two components were identified as *o*-nitrophenol (0.13 g) and *o*-methoxyphenol (0.03 g) by comparison with authentic standards.

o-*Nitroanisole/CN^-*

A solution of $\sim 5 \times 10^{-3}$ M *o*-nitroanisole (0.27 g) and 0.1 M KCN (2.28 g) in 1:1 *tert*-butanol/water (350 mL) was irradiated for 16 h. After irradiation, the solution was extracted with ether. The organic layer was dried over $MgSO_4$ and the solvent evaporated *in vacuo* on a rotary evaporator. The residue was chromatographed on a Waters alumina SEP-PAK cartridge, eluting with toluene. This procedure yielded a white solid (0.09 g), 3-methoxy-4-nitrobenzonitrile **14**; mp 150–151°C (lit. (16) mp 151°C); IR: 2230 (CN) cm^{-1}; NMR δ: 4.06 (s, 3H), 7.23 (d, 1H), 7.87 (dd, J=10 Hz, J=2 Hz, 1H), 8.18 (d, J=2 Hz, 1H) ppm; MS m/e: 178(M^+, 35), 148(33), 131(100), 117(71), 102(77), 89(37), 76(33), 62(56).

o-*Nitroanisole/diethylamine*

A solution of $\sim 5 \times 10^{-3}$ M *o*-nitroanisole (2.4 mL) and 0.1 M diethylamine (44 mL) in 1:1 tetrahydrofuran/water (300 mL) was irradiated for 25 h. The organic solvent was evaporated under reduced pressure. The aqueous layer was extracted with dichloromethane, and yielded unconsumed *o*-nitroanisole and one other component. The two were separated on alumina, eluting with 20% petroleum ether/toluene. The base extract yielded a single component, which, when purified on alumina with 20% petroleum ether/toluene, turned out to be the same compound separated in the neutral fraction. The compound was identified as *o*-methoxyphenol (0.1 g) upon comparison with an authentic sample.

3-Nitroveratrole/OH^-

A solution of 0.01 M 3-nitroveratrole (0.037 g) and 0.1 M NaOH (0.08 g) in 65:35 acetonitrile/water (20 mL) was irradiated in the Rayonet photoreactor (λ = 254 nm) for 30 min. After irradiation, the organic solvent was removed under reduced pressure. The aqueous solution was extracted with ether. The organic layer was dried over $MgSO_4$ and the solvent evaporated under reduced pressure to yield 3-nitroveratrole. The aqueous layer was acidified and reextracted with ether. The organic layer was dried over $MgSO_4$ and the solvent removed as above. It yielded a yellow liquid. Purification on a Waters silica SEP-PAK cartridge eluting with toluene yielded a pale yellow solid, 2-methoxy-3-nitrophenol (0.02 g); mp 93–101°C (lit. (18) mp

102–103°C); IR: 1340, 1528 (NO_2), 3489 (br), 3620 (OH) cm^{-1}; NMR δ: 3.98 (s, 3H), 6.12 (br, 1H), 7.12 (t, 1H), 7.25 (dd, J=8 Hz, J=2 Hz, 1H), 7.47 (dd, J=8 Hz, J=2 Hz, 1H) ppm; MS m/e: 169 (M^+, 80), 152(3), 139(4), 126(9), 107(71), 94(55), 77(41), 65(100).

3-Nitroveratrole/CN^-

A solution of 0.01 M 3-nitroveratrole (0.037 g) and 0.1 M KCN (0.14 g) in 65:35 acetonitrile/water (20 mL) was irradiated for 30 min in the Rayonet photoreactor (λ = 254 nm). After irradiation, the organic solvent was removed *in vacuo* on a rotatory evaporator. The aqueous layer was extracted with ether. The organic extracts were dried over $MgSO_4$ and the solvent evaporated once more. Evaporation yielded a brownish solid, which was chromatographed on a Waters silica gel SEP-PAK cartridge eluting with toluene. Evaporation of the solvent yielded a white solid (0.03 g) identified as 2-methoxy-3-nitrobenzonitrile, **13**; mp 101.5–103°C (lit. (16) mp 104–105°C); IR: 1350, 1543 (NO_2), 2233 (CN) cm^{-1}; NMR δ: 4.23 (s, 3H), 7.35 (t, 1H), 7.87 (dd, J=12 Hz, J=4 Hz, 1H), 8.05 (dd, J=8 Hz, J=4 Hz, 1H) ppm; MS m/e: 178 (M^+, 30), 148(82), 131(74), 117(100), 102(76), 90(60), 77(73), 62(96).

*3-Nitroveratrole/*n*-butylamine*

A solution of 0.01 M 3-nitroveratrole (0.037 g) and 0.2 M *n*-butylamine (0.4 mL) in 65:35 acetonitrile/water (20 mL) was irradiated for 10 h in the Rayonet photoreactor (λ = 300 nm). After irradiation, the organic solvent was evaporated and the aqueous layer extracted with ether. The organic layer was dried over $MgSO_4$ and the solvent evaporated *in vacuo* on a rotary evaporator. The residue was dissolved in a minimum amount of 65:35 methanol/water. The components were separated by semi-preparative HPLC. The mobile phase, 65:35 methanol/water, was delivered at a flow rate of 3.0 mL/min. Three components were separated: 3-nitroveratrole, *N*-butyl-2-methoxy-6-nitroaniline (0.0024 g) **15**, and *N*-butyl-2-methoxy-3-nitroaniline (0.0019 g) **16**. For **15**, IR: 1340, 1525 (NO_2), 3357, 3450 (NH) cm^{-1}; NMR δ: 0.93 (t, 3H), 1.40 (sextet, 2H), 1.58 (quintet, 2H), 3.54 (t, 2H), 3.85 (s, 3H), 6.62 (t, 1H), 6.91 (dd, J=8 Hz, J=2 Hz, 1H), 7.71 (dd, J=8 Hz, J=2 Hz, 1H) ppm; MS m/e: 224(M^+, 11), 207(1), 190(18), 181(100), 173(4), 162(65), 147(27), 134(62), 120(26), 106(55), 92(34), 77(58), 65(70). For **16**, IR: 1340, 1525 (NO_2), 3419, 3510 (NH) cm^{-1}; NMR δ: 0.98 (t, 3H), 1.46 (sextet, 2H), 1.64 (quintet, 2H), 3.15 (q, 2H), 3.62 (s, 3H), 6.80 (dd, J=8 Hz, J=2 Hz, 1H); 7.05 (t, J=8 Hz, 1H), 7.10 (dd, J=8 Hz, J=2 Hz, 1H) ppm; MS m/e: 224 (M^+, 37), 208(2), 193(1), 181(100), 161(3), 151(18), 134(24), 120(49), 106(43), 91(18), 77(35), 65(36).

Determination of quantum yields

Quantum yields were determined in duplicate using the method of Bunce, LaMarre, and Vaish (23) in which azoxybenzene in 95% ethanol was used as the actinometer. The method involved simultaneous irradiation of three solutions placed in 8 mm o.d. quartz ampoules held vertically in quartz test tubes of 16 mm o.d. The ampoules were filled with 2.0 mL of solution A. The test tube was filled to the same level with solution B. The solutions concerned were 1. A = test solution, B = water; 2. A = azoxybenzene, B = water; 3. A = azoxybenzene, B = test solution. All samples were irradiated in the Rayonet photoreactor using 300-nm lamps. The photoreactor was equipped with a "merry-go-round" to ensure equal illumination of all samples. After irradiation, solutions 2A and 3A were appropriately diluted with 1 M alcoholic KOH. The absorbance of these solutions at 458 nm was recorded. The difference in the absorbances of solutions 2A and 3A were used to calculate the amount of light absorbed by test solution 1A.

Kinetic irradiations

The conditions of irradiation used for mechanistic investigations mimicked those for the determination of quantum yields. The solution of interest (2.0 mL) was contained in an 8 mm o.d. quartz ampoule. Substrate loss and product formation were monitored by HPLC using the external standard method. All analyses were performed in duplicate with values agreeing to within 5%.

Acknowledgement

We thank the Natural Sciences and Engineering Research Council of Canada for financial support.

1. J. Cornelisse and E. Havinga. Chem. Rev. **75**, 353 (1975).
2. E. Havinga and J. Cornelisse. Pure Appl. Chem. **47**, 1 (1976).
3. J. Cornelisse, G. Lodder, and E. Havinga. Rev. Chem. Intermed. **2**, 231 (1979).
4. K. Mutai, R. Nakagaki, and H. Tukada. Bull. Chem. Soc. Jpn. **58**, 2066 (1985).
5. N. J. Bunce, S. R. Cater, J. C. Scaiano, and L. J. Johnston. J. Org. Chem. **52**, 4214 (1987).
6. R. L. Letsinger and J. H. McCain. J. Am. Chem. Soc. **91**, 6425 (1969).
7. R. Pschorr and C. Sumuleanu. Chem. Ber. **32**, 3407 (1899).
8. J. M. Gulland. J. Am. Chem. Soc. **26**, 2872 (1931).
9. P. Beak and V. Snieckus. Acc. Chem. Res. **15**, 306 (1982).
10. H. Gilman, J. Swiss and L. Cheney. J. Am. Chem. Soc. **62**, 1963 (1940).
11. P. Spagnolo, and P. Zanirato. J. Org. Chem. **43**, 3539 (1978).
12. J. N. Reed and V. Snieckus. Tetrahedron Lett. **24**, 3975 (1983); P. Spagnolo and P. Zanirato. J. Org. Chem. **47**, 3177 (1982).
13. R. Rolla. J. Org. Chem. **47**, 4327 (1982).
14. J. C. Stowell. J. Org. Chem. **36**, 3055 (1971).
15. G. L. Agrawal and A. K. Bhattacharya. Indian J. Chem. Sect. A, **16**, 900 (1978).
16. R. L. Letsinger and J. H. McCain. J. Am. Chem. Soc. **88**, 2884 (1966).
17. N. J. Bunce, J. P. Bergsma, and J. L. Schmidt. J. Chem. Soc. Perkin Trans. 2, 713 (1981).
18. T. J. F. Mattaar. Recl. Trav. Chim. Pays-Bas, **41**, 24 (1922).
19. K. Mizuno, C. Pac, and H. Sakurai. J. Chem. Soc. Chem. Commun. 353 (1975).
20. R. L. Letsinger, O. B. Ramsay, and J. H. McCain. J. Am. Chem. Soc. **89**, 2945 (1967).
21. D. Döpp. Top. Curr. Chem. **55**, 49 (1975).
22. S. R. Cater. Ph.D. thesis, University of Guelph. 1986.
23. N. J. Bunce, J. LaMarre, and S. P. Vaish. Photochem. Photobiol. **39**, 531 (1984).
24. H. F. Morley and M. M. P. Muir. *In* Watt's Dictionary of chemistry. Vol. 3. Longmans, Green and Co., London. 1912. p. 518.
25. J. H. Buckingham. Dictionary of organic compounds. 5th ed. Vol. 2. Chapman and Hall, New York. 1982. p. 2052.
26. J. H. Buckingham. Dictionary of organic compounds. 5th ed. Vol. 1. Chapman and Hall, New York. 1982. p. 672.
27. W. E. Doering and C. H. Depuy. J. Am. Chem. Soc. **75**, 5956 (1953).
28. L. F. Fieser and M. Fieser. Reagents for organic synthesis. Wiley, New York. 1967. p. 142.

Can. J. Chem. Downloaded from www.nrcresearchpress.com by 122.72.124.2 on 09/07/12
For personal use only.

An acidity scale, $[H^+]^{h\nu}$, for proton quenching of excited states

J. A. PINCOCK AND P. R. REDDEN
Department of Chemistry, Dalhousie University, Halifax, N.S., Canada B3H 4J3
Received April 28, 1988

J. A. PINCOCK and P. R. REDDEN. Can. J. Chem. **67**, 227 (1989).

An acidity scale for excited state protonation kinetics in 20% ethanol:80% aqueous sulfuric has been developed using 1-cyanonaphthalene as a fluorescent indicator. The utility of this new scale is demonstrated using the proton quenching of fluorescence of a variety of chromophores. These include 1- and 2-cyanonaphthalenes, 1- and 2-methoxynaphthalenes, benzyl alcohols, toluenes, and 2-vinylnaphthalene.

Key words: acidity scale, fluorescence quenching, excited state basicity.

J. A. PINCOCK et P. R. REDDEN. Can. J. Chem. **67**, 227 (1989).

Utilisant le cyano-1 naphtalène comme indicateur fluorescent, on a développé une échelle d'acidité pour la cinétique de la protonation de l'état excité dans un mélange éthanol/acide sulfurique 20/80. On démontre l'utilité de cette nouvelle échelle en utilisant l'extinction par les protons de la fluorescence d'une grande variété de chromophores, dont les cyano-1 (et -2) et méthoxy-1 (et -2) naphtalènes, les alcools benzyliques, les toluènes et le vinyl-2 naphtalène.

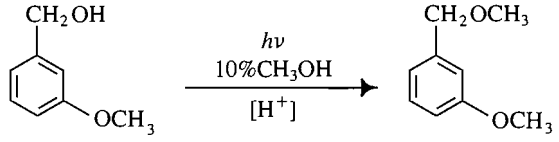
Mots clés : échelle d'acidité, extinction de la fluorescence, basicité de l'état excité.

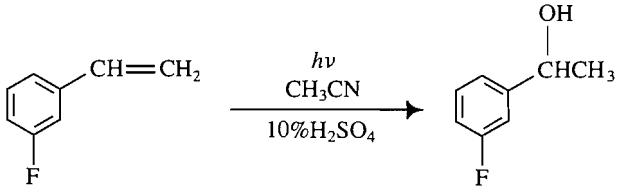
[Traduit par la revue]

Can. J. Chem. Downloaded from www.nrcresearchpress.com by 122.72.124.2 on 09/07/12
For personal use only.

Introduction

We have recently outlined in a preliminary communication a procedure for establishing an acidity scale, $[H^+]^{h\nu}$, for proton quenching of excited states (1). It proved to be a useful method of linearizing otherwise non-linear Stern–Volmer fluorescence quenching plots and, along with lifetimes of the excited singlet states, obtaining quenching rate constants. Moreover, the results sugested that $[H^+]^{h\nu}$ may be a fundamental property of the medium independent of the functional group being protonated. The method relies on the fact that a functional group may have increased basicity in its excited singlet state (2). Recent studies have also demonstrated that, after excited state protonation, reaction may occur. Examples of this are the studies by Wan and Turro (3, 4) on the photosolvolysis of benzyl alcohols, eq. [1], and Yates *et al.* (5–7) on the photohydrations of alkenes and alkynes, eq. [2]. In these cases, rate-determining excited

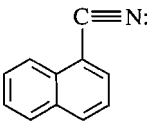
[1] 

[2] 

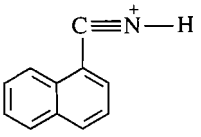
singlet state protonation was easily monitored by either quenching of the substrate fluorescence or by product formation. Determination of the quenching rate constant, k_q, is simple if the quenching occurs in a region where the concentration of the protons gives a reasonable estimate of the proton activity. However, in many cases, appreciable quenching does not occur until higher proton concentrations are reached and Stern–Volmer plots of either fluorescence intensity I^0/I, or reaction quantum yield Φ^0/Φ, versus proton concentration are curved. An acidity scale approach would seem to be the next logical step to follow. Neither of these previous studies discuss this obvious possibility of using well established ground state scales (8, 9) and, therefore, we assumed that correlations attempted were unsuccessful (*vide infra*).

Ground state acidity scales and their application to acid-catalyzed reactions have been extensively studied (for a review, see refs. 10, 11). These ground state scales were initially determined by the Hammett assumption of the cancellation of indicator activity coefficient ratios in acid–base equilibria, i.e. the zero'th order approximation (for a review, see ref. 10). Later approaches such as the Bunnett–Olsen method (12, 13) or excess acidity (14) are based on the assumption that, for different bases, activity coefficient ratios of the form log $(f_B f_{H^+}/f_{BH^+})$ are linear functions of one another, i.e. the first order approximation. An excited state scale may be inherently different in that the measurable quantities such as Φ_F or Φ_R are always ratios relative to other processes of the same excited state. Moreover, excited state protonations for the example reactions, eq. [1] and eq. [2], seem to be irreversible. Although cases of reversible excited state acid–base equilibria are well known (2), evidence against reversibility is reported for the styrene substrates, eq. [2], since no hydrogen–deuterium substrate–solvent exchange was observed (15) at acidities where the excited state was efficiently quenched. Therefore, since these excited state protonations occur for reactions proceeding by the mechanism of kinetic rate-determining proton catalysis rather than pre-equilibrium proton catalysis, a different approach is necessary.

In this paper, we report full details of our previous communication (1) on a method to establish an acidity scale in 20% ethanol: 80% aqueous sulfuric acid for protonation of excited states, using 1-cyanonaphthalene, **1**, as a fluorescent indicator.



1



18

This particular acidic medium was chosen because it has a well defined ground-state H_0 scale (13, 16) and because the substrates we wished to examine had better solubility in it than in aqueous sulfuric acid alone. The choice of indicator was

TABLE 1. Fluorescence quenching values in 20% ethanol:80% aqueous sulfuric acid for compounds **1–5**

		$I^0/I^{a,b}$				
$[H^+]^c$	$C_{H^+}{}^d$	**1**	**2**	**3**	**4**	**5**
0.100	0.065	1.05	1.04	1.02	1.03	1.03
0.250	0.151	1.11(1.09)	1.08(1.08)	1.04	1.06	1.07
0.350	0.209	1.16	1.12	1.09	1.10	1.09
0.513	0.302	1.23(1.20)	1.15(1.10)	1.13	1.14	1.14
0.782	0.456	1.35(1.36)	1.23(1.17)	1.23	1.19	1.22
0.977	0.569	1.43(1.45)	1.31(1.23)	1.29	1.25	1.29
1.175	0.683	1.52(1.61)	1.43(1.53)	1.32	1.30	1.36
1.448	0.840	1.74	1.52	1.42	1.43	1.52
1.992	1.15	2.14	1.82	1.65	1.65	1.81
2.653	1.53	2.78	2.21(2.19)	2.05	2.06	2.26
2.963	1.73	3.15	2.44	2.29	2.21	2.53
3.960	2.31	4.65	3.52	3.28	3.27	3.62
5.130	2.98	7.38	5.09	5.04	5.04	5.86
5.939	3.45	10.0	7.04	6.73	7.00	8.12
6.851	3.97	13.8	9.59	10.6	10.8	11.9
7.748	4.49	20.5	14.1	15.0	16.2	17.8
8.455	4.89	28.3	19.7	21.5	23.1	25.6
9.303	5.38	40.9	27.4	34.0	32.6	36.1
10.24	5.91	56.0	36.4	42.7	45.3	49.2
11.16	6.43	78.0	50.0	60.8	68.5	73.9
12.05	6.94	102	69.2	81.5	88.5	95.0

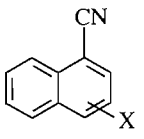
[a] I^0 refers to fluorescence intensity in 20% ethanol:80% water.
[b] Lifetime ratios as determined by single photon counting are given in parentheses.
[c] Determined by titration.
[d] C_{H^+} values were determined by interpolation of data in aqueous sulfuric acid from ref. 14.

based on the reported observation that 1-cyanonaphthalene has a high quantum yield of fluorescence (Φ_F = 0.37) and yet its fluorescence begins to be quenched in moderately acidic solutions (17). Moreover, estimates of the ground-state pK (~ −10) of its conjugate acid, **18**, indicate that ground-state protonation will not occur even in quite concentrated acidic solutions (18).

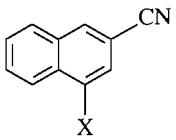
Results

The following compounds were studied. Compounds **1**, **6**, **9**, **12**, **13**, **14**, **15**, and **16** are commercially available (Aldrich). The preparation of **2**, **5**, **7**, **8**, and **11** have been described in previous work from this laboratory (19). Compounds **10** (20), **4** (21), and **3** (22) were prepared as reported in the literature.

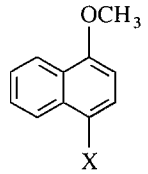
Fluorescence quenching values and, in some cases, singlet lifetimes as a function of acidity in 20% ethanol:80% aqueous sulfuric acid are reported in Table 1 (**1–5**), Table 2 (**6–11**), and Table 3 (**12–16**). All results are at 25.0 ± 0.1°C. Since very small amounts of contaminating impurities in these compounds could have fluorescence that was unquenched by protons and therefore lead to erroneous results, no I^0/I values over 100 were used.



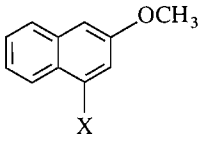
1 X = H
2 X = 4-CH_3
3 X = 3-CH_3



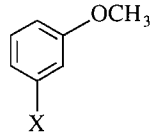
4 X = H
5 X = CH_3



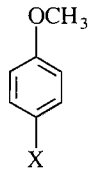
6 X = H
7 X = CH_3
8 X = CH_2OH



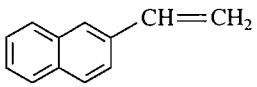
9 X = H
10 X = CH_3
11 X = CH_2OH



12 X = CH_3
13 X = CH_2OH



14 X = CH_3
15 X = CH_2OH



16

Discussion

Empirical evaluation of $[H^+]^{h\nu}$ and its application to Stern–Volmer plots

The fluorescence quenching data for **1** are plotted versus titratable proton concentration in Fig. 1. The lower line in the inset shows an expansion of the region up to 1.2 M in proton concentration as determined by titration. The least squares slope of this line is equal to 0.442 + 0.002 M^{-1}. Obviously, below 1.2 M the normal Stern–Volmer relationship, $I^0/I = 1 + K_{SV}[H^+]$ holds. (In this paper the symbol $[H^+]$ is used to define the concentration of protons as determined by titration, i.e., the normality of sulfuric acid. It is not the same as C_{H^+}, the concentration of free protons in the solution (*vide infra*). We have chosen to use $[H^+]$ as a measure of the acid concentration because it is a determinable experimental quantity.) As can be

Can. J. Chem. Downloaded from www.nrcresearchpress.com by 122.72.124.2 on 09/07/12
For personal use only.

TABLE 2. Fluorescence quenching values in 20% ethanol:80% aqueous sulfuric acid for compounds **6–11**

	$I^0/I^{a,b}$					
$[H^+]^c$	**6**	**7**	**8**	**9**	**10**	**11**
0.100	2.20	2.45	2.25	1.03	1.05	1.01
0.250	3.86	6.45	3.92(3.23)	1.04	1.08	1.03
0.350	4.92	8.49	5.08(5.71)	1.03	1.11	1.06
0.513	7.12	11.6	6.74	1.02	1.13	1.07
0.782	10.0	17.7	9.63	1.03	1.20	1.14
0.977	12.4	23.2	12.0	1.07	1.23	1.16
1.175	14.7	27.3	13.7	1.06	1.29	1.20
1.448	18.6	32.4	17.0	1.07	1.41	1.23
1.992	23.3	44.9	24.1	1.13	1.58	1.42
2.653	34.1	60.0	32.2	1.18	1.90	1.57
2.963	37.8	62.9	36.4	1.24	2.07	1.65
3.960	41.9	88.0	73.9	1.43	2.78	2.19
5.130	70.2		91.7	1.74	3.96	3.05
5.939	83.3			2.07	5.34	4.29
6.851				2.58	7.28	5.70
7.748				3.25	10.0	8.67
8.455				4.40	12.5	11.9
9.303				6.59	20.8	18.1
10.24				8.71	27.2	26.3
11.16				11.7	39.7	35.1
12.05				15.5	50.7	44.5

[a]I^0 refers to fluorescence intensity in 20% ethanol:80% water.
[b]Lifetime ratios as determined by single photon counting are given in parentheses.
[c]Determined by titration.

TABLE 3. Fluorescence quenching values in 20% ethanol:80% aqueous sulfuric acid for compounds **12–16**

	$I^0/I^{a,b}$				
$[H^+]^c$	**12**	**13**	**14**	**15**	**16**
0.100	1.08	1.84	1.10	1.01	1.04
0.250	1.12	2.84	1.12	1.03	1.07(1.07)
0.350	1.31	3.51	1.13	1.07	1.10
0.513	1.35	4.58	1.12	1.07	1.18(1.13)
0.782	1.57	6.67	1.17	1.09	1.16(1.18)
0.977	1.71	8.03	1.18	1.11	1.20(1.17)
1.175	1.73	9.54	1.20	1.12	1.19(1.20)
1.448	2.10	11.6	1.28	1.17	1.23(1.23)
1.992	2.63	16.2	1.42	1.22	1.24(1.32)
2.653	3.12	22.6	1.57	1.31	1.31(1.37)
2.963	3.56	27.3	1.67	1.39	1.36(1.43)
3.960	5.21	38.6	2.07	1.53	1.67(1.66)
5.130	7.92	57.9	2.63	2.05	2.00(2.15)
5.939	10.8	68.6	3.43	2.57	2.90(2.66)
6.851	15.1	91.7	4.71	3.23	3.52(3.53)
7.748	18.3		5.64	3.99	4.21(4.75)
8.455	24.8		8.88	5.16	5.86(6.31)
9.303	36.3		12.7	7.27	10.6(8.63)
10.24	42.5		16.1	9.09	12.8(11.6)
11.16	56.6		22.9	12.1	18.5(16.9)
12.05	68.6		28.9	15.3	23.3(21.5)

[a]I^0 refers to fluorescence intensity in 20% ethanol:80% water.
[b]Lifetime ratios as determined by single photon counting are given in parentheses.
[c]Determined by titration.

seen from Fig. 1, above 1.2 *M* the plot becomes curved. This curvature begins as the activity of the protons becomes very different from the concentration.

In an attempt to obtain a straight line, I^0/I fluorescence values for **1** were plotted versus h_0, the ground state acidity function (16), as shown in Fig. 2. The plot, overall, is not linear, indicating that the ground state acidity function is not useful in this case. The more general excess acidity scale (14) is not available for 20% ethanol:80% aqueous sulfuric acid so a correlation could not be attempted.

However, as has been demonstrated (13), the general function (H_0 + log C_{H^+}) where C_{H^+} is the molarity of sulfuric acid, as determined by titration, is a useful way of correlating data for this mixed solvent.[1] In fact, in purely aqueous sulfuric acid $H_0 + \log C_{H^+} \simeq -X$ (23). The assumption used here is the original Bunnett/Olsen one (12), that sulfuric acid is monodissociated so that C_{H^+} is half the concentration of titratable protons. As shown in column 2 of Table 1 this is not quite true for purely aqueous sulfuric acid (14). Values are not known for most mixed organic solvent/aqueous media such as the 20% ethanol/80% aqueous sulfuric acid used here.

Although Stern–Volmer kinetic experiments are not usually treated using logarithmic scales of concentration, rearrangement is possible giving eq. [3]. Since $k_qC_{H^+}$ corresponds to k_ψ, the observable pseudo-first order rate constant in an $A\text{–}S_E2$ type mechanism, eq. [4] can be derived (24) where ϕ^*, the slope

$$[3] \quad (I^0/I - 1)/\tau^0 = k_qC_{H^+}$$

[1]We thank a referee for this suggestion.

Can. J. Chem. Downloaded from www.nrcresearchpress.com by 122.72.124.2 on 09/07/12
For personal use only.

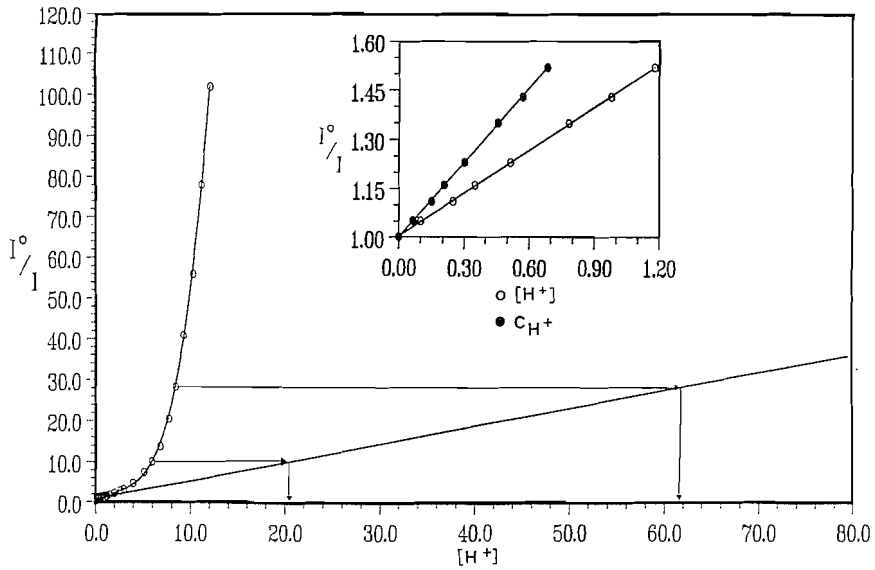


FIG. 1. Stern–Volmer quenching plot for 1-cyanonaphthalene of fluorescence intensity versus titratable $[H^+]$ in 20% ethanol:80% aqueous H_2SO_4 at 25°C. The lower line in the inset is for the region below $[H^+] = 1.20\ M$; the upper line is for the same data using C_{H^+}.

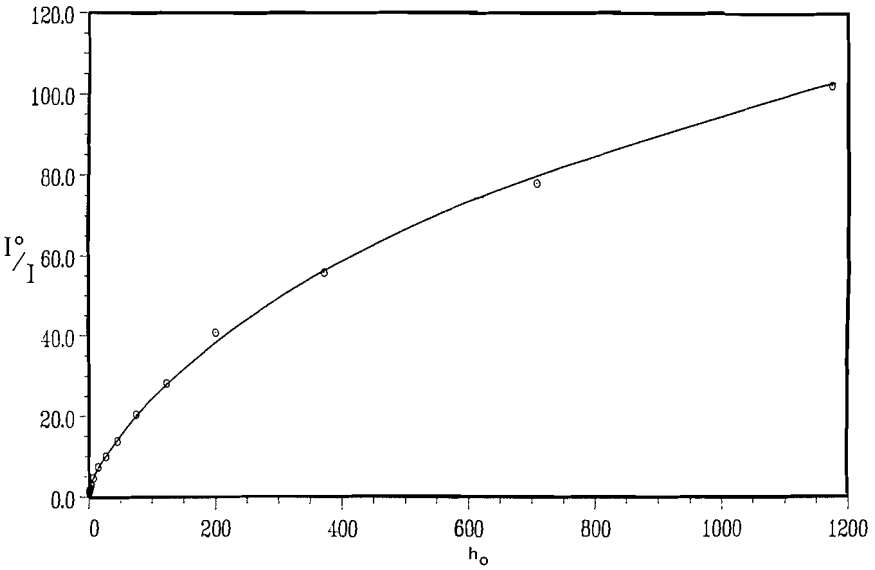


FIG. 2. Fluorescence intensity of 1-cyanonaphthalene versus h_0, the ground-state acidity function in 20% ethanol:80% aqueous H_2SO_4.

[4] $$\log\{(I^0/I - 1)/\tau^0\} + H_0 = \phi^*(H_0 + \log C_{H^+}) + \log k_q$$

parameter, is a measure of the solvation requirements of the transition state for protonation. The values required for this type of plot are in Table 4 for 1-cyanonaphthalene and the data is plotted in Fig. 3. A difficulty with this method becomes apparent. The experimentally most reliable values in Stern–Volmer plots are in the range of I^0/I from 1 to 10. Over this range the term ($\log k_\psi + H_0$) hardly changes and the points are all clustered in the top right of the plot with essentially zero slope. A least-squares correlation for all points gives an intercept of 8.11 ($r^2 = 0.983$) leading to $k_q = 13 \times 10^7\ M^{-1}\ s^{-1}$. Treatment of the results for all other compounds leads to very similar plots. The values of k_q that result are in Table 5.

Our method of evaluating an excited state acidity scale, $[H^+]^{h\nu}$, which is a linear rather than a logarithmic scale, was accomplished in the following manner. The linear portion of the Stern–Volmer fluorescence quenching plot for **1** (Fig. 1; lower line of inset) was extended well beyond the linear region. Evaluation of $[H^+]^{h\nu}$ at any $[H^+]$ involved only a projection from the quenching curve to the line obtained by extrapolating the slope of the linear region determined at low $[H^+]$ concentration. This is shown pictorially in Fig. 1. Mathematically, the values were determined from the Stern–Volmer slope. Values of $[H^+]^{h\nu}$, given in Table 4, represent the real quenching behavior of the acid media, at least for 1-cyanonaphthalene. Note that although most acidity scales are logarithmic, we have established the scale in concentration units in order for it to be compatible with photochemists' Stern–Volmer treatments.

The first obvious concern is that the projections required are long and the scale may, therefore, be unreliable. Table 4 shows that $[H^+]^{h\nu}$ values are between one and two orders of magnitude larger than the corresponding values of titratable protons. Moreover, the values are different from the corresponding

Can. J. Chem. Downloaded from www.nrcresearchpress.com by 122.72.124.2 on 09/07/12
For personal use only.

TABLE 4. Excited state acidity data derived from the fluorescence quenching of 1-cyanonaphthalene

wt%[a]	$[H^+]^b$	I^0/I	h_0[c]	H_0[d]	$H_0 + \log C_{H^+}$[e]	$\log k_\psi + H_0$[f]	$[H^+]^{h\nu}$[g]
0.53	0.100	1.05					0.100
1.32	0.250	1.10	0.178	+0.75	−0.153	7.76	0.250
1.84	0.350	1.16	0.251	+0.60	−0.157	8.02	0.350
2.64	0.513	1.23	0.355	+0.45	−0.140	8.03	0.513
4.08	0.782	1.35	0.562	+0.25	−0.158	8.01	0.782
5.18	0.977	1.43	0.708	+0.15	−0.161	8.00	0.977
5.94	1.175	1.52	0.891	+0.05	−0.181	7.98	1.18
7.69	1.448	1.74	1.12	−0.05	−0.190	8.03	1.67
10.1	1.992	2.14	1.78	−0.25	−0.252	8.02	2.58
13.4	2.653	2.78	2.82	−0.45	−0.327	8.02	4.03
14.9	2.963	3.15	3.39	−0.53	−0.354	8.02	4.86
19.3	3.960	4.65	6.76	−0.83	−0.533	7.95	8.26
24.5	5.130	7.38	14.8	−1.17	−0.761	7.85	14.4
27.8	5.939	10.0	26.9	−1.43	−0.957	7.74	20.4
31.8	6.851	13.8	44.7	−1.65	−1.12	7.67	29.0
35.6	7.748	20.5	74.1	−1.87	−1.28	7.63	44.1
39.2	8.455	28.3	123	−2.09	−1.46	7.56	61.8
42.8	9.303	40.9	200	−2.30	−1.63	7.52	90.3
46.1	10.24	56.0	372	−2.57	−1.86	7.39	124
49.3	11.16	78.0	708	−2.85	−2.10	7.25	174
52.5	12.05	102	1175	−3.07	−2.29	7.15	228

[a]Weight percent sulfuric acid assuming 100% sulfuric acid.
[b]Determined by titration.
[c]$h_0 = 10^{-H_0}$.
[d]See ref. 16.
[e]C_{H^+} values are the total sulfuric acid concentration as determined by titration (i.e. 1/2 the concentration of titratable protons). See ref. 13.
[f]log k_ψ values are determined from the expression log $\{(I^0/I - 1)/\tau\}$.
[g]From the expression $[H^+]^{h\nu} = (I^0/I - 1)/0.442 \pm 0.001\ M^{-1}$.

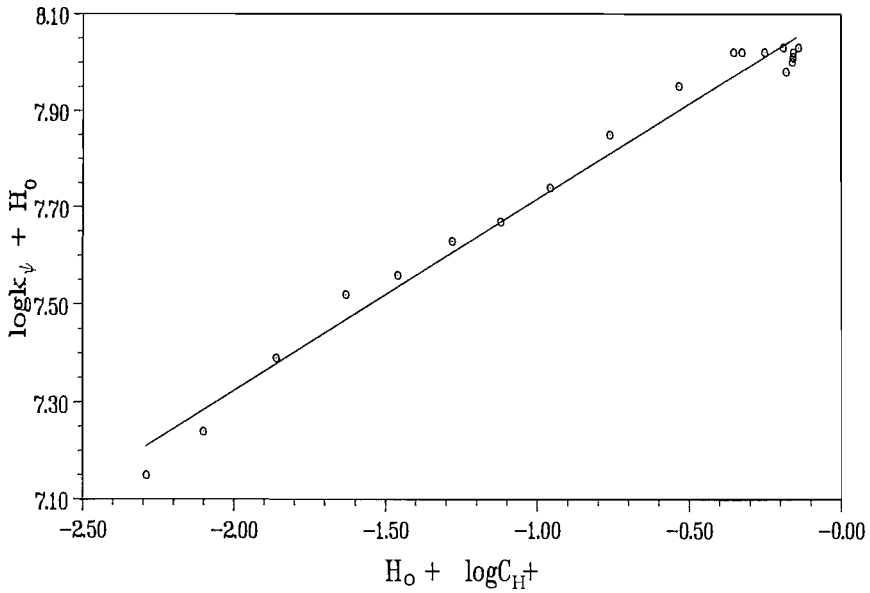


FIG. 3. A plot of log $k_\psi + H_0$ versus $H_0 + \log C_{H^+}$ for 1-cyanonaphthalene.

ground state acidity function, h_0. In fact, h_0 seems to undercorrect at low acidities but overcorrect at higher values. This shows that $[H^+]^{h\nu}$ is indeed a different type of scale and, therefore, tests of its applicability to other substrates are required.

In the previous communication (1), a variety of naphthalene substrates were studied including a series of 1-methoxy- (**6–8**) and 2-methoxy- (**9–11**) naphthalene derivatives. The plots of I^0/I versus $[H^+]^{h\nu}$ were all linear with very good correlation coefficients. These substrates were re-examined here at a constant temperature of 25.0 ± 0.1°C and over a larger range of acidic solutions. Normal Stern–Volmer plots versus titratable proton concentration were obtained for **6–8** (Fig. 4) in the low acid concentration region (<1.2 *M*). The Stern–Volmer slopes, K_{SV}, are given in Table 5. For compounds **9–11**, however, appreciable quenching occurred only at higher acidities (Fig. 5; inset). Normal Stern–Volmer plots in the low acid region are

Can. J. Chem. Downloaded from www.nrcresearchpress.com by 122.72.124.2 on 09/07/12
For personal use only.

TABLE 5. Table of singlet lifetimes and Stern–Volmer results for various naphthalene derivatives

Compound	τ^a (ns)	$K_{SV}{}^{b,c,d}$ (M^{-1})	$10^{-9}\ k_q$ ($M^{-1}\ s^{-1}$)	$K_{SV}{}^{c,e}$ (M^{-1})	$10^{-7}\ k_q{}^f$ ($M^{-1}\ s^{-1}$)	$10^{-7}\ k_q{}^g$ ($M^{-1}\ s^{-1}$)
1[h]	6.1 ± 0.1	0.442 ± 0.002 (0.9998)	—	—	13 ± 0.1	13 ± 1 (0.983)
2	4.6 ± 0.1	0.299 ± 0.014 (0.991)	0.11	0.292 ± 0.001 (0.999)	11 ± 0.1	12 ± 1 (0.986)
3	6.3 ± 0.1	0.298 ± 0.016 (0.991)	0.081	0.350 ± 0.003 (0.999)	9.7 ± 0.1	6.8 ± 0.3 (0.910)
4[i]	14.6 ± 0.1	0.280 ± 0.017 (0.979)	0.033	0.381 ± 0.002 (0.998)	4.52 ± 0.02	2.9 ± 0.2 (0.959)
5	11.9 ± 0.1	0.347 ± 0.021 (0.977)	0.050	0.411 ± 0.004 (0.999)	5.97 ± 0.04	4.2 ± 0.2 (0.946)
6[j]	10.8 ± 0.1	11.9 ± 0.2 (0.998)			190 ± 2	210 ± 8 (0.988)
7	9.8 ± 0.1	22.2 ± 0.4 (0.998)			400 ± 5	440 ± 17 (0.984)
8	8.8 ± 0.1	10.9 ± 0.1 (0.999)			210 ± 2	220 ± 14 (0.923)
9[k]	10.3 ± 0.1	0.033 ± 0.010 (0.67)	~0.005	0.0630 ± 0.001 (0.999)	1.06 ± 0.01	0.79 ± 0.08 (0.930)
10	13.1 ± 0.1	0.249 ± 0.017 (0.973)	<0.03	0.218 ± 0.001 (0.998)	2.87 ± 0.01	3.4 ± 0.2 (0.987)
11	10.9 ± 0.1	0.169 ± 0.007 (0.989)	/0.04	0.195 ± 0.002 (0.998)	3.10 ± 0.02	2.3 ± 0.1 (0.961)
12	5.3 ± 0.1	0.715 ± 0.018 (0.996)			23 ± 1	22 ± 1 (0.983)
13[l]	4.1 ± 0.1	7.25 ± 0.06 (0.999)			310 ± 1	320 ± 9 (0.995)
14	4.1 ± 0.1	0.117 ± 0.015 (0.912)	0.049	0.123 ± 0.001 (0.999)	5.2 ± 0.1	9.0 ± 1.2 (0.893)
15	4.0 ± 0.1	0.104 ± 0.010 (0.946)	0.045	0.063 ± 0.001 (0.999)	2.8 ± 0.1	4.8 ± 0.2 (0.965)
16[m]	71.2 ± 0.1	~0.12 ± 0.02 (0.84)	<0.003	0.0986 ± 0.0015 (0.995)	0.240 ± 0.002	0.38 ± 0.06 (0.855)
		~0.14 ± 0.03[n] (0.92)	<0.003	0.0892 ± 0.0011 (0.999)	0.218 0.002	

[a]By single photon counting.
[b]I^0/I versus titratable protons, $[H^+]$.
[c]Errors are standard deviations of least squares line with correlation coefficients given in parentheses.
[d]Calculated from points up to $[H^+] = 1.20\ M$.
[e]I^0/I versus $[H^+]^{h\nu}$.
[f]Calculated from eq. [20] assuming $k_q^1\tau^{0l} = 1.73\ M^{-1}$.
[g]Determined from the least squares intercept of the log $\{(I^0/I - 1)/\tau^0\} + H_0$ versus $H_0 + \log C_{H^+}$ plot.
[h]Values of 4.4 ns, 0.28 M^{-1} and $6.4 \times 10^7\ M^{-1}\ s^{-1}$ are reported in 20% CH_3CN:80% water (17).
[i]Values of 12 ns, 0.29 M^{-1} and $2.4 \times 10^7\ M^{-1}\ s^{-1}$ are reported in 20% CH_3CN:80% water (17).
[j]Values of 8.9 ns, 9.6 M^{-1} and $1.08 \times 10^9\ M^{-1}\ s^{-1}$ are reported in 20% CH_3CN:80% water (17).
[k]Values of 10 ns, <0.03 M^{-1} and $<3 \times 10^6\ M^{-1}\ s^{-1}$ are reported in 20% CH_3CN:80% water (17).
[l]Values of 4.4 ± 0.3 ns, 16.2 ± 0.1 M^{-1} and $3.7 \pm 0.2 \times 10^9\ M^{-1}\ s^{-1}$ are reported in aqueous acid (3).
[m]Values of 58.2 ns and $4.6 \times 10^6\ M^{-1}\ s^{-1}$ from fluorescence quenching and $4.5 \times 10^6\ M^{-1}\ s^{-1}$ from lifetime measurements are reported for aqueous H_2SO_4 (5).
[n]Based on τ^0/τ versus $[H^+]$.

unreliable because quenching occurs only to a very small extent. If the quenching data are plotted versus $[H^+]^{h\nu}$, very good linear results are obtained (Fig. 5). Now the Stern–Volmer slopes can be determined with much more precision and are given in Table 5 along with the correlation coefficients.

Another series of naphthalene compounds studied include 1-cyano- (**1**–**3**) and 2-cyano- (**4**, **5**) naphthalenes. The fluorescence quenching data for these compounds are shown in Fig. 6; inset. In all cases, plots using $[H^+]^{h\nu}$ are linear (Fig. 6). The Stern–Volmer slopes are given in Table 5.

Clearly the results to this point indicate that the scale is useful in linearizing non-linear Stern–Volmer plots. The question of whether chemically reasonable k_q values can be obtained will be addressed later. Since only naphthalene derivatives had been studied thus far the generality of the procedure was not yet clear. Substrates with different chromophores were required. Two of the methoxy-substituted compounds, 3- and 4-methoxy benzyl alcohol **13**, **15**, studied by Wan and Turro (3, 4) were re-examined here along with 3- and 4-methoxy toluene **12**, **14**. The fluorescence quenching data for these compounds is shown in Figs. 4 and 7. For compounds **12** and **13** extensive quenching occurred in the low acid region and Stern–Volmer slopes can be obtained by normal plots versus titratable proton concentration. These are given in Table 5.

For the *para*-substituted compounds **14** and **15** attempts to evaluate the Stern–Volmer slopes were very unreliable due to

Can. J. Chem. Downloaded from www.nrcresearchpress.com by 122.72.124.2 on 09/07/12
For personal use only.

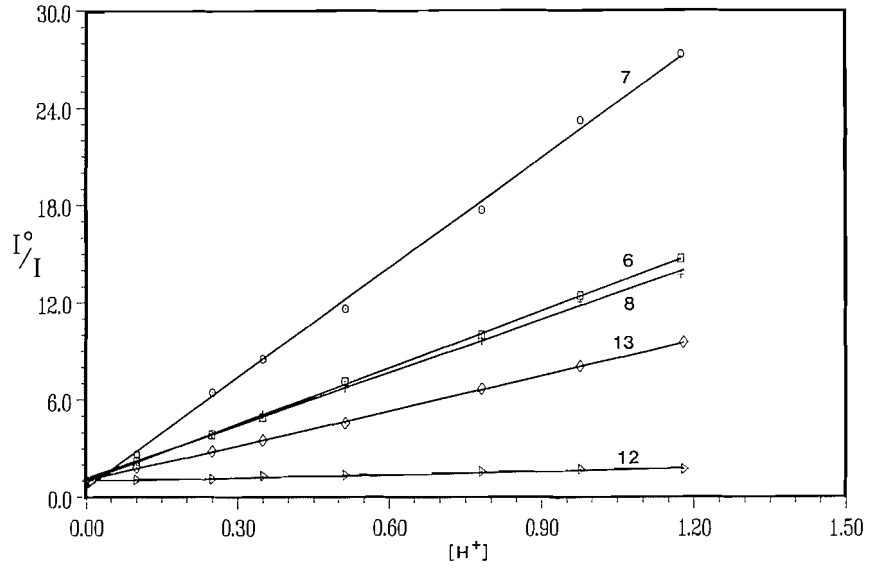


FIG. 4. Stern–Volmer quenching plots of fluorescence intensity versus titratable $[H^+]$ for **6**, **7**, **8**, **12**, and **13**.

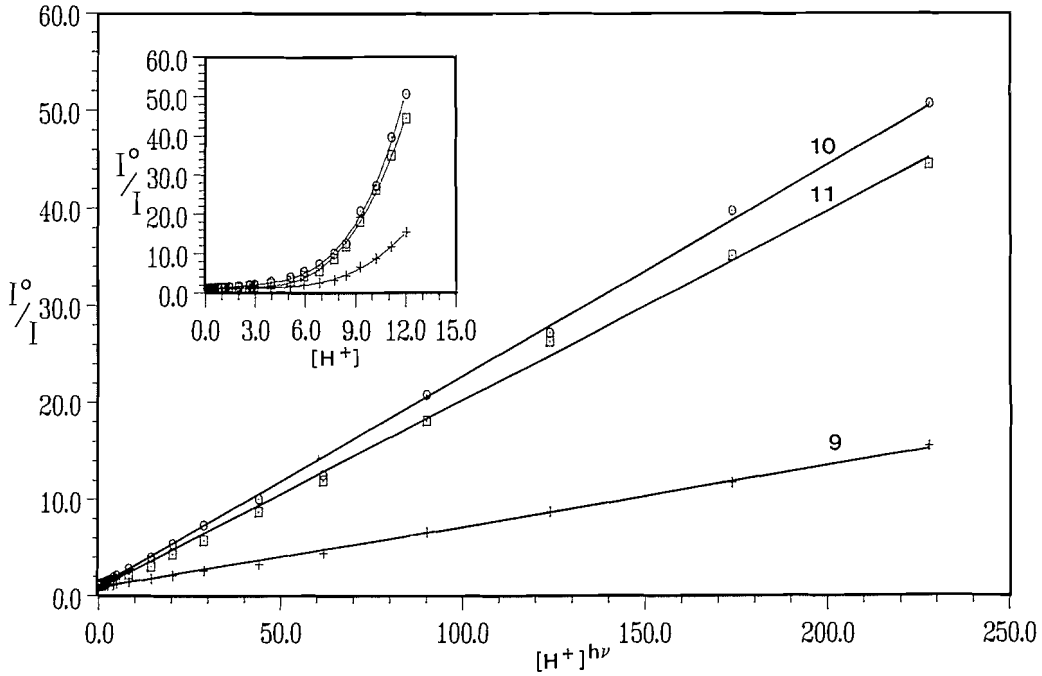


FIG. 5. Stern–Volmer quenching plots of fluorescence intensity versus $[H^+]^{h\nu}$ for **9**, **10**, and **11**. The inset shows the fluorescence intensity versus titratable $[H^+]$.

very little quenching. When I^0/I is plotted versus $[H^+]^{h\nu}$ as shown in Fig. 7 the correlation obtained is as good as it was for the naphthalene cases.

To test the usefulness and validity of the $[H^+]^{h\nu}$ scale further, the fluorescence quenching of 2-vinylnaphthalene, **16**, was studied. It is now well established that for many aromatic alkenes proton quenching of the excited state occurs at the double bond (5). For this particular compound the site of protonation is known to be at the beta carbon. As shown in Fig. 7 the results can again be correlated well using $[H^+]^{h\nu}$.

Derivation of the form of $[H^+]^{h\nu}$ using acidity scale concepts

In the previous section, we have demonstrated that a single indicator, 1-cyanonaphthalene, can be used to generate an empirical acidity scale. Surprisingly, this scale gave linear correlations for the proton quenching of a variety of functional groups. This is, in general, not true for ground state protonations and has resulted in different acidity scales for each functional group. Although some have called this "acidity function failure" (25), the development of the more general excess acidity scale (14) has shown that there is a relationship between the various scales. Our observation that there is an easily obtainable function, $f\{[H^+]\}$, which correlates data for excited state protonations, eq. [5], is therefore of interest.

$$[5] \quad I_F^0/F_F = 1 + K_{SV}f\{[H^+]\}$$

A derivation of the form of this function follows from the

Can. J. Chem. Downloaded from www.nrcresearchpress.com by 122.72.124.2 on 09/07/12
For personal use only.

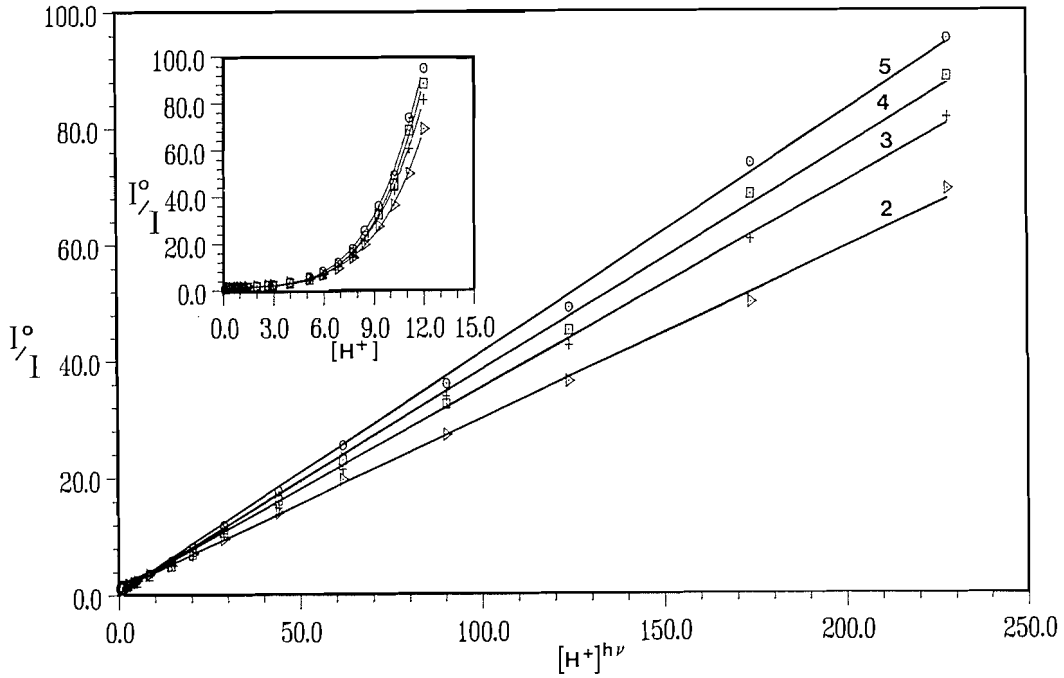


FIG. 6. Stern–Volmer quenching plots of fluorescence intensity versus $[H^+]^{h\nu}$ for **2**, **3**, **4**, and **5**. The inset shows the fluorescence intensity versus titratable $[H^+]$.

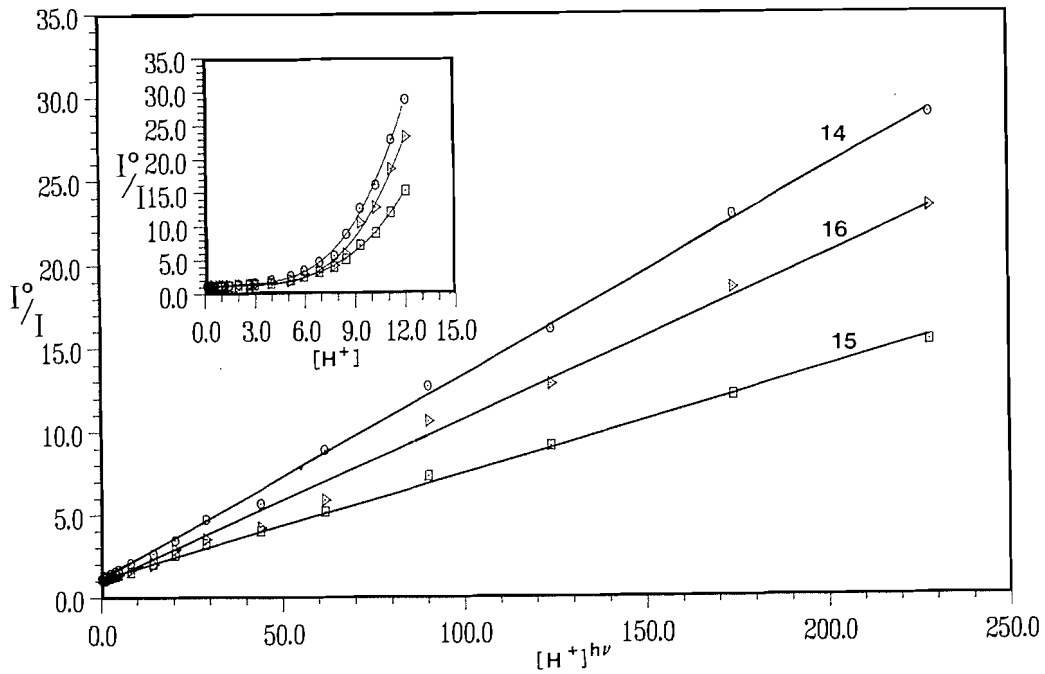


FIG. 7. Stern–Volmer quenching plots of fluorescence intensity versus $[H^+]^{h\nu}$ for **14**, **15**, and **16**. The inset shows the fluorescence intensity versus titratable $[H^+]$.

kinetic expression for excited state protonation using transition state theory in a way analogous to that for the kinetic expressions derived for ground state protonations (26).

In Scheme 1, S_0 is the ground state of the substrate, S_1 is the first excited singlet state, T is the triplet state, $[S_1—H^+]^{\ddagger}$ is the transition state for protonation of the excited singlet state, k_f is the rate constant for fluorescence, k_{ic} is the rate constant for internal conversion back to the ground state, k_{isc} is the rate constant for intersystem crossing to the triplet, and k_q is the bimolecular quenching rate constant.

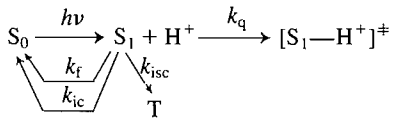
At any given acidity the decay of S_1 is pseudo-unimolecular according to eq. [6] where τ, the lifetime of the excited state, is the reciprocal of the sum of all the rate constants that lead to loss of S_1, eq. [7].

$$[6] \quad -d[S_1]/dt = (1/\tau)[S_1]$$

$$[7] \quad 1/\tau = k_f + k_{ic} + k_{isc} + k_q f\{[H^+]\}$$

From transition state theory, eq. [6] can be rewritten as eq. [8], assuming that k_q is the only activated process (27) described

Can. J. Chem. Downloaded from www.nrcresearchpress.com by 122.72.124.2 on 09/07/12
For personal use only.



SCHEME 1

by transition state theory. In eq. [9], $K^{\ddagger}$ is the transition state equilibrium constant for the protonated singlet and f is the activity coefficient of the species indicated. Now eq. [8] can be rewritten as eq. [10].

$$[8] \quad -d[S_1]/dt = (k_{ic} + k_f + k_{isc})[S_1] + (kT/h)[S_1—H^+]^{\ddagger}$$

$$[9] \quad K^{\ddagger} = [S_1—H^+]^{\ddagger} f_{\ddagger}/[S_1] f_{S_1} a_{H^+}$$

$$[10] \quad -d[S_1]/dt = (k_{ic} + k_f + k_{isc})[S_1] + (kT/h)K^{\ddagger}[S_1] a_{H^+}(f_{S_1}/f_{\ddagger})$$

This then can be simplified to eq. [11]. In the absence of quencher the reaction rate is a function only of the lifetime of the singlet, eq. [12].

$$[11] \quad -d[S_1]/dt = [k_{ic} + k_f + k_{isc} + k_q a_{H^+}(f_{S_1}/f_{\ddagger})][S_1] = 1/\tau[S_1]$$

$$[12] \quad -d[S_1]/dt = (k^0_{ic} + k^0_f + k^0_{isc})[S_1] = 1/\tau^0[S_1]$$

Since the quantum yield of fluorescence is related to the intensity of fluorescence and to the lifetime of the singlet as shown in eq. [13], division of eq. [11] by eq. [12] yields the expression in eq. [14]. This is the normal expression obtained

$$[13] \quad I^0_F/I_F = \Phi^0_F/\Phi_F = \tau^0/\tau$$

$$[14] \quad \tau^0/\tau = I^0_F/I_F = 1 + k_q\tau^0(a_{H^+} f_{S_1}/f_{\ddagger})$$

for a Stern–Volmer analysis with the exception that the term in parentheses is the desired function of proton concentration. Our definition of the acidity scale is then given in eq. [15] where all the terms have their usual meaning except the superscript I refers to the indicator 1-cyanonaphthalene. By rearranging eq. [15] to eq. [16] and substituting for the activity of the protons in eq. [14], we obtain eq. [17] which shows the connection between the empirically derived $[H^+]^{h\nu}$ scale for the indicator and the quenching equation for other substrates. Our observation of linear Stern–Volmer plots for these substrates is defined by eq. [18]. Therefore, the connection between eq. [17] and eq. [18] gives eq. [19].

$$[15] \quad [H^+]^{h\nu} K^I_{SV} = k^I_q\tau^{0I}(a_{H^+} f^I_{S_1}/f^I_{\ddagger})$$

$$[16] \quad a_{H^+} = [H^+]^{h\nu}(K^I_{SV}/k^I_q\tau^{0I}) f^I_{\ddagger}/f^I_{S_1})$$

$$[17] \quad I^0_F/I_F = 1 + k_q\tau^0(K^I_{SV}/k^I_q\tau^{0I})(f_{S_1}/f_{\ddagger} \cdot f^I_{\ddagger}/f^I_{S_1})[H^+]^{h\nu}$$

$$[18] \quad I^0_F/I_F = 1 + K_{SV}[H^+]^{h\nu}$$

$$[19] \quad K_{SV} = k_q\tau^0(K^I_{SV}/k^I_q\tau^{0I})(f_{S_1}/f_{\ddagger} \cdot f^I_{\ddagger}/f^I_{S_1})$$

The activity coefficient term in the parentheses of eq. [19] is the only term that could vary with acid concentration. The fact that linear plots are obtained, i.e. K_{SV} is a constant, demands that this term also be a constant (at least within experimental error) over the range of acidities examined. Note that this is quite different from the usual first-order approximation in ground state systems where log $(f_B f_{H^+}/f_{BH^+})$ terms are linearly related for different bases. Of course, if this method is to be used to obtain k_q values, then it is not enough that this term be a constant. It must be unity as in the Hammett cancellation assumption. As is now well established, this is not, in general, true for ground state reactions (10).

Although there is considerable information available about individual activity coefficients for substrates and transition states in ground state reactions (28) in purely aqueous acidic media, such results are unavailable for mixed solvents such as the 20% ethanol medium used here. Moreover, there would be no obvious way of determining activity coefficient values for excited states which, because of changes in dipole moment upon excitation, would change from the ground state values. It is worth noting that if the quenching process is exothermic the transition state might be early and, as such, be reactant-like. In fact, activation energies have been measured for the protonation of excited 1-methoxynaphthalene (17) and the very low value of 0.5 kcal/mol in 4:1 H_2O:CH_3CN suggests that the transition state for protonation and the excited singlet may be very similar in structure and therefore in activity coefficient. Therefore the term in brackets in eq. [19], which must be a constant, could be close to unity for all substrates. Results in aqueous perchloric acid, a medium in which measurement of these ratios is possible, indicate that this suggestion is very nearly true for most substrates (29). Although only a working hypothesis, the simplification of eq. [19] to eq. [20] seems justified on this basis.

$$[20] \quad K_{SV} = k_q\tau^0 K^I_{SV}/k^I_q\tau^{0I}$$

Using eq. [20] to obtain k_q values is only possible if a value is known for the indicator i.e. k^I_q. In the dilute acid region (up to $[H^+]$ of 1.20 M) the Stern–Volmer plot for 1-cyanonaphthalene is linear. Therefore, the more general eq. [14] can be simplified to eq. [21]

$$[21] \quad I^{0I}_F/I^I_F = 1 + k^I_q\tau^{0I}C_{H^+}$$

where the activity coefficient terms have been removed and where C_{H^+} is now the concentration of free protons in the acidic medium. As discussed above, the assumption has been made in the 20% ethanol medium used here that C_{H^+} is equal to $(1/2)[H^+]$ (13). More recent estimates in purely aqueous sulfuric acid, Table 1, indicate that this is not quite true (14). We have chosen to use the more recent values.

At this point it is worth noting that $[H^+]^{h\nu}$ could have been defined relative to C_{H^+} from the start rather than $[H^+]$. However, this would require an assumption about the extent of ionization for any given acid in any given medium. If knowledge about the extent of ionization improved, changes in the scale would be required. Defining the scale with respect to the experimentally determinable $[H^+]$ means that the scale will remain the same and only derived k_q values would change. Of course, the relative magnitude of k_q values which is often of more interest than the absolute values themselves would still be correct.

At any rate, assuming the C_{H^+} values in Table 1, the quenching data for 1-cyanonaphthalene gives an excellent Stern–Volmer plot (upper line in inset of Fig. 1) with $k_q\tau^0 = 1.73 \pm 0.01\ M^{-1}$, correlation coefficient = 0.9998. Using this value in eq. [20] allows calculation of all k_q values. These are listed in Table 5.

As mentioned earlier in the discussion section of this paper, the fluorescence quenching data for all compounds was also correlated using eq. [4] and the k_q values are in Table 5. In general, the agreement between the two methods is very good. The $[H^+]^{h\nu}$ method would seem to be statistically more precise based on the standard deviations. Whether it is more accurate or not is difficult to know since systematic error is not easy to compare in the two methods. Systematic error in the $[H^+]^{h\nu}$

Can. J. Chem. Downloaded from www.nrcresearchpress.com by 122.72.124.2 on 09/07/12
For personal use only.

Can. J. Chem. Downloaded from www.nrcresearchpress.com by 122.72.124.2 on 09/07/12
For personal use only.

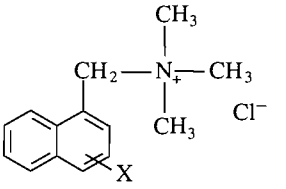
method is probably determined mainly by the cancellation of the activity coefficient term in eq. [19].

Some comment is also required about the possibility of static quenching. At high concentrations of a quencher, the excited state will be generated in "contact" with a quencher and diffusion is no longer required. Thus, the rate of quenching can exceed that of diffusion (30). For 1-cyanonaphthalene, the indicator used to establish $[H^+]^{h\nu}$, $k_q = 13 \times 10^7\ M^{-1}\ s^{-1}$ which is considerably slower than the diffusional rate of $3.3 \times 10^9\ M^{-1}\ s^{-1}$ calculated (31) using the viscosity, 18.1 mpoise at 25°C (32) for 20% ethanol:80% water. Although addition of sulfuric acid to water will raise the viscosity, even for the most acidic solution used here (52.5%), the diffusional rate constant can be estimated from the value in 50% aqueous sulfuric acid as $1.6 \times 10^9\ M^{-1}\ s^{-1}$ based on a viscosity of 38 mpoise (33). Therefore, the rate of quenching for 1-cyanonaphthalene is still considerably below diffusional and is determined by the activation barrier even for "contact" protons. For the most reactive substrate here, 1-methoxy-4-methylnaphthalene (**7**), $k_q = 4.0 \times 10^9\ M^{-1}\ s^{-1}$, which is now close to or even exceeding the rate of diffusion. Fortunately, the quenching process is now efficient enough to occur in dilute acid, so that static quenching may not affect the results. Note that even at 1 *M* quencher, the average diameter of the sphere containing a proton is 1.2–1.5 nm which is reasonably close to the estimated width across the long dimension of a naphthalene ring, ~0.7 nm. Interestingly, if a plot for **7** is made at higher acidities than those shown in Fig. 3 and a correlation is attempted versus $[H^+]^{h\nu}$, the plot begins to curve downward whereas an upward curvature would be expected if excess static quenching was occurring.

It is possible to check for complications of static quenching by comparing I^0/I plots versus τ^0/τ plots. Unfortunately, most of the substrates studied here have singlet lifetimes which are too short to measure over a wide range of acidities by nanosecond single photon counting. However, the lifetime ratios τ^0/τ obtained for 1-cyanonaphthalene were very similar to the fluorescence intensity ratio values (Table 1). This indicates that the quenching is dynamic at least in the low acid region. For 2-vinylnaphthalene, $\tau^0 = 71.2$ ns, a more complete τ^0/τ quenching plot is possible. As expected for a compound that has a slow rate of quenching, this plot gives $k_q = 2.18 \times 10^6\ M^{-1}\ s^{-1}$ (Table 5) which is very similar to that obtained from the I^0/I plot. This confirms that the quenching mechanism is dynamic for this substrate even in the most acidic solutions. Note as well, the reasonable agreement between the k_q value obtained by the $[H^+]^{h\nu}$ method and the literature value of $4.6 \times 10^6\ M^{-1}\ s^{-1}$ (5) considering that this value must have been very difficult to obtain since 2-vinylnaphthalene is quenched only to a very small extent in the region where the normal Stern–Volmer relationship applies.

Analysis of quenching rate Constants

Our interest in the work presented in this paper was initially stimulated by the observation of Turro and Wan (2, 3) that the proton-catalyzed photosolvolysis of benzyl alcohols showed large rate versus substituent effects. For instance, 3-methoxybenzyl alcohol, **13**, is quenched by protons 110 times faster than 4-methoxybenzyl alcohol, **15**, as determined by our acidity scale method (Table 5). This result was rationalized as a clear example of the photochemical "*meta*" effect as outlined by Zimmerman (34, 35) in his pioneering work on photosolvolysis. In contrast to this observation, we had not observed an enhanced rate of photosolvolysis for the 3-methoxy versus the 4-methoxy



17

X = H, 4-CH_3O, 3-CH_3O, 4-CN, 3-CN

substituent in a study of the photosolvolysis of (1-naphthylmethyl)trimethylammonium chlorides, **17** (19). In fact, the 4-methoxy compound reacted about 3.4 times as fast as the 3-methoxy one. Upon attempting to obtain proton quenching rate constants for a number of benzylic alcohols we immediately encountered the acidity function problem that prevented the determination of reliable rate constants for proton quenching. The $[H^+]^{h\nu}$ approach was developed to solve this problem. The last section of this paper will present an analysis of the rate constants thus obtained, including a discussion of the site of protonation for various excited state functional groups.

We initially examined the 1-naphthylmethyl alcohols **8** and **11** which are the naphthyl analogues of the benzylic alcohols **13** and **15** studied by Wan and Turro. In direct contrast to their results, the 4-methoxy isomer had a rate constant for proton quenching that was 66 times faster than the 3-methoxy isomer (Table 5). Moreover, it had been reported in the literature (17) that 1-methoxynaphthalene is quenched faster than 2-methoxynaphthalene by a factor greater than 300 in 20% CH_3CN/80% water and we have confirmed this relative rate for the same two compounds in 20% ethanol:80% water with a value of 160. It is well established by deuterium exchange experiments that the proton quenching of 1-methoxynaphthalene occurs by ring protonation, predominantly at C-5 (17). Probably the other 1-methoxy isomers, **7** and **8**, which are quenched at similar rates are also reacting by ring protonation. Since the 2-methoxy isomers, **9**, **10** and **11**, are also all quenched at similar rates but about a factor of 10^2 slower than the 1-isomers, the most likely process is again ring protonation. MO calculations (17) of excited state electron densities for 1- and 2-methoxynaphthalenes support this idea that the 1-methoxy isomers should be quenched more rapidly.

This observation prompted us to examine similar comparisons for the benzene cases. Surprisingly, in this case 3-methoxy toluene, **12**, was quenched more rapidly than the 4-methoxy isomer, **14**, by a factor of 5. Moreover, quenching of 3-methoxybenzyl alcohol was faster than 3-methoxy toluene by a factor of 13. This suggests that there really is a special excess reactivity for 3-methoxybenzyl alcohol which leads to photosolvolysis and that the "*meta*" effect is the explanation.

The reason for the difference in substituent effects between the benzene and naphthalene derivatives is not obvious. One suggested explanation is that the extra delocalization available for the naphthalene cases allows the changes in charge that occur on excitation to be distributed over a number of carbon atoms. Thus, although a 3-methoxy substituent is predicted to increase electon density at C-1 of naphthalene in the excited state, it also increases electron density at C-4, C-5, C-6, and C-7. The fastest rate may therefore be ring protonation and not enhanced photosolvolysis at the naphthylmethyl carbon. These questions can only be answered by a detailed study of the relative rates of hydrogen exchange versus photosolvolysis.

Can. J. Chem. Downloaded from www.nrcresearchpress.com by 122.72.124.2 on 09/07/12
For personal use only.

Considering, finally, the naphthylnitriles, **1–5**, the site of protonation seems very likely to be on the nitrile group. Electron density is well known to increase on the functional group upon excitation of aromatic rings having electron withdrawing substituents (2). Moreover, at least in the gas phase, the excited state of benzonitrile is reported to be protonated on nitrogen (36). Recent MO calculations on the excited states of simple nitrile functional groups suggest that C protonation is also possible (37). Yates and Haley (38) have searched without success for enhanced photohydrolysis of nitrile groups by excited state protonation. However, they point out that this type of catalysis is not likely for reactions that do not proceed by mechanisms involving rate-determining protonation. Again, only detailed hydrogen-deuterium exchange studies can give information (even if only negative evidence) on where aromatic nitriles in their excited states react with protons. The range of rate constant values for the nitrile protonations is quite small so that analysis of the small changes is more likely to be difficult. However, there are several interesting observations. First, the 2-cyanonaphthalenes, **4** and **5**, are quenched more slowly than the 1-cyanonaphthalenes, **1**, **2**, and **3**. Second, for 1-cyano-naphthalenes methyl substitution seems to slow down the rate of quenching whereas for the 2-cyano case methyl substitution increased the rate.

Summary

The important point of these findings is that an acidity scale to analyze excited state protonations can be obtained using a single fluorescent indicator. Since such a scale can be obtained easily and quickly in any solvent system at any temperature, this method should be very useful to researchers interested in this area. Secondly, a single scale seems to be sufficient to analyze protonation of a variety of chromophores. The ones studied here include aromatic ring carbons, nitriles, alkenes and alcohols. This suggests that $[H^+]^{h\nu}$ may be a fundamental property of the medium but analysis of results from an acidic medium simpler than sulfuric acid in 80% water:20% ethanol is required before this possibility can be confirmed. Such work is in progress.

Experimental

The 20% v/v ethanol:aqueous sulfuric acid solutions were prepared as follows. Commercial grade 95% ethanol and water were distilled twice before using. Sulfuric acid, 96–98%, was used directly as supplied by Mallinckrodt Inc. without further purification. To a series of 500 mL volumetric flasks 80.54 ± 0.05 g of 95% ethanol was added. Aqueous sulfuric acid was added to the flasks with the amount of acid added increasing to give a series of increasingly acidic solutions. Since a tremendous amount of heat was evolved upon addition of the acid the flasks were left to sit at room temperature overnight and then filled to the mark with water. They were tested by uv absorption and shown to have a flat baseline down to 230 nm. The normality of sulfuric acid equal to the molarity of titratable protons was determined by NaOH titration and the values are given in Tables 1–4.

All fluorescence values were measured using an Aminco–Bowman spectrofluorimeter whose sample holder was maintained at 25.0 ± 0.1°C. Solutions were prepared so as to have an approximate concentration of 10^{-4} *M* by pipetting 3 mL of the ethanolic acidic solutions into a fluorescent cuvette designed to be attached to a vacuum line and then adding 5 μL of a stock solution of the substrate. A blank solution containing 20% ethanol:80% water and 5 μL of the substrate was also prepared. All solutions were thoroughly degassed by three freeze–pump–thaw cycles. The fluorescence of all substrates was measured at their strongest emitting wavelength. The intensity ratio, I^0/I, was obtained by measuring the emission of the blank over the emission in the acidic solution. Five readings of each sample were taken and the values reported are averages.

All singlet lifetimes were determined by single photon counting using a PRA instrument.

Substrates **1**, **6**, **9**, and **12–15** are commercially available from Aldrich and were either recrystallized or vacuum distilled prior to use.

2-Methoxy-4-methylnaphthalene, **10**, was prepared as outlined by Baccolini *et al.* (20); mp 37–38°C, lit. 48–49°C; nmr ($CDCl_3$) δ2.60 (s, 3H) 3.86 (s, 3H) 7.00 (s, 1H) 7.3–8.0 (m, 6H).

2-Cyanonaphthalene, **4**. The procedure followed was that as outlined by Friedman and Schechter (39); mp 60–62°C lit. 66°C (40); nmr ($CDCl_3$) δ7.5–7.7 (m, 3H) 7.8–8.0 (m, 3H) 8.25 (s, 1H).

1-Cyano-3-methylnaphthalene, **3**, was prepared as outlined by Yoshida and Nagase (22); mp 51–52°C, lit. 52.5–53.5°C; nmr ($CDCl_3$) δ7.5–8.2 (m, 6H) 2.55 (s, 3H); uv (CH_3OH) λ_{max} = 297 nm; ms 167(100), 166(77), 141(77), 140(39), 139(48), 115(26), 75(25), 71(26), 69(35).

Acknowledgements

This work was supported by a grant from NSERC of Canada and a Dalhousie University Faculty of Graduate Studies Award (including a Walter C. Sumner fellowship) to P.R.

1. W. Brandon, A. L. Pincock, J. A. Pincock, P. Redden, and C. Sehmbey. J. Am. Chem. Soc. **109**, 2181 (1987).
2. J. F. Ireland and P. A. H. Wyatt. Adv. Phys. Org. Chem. **12**, 131 (1976).
3. N. J. Turro and P. Wan. J. Photochemistry, **28**, 93 (1985).
4. P. Wan. J. Org. Chem. **50**, 2583 (1985).
5. P. Wan, S. Culshaw, and K. Yates. J. Am. Chem. Soc. **104**, 2509 (1983).
6. P. Wan and K. Yates. J. Org. Chem. **48**, 869 (1983).
7. J. McEwen and K. Yates. J. Am. Chem. Soc. **109**, 5800 (1987).
8. R. A. Cox and K. Yates. Can. J. Chem. **59**, 2116 (1980).
9. L. P. Hammett and A. J. Deyrup. J. Am. Chem. Soc. **54**, 2721 (1932).
10. R. A. Cox and K. Yates. Can. J. Chem. **61**, 2225 (1983).
11. R. A. Cox and K. Yates. Can. J. Chem. **57**, 2944 (1979).
12. J. F. Bunnett and F. P. Olsen. Can. J. Chem. **44**, 1899 (1966).
13. C. Capobianco, F. Magno, and G. Scorrano. J. Org. Chem. **44**, 1654 (1979).
14. R. A. Cox and K. Yates. J. Am. Chem. Soc. **100**, 3861 (1978).
15. K. Yates and M. K. Boyd. Unpublished results.
16. A. J. Kresge and H. Chen. J. Am. Chem. Soc. **94**, 8192 (1979).
17. H. Shizuka and J. Tobita. J. Am. Chem. Soc. **104**, 6919 (1972).
18. E. M. Arnett. Prog. Phys. Org. Chem. Intersci. **1**, 223 (1963).
19. B. Foster, B. Gaillard, N. Mathur, A. L. Pincock, J. A. Pincock, and C. Sehmbey. Can. J. Chem. **65**, 1599 (1987).
20. G. Baccolini, G. Bartoli, M. Bosco, and R. Dalpozzo. J. Chem. Soc. Perkin Trans. II, 363 (1984).
21. M. S. Newman and H. Boden. J. Org. Chem. **26**, 2525 (1961).
22. K. Yoshida and S. Nagase. J. Am. Chem. Soc. **101**, 4268 (1979).
23. V. Lucchini, G. Modena, G. Scorrano, R. A. Cox, and K. Yates. J. Am. Chem. Soc. **104**, 1958 (1982).
24. V. Lucchini, G. Modena, G. Scorrano, and U. Tanellato. J. Am. Chem. Soc. **99**, 3387 (1977).
25. E. M. Arnett and G. W. Mach. J. Am. Chem. Soc. **88**, 1177 (1966).
26. R. A. Cox and K. Yates. Can. J. Chem. **57**, 2944 (1979).
27. N. J. Turro. *In* Modern molecular photochemistry. Benjamin/Cummings, Menlo Park, CA. 1978. p. 187.
28. K. Yates and R. A. McClelland. Prog. Phys. Org. Chem. Intersci. **11**, 323 (1974).
29. J. A. Pincock and P. R. Redden. Can. J. Chem. Submitted.
30. N. J. Turro. *In* Modern molecular photochemistry. Benjamin/Cummings, Menlo Park, CA. 1978. p. 317.
31. N. J. Turro. *In* Modern molecular photochemistry. Benjamin/Cummings, Menlo Park, CA. 1978. p. 314.

32. E. W. WASHBURN (*Editor*). Natl. Bur. Stand. Int. Crit. Tables, **5**, 22 (1929).
33. E. W. WASHBURN (*Editor*). Natl. Bur. Stand. Int. Crit. Tables, **5**, 13 (1929).
34. H. E. ZIMMERMAN and V. R. SANDEL. J. Am. Chem. Soc. **85**, 915 (1963).
35. H. E. ZIMMERMAN and V. R. SANDEL. J. Am. Chem. Soc. **85**, 922 (1963).
36. B. S. FREISER and J. L. BEAUCHAMP. J. Am. Chem. Soc. **99**, 3214 (1977).
37. P. S. MARTIN, K. YATES, and I. CSIZMADIA. J. Mol. Struct. Theochem. In Press.
38. M. F. HALEY and K. YATES. J. Org. Chem. **52**, 1817 (1978).
39. L. FRIEDMAN and H. SHECHTER. J. Org. Chem. **26**, 2522 (1961).
40. C. WEAST (*Editor*) *In* Handbook of chemistry and physics. 56th ed. CRC Press, Cleveland, OH. 1974.

Can. J. Chem. Downloaded from www.nrcresearchpress.com by 122.72.124.2 on 09/07/12
For personal use only.

Some physicochemical studies on organic eutectics and 1:1 addition compound; *p*-phenylenediamine – benzoic acid system

U. S. RAI AND K. D. MANDAL

Chemistry Department, Banaras Hindu University, Varanasi – 221 005, U.P., India

Received June 8, 1988

U. S. RAI and K. D. MANDAL. Can. J. Chem. **67**, 239 (1989).

The phase diagram of *p*-phenylenediamine – benzoic acid system, determined by the thaw–melt method, shows the formation of two eutectics and a 1:1 addition compound. The linear velocity of crystallization of pure components, eutectics and addition compound, determined by measuring the movement of growth front in a capillary, suggests that crystallization data obey the Hillig–Turnbull equation. Using experimental values of heats of fusion, entropy of fusion and excess thermodynamic functions were calculated and the results are explained on the basis of cluster formation in the melts. X-ray diffraction data infer that these eutectics are not simply the mechanical mixture of the two components and there is preferential ordering of atomic planes during their formation. The infrared spectral studies suggest the formation of intermolecular hydrogen bonding between the components forming the molecular complex.

Key words: organic eutectics, growth kinetics, phase diagram, thermochemistry, X-ray diffraction studies.

U. S. RAI et K. D. MANDAL. Can. J. Chem. **67**, 239 (1989).

Le diagramme de phase du système *p*-phénylènediame/acide benzoïque, déterminé par la méthode de liquéfaction, montre qu'il y a formation de deux eutectiques et d'un composé d'addition 1:1. La vitesse linéaire de cristallisation des produits purs, des eutectiques ainsi que du produit d'addition, telle que déterminée par le mouvement du front de croissance dans un capillaire, suggère que les données de cristallisation obéissent à l'équation de Hillig–Turnbull. Utilisant les valeurs expérimentales pour les chaleurs de fusion, on a calculé l'entropie de fusion ainsi que les fonctions thermodynamiques en excès et on a expliqué les résultats expérimentaux en se basant sur la formation d'agrégats dans les produits de fusion. Les données de la diffraction des rayons-X suggèrent que les eutectiques ne sont pas simplement des mélanges mécaniques des deux produits et qu'il existe un ordre préférentiel des plans atomiques au cours de leur formation. Des études réalisées par spectroscopie infrarouge suggèrent qu'il y a formation de ponts hydrogènes intramoléculaires entre les produits formant le complexe moléculaire.

Mots clés: eutectiques organiques, cinétique de croissance, diagramme de phase, thermochimie, études par diffraction des rayons-X.

[Traduit par la revue]

Can. J. Chem. Downloaded from www.nrcresearchpress.com by 122.72.124.2 on 09/07/12
For personal use only.

1. Introduction

Since the early sixties, the chemistry (1–5) of eutectics and addition compounds has been a field of potential interest due to their unusual physical properties not normally shown by the parent components. The metallic (6, 7) eutectics and intermetallic compounds constitute an active area of present investigation in metallurgy and materials science. However, the various studies carried out on these systems are inadequate and incomplete as high transformation temperature, opacity, and difficulties involved in purification present serious problems. Apart from these, wide difference in densities of the two components forming the metal eutectics causes density-driven convection effects, which in turn, affect their solidification. Due to low transformation temperature, ease in purification, transparency, low convection effects, and wider choice of materials, organic systems (8–12) are more suitable and are being used as model systems for detailed investigation of the parameters which control solidification. Further, the experimental techniques required for their investigation are simpler and more convenient as compared to those adopted in metallic systems.

Most of the organic systems studied in the past are simple eutectic type. There is only a limited number of cases in which two components form a molecular complex (13–15) with congruent melting point. Such systems are of potential technical interest since these are quite common in metallurgical systems. Organic systems, giving addition compounds which are organic analogues of intermetallic compounds, are important to material and metallurgical sciences since they permit visual observation of phase transformation and process during solidification. The formation of such molecular compounds can be established on the basis of phase diagrams which exhibit a characteristic maximum, surrounded by two eutectics, corresponding to the stoichiometry of the addition compounds formed. The growth morphology of eutectics and molecular compounds depend on the growth characteristics of individual constituent phases which can solidify either with faceted or with non-faceted interfaces. This behaviour is related to the nature of solid–liquid interface and can be predicted for pure materials from their entropy of fusion data. A unique crystallographic orientation relationship between the constituent phases and their mating planes was established by Hogan *et al.* (16). Gruzleski and Winegard (17) observed perfect lamellar grains in Sn—Cd eutectics but in a number of other systems, the eutectic grains did not exhibit a fixed crystal orientation with respect to external lines of forces. Bassi and Sharma (18) studied the infrared spectra of naphthalene – benzoic acid eutectic system and inferred that there exists a specific orientation between the constituents with respect to each other.

With a view to elucidate the chemistry of organic eutectics and the 1:1 addition compound, *p*-phenylenediamine (PPD) – benzoic acid (BA) system was undertaken and its phase diagram, linear velocity of crystallization and heat of fusion were studied. From the heats of fusion data the enthalpy of mixing, entropy of fusion, and excess thermodynamic functions were calculated to throw light on the nature of interactions among the components forming the melts. The structure of eutectics and molecular compound was also studied by infrared and X-ray methods.

2. Experimental

2.1. Materials and purification

p-Phenylenediamine (High Purity Chemicals, India) was purified by repeated distillation under vacuum and was stored in coloured bottles to avoid exposure to light. Benzoic acid (BDH) was recrystallised

from boiling water. The purity of the compounds was confirmed by determining their melting points which were in good agreement with literature values.

2.2 Phase diagram study

Phase diagram of *p*-phenylenediamine – benzoic acid system was determined (19, 20) by the thaw–melt method. Mixtures of various proportion covering the entire range of composition were taken in long-necked glass test tubes and were sealed. The mixtures were subjected to number of alternate melting in liquid paraffin followed by chilling in ice to make it homogeneous. The mixtures were taken out by breaking the test tubes and were further homogenized by grinding in a mortar with due care to avoid moisture or any other contamination. The melting and thaw temperatures were determined by Toshniwal Melting Point Apparatus.

2.3 Linear velocity of crystallization

The linear velocity of crystallization of pure components, eutectics and addition compound was determined (21, 22) by measuring the rate of movement of growth front in a capillary. The experimental details are reported earlier (22).

2.4. Heats of fusion

The heats of fusion of pure components, eutectics, and 1:1 addition compound were determined (23, 24) by their DTA patterns obtained from Stanton Redcroft STA-780 Series Unit. All the runs were carried out with heating rate 2°C/min, chart speed 10 mm/min, and chart sensitivity, 100 μV/10 mV. The sample weight range was 5–10 mg for each estimation. Using phenanthrene as a standard substance, the heats of fusion of unknown compounds were determined by the following equation:

$$[1] \qquad \Delta H = \Delta H_s \times \frac{W_s}{W} \times \frac{A}{A_s}$$

where ΔH is the heat of transition of unknown sample and ΔH_s is the heat of fusion of standard substance. W and A are weight and peak area, respectively.

2.5. Infrared studies

The infrared spectra of the pure components and adduct were recorded (25) in Nujol mull in the region 4000–600 cm^{-1}, on a Perkin–Elmer 783 Infrared Spectrophotometer.

2.6. X-ray diffraction studies

X-ray diffraction patterns of pure components, eutectics and 1:1 addition compound were recorded (24) on a computerized X-ray diffraction unit, PW 1710 model, using Cu-K_α radiation.

3. Results and discussion

3.1. Phase diagram

Phase diagram of *p*-phenylenediamine – benzoic acid system, given in Fig. 1, shows the formation of one 1:1 addition compound with congruent melting point surrounded by the two eutectics E_1 and E_2 having 0.228 and 0.807 mole fraction of benzoic acid, respectively. The melting temperatures of molecular compound and eutectics E_1 and E_2 are 145.0, 124.5, and 107.0°C, respectively. For each eutectic, the addition compound serves as one of the components. The flat maximum, observed in this system, suggests (13) that the addition compound dissociated in the molten state. From the phase diagram it can also be inferred that the addition compound is capable of existing as a solid compound in equilibrium with a liquid of the same composition. From the first eutectic point E_1 onwards, on addition of the second component, the melting point again rises, attains a maximum at C, where the composition of liquid and solid phases are identical. The existence of an eutectic point on either side of the maximum provides an information about the large stability of the molecular complex formed.

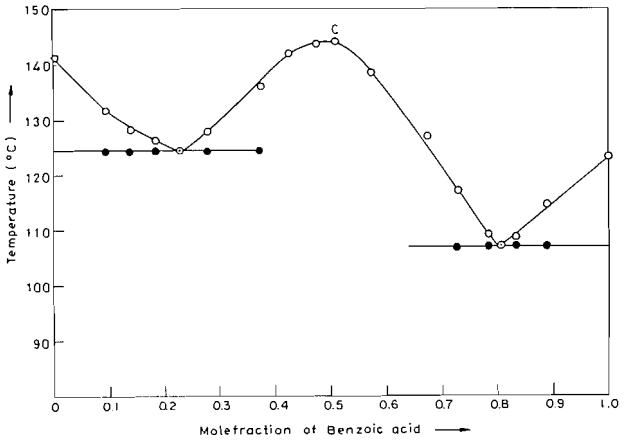


FIG. 1. Phase diagram of *p*-phenylendiamine – benzoic acid system. ○, Melting temperature; ●, thaw temperature.

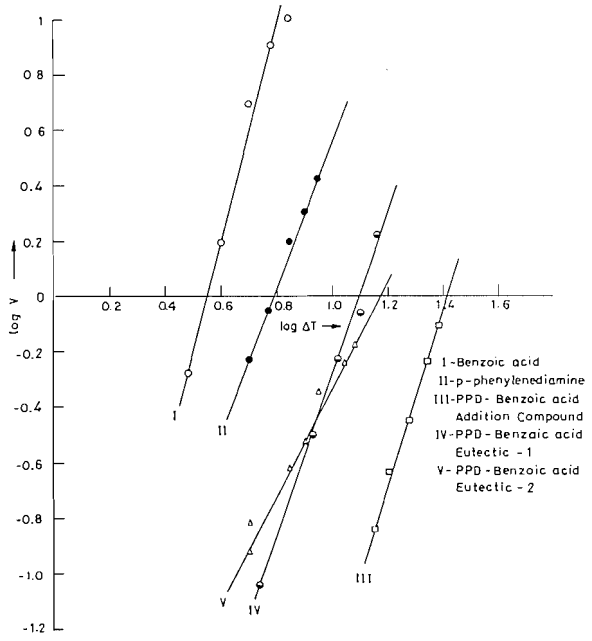


FIG. 2. Linear velocity of crystallization of pure components, eutectics and 1:1 addition compound at different undercoolings.

3.2. Growth kinetics

The linear velocity of crystallization, v, of pure components, eutectics and 1:1 addition compound, determined by measuring the rate of movement of growth front in a capillary at different undercoolings, ΔT, is given in Fig. 2 in the form of log v versus log ΔT. The linear dependence of growth velocity and undercooling suggests that the crystallization data obey Hillig–Turnbull (26) relation:

$$[2] \qquad v = u(\Delta T)^n$$

where u and n are constants depending on the nature of solidification of the sample under investigation. The experimental values of these constants are given in Table 1. The values of n being close to 2 suggest a square relationship between the linear growth velocity and undercooling. The slight deviations (20) in the values of n from 2, observed in some cases, may

Can. J. Chem. Downloaded from www.nrcresearchpress.com by 122.72.124.2 on 09/07/12
For personal use only.

TABLE 1. Values of u and n

Compound	u (mm/s deg)	n
p-Phenylenediamine	0.010230	2.60
Benzoic acid	0.007244	2.42
Eutectic-1	0.000794	2.71
Eutectic-2	0.005129	2.00
1:1 Addition compound	0.000071	2.87

be due to the difference between the bath temperature and the temperature of growing interface.

It is evident from the values of u, given in Table 1, that the crystallization velocity of eutectic-1 (E_1) and eutectic-2 (E_2) are lower than those of pure components and higher than the addition compound. The first eutectic (E_1), having a low molar concentration of benzoic acid, solidifies more slowly than the second eutectic (E_2) with a high molar concentration of benzoic acid. These results may be explained on the basis of the mechanism proposed by Winegard *et al.* (27). According to them, in binary system the eutectic solidification begins with the formation of the nucleus of one of the phases. This would grow until the surrounding liquid becomes rich in the other component and a stage is reached when the second component also starts nucleating. Now there are two possibilities. First, the two initial crystals may grow side by side. This explains the case in which the rates of solidification of eutectics are not lower than those of the parent components. The second possibility is that there may be alternate nucleation of the two components. This explains the solidification phenomena, in cases, where the crystallization velocity of the eutectics is lower than that of the parent components. Thus, the solidification of E_1 and E_2 takes place by side by side growth of the two components. For both eutectics, addition compound acts as one of the components and nucleates first. Thus, *p*-phenylenediamine and addition compound act as the parent components for E_1, while the molecular complex and benzoic acid do so for eutectic E_2. For E_1 and E_2 the nucleation of addition compound is followed by the nucleation of *p*-phenylenediamine and benzoic acid, respectively.

From the values of u, given in Table 1, it can be inferred that the 1:1 addition compound of *p*-phenylenediamine with benzoic acid crystallizes at a rate slower than that of pure components and both eutectics. Studies (14) on crystal morphology of the addition compounds indicate that they crystallize as a definite chemical entity. However, during crystallization, the two components from the melt have to enter the crystal lattice, simultaneously, in such a way that the composition of the melt corresponds to a 1:1 molar ratio of the two components. Due to this, the linear velocity of crystallization of the addition compounds may be expected to be of the order of the velocity of the species crystallizing at a slower rate.

3.3. Thermochemistry

The experimentally determined values of heats of fusion of parent components, eutectics, and addition compound are given in Table 2. If the eutectics were a simple mechanical mixture of the two components involving no heat of mixing or any type of association in the melt, the heats of fusion, $(\Delta_f h)_e$, would simply be given by the mixture law (28):

$$[3] \quad (\Delta_f h)_e = x_1 \Delta_f h_1 + x_2 \Delta_f h_2$$

where x_1 and x_2 are the mole fraction and $\Delta_f h_1$ and $\Delta_f h_2$ are the experimental values of heats of fusion of parent components 1 and 2, respectively. The heats of fusion, calculated from the mixture law, are also given in the same table. It is evident from the table that the values of heat of fusion calculated from eq. [3] are higher than the experimental values. This difference can be attributed to the formation of clusters in the eutectic melt. It can be imagined that during cluster formation, heat liberated may lower the actual value of heat of fusion. The cluster formation will be favoured if the molecules can associate themselves by certain weak intermolecular forces. In eutectic systems where one or both components contain hydroxyl groups, there would be a tendency to form hydrogen bonds and as a result, the cluster formation will be favoured. This is one of the reasons why the experimental values of heat of fusion are lower than those calculated from eq. [3]. The experimental value of heat of fusion of addition compound and its theoretical value, calculated by the mixture law, is also given in the Table 2. It is evident that the calculated value is higher than the experimental value. A similar type of cluster formation and explanation can also be suggested to justify this observation.

Heat of mixing (ΔH_m) which is the difference between the experimental and calculated values of heats of fusion is given by

$$[4] \quad \Delta H_m = (\Delta_f h)_{exp} - \Sigma x_i \Delta_f h_i$$

where $(\Delta_f h)_{exp}$ is the heat of fusion of the eutectic, determined experimentally, x_i and $\Delta_f h_i$ are the mole fraction and heat of fusion of the end components, respectively. It is evident from Table 2 that in all cases the heats of mixing are negative. Thermochemical studies suggest that the structure of eutectic melt depends on the sign and magnitude of the enthalpy of mixing. Three types of structures (29) are suggested; quasi-eutectic for $\Delta H_m > 0$, clustering of molecules for $\Delta H_m < 0$, and molecular solutions for $\Delta H_m = 0$. The negative values of ΔH_m of eutectics of system under investigation, suggest clustering of molecules in the eutectic melt and substantiate our earlier conclusion drawn on the basis of the mixture law. It is also very interesting to note that the molecular complex and one of the eutectics have low values of enthalpy of mixing, and one might argue for the possibility of simple molecular solutions instead of weak interactions. These results (30) are quite different from those of simple eutectic systems where merely ordering of the parent phases has been suggested in the melts. It seems that there is considerable enhancement in the interactions due to the presence of molecular complex in the eutectic melts.

In order to know the nature of interaction between the components forming the eutectics in the present systems, some thermodynamic functions, such as excess free energy, g^E, excess enthalpy of mixing, h^E, and excess entropy of mixing, S^E, were calculated using the following equations:

$$[5] \quad -\ln x_i^l \gamma_i^l = \frac{\Delta_f h_i^0}{R}\left(\frac{1}{T} - \frac{1}{T_i^0}\right)$$

$$[6] \quad g^E = RT(x_1 \ln \gamma_1^l + x_2 \ln \gamma_2^l)$$

$$[7] \quad h^E = -RT^2\left(x_1 \frac{\partial \ln \gamma_1^l}{\partial T} + x_2 \frac{\partial \ln \gamma_2^l}{\partial T}\right)$$

$$[8] \quad s^E = -R\left(x_1 \ln \gamma_1^l + x_2 \ln \gamma_2^l + x_1 T \frac{\partial \ln \gamma_1^l}{\partial T} + x_2 T \frac{\partial \ln \gamma_2^l}{\partial T}\right)$$

Can. J. Chem. Downloaded from www.nrcresearchpress.com by 122.72.124.2 on 09/07/12
For personal use only.

TABLE 2. Heat of fusion and entropy of fusion

Material		Heat of fusion (kJ/mol)	Enthalpy of mixing (kJ/mol)	Entropy of fusion ($kJ\ mol^{-1}\ K^{-1}$)	Roughness parameter $\left(\frac{\Delta S}{R}\right)$
p-Phenylenediamine		24.860		0.0597	7.21
Benzoic acid		17.317		0.0437	5.28
Eutectic-1	(Expt.)	17.111	−6.03	0.0430	5.19
	(Calc.)	23.140			
Eutectic-2	(Expt.)	15.910	−2.86	0.0419	5.06
	(Calc.)	18.770			
1:1 Addition compound	(Expt.)	19.460	−1.63	0.0467	5.64
	(Calc.)	21.089			

TABLE 3. Excess thermodynamic functions for eutectic-1 and eutectic-2

Material	g^E (J/mol)	h^E (J/mol)	s^E ($J\ mol^{-1}\ K^{-1}$)
Eutectic-1	927.53	21526.17	51.82
Eutectic-2	563.01	8484.05	20.84

where γ_i and T_i^0 are activity coefficient and melting temperature of the component indicated by the suffix and T and R are the eutectic temperature and gas constant, respectively. Equation [5] is obtained by considering the general condition of phase equilibrium for the two phases and assuming that heat of fusion is independent of temperature and the two components are miscible in the liquid phase only. This equation was used to calculate the activity coefficient of the end members at the eutectic point. The values of $\partial \ln \gamma_i^l / \partial T$ were calculated by differentiating eq. [5] and taking slope of the liquidus line near the eutectic point. The details of calculation of excess thermodynamic functions are reported earlier (28). Values of excess functions are given in Table 3. The positive values of excess free energy give measure of the departure of the system from ideal behaviour and suggest interaction among the components forming the eutectic melt. The values of h^E and s^E of Table 3 correspond to the excess free energy and are measures of excess enthalpy of mixing and excess entropy of mixing, respectively.

The entropies of fusion, ΔS, of pure components, eutectics and addition compounds were calculated using the following relation:

$$[9] \quad \Delta S = \frac{\Delta_f h}{T}$$

where $\Delta_f h$ is the heat of fusion and T is the fusion temperature, and are given in Table 2. In all the cases ΔS values are positive, indicating an increase of randomness during melting. According to Hunt and Jackson (1), the type of growth from a eutectic melt depends upon a factor α as defined by equation:

$$[10] \quad \alpha = \xi \frac{\Delta S}{R}$$

where ξ is a crystallographic factor depending upon the geometry of the molecules and has the values less than or equal to one. $\Delta S/R$, also known as Jackson's roughness parameter,

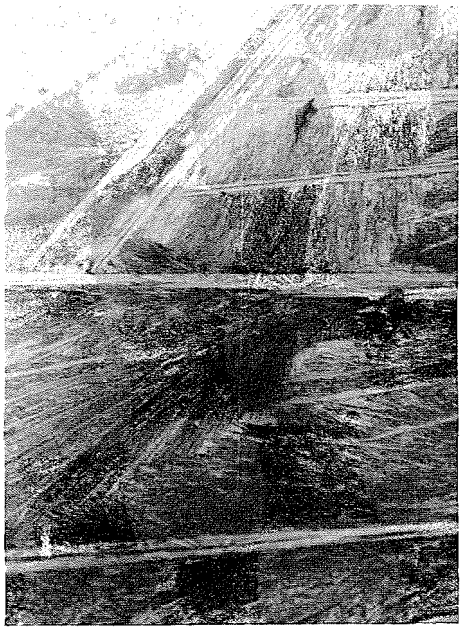


FIG. 3. Microstructure of eutectic E_1 (×200).

is the entropy of fusion in dimensionless unit and R is the gas constant. When $\alpha < 2$, non-faceted growth occurs whereas a faceted growth appears if $\alpha > 2$. In all cases, $\Delta S/R$ values are greater than 2, which indicate that they exhibit faceted growth. The microstructures of eutectic, recorded on a microscope (Leitz Laborlux D, West Germany) are given in Figs. 3 and 4, confirm this conclusion.

3.4. Infrared studies

The infrared spectrum of *p*-phenylenediamine shows a strong band at 3380 cm^{-1}. In the case of pure benzoic acid, there is no peak in the 3000–4000 cm^{-1} region. But the 1:1 addition compound of *p*-phenylenediamine with benzoic acid has three bands at 3230, 3340, and 3460 cm^{-1} in this range. The strongest band being at 3340 cm^{-1} shows a negative shift of 40 cm^{-1} as compared to the strong band observed in PPD at 3380 cm^{-1}. The other two bands in the 1:1 addition compound are attributed to free $—NH_2$ group present therein which is not involved in hydrogen bonding with benzoic acid. A band observed at 1690 cm^{-1} due to C=O stretching of benzoic acid was found to shift to 1640 cm^{-1} in the addition compound. These observations clearly indicate the formation of intermolecular

Can. J. Chem. Downloaded from www.nrcresearchpress.com by 122.72.124.2 on 09/07/12
For personal use only.

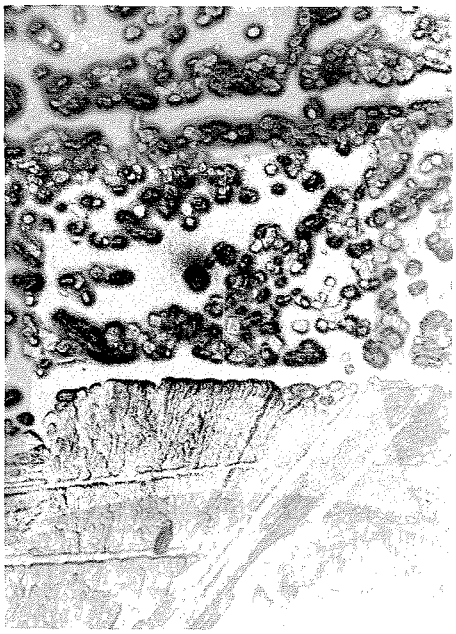
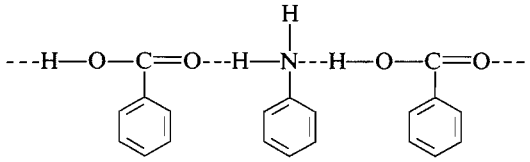


FIG. 4. Microstructure of eutectic E_2 (×200).

hydrogen bonding between the two components, which is represented below:



3.5. X-ray diffraction studies

Experimental results on some preliminary investigations of X-ray diffraction of pure components, eutectics, and addition compound are reported in Tables 4 and 5. It can be observed from the X-ray diffraction data that for a particular *d* value there is marked difference in the relative intensity of the components. This may be explained on the basis of the structure considerations of the compounds under investigation. It is evident from Tables 4 and 5 that the number of reflections of E_1, E_2, and addition compound are comparable. This suggests that they belong to the same crystal system and have similar lattices. In general, common reflections of benzoic acid and eutectic E_2 have smaller intensities in the case of eutectic. Common reflections of addition compound and eutectic E_2 also show decrease in intensities in the eutectic. Strong reflections of benzoic acid show a drastic decrease in intensity in the eutectic phase showing that the structure of the two differ very significantly. Whereas this is not true for the eutectic and addition compound. The structure of eutectic seems to be governed more by the addition compound as compared to benzoic acid because the high angle Bragg reflections are absent, both in addition compound and eutectic while they are present in benzoic acid. A drastic decrease of intensity of strong common reflections and the absence of high angle Bragg reflections are also observed in eutectic E_1 containing *p*-phenylenediamine as one of the components. There is no regular change of intensity of reflections of E_1 and addition compound but the tendency of decrease of intensity in the addition compound is dominant. Moreover the intensity of strong reflections of addition compound show drastic decrease in the eutectic E_1.

TABLE 4. Preliminary X-ray data (*i*)

p-Phenylenediamine		Eutectic-1		Addition compound	
d (Å)	Relative intensity	*d* (Å)	Relative intensity	*d* (Å)	Relative intensity
—	—	15.50	19	—	—
—	—	11.79	44	11.79	100
11.60	10	—	—	—	—
—	—	8.50	8	8.80	7
—	—	6.58	100	—	—
—	—	—	—	5.90	11
5.74	100	—	—	5.65	23
—	—	4.85	47	4.87	35
4.75	70	4.69	28	4.69	13
—	—	4.55	24	4.57	34
4.42	90	4.41	45	—	—
4.18	30	4.18	24	4.19	16
4.02	80	4.01	52	—	—
—	—	3.93	52	3.95	81
3.87	60	3.85	45	—	—
3.78	50	3.77	20	—	—
3.65	10	3.63	16	3.64	15
3.48	70	—	—	—	—
3.37	20	—	—	3.36	14
3.31	20	3.33	20	—	—
3.27	60	3.27	42	—	—
3.08	60	3.06	19	3.04	13
3.01	20	—	—	—	—
2.88	20	2.87	14	—	—

TABLE 5. Preliminary X-ray data (*ii*)

Benzoic acid		Eutectic-1		Addition compound	
d (Å)	Relative intensity	*d* (Å)	Relative intensity	*d* (Å)	Relative intensity
—	—	11.79	42	11.79	100
11.00	20	10.91	100	—	—
—	—	—	—	8.80	7
—	—	—	—	5.90	11
5.60	25	5.70	8	5.65	23
—	—	5.47	36	—	—
5.20	80	5.15	50	—	—
—	—	4.87	14	4.87	35
4.66	20	4.65	15	4.69	13
—	—	4.55	14	4.57	34
4.20	12	—	—	4.19	16
—	—	4.00	40	3.95	81
3.75	80	3.74	12	3.64	15
3.45	100	3.45	10	3.36	14
3.21	60	3.20	8	—	—
2.98	50	2.96	7	3.04	13
2.74	2	—	—	—	—
2.58	12	2.58	6	—	—

It is clear from Tables 4 and 5 that the intensities of the reflections diminish with decreasing *d* values. It is also noted from both the tables that some reflections of pure components and addition compound are absent in the corresponding eutectic. The first eutectic (E_1) formed between *p*-phenylenediamine and the addition compound has some strong reflections having *d* values 11.79, 6.58, 4.85, 4.41, 4.01, 3.93, and 3.85 Å whereas some reflections of PPD and molecular complex are missing in

Can. J. Chem. Downloaded from www.nrcresearchpress.com by 122.72.124.2 on 09/07/12
For personal use only.

it. In the case of the second eutectic (E_2), formed between benzoic acid and the molecular complex, a similar trend is observed and strong reflections correspond to *d* values 11.79, 10.91, 5.15, and 4.00 Å. These experimental results infer that the eutectics are not simply the mechanical mixture of the two components. In them, there is orientation (30) of some atomic planes and preferential ordering also takes place during their formation. These findings are in accordance with our earlier conclusions drawn in the case of *p*-phenylenediamine–catechol system reported earlier (23).

Acknowledgements

Thanks are due to Professor I. S. Ahuja, Head, Chemistry Department, Banaras Hindu University, Varanasi, for providing laboratory facilities. The authors are also thankful to CSIR, New Delhi, for financial assistance.

1. K. A. Jackson and J. D. Hunt. Trans. Met. Soc. AIME, **236**, 1129 (1966).
2. N. B. Singh and K. D. Dwivedi. J. Sci. Ind. Res. **41**, 96 (1982).
3. K. Pigon and A. Krajewska. Thermochim. Acta, **58**, 299 (1982).
4. R. P. Rastogi, D. P. Singh, Namwar Singh, and Narsingh B. Singh. Mol. Cryst. Liq. Cryst. **73**, 7 (1981).
5. N. B. Singh and Narsingh B. Singh. J. Cryst. Growth, **28**, 267 (1975).
6. R. M. Jordan and J. D. Hunt. Met. Trans. **2**, 3401 (1971).
7. R. Elliott. Int. Met. Rev. **22**, 161 (1977).
8. B. Derby and J. J. Favier. Acta Metall. **31**, 1123 (1983).
9. R. N. Grugel and A. Hellawell. Met. Trans. **15A**, 1626 (1984).
10. J. E. Smith, D. O. Frazier, and W. F. Kaukler. Scr. Metall. **18**, 677 (1984).
11. M. E. Glicksman, N. B. Singh, and M. Chopra. Manuf. Space, **11**, 207 (1983).
12. P. E. Arndt, J. G. Dunn, and R. L. S. Willix. Thermochim. Acta, **79**, 55 (1984).
13. B. M. Shukla, N. P. Singh, and Narsingh B. Singh. Mol. Cryst. Liq. Cryst. **104**, 265 (1984).
14. R. P. Rastogi, N. B. Singh, and K. D. Dwivedi. Ber. Bunsenges Phys. Chem. **85**, 85 (1981).
15. A. Krajewska and K. Pigon. Thermochim. Acta, **41**, 187 (1980).
16. L. M. Hogan, R. W. Kraft, and F. D. Lamkey. Advances in materials research. Vol. 1. H. Herman Edition. New York. 1971.
17. J. E. Gruzleski and W. C. Winegard. J. Inst. Metals, **96**, 301 (1968).
18. P. S. Bassi and N. K. Sharma. Indian J. Chem. **14A**, 692 (1976).
19. N. P. Singh and B. M. Shukla. Cryst. Res. Technol. **20**, 345 (1985).
20. N. B. Singh, U. S. Rai, and O. P. Singh. J. Cryst. Growth, **71**, 353 (1985).
21. U. S. Rai, O. P. Singh, and N. B. Singh. J. Chim. Phys. **84**, 483 (1987).
22. N. B. Singh and Narsingh B. Singh. Krist. Techn. **13**, 1175 (1978).
23. U. S. Rai and K. D. Mandal. Thermochim. Acta. In press.
24. U. S. Rai and K. D. Mandal. Crystal Res. Technol. **23**, 871 (1988).
25. U. S. Rai and K. D. Mandal. Z. Phys. Chem. In press.
26. W. B. Hillig and D. Turnbull. J. Chem. Phys. **24**, 914 (1956).
27. W. C. Winegard, S. Mojka, B. M. Thall, and B. Chalmers. Can. J. Chem. **29**, 320 (1951).
28. U. S. Rai, O. P. Singh, N. P. Singh, and Narsingh B. Singh. Thermochim. Acta, **71**, 373 (1983).
29. Namwar Singh, Narsingh B. Singh, U. S. Rai, and O. P. Singh. Thermochim. Acta, **95**, 291 (1985).
30. N. P. Singh, B. M. Shukla, Namwar Singh, and Narsingh B. Singh. J. Chem. Eng. Data, **30**, 49 (1985).

Can. J. Chem. Downloaded from www.nrcresearchpress.com by 122.72.124.2 on 09/07/12
For personal use only.

Esterification of 1,4-dichlorobutane with sodium formate under solid–liquid phase transfer catalysis. A kinetic study

HAYDER A. ZAHALKA[1] AND YOEL SASSON
Casali Institute of Applied Chemistry, The Hebrew University of Jerusalem, 91904 Jerusalem, Israel

Received May 27, 1988

HAYDER A. ZAHALKA and YOEL SASSON. Can. J. Chem. **67**, 245 (1989).

Kinetic data are reported regarding the esterification of 1,4-dichlorobutane with sodium formate catalyzed by quaternary ammonium salts as a model for reactions in series, under solid–liquid phase transfer conditions. The process was found to follow a consecutive first-order mechanism of the general type A → R → S. The reactivity of the quaternary ammonium salts with regard to the counteranion was $Cl^- > Br^- > I^- > HSO_4^-$. The reaction rate was linearly dependent on catalyst concentration up to 12 mol% of catalyst relative to the substrate. Above this concentration the rate was constant and independent of the amount of the catalyst. The activation energy of the two consecutive steps was found to be similar (21 kcal/mol). Therefore, the product distribution (R/S) is not appreciably affected by temperature. A mechanism termed "Thin aqueous boundary layer" is suggested for nucleophilic displacement reactions under solid–liquid phase transfer conditions.

Key words: phase transfer catalysis, series reactions, kinetic study.

HAYDER A. ZAHALKA et YOEL SASSON. Can. J. Chem. **67**, 245 (1989).

Dans le but de développer un modèle pour des réactions en série effectuées dans des conditions de transfert de phase solide–liquide, on a déterminé les données cinétiques relatives à l'estérification, catalysée par des sels d'ammonium quaternaires, du dichloro-1,4 butane par le formate de sodium. On a trouvé que le processus est une réaction consécutive du premier ordre du type général A → R → S. La réactivité des sels d'ammonium quaternaires en fonction des contre-ions est $Cl^- > Br^- > I^- > HSO_4^-$. Jusqu'à 12 mol% de catalyseur par rapport au substrat, la vitesse de la réaction varie d'une façon linéaire avec la concentration du catalyseur. Au-dessus de cette concentration, la vitesse est constante et elle est indépendante de la quantité de catalyseur. On a trouvé que les énergies d'activation des deux étapes consécutives sont semblables (21 kcal/mol). La distribution des produits (R/S) n'est donc pas très affectée par la température. On suggère un mécanisme appelé «limité par une mince couche aqueuse» pour les réactions de substitutions nucléophiles effectuées dans des conditions de transfert de phase solide–liquide.

Mots clés : catalyse de transfert de phase, réactions en série, étude cinétique.

[Traduit par la revue]

Introduction

The traditional phase transfer catalyzed ester synthesis, where a carboxylate anion in aqueous solution reacts with an alkyl halide in the presence of a lipophilic onium salt (1, 2), cannot be applied in the case of the hydrophilic formate anion (3–5) due to the high susceptibility of the heterogeneous displacement process (eq. [1]) to catalyst poisoning (3) and to deactivation of the phase transfer catalyst by extraction of free acids via hydrogen bonding (4). We observed (6, 7) that quantitative conversions in chloride–formate exchanges were obtained only by the use of highly concentrated aqueous solutions of the formate salts, namely, under the conditions known as solid–liquid phase transfer catalysis (S–L PTC) in the presence of catalytic amounts of water, e.g., 0.20% water content of sodium formate (5), which were shown to be essential for the chloride–formate exchange (eq. [1]):

$$[1]\quad RCl_{org} + HCOONa_{aq.\ or\ S} \xrightarrow{PT_{catalyst}} HCOOR_{org} + NaCl_{aq.\ or\ S}$$

There have been no publications, to our knowledge, on the kinetics of complex substitution reactions (e.g., reactions in series) under S–L PTC conditions, although some reports on the kinetics of simple substitution reactions have appeared in the literature (7, 8). Therefore, we found it imperative to study systematically the various kinetic aspects of the esterification of 1,4-dichlorobutane with sodium formate (eq. [2]) in a solid–liquid system as a model for reactions in series under S–L PTC conditions, and to discuss the mechanistic implications of the results.

$$[2]\quad \underset{A}{Cl(CH_2)_4Cl} + HCOONa \xrightarrow[QX]{k_1} \underset{R}{Cl(CH_2)_4OOCH} + NaCl$$

$$\underset{R}{Cl(CH_2)_4OOCH} + HCOONa \xrightarrow[QX]{k_2} \underset{S}{HCOO(CH_2)_4OOCH} + NaCl$$

(QX ≡ quaternary ammonium salt)

Results

Reaction profile

The displacement reaction (eq. [2]) was studied under varying conditions of mechanical stirring speed, catalyst structure, catalyst concentration, catalyst counterion, and temperature. Standard reaction conditions consisted of 1.37 M 1,4-dichlorobutane in chlorobenzene, 80.6 mmol sodium formate containing 0.2% (w/w) water, 2.5 mmol tetrabutyl ammonium bromide ($Bu_4N^+Br^-$), 115°C, and a stirring speed of 1000 rpm.

The progress of the reaction was followed by gas-chromatographic analysis of samples that were taken from the organic phase at constant intervals. Figure 1 shows the composition–time curves for the three components (A, R, and S) in a typical run. It is apparent from Fig. 1 that A decreases exponentially, R rises to a maximum (R_{max}) and then falls, and that S rises continuously. These curves are consistent with the behaviour expected for consecutive first-order reactions (9). Figure 2 presents a kinetic profile of the first step (A → R) of reaction [2] plotted as a first-order reaction. It is clear that the behaviour is in excellent agreement with a first-order rate equation. The order of the second step (R → S) was determined by examination

[1]Author to whom correspondence may be addressed. Current address: Division of Chemistry, National Research Council of Canada, Ottawa, Ont., Canada K1A 0R6.

Can. J. Chem. Downloaded from www.nrcresearchpress.com by 122.72.124.2 on 09/07/12
For personal use only.

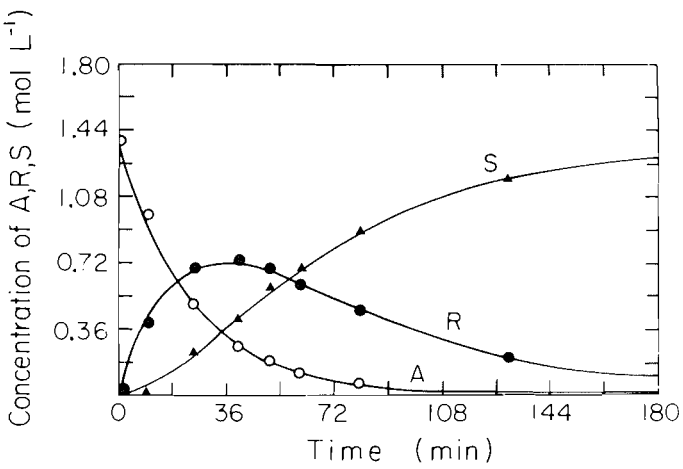


FIG. 1. Concentration–time curves for reaction [2]. Reaction conditions: 1,4-dichlorobutane (27.4 mmol), 99.8% sodium formate (80.6 mmol), tetra-*n*-butylammonium bromide (2.5 mmol), and chlorobenzene (17 mL) at 115°C with mechanical stirring at 1000 rpm. The concentration of S was calculated from the difference in the concentration of the reacting components by $C_S = C_{A_0} - (C_A + C_R)$.

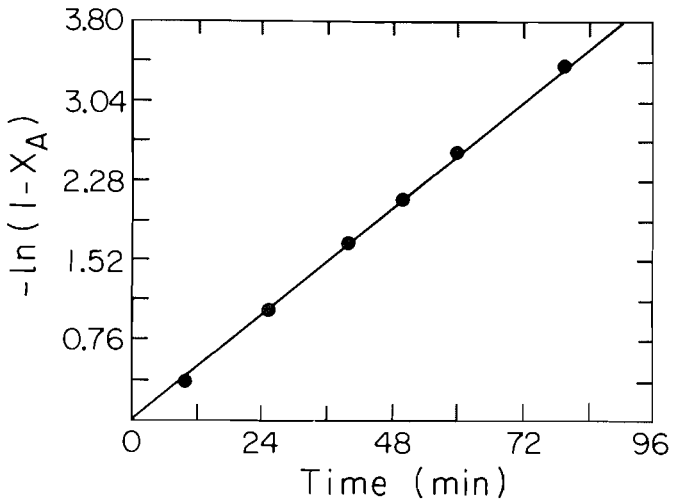


FIG. 2. Test for first order for the first step A → R in reaction [2]. Conditions, see Fig. 1.

of the variation in $C_{R,max}/C_{A_0}$ as a function of C_{A_0}: 1.37, 2.42, and 3.76 M. We obtained a constant ratio, viz. 0.5. Thus $C_{R,max}/C_{A_0}$ is independent of C_{A_0} and therefore the second step of the series (R → S) is first order as well (9).

Effect of stirring speed

Figures 3a and 3b show that the observed pseudo-first-order rate constants k_1 and k_2 are increased by increasing the stirring speed up to 400 rpm, and that they remain constant beyond this value. The curves exhibited in these figures are similar to those reported for liquid–liquid PTC systems (L–L PTC) (10, 11), in that the reaction rates are shown to increase upon increasing the stirring speed up to 300 rpm, and to remain constant beyond this value. It can safely be argued that the rate of mass transfer does not play a role in the substitution reaction if mixing above 400 rpm is applied.

Effect of catalyst structure

We studied the effect of catalyst structure on the observed rate constants of reaction [2]; the results are summarized in

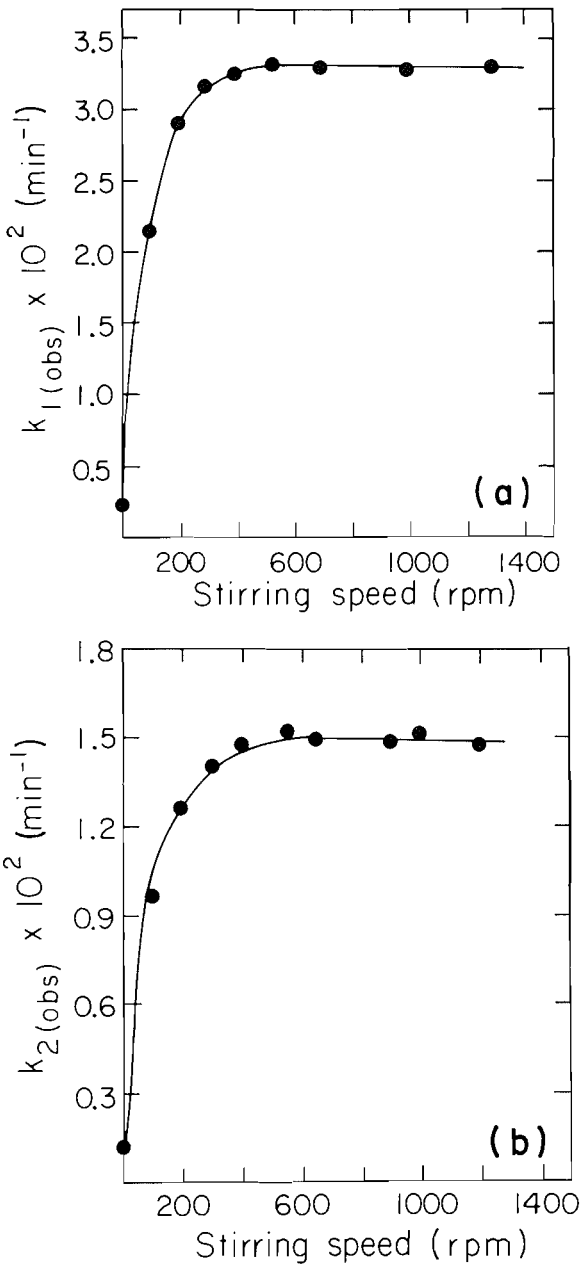


FIG. 3. Dependence of (a) $k_{1(obs)}$ and (b) $k_{2(obs)}$ on stirring speed. Reaction conditions: 1,4-dichlorobutane (27.4 mmol), 99.8% sodium formate (80.6 mmol), tetra-*n*-butylammonium bromide (1.6 mmol), chlorobenzene (17 mL) at 115°C.

Table 1. The data revealed similar catalytic activity for each of the various symmetrical tetra-*n*-alkylammonium bromides, $(C_nH_{2n+1})_4N^+Br^-$. The ammonium salts where the alkyl chain contained four or more carbons gave the maximum rate: $k_{1(obs)} = (3.2 \pm 0.1) \times 10^{-2}\,min^{-1}$, $k_{2(obs)} = (1.5 \pm 0.1) \times 10^{-2}\,min^{-1}$. This behaviour was expected due to the fact that the catalysts with $n \geq 4$ reside entirely in the organic phase (12). Thus, above the tetra-*n*-butyl cation the length of the alkyl chain has no marked effect on the reaction rate. In addition, it can be seen that symmetrical catalysts are much more efficient than unsymmetrical ones, e.g., Aliquat 336.

The catalysts TEBA-Cl and TEBA-Br were not found to be very effective as compared to other catalysts employed in this study (Table 1). This is mainly due to the poor solubility of the TEBA-Cl and -Br^- in the organic phase.

Can. J. Chem. Downloaded from www.nrcresearchpress.com by 122.72.124.2 on 09/07/12
For personal use only.

TABLE 1. Dependence of the observed rate constants of reaction [2] on catalyst structure

Catalyst*	$k_{1(obs)} \times 10^2$ (min^{-1})	$k_{2(obs)} \times 10^2$ (min^{-1})
—	0	0
$Bu_4N^+Br^-$	3.25	1.52
$Hep_4N^+Br^-$	3.31	1.60
$OCt_4N^+Br^-$	3.14	1.47
Aliquat 336	2.12	0.98
TEBA-Br	0.81	0.39
TEBA-Cl	0.99	0.47

Reaction conditions, see Fig. 3; stirring speed, 1000 rpm.
*$Bu_4N^+Br^-$ = tetra-*n*-butylammonium bromide; $Hep_4N^+Br^-$ = tetra-*n*-heptyl ammonium bromide; $OCt_4N^+Br^-$ = tetra-*n*-octylammonium bromide; Aliquat = tricaprylmethyl ammonium chloride; TEBA-Br = triethylbenzyl ammonium bromide; TEBA-Cl = triethylbenzyl ammonium chloride.

Effect of catalyst counteranion

The effect of the counteranion of the quaternary ammonium salts is presented in Table 2. It is clear that the halide anion (entries 2–4) behaved as would be expected, $Cl^- > Br^- > I^-$, but the hydrogen sulfate catalyst, which is usually considered as the catalyst of choice in L–L PTC systems (13), performed very poorly in the S–L PTC esterification. It is important to note that the reaction rate decreases on increasing the hydrogen sulfate concentration (entries 5, 6) while the total concentration of the catalyst was constant.

The poor performance of the bisulfate catalyst in the S–L PTC esterification with formate salts could be attributed to the *in situ* formation of formic acid, according to eq. [3]:

[3] $$HCOO^- + HSO_4^- \rightarrow HCOOH + SO_4^{2-}$$

The formic acid present in the system is extracted into the organic phase together with the ion pairs $HCOO^-Q^+$, via hydrogen bonding (eq. [4]), and inhibits the normal PTC substitution process (4).

[4] $$HCOOH_{aq.} + HCOO^-Q^+_{org} \rightarrow HCOOH\cdots HCOO^-Q^+_{org}$$

Effect of catalyst concentration

The catalyst $Bu_4N^+Br^-$ was used as reference compound for the kinetic study. This commercial and inexpensive catalyst was found to be very effective (Table 1) and less hygroscopic than the chloride counterpart.

The observed rate constants k_1 and k_2, Figs. 4a and 4b respectively, are linearly dependent on catalyst concentration up to 0.16 M, and remain constant beyond this value. We visualize that above 12 mol% of catalyst relative to the substrate (1,4-dichlorobutane) the interface is already saturated with the quaternary ammonium cations. Therefore, increasing the catalyst concentration swamps the interface. However, there is an optimal cation (Q^+) concentration that can participate in the phase transfer process. It is important to note that in the range of catalyst concentration examined (0.02–0.4 M), full solubility of the catalyst was observed in the organic phase.

Effect of temperature

The activation energies for the two consecutive steps (eq. [2]) were determined from the Arrhenius plots presented in Figs. 5a and 5b. The data yield 20.6 kcal/mol for the first step (A → R) and 21.5 kcal/mol for the second step (R → S). An activation energy of about 21 kcal/mol is typical for chemically controlled reactions (9).

The product distribution (R/S) is not appreciably affected by temperature. Therefore, the actual mode of operation for obtaining high selectivity towards the desired product in consecutive reactions, e.g., for the intermediate R, depends on the economics of the system under study.

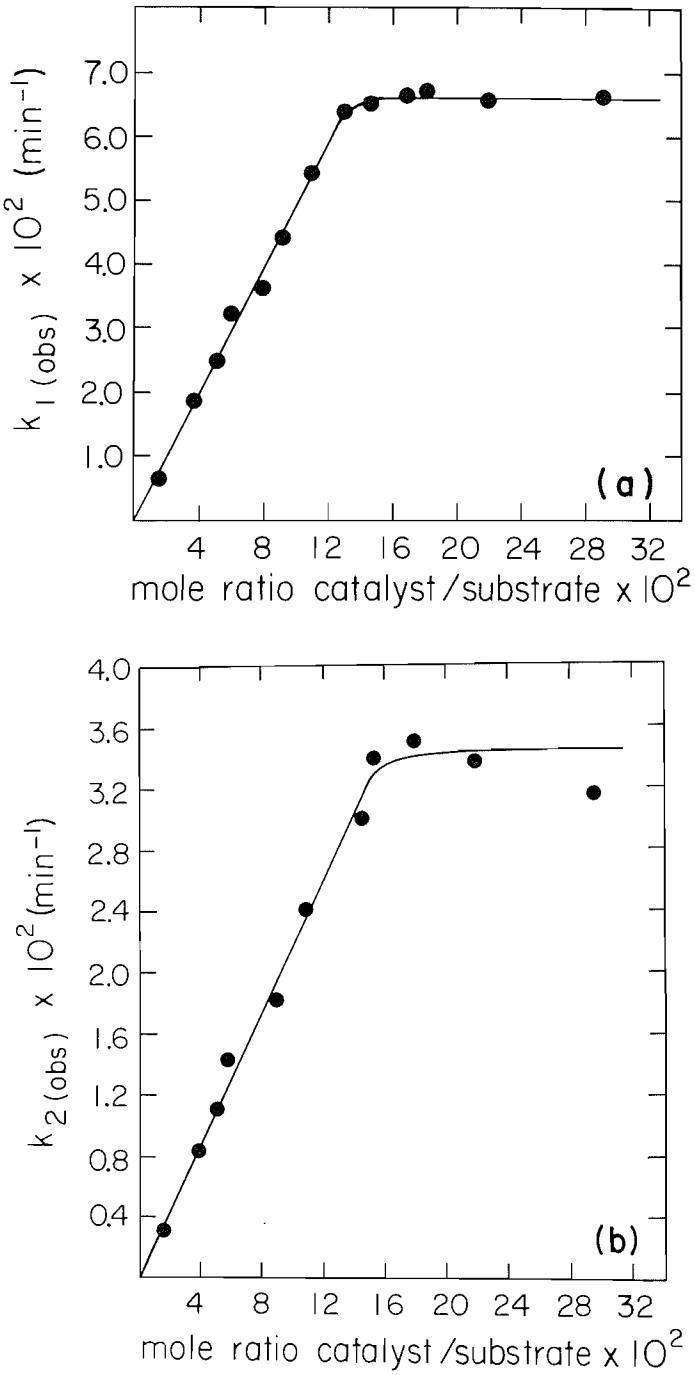


FIG. 4. Dependence of (a) $k_{1(obs)}$ and (b) $k_{2(obs)}$ on catalyst concentration.

Discussion

Analysis of the different variables examined in this study and in a previous report (5), regarding the critical importance of traces of water for chloride–formate exchange under S–L PTC conditions, suggests a detailed mechanism for substitution reactions catalyzed by quaternary onium salts under S–L conditions. We have termed the proposed mechanism "Thin aqueous boundary layer", as represented in Scheme 1.

Can. J. Chem. Downloaded from www.nrcresearchpress.com by 122.72.124.2 on 09/07/12
For personal use only.

TABLE 2. Dependence of the observed rate constants of reaction [2] on catalyst counteranion

Entry	Catalyst*	$k_{1(obs)} \times 10^2$ (min^{-1})	$k_{2(obs)} \times 10^2$ (min^{-1})
1	$Bu_4N^+HSO_4^-$	0.61	0.29
2	$Bu_4N^+Cl^-$	5.52	2.38
3	$Bu_4N^+Br^-$	3.25	1.52
4	$Bu_4N^+I^-$	1.02	0.49
5	*$Bu_4N^+Br^-$: Br^-(50%), HSO_4^-(50%)	1.93	0.83
6	*$Bu_4N^+Br^-$: Br^-(20%), HSO_4^-(80%)	0.82	0.37

*The values indicated in parentheses show the mol% of the counteranion from the total amount of catalyst, kept constant at 1.6 mmol. For reaction conditions, see Fig. 3.

Can. J. Chem. Downloaded from www.nrcresearchpress.com by 122.72.124.2 on 09/07/12
For personal use only.

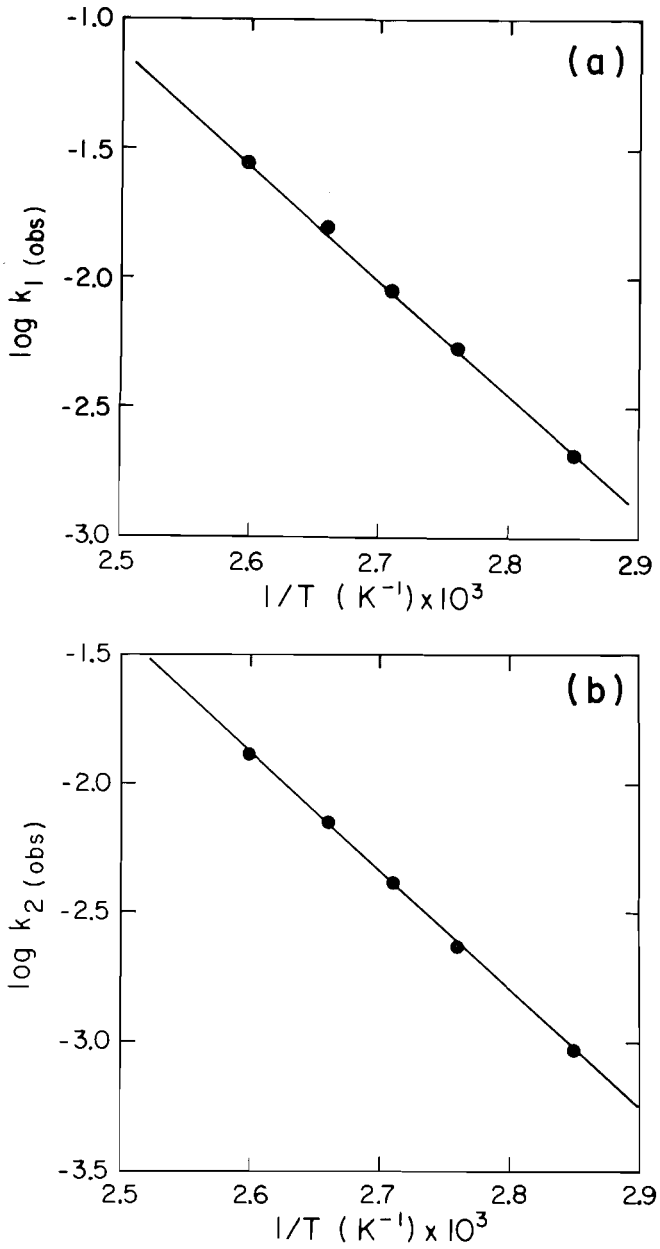


FIG. 5. Arrhenius plot: Dependence of (a) $k_{1(obs)}$ and (b) $k_{2(obs)}$ on temperature.

The first step involves activation of the formate ions by partial dissolution of the solid lattice molecules in the thin aqueous layer. In the second step the catalyst cation exchanges anions at the interface. The ion pair $HCOO^-Q^+$ reacts in the organic phase with the substrate and releases chloride (Cl^-), which combines with the cation (Q^+) and exchanges with formate anion at the interface. In a previous report (3) we demonstrated that highly concentrated aqueous solutions of sodium formate do not dissolve sodium chloride nor sodium bromide. Thus the chloride released during the course of reaction [2] precipitates as sodium chloride (Scheme 1) and does not participate in the phase transfer process. Therefore, the assumption that $[HCOO^-Q^+]_{org}$ is constant throughout the reaction is valid for the system under investigation.

According to the thin aqueous boundary layer mechanism and the experimental results, which are consistent with the suggested mechanism, we can write the rate equations of reaction [2] as:

$$[5] \quad \frac{-d[A]}{dt} = k_1[A]_{org}[HCOO^-Q^+]_{org}$$

$$[6] \quad \frac{d[R]}{dt} = k_1[A]_{org}[HCOO^-Q^+]_{org} - k_2[R]_{org}[HCOO^-Q^+]_{org}$$

$$[7] \quad \frac{d[S]}{dt} = k_2[R]_{org}[HCOO^-Q^+]_{org}$$

Since $[HCOO^-Q^+]_{org}$ = constant, eqs. [5]–[7] can be rewritten as:

$$[8] \quad \frac{-d[A]}{dt} = k_{1(obs)}[A]$$

$$[9] \quad \frac{d[R]}{dt} = k_{1(obs)}[A] - k_{2(obs)}[R]$$

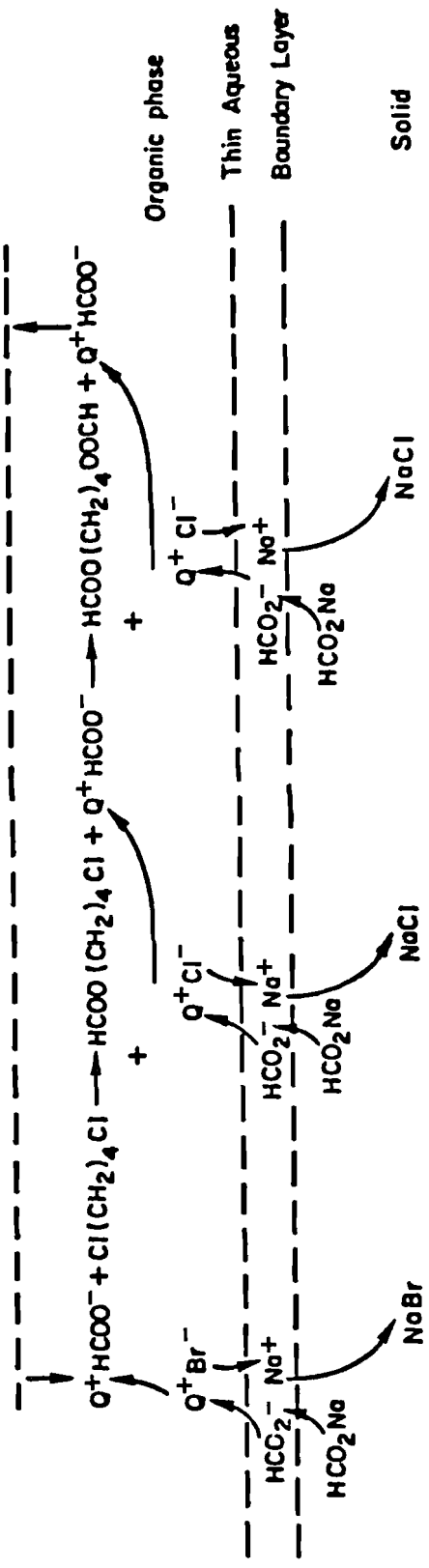
$$[10] \quad \frac{d[S]}{dt} = k_{2(obs)}[R]$$

where $k_{1(obs)} = k_1[HCOO^-Q^+]_{org}$ and $k_{2(obs)} = k_2[HCOO^-Q^+]_{org}$.

Experimental

All materials were commercially available at >99% purity. Analytical purity of chlorobenzene and 1,4-dichlorobutane were confirmed by

Can. J. Chem. Downloaded from www.nrcresearchpress.com by 122.72.124.2 on 09/07/12
For personal use only.



SCHEME 1. Mechanism of esterification of 1,4-dichlorobutane with sodium formate under S–L PTC conditions.

gc analysis. Anhydrous AR grade sodium formate was freeze-dried prior to the experiment. The precise amount of water in the formate salt was determined by thermogravimetric analysis. The particle size of sodium formate was below 5 μm.

Gas chromatographic determinations were performed on a Gow-Mac gas chromatograph (TC detector) equipped with a 2-m 15% OV-17 on Chromosorb W column operating at 110°C. From the appropriate calibration, concentrations of $Cl(CH_2)_4Cl$, $HCOO(CH_2)_4Cl$, and $HCOO(CH_2)_4OOCH$ in the reaction mixture were obtained. The reaction temperature was maintained ±0.5°C by a thermostatted bath. Stirring was provided by a Heidolph mechanical stirrer with appropriate gears attached to a flat-bladed Teflon paddle (36 mm length). The stirring speed was determined by a Jaquet tachometer to ±10 rpm.

In a typical reaction, a 50-mL round-bottomed flask with a side arm for sampling was charged with 5.481 g (80.6 mmol) sodium formate 99.8% w/w, 516 mg (1.6 mmol) $Bu_4N^+Br^-$, and with 27.4 mmol 1,4-dichlorobutane in 20 mL of chlorobenzene solution (1.37 M). The mixture was stirred with a mechanical stirrer at 115°C; at regular intervals, 20-μL samples of the organic phase were taken and immediately injected into the gas chromatograph. Phase separation was almost immediate after the stirring was stopped.

The rate constants were calculated by fitting the experimental data for A, R, and S to the appropriate kinetic equations (ref. 9, pp. 58, 59) by means of the least-squares method (14). The goodness of fit was estimated by calculation of χ^2, which was at least 0.98.

1. E. V. DEHMLOW and S. S. DEHMLOW. Phase transfer catalysis. 2nd ed. Verlag Chemie, Weinheim. 1983.
2. C. M. STARKS and C. LIOTTA. Phase transfer catalysis. Academic Press, New York. 1978.
3. Y. SASSON and H. A. ZAHALKA. J. Chem. Soc. Chem. Commun. 1347 (1983).
4. H. A. ZAHALKA and Y. SASSON. J. Chem. Soc. Chem. Commun. 1581 (1984).
5. H. A. ZAHALKA and Y. SASSON. J. Chem. Soc. Chem. Commun. 1652 (1984).
6. H. A. ZAHALKA and Y. SASSON. Synthesis, 763 (1986).
7. O. ARRAD and Y. SASSON. J. Am. Chem. Soc. **110**, 185 (1988), and references therein.
8. G. D. YADAV and M. M. SHARMA. Ind. Eng. Chem. Process Des. Dev. **20**, 385 (1981).
9. O. LEVENSPIEL. Chemical reaction engineering. J. Wiley, New York. 1972.
10. C. M. STARKS and R. M. OWENS. J. Am. Chem. Soc. **95**, 3613 (1973).
11. M. HALPERN, Y. SASSON, and M. RABINOVITZ. J. Org. Chem. **48**, 1022 (1983).
12. R. BAR, L. BAR, Y. SASSON, and J. BLUM. Anal. Chim. Acta, **154**, 203 (1983).
13. L. LINDBLOM and M. ELANDER. Bofors Nobel Kemi, Sweden. October 1980.
14. P. R. BEVINGTON. Data reduction and error analysis for the physical sciences. McGraw–Hill, New York. 1969. pp. 204–205.

The identification of structural fragments of enolic monoterpenes, enolic pheromones, and related natural products, from OH stretching vibration frequencies and relative intensities

JOHN F. BACON AND JOHN H. VAN DER MAAS[1]

Laboratory for Analytical Chemistry, University of Utrecht, Croesestraat 77A, 3522 AD Utrecht, The Netherlands

Received September 6, 1988

JOHN F. BACON and JOHN H. VAN DER MAAS. Can. J. Chem. **67**, 250 (1989).

The OH stretching frequency has proved to be a powerful tool for structural investigations of enolic natural products containing diverse structural elements. The position of unsaturation can in many cases be determined directly from frequency measurements. Primary, secondary, and tertiary α–β and β–γ unsaturation can unambiguously be identified due to the possession of OH bands arising from an interaction of the OH proton with the π system. Frequently, unsaturation further removed than the γ position can be identified, particularly when a double bond is present, intermediate between the distal π system and the OH group. The identification of long-range OH–π system interactions relies on the observation that an intermediate double bond reduces the rotational freedom of the molecule. This reduction in entropy is assumed to be responsible for a significant population of the conformation in which the OH group is associated with the π system.

Key words: infrared, conformation, natural products, alcohols, molecular structure.

JOHN F. BACON et JOHN H. VAN DER MAAS. Can. J. Chem. **67**, 250 (1989).

La fréquence de la vibration d'élongation OH s'avère un outil puissant dans les études de structures des produits naturels énoliques comportant divers éléments de structure. Dans plusieurs cas, les mesures de fréquence permettent de déterminer directement la position de l'insaturation. En se basant sur la présence de bandes OH provenant d'une interaction entre le proton du OH et le système π, on peut identifier sans ambiguïtés les insaturations α–β ainsi que β–γ, tant primaire que secondaire ou tertiaire. On peut fréquemment identifier des insaturations dont la position est plus éloignée que la position γ; cette affirmation est particulièrement vraie lorsqu'il existe une double liaison entre le système π éloigné et le groupement OH. L'identification des interactions OH–π à distance est basée sur l'observation qu'une double liaison intermédiaire réduit la liberté de rotation de la molécule. On fait l'hypothèse que cette réduction de l'entropie est responsable de la présence d'une population importante de la conformation dans laquelle le groupement OH est associé avec le système π.

Mots clés : infrarouge, conformation, produits naturels, alcools, structure moléculaire.

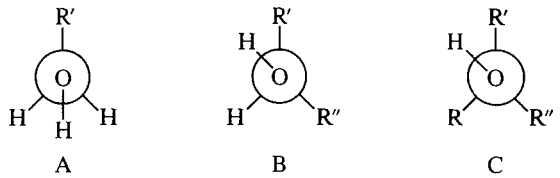
[Traduit par la revue]

Introduction

The enols are diversely represented amongst physiologically active compounds (1–8). Many important pheromones of the sex attractant (2–4) and the insect feedant types (1) possess enolic functions. It has been shown that the position and configuration of the double bonds are responsible for the structure–reactivity relationship (2). In addition, a large number of retinols and monoterpenes possess the hydroxy-isoprene unit (5–8).

Modern methods of structural elucidation of the positions of enolic functions contained within these natural products have relied mainly upon the use of NMR (1–4, 7, 8), HPLC (3, 6), mass spectrometry (2), TLC (1), and UV–visible spectrometry (6). Classically, the infrared spectra of naturally occurring alcohols have been measured as concentrated solutions or mulls etc., conditions under which molecular association increases the number of conformational isomers and complicates the conformational analysis. Structural elucidation has therefore depended upon assignment of numerous vibrational bands with known structures, in conjunction with GLC and NMR analyses (9, 10).

Recent advances in the study of the OH stretching frequency in dilute solution, using FT–IR, have allowed structural correlation with band position to be made with great accuracy (12–14, 23), and structural elucidations of certain natural products have been made (11). The purpose of this paper is to show that measurement of the OH stretching frequency, alone, is capable of giving detailed information regarding the nature of the OH group and the positions and configurations of neighbouring double bonds.



Primary alcohols: A and B type rotamers
Secondary alcohols: B and C type rotamers
Tertiary alcohols: C type rotamer

FIG. 1. Projection along the C—O bonds of alcohols at an sp^3 carbinol carbon atom, showing the three possible rotamer types for primary, secondary, and tertiary alcohols.

We recently described the influence of structural changes on the OH stretching vibrations of allylic and β–γ enols in dilute solution in CCl_4 (12, 13). It was shown that equilibria exist between conformations in which the OH proton is associated with the π system and those in which it is free. The relative abundances of these conformations differ appreciably from those found in the vapour state (14–22). The OH stretching frequencies and relative intensities of the OH bands are dependent upon the conformations, which in turn are influenced by substitution in the vicinity of the carbinol and olefinic carbons.

For OH groups substituted at an sp^3 carbon atom, three rotamers are possible, due to rotation about the C—O bond (Fig. 1). For the allylic and β–γ enols, only the B or C rotamers are sterically capable of associating with the π system.

[1]Author to whom correspondence may be addressed.

Can. J. Chem. Downloaded from www.nrcresearchpress.com by 122.72.124.2 on 09/07/12
For personal use only.

TABLE 1. The OH stretching frequencies of primary (P), secondary (S), and tertiary (T) saturated alcohols and of α–β and β–γ enols in CCl_4 solution

	OH stretching frequencies of different rotamer types				
Alcohol type	Free (A)	Free (B)	Free (C)	Bonded (B)	Bonded (C)
Saturated (P)	3641–3638	3628–3625	—	—	—
Saturated (S)	—	3628–3625	3617–3612	—	—
Saturated (T)	—	—	3620–3616	—	—
α–β enols (P)	3638–3632	—	—	3622–3619	—
α–β enols (S)[e]	—	—	—	3623–3617	3607–3601
α–β enols (T)	—	—	—	—	~3610[c]
β–γ enols (P)	3636–3635[d]	3627–3624	—	3586–3581[a] 3596–3591	—
β–γ enols (S)	—	3629–3626	3613–3608	3586–3581[a] 3596–3591	—
β–γ enols (T)	—	—	—	~3611[b,c]	—

Data from refs. 12–14, and 23. Frequencies in cm^{-1}, measured in dilute (<0.004 M) CCl_4 solution. Frequencies underlined correspond to the rotamer band with the highest intensity.

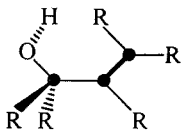
[a]Frequency range for conformations that are methyl substituted at the β carbon atom.

[b]Unpublished data.

[c]Approximated from limited data available.

[d]Relative intensity of rotamer bands depends upon degree of substitution at the carbinol and olefinic carbons (12).

[e]The secondary alcohols exhibit no bands that can be attributed to conformations in which the OH is free, except in the case of severe steric interactions in the eclipsed (E) conformation (13).



R = an alkyl group or hydrogen
The hydroxy proton has a *gauche* position (B or C rotamer), while the C=C bond eclipses the C—O bond

FIG. 2. Generalized conformation of allylic alcohols.



Primary alcohols, R = H; secondary alcohols, R = alkyl
Conformation **i**. R′ = H; conformation **ii**. R′ = alkyl

FIG. 3. Projections along C3—C2 bond of β–γ enols, showing the lowest energy rotamers of the alkene group of β–γ enols in which intramolecular hydrogen bonding occurs.

Figure 2 shows the typical intramolecularly hydrogen bonded conformation for allylic alcohols. Thus the allylic alcohols usually exhibit a composed OH stretching vibration band, which can be resolved into two bands by bandsplitting techniques (13). Typical OH stretching vibration frequencies are given in Table 1. The β–γ enols possess two types of intramolecularly hydrogen bonded conformations (**i** and **ii**, Fig. 3), which are mutually exclusive. Substitution at the β carbon atom determines which conformation is adopted (12).

In contrast with the allylic alcohols, the intensity ratios of free and bonded OH conformations are far more dependent upon the alkyl chain length and also upon the primary, secondary, or tertiary nature of the carbinol carbon. Unlike the allylic alcohols, it is possible for the A, B, and C type OH rotamers to exist in the free OH form. The OH stretching frequencies of these free OH rotamers are almost identical to the saturated analogues (Table 1). Therefore the OH stretching frequencies and relative intensities can be used to easily distinguish between α–β enols, β–γ enols, and saturated alcohols.

A large number of naturally occurring hydroxy monoterpenes possess unsaturation at the α–β or β–γ positions, frequently in conjunction with unsaturation further removed. Similarly, many pheromones of the sex attractant type are enolic, the position of saturation being somewhat variable. Such molecules may be primary, secondary, or tertiary alcohols. Based on results obtained so far, the use of the OH stretching frequency bands alone should be able to give detailed information regarding the configuration and conformation of certain structural elements that may be contained within the molecule. It is therefore useful to extend the study of the OH–π system interaction to a diverse variety of enolic natural compounds (Table 2), for the purpose of structural unit identification.

Experimental

The alcohols **1**–**12** were obtained commercially (**1**–**9** and **11**, Aldrich; **10**, Sigma); **13** was provided by Dr. L. Jirovetz, Institute for Organic Chemistry, University of Vienna. Trace water was removed with molecular sieves (3A). Infrared spectra were recorded for dilute (<0.004 M) solutions in CCl_4 (Merck) on a Perkin Elmer 1800 FT-IR spectrometer using 1-cm Infrasil quartz cells, resolution 1 cm^{-1}, number of scans 18. Accuracy is believed better than $+/-0.5$ cm^{-1}. Solvent subtraction was performed on a Perkin Elmer 7500 data station. Perkin Elmer interaction self-enhancement software was employed on the data station. The enhancement does the equivalent of a Fourier deconvolution by an operation that acts directly on the frequency spectrum. This convolution routine replaces each point in the spectrum with a weighted average of neighbouring points. The procedure is similar to smoothing, except that the coefficients for the weighted average are calculated to cause line narrowing. The

Can. J. Chem. Downloaded from www.nrcresearchpress.com by 122.72.124.2 on 09/07/12
For personal use only.

TABLE 2. Correlation of OH stretching frequencies of primary (P), secondary (S), and tertiary (T) alcohols **1–13**, with rotamer types of α–β and β–γ enols in CCl_4 solution

Compound no.	type	Position of unsaturation	Rotamer types for rotation about C—O bond: Free (A) rotamer	Free (B) rotamer	Free (C) rotamer	Bonded (B) rotamer	Bonded (C) rotamer	Other bands
1	P	α–β, ε–ζ	*3633.5*[a]	—	—	3621.0[a]	—	3552.0
2	P	ε–ζ	3637.0[a]	3626.0[a]	—	—	—	*3550.5*
3	P	α–β, ε–ζ	3633.5[a]	—	—	3623.0[a]	—	—
4	T	α–β, γ–δ	—	—	—	—	3610.5	3544.0
5	T	α–β, γ–δ	—	—	—	—	3611.0	3539.5
6	S	α–β, β–γ	—	—	—	3616.0	—	3573.5
7	S	β–γ, β–γ	—	3624.5	—	3590.5	—	—
8	P	γ–δ	3639.5[a]	3626.5[a]	—	*3592.0*[a]	—	—
9	P	γ–δ	3639.5[a]	3627.0[a]	—	—	—	—
10	P	δ–ε	3638.0[a]	3628.0[a]	—	—	—	—
11	T	β–γ	—	—	3611.0	—	—	3568.0
12	P	ε–ζ	—	—	3616.0	—	—	—
13	P	α–β	3635.0[a]	—	—	3620.5[a]	—	—

Frequencies in cm^{-1}. Frequencies underlined correspond to the rotamer band with the highest intensity. Frequencies in italics have intensities less than 10% of the band with the highest intensity.

[a]Determined by self-enhancement.

Can. J. Chem. Downloaded from www.nrcresearchpress.com by 122.72.124.2 on 09/07/12
For personal use only.

coefficients used depend upon the values selected for two parameters "WIDTH" and "FACTOR".

Results and discussion

The OH stretching frequencies of various unsaturated alcohols **1–13** are shown in Table 2. The structural relationships of the alcohols are shown in Fig. 4 and the observed spectra in the OH stretching region are shown in Fig. 5.

Correlations with α–β and (or) β–γ OH stretching frequencies

Compounds 1–3, 12, and 13

1 and **3** clearly possess a primary OH and a double bond at the α–β position, the A (free) and B (bonded) rotamer bands having typical frequencies and intensities. **2** does not possess α–β unsaturation and accordingly exhibits A (free) and B (free) OH rotamers. **1**, **2**, and **3** possess a double bond at the ε–ζ position. However, only alcohols **1** and **2** exhibit a band that could be correlated to an intramolecular association between the OH proton and the π system at an ε–ζ position. The frequency of this band is very similar in each alcohol (3552.0 cm^{-1} and 3550.5 cm^{-1}), although its intensity is greater in **1** than in **2**. In **3** (Fig. 4), the configuration of the α–β double bond is *trans*, while that of **2** is *cis*. Consequently it is impossible for the OH proton of **3** to interact with the π system at the ε–ζ position.

The difference in intensity of the band due to the ε–ζ double bond interaction with the OH proton is the result of the larger number of degrees of rotational freedom that **2** possesses compared with **1**. The presence of the double bond at the α–β position reduces the number of degrees of rotational freedom, making an interaction with the π system more probable. Thus the relative intensity of this band between the two alcohols is a function of the entropy of the systems. **13** possesses an α–β double bond; accordingly, the OH stretching frequencies are typical for the A (free) rotamers and B (bonded) rotamer. The π system present in the norbornyl skeleton is sterically hindered from an interaction with the OH proton.

The OH stretching frequency of **12** is typical of a saturated tertiary alcohol; the band cannot be resolved by self-enhancement, since the A/B (free) and C (free) OH rotamers are separated by too-small frequency differences. There is no band present that can be correlated with an association between the OH proton and the π system substituted at the ε–ζ position. The presence of five single bonds between the carbinol carbon and the double bond has a large entropy effect in favour of the free OH conformations. Consequently, no interaction between the OH proton and the π system can occur.

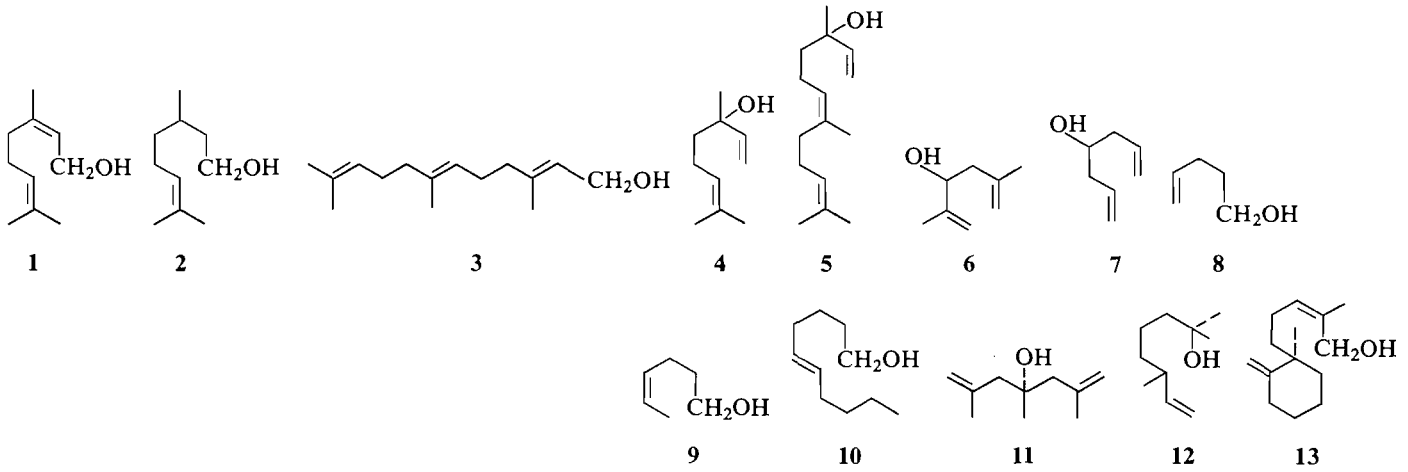
Compounds 4 and 5

The OH stretching frequencies of **4** and **5** correspond to those of a tertiary alcohol in which a C rotamer is intramolecularly hydrogen bonded with a double bond at the α–β position. In addition, another band is present for both alcohols, which can be attributed to the interaction of the OH proton with the double bond at the γ–δ position. The OH stretching frequencies are similar (3539.5 cm^{-1} and 3544.0 cm^{-1}). Inspection of the structures of **4** and **5** shows that the molecule **4** is a structural unit contained within the molecule **5**. In addition to this unit, **5** possesses another structural unit containing a double bond. Evidently, this double bond is too far away from the OH proton to be involved in a hydrogen bonding interaction.

Compounds 6 and 7

7 possesses OH stretching bands due to B (free) and B (bonded) rotamers, the latter being due to an interaction with the double bond at the β–γ position. The frequency of 3590.5 cm^{-1} indicates that there is no substitution at the β carbon. The presence of two β–γ double bonds cannot be proved, but can be inferred from the much lower than normal relative intensity of the free secondary OH rotamer. Thus an entropy effect is responsible for the increased relative intensity of the intramolecularly hydrogen bonded OH band.

6 has an OH stretching band at 3616.0 cm^{-1}, slightly lower than the normal frequency for a tertiary rotamer that is hydrogen



1 = nerol {*cis*-2,6-dimethyl-2,6-octadien-8-ol}
2 = 3,7-dimethyl-6-octen-1-ol
3 = *trans,trans*-farnesol {*trans,trans*-3,7,11-trimethyl-dodecatrien-1-ol}
4 = linalool {2,6-dimethyl-2,7-octadien-6-ol}
5 = nerolidol {*cis*-3,7,11-trimethyl-1,6,10-dodecatrien-3-ol}
6 = 2,5-dimethyl-1,5-hexadien-3-ol
7 = 1,6-heptadien-4-ol
13 = β-santanol {2-methylene, 3-methyl, 3-(2-methyl-3-penten-1-ol)-[2.2.1]bicycloheptane}
8 = 1-penten-5-ol
9 = 5-hexen-1-ol
10 = *trans*-5-decen-1-ol
11 = 2,4,6-trimethyl-1,6-heptadien-4-ol
12 = dihydromyrcenol{2,6-dimethyl-7-octen-2-ol}

FIG. 4. The structural relationships of compounds **1**–**13**.

bonded to an α–β double bond. The OH band due to the interaction of the OH proton with the β–γ double bond occurs at a frequency of 3573.5 cm^{-1}. Taking into consideration the methyl substitution at the β carbon, we would anticipate an OH stretching frequency in the range 3581.0–3586.0 cm^{-1}. Evidently the usual rotamer positions are somewhat perturbed by repulsive forces between the two π systems. This lowering of the OH stretching frequencies is therefore of help in the identification of two π systems that, due to their proximity, apparently perturb the usual rotamer positions.

Compound 11

11 possesses an OH group placed symmetrically between two β–γ double bonds. No recent data for tertiary β–γ enols is available, therefore this data must be treated as empirical. Two OH bands have been resolved, as 3611.0 cm^{-1} and 3568.0 cm^{-1}. The proximity of the two π systems results in a considerable interaction between them, which would be expected to influence the conformation in two ways: (*i*) The double bonds will orientate themselves so that the *p* orbitals of each are, as far as possible, directed away from each other. (*ii*) Orientation of the OH group will be to minimize the lone pair – π system repulsion and to optimize the OH proton – π system attraction.

On the basis of our previous knowledge, we presume that the OH band at 3611.0 cm^{-1} is due to a free OH rotamer, while the band at 3568.0 cm^{-1} must be due to a bonded OH rotamer, although the rotamer positions are difficult to assign from the limited data.

Compounds 8–10

Structurally, **8** and **9** are very similar; both are primary alcohols with a double bond at the γ–δ position. The only difference between the two is the substitution of a methyl for a hydrogen at the δ carbon in **9**. Both alcohols show rotamer bands due to free primary and secondary OH rotamers. In addition, however, **7** possesses a band of very low relative intensity at 3592.0 cm^{-1}, which can only be attributed to an interaction of the OH proton with the π system. The absence of this band in **9** must be due to the presence of the methyl group at the δ carbon.

The very low relative intensity of the band at 3592.0 cm^{-1} suggests that this conformation is of very low relative population, i.e., it is highly unfavoured relative to the free OH conformations. The additional steric interactions that are created on substitution of a methyl group at the δ carbon are apparently sufficient to reduce the population of intramolecularly hydrogen bonded conformations to undetectable concentrations.

10 possesses a double bond at the δ–ε position and, like **9**, shows OH stretching bands that are typical of saturated alcohols. The π system is therefore too far removed to interact with the OH proton.

For primary alcohols, the double bond at the γ–δ position seems to be the limit of the distance between the OH group and the π system. The formation of the intramolecular hydrogen bond in this system represents the formation of a 6- or 7-membered ring depending upon the site of interaction of the OH proton with the π system. As explained above, the entropy of this system is reduced if double bonds are present intermediate between the OH group and the distal π system.

Conclusions

The OH stretching vibration frequencies of unsaturated alcohols can provide detailed information regarding the nature, position, and rotational conformation of the OH group and its steric relation to the double bonds.

Long-range interactions between the OH proton and the π system can in certain instances be used to determine exactly the

Can. J. Chem. Downloaded from www.nrcresearchpress.com by 122.72.124.2 on 09/07/12
For personal use only.

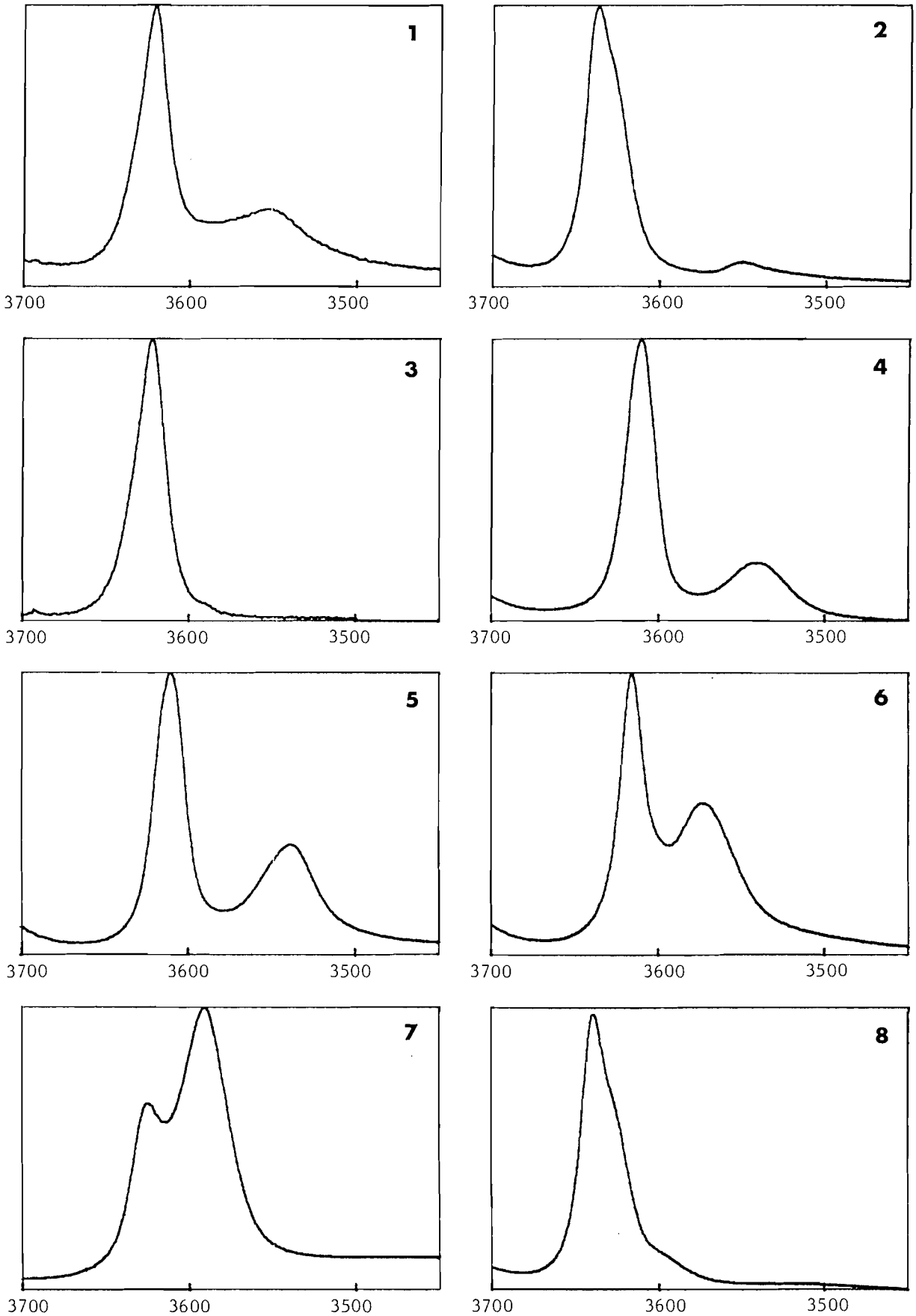
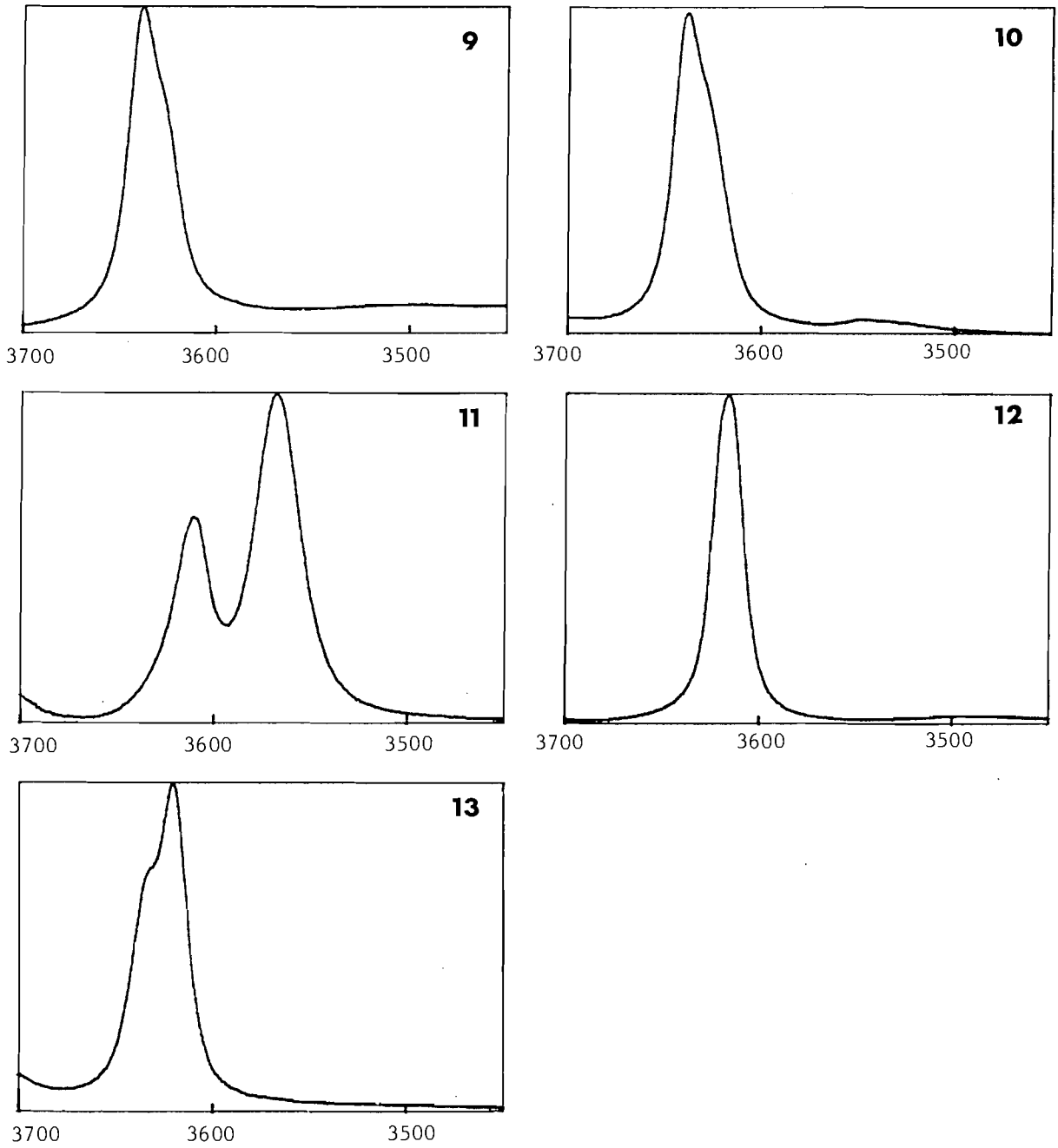


FIG. 5. Infrared spectra of the OH stretching region of compounds **1–13**. The spectra are adjusted to have an absorbance of 1.0. Abscissa: cm^{-1}; ordinate: absorbance.

Can. J. Chem. Downloaded from www.nrcresearchpress.com by 122.72.124.2 on 09/07/12
For personal use only.



Can. J. Chem. Downloaded from www.nrcresearchpress.com by 122.72.124.2 on 09/07/12
For personal use only.

positions of unsaturation and, frequently, the proximity of two π systems. As a consequence of the "short"- and "long"-range hydrogen bonding interaction of the OH proton with the π system, the conformations of the molecules as shown in Fig. 3 are in many cases misleading. Conformations in which the OH is associated with the π system and those in which the OH is free are of course in an equilibrium, the predominant conformation being dependent upon the nature and position of substituted alkyl groups. For alcohols containing more than one π system, a number of distinct intramolecularly hydrogen bonded species are in equilibrium with the free OH forms. It is therefore necessary to undertake a detailed spectroscopic study, to establish the minimum energy conformations. It has been shown, however, that the "standard" data presented in Table 1, and extended in Table 2, can be used for the structural elucidation of unsaturated alcohols.

1. S. V. Ley, D. Santafianos, W. M. Blaney, and M. S. J. Simmonds. Tetrahedron Lett. **28**, 221 (1987).
2. M. Bengtsson, T. Liljefors, and B. Hansson. Bioorg. Chem. **15**, 409 (1987).
3. E. Alvarez, T. Cuvigny, C. Herve du Penhoat, and M. Julia. Tetrahedron, **44**, 119 (1988).
4. A. D. Buss, N. Greeves, R. Mason, and S. Warren. J. Chem. Soc. Perkin Trans. 1, 2569 (1987).
5. K. D. Hope, C. Y. Robinson, M. F. Vaezi, W. J. Brouillette, and D. D. Muccio. Magn. Reson. Chem. **25**, 1040 (1987).

6. E. MÄRTI-FISCHER and C. H. EUGSTER. Helv. Chim. Acta, **70**, 1988 (1987).
7. F. BOHLMANN, R. ZEISBURG, and E. KLEIN. Org. Magn. Reson. **7**, 426 (1975).
8. E. WENKERT, M. J. GASIC, E. W. HAGAMAN, and L. D. KWART. Org. Magn. Reson. **7**, 51 (1974).
9. B. M. MITZNER, V. J. MANCINI, S. LEMBERG, and E. T. THEIMER. Appl. Spectrosc. **22**, 34 (1968).
10. B. CURRY, I. PALINGS, A. BROEK, J. JOHANNES, A. PARDOEN, P. P. J. MULDER, J. LUGTENBURG, and R. MATHIES. J. Phys. Chem. **88**, 688 (1984).
11. E. T. G. LUTZ, P. A. VAN DER SCHAAF, and J. H. VAN DER MAAS. Appl. Spectrosc. **41**, 1251 (1987).
12. J. F. BACON and J. H. VAN DER MAAS. Spectrochim. Acta, Part A. In press.
13. J. F. BACON and J. H. VAN DER MAAS. Spectrochim. Acta, Part A. In press.
14. J. H. VAN DER MAAS and E. T. G. LUTZ. Spectrochim. Acta, Part A. **30A**, 2005 (1974).
15. J. KAO and T. KATZ. J. Mol. Struct. **108**, 229 (1984).
16. W. CAMANATI and A. FANTONI. Chem. Phys. **105**, 59 (1986).
17. F. VANHOUTEGHEM, W. PYCKHOUT, C. VAN ALSENOY, L. VAN DEN ENDEN, and H. J. GEISE. J. Mol. Struct. **140**, 33 (1986).
18. W. CAMINATI, A. C. FANTONI, and B. VELINO. Mol. Phys. **61**, 1269 (1987).
19. S. D. KAHN and W. J. HERE. J. Am. Chem. Soc. **109**, 666 (1987).
20. Z. SMITH, N. CARBALLO, E. B. WILSON, K. MARSTOKK, and H. MØLLENDALL. J. Am. Chem. Soc. **107**, 1951 (1985).
21. P. ARNAUD and Y. C. R. ARMAND. C.R. Hebd. Séances Acad. Sci. **253**, 1547 (1961); Ann. Chim. (Paris), **9**, 433 (1964).
22. H. BADAWI, P. LORENCAK, K. W. HILLIG II, M. IMACHI, and R. L. KUCZKOWSKI. J. Mol. Spectrosc. **162**, 247 (1987).
23. F. A. J. SINGELENBURG, E. T. G. LUTZ, and J. H. VAN DER MAAS. Appl. Spectrosc. **40**, 1093 (1986).

Can. J. Chem. Downloaded from www.nrcresearchpress.com by 122.72.124.2 on 09/07/12
For personal use only.

Limonoids from the Fijian medicinal plant *Dysoxylum richii*

MADHU K. JOGIA[1] AND RAYMOND J. ANDERSEN[2]

Departments of Chemistry and Oceanography, University of British Columbia, Vancouver, B.C., Canada V6T 1W5

Received August 5, 1988

MADHU K. JOGIA and RAYMOND J. ANDERSEN. Can. J. Chem. **67**, 257 (1989).

Three new limonoids have been isolated from the Fijian medicinal plant *Dysoxylum richii*. Dried *D. richii* leaves collected at Suva yielded the known limonoid dysoxylin (**1**) as well as the previously unreported dysoxylone (**2**). A Taveuni collection of leaves contained the two new metabolites tigloyldysoxylin (**3**) and 6α-acetoxyobacunol acetate (**4**). The structures of all three new compounds were determined by spectroscopic analysis.

Key words: *Dysoxylum richii*, limonoid, dysoxylone, tigloyldysoxylin, 6α-acetoxyobacunol acetate.

MADHU K. JOGIA et RAYMOND J. ANDERSEN. Can. J. Chem. **67**, 257 (1989).

On a isolé trois nouveaux limonoïdes à partir de la plante médicinale Fidjienne *Dysoxylum richii*. On a récolté des feuilles séchées de *D. richii* à Suva et elles ont fourni le nouveau limonoïde dysoxyline (**1**) ainsi qu'un autre qui n'avait pas été rapporté antérieurement, la dysoxylone (**2**). Une collection de feuilles de Taveuni contenait deux nouveaux métabolites : la tygloyldysoxyline (**3**) et l'acétate de l'acétoxy-6α obacunol (**4**). On a déterminé les structures des trois nouveaux composés en faisant appel à des analyses spectroscopiques.

Mots clés : *Dysoxylum richii*, limonoïde, dysoxylone, tygloyldysoxyline, acetate de l'acétoxy-6α obacunol.

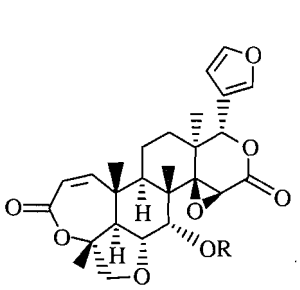
[Traduit par la revue]

Can. J. Chem. Downloaded from www.nrcresearchpress.com by 122.72.124.2 on 09/07/12
For personal use only.

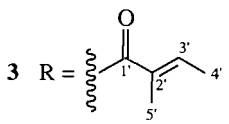
Introduction

The leaves of *Dysoxylum richii* (Gray) C.D.C. are used by natives of Fiji for medicinal purposes. A drink made by adding chopped *D. richii* leaves to a little boiling water is considered to be a cure for most aches and pains (1). We have investigated the extracts of *D. richii* as part of a survey of the chemical constituents of Fijian plants (2). From an initial collection of plant material, made at Suva in December 1985, we isolated dysoxylin (**1**), a new limonoid (3). A subsequent collection of *D. richii* leaves, made at Suva in December 1987, contained dysoxylin (**1**) and a second new limonoid dysoxylone (**2**), while a July 1987 collection of *D. richii* leaves from Taveuni contained the two new limonoids tigloyldysoxylin (**3**) and 6α-acetoxyobacunol acetate (**4**). The structures of the new metabolites **2**, **3**, and **4** are reported here.

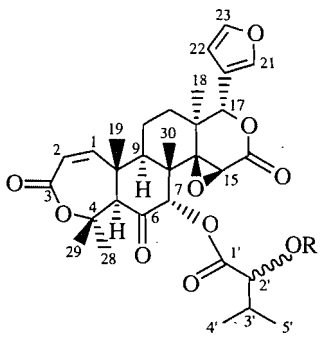
Dysoxylone (**2**) was obtained as an amorphous white solid (mp 203–207°C) that gave a parent ion in the HREIMS at *m/z* 570.2450 daltons appropriate for a molecular formula of $C_{31}H_{38}O_{10}$ (ΔM −1.5 mmu). The ^1H (Table 1) and ^{13}C (Table 2) nmr spectra of dysoxylone (**2**) showed a number of similarities to the data reported for obacunol (**5**) (4) and obacunone (5), suggesting that all three molecules possess the same tetranortriterpenoid carbon skeleton as well as the same ring A, ring D, and furan functionalities. These readily identifiable fragments accounted for 26 of the 31 carbon atoms and six of the 10 oxygen atoms in the molecular formula of dysoxylone (**2**). An OH stretching band at 3400 cm^{-1} in the ir spectrum of **2** indicated that at least one of the remaining oxygen atoms was an alcohol. Dysoxylone (**2**) formed a monoacetate **6** upon treatment with acetic anhydride and pyridine. The ^1H nmr spectrum of the monoacetate revealed that one of the methine resonances had undergone an acetylation shift (δ 4.21 in **2**; δ 4.73 in **6**) consistent with the presence of a secondary alcohol in **2**. It was possible to identify the functionality containing the remaining three oxygen atoms from the ^{13}C nmr data (Table 2). Resonances at δ 165.7, 166.7, and 173.7 were assigned to ester carbonyl carbons and a resonance at δ 203.0 was assigned to a ketone carbonyl carbon. Two of the esters could be accounted for by the ring A and ring D lactones. Together, the remaining ester and the ketone accounted for the final three oxygen atoms in **2**.



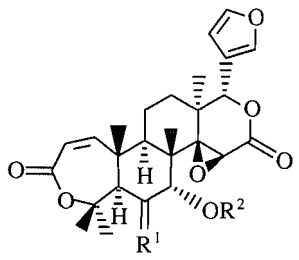
1 R = H

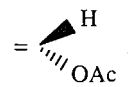


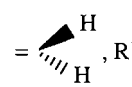
3 R =

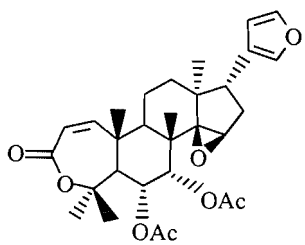


2 R = H
6 R = Ac



4 R^1 =  , R^2 = Ac

5 R^1 =  , R^2 = H



7

A combination of ^1H double resonance and SINEPT (6) nmr experiments demonstrated that the third ester functionality was

[1]On leave from the Department of Chemistry, University of the South Pacific, Suva, Fiji.

[2]Author to whom correspondence may be addressed.

TABLE 1. The ^{1}H nmr assignments for dysoxylin (**1**), dysoxylone (**2**), tigloyl dysoxylin (**3**), 6α-acetoxyobacunol acetate (**4**), and obacunol (**5**). All spectra were recorded in $CDCl_3$ at 400 MHz. Chemical shifts are in ppm from internal TMS

Proton on carbon no.	Compound				
	1	**2**	**3**	**4**	**5**
1	6.33, d, 12 Hz	6.20, d, 12.9 Hz	6.34, d, 12.6 Hz	6.57, d, 12 Hz	6.47, d, 12 Hz
2	5.85, d, 12 Hz	5.89, d, 12.9 Hz	5.92, d, 12.6 Hz	5.95, d, 12 Hz	5.87, d, 12 Hz
5	3.01, d, 12 Hz	3.85, s	2.90, d, 12.4 Hz	2.64, d, 12.4 Hz	2.76, dd, 3, 13 Hz
6	4.01, dd, 12, 2 Hz	—	4.11, dd, 12, 2 Hz	5.12, dd, 12.4, 2.4 Hz	—
7	3.64, d, 2 Hz	4.12, s	5.12, d, 2 Hz	4.92, d, 2.4 Hz	3.51, m
9	2.48, dd, 8, 8 Hz	2.92, dd, 11, 4 Hz	2.52, dd, 8, 8 Hz	2.56, dd, 11.9, 5.8 Hz	2.52, dd, 7, 11 Hz
15	3.95, s	3.51, s	3.80, s	3.63, s	3.84, s
17	5.58, s	5.60, s	5.56, s	5.60, s	5.59, s
18	1.21, s	1.32, s	1.14, s	1.25, s*	1.24, s
19	1.28, s	1.22, s	1.31, s	1.46, s*	1.31, s
21	7.39, m	7.40, m	7.43, m	7.42, m	7.40, m
22	6.33, d, 1 Hz	6.34, d, 1 Hz	6.32, d, 1 Hz	6.32, d, 1 Hz	6.34, d, 1 Hz
23	7.39, m	7.40, m	7.43, m	7.42, m	7.40, m
28	3.82, d, 9 Hz 4.33, d, 9 Hz	1.37, s	3.75, d, 9 Hz 4.19, d, 9 Hz	1.5, s	1.43, s*
29	1.60, s	1.56, s	1.57, s	1.43, s	1.45, s*
30	1.08, s	1.12, s	1.18, s	1.26, s*	1.06, s
2′	—	2.1, m	—		
3′	—	4.21, bm	6.88, qq, 7, 1.5 Hz		
4′	—	0.98, d, 7 Hz*	1.81, dq, 7, 1 Hz		
5′	—	1.08, d, 7 Hz*	1.88, dq, 1.5, 1 Hz		
OAc				2.01, s	
OAc				2.15, s	

*May be interchanged.

part of a 2-hydroxy-3-methylbutanoate fragment. Irradiation of the carbinol methine resonance at δ 4.21 (H2′) simplified the complex multiplet at δ 2.1 (H3′) to a septet ($J = 7$ Hz) and irradiation of either of the methyl doublets at 0.98 and 1.08 (Me4′ and Me5′) simplified the multiplet at δ 2.1 (H3′) to a quintet ($J = 7$ Hz). A SINEPT experiment, optimized for polarization transfer through a $J_{C,H}$ of 7 Hz, demonstrated a two-bond coupling between the methine proton at δ 4.21 (H2′) and the ester carbonyl carbon at δ 173.7 (C1′).

A series of nOe experiments facilitated a complete assignment of the ^{1}H nmr spectrum of dysoxylone (**2**) and established the locations of the ketone functionality and the 2-hydroxy-3-methylbutanoate fragment. Irradiation of the methyl resonance at δ 1.22, assigned to Me19, induced nOe's into the olefinic resonance at δ 6.20 (H1), the methyl resonance at δ 1.12 (Me30), and the methyl resonance at δ 1.56 (Me29). Irradiation of the Me29 resonance at δ 1.56 induced nOe's into the C19 methyl resonance at δ 1.22 and into a methyl resonance at δ 1.37 assigned to Me28. Irradiation of the Me28 resonance (δ 1.37) induced a strong nOe into a methine singlet at δ 3.85 assigned to H5. The lack of coupling to the H5 resonance and its downfield chemical shift relative to the corresponding resonance in dysoxylin (**1**) (δ 3.85 in **2**; 3.01 in **1**) were consistent with the placement of the ketone functionality at C6 in dysoxylone (**2**). Irradiation of H5 (δ 3.85) in a SINEPT experiment showed polarization transfer to C4 (δ 81.5), C10 (δ 50.4), and C6 (δ 203.0) in agreement with the proposed arrangement of functionality. A strong nOe between the C30 methyl resonance at δ 1.12 and a methine singlet at δ 4.12 (H7β) suggested that the 2-hydroxy-3-methylbutanoate fragment was attached in the α orientation at C7. The nOe's between H7 (δ 4.12) and H15 (δ 3.51), between H2′ (δ 4.21) and H15 (δ 3.51), and between H2′ and H5 (δ 3.85) were consistent with the expected spatial proximities resulting from the attachment of the butanoate fragment at C7α. Finally, irradiation of the resonance at δ 2.92 (H9, dd, $J = 4$, 11 Hz) induced nOe's into H5 (δ 3.85) and into a methyl singlet at δ 1.32, which could then be assigned to Me18. The proposed structure **2** for dysoxylone effectively accommodates all the observed spectral data.

Tigloyldysoxylin (**3**) was obtained as a white solid that showed a parent ion in the HREIMS spectrum at m/z 552.2356 daltons appropriate for a molecular formula of $C_{31}H_{36}O_9$(ΔM −0.4 mmu). The similarity between the ^{1}H and ^{13}C nmr data recorded for tigloyldysoxylin (**2**) (Tables 1 and 2) and the nmr data previously found for dysoxylin (**1**) immediately suggested that **3** was simply a C7 acylated derivative of dysoxylin (**1**) (H7: δ 3.64 in **1**; δ 5.12 in **3**). Mass spectral fragments at m/z 453.1900 ($C_{26}H_{29}O_7$: ΔM −1.3 mmu) and 452.1866 ($C_{26}H_{28}O_7$: ΔM +3.1 mmu) daltons supported this assumption and, in conjunction with a companion fragment ion at m/z 83 daltons, revealed that acyl group had a formula of C_5H_7O. An olefinic methine resonance at δ 6.88 (qq, J = 1.5, 7 Hz, H3′) and two olefinic methyl resonances at δ 1.81 (dq, J = 7, 1 Hz, Me4′) and δ 1.88 (dq, J = 1.5, 1 Hz, Me5′) along with ^{13}C resonances at δ 127.8 (C2′), 139.1 (C3′), 14.7 (C4′), and 12.4 (C5′) demonstrated that **3** was a tiglate ester of dysoxylin (7). We used nOe, ^{1}H double resonance, and HETCOR experiments to assign the ^{1}H and ^{13}C nmr spectra (Tables 1 and 2) and to confirm the proposed structure of tigloyldysoxylin (**3**). All the data were consistent wih the proposed structure. In particular, irradiation of H7 (δ 5.12) induced nOe's into the H15 (δ 3.80) and Me30 (δ 1.18) resonances, as expected for an acylated derivative of dysoxylin.

6α-Acetoxyobacunol acetate (**4**), obtained as a very unstable

Can. J. Chem. Downloaded from www.nrcresearchpress.com by 122.72.124.2 on 09/07/12
For personal use only.

TABLE 2. The ^{13}C nmr data for dysoxylin (**1**), dysoxylone (**2**), tigloyldysoxylin (**3**), and obacunol (**5**). All spectra were run in $CDCl_3$ at 75 MHz. Chemical shifts are reported in ppm from internal TMS

Carbon no.	1[a,c]	2[a]	3[a,b]	5[d]
1	149.8	147.1#	149.4	156.9
2	119.4	118.3	119.7	120.8
3	167.7*	166.7*	167.0*	167.8*
4	84.9	81.5	84.4	84.9
5	52.4	60.6	54.5	47.9
6	77.5	203.0	76.2	30.9
7	69.6	81.4	70.8	69.4
8	43.3	46.6	43.3	43.7
9	40.4	42.3	42.3	39.8
10	44.8	50.4	44.6	42.7
11	15.4	17.0	15.5	16.5
12	26.0	25.6	25.8	26.8
13	38.5	39.2	38.9	37.7
14	69.6	69.0	69.4	69.8
15	58.1	57.8	56.4	57.2
16	165.6*	165.7*	165.3*	167.0*
17	78.1	78.1	77.7	78.5
18	17.5	16.4†	17.2	16.0#
19	17.2	16.8†	18.6	18.2#
20	120.5	120.0	120.2	120.4
21	143.0	143.2#	143.0	143.0
22	109.9	109.8	109.8	109.9
23	141.2	141.3#	141.2	141.1
28	81.3	16.3†	81.3	18.5#
29	23.5	25.6†	23.3	26.9#
30	17.9	29.7†	17.6	32.2#
1′	—	173.7	166.0*	—
2′	—	75.6	127.8	—
3′	—	32.1	139.1	—
4′	—	17.6†	14.7	—
5′	—	19.1†	12.4	—

*, #, † may be interchanged.
[a]Proton attachments were determined by APT (10).
[b]Assignments partially based on one-bond HETCOR (11) results.
[c]Assignments partially based on one-bond HETCOR results.
[d]Assignments made by comparison to values for related compounds.

white amorphous solid, gave an unsatisfactory EI high resolution mass spectrum. The largest ion in the spectrum appeared at a mass of m/z 433.2209 daltons, corresponding to an elemental composition of $C_{24}H_{33}O_7$ (ΔM −1.7 mmu). It was apparent from the ^1H and ^{13}C nmr spectra of **4** (Table 1 and Experimental) that the molecule was a limonoid whose structure was closely related to obacunol (**5**) and dysoxylin (**1**). It was clear, therefore, that the ion at m/z 433 could not be a parent ion. A common mass spectral fragmentation pathway in all limonoids of this general structure leads to relatively intense $M^+ - 123$ ($C_6H_3O_3$) peaks (8). We assumed that the formation of the m/z 433 ion occurred via this pathway and therefore concluded that the molecular formula of **4** was $C_{30}H_{36}O_{10}$. The ^1H and ^{13}C nmr data recorded for **4** (Table 1 and Experimental) were in complete agreement with this conclusion.

Two deshielded methyl singlets at δ 2.01 and 2.15 in the ^1H nmr spectrum (Table 1) indicated that **4** was a diacetate. A series of three methine resonances at δ 2.64 (d, J = 12.4 Hz), 5.12 (dd, J = 12.4, 2.4 Hz), and 4.92 (d, J = 2.4 Hz) could be assigned to H5α, H6β, and H7β by comparison of their coupling constants to those observed for the same spin system in dysoxylin (**1**) (Table 1). The downfield shifts of H6 (δ 5.12 in **4**; 4.01 in **1**) and H7 (δ 4.92 in **4**; 3.64 in **1**) in **4** relative to their positions in **1** suggested that the oxygen atoms at C6 and C7 had been acetylated. The upfield shift of H15 in **4** (δ 3.63) relative to its position in obacunol (**5**) (δ 3.84) parallels the upfield shift of H15 in dysoxylin acetate (δ 3.69) (3) relative to its position in dysoxylin (**1**) (δ 3.95), offering further evidence of acetylation at C7. The remainder of the ^1H (Table 1) and ^{13}C (Experimental) nmr data was in complete agreement with the proposed structure **4**. 6α-Acetoxyobucanol (**4**) is closely related to surenin (**7**), which was isolated from leaves of *Toona sureni* (9).

The three new limonoids reported here were isolated from *D. richii* at two different locations in Fiji and at different times of the year. Further work is in progress to determine the extent of geographical and seasonal variation in the limonoid content of Fijian specimens of *D. richii*.

Experimental

The nmr spectra were recorded on Varian XL 300 and Bruker WH 400 spectrometers. Tetramethylsilane was used as an internal standard. Low resolution mass spectra were recorded on an AEI MS 902 spectrometer and high resolution mass spectra were recorded on an AEI MS 50 spectrometer. Infrared spectra were recorded on a Perkin–Elmer 1710 Fourier transform spectrometer. Merck silica gel 230–400 mesh was used for flash chromatography and Whatman Magnum-9 Partisil-10 and ODS-3 columns were used for preparative hplc. Sephadex LH 20 was used for molecular exclusion chromatography.

Isolation and extraction

Fresh leaves of *Dysoxylum richii* were collected at Suva and Taveuni, Fiji, in December and July 1987 respectively. A voucher specimen of this plant has been deposited at the South Pacific Regional Herbarium, Institute of Natural Resources, University of the South Pacific, Suva, Fiji.

Air-dried leaves (300 g) were soaked in methanol (1.5 L) for 3–5 days, the methanol extract was concentrated *in vacuo* to a gum, water was added, and the resulting suspension was extracted successively with hexane and chloroform. The chloroform layers were concentrated *in vacuo* and the residue was dissolved in ethyl acetate and stirred with alumina to decolorize it. Filtration of the suspension and evaporation of the ethyl acetate filtrate gave a gum (approximately 4 g). Fractionation of the gum by silica gel flash chromatography (step gradient: hexane to ethyl acetate) gave fractions containing crude dysoxylin (**1**) and dysoxylone (**2**) from the Suva collections, and fractions containing crude tigloyldysoxylin (**3**) and 6α-acetoxyobacunol acetate (**4**) from the Taveuni collections. Final purification of all four limonoids was accomplished by normal phase hplc (7:3 ethyl acetate/hexane).

Dysoxylone (**2**): white amorphous solid (yield, 0.003% dry wt.); mp 203–207°C; $[\alpha]_D^{25}$ −10° ($CHCl_3$, c 0.3); ir ($CHCl_3$): 1748, 1720, and 1685 cm^{-1}; ^1H nmr, see Table 1; ^{13}C nmr, see Table 2; HREIMS, M^+: 570.2450, $C_{31}H_{38}O_{10}$ (ΔM −1.5 mmu); LREIMS, m/z (rel. intensity): 570(1), 527(4), 358(20), 329(100), 143(76), 95(29), 55(57), 43(89).

Dysoxylone acetate (**6**): Dysoxylone (**2**) (3 mg) was stirred overnight at room temperature with pyridine (0.5 mL) and acetic anhydride (0.3 mL). Evaporation of the acetylation reagents *in vacuo* gave dysoxylone acetate (**6**) as a gum; ^1H nmr ($CDCl_3$) δ: 7.43 (m, 2H), 6.34 (d, J = 1 Hz), 6.19 (d, J = 12.9 Hz), 5.91 (d, J = 12.9 Hz), 5.58 (s), 4.73 (d, J = 6 Hz), 4.02 (s), 3.97 (s), 3.50 (s), 2.98 (dd, J = 11.4 Hz), 2.15 (s), 1.54 (s), 1.37 (s), 1.32 (s), 1.21 (s), 1.09 (s), 1.07 (d, J = 7 Hz), 1.05 (d, J = 7 Hz); HREIMS, M^+: 612.2569, $C_{33}H_{40}O_{11}$ (ΔM −0.3 mmu); LREIMS, m/z (rel. intensity): 612(0.5), 569(0.2), 469(2), 358(5), 329(36), 143(53), 115(52), 43(100).

Tigloyldysoxylin (**3**): amorphous white solid (yield, 0.1% dry wt.); mp 200–205°C; $[\alpha]_D^{25}$ +26° ($CHCl_3$, c 0.4); ir ($CHCl_3$): 1745, 1715, and 1695 cm^{-1}; ^1H nmr, see Table 1; ^{13}C nmr, see Table 2; HREIMS, M^+: 552.2356, $C_{31}H_{36}O_9$ (ΔM −0.4 mmu); LREIMS, m/z (rel. intensity): 552(1), 453(2), 429(2), 329(26), 95(27), 83(100), 55(86).

6α-Acetoxyobacunol acetate (**4**): amorphous white solid (yield 0.04% dry wt.); mp 236–238°C; ir ($CHCl_3$): 1745, 1700, and 1235 cm^{-1}; ^1H

Can. J. Chem. Downloaded from www.nrcresearchpress.com by 122.72.124.2 on 09/07/12
For personal use only.

nmr, see Table 1; ^{13}C nmr ($CDCl_3$: not all carbons were observed due to the low concentration), δ: 15.7, 16.2, 17.7, 18.7, 21.0, 26.4, 26.5, 34.8, 38.4, 41.0, 42.3, 43.1, 52.8, 55.3, 69.2, 69.4, 71.7, 78.1, 84.7, 109.7, 120.0, 123.1, 141.2, 143.2, 159.4, 167.3, 169.7; LREIMS, *m/z* (rel. intensity): 433(11), 373(4), 313(13), 95(25), 43(100).

Acknowledgements

Financial support was provided by a Natural Sciences and Engineering Research Council of Canada grant to R.J.A. M.K.J. was supported by a CIDA/NSERC Fellowship. The authors wish to thank Mr. Saula Vodonaivalu, University of the South Pacific, for collection of the plant material.

1. H. B. R. PARHAM. Polynesian Soc. Mem. **16**, 1 (1943).
2. (*a*) J. J. BROPHY and M. K. JOGIA. Flavour Fragrance J. **1**, 53 (1986); (*b*) J. Nat. Prod. **49**, 730 (1986); (*c*) Fiji Agric. J. **46**(1), 21 (1984); and (*d*) M. K. JOGIA. Fiji Agric. J. **46**(2), 9 (1984).
3. M. K. JOGIA and R. J. ANDERSEN. Phytochemistry, **26**, 3309 (1987).
4. D. L. DREYER. J. Org. Chem. **33**, 3577 (1968).
5. D. L. DREYER and R. D. BENNETT. Tetrahedron, **32**, 2367 (1976).
6. A. BAX. J. Magn. Reson. **57**, 314 (1984).
7. A. KLENK, M. BOKEL, and W. KRAUS. J. Chem. Soc. Chem. Commun. 523 (1986).
8. M. A. BALDWIN, A. G. LOUDON, A. MACCOLL, and C. W. L. BEVAN. J. Chem. Soc. (C), 1026 (1967).
9. W. KRAUS and K. KYPKE. Tetrahedron Lett. 2715 (1979).
10. S. L. PATT and J. N. SHOOLERY. J. Magn. Reson. **46**, 535 (1982).
11. A. BAX. *In* Topics in carbon-13 NMR spectroscopy. Vol. 4. *Edited by* G. C. Levy. Wiley, New York. 1984. Chap. 8. pp. 197–238, and references therein.

Can. J. Chem. Downloaded from www.nrcresearchpress.com by 122.72.124.2 on 09/07/12
For personal use only.

A total synthesis of a protected form of the secoxyloganin aglucone[1]

PETER T. W. CHENG AND STEWART MCLEAN
Department of Chemistry, University of Toronto, Toronto, Ont., Canada M5S 1A1

Received August 5, 1988

PETER T. W. CHENG and STEWART MCLEAN. Can. J. Chem. **67**, 261 (1989).

A synthesis is described that leads from cyclopentadiene through 5-norbornen-2-one to the monosubstituted cyclopentenone **5**; a vinyl substituent is attached by the reaction of a cuprate, and the enolate intermediate is trapped as the silyl enol ether **4**, which is converted to **19**, a product with the 10-carbon framework and stereochemistry of the secoxyloganin aglucone, and with all functional groups differentially protected and in the correct oxidation state. Explorations of the cuprate reaction required to convert the cyclopentenone **5** to the siloxycyclopentene **4** and of the reactions required for the oxidative cleavage of **4** reveal problems with these reactions when they are applied to compounds that are cyclopentane derivatives. The resolution of these problems leads to reaction sequences that proceed with high yields and excellent diastereoselectivity.

Key words: synthesis, secoxyloganin, vinyl cuprate, oxidative cleavage.

PETER T. W. CHENG et STEWART MCLEAN. Can. J. Chem. **67**, 261 (1989).

On décrit une méthode de synthèse qui conduit du cyclopentadiène à la cyclopenténone **5** en passant par la norbornène-5 one-2. On attache un substituant vinyle par le biais de la réaction d'un cuprate et on procède au piégeage de l'intermédiaire énolique sous la forme de l'éther énolique silylé **4** qui est ensuite transformé en produit **19**, un produit comportant le squelette à 10 atomes de carbone et la stéréochimie de l'aglycone de la secoxyloganine ainsi que tous les groupements fonctionnels dans l'état d'oxydation approprié et protégés de façons différentes. Afin d'explorer la réaction avec le cuprate, il s'est avéré nécessaire de transformer la cyclopenténone **5** en siloxycyclopentène **4**; par ailleurs, un examen des réactions nécessaires pour réaliser le clivage oxydant du composé **4** révèle que ces réactions donnent lieu à des problèmes lorsqu'on les applique à des dérivés cyclopentaniques. La solution de ces problèmes a permis d'établir une séquence de réactions qui conduit à des rendements élevés et à une excellent diastéréosélectivité.

Mots clés : synthèse, secoxyloganine, cuprate vinyle, clivage oxydant.

[Traduit par la revue]

Can. J. Chem. Downloaded from www.nrcresearchpress.com by 122.72.124.2 on 09/07/12
For personal use only.

The central role of the secoiridoid secologanin (**1**) in the biosynthesis of several families of alkaloids was predicted and demonstrated about 20 years ago by Battersby *et al.* (1), who had prepared it from menthiafolin. Its direct isolation from a plant source soon followed (2). Many subsequent studies served to confirm the unique position of secologanin as the last non-nitrogenous precursor in the biosynthesis of a vast array of alkaloids (3). Although its importance has been recognized for a considerable length of time, no total synthesis of secologanin has yet been reported. The dense array of functional and stereochemical centres in a relatively small molecule presents obvious synthetic difficulties; there are, for example, four aldehyde or crypto-aldehyde centres, two of which are chiral. A less obvious difficulty is the instability of the aglucone, which undergoes a series of rearrangements under extremely mild conditions (3). Two syntheses of a protected form of the aglucone (4, 5) and a synthesis of a rearranged form of the aglucone (6) have been reported. Although much progress has been made in developing highly selective glucosidation reactions (7), no report of the glucosidation of the fragile secologanin aglucone has yet appeared.

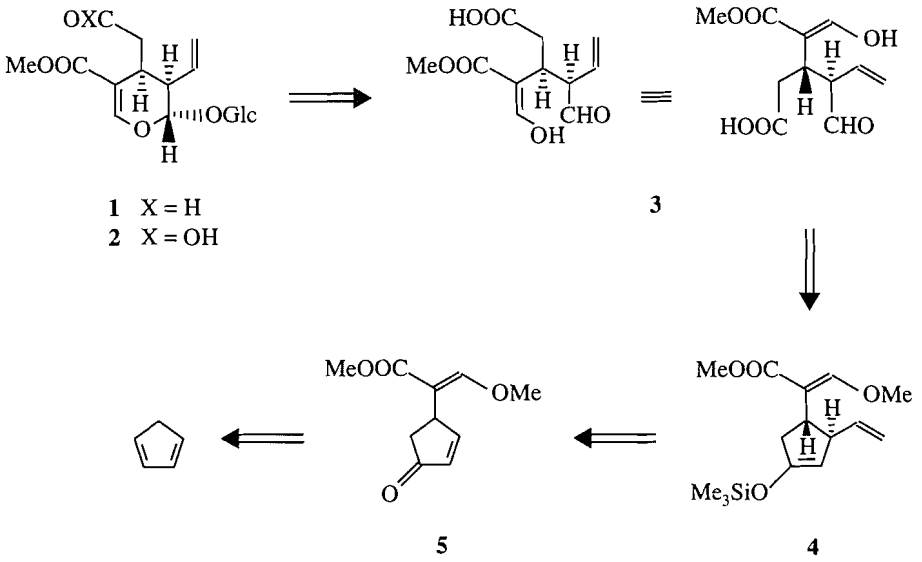
The strategy we chose in our synthetic approach to secologanin set the aglucone of the iridoid secoxyloganin (**2**) as the first target. The aglucone, shown in its acyclic form (**3**), has all of the required functionality suitably differentiated and incorporates the stereochemical information that is crucial for further synthetic development. Besides being a precursor to the iridoids, **3** itself provides the proper ten-carbon unit corresponding to the secologanin-derived portion of a range of alkaloids, and its differentiated functionality could be used to couple it with tryptamine, for example, and open a synthetic route to the indole alkaloids of the Corynanthé–Strychnos biosynthetic group. Retrosynthetic logic (Scheme 1) shows that it should be possible to synthesize **3** in three stages from readily available starting materials derived from cyclopentadiene. In essence, in the synthesis two side chains, one equivalent to a formylacetate unit and the other a vinyl group, are to be attached to a cyclopentanoid framework and the five-membered ring is to be opened oxidatively.

Synthesis of the monosubstituted cyclopentenone 5

Ideally, the formylacetate unit should be incorporated intact. A slight modification of Trost's palladium-catalyzed reaction of dimethyl malonate with cyclopentadiene monoepoxide (8) provided the diester **6** in 90% yield. The corresponding reaction with the *N*,*N*-dimethylhydrazone of methyl formylacetate gave **7** with the side chain at the correct oxidation level, but the yield was only 47% and, in the next step, all attempts to oxidize the allylic alcohol selectively to the corresponding cyclopentenone failed. Attempts to achieve a selective partial reduction of diester **6** also failed, and it became apparent that the plan to introduce an intact formylacetate unit would have to be abandoned in favor of a stepwise process. It was possible to monodecarbomethoxylate the diester under the Krapcho conditions (9) after the hydroxyl group had been protected. The yield of monoester **8** was excellent, but an alternative route to **8** through 5-norbornen-2-one (**9**) was experimentally more convenient for scaling up. Moreover, since both enantiomers of **9** may be prepared from cyclopentadiene by the use of chiral dienophiles, this route can readily be adapted to the synthesis of compounds with either the natural or the unnatural configuration.

The Baeyer–Villiger oxidation of a norbornenone to provide intermediates corresponding to **8** has been a key reaction in several syntheses (10–12). The well-recognized difficulty with

[1]Taken from the Ph.D. thesis of Peter T. W. Cheng, University of Toronto, Toronto, Ont., 1988. A preliminary account of some of this work has been reported (30).



1 X = H
2 X = OH

3

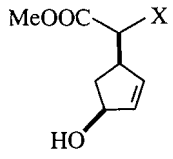
5

4

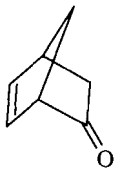
SCHEME 1

the reaction is that the oxidation product forms the rearranged lactone **10** (13) with extreme ease once the free hydroxy acid is liberated. The Baeyer–Villiger oxidation must, therefore, be carried out with alkaline peroxide; Le Drian and Greene (12) avoided forming the free acid by using an alkylating agent to trap the carboxylate ion. In our hands, however, the methyl ester was best prepared by very careful acidification of the intermediate followed by immediate treatment with diazomethane. Some of the lactone **10** inevitably formed, but the ester **8** could be obtained from the norbornenone in yields of about 45% on a preparative scale.

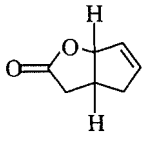
The hydroxyl group of **8** had to be protected before the C-formylation step, and the choice of protecting group proved to be critically important. One limiting factor was the extreme susceptibility of the cyclopentenol derivatives to rearrangement and elimination reactions under acidic conditions. The tetrahydropyranyl (THP) derivative was readily prepared, but it did not react with methyl formate when lithium diisopropylamide (LDA), even in excess, was used as the base. Suppression of the expected reaction in related cases has been attributed to a "complex-induced proximity effect" (14); the complex formed by LDA and the THP group sterically inhibits deprotonation of the ester by further LDA. The *tert*-butyldimethylsilyl ether was readily C-formylated by methyl formate and one equivalent of LDA, but attempts to desilylate in a later step led to decomposition of the molecule. The ethoxyethyl (EE) derivative did not react with methyl formate when one equivalent of LDA in the presence of hexamethylphosphoramide (HMPA) was used as base, but the simple expedient of using two equivalents of LDA led to a successful reaction. The complex with the first equivalent of LDA may have formed as in the THP case, but not have been bulky enough to inhibit the deprotonation step. The C-formylated compound was immediately treated with dimethyl sulfate and potassium carbonate, and the product was isolated in 80% yield for the two steps as a 10:1 mixture of *E* and *Z* isomers. These were separated, and only the *E* isomer (**11**) was carried forward. Treatment with pyridinium *p*-toluenesulfonate in acetone at room temperature removed the EE group, but even here extreme care was required to prevent degradation. Oxidation to the desired cyclopentenone **5** was carried out with pyridinium dichromate in the presence of 4-A molecular sieves in ethyl acetate.



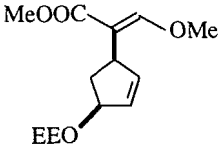
6 X = COOMe
7 X = CH=NNMe$_2$
8 X = H



9



10

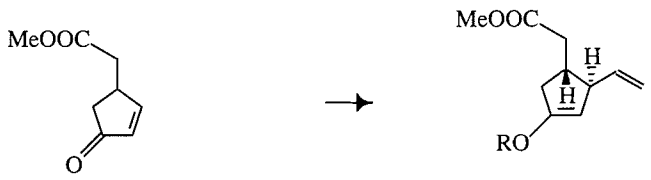


11

Stereoselective attachment of the vinyl side chain

The first major stage of the projected synthesis, the construction of the cyclopentenone carrying a protected formylacetate side chain, was complete, and **5** was available in an overall yield of 13% from the norbornenone. The next stage of the synthesis required the introduction of the vinyl side chain by a cuprate reaction and trapping of the enolate formed with a silylating agent. Reactions of this type have recently received a considerable amount of attention in several laboratories. We undertook first to explore some of the variants of the reaction. Oxidation of the cyclopentenol **8** provided **12**, which served as a model cyclopentenone; furthermore, the anticipated product (**13**) of the cuprate reaction of **12** offered a tactical variation for the synthetic plan, the possibility of carrying out the C-formylation step after both side chains had been introduced. Treatment of enone **12** with the cuprate derived from two equivalents of vinylmagnesium bromide and one equivalent of cuprous iodide, and then trapping the enolate with trimethylsilyl chloride in the presence of HMPA (15) provided **13** (R = SiMe$_3$) in 55% yield. It has recently become apparent that having the silylating agent present during the reaction with the cuprate can lead to enhanced

Can. J. Chem. Downloaded from www.nrcresearchpress.com by 122.72.124.2 on 09/07/12
For personal use only.



12 13

reaction rates, yields, and selectivity (16–19). When the enone **12** and an excess of trimethylsilyl chloride in tetrahydrofuran (THF) were added slowly to a solution of vinylmagnesium bromide and a catalytic amount of cuprous iodide in THF at −78°C, and 4-(dimethylamino)pyridine (DMAP) and triethylamine were then added sequentially, the yield of **13** was raised to 70% and no trace of a second stereoisomer could be detected by ^1H and ^{13}C nmr spectroscopy in **13** (R = $SiMe_3$) or in the ketone obtained by desilylation of **13**, and the ketone was homogeneous on gas chromatography. Much less satisfactory results were obtained if DMAP was not added.

Attempts to prepare the analog **13** (R = $SiMe_2t$-Bu) by these methods with a more robust protecting group failed. We turned, therefore, to the use of cuprates derived from vinyllithium and, after a considerable amount of experimentation, found conditions suitable for the purpose. First, it was necessary to use very pure vinyllithium prepared from tetravinyltin (20). Of the various cuprous salts that have recently been recommended for preparing organocuprates, we found the cyanide (21) to be clearly the best for the present purpose. The "higher order" cuprate (21) prepared from two equivalents of vinyllithium and one equivalent of cuprous cyanide reacted readily at −78°C with enone **12** (the vinylated cyclopentanone could be isolated in 85% yield), but the enolate could not be trapped with *tert*-butyldimethylsilyl chloride unless DMAP was present along with HMPA and triethylamine; under the latter conditions, the product isolated in 75% yield was a 5:1 mixture of **13** (R = $SiMe_2t$-Bu) and its *cis* isomer. The ratio, determined by ^1H nmr spectroscopy, showed that the stereoselectivity had been relatively poor.

Neither **13** (R = $SiMe_3$) nor **13** (R = $SiMe_2t$-Bu) was successfully C-formylated, but the conditions developed for preparing **13** (R = $SiMe_3$), viz., the use of vinylmagnesium bromide, a catalytic amount of cuprous iodide (the preferred salt in this case), trimethylsilyl chloride, HMPA, and DMAP, successfully converted enone **5** to the trimethylsilyl enol ether **4**; yields varied from 75% to 100% and the stereoselectivity was practically complete since no trace of an isomer could be detected spectroscopically in the product or the ketone obtained on desilylation, and gas chromatography showed that the ketone was homogeneous.

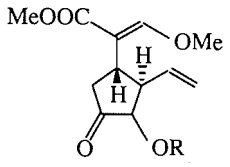
Selective oxidative cleavage of 4

The final major operation of the synthesis required the selective oxidative cleavage of **4** to give **3**. In our original plan this oxidation was to be carried out stepwise by the use of a peracid to oxidize **4** to the hydroxy ketone **14** and then periodate to cleave **14**. To prepare for this operation, we explored oxidations of the model compounds of formula **13** and of silyl enol ethers of cyclopentanone itself, and problems soon became apparent. Peracids such as *m*-chloroperbenzoic acid (mCPBA) oxidize trimethylsilyl enol ethers derived from cyclohexanones (and other unstrained ketones) to the siloxy epoxides (22), which generally rearrange immediately to the α-siloxy ketones (23). However, when we treated trimethylsilyl enol ethers derived from cyclopentanones with mCPBA a mixture was obtained in which the *m*-chlorobenzoate ester of the α-hydroxycyclopentanone was the major component. Rubottom, Boeckman, and co-workers (24) have demonstrated that, under certain conditions, the reaction of the trimethylsilyl enol ether of cyclohexanone with mCPBA can be caused to give the *m*-chlorobenzoate of α-hydroxycyclohexanone. Their mechanistic rationale was that the peracid reacted with the enol ether to give the siloxy epoxide and *m*-chlorobenzoic acid, and the carboxylic acid then opened the epoxide to form an intermediate of type **15**; in the next step the silyl group normally migrates to the hydroxyl site and the carboxylic acid is eliminated, leading to the formation of the α-siloxy ketone. However, the alternative process, migration of the ester and elimination of the silanol, can become competitive under some conditions. Our results indicate that the second process, leading to an acyloxy ketone, is dominant even under standard reaction conditions when the substrates are cyclopentanone derivatives. It seems probable that the difference in the behavior of cyclohexanone and cyclopentanone derivatives has a steric explanation; if the acyloxy and hydroxy substituents in **15** are *cis* to each other on a five-membered ring, the acyl group can migrate much more easily than the silyl group. If the siloxy epoxide is, indeed, an obligatory intermediate, the formation of **15** with the acyloxy and hydroxy substituents *cis* to each other implies that the carboxylic acid has opened the epoxide by a synchronous process in which the oxygen is protonated and the incipient siloxycarbonium ion is carboxylated. Whatever the mechanism may be, our results showed that our proposed route to an α-hydroxycyclopentanone through the siloxy ketone was not available. Jones and Denmark (15) have noted briefly that peracid oxidations are not applicable to silyl enol ethers of cyclopentanones.

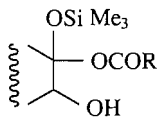
The careful oxidation of the trimethylsilyl enol ether of cyclopentanone with one equivalent of *tert*-butyl hydroperoxide in the presence of $MoO_2(acac)_2$ in benzene (26) provided α-(trimethylsiloxy)cyclopentanone in 55% yield, but this oxidizing system did not give satisfactory results with *tert*-butyldimethylsilyl enol ethers or, more importantly, with our key intermediate **4**.

In the light of our results with model systems, we undertook to oxidize the trimethylsilyl enol ether **4** with mCPBA and then seek conditions that would selectively hydrolyze the expected *m*-chlorobenzoate **16** to the hydroxy ketone **14**. However, mCPBA reacted extremely sluggishly with **4** under standard conditions, and very little of the expected product was obtained; hydrolysis of the silyl enol ether to the parent ketone appeared to be the main reaction. Increasing the relative amount of mCPBA in the reaction did not improve the yield of **16**, but a new product was isolated in 13% yield. This compound proved to be **17**, the Baeyer–Villiger oxidation product of **16**, and was extremely important for several reasons. First, the oxidative cleavage of **4** had been accomplished, and **17** was a protected form of the target compound **3**. Secondly, we could, for the first time, use ^1H nmr spectroscopy with confidence to confirm the stereochemistry assigned to intermediates on the reasonable expectation that the cuprate reaction of cyclopentenones such as **5** would lead stereoselectively to *trans* products such as **4**. The key vicinal coupling constants in the spectrum of **17** are $J_{a,b}$ = 11.5 Hz, showing that the side chains are *trans*-diequatorial, and $J_{b,c}$ = 2.7 Hz; since H_b is axial, the latter value must be an axial–equatorial coupling, and the ester substituent must,

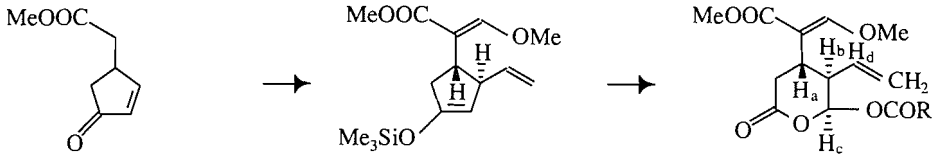
Can. J. Chem. Downloaded from www.nrcresearchpress.com by 122.72.124.2 on 09/07/12
For personal use only.



14 R = H
16 R = *m*-ClC_6H_4CO
18 R = CH_3CO



15



5 **4**
17 R = *m*-ClC_6H_4
19 R = CH_3

consequently, be axial and *cis* to the vinyl group. The further coupling, J = 10.9 Hz, exhibited by H_b was shown to be with H_d in the vinyl side chain.

Because it seemed possible that the *m*-chlorobenzoic acid produced in the reaction was responsible for the poor yields obtained in the oxidation of **4** with mCPBA, we sought a peracid that would produce a weaker carboxylic acid. Peracetic acid is usually a less convenient oxidizing agent than mCPBA, but for the present purpose it proved to be clearly superior. Commercial 32% peracetic acid was first treated with sodium carbonate and sodium acetate to remove traces of mineral acid, and then it was used to oxidize the trimethylsilyl enol ether **4**. When one equivalent of peracetic acid was used, a single product, the α-acetoxy ketone **18**, was isolated in 63% yield. When the amount of peracetic acid was increased, two equivalents were consumed and the Baeyer–Villiger product **19** was obtained in 71% yield as the only isolable product. All of the spectroscopic properties of **19** are in accord with the assigned structure, and the ^1H and ^{13}C nmr spectra show that it is a single isomer. As was the case with **17**, its stereochemistry is confirmed by its ^1H nmr spectrum; the critical coupling constants for **19** are $J_{a,b}$ = 11.4 Hz (axial–axial) and $J_{b,c}$ = 2.9 Hz (axial–equatorial); $J_{b,d}$ = 8.7 Hz.[2] It may be noted that if the conversion of **18** to **19** is, indeed, a Baeyer–Villiger oxidation that proceeds with the normal retention of configuration, the complete stereochemistry of **18** is also defined. The spectroscopic properties of **18** were in accord with its being a single isomer. The same observations were made with the mCPBA oxidation products **16** and **17**, but the much inferior yields in that series made the corresponding conclusions less secure.

Products **17** and **19** are protected forms of the target aglucone **3**, incorporating the proper 10-carbon framework, differentially protected functional groups, and stereochemistry. The yield for the conversion of **5** to **19** was 55–60% (about 7.5% from the norbornenone precursor) and diastereoselectivity was extremely high. The material in hand is racemic, but the route is now available to synthesize both enantiomers starting from the corresponding enantiomer of the norbornenone **9** (12). A route leading towards natural or unnatural enantiomers of secoiridoids and alkaloids is, consequently, opened.

[2]Since **17** and **19** are lactones, they clearly cannot adopt a simple chair conformation. A consequence of the flattening of the molecule by the carbonyl group can be seen in the coupling constants of H_a with the two protons in the adjacent methylene group. These do not have the usual axial–axial and axial–equatorial values; e.g., in **19** their values are 7.8 and 8.9 Hz. Nevertheless, the $J_{a,b}$ and $J_{b,c}$ values clearly define the stereochemical relationship of the substituents.

Experimental

Infrared spectra were obtained on a Nicolet 5DX FT spectrometer with samples as liquid films; selected absorptions are reported in wavenumber units (cm^{-1}). The spectra were obtained with samples dissolved in $CDCl_3$; Varian T-60, XL-200, and XL-400 spectrometers were used for ^1H spectra, and chemical shifts (for 60-MHz spectra unless otherwise indicated) are reported on the δ_H scale, followed in parentheses with an abbreviation showing the multiplicity of the signal, J values in Hz units, and the number of protons assigned to the signal; Varian XL-200 and XL-400 spectrometers were used for ^{13}C spectra, and chemical shifts are reported on the δ_C scale, followed by (e) to show 0 or 2 attached protons or (o) to show 1 or 3 attached protons as determined by the Attached Proton Test (APT) (27). A VG 70-250S mass spectrometer was used to obtain mass spectra and exact mass measurements. Analytical gas–liquid chromatography was carried out on a Varian 3400 chromatograph with fused silica capillary columns coated with DBWax or OV101 and hydrogen as the carrier gas. Merck 40–60 μm (grade 60) silica gel was used for flash chromatography (28).

Pd-catalyzed reactions of cyclopentadiene monoepoxide (ref. 8)

Diester 6

A solution of dimethyl malonate (5.00 g; 37.8 mmol) in 20 mL of dry THF was deoxygenated with Ar and added to $Pd(PPh_3)_4$ (1.00 g; 0.87 mmol) contained under Ar in a thoroughly dried 50-mL 2-necked flash equipped with a rubber septum and an Ar inlet, and the mixture was cooled to −2°C. A solution of cyclopentadiene monoepoxide (7.50 g; 91.3 mmol) in 5 mL of dry THF was deoxygenated by four freeze–pump–thaw cycles, and then added dropwise over 25 min by syringe to the stirred reaction mixture. The flask was protected from light by Al foil, and after 20 min the solution was allowed to warm to room temperature. After it had been stirred for 12 h, the solution was poured into 50 mL of saturated brine, and the mixture was thoroughly extracted with ether. The extract was worked up to provide a residue, which was dissolved in ether and passed through a Florisil plug; flash chromatography (1:1 hexane – ethyl acetate) gave the hydroxy diester **6** (8) as an oil (7.33 g; 34.3 mmol); ir: 3420 (br), 1740; ^1H nmr: 1.28–3.44 (complex, 5H), 3.76 (s, 6H), 4.75 (m, 1H), 5.88 (s, 2H); ^{13}C nmr: 169.2 (e), 168.9 (e), 135.8 (o), 134.1 (o), 76.5 (o), 55.9 (o), 52.5 (o), 52.5 (o), 43.8 (o), 37.2 (e).

Dimethylhydrazone 7

The dimethylhydrazone of methyl formylacetate was prepared by

Can. J. Chem. Downloaded from www.nrcresearchpress.com by 122.72.124.2 on 09/07/12
For personal use only.

Can. J. Chem. Downloaded from www.nrcresearchpress.com by 122.72.124.2 on 09/07/12
For personal use only.

treating the dimethylhydrazone of acetaldehyde with LDA and then dimethyl carbonate. The product was a yellowish oil. This material (0.50 g; 3.47 mmol) in 2 mL of THF was treated with $Pd(PPh_3)_4$ (0.15 g; 0.13 mmol) and cyclopentadiene monoepoxide (1.50 g; 18.3 mmol) by the same procedure as above except that the reaction mixture was heated to reflux for 13 h. The product **7** (0.37 g; 1.64 mmol) was isolated as an unstable yellow oil; ir: 3410 (br), 1732; ^{1}H nmr: 1.27–3.33 (complex, 5H), 2.81 (s, 6H), 3.73 (s, 3H), 4.77 (m, 1H), 5.85 (m, 2H), 6.52 (m, 1H). *Exact Mass* calcd. for $C_{11}H_{18}O_3N_2$: 226.1317; found: 226.1314.

Methyl cis*-(4-hydroxy-2-cyclopenten-1-yl)acetate 8*

A solution of sodium hydroxide (5.68 g; 140 mmol) in 50 mL of water at 0°C was added to a cooled (0°C) solution of 5-norbornen-2-one (12.80 g; 119 mmol) in 50 mL of ether. Hydrogen peroxide (30% aqueous; 29 mL; 260 mmol) was added dropwise over 45 min to the vigorously stirred reaction mixture, which was maintained at 10–25°C. The mixture was stirred for a further 15 min, and then allowed to warm to room temperature. The aqueous layer was extracted with ether (3 × 25 mL), cooled to 0°C, and brought to pH 5 (pH paper) by dropwise addition of concentrated hydrochloric acid. Saturated aqueous sodium sulfite was cautiously added to the cooled solution to destroy excess peroxide. Ethyl acetate (50 mL) was added and the cooled (0°C) aqueous solution was brought to pH 3 by the addition of concentrated hydrochloric acid. The organic layer was separated, the aqueous layer was extracted with ethyl acetate (5 × 100 mL), and the combined organic layers were dried (Na_2SO_4) and concentrated at room temperature on a rotary evaporator to a viscous oil. The oil was dissolved in ether (100 mL), cooled to 0°C, and a cold ethereal solution of diazomethane was slowly added until a slight yellowish color persisted. Excess diazomethane was destroyed with acetic acid, the solution was washed with saturated $NaHCO_3$ (2 × 50 mL), dried (Na_2SO_4), and worked up. The product was flash chromatographed (2:1 hexane – ethyl acetate) and **8** (7.76 g; 54 mmol) was isolated as a clear mobile oil (11); ir: 3400 (br), 1734; ^{1}H nmr: 1.3–3.2 (complex, 6H), 3.65 (s, 3H), 4.77 (m, 1H), 5.80 (s, 2H).

The monosubstituted cyclopentenone 5

Pyridinium *p*-toluenesulfonate (2 g; 8 mmol) was added to a solution of the hydroxy ester **8** (7.76 g; 54 mmol) and ethyl vinyl ether (10.5 mL; 110 mmol) in dry dichloromethane at 0°C. The stirred reaction mixture was allowed to warm to room temperature and stirring was continued a further 4 h. The solution was diluted with 250 mL of ether, washed with 10% aqueous $NaHCO_3$ (3 × 50 mL), dried ($MgSO_4$), and evaporated to provide the EE derivative of **8** as an oil (9.83 g; 43 mmol). This material was used in the next step; in one run a sample was flash chromatographed (5:1 hexane – ethyl acetate) and a colorless liquid was obtained; ir: 1739; ^{1}H and ^{13}C nmr showed that the sample was a 1:1 mixture of diastereoisomers (epimeric in EE group).

The EE derivative (9.83 g; 43 mmol) in 20 mL of dry THF was added dropwise over 1 h to a stirred solution of LDA (prepared from *n*-butyllithium (116 mmol) and diisopropylamine (139 mmol)) in 120 mL of THF at −78°C under Ar. The solution was allowed to warm slowly (75 min) to −2°C, stirring was continued for 30 min more, and the solution was then recooled to −78°C. Methyl formate (13.0 mL; 210 mmol) in 10 mL of THF was added dropwise over 15 min, and the mixture was stirred at −78°C for 15 min, allowed to warm to −45°C over 15 min, stirred for a further 30 min, and then poured into 100 mL of ice-cold water. The aqueous phase was separated, extracted with ether (2 × 100 mL), acidified with concentrated hydrochloric acid, and reextracted with dichloromethane (4 × 50 mL). The combined organic extracts were dried (Na_2SO_4) and evaporated to afford the C-formyl derivative as a dark oil (19.5 g). The oil was dissolved in 150 mL of acetone, K_2CO_3 (20 g) and dimethyl sulfate (5.0 mL; 53 mmol) were added, and the suspension was stirred vigorously under Ar for 23 h. After filtration, the solution was concentrated on a rotary evaporator without heating, and the residue was partitioned between 200 mL of ether and 50 mL of water. The organic phase was washed with water (4 × 40 mL), dried ($MgSO_4$), and evaporated to a dark oil. Flash chromatography (3:1 hexane – ethyl acetate) of the oil provided two products: **11** (8.52 g; 31.6 mmol) was obtained as a yellowish oil (a mixture of EE epimers); ir: 1706, 1639; ^{1}H nmr (400 MHz): 1.17 (t, *J*, 7.1; 3H), 1.30 (d, *J*, 5.4; 3H), 1.74 (m, 1H), 2.50 (m, 1H), 3.46 (m, 1H), 3.6–3.7 (complex, 2H), 3.65 (s, 3H), 3.75 (s, 3H), 4.77 (m, 2H), 5.72 (m, 1H), 5.79 (m, 1H), 7.28 (s, 1H), ^{13}C nmr: 168.2 (e), 159.5 (o), 136.4 and 136.3 (o), 130.7 and 130.2 (o), 111.3 (e), 98.7 and 98.5 (o), 79.9 and 79.7 (o), 61.4 (o), 60.3 and 60.0 (e), 50.8 (o), 39.3 and 39.2 (o), 38.5 and 37.8 (e), 20.5 (o), 15.1 (o). The second product was the *Z* isomer of **11** (0.84 g; 3.1 mmol); ir: 1720, 1690, 1642; ^{1}H nmr: 1.21 (t, *J*, 6; 3H), 1.31 (d, *J*, 5.5; 3H), 1.57 (m, 1H), 2.71 (m, 1H), 3.2–3.9 (complex, 3H), 3.71 (s, 3H), 3.76 (s, 3H), 4.77 (m, 2H), 5.76 (complex, 2H), 6.35 (s, 1H).

The EE protecting group was removed by stirring a solution of **11** (8.52 g; 31.6 mmol) in 270 mL of acetone with pyridinium *p*-toluenesulfonate (7.92 g; 31.6 mmol) under Ar at room temperature for 7 h. The suspension was filtered, the filtrate was evaporated under reduced pressure (it was necessary to avoid heating the material), and the residue was partitioned between 100 mL of water and 100 mL of ethyl acetate. The aqueous phase was further extracted with ethyl acetate (3 × 50 mL), the organic phases were combined, washed with saturated aqueous $NaHCO_3$ (2 × 50 mL) and dried (Na_2SO_4), and the solvent was removed under reduced pressure. The cyclopentenol was isolated as an orange oil (5.66 g; ca. 28 mmol), which was used in the next step. In one run a sample was flash chromatographed (2:1 hexane – ethyl acetate) to give an oil; ir: 3471 (br), 1697, 1635; ^{1}H nmr (400 MHz): 1.64 (m, 1H), 2.55 (m, 1H), 3.63 (s, 3H), 3.79 (br, 1H), 3.82 (s, 3H), 3.84 (m, 1H), 4.67 (m, 1H), 5.62 (m, 1H), 5.89 (m, 1H), 7.16 (s, 1H), ^{13}C nmr: 167.7 (e), 159.0 (e), 134.8 (o), 133.4 (o), 111.4 (e), 77.0 (o), 61.3 (o), 50.8 (o), 38.4 (o), 28.1 (e). *Exact Mass* calcd. for $C_{10}H_{14}O_4$: 198.0892; found: 198.0882.

The cyclopentenol (5.66 g) was dissolved in 20 mL of ethyl acetate and added to a suspension of pyridinium dichromate (16.1 g; 43 mmol) and activated 4-A molecular sieves in 300 mL of ethyl acetate, and the mixture was stirred under Ar for 22 h. Solids were removed by filtration and washed well with ethyl acetate. The combined organic solutions afforded a dark oil, which was flash chromatographed (3:1 hexane – ethyl acetate) to provide the cyclopentenone **5** (3.70 g; 19 mmol) as a yellowish oil; ir: 1710, 1640; ^{1}H nmr (400 MHz): 2.37 (ddd, *J*, 1, 3, 18.5; 1H), 2.58 (ddd, *J*, 1, 7, 18.5; 1H), 3.66 (s, 3H), 3.80 (s, 3H), 4.15 (m, 1H), 6.15 (dd, *J*, 2.5, 5.5; 1H), 7.36 (s, 1H), 7.45 (dd, *J*, 2.5, 5.5; 1H); ^{13}C nmr: 209.8 (e), 167.3 (3), 166.0 (o), 160.4 (o), 132.8 (o), 108.6 (e), 61.8 (o), 51.3 (o), 40.4 (e), 37.1 (o). *Exact Mass* calcd. for $C_{10}H_{12}O_4$: 196.0736; found: 196.0724.

Reactions with vinyl cuprates

Synthesis of ***13*** *(R = $SiMe_3$)*

The cyclopentenol **8** was oxidized to the cyclopentenone **12** in the manner just described. Recrystallized (29) CuI (0.25 g; 1.2 mmol) was added under Ar to a cold (−3°C) solution of vinylmagnesium bromide prepared from Mg turnings (0.39 g; 16 mmol) and vinyl bromide in 30 mL of THF under Ar. After 3 min, hexamethylphosphoramide (HMPA) (3.0 mL; 27 mmol) was added, the solution was stirred for another 3 min, and then cooled to −78°C. A solution of **12** (0.50 g; 3.2 mmol) and chlorotrimethylsilane (3.0 mL; 24 mmol) in 10 mL of THF was added dropwise over 50 min to the stirred reaction mixture. Stirring at −78°C was continued for a further 3 h, and 4-(dimethylamino)pyridine (DMAP) (0.46 g; 3.9 mmol) in 5 mL of THF was then added. After this mixture had been stirred at −78°C for 10 h, triethylamine (4.0 mL) was added dropwise and stirring was continued for 3 h longer. The reaction mixture was poured into 100 mL of ice-cold saturated aqueous $NaHCO_3$, 100 mL of water and 10 mL of hexane were added, and the mixture was then shaken and filtered through Celite. The filter cake was washed well with hexane, the aqueous layer was separated and extracted with hexane (3 × 25 mL), and the combined organic solutions were washed with saturated aqueous $NaHCO_3$ (2 × 25 mL), dried ($MgSO_4$), and evaporated to a yellow oil. The oil was partitioned between 50 mL of hexane and 25 mL of dimethyl sulfoxide, the dimethyl sulfoxide layer was extracted with hexane (5 × 20 mL), and the combined hexane extracts were washed

with water (2 × 25 mL) and saturated aqueous $NaHCO_3$ (2 × 25 mL), dried ($MgSO_4$), and worked up. The trimethylsilyl enol ether **13** (R = $SiMe_3$) was obtained as an oil (494 mg; 1.94 mmol); ir: 1739, 1644; ^1H nmr: 0.22 (s, 9H), 1.8–3.0 (complex, 6H), 3.63 (s, 3H), 4.47 (br, 1H), 4.8–5.1 (complex, 2H), 5.73 (m, 1H); ^{13}C nmr: 172.7 (e), 154.0 (e), 141.8 (o), 113.1 (e), 103.6 (o), 51.8 (o), 50.7 (o), 38.9 (e), 38.6 (o), 38.4 (e), −0.7 (o). *Exact Mass* calcd. for $C_{13}H_{22}O_3Si$: 254.1338; found: 254.1340. A sample of **13** was desilylated in a mixture of saturated aqueous NH_4Cl and dichloromethane, and the ketone was obtained as an oil, which analytical glc showed to be homogeneous and contain <2% of impurities. Material purified by flash chromatography (4:1 hexane – ethyl acetate) showed ir:1747, 1733, 1645; ^1H nmr: 1.7–2.9 (complex, 8H), 3.62 (s, 3H), 4.9–5.2 (complex, 2H), 5.68 (m, 1H); ^{13}C nmr: 215.7 (e), 172.4 (e), 138.4 (o), 116.8 (e), 51.5 (o), 46.9 (o), 44.9 (e), 44.3 (e), 38.5 (o), 37.2 (e). *Exact Mass* calcd. for $C_{10}H_{14}O_3$: 182.0943; found: 182.0927.

*Synthesis of **13** (R = $SiMe_2$-Bu)*

Cuprous cyanide (460 mg; 5.1 mmol) and 5 mL of dry toluene were placed in a thoroughly dried 100-mL 3-necked flask equipped with a gas inlet, pressure-equalizing addition funnel, rubber septum, and stirring bar (assembled under Ar). The toluene was removed by vacuum distillation at room temperature to dry the CuCN. Ether (5 mL) was added and the slurry was cooled to −78°C. A 0.78 M ethereal solution of vinyllithium (13.0 mL; 10.1 mmol) prepared from tetravinyltin (20) was added dropwise over 20 min. The suspension was allowed to warm to −40°C over 25 min, and then to −23°C over 10 min. The clear solution so formed was stirred and cooled to −78°C. A solution of the cyclopentenone **12** (605 mg; 3.9 mmol) in 5 mL of ether was added dropwise over 13 min, and stirring was continued at −78°C for 1 h. A solution of *tert*-butyldimethylsilyl chloride (1.45 g; 9.6 mmol), DMAP (0.1 g; 0.8 mmol), HMPA (2.0 mL), and triethylamine (2.0 mL) in 25 mL of dry THF was added dropwise over 10 min. The mixture was stirred at −78°C for 1 h, allowed to warm to room temperature, stirred for 16 h, and then cooled to 0°C. Water (100 mL) was added dropwise over 15 min, stirring was continued for 30 min, and 100 mL of ether was then added. The resulting emulsion was filtered through Celite, and the filter cake was washed with water (2 × 50 mL) and with ether (2 × 50 mL). The aqueous layer was separated and washed with ether (4 × 100 mL), and the ether solutions were combined, washed with water (4 × 50 mL), dried (Na_2SO_4), and worked up to provide a yellow oil. The ^1H nmr spectrum of this material showed it to be a 5:1 mixture of isomers. Flash chromatography (30:1 hexane – ethyl acetate) provided silyl enol ether **13** (R = $SiMe_2t$-Bu) (837 mg; 2.8 mmol); ir: 1742, 1645; ^1H nmr (400 MHz):0.12 (s, 3H), 0.13 (s, 3H), 0.88 (s, 9H), 2.0–2.9 (complex, 6H), 3.62 (s, 3H), 4.46 (m, 1H), 4.93–4.97 (complex, 2H), 5.77 (m, 1H); ^{13}C nmr: 173.3 (e), 154.5 (e), 142.1 (o), 113.5 (e), 104.5 (o), 52.4 (o), 51.4 (o), 39.5 (e), 39.2 (o), 39.0 (e), 25.6 (o), 18.1 (e), −4.7 (2 signals; o).

*Synthesis of **4***

The procedure used for the synthesis of **13** (R = $SiMe_3$) was applied to the cyclopentenone **5** (0.55 g; 2.8 mmol); vinylmagnesium bromide (16 mmol), CuI (0.15 g; 0.8 mmol), HMPA (5 mL), chlorotrimethylsilane (6.0 mL; 47 mmol), and DMAP (0.31 g; 2.6 mmol) were used. The trimethylsilyl enol ether **4** (0.62 g; 2.1 mmol) was obtainable as a mobile liquid; ir: 1708, 1643; ^1H nmr: 0.23 (s, 9H), 2.1–3.6 (complex, 4H), 3.70 (s, 3H), 3.80 (s, 3H), 4.60 (br, 1H), 4.7–5.0 (complex, 2H), 5.73 (m, 1H), 7.29 (s, 1H); ^{13}C nmr: 168.4 (e), 159.7 (o), 154.0 (e), 143.0 (o), 112.6 (e), 111.5 (e), 105.2 (o), 61.4 (o), 51.3 (o), 51.0 (o), 38.4 (o), 38.2 (e), 0.00 (o). *Exact Mass* calcd. for $C_{15}H_{24}O_4Si$: 296.1444; found: 296.1447. A sample of **4** was desilylated by the procedure used for **13** (R = $SiMe_3$), and analytical glc showed that the ketone obtained was homogeneous. Flash chromatography (4:1 hexane – ethyl acetate) provided material that showed ir: 1747, 1702, 1637; ^1H nmr (200 MHz): 2.06 (m, 1H), 2.30 (m, 1H), 2.48 (m, 1H), 2.71 (m, 1H), 3.1–3.2 (complex, 2H), 3.66 (s, 3H), 3.80 (s, 3H), 4.96 (m, 1H), 4.97 (m, 1H), 5.69 (m, 1H), 7.38 (s, 1H); ^{13}C nmr: 216.7 (e), 167.4 (e), 160.4 (o), 139.0 (o), 114.8 (e), 108.1 (e), 61.4 (o), 50.8 (o), 44.6 (e), 43.8 (o), 41.9 (e), 38.2 (o). *Exact Mass* calcd. for $C_{12}H_{16}O_4$: 224.1049; found: 224.1054.

*Peracid oxidations of silyl enol ether **4***

m-*Chloroperbenzoic acid*

A solution of **4** (700 mg; 2.36 mmol) in 25 mL of hexane was added dropwise over 1 h to a stirred suspension of commercial 85% *m*-chloroperbenzoic acid (530 mg; 2.6 mmol) in 25 mL of hexane at −23°C under Ar. The mixture was allowed to warm to room temperature and was stirred for 36 h. The suspension was filtered, and the filtrate was diluted with 50 mL of ether and washed with aqueous $NaHCO_3$ (3 × 25 mL). The organic solution afforded an oil, which was flash chromatographed (2:1 hexane – ethyl acetate) to afford the pentanolide derivative **17** (118 mg; 0.3 mmol) as a gum; ir: 1756, 1736; ^1H nmr (200 MHz):2.85 (dd, *J*, 7.4, 17.8; 1H), 2.92 (dd, *J*, 9.3, 17.8; 1H), 3.25 (ddd, *J*, 2.7, 10.9, 11.5; 1H), 3.76 (m, 1H), 3.70 (s, 3H), 3.86 (s, 3H), 5.1–5.2 (complex, 2H), 5.48 (m, 1H), 6.63 (d, *J*, 2.7; 1H), 7.39 (s, 1H), 7.4–7.6 (complex, 2H), 7.9–8.0 (complex, 2H); ^{13}C nmr: 168.9 (e), 167.3 (e), 163.0 (e), 160.9 (o), 134.7 (e), 133.8 (o), 133.1 (o), 130.6 (e), 130.0 (o), 129.9 (o), 128.1 (o), 120.4 (e), 109.2 (e), 94.6 (o), 62.0 (o), 51.4 (o), 44.2 (o), 33.8 (e), 28.1 (o). *Exact Mass* calcd. for $C_{19}H_{19}O_7Cl$: 394.0819; found: 394.0778.

Peracetic acid (1 equiv.)

Commercial 32% peracetic acid (1.0 mL; 4.75 mmol), anhydrous Na_2CO_3 (2.0 g; 19 mmol), and anhydrous sodium acetate (0.5 g; 6 mmol) were stirred in 40 mL of dichloromethane under Ar for 1 h, and the mixture was then cooled in an ice – water bath. A solution of **4** (1.29 g; 4.35 mmol) in 20 mL of dichloromethane was added dropwise over 1 h to the stirred reaction mixture, which was then allowed to warm to room temperature. Further pretreated peracetic acid (1.9 mmol) was added dropwise while the progress of the reaction was followed by tlc, and after 1 h no **4** remained. The mixture was filtered through Celite, and the filter cake was washed with dichloromethane. The combined filtrate was worked up to provide the α-acetoxy ketone **18** as a yellow oil (680 mg; 2.4 mmol). Flash chromatography (2:1 hexane – ethyl acetate) gave material that showed ir: 1758, 1748, 1703, 1640; ^1H nmr (400 MHz):2.06 (s, 3H), 2.46 (dd, *J*, 9.0, 18.7; 1H), 2.72 (dd, *J*, 8.5, 18.7; 1H), 3.25 (m, 1H), 3.48 (m, 1H), 3.67 (s, 3H), 3.81 (s, 3H), 5.06 (d, *J*, 9.9; 1H), 5.07 (d, *J*, 18.1; 1H), 5.28 (d, *J*, 7.8; 1H), 5.61 (m, 1H), 7.36 (s, 1H); ^{13}C nmr: 211.5 (e), 169.4 (e), 167.3 (e), 160.3 (o), 133.5 (o), 117.5 (e), 109.2 (e), 74.9 (o), 61.5 (o), 50.9 (o), 48.0 (o), 39.2 (e), 34.3 (o), 20.3 (o). *Exact Mass* cald. for $C_{14}H_{18}O_6$: 282.1103; found: 282.1101.

Peracetic acid (excess)

An ice-cold mixture of peracetic acid (1.2 mmol), Na_2CO_3 (0.4 g), and sodium acetate (0.1 g) in 5 mL of dichloromethane was prepared as described above. A solution of **4** (107 mg; 0.36 mmol) in 5 mL of dichloromethane was added dropwise over 15 min to the stirred mixture, and stirring was continued for 1 h further. The stirred mixture was allowed to warm to room temperature, and the progress of the reaction was followed by tlc. After 4 h the mixture was worked up as described above, and the product **19** (77 mg; 0.26 mmol) was obtained as a glass that, on recrystallization from ether, afforded white crystals, mp 99–101°C; ir: 1749, 1692; 1639; ^1H nmr (400 MHz): 2.15 (s, 3H), 2.88 (dd, *J*, 7.8, 17.8; 1H), 2.93 (dd, *J*, 8.9, 17.8; 1H), 3.27 (ddd, *J*, 2.9, 8.7, 11.4; 1H), 3.65 (ddd, *J*, 7.8, 8.9, 11.4; 1H), 3.79 (s, 3H), 3.96 (s, 3H), 5.15 (d, *J*, 10.3; 1H), 5.16 (d, *J*, 17.5; 1H), 5.25 (ddd, *J*, 8.7, 10.3, 17.5; 1H), 6.52 (d, *J*, 2.9; 1H), 7.48 (s; 1H); ^{13}C nmr: 169.0 (e), 168.5 (e), 167.2 (e), 160.7 (o), 133.2 (o), 119.8 (e), 109.0 (e), 93.6 (o), 61.7 (o), 51.1 (o), 43.4 (o), 33.5 (e), 27.8 (o), 20.6 (o). *Exact Mass* calcd. for $C_{14}H_{18}O_7$: 298.1052; found: 298.1025.

Acknowledgements

Financial support from the Natural Sciences and Engineering Research Council of Canada and from the Government of Ontario is acknowledged.

Can. J. Chem. Downloaded from www.nrcresearchpress.com by 122.72.124.2 on 09/07/12
For personal use only.

1. A. R. BATTERSBY, A. R. BURNETT, and P. G. PARSONS. J. Chem. Soc. (C), 1187 (1969).
2. I. SOUZU and H. MITSUHASHI. Tetrahedron Lett. 191 (1970).
3. L.-F. TIETZE. Angew. Chem. Int. Ed. Engl. **22**, 828 (1983).
4. L.-F.TIETZE. J. Am. Chem. Soc. **96**, 946 (1974).
5. C. R. HUTCHINSON, K. C. MATTES, M. NAKANE, J. J. PARTRIDGE, and M. R. USKOKOVIC. Helv. Chim. Acta, **61**, 1221 (1978).
6. R. T. BROWN, and M. F. JONES. J. Chem. Soc. Chem. Commun. 1818 (1986).
7. L.-F. TIETZE, R. FISCHER, and G. REMBERG. Liebigs Ann. Chem. 971 (1987).
8. B. M. TROST and G. A. MOLANDER. J. Am. Chem. Soc. **103**, 5969 (1981).
9. A. P. KRAPCHO, J. F. WEIMASTER, J. M. ELDRIDGE, E. G. E. JAHNGEN, A. J. LOVEY, and W. P. STEPHENS. J. Org. Chem. **43**, 138 (1978).
10 N. M. WEINSHENKER and R. STEPHENSON. J. Org. Chem. **37**, 3741 (1972).
11. A. BARCO, S. BENETTI, G. P. POLLINI, P. G. BARALDI, and C. GANDOLFI. J. Org. Chem. **45**, 4776 (1980).
12. C. LE DRIAN and A. E. GREENE. J. Am. Chem. Soc. **104**, 5473, (1982).
13. J. MEINWALD, M. C. SEIDEL, and B. CADOFF. J. Am. Chem. Soc. **80**, 6303 (1958).
14. P. BEAK and A. I. MEYERS. Acc. Chem. Res. **19**, 356 (1986).
15. R. L. FUNK and K. P. C. VOLLHARDT. J. Am. Chem. Soc. **102**, 5253 (1980).
16. E. J. COREY and N. W. BOAZ. Tetrahedron Lett. **26**, 6015, 6019 (1985).
17. A. ALEXAKIS, J. BERLAN, and Y. BESACE. Tetrahedron Lett. **27**, 1047 (1986).
18. Y. HORIGUCHI, S. MATSUZAWA, E. NAKAMURA, and I. KUWAJIMA. Tetrahedron Lett. **27**, 4025 (1986).
19. C. R. JOHNSON and T. J. MARREN. Tetrahedron Lett. **28**, 27 (1987).
20. P. A. BARTLETT, J. D. MEADOWS, and E. OTTOW. J. Am. Chem. Soc. **106**, 5304 (1984).
21. B. H. LIPSHUTZ, R. S. WILHELM, and J. A. KOZLOWSKI. Tetrahedron, **40**, 5005 (1984).
22. L. A. PAQUETTE, H.-S. LIN, and J. C. GALLUCCI. Tetrahedron Lett. **28**, 1363 (1987).
23. G. M. RUBOTTOM and J. M. GRUBER. J. Org. Chem. **43**, 1599 (1978).
24. G. M. RUBOTTOM, J. M. GRUBER, R. K. BOECKMAN, JR., M. RAMAIAH, and J. B. MEDWID. Tetrahedron Lett. 4603 (1978).
25. T. K. JONES and S. E. DENMARK. J. Org. Chem. **50**, 4037 (1985).
26. K. KANEDA, N. KII, K. JITSUKAWA, and S. TERANISHI. Tetrahedron Lett. **22**, 2595 (1981).
27. S. L. PATT and J. N. SHOOLERY. J. Magn. Reson. **46**, 535 (1982).
28. W. C. STILL, M. KAHN, and A. MITRA. J. Org. Chem. **43**, 2923 (1978).
29. G. B. KAUFFMAN and L. A. TETER. Inorg. Synth. **7**, 9 (1963).
30. P. T. W. CHENG and S. McLEAN. Tetrahedron Lett. **29**, 3511 (1988).

Can. J. Chem. Downloaded from www.nrcresearchpress.com by 122.72.124.2 on 09/07/12
For personal use only.

Microbial hydroxylation of steroids. Part 12. Hydroxylation of testosterone and related steroids by *Gnomonia fructicola* ATCC 11430

HERBERT L. HOLLAND, FRANCES M. BROWN, P. CHINNA CHENCHAIAH, MICHAEL J. CHERNISHENKO, SHAHEER H. KHAN, AND J. APPA RAO

Department of Chemistry, Brock University, St. Catharines, Ont., Canada L2S 3A1

Received August 24, 1988

HERBERT L. HOLLAND, FRANCES M. BROWN, P. CHINNA CHENCHAIAH, MICHAEL J. CHERNISHENKO, SHAHEER H. KHAN, and J. APPA RAO. Can. J. Chem. **67**, 268 (1989).

The fungus *Gnomonia fructicola* ATCC 11430 hydroxylates testosterone at C-2β in 40–60% yield. The enzyme involved has been shown to be an inducible CO sensitive, cyanide insensitive oxygenase, with a requirement for the Δ^4-3-ketosteroid substrate functionality. The use of 2α- and 2β-deuterium labelled substrates has shown that hydrogen loss from C-2 during 2β hydroxylation is isotope dependent and non-stereospecific. This is interpreted in terms of a $\Delta^{2,4}$-dienolic enzyme-bound intermediate form of the substrate.

Key words: *Gnomonia fructicola*, hydroxylation, steroids, testosterone.

HERBERT L. HOLLAND, FRANCES M. BROWN, P. CHINNA CHENCHAIAH, MICHAEL J. CHERNISHENKO, SHAHEER H. KHAN et J. APPA RAO. Can. J. Chem. **67**, 268 (1989).

Le champignon *Gnomonia fructicola* ATCC 11430 provoque une hydroxylation en position C-2β de la testostérone, avec un rendement de 40–60%. On a démontré que l'enzyme implique une oxygénase qui peut être induite, qui est sensible au CO et insensible au cyanure et dont le substrat doit contenir une fonctionnalité Δ^4-céto-3 stéroïde. Utilisant des substrats marqués au deutérium dans les positions 2α et 2β, on a pu démontrer que l'hydroxylation dépend de l'isotope et qu'elle n'est pas spécifique. On peut interpréter ce résultat, en suggèrant que le substrat est lié à l'enzyme par le biais d'une forme intermédiaire $\Delta^{2,4}$-diénolique.

Mots clés : *Gnomonia fructicola*, hydroxylation, stéroïdes, testostérone.

[Traduit par la revue]

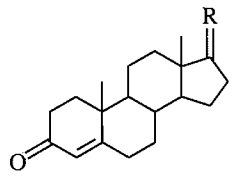
Can. J. Chem. Downloaded from www.nrcresearchpress.com by 122.72.124.2 on 09/07/12
For personal use only.

The introduction of a hydroxyl functionality into a steroid molecule by fungal biotransformation, first discovered over 40 years ago (1), is still the most efficient route for the preparation of many hydroxysteroids, particularly in the corticosteroid family.

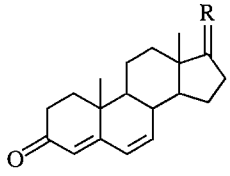
The enzymes responsible for this reaction were slow to yield their secrets, but their essential nature is now understood (2). Their characterization as cytochrome P-450 dependent monooxygenases preceded investigation of enzyme–substrate interactions: the latter have centred on the nature of enzyme–substrate binding through existing electronegative substituents such as substrate carbonyl or hydroxyl groups (2), and on the activation of ketosteroids towards electrophilic hydroxylation at positions adjacent or vinylogous to carbonyl by substrate enolization (3).

A report of the hydroxylation of testosterone (**1**) at C-2β by *Gnomonia fructicola* ATCC 11430 in unspecified yield (4), and the continued question of the intermediacy of a 2β-hydroxylation step in the conversion of testosterone to estradiol by the human aromatase enzyme (5, 6), suggesting a possible role for enzymic 2β hydroxylation of steroids in the control of human breast tumour cell proliferation (7, 8), prompted us to examine both mechanistic and synthetic parameters of the fungal hydroxylation of testosterone at C-2β by *G. fructicola*. In addition, hydroxylation of testosterone at C-2β by mammalian liver enzymes represents one of the major routes of testosterone metabolism in the liver (9, 10), suggesting a further role for the fungal biotransformation as a possible model for mammalian metabolism.

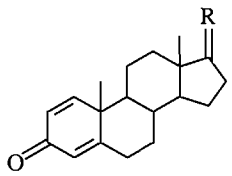
The original report of the steroidal 2β hydroxylating capacibility of *G. fructicola* was concerned largely with the use of Δ^4-3-ketopregnane substrates, reporting 2β hydroxylation of cortexone in 40% isolated yield (4, 11), with a more complex pattern of metabolism for progesterone, including hydroxylation at the C-2β, -6β, -14α, and -16β positions (11). To establish the best substrate for mechanistic purposes, we first investigated the fungal metabolism of the simple Δ^4-3-keto-steroids **1**–**4**, using a simplified procedure for biotransformation that replaced the original conditions (incubation in a complex growth medium (11)) with growth in a simpler medium followed by replacement culture incubation with resting cells in distilled water (for details, see experimental section). Under our conditions, testosterone was routinely converted to the 2β-hydroxy derivative **23** in isolated yields of 40–60%, accompanied by a trace of oxidation at C-17 to give the dione **4**. The results of this and other incubations are summarized in Table 1. Testosterone



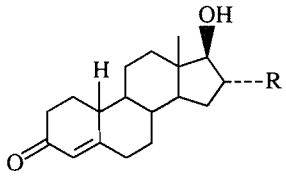
1 R = αH, βOH
2 R = αH, βOAc
3 R = O
4 R = αH, βCOCH$_3$



5 R = αH, βOH
6 R = O



7 R = αH, βOH
8 R = O



9 R = H
10 R = OH

TABLE 1. Transformations of steroids by *G. fructicola*

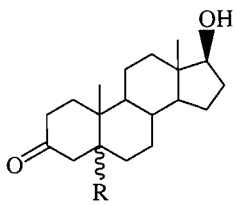
Substrate	Product (%)
1	**3** (1), **23** (40–60)
2	**3** (1), **23** (30), **31** (2)
3	**28** (4), **30** (5)
4	**32** (5), **33** (8), **34** (12), **35** (21)
5	**6** (16)
7	**8** (7)
9	**10** (6)
11	**36** (3), **37** (20), **38** (3)
12	**39** (7), **40** (19), **41** (17)
13	None
14	**13** (28)
15	None
16	None
17	**1** (2), **3** (1), **23** (17), **28** (2)
18	**19** (5)
18*	**19** (5), **42** (8)
20	**21** (3), **22** (10)

*Following enzyme induction by testosterone.

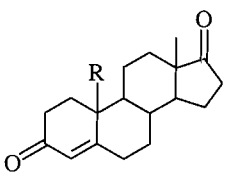
acetate is similarly transformed but in lower yield, presumably following enzymic hydrolysis of the ester function at C-17, but androst-4-ene-3,17-dione (**3**) underwent oxidation predominantly in the D-ring, yielding the 17β-hydroxy-16-ketone **30**. This compound may be formed by the rearrangement of an intermediate but not isolated 16-hydroxy-17-ketosteroid, a common phenomenon during fungal biotransformation (12). The biotransformation of progesterone gave, as originally reported (11), a mixture of products, from which the 2β and 14α alcohols and 2β,6β and 6β,14α diols were identified.

In view of the experiments outlined above, further work concentrated on steroids of the androstane skeleton, which carried the 17β-alcohol functionality. Substrate specificity was investigaed by using a series of substrates (**5**, **7**, **9**, and **11**–**17**); in only one instance (**11**) was 2β hydroxylation observed, and then in minor amount together with other reactions. Alternative modes of biotransformation that were noted included alcohol oxidation (for **5**, **7**, **12**, and **17**), carbonyl reduction (for **11**, **12**, and **14**), 16α hydroxylation (for **9** and **11**), and 5β hydroxylation of **12**.

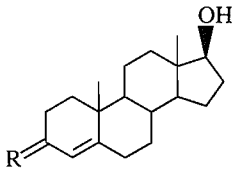
Product structure determination relied heavily on the interpretation of ^{13}C nmr data (see Experimental), the following shifts being particularly characteristic: for 16α hydroxylation (products **10**, **37**, and **38**) the regiochemistry of hydroxylation is given by downfield shifts of signals assigned to C-17 and C-15 compared with their position in the corresponding 16-unsubstituted steroids (13), and stereochemistry is confirmed by a γ upfield shift at C-14 of 2.8–3.3 ppm; for 5β hydroxylation (products **40** and **41**), regiochemistry is reflected in downfield shifts at C-4 and C-6, together with a γ upfield shift at C-1, and stereochemistry by the latter and by the characteristic C-9 signal of 5β steroids (13); for 2β hydroxylation (products **23**, **28**, **34**, and **38**), regiochemistry is given by upfield shifts at C-1, and characteristic shifts at C-4, -5, -9, and -10, and stereochemistry by a downfield shift of the C-19 signal by 3–5 ppm (13).



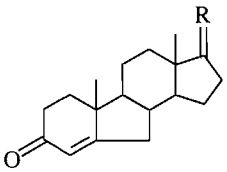
11 R = αH
12 R = βH



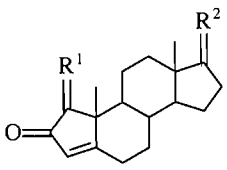
13 R = CH_2OH
14 R = CHO



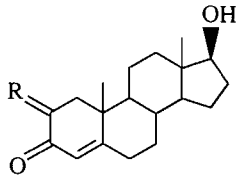
15 R = H_2
16 R = CH_2
17 R = αH, βOH



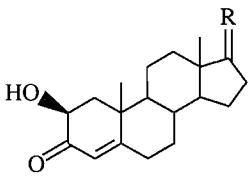
18 R = αH, βOH
19 R = O



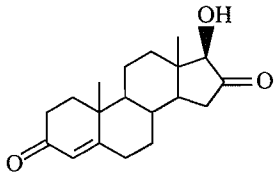
20 R^1 = H_2, R^2 = αH, βOH
21 R^1 = H_2, R^2 = O
22 R^1 = R^2 = αH, βOH



23 R = αH, βOH
24 R = αH, βD
25 R = αD, βH
26 R = αD, βOH
27 R = αH, β^{18}OH



28 R = O
29 R = αH, βOAc



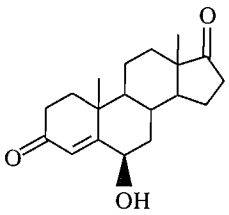
30

The α stereochemistry of reduction of the C-3 carbonyl group in 5α steroids (product **38**) is reflected in γ upfield shifts for C-1 and C-5, while the β stereochemistry of reduction (products **36** and **37**) is apparent from direct comparison with literature values reported for C-1–C-5, C-10, and C-19 for 3β-hydroxy-5α-androstanes (13). The stereochemistry of reduction at C-3 in the 5β-androstane series, giving the 3α-hydroxy product **41**, is confirmed by the absence of a γ-*gauche* upfield shift on the C-1 resonance in the spectrum of **41** compared with that of **40**.

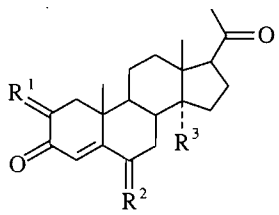
It is apparent from the above that the 2β-hydroxylase enzyme requires a Δ^4-3-keto steroid substrate with a C-19 methyl group for normal activity. It is noteworthy that neither 19-nortestosterone (**9**) nor the 19-functionalized steroids **13** and **14** are substrates for this enzyme. Complete removal of the C-3 oxygen function (compounds **15** and **16**) produces steroids that are not hydroxylated, while reduction at C-3 (compound **17**) is reversed by fungal oxidoreductases prior to hydroxylation (see Table 1).

The occurrence of 16α hydroxylation (substrates **9**, **11**, and possibly **3**) may involve the 2β-hydroxylase enzyme binding the substrate in an inverted manner, a common phenomenon for fungal steroid hydroxylases (2), and other steroid metabolizing enzymes (14) as suggested in Fig. 1, but in the absence of

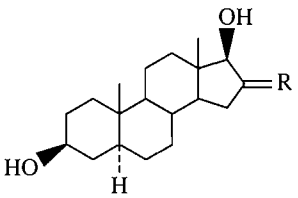
Can. J. Chem. Downloaded from www.nrcresearchpress.com by 122.72.124.2 on 09/07/12
For personal use only.



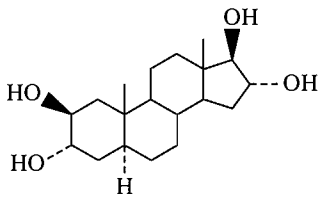
31



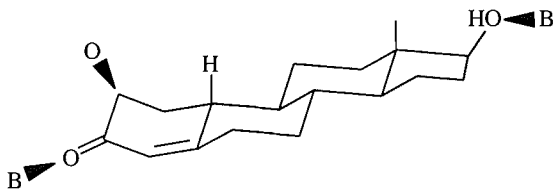
32 R^1 = αH, βOH, R^2 = H_2, R^3 = H
33 R^1 = R^2 = H_2, R^3 = OH
34 R^1 = R^2 = αH, βOH, R^3 = H
35 R^1 = H_2, R^2 = αH, βOH, R^3 = OH



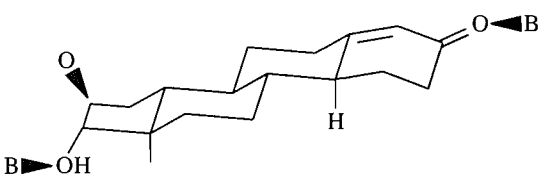
36 R = H_2
37 R = αH, βOH



38



Normal binding

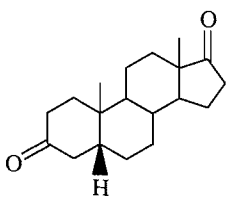


Inverted binding

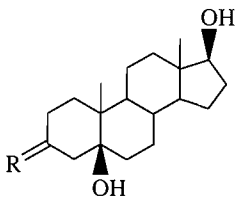
B = binding site
O = oxidation site

FIG. 1. Possible method for 16α hydroxylation by a 2β-hydroxylase.

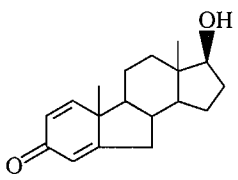
isolated enzymes this proposal must remain speculative. As previously noted (4), the 2β hydroxylase is able to tolerate an *A*-nor-$\Delta^{3(5)}$-2-one skeleton such as that of *A*-nortestosterone (**20**), giving a low yield of hydroxylation product **22**, analogous in structure to that observed for the normal Δ^4-3-keto skeleton. The *B*-norsteroid **18** was not hydroxylated under normal incubation conditions, the only biotransformation product (**19**) being the result of oxidation at C-17, but when testosterone was used as an enzyme inducer during the fungal growth period, as described in the experimental section, and **18** subsequently used as substrate, a low yield of the *B*-nor-$\Delta^{1,4}$-diene **42** was



39



40 R = O
41 R = αH, βOH



42

obtained. This may have arisen by acid-catalysed dehydration of a 2β-hydroxy intermediate in the growth medium (pH 4.6 at the end of the incubation), but in the absence of an isolated intermediate this proposal is speculative. The use of testosterone as an enzyme inducer was also investigated for incubations with substrates **7**, **9**, **11**, and **20**, but in each case the products were the same as those obtained from non-induced fungus.

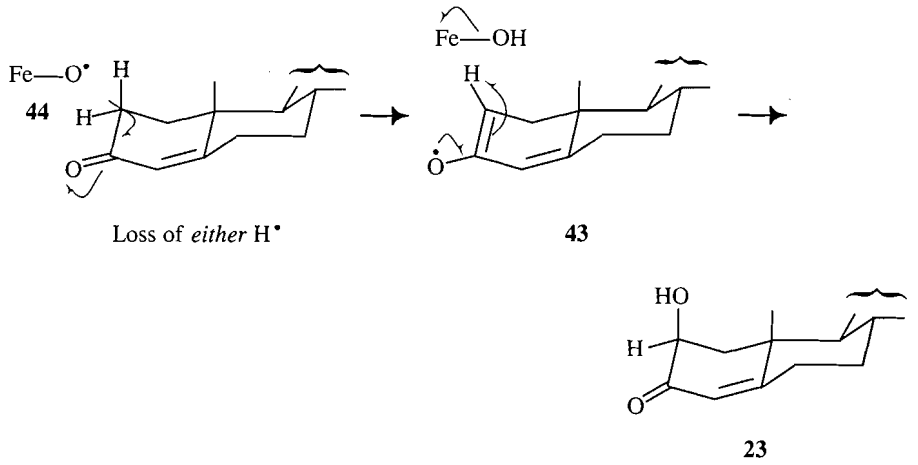
We have addressed the question of enzymic activation of the substrate towards electrophilic oxidation via formation of the $\Delta^{2,4}$-dienol **43** (Scheme 1) by the use of testosterone substrates labelled with deuterium at C-2β and C-2α (**24** and **25**, respectively), and the results of these experiments are summarized in Table 2. A meaningful interpretation depends upon a fuller knowledge of the nature of the 2β-hydroxylase enzyme, and to this end the experiments summarized in Table 3 were performed.

The enzyme uses molecular oxygen as the source of hydroxyl, giving 2β-hydroxytestosterone-2-^{18}O (**27**, ^{18}O content 50%) when the reaction was performed under an $^{18}O_2$ enriched atmosphere (^{18}O content 62%); it is insensitive to the presence of cyanide but is inhibited by carbon monoxide at saturation concentration in water, and is substrate inducible, the reaction being completely suppressed by the presence of the protein synthesis inhibitor, cycloheximide, unless preinduction with testosterone was carried out. All of these properties are consistent with the 2β-hydroxylase enzyme being a cytochrome P-450 dependent mono-oxygenase (15*a*), although in the absence of an isolated, purified enzyme this cannot be definitively proven.

The active site species of cytochrome P-450 dependent mono-oxygenases has been formulated as the ironoxy radical complex **44** of Schemes 1 and 2, and the current consensus of opinion favours the radical abstraction/recombination mechanism for hydroxylation outlined in Scheme 2 (15*b*). The data presented in Table 2 can now be interpreted on the basis of this mechanistic outline.

The substrates whose hydroxylation is summarized in Table 2 were prepared as described elsewhere (16). The β-labelled isomer (62% d_1, 85% of label in the β position (16)) was hydroxylated to give a product that contained 39% d_1 species, the location of label at C-2α being apparent from ^{1}H nmr integration, and from ^{2}H nmr and ^{13}C nmr data. The α-labelled isomer (80% d_1, 87% of label in the α position (16)) was hydroxylated to give 2β-hydroxytestosterone with 75% d_1 in the 2α position. It is therefore apparent that, within error, label originally present at C-2α is maintained during the hydroxyla-

Can. J. Chem. Downloaded from www.nrcresearchpress.com by 122.72.124.2 on 09/07/12
For personal use only.



SCHEME 1. Possible route for 2β hydroxylation of testosterone.

TABLE 2. Transformations of deuterium labelled testosterones by *G. fructicola*

Substrate (% composition)*	2β-hydroxytestosterone (% composition)*	% ^{2}H retention
1 (38) + **24** (53) + **25** (9)	**23** (61), **26** (39)	63
1 (20) + **24** (10) + **25** (70)	**23** (25), **26** (75)	94

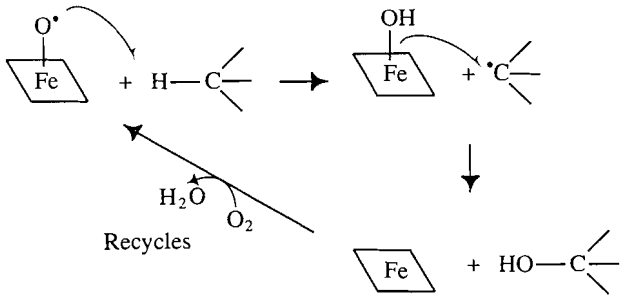
*±2.5%

TABLE 3. Transformations of testosterone by *G. fructicola*

Conditions of incubation	Product (%)
Normal	**23** (40–60)
Under $^{18}O_2$ atmosphere	**27** (58)
In 5 × 10^{-4} M KCN	**23** (50)
Under 15% CO atmosphere	0
In 3 × 10^{-4} M cycloheximide	0
In 3 × 10^{-4} M cycloheximide, cells preinduced with testosterone	**23** (10)

tion (94% retention). While this result alone would indicate hydroxylation with retention of configuration (the mode of cytochrome P-450 dependent hydroxylation most commonly observed (15*b*)), the data obtained from the β-labelled substrate, which retains 63% of the original label, show that this cannot be the case.

The analysis of the data of Table 2 depends on the relationship between stereoelectronic effects (SEE) (favouring axial (β) loss or addition of groups from C-2 (17)), and the intramolecular kinetic isotope effect (KIE) favouring loss of H over D, by a factor that may be as large as 11 in cytochrome P-450 hydroxylations (18). As outlined in Scheme 1, the loss of H from C-2 to the enzyme would be exclusively from the β face if the KIE and SEE are cooperative (for 2α-deuterium labelled substrate, **25**). However, these effects become counteractive for the C-2β labelled substrate, **24**, in which case the ratio of loss from the α and β sides is the result of an SEE/KIE competition. In both the cases reported in Table 2, recovered substrate shows no loss or epimerization of label, confirming that the phenomena reported are indeed a consequence of the hydroxylation process. The final stereochemistry of hydroxylation (conversion



SCHEME 2. Mechanism of C hydroxylation by cytochrome P-450 dependent mono-oxygenase enzymes.

of **43** to **23**) would be expected, proceeding under SEE control, to produce exclusive β product (17).

The magnitude of the SEE for hydrogen loss from C-2 during enolization of Δ^4-3-ketosteroids has been estimated at 4:1 (β:α) (17). The data of Table 2 suggest that, of the 39% d_1 species obtained from the β-labelled isomer, 30% was formed by epimerization of label from the β to the α position during the reaction (the remaining 9% being obtained from the 9% of **25** originally present). In this event, the ratio of β:α loss from C-2 of **24** can be estimated as (53–30):30 or 1:1.3, requiring an intramolecular KIE of ca. 1.3 × 4 or 5.2, well within the observed range of such effects (18, 19). The above analysis is approximate, ignoring as it does the role of intermolecular KIE's, but as these are usually close to unity in cytochrome P-450 dependent hydroxylation (19, 20), their contribution is generally small.

The phenomenon of non-stereospecific hydrogen loss followed by stereospecific hydroxylation is one that we have previously reported for enzymic hydroxylation (19, 20), and the present analysis is analogous to that given by us for the steroid 6β-hydroxylase enzyme of *Rhizopus arrhizus* (3, 12), where the stereochemistry of hydrogen loss is also isotope-dependent. This phenomenon may be a general one for hydroxylations at sites subject to stereoelectronic effects due to their proximity to carbonyl groups or other centres of π-electron density.

The data reported herein for the 2β-hydroxylase enzyme of *G. fructicola* therefore suggest that this enzyme is a cytochrome P-450 dependent mono-oxygenase, operating via a stepwise oxidation mechanism, the stereochemical details of which are subject to substrate stereoelectronic and kinetic isotope effects.

Can. J. Chem. Downloaded from www.nrcresearchpress.com by 122.72.124.2 on 09/07/12
For personal use only.

Can. J. Chem. Downloaded from www.nrcresearchpress.com by 122.72.124.2 on 09/07/12
For personal use only.

Experimental

Apparatus, material, and methods

Melting points were determined on a Kofler heating stage and are uncorrected. Infrared spectra were recorded with an Analect 6260FX spectrometer. Proton nmr spectra were recorded at 80 MHz with a Bruker WP80CW or at 200 MHz with an AC200 spectrometer, using CDCl, as solvent (except where stated) and TMS as internal standard. Carbon spectra were recorded at 50.3 MHz (JMOD mode) using the latter instrument with chloroform as solvent and internal standard. Deuterium spectra were recorded at 30.72 MHz (AC200) or at 76.8 MHz (Bruker AM500, McMaster University), using chloroform as solvent and natural abundance $CDCl_3$ as internal standard. Mass spectra were obtained with an AEI MS30/Kratos DS55 system. Isotopic abundances were determined from the molecular ion or M − H_2O spectral regions following standard correction procedures for natural ^{13}C abundances, and are accurate to ±2.5%. Thin-layer chromatography was performed on Merck silica gel 60F-254, and flash column chromatography on silica gel (230–400 mesh, Merck 9385).

Maintenance of microorganisms

Gnomonia fructicola ATCC 11430 was grown at 24–26°C on slopes of potato dextrose agar containing 0.5% strawberry petiole extract (21), then stored at 4°C and transferred at intervals not exceeding 8 weeks.

Preparation of substrates

With the exception of those listed below, the substrates used were commercial samples. Hitherto unreported spectral data are tabulated below for substrates not commercially available. 3-Deoxytestosterone (**15**): preparation, ref. 22; ^{13}C nmr, δ: 11.0 (C-18), 19.3 (C-2), 19.5 (C-19), 21.0 (C-11), 23.4 (C-15), 25.8 (C-6), 30.5 (C-16), 32.0, 32.5 (C-3, C-7) 36.0 (C-8), 36.8 (C-12), 37.1 (C-10), 37.9 (C-1), 42.7 (C-13), 50.9 (C-14), 54.6 (C-9), 81.7 (C-17), 117.2 (C-4), and 144.0 (C-5) ppm. 3-Methyleneandrost-4-en-17β-ol (**16**): preparation, ref. 23; ^{13}C nmr, δ: 11.1 (C-18), 18.6 (C-19), 21.1 (C-11), 23.5 (C-15), 27.3 (C-2), 30.6 (C-16), 32.4 (2C, C-6, C-7), 36.1 (C-8), 36.8 (C-12), 37.4 (C-1), 37.7 (C-10), 43.0 (C-13), 50.9 (C-14), 54.4 (C-9), 82.0 (C-17), 108.0 (=CH_2), 122.8 (C-4), 144.0 (C-3), and 149.0 (C-5) ppm. Androst-4-ene-3β,17β-diol (**17**): preparation, ref. 24; ^{13}C nmr, δ: 11.0 (C-18), 19.0 (C-19), 20.6 (C-11), 23.4 (C-15), 29.5 (C-2), 30.5 (C-16), 32.1, 32.6 (C-6, C-7), 35.4 (C-1), 36.0 (C-8), 36.6 (C-12), 37.4 (C-10), 42.9 (C-13), 50.8 (C-14), 54.6 (C-9), 67.9 (C-3), 81.8 (C-17), 123.5 (C-4), and 147.4 (C-5) ppm. *B*-Norandrost-4-en-17β-ol-3-one (**18**): preparation, ref. 25. *A*-Norandrost-4-en-17β-ol-3-one (**20**): preparation, ref. 26. Androst-4-en-17β-ol-3-one-2β-d_1 (**24**): preparation, ref. 16. Androst-4-en-17β-ol-3-one-2α-d_1 (**25**): preparation, ref. 16.

Fungal biotransformations

General procedure

G. fructicola was grown in a medium of potato dextrose broth (200 mL) in a 1-L Erlenmeyer flask, maintained on a rotary shaker (180 rpm) at 24–26°C. After a growth period of 5 days, the fungus was collected by centrifugation and resuspended in distilled water (200 mL) in a 1-L Erlenmeyer flask. In a typical procedure, 15 such flasks were used to transform 1 g of substrate, added at the rate of 70 mg in 2 mL 95% ethanol per flask. Incubations with substrate were then performed under conditions identical with those described above (24–26°C, 180 rpm), for a 5-day period, following which the fungus was removed by filtration and products isolated by continuous extraction of the aqueous medium (methylene chloride), and purified by column chromatography. Extraction of the fungal biomass led to the recovery of starting material in most cases. This latter process was not routinely performed and was not quantified.

Controlled atmosphere and inhibitor experiments

The experiments summarized in Table 3 were performed in closed 1-L vessels ($^{18}O_2$ and 15% CO atmospheres), or by replacement of distilled water in the above procedure by the appropriate inhibitor solution. Preinduction of enzymes by testosterone was carried out by the addition of testosterone (4 mg in 1 mL 95% ethanol per flask) to the growing fungus 4 days after inoculation, followed by a further 24-h growth period. Subsequent procedures were carried out as described above. In all cases, yields reported in Table 3 refer to isolated, purified products.

Substrates

Isolated yields of products are listed in Tables 1 and 2. The following paragraphs contain (in order) substrate; recovered substrate from aqueous medium (%); products (%), in order of elution from column chromatography, together with hitherto unpublished spectral and (or) analytical data.

Androst-4-en-17β-ol-3-one (testosterone, **1**), 17; androst-4-ene-3,17-dione (**3**), 1, identified by comparison with authentic material; androst-4-ene-2β,17β-diol-3-one (**23**), 40–60; ^{13}C nmr, δ: 11.3 (C-18), 22.5 (C-11), 22.8 (C-19), 23.3 (C-15), 30.4 (C-16), 33.0 (C-7), 34.5 (C-6), 35.8 (C-8), 36.5 (C-12), 39.5 (C-1), 41.4 (C-10), 43.4 (C-13), 50.3, 50.5 (C-9, C-14), 68.6 (C-2), 81.4 (C-17), 118.8 (C-4), 175.2 (C-5), 199.9 (C-3) ppm, identified by comparison with authentic material (27).

Androst-4-en-17β-ol-3-one, 2β-d_1 (**24**), 9; ^2H nmr, δ: 2.40 (C-2β^2H) ppm; androst-4-ene-2β,17β-diol-3-one, 2α-d_1 (**23** + **26**), total 25, ^1H nmr included signals at δ: 3.63 (1H, t, C-17αH), 4.15 (0.61 H, dd, C-2αH), and 5.78 (1H, s, C-4H) ppm; ^2H nmr δ: 4.16 (C-2α^2H) ppm.

Androst-4-en-17β-ol-3-one, 2α-d_1 (**25**), 9; ^2H nmr, δ: 2.32 (C-2α^2H) ppm; androst-4-ene-2β,17β-diol-3-one, 2α-d_1, (**23** + **26**), total 20; ^1H nmr included signals at δ: 3.63 (1H, t, C-17αH), 4.15 (0.25 H, dd, C-2αH), and 5.79 (1H, s, C-4H) ppm; ^2H nmr δ: 4.16 (C-2α^2H) ppm.

Androst-4-en-17β-ol-3-one, 17 acetate (testosterone acetate, **2**), 0; androst-4-ene-3,17-dione, 1; androst-4-ene-2β,17β-diol-3-one (**23**), 30; androst-4-en-6β-ol-3,17-dione (**31**), 2, identified by comparison with authentic material (20).

Androst-4-ene-3,17-dione (**3**), 5; androst-4-en-2β-ol-3,17-dione (**28**), 4, identified by comparison with an authentic sample (27); androst-4-ene-17β-ol-3,16-dione (**30**), 5; ^1H nmr included signals at δ: 0.78 (3H, s, C-18H), 1.2 (3H, s, C-19H), 3.75 (1H, s, C-17αH) and 5.7 (1H, s, C-4H) ppm, identified by spectral, tlc, and mp comparisons with data from authentic material (28).

Pregn-4-ene-3,20-dione (progesterone, **4**), 10; pregn-4-en-2β-ol-3,20-dione (**32**), 5, identified by comparison of spectral and physical data with those reported (11); pregn-4-en-14α-ol-3,20-dione (**33**), 8, identified by comparison with reported spectral data (29, 30); pregn-4-ene-2β,6β-diol-3,20-dione (**34**), 12; ^1H nmr including δ: 0.68 (3H, s, C-18H), 1.48 (3H, s, C-19H), 2.1 (3H, s, C-21H), 4.2–4.4 (2H, m, C-2 and -6 H's), and 5.82 ppm, obtained in admixture with pregn-4-ene-6β,14α-diol-2,20-dione (**35**), 21. The latter compound was purified by repeated chromatography and had physical and spectral data identical with those reported (29, 30).

Androsta-4,6-dien-17β-ol-3-one (**5**), 25; androsta-4,6-diene-3,17-dione (**6**), 16, identical with an authentic commercial sample.

Androsta-1,4-dien-17β-ol-3-one (**7**), 15; androsta-1,4-diene-3,17-dione (**8**), 7, identical with an authentic samples prepared by Jones' oxidation of **7**.

19-Norandrost-4-en-17β-ol-3-one (19-nortestosterone, **9**), 12; 19-norandrost-4-ene-16α,17β-diol-3-one (**10**), 6, mp 172–174°C (lit. (31) mp 185–186°C); ^1H nmr included peaks at δ: 0.78 (3H, s, C-18H), 3.49 (1H, t, C-16βH), 4.10 (1H, br s, C-17αH), and 5.81 (1H, s, C-4H) ppm; ^{13}C nmr δ: 12.2 (C-18), 25.7 (C-11), 26.5 (C-1), 30.6 (C-7), 33.7 (C-15), 35.4 (C-6), 36.4 (2C, C-2 and C-12), 40.0 (C-8), 42.6 (C-10), 43.6 (C-13), 47.6 (C-14), 49.5 (C-9), 78.4 (C-16), 89.7 (C-17), 124.7 (C-4), 166.5 (C-5), and 200.0 (C-3) ppm; ms *m/z* (%): 290 ($M^{+\cdot}$, 90), 272 (100), 257 (25), 254 (35).

5α-Androstan-17β-ol-3-one (**11**), 12; 5α-androstane-3β,17β-diol (**36**), 3, analytical and spectral data identical with those reported (13); 5α-androstane-3β,17β,16α-triol (**37**), 20, mp 238–240°C (lit. (32) mp 256–260°C corr.); ^1H nmr included signals at δ: 0.66 (3H, s, C-18H), 0.73 (3H, s, C-19H), 3.26 (d, J = 5.6 Hz, C-17αH), 3.30–3.45 (1H,

Can. J. Chem. Downloaded from www.nrcresearchpress.com by 122.72.124.2 on 09/07/12
For personal use only.

m, C-3αH), and 3.88 (1H, d of t, J = 2.1, 5.6 Hz, C-16βH) ppm; ^{13}C nmr δ: 11.5, 11.7 (C-18, C-19), 19.6 (C-11), 27.8 (C-6), 30.8, 30.9 (C-2, C-7), 33.1 (C-15), 34.3 (C-8), 34.8 (C-10), 36.2 (2C, C-1 and C-12), 37.5 (C-4), 42.7 (C-13), 44.1 (C-5), 48.0 (C-14), 53.8 (C-9), 69.6 (C-3), 77.3 (C-16), and 88.9 (C-17) ppm; converted to the triacetate, mp 172–175°C (lit. (32) mp 174–176°C); ^{1}H nmr included signals at δ: 0.75, 0.77 (each 3H, s, C-18H and C-19H), 2.0, 2.01, 2.04 (each 3H, s, $COCH_3$), 4.5–4.75 (1H, m, C-3αH), 4.89 (1H, d, J = 5.6 Hz, C-16βH) ppm; ^{13}C nmr δ: 12.2 (C-19), 13.0 (C-18), 20.4 (C-11), 21.0, 21.1, 21.4 (acetyl CH_3) 27.5 (C-2), 28.4 (C-6), 31.4 (C-7), 32.3 (C-15), 34.0 (C-4), 34.9 (C-8), 35.6 (C-10), 36.7, 36.8 (C-1, C-12), 43.6 (C-13), 44.7 (C-5), 49.1 (C-14), 54.1 (C-9), 73.6 (C-3), 78.1 (C-16), 86.3 (C-17), 170.6, 170.6, 170.7 (acetyl CO) ppm; 5α-androstane-2β,3α,16α,17β-tetrol (**38**), 3, mp 247–250°C; ^{1}H nmr included signals at δ: 0.63 (3H, s, C-18H), 0.88 (3H, s, C-19H), 3.28 (1H, d, J = 5.4 Hz, C-17αH), 3.35–3.7 (2H, complex m, C-2α and C-3β H's), and 3.90 (1H, d of t, J = 2, 5.4 Hz, C-16βH) ppm; ^{13}C nmr (DMSO-d_6) δ: 11.9 (C-18), 13.7 (C-19), 19.4 (C-11), 27.6 (C-6), 31.1 (C-4), 30.9 (C-7), 33.1 (C-15), 33.9 (C-8), 35.2 (C-10), 36.4 (C-12), 38.3 (C-1), 43.0 (C-13), 48.2 (C-14), 54.8 (C-9), 69.5, 70.6 (C-2, C-3), 77.2 (C-16), and 89.2 (C-17) ppm; the signal from C-5 was obscured by solvent peaks; ms, m/z (%): 324 ($M^{+\cdot}$), (25), 306 (80), 291 (40), 288 (45), 273 (40), 262 (43), 249 (75), 231 (100). **38** converted to the tetraacetate, mp 82–84°C from methanol; ^{1}H nmr included signals at δ: 0.76 (3H, s, C-18H), 0.87 (3H, s, C-19), 2.00, 2.03, 2.035, 2.04 (total 12H, each s, $COCH_3$), 4.87 (2H, br s, C-17α and C-2α or C-3β H), 4.75–5.0 (1H, m, C-2α or C-3β H), and 5.10 (1H, d of t, J = 2, 5.5 Hz, C-16β H) ppm; ^{13}C nmr δ: 13.0 (C-18), 13.7 (C-19), 20.0 (C-11), 21.1, 21.2, 21.3 (2C) (acetyl CH_3), 27.7 (C-6), 29.3 (C-4), 31.2 (C-7), 32.3 (C-15), 34.4 (C-8), 35.1 (C-10), 36.7 (C-12), 37.7 (C-1), 39.6 (C-5), 43.6 (C-13), 49.0 (C-14), 54.7 (C-9), 69.8, 70.2 (C-2, C-3), 78.1 (C-16), 86.2 (C-17), 169.6, 169.8, 170.7, 170.9 (acetyl CO) ppm.

5β-Androstan-17β-ol-3-one (**12**), 7; 5β-androstane-5,17β-diol-3-one (**40**), 19, mp 154–165°C (dec.); ^{1}H nmr included signals at δ: 0.75 (3H, s, C-18H), 1.0 (3H, s, C-19H), 3.0 (1H, half of ABq, J = 15 Hz, C-4H), and 3.65 (1H, t, J = 8 Hz, C-17α H) ppm; ^{13}C nmr δ: 11.1 (C-18), 16.2 (C-19), 21.4 (C-11), 23.4 (C-15), 28.7 (C-17), 30.6 (C-16), 31.2 (C-1), 35.0 (C-8), 36.6 (C-12), 37.0, 37.3 (C-2, C-6), 40.4 (C-10), 43.1 (C-13), 44.1 (C-9), 49.4 (C-4), 51.3 (C-14), 78.6 (C-5), 81.7 (C-17), and 210.8 (C-3) ppm; ms, m/z (%): 288 ($M - H_2O$, 10), 274 (10), 246 (10), 236 (18) relative to 71 (100); converted to the 17-monoacetate, mp 174–176°C (lit. (33) mp 176–178°C); ^{1}H nmr included signals at δ: 0.78 (3H, s, C-18H), 0.98 (3H, s, C-19H), 2.02 (3H, s, $COCH_3$), 3.0 (1H, half of ABq, J = 15 Hz, C-4H), and 4.57 (1H, t, J = 8 Hz, C-17αH) ppm; ^{13}C nmr δ: 12.1 (C-18), 16.2 (C-19), 21.1 (acetyl CH_3), 21.3 (C-11), 23.6 (C-15), 27.6 (C-16), 28.7 (C-7), 31.2 (C-1), 34.7 (C-8), 36.3, 36.9 (C-6, C-12), 37.3 (C-2), 40.8 (C-10), 42.7 (C-13), 44.0 (C-9), 49.5 (C-4), 51.0 (C-14), 78.5 (C-5), 82.6 (C-17), 170.8 (acetyl CO), and 210.6 (C-3) ppm; 5β-androstane-3α,5,17β-triol (**41**), 17; mp 218–221°C (lit. (34) mp 220–223°C); ^{1}H nmr included signals at δ: 0.73 (3H, s, C-18H), 0.90 (3H, s, C-19H), 3.4–3.7 (1H, m, C-3β H), and 3.64 (1H, t, J = 8 Hz, C-17α H) ppm; ^{13}C nmr δ: 11.1 (C-18), 16.4 (C-19), 20.8 (C-11), 23.4 (C-15), 28.2 (C-7), 29.8, 30.1 (2C) (C-1, C-2, C-16), 35.1 (C-8), 36.7, 36.9 (C-6, C-12), 39.8 (C-10), 42.0 (C-9), 43.0 (C-13), 43.5 (C-4), 51.2 (C-14), 68.1 (C-3), 75.7 (C-5), and 81.8 (C-17) ppm; ms, m/z (%): 308 (2), 290 (26), 275 (10), 273 (10), 272 (30), 257 (15), 236 (100).

Androst-4-en-19-ol-3,17-dione (**13**) was recovered quantatively and unchanged from incubation with *G. fructicola*.

Androst-4-en-19-al-3,17-dione (**14**) was converted to the alcohol **13** in 85% isolated yield by *G. fructicola*.

Androst-4-en-17β-ol (**15**) and 3-methyleneandrost-4-en-17β-*ol* (**16**) were recovered unchanged in yields of 28 and 36% respectively from the aqueous medium following incubation with *G. fructicola*. Extraction of the fungal biomass yielded the balance of the substrates.

Androst-4-ene-3β,17β-diol (**17**), 0; androst-4-en-17β-ol-3-one (**1**), 2; androst-4-ene-3,17-dione (**3**), 1; androst-4-ene-2β,17β-diol-3-one (**23**), 17; and androst-4-en-2β-ol-3,17-dione (**28**), 2; all of which were identified by comparison with authentic samples (see above).

B-*Norandrost-4-en-17β-ol-3-one* (**18**), 24; *B*-norandrost-4-ene-3,17-dione (**19**), 5; spectral data identical with those reported (25).

B-*Norandrost-4-en-17β-ol-3-one* (**18**), with induced enzymes, 45; *B*-norandrost-4-ene-3,17-dione (**19**), 5, identified as reported above; *B*-norandrosta-1,4-dien-17β-ol-3-one (**42**), 8, mp 156–159°C (lit. (35) mp 157–159°C); ^{1}H nmr included signals at δ: 0.80 (3H, s, C-18H), 1.10 (3H, s, C-19H), 3.68 (1H, t, J = 8 Hz, C-17αH), 6.0 (1H, s, C-4H), 6.15 and 7.02 (2H, ABq, C-2 and C-1 H's) ppm; ^{13}C nmr δ: 11.5 (C-18), 20.5 (C-19), 20.8 (C-11), 23.9 (C-15), 30.6 (C-16), 32.7 (C-6), 36.4 (C-12), 38.5 (C-8), 44.9 (C-13), 48.2 (C-10), 50.6 (C-14), 53.4 (C-9), 81.3 (C-17), 123.7 (C-4), 128.4 (C-2), 152.6 (C-1), 174.1 (C-5), and 186.7 (C-3) ppm.

A-*Norandrost-3(5)-en-17β-ol-2-one* (*A*-nortestosterone, (**20**), 60; *A*-norandrost-3(5)-ene-2,17-dione (**21**), 3, mp 163–166°C (lit. (36) mp 166–166.5°C), identified by comparison with an authentic sample produced by Jones' oxidation of *A*-nortestosterone; *A*-norandrost-3(5)-ene-1β,17β-diol-2-one (**22**), 10, mp 236–238°C (lit. (37) mp 240–243°C); ^{1}H nmr included peaks at δ: 0.80 (3H, s, C-18H), 1.10 (3H, s, C-19H), 3.62 (1H, t, J = 8 Hz, C-17α H), 3.75 (1H, s, C-1H), and 5.80 (1H, s, C-4H) ppm; ^{13}C nmr δ: 11.1 (C-18), 15.5 (C-19), 23.0 (C-11), 23.3 (C-15), 28.1 (C-6), 30.0 (C-16), 31.5 (C-7), 35.7 (C-8), 36.4 (C-12), 43.4 (C-13), 50.0 (C-10), 50.4 (C-14), 53.7 (C-9), 81.6 (C-17), 83.0 (C-1), 122.1 (C-3), 186.3 (C-5), and 207.4 (C-2) ppm; ms, m/z (%): 290 (78), 275 (52), 259 (20), relative to 57 (100).

Acknowledgements

Financial support was provided by the Natural Sciences and Engineering Research Council of Canada. We are grateful to Mr. T. Jones and Mrs. D. Vukmanic (Brock) and to Dr. D. W. Hughes (McMaster) for assistance with the acquisition of spectral data.

1. J. Horvath and A. Kramli. Nature, **162**, 619 (1948).
2. H. L. Holland. Chem. Soc. Rev. **11**, 371 (1982).
3. H. L. Holland. Acc. Chem. Res. **17**, 398 (1984).
4. A. I. Laskin, J. Fried, and P. A. Diassi. U.S. Patent 3,063,992 (13 Nov 1962); Chem. Abstr. **58**, 5011b (1963).
5. E. F. Hahn and J. Fishman. J. Biol. Chem. **259**, 1689 (1984).
6. E. Caspi, J. Wicha, T. Arunachalam, P. Nelson, and G. Spiteller. J. Am. Chem. Soc. **106**, 7282 (1984).
7. A. M. Soto and C. Sonnenschein. J. Steroid Biochem. **23**, 87 (1985).
8. C. J. Newton, D. L. Samuel, and V. H. T. James. J. Steroid Biochem. **24**, 1033 (1986).
9. J. J. Sheets and R. W. Estabrook. Biochemistry, **24**, 6591 (1985).
10. A. J. Sonderfan, M. P. Arlotto, D. R. Dutton, S. K. McMillen, and A. Parkinson. Arch. Biochem. Biophys. **255**, 27 (1987).
11. A. I. Laskin, J. Fried, A. I. Cohen, C. Meyers, P. Grabowich, B. Junta, R. M. Palmere, and P. A. Diassi. Steroids, **5**, 57 (1965).
12. H. L. Holland, P. C. Chenchaiah, E. M. Thomas, B. Mader, and M. J. Dennis. Can. J. Chem. **62**, 2740 (1984).
13. J. W. Blunt and J. B. Stothers. Org. Magn. Reson. **9**, 439 (1977).
14. S. Kashino, H. Katz, J. P. Glusker, R. M. Pollack, and P. L. Bounds. J. Am. Chem. Soc. **109**, 6765 (1987).
15. P. R. Ortiz de Montellano and N. O. Reich. *In* Cytochrome P-450. *Edited by* P. R. Ortiz de Montellano. Plenum, New York. 1986. (*a*) p. 273; (*b*) p. 217.
16. H. L. Holland, J. A. Rao, and P. C. Chenchaiah. J. Chem. Soc. Perkin Trans. 1, 2027 (1988).
17. S. K. Malhotra and H. J. Ringold. J. Am. Chem. Soc. **86**, 1997 (1964).

18. L. M. HJELMELAND, L. ARONOW, and J. R. TRUDELL. Biochem. Biophys. Res. Commun. **76**, 541 (1977).
19. H. L. HOLLAND, F. M. BROWN, B. MUNOZ, and R. W. NINNISS. J. Chem. Soc. Perkin Trans. 2, 1557 (1988).
20. H. L. HOLLAND and P. R. P. DIAKOW. Can. J. Chem. **56**, 694 (1978).
21. C. O. GOURLEY. Can. J. Bot. **50**, 49 (1972).
22. K. HEUSLER, J. KALVODA, P. WIELAND, G. ANNER, and A. WETTSTEIN. Helv. Chim. Acta, **45**, 2575 (1962).
23. S. MIYAIRI and J. FISHMAN. J. Biol. Chem. **261**, 6772 (1987).
24. W. G. DAUBEN and J. W. ASHMORE. Tetrahedron Lett. 4487 (1978).
25. H. L. HOLLAND. Can. J. Chem. **59**, 1651 (1981).
26. F. L. WEISENBORN, D. C. REMY, and T. L. JACOBS. J. Am. Chem. Soc. **76**, 552 (1954).
27. R. D. BURNETT and D. N. KIRK. J. Chem. Soc. Perkin Trans. 1, 1830 (1973); 284 (1974).
28. R. M. DOBSON and S. MIZUBA. J. Org. Chem. **27**, 698 (1962).
29. J. F. TEMPLETON, V. P. S. KUMAR, K. MARAT, R. S. KIM, and F. S. LABELLA. J. Nat. Prod. **50**, 463 (1987).
30. K. M. MADYASTHA and J. SRIVATSAN. Can. J. Microbiol. **33**, 361 (1987).
31. J. DE FLINES, W. F. VAN DER WAARD, W. J. MIJS, and S. A. SZPILFOGEL. Recl. Trav. Chim. Pays-Bas, **82**, 121 (1963).
32. G. F. MARRIAN and G. C. BUTLER. Biochem. J. **38**, 322 (1944).
33. P. KELLER, F. G. EGGART, H. WEHRLI, K. SCHAFFNER, and O. JEGER. Helv. Chim. Acta, **50**, 2259 (1967).
34. B. CAMERINO and D. CATTAPAN. Farm. Ed. Sci. **13**, 39 (1958).
35. J. JOSKA, J. FAJKOS, and F. SORM. Collect. Czech. Chem. Commun. **38**, 270 (1973).
36. F. L. WEISENBORN and H. E. APPLEGATE. J. Am. Chem. Soc. **81**, 1960 (1959).
37. K. YOSHIDA and T. KUBOTA. Chem. Pharm. Bull. (Tokyo), **13**, 156 (1965).

Can. J. Chem. Downloaded from www.nrcresearchpress.com by 122.72.124.2 on 09/07/12
For personal use only.

Nouveaux alcaloïdes bisbenzylisoquinoléiques biphényliques de *Crematosperma* sp.[1]

JAIRO SAEZ ET ESTELLA FERNANDEZ
Universidad de Antioquia, Departamento de Quimica, AA 1226 Medellin, Colombia

AKINO JOSSANG ET ANDRÉ CAVÉ[2]
Laboratoire de pharmacognosie, Unité associée 496 du Centre national de la recherche scientifique, Faculté de pharmacie, Université Paris-Sud, 92296 Châtenay-Malabry CEDEX, France

ET

ADRIEN CAVÉ
Centre de pharmacologie et endocrinologie, Institut national de la santé et de la recherche médicale, Centre national de la recherche scientifique, 34033 Montpellier CEDEX, France

Reçu le 14 juillet 1988

JAIRO SAEZ, ESTELLA FERNANDEZ, AKINO JOSSANG, ANDRÉ CAVÉ et ADRIEN CAVÉ. Can. J. Chem. **66**, 275 (1988).

Quatre nouveaux alcaloïdes : la (−)-cordobine **1**, la (−)-montérine **2**, la (−)-granjine **3** et la (−)-cordobimine **4** ont été isolés d'une Annonacée de Colombie, *Crematosperma* sp. Leurs structures ont été élucidées par analyse des données spectrales et par réactions chimiques. Ils constituent les premiers alcaloïdes possédant la configuration absolue 1*R*, 1′*S* dans les groupe des bisbenzyltétrahydroisoquinoléines liées par un pont diaryléther 8,7′ et par un pont biphénylique 11,11′.

Mots clés : Annonaceae, *Crematosperma*, alcaloïdes, biphénylbisbenzylisoquinoléines.

JAIRO SAEZ, ESTELLA FERNANDEZ, AKINO JOSSANG, ANDRÉ CAVÉ, and ADRIEN CAVÉ. Can. J. Chem. **66**, 275 (1988).

Four new alkaloids, (−)-cordobine **1**, (−)-monterine **2**, (−)-granjine **3**, and (−)-cordobimine **4** have been isolated from a Colombian Annonaceous plant, *Crematosperma* sp. Structures were elucidated from spectral data and chemical reactions. These alkaloids are the first 1*R*, 1′*S* bisbenzyltetrahydroisoquinolines including 8,7′ ether and 11,11′ biphenyl linkages.

Key words: Annonaceae, *Crematosperma*, alkaloids, biphenylbisbenzylisoquinolines.

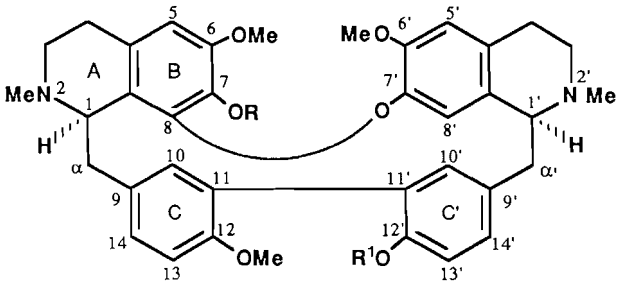
Le genre *Crematosperma*, Annonacées, est représenté, selon Fries, par 17 espèces sud-américaines (1). Jusqu'ici une seule d'entre elles, *C. polyphlebum*, a été étudiée; un alcaloïde bisbenzylisoquinoléique biphénylique, la phlebicine, en a été isolé (2). L'espèce étudiée ici, *Crematosperma* sp., est originaire de Colombie et a été récoltée à Urrao.

Des écorces de ce *Crematosperma*, quatre alcaloïdes nouveaux ont été isolés, la (−)-cordobine **1**, la (−)-montérine **2**, la (−)-granjine **3** et la (−)-cordobimine **4**. Les spectres uv de ces alcaloïdes sont caractéristiques des benzyltétrahydroisoquinoléines, et leurs spectres de masse, avec le pic moléculaire entre *m/z* 592 et 636, indiquent une structure de dimère (3, 4).

La (−)-cordobine **1**, obtenue amorphe, $[\alpha]_D^{20}$ −140($CHCl_3$), répond à la formule brute $C_{37}H_{40}N_2O_6$ ($M^{+\cdot}$ 608) déduite de son spectre de masse. Un léger effet bathochrome en milieu alcalin sur le spectre uv indique la présence d'une fonction phénolique. Le spectre de rmn ^1H (360 MHz) (Tableau 1) indique la présence de deux groupements N-méthyle à 2,42 et 2,64 ppm, trois groupes méthoxyle et neuf protons aromatiques. Les fragmentations du spectre de masse résultant d'une coupure 1-α et 1′-α′, pics à *m/z* 382, 381 et 191, correspondent aux ions monochargés et doublement chargés d'une *N,N′*-diméthylbistétrahydroisoquinoléine diméthoxylée et hydroxylée comportant un pont éther-oxyde (5). Le troisième méthoxyle est donc porté par la partie benzylique.

Les six protons aromatiques résonnant en deux systèmes ABX, 3H en 13, 14, 10 et 3H en 13′, 14′, 10′, révèlent surtout la présence d'une liaison biphénylique C-11, C-11′ entre les cycles C et C′ et les substitutions en C-12 et C-12′. Les positions des trois méthoxyles en 6, 6′ et 12 et des deux fonctions phénol en 7 et 12′ ont été établies grâce à des mesures de nOe. La structure plane de la (−)-cordobine **1** est ainsi établie et se révèle identique à celle de la (+)-antioquine (6).

La valeur du pouvoir rotatoire de la (−)-cordobine **1** ($[\alpha]_D^{20}$ −140) est de valeur comparable à celle de l'antioquine mais de signe opposé ($[\alpha]_D$ +214). De plus la courbe de dichroïsme circulaire de la (−)-cordobine **1** est l'inverse de celle de la (+)-antioquine. La configuration absolue de la (−)-cordobine **1** est donc 1*R*,1′*S*, énantiomère de la (+)-antioquine dont la stéréochimie a été établie comme étant 1*S*,1′*R* par une étude de diffraction de rayons X (6). Le spectre de rmn ^1H de la (−)-cordobine **1** est en accord avec cette conclusion. On observe en effet que l'ensemble des protons aromatiques résonnent entre 6,36 et 7,44 ppm, ce qui est caractéristique des bisbenzyltétrahydroisoquinoléines possédant ce type de liaison (pont éther-oxyde 8,7′, pont biphényle 11,11′) et ayant la configuration «*syn*» (8). La position du signal correspondant au proton en 10 à 7,17 ppm corrobore également cette configuration, le proton en 10 des produits de configuration «*anti*» résonnant à des champs nettement plus faibles, vers 7,55 ppm (8).



(-)-Cordobine **1** : R = R¹ = H
(-)-Montérine **2** : R = H, R¹ = Me
(-)-Granjine **3** : R = R¹ = Me

1. Partie 90 dans le série «Alcaloïdes des Annonacées». Pour la partie 89 voir: S. Berthou, M. Lebœuf, A. Cavé et H. Guinaudeau. J. Nat. Prod. Sous presse.

2. Auteur à qui adresser toute correspondance.

Printed in Canada / Imprimé au Canada

Can. J. Chem. Downloaded from www.nrcresearchpress.com by 122.72.124.2 on 09/07/12
For personal use only.

TABLEAU 1. Spectres de rmn ^1H des composés **1–6** ($CDCl_3$, 360 MHz)

		2		**3**				
	1	*a*	*b*	*a*	*b*	**4**	**5**	**6**
NCH_3-2	2,42	2,27	2,38	2,31	2,42	2,28	2,38	2,34
NCH_3-2′	2,64	2,56	2,62	2,60	2,67	—	NH	NH
CH_3O-6	3,82	3,79	3,77	3,78	3,80	3,82	3,83	3,83
CH_3O-6′	3,52	3,46	3,44	3,50	3,45	3,42	3,49	3,33
CH_3O-7	OH	OH	OH	3,27	3,42	OH	OH	OH
CH_3O-12	3,89	3,73	3,76	3,74	3,76	3,94	3,88	3,88
CH_3O-12′	OH	3,80	3,70	3,81	3,71	OH	OH	OH
H-1m	4,16	4,26	3.92	4,26	3,90	4,09	3,97	4,13
H-1′m	3,80	3,52	3,75	3,55		—	4,45	4,37
H-5	6,36	6,31	6,30	6,33	6,26	6,37	6,37	6,38
H-5′	6,50	6,57	6,30	6,57	6,33	6,43	6,48	6,40
H-8′	6,84	6,36	7,15	6,33	7,08	7,77	7,15	7,28
H-10 d	7,17	7,67	6,60	7,66	6,60	7,64	6,91	7,62
H-13 d	6,87	6,70	6,78	6,72	6,78	6,88	6,88	6,86
H-14 dd	7,44	7,10	7,25	7,10	7,27	7,26	7,42	7,27
H-10′ d	6,53	6,15	6,80	6,16	6,75	7,41	6,85	7,09
H-13′ d	6,89	6,90	6,68	6,90	6,68	6,79	6,86	6,84
H-14′ dd	7,23	7,20	7,18	7,21	7,19	7,15	7,20	7,21

J_o = 8,5 Hz; J_m = 2,2 Hz.

TABLEAU 2. Spectres de rmn ^1H de **2** et **3** à température variable (pyridine-d_5, 250 MHz)

	Montérine **2**		Granjine **3**	
	21°C	90°C	21°C	90°C
NCH_3-2	2,28 et 2,48	2,46	2,28 et 2,45	2,49
NCH_3-2′	2,53 et 2,56	2,63	2,58 et 2,60	2,64
CH_3O-6	3,68	3,75	3,72	3,76
CH_3O-6′	3,34 et 3,43	3,49	3,48 et 3,54	3,55
CH_3O-7	—	—	3,32 et 3,43	3,44
CH_3O-12	3,55	3,56	3,57	3,66
CH_3O-12′	3,72	3,78	3,74	3,78
9 H ar.	6,33–7,70	6,30–7,60	6,35–7,67	6,30–7,45

La (−)-montérine **2**, obtenue amorphe, $[\alpha]_D^{20}$ −135, a une structure apparentée à celle de la (−)-cordobine **1**. Son spectre de masse montre un pic moleculaire à m/z 622 ($C_{38}H_{42}N_2O_6$) indiquant 14 uma supplémentaires et des fragments à m/z 382, 381 et 191, correspondant à la partie bisisoquinoléique, identiques à ceux observés sur le spectre de la (−)-cordobine **1**. Donc, le méthoxyle supplémentaire doit se trouver en position 12′. La parenté avec la (−)-cordobine ainsi que la position du méthoxyle supplémentaire en 12′ sont confirmées par l'examen du spectre de rmn ^1H. Celui-ci présente des signaux dédoublés à température ambiante dus à l'existence de conformères stables *a* et *b* dans une proportion égale. Ceci est confirmé par la simplification du spectre enregistré à 90°C dans la pyridine-d_5 (Tableau 2). Une attribution complète des signaux des protons a été effectuée par une étude des découplages sélectifs et des nOe. La configuration 1*R*, 1′*S* de la (−)-montérine **2** est déduite de sa courbe de dc superposable à celle de la (−)-cordobine **1**.

La (−)-granjine **3**, également obtenue amorphe, $[\alpha]_D^{20}$ −63, possède une masse moléculaire $M^{+\bullet}$ à m/z 636 compatible avec la formule brute $C_{39}H_{44}N_2O_6$. Les fragments à m/z 396, 395 et 198 montrent que la (−)-granjine **3** comporte 14 uma de plus que la (−)-montérine **2**. Son spectre de rmn ^1H est très voisin de celui de la (−)-montérine **2** et également dédoublé en raison de la présence de conformères *a* et *b* dans une proportion 2 : 1. Il comporte un signal dédoublé à 3,27 et 3,42 ppm correspondant au méthoxyle en 7, en plus de ceux figurant sur le spectre de la (−)-montérine **2**. Les signaux correspondant aux protons de la (−)-granjine **3** ont été attribués par une étude de découplage sélectif et par comparaison aux valeurs déterminées pour la (−)-montérine **2**. Le spectre de dc, identique à celui de la (−)-cordobine **1**, indique la même configuration 1*R*, 1′*S* pour la (−)-granjine.

Il est à noter que les alcaloïdes biphényliques, lorsque la position 7 ou les deux positions 12 et 12′ sont substituées par un méthoxyle, donnent lieu à l'existence de conformères stables, ceci étant lié à l'encombrement stérique de la molécule. Les règles établies pour fixer les configurations en 1 et 1′ (8) présentent alors des exceptions pour l'un des deux conformères (6).

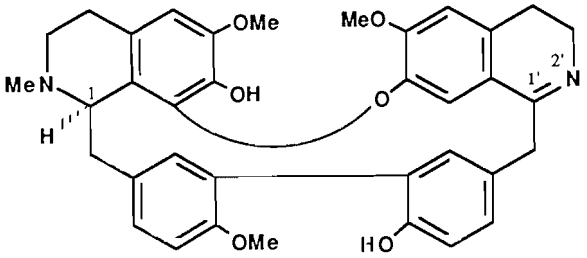
La corrélation entre ces trois alcaloïdes a été effectuée par O-méthylation de la (−)-cordobine **1** et de la (−)-montérine **2**, qui a fourni la *O*,*O*-diméthylcordobine et la *O*-méthylmontérine en tous points identiques à la (−)-granjine **3**.

La (−)-cordobimine **4**, amorphe, $[\alpha]_D^{20}$ −185, est un alcaloïde nouveau, de formule brute $C_{36}H_{36}N_2O_6$ déduite de son

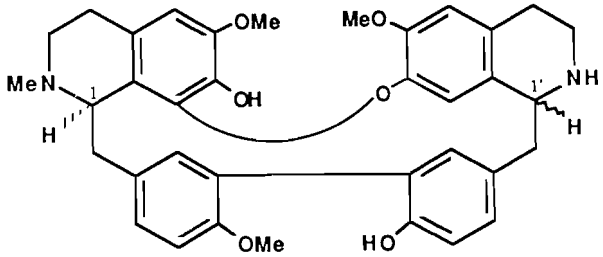
Can. J. Chem. Downloaded from www.nrcresearchpress.com by 122.72.124.2 on 09/07/12
For personal use only.

spectre de masse ($M^{+\bullet}$ 592). Le spectre uv, caractéristique de celui des benzylisoquinoléines, montre un épaulement supplémentaire à 308 nm et présente un important effet bathochrome en milieu acide à 346 nm caractéristique d'une dihydro-3,4 isoquinoléine, indiquant ainsi la présence d'une fonction imine. Le spectre ir confirme la présence d'une fonction imine conjuguée (bande à 1620 cm^{-1}).

Le spectre de rmn ^1H montre la présence de trois groupes méthoxyle et présente un seul signal de N-méthyle à 2,28 ppm, donc en 2, indiquant que la fonction imine se trouve sur la partie droite de la molécule, en 1′,2′. Par conséquent le singulet déblindé à 7,77 ppm est attribué au proton en 8′. La présence de deux autres singulets à 6,37 et 6,43 ppm et de deux systèmes ABX de six protons appartenant aux cycles C et C′, indique que la (−)-cordobimine **4** possède également une structure de bisbenzyltétrahydroisoquinoléine, comportant un pont éther-oxyde 8,7′ et un pont biphénylique 11,11′. Un découplage sélectif et une étude des nOe a permis de placer les trois groupes méthoxyle dans les positions 6, 6′ et 12 et par suite les deux hydroxyles en 7 et 12′.



(-)-Cordobimine **4**



(-)-Dihydrocordobimine **5** : 1′S

(-)-Dihydrocordobimine **6** : 1′R

Le signe négatif du pouvoir rotatoire indique que la (−)-cordobimine possède la configuration 1*R*, ce que confirme la courbe de dichroïsme circulaire. La réduction de la (−)-cordobimine **4** par $NaBH_4$ donne naissance à deux amines secondaires nouvelles, la dihydrocordobimine 1′*S* **5** et la dihydrocordobimine 1′*R* **6**, en proportion 1 : 2. Le composé **5**, *F* 205–209°C (MeOH), $[\alpha]_D^{20}$ −215, présente une courbe de dichroïsme circulaire superposable à celle de la (−)-cordobine **1**. Le dérivé N′-méthylé de **5** s'est révélé identique à la (−)-cordobine **1**, 1*R*, 1′*S*. La configuration 1*R* de la (−)-cordobimine est ainsi doublement confirmée. Le composé **6**, *F* 185–190°C (MeOH), $[\alpha]_D^{20}$ −9, doit donc avoir la configuration absolue 1*R*, 1′*R*, ce que montre la courbe de dc bien différente de celles de la (−)-cordobine **1**, de la (+)-antioquine et inverse de celle de la (+)-guattaguianine 1*S*, 1′*S* (8).

Trois autres Annonacées sud-américaines, *Crematosperma polyphlebum* (2), *Pseudoxandra sclerocarpa* (7) et *Guatteria guianensis* (8) contiennent le même type de bisbenzylisoquinoléines biphényliques, mais avec la configuration 1*S*, 1′*R* ou 1*S*, 1′*S*. *Crematosperma* sp. RC 3110 se caractérise par la configuration 1*R* de ses alcaloïdes, la (−)-cordobine **1**, la (−)-montérine **2** et la (−)-granjine **3**, qui constituent ainsi les premiers alcaloïdes possédant la configuration absolue 1*R*, 1′*S* dans le groupe des bisbenzyltétrahydroisoquinoléines liées par un pont diaryléther 8,7′ et un pont biphénylique 11,11′. Par contre, cette configuration a été trouvée dans le cas de bisbenzyltétrahydroisoquinoléines biphényliques comportant deux ponts diaryléther telles la tiliacorine (9) et la dinklacorine (10) isolées d'une Ménispermacée. La (−)-cordobimine **4** est également le premier alcaloïde présentant une configuration 1*R* du groupe des imino-bisbenzylisoquinoléines biphényliques.

Partie expérimentale

Points de fusion déterminés sur microscope Reichert. Pouvoirs rotatoires mesurés sur polarimètre Schmidt–Haensch, type Polartronic 1. Spectres enregistrés sur les appareils suivants : uv, Unicam SP 1800; ir, Perkin–Elmer 257; rmn ^1H, Cameca (250 MHz) et Bruker (360 MHz); sm, VG Micromass 70; dc, Auto-Dichrograph Mark V. Chromatographies sur colonne réalisées sur Kieselgel 60 (Merck 7734) ou 60H (Merck 7736); ccm analytiques sur DC Alufolien Kieselgel 60 F 254 (Merck 554); ccm préparatives sur Kieselgel 60 GF 254 (Merck 7730).

Matériel végétal

Les écorces de tiges de *Crematosperma* sp. ont été récoltées à Urrao (Antioquia), Colombie, en décembre 1986. Un échantillon d'herbier est déposé sous le numéro RC 3110 à l'Université d'Antioquia à Medellin et à Rijks Universiteit à Utrecht (en cours d'identification par le Pr. P. J. M. Maas; espèce nouvelle?).

Extraction et isolement des alcaloïdes

La poudre sèche des écorces de *Crematosperma* (1,07 kg) a été dégraissée par l'éther de pétrole. Le marc a été extrait au MeOH contenant 3% d'acide citrique par percolation jusqu'à réaction de Mayer négative. Après l'évaporation du MeOH, l'extrait alcaloïdique a été extrait par HCl à 2%. Les phases aqueuses ont été alcalinisées par l'ammoniaque et extraites au CH_2Cl_2. Après évaporation du solvant, on obtient les alcaloïdes totaux non quaternaires (21,4 g; 2%).

Les alcaloïdes totaux ont été chromatographiés sur colonne de silice. L'élution par le mélange hexane–CH_2Cl_2–diéthylamine (6 : 3 : 1) a fourni 2,00 g de (−)-granjine **3**, 5,35 g de (−)-montérine **2**, 3,20 g de (−)-cordobine **1** et, à la fin, 6,40 g de (−)-cordobimine **4**.

(−)-Cordobine 1

$C_{37}H_{40}N_2O_6$, amorphe; $[\alpha]_D^{20}$ −140 (*c* 0,7, $CHCl_3$); uv, λ_{max} (MeOH) : 213 (log ε 4,60), 238 (log ε 4,32) (épaule), 285 (log ε 3,99); dc (MeOH) : $\Delta\varepsilon_{218}$ +31,6, $\Delta\varepsilon_{231}$ 0, $\Delta\varepsilon_{246}$ −12,8, $\Delta\varepsilon_{260}$ 0, $\Delta\varepsilon_{285}$ −4,9 $\Delta\varepsilon_{305}$ 0, $\Delta\varepsilon_{320}$ +0,9, $\Delta\varepsilon_{335}$ 0; rmn ^1H, $CDCl_3$, nOeds (la solution a été dégazée sous pression réduite à la température de l'azote liquide, puis saturée par de l'argon) : NMe-2 → H-1 (10%), H-1 → NMe-2 (2), H-1 → H-10 (5), H-5 → OMe-6 (5), OMe-6 → H-5 (14), H-5′ → OMe-6′ (5), OMe-6′ → H-5′ (9), NMe-2′ → H-1′ (6), OMe-12 → H-13 (7), H-13 → OMe-12 (3); sm (ie), *m/z* (%) : 608 ($M^{+\bullet}$, 21), 607 (21), 593 (3), 577 (2), 382 (30), 381 (70), 367 (21), 353 (13), 192 (47), 191 (100), 174 (26).

O,O-*Diméthylcordobine*

Composé **1** (10 mg) dans 3 mL MeOH a été traité par 5 mL de CH_2N_2–Et_2O pendant 24 h. Après évaporation de l'éther, le résidu a été purifié sur ccm préparative (éluant : CH_2Cl_2–MeOH–ammoniaque (95 : 5 : 0,1)) et on a obtenu 9 mg d'un produit identique à la (−)-granjine **3** (ccm, sm, rmn ^1H, $[\alpha]_D$, dc).

(−)-Montérine 2

$C_{38}H_{42}N_2O_6$, amorphe; $[\alpha]_D^{20}$ −135 (*c* 0,4, $CHCl_3$); uv, λ_{max} (MeOH) : 213 (log ε 4,53), 238 (log ε 4,16) (épaule), 285 (log ε 3,75); dc (MeOH) : $\Delta\varepsilon_{225}$ +37,1, $\Delta\varepsilon_{233}$ 0, $\Delta\varepsilon_{246}$ −44,2, $\Delta\varepsilon_{264}$ 0, $\Delta\varepsilon_{283}$ −14,5, $\Delta\varepsilon_{305}$ 0; rmn ^1H, $CDCl_3$, 0°C, nOeds (% du conformère *a* est

Can. J. Chem. Downloaded from www.nrcresearchpress.com by 122.72.124.2 on 09/07/12
For personal use only.

souligné) : NMe-2 → H-1 (8%, 13%), NMe-2′ → H-1′ (6), H-1 → H-10 (6), H-10 → H-1 (6), H-10 → H-10′ (5), H-10 → H-8′ (4), H-10′ → H-10 (3, 7), H-10′ → H-8′ (4), H-1′ → H-8′ (4), CH_3O-12 → H-13 (12, 12), CH_3O-12′ → H-13′ (16), NMe-2 → H-14 (4), H-14 → H-13 (6), NMe-2′ → H-14′ (5), H-14′ → H-13′ (7), CH_3O-6 → H-5 (6), CH_3O-6′ → H-5′ (9, 6); sm (ie), m/z : 622 ($M^{+\bullet}$, 47), 621 (34), 607 (7), 591 (4), 382 (37), 381 (100), 367 (30), 192 (14), 191 (53), 175 (5), 174 (10).

O-*Méthylmontérine*

Composé **2** (10 mg) dans 3 mL de MeOH a été traité par 5 mL de CH_2N_2–Et_2O pendant 48 h. Après purification du résidu comme indiqué ci-dessus, on a obtenu 8 mg d'une substance identique à la (−)-granjine **3** (ccm, sm, rmn ^1H, $[\alpha]_D$, dc).

(−)-Granjine 3

$C_{39}H_{44}N_2O_6$, amorphe; $[\alpha]_D^{20}$ −63 (*c* 0,6, $CHCl_3$); uv, λ_{max} (MeOH) : 211 (log ε 4,61), 238 (log ε 4,28) (épaule), 284 (log ε 3,92); dc (MeOH) : $\Delta\varepsilon_{227}$ +22, $\Delta\varepsilon_{235}$ 0, $\Delta\varepsilon_{246}$ −30,0, $\Delta\varepsilon_{282}$ −10,4, $\Delta\varepsilon_{310}$ 0; sm, ie, m/z: 636 ($M^{+\bullet}$, 27), 635 (16), 621 (3), 396 (21), 395 (54), 381 (17), 199 (30), 198 (100), 175 (34), 174 (30).

(−)-Cordobimine 4

$C_{36}H_{36}N_2O_6$; amorphe; $[\alpha]_D^{20}$ −185 (*c* 0,5, $CHCl_3$); uv, λ_{max} (MeOH) : 218 (log ε 4,64), 284 (log ε 4,07), 308 (log ε 3,85) (épaule); MeOH–NaOH : 230, 302; MeOH–HCl : 218, 245 ép., 288, 346; dc (MeOH) : $\Delta\varepsilon_{215}$ +20,0, $\Delta\varepsilon_{226}$ −35,5, $\Delta\varepsilon_{250}$ −35,2, $\Delta\varepsilon_{260}$ 0, $\Delta\varepsilon_{269}$ +10,4 $\Delta\varepsilon_{279}$ 0, $\Delta\varepsilon_{301}$ −36,0, $\Delta\varepsilon_{337}$ 0; ir, ν (KBr): 1620 cm^{-1}; rmn ^1H, $CDCl_3$, nOeds : H-10 → H-1 (2%), H-1 → NMe-2 (3), H-5 → OMe-6 (4), OMe-6 → H-5 (15), OMe-12 → H-13 (14), H-10 → H-10′ (7), OMe-6′ → H-5′ (13), H-5′ → OMe-6′ (5), H-8′ → H-10′ (12), H-10′ → H-8′ (12); sm, ie, m/z : 592 ($M^{+\bullet}$, 100), 591 (89), 577 (18), 561 (22), 367 (2), 296 (15), 192 (7), 191 (12), 190 (13).

Reduction de la (−)-cordobimine 4

Composé **4** (130 mg) dans du MeOH a été réduit par 80 mg de $NaBH_4$. Après évaporation du solvant, le résidu a été acidifié par HCl, alcalinisé par de l'ammoniaque et extrait au CH_2Cl_2. Le résidu soumis à une ccm préparative sur silice (éluant : CH_2Cl_2–MeOH–ammoniaque (90 : 10 : 0,5)) a fourni 25 mg de dihydrocordobimine 1′*S* **5** et 54 mg de dihydrocordobimine 1′*R* **6**.

Dihydrocordobimine 1′S 5

$C_{36}H_{38}N_2O_6$, *F* 205–209°C (MeOH); $[\alpha]_D^{20}$ −215 (*c* 1, $CHCl_3$); uv, λ_{max} (MeOH) : 215 (log ε 4,44), 238 (log ε 4,16) (épaule), 286 (log ε 3,83); dc (MeOH) : $\Delta\varepsilon_{217}$ +18,4, $\Delta\varepsilon_{225}$ 0, $\Delta\varepsilon_{244}$ −26,3, $\Delta\varepsilon_{284}$ −8,9, $\Delta\varepsilon_{315}$ 0; rmn ^1H, $CDCl_3$, nOeds : H-1 → NMe-2 (1%), OMe-6 → H-5 (6), OMe-6′ → H-5′ (5), OMe-12 → H-13 (7); sm, ie, m/z : 594 ($M^{+\bullet}$, 40), 593 (42), 580 (4), 579 (9), 559 (7), 368 (36), 367 (68), 353 (43), 208 (16), 192 (62), 191 (36), 190 (25), 184 (100).

N-*Méthyldihydrocordobimine 1′S = (−)-cordobine 1*

Composé **5** (15 mg) dans 1 mL de MeOH a été traité par 0,1 mL de HCHO à 30% à 20°C, 30 min, puis réduit par $NaBH_4$. Après extraction, on a obtenu 13 mg d'alcaloïde identique à la (−)-cordobine **1** (sm, rmn ^1H, ccm, $[\alpha]_D$, dc).

Dihydrocordobimine 1′R 6

$C_{36}H_{38}N_2O_6$, *F* 185–190°C (MeOH): $[\alpha]_D^{20}$ −9 (*c* 1, $CHCl_3$); uv, λ_{max} (MeOH) : 220 (log ε 4,60), 238 (log ε 4,40) (épaule), 286 (log ε 4,05); dc (MeOH) : $\Delta\varepsilon_{226}$ −38,0, $\Delta\varepsilon_{238}$ 0, $\Delta\varepsilon_{243}$ +3,5, $\Delta\varepsilon_{246}$ 0, $\Delta\varepsilon_{254}$ −13,3, $\Delta\varepsilon_{273}$ 0, $\Delta\varepsilon_{296}$ −5,1, $\Delta\varepsilon_{320}$ 0; rmn ^1H, $CDCl_3$, nOeds : H-1 → NMe-2 (2%), NMe-2 → H-1 (9), H-1 → H-10 (6), H-10 → H-1 (7), H-5 → OMe-6 (4), OMe-6 → H-5 (14), H-10 → H-10′ (9), H-10′ → H-10 (9), OMe-12 → H-13 (13), H-1′ → H-8′ (2), H-5′ → OMe-6′ (4), OMe-6′ → H-5′ (12); sm, ie, m/z : 594 ($M^{+\bullet}$, 42), 593 (44), 580 (5), 579 (9), 563 (3), 368 (36), 367 (64), 353 (40), 208 (13), 192 (43), 191 (22), 190 (15), 184 (100).

Remerciements

Les auteurs expriment leur vive gratitude à M. R. Callejas (Université d'Antioquia, Colombie) pour la récolte du matériel végétal et à M. C. Mérienne (Faculté des Sciences d'Orsay, France) pour l'enregistrement des spectres de rmn du proton à 250 MHz.

1. R. E. Fries. Annonaceae, in die Natürlichen Pflanzen Familien. 2e ed., Vol. 17 a II. *Éditeurs* : A. Engler and K. Prantl. Dunker and Humbolt, Berlin. 1959.
2. M. P. Cava, K. Wakisaka, I. Noguchi, D. L. Edie et A. I. Darocha. J. Org. Chem., **39**, 3588 (1974).
3. K. P. Guha, B. Mukherjee et R. Mukherjee. J. Nat. Prod. **42**, 1 (1979), et références citées.
4. P. L. Schiff, Jr. J. Nat. Prod., **50**, 529 (1987), et références citées.
5. M. Tomita, T. Kikuchi, K. Fujitani, A. Kato, H. Furukawa, Y. Aoyagi, M. Kitano et T. Ibuka. Tetrahedron Lett. 857 (1966).
6. D. Cortes, J. Saez, R. Hocquemiller, A. Cavé et Ad. Cavé. J. Nat. Prod., **48**, 76 (1985).
7. D. Cortes, R. Hocquemiller, A. Cavé et J. Saez. J. Nat. Prod. **49**, 854 (1986).
8. S. Berthou, A. Jossang, H. Guinaudeau, M. Leboeuf et A. Cavé. Tetrahedron, **44**, 2193 (1988).
9. D. S. Bhakuni, A. N. Singh, S. Jain et R. S. Kapil. J. Chem. Soc. Chem. Commun. 226 (1978).
10. D. Dwuma-Badu, S. F. Withers, S. A. Ampofo, M. M. El-Azizi, D. J. Slatkin, P. L. Schiff, Jr. et J. E. Knapp. J. Nat. Prod. **42**, 116 (1979).

Can. J. Chem. Downloaded from www.nrcresearchpress.com by 122.72.124.2 on 09/07/12
For personal use only.

Formation of hexacyanomanganate(II) in cyanide medium and kinetics and mechanism of its oxidation by chromate

GUILLERMO LÓPEZ-CUETO[1] AND MIGUEL DUARTE
Analytical Chemistry Division, University of Alicante, Apdo. 99, 03080 Alicante, Spain

Received April 30, 1987[2]

GUILLERMO LÓPEZ-CUETO and MIGUEL DUARTE. Can. J. Chem. **67**, 279 (1989).

The rate of formation of hexacyanomanganate(II) is first-order in Mn(II) and depends on both the cyanide and hydroxide concentrations. The experimental results agree with a reaction mechanism which involves manganese(II) cyano- and hydroxo-complexes. Chromate slowly oxidizes hexacyanomanganate(II). The kinetics of this reaction is first-order on hexacyanomanganate(II), and the experimental rate constant depends on the chromate concentration according to the equation $k_{exp} = 3kK[Cr(VI)]/(1 + K[Cr(VI)])$. The effect of both the CN^- and the OH^- ions is slighter. A tentative mechanism is proposed which involves a pre-equilibrium with the formation of a hexacyanomanganate(II)–chromate complex, followed by a monomolecular decomposition. By comparing this reaction mechanism with that of other one-electron chromate reductions, it appears that hexacyanomanganate(II) behaves like octacyanomolybdate(IV) rather than like hexacyanoferrate(II) and other substitution-inert reductants. Both the equilibrium constants for the complex formation and the rate constant for its decomposition are evaluated, and voltammetric evidence of the formation of hexacyanomanganate(III)–chromate complexes is also presented.

Key words: hexacyanomanganate(II), formation rate, oxidation with chromate, kinetics, mechanism.

GUILLERMO LÓPEZ-CUETO et MIGUEL DUARTE. Can. J. Chem. **67**, 279 (1989).

La vitesse de formation de l'hexacyanomanganate(II) est du premier ordre en Mn(II) et dépend à la fois de la concentration en cyanure et en hydroxyde. Les résultats expérimentaux sont en accord avec un mécanisme réactionnel impliquant des complexes cyano- et hydroxy- manganèse(II). Le chromate oxyde lentement l'hexacyanomanganate(II). La cinétique de la réaction est du premier ordre en hexacyanomanganate(II) et la constante expérimentale de vitesse est reliée à la concentration en chromate par l'équation suivante : $k_{exp} = 3kK[Cr(VI)]/(1 + K[Cr(VI)])$. Les effets des ions CN^- et OH^- sont plus faibles. On propose un mécanisme impliquant un pré-équilibre, avec la formation d'un complexe hexacyanomanganate(II)–chromate, qui est suivi par une décomposition monomoléculaire. En comparant ce mécanisme réactionnel avec celui d'autres réductions effectuées par le chromate et impliquant un électron, il semble que l'hexacyanomanganate(II) se comporte plutôt comme l'octacyanomolybdate(IV) que comme l'hexacyanoferrate(II) et d'autres réducteurs qui sont inertes par rapport à la substitution. On a évalué la constante d'équilibre pour la formation du complexe ainsi que la constante de vitesse de sa décomposition; de plus, on présente des données voltamétriques concernant la formation de complexes hexacyanomanganate(III)–chromate.

Mots clés : hexacyanomanganate(II), vitesse de formation, oxydation par le chromate, cinétique, mécanisme.

[Traduit par la revue]

Introduction

Manganese(II) in cyanide solution forms a reducing complex. The standard potential of the $Mn(CN)_6^{3-}/Mn(CN)_6^{4-}$ couple is about −0.24 V (1), but not much is known about its reactions. In the presence of cyanide, manganese(II) readily reacts with several oxidizing substances, such as atmospheric oxygen, hydrogen peroxide, peroxydisulfate, vanadate, and hexacyanoferrate(III). The reaction with $Fe(CN)_6^{3-}$, which is very fast, has been studied for analytical purposes, and has been applied to both the coulometric titration of hexacyanoferrate(III) (2) and the volumetric and coulometric titration of manganese(II) (3). Chromate also oxidizes manganese(II) in cyanide medium but this reaction is slow. This paper is concerned primarily with the kinetics and mechanism of this reaction, in order to contribute to the knowledge of the redox behavior of manganese(II) in cyanide medium. This is the first kinetic study that has been reported about a redox reaction of manganese(II) in this complexing medium. Moreover, some aspects of the kinetics of formation of the hexacyanomanganate(II) ion are studied. In this medium manganese(II) is easily oxidized if oxygen is present; therefore, the monitoring technique must necessarily let us operate properly in an inert atmosphere. Amperometry with a rotating disc platinum electrode was used for the kinetic measurements.

Experimental

Reagents

Manganese(II) solutions were prepared with $MnSO_4.H_2O$ and were standardized with $K_3Fe(CN)_6$ standard solution to a potentiometric end point (3). Chromate solutions were prepared with K_2CrO_4 and were standardized by back titration with standard Fe(II) and $K_2Cr_2O_7$ solutions. NaCN, NaCl, and NaOH were also used in the preparation of the solutions. All of the chemicals used were of reagent grade.

Apparatus

A 506 E Metrohm polarograph provided with a three-electrode circuit has been used to obtain both the current–voltage and the current–time curves. The indicator electrode was a 628-10 Metrohm rotating disc platinum electrode, the reference electrode was a home-made saturated calomel electrode and the auxiliary electrode was a platinum wire.

A 50 mL EA 880 Metrohm vessel was used as the reaction cell. The temperature was kept constant within ±0.1°C by means of a Haake K circulation bath. Nitrogen was used to remove previously the dissolved oxygen.

Procedure

The required amounts of solid NaCN and NaCl were dissolved in the adequate volume of NaOH solution. After dilution to 50 mL, a gentle nitrogen stream was bubbled through the solution for 15–20 min. Then, 1 mL of the Mn(II) solution was added, and the anodic limiting current was measured at 0 V on the recorder chart. The appearance of a cathodic component in the current–voltage curves revealed that a certain amount of manganese(II) was oxidized by the dissolved oxygen introduced with the Mn(II) solution. However, no effect was observed

[1]To whom correspondence should be addressed.
[2]Revision received October 7, 1988.

Can. J. Chem. Downloaded from www.nrcresearchpress.com by 122.72.124.2 on 09/07/12
For personal use only.

from the Mn(III) on the kinetics, and therefore it was not necessary to carry out a more rigorous deaeration. Once the current has been stabilised, 1 mL of the CrO_4^{2-} solution was added and the current was continuously recorded against time.

The rate of formation of the $Mn(CN)_6^{4-}$ complex was monitored by recording the anodic limiting current measured at -0.3 V from the addition of manganese(II) to the cyanide solution.

Kinetic experiments were made at 25°C and at 1.0 *M* ionic strength excepting when the effects of these variables were studied.

Results and discussion

The formation of $Mn(CN)_6^{4-}$

Formation of the $Mn(CN)_6^{4-}$ complex is not an instantaneous reaction. Current–voltage curves of fresh cyanide solutions of manganese(II) at different times are shown in Fig. 1. The early voltammograms consist of several anodic waves. The first one, with a halfwave potential of about -0.5 V, is well defined and increases with time, while the other poorly defined waves decrease. When the equilibrium has been reached, only the first wave remains. This wave is probably due to the anodic oxidation of the $Mn(CN)_6^{4-}$ to $Mn(CN)_6^{3-}$, while the other waves would probably be due to the anodic oxidation of some transient Mn(II) cyanide complexes with a lower cyanide content. This behavior agrees with that observed by Kemula *et al.* (4) in the polarographic reduction of Mn(II) in cyanide medium. These authors reported two cathodic waves with half-wave potentials of -1.33 and -1.61 V, attributed to the reduction of $Mn(CN)_6^{4-}$ and of other complexes of smaller coordination number, respectively.

When the limiting current measured at -0.3 V is recorded against time after the reaction has been started by the manganese(II) addition, formation curves as that of the Fig. 2 are obtained. The experimental curves are fairly fitted to the equation

$$[1] \quad \ln \frac{i_\infty - i}{i_\infty} = -kt$$

which reveals a pseudo-first-order dependence, in accordance with the results of Kemula *et al.* (4). The pseudo-first-order rate constant reported by Kemula *et al.* in a 1.0 *M* KCN solution at 20°C was $3 \times 10^{-2}\ s^{-1}$. We found a value of $8.4 \times 10^{-3}\ s^{-1}$ in a 1.0 *M* NaCN and 0.01 *M* NaOH solution at 25°C. We believe that the difference can be attributed chiefly to the higher alkalinity of our solution. Indeed, the pseudo-first-order rate constant is influenced by both the cyanide and the hydroxide concentrations (Table 1). A rapid rise in the value of the rate constant is produced when the sodium cyanide concentration increases between 0.3 and 1.0 *M*, while an increase of the sodium hydroxide concentration from 0.01 to 0.09 *M* causes a decrease in the rate constant. The dependence of the rate constant on both the CN^- and the OH^- concentrations seems to reflect that some equilibria between manganese(II) cyano- and hydroxocomplexes are involved in the formation of hexacyanomanganate(II). The expected reaction scheme would have the following general form[3]

$$[2] \quad Mn^{2+} + pCN^- \xrightarrow{\text{fast}} Mn(CN)_p$$

$$[3] \quad Mn(CN)_p + (n-1)CN^- \overset{K_a}{\rightleftharpoons} Mn(CN)_{p+n-1}$$

[3]The authors are grateful to a reviewer for his valuable suggestions on the reaction scheme.

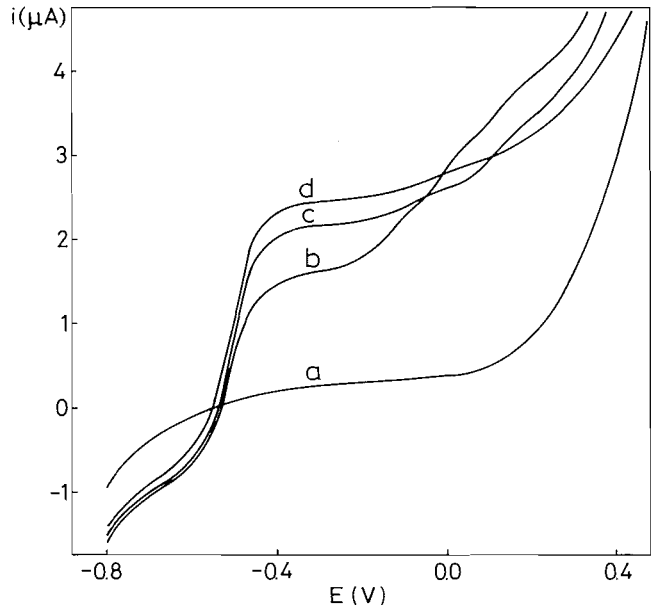


FIG. 1. Evolution of the current–voltage curves of a fresh solution of manganese(II) in the presence of cyanide: NaCN, 1.0 *M*; NaOH, 0.01 *M*; *T*, 25°C. (*a*), supporting electrolyte alone; (*b*), (*c*), and (*d*), Mn(II) 10^{-4} *M* at 2, 5, and 8 min, respectively. (The cathodic component indicates that some Mn(II) has been oxidized to Mn(III) by a trace of dissolved oxygen.)

TABLE 1. Kinetics of formation of hexacyanomanganate(II): experimental and calculated rate constants for different CN^- and OH^-: concentrations, Mn(II), 10^{-4} *M*; *T*, 25°C; *I*, 1.1 M

CN^- (*M*)	OH^- ($M \times 10^2$)	k_{exp} ($s^{-1} \times 10^3$)	k_{calc} ($s^{-1} \times 10^3$)	k_{calc}/k_{exp}
0.3	1.0	1.19	1.17	0.98
0.4	1.0	1.51	1.47	0.97
0.5	1.0	2.14	1.95	0.91
0.6	1.0	2.72	2.68	0.99
0.7	1.0	3.79	3.69	0.97
0.8	1.0	4.34	5.04	1.16
0.9	1.0	6.77	6.77	1.00
1.0	1.0	8.35	8.93	1.07
1.0	1.0	8.42	8.93	1.06
1.0	2.0	6.61	6.31	0.95
1.0	3.0	5.27	5.15	0.98
1.0	4.0	4.45	4.46	1.00
1.0	5.0	3.96	3.99	1.01
1.0	6.0	3.89	3.64	0.94
1.0	7.0	3.44	3.37	0.98
1.0	8.0	3.24	3.16	0.98
1.0	9.0	3.11	2.98	0.96
			Average:	0.99 ± 0.01

$$[4] \quad Mn(CN)_{p+n-1} + OH^- \overset{K_b}{\rightleftharpoons} Mn(CN)_{p+n-1}(OH)$$

$$[5] \quad Mn(CN)_{p+n-1} + CN^- \underset{k_{-1}}{\overset{k_1}{\rightleftharpoons}} Mn(CN)_{p+n}$$

where $p + n = 6$. Step [5] is rate-determining. This general mechanism leads to a pseudo-first-order rate equation where the pseudo-first-order constant takes the form

Can. J. Chem. Downloaded from www.nrcresearchpress.com by 122.72.124.2 on 09/07/12
For personal use only.

Can. J. Chem. Downloaded from www.nrcresearchpress.com by 122.72.124.2 on 09/07/12
For personal use only.

TABLE 2. Kinetics of the hexacyanomanganate(II)–chromate reaction. Pseudo-first-order rate constants for different Mn(II), CrO_4^{2-}, CN^-, and OH^- concentrations. Runs 1–22, NaCN, 1.0 *M*; NaOH, 0.01 *M*; Runs 23–39, Mn(II), 10^{-4} *M*; CrO_4^{2-}, 2×10^{-3} *M*; all runs were made at 25°C and at I = 1.1 M

Run No.	Mn(II) ($M \times 10^4$)	CrO_4^{2-} ($M \times 10^3$)	k_{exp} ($s^{-1} \times 10^3$)	k_{calc} ($s^{-1} \times 10^3$)	k_{calc}/k_{exp}	Run No.	CN^- (M)	OH^- ($M \times 10^2$)	k_{exp} ($s^{-1} \times 10^3$)
1	1.0	0.2	0.17	0.17	1.00	23	0.3	1.0	1.12
2	1.0	1.0	0.75	0.79	1.05	24	0.4	1.0	1.14
3	1.0	2.0	1.37	1.46	1.07	25	0.5	1.0	1.27
4	1.0	2.0[a]	1.54	1.46	0.95	26	0.6	1.0	1.35
5	1.0	2.0[b]	1.56	1.46	0.94	27	0.7	1.0	1.38
6	1.0	2.0[c]	1.49	1.46	0.98	28	0.8	1.0	1.39
7	0.1	2.0	1.30	1.46	1.12	29	0.9	1.0	1.39
8	0.2	2.0	1.68	1.46	0.87	30	1.0	1.0	1.34
9	0.5	2.0	1.57	1.46	0.93	31	1.0	1.0	1.37
10	1.0	2.0	1.47	1.46	0.99	32	1.0	2.0	1.30
11	1.5	2.0	1.61	1.46	0.91	33	1.0	3.0	1.18
12	2.0	2.0	1.50	1.46	0.97	34	1.0	4.0	1.12
13	2.5	2.0	1.44	1.46	1.01	35	1.0	5.0	1.10
14	3.0	2.0	1.31	1.46	1.11	36	1.0	6.0	1.03
15	1.0	3.0	1.88	2.06	1.10	37	1.0	7.0	1.00
16	1.0	4.0	2.46	2.58	1.05	38	1.0	8.0	0.97
17	1.0	5.0	3.00	3.04	1.01	39	1.0	9.0	0.95
18	1.0	6.0	3.41	3.46	1.01				
19	1.0	7.0	3.88	3.83	0.99				
20	1.0	8.0	4.43	4.16	0.94				
21	1.0	9.0	4.67	4.47	0.96				
22	1.0	10.0	5.26	4.75	0.90				
				Average:	0.99 ± 0.01				

[a] Cr(III), 10^{-5} *M*.
[b] Cr(III), 10^{-4} *M*.
[c] Cr(III), 10^{-3} *M*.

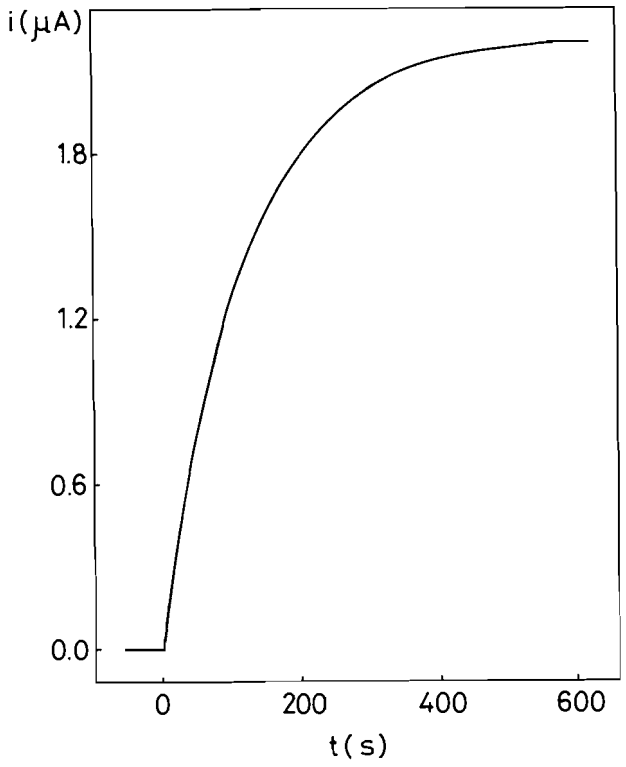


FIG. 2. Formation of $Mn(CN)_6^{4-}$. Variation of the anodic current measured at −0.3 V during the reaction: Mn(II), 10^{-4} *M*; NaCN, 1.0 *M*; NaOH, 0.01 *M*; *T*, 25°C.

$$[6] \quad k = \frac{k_1 K_a [CN^-]^n}{1 + K_a [CN^-]^{n-1}(1 + K_b [OH^-])} + k_{-1}$$

The experimental results can be fitted to this equation for $n = 3$, and the following values can be calculated

$$k_1 K_a = (1.00 \pm 0.02) \times 10^{-2}\ L^3\ mol^{-3}\ s^{-1}$$

$$K_a K_b = 45.5 \pm 1.8\ L^3\ mol^{-3}$$

$$\frac{1 + K_a}{k_1 K_a} = 101 \pm 8\ s$$

$$k_{-1} = (9.3 \pm 0.1) \times 10^{-4}\ s^{-1}$$

The individual values for the constants k_1, K_a, and K_b cannot be determined from the disposable data, because $K_a \ll 1$. The calculated values of the pseudo-first-order constant agree with the experimental ones (Table 1).

The $Mn(CN)_6^{4-}$–CrO_4^{2-} reaction

Kinetics of reaction

It has been found that the kinetics of the $Mn(CN)_6^{4-}$–CrO_4^{2-} reaction is first-order on the hexacyanomanganate(II) ion at least for the 95% of reaction. The pseudo-first-order constant over a range of initial Mn(II) concentrations from 0.1 to 3.0×10^{-4} *M* was $(1.48 \pm 0.05) \times 10^{-3}\ s^{-1}$ for 2×10^{-3} *M* CrO_4^{2-}, 1.0 *M* CN^-, 0.01 *M* OH^- and 25°C (Table 2). At low chromate concentrations the experimental rate constant increases almost linearly with the chromate concentrations (Table 2); however, the slope of the k_{exp} vs. $[CrO_4^{2-}]$ plot decreases as the $[CrO_4^{2-}]$ increases. Experimental values can be correlated quite well to

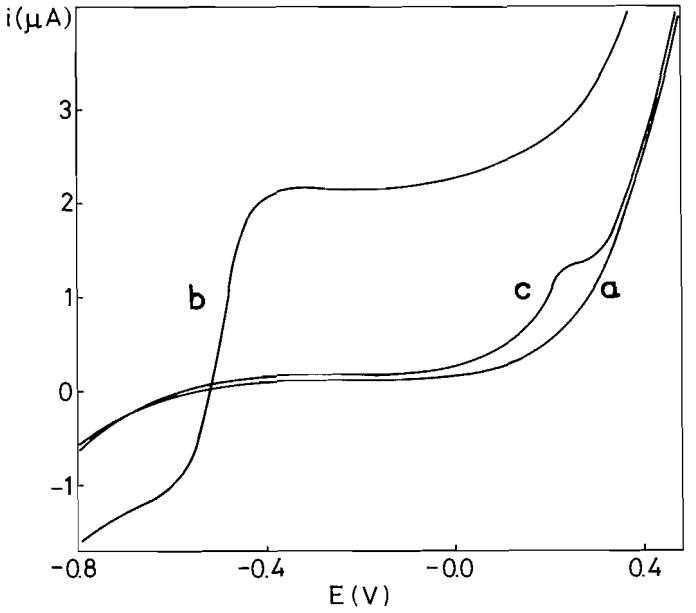


FIG. 3. Oxidation of $Mn(CN)_6^{4-}$ by CrO_4^{2-}. Current–voltage curves: NaCN, 1.0 *M*; NaOH, 0.01 *M*; *T*, 25°C. (*a*), supporting electrolyte alone; (*b*), $Mn(CN)_6^{4-}$, 10^{-4} *M* ($Mn(CN)_6^{4-}$ has been partially oxidized by dissolved oxygen); (*c*), after addition of 2×10^{-3} *M* CrO_4^{2-}, once the redox equilibrium has been reached.

the equation

$$[7] \quad -\frac{d[Mn(CN)_6^{4-}]}{dt} = \frac{[CrO_4^{2-}]}{A + B[CrO_4^{2-}]}[Mn(CN)_6^{4-}] = k_{exp}[Mn(CN)_6^{4-}]$$

where $A = 1.18 \pm 0.01$ L^{-1} mol s and $B = 93 \pm 11$ s in 1.0 *M* NaCN, 0.01 *M* NaOH and at 25°C. Observed and calculated values of the rate constant are given in Table 2.

It appears that the Mn(III) and the Cr(III) produced do not affect to the reaction kinetics and, on the other hand, only a slight effect has been observed from both the CN^- and the OH^- concentrations (Table 2). When the cyanide concentration is lower than 0.6 *M*, a small decrease on the experimental rate constant is produced, while the constant slightly decreases as the hydroxide ion concentration increases. The effect of the CN^- and the OH^- concentrations may be interpreted in terms of solution equilibria involving both aquo- and hydroxo-complexes, besides the hexacyanomanganate(II).

Stoichiometry of reaction

The stoichiometry of the reaction was determined by measuring amperometrically the decrease of the anodic wave of $Mn(CN)_6^{4-}$ after addition of measured chromate amounts to an excess of manganese(II) in sodium cyanide solution. Chromate and manganese(II) reacted by a ratio close to 1:3. The nature of the reaction products has not been well established. The oxidation product of Mn(II) seems not to be the $Mn(CN)_6^{3-}$ ion, as happens when the $Mn(CN)_6^{4-}$ is oxidized by other oxidizing substances, such as oxygen or hexacyanoferrate(III). Indeed, a composite reversible wave, with a half-wave potential of about −0.5 V, is usually obtained at a platinum electrode when both the $Mn(CN)_6^{3-}$ and the $Mn(CN)_6^{4-}$ ions are present in a cyanide solution. However, the products of the $Mn(CN)_6^{4-}$–CrO_4^{2-} reaction do not give any cathodic wave, but a poorly-defined anodic peak at about 0.2 V (Fig. 3). From this, it is apparent that the $Mn(CN)_6^{3-}$ ion has been masked by some species present in the solution. Masking of the products of chromate oxidations of $Fe(CN)_6^{4-}$, $Fe(bip)(CN)_4^{2-}$, and $Fe(bip)_2(CN)_2$ (bip = 2,2′-bipyridine) has been reported to occur, and this has been attributed to the formation of binuclear complexes with Cr(III) (5). Nevertheless, according to the reaction stoichiometry only one third of the Fe(III) is masked by Cr(III). In our case, the $Mn(CN)_6^{3-}$ cathodic wave did not appear at all, which indicates that the $Mn(CN)_6^{3-}$ ion was completely masked. A voltammogram similar to curve (*c*) in Fig. 3 was obtained when an excess of CrO_4^{2-} was added to a $Mn(CN)_6^{3-}$ solution. However, if a $Mn(CN)_6^{4-}$ solution is oxidized by an air stream in the presence of Cr(III), no interaction is observed to be produced between Mn(III) and Cr(III). Undoubtedly, the substitution-inert Cr(III) cannot share in such a reaction. These facts seem to reflect that the interaction takes place between the hexacyanomanganate(III) and the chromate ions. A similar interaction has been reported between Fe(III) and Cr(VI), which form a cationic complex of formula $FeCrO_4^+$ (6). Of course, the conditions in which these two reactions take place are quite different, and the product of the $Mn(CN)_6^{3-}$–CrO_4^{2-} interaction will surely have a different structure from that of the $FeCrO_4^+$ ion, probably a CN^-–bridged Mn—Cr binuclear compound. No attempt has been made to elucidate the nature of the electrode reaction responsible for the anodic peak appeared at about 0.2 V.

Mechanism of reaction

Oxidations of one-electron reductants by chromate proceed generally by three consecutive one-electron steps (5, 7, 8). The kinetics of these reactions are either first or second-order on the reductant, depending on whether the determining step is the reduction of Cr(VI) to Cr(V) (without change in the coordination number) or the reduction of Cr(V) to Cr(IV) (accompanied by a change in the coordination number from 4 to 6) (5, 6). The first type of behavior is followed by substitution-inert reductants, such as $Fe(phen)_3^{2+}$ (phen = 1,10-phenanthroline) (6), $Fe(CN)_6^{4-}$, $Fe(bip)(CN)_4^{2-}$, $Fe(bip)_2(CN)_2$, and $Fe(bip)_3^{2+}$ (5), and the reduction of Cr(VI) proceeds by an outer-sphere mechanism. On the other hand, substitution-labile reductants, such as $Fe(H_2O)_6^{2+}$ (6), show a behavior of the second type, and an inner-sphere mechanism involving an oxygen-bridged transition state takes place in the reaction with Cr(VI). Although these correlations between rate equation, lability or inertness of the reductant and mechanism has been proved to be significant for a series of one-equivalent chromium(VI) reductions, it appears that they can be not generalized. Octacyanomolybdate(IV) is a substitution-inert complex, its reaction with chromium(VI) shows a pseudo-first-order kinetics, and there is evidence that it proceeds via the formation of a CN^--bridged $Mo(CN)_8^{4-}$–CrO_4^{2-} binuclear complex in an inner-sphere mechanism (9). On the basis of these results, McKnight and Haight considered that the cyanocomplexes which coordinate directly to Cr(VI) through CN^- bridges form a third type of one-electron reductants against chromium(VI) (9).

The rate equation [7] for the $Mn(CN)_6^{4-}$–CrO_4^{2-} reaction is first-order on the reductant. Hexacyanomanganate(II) is more labile than both the isoelectronic hexacyanoferrate(III) and hexacyanoferrate(II), but it can be considered a rather inert complex (10). From this viewpoint, it can be expected that the $Mn(CN)_6^{4-}$–Cr(VI) reaction proceed via an outer-sphere mechanism, as does the $Fe(CN)_6^{4-}$–Cr(VI) reaction (5). On the other hand, the possibility of formation of a binuclear Mn(II)—Cr(VI) complex with a CN^- bridge allows for an inner-sphere mechanism like that observed in the $Mo(CN)_8^{4-}$–

Can. J. Chem. Downloaded from www.nrcresearchpress.com by 122.72.124.2 on 09/07/12
For personal use only.

Cr(VI) reaction (9). The generalized rate expression for the one-electron reduction of chromium(VI) is obtained by assuming that Cr(V) reaches a steady-state concentration (5, 8), and a first-order dependence on the reductant is obtained when the rate-determining step is the Cr(VI) to Cr(V) reduction. The kinetics of the $Mn(CN)_6^{4-}$–CrO_4^{2-} reaction cannot completely be explained by such a mechanism. The rate law given by eq. [7], in which a slight inhibiting effect from the CrO_4^{2-} is observed, suggests a preequilibrium in which a complex is formed between the reactants, followed by an inner-sphere electron transfer as the rate-determining step:

$$[8] \quad Mn(II) + Cr(VI) \overset{K}{\rightleftharpoons} [Mn(II).Cr(VI)]$$

$$[9] \quad [Mn(II).Cr(VI)] \overset{k}{\longrightarrow} [Mn(III).Cr(V)]$$

$$[10] \quad [Mn(III).Cr(V)] + Mn(II) \overset{fast}{\longrightarrow} [Mn(III).Cr(IV)] + Mn(III)$$

$$[11] \quad [Mn(III).Cr(IV)] + Mn(II) \overset{fast}{\longrightarrow} [Mn(III).Cr(III)] + Mn(III)$$

$$[12] \quad 2Mn(III) + 2Cr(VI) \overset{fast}{\longrightarrow} 2[Mn(III).Cr(VI)]$$

The successive Mn—Cr compounds are probably binuclear CN^--bridged complexes, including the [Mn(III).Cr(VI)] compound introduced in the last step to explain the masking that involves the $Mn(CN)_6^{3-}$ ion. Although only binuclear complexes have been considered in the mechanism, one cannot discount the possible formation of polycoordinated Mn(III)–Cr(III) compounds as those obtained as a product of the $Mo(CN)_8^{4-}$–CrO_4^{2-} reaction (9). From the proposed scheme the following rate equation may be derived

$$[13] \quad -\frac{d[Mn(II)]}{dt} = \frac{3kK[Cr(VI)]}{1 + K[Cr(VI)]}[Mn(II)]$$

which is in good agreement with the experimental results represented by equation [7]. The suggested mechanism approaches to that proposed for the $Mo(CN)_8^{4-}$–CrO_4^{2-} reaction, and the rate equation [13] takes a simplified second-order form for low CrO_4^{2-} concentration

$$[14] \quad -\frac{d[Mn(II)]}{dt} = 3kK[Cr(VI)][Mn(II)]$$

which is equivalent to the rate equation reported for the $Mo(CN)_8^{4-}$–CrO_4^{2-} reaction at a constant pH value (9). By comparison of eqs. [7] and [13] the values for both the equilibrium and the rate constants are calculated: $K = 79 \pm 9\,L\,mol^{-1}$ and $k = (3.6 \pm 0.4) \times 10^{-3}\,s^{-1}$.

Effects of ionic strength and temperature

When the ionic strength is increased from 1.0 to 5.0 *M* by addition of sodium chloride, a slight increase is produced in the pseudo-first-order constant. From the dependence of the experimental rate constant on the temperature, a value of $56.8 \pm 1.4\ kJ\ mol^{-1}\ K^{-1}$ has been obtained for the apparent energy of activation.

1. W. D. Treadwell and W. E. Raths. Helv. Chim. Acta, **35**, 2259 (1952).
2. J. Hernandez-Mendez, G. Lopez-Cueto, and F. Lucena-Conde. Quim. Anal. **28**, 300 (1974).
3. G. Lopez-Cueto and J. E. Gil-Perez. Analyst, **109**, 637 (1984).
4. W. Kemula, S. Siekierski, and E. Siekierska. Rocz. Chem. **29**, 966 (1955).
5. J. P. Birk. J. Am. Chem. Soc. **91**, 3189 (1969).
6. J. H. Espenson and E. L. King. J. Am. Chem. Soc. **85**, 3328 (1963).
7. J. H. Espenson. Acc. Chem. Res. **3**, 347 (1970).
8. K. E. Howlett and Y. Sulfab. Inorg. Chim. Acta, **17**, 129 (1976).
9. G. F. McKnight and G. P. Haight, Jr. Inorg. Chem. **12**, 1619 (1973).
10. A. G. Sharpe. The chemistry of the cyanocomplexes of the transition metals. Academic Press, New York. 1976.

Can. J. Chem. Downloaded from www.nrcresearchpress.com by 122.72.124.2 on 09/07/12
For personal use only.

Dielectric polarization and molecular interaction. Part II. Acetylacetone, benzoylacetone, and dibenzoylmethane – triethyl amine – cyclohexane systems

GAMAL R. SAAD, MAGDI M. NAOUM, AND HANNA A. RIZK[1]
Department of Chemistry, Faculty of Science, University of Cairo, Cairo, Egypt

Received July 6, 1988

GAMAL R. SAAD, MAGDI M. NAOUM, and HANNA A. RIZK. Can. J. Chem. **67**, 284 (1989).

A modified form of Few and Smith equation applicable to dilute solutions of acetylacetone, benzoylacetone, and dibenzoylmethane in constant-ratio mixtures of triethylamine in cyclohexane is confirmed. The changes in dielectric polarization of diketones with amine concentration in the mixed solvents are used to deduce the equilibrium constants of the association process, and the dipole moments of the complexes formed. Further, an inference is made of the relative polarities of the keto and enol tautomers of these diketones, and of the ketoanilides previously investigated (1).

Key words: dielectric polarization, molecular interaction, β-diketones, triethylamine.

GAMAL R. SAAD, MAGDI M. NAOUM et HANNA A. RIZK. Can. J. Chem. **67**, 284 (1989).

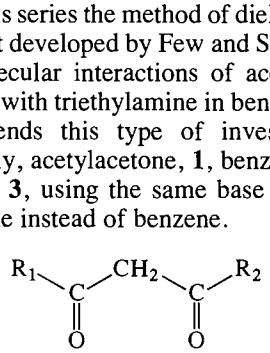
On a confirmé l'utilité d'une forme modifiée de l'équation de Few et Smith pour étudier des solutions diluées d'acétylacétone, de benzoylacétone et de dibenzoylméthane dans des mélanges à rapport constant de triéthylamine dans le cyclohexane. On utilise les changements de polarisation diélectrique des dicétones en fonction de la concentration d'amine dans les solvants mixtes pour déduire les constantes d'équilibre du processus d'association ainsi que les moments dipôlaires des complexes formés. De plus, on peut déduire les polarités relatives des tautomères cétoniques ou énoliques de ces dicétones ainsi que des cétoanilides étudiés antérieurement (1).

Mots clés : polarisation diélectrique, interaction moléculaire, β dicétones, triéthylamine.

[Traduit par la revue]

Can. J. Chem. Downloaded from www.nrcresearchpress.com by 122.72.124.2 on 09/07/12
For personal use only.

In part I (1) of this series the method of dielectric polarization measurements, first developed by Few and Smith (2), was used to investigate molecular interactions of acetoacetanilide and benzoylacetanilide with triethylamine in benzene solution. The present work extends this type of investigation to three β-diketones, namely, acetylacetone, **1**, benzoylacetone, **2**, and dibenzoylmethane, **3**, using the same base and the non-polar solvent cyclohexane instead of benzene.



1, $R_1 = R_2 = CH_3$; **2**, $R_1 = CH_3$, $R_2 = C_6H_5$; **3**, $R_1 = R_2 = C_6H_5$

However, since in an inert solvent, S, the acid, A, whether it is a β-diketones as in the present investigation, or β-ketoanilide as in the previous (1) one, exists in solution as an equilibrium mixture of the keto and enol tautomers, the presence of an interacting base, B, such as triethylamine will not only cause complexation through hydrogen bonding between the enolic OH group and the amine nitrogen, but also a shift in the position of equilibrium towards enol formation (3) as a consequence. This, in turn, might lead one to suggest that the standard value of polarization of the solute, which does not involve short-range interactions leading to complex formation (2, 4, 5), would be better taken as the extrapolated value of the polarization, P^*_A, in the solvent mixture, BS, in the limit when the concentration of the interacting base, B, approaches zero, rather than the polarization, P_A, in the non-polar solvent, S, as previously suggested (1, 2). Thus denoting $(P^*_A)_{w_B=0}$ as P'_A, where w_B is the weight fraction of the base in the constant-ratio solvent mixture, the equation of Few and Smith (2) can easily modified into

$$[1] \quad \frac{\Delta P}{P^*_A - P'_A} = 1 + \frac{M_B}{K w_B d}$$

where $\Delta P = P_{AB} - P'_A - P_B$, the other terms having their usual significance (1).

This equation has, therefore, been preferentially used in the present work for the calculation of both the equilibrium constants, K's of the association process between the β-diketone (**1**–**3**) and triethylamine in cyclohexane, and the dipole moments μ_{AB}'s, of the complexes formed. Recalculation of these two parameters has also been made for acetoacetanilide, **4**, and benzoylacetanilide, **5**, which were previously investigated (1).

Experimental and results

Acetylacetone (PROLABO, France) was purified by repeated distillation, benzoylacetone and dibenzoylmethane (HOPKINS & WILLIAMS, England) by two-fold crystallization from ethanol, and cyclohexane and triethylamine according to recommended procedures (6). The purity of compounds was checked by comparing their physical constants with those cited in literature (6).

Preparation of solutions and measurements of dielectric constant, ϵ, density, d, and refractive index for the sodium-D line, n_D, were carried out as described before (1, 7).

For the calculation of the equilibrium constant, K, of the association process and the dipole moment, μ_{AB}, of the complex, eq. [1] was used, the value of P'_A being first obtained by graphical extrapolation of P^*_A at $w_B = 0$.

The results obtained are summarized in Tables 1–3 for acetylacetone-, benzoylacetone-, and dibenzoylmethane–triethylamine–cyclohexane systems, respectively.[2]

Furthermore, since triethylamine has an appreciable dipole moment in cyclohexane, which is 0.83 D as determined in the present work, use was made of the modified Onsager equation (8, 9) for the determination of the apparent solution moment,

[1]Author to whom correspondence should be addressed.

[2]Tables 4 to 13 of original data have been deposited, A complete set may be purchased from the Depository of Unpublished Data, CISTI, National Research Council of Canada, Ottawa, Ont., Canada K1A 0S2.

TABLE 1. Polarization data of acetylacetone (A) in triethylamine (B) – cyclohexane (S) mixtures

% amine ($= w_B$)	d_{BS} (g/cm^3)	P^*_A (cm^3)	R^*_A (cm^3)	$1/(P^*_A - P'_A)$	$1/w_B d_{BS}$	μ_2 (D)
0.000	0.7698	201.7	—	—	—	—
2.032	0.7687	202.3	29.05	0.0838	63.99	2.92
3.308	0.7680	210.0	29.09	0.0510	39.34	2.98
4.005	0.7676	212.6	29.11	0.0451	32.51	3.00
5.431	0.7669	214.4	29.11	0.0417	23.99	3.02
6.845	0.7661	219.4	29.23	0.0345	19.05	3.06

$M_B/K\Delta P$ (slope)	$1/\Delta P$ (intercept)	ΔP (cm^3)	K (cm^3/mol)	P_{AB} (cm^3)	P'_A (cm^3)	R_{AB} (cm^3)	μ_{AB} (D)
1.07×10^{-3}	0.0128	78.3	1203	314.0	190.4	29.1	3.74

TABLE 2. Polarization data of benzoylacetone (A) in triethylamine (B) – cyclohexane (S) mixtures

% amine ($= w_B$)	d_{BS} (g/cm^3)	P^*_A (cm^3)	R^*_A (cm^3)	$1/(P^*_A - P'_A)$	$1/w_B d_{BS}$	μ_2 (D)
0.000	0.7698	231.4	—	—	—	—
2.542	0.7682	255.8	53.2	0.0344	51.69	3.16
5.409	0.7669	278.1	52.25	0.0195	24.33	3.33
6.413	0.7663	285.3	50.5	0.0171	20.31	3.40
8.413	0.7627	289.4	47.7	0.0159	15.73	3.45
9.663	0.7646	298.3	47.9	0.0140	13.66	3.51

$M_B/K\Delta P$ (slope)	$1/\Delta P$ (intercept)	ΔP (cm^3)	K (cm^3/mol)	P_{AB} (cm^3)	P'_A (cm^3)	R_{AB} (cm^3)	μ_{AB} (D)
5.41×10^{-4}	6.35×10^{-3}	157.1	1178	429.1	226.7	49.5	4.32

TABLE 3. Polarization data of dibenzoylmethane (A) in triethylamine (B) – cyclohexane (S) mixtures

% amine ($= w_B$)	d_{BS} (g/cm^3)	P^*_A (cm^3)	R^*_A (cm^3)	$1/(P^*_A - P'_A)$	$1/w_B d_{BS}$	μ_2 (D)
0.000	0.7698	241.1	—	—	—	—
1.883	0.7688	245.2	80.9	0.0982	69.73	2.92
3.772	0.7678	254.2	79.7	0.0521	34.85	2.98
4.985	0.7671	285.1	78.9	0.0433	26.40	3.00
6.088	0.7665	260.9	78.2	0.0371	21.63	3.02
8.339	0.7653	267.7	77.1	0.0306	15.83	3.06

$M_B/K\Delta P$ (slope)	$1/\Delta P$ (intercept)	ΔP (cm^3)	K (cm^3/mol)	P_{AB} (cm^3)	P'_A (cm^3)	R_{AB} (cm^3)	μ_{AB} (D)
1.27×10^{-3}	9.78×10^{-3}	102.2	777.2	382.5	235.0	78.4	3.87

μ_2, of the β-diketone in the constant-ratio solvent mixtures of the amines and cyclohexane. The results obtained are summarized in Tables 14–16.

Discussion

First, since the equilibrium position between the keto and enol tautomers of the acid A (whether a diketone in cyclohexane or ketoanilide in benzene) is shifted in favour of the enol form in the presence of triethylamine, owing to the hydrogen bonding between the enolic OH group and the nitrogen lone pair of electrons, we would expect that its polarization, P_A, at infinite dilution in the non-polar solvent, S, should be either higher or lower than its polarization, P'_A, at infinite dilution in the solvent mixture, BS, in the limit when the concentration of the base approaches zero, depending upon the relative polarities of the two tautomers. That is, if the keto form of the acid is of more polarity than the enol form, P_A will be greater than P'_A and vice versa. Based on this, an inspection of the results obtained as

Can. J. Chem. Downloaded from www.nrcresearchpress.com by 122.72.124.2 on 09/07/12
For personal use only.

TABLE 14. Apparent solution moments of acetylacetone in triethylamine–cyclohexane mixtures using modified Onsager's equation

% amine (w_B)	μ_1 (D)	V_1 (cm^3)	C_1^0	n_2^2	V_2 (cm^3)	$\left(\frac{d\epsilon_{12}}{dC_2}\right)_{C_2=0}$	F_2	μ_2 (D)
2.032	0.108	110	9.103	2.039	105	0.049	0.832	2.96
3.308	0.138	110	9.075	2.036	106	0.992	0.833	3.03
4.005	0.152	111	9.060	2.044	105	1.007	0.831	3.04
5.431	0.177	111	9.030	2.031	106	1.018	0.834	3.07
6.845	0.119	111	8.998	2.029	107	1.047	0.835	3.11

TABLE 15. Apparent solution moments of benzoylacetone in triethylamine–cyclohexane mixtures using modified Onsager's equation

% amine (w_B)	μ_1 (D)	V_1 (cm^3)	C_1^0	n_2^2	V_2 (cm^3)	$\left(\frac{d\epsilon_{12}}{dC_2}\right)_{C_2=0}$	F_2	μ_2 (D)
2.542	0.121	110	9.108	2.305	152	1.171	0.832	3.16
5.409	0.177	111	9.046	2.276	153	1.296	0.834	3.35
6.485	0.193	111	9.023	2.232	153	1.337	0.835	3.42
8.413	0.221	112	8.951	2.170	152	1.354	0.836	3.49
9.663	0.237	112	8.954	2.168	153	1.416	0.836	3.55

TABLE 16. Apparent solution moments of dibenzoylmethane in triethylamine–cyclohexane mixtures using modified Onsager's equation

% amine (w_B)	μ_1 (D)	V_1 (cm^3)	C_1^0	n_2^2	V_2 (cm^3)	$\left(\frac{d\epsilon_{12}}{dC_2}\right)_{C_2=0}$	F_2	μ_2 (D)
1.883	0.104	110	9.106	2.483	200	1.046	0.832	2.88
3.772	0.147	110	9.066	2.461	200	1.105	0.835	2.97
4.985	0.170	111	9.039	2.447	199	1.123	0.835	3.01
6.088	0.180	111	9.015	2.435	199	1.141	0.835	3.04
8.339	0.220	112	8.966	2.410	200	1.182	0.837	3.11

TABLE 17. Some physical properties of compounds **1** to **5**

Compound number	P_A (cm^3)	P'_A (cm^3)	μ'_A (D)	μ_{enol} (D)	μ_{keto} (D)	δm (D)	K (cm^3/mol)	pK_a^*	$\Delta\mu$ (D)	$-\Delta G^0$ (kJ/mol)
1	201.7	190.4	2.87	2.89	3.62	1.20	1203	14.15	1.90	0.47
2	231.4	226.7	2.97	2.95	3.49	1.29	1178	14.25	2.35	0.41
3	241.1	235.0	2.74	2.74	—	1.89	777	15.20	1.79	−0.64
4	267.0	273.0	3.35	3.97	3.06	—	364	11.45	1.75	−2.54
5	335.0	248.2	3.64	4.07	3.09	—	720	9.80	2.24	−0.83

*Measured in 50% dioxane water mixture (12).

TABLE 18. Fractions of the diketone introduced in triethylamine–cyclohexane mixtures which pass into the form of complex at infinite dilution

Acetylacetone		Benzoylacetone		Dibenzoylmethane	
% amine (w_B)	$\left(\frac{\Delta w_A}{w_A}\right)_{w_A=0}$	% amine (w_B)	$\left(\frac{\Delta w_A}{w_B}\right)_{w_A=0}$	% amine (w_A)	$\left(\frac{\Delta w_A}{w_A}\right)_{w_A=0}$
2.032	0.152	2.542	0.185	1.883	0.134
3.308	0.251	5.409	0.327	3.772	0.242
4.005	0.283	6.413	0.373	4.985	0.289
5.431	0.306	8.413	0.399	6.088	0.335
6.845	0.371	9.663	0.456	8.339	0.404

Can. J. Chem. Downloaded from www.nrcresearchpress.com by 122.72.124.2 on 09/07/12
For personal use only.

Can. J. Chem. Downloaded from www.nrcresearchpress.com by 122.72.124.2 on 09/07/12
For personal use only.

shown in Table 17 would lead to the inference that whilst the keto tautomer is more polar than the enol in the case of β-diketones, the opposite takes place in the case of β-ketoanilides, which is consistent with previous findings (10). Subsequently, use can be made of the value P'_A to calculate by the refractivity method, the corresponding molecular dipole moment, μ'_A. Thus the results obtained are also listed in Table 17, together with the dipole moments, μ_{enol} and μ_{keto}, which were previously (10) deduced from other lines of evidence.

It will be evident from this table that in the case of diketones there is a fair agreement between the values of μ'_A and μ_{enol}, and that in the case of ketoanilides there is a marked difference between these values, namely, μ'_A are appreciably lower than μ_{enol}. This in turn might suggest that in extreme dilute solutions of the acid A, the effect of the base B through the hydrogen bonding action is either to cause practically complete conversion of this acid into its enol form if it is a diketone in cyclohexane solution, or to shift largely the position of equilibrium in favour of the enol form (but not to completion) if it is a ketoanilide in benzene solution.

This conclusion might be accepted in view of the experimental facts (10, 11) that in the case of β-diketones the amount of enol present at infinite dilution in cyclohexane (as well as in carbon tetrachloride) is of the order of 98–100 mol%, whereas in the case of β-ketoanilides at infinite dilution in the less inert solvent benzene, in which preferential solvation of the keto tautomer takes place, it is less than 40 mol%.

Consequently, in the case of diketones a rough estimate has been made of the dipole moment, δm, of the intramolecular hydrogen bond of the enol tautomer by applying the method of bond moments (11) and making use of the value μ'_A which was taken as equal to μ_{enol}. The results obtained are again listed in Table 17. It will be evident from this table that δm increases in the order

[2] **1 < 2 < 3**

signifying that the acidity of the diketones decreases in the opposite order; that is,

[3] **1 > 2 > 3**

This is consistent with the observations that the values (12) of pK_a increase in the order given by eq. [2], whereas those of the equilibrium constant, K, as determined in the present work, decreases in the sequence given by eq. [3] (again see Table 17).

It may be pointed out here that in the case of ketoanilides an estimate of the dipole moment of the intramolecular hydrogen bond of the enol form could not be made as in the case of diketones, since μ'_A cannot be equated to μ_{enol}, as noted above. Also that the values of the equilibrium constant, K, of the association process in benzene solution, as obtained by applying eq. [1], which is a modified form of Few and Smith (2) original equation, are 364 and 720 cm^3/mol for acetoacetanilide and benzoylacetanilide, respectively. These values might be regarded as more correct than those previously (1) obtained. On the other hand, the fact that they are still much lower than those of the association process of the diketones with the same amine in cyclohexane solution (see Table 17) although the ketoanilides are of higher acidity, as can be evidenced from the pK_a values, can be accounted for on the basis that since benzene is more active than cyclohexane the formation of hydrogen bonded complexes in the former solvent necessitates the breaking of the bonds which the ketoanilides (and probably the base triethylamine) form with it.

It might be added here that although the apparent solution moments, μ_2's, of the diketones in the various constant-ratio mixtures obtained by either the usual Debye equation, or the modified Onsager (8, 9) equation could be regarded "incorrect", owing to the fact that no account is taken in any of these equations of the short-range forces that lead to complex formation, their apparent increase with increasing concentration of the amine (see Tables 1–3, and 14–16) suggests an increase in complex formation. An estimate of this increase can, in turn, be made by the calculation of the fraction, $\Delta w_A/w_A$, of the diketone introduced in the constant-ratio mixture of triethylamine and cyclohexane, which is complexed with the amine at infinite dilution. For this purpose, the following equation also suggested by Few and Smith (2) except that P'_A is substituted for P_A, as pointed out above, has been used.

[4] $$P^*_A - P'_A = \Delta P(\Delta w_A/w_A)$$

The results obtained are shown in Table 18. It is obvious from this table that an increase in the proportion of triethylamine in the solvent mixture favours complex formation; as is to be expected. Moreover, for a given solvent mixture, the tendency toward complex formation with the amine is highest for acetylacetone, **1**, and least with dibenzoylmethane, **3**. This agrees with the above conclusion drawn from the values of the dipole moment, δm, of the intramolecular hydrogen bond, as well as from those of the equilibrium constant, K, of complexation, and of the acidity, pK_a, of the diketones.

Owing to the limited number of investigated compounds in the present work, it is difficult to investigate the effect of change in acidity of these compounds in a given solvent upon the equilibrium constant of the association process. For the same reason, it is also difficult to check whether there is a correlation between the magnitude, $\Delta\mu$, of the dipole moment change associated with the formation of the intermolecular hydrogen bond, N---H—O, and the equilibrium constant expressed in terms of the free energy change, ΔG^0, of formation of the complex.

If, however, in a preliminary investigation one confines oneself just to the three diketones investigated here, it can be easily seen from Table 17 that there is a correlation between ΔG^0, and the acidity, pK_a, the trend being given by the relation

[5] $$\Delta G^0 = -15.6 + 1.07pK_a$$

and that there is no correlation between $\Delta\mu$, which was roughly calculated by the vector summation method of bond moments (11, 13–15), and ΔG^0. This is to be expected on the basis that a breaking of the intramolecular hydrogen bond in the enol tautomer of the acid should precede the formation of the intermolecular hydrogen bond.

Obviously, a clear justification of these inferences could only be obtained by extending measurements on a larger number of compounds.

1. M. M. Naoum, G. R. Saad, M. M. Abdel Moteleb, H. G. Shinouda, and H. A. Rizk. Can. J. Chem. **65**, 2760 (1987).
2. A. V. Few and J. W. Smith. J. Chem. Soc. 2781 (1949).
3. L. W. Reeves. Can. J. Chem. **35**, 1351 (1957).
4. D. P. Earp and S. Glasstone. J. Chem. Soc. 1709 (1935).
5. D. L. Hammick, A. Norris, and L. E. Sutton. J. Chem. Soc. 1755 (1938).
6. A. Weissberger and E. Proskauer. Organic solvents, physical constants and methods of purification. The Clarendon Press, Oxford. 1935.

7. A. R. TURKY, H. A. RIZK, and Y. M. GIRGIS. J. Phys. Chem. **64**, 565 (1960).
8. L. ONSAGER. J. Am. Chem. Soc. **58**, 1486 (1936).
9. H. A. RIZK and I. M. ELANWAR. Can. J. Chem. **46**, 507 (1968); H. A. RIZK, N. Y. YOSSEF, and H. GRACE. Can. J. Chem. **47**, 3767 (1969).
10. M. M. NAOUM, H. G. SHINOUDA, A. S. SHAWALI, and H. A. RIZK. J. Chim. Phys. **78**, 155 (1981); M. M. NAOUM and M. M. ABDEL MOTELEB. Gazz. Chim. Ital. **111**, 473 (1981); M. M. NAOUM and G. R. SAAD. Indain J. Chem. **26**, 510 (1987); M. M. NAOUM and G. R. SAAD. J. Soln. Chem. **17**, 67 (1988); M. M. NAOUM and M. G. BOTROS. Indain J. Chem. **25**, 427 (1986); M. M. NAOUM and M. G. BOTROS. Indain J. Chem. **26**, 607 (1987).
11. C. P. SMYTH. Dielectric behaviour and structure. McGraw-Hill, London. 1955.
12. H. J. HARRIES, R. K. HUGHES, and T. SMITH. J. Inorg. Nucl. Chem. **34**, 1609 (1972).
13. A. COULSON. *In* Hydrogen bonding. *Edited by* D. Hadzi and H. W. Thompson. Pergamon Press. New York. 1959. p. 339.
14. W. BLACK, J. G. D. DE JONGH, TH.G. OVERKEEK, and M. J. SPARNEAY. Trans. Faraday Soc. **56**, 1597 (1960).
15. P. L. HUYSKENS, W. CLEUREN, H. M. VAN BRADANT-GOVAERTS, and M. A. VUYLSTEKA. J. Chem. Phys. **84**, 2740 (1980).

Can. J. Chem. Downloaded from www.nrcresearchpress.com by 122.72.124.2 on 09/07/12
For personal use only.

Thermodynamic aspects in the adsorption of polynuclear aromatic hydrocarbons on chrysotile and silica – possible relation to synergistic effects in lung toxicity

JEANINE FOURNIER
Laboratoire de Réactivité de Surface et Structure, UA 1106, C.N.R.S., Université P. et M. Curie, Tour 54-55, 4 Place Jussieu, 75252 Paris Cédex 05, France
BICE FUBINI AND VERA BOLIS
Dipartimento di Chimica Inorganica, Chimica Fisicae Chimica dei Materiali, Facolta di Farmacia, Universita di Torino, Via Pietro Giuria, 9 – 10125 Torino, Italy
AND
HENRI PEZERAT
Laboratoire de Réactivité de Surface et Structure, UA 1106, C.N.R.S., Université P. et M. Curie, Tour 54-55, 2ème étage, 4 Place Jussieu, 75252 Paris Cédex 05, France

Received April 11, 1988

JEANINE FOURNIER, BICE FUBINI, VERA BOLIS, and HENRI PEZERAT. Can. J. Chem. **67**, 289 (1989).

This study is to compare the adsorption of phenanthrene — a polynuclear aromatic hydrocarbon — (apolar molecule) and water (polar molecule) on chrysotile, a mainly ionic solid and on one silica (Aerosil), a covalent solid. The adsorption of water shows that the adsorption capacity and the interaction energies are much higher for chrysotile than for silica. With phenanthrene, the adsorption mechanism on these two materials is very different: on chrysotile — a solid with a surface having a basic character — there is a multilayer adsorption, with lateral interactions between PAH molecules vertically oriented with regard to solid surface, whereas on silica (acidic solid), the PAH molecules are adsorbed flat and form only one layer. Chrysotile turns out to be a much more powerful adsorbent than silica towards both polar molecules and apolar molecules. The calorimetric data concerning the adsorption of phenanthrene on chrysotile in xylene reveal three thermal stages, showing the influence of preadsorbed water and solvent and permit to propose a model of adsorption mechanism. The formation of multilayers of phenanthrene on chrysotile converts its marked hydrophilic surface into a hydrophobic one which may act as a carrier of organic molecules and slowly release them into the biological medium. These phenomena may provide a possible interpretation for some synergistic effects concerning lung cancers observed after asbestos and cigarette-smoke exposure.

Key words: adsorption, phenanthrene, chrysotile, silica, water.

JEANINE FOURNIER, BICE FUBINI, VERA BOLIS et HENRI PEZERAT. Can. J. Chem. **67**, 289 (1989).

La comparaison des propriétés d'adsorption d'un solide ionique, le chrysotile avec celles d'un solide covalent, une silice (Aérosil), est fondée sur l'étude de l'adsorption d'un hydrocarbure polycyclique aromatique, le phénanthrène (molécule apolaire) dans le xylène et d'une molécule polaire à l'état gazeux, l'eau. L'adsorption de l'eau montre que la capacité d'adsorption et l'énergie d'interaction (solide-H_2O) sont beaucoup plus importantes dans le cas du chrysotile que dans le cas de la silice. L'adsorption du phénanthrène diffère selon le matériau étudié. En effet, pour le chrysotile dont la surface présente un caractère basique, les isothermes révèlent une adsorption en multicouches avec la présence d'interactions latérales entre les molécules adsorbées, ces molécules étant orientées verticalement par rapport à la surface. Par contre, pour la silice, seule une monocouche est formée avec des molécules adsorbées à plat. Tous ces résultats font apparaître que le chrysotile a une capacité d'adsorption pour le phénanthrène et pour l'eau très supérieure à celle de la silice. La présence de trois étapes thermiques lors de l'adsorption du phénanthrène sur le chrysotile révèle l'influence du solvant et de l'eau préadsorbée. Ces données calorimétriques permettant de proposer un modèle de mécanisme d'adsorption. La surface du chrysotile, initialement hydrophile devient hydrophobe du fait de la présence de multicouches de phénanthrène. Le chrysotile peut être considéré comme un collecteur et un transporteur de molécules organiques qui sont ainsi introduites dans le milieu biologique. Cette étude peut contribuer à expliquer, du moins en partie, les effets de synergie observées entre amiante et fumée de cigarette dans l'initiation de cancer du poumon.

Mots clés : adsorption, phénanthrène, chrysotile, silice, l'eau.

[Traduit par la revue]

Introduction

It is well known that the risk of bronchopulmonary cancers upon exposure to asbestos is much greater in people with smoking habits. Several epidemiological studies have in fact shown an effect of synergy between asbestos and cigarette smoke (1, 2). Among the carcinogenic organic compounds present in cigarette smoke, an important role is generally attributed to some polynuclear aromatic hydrocarbons (PAH).

The synergistic effect between PAH (e.g. benzo(*a*)pyrene or dimethyl-7,12-benzanthracene) and different varieties of asbestos has been confirmed by animal experimentations when the PAH preadsorbed on asbestos was introduced by intratracheal injection (3, 4). These studies have shown a great rate of bronchopulmonary cancers for preadsorbed PAH by comparison with solid PAH introduced alone.

Furthermore, several works *in vitro* (5, 6) confirm the results of epidemiology and of experimentations *in vivo*. The *in vitro* results have in fact revealed that the kinetics of PAH uptake in the hydrophobic zone of cells vary depending on whether PAH is previously adsorbed on asbestos.

The mechanisms of this synergy have not yet been clarified. We can suppose that the synergy involves either some complex interplay between the two pathological processes initiated by the two toxic agents as in the model proposed by Cohen (7) or some interaction between the inorganic solid and the PAH which could increase the intrinsic carcinogenic activity of one or both compounds. In the latter hypothesis, a detailed surface study on the adsorption properties of the solid is required. Both mechanisms, however, can act together.

In parallel with what happens in liquid–liquid interactions, it

Can. J. Chem. Downloaded from www.nrcresearchpress.com by 122.72.124.2 on 09/07/12
For personal use only.

Can. J. Chem. Downloaded from www.nrcresearchpress.com by 122.72.124.2 on 09/07/12
For personal use only.

is generally accepted that polar molecules will be preferentially adsorbed on ionic solids whereas apolar molecules will be preferentially adsorbed on covalent ones. In this respect, several studies (8–10) have shown that long-chain *n*-alkanes in apolar solvents are strongly preferentially adsorbed onto graphitised carbon black and also that the adsorption of acids or alcohols from aqueous solutions on a type of carbon (Spheron) increased with chain length of the solute.

In previous studies by some of us (11, 12), we have revealed that several inorganic solids such as asbestos are very good adsorbents for polynuclear aromatic hydrocarbons (PAH) like phenanthrene and dimethylbenzanthracene in organic solvent, phenomena in agreement with the study of Gerde and Scholander (13), and in spite of that their surface has to be considered mainly ionic. With these materials, we have obtained adsorption isotherms with multisteps which indicated the formation of bidimensional condensed layers (2D) at the surface of substrates.

If we take the example of chrysotile, an asbestos variety, the studies of Bonneau *et al.* (14, 15) have shown the presence of electron donor surface sites. Chrysotile, a magnesium silicate, presents an external surface (brucitic sheet) having hydroxyl ions in low coordination, at least at the exposed surface.

The present work compares the adsorptive properties of chrysotile with ones that are found for an amorphous silica of relatively low surface area, considered mainly as a covalent solid. Silicas have surface properties which strongly depend upon thermal pretreatments, crystallinity, and particle size (16, 17). Their capacity for adsorbing polar molecules is rather poor and decreases when siloxane (Si—O—Si) bridges present at the surface replace silanol couples[1] (18).

Two different kinds of molecules have been used as adsorptive surface probe: phenanthrene, as a typical apolar polynuclear aromatic hydrocarbon and water, as a typical polar molecule.

In order to assess both adsorptive capacity and interaction energy, calorimetric measures were carried out in parallel with traditional evaluation of adsorption isotherms.

In the case of water the two measurements were realized simultaneously, by dosing small amounts of water vapour onto the solid placed into the calorimetric vessel. This technique has already been used for the evaluation of hydrophilicity and hydrophobicity of a material[1] (19).

The adsorption isotherms of phenanthrene, already reported for chrysotile (12), were obtained using xylene solutions of phenanthrene in a wide range of concentrations. The corresponding heat of interaction in equilibrium conditions could not be obtained because of kinetic reasons. Thermokinetic data, obtained upon contact between the solid and the solutions, will be reported and will allow a useful insight into the thermodynamics of the early stages of adsorption and on the role of surface impurities on the adsorption mechanisms.

A model will be proposed which accounts for the role of solvent and surface preadsorbed species on the adsorption mechanism. This model presents evidence that chrysotile, a very powerful adsorbent for PAH, in spite of its ionic character, can act as a possible collector and carrier of PAH into the lungs.

Experimental

Materials

Two inorganic solids were used: (*i*) Rhodesian chrysotile, consisting of asbestos fibres, provided by UICC (International Union Against Cancer) with BET specific surface area (nitrogen) of 24 $m^2 g^{-1}$ for batch 1 and of 18 $m^2 g^{-1}$ for batch 2. (*ii*) Amorphous silica, Aerosil OX 50 (Degussa) obtained by pyrolisis of $SiCl_4$, with BET specific surface area (nitrogen) of 50 $m^2 g^{-1}$.

The solvents, xylene and *n*-hexane (Merck) and the solute, phenanthrene (Aldrich) are products of high purity.

The water used for vapour adsorption was gas-free, having been distilled several times *in vacuo*.

Methods

(i) Adsorption isotherms of phenanthrene in xylene medium

At room temperature, the adsorption of phenanthrene has been performed by contacting chrysotile (250 mg, batch 1) with solutions (50 mL) of different concentrations of PAH according to a process previously described (11).

The scale of concentrations in xylene used varies from 1×10^{-3} to 1 mol L^{-1}. This highest concentration value is very close to the one at saturation (C_S = 1.17 mol L^{-1}).

The analysis of the residual concentration of PAH after adsorption was performed by means of UV spectrofluorometry (Perkin Elmer, Hitachi MPF 3). This enables a plot of PAH adsorbed quantities (n_a in 10^{-6} mol m^{-2}) as a function of equilibrium concentrations (C_{eq} in 10^{-3} mol L^{-1}).

Standard conditions mean that the solvent and the solid have not been dried or degassed. For the study in dried and degassed medium, both substrate and solvent, which has been previously dried over potassium carbonate, were degassed under a nitrogen stream. During adsorption, the solid suspension was kept under nitrogen.

Desorption has been carried out by adding pure xylene to a suspension after the PAH adsorption stage. After every addition, the equilibrium concentration was measured.

(ii) Heat of interaction of phenanthrene with chrysotile

The adsorption of phenanthrene in liquid medium has been realized at fixed temperature (306 K) by adding the solution of PAH (2 mL) to chrysotile, batch 2 (100 mg). The initial concentration of PAH was 0.5 mol L^{-1} in xylene and 0.25 mol L^{-1} in *n*-hexane. The concentration in *n*-hexane is lower than in xylene because the 0.5 mol L^{-1} value corresponds to the saturated concentration in this solvent.

A microcalorimeter Calvet type (C-80 Setaram) was used: it is a turn flow calorimeter which in the present case was operated at 306 K. The calorimetric cells employed mainly consist of two concentric vessels which can be filled separately with two reactants. In the "measure" cell the solid was placed in the central vessel and the solution in the external vessel. The two compartments were separated, but in equilibrium with the same gas phase. The "reference" cell was filled only with the solid. Both cells were placed into the calorimeter and when the equilibrium was attained, an automatic mechanism for continuous alternative reversing of the calorimeter allowed the mixing of the reactants initially separated. A calorimetric signal was then recorded.

Calorimetric measurements were also performed in dried and degassed conditions, similar to the above-mentioned ones: both substrate and solvent previously dried on dehydrated zeolites were degassed under an argon stream.

(iii) Heat of adsorption of water vapour and related isotherms

For adsorption of water vapour, chrysotile (batch 2) and Aerosil have been outgassed in vacuum into a Tian Calvet microcalorimeter at the temperature of adsorption (303 K) until no endothermic deviation from the baseline was detectable, i.e., no more preadsorbed gases from the atmosphere could be desorbed.

Stepwise adsorption of water was performed following a technique previously described (20), by admitting successive small doses of H_2O vapour onto the sample up to an equilibrium pressure of ~10 Torr. For each dose the adsorbed amount and released heat were evaluated. The sample was then evacuated and a second adsorption run was performed in order to evaluate, by comparing the first and the second adsorption, if any H_2O was irreversibly held at the surface.

[1]V. Bolis, F. Fubini, S. Coluccia and L. Marchese. To be published.

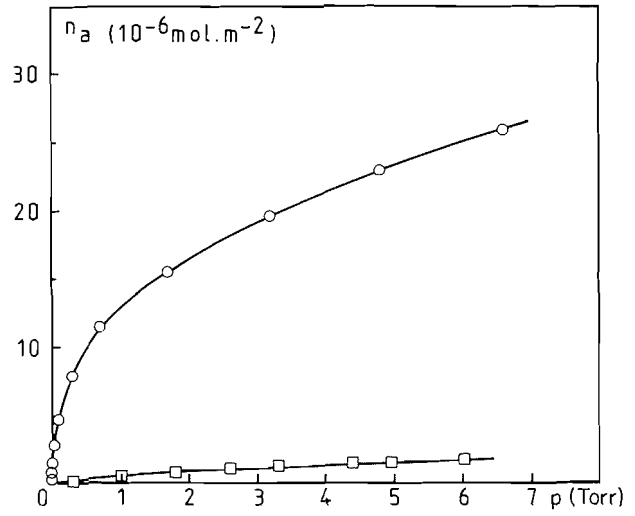


FIG. 1. Adsorption isotherm of water vapour on chrysotile (○) and amorphous silica (□) at 303 K.

Results

(a) Adsorption of water

Figure 1 reports the adsorption isotherms of water on chrysotile (batch 2) and amorphous silica (Aerosil 50) as adsorbed molecules, as a function of the equilibrium pressure of water.

Both isotherms exhibit the typical trend for adsorption of water on hydrophilic heterogeneous surfaces where adsorption in multilayers takes place. The isotherm shows a continuous increase with pressure and no plateau is detectable.

A marked difference in the adsorptive capacity of the two solids appears when we compare the adsorbed amounts per unit surface at the same pressure. At the equilibrium pressure of 5 Torr the uptake on silica is 1.5×10^{-6} mol m^{-2} whereas on chrysotile it is 23×10^{-6} mol m^{-2}. On chrysotile, densely packed layers of H_2O molecules are fixed on the brucitic hydroxyl exposed on the surface. On the pyrogenic amorphous silica, where only isolated patches of silanols are present,[1] much less water molecules per unit surface area are fixed, on top of silanols.

The molar enthalpy measured upon adsorption of each subsequent H_2O vapour dose is reported in Fig. 2 as a function of adsorbed amounts.

Chrysotile exhibits a small fraction of very strong sites (0.5×10^{-6} mol m^{-2}) which likely dissociates H_2O at the beginning of the experiment. From that point on, a regular trend (normal for an heterogeneous hydrophilic surface) is found, the $-\Delta H_{ads}$ value decreasing regularly from ~100 kJ mol^{-1} down to ~60 kJ mol^{-1}. Water is adsorbed via two H-bonds onto surface hydroxyls. The monolayer coverage is attained (with the hypothesis of one water molecule per two adjacent OH and 1.2×10^{19} (OH) groups per m^2 (15)), for an adsorption of 15×10^{-6} mol m^{-2}. Then the adsorption involves multilayers of H_2O molecules with a heat of ~60 kJ mol^{-1}, approximately constant with coverage.

A similar trend is found on silica with the following exceptions: (*i*) a much lower coverage interval of heterogeneity is detected (0.05×10^{-6} mol m^{-2}); (*ii*) the plateau value, corresponding to multilayer adsorption is much lower than on chrysotile, being near 44 kJ mol^{-1}, i.e. the latent heat of liquefaction of water.

This indicates that a strong surface field is present on chrysotile, so that even in multilayer adsorption, the energy of the process is much higher than the heat of liquefaction, whereas on silica, once the monolayer on hydroxylated patches is attained, multilayer condensation mainly occurs as in water liquefaction.

(b) Adsorption isotherms of phenanthrene

Figure 3 reports the adsorption isotherms of phenanthrene on chrysotile (*a*) and Aerosil (*b*) in xylene medium (standard conditions).

The two curves have a different shape and the isotherm (*b*) is situated in the scale of high concentrations by comparison with the isotherm (*a*).

The shape (S type) for chrysotile reveals the presence of lateral interactions between adsorbed molecules (21). This curve shows successive plateaus corresponding to a defined degree of coverage (θ).

By reference to Giles and McKay (22) on the adsorption studies of several PAH in liquid medium, the presence of lateral interactions between adsorbed molecules involves an orientation end-on of the PAH molecule onto the solid surface. Taking into account the basic character of this mineral surface (15), we had proposed this type of orientation with the most electrophilic C—C bond parallel to the solid surface (11). This orientation, very close to one encountered in the molecular structure of solid phenanthrene (23), involves an area of overlap of 33 Å^2.

With this value and the BET area, the two plateaus corresponded to the successive formation of a monolayer ($\theta = 1$) and then a bilayer ($\theta = 2$). We have obtained a multilayer curve with the formation of bidimensional condensed layers (2D), this phenomenon continuing after the second plateau (12).

Unlike chrysotile, silica exhibits an isotherm of Langmuir type. In this case, the molecule of phenanthrene is adsorbed flat onto surface, without lateral interactions between adsorbed molecules (24). In this position, the PAH molecule with its π electrons delocalized plays a nucleophilic role on the acidic surface of silica. With this orientation, the area of overlap is 92 Å^2. The plateau of the curve (*b*) corresponds to the formation of a monolayer ($\theta = 1$), in a field of concentrations very close to the saturated concentration C_s ($\ln C_{eq}/C_s \rightarrow 0$).

By comparison with chrysotile, the adsorption capacity is lower for silica, and very high concentrations of PAH are needed in order to initiate the adsorption process (Fig. 3).

Figure 4 compares the adsorption isotherms of phenanthrene on chrysotile in xylene under standard conditions of Fig. 1 (curve *a*) with the one obtained under dried and degassed conditions (curve *b*). Isotherm (*b*) shows an increase of the adsorbed quantity for a fixed concentration at equilibrium and the presence of only one short plateau. According to the criteria previously established, this plateau corresponds to the direct formation of a bilayer ($\theta = 2$). These phenomena are due to the partial elimination of preadsorbed molecules such as H_2O, O_2, CO_2 originated by contact of the solid with the atmosphere.

(c) Adsorption–desorption hysteresis

An hysteresis is found when adsorption of a first monolayer phenanthrene in standard conditions is followed by desorption (Fig. 5). In the whole concentration range covered, the desorption curve lies above the adsorption one. This fact which is reminiscent of phenomena related to capillary condensation is rather unusual, the hysteresis involving the monolayer range and not the multilayer one as in capillary condensation.

Can. J. Chem. Downloaded from www.nrcresearchpress.com by 122.72.124.2 on 09/07/12
For personal use only.

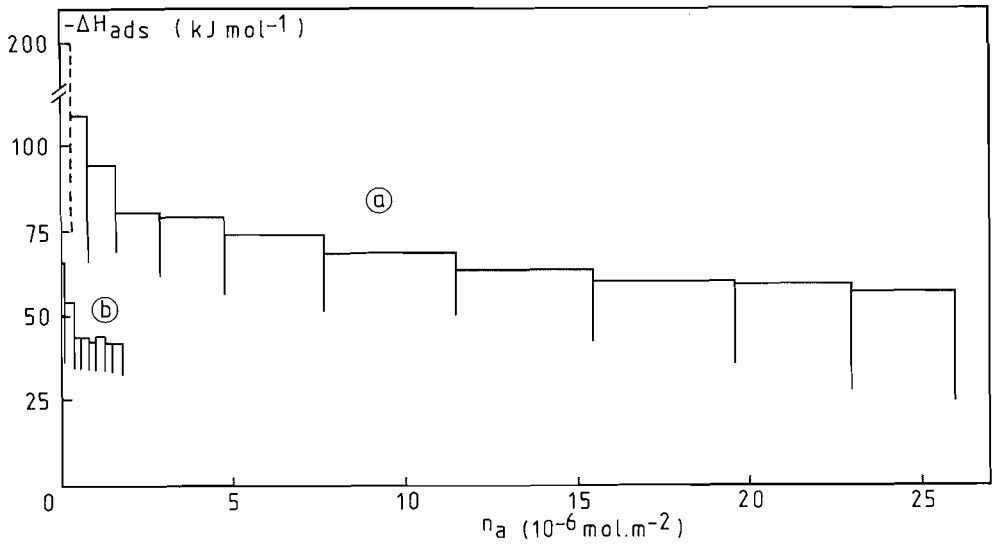


FIG. 2. Partial molar enthalpy of adsorption as a function of coverage (adsorbed moles) as measured in each admitted dose: (*a*) chrysotile; (*b*) amorphous silica.

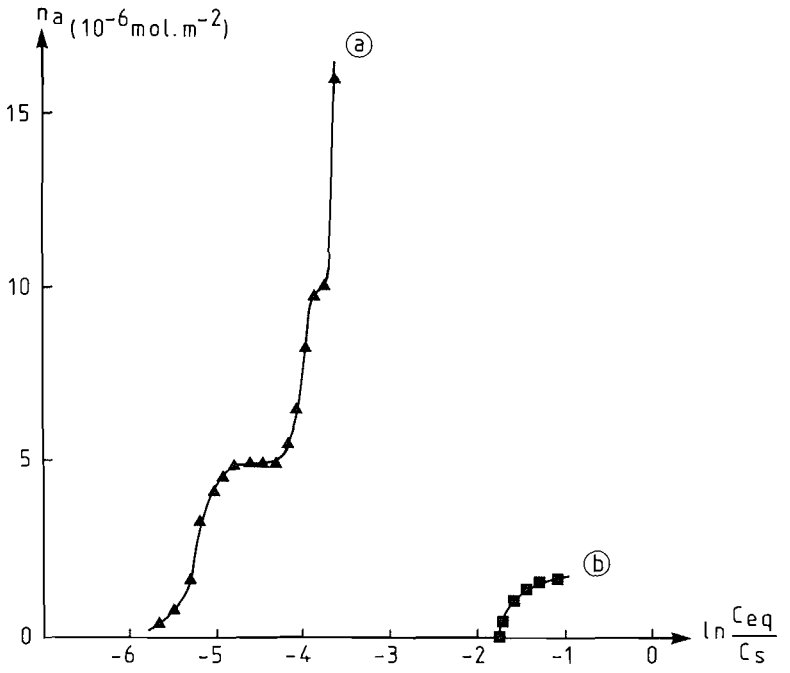


FIG. 3. Adsorption isotherms of phenanthrene in xylene (standard conditions): (*a*) chrysotile (batch 1); (*b*) Aerosil.

(d) Calorimetric data for phenanthrene adsorption on chrysotile

The calorimetric data concern, in this case, only the first stages of the adsorption phenomena and not the formation of multilayers of PAH on chrysotile.

Figure 6 presents thermokinetic curves obtained upon contact of phenanthrene solutions, with chrysotile (batch 2) in the calorimeter. The three curves refer to three different experiments. (*a*): Chrysotile, solution of phenanthrene in xylene (0.5 mol L^{-1}) under standard conditions; (*b*): chrysotile treated under argon, solution of phenanthrene in dried xylene (0.5 mol L^{-1}); (*c*): chrysotile, solution of phenanthrene in *n*-hexane (0.25 mol L^{-2}) under standard conditions.

These experiments were conducted under conditions clearly different from that used for the adsorption isotherms, because the vessel volume in calorimetry was small (2 mL), the thermic phenomenon was at the limit of sensitivity, and therefore we have increased the ratio: mass of solid/volume of solution (ratio m/v) which is raised from 5 (adsorption isotherms) to 25, and we have chosen a high value for the phenanthrene concentration in xylene (0.5 mol L^{-1}).

Under these experimental conditions we are not capable of reaching the equilibrium during the calorimetric experiment time. Indeed, the increase of the m/v ratio allows an increase of the water quantity in the medium and a slackening of the adsorption kinetics as illustrated by the data of Table 1 and Fig. 7. In Table 1 the adsorbed quantities of PAH (n_a) are measured for two values of m/v (5 and 25) after 1 h of contact of a PAH solution (8×10^{-3} mol L^{-1}) with chrysotile (batch 1). In

Can. J. Chem. Downloaded from www.nrcresearchpress.com by 122.72.124.2 on 09/07/12
For personal use only.

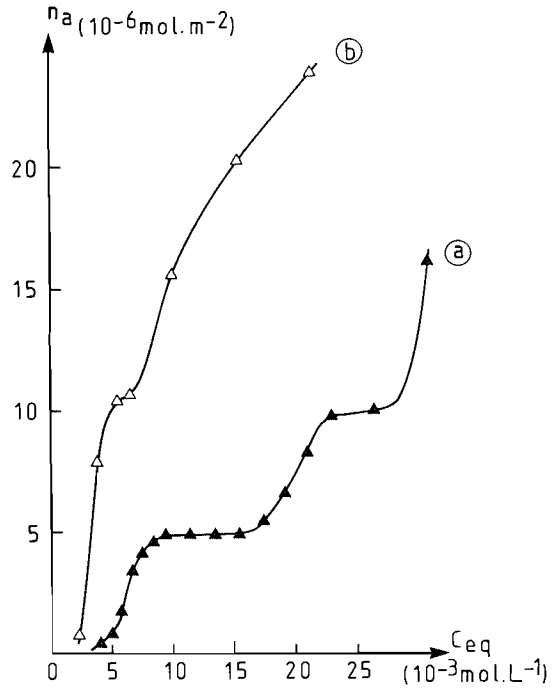


FIG. 4. Adsorption isotherms of phenanthrene in xylene on chrysotile (batch 1): (*a*) standard conditions; (*b*) substrate dried under nitrogen; solvent dried and degassed.

standard conditions, we observe that for the larger m/v (m/v = 25), we obtain the smaller value of n_a, whereas after a previous treatment of drying, the difference between the degrees of coverage (θ) for the two ratios is reduced and becomes insignificant when the dried system is degassed. In Fig. 7, with the same conditions as for the calorimetric experiment represented in Fig. 6(*a*), we observe that the equilibrium is reached only after a time of about 150 h, as against less than 1 h with a m/v ratio of 5 (adsorption isotherms). In dry medium (Fig. 6(*b*)), it is also very probable that we are far from the equilibrium conditions.

A third factor unfavorable for these calorimetric experiments is the use of chrysotile of batch 2, because of the exhausting batch 1 stock. Batch 2 has a weaker density of basic sites and a higher water content of hydration than batch 1 (H. Suquet, to be published). This involves for batch 2 a very weak adsorptive capacity towards PAH, but the adsorption mechanism is similar to the one observed with batch 1 (24).

Consequently the calorimetric results of Fig. 6 do not allow us to evaluate the heats of adsorption but only the three initial successive stages (exothermic, endothermic, exothermic) of the adsorption phenomena. The first step appears when the solution is brought into contact with the solid. The exothermic peak is more or less large according to the experimental conditions. This is due to the presence of endothermic phenomenon following the exothermic peak. By comparison with standard conditions (*a*) in xylene, the endothermic step and also the following exothermic phenomena are much less marked in dried medium (*b*). The drying of system reveals an influence of preadsorbed water on the endothermic phenomenon and on the following exothermic part.

Under standard conditions, the endothermic effect is also much strongly marked for xylene solution (*a*) than for *n*-hexane solution (*c*). This reveals the influence of solvent on the phenomenon of adsorption of PAH on chrysotile.

Discussion

All the results obtained from adsorption of both water and phenanthrene indicate a remarkable difference in surface properties between silica and chrysotile. Chrysotile appears as being a much more powerful adsorbent than silica towards both the molecules chosen (water and phenanthrene).

(1) Adsorption of water

As expected from the more ionic character of the chrysotile surface by comparison with silica, adsorptive capacity and interaction energy are higher on chrysotile than on silica. At the same equilibrium pressure the adsorption value is ~20 times larger on chrysotile than on Aerosil (Fig. 1). The interaction energy is much larger on chrysotile than on silica, both in the heterogeneous first part of the differential heat curve (Fig. 2) and at the plateau value which is ~60 kJ mol^{-1} on chrysotile and

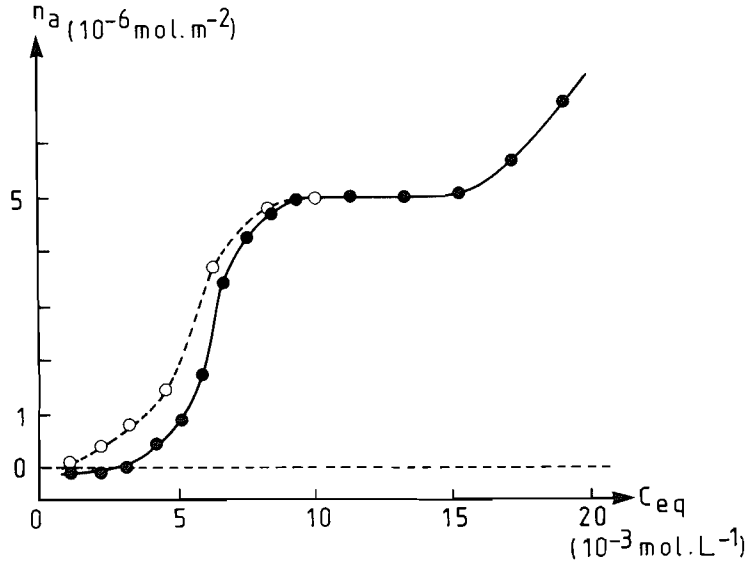


FIG. 5. Adsorption–desorption isotherms of phenanthrene on chrysotile (batch 1) in xylene (standard conditions). ● adsorption; ○ desorption.

Can. J. Chem. Downloaded from www.nrcresearchpress.com by 122.72.124.2 on 09/07/12
For personal use only.

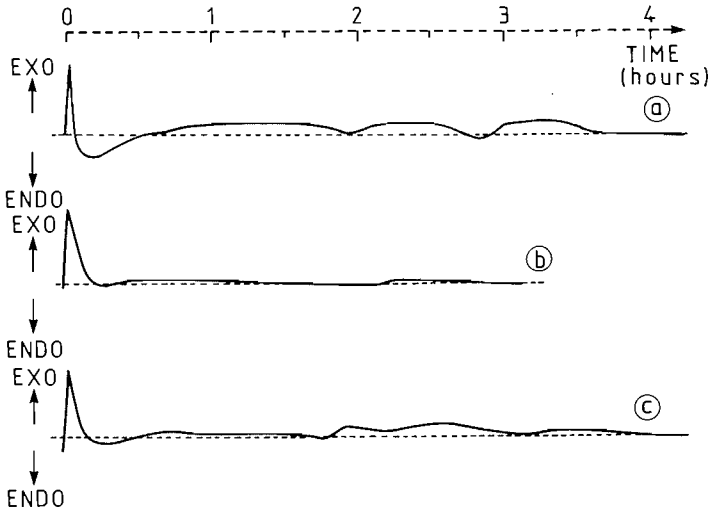


FIG. 6. Calorimetric curves for the first stages of adsorption of phenanthrene on chrysotile (batch 2) in liquid medium (arbitrary units in ordinate): (*a*) chrysotile, solution of phenanthrene in xylene (0.5 mol L^{-1}) in standard conditions; (*b*) chrysotile treated under argon, solution of phenanthrene in dried xylene (0.5 mol L^{-1}); (*c*) chrysotile, solution of phenanthrene in *n*-hexane (0.25 mol L^{-1}) in standard conditions.

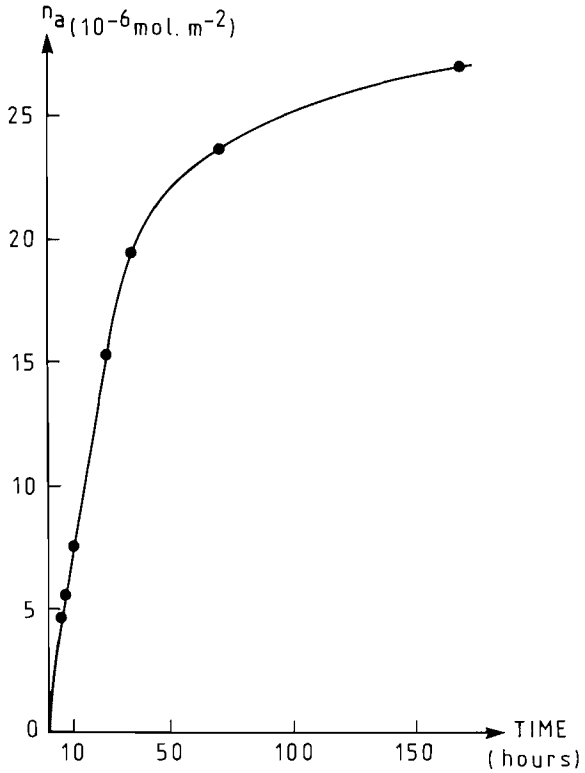


FIG. 7. Adsorption kinetic of phenanthrene in xylene (0.5 mol L^{-1}) on chrysotile (batch 2) in standard conditions, with ratio m/v = 25.

close to the latent heat of liquefaction of water (44 kJ mol^{-1}) on Aerosil 50. This latter finding is in agreement with that reported by Zettlemoyer *et al.* (25) for the overall heat of adsorption of water on chrysotile (67 kJ mol^{-1}).

However, it has to be pointed out that the affinity of Aerosil 50 for water is very poor even when compared with results on other silicas.[1]

(2) Adsorption of phenanthrene

Phenanthrene being an apolar aromatic hydrocarbon, one would expect that upon adsorption, this molecule would behave

TABLE 1. Phenanthrene adsorption on chrysotile (batch 1) after 1 h of contact with a solution 8×10^{-3} mol L^{-1} in xylene; effect of pretreatment on n_a and θ values for two values m/v

Experimental conditions*	m/v (mg mL^{-1})	n_a (10^{-6} mol m^{-2})	θ
a	5	2.92	1.58
	25	0.125	0.02
b	5	3.75	0.74
	25	1.625	0.32
c	5	5.33	1.06
	25	5.42	1.08

**a*, Standard conditions; *b*, substrate treated under N_2, solvent dried; *c*, substrate treated under N_2, solvent dried and degassed.

in the opposite way of water, i.e. be preferentially adsorbed on the less ionic solid, namely silica. This is not the case, as clearly shown by data in Fig. 3, because of the large polarisability of the molecule itself and of the basic character of the chrysotile surface which determine the mode of adsorption. As a consequence multilayers are only formed on chrysotile whereas on silica where the Langmuir model is followed, only a single layer of adsorption is possible.

Chrysotile, having electron donor sites on the surface (15) vertically adsorbs phenanthrene at the C_2–C_3, the most electrophilic bond (11). As a consequence, the molecule is polarized, lateral interactions between adsorbed molecules take place, and the strong surface field allows multilayer formation. The multistep isotherm of Fig. 3 is typical for this model of adsorption. Silica is an acidic covalent solid which implies molecule adsorption on flat. In this case, there are no lateral interactions and thus only one monolayer is formed. This orientation has been reported for the adsorption of aromatic compounds on graphon (26, 27).

The adsorption of phenanthrene on chrysotile however is not such a simple phenomenon as indicated by three main experimental facts whose interpretation is not straightforward: (*i*) the presence of an endothermic step upon adsorption whose

Can. J. Chem. Downloaded from www.nrcresearchpress.com by 122.72.124.2 on 09/07/12
For personal use only.

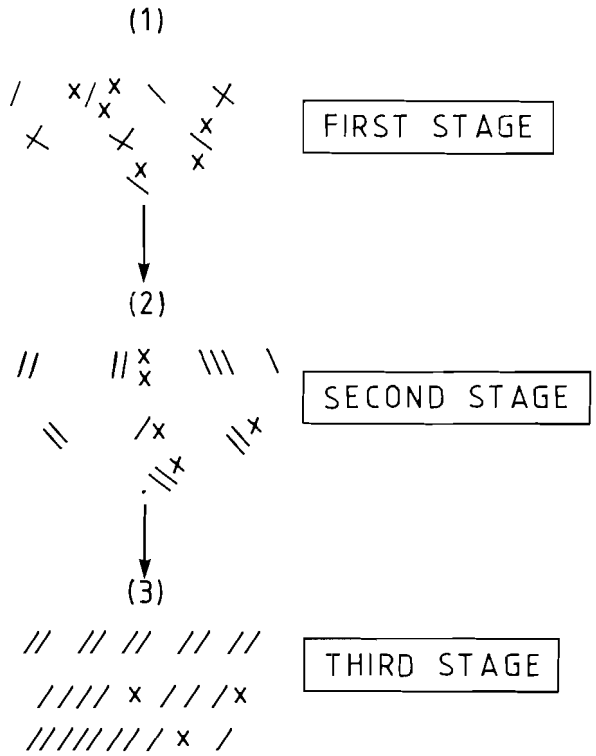


FIG. 8. Model of adsorption mechanism on chrysotile in standard conditions: / molecule of PAH; × preadsorbed molecule.

magnitude is related both to preadsorbed molecules (likely water) and to the solvent employed; (*ii*) the presence of an hysteresis in adsorption–desorption in the monolayer region; (*iii*) an enhancement of adsorption when a low mass of solid/volume of solution ratio is used which appears to be related to the presence of preadsorbed molecules on the solid surface (Table 1).

The endothermic step can be explained as follows: after the first contact between solid and solution which is always exothermic (phenomenon of wetting), phenanthrene displaces from the surface both the solvent molecules just adsorbed, and the pollutant molecules preadsorbed, mainly water. At this stage this process is endothermic, the energy of adsorption of water being likely higher than the one of phenanthrene because of strong hydrogen bonding. Adsorption of phenanthrene at this stage occurs for entropic reasons, taking into account that the number of phenanthrene molecules in the system largely exceeds the one of water molecules and that the molecular size of PAH being larger than H_2O, xylene and *n*-hexane, several molecules of H_2O or solvent will be displaced by one single PAH molecule. When the PAH concentration on the surface increases, lateral interactions take place and the adsorption becomes exothermic. This latter process continues for very long periods in the experimental conditions adopted (Fig. 6) and is not accomplished in the calorimetric experiment. Thus, unfortunately, the overall heat of adsorption in equilibrium conditions could not be measured. The endothermic step is very small if the experiment is carried out in dry conditions (Fig. 7(*b*)) because much less water will be fixed on the surface. If the experiment is carried out from *n*-hexane solution, *n*-hexane being an apolar molecule will be much less competitive for surface sites than xylene (24). In this case, therefore, the lower endothermicity recorded with respect to xylene solutions will be due to a lesser displacement of solvent because of its poor affinity for the surface.

In standard conditions, not all preadsorbed water molecules are displaced by phenanthrene. In fact, the difference between isotherms of Fig. 4 indicates that the presence of preadsorbed molecules in equilibrium conditions involves the edification of one monolayer followed by the second one whereas in dried conditions, the second layer is probably built up before the end of the first layer formation and for lower values of C_{eq} than those in standard conditions. Moreover, the quantity of pollutant molecules in the medium is more or less important according to the m/v ratio. For a high value of m/v, adsorption of PAH occurs only on isolated sites at a low extent. This situation is less favourable to adsorption. By either decreasing the m/v ratio or eliminating preadsorbed molecules, lateral interactions can take place, thus adsorption occurs at a much larger extent (Table 1).

Taking into account all the above data, we propose the following model (schematized in Fig. 8) for the adsorption features of phenanthrene onto chrysotile in standard conditions: (*1*) Isolated adsorption: in spite of the initial ionic character of chrysotile, there is the intervention of two parallel phenomena: (*i*) direct adsorption of PAH molecule on an electron donor site which is not poisoned by water or other pollutants; (*ii*) displacement of preadsorbed molecules by a PAH molecule which in turn is adsorbed onto an active site. In the two cases, the PAH molecules are fixed individually, i.e. one molecule for one active site, and these molecules are strongly polarized by the solid surface. (*2*) Cooperative phenomenon: lateral interactions between adsorbed PAH molecules are established and the formation of little "blocks" of PAH molecules appears. These "blocks" could grow either by the inclusion of new adsorbed molecules or by the displacement of the surrounding preadsorbed molecules. (*3*) The last step corresponds to the end of the monolayer. After the elimination of a great part of preadsorbed molecules, the "blocks" merge together, the driving force being the presence of lateral interactions. This stage involves the formation of a condensed layer (2D).

During stages *2* and *3*, the union of the PAH "blocks" implies that the global energetic term of lateral interactions increases.

Desorption will follow a different path from adsorption. In fact, at the same coverage, the presence of preadsorbed molecules during adsorption is a limiting factor for lateral interactions whereas upon desorption, when most preadsorbed molecules will be eliminated, more lateral interactions will be operating. As a consequence at any coverage below monolayer $C_{eq_{des}} < C_{eq_{ads}}$.

The thermodynamic descripiton of the process will be $\Delta G_{ads} < 0$, because in all cases adsorption occurs. At low coverage, phenanthrene will displace solvent and preadsorbed molecules. $\Delta H_{disp} > 0$, $T\Delta S_{disp} > 0$, displacement occurs for entropic reasons only.

At high coverage, strong lateral interactions will be established between adsorbed molecules of PAH:

$$\Delta H_{ads} < 0, \qquad T\Delta S_{ads} < 0$$

As a consequence, chrysotile will be covered by several layers, as in bulk phenanthrene, but probably with a high degree of disorder.

Conclusions

In spite of the ionic character of its external surface (brucitic sheet) chrysotile acts as a very powerful adsorbent for PAH, being able to adsorb at its surface several layers (2D) of apolar

Can. J. Chem. Downloaded from www.nrcresearchpress.com by 122.72.124.2 on 09/07/12
For personal use only.

molecules. Inversely, with the covalent character of its surface, Aerosil is only able to adsorb one layer of PAH molecules. Multilayer adsorption of PAH converts the marked hydrophilic surface of chrysotile into a hydrophobic one, which can facilitate the interaction of the asbestos particles with the external membrane of the cells (28).

The multilayer adsorption of PAH on asbestos can explain the observations of Chang *et al.* (5) and Eastman *et al.* (6) who have shown that the uptake kinetics of PAH (e.g. benzo(*a*)pyrene preadsorbed on asbestos) toward the hydrophobic zone of cells is different from that which occurs when the PAH is introduced into the cell culture as a solid phase or in solution in a solvent medium.

Eastman *et al.* observed a longer uptake time and a more marked DNA alkylation, with B(*a*)P adsorbed on chrysotile.

Our results suggest that in the first period of contact with cells, the high surface of the adsorbed PAH can allow a rapid uptake, but that the more strongly adsorbed molecules of the monolayer will be solubilized in the hydrophobic zone of the cells with difficulty and more slowly, from which the metabolisation of these latter molecules can appear delayed in time.

Therefore, the preadsorption of PAH on inorganic solids plays a role in the distribution and the availability of these PAH in biological medium, which also explains the results of the animal experiments (3, 4) where a great percentage of broncho-pulmonary cancers is observed when the PAH is introduced as preadsorbed on a basic, inorganic solid by intratracheal injection.

For asbestos, we must add a role of collector of air pollution and thus a role of carrier of these organic pollutants toward the pulmonary medium. These two roles depend directly on the adsorption properties of the inorganic solids.

This fact may provide a possible interpretation for some synergistic effects observed, for example between asbestos and cigarette-smoke exposure.

1. J. J. SELIKOFF, E. C. HAMMOND, and J. CHURG. J. Am. Med. Assoc. **204**, 106 (1968).
2. I. J. SELIKOFF, H. SEIDMAN, and E. C. HAMMOND. J. Natl. Cancer Inst. **65**, 507 (1980).
3. L. M. SHABAD, L. N. PYLEV, L. W. KRIVOSHEERA, T. F. KULAGINA, and B.M. NEMENKO. J. Natl. Cancer Inst. **52**, 1175 (1974).
4. D. C. TOPPING and P. NETTESHEIM. J. Natl. Cancer Inst. **65**, 627 (1980).
5. M. J. W. CHANG and R. W. HART. Seventh International Symposium on PAH. *Edited by* Coolle, Dennis, and Anthony. Batelle Press, Columbus. 1983. p. 293.
6. A. EASTMAN, B. T. MOSSMAN, and E. BRESNICK. Cancer Res. **43**, 1251 (1983).
7. B. COHEN. Lancet ii:, 1024 (1978).
8. J. J. KIPLING and E. H. M. WRIGHT. J. Chem. Soc. 885 (1962).
9. C. G. ARMISTEAD, A. J. TYLER, and J. A. HOCKEY. Trans. Faraday Soc. **67**, 493 (1971).
10. M. LIPHARD, P. GLANZ, G. PILAR, and G. H. FINDENEGG. Prog. Colloid. Polymer Sci. **67**, 131 (1980).
11. J. FOURNIER and H. PEZERAT. J. Chim. Phys. Phys. Chim. Biol. **79**, 589 (1982).
12. J. FOURNIER and H. PEZERAT. Environ. Res. **41**, 276 (1986).
13. P. GERDE and P. SCHOLANDER. Adsorption of polycyclic aromatic hydrocarbons onto asbestos and man-made mineral fibers in the gas phase. Symposium IARC, Lyon, Sept. 1987. In press.
14. L. BONNEAU and H. PEZERAT. J. Chim. Phys. Phys. Chim. Biol. **80**, 275 (1983).
15. L. BONNEAU, H. SUQUET, C. MALARD, and H. PEZERAT. Environ. Res. **41**, 251 (1986).
16. R. K. ILER. The chemistry of silica. Wiley, New York. 1967.
17. V. BOLIS, B. FUBINI, and G. VENTURELLO. J. Thermal Anal. **28**, 249 (1983).
18. V. BOLIS, B. FUBINI, S. COLUCCIA, and E. MOSTACCI. J. Thermal Anal. **30**, 1283 (1986).
19. B. FUBINI, V. BOLIS, and E. GIAMELLO. Thermochim. Acta, **85**, 23 (1985).
20. B. FUBINI. Rev. Gen. Therm. **18**, 297 (1979).
21. C. H. GILES. Surf. Sci. **11**, 143 (1981).
22. C. H. GILES and R. B. MCKAY. J. Chem. Soc. 58 (1961).
23. J. TROTTER. Acta Crystallogr. **16**, 605 (1963).
24. J. FOURNIER. Adsorption des hydrocarbures polycycliques aromatiques sur des solides donneurs d'électrons. Thesis, Paris. 1987.
25. A. C. ZETTLEMOYER, C. J. YOUNG, J. J. CHESSIK, and F. H. HEALEY. J. Phys. Chem. **57**, 649 (1953).
26. E. H. M. WRIGHT and A. V. POWELL. J. Chem. Soc. Faraday Trans. 1, **68**, 1908 (1972).
27. G. D. PARFITT and C. H. ROCHESTER. Adsorption from solution at the solid/liquid interface. *Edited by* G. D. Parfitt and C. H. Rochester. Academic Press, New York. 1983. p. 3.
28. P. GERDE and P. SCHOLANDER. Ann. Occup. Hyg. **31**, 3 (1987).

Can. J. Chem. Downloaded from www.nrcresearchpress.com by 122.72.124.2 on 09/07/12
For personal use only.

The ion-pair mechanism and bimolecular displacement at saturated carbon. VII. Racemization of substituted 1-phenylbromoethanes; ionic strength effects

ALLAN R. STEIN

Department of Chemistry, Memorial University of Newfoundland, St. John's, Nfld., Canada A1B 3X7

Received May 8, 1988

ALLAN R. STEIN. Can. J. Chem. **67**, 297 (1989).

No, or at most very small, salt effects have been detected for second-order racemizations of various 1-phenylbromoethanes, confirming that the "mixed kinetics", previously reported for 4-methyl- and 3,4-dimethylphenylbromoethanes with tetrabutylammonium bromide in acetonitrile and nitromethane, did not reflect a salt effect on a unimolecular reaction. Thus the uni- and bimolecular rate components can be evaluated using the equation:

$$\text{observed rate} = k_1 + k_2'[Bu_4NBr]$$

where k_1 = first-order or unimolecular rate constant, the intercept, and $k_2' = 2k_2$, the latter being the rate constant for the bimolecular substitution. A "special salt effect" was found for the unimolecular component; it was especially pronounced for 3,4-dimethyl substrate in acetonitrile with Bu_4NClO_4 as the electrolyte. In acetone, where no unimolecular reaction component was detected even with those substrates giving the most stable carbocations, the only salt effect was a common ion, Bu_4N^+, effect on the incomplete dissociation of Bu_4NBr. From an iterative best fit for plots of observed rate versus calculated bromide ion activity for unsubstituted, 4-methyl, and 3,4-dimethyl substrates, $K_{assoc} \sim 15 \pm 1$ at 40°C. The results are interpreted as additional support for a progression of mechanism with nucleophilic attack possible at any stage of the series of equilibria: substrate $\rightleftharpoons$ contact ion pair $\rightleftharpoons$ various solvated ion pairs $\rightleftharpoons$ dissociated ions.

Key words: special salt effects, ionic strength effects, racemization of 1-phenylbromoethanes, mechanism of nucleophilic substitution, ion pair mechanism.

ALLAN R. STEIN. Can. J. Chem. **67**, 297 (1989).

Pour les racémisations du deuxième ordre de divers phényl-1 bromoéthanes, on n'a détecté aucun, ou tout au plus de très faibles, effet de sels; ces résultats confirment que les « cinétiques mixtes » qui ont été observées antérieurement lors des réactions des méthyl-4 et diméthyl-3,4 phénylbromoéthanes avec le bromure de tétrabutylammonium dans l'acétonitrile et le nitrométhane, ne sont pas le reflet d'un effet de sel sur une réaction unimoléculaire. On peut donc évaluer les composantes uni- et bi-moléculaires de la vitesse en utilisant l'équation

$$\text{vitesse observée} = k_1 + k_2'[Bu_4NBr]$$

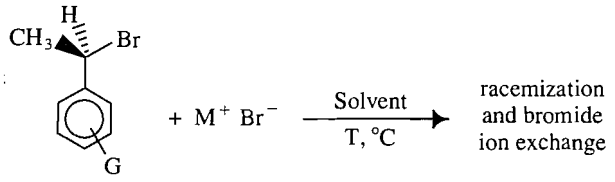
dans laquelle k_1 = constante de vitesse du premier ordre ou unimoléculaire, l'ordonnée à l'origine, et $k_2' = 2k_2$ où k_2 est la constante de vitesse de la substitution bimoléculaire. On a observé un « effet de sel spécial » sur la composante unimoléculaire; cet effet était particulièrement prononcé pour le substrat diméthyle-3,4, dans l'acétonitrile, avec le Bu_2NClO_4 comme électrolyte. Dans l'acétone, on n'a détecté aucune composante reliée à une réaction unimoléculaire (même pas avec les substrats qui donnent les carbocations les plus stables) et le seul effet de sel qui a pu être observé est celui d'un ion commun, Bu_4N^+, dû à une dissociation incomplète du Bu_4NBr. En se basant sur des itérations des courbes des vitesses observées versus l'activité calculée de l'ion bromure pour les réactions des substrats méthyle-4, diméthyl-3,4 ou non-substitués, on a évalué que $K_{assoc} \sim 15 \pm 1$, à 40°C. On interprète les résultats en fonction d'un support additionnel pour une progression du mécanisme avec l'attaque nucléophile qui est possible à tous les stages des séries d'équilibre: substrat $\rightleftharpoons$ paire d'ion de contact $\rightleftharpoons$ diverses paires d'ions solvatés $\rightleftharpoons$ ions dissociés.

Mots clés : effets de sel spécials, effets de force ionique, racémisation de phényl-1 bromoéthane, mécanisme de substitution nucléophile, mécanisme de paires d'ions.

[Traduit par la revue]

Chemists have long been aware that an important factor in medium effects is ionic strength, which, among other things, changes the dielectric constant and increases ionizing power (1). For reactions in which the ionic strength is changing during the reaction, that is for ion creating (for example, solvolysis of alkyl halides or esters) or ion destroying reactions (for example, ion combination reactions and some additions), ionic strength and hence the medium changes throughout the reaction. To facilitate mechanistic interpretation, it is the usual practice to use high concentrations of inert electrolyte to overwhelm the reaction's contribution to ionic strength.

For reactions such as the Finkelstein Reaction, especially an "identity process" such as $Br^- + RBr^* \rightarrow BrR + Br^{*-}$ as is the case for the studies in the current series of publications, as outlined in Scheme 1, there is no change in ionic strength nor, indeed, in the concentration of any species during the reaction. The addition of inert electrolyte is less critical. Still, even for these reactions, there is a change in charge or charge density in going from reactants to transition state whether the reaction follows the S_N2, S_N1, or an ion-pair mechanism. Consequently, the ability of the medium to support ionic charges, its ionizing power, and hence its ionic strength, can be important. Obviously, varying the concentration of the bromide ion, that is of M^+Br^-, to establish reaction order (2) and to permit separation of uni- and bimolecular components (2, 3), changes the ionic strength, and hence ionizing power, unless inert electrolyte is used to maintain constant ionic strength. Of course, if comparisons of,



G = H, 4-(CH_3, Br, or NO_2), 3-CH_3, 3,4-$(CH_3)_2$

SCHEME 1

Can. J. Chem. Downloaded from www.nrcresearchpress.com by 122.72.124.2 on 09/07/12
For personal use only.

Can. J. Chem. Downloaded from www.nrcresearchpress.com by 122.72.124.2 on 09/07/12
For personal use only.

say racemization and bromide–*radio*-bromide exchange rates, or of one substrate with another, are made at the same M^+Br^- concentrations and temperatures, fixed ionic strengths may not be required. Still, ideally, even for identity processes such as ours, working at constant ionic strength is desirable.

For our initial study of the racemization of chiral 1-phenylbromoethane in acetone with added LiBr, we used $LiNO_3$ to maintain constant lithium ion concentration and, hence, ionic strength (4). The apparent rate constant decreases with increasing LiBr concentration in the absence of added electrolyte but is constant at fixed ionic strength, that is, with constant lithium ion concentration. The falloff in the apparent rate constant with LiBr concentration was assigned to incomplete dissociation; the activity coefficient of Br^- decreases with increasing LiBr concentration. This was later confirmed by using data of Beronius *et al.* (5) for the association of LiBr in acetone to correct for bromide ion activity (2). Beronius and Gupta have reported similar behavior for methyl iodide and Et_4NBr (6).

To follow the bromide–*radio*-bromide exchange kinetics, the silver electrodeposition method of Beronius has been employed (7). Unfortunately, the various lithium salts tested (chlorate, perchlorate, nitrate, picrate...) either interfered with the silver bromide electrodeposition, were themselves incompletely dissociated, or both (4), so that attempts to work at constant ionic strength were abandoned; all subsequent kinetics were done at the same fixed concentrations ranging from 5.00 to 100.00×10^{-4} M in bromide ion. With the extension of the study to the more polar solvents acetonitrile and nitromethane, we found that tetrabutylammonium bromide, Bu_4NBr, was apparently completely dissociated over the concentration range used: plots of observed racemization rate versus Bu_4NBr concentration were linear (3). (In acetone, Bu_4NBr is partially associated, as is LiBr in the two more polar solvents.)

In acetonitrile and nitromethane, those substrates that are able to form more stable carbocations, the 3,4-dimethyl- and the 4-methylphenylbromoethane, racemize at a rate that increases linearly with Bu_4NBr concentration but with a large positive intercept (3). Equation [1] thus applies; k_1 is the intercept that is the first-order or unimolecular rate constant while k_2' is the slope or second-order rate constant for racemization. Since the rate of racemization is twice the inversion rate, $k_2' = 2k_2$ where k_2 is the rate constant for the bimolecular substitution.

$$[1] \quad \text{Observed rate} = k_1 + k_2'[Bu_4NBr]$$

There are, however, problems in apportioning the observed rate in this fashion. Ionization processes are prone to ionic strength effects, normally increasing with ionic strength, an effect that can be quite large in nonpolar solvents but would most likely be only moderate here (*1a*, *1f*). Thus questions remain to be answered. What is the ionic strength effect on the unimolecular process? How significant a contribution does that make to the apparent bimolecular rate? (In the extreme case, all of the apparent bimolecular component could be an ionic strength effect on a unimolecular, carbocation process.) Finally, what is the ionic strength effect on the bimolecular process? (It would be expected to be relatively small and probably negative.)

Unlike the silver bromide electrodeposition used to follow exchange kinetics, racemization studies can readily be done with added electrolyte. Thus the racemizations of the substrates that showed mixed kinetics and several that showed only bimolecular kinetics (3) were reexamined in acetonitrile and in nitromethane at constant and at varying ionic strengths using several electrolytes. In acetone, all substrates racemize with bimolecular kinetics with, at most, a very small unimolecular component (2). The 4-methyl substrate shows considerable internal return with racemization, presumably from a solvated ion pair, while the 3,4-dimethyl substrate shows stereochemical behavior halfway between that expected for an S_N1 and an S_N2 substitution.[1] The ionic strength effect study was extended to acetone solution since, for example, "special salt effects" are possible for those substrates (*1c*, 8, 9).

Finally, while ionic strength or salt effect studies are numerous, especially for solvolyses (1), there are almost none for identity processes such as ours (4, 6). Obviously, studying such effects for strictly bimolecular processes presents problems since very low ionic strengths cannot be used. Without added nucleophile (salt) there can be no substitution. Unimolecular processes or the unimolecular portion of reactions showing mixed kinetics should be more amenable to scrutiny and might show special salt effects (1, 8, 9).

Results

In Tables 1–3 and Figs. 1 and 2 the racemization rate behavior of various substrates, as a function of tetrabutylammonium bromide concentration in acetone, acetonitrile, and nitromethane, are presented. The data is for 40.00 ± 0.05 or 30.00 ± 0.05°C as indicated. With each substrate in each solvent, Bu_4NBr concentrations of 0.0000, 2.500, 5.000, 10.00, 15.00, 20.00, and 25.00×10^{-3} M were used, both without added electrolyte, and at constant ionic strength, i.e., Bu_4N^+ concentration of 25.00×10^{-3} M using ClO_4^- and BF_4^- counterions. In a number of cases, lower concentrations of Bu_4NBr, 0.500, 1.000, 1.500, 2.000, 2.500, 3.000, 3.500, 4.000, and 4.500×10^{-3} molar were also used. When no systematic deviations from linearity for a plot of observed racemization rate versus Bu_4NBr concentration were found, linear regression analysis was applied to the data to extract the second-order or bimolecular substitution rate constant, k_2 (k_2 = slope/2) and the first-order or unimolecular racemization rate constant, k_1 (intercept). These are reported, with the standard deviations, in Table 1. Correla-

[1] A referee has pointed out that the origin of the low $k_{rac}:k_{exch}$ value of 1.52 for 1-(3′,4′-dimethylphenyl)bromoethane in acetone could be quite different from that suggested in ref. 2. The low optical activity, and hence high substrate concentrations, required for the racemizations, together with a little pre-reaction elimination (with concomitant HBr formation), could result in a significant reduction in bromide ion activity through the equilibrium $HBr + Br^- \rightleftharpoons HBr_2^-$ (see, for example, ref. 13). Comparison of the racemization and bromide exchange rates at the same concentrations of LiBr could give the low rate ratio reported. Similar but lesser factors would apply to the *p*-methyl substrates; the actual ratio could be higher than the reported value of 2.36.

Using nmr, F. Y. Fujiwara and J. S. Martin (14) estimated the equilibrium constant for the above equilibrium as $K \approx 200$ in symmetrical tetrachloroethane. They were unable to obtain a value in acetonitrile because of solvent protonation, that is HBr dissociation (see also ref. 15). Like acetonitrile, acetone and nitromethane are "bases" so at least partial dissociation would be expected. Additionally, HCl has been shown to catalyze racemization and chloride exchange with 1-phenylchloroethane in nitromethane according to the equation, rate = $k_1[RCl] + k_2[RCl][HCl]$ (16). It should be noted that if the HBr formed reduces the bromide ion activity, the reaction rate should decrease, not increase, with time as the parallel elimination reaction proceeds. Finally, for the acetone results, LiBr was used; it is incompletely dissociated in that solvent. Bromide ion would be, in effect, "buffered" by the equilibrium $LiBr \rightleftharpoons Li^+ + Br^-$.

Obviously the effect of elimination on the $k_{rac}:k_{exch}$ rate ratio is not simple nor is it easily predicted. Additional work is planned in this area.

TABLE 1. Racemization rate as a function of tetrabutylammonium bromide concentration at fixed (added electrolyte) and varying (no added electrolyte) ionic strengths

Set number	Substrate PhEtBr	Electrolyte used	T (°C)	$k_2(\times 10^{-3}\,L\,mol^{-1}\,s^{-1})$ (slope/2)	$k_1(\times 10^{-5}\,s^{-1})$ (intercept)
Nitromethane solutions					
1	p-NO_2	Bu_4NBF_4	40	4.90±0.04[a]	0.01±0.12
2	p-NO_2	Bu_4NClO_4	40	4.73±0.05[a]	0.03±0.15
3	p-NO_2	—	40	4.80±0.01[a]	0.21±0.05
4	p-CH_3[b,c]	Bu_4NBF_4	40	18.92±0.62	24.50±1.77
5	p-CH_3[b,c]	Bu_4NClO_4	40	19.49±0.46	21.30±1.23
6	p-CH_3	—	40	19.35±0.45	22.41±1.32
7	3,4-diMe[c]	Bu_4NBF_4	30	11.06±0.18	20.78±0.53
8	3,4-diMe[c]	Bu_4NClO_4	30	11.06±0.18	20.26±1.19
9	3,4-diMe	—	30	11.62±0.24	19.96±0.61
Acetonitrile solutions					
10	p-NO_2	Bu_4NBF_4	40	7.93±0.04[d]	0.13±0.11[d]
11	p-NO_2	Bu_4NClO_4	40	7.89±0.05[d]	0.05±0.14[d]
12	p-NO_2	—	40	7.90±0.06[d]	0.18±0.20[d]
13	p-CH_3[c]	Bu_4NBF_4	40	20.74±0.47	6.92±1.33
14	p-CH_3[c]	Bu_4NClO_4	40	21.40±0.54	6.21±1.65
15	p-CH_3	—	40	21.83±0.37	5.00±1.13
16	3,4-diMe[c,e]	Bu_4NBF_4	30	13.63±0.36	3.25±1.19
17	3,4-diMe[c,f]	Bu_4NClO_4	30	12.09±0.03	7.40±0.06
18	3,4-diMe	—	30	12.89±0.24	5.72±0.69
Acetone solutions[g]					
19	Unsubstituted	Bu_4NBF_4	40	17.62±0.18	0.40±0.43
20	p-CH_3	Bu_4NBF_4	40	33.32±0.15	0.79±0.35
21	3,4-diMe	Bu_4NBF_4	40	40.98±0.35	0.32±0.92

[a]Average rate constant from kinetic runs: constant ionic strength, $k_2 = (4.894 \pm 0.006) \times 10^{-3}$ L mol^{-1} s^{-1}; no added electrolyte, $k_2 = (4.901 \pm 0.005) \times 10^{-3}$ L mol^{-1} s^{-1}.
[b]Rate deviates upward for low Bu_4NBr concentration but high ionic strength; for $[Bu_4NBr] = 0$, $[Bu_4NClO_4] = 0.000 \rightarrow 0.025$ M, average $k_{obs} = (26.13 \pm 0.38) \times 10^{-5}$ s^{-1}.
[c]Lowest Bu_4NBr concentrations omitted because of upward deviation of rate.
[d]Average rate constants from three data sets: $k_2 = (7.90 \pm 0.03) \times 10^{-3}$ L mol^{-1} s^{-1}; $k_1 = (0.122 \pm 0.084) \times 10^{-5}$ s^{-1}.
[e]Values below $[Bu_4NBr] = 0.010$ M omitted.
[f]Values below $[Bu_4NBr] = 0.015$ M omitted.
[g]Other sets show deviations from linearity throughout, see Figs. 3 and 4.

TABLE 2. Observed rates of racemization of 4-methylphenylbromoethane in acetone at 40°C

	Observed rate constant ($\times 10^{-5}$ s^{-1})		
		Constant ionic strength = 0.0250 M	
$[Bu_4NBr]$, M	No added electrolyte	Bu_4NBF_4	Bu_4NClO_4
0.0250	168.41±0.37	168.41±0.37	168.41±0.37
0.0200	139.17±0.49	135.55±0.22	132.70±0.36
0.0150	107.38±0.26	99.47±0.15	98.43±0.14
0.0100	78.01±0.10	66.15±0.16	64.87±0.17
0.0050	41.98±0.08	34.31±0.08	31.79±0.04
0.0025	22.87±0.10	17.29±0.04	15.25±0.02
0.0020	18.13±0.04	13.48±0.02	—
0.0015	14.02±0.03	10.78±0.01	—
0.0010	9.66±0.04	7.90±0.02	—
0.0005	5.18±0.03	4.34±0.03	—
0.0000	0.24±0.04	1.17±0.06	0.23±0.02

tion coefficients ranged from excellent for 4-nitrophenylbromoethane (R = 0.9998–0.99998) and phenylbromoethane (R = 0.9996–0.9999) to fair for 3,4-dimethylphenylbromoethane (R = 0.997–0.9995). In obtaining the initial rate data, that is, the individual observed rates for the lowest bromide ion concentrations with the methyl- and dimethyl-substituted substrates, initial slopes were used. Sometimes as little as one sixth of a half-life was used because elimination, a competing reaction, results in increasing bromide ion concentration and, hence, an increase of racemization rate with time (refs. 2, 3. See also footnote 1). Even with the above substrates at higher bromide ion concentrations, generally two to three half-lives were used and, with the nitro- and unsubstituted substrates, three to five.

Results for several systems that did not show good linear observed rate of racemization versus Bu_4NBr concentration behavior are presented in Figs. 1–4. Figure 1 shows the rate behaviour of 1-(3′,4′-dimethylphenyl)bromoethane in nitromethane (set of curves with the higher intercepts) and in acetonitrile (set of curves with the lower intercepts) with curves labelled A through E for Bu_4NBr alone (A), for Bu_4NBr at constant ionic strength with Bu_4NClO_4 (B), for Bu_4NBr with Bu_4NBF_4 (C), for Bu_4NClO_4 alone (D), and finally for Bu_4NBF_4 alone (E). The greatest deviations were found for the same substrate in acetonitrile with Bu_4NClO_4 as electrolyte, so these results are shown separately in Fig. 2. Curves labelled A, B, and D are analogous to those in the previous figure, curve E is the racemization rate versus $[Bu_4NClO_4]$ at $[Bu_4NBr]$ = 0.00100 M. Results for various substrates in acetone are presented in Figs. 3 and 4. Rate data for specific concentrations

Can. J. Chem. Downloaded from www.nrcresearchpress.com by 122.72.124.2 on 09/07/12
For personal use only.

TABLE 3. Racemization data in acetone at 40°C corrected for association of Bu_4NBr, K_{assoc} = 15; no added electrolyte

Bu_4NBr ($\times 10^{-3}$ M)	Free Br^- ($\times 10^{-3}$ M)	Observed rate constant ($\times 10^{-5}$ s^{-1})		
		Unsubstituted	4-CH_3	3,4-diMe
25.0	19.37	88.70	168.41	207.31
20.0	16.11	74.04	139.17	164.72
15.0	12.61	56.59	107.38	136.11
10.00	8.83	40.55	78.01	92.24
5.00	4.67	21.845	41.98	49.14
2.50	2.41	12.157	22.87	25.19
2.00	1.94	9.784	18.13	21.41
1.50	1.47	7.752	14.02	17.59
1.00	0.985	5.289	9.66	11.18
0.500	0.496	2.771	5.18	7.10
0.000	0.000	0.200	0.24	0.40
Slope ($2k_2 \times 10^{-3}$ L mol^{-1} s^{-1})		45.24±0.24	85.83±0.45	104.96±1.10
Intercept ($k_1 \times 10^{-5}$ s^{-1})		0.73±0.22	1.25±0.41	0.84±1.00
Corr. coefficient		0.99987	0.99988	0.99950

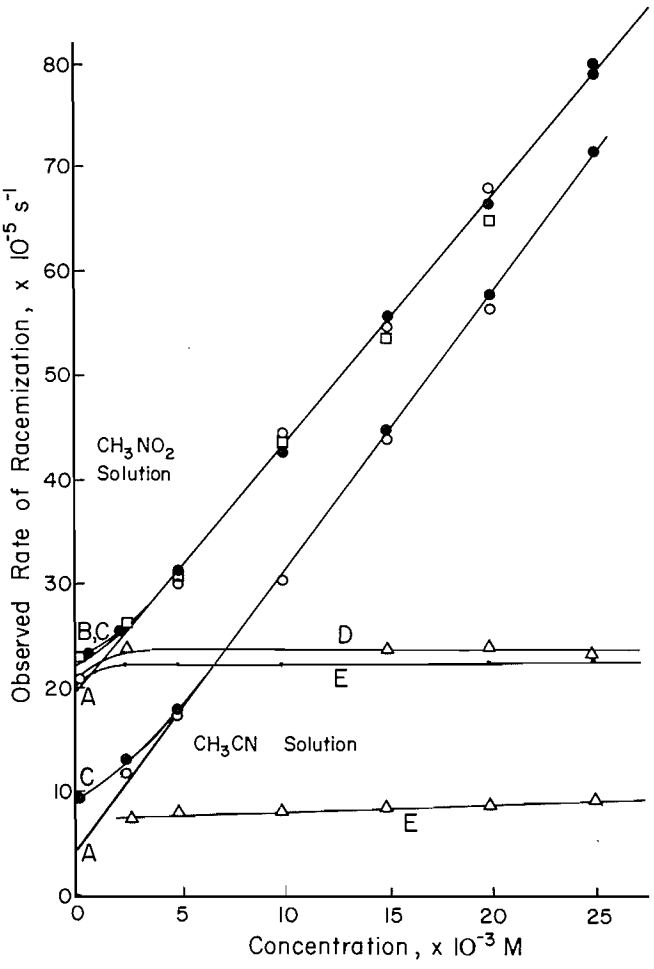


FIG. 1. Observed rate of racemization of 3,4-diMe substrate versus concentration of salt, in CH_3NO_2 and in CH_3CN at 30°C. A, vs. [Bu_4NBr], no added electrolyte; B, vs. [Bu_4NBr], ionic strength = 0.025 M with Bu_4NClO_4; C, vs. [Bu_4NBr], ionic strength = 0.025 M with Bu_4NBF_4; D, vs. [Bu_4NClO_4], no added Bu_4NBr; E, vs. [Bu_4NBF_4], no added Bu_4NBr.

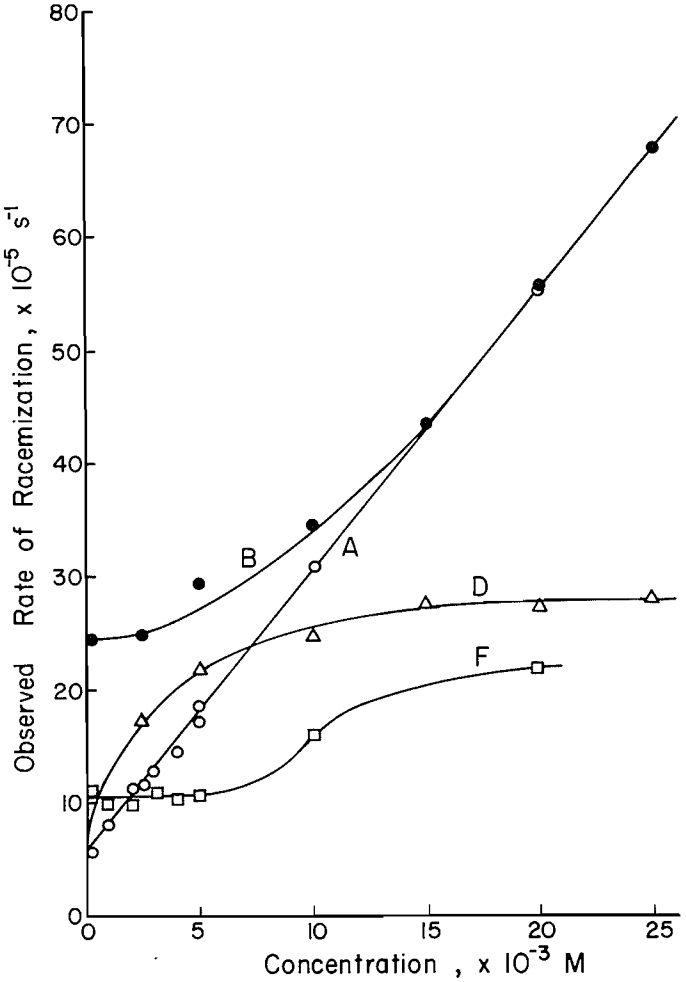


FIG. 2. Observed rate of racemization of 3,4-diMe substrate versus concentration of salt, in CH_3CN at 30°C. A, vs. [Bu_4NBr], no added electrolyte; B, vs. [Bu_4NBr], ionic strength = 0.025 M with Bu_4NClO_4; D, vs. [Bu_4NClO_4], no added Bu_4NBr; F, vs. [Bu_4NClO_4] with [Bu_4NBr] = 0.00100 M.

Can. J. Chem. Downloaded from www.nrcresearchpress.com by 122.72.124.2 on 09/07/12
For personal use only.

Can. J. Chem. Downloaded from www.nrcresearchpress.com by 122.72.124.2 on 09/07/12
For personal use only.

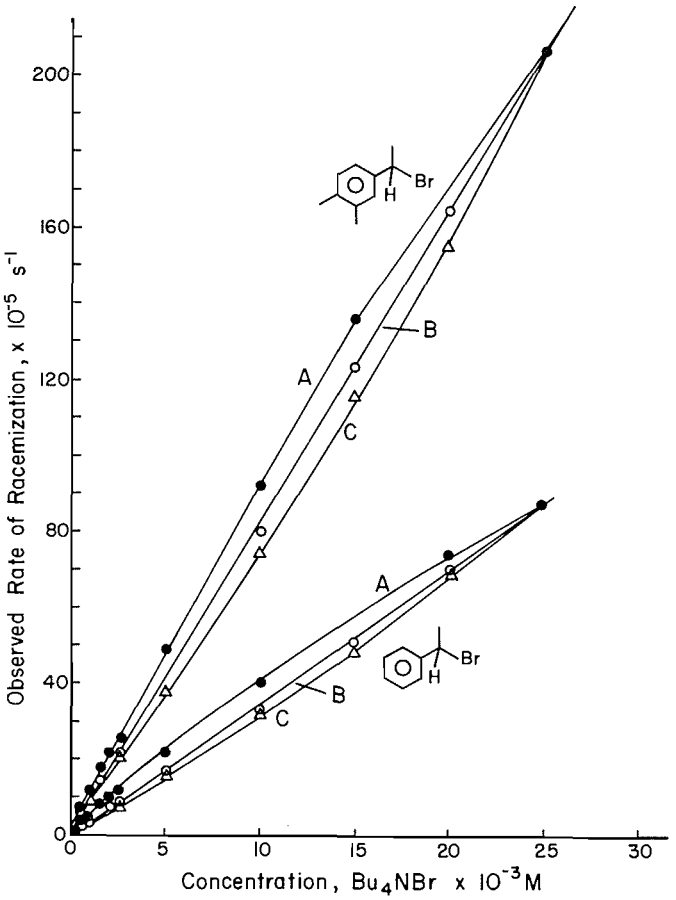


FIG. 3. Observed rate of racemization of 3,4-dimethyl and unsubstituted substrate versus concentration of Bu_4NBr in acetone, 40°C. A, no added electrolyte; B, ionic strength = 0.025 M with Bu_4NBF_4; C, ionic strength = 0.025 M with Bu_4NClO_4.

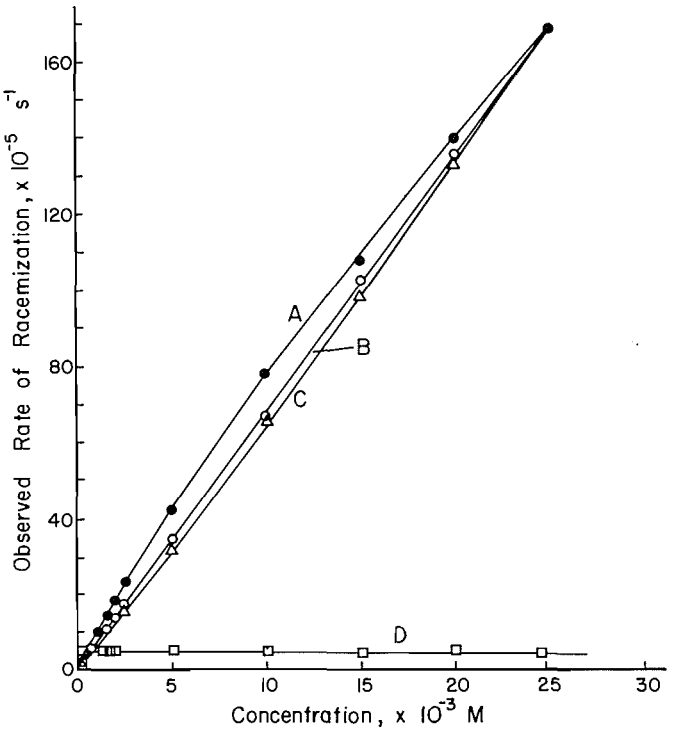


FIG. 4. Observed rate of racemization of 4-methyl substrate versus concentration of salt in acetone, 40°C. A, vs [Bu_4NBr], no added electrolyte; B, vs. [Bu_4NBr], ionic strength = 0.025 M with Bu_4NBF_4; C, vs. [Bu_4NBr], ionic strength = 0.025 M with Bu_4NClO_4; D, vs. [Bu_4NBF_4], [Bu_4NBr] = 0.00050 M.

of Bu_4NBr and of electrolyte in acetone are presented in Tables 2 and 3.

Discussion

Incomplete dissociation

In acetonitrile and nitromethane, even at the highest concentration used, 0.025 M, the Bu_4NBr is apparently completely dissociated. With the 4-nitro substrate, excellent linearity is obtained in the plot of observed rate vs. [Bu_4NBr] and the plots for constant and variable ionic strength are coincident as can be seen from the data presented in Table 1 (Sets 1, 2, 3, and 10, 11, 12). The intercept in all cases is, essentially, zero; there is at most a negligible unimolecular component.

In acetone the Bu_4NBr is not completely dissociated. Figures 3 and 4, curves A, show that in the absence of added electrolyte the rate falls off with increasing Bu_4NBr concentration due to partial association of the salt, probably simply as ion pairs (1*a*). Use of an iterative method for best fit with the data for each of the three substrates allows estimation of $K_{assoc} = 15 \pm 1$ for Bu_4NBr in acetone at 40°C. Table 3 contains the actual rate constants, the calculated activity for the bromide ion, and the resultant slopes and intercepts and correlation coefficients for unsubstituted, 4-methyl-, and 3,4-dimethyl-phenylbromoethanes.

As Figures 3 and 4 also show, the effect of working at constant ionic strength in acetone is also different from that for the 4-nitro substrate in acetonitrile or nitromethane. In acetone, good linearity of rate vs. [Bu_4NBr] is obtained if Bu_4NBF_4 is used as the electrolyte to maintain constant ionic strength (Figs. 3 and 4, curves B; Table 1, sets 19, 20, 21). With Bu_4NClO_4, the rate profile is concave (Figs. 3 and 4, curves C). These results suggest that the association constant for Bu_4NBF_4 is about equal to that of Bu_4NBr. Constant ionic strength would then maintain constant Bu_4N^+ activity and hence Br^- activity would vary linearly with Bu_4NBr concentration, resulting in the observed rate behavior. By contrast, the association constant for the perchlorate salt is less than that for Bu_4NBr. Consequently, the higher activity of Bu_4N^+ leads to association of more of the bromide, reduced Br^- activity, and a dip in the rate profile.

Ionic strength effects

For all data sets in acetone, whether the rate ratio of racemization to bromide–*radio*-bromide exchange is 2.0 as for unsubstituted, 2.4 as for 4-methyl, or 1.5 as for 3,4-dimethyl substrate (2, 3), there is no or very little apparent ionic strength effect other than that due to incomplete dissociation of the nucleophile (see above). As Figs. 3 and 4 show, all substrates give essentially a zero intercept both with and without added electrolyte. Also, the lower line of Fig. 4, curve D, illustrates the typical behavior of racemization rate with added electrolyte. For the 4-methyl substrate at [Bu_4NBr] = 5.00×10^{-4} M, the observed rate constant changes from 5.38 ± 0.04 through 5.19 ± 0.01 to 4.34 ± 0.03 for ionic strengths of 0.500, 2.500, and 25.00 $\times 10^{-3}$ M (with BF_4^- counterion).[2] This very small

[2]Linear regression for the observed rate constant vs. ionic strength gives an intercept (k_{obs}) of $(5.33 \pm 0.04) \times 10^{-5}$ s^{-1} and a slope of $(-4.31 \pm 0.39) \times 10^{-4}$ L mol^{-1} s^{-1} for Winstein's *b*-value (ref. 1*c*).

Can. J. Chem. Downloaded from www.nrcresearchpress.com by 122.72.124.2 on 09/07/12
For personal use only.

decrease in observed rate upon going from a Br^- to BF_4^- ratio of infinity to very low (2×10^{-2}) and an ionic strength increase of 50-fold, could arise from a very small negative salt effect or, perhaps equally likely, from a small change in bromide ion activity as the Bu_4N^+ concentration was changed, also 50-fold.

Similarly, for the 4-nitro substrate in acetonitrile and in nitromethane (Table 1, sets 1, 2, 3, and 10, 11, 12 respectively), there is no evidence of a significant ionic strength effect. With no bromide salt added, there is no change in optical rotation for hours whether the solution is 0.00 or 25.00×10^{-3} M in electrolyte, and the constant and varying ionic strength plots of observed rate versus [Bu_4NBr] are coincident throughout. Clearly the observed rate constants are unaffected by added electrolyte.

For those substrates showing mixed kinetics in acetonitrile and nitromethane, a different picture emerges. For 3,4-dimethyl substrate for example, as shown in Fig. 1, good colinearity for the observed rate of racemization at fixed and with varying ionic strength still applies at all but the lowest Bu_4NBr concentrations in nitromethane with Bu_4NBF_4 and Bu_4NClO_4 and in acetonitrile with Bu_4NBF_4. The data points that deviate significantly upwards from the line at low Bu_4NBr concentration were omitted in calculating the first- and second-order rate constants reported in Table 1 (sets 4–9, 13–18). Deviations are most pronounced for 3,4-dimethylphenylbromoethane in acetonitrile with Bu_4NClO_4, so the results illustrated in Fig. 2 will be considered first.

Curve A of Fig. 2, despite some scatter at low concentrations of Bu_4NBr, shows that the reaction rate increases linearly with nucleophile concentration. When Bu_4NClO_4 is used to maintain fixed ionic strength (curve B), the rate deviates markedly upward for low Br^-, high ClO_4^- concentrations. Since perchlorate ion is unlikely to serve as a nucleophile—ClO_4^- is recognized as an extremely poor nucleophile and alkyl perchlorates are very reactive (1, 10)—the deviation represents a salt effect. At higher bromide ion concentrations, the curves for fixed ionic strength and for no added electrolyte converge. Thus using the three highest Bu_4NBr concentration points for the constant ionic strength data set and all data points for the set with no added electrolyte gives slopes differing by only about six percent (Table 1, sets 17, 18). This establishes that the salt effect is principally in the unimolecular component of the reaction.

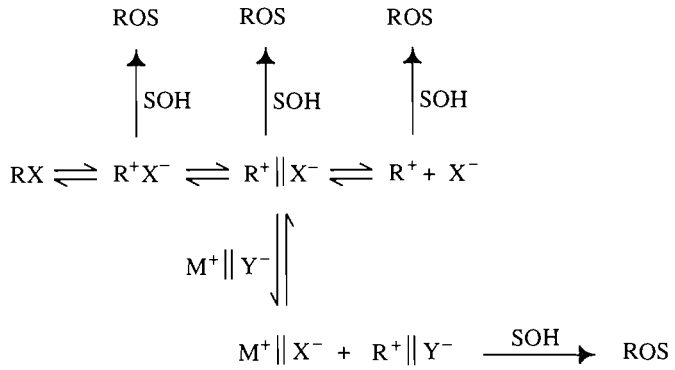
Special salt effects

There is apparently a special salt effect (1*c*) operating. Curve D of Fig. 2 shows the rate profile without any Bu_4NBr added as a function of ionic strength, i.e., concentration of Bu_4NClO_4 in acetonitrile. Initial rates of racemization were used because the liberated bromide ion from elimination serves as a nucleophile in racemization and the rate accelerates with time (ref. 2, see also footnote 1). For the data of curve D, generally only one fifth to one tenth of a half-life was used. Similarly, for the data of curve F and the lower bromide ion concentrations of curves A and B initial slopes were used but generally from larger fractions of a half-life. The short runs and the accelerating rates account for the scatter and poorer reproducibility. Still, the concentration – rate profiles of curves B and D clearly show a special salt effect.

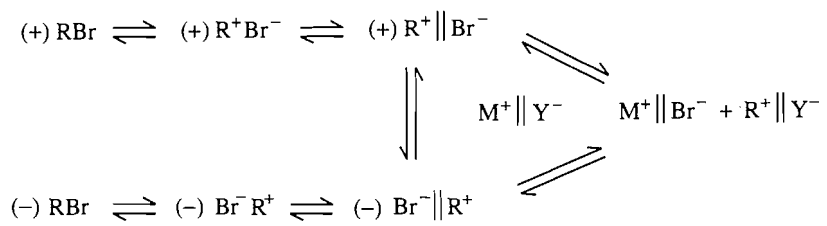
Special salt effects have been observed regularly since Winstein *et al.* first reported them about 35 years ago (1*c*). They are most commonly reported for solvolysis reactions with substrate giving quite stable carbocations, such as benzhydryl (8*f*) and 4-methyl or methoxybenzyl carbocations (1*c*), and carbocations that are sterically hindered to back-side nucleophilic attack, such as cholesteryl (1*a*), norbornyl (1*c*), and β-phenylethyl systems that react, at least in part, with assistance by the phenyl group (1*c*, 8*b*,*d*). Special salt effects have been reported for the addition of aryl sulfenyl chlorides, ArSCl, to rigid alkenes (8*e*) where the resultant ion pair must solvate so the chloride ion can migrate to the carbocation centre and, also, for other ArSCl reactions (8*g*). In all of these cases, the special salt effect is manifest kinetically as a marked rate acceleration at low ionic strengths. Recently special salt effects that manifest themselves as a marked rate deceleration have been reported for photolysis or pulsed radiolysis generated ion pairs (9). Thus time-resolved or picosecond spectroscopy of photogenerated charge-transfer ion pairs, from aromatic hydrocarbons and tetranitromethane (9*a*), and from benzophenones and dialkylanilines (9*b*), show special salt effects that markedly extend the lifetime of the ion pairs. Here, as for the solvolysis studies, special salt effects manifest themselves when ion pair exchange gives a new ion pair for which collapse is undesirable. Ion lifetimes are increased and, sometimes, other reaction pathways can compete with initial ion-pair collapse. For the solvolysis studies, the effects were noted in moderately ionizing but weakly nucleophilic solvents, especially in acetic acid. For the other studies, solvents were generally aprotic, ranging in polarity from ethers and dimethoxyethane through dichloromethane to acetonitrile and nitromethane.

Winstein's explanation of the special salt effect has stood the test of time (1*c*). Briefly, in a solvolysis situation, such effects reflect interception of an ion pair, formed reversibly from the substrate, by ion-pair exchange with a non-nucleophilic salt, typically $LiClO_4$. The carbocation–perchlorate ion pair then proceeds to give solvolysis products as illustrated in Scheme 2.

A similar mechanism is, no doubt, operating in our case. The ion pair formed from the 3,4-dimethylphenylbromoethane exists as various solvated ion pairs in equilibrium with the substrate. In the absence of any nucleophile, racemization requires a moderate degree of ion-pair separation and solvation to facilitate bromide ion migration or carbocation rotation and hence collapse of the ion pair with racemization. Added non-nucleophilic salt such as Bu_4NClO_4 facilitates such ion-pair separation and bromide ion migration by "ion-pair exchange," resulting in a marked increase in the observed rate of racemization. This mechanism is confirmed by the "competition" between added nucleophile, Bu_4NBr, and inert electrolyte, Bu_4NClO_4, as shown in Fig. 2, Curve F. Even at very low concentrations, the bromide ion competes very effectively with the perchlorate special salt effect: the rate is independent of



SCHEME 2. Special salt effects in solvolysis.



SCHEME 3. Special salt effects on internal return with racemization.

perchlorate concentration until it is more than five times that of the bromide ion.

Simon and Peters (9*b*) have presented evidence that the species most efficient at undergoing ion-pair exchanges are ones with similar degrees of separation; contact ion pairs exchange best with contact ion pairs, solvent separated ion pairs with solvent separated ones. Other results are also best interpreted in this fashion (8*f*, 9*c*). Thus a possible explanation of the special salt effect in our racemization studies is presented in Scheme 3. For simplicity, only two types of ion pairs, contact (R^+Br^-) and solvent separated ($R^+||Br^-$), are included even though dissociation of contact ion pairs must be progressive or stepwise with one, two, three ... "layers" of solvent separating the ions.

With Scheme 3 as a model, the solvent separated ion pairs must return to substrate faster than they undergo inversion and, hence, return with racemization, possibly because quite-well-separated ions are required for the carbocation inversion (or bromide ion migration). The presence of an "inert" ion pair, $Bu_4N^+||ClO_4$, introduces a new, faster-pathway, ion-pair exchange–reexchange to facilitate the racemization. With added bromide ion, an additional pathway for racemization/inversion, a nucleophile assisted one, is introduced. This latter pathway, which is not included in Scheme 3, competes very successfully with the special salt effect as shown by curve F of Fig. 2.

The special salt effects with Bu_4NBF_4 are much less pronounced in acetonitrile and in nitromethane. In the latter solvent, as can be seen in Fig. 1, deviations from linearity, from the line with no added electrolyte (curve A), are much smaller with either Bu_4NClO_4 (curve B) or Bu_4NBF_4 (curve C). As in acetonitrile, in nitromethane Bu_4NClO_4 shows the greater, if reduced, special salt effect (curve D vs. curve E). If Simon and Peters (9*b*) are correct, less of the Bu_4NBF_4 than of the Bu_4NClO_4 is in the appropriately solvated ion pair in both acetonitrile and nitromethane, but both salts have less of that ion pair in the latter solvent. The special salt effect pathway of Scheme 2 is thus less competitive with the "unassisted" pathway.

The salt effects and special salt effects for 4-methylphenylbromoethane with Bu_4NClO_4 in acetonitrile and nitromethane are analogous but considerably less marked. For the other substrates and for all substrates in acetone, no salt effect other than those attributable to incomplete dissociation of Bu_4NBr is found. This is presumably because the separation of contact ion pairs to solvated ones is too limited. Racemization requires nucleophile involvement of ionic bromide.

Conclusions

Special salt effects have traditionally been observed for solvolysis reactions that are forced to go via a unimolecular mechanism, *exo*-norbornyl toluenesulfonate for example (1*c*), or for which a carbocation is especially stable, 2-(4-methoxyphenyl)ethyl toluenesulfonate for example (8*d*). Thus it is not surprising that special salt effects appear only in the racemization of 3,4-dimethyl- and 4-methylphenylbromoethanes in the moderately ionizing solvents, acetonitrile and nitromethane, and then only in the absence of appreciable concentrations of bromide ion nucleophile, that is, for the unimolecular racemization. No other salt effect was detected in these more polar solvents. In acetone, a common ion effect by Bu_4N^+ on the dissociation of Bu_4NBr leads to a rate depression at high electrolyte concentrations, but no other salt effect was noted.

These results establish the validity of the separation of uni- and bimolecular components using eq. [1] (3). They also lend further support for racemization via internal return from solvated ion pairs. Additionally, the very successful competition of bromide ion with Bu_4NClO_4 or Bu_4NBF_4 for the substrate ion pair from 3,4-dimethyl- and 4-methylphenylbromoethane in acetonitrile and in nitromethane suggests there is an ion-pair process involved in the bimolecular racemization as well.

Together with our previously published results, these studies support a mechanistic progression for nucleophilic substitution at saturated carbon. Using bromide ion as the nucleophile with arylbromoethanes, we find systems showing cleanly bimolecular kinetics where there is a one-to-one correlation of bromide substitution and inversion of stereochemistry (e.g., phenylbromoethane in acetone (2, 4) or other solvents (3)), where there is an excess of inversion (i.e., internal return with racemization also occurs, e.g., 4-methylphenylbromoethane in acetone (2)), and where there is "mixed stereochemistry" (i.e., exchange with racemization accompanies exchange with inversion, e.g., 3,4-dimethylphenylbromoethane in acetone (2)). Other reactions show mixed unimolecular and bimolecular kinetics, ranging from almost exclusively bimolecular (e.g., 3-methylphenylbromoethane in acetonitrile (3)) to those having a major unimolecular component (e.g., 3,4-dimethylphenylbromoethane in nitromethane (3)), and now we have shown that the unimolecular reaction can be markedly accelerated by the addition of inert electrolyte. Thus, depending upon substrate, nucleophile, leaving group, medium, and other factors, nucleophilic substitution can, and presumably does, occur at any stage of the ionization/dissociation process, substrate $\rightleftharpoons$ intimate ion pair $\rightleftharpoons$ variously solvated ion pairs $\rightleftharpoons$ dissociated or free ions. Kinetics and stereochemistry run the gamut from those expected for the classical S_N2 to the classical S_N1 mechanisms with, apparently, no clear demarcations between them. Such conclusions are in broad agreement with those of others (12).

Experimental

Reagent, Analar, or HPLC grade solvents were stored over and freshly distilled, with moderate reflux ratio, from calcium hydride under tank dry nitrogen, which was further dried by bubbling through concentrated sulfuric acid followed by a column of type 3A molecular sieves. Analytical or reagent grade tetrabutylammonium bromide (Eastman), perchlorate (Baker), and fluoroborate (Aldrich) were dried

Can. J. Chem. Downloaded from www.nrcresearchpress.com by 122.72.124.2 on 09/07/12
For personal use only.

by pumping overnight at <0.1 Torr (1 Torr = 133.3 Pa) at 50–60°C. The salts were stored under vacuum or, for relatively short periods, tightly stoppered in the dry nitrogen filled glove box. After distillation and (or) drying, all weighings, transfers, and dilutions were done in the glove box using oven-dried glassware throughout. Stock solutions, $(2.500 \pm 0.005) \times 10^{-2}$ M, of the various salts were prepared and stored for up to several weeks in hypo-vials with Teflon coated septa. The chiral arylbromoethanes were prepared as previously described (11).

Racemization kinetics were followed using a Perkin–Elmer model 141MC polarimeter equipped with a potentiometric recorder. Solutions were prepared by directly pipetting a total of 5 mL of the appropriate stock or diluted stock solution(s) and (or) solvent into the 10-cm jacketted quartz cell. A known mass of substrate, 20–100 mg depending on the optical activity as previously described (2), was then added by syringe. The Teflon stoppers were inserted, the cell was removed from the glove box and connected to the circulatory constant-temperature bath operating at 30.00 or 40.00 ± 0.05°C. While the cell was equilibrating, the contents were thoroughly mixed by tilting and shaking the cell for several minutes. The cell was inserted into the polarimeter and the rotation change followed for usually 4–5 half-lives at 365 nm or, with nitromethane solutions or 4-nitrophenylbromoethane, at 434 nm. Infinity values differed very little from the no-cell zero value, so the latter was used in determining k_{obs}, i.e., the slope from the standard linear regression treatment of rotation vs. time data (as read from the recorder chart output) for the pseudo-first-order reactions.

1. (*a*) C. K. INGOLD. Structure and mechanisms in organic chemistry. 2nd ed. Bell and Sons Ltd., London. 1969. pp. 483–508; (*b*) L. P. HAMMETT. Physical organic chemistry. McGraw-Hill, New York. 1940. pp. 89–95; 2nd ed. 1970. Chap. 7, pp. 187–219; (*c*) S. WINSTEIN, B. APPEL, R. BAKER, and A. DIAZ. Organic reaction mechanisms. Special Publication No. 19, Chemical Society, London. 1965. p. 109; (*d*) D. J. RABER, J. M. HARRIS and P. V. R. SCHLEYER. *In* Ions and ion pairs in organic reactions. Vol. 2. *Edited by* M. Swarc. Wiley–Interscience, New York. 1974. p. 247; (*e*) J. M. HARRIS. Prog. Phys. Org. Chem. **11**, 89 (1974); (*f*) C. A. BUNTON, T. W. DELPESCO, A. M. DUNLOP, and K.-U. YANG. J. Org. Chem. **36**, 887 (1971).
2. A. R. STEIN and E. A. MOFFATT. Can. J. Chem. **63**, 3433 (1985).
3. A. R. STEIN. Can. J. Chem. **65**, 363 (1987).
4. A. R. STEIN. J. Org. Chem. **41**, 519 (1976); **38**, 4022 (1973).
5. P. BERONIUS, U. ISACSSON, and A.-M. NILSSON. Acta Chem. Scand. **24**, 189 (1970).
6. P. BERONIUS and R. P. GUPTA. Acta Chem. Scand. Ser. A: **A30**, 477 (1976).
7. P. BERONIUS. Trans. R. Inst. Technol. Stockholm. No. 213. 1963.
8. (*a*) L. P. HAMMETT. Physical organic chemistry. 2nd ed. McGraw-Hill, New York. 1970, pp. 165–167; (*b*) L. S. MILLER, D. ZAZZARON, and J. J. DANNENBERG. J. Org. Chem. **45**, 641 (1980); (*c*) V. P. VITULLO and F. P. WILGIS. J. Am. Chem. Soc. **103**, 1982 (1981); **103**, 880 (1981); **97**, 458 (1975); (*d*) R. FUJIYAMA, S. KIYOOKA, K. FUNATSU, M. FUJIO, and Y. TSUNO. Mem. Fac. Sci. Kyushu Univ. Ser. C: **13**, 117 (1981); M. FUJIO, Y. SEKI, R. FUJIYAMA, M. MISHIMA, and Y. TSUNO. Mem. Fac. Sci. Kyushu Univ. Ser. C: **13**, 71 (1981); (*e*) M. I. VINNIK, N. S. ZEFIVOV, I. S. KISLINA, A. S. KOZ'MIN, R. CAPLE, and A. G. NIKITIN. Dokl. Akad. Nauk SSSR, **277**, 1142 (1984); (*f*) E. A. PONOMAREVA, T. L. PERVISHKO, G. F. DVORKO, and A. I. VASIL'KEVICH. Org. React. (Tartu), **21**, 70 (1984) and references therein; (*g*) E. N. GIVENS and J. J. KWART. J. Am. Chem. Soc. **90**, 378 (1968); **90**, 386 (1968); E. CIUFFARINS and F. GRISELLI. J. Am. Chem. Soc. **92**, 6015 (1970).
9. (*a*) S. SANKARARAMAN, W. A. HANEY, and J. K. KOCHI. J. Am. Chem. Soc. **109**, 7824 (1987); J. M. MASNOVI, A. LEVINE, and J. K. KOCHI. J. Am. Chem. Soc. **107**, 4356 (1985); **107**, 7880 (1985); (*b*) J. D. SIMON and K. S. PETERS. J. Am. Chem. Soc. **105**, 4875 (1983); **104**, 6142 (1982); (*c*) Y. YAMAMOTO, S. NISHIDA, and K. HAYASHI. J. Chem. Soc. Faraday Trans. 1, **83**, 1795 (1987).
10. R. E. ROBERTSON, A. ANNESA, and J. M. W. SCOTT. Can. J. Chem. **53**, 3106 (1975).
11. A. R. STEIN, R. D. DAWE, and J. R. SWEET. Can. J. Chem. **63**, 3443 (1985).
12. (*a*) T. H. LOWRY and K. S. RICHARDSON. Mechanism and theory in organic chemistry. 3rd ed. Harper and Row, New York. 1987. pp. 341–349; (*b*) A. R. KATRITZKY and B. E. BRYCKI. J. Phys. Org. Chem. **1**, 1 (1988); (*c*) D. J. MCLENNAN, A. R. STEIN, and B. DOBSON. Can. J. Chem. **64**, 1201 (1986).
13. D. N. KEVILL and N. H. CROMWELL. J. Am. Chem. Soc. **83**, 3812 (1961); **83**, 3815 (1961).
14. F. Y. FUJIWARA and J. S. MARTIN. J. Am. Chem. Soc. **96**, 7625 (1974); J. Chem. Phys. **56**, 4091 (1972).
15. J. F. COETZEE. Prog. Phys. Org. Chem. **4**, 45 (1967).
16. Y. POCKER, W. A. MUELLER, F. NASCO, and G. TOCCHI. J. Am. Chem. Soc. **86**, 5012 (1964).

Can. J. Chem. Downloaded from www.nrcresearchpress.com by 122.72.124.2 on 09/07/12
For personal use only.

Counterion micellar effects upon the reaction of low-spin diimine iron(II) complexes

FRANCISCO ORTEGA AND ELVIRA RODENAS[1]

Departamento de Química Física, Universidad de Alcalá de Henares, Alcalá de Henares, Madrid, Spain

Received August 25, 1987[2]

FRANCISCO ORTEGA and ELVIRA RODENAS. Can. J. Chem. **67**, 305 (1989).

The rate of reaction of tris(1,10-phenanthroline)iron(II) ion (**1***a*), tris(3,4,7,8-tetramethyl-1,10-phenanthroline)iron(II) ion (**1***b*), and tris(4,7-diphenyl-1,10-phenanthroline)iron(II) ion (**1***c*) with hydroxide ion, in cationic micelles, is strongly affected by the concentration of micellar counterion in solution. The reaction of **1***a* in CTACl is modestly speeded up by the addition of added KCl, while the reactions of **1***b* and **1***c* are strongly inhibited by the addition of large amounts of KCl and KBr to micellar solutions of CTACl and CTABr, respectively. These rate effects fit the pseudophase-ion exchange model, assuming the binding of the substrates to the micelles depends upon the counterion concentration.

Key words: counterion micellar effects, low-spin diimine iron(II) complexes.

FRANCISCO ORTEGA et ELVIRA RODENAS. Can. J. Chem. **67**, 305 (1989).

La vitesse de réaction de l'ion hydroxyde avec les ions tris(phénanthroline-1,10)fer(II) (**1***a*), tris(tétraméthyl-3,4,7,8 phénanthroline-1,10)fer(II) (**1***b*) et tris(diphényl-4,7 phénanthroline-1,10)fer(II) (**1***c*), dans des micelles cationiques, est fortement influencée par la concentration des contre-ions dans la solution micellaire. La vitesse de la réaction du composé **1***a*, dans le CTACl, est légèrement plus rapide lorsqu'on ajoute du KCl; par ailleurs, les vitesses de réaction des composés **1***b* et **1***c* sont fortement inhibées par l'addition de grandes quantités de KCl et de KBr à des solutions respectivement de CTACl et de CTABr. Si l'on fait l'hypothèse que la liaison des substrats aux micelles dépend de la concentration du contre-ion, ces effets sur les vitesses des réactions sont en accord avec le modèle d'échange ionique pseudophase.

Mots clés : effets des contre-ions dans des micelles, complexes de diimine fer(II) « low-spin ».

[Traduit par la revue]

Introduction

The rates of many bimolecular reactions are known to be affected by micellized aqueous surfactant. It is now generally accepted that this effect arises primarily from the concentration of both reactants in the small volume of the Stern-layer of micelles (1–6).

For a large number of bimolecular reactions, micellar effects have been interpreted using the pseudophase-ion exchange model (2, 5), assuming that the fraction β of micellar bound counterions is constant and independent of counterion and surfactant concentration. However, several different physical measurements suggest that β increases on addition of counterions (7, 8), and a variety of kinetic results in the literature either at high counterion concentration (9–11) or with hydrophilic reactive counterions (12–14) cannot be explained by this model.

In earlier papers (15, 16) we published results on the reaction of some diimine iron(II) complexes with hydroxide and cyanide ions in cationic micelles (CTABr, CTACl, CTAOH, and CTACN, where CTA is cetyltrimethylammonium). The results were interpreted using the pseudophase-ion exchange and mass-action models, taking into account the very important "salting-out" of the substrates into the micelles. In view of these results, we studied the effect of added counterions, Br^- and Cl^-, on the reaction of tris(1,10-phenanthroline)iron(II) ion (**1***a*), tris(3,4,7,8-tetramethyl-1,10-phenanthroline)iron(II) ion (**1***b*) and tris(4,7-diphenyl-1,10-phenanthroline)iron(II) ion (**1***c*) with hydroxide ion in presence of CTAB and CTACl micelles. Our aim was to test the pseudophase-ion exchange model at high counterion concentration and if possible to correlate added counterion effects with the interaction between cationic micelles and cationic substrates of different hydrophobicities.

[1]To whom all correspondence should be addressed.

[2]Revision received October 11, 1988.

Experimental

Materials

Solutions of **1***a* and **1***c* were prepared "in situ", by mixing stoichiometric amounts of iron(II) sulphate (Merck) and ligand (Calo Erba). Substrate **1***b* (G. Frederick Smith Chemical Co.) was dissolved in water.

CTABr (Merck) was recrystallized from $MeOH/Et_2O$ mixture (17). CTACl was prepared by ion-exchange from CTABr using Amberlite 21K anionic resin (15), and MeOH as solvent. The absence of Br^- was tested with fluorescein. CTACl was recrystallized from $MeOH/Et_2O$ mixture. Here the cmc (critical micelle concentration) are as follows: cmc(CTAB) = 9×10^{-4} *M*, cmc(CTACl) = 1.2×10^{-4} *M*.

Kinetics

All reactions were run at 25 ± 0.1°C in a thermostated Spectronic 2000 Bausch and Lomb spectrophotometer. The reactions were followed at 513, 479, and 353 nm for substrates **1***a*, **1***b*, and **1***c*, respectively. Substrate stock solution, 0.1 *M*, was added to mixtures of CTAB (CTACl), NaOH and KBr (KCl) at given concentrations in the thermostated cuvettes of the spectrophotometer. The final complex concentration was 5×10^{-5} *M*.

The hydroxide ion was always in large excess over substrate and pseudo-first order rate constants were obtained by least-squares fits with correlation coefficients greater than 0.999.

Results and discussion

Second-order rate constants for reaction of both substrates **1***a* and **1***b*, in absence of surfactant, were obtained directly from the kinetic data in aqueous solution with values 1.06×10^{-2} and 6.05×10^{-4} M^{-1} s^{-1}, respectively. Substrate **1***c* is not soluble in pure water and the second order rate constant in water was obtained from rate constants in $MeOH/H_2O$ mixtures by extrapolation to zero concentration of methanol. The value obtained was 2.09×10^{-3} M^{-1} s^{-1}.

Rate constant – surfactant concentration profiles for the reaction of substrates **1***a* nd **1***b* with OH^- in CTACl and CTABr are shown in Figs. 1 and 2 at 0.1 *M* added KBr and no added

Can. J. Chem. Downloaded from www.nrcresearchpress.com by 122.72.124.2 on 09/07/12
For personal use only.

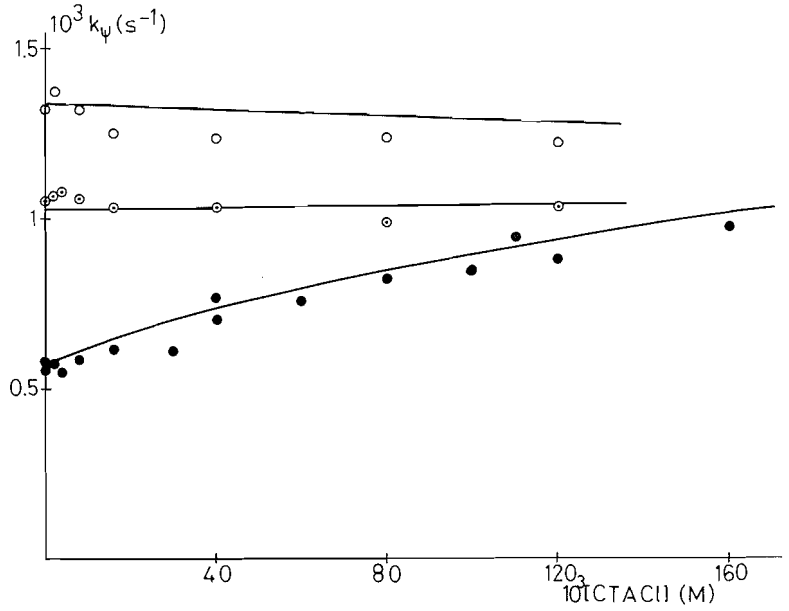


FIG. 1. Variation of the pseudo-first order rate constant, k_ψ, with CTACl concentration for reaction of **1***a* with OH^- (0.08 *M*): ○ in absence of added KCl; ⊙ [KCl] = 0.1 *M*; ● [KCl] = 0.4 *M*. Lines are predicted values from eqs. [1], [2], and [3] and parameters in Table 1.

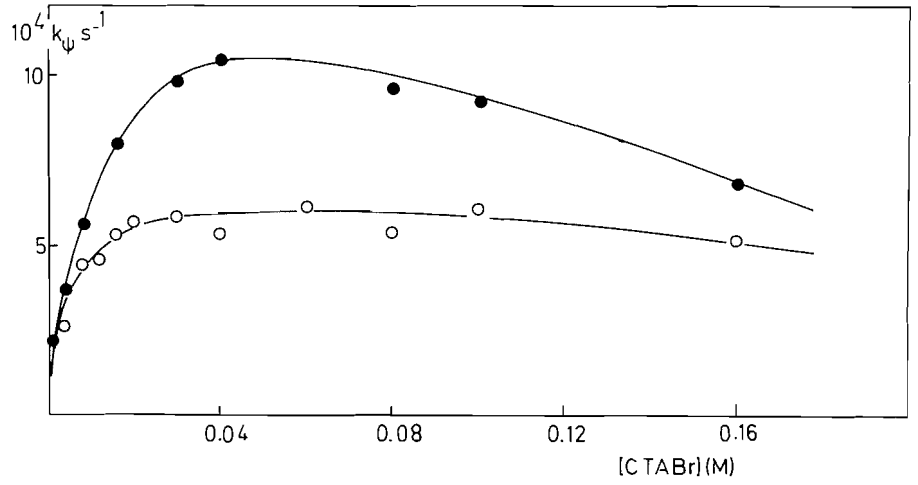


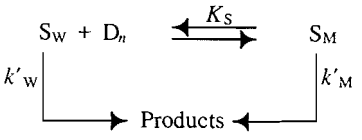
FIG. 2. Variation of the pseudo-first order rate constant, k_ψ, with CTABr concentration for substrate **1***b* with OH^- (0.04 *M*): ● in absence of added KBr; ○ [KBr] = 0.1 *M*. Lines are predicted values from eqs. [1] and [2] and parameters in Table 2.

counterion. Figures 3 and 4 show the rate constant – counterion concentration profiles for reaction of substrates **1***b* and **1***c* at a fixed surfactant concentration.

In the absence of added counterion the reaction rate for substrate **1***a* (Fig. 1) is not appreciably affected by micelles of CTACl. But in 0.4 *M* of KCl, added CTACl produces a small catalytic effect. In the case of substrates **1***b* and **1***c*, different counterion effects are observed. Both reactions are inhibited by added KBr while the reaction rate of **1***b* in CTACl is enhanced by 0.1 *M* KCl (Fig. 3).

We attempted to simulate all of these results using the pseudophase ion-exchange model developed by Bunton (4) and Romsted (2, 18).

The total volume of micelles is treated as a separate phase, uniformly distributed in the aqueous phase, with the reaction occurring in both phases according to Scheme 1.



SCHEME 1

D_n is the concentration of micellized surfactant equal to the stoichiometric surfactant concentration minus the cmc, K_S is the binding constant of substrate to the micelle, and k'_W and k'_M are pseudo-first order rate constants for the reaction in aqueous and micellar phases, given by $k'_W = k_W[OH^-_W]$ and $k'_M = k_M[OH^-_M]/[D_n]$.

Romsted (2, 18) proposed that when two ions compete for the micellar surface the distribution of counterions between the

Can. J. Chem. Downloaded from www.nrcresearchpress.com by 122.72.124.2 on 09/07/12
For personal use only.

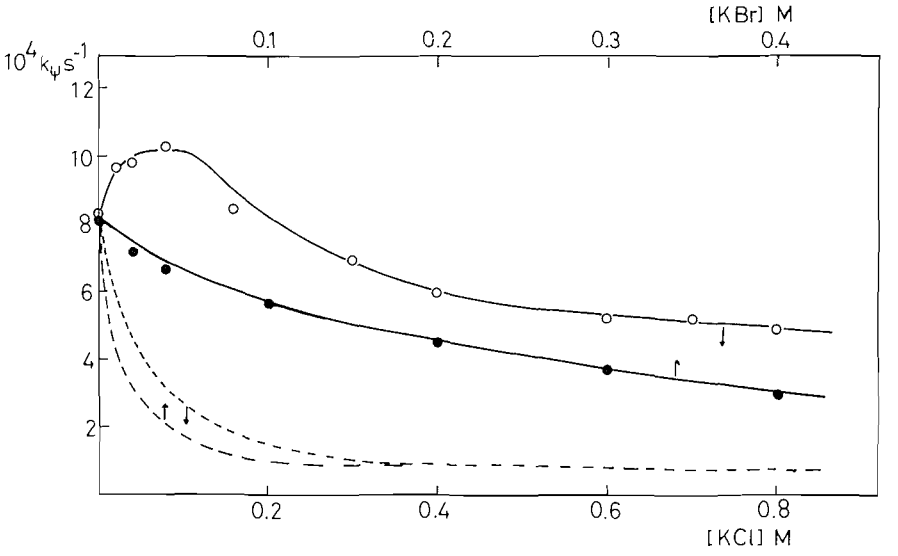


FIG. 3. Variation of the pseudo-first order rate constant, k_ψ, with micellar counterion concentration for the reaction of substrate **1***b*: ○ [NaOH] = 0.04 *M*, [CTACl] = 0.02 *M*; ● [NaOH] = 0.04 *M*, [CTABr] = 0.02 *M*. Dashed lines are predicted by eqs. [1] and [2] and continuous lines by eqs. [1], [2], [4], [5], and [6] with parameters given in Table 2 and [KBr + CTABr]: $A = 3500\ M^{-2}$, $p = 3$, $K_S^0 = 7.1\ M^{-1}$, and $\beta_0 = 0.8$; [KCl + CTACl]: $A = 200\ M^{-1}$; $p = 1$; $K_S^0 = 3.2\ M^{-1}$, and $\beta_0 = 0.71$.

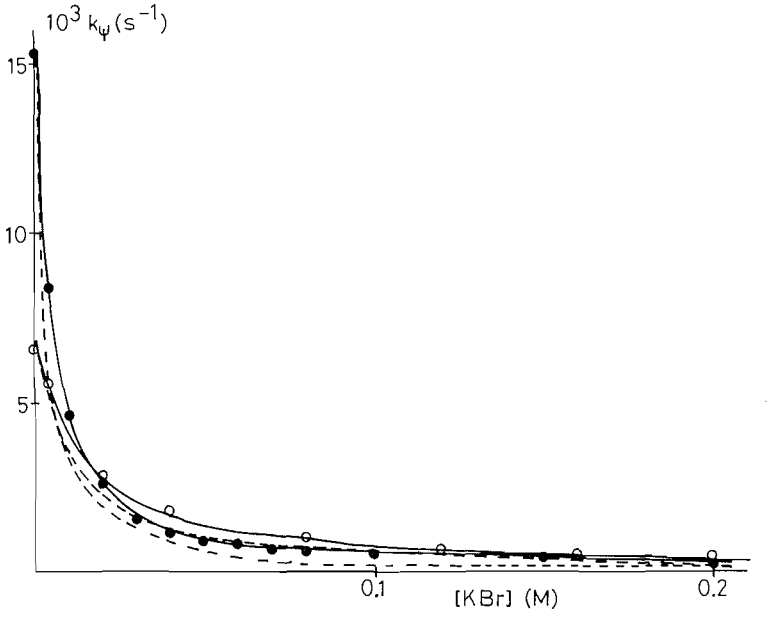


FIG. 4. Variation of the pseudo-first order rate constant, k_ψ, with micellar counterion concentration for the reaction of substrate lc: ○ [NaOH] = 0.04 *M*, [CTABr] = 0.020 *M*; ● [NaOH] = 0.04 *M*, [CTABr] = 0.002 *M*. Dashed lines are predicted from eqs. [1] and [2] and continuous lines by eqs. [1], [2], [5], and [6] with parameters given in Table 2 and $A = 1.5 \times 10^5\ M^{-1}$, $K_S^0 = 800\ M^{-1}$, $p = 0$, and $\beta_0 = 0.8$.

micelle surface and the aqueous phase is governed by an ion-exchange equilibrium as:

$$OH_M^- + Br_W^- \overset{K_{Br}^{OH}}{\rightleftharpoons} OH_W^- + Br_M^-$$

with the fraction of micellar head groups neutralized, β, constant.

According to this model the pseudo-first order rate constant is given by:

$$[1] \quad k_\psi = \frac{k_W[OH^-]_T + (k_M K_S - k_W) m_{OH}[D_n]}{1 + K_S[D_n]}$$

where m_{OH} can be obtained by:

$$[2] \quad m_{OH}^2 + m_{OH}\left[\frac{[OH^-]_T + K_{Br}^{OH}[Br^-]_T}{(K_{Br}^{OH} - 1)[D_n]} - \beta\right] - \frac{\beta[OH^-]_T}{(K_{Br}^{OH} - 1)[D_n]} = 0$$

This model predicts that the addition of counterion to micellar solutions should decrease the pseudo-first order rate constant by displacement of the reactive ion from the micellar to the aqueous phase. Thus, assuming K_S is constant, this treatment cannot account for the increase in k_ψ with added counterion for substrates **1***a* and **1***b* (Figs. 1 and 3).

Can. J. Chem. Downloaded from www.nrcresearchpress.com by 122.72.124.2 on 09/07/12
For personal use only.

TABLE 1. Parameters that best fit experimental results for the reaction of $[Fe(Phen)_3]^{2+}$ with OH^- (0.08 *M*) in CTACl

[KCl] (*M*)	k_M (s^{-1})	K_S (M^{-1})	K_{Cl}^{OH}	β
0.00	0.07	0.10	5	0.71
0.10	0.07	0.14	5	0.78
0.40	0.07	1.3	5	0.99

TABLE 2. Parameters[a] that best fit experimental results for the reaction of $[Fe((Me)_4Phen)_3]^{2+}$ and $[Fe((Ph)_2Phen)_3]^{2+}$ with OH^- in CTABr and CTACl

Substrate	Surfactant	[OH^-] (*M*)	[KX] (*M*)	k_M (s^{-1})	K_S (M^{-1})	K_X^{OH}	β
1*b*	CTABr	0.040	0.00	0.068	7.1	40	0.8
1*b*	CTABr	0.040	0.10	0.068	250	40	0.98
1*b*	CTACl	0.040	0.00	0.068	3.2	6.4	0.71
1*c*	CTABr	0.050	0.00	0.072	900	35	0.8

[a]Data in absence of added KX, taken from ref 15.

These results can be explained by considering counterion effects upon both the substrate binding to micelles and the fraction of neutralized micellar head groups (9, 11, 16, 19). The values of parameters that best fit the experimental results for substrate **1***a* in CTACl micelles are in Table 1; the solid lines in Fig. 1 represent the values of k_ψ calculated from eqs. [1] and [2]. In the calculation, the salt effect on the reaction in water is accounted for by the empirical equation:

$$[3] \quad k_W = 10^{(-\log k_W^0 - 0.92[KCl]^{0.5})}$$

where k_W^0 is the second order rate constant at ionic strength 0.2 *M*, obtained using 0.08 *M* hydroxide ion concentration and the appropriate amount of KCl to yield 0.2 *M*.

The reaction of substrate **1***a* in the absence of KCl or at 0.1 *M* occurs almost completely in the water phase as can be seen in Fig. 1. This indicates the absence of significant substrate binding to CTACl micelles. All the results can be explained by assuming a large variation in K_S and in the fraction of micellar head groups neutrallized, β, as can be seen from the parameters in Table 1. Solid lines in Fig. 1 correspond to calculated values with eqs. [1] and [2] and the given values of parameters.

The values of K_S and β must be adjusted to fit the results for substrates **1***b* and **1***c*. In Figs. 3 and 4, dashed lines correspond to k_ψ values calculated with parameters obtained for reactions carried out in absence of added counterion (Table 2). To fit the results in the presence of added 0.1 *M* KBr, larger values of K_S and β are needed (Table 2 and Fig. 2). The solid lines in Figs. 3 and 4 correspond to calculated values using the following empirical variations in K_S and β:

$$[4] \quad K_S = K_S^0(1 + a[Br^-]^2)$$

or

$$[5] \quad K_S = K_S^0(1 + A[Cl^-])$$

and

$$[6] \quad \beta = \beta_0(1 + p[X^-])$$

where K_S^0 and β_0 correspond to the values of K_S and β found in absence of added electrolyte, and the parameter, *a*, *A*, and *p* are given in the captions of Figs. 2 and 3. β_0 is 0.71 for CTACl and 0.8 for CTAB.

From these results we conclude that the binding of these like-charged substrates to micelles increases with added salt and from the variation obtained with substrate **1***b* it can be deduced that Br^-, a more hydrophobic ion, promotes the binding of these cationic substrates better than a hydrophilic ion such as Cl^-. As discussed previously (15) two opposing forces contribute to the binding of these substrates to micelles, hydrophobic attraction, and coulombic repulsion. At high salt concentration the coulombic repulsion is screened and the hydrophobic effect becomes more important. This is consistent with results in the literature (20) for other substrates, for which an increase in K_S was also found using fluorescence quenching measurements. The results can be explained by a decrease in the net micellar surface potential with increasing salt concentration.

This salt effect is less important for substrate **1***c*, for which hydrophobic forces are more important than electrostatic ones in the binding to cationic micelles. For this substrate any kind of variation of K_S with salt concentration, linear or quadratic, could fit the experimental results.

A similar variation in K_S with ions was observed for non-charged substrates and rationalized as a salting-out effect (21). Different effects have been found for substrates of opposite charge to the surfactant, for which kinetic results at high counterion concentration have been explained by a displacement of substrates from the micellar to the aqueous phase, resulting in a decrease in the K_S value (22).

A simple variation in K_S is not enough to explain all the kinetic data; an increase in the fraction of micellar bound counterions with salt concentration is necessary to obtain results that agree with a variety of different physical measurements (7, 8, 23–25). The influence of micellar counterions on these reactions is due to competition between three different effects: displacement of the substrate from the aqueous to the micellar phase, displacement of reactive ions by counterions from the micellar phase and an increase in the fraction of micellar group neutralized.

We recognize that some other kind of empirical variation could also explain the experimental data, but our approach agrees with other results in literature and makes it possible to see how much the results depart from the model.

At high salt concentrations the value of β does not have any physical sense that can be related to changes in micellar structure because added salt induces micelle growth from spherical to ellipsoidal (23–25). Even so the variation in K_S and in β necessary to fit the results cannot be accommodated by perturbations in the model. We must recognize that the pseudophase ion-exchange model fails to explain results at high salt concentrations, and other theoretical treatments to account for these effects need to be developed.

1. J. H. FENDLER and E. J. FENDLER. Catalysis in micellar and macromolecular system. Academic Press, New York. 1975.
2. L. S. ROMSTED. *In* Micellization, solubilization and microemulsions. *Edited by* K. L. Mittal. Plenum Press, New York. 1977. p. 509.
3. K. MARTINEK, A. K. YATSIMIRSKI, A. V. LEVASHOV, and I. V. BEREZIN. *In* ref. 2, p. 489.
4. C. A. BUNTON. Catal. Rev. Sci.-Eng. **20**, 1. (1979).
5. L. S. ROMSTED. *In* Surfactants in solutions. *Edited by* K. L. Mittal and B. Lindman. Plenum Press, New York. 1984. p. 1015.
6. F. H. QUINA and H. CHAIMOVICH. J. Phys. Chem. **83**, 1844

Can. J. Chem. Downloaded from www.nrcresearchpress.com by 122.72.124.2 on 09/07/12
For personal use only.

(1979); H. CHAIMOVICH, J. B. S. BONILHA, M. J. POLITI, and F. H. QUINA. J. Phys. Chem. **83**, 1851 (1979).
7. A. RODHE and E. J. SACKMAN. J. Colloid Interface Sci. **70**, 494 (1979); J. Phys. Chem. **84**, 1598 (1980).
8. J. P. KRATOHVIL. J. Colloid Interface Sci. **75**, 271 (1980).
9. E. RODENAS. An. Quim. **79**, 638 (1983).
10. C. A. BUNTON, L. S. ROMSTED, and G. SAVELLI. J. Am. Chem. Soc. **101**, 1253 (1979).
11. F. NOME, A. F. RUBIRA, C. FRANCO, and L. G. Ionescu. J. Phys. Chem. **86**, 1881 (1982); E. STEDLER, D. ZANETTE, M. C. REZENDE, and F. NOME. J. Phys. Chem. **88**, 1982 (1984).
12. C. A. BUNTON, L. S. ROMSTED, and G. SAVELLI. J. Am. Chem. Soc. **101**, 1253 (1979).
13. C. A. BUNTON, L. S. ROMSTED, and C. THAMAVIT. J. Am. Chem. Soc. **102**, 3900 (1980).
14. H. AL-LOHEDAN and C. A. BUNTON. J. Org. Chem. **47**, 1160 (1982).
15. F. ORTEGA and E. RODENAS. J. Phys. Chem. **90**, 2408 (1986).
16. F. ORTEGA and E. RODENAS. Transition Met. Chem. **11**, 351 (1986).
17. E. DUYNSTEE and E. GRUNDWALD. J. Am. Chem. Soc. **81**, 4570 (1958).
18. L. S. ROMSTED. Ph.D. Thesis. Indiana University, Bloomington, IN. 1975.
19. H. AL-LOHEDAN, C. A. BUNTON, and L. S. ROMSTED. J. Phys. Chem. **85**, 2123 (1981).
20. L. MIOLA, R. B. ABAKERLI, M. F. GINANI, P. B. FILHO, V. G. TOSCANO, and F. H. QUINA. J. Phys. Chem. **87**, 4417 (1983).
21. C. OTERO and E. RODENAS. Can. J. Chem. **63**, 2892 (1985).
22. S. VERA and E. RODENAS. J. Phys. Chem. **90**, 3414 (1986).
23. P. J. MISSEL, N. A. MAZER, G. B. BENEDEK, and C. Y. YOUNG. J. Phys. Chem. **84**, 1044 (1980); G. PORTE and J. APPELL. J. Phys. Chem. **85**, 2511 (1981); S. IKEDA, S. OZAKI, and S. HAYASHI. Biophys. Chem. **11**, 417 (1980); M. CORTI and V. DEGIORGIO. J. Phys. Chem. **85**, 711 (1981); H. HOFFMANN, H. REHAGE, W. SCHORR, and H. THURN. *In* Surfactants in solutions. Vol. 1. *Edited by* K. L. Mittal and B. Lindman. Plenum Press, New York. 1984. p. 245.
24. R. DORSHOW, J. BRIGGS, C. A. BUNTON, and D. F. NICOLI. J. Phys. Chem. **86**, 2388 (1982).
25. R. DORSHOW, C. A. BUNTON, and D. F. NICOLI. J. Phys. Chem. **87**, 1409 (1983); D. F. NICOLI, V. ATHANASSAKIS, J. R. MOFFAT, C. A. BUNTON, R. B. DORSHOW, and G. SAVELLI. Surfactants in solutions. Vol. 4. *Edited by* K. L. Mittal and P. Bothorel. Plenum Press, New York. 1986. p. 203.

Can. J. Chem. Downloaded from www.nrcresearchpress.com by 122.72.124.2 on 09/07/12
For personal use only.

Analysis of wood vacuum pyrolysis solid residues by diffuse reflectance infrared Fourier transform spectrometry

H. PAKDEL, J. L. GRANDMAISON, AND C. ROY

Chemical Engineering Department, Université Laval, Pavillon Adrien-Pouliot, Ste-Foy, P.Q., Canada G1K 7P4

Received June 27, 1988

H. PAKDEL, J. L. GRANDMAISON, and C. ROY. Can. J. Chem. **67**, 310 (1989).

Vacuum pyrolysis of wood furnishes high yields of oils which are a source of liquid fuels and chemicals. Wood charcoal is a solid residual by-product. Solid residues produced at 200, 263, 327, 363, 401, and 448°C in a Process Development Unit were analyzed using wet chemical methods and chromatography and infrared spectrometry.

A Diffuse Reflectance Infrared Fourier Transform (DRIFT) study of the solid residues which contained various proportions of organic polymeric constituents consisting of unconverted lignin, polysaccharides, and recondensed materials was performed. Polysaccharide contents were determined by hydrolysis in trifluoroacetic acid followed by derivatization and gas-chromatographic analysis. The DRIFT study showed that the solid residue retained its wood nature below 263°C. Significant degradation, decomposition, and recondensation reactions occurred with increasing temperature and coal-like nature prevailed above 327°C. Occurrence of a new band at 1700 cm^{-1} in samples produced at 363°C and above was found to be indicative of a new carbonyl group, presumably in recondensed material.

A series of equations were also developed to predict semiquantitatively Klason residue, glucose and xylose content of the solid residues. The usefulness of each equation is discussed in the article.

Key words: wood, vacuum pyrolysis, solid residue, DRIFT, spectrometry.

H. PAKDEL, J. L. GRANDMAISON et C. ROY. Can. J. Chem. **67**, 310 (1989).

Lorsqu'on pyrolyse du bois sous vide, on obtient des rendements élevés d'huiles qui sont une source de combustibles et de produits chimiques. On obtient aussi du charbon de bois comme sous-produit résiduel solide. Faisant appel à des méthodes chimiques humides ainsi qu'à la chromatographie et à la spectrométrie infrarouge, on a analysé les résidus solides obtenus par traitement à 200, 263, 327, 363, 401 et 448°C, dans une unité de développement de procédé.

On a réalisé une étude de réflexion diffuse par infrarouge transform de Fourier (DRIFT) des résidus solides qui contenaient diverses proportions de constituants organiques polymériques formées de lignine non-transformée, de polysaccharides et de matériaux recondensés. On a déterminé la teneur en polysaccharides en procédant à une hydrolyse dans de l'acide trifluoroacétique, puis à la formation de dérivés et finalement à une analyse par chromatographie en phase gazeuse. L'étude par la méthode DRIFT a permis de démontrer que, à des températures inférieures à 263°C, le résidu solide garde sa nature ressemblant à celle du bois. Avec une augmentation de la température, on observe de plus en plus de réactions de dégradation, de décomposition et de recondensation et, au-dessus de 327°C, le résidu obtenu est principalement d'une nature ressemblant à celle du charbon. Dans les échantillons de résidus obtenus à des températures supérieures à 363°C, on observe une nouvelle bande à 1700 cm^{-1}; celle-ci suggère la présence d'un nouveau groupement carbonyl qui provient probablement d'un produit de recondensation.

On a aussi développé une série d'équations qui permettent de prédire d'une façon semi-quantitative les teneurs en résidu de Klason, en glucose et en xylose des résidus solides. On discute de l'utilité de chacune de ces équations.

Mots clés : bois, pyrolyse sur vide, résidu solide, DRIFT, spectrométrie.

[Traduit par la revue]

Introduction

Vacuum pyrolysis of wood enables the production of high yields of oils which are a source of liquid fuels and chemicals (1, 2). Wood charcoal is a by-product of the vacuum pyrolysis reactions. This solid residue has been found to be rather reactive (3). Two recent studies of wood charcoal have used ESCA (4) and fluorescence and reflectance (5) measurements to investigate the mechanism of wood pyrolysis. This article presents new data obtained using the DRIFT technique. The specific advantages of DRIFT are discussed in this article.

The composition of solid residues from pyrolysis reactions of wood has been investigated by several researchers. Authors reported wet chemistry methods for the determination of moisture, insoluble and soluble lignins and carbohydrates (6–8). Schulz *et al.* (9) used the FTIR method with diffuse reflectance cell to determine the three major components of pretreated lignocellulosic materials at temperatures ranging from 140 to 280°C. Recently, this approach has been extended for qualitative and semiquantitative studies of thermally modified lignocellulosic constituents of *Populus tremuloïdes* produced by supercritical extraction (SCE) at 350°C under various pressures and flow rates (10). An ESCA study was also performed on the same SCE samples (11).

Until recently, infrared spectrometric measurements of carbonaceous materials have used the KBr pellet technique in transmission mode (12). The KBr technique has some drawbacks including a high scattering background and the possibility of strong Christiansen effects which are associated with preparation of the pellets (13). The DRIFT technique can alleviate these problems and provides more spectral information. In addition, it can be used to perform *in situ* studies (e.g. oxidation) using an appropriate chamber. Useful spectra may be obtained using neat samples (undiluted) (10, 14) but the best spectra are usually obtained in a non-absorbing matrix like KCl (15). Nevertheless, there are various problems associated with qualitative and quantitative DRIFT analysis in particular. Due to the assumptions made, Kubelka-Munk equation for diffuse reflectance measurements has been reported to be valid for dilute dispersion of an analyte in non-absorbing matrices (16, 17). Its linearity could be further improved by improving sample preparation technique (18, 19) and optical geometry of the system (20).

Can. J. Chem. Downloaded from www.nrcresearchpress.com by 122.72.124.2 on 09/07/12
For personal use only.

TABLE 1. Chemical analysis of vacuum pyrolysis solid residues (% by weight, dry basis)

Sample designation	Pyrolysis temperature	Klason residue	TFA soluble	Total sugars		
				Glucose	Xylose	Others*
Raw wood		11.6	87.4	35.1	10.4	3.5
H-I	200	13.6	87.5	34.9	9.1	3.3
H-II	263	27.2	79.4	32.7	4.5	2.1
H-III	327	94.3	7.7	0.4	Traces	Traces
H-IV	363	99.2	3.3	0.1	Traces	Traces
H-V	401	94.1	5.5	0.1	Traces	Traces
H-VI	448	92.5	7.6	0.2	Traces	Traces

*Composed of arabinose, levoglucosan, and mannose.

Can. J. Chem. Downloaded from www.nrcresearchpress.com by 122.72.124.2 on 09/07/12
For personal use only.

This work contributes to the knowledge of thermal conversion solid residue characteristics and extends the previously reported semiquantitative infrared approach to wood charcoals produced under vacuum pyrolysis (VP) conditions within a higher range of temperatures. Emphasis has been made on usefulness of DRIFT technique in fast determination of constituents of many lignocellulosic solid residues obtained by various liquefaction techniques.

Experimental

Debarked *Populus deltoïds* (Forintek clone D-38) wood chips sieved to 1/4″ to 1/2″ Tyler mesh sizes were pyrolysed in a Process Development Unit vacuum pyrolysis multiple hearth furnace. The mass flowrate through the six hearth reactor was 3.5 kg h^{-1}. In this process, the organic vapor and gas products are removed from the reactor chamber by a mechanical vacuum pump and are subsequently condensed in a series of receivers. Charcoal is collected at the bottom of the reactor. The reactor hearth temperatures were stabilized at 200, 263, 327, 363, 401, and 448°C from top to bottom of the reactor respectively (hearths H-I to H-VI). The radial temperature gradient for any heating plate was lower than 5° during a run. At the end of the run, a few particles of wood charcoal were left behind on top of each heating plate. Such solid residues along with the raw wood sample were analyzed as described below, using wet chemistry as well as chromatographic and IR spectroscopic methods. Operation of the Process Development Unit has been described elsewhere (21).

Hydrolyses of the residual polysaccharides were performed in trifluoroacetic acid (TFA) following the Fengel and Wegener procedure (22). About 100 mg of the charcoal sample was soaked in 10 g TFA overnight at room temperature. The mixture was then heated in an oil bath under reflux for 1 h, diluted to 80% (w/w) TFA in water and refluxed for 15 min. The mixture was further diluted to 30% (w/w) TFA, refluxed for 2 h, and filtered. The residue was washed with 100 mL of water and the filtrate was mixed with the mother liquors and evaporated in a rotary vacuum evaporator at 50°C to dryness to yield hydrolyzate. Approximately 30 mL of water was added to the hydrolyzate which was subsequently evaporated to dryness in order to completely eliminate any TFA traces. The hydrolyzate was finally derivatized using trimethylsilylimidazole (TMSI) in pyridine.

Gas-chromatographic analyses of the derivatized samples are presented in Table 1. Analyses were performed using a Varian 6000 chromatograph with 30 m × 0.25 mm i.d. DB-5 capillary column and split/splitless injector with 1:100 split ratio. He and N_2 were used as carrier and make-up gas, respectively. The FID and injector temperatures were set at 290 and 300°C, respectively. The column temperature was maintained at 150°C for 2 min then programmed to 190°C at 20°C min^{-1} and then to 290°C at 30°C min^{-1}.

Samples were dried for spectrometric analysis at 105°C for 12 h and ground in a SPEX stainless steel mill in air (30 min for wood and samples 1 and 2, and 10 min for samples 3 to 6). The samples were then further ground for an additional minute with dry KCl (Anachemia) in 1:100 ratio and analyzed immediately. FTIR spectra were obtained with a Digilab FTS-60 spectrometer equipped with a DTGS detector. A Harrick-2CE diffuse reflectance cell was used with coadding of 250 scans at 4000–700 cm^{-1} frequency range, 2 cm^{-1} resolution and triangular apodization.

Results and discussion

Table 1 presents wet chemistry (Klason residue and TFA soluble) and GC (total sugars) analytical results obtained for the raw material and the six solid pyrolysis residues. TFA treatment of the solid residues partially hydrolyzed the carbohydrates into monosaccharides. The remaining carbohydrates were degraded into water soluble non-carbohydrates e.g. furanic-type compounds. Despite a comparable Klason residue content of the solid residues determined by both sulfuric and TFA methods (8), the TFA method was preferred due to the ease of complete TFA removal by evaporation after hydrolysis. Since the solid residues obtained by relatively severe thermochemical conversion process are composed of unconverted and structurally modified lignin, therefore the term "Klason residue" is used instead of "Klason lignin" (8). The solid residue left on H-IV (Table 1) contained a high percentage of Klason residue (TFA insoluble) and a low content of TFA soluble monosaccharides produced by both pyrolysis and hydrolysis. Earlier, Wayman and Chua (23) suggested that carbohydrates and lignin as well as furfural type compounds participate in recondensation reactions.

DRIFT spectra of the original wood and of the solid residues from hearth H-I to H-VI are shown in Fig. 1 (designated as H-I to H-VI, respectively). Comparison of IR spectra of wood feedstock with H-I (200°C) and H-II (263°C) charcoals shows the wood-like nature of the solid residues with characteristic vibrational bands at 895 cm^{-1} (β-pyranose ring in cellulose, (24)); 1740 cm^{-1} (uronic acid and acetyl group in hemicellulose, (24)); 1235 to 1605 cm^{-1}, and 1505 cm^{-1} in particular (typical of lignin aromatic ring vibration, (25)) and 950 to 1100 cm^{-1} (mainly carbohydrate C—O vibrations, (24)). As the temperature increases from 263°C (H-II) to 327°C (H-III), significant differences appear in the IR spectra of H-II and H-III, associated with severe degradation, decomposition and recondensation reactions. Evolution of a coal-like pattern could be observed by disappearance of lignin (1235 to 1605 and 1505 cm^{-1}) and carbohydrate (e.g. 1740 and 895 cm^{-1}) bands as the reactor bed temperature was further increased from 327°C (H-III) to 448°C (H-VI). Interestingly, the moderate intensity band at about 1740 cm^{-1} in the raw material and H-I (200°C) and H-II (263°C) spectra disappeared which is probably due to

Can. J. Chem. Downloaded from www.nrcresearchpress.com by 122.72.124.2 on 09/07/12
For personal use only.

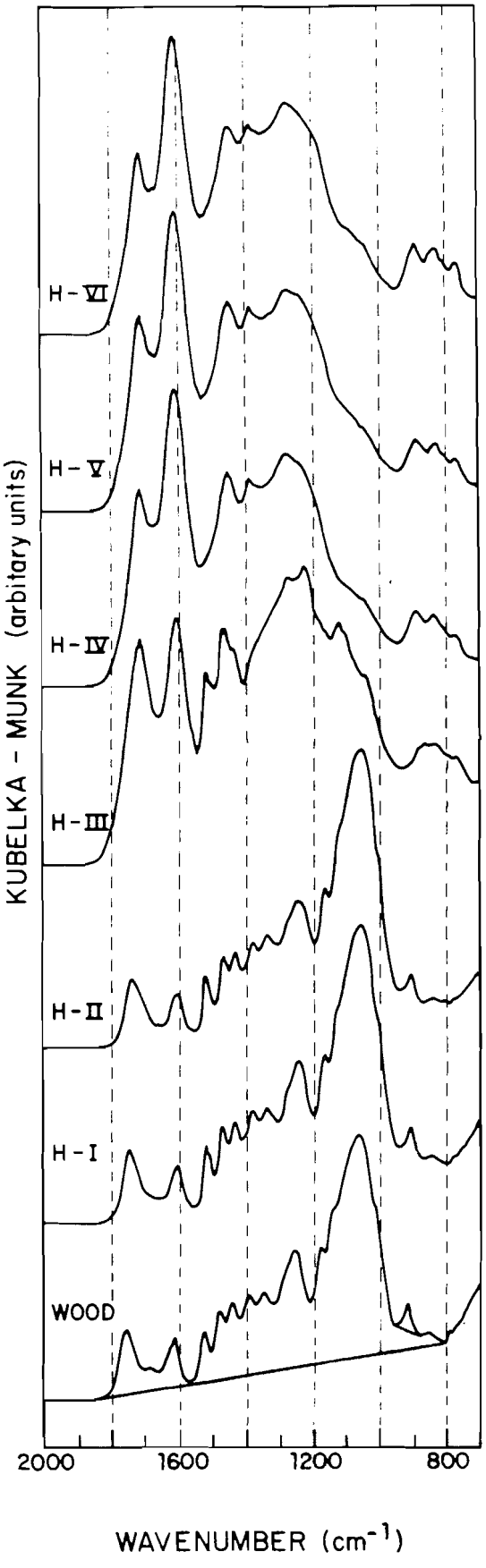


FIG. 1. DRIFT spectra of *Populus deltoïdes* and solid residues from six reactor hearths produced at different temperatures.

decarboxylation and a new band appeared instead near 1700 cm^{-1} in H-III (327°C) to H-VI (448°C) which is attributed to a new carbonyl group (Fig. 1). Occurrence of a band near 1700 cm^{-1} in Klason extracts of wood SCE residues was attributed to the conjugated carbonyl structure (8). Occurrence of the band at 1700 cm^{-1} in H-III to H-VI with a similar intensity on the other hand seemed to be more specifically indicative of various recondensation reactions during pyrolysis reactions or rearrangement of wood carbonyl or carboxyl group between 263°C and 327°C. Earlier we performed KBr pellet IR analysis of the same solid samples without milling and prior drying (26). A similar band at 1700 cm^{-1} was observed for H-III to H-VI samples instead of 1740 cm^{-1} in H-I and H-II. Although this may not completely rule out any possible post-pyrolysis oxidation of the solid samples, but indicates the absence of any significant effect due to drying and milling processes on 1700 cm^{-1} band. Further works are under investigation to characterize the nature of the 1700 cm^{-1} band in our laboratory. Increased intensity of band near 1700 cm^{-1} has been found also in early stages of aerial oxidation of Wyodak coal (12).

Recently ESCA analysis showed that recondensed materials are the main constituents of vacuum pyrolysis of *Populus deltoïdes* chars produced at 315°C (4). Change in the nature of IR spectra was also observed previously in SCE solid residues which have some IR spectral pattern similarities to VP solid residues (10). The SCE residues were prepared at 250, 300, and 350°C and various flow rates and pressures of the supercritical solvent. The SCE residue which was obained at 250°C showed a wood-like infrared pattern and its Klason residue content (measured by thioglycolic acid) was representative of the unconverted lignin. In contrast, samples obtained at 300 and 350°C showed coal-like IR patterns and their Klason residues were recondensed materials with possible polycyclic aromatic nature. Their aromaticity increased with the increase of the extraction temperature and pressure which was demonstrated by IR and ESCA analyses (27). Unlike the SCE samples, the VP solid residues obtained at 327°C and above gave rise to an enhanced band at about 1595–1600 cm^{-1}. This band is attributed to the aromatic vibrational band with methylene, ether, and carbonyl linkage (27).

The change in infrared spectra of wood-like and coal-like VP solid residues was found to be in good agreement with the results obtained previously using optical measurements of wood charcoals derived from *Populus tremuloïdes*. The VP solid residues were prepared in a bench scale batch reactor at temperatures ranging from 207 to 534°C, with about 40°C intervals (5). Raw wood and residual materials obtained below 287°C were characterized by their fluorescence properties. Those obtained above 287°C were characterized by their reflectance. It was concluded that an increase in reflectance from 0.13 to 2.19% is associated with aromatization of the molecular structure. In vacuum pyrolysis process, the woody material was transformed into a vitrinite-like substance which resembled the cell tissues encountered in peats and low rank coals.

Recently a series of equations were published to calculate Klason residue, unconverted lignin, recondensed material as well as glucose and xylose contents of SCE residues using a nonlinear least-squares regression analysis (10). Such correlation is further extended in this paper to VP solid residues for the calculation of Klason residue and glucose and xylose contents. Intensity of twelve bands between 1595 and 895 cm^{-1} were

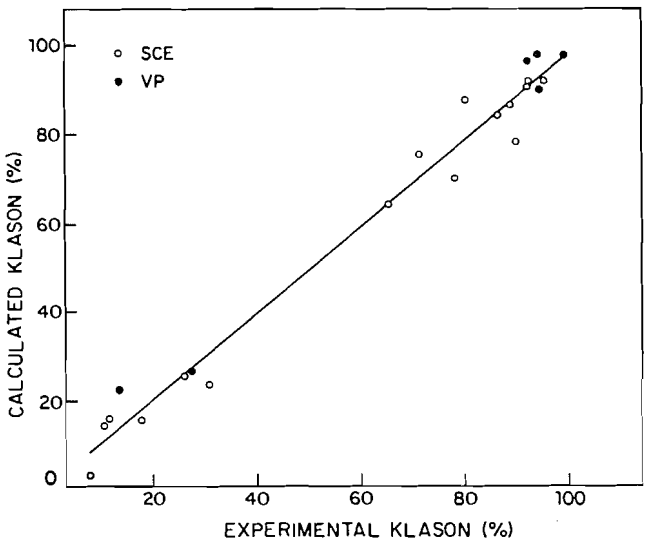


FIG. 2. Klason residue content, measured by standard procedure, vs. Klason residue content calculated by DRIFT spectrometry.

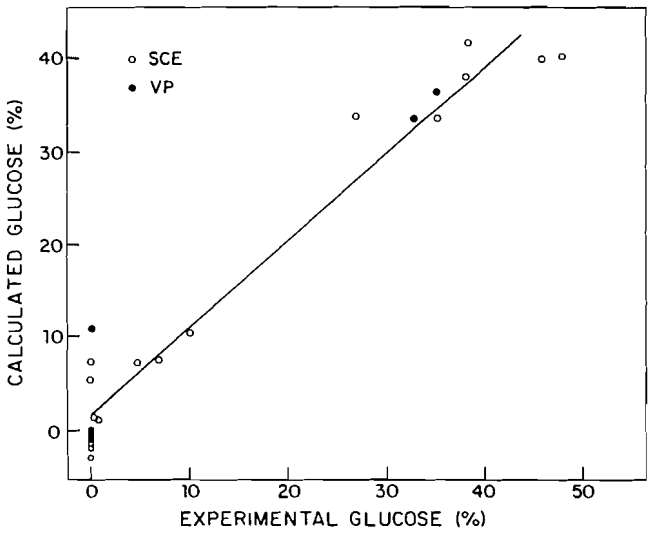


FIG. 3. Glucose content, measured by standard procedure, vs. glucose content calculated by DRIFT spectrometry.

measured by defining the IR base line as shown in Fig. 1. The regression equations as function of possible combinations of intensity ratios of twelve bands against Klason residue, glucose and xylose values (Table 1) as well as the previously published data of SCE residues (27) are as following:

$$[1]\quad \%\text{Klason residue} = 106.3 + \left(13.0 \times \frac{I_{1220}}{I_{1100}}\right) - \left(50.95 \times \frac{I_{1035}}{I_{1100}}\right) - \left(164.3 \times \frac{I_{895}}{I_{1100}}\right)$$

$$[2]\quad \%\text{glucose} = 1.43 + \left(27.77 \times \frac{I_{1505}}{I_{1210}}\right) - \left(23.1 \times \frac{I_{1370}}{I_{1210}}\right) + \left(15.6 \times \frac{I_{1035}}{I_{1210}}\right)$$

$$[3]\quad \%\text{xylose} = -11.66 + \left(29.65 \times \frac{I_{1260}}{I_{1595}}\right) - \left(24.10 \times \frac{I_{1210}}{I_{1595}}\right) + \left(9.33 \times \frac{I_{1160}}{I_{1595}}\right) - \left(33.79 \times \frac{I_{895}}{I_{1595}}\right)$$

The correlation between Klason content as calculated by eq. [1] and the conventional analysis on both VP and SCE solid residues is shown in Fig. 2. A good correlation coefficient with a value of 0.981 and a standard error of 7.6% was obtained. Klason content can be used to estimate the lignin content (unconverted lignin) of wood-like samples (treated at lower temperatures). Klason residue of the samples produced above 327°C represent the sum of unconverted lignin and recondensed material. Figure 3 shows the plot of glucose content measured by chromatographic procedure against the value as predicted by DRIFT (eq. [2]). A correlation factor of 0.976 with a high standard error of 27.9% was found for Fig. 3. Coal-like samples with less than 10% glucose content exhibit a non-linear correlation (low value) with high standard error. We concluded that DRIFT technique will be less accurate to predict glucose content of coal-like residues. Similarly, Fig. 4 shows the plot of xylose content against the value predicted by DRIFT (eq. [3]).

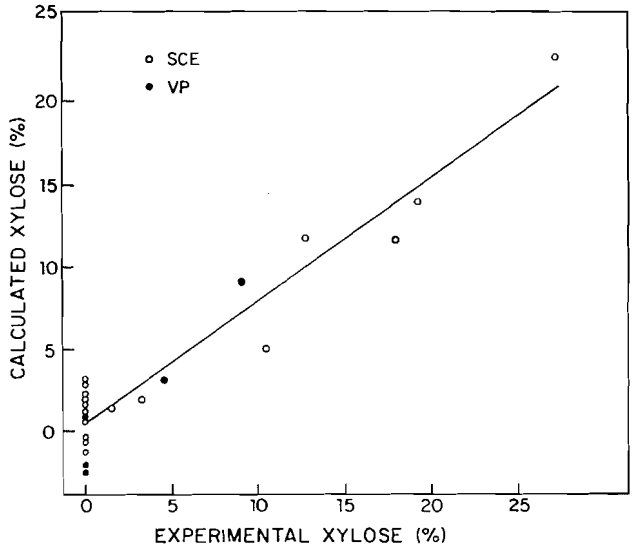


FIG. 4. Xylose content, measured by standard procedure, vs. xylose content calculated by DRIFT spectrometry.

A correlation factor of 0.957 and a standard error of 38.0% was obtained in this case. It is concluded that the xylose content also shows significant divergence from the straight line for coal-like samples containing 3% or less xylose. Glucose and xylose contents of wood-like samples on the other hand, show a good correlation and could be predicted by eq. [2] and eq. [3], respectively.

Conclusion

Solid residues were produced by vacuum pyrolysis of wood at different temperatures. Their composition was studied by wet chemistry and DRIFT techniques. Klason residue of the charcoals obtained by vacuum pyrolysis and SCE techniques was positively predicted by a regression equation derived from IR information. The usefulness of the two other equations has also been shown for the prediction of glucose and xylose content of low-temperature charcoals. The DRIFT study showed that the solid residues containing more than 10% glucose and 3%

Can. J. Chem. Downloaded from www.nrcresearchpress.com by 122.72.124.2 on 09/07/12
For personal use only.

xylose retain their wood-like nature below 263°C. Degradation, decomposition, and recondensation reactions proceed as the reactor hearth temperature increases. Ultimately, coal-like nature prevails above 327°C. Occurrence of a new IR band at 1700 cm^{-1} in samples produced at 363°C and above was found to be rather characteristic of vacuum pyrolysis solid residues and was attributed to a new carbonyl group formed by recondensation reactions.

Depending on the liquefaction process, wood experiences extensive degradation and modification. Thus, the DRIFT technique with its fast analysis capability could be further modified to study solid residues obtained by various liquefaction techniques.

Acknowledgment

Thanks are due to Professor S. Kaliaguine for access to the FTIR spectrometer and useful discussion.

1. C. Roy, B. de Caumia and H. Pakdel. Research in thermochemical biomass conversion. *Edited by* J. Kuester and T. Bridgewater. Elsevier Applied Science Publishers B.V. In press.
2. H. Pakdel and C. Roy. Biomass. **13**, 155 (1987).
3. P. Plante, C. Roy, and E. Chornet. Can. J. Chem. Eng. **66**, 307 (1988).
4. A. Ahmed, H. Pakdel, C. Roy, and S. Kaliaguine. J. Anal. Appl. Pyrolysis. In press.
5. W. Kalkreuth, D. Brouillard, and C. Roy. Biomass. **10**, 27 (1986).
6. E. McDonald and J. Howard. Fourth Bioenergy R & D Seminar, Winnipeg, Canada, March 29–31, 1982. p. 397.
7. C. J. Biermann, T. P. Schultz, and G. D. McGinnis. J. Wood Chem. Technol. **4**, 111 (1984).
8. A. Ahmed, J. L. Grandmaison, and S. Kaliaguine. J. Wood Chem. Technol. **6**, 219 (1986).
9. T. P. Schultz, M. C. Templeton, and G. D. McGinnis. Anal. Chem. **57**, 2867 (1985).
10. J. L. Grandmaison, J. Thibault, S. Kaliaguine, and P. D. Chantal. Anal. Chem. **59**, 2153 (1987).
11. A. Ahmed, A. Adnot, and S. Kaliaguine. J. Appl. Poly. Sci. **34**, 359 (1987).
12. N. R. Smyrl and E. L. Fuller, Jr. Coal and coal products: analytical characterization. *Edited by* E. L. Fuller, Jr. ACS Symp. Series 205, Division of Analytical Fuel and Colloid and Surface Chemistry. 1982. p. 133.
13. K. Krishnan and J. R. Feraro. Fourier transform infrared spectroscopy. *Edited by* J. R. Feraro and L. J. Basile. Academic Press, New York. 1982. p. 149.
14. M. P. Fuller and P. R. Griffiths. Anal. Chem. **50**, 1906 (1978).
15. M. P. Fuller and P. R. Griffiths. App. Spectrosc. **34**, 533 (1980).
16. P. R. Griffiths and M. P. Fuller. Advances in infrared and Raman Spectroscopy. vol. 9. *Edited by* R. J. H. Clark and R. E. Hester. Heyden, London. 1982. p. 82.
17. P. J. Brimmer and P. R. Griffiths. Anal. Chem. **58**, 2179 (1986).
18. S. A. Yeboah, S. H. Wang, and P. R. Griffiths. Appl. Spectrosc. **33**, 259 (1984).
19. I. M. Hamadeh, S. A. Yeboah, K. A. Trumbull, and P. R. Griffiths. Appl. Spectrosc. **38**, 486 (1984).
20. P. J. Brimmer and P. R. Griffiths. Appl. Spectrosc. **42**, 242 (1988).
21. C. Roy, R. Lemieux, B. de Caumia, and D. Blanchette. Pyrolysis oils from biomass: production, analysis and upgrading. *Edited by* Ed J. Soltes and T. A. Milne. ACS Symposium Series 376, 1988, p. 16.
22. D. Fengel and G. Wegener. ACS Advances in Chemistry Series No. 181, 145 (1979).
23. M. Wayman and M. G. S. Chua. Can. J. Chem. **57**, 2599 (1979).
24. K. Nakanishi. Infrared absorption spectroscopy—Practical. Holden-Day, San Francisco, CA. 1962.
25. H. L. Hergert. Lignins, occurrence, formation, structure and reactions. *Edited by* K. V. Sarkanen and C. H. Ludwig. Wiley New York. 1971. p. 267.
26. H. Pakdel and C. Roy. Pyrolysis oils from biomass: production, analysis and upgrading. *Edited by* Ed J. Soltes and T. A. Milne. ACS Symposium Series 376, 1988. p. 203.
27. J. L. Grandmaison, A. Ahmed, and S. Kaliaguine. Pyrolysis oils from biomass: production analysis and upgrading. *Edited by* Ed. J. Soltes and T. A. Milne. ACS Symposium Series 376, 1988, p. 139.

Can. J. Chem. Downloaded from www.nrcresearchpress.com by 122.72.124.2 on 09/07/12
For personal use only.

Deprotonation and transfer energetics of glycine in aqueous mixtures of urea and glycerol from emf measurements at different temperatures

HIMANSU TALUKDAR, SIBAPRASAD RUDRA, AND KIRON K. KUNDU[1]
Physical Chemistry Laboratories, Jadavpur University, Calcutta 700 032, India
Received July 15, 1988

HIMANSU TALUKDAR, SIBAPRASAD RUDRA, and KIRON K. KUNDU. Can. J. Chem. **67**, 315 (1989).

Deprotonation constants, $K_a(RH_2^+)$ and $K_a(RH^\pm)$, of glycine ($RH^\pm$) have been determined at five equidistant temperatures ranging from 15 to 35°C by measuring the emf of galvanic cells comprising Pt/H_2 and Ag–AgCl electrodes in aqueous mixtures of protophilic protic urea (UH) and protophobic protic glycerol (GL). Medium effects on deprotonation of the acid: $\delta(\Delta X^0_{diss}{}^N) = {}_s\Delta X^0 - {}_w\Delta X^0$ ($X = G$ or S) have been dissected into transfer free energies ($\Delta G^0_t(i)$) and entropies ($\Delta S^0_t(i)$) of the species involved as obtained by measuring the transfer energetics ΔX^0_t of $RH^\pm$ from solubility measurements at different temperatures and of H^+ based on tetraphenylarsonium tetraphenylborate (TATB) reference electrolyte assumption determined earlier. The $\Delta G^0_{t,ch}(i)$ values obtained after due correction from the cavity effect based on scaled particle theory (SPT) and electrostatic effects including Born and ion–dipole effects for the charged species involved in the two deprotonation equilibria enable better understanding of the solvent effect on the deprotonation constants. Moreover, the $T\Delta S^0_{t,ch}(i)$–composition profiles are found to exhibit similar characteristic maxima and minima as for simple cations and anions in these solvent systems, thus providing useful information on the structural characteristic of these cosolvents.

Key words: deprotonation energetics, glycine, aqueous urea, aqueous glycerol, EMF measurements.

HIMANSU TALUKDAR, SIBAPRASAD RUDRA et KIRON K. KUNDU. Can. J. Chem. **67**, 315 (1989).

Faisant appel à des mesures de fem des cellules galvaniques formées par des électrodes de Pt/H_2 et de Ag–AgCl et opérant dans des mélanges aqueux d'urée protique protophile (UH) et de glycérol protique protophobe, on a déterminé les constantes de déprotonation, $K_a(RH_2^+)$ et $K_a(RH^\pm)$, de la glycine à cinq températures équidistantes entre 15 et 35°C. On a divisé les effets du milieu sur la déprotonation de l'acide, $\delta(\Delta X^0_{diss}{}^N) = {}_s\Delta X^0 - {}_w\Delta X^0$ ($X = G$ ou S), en énergies ($\Delta G^0_t(i)$) et en entropies ($\Delta S^0_t(i)$) libres de transfert des espèces impliquées; pour ce faire, on a déterminé les énergies de transfert ΔX^0_t du $RH^\pm$ à partir de mesures de solubilité à diverses températures ainsi que celles du H^+ en se basant sur l'hypothèse de l'électrolyte de référence tétraphénylborate tétraphénylarsonium (TBTA) qui a été proposée antérieurement. Les valeurs de $\Delta G^0_{t,ch}(i)$ qui sont obtenues après avoir effectué une correction pour l'effet de cavité, qui est évaluée à l'aide de la théorie de la particule scalaire (TPS), et pour les effets électrostatiques, y compris les effets de Born et d'ion–dipôle des espèces chargées impliquées dans les deux équilibres de déprotonation, fournissent une meilleure compréhension de l'effet de solvant sur les constantes de déprotonation. De plus, on a trouvé que les profils des $T\Delta S^0_{t,ch}(i)$ vs la composition présentent des maxima et des minima caractéristiques semblables à ceux observés avec des cations et des anions simples dans ces solvants; on peut en tirer des réflexions utiles sur la caractéristique structurale de ces cosolvants.

Mots clés : énergies de déprotonation, glycine, urée aqueuse, glycérol aqueux, mesures de FEM.

[Traduit par la revue]

Introduction

Deprotonation constants and the associated energetics of amino acids and peptides in water and aqueous mixtures of ionic and non-ionic cosolvents form vital thermochemical quantities that will help understand the role of these key biochemicals in biological systems. Unfortunately, despite unusual interests the knowledge of deprotonation energetics of amino acids and peptides is quite limited in aqueous mixtures of ionic and non-ionic cosolvents except for some studies by Roy *et al.* (1) and others (2, 3). It is well known that glycine exists in aqueous solution predominantly in the zwitterionic form, $H_3N^+—CH_2—COO^-$ (symbolised as $RH^\pm$). In acidic solution, it is present as $H_3N^+—CH_2—COOH$ (symbolised as RH_2^+), whereas in alkaline solution it is present as $H_2N—CH_2—COO^-$ (symbolised as R^-). The contributions of these species at different pH in aquo-organic and biological systems are still an involved problem as the knowledge of the protolytic dissociations of these species in different solvents is yet fairly limited. The change in pK_a as a function of the properties of solvent is likely to provide useful information not only in the identification of the nature of the solute–solvent interaction patterns (in binary solvent systems) but also in the interaction of the carboxylate site ($NH_2.CH_2.COO^-$) and the nitrogen site ($\overset{+}{N}H_3.CH_2.COOH$) of glycine with water and with the components of binary solvent systems.

With this in mind, we report here the first and second deprotonation constants, ($K_a(RH_2^+)$ and $K_a(RH^\pm)$, of glycine as represented by [1] and [2]

$$[1] \quad RH_2^+ \underset{}{\overset{K_a(RH_2^+)}{\rightleftharpoons}} H^+ + RH^\pm$$

$$[2] \quad RH^\pm \underset{}{\overset{K_a(RH^\pm)}{\rightleftharpoons}} H^+ + R^-$$

in the aqueous mixtures of 10, 30, and 50 wt.% glycerol (GL) and 11.52, 20.31, and 29.64 wt.% urea (UH) and the related thermodynamic quantities. These have been determined using the Harned–Ehler type cells (4) [P] and [Q], respectively

[P] Pt; H_2(g, 1 atm)/$RH_2^+Cl^-(m_1)$, $RH^\pm(m_2)$, solvent/AgCl(S)–Ag

[Q] Pt; H_2(g, 1 atm)/$RH^\pm(m_1)$, $Na^+R^-(m_2)$, NaCl(m_3), solvent/AgCl(S)–Ag

at five equidistant temperatures ranging from 15 to 35°C. To evaluate the thermodynamic parameters of the species involved in processes [1] and [2], the free energies of transfer (ΔG^0_t) and entropies of transfer (ΔS^0_t) values of $RH^\pm$ and H^+ in these solvents were taken from our previous papers (5). We chose

[1]Author to whom all correspondence should be addressed.

Can. J. Chem. Downloaded from www.nrcresearchpress.com by 122.72.124.2 on 09/07/12
For personal use only.

TABLE 1. pK_a values ($pK_a(RH_2^+) = 1$ and $pK_a(RH^\pm) = 2$) (molal scale) of glycine in water, GL + H_2O, and UH + H_2O systems at different temperatures

Cosolvent	Wt.% of cosolvent	pK_a[a] 15°C	20°C	25°C	30°C	35°C
H_2O	0	(1) (2.38)	(2.37)	2.35 (2.35)	(2.34)	(2.33)
		(2) (10.05)	(9.91)	9.78 (9.78)	(9.65)	(9.53)
GL	10	(1) 2.39	2.35	2.31	2.30	2.29
		(2) 10.08	9.94	9.81	9.67	9.55
	30	(1) 2.56	2.54	2.52	2.49	2.46
		(2) 10.11	9.98	9.86	9.73	9.59
	50	(1) 2.80	2.76	2.75	2.72	2.71
		(2) 10.18	10.06	9.92	9.78	9.62
UH	11.52	(1) 1.78	1.77	1.76	1.75	1.74
		(2) 9.37	9.25	9.12	8.94	8.86
	20.31	(1) 1.62	1.61	1.60	1.59	1.58
		(2) 9.01	8.89	8.76	8.63	8.52
	29.64	(1) 1.42	1.41	1.40	1.39	1.35
		(2) 8.87	8.72	8.58	8.45	8.31

[a]Values in parentheses are taken from ref. 9.

these solvent systems because urea is a well known denaturant of proteins (6) while glycerol stabilizes them (7). It is hoped that knowing the thermodynamic behaviour of the species might be useful in finding out the behaviour of the cosolvents urea and glycerol.

Experimental

Purification of glycine (E Merck, GR grade) and the solvents has been described (5). For the first dissociation process, a stock solution of glycine was prepared by dissolving weighed amounts of glycine in known amounts of the solvent for a particular composition. Stock HCl (GR) solutions were prepared separately and their molalities were obtained by alkali–metric titration using phenolphthalein as indicator. The stock cell solutions were prepared by mixing appropriate weighed amounts of each of the two solutions and those of different ionic strengths (μ) by mass dilution with the solvents, which varied from 0.01 to 0.10 unit. For the second dissociation process, stock solutions of both glycine and NaCl (GR, E Merck) were similarly prepared, stock NaOH (E Merck, GR) solutions were also prepared separately, the molalities of which were determined titrimetrically with phenolphthalein as indicator. The stock cell solutions were then prepared by mixing appropriate weighed amounts of these three solutions and also those of different ionic strengths by mass dilution.

General experimental procedures including the preparation of the Ag–AgCl and H_2(Pt) electrodes, and the measurements of emf were similar to those described earlier (8). The equilibrium was attained in about 2–3 h. We assume equilibrium when the emf readings was constant to about ±0.1 mV per h. The pK_a data of glycine in water were taken from previous experiments (9) since the results obtained at 25°C by the above method (see Table 1) were found in good agreement with King's data (9).

Results

The measured emf of cells [P] and [Q] corrected to $P_{H_2} = 1$ atm gave the values of E. $pK_a(RH_2^+)$ values of the acid salt in those mixtures were then obtained at different molalities (m) using the following relation

$$[3] \quad \frac{E - E^0}{k} + \log \frac{m_{RH_2^+} . m_{Cl^-}}{m_{RH^\pm}} - 2A\sqrt{\mu} = pK_a(RH_2^+) + f(\mu)$$

where $k = 2.303RT/F$, $A = 1.824 \times 10^6 (\epsilon_s T)^{-3/2} d_s^{1/2}$ and μ = ionic strength = $\frac{1}{2}(m_{RH_2^+} + m_{Cl^-}) = m_1$. The required E^0 values, dielectric constants (ϵ_s), and densities (d_s) at different temperatures in GL + H_2O (10–12) and UH + H_2O (13) are taken from previous studies.

The plot of the left-hand side of eq. [3] against μ in each solvent mixture are found to be straight lines, which on extrapolation to $\mu = 0$, yield the values of $pK_a(RH_2^+)$. Notably, as the acid RH_2^+ is partially dissociated into H^+ and $RH^\pm$, $m_{RH^\pm} = m_2 + m_{H^+}$ and $m_{RH_2^+} = m_1 - m_{H^+}$. The values of m_{H^+} i.e., the H^+ ion concentrations, have been obtained from eq. [4].

$$[4] \quad -\frac{RT}{F} \ln m_{H^+} = E - E^0 + \frac{RT}{F} \ln m_{Cl^-} - 2kA\sqrt{\mu}$$

Similarly, for the second dissociation constants for cell [Q], the left-hand side of eq. [5] i.e.,

$$[5] \quad \frac{E - E^0}{k} + \log \frac{m_{RH^\pm} . m_{Cl^-}}{m_{R^-}} = pK_a(RH^\pm) + f(\mu)$$

was plotted against μ and the intercept for $\mu = 0$ gives $pK_a(RH^\pm)$. The emf data (E) of cells [P] and [Q] at different temperatures and the corresponding molalities of Cl^-, RH_2^+, $RH^\pm$ for cell [P] and those of NaCl, $RH^\pm$, and R^- for cell [Q] for the different solvent mixtures are deposited with the Depository of Unpublished Data.[2] The observed deprotonation constants of the acids (on molal scale) correct to ±0.01 unit are listed in Table 1.

These pK_a values in each of the solvents were then fitted into Harned–Robinson (14) type expression [6], although there is no complete agreement as to its correct form (15).

$$[6] \quad pK_a = AT^{-1} + B + CT$$

The maximum deviation of the pK_a values was found to be ±0.01. The thermodynamic parameters, namely standard Gibbs free energy (ΔG^0_{diss}) and entropy (ΔS^0_{diss}) accompanying deprotonation of the acids were then evaluated on the molal scale (m) by using the standard relations [7], [8]

[2]A complete set of the data may be purchased from the Depository of Unpublished Data, CISTI, National Research Council of Canada, Ottawa, Ont., Canada K1A 0S2.

Can. J. Chem. Downloaded from www.nrcresearchpress.com by 122.72.124.2 on 09/07/12
For personal use only.

TABLE 2. Coefficients of eq. [6] and $\Delta G^{0,N}_{diss}$, $\delta(\Delta G^{0,N}_{diss})$, $T\Delta S^{0,N}_{diss}$, and $T\delta(\Delta S^{0,N}_{diss})$ values in kJ mol^{-1} for the deprotonations of glycine in water, GL + H_2O, and UH + H_2O systems at 25°C[a]

Cosolvent	Wt.% of cosolvent		A/K	B	$C \times 10^2/k^{-1}$	$\Delta G^{0,N}_{diss}$	$\delta(\Delta G^{0,N}_{diss})$	$T\Delta S^{0,N}_{diss}$	$T\delta(\Delta S^{0,N}_{diss})$
H_2O	0	(1)	1500.86	−7.0080	1.4500	23.38	—	−19.32	—
		(2)	3019.48	−2.7340	0.8000	65.81	—	−21.59	—
GL	10	(1)	4600.31	−27.1230	4.7000	23.00	−0.38	−14.91	4.41
		(2)	817.07	12.1350	−1.7001	65.76	−0.05	−21.16	0.43
	30	(1)	−2309.06	19.5060	−3.1000	23.66	0.28	−15.11	4.21
		(2)	−3019.48	37.8781	−6.0000	65.60	−0.21	−21.27	0.32
	50	(1)	3010.76	−16.1513	2.9500	24.34	0.96	−16.91	2.41
		(2)	−6038.96	58.8000	−9.6021	65.35	−0.46	−17.57	4.02
UH	11.52	(1)	0.00	2.3563	−0.2001	19.80	−3.58	−16.40	2.92
		(2)	−1456.54	26.5280	−4.2000	61.84	−3.97	−18.23	3.36
	20.31	(1)	0.00	2.1963	−0.2001	18.72	−4.66	−15.31	4.01
		(2)	17.76	16.1540	−2.5000	59.61	−6.20	−16.70	4.89
	29.64	(1)	−4600.31	33.2300	−5.5010	17.39	−5.99	−11.86	7.46
		(2)	3019.48	−3.3381	0.6020	58.38	−7.43	−10.75	10.84

[a](1) and (2) refer to same as indicated in Table 1. The estimated uncertainties in the values of ΔG^0 and $T\Delta S^0$ are of the order: ±0.06 kJ mol^{-1} and ±0.60 kJ mol^{-1}, respectively.

[7] $$\Delta G^{0,m}_{diss} = 2.303R[A + BT + CT^2]$$

[8] $$\Delta S^{0,m}_{diss} = -2.303R[B + 2CT]$$

These values were then obtained on the mole fraction scale (N) by eq. [9] viz.,

[9a] $$\Delta G^{0,N}_{diss} = \Delta G^{0,m}_{diss} + RT \ln \frac{1000}{M_s}$$

and

[9b] $$\Delta S^{0,N}_{diss} = \Delta S^{0,m}_{diss} - R \ln \frac{1000}{M_s}$$

where M_s = mean molar mass of the solvent mixtures. The values of $\Delta X^{0,N}_{diss}$ ($X = G, S$), A, B, and C for both the dissociations are listed in Table 2. The solvent effects on deprotonation constants of the acids RH_2^+ and $RH^\pm$ relative to that in water, $\delta(\Delta X^{0,N}_{diss})$ were computed on mole fraction scale using relations [10] and [11] (see Table 2).

[10] $$\delta\Delta X^{0,N}_{diss}(RH_2^+) = {}_s\Delta X^{0,N}_{diss}(RH_2^+) - {}_w\Delta X^{0,N}_{diss}(RH_2^+)$$
$$= \Delta X^0_t(H^+) + \Delta X^0_t(RH^\pm) - \Delta X^0_t(RH_2^+)$$

[11] $$\delta\Delta X^{0,N}_{diss}(RH^\pm) = {}_s\Delta X^{0,N}_{diss}(RH^\pm) - {}_w\Delta X^{0,N}_{diss}(RH^\pm)$$
$$= \Delta X^0_t(H^+) + \Delta X^0_t(R^-) - \Delta X^0_t(RH^\pm)$$

where the subscripts w and s denote water and aqueous cosolvent and $\Delta X^0_t(i)$ represents the transfer parameter of any species (i) from the standard state in the reference solvent water (w) to the standard state of any of the compositions of the aqueous solvent(s). Since $\Delta X^0_t(H^+)$ values have been recently evaluated (5*b*) by a reasonable extrathermodynamic assumption such as the widely used tetraphenylarsonium tetraphenylborate (Ph_4AsBPh_4 = TATB) reference electrolyte (RE) assumption (16): $\Delta X^0_t(Ph_4As^+) = \Delta X^0_t(Ph_4B^-) = \frac{1}{2}\Delta X^0_t(TATB)$ and $\Delta X^0_t(RH^\pm)$ values are already known (5*a*), $\Delta X^0_t(RH_2^+)$ and $\Delta X^0_t(R^-)$ values were easily evaluated by eqs. [10] and [11], and were shown in Table 3.

Discussion

Table 1 shows that pK_a values of glycine increase with increasing GL concentration in the mixtures, pK_a values in UH + H_2O mixtures decrease with increasing UH concentration, while the dielectric constant of the cosolvent decreases and increases, respectively. Moreover, although the magnitude of this variation is much smaller than those of the corresponding carboxylic acids, the temperature coefficients of the pK_a values are practically negligible, particularly in the case of $pK_a(RH_2^+)$. Thus, as in HA-type acids (17), the variation of $pK_a(RH^\pm)$ with temperature is not significant, the small variation of $pK_a(RH_2^+)$ with temperature unlike BH^+-type acids (17) (for which the deprotonation is an isoelectric one) is an involved one in both the cosolvent systems. Evidently, the relative solvation of each species in the deprotonation equilibria and their induced structural changes factors to be considered.

Free energies of transfer

Figure 1 ilustrates the $\delta(\Delta G^{0,N}_{diss})$–composition profiles of both RH_2^+ and $RH^\pm$ in different solvent systems at 25°C. Notably $\delta(\Delta G^{0,N}_{diss})$ values for both acids are increasingly negative in UH + H_2O mixtures as expected from the increased basicity (13) and/or the dielectric constant of the solvents (13). However, in GL + H_2O mixtures, $\delta(\Delta G^{0,N}_{diss})$ values remain more or less invariant with cosolvent composition in spite of the decreased basicity (18) and dielectric constant of the medium (12). To understand the overall dissociation behaviour of these acids, analysis of the behaviour of the individual species is in order.

Moreover, as discussed in our previous papers (5, 8, 19), transfer energetics ΔX^0_t may be factorized into cavity forming effect $\Delta X^0_{t,cav}$ (especially for large-sized molecular species), Born-type electrostatic effect $\Delta X^0_{t,Born}$, and the chemical interaction effect $\Delta X^0_{t,ch}$, i.e.,

[12] $$\Delta X^0_t(i) = \Delta X^0_{t,cav}(i) + \Delta X^0_{t,Born}(i) + \Delta X^0_{t,ch}(i)$$

Thus the discussion of chemical transfer free energies of the

Can. J. Chem. Downloaded from www.nrcresearchpress.com by 122.72.124.2 on 09/07/12
For personal use only.

TABLE 3. Values of standard free energies of transfer $\Delta G_t^0(i)$, $\Delta G_{t,cav}^0(i)$, $\Delta G_{t,Born}^0(i)$, and $\Delta G_{t,ch}^0(i)$ with $\Delta G_{t,id}^0(i)$ and entropies of transfer $T\Delta S_t^0(i)$, $T\Delta S_{t,cav}^0(i)$, $T\Delta S_{t,Born}^0(i)$, and $T\Delta S_{t,ch}^0(i)$ (mole fraction scale) in kJ mol^{-1} of RH_2^+ and R^- of glycine from water to aqueous mixtures of glycerol and urea at 25°C

Cosolvent	Wt.% of cosolvent	$\Delta G_t^0(i)$		$\Delta G_{t,cav}^0(i)^a$	$\Delta G_{t,born}^0(i)^b$		$\Delta G_{t,ch}^0(i)$		$\Delta G_{t,id}^0(i)^c$		$T\Delta S_t^0(i)$		$T\Delta S_{t,cav}^0(i)^a$	$T\Delta S_{t,Born}^0(i)^b$		$T\Delta S_{t,ch}^0(i)$	
		RH_2^+	R^-		RH_2^+	R^-	RH_2^+	R^-	RH_2^+	R^-	RH_2^+	R^-		RH_2^+	R^-	RH_2^+	R^-
GL	10	1.0	−0.1	−0.3	0.2	0.3	1.1	−0.1	0.2	0.2	−6.8	4.1	3.9	−0.8	−1.0	−9.9	1.2
	30	1.1	−0.1	−0.9	0.7	0.9	1.3	−0.1	0.6	0.8	−3.6	−3.2	6.6	−1.8	−2.1	−8.4	−7.7
	50	1.1	−0.2	−1.9	1.4	1.6	1.6	0.1	1.2	1.6	−5.0	8.5	11.3	−2.7	−3.1	−13.6	0.3
UH	11.52	2.1	−2.4	1.6	−0.4	−0.4	0.9	−3.6	−1.1	−1.1	16.3	−20.9	8.2	0.7	0.8	7.4	−29.9
	20.31	2.2	−3.4	2.8	−0.6	−0.7	0.0	−5.5	−2.1	−2.1	1.3	−4.0	5.0	1.2	1.4	−4.9	−10.4
	29.64	1.5	−2.6	4.2	−0.8	−1.0	−1.9	−5.8	−3.4	−3.4	2.3	−7.0	3.1	1.7	2.0	−2.5	−12.1

[a]These values are taken to be same with that of $RH^{\pm}$ from ref. 5*a*, since the required diameter in the cavity calculation for RH_2^+, R^-, and $RH^{\pm}$ for glycine may be assumed to be equal.

[b]Since the charges are localised at one end, radius used for computing Born effect for $RH_2^+ \equiv 0.148$ nm which is being equal to N—H bond distance of NH_4^+ (28) and for R^- taken to be equal to 0.126 nm (as C—O bond distance in COO^- of the zwitterion) (29).

[c]The required diameters of the species are obtained from the corresponding radii of the species as indicated in *b*. Instead of using tetra-coordination round the ions as assumed by Kim *et al.* (22) for Ph_4B^-, tri-coordination has been assumed in these cases.

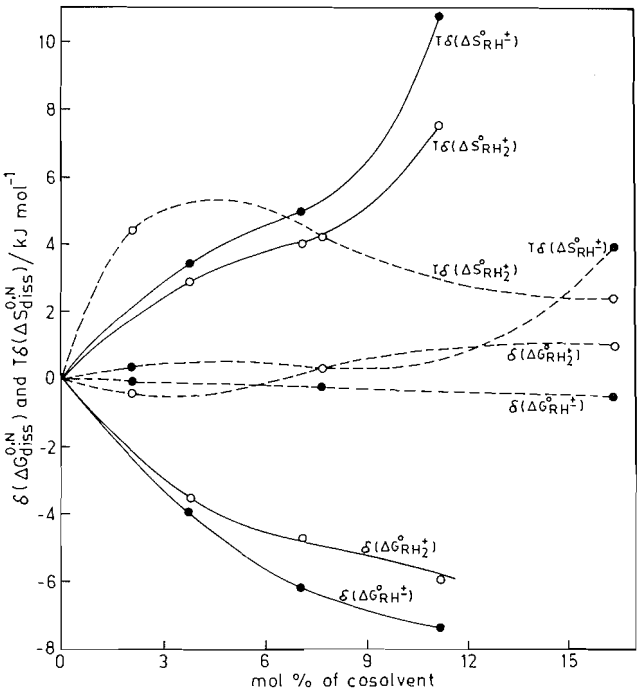


FIG 1. Variation of $\delta(\Delta G_{diss}^{0,N})$ and $T\delta(\Delta S_{diss}^{0,N})$ of glycine ($RH^{\pm}$) for the dissociation of RH_2^+(○) and $RH^{\pm}$(●) with cosolvent composition in the aqueous mixtures of urea (—) and glycerol (---) at 25°C.

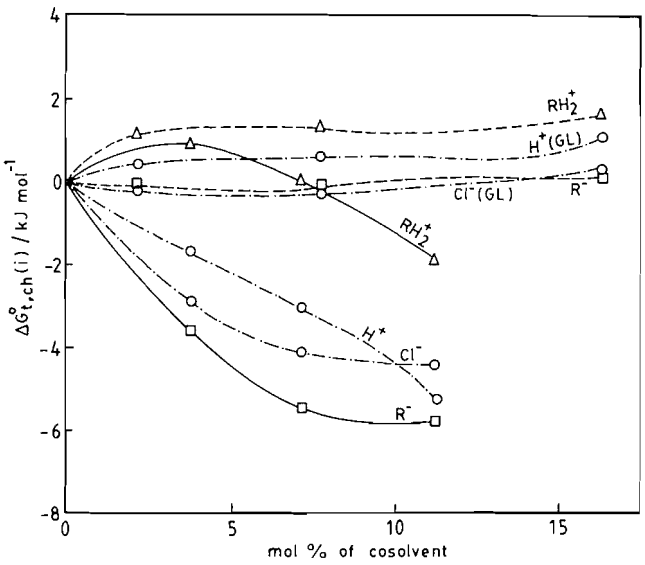


FIG 2. Variation of $\Delta G_{t,ch}^0(i)$ of RH_2^+(△) and R^-(□) of glycine and of H^+, Cl^- (·····) with cosolvent composition in the aqueous mixtures of UH (—) and GL (----) at 25°C.

species RH_2^+, R^-, and $RH^{\pm}$ i.e., $\Delta G_{t,ch}^0(i)$ rather than $\Delta G_t^0(i)$ should be more informative. Consequently, we have tentatively computed $\Delta G_{t,Born}^0$ of RH_2^+ and R^- by using simple Born equation (20) and also $\Delta G_{t,cav}^0(i)$ of RH_2^+ and R^- by scaled particle theory (SPT) (21) as formulated in the previous papers (5, 8, 19). The required solvent parameters are obtained from ref. 5*a*. The values of $\Delta G_{t,Born}^0(i)$, $\Delta G_{t,cav}^0(i)$, and $\Delta G_{t,ch}^0(i)$ so obtained are given in Table 3.

Figure 2 illustrates the $\Delta G_{t,ch}^0(i)$–composition profiles of the said species including H^+ and Cl^- ions (for comparison) (5*b*) in

Can. J. Chem. Downloaded from www.nrcresearchpress.com by 122.72.124.2 on 09/07/12
For personal use only.

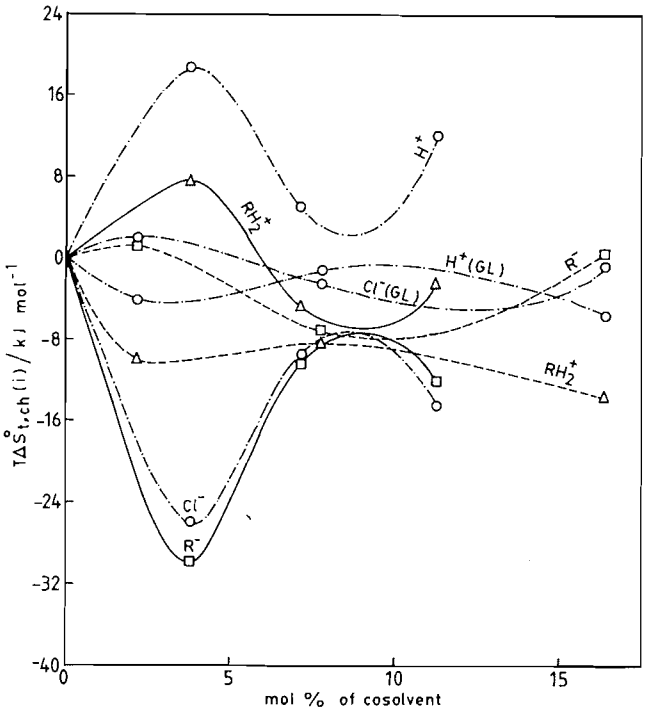


FIG 3. Variation of $T\Delta S^0_{t,ch}(i)$ of RH_2^+(△) and R^-(⊡) of glycine and of H^+, Cl^- (·····) with cosolvent composition in the aqueous mixtures of UH (—) and GL (----) at 25°C.

the aqueous mixtures of glycerol and urea, which will be largely guided by the cosolvent's acid–base properties, ion–dipole and dispersion interactions. The nature of $\Delta G^0_{t,ch}(RH^{\pm})$–composition profiles in both systems has already been described (5*a*).

Table 3 shows that in the GL + H_2O solvent system, whilst $\Delta G^0_{t,cav}$ values for RH_2^+ and R^- are increasingly negative with cosolvent composition, the reverse is true for Born effects for RH_2^+ and R^-. Consequently the $\Delta G^0_{t,ch}$–composition profiles (dotted lines) in Fig. 2 of RH_2^+ become increasingly positive, and slightly negative or invariant for R^-. Hence, while the RH_2^+ profile resembles that of H^+ (5*b*) the observed slight stabilisation of R^-, like Cl^- (5*b*), evidently results partly from the effect of increased ion–dipole or ion – induced dipole effect as indicated earlier in the case of Ph_4B^- (19). Since the contribution of ion – induced dipole interaction is negligibly small, we have tentatively computed only the ion–dipole (id) effect i.e. $\Delta G^0_{t,id}$ for RH_2^+ and R^- in each of the cosolvents of glycerol and urea according to the formulations adopted by Kim *et al.* (22). These values are given in Table 3. Thus the values of $\Delta G^0_{t,id}$ in GL + H_2O system indicate that the ion–dipole effect contributes positively, and opposes the combined effect of increased acidity (18) and dispersion interaction thus explaining the slightly negative profile or invariant nature of R^- in Fig. 2. Again, the $\Delta G^0_{t,ch}(RH_2^+)$–composition profile suggests that solvation of RH_2^+ is chiefly guided by increased dispersion interactions but opposed by the effect of decreased basicity as indicated by the upward trend of $\Delta G^0_{t,ch}(H^+)$–composition profile (5*b*, 18), thus resulting in the observed near invariance of relative solvation of RH_2^+ at those compositions. Moreover, it can also be observed that the combined effect of Born and ion–dipole interactions of RH_2^+ opposes the cavity effect (see Table 3) which indicates that the $\Delta G^0_{t,ch}(RH_2^+)$ values are invariant as a result of opposing effects of increased dispersion interaction and decreased basicity of GL + H_2O mixtures.

Similarly, in the case of UH + H_2O mixtures apart from the differences in magnitudes, the general features of $\Delta G^0_{t,ch}(i)$ of simple cation like H^+ (5*b*) and anion like Cl^- (5*b*) in this solvent system are retained in both the cationic RH_2^+ and the anionic R^- respectively, as shown in Fig. 2 (solid lines). Thus, $\Delta G^0_{t,ch}(i)$–composition profile of R^-, like Cl^-, becomes increasingly negative and then tends to become nearly invariant after ~7 mol% urea, that for RH_2^+ becomes increasingly more negative after an upward trend at initial composition like that of K^+ (5*b*). This implies that like Cl^-, R^- is seemingly stabilised by increased ion–dipole (see Table 3) and acid–base type interactions (5*b*, 23) of the negative charge centre of R^- with the zwitterionic form $NH_2{=}C(NH_2)O^-$, the predominant contributor to the resonating structure of urea (24). Similarly, the behaviour of RH_2^+ is seemingly guided by the increased basicity, ion–dipole (see Table 3) and dispersion effects at higher compositions of urea. The observed initial positive trends for $\Delta G^0_{t,ch}(RH_2^+)$ like that of K^+ (5*b*) is possibly indicative of the effect of possible steric hindrance of hydrogen-bonded UH + H_2O complexes (25, 26) which perhaps reduce the actual number of these interacting solvent complexes compared to that in pure water (5*b*, 23).

Thus, following the relative magnitudes of $\Delta G^0_{t,ch}(i)$ values of RH_2^+ and R^- of glycine, it can be inferred that while in GL + H_2O system the probable peptide–water interaction is appreciable, in UH + H_2O system the UH–peptide interaction is predominant, particularly at high UH content.

Entropies of transfer

The $T\delta(\Delta S^{0,N}_{diss})$–composition profiles for GL + H_2O and UH + H_2O mixtures are shown in Fig. 1. It can be noted that while the total entropy changes in both the deprotonation processes are similar in UH + H_2O system (solid lines), they differ appreciably in GL + H_2O system (dotted lines). As in the cases of free energies of deprotonation, to understand the overall behaviour of $T\delta(\Delta S^{0,N}_{diss})$, the entropic contributions of RH_2^+, R^-, and $RH^{\pm}$ are required. Moreover, for a better understanding of the entropic effects, tentative estimates of both the cavity and Born-type electrostatic effects towards the total $T\Delta S^0_t(i)$ of RH_2^+, R^-, and $RH^{\pm}$ have been made as in earlier papers (5, 8, 27). These values, along with $T\Delta S^0_{t,ch}(i)$ values, are listed in Table 3. Since the radius of glycine hardly differ within this small range of temperature, the ion–dipole effect towards $T\Delta S^0_{t,ch}(i)$ was considered negligible.

Figure 3 illustrates the $T\Delta S^0_{t,ch}(i)$–composition profiles of RH_2^+ and R^- and those of H^+ and Cl^- (for comparison) (5*b*) in GL + H_2O and UH + H_2O mixtures. The profiles for $RH^{\pm}$ of glycine has already been discussed in a previous paper (5*a*). Incidentally, while the profiles for RH_2^+ resemble the profiles of simple cations like H^+, the profiles for R^- resemble those of simple anions like Cl^- in each of the solvent systems. Thus, while the $T\Delta S^0_{t,ch}(i)$–composition profiles of RH_2^+, like H^+ or K^+ (5*b*), exhibit the "characteristic maxima" and that of R^-, like Cl^- (5*b*), exhibit the "characteristic minima" in UH + H_2O system as well as in other aquo-organic (5*b*, 27) and aquo-ionic systems (27), the reverse is true in the GL + H_2O system as well as in aqueous methanol system (5*b*). Evidently, fluctuations of these profiles are expected because of the structural variations in the solvent mixtures. Thus, the structural changes induced by the charged species in these cosolvents are similar to the changes induced by simple cations and anions. An opposite behaviour has been discussed earlier not only in these systems

Can. J. Chem. Downloaded from www.nrcresearchpress.com by 122.72.124.2 on 09/07/12
For personal use only.

(5*b*) but also in an aquo-ionic system (27). The observations substantiated the earlier contention that urea acts as a three-dimensional (3D) water structure breaker right from the initial composition but induces some structural order due to the possible formation of UH + H_2O and biurate complexes (25, 26) around 4–10 mol% UH, while small amounts of glycerol slightly promote the 3D water structure initially and large amounts break up the same afterwards. Moreover, the transfer process of all the species of glycine appeared to be non-spontaneous because of a large decrease in the entropy term in these systems as expected.

Acknowledgement

Thanks are due to UGC, Govt. of India, New Delhi, for financial assistance.

1. (*a*) R. N. Roy, J. J. Gibbons, and R. Snelling. J. Soln. Chem. **6**, 475 (1977); (*b*) R. N. Roy, J. J. Gibbons, G. Lacross, Jr., and C. W. Krueger. J. Soln. Chem. **5**, 333 (1975).
2. (*a*) A. K. Chattopadhyay and S. C. Lahiri. Ind. J. Chem. **15**A, 930 (1977); (*b*) B. P. Dey, S. Dutta, and S. C. Lahiri. Ind. J. Chem. **21**A, 886 (1982).
3. V. P. Vasil'ev, N. K. Grechina, and G. A. Zaitseva. Zh. Obshch. Khim. **53**, 199 (1983).
4. H. S. Harned and R. W. Ehlers. J. Am. Chem. Soc. **54**, 1350 (1932).
5. H. Talukdar, S. P. Rudra, and K. K. Kundu. (*a*) Can. J. Chem. **66**, 461 (1988); (*b*) Can. J. Chem. **67**, 315 (1989).
6. Y. Nozaki and C. Tanford. J. Biol. Chem. **238**, 4074 (1963).
7. K. Gekko. J. Biochem. **90**, 1633 (1981).
8. S. P. Rudra, H. Talikdar, B. P. Chakraborty, and K. K. Kundu. Can. J. Chem. **64**, 1960 (1986).
9. E. J. King. J. Am. Chem. Soc. **73**, 155 (1951).
10. I. N. Basumallick and K. K. Kundu. Can. J. Chem. **57**, 961 (1979).
11. E. W. Washburn (*Editor*). International critical tables of numerical data, Physics, Chemistry and Technical Tables Vol. III. McGraw Hill (1928).
12. G. Akerlof. J. Am. Chem. Soc. **54**, 4125 (1932).
13. K. K. Kundu and K. Majumdar. J. Chem. Soc. Faraday Trans. I. **69**, 806 (1973).
14. H. S. Harned and R. A. Robinson. Trans. Faraday Soc. **36**, 973 (1941).
15. D. J. G. Ives and P. G. N. Moseley. J. Chem. Soc. Faraday Trans. I. **72**, 1132 (1976).
16. B. G. Cox, R. R. Hedwig, A. J. Parker, and D. W. Watts. Aust. J. Chem. **27**, 477 (1974).
17. H. S. Harned and B. B. Owen. The physical chemistry of electrolytic solutions. 2nd ed. Reinhold, New York. 1958. Chap. 15.
18. I. N. Basumallick and K. K. Kundu. Can. J. Chem. **58**, 79 (1980).
19. S. P. Rudra, B. P. Chakraborty, I. N. Basumallick, and K. K. Kundu. Z. Phys. Chem. (Neue Folge), **150**, 211 (1986).
20. M. Born. Z. Physik. **1**, 45 (1920).
21. R. A. Pierotti. J. Phys. Chem. **67**, 1840 (1963); **69**, 281 (1965); Chem. Rev. **76**, 717 (1976).
22. J. I. Kim, A. Cocal, H. J. Born, and E. A. Comaa. Z. Phys. Chem. (Neue Folge), **110**, 209 (1978).
23. K. K. Kundu and A. K. Das. J. Soln. Chem. **8**, 259 (1979).
24. A. L. De and A. K. Atta. Can. J. Chem. **64**, 1521 (1986).
25. T. S. Sarma and J. C. Ahluwalia. Chem. Soc. Rev. **2**, 203 (1973).
26. A. K. Das and K. K. Kundu. J. Phys. Chem. **79**, 2604 (1975) and references therein.
27. S. P. Rudra, H. Talukdar, and K. K. Kundu. Can. J. Chem. **65**, 2595 (1987).
28. Y. Marcus. Ion solvation. Wiley-Interscience, Chichester. 1985.
29. R. C. Weast (*Editor*). Handbook of chemistry and physics, 52nd ed. Cleveland, 1971–1972.

Can. J. Chem. Downloaded from www.nrcresearchpress.com by 122.72.124.2 on 09/07/12
For personal use only.

Single-ion transfer energetics of some ions using tetraphenylarsonium tetraphenylborate reference electrolyte assumption in aqueous mixtures of urea and glycerol

HIMANSU TALUKDAR, SIBAPRASAD RUDRA, AND KIRON K. KUNDU[1]
Physical Chemistry Laboratories, Jadavpur University, Calcutta 700 032, India

Received July 20, 1988

HIMANSU TALUKDAR, SIBAPRASAD RUDRA, and KIRON K. KUNDU. Can. J. Chem. **67**, 321 (1989).

Single-ion transfer free energies [$\Delta G_t^0(i)$] and entropies [$\Delta S_t^0(i)$] of some ions from water to aqueous mixtures of urea and glycerol have been determined using the widely used tetraphenylarsonium tetraphenylborate reference electrolyte assumption from solubility and emf measurements of some appropriate electrolytes at five different temperatures (15 to 35°C). Analysis of $\Delta G_t^0(i)$ and $T\Delta S_t^0(i)$ values of the ions as well as their respective "chemical" effect, $\Delta G_{t,ch}^0(i)$ and $T\Delta S_{t,ch}^0(i)$, as obtained after correcting for their cavity and Born-type electrostatic effects, estimated by the scaled particle theory (SPT) and simple Born equation, respectively, show a complex dependence upon solvent composition. Attempts have been made to explain the observed mirror-image entropic behaviour of simple cations and anions in the light of Kundu *et al.*'s four-step transfer process and to compare the results with those obtained in other aquo-ionic and nonionic systems.

Key words: single ion, transfer energetics, TATB assumption, aqueous glycerol, aqueous urea.

HIMANSU TALUKDAR, SIBAPRASAD RUDRA et KIRON K. KUNDU. Can. J. Chem. **67**, 321 (1989).

Opérant à cinq températures différentes (de 15 à 35°C), en se basant sur des mesures des solubilités et des fem de quelques électrolytes appropriés et utilisant le tétraphénylborate de tétraphénylarsonium comme électrolyte de référence, on a déterminé les énergies libres [$\Delta G_t^0(i)$] ainsi que les entropies [$\Delta S_t^0(i)$] de transfert de quelques ions de l'eau à des mélanges aqueux d'urée et de glycérol. En se basant sur une analyse des valeurs de [$\Delta G_t^0(i)$] et de [$\Delta S_t^0(i)$] des ions ainsi que de leurs effets «chimiques» respectifs, [$\Delta G_{t,ch}^0(i)$] et de [$\Delta S_{t,ch}^0(i)$], qui ont été obtenus après avoir apporté des corrections pour leur cavité et pour les effets électrostatiques du type de Born qui ont été évaluées respectivement par la théorie de la particule réduite (SPT) et par une équation simple de Born, on a pu déduire qu'elles présentent une relation complexe avec la composition du solvant. On a tenté d'utiliser le processus de transfert en quatre étapes proposé par Kundu pour expliquer le comportement entropique en image dans un miroir qui a été observé avec quelques cations et anions simples; on a aussi tenté de comparer ces résultats avec ceux obtenus dans d'autres systèmes aquo-ioniques ainsi que non-ioniques.

Mots clés : seul ion, énergétique de transfert, hypothèse TATB, glycérol aqueux, urée aqueuse.

[Traduit par la revue]

Can. J. Chem. Downloaded from www.nrcresearchpress.com by 122.72.124.2 on 09/07/12
For personal use only.

Introduction

It is now well recognised that transfer enthalpies (ΔH_t^0) and entropies (ΔS_t^0) of electrolytes and non-electrolytes often provide useful information regarding the relative structuredness of solvents. However, the interpretation of the experimental results on ΔS_t^0 lately proved somewhat difficult and conflicting with the general recognition that the entropic behaviour of the oppositely charged species like H^+ and X^- (X = Cl, Br, or I) as based on the widely used tetraphenylarsonium tetraphenylborate (TATB) reference electrolyte (RE) assumption (1) show nearly mirror-image behaviour in some aquo-organic (2–6) and aquo-ionic (7) systems imparting more refined information on the solvent structural features.

Evidently, it should be of particular interest to extend this type of study to some other aquo-organic solvents and especially urea (UH) + H_2O and glycerol (GL) + H_2O systems, since it is well known that these two co-solvents exhibit opposite behaviour towards the conformational stability of proteins and enzymes. Moreover, while urea acts more like a statistical structure breaker in water (8), glycerol lies on the border line of the structure-making mono-ols and structure-breaking poly-ols (9).

Hence, with a view to have detailed reflection on the structuredness of these two cosolvents, the $\Delta P_t^0(i)$ (P = G, S, or H) of some cations like Ph_4As^+ (Ph = phenyl), K^+, H^+, and some anions like Pi^- (Pi = picrate), Ph_4B^-, and Cl^- from water to the aqueous mixtures of 11.52, 20.31, 29.64 wt% UH and 10, 30, and 50 wt% GL have been determined by the RE assumption. The required solubility data of $KBPh_4$, KPi, and Ph_4AsPi at different temperatures and also of ΔP_t^0 values of KCl computed from the standard emf's (ΔE^0) of the double cell (A)

[A] Ag–AgCl/KCl(m), solvent/K(Hg)/KCl(m), water/AgCl–Ag

were obtained at different temperatures ranging from 15 to 35°C since the corresponding data for HCl are already known in the literature (10, 11). The usual formulations regarding the RE assumption has been described earlier (1).

Experimental

The quality and method of purifications of the solvents and solutes have already been described (10–12). The general experimental procedure for measuring the emf's of the cell (A) were also exactly similar to those of our previous measurements (12).

Preparation of the salts $KBPh_4$, Ph_4AsPi, and KPi and measurements of their saturated solubilities at different temperatues by spectrophotometric method were essentially similar to those described earlier (12). Constancy of the absorbance to within 1% was taken as the criterion of the attainment of the saturated solubility of the salts. At least two sets of measurements were made for all the solutes and the results were found to agree to within 1%. The molar extinction coefficient (ϵ) values of the salts in the media and the wavelengths of light used are given elsewhere (12*a*, 13). Notably, in the case of GL + H_2O systems, all solubility measurements were made at five different temperatures ranging from 15 to 35°C while that for UH + H_2O mixtures were done in the temperature range 10 to 30°C (except for $KBPh_4$, which was done in the range of 5 to 25°C) to avoid the possible effect of irreversible change undergone by UH + H_2O mixtures above 30°C (14).

[1]Author to whom all correspondence should be addressed.

TABLE 1. Values of ΔE_m^0/V at different temperatures, coefficients A, B, and C of eq. [3] and ΔG_t^0, $T\Delta S_t^0$ (kJ mol^{-1} and in mole fraction scale) of KCl in aqueous mixtures of UH and GL at 25°C[a]

	Wt% of cosolvent	ΔE_m^0/V 15°C	20°C	25°C	30°C	35°C	A (kJ mol^{-1})	B (kJ mol^{-1} K^{-1})	C (kJ mol^{-1} K^{-1})	ΔG_t^0	$T\Delta S_t^0$
UH	11.52	0.0005	0.0008	0.0010	0.0016	0.0020	28.49	−0.6789	0.1022	−0.31	−1.67
	20.31	0.0014	0.0016	0.0025	0.0032	0.0036	7.01	−0.2194	0.0341	−0.48	−2.68
	29.64	0.0040	0.0052	0.0060	0.0068	0.0075	−60.20	1.2678	−0.1874	−0.55	−3.78
GL	10	0.0080	0.0084	0.0086	0.0086	0.0088	−35.79	0.8010	−0.1193	0.36	−0.59
	30	0.0220	0.0240	0.0260	0.0270	0.0280	−153.42	3.3338	−0.4941	1.12	−7.27
	50	0.0450	0.0460	0.0480	0.0500	0.0520	95.91	−2.2560	0.3407	2.04	−7.71

[a]Maximum uncertainties in ΔE_m^0 values are ±0.5 mV and those in ΔG_t^0 and $T\Delta S_t^0$ values are within ±0.05 and ±0.6 kJ mol^{-1}, respectively.

Can. J. Chem. Downloaded from www.nrcresearchpress.com by 122.72.124.2 on 09/07/12
For personal use only.

Results

The observed emf (ΔE) values of cell (A) at different molalities, m (mol kg^{-1}) of KCl for the different solvent mixtures at different temperatures are given elsewhere.[2] The standard ΔE^0 values (Table 1) were obtained by extrapolating the function $\Delta E^{0\prime}$ defined by eq. [1] against m to $m = 0$

$$[1] \quad \Delta E^{0\prime} = \Delta E - 2k[f_s(m) - f_w(m)] = \Delta E^0 - 2k\Delta bm$$

where $f(m) = -A_0B_0m^{1/2}(1 + a_0B_0m^{1/2})^{-1} + \ln(1 + 0.002Mm)$ and the symbols have their usual significance (12). The required densities and dielectric constants at different temperatures were taken from the literature (10, 15). The estimated standard deviations in ΔE^0 values for all the cases lie within ±0.5 mV.

Standard free energies of transfer, ΔG_t^0, of KCl from water to the mixed solvents on mole fraction scale (N) were derived at each temperature from eq. [2]

$$[2] \quad \Delta G_t^0 = F\Delta E^0 - 2RT \ln (M_s/M_w)$$

where M_w and M_s are the molar and mean molar masses of pure water and the solvent mixtures, respectively. The ΔG_t^0(KCl) values at different temperatures were then fitted to eq. [3]

$$[3] \quad \Delta G_t^0 = A + BT + CT \ln T$$

where A, B, and C are constants and thus the ΔS_t^0 values on the mole fraction scale were obtained by eq. [4]

$$[4] \quad \Delta S_t^0 = -[B + C(1 + \ln T)]$$

These values along with the constants A, B, and C were listed in Table 1.

For salts $KBPh_4$, Ph_4AsPi, and KPi, the observed saturated solubilities (S) in mol dm^{-3} in both UH + H_2O and GL + H_2O systems are given elsewhere.[2] The ΔG_s^0 values at different temperatures were calculated on the molar scale using

$$[5] \quad \Delta G^0 = -2RT \ln S \qquad \gamma_\pm = 2.303RT\, pK_{sp}$$

where $\gamma_\pm$ is the mean molar activity coefficient of the electrolyte which was computed using the extended Debye–Hückel equation as before (12). pK_{sp}^c values thus obtained on molar scale (c) at different temperatures were listed in Table 2. The same in water has been obtained from our previous experiments (7*b*). The ΔG_s^0 values were then fitted to the temperature equation

TABLE 2. Solubility products (pK_{sp}^c) of Ph_4BK, Ph_4AsPi, and KPi in UH + H_2O and GL + H_2O mixtures at different temperatures (°C)

Solute	pK_{sp}^c 5°C	10°C	15°C	20°C	25°C	30°C
			11.52 wt% UH			
Ph_4BK	8.47	8.31	8.15	7.95	7.76	—
Ph_4AsPi	—	8.31	8.25	8.17	8.12	8.03
KPi	—	3.38	3.33	3.25	3.15	3.06
			20.31 wt% UH			
Ph_4BK	8.10	8.02	7.91	7.79	7.64	—
Ph_4AsPi	—	7.79	7.69	7.59	7.45	7.39
KPi	—	3.17	3.12	3.04	2.97	2.89
			29.64 wt% UH			
Ph_4BK	7.93	7.85	7.76	7.65	7.49	—
Ph_4AsPi	—	7.41	7.31	7.21	7.14	7.03
KPi	—	2.96	2.87	2.79	2.70	2.60

Solute	pK_{sp}^c 15°C	20°C	25°C	30°C	35°C
		10 wt% GL			
Ph_4BK	7.64	7.57	7.51	7.44	7.40
Ph_4AsPi	8.96	8.83	8.67	8.55	8.44
KPi	3.69	3.55	3.41	3.25	3.09
		30 wt% GL			
Ph_4BK	7.61	7.54	7.51	7.42	7.38
Ph_4AsPi	8.65	8.51	8.40	8.25	8.10
KPi	3.74	3.62	3.47	3.31	3.15
		50 wt% GL			
Ph_4BK	7.55	7.50	7.47	7.40	7.37
Ph_4AsPi	8.32	8.17	8.06	7.90	7.74
KPi	3.79	3.67	3.52	3.37	3.23

of the form

$$[6] \quad \Delta G_s^0 = a + bT + CT \ln T$$

The values of these coefficients (a, b, and c) were presented in Table 3. These are found to reproduce the experimental data within ±0.02 kJ. The ΔG_t^0 and ΔS_t^0 of the salts were calculated

[2]A complete set of the experimental data may be purchased from the Depository of Unpublished Data, CISTI, National Research Council of Canada, Ottawa, Ont., Canada K1A 0S2.

TABLE 3. Values of coefficients (a, b, and c) of eq. [6] for Ph_4BK, Ph_4AsPi, and KPi and transfer energetics (ΔG_t^0 and $T\Delta S_t^0$) (kJ mol^{-1} and in mole fraction scale) of the salts and HCl[a] from water to aqueous mixtures of urea and glycerol at 25°C

Salts of RE	a (kJ mol^{-1})	b (kJ mol^{-1} K^{-1})	c (kJ mol^{-1} K^{-1})	ΔG_t^0	$T\Delta S_t^0$
		Water			
Ph_4BK	121.5810	−2.1522	0.3315	—	—
Ph_4AsPi	−102.2828	3.3148	−0.4916	—	—
KPi	30.4168	0.4290	−0.0818	—	—
		11.52 wt% UH			
Ph_4BK	−317.8422	8.6216	−1.3000	1.03	45.98
Ph_4AsPi	−106.5414	3.0257	−0.4411	−4.93	−14.39
KPi	−300.3716	7.4333	−1.1172	−1.59	−20.49
HCl[a]	—	—	—	−4.03	0.11
		20.31 wt% UH			
Ph_4BK	−429.2326	10.8006	−1.6173	0.07	30.15
Ph_4AsPi	80.5231	−1.0275	0.1581	−8.67	−2.23
KPi	−160.0653	4.1604	−0.6260	−2.91	−25.32
HCl[a]	—	—	—	−6.01	0.89
		29.64 wt% UH			
Ph_4BK	−507.7068	12.5694	−1.8820	−0.96	31.63
Ph_4AsPi	−5.3146	0.8525	−0.1225	−10.92	−2.16
KPi	−113.1219	3.2000	−0.4860	−4.76	−18.27
HCl[a]	—	—	—	−7.83	2.27
		10 wt% GL			
Ph_4BK	125.3863	−2.2772	0.3511	−0.47	−1.57
Ph_4AsPi	189.3672	−3.2307	0.4847	−1.71	2.28
KPi	−225.0757	6.0992	−0.9265	−0.15	−3.50
HCl[a]	—	—	—	0.16	0.03
		30 wt% GL			
Ph_4BK	−19.1644	0.9515	−0.1305	−1.22	−1.99
Ph_4AsPi	−222.0740	6.0361	−0.9005	−4.07	5.99
KPi	−309.9840	8.0020	−1.2103	−0.46	−3.58
HCl[a]	—	—	—	0.55	0.59
		50 wt% GL			
Ph_4BK	−14.5043	0.7681	−0.1012	−2.40	−4.67
Ph_4AsPi	−254.0244	6.7931	−1.0157	−7.13	11.67
KPi	−162.0120	4.6321	−0.7058	−1.35	−5.14
HCl[a]	—	—	—	1.25	−0.48

[a]Data for UH + H_2O, ref. 10; for GL + H_2O, ref. 11. Maximum uncertainties in ΔG_t^0 and $T\Delta S_t^0$ values are within ±0.05 and ±0.6 kJ mol^{-1}, respectively.

on the mole fraction scale using

$$[7]\quad \Delta G_t^0 = {}_s\Delta G_s^0 - {}_w\Delta G_s^0 = 2.303RT[p_sK_{sp} - p_wK_{sp}] - 2RT \ln (M_s d_w/M_w d_s) = (a_s - s_w) + (b_s - b_w)T + (c_s - c_w)T \ln T - 2RT \ln (M_s d_w/M_w d_s)$$

and

$$[8]\quad \Delta S_t^0 = (b_w - b_s) + (c_w - c_s) + (c_w - c_s) \ln T + 2R \ln (M_s d_w/M_w d_s) + 2RT(\mathrm{d} \ln d_w/\mathrm{d}T - \mathrm{d} \ln d_s/\mathrm{d}T)$$

where T = 298.15 K and subscripts s and w refer to co-solvent and water, respectively. The values were tabulated in Table 3. These were then utilised to compute ΔP_t^0 of the RE with the help of eq. [9].

$$[9]\quad \Delta P_t^0(Ph_4AsBPh_4) = \Delta P_t^0(Ph_4AsPi) + \Delta P_t^0(KBPh_4) - \Delta P_t^0(KPi)$$

These were then apportioned into individual ionic contributions by TATB assumption (1). $\Delta P_t^0(i)$ values of other ions were then estimated by the additivity rule from the ΔP_t^0 values of the appropriate electrolytes which were listed in Table 4.[2] $\Delta P_t^0(HX)$ values were taken from previous papers (10, 11).

Discussion

Free energies of transfer

Figures 1 and 2 illustrate the variation of the $\Delta G_t^0(i)$–composition profiles (solid lines) of the individual ions with

Can. J. Chem. Downloaded from www.nrcresearchpress.com by 122.72.124.2 on 09/07/12
For personal use only.

co-solvent composition in UH + H_2O and GL + H_2O mixtures, respectively. Evidently, the profiles vary to a very little extent with that of previous experiments (12*a*, 13) which indicate the consistency of the experimental results in both the cases.

However, the discrepancies between the $\Delta G_t^0(H^+)$ values (so also for the other ions) obtained by Wells' method (16) and the present TATB method in these co-solvent systems have already been discussed earlier (12*a*). It was concluded that Wells equated $\Delta G_t^0(H^+)$ with the Born-type electrostatic contribution only, neglecting the chemical or basicity effects, thereby accounting in part for the disagreement between the transfer parameters. Not only that, recently both Blandamer (17) and Marcus (18) have pointed out some important shortcomings of the Wells' method and preferred the TATB assumption among the various existing extrathermodynamic assumptions for the estimation of single ion transfer properties not only at 25°C but also at other temperatures too.

As per discussions in our previous papers (7, 19), transfer energetics ΔP_t^0 can be taken to comprise cavity forming effect $\Delta P_{t,cav}^0$, long-range Born-type electrostatic effect, $\Delta P_{t,Born}^0$, and the chemical effect $\Delta P_{t,ch}^0$ i.e.

$$[10] \quad \Delta P_t^0(i) = \Delta P_{t,cav}^0(i) + \Delta P_{t,Born}^0(i) + \Delta P_{t,ch}^0(i)$$

Thus, the discussions of chemical transfer free energies of ions (which result from short-range interactions like ion–dipole, ion–quadrupole, dispersion, acid–base, H-bonding, specific, if any) i.e. $\Delta G_{t,ch}^0(i)$ should be more informative. Consequently, we have tentatively computed $\Delta G_{t,Born}^0(i)$ and $\Delta G_{t,cav}^0(i)$ terms for the different ions as per formulations described and referred to in the previous papers (7, 19). The values so obtained are given in Table 4 and depicted by dotted lines in Figs. 1 and 2.

Significantly enough, in the case of small-sized ions, the cavity effect is less and in fact gets nullified to a larger extent by the opposing Born effect, resulting in similar profiles for $\Delta G_t^0(i)$ and $\Delta G_{t,ch}^0(i)$. In the case of big ions, the cavity interaction term plays an important role as expected in both co-solvents as also observed in the case of $NaNO_3$ solutions (7).

Thus, in the UH + H_2O system, the $\Delta G_{t,ch}^0$–composition profile of H^+ indicates increased basicity and that of Cl^- indicates increased acidity of the co-solvent as before (13). Although there are several reasons for the nature of the observed $\Delta G_{t,ch}^0(H^+)$–composition profile as evidenced from various experiments (20, 21), the same reasoning for Cl^- might seem confusing. However, this may be possible in the sense that though UH molecules bring in "statistical structure breaking" (8) of water releasing free more monomeric water molecules, those water molecules are engaged in the formation of H-bonded urea–water clusters (10, 22), thus depleting the number of free water molecules. But then again it is difficult to understand why the alkali metal cation like K^+ should be hydrated more in pure water as reflected in Fig. 1. On the other hand, if one assumes, which is not quite unlikely either, that due to possible steric hindrance, the number of H-bonded UH + H_2O complexes interacting with these small sized K^+ ion is much less than that in pure water, and hence the resulting $\Delta G_{t,ch}^0(i)$ values of K^+ ion would be increasingly positive. The fact that $\Delta G_t^0(K^+)$ values obtained by the RE method are also increasingly positive in aqueous mixture of methanol (23), ethanol (24), and ethylene glycol (25) seemingly indicate such possibility.

Besides, since the dipole moment (μ) of urea is greater than that of water (μ_{UH} = 4.56 D; μ_{H_2O} = 1.87 D) (26), the other electrostatic effects like ion–dipole, ion – induced dipole etc. might also affect the solvation of these ions. Hence, in order

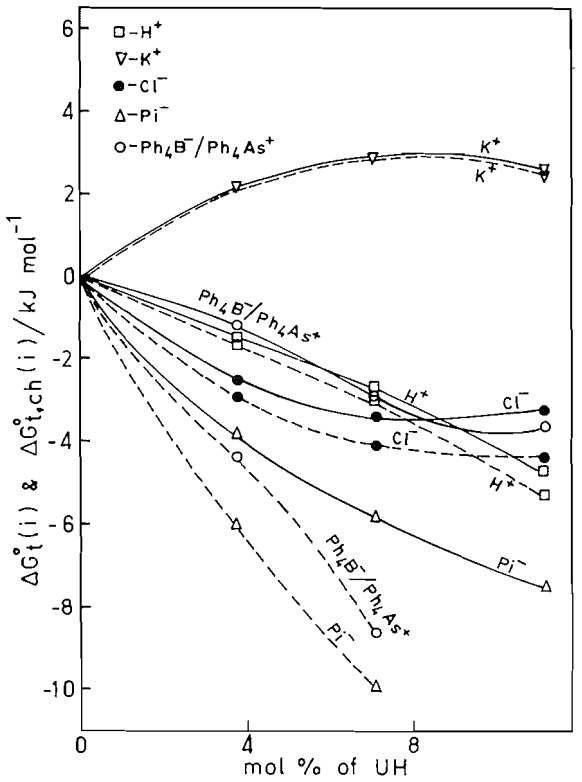


FIG. 1. Variation of $\Delta G_t^0(i)$ (solid lines) and $\Delta G_{t,ch}^0(i)$ (dotted lines) of different ions with mol% of urea (UH) at 25°C.

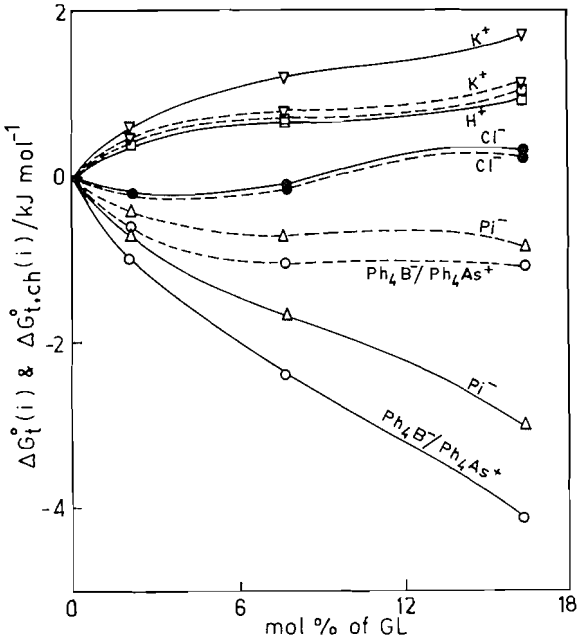


FIG. 2. Variation of $\Delta G_t^0(i)$ (solid lines) and $\Delta G_{t,ch}^0(i)$ (dotted lines) of different ions with mol% of glycerol (GL) at 25°C.

to have a picture about these interactions, the ion–dipole (id) effects have only been computed by the formulations of Kim (27) as has been done in a recent paper (19). The estimated $\Delta G_{t,id}^0(i)$ values were shown in Table 4. It is evident from this table that all ions, particularly small ions, are stabilised appreciably due to the id effect in the UH + H_2O system and this effect increases as the UH content in water increases. As a result, one can easily measure the chemical effect arising from

Can. J. Chem. Downloaded from www.nrcresearchpress.com by 122.72.124.2 on 09/07/12
For personal use only.

Can. J. Chem. Downloaded from www.nrcresearchpress.com by 122.72.124.2 on 09/07/12
For personal use only.

acid–base and other properties of this co-solvent which guide the behaviour of these small ions.

Unlike in UH + H_2O, in the case of GL + H_2O system, all the $\Delta G^0_{t,ch}(i)$–composition profiles for small ions are shifted towards the zero axis, indicating that the effect of chemical interactions of ions in the solvent mixtures are more or less the same as that in water. Moreover, the observed behaviour of these profiles is seemingly due partly to the decreased basicity and increased acidity of the solvent molecule glycerol compared to the water molecule, and partly to the id effect as evidenced from Table 4. For this reason, the decreased stabilization of Cl^- at high concentration of glycerol is mainly due to the positive contribution of $\Delta G^0_{t,id}(Cl^-)$ (see Table 4) as expected. Thus the observed increasing destabilization on cations like H^+ and K^+ and comparatively less stabilization of anion like Cl^- also conform to what is expected from the acid–base type interactions in this co-solvent as has already been described (12*a*). Moreover, if $\Delta G^0_{t,id}(i)$ values are subtracted from the corresponding $\Delta G^0_{t,ch}(i)$ values, it will be seen that all profiles are shifted nearer to zero axis (except for big ions) which indicate that glycerol though initially appears to be acidic, actually behaves more like an inert solvent (or slightly acidic) when various interactions are considered, as is done in the present case.

On the other hand, the increasing negative magnitudes of $\Delta G^0_{t,ch}(i)$ for Ph_4B^-/Ph_4As^+ in both these co-solvent mixtures can be attributed, as in other co-solvent systems (23–25), to the dispersion interaction of four phenyl groups with the co-solvent molecules. Moreover, the relative positions of $\Delta G^0_{t,ch}(i)$–composition profiles of Ph_4B^-/Ph_4As^+ and Pi^- in both UH + H_2O and GL + H_2O systems appear to suggest that like other aquo-organic solvents, UH + H_2O mixtures show more dispersion interactions with hydrocarbon moieties of Ph_4B^-/Ph_4As^+ or Pi^- compared to GL + H_2O mixtures. This appears to suggest that in GL + H_2O system hydrophobic solutes are likely to be relatively less solvated and hence more prone to undergo hydrophobic interactions among themselves than in the UH + H_2O system. Besides, the observed tentatively increased stabilization of Pi^- compared to Ph_4B^-/Ph_4As^+ in UH + H_2O mixtures is probably the result of pronounced H-bonding stabilization of Pi^- through three NO_2-groups with the zwitterionic form of UH molecule. On the other hand, the reverse relative behaviour of these ions in GL + H_2O mixtures is indicative of the larger hydrophobic interaction of Ph_4B^-/Ph_4As^+ than the acidity effect on Pi^-.

Entropies of transfer

Figures 3 and 4 (solid lines) illustrate the $T\Delta S^0_t(i)$–composition profiles of the single ions in UH + H_2O and GL + H_2O mixtures, respectively. Notably, while the profiles for cations (H^+, K^+) for aqueous urea system like other aquo-organic (2–6) and aquo-ionic (7) systems exhibit roller-coaster type behaviour with a maximum around 5 mol% urea followed by a minimum around 8–9 mol% urea, that for anions (Cl^-, Pi^-) exhibit exact mirror-image projection. But that for Ph_4B^-, however, exhibits an increasing positive trend up to 5 mol% UH beyond which it takes a downward trend.

In the case of GL + H_2O system, unlike the UH + H_2O system but as in the MeOH + H_2O system (a comparison of $T\Delta S^0_t(i)$–composition profiles in some aquo-organic systems (2, 3, 6) have been shown in Fig. 5) while the profiles for H^+ and Cl^- show reverse mirror-image behaviour as that observed in UH + H_2O mixtures, that for K^+ shows an increasingly negative trend and those for both Pi^- and Ph_4B^- show an increasingly upward trend.

Before we analyse the implications of the observed behaviours, let us make, at least a tentative estimate of $\Delta S^0_{t,ch}(i)$ which has been obtained after subtracting $\Delta S^0_{t,cav}(i)$ and $\Delta S^0_{t,Born}(i)$ from the total $\Delta S^0_t(i)$, exactly similar to what has been done in the case of $NaNO_3$ solution (7). The calculated values have been shown in Table 4 and illustrated by dotted lines in Figs. 3 and 4. Evidently, there are little differences between $T\Delta S^0_t(i)$– and $T\Delta S^0_{t,ch}(i)$–composition profiles for most of the ions save Pi^- and Ph_4B^-/Ph_4As^+ which become more negative, particularly in the GL + H_2O system (Fig. 4).

Now, as before (7), by following Kundu *et al.*'s four-step transfer process, $\Delta S^0_{t,ch}(i)$ may be formulated as

$$[11]\quad \Delta S^0_{t,ch}(i) = \Delta S^0_1 - \Delta S^0_2 + \Delta S^0_3 - \Delta S^0_4$$

It was also indicated (7) that for small cations like H^+, K^+ etc., $(\Delta S^0_1 - \Delta S^0_2)$ may be considered to be a constant positive quantity and the same will be a constant negative quantity for anions like Cl^-, Br^- etc., since ΔS^0_1 and ΔS^0_2 are both referred to water only (7); the implications for ΔS^0_3 and ΔS^0_4 referred to the solvents, however, would be as follows.

In the case of the UH + H_2O system, which may be assumed to comprise three distinct regions (Fig. 3), the $\Delta S^0_3 = 0$ for cations in the initial water-rich region since, addition of small amount of urea causes the breakdown of water structure (10, 22) leaving free monomeric H_2O and UH molecules to solvate the incoming cations. Also, since the translational degrees of freedom of both H^+ and K^+ are arrested in step 4 of the process, $-\Delta S^0_4$ would be increasingly negative. Consequently, the increasingly negative $(\Delta S^0_3 - \Delta S^0_4)$ would nullify the positive $(\Delta S^0_1 - \Delta S^0_2)$, thus resulting in a maximum in the profiles for cations (7), as observed. Beyond the intermediate region, the possible formation of UH + H_2O clusters and particularly the biurate complexes (22) contribute positively to ΔS^0_3, resulting in a positive trend of the said profiles for cations at higher compositions of urea.

Similarly, for anions, since $\Delta S^0_3 = 0$, $T\Delta S^0_{t,ch}(i)$ will be increasingly negative, from the initial composition (7). However, after about 5 mol% UH, ΔS^0_3 would be an increasingly positive quantity as the free species are now replaced by UH + H_2O clusters. Evidently, after the intermediate region $(\Delta S^0_3 - \Delta S^0_4)$ would become increasingly positive, and consequently, the opposing effects of $(\Delta S^0_1 - \Delta S^0_2)$ and $(\Delta S^0_3 - \Delta S^0_4)$ will result in a minimum in $T\Delta S^0_{t,ch}(i)$–composition profiles for the anions. At still higher compositions, the downward trend of the profiles of Cl^- indicate that Cl^- is probably unable to break the proposed UH—UH aggregates (22), so that $\Delta S^0_3 = 0$ as is evident from the invariant nature of $\Delta G^0_{t,ch}(Cl^-)$–composition profiles after 7 mol% UH (Fig. 1) which indicate that Cl^- prefers the more water-like environment in this region.

In the case of large ions, Pi^- shows predominating effect of anionic character (Fig. 3), while for more larger Ph_4B^-, transfer to the mixed solvents leads to considerable increase in $T\Delta S^0_{t,ch}(i)$ values similar to that observed in other co-solvents like ACN (4), DMF (5), and MeOH (6). The ions are presumably preferentially solvated by urea as indicated by large $-\Delta G^0_{t,ch}(i)$ values, dismantling the possible clusters, resulting in positive entropy changes in the transfer process.

As indicated earlier, the same observations in the present GL + H_2O system are somewhat unusual as they are also found in the MeOH + H_2O system (Fig. 5), some considerations about the solvent structure may be taken up for the sake of simplicity

Can. J. Chem. Downloaded from www.nrcresearchpress.com by 122.72.124.2 on 09/07/12
For personal use only.

TABLE 4. Values of free energies and enthalpies of cavity formation ($\bar{G}_c$) and ($\bar{H}_c$), standard free energies of transfer $\Delta G_t^0(i)$, $\Delta G_{t,cav}^0(i)$, $\Delta G_{t,Born}^0(i)$, and $\Delta G_{t,ch}^0(i)$ with $\Delta G_{t,id}^0(i)$ and entropies of transfer $T\Delta S_t^0(i)$, $T\Delta S_{t,cav}^0(i)$, $T\Delta S_{t,Born}(i)$, and $T\Delta S_{t,ch}(i)$ (mole fraction scale) in kJ mol^{-1} of the individual ions and the required solvent parameter α in the aqueous mixtures of UH and GL at 25°C

Ions	$\bar{G}_c{}^a$ (water)	$\bar{G}_c{}^a$ (solvent)	$\bar{H}_c{}^a$ (water)	$\bar{H}_c{}^a$ (solvent)	$\Delta G_t^0(i)^c$	$\Delta G_{t,cav}^0(i)^a$	$\Delta G_{t,Born}^0(i)^b$	$\Delta G_{t,ch}^0(i)$	$\Delta G_{t,id}^0(i)^a$	$T\Delta S_t^0(i)$	$T\Delta S_{t,cav}^0(i)^a$	$T\Delta S_{t,Born}^0(i)^b$	$T\Delta S_{t,ch}^0(i)$
					11.52 wt% UH; $\alpha = 531 \times 10^{-6}$ K^{-1} [a]								
H^+	13.5	14.1	1.8	4.6	−1.5	0.4	−0.2	−1.7	−1.5	21.7	2.4	0.4	18.9
K^+	13.1	13.6	1.7	4.5	2.2	0.4	−0.4	2.2	−1.5	19.9	2.2	0.8	16.9
Cl^-	20.7	21.5	2.8	7.3	−2.5	0.7	−0.3	−2.9	−1.5	−21.6	3.8	0.6	−26.0
Pi^-	67.2	69.8	9.7	25.1	−3.8	2.4	−0.2	−6.0	−1.0	−40.4	13.0	0.3	−53.7
Ph_4B^-/Ph_4As^+	88.9	92.2	12.9	33.5	−1.2	3.2	−0.1	−4.3	−0.9	26.0	17.4	0.2	8.4
					20.31 wt% UH; $\alpha = 435 \times 10^{-6}$ K^{-1} [a]								
H^+	—	14.5	—	4.0	−2.6	0.8	−0.4	−3.0	−2.9	7.1	1.5	0.6	5.0
K^+	—	14.0	—	3.9	2.9	0.7	−0.7	2.9	−2.9	3.5	1.4	1.3	0.8
Cl^-	—	22.1	—	6.4	−3.4	1.2	−0.5	−4.1	−2.7	−6.2	2.3	1.0	−9.5
Pi^-	—	71.9	—	21.9	−5.8	4.4	−0.3	−9.9	−1.9	−28.9	7.8	0.5	−37.2
Ph_4B^-/Ph_4As^+	—	95.0	—	29.3	−2.9	5.9	−0.2	−8.6	−1.7	26.6	10.5	0.4	15.7
					29.64 wt% UH; $\alpha = 390 \times 10^{-6}$ K^{-1} [a]								
H^+	—	15.0	—	3.9	−4.7	1.1	−0.5	−5.3	−4.5	13.8	1.0	0.9	11.9
K^+	—	14.5	—	3.8	2.6	1.1	−1.0	2.5	−4.5	7.8	0.9	1.9	5.0
Cl^-	—	22.9	—	6.1	−3.2	1.9	−0.7	−4.4	−4.3	−11.5	1.4	1.4	−14.3
Pi^-	—	74.3	—	21.2	−7.4	6.7	−0.4	−13.7	−3.0	−26.0	4.8	0.7	−31.5
Ph_4B^-/Ph_4As^+	—	98.2	—	28.3	−3.6	9.0	−0.3	−12.3	−2.7	23.9	6.4	0.6	16.9

Can. J. Chem. Downloaded from www.nrcresearchpress.com by 122.72.124.2 on 09/07/12
For personal use only.

TABLE 4. (*concluded*)

Ions	$\bar{G}_c^a$ (water)	$\bar{G}_c^a$ (solvent)	$\bar{H}_c^a$ (water)	$\bar{H}_c^a$ (solvent)	$\Delta G_t^0(i)^c$	$\Delta G_{t,cav}^0(i)^a$	$\Delta G_{t,Born}^0(i)^b$	$\Delta G_{t,ch}^0(i)$	$\Delta G_{t,id}^0(i)^a$	$T\Delta S_t^0(i)$	$T\Delta S_{t,cav}^0(i)^a$	$T\Delta S_{t,Born}^0(i)^b$	$T\Delta S_{t,ch}^0(i)$
H^+	—	13.5	—	2.8	0.4	−0.1	0.1	0.4	0.2	−3.0	1.2	−0.4	−3.8
K^+	—	13.1	—	2.7	0.6	−0.1	0.3	0.4	0.2	−3.7	1.1	−0.9	−3.9
Cl^-	—	20.7	—	4.5	−0.2	−0.2	0.2	−0.2	0.1	3.1	1.8	−0.7	2.0
Pi^-	—	67.0	—	15.4	−0.7	−0.4	0.1	−0.4	0.0	0.2	6.0	−0.3	−5.5
Ph_4B^-/Ph_4As^+	—	88.5	—	20.5	−1.0	−0.5	0.1	−0.6	0.0	2.1	8.0	−0.3	−5.6
30 wt% GL; $\alpha = 398 \times 10^{-6}\ K^{-1}$ [a]													
H^+	—	13.6	—	3.5	0.6	−0.4	0.4	0.6	0.9	2.1	2.1	−1.0	1.0
K^+	—	13.2	—	3.3	1.2	−0.4	0.8	0.8	0.9	−5.8	2.0	−2.0	−5.8
Cl^-	—	20.6	—	4.4	−0.1	−0.5	0.6	−0.2	0.5	−1.5	2.1	−1.5	−2.1
Pi^-	—	66.5	—	18.6	−1.7	−1.3	0.3	−0.7	0.0	2.2	10.2	−0.7	−7.3
Ph_4B^-/Ph_4As^+	—	87.8	—	24.8	−2.4	−1.6	0.3	−1.1	0.0	3.8	13.5	−0.6	−9.1
50 wt% GL; $\alpha = 497 \times 10^{-6}\ K^{-1}$ [a]													
H^+	—	13.6	—	4.6	0.9	−0.9	0.7	1.1	1.9	−3.5	3.7	−1.4	−5.8
K^+	—	13.2	—	4.4	1.7	−0.9	1.5	1.1	1.9	−10.7	3.5	−2.9	−11.3
Cl^-	—	20.5	—	7.2	0.3	−1.1	1.1	0.3	1.1	3.0	5.4	−2.2	−0.2
Pi^-	—	65.5	—	24.4	−3.0	−2.7	0.6	−0.9	0.1	5.6	17.4	−1.1	−10.7
Ph_4B^-/Ph_4As^+	—	86.4	—	32.5	−4.1	−3.5	0.5	−1.1	0.0	6.1	23.1	−0.9	−16.1

[a]The required diameters of H_2O, UH, and GL molecules are 0.276 nm (7), 0.441 nm (32), and 0.498 (32), respectively. The values for the scale effect i.e. $RT \ln V_w/V_s$ are obtained from density (d_s) and M_s data of the solvents (10, 11). α (= $-$d ln d_s/dT) values for water and for the solvent mixtures are taken from ref. 33. The required diameters of the solute species are $b_{Ph_4B^-}$ = 0.84 nm (7), b_{Pi^-} = 0.72 nm as tentatively taken to be equal to that of *p*-nitroaniline (pNA) given in ref. 7, b_{Cl^-} = 0.362 nm (7), b_{K^+} = 0.270 (7), $b_{H_3O^+}$ = 0.276 nm (7). The required dipole moments (μ) in computing $\Delta G_{t,id}^0(i)$ are μ_{H_2O} = 1.87 D (26), μ_{UH} = 4.56 D (26), and μ_{GL} = 2.68 D (19).

[b]The required radii of the ionic species are obtained from the corresponding diameters of the species as indicated in *a* and that of H^+ as equal to 0.276 nm (7).

[c]The estimated uncertainties in $\Delta G_t^0(i)$ and $T\Delta S_t^0(i)$ values are within ±0.05 and ±0.6 kJ mol^{-1}, respectively.

Can. J. Chem. Downloaded from www.nrcresearchpress.com by 122.72.124.2 on 09/07/12
For personal use only.

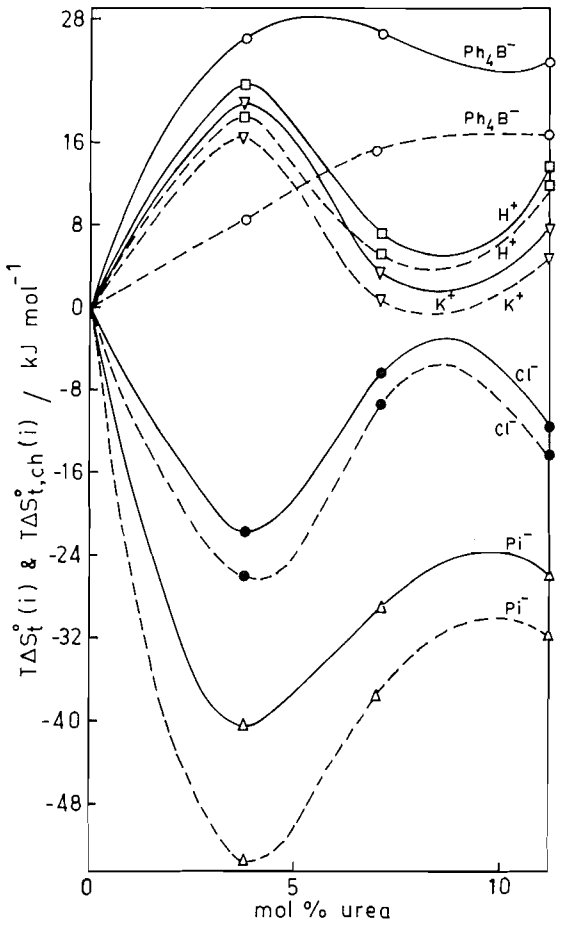


FIG. 3. Variation of $T\Delta S_t^0(i)$ (solid lines) and $T\Delta S_{t,ch}^0(i)$ (dotted lines) of different ions in the aqueous mixtures of urea at 25°C.

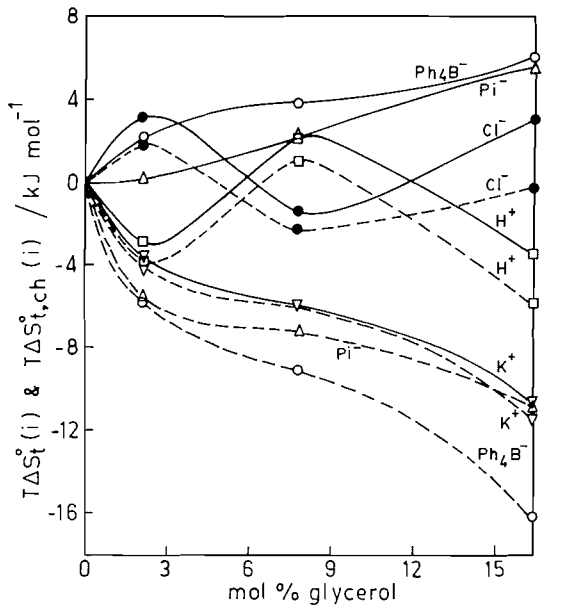


FIG. 4. Variation of $T\Delta S_t^0(i)$ (solid lines) and $T\Delta S_{t,ch}^0(i)$ (dotted lines) of different ions in the aqueous mixtures of glycerol at 25°C.

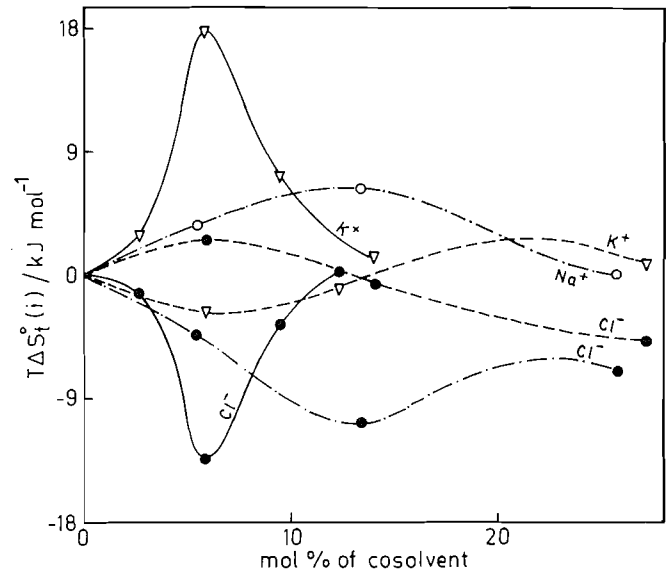


FIG. 5. Variation of $T\Delta S_t^0(i)$ of K^+ (▽), Na^+ (○), and Cl^- (●) with cosolvent composition in aqueous mixtures of *t*-BuOH (—), MeOH (----), and DMSO (·-·-·-·) at 25°C.

of the explanation, although both the co-solvents hardly affect the structure of water (9, 28). Hence, just as in ACN + H_2O (4*a*), in the water-rich region of GL, the voids inside the aqueous framework of the water lattice may be assumed to be progressively filled with GL molecules, since the "O—O" distance in GL molecule (4.75 Å) (29) is comparable with zero-spacing in water, resulting no significant enhancement of 3D water lattice. This region may, therefore, be stated as "essentially aqueous". In the intermediate region, on the other hand, the large aggregates formed in the former region are considered to be progressively broken down into smaller ones after filling up the voids. Thus, the mixed solvent can be regarded as slightly "structure maker" of the water lattice initially and a "structure breaker" in the intermediate region as observed previously (11).

Now, recalling Kundu *et al.*'s four-step transfer process, since cations (such as H^+, K^+) are expected to be solvated mainly by water as reflected in the $\Delta G_{t,ch}^0(i)$ values, the observed decrease in $T\Delta S_{t,ch}^0(H^+, K^+)$ values from the initial position, though somewhat abnormal, could be ascribed to some "preferential" solvation by monomeric water dipoles, this results in negative $(\Delta S_3^0 - \Delta S_4^0)$ values which probably exceed the positive magnitudes of $(\Delta S_1^0 - \Delta S_2^0)$, giving rise to negative $T\Delta S_{t,ch}^0$–composition profiles from initial composition. However, the observed positive hump for H^+ or H_3O^+ at the intermediate region is not surprising as either this small H^+ or H_3O^+ ion can occupy an interstitial location in the structure, resulting in $(\Delta S_3^0 - \Delta S_4^0) \sim 0$.

For the anions, since these are expected to be more solvated in the GL + H_2O system than in water by breaking down the possible water-lattice in the water-rich region, the contribution of ΔS_3^0 will be large and hence $(\Delta S_3^0 - \Delta S_4^0)$ would be increasingly positive quantity. This $(\Delta S_3^0 - \Delta S_4^0)$, however, is not expected to exceed the constant negative magnitude of $(\Delta S_1^0 - \Delta S_2^0)$ for the anions. But this has happened in this case for Cl^- as is observed by the low positive magnitude of $T\Delta S_{t,ch}^0(i)$ values (compared to that in UH + H_2O system) in this region (maximum nearly ~2 kJ). But near the intermediate

region ΔS_3^0 would be zero since the clusters have already been broken down. Evidently, the combined effect $(\Delta S_1^0 - \Delta S_2^0) + (\Delta S_3^0 - \Delta S_4^0)$, i.e., $T\Delta S_{t,ch}^0(i)$–composition profile will be increasingly negative.

In the solvent-rich region, $T\Delta S_{t,ch}^0(i)$ values do not rise sharply. This region may be interpreted as one in which GL molecules begin to penetrate the inner hydration structure of the ions, with preferential solvation becoming important above the observed minimum. Although Cl^- is relatively small, the orienting electrostatic effects of high fields may be much more important than the structural effects arising from changing the H-bond network in aqueous glycerol, relative to pure water (30).

Regarding the behaviour of Ph_4B^-/Ph_4As^+ and Pi^-, as found by Abraham *et al.* for transfer to MeOH + H_2O system (6), values of $T\Delta S_t^0(i)$ for these hydrophobic ions in GL + H_2O are all the more positive than for the small ions. The relative positions of the composition profiles of $T\Delta S_t^0(i)$ and $T\Delta S_{t,ch}^0(i)$ in this system for Ph_4B^-/Ph_4As^+ and Pi^- suggest that the cavity effect plays an important role (see Table 4). Moreover, the nature of the latter profiles, in contrast to the profiles of Cl^-, is indicative that entropic contribution of the characteristic features of the hydrophilic anions as discussed above, are largely subdued by the opposing hydrophobic/solvophilic effects of the aromatic rings of Pi^- and Ph_4B^-.

Therefore, similar to the observation by Dollet *et al.* (31) in aqueous *t*-butanol and also by others in some other aquo-organic solvents (2–6), it must be true that anions and cations are not accommodated in the same way in both UH + H_2O and GL + H_2O systems, as in other aquo-organic systems.

Can. J. Chem. Downloaded from www.nrcresearchpress.com by 122.72.124.2 on 09/07/12
For personal use only.

Acknowledgement

Thanks are due to the University Grants Commission, New Delhi, Government of India, for financial assistance.

1. B. G. Cox, C. R. Hedwig, A. J. Parker, and D. W. Watts. Aust. J. Chem. **27**, 477 (1974) and references therein.
2. (*a*) J. Juillard. J. Chem. Soc. Faraday Trans. I, **78**, 43 (1982); (*b*) J. Juillard, C. Tissier, J. Barczynska, J. Mokrzan, and S. Taniewska-Osinska. J. Chem. Soc. Faraday Trans. I, **81**, 3081 (1985).
3. (*a*) P. K. Biswas and M. N. Das. J. Chem. Soc. Faraday Trans. I, **82**, 1973 (1986); (*b*) R. Fuchs, C. P. Hagen, and R. F. Rodewald. J. Phys. Chem. **78**, 1509 (1974).
4. (*a*) K. Miyaji and K. Morinaga. Bull. Chem. Soc. Jpn. **59**, 1695 (1986); (*b*) B. G. Cox, R. Natarajan, and W. S. Waghorne. J. Chem. Soc. Faraday Trans. I, **75**, 86 (1979).
5. M. Booij and G. Somsen. Electrochim. Acta, **28**, 1883 (1983).
6. M. H. Abraham, T. Hill, H. C. Ling, R. A. Schulz, and R. A. C. Watt. J. Chem. Soc. Faraday Trans. I, **80**, 489 (1984).
7. S. P. Rudra, H. Talukdar, and K. K. Kundu. Can. J. Chem. (*a*) **64**, 1960 (1986); (*b*) **65**, 2595 (1987); (*c*) **65**, 2843 (1987).
8. H. S. Frank and F. Franks. J. Chem. Phys. **48**, 4746 (1968).
9. G. Dipaola and B. Belleau. Can. J. Chem. **55**, 3825 (1977); **56**, 848 (1978).
10. K. K. Kundu and K. Majumder. J. Chem. Soc. Faraday Trans. I, **69**, 806 (1973); **74**, 1051 (1978).
11. I. N. Basu-Mullick and K. K. Kundu. Can. J. Chem. **57**, 961 (1979).
12. (*a*) I. N. Basu-Mullick and K. K. Kundu. Can. J. Chem. **58**, 79 (1980); (*b*) K. Das, A. K. Das, and K. K. Kundu. Electrochim. Acta, **26**, 471 (1981).
13. A. K. Das and K. K. Kundu. J. Soln. Chem. **8**, 259 (1979).
14. J. Wyman, Jr. J. Am. Chem. Soc. **55**, 4116 (1933).
15. (*a*) E. W. Washburn (*Editor*). International critical tables of numerical data. Physics, chemistry and technical tables. Vol. III. McGraw Hill. 1928; (*b*) G. Akerlof. J. Am. Chem. Soc. **54**, 4125 (1932).
16. (*a*) C. F. Wells. Aust. J. Chem. **36**, 1739 (1983); (*b*) G. S. Groves and C. F. Wells. J. Chem. Soc. Faraday Trans. I, **81**, 3091 (1985).
17. M. J. Blandamer and co-workers. J. Chem. Soc. Faraday Trans. I, **82**, 1471 (1986).
18. Y. Marcus. Pure Appl. Chem. **58**, 1721 (1986).
19. S. P. Rudra, B. P. Chakravarty, K. K. Kundu, and I. N. Basu-Mullick. Z. Phys. Chem. (Neue Folge), **150**, 211 (1986).
20. N. B. Bull, K. Brease, G. L. Ferguson, and C. A. Swenson. Arch. Biochem. Biophys. **104**, 297 (1964).
21. R. C. Paul and S. L. Chadha. Spectrochim. Acta, **23**, 1243 (1967).
22. A. K. Das and K. K. Kundu. J. Phys. Chem. **79**, 2604 (1975) and references therein.
23. O. Popovych. Anal. Chem. **46**, 2009 (1974).
24. O. Popovych, A. Gibofsky, and D. H. Berne. Anal. Chem. **44**, 811 (1972).
25. A. K. Das and K. K. Kundu. Ind. J. Chem. **16A**, 467 (1978).
26. R. C. Weast (*Editor*). Handbook of chemistry and physics. 52nd ed. Cleveland. 1971–72.
27. (*a*) J. I. Kim. J. Phys. Chem. **82**, 191 (1978); (*b*) J. I. Kim, A. Cocal, H. J. Born, and E. A. Comaa. Z. Phys. Chem. (Naue Folge), **110**, 209 (1978).
28. F. Franks and D. J. G. Ives. Q. Rev. London, **20**, 1 (1966).
29. D. T. Warner. Nature, **196**, 1055 (1962).
30. J. H. Stern and S. L. Hansen. J. Phys. Chem. **85**, 3713 (1981).
31. N. Dollet, J. Juillard, and R. Zana. J. Soln. Chem. **9**, 827 (1980).
32. J. Datta and K. K. Kundu. (*a*) J. Phys. Chem. **86**, 4055 (1982); (*b*) Can. J. Chem. **61**, 625 (1983).

Vinylogous nucleophilic catalysis. The tertiary amine promoted reaction of ethenesulfonyl chloride with alcohols[1]

JAMES FREDERICK KING,[2] SHEENA MAY LOOSMORE, JOHN HENRY HILLHOUSE, AND KISHAN CHAND KHEMANI
Department of Chemistry, University of Western Ontario, London, Ont., Canada N6A 5B7

Received August 15, 1988

JAMES FREDERICK KING, SHEENA MAY LOOSMORE, JOHN HENRY HILLHOUSE, and KISHAN CHAND KHEMANI. Can. J. Chem. **67**, 330 (1989).

Ethenesulfonyl chloride (**1**) reacts with alcohols in the presence of tertiary amines to give a mixture of the alkyl ethenesulfonate (**5**) and the alkyl betylate ($R_3'N^+CH_2CH_2SO_2OR\ Cl^-$). With pyridine and neopentyl alcohol the product composition from the reaction of **1** is identical to that from the pyridinio-sulfonyl chloride (**9**). These results, when taken with experiments with deuterium labelled reagents, lead to the conclusion that the major (~80%) reaction pathway involves conversion of **1** or **9** to the sulfene **8**, which reacts with the alcohol to form **5** or the betylate, and hence vinylogous nucleophilic catalysis is the major process leading to **5**. The labelling experiments disclosed a minor pathway, evidently involving interconversion of **1** and **9**. Examination of possible mechanisms leads to the suggestion that the sulfene is formed from **1** or **9** by way of the carbanion (**14**), i.e., that **9** reacts by an E1cB process, and that the minor pathway is simply the result of side reactions of the carbanion (**14**).

Key words: sulfenes, sulfonyl transfer mechanisms, vinylogous nucleophilic catalysis.

JAMES FREDERICK KING, SHEENA MAY LOOSMORE, JOHN HENRY HILLHOUSE et KISHAN CHAND KHEMANI. Can. J. Chem. **67**, 330 (1989).

Le chlorure d'éthènesulfonyle (**1**) réagit avec les alcools, en présence d'amines tertiaires, pour conduire à un mélange d'éthènesulfonate d'alkyle (**5**) et de bétylate d'alkyle ($R_3'N^+CH_2CH_2SO_2OR\ Cl^-$). La réaction du composé **1** avec l'alcool néopentylique en présence de pyridine conduit à un mélange dont la composition est identique à celle obtenue à partir du chlorure de pyridinio-sulfonyle (**9**). Lorsqu'on considère ces résultats de concert avec les expériences effectuées à l'aide de réactifs marqués au deutérium, on arrive à la conclusion que la principale voie réactionnelle (~80%) implique la transformation des composés **1** ou **9** en sulfène **8** qui réagit avec l'alcool pour former le composé **5** ou le bétylate; on en déduit que la catalyse nucléophile vinylogue est le processus principal conduisant au produit **5**. Les expériences de marquage ont mis en évidence l'existence d'une voie secondaire impliquant évidemment une interconversion des composés **1** et **9**. Un examen des divers mécanismes possibles conduit à suggérer que le sulfène se forme à partir des composés **1** ou **9** par le biais du carbanion **14**, c'est-à-dire que le composé **9** réagit par un processus E1cB et que le produit mineur n'est que le résultat de réactions secondaires du carbanion **14**.

Mots clés : sulfènes, mécanismes de transfert sulfonyle, catalyse nucléophile vinylogue.

[Traduit par la revue]

Can. J. Chem. Downloaded from www.nrcresearchpress.com by 122.72.124.2 on 09/07/12
For personal use only.

Introduction

In the context of a continuing study of the mechanisms of the reactions of sulfonyl chlorides and related species (5, 6), it became evident some years ago that current knowledge of the mechanisms of reactions of alkanesulfonyl and arenesulfonyl chlorides did not predict the mode of reaction of 1-alkenesulfonyl chlorides. As may be seen in Scheme 1, the reaction of ethenesulfonyl chloride (**1**) with an alcohol and a tertiary amine might well be imagined to proceed by way of any of three different intermediates (**2**, **3**, and **4**), or even by a fourth process involving a one-step, general base-assisted direct displacement. The first two pathways correspond to the usual reactions of the alkane- and arenesulfonyl chlorides (6–10), while the third is a variation on nucleophilic catalysis, labelled "vinylogous nucleophilic catalysis" (11, 12). This last process was unknown at the time, but we have subsequently shown that this can be the chief route of the tertiary amine promoted hydrolysis of 1-alkenesulfonyl chlorides (11, 12). The present paper describes extension of this work to the reaction of alcohols with tertiary amines and 1-alkenesulfonyl chlorides; a preliminary report of the earliest stages has appeared (13).

Results and discussion

Initial experiments and related work

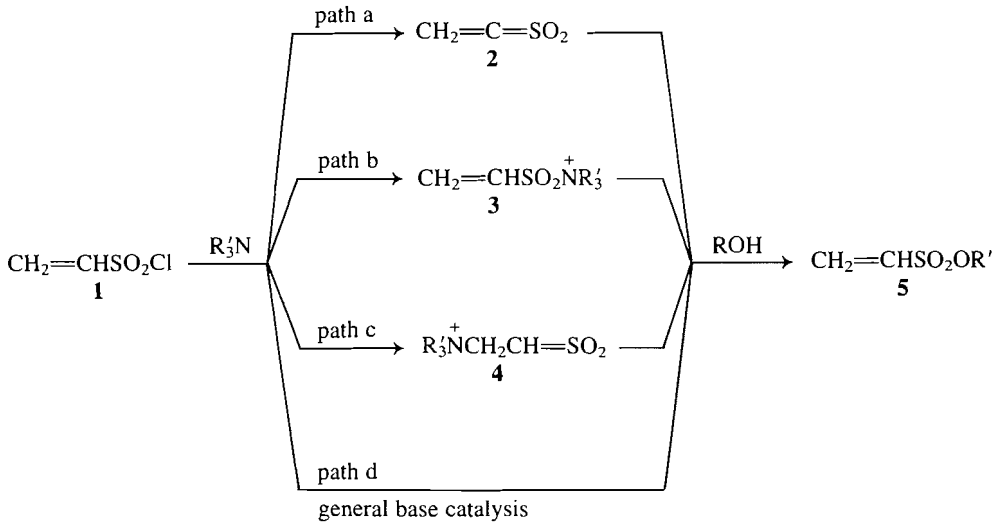
We were unable to find any reports of the preparation of ethenesulfonate esters by the direct base-promoted reaction of **1** with alcohols. These esters had been prepared, however, under similar conditions from 2-chloroethanesulfonyl chloride (14, 15), which is known to yield **1** on treatment with 2,6-lutidine (16). In addition, Truce and Campbell (8) had looked at the action of triethylamine and alcohols on 1-propene-1-sulfonyl chloride and had noted the formation of both the 1-propene- and 2-propenesulfonate esters, $CH_3CH{=}CHSO_2OR$ and $CH_2{=}CHCH_2SO_2OR$.

In our first experiments (13), simple mixing of **1** with 2-propanol in the presence of pyridine or trimethylamine followed by conventional work-up gave the ethenesulfonate ester (**5**, R = Pr^i) in mediocre (40–50%) yield. To find out what had happened to the rest of the material, we examined the product directly by ^{1}Hmr, which showed the presence of about 60% of the ester (**5**, R = Pr^i) along with another product (~40%), which appeared to be $Me_3N^+CH_2CH_2SO_2OPr^i\ Cl^-$ (**6**), i.e. what we subsequently called the [2]betylate ester (17); this was verified by synthesis of **6**. Since the betylate **6** was found to be converted to **5** with aqueous sodium carbonate, the conversion of **1** into **5** was then readily carried out in good yield (≥90%) by incorporating a sodium carbonate wash in the work-up (17). When the reaction of **1** with 2-propanol was carried out with pyridine, we saw a second set of peaks also ascribable to the corresponding betylate, $C_5H_5N^+CH_2CH_2SO_2OPr^i\ Cl^-$ (**7**). Synthesis of **7** by a route analogous to that of **6** was not feasible and the assignment at this point was based on the ^{1}Hmr spectrum.

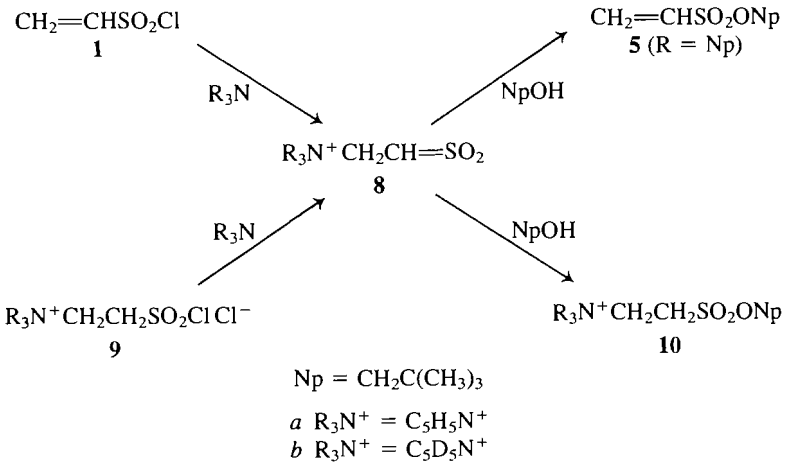
Rough estimates of rates by titration or by working up reaction products at different times and temperatures showed

[1]Part 30 in the series Organic Sulfur Mechanisms; for part 29 see ref. 1. Owing to delays in the preparation of the manuscript this paper appears after parts 31, 32, and 33, respectively, refs. 2, 3, and 4.

[2]Author to whom correspondence may be addressed.



SCHEME 1



SCHEME 2

the patterns expected of nucleophilic attack of the amine at C–2 of the sulfonyl chloride, specifically, a roughly 10^4-fold greater rate for pyridine vs. 2,6-lutidine in reaction with **1** (to give a mixture of **5** and the presumed betylate), and an approximately 500-fold slower reaction of 1-propene-1-sulfonyl chloride ($CH_3CH{=}CHSO_2Cl$) than **1** with pyridine (at −70°C).

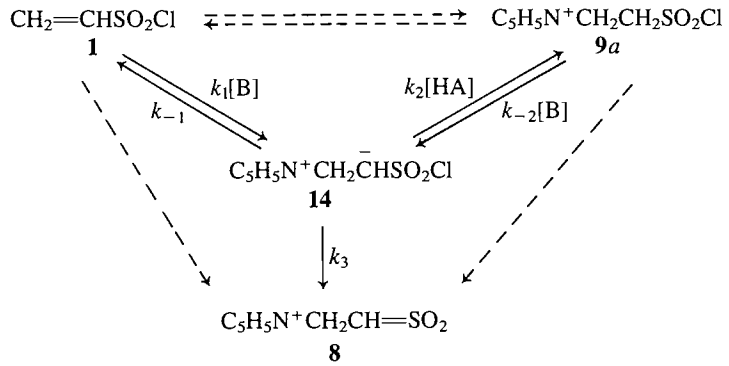
At this stage work on this project was channeled into two other directions, first to examine the usefulness of betylates as alkylating agents (17), and second to study the reaction of **1** with tertiary amines in an aqueous medium (11, 12). We then returned to the topic of the present paper, namely, the reaction of alcohols in an organic medium, a process of significance from the point of view of synthetic use. The key question was, does the reaction with alcohols in an organic medium proceed by a pathway exactly analogous to that of the aqueous system, i.e., as in Scheme 2, or does it differ? The short answer is that the hydrolysis and esterification reactions evidently have much the same overall mechanism but there are differences in detail.

Evidence for the principal pathway

For reasons detailed elsewhere (2), the more recent experiments were carried out with neopentyl alcohol in CD_3NO_2. Reaction of **1** with pyridine-d_5 and the alcohol for 1 min at 37°C gave a mixture of **5** (R = Np) and the betylate (**10***b*), in the ratio 67:33. The product ratio was not visibly altered on standing for 0.5 h, but on longer standing the ethenesulfonate ester (**5**, R = Np) was gradually converted to the betylate (**10***b*), and after 45 h the betylate made up 88% of the reaction mixture. This latter reaction, which is presumably a simple Michael addition to the electrophilic double bond of **5** (R = Np), made it possible to obtain a pure crystalline sample of the betylate (**10***a*), which was characterized by spectra and elemental analyses. The ^{1}Hmr spectrum of **10***a* was similar to that provisionally ascribed above to the corresponding isopropyl betylate (**7**) and served to confirm the earlier assignment.

Similar reaction of the pyridinio-sulfonyl chloride (**9***a*) gave exactly the same proportion of the ethenesulfonate and betylate esters, 67% of **5** (R = Np) and 33% of **10***b*; this on long standing also changed to the 12:88 ester mixture. As in the case of the corresponding reaction in water (12), this observation points strongly to a common pathway for the two reactions. For the aqueous system mentioned earlier it was possible to show, from appropriate labelling experiments, that essentially all of the products were formed via the sulfene (**8**) with no detectable interconversion between **1** and **9***a*. We accordingly carried out the analogous labelling test with the present esterification reaction. With the pyridinio-d_5-sulfonyl chloride (**9***b*) and ordinary (protiated) pyridine (in 6-fold excess) the betylate produced was largely (~80%) the deuterated product (**10***b*) with about 20% of the undeuterated betylate (**10***a*). We conclude that

Can. J. Chem. Downloaded from www.nrcresearchpress.com by 122.72.124.2 on 09/07/12
For personal use only.



SCHEME 3

about 20% of the starting material (**9***b*) undergoes elimination to ethenesulfonyl chloride (**1**), which subsequently reacts with ordinary pyridine to form the undeuterated ester (**10***a*).

To obtain further information about the mechanism, ethenesulfonyl chloride (**1**) was treated with pyridine-d_5 and neopentyl alcohol-*d* (93% D). The product consisted of a mixture of (*i*) neopentyl ethenesulfonate (total 67%) of which 80% was the undeuterated ester (**5**, R = Np) and 20% the monodeuterated ester, $CH_2{=}CDSO_2ONp$ (**11**), and (*ii*) the betylate (total 33%) consisting (as judged by its ^{1}Hmr spectrum) of about 80% $C_5D_5N^+CH_2CHDSO_2ONp$ (**12**) and 20% of the α-dideuterated ester $C_5D_5N^+CH_2CD_2SO_2ONp$ (**13**). Again, most of the reaction proceeds by direct formation of the sulfene (**8**), which is immediately trapped by NpOD to give the undeuterated ethenesulfonate (**5**, R = Np) and the α-monodeuterated betylate (**12**). The extra deuterium in **11** and **13** may be presumed to have arisen from the α-monodeuterated pyridinio-sulfonyl chloride, $C_5D_5N^+CH_2CHDSO_2Cl\ Cl^-$. We reiterate that the reaction in water gave neither $CH_2{=}CDSO_3^-$ nor $C_5D_5N^+CH_2CD_2SO_3^-$, and a simple formation of **8** from either **1** or **9** (without any conversion of **1** to **9** or **9** to **1**) accounted for all of the products. With the esterifications, however, it is evident that although the principal reaction mode corresponds to that in water, some interconversion of **1** and **9** may occur. Consideration of how this latter reaction might take place leads to a circumstantial case for the detailed mechanism of the formation of the sulfene (**8**) in this system, as described in the next section.

The detailed mechanisms

It should be recalled that the pyridinio-sulfonyl chloride (**9**) is prepared simply by mixing ethenesulfonyl chloride and pyridinium chloride in dichloromethane solution and collecting the crystals of **9** (12). The reaction is very facile and neither the formation of **9** nor its reversal to **1** and $C_5H_5NH^+$ under the conditions of the present study should occasion surprise.

In this context we suggest the sequence shown by the solid arrows in Scheme 3, where B and HA are the base (e.g., pyridine) and proton source, e.g., NpOH and (or) $C_5H_5N^+H$. From the deuteration experiments we may obtain[3] values of $k_3/k_{-1} = 4$ and $k_3/k_2[HA] \approx 3 \pm 1$; such low rate ratios are in accord with what one would expect with a very short-lived intermediate such as **14**. Previous work with alkanesulfonyl chlorides has concluded that these substrates probably react by way of an E1cB-like E2 mechanism (5), though the closely related $(E1cB)_I$ process has been demonstrated or implicated in reactions with other leaving groups (18–20). With such a strongly nucleofugal leaving group as chloride we would expect the E1cB process to become favoured only with particular stabilization of the α-sulfonyl carbanion. Thomas and Stirling (21), however, have shown that the ease of formation of such carbanions is remarkably facilitated by electron-withdrawing β-substituents,[4] and hence **14** is as likely as most α-chlorosulfonyl carbanions to be sufficiently long-lived to be an actual intermediate in the formation of a sulfene.

Other possible pathways, however, could conceivably account for the observed products. The broken arrows in Scheme 3 show another way of getting to the same compounds, but on closer examination it is difficult to devise a likely route for the reaction **1** → **9***a* that does not involve **14** as intermediate. Once **14** is accepted as a component of the reaction mixture there then seems to be no rational basis for excluding formation of **8** from **14** while at the same time permitting the direct (concerted) processes **1** → **8** and **9***a* → **8**. This situation is simply another example of the general question of the coexistence of concerted and stepwise carbanion eliminations, a point that seems to have first been brought to notice by a comment by Breslow (22), and which has been the subject of a very recent paper by Fishbein and Jencks (23). These authors concluded after detailed analysis that their results (at least in the case of the reactions of β-cyanothioethers) provided evidence against the coexistence of stepwise and concerted mechanisms, and in the face of this we favour the relatively simple process involving only the solid arrows in Scheme 3.

Another possibility is that the dideuterated product **13** arises by trapping of the sulfene (**8***b*) with pyridine-d_5 to form $C_5D_5\overset{+}{N}CH_2\overset{-}{C}HSO_2\overset{+}{N}C_5D_5$ (**15**), which in turn can exchange the α-hydrogen for deuterium in a manner analogous to that proposed for the hydrogen multiexchange reaction found with methanesulfonyl chloride and small tertiary amines (6). This reaction would explain the formation of **11** and **13** but would not, in itself, account for the formation of **10***a* from **9***b*. The latter reaction would require either (*a*) that the scheme be

[3]In the experiment starting with **9***b* and ordinary pyridine k_3/k_{-1} is equal to the product ratio [**10***b*]/[**10***a*], which was found to be 4. Defining the product ratio r = [**5**, R = Np]/[**11**] = [**12**]/[**13**] for the experiment with **1** and NpOD, we find that

$$r = (1 + k_{2D}/k_{2H})k_3/k_2$$

From the observation that $r = 4$ and the restriction of k_{2H}/k_{2D} to values ≥ 1, $k_3/k_2[HA]$ is limited to the range 2–4, i.e., 3 ± 1. (Since [HA] may change during the reaction, this represents an average value for the whole reaction.)

[4]Correlation with σ* of the rate of detritiation of $PhSO_2CHTCH_2Z$ with ethoxide in ethanol gave $\rho^* = 4.89$ (21). A very similar strong dependence of the rate of the reaction $XCH_2CH_2SO_2Cl + Et_3N \rightarrow XCH_2CH{=}SO_2$ on X has been observed in these laboratories (J. F. King and L. Lyubechansky, unpublished work).

Can. J. Chem. Downloaded from www.nrcresearchpress.com by 122.72.124.2 on 09/07/12
For personal use only.

supplemented with the concurrent conversion of **9***b* to **1**, and would therefore also suffer from the difficulties associated with the coexistence of the concerted and stepwise processes, or (*b*) that **15** be able to exchange the pyridine attached to C-2 via $CH_2{=}CHSO_2N^+C_5D_5$. The latter possibility, though appearing to be rather complex, does not seem to be excluded by our present results.

We may conclude by noting that the mechanism shown by the solid arrows in Scheme 3 accounts very simply for the products and is fully consistent with earlier work. It cannot be regarded at this stage as proved, however, and a definitive description of mechanism must await further study.

As a final comment we note that although the formation of a minor amount of the monodeuterated ethenesulfonate ester (**11**) could be taken as evidence for formation of some of the cumulated sulfene (**2**), we exclude this for two reasons. First, such a mechanism leaves unexplained the formation of the dideuterated betylate (**13**) in the same reaction. Second, and more seriously, this constitutes another route from **1** to **5** that is unavailable to the pyridiniosulfonyl chloride (**9**); such a circumstance would not give the identical products that have been consistently observed starting from either **1** or **9**.

Experimental

Instrumentation, methods, and provenance of most of the starting materials and comparison compounds have been previously described (2, 12, 17).

Reaction of ethenesulfonyl chloride (1) with 2-propanol and tertiary amines

A series of small-scale experiments was carried out in which **1** (50–100 mg) and 2-propanol (10–20 equiv.) in CH_2Cl_2 (1–10 mL) were mixed with pyridine (~5 equiv.) at temperatures varying from 0°C to room temperature and allowed to stand for times varying from 0.5 to 4 h. Work-up by washing with dilute HCl, drying over Na_2SO_4, and evaporation of the solvent gave consistently 40–50% yields of isopropyl ethenesulfonate (**5**, R = Pr^i), identified by the ^{1}Hmr signals ($CDCl_3$) at δ 1.4 (d, 6H), 4.8 (septet. 1H), and a characteristic ABC multiplet in the range 5.9–6.7 (3H) (cf. ref. 17). The same product and yield were obtained similarly from 2-chloroethanesulfonyl chloride (15), and from **1** with Me_3N, Et_3N, diisopropylethylamine, 2,6-lutidine, 2-picoline, and 1,4-diazabicyclooctane. 2-Propanol-*d* instead of the ordinary alcohol also gave a product with the ^{1}Hmr spectrum (T-60) exactly as above with all amines tested (Me_3N, Et_3N, pyridine, and 2,6-lutidine).

When the reaction of **1** (31 mg) with 2-propanol (21 μL) and pyridine (20 μL) in $CDCl_3$ (~0.5 mL) at 0°C was observed by ^{1}Hmr, after about 15 min the signals due to **5** (R = Pr^i) at δ 1.4, 4.8, and 6.0–6.8 were accompanied by peaks at δ 1.2 and 4.0 due to unreacted 2-propanol and, in addition, by new peaks at δ 1.3 (d), 5.0 (partly obscured septet), 4.3 and 5.6 (apparent triplets), and pyridinio signals from 7.5 to 9.5 ppm, assigned to the pyridiniobetylate (**7**); ratio **5**:**7**, about 60:40. Addition of D_2O removed the signals assigned to **7** (and the pyridinium ion) leaving those of **5** (R = Pr^i) and 2-propanol.

Reaction of **1** in $CDCl_3$ in an nmr tube as above except that Me_3N replaced the pyridine gave a spectrum showing **5** (R = Pr^i), unreacted 2-propanol, Me_3NH^+ (δ 3.0, d), and signals at δ 1.5 (d), 3.5 (br s), 4.1 (br s), and 5.1 (apparent septet) assignable to the [2]betylate (**6**). An authentic sample of isopropyl [2]betylate fluorosulfate was prepared as follows (cf. ref. 17). Isopropyl ethenesulfonate (**5**, R = Pr^i) (155 mg) in CH_2Cl_2 was treated with excess Me_2NH for 10 min and the solvent and unreacted amine evaporated. Addition of methyl fluorosulfate (115 mg) and CH_2Cl_2, and, after 20 min, evaporation of the CH_2Cl_2, gave the [2]betylate ester; ^{1}Hmr (CD_3CN) δ: 1.4 (d, 6H), 3.2 (br s, 9H), 3.7 (br s, 4H), 5.0 (septet, 1H); with the addition of ~2 equiv. of Et_4N^+ Cl^- the two singlets are shifted downfield to δ 3.4 and 4.0, respectively (the other two signals also move downfield by about 0.05 ppm).

The reaction of **1** (50 mg) and 2-propanol (0.5 mL) with pyridine (0.15 mL) in CH_2Cl_2 (50 mL) was allowed to proceed for 36 s at −70°C and then quickly quenched by addition of excess HCl in CH_2Cl_2 (at −70°C). The ^{1}Hmr spectrum (T-60) showed the presence of **5** (R = Pr^i) and unreacted **1** in the ratio 67:33 by comparison of the integral of the complex signal from 5.8 to 7.3 (due to **1** plus **5**) with that of the methyl doublet (δ 1.4) due to **5** (R = Pr^i) alone. Similar reaction for 18 s gave a 52:48 mixture of **5** (R = Pr^i) and **1**; estimated $k_{obs} \approx 3.5 \times 10^{-2}$ s^{-1} (at −70°C). With 2,6-lutidine instead of pyridine as above, ratios of 25:75 after 10 min at −20°C and 50:50 after 5 min at 0°C, were found; estimated $k_{obs} \approx 3 \times 10^{-6}$ s^{-1} (at −70°C).

Reaction of trans*-1-propene-1-sulfonyl chloride with 2-propanol and pyridine*

Pyridine (0.14 mL) in CH_2Cl_2 (1 mL) was added to a solution of the sulfonyl chloride (50 mg, 0.36 mmol) and 2-propanol (0.43 mL) in CH_2Cl_2 (4 mL) at 0°C and the mixture stirred for 5 min. Work-up as above gave a product clearly identifiable as isopropyl *trans*-1-propene-1-sulfonate by ^{1}Hmr signals at δ 1.4, (6H, d, J = 6 Hz), 2.0 (3H, d of d, J = 7 and 2 Hz), 4.8 (1H, septet, J = 6 Hz), plus an AB quartet of 1:3:3:1 quartets (total 2H) δ 7.2 (J_{AB} = 15 Hz, J_{Me} = 2 Hz), and 5.9 (J_{Me} = 7 Hz). The above reaction after 60 s at −20°C showed an ester to unreacted chloride ratio of 23:77, and after 4.75 h at −70°C a ratio of 57:43 (corresponding to $k_{obs} \approx 5 \times 10^{-5}$ s^{-1} at −70°C). 2-Propanol-*d* instead of ordinary 2-propanol gave no detectable change in the ^{1}Hmr spectrum (T-60) of the product.

N-*[2-(2′,2′-Dimethylpropoxysulfonyl)ethyl]pyridinium chloride (10*a*)*

Ethenesulfonyl chloride (**1**) (880 mg, 7.0 mmol) was combined with neopentyl alcohol (650 mg, 7.4 mmol) in methylene chloride (30 mL) at room temperature. Pyridine (2.5 mL, 31 mmol) was injected and the solution allowed to stand for 8 days; the reaction mixture turned orange and deposited colorless needles during this time. The precipitate of **10***a* was filtered and recrystallized from dry acetonitrile (1.3 g, 65%), mp 154–155°C; ir (Nujol): 3130 (w), 3075 (m), 1635 (m), 1335 (s), 1268 (s), 1200 (vs), 1135 (s), 1050 (s), 950 (s) cm^{-1}; ^{1}Hmr (CD_3CN) δ: 0.93 (s, 9H), 4.01 (s, 2H), 4.21 (t, 2H), 5.18 (t, 2H), 8.11 (t, 2H), 8.60 (t, 1H), 9.28 (d, 2H); ^{1}Hmr (CD_3NO_2) δ: 0.92 (s, 9H), 4.02 (s, 2H), 4.26 (t, 2H), 5.36 (t, 2H), 8.22 (t, 2H), 8.62 (m, 1H), 9.36 (d, 2H). *Anal.* calcd. for $C_{12}H_{20}ClNO_3S$: C 49.06, H 6.86, N 4.77, S 10.91, Cl 12.07; found: C 49.25, H 6.82, N 4.83, S 10.99, Cl 12.01.

Reaction of ethenesulfonyl chloride (1) with pyridine-d_5 *and neopentyl alcohol*

Ethenesulfonyl chloride (**1**) (17 mg, 0.13 mmol) was dissolved in nitromethane-d_3 (0.25 mL) containing neopentyl alcohol (20 mg, 0.23 mmol) and placed in an nmr tube. To this solution (at 37°C, probe temperature) pyridine-d_5 (60 μL, 0.7 mmol) was injected and the solution thoroughly mixed. The ^{1}Hmr spectrum was obtained immediately (≈1 min after mixing), and showed absorptions at δ 3.8 and 4.0 (singlets), a triplet at 5.3, and a multiplet of the characteristic pattern observed with **5** (R = Np) from 6.0 to 7.0 ppm. The peaks were identified as characteristic of neopentyl ethenesulfonate (**5**, R = Np) and the neopentyl betylate chloride (**10***b*), by comparison with ^{1}Hmr spectra of authentic specimens. The ratio of **5** (R = Np) to **10***b* was found, by integration of the singlets at 3.8 and 4.0 ppm, to be 33:67. After 6 days at 37°C the relative proportion of the betylate ester was found to be 88%, with the signal at 5.3 appearing as a superposition of a doublet on the original triplet, pointing to the presence of **12** ($C_5D_5N^+CH_2CHDSO_2ONp$ Cl^-) as well as **10***b*.

Reaction of N*-[2-chlorosulfonylethyl]pyridinium chloride (9) with neopentyl alcohol and pyridine-*d_5

The sulfonyl chloride (**9***a*) (25 mg, 0.1 mmol) was mixed with neopentyl alcohol (14 mg, 0.16 mmol) and nitromethane-d_3 (250 μL) in an nmr tube at 37°C. To this mixture pyridine-d_5 (45 μL), 0.53 mmol) was injected. After thorough mixing, the ^{1}Hmr spectrum was obtained (~1 min after injection of pyridine). The spectrum showed

Can. J. Chem. Downloaded from www.nrcresearchpress.com by 122.72.124.2 on 09/07/12
For personal use only.

absorptions identical to those described above, indicating the presence of neopentyl ethenesulfonate (**5**, R = Np) and the neopentyl betylate chloride (**10***a*) in relative proportions 67 and 33%, respectively. After 45 h at 37°C the ^{1}Hmr spectrum of the solution showed a relative proportion of **10** of 88%, with partial deuteration as before, and no other products.

Reaction of N-*[2-chlorosulfonylethyl]pyridinium*-d_5 *chloride (9b) with pyridine*

Freshly prepared pyridinio-d_5-sulfonyl chloride (**9***b*) (27 mg, 0.11 mmol) was mixed with neopentyl alcohol (17 mg, 0.19 mmol) and nitromethane-d_3 (400 μL) at 37°C in an nmr tube. Pyridine (50 μL, 0.62 mmol) was injected and the mixture thoroughly shaken, and the ^{1}Hmr spectrum of the resulting solution obtained immediately. The absorptions in the spectrum indicated the presence of neopentyl ethenesulfonate (**5**, R = Np) and the pyridine-d_5 betylate (**10***b*), along with the absorption around 9.4 ppm that was ascribed to the completely protiated betylate (**10***a*). Comparison of the multiplet at δ 9.4 with the singlet at 4.0 (for **10***a* and **10***b*) gave the proportion of **10***a* as 20% of the total amount of **10** formed in the reaction.

Neopentyl ethenesulfonate (5, R = Np) with pyridine-d_5 *and neopentyl alcohol*

Neopentyl ethenesulfonate (**5**, R = Np) (30 mg, 0.17 mmol) was dissolved in nitromethane-d_3 (0.40 mL) containing neopentyl alcohol (60 mg, 0.68 mmol) at room temperature. Pyridine-d_5 (0.075 mL, 0.90 mmol) was added, and the solution monitored by ^{1}Hmr spectroscopy for 24 h, after which period no reaction was observed. To this solution pyridinium-d_5 chloride (40 mg, 0.33 mmol) was added, and the solution monitored for a further 22 h. The presence of the neopentyl betylate chloride (**10***b*) was initially observed in the ^{1} Hmr spectrum after 2 h, eventually making up ~85% of the mixture of **5** (R = Np) and **10** after 22 h at room temperature (signals due to both **10***b* and **12** were observed).

Reaction of ethenesulfonyl chloride (1) with pyridine-d_5 *and neopentyl alcohol*-d

When the reaction of **1** (63 mg, 0.50 mmol) and pyridine-d_5 (215 μL, 2.5 mmol) in CD_3NO_2 was carried out as above with neopentyl alcohol-*d* (93% D, 223 mg, 2.5 mmol), the singlets in the ^{1}Hmr spectrum (XL-200) at δ 3.8 and 4.0 gave the ratio of total neopentyl ethenesulfonate (**5**, R = Np, plus **11**) to the betylate total (**12** plus **13**) as 67:33. The 6–7 ppm region showed 1:1:1 triplets at 6.13 and 6.19 ppm ascribable to about 20 ± 5% of **11** in the total neopentyl ethenesulfonate. Examination of the $-N^+CH_2$ signal (around 5.4 ppm) of the betylate showed a (broadened) doublet at δ 5.45 due to **12**, and a small singlet about 1 Hz upfield from the doublet and consistent with the presence of roughly 20 ± 10% of **13**; there was no sign of any triplet appropriate to **10***b*. The poorly resolved apparent triplet of 1:1:1 triplets at δ 4.35 due to $CHDSO_2$ was consistent with this assignment though the signal could not be integrated accurately because it was partly obscured by the solvent (CD_2HNO_2) signal. In another experiment using a 1:1 mixture of NpOH and NpOD the superimposed peaks at 5.4–5.5 ppm due to **10***b* and **12** were clearly seen, with the triplet for **10***b* about 1 Hz downfield from the doublet for **12**.

Acknowledgement

We thank the Natural Sciences and Engineering Research Council of Canada for financial support of this work.

1. J. F. KING and S. SKONIECZNY. Phosphorus Sulfur, **25**, 11 (1985).
2. J. F. KING, J. H. HILLHOUSE, T. M. LAURISTON, and K. C. KHEMANI. Can. J. Chem. **66**, 1109 (1988).
3. J. F. KING, M. R. WEBSTER, N. CHIBA, J. K. ALLEN, K. J. M. PARKER, R. RATHORE, and S. SKONIECZNY. Phosphorus Sulfur, **31**, 161 (1987).
4. J. F. KING and R. RATHORE. Phosphorus Sulfur, **33**, 165 (1987).
5. J. F. KING. Acc. Chem. Res. **8**, 10 (1975).
6. J. F. KING, S. SKONIECZNY, K. C. KHEMANI, and J. D. LOCK. *In* Nucleophilicity. *Edited by* J. M. Harris and S. P. McManus. Adv. Chem. Ser. **215**, Chap. 27, pp. 385–398 (1987).
7. J. F. KING and T. DURST. J. Am. Chem. Soc. **87**, 5684 (1965).
8. W. E. TRUCE and R. W. CAMPBELL. J. Am. Chem. Soc. **88**, 3599 (1966).
9. O. ROGNE. J. Chem. Soc. B, 727 (1970).
10. O. ROGNE. J. Chem. Soc. B, 1334 (1971).
11. J. F. KING and J. H. HILLHOUSE. J. Chem. Soc. Chem. Commun. 454 (1979).
12. J. F. KING, J. H. HILLHOUSE, and S. SKONIECZNY. Can. J. Chem. **62**, 1977 (1984).
13. J. F. KING and S. M. LOOSMORE. J. Chem. Soc. Chem. Commun. 1011 (1976).
14. W. F. WHITMORE and E. F. LANDAU. J. Am. Chem. Soc. **68**, 1797 (1946).
15. H. DISTLER. Angew. Chem. Int. Ed. Engl. **4**, 300 (1965).
16. C. S. RONDESTVEDT. J. Am. Chem. Soc. **76**, 1926 (1954).
17. J. F. KING, S. M. LOOSMORE, M. ASLAM, J. D. LOCK, and M. J. MCGARRITY. J. Am. Chem. Soc. **104**, 7108 (1982).
18. M. B. DAVY, K. T. DOUGLAS, J. S. LORAN, A. STELTNER, and A. WILLIAMS. J. Am. Chem. Soc. **99**, 1196 (1977).
19. J. F. KING and R. P. BEATSON. Tetrahedron Lett. 973 (1975).
20. L. O. FARNG and J. L. KICE. J. Am. Chem. Soc. **103**, 1137 (1981).
21. P. J. THOMAS and C. J. M. STIRLING. J. Chem. Soc. Perkin Trans. 2, 1909 (1977).
22. R. S. BRESLOW. Tetrahedron Lett. 399 (1964).
23. J. C. FISHBEIN and W. P. JENCKS. J. Am. Chem. Soc. **110**, 5075 (1988).

Can. J. Chem. Downloaded from www.nrcresearchpress.com by 122.72.124.2 on 09/07/12
For personal use only.

Bromophloroglucinols and their methyl ethers[1]

E. KIEHLMANN AND R. W. LAUENER
Department of Chemistry, Simon Fraser University, Burnaby, B.C., Canada V5A 1S6

Received August 25, 1988

E. KIEHLMANN and R. W. LAUENER. Can. J. Chem. **67**, 335 (1989).

All 16 bromination products of phloroglucinol and its methyl ethers, as well as five bromoresorcinols and three of their dimethyl ethers, were synthesized and analyzed by nuclear magnetic resonance spectroscopy. Two or three equivalents of bromine convert phloroglucinol to di- and tribromophloroglucinol, 5-methoxyresorcinol to the tri- and 2,4-dibromo, 3,5-dimethoxyphenol to the tri- and 2,6-dibromo, and 1,3,5-trimethoxybenzene to the dibromo compound. With one equivalent of bromine, 3,5-dimethoxyphenol reacts preferentially at C-2 while 5-methoxyresorcinol gives both monobromo isomers. Partial debromination with sodium sulfite yields successively 2,4-dibromo- and 2-bromo-5-methoxyresorcinol from the tribromo compound but fails with brominated 3,5-dimethoxyphenol. In the resorcinol series, C-2 is invariably the least reactive position. 4,6-Dibromo-5-methoxyresorcinol and 2,4-dibromo-3,5-dimethoxyphenol are accessible by methylation of dibromophloroglucinol, obtained from 3,5-dibromo-2,4,6-trihydroxybenzoic acid by decarboxylation. In contrast to resorcinol and tribromoresorcinol, the partial bromination of phloroglucinol and debromination of tribromophloroglucinol are not selective. The ^{13}Cmr spectra of bromophloroglucinol methyl ethers show characteristic downfield shifts for methoxy groups orthogonal to the aromatic ring plane.

Key words: bromophloroglucinols, synthesis, nmr, and debromination; bromo-5-methoxyresorcinols, synthesis, nmr, and debromination; bromo-3,5-dimethoxyphenols, synthesis and nmr.

E. KIEHLMANN et R. W. LAUENER. Can. J. Chem. **67**, 335 (1989).

On a effectué la synthèse des 16 produits de bromination du phloroglucinol et de ses éthers méthyliques ainsi que de cinq bromorésorcinols et de trois de leurs éthers diméthyliques et on a pu effectuer une analyse de tous ces dérivés par spectroscopie en résonance magnétique nucléaire. Deux ou trois équivalents de brome transforment le phloroglucinol en di- et en tri-bromophloroglucinols, le méthoxy-5 résorcinol en dérivés tribromo et dibromo-2,4, le diméthoxy-3,5 phénol en dérivés tribromo et dibromo-2,6 et le triméthoxy-1,3,5 benzène en composé dibromé. Avec un équivalent de brome, le diméthoxy-3,5 phénol réagit préférentiellement en C-2 alors que le méthoxy-5 résorcinol fournit les deux isomères monobromés. Si on soumet le dérivé tribromé à une débromation partielle à l'aide de sulfite de sodium, on obtient successivement le dibromo-2,4 et le bromo-2 méthoxy-5 résorcinol; toutefois, on ne peut effectuer de débromation partielle sur le diméthoxy-3,5 phénol bromé. Dans la série du résorcinol, la position C-2 est toujours la moins réactive. Les dibromo-4,6 méthoxy-5 résorcinol et dibromo-2,4 diméthoxy-3,5 phénol sont accessibles par méthylation du dibromophloroglucinol qui est obtenu par décarboxylation de l'acide dibromo-3,5 trihydroxy-2,4,6 benzoïque. Par opposition avec ce qui est observé avec le résorcinol et le tribromorésorcinol, la bromation partielle du phloroglucinol et la débromation du tribromophloroglucinol ne sont pas sélectives. Dans les spectres rmn du ^{13}C des éthers méthyliques des bromophloroglucinols, les groupements méthoxyles orthogonaux par rapport au plan du cycle aromatique présentent des déplacements caractéristiques vers les bas champs.

Mots clés : bromophloroglucinols, synthèse, rmn et débromation; bromo méthoxy-5 résorcinol, synthèse, rmn et débromation; bromo diméthoxy-3,5 phénol, synthèse et rmn.

[Traduit par la revue]

Introduction

Catechin or epicatechin (**1**) is the terminal unit of most condensed tannins found in various plant tissues. It contains a phloroglucinol-type A-ring with two centers of high nucleophilicity (C-6 and C-8) that, on reaction at the electrophilic C-4 carbon of the heterocyclic ring of flavan-3,4-diols, yield oligomeric polyhydroxy flavanoids. The regiospecific synthesis of a diflavanoid tannin precursor requires temporary blockage of C-6 (or C-8) of catechin with an easily removable protecting group such as bromine. This objective has been partially met by the synthesis of 6-bromocatechin via dibromination of catechin followed by regioselective bromine removal from C-8 with sodium sulfite (1).

To gain a better understanding of the factors determining the regiochemistry of bromination and debromination, with the goal of developing an efficient procedure for the synthesis of 8-bromocatechin, and to assist in the structure elucidation of halogenated flavanoids (2, 3), we prepared and studied the nmr spectra of mono-, di-, and tribromophloroglucinol and their 13 methyl ethers as well as a series of brominated resorcinol derivatives.

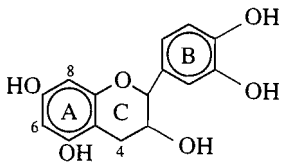
Results and discussion

The three phloroglucinol methyl ethers used as starting materials are readily accessible by methylation of phloroglucinol (**2***a*). With methanol and dry HCl, only 5-methoxyresorcinol (**3***a*) and 3,5-dimethoxyphenol (**4***a*) are formed (4), probably via a hemiketal intermediate (5). They have also been obtained by methylation and decarboxylation of phloroglucylic acid (**6***a*) (6) and by partial demethylation of 1,3,5-trimethoxybenzene (**5***a*) with boron trichloride (7). With excess dimethyl sulfate or methyl iodide in alkaline medium, phloroglucinol is converted to **5***a* (4*a*, 8).

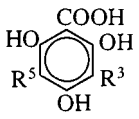
Considering the strong activating effect of three *meta*-oriented hydroxy and (or) methoxy groups toward electrophilic aromatic substitution at their respective *ortho* and *para* positions, it is not surprising that tribromination occurs rapidly, and that most of the mono- and dibromo compounds have not been described in the literature. Thus, tribromophloroglucinol (**2***d*) (9), frequently accompanied by penta- and hexabromo-1,3,5-cyclohexatrione (10), results from the reaction of phloroglu-

[1]Presented in part at the 43rd ACS Northwest Regional Meeting, 30 June 1988, Spokane, Washington.

Can. J. Chem. Downloaded from www.nrcresearchpress.com by 122.72.124.2 on 09/07/12
For personal use only.

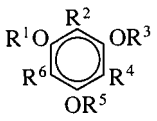


1

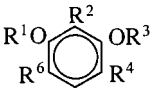


6

R^3/R^5 = H or Br



$R^2/R^4/R^6$ = H or Br
2, $R^1 = R^3 = R^5$ = H
3, $R^1 = R^3$ = H, R^5 = Me
4, R^1 = H, $R^3 = R^5$ = Me
5, $R^1 = R^3 = R^5$ = Me



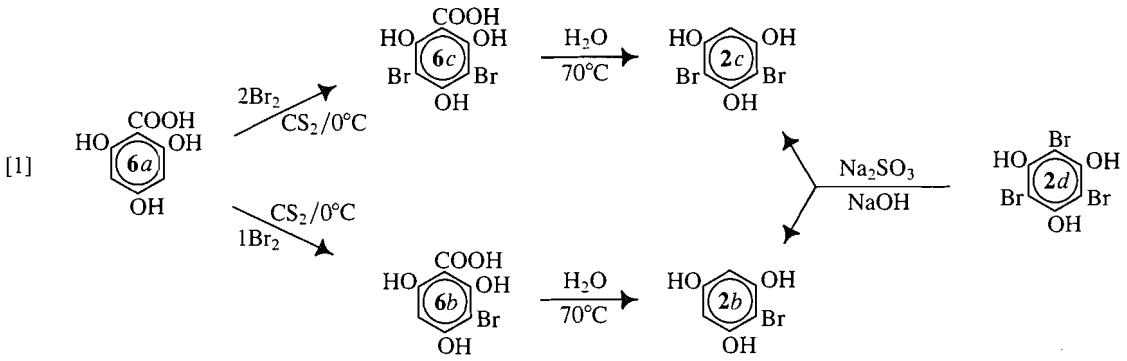
$R^2/R^4/R^6$ = H or Br
7, $R^1 = R^3$ = H
8, $R^1 = R^3$ = Me

cinol (**2***a*) with excess bromine in glacial acetic acid or in aqueous solution. It is also the major product when only two equivalents of bromine are added to an ice-cooled suspension of **2***a* in carbon disulfide, i.e., under conditions that permit the partial bromination of resorcinol (11). Small samples of the minor components monobromophloroglucinol (**2***b*) and dibromophloroglucinol (**2***c*) can be isolated from the crude product mixture by fractional crystallization (from benzene) and chromatography. However, the partial debromination of **2***d* with one molar equivalent of sodium sulfite in the presence of sodium bicarbonate is a more satisfactory procedure, yielding mainly **2***b* (32%) and **2***c* (42%). The best route to **2***c* (eq. [1]) involves bromination of 2,4,6-trihydroxybenzoic acid (phloroglucylic acid) followed by decarboxylation (12). This reaction sequence is also applicable to the preparation of **2***b* although the lack of selectivity in the initial bromination step leads to a mixture of mono- and dibromophloroglucylic acid (**2***b* and **2***c*), which cannot be separated without concomitant loss of carbon dioxide. The acetylation of **2***b* gives 1,3,5-triacetoxy-2-bromobenzene with spectral properties identical to those reported by Glombitza and Gerstberger (13) for a component of an acetylated extract from brown algae, thereby verifying their structure assignment. Dibromophloroglucinol (**2***c*) has also been found in marine organisms (14) but neither **2***b* nor **2***c* has been previously synthesized and spectroscopically characterized.

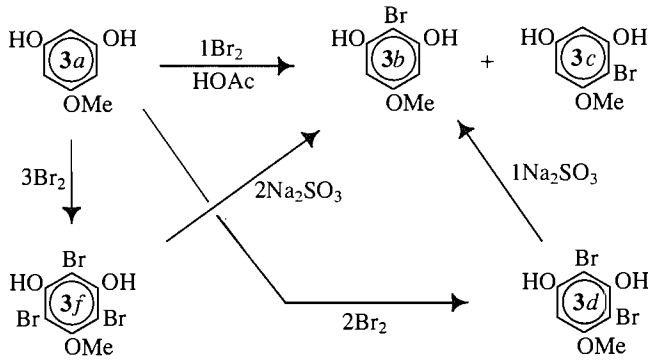
Only one of the five possible bromination products of the slightly less reactive 5-methoxyresorcinol, namely tribromo-5-methoxyresorcinol (**3***f*), has been reported in the literature (15). Monobromination is not regiospecific (eq. [2]) and gives mainly the two monobromo compounds (**3***b* and **3***c*) as well as smaller amounts of 2,4-dibromo-5-methoxyresorcinol (**3***d*) and **3***f* but none of the 4,6-dibromo isomer (**3***e*) of **3***d*. With two equivalents of bromine in acetic acid, **3***d* (accompanied by some **3***f*) is obtained in 90% yield. The absence of **3***e* shows that C-6 of 4-bromo-5-methoxyresorcinol is considerably less nucleophilic than C-2, which emphasizes the importance of coplanarity of the methoxy group with the aromatic ring for effective charge delocalization (*ortho*/*para* activation). The same reason appears to be responsible for the preferred removal of bromine from C-4 and C-6 to provide predominantly 2-bromo-5-methoxyresorcinol (**3***b*) when **3***f* or **3***d* is treated with sodium sulfite (eq. [2]). The latter reaction parallels the regioselective debromination of 6,8-dibromocatechin at C-8 under comparable conditions (1) and suggests that stabilization of the proposed α-hydroxysulfonate intermediate (16, 17) or the final product by OH....Br hydrogen bonding (18) is also a contributing factor.

To gain further insight into its mechanism and to optimize the reaction conditions, we reexamined the debromination of 2,4,6-tribromoresorcinol (**7***f*) (9*c*, 10*b*, 19) with sodium sulfite (eq. [3]), studied originally by Davis and Harrington (20), and confirmed the formation of 2-bromoresorcinol (**7***b*) (12*b*, 21) and 2,4-dibromoresorcinol (**7***d*) (12*b*, 22). The application of this method to 4,6-dibromoresorcinol (**7***e*) (11, 23) constitutes a good alternative synthesis for 4-bromoresorcinol (**7***c*) (16), which can also be prepared by decarboxylation of 5-bromo-2,4-dihydroxybenzoic acid (11, 12*b*, 24), or by bromination of resorcinol with *N*-bromosuccinimide in dimethylformamide (25) or with dioxane dibromide in ether (23*a*). Using two moles of sodium sulfite per mole of tribromoresorcinol (**7***f*), or a mixture of one mole of sodium sulfite and one mole of sodium hydroxide, we obtained **7***d* in high yield while only **7***b* was formed with the reagents Na_2SO_3/NaOH/**7***f* in the molar ratio 2:2:1. When sodium sulfite is replaced by sodium thiosulfate, no reaction takes place; the addition of base leads to the slow formation of **7***d* and partial decomposition. With sodium hydroxide alone, both tribromophloroglucinol and tribromo-

[1]



Can. J. Chem. Downloaded from www.nrcresearchpress.com by 122.72.124.2 on 09/07/12
For personal use only.

[2] 

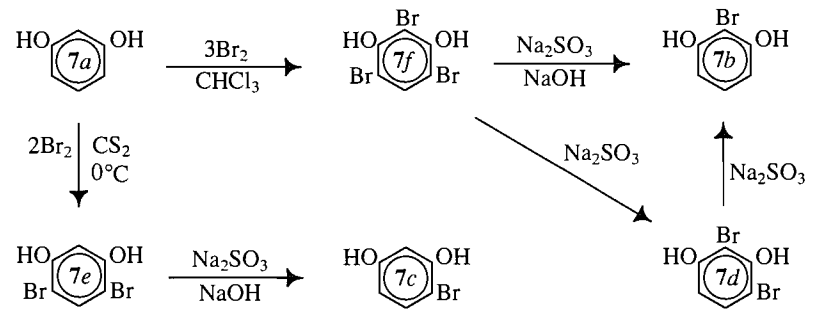
resorcinol undergo rapid decomposition (9*a*). As observed for tribromo-5-methoxyresorcinol (**3***f*), the bromine atom *ortho* to both hydroxy groups is removed less easily than Br-4 and Br-6; i.e., the reaction is regiospecific, proceeds in a stepwise fashion, and yields resorcinol with excess sulfite and base. 4,6-Dibromo-3-methoxyphenol (16), 4,6-dibromo-1,3-dimethoxybenzene (**8***b*), 2,4-dibromo-1,3,5-trimethoxybenzene (**5***c*), 2,6-dibromo-3,5-dimethoxyphenol (**4***e*), 2,4,6-tribromo-3,5-dimethoxyphenol (**4***f*), and 6,8-dibromocatechin tetramethyl ether were found to resist debromination under these conditions, even when refluxed for several hours in aqueous methanol.

These experimental results suggest a mechanism similar to that proposed for the dehalogenation of bromouracil (26) and of 4-bromo-3-arylsydnones (27). Either sulfite adds at the carbonyl carbon of an initially formed "ketobromide" tautomer of the starting material to give an α-hydroxysulfonate intermediate, which undergoes oxidation at sulfur and halide elimination at the α-carbon (16), or it attacks the bromine atom of the α-haloketone directly. In view of recent spectroscopic evidence for a phloroglucinol/sulfite adduct (17), we favor the former route. According to this scheme, sulfite serves as base to catalyze enol/keto equilibration (28), as nucleophile to protect the intermediate α-bromoketone by complexation, as reducing agent to abstract the halogen, and again as base to neutralize the bisulfate formed in the reduction step. The latter function explains why, in the absence of sodium hydroxide, two moles of sulfite are required for the removal of one halogen, i.e., the reaction succeeds only in alkaline medium. Neutral aqueous thiosulfate fails to react but is slowly converted to sulfite in the presence of base. We attribute the failure of monohydric bromophenols to react by this mechanism to their lower acidity, which renders the concentration of their keto tautomers negligibly small at a given pH.

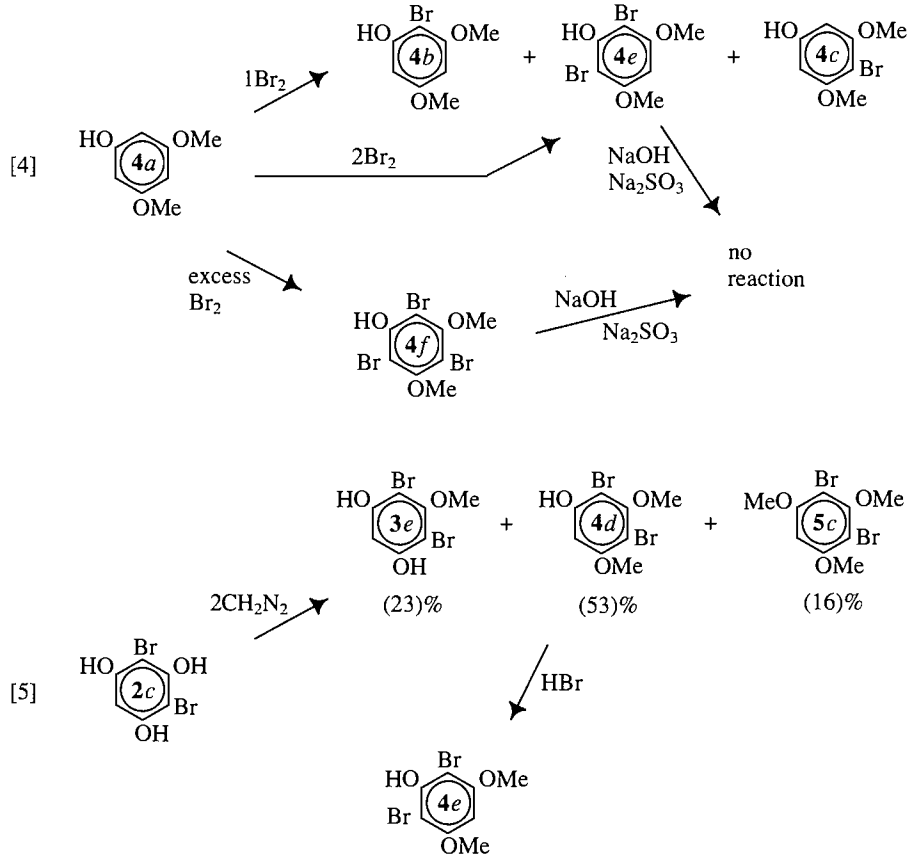
The bromination of 3,5-dimethoxyphenol (**4***a*) (eq. [4]) with two or three equivalents of elemental bromine in chloroform or methylene chloride gives 2,6-dibromo-3,5-dimethoxyphenol (**4***e*) (29) and tribromo-3,5-dimethoxyphenol (**4***f*), respectively, in high yields. The latter can be readily separated from the former on account of its higher solubility in benzene and aqueous bicarbonate solution. With one equivalent of bromine, 2-bromo-3,5-dimethoxyphenol (**4***b*) (29) is formed as the main product (44% yield) together with lesser amounts of **4***e* (8%) and the 4-bromo isomer (**4***c*, 5%). As expected, electrophilic substitution occurs preferentially at the sterically more accessible C-2 and C-6 positions. No 2,4-dibromo-3,5-dimethoxyphenol (**4***d*) was detected, since the elimination of a proton from the cation formed by electrophilic attack of bromine at C-4 of **4***b* would force the 3-methoxy carbon to rotate out of the aromatic ring plane. To synthesize this elusive compound, we treated dibromophloroglucinol (**2***c*) with a limited quantity of diazomethane and obtained a product mixture that, much to our surprise, contained **4***d* as major and 4,6-dibromo-5-methoxyresorcinol (**3***e*) and 2,4-dibromo-1,3,5-trimethoxybenzene (**5***c*) as minor components (eq. [5]). Clearly the hydroxy group flanked by two *ortho*-bromo substituents exhibits enhanced nucleophilicity toward the methylating agent. This result is analogous to the formation of 3-methoxy-2,4-dibromophenol from 2,4-dibromoresorcinol and dimethyl sulfate, as reported by Rice (12*b*), and parallels the enhanced reactivity of *ortho*-disubstituted anisoles toward dealkylating agents (7, 30). In the presence of hydrogen bromide, **4***d* rearranges to the more stable 2,6-dibromo isomer (**4***e*), and both compounds were found to undergo slow debromination as well as H/D exchange at the unsubstituted ring carbon after several days of exposure to hydrochloric acid in acetone-d_6 solution (monitored by nmr).

The results of the bromination of 1,3,5-trimethoxybenzene (**5***a*) are primarily a function of bromine quantity, reaction time, and temperature (31), yielding mainly 2-bromo-1,3,5-trimethoxybenzene (**5***b*) (32) with one equivalent (2 h at 25°C), 2,4-dibromo-1,3,5-trimethoxybenzene (**5***c*) (33) with three equivalents (1 h at 25°C), and 2,4,6-tribromo-1,3,5-trimethoxybenzene (**5***d*) (**4***a*, 34) with excess neat bromine.

Systematic analysis of the nmr data summarized in Tables 1 and 2 (^{1}Hmr and ^{13}Cmr of 32 compounds in acetone-d_6) and in Table 3 (^{1}Hmr of 19 methyl ethers in chloroform-*d*) reveals interesting trends, which parallel similar observations for

[3] 

Can. J. Chem. Downloaded from www.nrcresearchpress.com by 122.72.124.2 on 09/07/12
For personal use only.



flavans with phloroglucinol-type A-rings (2, 3, 35) and are potentially useful for the structure elucidation of naturally occurring polyphenols. Ten of the 18 brominated phloroglucinol derivatives are new compounds and, to the best of our knowledge, ^{1}Hmr parameters have been previously reported only for 2,6-dibromo-3,5-dimethoxyphenol (**4***e*) (36), monobromo- (**5***b*) (37), dibromo- (**5***c*) (31, 33*d*, 38), and tribromo-1,3,5-trimethoxybenzene (**5***d*) (31, 34), and ^{13}Cmr data only for **5***b* (37). Although the following discussion focuses mainly on the 16 bromophloroglucinols and their methyl ethers, dissolved in acetone-d_6, similar conclusions may be drawn for the corresponding resorcinol (**7** and **8**) and phloroglucylic acid (**6**) derivatives.

The proton assignments for 2-bromo-3,5-dimethoxyphenol (**4***b*) and 4-bromo-5-methoxyresorcinol (**3***c*) are based on nuclear Overhauser effect (nOe) studies (2). In the former compound, saturation at the MeO-3, OH, and MeO-5 frequencies increases the peak intensities of H-4, H-6, and both H-4 and H-6, respectively. In the latter compound, only H-6 is enhanced when the methoxy protons are irradiated. In the presence of cadmium nitrate (2, 39), the two hydroxy peaks of 2,4-dibromo-5-methoxyresorcinol (**3***d*) are well separated, and saturation at 9.03 ppm leads to more efficient H-6 relaxation than saturation at 8.25 ppm. Thus double irradiation for the short duration of 1 s minimizes saturation transfer between the two hydroxy groups, yet produces a sufficiently strong nOe to permit assignment of the downfield signal to OH-1. In the 1,3-dimethoxy-4,6-dibromo compounds **4***e*, **5***c*, and **8***b* the methoxy protons resonate at relatively high frequencies (3.91–3.93 ppm) and H-2 experiences a large upfield shift (by 0.35 ± 0.02 ppm) when the solvent is changed from acetone to chloroform, indicating strong nonbonding interactions in the favored planar "crab" (or *cis*) conformation, which places four of the six methyl protons into the immediate vicinity of the aryl hydrogen. In general, the ^{1}Hmr spectra of the title compounds show the expected downfield shifts for *meta* protons on bromination (by about 0.2 ppm) and for *para* protons on O-methylation (by 0.06–0.12 ppm). The latter effect is particularly strong (0.21–0.22 ppm) when the hydroxy group is located between two *ortho*-bromo substituents that force the methoxy carbon into a position orthogonal to the aromatic ring plane. This rotation interferes with effective resonance delocalization of an oxygen lone pair and thereby reduces the electron density at the *para* hydrogen, as observed for **3***d* → **4***d*, **2***c* → **3***e*, and **4***e* → **5***c*.

The ^{13}Cmr spectra show even stronger evidence for such stereoelectronic substituent effects (3). To arrive at reliable peak assignments as an essential prerequisite for subsequent correlations, we first recorded the spectra of the bromine-free parent compounds and found good agreement with published literature values for phloroglucinol (17, 28, 40) and its three methyl ethers (**3***a*, **4***a*, **5***a*) (37, 41). High molecular symmetry and the large chemical shift differences between oxygenated, brominated, and unsubstituted ring carbons lead to facile identification of the peaks for tribromophloroglucinol (**2***d*), its trimethyl ether (**5***d*), and tribromoresorcinol (**7***f*) as well as for 4,6-dibromoresorcinol (**7***e*) and its dimethyl ether (**8***b*). The distinction between the oxygenated ring carbons of phloroglucylic acid (**6***a*), dibromophloroglucylic acid (**6***c*), mono- and dibromophloroglucinol (**2***b* and **2***c*), 4,6-dibromo- and tribromo-5-methoxyresorcinol (**3***e* and **3***f*), 2,6-dibromo- and tribromo-3,5-dimethoxyphenol (**4***e* and **4***f*), and dibromo-1,3,5-trimethoxybenzene (**5***c*) is based on the different intensities of their resonance signals in inverse-gated proton-decoupled spectra as well as on the larger magnitude of bromination shift increments for *ortho* (upfield by 3.3–5.5 ppm) than for *para* carbons (upfield by 0.5–1.7 ppm), as previously reported (3) for

Can. J. Chem. Downloaded from www.nrcresearchpress.com by 122.72.124.2 on 09/07/12
For personal use only.

Can. J. Chem. Downloaded from www.nrcresearchpress.com by 122.72.124.2 on 09/07/12
For personal use only.

bromocatechin derivatives. Using monobromophloroglucinol (**2***b*) as reference compound and the general rule (41*b*) that in the absence of steric hindrance O-methylation has a negligible effect on the chemical shift of the *meta* carbon, the absorption peaks of the monobromophloroglucinol methyl ethers at 156 ppm must be assigned to C-1 (**3***b* and **4***b*) and C-3 (**3***c*), those at 159.0 and 159.5 ppm, respectively, to C-1 (**3***c* and **4***c*), the signals at 161–162 ppm to C-5 (**3***b*, **4***b*, and **5***b*), and, consequently, those near 158.5 ppm to the methoxy-substituted carbons *ortho* to bromine (**3***c*, **4***b*, **4***c*, and **5***b*). Similarly, **3***d*, **3***e*, and **4***d* can be considered as O-methylation products of dibromophloroglucinol (**2***c*), i.e., the resonance lines near 152.8 and 155.5 ppm are due to C-3 (**3***d*) and C-1, respectively. Brominated carbons are characterized by very weak absorptions, on account of their long spin-lattice relaxation times (42), and unsubstituted ring carbons by their doublets in proton-coupled spectra. Since three-bond coupling to the methoxy and two-bond coupling to the *ortho* proton are of approximately equal magnitude (4 Hz), the broad quintet patterns centered near 157.5 ppm established the resonance frequencies for C-5 of **3***d* and **4***d*, C-3 of **4***e*, and C-1 of **5***c*. This analysis leaves only the assignments for C-2 and C-4 of 2,4-dibromo-5-methoxyresorcinol (90.5 vs. 91.2 ppm) uncertain and suggests a reversal of the C-1 (157.4 ppm in $CDCl_3$) and C-5 (160.5 ppm) assignments for **5***b* published by Fischer and Henderson (37).

In their recent paper (43) on the non-additivity of ^{13}Cmr substituent chemical shifts (SCS) for 1,3-disubstituted benzenes Bromilow *et al.* noted the large deviations from additivity observed for molecules with conformationally flexible substituents such as methoxy. They excluded bromine from their considerations because of its anisotropic contributions to paramagnetic screening, and pointed out that *meta* SCS values are always small because of the absence of direct mesomeric interactions between the substituents. In *meta*- and *para*-substituted phenols and phenoxides, ipso effects are largely governed by substituent electronegativities, and the superposition of electronic and steric effects makes SCS calculations for *ortho*-disubstituted benzenes particularly difficult (44). While we agree with these observations, our results indicate that limited chemical shift predictions are possible for polysubstituted aromatic compounds as long as structural variations are kept to a minimum (45).

The operation of steric effects is clearly evident from the chemical shift difference of 1.7 ppm for C-6 of 2- and 4-bromo-5-methoxyresorcinol (**3***b* and **3***c*) and of 5.6 ppm for C-2 of the two isomeric dibromo-3,5-dimethoxyphenols (**4***d* and **4***e*). The extra shielding observed for **3***c* is common for anisoles and has been attributed to steric enhancement of resonance by the methoxy group (46), which tries to achieve coplanarity with the benzene ring. In the case of **4***d*, the two large bromine atoms force the methoxy carbon at C-3 into a perpendicular orientation relative to the ring plane, which interferes with effective delocalization of an oxygen electron pair. Therefore, the electron density at the *ortho* and *para* carbons is reduced. The calculation of bromination shift increments leads to the same conclusion: Bromine introduced at C-6 of 2-bromo-3,5-dimethoxyphenol (**4***b*) has a net shielding effect on the ring carbons that is felt most strongly at the ipso and *ortho* positions (−3.1, −3.6, and −3.8 ppm). Bromination at C-4, on the other hand, deshields C-2 (+6.4 ppm), C-4 (+5.5 ppm), and C-6 (+2.4 ppm) since these three carbons are *ortho* and *para* to the MeO-3 group, which rotates out of the ring plane and thereby loses its electron-releasing effect. In general, this

TABLE 1. Bromo-phloroglucinols and -resorcinols: nmr data (in acetone-d_6)[a]

Compound name[b]	No.	δ(Ar-*H*)[c,d]	Carbon-13 chemical shifts (and $^1J_{CH}$ (Hz)) C-1/3/5[c]	C-2/4/6[c]	Coupling constants other than $^1J_{CH}$ (Hz)
Phloroglucinol	**2***a*	5.83	159.9	95.4(158.8)	C2/H4:4.8
2-Bromo-	**2***b*	6.08	156.2/158.6	89.2/96.1(160.7)	C4/H6:3.5; C5/H4:3.1
2,4-Dibromo-	**2***c*	6.35	155.2/152.8	90.2/96.6(161.7)	
2,4,6-Tribromo-	**2***d*	—	151.8	91.2	
Phloroglucylic acid	**6***a*	5.93	94.1/96.1(162.2)	163.6/165.3	δ(COOH):172.1 ppm
3-Bromo-	**6***b*	6.16	95.2/89.6/95.9(163.0)	160.7/161.5[e]/161.7[e]	δ(COOH):172.7 ppm
3,5-Dibromo-	**6***c*	—	95.6/90.2	159.3/158.1	δ(COOH):171.3 ppm
Resorcinol	**7***a*	6.33/6.30/6.96	159.2/130.7(157.3)	103.5(156.6)/107.6(160.0)	C1/H5:10.6; C4/H2:5; C4/H6:7
2-Bromo-	**7***b*	6.49/6.98	156.1/129.0(160.0)	99.2/108.2(161.8)	C1/H5:10.9; C4/H6:8.1
4-Bromo-	**7***c*	6.52/7.24/6.31	157.8/154.8/133.5(164.0)	104.0(159.0)/99.4/108.9(163.0)	C1/H5:11.0; C3/H5:8.6; C2/H6:4.8; C6/H2:5
2,4-Dibromo-	**7***d*	6.54/7.31	152.2/155.6/132.0(166.0)	100.3/109.6(164.8)/100.3	C1/H5:8.4; C3/H5:11
4,6-Dibromo-	**7***e*	6.71/7.54	155.1/135.9(168.8)	105.2(160.5)/100.6	C1/H5:8.8; C4/H2:8.1; C4/H5:5.3
2,4,6-Tribromo-	**7***f*	7.67	152.0/134.2(171.4)	101.4/101.3	C1/H5:8.9

[a]In ppm downfield from TMS (Me of acetone at 2.04 and 29.80 ppm).
[b]Phenolic OH: δ 8.1–9.3 ppm.
[c]Listed in order of decreasing nomenclature priority.
[d]J_{meta} (Hz) = 2.3 (**7***a*), 2.7 (**7***c*); J_{ortho} (Hz) = 8.0 (**7***a*), 8.6 (**7***c*), 8.8 (**7***d*).
[e]Assignments may be interchanged.

Can. J. Chem. Downloaded from www.nrcresearchpress.com by 122.72.124.2 on 09/07/12
For personal use only.

TABLE 2. Bromo-phloroglucinol and -resorcinol methyl ethers: nmr data (in acetone-d_6)[a]

Compound name[b]	No.	Proton chemical shifts		Carbon-13 chemical shifts (and $^1J_{CH}$ (Hz))			Coupling constants other than $^1J_{CH}$
		Ar-H[c,d]	MeO-1/3/5[c]	C-1/3/5[c]	C-2/4/6[c]	OMe[c]	
5-Methoxyresorcinol	**3***a*	5.96/5.92	3.66	160.0/163.0	96.4(158.6)/94.0(159.3)	55.2(143.7)	
2-Bromo	**3***b*	6.14	3.68	156.3/161.3	90.6/94.8(161.0)	55.6(144.1)	C5:3.7[f]
4-Bromo-	**3***c*	6.18/6.10	3.77	159.0/156.3/158.5	96.9(160.6)/89.8/93.1(160.6)	56.3(144.7)	C2/H6:5.0; C6/H2:5.1
2,4-Dibromo-	**3***d*	6.37	3.80	155.7/152.8/157.2	91.2[e]/90.5[e]/93.3(162.3)	56.6(145.1)	C5:3.8[f]; C4/H6:8.2
4,6-Dibromo-	**3***e*	6.56	3.78	155.6/156.4	100.7(161.8)/96.7	60.4(145.5)	C4/H2:7.9
2,4,6-Tribromo-	**3***f*	—	3.83	152.3/155.3	96.4/97.9	60.8(145.9)	C5/OMe:3.8
3,5-Dimethoxyphenol	**4***a*	6.01/5.98	3.70	160.0/162.7	94.9(159.7)/92.7(160.2)	55.4(143.8)	C1/H2:3; C3/OMe:3.1; C4/H2:4.5
2-Bromo-	**4***b*	6.19/6.23	3.82/3.74	156.4/158.6/161.4	91.4/92.3(161.6)/95.3(161.2)	56.4(144.9)/55.6(144.2)	C5/OMe:4.5; C4/H6:5.1
4-Bromo-	**4***c*	6.21	3.78	159.5/158.5	94.0(160.3)/90.8	56.5(144.7)	
2,4-Dibromo-	**4***d*	6.59	3.81/3.79	155.9/156.5/157.5	97.8/97.8/97.6(161.8)	60.5(145.6)/56.8(145.4)	C4/H6:8.8; C5:4[f]
2,6-Dibromo-	**4***e*	6.49	3.91	152.8/157.6	92.2/90.8(162.6)	57.0(145.5)	C3:4[f]; C2/H4:9.0
2,4,6-Tribromo-	**4***f*	—	3.84	152.8/155.7	103.4/104.7	60.9(146.0)	C3/OMe:3.8
1,3,5-$C_6H_3(OMe)_3$	**5***a*	6.07	3.73	162.6	93.6(160.1)	55.5(144.0)	C2/H4:4.2
2-Bromo-	**5***b*	6.31	3.85/3.82	158.6/161.9	92.2/92.6(161.0)	56.6(144.9)/55.9(144.3)	C5:4.3[f]; C2/H4:7.5; C4/H6:5
2,4-Dibromo-	**5***c*	6.71	3.93/3.81	157.8/156.6	98.8/94.6(161.9)	57.1(145.4)/60.6(145.6)	C1:3.7[f]; C3/OMe:3.6; C2/H6:8.3
2,4,6-Tribromo-	**5***d*	—	3.85	156.2	110.7	61.0(146.2)	C1/OMe:3.8
1,3-Dimethoxybenzene	**8***a*	6.46/6.49/7.17	3.75	161.9/130.7(158.6)	101.0(158.0)/106.8(160.8)	55.4(143.8)	C2/H4:4; C4/H2:5.7
4,6-Dibromo-	**8***b*	6.86/7.64	3.93	157.5/136.2(169.5)	99.2(160.7)/102.4	57.1(145.4)	C4/H2:8.6; C4/H5:4.9
2,4,6-Tribromo-	**8***c*	7.88	3.86	156.0/135.9(173.8)	116.0/113.9	61.0(146.1)	

[a,b,c,e]See Table 1.
[d]J_{meta} (Hz) = 2.1(**3***a*, **4***a*), 2.3 (**8***a*), 2.5 (**3***c*), 2.7 (**4***b*); J_{ortho} (Hz) ≈ 8.0(**8***a*).
[f]Two-bond coupling to ArH and three-bond coupling to OMe.

TABLE 3. Proton chemical shifts (in $CDCl_3$)[a]

Compound name[b]	No.	Chemical shift Ar-H[c]	Chemical shift OMe[c]
5-Methoxyresorcinol	**3***a*	5.96/6.00	3.75
2-Bromo-	**3***b*	6.21	3.74
4-Bromo-	**3***c*	6.19/6.06	3.84
2,4-Dibromo-	**3***d*	6.31	3.84
4,6-Dibromo-	**3***e*	6.60	3.87
2,4,6-Tribromo-	**3***f*	—	3.87
3,5-Dimethoxyphenol	**4***a*	6.03/6.07	3.74
2-Bromo-	**4***b*	6.25/6.10	3.76/3.84
4-Bromo-	**4***c*	6.10	3.80
2,4-Dibromo-	**4***d*	6.49	3.86[d]/3.87[d]
2,6-Dibromo-	**4***e*	6.16	3.90
2,4,6-Tribromo-	**4***f*	—	3.88
1,3,5-Trimethoxybenzene	**5***a*	6.09	3.77
2-Bromo-	**5***b*	6.17	3.87
2,4-Dibromo-	**5***c*	6.35	3.87
2,4,6-Tribromo-	**5***d*	—	3.88
1,3-Dimethoxybenzene	**8***a*	6.47/6.52/7.19	3.80
4,6-Dibromo-	**8***b*	6.49/7.65	3.87
2,4,6-Tribromo-	**8***c*	7.73	3.90

[a]In ppm downfield from TMS ($CHCl_3$ at 7.26 ppm).
[b]Phenolic OH: δ 5.0–6.1 ppm.
[c]Listed in order of decreasing nomenclature priority.
[d]Assignments may be interchanged.

conformational change is associated with a downfield shift of 5.5–7.3 ppm for each CBr carbon (0.7–1.5 ppm when coplanarity can be maintained). The most dramatic illustration of *ortho/para* deshielding by steric inhibition of resonance is seen in the high δ value of 110.7 ppm for the three brominated carbons of tribromo-1,3,5-trimethoxybenzene (**5***d*). Comparison of the chemical shift sums for the six ring carbons shows that O-methylation of phloroglucinol changes the electron density very little (765.8 → 768.5 ppm), and that tribromination leads to shielding (765.8 → 728.8). However, the loss of mesomeric interaction with three oxygen atoms that accompanies the trimethylation of tribromophloroglucinol (**2***d*) results in deshielding by more than 70 ppm (728.8 → 800.6 ppm). The low reactivity of dibromo-1,3,5-trimethoxybenzene (**5***c*) toward excess bromine is, of course, but another manifestation of the reduced *ortho/para* activating effect of orthogonal methoxy groups (31). The primary deuterium isotope effect found (31) for the bromination of mono- and dibromo-1,3,5-trimethoxybenzene (but not for the monobromination of 1,3,5-trimethoxybenzene) shows that in these cases proton loss from the initially formed carbocation intermediate becomes the rate-determining step. Contrary to expectation, the methoxy peaks also shift downfield (by 4–5 ppm) when two bulky *ortho* substituents prevent free rotation (47), so that their chemical shifts may serve as sensitive probes to distinguish between crowded and uncrowded polysubstituted aromatic rings. Examining the oxygenated ring carbons, we found that their chemical shifts fall into narrow, non-overlapping regions that depend on the number of *ortho*-bromo substituents: each bromine atom shields the adjacent carbon by 1.5–4.5 ppm. The internal consistency of the observed SCS values lends further support to the initial peak assignments.

Finally, the one-bond coupling constants increase gradually with increasing bromine substitution: from 143.7 to 146.2 Hz for the methoxy and from 158.8 to 162.6 Hz for the aromatic protons in the phloroglucinol series (157.3–173.8 Hz for C-5 of resorcinol derivatives). Since bromine consistently affects *ortho*-methoxy coupling more strongly (by 0.6–1.3 Hz) than *para* (0.3–0.7 Hz), this trend may be used as an alternative to selective heteronuclear decoupling to distinguish MeO-3 (56.4 ppm, *J* 144.9 Hz) from MeO-5 (55.6 ppm, *J* 144.2 Hz) in 2-bromo-3,5-dimethoxyphenol (**4***b*). Long-range carbon/hydrogen coupling constants range from 3.1–4.3 Hz for RO—*C*—C—H and *C*—O—CH_3 to 4.2–5.1 Hz for *C*—C—C—H and 7.5–9.0 Hz for Br—*C*—C—C—H, in agreement with literature values (42).

In summary, all 16 bromophloroglucinols and their methyl ethers are readily accessible by simple bromination, debromination, and methylation reactions. Their spectral properties are similar to those reported for bromocatechins (2, 3), featuring substantial deshielding for aromatic protons, and for methoxy carbon and ring carbon atoms *ortho* and *para* to methoxy groups that have been forced out of the ring plane by two adjacent bromine atoms. Successive bromination shifts oxygenated sp^2 carbon-13 signals gradually upfield; the magnitude of SCS values is not only a function of electronic substituent effects but varies also with conformational changes induced by the new bromine substituent.

Experimental

Commercial phloroglucinol dihydrate was dried *in vacuo* over P_2O_5 (110°C/12 h); 2,4,6-trihydroxybenzoic acid monohydrate (phloroglucylic acid), 1,3-dimethoxybenzene, 1,3,5-trimethoxybenzene, and resorcinol were used as commercially supplied (Aldrich). Melting points (uncorrected) were recorded on a Fisher–Johns melting point apparatus, mass spectra (70 eV) on an HP-5985 quadrupole instrument, and nmr spectra on a Bruker spectrometer (400 MHz). Gas chromatographic analyses were carried out on a Hewlett–Packard instrument (model HP-5890A) with integrator (model HP-3392A) and 15-m DB-1 capillary column (temperature programmed to increase between specified values at 20°/min; carrier gas, helium). For other chromatographic separations we used the following systems: (a) analytical tlc in $CHCl_3$/MeOH/HOAc/H_2O (85:15:10:3 v/v, solvent A, or 90:5:3:2, solvent B), petroleum ether (30–60°C)/EtOAc (1:1, solvent C), and $CHCl_3$/MeOH/HOAc (90:6:4, solvent D) on Merck Kieselgel 60F-254 (0.2 mm) DC-Plastikfolien; (b) preparative tlc on Merck Silica Gel 60HF254/366, and (c) flash chromatography on Kieselgel 60 (230–400 mesh) with the same solvents. Elemental analyses were performed on a Carlo Erba Elemental Analyzer model 1106. A 3:1 (v/v) mixture of petroleum ether (65–110°C) and chloroform (solvent E) was used for several recrystallizations.

Methylation of phloroglucinol (2a)

5-Methoxyresorcinol (**3***a*) and 3,5-dimethoxyphenol (**4***a*) were obtained in 41 and 10% yield, respectively, by methylation of anhydrous phloroglucinol in methanol saturated with hydrogen chloride, as described in the literature (4*b*), and purified by distillation and recrystallization from benzene (**3***a*: bp 160°C/0.3 Torr (1 Torr = 133.3 Pa); mp 74–76°C (lit. (4*b*) mp 75–78°C); **4***a*: bp 130–140°C/0.3 Torr; mp 37–39°C (lit. (4*b*) mp 36–38°C).

Bromination of phloroglucinol (2a)

(a) Tribromophloroglucinol (2d)

To a stirred suspension of 5.21 g (41.3 mmol) anhydrous phloroglucinol in 130 mL dichloromethane was added dropwise (1 h/25°C) a solution of 19.8 g (124 mmol) bromine in 20 mL dichloromethane. Solvent evaporation from the clear yellow solution and recrystallization of the beige residue (14.55 g, 97%) from 100 mL benzene gave 8.95 g (60%) pure **2***d*, long colorless needles, mp 151–152°C (lit. (9*b*) mp 148–149°C).

Can. J. Chem. Downloaded from www.nrcresearchpress.com by 122.72.124.2 on 09/07/12
For personal use only.

Can. J. Chem. Downloaded from www.nrcresearchpress.com by 122.72.124.2 on 09/07/12
For personal use only.

(b) Partial bromination

The dropwise addition (4.5 h) of a solution of 13.5 g bromine (84.4 mmol) in 20 mL carbon disulfide to a stirred, ice-cooled suspension of 5.32 g (42.2 mmol) anhydrous phloroglucinol in 300 mL carbon disulfide led to instant decolorization and precipitation of a fluffy white solid. Solvent evaporation left a solid residue (11.64 g) containing **2***d* and dibromophloroglucinol (**2***c*) as major and monobromophloroglucinol (**2***b*) and unreacted phloroglucinol as minor components (by ^{1}Hmr, tlc, and glc at 160–240°C). Trituration with hot benzene (3 × 150 mL) and cooling gave three crops of crystals containing mainly **2***d* and **2***c* (3.81 g, first fraction), **2***c* and **2***b* (1.70 g, second fraction), **2***b* and **2***a* (0.53 g, third fraction), and an insoluble residue (mainly **2***a*). A small sample of pure **2***b* (R_f 0.44) was obtained from the third fraction (**2***b*/**2***a* molar ratio 6:1, with traces of **2***c* (R_f 0.75)) by preparative tlc (solvent A); mp 162.5–163.5°C; *m/z*: 206 (100), 204 (91), 188 (4.7), 186 (5.3), 177 (4.2), 175 (4.0), 97 (19), 85 (11), 79 (11), 78 (14), and 69 (88). *Anal.* calcd. for $C_6H_5BrO_3$: C 35.12, H 2.44%; found: C 35.25, H 2.38%.

*Partial debromination of tribromophloroglucinol (2*d*)*

A solution of 1.0 mmol Na_2SO_3 and 2.0 mmol $NaHCO_3$ in 3 mL water was added to a suspension of 1.0 mmol **2***d* in 3 mL aqueous methanol (2:1 v/v) and magnetically stirred for 15 min at 25°C. After acidification with 10% HCl, evaporation of the methanol *in vacuo* (50°C/15 min), extraction with ether (6 × 4 mL), drying ($MgSO_4$), and ether evaporation, the solid residue (210 mg) was dried *in vacuo* over P_2O_5 (1 h/25°C) and found by ^{1}Hmr and glc (160–240°C) analysis to contain 32% **2***b*, 42% **2***c*, and 6% **2***a* as well as some unreacted starting material and unidentified decomposition products. With different ratios of reducing agent and base, we obtained the following results (sulfite/base ⇢ yields): 1.0 mmol Na_2SO_3/1.0 mmol NaOH → 20% **2***b*/30% **2***c*/35% **2***a*; 1.0 mmol Na_2SO_3/1.0 mmol $NaHCO_3$ → 10% **2***b*/40% **2***c*/4% **2***a*. With Na_2SO_3 alone, only **2***a* and **2***d* were detected, and the ^{1}Hmr spectrum of the brown, tarry product formed with NaOH alone (no Na_2SO_3) showed no identifiable peaks. Because of slow H/D exchange with the nmr solvent (acetone-d_6), the yields reported above are only approximate.

*Dibromophloroglucylic acid (6*c*) and dibromophloroglucinol (2*c*)*

A solution of 3.26 g (20.4 mmol) bromine in 50 mL carbon disulfide was dropped into a stirred suspension of 1.88 g (10.0 mmol) phloroglucylic acid monohydrate (**6***a*) in 100 mL carbon disulfide at 5°C. After stirring for 1 h at 25°C, the white solid was filtered off, washed with ice-cold water (3 × 20 mL), ground in a mortar, and dried *in vacuo* over KOH (8 h/56°C) to give 2.39 g (73%) **6***c*, mp 199–200°C (dec.). *Anal.* calcd. for $C_7H_4Br_2O_5$: C 25.64, H 1.23%: found: C 25.55, H 1.21%. Heating a solution (orange) of 2.10 g **6***c* in 150 mL water at 75°C for 2 h (until acidity drops from pH 2 to pH 6), refrigeration (12 h/4°C), filtration, and drying *in vacuo* over P_2O_5 (48 h/25°C) yielded long beige needles (1.74 g, 83%) of **2***c*, mp 170–172°C (recrystallized from water) (lit. (12*a*) mp 171–172°C; *m/z*: 286 (50), 284 (100), 282 (54), 268 (5.4), 266 (11.6), 264 (5.8), 206 (5.5), 204 (5.9), 177 (4.0), 175 (5.3), 159 (5.3), and 157 (5.7). *Anal.* calcd. for $C_6H_4Br_2O_3$: C 25.38, H 1.42%; found: C 25.34, H 1.57%.

*Partial bromination of phloroglucylic acid (6*a*)*

A solution of 1.60 g (10.0 mmol) bromine in 50 mL carbon disulfide was dropped slowly (2.5 h) into a stirred, ice-cooled suspension of 1.98 g (10.0 mmol) phloroglucylic acid monohydrate in 100 mL carbon disulfide. After another 80 min of stirring at 25°C, the colorless reaction mixture was filtered through a sintered glass funnel, and the precipitate washed with water (2 × 20 mL, removal of **6***c*, loss of some **6***b*) and dried in air on clay (12 h) to give 0.83 g of a mixture of bromophloroglucylic acid (**6***b*) and unreacted starting material (molar ratio 11:5). Purification of **6***b* by tlc failed because of slow decarboxylation on silica. However, evaporation to dryness (at 70°C) of an aqueous solution of the crude product yielded a mixture of monobromophloroglucinol (**2***b*) and phloroglucinol, which could be readily separated by preparative tlc (solvent A) and purified (**2***b*) by recrystallization from benzene.

1,3,5-Triacetoxy-2-bromobenzene

Acetylation of monobromophloroglucinol (**2***b*) with acetic anhydride and pyridine (16) gave the triacetate in 72% yield (recrystallized from ethanol), mp 107–108°C; ^{1}Hmr (ppm, acetone-d_6): 7.06 (2H, ArH), 2.32 (6H, AcO-1,3), and 2.26 (3H, AcO-5); ^{13}Cmr (ppm, acetone-d_6): 169.0 (AcO-5), 168.4 (AcO-1,3, ^2J = 7.2 Hz), 151.4 (C-5), 150.6 (C-1,3), 116.3 (C-4,6, ^1J = 169.4 Hz, ^3J = 5.0 Hz), 108.7 (C-2), 20.8 (AcO-5, ^1J = 130.5 Hz), and 20.6 (AcO-1,3, ^1J = 130.5 Hz). The ^{1}Hmr chemical shifts in $CDCl_3$ and the mass spectrum are identical to those reported in the literature (13). *Anal.* calcd. for $C_{12}H_{11}BrO_6$: C 43.53, H 3.35%; found: C 43.76, H 3.37%.

*Bromination of 5-methoxyresorcinol (3*a*)*

A solution of 1.17 g (7.31 mmol) bromine in 5 mL glacial acetic acid was added dropwise to a stirred, cooled solution of 1.00 g (7.14 mmol) **3***a* in 10 mL acetic acid. Evaporation of the solvent and vacuum drying gave 1.83 g of a brown oil that was found to contain 2-bromo- (**3***b*), 4-bromo- (**3***c*), 2,4-dibromo- (**3***d*), tribromo-5-methoxyresorcinol (**3***f*), and unreacted starting material in the approximate molar ratio 6:5:4:1:4 (analysis by glc at 120–200°C and by ^{1}Hmr). With 2.33 g (14.6 mmol) bromine and 1.02 g (7.3 mmol) **3***a*, the same procedure gave 2.46 g of a light brown solid containing **3***d* and **3***f* (ratio 9:1) from which pure **3***d* was obtained by recrystallization from petroleum ether (65–110°C)/$CHCl_3$ (1:1 v/v) and hexane. For **3***d*, mp 109–111°C; *m/z*: 300/298/296 (base peak, molecular ion), dibromo fragments at 285/283/281, 271/269/267, 270/268/266, and 257/255/253, and monobromo fragments at 219/217, 204/202, 203/201, 191/189, 190/ 188, 189/187, 176/174, and 175/173. *Anal.* calcd. for $C_7H_6Br_2O_3$: C 28.22, H 2.03%; found: C 28.44, H 1.98%. With excess bromine, **3***f* was isolated in 69% yield after two recrystallizations from benzene and petroleum ether/$CHCl_3$ (3:1), mp 122–123°C (lit. (15) mp 123°C).

*Partial debromination of 2,4-dibromo-5-methoxyresorcinol (3*d*) and tribromo-5-methoxyresorcinol (3f)*

A solution of 252 mg (2.00 mmol) Na_2SO_3 in 3 mL water was added dropwise to a stirred solution of 300 mg (1.01 mmol) **3***d* in 10 mL aqueous methanol (1:1 v/v). After acidification with 10% HCl and flash evaporation of the methanol (5 min/50°C), the residual yellow aqueous solution was extracted with ether (4 × 10 mL). Drying ($MgSO_4$) and solvent evaporation gave 140 mg of crude product containing 2-bromo-5-methoxyresorcinol (**3***b*) and **3***a* (molar ratio 5:2) and a trace of the 4-bromo isomer (**3***c*) from which **3***b* was isolated by flash chromatography (solvent C). For **3***b*, mp 73–75°C; *m/z*: 220/218 (base peak, molecular ion), 191/189, 190/188, 177/175, 172/170, 140, 111, 110, 95, and 69. *Anal.* calcd. for $C_7H_7BrO_3$: C 38.38, H 3.22%; found: C 38.50, H 3.02%.

With 2.68 g (21.2 mmol) Na_2SO_3 in 25 mL water and 2.00 g (5.31 mmol) **3***f* in 50 mL aqueous methanol, the same procedure gave 1.10 g of a light brown oil containing **3***a*, **3***b*, and **3***c* in the approximate molar ratio 5:3:2 (also traces of **3***d*) from which a small sample of pure 4-bromo-5-methoxyresorcinol was obtained by flash chromatography (solvent B) and recrystallization from hexane. For **3***c*, mp 117–118°C; mass spectrum nearly identical to that of **3***b* (172/170 fragment absent). *Anal.* found: C 38.66, H 3.10% (for calcd. values, see **3***b* above). The two isomeric monobromo-5-methoxyresorcinols **3***b* and **3***c* were clearly distinguished by their different melting points, nmr spectra (Tables 2 and 3), and glc retention times (2.98 and 3.82 min at 160–240°C). When only 2 mmol Na_2SO_3 (with or without additional NaOH) was used per mmol **3***f*, the reaction remained incomplete, **3***b* was formed as major product (together with **3***d*), and no **3***c* was detected in the product mixture.

*Partial debromination of 2,4,6-tribromoresorcinol (7*f*)*

To synthesize the known (18–25) bromoresorcinols and record their nmr spectra, we reinvestigated and optimized the reaction conditions reported by Davis and Harrington (20) for the debromination of tribromoresorcinol (**7***f*). Starting from 1.00 mmol **7***f* (19*b*) in 3 mL aqueous methanol (2:1 v/v) and 2.00 mmol Na_2SO_3 in 3 mL water, and following the standard procedure described for the partial debromination of tribromophloroglucinol (see above), 2,4-dibromoresorcinol

Can. J. Chem. Downloaded from www.nrcresearchpress.com by 122.72.124.2 on 09/07/12
For personal use only.

(**7***d*) was obtained in 94% yield. Both **7***d* (56%) and 2-bromoresorcinol (**7***b*, 31%) were formed when the methanol/water ratio was increased from 1:5 to 1:1 (v/v) and the reaction mixture stirred for 18 h, while the use of 2 mmol Na_2SO_3 and 2 mmol NaOH under standard conditions (15 min reaction time, solvent composition $MeOH/H_2O$ = 1:5) led to the exclusive formation of **7***b* (98%). Other reagent combinations (per mmol **7***f*) resulted in the following product yields: 4 mmol $Na_2SO_3 \rightarrow$ 31% **7***b* and 37% **7***d*; 1 mmol Na_2SO_3/1 mmol NaOH → 80% **7***d*; 1 mmol Na_2SO_3/2 mmol $NaHCO_3 \rightarrow$ 67% **7***d*; 2 mmol $Na_2S_2O_3 \rightarrow$ 67% **7***d*; 2 mmol $Na_2S_2O_3$/2 mmol NaOH → 50% **7***d*.

*Bromination of 3,5-dimethoxyphenol (***4***a)*

A solution of 5.84 g (36.6 mmol) bromine in 20 mL dichloromethane was added dropwise (65 min) to a stirred solution of 2.00 g (13.3 mmol) **4***a* in 40 mL dichloromethane. Solvent evaporation after an additional 15 min of stirring, and vacuum drying of the residue gave 4.99 g of a crude pink product, which was found (by ^{1}Hmr) to contain 65% tribromo- (**4***f*) and 35% 2,6-dibromo-3,5-dimethoxyphenol (**4***e*). Recrystallization from benzene (15 mL) yielded 1.00 g **4***e*, which was further purified by sublimation and recrystallization from solvent E, mp 164–165°C (lit. (29) mp 165–167°C). The filtrate of the first recrystallization (from C_6H_6) was evaporated to dryness, the residue dissolved in 5% aqueous $NaHCO_3$ and washed with ether. Acidification of the aqueous layer, extraction with ether, solvent evaporation, and recrystallization (solvent E) gave 1.53 g **4***f*, white crystals, mp 73–75°C; *m/z*: 394/392/390/388 (base peak, molecular ion), tribromo fragments at 379/377/375/373, 351/349/347/345, and 336/334/332/330, dibromo fragments at 298/296/294, 297/295/293, 283/281/279, 269/267/265, and 255/253/251, and 232/230 (M − 2Br). *Anal.* calcd. for $C_8H_7Br_3O_3$: C 24.58, H 1.81%; found: C 24.58, H 1.80%. The bromination of 1.00 g (6.49 mmol) **4***a* with 2.07 g (12.94 mmol) bromine in dichloromethane gave 1.39 g (69%) pure **4***e* after recrystallization of the crude product (1.91 g, 93%) from solvent E. With equimolar amounts of **4***a* and bromine (6.5 mmol) a dark red solid was obtained, which on treatment with charcoal in boiling benzene, cooling, and filtration gave 1.10 g (75%) of crude product (red) consisting of 19% **4***a*, 44% 2-bromo- (**4***b*), 5% 4-bromo-3,5-dimethoxyphenol (**4***c*), and 8% **4***e*. A mixture (1:1) of **4***a* and **4***c* and a sample of pure **4***b*, mp 79–81°C (from hexane (lit. (29) mp 79–81°C) were isolated by preparative tlc (solvent B). The two isomeric monobromo-3,5-dimethoxyphenols (**4***b* and **4***c*) had nearly identical mass spectra (gc–ms, 120–240°C) but were clearly distinguished by their different glc retention times (5.50 and 7.65 min, respectively) and nmr spectra (Tables 2 and 3). For **4***c*, *m/z*: 234/232 (base peak, molecular ion), 191/189, 176/174, 138, 125, 124, 123, 108, 95, 93, and 69.

*Methylation of dibromophloroglucinol (***2***c)*

A solution of 852 mg (3.00 mmol) **2***c* in10 mL ether was methylated by slow addition of an ethereal solution (10 mL) of diazomethane prepared from 927 mg (9.00 mmol) *N*-nitroso-*N*-methylurea and 3 mL 40% KOH at 5°C. The residue left after solvent evaporation was taken up in 20 mL 0.3 N KOH and extracted with ether (3 × 25 mL), the organic layers were dried ($MgSO_4$), and the solvent evaporated to give 162 mg (0.50 mmol) dibromo-1,3,5-trimethoxybenzene (**5***c*). Acidification of the green aqueous layer, ether extraction (4 × 40 mL), washing with 0.4 M aqueous $NaHSO_3$ (10 mL) to pH 4, drying ($MgSO_4$), and solvent evaporation gave a mixture (740 mg) containing 2,4-dibromo-3,5-dimethoxyphenol (**4***d*) and 4,6-dibromo-5-methoxyresorcinol (**3***e*) in the approximate molar ratio 7:3 (by glc at 120–200°C and ^{1}Hmr) together with traces (<3%) of **3***d*, **4***e*, and **2***c*. The two major products were separated by preparative tlc (solvent D). For **3***e* (R_f 0.45), mp 103–106°C; gc–ms (retention time 4.18 min) *m/z*: 300/298/296 (base peak, molecular ion), 257/255/253, 219/217, 204/202, 203/201, 175/173, 138, 131, 110, and 69. *Anal.* calcd. for $C_7H_6Br_2O_3$: C 28.22, H 2.03%; found: C 27.70, H 2.25%; for **4***d* (R_f 0.74), gc–ms (retention time 4.90 min) *m/z*: 314/312/310 (base peak molecular ion), 271/269/267, 218/216, 217/215, 203/201, 175/173, 152, 131, 124, and 69. *Anal.* calcd. for $C_8H_8Br_2O_3$: C 30.80, H 2.58%; found: C 31.71, H 2.70%. 2,4-Dibromo-3,5-dimethoxyphenol (**4***d*) was not obtained in crystalline form. Storage in a vial (8 months) led to partial, exposure to HBr (48 h, desiccator) to complete, rearrangement to 2,6-dibromo-3,5-dimethoxyphenol (**4***e*), as shown by nmr spectroscopy. The addition of 4 μL concentrated HCl to a solution of the partially rearranged sample in acetone-d_6 resulted in slow debromination (monitored by ^{1}Hmr over a period of 4 days) of both compounds to 3,5-dimethoxyphenol (δ(OMe) 3.69 ppm), presumably by bromine transfer to the solvent.

*Bromination of 1,3,5-trimethoxybenzene (***5***a)*

A solution of 502 mg (3.14 mmol) bromine in 10 mL dichloromethane was added dropwise (2 h) to a stirred solution of 556 mg (3.31 mmol) **5***a* in 10 mL dichloromethane. Washing with 5% aqueous Na_2SO_3 and water, drying ($MgSO_4$), and solvent evaporation gave 820 mg of a white solid containing 2-bromo-1,3,5-trimethoxybenzene (**5***b*) and **5***a* in the approximate molar ratio 7:2 (by glc at 160°C and ^{1}Hmr). Recrystallization from heptane yielded 475 mg (58%) **5***b*, which was purified by a second recrystallization (from 50% aqueous EtOH), mp 95–97°C (lit. (32*a*) mp 97–99°C). With 3 mmol bromine per mmol **5***a*, 2,4-dibromo-1,3,5-trimethoxybenzene (**5***c*), mp 129–130°C (from solvent E) (lit. (33*c*) mp 129–130°C), was obtained in quantitative yield by the same procedure. In refluxing chloroform, a 1:1 mixture of **5***c* and tribromo-1,2,4-trimethoxybenzene (**5***d*) was formed in 84% yield from 1 mmol **5***a* and 5 mmol bromine. Since the preparative separation of these two compounds proved difficult, we prepared **5***d* by adapting Will's method (4*a*): Excess neat bromine (13.4 mmol) is added in two portions to **5***a* (2.0 mmol), the bromine excess is allowed to evaporate, and the crude product is dissolved in ether and washed with 5% aqueous Na_2SO_3 and water. Drying ($MgSO_4$) and solvent evaporation gives 645 mg **5***d* (80%), mp 142–143°C (from 95% EtOH) (lit. (4*a*) mp 145°C).

*Bromination of 1,3-dimethoxybenzene (***8***a)*

A solution of 3.20 g (20.0 mmol) bromine in 30 mL dichloromethane was added dropwise (1 h) to a stirred solution of 1.38 g (10.0 mmol) **8***a* in 30 mL dichloromethane. Evaporation of the solvent gave 2.94 g (99%) 4,6-dibromo-1,3-dimethoxybenzene (**8***b*), mp 139–141°C (from $MeOH/C_6H_6$ 4:1) (lit. (12*b*) mp 141°C). 2,4,6-Tribromo-1,3-dimethoxybenzene (**8***c*) was obtained from **8***a* and excess neat bromine by Will's method (ref. 4*a*, see above) in 86% yield, white needles, mp 69–70° (from 95% EtOH) (lit. (48) mp 68–69°C).

Acknowledgements

We thank I. Micallef, C. Schafmeister, and N. Lehto for technical assistance, the Government of British Columbia for two Youth Employment Grants, and the Natural Sciences and Engineering Research Council of Canada for an Undergraduate Research Award and instrument support.

1. E. KIEHLMANN, P. J. VAN DER MERWE, and H. K. L. HUNDT. Org. Prep. Proced. Int. **15**, 341 (1983).
2. E. KIEHLMANN and A. S. TRACEY. Can. J. Chem. **64**, 1998 (1986).
3. E. KIEHLMANN and A. S. TRACEY. Magn. Reson. Chem. **26**, 204 (1988).
4. (*a*) W. WILL. Chem. Ber. **21**, 603 (1888); (*b*) H. WEIDEL and J. POLLACK. Monatsh. Chem. **18**, 347 (1897); **18**, 736 (1897).
5. J. C. TOUCHSTONE, J. ASHMORE, and M. N. HUFFMAN. J. Am. Chem. Soc. **78**, 5643 (1956).
6. J. HERZIG and F. WENZEL. Monatsh. Chem. **22**, 227 (1901).
7. C. F. CARVALHO, A. V. RUSSO, and M. V. SARGENT. Aust. J. Chem. **38**, 777 (1985).
8. (*a*) J. HERZIG and F. WENZEL. Monatsh. **27**, 785 (1906); (*b*) K. FREUDENBERG. Chem. Ber. **53**, 1416 (1920); (*c*) J. W. CLARK-LEWIS. Aust. J. Chem. **10**, 505 (1957).
9. (*a*) J. HERZIG. Monatsh. Chem. **6**, 863 (1885); **6**, 884 (1885); (*b*) J. HERZIG and H. KASERER. Monatsh. Chem. **23**, 573 (1902); (*c*) S. BITTNER and M. IDELSOHN. Chem. Ind. (London), **19**, 840 (1975).

10. (*a*) T. ZINCKE and O. KEGEL. Chem. Ber. **23**, 1706 (1890); (*b*) A. W. FRANCES and A. J. HILL. J. Am. Chem. Soc. **46**, 2503 (1924).
11. J. ZEHENTER. Monatsh. Chem. **8**, 293 (1887).
12. (*a*) F. V. HEMMELMAYR. Monatsh. Chem. 23, 773 (1911); (*b*) G. P. RICE. J. Am. Chem. Soc. **48**, 3125 (1926).
13. K. W. GLOMBITZA and G. GERSTBERGER. Phytochemistry, **24**, 543 (1985).
14. A. J. BLACKMAN and D. J. MATTHEWS. Phytochemistry, **21**, 2141 (1982).
15. J. HERZIG and F. AIGNER. Monatsh. Chem. **21**, 433 (1900).
16. E. KIEHLMANN, N. LEHTO, and D. CHERNIWCHAN. Can. J. Chem. **66**, 2431 (1988).
17. R. J. HIGHET and I. V. EKHATO. J. Org. Chem. **53**, 2843 (1988).
18. (*a*) T. SCHAEFER and J. B. ROWBOTHAM. Can. J. Chem. **54**, 2228 (1976); (*b*) P. N. KARPOV and V. A. GRANZHAN. J. Struct. Chem. **19**, 170 (1978).
19. (*a*) H. HLASIWETZ and L. BARTH. Liebigs Ann. Chem. **130**, 354 (1864); (*b*) T. L. DAVIS. J. Am. Chem. Soc. **51**, 501 (1929).
20. T. L. DAVIS and V. F. HARRINGTON. J. Am. Chem. Soc. **56**, 129 (1934).
21. (*a*) R. A. EADE, J. F. MCDONALD, and PHUNG PHAM HUU. Aust. J. Chem. **31**, 2699 (1978); (*b*) N. SCHAMP and H. DEPOOTER. Bull. Soc. Chim. Belg. **75**, 391 (1966).
22. J. ZEHENTER. Monatsh. Chem. **2**, 468 (1881).
23. (*a*) L. A. YANOVSKAYA, A. P. TERENTYEV, and L. I. BELENKY. Zh. Obshch. Khim. **22**, 1594 (1952); (*b*) M. KOHN and G. LOFF. Monatsh. Chem. **45**, 589 (1924); (*c*) K. W. ROSENMUND and W. KUHNHENN. Chem. Ber. **56**, 1262 (1923); (*d*) M. KOHN and L. STEINER. J. Org. Chem. **12**, 30 (1947).
24. R. B. SANDIN and R. A. MCKEE. Org. Synth. Coll. Vol. **II**, 100 (1943).
25. R. H. MITCHELL, Y. H. LAI, and R. V. WILLIAMS. J. Org. Chem. **44**, 4733 (1979).
26. F. A. SEDOR and G. E. SANDER. Arch. Biochem. Biophys. **161**, 632 (1974).
27. K. TURNBULL and M. SALJOUGHIAN. Synth. Commun. **16**, 461 (1986).
28. P. K. AGRAWAL and H. J. SCHNEIDER. Tetrahedron Lett. **24**, 177 (1983).
29. J. MACMILLAN. J. Chem. Soc. 2585 (1954).
30. P. W. JARDON, E. H. VICKERY, L. F. PAHLER, N. POURAHMADY, G. J. MAINS, and E. J. EISENBRAUN. J. Org. Chem. **49**, 2130 (1984).
31. E. HELGSTRAND. Acta Chem. Scand. **18**, 1616 (1964); **19**, 1583 (1965).
32. (*a*) W. MAYER, R. FIKENTSCHER, J. SCHMIDT, and O. T. SCHMIDT. Chem. Ber. **93**, 2761 (1960); (*b*) O. HESSE. Liebigs Ann. Chem. **276**, 328 (1893).
33. (*a*) ST. V. KOSTANECKI and V. LAMPE. Chem. Ber. **39**, 4007 (1906); **40**, 4910 (1907); (*b*) K. FREUDENBERG, L. ORTHNER, and H. FIKENTSCHER. Liebigs Ann. Chem. **436**, 286 (1924); (*c*) H. LEUCHS. Liebigs Ann. Chem. **460**, 1 (1928); (*d*) A. M. CHEVOLOT-MAGUEUR, A. CAVE, P. POTIER, J. TESTE, A. CHIGRONI, and C. RICHE. Phytochemistry, **15**, 767 (1976).
34. L. ENGMAN and J. S. E. HELLBERG. J. Organomet. Chem. **296**, 357 (1985).
35. P. K. AGRAWAL and R. P. RASTOGI. Heterocycles, **16**, 2181 (1981).
36. J. A. DONNELLY and F. POLICKY. Chem. Ind. (London), 1338 (1965).
37. A. FISCHER and G. N. HENDERSON. Can. J. Chem. **61**, 1045 (1983).
38. G. P. CROWTHER, R. J. SUNDBERG, and A. M. SARPESHKAR. J. Org. Chem. **49**, 4657 (1984).
39. Y. SUZUKI and I. ANAZAWA. Bunseki Kagaku, **31**, 498 (1982); Chem. Abstr. **98**, 16 360 (1983).
40. (*a*) J. KNUUTINEN, R. LAATIKAINEN and J. PAASIVIRTA. Org. Magn. Reson. **14**, 360 (1980); (*b*) P. ÄYRÄS and C.-J. WIDÉN. Planta Med. **34**, 144 (1978); (*c*) V. B. VASILJEV, V. Y. KOMAROV, L. B. VETKOVA, and B. I. IONIN. Zh. Obsch. Khim. **52**, 524 (1982); (*d*) J. S. CRAIGIE, A. G. MCINNES, M. A. RAGAN, and J. A. WALTER. Can. J. Chem. **55**, 1575 (1977).
41. (*a*) B. H. ARISON, N. L. WENDLER, D. TAUB, R. D. HOFFSOMMER, and C. H. KUO. J. Am. Chem. Soc. **85**, 627 (1973); (*b*) M. A. RAGAN. Can. J. Chem. **63**, 291 (1985); (*c*) J. H. BOWIE, J. RONAYNE, and D. H. WILLIAMS. J. Chem. Soc. B, 785 (1966); (*d*) A. ZWEIG, J. E. LEHNSEN, J. E. LANCASTER, and M. T. NEGLIA. J. Am. Chem. Soc. **85**, 3940 (1963); (*e*) P. ÄYRÄS and C. J. WIDÉN. Finn. Chem. Lett. 264 (1978).
42. R. S. NORTON, K. D. CROFT, and R. J. WELLS. Tetrahedron, **37**, 2341 (1981).
43. J. BROMILOW, R. T. C. BROWNLEE, D. J. CRAIK, and M. SADEK. Magn. Reson. Chem. **24**, 862 (1986).
44. F. GUILLAUME, J. P. SEQUIN, L. NADJO, R. UZAN, F. MEMBREY, and J. P. DOUCET. J. Chem. Soc. Perkin Trans. 2, 1139 (1984).
45. (*a*) G. W. BUCHANAN, G. MONTAUDO, and P. FINOCCHIARO. Can. J. Chem. **52**, 767 (1974); (*b*) D. J. CALVERT, R. C. CAMBIE, and B. R. DAVIS. Org. Magn. Reson. **12**, 583 (1979).
46. (*a*) A. MAKRIYANNIS and S. FESIK. J. Am. Chem. Soc. **104**, 6462 (1982); (*b*) K. S. DHAMI and J. B. STOTHERS. Can. J. Chem. **44**, 2855 (1966); (*c*) W. KITCHING, I. DEJONGE, W. ADCOCK, and A. N. ABEYWICKREMA. Org. Magn. Reson. **14**, 502 (1980).
47. J. N. ROITMAN and L. F. JAMES. Phytochemistry, **24**, 835 (1985).

Can. J. Chem. Downloaded from www.nrcresearchpress.com by 122.72.124.2 on 09/07/12
For personal use only.

Solvent effects on S_N2 transition state structure. II: The effect of ion pairing on the solvent effect on transition state structure

KENNETH CHARLES WESTAWAY[1] AND ZHU-GEN LAI
Chemistry Department, Laurentian University, Sudbury, Ont., Canada P3E 2C6

Received October 6, 1987[2]

KENNETH CHARLES WESTAWAY and ZHU-GEN LAI. Can. J. Chem. **67**, 345 (1989).

Identical secondary α-deuterium kinetic isotope effects (transition state structures) in the S_N2 reaction between *n*-butyl chloride and a free thiophenoxide ion in aprotic and protic solvents confirm the validity of the Solvation Rule for S_N2 Reactions. These isotope effects also suggest that hydrogen bonding from the solvent to the developing chloride ion in the S_N2 transition state does not have a marked effect on the magnitude of the chlorine (leaving group) kinetic isotope effects. Unlike the free ion reactions, the secondary α-deuterium kinetic isotope effect (transition state structure) for the S_N2 reaction between *n*-butyl chloride and the solvent-separated sodium thiophenoxide ion pair complex is strongly solvent dependent. These completely different responses to a change in solvent are rationalized by an extension to the Solvation Rule for S_N2 Reactions. Finally, the loosest transition state in the reactions with the solvent-separated ion pair complex is found in the solvent with the smallest dielectric constant.

Key words: ion pairs, transition state, solvent effects, nucleophilic substitution, isotope effects.

KENNETH CHARLES WESTAWAY et ZHU-GEN LAI. Can. J. Chem. **67**, 345 (1989).

Les effets isotopiques cinétiques secondaires des deutérium en α (états de transition ressemblant aux structures) qui sont observés au cours de la réaction S_N2 du chlorure de *n*-butyle avec l'ion thiophénolate libre sont identiques que les solvants soient aprotique ou protique; ces résultats confirment la validité de la règle de solvatation pour les réactions S_N2. Ces effets isotopiques suggèrent aussi que la liaison hydrogène qui se développe, dans l'état de transition S_N2, entre le solvant et l'ion chlorure qui se forme n'a pas d'influence marquée sur l'amplitude des effets isotopiques cinétiques du chlore (groupement nucléofuge). Par opposition avec ce qui est observé lors des réactions des ions libres, l'effet isotopique cinétique secondaire des deutérium en α (structure ressemblant à l'état de transition) qui caractérise la réaction S_N2 entre le chlorure de *n*-butyle et la paire d'ions complexe de l'ion thiophénolate de sodium séparé par le solvant dépend fortement sur le solvant. Pour rationaliser ces réponses complètement différentes à un changement de solvant, on fait appel à une extension de la règle de solvatation pour les réactions S_N2. Enfin, dans les réactions comportant une paire d'ions complexe séparée par le solvant, c'est avec le solvant possédant la plus faible constante diélectrique qu'on observe l'état de transition le plus lâche.

Mots clés : paires d'ions, état de transition, effets du solvant, substitution nucléophile, effets isotopiques.

[Traduit par la revue]

Can. J. Chem. Downloaded from www.nrcresearchpress.com by 122.72.124.2 on 09/07/12
For personal use only.

Introduction

In an earlier paper (1), a "Solvation Rule for S_N2 Reactions" was proposed. This rule states that "a change in solvent will not lead to a change in the structure of an S_N2 transition state if the charges on the two nucleophiles in the transition state are the same (a Type I reaction) but will lead to a change in structure of the transition state when a negatively charged nucleophile and a neutral nucleophile (a Type II reaction) are present in the transition state." Although this theory was based on many experimental results, one of the strongest pieces of supporting evidence was the constant chlorine (leaving group) kinetic isotope effects, Table 1, found for the S_N2 reaction between *n*-butyl chloride and sodium thiophenoxide, eq. [1], in a wide

[1] $CH_3CH_2CH_2CL_2—Cl + C_6H_5S^- Na^+ \rightarrow CH_3CH_2CH_2CL_2—SC_6H_5 + Na^+ Cl^-$ L = H, D

range of aprotic and protic solvents (2). The constant chlorine kinetic isotope effects were taken as evidence that the length of the α-carbon–chlorine transition state bond and the transition state did not change when the solvent was altered. However, theoretical calculations by Sims and co-workers (3, 4) suggest that hydrogen bonding to the developing chloride ion by solvent in the transition state can reduce significantly, or even level, the chlorine kinetic isotope effect and mask changes that occur in the length of the α-carbon–chlorine transition state bond. If this is the case, the constant chlorine kinetic isotope effects do not mean that the transition state remains constant when the solvent is altered in the *n*-butyl chloride – sodium thiophenoxide reaction, and the Solvation Rule for S_N2 Reactions might not be valid.

TABLE 1. The second-order rate constants and chlorine kinetic isotope effects found in several protic and aprotic solvents for the S_N2 reaction between *n*-butyl chloride and sodium thiophenoxide at 20°C

Solvent	Rate constant[a] (L mol^{-1} s^{-1})	$(k^{35}/k^{37})^{a,b}$
DMSO	2.6×10^{-2}	1.00964
DMF	4.1×10^{-2}	1.00953
Tetraglyme	1.1×10^{-2}	1.00942
Diglyme	3.5×10^{-3}	1.00949
Methanol	2.2×10^{-5}	1.00930
1-Propanol	6.2×10^{-5}	1.00931
1-Amyl alcohol	4×10^{-5}	1.00942
		Average 1.00944±0.00012[c]

[a]This data is taken from ref. 2.
[b]The error in each chlorine isotope effect is ±0.00015.
[c]Standard deviation.

If the Solvation Rule holds for the S_N2 reaction between *n*-butyl chloride and thiophenoxide ion (a Type I reaction with a negatively charged nucleophile and leaving group), the secondary α-deuterium kinetic isotope effect (transition state structure) will not be altered when the solvent is changed. If, on the other hand, the transition state shifts with a change in solvent, the secondary α-deuterium kinetic isotope effects will be different in each solvent. The secondary α-deuterium kinetic

[1]Author to whom correspondence may be addressed.
[2]Revision received November 2, 1988.

TABLE 2. The secondary α-deuterium kinetic isotope effects[a] for the S_N2 reaction between *n*-butyl chloride and free thiophenoxide ion in DMSO, DMF, and methanol at 20°C

Solvent	k_H (L mol^{-1} s^{-1})	k_D (L mol^{-1} s^{-1})	$(k_H/k_D)_\alpha$
DMSO	$(3.168\pm0.005)^b \times 10^{-2}$	$(2.844\pm0.021)^b \times 10^{-2}$	1.114 ± 0.007^c
	$(2.927\pm0.017) \times 10^{-2}$	$(2.617\pm0.013) \times 10^{-2}$	1.118 ± 0.009^c
			Average 1.116 ± 0.003^d
DMF	$(6.131\pm0.043) \times 10^{-2}$	$(5.432\pm0.033) \times 10^{-2}$	1.129 ± 0.010
	$(6.136\pm0.045) \times 10^{-2}$	$(5.457\pm0.006) \times 10^{-2}$	1.124 ± 0.008
			Average 1.127 ± 0.004^d
Methanol	$(3.396\pm0.002) \times 10^{-5}$	$(3.001\pm0.017) \times 10^{-5}$	1.132 ± 0.010
			Average for all solvents 1.125 ± 0.008^d

[a]Each isotope effect was determined with a different batch of solvent and by a different worker.
[b]Standard deviation from at least three different kinetic runs.
[c]The error is $1/k_D[(\Delta k_H)^2 + (k_H/k_D)^2 \times (\Delta k_D)^2]^{1/2}$ where Δk_H and Δk_D are the standard deviations for the rate constants for the undeuterated and deuterated substrates, respectively (5).
[d]Standard deviation for the average isotope effect.

isotope effects for the *n*-butyl chloride – sodium thiophenoxide reaction have been measured in three different solvents, DMSO, DMF, and methanol, to determine whether the transition state of this S_N2 reaction changes when the solvent is altered. The results will establish or refute the validity of the Solvation Rule.

Finally, the secondary α-deuterium kinetic isotope effects have also been determined for the S_N2 reaction between *n*-butyl chloride and the solvent-separated sodium thiophenoxide ion pair complex (5) to learn how the form of the reacting nucleophile affects the solvent effects on transition state structure for an S_N2 reaction.

Results and discussion

Graczyk *et al.* reported that the S_N2 reaction between *n*-butyl chloride and sodium thiophenoxide gave only the substitution products *n*-butyl phenyl sulfide and chloride ion, and was not complicated by a competing elimination reaction (2). This was confirmed when HPLC analyses of reaction mixtures for the substitution product, *n*-butyl phenyl sulfide, showed that substitution accounted for 100 ± 1% of the product in each solvent. Conductivity studies and uv spectroscopic studies of alkali metal thiophenoxide solutions, as well as secondary α-deuterium kinetic isotope effect measurements in the presence and absence of 15-crown-5 ether, have shown that *n*-butyl chloride reacts with a free thiophenoxide ion at some sodium thiophenoxide concentrations and with a solvent-separated sodium thiophenoxide ion pair complex at other concentrations in DMSO, DMF, and methanol (5).

The presence of the solvent-separated ion pair complex at high sodium thiophenoxide concentrations in DMSO, DMF, and methanol (5) was indicated by (*i*) the decrease in the slope of the conductance versus concentration plot at a particular sodium thiophenoxide concentration, (*ii*) the rapid change in the uv spectrum with concentration at this same concentration, and (*iii*) because 15-crown-5 ether caused the same changes as dilution in the uv spectrum of sodium thiophenoxide solutions. The cation independent λ_{max} of the uv spectra of lithium, sodium, and cesium thiophenoxide solutions at concentrations where the salts were known to exist as the ion pair complex in DMSO, DMF, and methanol demonstrated that the nucleophilic reactant in these three solvents is a solvent-separated ion pair (6). Finally, the extremely sharp change in the uv spectrum, and in the secondary α-deuterium kinetic isotope effects, with concentration indicates that the solvent-separated ion pair must exist as a complex consisting of several solvent-separated sodium thiophenoxide ion pairs, eq. [2].

$$[2] \quad m\mathrm{Na}^+ + m\mathrm{SC_6H_5}^- \rightleftarrows (\mathrm{Na}^+(\mathrm{solvent})_n(\mathrm{SC_6H_5}^-))_m$$

All of the experimental findings are consistent with such an equilibrium. First, the form of the reacting anion would change rapidly with concentration if this equilibrium existed. Also, the rapid change in the uv spectra and in the secondary α-deuterium kinetic isotope effects with concentration are expected. The conductivity data are also consistent with the formation of the ion pair complex because the conductance of the ion pair complex is lower than that of the free ions (7). Finally, the secondary α-deuterium kinetic isotope effects found at high sodium thiophenoxide concentrations in the 15-crown-5 ether reactions are identical to those found in the free ion reactions because the 15-crown-5 ether complexes the sodium ions (8) and the ion pair complex cannot form.

Testing the Solvation Rule for S_N2 reactions

The secondary α-deuterium kinetic isotope effects found for the S_N2 reaction between *n*-butyl chloride and the free thiophenoxide ion in three different solvents, Table 2, are the same within experimental error. These identical kinetic isotope effects are impressive because the rate constant changes by 1400 times when the solvent is changed from DMF to methanol. A change in the length of either the nucleophile–α-carbon and (or) α-carbon – leaving group bonds in the S_N2 transition state would change the steric crowding around the α carbon and alter the frequencies of the C_α–H(D) out-of-plane bending vibrations, which primarily determine the magnitude of the secondary α-deuterium kinetic isotope effect (9, 10). Thus, the simplest explanation is that the transition states do not change when the solvent is altered in the free ion S_N2 reaction, i.e., the identical isotope effects indicate that the transition states are identical in all three solvents.

Although other factors such as a change in the amount of conjugation to the phenyl ring on the α carbon (3, 12), changes in the reaction coordinate motion (13, 14), tunnelling (13, 14), and changes in product composition (15) can affect the magnitude of secondary α-deuterium kinetic isotope effects, the simplest explanation for the identical isotope effects in the free ion reaction is preferred because (*i*) the substrate is saturated,

Can. J. Chem. Downloaded from www.nrcresearchpress.com by 122.72.124.2 on 09/07/12
For personal use only.

TABLE 3. The secondary α-deuterium kinetic isotope effects[a] for the S_N2 reaction between *n*-butyl chloride and the solvent-separated sodium thiophenoxide ion pair complex in DMSO, DMF, methanol, and diglyme at 20°C

Solvent	k_H (L mol^{-1} s^{-1})	k_D (L mol^{-1} s^{-1})	$(k_H/k_D)_\alpha$
DMSO	$(3.424\pm0.004)^b \times 10^{-2}$	$(3.311\pm0.006)^b \times 10^{-2}$	1.034 ± 0.002^c
DMF	$(4.503\pm0.063) \times 10^{-2}$	$(4.156\pm0.068) \times 10^{-2}$	1.083 ± 0.023
	$(4.352\pm0.022) \times 10^{-2}$	$(4.011\pm0.034) \times 10^{-2}$	1.085 ± 0.011
			Average 1.084 ± 0.001^d
Methanol	$(2.457\pm0.016) \times 10^{-5}$	$(2.233\pm0.011) \times 10^{-5}$	1.100 ± 0.009
	$(2.408\pm0.011) \times 10^{-5}$	$(2.190\pm0.004) \times 10^{-5}$	1.100 ± 0.005
			Average 1.110 ± 0.002^d
Diglyme	$(3.235\pm0.120) \times 10^{-3}$ [e]	$(2.839\pm0.200) \times 10^{-3}$ [e]	1.139 ± 0.091
	$(4.009\pm0.054) \times 10^{-3}$	$(3.501\pm0.112) \times 10^{-3}$	1.145 ± 0.039
	$(4.825\pm0.140) \times 10^{-3}$	$(4.238\pm0.085) \times 10^{-3}$	1.139 ± 0.040
	$(5.627\pm0.087) \times 10^{-3}$	$(4.927\pm0.031) \times 10^{-3}$	1.142 ± 0.019
			Average 1.141 ± 0.003^d

[a]Each isotope effect was determined with a different batch of solvent and by a different worker except for the isotope effects in methanol.

[b]Standard deviation from at least three kinetic runs.

[c]The error is $1/k_D[(\Delta k_H)^2 + (k_H/k_D)^2 \times (\Delta k_D)^2]^{1/2}$ where Δk_H and Δk_D are the standard deviations for the rate constants for the undeuterated and deuterated substrates, respectively (5).

[d]Standard deviation on the average isotope effect.

[e]The different rate constants were found at different times and at different sodium thiophenoxide concentrations. The variation in the rate constants is probably due to a small salt effect.

(*ii*) quantitative yields of the S_N2 product are found in these reactions (2, *vide supra*), and (*iii*) the secondary α-deuterium kinetic isotope effects for the free ion reactions ($k_H/k_D = 1.06$/α-D) are well within the range expected for an S_N2 reaction of an alkyl chloride (16, 17). Since large secondary α-deuterium kinetic isotope effects, significantly greater than the equilibrium isotope effect, are found when changes in the reaction coordinate motion and (or) tunnelling affect the magnitude of the isotope effect (13, 14), it seems unlikely that these factors affect the magnitude of these secondary α-deuterium kinetic isotope effects significantly. As a result, the most likely explanation is the simple one, i.e., that the magnitude of the isotope effects is related to the structure of the transition state and that the identical isotope effects indicate that the S_N2 transition states do not change with solvent when the reacting nucleophile is a free ion.

The failure to detect a change in the secondary α-deuterium kinetic isotope effect (structure of the S_N2 transition state), even though the change in solvent markedly changes the rate constant for the reaction, is, in fact, predicted by the Solvation Rule for S_N2 Reactions because both the thiophenoxide ion and the developing chloride ion are negatively charged in the transition state. Thus, one is forced to conclude that the Solvation Rule for S_N2 Reactions is valid.

The effect of solvation on chlorine kinetic isotope effects

The secondary α-deuterium kinetic isotope effects found in this study are also useful because they support the contention (2) that chlorine (leaving group) kinetic isotope effects can be used for determining the relative length of the C_α—Cl transition state bonds in S_N2 reactions. The identical secondary α-deuterium kinetic isotope effects indicate that the transition state for the S_N2 reaction between *n*-butyl chloride and sodium thiophenoxide does not change when the solvent is changed from the dipolar aprotic solvents, DMF or DMSO, to a protic solvent, methanol. This observation is important because it confirms that the length of the α-carbon–chlorine bond does not change appreciably in these transition states when the solvent is altered. Thus, the virtually identical chlorine isotope effects found by Graczyk *et al.* for this S_N2 reaction (2) do reflect accurately the length of the α-carbon–chlorine transition state bond and the magnitude of the chlorine kinetic isotope effects for S_N2 reactions are not lowered as much by hydrogen bonding with the solvent as the theoretical calculations suggest (3, 4). In fact, a close examination of the chlorine kinetic isotope effects in Table 1 suggests that hydrogen bonding of the developing chloride ion has only a very small (within experimental error) effect on the magnitude of the chlorine kinetic isotope effect. The chlorine isotope effects for the reactions in dipolar aprotic and aprotic solvents, where the developing chloride ion is only weakly solvated (relative to its solvation energy in protic solvents) (1, 18), are only slightly larger (1.00952 ± 0.00009) than those found in the protic solvents (1.00934 ± 0.00007) where hydrogen bonding to the developing chloride ion could lower the magnitude of the chlorine isotope effect. In fact, the difference of 0.00018 between the average kinetic isotope effects in the aprotic and protic solvents is barely outside the error of 0.00015 reported for the individual isotope effects (2) and one is forced to conclude that hydrogen bonding to the developing chloride ion has only a very small effect on the chlorine kinetic isotope effect for S_N2 reactions. This conclusion is particularly important because the chlorine kinetic isotope effects for this reaction are near the maximum found for S_N2 reactions. Thus, the amount of C_α—Cl bond rupture in the transition state and the effect of hydrogen bonding by solvent must be at or near the maximum for S_N2 reactions. This suggests that chlorine (leaving group) isotope effects can be used as a probe of transition state structure for S_N2 reactions. It is important to note, however, that hydrogen bonding to the developing chloride ion by solvent in the transition state should cause a greater reduction in, and may

Can. J. Chem. Downloaded from www.nrcresearchpress.com by 122.72.124.2 on 09/07/12
For personal use only.

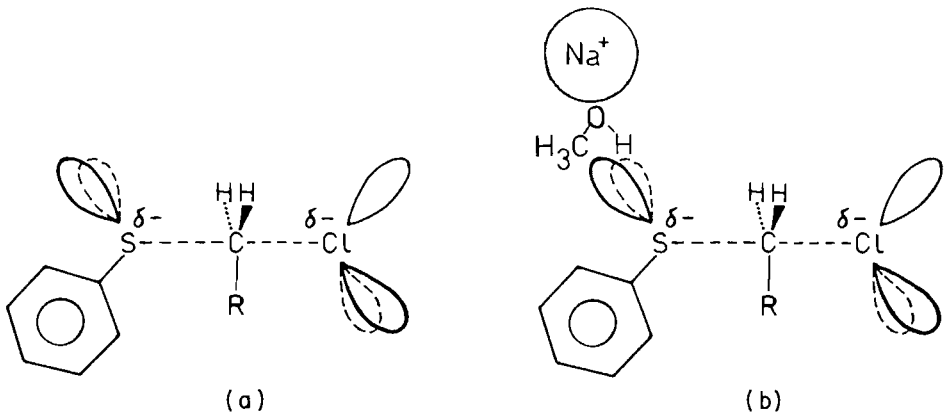


FIG. 1. The S_N2 transition states for the reaction between *n*-butyl chloride and (a) the free thiophenoxide ion; (b) the solvent-separated sodium thiophenoxide ion pair complex.

even level, the chlorine isotope effects of carbocation S_N reactions that have looser transition states with more α-carbon–chlorine bond rupture (19–22).

The effect of ion pairing on the solvent effects on transition state structure

The results in Tables 2 and 3 indicate that the secondary α-deuterium kinetic isotope effect and transition state structure for the S_N2 reaction between *n*-butyl chloride and sodium thiophenoxide are affected very differently by a change in solvent when the sodium thiophenoxide reacts as a solvent-separated ion pair complex (ref. 5, *vide supra*) and as a free ion. While the secondary α-deuterium kinetic isotope effects in the free ion reactions are identical in both aprotic and protic solvents, the α-deuterium kinetic isotope effects in the reactions where the reacting nucleophile is the solvent-separated ion pair complex are different in each solvent. In fact, these kinetic isotope effects cover the range from much smaller ($(k_H/k_D)_\alpha$ = 1.034) to slightly larger ($(k_H/k_D)_\alpha$ = 1.141) than the average secondary α-deuterium kinetic isotope effect of 1.125 ± 0.008 found in the free ion reactions. Moreover, the average kinetic isotope effects for the reactions with the solvent-separated ion pair complex, Table 3, are significantly different in each solvent. Thus, one must conclude that the transition state structure (the secondary α-deuterium kinetic isotope effect) changes significantly when the solvent is changed in the S_N2 reaction between *n*-butyl chloride and the solvent-separated sodium thiophenoxide ion pair complex.

The very different solvent effects on the secondary α-deuterium kinetic isotope effects and transition state structures for the free ion and ion pair reactions can be rationalized with the Solvation Rule for S_N2 Reactions. The S_N2 transition states for the free ion and ion pair complex reactions, Fig. 1, are very different from the point of view of solvation. The S_N2 transition state for the free ion reaction will be mainly, if not exclusively, solvated at the two negatively charged nucleophiles, the sulfur of the thiophenoxide ion and the developing chloride ion. Since the charges, and perhaps the charge density, on these two nucleophiles are the same in the S_N2 transition state, a change in solvent will cause the same changes in solvation at the two nucleophiles. For example, if the solvent is changed from methanol to DMSO, the solvation at both nucleophiles changes in the same way, i.e., from hydrogen bonding in methanol to an ion–dipole interaction in DMSO. As a result, the relative nucleophilicity of the two nucleophiles will not be changed by a change in solvent, and the transition state will not be altered (1).

The variable secondary α-deuterium kinetic isotope effects in the solvent-separated ion pair complex reactions are consistent with a tight solvent-separated ion pair. In a tight S_N2 ion pair transition state (an approximation of the transition state is shown in Fig. 1(b)) the solvation will be mainly at the sodium ion, which has a full positive charge, and the developing chloride ion, which has a partial negative charge. More important, however, the sodium ion blocks the normal solvation of the partially charged sulfur anion. As a result, changing from the protic solvent, methanol, to the dipolar aprotic solvent, DMSO, will have very different effects on the solvation and nucleophilicity at the sulfur and chloride ions in the ion pair S_N2 transition state.

The solvent change from methanol to DMSO changes the solvation from hydrogen bonding to an ion–dipole interaction at the negatively charged chloride ion. Since hydrogen bonding lowers the electron density of an anion, the loss of hydrogen bonding to the developing chloride ion will increase the electron density (the nucleophilicity) of the chloride ion.

The methanol molecule(s) in a tight solvent-separated ion pair complex could not hydrogen bond to the sulfur anion in the tight ion pair S_N2 transition state because the distance between the sodium and sulfur ions would be too small to form linear hydrogen bonds to methanol. Thus, no hydrogen bonding is lost when the solvent changes, i.e., the change in solvent from methanol to DMSO only changes one dipole–ion interaction for another at the sulfur ion. As a result, the electron density on the sulfur anion is not markedly affected by the change in solvent.

Since the solvent change alters the charge density on the chloride anion much more than that on the sulfur ion, the relative nucleophilicity of the chloride and sulfur anions is altered significantly by a change in solvent. As a result, the ion pair S_N2 transition state behaves like a Type II system (1) and the transition state structure (the secondary α-deuterium kinetic isotope effect) is altered by a change in solvent. An extension of the Solvation Rule for S_N2 Reactions states that the structure of the transition state containing a tight, solvent-separated ion pair nucleophile and a negatively charged leaving group will be altered by a change in solvent (behave like a Type II transition state) because the cation in the tight ion pair alters the solvation of the nucleophile.

Finally, the smallest secondary α-deuterium kinetic isotope effect and tightest transition state in the ion pair complex reactions are found in the most polar solvent, DMSO, and the largest isotope effect and loosest transition state are found in the least polar solvent, diglyme, Table 4. In fact, the correlation

Can. J. Chem. Downloaded from www.nrcresearchpress.com by 122.72.124.2 on 09/07/12
For personal use only.

TABLE 4. The dielectric constant of the solvent and the secondary α-deuterium kinetic isotope effects for the S_N2 reaction between *n*-butyl chloride and the solvent-separated sodium thiophenoxide ion pair complex in DMSO, DMF, methanol, and diglyme at 20°C

Solvent	Dielectric constant[c]	$(k_H/k_D)_\alpha$
DMSO	46.6	1.034±0.002[a]
DMF	36.7	1.084±0.001[b]
Methanol	32.6	1.100±0.000[b]
Diglyme	7.3	1.141±0.003[b]

[a]The error is $1/k_D[(\Delta k_H)^2 + (k_H/k_D)^2 \times (\Delta k_D)^2]^{1/2}$ where Δk_H and Δk_D are the standard deviations for the rate constants for the undeuterated and deuterated substrates, respectively (5).
[b]Standard deviation for the average isotope effect, see Table 3.
[c]Taken from ref. 24.

coefficient for the plot of the secondary α-deuterium kinetic isotope effect versus the dielectric constant of the solvent is 0.95. This crude relationship is presumably found because the influence of the negatively charged sulfur of the thiophenoxide ion pair complex is transmitted for greater distances through the less polar solvent, i.e., the charge on the sulfur atom is felt by the α carbon at larger distances when the dielectric constant (polarity) of the solvent is lower (11). In the more polar solvents, the sulfur anion has to come closer to the α carbon before it distorts the α-carbon–chlorine bond and causes reaction.

Conclusion

The identical secondary α-deuterium kinetic isotope effects found in aprotic and protic solvents for the S_N2 reaction between *n*-butyl chloride and the free thiophenoxide ion demonstrate that the Solvation Rule for S_N2 Reactions (1) is valid. The identical isotope effects (transition states) in the different solvents also support the contention by Graczyk *et al.* (2) that hydrogen bonding to the developing chloride ion by solvent in an S_N2 transition state does not have a significant effect on the magnitude of chlorine leaving group kinetic isotope effects, as theoretical calculations suggest (3, 4). In fact, the changes in the chlorine isotope effect for this reasonably loose S_N2 transition state are almost within the experimental error when the solvent is changed from a poorly solvating aprotic solvent to a strongly solvating hydrogen-bonding solvent.

The large solvent effect on the secondary α-deuterium kinetic isotope effects (transition state structure) for the S_N2 reaction between *n*-butyl chloride and the solvent-separated sodium thiophenoxide ion pair complex is completely different from the effect on the corresponding free ion reaction. These differences are consistent with the Solvation Rule for S_N2 Reactions if one considers that the metal cation changes the normal solvation of the ion pair nucleophile in the transition state. Finally, the loosest transition state in the reactions with the ion pair complex is found in the solvent with the smallest dielectric constant. This presumably occurs because the charge on the nucleophilic sulfur atom distorts the electron density in the α-carbon–chlorine bond and causes reaction at a greater distance in the less polar solvent.

Experimental

Preparation of reagents

The purification of the solvents and the preparation of the sodium thiophenoxide and the deuterated and undeuterated substrates are described elsewhere (5).

Kinetic method

The kinetic methods in the various solvents are described in ref. 5.

HPLC analysis

The percent yield of *n*-butyl phenyl sulfide was determined by using diphenyl ether as the internal standard (23). The separation was done isocratically with 67% methanol – 33% water on a Waters 5PAH 10 Radial Pak column at a flow rate of 2 mL/min. A Waters model 600 and a Waters 490 uv detector set at 275 nm were used for the analysis.

Acknowledgement

The authors gratefully acknowledge the financial support provided by the Natural Sciences and Engineering Research Council of Canada.

1. K. C. WESTAWAY. Can. J. Chem. **56**, 2691 (1978).
2. D. G. GRACZYK, J. W. TAYLOR, and C. R. TURNQUIST. J. Am. Chem. Soc. **100**, 7333 (1978).
3. D. M. BRUBAKER. Ph.D. dissertation, University of Arkansas, Fayetteville, AR. 1978.
4. G. W. BURTON, L. B. SIMS, J. C. WILSON, and A. FRY. J. Am. Chem. Soc. **99**, 3371 (1977).
5. K. C. WESTAWAY and Z. G. LAI. Can. J. Chem. **66**, 1263 (1988).
6. E. BUNCEL, B. C. MENON, and J. P. COLPA. Can. J. Chem. **57**, 999 (1979).
7. R. J. WILLIAMS, J. N. PHILLIPS, and K. J. MYSELS. Trans. Faraday Soc. **51**, 728 (1955).
8. J. J. CHRISTENSEN, D. J. EATOUGH, and R. M. IZATT. Chem. Rev. **74**, 351 (1974).
9. K. C. WESTAWAY and Z. WASZCZYLO. Can. J. Chem. **60**, 2500 (1982).
10. V. J. SHINER, JR., M. W. RAPP, E. A. HALEVI, and M. WOLFSBERG. J. Am. Chem. Soc. **90**, 7171 (1968).
11. J. E. GORDON. The organic chemistry of electrolyte solutions. J. Wiley and Sons, Toronto. 1975. p. 372.
12. Z. WASZCZYLO and K. C. WESTAWAY. Tetrahedron Lett. **23**, 143 (1982).
13. W. P. HUSKEY and R. L. SCHOWEN. J. Am. Chem. Soc. **105**, 5704 (1983).
14. W. H. SAUNDERS, JR. J. Am. Chem. Soc. **106**, 2223 (1984).
15. D. J. MCLENNAN and P. M. W. GILL. Isr. J. Chem. **26**, 378 (1985).
16. K. C. WESTAWAY. Tetrahedron Lett. 4229, 1975.
17. V. J. SHINER, JR. Isotope effects in chemical reactions. *Edited by* C. J. Collins and E. S. Bowman. Van Nostrand-Reinhold, New York, NY. 1971. Chap. 2. p. 137.
18. A. J. PARKER. Chem. Rev. **69**, 1, (1969).
19. D. G. GRACZYK and J. W. TAYLOR. J. Am. Chem. Soc. **96**, 3255 (1974).
20. J. BIGELEISEN and M. WOLFSBERG. J. Chem. Phys. **22**, 1264 (1954).
21. T. H. CROMARTIE and C. G. SWAIN. J. Am. Chem. Soc. **98**, 545 (1976).
22. T. H. CROMARTIE and C. G. SWAIN. J. Chem. Soc. **98**, 2962 (1976).
23. S. DAL NOGARE and R. S. JUVET, JR. Gas–liquid chromatography. J. Wiley and Sons, Interscience, New York, NY. 1962. p. 256.
24. J. F. COETZEE and C. D. RITCHIE. Solute–solvent interactions. Marcel Dekker, New York, NY. 1969. p. 52.

Can. J. Chem. Downloaded from www.nrcresearchpress.com by 122.72.124.2 on 09/07/12
For personal use only.

The degradation of Indulin ATR by *Streptomyces*: chemical characterization of the water soluble acid precipitable products

P. F. VIDAL,[1] J. BOUCHARD, E. CHORNET, AND R. P. OVEREND
Department of Chemical Engineering, University of Sherbrooke, Sherbrooke, P.Q., Canada J1K 2R1
AND
H. GIROUX AND F. LAMY
Department of Biochemistry, University of Sherbrooke, Sherbrooke, P.Q., Canada J1K 2R1

Received March 31, 1988[2]

P. F. VIDAL, J. BOUCHARD, E. CHORNET, R. P. OVEREND, H. GIROUX, and F. LAMY. Can. J. Chem. **67**, 350 (1989).

Two strains of *Streptomyces*, *S. badius* and *S. virdosporus*, when incubated with kraft lignin (Indulin ATR) produce water soluble acid precipitable compounds. We show by a combination of elemental analysis, amino acid analysis, and FTIR that these are complexes of lignin fragments strongly associated with proteins. The latter, which can be separated by solvent extraction, are added by the microorganisms themselves. The lignin fraction, which represents approximately 60% of the complex weight, consists of lower molecular weight, lower methoxyl content Indulin fragments.

Key Words: lignin, Indulin, lignin–protein complexes, Fourier transform infrared spectrophotometry, high performance size exclusion chromatography, *Streptomyces*.

P. F. VIDAL, J. BOUCHARD, E. CHORNET, R. P. OVEREND, H. GIROUX et F. LAMY. Can. J. Chem. **67**, 350 (1989).

Lorsque incubées avec une lignine kraft (Indulin ATR), deux souches de *Streptomyces : S. badius* et *S. viridosporus* produisent des composés solubles dans l'eau qui précipitent en milieu acide. Ceux-ci sont des complexes formés de lignine fortement associée à des protéines qui peuvent être dissociés par solubilisation séquentielle. La fraction ligneuse qui représente environ 60% de la masse du complexe est constituée de fragments d'Indulin ATR de plus faibles poids moléculaires et teneur en méthoxyles.

Mots clés: lignine, Indulin, complexes lignine–protéine, spectrophotométrie infra-rouge à transformé de Fourier, chromatographie d'exclusion stérique haute performance, *Streptomyces*.

Can. J. Chem. Downloaded from www.nrcresearchpress.com by 122.72.124.2 on 09/07/12
For personal use only.

Introduction

The biodegradation of lignin, the second most abundant biopolymer found in vascular plants, has been studied for many years in the laboratories of Nord (1), Eriksson (2), and Kirk (3). These studies were mainly concerned with the degradation of lignocellulose under the influence of white-rot fungi, leading to the isolation, from *Phanerochaete chysosporium*, of an enzyme able to cleave the C_α—C_β bond in lignin model compounds (4). Later, it was shown that this enzyme was a peroxidase, catalysing electron transfer processes (5, 6). The mechanism of lignocellulose degradation by bacteria, especially by actinomycetes, is as yet not understood. It has been shown by Broda and co-workers (7, 8) and by Crawford and co-workers (9–12) that several species of actinomycetes could solubilize the insoluble substrate, but so far no bacterial ligninolytic enzyme has been found.

We have shown recently that *Streptomyces viridosporus* and *Streptomyces badius*, the two species extensively used in Crawford's laboratory, could solubilize a commercial kraft lignin, Indulin (13). The amounts of Indulin solubilized (7%), recovered as a water soluble, Acid Precipitable Polymeric Lignin (APPL), were comparable to the amounts reported by Crawford with a lignocellulosic substrate; 3.7% for spruce, 8.6% for maple, and 13.4% for corn stover (12). When the extra- and intra-cellular bacterial proteins were incubated with Indulin, a solubilization of the substrate was observed that, in the case of *S. badius*, was enhanced by H_2O_2. Some of the results collected do not support the enzyme hypothesis and, therefore, in this paper a second, new hypothesis will be proposed and discussed.

[1]Author to whom correspondence may be addressed.
[2]Revision received November 9, 1988.

Material and methods

Lignin preparation

Indulin AT lignin was obtained from Westvaco chemical division, Charleston, SC, USA, and before use it was treated according to the manufacturer's specifications—essentially an acid washing overnight—to produce Indulin ATR.

Bacterial growth and APPL recovery

The cultures of *S. badius* 252 (ATCC39115) and *S. viridosporus* T7A (ATCC 39117) were carried out with agitation, at pH 7.5 and 37°C, in salt media containing Indulin at a concentration of 0.5% (w/vol), glucose (0.2%), and yeast extract (0.6%) (13, 17). The APPL samples used in our characterization studies were recovered after 35 days incubation as described in ref. 7. In some experiments the yeast extract was replaced with NH_4Cl (0.02%) (see results and discussion).

Elemental analyses

The percentages of carbon, hydrogen, and nitrogen present in the APPLs were determined with a Perkin–Elmer 240C elemental analyzer. The oxygen content was calculated by difference.

Carbohydrate analyses

We used a milder version of the standard method for wood hydrolysis (14). Fifty milligrams of APPL was suspended in 1 mL of 24.0 N H_2SO_4 for 1 h at 30°C. This solution was diluted with distilled water to an acid concentration of 0.8 N and autoclaved for 1 h at 120°C. Neutralization was carried out with a saturated solution of $Ba(OH)_2$ and the $BaSO_4$ precipitate removed by centrifugation. After the supernatant was evaporated until completely dry, the monosaccharides were converted into their trimethylsilyl ether derivatives using trimethylsilyl imidazole (Sigma Chem. Co.) (15), and were subjected to quantitative gas–liquid chromatography using the sorbitol derivative as the internal standard. The glc analyses were performed using a Hewlett–Packard HP-5880 A instrument equipped with a flame ionization detector (FID). The column (530 μm × 10 m) was coated with methyl silicone gum and temperature programmed at 3°C/min from 100°C to 250°C.

Methoxyl group quantification

The methoxyl content of the different samples was determined using a modified Zeisel procedure (16). The alkyl iodides formed were measured by glc using a methyl silicone phase (SP-2100 10% on Supelcoport, Supelco) on a 4 mm × 2 m column. The chromatograph (HP-5706A) was programmed for an isotherm of 4 min at 30°C and heated to 100°C at 32°C/min. Detection was made by FID. The calibration was done using vanillic acid, and decane as used was the internal standard.

Amino acids analyses

These analyses were carried out as described in Giroux *et al.* (13) with a pre-column derivatization of the protein hydrolysates to form PTC (phenylthiocarbamide) amino acid derivatives and a subsequent separation of these on C-18 μ-Bondapak column.

Sequential solubilization by tetrahydrofuran (THF) and dimethylformamide (DMF)

About 100 mg of APPLs was suspended in 20 mL of THF (Anachemica Co.) for 5 h. After centrifugation, the filtrate was evaporated to dryness and weighed. The residue was then resuspended in the same volume of the subsequent solvent mixture for 5 h and this procedure was repeated to the obtention of the final residue. The solvent sequence was the following: THF, THF:DMF (85:15), THF:DMF (50:50), and DMF (Aldrich Co.).

Fourier transform infrared analysis

A 5-DXB Nicolet system with a TGDS detector was used at a resolution of 4 cm^{-1}. The samples were mixed with pure KBr (Aldrich) at a concentration of 1–2% (w/w), milled in a steel ball mill for 40 s, and pressed in pellets with a vacuum dye. Sixty-four scans were collected and pure KBr was used as a background spectrum.

High performance size exclusion chromatography (HPSEC)

A Varian model 5000 liquid chromatograph equipped with a variable wavelength UV-100 detector was used. Two columns in series were used (PLgel 300 × 7.5 mm, particle size 5 μm, Polymer Laboratories), the first having a porosity of 50 Å and the second of 500 Å. The linearity of the calibration curve for this system is effective from a peak average molecular weight (M_p) of 100 to a M_p of 20 000 as evaluated with low dispersity polystyrene standards ($M_w/M_n < 1.10$). Filtered and degassed THF was eluted at room temperature and at a flow rate of 1.0 mL/min. Ten-microlitre samples (0.1% in THF) were injected and detection was made at 280 nm. Preparative APPL fractionation for further FTIR characterization was performed in the same apparatus using a 200-μL loop, a sample concentration of 1%, and a Gilson fraction collector.

Results

Part I: Crude APPL analysis

The elemental composition and methoxyl content of Indulin ATR and of the APPLs are presented in Table 1. The APPLs have a substantial amount of nitrogen compared to the very low value initially present in Indulin ATR. To determine where this nitrogen fraction originates, we carried out amino acid analyses, which are summarized in Table 2. They show clearly that proteins are indeed found associated with APPL collected from cultures of either *S. badius* or *S. viridosporus*. The main point to note is that the amino acid compositions are similar for the two APPLs and that they are not influenced by the presence or absence of yeast extract in the culture media. Some differences can be found in yeast extract and the APPL. For example, the ratio Polar amino acid/Aliphatic amino acid (A.A.) is equal to 0.9 in the extract while it is 0.6 ± 0.1 for the APPL (all values pooled). On the other hand, the values for the ratios Aliphatic A.A./Hydroxylated A.A. are very similar: 3.14 for yeast extract and 3.5 ± 0.3 for the APPL. The difference found in the overall recovery of amino acids in the analyses (11 ± 1 pmol L^{-1} in the APPL and 19 pmol L^{-1} in the yeast extract) is due to the fact that identical sample weights (10 mg) were initially hydrolyzed in 6 N HCl. The true weights of the APPL protein fractions were of course lower due to the presence of the lignin fragments.

TABLE 1. Elemental analyses and methoxyl group quantification of Indulin ATR and of the APPLs

Sample	%N	%C	%H	%O*	$\%OCH_3$
Indulin ATR	0.2	66.1	5.9	27.8	13.7
APPL *S.bad*	6.1	51.6	5.6	36.7	6.8
APPL *S.vir*	6.0	54.2	5.8	34.1	6.5

*Percentage of oxygen is calculated by difference.

TABLE 2. Amino acid composition of the yeast extract and of the APPL associated proteins

	Amino acid concentrations (pmol L^{-1})				
		APPL (+) yeast extract		APPL (−) yeast extract	
Amino acid categories	Yeast extract	S.bad	S.vir	S.bad	S.vir
Polar	7.23	3.16	4.27	3.85	2.81
Aliphatic	8.31	5.36	5.31	6.30	5.30
Aromatic	0.95	0.68	0.64	0.73	0.62
Hydroxylated	2.65	1.71	1.59	1.61	1.52
Total	19.14	10.91	11.81	12.49	10.25

*Initial freeze-dried samples, hydrolyzed in 6.0 N HCl, had identical weights (10 mg).

Since the protein fractions are methoxyl-free, it appears that the APPL fractions have a lesser methoxyl content when compared to the starting material, the decrease being 14% for *S. badius* and 19% for *S. viridosporus*.

The percentage of carbohydrates in Indulin ATR and in the APPLs is given in Table 3. Despite the variations among the five analyzed sugars, the summative percentages of carbohydrates remain constant, with carbohydrates being less than 1% on a weight basis.

The Fourier transform infrared spectra of the APPLs, depicted in Fig. 1, show similar patterns for the APPLs produced by *S. viridosporus* and *S. badius* but are quite different from the spectrum of Indulin ATR in the 1800–800 cm^{-1} area. Figure 2 is an expansion of this area for Indulin ATR and the APPLs produced by *S. badius* in culture media containing yeast extract or NH_4Cl as nitrogen source. The same patterns (not shown) were obtained from the APPLs derived from *S. viridosporus*.

All of the Indulin ATR infrared bands (we used the empirical assignment of lignin ir bands proposed by Hergert (18)) may be identified in the APPL spectra but variations in relative intensity and displacement of frequencies of the bands are noticeable. In the 3600–2500 cm^{-1} area, the difference between APPLs and lignin may be summarized as firstly, the existence of shoulders around 3290 and 3080 cm^{-1} in APPLs, representing peptidic bonds, and secondly, the variation in the relative intensity of bands related to alkyl groups, especially at 2965 and 2845 cm^{-1}.

From Fig. 2, the important increase of the 1700 and 1660 cm^{-1} bands, related respectively to unconjugated and conju-

Can. J. Chem. Downloaded from www.nrcresearchpress.com by 122.72.124.2 on 09/07/12
For personal use only.

TABLE 3. Carbohydrate analyses of Indulin ATR and of the APPLs

Sample	Arabinose	Xylose	Mannose	Galactose	Glucose	Total
Indulin ATR	0.11	0.17	0.06	0.23	0.23	0.80
APPL *S.bad*	0.16	0.00	0.16	0.11	0.27	0.70
APPL *S.vir*	0.00	0.00	0.18	0.12	0.35	0.60

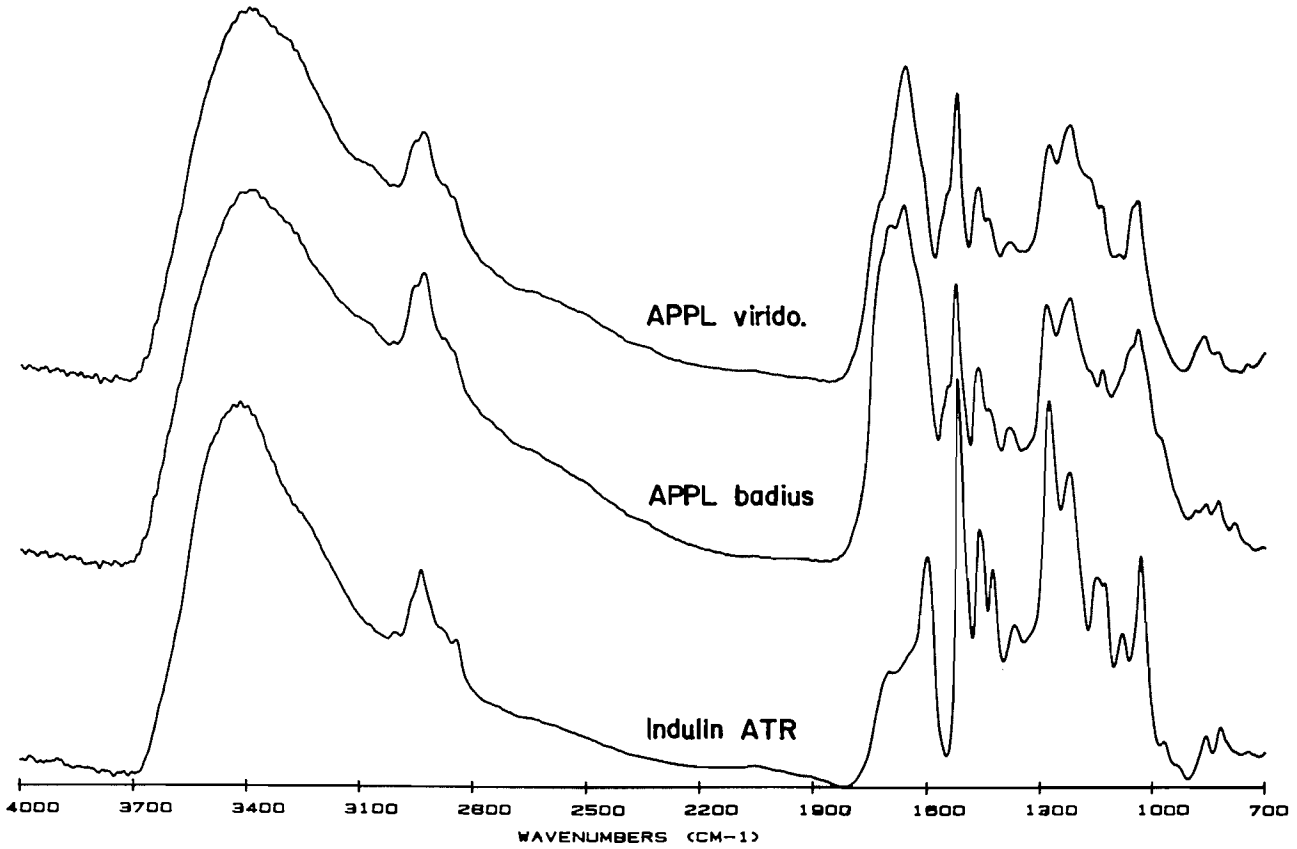


FIG. 1. FTIR spectra of Indulin ATR and of the APPLs produced by *S. badius* and *S. viridosporus*.

gated carbonyl in lignin, can be seen. Consequently, the lignin aromatic ring band at 1595 cm^{-1} is overlapped. The appearance of the 1540 cm^{-1} band, related to amide groups, does not affect the aromatic ring band at 1515 cm^{-1}.

The following four bands: 1460, 1427, 1370, and 1270 cm^{-1}, respectively assigned to alkyl, aromatic ring, alkyl and (or) hydroxyl, and finally aryl C—O of aryl–alkyl ethers in lignin, are only distorted in the APPLs spectra. The intensities of the five subsequent bands: 1220, 1150, 1130, 1080, and 1030 cm^{-1}, are strongly modified. These bands, related to C—H and C—O vibrations of syringyl and guaiacyl units, are overlapped with similar vibrations of different intensities from protein. Finally, new bands appear at 887 and 783 cm^{-1} in the APPLs spectra due to aromatic ring and amine group absorptions of some of the amino acids that compose the protein fraction.

Part II: Dissociation of the protein–polyphenolic complex and characterization of the polyphenolic fraction

The main objective of the dissociation of the protein–polyphenolic complex is to obtain the polyphenolic fraction as pure as possible for characterization purposes and to determine the extent of depolymerization. On the assumption that the complex is not strongly bound, we tried to dissociate by preferential solubilization.

Indulin ATR is almost totally soluble in THF (about 95%) and is routinely analysed by size exclusion chromatography using THF as eluent. The solubility of APPL in THF is quite low: 8.0% and 2.3% for the APPL produced by *S. badius* and *S. viridosporus* respectively, by comparison with that in DMF: 95%. These results indicate that a combination of these solvents may be able to dissociate the complex.

As shown in Table 4, we solubilized the APPLs sequentially with different ratios of THF:DMF. The quantification of each fraction as percentage of the starting material shows that the solubility distribution is different for each APPL.

In both cases, an important residue is obtained, indicating that the association of the fractions solubilized by the THF-rich solvents is required for complete solubilization of APPL in DMF.

The nitrogen quantification by elemental analysis of each fraction indicates an increase in nitrogen content as the sequential solubilization proceeds, with a maximum between

Can. J. Chem. Downloaded from www.nrcresearchpress.com by 122.72.124.2 on 09/07/12
For personal use only.

Can. J. Chem. Downloaded from www.nrcresearchpress.com by 122.72.124.2 on 09/07/12
For personal use only.

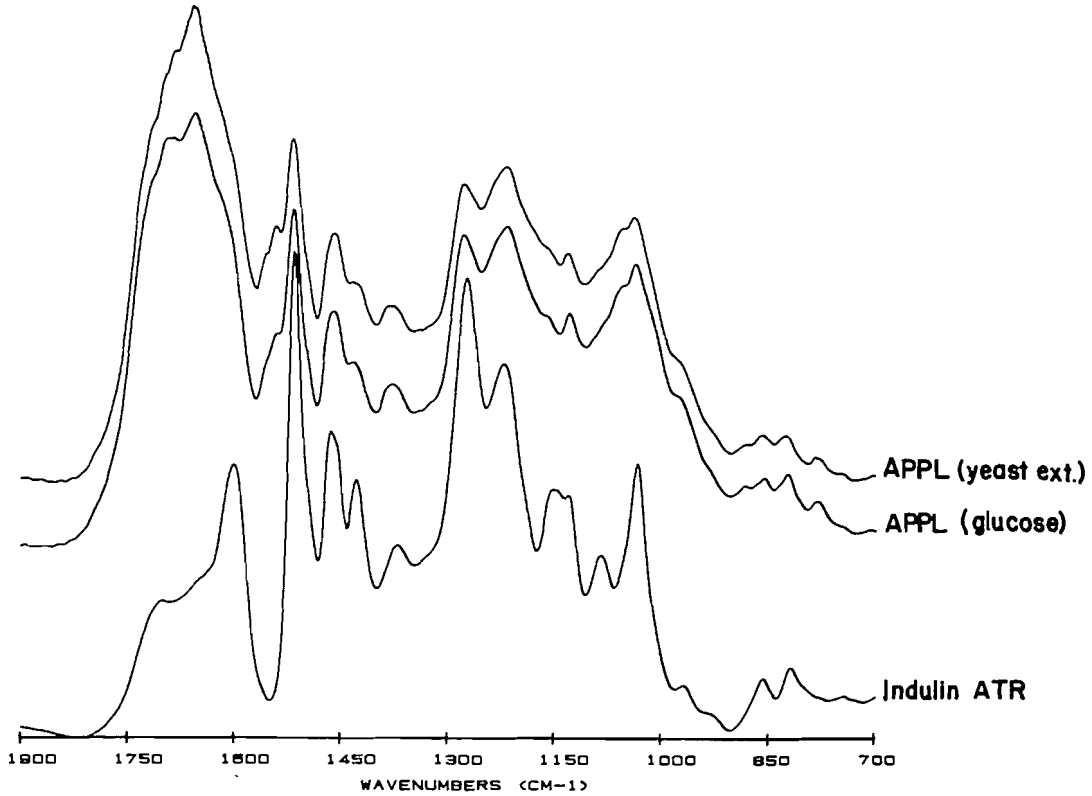


FIG. 2. FTIR spectra (1900–700 cm^{-1}) of Indulin ATR and of the APPLs produced by *S. badius* with or without yeast extract.

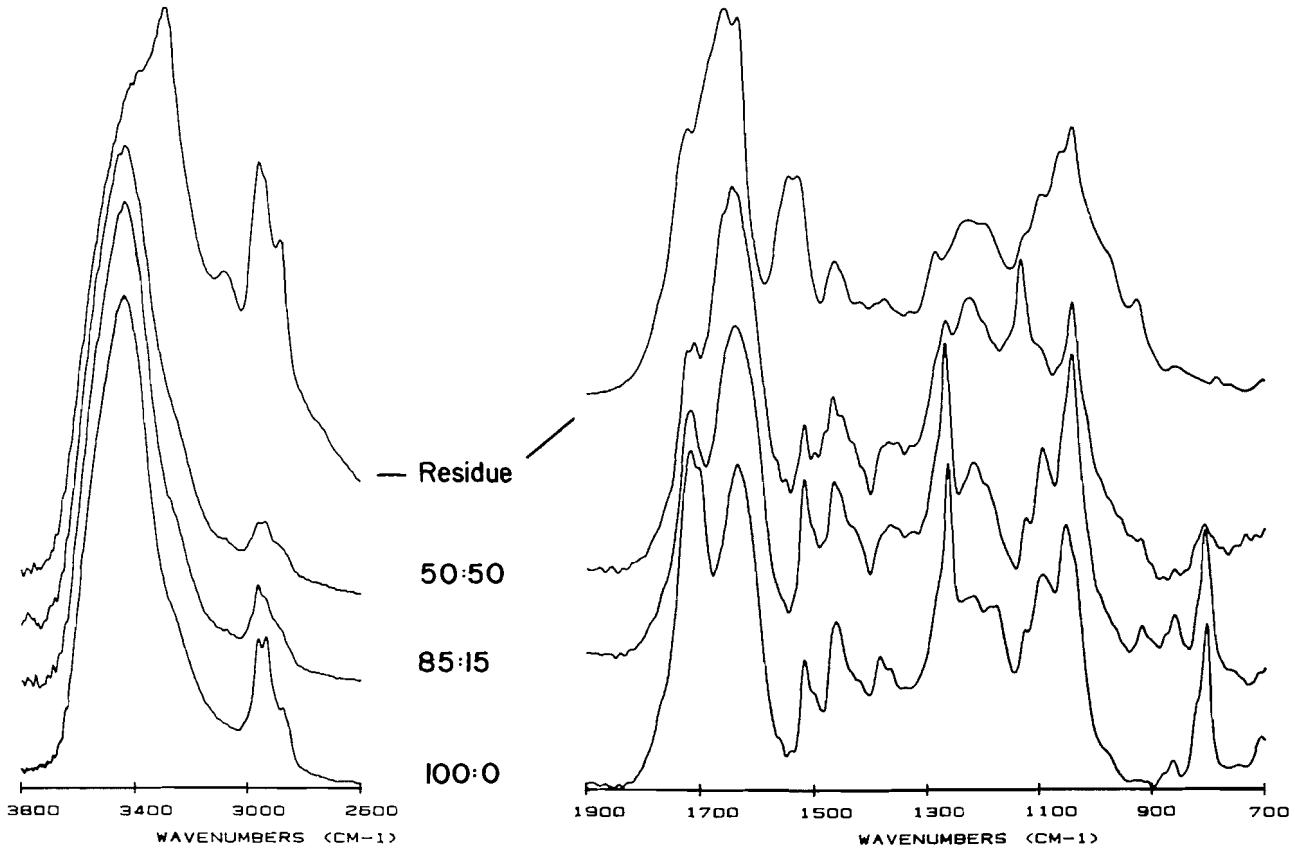


FIG. 3. FTIR spectra of the fractions and of the insoluble residue obtained by sequential solvent solubilization. The fractions are identified by the THF:DMF ratio used.

TABLE 4. Elemental analyses of the fractions obtained by sequential solvent solubilization with THF and DMF of the APPLs derived from *S. badius* and *S. viridosporus*

Sample	THF:DMF	Percentage of starting material	%N	%C	%H	%O*
APPL *S.bad*	100:0	8.0	1.0	67.4	7.1	24.5
	85:15	21.1	2.7	61.7	6.1	29.5
	50:50	19.0	4.8	58.6	6.4	30.2
	0:100	9.8	4.3	57.2	5.7	32.8
	Residue	42.1	8.7	49.6	6.5	35.2
APPL *S.vir*	100:0	2.3	—	—	—	—
	85:15	4.3	2.0	65.8	7.1	25.1
	50:50	36.3	3.3	61.7	6.6	28.4
	0:100	2.8	4.0	57.2	5.1	33.7
	Residue	54.3	9.9	49.6	6.9	33.6

*Percentage of oxygen is calculated by difference.

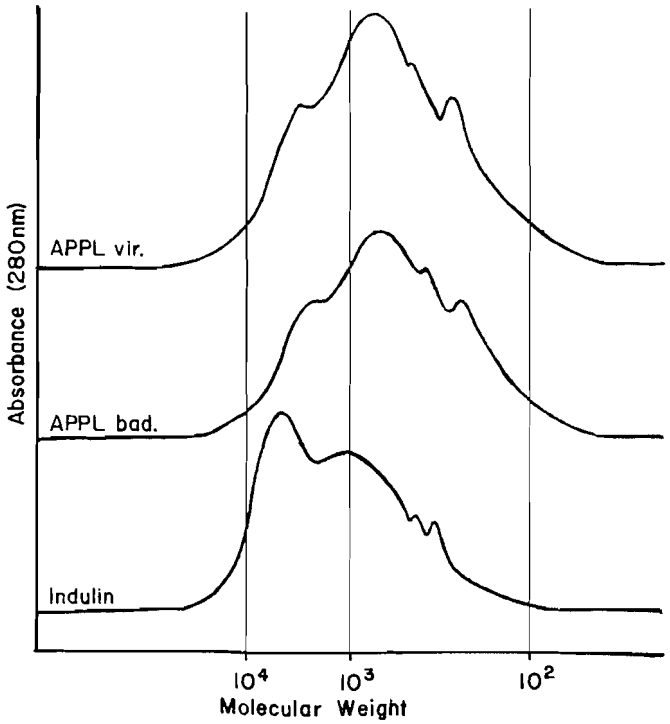


FIG. 4. High performance size exclusion chromatography of Indulin ATR and of the THF soluble fraction of each APPL.

8.7% and 9.9% for the insoluble residues. It thus appears that the THF fraction is the more polyphenolic, with only 1% nitrogen, and the residue is more protein-like, with about 9% nitrogen. These features become more obvious from the FTIR spectra for each fraction of *S. badius* APPL (Fig. 3). As the fractionation proceeds with increasing solvent polarity, the characteristic lignin bands: 1515, 1460, 1265, 1095, 1035, and 810 cm^{-1}, disappear and the characteristic amide bands at 3290 and 3080 cm^{-1} appear.

The THF-soluble fractions of each APPL and Indulin ATR were subjected to high performance size exclusion chromatography using THF as eluent. The data are reported in Fig. 4. THF-soluble fractions of the APPLs derived from *S. viridosporus* and *S. badius* consisted of a broad range of molecular weights, the distribution being similar to that of Indulin ATR, with the difference that the proportion of high MW was lower in the APPL fractions. For both there was a significant increase in the amount of the middle MW range (MW 1000) accompanied by a decrease in the amount of high molecular weight material (MW > 2500).

Moreover, all the fractions obtained after HPSEC fractionation and analyzed by FTIR are chemically equivalent and are similar to the parent Indulin ATR (data not shown).

Discussion

This paper deals with the chemical characterization of acid precipitable intermediates found in the cultures of *S. badius* and *viridosporus* grown with Indulin ATR lignin as a carbon source. We have shown in a previous paper (13) that about 7% of the initial Indulin ATR could be recovered as water soluble acid precipitable intermediates in the medium of 35-day bacterial cultures of these *Streptomyces*. Furthermore, bacterial intra- and extra-cellular proteins incubated with Indulin ATR also brought about a partial solubilization of the substrate. Given the fact that an increase of the bacterial biomass was observed during the incubation of Indulin ATR for both *Streptomyces*, we can conclude that a kraft lignin can be degraded by such species, as has been shown by Crawford *et al.* with lignocellulosics, their work being quoted and accepted as evidence. The most widely accepted hypothesis is one that states that the degradation is due to enzymatic attack. Despite their extensive studies, Crawford *et al.* have not reported the isolation of ligninolytic enzymes.

The most important result presented in this paper, which will lead us to a second, new hypothesis, is that the APPL intermediates are in fact associative complexes of lignin and protein. The first indication that led to such a conclusion is the high percentage of nitrogen detected by elemental analysis in the crude APPLs, the possibility of an association being confirmed first by an amino acid analysis, then by FTIR and sequential solubilization. The presence of characteristic lignin bands in the APPLs infrared spectra indicates that, indeed, the intermediates contain Indulin ATR fragments, while other bands characteristic of amino acids confirm the presence of a protein fraction associated with the lignin part. The fact that yeast extract is not a source of contamination is supported both by the amino acid and the FTIR analyses of the APPLs obtained from a medium with or without extract.

Both the yields and the distribution of the amino acids recovered in the analyses are similar (Table 2). Furthermore, a significant difference is found in the ratio polar/aliphatic A.A. determined for the yeast extract as compared to the same ratio in the case of proteins associated with the soluble intermediates.

The FTIR spectra in each case, with and without, are identical. This indicates that the protein fraction is indeed added by the microorganisms themselves and is not taken from the incubation medium.

The protein-free fraction represents approximately 60% of the APPL weight. Thus, the corrected yield of APPL production after a 35-day incubation is about 3.5–4% and is very close to that obtained when *S. viridosporus* was grown on spruce lignocellulose (9).

Despite the variations among the five analyzed sugars, the summative percentage of carbohydrates remains constant with carbohydrates being less than 1% of the mass. This result shows that APPLs are not significantly complexed with polysaccharides, in agreement with Crawford (11), who found that neither *S. viridosporus* nor *S. badius* cells produce substantial amounts of extracellular polysaccharides.

Can. J. Chem. Downloaded from www.nrcresearchpress.com by 122.72.124.2 on 09/07/12
For personal use only.

The fact that proteins are detected in the intermediates suggests that they may be responsible for a detergent-like action. This new hypothesis states that these proteins associate themselves with smaller, pre-existing lignin fragments found in Indulin ATR (19) in much the same way that detergent surrounds oil. This action causes the lignin fragments to go into solution in the form of a complex.

Observations such as differences in the HPSEC chromatograms and methoxyl content between the starting material and the lignin part of the intermediates can be explained by the hypothesis of detergent-like action as well as by that of enzymatic attack.

The enzymatic degradation of Indulin should *a priori* cause a shift in the molecular weight distribution of the lignin derivatives towards smaller values. To obtain this distribution it is necessary to initially dissociate the soluble complexes so as to obtain as pure a polyphenolic fraction as possible. Table 4 shows that pure THF solubilizes a small amount of material with a low percentage of nitrogen. A series of subsequent extractions using mixtures of THF:DMF that grow progressively richer in DMF leads to fractions with a higher nitrogen content. Finally in 100% DMF the insoluble residue contains 9–10% nitrogen. Thus, in this system, the Indulin fragments are progressively washed out. This is confirmed by the infrared analyses (Fig. 4) in which we see the progressive disappearance of the characteristic lignin bands and the appearance of the amide bands as the polarity of the solvent increases. Although it is clear that proteins and Indulin fragments are not covalently bound, the separation of the two constituents of the complex is difficult and only the fraction soluble in pure THF contains reasonably pure lignin. Size exclusion chromatography of these fractions derived from APPL produced in cultures of *S. badius* and *S. viridosporus* (Fig. 4) reveals polydisperse distributions, the largest difference between these data and Indulin ATR being that the predominant high molecular weight lignol detected in the APPL is DP 16 while in Indulin ATR it is DP 32. This does not necessarily indicate that the APPL lignin fragments are depolymerized Indulin ATR resulting from a specific enzymatic attack since they only represent a fraction of the APPL, which is also a fraction of the starting material. These lower molecular weight fragments could also result from a preferential Indulin solubilization.

The decrease in the methoxyl content could be explained as well by the existence of demethoxylating enzymes or by preferential solubilization of low methoxyl content fragments via a detergent-like mechanism.

Since we cannot prove conclusively which is the correct hypothesis to explain the APPL formation, further experiments must be planned to determine if one or the other hypothesis, or a combination of both, could explain the phenomenon. Meanwhile, we believe that these two theories are not contradictory. Moreover, the fact that the bacterial biomass increases cannot be a result of anything other than the use of Indulin ATR as a carbon source, this certainly due to an enzymatic attack. The production of APPL in itself being a side effect is probably due to surfactant-like reaction, as the presence of proteins would seem to indicate.

Can. J. Chem. Downloaded from www.nrcresearchpress.com by 122.72.124.2 on 09/07/12
For personal use only.

Acknowledgements

The authors are indebted to the Bioenergy division of the Ministry of Energy, Mines and Resources (Canada) and to the Ministry of Education (Québec, FCAR) for financial support. We are grateful to N. Basora for typing this manuscript.

1. W. J. SCHUBERT and F. F. NORD. *In* Advances in enzymology. Vol. 18, *Edited by* F. F. Nord. Interscience, New York. 1957. pp. 349–378.
2. P. ANDER and K. E. ERIKSSON. Progress in industrial microbiology. *Edited by* M. J. Bull. Elsevier, Amsterdam. 1978.
3. T. K. KIRK and M. SHIMADA. Biosynthesis and degradation of wood components. *Edited by* T. Higushi. Academic Press, New York. 1985. pp. 579–605.
4. M. TIEN and T. K. KIRK. Proc. Natl. Acad. Sci. U.S.A. **81**, 2280 (1984).
5. P. J. HARVEY, H. E. SHOEMAKER, A. M. BOWEN, and J. M. PALMER. FEBS Lett. **183**, 13 (1985).
6. H. E. SHOEMAKER, P. J. HARVEY, A. M. BOWEN, and J. M. PALMER. FEBS Lett. **183**, 7 (1985).
7. A. J. MCARTHY and P. BRODA. J. Gen. Microbiol. **130**, 2905 (1984).
8. A. J. MCARTHY, A. PATERSON, and P. BRODA. Appl. Microbiol. Biotechnol. **24**, 347 (1986).
9. S. P. ANTAI and D. L. CRAWFORD. Appl. Environ. Microbiol. **42**, 378 (1981).
10. J. R. BORGMEYER and D. L. CRAWFORD. Appl. Environ. Microbiol. **49**, 273 (1985).
11. D. L. CRAWFORD. **35**, 1041 (1978).
12. D. L. CRAWFORD, A. L. POMETTO III, and A. L. CRAWFORD. Appl. Environ. Microbiol. **45**, 898 (1983).
13. H. GIROUX, P. F. VIDAL, J. BOUCHARD, and F. LAMY. Appl. Environ. Microbiol. In press.
14. W. D. MOORE and D. B. JOHNSON. Procedure for the chemical analysis of wood and wood products. U.S. Products Lab., Dept. of Agriculture, Madison WI. 1967. pp. 9–20.
15. A. E. PIERCE. Sililation of organic compounds. Pierce Chem. Co., Rockford, IL. 1968. pp. 259–331.
16. J. P. HALUK and M. METCHE. Cellul. Chem. Technol. 20, 31 (1986).
17. H. A. KREBS. Biochem. Acta, **4**, 249 (1950).
18. H. L. HERGERT. *In* Lignins. *Edited by* K. V. Sarkanen and C. H. Ludwig. Wiley Interscience, New York. 1971.
19. T. OBIAGA and M. WAYMAN. Can. J. Chem. **52**, 2102 (1974).

Hydration studies on some polyhydroxy non-electrolytes and non-ionic surfactants

S. P. MOULIK AND SYAMASRI GUPTA
Department of Chemistry, Jadavpur University, Calcutta 700032, India
AND
A. R. DAS
Polymer Science Unit, Indian Association for the Cultivation of Science, Jadavpur, Calcutta 700032, India

Received July 12, 1988

S. P. MOULIK and SYAMASRI GUPTA. Can. J. Chem. **67**, 356 (1989).

The hydration numbers of some polyhydroxy non-electrolytes and polyoxyethylenated non-ionic surfactants have been determined and found to depend considerably on the method used, the general order being conductometry < ultrasonic interferometry < ir, spectrophotometry. PEG and Tx-100 are exceptions to this trend. The results from ultrasonic interferometry study strongly depend on the data treatment. The maximum hydration obtained using the ir method shows fair agreement with recent nmr and low angle light scattering results on similar compounds. The results indicate the existence of both strongly and loosely bound water molecules with the micelles as well as the penetration of water in the non-polar micellar region.

Key words: hydration, non-electrolytes, non-ionic surfactants, conductometry, ultrasonic, near infrared.

S. P. MOULIK et SYAMASRI GUPTA. Can. J. Chem. **67**, 356 (1989).

On a déterminé les nombres d'hydratation de quelques composés non-électrolytes polyhydroxylés et de quelques agents de surface non-ioniques polyoxyéthylénés et on a trouvé que ces valeurs dépendent grandement de la méthode utilisée pour les déterminer et que l'ordre général est le suivant : conductimétrie < interférométrie ultrasonique < spectrophotométrie ir. Le PEG et le Tx-100 sont des exceptions à cette tendance. Les résultats obtenus à l'aide de l'interférométrie ultrasonique dépendent beaucoup de la façon dont les données sont traitées. L'hydratation maximale qui est réalisée par la méthode ir présente une bonne corrélation avec celle obtenue récemment par rmn et par diffusion de la lumière sur des composés semblables. Les résultats suggèrent l'existence de molécules d'eau tant fortement que faiblement liées aux micelles ainsi que la pénétration de l'eau dans la région non-polaire de la micelle.

Mots clés : hydratation, non-électrolytes, agents de surface non-ioniques, conductimétrie, ultrasonique, infrarouge proche.

[Traduit par la revue]

Ions and non-polar molecules interact with water so that the molecules of the latter get attached to the former, lose their identity from the bulk water and ultimately yield separate kinetic entities. Polyhydroxy compounds readily hydrate and non-ionic surfactants with polyhydroxy groups are solubilised in water through hydration at their available hydroxy centres. The outer mantle of the micelle is protected through hydration, their microscopic properties such as catalysis, local viscosity, solubilisation etc. are functions of hydration and the vicinal water structure. In our effort to characterise micelles and polyhydroxy compounds in aqueous medium we have been interested in their hydration behaviour (1, 2). Informations on small hydroxy non-electrolytes are available but those on relatively large molecules are rather meager. Different methods (3–6) such as viscosity, diffusion, light scattering, etc. have been mostly used for this purpose. Nuclear magnetic resonance studies (7, 8) have also been found suitable. We have used conductometry, ultrasonic interferometry, and near-ir spectrophotometry as experimental approaches. In some recent and earlier studies (9–15) similar methods have been used. The results of investigations are likely to depend on the methodology (7), particularly so if different methods are based on equilibrium or non-equilibrium principles. If the hydrated entities are under constant shearing stress (as in viscosity) or are under constant influence of compression and rarefaction (as in ultrasound) the method would essentially monitor the strongly attached water molecules. On the other hand an unperturbed equilibrium method (as ir spectrophotometry) should yield the total hydration, which includes both strongly and weakly bound water molecules. A comprehensive single study employing equilibrium as well as non-equilibrium methods is therefore warranted. The present article is an attempt to achieve this.

The polyhydroxy compounds studied include D-fructose, D-glucose, sucrose, two polyethylene glycols, and five non-ionic surfactants containing polyoxyethylene residues. Such surfactants find extensive applications in biomedical, pharmaceutical, and industrial fields.

Experimental

Materials

D-Fructose, D-glucose, sucrose, the two polyethylene glycols of average molecular weights 400 and 600, respectively, and *p-tert*-octyl phenoxy polyoxyethylene ether (Triton-100) were of BDH pure grade and used without further purification. Polyoxyethylene sorbitan monolaurate (PSML), polyoxyethylene sorbitan monopalmilate (PSMP), polyoxyethylene sorbitan menostearate (PSMS), and polyoxyethylene sorbitan mono oleate (PSMO) were products of Sigma Chemical Company, USA. All the compounds contained 20 oxyethylene units and 27 oxygen centres. They were purified by partitioning between water and chloroform. Thin layer chromatography (6, 16) of the purified samples and Tx-100 with water-saturated butanol as the mobile phase indicated the absence of free polyethylene glycols. Microanalysis of the elements carbon, hydrogen, and oxygen agreed on the average to within 1% of the calculated values.

The critical micelle concentrations of the surfactants were measured by surface tension method and compared with the literature values (17, 18) (PSML, 0.05 m*M*, lit. 0.05 m*M*; PSMP 0.02 m*M*, lit. 0.023 m*M*; PSMP 0.019 m*M*, lit. 0.021 m*M*; PSMO 0.012 m*M*, lit. 0.01 m*M*; Tx-100, 0.22 m*M*, lit. 0.20 m*M*).

Techniques

All the solutions were made with double distilled conductivity water

Can. J. Chem. Downloaded from www.nrcresearchpress.com by 122.72.124.2 on 09/07/12
For personal use only.

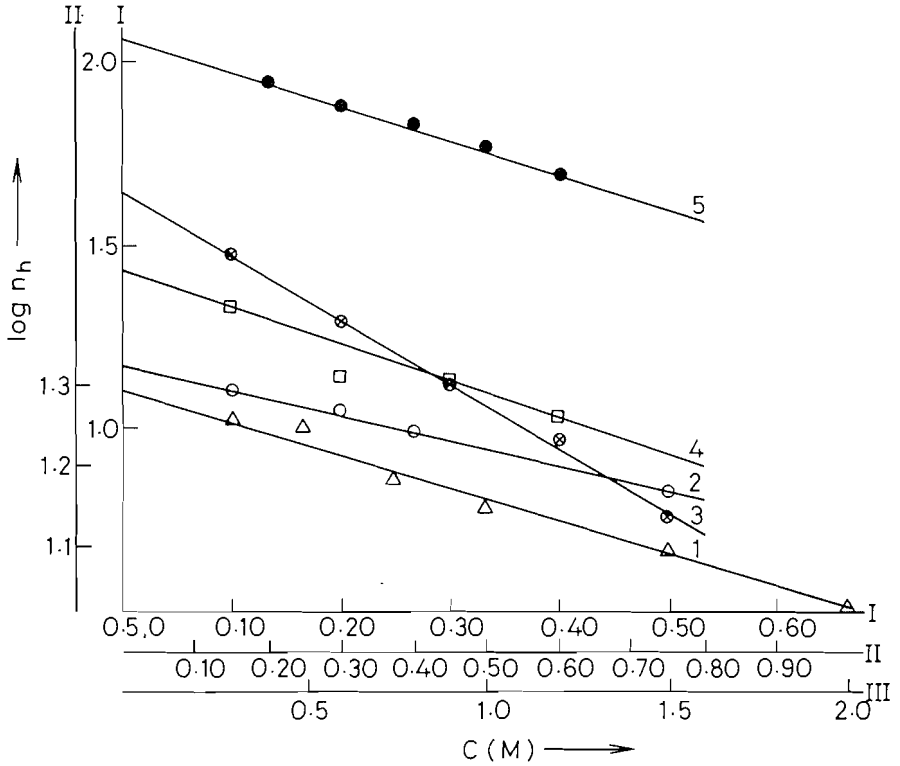


FIG. 1. Concentration-dependent hydration obtained by the near ir method. Lines 1–5 represent Sucrose (II–III), PEG 400 (I–I), Tx-100 (I–I), PEG 600 (I–I), PSML (I–II).

of specific conductance 1.0–2.0 μmho cm^{-1} at 303 K. The experimental temperature was maintained at 303 ± 0.10 K. The near-ir spectrophotometric measurements were recorded at 958 nm in a Carey 17 D apparatus using a 5 mL stoppered quartz cell. The absorbances of pure water and solution were measured against air in a set. Each set was duplicated and the mean absorbance used in the calculation.

The ultrasonic velocities were measured at a frequency of 1 MHz in an ultrasonic interferometer of Mittal Enterprises, New Delhi, India. The instrument generated ultrasound waves by a pulsating quartz crystal. The average of at least 20 readings was considered for each concentration in a set. The sets were duplicated to minimise experimental errors.

The conductance measurements were taken with a PR 9500 Philips India conductivity bridge using a cell of cell constant 1.0 cm^{-1}. The calibration of the bridge was checked against a standard resistance. At least duplicate measurements were made and the average value used in the calculation. For the procedural details please see our earlier publications (1, 9, 10). The densities of the solutions were measured in a calibrated pycnometer (1) of long uniform neck with close graduations.

The standard deviations of absorbance, sound velocity, specific conductance, and density were ±0.5%, ±0.36%, ±1%, and ±0.006%, respectively.

Treatment of data

Infrared spectrophotometry

The spectrophotometric data were processed following the procedure of Bonner and Woolsey (14) and Hollenberg and Ifft (15). The relevant equation is given by

$$[1] \quad A_d = A_r - A_s = k_1\{[H_2O]_r - [H_2O]_s\} + k_2(1-f)[X]_r$$

where A_r and A_s refer to the absorbances of the reference (pure water) and the solution, respectively. $[H_2O]_r$, $[H_2O]_s$, and $[X]_r$ are the concentrations of water monomers in reference medium, water monomers in the solution and the hydrogen bonded or polarized water in reference medium respectively, k_1 and k_2 are the respective molar absorptivities multiplied by path length ($k = \epsilon L$) of water monomer and hydrogen-bonded water, and f is the volume fraction of water in the solution. Bonner and Woolsey (14) have shown how $k_1[H_2O]_r$ and $k_2[X]_r$ can be evaluated from the absorbance of pure water and that of a saturated solution of a non-absorbing solute. Such values when used in eq. [1] can yield the value of $k_1[H_2O]_s$.

The hydration number is envisaged as the fraction of monomeric water molecules removed by a mole of solute in 1000 g solvent. If Y is the fraction of monomeric water removed due to hydration of the solute, then

$$[2] \quad Y = \frac{k_1[H_2O]_r - k_1[H_2O]_s}{k_1[H_2O]_r}$$

and the hydration number

$$[3] \quad n_h = \frac{Y(55.5)}{m} = \frac{55.5}{m}\left(\frac{k_1[H_2O]_r - k_1[H_2O]_s}{k_1[H_2O]_r}\right)$$

where m is the molal concentration of the solute. The reported n_h values are obtained by plotting log n_h vs. m, extrapolated to zero concentration (Fig. 1).

Ultrasonic interferometry

The velocity of sound wave u was determined (19) from the relation

$$[4] \quad u = \lambda F$$

where F is the frequency and λ is the wavelength.

The adiabatic compressibilities of the solvent water and the solution were determined from the relationship,

$$[5] \quad \text{Compressibility} = -\left(\frac{\partial v}{\partial P}\right)_T \frac{1}{V} = \frac{1}{\rho u^2}$$

Can. J. Chem. Downloaded from www.nrcresearchpress.com by 122.72.124.2 on 09/07/12
For personal use only.

TABLE 1. Hydration numbers[g] (mole/mole) of the polyhydroxy non-electrolytes by different methods at 303 K

			Ultrasonic			
			Solute incompressible		Solute compressible	
Compound (1)	Near-ir (2)	Conductance (3)	Eq. [6] (4)	Eq. [8] (5)	Eq. [9] (6)	Eq. [11] (7)
D-Fructose C = 6; O = 6	21.9	2.5		3.8[c]		
D-Glucose[d] C = 6; O = 6	20.0(10.0[a])	3.2	6.8	1.4 (3.5,[c] 4.3[b]) (4.0[d])		
Sucrose[d] C = 12; O = 11	22.4(21.0[a])	7.5	12.3	1.3 (3.8[c]) (5.0[d])		
PEG (400) C = 18; O = 10	14.8	20.0	13.6		24.7	31.0
PEG (600) C = 26; O = 14	26.9	28.0	22.5		34.5	47.5
Tx-100 C = 34; O = 11	43.6	(7.9[e])	4.6		6.7	35.8
PSML C = 58; O = 27	114.8	(30.0[f])	28.8		60.3	87.0
PSMP C = 62; O = 27	138.0	19.0	28.2		65.8	83.0
PSMS C = 64; O = 27	158.5	22.0	25.0		63.3	91.0
PSMO C = 64; O = 27	177.8	14.5[e]	18.6		35.8	84.5

[a]Reference 14.
[b]Reference 12.
[c]Reference 11.
[d]Reference 3.
[e]Reference 1.
[f]Reference 2.
[g]The uncertainty limits of the ir spectrophotometric, ultasonic, and conductance methods are ±1%, ±2%, and ±1%, respectively. It is the maximum probable uncertainty obtained by combining all estimated experimental uncertainties in the same direction.

where V, P, ρ, and u stand for the volume, pressure, density, and sound velocity, respectively. The hydration numbers were computed from the following relation (20)

$$[6] \quad n_h = \frac{n_w}{n_s}\left(1 - \frac{\beta}{\beta_0}\right)$$

where n_w and n_s are the number of moles of water and solute, respectively, present in solution; β and β_0 represent the compressibilities of solution and water, respectively. The n_h values were calculated for different concentrations using eq. [6]. The values reported in Table 1 are the extrapolated values of n_h vs. c plots shown in Fig. 4 (unprimed numbers). Equation [6] is applicable to only small molecules and ions assuming them to be incompressible. Except for the carbohydrates, most of the solutes used in our study were compressible. Thus a more judicious choice would be the equation of Shiio (11) valid for both compressible and non-compressible solutes.

$$[7] \quad (\beta/\beta_0 - V_0)/C = (\beta_1/\beta_0)\frac{1}{\rho_1} - \left(v_0 - \frac{v_2\beta_2}{\beta_0}\right)\Big/ C$$

where β, β_0, β_1, and β_2 represent adiabatic compressibilities of the solution, solvent, solute, and bound water respectively, v_0, v_2 and V_0 are the apparent specific volume fraction of bound water, specific volume fraction of bound water and apparent specific volume fraction of the total solvent, respectively. ρ_1 is the density of the solute and C is the concentration of the solute in g/mL of solution. Gekko and Noguchi (21) have recently used this equation for polymeric carbohydrates. For a non-compressible solute $\beta_1 = 0$, hence eq. [7] becomes

$$[8] \quad (\beta/\beta_0 - V_0)/C = -(v_0 - v_2\beta_2/\beta_0)/C$$

Equation [7] can be rearranged as

$$[9] \quad (\beta/\beta_0 - V_0)/C - \left(\frac{\beta_1}{\beta_0}\right)\frac{1}{\rho_1} = -(v_0 - v_2\beta_2/\beta_0)/C$$

and used for compressible solutes. The left hand side of eqs. [7] and [8] has been plotted against concentration for compressible and non-compressible solutes, respectively, and the extrapolated values used to calculate hydration. A representative presentation on the basis of eq. [8] is shown in Fig. 2. In the

Can. J. Chem. Downloaded from www.nrcresearchpress.com by 122.72.124.2 on 09/07/12
For personal use only.

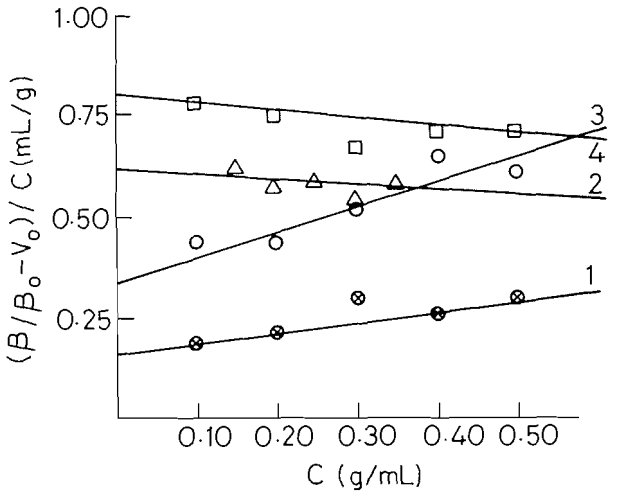


FIG. 2. $(\beta/\beta_0 - V_0)/C$ versus C plots from ultrasonic measurements; lines 1–4 represent PEG (600), PSMS, PSMP, Tx-100.

calculation v_2 has been assumed identical with the compressibility of ice (12, 21) i.e. 18×10^{-12} cm^2/dyn. β used in eq. [6] can be corrected for the solute compressibility by an alternative treatment of the ultrasonic data. The term β of eq. [6] must include the compressibility of the hydrated solute over and above that of free water. The ratio β/β_0 is therefore greater than that obtained and derived hydration is thus lower than the actual value.

The observed compressibility β may be written as

$$[10] \quad \beta = \beta_0 v_0^f + \beta_1 v_1^f$$

where β_0 and β_1 are the compressibilities of pure water and solute respectively; v_0^f and v_1^f are their respective volume fractions. The required quantity for the calculation of hydration using eq. [6] is the compressibility of the unbound water, $\beta_0 v_0^f = (\beta - \beta_1 v_1^f)$ and not β. By eqs. [6] and [10] we have

$$[11] \quad n_h = \frac{n_w}{n_s}\{1 - (\beta - \beta_1 v_1^f)/\beta_0\}$$

The hydration numbers calculated by eq. [11] have been plotted against concentration (primed numbered lines of Fig. 4) and the extrapolated values are presented in column 7 of Table 1.

Conductometry

The hydration values were obtained using the equation

$$[12] \quad K'/K = 1 - 1.98\, v_h(K'C/K)$$

where K' and K are the specific conductances of a non-interacting strong electrolyte in the presence and absence of a solute having hydrated specific volume, v_h, respectively: C is the concentration in g/mL. The v_h values have been obtained from the slopes of the linear plot of K'/K against $K'C/K$ (Fig. 3). Subtraction of the anhydrous specific volume from v_h has yielded the hydration values presented in Table 1. Equation [12] is valid in low concentration range (9), therefore the reported hydration is considered independent of concentration.

Partial molal quantities

The apparent molal volume $\bar{V}_1$ of the solute has been calculated from the following relation

$$[13] \quad \bar{V}_1 = \frac{M}{d} + \left(\frac{d_0 - d}{Mdd_0}\right) \times 10^3$$

where d_0 is the density of water, d is that of the solution, and M is the molecular weight of the solute. The partial molal volume of the solute $\bar{V}_1^0$ has been obtained from the extrapolated value of the linear plot of $\bar{V}_1$ vs. m.

The partial specific compressibility of the solute $\bar{\beta}_1^0$ has been calculated from the relation

$$[14] \quad \bar{\beta}_1^0 = (\beta_0/\bar{v}_1^0) \lim_{C \to 0} \left(\frac{\beta}{\beta_0} - V_0\right)\Big/ C$$

where the new term $\bar{v}_1^0$ is the partial specific volume of the solute, given by the relation

$$[15] \quad \bar{v}_1^0 = \lim_{C \to 0} (1 - V_0)/C$$

The partial molal compressibility $\bar{V}_1^0\bar{\beta}_1^0$ has been then calcu-

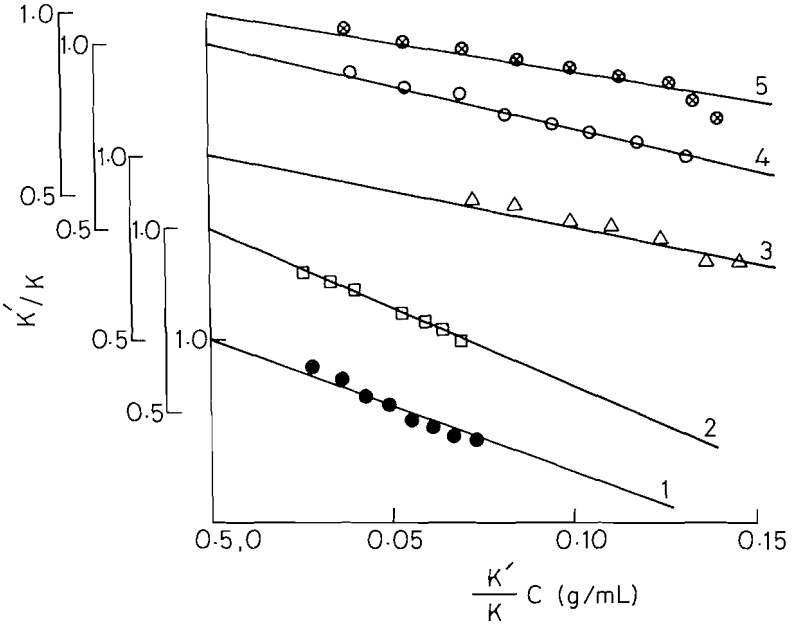


FIG. 3. K'/K versus $K'C/K$ plots from conductance measurements; lines 1–5 represent glucose (I), PEG (400) (II), Tx-100 (III), PEG (600) (IV), PSML (V).

Can. J. Chem. Downloaded from www.nrcresearchpress.com by 122.72.124.2 on 09/07/12
For personal use only.

TABLE 2. Comparison of results from different authors

Authors	Method	Compound	mol H_2O/mol O_2
Lindman and Nilsson (7)	NMR	penta- and octaoxyethylene dodecylether	4.0–6.0
		PEG (mw 20 000)	
Saito and Sato (6)	L.S.	Polyoxyethylene monostearate of ethylene oxide residues	
		20	3.70
		25	3.41
		30	4.78
		40	6.48
		45	4.82
		55	7.32
This work	IR	Tx-100	4.0
		PSML	4.42
		PSMP	5.30
		PSMS	6.07
		PSMO	8.84
		PEG (MW 400)	1.53
		PEG (MW 600)	1.93

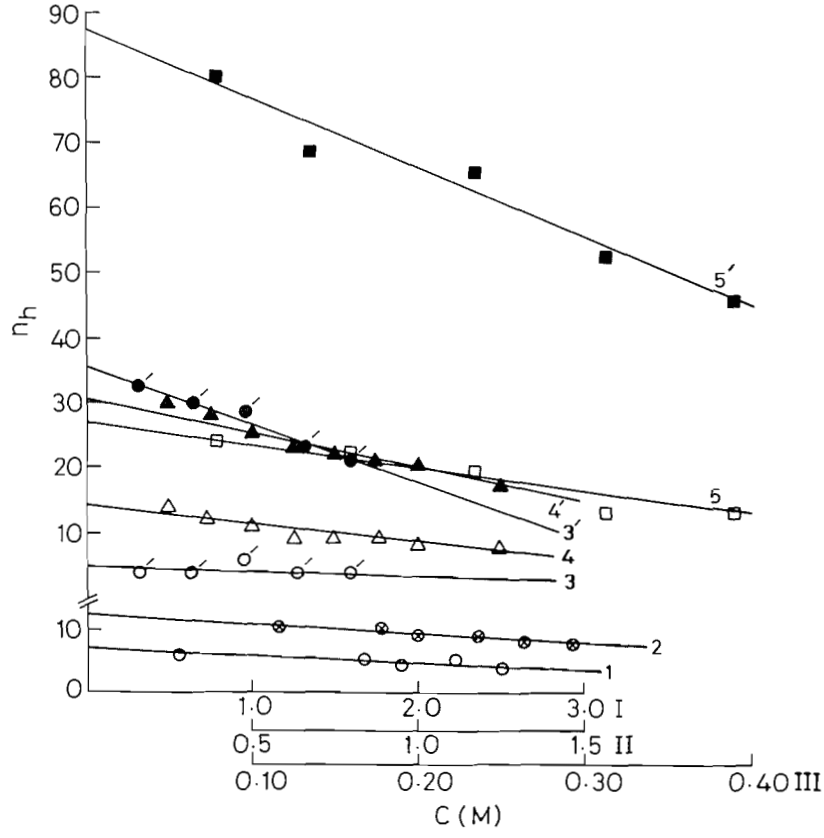


FIG. 4. n_h versus C plots for a comparative look between incompressible and compressible solutes. Line 1, glucose (I); line 2, sucrose (II); lines 3, 3′, Tx-100 (III); lines 4, 4′, PEG (400) (III); lines 5, 5′ PSMP (III). Unprimed and primed numbers represent data treatment according to eq. [6] and eq. [11], respectively.

lated. It signifies the pressure-dependent differential coefficient of the partial molal volume.

Results and discussion

Comparison of the methods

This work is a comprehensive approach of determining hydration using equilibrium as well as non-equilibrium methods. Representative graphs for the three methods are presented in Figs. 1, 3, and 4 which signify that individual methods are applicable to the solid compounds D-fructose, D-glucose, and sucrose as well as to the liquid compounds, the polyethylene glycols, Tx-100, and the polyoxyethylene sorbitan class (the tweens). Columns 2–4 of Table 1 show that except for the polyethylene glycols, the infrared spectrophotometry has given

Can. J. Chem. Downloaded from www.nrcresearchpress.com by 122.72.124.2 on 09/07/12
For personal use only.

Can. J. Chem. Downloaded from www.nrcresearchpress.com by 122.72.124.2 on 09/07/12
For personal use only.

significantly higher hydration numbers than either conductometry or ultrasonic interferometry. There is no general agreement between the last two methods, particularly for compressible solutes. The degree of disagreement depends on the ways of accounting for the compressibility of the solutes. The hydration numbers are found to depend on the methodology.

The analysis of the results obtained by the non-equilibrium method of conductometry is based on the concept of obstruction (22–24) to the ionic transport offered by the hydrated solutes or surfactant micelles. When obstructed, the ions take a detour, resulting in an increase in the overall resistance of the solution. They may, however, penetrate (22) the loosely solvated portion of the solute. This may lead to lower hydration that corresponds to the primary hydration envisaged by Frank and Evans (25). In the equilibrium ultrasonic method, the solvent molecules in the bulk as well as in the loosely attached portion of the hydration envelope undergo repeated compression and rarefaction, the strongly held portion being least affected. This method would thus monitor only a part of the total hydration. On the other hand, the near-ir equilibrium spectrophotometric method remains unperturbed by any of the above effects, and should thus monitor both the rigidly and loosely held water molecules by the solute. The results obtained support this view.

There is an apparent agreement between the conductance and ultrasonic results of hydration when eq. [6] is used. Except for the carbohydrates, all the other compounds studied are large and compressible. Shiio's equation [9] is applicable to these. The hydration derived from eq. [9] is greater than that from eq. [6].

The hydration numbers calculated by eq. [11] (column 7 of Table 1) show improvement over the values obtained by using eq. [6] as well as eq. [9] (cf. Fig. 4). They are considered reasonable but do not satisfactorily agree with the results from the ir method. It is to be noted that the hydration results evaluated by the ultrasonic interferometry strongly depend on the data treatment. We may mention here that the simple proportional contributions of the solvent and the solute to the overall compressibility, considered in eq. [11] is a limitation of the approach. The assumption of comparable compressibilities of ice and hydrated water in the calculation (12, 21) is also not above criticism. In principle the compressibility of water bound to a solute is expected to be different from the compressibility of water in ice (18×10^{-12} cm^2/dyn). For lack of such data the overall compressibility of ice has been used in the calculation.

The hydration numbers of the solutes have been found to significantly depend on the method, the general order being conductometry < ultrasonic interferometry < ir spectrophotometry. Tx-100 and PEG are exceptions; they do not fit into this trend. We are unable to explain this discrepancy.

Solute-dependent hydration

The hydration behaviours of carbohydrates studied by different methods show rather wide variations. Ultrasonic results by Shiio *et al.* (12) resemble the conductance results. The hydration values of D-glucose and sucrose estimated by conductometry are comparable to those reported using the non-equilibrium viscosity method (3). From thermodynamic considerations, Stokes and Robinson (26) have shown the hydration of sucrose to be 11, and other carbohydrates are expected to bind water molecules equivalent to the number of oxygen atoms present in the molecule. The hydration results of sucrose and glucose from the ultrasonic method (eq. [6]) lend support to this view. However, these values are higher than those reported by Shiio *et al.* (11,12) (column 5, Table 1). The spectrophotometric results on sucrose, nevertheless, show fair agreement with that reported by Bonner and Woolsey (14). The subsequent discussion on surfactants is based on the results by ir spectrophotometry. It will be seen that these are consistent with the recent light scattering and nmr results on similar compounds.

In recent years, there has been much controversy over micellar hydration, particularly in the matter of water penetration into the micelles. Hartley's original model (27) of a water-free "oil droplet surrounded by an ionic coat" has been seriously questioned. Menger (28) has proposed the porous cluster model which portrays the micelle as a loose cluster of surfactant molecules with water-filled cavities. A few experimental evidence supports water penetration (29–33). Cabane (34) has presented a critical study of different micellar models. In this context reliable hydration studies are considered primary prerequisites. The present investigation is an attempt in this direction.

The experimental concentration of the surfactants studied are well above their cmc's and the hydration behaviour, therefore, ought to be considered as the weighted contributions of the monomers and the micelles. If phase separation model of the micelles is considered, the monomer concentration may be taken as constant at all concentrations above the cmc. Well above cmc, the monomer concentration is not only constant but also much smaller than the concentration of the surfactants in the micellar state. To minimize the effect of intermicellar interaction on hydration, graphical extrapolation up to cmc is required. Since measurements were taken at concentrations fairly much higher than cmc, the extrapolated to zero concentration hydration values essentially correspond to the hydration of the surfactants in their micellar state.

Nilsson and Lindman (7) have studied self-diffusion coefficient of D_2O in penta- and octaoxyethylene dodecyl ether solutions by nmr and have obtained 4.0 to 6.0 water molecules bound per oxygen of the surfactant molecules. Similar value per oxygen for a polyethylene glycol of molecular weight 20 000 has been also obtained. The increased hydration over and above the two water molecules per oxygen atom has been attributed to the ordering of water molecules around the polyoxyethylene chain. Minor temperature dependence of hydration has been observed. Saito and Sato (6) have reported light scattering studies on the water binding capacities per gram of several non-ionic surfactants such as polyoxyethylene monostearates and also polyoxyethylene octylether having 20, 30, 40 units of ethylene oxide residues, respectively (Table 2). The present hydration values from the ir method for polyoxyethylene containing surfactants (Table 2) are in reasonable agreement with the above mentioned nmr and light scattering results (6, 7). The moles of water bound per mole of oxygen are 4.0 for Tx-100, 4.42 for PSML, 5.30 for PSMP, 6.07 for PSMS, 8.84 for PSMO, 1.53 for PEG 400, and 1.93 for PEG (600). Polyoxyethylene residues present in the surfactant micelles bind more water than when they are free. The last four surfactants (Table 2) have identical hydrophilic head groups but differ in their non-polar tails. With increasing molecular length the micellar aggregation number decreases and the overall micellar size increases (6, 35–38). Large micelles trap more water. PSMS and PSMO have the same number of carbon and oxygen atoms but the latter contains unsaturation in the hydrocarbon chain. But the increased hydration of PSMO compared to PSMS is difficult to rationalize. The conductance results claim about 15% of the (maximum) hydration obtained from the ir method. This may be the strongly attached fraction of the total hydration. About 50% reduced hydration obtained by the ultrasonic method (eq. [11]) suggests that nearly one half of the total

TABLE 3. Molal volume (MV), partial molal volume $\bar{V}_1^0$, excess volume (Δv), adiabatic compressibility (β), partial specific compressibility ($\bar{\beta}_1^0$), and partial molal compressibility ($\bar{V}_1^0\bar{\beta}_1^0$) of the polyhydroxy non-electrolytes at 303 K

Compounds	MV (mL)	$\bar{V}_1^0$ (mL)	$-\Delta v$ (mL)	$\beta_1 \times 10^{12}$ ($cm^2\,dyn^{-1}$)	$\bar{\beta}_1^0 \times 10^{12}$ ($cm^2\,dyn^{-1}$)	$\bar{V}_1^0\bar{\beta}_1^0 \times 10^8$ ($mL\,cm^2\,dyn^{-1}$)
D-Glucose	115.2	109.4 (112.04[a])	5.8	0	−5.77	−0.063 (−0.1750[a])
Sucrose	216.4	208.2 (211.32[a])	8.2	0	−2.66	−0.033 (−0.1246[a])
PEG (400)	363.3	339.8	23.5	37.3	6.96	0.237
PEG (600)	537.6	498.0	39.6	36.6	8.43	0.420
Tx-100	580.6	568.8	11.8	42.4	37.88	2.155
PSML	1151.2	1046.5	105.2	40.6	18.55	1.941
PSMP	1183.8	987.1	196.6	40.2	18.44	1.820
PSMS	1262.8	1008.7	254.1	42.5	25.14	2.536
PSMO	1265.2	1125.0	139.0	39.7	31.43	3.536

[a]Reference 40.

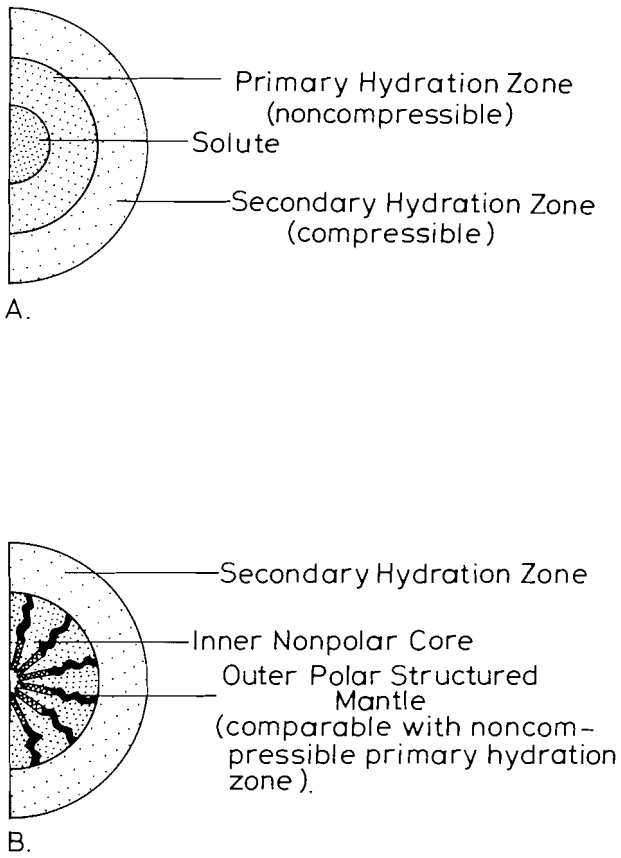


FIG. 5. Model two dimensional half profile representations of hydrated solute and micelle. *A*: a hydrated non-micelle forming solute molecule; *B*: a hydrated nonionic micelle.

hydration is softly bound, which can be melted by applying pressure. According to the recent statistical theory of Flory and Dill (39), based on lattice model, "Spectroscopic methods measure the proximity of the probe to water, interfacial and internal; whereas measurement of thermodynamic and transport properties measure only the amount of water bound internally in the core" of the micelles. In the ir method the absorbance of the water monomer in the solutions are monitored and we believe that the hydration results manifest the total water, penetration, interfacial, and internal in the micelles. The hydration values by the ir method are thus higher than those by other methods. Probable models of hydrated solutes and micelles are presented in Fig. 5. A general correlation of hydration with the total number of carbons is depicted in Fig. 6. Similar correlation with the number of oxygen atoms embracing all the solutes has not been observed. The contribution of the overall length of the molecule towards hydration is anticipated. The enthalpies of hydration of Tx-100, PSML, and PSMS have been evaluated conductometrically and found to be in the range of 20–28 kJ mol^{-1}. Shiio (11) has reported values of nearly 50 kJ mol^{-1} for carbohydrates. This appreciable enthalpy of hydration is in contrast to the results of Nilsson (7) and Lindman (6) who have observed a minor temperature dependence of hydration.

Molal and partial molal quantities

The molal volumes, partial molal volumes, excess volumes, and the partial specific and partial molal compressibilities of the solutes are presented in Table 3. The partial molal volumes are all less than molal volumes, thus the excess volumes are all negative. PSML, PSMP, PSMS, and PSMO have shown large change in volume, the last member being odd in the series. It has also shown irregularities in hydration (Table 1). We have found partial molal compressibilities of glucose and fructose to be negative, an observation similar to that of Milero *et al.* (40) who have attributed the negative compressibility for the large extent of hydration of the molecules. Their results are shown in Table 3 for comparison. The partial molal compressibilities of the other compounds are positive. The trend in the excess volume gives the order of interaction with water. The compounds of the carbohydrate family have shown negative partial molal compressibilities in good solvents (11, 18) while other polymeric compounds have shown positive partial molal compressibilities (21, 41, 42). The positive values originate from the deorganisation and the release of loosely bound water molecules from the hydrated micelles by the application of pressure. The configurational changes of the polymeric compounds may also add to this effect.

Can. J. Chem. Downloaded from www.nrcresearchpress.com by 122.72.124.2 on 09/07/12
For personal use only.

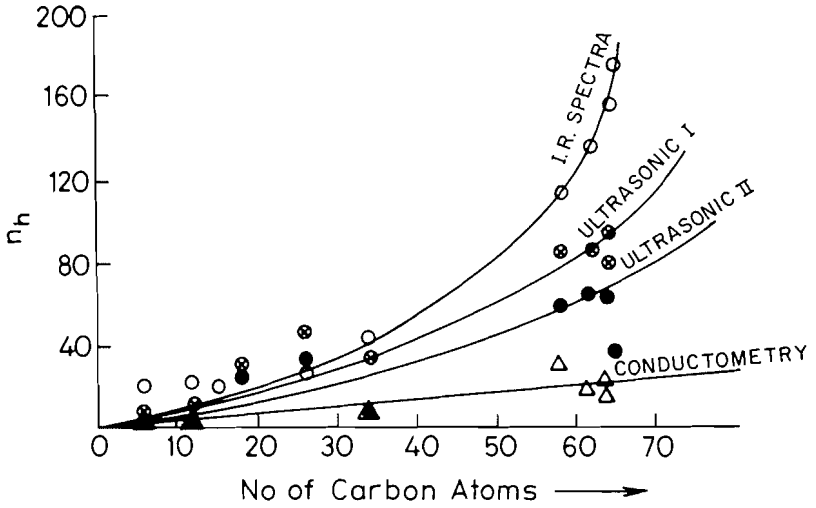


FIG. 6. Dependence of hydration numbers on the number of carbon atoms of the solutes. I and II represent results of columns 7 and 6 in Table 1.

Acknowledgement

Syamasri Gupta thanks the Council of Scientific and Industrial Research for a Research Associateship to carry out this work.

1. S. P. MOULIK, A. B. MANDAL, A. M. BISWAS, and S.RAY. J. Phys. Chem. **34**, 856 (1980).
2. S. P. MOULIK, A. B. MANDAL, and S. GUPTA. Ind. J. Chem. A**24**, 670 (1985).
3. R. H. STOKES and R. MILLS. *In* International encyclopaedia of physical chemistry and chemical physics. *Edited by* E. A. Guggenheim, J. E. Meyer, and F. C. Tompkins. 1965. Chap. 5.
4. R. J. ROBSON and F. A. DENNIS. J. Phys. Chem. **81**, 1075 (1977).
5. L. M. KUSHNER and W. D. HUBBARD. J. Phys. Chem. **58**, 1163 (1954).
6. Y. SAITO and T. SATO. J.Phys. Chem. **89**, 2110 (1985).
7. P. G. NILSSON and B. LINDMAN. J. Phys. Chem. **87**, 4756 (1983).
8. P. G. NILSSON, B. LINDMAN, and R. G. LAUGHLIN. J. Phys. Chem. **88**, 6357 (1984).
9. S. P. MOULIK. Electrochim. Acta, **18**, 981 (1973).
10. S. P. MOULIK and D. P. KHAN. Carbohydrate Res. **36**, 147 (1974).
11. H. SHIIO. J. Am. Chem. Soc. **80**, 70 (1958).
12. H. SHIIO, T. OGAWA, and H. YOSHIHASHI. J. Am. Chem. Soc. **77**, 4980 (1955).
13. J. AUTOSLEWIEZ, A. JUZKIEWIEZ, and D. SHUGAR. J. Phys. Chem. **86**, 4831 (1982).
14. O. D. BONNER and G. B. WOOLSEY. J. Phys. Chem. **72**, 899 (1968).
15. J. H. HOLLENBERG and J. B. IFFT. J. Phys. Chem. **86**, 1938 (1982).
16. K. SHINODA, T. NAKAGAWA, B. I. TAMAMUSHI, and T. ISEMURA. *In* Colloidal surfactants. Some physicochemical aspects. Academic Press, New York. 1963, Chap. 2.
17. W. L. HINZE. Separation science. Am. Chem. Soc. Symp. Ser. No. 342, 1987. Chap. 1 pp. 1–82.
18. M. J. SCHICK (*Editor*). Non-ionic surfactants. Marcel Dekker, Inc., New York. 1967. Surfactant Science Series Vol. 1, Chap. 15, p. 481.
19. P. K. DASGUPTA and S. P. MOULIK. J. Phys. Chem. **91**, 5826 (1987).
20. J. O. M. BOCKRIS and A. K. N-REDDY. Modern electrochemistry. Vol. I. Plenum Press, New York. 1977. p. 127.
21. K. GEKKO and H. NOGUCHI. Biopolymer, **10**, 1513 (1971).
22. H. FRICKE. Phys. Rev. **24**, 575 (1923); **25**, 692 (1924).
23. B. N. GHOSH, S. BANDOPADHYA, and S. P. MOULIK. Proc. Natl. Inst. Sci. India **27**A, 193 (1961).
24. R. H. STOKES and R. MILLS. *In* International encyclopaedia of physical chemistry and chemical physics. *Edited by* E. A. Guggenheim, J. E. Meyer, and F. C. Tompkins. 1965. Topic 16, Chap. 6.
25. H. S. FRANK and M. W. EVANS. J. Chem. Phys. **13**, 507 (1945).
26. R. H. STOKES and B. A. ROBINSON. J. Phys. Chem. **70**, 2126 (1966).
27. G. S. HARTLEY. Trans. Faraday Soc. **30**, 444 (1934).
28. F. M. MENGER. Acc. Chem. Res. **12**, 111 (1979).
29. F. M. MENGER, J. M. JERKUNICA, and J. C. JOHNSTON. J. Am. Chem. Soc. **100**, 4676 (1978).
30. N. MÜLLER and H. SIMSOHN. J. Phys. Chem. **75**, 942 (1971).
31. J. ULMINUS and B. LINDMAN. J. Phys. Chem. **85**, 4131 (1981).
32. B. CABANE. J. Phys. Chem. (Orsay, France) **6**, 848 (1981).
33. F. M. MENGER, H. YOSHINAGA, K. S. VENKATSUBBAN, and A. R. DAS. J. Org. Chem. **46**, 415 (1981).
34. B. CABANE. J. Phys. Chem. (Orsay, France) **42**, 847 (1981).
35. P. BECHER and H. ARAI. J. Coll. Interface Sci. **27**, 634 (1968).
36. R. H. ELWORTHY and G. B. MACFARLANE. J. Chem. Soc. 537 (1962).
37. A. ARNANSON and R. H. ELWORTHY. J. Pharm. Pharmacol. **34**, 87 (1982).
38. P. BEEHER. J. Coll. Interface Sci. **16**, 49 (1961).
39. P. J. FLORY and K. A. DILL. Proc. Natl. Acad. Sci. USA, 78, 676 (1971).
40. A LO SARDO, C. SHIN, and F. J. MILERO. J. Chem. Eng. Data, **23**, 197 (1978).
41. H. MOMURA and Y. MIYAHARA. J. Appl. Polym. Sci. **8**, 1643 (1964).
42. K. GEKKO and H. NOGUCHI. Macromolecules, **7**, 224 (1974).

Can. J. Chem. Downloaded from www.nrcresearchpress.com by 122.72.124.2 on 09/07/12
For personal use only.

Ryoichi Nakagaki, Kiyoshi Mutai, Mitsuo Hiramatsu, Hideyuki Tukada, and Saburo Nagakura. Magnetic field effects upon photochemistry of bichromophoric chain molecules containing nitroaromatic and arylamino moieties: Elucidation of reaction mechanism and control of reaction yields. Can. J. Chem. **66**, 1989 (1988).

Page 1989. In lines 13, 17, and 26, Nakakura should be Nagakura.

Can. J. Chem. Downloaded from www.nrcresearchpress.com by 122.72.124.2 on 09/07/12
For personal use only.

Isotherme d'adsorption du phénanthrène et de ses dérivés hydrogénés sur du nickel de Raney

FRANÇOIS BOSSÁNYI, CHAKIB AMEZIANE HASSANI, HUGUES MÉNARD[1] ET JEAN LESSARD
Département de chimie, Faculté des sciences, Université de Sherbrooke, Sherbrooke (Qué.), Canada J1K 2R1

Reçu le 19 avril 1988

FRANÇOIS BOSSÁNYI, CHAKIB AMEZIANE HASSANI, HUGUES MÉNARD et JEAN LESSARD. Can. J. Chem. **67**, 365 (1989).

Des études chromatographiques ont permis de déterminer les isothermes d'adsorption du phénanthrène et de ses dérivés hydrogénés, du naphtalène et de la tétraline sur le nickel de Raney. L'adsorption de ces molécules sur le nickel de Raney dépend du nombre d'électrons π, de la position et de l'orientation des hydrogènes pouvant empêcher ou diminuer l'interaction des électrons π avec le catalyseur.

Mots clés : adsorption, phénanthrène, études chromatographiques.

FRANÇOIS BOSSÁNYI, CHAKIB AMEZIANE HASSANI, HUGUES MÉNARD, and JEAN LESSARD. Can. J. Chem. **67**, 365 (1989).

The adsorption isotherms of phenanthrene and its hydrogenated derivatives, of naphthalene, and of tetralin on Raney nickel have been determined by chromatographic studies. The adsorption of these molecules on Raney nickel depends on the number of π electrons and on the position and orientation of hydrogen atoms that can interfere with the interaction of the π electrons with the catalyst.

Key words: adsorption, phenanthrene, chromatographic studies.

Can. J. Chem. Downloaded from www.nrcresearchpress.com by 41.223.56.140 on 09/07/12
For personal use only.

Introduction

Lors de l'hydrogénation ou de l'électrohydrogénation catalytique d'un composé organique insaturé sur un catalyseur, Horiuti et Polanyi (1) et Lessard et ses collaborateurs (2, 3) décrivent les mécanismes de réaction à la surface comme suit :

[1] $2H_2O + M + 2e \rightleftarrows 2M \ldots H + 2OH^-$

[2] $M + H_2 \rightleftarrows 2M \ldots H$

[3] $M + Y = Z \rightleftarrows M \ldots (Y = Z)$

[4] $2M \ldots H + M \ldots (Y = Z) \rightleftarrows M \ldots (YH - ZH)$

[5] $M \ldots (YH - ZH) \rightleftarrows YH - ZH + M$

Dans un premier temps, il y a formation d'hydrogène adsorbé à la surface du catalyseur obtenu par réduction de l'eau (éq. [1]) dans le cas d'une électrohydrogénation, ou par adsorption dissociative de l'hydrogène moléculaire, souvent sous pression (éq. [2]), dans le cas d'une hydrogénation catalytique. Par la suite, on a adsorption du substrat sur le catalyseur (éq. [3]) et réaction de ce dernier avec l'hydrogène adsorbé (éq. [4]). Finalement, il y a désorption du substrat (éq. [5]). Mitsui *et al.* (4–6) ont suggéré que l'étape déterminante d'une hydrogénation sur le nickel de Raney est l'adsorption du substrat sur le catalyseur.

Dans la présente étude, nous allons tracer les isothermes d'adsorption du phénanthrène et de ses dérivés hydrogénés, du naphtalène et de la tétraline sur le nickel de Raney dans le but d'identifier les facteurs qui influencent l'adsorption de ces composés. Les isothermes ont été obtenus par chromatographie en phase liquide et l'approche mathématique, pour le calcul de ces isothermes, était la même que celle utilisée par Ménard *et al.* (7) à partir de la méthode de Chuduk *et al.* (8).

Section expérimentale

Appareillage

L'équipement utilisé pour cette étude consiste en une pompe HPLC Beckman modèle 100-A, couplé avec un détecteur UV Altex Hitachi, modèle 100-40, muni d'une cellule de détection de 20 µL, relié à un enregistreur (Varian modèle FE-2). L'acquisition et le traitement des données ont été faits à l'aide d'un micro-ordinateur de type RX-8800, tel qu'utilisé par Noël (9).

Le remplissage des colonnes a été effectué avec une pompe Haskel. Les colonnes ont une longueur de 3,5 cm avec un diamètre interne de 4,6 mm.

Réactifs

Le naphthalène purifié a été obtenu de la compagnie Fisher Scientifique, le phénanthrène (≥95%) de la compagnie BDH, et le dihydrophénanthrène (≥97%) de la compagnie (Aldrich Chemical. L'octahydrophénanthrène symétrique (≥95,4%) et asymétrique (≥97,5%) ont été obtenus à partir de l'électrohydrogénation catalytique du phénanthrène sur le nickel de Raney et séparés sur colonne chromatographique. Le tétrahydrophénanthrène (≥99%) a été obtenu à partir du naphtalène selon la synthèse décrite par Haworth (10). Le nickel de Raney a été obtenu de la compagnie Aldrich Chemical.

Le dichlorométhane et l'hexane de qualité Accusolve ont été obtenus de la compagnie Anachemia. Les solvants ont été séchés sur tamis moléculaire (Type 3 Å, Grade 564) de la compagnie Fisher Scientifique.

Procédure

Tous les solvants utilisés pour le HPLC ont été désoxygénés sous vide pendant une période de 15 min et une légère surpression d'azote sec circulait au-dessus du solvant pendant la durée de l'expérience.

Le nickel de Raney, de granulométrie 53–105 µm (−140 à +270 mesh), a été lixivié par une solution de NaOH 30% pendant 7 h à 70°C. Le nickel de Raney d'activité W_4 (11) résultant a été lavé à l'eau jusqu'à la neutralité, puis 2 fois au méthanol. Finalement, on a séché sous vide pour éliminer l'hydrogène présent sur le catalyseur.

La colonne et la buse ont été remplies et compactées à sec avec le nickel de Raney W_4 et par la suite, du propanol a été pompé sous pression (31 MPa) à travers la colonne et la buse par une pompe Haskel. La colonne a été placée dans un cyclindre thermostaté à 25°C ± 0,1°C et reliée au HPLC. Le débit de l'éluant était de 0,2 mL/min.

Le HPLC a été utilisé avec une boucle d'échantillonnage de 50 µL, et les concentrations injectées étaient comprises entre 100 et 500 nmol pour tous les solutés dilués dans le toluène et entre 20 et 100 nmol pour les solutés dilués dans le dichlorométhane.

Résultats et discussion

La figure 1 représente les isothermes obtenus pour le phénanthrène, le dihydrophénanthrène, le naphtalène et la tétraline sur un catalyseur de type nickel de Raney ayant une

1. Auteur à qui adresser toute correspondance.

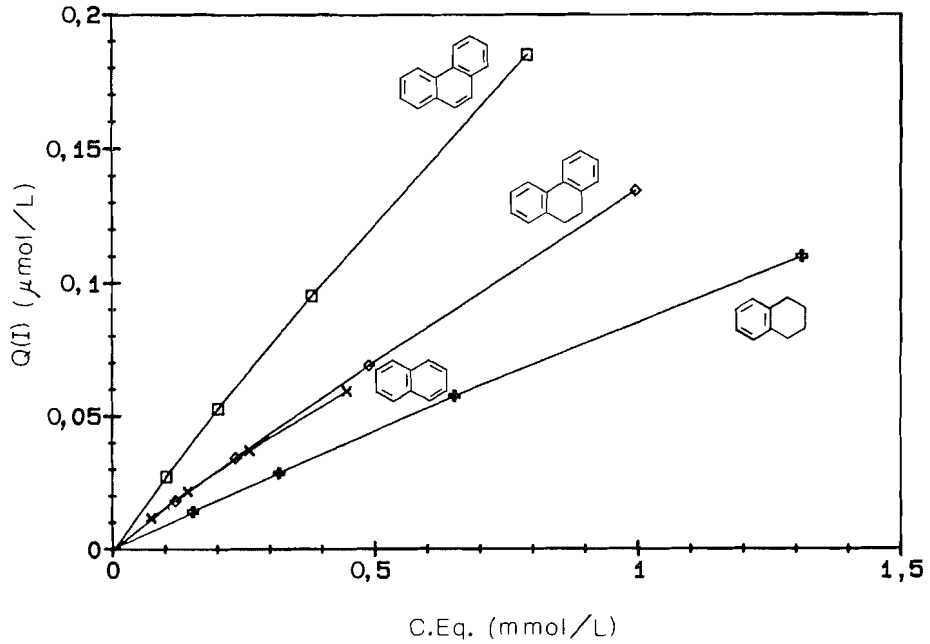


FIG. 1. Isotherme d'adsorption du phénanthrène, du dihydrophénanthrène, du naphtalène et de la tétraline sur du nickel de Raney (activé) à 25°C dans l'hexane comme solvant.

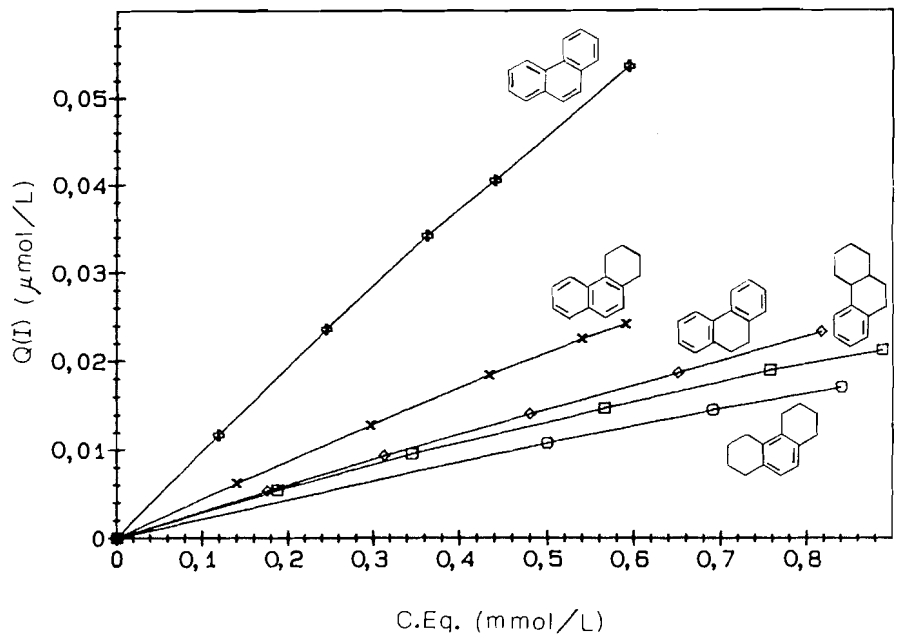


FIG. 2. Isotherme d'adsorption du phénanthrène, du tétrahydrophénanthrène, du dihydrophénanthrène et des octahydrophénanthrènes (asymétrique et symétrique) sur nickel de Raney (désactivé) à 25°C dans le dichlorométhane comme solvant.

granulométrie inférieure à 105 μm. Le solvant utilisé est l'hexane. Nous remarquons que le phénanthrène est très fortement adsorbé par rapport au naphtalène. Le dihydrophénanthrène présente une adsorption comparable à celle du naphtalène tandis que la tétraline est le composé le moins fortement adsorbé. La force d'adsorption de ces molécules dépend donc du nombre d'électrons π (14 pour le phénanthrène, 10 pour le naphtalène et six pour la tétraline).

Dans la figure 2, nous avons le tracé des isothermes d'adsorption du phénanthrène et de ses dérivés hydrogénés sur un catalyseur de type nickel de Raney ayant une granulométrie de 53–105 μm. Dans le tableau 1 sont indiquées les valeurs de la constante de Henry. Le dichlorométhane a été utilisé comme solvant. Les résultats montrent que l'adsorption dépend là encore du nombre d'électrons π. En effet les octahydrophénanthrènes avec six électrons π sont moins fortement adsorbés que le tétrahydrophénanthrène qui en compte 10. Cependant, le nombre d'électrons π n'est pas le seul facteur influençant l'adsorption puisque le dihydrophénanthrène qui comporte 12 électrons π est moins fortement adsorbé que le tétrahydrophénanthrène qui en compte 10.

L'adsorption de ces molécules fait donc intervenir une interaction entre les électrons π et le métal. Plus il y a d'électrons π en contact avec le métal, plus l'adsorption devait être forte. Il

Can. J. Chem. Downloaded from www.nrcresearchpress.com by 41.223.56.140 on 09/07/12
For personal use only.

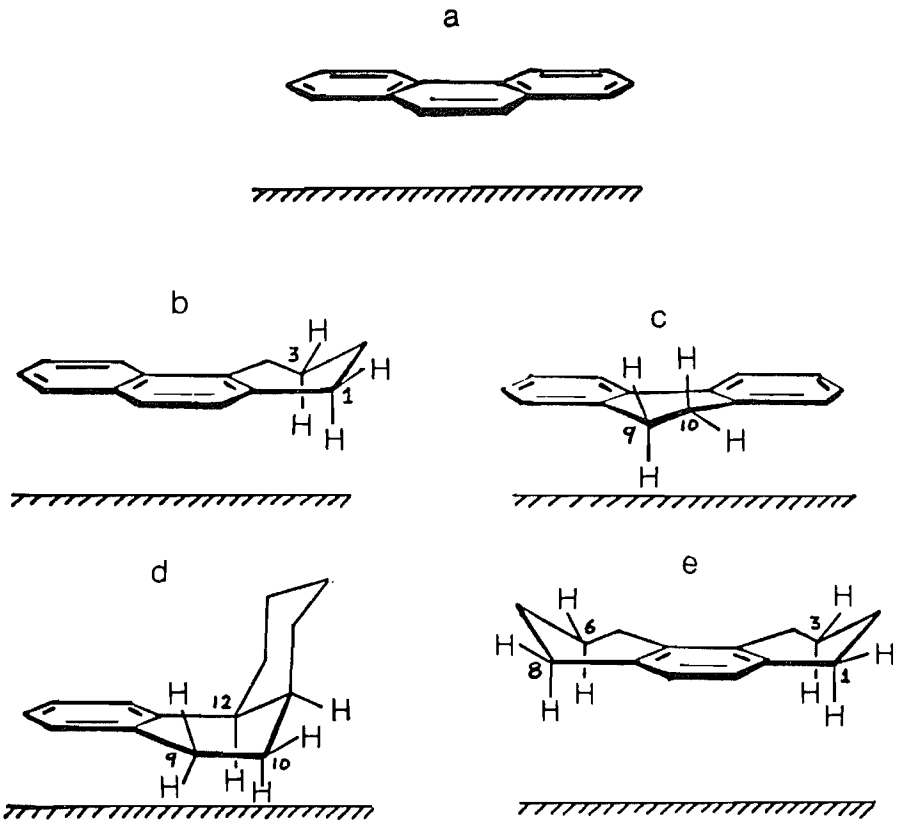


FIG. 3. Modèle moléculaire d'adsorption sur catalyseur de nickel de Raney : (a) phénanthrène; (b) tétrahydrophénanthrène; (c) dihydrophénanthrène; (d) octahydrophénanthrène asymétrique; (e) octahydrophénanthrène symétrique.

TABLEAU 1. Valeur de la constante de Henry (K_H) pour l'adsorption du phénanthrène et de ses dérivés hydrogénés sur du nickel de Raney dans le chlorure méthylène à 25°C

Substrat	K_H (cm^3/m^2)
Phénanthrène	0,0058
Dihydro-9,10 phénanthrène	0,0018
Tetrahydrophénanthrène	0,0026
Octahydrophénanthrène asymétrique	0,0016
Octahydrophénanthrène symétrique	0,0011

n'y a rien qui empêche des molécules planaires comme le phénanthrène et le naphtalène de se coucher sur la surface du catalyseur de façon à ce que tous les électrons π interviennent dans l'adsorption tel qu'illustré à la figure 3(a) dans le cas du phénanthrène[2]; ce dernier, avec ses 14 électrons π, est alors beaucoup plus fortement adsorbé que le naphtalène qui n'en compte que 10.

Eltekov et Khopina (12) ont montré par HPLC que l'adsorption des composés aromatiques sur le gel de silice dépend du nombre d'électrons π et de la longueur de la molécule selon la relation linéaire [6] :

[6] $\log K = A + B(n_\pi + n_\pi/1)$

où $K = Q(I)/C_{éq}$ *où* $Q(I)$ est la quantité adsorbée par unité de surface et $C_{éq}$ la concentration à l'équilibre, A et B sont des constantes, n_π le nombre d'électrons π, et l la longueur de la molécule selon l'axe le plus long. Cette relation, strictement parlant, devrait plutôt avoir la forme [7] :

[7] $\log K = A + Bn_\pi + Cn_\pi/1$

où C est une constante. Les auteurs ont supposé, de façon arbitraire, que les constantes B et C avaient la même valeur.

L'adsorption du dihydrophénanthrène, du tétrahydrophénanthrène et des octahydrophénanthrènes ne peut dépendre uniquement du nombre d'électrons π et de la longueur de la molécule mais doit être influencée également par la gêne stérique causée par les hydrogènes des sites saturés (voir figure 3)[2]. En effet, la molécule de dihydrophénanthrène et celle du tétrahydrophénanthrène ont sensiblement la même longueur et même si le dihydrophénanthrène a plus d'électrons π que le dérivé tétrahydro, il est moins fortement adsorbé que ce dernier. La gêne stérique causée par les hydrogènes aux positions 9 et 10 du dihydrophénanthrène doit être plus grande que celle causée par les hydrogènes aux positions 1 et 3 du dérivé tétrahydro (voir figure 3 (b et c)). Les effets stériques doivent être aussi responsables du fait que l'octahydrophénanthrène symétrique est moins fortement adsorbé que son isomère asymétrique. En étant au centre de la molécule, le noyau aromatique du dérivé symétrique ne peut pas s'approcher aussi facilement de la surface du catalyseur (interférence des hydrogènes aux positions 1, 3, 6 et 8) que le noyau aromatique situé à l'extrémité de la molécule du dérivé asymétrique (voir figure 3 (e et d)), car une légère inclinaison de la molécule de l'octahydrophénanthrène asymétrique devrait permettre de minimiser l'interférence des hydrogènes aux positions 9, 10 et 12.

2. La figure 3 est basée sur l'étude des modèles moléculaires de type Dreiding et nous n'avons pas mesuré expérimentalement l'orientation des molécules adsorbées à la surface du catalyseur.

Can. J. Chem. Downloaded from www.nrcresearchpress.com by 41.223.56.140 on 09/07/12
For personal use only.

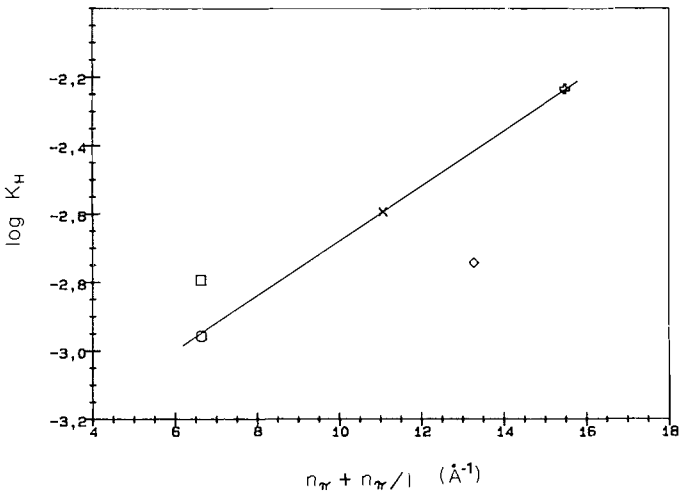


FIG. 4. Rapport de log K sur $n_\pi + n_\pi/l$ pour le phénanthrène (+), le tétrahydrophénanthrène (X), le dihydrophénanthrène (◇), l'octahydrophénanthrène asymétrique (□) et l'octahydrophénanthrène symétrique (○).

Lorsque l'on porte en graphique la quantité de molécules adsorbées en fonction du nombre d'électrons π et de la longueur de la molécule selon l'équation [6] pour l'adsorption du phénanthrène et de ses dérivés hydrogénés sur le nickel de Raney, on obtient le graphique de la figure 4. Dans la série phénanthrène, tétrahydrophénanthrène et octahydrophénanthrène symétrique, la variation des effets stériques est telle que la relation est tout-à-fait linéaire. Il s'agit évidemment d'une coïncidence. La figure illustre bien que les effets stériques sont plus importants dans le cas du dihydrophénanthrène et moins importants dans le cas de l'octahydrophénanthrène asymétrique.

Conclusion

L'obtention des isothermes d'adsorption du naphtalène, de la tétraline, du phénanthrène et de ses dérivés hydrogénés sur le nickel de Raney, montrent que l'adsorption des molécules dépend du nombre d'électrons π mais aussi de la disposition de ses électrons π dans la molécule lorsque des hydrogènes peuvent créer des interférences stériques entre la molécule et le catalyseur.

Remerciements

Les auteurs remercient le Fonds pour la formation de chercheurs et l'aide à la recherche du Québec pour le financement du projet et Monsieur Yvon Couture pour la synthèse du tétrahydrophénanthrène.

1. I. HORIUTI et M. POLANYI. Trans. Faraday Soc. **30**, 1164 (1934).
2. G. BELOT, S. DESJARDINS et J. LESSARD. Tetrahedron Lett. **25**, 5347 (1984).
3. M. COMTOIS. Mémoire de maîtrise, Université de Sherbrooke, 1986.
4. S. MITSUI, K. GOHKE, H. SAITO, A. NANBU et Y. SENDA. Tetrahedron, **29**, 1523 (1973).
5. S. MITSUI, S. IMAIZUMI, A. NANBU et Y. SENDA. J. Catal. **36**, 333 (1973).
6. S. MITSUI, M. ITO, A. NANBU et Y. SENDA. J. Catal. **36**, 119 (1975).
7. H. MÉNARD, L. NOËL, F. M. KIMMERLE, L. TOUSIGNANT et M. LAMBERT. Anal. Chem. **56**, 1240 (1984).
8. N. A. CHUDUK, YU A. ELTEKOV et A. V. KISELEV. J. Colloid Interface Sci. **84**, 149 (1981).
9. L. NOËL. Thèse de doctorat, Université de Sherbrooke, 1986.
10. P. D. HAWORTH. J. Chem. Soc. 1125 (1932).
11. R. L. AUGUSTINE. Catalytic hydrogenation. M. Dekker Inc., New York, NY. 1965.
12. Y. A. ELTEKOV et V. V. KHOPINA. Langmuir, **3**, 957 (1987).

Can. J. Chem. Downloaded from www.nrcresearchpress.com by 41.223.56.140 on 09/07/12
For personal use only.

The synthesis and reactivity of α-oxosulfines[1]

IAN W. J. STILL,[2] DONALD V. FRAZER, DONNA K. T. HUTCHINSON, AND JEFFERY F. SAWYER
Department of Chemistry, University of Toronto, 80 St. George Street, Toronto, Ont., Canada M5S 1A1

Received June 9, 1988

IAN W. J. STILL, DONALD V. FRAZER, DONNA K. T. HUTCHINSON, and JEFFERY F. SAWYER. Can. J. Chem. **67**, 369 (1989).

Thiochroman-4-one and cyclohexanone have been converted into the corresponding α-oxosulfines and the behaviour of these reactive intermediates with a range of alkenes and alkynes has been examined. In contrast to some earlier work, the major reaction pathway does not involve formation of the initially expected Diels–Alder adducts but instead a series of adducts involving electrophilic addition to the alkene or alkyne, with concomitant deoxygenation and incorporation of chlorine. The structures of these adducts have been determined by the usual spectroscopic means and, in two representative cases, by X-ray crystallographic analysis. The crystal structures, which include unusual features such as relatively short S...O nonbonding contacts, are discussed in detail.

Key words: (α-oxo)sulfines, sulfenic acids, X-ray analysis, electrophilic addition.

IAN W. J. STILL, DONALD V. FRAZER, DONNA K. T. HUTCHINSON et JEFFERY F. SAWYER. Can. J. Chem. **67**, 369 (1989).

On a transformé la thiochromanone-4 ainsi que la cyclohexanone en α-oxosulfines correspondantes et on a étudié le comportement de ces intermédiaires réactifs avec un certain nombre d'alcènes et d'alcynes. La réaction principale diffère de celles qui ont été observées aux cours de travaux antérieurs; elle n'implique pas la formation initiale des adduits de Diels–Alder attendus, mais plutôt une série de produits impliquant une addition électrophile sur l'alcène ou sur l'alcyne accompagnée d'une déoxygénation concomitante et de l'incorporation du chlore. On a déterminé la structure de ces adduits en faisant appel aux méthodes spectroscopiques habituelles et, dans deux cas représentatifs, à la diffraction des rayons-X. On présente une discussion détaillée des structures qui comportent des caractéristiques inhabituelles comme des contacts non-liants S...O qui sont très courts.

Mots clés : (α-oxo)sulfines, acides sulfeniques, diffraction des rayons-X, addition électrophile.

[Traduit par la revue]

Can. J. Chem. Downloaded from www.nrcresearchpress.com by 41.223.56.140 on 09/07/12
For personal use only.

Introduction

While the chemistry of the class of organosulfur compounds known as sulfines has been thoroughly investigated in the last 25 years since their first unambiguous characterization (1) and has been reviewed recently by Zwanenburg (2), the availability of an interesting sub-class of sulfine, the α-oxosulfines, $R^1C(=O)C(=SO)R^2$ was only recently reported, independently, by the research groups of Still and Ablenas (3) and Zwanenburg and co-workers (4). Matturo and Reynolds (5) have very recently generated a vinylogous oxosulfine by the thermal decomposition of a thioozonide, the endoperoxide from 2,5-dimethylthiophene (6).

Interest in the ability of various thione and sulfine units to function as components of cycloaddition reactions, leading to a variety of heterocyclic ring systems, has recently been intense. Huisgen and Rapp (7), for example, have reported the successful addition of thiobenzophenone *S*-sulfide (a thiosulfine) with various dipolarophiles. Steliou *et al.* (8) have examined the generation and Diels–Alder dienophile reactivity of disulfur (S_2). Ando and co-workers (9) have successfully trapped 1,2-dithiones with suitable olefins although, interestingly, a 1,2-dithione prepared by Cava and Atwood (10) was unreactive towards both electron-rich and electron-poor dienophiles. In another interesting contrast, Huisgen and Peng (11) showed that thionitroso *S*-sulfides (thiosulfinylamines) react as 1,3-dipoles with suitable alkenes to give 1,2,3-dithiazolidines, whereas Zoller and Rona (12) have found that *N*-sulfinylanilines react as *dienes* in Diels–Alder reactions with benzalanilines to give six-membered thiadiazine derivatives.

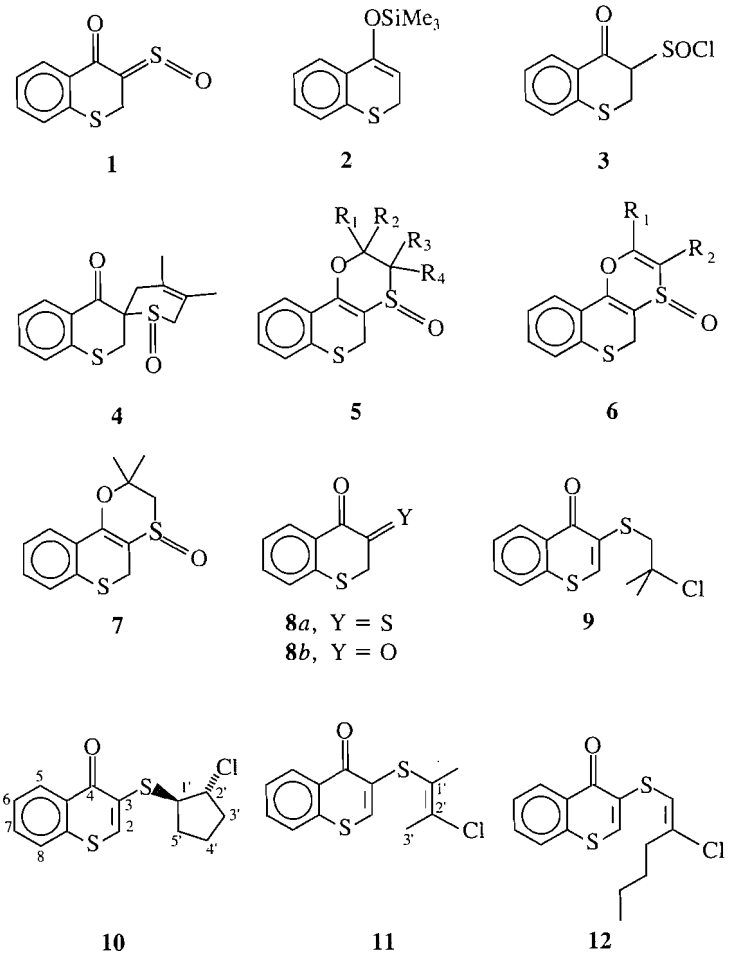
While C=S units in both simple sulfines (2, 13) and α-oxosulfines (3, 4, 14) have been observed to function as *dienophiles* in the Diels–Alder reaction with conjugated dienes such as 2,3-dimethyl-1,3-butadiene, we were interested in examining the potential use of α-oxosulfines as *dienes* in this type of reaction (14). Since we expected α-oxosulfines to be basically electron-poor, we have examined the use of various electron-rich alkenes and alkynes for this purpose. The "inverse-demand" Diels–Alder reactions which might be expected to result would lead to 5,6-dihydro-1,4-oxathiins or 1,4-oxathiins, respectively, — compounds of considerable potential interest for their fungicidal activity (15, 16). We now present our findings involving two separate series of α-oxosulfines and their behaviour towards various alkenes and alkynes. Surprisingly, and in sharp contrast to earlier results (3, 14), the products observed do not result from the Diels–Alder reaction.

Results and discussion

We decided to first prepare 3-sulfinylthiochroman-4-one **1** by modifying our successful approach to the synthesis of the 3-alkylidene analogues (17), using the trimethylsilyl enol ether **2** as the starting point. It is well known that activated methylene compounds react directly with thionyl chloride in many cases (18, 19) and this subject has been comprehensively reviewed by Oka (20), but mixtures of products are frequently formed and the reactions are notoriously sensitive to the reaction conditions employed. The initially expected α-sulfinyl chloride **3**, arising from C-sulfinylation of **2**, would be expected to rapidly lose HCl (20) to form the α-oxosulfine **1**. This elimination was found to proceed even in the absence of base, but best results were achieved using 2,2,6,6-tetramethylpiperidine (1 equiv.) at low temperatures. Since the α-oxosulfine did not precipitate from the reaction mixture, and hence was expected to be unstable (14), its presence was first confirmed by trapping with 2,3-dimethyl-1,3-butadiene to form the expected Diels–Alder adduct **4**. Compound **4** showed the expected C=O and S=O

[1]Taken in part from the M.Sc. thesis of D. K. T. Hutchinson, University of Toronto, 1987.

[2]Author to whom correspondence may be addressed.



1 2 3

4 5 6

7 8*a*, Y = S 8*b*, Y = O 9

10 11 12

bands in the ir spectrum at 1670 and 1052 cm^{-1}, respectively. Its ^1H nmr spectrum (see Experimental) was also in accord with expectation and the molecular formula ($C_{15}H_{16}O_2S_2$) was confirmed by high-resolution mass spectral analysis. (The intermediate sulfine **1** is assumed to possess the *Z*-configuration shown, since the corresponding *E*-isomer would exhibit a very unfavourable dipole–dipole repulsion.) Some of the ketone corresponding to the enol ether **2** was also isolated in the above reaction, due either to hydrolysis and desulfonylation (21) of unreacted α-oxosulfine during work-up or to hydrolysis of unreacted silyl enol ether.

Having demonstrated the effectiveness of this approach to the generation of the α-oxosulfine we then proceeded to examine the behavior of **1**, a potential electron-deficient *diene* component, in the Diels–Alder reaction with a number of relatively electron-rich alkene and alkyne dienophiles (3, 4). Added interest derived from the fact that success in this endeavour might produce novel 1,4-oxathiins such as **5** and **6**. This type of ring system was virtually unknown until our earlier work with the thiochroman-4-one 1,1-dioxide analogs (3).

Our first attempt at this type of trapping of **1** employed an excess of 2-methylpropene at −78°C under similar conditions to those used to prepare **4**. On the basis of the charge densities in both the diene and the dienophile, it was predicted that the regiochemistry of the Diels–Alder reaction of **1** and 2-methylpropene would lead to **7**. After extensive purification by crystallization, two products — a yellow solid *A*, mp 87–88°C (19%), and tan needles *B*, mp 156–157°C, were isolated. Five aromatic protons and two singlets corresponding to six and two protons, respectively, were observed in the ^1H nmr spectrum of *A*. This did not correlate with the spectrum expected for **7**. The mass spectrum of *A* showed two peaks corresponding to mass units 284 and 249, with relative intensities of 5 and 41% respectively. Compound **7** ($C_{13}H_{14}O_2S_2$) would have an expected molecular ion peak at m/z = 266. The observed ion at m/z 284, however, indicates a product of formula $C_{13}H_{13}ClOS_2$ (^{35}Cl isotope). The peak at m/z 249 could then be attributed to loss of chlorine. Sodium fusion and Beilstein tests independently confirmed the presence of chlorine in *A*. In the infrared spectrum of *A*, there was, in addition, no peak indicating the presence of a sulfoxide group. Confirmation of the molecular formula of *A* as $C_{13}H_{13}ClOS_2$ was also obtained from the elemental analysis.

Compound *B*, the other product isolated from the reaction mixture above, remains unidentified. However, evidence from the ^1H nmr, ir, and mass spectra and elemental analysis indicates that *B* is probably a low molecular weight polymer of 3-thioxothiochroman-4-one, **8***a*. Loss of oxygen from the *S*-oxide probably occurs in the α-oxosulfine **1** itself, or possibly after polymerization.

An analogous trapping reaction of the α-oxosulfine **1** with cyclopentene was also carried out. The spectral evidence (^1H nmr, ir, mass spectrum) and elemental analysis once again indicated that the product (41%) was *not* a Diels–Alder adduct of type 5 — but a compound with the composition $C_{14}H_{13}ClOS_2$. The ^1H nmr spectrum showed a multiplet at δ 2.1 corresponding to the six methylene protons of a 1,2-disubstituted cyclopentane and two multiplets at δ 3.7 and 4.2. Three aromatic protons

Can. J. Chem. Downloaded from www.nrcresearchpress.com by 41.223.56.140 on 09/07/12
For personal use only.

TABLE 1. 2D nmr (HETCOR)[a] (22) analysis of **10** ($CDCl_3$)

^1H (δ)	^{13}C nmr (δ)	Position
1.9	22.45	C-4′
2.0, 2.4	29.84	C-5′
1.7, 2.5	34.93	C-3′
3.8	51.86	C-1′
4.2	65.68	C-2′
7.5–7.6	126.22, 127.74, 131.30	C-6, C-7, C-8
7.8	131.57	C-2
8.5	129.07	C-5

[a]The 2D nmr spectra were recorded on a different spectrometer from the original ^1H and ^{13}C nmr spectra, accounting for the slight differences in chemical shift observed.

appeared as a multiplet at δ 7.4 and additional signals were observed in this region as a singlet at δ 7.7 and a multiplet at 8.5. At this stage a single-crystal X-ray analysis was carried out (*vide infra*) which confirmed that the product was the 3-substituted thiochromone **10**. Independent proof of structure was obtained from a 2D nmr (HETCOR) analysis (22) of **10**, to correlate the protons with the carbons to which they are attached (see Table 1).

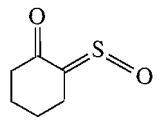
Some of the parent ketone corresponding to **2**, thiochroman-4-one, was recovered from the reaction mixture during chromatography of the crude product and indeed from all the reactions in this series. Under aqueous conditions, α-oxosulfines are known to be hydrolysed to the parent ketone, or to the corresponding α-diketone (21). In our case, it is probable that hydrolysis to thiochroman-4-one occurred on silica gel during chromatography. The alternative product of acid-catalyzed hydrolysis, the α-diketone **8***b*, was not detected in the reaction mixture.

Re-examination of the spectral data for the adduct from the previous reaction of **1** with 2-methylpropene, in the light of the very detailed structural examination of **10**, leads us to identify the analogous structure **9** as the correct one for this adduct.

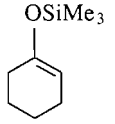
With the successful formation of the cyclopentene adduct **10**, analogous preparations of the corresponding cyclohexene and cyclooctene adducts were attempted. The presence of adducts analogous to **10** could be detected in the respective reaction mixtures by ^1H nmr, but these products proved incapable of isolation in a pure state. They appear to decompose during chromatography on either silica gel or alumina. The reasons for the apparent instability of these cycloadducts are not at all clear but may be due in part to the larger, more conformationally mobile, alicyclic rings present.

Trapping of the α-oxosulfine **1** was also attempted with various alkynes to verify the generality of the above reactions. When **1** was reacted with 2-butyne at −78°C, the now expected *E*-3-(2′-chloro-1′-methyl-1′-propenylthio)thiochromone[3] **11** was isolated in 26% yield. Interestingly, this reaction was unsuccessful when attempted at −23°C. The only product isolated at the higher temperature was a tan solid which had similar physical and spectroscopic properties to those of solid *B* in the 2-methylpropene trapping experiment (*vide supra*). The ^1H nmr spectrum of **11** shows two peaks at δ 2.5 and 2.1, corresponding to the two methyl groups. A singlet for the C-2 proton appears at δ 7.3. Three aromatic protons appear as a multiplet at δ 7.5 and a further multiplet at 8.5 is assigned

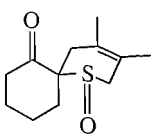
[3]The *E*-geometry of **11** is assigned by analogy with the structure of the 2-butyne adduct in the 2-sulfinylcyclohexanone series (*vide infra*).



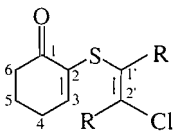
13



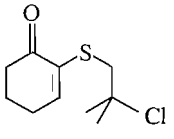
14



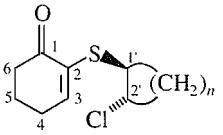
15



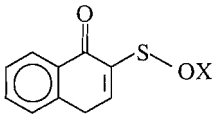
16*a*, R = Me
16*b*, R = Ph



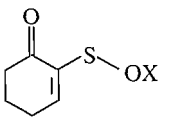
17



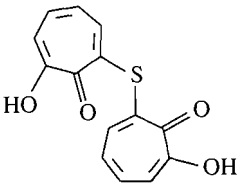
18*a*, *n* = 3
18*b*, *n* = 4
18*c*, *n* = 6



19*a*, X = H
19*b*, X = SOCl



20*a*, X = H
20*b*, X = SOCl



21

to the C-5 proton. The ^{13}C nmr spectrum (see Experimental) confirmed the presence of two methyl groups, five sp^2 *CH* carbons and six sp^2 quaternary carbons, in agreement with the assigned structure.

The trapping of **1** was also attempted using an unsymmetrically substituted alkyne, 1-hexyne. A mixture of regioisomers was isolated as a red oil, in 20% yield, in a ratio of 4:1. Only the major regioisomer **12** could be isolated in crystalline form. The ^1H nmr spectrum of **12** shows a multiplet for four aromatic protons at δ 7.5 and a peak corresponding to one proton at 8.5. The side-chain vinylic proton appears as a sharp singlet at δ 6.5. The signal for the methyl group appears as a triplet at δ 0.95 and the six methylene protons are observed as two distinct signals, a triplet (2H) at 2.5 and a multiplet (4H) at 1.5. The assignment of the structure of **12** is based on analogy with the adduct **9** from 2-methylpropene. We will return to this point later in the discussion of a probable mechanism for formation of these adducts.

We have also examined the behaviour of a much simpler α-oxosulfine **13**, derived from cyclohexanone via the usual trimethylsilyl enol ether precursor **14**, followed by reaction with thionyl chloride in the presence of 2,6-dimethylpyridine (2,6-lutidine). The expected formation of the α-oxosulfine **13** was confirmed as in the series above by a simple trapping experiment with 2,3-dimethyl-1,3-butadiene. A product ($C_{12}H_{18}O_2S$), which showed the expected bands in the ir spectrum at 1707 (C=O) and 1050 (S=O) cm^{-1}, was formed in 46% yield. In the ^1H nmr spectrum, the most downfield signal observed was at δ 3.30, in sharp contrast to the ^1H nmr spectra of the adducts formed from simple alkenes and alkynes (*vide infra*). These data strongly indicate the expected spiro-ketone **15** as the structure of this adduct and hence **13** as the structure of the intermediate α-oxosulfine.

Trapping reactions were first carried out on **13** with a series of simple alkenes — 2-methylpropene, cyclopentene, cyclo-

Can. J. Chem. Downloaded from www.nrcresearchpress.com by 41.223.56.140 on 09/07/12
For personal use only.

TABLE 2. 2D nmr (HETCOR)[a] (22) analysis of **16***a* ($CDCl_3$)

^{1}H nmr (δ)	^{13}C nmr (δ)	Position
1.96	21.26	CH_3(C-1′)
1.95	22.47	C-5
2.25	24.04	CH_3(C-2′)
2.38	26.82	C-4
2.45	38.22	C-6
6.47	143.03	C-3

[a]The 2D nmr spectra were recorded on a different spectrometer from the original ^{1}H and ^{13}C nmr spectra, accounting for the slight differences in chemical shift observed.

hexene, and cylcooctene. Adducts which were liquids at 25°C were obtained in all cases. All four products displayed a very strong ir band in the range 1682–1688 cm^{-1}, indicative of an unsaturated carbonyl group, and a triplet signal far downfield in the ^{1}H nmr spectrum, in the range δ 6.90–7.05, indicative of a vinylic proton. As in the thiochromanone series above, these data clearly did not accord with expectation for a Diels–Alder adduct. Since the four adducts so obtained were liquids, however, we decided to examine the analogous reactions of **13** with simple alkynes in the hope that the more rigid structures so obtained would be more likely to provide us with a crystalline product for X-ray analysis.

When the α-oxosulfine **13**, generated in the same manner as for the above cycloadditions, was allowed to react with a two-fold excess of 2-butyne between −78° and 25°C, a pale yellow crystalline solid, mp 42–44°C, was obtained in 35% yield, after initial purification by flash chromatography. This product possessed an ir band at 1689 cm^{-1}, similar to that in the alkene adducts above, and also showed the distinctive downfield triplet (J = 4 Hz) in the ^{1}H nmr spectrum, albeit slightly further upfield at δ 6.60. The formula $C_{10}H_{13}ClOS$ for this adduct was confirmed by elemental analysis. ^{13}C nmr analysis with APT-editing indicated the presence of two CH_3 groups (at δ 21.6 and 24.4), three CH_2 groups (at δ 22.8, 27.1, and 38.5), one sp^2-CH (at δ 143.0), and four other quaternary sp^2 carbons (three in the range δ 122.0–134.4 and what appeared to be a carbonyl carbon at δ 195.7). A two-dimensional, ^{1}H–^{13}C shift-correlated nmr (HETCOR) analysis (22) confirmed the respective assignments (see Table 2) and in particular the matching of the proton signal at δ 6.60 with the sp^2 carbon at δ 143.0.

A very similar result was obtained when diphenylacetylene was used as the trapping species, although the adduct in this case was a colourless, viscous oil and the yield of purified adduct was very low. Preliminary examination of the trapping reaction with 1-hexyne and with acetylene itself also yielded crude products which showed the now characteristic ir band at 1682 cm^{-1} and a downfield triplet in the ^{1}H nmr spectra at δ 6.70 and 6.90, respectively. Extensive purification was not carried out on these adducts, however, since we were by now convinced that these products were fully analogous to the above adduct from 2-butyne.

Since we had obtained a crystalline sample of the 2-butyne adduct of **13** and since more than one structure was potentially consonant with the spectral data presented above, we subjected the 2-butyne adduct to single crystal X-ray analysis (*vide infra*). As a result, this adduct has now been unambiguously identified as *E*-2-(2′-chloro-1′-methyl-1′-propenylthio)-2-cyclohexenone **16***a* (see Fig. 1). By analogy, the diphenylacetylene adduct above is assigned structure **16***b* and, more tentatively, we can assign the impure adducts from 1-hexyne and acetylene to the same structural class. Because of the close correspondence of the ir and ^{1}H nmr data in these cases, it also seems reasonable to assign structures **17** and **18***a–c*, respectively, to the (liquid) 2-methylpropene and cycloalkene adducts described above. Structure **18***a* was also confirmed by nmr (HETCOR) analysis similar to those described earlier for **10** and **16***a* (see Table 3).

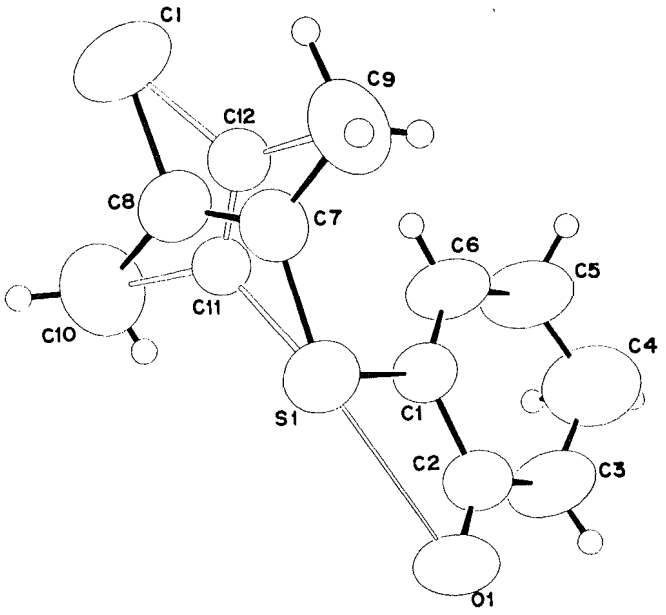


FIG. 1. ORTEP view of compound **16***a* showing the crystallographic numbering scheme. Thermal ellipsoids are drawn at the 50% probability level; hydrogen atoms with uniform isotropic temperature factors. Both arrangements of the disordered chloro-methylpropenyl moiety are indicated. The close S...O contact referred to in the discussion is indicated by the thinner unfilled bond.

TABLE 3. 2D nmr (HETCOR)[a] (22) analysis of **18***a* ($CDCl_3$)

^{1}H nmr (δ)	^{13}C nmr (δ)	Position
1.75, 1.85[b]	22.20	C-4′[b]
1.95[b]	22.39	C-5[b]
2.40	26.86	C-4
1.50, 2.35	29.78	C-5′
1.85, 2.20	34.47	C-3′
2.45	38.14	C-6
3.46	51.08	C-1′
4.10	65.47	C-2′
6.82	145.02	C-3

[a]The 2D nmr spectra were recorded on a different spectrometer from the original ^{1}H and ^{13}C nmr spectra, accounting for the slight differences in chemical shift observed.
[b]These signals may be interchanged.

Discussion of crystal structures

X-ray analyses have indicated that compound **16***a* and both independent molecules in the asymmetric unit of compound **10** do not contain conjugated ring systems but instead consist of

Can. J. Chem. Downloaded from www.nrcresearchpress.com by 41.223.56.140 on 09/07/12
For personal use only.

Can. J. Chem. Downloaded from www.nrcresearchpress.com by 41.223.56.140 on 09/07/12
For personal use only.

thioether linked molecules. In **16***a* the sulfur atom bridges between cyclohexenone and chloro-methylpropenyl moieties, while in **10** 2-chlorocyclopentane and thiochromone moieties are bridged. In **16***a*, the cyclohexenone ring exists in a flattened envelope conformation with C(4) and C(5) −0.440(10) and −0.089(8) Å respectively above the planar C(1)—C(2)—C(3)—C(6) section of the ring.[4,5] Similarly, S(1) and O(1) are 0.087(1) and 0.021(4) Å, respectively, out of this plane. The chloro-methylpropenyl moiety in this molecule is slightly disordered, with the double bond in ca. 15% of molecules in the unit cell rotated by 90° with respect to the major orientation, while preserving the positions of the peripheral S, Cl, and Me atoms (Fig. 1). A least-squares mean plane through these peripheral atoms and both orientations of the double bond indicate that these atoms remain planar to ±0.059(26) Å. A similar disordered arrangement has been observed for dimethylstilbene (23) and has been suggested for *trans*-stilbene (with ca. 20% probability of disorder (calculated) at room temperature) (24). The observed C(7)=C(8) double bond and C(8)—Cl distances for the major orientation (1.299(10) and 1.759(5) Å (Table 4)) are generally comparable with values observed for *E*-1-chloro-2-methoxy-1,2-diphenylethene (1.336(4) and 1.737(3) Å) (25) and 2,2′-(2,2-dichlorovinylidene)bis(4-chloro-6-nitrophenol) (1.330(12) and 1.719(5) Å) (26), while the carbon–chlorine distances in the two molecules of compound **10** are 1.798(16) and 1.777(23) Å (major component).

The two S—C(sp^2) distances (1.771(3) and 1.797(6) Å (major orientation)) are somewhat longer and the C(7)—S(1)—C(1) angle somewhat smaller (101.5(2)°) than distances and angles in compounds such as bis(3-phenyl-1,4-benzodioxin-2-yl) sulfide (1.749(2) Å, 103.2(2)°) (27) and bis(3-hydroxy-2-oxo-cyclohepta-3,5,7-trienyl) sulfide **21** (C—S = 1.75, 1.76, 1.78 and 1.83(1) Å and CSC = 103.5° and 102.1(5)° (two independent molecules)) (28). In **10** the S—C(sp^2) and S—C(sp^3) distances and the C(n3)—S(n2)—C(n9) angles at the bridging atom are 1.754(16) Å (1.729(17) Å) and 1.810(17) Å (1.791(21) Å) and 103.8(8)° (103.4(9)°) in the two independent molecules (Table 4).

A notable feature of the structure of **16***a* is the close intramolecular S...O contact distance of 2.829(3) Å. This distance is significantly shorter than the van der Waals distance (3.25 Å) and ca. 0.13 Å shorter than a distance calculated with "normal" (120°) SCC and CCO angles. The 14° difference in the S(1)—C(1)—C(2) and S(1)—C(1)—C(6) bond angles is in the direction of pushing S towards O, although contacts involving H(61) and atoms in the chloropropenyl group are as short as 2.550 Å (C(7)...H(61)).[6] Both of the angles C(7)—S(1)...O(1) and C(11)—S(1)...O(1) are somewhat distorted from 180° (156.7(1) and 148.0(8)°). Similarly, the O(1)—C(2) bond length (1.215(4) Å) is slightly longer than that observed in 2,6-dimethyl-4*H*-1-thiopyran-4-one (1.189(4) Å) (29) but comparable to that observed in 2-(1,3-dithiol-2-ylidene)cyclopent-4-ene-1,3-dione (1.213(3) Å), a molecule with a close S...O contact of length 2.944(3) Å (30). In the sulfide **21** above, the shortest intramolecular S...O contacts have been calculated as 2.731 and 2.664 Å and the two carbonyl bonds involved have lengths of 1.22 and 1.24(1) Å (27).

The crystal packing of **16***a* consists of layers of molecules in the (10$\bar{1}$) plane (Fig. 2). The shortest intermolecular contacts are S(1)...H(42) $(-\frac{1}{2} + x, \frac{1}{2} - y, -\frac{1}{2} + z) = 3.02$ Å, Cl...H(52) $(-\frac{1}{2} + x, \frac{3}{2} - y, -\frac{1}{2} + z) = 3.19$ Å and O(1)...H(31) $(1 - x, -y, 1 - z) = 2.88$ Å.

In **10** the quality of the crystals has limited the precision of the geometrical parameters of both molecules. However, both molecules contain sulfur-linked 2-chlorocyclopentane and thiochromone ring systems. Both thiochromone rings are essentially planar, although the maximum deviation of atom C(113) (0.134(17) Å) and the deviation of S(12) (0.250(5) Å) from the least-squares mean plane are significantly larger than those values obtained for the second molecule, which is planar, to 0.056(13) Å and S(22) is 0.106(6) Å out of plane. Where the two molecules differ most is in the orientation of the cyclopentane rings with respect to the thiochromone moieties, the change in configuration at the chloro-substituted atom C(n13) and the presence of a small amount (ca. 15%) of disorder of the Cl atom in molecule **2**. Thus, in molecule **1**, the Cl is pseudoaxial and *anti* to the S(12)—C(19) bond (τ (S(12)—C(19)—C(113)—Cl) = −164(1)°), whereas in molecule **2** the Cl is on the opposite side of the cyclopentane ring in a pseudoequatorial configuration, with τ (S(22)—C(29)—C(213)—Cl) = 82(2)°. The disorder in molecule **2** places the alternative Cl position (ca. 15%) on C(29). Similarly, the difference in the torsion angles τ (S(12)—C(19)—C(110)—C(111)) = −93(2)° and τ (S(22)—C(29)—C(213)—C(212)) = −159(2)° would indicate that the cyclopentane ring in molecule **2** is rotated by ca. 66° towards a more "perpendicular" arrangement with respect to the thiochromone plane (Fig. 3). Internal torsion angles (Table 5), however, indicate that both pentane rings have the same conformation within the measured standard deviations.

As with compound **16***a*, both molecules contain S(n2)...O(n1) intramolecular contacts (2.778 and 2.775(13) Å) slightly shorter in length than the S...O distance in **16***a* above. Although the errors are quite large, it does appear that the C(n4a)—C(n4)—O(n1) angles (122.7(16) and 123.5(16)°) are slightly larger than the C(n3)—C(n4)—O(n1) angles (117.5(16) and 115.1(16)°). In the thiochromone rings the bond lengths and bond angles for the thiopyranone moiety are substantially different from those observed in 2,6-dimethyl-[4*H*]-1-thiopyran-4-one (29), in which a localised valence bond structure predominates, but are more consistent with the dimensions of the thiopyranone ring in 3-[2(*Z*)-(benzylthio)-2-phenylethenyl]-2,6-diphenyl-[4*H*]-thiopyran-4-one (31) (Fig. 4). The authors concluded that bond lengths in the latter structure were consonant with contributions in a 2:1 ratio of localised and delocalised valence bond structures (31). The presence of the negative charge on O in the delocalised structure presumably favours the S...O contacts.

Apart from the S...O contacts mentioned above, similar contacts have been noted in a variety of compounds over a spectrum of S...O distances, especially when the contact results in a 5-membered ring system (32), and have been the subject of theoretical calculations (33). Notably, there are several structures, including **21** above, in which the significance of similar contacts has been overlooked.

[4]The crystallographic numbering schemes used to identify atoms as indicated in Figs. 1 and 3 are used throughout the following discussions of the structures of **10** and **16***a*. In **10** the first digit in any atom number refers to molecule **1** or molecule **2**.

[5]A complete set of data may be purchased from the Depository of Unpublished Data, CISTI, National Research Council of Canada, Ottawa, Ont., Canada K1A 0S2.

[6]Cf. H(61) contacts with S(1), C(9), C(11), and C(12) of lengths 2.881, 2.947, 2.732, and 2.861 Å, respectively.

TABLE 4. Bond lengths (Å) and bond angles (deg) for compounds **16***a* and **10**

(*i*) Compound **16***a*

Bond	Length	Bond	Length
S(1)—O(1)	2.829(3)	C(8)—C(10)	1.499(8)
S(1)—C(1)	1.771(3)	C(9)—C(12)	1.469(29)
S(1)—C(7)	1.797(6)	C(10)—C(11)	1.666(29)
S(1)—C(11)	1.781(28)	C(11)—C(12)	1.287(53)
Cl—C(8)	1.759(5)	Contacts	
Cl—C(12)	1.831(29)	C(7)—C(11)	0.897(26)
O(1)—C(2)	1.215(4)	C(7)—C(12)	0.842(28)
C(1)—C(2)	1.469(5)	C(8)—C(11)	0.879(26)
C(1)—C(6)	1.309(4)	C(8)—C(12)	1.041(28)
C(2)—C(3)	1.490(6)	Range C—H distances	
C(3)—C(4)	1.411(8)	C—H	0.79(5)—1.18(17)
C(4)—C(5)	1.437(8)		
C(5)—C(6)	1.499(5)		
C(7)—C(8)	1.299(10)		
C(7)—C(9)	1.513(7)		

Bonds	Angle	Bonds	Angle
C(1)—S(1)—O(1)	55.4(1)	C(7)—C(8)—Cl	117.3(4)
C(7)—S(1)—O(1)	156.7(1)	C(10)—C(8)—Cl	114.5(5)
C(7)—S(1)—C(1)	101.5(2)	C(11)—C(8)—Cl	160.5(21)
C(11)—S(1)—O(1)	148.0(8)	C(11)—C(8)—C(7)	43.5(19)
C(11)—S(1)—C(1)	104.1(7)	C(11)—C(8)—C(10)	84.7(20)
C(11)—S(1)—C(7)	29.0(9)	C(12)—C(8)—Cl	77.0(18)
C(2)—O(1)—S(1)	71.5(2)	C(12)—C(8)—C(7)	40.3(17)
C(2)—C(1)—S(1)	112.7(2)	C(12)—C(8)—C(10)	168.5(20)
C(6)—C(1)—S(1)	126.7(3)	C(12)—C(8)—C(11)	83.8(29)
C(6)—C(1)—C(2)	120.6(3)	C(12)—C(9)—C(7)	32.8(11)
C(1)—C(2)—O(1)	120.4(3)	C(8)—C(10)—C(11)	31.7(9)
C(3)—C(2)—O(1)	122.0(3)	S(1)—C(11)—C(7)	76.5(20)
C(3)—C(2)—C(1)	117.5(3)	S(1)—C(11)—C(8)	168.0(27)
C(4)—C(3)—C(2)	114.9(4)	C(7)—C(11)—C(8)	94.1(32)
C(5)—C(4)—C(3)	120.3(6)	S(1)—C(11)—C(10)	125.3(18)
C(6)—C(5)—C(4)	112.6(4)	C(7)—C(11)—C(10)	157.4(30)
C(5)—C(6)—C(1)	123.9(4)	C(8)—C(11)—C(10)	63.6(18)
C(8)—C(7)—S(1)	116.6(4)	C(9)—C(11)—C(10)	149.0(17)
C(9)—C(7)—S(1)	119.5(4)	S(1)—C(11)—C(12)	117.1(24)
C(9)—C(7)—C(8)	123.8(6)	C(7)—C(11)—C(12)	40.7(17)
C(11)—C(7)—S(1)	74.5(20)	C(8)—C(11)—C(12)	53.5(22)
C(11)—C(7)—C(8)	42.4(19)	C(10)—C(11)—C(12)	117.1(26)
C(11)—C(7)—C(9)	165.9(22)	Cl—C(12)—C(7)	156.0(31)
C(12)—C(7)—S(1)	169.3(22)	Cl—C(12)—C(8)	69.4(16)
C(12)—C(7)—C(8)	53.1(21)	C(7)—C(12)—C(8)	86.6(31)
C(12)—C(7)—C(9)	70.7(22)	Cl—C(12)—C(9)	127.5(21)
C(12)—C(7)—C(11)	95.4(32)	C(8)—C(12)—C(9)	163.1(31)
		Cl—C(12)—C(11)	112.1(23)
		C(7)—C(12)—C(11)	43.9(22)
		C(8)—C(12)—C(11)	42.8(16)
		C(9)—C(12)—C(11)	120.4(28)

(*ii*) Compound **10**

	Length			Angle	
Bond	$n = 1$	$n = 2$	Bonds	$n = 1$	$n = 2$
S(1)—C(2)	1.684(17)	1.690(17)	C(1a)—S(1)—C(2)	102.7(8)	103.3(9)
S(1)—C(1*a*)	1.724(16)	1.737(17)	C(9)—S(2)—C(3)	103.8(8)	103.4(9)
S(2)—C(3)	1.754(16)	1.729(17)	S(1)—C(2)—C(3)	126.5(14)	127.7(15)
S(2)—C(9)	1.810(17)	1.791(21)	S(2)—C(3)—C(2)	124.9(13)	125.7(14)
C(13)—Cl	1.798(16)	1.777(23)	S(2)—C(3)—C(4)	113.0(12)	114.1(13)
C(9)—Cl*		1.29(8)			
C(4)—O(1)	1.225(17)	1.263(18)	C(2)—C(3)—C(4)	121.9(15)	120.2(16)
C(2)—C(3)	1.369(19)	1.347(20)	O(1)—C(4)—C(3)	117.5(16)	115.1(16)

Can. J. Chem. Downloaded from www.nrcresearchpress.com by 41.223.56.140 on 09/07/12
For personal use only.

TABLE 4 (*concluded*)

Bond	Length		Bonds	Angle	
	$n = 1$	$n = 2$		$n = 1$	$n = 2$
C(3)—C(4)	1.476(21)	1.500(22)	O(1)—C(4)—C(4a)	122.7(16)	123.5(16)
C(4)—C(4a)	1.448(21)	1.426(21)	C(3)—C(4)—C(4a)	119.8(15)	121.3(16)
C(1a)—C(4a)	1.359(20)	1.374(21)	S(1)—C(1a)—C(4a)	125.0(14)	123.3(14)
C(1a)—C(8)	1.454(21)	1.387(22)	S(1)—C(1a)—C(8)	115.6(12)	115.5(14)
C(4a)—C(5)	1.424(20)	1.432(22)	C(4a)—C(1a)—C(8)	119.4(16)	121.2(16)
C(5)—C(6)	1.342(21)	1.380(22)	C(4)—C(4a)—C(1a)	123.5(16)	124.0(16)
C(6)—C(7)	1.372(22)	1.349(24)	C(4)—C(4a)—C(5)	116.5(15)	115.5(16)
C(7)—C(8)	1.363(22)	1.387(24)	C(1a)—C(4a)—C(5)	119.9(16)	120.5(16)
C(9)—C(10)	1.513(22)	1.462(31)	C(4a)—C(5)—C(6)	120.4(17)	116.6(18)
C(9)—C(13)	1.535(22)	1.617(27)	C(5)—C(6)—C(7)	120.0(18)	122.0(20)
C(10)—C(11)	1.556(22)	1.657(29)	C(6)—C(7)—C(8)	122.8(19)	122.2(21)
C(11)—C(12)	1.519(22)	1.325(29)	C(1a)—C(8)—C(7)	117.4(17)	117.5(19)
C(12)—C(13)	1.510(21)	1.527(30)	S(2)—C(9)—C(10)	106.8(12)	120.7(19)
			S(2)—C(9)—C(13)	110.5(12)	108.2(14)
			C(10)—C(9)—C(13)	103.4(14)	100.7(19)
			C(9)—C(10)—C(11)	107.7(15)	111.0(20)
			C(10)—C(11)—C(12)	105.1(14)	99.3(20)
			C(11)—C(12)—C(13)	106.2(15)	117.3(24)
			Cl—C(13)—C(9)	107.9(11)	110.2(15)
			Cl—C(13)—C(12)	110.1(11)	113.2(18)
			C(9)—C(13)—C(12)	104.9(14)	99.3(18)
			Cl*—C(9)—S(2)		112(4)
			Cl*—C(9)—C(10)		118(4)
			Cl*—C(9)—C(13)		91(4)

TABLE 5. Selected torsion angles (deg)

(*a*) Compound **16***a*

Bonds	Angle	Bonds	Angle
S(1)—C(1)—C(2)—O(1)	−1.4(4)	C(3)—C(4)—C(5)—C(6)	33.7(5)
C(6)—C(1)—C(2)—O(1)	−179.0(3)	C(4)—C(5)—C(6)—C(1)	−12.0(5)
S(1)—C(1)—C(2)—C(3)	176.8(3)	C(5)—C(6)—C(1)—C(2)	−3.4(5)
C(2)—C(1)—S(1)—C(7)	178.1(2)	S(1)—C(7)—C(8)—Cl	176.6(3)
C(2)—C(1)—S(1)—C(11)	−152.3(8)	S(1)—C(7)—C(8)—C(10)	−4.1(6)
C(6)—C(1)—S(1)—C(7)	−4.5(3)	C(9)—C(7)—C(8)—Cl	0.9(5)
C(6)—C(1)—S(1)—C(11)	25.2(9)	C(9)—C(7)—C(8)—C(10)	−179.9(5)
C(1)—S(1)—C(7)—C(8)	103.9(4)	S(1)—C(11)—C(12)—Cl	−174.5(14)
C(1)—S(1)—C(7)—C(9)	−80.2(4)	S(1)—C(11)—C(12)—C(9)	6.3(25)
C(1)—S(1)—C(11)—C(10)	98.4(16)	C(10)—C(11)—C(12)—Cl	−3.0(20)
C(1)—S(1)—C(11)—C(12)	−90.9(21)	C(10)—C(11)—C(12)—C(9)	177.8(19)
C(6)—C(1)—C(2)—C(3)	−0.8(4)		
C(1)—C(2)—C(3)—C(4)	20.7(5)		
C(2)—C(3)—C(4)—C(5)	−38.4(7)		

(*b*) Compound **10**

Bonds	Angle		Bonds	Angle	
	$n = 1$	$n = 2$		$n = 1$	$n = 2$
S(2)—C(9)—C(13)—Cl	−164(1)	82(2)	C(13)—C(9)—C(10)—C(11)	24(2)	23(2)
S(2)—C(9)—C(13)—C(12)	79(1)	−159(2)	C(9)—C(10)—C(11)—C(12)	−4(2)	−3(2)
S(2)—C(9)—C(10)—C(11)	−93(2)	142(2)	C(10)—C(11)—C(12)—C(13)	−18(2)	−21(3)
C(3)—S(2)—C(9)—C(10)	−172(1)	85(2)	C(11)—C(12)—C(13)—C(9)	33(2)	36(2)
C(3)—S(2)—C(9)—C(13)	76(2)	−160(2)	C(12)—C(13)—C(9)—C(10)	−35(2)	−32(2)

Can. J. Chem. Downloaded from www.nrcresearchpress.com by 41.223.56.140 on 09/07/12
For personal use only.

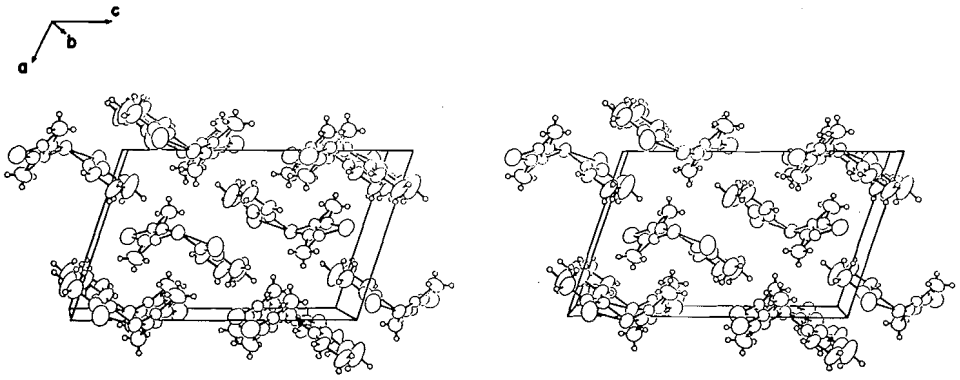


FIG. 2. The crystal packing in compound **16***a* as viewed down ***b***.

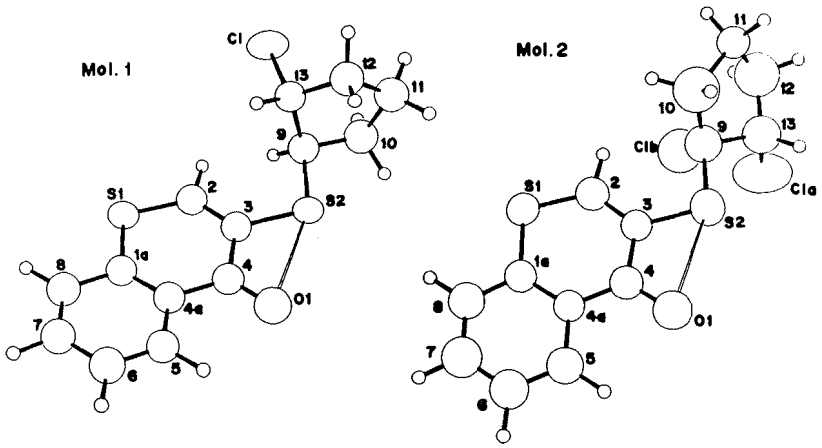


FIG. 3. ORTEP view of the two molecules of compound **10**. The close S...O contacts are indicated by the thinner unfilled bonds.

A view of the crystal packing is given in Fig. 5. The shortest intermolecular contacts of note are the S(11)...S(12)′ and S(22)...S(22)″ contacts of lengths 3.92 and 4.13 Å, S(11)...Cl(11)‴ = 3.46 Å, Cl(11)...H(11) = 3.00, Cl(21)...H(15) = 2.92, Cl(21)...H(19) = 3.02, S(21)...H(12) = 2.81, S(22)...H(213) = 3.02 and O(11)...H(21) = 2.31 Å.

Conclusions

Mechanistically, the formation of adducts such as **16**, **17**, and **18** from **13** can be rationalized in a number of ways. We think it quite plausible, however, that both the α-oxosulfines studied, **1** and **13**, may initially tautomerize to the unsaturated sulfenic acid species **19***a* or **20***a*, respectively. Formation of the corresponding mixed anhydride derivatives may occur with the excess $SOCl_2$ present, to form **19***b* or **20***b* respectively. Well precedented, stereospecific electrophilic addition of such reactive species (34) to the respective alkyne or alkene would then be expected to occur, possibly by way of an intermediate thiirenium or thiiranium ion (35) (see Scheme 1). While the α-oxosulfine **1** appears to undergo similar tautomerization, and hence reacts via the non-Diels–Alder pathway, it should be noted that **13** is, to our knowledge, the first example of a purely aliphatic α-oxosulfine to be studied. Whatever the reason, the α-oxosulfine systems of **1** and **13** are simply too short-lived or, possibly, too conformationally mobile, to follow the Diels–Alder reaction pathway, at least with those dienophiles reported here.

Further studies to delineate the scope of the Diels–Alder reaction of α-oxosulfines, and to explore further the chemistry and novel structural features of the adducts reported in the present work, are presently under way.

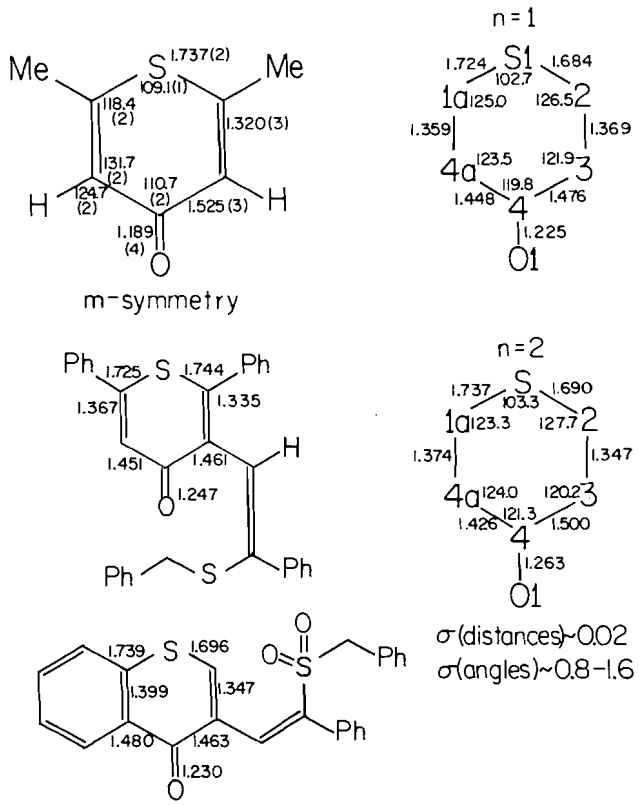


FIG. 4. Principal bond lengths and some bond angles in the thiochromone rings of compound **10** and some related molecules (see text for appropriate references).

Can. J. Chem. Downloaded from www.nrcresearchpress.com by 41.223.56.140 on 09/07/12
For personal use only.

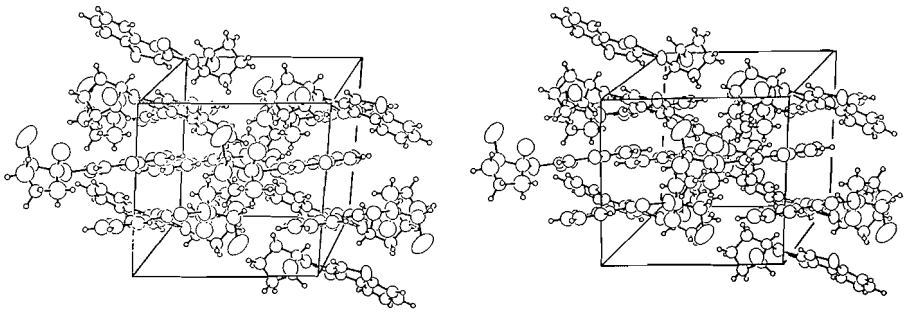
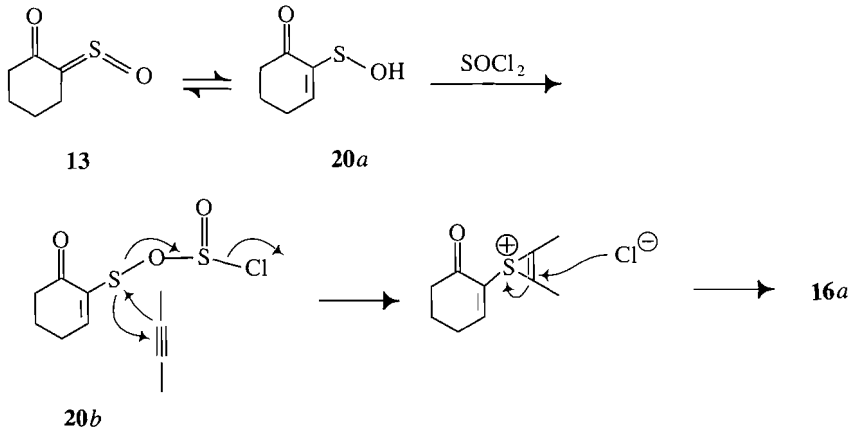


FIG. 5. The crystal packing in compound **10**.



SCHEME 1

Can. J. Chem. Downloaded from www.nrcresearchpress.com by 41.223.56.140 on 09/07/12
For personal use only.

Experimental

Infrared spectra were recorded as KBr discs (solids) or as neat films (liquids), using a Nicolet 5DXB FT-IR spectrometer. The ^{1}H nmr spectra were obtained on a Varian EM-360L spectrometer in $CDCl_3$ solution, unless otherwise indicated. High field ^{1}H nmr and ^{13}C nmr spectra were obtained on Varian XL-400 or XL-200 spectrometers. High- and low-resolution mass spectra were recorded on a VG-70-250S mass spectrometer. Column chromatography was carried out on grade 60, 60 Å silica gel supplied by E. Merck (Darmstadt). Elemental analyses were performed by the Scandinavian Microanalytical Laboratory, Box 25, 2730 Herlev, Denmark.

Dichloromethane and chloroform were dried by distillation over phosphorus pentoxide and stored over 4 Å molecular sieves. Diethyl ether was dried by distillation from sodium benzophenone ketyl. Triethylamine was dried by distillation over calcium hydride and thionyl chloride was purified by distillation over triphenyl phosphite. Potassium iodide was dried at ~140°C for 3 h.

4-Trimethylsilyloxythiochrom-3-ene **2** *(17)*

Dry chloroform (60 mL) was added to potassium iodide (65.70 g, 0.40 mol) with stirring under nitrogen. The mixture was cooled to 0°C and chlorotrimethylsilane (18.0 mL, 0.14 mol) was added. A solution of thiochroman-4-one (9.64 g, 0.059 mol) and triethylamine (33.1 mL, 0.24 mol) in dry chloroform (50 mL) was then added dropwise. The mixture was allowed to warm to room temperature, then the flask was covered with foil paper and refluxed in the dark for 16 h. The reaction mixture was diluted with diethyl ether. The precipitated solid was removed by vacuum filtration and the filtrate was dried ($MgSO_4$). Removal of the solvents on the rotary evaporator yielded **2** as a brown oil (13.5 g, 97%) (36). This was distilled (Kugelrohr) at 180–190°C/0.5 mbar, or used without further purification; ir: ν 1638 (C=C), 1255 (C—O) cm^{-1}: ^{1}H nmr: δ0.2 (s, 9H), 3.4 (d, J = 5 Hz, 2H), 5.2 (t, J = 5 Hz, 1H), 7.1 (m, 3H), 7.5 (m, 1H). (For literature values, see ref. 36.)

2-Benzo-9,10-dimethyl-4,7-dithiaspiro[5.5]undec-9-en-1-one 7-oxide, **4**

A solution of **2** (1.50 g, 6.35 mmol) in dry diethyl ether (5 mL) was cooled to −23°C with stirring under nitrogen. 2,2,6,6-Tetramethylpiperidine (0.90 g, 6.35 mmol) and 2,3-dimethyl-1,3-butadiene (3 mL, 26.5 mmol) were added to the solution. Thionyl chloride (0.76 g, 6.35 mmol) in diethyl ether (3 mL) was then added dropwise. After stirring at −23°C for 6 h, the mixture was allowed to warm to 25°C and stirred for an additional 16 h. The yellow reaction mixture was diluted with diethyl ether. The hydrochloride salt of the base was then removed by vacuum filtration and the filtrate was dried ($MgSO_4$). Removal of the solvent yielded an impure yellow solid (1.42 g). The solid was washed with cold carbon tetrachloride and thiochroman-4-one was recovered from the filtrate. Recrystallization of the remaining solid from CH_2Cl_2/pentane gave tan crystals (0.27 g, 15%) mp 125–126°C; ir: ν 1670 (C=O), 1052 (S=O) cm^{-1}; ^{1}H nmr: δ1.7 (s, 6H), 2.6 (d, J = 4 Hz, 2H), 3.2 (m, 3H), 3.8 (d, J = 14 Hz, 1H), 7.3 (m, 3H), 8.0 (d, J = 6 Hz, 1H); ms m/z (% rel. int.): 274 (33), 273 (42), 272 (100), 257 (28), 255 (38), 243 (89), 229 (19), 227 (29), 201 (32), 147 (18), 136 (31), 121 (15), 100 (27), 91 (16). High-resolution ms: exact mass calcd. for $C_{15}H_{16}O_2S_2$: 292.0592; found: 292.0584.

3-(2'-Chloro-2'-methylpropylthio)thiochromone, **9**

Thionyl chloride (0.62 mL, 8.46 mmol) and 2,6-lutidine (1.0 mL, 8.46 mmol) in dry dichloromethane (4 mL) were cooled to −78°C with stirring under nitrogen. A solution of **2** (2.0 g, 8.46 mmol) in dichloromethane (8 mL) was added dropwise. After 45 min isobutylene was bubbled into the mixture for 5 min and the mixture allowed to warm to 25°C. After 30 h, the mixture was washed with dilute hydrochloric acid, followed by saturated sodium bicarbonate, and

Can. J. Chem. Downloaded from www.nrcresearchpress.com by 41.223.56.140 on 09/07/12
For personal use only.

dried ($MgSO_4$). Filtration and removal of the solvent gave a yellow–brown solid (1.74 g). The nmr spectrum of the crude product indicated the presence of some of the ketone corresponding to **2**. Purification by recrystallization from CH_2Cl_2/pentane yielded tan needles of *B* (see Results and discussion). Further cooling of the filtrate yielded yellow crystals of **9**(*A*), mp 87–88°C (0.45 g, 19%); ir: ν 1596(m), 1582(s) cm^{-1}; ^1H nmr: δ1.7 (s, 6H), 3.4 (s, 2H), 7.6 (m, 3H), 7.9 (s, 1H), 8.6 (m, 1H); ^{13}C nmr ($CDCl_3$): δ31.84q (CH_3's)), 47.32t (SCH_2), 69.46s (CCl), 126.27d, 127.81d, 129.01d, 130.40s, 131.24d, 131.92s, 133.85d, 136.60s, 174.0s (C=O): ms *m/z* (% rel. int.): 286 (2), 284 (5), 249 (41), 248 (38), 215 (31), 194 (100), 162 (21), 149 (33), 136 (24), 121 (17), 112 (32), 108 (16). *Anal.* calcd. for $C_{13}H_{13}ClOS_2$: C 54.82, H 4.60, Cl 12.45, S 22.51; found: C 54.94, H 4.61, Cl 12.00, S 22.02.

trans-*3-(2'-Chlorocyclopentylthio)thiochromone,* ***10***

A solution of **2** (1.50 g, 6.35 mmol) in dry dichloromethane (5 mL) was stirred at −23°C under nitrogen. 2,2,6,6-Tetramethylpiperidine (0.90 g, 6.35 mmol) and cyclopentene (2.0 mL, 22.7 mmol) were added. Thionyl chloride (0.76 g, 6.35 mol) in dichloromethane (3 mL) was added dropwise to the reaction mixture. The hydrochloride salt of the base was removed by vacuum filtration, the filtrate dried ($MgSO_4$), and the solvent removed. The resultant brick-red mixture was stirred at −23°C for 6 h then allowed to warm to 25°C. After 14 h, the mixture was diluted with diethyl ether and the resultant solid (1.98 g) flash chromatographed on silica gel. Dichloromethane eluted a brown oil (1.58 g). Crystallization from CH_2Cl_2/pentane gave yellow needles of **10**, mp 79.5–80.5°C (0.77 g, 41%). (The ^1H nmr spectrum showed that thiochroman-4-one was also recovered by chromatography.) Infrared: ν 1603(s), 1586(s) cm^{-1}; ^1H nmr: δ2.1 (m, 6H), 3.7 (m, 1H), 4.2 (m, 1H), 7.4 (m, 3H), 7.7 (s, 1H), 8.5 (m, 1H); ^{13}C nmr ($CDCl_3$): δ22.58t (C-4'), 30.05t (C-5'), 35.05t (C-3'), 52.05d (C-1'), 65.73d (C-2'), 126.33d, 127.87d, 129.13d, 131.29d, 131.71d, 132.52s, 136.20s, 136.87s, 176.98s (C=O); ms *m/z* (% rel. int.): 299 (27), 297 (65), 262 (13), 261 (35), 260 (100), 227 (19), 194 (62), 149 (14), 136 (12), 121 (19), 108 (11), 89 (9). *Anal.* calcd. for $C_{14}H_{13}ClOS_2$: C 56.65, H 4.41, Cl 11.94, S 21.60; found: C 56.91, H 4.53, Cl 12.16, S 21.42.

E-*3-(2'-Chloro-1'-methyl-1'-propenylthio)thiochromone,* ***11***

A solution of **2** (1.50 g, 6.35 mmol) in dry dichloromethane (5 mL) was stirred at −78°C under nitrogen. 2,2,6,6-Tetramethylpiperidine (0.90 g, 6.35 mmol) and 2-butyne (2.0 mL, 25.6 mmol) were added. Thionyl chloride (0.76 g, 6.35 mmol) in dichloromethane (4 mL) was added dropwise. After stirring at −78°C for 6 h, the reaction mixture was allowed to warm to 25°C and stirred for an additional 14 h before diluting with diethyl ether. The hydrochloride salt of the base was then removed by vacuum filtration, the filtrate was dried ($MgSO_4$) and the solvent removed, resulting in a brown liquid (1.84 g). Flash chromatography on silica gel afforded **11** (0.46 g, 26%). (The ^1H nmr spectrum showed that thiochroman-4-one was also recovered by chromatography.) Dichloromethane/hexane (53:47) eluted a product, recrystallized from CH_2Cl_2/pentane, as off-white crystals of **11**, mp 131–132°C; ir: ν 1615 (s) 1585 (s) cm^{-1}; ^1H nmr: δ2.1 (d, J = 1 Hz, 3H), 2.5 (d, J = 1 Hz, 3H), 7.3 (s, 1H), 7.5 (m, 3H), 8.5 (m, 1H); ^{13}C nmr ($CDCl_3$): δ21.85q, 24.58q, 121.98s, 126.34d, 127.78d, 127.93d, 128.91d, 130.08s, 131.32d, 131.73s, 137.13s, 138.47s, 176.78s; ms *m/z* (% rel. int.): 284 (1), 282 (2), 257 (5), 247 (8), 196 (7), 195 (17), 194 (69), 193 (100), 162 (73), 149 (48), 136 (47), 121 (20), 108 (32), 89 (47). *Anal.* calcd. for $C_{13}H_{11}ClOS_2$: C 55.21, H 3.92, Cl 12.54, S 22.68; found: C 55.48, H 4.19, Cl 12.61, S 22.55.

E-*3-(2'-Chloro-1'-hexenylthio)thiochromone,* ***12***

A solution of **2** (1.50 g, 6.35 mmol) in dry dichloromethane (5 mL) was stirred at −78°C under nitrogen. 2,2,6,6-Tetramethylpiperidine (0.90 g, 6.35 mmol) and 1-hexyne (2.0 mL, 17.4 mmol) were added. Thionyl chloride (0.76 g, 6.35 mmol) in dichloromethane (3 mL) was added dropwise. After stirring at −78°C for 6 h, the reaction mixture was allowed to warm to 25°C and stirred a further 14 h. The mixture was diluted with diethyl ether and the hydrochloride salt of the base removed by vacuum filtration. The filtrate was dried ($MgSO_4$) and the solvent removed, giving a brown oil (1.63 g). Flash chromatography on silica gel (CH_2Cl_2) yielded a dark red oil (0.39 g, 20%). The nmr spectrum showed this to be a mixture (4:1) of the two possible regioisomers. (Thiochroman-4-one was also recovered after chromatography.) Recrystallization from dichloromethane/pentane gave **12**, mp 64–65°C; ir: ν 1600 (m) 1584 (s) cm^{-1}; ^1H nmr: δ0.95 (t, J = 6 Hz, 3H), 1.5 (m, 4H), 2.5 (t, J = 7 Hz, 2H), 6.5 (s, 1H), 7.5 (m, 4H), 8.5 (m, 1H); ms *m/z* (% rel. int.): 312 (9), 310 (19), 277 (12), 276 (20), 275 (100), 247 (9), 196 (10), 195 (16), 194 (96), 149 (28), 136 (36), 121 (32), 108 (35), 89 (56). *Anal.* calcd. for $C_{15}H_{15}ClOS_2$: C 57.96, H 4.86, Cl 11.40, S 20.63; found: C 57.99, H 5.04, Cl 11.71, S 20.33.

9,10-Dimethyl-7-thia-spiro[5.5]undec-9-en-1-one 7-oxide, ***15***

To a solution of 1-trimethylsilyloxycyclohexene **14** (1.00 g, 5.88 mmol) 2,6-lutidine (0.629 g, 0.68 mL, 5.88 mmol) and excess 2,3-dimethyl-1,3-butadiene (2.9 g, 35.4 mmol) in dry CH_2Cl_2 (25 mL) at room temperature, was added thionyl chloride (0.7 g, 5.88 mmol) in dry CH_2Cl_2 (5 mL), dropwise over 10 min with vigorous stirring. The reaction mixture was then stirred at 25°C for 24 h before being washed with water twice. The aqueous layers were combined and re-extracted with CH_2Cl_2. All the CH_2Cl_2 phases were then combined, washed (20 mL 5% $NaHCO_3$), dried ($MgSO_4$), filtered, and concentrated to yield a brown oil (1.0 g) which, upon flash chromatography (EtOAc), yielded the product **15** as a slightly brown oil (0.61 g, 46%); ir: ν 1707 (C=O), 1050 (S=O) cm^{-1}; ^1H nmr: δ1.77 (s, 6H, CH_3), 1.85–2.30 (m, 6H), 2.43 (s, 4H), 3.30 (s, 2H).

E-*2-(2'-Chloro-1'-methyl-1'-propenylthio)-2-cyclohexenone,* ***16***a

A 100 mL flask containing **14** (1.5 g, 8.82 mmol), dissolved in dry CH_2Cl_2 (30 mL) was cooled to −78°C, whereupon 2,6-lutidine (1.1 g, 10.3 mmol) was added in one portion, followed by thionyl chloride (1.63 g, 13.7 mmol) in one portion after 10 min. The solution was then stirred for 30–40 min (during which time it became yellow), before a solution of 2-butyne (1.04 g, 19.2 mmol) in dry CH_2Cl_2 (10 mL) was added dropwise over 10–15 min. After maintaining the reaction temperature at −78°C for 4–5 h the reaction mixture was allowed to warm to room temperature and stirred for a further 16 h. The organic phase was then successively washed with 1 *M* HCl (3 times), saturated $NaHCO_3$ (3 times) and saturated NaCl, before being dried (Na_2SO_4), filtered, and concentrated to yield the crude product as a light brown oil (1.54 g). Purification by flash chromatography (hexane:CH_2Cl_2 = 4:6) yielded a yellow oil (1.0 g) which subsequently crystallized. Recrystallization from pentane yielded pale yellow crystals (0.67 g, 35%) of ***16a***, mp 42–44°C; ir (CCl_4): ν 1689 (C=O), 1596 cm^{-1}; ^1H nmr: δ1.93 (m, 5H), 2.30 (m, 7H), 6.53 (t, J = 4 Hz, 1H); ^{13}C nmr ($CDCl_3$): δ21.59q, 22.78 (C-5), 24.39q, 27.07 (C-4), 38.50t (C-6), 122.03s (C-1'), 134.36s (C-2'), 136.41s (C-2), 143.03d (C-3), 195.75s (C-1). *Anal.* calcd. for $C_{10}H_{13}ClOS$: C 55.42, H 6.00, Cl 16.39, S 14.78; found: C 55.42, H 6.11, Cl 16.30, S 14.76.

Test for ionic Cl

The adduct was dissolved in ethanol and treated with a 3% solution of $AgNO_3$ in ethanol (10–15 drops). After 15 min at 25°C a bulky white precipitate had formed.

E-*2-(2'-Chloro-1',2'-diphenylethenylthio)-2-cyclohexenone,* ***16***b

1-Trimethylsilyloxycyclohexene **14** (1.0 g, 5.87 mmol), 2,6-lutidine (0.70 g, 6.54 mmol) and diphenylacetylene (3.14 g, 17.6 mmol) were dissolved in dry CH_2Cl_2 (30 mL). Thionyl chloride (0.17 g, 5.96 mmol) in dry CH_2Cl_2 (5 mL) was added dropwise over 10 min. The solution immediately turned yellow and was stirred at room temperature for 24 h. After washing the reaction mixture twice with water, the aqueous layers were combined and re-extracted with CH_2Cl_2. The CH_2Cl_2 phases were then combined and washed with 5% $NaHCO_3$ (3 × 20 mL), dried ($MgSO_4$), filtered, and concentrated to yield a yellow solid. Purification by flash chromatography (CH_2Cl_2) yielded the crude product as a brown oil (0.75 g). Further purification by flash chromatography (CH_2Cl_2: hexane = 3:1) yielded a viscous brown oil (0.23 g). A third and final purification by flash chromatography

TABLE 6. Crystal data, details of intensity measurements[a] and structure refinements

Compound	$C_{10}H_{13}ClOS$, **16***a*	$C_{14}H_{13}ClOS_2$, **10**
System	Monoclinic[b]	Triclinic
a (Å)	10.620(2)	10.79(2)
b (Å)	6.571(3)	11.37(2)
c (Å)	16.832(4)	11.97(2)
α (deg)	90.0	88.8(1)
β (deg)	108.17(2)	68.9(2)
γ (deg)	90.0	84.5(1)
V (Å^3)	1116	1364
fw/F(000)	216.7/456	296.81/616
Z/D_{calc} (g cm^{-3})	4/1.29	4(2 ind. mols)/1.445
μ(Mo Kα) (cm^{-1})	4.8	5.6
Space group	$P2_1/n$	$P\bar{1}$
Reflections used in cell determination (No./θ range)	$25/9.4 < \theta < 14.9°$	$23/4.0 < \theta < 11.6°$
Mode/maximum 2θ (deg)	ω:2θ/55	ω:2θ/40
Scan ranges (deg)	0.70 + 0.35 tan θ	0.95 + 0.35 tan θ
Maximum scan time (s)[c]	65	42
Standard reflections (No./interval in s)	3/4000[d]	2/5200[d]
Quadrants	$h, k, \pm l$	$h, \pm k, \pm l$
Number of data collected	3125 (including standards)	3630 (including standards)
No. non-zero data	2279[e]	2831[f]
Structure solution	Direct methods (SHELX), least-squares, Fourier + ΔF Fourier	
No. observed data used in refinements	1461 ($I \geq 3\sigma(I)$)	1356 ($I \geq 2.5\sigma(I)$)
R-factors: $R(wR)$	0.054 (0.060)[g]	0.098 (0.099)[h]
Maximum Δ/σ	0.20	0.29
Weighting scheme	$[\sigma^2(F) + 0.00062F^2]^{-1}$	$[\sigma^2(F) + 0.00248F^2]^{-1}$
Final difference Fourier Maximum peaks (e Å^{-3})	0.37 (near (0.9 Å) S)	0.58 (middle of pentane ring of mol. **2**)
Scattering factors	0.37 (near (0.9 Å) Cl)	0.57 (near O(21))
Programs	From International tables for X-ray crystallography SHELX and Enraf-Nonius SDP package on PDP 11/23 computer	

[a]Enraf-Nonius CAD4 diffractometer: MoKα radiation (graphite monochromator), λ = 0.71069 Å; T = 298 K.

[b]The $P2_1/c$ and $P2_1/n$ cells have very similar dimensions so that the transformation (100/102/0–10) defines a paraorthorhombic C centred cell of dimensions 10.620 × 31.943 × 6.571 with γ = 90.12°, but without the required higher Laue symmetry.

[c]Prescan at 10 deg min^{-1}, other scan speeds chosen to give $I/\sigma(I) \geq 25$ within maximum scan time specified. Backgrounds were obtained by extending scan by 25% on either side of peak and were measured for half the time taken to collect peak.

[d]Declines of 23% and 8.5% in the measured intensities of the standard reflections of **16***a* and **10**, respectively, were corrected for after data reductions (maximum rescale factor on F = 1.441 (1.179) for **16***a*, **10**, respectively).

[e]Rejection of 168 standards and 549 systematically absent or zero F_{obs} data and averaging 220 symmetry equivalent data ($R_{merge}(F)$ = 0.031) gave the indicated number of non-zero data.

[f]Rejection of 78 standards and 721 reflections with F_{obs} = 0.0 gave the indicated number of non-zero data.

[g]Sum of population parameters of disordered double bond atoms constrained to equal 1.0; all non-hydrogen atoms except C(10) and C(11) anisotropic; H-atom parameters allowed to refine (179 variables).

[h]One peak close to atom C(29) and the significantly higher temperature factor for the Cl atom in the second molecule suggested the possibility of some disorder. These two positions were therefore allowed to refine such that the sum of their population parameters was 1.0. Refinement of the second peak position with isotropic thermal motion indicated that it represented ca. 16(2)% of an alternative chlorine position.

Can. J. Chem. Downloaded from www.nrcresearchpress.com by 41.223.56.140 on 09/07/12
For personal use only.

(CH_2Cl_2) yielded **16***b* as a colorless viscous oil (0.050 g, 2.5%). (Lowering the reaction temperature in this case did not markedly improve the yield.) Infrared (CCl_4): ν 1689 (C=O), 1596 cm^{-1}; ^{1}H nmr: δ1.67 (m, 2H), 2.11 (br q, 4H), 6.82 (t, J = 4 Hz, 1H), 7.33 (m, 8H), 7.63 (m, 2H); ms m/z (% rel. int.): 342 (39), 340 (100), 305 (84), 249 (17), 210 (11), 178 (47), 121 (14), 105 (20); high-resolution ms: exact mass calcd. for $C_{20}H_{17}ClOS$: 342.0653, 340.0683; found: 342.0699, 340.0707.

2-(2′-Chloro-2′-methylpropylthio)-2-cyclohexenone, 17

1-Trimethylsilyloxycyclohexene **14** (1.0 g, 5.88 mmol) in dry CH_2Cl_2 (10 mL) was cooled to −78°C. Thionyl chloride (1.22 g, 10.3 mmol) and 2,6-lutidine (0.69 g, 6.44 mmol) were added in one portion and after 30 min isobutylene was bubbled through the solution for 5 min. The mixture was stirred for a further 60 h. The reaction mixture was washed successively with 1 *M* HCl (twice), saturated $NaHCO_3$ (3 times), dried (Na_2SO_4), filtered, and concentrated to afford a light brown oil (0.56 g, 44%); ir (CCl_4): ν 1688 (C=O) cm^{-1}; ^{1}H nmr: δ1.65 (s, 6H, *CH*$_3$), 1.8–2.8 (br m, 6H), 3.10 (s, 2H, *SCH*$_2$), 7.00 (t, J = 4 Hz, 1H, = *CH*); ms m/z (% rel. int.): 182 (100) (M^+ − HCl).

trans-*2-(2′-Chlorocyclopentylthio)-2-cyclohexenone, 18*a

A solution of **14** (1.5 g, 8.82 mmol) in dry CH_2Cl_2 (35 mL) was cooled to −78°C. 2,6-Lutidine (1.1 g, 10.3 mmol) was added in one portion, followed 20 min later by thionyl chloride (1.63 g, 13.7 mmol), also added in one portion. The solution was then stirred for 45 min (solution became yellow) before adding cyclopentene (1.31 g, 19.2 mmol) in dry CH_2Cl_2 (10 mL) dropwise over 20 min. After stirring at −78°C for 4 h, the reaction mixture was allowed to

TABLE 7. Table of final positional ($\times 10^4$) and thermal ($\times 10^3$) parameters[a]

(*i*) Compound **16***a*, $C_{10}H_{13}ClOS$

Atom	*x*	*y*	*z*	U/U_{eq} (Å^2)
S(1)	4936(1)	2316(1)	2805(1)	68.5(3)
Cl	5347(1)	7269(2)	1234(1)	103.0(5)
O(1)	5661(3)	−423(4)	4168(2)	93.5(13)
C(1)	5926(3)	2957(5)	3832(2)	53.3(10)
C(2)	6153(4)	1222(5)	4409(2)	65.4(13)
C(3)	7034(6)	1550(8)	5281(3)	96(2)
C(4)	7191(9)	3601(10)	5541(3)	136(3)
C(5)	7290(7)	5169(8)	4969(3)	97(2)
C(6)	6471(4)	4724(6)	4086(2)	72.3(13)
C(7)[b]	4804(4)	4728(8)	2284(3)	58(2)
C(8)[b]	5528(4)	4973(7)	1795(3)	64(2)
C(9)	3814(5)	6282(9)	2384(4)	90(2)
C(10)	6530(7)	3541(12)	1647(5)	103(3)
C(11)[b]	5451(26)	4056(43)	2156(15)	47(8)
C(12)[b]	4817(26)	5749(48)	1984(15)	53(9)

[a]All atoms refined anisotropically except C(11) and C(12): U_{eq} = (1/3)trace *U*.
[b]Population parameters: C(7) and C(8) = 0.85(2), C(11) and C(12) = 0.15(2).

(*ii*) Compound **10**, $C_{14}H_{13}ClOS_2$

Atom	*x*	*y*	*z*	U/U_{eq} (Å^2)
S(11)	7886(5)	690(5)	−2338(4)	67(2)[a]
S(12)	5384(4)	914(5)	1467(4)	61(2)[a]
Cl(11)	9264(5)	−200(5)	1644(5)	87(3)[a]
O(11)	4057(13)	2235(10)	188(11)	74(4)
C(12)	7232(17)	561(15)	−840(14)	56(5)
C(13)	6052(16)	1114(14)	−86(14)	52(5)
C(14)	5146(17)	1864(14)	−539(15)	55(5)
C(11a)	6760(16)	1721(14)	−2622(15)	52(5)
C(14a)	5582(17)	2168(14)	−1793(15)	53(5)
C(15)	4749(17)	3041(15)	−2127(15)	57(5)
C(16)	5120(18)	3430(16)	−3256(16)	67(5)
C(17)	6302(18)	2974(16)	−4100(17)	64(5)
C(18)	7160(18)	2151(16)	−3841(16)	63(5)
C(19)	6698(17)	24(15)	1784(15)	59(5)
C(110)	6124(19)	−327(16)	3083(16)	72(6)
C(111)	6445(18)	612(15)	3841(16)	69(6)
C(112)	7295(17)	1438(15)	2935(14)	65(5)
C(113)	7816(16)	781(15)	1749(15)	56(5)
S(21)	11158(5)	2982(5)	−107(4)	66(2)[a]
S(22)	9981(5)	3864(5)	3683(5)	83(3)[a]
Cl(21)[b]	10848(9)	1576(10)	5413(10)	158(6)[a]
Cl(22)[b]	11793(82)	2129(77)	3339(69)	247(48)
O(21)	7804(13)	4495(11)	3009(11)	84(4)
C(22)	11075(19)	3216(15)	1309(15)	66(5)
C(23)	10012(17)	3659(14)	2246(15)	56(5)
C(24)	8723(18)	4060(16)	2083(16)	64(5)
C(21a)	9557(17)	3455(15)	−51(15)	59(5)
C(24a)	8551(16)	3884(15)	974(15)	55(5)
C(25)	7233(19)	4201(16)	975(18)	74(6)
C(26)	7049(21)	4065(17)	−96(18)	83(6)
C(27)	8059(21)	3672(18)	−1100(20)	92(7)
C(28)	9332(20)	3332(16)	−1111(17)	77(6)
C(29)	11597(21)	3238(22)	3607(19)	85(7)
C(210)	12745(29)	3937(25)	3192(25)	144(10)
C(211)	13729(18)	3641(16)	3972(16)	65(5)
C(212)	13015(28)	2896(26)	4752(25)	148(10)
C(213)	11530(21)	2945(20)	4954(20)	91(7)

[a]Atom refined anisotropically: U_{eq} = (1/3)trace *U*.
[b]Population parameters: Cl(21) = 0.83(2), Cl(22) = 0.16(2).

warm to 25°C and stirred a further 12 h. The CH_2Cl_2 phase was then washed successively with 1 *M* HCl (3 times), saturated $NaHCO_3$ (3 times) and saturated NaCl (3 times), dried (Na_2SO_4), filtered, and concentrated to yield the crude product as a brown oil (1.67 g). Purification by flash chromatography (ethyl acetate:hexane = 1:9) yielded a yellow liquid (1.0 g, 46%); ir: ν 1682 (C=O), 1589 cm^{-1}; ^{1}H nmr: δ1.7–2.3 (br m, 7H), 2.50 (br q, 5H), 3.55 (m, 1H, *SCH*), 4.20 (m, 1H, Cl*CH*), 6.90 (t, J = 4 Hz, 1H, =CH); ^{13}C nmr: δ22.04t (C-4′), 22.23t (C-5), 26.85t (C-4), 29.58t (C-5′), 34.47t (C-3′), 38.09t (C-6), 50.80d (C-1′), 65.24d (C-2′), 135.00s (C-2), 145.13d (C-3), 195.27s (C-1).

trans-*2-(2′-Chlorocyclohexylthio)-2-cyclohexenone*, ***18***b

A solution of dry CH_2Cl_2 (35 mL) containing **14** (1.5 g, 8.82 mmol) was cooled to −78°C before 2,6-lutidine (1.1 g, 10.3 mmol) was added in one portion. After 20 min thionyl chloride (1.63 g, 13.7 mmol) was added in one portion and the mixture stirred for 1 h (became yellow), whereupon cyclohexene (1.57 g, 19.2 mmol) in dry CH_2Cl_2 (10 mL) was added dropwise over 20–30 min. The reaction mixture was then stirred at −78°C for 4–5 h, followed by 18 h at 25°C. The CH_2Cl_2 phase was successively washed with 1 *M* HCl (3 times), saturated $NaHCO_3$ (3 times) and saturated NaCl (3 times), dried (Na_2SO_4), filtered, and concentrated. This yielded a brown oil containing the desired product (1.7 g). Purification by flash chromatography (CH_2Cl_2) yielded a yellow oil (0.55 g, 26%); ir: ν 1682 (C=O), 1589 cm^{-1}; ^{1}H nmr: δ1.2–2.8 (br m, 14H), 3.35 (br q, 1H, *SCH*), 4.20 (m, 1H, Cl*CH*), 7.07 (t, J = 4 Hz, 1H, =CH).

trans-*2-(2′-Chlorocyclooctylthio)-2-cyclohexenone*, ***18***c

A solution of **14** (1.5 g, 8.82 mmol) in dry CH_2Cl_2 (30 mL) was cooled to −78°C. 2,6-Lutidine (1.1 g, 10.3 mmol) was added in one portion, followed 20 min later by thionyl chloride (1.63 g, 13.7 mmol), also added in one portion. After stirring for 1 h, cyclooctene (2.1 g, 19.2 mmol) in dry CH_2Cl_2 (10 mL) was added dropwise over 10–15 min to the now yellow reaction mixture. After 4–5 h at −78°C the reaction mixture was allowed to warm to room temperature and stirred for a further 22 h. The reaction mixture was successively washed with 1 *M* HCl (3 × 30 mL), saturated $NaHCO_3$ (3 × 30 mL) and saturated NaCl (3 × 30 mL), before being dried (Na_2SO_4), filtered, and concentrated to yield the crude product as a brown oil (2.20 g). Purification by flash chromatography (hexane:CH_2Cl_2 = 4:6) yielded the desired product as a yellow oil (1.3 g, 54%); ir: ν 1682 (C=O), 1589 cm^{-1}; ^{1}H nmr: δ1.2–2.4 (br m, 14H), 2.5 (br q, 4H), 3.5 (br m, 1H, S*CH*), 4.2 (br m, 1H, Cl*CH*), 7.00 (t, J = 4 Hz, 1H, =*CH*).

X-ray crystallography

Crystals of **16***a* suitable for X-ray work were obtained from pentane as low mp colourless or slightly yellow plates or flakes with a waxy appearance and somewhat rounded edges. A crystal of maximum dimensions 0.30 × 0.42 × 0.12 mm in the ***a***, ***b***, ***c*** directions was used throughout. Crystals of **10** were cloudy white rhombs. Despite the crystal used being of more than sufficient size (0.113 × 0.16 × 0.275 mm), diffraction intensities from this crystal were weak and very broad. Consequently it was difficult to centre even the low angle reflections of sufficient intensity. This has resulted in a somewhat inaccurate cell and led to the decision not to extend the data collection beyond $2\theta_{max}$ of 42°. Further work on the diffractometer gave the crystal data for both compounds summarized in Table 6, which also contains a summary of the intensity measurements and structure refinements undertaken. A slow steady decline in the intensities of the standard reflections for both crystals was observed during the data collections and at the end the crystal of **16***a* had turned slightly cloudy. Lorentz, polarization, and corrections for crystal decay were applied to all data collected. The structures were solved by the use of direct methods. Towards the end of the refinement of **16***a* two residual peaks clearly indicated that there was some disorder in the arrangement of the double bond with respect to S, Cl, and the two methyl groups. Similar disordered arrangements of stilbene and related molecules have been observed. For compound **10** the small number of observed data (even with the criterion $I \geq 2.5\sigma(I)$) has limited the refinement of anisotropic thermal parameters to only the S and Cl atoms.

Can. J. Chem. Downloaded from www.nrcresearchpress.com by 41.223.56.140 on 09/07/12
For personal use only.

A significant difference in the thermal parameters for the Cl atoms and the observation of a significant peak near C(29) in the second molecule has been refined as a 85:15 disordered arrangement of the Cl(2) atom. Hydrogen atoms have been placed in calculated positions. Least-squares refinements minimizing $\Sigma w \Delta F^2$ with the conditions specified have converged to the indicated residuals (Table 6). The final atomic positional and equivalent isotropic thermal parameters are given in Table 7. Tables of anisotropic thermal parameters, calculated hydrogen atom positions, least-squares mean planes, and final structure factor amplitudes for the observed reflections for both compounds have been deposited.[5]

1. J. F. KING and T. DURST. Tetrahedron Lett. 585 (1963).
2. B. ZWANENBURG. Recl. Trav. Chim. Pays-Bas. **101**, 1 (1982).
3. I. W. J. STILL and F. J. ABLENAS. J. Chem. Soc. Chem. Commun. 524 (1985).
4. B. G. LENZ, H. REGELING, and B. ZWANENBURG. Tetrahedron Lett. **25**, 5947 (1984).
5. M. G. MATTURO and R. P. REYNOLDS. Tetrahedron Lett. **28**, 4981 (1987).
6. K. GOLLNICK and A. GRIESBECK. Tetrahedron Lett. **25**, 4921 (1984).
7. R. HUISGEN and J. RAPP. J. Am. Chem. Soc. **109**, 902 (1987).
8. K. STELIOU, P. SALAMA, D. BRODEUR, and Y. GAREAU. J. Am. Chem. Soc. **109**, 926 (1987).
9. W. ANDO, Y. KUMAMOTO, and N. TOKITOH. Tetrahedron Lett. **28**, 4833 (1987).
10. M. V. LAKSHMIKANTHAM, M. S. RAASCH, M. P. CAVA, S. G. BOTT, and J. L. ATWOOD. J. Org. Chem. **52**, 1874 (1987).
11. R. HUISGEN and X. PENG. Tetrahedron Lett. **27**, 6063 (1986).
12. U. ZOLLER and P. RONA. Tetrahedron Lett. **26**, 2813 (1985).
13. A. A. FREER, G. W. KIRBY, and R. A. LEWIS. J. Chem. Soc. Chem. Commun. 718 (1987).
14. B. G. LENZ, H. REGELING, H. L. M. VAN ROZENDAAL, and B. ZWANENBURG. J. Org. Chem. **50**, 2930 (1985).
15. J. MATTAY and C. DITTMER. J. Org. Chem. **51**, 1894 (1986).
16. W. S. LEE, O. S. PARK, J. K. CHOI, and K. D. NAM. J. Org. Chem. **52**, 5374 (1987).
17. I. W. J. STILL and F. J. ABLENAS. Can. J. Chem. **62**, 2535 (1984).
18. I. W. J. STILL and G. W. KUTNEY. J. Org. Chem. **46**, 4911 (1981).
19. T. C. BRITTON, T. J. LOBL, and C. G. CHIDESTER. J. Org. Chem. **49**, 4773 (1984).
20. K. OKA. Synthesis, 661 (1981).
21. J. STRATING, L. THIJS, and B. ZWANENBURG. Recl. Trav. Chim. Pays-Bas. **86**, 641 (1967).
22. (*a*) A. BAX and G. A. MORRIS. J. Magn. Reson. **42**, 501 (1981); (*b*) A. BAX. J. Magn. Reson. **53**, 517 (1983).
23. G. VALLE, V. BUSETTI, and G. GALIAZZO. Cryst. Str. Commun. **10**, 867 (1981).
24. J. BERNSTEIN and K. MIRSKY. Acta Crystallogr. A**34**, 161 (1978).
25. A. J. KRESGE, J. F. SAWYER, and T. I. YOUSAF. Acta Crystallogr. C**44**, 1590 (1988).
26. D. G. HAY, P. DEMUNK, and M. F. MACKAY. Aust. J. Chem. **34**, 559 (1981).
27. W. ADAM, E. M. PETERS, K. PETERS, E. SCHMIDT, and H. G. VON SCHNERING. Chem. Ber. **116**, 1686 (1983).
28. K. GORLER, W. MOLLS, H. U. SIEHL, J. STRAHLE, and C. WESTPHAL. Justus Liebig's Ann. Chem. 1006 (1982).
29. A. BANERJEE, C. J. BROWN, and P. C. JAIN. Acta Crystallogr. C**41**, 1505 (1985).
30. W. H. WATSON, J. GALLOY, D. A. GROSSIE, and J. NAKAYAMA. Acta Crystallogr. C**40**, 190 (1984).
31. C. H. CHEN, G. A. REYNOLDS, D. L. SMITH, and J. L. FOX. J. Org. Chem. **49**, 5136 (1984).
32. (*a*) T. R. LYNCH, I. P. MELLOR, and S. C. NYBURG. Acta Crystallogr. B**27**, 1948 (1971); (*b*) A. ATKINSON, A. G. BREWSTER, S. V. LEY, R. S. OSBORN, D. ROGERS, D. J. WILLIAMS, and K. A. WOODE. J. Chem. Soc. Chem. Commun. 325 (1977).
33. J. G. ÁNGYÁN, R. A. POIRIER, A. KUCSMAN, and I. G. CSIZMADIA. J. Am. Chem. Soc. **109**, 2237 (1987).
34. E. KÜHLE. The chemistry of the sulfenic acids. G. Thieme, Stuttgart, West Germany. 1973. pp. 44–55.
35. G. H. SCHMID, M. STRUKELJ, and S. DALIPI. Can. J. Chem. **65**, 1945 (1987) and references therein.
36. L. H. HELLBERG and A. JUAREZ. Tetrahedron Lett. 3553 (1974).

Can. J. Chem. Downloaded from www.nrcresearchpress.com by 41.223.56.140 on 09/07/12
For personal use only.

Fermi level pinning or semiconductor electrodes in aqueous and non aqueous electrolytes: influence of the modification of the electrode surface

O. SAVADOGO

Département de Génie Métallurgique, École Polytechnique de Montréal, C.P. 6079, succ. "A", Montréal (Qué.), Canada H3C 3A7

Received May 25, 1988

O. SAVADOGO. Can. J. Chem. **67**, 382 (1989).

Modification of several semiconductors material surfaces with $H_4SiW_{12}O_{40}.nH_2O$ have been carried out to produce an increase in the open circuit photopotential at the semiconductor/electrolyte interface (V_{oc}) without changing the flat-band potential. The augmentation of V_{oc} is shown to be attributed to a decrease of the minority carriers recombination at the semiconductor/electrolyte interface along with the suppression of Fermi level pinning. The enhancement of V_{oc} and the electrocatalytic activity of the hydrogen evolution reaction in acidic medium of the derivatized electrodes is attributed to the Fermi level unpinning.

Key words: photoelectrodes, photoelectrocatalysis, pinning, modification improvement.

O. SAVADOGO. Can. J. Chem. **67**, 382 (1989).

La modification des surfaces de matériaux semiconducteurs avec $H_4SiW_{12}O_{40}.nH_2O$ conduit à une augmentation de la tension en circuit ouvert des cellules photoélectrochimiques (V_{oc}) et à une diminution de la surtension des cellules photoélectrocatalytiques pour la réaction de dégagement d'hydrogène en milieu acide. Les potentiels de bandes plates des matériaux ne sont pas influencés par cette modification. Ces résultats sont attribués à une diminution du taux de recombinaison des porteurs minoritaires due à la suppression de l'ancrage du niveau de Fermi des matériaux.

Mots clés : photoélectrodes, photoélectrocatalysis, accrochage, modification amelioration.

Can. J. Chem. Downloaded from www.nrcresearchpress.com by 41.223.56.140 on 09/07/12
For personal use only.

Introduction

Because of their acidic and redox properties, the heteropoly compounds (HPCs) have been recognized and used as heterogeneous catalysts (1–6). The homogeneous catalytic properties of HPCs have also been investigated and related to their redox properties (7–12). Further, other electrochemical studies have shown that formation of various HPC complexes (13, 14) was possible by changing the pH, and their analytical properties have been considered (15–18). In view of these interesting properties they appeared to be valuable candidates for conversion and for storing high energy (19–22).

The activation of electrodes surfaces by HPCs has been established and the electrocatalysis of the hydrogen evolution reaction at modified electrodes by heteropolyanions have been studied (23). Hence, the exchange current densities for the hydrogen reaction on various electrode materials improved after derivatization of the electrodes with heteropolyanions (23–26); the potential also improved. In general, it has been found that heteropolyanions (HPA), isopolyanions (IPA), and monotungstate (MW) electrolytes can modify metal or semiconductor electrode surfaces (26). In particular, the reduction of oxygen on HPA modified glassy carbon electrode has been investigated with improvements in exchange current density and decrease in overpotential of the oxygen reduction reaction (27).

The effect of acidity on the behaviour of cyclic voltammetric curves of phosphotungstic and silicotungstic heteropolyanions in water and *N*-dimethylformamide which are in contact with a glassy carbon electrode has been determined by Keita and Nadjo (28). They showed that the evolution of the voltammetric pattern for several heteropolycompounds appeared to be largely dominated by acido-basic properties. Further, their study of the reduction process of silicotungstic species by cyclic voltammetry in strongly acidic aqueous solutions and in dimethylformamide with stepwise increase of perchloric acid shows important morphological changes in the waves. These observations were explained on the basis of solvent effects. Hence, solvation and ion pairing of silicotungstic and phosphotungstic species in acidic concentrated aqueous solutions of alkali-metal salts have shown that $SiW_{12}O_{40}^{4-}$ and $PW_{12}O_{40}^{3-}$ were suitable reference redox systems in acidic aqueous solutions (29). This study of the reduction currents of heteropolyanions shows that $SiW_{12}O_{40}^{4-}$ appears to be a good discriminating probe for the structure of electrolytes in aqueous solutions (30).

The purpose of this paper is to present the results of a study on the behaviour of the flat band potentials of several semiconductors derivatized by silicotungstic acid in aqueous solution. For comparison, the flat band potentials of modified electrodes have been measured in 1,2-dichloroethane with tetra-*n*-butylammonium perchlorate as supporting electrolyte.

Experimental

Electrodes

The reference electrode was a saturated calomel electrode (SCE). The counter electrode was a platinum gauze of large surface area, and the working electrode, monocrystalline semiconductors. These semiconductor crystals employed were n- and p-GaAs, n- and p-InP, n-GaP, and n- and p-Si. The sources of the single crystals, their doping density, and the etching procedures are given in Table 1.

Each experiment to determine current–potential and capacitance–potential characteristics were carried out at least three times to insure reproducibility of the data.

Electrochemical equipment and apparatus

The capacitance of the electrode/electrolyte interface at various electrode potentials was measured with a PARC frequency response analyzer (Model 378) and a PARC electrochemical interface (Model 276).

Chemicals

All chemicals were reagent grade quality, $H_4SiW_{12}O_{40}.nH_2O$ (Fisher Scientific) and H_2SO_4 (BDH) were used. Pure water was obtained by bidistillation. 1,2-Dichloroethane with tetra-*n*-butyl ammonium perchlorate (TBAP) (Fisher Scientific) was used for non-aqueous medium and was not purified before use.

pH variation

The variation of the pH in the 1,2-dichloroethane electrolyte was obtained by a method described elsewhere (31). Briefly, changes of the

TABLE 1. Electrodes and etching processes

Semiconductor	Density (n or p) (in cm^{-3})	Origin	Etching
p-Si n-Si	$\sim 10^{15}$, $\sim 10^{18}$ $\sim 5 \times 10^{14}$ $\sim 10^{18}$	Rhône–Siltec	HNO_3:CH_3COOH:HF (3:1:3 by volume) followed by HF 49% and rinsed with distilled water
p-GaAs n-GaAs	$\sim 10^{18}$	Radiotechnique Compelec	Trichloroethylene for 30 s, $H_2SO_4+H_2O_2$ (30%) (3:1 by volume) for 10 s then rinsed with distilled water
p-InP n-InP n-GaP	$\sim 10^{18}$ $\sim 10^{18}$ $\sim 10^{19}$	Centre National d'Etude et de Télécommunication Radiotechnique Compelec	Trichloroethylene for 30 s, Br_2 (5%) + CH_3OH for 15 s, and CH_3OH for 30 s, then rinsed with distilled water

TABLE 2. Derivatization potentials and times of the different electrodes in 1 M H_2SO_4 with 5×10^{-4} M $H_4SiW_{12}O_{40}.nH_2O$

Semiconductor	Potential (in V/SCE)	Time (in min)
p-Si	−1.0	~30
n-Si	−1.2	~30
p-GaAs	−1.1	~45
n-GaAs	−1.3	~45
p-InP	−1.1	~45
n-InP	−1.0	~45
n-GaP	−2.0	~25

pH toward more acidic values were obtained by saturating the electrolyte with gaseous HCl. The HCl solubility was determined by measuring the pH of a known volume of pure water equilibrated with a saturated HCl solution in 1,2-dichlorethane. At room temperature HCl is soluble up to 5×10^{-2} M. Measurements were carried out after stirring the two phases and waiting for their separation.

Results and discussion

Electrodes derivatization and electrocatalysis

The modification of the material surfaces was performed under potentiostatic conditions during illumination of the surface for p-type materials and under darkness for n-type materials. The supporting electrolyte for derivatization was 1 M H_2SO_4 which contains 5×10^{-4} M $H_4SiW_{12}O_{40}.nH_2O$ in a nitrogen atmosphere. The modifications were achieved with very negative potentials to the cathodic–anodic transition potential. The derivatization procedure of Keita and Nadjo (23) was employed.

During the derivatization process the observed current gradually increased with gas evolution. The time derivatization was determined after stabilisation of the current. For p-type electrodes, power input of 50 mW cm^{-2} with a He–Ne laser was used to achieve the modifications. The derivatization times and potentials of the different electrodes are collected in Table 2. Typical examples of cyclic voltammetry patterns obtained during the surface modification of p-type GaAs and p-type InP

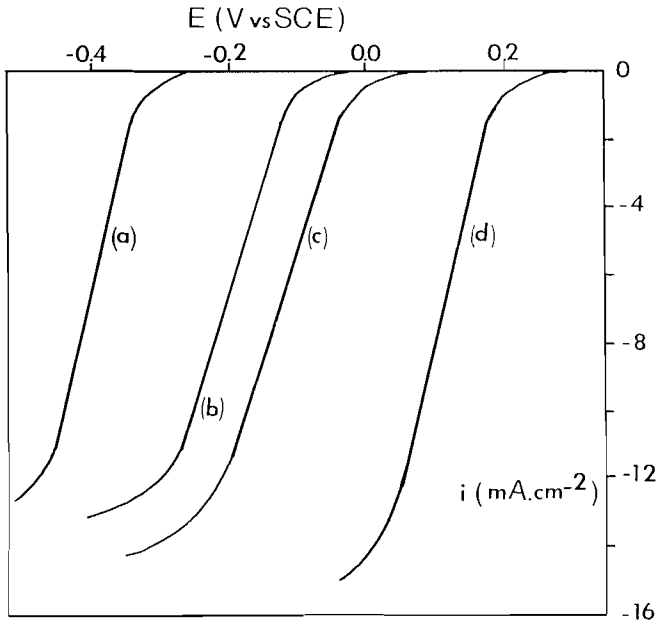


FIG. 1. Current–potential curves obtained in stirred solutions at a potential sweep of 100 mV/s. (*a*) and (*c*) cathodic: current–potential (I–V) curve for p-type GaAs and p-type InP electrodes in 1 M HCl alone; (*b*) and (*d*): cathodic I–V curve for p-type GaAs and p-type InP electrodes in 1 M HCl, following derivatization with 5×10^{-4} M $SiW_{12}O_{40}^{4-}$ in a supporting electrolyte of 1 M H_2SO_4.

are shown in Fig. 1. As indicated the successive cycles obtained after derivatization showed longer increases in cathodic current than those measured before derivatization. The cathodic electrocatalysis were even maintained after transferring the electrode to a supporting electrolyte without $H_4SiW_{12}O_{40}.nH_2O$. As for other published data (23, 24), stability of the derivatization is observed.

The improvement in overpotential for hydrogen evolution on p-type materials has been determined by measuring the potential shift between modified photocathodes and base photocathodes (ΔV) at a light power input of 50 mW cm^{-2} and a current density

Can. J. Chem. Downloaded from www.nrcresearchpress.com by 41.223.56.140 on 09/07/12
For personal use only.

Can. J. Chem. Downloaded from www.nrcresearchpress.com by 41.223.56.140 on 09/07/12
For personal use only.

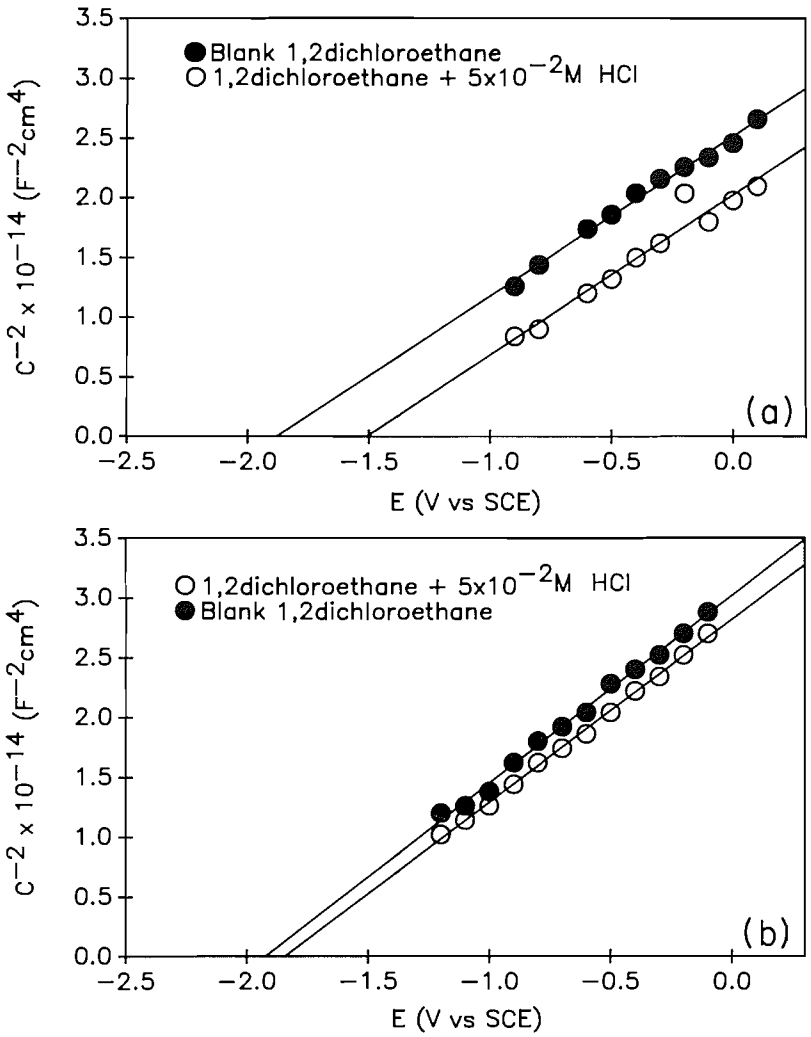


FIG. 2. (*a*) Schottky–Mott plots for n-GaP in contact with 1,2-dichloroethane charged with 0.1 *M* TBAP before modification with $H_4SiW_{12}O_{40}.nH_2O$. (*b*) Schottky–Mott plots for n-GaP in contact with 1,2-dichloroethane charged with 0.1 *M* TBAP after modification with $H_4SiW_{12}O_{40}.nH_2O$. In the two cases, measurements were performed at 6.3 kHz.

TABLE 3. Improvements in overpotential ΔV for the hydrogen evolution reaction of different photocathodes modified by $H_4SiW_{12}O_{40}.nH_2O$ at light power illumination of 50 mW cm^{-2} and a current density of 5 mA cm^{-2}

Materials	ΔV (V)
p-GaAs	0.20–0.25
p-InP	0.25–0.30
p-Si	0.35–0.40

TABLE 4. V_{fb} (V/SCE) of various materials in HCl before and after modification by $H_4SiW_{12}O_{40}.nH_2O$

	Electrode			
	Not modified		Modified in $H_4SiW_{12}O_{40}.nH_2O$	
Material	1 *M* HCl	10^{-3} *M* HCl	1 *M* HCl	10^{-3} *M* HCl
p-Si	~ +0.07	~ −0.18	+0.05	0.00
n-Si	~ −0.50	~ −0.75	−0.60	−0.65
n-GaP	−1.45	−1.70	−1.35	−1.40
p-GaAs	−0.05	−0.25	+0.10	+0.05
n-GaAs	−0.80	−1.0	−0.80	−0.75
p-InP	+0.90	+0.55	+0.80	+0.75
n-InP	−0.35	−0.50	−0.40	−0.45

of 5 mA cm^{-2} (see Table 3). The stability of the improvement in potential for hydrogen evolution reaction (h.e.r.) has been checked by comparing the measurements done at one month interval. Experiments over longer periods of time would be necessary to further support their stability. This variation in overpotential is not atributed to certain thermodynamics consideration but to certain kinetics phenomena. In particular, a decrease of the available minority carrier recombination at the semiconductor/electrolyte interface can account for the results. This is favored by electrode surface modifications. Analogous results have been obtained on p-type GaAs modified with cobalt (32). Thus, a systematic comparison of other photoelectrocatalytic and electrocatalytic properties of the modified p-type GaAs and p-type InP to efficient hydrogen cathodes or photocatocathodes is planned.

TABLE 5. Open circuit photopotentials V_{oc} (V/SCE) in 0.1 *M* HCl of some semiconductors after modification by $H_4SiW_{12}O_{40}.nH_2O$

	V_{oc}						
Material	$Eu^{2+/3+}$	$V^{2+/3+}$	$Sn^{2+/4+}$	I/I_2	$Fe(CN)^{4-/3-}$	$Fe^{2+/3+}$	$Ce^{3+/4+}$
n-GaAs	0.10	0.25	0.50	0.65	0.75	0.85	1.10
n-InP	0.05	0.20	0.45	0.70	0.80	0.90	1.05

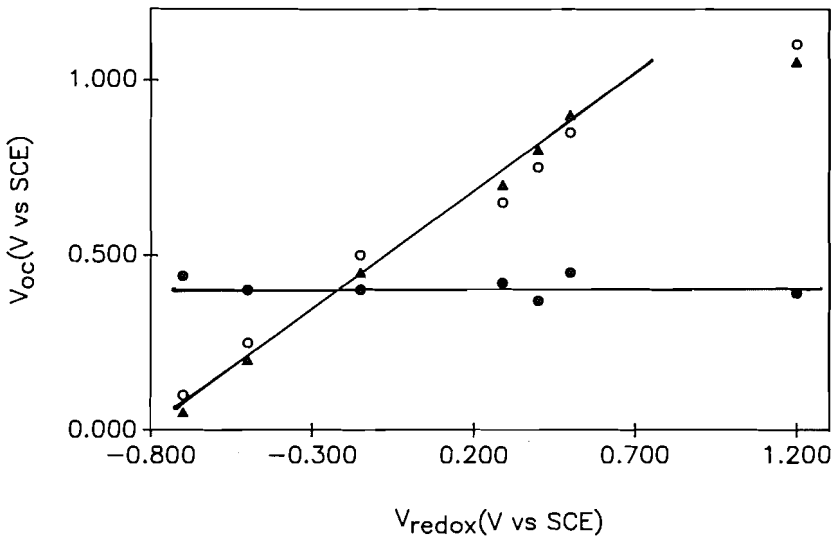


FIG. 3. Variation of V_{oc} with V_{redox} using data of Tables 5 and 7, ○, n-GaAs; ▲, n-InP after derivatization with $H_4SiW_{12}O_{40}.nH_2O$; ●, n-GaAs before derivatization with $H_4SiW_{12}O_{40}.nH_2O$.

Effect of the derivatization on the flat band potential and the open circuit photopotential of the photoelectrodes

The energy levels of the materials were determined from the knowledge of the flat band potential (V_{fb}). The V_{fb} was deduced from impedance measurements. Plots of C^{-2} vs. V are straight lines in a large potential interval (see Fig. 2). Thus the Schottky–Mott (S–M) model is verified for these interfaces, i.e. the following equation applies:

$$[1] \quad \frac{1}{C^2} = \frac{2}{e \in \epsilon_0 N}\left(V - V_{fb} - \frac{kT}{e}\right)$$

Here C is the interface capacitance per unit area, e the electron charge (1.6×10^{-19} C), $\in$ the semiconductor dielectric constant, ϵ_0 the vacuum permittivity (8.85×10^{-14} F/cm), and N, the donor (n-type) or acceptor (p-type) density. From the measurement, V_{fb} was determined with an accuracy of ±0.100 V.

(1) Studies in aqueous acidic medium

The flat band potential values in darkness are collected in Table 4. For the p-type silicon, capacitance–voltage measurements were done after stabilization of the p-Si/electrolyte interface by cycling the electrode between −0.5 V and −1.5 V vs. SCE until no further change in current potential curve was observed. Here, no significant difference exists in the reproducibility of the capacitance–voltage curves measured with and without $[Fe(CN)_6]^{3-}$. The measurements were carried out in the electrolyte with and without $[Fe(CN)_6]^{3-}$. $[Fe(CN)_6]^{3-}$ was added because it has been shown that this species produces reproducibility (33). Hence, under our experimental conditions, cycling of the interface is an efficient means of obtaining reproducible capacitance–voltage curves. Since illumination has no influence on V_{fb} the data obtained under illumination are not shown. As can be seen in Table 4 there is a remarkable variation of V_{fb} with the (H_3O^+) species before modification of the electrode surface. This variation of V_{fb} with (H_3O^+) is generally attributed to the adsorption of H_3O^+ or OH^- ions on the electrode surface (34, 35) depending on the acid–base character of the surface. On the other hand, modification of the surface with $H_4SiW_{12}O_{40}.nH_2O$ (with an acidic character (7–12)) did not result in variation of V_{fb} with (H_3O^+). From these data it can be concluded that modification of the electrodes results in the adsorption of species at the surface, thus preventing the adsorption of (H_3O^+). Further they confirm that the acid–base of $H_4SiW_{12}O_{40}.nH_2O$ determine the behaviour of the interface. A systematic study using electrochemical techniques and Scanning Auger Microscopy is planned to monitor the chemical nature of the electrode surfaces before and after derivatization.

The presence of either $Eu^{2+/3+}$, $V^{2+/3+}$, $[Fe(CN)_6]^{4-/3-}$, $Fe^{2+/3+}$, or $Ce^{3+/4+}$ as redox couple in the electrolyte was shown to have no effect on V_{fb} after electrode derivatization, and thus the data obtained with redox couples are not shown. This can be attributed to Fermi level unpinning (36, 37). Further support to this conclusion can be found through measuring the open circuit photopotentials V_{oc} of the modified photoelectrodes. V_{oc} is the barrier height of semiconductor/liquid junction. It varies with the electrochemical potential of the redox couple, V_{redox}, according to eq. [2]. The V_{oc} values were determined with an accuracy of ±0.100 V under an illumination of 50 mW cm^{-2}. As can be seen in Table 5, V_{oc} is clearly

Can. J. Chem. Downloaded from www.nrcresearchpress.com by 41.223.56.140 on 09/07/12
For personal use only.

TABLE 6. V_{fb} (V/SCE) of some semiconductors in 1 *M* HCl without modification

	V_{fb}				
Material	$Eu^{2+/3+}$	$V^{2+/3+}$	$[Fe(CN)_6]^{4-/3-}$	$Fe^{2+/3+}$	$Ce^{3+/4+}$
n-GaAs	−1.55	−1.40	−0.85	−0.80	+0.05
n-InP	−0.95	−0.75	−0.30	−0.25	+0.5

TABLE 7. Open-circuit photopotentials V_{oc} (V/SCE) in 0.1 *M* HCl of some semiconductors without modification by $H_4SiW_{12}O_{40}.nH_2O$

	V_{oc}				
Material	$Eu^{2+/3+}$	$V^{2+/3+}$	$[Fe(CN)_6]^{4-/3-}$	$Fe^{2+/3+}$	$Ce^{3+/4+}$
n-GaAs	0.39	0.45	0.42	0.40	0.44
n-InP	0.19	0.15	0.20	0.25	0.15

TABLE 8. Variations of V_{fb} (V/SCE) in a 1,2-dichloroethane medium with and without modification by $H_4SiW_{12}O_{40}.nH_2O$

	Not modified		Modified	
Material	"Neutral"	$+ 5 \times 10^{-2}$ *M* HCl	"Neutral"	$+ 5 \times 10^{-2}$ *M* HCl
n-GaP	−1.90	−1.50	−1.75	−1.80
n-GaAs	−1.00	−0.80	−0.95	−0.90
p-GaAs	+0.45	+0.10	+0.35	+0.40
n-InP	−0.80	−0.60	−0.70	−0.75
p-InP	+0.35	+0.05	+0.45	+0.40
n-Si	+0.00	—	+0.10	—
p-Si	+0.60	—	+0.40	+0.50

dependant on V_{redox}. Thus, if Fermi level unpinning is to be occurred, V_{fb} will not (and does not) change with V_{redox}. Because V_{oc} varies as $(V_{fb} - V_{redox})$ (36, 38, 39), it will also vary with V_{redox} as shown by the results.

[2] $V_{oc} = |V_{fb} - V_{redox}|$

As can be seen in Fig. 3, a slope of unity is obtained with n-GaAs and n-InP. According to eq. [2], this implies an important suppression of the Fermi level pinning.

It should be pointed out that the measurements of V_{fb} and V_{oc} obtained with the same electrodes in acidic medium, but without modification of the surface, show that V_{fb} varies with the redox couples (see Table 6) whereas V_{oc} is independent over a large range of V_{redox} (see Table 7). It should be pointed out that constant V_{oc} values are found for n-GaAs (E_g = 1.43 eV), and n-InP (E_g = 1.27 eV) cells for a large number of redox (see Fig. 3 for n-GaAs) systems whose V_{redox} span a range of 2.1 V. Moreover, the potential range over which V_{oc} is independant of V_{redox} is considerably wider than the band gap energy values. This implies Fermi level pinning which is believed to be due to the presence of a high density of interface or surface states (36, 38, 40, 41) or carrier injection due to a sufficient band bending to change the relative carrier density (42–44). Analogous to other published data obtained in non-aqueous (36, 38, 41, 44) and aqueous (35, 40, 45–47) solvents, it could be concluded that a "surface-controlled model" appears to be appropriate to explain these experimental results. We are in the process of determining the effect of material surface chemistry on Fermi level energy. The unpinning of the Fermi level, which occurred after the derivatization, suggests that the effects of the high density of the interface states are suppressed. Thus Fermi level behaviour is governed by material surface chemistry.

Analogous to other published data (31), it is interesting to note that the flat band potential values after modification of n-type ($V_{fb}^{(n)}$) and p-type ($V_{fb}^{(p)}$) Si, with doping density of $\sim 10^{15}$ cm^{-3} and 5×10^{14} cm^{-3}, are +0.05 and −0.60 V/SCE. Thus the difference between these two potentials, i.e. $|eV_{fb}^{(p)} - eV_{fb}^{(n)}|$ equals 0.65 eV. This value compares well with the theoretical value of

[3] $E_g - (\mu_1 + \mu_2) = 0.60$ eV

Here E_g is the energy of the material bang gap, μ_1 is the energy difference between the top of the valence band (E_{Vb}) and the Fermi level (E_F) for the p-type material, and μ_2 the difference of energy between the top of the conduction band (E_{cb}) and E_F. μ_1 and μ_2 can be calculated if the effective state density in the conduction band (N_c) and that in the valence band (N_v) are known (34, 35). For silicon, the values of N_c and N_v are 2.8×10^{19} cm^{-3} and 1.04×10^{19} cm^{-3}, respectively (48). Further, from the n and p values given in Table 1, μ_1 and μ_2 equal 0.25 eV. For n-type and p-type silicons with doping density of 10^{18} cm^{-3} the experimental values of the flat band potential are −0.40 V/SCE $V_{fb}^{(n)}$ and +0.80 V/SCE $V_{fb}^{(p)}$. The difference between these two potentials is 1.20 eV, which is close to the

Can. J. Chem. Downloaded from www.nrcresearchpress.com by 41.223.56.140 on 09/07/12
For personal use only.

TABLE 9. V_{fb} (V/SCE) of modified semiconductors with $H_4SiW_{12}O_{40}.nH_2O$ in "neutral" 1,2-dichloroethane containing different redox couples

	V_{fb}			
Material	$Fe(Cp)^{0/+}$	I^-/I_2	$Perylene^{0/+}$	(Pn^0/Pn^+)
p-GaAs	−0.40	−0.60	−0.45	Pn^+ is quasi
n-GaAs	−0.90	−1.05	−0.95	insoluble in 1,2-
n-InP	−0.75	−0.85	−0.80	dichloroethane

TABLE 10. Open-circuit photopotentials V_{oc} (V/SCE) of modified semiconductors by $H_4SiW_{12}O_{40}.nH_2O$ in "neutral" 1,2-dichloroethane containing different redox couples

	V_{oc}			
Material	I^-/I_2	$Fe(Cp)^{0/+}$	$Perylene^{0/+}$	(Pn^0/Pn^+)
n-GaAs	0.65	0.85	1.10	Pn^+ is quasi
p-GaAs	0.45	0.65	0.90	insoluble in 1,2-
n-InP	0.30	0.55	0.80	dichloroethane

theoretical value of E_g (i.e. 1.12 eV). For InP it is also found that the experimental value agrees with the theoretical value (1.20 eV vs. 1.27 eV). All these findings are similar to those obtained without electrodes modifications in 1,2-dichloroethane media (31), aqueous media (49, 50) or ammonia media (51). Thus, they confirm that the observed variation of the flat band potentials is independent of the conductivity type of the material. In other words, the modification of the electrodes does not change the type of conductivity. Furthermore, the experimental results show that also V_{fb} for modified electrodes does not vary with redox species in the electrolyte.

(2) Studies in 1,2-dichloroethane

The flat band potentials of several materials in 1,2-dichloroethane and acidic pH are given in Table 8. The variations of V_{fb} with different redox species in the electrolyte are presented in Table 9 for modified electrodes.

As can be seen in Table 8 the flat band potential does not change with the presence of (H_3O^+) in the electrolyte after modification of the electrode. Table 9 shows that the band edges at the semiconductor/electrolyte interfaces remain fixed in the presence of different redox couples as in aqueous acidic medium. Again, this can be attributed to Fermi level unpinning (39). A support to this conclusion can also be found through the measurements of the open-circuit photopotentials V_{oc} which are shown in Table 10. In view of the above results, the same conclusions other than those obtained with the study in the aqueous medium, apply.[1]

Conclusion

Based on the results reported here, it can be concluded that the modification of semiconductor materials with $H_4SiW_{12}O_{40}.nH_2O$ decreases the overpotential of hydrogen evolution at the photocathodes along with improvement of the open circuit photopotentials of the photoelectrochemical cells. It was also shown that suppression of Fermi level pinning is possible. This suppression is accomplished by surface electrode modifications. It is therefore necessary to understand the origin of Fermi level pinning at semiconductor/electrolyte interfaces. A systematic work in this area is planned.

[1]It should be pointed out that previous experiments (31) carried out with similar electrodes in 1,2-dichloroethane, but without modification of the surface, has shown Fermi level pinning due to the presence of a high density of surface states. Accordingly, the band edges at the semiconductor/electrolyte interface varied as a function of different redox couples, whereas V_{oc} was relatively independent of V_{redox} (52).

Acknowledgements

The author would like to express his gratitude to Dr. N. Marchand for his helpful discussions. The Natural and Engineering Research Council of Canada and "le programme action structurante du gouvernement du Québec" are acknowledged for financial support.

1. M. T. POPE. Heteropoly and isopoly oxometalates. Springer Verlag, Berlin, Heidelberg. 1983.
2. K. EGUCHI, I. ASO, N. YAMAZOE, and T. SAIYAMA. Chem. Lett. 1345 (1979).
3. M. AKIMOTO, Y. TSUCHIDA, K. SATO, and E. ECHIGOYA. J. Catal. **83**, 72 (1981).
4. N. MIZUMO, T. WATANABE, and M. MISONO. J. Phys. Chem. **89**, 80 (1985).
5. H. HAYASHI and J. B. MOFFAT. J. Catal. **77**, 473 (1982).
6. M. AI. Appl. Catal. **4**, 245 (1982).
7. H. HAYASHI and J. B. MOFFAT. J. Catal. **83**, 292 (1983).
8. I. V. KHOZHEVNIKOV and K. I. MATNEEV. Appl. Catal. **5**, 135 (1983).
9. M. AKIMOTO, H. IKEDA, A. OKEBE, and E. ECHIGOYA. J. Catal. **89**, 196 (1984).
10. M. AKIMOTO, Y. TSCHIDA, Y. SATO, and E. ECHIGOYA. J. Catal. **72**, 83 (1981).
11. M. AKIMOTO, K. SHIMA, H. IKEDA, and E. ECHIGOYA. J. Catal. **86**, 173 (1984).
12. H. HAYASHI and J. B. MOFFAT. J. Catal. **81**, 61 (1983).
13. G. A. TSIGINOS. *In* Topics in Current Chemistry. Vol. 76. M. J. J. DEWAR. Springer, Berlin. (1978) p. 1.
14. T. J. R. WEAKLY. *In* Structure and bonding. Vol. 18. *Edited by* J. D. Dunits. Springer, Berlin. 1974. p. 131.
15. J. P. LANNAY, R. MASSART, and P. SOUCHAY. J. Less Common Met. **36**, 139 (1974).

Can. J. Chem. Downloaded from www.nrcresearchpress.com by 41.223.56.140 on 09/07/12
For personal use only.

16. G. HERVÉ. Ann. Chim. Paris, **6**, 219 (1971).
17. G. HERVÉ. Ann. Chim. Paris, **6**, 287 (1971).
18. J. M. FRUCHART and G. HERVÉ. Ann. Chim. **6**, 337 (1971).
19. R. AKID and J. DARVENT. J. Chem. Soc. Dalton Trans. 395 (1985).
20. D. DIMOTIKALI and E. PAPACONSTANTINOV. Inorg. Chem. Acta, **87**, 177 (1984).
21. T. YAMASSE. Inorg. Chim. Acta, **76**, L 25 (1983).
22. T. YAMASSE. Inorg. Chim. Acta, **64**, L 155 (1982).
23. B. KEITA and L. HADJO. J. Electroanal. Chem. **191**, 411 (1985).
24. A. J. MCEVOY and M. GRATZEL. J. Electroanal. Chem. **209**, 391 (1986).
25. B. KEITA and L. NADJO. J. Electroanal. Chem. **199**, 229 (1986).
26. B. KEITA and L. NADJO. J. Electroanal. Chem. **223**, 287 (1987).
27. B. KEITA and L. NADJO. J. Electroanal. Chem. **227**, 265 (1987).
28. B. KEITA and L. NADJO. J. Electroanal. Chem. **227**, 77 (1987).
29. B. KEITA and L. NADJO. J. Electroanal. Chem. **230**, 267 (1987).
30. B. KEITA and L. NADJO. J. Electroanal. Chem. **208**, 343 (1986).
31. O. SAVADOGO, M. ETMAN, M. HERLEM, F. CHENG, and J. JORDAN. To be published.
32. O. SAVADOGO and A. DESCHANVRES. C.R. Acad. Sci. Paris, **296**, 827 (1983).
33. M. J. MADOU, B. H. LOO, K. W. FRESE, and S. ROY MORRISON. Surf. Sci. **108**, 135 (1980).
34. S. R. MORRISSON. Electrochemistry on semiconductors and oxidized metals. Plenum Press, New York. 1980.
35. O. SAVADOGO. Thèse d'État. University of Caen, France. 1985.
36. A. J. BARD, A. B. BOCARSLY, F. F. FAN, E. G. WALTON, AND M. S. WRIGHTON. J. Am. Chem. Soc. **102**, 3671 (1980).
37. R. NOUFI, D. TENCH, and L. F. WARREN. J. Electrochem. Soc. **127**, 2310 (1980).
38. LUNN, F. SCHNEEMEYER, and M. S. WRIGHTON. J. Am. Chem. Soc. **102**, 6964 (1980).
39. O. SAVADOGO, J. YAZBECK, and A. DESCHANVRES. Mat. Res. Bull. **11**, 18, 1455 (1983).
40. F. R. FAN and A. J. BARD. J. Am. Chem. Soc. **10**, 3677 (1980).
41. A. B. BOCARSLY, D. C. BOOKBINDER, R. N. DOMINEY, N. S. LEWIS, and M. S. WRIGHTON. J. Am. Chem. Soc. **102**, 3683 (1980).
42. J. GOBRECHT, H. GERISCHER, and H. TRIBUTSLH. Ber. Bunseng. Phys. Chem. **82**, 1331 (1978).
43. J. A. TURNER, J. MANASSEN, and A. J. NOZIK. J. Appl. Phys. Lett. **37**, 488 (1980).
44. R. N. DOMINEY, N. S. LEWIS, and M. S. WRIGHTON. J. Am. Chem. Soc. **103**, 1261 (1981).
45. J. J. KELLY and R. MEMMING. J. Electrochem. Soc. **129**, 730 (1982).
46. D. VANNEACHELBERGH, W. P. GOMES, and F. CARDON. Ber. Bunsengese. Phys. Chem. **89**, 994 (1985) and references therein.
47. R. MEMMING. Ber. Bunsenges. Phys. Chem. **91**, 353 (1987) and references therein.
48. R. A. SMITH. Semiconductors. Cambridge Univ. Press, 1968. p. 83.
49. O. SAVADOGO. Thèse de 3e cycle. University of Caen, France. 1982.
50. F. EL HALOUANI. Thèse d'État. University of Caen, France. 1980.
51. J. NELLONI, G. V. AMERONGEN, R. HEINDL, M. HERLEM, and J. L. SCULFORT. C. R. Acad. Sci. Paris, **288**, 288 (1979).
52. G. NAGASUBRAMANIA, B. L. WHEELER, and A. J. BARD. J. Electrochem. Soc. **130**, 1680 (1983).

Can. J. Chem. Downloaded from www.nrcresearchpress.com by 41.223.56.140 on 09/07/12
For personal use only.

Protected porous polymers

CAI-YING WU[1] AND WALTER A. AUE[2]
Department of Chemistry, Dalhousie University, Halifax, N.S., Canada B3H 4J3

Received June 7, 1988

CAI-YING WU and WALTER A. AUE. Protected porous polymers. Can. J. Chem. **67**, 389 (1989).

This study was designed to answer the question whether the chromatographic performance of porous polymers — serving here as a model system for pressure-sensitive separation media of relatively large mass transfer resistance — could be improved (*a*) by imposing on them a chromatographically favorable, extrinsic macrostructure and (*b*) by protecting that macrostructure against physical deformation. Packed-column gas chromatography was used as the test system.

Protected porous polymers (PPP's) were synthesized from pure divinylbenzene (DVB) inside conventional diatomaceous supports, using various amounts and types of porogens. The non-extractable polymer loads ranged from 10 to 40% and conformed to (i.e. formed layers on) the diatomaceous macrostructures. The best plate numbers were in excess of 4000/m on a 100/120 mesh Chromosorb W base. The mass transfer resistance of these materials was very low and permitted high flow rates. The PPP's could be used up to 280°C and did not appear to suffer deformation; in fact, the polymer appeared to shield the diatom supports from abrasion. The data indicate that the porous polymer deposits had relatively high specific surface areas, and produced a relatively large value for the free energy of sorption per methylene group, as compared with conventional porous polymer beads. Otherwise, protected and unprotected types of porous polymers had similar chromatographic characteristics.

Key words: porous polymer, poly(divinylbenzene), gas chromatography, protected polymer, diatoms.

CAI-YING WU et WALTER A. AUE. Protected porous polymers. Can. J. Chem. **67**, 389 (1989).

On a réalisé cette étude dans le but de déterminer s'il est possible d'améliorer la performance chromatographique de polymères poreux — servant ici de système modèle pour un milieu de séparation sensible à la pression et possédant une résistance au transfert de masse qui est relativement importante — (*a*) en leur imposant une macrostructure extrinsèque qui est favorable d'un point de vue chromatographique et (*b*) en protégeant cette macrostructure contre les déformations physiques. Comme système de vérification, on a utilisé la chromatographie gazeuse à l'aide de colonnes remplies.

On a synthétisé les polymères poreux protégés (PPP) à l'intérieur de supports diatomées conventionnels, à partir du divinylbenzène (DVB) et utilisant diverses quantités et divers types de porogènes. Les quantités ajoutées de polymère qui ne peuvent être extraits varient de 10 à 40% et elles se conforment (c'est-à-dire qu'elles forment des couches sur) aux macrostructures de diatomées. Sur une base de Chromosorb W, 100/120 mesh, les meilleurs nombres de plateaux dépassaient 4000/m. La résistance au transfert de masse de ces matériaux est très faible et ils permettent des vitesses d'écoulement élevées. On peut utiliser les PPP jusqu'à 280°C et ils ne donnent pas de signes de déformation; en fait, il semble que le polymère protège le support diatomée contre l'abrasion. Les données indiquent que les dépots de polymère poreux possèdent des surfaces spécifiques relativement élevées et que, comparées aux valeurs correspondantes pour des billes conventionnelles de polymère poreux, leur énergie libre de sorption par groupement méthylène est relativement élevée. Autrement, les polymères poreux protégés et non-protégés possèdent des caractéristiques chromatographiques semblables.

Mots clés : polymères poreux, polydivinylbenzène, chromatographie gazeuse, polymères protégés, diatomées.

[Traduit par la revue]

Introduction

As both scientific literature and scientific supply catalogues will readily demonstrate, the so-called "porous polymers" occupy a steady if somewhat specialized niche in the chromatographer's arsenal. These separation media usually come in the form of porous beads that are made by polymerizing in emulsion, together with a porogen (diluent), a variety of olefinic materials, e.g. styrene/divinylbenzene. Porous polymers can also be produced in bulk and ground, or be coated or synthesized inside chromatographic supports or capillaries. Reference 1 presents an overview of the area, refs. 2 to 4 deal with synthesis and chromatographic behavior, ref. 5 investigates the basic polymer chemistry, and refs. 6 to 8 discuss aspects of porous polymers that are of particular relevance to this study. There are, of course, many more references — indeed far too many to cite.

The main advantage of porous polymers in gas chromatography is their strong retention of various gases and non-protic organics, coupled with a relatively short retention of, and good chemical resistance to, water. The main disadvantage — in the conventional bead form — is their generally poor chromatographic efficiency (plate number), coupled with a relatively low dimensional stability.

Although this is not commonly done, we were interested in producing some porous polymers by and for ourselves. However, we wanted to obtain high efficiency phases that would not shrink inside the gas chromatographic column. More importantly, we wanted to find out whether the comparatively low plate numbers of porous polymers were intrinsic and therefore inevitable (e.g. originating from the slow diffusion of solute into the cross-linked polymer) — or whether they were accidental and therefore remediable (e.g. by preserving the dominant retention while reducing the dominant dispersion process).

The point has been made that the plate numbers of porous polymer beads are comparatively low — that is, low *in comparison to* typical gas–liquid chromatography involving thin layers of liquid phases on low-surface area supports. Now, the pores of the former are much smaller than the open internal spaces of the latter. Resistance to mass transfer in the mobile phase is therefore the most likely major contributor to the poor efficiency of porous polymers. The second contributor may be

[1]Present address: Department of Chemistry, Wuhan University, Wuhan, People's Republic of China.

[2]To whom correspondence should be addressed.

Can. J. Chem. Downloaded from www.nrcresearchpress.com by 122.72.124.2 on 09/07/12
For personal use only.

Can. J. Chem. Downloaded from www.nrcresearchpress.com by 122.72.124.2 on 09/07/12
For personal use only.

physical deformation. High pressure, or even relatively low pressure at high temperature, can deform soft beads and hence their pores.

One of the most obvious ways of improving mass transfer in the mobile phase is to use porous polymers in a geometry patterned after that of the traditional stationary phase in gas–liquid chromatography. That is, one would want the narrow-pore polymer to form thin layers inside a wide-pore support structure; thus effectively uncoupling the retention effect of large surface areas and narrow pores from the mass transfer resistance effect of very long, tortuous and constricted passages.

Inside a wide-pore silicic structure of suitable physical strength, the porous polymers would also be protected from the detrimental effect of pressure. Note that this detrimental effect is due to the differential, not the absolute, pressure on a particular particle. Thus, a soft gel bed (as, for instance, in Sephadex chromatography) may be compressed longitudinally by a relatively low flow/pressure regime. Yet, beads of such a gel, when simply suspended in water and not pressed against each other, would be stable at any pressure — much as jellyfish retain their shape at various ocean depths. The question of what types of chromatographic beds are stable against pressure is therefore the question of what material provides the counter-force to the force of the moving mobile phase — not what material produces the chromatographic separation. This seems obvious for conventional gas–*liquid* chromatography — and it should also be correct for a soft porous polymer nestled inside a hard inorganic framework.

It would stand to reason that the most important consequences of a (successful) attempt to protect soft separation media in this manner should occur in chromatographic techniques characterized by high pressure and/or the need to use very soft phases. However, for a demonstration of principle it seemed advisable to choose the easiest handled system: In our case, that was packed-column gas chromatography on porous polymers. For a first try, styrene–divinylbenzene on Chromosorb W appeared to be the obvious choice. As had been the case on several occasions earlier on, a methodology successfully developed on packed columns would likely find itself transferred without too much delay to other chromatographic modes of higher power and price.

To recapitulate, the incorporation of a porous polymer into a Chromosorb particle should be helpful in two ways: not only should the diatomaceous structure of the host provide a template for the physical shape of the polymer and allow easy access to its innermost deposits, but it should also protect it from the deleterious effects of deformation by the longitudinal column pressure gradient. Even if the polymer layer were to shrink, the column bed would still stay intact (as long as the carrier particles did not abruptly deform, i.e. break). Following this line of thought, one might want to refer to such materials as "protected porous polymers" (PPP's).

Incorporating or suspending an active medium on the high-surface area structure of a support is an approach found in several areas of chemistry, e.g. in the synthesis of supported catalysts. In the chromatographic realm — where supports and polymers play crucial roles — the work closest to our interests is that of Fuller (7). He focussed primarily on polymer characterization and described the physical bonding to Chromosorb of porous copolymers from mixtures of divinylbenzene, ethylvinylbenzene, and styrene. Straight-chain alkanes gave particular high efficiencies (a H_{min} of ca. 0.48 mm for pentane, i.e. close to 2100 plates/m) — although branched hydrocarbons did not do as well, and polar solutes tailed.

Our first attempts at producing polymers from styrene and DVB (divinylbenzene) inside Chromosorb particles resulted in extraction- and heat-resistant materials but little else. Early plate numbers ranged below 2000/m; some significantly worse, in fact, than Fuller's data. By a series of modifications to the synthetic technique, the plate numbers could be raised above 4000/m on a 100/120 mesh support, and a wide variety of different compounds could be satisfactorily chromatographed. At that point, mindful of diminishing returns and the theoretical limits on column efficiencies, we considered that the study had essentially reached its goal.

Experimental

Materials

Chromosorbs W and G (in commercial AW and AW-DMCS forms) and Chromosorb 101 were all Johns-Manville products received as 100/120 mesh cuts. Poropak Q was obtained from Waters. The conventional divinylbenzene mixture (about 50 to 60% DVB in ethylvinylbenzene plus other materials) was supplied by BDH Chemicals. Neat (i.e. non-diluted but stabilized) divinylbenzene was purchased from Pfaltz and Bauer, 2,2-azobis(isobutyronitrile) from PolyScience, dimethyldichlorosilane from Aldrich, vinyldimethylchlorosilane from Petrarch, and 1,2,3,4-tetrahydronaphthalene (tetralin) from Fisher. Other chemicals were ACS grade or better.

Divinylbenzene (the "pure" material) was distilled in vacuum under nitrogen at 36 to 40°C and stored under nitrogen in the refrigerator before use. Other solvents and reagents were used as received.

Typical synthesis of a protected porous polymer

While the ingredients varied widely, most other synthesis conditions — in particular time and temperature of polymerization — remained the same. In the following paragraphs a fairly detailed procedure is given for the production of a high-efficiency, low-load support (PPP # 7 of Table 1, the best characterized of the protected porous polymers).

Five gram of Chromosorb W-AW-DMCS, 100/120 mesh (the commercial material), was placed into a Buchner flask fitted with a separatory funnel. The flask was evacuated to oil pump vacuum for about half an hour.

A reagent mixture was prepared by dissolving 0.28 g azobis(isobutyronitrile) in 12 mL acetone and adding 56 mL tetralin and 10 mL DVB (for similar types of synthesis, only the amount of tetralin was changed). This solution was poured into the separatory funnel, the vacuum line closed, and then the stopcock of the funnel opened. (On occasion, vacuum was again applied for a short time and released, in order to ensure, as far as possible, penetration of the monomer solution into the Chromosorb particles.)

The contents of the flask were shaken thoroughly and allowed to settle for 30 min. The excess of monomer solution was decanted and the rest removed by filtration, using a minimum of vacuum and time, on Whatman # 1 filter paper held by a frit. Larger sheets of this paper were then used to further blot the support, repeatedly, until it became free-flowing. (The latter operation was conveniently carried out in a flat pan or on a large, fine sieve in order to avoid losses of support. It prevented the particles from sticking together later on. While "drying" the support in this manner could be considered a haphazard undertaking, apt to result in uncontrollably varying polymer loads, the operation is actually quite reproducible.)

The coated support was transferred to a thick-walled glass bottle with septum and crimped cap, the air in the bottle replaced by nitrogen under slight overpressure, and the bottle placed into a GC oven. The oven was then programmed to heat up from 30 to 80°C at 0.5°/min and remain at the upper temperature for 40 h.

After cool-down the contents of the bottle were subjected to soxhlet extraction by benzene for 6 h, followed by acetone for another 5 h. The PPP material was then transferred, filtered, and washed by using two portions of fresh acetone, and dried in a heated desiccator at 100°C

under oil-pump vacuum over night. The dried product was resieved to ensure a 100/120 mesh fraction.

Gas chromatographic testing

The PPP phases were filled into 100 × 0.20 cm i.d. borosilicate glass U-tubes and tested with nitrogen as carrier gas, using flame ionization detection in a Bendix 2500 floor model gas chromatograph. Other conditions are given in the legends or in the text.

Other tests

Initial trends in polymer load were assessed — very roughly — through measuring the apparent ("free fall") density by filling 5 mL of a 10 mL graduate cylinder with slight tapping, and by weighing the phase; as well as by oxidative pyrolysis (to weight constancy) in a muffle furnace at 650°C. Occasionally, load was also determined by C, H analysis (Guelph Chemical Laboratories or Wuhan University).

Infrared spectra were run on HF-treated phases in KBr discs on a PE 2838 spectrometer, courtesy of the Atlantic Regional Laboratory of the National Research Council. Carbon-13 NMR spectra were obtained on a Bruker MSL-200 spectrometer, courtesy of Professor R. Wasylishen. Scanning electron micrographs were taken on a Bausch and Lomb Nanolab 2000 instrument after coating the phases with 60:40% Au:Pd.

Results and discussion

The primary interest of this study was to find out whether a change in macrostructure (thickness, shape), and the protection of that macrostructure against deformation by pressure, would lead to an improved chromatographic performance of relatively soft separation media. Although gel chromatography would have provided a more challenging model system and, with experiments successful, might have elicited greater general interest, this study focussed on porous polymers in packed-column gas chromatography as the easiest modified and fastest tested model system. Theoretical plate numbers were to be used as the primary criterion of improvement; temperature limitations as the secondary one. That is, chromatographic efficiency alone was to guide variations in synthetic procedure: only if the phases reached satisfactory plate numbers would their behaviour at a high temperature — where pressure deformation is most likely to occur — be further investigated.

A significantly greater number of syntheses were carried out than can be reported here in detail: however, their results all appeared to follow the general trends discussed below. The variation of synthesis conditions was stopped when the best PPP phases exceeded 4000 plates/m, even though limited improvement might still have been possible. There does exist some uncertainty about the precise theoretical HETP limit for a given particle size; however, considering the fact that, say, 5000 plates/m would have been equivalent to an HETP of less than one-and-a-half particle diameters (the average diameter of a 100/120 mesh particles is ca. 140 micron), protracted further effort would have meant staying in a game of rapidly decreasing odds.

Within this reasonable constraint, then, the following variations of synthesis proved to be the most significant.

Monomer selection

The only monomers used were styrene, divinylbenzene (DVB), and the materials contained in the conventional "DVB" material as used by industry (typically about 56% divinylbenzene, 38% ethylstyrene, and 6% of diethylbenzene and other saturated compounds, all as isomer mixtures). This is not to say that other vinyl monomers — or, for that matter, other types of monomers — would not have worked just as well or better, but simply that we wanted to restrict the initial study to the most basic and most frequently used of the porous polymer systems.

In our hands, styrene/DVB(mixture) systems gave rather low chromatographic efficiencies (measured in earlier experiments with benzene, in later experiments with the somewhat more efficient *n*-butanol). Matters improved when the DVB(mixture) was used without additional styrene, and again when DVB(neat) replaced DVB(mixture) as the only monomer source. It is not common procedure, of course, to use a cross-linker by itself, but here that came about simply as a matter of optimization guided by plate numbers. It may also be mentioned that Pollock *et al.* employed 95% DVB for stronger retention and separation of N_2, O_2, Ar, and CO at ambient temperature conditions (8).

Porogen (diluent) selection

Two types of porogens are commonly used: solvating aromatics like toluene and non-solvating aliphatics like heptane or decane. As is well known, the latter produce higher porosities. Under our initial conditions, toluene worked better than octane. Following a hunch that had to do with aromatic/aliphatic character, solubility, volatility, and molecular size (but was never validated by experiment), tetralin (1,2,3,4-tetrahydronaphthalene) was used and worked better than toluene. No further porogens were tried.

The amount of toluene and tetralin were varied within relatively wide limits as shown in Table 1, which presents selected but typical data of the best characterized and/or most important phases. The top performance was obtained with 75% tetralin; however, only one higher percentage was tested.

Figure 1 shows the number of theoretical plates — measured with *n*-butanol at or close to optimum flow — as it relates to polymer load. The term "polymer load" is chosen here for its analogy to the stationary phase load of GLC; it is simply the percent weight loss incurred by heating the material in air at 650°C to weight constancy. Table 1 shows some of these numbers, augmented in strategic cases by conventional combustion analysis for carbon and hydrogen (the latter values do not quite add up to the "polymer load", likely due to the silicic structure losing some additional water in the muffle furnace).

The chromatographic efficiency, not surprisingly, increases fairly steadily with decreasing polymer load. Eventually, of course, there has to be a downturn: whether that indeed occurs at a polymer load of about 10% is open to question. Only a far more detailed and time-consuming series of experiments could establish that. The numbers, if taken at face value, are not unreasonable though. A 10% load on Chromosorb W is comparatively high for a conventional stationary liquid phase (the nominal layer thickness is about 1000 Å). However, one would expect a porous polymer, which relies on adsorption rather than, as the liquid phase, on partition, to need thicker layers for maximum efficiency. (The argument presumes, of course, an *evenly distributed* separation medium — which often might not be present. Note also that the strongest mass transfer resistance terms of this comparison likely concern different phases: diffusion in the stationary *liquid* for classical GLC, diffusion in the more or less stagnant *gas* that fills the pores for the bead-type porous polymer.) In the protected and spread-out porous polymer, though, the resistance to mass transfer in and out of the polymer pores should be very small, as one can appreciate from the fact that the nominal layer thickness of the PPP is about a thousand times smaller than the radius of the porous polymer bead.

Aside from its effect on porosity, the amount of porogen also regulates the polymer load in our particular type of preparation: the larger the volume of porogen, the larger the total volume of

Can. J. Chem. Downloaded from www.nrcresearchpress.com by 122.72.124.2 on 09/07/12
For personal use only.

TABLE 1. Effects of support and porogen

#	Support[a]	Porogen	Percent porogen[b]	A.D.[c] g/mL	Load[d] %	%C	%H	Plates per m[e]	S.A. m^2/g[f]
1	W-AW-DMCS	Tetralin	19	0.49	30.9			2080	
2	W-AW-DMCS	Tetralin	31	0.44	26.2	23.9	2.09	2600	242
3	W-AW-DMCS	Toluene	31	0.43	20.1			2360	
4	W-AW-DMCS	Tetralin	48	0.43	21.1	18.4	1.53	3150	224
5	W-AW-DMCS	Toluene	48	0.40	14.5			2600	
6	W-AW-DMCS	Tetralin	55	0.41	19.8	17.2	1.49	3660	195
7	W-AW-DMCS	Tetralin	75	0.38	11.1	9.28	0.82	4200	79
8	W-AW	Tetralin	75	0.36	12.0			2430	
9	G-AW-DMCS	Tetralin	75	0.64	5.64	4.40	0.34	4140	
10	G-AW	Tetralin	75	0.64	5.53			2930	
11	W-AW-DMCS	Tetralin	85	0.35	8.1	6.93	0.54	3070	72
Conventional porous polymers (as received):									
Porapak Q (Waters)								1500	510
Chromosorb 101 (Johns-Manville)								2270	46

[a]100/120 mesh.
[b]Weight percent porogen (diluent) in DVB/acetone/catalyst/porogen mixture.
[c]Apparent density (see text).
[d]Weight loss after heating to 650°C in air to weight constancy.
[e]Number of theoretical plates per meter, measured with *n*-butanol.
[f]Surface area measured by BET method with nitrogen.

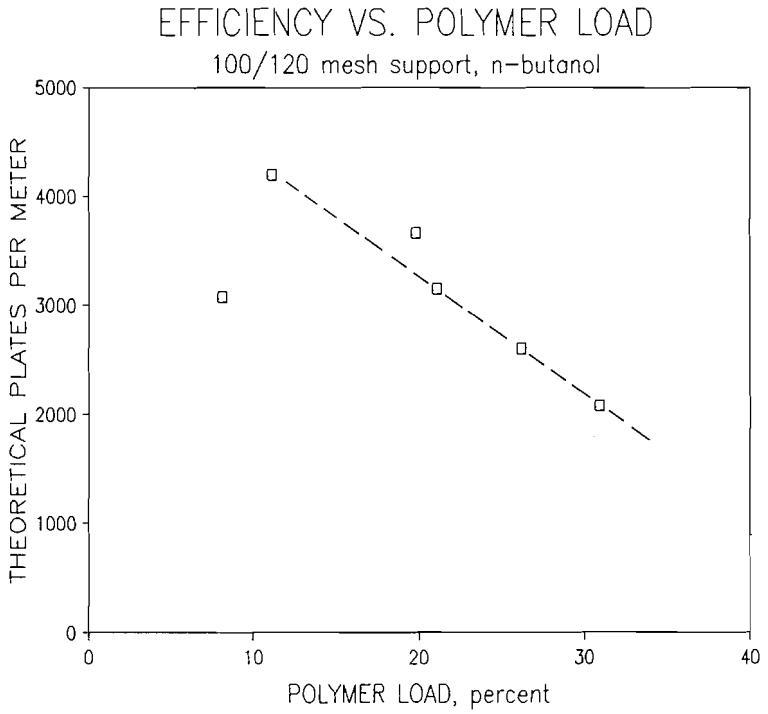


FIG. 1. Dependence of efficiency on polymer load. Chromosorb W-AW-DMCS, 100/120 mesh as support, pure DVB as monomer, tetralin as porogen. Theoretical plates determined with *n*-butanol as test compound at 130°C in nitrogen at or close to the minimum of the Van Deemter curve. See text for determination of polymer load.

monomer + porogen + catalyst, and the smaller the amount of DVB the support can hold on to for subsequent polymerization.

Figure 2 shows the correlation of the percentage of porogen in the initial monomer solution versus the resulting polymer load. The data appear to be perhaps more consistent than they really were — considering, for instance, the vagaries of blotting wet support with filter paper. However, the control over synthesis conditions is clearly adequate and the overall trend is unmistakable: the larger the amount of porogen, the smaller the polymer load.

Support pretreatment

Not surprisingly, an acid-washed support produced better performance than a support not so treated (although this was checked only in one case). What was surprising was the significantly better performance of DMCS-treated materials, as can be seen by comparing phases # 7 and # 8, as well as # 9 and # 10, from Table 1 (and, in addition, several other phases not listed therein).

The surprise came from the fact that, while treatment of the support surface with dimethyldichlorosilane, as most other

Can. J. Chem. Downloaded from www.nrcresearchpress.com by 122.72.124.2 on 09/07/12
For personal use only.

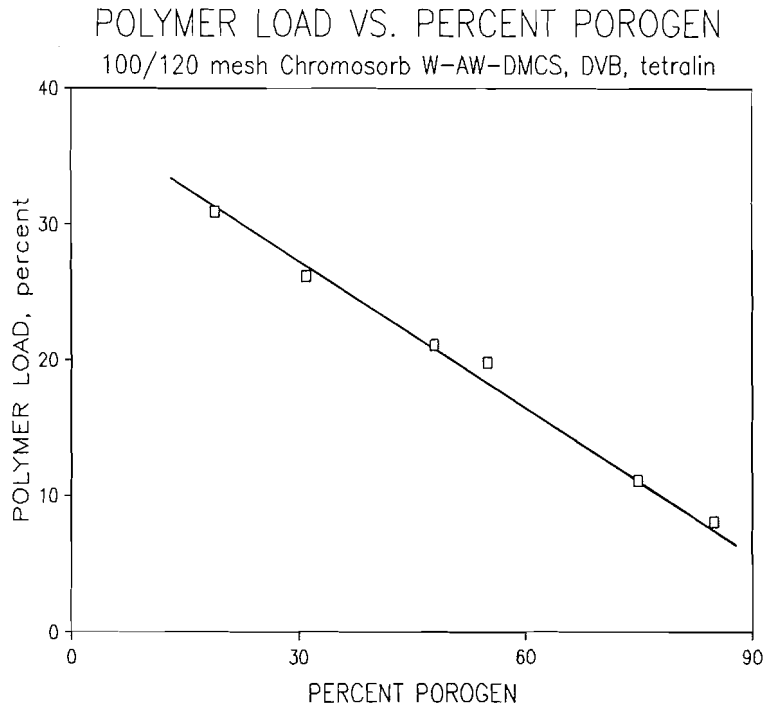


FIG. 2. Polymer load vs. percent porogen used in monomer formulation.

types of silanizations, often has a beneficial effect on plate numbers in GLC — by (presumably) reducing the interaction of surface silanol groups with, particularly, polar solutes — this effect was not expected to play a significant role in the case of porous polymers. The support surface, in the role of an adsorbent, can compete with a conventional liquid phase, but not with a porous polymer, in retentive strength (as one can easily demonstrate by chromatographing the same compounds on both a porous polymer and on a plain support, or easily deduce by considering the large differences in surface areas and elution temperatures between typical GLC and porous polymer GSC systems). In other words, the state of the diatomaceous support surface should be of little direct chromatographic consequence with all but the most polar and adsorptive solutes.

Why, then, do DMCS-treated supports lead to better chromatographic performance in the end? At this point, only speculation can be offered. As the monomer mixture initially coats the diatomaceous caverns of the Chromosorb particle, and as, later, polymerization starts and polymer and porogen separate, the physical form of the emerging polymer will strongly depend on its interaction with the surface. Does it initially "wet" the surface? And, if so, does the effect remain strong enough to make it accept the diatomaceous template throughout polymerization? Or does the polymer in statu nascendi coalesce into small droplets? Obviously, evenly distributed layers of diatom reciprocals would be far preferable to a few unextractable blobs of resin found here and there.

It may also be mentioned in this context that phases based on AW-DMCS type supports did produce peaks of less asymmetry than those based on AW type supports. In conventional GLC, peak asymmetry is usually attributed to the interaction of solute with the support surface, particularly when protic and/or polar substances tail while non-polar ones don't. The available evidence in the case of PPP's in this regard is not completely consistent and would have to be clarified by further experiments — but, on the whole, it appears that the tailing in the case of non-DMCS treated supports affects all types of compounds, not just protic and/or polar ones. Asymmetry, particularly of the sort that can be observed with both polar and non-polar types of analytes, could for instance arise from an uneven distribution of the retentive porous polymer inside its protective support.

For this study, the beneficial effect of DMCS was appreciated, exploited, and not explained. It may be added that the effect is also evident when the DMCS treatment of the support is carried out in the lab (as opposed to using the commercially treated support). However, a similar treatment with vinyldimethylchlorosilane did not provide the same benefit. As an aside in regard to the possibility of "bonding", the use of DMCS as a pretreatment for the easy *release* of bulk-polymerized styrene–DVB copolymers from glass tubes has been mentioned in the literature (5).

Polymer characteristics

A detailed characterization of the polymer part of the PPP phases is precluded for a simple, exploratory study such as this, not only by our dearth of suitable instrumentation but also by a dilemma inherent in the task: If the polymer is examined in situ, the presence of the diatomaceous support may influence the results; if the diatomaceous support is removed from the polymer prior to characterization, new surfaces are created and perhaps new internal regions become accessible that would not have made their presence felt in the chromatographic tests; and, finally, if the polymer is produced from the same monomer formulation but in the absence of the diatomaceous support, it is highly questionable whether a material with the same properties as the nominally corresponding PPP will emerge.

Consequently we shall make use only of data already available from the optimization studies, and do so mainly to establish a speculatory framework for later comparison with chromatographic behaviour.

One of the most important characteristics of the polymer is its surface area. A number of PPP phases were measured by BET nitrogen adsorption, and the results are shown in Table 1. It is well recognized that such data have to be interpreted with some

Can. J. Chem. Downloaded from www.nrcresearchpress.com by 122.72.124.2 on 09/07/12
For personal use only.

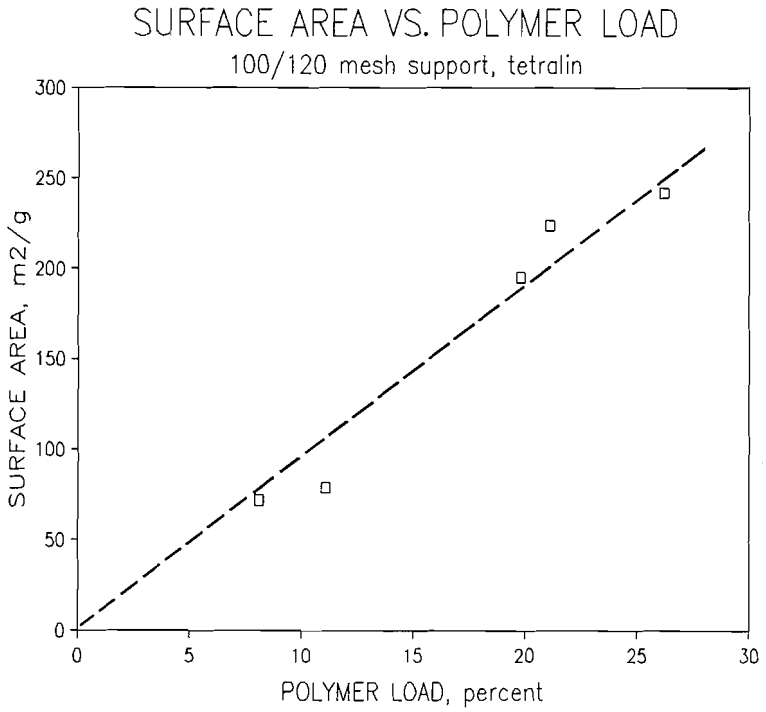


FIG. 3. Surface area of PPP's vs. polymer load. Pure DVB, tetralin. Surface area by BET (N_2).

caution (5). However, the trends shown by the numbers are very clear. Also, the commercial beads Porapak Q and Chromosorb 101 were run alongside and the results fell within the ranges given in the literature.

Figure 3 shows that (within the all-too-obvious error limit) the surface area turns out to be a linear function of polymer load. That is somewhat surprising since, as Fig. 2 has demonstrated, polymer load in our synthetic procedure was essentially determined by the amount of porogen added to an otherwise constant monomer mixture. And it is well known that the concentration of porogen can influence the surface area. Thus one might have expected to see a curve, not a straight line, appearing in Fig. 3. However, if it is truly a straight line, going through the origin — or, rather, through a negligible 1 m^2/g (the latter being the surface area of the clean support) — it would mean that the poly(divinylbenzene) fractions of *all* the samples have the *same* specific surface area (m^2/g of polymer) regardless of the amount of porogen and/or the polymer load used in their synthesis. Perhaps such behaviour is related to a very early phase separation during the polymerization process, promoted both by the alicyclic part of the tetralin porogen and the exclusive use of a cross-linking monomer (c.f. ref. 5).

If the specific surface area of the polymer itself (and, presumably, the chemical nature of its surface) remains constant, then retention must become a linear function of the amount of polymer present in the column. Or, since all GC test columns used in this study have similar lengths and volumes, retention should be a linear function of what one might call the "apparent polymer density", i.e. the grams of polymer present in one cubic centimeter of the PPP column packing. The latter number is easily estimated from the apparent or free-fall density of the packing and its polymer load (Table 1). It can be used to plot the retention times obtained from separating on various packings a standard test mixture (made up of four substances with boiling points all within 3°C of each other). The plot is shown in Fig. 4 and it is indeed linear and starts from the origin. Within (the fairly wide) error limits, then, the *specific* surface area of the polymer appears independent of the concentration of porogen used in its synthesis.

Which, in turn, raises the question what that specific surface area of the polymer itself is likely to be. It can be rather easily estimated by assuming that the support does not contribute to the surface area (its area is very small and, besides, most of it should be covered by the polymer), and that the polymer load (the weight loss on ignition) correctly describes the weight percent of polymer. Such estimates (using the few data available from Table 1) lead to very high numbers, with an average specific surface area close to 900 square meter per gram of polymer. While the spread in the numbers is very large (from 710 to 1060) and while that does not allow recognition of a possible (minor) extent of correlation with the porogen concentration, it is nevertheless clear that the specific surface areas of the porous polymer of this study are higher than those of the conventional bead types. This may be quite reasonable considering that the monomer is a pure crosslinking agent and the porogen a molecule with both solvating and non-solvating features. It is surprising only to the extent that one is accustomed to thinking of porous polymers in bead form — and, in a conventionally sized bead, such a high surface area (such narrow pores) would likely engender severe peak broadening and thus make the material unsuitable for most chromatographic uses.

Gas chromatographic performance

The perhaps most important chromatographic property of PPP's has already been mentioned: their significantly improved efficiency. The highest efficiency measured was 4200 plates/m, corresponding to a theoretical plate height of 0.24 mm. This was achieved with PPP # 7 (Table 1), whose polymer load is about 11% and (total phase) surface area 80 m^2/g; and whose synthesis is described in the Experimental part. A variety of different chromatographic tests were carried out with this and other columns, often in comparison with benchmark porous

Can. J. Chem. Downloaded from www.nrcresearchpress.com by 122.72.124.2 on 09/07/12
For personal use only.

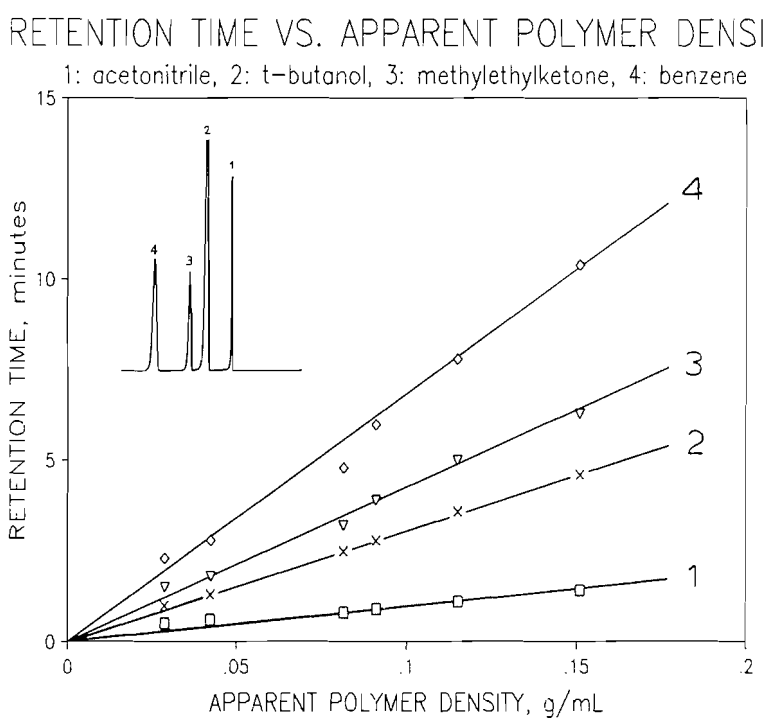


FIG. 4. Retention vs. apparent polymer density. Probes: *1*, acetonitrile; *2*, *t*-butanol; *3*, methylethyl ketone; *4*, benzene. See text for calculation of apparent polymer density.

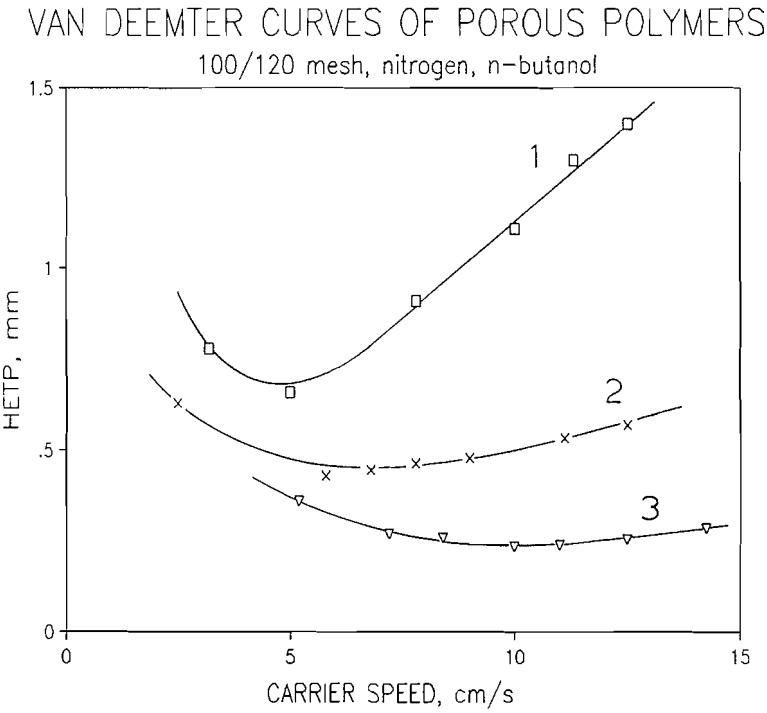


FIG. 5. Van Deemter curve of protected and conventional porous polymers. Carrier: nitrogen at 130°C, probe: *n*-butanol. All phases 100/120 mesh. Phases: *1*, Porapak Q; *2*, Chromosorb 101; *3*, PPP # 7 (Table 1).

polymers of the bead type such as Porapak Q or Chromosorb 101.

Van Deemter curve

In Fig. 5, Van Deemter curves for *n*-butanol at 130°C in nitrogen are plotted for PPP # 7, Porapak Q, and Chromosorb 101. Column # 7 is comparable in chromatographic efficiency with a very good, conventional GLC column filled with a packing of the same particle size (100/120 mesh). Its minimum HETP is about 0.24 mm (4200 plates/m). The low mass transfer resistance means that higher flow rates can be used with only a minor loss in efficiency, an advantage particularly welcome when working with porous polymers.

For purpose of comparison, PPP # 7 is a pure DVB polymer,

Can. J. Chem. Downloaded from www.nrcresearchpress.com by 122.72.124.2 on 09/07/12
For personal use only.

Can. J. Chem. Downloaded from www.nrcresearchpress.com by 122.72.124.2 on 09/07/12
For personal use only.

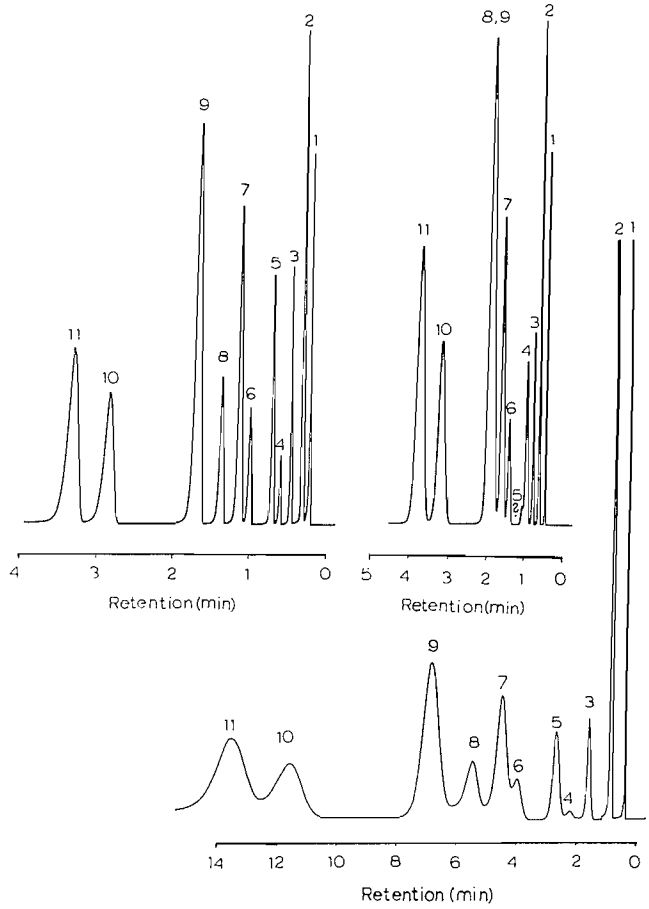


FIG. 6. Separation of C_1 to C_5 alcohols. Top left: PPP # 7 (Table 1); top right: Chromosorb 101; bottom: Porapak Q. Solutes: *1*, methanol; *2*, ethanol: *3*, *i*-propranol; *4*, *n*-propanol; *5*, *t*-butanol; *6*, *s*-butanol; *7*, *i*-butanol; *8*, *n*-butanol; *9*, *t*-pentanol; *10*, *i*-pentanol; *11*, *n*-pentanol.

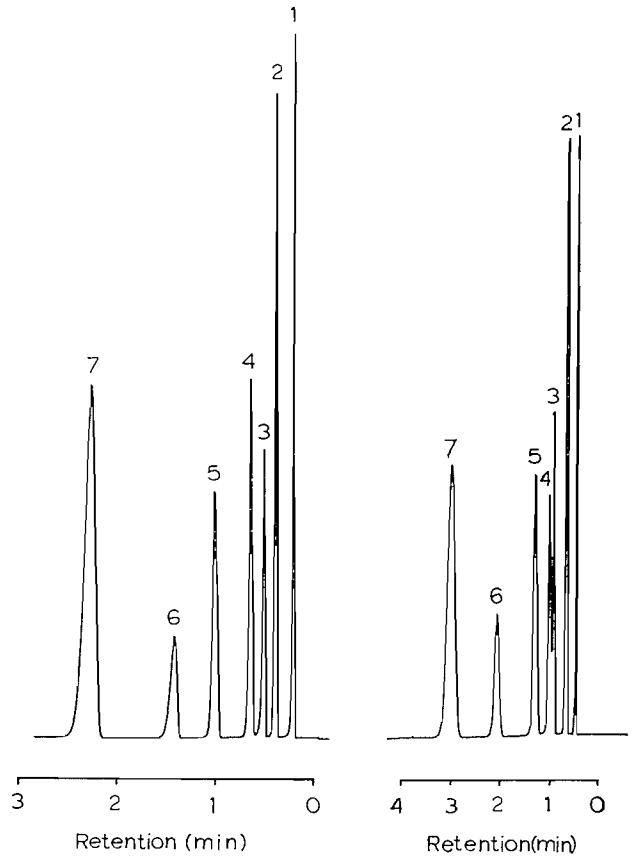


FIG. 7. Separation of various organic compounds. Left: PPP # 4 (Table 1); right: Chromosorb 101. Solutes: *1*, methanol; *2*, ethanol; *3*, acetonitrile; *4*, acetone; *5*, cyclopentane; *6*, chloroform; *7*, benzene.

Chromosorb 101 is a styrene-DVB co-polymer and Porapak Q is an ethylvinylbenzene–DVB copolymer (but *Q*-type materials are also listed as styrene–DVB as in the PoraPLOT *Q* column (6) or plain DVB as in the HayeSep *Q* material (9) and, furthermore, it should be realized that, as one of the referees of this manuscript poignantly put it, "there is no proof that they are, or should be, similar (like Coca Cola and Pepsi Cola)"). Surface areas do vary, but a recent book, with a cautionary note to that effect, lists 50 m^2/g for Chromosorb 101 and 500 to 700 m^2/g for Porapak Q (10). (Our own measurements on the materials we used for comparison yielded values of 46 and 510 m^2/g, respectively).

Some separations

A small number of separations are presented here for visual comparison and assessment. Figure 6 shows the chromatography of C-1 to C-5 alcohols, done on the three columns characterized by their Van Deemter profiles in Fig. 5. The alcohols display the shortest retention times on PPP # 7, closely followed by Chromosorb 101, but rather far from Porapak Q. Similar behaviour is also shown by other types of compounds. This is demonstrated in Fig. 7 by seven compounds hailing from six different chemical families, separating on PPP # 4 (a more retentive column with a polymer load of 21.1%) and Chromosorb 101. The peak sequences are similar though not identical on the various columns of Figs. 6 and 7 — not surprisingly so in light of the different chemical structure, polarity and porosity of the polymers that are being compared.

Free energy plots

The familiar log t_R' vs. #C plots, linear for homologous series, relate to the free energy of sorption and are helpful in comparing different types of chromatographic systems. For this reason we have tested PPP # 7 together with the two commercial porous polymers Chromosorb 101 and Porapak Q, by using the *n*-alkane, *n*-alkylbenzene, 2-alkanone, methyl-*n*-alkanoate, and *n*-alkanol(1) homologous series, i.e. paraffins, aromatics, ketones, esters, and alcohols. The results are quite interesting. (To avoid the proliferation of figures and, since Chromosorb 101 and Porapak Q have been well described in the literature, only the PPP # 7 plot is shown in Fig. 8. However, the following comparison is based on our own, not literature data; all obtained at 170°C and under identical chromatographic conditions).

What is striking about the comparison is that, despite the fact that the PPP and Chromosorb 101 have relatively similar retention capability, the PPP shows a considerably steeper slope (the difference in log t_R' per methylene group) — steeper, in fact, than even Porapak Q. The three slopes are 0.38, 0.34, and 0.28 for PPP # 7, Porapak Q and Chromosorb 101. This means that the later eluting one of two adjacent members of a homologous series will have isothermal retention times 2.4, 2.2, and 1.9 times longer than the earlier eluting one, respectively.

In chromatographic terms, this is important because it —

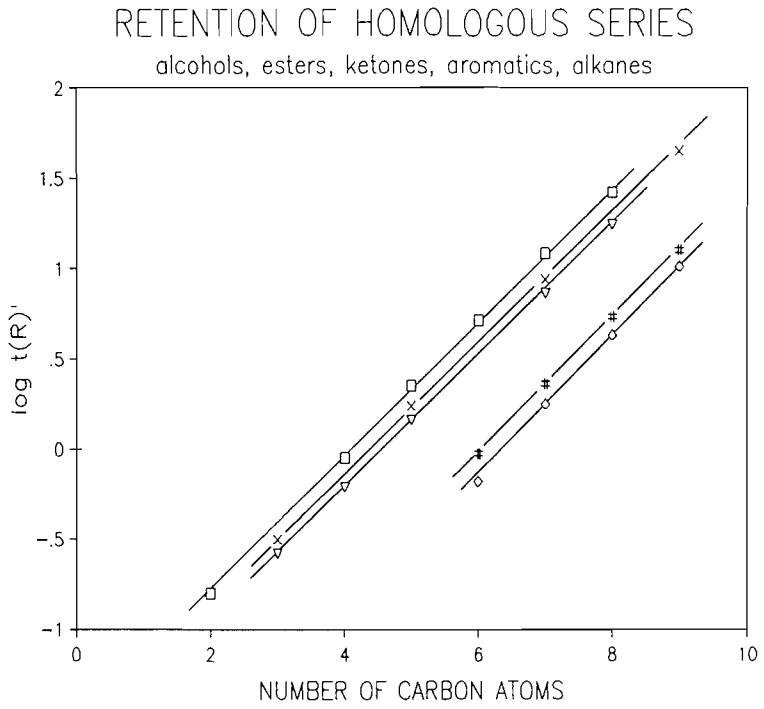


FIG. 8. Retention of homologous series. □, *n*-alcohols; ×, methyl esters; ▽, methyl ketones; #, *n*-alkyl benzenes; ◇, *n*-alkanes.

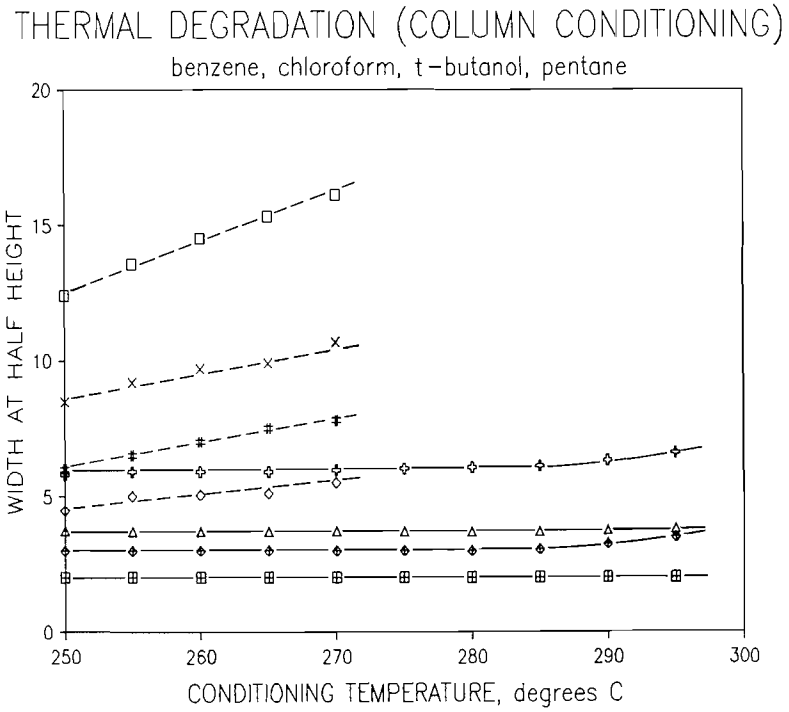


FIG. 9. Thermal degradation of protected and unprotected porous polymers. Dashed line: Porapak Q; full line: PPP # 6 (Table 1). Test compounds (from top to bottom): benzene, chloroform, *t*-butanol, pentane.

together with plate numbers, of course — determines the numbers of peaks that can be squeezed between two neighbouring alkanes (the Trennzahl or separation number). Thus, the PPP material offers both a high efficiency and a large retention interval per methylene group — or, differently put, it allows a narrower fraction of the boiling-point range to be separated within a given retention window.

It is interesting to speculate in polymer terms why this should be so. First, there could simply be a better *chemical* match, i.e. a larger interaction, between the methylene group and the polymer matrix. This would be analogous to non-polar liquid phases having steeper slopes than polar ones in log t_R'/#C GLC plots. However, neither the absolute retention nor the "polarity" of these phases suggests this to be the case (the "polarity", as can

Can. J. Chem. Downloaded from www.nrcresearchpress.com by 122.72.124.2 on 09/07/12
For personal use only.

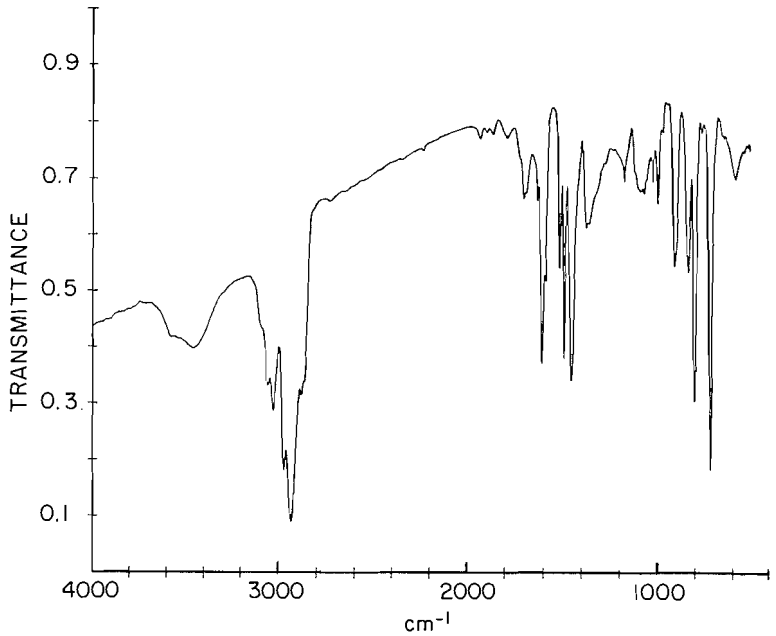


FIG. 10. Infrared absorption spectrum of pure DVB porous polymer. Diatomaceous support dissolved in HF, residual polymer pelletized with KBr.

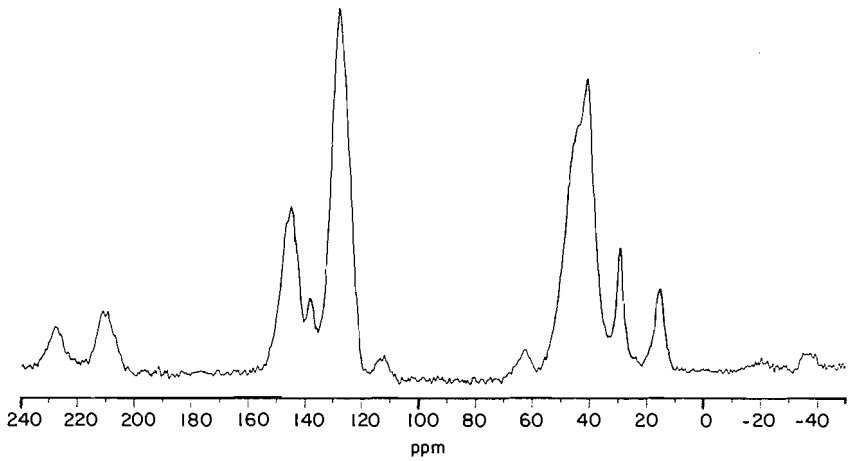


FIG. 11. ^{13}C NMR spectrum of intact PPP.

be roughly judged from the plots, shows PPP # 7 *between* the more polar Chromosorb 101 and the less polar Porapak Q — but all three are, as would be expected, fairly close to one another).

Second, there could simply be a better *physical* match between the test chromatographic solutes and the dimensions and distribution of polymer pores. Although this is not a separation on the basis of molecular size, the size of pores — particularly when they are relatively narrow — will affect sorption behaviour. One would expect that the most preferable situation, i.e. the steepest slope in the log $t_R'/\#C$ plot, will occur when the pore size distribution is narrow (and the pores themselves are narrow as well). It could be argued that a polymer made from *only* a cross-linker should be closest to fulfilling these conditions. This reasoning fits well to an experimental estimate, made earlier, that the porous polymer part of the PPP does, in fact, have a very high specific surface area. On the basis of that argument, then, one could indeed have predicted that the slopes should follow the sequence of the (polymers') specific surface areas, i.e. PPP > Poropak Q > Chromosorb 101. Still, in the absence of more — and perhaps different types of — data from a still larger number of systems, the argument must remain speculatory.

Sample capacity

In an adsorption mechanism, sample capacity should be related primarily to surface area (really: area active in retention) per column volume. One would therefore not expect large differences among PPP and conventional bead phases of comparable surface area. However, one always likes to be assured about the linearity of *ad*sorption isotherms. Besides, it is not clear what effect, if any, is produced by polymerizing within range of surface forces and whether the observed conditions lead to significant differences in pore size distributions. All of these factors could conceivably influence the sample capacity.

PPP # 7 was used as a test phase — in part because it showed

Can. J. Chem. Downloaded from www.nrcresearchpress.com by 122.72.124.2 on 09/07/12
For personal use only.

Can. J. Chem. Downloaded from www.nrcresearchpress.com by 122.72.124.2 on 09/07/12
For personal use only.

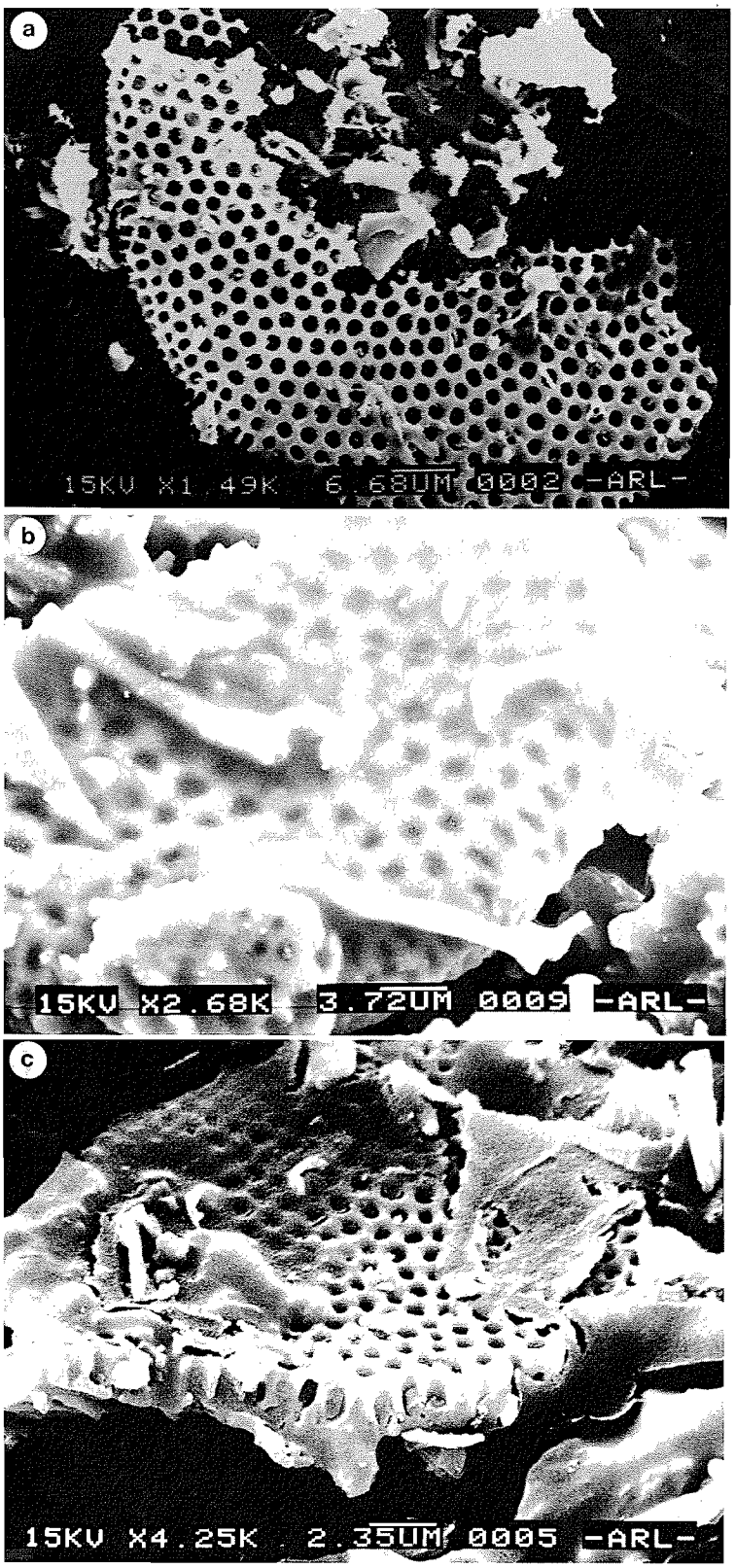


FIG. 12. Scanning electron micrographs of similar bare and porous-polymer-covered diatom structures. Corresponding polymer load: *a*, 0%; *b*, 37%; *c*, 11% (PPP # 7).

the highest plate number, in part because its polymer load was comparatively low (11.1%). In the tests PPP # 7 was compared to Chromosorb 101 (which is far closer in plate number and overall surface area than Porapak Q would have been). The tests did not show any great difference between the two phases. Under similar (and conventional) circumstances, both phases were capable of handling (single peak) samples of up to about 30 μg.

Temperature range

Similar to sample capacity, the useable temperature range of chromatographic separation media has no unambiguous definition, since it depends to some extent on what one wants to do with the phase — i.e. with what types of samples, in what concentration ranges, and with what detector it is going to be used. Furthermore, column performance at high temperatures can depend on the conditioning procedures, the purity of the carrier gas, the purity of the polymer (often: the purity of the monomer used to synthetize the phase), etc. In addition, porous polymers are subject to deformation at high temperatures — an effect that should be minimal for materials fitted with a diatomaceous exoskeleton.

We therefore chose to monitor the column bleed rate and probe peak width in a high-temperature range. Figure 9 shows selected but typical data from the more sensitive peak width study, with measurements on PPP # 6 (3660 plates, 19.8% polymer load) being carried out repeatedly at 130°C, *after* the various steps of the conditioning regime. The initial conditioning (after the routine conditioning carried out with *all* columns) lasted for 8 h at 250°C, then came 5 h at 255°C, then successive 1-h conditioning periods at 260, 265, etc., up to 295°C.

The peak width at half-height is a very sensitive indicator of any deterioration in performance, and it shows the first, slight change for the PPP phase at 290°C. Consequently we suggest that 280°C should be a safe upper limit. The bleed rates show only a slow rise and do not contradict this estimate. Yet it needs to be added that the question of thermal stability has been tested only in a perfunctory manner in this study, and may have to be re-evaluated in light of a particular intended usage.

It is safe to assert, however, that the highly cross-linked, relatively pure, and diatomaceously protected phases of this study show excellent thermal stability. This is particularly important in light of the typically strong retention ability of such porous polymers, i.e. of the limited volatility range of analytes that can be processed.

Mechanical stability

Almost by definition, there should be little if any pressure deformation of the polymer and/or settling of the column packing in the case of a diatomaceously encased porous polymer — unless the diatomaceous support should happen to break. And it is, indeed, well known that the fragility of various Chromosorbs can strongly contribute to poor performance of conventional GLC columns. In this regard, the protection afforded the porous polymer by the Chromosorb appears to have been reciprocated in kind: while a support like bare Chromosorb W is easily reduced to dust by rough treatment, it is far more resistant to abrasion when covered by the porous polymer. Polymer coatings have, of course, often been used to reduce or modify breakage of various inorganics (e.g. on car windshields, vacuum desiccators, and fused-quartz capillaries) Although we did not attempt to quantify the effect, it was clearly apparent and, for packing characteristics and lifetimes of columns, clearly beneficial.

Ancillary methods of characterization

Figure 10 shows the infrared spectrum of a pure-DVB protected polymer (for taking the IR spectra from a KBr disk, the diatomaceous protection had to be removed by a treatment with hydrofluoric acid). The spectrum is very similar to that of Porapak Q. The number of vinyl groups appears relatively low, as judged from the C—H stretch at 3085 and 3060 cm^{-1} and the C—H out-of-plane bending a 990 and 910 cm^{-1}.

Figure 11, for general interest, presents the ^{13}C NMR spectrum obtained on the intact phase with cross polarization and magic angle spinning. The spectrum shows only negligible differences from that of Porapak Q or that of DVB polymerized in bulk.

Figure 12 presents some scanning electron micrographs in order to illustrate — as opposed to define — (*a*) the mutual stabilization that support and porous polymer can offer one another, and (*b*) the easy chromatographic access that their interaction affords the solute molecules. The honeycomb-like structure of particular types of diatoms, which is commonly found in diatomaceous earths, was selected here to illustrate these two points. Figure 12*a* shows the diatom uncovered, Figs. 12*b* and 12*c* show it fully and partially covered. Figure 12*a* is a look at a speck of pure Chromosorb dust, while Figs. 12*b* and *c* are detail shots of the outside of particles with a 37% (not in Table 1) and 11% (#7 in Table 1) average polymer loads. It should be noted that coverages are not necessarily uniform throughout or among particles; nor need heavy loads of polymer appear everywhere as thick and smooth as they do in Fig. 12*b*. Cracks often appear in the polymer and it is not unusual, particularly at lower loads, to see the polymer half-filling the holes and cracking away from the walls (Fig. 12*c*, lower middle). It should be further realized that these scanning electron micrographs show only a small segment of the whole particle. Chromosorb particles are very loose conglomerates from diatoms of a wide variety of structures and sizes: that means essentially free access from/to the gas phase for the adsorbing/desorbing solutes, and only short diffusion paths (compared to a bead-type phase) through narrow polymer pores.

Conclusions

Protected porous polymers, at least as far as DVB-based materials are concerned, can be easily produced in the laboratory. They provide excellent column efficiency and pressure resistance. Beyond these practical advantages, they also offer evidence that porous polymers are not intrinsically less efficient than conventional GLC phases — provided their geometry permits facile access of carrier gas and solute molecules.

The optimization procedure used in this study was very crude and chromatographic performance could likely be further improved. Beyond DVB, other types of polymer systems could probably be deployed in similar fashion. It might also be worthwhile to attempt transferring some of the in-situ polymerization technique developed here, to other protective geometries commonly used in high performance and/or high pressure chromatographic systems.

Acknowledgements

We are grateful to P. Seto of the NRC Atlantic Regional Laboratory for the IR spectra, to R. Wasylishen and M. McKinnon for the solid-state NMR spectra, to J. Müller for the aesthetically and functionally superior glassware needed for some of the experiments, and to A. McMahon and Y. Z. Tang for their ever so patient help with administration and communi-

Can. J. Chem. Downloaded from www.nrcresearchpress.com by 122.72.124.2 on 09/07/12
For personal use only.

cation problems. This research was made possible by a sabbatical leave grant from Wuhan University (to C.Y.W.), and by an operating grant from NSERC (to W.A.A.).

1. G. E. BAIULESCU and V. A. ILIE. Stationary phases in gas chromatography. Pergamon Press, Toronto. pp. 295–312.
2. O. L. HOLLIS. J. Chromatogr. Sci. **11**, 335 (1973).
3. O. L. HOLLIS. Anal. Chem. **38**, 309 (1966).
4. S. B. DAVE. J. Chromatogr. Sci. **7**, 389 (1969).
5. G. J. HOWARD and C. A. MIDGLEY. J. Appl. Polymer Sci. **26**, 3845 (1981).
6. J. DE ZEEUW, R. C. M. DE NIJS, J. C. BUIJTEN, J. A. PEENE, and M. MOHNKE. American Laboratory. October 1987. p. 82.
7. E. N. FULLER. Anal. Chem. **44**, 1747 (1972).
8. G. E. POLLOCK, D. O'HARA, and O. L. HOLLIS. J. Chromatogr. Sci. **22**, 343 (1984).
9. Chromatographic Specialties Inc., Brockville, Ontario, 1987 catalogue.
10. C. F. POOLE and S. A. SCHUETTE. Contemporary practice of chromatography. Elsevier, Amsterdam. 1984. p. 69.

Can. J. Chem. Downloaded from www.nrcresearchpress.com by 122.72.124.2 on 09/07/12
For personal use only.

Transformation and transmission of organotin compounds inside a gas chromatograph[1]

WALTER A. AUE,[2] BERNARD J. FLINN, CHRISTOPHER G. FLINN, VELUPPILLAI PARAMASIGAMANI, AND KATHLEEN A. RUSSELL

Department of Chemistry, Dalhousie University, Halifax, N.S., Canada B3H 4J3

Received August 31, 1988

WALTER A. AUE, BERNARD J. FLINN, CHRISTOPHER G. FLINN, VELUPPILLAI PARAMASIGAMANI, and KATHLEEN A. RUSSELL. Can. J. Chem. **67**, 402 (1989).

A wide variety of mono-, di-, and tri-substituted tin compounds are transformed to, and transmitted as, chlorides, bromides, or iodides on injection into a gas chromatographic system doped with HCl, HBr, or HI, respectively. This transformation occurs directly from some thirty-odd analytes such as organotin oxides, hydroxides, organic esters, and other halides including fluorides. Three germanium compounds appear to behave similarly. A conventional, packed-column gas chromatographic set-up with flame photometric or flame ionization detector can tolerate the necessary acid doping. Compounds such as bis(tributyltin) oxide will elute, as halides, in subpicogram amounts. If the dopant flow is turned off, the packed column can act as a hydrogen halide reservoir for several days of operation. The transformations of tributyltin species into the halide form are generally fast on the timescale of chromatographic processes, i.e. sharp peaks result from the use of mixed hydrogen halides, and the retention time of mixed-halide peaks can be adjusted by varying the dopant composition.

Key words: organotins, gas chromatography, derivatization, acid doping, photometric detection.

WALTER A. AUE, BERNARD J. FLINN, CHRISTOPHER G. FLINN, VELUPPILLAI PARAMASIGAMANI et KATHLEEN A. RUSSELL. Can. J. Chem. **67**, 402 (1989).

Lorsqu'on injecte une grande variété de composés mono-, di- et tri-substitués de l'étain dans un système de chromatographie en phase gazeuse dopé par du HCl, du HBr ou du HI, ils sont respectivement transformés en, et transmis sous la forme de, chlorures, bromures ou iodures. Ces transformations se produisent directement à partir d'environ trente dérivés comme des oxydes, des hydroxydes, des esters organiques et d'autres halogénures (y compris les fluorures) organiques de l'étain. Il semble que trois composés du germanium se comportent de la même manière. Une colonne régulière de chromatographie en phase gazeuse remplie, munie d'une détecteur photométrique à flamme ou à ionisation à flamme, peut tolérer le dopage acide approprié. Des composés comme l'oxyde de bis(tributylétain) seront élués sous la forme d'halogénure, les quantités formées seront inférieures au picogramme. Lorsqu'on arrête l'écoulement de l'agent de dopage, la colonne remplie agit pendant plusieurs jours comme réservoir d'halogénure d'hydrogène. Les transformations des espèces tributylétain en dérivés halogénés sont généralement rapides si on les compare à l'échelle de temps des processus chromatographiques, c'est-à-dire que, lorsqu'on utilise des mélanges d'halogénures d'hydrogène, on observe des pics fins et le temps de rétention des pics provenant d'halogénures mixtes peut être ajusté en faisant varier la composition de l'agent de dopage.

Mots clés : composés organiques de l'étain, chromatographie en phase gazeuse, dérivatisation, dopage d'acide, détection photométrique.

[Traduit par la revue]

Can. J. Chem. Downloaded from www.nrcresearchpress.com by 41.223.56.140 on 09/07/12
For personal use only.

Introduction

This study arose from a chance observation. We had attempted to use organotin hydrides (prepared by treating typical tin-containing biocides in methanol with silane gas) for gas chromatographic trace analysis with a flame photometric detector (1). In the picogram range, decomposition became apparent. Turning to a common remedy (c.f. ref. 2), we attempted to treat the column with dimethyldichlorosilane, a compound traditionally used to deactivate the silanol groups of the chromatographic support. The hydride peaks were not improved, but new peaks started to appear. The latter were traced to the action of the deactivation by-product HCl on tin-containing non-volatiles in the injection port. Since the presence of — chemisorbed or physisorbed — hydrogen chloride was apparently able to transform organotin compounds *in situ* to chlorides, and allow them to migrate in that state through the column at picogram levels, the conclusion appeared obvious that deliberate doping of the gas chromatographic system with HCl — or, perhaps, with HBr or HI — might prove interesting and useful.

Although it appeared surprising at first sight, the formation of organotin chlorides under these circumstances might have been predicted. Organotin halides are easily produced in solution — a fact that has often been used for analytical ends by extracting them from a complex sample matrix — and they elute at conveniently low temperatures from gas chromatographic columns. In fact, the earliest reports concerned with the gas chromatographic separation of organotin halides date back to 1965 (3, 4). The general literature on organotin compounds is extensive; we are mentioning here only a few, selected papers (refs. 5–17 and references cited therein), to set the stage and focus on aspects relevant to this study.

Despite the easy formation and adequate volatility of organotin halides, they have often taken second or third place to fully alkylated (Grignard) or hydride ($NaBH_4$) derivatives for various types of analysis, particularly those of the trace variety. This is not surprising since the fast, quasi-ionic reactions of organotin halides also imply interaction with various materials in the gas chromatographic system (presumedly metal oxides, silanol groups on glass tubes or phase supports, trace amounts of water, etc.). Obviously, the detrimental effects of these interactions

[1]Material taken in part from the doctoral thesis of C. G. Flinn (Dalhousie University, 1979); and presented at the 62nd CIC Conference, Vancouver, June 1979. Further material taken from Co-op Summer Work Term Report of B. J. Flinn (Dalhousie University, 1983).

[2]To whom correspondence should be addressed.

are the more acutely felt the lower the amount of the organotin halide and the larger the number of hydroxide and other groups in the chromatographic system with which it can react.

In fact, it is useful to consider the chromatographic system as being governed by a network of equilibria such as

$$2but_3SnCl + H_2O \rightleftarrows (but_3Sn)_2O + 2HCl$$

with water being representative of a wide variety of similarly reactive, stationary or mobile chemical structures; and but_3Sn representative of the organotin moiety. (Note that bis(tri-*n*-butyltin) oxide, aka TBTO, is a much used and much researched marine antifouling agent.)

The equilibrium is useful for illustrating two points. First, to keep tributyltin in the chloride form and hence migrating through the column, a low level of water and a high level of hydrogen chloride (more general: a low level of ROH and a high level of HX) is advantageous. Second, at an appropriately high level of hydrogen chloride, analytes of low volatility such as TBTO can be directly injected into the chromatographic system for conversion to, and migration as, chlorides. Of course, the rate at which organotins approach the various *chemical* equilibria should be faster than the rate at which transport and diffusion establish the *physical* equilibria typical of chromatographic migration — in other words, the organotin kinetics should not unduly increase the peak dispersion beyond its purely chromatographic value.

The present study was designed to probe the feasibility, characteristics, range, and limitations of organotin transformations to, and gas chromatographic transmissions in, halide form. Analytical relevance was used as an important criterion in designing the experiments, but no attempt was made to focus on a particular compound or type of sample. Since organotins serve a wide variety of interests in industry and agriculture (5), they need to be determined at both high and low levels in vastly disparate matrices. In the context of doping a gas chromatographic system with a gas as reactive as hydrogen chloride, high levels of a (non-volatile) organotin analyte require more hydrochloric acid for conversion and may therefore represent a more severe test of the gas chromatograph's and particularly the column's ability to stomach large amounts of both analyte and dopant.

If the analyst is interested mainly in tin compounds, a selective detector is likely to be the correct choice; e.g. the flame photometric (7, 9, 10, 11, 13, 14), the hydrogen-rich flame ionization (8), or the electron capture detector (15, 16). Alternatively, one of the hyphenated-type instruments such as GC-MS (12), or machines capable of sample atomization and optical or mass spectral analysis (17) can be used. Here the flame photometric detector demonstrates detection at the sub-picogram level and, for higher analyte levels and the more general chemical objectives of most of this study, the non-selective flame ionization detector is used. Since the latter responds to the presence of CH in the analyte, essentially all volatile organic compounds will show up — whether they contain tin, another metal or metalloid, or no heteroatoms at all. This is important in the context of conversion rates, possible by-products, the behaviour of non-tin organometallics, and the correlation to hydrocarbon retention standards — all of which play a role in this study.

The questions that first spring to mind are these: Will a typical gas chromatograph — in particular, will typical stationary phases — stand up to hydrogen halide doping? Will the hydrogen halide really provide the expected benefits of *in situ* conversion and efficient chromatographic migration of the organotin moiety, both at high and low levels of analyte? What types of organotin compounds can be processed in this manner? Will the choice of hydrogen chloride vs. hydrogen bromide vs. hydrogen iodide make any difference? (Hydrogen fluoride was disregarded for a couple of fairly obvious reasons.) Will the exchange reactions be fast enough not to degrade peak shape? What levels of hydrogen halide are necessary for a well-functioning system? Will the gas chromatographic system retain larger amounts of hydrogen halides once their supply is turned off? Will retention times vary with the composition of dopant mixtures of different hydrogen halides? Will the presence of hydrogen halide in the hot gas chromatograph lead to undesirable degradation of the organotin structure, i.e. can the latter lose one or more alkyl or aryl groups? Can the developed methodology be extended to compounds of germanium and perhaps further elements?

Experimental

For experiments involving flame *photometric* detection, a Shimadzu GC-4BMPF gas chromatograph with a flame photometric detector was used. The quartz chimney of the detector was slightly modified to permit increased contact of the hot flame gases with the quartz surface — either on a radial quartz rod or on a wad of quartz wool (10) situated above the flame. The blue surface emission (together with the weaker, greenish SnOH and the red SnH gas-phase emissions) were monitored by the conventional Hamamatsu R-268 photomultiplier tube without additional spectral discrimination beyond that defined by its response profile.

Doping with hydrogen halides was carried out by adding HCl or HBr gas into the nitrogen line just before it entered the injection port, or by injecting into the chromatograph a few microliters of dilute solutions of HCl or HBr in methanol. In the former case, the flow of hydrogen halide gas was kept very low through a restrictor made by hammering a capillary steel tube until it was almost closed off, or by a stainless steel very fine metering valve (Nupro), or both.

In experiments involving flame *ionization* detection, a Tracor 550 gas chromatograph was used. The most common column packing was 10% Apiezon L on Chromosorb W, 45/60 mesh, in a 100 × 0.2 cm i.d. borosilicate tube. The doping gases hydrogen chloride and hydrogen bromide were usually diluted with nitrogen to 1 to 3% (for easier flow control) in a high pressure cylinder and slowly bled into the nitrogen carrier gas line before the injection port. Pressure controllers, valves, etc. were acid resistant (Matheson). The concentration of starting mixtures, as well as the amount of HX leaving the detector, were determined by titration. In some experiments involving HCl or HBr, and in all experiments using HI, the hydrogen halide was discontinuously introduced by injecting it in methanol solution. Depending on the analyte load, the flame ionization detector was cleaned of SnO_2 residues every two to four weeks.

Results and discussion

High-sensitivity experiments (flame photometric detection)

The experiments involving the modified Shimadzu photometric detector demonstrate that tri-organotins such as bis(tributyltin) oxide, triphenyltin hydroxide, and tricyclohexyltin hydroxide can be easily converted to the volatile halides by injecting them into the doped chromatograph. Either gas or solution doping work well.

Figure 1 shows the chromatography following injection of one *picogram* each of bis(tripropyltin) and bis(tributyltin) *oxides* into a chromatograph doped with HCl gas. The response indicates that most of the injected tin has reached the detector. (Note also that the small peak just prior to but_3SnCl implies

Can. J. Chem. Downloaded from www.nrcresearchpress.com by 41.223.56.140 on 09/07/12
For personal use only.

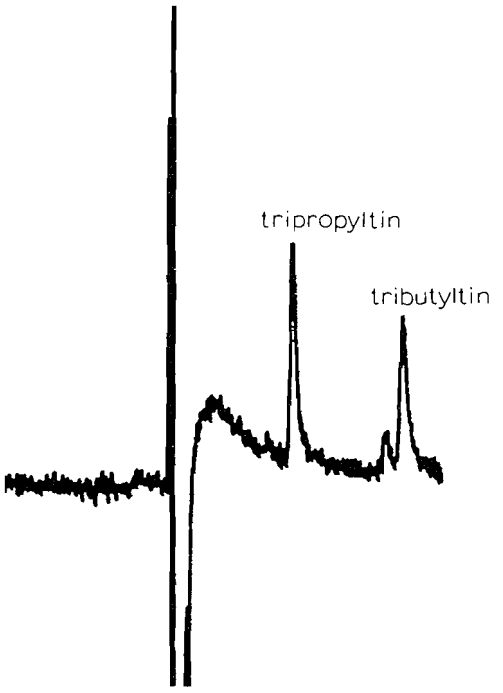


FIG. 1. Gas chromatogram of 1 picogram injected of each of bis(tripropyltin) and bis(tributyltin) oxides, detected as the respective chlorides in a flame photometric detector by quartz-surface luminescence. HCl (gas) rate of introduction ca. 4×10^{-7} mol/min.

some minor decomposition to but_2SnCl_2). Thus it appears that, even with the flame photometric detector close to its most sensitive state — it is no longer the *column* that restricts the limit of detection. That is highly significant: the 1 pg level is several orders of magnitude lower than what can be achieved in the gas chromatography of organotin halides *without* acid doping.

The column, incidentally, is a 50 × 0.3 cm i.d. borosilicate tube filled with Carbowax-20M modified (18) Chromosorb W, 80/100 mesh — a packing whose organic layer is only a nominal 15 Å thick and of which, since it is a polyether, one might not have expected satisfactory performance under acid doping conditions. It might be added that acid doping on the Shimadzu chromatograph was carried out (with a variety of columns) for about one year (1978/79). Aside from the bonded Carbowax column mentioned above, the liquid phases were usually of the dimethylpolysiloxane variety, e.g. OV-101. None of the columns suffered any obvious damage due to HCl or HBr, and the chromatograph and its photometric detector are still working well today.

In the experiments using the flame photometric detector (which preceded those using the flame ionization detector), di- and mono-substituted tin compounds were only superficially investigated and then only at levels above 100 pg injected. A variety of derivatives were obtained, but it was also obvious that, as is well known, the analytical difficulties decreased from mono- to di- to tri-organotin structures. The larger the number of halide atoms required for a particular analyte molecule, the heavier a dopant level was necessary for successful chromatography.

Depending on the dopant level and the temperature, it was also obvious that some degradation could occur (the term degradation is used here to describe the loss of alkyl or aryl substituents from tin). Under heavy doping conditions, for example, significant amounts of diphenyltindichloride and dicyclohexyltindichloride were obtained from the triphenyltin and tricyclohexyltin hydroxides, respectively. Even tetrabutyltin — but not the faster-eluting tetrapropyltin — would occasionally form minor amounts of tributyltinchloride. Judged merely by chromatogram, the degradation of organotins in injection port and early column can mimic the results of their degradation in the biosphere; and particular attention has to be paid to that fact in the analysis of environmental samples.

It can be assumed from basic principles that higher temperatures and stronger retention are generally helpful in terms of derivatization, harmful in terms of degradation. This actually happened to be the case. For instance, we had to use longer, more retentive columns for the very volatile methylated tin compounds, so the higher temperatures would speed up derivatization equilibria and maximize chromatographic efficiency. But we had to use shorter and less retentive columns for the much heavier analytes such as triphenyltinchloride and dioctyltindichloride, so the lower temperatures would minimize degradation.

(Note that, in case of derivatization *prior* to injection into the gas chromatograph — as in a CH_3OH/HX solution — one would not have to worry about *initial* derivatization. But one would have to worry about degradation, and about keeping the derivative in its halide form — i.e. about continuous and speedy *re*-derivatization, so to speak — because organotin species revert easily to non-volatile forms by reaction with components of the gas chromatographic system. Obviously, the overall analytical effort would be wasted if equilibrium conditions were to favor the derivative only in the injected sample, not in the chromatographic column.)

Notwithstanding such caveats, the important result of the experiments using the photometric detector is the demonstrated ability to derivatize, separate and detect, in *one* operation, extremely *small* amounts of a wide variety of organotin compounds.

Low-sensitivity experiments (flame ionization detection)

In contrast, the experiments using the Tracor gas chromatograph with the flame ionization detector were carried out with much larger amounts of organotins. This was done for a variety of purposes (besides being mandated by the general but much less sensitive response of the detector). First, a good deal of present-day organotin analysis is concerned with relatively large amounts of tin compounds, as they occur, for instance, in biocide or polymer stabilizer formulations. Second, the larger amounts of dopants necessary for larger amounts of analyte, as well as for *mono*- and *di*-organotins, present a greater challenge to the chromatographic system. Third, we needed to use a detector capable of monitoring hydrocarbons — e.g. for Kovats retention index measurements, for assessment of column degradation and chemical noise, etc. Yet it must be stressed in this context that our move to the flame ionization detector was solely for this fairly basic investigation — for most *analytical* tasks, a selective detector such as the flame photometric would do a far better job. The flame ionization detector is not only much less sensitive than the flame photometric detector, it also needs to be cleaned frequently when used for organotin halides — and its fits of electrical noise, caused by the dusty and corrosive environment, can reduce sensitivity further and lead to the occasional loss of data.

Bromide derivatives

In the first series of experiments with the flame ionization detector, HBr (gas) was used as the dopant. Its flow was

Can. J. Chem. Downloaded from www.nrcresearchpress.com by 41.223.56.140 on 09/07/12
For personal use only.

measured before and after the experiments: it had remained fairly steady throughout the experiments at about 1.3×10^{-6} mol/min. This was considered a fairly heavy doping level and it served well to define the chemical challenge to the chromatographic system and to the analytes.

The first demonstration with the HBr (gas) system was concerned with one of those groups of organotin compounds that are expected to yield the *same* derivative, i.e. one peak of nonvariant retention time. The following tributyltin type structures were used: bis(tributyltin) oxide and sulfide, hexabutylditin, and tributyltin fluoride, chloride, bromide, acetate, and linoleate. They all gave a single, large peak of precisely the same retention time, i.e. that of tributyltin bromide. Other experiments agree with this result: none of the common tributyltin compounds at our disposal ever showed a different behaviour. We must therefore conclude that the transformation to halides occurs easily from many different types of structures. (Note again that this is not too surprising: organotin carboxylates, for instance, convert to the chlorides simply on being treated with a solution of sodium chloride in water (19). The only surprise is, perhaps, how well this works inside the arid gas chromatograph.)

However, how quantitative is the conversion inside the gas chromatograph? To answer this question, the response was calculated per weight of tributyltin moiety (not original compound) injected. It turned out to be (normalized to the fluoride) 0.98 (oxide), 1.00 (sulfide), 0.86 (ditin), 1.00 (fluoride), 1.14 (chloride), 0.86 (bromide), 1.02 (acetate), and 0.74 (linoleate). Given that these responses were similar in magnitude to those of non-derivatizable compounds such as tetrabutyltin; and given the questionable purity of most tin compounds, their slow degradation in storage, and the errors involved in sample preparation, injection, and response assessment; it seems reasonable to assume that the conversions were, in essence, quantitative.

This is relevant not only from a chemical but also from a biological point of view: the *biocidal* structure is the tributyltin moiety and it is the one that is being determined here — regardless of the remaining labile group used in the formulation. To demonstrate this behaviour, calibration curves were measured for three different tributyltin compounds. The composite result is shown in Fig. 2: all three calibration curves *coincide*.

Analogous experiments were conducted with dibutyl and monobutyl tin compounds; though we had only a smaller number of such compounds available for testing. Similar to the tributyltin compounds, the dibutyltin species in oxide, dichloride, dilaurate, and dibromide form produced peaks of precisely the same retention time (i.e. that of dibutyltindibromide). Three of the compounds were used for the "mixed" calibration curve shown in Fig. 3. Again, the conversions and determinations appear to be essentially quantitative.

Only two monobutyl compounds were available: monobutyltin hydroxide oxide (butylstannoic acid) and butyltintrichloride. Both gave the same peak (butyltintribromide). Figure 4 shows this peak (originating from the trichloride), together with the peaks of dibutyltindibromide (from the dilaurate) and tributyltinbromide (from the linoleate) in a temperature-programmed separation.

A number of further organotins were injected under HBr(gas)-doped conditions, simply to see whether sharp, essentially single peaks of about the correct size and retention could be obtained. The compounds that produced such peaks were:

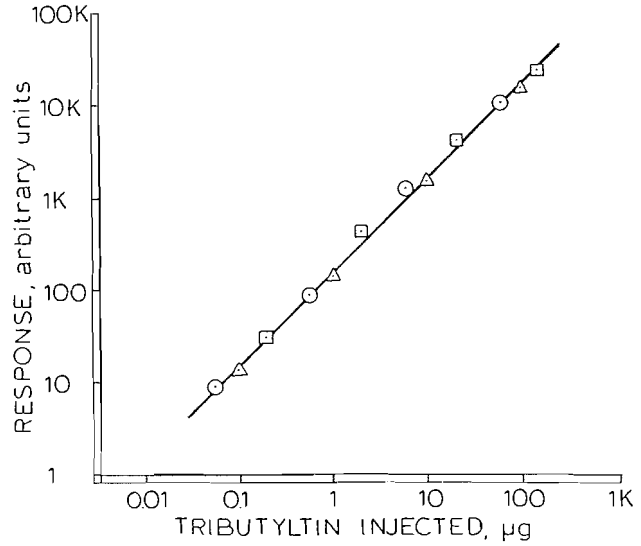


FIG. 2. Calibration curve of bis(tributyltin) oxide (○), tributyltin linoleate (△), and tributyltin fluoride (□), measured as tributyltin bromide in a flame ionization detector and plotted per μg of tributyltin injected. HBr (gas) rate of introduction 1.4×10^{-6} mol/min.

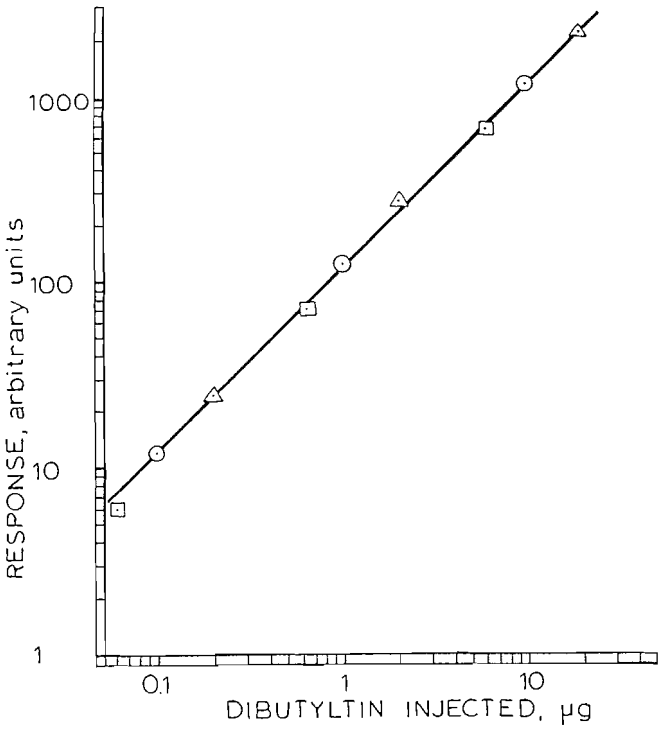


FIG. 3. Calibration curve of dibutyltindimethoxide (□), dibutyltindilaurate (○), and dibutyltindichloride (△), measured as dibutyltindibromide in a flame ionization detector and plotted per μg of dibutyltin injected. HBr (gas) introduction rate 1.4×10^{-6} mol/min.

phenyltintrichloride, diphenyltindichloride, triphenyltin chloride, triphenyltin hydroxide, bis(triphenyltin) oxide; dimethyltindichloride, dimethyltin oxide, trimethyltin chloride, trimethyltin hydroxide; bis(tripropyltin) oxide; dioctyltindichloride, diphenyltindichloride; cyclohexylstannoic acid, dicyclohexyltindibromide, dicyclohexyltin oxide, tricyclohexyltin bromide, and tricyclohexyltin hydroxide.

For exploratory interest only, a few organic derivatives of

Can. J. Chem. Downloaded from www.nrcresearchpress.com by 41.223.56.140 on 09/07/12
For personal use only.

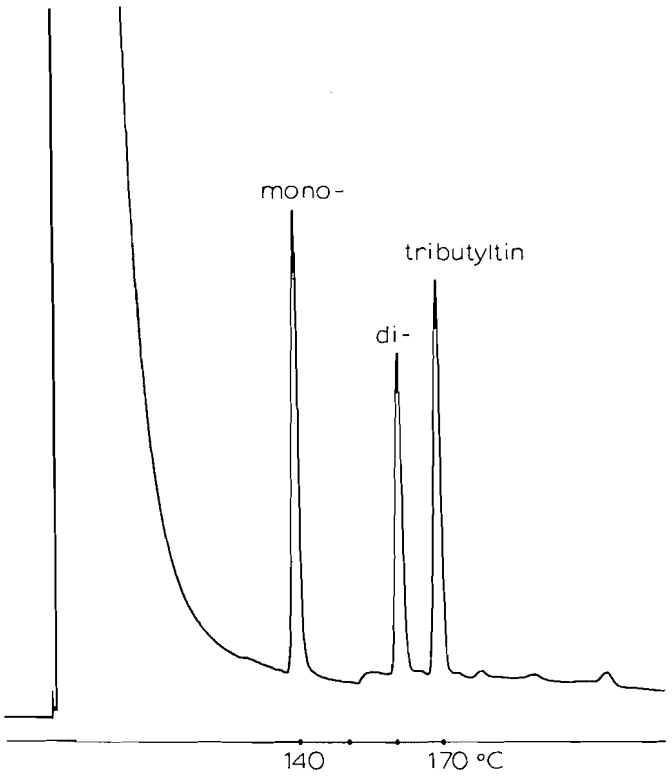


FIG. 4. Temperature-programmed chromatography of 0.5 μg injected of each of butyltintrichloride, dibutyltindilaurate, and tributyltin linoleate, separated and detected by flame ionization as butyltintribromide, dibutyltindibromide, and tributyltin bromide, respectively. HBr (gas) introduction rate 1.4×10^{-6} mol/min.

metals other than tin were also injected. Peaks were obtained — although not always sharp ones — from the three germanium compounds bis(trimethylgermanium) oxide, tributylgermanium chloride, and diphenylgermanium oxide, and from two arsenic species, phenylarsine oxide and phenylarsonic acid. We have no information on the identity of the peaks or the purity of the starting reagents, and we did not seek to explore the situation further. The only reason these seemingly positive results are mentioned here — and we should note that they were accompanied by seemingly negative results from further four compounds (another two arsenicals as well as an antimony and a lead compound) — is to demonstrate that there does exist a good possibility that organometallics other than those of tin may be amenable to acid-doped gas chromatography.

During the experimental series, i.e. during about three hot summer months of doping at a rate of 1.3×10^{-6} mol HBr/min, the color of the column packing (10% Apiezon L on Chromosorb W, 45/60 mesh) slowly changed from white to light yellowish-brown — but its ability to produce sharp, symmetrical peaks was not reduced.

Chloride derivatives

Further series of experiments were done with hydrogen chloride (gas) as the dopant. The first task was to establish that similar results could be obtained by doping with HCl as had been reported above for doping with HBr.

This was indeed the case. *All* thirty-odd organotin compounds that had given peaks with HBr, also gave peaks with HCl. The calibration curves of tributyltin chloride, tributyltin linoleate, and bis(tributyltin) oxide were identical within error margins (when plotted on a tributyltin basis) in the HCl gas system. Though the investigation of the quantitative aspects of organotin transformation and transmission was less extensive for HCl than for HBr doping, no serious differences were found.

Again as a sideline, the same non-tin organometallics earlier treated with HBr, were now exposed to HCl. The results were fairly similar. The three germanium compounds all gave peaks. Phenylarsine oxide again gave a peak, and a peak was also obtained from triphenylantimonydiacetate, which had not responded earlier in HBr. On the other hand, no peak was obtained for phenylarsonic with HCl. Based on these very sparse data we assume that organogermanium compounds behave fairly similar to tin compounds. Other peaks, such as those arising from certain arsenicals and antimonials, would need further work to identify. They might not even contain metal but might simply represent volatile decomposition products of the analyte (to which the flame ionization detector would respond equally well).

Halide exchange

Coming back to the primary targets of this study, namely the organotin compounds, we considered it interesting to investigate further the switch-over from HBr to HCl doping conditions and vice versa. The fact that sharp peaks are obtained from the injection of non-volatile analytes with either HCl or HBr suggests that the transformation (initial derivatization) to volatile chromatographic solutes must occur in the injection port or at the very front of the column, and that it occurs fast (fast, that is, on the timescale of separation kinetics). Furthermore, the peaks obviously stay sharp as they migrate through the rest of the column, and this suggests that the various equilibria (occasional hydrolysis, re-derivatization) are also fast compared to chromatographic peak dispersion. If the various equilibria are indeed reached fast enough in both HCl and HBr systems, then it is reasonable to assume that a mixture of HCl and HBr would lead to similarly fast derivatization and re-derivatization — and that the additional halide exchange equilibrium in the column, either directly

$$but_3SnCl + HBr \rightleftarrows but_3SnBr + HCl$$

or via oxygen-containing structures, would likewise be fast enough to satisfy chromatographic desiderata.

If so, then the equilibrium concept suggests that mixtures of dopants should not only produce sharp peaks, but that these peaks should migrate with speeds intermediate to those obtained by using pure dopants. In other words, chromatographic retention should become a function of the ratio of different dopant concentrations inside the chromatographic column. If a system is started, say, under HCl doping, and a peak is obtained at a particular retention time, that retention time should start to change smoothly upon the incessant introduction of HBr — until, when all reactive chloride in the column has been replaced by bromide, the peak again resumes constancy of retention (though now at a different value). Non-volatile organotin compounds that derivatize (fast) to the *same* chromatographic solute should behave identically in terms of retention time changes during such a switch-over.

An experiment along these lines was set up with three compounds: bis(tributyltin) oxide, hexabutylditin, and tetrabutyltin. The first two should derivatize to the same product. The third should not derivatize at all, hence its peak should remain at the same position in the chromatogram during dopant changes. The actual experiment involved a round trip from HCl to HBr and then back again to HCl (all injected in methanol).

Can. J. Chem. Downloaded from www.nrcresearchpress.com by 41.223.56.140 on 09/07/12
For personal use only.

The duration of this lengthy journey and the day-to-day changes in chromatographic conditions made it advisable to use not the raw retention times of the peaks but their Kovats retention indices.

The system performed precisely as expected. The Kovats indices of the first two compounds changed in unison from 1607 +/−4 to 1651 +/−2 and back again to 1607 +/−4. The index of tetrabutyltin stayed constant at 1601 +/−2. All peaks remained sharp and single throughout the experiment.

While the tributyltin peaks remained sharp through the switch-overs, this was not necessarily the case for other types of compounds. To gain some appreciation of possible effects, dibutyltindichloride was also injected from time to time. During both switch-overs, the peak became broad and tailed. Its position changed in the expected direction and it was situated in a retention range bordered by the pure chloride and bromide derivatives. As was mentioned earlier, the dibutyltins need more acid to yield sharp peaks, not surprisingly so since *two* halide atoms have to be introduced and the equilibrium constants are presumedly less favorable than those for the tributyltin analogues. Furthermore, in the switch-over, *three* volatile forms are possible (but_2SnCl_2, $but_2SnClBr$, and but_2SnBr_2), and additional equilibria are introduced, e.g.

$$but_2SnCl_2 + but_2SnBr_2 \rightleftarrows 2but_2ClBr$$

This makes it even more difficult for the migrating dibutyltin to approach the compound equilibrium fast enough to produce a sharp peak. In other words, the interchange among the three migrating halides themselves, as well as among them and the reactive halide and reactive hydroxyl populations in the column, must be so fast that each dibutyltin moiety travels with the same effective speed (which is the weighted average of the different speeds of the three pure dihalides) within distances that should presumedly not be much larger than the most important perturbation parameter, i.e. the particle diameter of the chromatographic support. It should be noted in this context that the occurrence of broad peaks for *di*-organotins has been mentioned several times in the literature, and that the kinetic explanation developed here for a special case is by no means the only one possible.

(For completeness' sake we should also mention that the concentration ratio [Cl]/[Br] is *not* constant along the length of the column in our experiment: the last injected hydrogen halide must dominate in the first segments of the column. In terms of chromatographic peak dispersion, however, a purely axial gradient is inconsequential.)

The change from chloride to bromide and back to chloride derivatives is interesting from both basic and applied viewpoints. We therefore tried to apply the idea to a second system, i.e. to the switchover from chloride to iodide and back to chloride. A new Apiezon L column was used for this purpose, mainly to check reproducibility in the chloride mode, and to ascertain thereby that the old column had not changed its characteristics during the long period of being subjected to chemical brainwashing. The dopants were HCl (gas) dissolved in methanol; and hydroiodic acid, dissolved in methanol and treated with $MgSO_4$.

Iodide derivatives

The results of the Cl → I → Cl exchange were similar to those observed for the Cl → Br → Cl switching sequence. Retention indices increased when HI was introduced — more so than with HBr, obviously — and the system could be returned to its initial state by re-injecting HCl. The retention of tetrabutyltin remained constant, of course. The tributyltin peaks were sharp throughout. Again, when dibutyltindichloride was injected, it required more of either acid than the tributyltin structures in order to produce a sharp peak. Also, organotin peaks sometimes appeared larger in the iodide than in the chloride system.

TABLE 1. Retention and response*

Compound	HCl		HBr		HI	
	KI	R	KI	R	KI	R
Bis(tributyltin) oxide	1608		1651	400		
	1596	336			1715	340
Hexabutylditin	1605		1651	310		
	1598	260			1715	256
Tetrabutyltin	1603		1600	315		
	1600	402			1595	400

*KI, Kovats index; R, response, in arbitrary units of peak area, per weight of original compound injected. Note: The two lines of values for each compound represent the Cl > Br > Cl and Cl > I > Cl dopant changes, respectively; with the latter being done on a new column.

Table 1 combines the retention indices of the two tributyltins and the standard tetrabutyltin, from the two experimental series mentioned above. Note that two columns were used, and that there exist therefore two sets of data for the chloride system. The retention ranges in the three dopant systems are clearly distinguished from each other, and the increased retention in the sequence Cl < Br < I is in accordance with expectation.

Table 1 also lists responses, in peak area per weight of (underivatized) substance injected. Responses from the hydrogen flame ionization detector, which monitors CH-containing species, should remain roughly the same for a particular (initial) analyte, regardless of whether the compound entering the detector had travelled and arrived in a chloride, bromide, or iodide system and form.

In this context it should be noted that the flame ionization detector is being severely challenged by experimental circumstances. Not only is it under the high-temperature assault of various strong acids, but the heavy amounts of tin compounds attempt to cover it with semiconducting debris (presumably SnO_2). Depending on injection load and other conditions, the detector had to be cleaned every two to four weeks — yet, it was still given to display interim fits of noise, and the time at which a particular value was measured may have had a bearing on the result. That this is so can be seen from the response of tetrabutyltin, which serves as a tin-containing standard not only for retention but also for response assessment.

With these caveats in mind, one can now examine the final data given in Table 1. They show that the response for each structure remains roughly comparable in the three dopant systems. Also, the response from the *reacting* tributyltin analytes is not significantly different from that of the *non-reacting* tetrabutyltin. That is a very strong indication indeed that the transformation and transmission of the tributyltin species is essentially quantitative in all three hydrogen halide-doped systems.

The experiments further suggest that iodide derivatives, just as chlorides and bromides, may be pressed into chromatographic service. To demonstrate that, a composite calibration curve of three of the (more difficult to chromatograph) *di*butyltins was measured and is shown in Fig. 5. Except for the different

Can. J. Chem. Downloaded from www.nrcresearchpress.com by 41.223.56.140 on 09/07/12
For personal use only.

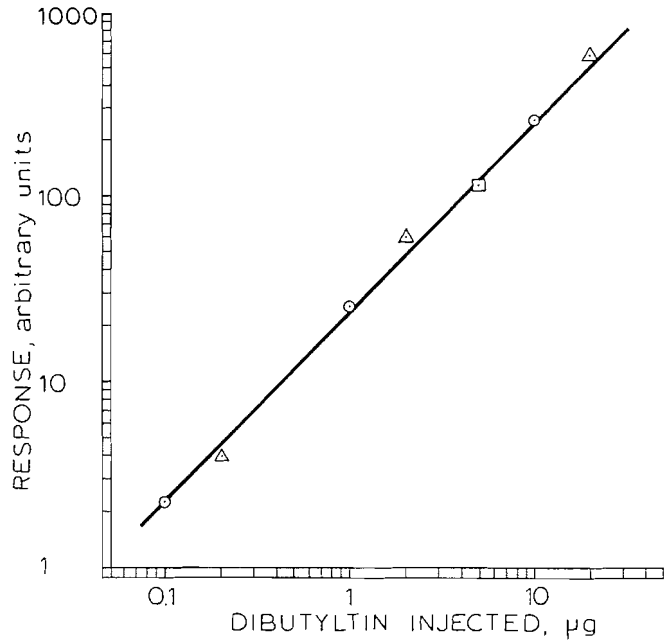


FIG. 5. Calibration curve of dibutyltindimethoxide (□), dibutyltindilaurate (○), and dibutyltindichloride (△), measured as dibutyltindiiodide in a flame ionization detector and plotted per μg of dibutyltin injected. Amount of HI injected (in methanol) ca. 8×10^{-5} mol.

dopant, it is comparable to Fig. 3. Still, the iodide experiment was only added as an afterthought, and no comparative studies were done on the wide variety of thirty-odd tin (and other) compounds as with chlorides and bromides.

During the doping experiments, a record was kept of the total amount of each acid injected. The value of this total amount was dependent on several criteria: in the beginning of the experimental series, acid was introduced until the tributyltins showed sharp peaks, then further acid was injected until dibutyltindichloride did the same. In the switch-overs, the new acid was added until the retention of the tributyltins became constant and dibutyltindichloride produced a sharp peak. Although these criteria are fairly subjective (and our protocol for complying with them was fairly lax), it is still interesting to note the approximate amount of each acid required for the task. On the five occasions that track was kept, this amount ranged between 3 and 10×10^{-5} moles of acid per initial doping or switch-over. We shall discuss the implications of this range later.

HCl retention and depletion

The final experiment of this study was designed to deal with the retention of HCl gas (really: reactive chloride) by the chromatographic system, and with the question of how much of it is necessary for adequate tributyltin transformation and transmission.

Obviously, the question can be answered only for a defined set of analyte and conditions — with the hope that the results will be fairly typical, hence applicable to other systems. The retention of the dopant will depend, *inter alia*, on the nature and amount of retentive materials in the gas chromatograph. For example, one would assume that a large-diameter packed column had a much larger capacity for halide retention than a capillary; or that a porous polymer packing might differ from one using a diatomaceous earth support; or that various tubing materials may act in a disparate manner. Furthermore, different organotin compounds and different dopants are wont to react with different degrees of effectiveness — as both kinetic and thermodynamic aspects are coming to the fore under suitable conditions — and the whole system is, furthermore, subject to the influence of temperature, flow rates, etc. Still, to have *some* idea of what is a useable/desirable dopant level may be quite helpful — as can be readily appreciated from the fact that at least part of this very study had been flying blind: The dopant levels of HCl or HBr in gaseous form were established in the beginning by guess and chance (we have not quite mastered yet the art of setting, and maintaining, a very low, precise flow of a highly reactive gas). Consequently, the steady-state hydrogen halide effluent from the column was occasionally measured by titration, but it was never optimized for a particular group of analytes or a particular gas chromatographic set-up.

By measuring the steady rate at which HCl emerges from the column, a particular dopant level can be correlated with chromatographic performance, i.e. peak area and shape. Furthermore, the amount of reactive chloride held by the column can be estimated.

An experiment of this sort was carried out by doping the one-meter, 10% Apiezon L on Chromosorb W column with a continuous flow of HCl that, measured as the (constant) column effluent rate, was 1.8×10^{-7} mol/min. The HCl tank was then shut off, allowing the gas that remained in the lines to bleed slowly through the restrictor valve and thereby provide an exponentially decreasing halide input. The column output of HCl was titrated again when the HCl input reached zero (as judged from a pressure gauge), and then titrated a few times more until it became too low to measure. From about the time of zero input (day 5) on, effluent HCl originated only from the column, which acted thus as a reservoir by equilibrating its HCl content with the nitrogen carrier gas stream flowing through it.

Throughout the experiment, tributyltin linoleate was injected a few times per day (weekends excepted) to check for chromatographic performance. The peak width started to broaden soon after the HCl tank was shut off; by the time no new HCl entered the column (day 5), it had reached about double the initial value. (The peak area, on the other hand, had remained essentially constant.) At that point in time, HCl emerged from the column at the rate of 6.4×10^{-9} mol/min.

The fact that the peaks started to broaden soon after the HCl tank was shut off indicates that the initial HCl input was just enough, or even a bit too low, for producing the sharpest peaks obtainable from tributyltin linoleate (really: tributyltin chloride). Note that the initial dopant concentration was almost an order of magnitude lower than that used earlier in some of the HBr (gas) experiments. The fact that the peak area stayed constant suggests that all of the analyte made it to the detector, but that the analyte derivatization rate (initial and/or in the column) became slow enough to broaden the peak.

It may be interesting to ask how much reactive chloride the column contained at this point. Figure 6 shows the drop in HCl output in a semilogarithmic plot. If, for the purpose of a rough estimate, one assumes that a strictly exponential function applies

$$r = r_0 \exp(-kt)$$

where r is the output rate at time t and r_0 is the initial output rate, then the integral to infinite time is r_0/k (the constant k is the slope in Fig. 6). If one assumes r_0 to have the value of day 5 (no further HCl input) and accepts the slope of the straight

Can. J. Chem. Downloaded from www.nrcresearchpress.com by 41.223.56.140 on 09/07/12
For personal use only.

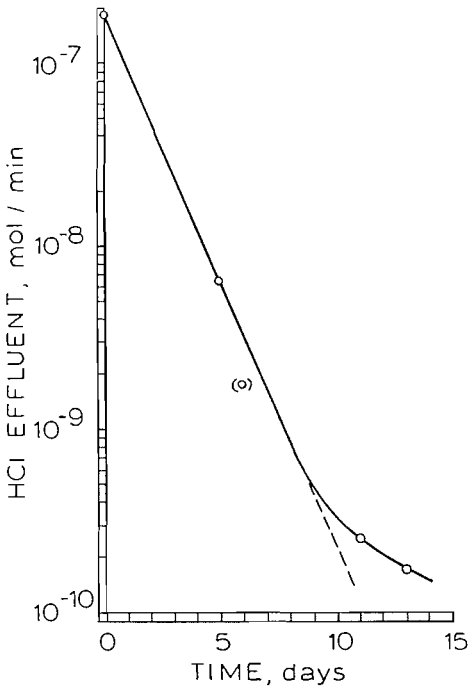


FIG. 6. Effluent rate of HCl (gas) over two weeks. See text for explanation. Titration at day 6 was prematurely terminated, resulting in only a minimum value.

line (as extrapolated in dashes), then the amount of elutable chloride from day 5 on is about $(6.4 \times 10^{-9}$ mol/min)/$(4.7 \times 10^{-4}$ min$^{-1}) = 1.4 \times 10^{-5}$ mol. (The actual amount is most likely higher, not only because the curve deviates from the pure exponential, but also because the column net loss started *before* the HCl input finally stopped on day 5, and because the injections of tributyltin linoleate consumed some additional HCl. However, this should not matter much in an order-of-magnitude calculation.)

It is interesting to compare this number (1.4×10^{-5} mol) with earlier measured amounts of acid necessary to condition the column or to switch halide (3 to 10×10^{-5} mol). Given that the first number is low (peak broadening of tributyltin linoleate is already apparent) and the second is high (not only tributyltin linoleate but also dibutyltindichloride produces a sharp peak), the amount of hydrogen halide typically necessary for this particular column and chromatographic system appears consistent in the two types of experiments.

One can further compare the overall range of 1 to 10×10^{-5} mol HX to the surface area, about 1.3 m^2, of the Chromosorb W support typically contained in the column. If one uses, for instance, an area of 12 Å^2 per halide, that area translates to about 1.8×10^{-5} mol of halide. In other words, this order-of-magnitude calculation would be consistent with the idea that the available (reactive) surfaces have to be more or less covered by chemically or physically sorbed hydrogen halide.

As the active chloride concentration further dropped in the column, the peak width continued to broaden. On the next day (day 6), peaks started to exhibit asymmetry. This is consistent with HCl being slowly swept from the column — the effect being most strongly felt at the start of the chromatographic path, i.e. in the injection port. The peak area, on the other hand, still remained about the same.

In fact, the peak area remained fairly constant — while peaks continued to broaden to about *four times* the original peak width — up to about day 13. Then it, too, started to deteriorate. By day 18 the peaks had become genuinely irreproducible and the experiment was terminated.

(It should be noted that this experiment, while quite rich in information content, was intrinsically unable to provide *precise* measurements of such parameters as peak broadening. The reason lies in the equilibria and the extent of interference that repeated testing brings to them. For instance, the injection of tributyltin linoleate consumes reactive chloride in the injection port and the beginning of the column. Some of the HCl is being replenished by diffusion of HCl from positions upstream (and, perhaps to a minor extent, downstream) in the flow path, i.e. the local equilibria slowly re-establish themselves. In agreement with this scenario, a rapid sequence of repeated injections will successively broaden peaks. If the chromatograph is then given some time to recuperate, its performance improves: the peak will be sharper now than the last peak of the rapid sequence run earlier — even though the effluent rate, and the total amount of reactive chloride in the column, keep continually decreasing.)

The rate of HCl effluence shown in Fig. 6 was governed not by a single but by a variety of processes. During the first days of the experiment, the rate simply reflected the exponentially decreasing HCl input. As the latter gradually ceased, the rate became dominated by condensed-phase/gas-phase equilibria. Overlaying these, and particularly important toward the end of the experiment, might have been the substitution of active surface chloride by hydroxyl from traces of water in the carrier gas (and/or the physical displacement of adsorbed HCl by H_2O). Although care was taken to dry the carrier nitrogen as far as possible (Linde molecular sieve 5A followed by a Supelco heated O_2/H_2O scavenger cartridge), it is likely that the residual moisture in the carrier gas could not be depressed much below the 1 ppm level — not to mention the possibility of moisture diffusing into the chromatograph from the atmosphere. A short calculation shows that a 1 ppm level of hydrogen chloride in the carrier gas (which corresponds, reactionwise, to 0.5 ppm water) amounts to about 10^{-9} mol HCl/min, i.e. a rate well within the range of the experiment. Therefore, the possible influence of even traces of moisture in the carrier gas cannot be lightly dismissed.

In any case, it is clear that the retention of HX by a packed-column chromatographic system can be extensive. This is, of course, the reason why the effect has been found in the first place. It enables the system to provide good chromatography under *dis*continuous doping, with the sharpness of the analyte peak (c.f. refs. 15, 16) serving as a quality control (halide concentration) indicator.

Beyond obvious analytical implications of the equilibria defining desirable doping levels in a gas chromatographic system, the halide transformation/transmission effects could also surface in other contexts. Imagine, for instance, a mass spectrometer's direct probe whose walls, courtesy of a prior sample, had acquired a chloride coating, and which was asked to procure a spectrum of TBTO: some of the sample might enter the source not as the oxide but as the chloride. Chromatographically, the migration of organotin structures as mixed halides is interesting in that it allows, within limits, a continual adjustment of retention relative to other compounds. Since analyte retention depends on the average composition of the migrating organotin halide, and since peak dispersion, given the right circumstances, includes *chemical* rate constants, certain kinetic data could also be derived from such a chromatographic

Can. J. Chem. Downloaded from www.nrcresearchpress.com by 41.223.56.140 on 09/07/12
For personal use only.

system. Furthermore, it is unlikely that the effects should be restricted to organo*tin* compounds. Compounds of germanium will likely show similar behaviour. Halide exchanges occur easily among inorganic compounds of various elements, as documented by isotope exchange (e.g. 20). The benefit of doping a column with mercuric chloride for the efficient chromatography of organomercurials has been partly attributed to analogous processes (21). There must surely exist a variety of organic (as opposed to organometallic) compounds that are prone to exchange labile halide during gas chromatography. It is, furthermore, possible to envision the synthetic use of (preparative) gas chromatography for obtaining small amounts of particular (e.g. isotope-enriched) organometallic halides. Finally, it may be advantageous to use the volatilization of analyte in an HX stream for preconcentration of organotin and other organometallic compounds.

Acknowledgements

We appreciate the most helpful assistance of Wayne LeMoine in electronics, Jürgen Müller in glassblowing, and Reg Myatt in machining. This study was supported by NSERC operating grant A-9604 and by two NSERC undergraduate summer scholarships (to B. J. Flinn and K. A. Russell).

1. C. G. Flinn. Ph.D. Thesis. Dalhousie University, Halifax, N.S. 1979.
2. W. O. Gauer, J. N. Seiber, and D. G. Crosby. Agr. Food Chem. **22**, 252 (1974).
3. H. Geissler and H. Kriegsmann. Z. Chem. **5**, 423 (1965); Chem. Abstr. **64**, 11834d (1966).
4. B. L. Tonge. J. Chromatogr. **19**, 182 (1965).
5. W. T. Piver. Env. Health Persp. 61 (1973).
6. R. D. Steinmeyer, A. F. Fentiman, and E. J. Kahler. Anal. Chem. **37**, 520 (1965).
7. W. A. Aue and C. G. Flinn. J. Chromatogr. **142**, 145 (1977).
8. D. R. Hansen, T. J. Gilfoil, and H. H. Hill, Jr. Anal. Chem. **53**, 857 (1981).
9. S. Kapila and C. R. Vogt. J. Chromatogr. Sci. **18**, 144 (1980).
10. C. G. Flinn and W. A. Aue. Can. J. Spectrosc. **25**, 141 (1980).
11. R. S. Braman and M. A. Tompkins. Anal. Chem. **51**, 12 (1979).
12. H. A. Meinema, T. Burger-Wiersma, G. Versluis-de-Haan, and E. C. Gevers. Env. Sci. Techn. **12**, 288 (1978).
13. B. W. Wright, M. L. Lee, and G. M. Booth. J. High Res. Chromatogr. Chromatogr. Commun. April 1979. p. 189.
14. R. J. Maguire and H. Huneault. J. Chromatogr. **209**, 458 (1981).
15. G. A. Junk and J. J. Richard. Proceedings of Oceans 86. Vol. 4. Organotin Symposium. 1986. p. 1160.
16. M. Takeuchi, K. Mizuishi, H. Yamanobe, and Y. Watanabe. Bunseki Kagaku, **36**, 138 (1987).
17. K. W. M. Siu and S. Berman. Symposium on Organometallics in the Environment. Third Chemical Congress of North America, Toronto, Ont. June 1988. Abstract GEOC #74.
18. M. M. Daniewski and W. A. Aue. J. Chromatogr. **147**, 119 (1978).
19. K. N. Somasekharan and R. V. Subramanian. Am. Chem. Soc. Org. Coatings Plast. Chem. (Preprints) **40**, 167 (1979).
20. Y. Makide and N. Saito. Abstracts, IUPAC International Congress on Analytical Chemistry, Kyoto, Japan. 1972.
21. J. E. O'Reilly. J. Chromatogr. **238**, 433 (1982).

Can. J. Chem. Downloaded from www.nrcresearchpress.com by 41.223.56.140 on 09/07/12
For personal use only.

Soluble polymer supported synthesis of a monosubstituted tetraaryl porphyrin

Y. TAKAHASHI,[1] J. E. GUILLET, AND M. A. WINNIK
Department of Chemistry, University of Toronto, Toronto, Ont., Canada M5S 1A1

Received August 8, 1988

Y. TAKAHASHI, J. E. GUILLET, and M. A. WINNIK. Can. J. Chem. **67**, 411 (1989).

A new synthesis of monosubstituted tetraarylporphines is described based upon the soluble polymer supported synthesis strategy. Low molecular weight poly(ethylene glycol) is chloromethylated at both ends. These ends are then used to build up the polymer-bound ether of 5-(4′-hydroxymethyl)-10,15,20-tritolylporphine, which, after purification of the polymer, can be cleaved in high yield with $TiCl_4$. While the method offers useful conveniences, such as the ease of separation and purification of the desired material, the overall yield is low: 100 mg from 40 g of polymer. Oligomerization of the polymer during chloromethylation increases the polymer molecular weight and thereby decreases the number of end groups per gram of polymer.

Key words: porphyrin, tetraaryl, monosubstituted poly(ethylene glycol) oligomerization, polymer-supported synthesis.

Y. TAKAHASHI, J. E. GUILLET et M. A. WINNIK. Can. J. Chem. **67**, 411 (1989).

On a mis au point une nouvelle méthode de synthèse des tétraarylporphyrines monosubstituées qui est basée sur l'emploi d'un polymère soluble comme support. On a procédé à la chlorométhylation des deux extrémités d'un poly(éthylène glycol) de bas poids moléculaire. Ces extrémités sont alors utilisées pour construire l'(hydroxy-4′ méthyl)-5 tritolyl-10,15,20 porphine reliée au polymère par une liaison éther; après purification du polymère, on peut effectuer le clivage de cet éther avec de très bons rendements en utilisant du $TiCl_4$. Même si cette méthode offre plusieurs avantages, comme la facilité de séparation et de purification du produit désiré, le rendement global est faible : 100 mg à partir de 40 g de polymère. L'oligomérisation du polymère durant la chlorométhylation augmente le poids moléculaire du polymère et diminue ainsi le nombre de groupements terminaux par gramme de polymère.

Mots clés : porphyrine, tétraaryl, oligomérisation du poly(éthylène glycol) monosubstituée, synthèse basée sur l'emploi d'un polymère comme support.

[Traduit par la revue]

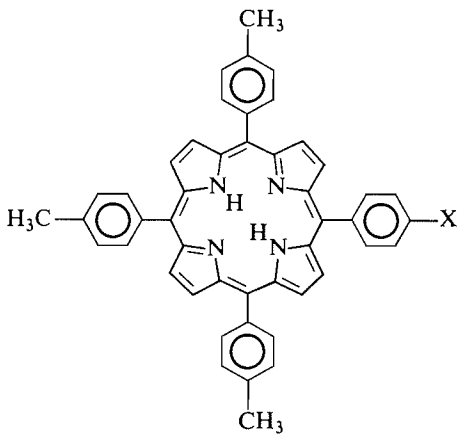
Can. J. Chem. Downloaded from www.nrcresearchpress.com by 41.223.56.140 on 09/07/12
For personal use only.

For many years we have been concerned with the problem of designing polymers that could serve as a mimic of the light-harvesting chlorophylls in a chloroplast (1). Porphyrins (Por) are ideal candidates for this function. Their spectroscopy is well understood (2). Certain derivatives are quite stable under many of the conditions under which a photosynthetic device might be operated and, most important, the R_0 value for self-energy transfer (Por* + Por → Por + Por*) by the dipole-coupling mechanism is suitably large (3).

To attach a porphyrin to a synthetic polymer, one needs a derivative with a single functional group. A monoacrylate or methacrylate derivative would allow porphyrins to be introduced as comonomers into a polymer chain by free radical copolymerization. Some such derivatives are not difficult to prepare, although in low yield, but they pose certain problems in their eventual application as antenna groups in the polymer. One could avoid these problems with other derivatives, but they are much more difficult to synthesize, isolate, and purify.

For example, one of the easiest monosubstituted tetraphenylporphyrin derivatives to obtain is the mono-4-hydroxy derivative **1***a*. It can be prepared by a mixed condensation of pyrrole, benzaldehyde, and *p*-hydroxybenzaldehyde. The yield is terrible (<5%) but the isolation and purification steps are not too difficult. Nevertheless, esters of **1***a* attached to water-soluble polymers experience two problems. The first is hydrolysis of the aromatic ester, which occurs much too quickly in water; and the second is the problem of photo-Fries reactions competing with the processes of interest. These particular problems could be overcome in a molecule such as **1***b* where the -OH is separated from the phenyl group by the $-CH_2-$ spacer.

There is a wide interest in the synthesis of porphyrins, often



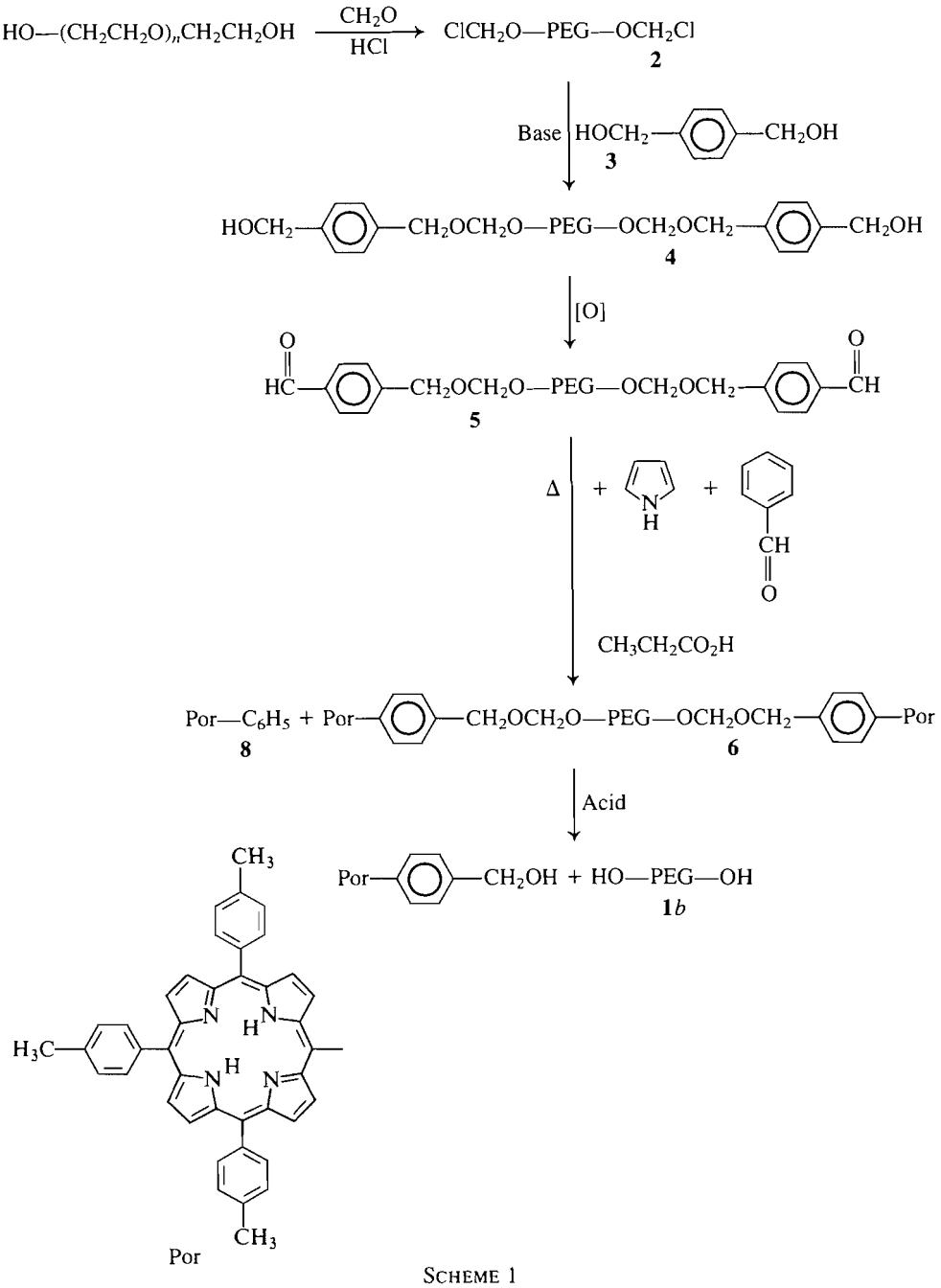
1*a* X = OH
b X = CH_2OH
c X = $CH_2OC(=O)C(CH_3)=CH_2$

for the purpose of mimicking natural systems such as oxygen-binding proteins. These efforts have led to synthetic strategies that can be categorized into three groups. The mixed benzaldehyde condensation mentioned above (4) works well for symmetrical tetraaryl porphyrins. For monosubstituted derivatives the method has limited utility, since the separation of the desired product is successful only for tetraaryl porphyrins containing a strongly polar group such as HO, NO_2, and CO_2H.

Another approach involves substitution reactions on the porphyrin nucleus (5). This method usually results in a complex mixture of mono- and multi-substituted isomers. In exceptional cases, monosubstituted derivatives can be isolated from these reactions.

The most general route involves step-by-step synthesis (6).

[1]Permanent address: Oji Paper Co., Ltd., 1-10-6 Shinonome Koto-ku, Tokyo, Japan.



SCHEME 1

One starts with a single pyrrole and adds bridging methylene and successive pyrrole units to construct a linear tetrapyrrole. This species is then condensed with an appropriate aldehyde to give the porphyrin. The disadvantage of this method is one associated with all multistep syntheses: the skill required by the experimenter and the large number of isolation and purification steps involved in the transformation.

The other alternative is a synthetic scheme based upon polymer supported synthesis (7). This can be either of solid supported type employing crosslinked polymer beads (7, 8) or of the soluble polymer type (9). These methods simplify the steps of product isolation and purification, since the by-products and impurities are normally small molecules.

Leznoff and Svirskaya (8) used an insoluble support (crosslinked polystyrene) to prepare unsymmetrical tetrarylporphyrins. They attached an aromatic aldehyde to the polystyrene bead via a substituent in the *para* position. The polymer-bound derivative was condensed with an excess of pyrrole and benzaldehyde to provide a mixture of tetraphenylpyrrole and the desired product, bound to the particles. The separation and purification steps required for the product were somewhat more onerous than one might have anticipated. Later the authors applied this scheme to prepare unsymmetrical phthalocyanines (10).

An alternative approach involves synthesis on a soluble polymer support. For instance, poly(ethylene glycol) was used as a support for N-protected amino acids in peptide synthesis (9*a*). In the case of application of solvent-soluble supports, the low molecular weight reactants and by-products were separated by either ultrafiltration or selective precipitation.

Can. J. Chem. Downloaded from www.nrcresearchpress.com by 41.223.56.140 on 09/07/12
For personal use only.

Can. J. Chem. Downloaded from www.nrcresearchpress.com by 41.223.56.140 on 09/07/12
For personal use only.

We have chosen to examine a soluble polymer supported synthesis of 4-hydroxymethylphenyl-triphenyl porphyrin. While our approach did work, and is described in the sections that follow, success did not come as smoothly and simply as we had anticipated. Some of the problems we encountered are actually quite interesting from a polymer chemistry point of view. Those aspects are also examined in this paper.

Strategy

Polyethylene glycol (PEG) of sufficient molecular weight is insoluble in diethyl ether. If one uses the HO groups on the chain ends as points of attachment for chemical transformations, then the work-up of each step would involve filtration to remove unwanted solids, precipitation of the polymer into ether, followed by filtration to remove unwanted solvent and soluble by-products. This property suggested to us that if we could prepare a PEG sample containing an appropriate 4-substituted benzaldehyde at each end, this group could be incorporated into a porphyrin by cocondensation of the polymer with benzaldehyde and pyrrole. A vast excess of tetraphenylporphyrin would be produced as a by-product, but this could be removed by filtration from the soluble polymer-bound porphyrin. In Scheme 1, given below, the desired porphyrin could be cleaved from the polymer by treatment with acid.

We presumed that PEG could be chloromethylated using conditions similar to that used by Corey *et al.* (11) in their synthesis of the protecting group precursor $CH_3OCH_2CH_2OCH_2Cl$ (MEM-Cl). Reaction of the chloromethylated polymer **2** with an excess of the diol **3** in DMF containing sodium hydride should yield the difunctional polymer **4**, which could be oxidized in turn to the bisbenzaldehyde derivative **5**. Model studies indicated that the formaldehyde acetal linkage (as in **4** and **5**) was stable to the reaction conditions (refluxing propionic acid) necessary for the pyrrole–benzaldehyde condensation. As a consequence, we envisaged no problem with the condensation step **5** → **6**. Cleavage of the purified polymer **6** with $TiCl_4$ should lead to the desired porphyrin **1***b*.

Results and discussion

Experiments began with polyethylene glycol (PEG) of $M_w \approx 2000$ ($\bar{M}_n/\bar{M}_w = 1.1$). It was chloromethylated by treatment with s-trioxane and HCl gas in dry methylene chloride. The product, substituted at both chain ends ($ClCH_2O$—PEG—OCH_2Cl, **2**), was precipitated from diethyl ether. Analysis of the product by gel permeation chromatography (gpc), however, indicated a large increase in polymer molecular weight. This point is examined in more detail below.

The transformation of **2** to **4** introduces an aromatic ring whose uv absorption allows the extent of incorporation to be monitored. Thus treatment of **2** in THF with a large excess of *p*-di(hydroxymethyl)benzene in the presence of sodium hydride gave a polymer with uv-absorbing groups attached. This reaction could be monitored by gpc. Like PEG itself, the precursor polymer **2** gives a signal only in the differential refractive index detector (ri), whereas the product **4** shows a response in both the ri and uv (250 nm) detectors.

The most striking feature, which is apparent in comparing the traces in Fig. 1, is the shift of the elution volume and elution profile of the polymer. The sharp peak for PEG is broadened in **2** and appears at much shorter times. The gpc analysis confirms that molecular weight changes occur during chloromethylation. We presume that the oxacarbocation intermediate can be

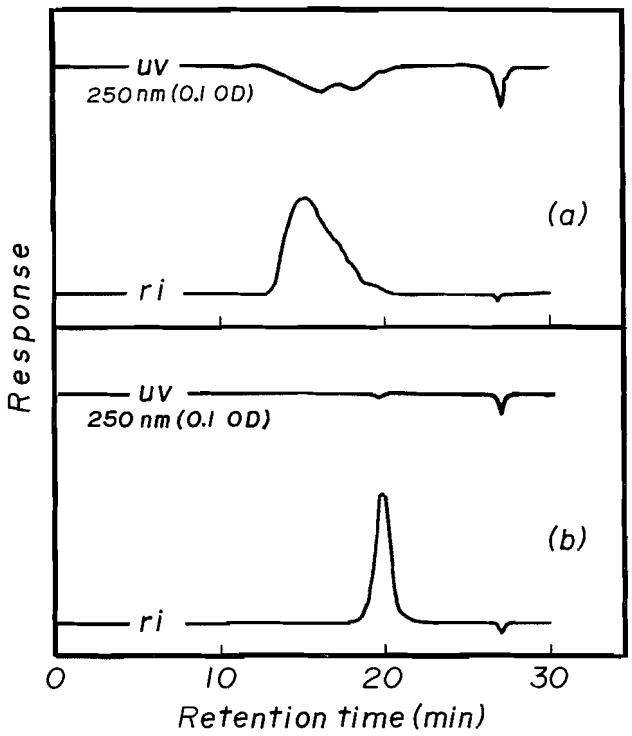


FIG. 1. Gel permeation chromatography traces (a) of $HOCH_2$—$C_4H_4OCH_2OPEGOCH_2OC_6H_4$—$CH_2OH$ (**4**) and (b) of the PEG sample used in its synthesis. Solvent: toluene. Detectors: ri, differential refractive index; uv, absorption at 250 nm.

trapped by reaction with a second PEG in competition with its reaction with chloride.

$$HO—PEG—OH \rightarrow [HO—PEG—O\overset{+}{C}H_2] \rightleftharpoons HO—PEG—OCH_2Cl$$

$$\downarrow \; HO—PEG—OH$$

$$HO—PEG—OCH_2O—PEG—OH$$

As a consequence of oligomerization, the number of functional groups available for synthetic use are reduced. The product distribution was remarkably insensitive to changes in the reaction conditions. If we estimate the polymer $\bar{M}_n$ from gpc to be 8000, uv analysis indicates that 85% of the chain ends contain benzyl alcohol groups.

The polymer **4** was treated with CrO_3/pyridine in dichloromethane to oxidize the $-CH_2OH$ groups to the aldehyde. The uv spectrum of the product is identical to that of benzaldehyde. Quantitative evaluation of the spectrum (using $\epsilon(250\text{ nm}) = 15\,700\text{ L mol}^{-1}\text{ cm}^{-1}$ for benzaldehyde) indicated essentially quantitative conversion.

The next step was to form the porphyrin nucleus by taking advantage of Adler's porphyrin synthesis (12). A 50-fold excess of pyrrole and tolualdehyde was mixed with the polymer **5** and refluxed in propionic acid for 30 min. The tetratolylporphine by-product, which precipitated from the solution, was filtered out of the mixture. The dark brown propionic acid solution was gradually added to diethyl ether to precipitate the polymer (**6**). Polymer **6** was repeatedly purified by dissolution and reprecipitation. Figure 2 displays the result of the gpc measurement. A strong response detected on the uv–vis detector monitored

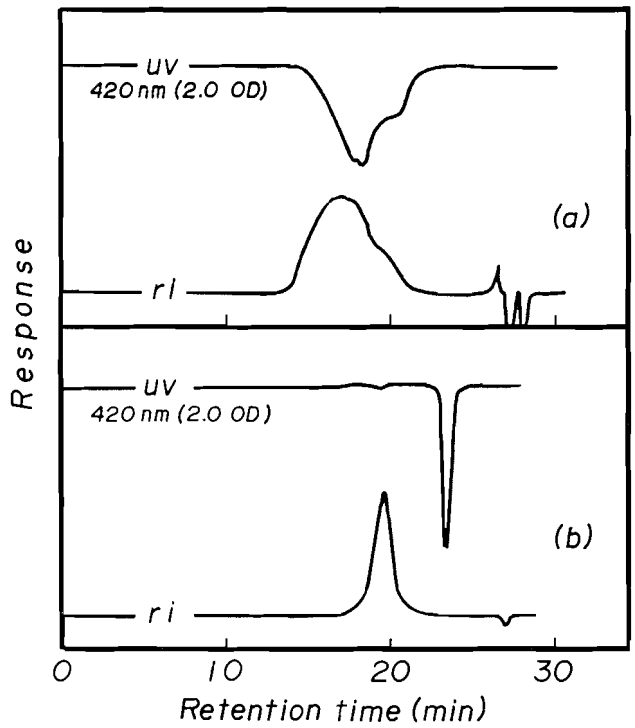


FIG. 2. Gel permeation chromatography traces (a) of PEG-bound porphyrin **6** and (b) of the polymer resulting from cleavage of the end groups with $TiCl_4$. Detectors: ri and uv–visible absorption at 420 nm.

in the visible region suggests the successful conversion of polymer-attached aldehydes (**5**) to visible light-absorbing chromophores, and the absence of small molecule contaminants. The absorption spectrum of polymer **6** displayed in Fig. 3 is characteristic of the porphyrin moiety. These data indicate that we have succeeded in the synthesis of porphyrin-attached PEG in this stage. By uv analysis only 10% of the polymer-bound aldehyde groups were converted to porphyrins. This result, though disappointing, is not surprising. The Alder synthesis normally gives low yields of symmetrical porphyrins, viz. the 15% yield of tetratolylporphine that precipitates from this reaction mixture. Thus, while product recovery here is not difficult, the yield of polymer-bound porphyrin is low.

To perform the cleavage (or deprotection) reaction to obtain the unsymmetric porphyrin **1***b*, the purified and dried polymer **6** was treated with $TiCl_4$ in dichloromethane at room temperature ($ZnBr_2$ did not work). This procedure not only successfully cleaved PEG-porphyrin to free unsymmetrical porphyrin but also cleaved chemical bonds that were responsible for the oligomerization of PEG. Figure 2 also illustrates the result of gpc measurements after the cleavage reaction, which shows (*i*) no uv/vis absorbing chromophore attached to the polymer, and (*ii*) regenerated, monodisperse distribution of the polymer molecular weight. Thus, we conclude that $TiCl_4$ selectively attacks the PEG—CH_2—O—CH_2—O—CH_2—R (R = porphyrin) function. This reaction presumably involves the special coordination configuration suggested by Corey (11).

The black solution produced by the cleavage reaction was concentrated and column chromatographed through silica. It was first eluted with chloroform, to get rid of the small amount of tetratolylporphine present, then with chloroform–THF mixed solvent (95:5 v/v). The desired compound (uv–vis spectrum, Fig. 3) was eluted as a major band, which was collected and dried to give purple crystals of **1***b*.

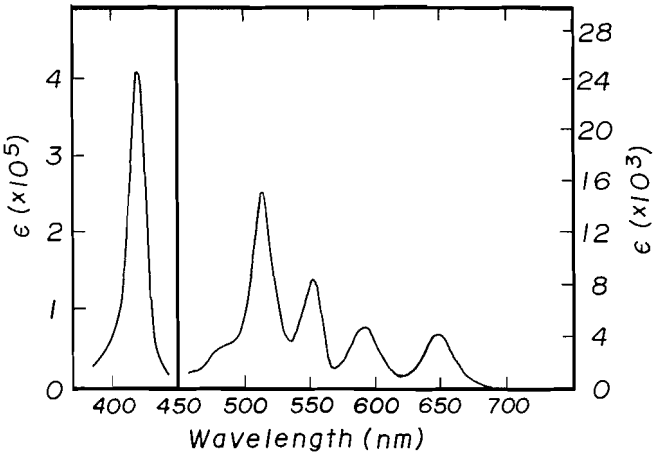


FIG. 3. Ultraviolet–visible spectrum of **1***b* in $CHCl_3$. The polymer-bound precursor **6** has an identical spectrum.

The methacrylate of **1***b* (**1***c*) could be prepared in a straightforward manner by its reaction with methacryloyl chloride, and incorporated into polymers by free radical copolymerization. The synthesis of these polymers and their fluorescence properties will be reported in due course.

Summary

A synthesis of 5-(4′-hydroxymethylphenyl)-10,15,20-tritolylporphine is reported, using a soluble polymer supported synthetic methodology. The key step involves the condensation of a PEG polymer containing appropriate aromatic aldehyde groups at both chain ends with an excess of pyrrole and tolualdehyde. The separation of the polymer-bound porphyrin from the excess tetratolylporphyrin by-product was simple, justifying the strategy of the method.

The yield of aldehyde-to-porphyrin conversion was low, only 10% for the polymer-bound aldehyde. As a consequence, one needs large amounts of polymer to produce small amounts of porphyrin. This problem is exacerbated by the first step in the polymer supported synthesis: chloromethylation of the chain ends led to coupling of the oligomers, producing material with fewer chain ends per gram of polymer. The synthetic scheme is less convenient than one might have hoped. Even though the reagents are not expensive, it still takes ca. 40 g of polymer to produce 0.1 g of purified porphyrin derivative. The major value of this approach to porphyrin synthesis is in the ease of purification of the unsymmetric porphyrin derivative.

Experimental

The ^1H nmr spectra were run on Varian T-60 and Varian XL 200 spectrometers and the ultraviolet–visible spectra on a Hewlett–Packard model 8451A diode-array spectrometer. The gpc measurements were made using a Waters model 6000 pump in conjunction with Waters 10^3 and 500 Å Ultrastyragel columns (THF as eluent), with a Waters model R401 differential refractive index detector and a Hitachi model 100-40 variable wavelength uv–vis detector.

Solvents and reagents

Poly(ethylene glycol) (Carbowax, Union Carbide, MW ~ 2000) was dried by azeotropic distillation of a toluene solution, precipitated into dry diethyl ether, and then dried under vacuum. Diethyl ether (Caledon) was refluxed over sodium metal using benzophenone as an indicator of dryness. Tetrahydrofuran (THF, Caledon) was dried in the same manner as diethyl ether. Dichloromethane (Caledon) was washed with concentrated H_2SO_4, then with water, and with saturated aqueous

Can. J. Chem. Downloaded from www.nrcresearchpress.com by 41.223.56.140 on 09/07/12
For personal use only.

Can. J. Chem. Downloaded from www.nrcresearchpress.com by 41.223.56.140 on 09/07/12
For personal use only.

solutions of NaCl. After being dried over 4 Å molecular sieves, dichloromethane was fractionally distilled and stored over 4 Å molecular sieves. Pyridine (Caledon) was refluxed and distilled over BaO. s-Trioxane (Aldrich) was used as received. Hydrogen chloride gas (Matheson practical grade) was dried by bubbling through concentrated H_2SO_4. Chromium trioxide (Fisher) was dried over P_2O_5 under vacuum. Dihydroxymethylbenzene (Aldrich) was used as received. Pyrrole (Aldrich) was distilled immediately before use. Tolualdehyde (Aldrich) was distilled under reduced pressure immediately before use. Propionic acid (Aldrich) and titanium tetrachloride (Fisher) were used as received.

Synthesis of chloromethylene-terminated PEG (2)

A mixture of 50 g of PEG (MW ~ 2000, 25 mmol) and 3.9 g of s-trioxane (47 mmol) was dissolved in 30 mL of dry dichloromethane. Dry hydrogen chloride was bubbled through this solution for 2 h. The exhaust gas was directed into a suction flask filled with aqueous ammonium hydroxide solution to quench any excess amount of HCl gas coming from the reactor. Subsequently, dry nitrogen gas was bubbled through the reaction mixture to get rid of dissolved HCl until little formation of ammonium chloride (white solid) was observed in the quenching flask (24–48 h). While bubbling with N_2, dichloromethane was continuously added to the mixture to avoid complete evaporation of the solvent. The methylene chloride solution of the polymer was then slowly added to the rapidly stirred dry diethyl ether (1.6 L) to precipitate the polymer (**2**). This process was repeated twice by using dry THF as a good solvent with dry diethyl ether as a poor solvent. The polymer was filtered and dried under vacuum. The gpc analysis showed oligomerization of the PEG at this stage. The amount of the polymer recovered was 48 g. Yield recovery of the polymer was 96%. This polymer was immediately used in the following reaction (within 24 h) because of suspected instability of the terminal chloromethyl groups.

Synthesis of benzylalcohol-terminated PEG (4)

(i) Preparation of sodium di(hydroxymethyl)benzene

To 27 g of *p*-di(hydroxymethyl)benzene (196 mmol) dissolved in 150 mL of dry THF under an inert atmosphere (nitrogen), 7 g of sodium hydride (292 mmol, 15 g of 50% suspension in mineral oil, washed twice with 15 mL each of dry pentane) was added at once. A white-grey solid precipitated, with formation of hydrogen gas, at the bottom of a 500-mL two-necked flask equipped with a magnetic stirrer and a refluxing condenser. The mixture was refluxed for 3 h.

(ii) Synthesis of benzylalcohol-terminated PEG (4)

To the cooled mixture of sodium di(hydroxymethyl)benzene in THF at 0–5°C, 48 g of chloromethylene-terminated PEG (**2**) dissolved in 250 mL of dry THF was gradually added with stirring, under an inert atmosphere. Upon addition of the PEG-CH_2Cl, the sodium salt started to dissolve. After addition was completed, the ice bath was removed and the mixture was gradually heated to reflux. It was refluxed for 24 h under an inert atmosphere. The cooled reaction mixture was then filtered through a sintered glass filter. The filtrate was gradually added to rapidly stirred dry diethyl ether (1.6 L) to precipitate the polymer (**4**). Precipitation was repeated twice, and after filtration the white polymer obtained was dried under vacuum. Yield (recovery of the polymer) was 45 g (94%). Chemical yield (based on uv analysis), 85%.

Synthesis of benzaldehyde-terminated PEG (5)

To a magnetically stirred solution of dry pyridine (19 g, 240 mmol) in 180 mL of dry dichloromethane, placed in a 500-mL round-bottom flask equipped with a magnetic stirrer and a drying tube, chromium trioxide (12 g, 120 mmol) was added in one portion. After 15 min of stirring, 45 g of the benzylalcohol-terminated PEG (**4**) dissolved in 60 mL of dry dichloromethane was added at once. Immediately after mixing, the color of the solution changed from burgundy to pale brown with formation of a black precipitate. After 30 min reaction at room temperature, dichloromethane was removed (rotary evaporator), leaving a dark-brown, viscous liquid. This was dissolved in 500 mL of toluene, then decanted, leaving a black precipitate. The liquid phase was centrifuged and then filtered through a 2 cm thick Celite bed to give a pale brown colored toluene solution, which was slowly added to rapidly stirred dry diethyl ether (1.6 L) to give 41 g of beige polymer (**5**). After two reprecipitations, the yield (recovery of polymer) was 91%. The chemical yield, based on uv analysis, was 96%.

Synthesis of porphyrin-terminated PEG (6)

To a magnetically stirred and refluxing mixture of 25 g of benzaldehyde-terminated PEG (3 mmol) and 20 g of tolualdehyde (160 mmol) dissolved in 500 mL of propionic acid, 10.6 g (160 mmol) of pyrrole was added dropwise over a period of 15 min. After an additional 30 min of refluxing, 250 mL of propionic acid was quickly distilled off under reduced pressure. Then, the rapidly cooled (with ice) mixture was filtered through a sintered glass funnel to collect tetratolylporphine (by-product, 4.0 g, yield 15%). The filtrate was repeatedly filtered to remove all solid components, then gradually added to rapidly stirred diethyl ether (2 L) to precipitate the polymer. The dark brown polymer (**6**) thus obtained was purified by repeated reprecipitation, then collected and air dried. It was then dried by azeotropic distillation of a toluene solution, followed by precipitation into dry diethyl ether. Yield (recovery of the polymer), 95%. Chemical yield (based on uv analysis), 10%.

Cleavage reaction of porphyrin-terminated PEG

To a magnetically stirred solution of porphyrin-terminated PEG (16 g) in 300 mL of dry dichloromethane, 10 mL of titanium tetrachloride was added over a period of 10 min. During this addition the viscosity of the solution increased and then decreased. A black precipitate appeared. The mixture was stirred overnight and then quenched by the addition of 100 mL of 10% aqueous ammonium hydroxide solution. The decanted liquid was combined with 50 mL of chloroform, and transferred to a separatory funnel. The organic phase was separated and washed repeatedly with distilled water and then dried over anhydrous magnesium sulfate. The black solid obtained was dissolved in 20 mL of chloroform and chromatographed on 400 g of silica gel. A small amount of tetratolylporphine (R_f = 1.0, $CHCl_3$) was eluted in chloroform. The desired product eluted in a mixture (95:5 v/v) of chloroform and THF. The major portion (R_f = 0.63 $CHCl_3$, R_f = 0.73 95:5 v/v $CHCl_3$–THF) was collected and evaporated to give 100 mg of purple crystals; ^{1}H nmr ($CDCl_3$): pyrrole CH (8H) δ 8.84, ArCH (hydroxymethyl phenyl-2,6) (2H) δ 8.20 (d, 8 Hz), ArCH (tolyl-2,6) (6H) δ 8.08 (d, 8 Hz), ArCH (hydroxymethyl phenyl-3,5) (2H) δ 7.73 (d, 8 Hz), ArCH (tolyl-3,5) (6H) δ 7.54 (d, 8 Hz), OCH_2 (2H) δ 5.05, CH_3 (tolyl) (9H) δ 2.69, NH (2H) δ −2.79. The peaks assigned to pyrrole CH, ArCH, and CH_3 (tolyl) are essentially identical to those reported for 5-(carbomethoxyphenyl)-10,15,20-tritolylporphine (*4b*). It proved impossible to obtain a reliable mass spectrum by electron impact ionization. It was, however, possible to obtain a low resolution spectrum by field desorption mass spectroscopy (Oji Paper Co., Tokyo, Japan), which gave exclusively the molecular ion at *m/e* 686.

Esterification of ***1*** b–***1*** c

To a magnetically stirred mixture of 50 mg of **1***b* and 2 mL of dry pyridine in 5 mL of dry THF, 0.5 mL of freshly distilled methacryloyl chloride was added over a period of 2 min at 0–5°C. The mixture was stirred at this temperature for 1 h, then heated to reflux for 5 h. The cooled mixture was combined with 50 mL of $CHCl_3$, then washed with 2 × 10 mL of dilute aqueous ammonium hydroxide. The separated organic layer was dried over anhydrous magnesium sulphate ($MgSO_4$), concentrated, and chromatographed on 40 g of silica gel with a 95:5 v/v mixture of $CHCl_3$ and THF. The desired compound (**6**) was eluted as the first band. Yield, 70%; ^{1}H nmr ($CDCl_3$): pyrrole CH (8H) δ 8.84, ArCH (methacryloxymethylphenyl-2,6) (2H) δ 8.20 (d, 8 Hz), ArCH (tolyl) (6H) δ 8.08 (d, 8 Hz), ArCH (methacryloxymethylphenyl-3,5) (2H) δ 7.73 (d, 8 Hz), ArCH (tolyl) (6H) δ 7.54 (d, 8 Hz), $=CH_2$ (1H) δ 6.34 (m), $=CH_2$ (1H) δ 5.70 (m), OCH_2 δ 5.55, CH_3 (tolyl) (9H) δ 2.70, CH_3—C= (3H), NH (2H) δ −2.80.

Acknowledgements

The authors thank the Natural Sciences and Engineering

Research Council of Canada for their support of this research. Y.T. wishes to express his appreciation to the Oji Paper Company, Tokyo, Japan, for their support of his Ph.D. studies in Toronto.

1. (*a*) C. E. HOYLE and J. E. GUILLET. J. Polym. Sci. Polym. Lett. Ed. **16**, 185 (1978); (*b*) D. A. HOLDEN and J. E. GUILLET. Macromolecules, **13**, 289 (1980); (*c*) D. NG and J. E. GUILLET. Macromolecules, **15**, 724 (1982); (*d*) D. A. HOLDEN, W. A. RENDALL, and J. E. GUILLET. Ann. N.Y. Acad. Sci. **366**, 11 (1981).
2. P. SAYER, M. GOUTERMAN, and C. R. CONNELL. Acc. Chem. Res. **15**, 73 (1982), and references therein.
3. (*a*) TH. FORSTER. Fluoreszenz organischer Verbindungen. Vandenhoek und Rupprecht, Göttingen, Germany. 1951; (*b*) Disc. Faraday Soc. **27**, 7 (1959).
4. (*a*) A. D. ADLER, F. R. LONG, J. D. FINARELLI, J. GOLDMACHER, J. ASSOUR, and L. KORSAKOFF. J. Org. Chem. **32**, 476 (1967); (*b*) J. A. ANTON, J. KWONG, and P. A. LOACH. J. Heterocycl. Chem. **13**, 717 (1976); (*c*) J. A. ANTON and P. A. LOACH. J. Heterocycl. Chem. **12**, 573 (1975); (*d*) E. HASEGAWA, J. NEMOTO, T. KANAYAMA, and E. TSUCHIDA. Eur. Polym. J. **14**, 123 (1978).
5. R. GRIGG. J. Chem. Soc. C, 3664 (1971).
6. D. DOLPHIN (*Editor*). The porphyrins. Vol. 1. Academic Press, New York. 1978.
7. N. K. MATHUR, C. K. NARANG, and R. E. WILLIAMS. Polymers as aids in organic chemistry. Academic Press, New York. 1980; (*b*) R. B. MERRIFIELD. J. Am. Chem. Soc. **85**, 2149 (1963).
8. C. C. LEZNOFF and P. I. SVIRSKAYA. Angew. Chem. Int. Ed. Engl. **17**, 947 (1978).
9. (*a*) K. G. GECKELER, V. N. R. PILLAI, and M. MUTTER. Adv. Polym. Sci. **38**, 65 (1981); (*b*) M. MUTTER, H. HAGENMAIER, and E. BAYER. Angew. Chem. Int. Ed. Engl. **10**, 811 (1971).
10. C. C. LEZNOFF and T. W. HALL. Tetrahedron Lett. **23**, 3023 (1982).
11. E. J. COREY, J.-L. GRAS, and P. ULRICH. Tetrahedron Lett. **11**, 809 (1976).
12. R. G. LITTLE, J. A. ANTON, P. A. LOACH, and J. A. IBERS. J. Heterocycl. Chem. **12**, 343 (1975).

Can. J. Chem. Downloaded from www.nrcresearchpress.com by 41.223.56.140 on 09/07/12
For personal use only.

Coprinolone and Δ^6-coprinolone: new sesquiterpenes from *Coprinus psychromorbidus*[1]

ALVIN N. STARRATT AND EDMUND W. B. WARD
Agriculture Canada Research Centre, 1400 Western Road, London, Ont., Canada N6G 2V4
AND
J. B. STOTHERS
Department of Chemistry, The University of Western Ontario, London, Ont., Canada N6A 5B7

Received September 6, 1988

ALVIN N. STARRATT, EDMUND W. B. WARD, and J. B. STOTHERS. Can. J. Chem. **67**, 417 (1989).

The structure of coprinolone (**1**), an oxygen-bridged protoilludane from the W2 isolate of the fungus *Coprinus psychromorbidus*, has been elucidated by chemical transformations and detailed ^1H and ^{13}C magnetic resonance studies, including homo- and heteronuclear correlation spectra. The $^1H-^1H$ coupling data and nuclear Overhauser difference spectra for **1** and derived isomers led to the establishment of its stereochemistry. A second metabolite was identified as Δ^6-coprinolone (**20**) by spectroscopic results. Confirmatory evidence in support of the structures was obtained from the labelling patterns of the compounds from cultures supplemented with sodium [1,2-$^{13}C_2$]acetate.

Key words: coprinolone, Δ^6-coprinolone, protoilludane, sesquiterpenes, NMR.

ALVIN N. STARRATT, EDMUND W. B. WARD et J. B. STOTHERS. Can. J. Chem. **67**, 417 (1989).

En se basant sur des transformations chimiques et des études détaillées de résonance magnétique nucléaire du ^1H et du ^{13}C, y compris des spectres de corrélation homo- et hétéronucléaires, on a élucidé la structure de la coprinolone (**1**), un protoilludane portant un pont oxygène qui a été isolé de l'extrait W2 du champignon *Coprinus psychromorbidus*. L'utilisation de données de couplage $^1H-^1H$ et de spectres Overhauser nucléaires de différence obtenus à partir du composé **1** et d'isomères qui en dérivent ont permis d'établir sa stéréochimie. Sur la base de données spectroscopiques, on a pu identifier un second métabolite, la Δ^6-coprinolone (**20**). En se basant sur les patrons de marquage des composés obtenus à partir de cultures auxquelles on avait ajouté de l'acétate-[$^{13}C_2$-1,2], on a obtenu des données qui ont permis de confirmer les structures.

Mots clés : coprinolone, Δ^6-coprinolone, protoilludane, sesquiterpènes, RMN.

[Traduit par la revue]

Can. J. Chem. Downloaded from www.nrcresearchpress.com by 41.223.56.140 on 09/07/12
For personal use only.

Introduction

The production of hydrogen cyanide by the W2 isolate of a low-temperature basidiomycete (1), now classified as *Coprinus psychromorbidus* (2, 3), which causes extensive snow mold damage to overwintering cereals, grasses, and legumes in western Canada, has been the subject of several studies (4–7). During our investigation, we observed the presence of a new metabolite that we have named coprinolone (8) in extracts of both the culture filtrate and the mycelium. This compound is a member of a small class of sesquiterpenes produced by various basidiomycetes that possess the protoilludane skeleton. It showed no evidence of phytotoxicity when tested on seedlings of winter wheat and soybeans at a concentration of 10^{-3} M and was also inactive when tested against fungi and bacteria. In this paper, we describe the isolation and the full experimental evidence leading to the structures of coprinolone (**1**) and a related metabolite Δ^6-coprinolone (**20**).

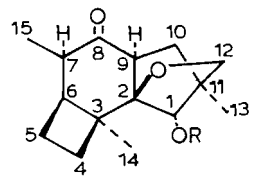
Results and discussion

Structure of coprinolone

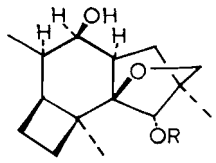
Crystalline coprinolone, isolated by silicic acid – Celite chromatography of the extracts of the W2 isolate of *Coprinus psychromorbidus*, was the major metabolite, obtained in overall yields of ca. 100 mg/L from cultures grown for 21–24 days. Recrystallization from light petroleum afforded material melting at 105–107°C having an optical rotation of $[\alpha]_D^{23}$ −95°. Its empirical constitution of $C_{15}H_{22}O_3$, established by microanalysis and precise mass measurement, was indicative of a sesquiterpene. The ir spectrum included hydroxyl (3510 cm^{-1}) and ketonic carbonyl (1700 cm^{-1}) absorptions. The ^1Hmr spectrum in C_6D_6 solution exhibited signals for two tertiary methyl groups (δ 0.64 and 1.20), a secondary methyl group (δ 1.04, d, J = 6.7 Hz) coupled to a methine proton at δ 1.95 (ddq, J = 1.4, 9.0, 6.7 Hz), a $\diagdown\!\!\diagup$CHO— (δ 3.21, d, J = 0.9 Hz) and a —CH_2O— grouping, δ_A 3.56 (d, J = 6.7 Hz) and δ_B 3.27 (dd, J = 3.2, 6.7 Hz). In addition, a $\diagdown\!\!\diagup$CH—CH_2 unit was evident as an ABX pattern in which each proton exhibited an additional coupling. The methine proton, δ_X 2.91, J_{AX} = 10.6, J_{BX} = 3.9 Hz, was found to be coupled to the proton at δ 1.95 (J = 1.4 Hz) and the methylene protons, δ_A 1.52, δ_B 2.38, J_{AB} = 12.3 Hz, are coupled to the protons at δ 3.27 (J = 3.2 Hz) and 3.21 (J = 0.9 Hz), respectively. The ^{13}Cmr spectrum in C_6D_6 solution contained signals for a carbonyl carbon (δ_C 210.1), quaternary, methine, and methylene carbons bearing oxygen (93.3, 81.7, 75.5), as well as three methyl (10.1, 13.7, 24.8), three methylene (20.7, 27.7, 30.6), three methine (43.7, 51.1, 51.9), and two quaternary (41.8, 47.3) absorptions at higher field. Since there was no olefinic unsaturation, the compound is tetracyclic.

Acetylation of coprinolone (**1**) provided a monoacetyl derivative **2** exhibiting infrared absorption attributable to keto and acetyl groupings (1715, 1734 cm^{-1}). Treatment of **1** with sodium borohydride gave a more polar substance lacking carbonyl absorption in the ir spectrum. Acetylation of this new diol **3** furnished a monoacetyl derivative **4**, which is identical to that produced upon sodium borohydride reduction of **2**. As expected, coprinolone acetate (**2**) is formed by oxidation of **4**

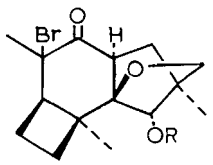
[1]Part 139 of ^{13}Cmr studies: for Part 138 see ref. 24.



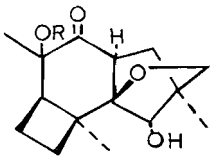
1 R = H
2 R = Ac



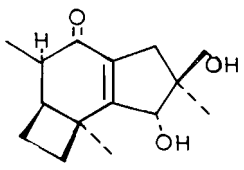
3 R = H
4 R = Ac



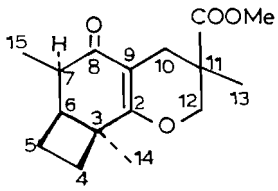
5 R = H
6 R = Ac



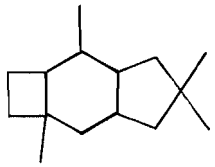
7 R = OH
8 R = H



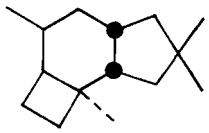
9



10



11



12

with pyridinium chlorochromate (9). Clearly, the hydroxyl group formed upon reduction of the ketonic carbonyl in **1** is more hindered than the original hydroxyl function.

Both **1** and **2** yield monobromo derivatives, **5** and **6**, respectively, upon treatment with *N*-bromosuccinimide (NBS) in refluxing carbon tetrachloride. The appearance of a third methyl singlet replacing the methyl doublet in the ^{1}Hmr spectrum and the replacement of a methine signal with a new quaternary carbon peak in the ^{13}C spectrum indicated that the secondary methyl group in **1** is α to the carbonyl group. Acetylation of **5** affords bromocoprinolone acetate (**6**).

A crystalline compound precipitated from benzene solutions of **1** that had been at room temperature for extended periods. On chromatograms, this substance **7** gave color reactions typical of peroxides. Its ^{1}H spectrum contained three methyl singlets, δ 1.00, 1.10, and 1.39, and a new quaternary signal replaced one of the methine peaks in the ^{13}C spectrum. These changes and the shielding differences for the two other methine carbons indicated that peroxidation occurred at the same α carbon as that involved in the bromination with NBS. As expected, **7** was converted to a ketodiol **8** upon reduction in acetic acid with activated zinc dust.

Mild base treatment of **1** gave a more polar, crystalline compound **9** for which absorption at 1652 cm^{-1} in the infrared and at 252 nm in the ultraviolet spectrum indicated the presence of an α,β-unsaturated ketone. The ^{13}C spectrum contained signals for a carbonyl carbon (δ_C 200.1), two fully substituted olefinic carbons (135.5, 162.1), methine (80.8) and methylene (69.8) carbons bearing oxygen as well as for three methyl (10.5, 17.4, 25.2), three methylene (19.4, 30.8, 37.0), two methine (39.8, 47.8), and two quaternary carbons (40.5, 47.0). These features are accounted for by base-catalyzed opening of an oxide ring β to the carbonyl yielding an α,β-unsaturated ketone with a primary alcohol group. The relationship between the functional groups in **1** was further revealed upon isolation of a less polar compound with λ_{max} 266 nm after ketodiol **9** was oxidized with 4-(dimethylamino)pyridinium chlorochromate (10), a selective reagent for oxidation of allylic hydroxyl groups.

Oxidation of **1** in acetone with chromic acid yielded a carboxylic acid, which was converted to methyl ester **10** for characterization. The presence of a fully substituted enone unit bearing β oxygen was indicated by the uv absorption, λ_{max} 260 nm (ε 9080), and ^{13}C peaks at δ_C 109.3, 174.7, and 197.1. Thus, we could conclude that the generation of these two enones, **9** and **10**, involved β cleavage of a C—O bond with base and a C—C bond by oxidation, respectively.

The mass spectra of coprinolone and related compounds showed a strong peak at $M^+ - 28$, which was found by precise mass measurements to be due to the loss of ethylene and not carbon monoxide. Facile loss of ethylene from a cyclobutane ring has been found (11, 12) to be a characteristic feature for the sterpurane **11** and protoilludane **12** skeletons. Only the latter can accommodate a secondary methyl α to a carbonyl group, and the results of a series of nmr experiments showed that this is the carbon skeleton of coprinolone.

For each of the ^{13}C signals arising from protonated carbons, the absorptions for the directly bonded protons were identified through a ^{13}C–^{1}H heteronuclear correlation (COSY) spectrum. An important finding from this spectrum was the fact that the methine and methylene carbons at δ_C 51.1 and 30.6, respectively, are those bearing the protons giving rise to the ABX system noted above. Two- and three-bond proton–carbon couplings were revealed through long-range heteronuclear correlation experiments utilizing the XCORFE sequence (13). From the results for C_6D_6 solutions, it was found that the methyl protons at δ 1.04, bonded to the methyl carbon at δ_C 10.1, are coupled to the methine carbons at δ 51.9 and 43.7. The latter carbon bears the methine proton at δ 1.95. The methine carbon, δ_C 51.9, is vicinally coupled to the methyl protons at δ 1.20 (δ_C 24.8), which are also coupled to the quaternary carbon (δ_C 41.8) and the methylene carbon, δ_C 27.7. The protons for the third methyl group, δ 0.64 (δ_C 13.7), were found to be coupled to the quaternary carbon at δ_C 47.3, the carbinyl methine, δ_C 81.7, and methylene carbons at δ_C 30.6 and 75.5. It was also found that the proton bonded to the methine carbon at δ_C 51.1 is coupled to the quaternary carbons at δ_C 93.3 and 41.8. Additional information on the carbon–carbon connectivities was obtained from one- and two-dimensional double quantum coherence (INADEQUATE) spectra (14). A major observation from the 1D-INADEQUATE spectrum was the J_{CC} value of 10 Hz common to the methine carbons absorbing at δ_C 43.7 and 51.1; this is a typical geminal coupling between carbons flanking a carbonyl group and thus identified the α carbons in **1**. Further-

Can. J. Chem. Downloaded from www.nrcresearchpress.com by 41.223.56.140 on 09/07/12
For personal use only.

Can. J. Chem. Downloaded from www.nrcresearchpress.com by 41.223.56.140 on 09/07/12
For personal use only.

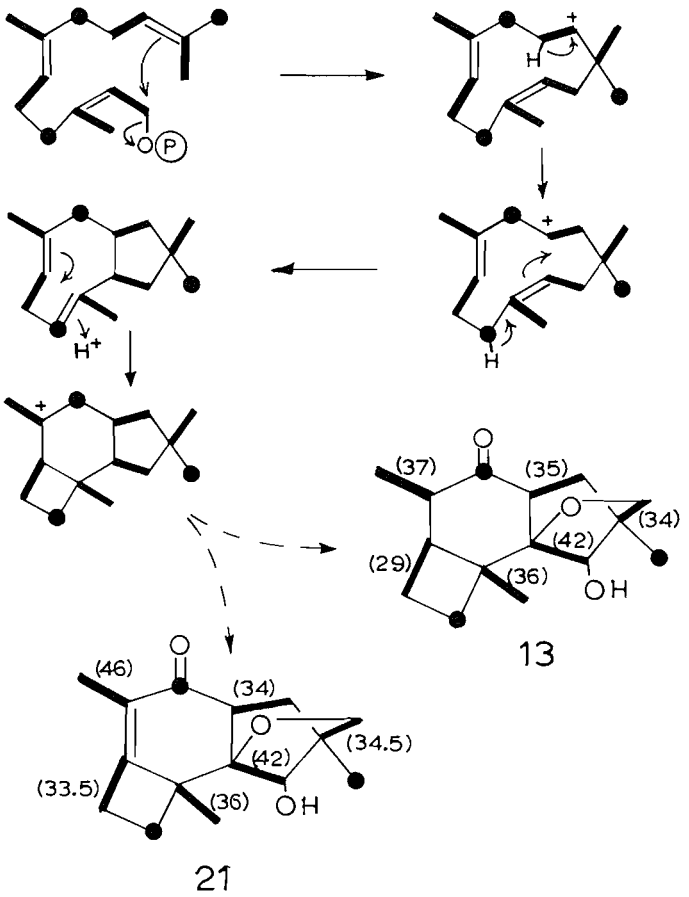


FIG. 1. Possible biosynthetic sequence leading to coprinolone and Δ^6-coprinolone from farnesyl pyrophosphate, illustrating the ^{13}C labelling patterns from [1,2-$^{13}C_2$]acetate incorporation.

more the protons bonded to these carbons exhibited a long-range coupling of 1.4 Hz. In addition to confirming the linkages found from the XCORFE spectra, the 2D-INADEQUATE experiment showed that the methylene carbons at δ_C 20.7 and 27.7 are directly bonded, as are the quaternary (93.3) and carbinyl (81.7) carbons. All of these data are consistent with structure **1** for coprinolone in planar projection.

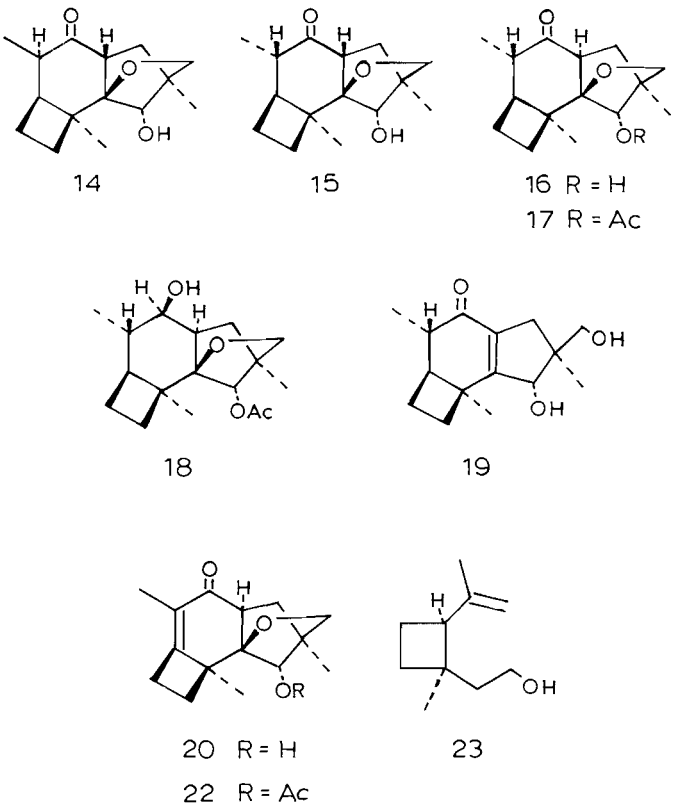
To confirm the proposed structure, coprinolone was isolated from cultures of *C. psychromorbidus* that had been amended with sodium [1,2-$^{13}C_2$]acetate at the time of maximum production of the metabolite. The ^{13}Cmr spectrum of **1**-$^{13}C_x$ isolated on day 13 showed that all carbons were labelled (4.0% specific incorporation) in the pattern **13**, possibly arising from the sequence outlined in Fig. 1, a pathway analogous to that proposed for illudins S and M (15). The heavy bonds in **13** represent intact acetate units for which the observed J_{CC} values are indicated in Hz, while the dark circles denote carbons arising from C-2 of the three mevalonate units. The relatively high enrichment level signals the formation of multilabelled species, the presence of which will increase the probability of ^{13}C incorporation at contiguous carbons in **1** that arise from different acetate units. Thus, additional information on the carbon connectivities was sought through a two-dimensional $^{13}C-^{13}C$ COSY spectrum. This experiment provided confirmation of direct bondings of C-4 with C-3 and C-5, C-7 with C-6 and C-8, C-9 with C-2 and C-8, and C-11 with C-1, C-10, and C-13.

The ^1H and ^{13}C shielding data are collected in Tables 1 and 2 for C_6D_6 and CD_2Cl_2 solutions while the observed coupling constants are listed in Table 3. Although solvent effects are minimal for the ^{13}C spectra, some distinctive shift differences, which aided the specific assignments by clarifying the multiplicities of certain absorption patterns, were observed for the ^1H spectra. A detailed discussion of the proton data is presented later.

Structures **2–10** for the compounds derived from **1**, as described above, follow directly and their nmr data are collected in Tables 1–3. The specific assignments followed from $^1H-^1H$ and $^{13}C-^1H$ correlation spectra analogous to those employed for the analysis of **1**.

Stereochemistry of 1

In the early stages of this study, attempts to isolate coprinolone from culture extracts by chromatography on alumina led to the isolation of two slightly more polar isomers of **1**, which could be partially separated by chromatography over silicic acid – Celite and were purified by crystallization. Neither of these isomers **14** and **15** was acetylated under the conditions leading to the formation of **2** from **1**, indicating that the hydroxyl group in each is more hindered than that in **1**. A small amount of a third isomer **16**, which could be readily acetylated, was obtained from the mother liquors from recrystallization of **1**. Reduction of this isomeric acetate **17** with sodium borohydride afforded **18**, an isomer of **4**. It may be noted that our initial nmr examination of **1** in $CDCl_3$ revealed the slow formation of small amounts of a second component upon standing for several hours. The subsequent isolation of **16** established that this slow process in $CDCl_3$ is an isomerization. Similarly the initial nmr sample of **14** in $CDCl_3$ solution was found to give a 50:50 mixture of **14** and **15** upon standing. Consequently, C_6D_6 was chosen for this study with several samples also run in CD_2Cl_2 solutions to alter the signal dispersion in the ^1Hmr spectra. Thus, four isomers having the same carbon skeletons were in hand and, on the basis of their behaviour under acetylation



Can. J. Chem. Downloaded from www.nrcresearchpress.com by 41.223.56.140 on 09/07/12
For personal use only.

TABLE 1. ^{1}H shieldings[a] for coprinolone, its isomers, and derivatives

Compound	Solvent[b]	H-1	H-4	H-5	H-6	H-7	H-9	H-10		H-12[c]		3-Me	7-Me	11-Me	Other
								α	β	*syn*	*anti*				
1	a	3.214	1.45 2.15	1.57 2.08	2.420	1.953	2.910	1.52	2.38	3.266	3.555	1.205	1.037	0.636	
	b	3.785	1.6 2.0	1.6 1.7	2.760	2.393	3.181	~1.6	2.159	3.525	3.494	1.423	0.867	1.009	
2	a	5.126	1.45 2.13	1.50 2.00	2.37	1.980	2.803	1.43	2.423	3.305	3.495	1.038	1.024	0.696	1.632
	b	5.042	1.60 1.70	1.60 2.02	2.77	2.39	3.191	1.58	2.227	3.627	3.533	1.244	0.869	0.953	2.061
3	a	3.170	1.57 2.38	1.84 2.07	2.09	1.52	2.07	1.77	1.87	3.273	3.493	1.119	1.190	0.707	3.760(H-8)
	a/b	3.393	1.53 2.28	1.75 1.95	2.00	1.33	2.14	1.80	1.75	3.34	3.50	1.199	1.013	0.827	3.630(H-8)
4	a	5.076	1.49 2.33	1.75 2.00	2.06	1.367	1.978	1.621	1.863	3.285	3.419	0.958	1.167	0.721	3.713(H-8) 1.620
5	a	3.160	1.36 1.95	1.62 2.05	3.010	—	4.268	1.58	2.340	3.205	3.440	1.382	1.769	0.573	
6	a	5.114	1.30 2.00	1.50 1.96	2.960	—	4.274	1.56	2.378	3.243	3.409	1.251	1.744	0.644	1.565
7	c	3.678	1.54 2.02	1.60 1.79	2.390	—	3.951	1.65	2.08	3.51	3.49	1.393	1.101	1.005	
8	a/b	3.415	1.35 1.90	1.45 1.55	2.308	—	3.696	1.480	2.030	3.305	3.373	1.253	0.970	0.763	

Can. J. Chem. Downloaded from www.nrcresearchpress.com by 41.223.56.140 on 09/07/12
For personal use only.

TABLE 1 (*concluded*)

Compound	Solvent[b]	H-1	H-4	H-5	H-6	H-7	H-9	H-10 α	H-10 β	H-12[c] *syn*	H-12[c] *anti*	3-Me	7-Me	11-Me	Other
9	d	4.720	1.8 1.9	1.5 1.85	2.55	2.55	—	(2.238) (2.350)		(3.440) (3.524)		1.414	0.964	1.089	
10	a	—	1.58 1.87	1.55 1.60	2.14	2.18	—	2.742	2.633	3.901	3.616	1.173	1.105	0.991	3.222
14	a	3.326	1.67 2.52	1.81 1.27	2.198	2.764	2.579	2.126	1.823	3.26	3.28	1.280	1.014	0.649	
	b	3.706	1.72 2.31	1.31 2.03	2.437	2.718	2.623	1.96	1.96	3.54	3.53	1.326	0.888	1.008	
15	a	3.301	1.70 2.50	1.20 2.21	1.70	2.080	2.60	2.60	1.267	3.279	3.221	1.344	1.025	0.630	
	b	3.586	1.63 2.57	1.60 2.55	1.77	2.51	2.913	2.43	1.50	3.548	3.521	1.372	0.967	1.014	
16	a	3.186	1.50 2.85	1.45 2.08	1.55	2.618	2.646	1.754	2.135	3.273	3.320	1.218	1.076	0.600	
17	a	5.095	1.44 2.80	1.41 2.05	1.50	2.585	2.473	1.652	2.135	3.301	3.283	1.070	1.073	0.658	1.616
18	a	5.107	1.50 2.62	1.70 2.00	1.40	1.95	2.08	1.65	1.95	3.338	3.410	1.062	0.910	0.755	3.54(H-8) 1.632
19	d	4.72	1.5–2.0		2.33	2.18	—	~2.28		3.43 3.51		1.422	1.078	1.070	
20	b	3.826	1.68 2.44	2.60 3.06	—	—	3.300	1.810	1.964	3.512	3.390	1.560	1.588	1.010	
22	a	5.121	1.40 2.6	2.33 2.6	—	—	3.096	1.720	2.292	3.29	3.27	1.158	1.782	0.663	1.600

[a]In ppm from internal TMS; the precision of the data for well-defined patterns is judged to be ±0.002 ppm and ±0.01 ppm for overlapping multiplets.
[b]Solvents: a = C_6D_6; b = CD_2Cl_2; c = CD_3OD; d = $CDCl_3$.
[c]Distinguished as *syn* and *anti* relative to C-1.

Can. J. Chem. Downloaded from www.nrcresearchpress.com by 41.223.56.140 on 09/07/12
For personal use only.

TABLE 2. ^{13}C shielding data[a] for coprinolone, its isomers, and several derivatives

Compound	Solvent[b]	C-1	C-2	C-3	C-4	C-5	C-6	C-7	C-8	C-9	C-10	C-11	C-12	C-13	C-14	C-15	Other
1	a	81.7	93.3	41.8	27.7	20.7	51.9	43.7	210.1	51.1	30.6	47.3	75.5	13.7	24.8	10.1	
	b	81.9	93.7	41.9	27.5	20.7	52.0	43.9	211.3	51.2	30.6	47.5	75.7	13.8	24.8	9.7	
2	a	81.4	92.1	41.5	27.4	20.7	51.3_1	43.7	207.9	51.3_4	31.3	47.3	75.3	13.9	24.0	10.0	
	b	81.5	92.7	41.8	27.4	20.7	51.7	44.0	210.2	51.7	31.3	47.6	75.8	14.2	24.2	9.7	
3	a	80.8	89.7	41.3	30.0	22.7	47.6	35.0	73.9	41.7	34.0	46.2	75.9	13.7	25.3	14.4	
	a/b	80.9	90.1	41.5	29.9	22.6	47.6	34.9	74.5	41.7	34.3	46.5	76.4	14.0	25.4	14.1	
4	a	80.4	89.0	41.2	29.9	22.9	47.5	35.2	73.5	42.6	34.8	46.5	75.9	14.2	24.6	14.5	20.8 169.1
5	a	81.4	92.8	42.5	27.6	24.4	59.7	66.3	202.1	46.7	30.5	47.0	75.6	13.3	24.5	23.4	
6	a	80.9	91.8	42.3	27.2	24.4	59.4	66.3	200.9	47.1	31.3	47.1	75.5	13.6	23.7	23.3	20.4 169.3
7	c	82.3	94.5	42.8	28.5	21.6	55.8	89.1	210.9	48.7	31.1	48.1	76.6	14.0	25.8	14.7	
8	a/b	81.6	93.2	41.7	27.8	21.3	58.0	76.3	208.7	46.8	30.3	47.4	75.7	13.7	25.3	19.9	
9	d	80.8	162.1	40.5	30.8	19.4	47.8	39.8	200.1	135.5	37.0	47.0	69.8	17.4	25.2	10.5	
10	a	—	174.7	41.0	31.0	19.9	44.4	38.3	197.1	109.3	29.2	39.8	71.1	20.1	23.7	11.4	51.5 169.3
14	a	79.8	88.4	38.2	27.4	19.7	44.6	45.0	214.8	53.1	37.6	45.9	75.3	13.4	25.4	11.7	
	b	80.0	88.8	38.3	27.2	19.6	44.7	45.1	216.6	53.2	37.6	46.3	75.6	13.7	25.8	11.4	
15	a	81.9	93.5	38.3	29.4	27.1	50.6	47.8	209.7	53.2	31.6	45.1	76.2	13.4	22.7	13.3	
	b	82.0	93.9	38.3	29.3	27.3	50.8	48.1	211.0	53.3	31.7	45.3	76.5	13.7	22.5	13.0	
16	a	80.3	88.0	39.6	26.3	22.0	47.4	47.0	212.1	50.7	32.4	47.6	75.4	13.7	23.9	14.0	
17	a	80.0	87.2	39.3	26.0	21.9	47.1	46.9	211.1	51.3	33.3	47.7	75.4	14.0	23.0	13.8	
18	a	80.5	88.0	40.1	27.8	23.4	46.8	41.1	74.4	39.7	33.0	46.8	75.4	14.3	24.1	19.7	20.6 169.3
19	d	81.1	162.8	27.2	31.6	21.7	48.4	44.3	201.7	133.9	37.0	46.8	70.0	17.4	27.2	19.5	
20	b	81.3	91.2	49.8	26.5	29.5	164.5	125.6	199.5	49.9	32.3	47.6	75.8	13.8	19.7	9.7	
22	a	80.9	89.6	49.2	26.3	29.1	161.9	126.2	196.9	50.3	33.0	47.1	75.4	13.9	18.7	10.0	20.5 169.4

[a]In ppm from internal TMS: estimated precision is ±0.05 ppm.
[b]Solvents: a = C_6D_6; b = CD_2Cl_2; c = CD_3OD; d = $CDCl_3$.

TABLE 3. Selected $^1H-^1H$ coupling constants[a] for coprinolone, its isomers, and derivatives

Compound	Solvent[b]	^2J		^3J						^4J			
		$J_{10,10}$	$J_{12,12}$	$J_{6,7}$	$J_{7,Me}$	$J_{7,8}$	$J_{8,9}$	$J_{9,10\alpha}$	$J_{9,10\beta}$	$J_{7,9}$	$J_{10\alpha,12}$	$J_{1,9}$	$J_{1,10\beta}$
1	b	12.3	6.7	9.0	6.7	—	—	10.6	3.9	1.4	3.2		0.9
2	b	12.2	6.8	9.0	6.7	—	—	10.6	3.8	1.4	3.5		0.9
3	a/b	12.0	6.5	11.0	7.0	3.3	3.2	11.0	6.2		3.0		
4	a	12.2	6.7	8.0	6.3	3.3	3.3	11.6	5.5		3.0		
5	a	12.8	6.8	—	—	—	—	10.7	3.8	—	3.4		0.8
6	a	12.0	6.9	—	—	—	—	10.8	3.8	—	3.6		1.0
8	a/b	12.0	6.7	—	—	—	—	10.7	4.0	—	3.3		
9	d	16.0	10.6		6.5	—	—	—	—	—		—	
10	a	16.8	10.6	4.5	6.7	—	—	—	—	—	1.8	—	
14	a	12.5	6.5	5.4	6.9	—	—	5.1	10.2		2.8	0.9	1.0
15	b	14.5	7.0	8.8	6.6	—	—	5.1	8.9	1.5	3.1	0.7	
16	a	12.5	7.0	9.6	7.0	—	—	11.5	4.0		3.2		
17	a	12.2	7.0	10.0	7.1	—	—	11.6	4.1		3.4		1.2
20	b	12.5	6.7	—	—	—	—	11.6	4.8	—	3.2		0.8
22	a	12.3	6.7	—	—	—	—	11.6	4.8	—	3.0		1.0

[a]In Hz.
[b]Solvents: a = C_6D_6; b = CD_2Cl_2; d = $CDCl_3$.

conditions and in $CDCl_3$ solutions, these could be paired as **1** with **16** and **14** with **15**; the isomerizations presumably involve configuration differences at C-7 and -9. Examination of the ^{13}C spectra of these isomers did not reveal any clear trends that would indicate the relative stereochemistry at these centres, but the ^1H spectra allowed definitive assignments for each.

The protoilludane skeleton is characterized by the *cis–anti–cis* stereochemistry of the carbocyclic ring system as in **12** (16). Consideration of the long-range $^1H-^1H$ coupling interactions resolved in the spectra of **1** and **14–16**, together with the results from nOe difference spectra, revealed the relative stereochemistry at the two epimeric centres, C-7 and -9. The absorption patterns for H-9 were particularly informative. For **1**, this proton gave rise to a six-line multiplet through vicinal coupling to the 10-methylene protons, J = 3.9 and 10.6 Hz, and a long-range coupling of 1.4 Hz with H-7. The corresponding pattern for H-9 in **15** contained similar couplings with the 7 and 10 protons, J = 1.5, 5.1, and 8.9 Hz, as well as a long-range interaction of 0.7 Hz with H-1. A comparable coupling of 0.9 Hz was evident for H-9 with H-1 in **14**, for which $J_{9,10}$ = 5.1 and 10.2 Hz with no resolved coupling between H-9 and -7. For **16**, the H-9 pattern was a clean doublet of doublets $J_{9,10}$ = 4.0 and 11.5 Hz. From the nOe difference spectra, it was found that irradiation of the 3-methyl protons enhanced the H-9 absorptions in **1** and **16** but not in **14** and **15**, while the H-1 and -6 patterns were enhanced in all cases. Furthermore, irradiation of the H-9 patterns increased the intensity of the H-7 absorptions for **1** and **15** but not for **14** and **16**. Irradiation of the 7-methyl doublet revealed enhancement of the H-7 absorption in all cases, as expected, but only the H-6 patterns in **15** and **16**. From these results, we can conclude that H-9 is α in **1** and **16**, β in **14** and **15**, while H-7 is α in **1** and **14** but β in **15** and **16**.

Models show that H-1β and -9β in this skeleton are in the W arrangement conducive to four-bond coupling in saturated systems, nicely accounting for the long-range interaction observed for **14** and **15**. With a 1β-hydroxyl group, one would not expect to observe long-range coupling between the 1α and 9 protons. From models, this *cis* C-2,9 ring junction appears to increase the steric congestion around the α-hydroxyl group, in agreement with the fact that **14** and **15** are not readily acetylated. This orientation of the hydroxyl group is the same as that found for other members of the protoilludane family of sesquiterpenes, which are oxygenated at C-1 (17).

In the tetracyclic compounds **1–8** and **14–18**, the 12-methylene protons, denoted in Table 1 as *syn* and *anti* with respect to C-1, gave rise to an AB pattern, J_{AB} = 6.7 ± 0.2 Hz, with an additional coupling of 3.2 ± 0.4 Hz to one of the protons. The latter coupling interaction involves the 10α proton, which was identified by the magnitude of its vicinal coupling with H-9. For **1** and **16**, the dihedral angle relating the 9α and 10α protons is near zero and the J values are 10.6 and 11.5 Hz, respectively, while for **14** and **15** this angle between the 9β and 10α protons is near 120° with J = 5.1 Hz for each. With the heterocyclic ring bridged through a 2β oxygen, the 10α proton is in the zigzag, or W arrangement, with respect to *syn* H-12, accounting for the observed long-range coupling. The alternative 2α-oxygen bridge would place the 10β proton in a comparable orientation. It may be noted that a 1β-hydroxyl group would place H-1α in a W arrangement with respect to *anti* H-12 and lead to long-range coupling, contrary to the facts. Thus, the relative stereochemistry as shown for **1** and **14–16** was established. The $^1H-^1H$ coupling constants are collected in Table 3.

An attempt was made to determine if the isomers of **1** were present in the initial culture extracts. Coprinolone and its isomers, **14–16**, could be distinguished by capillary gas chromatography, having retention times of 4.0 (**15**), 4.6 (**16**), 4.8 (**1**), and 5.4 min (**14**). Two culture filtrate extracts showed, in addition to a major peak for **1**, many minor peaks of which one coincided with the retention time of **16**. In both cases, the area of this peak was ca. 8% of that for **1**. Although this provides evidence for **16** at an early stage of isolation, it does not exclude isomerization during the extraction steps. Isomer **14** was not detected but a composite peak was observed at the retention time of **15** with an area ca. 1% of that for **1**.

When coprinolone was chromatographed over alumina or exposed in refluxing benzene to alumina, ketodiol **9** also formed from opening of the oxide ring. Thin-layer chromatographic examination showed that this product was a mixture of two

Can. J. Chem. Downloaded from www.nrcresearchpress.com by 41.223.56.140 on 09/07/12
For personal use only.

components, only one of which, **9**, crystallized. The same mixture was formed when **1**, **14**, or **15** was treated with methanolic potassium hydroxide. The ^{13}C spectrum of the noncrystalline component is remarkably similar to that of **9** and its ^1H spectrum contained a methyl doublet, δ 1.08, $J = 7.5$ Hz; two methyl singlets, 1.07 and 1.42; a 1-proton singlet, 4.72; an AB pattern, 3.43, 3.51, $J_{AB} = 10$ Hz; and a series of overlapping multiplets arising from eight protons, δ 1.5–2.4. These data (Tables 1 and 2) indicated that this material formed with **9** is ketodiol **19**.

Structure of Δ^6-coprinolone

A study to determine the period of most active synthesis of **1** by *C. psychromorbidus* revealed that a second major metabolite, slightly more polar than **1** on silica gel tlc plates, was present in relatively young cultures. The amount of this substance, however, declined in cultures after 15 days' growth and was not detected by tlc in extracts of 21- to 24-day-old cultures, the age at which cultures were normally used for the production of **1**. This compound, which could easily be separated from **1** by chromatography, melted at 186–187°C and had an optical rotation of $[\alpha]_D^{20}$ −105°. Its constitution as $C_{15}H_{20}O_3$ was established by microanalysis and precise mass measurement. The ketonic carbonyl absorption (1646 cm^{-1}) and uv maximum (λ_{max} 248, ε 11 760) are very similar to those found for ketodiol **9** and are indicative of an α,β-unsaturated ketone. The proton spectrum included three methyl singlets, δ 1.01, 1.56, 1.59, and absorption patterns closely resembling those exhibited by H-1, -9, -10, and -12 for **1** but with the absence of long-range coupling for H-9. These data point to structure **20** for this metabolite, Δ^6-coprinolone, and the ^{13}C spectrum was entirely consistent with this proposal; the nmr data are collected in Tables 1–3. In addition, a long-range $^{13}C-^1H$ COSY experiment confirmed the linkages of C-11 with C-1, C-10, C-12, and C-13, and of C-3 with C-2, C-4, and C-14. Further support for this structure was provided by the ^{13}C spectrum of the labelled material isolated from the [1,2-$^{13}C_2$]acetate incorporation experiment described earlier. All carbons were enriched (4.0% specific incorporation) in the labelling pattern **21** (Fig. 1) in which the J_{CC} values in Hz for the intact acetate units incorporated are indicated. As in the case of **1**-$^{13}C_x$, a $^{13}C-^{13}C$ COSY experiment with **20**-$^{13}C_x$ provided confirmation of the direct bondings of C-4 with C-3 and C-5, C-2 with C-3 and C-9, and C-11 with C-1, C-10, and C-13. Treatment with acetic anhydride – pyridine gave a monoacetyl derivative **22**, a structure fully supported by the nmr results (Tables 1–3).

Concluding remarks

It was proposed earlier (8) that the isolation of **1** from the W2 isolate may have taxonomic significance and might be of value because of the difficulty of identifying *C. psychromorbidus* owing to its failure to produce fruiting bodies in culture. However, only trace quantities, if any, of coprinolone were detected in cultures of three other isolates of *C. psychromorbidus* (W1, 1291, 1292) that can be distinguished from W2 on the basis of physiological and morphological characteristics (1, 2). The possibility remains, however, that **1** may be produced by other isolates of this fungus exhibiting properties more closely resembling those of W2.

The absolute configuration of **1** was not determined but very probably corresponds to that of other naturally occurring protoilludanes (17*d*, 18). If so, it may be possible to degrade **1**, perhaps by conversion to **8**, base-catalyzed opening of the oxide ring, and oxidation, to an intermediate containing the cyclobutyl ring, which could be transformed to (+)-grandisol (**23**), an aggregation pheromone of the cotton boll weevil (19). Grandisol, of undetermined absolute stereochemistry, has also been reported as a pheromone component of several other insects (20).

Experimental

Melting points were measured on a Kofler hot stage and are uncorrected. Microanalyses were performed by Dr. C. Daesslé, Montreal, and Guelph Chemical Laboratories, Guelph. Infrared spectra of compounds, in KBr unless otherwise indicated, were recorded on a Pye Unicam PU9516 spectrophotometer. Ultraviolet spectra were recorded on a Shimadzu UV-240 instrument and mass spectra were determined with either a Varian MAT 311A or a Finningan MAT 8230 system. Optical rotations were determined in chloroform on Schmidt–Haensch or Perkin–Elmer 241 polarimeters. Gas chromatography was done at 180°C using a Hewlett–Packard 5880A instrument equipped with a 10 m × 0.2 mm i.d. fused silica capillary column, coated with dimethyl silicone fluid (Hewlett–Packard), and a flame ionization detector. Thin-layer chromatography (tlc) was carried out on Macherey–Nagel silica gel precoated plastic sheets (Polygram Sil G/UV_{254}) and Whatman high performance silica gel plates (LHP-KF). Vanillin – phosphoric acid spray was used routinely for visualization. Light petroleum refers to the fraction with bp 35–60°C unless otherwise stated.

The nmr spectra were recorded with Varian XL-200 and -300 systems. Although initially some selective decoupling experiments were done to aid analysis of the proton spectra, all of the coupling interactions were identified by $^1H-^1H$ homonuclear correlation using the HOMCOR sequence of the XL software. The correlated spectra were obtained using a 1024 × 512 data matrix transforming 1024 points in both domains with a spectral width of 1000 Hz in both. A series of nOe difference spectra were recorded for **1** and **14**–**16** with a spectral width of 1000 Hz, 90° pulses, and acquisition time of 3 s with a delay of 10 s. A total of 15 16-transient blocks, each with four steady-state pulse cycles, was collected at various (6–10) irradiation frequencies, one of which was 5 kHz off-resonance. Subtraction of the latter FID from each of the others containing a saturated absorption before 16 K transformation gave the required difference spectra. Several examples were done with the irradiating frequency cycled through the lines of a multiplet for saturation. The ^{13}Cmr spectra were all obtained at 75.4 MHz and the protonated carbons distinguished with the APT technique (21). Heteronuclear $^{13}C-^1H$ correlation spectra were recorded to establish the one-bond correlations using the HETCOR sequence of the XL software, using a 2048 × 128 data matrix transforming 2048 and 512 points for ^{13}C and ^1H respectively, with sweep widths of 6700 (^{13}C) and 1000 Hz (^1H). The same parameters were employed for the XCORFE sequence (13) to obtain the two- and three-bond correlations using fixed delays of 0.064–0.128 s. The INADEQUATE spectra (14) for **1** were obtained with the XL software sequences using a 6700-Hz sweep width; for the 2D spectrum a 2048 × 128 data matrix transforming 2048 and 512 points was used. The ^{13}C COSY spectra for **1**-$^{13}C_x$ and **2**-$^{13}C_x$ were obtained with the HOMCOR sequence and a 1024 × 256 data matrix, transforming 1024 points in each domain with 6700- and 15 000-Hz sweep widths for each of two experiments.

Cultural conditions and extraction of metabolites

The W2 isolate of a low-temperature basidiomycete (1) was routinely grown at 15°C for 21–24 days in 1-L Roux bottles on a synthetic medium (150 mL /bottle) as described previously (4). After removal of the mycelium by filtration, the culture fluid from bottles was extracted with ethyl acetate. At this stage, the addition of ethyl alcohol and saturated NaCl solution (both 10% by volume) aided in the separation of the organic and aqueous layers. The extracts were combined, washed with saturated sodium chloride solution, and dried over anhydrous sodium sulfate. Removal of the solvent gave a thick brown oil (750 mg). Extraction of cultures with ether afforded a smaller quantity (430 mg) of a lighter coloured oil. Similar yields were

Can. J. Chem. Downloaded from www.nrcresearchpress.com by 41.223.56.140 on 09/07/12
For personal use only.

Can. J. Chem. Downloaded from www.nrcresearchpress.com by 41.223.56.140 on 09/07/12
For personal use only.

obtained when this fungus was cultured on malt extract – yeast extract – glucose (5 g, 5 g, 15 g/L) medium.

Wet mycelium from 10 bottles was mixed with ethyl alcohol (50 mL) and ethyl acetate (100 mL) and homogenized in a Waring blender. The resulting paste was diluted with water and filtered through a pad of Celite. After washing the Celite thoroughly with ethyl acetate, the organic and aqueous phases of the filtrate were separated and the latter was further extracted with ethyl acetate. The combined extracts were washed with saturated sodium chloride solution and dried over sodium sulfate. After removal of solvent, a typical yield was 250 mg of a dark oil.

Three other isolates, W1 (1), 1291, and 1292 (2), were grown on synthetic media under the same conditions as W2. The culture filtrates were extracted with ether and, in each case, the yield of extracts was ca. 20 mg. To test for the presence of **1**, extracts were separated on silica gel sheets using chloroform–methanol (19:1), and the material in the zone corresponding to the sesquiterpenes was analyzed by gas chromatography. Trace amounts of a substance with a retention time corresponding to that of **1** were detected in extracts of W1 and 1291 but none was observed in the extract of 1292.

In a time course study, cultures from two bottles were extracted every second day between days 7 and 25 after inoculation, essentially as described above except that the mycelium was not separated. After the addition of ethyl alcohol (30 mL) and ethyl acetate (100 mL), the cultures were homogenized for 1.5 min and the resulting mixture was filtered through Celite. The Celite was washed well with ethyl acetate and the aqueous portion of the extracts was extracted twice with ethyl acetate (100-mL portions) after the addition of saturated sodium chloride solution (100 mL). Removal of the ethyl acetate after washing and drying yielded the metabolites. Inspection of a tlc of the extracts under short wavelength uv light revealed the presence of a second major metabolite, slightly more polar than coprinolone, which peaked in concentration around days 13–15 and declined thereafter. In contrast, the total amount of extract as well as the level of coprinolone, as judged by tlc, peaked at day 15 and remained relatively constant throughout the remaining period.

*Isolation of coprinolone (**1**)*

The crude extracts were chromatographed over silicic acid – Celite (4:1) using methylene chloride as eluent. In a typical separation, the culture filtrate extract (425 mg) was chromatographed over 30 g adsorbant (20 × 1.8 cm column). After examination by tlc (silica gel; chloroform–methanol, 19:1), fractions containing the major metabolite were pooled, yielding crystalline material (167 mg). Recrystallization from ether – light petroleum provided coprinolone, mp 105– 107°C; $[\alpha]_D^{23}$ −95° (*c* 1.03); ir: 3510, 1700 cm^{-1}. *Exact Mass* calcd. for $C_{15}H_{22}O_3$ (M^+): 250.1568; found: 250.1565. *Exact Mass* for $C_{13}H_{18}O_3$ (M^+ −28): 222.1255; found: 222.1253. *Anal.* calcd. for $C_{15}H_{22}O_3$: C 71.97, H 8.86; found: C 71.73, H 9.04.

Chromatography of a mycelial extract (252 mg) in the same way yielded fractions containing mainly coprinolone (38 mg), preceded by fractions containing another substance (85 mg) that had approximately the same R_f when analyzed by tlc. In contrast to coprinolone, this substance could be detected by viewing the tlc plates under uv light. Recrystallization from ether–methanol afforded plates, mp 149–152°C; $[\alpha]_D^{22}$ −116° (*c* 0.9); this substance was indistinguishable from ergosterol by tlc, uv, ir, and mixture mp.

*Coprinolone acetate (**2**)*

Coprinolone (56 mg) in pyridine (0.5 mL) was treated with acetic anhydride (0.25 mL) for 16 h at room temperature. Chromatography of the product over silicic acid – Celite (4:1) using methylene chloride yielded a substance that was recrystallized from light petroleum (60–80°C) to give acetate **2**, mp 102–103°C; $[\alpha]_D^{20}$ −50° (*c* 1.18); ir: 1734, 1715 cm^{-1}. *Anal.* calcd. for $C_{17}H_{24}O_4$: C 69.83, H 8.27; found: C 69.58, H 8.22.

*Diol **3***

Sodium borohydride (58 mg) was added to a stirred solution of coprinolone (250 mg) in methanol (5 mL). After 1.5 h, additional reagent (39 mg) was added as tlc showed the presence of starting material. Stirring was continued for a further 3.5 h, water was added, and the product was extracted into methylene chloride. Recrystallization from ether–hexane removed a small amount of coprinolone, which was further treated with sodium borohydride. Combination of the products and recrystallization from ether–hexane gave diol **3** (210 mg), mp 137–138°C; $[\alpha]_D^{24}$ −38° (*c* 0.84); ms 252 (M^+). *Anal.* calcd. for $C_{15}H_{24}O_3$: C 71.39, H 9.59; found: C 71.56, H 9.53.

*Hydroxyacetate **4***

Diol **3** (179 mg) in pyridine (1 mL) was treated overnight at room temperature with acetic anhydride (0.5 mL). After purification by chromatography over silicic acid – Celite (4:1) with methylene chloride as eluent, the product was recrystallized from hexane to give hydroxyacetate **4**, mp 73–74°C; $[\alpha]_D^{22}$ +4° (*c* 1.04); ir: 3478, 1742 cm^{-1}. *Anal.* calcd. for $C_{17}H_{26}O_4$: C 69.36, H 8.90; found: C 69.25, H 8.89.

Hydroxyacetate **4** was also formed when coprinolone acetate (**2**) was treated with sodium borohydride. Oxidation of **4** in methylene chloride with pyridinium chlorochromate (9) yielded coprinolone acetate (**2**).

*Bromocoprinolone (**5**)*

Coprinolone (37 mg) was treated with *N*-bromosuccinimide (32 mg) in refluxing carbon tetrachloride (4 mL) for 30 min. Removal of the solvent after washing twice with water yielded material that was recrystallized from ether–hexane to give **5**, as needles, mp 145–148°C (dec.); $[\alpha]_D^{24}$ +127° (*c* 1.02); ir: 3562, 1713 cm^{-1}. *Anal.* calcd. for $C_{15}H_{21}O_3Br$: C 54.72, H 6.43; found: C 54.34, H 6.77.

*Bromocoprinolone acetate (**6**)*

Coprinolone acetate (**2**; 13 mg) was treated with *N*-bromosuccinimide (10 mg) in carbon tetrachloride (2 mL) as above. Isolation of the product and recrystallization from ether–hexane yielded bromoacetate **6**, mp 121–122°C; $[\alpha]_D^{22}$ +125° (*c* 0.51); ir: 1743, 1724 cm^{-1}. *Anal.* calcd. for $C_{17}H_{23}O_4Br$: C 54.99, H 6.24; found: C 54.82, H 5.97. The same substance was obtained when bromocoprinolone (**5**) was acetylated using acetic anhydride – pyridine.

*Hydroperoxide **7***

A solution of coprinolone (509 mg) in C_6D_6 deposited crystals during standing at room temperature for 4 weeks. Thin-layer chromatography of this material (25 mg) showed that it was more polar than coprinolone. Recrystallization from methanol yielded crystals, mp 181–183°C (vigorous gas evolution); ir: 3510, 3340, 1722 cm^{-1}; ms: 282 (M^+). Chromatograms of **7** showed a characteristic spot for a peroxide with potassium iodide – starch and ferrous thiocyanate sprays (22).

Treatment of **7** (10.1 mg) in acetic acid (2 mL) with freshly activated zinc dust (37 mg) by stirring for 16 h yielded a new compound, which was recrystallized from methylene chloride – hexane to give alcohol **8**, mp 170–173°C; ir: 3470, 1714 cm^{-1}. *Exact Mass* calcd. for $C_{15}H_{22}O_4$: 266.1517; found: 266.1517.

*Ketodiol **9***

Methanolic potassium hydroxide (1 N, 0.2 mL) was added to a solution of coprinolone (10 mg) in methanol (1 mL) under nitrogen. No starting material remained after 23 h at room temperature (tlc evidence). After addition of water, the product (7.8 mg) was extracted into methylene chloride. Recrystallization from ethyl acetate – hexane yielded ketodiol **9**, mp 144–146°C; $[\alpha]_D^{25}$ −27° (*c* 0.81); ir: 3410, 1652 cm^{-1}; uv(EtOH): 252 nm (ϵ 8490). *Exact Mass* calcd. for $C_{15}H_{22}O_3$: 250.1568; found: 250.1567.

Ketodiol **9** (6.8 mg) in 2 mL of methylene chloride was oxidized with 4-(dimethylamino)pyridinium chlorochromate (44 mg) in methylene chloride (1 mL) for 1 h at room temperature (10). Isolation of product and separation from starting material by tlc yielded a new substance (1.7 mg), uv(EtOH): 266 nm.

Oxidation of coprinolone

Coprinolone (44 mg) in acetone (10 mL) was treated at room temperature for 4 h with an excess of oxidant (23) prepared by dissolving chromium trioxide (3 g) in water (15 mL) and concentrated H_2SO_4 (2.7 mL). Reaction of the polar oxidation product with a solution of diazomethane in ether and recrystallization of the product

from ether–hexane yielded methyl ester **10**, mp 110–111°C; $[\alpha]_D^{22}$ +21° (*c* 1.00); ir: 1730, 1638, 1610 cm^{-1}; uv(EtOH): 260 nm (ε 9080); ms 278 (M^+) *Anal.* calcd. for $C_{16}H_{22}O_4$: C 69.04, H 7.97; found: C 68.82, H 7.50.

Isomerization of coprinolone on alumina

Chromatography of culture filtrate extracts on alumina (neutral, Grade III) yielded, in addition to coprinolone, several new compounds not initially present in the mixture (tlc evidence). To determine the source of these substances, coprinolone was applied in benzene to a similar column. Analysis (tlc) of material eluted after 27 h with ether showed that most of the coprinolone had disappeared and two slightly more polar compounds, which did not acetylate when treated with acetic anhydride – pyridine at room temperature, had formed. Rechromatography of fractions from alumina chromatography containing these two substances, over silicic acid – Celite (4:1) using methylene chloride, gave partial separation. Recrystallization of fractions rich in the less polar component, from aqueous methanol, yielded isomer **14**, mp 163–164°C; $[\alpha]_D^{18}$ −239° (*c* 1.06) ; ir: 3475, 1691 cm^{-1}. *Exact Mass* calcd. for $C_{15}H_{22}O_3$: 250.1568; found: 250.1567. Recrystallization of fractions rich in the other component, from hexane, yielded isomer **15**, mp 168–169°C; $[\alpha]_D^{17}$ −16° (*c* 0.32); ir: 3488, 1704 cm^{-1}. *Exact Mass* calcd. for $C_{15}H_{22}O_3$: 250.1568; found: 250.1562.

Isomer **14** in $CDCl_3$ at 4°C for 8 days isomerized to give approximately equal parts of isomers **14** and **15** (tlc evidence; high performance silica gel with ether – light petroleum – acetic acid, 40:60:1). No further change was noted when this mixture was treated with $CHCl_3$ at reflux for 1 h.

Longer contact with alumina resulted in the production of a polar material, which on plates containing fluorescent indicator was visible under uv light. Subsequent chromatography on a Whatman high performance silica gel plate using repeated development with ether – light petroleum – acetic acid (60:40:1) indicated that this material consisted of at least two components, one of which corresponded to keto diol **9**. This mixture was also obtained as the main product when coprinolone (20 mg) was exposed to alumina (1 g, Grade III neutral) in refluxing benzene for 1.3 h. The same mixture was obtained when isomers **14** and **15** were treated with methanolic potassium hydroxide as described above for **1**. Recrystallization yielded keto diol **9** (nmr evidence) corresponding chromatographically to the less polar component. A small quantity of the noncrystalline second component **19** was obtained from the mother liquors by preparative tlc on silica gel G using the ether – light petroleum – acetic acid system. Reinvestigation showed that coprinolone also afforded **19** in addition to **9** when treated with methanolic potassium hydroxide.

*Isomer **16***

Chromatography of material in mother liquors from recrystallization of coprinolone over 12 g silicic acid – Celite (4:1) with methylene chloride as eluent yielded fractions containing coprinolone followed by a mixture and then by a substance (6 mg) slightly more polar on tlc than coprinolone. Recrystallization from light petroleum gave isomer **16**, mp 80–105°C. *Exact Mass* calcd. for $C_{15}H_{22}O_3$: 250.1568; found: 250.1565.

*Acetate **17***

Material (93 mg) in mother liquors from recrystallization of coprinolone was acetylated (acetic anhydride – pyridine, room temperature) and the product chromatographed over 10 g silicic acid – Celite (4:1) with toluene to give coprinolone acetate (**2**), followed by fractions containing a second substance (18 mg) distinguishable from **2** by tlc (Whatman high performance silica gel plate developed three times with toluene). Recrystallization from hexane afforded acetate **17**, mp 64–66°C. *Exact Mass* calcd. for $C_{17}H_{24}O_4$: 292.1674; found: 292.1671.

Treatment of acetate **17** in methanol with sodium borohydride afforded a more polar substance **18**, ir($CHCl_3$): 3460, 1738 cm^{-1}, which could not be induced to crystallize.

*Δ^6-Coprinolone (**20**)*

Chromatography of the product (200 mg) obtained from 15-day cultures (see above description of time course experiment), over 30 g silicic acid – Celite (4:1) with methylene chloride, separated coprinolone (33 mg) from a new compound (31 mg), which was recrystallized from methylene chloride – ethyl acetate to give Δ^6-coprinolone, mp 186–187°C; $[\alpha]_D^{20}$ −105° (*c* 0.98); ir: 3400, 1646 cm^{-1}; uv(EtOH): 248 nm (ε 11 760). *Exact Mass* calcd. for $C_{15}H_{20}O_3$: 248.1412; found: 248.1416. *Anal.* calcd. for $C_{15}H_{20}O_3$: C 72.55, H 8.12; found: C 72.75, H 8.51.

Yields of coprinolone and Δ^6-coprinolone from the 13-day-old cultures were 10 and 15 mg respectively.

*Δ^6-Coprinolone acetate (**22**)*

Acetylation (acetic anhydride – pyridine, room temperature) of Δ^6-coprinolone (**20**) and recrystallization of the product from light petroleum yielded the acetate **22**, mp 82–87°C; ir($CHCl_3$): 1740, 1660 cm^{-1}. *Exact Mass* calcd. for $C_{17}H_{22}O_4$: 290.1517; found: 290.1518.

[1,2-$^{13}C_2$]Acetate incorporation study

A sterile solution (5 mL of sodium [1,2-$^{13}C_2$]acetate (0.06 M; 99.4 at.% ^{13}C) from MSD Isotopes, Point Claire – Dorval, was added to each of five Roux bottle cultures on days 8 and 10 after inoculation. The cultures were extracted, as described for the time course study, on day 13. Chromatography of the product (509 mg) over silicic acid – Celite (4:1) using methylene chloride gave coprinolone (155 mg) and Δ^6-coprinolone (50 mg). Recrystallization afforded ^{13}C-enriched coprinolone, mp 104–105°C, and Δ^6-coprinolone, mp 185–186°C.

Acknowledgements

We wish to acknowledge the financial support of the Natural Sciences and Engineering Research Council of Canada and the excellent technical assistance of A. Gaidauskas, D. Hairsine, V. Richardson, M. E. Stevens, and S. Wilson. We also thank Dr. J. A. Traquair, Agriculture Canada Research Station, Harrow, Ont., for providing isolates 1291 and 1292 of *C. psychromorbidus*.

1. E. W. B. Ward, J. B. Lebeau, and M. W. Cormack. Can. J. Bot. **39**, 297 (1961).
2. J. A. Traquair. Can. J. Plant Pathol. **2**, 105 (1980).
3. S. A. Redhead and J. A. Traquair. Mycotaxon, **13**, 373 (1981).
4. E. W. B. Ward and G. D. Thorn. Can. J. Bot. **44**, 95 (1966).
5. E. W. B. Ward, G. D. Thorn, and A. N. Starratt. Can. J. Microbiol. **17**, 1061 (1971).
6. E. W. B. Ward, A. N. Starratt, and J. R. Robinson. Can. J. Bot. **55**, 2065 (1977).
7. B. A. Tapper and M. A. MacDonald. Can. J. Microbiol. **20**, 563 (1974).
8. A. N. Starratt, J. B. Stothers, and E. W. B. Ward. J. Chem. Soc. Chem. Commun. 590 (1988).
9. E. J. Corey and J. W. Suggs. Tetrahedron Lett. 2647 (1975).
10. F. S. Guziec and F. A. Luzzio. J. Org. Chem. **47**, 1787 (1982).
11. W. A. Ayer and M. H. Saeedi-Ghomi. Can. J. Chem. **59**, 2536 (1981).
12. S. Nozoe, H. Kobayashi, S. Urano, and J. Furakawa. Tetrahedron Lett. 1381 (1977).
13. W. F. Reynolds, D. W. Hughes, and M. Perpick-Dumont. J. Magn. Reson. **63**, 413 (1985).
14. A. Bax, R. Freeman, and S. P. Kempsell. J. Am. Chem. Soc. **102**, 4849 (1980); A. Bax, R. Freeman, T. A. Frankiel, and M. H. Levitt. J. Magn. Reson. **43**, 478 (1981).
15. A. P. W. Bradshaw, J. R. Hanson, and I. H. Sadler. J. Chem. Soc. Perkin Trans. 1, 2445 (1982).
16. W. A. Ayer and L. M. Browne. Tetrahedron, **37**, 2199 (1981).
17. (*a*) D. M. X. Donnelly, D. J. Coveney, and J. Polonsky. Tetrahedron Lett. **26**, 5343 (1985); (*b*) A. Arnone, R. Cardillo, and G. Nasini. Phytochemistry, **25**, 471 (1986); (*c*) D. M.

Can. J. Chem. Downloaded from www.nrcresearchpress.com by 41.223.56.140 on 09/07/12
For personal use only.

X. DONNELLY, P. F. QUIGLEY, D. J. COVENEY, and J. POLONSKY. Phytochemistry, **26**, 3075 (1987); (*d*) A. ARNONE, R. CARDILLO, G. NASINI, and S. V. MEILLE. J. Chem. Soc. Perkin Trans. 1, 503 (1988); (*e*) A. ARNONE, R. CARDILLO, V. DI MODUGNU, and G. NASINI. Gazz. Chim. Ital. **118**, 517 (1988); (*f*) A. ARNONE, R. CARDILLO, and G. NASINI. Gazz. Chim. Ital. **118**, 523 (1988).

18. D. M. X. DONNELLY, J. POLONSKY, T. PRANGÉ, G. SNATZKE, and U. WAGNER. J. Chem. Soc. Chem. Commun. 222 (1984); A. ARNONE, G. NASINI, G. ASSANTE, H. J. ROEIJMANS, and G. W. VAN EIJK. Phytochemistry, **26**, 1739 (1987).
19. J. H. TUMLINSON, D. D. HARDEE, R. C. GUELDNER, A. C. THOMPSON, P. A. HEDIN, and J. P. MINYARD. Science, **166**, 1010 (1969); P. D. HOBBS and P. D. MAGNUS. J. Chem. Soc. Chem. Commun. 856 (1974).
20. D. C. BOOTH, T. W. PHILLIPS, A. CLAESSON, R. M. SILVERSTEIN, G. N. LANIER, and J. R. WEST. J. Chem. Ecol. **9**, 1 (1983); T. W. PHILLIPS, J. R. WEST, J. L. FOLTZ, R. M. SILVERSTEIN, and G. N. LANIER. J. Chem. Ecol. **10**, 1417 (1984); W. FRANCKE, M.-L. PAN, W. A. KÖNIG, K. MORI, P. PUAPOOMCHAREON, H. HEUER, and J. P. VITÉ. Naturwissenschaften, **74**, 343 (1987).
21. S. L. PATT and J. N. SHOOLERY. J. Magn. Reson. **46**, 535 (1982).
22. K. G. KREBS, D. HEUSSER, and H. WIMMER. *In* Thin-layer chromatography. 2nd ed. *Edited by* E. Stahl. Springer-Verlag, New York. 1969. p. 854.
23. K. BOWDEN, I. M. HEILBRON, E. R. H. JONES, and B. C. L. WEEDON. J. Chem. Soc. 39 (1946).
24. S. PEIRIS, J. B. STOTHERS, and S. E. THOMAS. Can. J. Chem. **67**, 187 (1989).

Can. J. Chem. Downloaded from www.nrcresearchpress.com by 41.223.56.140 on 09/07/12
For personal use only.

Rate and equilibrium studies of the deprotonation of benzylic ketones bearing pyridinium cations

JOHN W. BUNTING AND DIMITRIOS STEFANIDIS
Department of Chemistry, University of Toronto, Toronto, Ont., Canada M5S 1A1

Received September 5, 1988

JOHN W. BUNTING and DIMITRIOS STEFANIDIS. Can. J. Chem. **67**, 428 (1989).

Rates and equilibria for the deprotonation of four benzylic ketones containing pyridinium substituents (**1**, **2**, **5**, and **6**) have been investigated in basic aqueous solution (ionic strength 0.1) over the range 15–45°C, and thermodynamic and activation parameters have been evaluated. Similar data are also reported for the deprotonation of nitroethane. The kinetic preference for hydroxide ion addition to the carbonyl group in competition with the thermodynamically preferred enolate ion formation, which was previously reported for the 1-methyl-4-phenylacetylpyridinium cation (**1**) and its 3-phenylacetyl isomer (**2**), is also found for the 1-(1-methyl-2-oxo-2-phenylethyl)pyridinium cation (**6**). Rates of equilibration of the 1-(2-oxo-2-phenylethyl)-pyridinium cation (**5**) with its enolate ion conjugate base are too rapid to allow investigation by stopped-flow spectrophotometry. For the hydroxide ion catalyzed deprotonation of each of **1**, **2**, **6**, and nitroethane, $\Delta S_d^{\ddagger}$ is more negative than ΔS^0. This difference, which represents the entropy of activation for protonation of the conjugate base of each of these carbon acids by water, is approximately constant at $\Delta S_p^{\ddagger} = -4.9 \pm 0.5$ cal deg^{-1} mol^{-1}.

Key words: carbon acids, kinetic studies, deprotonation, activation parameters, pK_a values.

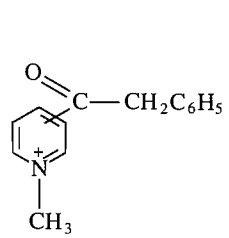
JOHN W. BUNTING et DIMITRIOS STEFANIDIS. Can. J. Chem. **67**, 428 (1989).

Opérant à des températures allant de 15 à 45°C, en solutions basiques aqueuses (force ionique de 0,1), on a déterminé les vitesses de déprotonation ainsi que les équilibres de quatre cétones benzyliques contenant des substituants pyridinium (**1**, **2**, **5** et **6**) et on a évalué les paramètres thermodynamiques et d'activation. On rapporte aussi des données semblables relatives à la déprotonation du nitroéthane. Il a été établi antérieurement, avec la cation méthyl-1 phénylacétyl-4 pyridinium (**1**) et avec son isomère phénylacétyle-3 (**2**), que d'un point de vue cinétique l'ion hydroxyde s'additionne sur le groupement carbonyle plutôt que de donner lieu à la formation de l'ion énolique qui est favorisée d'un point de vue thermodynamique; on a trouvé que cette conclusion vaut aussi pour le cation (méthyl-1 oxo-2 phényl-2 éthyl)-1 pyridinium (**6**). La vitesse d'équilibration du cation (oxo-2 phényl-2 éthyl)-1 pyridinium (**5**) avec sa base conjuguée, l'ion énolate, est trop rapide pour permettre une étude par spectrophotométrie à flux stoppé. Pour la déprotonation catalysée par l'ion hydroxyde des composés **1**, **2**, **5**, **6** et du nitro-éthane, les $\Delta S_d^{\ddagger}$ sont plus négatifs que les ΔS^0. On a observé que cette différence, qui représente l'entropie d'activation pour la protonation de la base conjuguée de chacun de ces acides carbonés par l'eau, est approximativement constante à $\Delta S_p^{\ddagger} = -4{,}9 \pm 0{,}5$ cal deg^{-1} mol^{-1}.

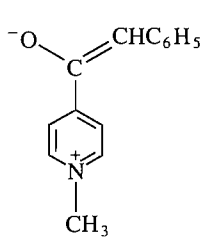
Mots clés : acides carbonés, études cinétiques, déprotonation, paramètres d'activation, valeurs de pK_a.

[Traduit par la revue]

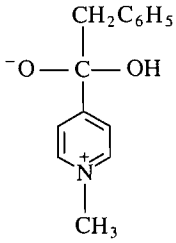
We recently reported (1) upon the kinetics of deprotonation of several series of benzylic ketones in aqueous solutions. While the *N*-methyl phenylacetylpyridinium cations **1** (pK_a = 9.02) and **2** (pK_a = 10.32) undergo deprotonation in a hydroxide ion catalyzed process, this deprotonation is not the kinetically controlled reaction when neutral aqueous solutions of these cations are adjusted to pH >11. In these basic solutions, the addition of hydroxide ion to the carbonyl group to give the *gem* diol anion (e.g., **4**) is faster than hydroxide ion catalyzed enolate ion formation (e.g., **3**), although the enolate ion is the thermodynamically favoured species in basic aqueous solutions of both **1** and **2**.



1: 4-pyridyl
2: 3-pyridyl

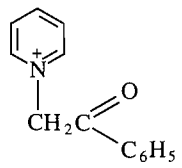


3

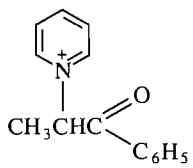


4

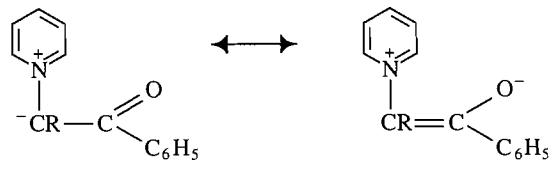
It seems likely that a similar competition between the products of kinetic and thermodynamic control may also exist for other carbonyl-activated carbon acids that contain similar pyridinium units. The methylene group of the *N*-phenacyl pyridinium cation (**5**) (1-(2-oxo-2-phenylethyl)pyridinium cation) is reported (2, 3) to be reasonably acidic in aqueous solution,



5



6



7

although we have been unable to locate any report of the kinetic acidity of either this species or any closely related species. We have now found that the thermodynamic acidity of **5** is readily measured in aqueous solution, but its equilibration with its enolate anion (**7**; R = H) is too rapid to allow investigation by stopped-flow spectrophotometry. However, both the kinetic and thermodynamic acidities of the methyl derivative **6** (1-(1-methyl-2-oxo-2-phenylethyl)pyridinium cation) are readily accessible in aqueous solution, and **6** does display the above noted competition between deprotonation and hydroxide ion addition in aqueous base.

We also report the temperature dependences of the rate and equilibrium constants for the deprotonation of **1**, **2**, **5** (equilibrium only), and **6**, and a reinvestigation of the deprotonation of

Can. J. Chem. Downloaded from www.nrcresearchpress.com by 41.223.56.140 on 09/07/12
For personal use only.

TABLE 1. Temperature dependence of pK_a values for carbon acids[a]

Acid	Temperature (°C)	pK_a	ΔH^0 (kcal mol^{-1})	ΔS^0 (cal deg^{-1} mol^{-1})
1	15	9.21		
	20	9.12		
	25	9.01		
	35	8.89		
	40	8.84		
	45	8.74	+6.3 ± 0.2	−20.0 ± 0.6
2	20	10.46		
	25	10.33		
	30	10.30		
	35	10.14		
	40	10.07	+8.2 ± 0.4	−20.0 ± 1.3
5	15	11.21		
	25	11.02		
	35	10.79		
	45	10.56		
	55	10.38	+9.2 ± 0.3	−19.6 ± 0.9
6	25	11.65		
	35	11.44		
	45	11.28	+8.0 ± 0.5	−26.3 ± 1.6
$CH_3CH_2NO_2$	25	8.44		
	35	8.37		
	45	8.31	+2.8 ± 0.2	−29.2 ± 0.5[b]

[a]All data at ionic strength 0.1. Standard errors in pK_a are always within ±0.03.
[b]Literature data (15) at ionic strength 0: pK_a (25°C) = 8.53; ΔH^0 = 2.40 kcal mol^{-1}; ΔS^0 = −31.0 cal deg^{-1} mol^{-1}.

nitroethane, which surprisingly is the only carbon acid for which we have been able to locate *both* thermodynamic *and* activation paramaters for hydroxide ion catalyzed deprotonation in aqueous solution (4).

Experimental

The bromide salts of **1** and **2** were available from a recent study (1). Nitroethane (99.5% from Aldrich Chemical Co.) was redistilled before use. The bromide salts of **5** and **6** were prepared by treatment of pyridine with 2-bromoacetophenone and 2-bromopropiophenone, respectively, in benzene solution (5). The bromide salts, which precipitated from the reaction mixtures, were recrystallized several times from ethanol and appeared pure by ^{1}H nmr spectroscopy.

The pK_a values for **1**, **2**, and **6** were obtained spectrophotometrically, while pK_a values for **5** and nitroethane were calculated from potentiometric titrations (6). All kinetic data were obtained in aqueous solutions of ionic strength 0.1 on the Durrum–Gibson stopped-flow spectrophotometer, with the temperature controlled to ±0.1°C. Stock solution syringes were thermostatted for 20 min to ensure thermal equilibration before the initiation of reactions. Kinetic studies employed the following wavelengths and concentrations of the carbon acids: **1**, 445 nm, 0.02 mM; **2**, 360 nm, 0.02 mM; **6**, 400 nm, 0.2 mM; nitroethane, 250 nm, 0.2 mM. Data collection and analysis closely followed the methods previously described (1).

Spectral data for stable species were obtained on a Cary 210 spectrophotometer. All pH measurements and potentiometric titrations utilized a Radiometer PHM82 pH meter, which was calibrated with standard buffer solutions thermostatted at the appropriate temperature. All pH measurements were made in a cell thermostatted at the temperature under investigation.

Results

Basic aqueous solutions (pH >11) of each of the cations **5** and **6** show long wavelength absorption maxima in the vicinity of 400 nm. However, these solutions are unstable, and this long wavelength absorption decays in a base-catalyzed process. We have not investigated this decomposition in any detail at the present time, but note that the alkaline cleavage of *N*-(β-ketoalkyl)pyridinium cations to a carboxylate anion and an alkylpyridinium cation has been reported previously (3, 7–9). From the data of Pearson and Dillon (3), we calculate a half-time of 97 min for the decomposition of **5** at pH 12 at 25°C. This decomposition occurs sufficiently slowly that we have been able to obtain a clean potentiometric titration of **5** with aqueous base and thus evaluate the pK_a value. Table 1 contains pK_a values evaluated for the acid–base equilibration of **5** with its conjugate base at a number of temperatures, and also the thermodynamic parameters for this process that have been calculated from the van't Hoff equation.

When a neutral aqueous solution of **5** is mixed with basic buffers in the stopped-flow spectrophotometer, the development of the absorbance in the vicinity of 400 nm is complete within the mixing time of this instrument. When a neutral aqueous solution of **6** is mixed with basic buffers in the stopped-flow spectrophotometer, the absorbance in the vicinity of 400 nm is observed to increase to a maximum value, prior to a much slower decay of this absorbing species. The pH dependence of this maximum absorbance describes a simple acid–base equilibration of **6** with its conjugate base, and pK_a values and thermodynamic parameters for this process are included in Table 1.

The increase in absorbance of a basic solution of **6** to its maximum value at that pH is consistent with a process that is kinetically first order in [**6**]. The pseudo-first-order rate constant (k_{obs}) for the equilibration of **6** with its conjugate base was evaluated as a function of pH over the range pH 11–13. The equilibration of a carbon acid (CH) with its conjugate base

Can. J. Chem. Downloaded from www.nrcresearchpress.com by 41.223.56.140 on 09/07/12
For personal use only.

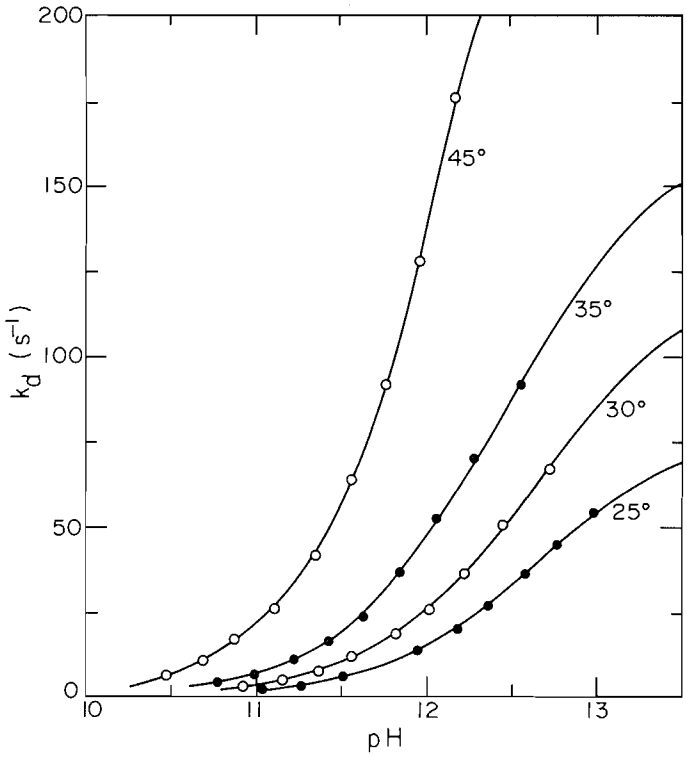


FIG. 1. The pH dependence of the pseudo-first-order rate constants for deprotonation of **6** at several temperatures. Curves are calculated from eq. [5] using the parameters in Table 2.

(C^-) is described by eq. [1], with k_{obs} being the sum of the individual rate constants for deprotonation (k_d) and protonation (k_p) at constant pH.

$$[1]\quad CH \underset{k_p}{\overset{k_d}{\rightleftharpoons}} C^-$$

$$[2]\quad k_{obs} = k_d + k_p$$

$$[3]\quad K_a = \frac{[H^+][C^-]}{[CH]} = k_d[H^+]/k_p$$

$$[4]\quad k_d = k_{obs}/(1 + [H^+]/K_a)$$

Individual values of k_d and k_p were calculated from each k_{obs}, and the pH dependences of these individual pseudo-first-order rate constants are shown in Fig. 1. The value of k_d increases with increasing pH, but appears to approach a limiting value in the most basic solutions. We have recently reported (1) similar observations for the hydroxide ion catalyzed deprotonation of both **1** and **2**, and have shown that this phenomenon is consistent with Scheme 1. In this scheme, the formation of the thermodynamically more stable conjugate base C^- of CH competes with the acid–base equilibration of CH with Z^- as the kinetically preferred process.

Analysis of Scheme 1, with the assumption that the K_z equilibrium is established much more rapidly than the formation of C^-, produces eq. [5].

$$[5]\quad k_d = k_{OH}[^-OH]/(1 + K_z[^-OH]/K_w)$$
$$= k_{OH}K_w/([H^+] + K_z)$$

Values of k_{OH} and K_z were evaluated from the pH dependence of k_d, and are collected in Table 2. Activation parameters for k_{OH} and thermodynamic parameters for the K_z process are given in Table 3.

$$H^+ + Z^- \overset{K_z}{\rightleftharpoons} CH \underset{k_{H_2O}}{\overset{k_{OH}[^-OH]}{\rightleftharpoons}} C^- + H_2O$$

SCHEME 1

TABLE 2. Temperature dependence of kinetic parameters for the deprotonation of carbon acids[a]

Acid	Temperature (°C)	k_{OH} ($M^{-1}s^{-1}$)	pK_z	k_{H_2O}(s^{-1})[b]
1	20	616	11.89	0.0056
	25	788	11.87	0.0081
	30	1120	11.75	0.015
	35	1500	11.67	0.024
	40	2350	11.52	0.047
	45	3040	11.43[c]	0.067
2	20	481	12.39	0.094
	25	620	12.33	0.13
	30	875	12.25	0.26
	35	1230	12.18	0.35
	45	2400	12.03[d]	0.89
5[e]	25	$>2 \times 10^4$		
6	25	1680	12.68	7.5
	30	2120	12.60	11
	35	3080	12.42	18
	45	4920	12.35[f]	37
$CH_3CH_2NO_2$	25	5.96		
	35	11.4		
	45	21.4		
	50	31.0		

[a]All data in aqueous solution at ionic strength 0.1.
[b]Calculated from $k_{H_2O} = k_{OH}K_w/K_a$.
[c]From the temperature dependence of pK_z for **1**: $\Delta H^0 = 8.3 \pm 0.8$ kcal mol^{-1}; $\Delta S^0 = -26 \pm 2$ cal deg^{-1} mol^{-1}.
[d]From the temperature dependence of pK_z for **2**: $\Delta H^0 = 6.2 \pm 0.2$ kcal mol^{-1}; $\Delta S^0 = -35.6 \pm 0.6$ cal deg^{-1} mol^{-1}.
[e]The estimation of k_{OH} for **5** is described in the text.
[f]From the temperature dependence of pK_z for **6**: $\Delta H^0 = 7.5 \pm 1.6$ kcal mol^{-1}; $\Delta S^0 = -33 \pm 5$ cal deg^{-1} mol^{-1}.

We have also investigated the temperature dependence of both the rate and equilibrium constants for enolate ion formation from **1** and **2**. The experimental kinetic data were analyzed in terms of Scheme 1 as previously described (1). The experimental rate and equilibrium constants, and the derived thermodynamic and activation parameters, are included in Tables 1–3. These tables also contain analogous data from our brief reinvestigation of the temperature dependence of the rates and equilibria for the deprotonation of nitroethane. The observed pseudo-first-order rate constants for the deprotonation of this latter carbon acid are cleanly proportional to hydroxide ion concentration over the range pH 11–13.

Discussion

Deprotonation of N-*(phenacyl)pyridinium cations*

N-(Phenacyl)pyridinium cations undergo deprotonation to their ylidic enolate ion conjugate bases (**7**) in basic solution (2, 3, 5). We have been unable to locate any previous potentiometric or spectrophotometric measurements of the pK_a values

Can. J. Chem. Downloaded from www.nrcresearchpress.com by 41.223.56.140 on 09/07/12
For personal use only.

TABLE 3. Thermodynamic and activation parameters for the reaction[a]

$$CH + {}^{-}OH \rightleftharpoons C^{-} + H_2O$$

Acid	ΔH^0	ΔS^0	$\Delta H_d^{\ddagger}$	$\Delta S_d^{\ddagger}$	$\Delta H_p^{\ddagger}$	$\Delta S_p^{\ddagger}$
1	−6.9	−0.7	11.6 ± 0.4	−6.3 ± 0.9	18.6	−5.6
2	−5.1	−0.7	12.1 ± 0.3	−5.3 ± 0.9	17.2	−4.6
5	−4.1	+0.3				
6	−5.3	−7.0	9.6 ± 0.5	−11.6 ± 1.5	14.9	−4.6
$CH_3CH_2NO_2$	−10.5	−9.9	12.0 ± 0.3	−14.7 ± 0.9	22.5	−4.8
	−12.2[b]	−18.3[b]	12.1[b]	−15.5[b]	24.3[b]	+3.0[b]

[a]All data in aqueous solution at ionic strength 0.1. ΔH^0 and ΔS^0 are calculated from the data in Table 1, using $\Delta H^0 = -13.3$ kcal mol^{-1} and $\Delta S^0 = 19.3$ cal deg^{-1} mol^{-1} for the ionization of water (17). $\Delta H_d^{\ddagger}$ and $\Delta S_d^{\ddagger}$ refer to deprotonation of CH by hydroxide ion; $\Delta H_p^{\ddagger}$ and $\Delta S_p^{\ddagger}$ refer to protonation of C^- by water; $\Delta H_p^{\ddagger} = \Delta H_d^{\ddagger} - \Delta H^0$; $\Delta S_p^{\ddagger} = \Delta S_d^{\ddagger} - \Delta S^0$.
[b]Data from ref. 3.

Can. J. Chem. Downloaded from www.nrcresearchpress.com by 41.223.56.140 on 09/07/12
For personal use only.

of either **5** or **6** in aqueous solution, although Pearson and Dillon (3) report $pK_a = 10.51$ (at 31.5°C) for **5** based upon a kinetic analysis of its decomposition in aqueous base. This value is reasonably consistent with our measurement of $pK_a = 10.79$ at 30°C (Table 1). The acidity of **5** in aqueous solution is somewhat less than that reported by Phillips and Ratts (5) in methanolic solution ($pK_a = 9.7$).

We have been unable to locate any previous measurements of the acidity of **6**, which we find to be 0.63 pK_a units less acidic than **5** at 25°C. This decrease in acidity upon methylation α to the carbonyl group is considerably smaller than the decreases in acidity by $\Delta pK_a = 1.6$ and 2.3 that have been reported upon α-methylation of ethyl acetoacetate (10) and acetylacetone (11), respectively. The cationic ketone **5** is only a slightly weaker acid than ethyl acetoacetate ($pK_a = 10.65$ at 25°C (10)) in aqueous solution.

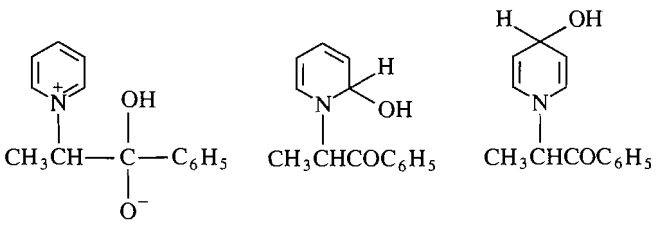
The rates of deprotonation of **5** were found to be too rapid to be measured by stopped-flow spectrophotometry. This observation requires $t_{1/2} < 3$ ms at pH 12 where $k_{obs} \simeq k_d$, and allows an estimate of $k_{OH} > 2 \times 10^4$ M^{-1} s^{-1} for the hydroxide ion catalyzed deprotonation of **5**. The pH dependence of the pseudo-first-order rate constant (k_d) for the deprotonation of **6** (Fig. 1) is consistent with Scheme 1, and the derived eq. [5]. The second-order rate constant ($k_{OH} = 1680$ M^{-1} s^{-1} at 25°C) for the hydroxide ion catalyzed deprotonation of **6** is thus at least tenfold smaller than for deprotonation of **5**. α-Methylation of acetylacetone and ethyl acetoacetate results in decreases in k_{OH} by 200-fold and 60-fold, respectively (10, 11). For **6**, k_{OH} is considerably larger than $k_{OH} = 107$ M^{-1} s^{-1} (10) for the deprotonation of ethyl acetopropionate (**8**) ($pK_a = 12.25$), which is only a slightly weaker acid than **6**.

$CH_3COCH(CH_3)CO_2C_2H_5$

8

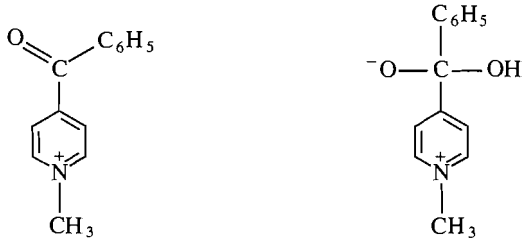
At present there is little direct experimental evidence relevant to the identity of the species Z^-, which is derived from **6** according to Scheme 1. However, in view of the structural simplicity of **6**, there are relatively few possibilities for Z^-. Since **6** has no significantly acidic protons other than the proton α to the carbonyl group, Z^- must be formed via hydroxide ion addition to **6**. The only reasonable sites for hydroxide ion addition to **6** are the carbonyl carbon atom, and the C-2 and C-4 carbon atoms of the pyridinium ring. Thus, **9**, **10**, and **11** would seem to be the only reasonable structures for Z^-.

The observed $pK_z = 12.68$ for the equilibration of Z^- with **6** is probably too low to be assigned as pK_{R^+} for formation of either of the pseudobases **10** or **11**. For the *N*-methyl pyridinium cation, pK_{R^+}, values of 18.2 and 20.5 have been estimated (12) for hydroxide ion addition to C-2 and C-4, respectively. For *N*-substituted heterocyclic cations, pK_{R^+} values are approximately correlated with σ^* for the *N*-substituent, with $\rho^* \simeq 4$ (13). Using $\sigma^* = 0.62$ for CH_3COCH_2 (14) as a reasonable approximation for $C_6H_5COCH(CH_3)$ allows the prediction of $pK_{R^+} \simeq 15.8$ and $\simeq 18.1$ for formation of **10** and **11**, respectively. These values are considerably larger than the experimental pK_z in Table 2, and seem to eliminate **10** and **11** as reasonable possibilities for the Z^- species.

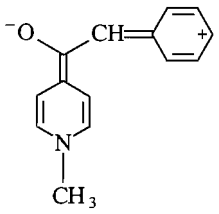


9 **10** **11**

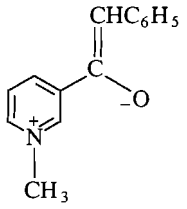
We are thus left with the geminal diol anion, **9**, as the most likely structure for Z^-. Analogous anions (e.g., **4**) were shown (1) to be consistent with the similar species Z^-, which was found necessary to describe the experimentally observed pH dependence of k_d for the deprotonation of both **1** and **2**. In an unpublished study, we have also observed the acid–base equilibration of the cationic ketone, **12**, with its geminal diol anion (**13**) ($pK_R = 12.25$). This further indicates the strong activating effect that an *N*-alkyl pyridinium cation has upon the susceptibility of such ketones to hydroxide ion addition. It appears that geminal diol anions are the kinetically controlled species that are formed upon basification of neutral aqueous solutions



12 **13**



14



15

of **1**, **2**, and **6** (and probably also **5**, although evidence for this is not currently available because of the very rapid deprotonation of this species).

For **6**, the $pK_a = 11.65$ (at 25°C) for deprotonation is sufficiently close to the kinetically determined $pK_z = 12.68$ (at 25°C) that equilibrated basic aqueous solutions of **6** will contain approximately a 10:1 ratio of enolate ion and Z^- (9).

Temperature dependence of deprotonation

The thermodynamic and activation parameters for the deprotonation of carbon acids by hydroxide ion are summarized in Table 3. Nitroethane is the only carbon acid for which we have been able to find literature data (4) for both the thermodynamic parameters and also the activation parameters for deprotonation by hydroxide ion. Since Pearson's study (4) for nitroethane was at only two temperatures (0°C and 5.2°C), we felt it appropriate to reinvestigate this species in the current study. In fact our data for $\Delta H_d^{\ddagger}$ and $\Delta S_d^{\ddagger}$ are quite close to the earlier results of Pearson (see Table 3), although Pearson's values of $\Delta H^0 = -12.2\,\text{kcal mol}^{-1}$ and $\Delta S^0 = -18.3\,\text{eu}$ for this reaction are quite different from more recent values (15).

The deprotonation of each of the carbon acids in Table 3 results in very extensive delocalization of negative charge. One would expect that there would be some rather dramatic solvent reorganizations upon the formation of the conjugate bases of these carbon acids. The magnitudes of ΔH^0 and ΔS^0, in particular, will be significantly influenced by such solvation changes, and it is difficult to comment upon the relative magnitudes of these parameters in any detail. However, of particular significance in this regard are the differences in ΔS^0 for **5** and **6**. Methylation of the acidic methylene group in **5** (to give **6**) would be expected to have a significant influence upon the solvation of the cationic charge of these carbon acids, and also upon solvation of the ylidic systems in the conjugate base species. The smaller ΔH^0 and more negative ΔS^0 for **6** than for **5** are in the same direction as the variation of these parameters upon successive α-methylation of nitromethane (15). Similar variations in ΔH^0 and ΔS^0 for deprotonation are also observed (16) upon successive *N*-methylations of ammonium ions.

It should also be noted that the similarity in the ΔS^0 parameters for the isomers **1** and **2** may be fortuitous, since two different factors have been proposed (1) to have an influence upon the stabilization of the conjugate bases of these two species. Resonance stabilization of the conjugate base of **1** via **14** is not expected to be significant for the conjugate base of **2**. On the other hand, the electrostatic interaction in **15** should be of little significance in the conjugate base of **1**.

For the deprotonation of each of **1**, **2**, **6**, and nitroethane by hydroxide ion, $\Delta S_d^{\ddagger}$ is more negative than ΔS^0. Interestingly, this difference, which represents $\Delta S_p^{\ddagger}$ for the protonation of the conjugate base by a water molecule, is approximately constant ($\Delta S_p^{\ddagger} = -4.9 \pm 0.5\,\text{cal deg}^{-1}\,\text{mol}^{-1}$), while $\Delta H_p^{\ddagger}$ is quite variable. While it is unreasonable to attempt to make any generalization on the basis of four cases, we note that these data do include acids and their conjugate bases having quite significant structural differences, and it will be interesting to see whether such a relationship persists as further data become available for other carbon acids. The much larger negative value for $\Delta S_d^{\ddagger}$ than for $\Delta S_p^{\ddagger}$ suggests that the solvation of the rate-determining transition state species is similar to the solvation of the conjugate base species from each of these carbon acids.

Acknowledgement

We appreciate the continued support of this work by the Natural Sciences and Engineering Research Council of Canada.

1. J. W. Bunting and D. Stefanidis. J. Am. Chem. Soc. **110**, 4008 (1988).
2. F. Krohnke. Chem. Ber. **68**, 1177 (1935).
3. R. G. Pearson and R. L. Dillon. J. Am. Chem. Soc. **70**, 1933 (1948).
4. R. G. Pearson. J. Am. Chem. Soc. **70**, 204 (1948).
5. W. G. Phillips and K. W. Ratts. J. Org. Chem. **35**, 3144 (1970).
6. A. Albert and E. P. Serjeant. The determination of ionization constants. 3rd ed. Chapman and Hall, London. 1984.
7. S. H. Babcock and R. C. Fuson. J. Am. Chem. Soc. **55**, 2946 (1933).
8. F. Krohnke. Chem. Ber. **66**, 604 (1933).
9. F. Krohnke and W. Heffe. Chem. Ber. **70**, 864 (1937).
10. R. Brouillard and J. E. Dubois. J. Org. Chem. **39**, 1137 (1974).
11. P. Alcais and R. Brouillard. J. Chem. Soc. Perkin Trans. 2, 1214 (1972).
12. J. W. Bunting. Tetrahedron, **43**, 4277 (1987).
13. J. W. Bunting and W. G. Meathrel. Can. J. Chem. **52**, 962 (1974).
14. D. D. Perrin, B. Dempsey, and E. P. Serjeant. pK_a prediction for organic acids and bases. Chapman and Hall, London. 1981. p. 116.
15. T. Matsui and L. G. Hepler. Can. J. Chem. **51**, 1941 (1973); **51**, 3789 (1973).
16. L. L. Schaleger and F. A. Long. Adv. Phys. Org. Chem. **1**, 1 (1963).
17. J. F. Coetzee and C. D. Ritchie. Solute solvent interactions. M. Dekker, New York. 1969. p. 5.

Can. J. Chem. Downloaded from www.nrcresearchpress.com by 41.223.56.140 on 09/07/12
For personal use only.

Synthesis and spectroscopic studies of some substituted 3-benzoylpyrroles and their tricarbonylchromium complexes

NIALL J. GOGAN,[1] ROBERT MCDONALD, HUGH J. ANDERSON, AND CHARLES E. LOADER
Department of Chemistry, Memorial University of Newfoundland, St. John's Nfld., Canada A1B 3X7

Received June 9, 1988

NIALL J. GOGAN, ROBERT MCDONALD, HUGH J. ANDERSON, and CHARLES E. LOADER. Can. J. Chem. **67**, 433 (1989).

3-Benzoylpyrroles with a substituent on the pyrrole ring have been synthesized. Both the iodination and chlorination gave only the 2,4 derivatives while isopropylation gave mixtures of the 2,4 and 2,3 compounds. No 3,4 compounds were obtained. Both steric and electronic effects seem to determine the substitution pattern. The $Cr(CO)_3$ complexes (Cr on the benzene ring) were prepared and these complexes, together with the uncomplexed pyrroles, were studied by IR, ^{1}H-NMR, and ESR of the radical anions from the *N*-methylpyrrole derivatives. For the 2,4 compounds, the substituent on the pyrrole ring has relatively little effect on the spectral parameters of the benzene ring indicating relatively little electron delocalization between the two rings. 3-Benzoyl-2-isopropylpyrrole, however, gives an ESR spectrum very different from the other compounds.

Key words: benzoylpyrroles, tricarbonylchromium, ESR, chlorination, isopropylpyrroles.

NIALL J. GOGAN, ROBERT MCDONALD, HUGH J. ANDERSON et CHARLES E. LOADER. Can. J. Chem. **67**, 433 (1989).

On a synthétisé des benzoyl-3 pyrroles portant un substituant sur le noyau pyrrole. Leur iodation ainsi que leur chloration ne conduisent qu'aux dérivés 2,4 alors que la réaction d'isopropylation conduit à un mélange des dérivés 2,4 ainsi que 2,3. On n'a pas obtenu de composés substitués en 3,4. Il semble que des effets tant stériques qu'électroniques soient responsables des patrons de substitution. On a préparé des complexes du $Cr(CO)_3$ (le Cr étant porté par le noyau benzénique) et on a déterminé les spectres ir ainsi que les spectres rmn du ^{1}H de ces complexes ainsi que des pyrroles non-substitués; de plus, on a déterminé les spectres rpe des radicaux anions obtenus à partir des dérivés *N*-méthylpyrroles. Dans les cas des composés 2,4, le substituant présent sur le noyau pyrrole n'a pratiquement pas d'influence sur les paramètres spectraux du noyau benzénique; ces données suggèrent qu'il y a peu de délocalisation électronique entre les deux noyaux. Toutefois, le benzoyl-3 isopropyl-2 pyrrole présente un spectre rpe qui est très différent de celui des autres composés.

Mots clés : benzoyl pyrroles, chrome tricarbonylé, RPE, chloration, isopropyl pyrroles.

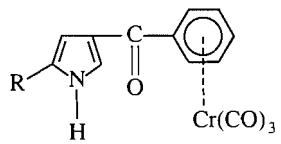
[Traduit par la revue]

Introduction

In a previous paper (1) we reported how the acylation of 1-(phenylsulfonyl)pyrrole led to the synthesis of a series of 3-aroylpyrroles. Subsequently these products were complexed on the benzenoid ring with a $Cr(CO)_3$ group and the resulting complexes and the parent pyrroles were studied by various spectroscopic techniques and molecular-orbital theory (2). These studies, together with ESR studies on the corresponding anions produced from the *N*-methyl derivatives (3), were very helpful in elucidating the electronic structures of these molecules. None of these compounds had a substituent on any of the pyrrole ring carbons.

Variation of substituents on the benzene ring or complexation by a $Cr(CO)_3$ group (on the benzene ring) resulted in no significant changes in the ^{1}H-NMR resonances of the pyrrole protons (2). In addition, the ESR spectra showed no hyperfine splittings (hfs) from the pyrrole ring. These results demonstrated that changes occurring on the benzene ring caused no measurable effects on the pyrrole ring. The opposite, however, could not be proven because the studies did not involve any changes on the pyrrole ring. A previously reported study of benzoylcyclopentadienyl manganese tricarbonyl complexes (4) showed that substituents on the cyclopentadienyl ring caused changes in the benzene ring proton hfs even though no hfs were observed for the cyclopentadienyl protons. The present study was carried out to see if changes on the pyrrole ring cause significant changes to various spectroscopic parameters of the benzene ring either in the complexes or in the parent pyrroles.

In general 2,4 substitution is preferred in each case so that effects can be directly compared. This structure is shown in



R = H, $CH(CH_3)_2$, Cl, I

FIG. 1. 2,4-Substitution of benzoylpyrroles.

Fig. 1. The isopropylation also yielded 3-benzoyl-2-isopropylpyrrole as a minor product which was useful in examining some steric effects. Friedel–Crafts isopropylation of 3-acetylpyrrole was explored in one of our laboratories (5). Hodge and Rickards (6) studied the chlorination of methylpyrrole-2-carboxylate and Farnier and Fournari (7) iodinated pyrrole-2-carboxaldehyde, These three studies were very helpful in enabling us to devise synthetic routes to the desired compounds.

This paper reports the synthesis of the 3-benzoylpyrroles and their $Cr(CO)_3$ complexes, IR and ^{1}H-NMR studies on these compounds, and ESR studies of the radical anions of the *N*-methyl derivatives.

Experimental

Melting points (°C) are uncorrected. Elemental analyses were performed by Canadian Microanalytical Service, Vancouver, B.C. The IR spectra were recorded in $CHCl_3$ solution on a Perkin-Elmer 283 spectrophotometer. ^{1}H-NMR spectra were determined using a Bruker WP-80 instrument and are expressed in ppm (δ values) relative to tetramethylsilane as internal reference in $CDCl_3$. Electron spin resonance spectra were recorded on a JEOLCO ME-3X spectrometer at room temperature (23°C).

The term "hexanes" refers to a mixture of isomers bp 65.8–69.0°C. 3-Benzoylpyrrole was prepared as described previously (8). Tricar-

[1]Author to whom correspondence should be addressed.

Can. J. Chem. Downloaded from www.nrcresearchpress.com by 122.72.124.2 on 09/07/12
For personal use only.

Can. J. Chem. Downloaded from www.nrcresearchpress.com by 122.72.124.2 on 09/07/12
For personal use only.

bonylchromium complexes were prepared from the parent pyrrole and $Cr(CO)_6$ in refluxing di-*n*-butyl ether as previously described (9). The *N*-methyl derivatives of the ligands and complexes were prepared by reaction with dimethyl sulfate using phase transfer catalysis as outlined previously (10). The radical anions were prepared from the *N*-methyl derivatives using potassium in 1,2-dimethoxyethane (DME) as described in an earlier paper (4).

4-Benzoyl-2-iodopyrrole

A mixture consisting of 3-benzoylpyrrole (1.5 g, 8.8 mmol), iodic acid (0.31 g, 1.8 mmol), iodine (0.89 g, 3.5 mmol), water (1.9 mL), glacial acetic acid (4.4 mL), concentrated sulfuric acid (six drops), and carbon tetrachloride (63 mL) was stirred for 24 h. The crude 4-benzoyl-2-iodopyrrole which had precipitated was then redissolved using a minimum of dichloromethane, and the aqueous and organic layers separated. The organic layer was washed with saturated aqueous sodium thiosulfate (two 50 mL portions), aqueous sodium bicarbonate (50 mL of the 5% solution), and saturated aqueous sodium chloride (50 mL). After drying the organic solution over anhydrous magnesium sulfate and evaporating the solvent, the residue was purified by flash chromatography, using 1:5 ethyl acetate/petroleum (30–60°C) as the eluting solvent. The product thus obtained was recrystallized from dichloromethane/petroleum (30–60°C), yielding 0.75 g (29%) of fibrous, pale yellow crystals of 4-benzoyl-2-iodopyrrole; mp 150–151°C (dec.). *Exact mass* calcd. for $C_{11}H_8NOI$: 296.96524; found: 296.9667, deviation 1.5 mmu.

4-Benzoyl-2-chloropyrrole

A solution of 3-benzoylpyrrole (4.00 g, 23.4 mmol) in ethyl ether (150 mL) was chilled to 0°C in an ice bath, to which was added, with stirring, sulfuryl chloride (3.47 g, 25.7 mmol) in ethyl ether (75 mL) over a period of 30 min. The solution was then stirred at room temperature for 20 h, after which the solvent was evaporated. The residue was purified by flash chromatography using 1:5 ethyl acetate:hexanes as the eluting solvent. Recrystallization from ethyl acetate/hexanes gave 3.23 g (67.2%) of colourless crystals of 4-benzoyl-2-chloropyrrole; mp 169–170°C (dec.). *Exact mass* calcd. for $C_{11}H_8NOCl$: 205.02939; found: 205.0306, deviation 1.2 mmu.

4-Benzoyl-2-isopropylpyrrole and 3-benzoyl-2-isopropylpyrrole[2]

3-Benzoylpyrrole (1.56 g, 9.11 mmol) was dissolved in dichloromethane (30 mL), to which was added rapidly anhydrous aluminum chloride (Fluka) (2.55 g, 19.1 mmol) and, dropwise, isopropyl chloride (0.69 g, 8.8 mmol). This mixture was stirred with heating for 2½ h, then poured onto ice and water (30 g). The purple organic layer was drawn off and the aqueous solution extracted with ethyl ether (three 15 mL portions). The combined organic layers were dried over anhydrous magnesium sulphate and the solvent evaporated. The gummy light-violet residue was shown by thin-layer chromatography to contain two distinct products which were separated using flash chromatography with 1:7 acetone:hexanes as the eluting solvent. The fractions containing the second component were evaporated and the residue recrystallized from methanol to give 1.38 g (73.5%) of colourless crystals of 4-benzoyl-2-isopropylpyrrole; mp 125–127°C. *Anal.* calcd. for $C_{14}H_{15}NO$: C 78.84, H 7.09, N 6.57; found: C 78.56, H 7.06, N 6.53. Recovery of the first mixture component in the same manner gave 0.23 g (12.3%) of colourless crystals of 3-benzoyl-2-isopropylpyrrole; mp 172–173°C. *Anal.* calcd. for $C_{14}H_{15}NO$: C 78.84, H 7.09, N 6.57; found: C 78.87, H 7.08, N 6.57.

A subsequent isopropylation of 3-benzoylpyrrole was attempted to obtain a greater yield of the minor product. The reaction conditions described above were reproduced exactly except that the reaction time was reduced to 20 min. After extraction, purification and recrystallization, yield was 1.22 g (65.0%) 4-benzoyl-2-isopropylpyrrole and 0.60 g (32.0%) 3-benzoyl-2-isopropylpyrrole.

[2]This compound would be named 4-benzoyl-5-isopropylpyrrole relative to the other compounds described in this paper.

TABLE 1. Infrared spectra (cm^{-1}, $CHCl_3$) of $RC_4H_3NCOC_6H_5Cr(CO)_3$

Substituents	$\nu_{CO}[Cr(CO)_3]$ A_1	E	ν_{CO}(ketone)	ν_{NH}
3-Benzoyl[a]	1986	1914	1636(1635)[b]	3470
4-Benzoyl-2-iodo	1985	1919	1635(1642)	3475
4-Benzoyl-2-chloro	1987	1920	1639(1639)	3460
4-Benzoyl-2-isopropyl	1982	1915	1630(1631)	3463
3-Benzoyl-2-isopropyl	1986	1919	1633(1633)	3475

[a]From ref. 8.
[b]Ligand values in parentheses.

Results and discussion

Synthesis

The synthetic routes to the substituted aroylpyrrole ligands were based on earlier work on other substituted pyrroles. In the case of the 2-iodo- and 2-chloro-4-benzoylpyrroles, the previous halogenations (6, 7) had been done on 2-substituted compounds to produce the 4-halo- compounds, thus the applications here depended upon steric and electronic factors to yield the desired products. It was hoped that the size of the benzoyl group of 3-benzoylpyrrole would prevent substitution onto the 2- or 4-positions of the pyrrole ring. The fact that electrophilic substitution at the 2- or 5-positions of the pyrrole ring is favoured seems to additionally favour the conversion of 3-benzoylpyrrole into 4-benzoyl-2-halopyrrole by the appropriate reaction, and this seems to have been borne out by the recovery of the products of only this substitution pattern.

The isopropylation reaction was based on the Friedel–Crafts alkylation for 3-acetylpyrrole (5), which itself yielded 4-acetyl-2-isopropylpyrrole almost exclusively as the product. Substitution should be determined by both electronic and steric factors with the latter being especially important because the *i*-propyl group is bulky. Thus 4-benzoyl-2-isopropylpyrrole is the predominant product as expected. It is surprising, however, that 3-benzoyl-2-isopropylpyrrole is a substantial component of the isolated product; here it is thought that attack of the alkyl chloride – aluminum chloride complex occurs at both the electronically-favoured 2- and 5-positions of the pyrrole ring, and that the isopropyl groups tend to migrate to the sterically favoured 2-position (where the 4-position is benzoylated). This would account for the greater yield of the minor product after a shorter reaction time. Even though there is a mixture of products, the yield of the major isomer was better for both trials of this reaction than for the isopropylation of 3-acetylpyrrole, and in both trials over 80% of the initial 3-benzoylpyrrole was isopropylated.

Infrared and nuclear magnetic resonance studies

Substituents on the pyrrole ring have a very small effect on the ν_{CO} of the $Cr(CO)_3$ group (Table 1) in keeping with results obtained for benzophenone $Cr(CO)_3$ and benzoylcyclopentadienyl $Cr(CO)_3$ complexes (11). Even though the effect is small, the lowest value for the more precise *A* mode is observed for the 2-isopropyl derivatives (1982 cm^{-1}) while the highest value observed is for the 2-chloro derivative (1987 cm^{-1}). This follows the same trend as observed for substituents on the benzene ring, i.e. the value of ν_{CO} is higher the more electron-withdrawing is the substituent. This is consistent with some π-electron delocalization between the two rings because this effect is dependent on changes in π-donation to the CO groups

TABLE 2. ^{1}H-NMR chemical shifts (δ, ppm) of $RC_4H_3NCOC_6H_5Cr(CO)_3$[a]

Substituents	Arene ring			Pyrrole ring			Isopropyl		
	o	*m*	*p*	(N)H	H^3	H^2	H^5	(C)H	$(C)H_3$
3-Benzoyl	6.10	5.36	5.56	8.67	6.81	6.81	7.59		
	(−1.75)	(−2.15)	(−1.83)	(0.00)	(0)	(0)	(−0.03)		
4-Benzoyl-2-iodo	6.13	5.37	5.60	8.75	6.84	—	7.54	—	—
	(−1.70)	(−2.15)	(−1.84)	(0.16)	(0.06)	—	(0.18)		
4-Benzoyl-2-chloro	6.08	5.34	5.60	8.57	6.61	—	7.48	—	—
	(−1.76)	(−2.20)	(−1.86)	(−0.03)	(0.01)	—	(0.26)		
4-Benzoyl-2-isopropyl	6.06	5.30	5.53	8.54	6.43	—	7.44	2.91	1.28
	(−1.76)	(−2.19)	(−1.88)	(−0.37)	(−0.04)	—	(0.26)	(−0.01)	(0.01)
3-Benzoyl-2-isopropyl	6.05	5.30	5.54	8.36	6.65	7.47	—	3.43	1.20
	(−1.74)	(−2.19)	(−1.87)	(−0.11)	(−0.01)	(0.40)	—	(−0.04)	(0.06)

[a]Numbers in parentheses are Δ values where Δ = δ (complex) − δ (ligand).

TABLE 3. Electron spin resonance data (Gauss) of *N*-methyl 2-substituted 4-benzoylpyrroles[a]

Substituent	A_p	A_o	(1/2)SW[b]	SW(ligand)/ SW(complex)
H	8.3	3.3	7.4	2.05
	(3.2)	(1.7)	(3.6)	—
I	8.0	3.5	7.5	—
Cl	8.0	3.5	7.5	2.20
	(3.6)	(1.7)	(3.4)	—
Isopropyl	8.0	3.3	7.3	2.02
	(3.5)	(1.7)	(3.6)	—

[a]Numbers in parentheses are the values for the $Cr(CO)_3$ complexes.
[b]SW = spectrum width.

of the $Cr(CO)_3$ moiety. Substituents change ν_{CO} (ketone) in the same direction for both ligand and complex suggesting that the orientation of the ketonic CO group with respect to the benzene ring is not significantly affected by complexation. Nuclear magnetic resonance resonances of the benzene protons (Table 2) show very little change with substituents on the pyrrole ring.

Complexation by a $Cr(CO)_3$ group has a small effect on ν_{CO} (ketone) but leaves ν_{N-H} unchanged with the exception of a 3 cm^{-1} increase for the 5-isopropyl compound. The benzene ^{1}H-NMR resonances show the usual upfield shift and the magnitude of this shift has little variation with substituent. The effect on the pyrrole resonances is small and does not follow a trend.

Electron spin resonance studies

The *N*-methyl derivatives were used in these studies because of the lability of the hydrogen attached to nitrogen as discussed in a previous paper (3). Solutions of the radical anions (5–8 × 10^{-3} *M* in DME) of the pyrroles are dark blue or purple whereas those of the complexes are yellow or orange. The ligands and complexes of the 2-substituted derivatives all show six lines consisting of a doublet split into triplets. This is the same pattern observed for the unsubstituted compounds (3) and the doublet is assigned to the *para* proton of the benzene ring and the triplet to the two equivalent *ortho* protons. No other splittings are observed leading to the conclusion that any unpaired electron (upe) density on the pyrrole ring is not great enough to be observed. The A_p in each case (Table 3) is 8.0 G for the uncomplexed substituted pyrroles compared to 8.3 G for the unsubstituted compound. The A_o values are greater for the I and Cl compounds than for the isopropyl which shows the same value as the unsubstituted compound. In the complexes, A_p is greater for the substituted compounds and A_o is the same for all three cases. The iodo complex did not give an ESR spectrum.

The ratio of spectrum width (ligand/complex) is given in Table 3. The greatest reduction of spectrum width on complexation occurs in the 2-chloro compound indicating that the electron-withdrawing effect of the chlorine is transmitted to the benzene ring.

It is concluded from these results that there is some electron delocalization between the two rings but it is not great enough to result in the observance of hfs from the pyrrole ring. This is in agreement with the SCCC-MO results obtained for 3-benzoylpyrrole and its $Cr(CO)_3$ complex (3) which indicated a small amount of upe on the pyrrole ring. It contrasts with the results obtained for substituted benzophenones and their complexes (13, 14) which showed significant and observable upe on both rings.

The ESR spectra of 3-benzoyl-2-isopropylpyrrole and its $Cr(CO)_3$ complexes were quite different from those of the 2-substituted compounds. For the uncomplexed compound, the spectral pattern is a quartet of quartets which would be expected from two sets of three equivalent protons. It is most likely that the hyperfine coupling constants of the *para* and *ortho* protons are equal, making up one equivalent set similar to what is observed for 2-methylbenzophenone (12). The other set may arise from three protons of one of the isopropyl methyl groups. Delocalization of upe density onto the methyl group could occur via direct interaction with the carbonyl oxygen. The values observed are $A_p = A_o = 4.5$ G and $A_{CH_3} = 1.1$ G. The spectrum of the complex is narrower and the lines are not sufficiently well resolved to give an unambiguous assignment.

Acknowledgements

We are grateful to the Natural Sciences and Engineering Research Council of Canada and to Memorial University for financial support. The assistance of Mrs. Sheila I. De Silva

Can. J. Chem. Downloaded from www.nrcresearchpress.com by 122.72.124.2 on 09/07/12
For personal use only.

with ESR spectra and the advice of Dr. Pardeep K. Sayal and Mr. L. Cameron Hopkins are gratefully acknowledged.

1. H. J. ANDERSON, C. E. LOADER, R-X. XU, N. LÊ, N. J. GOGAN, R. MCDONALD, and L. G. EDWARDS. Can. J. Chem. **63**, 896 (1985).
2. N. J. GOGAN, I. S. JAYASINGHE, and P. K. SAYAL. J. Organomet. Chem. **317**, 55 (1986).
3. N. J. GOGAN, I. S. JAYASINGHE, and P. K. SAYAL. J. Organomet. Chem. **336**, 137 (1987).
4. N. J. GOGAN, C. K. CHU, and G. W. GRAY. J. Organomet. Chem. **51**, 323 (1973).
5. H. J. ANDERSON and C. W. HUANG. Can. J. Chem. **45**, 897 (1967).
6. P. HODGE and R. W. RICKARDS. J. Chem. Soc. 459 (1965).
7. M. FARNIER and P. FOURNARI. Bull. Soc. Chim. Fr. 351 (1973).
8. R-X XU, H. J. ANDERSON, N. J. GOGAN, C. E. LOADER, and R. MCDONALD. Tetrahedron Lett. **22**, 4899 (1981).
9. N. J. GOGAN, J. DOULL, and J. EVANS. Can. J. Chem. **63**, 3147 (1985).
10. N. C. WANG, K. E. TEO, and H. J. ANDERSON. Can. J. Chem. **55**, 4112 (1977).
11. N. J. GOGAN, I. L. DICKINSON, and J. R. PATTERSON. J. Organomet. Chem. **214**, 65 (1981); N. J. GOGAN and C. K. CHU. J. Organomet. Chem. **132**, 103 (1977).
12. K. MARUYAMA, R. TANKIKOGA, and R. GATO. Bull. Chem. Soc. Jpn. **36**, 1141 (1963).
13. N. J. GOGAN, I. L. DICKINSON, J. DOULL, and J. R. PATTERSON. J. Organomet. Chem. **212**, 71 (1981).
14. A. CECCON, C. CORVAJA, G. GIACOMETTI, and A. VENZO. J. Chem. Soc. Perkin II, 283 (1978).

Can. J. Chem. Downloaded from www.nrcresearchpress.com by 122.72.124.2 on 09/07/12
For personal use only.

Pressure-dependent study of ultrasonic velocity of benzene + nitrobenzene system at 293.15, 303.15, and 313.15 K

J. D. PANDEY AND R. D. RAI
Department of Chemistry, University of Allahabad, Allahabad-211002, India

AND

R. K. SHUKLA
Department of Chemistry, V.S.S.D. Degree College, Nawabganj, Kanpur, India

Received May 12, 1988

J. D. PANDEY, R. D. RAI, and R. K. SHUKLA. Can. J. Chem. **67**, 437 (1989).

Various statistical and empirical theories of ultrasonic velocity have been applied to a binary liquid mixture (benzene + nitrobenzene) at elevated pressures and their validity have been tested. A pressure-dependent study of ultrasonic velocities has been made at three different temperatures (293.15, 303.15, and 313.15 K). The agreement between the theory and experiment is found to be satisfactory.

Key words: ultrasonic velocity, benzene + nitrobenzene, pressure dependent, theoretical evaluation, binary mixtures at elevated pressures.

J. D. PANDEY, R. D. RAI et R. K. SHUKLA. Can. J. Chem. **67**, 437 (1989).

On a appliqué diverses théories statistiques et empiriques de la vitesse ultrasonique à un mélange liquide binaire (benzène + nitrobenzène), à haute température, et on a évalué leur validité. Opérant à trois températures différentes (293,15, 303,15 et 313,15 K), on a réalisé une étude des vitesses ultrasoniques en fonction de la pression. On a trouvé que l'accord entre la théorie et l'expérience est satisfaisante.

Mots clés : vitesse ultrasonique, benzène + nitrobenzène, dépendant de la pression, évaluation, théorique, mélanges binaires à haute pression.

[Traduit par la revue]

Introduction

Successful attempts have been made in recent years (1–7) on the theoretical evaluation of ultrasonic velocity and its correlation with other thermodynamic properties in binary liquid mixtures using statistical and semi-empirical theories. Such studies have been limited to binary liquid systems at atmospheric pressure. Due to lack of experimental data on ultrasonic velocity at elevated pressure, such studies could not be extended at elevated pressures. For the first time, Takagi *et al.* (8–14) have carried out experimental measurements of ultrasonic velocity and related thermodynamic properties of a few binary liquid mixtures at elevated pressures over a wide range of temperatures (293.15, 303.15, and 313.15 K). In the present paper, we report results of theoretical calculations of ultrasonic velocity at elevated pressures using the above mentioned theories in mixture of benzene + nitrobenzene. Ultrasonic investigations of this system have been reported by Takagi and Teranishi (8). A comparative study has also been presented and correlated.

Theoretical

Flory–Patterson theory (15–17) in conjunction with the Auerbach relation (18) yields the following expressions for the ultrasonic velocity (C) in a binary liquid mixture.

$$[1]\quad C = \left(\frac{kP^{*2}T^{*}}{6.3 \times 10^{-4}\rho}\right)^{2/9} M\tilde{V}^{-5/3} - \left(\frac{\tilde{V}^{1/3}-1}{\tilde{V}^{2}}\right)\ln\left(\frac{V^{1/3}-0.5}{V^{1/3}-1.0}\right)^{2/3}$$

where k, P^*, T^*, ρ, $\tilde{V}$, and M are the Boltzman constant, characteristic pressure, characteristic temperature, mass density and reduced volume of the mixture, and fraction of nearest neighbours that a molecule loses moving from the bulk of the liquid to the surface. Here the value of M is 0.30 which is taken throughout the calculations. The characteristic and reduced parameters at elevated pressures have been evaluated by the usual procedure (15).

Van Dael (19), based on assumptions made by Richardson (20) and Blandamer and Waddington (21) obtained the expression for the ultrasonic velocity (C) in a binary liquid mixture which may be expressed as

$$[2]\quad \left(\frac{1}{X_1M_1 + X_2M_2}\right)\frac{1}{C^2} = \left[\frac{X_1}{M_1C_1^2} + \frac{X_2}{M_2C_2^2}\right]$$

where X_1, X_2, M_1, M_2, and C_1, C_2 are the mole fractions, molecular weight, and ultrasonic velocities of benzene and nitrobenzene, respectively.

Assuming the linearity of molecular sound velocity and additivity of molar volumes, Nomoto (22) suggested an empirical formula for the sound velocity in a binary liquid mixture.

$$[3]\quad C = \left(\frac{R}{V}\right)^3 = \left(\frac{X_1R_1 + X_2R_2}{X_1V_1 + X_2V_2}\right)^3$$

where R is the molar sound velocity and V is the molar volume of the mixture.

Schaaffs (23, 24) and Nutsch-Kuhnkies (25) developed an expression for evaluating sound velocity in binary liquid mixture

$$[4]\quad C = C_\infty(X_1S_1 + X_2S_2)\left(\frac{X_1B_1 + X_2B_2}{V}\right)$$

where $C_\infty = 1600\ \mathrm{ms}^{-1}$, S_1, S_2 and B_1, B_2 are the collision factors and actual volumes of the molecule per mole (benzene + nitrobenzene), respectively.

Printed in Canada / Imprimé au Canada

Can. J. Chem. Downloaded from www.nrcresearchpress.com by 41.223.56.140 on 09/07/12
For personal use only.

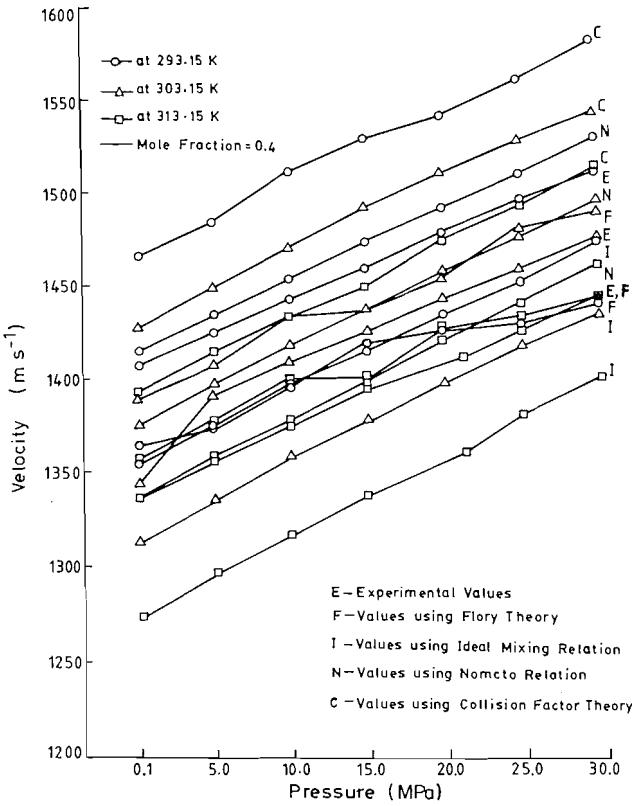


FIG. 1. Comparison between theoretical and experimental values of ultrasonic velocity of binary liquid mixture (benzene + nitrobenzene) at 293.15, 303.15, and 313.15 K at elevated pressure for mole fraction = 0.4 (benzene).

Results and discussion

Theoretical values of ultrasonic velocity computed from all the theories mentioned have been plotted against pressure at three different temperatures along with the experimental ultrasonic velocities at 0.4 mole fraction of benzene (Fig. 1). Figure 2 represents the variation of ultrasonic velocity with composition of benzene at three different temperatures (at 30 MPa). Both figures show linear or near linear behaviour for all the relations. Lack of smoothness in the figures are due to the interactions between the molecules at that instant. Interactions are the result of active collisions between the molecules. As temperature increases, collision between polar and non-polar molecules become more frequent hence increases the energy of activation. Further, high pressure adversely affects the temperature effect and figures seem to be more comprehensive. Non-linearity in Figs. 1 and 2 for the Flory approximation is also due to the computed values of thermal expansion coefficient (α) at elevated pressures using experimental data (8).

Table 1 contains the parameters for the pure component liquids at elevated pressures and temperatures where as Table 2 records the percentage deviations obtained from various theories. Percentage error of the measurement is not more than 0.3%. A close observation of Table 2 evinces that theoretical values of ultrasonic velocity agree satisfactorily with the experimental values. The average percentage deviations for Flory–Patterson theory, ideal mixing relation, Nomoto relation, and collision factor theory are 2.78, 2.60, 0.66, and 3.70 at 293.15 K, 1.75, 2.73, 0.72, and 3.83 at 303.15 K, and 1.66, 3.11, 0.48, and 3.74 at 313.15 K, respectively.

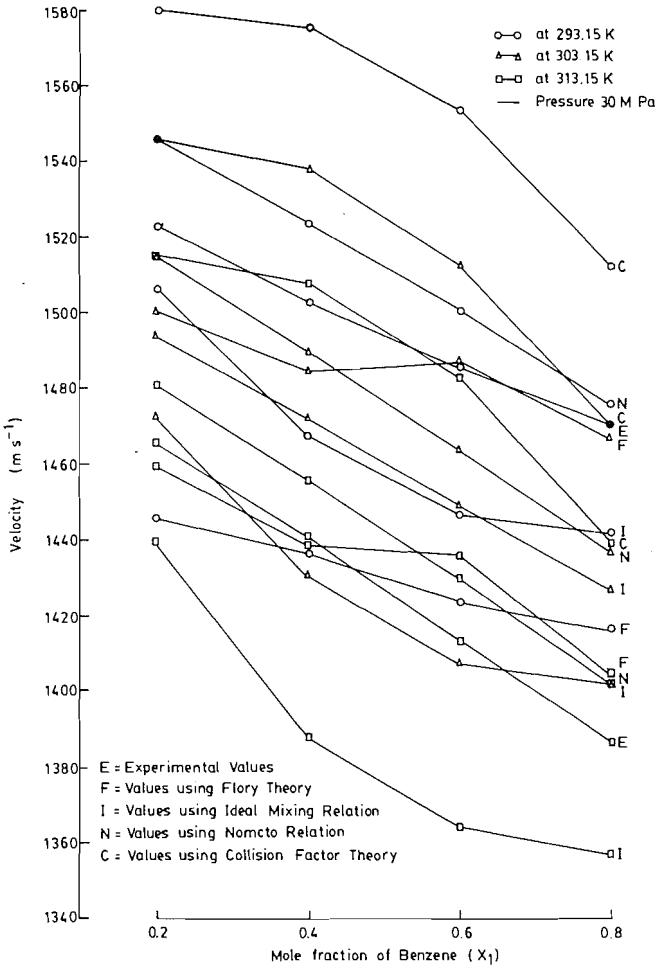


FIG. 2. Variation of ultrasonic velocities of binary liquid mixture (benzene + nitrobenzene) with the compositions of benzene at 293.15, 303.15, and 313.15 K at 30 MPa pressure.

In the collision factor theory, molecules are treated as real non-elastic substances which cause larger deviations. Benzene and nitrobenzene and organic volatile liquids which have weak intermolecular force of attraction. Hence, their collisions are likely to be elastic in nature.

It appears to be remarkable that it is the concentration of the nitrobenzene which causes interaction to an appreciable extent in binary liquid mixture. Nitrobenzene is supposed to be relatively complex molecule and its non-ideality in all probability may be due to the C—N as well as due to the polar nature of the group itself. As far as the contribution of the nitrogroup is concerned, it rotates freely along the C—N axis which is likely to activate the attached benzene ring. Larger deviations in the system may also result due to polar–nonpolar interactions, nonpolar–central forces and of structural origin. Consequently, in such system interactions are minimum. The intermolecular distance between the two parallel benzene rings may get reduced further due to the interaction with electron deficient rings of nitrobenzene which may be sandwiched between two aromatic benzene rings.

In conclusion, it appears from the preceding discussion that the Nomoto relation provides best result followed by the Flory theory, the theory of ideal mixing, and the collision factor theory for the benzene + nitrobenzene system at elevated pressures and temperatures.

Can. J. Chem. Downloaded from www.nrcresearchpress.com by 41.223.56.140 on 09/07/12
For personal use only.

TABLE 1. Parameters of the pure component liquids

Pressure (P) (MPa)	$\tilde{V}$ ($cm^3\ mol^{-1}$)	V^* ($cm^3\ mol^{-1}$)	$P^* \times 1.0^{-9}$ (dyn cm^{-2})	T^* (K)	Velocity (C) ($m\ s^{-1}$)	Density (ρ) ($g\ cm^{-3}$)
			293.15 K			
Benzene						
0.1	1.2895	68.9011	6.63	3607.66	1321.7	0.8792
5.0	1.2819	69.0038	6.67	3690.01	1345.9	0.8831
10.0	1.2743	69.1186	6.40	3776.97	1369.9	0.8869
15.0	1.2711	68.9957	6.65	3814.70	1391.3	0.8907
20.0	1.2635	69.1305	6.75	3908.48	1411.0	0.8943
25.0	1.2559	69.2838	6.46	4007.60	1429.4	0.8977
30.0	1.2529	69.1912	6.36	4049.39	1452.1	0.9011
Nitrobenzene						
0.1	1.1958	88.5724	6.57	5065.77	1471.6	1.2031
5.0	1.1935	85.5286	6.60	5118.44	1486.7	1.2060
10.0	1.1912	85.4854	6.73	5172.26	1502.4	1.2089
15.0	1.1890	85.4488	6.88	5226.99	1518.4	1.2117
20.0	1.1849	85.5534	6.69	5330.18	1534.6	1.2144
25.0	1.1827	85.5244	6.58	5388.26	1551.1	1.2171
30.0	1.1824	85.3609	6.57	5397.72	1567.8	1.2198
			303.15 K			
Benzene						
0.1	1.3002	69.1734	6.48	3617.69	1271.1	0.8685
5.0	1.2923	69.2618	6.50	3700.05	1300.4	0.8727
10.0	1.2844	69.3625	6.55	3787.01	1327.4	0.8768
15.0	1.2765	69.4824	6.27	3878.69	1347.6	0.8807
20.0	1.2732	69.3551	6.51	3918.54	1370.3	0.8846
25.0	1.2677	69.3685	6.18	3987.82	1390.1	0.8883
30.0	1.2598	69.5262	6.58	4090.74	1408.6	0.8918
Nitrobenzene						
0.1	1.2489	82.5607	9.12	4243.86	1438.1	1.1939
5.0	1.2466	82.5056	9.19	4278.02	1453.8	1.1969
10.0	1.2443	82.4511	9.39	4312.76	1470.1	1.1999
15.0	1.2421	82.4030	9.28	4347.85	1486.7	1.2028
20.0	1.2398	82.3555	9.49	4383.57	1503.7	1.2057
25.0	1.2375	82.3143	9.72	4419.65	1520.9	1.2085
30.0	1.2335	82.2571	9.48	4485.87	1538.4	1.2112
			313.15 K			
Benzene						
0.1	1.3110	69.4583	6.35	3627.64	1231.0	0.8578
5.0	0.3028	69.5315	6.35	3710.00	1256.4	0.8623
10.0	1.2946	69.6176	6.38	3796.95	1281.2	0.8667
15.0	1.2888	69.5955	6.51	3861.69	1305.7	0.8709
20.0	1.2830	69.5896	6.48	3928.47	1331.5	0.8749
25.0	1.2748	69.7234	6.36	4027.28	1353.4	0.8788
30.0	1.2715	69.6063	6.26	4069.69	1373.9	0.8826
Nitrobenzene						
0.1	1.2326	84.4160	7.90	4632.79	1403.2	1.1822
5.0	1.2331	84.2305	8.05	4643.78	1419.1	1.1853
10.0	1.2289	84.3055	8.10	4717.89	1435.6	1.1994
15.0	1.2226	84.5207	7.78	4832.90	1452.5	1.1914
20.0	1.2221	84.3414	6.05	4841.99	1469.7	1.1944
25.0	1.2216	84.1687	8.04	4850.77	1487.2	1.1973
30.0	1.2193	84.1284	7.93	4896.68	1505.1	1.2002

Can. J. Chem. Downloaded from www.nrcresearchpress.com by 41.223.56.140 on 09/07/12
For personal use only.

Can. J. Chem. Downloaded from www.nrcresearchpress.com by 41.223.56.140 on 09/07/12
For personal use only.

TABLE 2. Values of computed percentage deviations of ultrasonic velocity of binary liquid mixture (benzene + nitrobenzene) at elevated pressure at different temperatures

		293.15 K				303.15 K				313.15 K			
Pressure	Mole fraction	Flory theory eq. [1]	Ideal mixing relation eq. [2]	Nomoto relation eq. [3]	Collision factor theory eq. [4]	Flory theory eq. [1]	Ideal mixing relation eq. [2]	Nomoto relation eq. [3]	Collision factor theory eq. [4]	Flory theory eq. [1]	Ideal mixing relation eq. [2]	Nomoto relation eq. [3]	Collision factor theory eq. [4]
0.1	0.8	2.48	2.68	−0.03	−2.69	−2.90	3.03	0.14	−2.70	−3.42	2.90	−0.07	−3.14
5.0		1.21	2.44	−0.19	−2.73	−2.29	2.46	−0.30	−3.07	−3.21	2.67	−0.17	−3.18
10.0		1.71	2.25	−0.30	−3.17	−3.41	2.14	−0.52	−3.24	−3.68	2.78	−0.00	−2.93
15.0		1.15	1.91	−0.60	−3.38	−2.09	2.12	−0.51	−3.27	−2.74	2.57	−0.14	−2.77
20.0		1.29	2.20	−0.26	−2.65	−2.45	2.09	−0.47	−3.14	−2.60	2.26	−0.36	−3.13
25.0		1.57	2.21	−0.23	−2.57	−1.38	1.95	−0.59	−3.14	−1.34	2.83	−0.27	−2.33
30.0		0.68	1.94	−0.46	−2.92	−2.84	1.84	−0.68	−3.06	−1.21	2.16	−0.39	−3.04
0.1	0.6	2.21	3.81	−0.33	−4.14	−2.77	4.44	−0.03	−4.01	−3.40	4.08	−0.47	−4.87
5.0		2.32	3.56	−0.45	−4.08	−2.84	3.85	−0.36	−4.30	−3.30	3.77	−0.59	−4.88
10.0		2.34	3.24	−0.65	−4.75	−3.43	3.42	−0.65	−4.52	−3.41	3.81	−0.45	−4.64
15.0		1.89	3.16	−0.65	−4.63	−2.24	3.38	−0.61	−4.56	−2.45	3.52	−0.62	−4.38
20.0		2.14	2.97	−0.80	−4.22	−2.96	2.92	−0.99	−4.83	−2.01	3.79	−0.19	−4.13
25.0		3.09	2.80	−0.98	−4.43	−2.47	2.96	−0.91	−4.57	−2.05	3.00	−0.94	−4.69
30.0		4.05	2.57	−1.08	−4.62	−2.73	2.80	−1.04	−4.44	−1.59	2.75	−1.15	−4.95
0.1	0.4	3.08	3.75	−0.54	−4.17	−3.35	2.40	−2.28	−6.21	−1.49	4.67	−0.05	−4.21
5.0		3.55	3.43	0.71	−4.17	−1.15	3.97	−0.39	−4.14	−1.44	4.31	−0.20	−4.25
10.0		3.25	3.18	−0.83	−4.75	−1.74	3.55	−0.65	−4.34	−1.67	4.20	−0.20	−4.18
15.0		2.76	3.00	−0.92	−4.72	−0.82	3.29	−0.83	−4.59	−0.51	3.93	−0.33	−3.91
20.0		3.52	2.94	−0.93	−4.21	−1.28	3.04	−0.99	−4.64	−0.93	3.55	−0.58	−4.34
25.0		1.72	2.82	−1.00	−4.32	−1.47	2.84	−1.14	−4.64	−0.43	3.12	−0.94	−4.51
30.0		4.54	2.44	−1.30	−4.70	−0.89	2.70	−1.25	−4.50	0.01	2.85	−1.16	−4.79
0.1	0.2	3.40	2.66	−0.34	−2.64	−0.24	2.69	−0.56	−3.00	−1.05	2.93	−0.42	−3.07
5.0		4.02	2.42	−0.48	−2.68	0.18	2.66	−0.41	−2.79	−0.81	2.78	−0.41	−2.99
10.0		3.53	2.19	−0.60	−3.09	−0.25	2.42	−0.52	−2.86	−1.08	2.65	−0.46	−2.99
15.0		2.99	1.99	−0.74	−3.16	−0.30	2.43	−0.44	−2.83	−0.63	2.35	−0.65	−2.93
20.0		3.89	1.82	−0.86	−2.95	−0.21	1.97	−0.84	−3.17	0.23	2.19	−0.70	−3.09
25.0		4.57	1.50	−1.17	−3.28	−0.23	1.76	−1.01	−3.24	0.51	1.85	−0.99	−3.26
30.0		5.06	1.03	−1.58	−3.74	−0.41	1.32	−1.40	−3.47	0.42	1.78	−1.01	−3.32
Average percentage deviation		2.78	2.60	0.66	3.70	1.75	2.73	0.72	3.83	1.66	3.11	0.48	3.74

Acknowledgement

We are extremely thankful to C.S.I.R., New Delhi, for financial assistance.

1. J. D. PANDEY. J. Chem. Soc. Faraday Trans. II, **76**, 1215 (1980).
2. J. D. PANDEY, B. R. CHATURVEDI, and N. PANT. Acoustics Lett. **4**, 128 (1980).
3. J. D. PANDEY and ALEC D. M. DAVID. Chem. Scr. **19**, 39 (1982).
4. J. D. PANDEY. Electrochem. Acta, **27**, 1097 (1982).
5. J. D. PANDEY, R. K. UPADHYAY, and U. GUPTA. Acoustics Lett. **5**, 120 (1982).
6. J. D. PANDEY and U. GUPTA. Electrochem. Acta, **28**, 1047 (1983).
7. J. D. PANDEY, B. R. CHATURVEDI, and R. P. PANDEY. J. Phys. Chem. **85**, 1750 (1981).
8. T. TAKAGI and H. TERANISHI. J. Chem. Thermodyn. **14**, 1167 (1982).
9. T. TAKAGI and H. TERANISHI. J. Chem. Thermodyn. **14**, 577 (1982).
10. T. TAKAGI and H. TERANISHI. J. Chem. Thermodyn. **16**, 1031 (1984).
11. T. TAKAGI and H. TERANISHI. J. Chem. Thermodyn. **17**, 1057 (1985).
12. T. TAKAGI. J. Chem. Thermodyn. **12**, 277 (1980).
13. T. TAKAGI. J. Chem. Thermodyn. **12**, 1183 (1980).
14. T. TAKAGI. J. Chem. Thermodyn. **13**, 291 (1981).
15. P. J. FLORY. J. Am. Chem. Soc. **87**, 1833 (1965).
16. P. J. FLORY and A. ABE. J. Am. Chem. Soc. **87**, 1838 (1965).
17. D. PATTERSON and A. K. RASTOGI. J. Phys. Chem. **74**, 1067 (1970).
18. M. AUERBACH. Experientia, **4**, 473 (1948).
19. W. VAN DAEL. Experimental thermodynamics. Vol. II. Thermodynamic properties and the velocity of the sound. Butterworths & Co. Ltd., London. 1975. Chap. XI.
20. E. G. RICHARDSON. Ultrasonic physics. Elsevier, Amsterdam. 1962.
21. M. J. BLANDAMER and D. WADDINGTON. J. Phys. Chem. **74**, 2569 (1970).
22. O. NOMOTO. J. Phys. Soc. Jpn. **13**, 1528 (1958).
23. W. SCHAAFFS. Molekularakustik, Springer-Verlag-Berlin-Gottingen. Heidelberg. 1963. Chaps. XI and XII.
24. W. SCHAAFFS. Z. Phys. **114**, 110 (1939); **115**, 69 (1940).
25. R. NUTSCH-KUHNKIES. Acustica, **15**, 383 (1965).

Can. J. Chem. Downloaded from www.nrcresearchpress.com by 41.223.56.140 on 09/07/12
For personal use only.

Newton-variational solution of the Frank–Kamenetskii thermal explosion problem

AVYGDOR MOISE AND HUW O. PRITCHARD
Centre for Research in Experimental Space Science, York University, Downsview, Ont., Canada M3J 1P3

Received July 5, 1988

AVYGDOR MOISE and HUW O. PRITCHARD. Can. J. Chem. **67**, 442 (1989).

The Newton method was shown by Vatsya to be suitable for solving the generalised elliptic problem, and we show that this approach can be used to treat the Frank–Kamenetskii model of a thermal explosion, by using a variational solution of the sequence of linear equations that are encountered in the Newton method. Convergence to the desired solution is rapid in the case of spherical geometry. The method produces converging upper and lower bounds to the critical value of the dimensionless heat production rate, δ_c, and lower bounds to the dimensionless temperature excess distribution function θ and its critical form θ_c.

Key words: thermal explosions, Frank–Kamenetskii model.

AVYGDOR MOISE et HUW O. PRITCHARD. Can. J. Chem. **67**, 442 (1989).

Vatsya a démontré que la méthode de Newton permet de résoudre le problème elliptique généralisé et on montre que, si on fait appel à la solution variationnelle de la suite des équations linéaires rencontrées dans la méthode de Newton, cette approche peut être utilisée pour traiter le modèle de Franck–Kamenetskii d'une explosion thermique. Dans le cas d'une géométrie sphérique, la convergence de la solution désirée est rapide. La méthode fournit des limites supérieure et inférieure qui convergent vers la valeur critique de la vitesse de production de la chaleur (sans dimension), δ_c, ainsi que les limites inférieures de la fonction de distribution des températures en excès (sans dimension), θ, et sa forme critique θ_c.

Mots clés : explosions thermiques, modèle de Franck–Kamenetskii.

[Traduit par la revue]

Can. J. Chem. Downloaded from www.nrcresearchpress.com by 41.223.56.140 on 09/07/12
For personal use only.

Introduction

The theory of thermal explosions, as developed by Frank–Kamenetskii (1), requires the solution of the equation

$$[1] \quad \nabla_\xi^2\theta + \delta e^\theta = 0$$

where θ is the (dimensionless) difference in temperature between a point inside the system and that at the outer boundary, and δ is a parameter (in fact, the dimensionless measure of the heat-release rate). This equation has the property that a minimal positive solution can be found below a certain critical value of δ, i.e. δ_c, but not above: thus, δ_c is identified with the critical condition for explosion.

Equation [1] has been the subject of many studies: these have included the conversion from a boundary-value to an initial-value problem (2, 3), asymptotic expansions (4, 5), and generalised polynomial expansions (6, 7). These methods suffer from two major defects, one that long expansion lengths are needed to obtain sufficient accuracy and two, that multiple solutions exist, and the unwanted ones have to be discarded by appeal to intuitive arguments. Recently, Vatsya proposed the solution of this problem by the use of Newton's method (8), and showed that the explosion condition could be defined uniquely, without the need for arbitrary exclusion of alternative "non-physical" solutions. In this paper, we show that the Newton method converges quickly to the required result, in contrast to all of the preceding approaches. The use of the Newton method linearises the equation and, in principle, could give rise to asymptotic *analytic* approximations. However, we have not been able to find a purely analytic representation in this case, beyond the first iteration, and have resorted to the Bubnov–Garlerkin generalisation of the variational method (9), which is known to be a convergent procedure, to obtain numerical solutions for the higher Newton approximants. The use of both the Newton method and the variational method in the solution of non-linear problems is a novel feature of this work.

We begin by defining the differential operator $\mathcal{L}$ and a function $\phi(x;\lambda)$ as follows:

(*i*) Let $\mathcal{L}^2(D,dx)$ be the real Hilbert space of square integrable functions with respect to the Lebesgue measure dx on $D = (0,1)$, and let $L = -d^2/dx^2$ be an operator from $\mathcal{D}(L) \to \mathcal{L}^2(D,dx)$.

(*ii*) Let $\phi(x;\lambda)$ be twice differentiable with respect to x for all $x \in D = (0,1)$, and let $\phi(x,\lambda) = 0$, $x \in \partial D = \{0,1\}$, where $\phi(x;\lambda)$ is the minimal positive solution of

$$[2] \quad L\phi = \lambda f(\phi) \qquad x \in D$$

λ is a positive parameter and $f(\eta) \equiv f(x;\lambda;\eta(x;\lambda))$ is a continuous, positive, increasing and convex function of $\eta(x;\lambda) > 0$; i.e. the derivative $f'(\eta)$ with respect to η of $f(x;\lambda;\eta(x;\lambda))$ is continuous, positive and increasing on D for $\eta > 0$.

Then, whenever eq. [2] makes sense, i.e. has a definite minimal positive solution, we may use Newton's approximating formula to produce successive lower bounds to $\phi(x;\lambda)$ and upper bounds to λ^*, where λ^* is the bifurcation point (8).

Application of Newton's method

If we choose an initial value for $\phi_0(x;\lambda) = 0$ (a guaranteed lower bound to $\phi(x;\lambda)$, since $\phi(x;\lambda)$ is strictly positive) then Newton's approximating formula takes the form,

$$[3] \quad [L - \lambda f'(x;\lambda;\phi_n(x;\lambda))]\phi_{n+1}(x;\lambda) = \lambda[f(x;\lambda;\phi_n(x;\lambda)) - \phi_n(x;\lambda)f'(x;\lambda;\phi_n(x;\lambda))]$$

$n = 0, 1, 2, \ldots$, and we are assured (8) that $\phi_n(x;\lambda) \uparrow \phi(x;\lambda)$ uniformly with respect to $x \in \bar{D} = D \cup \partial D$ for each fixed $\lambda < \lambda^*$. Let λ^* be the critical point, i.e. $\lambda > \lambda^*$ implies that eq. [2] does not have a minimal positive solution. For each fixed n, $\phi_n(x;\lambda)$ is known to exist up to some point $\bar{\lambda}_{n-1} > \lambda^*$. Furthermore, we know (8) that $\bar{\lambda}_n \uparrow \lambda^*$, where $\bar{\lambda}_n$ is the smallest eigenvalue of

$$[L - \bar{\lambda}_n f(\phi_n)]\phi_{n+1} = 0$$

By restricting ourselves to spherical geometry, eq. [1] can be rewritten as (7)

$$[4] \quad \frac{d^2u}{d\xi^2} + \delta\xi e^{u/\xi} = 0$$

where $0 \le \xi \le 1$ is the (scaled) distance from the centre, and

$u = \xi\theta$. With $\delta = \lambda$, it has the required form

$$[5] \quad Lu = \delta f(u)$$

and has been shown, elsewhere (7, 10), to satisfy the above conditions: it may, therefore, be solved by the Newton method.

Let $\{u_n\}$ be Newton's sequence for $u(\xi,\delta)$, and let $u_0 = 0$ be our initial input function in eq. [3]; u_0 is a lower bound to $u(\xi,\delta)$, since we already know that u is positive and $u_n \uparrow u$. Then, expressing eq. [5] in terms of [4] and [3] gives

$$[6] \quad \left[-\frac{d^2}{d\xi^2} - \delta e^{u_n/\xi}\right] u_{n+1} = \delta[\xi e^{u_n/\xi} - u_n e^{u_n/\xi}]$$

With $n = 0$, this reduces to

$$\left[-\frac{d^2}{d\xi^2} - \delta\right] u_1 = \delta\xi$$

or

$$\frac{d^2u_1}{d\xi^2} = -\delta(\xi + u_1)$$

to which the solution

$$[7] \quad u_1(\xi,\delta) = \frac{\sin \xi\sqrt{\delta}}{\sin \sqrt{\delta}} - \xi$$

is already known (7). In principle, we may now re-substitute this closed form approximation u_1 for u in eq. [6] and solve for u_2, but we were unable to find a tractable solution, and so proceeded to employ numerical methods by which to extract higher order approximations for u.

The variational approximation

When the function $\phi(x;\lambda)$ (or its Newton approximant $\phi_n(x;\lambda)$) cannot be expressed in closed form, it is possible to produce a variational expansion for $\phi_n(x;\lambda)$ and $\phi(x;\lambda)$ given by

$$\phi_{n,m}(x;\lambda) = \sum_{j=1}^{m} \beta_{j,n}\tilde{\phi}_j(x;\lambda)$$

$$\phi_m(x;\lambda) = \sum_{j=1}^{m} \beta_j\tilde{\phi}_j(x;\lambda)$$

where $\beta_{j,n}$ and β_j are defined by

$$[8] \quad \sum_{j=1}^{m} (\tilde{\phi}_i, [L - \lambda f'(\phi_{n,m})]\beta_{j,n+1}\tilde{\phi}_j) = \lambda(\tilde{\phi}_i, [f(\phi_{n,m}) - \phi_{n,m}f'(\phi_{n,m})])$$

and

$$[9] \quad \sum_{j=1}^{m} (\tilde{\phi}_i, [L - \lambda f'(\phi_m)]\beta_j\tilde{\phi}_j) = \lambda(\tilde{\phi}_i, [f(\phi_m) - \phi_m f'(\phi_m)])$$

respectively, (the notation (,) denoting the scalar product of two vectors) $\{\tilde{\phi}_j(x;\lambda)\} \subset \mathcal{D}(L)$ is some linearly independent basis set and m is the chosen expansion length (10). For each (Newton iteration) n we have that

$$\lim_{m\to\infty} \phi_{n,m}(x;\lambda) = \phi_n(x;\lambda)$$

and

$$\lim_{n\to\infty} \phi_n(x;\lambda) = \phi(x;\lambda)$$

Also (8), if $\phi_{n,m_k} \leq \phi_{n,\infty} = \phi_n(x;\lambda)$ for each n, where $m_k < m$ selects only that sub-set of the sequence that is monotonically increasing, then ϕ_{n,m_k} yields successive lower bounds to ϕ as $m \to \infty$ followed by $n \to \infty$.

Application to the Frank–Kamenetskii model

Rather than producing a variational approximation to u_n, we make use of the fact that (7) eq. [7] represents the θ function to within about 5% up to values of $\delta = 3.3$. Notice that the first Newton approximant can also be obtained independently by the use of an inverse Laplace transformation of a time-variant Frank–Kamenetskii equation, with the exponential term approximated in the usual manner (6), and the steady-state limit of that solution is naturally expressible in terms of a sum of sine functions (10). For this reason, we chose the set $\{\sin j\pi\xi\}_{j=1}^{\infty} \subset \mathcal{D}(L)$, (which obviously forms a basis in the appropriate space) to represent, in our variational procedure, the difference $\Delta u_n = u_n - u_1$, in a two-pronged attempt to reduce the number of terms required for an accurate representation of u; it is shown elsewhere (10) that Δu_n also satisfies all the requirements for convergence described above.

We re-write eq. [5] in terms of $\Delta u = u - u_1$

$$L(u_1 + \Delta u) = \delta\xi e^{(u_1+\Delta u)/\xi}$$

$$L(\Delta u) = \delta\xi e^{(u_1+\Delta u)/\xi} - Lu_1$$

$$= \delta[\xi e^{(u_1+\Delta u)/\xi} - (\xi + u_1)]$$

Thus

$$f(\Delta u) = \xi e^{(u_1+\Delta u)/\xi} - (\xi + u_1)$$

and

$$f'(\Delta u) = e^{(u_1+\Delta u)/\xi}$$

whence Newton's approximating sequence for $\{\Delta u_n\}$ becomes

$$\left[-\frac{d^2}{d\xi^2} - \delta f'(\Delta u_n)\right]\Delta u_{n+1} = \delta[f(\Delta u_n) - (\Delta u_n)f'(\Delta u_n)]$$

We now transform this operator equation into an $m \times m$ dimensional matrix equation that represents the variational equation [8]

$$A_n \cdot B_{n+1} = G_n$$

where the elements of A_n and G_n are $\alpha_{(i,j),n}$ and $\gamma_{j,n}$, defined by

$$\alpha_{(i,j),n} = \int_0^1 \sin(i\pi\xi)\left[-\frac{d^2}{d\xi^2} - \delta e^{(u_1+\Delta u_n)/\xi}\right]\sin(j\pi\xi)d\xi$$

$$\gamma_{j,n} = \int_0^1 \sin(j\pi\xi)\delta[(\xi - \Delta u_n)e^{(u_1+\Delta u_n)/\xi} - (\xi + u_1)]d\xi$$

A solution vector $B_{n+1} = (\beta_{j,n+1})$ will exist for all values of $\delta < \delta_{c,n}$ (where $n = 1, 2, 3\ldots$ represents the nth Newton's approximation); conversely, for each fixed n we can find a $\delta_{c,n}$ for which a solution ceases to exist. The non-existence of a solution to the above matrix equation will manifest itself when the determinant $\det(A_n(\delta))$ becomes singular. Since we know (8, 10) that u_n exists, and is continuous as long as $\delta < \delta_{c,n-1}$, therefore, the positive normalised determinant

$$\det(\bar{A}_n(\delta)) = \frac{\det(A_n(\delta))}{\det(A_n(0))}$$

Can. J. Chem. Downloaded from www.nrcresearchpress.com by 41.223.56.140 on 09/07/12
For personal use only.

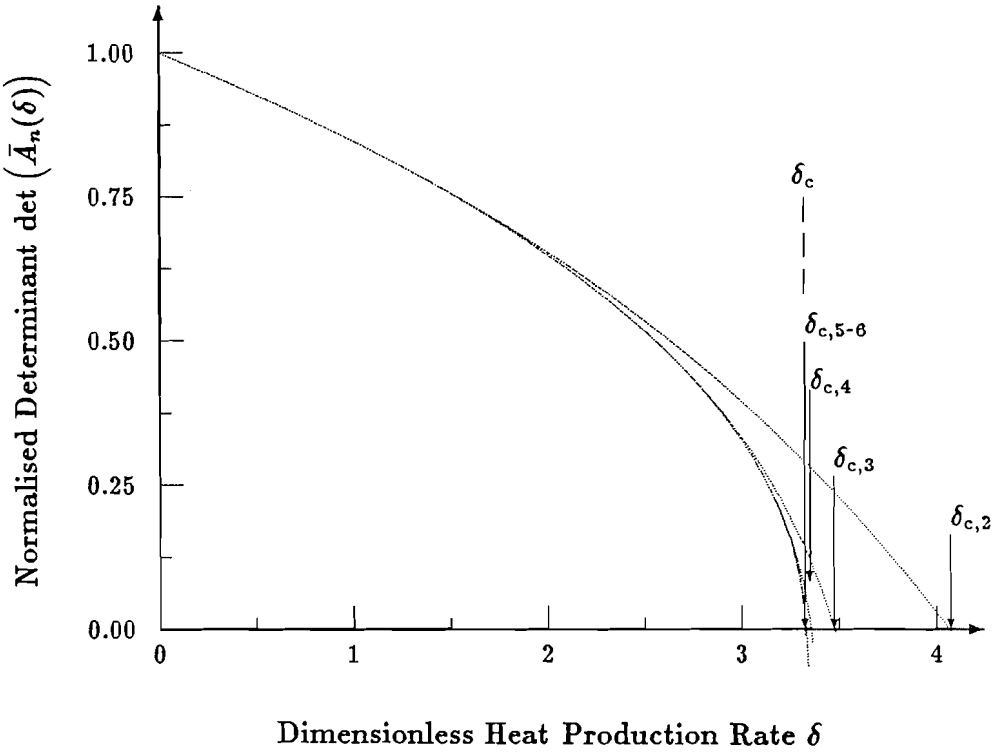


FIG. 1. Convergence characteristics of the normalised determinant det $(\bar{A}_n(\delta))$, using three basis functions and the initial value $\Delta u(\xi,\delta) = 0$.

will decrease towards zero as δ approaches $\delta_{c,n}$. Note that since $\lim_{\delta \to \delta_{c,n}} \det(\bar{A}_n(\delta)) = 0$, simply observing the sign and magnitude of the normalised determinant $\bar{A}_n(\delta)$ will enable us to compute successive upper and lower bounds to $\delta_{c,n}$.

Numerical implementation

The matrix and vector elements $\alpha_{(i,j),n}$ and $\gamma_{j,n}$ were computed by using a five-point Gauss–Legendre quadrature (11) applied to an integral number of sub-intervals in D. The number of intervals was chosen in such a manner as to ensure that there were at least four sub-intervals per integration segment for each zero crossing of any of the basis functions; this provides better accuracy than equal-interval formulae, without a significant increase in computational overhead.

The solution vector $B_{n+1}(\delta)$ was computed from the input matrix $A_n(\delta)$ and the vector $G_n(\delta)$ by using a standard Gauss–Jordan reduction method (11), which has the advantage of yielding simultaneously the required determinant det $(A_n(\delta))$. For each fixed value of δ, an initial guess for Δu_n, known to be less than Δu, was chosen and the Newton-variational method was applied repeatedly for $n = 1, 2, \ldots$ until either det $(\bar{A}_n(\delta))$ became negative, convergence was achieved to within some ϵ, defined by

$$\epsilon > \left|\frac{\det(\bar{A}_n(\delta)) - \det(\bar{A}_{n-1}(\delta))}{\det(\bar{A}_{n-1}(\delta))}\right| \text{ and } \left|\frac{\delta_{c,n+1} - \delta_{c,n}}{\delta_{c,n+1}}\right|$$

or else until a contradiction in the sense that det $(\bar{A}_n(\delta)) <$ det $(\bar{A}_{n-1}(\delta))$ was encountered.

In principle, for each new value of δ, one begins with $\Delta u_1(\xi,\delta) = 0$, but because $\Delta u_n < \Delta u$ for all n and Δu is a monotonically increasing function of δ, one can use the previous solution $\Delta u_n(\xi,\delta)$ as the initial guess for $\Delta u(\xi,\delta + d\delta)$, thereby reducing considerably the number of iterations required to achieve convergence.

TABLE 1. Comparison of Newton-variational approximations to the steady-state solution for a thermal explosion in a sphere, for expansion lengths of m = 4, 5, 8, and 10*

m	$\delta_{c,max}$	$\theta_c(\delta)\|_{\xi=0}$	$\frac{d\theta_c(\delta)}{d\xi}\|_{\xi=1}$
4	3.32199232	1.607	−2.001
5	3.32199224	1.6072	−2.0005
8	3.32199213	1.60714	−2.00008
10	3.32199212	1.60743	−2.00005
m	$\delta_{infl,max}$	$\theta_{infl}(\delta)\|_{\xi=0}$	$\frac{d\theta_{infl}(\delta)}{d\xi}\|_{\xi=1}$
10	3.11169729	1.06779	−1.55585

*Error criterion $\epsilon = 10^{-8}$.

Results

Figure 1 shows the behaviour of the normalised determinant det $(\bar{A}_n(\delta))$ when using only three basis functions, and an initial value of $\Delta u_1(\xi,\delta) = 0$. In the first numerical iteration, i.e. $n = 2$, the determinant remains positive up to a value of δ of about 4.1; the next iteration places the upper bound for δ_c at just below 3.5, and the Newton sequence converges between $n = 5$ and 6 to a value of δ_c just above 3.32, which is almost correct. Figure 2 shows the corresponding values for the dimensionless excess temperature at the centre of the vessel, for the highest value of δ that gave a valid solution, giving a maximum value, at

Can. J. Chem. Downloaded from www.nrcresearchpress.com by 41.223.56.140 on 09/07/12
For personal use only.

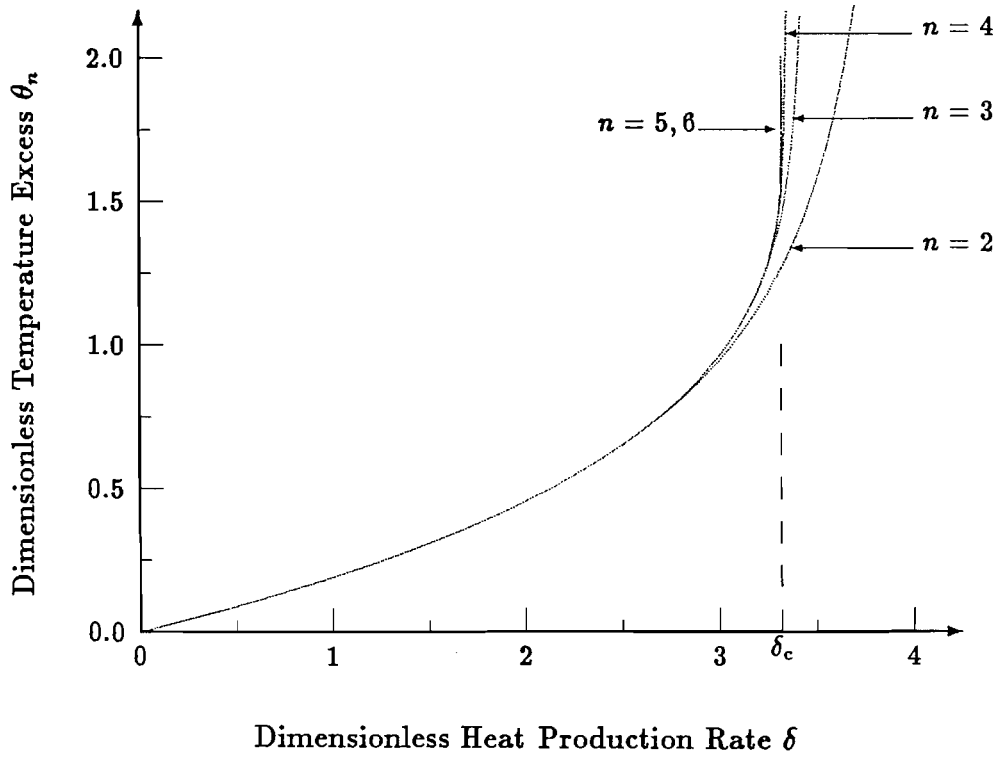


FIG. 2. Convergence characteristics of Newton's sequence $\{\theta_n(\xi,\delta)\}|_{\xi=0}$, using three basis functions and the initial value $\Delta u(\xi,\delta) = 0$.

TABLE 2. Coefficients for calculating the dimensionless temperature excess function θ for a sphere,* with a 10-term expansion, for the two critical values of δ, viz. δ_{infl} and δ_c

Term	Inflection point	Critical point
$\beta_{1,10}$	$7.71982282 \times 10^{-2}$	$1.99500111 \times 10^{-1}$
$\beta_{2,10}$	$4.61003792 \times 10^{-3}$	$1.51646033 \times 10^{-2}$
$\beta_{3,10}$	$-1.73666301 \times 10^{-4}$	$2.21632157 \times 10^{-4}$
$\beta_{4,10}$	$5.29551631 \times 10^{-5}$	$1.25306677 \times 10^{-4}$
$\beta_{5,10}$	$-1.64568766 \times 10^{-5}$	$-2.65487057 \times 10^{-5}$
$\beta_{6,10}$	$6.53680820 \times 10^{-6}$	$1.16056878 \times 10^{-5}$
$\beta_{7,10}$	$-2.99846054 \times 10^{-6}$	$-5.25620570 \times 10^{-6}$
$\beta_{8,10}$	$1.52954647 \times 10^{-6}$	$2.69028216 \times 10^{-6}$
$\beta_{9,10}$	$-8.45614420 \times 10^{-7}$	$-1.48783407 \times 10^{-6}$
$\beta_{10,10}$	$4.98409179 \times 10^{-7}$	$8.78419588 \times 10^{-7}$

*$u = \xi\theta = \lim_{m,n\to\infty} u_n$,

$$u_n \equiv u_n(\xi,\delta) = \frac{\sin(\xi\sqrt{\delta})}{\sin\sqrt{\delta}} - \xi + \sum_{j=1}^{m} \beta_{j,n}(\delta)\sin(j\pi\xi).$$

convergence, which is also very nearly correct. A full summary of these results and details of the algorithm are available elsewhere (10).

The results of calculations for 4, 5, 8, and 10 basis functions are compared in Table 1, where the rapid convergence of the method can be seen; the numbers in this table are to be interpreted as follows: the δ values are upper bounds, with the lower bound for that value of the expansion length m being within 10^{-8} below it and for the θ and $d\theta/d\xi$ values, the uncertainty is in the last digit quoted. The final results are in excellent agreement with the accepted values (12), but are superior in the sense that the present method provides converging upper and lower bounds to $\delta_{c,n}$; also the θ function, at convergence, is known to be a lower bound. The lower part of this table shows the conditions for the first appearance of an inflection in the $\theta(\xi)$ function, also in excellent agreement with the result of Boddington and Gray (12). Table 2 gives a list of the 10th order expansion coefficients, from which the appropriate temperature profiles for these two unique conditions may be constructed.

Acknowledgements

We would like to express our thanks to Raj Vatsya for introducing us to these methods of analysis, and to the Natural Sciences and Engineering Research Council of Canada for financial support.

1. D. A. FRANK-KAMENETSKII. Diffusion and heat exchange in chemical kinetics. 2nd ed. Princeton University Press. 1955.
2. S. CHANDRASEKHAR and G. W. WARES. Astrophys. J. **109**, 551 (1949).
3. P. L. CHAMBRÉ. J. Chem. Phys. **20**, 1975 (1952).
4. O. K. RICE. J. Chem. Phys. **8**, 727 (1940).
5. I. S. LYUBCHENKO and G. N. MARCHENKO. Russ. J. Phys. Chem. **54**, 517 (1980).
6. P. GRAY and M. E. SHERRINGTON. Specialist periodical Reports. Kinet. Energy Transfer, **2**, 331 (1977).
7. A. MOISE and H. O. PRITCHARD. Can. J. Chem. **60**, 2012 (1982).
8. S. R. VATSYA. J. Math. Phys. **22**, 2977 (1981).
9. S. G. MIKHLIN. Variational methods in mathematical physics. *Translated by* T. Boddington. Macmillan, New York. 1964. p. 448.
10. A. MOISE. Ph.D. Thesis. York University. 1988.
11. B. CARNAHAN, H. A. LUTHER, and J. O. WILKES. Applied numerical methods. John Wiley and Sons, New York. 1969.
12. T. BODDINGTON and P. GRAY. Proc. R. Soc. London Ser. A**320**, 71 (1970).

Can. J. Chem. Downloaded from www.nrcresearchpress.com by 41.223.56.140 on 09/07/12
For personal use only.

Viscosities of mixtures of chloroform + triethylamine: analysis in terms of three components (A, B, and AB)

RICHARD P. SCHUTTE, TERRY C. LIU, AND LOREN H. HEPLER
Department of Chemistry, University of Alberta, Edmonton, Alta., Canada T6G 2G2

Received August 22, 1988

RICHARD P. SCHUTTE, TERRY C. LIU, and LOREN H. HEPLER. Can. J. Chem. **67**, 446 (1989).

Viscosities and densities of highly non-ideal mixtures of chloroform (A) + triethylamine (B) have been measured at 25°C. It has been shown that the Grunberg equation (one adjustable parameter) can account for these viscosities over the whole range of compositions. It has also been shown that a new combination of the ideal associated solution model, based on consideration of an equilibrium of the type A + B = AB, with an ideal viscosity equation (also one adjustable parameter) accounts more accurately for all of the viscosities. This latter treatment also has the advantage of offering a clear pictorial model of the mixtures.

Key words: viscosity of solution, complex formation in solution, chloroform + triethylamine, triethylamine + chloroform.

RICHARD P. SCHUTTE, TERRY C. LIU et LOREN H. HEPLER. Can. J. Chem. **67**, 446 (1989).

Opérant à 25°C, on a mesuré les viscosités et les densités de mélanges de chloroforme (A) et de triéthylamine (B) qui s'écartent beaucoup de l'idéalité. On a montré que l'équation de Grunberg (avec un seul paramètre ajustable) peut expliquer les viscosités à toutes les compositions. On a aussi démontré qu'une nouvelle combinaison du modèle de la solution idéale associée, basé sur la considération d'un équilibre du type A + B = AB, avec une équation de viscosité idéale (qui est aussi adjustable avec un seul paramètre) permet de mieux expliquer toutes les viscosités. Ce traitement offre aussi l'avantage de présenter un modèle visuel clair des mélanges.

Mots clés : viscosité de la solution, complexé formation dans solution, chloroforme + triéthylamine, triéthylamine + chloroforme.

[Traduit par la revue]

Can. J. Chem. Downloaded from www.nrcresearchpress.com by 41.223.56.140 on 09/07/12
For personal use only.

1. Introduction

Viscosities of many mixtures or solutions are of considerable direct importance in connection with a wide variety of flow processes and are also important in connection with processes that involve diffusion or thermal conductivities. In addition, viscosities have often been regarded as a probe to be used to gain understanding of molecular interactions in mixtures and solutions.

Our immediate interest has been to use the mole fraction dependence of the viscosity of a non-electrolyte mixture as a means of testing and possibly extending earlier treatments of the thermodynamic properties of such mixtures. A longer range interest is the development of improved methods for estimating the viscosities of multi-component mixtures, such as bitumen or heavy oil containing diluent or dissolved gas.

Many earlier investigators (1–12) of viscosities of mixtures have expressed these viscosities as weighted sums of viscosities of pure components. Long ago (1887) Arrhenius recognized that logarithms of viscosities of liquids were approximately proportional to $1/T$ and therefore suggested that the logarithm of the viscosity of a mixture might be expressed as a weighted sum of the logarithms of the viscosities of the pure components at the same temperature. Subsequent investigators have taken the weighting factors to be volume fractions or (more often) mole fractions. On this basis we begin by expressing the viscosity of an ideal mixture as

$$[1] \quad \ln \eta_{id} = \Sigma X_i \ln \eta_i$$

in which η_{id} is the viscosity of an ideal mixture, X_i is the stoichiometric mole fraction of component i, and η_i is the viscosity of pure liquid component i. Possibly the most often used extension of the ideal eq. [1] to non-ideal solutions was originated by Grunberg (1, 2), who wrote

$$[2] \quad \ln \eta = X_A \ln \eta_A + X_B \ln \eta_B + X_A X_B d$$

for a mixture of components A and B. In eq. [2] d is a parameter that is related to the molecular interactions that are responsible for the non-ideal properties of the mixture. It has been found that d is typically small and negative for mixtures that exhibit positive deviations from Raoult's law and is positive (sometimes relatively large) for mixtures that exhibit negative deviations from Raoult's law. Later in this paper we consider eq. [2] in relation to our viscosities of chloroform + triethylamine mixtures.

Because of uncertainties about the specific theoretical relationship of d in eq. [2] to molecular interactions, we have also applied another approach as follows. Several previous investigations (13) have shown that the "ideal associated solution model" (defined below) provides an accurate and convenient description of the thermodynamic properties of some mixtures for which there is good evidence for the reality of complex formation of the type represented by

$$[3] \quad A + B = AB$$

It has also been shown (14, 15) that this ideal associated solution model is applicable to the thermodynamic properties of the chloroform + triethylamine system of present interest.

In the present application of the ideal associated solution model it is specified that all apparent deviations from ideality of the two component systems (A + B) can be explained in terms of ideal properties of the three component system (A, B, and AB) and the equilibrium mole fractions of A, B, and AB. We have therefore considered the measured viscosities of the chloroform (A) + triethylamine (B) system in terms of a three component extension of eq. [1]

$$[4] \quad \ln \eta = Z_A \ln \eta_A + Z_B \ln \eta_B + Z_{AB} \ln \eta_{AB}$$

in which Z represents the equilibrium (as contrasted to the stoichiometric) mole fraction and η_{AB} represents the viscosity of the hypothetical pure liquid AB. As shown later in this paper, an equation of the form of [4] is consistent with our measured viscosities and the previously evaluated equilibrium constant for the equilibrium represented by eq. [3].

[1] R. P. Schutte. Unpublished results, available on request.

Can. J. Chem. Downloaded from www.nrcresearchpress.com by 41.223.56.140 on 09/07/12
For personal use only.

2. Experimental

Materials

Triethylamine from Jannsen Chemica was refluxed for 1.5 h over potassium hydroxide in a nitrogen atmosphere, then fractionally distilled. Chloroform from Anachemia was washed 3–5 times with distilled water and then dried for 48 h over anhydrous calcium chloride. Finally, the chloroform was distilled in a nitrogen atmosphere and stored (maximum of 4 days storage) in a dark bottle in a closed cabinet. Throughout the purification procedure, care was taken to protect the chloroform from exposure to light.

Mixtures of chloroform + triethylamine were prepared by mixing weighed amounts of pure components; stoichiometric mole fractions were calculated from the masses and molecular weights.

Apparatus and procedure

Densities of the liquids were determined with glass pycnometers of 25 cm^3 approximate volume, calibrated with distilled water and suspended in a water bath at 25°C. The temperature of the water bath was controlled by a Thermomix 1460 and was known to ±0.01°C and stable to ±0.005°C as monitored with a platinum resistance thermometer.

Kinematic viscosities (ν) were measured with Cannon–Fenske viscometers (Fisher Scientific sizes 25 and 50) suspended in the same water bath as the pycnometers. The viscometers were calibrated with distilled water and chloroform to determine k and K to be used in

$$[5] \quad \nu = \eta/\rho = kt - K/t^2$$

where η is dynamic viscosity, ρ is density, and t the flow time measured in seconds. Equation [5] is the Hagen–Poiseuille equation corrected for kinetic energy effects for capillaries with trumpet-shaped ends (16). Flow times as measured with a stopwatch ranged from approximately 90 to 230 s.

3. Results and calculations

Compositions of mixtures (expressed in terms of the stoichiometric mole fraction of chloroform, X_A), densities, and absolute viscosities (η) of chloroform (A) + triethylamine (B) are summarized in Table 1. Each density is the average of three determinations and each viscosity is the averge of six determinations. Standard deviations of the densities and viscosities were all close to 0.0002 g cm^{-3} and 0.003 CP. Our densities are in good agreement with the more accurate values previously reported (15) as part of a thermodynamic investigation.

After our measurements and calculations were completed, we became aware of viscosities and densities measured by Wei and Rowley (17). Densities from the two investigations agree to within 0.4% over the entire range of compositions, while differences in the viscosities range from about 1–4%. More important for our purposes than this reasonably good numerical agreement is the fact that the general shapes of the viscosity versus composition curves from the two investigations are very similar, which means that the same conclusions can be drawn from both sets of experimental results.

A graph of our viscosities against stoichiometric mole fractions is shown in Fig. 1, where it can be seen that the actual viscosities are greater than expected on the basis of an ideal mixture of two components, as in eq. [1]. This qualitative observation of positive excess viscosities was expected on the basis of the very accurate negative excess volumes previously reported (15) or the less accurate (also negative) excess volumes that can be calculated from our densities.

Now we turn to analysis of our viscosities in terms of the ideal associated solution model. The basis of this model is the assumption that observed non-ideal thermodynamic properties (vapor pressures, enthalpies of mixing, heat capacities, volumes) are entirely due to the kind of equilibrium represented by

TABLE 1. Stoichiometric mole fractions (X), densities (ρ), viscosities (η), and equilibrium mole fractions (Z) for chloroform + triethylamine mixtures

X_A	ρ (g cm^{-3})	η (cP)	Z_A	Z_B	Z_{AB}
0.0000	0.7222	0.344	0.0000	1.0000	0.0000
0.0983	0.7706	0.389	0.0319	0.8945	0.0736
0.1979	0.8237	0.442	0.0761	0.7721	0.1518
0.2978	0.8824	0.503	0.1385	0.6346	0.2269
0.3989	0.9466	0.567	0.2273	0.4872	0.2855
0.4988	1.0160	0.618	0.3442	0.3474	0.3084
0.5829	1.0795	0.640	0.4607	0.2465	0.2928
0.6859	1.1618	0.631	0.6112	0.1509	0.2379
0.8008	1.2654	0.604	0.7704	0.0769	0.1527
0.9010	1.3673	0.574	0.8937	0.0321	0.0742
1.0000	1.4791	0.542	1.0000	0.0000	0.0000

eq. [3]. Because of this equilibrium, the actual mole fractions (of A, B, and AB) are not the same as the stoichiometric mole fractions (of A and B, no AB). It therefore follows that extension of this ideal associated solution model of thermodynamic properties to viscosities should be based on eq. [4], with the equilibrium mole fractions (Z) calculated from the known stoichiometric mole fractions (X) and the previously established (15) equilibrium constant ($K = 2.58$ at 25°C). For these calculations of Z values from X values and K, we set all activity coefficients equal to unity, as required by the model (13–15). The resulting equilibrium mole fractions (Z) are listed in Table 1.

If it were possible to measure the viscosity of the hypothetical pure liquid AB, it would then be possible to make a direct comparison of the calculated (by way of eq. [4]) viscosities of mixtures with the measured viscosities. But it is impossible to obtain pure liquid AB because mixtures of A + B all contain non-negligible amounts of all three species (A, B, and AB). We have therefore tested the applicability of eq. [4] as follows.

The effect of AB on the viscosities of mixtures of A + B is negligible near $X_A = 0$ and $X_A = 1$ where the equilibrium mole fractions of AB are very small, and is largest near $X_A \approx 0.5$ where the equilibrium mole fraction of AB is a maximum. (Later we consider in detail why the maximum in the graph of η against X_A is "off-centre".) The simplest procedure for evaluating the unknown viscosity of the hypothetical pure AB is to use the measured viscosity of one mixture (near the maximum in the curve in Fig. 1, $X_A = 0.5829$) with the corresponding values of Z_A, Z_B, and Z_{AB} and the known viscosities of the pure components to obtain a calculated viscosity of the hypothetical pure liquid AB to be $\eta_{AB} = 1.402$ cP. That is, we have forced a fit of eq. [4] at one stoichiometric composition. Then, with this value of η_{AB}, we have used eq. [4] in calculating the viscosities of mixtures having various compositions. The average difference between calculated and measured viscosities is 0.001_5 cP. It is therefore clear that our combination of the ideal associated solution model (13–15) with the ideal mixture viscosity equation [1] provides calculated viscosities that are in very good agreement (average deviation no larger than experimental uncertainties) with the experimental data.

Another, more elaborate, test of eq. [4] is based on choosing the value of the viscosity of the hypothetical pure liquid AB that will lead to the minimum average difference between all measured and calculated viscosities. In this way we have

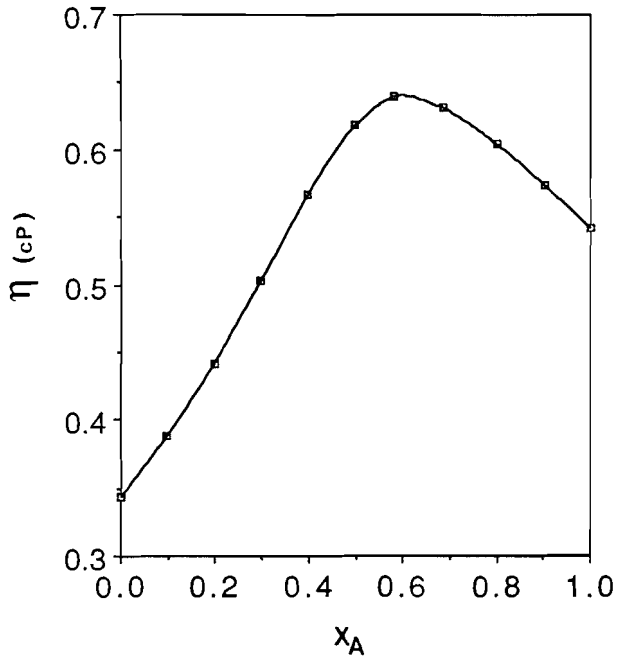


FIG. 1. Plot of absolute viscosity vs. stoichiometric mole fraction of chloroform.

obtained $\eta_{AB} = 1.386$ and thence obtain 0.001_1 cP as the average difference between measured and calculated viscosities. This procedure leads to an insignificant statistical improvement over the simpler treatment described in the preceding paragraph.

We now test eq. [2] from Grunberg (1, 2) in a way that is similar to our first test of eq. [4], as follows. We have used the measured viscosity of the mixture with $X_A = 0.5829$ to evaluate $d = 1.463$, and have then used this value of d in eq. [2] to calculate viscosities of the other mixtures. The average difference between these calculated viscosities and the measured viscosities is 0.019 cP, which is 13 times as large as the corresponding difference based on eq. [4], which also involves one adjustable parameter.

We have also tested the Grunberg eq. [2] by choosing the value of d that leads to the minimum average difference between all measured and calculated viscosities. In this way we have obtained $d = 1.333$ and 0.013 cP for the average difference between measured and calculated viscosities. This average difference between calculated and measured viscosities is 12 times as large as that found for the corresponding test of eq. [4].

Some of the thermodynamic properties (enthalpies of mixing and excess volumes) of chloroform + triethylamine mixtures are symmetrical about $X = 0.5$. Appropriate calculations (13–15) with the ideal associated solution model show that this observed symmetry is in accord with the model. In addition, it may be intuitively obvious that some effects caused by an equilibrium of the type [3] involving a 1:1 complex should be symmetrical about $X = 0.5$. On the other hand, it is clear from the compositions and viscosities listed in Table 1 and from the graph in Fig. 1 that the maximum in ln η (or in η) occurs at $X_A = 0.61$, rather than at the "expected" $X_A = 0.5$.

We first consider the shape (composition of the mixture with maximum viscosity) of ln η against X_A in terms of the Grunberg eq. [2]. To do so we substitute $X_B = 1 - X_A$ in eq. [2] and then differentiate with respect to X_A. The resulting d ln η/dX_A is set equal to zero and solved to obtain

$$[6] \quad X_A(\text{max. } \eta) = 0.5 + [\ln(\eta_A/\eta_B)]/2d$$

Using $d = 1.463$ and $d = 1.333$ and experimental values for η_A and η_B in eq. [6] leads to calculated $X_A(\text{max. } \eta) = 0.65_5$ and 0.67_1, in fair agreement with the observed $X_A(\text{max. } \eta) = 0.61$. Equation [6] shows that the maximum viscosity will occur at $X_A = 0.5$ only in the special case $\eta_A = \eta_B$.

We have also applied the same kind of procedure to eq. [4]. In this case the mathematics are much more complicated because eq. [4] is written in terms of the equilibrium mole fractions (Z), but we want to set d ln η/d$X_A = 0$. Details of this complicated derivation and subsequent calculation are available elsewhere;[1] results can be summarized by stating that eq. [4] leads to a maximum in ln η (or in η) at $X_A = 0.61_2$, in excellent agreement with the experimental results. Again we see that our combination of the ideal associated solution model with the ideal viscosity eq. [1] is more consistent with the experimental results than is the Grunberg equation.

4. Conclusions

It has been shown that the Grunberg equation (one adjustable parameter, d) can account for the composition dependence of the viscosities of highly non-ideal mixtures of chloroform+ triethylamine over the whole range of compositions. It has also been shown that a combination of the ideal associated solution model with the ideal viscosity equation (this combination also has one adjustable parameter, η_{AB}) provides a more accurate account of the viscosities of chloroform + triethylamine. In addition to providing an accurate quantitative representation of the viscosities over the entire range of compositions, this latter approach also has the appeal of offering a clear pictorial model of the mixtures.

Acknowledgment

We thank the Natural Sciences and Research Council of Canada for support of this and related research.

1. L. GRUNBERG and A.H. NISSAN. Nature, **164**, 799 (1949).
2. L. GRUNBERG. Trans. Faraday Soc. **50**, 1293 (1954).
3. R. J. FORT and W. R. MOORE. Trans. Faraday Soc. **62**, 1112 (1966).
4. G. DELMAS, P. PURVES, and P. DE SAINT-ROMAN. J. Phys. Chem. **79**, 1970 (1975).
5. M. P. KHOSLA, P. P. SINGH, and B. S. MAHL. Z. Phys. Chem. Leipzig, **256**, 1 (1975).
6. J. NATH and S. N. DUBEY. J. Phys. Chem. **85**, 886 (1981).
7. H. VOGEL and A. WEISS. Ber. Bunsenges. Phys. Chem. **86**, 193 (1982).
8. W. E. ACREE, JR., and G. L. BERTRAND. J. Solution Chem. **12**, 755 (1983).
9. D. J. G. IRWIN, R. JOHNSON, and R. PALEPU. Thermochim. Acta, **82**, 277 (1984).
10. R. PALEPU, J. OLIVER, and B. MACKINNON. Can. J. Chem. **63**, 1024 (1985).
11. A. V. ANATARAMAN. Can. J. Chem. **64**, 46 (1986).
12. H. PHUONG-NGUYEN and G. DELMAS. Can. J. Chem. **64**, 681 (1986).
13. D. V. FENBY and L. G. HEPLER. Chem. Soc. Rev. **3**, 193 (1974).
14. L. G. HEPLER and D. V. FENBY. J. Chem. Thermodyn. **5**, 471 (1973).
15. L. G. HEPLER, Z. S. KOONER, G. ROUX-DESGRANGES, and J.-P. E. GROLIER. J. Solution Chem. **14**, 579 (1985).
16. J. R. VAN WAZER, J. W. LYONS, K. Y. KIM, and R. E. COLWELL. Viscosity and flow measurement. Interscience Publishers (J. Wiley & Sons), New York, 1963. pp. 202–204.
17. I. C. WEI and R. L. ROWLEY. J. Chem. Eng. Data, **29**, 332 (1984).

Can. J. Chem. Downloaded from www.nrcresearchpress.com by 41.223.56.140 on 09/07/12
For personal use only.

Conformational analysis of configurationally isomeric dicyclohexano-12-crown-4 ethers and their lithium complexes in solution as studied via ^{13}C NMR spectroscopy

G. W. BUCHANAN,[1] R. A. KIRBY, AND K. BOURQUE

Ottawa–Carleton Chemistry Institute, Department of Chemistry, Carleton University, Ottawa, Ont., Canada K1S 5B6

Received August 2, 1988

G. W. BUCHANAN, R. A. KIRBY, and K. BOURQUE. Can. J. Chem. **67**, 449 (1989).

From ^{13}C NMR coalescence temperature measurements, the *cis-syn-cis* isomer of the title crown ether is shown to undergo a single degenerate ring inversion process with a barrier of 45.9 ± 0.3 kJ/mol. For the corresponding *cis-anti-cis* isomer, a second ring inversion process has been detected, giving rise to two conformations whose free energies differ by ca. 1.5 kJ/mol. The influence of lithium ion complexation on these barriers as well as on the ^{13}C spin-lattice relaxation times has been investigated.

Key words: crown ethers, dynamic stereochemistry.

G. W. BUCHANAN, R. A. KIRBY et K. BOURQUE. Can. J. Chem. **67**, 449 (1989).

En se basant sur des mesures de température de coalescence en RMN du ^{13}C, on a démontré que l'isomère *cis-syn-cis* de l'éther couronne mentionné dans le titre subit un seul processus dégénéré d'inversion de cycle, avec une barrière de 45,9 ± 0,3 kJ/mol. Pour l'isomère *cis-anti-cis* correspondant, on a détecté un deuxième processus d'inversion de cycle qui donne lieu à deux conformations dont les énergies libres diffèrent par environ 1,5 kJ/mol. On a étudié l'influence de la complexation par l'ion lithium sur ces barrières ainsi que sur les temps de relaxation spin réseau en RMN du ^{13}C.

Mots clés : éthers couronnes, stéréochimie dynamique.

[Traduit par la revue]

Can. J. Chem. Downloaded from www.nrcresearchpress.com by 122.72.124.2 on 09/07/12
For personal use only.

Introduction

Recent publications from these laboratories have dealt with the detection, via ^{13}C nuclear magnetic resonance at low temperature, of multiple conformational equilibria in stereoisomeric dicyclohexano-18-crown-6 (1) and -14-crown-4 (2, 3) ethers and their alkali metal ion complexes. In view of the current interest in lithium ion complexation by 12-crown-4 ether systems (4), we wish to report results of our studies concerning the corresponding dicyclohexano-12-crown-4 cases.

Results and discussion

Catalytic hydrogenation of dibenzo-12-crown-4 ether (5) yields a mixture of *cis-syn-cis*-dicyclohexano-12-crown-4, **1**, and the corresponding *cis-anti-cis* isomer, **2**, in a ratio of ca. 20:1. The configurations of **1** and **2** have been determined by X-ray crystallography.[2] Figure 1 depicts the structures and numbering schemes for these materials, with the dispositions of the cyclohexane rings being consistent with the X-ray data.

Chemical shifts and coalescence data

These data are collected in Table 1. Chemical shift assignments at 298 K are made as a result of two considerations. Initially, distinction between resonances for CH vs. CH_2 carbons bearing oxygen is made on the basis of results of the APT experiment (7). Distinction between resonances for C-7,10,17,20 vs. C-8,9,18,19 is made subsequently on the basis of the known β-deshielding effect of oxygen on cyclohexyl ring carbon resonances (7).

For **1**, reduction of the temperature produces ^{13}C NMR spectral changes (Fig. 2) consistent with a single degenerate process becoming slow on the NMR time scale. The four-line spectrum at 298 K shows eight lines in the slow exchange limit.

From the coalescence temperatures (T_c) and limiting chemical shift differences in Table 1, one can use the Eyring equa-

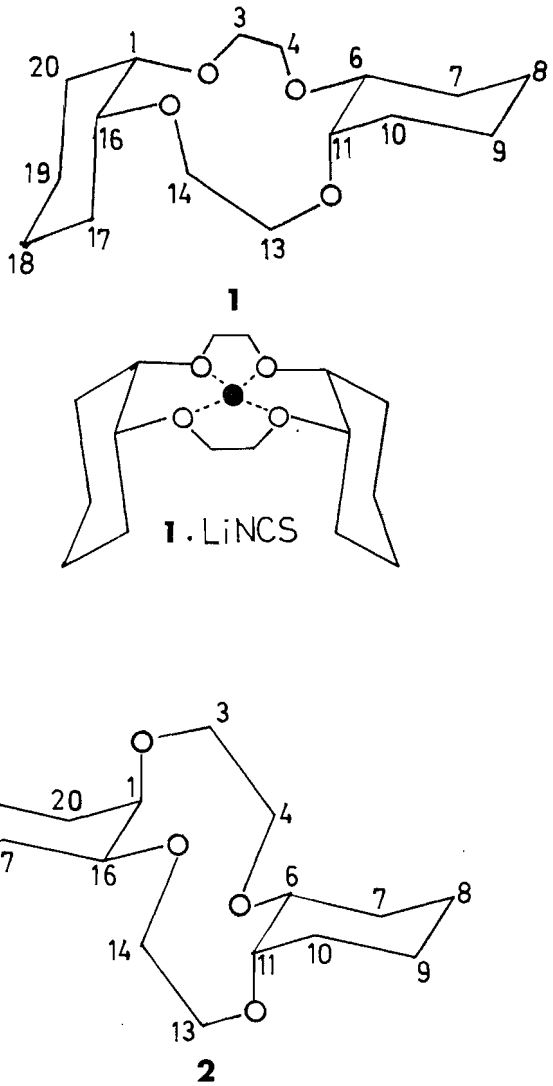


FIG. 1. Structures and numbering schemes for materials studied.

[1]Author to whom correspondence may be addressed.

[2]G. W. Buchanan, R. A. Kirby, and J. P. Charland. Unpublished observations.

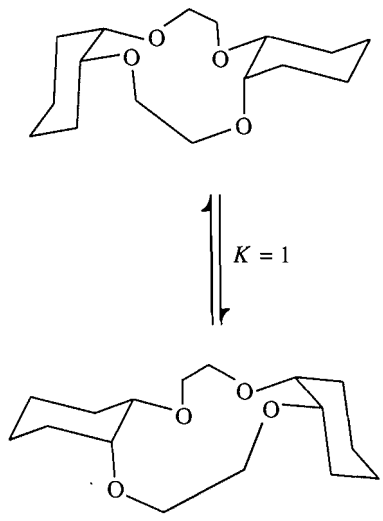
TABLE 1. ^{13}C Chemical shifts ($\delta_C \pm 0.01$) and coalescence data

Compound	Carbon	δ_C (at 298 K)	$\Delta\nu$ (Hz)[a]	T_c (K) ± 1	$\Delta G^{\ddagger}$ (kJ/mol)
1	1, 6, 11, 16	74.52	566.85	249	45.8
	3, 4, 13, 14	65.76	106.35	232	45.7
	7, 10, 17, 20	27.61	75.25	232	46.4
	8, 9, 18, 19	22.52	258.15	240	45.6
					Average = 45.9 ± 0.3[b,d]
1·LiNCS	1, 6, 11, 16	75.77	447.17	252	46.8
	3, 4, 13, 14	65.34	n.o.[c]		
	7, 10, 17, 20	27.00	58.85	230	46.5
	8, 9, 18, 19	21.75	272.63	245	46.5
					Average = 46.6 ± 0.1[b,d]
2	1, 6, 11, 16	78.35	328.96 (major)	225	42.3
			327.95 (minor)		
	3, 4, 13, 14	70.08	181.08 (major)	215	41.3
	7, 10, 17, 20	28.23	n.o.[c]		
	8, 9, 18, 19	22.47	285.70	220	41.5
					Average = 41.7 ± 0.4[b,d]
2 + 1 equiv. LiNCS	1, 6, 11, 16	77.76	223.84 (major)	220	42.0
	3, 4, 13, 14	66.66	n.o.[c]		
	7, 10, 17, 20	26.55	n.o.[c]		
	8, 9, 18, 19	21.64	271.62	223	42.6
					Average = 42.3 ± 0.3[b,d]

[a]At 50.3 MHz.
[b]Uncertainties in $\Delta G^{\ddagger}$ are standard deviations.
[c]Not observable due to resonance overlap.
[d]The close agreement between $\Delta G^{\ddagger}$ values at different temperatures indicates that $\Delta S^{\ddagger}$ must be near zero for these processes.

Can. J. Chem. Downloaded from www.nrcresearchpress.com by 122.72.124.2 on 09/07/12
For personal use only.

tion to calculate $\Delta G^{\ddagger}$, the free energy of activation for the process. The value obtained, 45.9 ± 0.3 kJ/mol, is 3–4 kJ/mol *higher* than that obtained for ring inversion in simple 1,2-disubstituted cyclohexanes (8), or in related dicyclohexano-18-crown-6 (1) and -14-crown-4 systems (2, 3). Apparently the constraints of the smaller bridging units in the dicyclohexano-12-crown-4 ether **1** have introduced additional rigidity into the molecule and hence increased the inversion barrier. We attribute the present results to the degenerate double cyclohexane ring inversion process as depicted below. In the slow exchange limit there is an exceptionally large chemical shift difference of



11.26 ppm between methine carbons bearing oxygen, the more deshielded resonance being attributed to the carbon bearing equatorial oxygen, i.e., C-6,16, by analogy with earlier work (1–3). The most shielded resonance, at $\delta_C = 19.92$, is assigned to C-9,19, which bear a *gauche*-γ relationship to the axial oxygens at positions 2 and 12 respectively (8). The sites that are *trans*-γ to equatorial oxygen, i.e., C-8,18, resonate at δ_C = 25.08 ppm in the slow exchange limit.

For **1**·LiNCS, the data in Table 1 indicate only a minor increase (i.e., <1 kJ/mol) in $\Delta G^{\ddagger}$ for the ring reversal process relative to free **1**. This is in marked contrast to the case for the corresponding isomer in the dicyclohexano-14-crown-4 series (3), where complexation induced an increase of ca. 5 kJ/mol. The X-ray crystallographic data[2] indicate that the four oxygens of the LiNCS complex of **1** do not lie in a plane and hence a less than ideal coordination geometry results. Furthermore, the 12-crown-4 effective cavity diameter is substantially less than that regarded as optimal for Li complexation, so that stabilities of 12-crown-4 lithium complexes are substantially lower than those for the corresponding 14-crown-4 ether systems (5). The less effective complexation of Li^+ by **1** than in the case of the 14-crown-4 analog is further manifest in the spin-lattice relaxation time results (*vide infra*).

For the *cis-anti-cis* isomer **2**, the spectra (Fig. 2) clearly indicate the presence of a second conformation in the low temperature limit. From relative peak intensity measurements, the equilibrium constant K is 2.6 ± 0.3, giving rise, via the equation $-\Delta G^0 = RT \ln K$, to a free energy difference between these forms of 1.5 ± 0.3 kJ/mol at 183 K. It is also evident

Can. J. Chem. Downloaded from www.nrcresearchpress.com by 122.72.124.2 on 09/07/12
For personal use only.

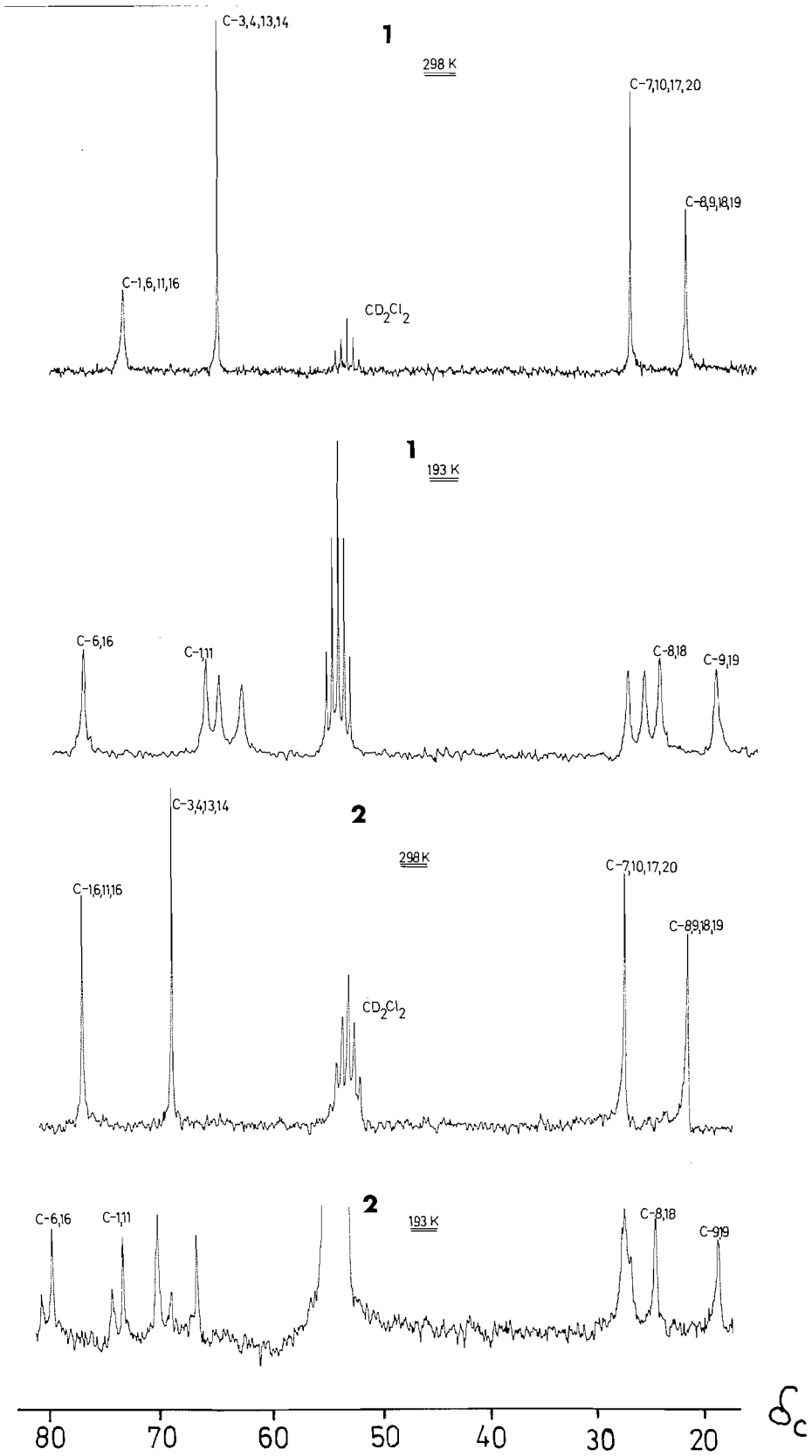
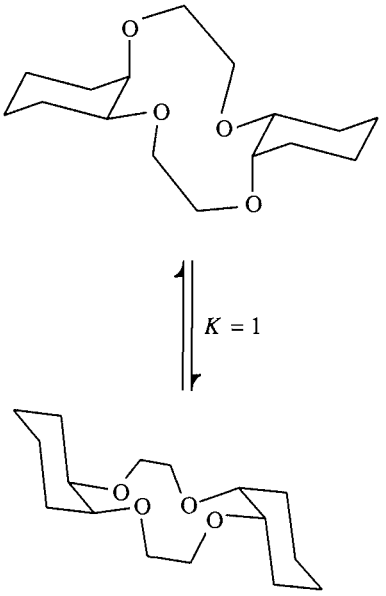


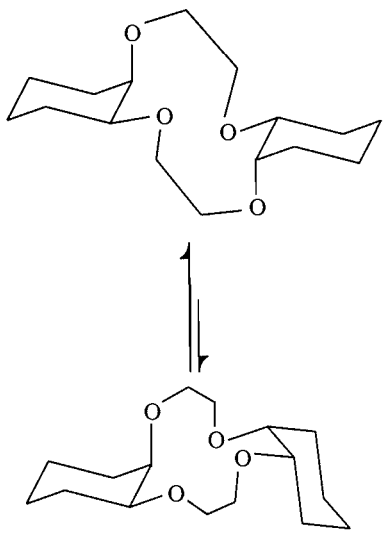
FIG. 2. The 50.3-MHz ^{13}C NMR spectra of **1** and **2** as a function of temperature.

from the spectra that peak overlap or accidental chemical shift equivalence renders the non-degenerate process invisible at the non-oxygenated carbons. For example, the C-8,9,18,19 resonance changes from a single line at 298 K appearing at δ_C = 22.47 to a pair of equal intensity lines at 19.23 and 24.91 ppm in the slow exchange limit. This observation indicates the presence of the degenerate double cyclohexane ring inversion process as depicted in the following scheme.



The free energy of activation for this process in **2** is significantly lower (ca. 4 kJ/mol) than that for **1**. This fact is reflected in the spectra of **1** and **2** at 298 K. There is already evidence of exchange broadening for the C-8,9,18,19 resonance of **1** despite the lower limiting chemical shift difference at this site than is found for **2**.

Although it is difficult to identify unambiguously the nature of the second dynamic process, we tentatively attribute it to the inversion of a single cyclohexane ring, accompanied by a reorganization of the macrocyclic geometry as shown below. The postulated structure of the minor conformation is such that the "chromophoric unit" is 1/2 a molecule, so that 8 carbons are anticipated for it in the limit of slow exchange. Unfortunately, accidental resonance overlap precludes observation of all the anticipated resonances for the conformers of **2**.



An alternative would be to suggest that 12-membered ring pseudorotation was the origin of the spectral changes, with no accompanying cyclohexane ring inversion. For 12-crown-4 itself, two dynamic conformational processes have been detected by low temperature ^1H and ^{13}C spectroscopy (9). The barriers for these processes, however, are ca. 26 and 23 kJ/mol respectively, which are substantially lower than observed in **2**. Accordingly, we suggest that it is the cyclohexane ring inversion that is rate limiting in the present case, with internal conformational changes in the 12-membered central ring remaining fast on the NMR time scale at 183 K. Notably, ΔG^0 of 1.5 kJ/mol between conformations of **2** is nearly identical to that found for the *cis-anti-cis* isomer of dicyclohexano-14-crown-4, a case where the nature of the second ring reversal process can be unambiguously identified (2, 3).

TABLE 2. ^{13}C Spin-lattice relaxation times (T_1)

Compound	Site	T_1 (s)
1	C-1, 6, 11, 16	1.76 ± 0.19
1·LiNCS	C-1, 6, 11, 16	1.29 ± 0.02
2	C-1, 6, 11, 16	2.84 ± 0.17
2 + 1 equiv. LiNCS	C-1, 6, 11, 16	2.06 ± 0.20
1	C-3, 4, 13, 14	0.79 ± 0.11
1·LiNCS	C-3, 4, 13, 14	0.78 ± 0.01
2	C-3, 4, 13, 14	1.72 ± 0.04
2 + 1 equiv. LiNCS	C-3, 4, 13, 14	1.23 ± 0.14
1	C-7, 10, 17, 20	0.82 ± 0.12
1·LiNCS	C-7, 10, 17, 20	0.82 ± 0.02
2	C-7, 10, 17, 20	1.68 ± 0.03
2 + 1 equiv. LiNCS	C-7, 10, 17, 20	1.49 ± 0.16
1	C-8, 9, 18, 19	0.82 ± 0.09
1·LiNCS	C-8, 9, 18, 19	0.76 ± 0.02
2	C-8, 9, 18, 19	1.52 ± 0.03
2 + 1 equiv. LiNCS	C-8, 9, 18, 19	1.42 ± 0.19

The lower ring inversion barriers in **2** relative to **1** and the presence of an additional conformation in **2** leads one to the conclusion that **2** is a more "mobile" species than **1** in solution at 298 K. Spin-lattice relaxation time data (*vide infra*) lend support to this thesis.

Although **2** does not form an isolable LiNCS complex, a solution of **2** containing 1 equivalent of LiNCS has been examined via low temperature ^{13}C NMR to detect any influence that solution interactions with the Li^+ species may have on the stereochemical equilibria. The results are included in Table 1. It is evident that there is only a minor influence on the barrier to degenerate double cyclohexane ring inversion, although the chemical shifts differ substantially between free **2** and the solution containing 1 molar equivalent of LiNCS. The spectra in the low field region do indicate the presence of a second conformation; however, peak overlap precludes determination of the ΔG^0 values between conformers.

^{13}C spin-lattice relaxation times (T_1)

These data were determined by the inversion–recovery method (10) and are presented in Table 2. Measurement of nuclear Overhauser enhancements indicated that spin-lattice relaxation in these molecules is dominated by the dipole–dipole mechanism to the extent of over 90% at all sites. In view of the molecular weights of **1** and **2** it is reasonable to assume that the motional narrowing conditions apply, hence the correlation time τ_c for the C—H vector is proportional to $1/T_1$.

Initially it is of interest to compare the T_1 data for uncomplexed **1** and **2**. At all carbons, the observed T_1's for **2** are substantially longer than for the corresponding carbons of **1**. This indicates a greater degree of mobility in the *cis-anti-cis* isomer **2** than in the *cis-syn-cis* counterpart **1**. Such behavioural differences between these isomers were suggested in the previous discussion, based on the lower ring inversion barriers found for **2** as well as the presence of a second conformational

Can. J. Chem. Downloaded from www.nrcresearchpress.com by 122.72.124.2 on 09/07/12
For personal use only.

isomer for **2**, which can be detected at temperatures below 200 K.

For the LiNCS complex of **1**, only the T_1 for the CH carbon bearing oxygen (i.e., C-1,6,11,16) is shortened relative to the data for free **1**. The relaxation times of the other sites are unchanged, indicating little alteration in the motional character of these C—H bonds as a result of lithium complexation. As a consequence of these apparently weak interactions of the lithium ion with **1**, the ring inversion barrier (Table 1) increases to only a minor extent. These findings are in marked contrast to the corresponding isomer in the 14-crown-4 series, where the T_1's were reduced to ca. 50% in the LiNCS complex relative to the free ligand, and lithium complexation increased the ring inversion barrier by ca. 5 kJ/mol (3).

The T_1 results for the solution of **2** and one equivalent of LiNCS indicate that the mobilities of both types of oxygenated carbon have been decreased upon addition of the Li^+ ion. By contrast, the T_1's for the non-oxygenated carbons are, within the limits of uncertainty, essentially identical. Hence there appears to be a weak specific solution binding interaction between **2** and the Li^+ ion despite the fact that no LiNCS or $LiClO_4$ complex is isolable. This weak binding interaction is manifest also in the minor increase in the ring inversion barrier noted for the solution of **2** and LiNCS.

For 12-crown-4 itself in methanol solution, the effects of complexation of Li^+, Ca^{2+}, and Mg^{2+} on the ^{13}C T_1's have been evaluated recently (11). The higher mobility of 12-crown-4 relative to the dicyclohexano analogs **1** and **2** is evident from the observed T_1 of ca. 6 s at 298 K. Upon complexation with LiCl this value is reduced to ca. 3 s, which reflects the expected reduction in the mobility of the crown ether carbons. Complexation effects on the T_1's of **1** and **2** are less pronounced than for 12-crown-4 itself. This is presumably due to the influence of the bulky cyclohexano groups, which prevent a facile reorganization of the 12-membered ring geometry to that most favorable for lithium ion complexation.

The 200-MHz ^1H spectra of **1**, **1**·LiNCS, and **2** are also temperature dependent; however, extensive resonance overlap in the spectra near $\delta = 3.6$ between the cyclohexyl methine protons and the methylene protons on C-3, 4, 13, and 14 precludes any detailed interpretation. It is clear for **2**, however, that the cyclohexyl methine protons decoalesce at a considerably higher temperature than do the methylene protons of the crown ether, and a degenerate process is observed. At 218 K, this is evident from the detection of distinct resonances of equal integrated intensity for the axial and equatorial methine protons with a chemical shift difference of ca. 1 ppm. Hence the ^{13}C NMR evidence for the degenerate double ring inversion in **2** at the higher temperatures is supported by the ^1H results.

At higher fields, i.e., 400 or 500 MHz, it may be possible to obtain useful information regarding the 12-membered ring conformations at lower temperatures in these materials, as has been carried out for 12-crown-4 itself (12) and a 2:1 12-crown-4:NaNCS complex (13). Such experiments are planned.

Experimental

Spectra

The ^{13}C NMR spectra were obtained using a Varian XL-200 spectrometer operating at 40.3 MHz. Sample concentrations were approximately 0.2 M in CD_2Cl_2 solutions contained in 5 mm o.d. tubes. Routinely spectra were recorded with complete ^1H noise decoupling. Normal operating conditions were as follows: sweep width = 5 kHz with 16K data points; pulse width = 6 μs (45°) and a repetition rate of 1.0 s. The number of accumulations for the low temperature spectra was typically 1000–2000. Temperatures were calibrated using a copper–constantan thermocouple in a dummy NMR tube.

For the T_1 measurements, the inversion–recovery sequence (10) was employed and data were processed using the standard XL-200 software.

Materials

Dibenzo-12-crown-4 ether was prepared via the published procedure (5) with the exception of the hydrolysis of 1,2-bis(*o*-methoxyphenoxy)ethane to 1,2-bis(*o*-hydroxyphenoxy)ethane. This was accomplished selectively using the trimethylsilyliodide reagent (14) as described previously (15).

Hydrogenation of dibenzo-12-crown-4 to a mixture of **1** and **2** was accomplished employing an American Instrument Co. 50 000 psi maximum pressure high pressure apparatus (1 psi = 6.9 kPa). A typical procedure follows. In 60 mL of dry 1-butanol was dissolved 2.0 g (0.0074 mol) of dibenzo-12-crown-4 and 0.40 g of 5% ruthenium on alumina catalyst. A pressure of H_2 gas of 1200 psi was used and the reaction was continued for 12 h at a temperature of 120°C. The catalyst was removed by filtration and the butanol by rotary evaporation at 70°C to yield 1.9 g (90%) of a dark oily mixture, which was estimated by ^{13}C NMR to contain two isomers in a ratio of ca. 20:1. Column chromatography was carried out on silica gel (70–230 mesh) with a 30:1 hexane:diethyl ether solvent mixture. Initial fractions contained a ca. 50:50 mixture of isomers while the latter ones contained an essentially pure isomer, mp 69–71°C. This was later shown by X-ray crystallography to be the *cis-syn-cis* compound **1**. The early fractions from several such columns were combined and subsequent column chromatography using the same solvent system yielded the minor (*cis-anti-cis*) isomer **2**, mp 101–103°C.

The LiNCS complex of **1** was prepared according to the following procedure. Equimolar amounts of **1** and LiNCS were dissolved in a minimum volume of dry methanol. Subsequently the solvent was removed via rotoevaporation to yield a thick oil. This oil was dissolved in dry methylene chloride and the solvent was allowed to evaporate slowly to yield white crystals of **1**·LiNCS, mp 202–204°C. The structure of this complex was verified by X-ray crystallography.[2]

1. G. W. Buchanan, K. Bourque, J. W. Bovenkamp, and A. Rodrigue. Can. J. Chem. **63**, 2747 (1985).
2. G. W. Buchanan and R. A. Kirby. Tetrahedron Lett. **28**, 1507 (1987).
3. G. W. Buchanan, R. A. Kirby, K. Bourque, and C. Morat. Can. J. Chem. **66**, 2204 (1988).
4. P. P. Power. Acc. Chem. Res. **21**, 147 (1988).
5. C. J. Pedersen. J. Am. Chem. Soc. **89**, 7017 (1967).
6. S. L. Patt and J. N. Shoolery. J. Magn. Reson. **46**, 535 (1982).
7. H.-J. Schneider and V. Hoppen. Tetrahedron Lett. 579 (1974).
8. N. K. Wilson and J. B. Stothers. Top. Stereochem. **8**, 1 (1973).
9. F. A. L. Anet, J. Krane, J. Dale, K. Daasvatn, and P. O. Kristiansen. Acta Chem. Scand. **27**, 3395 (1973).
10. R. L. Vold, J. S. Waugh, M. P. Klein, and D. E. Phelps. J. Chem. Phys. **48**, 383 (1968).
11. C. Erk. Spectrosc. Lett. **19**, 1175 (1986).
12. J. Borgen, J. Dale, K. Daasvatn, and J. Krane. Acta Chem. Scand. Ser. B: **B34**, 249 (1980).
13. J. Krane, E. Amble, J. Dale, and K. Daasvatn. Acta Chem. Scand. Ser. B: **B34**, 255 (1980).
14. M. E. Jung and M. A. Lyster. J. Org. Chem. **42**, 3761 (1977).
15. G. W. Buchanan, R. A. Kirby, and J. P. Charland. J. Am. Chem. Soc. **110**, 2477 (1988).

Can. J. Chem. Downloaded from www.nrcresearchpress.com by 122.72.124.2 on 09/07/12
For personal use only.

Phosphorus-31 solid-state nuclear magnetic resonance study of monophosphazenes

WILLIAM P. POWER, RODERICK E. WASYLISHEN,[1] AND RONALD D. CURTIS
Department of Chemistry, Dalhousie University, Halifax, N.S., Canada B3H 4J3

Received September 21, 1988

WILLIAM P. POWER, RODERICK E. WASYLISHEN, and RONALD D. CURTIS. Can. J. Chem. **67**, 454 (1989).

Simultaneous observation of anisotropic chemical shielding and dipolar coupling in polycrystalline monophosphazenes has been used to obtain information on the $^{31}P-^{14}N$ spin pair. Phosphorus-31 chemical shielding tensor components have been determined; the most shielded component was found to lie along the P=N bond. The $^{31}P-^{14}N$ dipolar coupling constants have provided P=N bond lengths from powder samples, equivalent for all compounds within experimental error; the value obtained for *N*-(triphenylphosphoranylidene)-aniline is in excellent agreement with that obtained in a recent X-ray diffraction study. Features of crystallographic significance have been determined from the solid-state nuclear magnetic resonance spectra for two of the compounds without resorting to diffraction techniques. Information on the magnitude and orientation of the ^{14}N electric field gradient tensor has been inferred from ^{31}P MAS spectra and *ab initio* calculations.

Key words: monophosphazenes, dipolar nmr, ^{31}P chemical shielding anisotropies, solid-state nmr.

WILLIAM P. POWER, RODERICK E. WASYLISHEN et RONALD D. CURTIS. Can. J. Chem. **67**, 454 (1989).

Dans le but d'obtenir de l'information sur la paire de spin $^{31}P-^{14}N$, on a observé simultanément le blindage chimique anisotropique et le couplage dipolaire de monophosphazènes polycristallins. On a déterminé les composantes du tenseur du blindage chimique du phosphore-31; la composante la plus blindée se trouve le long de la liaison P=N. Utilisant les constantes de couplages dipolaires $^{31}P-^{14}N$ déterminées à partir d'échantillons de poudres, on a pu évaluer les longueurs des liaisons P=N qui sont équivalentes pour tous les composés, aux erreurs expérimentales près; la valeur obtenue pour la *N*-(triphénylphospharanylidène)-aniline est en excellent accord avec celle qui a été obtenue dans une étude récente de diffraction des rayons-X. Sans recourir à des techniques de diffraction, mais en faisant appel à leurs spectres en résonance magnétique nucléaire, on a pu déterminer des caractéristiques cristallographiques importantes pour deux des composés. En se basant sur les spectres MAS du ^{31}P et des calculs *ab initio*, on a pu déduire des informations sur l'amplitude et l'orientation du tenseur du gradient du champ électrique du ^{14}N.

Mots clés : monophosphazènes, rmn dipolaire, anisotropies du blindage chimique de ^{31}P, rmn de l'état solide.

[Traduit par la revue]

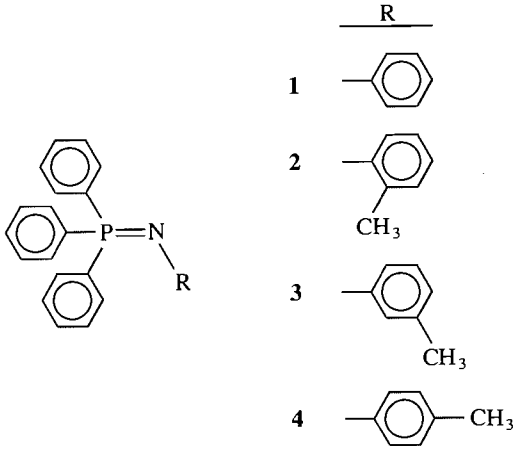
Introduction

Recent advances in the study of polycrystalline solids by nmr have led to an increase in the use of this technique to elucidate the structural and electronic characteristics of biological (1–5), organic (6–10), inorganic (11,12), and polymeric compounds (13, 14). In principle, the nmr spectrum of a solid contains much more information on the chemical nature of a compound than the corresponding solution spectrum. The solid-state spectrum defines the orientation dependence of various interactions, which in solution are either observed simply as their isotropic average, or not observed at all (15, 16).

In the simplest experiment, an isolated spin 1/2 nucleus is studied yielding its chemical shielding anisotropy, which arises from variations in the electronic screening of the nucleus with changes in the orientation of the molecule in the magnetic field (16). However, for powder samples, only the magnitudes of the principal components of the chemical shielding tensor are obtained and no information on the orientation of the tensor can be determined from an experiment of this type. Previously, the only methods by which the orientation could be derived were symmetry arguments, in favorable cases, or time-consuming single crystal analysis (17–20).

Recently, however, there have been several reports of determination of the orientation of the shielding tensor from a single experiment (1–14). This has been accomplished by studying an isolated spin pair where dipolar coupling exists between the two nuclei. The dipolar coupling is manifested in the overall lineshape, and provides a molecular frame of reference about which the chemical shielding tensor of one of the nuclei can be oriented.

Using this technique, we report both the magnitude of the principal components and the orientations of previously undetermined phosphorus-31 shielding tensors, as well as P=N bond lengths, in a series of monophosphazenes (**1**–**4**) by analysis of the solid-state ^{31}P spectra for a $^{31}P-^{14}N$ spin pair. With the exception of the diatomic molecule, PN (21), the anisotropy of ^{31}P shielding in compounds containing phosphorus–nitrogen bonds has not been previously investigated (22). The monophosphazene system is composed of a phosphorus(V) centre double-bonded to a nitrogen, and is of some importance with the recent development of inorganic polymers such as polyphosphazene (23).



[1]Author to whom correspondence may be addressed.

Can. J. Chem. Downloaded from www.nrcresearchpress.com by 41.223.56.140 on 09/07/12
For personal use only.

Can. J. Chem. Downloaded from www.nrcresearchpress.com by 41.223.56.140 on 09/07/12
For personal use only.

Theory

For an isolated $^{31}P-^{14}N$ spin pair, the ^{31}P nmr frequencies depend on the strength of the applied static magnetic field, B_0, the ^{31}P chemical shielding tensor, σ, and the magnitude of the $^{31}P-^{14}N$ dipolar coupling (16, 24). Work in our laboratory has described a theoretical treatment for such a spin 1/2 – spin 1 system (in that study, $^{13}C-^{14}N$) in the case of axial symmetry in the spin 1/2 chemical shielding where the unique axis of the shielding tensor is constrained to lie along the internuclear vector (25). Following that notation, the phosphorus spin Hamiltonian is given by

$$[1] \quad h^{-1}H = -\nu_P[1 - \sigma_{iso} + \Delta\sigma(1/3 - \cos^2\theta)]\hat{I}_z + R[(1 - 3\cos^2\theta)\hat{I}_z\hat{S}_z - (3\sin\theta\cos\theta)\hat{I}_z\hat{S}_x]$$

where

$$[2] \quad \nu_P = (\gamma_P/2\pi)B_0$$

$$[3] \quad \sigma_{iso} = (\sigma_{||} + 2\sigma_{\perp})/3$$

$$[4] \quad \Delta\sigma = \sigma_{||} - \sigma_{\perp}$$

and

$$[5] \quad R = \frac{\gamma_P\gamma_N\hbar}{2\pi}\left\langle\frac{1}{r_{PN}^3}\right\rangle\frac{\mu_0}{4\pi}$$

θ is the angle between the applied magnetic field and the internuclear dipolar vector, and r_{PN} is the P=N bond length.

However, eq. [1] does not hold in the case of nonaxial symmetry in the chemical shielding of the ^{31}P nucleus, nor when the internuclear vector does not lie along the unique shielding axis. Analysis of such cases has been performed on spin 1/2–spin 1/2 systems (e.g., $^{13}C-^{15}N$ spin pairs) to yield a completely general treatment when both chemical shielding and dipolar coupling are present (1, 3, 6, 26). If this treatment is extended along the lines of the previous work but now including nonaxially symmetric chemical shielding and allowing the internuclear vector to assume any orientation relative to the shielding tensor, new expressions are obtained. Following the method of Valentine *et al.* (1), the chemical shielding and dipolar interactions are given respectively by

$$[6] \quad \nu_{CS} = (\gamma_P/2\pi)B_0\{1 - [\sigma_{11}\sin^2\theta\cos^2\phi + \sigma_{22}\sin^2\theta\sin^2\phi + \sigma_{33}\cos^2\theta]\}$$

$$[7] \quad \nu_D = R[1 - 3(\sin\beta\sin\theta\cos(\phi - \alpha) + \cos\beta\cos\theta)^2]$$

where θ and ϕ are the polar and aximuthal angles relating the applied magnetic field to the chemical shielding tensor (see Fig. 1). The angles α and β relate the orientation of the chemical shielding tensor to the internuclear vector, in this case the P=N bond, thus providing a molecular frame of reference. The principal components of the shielding tensor, σ_{11}, σ_{22}, and σ_{33}, can be expressed in terms of chemical shifts, δ_{ii}'s, from the isotropic resonance of a suitable reference compound with values increasing to higher frequency such that $\delta_{11} > \delta_{22} > \delta_{33}$. Note that δ_{11} corresponds to σ_{11} using this convention.

To simulate the experimental spectra, the chemical shielding and dipolar contributions to the spectrum are given by eqs. [6] and [7] and combine as

$$[8] \quad \nu_m = \nu_{CS} - m_N\nu_D$$

where $m_N = -1, 0, +1$, the three possible spin states of ^{14}N. Subspectra corresponding to each of these states were obtained by integration over the angles θ and ϕ in one-degree intervals and then summed to give the total lineshape. A Gaussian broadening function, $g(\nu)$, was also included to account for residual line broadening inherent in the experiment. This allows a better fit between the simulated and experimental spectra, giving as the final operative equation

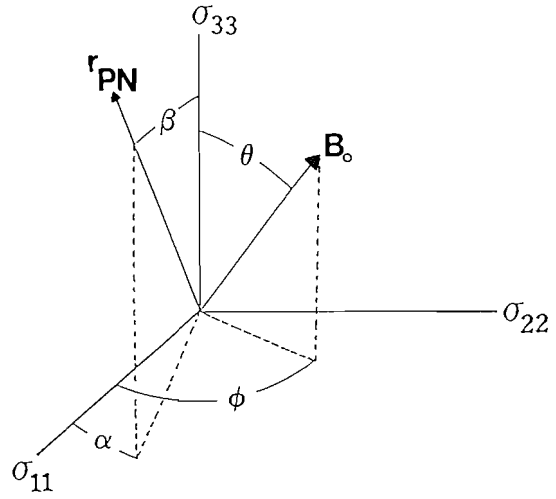


FIG. 1. The magnetic field vector, B_0, and the internuclear dipolar vector, r_{PN}, in the principal axis system of the chemical shielding tensor.

$$[9] \quad I(\nu) = \sum_{-I}^{+I}\int_0^{\pi/2}\int_0^{2\pi} g(\nu - \nu_m)\sin\theta\,d\theta\,d\phi$$

For the general case we have just treated, where the shielding is now no longer axially symmetric, the chemical shielding anisotropy is most conveniently expressed as the width of the entire lineshape, i.e.,

$$[10] \quad \Delta\sigma = \sigma_{33} - \sigma_{11} = \delta_{11} - \delta_{33}$$

and the asymmetry parameter, η, follows the usual convention as described by Spiess (27), Haeberlen (28), and others.

In this analysis, it has been assumed that the ^{14}N Zeeman spin functions are valid spin functions for this system. This may not be true, depending on the relative magnitude of the applied magnetic field and the ^{14}N nuclear quadrupole interaction. If the magnitude of the latter interaction is on the order of the ^{14}N Zeeman interaction, the high-field approximation breaks down and the Zeeman spin functions mix, introducing distortions in the nmr lineshape calculated from eq. [8]. Stoll *et al.* (29) have shown that provided the ratio of the ^{14}N Larmor frequency, $\nu_N = \gamma_N B_0/2\pi$, to the ^{14}N quadrupolar coupling constant, χ, is greater than 4, the high-field approximation results in relatively small errors when calculating the lineshape. If the electric field gradient (efg) is axially symmetric with the largest component oriented along the dipolar vector, the apparent dipolar splitting extracted from the spin 1/2 powder pattern corresponding to the $\theta = 0°$ and 90° orientations will have a negligible error provided $\nu_N/\chi \geq 3$ (25). Although nuclear quadrupolar coupling constants are unavailable for the ^{14}N of a P=N fragment, values are available for HN=SOF_2 (30), where the ^{14}N nuclear quadrupole coupling constant, χ, is 3.59 MHz. It is unlikely that χ in the monophosphazenes exceeds 4.0 MHz (*vide infra*), in which case $\nu_N/\chi \geq 3.6$.

TABLE 1. Principal components of the ^{31}P chemical shift tensor (ppm),[a] $^{31}P-^{14}N$ direct dipolar coupling constants (Hz), P=N bond lengths (Å), and the angles α and β (deg)

Compound	δ_{11}	δ_{22}	δ_{33}	δ_{iso}[b] Solid	δ_{iso}[b] Solution	Δσ	η	R[c]	r_{PN}	α[d]	β[d]
1	50	31	−85	−1 (−0.3)	−1.2	135	0.23	859	1.60	0	0
2	69	29	−72	9 (8.1)	−1.8	141	0.50	888	1.58	0	0
3	48	31	−91	−4 (−2.5, −4.8)	−2.1	139	0.20	875	1.59	0	0
4	49	35	−91	−2 (−1.7)	−1.7	140	0.16	889	1.58	0	0

[a]The shift tensor components can be converted to an absolute shielding scale as follows (22*b*): $\sigma_{ii}(^{31}P)$ = 356 ppm − $\delta_{ii}(^{31}P)$. The error in the reported ^{31}P chemical shift components is ±2 ppm. These values have not been corrected for bulk susceptibility effects.

[b]The values in parentheses were obtained from CP/MAS experiments. The error in the solid δ_{iso} is ±2 ppm, and ±0.2 ppm for the MAS and solution values.

[c]The error in the dipolar coupling constant is ±40 Hz, corresponding to ±0.02 Å for r_{PN}.

[d]The error in the angles α and β is estimated to be less than 10°.

Experimental

Compounds **1**–**4** were obtained from Aldrich Chemical Company and the Alfred Bader Library of Rare Chemicals. The compounds (approximately 0.3 g) were packed in aluminum oxide rotors under a nitrogen atmosphere. Solid-state spectra were recorded on a Bruker MSL-200 nmr spectrometer operating at 200.106 MHz for ^{1}H and 81.005 MHz for ^{31}P. All spectra were accumulated with high-power proton decoupling and cross-polarization. The $\pi/2$ pulses were 4.0 μs. The magic angle sample spinning (MAS) spectra were typically run with spinning rates of 3.0–3.5 kHz in a double-bearing axial spinner probe. All solid-state ^{31}P spectra were referenced to external $NH_4H_2PO_4$, which has a chemical shift of +1.0 ppm with respect to 85% H_3PO_4. Cross-polarization contact times were optimized for each compound in the MAS experiments, and were between 1.3 and 1.8 ms. Flipback of the ^{1}H magnetization was used to increase the sensitivity of the experiment (31). Recycle times were typically 50 s for both the static and MAS spectra. Normally, 32 scans were recorded for the MAS spectra, while up to 800 scans were recorded for some of the static spectra. Solution spectra were recorded on a Nicolet NB-360 spectrometer, operating at 146.15 MHz for ^{31}P. Solutions were 0.010 M in diethyl ether, with external 85% H_3PO_4 as the reference standard.

Simulations were performed using a computer program written in this laboratory based on the treatment outlined in the theory section. Computations were carried out an a VAX 8800 computer and a Perkin–Elmer 3230 computer, with plotting performed on Hewlett–Packard HP 7475A and Nicolet Zeta-12 plotters.

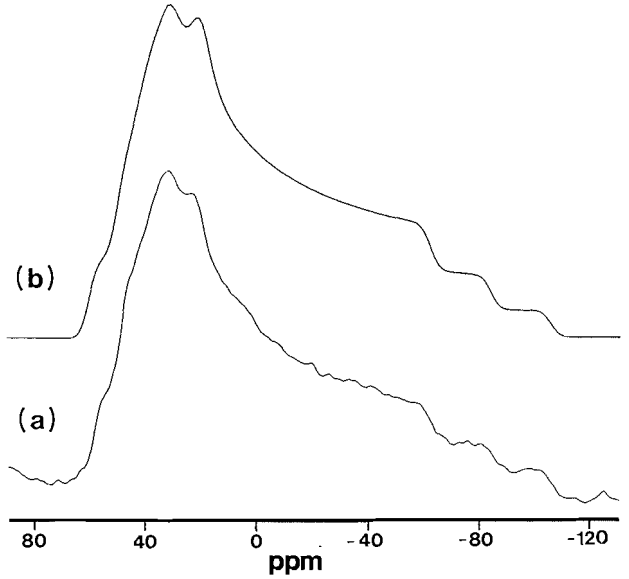


FIG. 2. Experimental (a) and simulated (b) ^{31}P powder spectra of the parent compound, **1**. The simulated spectrum included 200 Hz of Gaussian broadening to fit the experimental spectrum. This large line broadening results from $^{31}P-^{31}P$ intermolecular dipolar interactions.

Results and discussion

A ^{31}P nmr powder pattern typical of those obtained in these experiments is illustrated in Fig. 2(a) for **1**, the parent compound. This lineshape arises from the orientation dependence of both the chemical shift and the direct $^{31}P-^{14}N$ dipole–dipole interaction. Dipolar coupling with the ^{14}N splits the spectrum into three subspectra corresponding to each of the nitrogen spin states ($m_N = -1, 0, +1$). This splitting is clearly visible at the low frequency end of the spectrum. Shown in Fig. 2(b) is the simulation of the ^{31}P nmr spectrum for **1**. The simulation allows precise determination of the shift tensor components, the dipolar coupling constant (hence the P=N bond length), and the relative orientations of the principal components of these two interactions, a factor to which the lineshape is quite sensitive. The results from such analyses for compounds **1**–**4** are given in Table 1.

The parent compound, **1**, shows several characteristics that are consistent throughout this series of compounds. In all cases, the most shielded component of the chemical shift tensor, δ_{33}, was found to lie along the P=N bond. This indicates that the phosphorus nucleus is most shielded when the P=N bond axis is parallel to the applied magnetic field, B_0, a result in accord with other $R_3P{=}X$ systems, where X = O, S, and Se (32–34). However, the asymmetry in the shielding, η, is substantially greater for **1**–**4**, as would be expected for an asymmetric substituent like X = N—Ph. While the chemical shielding anisotropy varies little in this series, it is only 70% of that observed for $Ph_3P{=}O$ in the solid state (32–34) and is even less

Can. J. Chem. Downloaded from www.nrcresearchpress.com by 41.223.56.140 on 09/07/12
For personal use only.

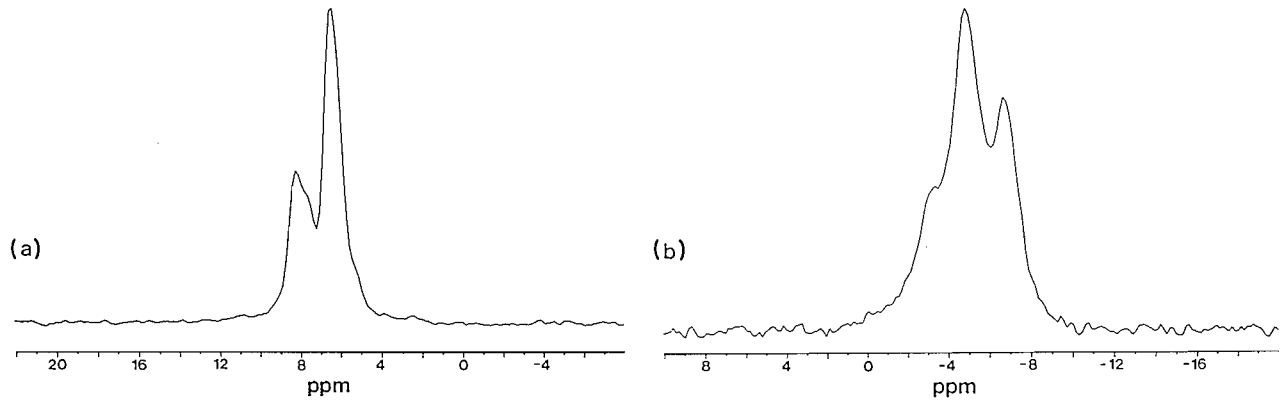


FIG. 3. ^{31}P MAS spectra of compounds **2** (a) and **3** (b). Note that the relative intensities of the components of the asymmetric doublet in **3** appear to be reversed compared to **2** and the other monophosphazenes examined in the present study.

Can. J. Chem. Downloaded from www.nrcresearchpress.com by 41.223.56.140 on 09/07/12
For personal use only.

than those for the corresponding sulfide and selenide compounds (33, 34).

The bond lengths we report for these compounds (**1–4**) were derived from the dipolar coupling constants and are equivalent for all four phosphazenes within experimental error. Note that these are determined from powder samples; there is no need for single crystals in this analysis. A recent X-ray diffraction study of **1** (35) has reported a P=N bond length of 1.602 Å, in excellent agreement with the value given here. Crystallographic data on other related compounds (36–38) establish a range of 1.55–1.61 Å for P=N bond lengths, indicating that those reported here are well within the expected limits. In determining bond lengths from dipolar coupling constants it is sometimes necessary to include contributions from anisotropy in the indirect (J) coupling (24). The small value for $J(^{31}P^{15}N)_{iso}$ in **1**, 32.9 Hz (39), leads one to expect negligible influence from such effects, so it could be safely ignored in this analysis.

Although there are general consistencies for these compounds, one obvious difference is present for the *ortho*-methyl substituted compound, **2**. The asymmetry in the ^{31}P shielding for this molecule is over twice as large as any of the other three. The two extreme components of the shielding, δ_{11} and δ_{33}, are substantially deshielded, leading to a 10-ppm shift to higher frequency for δ_{iso}. It should be noted that this is a solid-state effect; δ_{iso} for **2** in solution is similar to those for the other compounds. Presumably the *ortho*-methyl substitution has affected the crystal packing of this molecule, possibly by tilting the N-phenyl ring out of the PNC plane. However, as there are to our knowledge no available crystal structures of this compound, such conclusions are simply speculation at this point.

It has been possible to establish some crystallographic information for the *meta*-methyl substituted compound, **3**. Inspection of the ^{31}P MAS spectra for **2** and **3** (Figs. 3(a) and (b), respectively) indicates an apparent reversal in the intensity of the 2:1 "doublet" for **3**. Note that for compounds **1**, **2**, and **4** the asymmetric doublet had the same relative orientation. This asymmetric doublet has proven useful in elucidating structural characteristics for $^{13}C,^{14}N$ spin pairs (40–43), and results from a breakdown of the high-field approximation for the ^{14}N in the MAS technique. Under these conditions, magic angle sample spinning no longer completely suppresses the direct dipolar interaction involving ^{14}N and the splitting of the asymmetric doublet depends, among other things, on the orientation and magnitude of the ^{14}N efg tensor (40). It is unlikely that these parameters for the ^{14}N efg tensor in **3** would differ substantially from the corresponding values in **1**, **2**, and **4**; thus the apparent reversal of the asymmetric doublet for **3** must have a different origin. Notice, however, that a shoulder is present on the high frequency side of the doublet, indicating the possibility of nearly coincident resonances arising from magnetically nonequivalent molecules present in the unit cell. A subsequent ^{13}C MAS spectrum for **3** revealed a doubling of the methyl resonance, confirming this explanation. The utility of MAS experiments in identifying such crystal features has been pointed out recently by Harris *et al.* (44). To our knowledge, there have been no diffraction studies of this compound; however, it is unlikely that the nonequivalent molecules differ much in their overall shielding characteristics as the static ^{31}P powder pattern of **3** could be analyzed in terms of a single crystallographic site.

As previously mentioned, the asymmetric doublet observed in the ^{31}P MAS spectra contains information on the magnitude and orientation of the ^{14}N electric field gradient tensor, which should allow one to validate the high-field approximation. As there appear to be no values for this interaction in a ^{14}N=P(V) system available in the literature, estimates were derived from *ab initio* calculations and experimental values for a similar compound, HN=SOF_2 (30), where nitrogen is double bonded to a second row element, sulfur. Calculations were performed on this compound and on HN=PH_3 using the GAMESS *ab initio* calculation package (45) with 6-31G basis sets, to determine the characteristics of the ^{14}N efg tensor in both these compounds. It was found that while the orientation for the efg tensor was fairly accurately predicted by theory for HN=SOF_2 (within 10°), the magnitude of the principal component was overestimated by roughly 40%, common in such treatments when second row elements are involved (46). Subsequently the results for HN=PH_3 were used to establish the orientation of the ^{14}N efg tensor, and the magnitude was scaled according to the relationship between those for the experimental and calculated values for NH=SOF_2. This led to values for the HN=PH_3 system of χ = 3.17 MHz and η = 0.92. The calculated orientation placed the largest principal component of the efg tensor 17° from the P=N bond, with the smallest component lying roughly along the N—H bond. This is the same orientation that was determined experimentally for HN=SOF_2 (30). This information was then used to simulate the ^{31}P MAS

spectrum of **1** using reported routines (40), and a splitting of 154 Hz was calculated, compared to 140 ± 20 Hz observed. In this case, the ratio $\nu_N/\chi = 4.56$; thus for the analysis of the static spectrum, any error introduced by not accounting for the effect of the ^{14}N efg is negligible. While the number of parameters in these simulations does not allow a precise determination of the ^{14}N efg tensor for this system, it does provide a reliable estimate based on both theoretical and experimental methods.

There have been relatively few theoretical treatments of ^{31}P chemical shielding, most concentrating on P(III) species (47–51), while the majority of the experimental studies have been on phosphate and phospholipid systems that do not portray any similarities to the monophosphazenes. For P(III) species, the presence of the lone pair has a very substantial effect on the shielding of the phosphorus nucleus, an effect that is noticeably absent in the compounds studied here. In a recently investigated diphosphene (12), a chemical shielding anisotropy of 1239 ppm was reported, with the direction of greatest shielding not along the P═P bond, but perpendicular to the plane of the molecule, resembling the ^{13}C shielding for carbon nuclei involved in π-bonds (double bonding) of organic molecules (27). Theoretical (47) and experimental (21) work on the diatomic PN indicates an even larger anisotropy of 1376 ppm. Clearly the paramagnetic contribution to the ^{31}P shielding coming from the lone pair on the phosphorus is considerable, leading to the large observed anisotropies, though this is often overestimated by theory, as for ^{15}N in diazenes (52, 53).

In conclusion, the ^{31}P chemical shielding anisotropies observed for the monophosphazenes, approximately 140 ppm, are relatively small compared to those observed in P(III) compounds in which the phosphorus is involved in multiple bonding. As well, the orientation of the shift tensor is markedly different between the P(III) and P(V) oxidation states. The $\Delta\sigma$ values in **1**–**4** are comparable but slightly smaller than the values observed for analogous P(V) compounds where phosphorus forms a double bond to one of the chalcogens (O, S, and Se). It is hoped that the ^{31}P shielding constants reported here will stimulate the interest of theoretical chemists in understanding ^{31}P shielding in phosphorus(V) compounds. Also, the direct measurement of ^{14}N nuclear quadrupolar coupling constants and their orientation in monophosphazenes would clearly be of interest.

Can. J. Chem. Downloaded from www.nrcresearchpress.com by 41.223.56.140 on 09/07/12
For personal use only.

Acknowledgements

We wish to thank Dr. K. Darvesh and Professor R. J. Boyd for providing access to and assistance with the GAMESS program package. W.P.P. and R.D.C. are the holders of NSERC, Killam, and Sumner postgraduate scholarships. All nmr spectra were recorded at the Atlantic Region Magnetic Resonance Centre; we thank NSERC for supporting this centre and this research.

1. K. G. Valentine, A. L. Rockwell, L. M. Gierasch, and S. J. Opella. J. Magn. Reson. **73**, 519 (1987).
2. C. J. Hartzell, T. K. Pratum, and G. Drobny. J. Chem. Phys. **87**, 4324 (1987).
3. T. G. Oas, C. J. Hartzell, T. J. McMahon, G. P. Drobny, and F. W. Dahlquist. J. Am. Chem. Soc. **109**, 5956 (1987).
4. T. G. Oas, C. J. Hartzell, F. W. Dahlquist, and G. P. Drobny. J. Am. Chem. Soc. **109**, 5962 (1987).
5. Y. Hiyama, C.-H. Niu, J. V. Silverton, A. Bavoso, and D. A. Torchia. J. Am. Chem. Soc. **110**, 2378 (1988).
6. K. W. Zilm and D. M. Grant. J. Am. Chem. Soc. **103**, 2913 (1981).
7. A. M. Orendt, J. C. Facelli, A. J. Beeler, K. Reuter, W. J. Horton, P. Cutts, D. M. Grant, and J. Michl. J. Am. Chem. Soc. **110**, 3386 (1988).
8. M. Linder, A. Hoehener, and R. R. Ernst. J. Chem. Phys. **73**, 4959 (1980).
9. M. Munowitz, T.-H. Huang, and R. G. Griffin. J. Chem. Phys. **86**, 4362 (1987).
10. K. W. Zilm, A. J. Beeler, D. M. Grant, J. Michl, T.-C. Chou, and E. L. Allred. J. Am. Chem. Soc. **103**, 2119 (1981).
11. K. W. Zilm, G. A. Lawless, R. M. Merrill, J. M. Millar, and G. G. Webb. J. Am. Chem. Soc. **109**, 7236 (1987).
12. K. W. Zilm, G. G. Webb, A. H. Cowley, M. Pakulski, and A. Orendt. J. Am. Chem. Soc. **110**, 2032 (1988).
13. W. E. J. R. Maas, A. P. M. Kentgens, and W. S. Veeman. J. Chem. Phys. **87**, 6854 (1987).
14. T. Nakai, T. Terao, and H. Shirakawa. Chem. Phys. Lett. **145**, 90 (1988).
15. A. Abragam. Principles of nuclear magnetism. Oxford University Press, Oxford. 1961.
16. M. Mehring. Principles of high resolution NMR in solids. 2nd ed. Springer Verlag, New York. 1983.
17. (*a*) P. N. Tutunjian and J. S. Waugh. J. Magn. Reson. **49**, 155 (1982); (*b*) J. Chem. Phys. **76**, 1223 (1982).
18. A. Naito, D. L. Sastry, and C. A. McDowell. Chem. Phys. Lett. **115**, 19 (1985).
19. M.-R. Van Calsteren, G. I. Birnbaum, and I. C. P. Smith. J. Chem. Phys. **86**, 5405 (1987).
20. H. Hauser, C. Radloff, R. R. Ernst, S. Sundell, and I. Pascher. J. Am. Chem. Soc. **110**, 1054 (1988).
21. J. Raymonda and W. Klemperer. J. Chem. Phys. **55**, 232 (1971).
22. (*a*) J. B. Robert and L. Wiesenfeld. *In* Phosphorus-31 NMR spectroscopy in stereochemical analysis—Organic compounds and metal complexes. *Edited by* J. G. Verkade and L. D. Quin. VCH Publishers, Inc., Deerfield Beach, FL. 1987. p. 151; (*b*) C. J. Jameson. Specialist periodical report—NMR spectroscopy. Vol. 10–17. *Edited by* G. A. Webb. The Chemical Society, London. 1981–1988.
23. R. H. Neilson and P. Wisian-Neilson. Chem. Rev. **88**, 541 (1988).
24. D. L. VanderHart and H. S. Gutowsky. J. Chem. Phys. **49**, 261 (1968).
25. R. M. Dickson, M. S. McKinnon, J. F. Britten, and R. E. Wasylishen. Can. J. Chem. **65**, 941 (1987).
26. U. Haubenreisser, U. Sternberg, and A.-R. Grimmer. Mol. Phys. **60**, 151 (1987).
27. H. W. Spiess. NMR basic principles and progress. Vol. 15. *Edited by* P. Diehl, E. Fluck, and R. Kosfeld. Springer Verlag, New York. 1978.
28. U. Haeberlen. Advances in NMR spectroscopy. Suppl. 1. *Edited by* J. S. Waugh. Academic Press, New York. 1976.
29. M. E. Stoll, R. W. Vaughan, R. B. Saillant, and T. Cole. J. Chem. Phys. **61**, 2896 (1974).
30. P. Cassoux, A. Serafini, G. Fong, and R. L. Kuczkowski. Inorg. Chem. **17**, 1204 (1978).
31. J. Tegenfeldt and U. Haeberlen. J. Magn. Reson. **36**, 453 (1979).
32. L. Bemi, H. C. Clark, J. A. Davies, C. A. Fyfe, and R. E. Wasylishen. J. Am. Chem. Soc. **104**, 438 (1982).
33. J. B. Robert and L. Wiesenfeld. Mol. Phys. **44**, 319 (1981).
34. J. B. Robert and L. Wiesenfeld. J. Magn. Reson. **38**, 357 (1980).
35. E. Boehm, K. Dehnicke, J. Beck, W. Hiller, J. Straehle, A. Maurer, and D. Fenske. Z. Naturforsch. B: Anorg. Chem. Org. Chem. **43B**, 138 (1988).
36. M. J. E. Hewlins. J. Chem. Soc. (B), **1971**, 942 (1971).

37. A. F. CAMERON, I. R. CAMERON, and R. KEAT. Acta Crystallogr. Sect. B: Struct. Crystallogr. Cryst. Chem. **B35**, 1373 (1979).
38. C. W. ALLEN, D. E. BROWN, A. W. CORDES, and S. L. CRAIG. J. Chem. Soc. Dalton Trans. **1988**, 1405 (1988).
39. M. POMERANTZ, B. T. ZIEMNICKA, Z. M. MERCHANT, W.-N. CHOU, W. B. PERKINS, and S. BITTNER. J. Org. Chem. **50**, 1757 (1985).
40. (*a*) J. G. HEXEM, M. H. FREY, and S. J. OPELLA. J. Chem. Phys. **77**, 3847 (1982); (*b*) J. G. HEXEM. Ph.D. thesis, University of Pennsylvania. 1982.
41. (*a*) A. NAITO, S. GANAPATHY, and C. A. MCDOWELL. J. Chem. Phys. **74**, 5393 (1981); (*b*) J. Magn. Reson. **48**, 367 (1982).
42. N. ZUMBULYADIS, P. M. HENRICHS, and R. H. YOUNG. J. Chem. Phys. **75**, 1603 (1981).
43. A. C. OLIVIERI, L. FRYDMAN, and L. E. DIAZ. J. Magn. Reson. **75**, 50 (1987).
44. R. K. HARRIS, L. H. MERWIN, and G. HAEGELE. J. Chem. Soc. Faraday Trans. 1, **83**, 1055 (1987).
45. M. DUPUIS, D. SPANGLER, and J. J. WENDOLOSKI. GAMESS: General Atomic and Molecular Electronic Structure System. National Resource for Computations in Chemistry Software Catalog, Vol. 1, program QG01. Lawrence Berkeley Laboratory, USDOE. 1980.
46. R. D. BROWN and M. P. HEAD-GORDON. Mol. Phys. **61**, 1183 (1987).
47. P. LAZZERETTI and J. A. TOSSELL. J. Phys. Chem. **91**, 800 (1987).
48. V. GALASSO. Chem. Phys. **83**, 407 (1984).
49. T. WELLER, D. DEININGER, and R. LOCHMANN. Z. Chem. **21**, 105 (1981).
50. U. FLEISCHER, M. SCHINDLER, and W. KUTZELNIGG. J. Chem. Phys. **86**, 6337 (1987).
51. D. B. CHESNUT. *In* Phosphorus-31 NMR spectroscopy in stereochemical analysis—Organic compounds and metal complexes. *Edited by* J. G. Verkade and L. D. Quin. VCH Publishers, Inc., Deerfield Beach, FL. 1987. p. 185.
52. M. SCHINDLER. J. Am. Chem. Soc. **109**, 5950 (1987).
53. R. E. WASYLISHEN, W. P. POWER, G. H. PENNER, and R. D. CURTIS. Can. J. Chem. Submitted.

Can. J. Chem. Downloaded from www.nrcresearchpress.com by 41.223.56.140 on 09/07/12
For personal use only.

On the shape of spherically averaged Fermi-hole correlation functions in density functional theory. 1. Atomic systems

VINCENZO TSCHINKE AND TOM ZIEGLER[1]

Department of Chemistry, University of Calgary, Calgary, Alta., Canada T2N 1N4

Received April 27, 1988

VINCENZO TSCHINKE and TOM ZIEGLER. Can. J. Chem. **67**, 460 (1989).

We have compared, for atomic systems, the spherically averaged Fermi-hole correlation function $\bar{\rho}_x^{\alpha\alpha}(r_1, s)$ in the Hartree–Fock theory with the corresponding function $\bar{\rho}_{X\alpha}^{\alpha\alpha}(r_1, s)$ employed in local density functional theory. It is shown that, in contrast to $\bar{\rho}_x^{\alpha\alpha}(r_1, s)$, the function $\bar{\rho}_{X\alpha}^{\alpha\alpha}(r_1, s)$ behaves qualitatively incorrectly at positions r_1 of the reference electron far from the nucleus. Furthermore, we have shown that the qualitatively incorrect behaviour of $\bar{\rho}_{X\alpha}^{\alpha\alpha}(r_1, s)$ can be remedied by an approximate expansion of $\bar{\rho}_x^{\alpha\alpha}(r_1, s)$ in powers of s, where s is the inter-electronic distance. However, such an expansion must be conducted in two regions due to the discontinuity of $\bar{\rho}_x^{\alpha\alpha}(r_1, s)$ as a function of s at the atomic nucleus. Based on the two-region expansion of $\bar{\rho}_x^{\alpha\alpha}(r_1, s)$, we have developed an alternative approximate density functional expansion $\bar{\rho}_{PW}^{\alpha\alpha}(r_1, s)$ for the spherically averaged Fermi-hole correlation function. The corresponding exchange energy density functional yields values for the exchange energies of atoms in good agreement with Hartree–Fock results.

Key words: atomic exchange energy, density functional theory, Fermi hole.

VINCENZO TSCHINKE et TOM ZIEGLER. Can. J. Chem. **67**, 460 (1989).

Dans le cas de systèmes atomiques, on a comparé la moyenne sphérique de la fonction de corrélation de trou de Fermi $\bar{\rho}_x^{\alpha\alpha}(r_1, s)$ dans la théorie de Hartree–Fock avec la fonction correspondante $\bar{\rho}_{X\alpha}^{\alpha\alpha}(r_1, s)$ utilisée dans la théorie fonctionnelle de la densité locale. On démontre que, par rapport à la fonction $\bar{\rho}_x^{\alpha\alpha}(r_1, s)$, la fonction $\bar{\rho}_{X\alpha}^{\alpha\alpha}(r_1, s)$ se comporte qualitativement d'une façon incorrecte aux positions r_1 de l'électron de référence éloigné du noyau. De plus, on a démontré que l'on peut remédier au comportement qualitativement incorrect de la fonction $\bar{\rho}_{X\alpha}^{\alpha\alpha}(r_1, s)$ en utilisant une extension approximative de la fonction $\bar{\rho}_x^{\alpha\alpha}(r_1, s)$ en puissances de s, où s est la distance inter-électronique. Toutefois, à cause de la discontinuité de la fonction $\bar{\rho}_x^{\alpha\alpha}(r_1, s)$ comme fonction de s au niveau du noyau atomique, on doit procéder cette extension dans deux régions. En se basant sur une extension de la fonction $\bar{\rho}_x^{\alpha\alpha}(r_1, s)$ dans deux régions, on a développé une autre expression approximative de la densité fonctionnelle, $\bar{\rho}_{PW}^{\alpha\alpha}(r_1, s)$ qui peut s'appliquer comme moyenne sphérique de la fonction de corrélation de trou de Fermi. La densité fonctionnelle correspondante de l'énergie d'échange fournit des valeurs pour les énergies d'échange des atomes qui sont en bon accord avec les résultats de Hartree–Fock.

Mots clés : énergie d'échange des atomes, théorie fonctionnelle de la densité, trou de Fermi.

[Traduit par la revue]

I. Introduction

Hohenberg and Kohn (1) demonstrated in 1964 that the ground-state energy of an electronic system is an unique (albeit unknown) functional of the electron density. This remarkable theorem gave credence to previous work by Slater (2) and others (3), and initiated an extensive study (4, 5) into the relation between electronic energy and electron density, a field that now has become known as (energy) density functional theory.

In the last 15 years, due to a number of innovative implementations (6), it has become possible to carry out calculations based on approximate density functionals. Of the various approximate density functional methods, the Hartree–Fock–Slater (or Xα) scheme (7) is by far the most commonly used in chemistry. The accumulated experience with the HFS method seems to indicate that geometrical parameters (8), force constants (9), and spectroscopic energy differences (5*p*, 10) (ionization potentials and excitation energies) are in good to fair agreement with experiment. However, bond energies (8*a*–*b*, 11*a*) are not in general well represented by the HFS method as indicated in Table 1, where several of the theoretical values obtained from HFS calculations typically are too high in comparison with experiment.

The slightly more elaborate Local Spin Density method (LSD) (5*p*) provides geometrical parameters comparable to those obtained from HFS calculations (8*a*), whereas ionization potentials and excitation energies from LSD calculations (12) compare somewhat better with experiment than the corresponding HFS results. However, the LSD method does not uniformly improve (12) the quality of the calculated bond energies as indicated in Table 1.

The spherically averaged Fermi-hole correlation functions $\bar{\rho}_x^{\gamma\gamma}$ (to be defined in the next sections, with $\gamma\gamma = \alpha\alpha$ or $\beta\beta$) completely determine the exchange energies $E_x^{\gamma\gamma}$, one of the fundamental components of the total energy of an electronic system. Furthermore, the functions $\bar{\rho}_x^{\gamma\gamma}$ contain information on the correlated motion of like-spin electrons and several important properties of $\bar{\rho}_x^{\gamma\gamma}$ can be derived from general physical arguments. The functions $\bar{\rho}_x^{\gamma\gamma}$, and as a consequence, $E_x^{\gamma\gamma}$ are in the HFS and the LSD methods represented simply as local functions of the electron density, and most attempts to improve upon the two methods have involved the inclusion of correction terms depending on derivatives of the electron density in the representation of $E_x^{\gamma\gamma}$. However, in earlier investigations (13) the forms chosen for such correction terms were based on dimensional arguments rather than on an analysis of the functions $\bar{\rho}_x^{\gamma\gamma}$. Also, the expression for $E_x^{\gamma\gamma}$ in terms of electron-density derivatives, known as the gradient expansion of $E_x^{\gamma\gamma}$ or the non-local representation of $E_x^{\gamma\gamma}$, has met with considerable criticism (7), and it has been claimed that the gradient expansion of $E_x^{\gamma\gamma}$ in fact is divergent. It has been shown further (14) that potentials, $U_x^{\gamma\gamma}$, derived from the gradient expansion of $E_x^{\gamma\gamma}$ in certain cases are divergent.

In an important recent development, Becke (15*a*) has derived the lowest order gradient corrections to $\bar{\rho}_x^{\gamma\gamma}$, by expanding $\bar{\rho}_x^{\gamma\gamma}$ in powers of the inter-electronic distance s. This expansion affords in a transparent way a non-local expression for $E_x^{\gamma\gamma}$ in terms of electron density derivatives. Becke (15*c*) was in addition able to avoid divergencies of the related coulomb potentials $V_x^{\gamma\gamma}$,

[1]To whom all correspondence should be addressed.

Can. J. Chem. Downloaded from www.nrcresearchpress.com by 41.223.56.140 on 09/07/12
For personal use only.

Can. J. Chem. Downloaded from www.nrcresearchpress.com by 41.223.56.140 on 09/07/12
For personal use only.

TABLE 1.

(*a*) Dissociation energies (eV)

	HFS	LSD	Becke	Exp.
N_2[a]	9.09	11.2	9.81	9.76
O_2[a]	6.85	7.35	5.26	5.12
F_2[a]	3.18	3.34	1.81	1.60
CO[a]	11.84	12.68	10.81	11.08
NO[a]	7.03	8.36	6.66	6.62
Cr_2[b]	—	—	1.75	1.69
Mo_2[b]	—	—	4.03	4.18
$2CH \rightarrow C_2H_2$[a,c]	11.20	11.57	9.43	10.26
$2CH_2 \rightarrow C_2H_4$[a,c]	7.24	8.46	7.02	7.07
$2CH_3 \rightarrow C_2H_6$[a,c]	4.32	4.81	3.40	3.82

(*b*) Average bond energies (kJ mol^{-1})

	HFS	LSD	Becke	Exp.
H_2O[a]	435	497	429	459
CO_2[a]	869	946	768	799
CH_4[a]	385	434	397	411
NH_3[a]	345	415	372	385
NF_3[a]	385	443	290	283
$Cr(CO)_6$[d,e]	—	—	107	110
$Mo(CO)_6$[d,e]	—	—	126	151
$W(CO)_6$[e,e]	—	—	156	179

(*c*) Metal–ligand dissociation energies (kJ mol^{-1})

	HFS	LSD	Becke	Exp.
$HMn(CO)_5$[f]	—	—	225	213
$CH_3Mn(CO)_5$[f]	—	—	153	153
$HCo(CO)_4$[f]	—	—	230	238
$Cr(CO)_6$[g]	272[a]	276[a]	147[d]	162[d]
$Mo(CO)_6$[g]	226[a]	226[a]	119[d]	126[d]
$W(CO)_6$[g]	238[a]	247[a]	142[d]	166[d]
$Fe(CO)_5$[g]	263[a]	263[a]	185[d]	176[d]
$Ni(CO)_4$[g]	188[a]	192[a]	106[d]	104[d]

[a] See ref. 12.
[b] See ref. 11*b*.
[c] Dimerization energy.
[d] See ref. 11*d*.
[e] Average metal–carbonyl bond energy.
[f] Metal–hydrogen or metal–methyl bond energy; see ref. 11*c*.
[g] First metal–carbonyl dissociation energy.

due to $\bar{\rho}_x^{\gamma\gamma}$, by introducing an empirical cut-off factor, $f_x^{\gamma\gamma}$, in the exchange energy expansion. Bond energies (11, 12) based on Becke's functional are displayed in Table 1, and it follows from Table 1 that the result from Becke's functional constitute a significant improvement over the bond energies derived from HFS and LSD calculations. Other recently derived non-local density functionals (16) also seem to provide bond energies of high accuracy.

In view of the important role played by $\bar{\rho}_x^{\gamma\gamma}$ in density functional theory, we shall here initiate a detailed study of the spherically averaged Fermi-hole correlation functions $\bar{\rho}_x^{\gamma\gamma}$ (17). The present investigation (Section III) will be restricted to atomic systems for which $\bar{\rho}_x^{\gamma\gamma}$ is represented with high accuracy within the HF approximation. Section III provides further a similar analysis of the spherically averaged Fermi-hole correlation functions $\bar{\rho}_{x\alpha}^{\gamma\gamma}$ in the HFS (or Xα) theory, with special emphasis on the shortcomings of $\bar{\rho}_{x\alpha}^{\gamma\gamma}$ as a result of the simple local representation in terms of the electronic density. The expansion of $\bar{\rho}_x^{\gamma\gamma}$ in powers of s is discussed in Section IV and the origin of the divergent behaviour of $V_x^{\gamma\gamma}$ and the cut-off function $f_x^{\gamma\gamma}$ in Section VI. Finally, after an analysis of Becke's functional (Section V), we provide an alternative non-local representation of $\bar{\rho}_x^{\gamma\gamma}$ in Section VII.

II. The hole correlation functions

The total energy of a n-electron system can be expressed (18) in terms of the hole correlation functions $\rho_x^{\gamma\gamma'}(\boldsymbol{r}_1, \boldsymbol{r}_2)$ ($\gamma = \alpha, \beta$; $\gamma' = \alpha, \beta$), the one electron density matrix $\rho_1(\boldsymbol{r}_1, \boldsymbol{r}')$, and the one-electron density $\rho_1(\boldsymbol{r}_1)$, as

$$[1] \qquad E = \int_{r_1' \rightarrow r_1} h(\boldsymbol{r}_1)\rho_1(\boldsymbol{r}_1, \boldsymbol{r}_1')\delta\boldsymbol{r}_1 + \frac{1}{2}\int\frac{\rho_1(\boldsymbol{r}_1)\rho_1(\boldsymbol{r}_2)}{|\boldsymbol{r}_2 - \boldsymbol{r}_1|}\delta\boldsymbol{r}_1\delta\boldsymbol{r}_2 + \sum_{\gamma=\alpha}^{\beta}\sum_{\gamma'=\alpha}^{\beta} E_x^{\gamma\gamma'}$$

where

$$[2] \qquad E_x^{\gamma\gamma'} = -\frac{1}{2}\int\frac{\rho_1^{\gamma}(\boldsymbol{r}_1)\rho_x^{\gamma\gamma'}(\boldsymbol{r}_1, \boldsymbol{r}_2)}{|\boldsymbol{r}_2 - \boldsymbol{r}_1|}\delta\boldsymbol{r}_1\delta\boldsymbol{r}_2$$

and $h(\boldsymbol{r}_1)$ is the sum of the one-electron operators representing the kinetic energy of electron i and the attraction between electron i and the nuclei.

In the next sections we shall be dealing extensively with the spherically averaged hole correlation functions (19–21) $\bar{\rho}_x^{\alpha\alpha}$, $\bar{\rho}_x^{\alpha\beta}$, $\bar{\rho}_x^{\beta\alpha}$, $\bar{\rho}_x^{\beta\beta}$, in which all information about the relative orientation of two electrons at the fixed interelectronic distance $s \equiv |\boldsymbol{s}| = |\boldsymbol{r}_2 - \boldsymbol{r}_1|$ has been integrated out. The spherically averaged hole-correlation functions are defined (19–21) as

$$[3] \qquad \bar{\rho}_x^{\gamma\gamma'}(\boldsymbol{r}_1, s) = \frac{1}{4\pi}\int\rho_x^{\gamma\gamma'}(\boldsymbol{r}_1, \boldsymbol{r}_1 + \boldsymbol{s})\delta\Omega_s \qquad \text{with } \gamma = \alpha, \beta \text{ and } \gamma' = \alpha, \beta$$

where we have introduced the variable transformation $\boldsymbol{r}_2 = \boldsymbol{r}_1 + \boldsymbol{s}$, see Fig. 1*a*. The spherically averaged hole correlation functions $\bar{\rho}_x^{\gamma\gamma'}$ are useful since they, as discussed by Gunnarsson *et al.* (19–21), completely determine the expectation value of a scalar two-electron operator such as $1/|\boldsymbol{r}_2 - \boldsymbol{r}_1| = 1/s$. Thus, for $E_x^{\gamma\gamma'}$ of eq. [2] one has

$$[4] \qquad E_x^{\gamma\gamma'} = -2\pi\int\frac{\rho_1^{\gamma}(\boldsymbol{r}_1)\bar{\rho}_x^{\gamma\gamma'}(\boldsymbol{r}_1, s)}{s}(s^2\delta s)\delta\boldsymbol{r}_1$$

The spherically averaged hole correlation function $\bar{\rho}_x^{\alpha\alpha}(\boldsymbol{r}_1, s)$ is, Fig. 1*b*, centred around the reference electron at position $\boldsymbol{r}_1$. The function $\bar{\rho}_x^{\alpha\alpha}(\boldsymbol{r}_1, s)$ will to a larger or smaller extent exclude another electron of the same spin from approaching the reference electron at the distance $s = |\boldsymbol{r}_2 - \boldsymbol{r}_1|$, see Fig. 1*b*.

We shall on occasions write $E_x^{\gamma\gamma'}$ as

$$[5a] \qquad E_x^{\gamma\gamma'} = \frac{1}{2}\int\rho_1^{\gamma}(\boldsymbol{r}_1)V_x^{\gamma\gamma'}(\boldsymbol{r}_1)\delta\boldsymbol{r}_1$$

where

$$[5b] \qquad V_x^{\gamma\gamma'}(\boldsymbol{r}_1) = -4\pi\int\frac{\rho_x^{\gamma\gamma'}(\boldsymbol{r}_1, s)}{s}s^2\delta s$$

is the coulomb *potential* due to the spherically averaged hole correlation function $\rho_x^{\gamma\gamma'}(\boldsymbol{r}_1, s)$.

For the simple HF theory, where the many-electron wave function Ψ^0 is represented by a single normalized Slater

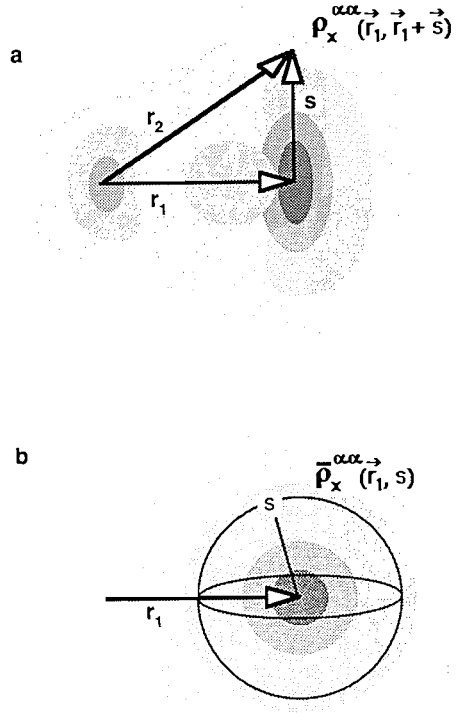


FIG. 1. Schematic representation of the hole correlation functions $\rho_x^{\alpha\alpha}(r_1, r_1 + s)$ and $\bar{\rho}_x^{\alpha\alpha}(r_1, s)$, for the reference electron at a fixed position r_1. Darker shaded areas correspond to larger values of the functions. (*a*) The hole correlation function $\rho_x^{\alpha\alpha}(r_1, r_1 + s)$; note the dependency on the distance $s \equiv |s|$ as well as on the orientation of the vector s. (*b*) The spherically averaged hole correlation function $\bar{\rho}_x^{\alpha\alpha}(r_1, s)$, which depends only on the distance $s \equiv |s|$.

determinant, as

$$[6a] \quad \Psi^0 = |\phi_1^\alpha, \phi_2^\alpha, \ldots, \phi_{n_\alpha}^\alpha, \phi_{n_\alpha+1}^\beta, \phi_{n_\alpha+2}^\beta, \ldots, \phi_{n_\alpha+n_\beta}^\beta|$$

and $\{\phi_i(r_i)\}$ is a set of one-electron HF orbitals, one finds readily that

$$[6b] \quad \rho_x^{\alpha\beta}(r_1, r_2) = \rho_x^{\beta\alpha}(r_1, r_2) = 0$$

and

$$[7] \quad \rho_{xHF}^{\alpha\alpha}(r_1, r_1 + s) = \rho_{xHF}^{\alpha\alpha}(r_1, r_2) = \sum_i^{n_\alpha} \sum_j^{n_\alpha} \frac{\phi_i^\alpha(r_1)\phi_i^\alpha(r_2)\phi_j^\alpha(r_1)\phi_j^\alpha(r_2)}{\rho_1^\alpha(r_1)}$$

A similar expression for $\rho_{xHF}^{\beta\beta}(r_1, r_2)$ is obtained by substituting α by β in eq. [7]. The negative hole correlation functions $-\rho_{xHF}^{\alpha\alpha}$ and $-\rho_{xHF}^{\beta\beta}$ are often referred to as exchange densities.

The following relations can be derived from eq. [7] for $\rho_x^{\alpha\alpha}(r_1, r_2)$ and $\rho_x^{\beta\beta}(r_1, r_2)$ of like spins:

$$[8] \quad \int \rho_x^{\alpha\alpha}(r_1, r_2)\delta r_2 = 1$$

and

$$[9a] \quad \rho_x^{\alpha\alpha}(r_1, r_1) = \rho_1^\alpha(r_1)$$

The relation in eq. [9*a*] is a rigorous result. However, we would like to demonstrate that $\rho_{xHF}^{\alpha\alpha}(r_1, r_1 + s)$ and $\rho_1^\alpha(r_1 + s)$ are close for small values of s. To this end let us, without approximations, write $\rho_{xHF}^{\alpha\alpha}(r_1, r_1 + s)$ of eq. [7] in terms of a set of localized orbitals $\{\lambda_i\}$ obtained from a unitary transformation of the set $\{\phi_i\}$, as

$$[9b] \quad \rho_{xHF}^{\alpha\alpha}(r_1, r_1 + s) = \frac{\sum_{i=1}^{n_\alpha} \sum_{j=1}^{n_\alpha} \lambda_i(r_1)\lambda_i(r_1 + s)\lambda_j(r_1)\lambda_j(r_1 + s)}{\sum_{k=1}^{n_\alpha} \lambda_k(r_1)\lambda_k(r_1)}$$

There are various ways (22) in which $\{\phi_i\}$ can be transformed into a set of localized orbitals $\{\lambda_i\}$, and the set of orbitals $\{\lambda_i\}$ obtained from the different methods are in general quite similar (23). Let us now assume that the set $\{\lambda_i\}$ is well localized in such a way that each λ_k represents a region. That is, with r_1 in region k one finds that $\lambda_i(r_1) \neq 0$ for $i = k$, whereas $\lambda_i(r_1) \sim 0$ for $i \neq k$. With this set of assumptions, the function $\rho_{xHF}^{\alpha\alpha}$ will reduce to

$$[9c] \quad \rho_{xHF}^{\alpha\alpha}(r_1, r_1 + s) \sim \lambda_i(r_1 + s)\lambda_i(r_1 + s)$$

with the reference electron positioned at r_1 in region i.

The relation in eq. [9*c*] would indicate, since $\rho_1^\alpha(r) = \lambda_i(r)\lambda_i(r)$ for r in region i, that $\rho_{xHF}^{\alpha\alpha}(r_1, r_1 + s)$ not only is identical to $\rho_1^\alpha(r_1 + s)$ for $s = 0$, as it must according to eq. [9*a*], but also, at least approximately, in a domain around $s = 0$ where $r_1 = s$ is inside region i.

The following relations hold for the spherically averaged hole-correlation functions $\bar{\rho}_x^{\alpha\alpha}$ and $\bar{\rho}_x^{\beta\beta}$ (19–21),

$$[10] \quad \int \bar{\rho}_x^{\gamma\gamma}(r_1, s)\delta s = 1; \qquad \gamma = \alpha, \beta$$

$$[11] \quad \bar{\rho}_x^{\gamma\gamma}(r_1, 0) = \rho_1^\gamma(r_1); \qquad \gamma = \alpha, \beta$$

$$[12] \quad \lim_{s\to\infty} \bar{\rho}_x^{\gamma\gamma}(r_1, s) = 0; \qquad \gamma = \alpha, \beta$$

and

$$[13] \quad \bar{\rho}_x^{\gamma\gamma}(r_1, s) > 0; \qquad \text{all } r_1, s; \qquad \gamma = \alpha, \beta$$

The way in which (spherically averaged) hole correlation functions are represented in approximate density functional theory will be the subject of the next section.

III. The spherically averaged hole correlation functions in the Hartree–Fock and HFS theories

We shall here primarily be concerned with the spherically averaged hole-correlation functions $\bar{\rho}_x^{\alpha\alpha}(r_1, s)$ and $\bar{\rho}_x^{\beta\beta}(r_1, s)$ corresponding to electrons of the same spins. We shall further, for the moment, restrict the discussion to atomic systems. Hole correlation functions for electrons of like spins are also referred to as Fermi-hole correlation functions.

In order to illustrate the properties of $\bar{\rho}_x^{\alpha\alpha}(r_1, s)$ and $\bar{\rho}_x^{\beta\beta}(r_1, s)$, we have plotted $\bar{\rho}_x^{\alpha\alpha}(r_1, s)$ for the simple He atom in Fig. 2. The plots in Fig. 2 are based on a single determinantal representation of the wave function Ψ^0 for He

$$[14a] \quad \Psi^0 = |\phi_{1s}(1)\alpha(1)\phi_{1s}(2)\beta(2)|$$

with

$$[14b] \quad \phi_{1s}(1) = \left[\frac{\sigma^3}{\pi}\right]^{1/2} \exp(-\sigma r_1)$$

and the hole correlation function $\rho_x^{\alpha\alpha}(r_1, r_2)$ has in this representation according to eq. [7] the following analytical form:

$$[15a] \quad \rho_x^{\alpha\alpha}(r_1, r_2) = \frac{\sigma^3}{\pi} \exp(-2\sigma r_2) = \frac{\sigma^3}{\pi} \exp(-2\sigma|r_1 + s|)$$

Can. J. Chem. Downloaded from www.nrcresearchpress.com by 41.223.56.140 on 09/07/12
For personal use only.

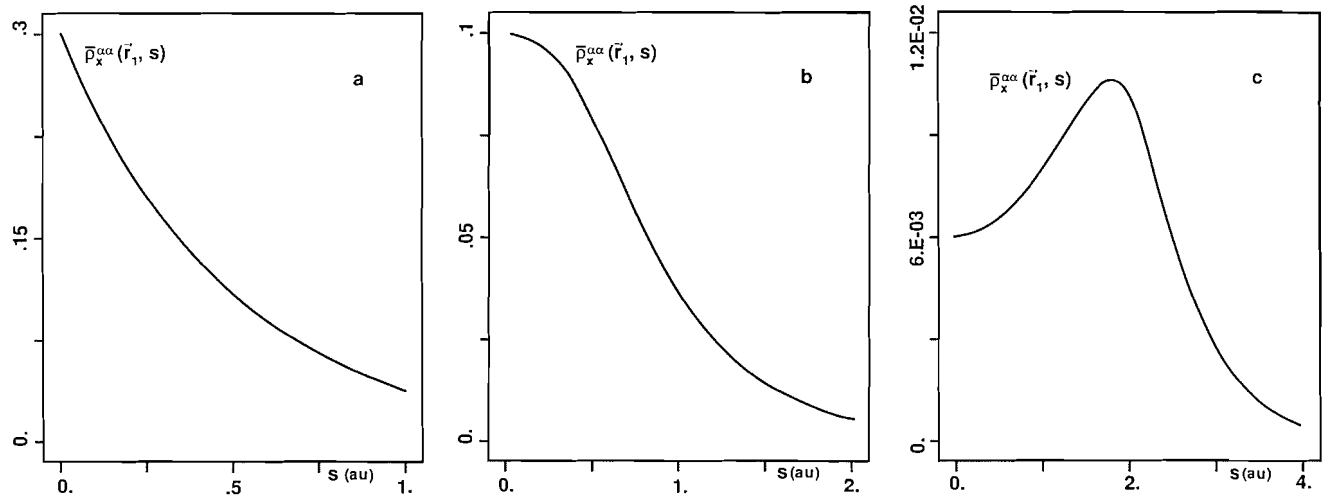


FIG. 2. The spherically averaged hole correlation function $\bar{\rho}_x^{\alpha\alpha}(r_1, s)$ for the He atom. (*a*) $r_1 = 0$ au; (*b*) $r_1 = 0.5$ au; (*c*) $r_1 = 2$ au.

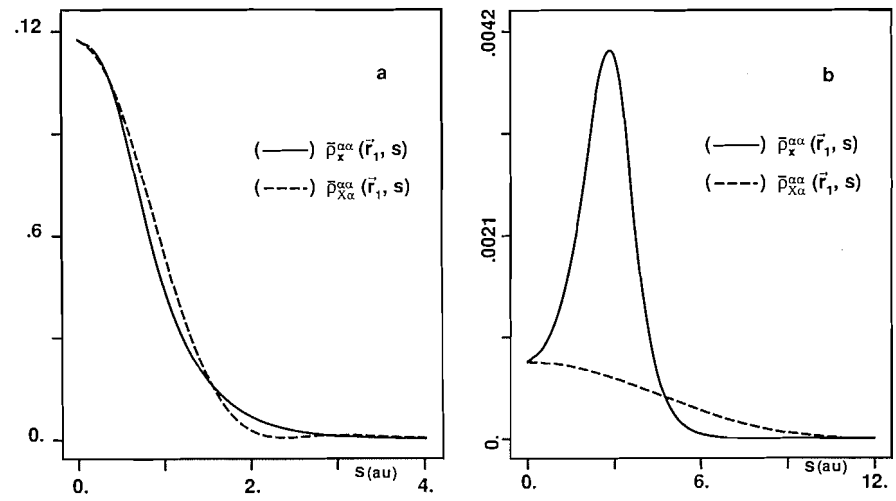


FIG. 3. The spherically averaged hole correlation functions $\bar{\rho}_x^{\alpha\alpha}(r_1, s)$ and $\bar{\rho}_{X\alpha}^{\alpha\alpha}(r_1, s)$ for the He atom. (*a*) $r_1 = 0.5$ au; (*b*) $r_1 = 3.0$ au.

whereas the spherically averaged hole correlation function $\bar{\rho}_x^{\alpha\alpha}$ is given by

$$[15b] \quad \bar{\rho}_x^{\alpha\alpha}(r_1, s) = \frac{\sigma}{4\pi r_1 s}\left\{\exp(-2\sigma|r_1 - s|)\left[\sigma|r_1 - s| + \frac{1}{2}\right] - \exp(-2\sigma|r_1 + s|)\left[\sigma|r_1 + s| + \frac{1}{2}\right]\right\}$$

where $|r_1 - s| = [(r_1 - s)^2]^{1/2}$. We shall on occasions refer to the simple He model in order to illustrate the salient concepts in our discussion.

The exponential function $\rho_x^{\alpha\alpha}(r_1, r_1 + s)$, defined in eq. [15*a*], has its maximum at $s = -r_1$. As a consequence, it is not surprising that the related function $\bar{\rho}_x^{\alpha\alpha}(r_1, s)$ has its maximum at $s = r_1$ for large values of r_1 (Fig. 2*c*), and its maximum at $s = 0$ (Fig. 2*a*) for $r_1 = 0$. It is perhaps surprising that $\bar{\rho}_x^{\alpha\alpha}(r_1, s)$ not only has its maximum at $s = 0$ for $r_1 = 0$ but also for somewhat larger values of r_1, see Fig. 2*b*. The behaviour of $\bar{\rho}_x^{\alpha\alpha}(r_1, s)$ in Fig. 2*b* can be readily understood from a numerical analysis. However, we shall postpone a detailed discussion to a later section.

The spherically averaged hole correlation function in the HFS method is modeled by writing $\bar{\rho}_x^{\alpha\alpha}(r_1, s)$ in the form

$$[16] \quad \bar{\rho}_x^{\alpha\alpha}(r_1, s) \sim \bar{\rho}_{X\alpha}^{\alpha\alpha}(r_1, s) = \rho_1^{\alpha}(r_1) f(k_f s)$$

where $k_f = [6\pi^2 \rho_1^{\alpha}(r_1)]^{1/3}$. The unknown function $f(k_f s)$ is subsequently determined in such a way that $\bar{\rho}_{X\alpha}^{\alpha\alpha}$ of eq. [16] will satisfy all four constraints given in eqs. [10]–[13] for a spherically averaged hole correlation function.

Several functions (24–26) have the properties given in eqs. [10]–[13] and $f(k_f s)$ is as a consequence not uniquely determined. The most commonly used form (24) for $f(k_f s)$, derived from electron gas theory, is given by

$$[17] \quad f_g(k_f s) = 9\frac{[\sin(k_f s) - (k_f s)\cos(k_f s)]^2}{(k_f s)^6}$$

We compare in Fig. 3, for the He atom, $\bar{\rho}_{X\alpha}^{\alpha\alpha}(r_1, s)$ of eq. [16], derived from the density $\rho_1^{\alpha}(r_1) = \frac{\sigma^3}{\pi}\exp[-2\sigma r_1]$ and the expression for $f(k_f s)$ given in eq. [17], with $\bar{\rho}_x^{\alpha\alpha}(r_1, s)$ of eq. [15*b*]. For small values of r_1, both $\bar{\rho}_x^{\alpha\alpha}(r_1, s)$ and $\bar{\rho}_{X\alpha}^{\alpha\alpha}(r_1, s)$ have a maximum at $s = 0$ and exhibit closely the same dependency on s, see Fig. 3*a*. However, the two functions

Can. J. Chem. Downloaded from www.nrcresearchpress.com by 41.223.56.140 on 09/07/12
For personal use only.

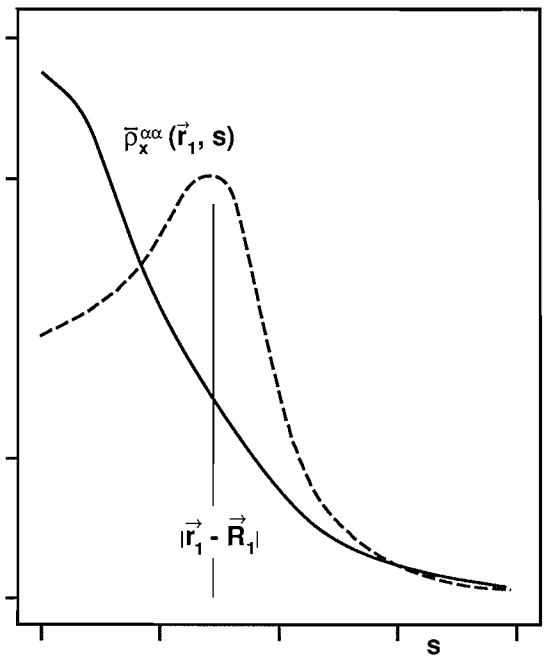


FIG. 4. Schematic representation of the spherically averaged hole correlation function $\bar{\rho}_x^{\alpha\alpha}(r_1, s)$ for an atomic system, with r_1 inside a given shell. (—) $\bar{\rho}_x^{\alpha\alpha}(r_1, s)$ for r_1 near the principal maximum R_1 (see text) within the shell. (-----) $\bar{\rho}_x^{\alpha\alpha}(r_1, s)$ for r_1 at the edge of the shell, with distance $|r_1 - R_1|$ from R_1.

differ qualitatively for large values of r_1 (Fig. 3*b*), where $\bar{\rho}_x^{\alpha\alpha}(r_1, s)$, as already mentioned, has a maximum at $s = r_1$, whereas $\bar{\rho}_{X\alpha}^{\alpha\alpha}(r_1, s)$ in this region, as for any other value of r_1, has its maximum at $s = 0$. That $\bar{\rho}_{X\alpha}^{\alpha\alpha}(r_1, s)$ has a maximum at $s = 0$ for all values of r_1 is of course related to the fact that $f(k_f s)$ of eq. [17] has its maximum at $s = 0$.

Investigations (17, 20) of $\bar{\rho}_x^{\alpha\alpha}(r_1, s)$, from HF calculations on atoms with more complicated shell structures than He, have revealed the following trends (see Fig. 4). When the reference electron is positioned (at r_1) near to a principal maximum R_i of the density in shell i, $\bar{\rho}_{xHF}^{\alpha\alpha}(r_1, s)$ is a decreasing function of s with a maximum at $s = 0$. On the other hand, the spherically averaged hole correlation function $\bar{\rho}_{xHF}^{\alpha\alpha}(r_1, s)$ has a principal maximum at $s = |r_1 - R_i|$ in the case where the reference electron is at the edge of shell i. By way of contrast, $\bar{\rho}_{X\alpha}^{\alpha\alpha}(r_1, s)$ exhibits for all r_1 a maximum at $s = 0$. Note that $R_1 = 0$ in the case of He.

It is readily shown (17*d*) that the qualitative incorrect behaviour of $\bar{\rho}_{X\alpha}^{\alpha\alpha}(r_1, s)$ at the edge of each shell results in exchange energies, $E_{X\alpha}^{\alpha\alpha} + E_{X\alpha}^{\beta\beta}$, that in absolute values are too low compared to exchange energies $E_{HFx}^{\alpha\alpha} + E_{HFx}^{\beta\beta}$ obtained by the HF method, see Table 2.

In the next section we shall discuss how the qualitatively incorrect behaviour of $\bar{\rho}_{X\alpha}^{\alpha\alpha}(r_1, s)$ at the edge of each shell can be alleviated. However, we would first like to point out that the so-called local density (LSD) method (5) has the same representation for $\bar{\rho}_{X\alpha}^{\alpha\alpha}$ and $\bar{\rho}_{X\alpha}^{\beta\beta}$ as the HFS scheme, and only differs from the latter method in the representation of the hole correlation functions of different spins. The shortcomings of the HFS scheme with respect to $\bar{\rho}_{X\alpha}^{\alpha\alpha}$ and $\bar{\rho}_{X\alpha}^{\beta\beta}$ applies thus as well to the LSD method.

IV. Expansion of the spherically averaged Fermi-hole correlation function in powers of s

The spherically averaged Fermi-hole correlation function $\bar{\rho}_x^{\alpha\alpha}(r_1, s)$ can be expanded in powers of s. For atoms, however, such an expansion must be carried out in two parts, one for $0 < s < |r_1|$ and one for $s > |r_1|$, since the Fermi-hole correlation function $\rho_x^{\alpha\alpha}(r_1, r_1 + s)$ has a cusp (27) at $|r_1 + s| = 0$. As a consequence, the functions $\rho_x^{\alpha\alpha}$ and $\bar{\rho}_x^{\alpha\alpha}$ will have discontinuous derivatives of s at $s = -r_1$.

For $0 < s < |r_1|$, as already discussed by Becke (15*a*), the expansion of the spherically averaged Fermi-hole correlation function $\bar{\rho}_x^{\alpha\alpha}(r_1, s)$ in powers of s has the form of a Taylor series

$$[18]\quad \bar{\rho}_x^{\alpha\alpha}(r_1, s) = \rho_1^{\alpha} + \sum_{i=1}^{\infty} \frac{s^{2i}}{(2i+1)!} \nabla_s^{2i} \rho_x^{\alpha\alpha}(r_1, r_1 + s)|_{s=0}, \quad 0 < s < |r_1|$$

The expansion of $\bar{\rho}_x^{\alpha\alpha}$ in the second region with $s > r_1$ is given by the Laurent series

$$[19]\quad \bar{\rho}_x^{\alpha\alpha}(r_1, s) = \sum_{j=-\infty}^{\infty} \frac{s^j}{2\pi i} \oint_C \frac{\bar{\rho}_x^{\alpha\alpha}(r_1, z)}{z^{j+1}} dz, \quad s > |r_1|$$

where i is the imaginary unit and z is a complex variable. Further, C is a circle of radius $R > |r_1|$.

For He, the spherically averaged hole correlation function is given by

$$[20a]\quad \bar{\rho}_x^{\alpha\alpha}(r_1, s) = \rho_1^{\alpha}(r_1) \sum_{i=0}^{\infty} \frac{1}{(2i+1)!} \left[1 - \frac{i}{\sigma r_1}\right] (2\sigma s)^{2i}, \quad 0 < s < r_1$$

and

$$[20b]\quad \bar{\rho}_x^{\alpha\alpha}(r_1, s) = \rho_1^{\alpha}(r_1) \sum_{i=-1}^{\infty} \frac{(-1)^i}{(i+1)!} \left[a_1 + \frac{a_2 i}{\sigma r_1}\right] (2\sigma s)^i, \quad s > r_1$$

where

$$a_1 = \frac{1}{2}\left(\frac{4\sigma^6}{\pi^2 \rho_1^{\alpha}} + 1\right)$$

and

$$a_2 = \frac{1}{4}\left(\frac{4\sigma^6}{\pi^2 \rho_1^{\alpha}} - 1\right)$$

The two series given in eq. [20] have been plotted in Fig. 5 for both small and large values of r_1.

For smaller values of r_1 ($r_1 < 1/\sigma$), Fig. 5*a*, we find that the Taylor series of eq. [20*a*] is, in its definition range ($0 < s < r_1$), a decreasing function of s, since all powers of s have negative coefficients. Outside its definition range at $s > r_1$, where the coefficients to all powers of s are negative ($r_1 < 1/\sigma$) and higher powers of s dominant, the Taylor series of eq. [20*a*] is a rapidly decreasing function of s, approaching $-\infty$. The function $\bar{\rho}_x^{\alpha\alpha}(r_1, s)$ is in the range $s > r_1$ represented by the Laurent series of eq. [20*b*] and the Laurent series too is seen, Fig. 5*a*, in this range with $r_1 < 1/\sigma$ to be a decreasing function of s. However, the Laurent series is approaching zero for large s. This is according to eq. [12] the proper limit for $\bar{\rho}_x^{\alpha\alpha}(r_1, s)$.

For large values of r_1 ($r_1 > 1/\sigma$), we find that the lowest powers of s in the Taylor expansion have positive coefficients whereas higher powers of s in eq. [20*a*] have negative coefficients. As a consequence, Fig. 5*b*, the Taylor expansion in eq. [20*a*] is at the onset (small values of s) an increasing function of s, since the lower powers of s are dominant. At the end of its definition range ($0 < s < r_1$), however, the series of

Can. J. Chem. Downloaded from www.nrcresearchpress.com by 41.223.56.140 on 09/07/12
For personal use only.

TABLE 2. Atom exchange energy[f]

Atom	Atom exchange energy					
	HF[a]	LSD[a]	GC[a]	Becke[b]	Kress[c]	PW[d]
H	−0.313	−0.268	−0.326	−0.310	−0.309	−0.306
He	−1.026	−0.884	−1.074	−1.027	−1.023	−1.014
Li	−1.781	−1.538	−1.843	−1.780	−1.771	−1.758
Be	−2.667	−2.312	−2.729	−2.669	−2.652	−2.638
B	−3.744	−3.272	−3.804	−3.744	−3.724	−3.709
C	−5.045	−4.459	−5.112	−5.050	−5.028	−5.013
N	−6.596	−5.893	−6.671	−6.608	−6.584	−6.569
O	−8.174	−7.342	−8.236	−8.192	−8.167	−8.158
F	−10.00	−9.052	−10.07	−10.04	−10.02	−10.01
Ne	−12.11	−11.03	−12.18	−12.16	−12.14	−12.14
Na	−14.02	−12.79	−14.06	−14.06	−14.03	−14.03
Mg	−15.99	−14.61	−16.01	−16.03	−16.01	−16.01
Al	−18.07	−16.53	−18.06	−18.10	−18.07	−18.08
Si	−20.28	−18.59	−20.25	−20.30	−20.27	−20.29
P	−22.64	−20.79	−22.60	−22.65	−22.63	−22.64
S	−25.00	−23.00	−24.93	−25.01	−24.98	−25.00
Cl	−27.51	−25.35	−27.43	−27.52	−27.49	−27.51
Ar	−30.19	−27.86	−30.08	−30.18	−30.16	−30.19
Kr	−93.89	−88.62	−93.32	−93.82	−93.81	−93.97
Xe	−179.2	−170.6	−177.9	−178.9	−178.8	−179.1
σ[e]	—	—	0.330	0.070	0.095	0.029

[a]Reference 15*a*.
[b]Reference 15*c*.
[c]Equation [6], ref. 16*a*.
[d]Present work: eq. [38].
[e]Standard deviation.
[f]Exchange energies calculated from spherically averaged atomic densities; Hartree–Fock (28) atomic orbitals used.

Can. J. Chem. Downloaded from www.nrcresearchpress.com by 41.223.56.140 on 09/07/12
For personal use only.

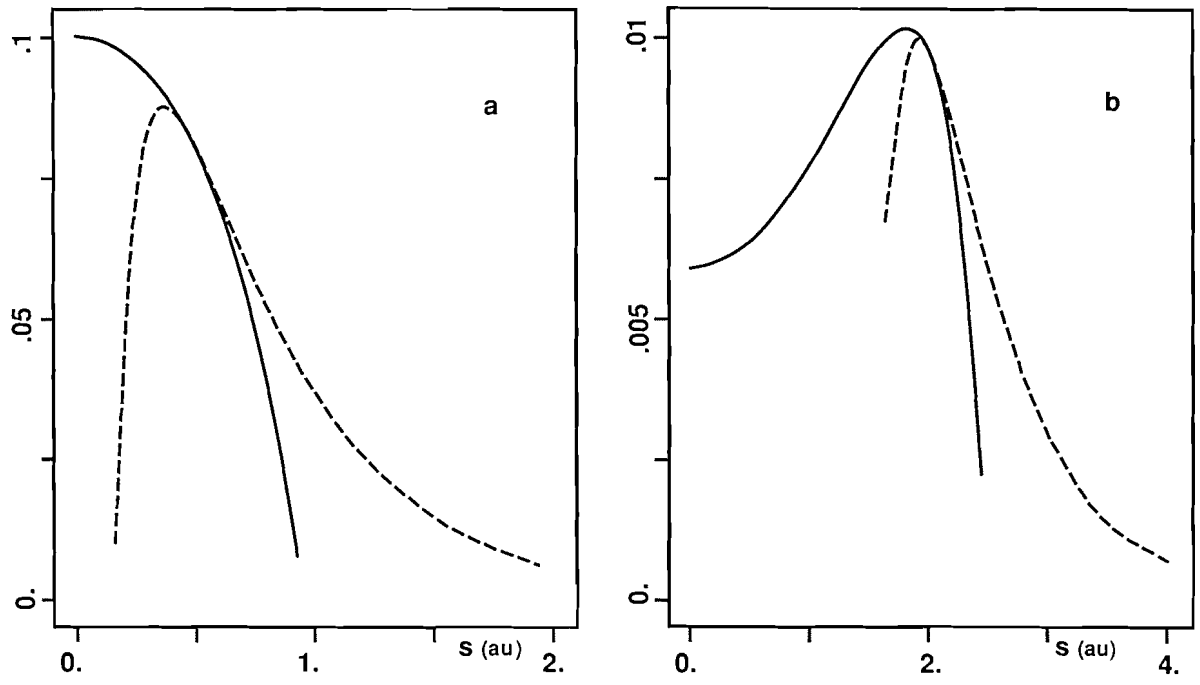


FIG. 5. He atom: Taylor expansion (—), defined for $0 < s < r_1$, and Laurent expansion (- - - - -), defined for $s > r_1$; of the spherically averaged hole correlation function $\bar{\rho}_x^{\alpha\alpha}(r_1, s)$. (*a*) $r_1 = 0.5$ au; (*b*) $r_1 = 2.0$ au.

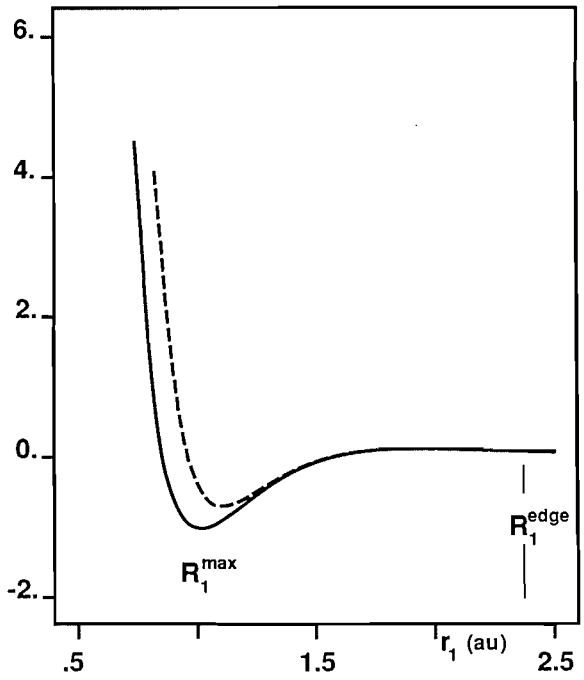


FIG. 6. Ar atom: plot of a_{HF} (—) and a_L (-----) as functions of r_1, for the M-shell ($n = 3$). The radius R_1^{max}, corresponding to the maximum of the density ρ_3 inside the shell, and the radius R_1^{edge}, at the edge of a shell, are indicated in the figure.

eq. [20a] will, after reaching a maximum, decrease due to the influence of higher powers of s. Outside its definition range ($s > r_1$), where higher powers of s are completely dominant, the Taylor expansion approaches $-\infty$. For $r_1 > 1/\sigma$, Fig. 5b, the Laurent expansion of eq. [20b] is, in its definition range ($s > r_1$), a decreasing function of s, with the correct asymptotic limit of zero for large values of s.

From the discussion up to this point, it follows that the shape of $\bar{\rho}_x^{\alpha\alpha}(r_1, s)$ (the position of the maximum) for different values of r_1, at least for He, is determined by the Taylor expansion of eq. [18]. Our analysis would thus indicate that one would have to include, in any approximate representation of $\bar{\rho}_x^{\alpha\alpha}(r_1, s)$ in which the shape of $\bar{\rho}_x^{\alpha\alpha}(r_1, s)$ as a function of r_1 is reproduced qualitatively correctly, at least some of the terms in the Taylor expansion of eq. [18]. The Taylor expansion of eq. [18] is, with terms up to s^2 included, given by:

$$[21] \quad \bar{\rho}_x^{\alpha\alpha}(r_1, s) = \rho_1^\alpha(r_1) + as^2 + \ldots, \qquad 0 < s < |r_1|$$

where a, according to eq. [20a], has the form

$$[22] \quad a = \tfrac{1}{6}[\nabla_s^2 \rho_x^{\alpha\alpha}(r_1, r_1 + s)|_{s=0}]$$

Becke (15a) has shown that the coefficient a in the expansion of $\bar{\rho}_{xHF}^{\alpha\alpha}(r_1, s)$ can be expressed as

$$[23a] \quad a \sim a_{HF} = \frac{1}{6}\left[\nabla_1^2 \rho_1^\alpha(r_1) - 2\tau_1^\alpha + \frac{1}{2}\frac{|\nabla_1 \rho_1^\alpha(r_1)|^2}{\rho_1^\alpha(r_1)}\right]$$

where τ_1^α is the kinetic energy density

$$[23b] \quad \tau_1^\alpha = \sum_{i=1}^{n_\alpha} |\nabla_1 \phi_i(r_1)|^2$$

Furthermore, under the simplifying assumptions of perfect localization according to eq. [9c], we have that

$$[23c] \quad a \sim a_L = \tfrac{1}{6}[\nabla_s^2 \rho_1^\alpha(r_1 + s)|_{s=0}] = \tfrac{1}{6}[\nabla_1^2 \rho_1^\alpha(r_1)]$$

Thus, the coefficient a in eq. [21] is seen to be related to the curvature of $\rho_1^\alpha(r_1)$. In Fig. 6, we give a_{HF} and a_L as a function of r_1 for the Ar atom in the M-shell ($n = 3$). It is seen that a_{HF} and a_L follow each other closely. Also, note that a_{HF} and a_L are negative where $\rho_1^\alpha(r_1)$ has its maximum (and a negative curvature), and positive at the edge of the shell where $\rho_1^\alpha(r_1)$ has a positive curvature.

V. Becke's approximate spherically averaged Fermi-hole correlation function

Becke (15a) has recently introduced an approximate hole correlation function $\bar{\rho}_B^{\alpha\alpha}(r_1, s)$ in which some of the qualitatively incorrect features, see Section III, of $\bar{\rho}_{X\alpha}^{\alpha\alpha}(r_1, s)$ were remedied. Becke's approximate expression is given by

$$[25] \quad \bar{\rho}_B^{\alpha\alpha}(r_1, s) = \begin{cases} (1 + a_B s^2 + b_B s^4)\bar{\rho}_{X\alpha}^{\alpha\alpha}(r_1, s); & k_f s < z \\ \bar{\rho}_{X\alpha}^{\alpha\alpha}(r_1, s); & k_f s > z \end{cases}$$

where $z = 4.4934$ represents the first zero (24) for $\bar{\rho}_{X\alpha}^{\alpha\alpha}$ as a function of $k_f s$. Becke (15a) obtained in addition, after some straightforward manipulations involving partial integration, the following approximate expression for the potential $V_x^{\alpha\alpha}$ of eq. [5b]

$$[26] \quad V_B^{\alpha\alpha}(r_1) = V_{X\alpha}^{\alpha\alpha}(r_1) - \frac{\beta}{2}\frac{|\nabla_1 \rho_1^\alpha(r_1)|^2}{(\rho_1^\alpha(r_1))^{7/3}}$$

whereas the energy expression $E_x^{\alpha\alpha}$ of eq. [4] takes on the form

$$[27] \quad E_B^{\alpha\alpha} = E_{X\alpha}^{\alpha\alpha} - \beta\int \frac{|\nabla_1 \rho_1^\alpha(r_1)|^2}{(\rho_1^\alpha(r_1))^{4/3}}\delta r_1$$

The constant β in eqs. [26]–[27] is given by $\beta = 0.00293$. The functional form of eq. [27] had already been derived by Herman *et al.* (13) from dimensional arguments, and by Sham (5r) on the basis of density functional theory. An interesting alternative nonlocal exchange functional was proposed by Gunnarsson *et al.* (21). These authors, rather than using a gradient expansion for $\bar{\rho}_x^{\alpha\alpha}(r_1, s)$, developed a general procedure to average the electron density around the reference electron. This average value was then inserted into the local Fermi-hole correlation function of eq. [17], thereby introducing a nonlocal dependency into the corresponding exchange energy functional.

The function $\bar{\rho}_B^{\alpha\alpha}(r_1, s)$ constitutes a considerable improvement over $\bar{\rho}_{X\alpha}^{\alpha\alpha}(r_1, s)$ in the tails of the atomic shells. However, it is, at variance with eq. [13], not positive for all s (17d), as shown in the Ar atom in Fig. 7.

Another shortcoming of the model proposed by Becke is the divergence as $(\rho_1^\alpha(r_1))^{-1/3}$ of the potential $V_B^{\alpha\alpha}(r_1)$ (13, 15a), in the tail of any exponentially decaying density $\rho_1^\alpha(r_1)$. Thus $V_B^{\alpha\alpha}(r_1)$ of eq. [26] will diverge for large r_1 in the atomic tail, as illustrated for He in Fig. 8. In order to overcome this problem, Becke (15c) multiplied the second term of $V_B^{\alpha\alpha}(r_1)$ and $E_B^{\alpha\alpha}$ by the cut-off function

$$[28a] \quad g_B(r_1) = (1 + \gamma y^2)^{-1}$$

where

$$[28b] \quad y = \frac{|\nabla_1 \rho_1^\alpha(r_1)|}{(\rho_1^\alpha(r_1))^{-4/3}}$$

and γ is an adjustable parameter ($\gamma = 0.0053$).

The modified potential is now well behaved as illustrated in Fig. 8, and the corresponding modified energy expression is

Can. J. Chem. Downloaded from www.nrcresearchpress.com by 41.223.56.140 on 09/07/12
For personal use only.

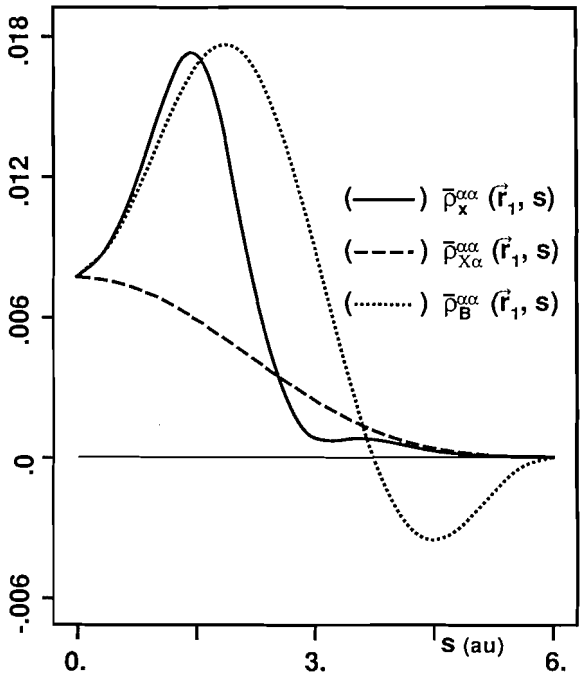


FIG. 7. Ar atom: the spherically averaged hole correlation functions $\bar{\rho}_x^{\alpha\alpha}(r_1, s)$, $\bar{\rho}_{X\alpha}^{\alpha\alpha}(r_1, s)$ and $\bar{\rho}_B^{\alpha\alpha}(r_1, s)$, for r_1 in the third atomic shell with $r_1 = 2.5$ au. Note that $\bar{\rho}_B^{\alpha\alpha}(r_1, s)$ assumes negative values for large s.

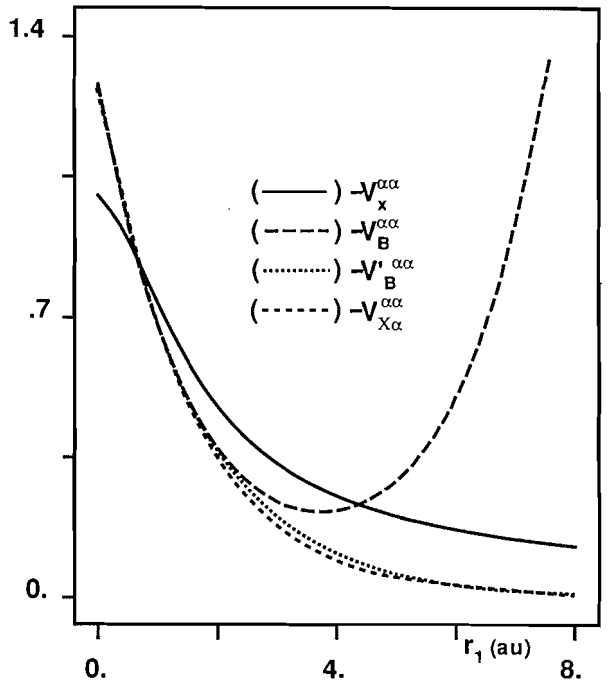


FIG. 8. He atom: the potentials $V_x^{\alpha\alpha}(r_1)$, $V_B^{\alpha\alpha}(r_1)$, and $V'^{\alpha\alpha}_B(r_1)$, as well as $V_{X\alpha}^{\alpha\alpha}(r_1)$. Note that the divergency of $V_B^{\alpha\alpha}(r_1)$ is eliminated by the cut-off factor (see text), present in $V'^{\alpha\alpha}_B(r_1)$.

given (15*c*) by

$$[28c] \quad E'^{\alpha\alpha}_B = E_{X\alpha}^{\alpha\alpha} - \beta \int (\rho_1^{\alpha}(r_1))^{4/3} y^2 (1 + \gamma y^2)^{-1} \delta r_1$$

DePristo and Kress (16*a*) have recently suggested an alternative cut-off function of the form

$$[29] \quad g_{DK}(r_1) = \beta_g (1 + a_{DK} y)(1 + b_{DK} y^2)^{-1}$$

in which a_{DK} and b_{DK} are adjustable parameters and $\beta_g = 0.001323$. The energy expression $E'^{\alpha\alpha}_B$ of eq. [28*c*] has been used with remarkable success to calculate bond energies and other properties in molecular systems (11, 12, 15*c*), and exploratory calculations indicate that the expression $E'^{\alpha\alpha}_{DK}$ based on eq. [29]) is equally appropriate. A gradient-type correction for the LSD exchange-correlation energy which leads to substantial improvements over the LSD results for atomic and solid-state systems was proposed earlier by Langreth and Mehl (5*e*). These authors also introduced an exponential cut-off factor (5*e*, 13) as a numerical tool in the evaluation of the integrals involved in their SCF calculations. Unlike the factors g_{DK} and g_B, this cut-off function does not influence the value of the calculated exchange energy (5*e*); also, dissociation energy values given by the Langreth and Mehl functional (15*c*) are in general less satisfactory than those given by Becke's functional.

The *ad hoc* introduction of a cut-off function is somewhat unsatisfactory and it is not quite clear what would be the form of the spherically-averaged hole correlation function corresponding to the expressions $E'^{\alpha\alpha}_B$ and $E'^{\alpha\alpha}_{DK}$. In the next sections, we shall illustrate the physical origin of the cut-off functions g_{DK} and g_B by proposing an approximate expression for the spherically averaged hole correlation functions, which automatically leads to potentials and energy expressions with a built-in cut-off function.

VI. The cut-off factor in the gradient correction to the HFS exchange energy

In Section IV, we have pointed out the necessity of expanding the Fermi-hole correlation functions of atoms in two regions, due to the presence of a cusp at $|s| = |-r_1|$. In this section we shall discuss the relation between the cusp at $|s| = |-r_1|$ and the origin of the cut-off factor introduced by Becke (15*c*) and DePristo *et al.* (16*a*). For an atom, we can expand the Fermi hole-correlation function as

$$[30] \quad \bar{\rho}_x^{\alpha\alpha}(r_1, s) = \begin{cases} \rho_1^{\alpha}(r_1) + as^2 + \ldots; & 0 < s < r_1 \\ [\rho_1^{\alpha}(r_1) + ar_1^2 + \ldots] f(r_1, s); & s > r_1 \end{cases}$$

with the coefficient a given by eq. [22]. Further, $f(r_1, s)$ can be immediately determined by recasting the expression for the spherically averaged Fermi-hole correlation function of eqs. [18], [19]). The function $f(r_1, s)$ is simply introduced here as a formal device that allows us to express $\bar{\rho}_x^{\alpha\alpha}$ in terms of its gradient expansion, for $s > r_1$.

Inserting eq. [30] into eq. [5*b*], and integrating over the s coordinate in the two different regions yields the coulomb potential expression

$$[31] \quad V_x^{\alpha\alpha}(r_1) = -\left[\frac{\pi}{2(6\pi^2)^{2/3}}(x_1)^2 + \frac{\pi}{6}F(r_1)\right](\rho_1^{\alpha}(r_1))^{1/3}$$
$$+ -\left[\frac{\pi}{4(6\pi^2)^{4/3}}(x_1)^4 + \frac{\pi}{2(6\pi^2)^{4/3}}(x_1)^2 F(r_1)\right]\frac{a}{(\rho_1^{\alpha}(r_1))^{4/3}} + \ldots$$

Can. J. Chem. Downloaded from www.nrcresearchpress.com by 41.223.56.140 on 09/07/12
For personal use only.

Can. J. Chem. Downloaded from www.nrcresearchpress.com by 41.223.56.140 on 09/07/12
For personal use only.

where $x_1 = k_f r_1 = (6\pi^2\rho_1^\alpha)^{1/3} r_1$. Further, the dimensionless factor F is defined as

$$F(\boldsymbol{r}_1) = (k_f)^2 \int_{r_1}^{\infty} s f(\boldsymbol{r}_1, s)\delta s$$

The first term on the r.h.s. of eq. [31] contains the potential given by the HFS approximation, multiplied by a dimensionless factor. Similarly, the second term contains the simple second order gradient correction $a/(\rho_1^\alpha)^{4/3}$, as obtained from the method by Becke (15*a*) (see Section V), also multiplied by a dimensionless factor. The contribution of the second order term to the potential is, according to eq. [31], given by

$$[33] \quad V_{NL}^{\alpha\alpha}(\boldsymbol{r}_1) = -\left[\frac{\pi}{4(6\pi^2)^{4/3}}(x_1)^4 + \frac{\pi}{2(6\pi^2)^{4/3}}(x_1)^2 F(\boldsymbol{r}_1)\right]\frac{a}{(\rho_1^\alpha(\boldsymbol{r}_1))^{4/3}}$$

Without the factor in brackets, the expression of eq. [33] would be divergent as $1/r_1$ (13) at the atomic nucleus, due to the singularity of the density laplacian contained in the coefficient a (see eq. [23*a*]). Furthermore, the expression of eq. [33] would be divergent as $(\rho_1^\alpha)^{-1/3}$ (13, 15*a*) in the atomic exponential tail, in the same way as the potential of eq. [26]. We shall now show that the bracketed factor in eq. [33] removes the two singularities. To this purpose, we point out that the term F of eq. [32] must be finite for any value of the Fermi-hole correlation function, in order to ensure that the exchange potential be finite.[2] Thus, both the first and the second term in brackets in eq. [33] are able to remove the singularity of $a/(\rho_1^\alpha)^{4/3}$ at the nucleus, through the factor r_1 in the x_1 term. Similarly, the factor $(\rho_1^\alpha)^{1/3}$ in x_1 removes the singularity in the atomic exponential tail.

The bracketed term in eq. [33] acts therefore as a cut-off function, much in the same way as the factor proposed by Becke (15*c*) and DePristo *et al.* (16*a*) to eliminate the divergence of the gradient corrected potential of eq. [26]. The cut-off factor of eq. [33] is zero at the atomic nucleus, larger than zero in intermediate atomic regions, and decays rapidly in the atomic exponential tail.

According to the above discussion, when the presence of the cusp in the Fermi-hole correlation function is taken into account, one can derive a gradient correction to the HFS potential, eq. [33], which is well-behaved and contains a cut-off factor. However, the value of eq. [33] is purely formal, since to evaluate the term F of eq. [32] it is necessary to know the exact Fermi-hole correlation function. In the next section we shall develop an approximate expression for the Fermi-hole correlation function, which leads to a gradient correction to the HFS exchange energy expression containing a cut-off factor.

[2]Since the spherically averaged Fermi-hole correlation function is always larger than or equal to zero (eq. [13]), the contributions to the potential $V_x^{\alpha\alpha}(\boldsymbol{r}_1)$ from the two regions of eq. [30], are of the same sign. Therefore, they both must be finite in order to ensure that $V_x^{\alpha\alpha}(\boldsymbol{r}_1)$ be finite. For $s > r_1$, the function $\bar{\rho}_x^{\alpha\alpha}(\boldsymbol{r}_1, s)$ is, according to eq. [30], given by

$$\bar{\rho}_x^{\alpha\alpha}(\boldsymbol{r}_1, s) = [\rho_1^\alpha(\boldsymbol{r}_1) + a r_1^2 + \ldots] f(\boldsymbol{r}_1, s)$$

The factor in brackets is just the value of $\bar{\rho}_x^{\alpha\alpha}(\boldsymbol{r}_1, s)$ when s encompasses the nucleus. Such a value is always larger than zero for an atom, due to the presence of the cusp at the nucleus. Thus the contribution to $V_x^\alpha(\boldsymbol{r}_1)$ of eq. [31] from the second region ($s > r_1$), is given by the term F of eq. [32], multiplied by a nonzero factor. Hence, the term F must be finite in order to ensure a finite value for the coulomb potential due to $\bar{\rho}_x^{\alpha\alpha}(\boldsymbol{r}_1, s)$.

The physical origin of the cut-off function has also been examined recently by Perdew (16*b*–*c*). This author proposed an interesting model for the Fermi-hole correlation function, which generates exchange energy and potential expressions containing a cut-off factor, based on a second order expansion for the inhomogeneous electron gas Fermi-hole correlation function. Perdew was able to enforce the condition of non-negativity (eq. [13]) by introducing a step-function factor which eliminates the negative-valued regions, and to enforce the normalization condition by imposing a cut-off radius. Our alternative model given in the next section satisfies automatically the exact conditions of eqs. [10]–[13] by reproducing the change in analytical structure of the Fermi-hole correlation function in atomic systems expressed by eq. [30].

VII. An alternative approximation to the spherically averaged Fermi-hole correlation function

In this section we shall attempt to develop an approximate expression for $\bar{\rho}_x^{\alpha\alpha}(\boldsymbol{r}_1, s)$, based on the expansion of eq. [30]. Making the variable substitution $x = k_f s$, we have, from eq. [30]

$$[34a] \quad \bar{\rho}_x^{\alpha\alpha}(\boldsymbol{r}_1, s) = \begin{cases} \rho_1^\alpha(\boldsymbol{r}_1) + a'x^2 + \ldots; & 0 < x < x_1 \\ [\rho_1^\alpha(\boldsymbol{r}_1) + a'x_1^2 + \ldots] g(\boldsymbol{r}_1, x); & x > x_1 \end{cases}$$

where $g(\boldsymbol{r}_1, x) = f(\boldsymbol{r}_1, s)$ and $a' = a/(k_f)^2$, with a defined by eq. [24*a*]. Further, $x_1 = k_f r_1$ in the exact expression of eq. [34*a*]. As a first approximation, we shall truncate the expansion of eq. [34*a*] to the second order term. Furthermore, we shall treat the variable x_1 as a parameter, larger than zero, to be determined by the normalization condition on $\bar{\rho}_x^{\alpha\alpha}(\boldsymbol{r}_1, s)$, and we shall substitute the function $g(\boldsymbol{r}_1, x)$ by a suitable approximate expression $g'(\boldsymbol{r}_1, x)$. The resulting expression is given by

$$[34b] \quad \bar{\rho}_{PW}^{\alpha\alpha}(\boldsymbol{r}_1, s) = \begin{cases} \rho_1^\alpha(\boldsymbol{r}_1) + a'x^2; & 0 < x < x_1 \\ [\rho_1^\alpha(\boldsymbol{r}_1) + a'x_1^2] g'(\boldsymbol{r}_1, x); & x > x_1 \end{cases}$$

where $\bar{\rho}_{PW}^{\alpha\alpha}$ denotes the present approximation. Note that the parameter x_1 will vary with the value of $\boldsymbol{r}_1$. The simplest possible expression for g' is the exponential form

$$[34c] \quad g'(\boldsymbol{r}_1, x) = \exp[-\alpha(x - x_1)]$$

where α is a parameter which varies with the value of $\boldsymbol{r}_1$, with the imposed condition $\alpha > 0$. The normalization condition on $\bar{\rho}_{PW}^{\alpha\alpha}$ is expressed by

$$[34d] \quad 4\pi \int_0^\infty \bar{\rho}_{PW}^{\alpha\alpha} s^2 \delta s = \frac{2}{3\pi}\left[\frac{x_1^3}{3} + \frac{x_1^2}{\alpha} + \frac{2x_1}{\alpha^2} + \frac{2}{\alpha^3}\right] + \frac{4\pi}{3!(6\pi^2)^{5/3}} \frac{a}{(\rho_1^\alpha(\boldsymbol{r}_1))^{5/3}}\left[\frac{x_1^5}{5} + \frac{x_1^4}{\alpha} + \frac{2x_1^3}{\alpha^2} + \frac{2x_1^2}{\alpha^3}\right] = 1$$

The parameter x_1 should follow approximately the function $k_f r_1$ in order to reproduce the Fermi-hole correlation function for an atomic system. As depicted in Fig. 9 for the Ar atom, the function $k_f r_1$ is zero at the nucleus, increases with r_1 in intermediate atomic regions, and then reduces asymptotically to zero in the exponential tail. In the following discussion, we shall assume the same general behaviour for the parameter x_1 as a function of r_1. In particular, x_1 must tend to zero both for $r_1 = 0$ and for $r_1 \to \infty$ in order to remove the singularities of the term $a/(\pi_1^\alpha(\boldsymbol{r}_1))^{5/3}$ of eq. [34*d*], which diverges as $-1/r_1$ at the atomic nucleus and as $(\rho_1^\alpha(\boldsymbol{r}_1))^{-2/3}$ in the atomic exponential

Can. J. Chem. Downloaded from www.nrcresearchpress.com by 41.223.56.140 on 09/07/12
For personal use only.

tail, as discussed in Section VI. Also, if we want the approximate expression of eq. [34*b*] to reproduce the exact expression of eq. [34*a*] qualitatively correctly, we must assume that in the limit $r_1 \rightarrow \infty$ we have the condition $x_1/k_f \rightarrow \infty$. Given the above conditions on the behaviour of x_1, it is possible to outline the behaviour of the parameter α both at the nucleus and in the exponential tail of an atom. At the atomic nucleus, assuming that the second term on the RHS of eq. [34*d*] vanishes, the value of $\alpha = \alpha_0 = (4/3\pi)^{1/3}$ is readily determined from the normalization condition of eq. [34*d*]. Also, in the exponential tail of atoms, since as $r_1 \rightarrow \infty$ we assume that $x_1/k_f \rightarrow \infty$, we must have that $\alpha \rightarrow \infty$, in order to satisfy the normalization condition of eq. [34*d*] and to remove the singularity of the term $a/(\rho_1^\alpha(\boldsymbol{r}_1))^{5/3}$.

We shall now express x_1 in terms of α, so that only one unknown parameter is to be determined from the normalization condition of eq. [34*d*]. If we assume that the parameter α be a monotonically increasing function of r_1, then a general dependency of x_1 on α can be established. Thus, x_1 will be zero at $\alpha = \alpha_0$, will increase for intermediate values of α, and will eventually tend asymptotically to zero as $\alpha \rightarrow \infty$. One relation that satisfies all the conditions stated above is,

$$[34e] \quad x_1 = \frac{\alpha - \alpha_0}{c_0 + c_1\alpha + c_2\alpha^2}$$

We shall make use of the form of eq. [34*e*] in the following discussion. In eq. [34*e*] c_1 and c_2 are adjustable parameters to be determined from a least square fit of the exchange energy of atoms, as discussed at the end of the present chapter. Furthermore, c_0 is determined by imposing that the potential expression obtained by substituting eq. [34*b*] into eq. [5*b*] reduce to the HFS expression when $a = 0$, i.e. in the case of homogeneous density. The value of α can readily be determined by numerical methods from the normalization equation, as a function of the dimensionless variable

$$[35] \quad \lambda = \frac{a}{(\rho_1^\alpha(\boldsymbol{r}_1))^{5/3}}$$

once the relation of eq. [34*e*] has been established.

We should point out that the function $\bar{\rho}_{PW}^{\alpha\alpha}$ satisfies, by construction, the four conditions of eqs. [10]–[13] pertaining to the exact function $\bar{\rho}_x^{\alpha\alpha}(\boldsymbol{r}_1, s)$.

For atoms, the expression[3] of eq. [34*b*] follows the exact function $\bar{\rho}_x^{\alpha\alpha}(\boldsymbol{r}_1, s)$ reasonably well, as shown for the Ar atom in Fig. 10. At the atomic nucleus, we have that $x_1 = 0$ and $\alpha = \alpha_0$. Thus, eq. [34*b*] reduces to a simple exponential, in excellent accord with the exact expression $\bar{\rho}_x^{\alpha\alpha}(\boldsymbol{r}_1, s)$, which at the nucleus is close to the 1*s* orbital, see Fig. 10*a*. The behaviour of the exact function $\bar{\rho}_x^{\alpha\alpha}(\boldsymbol{r}_1, s)$ at the maximum of the density within a shell (Fig. 10*b*) and at the edge of a shell (Fig. 10*c*) is qualitatively well reproduced by our approximate expression $\bar{\rho}_{PW}^{\alpha\alpha}$.

We shall now show that the model presented here (eq. [34*b*–*e*]), is sufficient to generate a cut-off factor in the second order correction to the HFS potential expression. To this purpose, we shall consider the normalization condition on $\bar{\rho}_{PW}^{\alpha\alpha}$,

[3]Following the procedure developed by Becke (15*b*), we have adopted the approximate expression

$$\frac{1}{6}a \sim -\frac{1}{18}\nabla_1^2\rho_1^\alpha(\boldsymbol{r}_1) + \frac{2}{27}\frac{|\nabla_1\rho_1^\alpha(\boldsymbol{r}_1)|^2}{\rho_1^\alpha(\boldsymbol{r}_1)}$$

for the second order coefficient in the expansion of $\bar{\rho}_x^{\alpha\alpha}(\boldsymbol{r}_1, s)$.

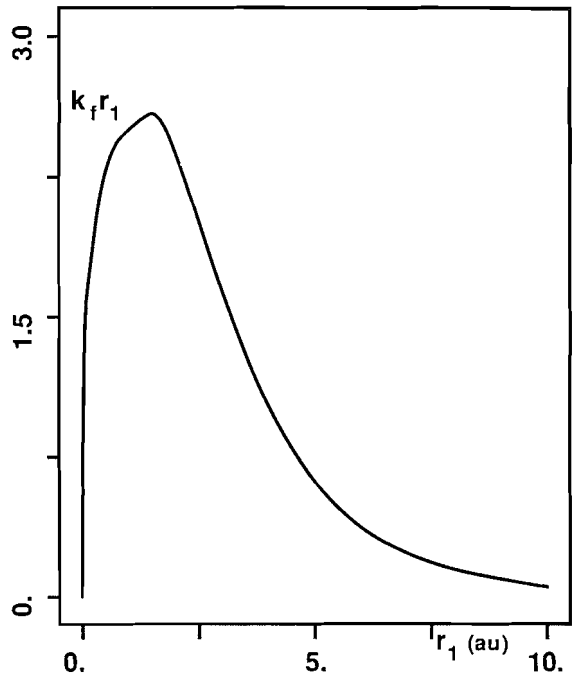


FIG. 9. Plot of $k_f r_1$ versus r_1 for the Ar atom.

given by eq. [34*d*], as well as the coulomb potential expression, obtained by inserting eq. [34*b*] into eq. [5*b*],

$$[36] \quad V_{PW}^{\alpha\alpha}(\boldsymbol{r}_1) = -\frac{4\pi}{(6\pi^2)^{2/3}}(\rho_1^\alpha(\boldsymbol{r}_1))^{1/3}\left[\frac{x_1^2}{2} + \frac{x_1}{\alpha} + \frac{1}{\alpha^2}\right] + -\frac{4\pi}{3!(6\pi^2)^{4/3}}\frac{a}{(\rho_1^\alpha(\boldsymbol{r}_1))^{4/3}}\left[\frac{x_1^4}{4} + \frac{x_1^3}{\alpha} + \frac{x_1^2}{\alpha^2}\right]$$

We shall now prove that the values of x_1 and α that satisfy the normalization condition of eq. [34*d*], and remove the two singularities of the term $a/(\rho_1^\alpha(\boldsymbol{r}_1))^{5/3}$, also lead to a well behaved expression for the potential of eq. [36], by removing the two singularities of the term $a/(\rho_1^\alpha(\boldsymbol{r}_1))^{4/3}$ in eq. [36], which diverges as $-1/r_1$ at the atomic nucleus and as $(\rho_1^\alpha)^{-1/3}$ in the atomic exponential tail, as discussed in Section V.

At the atomic nucleus, as the function α tends to the finite value α_0 and $x_1 \rightarrow 0$, we have the limit form

$$[37a] \quad x_1 = -\frac{\alpha_0^4 - 3\alpha_0^2(c_0 + c_1\alpha_0 + c_2\alpha_0^2)}{2b\lambda}; \qquad r_1 \sim 0$$

as it can be shown from eq. [34*d*–*e*], after some rather straightforward algebra. In eq. [37*a*] we have that $b = 4\pi/[3!(6\pi^2)^{5/3}]$ and λ is given by eq. [35]. The limit form of eq. [37*a*] is sufficient to remove the singularity of the term $a/(\rho_1^\alpha(\boldsymbol{r}_1))^{4/3}$ of eq. [36], leading to a well behaved potential expression at the atomic nucleus.

In the exponential tail of atoms, as $x_1 \rightarrow 0$ and $\alpha \rightarrow \infty$, we have from eq. [34*e*] the limit form

$$[37b] \quad x_1 = \frac{1}{c_2\alpha}; \qquad r_1 \gg 0$$

Thus the limit forms for the normalization equation and for the potential expression are given by

$$[37c] \quad 4\pi\int_0^\infty \bar{\rho}_{PW}^{\alpha\alpha}s^2\delta s = \text{const}_1 x_1^3 + \text{const}_2\frac{a}{(\rho_1^\alpha(\boldsymbol{r}_1))^{5/3}}x_1^5 = \text{const}_1 x_1^3 + \text{const}_2\lambda x_1^5 = 1; \qquad r_1 \gg 0$$

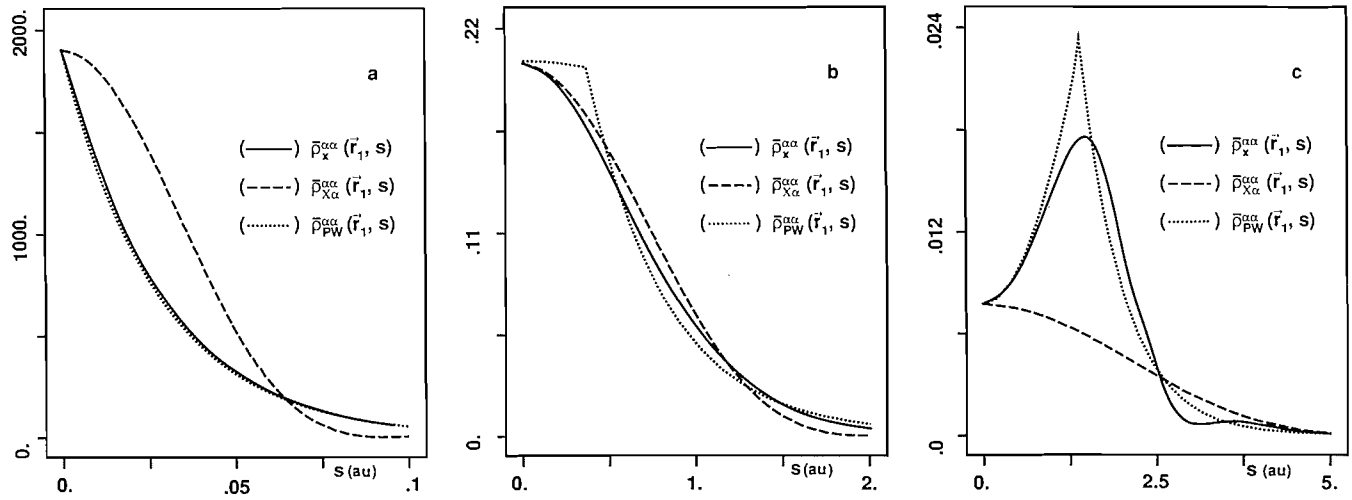


FIG. 10. Ar atom: the spherically averaged hole correlation functions $\bar{\rho}_x^{\alpha\alpha}(r_1, s)$, $\bar{\rho}_{X\alpha}^{\alpha\alpha}(r_1, s)$ and $\bar{\rho}_{PW}^{\alpha\alpha}(r_1, s)$. (*a*) for $r_1 = 0$ au; (*b*) for $r_1 = 1$ au; (*c*) for $r_1 = 2.5$ au.

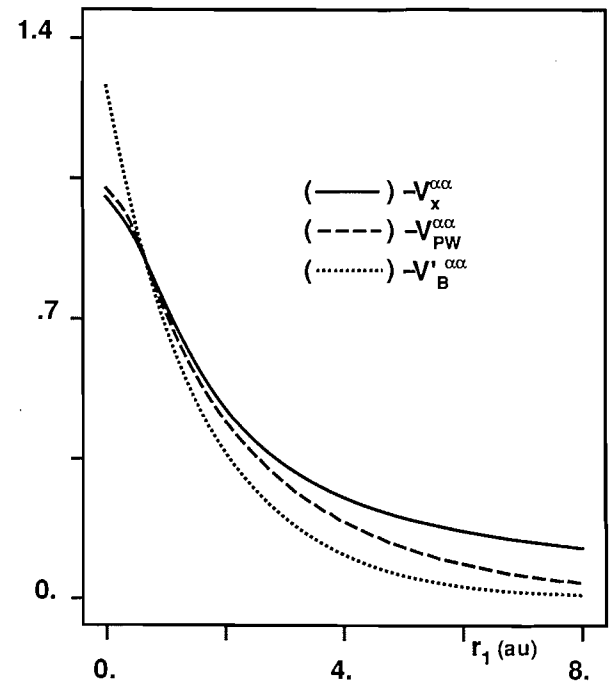


FIG. 11. He atom: the potentials $V_x^{\alpha\alpha}(r_1)$ and $V'^{\alpha\alpha}_B(r_1)$, as well as the present approximation $V_{PW}^{\alpha\alpha}(r_1)$.

and

$$[37d]\quad V_{PW}^{\alpha\alpha}(r_1) = -\text{const}_3(\rho_1^{\alpha}(r_1))^{1/3}x_1^2 - \text{const}_4\frac{a}{(\rho_1^{\alpha}(r_1))^{4/3}}x_1^4; \qquad r_1 \gg 0$$

Where the symbol const_n denotes a constant factor. From eq. [37*b*], it can immediately be shown that, as $x_1 \to 0$ and $\lambda \to \infty$, we have the limit form

$$[37e]\quad x_1 = \frac{1}{[\text{const}_2\lambda]^{1/5}} = \frac{1}{[(1/5 + c_2 + 2c_2^2 + 2c_2^3)b\lambda]^{1/5}}; \qquad r_1 \gg 0$$

where the value of const_2 is given explicitly. Also, the constant term b was defined in connection with eq. [37*a*]. The limit form given by eq. [37*e*] is sufficient to remove the singularity of the term $a/(\rho_1^{\alpha}(r_1))^{4/3}$ in the potential expression of eq. [37*d*], leading to a well behaved potential expression in the atomic exponential tail.

Thus, we have shown that our simple model $\bar{\rho}_{PW}^{\alpha\alpha}$ for the spherically averaged Fermi-hole correlation function, subject to the normalization condition of eq. [34*d*], leads to a well-behaved expression for the potential, eq. [36]. The expression of eq. [36] contains, as a factor of the term $a/(\rho_1^{\alpha}(r_1))^{4/3}$, a cut-off function analogous to the exact expression of eq. [33] and to the empirical expressions proposed by Becke (15*b*) and DePristo *et al.* (16*a*).

The behaviour of the potential expression of eq. [36] is depicted in Fig. 11, for the He atom. It appears that our model represents a qualitative improvement over the potential proposed by Becke (15*b*). It might be argued that such an improvement is due to the use of a realistic, albeit crude, model for the Fermi-hole correlation function which satisfies the exact conditions of eqs. [10]–[13], as already mentioned.

In the present approximation, the exchange energy is given by the expression

$$[38]\quad E_{PW}^{\alpha\alpha} = -\frac{2\pi}{(6\pi^2)^{2/3}}\int(\rho_1^{\alpha}(r_1))^{4/3}\left[\frac{x_1^2}{2} + \frac{x_1}{\alpha} + \frac{1}{\alpha^2}\right]\delta r_1 + -\frac{2\pi}{3!(6\pi^2)^{4/3}}\int\frac{a}{(\rho_1^{\alpha}(r_1))^{1/3}}\left[\frac{x_1^4}{4} + \frac{x_1^3}{\alpha} + \frac{x_1^2}{\alpha^2}\right]\delta r_1$$

obtained by substituting the potential of eq. [36] into eq. [5*a*].

Using the expression of eq. [38], we have calculated the exchange energies of the atomic systems from H to Ar, as well as Kr and Xe, for different values of the parameters c_0, c_1, and c_2. We have found that the lowest standard deviation relative to the Hartree–Fock exchange energies is given by the parameter values $c_0 = -0.195$, $c_1 = 0.290$, and $c_2 = 0.190$. The corresponding exchange energies are shown in Table 2. As indicated in Table 2, the values obtained from the present approximation compare favourably with the values obtained from the HFS exchange energy expression as well as the simple nonlocal expression of eq. [27] and the expressions containing

Can. J. Chem. Downloaded from www.nrcresearchpress.com by 41.223.56.140 on 09/07/12
For personal use only.

a cut-off factor due to respectively Becke (eq. [28*b*]) and DePristo *et al.* (eq. [29]).

VII. Concluding remarks

We have investigated various expressions based on the gradient expansion on the spherically averaged Fermi-hole correlation function $\bar{\rho}_x^{\alpha\alpha}(r_1, s)$ and the corresponding exchange energy expressions. In Section IV, we have shown that, for atomic systems, the expansion of $\bar{\rho}_x^{\alpha\alpha}(r_1, s)$ in powers of s must be carried out in two regions, for $0 < s < r_1$ where it is defined as a Taylor expansion, and for $s > r_1$ where it is defined as a Laurent expansion.

Becke (15*a*) has, as discussed in Section V, obtained an approximate expression, $\bar{\rho}_B^{\alpha\alpha}(r_1, s)$, for $\bar{\rho}_x^{\alpha\alpha}(r_1, s)$, without taking into account the properties of the expansion in the second region. The function $\bar{\rho}_B^{\alpha\alpha}(r_1, s)$ represents a partial improvement over the local density approximation $\bar{\rho}_{X\alpha}^{\alpha\alpha}(r_1, s)$, since it goes to a maximum as a function of s for r_1 at the edge of an atomic shell, in agreement with the behaviour of the exact expression $\bar{\rho}_x^{\alpha\alpha}(r_1, s)$. However, the coulomb potential $V_B^{\alpha\alpha}(r_1)$ corresponding to $\bar{\rho}_B^{\alpha\alpha}(r_1, s)$ is divergent in the exponential tail of atoms. A remedy for such a divergency was proposed by Becke (15*b*) in the form of an empirical cut-off factor for the second order gradient correction term in the potential expression. In Section VI, we have furnished a theoretical explanation for the origin of such a cut-off factor, based on the two-region expansion of $\bar{\rho}_x^{\alpha\alpha}(r_1, s)$. Finally, in Section VII, we have proposed an alternative approximate expression for the spherically averaged Fermi-hole correlation function $\bar{\rho}_{PW}^{\alpha\alpha}(r_1, s)$, derived from the two-region expansion of $\bar{\rho}_x^{\alpha\alpha}(r, s)$. The coulomb potential expression corresponding to $\bar{\rho}_{PW}^{\alpha\alpha}(r_1, s)$ contains a cut-off factor analogous to the function proposed by Becke and yields values for the exchange energies of atoms in good agreement with the Hartree–Fock results.

Can. J. Chem. Downloaded from www.nrcresearchpress.com by 41.223.56.140 on 09/07/12
For personal use only.

Acknowledgments

This investigation was supported by the Natural Sciences and Engineering Research Council of Canada (NSERC). We would like to thank Professor A. Becke, from Queens University, for many useful discussions.

1. P. HOHENBERG and W. KOHN. Phys. Rev. **136**, B864 (1964).
2. J. C. SLATER. Phys. Rev. **81**, 385 (1951).
3. (*a*) L. H. THOMAS. Proc. Camb. Phil. Soc. **23**, 542 (1927); (*b*) E. FERMI. Z. Physik. **48**, 73 (1928); (*c*) P. A. M. DIRAC. Proc. Camb. Phil. Soc. **26**, 376 (1930).
4. (*a*) J. P. DAHL and J. AVERY (*Editors*). Local density approximations in quantum chemistry and solid state physics. Plenum, New York. 1984; R. ERDAHL and V. H. SMITH, JR. (*Editors*). Density matrices and density functionals. Reidel, Dordrecht. 1987; (*c*) J. DA PROVIDENCIA (*Editor*). Density functional methods in physics. Plenum, New York. 1985.
5. (*a*) E. V. LUDENA and A. S. IERRALTA. Phys. Rev. A**32**, 19 (1985); (*b*) J. P. DAHL and M. SPRINGBORG. Mol. Phys. **47**, 1001 (1982); (*c*) E. ZAREMBA and K. STURM. Phys. Rev. Lett. **55**, 750 (1985); (*d*) J. E. HARRIMAN. Phys. Rev. A**30**, 19 (1984); (*e*) D. C. LANGRETH and M. J. MEHL. Phys. Rev. B**28**, 1809 (1983); (*f*) S. H. VOSKO, L. WILK, and M. NUSAIR. Can. J. Phys. **58**, 1200 (1980); (*g*) H. STOLL, E. GOLKA, and H. PREUSS. Theor. Chim. Acta, **55**, 29 (1980); (*h*) A. SAVIN, U. WEDIG, H. PREUSS, and H. STOLL. Phys. Rev. Lett. **53**, 2089 (1984); (*i*) E. H. LIEB. Phys. Rev. Lett. **46**, 457 (1981); (*j*) M. LEVY. Phys. Rev. A**26**, 1200 (1982); (*k*) J. P. PERDEW. Phys. Rev. B**33**, 8822 (1986); (*l*) N. H. MARCH. J. Phys. Chem. **86**, 2262 (1982); (*m*) R. G. PARR and L. J. BARTOLOTTI. J. Am. Chem. Soc. **104**, 3801 (1982); (*n*) E. S. KRYACHKO. Int. J. Quantum Chem. **21**, 1123 (1982); (*o*) U. VON BARTH and L. HEDIN. J. Phys. C**5**, 1629 (1972); (*p*) O. GUNNARSSON and R. O. JONES. Phys. Script. **21**, 394 (1980); (*q*) L. FRITSCHE and H. GOLLISCH, in ref. 4*a*, p. 245; (*r*) L. J. SHAM. *In* Computational methods in band theory. *Edited by* P. M. Markus, J. F. Janak, and A. R. Williams. Plenum, New York. 1971.
6. (*a*) E. J. BAERENDS, D. E. ELLIS, and P. ROS. Chem. Phys. **2**, 41 (1973); (*b*) A. ROSEN, D. E. ELLIS, H. ADACHI, and F. W. AVERILL. J. Chem. Phys. **65**, 3629 (1976); (*c*) H. SAMBE and R. H. FELTON. J. Chem. Phys. **62**, 1122 (1975); (*d*) K. H. JOHNSON. J. Chem. Phys. **45**, 3085 (1966); (*e*) B. DELLEY and D. E. ELLIS. J. Chem. Phys. **76**, 1949 (1982); (*f*) G. L. GUTSEV and A. A. LEVIN. Chem. Phys. **51**, 459 (1980); (*g*) O. GUNNARSSON, J. HARRIS, and R. O. JONES. Phys. Rev. B**15**, 3027 (1977); (*h*) B. I. DUNLAP, J. W. D. CONNOLLY, and J. F. SABIN. J. Chem. Phys. **71**, 3396 (1979).
7. J. C. SLATER. Adv. Quantum Chem. **6**, 1 (1972).
8. (*a*) A. C. BECKE. J. Chem. Phys. **76**, 6037 (1982); (*b*) B. I. DUNLAP. J. Phys. Chem. **90**, 5524 (1986); (*c*) T. ZIEGLER. Inorg. Chem. **25**, 2721 (1986); (*d*) L. VERSLUIS and T. ZIEGLER. J. Chem. Phys. In press.
9. (*a*) N. ROSCH, H. JORG, and B. I. DUNLAP. NATO ASI, C**176**, 179 (1986); (*b*) E. J. BAERENDS and A. ROZENDAAL. NATO ASI, C**176**, 159 (1986); (*c*) T. ZIEGLER, J. G. SNIJDERS, and E. J. BAERENDS. J. Chem. Phys. **74**, 1271 (1981).
10. (*a*) E. J. BAERENDS, J. G. SNIJDERS, C. A. DE LANGE, and G. JONKERS. *In* Local density approximations in quantum chemistry and solid state physics. *Edited by* J. P. Dahl and J. Avery. Plenum, New York. 1984. p. 415; (*b*) T. ZIEGLER, A. RAUK, and E. J. BAERENDS. Theor. Chim. Acta, **43**, 261 (1977); (*c*) U. VON BARTH. Phys. Rev. A**20**, 1693 (1979).
11. (*a*) T. ZIEGLER, V. TSCHINKE, and L. VERSLUIS. NATO ASI, C**176**, 189 (1986); (*b*) T. ZIEGLER, V. TSCHINKE, and A. BECKE. Polyhedron, **6**, 685 (1987); (*c*) T. ZIEGLER, V. TSCHINKE, and A. BECKE. J. Am. Chem. Soc. **109**, 1351 (1987); (*d*) T. ZIEGLER, V. TSCHINKE, and C. URSENBACH. J. Am. Chem. Soc. **109**, 4825 (1987).
12. V. TSCHINKE and T. ZIEGLER. *In* Density matrices and density functionals. *Edited by* R. Erdahl and V. H. Smith. Reidel, Dordrecht. 1987. p. 189.
13. F. HERMAN, J. P. VAN DYKE, and I. B. ORTENBURGER. Phys. Rev. Lett. **22**, 807 (1969).
14. K. SCHWARZ. Chem. Phys. **7**, 94 (1975).
15. (*a*) A. D. BECKE. Int. J. Quantum Chem. **27**, 1915 (1983); (*b*) A. D. BECKE. Phys. Rev. A**33**, 2786 (1986); (*c*) A. D. BECKE. J. Chem. Phys. **84**, 4524 (1986).
16. (*a*) A. E. DEPRISTO and J. D. KRESS. J. Chem. Phys. **86**, 1425 (1987); (*b*) J. P. PERDEW. Phys. Rev. Lett. **55**, 1655 (1985); (*c*) J. P. PERDEW and W. YUE. Phys. Rev. B**33**, 8800 (1986); (*d*) F. W. KUTZLER and G. S. PAINTER. Phys. Rev. Lett. **59**, 1285 (1987); (*e*) F. W. KUTZLER and G. S. PAINTER. Phys. Rev. B**37**, 285 (1988).
17. (*a*) R. J. BOYD and C. A. COULSON. J. Phys. B**7**, 1805 (1974); (*b*) J. P. PERDEW and A. ZUNGER. Phys. Rev. B**23**, 5048 (1981); (*c*) V. SAHNI, K. P. BOHNEN, and M. K. HARBOLA. Phys. Rev. A**37**, 1895 (1988); (*d*) V. TSCHINKE. Ph.D. Thesis, Calgary. 1989.
18. R. MCWEENEY and B. T. SUTCLIFFE. Methods of molecular quantum mechanics. Academic Press, New York. 1969.
19. O. GUNNARSSON and I. LUNDQUIST. Phys. Rev. B**10**, 1319 (1974).
20. O. GUNNARSSON and I. LUNDQUIST. Phys. Rev. B**13**, 4274 (1976).
21. O. GUNNARSSON, M. JONSON, and I. LUNDQUIST. Phys. Rev. B**20**, 3136 (1979).
22. (*a*) J. E. LENNARD-JONES and J. A. POPLE. Proc. R. Soc. London, A**202**, 166 (1950); (*b*) S. F. BOYS. Rev. Mod. Phys. **32**, 296 (1960); (*c*) S. F. BOYS and J. M. FOSTER. Rev. Mod. Phys. **32**, 300 (1960); (*d*) C. EDMISTON and K. RUEDENBERG. Rev.

Mod. Phys. **35**, 457 (1963); (*e*) S. F. BOYS. Quantum theory of atoms, molecules, and the solid state. *Edited by* P. O. Löwdin. Academic Press, New York. 1966; (*f*) W. VON NIESSEN. J. Chem. Phys. **56**, 4290 (1972).

23. (*a*) W. VON NIESSEN. Theoret. Chim. Acta, **27**, 9 (1972); (*b*) L. A. BURKE, G. LEROY, R. DAUDEL, and M. E. STEPHENS. Chem. Phys. Lett. **57**, 15 (1978).
24. J. C. SLATER. Quantum theory of atomic structure. Vol. 2. McGraw-Hill, New York. 1960. App. 22.
25. J. C. SLATER. The self consistent field of molecules and solids. Vol. 4. McGraw-Hill, New York. 1974. Chap. 1.
26. (*a*) M. S. GOPINATHAN, M. A. WHITEHEAD, and R. BOGDANOVIC. Phys. Rev. A**14**, 1 (1976); (*b*) J. L. GASQUEZ and J. KELLER. Phys. Rev. A**16**, 1358 (1977).
27. E. R. DAVIDSON. Reduced density matrices in quantum chemistry. Academic Press, New York. 1976.
28. E. CLEMENTI and C. ROETTI. Atm. Data Nucl. Data, **14**, 177 (1974).

Can. J. Chem. Downloaded from www.nrcresearchpress.com by 41.223.56.140 on 09/07/12
For personal use only.

Laser flash photolysis studies of 2,4,6-trialkylphenyl ketones[1]

B. GUERIN[2] AND L. J. JOHNSTON

Division of Chemistry, National Research Council of Canada, Ottawa, Ont., Canada K1A 0R6

Received September 26, 1988

B. GUERIN and L. J. JOHNSTON. Can. J. Chem. **67**, 473 (1989).

2,4,6-Triisopropylbenzophenone (**3**), 2,4,6-trimethylbenzophenone (**4**), and 2,4,6-trimethylacetophenone (**5**) have been examined by laser flash photolysis. Relatively long-lived triplets compared to similar mono-alkyl substituted ketones have been observed for each (280 ns, >2 μs and 220 ns in acetronitrile for **3**, **4** and **5**, respectively). Photoenol intermediates with λ_{max} 360 nm and 380 nm were also observed from ketones **3** and **5**, respectively. Ketone **3** yielded a mixture of approximately equal amounts of *Z* and *E* enols in hexane. The *Z* enol had a lifetime of ~4 μs while the *E* enol did not decay appreciably during 100 μs. Biradical intermediates were not observed from any of the three ketones. Quenching rate constants for several energy transfer and hydrogen donor substrates are reported. For example, ketones **3** and **4** react with 1,4-cyclohexadiene with rate constants of 2.8×10^7 and 3.7×10^7 M^{-1} s^{-1}, respectively, to yield ketyl radicals with λ_{max} ~480 nm.

Key words: photoenolization, trialkyl phenyl ketone, flash photolysis, triplets.

B. GUERIN et L. J. JOHNSTON. Can. J. Chem. **67**, 473 (1989).

On a étudié les triisopropyl-2,4,6 (**3**) et triméthyl-2,4,6 (**4**) benzophénones ainsi que la triméthyl-2,4,6 acétophénone (**5**) à l'aide de la photolyse éclair au laser. Pour chacun de ces composés, on a observé des triplets dont la vie est relativement longue (280 ns, >2 μs et 220 ns respectivement pour les composés **3**, **4** et **5**, dans l'acétonitrile) si on la compare à celle de cétones semblables monosubstituées par des groupements alkyles. Dans les cas des cétones **3** et **5**, on a aussi observé des intermédiaires photoénoliques dont les λ_{max} sont respectivement à 360 et à 380 nm. Dans l'hexane, la cétone **3** fournit un mélange, en quantités pratiquement égales, des deux énols *Z* et *E*. Le temps de vie de l'énol *Z* est d'environ ~4 μs alors que l'énol *E* ne se décompose pratiquement pas durant 100 μs. On n'a observé d'intermédiaires biradicalaires avec aucune de ces trois cétones. On rapporte les constantes de vitesse de piégeage pour plusieurs transferts d'énergie et plusieurs substrats donneurs d'hydrogène. Par exemple, les cétones **3** et **4** réagissent avec le cyclohexadiène-1,4 avec des constantes de vitesse respectives de $2{,}8 \times 10^7$ et $3{,}7 \times 10^7$ M^{-1} s^{-1} et elles fournissent des radicaux cétyles dont le λ_{max} est d'environ ~480 nm.

Mots clés : photoénolisation, phényl-cétone trialkylée, photolyse éclair, triplets.

[Traduit par la revue]

Introduction

The photoenolization of *o*-alkylphenyl ketones such as 2-methylacetophenone (**1**) and 2-methylbenzophenone (**2**) has been examined by conventional and laser flash photolysis by a number of groups (1–11). Despite some initial confusion, the mechanism for the reaction and the assignment of the various transients involved is now well-established. Briefly, intramolecular hydrogen abstraction from triplet **1** has been shown to give a rotationally equilibrated biradical (lifetime of 580 ns (3)) which then decays to a mixture of short- (*Z*) and long- (*E*) lived enols (2–5). In this case two kinetically distinct triplet states (0.5, 35 ns) have been observed with the shorter-lived *syn* conformer being the reactive species (3, 12). The long-lived *anti* conformer decays by bond rotation to the *syn* triplet followed by hydrogen abstraction. For ketone **2** the triplet is short-lived (~3.5 ns (11)) and yields a biradical with an approximately 30 ns lifetime in various solvents (2). The biradical again gives a mixture of two enols with lifetimes which vary with solvent. In both of these systems the net photochemistry (intra- or intermolecular) is inefficient since the primary decay pathway for the enol in the absence of trapping reagents is regeneration of the starting ketone (6, 13–15).

In contrast to ketones **1** and **2**, the intermediates involved in the photochemistry of 2,6-dialkylphenyl ketones have not been as well established. A variety of 2,4,6-trialkylacetophenones and benzophenones undergo photocyclization to benzocyclobutenols (reaction [1]) (16–19). For example, a quantum yield of 0.6 for photocyclization of 2,4,6-triisopropylbenzophenone (**3**) in benzene has been measured while a value of < 0.01 was determined for 2,4,6-trimethylbenzophenone, **4** (17, 18). Stern–Volmer quenching studies for these and related ketones have indicated that the triplet states are considerably longer-lived than those for ketones **1** or **2** (18), and the existence of two kinetically distinct triplets has been suggested for ketone **4** (18) and γ,2,4,6-tetramethylvalerophenone (15).

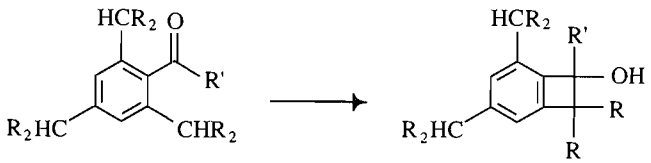
There are only several brief reports on transient measurements for trialkylphenyl ketones (3, 9, 20–22). For **3**, the transients observed by laser flash photolysis have been assigned to triplet **3** and the biradical formed by intramolecular hydrogen abstraction with lifetimes of 225 ns and 17 μs, respectively, in acetonitrile (20). Similar results were reported for 4′-substituted ketone **3** (21). Long-lived transients have been observed from several di- and trialkylbenzophenones but these have not been conclusively identified (8, 9, 22). The triplet state of 2,4,6-trimethylacetophenone (**4**) has been suggested to be relatively long-lived (ca. 300 ns) compared to **1** on the basis of Stern–Volmer analyses of methylnapthalene sensitization results and methyl viologen trapping (3). However, no definite conclusion as to the transients involved was reached.

We have examined ketones **3**, **4**, and **5** by laser flash photolysis in an attempt to identify the transients involved in the photoenolization. Our results confirm the presence of relatively long-lived triplet states for these ketones, as well as both short- and long-lived enols. However, no biradical intermediates were observed, which suggests that these intermediates have considerably shorter lifetimes than the triplet ketones and are, therefore, not detectable in our experiments. All three ketones have also been shown to undergo efficient hydrogen abstraction in the presence of good hydrogen donors.

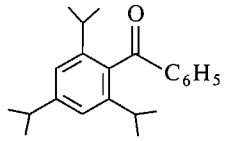
[1]NRCC No. 29864.

[2]Co-op student, University of Sherbrooke.

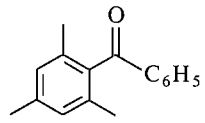
Can. J. Chem. Downloaded from www.nrcresearchpress.com by 41.223.56.140 on 09/07/12
For personal use only.

[1] 

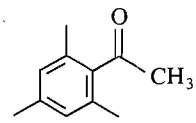
3; R = CH_3 R′ = Ph
4; R = H R′ = Ph



3



4



5

Results

Phosphorescence spectra

Phosphorescence spectra for ketones **3**, **4**, and **5** were measured in methylcyclohexane glasses at 77 K. Each gave a spectrum which showed the well-resolved vibrational structure typical of n,π* ketone triplets and which was not appreciably broader than the corresponding unsubstituted ketone. Triplet energies of 68.6, 68.4, and 72.1 kcal/mol were calculated from the 0,0 bands for **3**, **4**, and **5**, respectively. These may be compared to values of 68.6 and 73.7 kcal/mol for benzophenone and acetophenone in nonpolar solvents (23*a*). The phosphorescence spectrum of ketone **5** in a polar glass (9:1 ethanol/methanol) which would tend to favor a lowest π,π* triplet still showed the typical n,π* vibrational structure. Although these results are consistent with a n,π* lowest triplet, the measured lifetime of ~10 ms in methylcyclohexane at 77 K is somewhat longer than usual for n,π* states (23*b*). These results may indicate that the π,π* state is slightly lower in energy, with the emission arising from the nearby n,π* state.

Phosphorescence spectra for all three ketones could also be readily measured in solution at room temperature using an optical multichannel analyzer. Phosphorescence from ketone **5** in methanol showed vibrational structure similar to that at 77 K.

Transient photochemistry of **3**

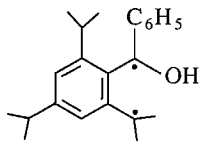
Excitation of ketone **3** at either 308 nm or 337 nm in methanol or acetonitrile (~3 m*M*) gave transient spectra similar to those previously reported (20). A short-lived transient with λ_{max} ~330 nm and a second broad band around 700 nm was observed on short timescales. This spectrum was replaced by a long-lived transient with λ_{max} = 360 nm (Fig. 1). Similar results were also obtained in hexane. In each solvent the decay of the short-lived transient could be monitored at 700 nm without any interference from other species. The decay kinetics at 700 nm corresponded very well to those of the growth of the long-lived signal at 360 nm (Fig. 1, insert) indicating that the first is the precursor of the second. The characterization of these two transients is discussed separately below.

(*a*) Triplet **3**. Lifetimes for the decay of the short-lived transient of 350, 280, 330, and 260 ns were measured at 700 nm in acetonitrile, methanol, benzene, and hexane, respectively. The decay kinetics at 325 nm agreed well with these results although there was a residual absorption due to the long-lived transient at this wavelength. The short-lived transient was confirmed to be triplet **3**, in agreement with the previous report (20), on the basis of the following observations.

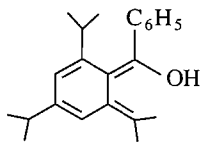
In acetonitrile the ketone showed readily detectable phosphorescence which was similar to the spectrum recorded in a glass at 77 K and which decayed with the same lifetime as that of the triplet–triplet absorption at 700 nm. Furthermore, the 700 nm transient was efficiently quenched by typical triplet quenchers such as oxygen and 1,3-cyclohexadiene. Plots of the triplet decay rate at 700 nm against quencher concentration gave rate constants (k_q) of $3.3 \times 10^9\ M^{-1}\ s^{-1}$ and $1.9 \times 10^8\ M^{-1}\ s^{-1}$ for 1,3-cyclohexadiene and oxygen, respectively (see Table 1). It should be noted that similar results could be obtained at either 325 or 700 nm. The triplet was also quenched by 1-methylnapthalene with concomitant production of its triplet state (λ_{max} ~420 nm) with $k_q = 2.0 \times 10^9\ M^{-1}\ s^{-1}$. In this experiment the rate of decay of triplet **3** at 700 nm was measured as a function of added methylnapthalene. The growth kinetics of the methylnapthalene triplet were complicated by the presence of the additional long-lived species at 360 nm. Quenching rate constants for several other substrates are also tabulated in Table 1.

An Arrhenius plot for the decay of triplet **3** over the temperature range 240–312 K gave $E_a = 6.1 \pm 0.3$ kcal/mol^{-1} and log (A, s^{-1}) = 11.1 ± 0.2. These Arrhenius parameters are rather unusual for decay of the triplet by intramolecular hydrogen abstraction (24, 25).

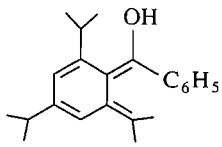
(*b*) Enols **7** and **8**. The long-lived signal at 360 nm had previously been assigned to biradical **6** (20). However, the results outlined below indicate that this transient is a mixture of the *Z* and *E* enols, **7** and **8**. The decay kinetics at 360 nm (Fig. 2)



6



7



8

in hexane show one component with a lifetime of ~4 μs in addition to a much longer-lived residual which does not decay significantly over a 100 μs timescale. The latter accounts for approximately 50% of the total signal. Spectra obtained at 1.5 μs and 50 μs after laser excitation for the short and long components are similar except for slightly enhanced absorption at shorter wavelengths for the latter (Fig. 2). Qualitatively similar results are found in acetonitrile and methanol although the lifetimes for the short component are lengthened to 20 μs in acetonitrile and ~40 μs in methanol. These results suggest that the 360 nm transient is a mixture of the *Z* and *E* enols since both spectral and kinetic evidence agree well with that for enols in related systems (2, 4, 26). Furthermore, based on the data available for similar systems, biradical **6** would be expected to have an absorption similar to that of the ketyl radical from **3** and to be considerably shorter-lived than the transient at 360 nm (27, 28). For example, biradicals produced by intramolecular hydrogen abstraction in 2,4-dimethylbenzophenone and 2-*tert*-butylbenzophenone show absorption maxima at 535 nm (2) and 465 nm (29), respectively.

Quenching studies are also consistent with the enol assignment since oxygen, methyl viologen, and di-*tert*-butyl nitroxide all failed to affect the lifetime of the transient. However, each of these quenchers did decrease the triplet lifetime as well as decreasing the yield of the enol. These substrates are all known to react with biradicals with rate constants in excess of $10^9\ M^{-1}\ s^{-1}$ (27, 28) and would, therefore, react with a biradical

Can. J. Chem. Downloaded from www.nrcresearchpress.com by 41.223.56.140 on 09/07/12
For personal use only.

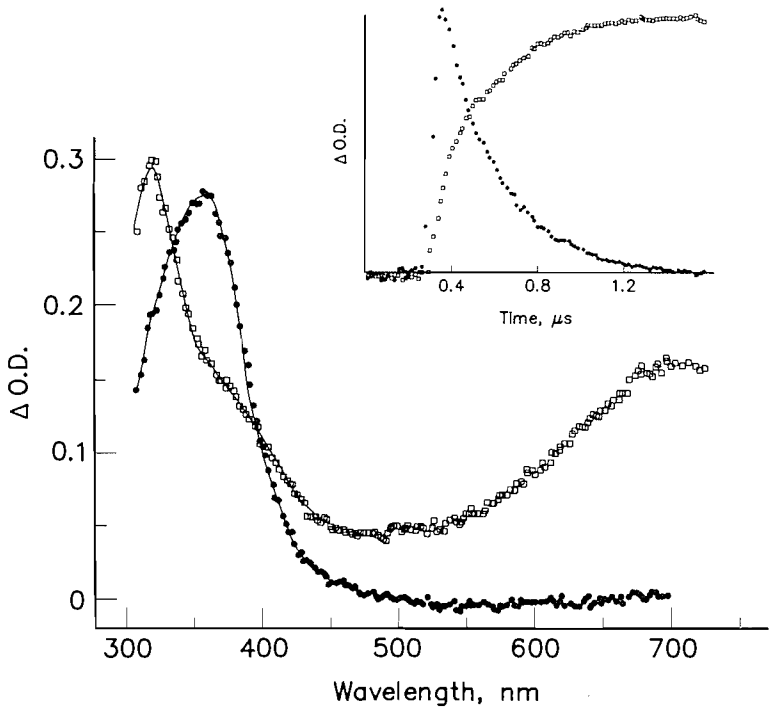


FIG. 1. Transient absorption spectra measured 0.10 μs (□) and 2 μs (●) after 308 nm excitation of ketone **3** in methanol. *Insert*. Decay of the transient absorption from **3** monitored at 700 nm (●) and 360 nm (□).

TABLE 1. Rate constants for quenching of triplet ketones

Quencher	Ketone	Solvent	k_q, M^{-1} s^{-1}[a]
Oxygen	**3**	Methanol	$(1.9\pm0.2)\times10^8$
1,3-Cyclohexadiene	**3**	Methanol	$(3.3\pm0.3)\times10^9$
1,4-Cyclohexadiene	**3**	Methanol	$(2.8\pm0.2)\times10^7$
1-Methylnaphthalene	**3**	Methanol	$(2.0\pm0.2)\times10^9$
Methyl viologen	**3**	Methanol	$(2.7\pm0.4)\times10^9$
Oxygen	**4**	Acetonitrile	$(4.6\pm0.7)\times10^8$
1,3-Cyclohexadiene	**4**	Acetonitrile	$(4.5\pm0.3)\times10^9$
1,4-Cyclohexadiene	**4**	Acetonitrile	$(3.7\pm0.3)\times10^7$
1-Methylnaphthalene	**4**	Acetonitrile	$(3.2\pm0.4)\times10^9$
Oxygen	**5**	Methanol	3.1×10^{9b}
1,3-Cyclohexadiene	**5**	Methanol	$(2.5\pm0.2)\times10^9$
1,4-Cyclohexadiene	**5**	Methanol	$<1\times10^6$
Tri-*n*-butyltin hydride	**5**	Methanol	$(7.6\pm0.6)\times10^7$

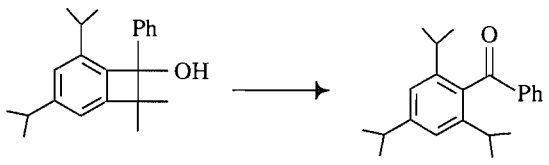
[a]At room temperature.
[b]Based on the triplet lifetime in oxygen-saturated solution.

of 17 μs lifetime at much lower quencher concentrations than those necessary to quench a 280 ns triplet. It is, thus, unreasonable to assign the observed species to biradical **6**.

Attempts to trap the proposed enols with typical dienophiles were unsuccessful since the triplet ketone was quenched by these substrates. For example, 0.01 *M* dimethylacetylene dicarboxylate was found to quench >50% of triplet **3**. The possibility of deuterium incorporation in recovered starting material was also investigated as a further test of the intermediacy of enols **7** and **8**. Accordingly, ketone **3** was photolysed to ~95% conversion in methanol and methanol-O-*d* with 350 nm light to prevent back reaction of the product cyclobutenol to starting material. The unreacted ketone was then examined by LC/MS to check for deuterium incorporation. The sample photolysed in deuterated solvent contained 30–40% monodeuterated ketone. Although this evidence suggests that deuterium incorporation may occur at the enol stage, the possibility of deuterium incorporation via the biradical cannot be ruled out.

(*c*) Attempted detection of biradical **6**. The above results suggest that although biradical **6** is probably formed from triplet **3**, it decays to enols **7** and **8** with a higher rate constant than that for triplet decay. No additional transients were observed on a short timescale in methanol, even at 65°C at which temperature the triplet lifetime has been shortened to ~70 ns. Similarly, no signals attributable to **6** were observed in the presence of sufficient 1,3-cyclohexadiene to substantially reduce the triplet lifetime.

Both direct and sensitized photolysis of benzocyclobutenol **9** have been reported to yield ketone **3**, presumably via biradical **6** (19). Accordingly **9** was investigated as an alternative source of



9

the biradical. Direct photolysis of **9** in acetonitrile gave very weak signals attributable to enols **7** and **8**. However, it was difficult to dissolve sufficient material to obtain a reasonable absorption of the starting material at the excitation wavelength (308 nm). Acetone sensitization at first appeared more promising since enols **7** and **8** were readily detectable upon 308 nm excitation of 0.15 *M* acetone in acetonitrile containing 0.05 *M* **9**. The growth of the enol signal was a function of the cyclobutenol concentration, as expected if it was produced from triplet **9** generated by energy transfer from acetone. Analysis of the enol growth as a function of [**9**] gave a rate constant for energy transfer of $\sim2\times10^7\ M^{-1}\ s^{-1}$, which agrees well with a previous estimate (19). This relatively slow rate constant made it impossible to add sufficient cyclobutenol to trap acetone

Can. J. Chem. Downloaded from www.nrcresearchpress.com by 41.223.56.140 on 09/07/12
For personal use only.

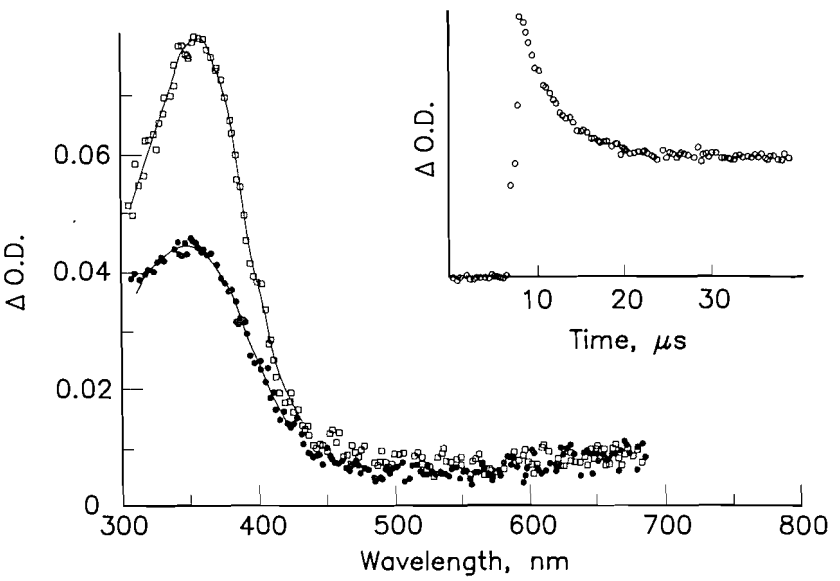


FIG. 2. Transient absorption spectra measured 1.5 μs (□) and 50 μs (●) after 308 nm excitation of **3** in hexane. *Insert*. Decay of the transient absorption at 360 nm.

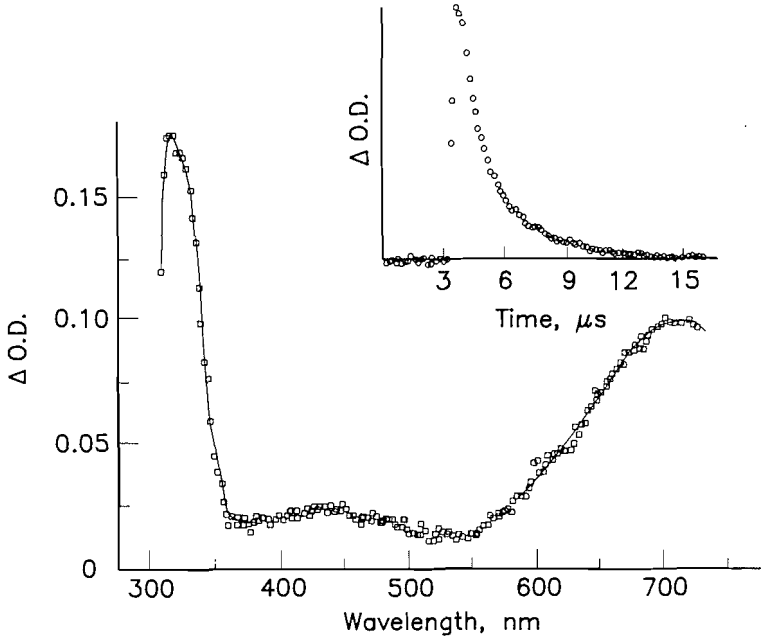


FIG. 3. Transient absorption spectrum produced by 308 nm excitation of ketone **4** in acetonitrile and measured 1 μs after the laser pulse. *Insert*. Decay of the transient absorption at 700 nm.

triplet sufficiently rapidly to detect signals from a short-lived biradical. Furthermore, the presence of relatively long-lived acetone triplets precluded the use of the commonly employed biradical trapping reagent, methyl viologen, as a means of determining the biradical lifetime.

2,4,6-Trimethylbenzophenone, **4**

Excitation of **4** at 308 nm in acetonitrile gave a spectrum which had λ_{max} at ~320 nm and a second broad band at 700 nm (Fig. 3) and which was very similar to that of triplet **3**. This transient was readily assigned to triplet **4** on the basis of its similarity to triplet **3**, its characteristic quenching by oxygen, 1,3-cyclohexadiene, and 1-methylnapthalene (Table 1) and the observation of phosphorescence at room temperature which decayed with the same lifetime as the transient absorption. Decay kinetics at either 320 or 700 nm gave lifetimes of ≥2 μs although the presence of a small second order component made it difficult to obtain a good first-order fit of the data. The second order component of the decay is attributable to triplet–triplet annihilation which is commonly observed for long-lived triplets at the transient concentrations produced by laser excitation.

In benzene, methanol, and hexane the triplet lifetimes were ≥4 μs, 850 ns, and 750 ns, respectively. Spectra in the latter two solvents showed a residual long-lived absorption in the 450–500 nm region which we attribute to ketyl radical formed by intermolecular hydrogen abstraction from solvent (see below; *vide infra*). The shorter triplet lifetimes in these solvents are, thus, readily explainable.

There was no evidence for the formation of any transients other than the triplet from ketone **4**. The long triplet lifetimes in

Can. J. Chem. Downloaded from www.nrcresearchpress.com by 41.223.56.140 on 09/07/12
For personal use only.

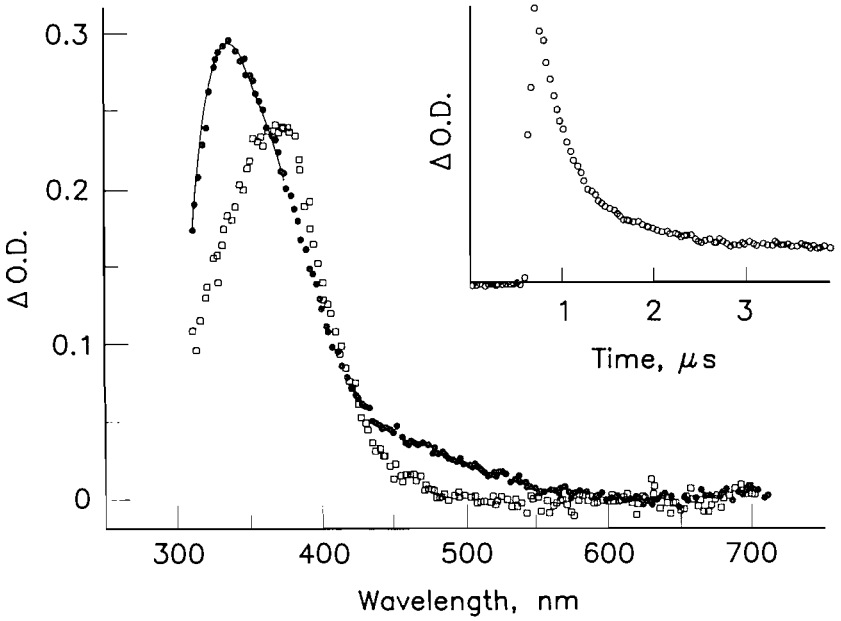


FIG. 4. Transient absorption spectra produced by 308 nm excitation of ketone **5** in methanol and measured 0.1 μs (●) and 2 μs (□) after the laser pulse. *Insert*. Decay of the transient absorption at 325 nm.

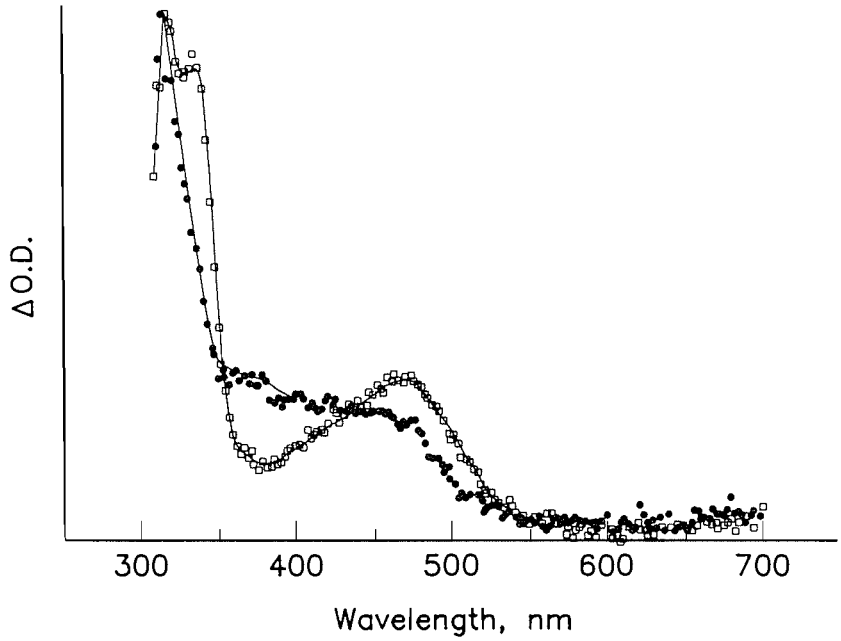


FIG. 5. Transient absorption spectra measured 1 μs after 308 nm excitation of ketone **3** in methanol + 1.1 *M* 1,4-cyclohexadiene (●) and of ketone **4** in acetonitrile + 0.21 *M* 1,4-cyclohexadiene (□).

inert solvents and the inefficient product formation (16) are consistent with the absence of biradical or enol signals in this system.

2,4,6-Trimethylacetophenone, **5**

Excitation at 308 nm of **5** in methanol produced a short-lived transient with $\lambda_{max} = 340$ nm and $\tau \sim 450$ ns. An additional weaker and longer-lived signal with $\lambda_{max} = 380$ nm was also observed (Fig. 4). Quenching experiments with oxygen and 1,3-cyclohexadiene (Table 1) confirmed that the short-lived signal was the triplet ketone. In these experiments, the triplet could be monitored conveniently at ~325 nm with only a small contribution (~15%) from the long-lived transient. Alternatively, the triplet absorbed weakly as 480 nm and could also be monitored at this wavelength. Triplet **5** was also quenched by 1-methylnapthalene although overlap of the signals due to triplet methylnapthalene, triplet **5**, and the 380 nm transient made it difficult to obtain an accurate rate constant in this case. Qualitatively similar results were obtained in benzene and acetonitrile where the triplet lifetimes were 100 and 220 ns, respectively.

The signal at 380 nm was assigned to the enol based on its similarity to the previous examples and on the following observations. There was sufficient overlap of the triplet and enol signals that, given the weak enol signals, it was not possible to observe the growth of the enol in methanol, acetonitrile, or benzene. However, quenching of the triplet with either oxygen

Can. J. Chem. Downloaded from www.nrcresearchpress.com by 41.223.56.140 on 09/07/12
For personal use only.

Can. J. Chem. Downloaded from www.nrcresearchpress.com by 41.223.56.140 on 09/07/12
For personal use only.

or diene did result in a concomitant decrease in the enol yield, although the decay kinetics remained unchanged. For example, in oxygenated acetonitrile the triplet lifetime was shortened to ~35 ns (vs. 220 ns under nitrogen; 84% of the triplets quenched by oxygen) and ~80% of the enol signal was eliminated. These results demonstrate that all (or at least most of) the enol is formed from the observed triplet.

In all three solvents the enol was long-lived (>50 μs) and there was no evidence for a shorter-lived component that could be distinguished from the triplet ketone. This may be due to the relative extinction coefficients of the triplet and the short-lived enol as well as a low yield of the latter. Even in aerated solvents where the triplet lifetime was decreased to ~100 ns, a short-lived enol was not observed.

Intermolecular hydrogen abstraction by triplet **3**, **4**, and **5**

The triplet lifetimes of all three ketones are sufficiently long to permit intermolecular reactions with efficient hydrogen donors. Triplets **3** and **4** reacted with 1,4-cyclohexadiene with rate constants of $(2.8 \pm 0.2) \times 10^7\ M^{-1}\ s^{-1}$ and $(3.7 \pm 0.3) \times 10^7\ M^{-1}\ s^{-1}$, respectively (Table 1). In both cases the quenching of the triplet was accompanied by the appearance of a new long-lived absorption at approximately 480 nm (Fig. 5). These results are consistent with hydrogen abstraction by the triplet ketones to give substituted diphenylketyl radicals. Note that the spectrum for **3** in the presence of the diene still shows a small amount of enol in the 350–400 nm region. The growth of the radical could not be observed due to overlap with the triplet signals.

Ketone **5** was not readily quenched by 1,4-cyclohexadiene ($k_q < 1 \times 10^6\ M^{-1}\ s^{-1}$) but did react with tri-*n*-butyltin hydride with a rate constant of $(7.6 \pm 0.6) \times 10^7\ M^{-1}\ s^{-1}$.

Discussion

Triplet ketones

Ketones **3** and **4** both have triplet spectra which are considerably different from that of benzophenone itself (λ_{max} ~520 nm for the visible band (30)). However, the strong broad absorption at ~700 nm has been observed previously for another sterically hindered ketone, 2-*tert*-butylbenzophenone (29). Furthermore, the characteristic quenching behavior and the agreement between room-temperature phosphorescence lifetimes and those based on triplet–triplet absorption leave no doubt as to the assignment.

The relatively long lifetime for triplet **3** has been attributed to the fact that rotation is required for hydrogen abstraction to occur (18). This hypothesis was based on several factors. Firstly, the crystal structure (18) of **3** showed the most stable conformation to be one with the substituted phenyl nearly completely twisted from the plane of the benzoyl group and with the two *ortho*-isopropyl methine hydrogens 2.88 and 2.97 Å from the carbonyl oxygen. This distance was suggested to be too far for hydrogen abstraction to occur.[3] Secondly, the activation energy of 9.09 kcal/mol measured by Stern–Volmer quenching of product formation was thought to be too large for hydrogen abstraction (18). The Arrhenius parameters measured in the present study using direct detection are probably more reliable than the previous values. However, the activation energy of 6.1 kcal/mol, while lower than the previous number, is still somewhat higher than that normally measured for hydrogen abstraction by triplet ketones. For example, hydrogen abstraction by triplet benzophenone from cyclohexane shows an activation energy of 2 kcal/mol (25). Finally, Ito's hypothesis of bond rotation determining the triplet lifetime of **3** was also supported by the low isotope effect and by substituent effects on τ_T (18).

Ketone **4** has a considerably longer triplet lifetime than **3** in inert solvents and appears to undergo little, if any, intramolecular hydrogen abstraction. It is tempting to assume that the two *ortho* substituents are again forcing the ketone to adopt a conformation where the hydrogens are not within reach of the carbonyl. Since ketone **4** could not be obtained in crystalline form this hypothesis could not be tested by determining the crystal structure. Although the methyl groups would not be expected to exert as large an effect as the more bulky isopropyl groups, the abstraction of a primary hydrogen in **4** versus a secondary in **3** may be responsible for the longer lifetime of the former. For example, the intramolecular Type II hydrogen abstraction rate for valerophenone (secondary hydrogen) is over an order of magnitude larger than that for butyrophenone (primary hydrogen abstracted) (32). Certainly the difference in reactivity for the triplets of 2-methylbenzophenone and 2-*tert*-butylbenzophenone ($\tau_T < 1$ ns for both) compared to triplets **3** and **4** is remarkable.

Trimethylacetophenone also has a relatively long-lived triplet which may again be the result of steric hindrance from the two *ortho*-methyls preventing the necessary conformation for hydrogen abstraction. The longer lifetime for 5,8-dimethyltetralone compared to 2-methylacetophenone (4.5 ns versus 0.5 ns) has been attributed to a decrease in reactivity caused by increased π,π^* character resulting from trialkyl substitution (3). Similar effects may be operative for triplet **5**. A relatively long-lived triplet has also recently been reported for 2,4-*tert*-butylacetophenone (130 ns in methanol) (33).

A comparison of our results with previous studies of diene quenching of product formation indicates that, at least for **3** (18) and **5** (16*b*), similar diene concentrations quench both the observable triplet and cyclobutenol formation. This suggests that the triplet observed by flash photolysis is the precursor for the products. For ketone **4**, some cyclobutenol may arise from a shorter-lived triplet than the one observed here, based on the previously observed nonlinear Stern–Volmer plots (18). We also note that cyclobutenol formation from a short-lived triplet has also been suggested for a ketone similar to **5** (15). A triplet with a lifetime of ≤5 ns would not have been readily detectable in our experiments.

Biradicals

No transients attributable to biradicals produced by hydrogen abstraction could be observed. Given the long triplet lifetimes for the ketones and the variety of transients involved this result is not unexpected. The biradicals from **3** and **4** would reasonably be expected to have quite short lifetimes based on the measured lifetime for the 2-methylbenzophenone biradical (~30 ns) (2). In any case the earlier conclusion of long-lived (≥5 μs) biradicals from ketone **3** should be revised.

Enols

Previous product studies (17) had not shown any evidence for the formation of enols from ketone **3** but the present results indicate that a substantial yield of both *Z* and *E* enols is produced. This observation is fully consistent with previous studies of photoenolization of related ketones (2, 26). The *Z* enol is considerably longer-lived in both polar and nonpolar solvents than some earlier examples but this may result from steric effects on the enol decay. The observed solvent depen-

[3]It has been suggested that the upper limit for hydrogen abstraction is 2.72 Å (31).

Can. J. Chem. Downloaded from www.nrcresearchpress.com by 41.223.56.140 on 09/07/12
For personal use only.

dence on enol decay agrees well with the literature data. The failure to observe products (17) derived from trapping of enols **7** and **8** is probably due to the fact that the typical dienophile concentrations required to trap other enols will also quench triplet **3** since it has a relatively long lifetime. We have in fact observed that 0.01 *M* dimethylacetylene dicarboxylate quenches >50% of triplet **3**. Although the reaction conditions for the attempted trapping of enols from **3** were not specified (17), we note that relatively high dienophile concentrations (>0.05 *M* (13)) are typically used in other examples. The reported rate constant for trapping of the enol from 2,4-dimethylbenzophenone is $10^2\ M^{-1}\ s^{-1}$ (9).

It is interesting to note that the yield of benzocyclobutenol product is quite high ($\Phi \leq 0.6$) for ketone **3** relative to **4** and **5** and other 2-alkyl aryl ketones. This raises the question of whether the product arises from the biradical or from one or the other of the enols. Although this question could be addressed by examining the benzocyclobutenol yield in the presence of a suitable enol trap, the complications resulting from the long-lived triplet prevent this approach. Furthermore, measurement of the quantum yields for enol formation in the transient experiments requires the enol extinction coefficient, a value which is not readily available.

The lack of enol signal from **4** is not surprising given its low reactivity towards intramolecular hydrogen abstraction. The previously observed and unidentified long-lived transient (8) from 2,6-dimethylbenzophenone in cyclohexane was most likely due to the ketyl radical not the enols. For ketone **5** only a long-lived enol was observed although it should be noted that a short-lived enol (<100 ns) would not have been readily detectable in this system. The observation of an enol transient in this system is consistent with the previous suggestion that deuterium incorporation in photolysed **5** occurs via the enol (16*a*). However, we again note that deuterium incorporation could occur at the biradical stage in both **3** and **5**.

Intermolecular reactivity

The measured rate constants for quenching of triplet **3** are all somewhat lower than for benzophenone itself (Table 1). For example, a rate constant of $7.4 \times 10^9\ M^{-1}\ s^{-1}$ has been reported for 1-methylnaphthalene quenching of benzophenone (26). For energy transfer quenchers such as 1,3-cyclohexadiene and 1-methylnapthalene these differences may be attributed to stereoelectronic effects which have been suggested in other systems where the π-systems of either the donor or acceptor are twisted such that the orbital overlap required for electron exchange is reduced (34). The results for the less hindered ketone **4** support this suggestion as the rate constants for quenching are consistently higher than those for **3**.

The rate of hydrogen abstraction from 1,4-cyclohexadiene for triplets **3** and **4** is approximately an order of magnitude lower than that for benzophenone ($k_q = 2.9 \times 10^8\ M^{-1}\ s^{-1}$) (25). This may also reflect steric effects of the *ortho* substituents although 4,4′-dialkyl substitution has also been found to decrease hydrogen abstraction rates for benzophenone (35). Twisting the rings away from planarity as in dibenzosuberone also produces the same effect as concluded from the fact that dibenzosuberone is less reactive than benzophenone in hydrogen abstraction reactions while dimethylanthrone is as reactive as benzophenone (36). The reactivity of triplets **3** and **4** towards hydrogen donors is in agreement with Ito's reports of shorter triplet lifetimes in hydrogen-donating solvents (e.g., mesitylene) based on Stern–Volmer studies (18). The low reactivity of triplet **5** towards 1,4-cyclohexadiene may reflect some π,π^* character for this triplet, since steric hindrance would not be expected to be as important here.

The spectra of ketyl radicals produced by intermolecular hydrogen abstraction for ketones **3** and **4** are considerably shifted from that of the diphenylketyl radical (λ_{max} ~540 nm) (37). This shift towards a more acetophenone ketyl-like spectrum probably reflects a decreased interaction between the two phenyl rings due to the presence of bulky *ortho* substituents. This is also consistent with the observation of λ_{max} ~465 nm for the 2-*tert*-butylbenzophenone biradical (29).

Conclusions

Ketones **3**, **4**, and **5** all have triplet states which are relatively long-lived (280 ns, >2 μs, and 220 ns, respectively) compared to similar 2-substituted ketones. For ketone **3** the long-lived transient previously assigned to biradical **6** (20) has been shown to be a mixture of *Z* and *E* enols, **7** and **8**. Biradical **6** was not detectable under our conditions indicating that its lifetime must be ≪100 ns rather than 17 μs as previously reported (20). For ketone **4** the long triplet lifetime is consistent with the absence of biradical or enol intermediates and with the inefficient photochemistry (17, 18). There was no evidence for more than one triplet state from any of the three ketones. All three ketones undergo relatively efficient quenching with energy transfer quenchers and hydrogen donors with, in some cases, decreases in rate constants which are consistent with steric or stereoelectronic effects resulting from the two *ortho* substituents. Ketyl radicals from **3** and **4** are readily detectable in the presence of 1,4-cyclohexadiene.

Experimental

Materials and general techniques

Ketones **3** (38) and **4** (39) were prepared by Friedel–Crafts acylation of 1,3,5-triisopropylbenzene and mesitylene, respectively, with benzoyl chloride and were purified by recrystallization from methanol and by chromatography, respectively. Ketone **5** was commercially available (Aldrich >99.5% by GC) and was used as received. Cyclobutenol **9** was synthesized by irradiation of **3** in benzene (350 nm) according to a literature procedure (16*a*). All solvents were spectrograde or Aldrich Gold Label and were used as received. 1,3-Cyclohexadiene and 1,4-cyclohexadiene were distilled before use and methyl viologen dichloride was recrystallized.

Phosphorescence spectra at 77 K were recorded on a Perkin–Elmer LS-5 spectrofluorimeter. Gas chromatographic analysis for purity of ketones **3**, **4**, and **5** and cyclobutenol **9** was done on a Perkin–Elmer 8320 gas chromatograph with a 12 m BPI on vitreous silica capillary column. LC/MS measurements were done on a Hewlett–Packard 5988A instrument with a reverse phase column with methanol/water mixtures as eluent.

Laser flash photolysis experiments

The laser flash photolysis facility has been described in detail elsewhere (40, 41). For these experiments either a Lumonics TE-860-2 excimer laser with a Xe–HCl gas mixture (308 nm, ~5 ns pulses, ≤20 mJ/pulse) or a Molectron UV-24 nitrogen laser (337 nm, ~8 ns pulses, ≤20 mJ/pulse) were used for excitation.

Samples were contained in $7 \times 7\ mm^2$ quartz cells and were deaerated by nitrogen purging. For oxygen quenching experiments samples were purged with oxygen/nitrogen mixtures of known composition prepared with a Matheson model 610 gas mixer.

Phosphorescence spectra at room temperature were recorded using an EG & G gated intensified optical multichannel analyzer (OMA) with either a 20 ns gate or a variable-time gate (>120 ns). Transient absorption spectra were also recorded using the OMA with the light from a 150 W xenon lamp as the monitoring beam.

Acknowledgements

We thank Mr. S. E. Sugamori for technical assistance and Dr. J. C. Scaiano for reading this manuscript.

1. P. G. Sammes. Tetrahedron, **32**, 405 (1976).
2. R. Haag, J. Wirz, and P. J. Wagner. Helv. Chim. Acta, **60**, 2595 (1977).
3. P. K. Das, M. V. Encinas, R. D. Small, and J. C. Scaiano. J. Am. Chem. Soc. **101**, 6965 (1979).
4. J. C. Scaiano. Chem. Phys. Lett. **73**, 319 (1980).
5. K. H. Grellmann, H. Weller, and E. Tauer. Chem. Phys. Lett. **95**, 195 (1983).
6. A. Beckett and G. Porter. Trans. Faraday Soc. **59**, 2051 (1963).
7. E. F. Ullman and K. R. Huffmann. Tetrahedron Lett. **23**, 1863 (1965).
8. G. Porter and M. F. Tchir. J. Chem. Soc. Chem. Commun. 1372 (1970).
9. G. Porter and M. F. Tchir. J. Chem. Soc. (A) 3772 (1971).
10. K. Uji-ie, K. Kikuchi, and H. Kokubun. J. Photochem. **10**, 145 (1979).
11. P. K. Das and J. C. Scaiano. J. Photochem. **12**, 85 (1980).
12. P. J. Wagner and C. P. Chen. J. Am. Chem. Soc. **98**, 239 (1976).
13. N. C. Yang and C. Rivas. J. Am. Chem. Soc. **83**, 2213 (1961).
14. N. D. Heindel, E. W. Sarver, and M. A. Pfau. Tetrahedron Lett. **32**, 3579 (1968).
15. P. J. Wagner. Pure Appl. Chem. **49**, 259 (1977).
16. (*a*) Y. Kitaura and T. Matsuura. Tetrahedron, **27**, 1597 (1971); (*b*) T. Matsuura and Y. Kitaura. Tetrahedron, **25**, 4487 (1969).
17. Y. Ito, Y. Umehara, T. Hijiya, Y. Yamada, and T. Matsuura. J. Am. Chem. Soc. **102**, 5917 (1980).
18. Y. Ito, H. Nishimura, Y. Umehara, Y. Yamada, M. Tone, and T. Matsuura. J. Am. Chem. Soc. **105**, 1590 (1983).
19. Y. Ito and T. Matsuura. J. Am. Chem. Soc. **105**, 5237 (1983).
20. H. Hayashi, S. Nagakura, Y. Ito, Y. Umehara, and T. Matsuura. Chem. Lett. 939 (1980).
21. Y. Ito, H. Nishimura, T. Matsuura, and H. Hayashi. J. Chem. Soc. Chem. Commun. 1187 (1981).
22. W. G. Herkstroeter, L. B. Jones and G. S. Hammond. J. Am. Chem. Soc. **88**, 4777 (1966).
23. (*a*) S. L. Murov. Handbook of photochemistry. Marcel Dekker Inc., New York. 1973. pp. 31, 33; (*b*) P. J. Wagner, M. J. May, A. Huang, and D. R. Graber. J. Am. Chem. Soc. **92**, 5269 (1970).
24. M. V. Encinas, E. A. Lissi, E. Lemp, A. Zanocco, and J. C. Scaiano. J. Am. Chem. Soc. **105**, 1856 (1983).
25. M. V. Encinas and J. C. Scaiano. J. Am. Chem. Soc. **103**, 6393 (1981).
26. W. C. Agosta, R. A. Caldwell, J. Jay, L. J. Johnston, B. R Venepalli, J. C. Scaiano, M. Singh, and S. Wolff. J. Am. Chem. Soc. **109**, 3050 (1987).
27. J. C. Scaiano. Landolt–Bornstein, New Series, Vol. 13e; *Edited by* H. Fischer. Springer–Verlag: Berlin. 1985. Chap. 11.
28. L. J. Johnston and J. C. Scaiano. Chem. Rev. In press.
29. P. J. Wagner, B. P. Giri, J. C. Scaiano, D. L. Ward, E. Gabe, and F. L. Lee. J. Am. Chem. Soc. **107**, 5483 (1985).
30. I. Carmichael and G. L. Hug. J. Phys. Chem. Ref. Data, **15**, 1 (1986).
31. J. R. Scheffer. Acc. Chem. Res. **13**, 283 (1980).
32. J. Grotewold, D. Soria, C. M. Previtali, and J. C. Scaiano. J. Photochem. **1**, 471 (1973/73).
33. P. J. Wagner, B. P. Giri, R. Pabon, and S. B. Singh. J. Am. Chem. Soc. **109**, 8104 (1987).
34. J. C. Scaiano, W. J. Leigh, M. A. Meador, and P. J. Wagner. J. Am. Chem. Soc. **107**, 5806 (1985).
35. P. J. Wagner, R. J. Truman, and J. C. Scaiano. J. Am. Chem. Soc. **107**, 7093 (1985).
36. J. C. Netto-Ferreira and J. C. Scaiano. Unpublished results.
37. E. J. Land. Proc. R. Soc. **305**, 457 (1968).
38. R. C. Fuson, E. M. Bottorff, R. E. Foster, and S. B. Speck. J. Am. Chem. Soc. **64**, 2573 (1942).
39. A. Fischer, B. A. Grigor, J. Packer, and J. Vaughan. J. Am. Chem. Soc. **83**, 4208 (1961).
40. J. C. Scaiano. J. Am. Chem. Soc. **102**, 7747 (1980).
41. J. C. Scaiano, M. Tanner, and D. Weir. J. Am. Chem. Soc. **107**, 4396 (1985).

Can. J. Chem. Downloaded from www.nrcresearchpress.com by 41.223.56.140 on 09/07/12
For personal use only.

Identification of domoic acid, a neuroexcitatory amino acid, in toxic mussels from eastern Prince Edward Island[1]

J. L. C. WRIGHT,[2] R. K. BOYD, A. S. W. DE FREITAS, M. FALK, R. A. FOXALL, W. D. JAMIESON, M. V. LAYCOCK, A. W. MCCULLOCH, A. G. MCINNES, P. ODENSE, V. P. PATHAK, M. A. QUILLIAM, M. A. RAGAN, P. G. SIM, P. THIBAULT, AND J. A. WALTER

Atlantic Research Laboratory, National Research Council of Canada, 1411 Oxford Street, Halifax, N.S., Canada B3H 3Z1

M. GILGAN

Department of Fisheries and Oceans, Inspection Services Branch, P.O. Box 550, Halifax, N.S., Canada B3J 2S7

D. J. A. RICHARD

Department of Fisheries and Oceans, Inspection Services Branch, P.O. Box 270, Black's Harbour, N.B., Canada E0G 1H0

AND

D. DEWAR

Canada Institute for Scientific and Technical Information, National Research Council of Canada, Ottawa, Ont., Canada K1A 0S2

Received August 15, 1988

J. L. C. WRIGHT, R. K. BOYD, A. S. W. DE FREITAS, M. FALK, R. A. FOXALL, W. D. JAMIESON, M. V. LAYCOCK, A. W. MCCULLOCH, A. G. MCINNES, P. ODENSE, V. P. PATHAK, M. A. QUILLIAM, M. A. RAGAN, P. G. SIM, P. THIBAULT, J. A. WALTER, M. GILGAN, D. J. A. RICHARD, and D. DEWAR. Can. J. Chem. **67**, 481 (1989).

The causative agent of toxicity in cultured mussels from a localized area of eastern Prince Edward Island has been identified as domoic acid, a neuroexcitatory amino acid. The toxin was isolated by a number of different bioassay-directed separation techniques including high-performance liquid chromatography, high-voltage paper electrophoresis, and ion-exchange chromatography, and characterized by a number of spectroscopic techniques including ultraviolet, infrared, mass spectrometry, and nuclear magnetic resonance. The isolation and purification methods are described in detail and some new analytical data for domoic acid are reported.

Key words: shellfish toxin, domoic acid, neurotoxin, bioassay-directed analysis.

J. L. C. WRIGHT, R. K. BOYD, A. S. W. DE FREITAS, M. FALK, R. A. FOXALL, W. D. JAMIESON, M. V. LAYCOCK, A. W. MCCULLOCH, A. G. MCINNES, P. ODENSE, V. P. PATHAK, M. A. QUILLIAM, M. A. RAGAN, P. G. SIM, P. THIBAULT, J. A. WALTER, M. GILGAN, D. J. A. RICHARD et D. DEWAR. Can. J. Chem. **67**, 481 (1989).

On a identifié l'agent qui est la cause de la toxicité des moules d'élevage provenant d'une zone localisée de la portion est de l'île du prince Edouard; il s'agit de l'acide domoïque, un acide aminé neuro-excitant. On a isolé la toxine en faisant appel à un certain nombre de techniques de séparation basées sur des essais biologiques parmi lesquelles on peut citer la chromatographie liquide à haute performance, l'électrophorèse sur papier à voltage élevé ainsi que la chromatographie d'échange ionique; on l'a caractérisée par un certain nombre de techniques spectroscopiques dont l'ultraviolette, l'infrarouge, la spectrométrie de masse et la résonance magnétique nucléaire. On décrit en détail les méthodes d'isolement et de purification et on présente des données analytiques nouvelles concernant l'acide domoïque.

Mots clés : toxine des coquillages, acide domoïque, neurotoxine, analyse basée sur des essais biologiques.

[Traduit par la revue]

Introduction

Shellfish poisons have been known since antiquity (1) and a recent review (2) lists the different families of marine toxins. From a Canadian perspective, the paralytic shellfish poisons (PSPs) have been of most significance to the shellfish industry (3). PSPs are products of the cold-water dinoflagellates, *Gonyaulax* spp., which are ingested by filter-feeding shellfish. Another group of marine toxins of potential significance to the Canadian shellfish industry are the diarrhetic shellfish poisons (DSPs). These toxins are produced by other cold-water dinoflagellates belonging to the genus *Dinophysis*, and although there is no unambiguous evidence that a DSP outbreak has occurred in Canada, there have been serious outbreaks in Japan and Europe (4).

Towards the end of 1987, an outbreak of poisoning in Canada was traced to cultured blue mussels (*Mytilus edulis* L.) from a localized area of eastern Prince Edward Island (P.E.I.). During this period (November 11 to December 12) 153 cases of acute intoxication related to ingestion of toxic mussels were documented (5), corresponding to about three cases per thousand portions of mussels consumed.[3] Symptoms included vomiting and diarrhea, which in some cases were followed by confusion, memory loss, disorientation, and even coma. Three elderly patients died. In the other most severely affected cases neurological symptoms still persist (5). The term Amnesic Shellfish Poison (ASP) has been proposed for this new shellfish toxin.[4]

Chemical analysis at ARL and other laboratories soon established that the toxicity was not due to any of the marine toxins that are usually monitored,[5] nor to any of the known anthropogenic xenobiotics (e.g., heavy metals,[6] pesticides, PCBs, and PAHs[7]). Significantly, extracts of contaminated mussels, when injected intraperitoneally into laboratory mice, produced a very characteristic and reproducible scratching syndrome and even-

[1]NRCC No. 29840.

[2]Author to whom correspondence may be addressed.

[3]F. Iverson, J. Truelove, E. Nera, L. Tryphonas, J. Campbell, and E. Lok. Submitted for publication.

[4]J. Hockin (HWC, Ottawa), personal communication.

[5]A. Cembella (DFO, Mont-Joli, PQ), personal communication.

[6]J. W. McLaren (NRC, Ottawa), personal communication.

[7]V. Zitko (DFO, St. Andrews, NB), personal communication.

Can. J. Chem. Downloaded from www.nrcresearchpress.com by 122.72.124.2 on 09/07/12
For personal use only.

tual death. In the interest of public health the entire East Coast shellfish industry was closed down.

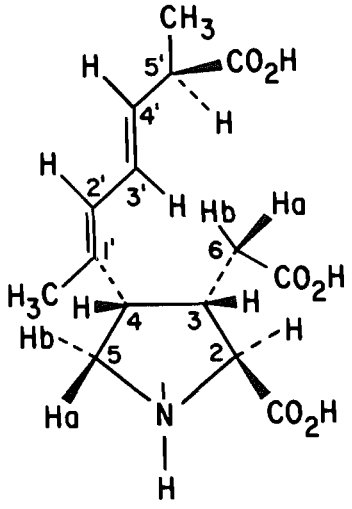
A task force was organized jointly by the Canadian Department of Fisheries and Oceans (DFO) and Health and Welfare Canada (HWC) to establish the extent of the contamination, the chemical nature of the toxin, and its origins. The Atlantic Research Laboratory (ARL) of the National Research Council of Canada, as part of the task force, was one of the laboratories that undertook the task of isolating and determining the chemical nature of the toxin. Within 5 days it was established at ARL that the mollusc toxin was domoic acid, a glutamate agonist (6) originally isolated some 30 years ago from the red alga *Chondria armata* Okamura (7, 8). This paper describes the methods used to isolate and identify domoic acid as the toxin in the contaminated mussels, and reports some new analytical and chemical data on this compound. The possible origin(s) of domoic acid in the 1987 outbreak are also discussed.

Results and discussion

Toxic mussels and control (nontoxic) mussels were supplied by DFO (Charlottetown, P.E.I.). In all cases extracts of both toxic and control mussels were taken through identical procedures. This was done to distinguish the effects of the unknown toxic factor in the bioassay from inherent salt toxicity in some fractions, and from possible interference of other factors such as chromatographic mobile phases. Furthermore, this parallel approach would highlight additional or unusual signals present only in chromatograms and spectra of toxic mussel fractions. Strict control over the dosage used in the mouse bioassay was an important element of the procedure. A preliminary dose–response curve indicated a narrow dynamic range, less than one order of magnitude, for the bioassay of the toxin(s). Extracts representing 0.3–2.5 g-equivalent of original wet tissue resulted in times of death (TOD) of 100–10 min after intraperitoneal injection respectively. Volumetric control was used to afford an intraperitoneal dose in the range of 1.2–2.5 g-equivalents original tissue, independent of the actual amount of nontoxic material extracted. In addition it was important to verify that the symptoms induced in the bioassay by toxic fractions were exactly the same as those observed with extracts of toxic mussels.

In initial experiments the digestive glands were separated from the remaining mussel tissue. Each tissue type was extracted with methanol:water (7:3 v/v), concentrated, and then partitioned against dichloromethane. In no case was organic-soluble toxicity found. Aqueous extracts of both tissue types from control mussels displayed no toxicity but the digestive-gland extracts of toxic mussels were found to be toxic. The remaining tissue of toxic mussels displayed some low-level toxicity but this was attributed to incomplete separation of the two tissue types. However, in the interest of time saving during very-large-scale extractions, the entire mussel was processed.

Later, when the toxin was firmly identified as domoic acid (**1**), other extraction procedures were studied. Quantitative extraction of **1** was achieved by boiling for 5 min, or by shaking for 24 h at room temperature, with either 50% aqueous methanol or water.[8] Interestingly, the standard Association of Official Analytical Chemists (AOAC) method (5 min boiling, 0.1 M HCl) for extracting PSPs for mouse bioassay (9) was less efficient (75–85% recovery). Moreover, the concentration of **1** in the extract was found to decrease upon storage at room temperature (up to 50% loss in 1 week), although this loss could be reduced by storage at −15°C. The feasibility of using the AOAC method for simultaneous monitoring for PSP and domoic acid has been examined.[9]



Domoic Acid

1

In the initial search for the toxin several methods of separation (high-performance liquid chromatography, hplc; high-voltage paper electrophoresis, hvpe; ion-exchange chromatography) were selected to avoid the possibility that in any one process the toxin might be obscured by other nontoxic compounds present in the extract. Furthermore, toxic fractions isolated by one scheme were cross-analyzed by another to verify that they were the same material, thus providing an internal check on the validity of the separation schemes.

Following cleanup of the toxic aqueous extract on an XAD-2 column, the resulting toxic fractions were subjected to hvpe. This approach has the advantage of separating the fraction into acidic, basic, or neutral components. By slicing the chromatogram into sections, followed by extraction with distilled water, it was found that *all* the toxicity moved towards the anode at pH 6.5, indicating that the toxin was acidic. By repeating this experiment and by taking narrower slices it was eventually apparent that the toxic activity was associated with a band that stained yellow with ninhydrin and migrated on the trailing edge of the red-staining band for glutamic acid.

Based on the premise that the toxic material was acidic and possibly a peptide, a reversed-phase hplc method was employed using a C_{18} stationary phase and gradient elution with water–acetonitrile mixtures containing 0.1% trifluoracetic acid (TFA) to suppress ionization of the carboxyl groups. Detection was provided by a diode-array detector (dad), which also allowed continuous acquisition of uv–visible spectra. The hplc profile of the toxic hvpe fraction obtained from the XAD-2 column, compared with the equivalent fraction from control mussels, is shown in Fig. 1. Initial runs were monitored by uv absorption at 210 nm since most peptides and organic acids absorb at this wavelength. The chromatogram for the toxic fraction showed a unique peak at retention time 12.1 min (peak D). The equivalent region in the control chromatogram showed no peak. Significantly, this same peak was consistently observed in other extracts of toxic mussels but could not be seen in any extracts

[8]M. A. Quilliam, P. G. Sim, A. W. McCulloch, and A. G. McInnes. Submitted for publication.

[9]J. F. Lawrence, C. F. Charbonneau, C. Menard, M. A. Quilliam, and P. G. Sim. Submitted for publication.

Can. J. Chem. Downloaded from www.nrcresearchpress.com by 122.72.124.2 on 09/07/12
For personal use only.

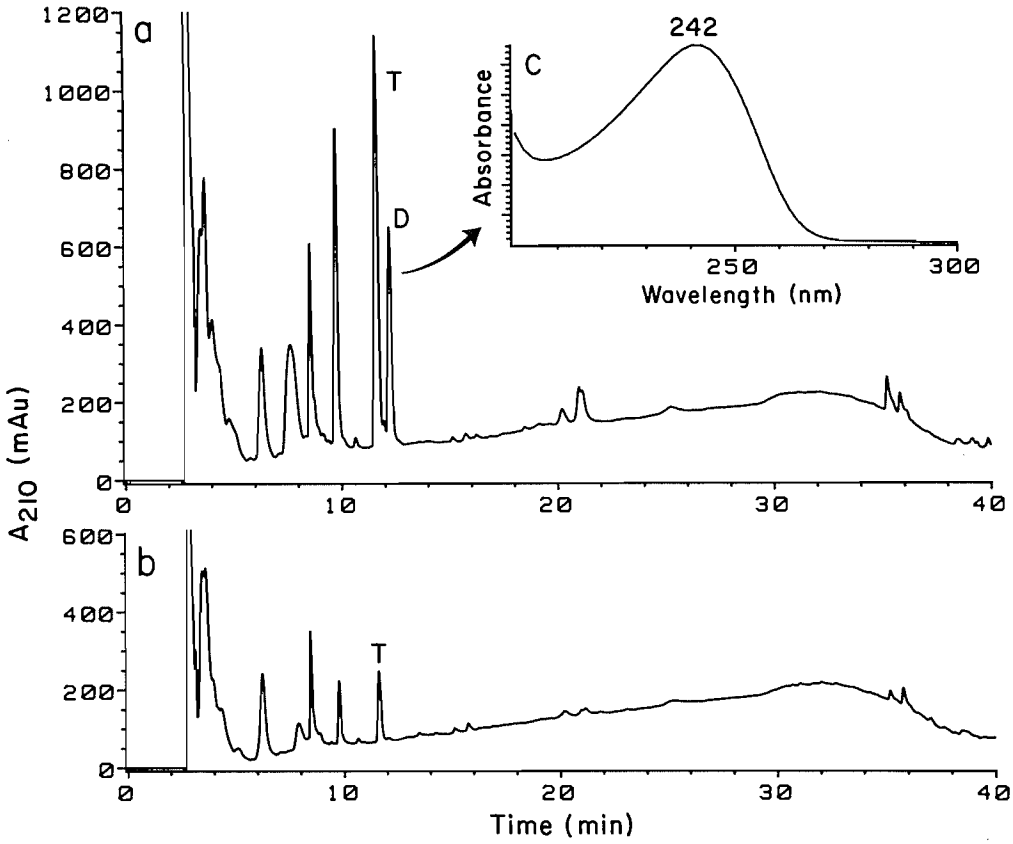


FIG. 1. Reversed-phase hplc chromatograms of XAD-2 cleaned extracts of (a) toxic and (b) control mussels. The inset (c) is the uv–visible spectrum acquired at the apex of peak D (domoic acid). Peak T is due to the amino acid tryptophan. Conditions: 25 cm × 2.1 mm i.d. 5-μm Vydac 201TP52 column at 40°C; 0.2 mL min^{-1} flow rate; gradient elution from TFA/H_2O (0.1:99.9) to CH_3CN/TFA/H_2O (50:0.1:49.9) in 25 min and then to CH_3CN/TFA (99.9:0.1) at 35 min and hold to 50 min; detection provided by absorption at 210 nm (20-nm bandwidth).

of control mussels. The uv–visible spectrum acquired at the apex of this peak revealed a single absorption maximum at 242 nm, suggesting the molecule contained two conjugated double bonds.

By employing the same chromatographic conditions on a preparative hplc scale it was possible to collect fractions corresponding to peak D as well as other regions of the chromatogram for bioassay and chemical analysis. However, all the fractions obtained in the first series of preparative runs displayed toxic effects both in the control and toxic samples, although the symptoms were different from those induced by toxic mussel extracts. This problem of general toxicity was resolved by replacing the rodenticide TFA used in the mobile phase with 1% acetic acid. The peak D fraction was then found to be toxic to mice, with the correct symptoms. All the other fractions from aqueous methanol extracts were nontoxic, even at a fivefold higher dose in terms of weight equivalents of original tissue. When the toxic hplc fraction was subjected to hvpe, a yellow band was observed at a position corresponding to where toxicity was previously observed. Bioassays of aqueous extracts of slices of this electrophoretogram revealed that only the yellow band was toxic. Conversely, this band obtained by preparative hvpe of crude extracts gave an hplc peak at the same retention time as peak D, and the same uv spectrum. The fact that such different fractionation schemes yielded the same toxic factor was very important to the certainty of the result.

Early on it was found the acidic toxin could also be eluted from a strongly basic ion-exchange resin (Dowex 1) using ammonia, and analysis of mussel extracts with a conventional amino acid analyser revealed an unusual peak present only in toxic samples. The compound eluted between methionine and isoleucine; the ninhydrin-reaction product absorbed strongly at 440 nm, consistent with a proline derivative. The acidic toxic factor could also be conveniently separated from a crude fraction using a weak anion-exchange resin. This proved to be a useful and facile method for purifying the toxin, and was also used to remove the toxin from the initial extract to assess the toxicity of the remaining residue. Concentrated residues from both toxic and control extracts obtained in this manner demonstrated some additional toxicity on mouse bioassay. However, the observed symptoms of general weakening and occasional cyanosis prior to death were quite different from those neurological symptoms induced by toxic mussel extracts. This additional toxic factor(s) was found to pass through a 500-Da ultrafilter membrane (Amicon YC-05) but once again the toxicity was the same for both control and toxic extracts. These symptoms of weakening, occasional cyanosis, and death have been observed with high salt concentrations; interestingly, similar symptoms have been observed in mice given intraperitoneal injections containing high (≥500 ppm) concentrations of zinc (10).

The ir spectra of the early toxic fractions from the preparative hplc runs were highly variable, due to dependence on the pH at which the films were deposited. Also, the spectrum of the toxin was partly masked by absorption bands due to acetate or trifluoracetate salts, contaminants originating from either acetic or trifluoroacetic acid used in the chromatographic separations. Both of these complications were removed by deposit-

Can. J. Chem. Downloaded from www.nrcresearchpress.com by 122.72.124.2 on 09/07/12
For personal use only.

Can. J. Chem. Downloaded from www.nrcresearchpress.com by 122.72.124.2 on 09/07/12
For personal use only.

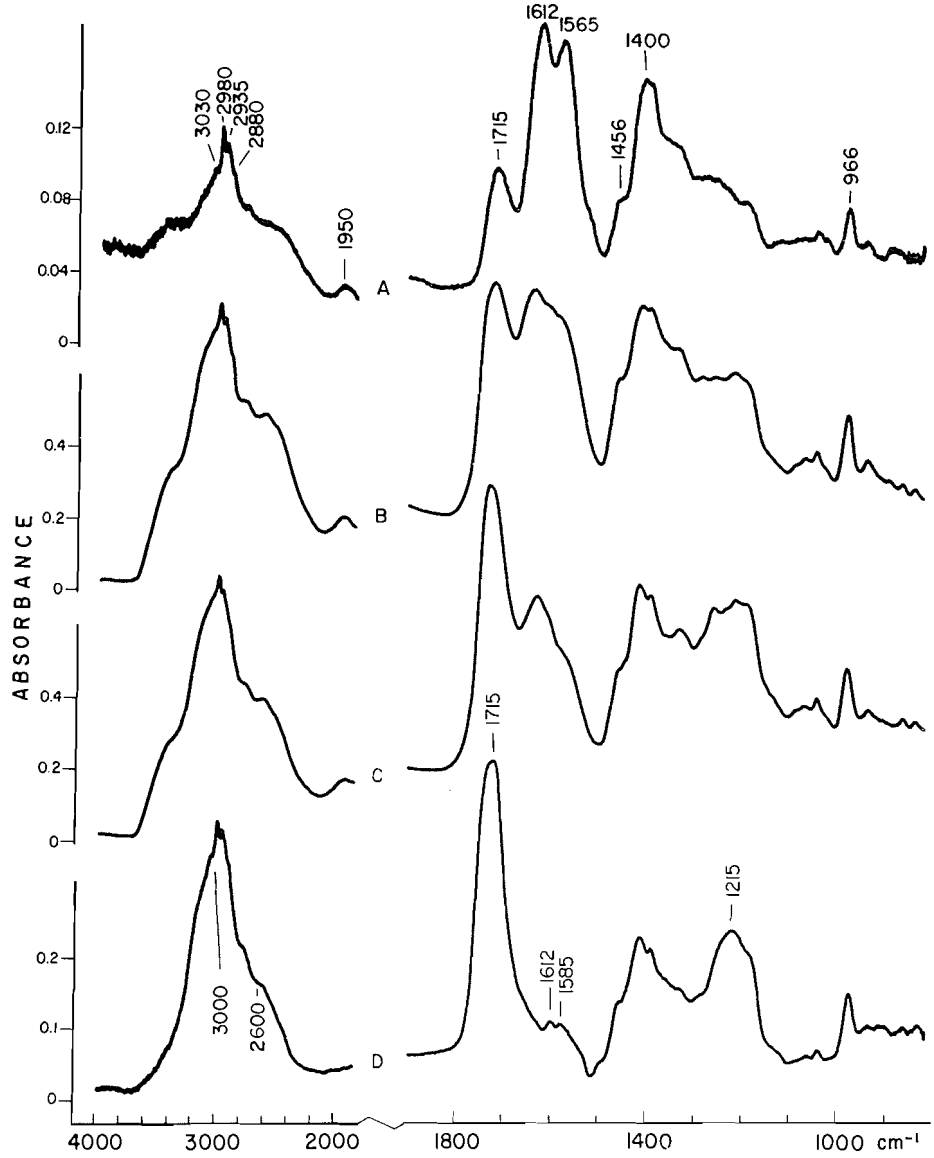


FIG. 2. Spectra of amorphous domoic acid films on a CaF_2 plate at increasing degrees of protonation from A to D.

ing the films from a solution of 0.1 M HCl. Acidification ensured a uniform and essentially complete protonation of the toxin molecules (shown by the absence of further spectral change upon evaporation from additional quantities of HCl). This procedure also replaced the acetate or trifluoracetate salts by the corresponding chlorides, which did not interfere with the spectrum, plus free acetic or trifluoroacetic acid, which rapidly evaporated during the preparation of the films. The spectrum of the toxin, when freed of such contaminants, contained absorption bands characteristic of non-ionized COOH (1215 and 1715 cm^{-1}, and a broad band with maxima at 3000, 2750, and 2600 cm^{-1}), ionized COO^- (1400 and 1612 cm^{-1}), NH_2^+ (1565–1585 and 1950 cm^{-1}), *trans* —CH=CH— (966 cm^{-1}), olefinic CH groups (3030 cm^{-1}), and aliphatic CH groups (2980, 2935, and 2880 cm^{-1}). Figure 2 shows a typical series of spectra obtained at pH varying from about 5.0 in Fig. 2A to about 1.0 in Fig. 2D, the molecule being fully protonated at the latter pH. Further details of the ir spectra and of vibrational assignments are discussed elsewhere (11).

Toxic and control fractions were continually screened by mass spectrometry (ms). In view of the water solubility of the toxin, ionization by fast atom bombardment (FAB) using a glycerol:water matrix (2:1 v/v) was selected. Since some early samples were heavily contaminated by chloride ions, the most useful spectra were initially obtained in the positive-ion mode where sodium adduct ions were the principal but less complicating problem. As the fractionation procedures succeeded in progressively concentrating the toxicity, the corresponding positive-ion mass spectra showed the increasing importance of an ion at *m/z* 312, which was absent from spectra of control samples. This observation, together with an ion at *m/z* 310 in the negative-ion spectra, suggested a molecular weight of 311 Da for the toxin.

Daughter-ion spectra of the positive FAB ions at *m/z* 312 displayed fragment ions at *m/z* 294, 266, 248, 220, and 74 (Fig. 3). An important feature of the daughter-ion spectra was the series of losses of 46 Da (presumably HCOOH) characteristic of protonated carboxylic acids including amino acids (12, 13). Because the even-electron ion at *m/z* 312 must contain an odd number of nitrogens, it appeared likely that this ion

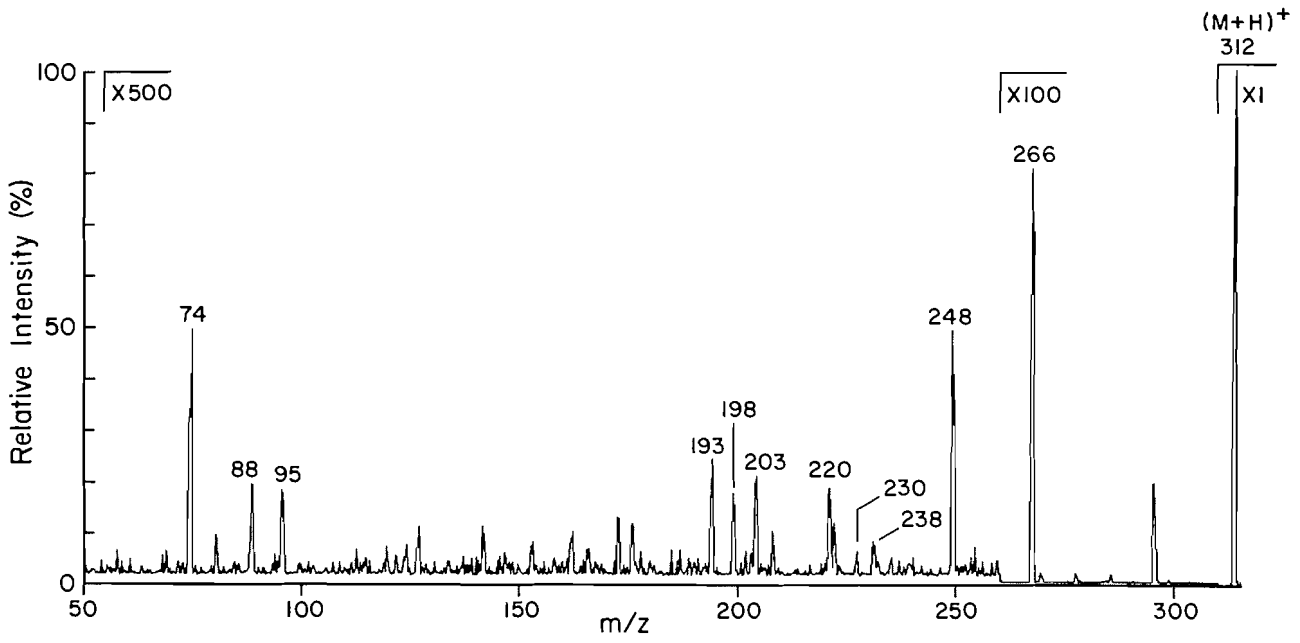


FIG. 3. Fragment-ion mass spectrum, for collision-induced dissociation in rf-only quadrupole, of MH^+ ions (m/z 312) formed by FAB ionization of the toxin in a glycerol/water matrix.

Can. J. Chem. Downloaded from www.nrcresearchpress.com by 122.72.124.2 on 09/07/12
For personal use only.

corresponded to a protonated molecule of a nitrogen-containing compound, perhaps an amino acid containing at least two carboxyl groups. This conclusion was substantiated by the successive losses of 44 Da (CO_2) from the $[M - H]^-$ anion.[10] Finally, in the positive-ion spectra, the intense signal at m/z 74 is characteristic of protonated α-amino acids and is ascribed (13) to the ion $H_2N{=}CH{-}COOH^+$. An alternative interpretation in terms of the odd-electron ion $C_3H_6O_2^{+\bullet}$ characteristic (14) of the substructure HOOC—$CH(CH_3)$— is unlikely to be valid for fragmentations of the even-electron species $[M + H]^+$ studied here.

Accurate mass measurement of the signal at m/z 312 gave a value of 312.146 ± 0.003 Da. Eleven molecular formulae are consistent with this value. However, by applying the additional restriction of an odd number of N atoms plus at least four oxygen atoms (at least two carboxyl groups, *vide infra*) the possibilities are reduced to just two, $C_{15}H_{22}NO_6$ and $C_{12}H_{26}NO_6S$, for the protonated molecule. In principle it should be possible to distinguish between these possibilities based on the relative intensities of the m/z 312, 313, and 314 signals. The intensity of the signal at m/z 313 invariably fell in the range 16–19% of that of the m/z 312 peak, favouring the $C_{15}H_{22}NO_6$ formula, but the intensity of the m/z 314 signal was highly variable due to beam-induced interaction of the analyte with the matrix.[10] Further support came from analysis by electron ionization (EI) of the *tert*-butyldimethylsilyl (TBDMS) derivative. Rapid (≤5 min) esterification of the three carboxyl groups gave a product whose spectrum displayed ions at m/z 653.395 ± 0.002 ($[M]^{+\bullet}$), 596.327 ± 0.002 ($[M - t\text{Bu}]^+$), and 494.314 ± 0.002 ($[M - t\text{BuMe}_2\text{SiO}_2\text{C}]^+$). After several hours reaction with the silylation reagent, intense signals were observed corresponding to a product in which the amine group was also derivatized: m/z 767.483 ± 0.002 ($[M]^{+\bullet}$), 710.414 ± 0.002 ($[M - t\text{Bu}]^+$), and 608.401 ± 0.002 ($[M - t\text{BuMe}_2\text{SiO}_2\text{C}]^+$).

[10]P. Thibault, M. A. Quilliam, W. D. Jamieson, and R. K. Boyd. Submitted for publication.

These data are consistent with a tricarboxylic amino acid of molecular formula $C_{15}H_{21}NO_6$.

The first useful ^1H nmr spectra of toxic fractions from preparative hplc were obtained with solutions in dry DMSO-d_6, this solvent having been chosen to avoid hydrogen exchange. Earlier ^1H nmr experiments using THF-d_8 had yielded broad spectra although, in retrospect, the domoic acid resonances are identifiable. The spectra in DMSO-d_6 showed the compound to be largely free of other organic impurities and enabled resonances characteristic of a vinylic methyl group (1.81 ppm, broad singlet) and an allylic methyl group (1.27 ppm, doublet) to be identified. The connectivity of the olefinic protons, H-5′, and the allylic methyl group was determined from their coupling patterns and a COSY experiment, establishing the partial structure CH_3—CH—CH=CH—CH=C—CH_3.

Throughout the structure analysis, the uv, ir, ms, and nmr data were continually updated and used to search the Chemical Abstracts and its accompanying Registry File on the STN International on-line database (16). The search, in which the partial structural data, toxicological data, and the marine origin of the toxin were used together, led at first to a long list of compounds. However, as the structural information became progressively more detailed this list shrank rapidly until the neuroexcitatory amino acid domoic acid (**1**) and its isomers emerged as likely candidates.

Meanwhile, ^1H nmr spectra of the toxin were found to sharpen when D_2O was added to the DMSO-d_6 solution, and in neat D_2O at pH 3.1 a ^1H spectrum was obtained that agreed in every respect (chemical shifts to 0.02 ppm, spin–spin couplings to 0.2 Hz) with detailed published data for domoic acid (15, 17), taking into account that the published data were obtained at an unspecified pH. It also became apparent that the ir and ms data for the toxin were consistent with the domoic acid structure, and further spectral data were collected that completed the final identification.

Further ^1H and ^{13}C nmr work (Table 1) was undertaken to confirm assignments and structural features of the toxin in D_2O

Can. J. Chem. Downloaded from www.nrcresearchpress.com by 122.72.124.2 on 09/07/12
For personal use only.

TABLE 1. Nuclear magnetic resonance data for domoic acid

Position	2	3	4	5α	5β	6a	6b	7	2-CO_2H
δ(^{1}H), ppm[a,b]	3.98	3.05	3.84	3.49	3.71	2.76	2.50		
Multiplicity[c]	d	dddd	ddd	dd	dd	dd	dd		
J_{HH}, Hz[d]	(2, 3) 8.1	(2, 3) 8.1 (3, 4) 8.4 (3, 6a) 5.8 (3, 6b) 9.1	(3, 4) 8.4 (4, 5α) 7.3 (4, 5β) 7.9	(4, 5α) 7.3 (5α, 5β), −12.2	(4, 5β), 7.9 (5α, 5β), −12.2	(3, 6a), 5.8 (6a, 6b), −16.7	(3, 6b), 9.1 (6a, 6b), −16.7		
% nOe produced when H irradiated[e]	None	H-4, 4.7	H-3, 6.4[g] H-3′, 14.9	H-5β, 12.5 1′-CH_3, 1.0	H-5α, 11.2[g]	H-6b, 5.8	H-6a, 9.0		
δ(^{13}C), ppm[a,f]	67.1	44.6	42.7	49.1		35.4		177.5	174.9
Multiplicity	bd	bd	bd	bt		bt		dt	dd
J_{CH}, Hz	149 ± 3	138 ± 4	133 ± 4	147.6 ± 2		12 ± 3		3.0 7.2	4.1

Position	1′	2′	3′	4′	5′	6′	1′-CH_3	5′-CO_2H
δ(^{1}H), ppm[a,b]		6.13	6.35	5.78	3.30	1.27	1.81	
Multiplicity[c]		d	dd	dd	dq	d	s	
J_{HH}, Hz[d]		(2′, 3′) 11.1	(2′, 3′) 11.1 (3′, 4′) 14.9	(3′, 4′) 14.9 (4′, 5′) 7.8	(4′, 5′) 7.8 (5′, 6′) 7.1	(5′, 6′) 7.1		
% nOe produced when H irradiated[e]		H-4′, 13.0 1′-CH_3, 1.5	H-4, 8.5 H-5′, 4.5	H-2′, 8.0 H-5′, 4.7	H-3′, 3.5 H-4′, 3.0	H-4′, 5.2 H-5′, 10.7	H-5α, 4.5 H-6b, 2.4 H-2′, 13.3	
δ(^{13}C), ppm[a,f]	133.8	132.8	128.6	135.2	44.9	18.6	23.5	181.9
Multiplicity	bm	bd	dd	bd	bd	qdd	qdd	m
J_{CH}, Hz		151 ± 8	153.5 5.1	161 ± 5	129 ± 4	129.3 ± 1.2 3.9 ± 1.2 3.9 ± 1.2	126.4 ± 1 6.8 5.0	

[a]Reference to TSP (sodium 3-trimethylsilylpropionate-2,2,3,3-D_4) solution in D_2O contained in a concentric tube. Domoic acid solution at pH 3.40 ± 0.05, temperature, 20.0°C.
[b]Error ca. ±0.02 ppm.
[c]s = singlet, d = doublet, t = triplet, q = quartet, m = multiplet, b = broad.
[d]Error ca. ±0.2 Hz. Spin–spin coupling connectivity confirmed by an ^{1}H COSY spectrum. Some couplings determined by simulation.
[e]Error ca. ±0.5% for single protons, ca. ±0.15% for methyl groups. Samples were not degassed or otherwise specially prepared for nOe measurements.
[f]^{13}C assignments determined from ^{13}C/^{1}H heterocorrelation experiment and ^{1}H-coupled ^{13}C spectrum.
[g]The nOe (if any) between H-4 and H-5β was not measurable in these experiments due to the closeness of the resonances.

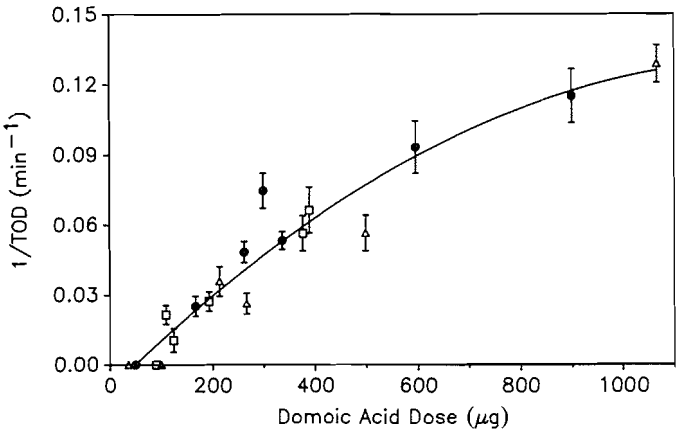


FIG. 4. Toxicity (expressed as reciprocal of time of death (TOD) of mouse) as a function of the amount of domoic acid injected into the mouse (as determined by hplc analysis). The toxicities of room temperature aqueous methanol (△) and boiling 0.1 M HCl (□) extracts of mussel tissue are similar to that of aqueous solutions of pure domoic acid (●). Each point is the mean of 2–4 replicate measurements of TOD for one solution, and the error bars represent an estimate of the standard deviation. The curve is a second-order polynomial least-squares regression on all data points.

solutions at pH 3.4. ^{1}H COSY spectra and spectral simulation showed that the published ^{1}H assignments (15, 17) were correct, as were ^{1}H–^{1}H spin–spin couplings apart from two minor differences probably resulting from our use of simulation to extract coupling constants. Homonuclear ^{1}H nuclear Overhauser enhancement (nOe) experiments with our sample of domoic acid (Table 1) confirmed the *Z,E* configuration of the conjugated double bond system in the side chain, as well as the *cis* relationship of H-3 and H-4 in the prolyl ring. The only nOe's between this side chain and the ring were those between the C-1′ methyl group and H-5α and H-6b, and between H-3′ and H-4. These are consistent with one orientation of the side chain, but rotation about the C-4—C-1′ bond is not necessarily precluded by the indetectability of nOe's that might be expected if rotation occurred. However, nOe between H-5′ and both H-3′ and H-4′ shows that rotation is possible about the C-4′—C-5′ bond.

Only sketchy details on the assignment of the ^{13}C nmr data of **1** have been published (7, 18) and a more complete account of the data and some reassignment is necessary. The ^{13}C nmr spectrum displayed 15 resonances composed of three carbonyl, four olefinic, and eight saturated carbons. All the carbons bearing hydrogen could be unequivocally assigned by a 2-D heterocorrelation experiment using the ^{1}H nmr shifts and coupling values previously assigned (15, 17) and reconfirmed in this work. Of the four remaining quaternary carbons the resonance at 133.8 ppm was assigned to C-1′. The high-resolution ^{13}C nmr data were used to distinguish the three remaining carboxyl resonances. The signal at 177.5 ppm ascribed to C-7 appeared as a doublet of triplets due to coupling with H-3 (J = 3.0 Hz) and with H-6a and H-6b (J = 7.2 Hz). The resonance for the C-2 carboxyl appeared as a doublet of doublets at 174.9 ppm (coupling to H-2 and H-3; J = 4.1 Hz) and the resonance for the C-5′ carboxyl appeared as a complex multiplet centred at 181.9 ppm (coupling to H-6′, H-5′, H-4′).

Finally, to determine if domoic acid accounted for all the observed toxicity, quantitative mouse and hplc assays were performed on a variety of extracts and on pure domoic acid solutions. The data, presented in Fig. 4 in the form of a dose–response curve, showed that no significant toxicity other than that due to domoic acid occurred in either the aqueous methanol or boiling acid (0.1 M HCl) extracts.

The intraperitoneal dose required for a 30-min death time in the mouse bioassay was about 10 mg kg^{-1} body weight (200 μg per average mouse). Pure domoic acid in aqueous solution produced the same symptoms in the mouse bioassay as did toxic-mussel extracts. The hplc assays have identified concentrations of domoic acid in toxic shellfish samples as great as 900 μg g^{-1} fresh tissue, although the levels varied greatly between batches and averaged about 300 μg g^{-1}.

This is the first report of domoic acid (**1**) in shellfish and the first known occurrence of human intoxication from ingesting the neurotoxin. Domoic acid was originally isolated from the warm-water red macro alga *Chondria armata* over 30 years ago (7, 8), and subsequently several isomers and derivatives of **1** have been isolated from the same algal source (17, 19). There are early reports (20) of the use of domoic acid as an anthelmintic for young children in Japan; however, the doses used were at the ~0.6 mg kg^{-1} level (20), an order of magnitude lower than those encountered by adult Canadians experiencing toxic effects from eating contaminated mussels.[4] Over the years there has been considerable interest in this group of metabolites because of their insecticidal properties (21) and because domoic acid (**1**) and the structurally related compound kainic acid (**2**) are potent members of a group of neurotoxic amino acids (22, 23). Biochemical, pharmacological, and physiological studies have shown that these excitatory amino acids act on three types of receptors in the brain, the hippocampus being the most sensitive structure in the central nervous system (CNS). These studies have been extensively reviewed (24–27). Very recently, the first electrophysiological evidence has been obtained that domoic acid activates kainate receptors and is more potent than kainic acid itself.[11] Furthermore, these electrophysiological results are in keeping with the clinical reports of patients hospitalized after ingesting the mussel toxin, and two post-mortem anatomopathological examinations are reported to reveal extensive damage of the hippocampus as well as spotty damage of thalamic and forebrain regions.[11]

Since domoic acid was not detected in mussels from elsewhere in P.E.I., it is unlikely that it is a metabolic product of the mussel itself. Moreover, toxic shellfish held in tanks of clean water for several weeks steadily purged themselves of domoic acid,[12] a phenomenon often associated with dietary products of shellfish (2). As efficient filter-feeding bivalves, mussels process huge volumes of water relative to their body size (28) and at least some of the toxin in their tissues could be derived from low (undetectable) levels of domoic acid in sea water. However, the food vector is probably much more important than the water vector to account for the substantial quantities of domoic acid found in contaminated mussels. It is estimated that the total amount of domoic acid in mussels from the affected area was probably in excess of 6 kg, with essentially all of the toxin body burden associated with digestive-gland tissue.

The major food items for cultured mussels are phytoplankton and other particulate detrital organic material such as fragmented seaweed tissue from benthic macrophytes and particulate organic material of terrestrial origin carried into the marine

[11]G. Dobennel, L. Beauchesne, and C. de Montigny. Submitted for publication.

Can. J. Chem. Downloaded from www.nrcresearchpress.com by 122.72.124.2 on 09/07/12
For personal use only.

Can. J. Chem. Downloaded from www.nrcresearchpress.com by 122.72.124.2 on 09/07/12
For personal use only.

environment by surface-water runoff. The available evidence on distribution and abundance of benthic macrophytes known to produce domoic acid, such as *Alsidium corallinum* C. Ag. (29), *Chondria armata* (6, 7), and its congener *C. baileyana* (Mont.) Harv. (unpublished result), effectively rule out these species as sources of the toxin in eastern P.E.I. Based on other shellfish toxin results, a more likely source of mussel contamination is the microalgal component of the plankton ingested by filter feeders.

Plankton tows made in early December 1987 by L. A. Hanic (University of Prince Edward Island) revealed an intense diatom bloom in the affected area. This diatom was subsequently identified as *Nitzschia pungens* Grun. f. *multiseries* Hasle.[13] When injected in mice, extracts of the plankton-tow samples produced symptoms identical to those produced by extracts from toxic mussels. As well, all toxic mussels harvested in December 1987 showed engorged digestive glands containing identifiable shell remnants of *N. pungens*; this was also true of toxic mussels harvested in late October and November, although no information is available on the plankton composition at that time. We observed domoic acid in plankton from the affected areas at levels sometimes in excess of 1% dry weight (30), sufficient to account for the levels observed in toxic mussels. This strong evidence that *N. pungens* was the major source of domoic acid in the toxic mussels is further supported by the demonstration of *de novo* production of domoic acid by laboratory cultures of *N. pungens* isolated from the affected area (34). Additional results from the St. Andrews Biological Station[14] and from the University of Rhode Island[15] document the very high probability that other phytoplankton such as *Amphora coffaeformis* (Ag.) Kütz. are also primary producers of domoic acid. In view of the importance of this new shellfish toxin to the Atlantic regional fisheries and the possibility that it may be more widespread, it is essential to determine what other marine organisms can synthesize domoic acid.

Experimental

All solvents were hplc grade from Anachemia. Distilled water was further purified by passage through a Millipore water-purification system (Milli-QR) equipped with ion-exchange and carbon filters. Trifluoroacetic acid (TFA) was purchased from BDH. Reference samples of domoic acid were obtained from Cambridge Research Biochemicals, England (Lot 12026), and Regis Chemical Company, Illinois, U.S.A. (Lot 2555). Melting points are corrected and were observed with a Kofler-type hot-stage apparatus. Optical rotations were measured using a Perkin Elmer model 141 polarimeter.

Infrared spectroscopy

Infrared spectra were recorded by microspectroscopic techniques using a BOMEM FT-IR spectrometer (model DA3.02) equipped with a "Spectroscope" microscope attachment made by Spectra-Tech Inc. The spectrometer was used with a KBr beamsplitter and a mercury – cadmium telluride detector. Spectra in the region 4000–700 cm^{-1} were recorded at a resolution of 2 cm^{-1} with 400 interferograms accumulated for each spectrum. A microgram quantity of domoic acid, dissolved in water and with the pH adjusted if necessary with dilute hydrochloric acid, was evaporated on a small AgCl or CaF_2 plate to yield a thin solid film approximately 3 mm in diameter and a few microns in thickness. Small circular areas of 0.1 mm diameter were visually selected, optically isolated by the microscope aperture, and their ir spectra recorded. The spectrum of an equivalent area of the empty plate was recorded as reference: the ratio of such spectral pairs yielded the transmittance spectrum, from which the absorbance spectrum was derived. Since the sample space was normally evacuated to a pressure of 0.2 Torr (26 Pa), the spectra obtained were those of anhydrous material.

Nuclear magnetic resonance spectroscopy

All nmr spectra were obtained with a Bruker MSL-300 spectrometer at room temperature (20°C), in 5-mm tubes, under the following conditions. ^1H spectra: 300.13 MHz, one-pulse sequence, spectral width (SW) 4505 Hz or 2403 Hz, acquisition time (AQ) 1.82 s or 3.41 s, 16 384 data points, delay between 45-deg rf pulses 8.6 s, data processed where necessary with exponential multiplication and zero-filling. Integrated intensities of signals were compared with those of a standard sucrose solution in D_2O using identical experimental conditions, allowing complete spin-lattice relaxation for quantitative estimation of concentrations. ^1H COSY spectra (31): SW 2401 Hz and 90-deg pulses. ^{13}C spectra: SW 16 667 Hz, AQ 0.983 s or 0.492 s, 30-deg pulses, and broadband ^1H-decoupling. ^{13}C coupled spectra used SW 13514 Hz and AQ 2.43 s. Nuclear Overhauser enhancements were obtained by irradiating selected resonances for 10 s between acquisitions at a power level just sufficient to cause saturation (ca. 180 mV peak–peak into a 50-ohm load via a directional coupler), and subtracting these spectra from one obtained under the same conditions but with irradiation well removed from any resonances. D_2O was used as a solvent and spectra were referred to TSP in a concentric tube. The concentration of domoic acid in the original preparation was estimated from the ^1H resonance areas to be 2.0(±0.1) mg in 0.7 mL D_2O, which was close to saturation at room temperature. A supersaturated solution of a later preparation of anhydrous domoic acid from mussels (9.4 mg in 0.6 mL D_2O) was used for ^{13}C–^1H correlation spectra. The ^1H and ^{13}C spectra reported in Table 1 were obtained from a saturated solution of the latter preparation at pH 3.4.

Mass spectrometry

All mass spectrometric measurements reported herein were conducted using a VG Analytical ZAB-EQ tandem hybrid mass spectrometer, or a VG Masslab 20-250 quadrupole mass spectrometer, each equipped with a VG11-250J datasystem. The FAB mass spectra were obtained using the ZAB-EQ instrument. Sample sizes in the range 10–100 nmol, in 1–10 μL of aqueous solution, were deposited on a gold probe tip, evaporated down to less than 1 μL, then mixed with about twice as much glycerol. Although this simple glycerol/water matrix kept the background to a minimum, the matrix was acidified with HCl when working in positive-ion mode. An 8-keV Xe^0 beam (Ion Tech FAB gun, 1-mA discharge current) was used. Conventional FAB mass spectra were obtained at a resolving power (10% valley) of 1500, scanning the range *m/z* 1300–50 Da with a cycle time of approximately 10 s. Mass assignments were reliable to within 0.1 Da. Masses of ions formed by FAB ionization were measured to better than 10 ppm by peak matching against either the matrix cluster ion at *m/z* 277 (3 glycerol molecules + H) or, in a separate determination for a sample doped with sodium iodide, the $Na_3I_2^+$ cluster at *m/z* 323; resolving power was 8000 (10% valley definition). Electron ionization (EI) spectra of the *tert*-butyldimethylsilyl derivatives formed by reaction of domoic acid in dimethylformamide with *N*-methyl-*N*-(*tert*-butyldimethylsilyl)trifluoracetamide (MTBSTFA, Regis Chemicals) were obtained using 70-eV nominal energy electrons. Accurate mass measurements of these EI ions were made by peak matching against perfluorokerosene at a resolving power of 8000. Tandem mass spectrometry experiments were done to obtain fragment-ion spectra of the ions at *m/z* 312 in the positive-ion FAB spectra. For these, the precursor ions were selected by the double-focusing BE stages of the instrument, decelerated, then focused into the rf-only quadrupole collision cell (q) containing argon at a pressure such that the intensity of the precursor ion signal was attenuated by 50–60% while the tandem quadrupole mass analyser (Q) was scanned. A collision energy (laboratory frame) of 30 eV was used. All tandem mass spectrometry data

[12]D. Scarratt (DFO, Halifax), personal communication.

[13]C. J. Bird (ARL) and M. Poulin (National Museum of Canada, Ottawa), personal communication.

[14]J. Martin (St. Andrews Biological Station, DFO), personal communication.

[15]Y. Shimizu (University of Rhode Island), personal communication.

Can. J. Chem. Downloaded from www.nrcresearchpress.com by 122.72.124.2 on 09/07/12
For personal use only.

were acquired in continuum mode, each spectrum representing the sum of at least 10 scans.

High voltage paper electrophoresis (hvpe)

Concentrated aqueous-methanol extract (approximately 1 mL) was streaked across the middle of a sheet of Whatman 3MM chromatography paper and air-dried. The paper on either side of the sample zone was wetted with pyridine–acetate buffer at pH 6.5 (pyridine:acetic acid:water, 25:1:225 by volume) and electrophoresis was carried out at 3 kV for 40 min in a Michl tank (32) with toluene as the heat exchanger. The paper was dried and vertical strips (1 cm wide) cut off and stained with cadmium acetate – ninhydrin (33). The remainder of the electrophoretogram was cut into horizontal zones, which were eluted with water and taken to dryness *in vacuo*.

Amino acid analysis

Dilute aqueous extracts (0.1 mL) were loaded on a Beckman 119CL automatic amino acid analyzer. The cation-exchange column (sulfonated polystyrene, 30 μm diameter) was equilibrated with 0.3 M sodium citrate buffer, pH 3.25, and eluted with 0.3 M sodium citrate buffers of pH 3.95 and pH 6.40. The dual-wavelength detector recorded absorbances of ninhydrin reaction products at 570 and 440 nm.

High performance liquid chromatography (hplc) and ultraviolet (uv) spectroscopy

Domoic acid determinations were performed on a Hewlett–Packard model 1090M hplc equipped with a ternary DR5 solvent delivery system, variable volume (1–25 μL) injector and autosampler, built-in HP1040 diode array detector (DAD), and HP79994 data system. A 25 cm × 2.1 mm i.d. 5-μm Vydac 201TP52 column (Separations Group, Hesperia, CA) was operated at 40°C with 0.5 mL min^{-1} 10% (v/v) acetonitrile in water with 0.1% (v/v) trifluoroacetic acid and 5-μL injection volumes. Detection was accomplished by monitoring absorption at both 210 and 242 nm with 10-nm bandwidths. Ultraviolet acquisition was either in the peak-triggered mode or in the continuous mode with a 640-ms scan interval. Prior to analysis, aqueous extracts (1–2 mL; pH 6–7) were applied to a prerinsed C_{18} solid-phase extraction cartridge (Supelco, Bellfonte, PA), eluted with 10% aqueous acetonitrile (3 mL) into a 5-mL volumetric, made up to volume, and filtered through a dry 0.22-μm filter. Calibration was accomplished using a solution of pure domoic acid isolated by heart-cutting the domoic acid peak from preparative hplc, and calculating domoic acid concentration from the literature molar absorptivity (7) at 242 nm (2.63×10^4) and the observed optical density at 242 nm. The molar absorptivity of purified domoic acid was later redetermined in our laboratory and found to be pH-dependent. The value is $(2.43 \pm 0.04) \times 10^4$ at pH 2.0 and $(2.61 \pm 0.04) \times 10^4$ at pH 7.0.

Isolation of domoic acid

(i) By ion-exchange chromatography

Digestive glands (572 g) were excised from frozen, cooked, mussel tissue (1826 g) (processed by North Ocean Enterprises Ltd., Souris, P.E.I.) and homogenized with a mixture of distilled water (450 mL) and methanol (650 mL). The homogenate was stirred and heated at 65°C for 10 min. The cooled mixture was centrifuged (3500 rpm for 10 min) and the supernatant decanted. The residue was washed twice with 50% aqueous methanol (1 × 600 mL; 1 × 300 mL). The combined supernatants were concentrated *in vacuo* to give a viscous golden-brown oily residue. This was taken up in water (200 mL); an aliquot (10 mL) was reevaporated to give a residue (1.62 g), shown by hplc to contain 35.8 mg of domoic acid.

The residue (30.8 g), obtained by evaporating the remaining solvent (190 mL), was triturated with methanol. This afforded an insoluble cream-coloured solid (11.13 g) and a methanol-soluble fraction (17.91 g).

The solid was dissolved in water (325 mL), the pH adjusted to 5.0, and the solution centrifuged. The supernatant was placed on a Bio-Rad AG 3-X4 column (2.5 × 25 cm; 107 mL resin; OH^- form). After washing with water (700 mL) and 2 M acetic acid (200 mL), fractions (400 mL) containing domoic acid were eluted from the column with 4 M acetic acid. Evaporation gave residue A (691 mg).

The methanol-soluble fraction above was dissolved in water (200 mL), extracted with dichloromethane (3 × 200 mL), placed on a Bio-Rad Ag 3-X4 column, and treated as described above. The domoic acid fraction (350 mL) was evaporated *in vacuo* to give residue B (889 mg).

Residues A and B were combined and crystallized from water to give domoic acid (208 mg), mp 200–205°C (subsequent crops gave an additional 273 mg of less pure material). Successive recrystallizations from water gave pure domoic acid dihydrate (180 mg), mp 215–216°C (lit. (8) mp 217°C). This melting point refers to loss of polarizing properties, and deformation, of the dihydrate crystal examined as soon as possible after preparation. Such crystals do not exhibit this well-defined behaviour on standing. $[\alpha]_D^{23}$ −120.5° for anhydrous material; reported value (29) for dihydrate, −108°, equivalent to −120.5° for the anhydrous compound. *Anal.* calcd. for $C_{15}H_{21}NO_6$: C 57.87, H 6.80, N 4.50%; found (after drying at 50°C for 18 h): C 57.54, H 6.98, N 4.16%.

(ii) By preparative hplc

Shucked frozen mussels (≈800 g wet wt) were homogenized with methanol:water (7:3 v/v; 3 L) and allowed to stand at room temperature for 24 h with occasional stirring. The slurry was filtered through glass-fibre paper and the filtrate concentrated *in vacuo*. The concentrate was partitioned twice against dichloromethane to yield an organic-soluble extract (12.4 g) and a water-soluble extract (≈65 g). Biological testing showed the toxicity to be present in the aqueous fraction. A portion of this aqueous extract (4 g) was applied to a column (40 × 3 cm) containing XAD-2 (Amberlite) resin. Fractions (200 mL) were collected during elution with a stepwise gradient from water through methanol. The toxicity was contained in the first two fractions. These were combined, concentrated *in vacuo*, and applied to a preparative reversed-phase column (Supelcosil LC-18 5 μm; 25 cm × 21.2 mm) and eluted with a linear gradient of 10% acetonitrile–water through 35% acetonitrile–water (1% acetic acid; flow rate 12 mL min^{-1}). The eluant was monitored at 242 nm and domoic acid (retention time 10.5 min) was collected following repeated injections. After concentration, the resulting yellowish oil was dissolved in the minimum volume of hot water and, upon cooling, straw-coloured crystals of domoic acid formed. Repeated crystallization yielded colourless needles, mp 212–214°C, identical (uv, ir, nmr) with authentic material.

Bioassays

The biological assays were performed using female mice (CD-1, Charles River Canada Inc.) weighing 16–23 g. Each was injected intraperitoneally with an extract (1 mL) and observed for up to 3 h. At least two mice were used for each test. The symptoms varied depending on the dose of domoic acid. Mice with death times of less than 13 min exhibited circling movements, occasional barrel rotation, and convulsions. Mice with longer death times exhibited loss of coordination, scratching of shoulder area with back legs alternating from one leg to the other at 3 to 20-s intervals, occasional aggressiveness, and gnawing or biting.

Acknowledgements

We acknowledge the efforts and cooperation of our DFO colleagues, particularly R. Bourque, J. Worms, and L. Lea (Gulf Region) and R. F. Addison and J. E. Stewart (Scotia-Fundy Region), and those of our HWC colleagues including H. B. S. Conacher, S. W. Gunner, J. F. Lawrence, and E. Todd. We thank L. A. Hanic, University of P.E.I., for phytoplankton samples, often collected under extreme weather conditions.

We would also like to thank our NRC colleagues, J. W. McLaren (Ottawa) for heavy metal analysis, C. J. Bird and J. L. McLachlan (Halifax) for biological examination of algal and mussel samples, A. M. Backman and A. R. Taylor, CISTI–ARL, for library services, and F. E. Isaacs, Public Relations and Information Services, for a magnificent job under enormous pressure. It is a particular pleasure to acknowledge the extraordinary efforts of the ARL staff throughout this work.

They include the following technical staff: C. A. Craft, E. W. Dyer, D. J. Embree, M. G. Flack, C. Gillis, M. Greenwell, W. R. Hardstaff, P. LeBlanc, N. I. Lewis, G. K. McCully, M. McInerney-Northcott, D. O'Neil, P. F. Seto, and D. F. Tappen, and the entire maintenance and administrative support staff, in particular K. V. Gray, W. J. Gray, H. O. Henderson, K. D. MacLeod, D. R. Robson, G. Saab, C. T. Vaughan, H. R. Watts, and B. Willis.

Finally, we thank Dr. Y. Ohfune, Suntory Institute for Bioorganic Research, Osaka, for the generous gift of a quantity of (−)-domoic acid obtained by total synthesis (ref. 15).

1. B. W. HALSTEAD. Poisonous and venomous marine animals of the world. Vol. 1. U.S. Government Printing Office, Washington, D.C. 1965.
2. E. P. RAGELIS. Seafood toxins. ACS Symposium Series 262. Washington, D.C. 1984.
3. A. W. WHITE. *In* Toxic red tides and shellfish toxicity in Southeast Asia. *Edited by* A. W. White, M. Anraku, and K. K. Hooi. IDRC, Ottawa, Canada. 1984. p. 110.
4. T. YASUMOTO, M. MURATA, Y. OSHIMA, M. SANO, G. K. MATSUMOTO, and J. CLARDY. Tetrahedron, **41**, 1019 (1985).
5. T. M. PERL, L. BEDARD, T. KOSATSKY, J. HOCKIN, and R. S. REMIS. Epidemic Intelligence Service Conference, Center for Disease Control, Atlanta, GA. 1988.
6. T. J. BISCOE, R. H. EVANS, P. M. HEADLEY, M. MARTIN, and J. C. WATKINS. Nature, **255**, 100 (1975).
7. T. TAKEMOTO and K. DAIGO. Chem. Pharm. Bull. **6**, 578 (1958).
8. T. TAKEMOTO and K. DAIGO. Arch. Pharm. (Weinheim), **293**, 627 (1960).
9. Official method of analysis. Association of Official Analytical Chemists, Arlington, VA. 18.086–18.092. 1984; W. N. ADAMS and J. J. MIESCIER. J. Assoc. Off. Anal. Chem. **63**, 1336 (1980).
10. R. K. BOYD, A. S. W. DE FREITAS, R. A. FOXALL, W. D. JAMIESON, M. V. LAYCOCK, A. W. MCCULLOCH, M. A. QUILLIAM, and J. L. C. WRIGHT. Atlantic Research Laboratory Tech. Report No. 54 (1988).
11. M. FALK. Can. J. Spectrosc. **33**, 117 (1988).
12. G. W. A. MILNE, T. AXENROD, and H. M. FALES. J. Am. Chem. Soc. **92**, 5170 (1970); P. A. LECLERQ and D. M. DESIDERIO. Org. Mass Spectrom. **7**, 515 (1973); M. MEOT-NER and F. H. FIELD. J. Am. Chem. Soc. **95**, 7207 (1973).
13. C. W. TSANG and A. G. HARRISON. J. Am. Chem. Soc. **98**, 1301 (1976).
14. F. W. MCLAFFERTY and R. VENKATURAGHAVAN. Mass spectral correlations. Advances in Chemistry. Ser. No. 40. ACS, Washington, D.C. 1982. p. 40.
15. Y. OHFUNE and M. TOMITA. J. Am. Chem. Soc. **104**, 3511 (1982).
16. Anonymous. CISTI News, **5**(4), 1 (1988).
17. M. MAEDA, T. KODAMA, T. TANAKA, H. YOSHIZUMI, T. TAKEMOTO, K. NOMOTO, and T. FUJITA. Chem. Pharm. Bull. **34**, 4892 (1986).
18. M. MAEDA, T. KODAMA, T. TANAKA, H. YOSHIZUMI, K. NOMOTO, T. TAKEMOTO, and T. FUJITA. Tennen Yuki Kagobutsu Toronkai Koen Yoshishu, **27th**, 616 (1985).
19. M. MAEDA, T. KODAMA, T. TANAKA, H. YOSHIZUMI, T. TAKEMOTO, K. NOMOTO, and T. FUJITA. Tetrahedron Lett. **28**, 633 (1987).
20. K. DAIGO. J. Jpn. Pharm. Assoc. **79**, 353 (1959).
21. M. MAEDA, T. KODAMA, T. TANAKA, Y. OHFUNE, K. NOMOTO, K. NISHIMURA, and T. FUJITA. J. Pestic. Sci. **9**, 27 (1984).
22. R. ZACZEK and J. T. COPYLE. Neuropharmacology, **21**, 15 (1982).
23. J. S. KIZER, C. B. NEMEROFF, and W. W. YOUNGBLOOD. Pharmacol. Rev. **29**, 301 (1978).
24. J. T. COYLE. J. Neurochem. **41**, 1 (1983).
25. R. A. SCHWARTZ and Y. BEN-ARI. Adv. Exp. Med. Biol. 203 (1986).
26. J. C. WATKINS and H. J. OLVERMAN. Trends Neurosci. **10**, 265 (1987).
27. C. ANGST and M. WILLIAMS. Transmissions, **3**, 1 (1987).
28. M. E. WARD and E. AIELLO. Physiol. Zool. **46**, 157 (1973).
29. G. IMPELLIZZERI, S. MANGIAFICO, G. ORIENTE, M. PIATELLI, S. SCUITO, E. FATTORUSSO, S. MAGNO, C. SANTACROCE, and D. SICA. Phytochemistry, **14**, 1549 (1975).
30. S. S. BATES, C. J. BIRD, R. K. BOYD, A. S. W. DE FREITAS, M. FALK, R. A. FOXALL, L. HANIC, W. D. JAMIESON, A. W. MCCULLOCH, P. ODENSE, M. A. QUILLIAM, P. G. SIM, P. THIBAULT, J. A. WALTER, and J. L. C. WRIGHT. Atlantic Research Laboratory Tech. Report No. 57 (1988).
31. A. BAX and R. FREEMAN. J. Magn. Reson. **44**, 542 (1981).
32. H. MICHL. Monatsh. Chem. **82**, 489 (1951).
33. J. HEILMANN, J. BAROLLIER, and E. WATZKE. Hoppe-Seyler's Z. Physiol. Chem. **309**, 219 (1957).
34. D. V. SUBBA RAO, M. A. QUILLIAM, and R. POCKLINGTON. Can. J. Fish. Aquat. Sci. **45**, 2076 (1988).

Can. J. Chem. Downloaded from www.nrcresearchpress.com by 122.72.124.2 on 09/07/12
For personal use only.

Synthetic antigenic determinants of the *Brucella* A polysaccharide: A disaccharide thioglycoside for block synthesis of pentasaccharide and lower homologues of α1,2-linked 4,6-dideoxy-4-formamido-α-D-mannose[1]

THOMAS PETERS[2] AND DAVID R. BUNDLE

Division of Biological Sciences, National Research Council of Canada, Ottawa, Ont., Canada K1A 0R6

Received August 4, 1988

THOMAS PETERS and DAVID R. BUNDLE. Can. J. Chem. **67**, 491 (1989).

Methyl glycosides **13**, **18**, and **22**, which represent potential antigenic determinants of the *Brucella* A polysaccharide, are the first synthetic analogues of this antigen. Their synthesis was necessitated by crystallographic studies of a Fab combining site obtained from a monoclonal antibody that binds the *Brucella* A antigen and synthetic pentasaccharide. Monosaccharide synthon **3** and disaccharide **7**, *S*-ethyl glycoside derivatives of 4-azido-4,6-dideoxy-D-mannose, have been used successfully as key intermediates in a convergent strategy to synthesize α1,2-linked homo-oligosaccharides of 4,6-dideoxy-4-formamido-D-mannose. The disaccharide thioglycoside **7** was activated by methyl triflate in the presence of selectively protected mono- or trisaccharide alcohols **1**, **6**, or **10** to give α1,2-linked tri- and pentasaccharides **8**, **9**, and **19**. Despite the non-participating glycosyl substituent at position two of the thioglycoside, 1,2-*trans* glycosidic products appeared to be formed exclusively. Conversion of **3** to the glycosyl bromide **5** by bromine under mild conditions provided routes to both the disaccharide building block **7** and a tetrasaccharide **15** using conventional silver triflate promoted glycosylation reactions. Deprotection was accomplished by transesterification, hydrogen sulphide reduction of azido groups, followed by *N*-formylation and finally hydrogenolysis of benzyl ethers.

Key words: *Brucella* A antigen, pentasaccharide synthesis, thioglycosides, oligosaccharide building units, 4,6-dideoxy-4-formamido-D-mannose, antibody combining sites.

THOMAS PETERS et DAVID R. BUNDLE. Can. J. Chem. **67**, 491 (1989).

Les glycosides de méthyle **13**, **18** et **22** qui représentent des déterminants antigéniques potentiels du polysaccharide de la *Brucella* A sont les premiers analogues de synthèse de cet antigène. On a dû réaliser leur synthèse pour effectuer des analyses de structure par diffraction des rayons-X sur un Fab cristallin combinant le site de liaison de l'antigène *Brucella* A et le pentasaccharide de synthèse. Le monosaccharide de synthèse **3** ainsi que le disaccharide **7**, des dérivés glycoside de *S*-éthyle de l'azido-4 didésoxy-4,6 D-mannose, ont été utilisés avec succès comme intermédiaires clés dans une stratégie convergente conduisant à la synthèse d'homo-oligosaccharides liés en α1,2 du didésoxy-4,6 formamido-4 D-mannose. On a activé le thioglycoside du disaccharide **7** par le triflate de méthyle en présence des mono- ou tri-saccharides alcools **1**, **6** ou **10**, protégés d'une façon sélective, et on a obtenu les tri- et penta-saccharides **8**, **9** ou **19** liés par les positions α1,2. Malgré la présence d'un substituant glycosyle non-participant en position deux du thioglycoside, il semble que les produits glycosidiques 1,2-*trans* se forment d'une façon exclusive. La transformation du composé **3** en bromure de glycosyle, par l'action du brome dans des conditions douces, fournit des voies pouvant conduire, par des réactions de glycosylation conventionnelles activées par le triflate d'argent, soit au disaccharide **7** ou au tétrasaccharide **15**. On a procédé à la déprotection par le biais d'une transestérification qui a été suivie d'une réduction des groupements azido par le sulfure d'hydrogène et d'une *N*-formylation et finalement d'une hydrogénolyse des éthers benzyliques.

Mots clés : antigène *Brucella* A, synthèse des pentasaccharides, thioglycosides, éléments d'édification des oligosaccharides, didésoxy-4,6 formamido-4 D-mannose, sites de liaison des anticorps.

[Traduit par la revue]

Introduction

Structural studies of the *Brucella* A and M antigens have shown these to be distinctive linear homopolymers of the rare monosaccharide 4,6-dideoxy-4-formamido-D-mannose (1, 2). The A antigen is an α1,2-linked polymer (1),

$$\rightarrow 2)\text{-}\alpha\text{-D-Rha4NFo}\,(1\rightarrow_n$$

while the M antigen possesses a repeating unit with four α1,2-linked and one α1,3-linked residues (2):

$$\rightarrow 2)\text{-}\alpha\text{-D-RhaNFo}(1\rightarrow 3)\text{-}\alpha\text{-D-Rha4NFo}(1\rightarrow 2)\alpha\text{-D-}$$
$$\text{Rha4NFo}(1\rightarrow 2)\text{-}\alpha\text{-D-Rha4NFo}(1\rightarrow 2)\text{-}\alpha\text{-Rha4NFo}(1\rightarrow$$

Despite their homology the A and M antigens may be distinguished by cross-absorbed antibody preparations and these are used to serologically differentiate *Brucella* strains (3–5). Monoclonal antibodies exhibiting similar specificity have been obtained (6)[3] and one crystalline Fab fragment has been successfully analyzed by X-ray diffraction.[4] To study the structural basis for the differentiation of the A and M antigen by antibodies and to map the antibody combining site by hapten binding studies, a series of oligomers containing from three to five saccharide residues was required.

The key intermediate **1** has been synthesized from D-mannose in 10 steps (7) and shown to be effective in the preparation of a disaccharide and trisaccharide using conventional silver salt promoted glycosylation reactions (7, 8). In this work we describe the utilization of **1** to prepare *S*-ethyl glycoside derivatives **3** and **7**, which undergo methyl triflate promoted glycosylation to provide 1,2-*trans*-linked oligomers of the *manno* series in both high yield and stereospecificity. A preliminary account of this work has appeared (9).

---

[1]Issued as NRCC No. 29853.

[2]NRCC Research Associate 1986–1987.

[3]Bundle, Gidney, and Meikle. Unpublished results.

[4]Bundle, Vorberg, and Rose. Unpublished results.

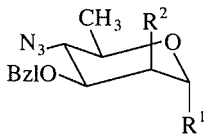
Can. J. Chem. Downloaded from www.nrcresearchpress.com by 41.223.56.140 on 09/07/12
For personal use only.

Can. J. Chem. Downloaded from www.nrcresearchpress.com by 41.223.56.140 on 09/07/12
For personal use only.

Results and discussion

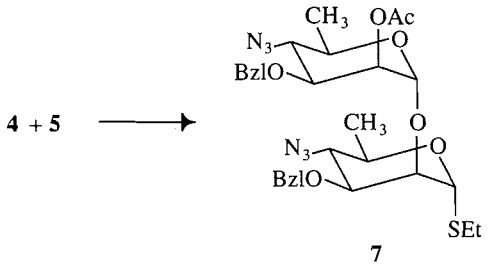
The successful convergent approach adopted here for the synthesis of α1,2-linked homo-oligomers of the rare sugar 4,6-dideoxy-4-formamido-D-mannose was made possible by the use of thioglycosides. This is, to our knowledge, the first time synthetic analogues of the *Brucella* A antigen have been prepared by utilizing thioglycosides as key intermediates. The target oligosaccharides were essential components for studies of antibody combining sites directed against the *Brucella* A antigen. A crystalline Fab fragment from one antibody also crystallizes in the presence of the synthetic pentasaccharide.

A high yield synthesis from D-mannose (7, 8) of the key intermediate methyl 4-azido-3-*O*-benzyl-4,6-dideoxy-α-D-mannopyranoside (**1**) provided the foundation of our work. Acetylation and subsequent mild acetolysis of **1** gave the 1,2-



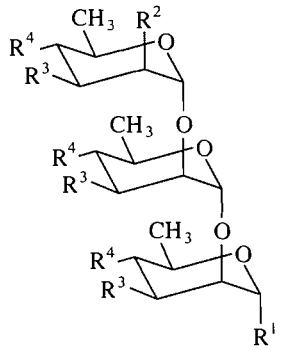
1 R^1 = OMe, R^2 = OH
2 R^1 = OAc, R^2 = OAc
3 R^1 = SEt, R^2 = OAc
4 R^1 = SEt, R^2 = OH
5 R^1 = Br, R^2 = OAc
6 R^1 = $O(CH_2)_8CO_2Me$, R^2 = OH

di-*O*-acetyl derivative **2** (8), which was converted to the corresponding *S*-ethyl glycoside **3** by reaction with Lewis acid and ethanethiol (10). Transesterification of **3** gave a selectively protected monosaccharide alcohol **4**, while reaction of **3** with bromine under mild conditions (11) provided a facile route to the glycosyl bromide **5**. Silver salt assisted glycosylation of **4** by **5** provided the crucial disaccharide **7**, which served as the building unit for oligosaccharide assembly. It was essential to utilize the glycosyl bromide **5**, because the more direct route to **7** from the two thioglycosides **3** and **4** utilizing methyl triflate activation causes concurrent activation of the glycosyl acceptor and the glycosyl donor.



7

The most attractive and direct route to synthesis of higher oligomers of 4,6-dideoxy-4-formamido-D-mannose involved block synthesis employing **7** as a glycosyl donor with mono- and trisaccharide acceptors such as **1** and **10**. The functionalized monosaccharide glycoside **6** provided access to an oligosaccharide that could be covalently attached to proteins (12). Trisaccharides **8** and **9** were prepared using disaccharide donor **7** and either of the selectively protected glycosides **1** or **6**. Methyl triflate activation (13, 14) of the *S*-ethyl disaccharide glycoside **7** in the presence of the monosaccharide alcohol in dichloromethane solution provided trisaccharides **8** and **9** in greater than 80% yield. A carbon-13 nmr spectrum indicated that the isolated product was exclusively α-linked by virtue of the one-bond heteronuclear coupling constant, $^1J_{C,H} \approx 170$ Hz

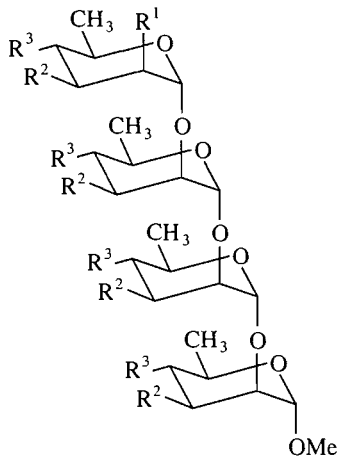


8 R^1 = OMe, R^2 = OAc, R^3 = OBzl, R^4 = N_3
9 R^1 = $O(CH_2)_8CO_2Me$, R^2 = OAc, R^3 = OBzl, R^4 = N_3
10 R^1 = OMe, R^2 = OH, R^3 = OBzl, R^4 = N_3
11 R^1 = OMe, R^2 = OH, R^3 = OBzl, R^4 = NH_2
12 R^1 = OMe, R^2 = OH, R^3 = OBzl, R^4 = NHCHO
13 R^1 = OMe, R^2 = R^3 = OH, R^4 = NHCHO
14 R^1 = $O(CH_2)_8CO_2Me$, R^2 = R^3 = OH, R^4 = NHCHO

(15). In contrast to the experience of Srivastava and Hindsgaul (19), who obtained a β-linked oligosaccharide from a 2-*O*-(α-D-mannopyranosyl)-α-D-mannopyranosyl halide, no β-linkage was found in our reaction products. The acetate group at O-2 of the terminal glycosyl residue of **7** serves as a latent site for chain extension after glycosylation of the saccharide acceptor **1**.

The trisaccharide methyl glycoside **8** was transesterified to yield the selectively protected alcohol **10**, which then served as the precursor for synthesis of either a tetrasaccharide or pentasaccharide. Silver triflate promoted glycosylation of **10** by the glycosyl bromide **5** gave the tetrasaccharide methyl glycoside **15** in 80% yield. Synthesis of the pentasaccharide **19** was accomplished by electrophilic activation of the disaccharide thioglycoside **7** with methyl triflate. This led over a 2-day period to 1,2-*trans* glycosidic bond formation with the trisaccharide alcohol **10**. Heteronuclear coupling constants (15) again confirmed the stereoselective and exclusive formation of α-linked roduct. Preparation of the trisaccharide **9** by a block synthesis involving the *S*-ethyl disaccharide glycoside **7** and the monosaccharide glycoside (**6**) led to a trisaccharide hapten **14** that could be covalently attached to protein (12).

Deprotection of the oligosaccharides **8**, **9**, **15**, and **19** was

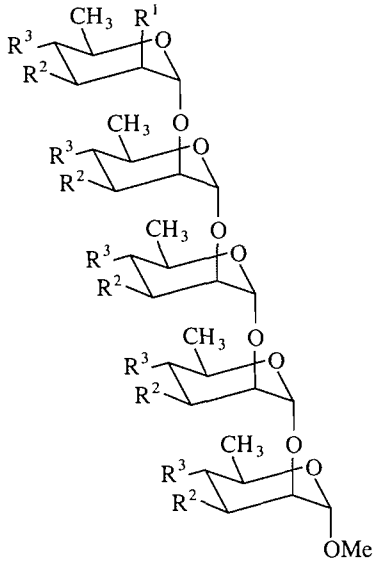


15 R^1 = OAc, R^2 = OBzl, R^3 = N_3
16 R^1 = OH, R^2 = OBzl, R^3 = N_3
17 R^1 = OH, R^2 = OBzl, R^3 = NHCHO
18 R^1 = R^2 = OH, R^3 = NHCHO

Can. J. Chem. Downloaded from www.nrcresearchpress.com by 41.223.56.140 on 09/07/12
For personal use only.

performed in a four-step process. Transesterification afforded intermediates **10**, **16**, and **20** containing only azido and benzyl protecting groups. The former were converted to amines by mild H_2S reduction (16) and these were in turn *N*-formylated by methyl formate, used in solvent quantities (17, 18) to yield **12**, **17**, and **21**. Attempts to reduce the azido group by hydrogenation and to simultaneously remove benzyl ether residues were unsuccessful. Finally, palladium catalyzed hydrogenolysis in acetic acid gave the deprotected trisaccharides **13**, **14**, tetrasaccharide **18**, and pentasaccharide **22**. The overall yields for the combined deprotection steps ranged from 65 to 80%.

The rotational isomerism of the formamido group results in complicated nmr spectra, particularly for the higher oligomers. However, the ^1H and ^{13}C nmr spectra of oligosaccharides **13**, **18**, and **22** were amenable to analysis with the assistance of



19 $R^1 = OAc$, $R^2 = OBzl$, $R^3 = N_3$
20 $R^1 = OH$, $R^2 = OBzl$, $R^3 = N_3$
21 $R^1 = OH$, $R^2 = OBzl$, $R^3 = NHCHO$
22 $R^1 = R^2 = OH$, $R^3 = NHCHO$

homo- and heteronuclear two-dimensional nmr spectroscopy at 500 MHz. The spectra were consistent with the assigned structures.

The use of oligosaccharides **13**, **14**, **18**, and **22** to map the combining sites of crystalline monoclonal antibody fragments will be reported separately.[4]

Experimental

General

Unless otherwise indicated, methods used were similar to those reported in an earlier paper (8).

Hexane refers to a mixture supplied by Home Oil Company, Wichita, Kansas. Solvents were distilled before use and were dried where necessary by literature procedures (20). Reactions performed with dried solvents were conducted under dry nitrogen.

Melting points were determined on a Fisher–Johns apparatus and are uncorrected. Optical rotations were measured with a Perkin–Elmer polarimeter.

The ^1H and ^{13}C nmr were recorded with Bruker AM 200 and AM 500 spectrometers. Solutions in organic solvents were referenced to internal tetramethylsilane and in D_2O solutions, relative to 1.0% v/v internal acetone (δ_H 2.225 ppm). Internal acetone (δ_C 30.50 ppm) was used as the internal ^{13}C reference for solutions in D_2O. Chemical shifts and coupling constants are first-order values. Assignments are based upon homo- and heteronuclear shift correlation spectroscopy (21–24).[5]

Ethyl 2-O-acetyl-4-azido-3-O-benzyl-4,6-dideoxy-1-thio-α-D-mannopyranoside **3**

Ethanethiol (6 mL, 81.02 mmol) and boron trifluoride etherate (6 mL, 48.78 mmol) were added to a stirred suspension of compound **2** (11.8 g, 32.56 mmol) (8) and powdered 4 Å molecular sieves (1.0 g) in dichloromethane (200 mL). After 2 h at room temperature (tlc, hexane – ethyl acetate 3:1 v/v) the reaction was stopped by dropwise addition of triethylamine (7 mL, 50.22 mmol). Filtration and removal of the solvents *in vacuo* afforded the crude reaction product, which was purified on a silica gel column (hexane – ethyl acetate 3:1 v/v) to give pure **3** (10.5 g, 88%) and a small amount of the β anomer (0.6 g, 5%). Pure **3**: syrup, $[\alpha]_D^{20}$ +179.22° (*c* 0.99, chloroform); ^1H nmr (200 MHz, $CDCl_3$) δ: 7.40–7.20 (m, 5H, Ph), 5.41 (dd, 1H, $J_{1,2}$ 1.6 Hz, $J_{2,3}$ 3.3 Hz, H-2), 5.19 (d, 1H, H-1), 4.67 (d, 1H, *J* 11.2 Hz, CH_AH_BPh), 4.51 (d, 1H, CH_AH_BPh), 3.89 (dq, 1H, $J_{4,5}$ 10.0 Hz, $J_{5,6}$ 6.4 Hz, H-5), 3.74 (dd, 1H, $J_{2,3}$ 3.3 Hz, $J_{3,4}$ 9.8 Hz, H-3), 3.43 (dd, 1H, H-4), 2.70–2.50 (m, 2H, SCH_2CH_3), 2.13 (s, 3H, OAc), 1.33 (d, 3H, H-6), 1.27 (dd, 3H, *J* 7.4 Hz, SCH_2CH_3); ^{13}C nmr (50 MHz, $CDCl_3$) δ: 82.30 (d, 1C, $J_{C1,H1}$ 166.0 Hz, C-1). *Anal.* calcd. for $C_{17}H_{23}N_3O_4S$: C 55.87, H 6.34, N 11.50; found: C 56.11, H 6.84, N 11.44. β anomer: syrup, $[\alpha]_D^{20}$ +107.66° (*c* 0.5, chloroform); ^1H nmr (500 MHz, $CDCl_3$) δ: 7.38–7.28 (m, 5H, Ph), 5.26 (d, 1H, $J_{1,2}$ 1.6 Hz, H-1), 5.02 (dd, 1H, $J_{2,3}$ 3.1 Hz, $J_{3,4}$ 10.1 Hz, H-3), 4.67 (d, 1H, *J* 12.2 Hz, CH_AH_BPh), 4.53 (d, 1H, CH_AH_BPh), 3.96 (dq, 1H, $J_{4,5}$ 10.0 Hz, $J_{5,6}$ 6.0 Hz, H-5), 3.94 (dd, 1H, H-2), 3.64 (dd, 1H, H-4), 2.61 (dq, 1H, $^2J_{gem}$ 13.0 Hz, $^3J_{vic}$ 7.8 Hz, $SCH_AH_BCH_3$), 2.55 (dq, 1H, $SCH_AH_BCH_3$), 2.07 (s, 3H, OAc), 1.35 (d, 3H, H-6), 1.25 (q, 3H, SCH_2CH_3); ^{13}C nmr (50 MHz, $CDCl_3$) δ: 81.60 (d, 1C, $J_{C1,H1}$ 155.0 Hz, C-1). *Anal.* calcd. for $C_{17}H_{23}N_3O_4S$: C 55.87, H 6.34, N 11.50; found: C 56.13, H 6.76, N 11.41.

Ethyl 4-azido-3-O-benzyl-4,6-dideoxy-1-thio-α-D-mannopyranoside **4**

Compound **3** (2 g, 6.18 mmol) in methanol (50 mL) was treated with 0.1 M sodium methoxide solution (1 mL). After 8 h, tlc (hexane – ethyl acetate 3:1, v/v) showed complete deacetylation of **3**. Neutralization was achieved with Amberlite IR-120 (H^+) ion exchange resin. Removal of the solvent under reduced pressure gave pure **4**; yield 1.9 g (95%), syrup, $[\alpha]_D^{20}$ +268.90° (*c* 4.1, chloroform); ^1H nmr (500 MHz, $CDCl_3$) δ: 7.41–7.20 (m, 5H, Ph), 5.28 (d, 1H, $J_{1,2}$ 1.2 Hz, H-1), 4.67 (d, 1H, *J* 11.4 Hz, CH_AH_BPh), 4.63 (d, 1H, CH_AH_BPh), 3.89 (d, 1H, $J_{4,5}$ 9.8 Hz, $J_{5,6}$ 6.0 Hz, H-5), 3.66 (dd, 1H, $J_{2,3}$ 3.0 Hz, $J_{3,4}$ 9.8 Hz, H-3), 4.02 (ddd, 1H, $J_{2,OH-2}$ 1.5 Hz, H-2), 3.45 (dd, 1H, H-4), 2.77 (d, 1H, OH-2), 2.58 (dq, 1H, $^2J_{gem}$ 12.6 Hz, $^3J_{vic}$ 7.2 Hz, $SCH_AH_BCH_3$), 2.54 (dq, 1H, $SCH_AH_BCH_3$), 1.31 (d, 3H, H-6), 1.26 (dd, 3H, SCH_2CH_3). *Anal.* calcd. for $C_{15}H_{21}N_3O_3S$: C 55.71, H 6.54, N 12.99; found: C 56.02, H 6.39, N 12.01.

2-O-Acetyl-4-azido-3-O-benzyl-4,6-dideoxy-α-D-mannopyranosyl bromide **5**

Bromine (0.1 mL) was added to a solution of the thioglycoside **3** (1.1 g, 3.01 mmol) in dichloromethane (20 mL) at 0°C and the solution was stirred for 1.5 h while the temperature was allowed to rise to 20°C (tlc, hexane – ethyl acetate 3:1, v/v). The reaction mixture was concentrated and codistilled three times with toluene to give pure **5** as a syrup (1.1 g, 95%); ^1H nmr (200 MHz, $CDCl_3$) δ: 7.42–7.22 (m, 5H, Ph), 6.28 (d, 1H, $J_{1,2}$ 1.7 Hz, H-1), 5.49 (dd, 1H, $J_{2,3}$ 3.0 Hz, H-2), 4.69 (d, 1H, *J* 11.1 Hz, CH_AH_BPh), 4.56 (d, 1H, CH_AH_BPh), 4.21 (dd, 1H, $J_{3,4}$ 10.2 Hz, H-3), 3.74 (dq, 1H, $J_{4,5}$ 10.0 Hz, $J_{5,6}$ 6.4 Hz, H-5), 3.50 (dd, 1H, H-4), 2.13 (s, 3H, OAc), 1.37 (d, 3H, H-6).

[5]Also, J. Jeener, Ampère Int. Summer School, Basko Polje, Yugoslavia 1971, unpublished.

*8-Methoxycarbonyloctyl-2-*O*-acetyl-4-azido-3-*O*-benzyl-4,6-dideoxy-α-*D*-mannopyranose* ***6***

8-Methoxycarbonyloctanol (300 mg, 1.59 mmol) was stirred with powdered 4 Å molecular sieves (300 mg) and silver triflate (500 mg, 2.0 mmol) for 1 h at 20°C in dichloromethane (10 mL). The freshly prepared bromide **5** (769 mg, 2.00 mmol) dissolved in dichloromethane (10 mL) was slowly dropped into this solution at −70°C. Stirring was continued overnight and the temperature allowed to rise slowly to 20°C (tlc, hexane – ethyl acetate 3:1, v/v). The reaction mixture was filtered through Celite, and the filtrate washed with saturated sodium hydrogen carbonate solution and concentrated. After column chromatography (hexane – ethyl acetate 4:1, v/v), pure **6** was obtained as a syrup (469 mg, 65%), $[\alpha]_D^{20}$ +57.81° (*c* 1.12, chloroform); ^{1}H nmr data was in accordance with the assigned structure. *Anal.* calcd. for $C_{25}H_{37}N_3O_7$: C 61.08, H 7.50, N 8.55; found: C 60.91, H 7.78, N 8.03.

*Ethyl 2-*O*-(2-*O*-acetyl-4-azido-3-*O*-benzyl-4,6-dideoxy-α-*D*-mannopyranosyl)-4-azido-3-*O*-benzyl-4,6-dideoxy-1-thio-α-*D*-mannopyranoside* ***7***

The aglycon **4** (0.895 g, 2.77 mmol) was stirred with powdered 4 Å molecular sieves (0.9 g) and silver triflate (0.9 g, 3.6 mmol) in dichloromethane (10 mL) under a nitrogen atmosphere at Dry Ice temperature for 1 h. Then the bromide **5** (1.1 g, 2.86 mmol) dissolved in dichloromethane (20 mL) was slowly dropped into the cooled solution. After another 2 h of stirring at −70°C (tlc, hexane – ethyl acetate 3:1, v/v), the reaction mixture was filtered through Celite, washed with saturated sodium hydrogen carbonate solution, and concentrated to a syrup. Column chromatography gave pure **7** as a syrup (1.3 g, 75%), $[\alpha]_D^{20}$ +140.7° (*c* 1.3, chloroform); ^{1}H nmr (500 MHz, $CDCl_3$) δ: 7.44–7.27 (m, 10H, Ph), 5.39 (dd, 1H, $J_{1',2'}$ 1.8 Hz, $J_{2',3'}$ 3.2 Hz, H-2′), 5.15 (d, 1H, H-1′), 4.81 (d, 1H, $J_{1,2}$ 2.0 Hz, H-1), 4.72 (d, 1H, *J* 11.0 Hz, CH_AH_BPh), 4.69 (d, 1H, *J* 11.6 Hz, $CH_{A'}H_{B'}$Ph), 4.58 (d, 1H, *J* 11.6 Hz, $CH_{A'}H_{B'}$Ph), 4.53 (d, 1H, *J* 11.0 Hz, CH_AH_BPh), 3.89 (dd, 1H, $J_{2,3}$ 3.0 Hz, H-2), 3.81 (dq, 1H, $J_{4,5}$ 10.0 Hz, $J_{5,6}$ 6.2 Hz, H-5), 3.80 (dd, 1H, $J_{3',4'}$ 9.8 Hz, H-3′), 3.65 (dd, 1H, $J_{3,4}$ 9.9 Hz, H-3), 3.62 (dq, 1H, $J_{4',5'}$ 10.0 Hz, $J_{5,6'}$ 6.2 Hz, H-5′), 3.34 (dd, 1H, H-4), 2.56 (m, 2H, SCH_2CH_3), 2.09 (s, 3H, OAc), 1.30 (d, 3H, H-6′), 1.28 (d, 3H, H-6), 1.25 (dd, 3H, *J* 7.4 Hz, SCH_2CH_3); ^{13}C nmr (125 MHz, $CDCl_3$) δ: 128.56, 128.52, 128.47, 128.09 (12C, Ph), 99.59 (1C, $J_{C1',H1'}$ 173.1 Hz, C-1′), 83.28 (1C, $J_{C1,H1}$ 165.8 Hz, C-1), 78.10 (C-5′), 76.29 (C-2), 75.33 (C-5), 72.17 (CH_2Ph), 71.57 (CH_2Ph), 67.72 (C-3), 67.59 (C-3′), 67.27 (C-2′), 64.41 (C-4), 63.87 (C-4′), 25.59 (SCH_2CH_3), 20.95 (OAc), 18.49 (C-6, C-6′). *Anal.* calcd. for $C_{40}H_{38}N_6O_7S$: C 57.49, H 6.11, N 13.41, S 5.12; found: C 57.60, H 6.14, N 13.26, S 5.23.

Methyl O*-(2-*O*-acetyl-4-azido-3-*O*-benzyl-4,6-dideoxy-α-*D*-mannopyranosyl)-(1→2)-*O*-(4-azido-3-*O*-benzyl-4,6-dideoxy-α-*D*-mannopyranosyl)-(1→2)-4-azido-3-*O*-benzyl-4,6-dideoxy-α-*D*-mannopyranoside* ***8***

Disaccharide **7** (1.0 g, 1.59 mmol), the alcohol **1** (0.47 g, 1.59 mmol), and powdered 4 Å molecular sieves (2 g) were stirred in dichloromethane (50 mL) for 1 h at 20°C. Methyl triflate (1.0 mL, 8.84 mmol) was added slowly to the stirred solution. After 48 h, tlc (hexane – ethyl acetate 3:1, v/v) showed complete conversion of the starting materials to the trisaccharide **8**. Triethylamine (5 mL, 35.87 mmol) was added dropwise at 0°C to the stirred solution, which was allowed to warm to room temperature with stirring over a 30-min period. The reaction mixture was filtered and washed with half-saturated sodium chloride solution. After concentration to a syrup and chromatography on silica gel (hexane – ethyl acetate 4:1, v/v), pure **8** (1.1 g, 80%) was obtained as a syrup; all physical data are identical with the literature data for the compound prepared by a silver triflate promoted reaction (8).

Methyl O*-(4-azido-3-*O*-benzyl-4,6-dideoxy-α-*D*-mannopyranosyl)-(1→2)-*O*-(4-azido-3-*O*-benzyl-4,6-dideoxy-α-*D*-mannopyranosyl)-(1→2)-4-azido-3-*O*-benzyl-4,6-dideoxy-α-*D*-mannopyranoside* ***10***

Trisaccharide **8** (200 mg, 0.233 mmol) in methanol (5 mL) containing 0.1 M sodium methoxide solution (0.1 mL) was deacetylated after 5 h at 20°C (tlc, hexane – ethyl acetate 3:1, v/v). Neutralization with Amberlite IR-120 (H^+) ion exchange resin and removal of the solvents under reduced pressure gave pure **10** as a syrup (188 mg, 99%), $[\alpha]_D^{20}$ +108.24° (*c* 0.56, chloroform); ^{1}H nmr (500 MHz, $CDCl_3$) δ: 7.44–7.24 (m, 15H, Ph), 4.97 (d, 1H, $J_{1',2'}$ 2.0 Hz, H-1′), 4.96 (d, 1H, $J_{1'',2''}$ 1.8 Hz, H-1″), 4.73 (d, 1H, *J* 11.2 Hz, CH_AH_BPh), 4.69 (d, 1H, *J* 11.2 Hz, CH_AH_BPh), 4.68 (d, 1H, *J* 11.6 Hz, $CH_{A'}H_{B'}$Ph), 4.64 (d, 1H, *J* 11.6 Hz, $CH_{A'}H_{B'}$Ph), 4.62 (d, 1H, *J* 11.4 Hz, $CH_{A''}H_{B''}$Ph), 4.59 (d, 1H, *J* 11.4 Hz, $CH_{A''}H_{B''}$Ph), 4.56 (d, 1H, $J_{1,2}$ 1.9 Hz, H-1), 3.99 (ddd, 1H, $J_{2'',3''}$ 3.2 Hz, $J_{2'',OH}$ 1.8 Hz, H-2″), 3.94 (dd, 1H, $J_{2',3'}$ 3.2 Hz, H-2′), 3.85 (dd, 1H, $J_{2,3}$ 3.4 Hz, H-2), 3.73 (dd, 1H, $J_{3',4'}$ 10.0 Hz, H-3′), 3.70 (dd, 1H, $J_{3'',4''}$ 9.6 Hz, H-3″), 3.69 (dd, 1H, $J_{3,4}$ 10.0 Hz, H-3), 3.54 (dq, 1H, $J_{4',5'}$ 10.0 Hz, $J_{5',6'}$ 6.2 Hz, H-5′), 3.51 (dq, 1H, $J_{4'',5''}$ 10.0 Hz, $J_{5'',6''}$ 6.4 Hz, H-5″), 3.43 (dq, 1H, $J_{4,5}$ 10.0 Hz, $J_{5,6}$ 6.2 Hz, H-5), 3.41 (dd, 1H, H-4″), 3.32 (dd, 1H, H-4′), 3.31 (s, 3H, OMe), 3.24 (dd, 1H, H-4), 2.29 (d, 1H, OH-2″), 1.30 (d, 3H, H-6), 1.29 (d, 3H, H-6′), 1.19 (d, 3H, H-6″). *Anal.* calcd. for $C_{40}H_{49}O_{10}N_9$: C 58.89, H 6.05, N 15.45; found: C 59.06, H 6.19, N 15.35.

Methyl O*-(3-*O*-benzyl-4,6-dideoxy-4-formamido-α-*D*-mannopyranosyl)-(1→2)-*O*-(3-*O*-benzyl-4,6-dideoxy-4-formamido-α-*D*-mannopyranosyl)-(1→2)-3-*O*-benzyl-4,6-dideoxy-4-formamido-α-*D*-mannopyranoside* ***12***

Compound **10** (200 mg, 0.245 mmol) was dissolved in pyridine (10 mL) and water (5 mL) and the solution was saturated with H_2S for 0.5 h at 40°C. Stirring for 12 h at this temperature afforded the amino compound **11** (tlc, chloroform–methanol–water 5:4:1, v/v/v). Nitrogen was bubbled through the reaction mixture to remove H_2S. After filtering and concentration *in vacuo* the crude product **11** was taken up in methyl formate (5 mL). Thin-layer chromatography (chloroform–methanol 5:1, v/v) showed that conversion to the *N*-formylated compound **12** was complete within 8 h at room temperature. The reaction mixture was filtered, concentrated *in vacuo*, and purified on a silica gel column (chloroform–methanol 30:1, v/v) to give pure **12** (170 mg, 84%) as a syrup, $[\alpha]_D^{20}$ +40.16° (*c* 1.02, chloroform); ^{1}H nmr showed an approximate *Z*/*E* ratio of 2:1; ^{1}H nmr (500 MHz, acetone-d_6) δ: 8.29–8.21 (14s, 2H, NHC*H*O-*Z*), 8.04–8.00 (9s, 1H, NHC*H*O-*E*), 7.46–7.24 (m, 15H, Ph), 5.27–5.17 (8d, 1H, $J_{1',2'}$ 1.8–2.0 Hz, H-1′), 5.08–4.93 (8d, 1H, $J_{1'',2''}$ 1.80–2.0 Hz, H-1″), 4.77–4.40 (m, 7H, 6 CH_2Ph, H-1), 4.25–3.65 (m, 11H, H-2, H-2′, H-2″, H-3, H-3′, H-3″, H-4-*Z*, H-4′-*Z*, H-4″-*Z*), 3.50–3.20 (m, 1H, H-4-*E*, H-4′-*E*, H-4″-*E*), 3.33–3.31 (3s, 3H, OMe), 2.82 (bs, 1H, OH-2″), 1.30–0.98 (16d, 9H, $J_{5,6}$ $J_{5',6'}$ $J_{5'',6''}$ 6.2–6.4 Hz, H-6, H-6′, H-6″). *Anal.* calcd. for $C_{43}H_{55}N_3O_{13}$: C 62.84, H 6.74, N 5.11; found: C 62.56, H 6.63, N 4.93.

Methyl O*-(4,6-dideoxy-4-formamido-α-*D*-mannopyranosyl)-(1→2)-*O*-(4,6-dideoxy-4-formamido-α-*D*-mannopyranosyl)-(1→2)-4,6-dideoxy-4-formamido-α-*D*-mannopyranoside* ***13***

Trisaccharide **12** (20 mg, 0.024 mmol) was dissolved in glacial acetic acid (5 mL) and hydrogenated over 5% palladium on charcoal (50 mg) at 5 kPa and 20°C. Conversion to the product **13** was completed within 4–5 h (tlc, chloroform–methanol–water 5:1:1, v/v/v). The reaction mixture was filtered and concentrated and the crude product was purified on a Biogel P2 column to give pure **13** (12 mg, 83%) as a syrup, $[\alpha]_D^{20}$ +48.7° (*c* 0.2, water); ^{1}H nmr showed an approximate *Z*/*E* ratio of 3.5:1; ^{1}H nmr (500 MHz, D_2O) δ: 8.22–8.19 (2s, 3H, NHC*H*O-*Z*), 8.04 (s, 3H, NHC*H*O-*E*), 5.21–5.18 (2bs, 1H, H-1″), 5.06 (bs, 1H, H-1′), 4.81–4.78 (2bs, 1H, H-1), 4.19–4.09 (m, 2H, H-2″, H-2′), 4.09–3.75 (m, 10H, H-2, H-3, H-3′, H-3″, H-4-*Z*, H-4′-*Z*, H-4″-*Z*, H-5, H-5′, H-5″), 3.41 (bs, 3H, OMe), 1.35–1.17 (m, 9H, H-6, H-6′, H-6″); ^{13}C nmr (125 MHz, D_2O) δ: 167.99 (1C, NH*C*HO-*E*), 165.10 (1C, NH*C*HO-*Z*), 102.17 (1C, C-1″), 100.81 (1C, C-1′), 99.73 (1C, C-1). *Anal.* calcd. for $C_{22}H_{37}N_2O_{13}$: C 47.97, H 6.76, N 7.62; found: C 47.97, H 6.65, N 7.60.

8-Methoxycarbonyloctanyl O*-(4,6-dideoxy-4-formamido-α-*D*-mannopyranosyl)-(1→2)-*O*-(4,6-dideoxy-4-formamido-α-*D*-mannopyranosyl)-(1→2)-4,6-dideoxy-4-formamido-α-*D*-mannopyranoside* ***14***

Trisaccharide **9** was synthesized starting from **6** (40 mg, 81 μmol)

Can. J. Chem. Downloaded from www.nrcresearchpress.com by 41.223.56.140 on 09/07/12
For personal use only.

Can. J. Chem. Downloaded from www.nrcresearchpress.com by 41.223.56.140 on 09/07/12
For personal use only.

and **7** (61 mg, 82 μmol) in analogous fashion to the preparation of **8**. Deprotection followed the procedure used for the conversion of **8** to **13**. The deblocked trisaccharide **14** (31 mg, 55%) was obtained as a syrup, $[\alpha]_D^{20}$ +20.3° (*c* 1.08, water); ^{1}H nmr showed an approximate *Z/E* ratio of 3.5:1; ^{1}H nmr (500 MHz, D_2O) δ: 8.22–8.18 (2bs, 3H, NHC*H*O-*Z*), 8.02 (bs, 3H, NHC*H*O-*E*), 5.20–5.17 (3bs, 1H, H-1″), 5.04 (bs, 1H, H-1′), 4.90–4.87 (2bs, 1H, H-1); ^{13}C nmr (125 MHz, D_2O) δ: 177.66 (1C, *C*OOMe), 168.03 (1C, NH*C*HO-*E*), 165.12 (1C, NH*C*HO-Z), 102.18 (1C, C-1″), 100.96 (1C, C-1′), 98.47 (1C, C-1). *Anal.* calcd. for $C_{31}H_{53}N_3O_{15}$: C 52.61, H 7.55, N 5.94; found: C 52.91, H 7.45, N 5.99.

Methyl O-*(2-*O*-acetyl-4-azido-3-*O*-benzyl-4,6-dideoxy-α-*D*-mannopyranosyl)-(1→2)-*O*-(4-azido-3-*O*-benzyl-4,6-dideoxy-α-*D*-mannopyranosyl)-(1→2)-*O*-(4-azido-3-*O*-benzyl-4,6-dideoxy-α-*D*-mannopyranosyl)-(1→2)-4-azido-3-*O*-benzyl-4,6-dideoxy-α-*D*-mannopyranoside **15***

Trisaccharide alcohol **10** (150 mg, 0.184 mmol), powdered molecular sieves (150 mg), and silver triflate (100 mg, 0.4 mmol) were stirred at room temperature in dichloromethane (10 mL) for 0.5 h. Freshly prepared bromide **5** (106 mg, 0.276 mmol) dissolved in dichloromethane (10 mL) was added dropwise to the stirred solution at −70°C. The reaction mixture was allowed to warm to room temperature and was stirred for another 5 h (tlc, hexane – ethyl acetate 3:1, v/v). The reaction mixture was then filtered over a layer of Celite, and the filtrate was washed with saturated sodium hydrogen carbonate solution and concentrated to a syrup. Column chromatography (hexane – ethyl acetate 4:1, v/v) gave pure **15** as a syrup (165 mg, 80%), $[\alpha]_D^{20}$ +95.2° (*c* 3.63, chloroform); ^{1}H nmr (500 MHz, $CDCl_3$) δ: 7.44–7.25 (m, 20H, Ph), 5.45 (dd, 1H, $J_{1''',2'''}$ 1.7 Hz, $J_{2''',3'''}$ 3.2 Hz, H-2‴), 4.98 (d, 1H, $J_{1'',2''}$ 2.0 Hz, H-1″), 4.93 (d, 1H, $J_{1',1''}$ 2.0 Hz, H-1′), 4.88 (d, 1H, H-1‴), 4.78–4.56 (m, 8H, CH_2Ph), 4.56 (d, 1H, $J_{1,2}$ 1.5 Hz, H-1), 3.91 (dd, 1H, $J_{2,3}$ 3.1 Hz, H-2), 3.87 (dd, 1H, $J_{2',3'}$ 3.1 Hz, H-2′), 3.86 (dd, 1H, $J_{2'',3''}$ 3.0 Hz, H-2″), 3.82 (dd, 1H, $J_{3''',4'''}$ 9.8 Hz, H-3‴), 3.77 (dd, 1H, $J_{3,4}$ 9.8 Hz, H-3), 3.74 (dd, 1H, $J_{3'',4''}$ 9.8 Hz, H-3″), 3.72 (dd, 1H, $J_{3',4'}$ 9.8 Hz, H-3′), 3.59–3.40 (m, 4H, H-5‴, H-5′, H-5″, H-5), 3.41 (dd, 1H, $J_{4''',5'''}$ 10.0 Hz, H-4‴), 3.37 (dd, 1H, $J_{4'',5''}$ 10.0 Hz, H-4″), 3.32 (s, 3H, OMe), 3.28 (dd, 1H, $J_{4',5'}$ 10.0 Hz, H-4′), 3.24 (dd, 1H, $J_{4,5}$ 10.0 Hz, H-4), 2.13 (s, 3H, OAc), 1.32 (d, 3H, $J_{5,6}$ 6.3 Hz, H-6), 1.31 (d, 3H, $J_{5',6'}$ 6.2 Hz, H-6′), 1.25 (d, 3H, $J_{5''',6'''}$ 6.2 Hz, H-6‴), 1.20 (d, 3H, $J_{5'',6''}$ 6.3 Hz, H-6″); ^{13}C nmr (125 MHz, $CDCl_3$) δ: 100.31 (1C, $J_{C1''',H1'''}$ 173 Hz, C-1‴), 100.03 (1C, $J_{C1'',H1''}$ 172 Hz, C-1″), 99.70 (1C, $J_{C1',H1'}$ 170 Hz, C-1′), 99.05 (1C, $J_{C1,H1}$ 171 Hz, C-1). *Anal.* calcd. for $C_{55}H_{66}N_{12}O_{14}$: C 59.02, H 5.94, N 15.02; found: C 58.91, H 5.89, N 15.01.

Methyl O-*(4-azido-3-*O*-benzyl-4,6-dideoxy-α-*D*-mannopyranosyl)-(1→2)-*O*-(4-azido-3-*O*-benzyl-4,6-dideoxy-α-*D*-mannopyranosyl)-(1→2)-*O*-(4-azido-3-*O*-benzyl-4,6-dideoxy-α-*D*-mannopyranosyl)-(1→2)-4-azido-3-*O*-benzyl-4,6-dideoxy-α-*D*-mannopyranoside **16***

Tetrasaccharide **15** (150 mg, 0.134 mmol) was deacetylated in methanol (5 mL) containing 0.1 M sodium methoxide solution (0.1 mL). The reaction was complete after 5 h at 20°C (tlc, hexane – ethyl acetate 3:1, v/v). Neutralization with Amberlite IR-120 (H^+) ion exchange resin and removal of the solvents under reduced pressure gave pure **16** as a syrup (141 mg, 98%), $[\alpha]_D^{20}$ +111.7° (*c* 0.23, chloroform); ^{1}H nmr (500 MHz, $CDCl_3$) δ: 7.44–7.24 (m, 20H, Ph), 4.98 (d, 1H, $J_{1''',2'''}$ 1.8 Hz, H-1‴), 4.95 (d, 1H, $J_{1'',2''}$ 1.7 Hz, H-1″), 4.90 (d, 1H, $J_{1',2'}$ 1.8 Hz, H-1′), 4.76–4.56 (m, 8H, CH_2Ph), 4.53 (d, 1H, $J_{1,2}$ 1.8 Hz, H-1), 4.00 (ddd, 1H, $J_{2''',3'''}$ 3.2 Hz, $J_{2''',OH}$ 2.0 Hz, H-2‴), 3.94 (dd, 1H, $J_{2'',3''}$ 3.2 Hz, H-2″), 3.83 (dd, 1H, $J_{2',3'}$ 3.3 Hz, H-2′), 3.82 (dd, 1H, $J_{2,3}$ 3.2 Hz, H-2), 3.77 (dd, 1H, $J_{3''',4'''}$ 9.9 Hz, H-3‴), 3.70 (dd, 1H, $J_{3'',4''}$ 9.8 Hz, H-3″), 3.69 (dd, 1H, $J_{3',4'}$ 9.8 Hz, H-3′), 3.68 (dd, 1H, $J_{3,4}$ 9.8 Hz, H-3), 3.56–3.39 (m, 4H, H-5‴, H-5″, H-5′, H-5), 3.42 (dd, 1H, $J_{4''',5'''}$ 9.9 Hz, H-4‴), 3.30 (dd, 1H, $J_{4'',5''}$ 9.8 Hz, H-4″), 3.30 (s, 3H, OMe), 3.25 (dd, 1H, $J_{4',5'}$ 9.8 Hz, H-4′), 3.20 (dd, 1H, $J_{4,5}$ 9.8 Hz, H-4), 2.28 (d, 1H, OH-2‴), 1.29 (d, 3H, $J_{5,6}$ 6.3 Hz, H-6), 1.27 (d, 3H, $J_{5',6'}$ 6.2 Hz, H-6′), 1.20 (d, 3H, $J_{5''',6'''}$ 6.3 Hz, H-6‴), 1.17 (d, 3H, $J_{5'',6''}$ 6.3 Hz, H-6″). *Anal.* calcd. for $C_{53}H_{64}N_{12}O_{13}$: C 59.10, H 6.00, N 15.60; found: C 59.21, H 6.04, N 15.54.

Methyl O-*(3-*O*-benzyl-4,6-dideoxy-4-formamido-α-*D*-mannopyranosyl)-(1→2)-*O*-(3-*O*-benzyl-4,6-dideoxy-4-formamido-α-*D*-mannopyranosyl)-(1→2)-*O*-(3-*O*-benzyl-4,6-dideoxy-4-formamido-α-*D*-mannopyranosyl)-(1→2)-3-*O*-benzyl-4,6-dideoxy-4-formamido-α-*D*-mannopyranoside **17***

Tetrasaccharide **16** (100 mg, 0.093 mmol) was dissolved in pyridine (5 mL) and water (2.5 mL) and the solution was saturated with H_2S for 0.5 h at 40°C. Stirring for 12 h at this temperature afforded the amino derivative (tlc, chloroform–methanol–water 5:4:1, v/v/v). Nitrogen was passed through the reaction mixture to remove H_2S. The solution was filtered and the filtrate was concentrated *in vacuo* to a crude product, which was taken up in methyl formate (5 mL). Complete conversion into the *N*-formylated compound **17** was seen within 8 h at 20°C (tlc, chloroform–methanol 5:1). The concentrated crude syrup was purified on a silica gel column (chloroform–methanol 30:1, v/v) to give pure **17** (83 mg, 82%) as a syrup, $[\alpha]_D^{20}$ +36.1° (*c* 0.31, chloroform); ^{1}H nmr showed an approximate *Z/E* ratio of 2:1; ^{1}H nmr (500 MHz, $CDCl_3$) δ: 8.19 (bs, 4H, NHC*H*O-*Z*), 8.02 (bs, 4H, NHC*H*O-*E*), 7.42–7.12 (m, 20H, Ph), 5.20–4.80 (m, 3H, H-1‴, H-1″, H-1′), 4.76–4.37 (m, 9H, CH_2Ph, H-1), 4.21–3.92 (m, 4H, H-2‴, H-2″, H-2′, H-2), 3.87–3.44 (m, 8H, H-5‴, H-5″, H-5′, H-5, H-4‴-*Z*, H-4″-*Z*, H-4′-*Z*, H-4-*Z*), 3.36 (s, 3H, OMe), 3.35 (s, 3H, OMe), 3.40–3.30 (m, 4H, H-4‴-*E*, H-4″-*E*, H-4′-*E*, H-4-*E*), 1.38–1.10 (m, 12H, H-6‴, H-6″, H-6′, H-6). *Anal.* calcd. for $C_{57}H_{72}N_4O_{17}$: C 63.09, H 6.69, N 5.16; found: C 62.81, H 6.76, N 5.06.

Methyl O-*(4,6-dideoxy-4-formamido-α-*D*-mannopyranosyl)-(1→2)-*O*-(4,6-dideoxy-4-formamido-α-*D*-mannopyranosyl)-(1→2)-*O*-(4,6-dideoxy-4-formamido-α-*D*-mannopyranosyl)-(1→2)-4,6-dideoxy-4-formamido-α-*D*-mannopyranoside **18***

Tetrasaccharide **17** (20 mg, 0.018 mmol) was hydrogenated as described for preparation of trisaccharide **13**. Pure **18** (11 mg, 81%) was obtained as a syrup, $[\alpha]_D^{20}$ +47.3° (*c* 0.27, water); ^{1}H nmr revealed an approximate *Z/E* ratio of 3.5:1; ^{1}H nmr (500 MHz, D_2O) δ: 8.23–8.19 (4bs, 4H, NHC*H*O-*Z*), 8.06–8.02 (3bs, 4H, NHC*H*O-*E*), 5.21–5.14 (m, 2H, H-1″, H-1′), 5.05 (bs, 1H, H-1‴), 4.80, 4.78 (2bs, 1H, H-1), 4.18–4.03 (m, 4H, H-2‴, H-2″, H-2′, H-5‴), 4.01–3.74 (m, 12H, H-2, H-3‴, H-3″, H-3′, H-3, H-5″, H-5′, H-5, H-4‴-*Z*, H-4″-*Z*, H-4′-*Z*, H-4-*Z*), 3.46–3.34 (m, 4H, H-4‴-*E*, H-4″-*E*, H-4′-*E*, H-4-*E*), 3.40 (bs, 3H, OMe), 1.30–1.18 (m, 12H, H-6‴, H-6″, H-6′, H-6); ^{13}C nmr (125 MHz, D_2O) δ: 168.05 (1C, HN*C*HO-*E*), 165.12 (1C, HN*C*HO-*Z*), 102.14 (1C, C-1‴), 100.78 (2C, C-1″, C-1′), 99.76 (1C, C-1).

Methyl O-*(2-*O*-acetyl-4-azido-3-*O*-benzyl-4,6-dideoxy-α-*D*-mannopyranosyl)-(1→2)-*O*-(4-azido-3-*O*-benzyl-4,6-dideoxy-α-*D*-mannopyranosyl)-(1→2)-*O*-(4-azido-3-*O*-benzyl-4,6-dideoxy-α-*D*-mannopyranosyl)-(1→2)-*O*-(4-azido-3-*O*-benzyl-4,6-dideoxy-α-*D*-mannopyranosyl)-(1→2)-4-azido-3-*O*-benzyl-4,6-dideoxy-α-*D*-mannopyranoside **19***

Disaccharide **7** (180 mg, 0.286 mmol), the trisaccharide alcohol **10** (234 mg, 0.287 mmol), and powdered 4 Å molecular sieves (300 mg) were stirred in dichloromethane (5 mL) for 1 h at 20°C. Then methyl triflate (0.3 mL, 2.7 mmol) was added to the stirred solution and, after 48 h, tlc (hexane – ethyl acetate 3:1, v/v) indicated complete conversion of the starting materials to the product **19**. Triethylamine (1 mL, 7.17 mmol) was added dropwise to the cooled, stirred reaction mixture at 0°C. After warming to 20°C, stirring was continued for another 0.5 h. The reaction mixture was filtered and washed with a 50% saturated sodium chloride solution. After concentration to a syrup and chromatography on silical gel (hexane – ethyl acetate 4:7, v/v), pure **19** (315 mg, 80%) was obtained as a syrup; $[\alpha]_D^{20}$ +95.9° (*c* 1.75, chloroform); ^{1}H nmr (500 MHz, $CDCl_3$) δ: 7.45–7.24 (m, 25H, Ph), 5.43 (dd, 1H, $J_{1''',2'''}$ 1.8 Hz, $J_{2''',3'''}$ 3.2 Hz, H-2‴), 4.97 (d, 1H, $J_{1',2'}$ 1.9 Hz, H-1′), 4.89 (d, 1H, $J_{1'',2''}$ 1.9 Hz, H-1″), 4.88 (d, 1H, $J_{1''',2'''}$ 1.8 Hz, H-1‴), 4.87 (d, 1H, H-1‴), 4.76–4.55 (m, 10H, CH_2Ph), 4.54 (d, 1H, $J_{1,2}$ 1.7 Hz, H-1), 3.90 (dd, 1H, $J_{2',3'}$ 3.2 Hz, H-2′), 3.86 (dd, 1H, $J_{2''',3'''}$ 3.2 Hz, H-2‴), 3.82 (dd, 1H, $J_{2'',3''}$ 3.2 Hz, H-2″),

3.80 (dd, 1H, $J_{3''',4'''}$ 9.8 Hz, H-3'''), 3.73 (dd, 1H, $J_{3',4'}$ 9.9 Hz, H-3'), 3.69 (dd, 1H, $J_{3'',4''}$ 9.8 Hz, H-3''), 3.69 (dd, 1H, $J_{3,4}$ 9.8 Hz, H-3), 3.67 (dd, 1H, $J_{3''',4'''}$ 9.8 Hz, H-3'''), 3.57–3.39 (m, 5H, H-5''', H-5''', H-5', H-5'', H-5), 3.39 (dd, 1H, $J_{4''',5'''}$ 10.0 Hz, H-4'''), 3.36 (dd, 1H, $J_{4',5'}$ 9.8 Hz, H-4'), 3.31 (s, 3H, OMe), 3.23 (dd, 1H, $J_{4,5}$ 9.8 Hz, H-4), 3.22 (dd, 1H, $J_{4'',5''}$ 9.8 Hz, H-4''), 3.21 (dd, 1H, $J_{4''',5'''}$ 9.8 Hz, H-4'''), 1.30 (d, 3H, $J_{5,6}$ 6.2 Hz, H-6), 1.27 (d, 3H, $J_{5''',6'''}$ 6.2 Hz, H-6'''), 1.23 (d, 3H, $J_{5''',6'''}$ 6.3 Hz, H-6'''), 1.20 (d, 3H, $J_{5',6'}$ 6.3 Hz, H-6'), 1.17 (d, 3H, $J_{5'',6''}$ 6.2 Hz, H-6''); ^{13}C nmr (125 MHz, $CDCl_3$) δ: 100.30 (1C, $J_{C1''',H1'''}$ 172 Hz, C-1'''), 100.75 (1C, $J_{C1''',H1'''}$ 170 Hz, C-1'''), 100.03 (1C, $J_{C1'',H1''}$ 171 Hz, C-1''), 99.73 (1C, $J_{C1',H1'}$ 171 Hz, C-1'), 99.08 (1C, $J_{C1,H1}$ 172 Hz, C-1). *Anal.* calcd. for $C_{68}H_{81}N_{15}O_{17}$: C 59.16, H 5.91, N 15.22; found: C 58.60, H 5.96, N 15.29.

Methyl O-*(4-azido-3-*O*-benzyl-4,6-dideoxy-α-*D*-mannopyranosyl)-(1→2)-*O*-(4-azido-3-*O*-benzyl-4,6-dideoxy-α-*D*-mannopyranosyl)-(1→2)-*O*-(4-azido-3-*O*-benzyl-4,6-dideoxy-α-*D*-mannopyranosyl)-(1→2)-*O*-(4-azido-3-*O*-benzyl-4,6-dideoxy-α-*D*-mannopyranosyl)-(1→2)-4-azido-3-*O*-benzyl-4,6-dideoxy-α-*D*-mannopyranoside* ***20***

Pentasaccharide **19** (200 mg, 0.145 mmol) was dissolved in methanol (5 mL) and treated with 0.1 M sodium methoxide solution (0.1 mL). Deacetylation was completed within several hours (tlc, hexane – ethyl acetate 3:1, v/v). Neutralization with Amberlite IR-120 (H^+) ion exchange resin and removal of the solvents under reduced pressure gave pure **20** (178 mg, 92%), $[\alpha]_D^{20}$ +96.2° (*c* 0.56, chloroform); ^{1}H nmr (500 MHz, $CDCl_3$) δ: 7.44–7.24 (m, 25H, Ph), 4.98 (d, 1H, $J_{1''',2'''}$ 1.6 Hz, H-1'''), 4.97 (d, 1H, $J_{1',2'}$ 1.6 Hz, H-1'), 4.89 (d, 1H, $J_{1'',2''}$ 1.7 Hz, H-1''), 4.88 (d, 1H, $J_{1''',2'''}$ 1.6 Hz, H-1'''), 4.76–4.55 (m, 10H, CH_2Ph), 4.52 (d, 1H, $J_{1,2}$ 1.6 Hz, H-1), 4.00 (ddd, 1H, $J_{2''',3'''}$ 3.1 Hz, $J_{2''',OH}$ 1.6 Hz, H-2'''), 3.94 (dd, 1H, $J_{2',3'}$ 3.2 Hz, H-2'), 3.84 (dd, 1H, $J_{2'',3''}$ 3.1 Hz, H-2''), 3.81 (2dd, 2H, $J_{2,3}$ 3.2 Hz, $J_{2''',3'''}$ 3.2 Hz, H-2, H-2'''), 3.74–3.64 (m, 5H, H-3, H-3', H-3'', H-3''', H-3'''), 3.56–3.38 (m, 6H, H-5, H-5', H-5'', H-5''', H-5''', H-4'''), 3.32 (dd, 1H, $J_{4',5'}$ 9.8 Hz, H-4'), 3.30 (s, 3H, OMe), 3.23 (dd, 1H, $J_{4,5}$ 9.8 Hz, H-4), 3.21 (dd, 1H, $J_{4'',5''}$ 9.9 Hz, H-4''), 3.19 (dd, 1H, $J_{4''',5'''}$ 9.8 Hz, H-4'''), 2.30 (d, 1H, OH-2'''), 1.29 (d, 3H, $J_{5,6}$ 6.3 Hz, H-6), 1.26 (d, 3H, $J_{5''',6'''}$ 6.2 Hz, H-6'''), 1.22 (d, 3H, $J_{5''',6'''}$ 6.3 Hz, H-6'''), 1.19 (d, 3H, $J_{5',6'}$ 6.3 Hz, H-6'), 1.15 (d, 3H, $J_{5'',6''}$ 6.2 Hz, H-6''). *Anal.* calcd. for $C_{66}H_{79}N_{15}O_{16}$: C 59.23, H 5.95, N 15.70; found: C 59.50, H 6.10, N 15.39.

Methyl O-*(3-*O*-benzyl-4,6-dideoxy-4-formamido-α-*D*-mannopyranosyl)-(1→2)-*O*-(3-*O*-benzyl-4,6-dideoxy-4-formamido-α-*D*-mannopyranosyl)-(1→2)-*O*-(3-*O*-benzyl-4,6-dideoxy-4-formamido-α-*D*-mannopyranosyl)-(1→2)-*O*-(3-*O*-benzyl-4,6-dideoxy-4-formamido-α-*D*-mannopyranosyl)-(1→2)-3-*O*-benzyl-4,6-dideoxy-4-formamido-α-*D*-mannopyranoside* ***21***

Pentasaccharide **20** (100 mg, 0.075 mmol) was converted to the formamido derivative **21** by a reaction sequence similar to that described for preparation of compound **16**. The formamido compound **21** (84 mg, 83%) was obtained as a syrup, $[\alpha]_D^{20}$ +37.0° (*c* 0.78, chloroform); the estimated (^{1}H nmr) *Z*/*E* ratio was 3:1; ^{1}H nmr (500 MHz, acetone-d_6) δ: 8.20–8.09 (m, 5H, NHC*H*O-*Z*), 7.95–7.87 (m, 5H, NHC*H*O-*E*), 7.45–7.25 (m, 25H, Ph), 5.14–4.86 (m, 4H, H-1''', H-1''', H-1'', H-1'), 4.68–4.42 (m, 11H, C*H*$_2$Ph, H-1), 4.24–3.62 (m, 23H, H-3''', H-3''', H-3'', H-3', H-3, H-4''', H-4''', H-4'', H-4', H-4, H-5''', H-5''', H-5'', H-5', H-5, OMe), 1.29–1.18 (m, 15H, H-6''', H-6''', H-6'', H-6', H-6). *Anal.* calcd. for $C_{71}H_{89}N_5O_{21}$: C 63.24, H 6.65, N 5.19; found: C 62.91, H 6.60, N 5.21.

Methyl O-*(4,6-dideoxy-4-formamido-α-*D*-mannopyranosyl)-(1→2)-*O*-(4,6-dideoxy-4-formamido-α-*D*-mannopyranosyl)-(1→2)-*O*-(4,6-dideoxy-4-formamido-α-*D*-mannopyranosyl)-(1→2)-*O*-(4,6-dideoxy-4-formamido-α-*D*-mannopyranosyl)-(1→2)-4,6-dideoxy-4-formamido-α-*D*-mannopyranoside* ***22***

Pentasaccharide **21** (30 mg, 0.022 mmol) was treated as described before for the synthesis of trisaccharide **13** and tetrasaccharide **18**. Pure **22** (17 mg, 85%) was obtained as a syrup, $[\alpha]_D^{20}$ +40.5° (*c* 0.11, water); ^{1}H nmr (500 Hz, D_2O) δ: 8.21 (bs, 5H, NHC*H*O-*Z*), 8.03 (bs, 5H, NHC*H*O-*E*), 5.23–5.11 (2bs, 3H, H-1''', H-1'', H-1'), 5.05 (bs, 1H, H-1'''), 4.80 (bs, 1H, H-1), 4.20–4.02 (m, 5H, H-2''', H-2''', H-2'', H-2', H-5'''), 4.01–3.70 (m, 15H, H-2, H-3''', H-3''', H-3'', H-3', H-3, H-5''', H-5'', H-5', H-5, H-4'''-*Z*, H-4'''-*Z*, H-4''-*Z*, H-4'-*Z*, H-4-*Z*), 3.46–3.34 (m, 5H, H-4'''-*E*, H-4'''-*E*, H-4''-*E*, H-4'-*E*, H-4-*E*), 3.40 (bs, 3H, OMe), 1.35–1.15 (m, 15H, H-6''', H-6''', H-6'', H-6', H-6); ^{13}C nmr (125 MHz, D_2O) δ: 168.01 (1C, NH*C*HO-*Z*), 165.11 (1C, NH*C*HO-*E*), 102.13 (1C, C-1'''), 100.74 (3C, C-1''', C-1'', C-1'), 99.73 (1C, C-1). *Anal.* calcd. for $C_{36}H_{59}N_5O_{21}$: C 48.16, H 6.62, N 7.80; found: C 48.22, H 6.59, N 7.79.

1. M. Caroff, D. R. Bundle, M. B. Perry, J. W. Cherwonogrodzky, and J. R. Duncan. Infect. Immun. **46**, 384 (1984).
2. D. R. Bundle, J. W. Cherwonogrodzky, and M. B. Perry. Biochemistry, **26**, 8717 (1987).
3. G. Wilson. *In* Principles of bacteriology, virology and immunity. Vol. 2. 7th ed. *Edited by* G. Wilson, A. Miles, and M. T. Parker. Edward Arnold, London. 1983. pp. 406–421.
4. G. S. Wilson and A. A. Miles. Br. J. Exp. Pathol. **13**, 1 (1932).
5. G. G. Alton, L. M. Jones, and D. E. Pietz. W.H.O. Monogr. Ser. No. 55 (1975).
6. D. R. Bundle, M. A. J. Gidney, M. B. Perry, J. R. Duncan, and J. W. Cherwonogrodzky. Infect. Immun. **46**, 389 (1984).
7. M. Gerken and D. R. Bundle. Tetrahedron Lett. **28**, 5067 (1987).
8. D. R. Bundle, M. Gerken, and T. Peters. Carbohydr. Res. **174**, 239 (1988).
9. T. Peters and D. R. Bundle. J. Chem. Soc. Chem. Commun. 1648 (1987).
10. R. J. Ferrier and R. H. Furneaux. Carbohydr. Res. **52**, 63 (1976).
11. F. Weygand, H. Ziemann, and H. J. Bestmann. Chem. Ber. **91**, 2534 (1958).
12. R. U. Lemieux, D. R. Bundle, and D. A. Baker. J. Am. Chem. Soc. **97**, 4076 (1975).
13. H. Lönn. Carbohydr. Res. **135**, 105 (1985).
14. H. Lönn. Carbohydr. Res. **139**, 115 (1989).
15. K. Bock and C. Pedersen. Acta. Chem. Scand. Ser. B, **29**, 258 (1975).
16. T. Adachi, Y. Yamada, I. Inoune, and M. Saneyoshi. Synthesis, 45 (1977).
17. B. C. McKusick and M. E. Hermes. Org. Synth. **41**, 14 (1961).
18. G. Moffat, M. V. Newton, and G. J. Papenmeir. J. Org. Chem. **27**, 4058 (1962).
19. O. P. Srivastava and O. Hindsgaul. Can. J. Chem. **64**, 2324 (1986).
20. D. D. Perrin, W. L. Armarego, and D. R. Perrin. Purification of laboratory compounds. Pergamon, London. 1966.
21. W. P. Aue, E. Bartholdi, and R. R. Ernst. J. Chem. Phys. **64**, 2229 (1976).
22. A. Bax, R. Freeman, and G. Morris. J. Magn. Reson. **42**, 164 (1981).
23. A. A. Maudsley and R. R. Ernst. Chem. Phys. Lett. **50**, 368 (1977).
24. A. Bax and G. Morris. J. Magn. Reson. **42**, 501 (1981).

Can. J. Chem. Downloaded from www.nrcresearchpress.com by 41.223.56.140 on 09/07/12
For personal use only.

Block synthesis of two pentasaccharide determinants of the *Brucella* M antigen using thioglycoside methodologies[1]

THOMAS PETERS[2] AND DAVID R. BUNDLE
Division of Biological Sciences, National Research Council of Canada, Ottawa, Ont., Canada K1A 0R6

Received August 4, 1988

THOMAS PETERS and DAVID R. BUNDLE. Can. J. Chem. **67**, 497 (1989).

Two frame shifted pentasaccharides containing 4,6-dideoxy-4-formamido-D-mannose (4-deoxy-4-formamido-D-rhamnose) have been synthesized by application of a strategy utilizing *S*-ethyl disaccharide glycoside building blocks **16** and **25**. The target molecules contain a single α1,3 linkage as either the first or last inter-residue linkage in an otherwise α1,2-linked homo-pentameric structure:

α-D-Rha4NFo(1→3)-α-D-Rha4NFo(1→2)-α-D-Rha4NFo(1→2)-α-D-Rha4NFo(1→2)-α-D-Rha4NFo-1→OCH_3

and

α-D-Rha4NFo(1→2)-α-D-Rha4NFo(1→2)-α-D-Rha4NFo(1→2)-α-D-Rha4NFo(1→3)-α-D-Rha4NFo-1→OCH_3

These structures represent possible biological repeating units of the *Brucella* M antigen and their synthesis is designed to facilitate the identification of the structural element that is polymerized to provide the intact polysaccharide antigen. The α1,2-linked tetrasaccharide component of each pentasaccharide was constructed by methyl triflate promoted activation of the α1,2-linked *S*-ethyl disaccharide glycoside **16**. Glycosylation of methyl 4-azido-2-*O*-benzyl-4,6-dideoxy-α-D-mannopyranoside **3** by **16**, followed by a second block extension, gave the pentasaccharide **22** with an α1,3 linkage at the reducing terminus. In analogous fashion the α1,3-linked *S*-ethyl derivative **25** was used in conjunction with methyl triflate to glycosylate the α1,2-linked trisaccharide **26**, and provided the pentasaccharide **27** that possesses a 1,3 linkage at its non-reducing end. The synthesis of an α1,3-linked disaccharide and a trisaccharide are also reported.

Key words: Brucella M antigen, synthesis of frame shifted pentasaccharides, thioglycoside building units, 4,6-dideoxy-4-formamido-D-mannose, biological repeating unit.

THOMAS PETERS et DAVID R. BUNDLE. Can. J. Chem. **67**, 497 (1989).

Faisant appel à une stratégie utilisant les disaccharides glycosides de *S*-éthyle **16** et **25** comme éléments d'édification, on a synthétisé deux pentasaccharides contenant du didésoxy-4,6 formamido-4 D-mannose (désoxy-4 formamido-4 D-rhamnose). Les molécules cibles contiennent une seule liaison α1,3 soit sur la première soit sur la dernière liaison inter-résidu d'une structure homo-pentamère autrement liée en α1,2 :

α-D-Rha4NFo(1→3)-α-D-Rha4NFo(1→2)-α-D-Rha4NFo(1→2)-α-D-Rha4NFo(1→2)-α-D-Rha4NFo-1→OCH_3

et

α-D-Rha4NFo(1→2)-α-D-Rha4NFo(1→2)-α-D-Rha4NFo(1→2)-α-D-Rha4NFo(1→3)-α-D-Rha4NFo-1→OCH_3

Ces structures représentent des unités biologiques qui pourraient se répéter dans l'antigène *Brucella* M et leur synthèse a été réalisée afin de faciliter l'identification de l'élément de structure qui est polymérisé pour fournir l'antigène polysaccharide intact. Afin de synthétiser les tétrasaccharides liés en α1,2 qui composent chacun des pentasaccharides, on a fait appel à une activation par le triflate de méthyle du disaccharide de glycoside de *S*-éthyle lié en α1,2 **16**. La glycosylation de l'azido-4 *O*-benzyl-2 didésoxy-4,6 α-D-mannopyranoside de méthyle (**3**) par le composé **16**, suivie par une deuxième extension, conduit au pentasaccharide **22** comportant une liaison α1,3 dans le terminus réducteur. D'une façon analogue, on a utilisé le dérivé *S*-éthyle lié en α1,3 (**25**) de concert avec le triflate pour effectuer la glycosylation du trisaccharide **26** lié en α1,2 et pour obtenir le pentasaccharide **27** qui possède une liaison 1,3 dans le terminus non-réducteur. On rapporte aussi la synthèse d'un disaccharide et d'un trisaccharide liés en α1,3.

Mots clés : antigène *Brucella* M, synthèse des pentasaccharides à structure décalée, éléments d'édification des thioglycosides, didésoxy-4,6 formamido-4 D-mannose, unité biologique répétitive.

[Traduit par la revue]

Introduction

The *Brucella* M antigen differs from the *Brucella* A antigen by the presence of several α1,3 linkages in an otherwise α1,2-linked homopolymer of 4,6-dideoxy-4-formamido-D-mannose (Rha4NFo) (1, 2). Evidence of detailed structural and immunochemical studies (3, 4) suggests that the biosynthetic assembly of these *O*-polysaccharides may occur by mechanisms that differ from those used by other Gram negative organisms such as the *Salmonella* (5). To assist immunochemical attempts to locate the position of the 1,3 linkages in the M polysaccharide antigen extracted from *Brucella* it was desirable to synthesize pentasaccharides in which the position of the 1,3 linkage was varied.

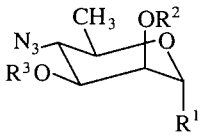
In this paper we report the synthesis of two pentasaccharides in which the 1,3 linkage is positioned at either the reducing or non-reducing end of the oligomer. In addition, the synthesis of a 1,3-linked disaccharide, α-D-Rha4NFo(1→3)-α-D-Rha4NFo, and a trisaccharide, α-D-Rha4NFo(1→2)-α-D-Rha4NFo(1→3)-α-D-Rha4NFo, are reported. The central chemistry of this approach involves the use of *S*-ethyl mono- and disaccharide glycosides, which also formed the basis of related work on synthetic analogues of the A antigen described in the preceding communication (6).

[1]NRCC No. 29854.
[2]NRCC Research Associate 1986–1987.

Can. J. Chem. Downloaded from www.nrcresearchpress.com by 122.72.124.2 on 09/07/12
For personal use only.

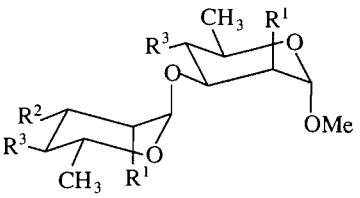
Results and discussion

To prepare an α1,3-linked disaccharide of 4-azido-4,6-dideoxy-D-mannopyranose, selective protection of glycoside **1** had to be accomplished. Two literature-based solutions to this problem were employed. Regioselective opening of a 2,3-ortho-acetate by aqueous acetic acid gave **2** (7, 8). Alternatively a phase transfer mediated benzylation of **1** gave **3**, as well as the minor 2,3-di-*O*-benzyl ether **4** (9).



1 R^1 = OMe, $R^2 = R^3$ = H
2 R^1 = OMe, R^2 = Ac, R^3 = H
3 R^1 = OMe, R^2 = Bzl, R^3 = H
4 R^1 = OMe, $R^2 = R^3$ = Bzl
5 R^1 = OMe, $R^2 = R^3$ = Ac
6 R^1 = OAc, $R^2 = R^3$ = Ac
7 R^1 = SEt, $R^2 = R^3$ = Ac
8 R^1 = SEt, $R^2 = R^3$ = H
9 R^1 = SEt, R^2 = Ac, R^3 = H
10 R^1 = Br, R^2 = Ac, R^3 = Bzl

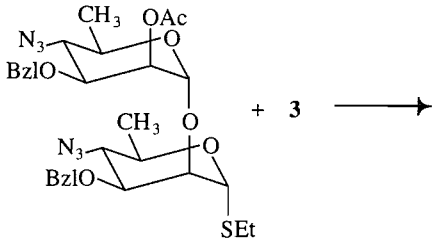
Conversion of **1** to the corresponding *S*-ethyl glycoside **7** provided the glycosyl donor for synthesis of α1,3-linked disaccharide building blocks. This was accomplished by acetylation of **1** to the diacetate **5** followed by acetolysis to the triacetate **6**, which was obtained from **1** in 95% yield. Lewis acid catalyzed generation of the acetoxonium ion and *in situ* reaction with ethanethiol (10) gave the thioglycoside **7**, from which an additional glycosyl acceptor **9** may be generated via **8**. The glycosyl acceptor **9** permits the synthesis of disaccharide glycosides that are themselves suitable for use as a disaccharide building unit. For such purposes the glycosyl bromide **10** described in the preceding paper (6) is an essential partner, whilst **7** may also act as a glycosyl donor for partners devoid of thioglycoside functionality. Thus activation of **7** by methyl triflate (11, 12) and reaction of the intermediate sulphonium ion with the monosaccharide alcohol **2** gave the crystalline α1,3-linked disaccharide glycoside **11** in 80% yield.



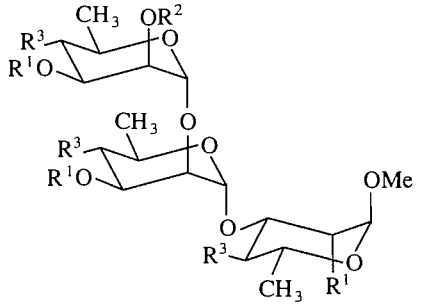
11 $R^1 = R^2$ = OAc, $R^3 = N_3$
12 $R^1 = R^2$ = OH, $R^3 = N_3$
13 $R^1 = R^2$ = OH, $R^3 = NH_2$
14 $R^1 = R^2$ = OH, R^3 = NHAc
15 $R^1 = R^2$ = OH, R^3 = NHCHO

When the disaccharide thioglycoside **16**, described in the previous paper (6), was used in a similar reaction with the related monosaccharide alcohol **3** an 84% yield of a trisaccharide **17** was obtained. This was in turn selectively transformed to a trisaccharide alcohol **18**, which was further glycosylated by disaccharide **16** to give a pentasaccharide **22**.

The disaccharide **11**, trisaccharide **17**, and pentasaccharide **22** were each subjected to a similar deprotection scheme that first saw the removal of *O*-acetates by transesterification to



16



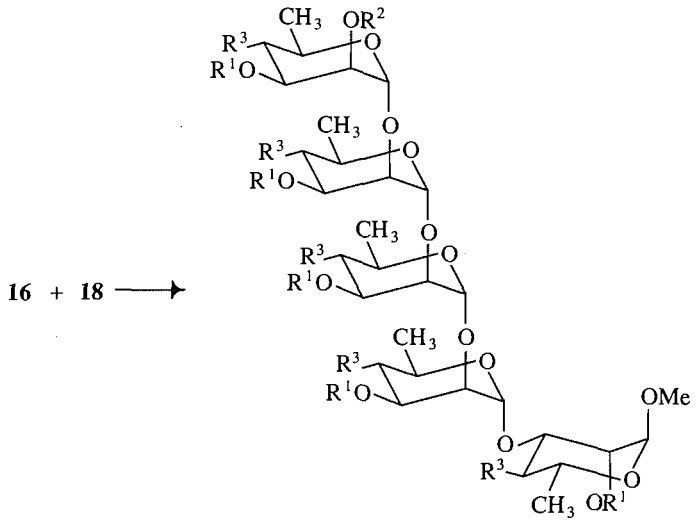
17 R^1 = Bzl, R^2 = Ac, $R^3 = N_3$
18 R^1 = Bzl, R^2 = H, $R^3 = N_3$
19 R^1 = Bzl, R^2 = H, $R^3 = NH_2$
20 R^1 = Bzl, R^2 = H, R^3 = NHCHO
21 $R^1 = R^2$ = H, R^3 = NHCHO

compounds **12**, **18**, and **23**. Reduction by H_2S provided the amino derivatives, which were not isolated but *N*-formylated by methyl formate (13), followed by catalytic hydrogenolysis to give respectively disaccharide **15**, trisaccharide **21**, and pentasaccharide **24**.

The second pentasaccharide was constructed from a trisaccharide alcohol **26**, the preparation of which was described in the preceding paper (6), and disaccharide **25**. The latter was synthesized from the glycosyl bromide **10** and the *S*-ethyl glycoside **9** in 83% yield. The disaccharide thioglycoside **25**, activated by methyl triflate in the presence of **26**, then gave the target pentasaccharide **27** in 64% yield. Compared to the disaccharide thioglycoside **16**, the disaccharide building block **25** is a much less reactive glycosyl donor, resulting in considerably longer reaction times and lower overall yields. Removal of blocking groups and conversion of the azido to formamido functionality to give deprotected pentasaccharide **28** (64% yield) used the strategy outlined for the other di-, tri-, and pentasaccharides **15**, **21**, and **24**.

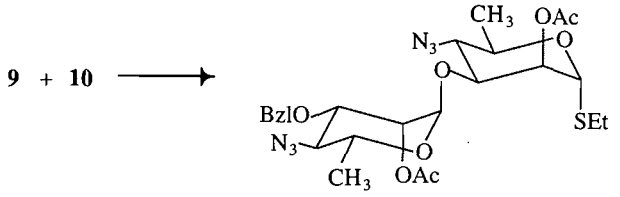
The one-bond heteronuclear coupling constants (14) measured for each anomeric carbon atom confirmed the anticipated stereochemistry of the anomeric linkages.

Can. J. Chem. Downloaded from www.nrcresearchpress.com by 122.72.124.2 on 09/07/12
For personal use only.



22 R^1 = Bzl, R^2 = Ac, R^3 = N_3
23 R^1 = Bzl, R^2 = H, R^3 = N_3
24 R^1 = R^2 = H, R^3 = NHCHO

The series of di-, tri-, and pentasaccharides **15**, **21**, **24**, and **28** have been used in immunochemical mapping of the combining sites of *Brucella* A and M specific monoclonal antibodies.



25

Experimental

The general experimental methods employed throughout this work are described in the preceding paper (6).

Methyl 4-azido-2-O-benzyl-4,6-dideoxy-α-D-mannopyranoside **3**

Benzyl bromide (0.63 mL, 5.00 mmol) and tetrabutylammonium bromide (50 mg) were added to a solution of the dialcohol **1** (1 g, 4.91 mmol) (6) in dichloromethane (20 mL) and this solution was stirred vigorously at room temperature for 30 h with aqueous NaOH solution (20% w/v). Two products (tlc, hexane – ethyl acetate 3:1, v/v) were obtained and these were purified by column chromatography (hexane – ethyl acetate 3:1, v/v) to give pure **3** (810 mg, 56%) and the minor product **4** (300 mg, 16%).

3; $[\alpha]_D^{20}$+8.54° (*c* 5.2, chloroform); ^{1}H nmr (500 MHz, $CDCl_3$) δ: 7.43–7.29 (m, 5H, Ph), 4.73 (d, 1H, $J_{1,2}$ 1.4 Hz, H-1), 4.73 (d, 1H, ^2J 11.9 Hz, CH_AH$_B$Ph), 4.58 (d, 1H, CH$_A$$H_B$Ph), 3.85 (bd, 1H, H-3), 3.69 (dd, 1H, $J_{2,3}$ 3.7 Hz, H-2), 3.51 (dq, 1H, $J_{4,5}$ 10.0 Hz, $J_{5,6}$ 6.0 Hz, H-5), 3.33 (s, 3H, OMe), 3.28 (dd, 1H, $J_{3,4}$ 10.0 Hz, H-4), 2.65 (bs, 1H, OH-3), 1.34 (d, 3H, H-6). *Anal.* calcd. for $C_{14}H_{19}N_3O_4$: C 57.33, H 6.53, N 14.33; found: C 57.09, H 6.37, N 14.08.

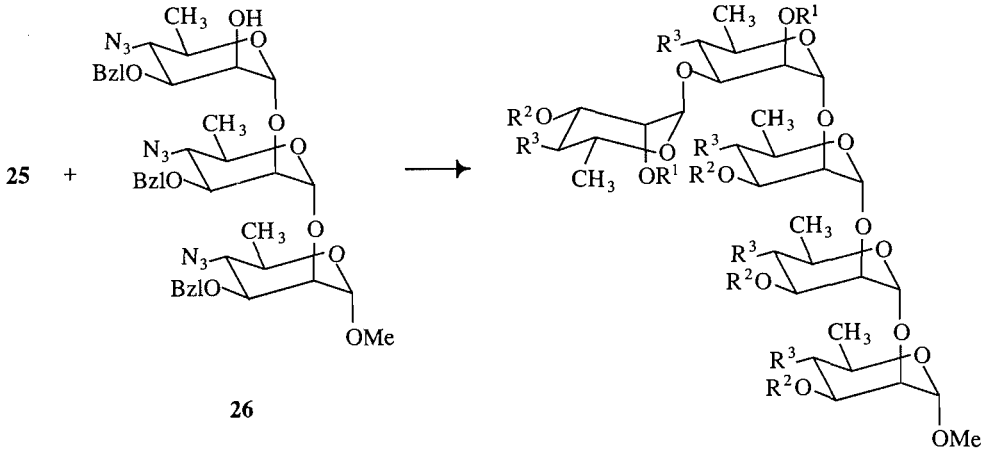
4; $[\alpha]_D^{20}$+ 65.9° (*c* 2.51, chloroform); ^{1}H nmr (500 MHz, $CDCl_3$) δ: 7.46–7.25 (m, 10H, 2Ph), 4.73 (d, 1H, ^2J 12.4 Hz, CH_AH$_B$Ph), 4.70 (d, 1H, $J_{1,2}$ 1.6 Hz, H-1), 4.70 (d, 1H, CH$_A$$H_B$Ph), 4.63 (d, 1H, ^2J 12.0 Hz, C$H_{A'}$H$_{B'}$Ph), 4.60 (d, 1H, CH$_{A'}$$H_{B'}$Ph), 3.77 (dd, 1H, $J_{2,3}$ 3.2 Hz, H-2), 3.75 (dd, 1H, $J_{3,4}$ 9.9 Hz, H-3), 3.63 (dd, 1H, $J_{4,5}$ 10.0 Hz, H-4), 3.50 (dq, 1H, $J_{5,6}$ 6.0 Hz, H-5), 3.32 (s, 3H, OMe), 1.37 (d, 3H, H-6). *Anal.* calcd. for $C_{21}H_{25}N_3O_4$: C 65.78, H 6.57, N 10.96; found: C 65.65, H 6.52, N 10.94.

Methyl 4-azido-2,3-di-O-acetyl-4,6-dideoxy-α-D-mannopyranoside **5**

The dialcohol **1** (5 g, 24.55 mmol) (6) was acetylated by standard procedures (acetic anhydride/pyridine) and crude **5** was subjected to column chromatography (hexane – ethyl acetate 3:1, v/v) to give pure crystalline **5** (6.7 g, 95%), mp 81–82°C; $[\alpha]_D^{20}$+111.68° (*c* 0.97, chloroform); ^{1}H nmr (200 MHz, $CDCl_3$) δ: 5.25–5.16 (m, 2H, H-2, H-3), 4.61 (d, 1H, $J_{1,2}$ 1.8 Hz, H-1), 3.66 (dq, 1H, $J_{4,5}$ 10.0 Hz, $J_{5,6}$ 6.0 Hz, H-5), 3.47 (dd, 1H, $J_{3,4}$ 10.0 Hz, H-4), 3.38 (s, 3H, OMe), 2.16 (s, 3H, OAc), 2.06 (s, 3H, OAc), 1.38 (d, 3H, H-6). *Anal.* calcd. for $C_{11}H_{17}N_3O_6$: C 45.99, H 5.96, N 14.63; found: C 46.11, H 6.09, N 14.78.

4-Azido-4,6-dideoxy-1,2,3-tri-O-acetyl-α-D-mannopyranose **6**

A solution of **5** (1 g, 3.48 mmol) in acetic anhydride – acetic acid – sulfuric acid (50:20:0.5, 20 mL) was stirred at 20°C for 4 h, then poured into ice-cold aqueous potassium carbonate. The product was extracted with dichloromethane, the extract was dried (Na_2SO_4), concentrated, and toluene was distilled from the residue to give **6** (1.1 g, ~100%), mp 69–70°C; $[\alpha]_D^{20}$+128.4° (*c* 1.1, chloroform); ^{1}H nmr (200 MHz, $CDCl_3$) δ: 6.01 (d, 1H, $J_{1,2}$ 1.8 Hz, H-1), 5.26–5.18 (m, 2H, H-2, H-3), 3.70 (dq, 1H, $J_{4,5}$ 10.0 Hz, $J_{5,6}$ 6.0 Hz, H-5), 3.55 (dd, 1H, $J_{3,4}$ 10.0 Hz, H-4), 2.08 (s, 3H, OAc), 1.38 (d, 3H, H-6). *Anal.* calcd. for $C_{12}H_{17}N_3O_7$: C 45.71, H 5.43, N 13.33; found: C 45.46, H 5.47, N 13.40.



26

27 R^1 = Ac, R^2 = Bzl, R^3 = N_3
28 R^1 = R^2 = H, R^3 = NHCHO

Can. J. Chem. Downloaded from www.nrcresearchpress.com by 122.72.124.2 on 09/07/12
For personal use only.

Can. J. Chem. Downloaded from www.nrcresearchpress.com by 122.72.124.2 on 09/07/12
For personal use only.

Ethyl 4-azido-2,3-di-O-acetyl-4,6-dideoxy-1-thio-α-D-mannopyranoside **7**

Compound **6** (5 g, 15.86 mmol) was stirred with powdered 4 Å molecular sieves (0.5 g), dichloromethane (100 mL), ethanethiol (3 mL, 40.51 mmol), and boron trifluoride etherate (2.5 mL, 20.32 mmol) for 2 h at 20°C (tlc, hexane – ethyl acetate 3:1, v/v). Dropwise addition of triethylamine (3.0 mL, 21.52 mmol), filtration, and removal of the solvents *in vacuo* afforded the crude reaction product, which was purified by column chromatography (hexane – ethyl acetate 3:1, v/v) to give **7** as a syrup (4.5 g, 90%); $[\alpha]_D^{20}$+194.73° (*c* 1.3, chloroform): ^{1}H nmr (200 MHz, $CDCl_3$) δ: 5.31 (dd, 1H, $J_{1,2}$ 1.6 Hz, $J_{2,3}$ 3.4 Hz, H-2), 5.19 (d, 1H, H-1), 5.14 (dd, 1H, $J_{3,4}$ 10.0 Hz, H-3), 4.03 (dq, 1H, $J_{4,5}$ 9.8 Hz, $J_{5,6}$ 6.0 Hz, H-5), 3.53 (dd, 1H, H-4), 2.65 (dd, 1H, ^2J 3.4 Hz, ^3J 7.4 Hz, $SCH_AH_B CH_3$), 2.58 (dd, 1H, $SCH_AH_B CH_3$), 2.15 (s, 3H, OAc), 2.06 (s, 3H, OAc), 1.37 (d, 3H, H-6), 1.28 (dd, 3H, SCH_2CH_3); ^{13}C nmr (50 MHz, $CDCl_3$) δ: 81.73 (C1, J_{C_1,H_1} 168.0 Hz). *Anal.* calcd. for $C_{12}H_{19}N_3SO_5$: C 45.42, H 6.03, N 13.24, S 10.10; found: C 45.24, H 5.94, N 13.11, S 10.28.

Ethyl 4-azido-4,6-dideoxy-1-thio-α-D-mannopyranoside **8**

The di-*O*-acetylated compound **7** (3.2 g, 10.08 mmol) was subjected to a standard deacetylation with sodium methoxide as described before (6) to give pure **8** as a syrup (2.3 g, 99%), $[\alpha]_D^{20}$+281.7° (*c* 0.33, chloroform); ^{1}H nmr (500 MHz $CDCl_3$) δ: 5.28 (d, 1H, $J_{1,2}$ 1.2 Hz, H-1), 4.03 (dd, 1H, $J_{2,3}$ 3.5 Hz, H-2), 4.00 (dq, 1H, $J_{4,5}$ 10.0 Hz, $J_{5,6}$ 6.2 Hz, H-5), 3.82 (m, 1H, H-3), 3.33 (dd, 1H, $J_{3,4}$ 10.0 Hz, H-4), 2.65 (dq, 1H, ^2J 13.0 Hz, ^3J 7.2 Hz, $SCH_AH_BCH_3$), 2.58 (dq, 1H, $SCH_AH_BCH_3$), 1.36 (d, 3H, H-6), 1.30 (dd, 3H, SCH_2CH_3). *Anal.* calcd. for $C_8H_{15}N_3SO_3$: C 41.19, H 6.48, N 18.01, S 13.74; found: C 40.98, H 6.45, N 17.89, S 13.58.

Ethyl 2-O-acetyl-4-azido-4,6-dideoxy-1-thio-α-D-mannopyranoside **9**

A solution of **8** (1.5 g, 6.43 mmol) in dry *N,N*-dimethylformamide (25 mL) was stirred with triethylorthoacetate (1.5 mL, 8.2 mmol) and *p*-toluenesulphonic acid (25 mg) for 2 h at 50°C. Triethylamine (1.5 mL) was added and the mixture was concentrated to a syrup, which was then dissolved in aqueous acetic acid (15 mL, 80%). After 10 min the mixture was concentrated and toluene was distilled several times from the residue to give **9** as crystals (1.7 g, 98%), mp 57–58°C; $[\alpha]_D^{20}$+170.4° (*c* 1.6, chloroform); ^{1}H nmr (200 MHz, $CDCl_3$) δ: 5.22 (d, 1H, $J_{1,2}$ 1.4 Hz, H-1), 5.16 (dd, 1H, $J_{2,3}$ 3.6 Hz, H-2), 3.97 (dd, 1H, $J_{3,4}$ 9.9 Hz, H-3), 3.95 (dq, 1H, $J_{4,5}$ 10.0 Hz, $J_{5,6}$ 6.2 Hz, H-5), 3.33 (dd, 1H, H-4), 2.61 (m, 1H, SCH_2CH_3), 2.17 (s, 3H, OAc), 1.36 (d, 3H, H-6), 1.28 (dd, 3H, *J* 7.6 Hz, SCH_2CH_3). *Anal.* calcd. for $C_{10}H_{17}N_3SO_4$: C 43.62, H 6.22, N 15.26, S 11.65; found: C 43.68, H 6.36, N 15.36, S 11.52.

Methyl 2-O-acetyl-4-azido-3-O-(4-azido-2,3-di-O-acetyl-4,6-dideoxy-α-D-mannopyranosyl)-4,6-dideoxy-α-D-mannopyranoside **11**

The alcohol **2** (100 mg, 0.408 mmol), the thioglycoside donor **7** (143 mg, 0.450 mmol), and powdered 4 Å molecular sieves (150 mg) were stirred in dichloromethane (10 mL) for 1 h at 20°C. Methyltriflate (0.1 mL, 0.884 mmol) was added to the stirred solution. After 50 h (tlc, hexane – ethyl acetate 3:1, v/v) the reaction was complete and triethylamine (0.5 mL, 0.359 mmol) was added carefully. The solution was stirred for another 0.5 h, then filtered and washed with a 50% saturated NaCl solution. The solution was concentrated to a syrup and purification was achieved by column chromatography (hexane – ethyl acetate 3:1, v/v). The product **11** was obtained as a crystalline solid (163 mg, 80%), mp 137–139°C; $[\alpha]_D^{20}$+114.95° (*c* 1.2, chloroform); ^{1}H nmr (200 MHz, $CDCl_3$) δ: 5.27 (dd, 1H, $J_{1',2'}$ 1.8 Hz, $J_{2',3'}$ 3.4 Hz, H-2'), 5.17 (dd, 1H, $J_{3',4'}$ 10.2 Hz, H-3'), 5.09 (dd, 1H, $J_{1,2}$ 1.8 Hz, $J_{2,3}$ 3.4 Hz, H-2), 5.02 (d, 1H, H-1'), 4.60 (d, 1H, H-1), 3.93 (dd, 1H, $J_{3,4}$ 9.6 Hz, H-3), 3.70 (dq, 1H, $J_{4',5'}$ 10.0 Hz, $J_{5',6'}$ 6.1 Hz, H-5'), 3.62–3.40 (m, 2H, H-4, H-5), 3.45 (dd, 1H, H-4'), 3.34 (s, 3H, OMe), 2.18 (s, 3H, OAc), 2.15 (s, 3H, OAc), 2.06 (s, 3H, OAc), 1.35 (d, 3H, $J_{5,6}$ 6.0 Hz, H-6), 1.34 (d, 3H, H-6'); ^{13}C nmr (125 MHz, $CDCl_3$) δ: 170.33 (CO), 169.71 (CO), 169.53 (CO), 99.29 (C-1', $J_{C1',H1'}$ 172 Hz), 98.17 (C-1, $J_{C1,H1}$ 170 Hz), 76.29 (C-3), 70.52 (C-2), 69.76 (C-3'), 69.05 (C-2'), 67.87 (C-5'), 66.90 (C-5), 64.50 (C-4), 62.27 (C-4'), 55.05 (OMe), 20.84 (OAc), 20.78 (OAc), 20.67 (OAc), 18.34 (C-6), 18.17 (C-6'). *Anal.* calcd. for $C_{19}H_{28}N_6O_{10}$: C 45.60, H 5.64, N 16.79; found: C 45.40, H 5.55, N 16.66.

Methyl 4-amino-3-O-(4-amino-4,6-dideoxy-α-D-mannopyranosyl)-4,6-dideoxy-α-D-mannopyranoside **13**

Disaccharide **11** (100 mg, 0.200 mmol) in methanol (5 mL) was treated with 0.1 M sodium methoxide solution (0.1 mL) at 20°C until tlc (hexane – ethyl acetate 1:1, v/v) indicated complete deacetylation. Neutralization with Amberlite IR-120 (H^+) ion exchange resin and concentration afforded the intermediate **12**, which was dissolved in pyridine (10 mL) and water (5 mL). The solution was saturated with H_2S at 40°C for 0.5 h and then stirred at this temperature for another 24 h (tlc, chloroform—methanol—water 5:4:1, v/v/v). Filtration and concentration of the filtrate gave the crude product, which was purified on a silica gel column (chloroform–methanol–water 5:4:1, v/v/v). The disaccharide **13** was obtained as a syrup (53 mg, 83%); $[\alpha]_D^{20}$+73.0° (*c* 0.87, water); ^{1}H nmr was consistent with the proposed structure and is reported elsewhere.[3] *Anal.* calcd. for $C_{13}H_{26}N_2O_7$: C 48.44, H 8.13, N 8.69; found: C 48.24, H 8.04, N 8.56.

Methyl 3-O-(4-acetamido-4,6-dideoxy-α-D-mannopyranosyl)-4-acetamido-4,6-dideoxy-α-D-mannopyranoside **14**

Acetic anhydride (0.2 mL) was added to a solution of **13** (20 mg, 0.062 mmol) in methanol (2 mL). After 2 h at 20°C the solution was concentrated and, codistilled with toluene, gave pure **13** (18 mg, 72%); $[\alpha]_D^{20}$+10.5° (*c* 1.0, water); ^{1}H nmr was consistent with the proposed structure and is reported elsewhere.[3] *Anal.* calcd. for $C_{17}H_{30}N_2O_9$: C 50.24, H 7.44, N 6.89; found: C 50.02, H 7.37, N 6.66.

Methyl 3-O-(4,6-dideoxy-4-formamido-α-D-mannopyranosyl)-4,6-dideoxy-4-formamido-α-D-mannopyranoside **15**

Disacharride **13** (20 mg, 0.062 mmol) was dissolved in methyl formate (2 mL) and kept at 20°C overnight. After concentration, pure **15** was obtained as a syrup (23 mg, 99%); $[\alpha]_D^{20}$+90.6° (*c* 0.12, water); ^{1}H nmr was in agreement with expectation and details will be reported elsewhere.[3] *Anal.* calcd. for $C_{15}H_{26}N_2O_9$: C 47.61, H 6.93, N 7.40; found: C 46.59, H 6.73, N 7.39.

Methyl O-(2-O-acetyl-4-azido-3-O-benzyl-4,6-dideoxy-α-D-mannopyranosyl)-(1→2)-O-(4-azido-3-O-benzyl-4,6-dideoxy-α-D-mannopyranosyl)-(1→3)-4-azido-2-O-benzyl-4,6-dideoxy-α-D-mannopyranoside **17**

Disaccharide **16** (1.0 g, 1.59 mmol) (6) and the selectively protected alcohol **3** (466 mg, 1.59 mmol) were reacted under similar conditions to those described for the preparation of the 1,2-linked trisaccharide **26** (6).

Trisaccharide **17** was obtained as a syrup (1.15 g, 84%); $[\alpha]_D^{20}$+67.7° (*c* 4.3, chloroform); ^{1}H nmr (200 MHz, $CDCl_3$) δ): 7.46–7.25 (m, 15H, Ph), 5.44 (dd, 1H, $J_{1'',2''}$ 1.9 Hz, $J_{2'',3''}$ 3.2 Hz, H-2''), 5.02 (d, 1H, $J_{1',2'}$ 1.7 Hz, H-1'), 4.91 (d, 1H, H-1''), 4.72 (d, 1H, $J_{1,2}$ 1.7 Hz, H-1), 4.81–4.53 (m, 6H, CH_2Ph), 4.07 (dd, 1H, $J_{2',3'}$ 3.2 Hz, H-2'), 3.86 (dd, 1H, $J_{2,3}$ 3.2 Hz, $J_{3,4}$ 10.0 Hz, H-3), 3.81 (dd, 1H, $J_{3'',4''}$ 9.9 Hz, H-3''), 3.78 (dd, 1H, $J_{3',4'}$ 9.8 Hz, H-3'), 3.66 (dd, 1H, H-2), 3.65–3.30 (m, 6H, H-4, H-5, H-4', H-5', H-4'', H-5''), 3.34 (s, 3H, OMe), 2.11 (s, 3H, OAc), 1.37 (d, 3H, $J_{5',6'}$, 5.9 Hz, H-6'), 1.35 (d, 3H, $J_{5,6}$ 6.0 Hz, H-6), 1.26 (d, 3H, $J_{5'',6''}$ 6.0 Hz, H-6''); ^{13}C nmr (50 MHz, $CDCl_3$) δ: 100.85 (C-1'', $J_{C1'',H1''}$ 171 Hz), 99.38 (C-1', $J_{C1',H1'}$ 171 Hz), 98.10 (C-1, 168 Hz). *Anal.* calcd. for $C_{42}H_{51}N_9O_{11}$: C 58.80, H 5.99, N 14.69; found: C 58.89, H 6.12, N 14.80.

Methyl O-(3-O-benzyl-4,6-dideoxy-4-formamido-α-D-mannopyranosyl)-(1→2)-O-(3-O-benzyl-4,6-dideoxy-4-formamido-α-D-mannopyranosyl)-(1→3)-2-O-benzyl-4,6-dideoxy-4-formamido-α-D-mannopyranoside **20**

Trisaccharide **17** (200 mg, 0.233 mmol) was deacetylated in methanol (5 mL) with 0.1 M sodium methoxide (0.1 mL) and neutralization was achieved with Amberlite IR 120 (H^+) ion exchange resin. After

[3]T. Peters and D. R. Bundle. Manuscript in preparation.

Can. J. Chem. Downloaded from www.nrcresearchpress.com by 122.72.124.2 on 09/07/12
For personal use only.

filtration and concentration pure alcohol **18** was obtained in quantitative yield (190 mg, 99%); $[\alpha]_D^{20}$ +87.9° (*c* 1.1, chloroform). *Anal.* calcd. for $C_{49}N_9O_{10}$: C 58.89, H 6.05, N 15.45; found: C 58.76, H 6.16, N 15.51. The azido derivative **18** (190 mg, 0.232 mmol) was then dissolved in pyridine (5 mL) and water (2.5 mL), H_2S was bubbled through the solution for 0.5 h at 40°C, and stirring at this temperature was continued for 24 h (tlc chloroform–methanol–water 5:4:1, v/v/v).

After filtration and concentration the crude reaction product **19** was taken up in methyl formate (5 mL) and kept at 20°C for 12 h (tlc chloroform–methanol 5:1, v/v). Concentration and purification on a silica gel column (chloroform--methanol 30:1, v/v) afforded pure **20** as a syrup (164 mg, 86%); $[\alpha]_D^{20}$ +34.6° (*c* 1.1, chloroform); ^{1}H nmr (200 MHz, $CDCl_3$) δ: 8.23–7.91 (m, 3H, NHC*H*O), 7.45–7.24 (m, 15H, Ph), 5.20–4.36 (m, 9H, H-1″, H-1′, H-1, CH_2Ph), 4.18–3.15 (m, 15H, H-2″, H-2′, H-2, H-3″, H-3′, H-3, H-4″, H-4′, H-4, H-5″, H-5′, H-5, OMe), 2.77 (bs, 1H, OH-2″), 1.36–1.00 (m, 9H, H-6″, H-6′, H-6). *Anal.* calcd. for $C_{43}H_{55}N_3O_{13}$: C 62.84, H 6.74, N 5.11; found: C 62.67, H 6.87, N 5.22.

Methyl O-*(4,6-dideoxy-4-formamido-α-D-mannopyranosyl)-(1→2)*-O-*(4,6-dideoxy-4-formamido-α-D-mannopyranosyl)-(1→3)-4,6-dideoxy-4-formamido-α-D-mannopyranoside* **21**

Trisaccharide **19** (21 mg, 0.025 mmol) was dissolved in glacial acetic acid (5 mL) and hydrogenated over 5% palladium on charcoal (50 mg) at 20°C and 5 kPa hydrogen pressure. Thin-layer chromatography (chloroform–methanol–water 5:4:1, v/v/v) indicated complete debenzylation after 5–6 h. After filtering the reaction mixture and concentration under reduced pressure, the crude product was purified on a Biogel P2 column to give **21** as a syrup (13 mg, 84%); $[\alpha]_D^{20}$ +80.5° (*c* 0.65, water); ^{1}H nmr showed an approximate *Z*/*E* ratio of 3.5:1.0; ^{1}H nmr (500 MHz, D_2O) δ: 8.24–8.20 (4s, 3H, NHC*H*O-*Z*), 8.06–8.02 (4s, 3H, NHC*H*O-*E*), 5.06–5.02 (m, 1H, H-1′), 5.02–4.99 (m, 1H, H-1″), 4.73 (d, 1H, $J_{1,2}$ 1.8 Hz, H-1), 4.13–3.80 (m, 12H, H-2″, H-2′, H-2, H-3″, H-3′, H-3, H-4″-*Z*, H-4′-*Z*, H-4-*Z*, H-5″, H-5′, H-5), 3.50–3.30 (m, 6H, H-4″-*E*, H-4′-*E*, H-4-E, OMe), 1.31–1.21 (m, 9H, H-6″, H-6′, H-6); ^{13}C nmr (125 MHz, D_2O) δ: 102.44 (C1′), 102.07 (C1″), 100.91 (C1). *Anal.* calcd. for $C_{22}H_{37}N_3O_{13}$: C 47.91, H 6.76, N 7.62; found: C 47.94, H 6.78, N 7.70.

Methyl O-*(2-O-acetyl-4-azido-3-O-benzyl-4,6-dideoxy-α-D-mannopyranosyl)-(1→2)*-O-*(4-azido-3-O-benzyl-4,6-dideoxy-α-D-mannopyranosyl)-(1→2)*-O-*(4-azido-3-O-benzyl-4,6-dideoxy-α-D-mannopyranosyl)-(1→2)*-O-*(4-azido-3-O-benzyl-4,6-dideoxy-α-D-mannopyranosyl)-(1→3)-4-azido-2-O-benzyl-4,6-dideoxy-α-D-mannopyranoside* **22**

Disaccharide thioglycoside **16** (185 mg, 0.294 mmol) and the trisaccharide alcohol **17** (232 mg, 0.284 mmol) were reacted by methyl triflate activation using the same procedure as described for the synthesis of the analogous pentasaccharide carrying only (1→2) linkages (6).

Pure **22** was obtained as a syrup (310 mg, 76%); $[\alpha]_D^{20}$ +80.0° (*c* 0.36, chloroform); ^{1}H nmr showed an approximate *Z*/*E* ratio of 3.5/1.0; ^{1}H nmr (500 MHz, $CDCl_3$) δ: 7.45–7.20 (m, 25H, Ph), 5.40 (dd, 1H, $J_{1''',2'''}$ 1.6 Hz, $J_{2''',3'''}$ 3.2 Hz, H-2′′′), 4.96 (d, 1H, $J_{1',2'}$ 1.6 Hz, H-1′), 4.92 (d, 1H, $J_{1'',2''}$, 1.6 Hz. H-1″), 4.91 (d, 1H, $J_{1'',2''}$ 1.7 Hz, H-1″), 4.84 (d, 1H, H-1′′′′) 4.73–4.51 (m, 10H, CH_2Ph), 4.68 (d, 1H, $J_{1,2}$ 1.5 Hz, H-1), 4.01 (dd, 1H, $J_{2',3'}$ 3.0 Hz, H-2′), 3.87 (dd, 1H, $J_{2'',3''}$ 3.1 Hz, H-2″), 3.82 (dd, 1H, $J_{2,3}$ 3.0 Hz, $J_{3,4}$ 10.0 Hz, H-3), 3.81 (dd, 1H, $J_{2''',3'''}$ 3.1 Hz, H-2′′′), 3.77 (dd, 1H, $J_{3''',4'''}$ 10.0 Hz, H3′′′′), 3.71 (dd, 1H, $J_{3',4'}$ 10.0 Hz, H-3′), 3.69 (dd, 1H, $J_{3'',4''}$ 10.0 Hz, H-3″), 3.66 (dd, 1H, $J_{3''',4'''}$ 10.0 Hz, H-3′′′), 3.60 (dd, 1H, H-2), 3.55–3.39 (m, 5H, H-5, H-5′, H-5″, H-5′′′, H-5′′′′), 3.54 (dd, 1H, $J_{4,5}$ 10.0 Hz, H-4), 3.36 (dd, 1H, $J_{4'''',5''''}$ 10.0 Hz, H-4′′′′), 3.32 (dd, 1H, $J_{4'',5''}$ 10.0 Hz, H-4″), 3.31 (s, 3H, OMe), 3.24 (dd, 1H, $J_{4''',5'''}$ 10.0 Hz, H-4′′′), 3.22 (dd, 1H, $J_{4',5'}$ 10.0 Hz, H-4′), 2.09 (s, 3H, OAc), 1.34 (d, 3H, $J_{5,6}$ 6.0 Hz, H-6), 1.28 (d, 3H, $J_{5''',6'''}$ 6.0 Hz, H-6′′′), 1.21 (d, 3H, $J_{5''',6''''}$ 6.0 Hz, H-6′′′′), 1.19 (d, 3H, $J_{5',6'}$ 6.0 Hz, H-6′), 1.14 (d, 3H, $J_{5'',6''}$ 6.0 Hz, H-6″); ^{13}C nmr (125 MHz, $CDCl_3$) δ: 100.97 (1C, $J_{C1''',H1'''}$ 170 Hz, C-1′′′′), 100.44 (1C, $J_{C1''',H1'''}$ 171 Hz, C-1′′′), 100.17 (1C, $J_{C1'',H1''}$ 172 Hz, C-1″), 99.13 (1C, $J_{C1',H1'}$ 171 Hz, C-1′), 98.24 (1C, $J_{C1,H1}$ 170 Hz, C-1). *Anal.* calcd. for $C_{68}H_{81}N_{15}O_{17}$: C 59.16, H 5.91, N 15.22; found: C 59.29, H 6.10, N 14.93.

Methyl O-*(4,6-dideoxy-4-formamido-α-D-mannopyranosyl)-(1→2)*-O-*(4,6-dideoxy-4-formamido-α-D-mannopyranosyl)-(1→2)*-O-*(4,6-dideoxy-4-formamido-α-D-mannopyranosyl)-(1→2)*-O-*(4,6-dideoxy-4-formamido-α-D-mannopyranosyl)-(1→3)-4,6-dideoxy-4-formamido-α-D-mannopyranoside* **24**

Pentasaccharide **22** (100 mg, 0.072 mmol) was subjected to a standard Zemplén deacetylation. The resulting syrup **23** was reduced by H_2S under identical conditions as described for the analogous 1,2-linked pentasaccharide (6) carrying only α1,2 linkages and also for the reduction of disaccharide **12** (this paper). *N*-Formylation was achieved using the standard procedure already described for preparation of disaccharide **15**. Hydrogenation under pressure was performed as described for the preparation of trisaccharide **21**.

The pentasaccharide **24** was a syrup (43 mg, 67%); $[\alpha]_D^{20}$ +74.2° (*c* 0.54, water); ^{1}H nmr shows an approximate *Z*/*E* ratio of 3.5:1; ^{1}H nmr (500 MHz, D_2O) δ: 8.22–8.19 (4s, 5H, NHC*H*O-*Z*), 8.05, 8.03 (2bs, 5H, NHC*H*O-*E*), 5.19, 5.12, 5.05, 5.01, 4.99 (5m, 4H, H-1′′′′, H-1′′′, H-1″, H-1′), 4.72 (m, 1H, H-1), 4.20–3.80 (m, 20H, H-2, H-2′, H-2″, H-2′′′, H-2′′′′, H-3, H-3′, H-3″, H-3′′′, H-3′′′′, H-4-*Z*, H-4′-*Z*, H-4″-*Z*, H-4′′′-*Z*, H-4′′′′-*Z*, H-5, H-5′, H-5″, H-5′′′, H-5′′′′), 3.50–3.34 (m, 8H, H-4-*E*, H-4′-*E*, H-4″-*E*, H-4′′′-*E*, H-4′′′′-*E*, OMe), 1.32–1.15 (m, 15H, H-6, H-6′, H-6″, H-6′′′, H-6′′′′); ^{13}C nmr (125 MHz, D_2O) δ: 168.07, 167.93 (5C, NCHO-*E*), 165.15, 164.63 (5C, NHCHO-*Z*), 102.28, 102.19, 101.07, 100.92, 100.71, (5C, C-1, C-1′, C-1″, C-1′′′, C-1′′′′). *Anal.* calcd. for $C_{36}H_{59}N_5O_{21}$: C 48.16, H 6.62, N 7.80; found: C 48.40, H 6.55, N 7.85.

Ethyl 3-O-*(2-O-acetyl-4-azido-3-O-benzyl-4,6-dideoxy-α-D-mannopyranosyl)-2-O-acetyl-4-azido-4,6-dideoxy-1-thio-α-D-mannopyranoside* **25**

The monosaccharide alcohol **9** (122 mg, 0.44 mmol) dissolved in dichloromethane (5 mL) was stirred with powdered 4 Å molecular sieves (120 mg) for 1 h at 20°C. Freshly prepared bromide **10** (192 mg, 0.50 mmol) (6) dissolved in dichloromethane (5 mL) was added dropwise into the solution of **9** at 0°C. The reaction mixture was stirred overnight at 20° when tlc (hexane – ethyl acetate 3:1, v/v) indicated complete conversion into the disaccharide **25**. After filtration through Celite, washing with saturated hydrogen carbonate solution, and concentration to a syrup, the reaction product was subjected to column chromatography (hexane – ethyl acetate 5:1, v/v) to give pure **25** as a syrup (211 mg, 83%); $[\alpha]_D^{20}$ +149.7° (*c* 0.62, chloroform); ^{1}H nmr (500 MHz, $CDCl_3$) δ: 7.40–7.28 (m, 5H, Ph), 5.44 (dd, 1H, $J_{1',2'}$ 1.8 Hz, $J_{2',3'}$ 3.2 Hz, H-2′), 5.21 (d, 1H, $J_{1,2}$ 1.6 Hz, H-1), 5.17 (dd, 1H, $J_{2,3}$ 3.5 Hz, H-2), 5.01 (d, 1H, H-1′), 4.68 (d, 1H, ^2J 11.2 Hz, CH_AH$_B$Ph), 4.51 (d, 1H, CH$_A$H$_B$Ph), 3.92 (dd, 1H, $J_{3,4}$ 10.0 Hz, H-3), 3.90 (dq, 1H, $J_{4,5}$ 10.0 Hz, $J_{5,6}$ 6.0 Hz, H-5), 3.75 (dd, 1H, $J_{3',4'}$ 9.8 Hz, H-3′), 3.53 (dq, 1H, $J_{4',5'}$ 10.0 Hz, $J_{5',6'}$ 6.0 Hz, H-5′), 3.52 (dd, 1H, H-4), 3.40 (dd, 1H, H-4′), 2.88–2.55 (m, 2H, SCH_2CH$_3$), 2.13 (s, 3H, OAc), 2.12 (s, 3H, OAc), 1.35 (d, 3H, H-6), 1.28 (d, 3H, H-6′), 1.28 (dd, 3H, SCH$_2$CH_3); ^{13}C nmr (125 MHz, $CDCl_3$) δ: 99.85 (C-1′, $J_{C1',H1'}$ 170.5 Hz), 81.88 (C-1, $J_{C1,H1}$ 168.0). *Anal.* calcd. for $C_{25}H_{34}N_6O_8S$: C 51.89, H 5.92, N 14.52, S 5.54; found: C 51.02, H 6.07, N 14.63, S 5.48.

Methyl O-*(2-O-acetyl-4-azido-3-O-benzyl-4,6-dideoxy-α-D-mannopyranosyl)-(1→3)*-O-*(4-azido-2-O-benzyl-4,6-dideoxy-α-D-mannopyranosyl)-(1→2)*-O-*(4-azido-3-O-benzyl-4,6-dideoxy-α-D-mannopyranosyl)-(1→2)*-O-*(4-azido-3-O-benzyl-4,6-dideoxy-α-D-mannopyranosyl)-(1→2)-4-azido-3-O-benzyl-4,6-dideoxy-α-D-mannopyranoside* **27**

Disaccharide **25** (91 mg, 0.16 mmol), the selectively protected trisaccharide alcohol **26** (117 mg, 0.14 mmol) (6), and powdered 4 Å molecular sieves (200 mg) were stirred in dichloromethane (5 mL) for 2 h at 20°C. Methyl triflate (0.3 mL, 2.65 mmol) was added and stirring was continued for another 4 days (tlc, hexane – ethyl acetate 3:1). The disaccharide donor **25** and the trisaccharide acceptor **26** were indistin-

guishable by tlc. Triethylamine (2 mL, 14.35 mmol) was added carefully and stirring was continued for another 0.5 h. The reaction mixture was filtered, and the filtrate was washed with a 50% saturated NaCl solution and then concentrated. Subsequently the crude reaction product was purified by column chromatography (hexane – ethyl acetate 6:1, v/v) and pure **27** was obtained as a syrup (143 mg, 64%); $[\alpha]_D^{20}$ +79.6° (*c* 2.19, chloroform); ^{1}H nmr ($CDCl_3$, 200 MHz) δ: 7.40–7.25 (m, 20H, Ph), 5.45 (dd, 1H, $J_{1'''',2''''}$ 1.8 Hz, $J_{2'''',3''''}$ 3.2 Hz, H-2''''), 5.17 (dd, 1H, $J_{1''',2'''}$ 1.7 Hz, $J_{2''',3'''}$ 3.2 Hz, H-2'''), 5.06 (d, 1H, H-1''''), 4.94 (d, 1H, $J_{1',2'}$ 1.6 Hz, H-1'), 4.88 (d, 1H, $J_{1'',2''}$ 1.8 Hz, H-1''), 4.84 (d, 1H, H-1'''), 4.74–4.46 (m, 9H, $4CH_2Ph$, H-1), 3.97 (dd, 1H, $J_{3''',4'''}$ 9.8 Hz, H-3'''), 3.87–3.12 (m, 20H, H-2, H-2', H-2'', H-3, H-3', H-3'', H-3''', H-4, H-4', H-4'', H-4''', H-4'''', H-5, H-5', H-5'', H-5''', H-5'''', OMe), 2.13 (s, 3H, OAc), 2.09 (s, 3H, OAc), 1.28 (d, 3H, $J_{5,6}$ 6.0 Hz, H-6), 1.27 (d, 3H, $J_{5''',6'''}$ 6.2 Hz, H-6'''), 1.26 (d, 3H, $J_{5'''',6''''}$ 6.0 Hz, H-6''''), 1.19 (d, 3H, $J_{5',6'}$ 6.0 Hz, H-6'), 1.17 (d, 3H, $J_{5'',6''}$ 6.0 Hz, H-6''); ^{13}C nmr (50 MHz, $CDCl_3$) δ: 100.37 (1C, $J_{C1'''',H1''''}$ 171 Hz, C-1''''), 99.99 (1C, $3J_{C1''',H1'''}$ 170 Hz, C-1'''), 99.79 (1C, $J_{C1'',H1''}$ 172 Hz, C-1''), 99.61 (1C, $J_{C1',H1'}$ 170 Hz, C-1'), 98.61 (1C, $J_{C1,H1}$ 171 Hz, C-1). *Anal.* calcd. for $C_{63}H_{77}N_{15}O_{18}$: C 56.79, H 5.82, N 15.77; found: C 56.77, H 5.88, N 15.57.

Methyl O-*(4,6-dideoxy-4-formamido-α-D-mannopyranosyl)-(1→3)*-O-*(4,6-dideoxy-4-formamido-α-D-mannopyranosyl)-(1→2)*-O-*(4,6-dideoxy-4-formamido-α-D-mannopyranosyl)-(1→2)*-O-*(4,6-dideoxy-4-formamido-α-D-mannopyranosyl)-(1→2)-4,6-dideoxy-4-formamido-α-D-mannopyranoside* **28**

Pentasaccharide **27** (20 mg, 0.014 mmol) was converted to the deblocked and *N*-formylated derivative **28** according to the procedure described for the conversion of pentasaccharide **22** to **24**. Pure **28** was obtained as a syrup (12 mg, 64%); $[\alpha]_D^{20}$ +35.8° (*c* 0.1, water); ^{1}H nmr shows an approximate *Z*/*E* ratio of 3.5:1; ^{1}H nmr (500 MHz, D_2O) δ: 8.22–8.19 (m, 5H, NHC*H*O-*Z*), 8.05–8.00 (m, 5H, NHC*H*O-*E*), 5.19, 5.17, 5.05, 5.00, 4.80 (5bs, 5H, H-1'''', H-1''', H-1'', H-1', H-1), 4.22–3.80 (m, 20H, H-2, H-2', H-2'', H-2''', H-2'''', H-3, H-3', H-3'', H-3''', H-3'''', H-4-*Z*, H-4'-*Z*, H-4''-*Z*, H-4'''-*Z*, H-4''''-*Z*, H-5, H-5', H-5'', H-5''', H-5''''), 3.48–3.34 (m, 8H, H-4-*E*, H-4'-*E*, H-4''-*E*, H-4'''-*E*, H-4''''-*E*, OMe), 1.36–1.15 (m, 15H, H-6, H-6', H-6'', H-6''', H-6''''). *Anal.* calcd. for $C_{36}H_{59}N_5O_{21}$: C 48.16, H 6.62, N 7.80; found: C 48.22, H 6.59, N 7.79.

1. M. Caroff, D. R. Bundle, M. B. Perry, J. W. Cherwonogrodzky, and J. R. Duncan. Infect. Immun. **46**, 384 (1984).
2. D. R. Bundle, J. W. Cherwonogrodzky, and M. B. Perry. Biochemistry, **26**, 8717 (1987).
3. P. A. Meikle, J. W. Cherwonogrodzky, M. B. Perry, and D. R. Bundle. Infect. Immun. Submitted.
4. D. R. Bundle, M. A. J. Gidney, P. A. Meikle, J. W. Cherwonogrodzky, and M. B. Perry. Infect. Immun. Submitted.
5. P. W. Robbins and A. Wright. *In* Microbial toxins. Vol. IV. Bacterial endotoxin. *Edited by* G. Weinbaum, S. Kadis, and S. J. Ajl. Academic Press, New York. 1971. p. 351.
6. T. Peters and D. R. Bundle. Can. J. Chem. **67**, 491 (1989).
7. P. J. Garegg and H. Hultberg. Carbohydr. Res. **72**, 276 (1979).
8. S. Josephson and D. R. Bundle. J. Chem. Soc. Perkin Trans. **1**, 297 (1980).
9. P. J. Garegg, T. Iverson, and S. Oscarson. Carbohydr. Res. **50**, C12 (1976).
10. R. J. Ferrier and R. H. Furneaux. Carbohydr. Res. **52**, 63 (1976).
11. H. Lönn. Carbohydr. Res. **135**, 105 (1985).
12. H. Lönn. Carbohydr. Res. **139**, 115 (1985).
13. G. Moffat, M. V. Newton, and G. J. Papenmeier. J. Org. Chem. **27**, 4058 (1962).
14. K. Bock and C. Pedersen. Acta Chem. Scand. Ser. B, **29**, 258 (1975).

Can. J. Chem. Downloaded from www.nrcresearchpress.com by 122.72.124.2 on 09/07/12
For personal use only.

A structural reinvestigation of 4,6-dinitrobenzofuroxan by ^1H, ^{13}C, and ^{15}N nuclear magnetic resonance

F. TERRIER, J. C. HALLE, P. MACCORMACK,[1] AND M. J. POUET

Laboratoire de physicochimie des solutions, École nationale supérieure de chimie de Paris, Unité associée au Centre national de la recherche scientifique, n° 403, 11 Rue Pierre et Marie Curie, 75231 Paris CEDEX 05, France

Received August 12, 1988

F. TERRIER, J. C. HALLE, P. MACCORMACK, and M. J. POUET. Can. J. Chem. **67**, 503 (1989).

A detailed nuclear magnetic resonance study of 4,6-dinitro-2,1,3-benzoxadiazole N-oxide (DNBF), which includes a 2D INADEQUATE analysis and experiments with samples ^{15}N-labelled at the NO_2 groups, is described. The results lead to an unambiguous assignment of the carbon and proton chemical shifts in various solvents. Some ^1H and ^{13}C data pertaining to 4,6-dinitro-2,1,3-benzoxadiazole (DNBZ), the deoxygenated analog of DNBF, are also reported, allowing the influence of the N-oxide group on the proton and carbon chemical shifts to be discussed. It is shown that all of the ^1H nmr evidence so far reported for the characterization of DNBF σ adducts as arising from nucleophilic addition to the 7-position, i.e., as structure **2***a*, has no significance. That complexation actually occurs at this position is, however, convincingly demonstrated by ^{15}N data. These also allow us to establish that this process is both kinetically and thermodynamically favored.

Key words: nitrobenzofuroxans, Meisenheimer complexes, ^{13}C nmr of benzofuroxans, 2,1,3-benzoxadiazole N-oxides, nitrobenzofuroxan σ-adducts.

F. TERRIER, J. C. HALLE, P. MACCORMACK et M. J. POUET. Can. J. Chem. **67**, 503 (1989).

Une étude en résonance magnétique nucléaire très détaillée du dinitro-4,6 benzoxadiazole-2,1,3 N-oxyde, plus connu sous le nom de dinitro-4,6 benzofuroxanne (DNBF), a été réalisée dans divers solvants. Elle comporte notamment une analyse 2D INADEQUATE et des mesures faites avec des échantillons marqués à l'azote 15 sur l'un ou sur les deux groupes NO_2. Les résultats permettent d'attribuer sans ambiguïté les déplacements chimiques des protons et des carbones du DNBF. Une comparaison avec les résultats obtenus pour le dinitro-4,6 benzoxadiazole-2,1,3 (DNBZ) révèle l'influence considérable du groupe N-oxyde sur certains déplacements chimiques. Il est montré que les arguments rmn précèdemment développés pour affirmer que le DNBF réagit avec les nucléophiles en formant des complexes-σ en position 7 (complexes **2***a*) sont peu convaincants. Seule l'analyse des résultats obtenus avec les échantillons marqués en ^{15}N permet d'étayer valablement cette conclusion. Cette analyse montre en outre que la formation des complexes **2***a* est cinétiquement et thermodynamiquement contrôlée.

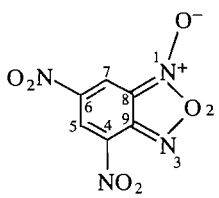
Mots clés : nitrobenzofuroxannes, complexes de Meisenheimer, rmn du ^{13}C des benzofuroxannes, benzoxadiazole-2,1,3 N-oxydes, σ-adduits des nitrobenzofuroxannes.

Can. J. Chem. Downloaded from www.nrcresearchpress.com by 122.72.124.2 on 09/07/12
For personal use only.

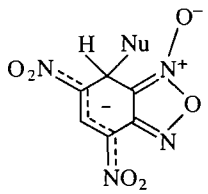
There is presently much interest in 4,6-dinitro-2,1,3-benzoxadiazole N-oxide, commonly known as 4,6-dinitrobenzofuroxan (DNBF). This compound exhibits an extremely high electrophilic character, which is useful in assessing the reactivity of very weak nucleophiles (1–7). So far, all reactions have been reported to involve covalent addition of the nucleophile to the carbocyclic ring, giving rise to stable σ adducts that have been formulated as having structure **2***a*, mainly on the basis of ^1H nmr.

As a continuation of our work in this field (3, 4, 6, 8), we have recently become interested in the reaction of DNBF with indene. In this instance, we have found a new product exhibiting none of the spectral and chemical characteristics of a σ complex that we could identify as being the dihydrooxazine N-oxide **3**. These results have recently been published (9) but our thorough nmr investigation has also led us to the surprising discovery that there are many contradictory assignments of the ^1H resonances of DNBF in the literature (2–5, 7, 10–12). Concomitantly, we realized that much of the ^1H nmr evidence reported for the characterization of the σ adducts **2***a* may be seriously questioned (2–5, 7, 10–12).

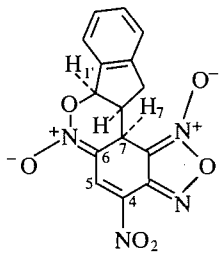
In this paper, we report a 2D INADEQUATE analysis of DNBF and we present the results of ^{15}N experiments carried out after ^{15}N labelling of the 6-NO_2 group or of both 4- and 6-NO_2 groups of this compound and its methoxide σ adduct. ^1H and ^{13}C results pertaining to 4,6-dinitro-2,1,3-benzoxadiazole (4,6-dinitrobenzofurazan or DNBZ), the deoxygenated analog of DNBF, are also included for purpose of comparison.



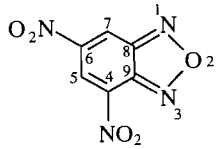
DNBF (**1***a*)



2*a*



3



DNBZ

Results

4,6-Dinitrobenzofuroxan (DNBF)

The ^1H spectrum of DNBF shows the H_A and H_X doublets of the AX system at 9.27 and 8.95 ppm, respectively, in dimethyl sulfoxide (Me_2SO; J_{HA-HX} = 1.9 Hz). On ^{15}N labelling of the 6-NO_2 group, the H_A and H_X resonances show coupling with

[1]Post doctoral fellow of the Consejo Nacional de Investigaciones Cientificas y Tecnicas de la Republica Argentina.

Printed in Canada / Imprimé au Canada

the nitrogen atom but, due to an insufficient separation of the inner lines of the resulting double doublets, they both appear as a triplet. From the separation of the outer lines, the J_{N6HA} and J_{N6HB} coupling constants were readily calculated: $J_{N6HA} = 2.4$; $J_{N6HB} = 1.6$ Hz. On further ^{15}N labelling at the 4-NO_2 group, the resonance of H_A remains unaffected while that of H_X undergoes additional splitting: $J_{N4HX} = 2.9$ Hz. These observations show unambiguously that H_A is H-7 and H_X is H-5 in Me_2SO.

Similar experiments have been carried out in various solvents (Table 1). In THF and acetone, it is the high-field resonance of the observed AX and AB patterns, respectively, that is split on ^{15}N labelling of the 4-NO_2 group. This indicates a sequence of the H-7 and H-5 resonances in these solvents that is the same as that found in Me_2SO. In contrast, it is the H_A resonance that is affected by labelling the 4-NO_2 group in nitromethane, methylene chloride, chloroform, benzene, and acetonitrile. This shows that the low-field doublet of the AX (or AB) system is ascribable to H-5 in these solvents. A particular situation is found in methanol where the two protons have quite identical chemical shifts.

^{13}C chemical shifts were obtained from proton noise-decoupled ^{13}C spectra. From selective irradiations of H-7 and H-5, the resonances at 120.8 ppm and 126.5 ppm in Me_2SO were readily assigned as being due to C-7 and C-5, respectively. Then, the complete elucidation of the carbon skeleton, in Me_2SO, was obtained from a two-dimensional analysis: 2D INADEQUATE (13). Using the C-7 and C-5 carbons at 120.8 and 126.5 ppm as reference points, the assignment of the various quaternary carbons of DNBF was completed. The ^{13}C chemical shifts together with the various J_{CH} coupling constants in Me_2SO are summarized in Table 2.

In methylene chloride where no 2D INADEQUATE analysis was performed, the C-5 and C-7 carbons of DNBF have been firmly assigned from selective proton decoupling. Other carbons were assigned by analogy with the results (δ, J) obtained in Me_2SO. These assignments are also given in Table 2.

4,6-Dinitrobenzofurazan (DNBZ)

The ^1H spectrum of DNBZ shows an AX system comparable to that of DNBF in Me_2SO: $\delta_{HA} = 9.80$; $\delta_{HX} = 9.04$; $J_{HA-HX} = 1.8$ Hz (Table 1). From selective proton irradiation and comparison of the measured $^1J_{CH}$ coupling constants with those determined for DNBF, correlated ^{13}C and ^1H resonances at 122.59 and 9.80 were assigned to C-7 and H-7, respectively, while those at 125.17 and 9.04 were assigned to C-5 and H-5, respectively. Other carbons were also assigned by analogy with the results obtained for DNBF. The data are collected in Table 2.

The methoxide adduct of DNBF

The ^1H spectrum of this adduct consists of an AX system with the H_A and H_X doublets at 8.70 and 5.89 ppm, respectively ($J_{HAHX} = 0.6$ Hz), and a methoxyl singlet at 3.35 ppm in Me_2SO. ^{15}N labelling of the 6-NO_2 group leaves the H_X resonance essentially unchanged while it causes a splitting of the H_A resonance, which appears as a double doublet: $J_{N6HA} = 2.6$ Hz. Further splitting of H_A occurs on labelling the 4-NO_2 group, resulting in the appearance of a multiplet ($J_{N4HA} = 1.9$ Hz). In addition, ^{13}C spectra of the adduct formed from (4,6-^{15}N)-DNBF show a vicinal J_{C4-N4} coupling constant of 22.2 Hz. These results show unambiguously that the adduct has the structure **2***a* rather than the isomeric structure **2***b* (Nu = OCH_3; see Scheme 1).

TABLE 1. Solvent effect on ^1H nmr data for ^{15}N labelled DNBF (4,6-di-$^{15}NO_2$) (a) and unlabelled DNBZ (b)[a]

Solvent		H5	H7
$(CD_3)_2SO$	(a)	8.94_9	9.27_3
	(b)	9.04_3	9.80_0
THF-d_8	(a)	9.04_3	9.16_4
$(CD_3)_2CO$	(a)	9.11_7	9.14_2
CD_3OD	(a)	9.07_1	9.07_1
CD_3NO_2	(a)	9.14_1	8.96_6
CD_3CN	(a)	8.98_6	8.90_1
CD_2Cl_2	(a)	9.13_0	8.86_3
	(b)	9.22_5	9.32_6
$CDCl_3$	(a)	9.12_0	8.82_3
C_6D_6	(a)	8.08_3	7.29_1

[a]Chemical shifts in ppm from internal TMS; $c \approx 0.06$ mol L^{-1} (DNBF); $c \approx 0.1$ mol L^{-1} (DNBZ). Solvent independent coupling constants in hertz (± 0.2); for ^{15}N labelled DNBF: $J_{H5-H7} = 1.9$, $J_{N4-H5} = 2.9$, $J_{N6-H5} = 1.6$, $J_{N6-H7} = 2.4$; for unlabelled DNBZ: $J_{H5-H7} = 1.8$.

Discussion

^1H chemical shifts of DNBF and DNBZ

In an early study by Katritzky and co-workers (14), it was found that the ^1H spectrum of DNBF consists of a single AB or AX pattern, which persists over a large temperature range in dioxan, acetonitrile, and dimethyl sulfoxide. This showed that neither of the two possible types of tautomerism from **1***a* to **1***b* (Scheme 1) or **1***a* to **1***a*′ (Scheme 2 with **1***a*′ ≡ **1***a* for unlabelled DNBF) is important. DNBF was thus formulated as **1***a* on the basis that steric, electrostatic, and mesomeric effects are expected to cause the equilibrium **1***a* ⇔ **1***b* to lie very predominantly on the side of the isomer **1***a* (10, 11, 14). Interestingly, **1***a* was later found by an X-ray crystallography study to be the structure of DNBF in the solid state (15). Another interesting observation of Katritzky dealt with the solvent dependence of the AX or AB pattern, but no attempt to assign the H_A and H_B (H_X) resonances to the H-7 and H-5 protons of **1***a* was made (14).

In all solvents employed in this work, a unique AB or AX pattern has been observed. In accordance with Katritzky's observations, our results in Table 1 emphasize the large dependence of the proton resonances of DNBF on the solvent. They further reveal that the individual chemical shifts of H-7 and H-5 may be affected to such a different extent that the sequence of these chemical shifts may be reversed on going from one solvent to another. However, there is no apparent correlation of chemical shifts with common solvent parameters like polarity.

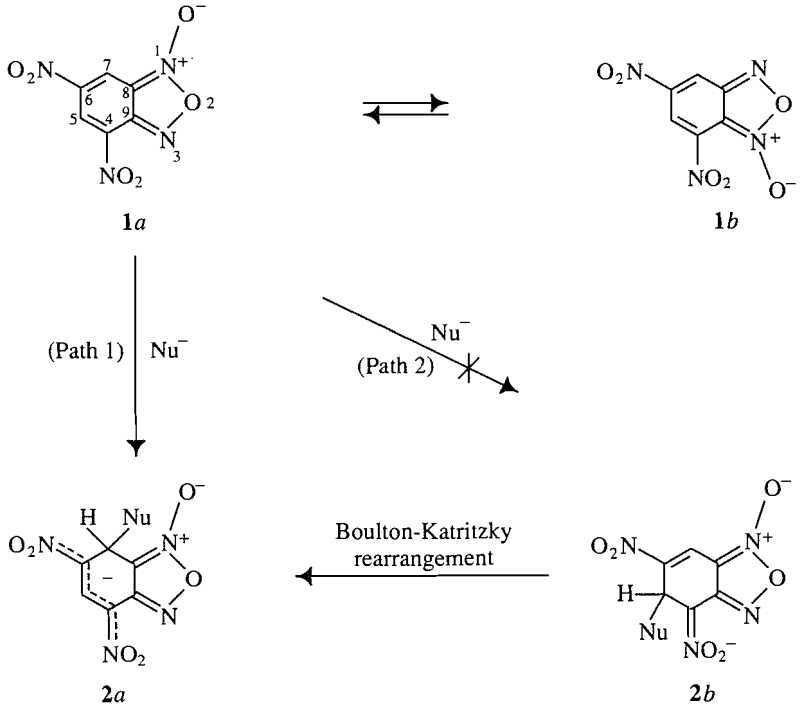
Because they can be related to previous work, some of our assignments are worthy of comment. From a comparison of the ^1H spectra of DNBF and its partially 5-deuterated analog, Brown and Keyes concluded in 1965 that the lower-field doublet of the AX pattern observed in methylene chloride corresponds to H-7 (10). As can be seen in Table 1, our ^{15}N experiments lead us to assign this doublet to H-5 and therefore to raise doubt about the validity of the structural characterization of the hydroxide adduct of DNBF reported by these authors (*vide infra*) (10). On the other hand, the majority of recent studies have been carried

Can. J. Chem. Downloaded from www.nrcresearchpress.com by 122.72.124.2 on 09/07/12
For personal use only.

TABLE 2. The ^{13}C nmr data for DNBF and DNBZ in $(CD_3)_2SO$ and in CD_2Cl_2[a]

	$(CD_3)_2SO$				CD_2Cl_2				
	DNBF[b]		DNBZ[d]		DNBF[c]		DNBZ[d]		
Carbon	δ	J	δ	J	δ	J	δ	J	
		1.7		1.7		nr		nr	$^4J_{C4H7}$
C4	136.7_2		136.8_1		137.9_6		137.8_8		
		5.9		5.7		nr		nr	$^2J_{C4H5}$
		5.5		5.6		5.5		5.6	$^3J_{C5H7}$
C5	126.5_2		125.1_7		125.8_3		124.5_0		
		176.8		177.0		176.6		176.9	$^1J_{C5H5}$
		4.9		4.8		nr		nr	$^2J_{C6H5}$
C6	144.8_3		148.7_3		144.8_5		148.8_0		
		4.9		4.8		nr		nr	$^2J_{C6H7}$
		4.7		4.5		4.9		4.7	$^3J_{C7H5}$
C7	120.8_0		122.5_9		119.5_3		122.2_2		
		184.5		184.0		182.6		181.8	$^1J_{C7H7}$
C8	116.6_4	2.1	150.0_0	0.9	116.1_2	nr	150.2_3	s	$^2J_{C8H7}$
		4.9		4.9		5.0		5.1	$^3J_{C9H7}$
C9	145.0_2		143.3_0		144.6_5		143.6_2		
		7.8		7.9		7.5		7.8	$^3J_{C9H5}$

[a]Chemical shifts (±0.03) in ppm from TMS; coupling constants in hertz (±0.5); nr, not resolved; s, singlet.
[b]Concentration is ≈0.7 mol L^{-1}.
[c]Concentration is ≈0.4 mol L^{-1}.
[d]Concentration is ≈0.2 mol L^{-1}.

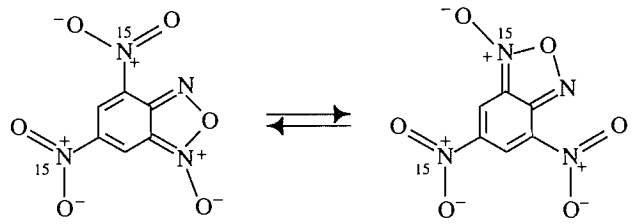


SCHEME 1

out in dimethyl sulfoxide (2–5). However, no unambiguous assignment of the two proton resonances is found in these papers. Our determination that the H_A and H_X resonances correspond to the H-7 and H-5 protons, respectively, in this solvent agrees with some reports but disagrees with many others. This uncertainty in the exact chemical shift sequence in Me_2SO has been a major drawback in our efforts to characterize the dihydrooxazine N-oxide **3** and has led to the present study (9).

Consistent with a previous study is the observation of

Can. J. Chem. Downloaded from www.nrcresearchpress.com by 122.72.124.2 on 09/07/12
For personal use only.



1a 1a'

SCHEME 2

close chemical shifts for H-7 and H-5 in acetone (14). Also remarkable is the coincidence of these chemical shifts in methanol.

Comparison of the ^1H spectra of unsubstituted benzofurazan and benzofuroxan has shown that the effect of adding an N-oxide oxygen atom is to cause a high-field shift of all the protons (16). This result has been attributed to a significant electron-donating influence of the N-oxide group, which is greater at the 4- and the 6- than at the 5-position, in agreement with theoretical expectation (Scheme 3). Due to an anisotropy effect of the N-oxide group, the 7-position suffers a much larger high-field shift. Interestingly, Table 3 shows that the shifts to high field are similar when the H-5, H-6, and H-7 resonances of 4-nitrobenzofurazan and 4-nitrobenzofuroxan are compared in acetone or Me_2SO (14). Table 3 also shows that a comparison of DNBF and DNBZ based on our assignments (from ^{15}N experiments) affords $\Delta\delta$ values for the H-7 and H-5 protons that are analogous to those found for unsubstituted or mononitro derivatives. This brings additional support for our assignments.

No assignment of the H-7 and H-5 resonances of DNBZ was previously made (17). Due to the absence of the influence of the N→O group mentioned above, the resonance of the H-7 proton of DNBZ appears at much lower field than that of DNBF. The result is that the sequence of the H-7 and H-5 chemical shifts of DNBZ is not solvent dependent despite notable variations in each of these chemical shifts on going from Me_2SO to CH_2Cl_2 (Table 1).

^{13}C chemical shifts and coupling constants of DNBF and DNBZ

Since it is based on a combination of the information accumulated from ^{15}N labelling, selective proton irradiation experiments, and a two-dimensional analysis, our assignment of the carbon resonances of DNBF in dimethyl sulfoxide given in Table 2 is unambiguous. In CD_2Cl_2, where no 2D-INADEQUATE analysis was performed, only the C-5 and C-7 carbons could be assigned with certainty but the validity of the assignments of the various quaternary carbons is indirectly confirmed by the observed consistency in the quoted carbon chemical shifts and J_{CH} coupling constants. It is also on grounds of analogy with DNBF that the quaternary carbons of DNBZ were assigned. Significantly, the results lead us to assign very similar chemical shifts to the C-9 carbons of these derivatives but very different chemical shifts to the C-8 carbons: in Me_2SO, C-8 is at ≈116 ppm for DNBF but at ≈150 ppm for DNBZ. This result agrees with a previous report by Anet and Yavari that addition of an oxygen to a nitrogen atom of benzofurazan causes a large upfield shift (≈40 ppm) of the resonance of the quaternary carbon (C-8) close to the N→O function, while that of the removed carbon (C-9) is only slightly affected (16). Here, the upfield shift observed on going from DNBZ to DNBF is ≈34 ppm and this supports our assignments of C-8 and C-9. This large substituent effect has been attributed to the presence of a partial negative charge on C-8 resulting from a significant

TABLE 3. Effect of the N-oxide oxygen atom on the chemical shifts of benzofurazan derivatives $\Delta\delta_{Hi} = \delta_{Hi}(N\text{-}O) - \delta_{Hi}(N)^a$

R	$\Delta\delta_{H4}$	$\Delta\delta_{H5}$	$\Delta\delta_{H6}$	$\Delta\delta_{H7}$
H[b]	−0.25	−0.09	−0.25	−0.50
4-NO_2[b]	—	−0.13	−0.36	−0.52
[c]	—	−0.08	−0.33	−0.48
4,6-diNO_2[d]	—	−0.09	—	−0.53

[a] δ in ppm.
[b] In acetone at room temperature, ref. 14.
[c] In Me_2SO-d_6 at 37°C, ref. 19.
[d] In Me_2SO-d_6; calculated from chemical shifts of Table 1 ($t \cong 20$°C).

contribution of the second resonance canonical form of DNBF described in Scheme 3 (16). Evidence for the importance of this structure is provided by the finding by X-ray crystallography that the C8N1 bond (1.40 Å) is appreciably longer than the C9N3 bond (1.37 Å) (15).

Concerning the coupling constants, the close analogy between the $^1J_{C7H7}$ and $^1J_{C5H5}$ values of DNBF and DNBZ is noteworthy since it is reminiscent of that found between the same coupling in the unsubstituted parents (16).

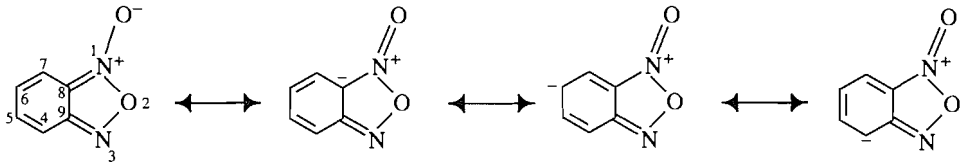
^1H nuclear magnetic resonance characterization of DNBF σ adducts

Since it is the H_A resonance of the AX system corresponding to the DNBF–methoxide σ complex which is split by ^{15}N labelling of both the 4- and 6-NO_2 groups of the parent molecule, the present work leaves no doubt that this adduct has the structure **2***a* (Scheme 1) and therefore that DNBF undergoes preferentially covalent nucleophilic addition at the 7-position. While this conclusion agrees with all reported formulations of DNBF σ adducts (1–12), it is important to emphasize why our results provide the first convincing evidence for structure **2***a*.

Changes in the ^1H nmr spectra that take place on reaction of DNBF with a large variety of nucleophiles may only be understood in terms of σ complexation since they are closely reminiscent of those described in the reactions involving covalent addition of the same nucleophiles to nitroaromatics like 1,3,5-trinitrobenzene (TNB) (1, 10, 11). Thus, all reactions are accompanied by a considerable shift to high field of one of the resonances forming the AX or AB pattern of DNBF, as anticipated for a change from sp^2 to sp^3 hybridization at one of the hydrogen-bearing carbons of the carbocyclic ring. Concomitantly, the second resonance is also moved to high field but to a much smaller extent, consistent with loss of aromaticity and increased negative charge in the resulting hetarenide ring. However, both structures **2***a* and **2***b* are consistent with the observed nmr changes and it is not possible to discriminate between the two on this basis irrespective of whether the exact sequence of the H-7 and H-5 resonances in the original spectra of DNBF is known or not. Nevertheless, the observation of a single set of two weakly coupled resonances in all reported ^1H spectra indicates that only one of the two isomers is important in the solutions studied.

So far, only one study has been especially designed to decide on the structure of the resulting isomer. It is the early comparison by Brown and Keyes of the changes in the ^1H spectra brought about by the addition of hydroxide ion to DNBF and its partially 5-deuterated analog in *water* (10). Since it was the signal not affected by the deuteration, attributed to

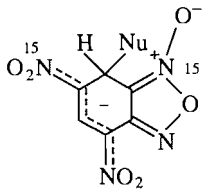
Can. J. Chem. Downloaded from www.nrcresearchpress.com by 122.72.124.2 on 09/07/12
For personal use only.



SCHEME 3

H-7 in CH_2Cl_2 (*vide supra*), which moved to high field, it was concluded that the corresponding adduct had structure **2***a* (Nu = OH). This formulation has never been questioned since it agreed with consideration of resonance forms that favor **2***a* over **2***b*, and in all subsequent studies DNBF σ adducts were characterized as having structure **2***a* on the basis only of the observation of the anticipated AX patterns in ^1H nmr (2–5, 7, 12). Obviously, the finding that Brown and Keyes' assignments of the two proton resonances of DNBF in methylene chloride were erroneous has the effect of making their structural characterization of **2***a* (Nu = OH) totally inconclusive. Therefore, the definitive demonstration by nmr that structure **2***a* is valid is an important result in DNBF chemistry (1).

A most interesting point, which also merges from ^{15}N data, deals with the mechanism of the complexation of DNBF. The question is whether the formation of the adducts **2***a* arises from



2*a'*

direct nucleophilic addition at the 7-position (Scheme 1) or from initial addition at the 5-position to give **2***b*, followed by rapid Boulton–Katritzky rearrangement (Scheme 2). Should the latter pathway occur (18), it is clear that experiments carried out with a DNBF sample labelled at the 4- and 6-NO_2 groups would give adducts **2***a'* having only the 6-NO_2 group labelled. In this case, the H_A resonance of **2***a'* should appear as a double doublet and not as the multiplet found experimentally for the methoxide adduct. We therefore conclude that the formation of adducts **2** occurs via path 1 to give **2***a* (Scheme 1), which is both kinetically and thermodynamically favored.[2]

Experimental

Nuclear magnetic resonance

The ^1H and ^{13}C nmr spectra were recorded on a Bruker AM-250 spectrometer equipped with an ASPECT 3000 computer. Chemical shifts are reported in parts per million (δ, *J* in hertz) relative to internal Me_4Si. The 2D INADEQUATE spectrum of DNBF was obtained with the basic sequence proposed by Mareci and Freeman (13).

Materials

4,6-Dinitrobenzofuroxan (DNBF) and 4,6-dinitrobenzofurazan (DNBZ) were prepared according to previously reported methods. DNBF: mp 173°C (lit. (20, 21) mp 172–174.5°C); DNBZ: mp 133°C (lit. (8, 17) mp 129–132°C). [6-^{15}N]-4,6-Dinitrobenzofuroxan was obtained as recently described (9).

[4,6-^{15}N]-4,6-Dinitrobenzofuroxan

A solution of 1 mL of 40% H $^{15}NO_3$ (Aldrich, 98% ^{15}N) in 4 mL of sulfuric acid (*d* = 1.84) was added dropwise to a stirred solution of 0.5 g of benzofuroxan (3.7 mmol) in 8 mL of sulfuric acid (*d* = 1.84) maintained at ice-bath temperature. The resulting mixture was kept at this temperature for 30 min, then slowly heated and maintained at 60–70°C for 3 h. After the mixture returned to room temperature, it was poured onto cracked ice and the resulting orange crystals were filtered, washed with water, and vacuum dried over P_2O_5; mp 175°C; mass spectrum (obsd.), *m/e*: 228, 212, 198, 152, 121; for comparison, DNBF mass spectrum (obsd.), *m/e*: 226, 210, 196, 150, 120.

[2]Reversible formation of **2***a* from DNBF after initial and reversible formation of **2***b* in a fast preequilibrium step is an alternative mechanism that is ruled out by the kinetic results obtained for many interactions (1, 6, 8).

Acknowledgements

The authors are indebted to Y. Besace for his technical assistance in carrying out "INADEQUATE analysis" experiments.

1. E. Buncel, M. R. Crampton, M. J. Strauss, and F. Terrier. *In* Electron-deficient aromatic and heteroaromatic base interactions. The chemistry of anionic sigma complexes. Elsevier, Amsterdam. 1984.
2. E. Buncel, R. A. Renfrow, and M. J. Strauss. J. Org. Chem. **52**, 488 (1987).
3. F. Terrier, J. C. Halle, M. J. Pouet, and M. P. Simonnin. J. Org. Chem. **51**, 409 (1986).
4. (*a*) F. Terrier, J. C. Halle, M. P. Simonnin, and M. J. Pouet. J. Org. Chem. **49**, 4369 (1984); (*b*) J. C. Halle, M. J. Pouet, M. P. Simonnin, and F. Terrier. Tetrahedron Lett. **26**, 1307 (1985).
5. M. J. Strauss, R. A. Renfrow, and E. Buncel. J. Am. Chem. Soc. **105**, 2473 (1983).
6. F. Terrier. Chem. Rev. **82**, 77 (1982).
7. (*a*) R. J. Spear, W. P. Norris, and R. W. Read. Tetrahedron Lett. **24**, 1555 (1983); (*b*) R. W. Read, R. J. Spear, and W. P. Norris. Aust. J. Chem. **37**, 985 (1984).
8. F. Terrier, A. P. Chatrousse, Y. Soudais, and M. Hlaibi. J. Org. Chem. **49**, 4176 (1984).
9. P. MacCormack, J. C. Halle, M. J. Pouet, and F. Terrier. J. Org. Chem. **53**, 4407 (1988).
10. N. E. Brown and R. T. Keyes. J. Org. Chem. **30**, 2452 (1965).
11. W. P. Norris and J. Osmundsen. J. Org. Chem. **30**, 2407 (1965).
12. F. Terrier, M. P. Simonnin, M. J. Pouet, and M. J. Strauss. J. Org. Chem. **46**, 3537 (1981).
13. T. H. Mareci and R. Freeman. J. Magn. Reson. **48**, 158 (1982).
14. R. K. Harris, A. R. Katritzky, S. Oksne, A. S. Bailey, and W. G. Paterson. J. Chem. Soc. 187 (1963).
15. C. K. Prout, O. J. R. Hodder, and D. Viterbo. Acta Crystallogr. Sect. B: Struct. Crystallogr. Cryst. Chem. **28**, 1523 (1972).
16. F. A. L. Anet and I. Yavari. Org. Magn. Reson. **8**, 158 (1976).
17. R. W. Read, R. J. Spear, and W. P. Norris. Aust. J. Chem. **36**, 1227 (1983).
18. (*a*) A. Gasco and A. J. Boulton. Adv. Heterocycl. Chem. **29**, 251 (1981); (*b*) P. B. Ghosh, B. Ternai, and M. Whitehouse. Med. Res. Rev. **1**, 159 (1981).
19. F. Terrier, F. Millot, A. P. Chatrousse, M. J. Pouet, and M. P. Simonnin. Org. Magn. Reson. **8**, 56 (1976).
20. P. Drost. Liebigs Ann. Chem. **307**, 49 (1899).
21. W. P. Norris, R. J. Spear, and R. W. Read. Aust. J. Chem. **36**, 897 (1983).

Can. J. Chem. Downloaded from www.nrcresearchpress.com by 122.72.124.2 on 09/07/12
For personal use only.

Effects of halide (X) and sulfoxide (R_2SO) replacement within the ruthenium(II) nitroimidazole complexes, $RuX_2(R_2SO)_m$ (nitroimidazole)$_n$, m = 1–3, n = 1 or 2: their characterization, solution chemistry, radiosensitizing activity, and related properties

PETER K. L. CHAN, BRIAN R. JAMES,[1] DAVID C. FROST,[1] PAUL K. H. CHAN,[2] AND HONG-LIANG HU
Department of Chemistry, University of British Columbia, Vancouver, B.C., Canada V6T 1Y6

AND

KIRSTEN A. SKOV[1]
Medical Biophysics Unit, British Columbia Cancer Research Centre, 601 West 10th Avenue, Vancouver, B.C., Canada V5Z 1L3

Received September 16, 1988

PETER K. L. CHAN, BRIAN R. JAMES, DAVID C. FROST, PAUL K. H. CHAN, and HONG-LIANG HU. Can. J. Chem. **67**, 508 (1989).

During our studies on metal–radiosensitizer complexes, a complex $RuCl_2(dmso)_2(4\text{-}NO_2Im)_2$ was found to show better radiosensitizing properties and lower toxicity than the free 4-nitroimidazole ligand; complexes with *N*-substituted-4-nitroimidazoles were less effective as radiosensitizers (Can. J. Chem. **66**, 117 (1988)). In the present study, the effects of replacement of the chloride ligand by bromide, and dimethylsulfoxide (dmso) ligand by tetramethylenesulfoxide (tmso), as well as the use of a wider variety of nitroimidazole ligands, are described. A series of ruthenium(II) complexes of formulation: $RuCl_2(dmso)_2L_2$ (L = a 2-nitroimidazole); $RuCl_2(tmso)_mL_n$ (L = a 2- or 4-nitroimidazole, m = 1–3 and n = 1 or 2); and $RuBr_2(dmso)_2L_n$ (L = a 4-nitroimidazole, n = 1 or 2), has been synthesized and characterized by spectroscopic methods, particularly ^1H nmr and X-ray photoelectron spectroscopy. The precursors used were $RuX_2(dmso)_4$, X = Cl, Br, and $RuCl_2(tmso)_4$. The *N*-methyl-4-nitroimidazole (NMe-4-NO_2Im) ligand of the complex $RuBr_2(dmso)_2$(NMe-4-NO_2Im) chelates through the imidazole-*N* and the oxygen of NO_2. Another substituted 4-nitroimidazole, RSU-3159,[3] in $RuCl_2(tmso)$ (RSU-3159), binds through the sulfur and is almost certainly chelated; the complex with a substituted 2-nitroimidazole, $RuCl_2(tmso)_2$(SR-2508), is five-coordinate and probably trigonal bipyramidal. The replacement of dmso by tmso does not markedly alter the redox properties and radiosensitizing ability of the 4-nitroimidazole complexes, but increases their lipophilicity. The tmso complexes (unlike the dmso analogues) do not bind to DNA, as evidenced by non-inhibition of restriction enzymes. The tmso/2-nitroimidazole complexes, in contrast to the dmso analogues, are stable in aqueous media. The substitution of Cl^- by Br^- reduces the radiosensitizing ability of the 4-NO_2Im complexes. At only 200 μM, the complexes $RuCl_2(tmso)_2(4\text{-}NO_2Im)_2$ and $RuCl_2(tmso)_2$(SR-2508) have promising sensitizing enhancement ratio values of 1.6 and 1.5, respectively, and require further biological assessment.

Key words: ruthenium, nitroimidazoles, sulfoxides, radiosensitizers.

PETER K. L. CHAN, BRIAN R. JAMES, DAVID C. FROST, PAUL K. H. CHAN, et HONG-LIANG HU. Can. J. Chem. **67**, 508 (1989).

Au cours de nos études sur les complexes métalliques radio-sensibilisateurs, on a trouvé un complexe – le $RuCl_2(dmso)_2(NO_2\text{-}4Im)_2$ – qui présente de meilleures propriétés radio-sensibilisatrices et une toxicité inférieure à celle du ligand nitro-4 imidazole libre; les complexes des nitro-4 imidazoles *N*-substitués présentent de moins bonnes propriétés comme radiosensibilisateurs (J. Can. Chim. **66**, 117 (1988)). Dans l'étude rapportée ici, on décrit les effets produits par la substitution du ligand chlorure par le bromure, la substitution du diméthylsulfoxyde (dmso) par le tétraméthylènesulfoxyde (tmso) ainsi que l'utilisation d'une plus grande variété de ligands nitroimidazoles. On a synthétisé une série de complexes du ruthénium(II) de formules $RuCl_2(dmso)_2L_2$ (L = un nitro-2 imidazole); $RuCl_2(tmso)_mL_n$ (L = un nitro-2 (ou -4) imidazole, m = 1 à 3 et n = 1 ou 2) et $RuBr_2(dmso)_2L_n$ (L = un nitro-4 imidazole, n = 1 ou 2) et on les a caractérisés par des méthodes spectroscopiques et, en particulier, par rmn du ^1H et par spectroscopie photoélectrique des rayons-X. On a utilisé le $RuX_2(dmso)_4$ (X = Cl et Br) et le $RuCl_2(tmso)_4$ comme précurseurs. Le ligand *N*-méthyl nitro-4 imidazole (NMe-4NO_2Im) du complexe $RuBr_2(dmso)_2$(NMe-4NO_2Im) se chélate par le N de l'imidazole et l'oxygène du NO_2. Un autre nitro-4 imidazole substitué, le RSU-3159[3] que l'on retrouve dans le complexe $RuCl_2(tmso)$ (RSU-3159), se complexe par le soufre et est vraisemblablement chélaté; le complexe issu d'un nitro-2 imidazole substitué, le $RuCl_2(tmso)_2$(SR-2508), est pentacoordonné et est probablement du type trigonal bipyramidal. Le remplacement du dmso par le tmso n'influence pratiquement pas les propriétés redox et radiosensibilisatrices des complexes nitro-4 imidazoles; toutefois, ces substitutions augmentent leurs propriétés lipophiles. Tel qu'on a pu le démontrer par le fait qu'ils n'inhibent pas les enzymes de restriction, les complexes du tmso (contrairement à leurs analogues dmso) ne se lient pas à l'ADN. Par opposition à leurs analogues du dmso, les complexes du tmso/nitro-2 imidazole sont stables en solutions aqueuses. La substitution d'un Cl^- par un Br^- réduit les propriétés radio-sensibilisatrices des complexes du 4-NO_2IM. A des niveaux de seulement 200 μM, les complexes du $RuCl_2(tmso)(4\text{-}NO_2Im)_2$ et du $RuCl_2(tmso)_2$(SR-2508) présentent des rapports d'augmentation de sensibilité de 1,6 et 1,5 respectivement et nécessitent d'autres examens biologiques.

Mots clés : ruthénium, nitroimidazoles, sulfoxydes, radio-sensibilisateurs.

[Traduit par la revue]

---

[1]Authors to whom correspondence should be addressed.

[2]Present address: Atomic Energy of Canada, Chalk River, Ont., Canada K0J 1J0.

[3]The ligand structures are given in Fig. 1.

Can. J. Chem. Downloaded from www.nrcresearchpress.com by 41.223.56.140 on 09/07/12
For personal use only.

Can. J. Chem. Downloaded from www.nrcresearchpress.com by 41.223.56.140 on 09/07/12
For personal use only.

Introduction

Our interest in ruthenium complexes containing nitroimidazole ligands as radiosensitizers has been detailed elsewhere (1). In essence, by using the DNA-binding properties of Ru to take the nitroimidazole to DNA, we are attempting to improve the radiosensitizing properties of these nitroimidazoles in radioresistant hypoxic cells. The effectiveness of the complexes is measured in cultured mammalian cells by the sensitizing enhancement ratio (SER value), which is defined as the ratio of X-ray doses between hypoxic control and drug to give 1% cell survival.

The complex *cis,cis,cis*-$RuCl_2(dmso)_2(4\text{-}NO_2Im)_2$, **1**, was found to (*i*) have an SER value of 1.6 in hypoxic Chinese hamster ovary (CHO) cells, compared to 1.2 for the free 4-nitroimidazole ligand, (*ii*) bind to DNA, and (*iii*) have low genotoxicity (1–4). These encouraging findings prompted us to explore further this type of ruthenium complex, particularly with the variation of the ligand sets. The present paper reports on some complexes containing bromide, tetramethylenesulfoxide, and other nitroimidazoles; the synthesis, characterization, solution chemistry, and biological properties are discussed. Other reports have focussed on using metals to transport the classic, "electron affinic" nitro-compound radiosensitizers to the DNA target: as well as Ru, systems of Pt (5–9) and Rh (8) have been tested thus far; however, not all complexes sensitize better than the nitro-containing ligand itself (7, 8).

Experimental section

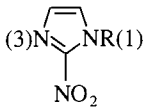
Chemicals and complexes

The sources and syntheses of $RuCl_3 \cdot 3H_2O$, *cis*-$RuCl_2(dmso)_4$, and some of the nitroimidazoles were given in an earlier paper (1). 2-Nitroimidazole (2-NO_2Im) and tetramethylenesulfoxide (tmso) were purchased from Sigma and Aldrich, respectively; 5-chloro-1-methyl-4-nitroimidazole (CMNI) was supplied by Dr. T. C. Jenkins (Medical Research Council, Harwell, Didcot, England); misonidazole (miso) and desmethylmisonidazole (De-miso) were donated by Roche Products Ltd; and etanidazole (SR-2508) was a gift from the US National Cancer Institute. All the imidazoles and tmso were used as received.

$RuCl_2(tmso)_4$, **2**. Some $RuCl_2 \cdot 3H_2O$ (3 g, 11 mmol) was added to previously dried methanol (50 mL), in a two-necked flask equipped with gas-inlet tube, reflux condenser, and magnetic stirrer. The solution was refluxed under H_2 (1 atm) overnight (approximately 16 h) to give a deep blue colour. To the Ru blue solution was added 3 mL of tmso. Refluxing under H_2 was continued for 6 h to yield an orange solution, which was cooled to room temperature (RT), when a yellow precipitate formed. No reaction was observed when the refluxing was carried out under N_2 or Ar. The solid was filtered off in air, washed with acetone, and dried *in vacuo* at RT (1.62 g, 70% yield). *Anal.* calcd. for $C_{16}H_{32}O_4S_4Cl_2Ru$: C 32.61, H 5.48, S 21.74; found: C 32.49, H 5.50, S 21.67. λ_{max} nm (log ϵ), H_2O: 343 (2.54), 303 (2.37). Infrared (Nujol): ν_{SO} 1133, 1094 cm^{-1}.

trans-$RuBr_2(dmso)_4$, **3**. Some $RuCl_2(dmso)_4$ (483 mg, 1 mmol) dissolved in CH_2Cl_2 (75 mL), and NaBr (205 mg, 2 mmol) dissolved in a minimum amount of water (approximately 3 mL), were mixed together, and sufficient methanol (approximately 40 mL) then added to

2-Nitroimidazoles



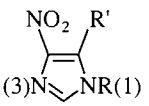
2-Nitroimidazole (2-NO_2Im): R = H

1-(2-Nitro-1-imidazolyl)-3-methoxypropanol, misonidazole (miso): R = CH_2—$CH(OH)CH_2OCH_3$

1-(2-Nitro-1-imidazolyl)-3-hydroxypropanol, desmethylmisonidazole (De-miso): R = CH_2—$CH(OH)CH_2OH$

1-{N-(2-hydroxyethyl)-acetamido}-2-nitroimidazole, etanidazole, SR-2508: R = CH_2—C(=O)—$NHCH_2CH_2OH$

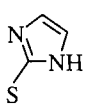
4-Nitroimidazoles



4-Nitroimidazole (4-NO_2Im): R = H, R′ = H

N-Methyl-4-nitroimidazole (NMe-4-NO_2Im): R = CH_3, R′ = H

1-Methyl-5-(2′-thioimidazolyl)-4-nitroimidazole, RSU-3159: R = CH_3, R′ =



5-Chloro-1-methyl-4-nitroimidazole, CMNI: R = CH_3, R′ = Cl

FIG. 1. Structural formulae and numbering scheme for the 2- and 4-nitroimidazole ligands.

Can. J. Chem. Downloaded from www.nrcresearchpress.com by 41.223.56.140 on 09/07/12
For personal use only.

make the two layers miscible. This mixture was refluxed overnight (approximately 16 h) under N_2 to give an orange solution, which was roto-evaporated to dryness. The resulting pale orange solid was dissolved in dmso (3 mL) and the solution heated for 1 h. Acetone (approximately 25 mL) was added to precipitate a pale orange solid, which was filtered off in air, washed with acetone/water mixture (2:1) and acetone, and then dried *in vacuo* at RT (0.34 g, 60% yield). *Anal.* calcd. for $C_8H_{24}O_4S_4Br_2Ru$: C 16.76, H 4.22, S 22.36; found: C 17.01, H 4.24, S 22.46. λ_{max} nm (log ϵ), H_2O: 465 (2.32), 314 (2.17). Infrared (Nujol): ν_{SO} 1080 cm^{-1}. Complex **3** has been made previously by treating $RuBr_3$ with dmso (10, 11).

$RuCl_2(dmso)_2(2\text{-}NO_2Im)_2$, ***4***. The ligand 2-$NO_2$Im (282 mg, 2.5 mmol) was added to $RuCl_2(dmso)_4$ (483 mg, 1 mmol) in dry methanol (15 mL), and the solution refluxed for 6 h under N_2. The resulting blue solution was cooled to RT, when slow addition of diethylether (40 mL) gave a blue precipitate, which was filtered off in air, washed with hexanes and diethylether, and dried *in vacuo* at RT (0.36 g, 65% yield. *Anal.* calcd. fØ $Ç_{10}H_{18}O_6N_6S_2Cl_2Ru$: C 21.66, H 3.25, N 15.16; found: C 21.32, H 3.37, N 15.31. λ_{max} nm (log ϵ), EtOH: 332 (3.72), 420 (2.34). Infrared (Nujol): ν_{SO} 1112, 1084, ν_{NO_2} 1560, 1548 (1567, 1559 cm^{-1} for the free ligand).

$RuCl_2(dmso)_2(miso)_2$, ***5***. The complex $RuCl_2(dmso)_4$ (483 mg, 1 mmol) was added to miso (402 mg, 2 mmol) dissolved in toluene (10 mL), and the mixture refluxed for 6 h under N_2. The resulting blue solution was reduced in volume, and hexanes (30 mL) added slowly to give a blue, oily product. The oily product was cooled in liquid N_2 to yield a blue precipitate, which was filtered in air, washed with diethylether, and dried *in vacuo* at RT (0.36 g, 50% yield). *Anal.* calcd. for $C_{18}H_{34}O_{10}N_6S_2Cl_2Ru$: C 29.63, H 4.69, N 11.51; found: C 29.81, H 4.95, N 11.86. λ_{max} nm (log ϵ), EtOH: 325 (3.82), 638 (1.84). Infrared (Nujol): ν_{SO} 1100, 1089, ν_{NO_2} 1520, 1500 (1528, 1512 cm^{-1} for the free ligand).

$RuCl_2(dmso)_2(De\text{-}miso)_2$, ***6***. Dry methanol (15 mL) was added to $RuCl_2(dmso)_4$ (483 mg, 1 mmol) and De-miso (374 mg, 2 mmol), and the mixture refluxed for 4 h under N_2. The resulting blue solution was filtered hot, and the filtrate cooled to RT to give a blue precipitate. This was filtered off in air, washed with diethylether (20 mL), and dried *in vacuo* at RT (0.55 g, 78% yield). *Anal.* calcd. for $C_{16}H_{30}O_{10}N_6S_2Cl_2Ru$: C 27.35, H 4.30, N 11.96; found: C 27.15, H 4.27, N 12.07. λ_{max} nm (log ϵ), EtOH: 332 (3.57), 584 (2.01). Infrared (Nujol): ν_{SO} 1105, 1078, ν_{NO_2} 1532, 1515 (1538, 1527 cm^{-1} for the free ligand).

$RuCl_2(tmso)_2(4\text{-}NO_2Im)_2$, ***7***. Dry methanol (15 mL) was added to **2** (588 mg, 1 mmol) and 4-NO_2Im (282 mg, 2.5 mmol), and the solution refluxed for 4 h under N_2. The resulting brown solution was roto-evaporated to a reduced volume (3 mL) and diethylether/hexane (1:1) mixture (30 mL) added slowly to precipitate out a brown product, which was filtered off in air, washed with acetone and diethylether, and dried *in vacuo* at RT (0.33 g, 55% yield). *Anal.* calcd. for $C_{14}H_{22}O_6N_6S_2Cl_2Ru$: C 27.72, H 3.65, N 13.86; found: C 27.84, H 3.48, N 13.95. λ_{max} nm (log ϵ), EtOH: 330 (3.88). Infrared (Nujol): ν_{SO} 1102, 1075, ν_{NO_2} 1557, 1537 (1560, 1550 cm^{-1} for the free ligand).

$RuCl_2(tmso)_2(NMe\text{-}4\text{-}NO_2Im)_2$, ***8***. Complex **2** (588 mg, 1 mmol) was suspended in a methanol solution (20 mL) of NMe-4-NO_2Im (254 mg, 2 mmol), and the mixture refluxed for 6 h under N_2. The resulting blue solution was filtered hot and cooled to RT; slow addition of diethylether (30 mL) yielded a blue solid, which was filtered off in air, washed with acetone, and diethylether, and dried *in vacuo* at RT (0.44 g, 69% yield). *Anal.* calcd. for $C_{16}H_{26}O_6N_6S_2Cl_2Ru$: C 30.28, H 4.13, N 13.25; found: C 30.45, H 4.26, N 13.59. λ_{max} nm (log ϵ), H_2O: 309 (3.92), 413 (2.87). Infrared (Nujol): ν_{SO} 1115, 1088, ν_{NO_2} 1554, 1538 (1565, 1545 cm^{-1} for the free ligand), ν_{NCH_2-H} 2809 (2815 cm^{-1} for the free ligand).

$RuCl_2(tmso)_2(De\text{-}miso)_2$, ***9***. The De-miso ligand (374 mg, 2 mmol) was added to **2** (588 mg, 1 mmol) in dry methanol (10 mL), and the mixture refluxed for 6 h under N_2. The resulting blue solution was cooled to RT and filtered; slow addition of diethylether (30 mL) to the filtrate yielded a blue solid, which was filtered off in air, washed with acetone, and dried *in vacuo* at RT (0.54 g, 72% yield). *Anal.* calcd. for $C_{20}H_{34}O_{10}N_6S_2Cl_2Ru$: C 31.83, H 4.54, N 11.13; found: C 32.22, H 4.84, N 11.29. λ_{max} nm (log ϵ), H_2O: 330 (3.24), 532 (1.93). Infrared (Nujol): ν_{SO} 1114, 1078, ν_{NO_2} 1534, 1515 cm^{-1}.

$RuCl_2(tmso)_2(SR\text{-}2508)$, ***10***. The SR-2508 ligand (428 mg, 2 mmol) was added to **2** (588 mg, 1 mmol) in dry methanol (10 mL), and the solution refluxed for 4 h under N_2. The resulting blue solution was filtered hot and diethylether (30 mL) added slowly to the cooled filtrate to precipitate a blue solid; this was filtered off in air, washed with acetone and diethylether, and dried *in vacuo* at RT (0.44 g, 74% yield). *Anal.* calcd. for $C_{15}H_{26}O_6N_4S_2Cl_2Ru$: C 30.30, H 4.41, N 9.43; found: C 30.38, H 4.73, N 9.04. λ_{max} nm (log ϵ), H_2O: 341 (3.39), 495 (1.82). Infrared (Nujol): ν_{SO} 1093, 1050, ν_{NO_2} 1532, 1508 (1538, 1517 cm^{-1} for the free ligand).

$RuCl_2(tmso)_3(CMNI)$, ***11***. The compound CMNI)322 mg, 2 mmol) was mixed with **2** (588 mg, 1 mmol) in dry methanol (10 mL), and the solution refluxed for 6 h under N_2. The resulting green solution was cooled to RT, and diethylether (30 mL) was added slowly to precipitate out a green product. This was filtered off, washed with acetone, and dried *in vacuo* at RT (70% yield). *Anal.* calcd. for $C_{16}H_{28}O_5N_3S_3Cl_3Ru$: C 29.74, H 4.37, N 6.50; found: C 30.01, H 4.42, N 6.75. λ_{max} nm (log ϵ), H_2O: 320 (3.71), 381 (2.71). Infrared (Nujol): ν_{SO} 1094, 1057, ν_{NO_2} 1593, 1574 (1587, 1568 cm^{-1} for the free ligand).

$RuCl_2(tmso)(RSU\text{-}3159)$, ***12***. Complex **2** (588 mg, 1 mmol) was added to RSU-3159 (450 mg, 2 mmol) in methanol (15 mL), and the mixture refluxed for 6 h under N_2. The resulting dark green solution was filtered hot, and diethylether (40 mL) added slowly to the cooled filtrate to precipitate a green solid; this was filtered off in air, washed with acetone and diethylether, and dried *in vacuo* at RT (0.31 g, 62% yield). *Anal.* calcd. for $C_{11}H_{15}O_3N_5S_2Cl_2Ru$: C 26.34, H 3.01, N 13.97; found: C 26.33, H 2.93, N 13.74. λ_{max} nm (log ϵ), H_2O: 330 (3.89). Infrared (Nujol): ν_{SO} 1106, 1079, ν_{NO_2} 1681, 1652 (1673, 1641 cm^{-1} for the free ligand).

$RuBr_2(dmso)_2(4\text{-}NO_2Im)_2$, ***13***. Dry methanol (15 mL) was added to **3** (573 mg, 1 mmol) and 4-NO_2Im (282 mg, 2.5 mmol), and the solution refluxed for 4 h under N_2. The resulting brown solution was cooled to RT and diethylether (40 mL) added slowly to precipitate out a brown product, which was filtered off in air, washed with acetone and diethylether, and dried *in vacuo* at RT (0.45 g, 70% yield). *Anal.* calcd. for $C_{10}H_{18}O_6N_6S_2Br_2Ru$: C 18.67, H 2.82, N 13.06; found: C 18.43, H 2.71, N 12.78. λ_{max} nm (log ϵ), EtOH: 347 (4.17). Infrared (Nujol): ν_{SO} 1099, 1084, ν_{NO_2} 1552, 1539 cm^{-1}.

$RuBr_2(dmso)_2(NMe\text{-}4\text{-}NO_2Im)$, ***14***. Complex **3** (572 mg, 1 mmol) was dissolved in a methanol solution (15 mL) of NMe-4-NO_2Im (254 mg, 2 mmol) and the mixture refluxed for 4 h under N_2. The resulting blue solution was cooled to RT, when a blue precipitate formed. This was collected, washed with diethylether (20 mL), and dried *in vacuo* at RT (0.38 g, 70% yield). *Anal.* calcd. for $C_8H_{17}O_4N_3S_2Br_2Ru$: C 17.65, H 3.15, N 7.72; found: C 17.72, H 3.31, N 7.84. λ_{max} nm (log ϵ), H_2O: 306 (4.28), 440 (3.01). Infrared (Nujol): ν_{SO} 1092, 1073, ν_{NO_2} 1542, 1521 cm^{-1}.

Microanalyses were performed by Mr. P. Borda of the Department of Chemistry, U.B.C.

Physical techniques and methods

Equipment and procedures have been described in earlier papers (1–4, 12), except that a new X-ray source (Philips RT 250, 250 kV, 0.5 mm Cu) was used in the radiosensitization experiments. Briefly, assessment of radiosensitization and toxicity of compounds was carried out using Chinese hamster ovary cells in suspension, with hypoxia produced by nitrogen flow, and colony-forming ability at 7 days being the survival end-point. DNA-binding was indicated by inhibition of restriction endonuclease activity on plasmid pSV2-gpt DNA (12). Reduction potentials were determined by polarography. Partition coefficients (P) of the complexes and ligands were measured by equilibrating aqueous PBS solutions (0.01 *M* phosphate-buffered saline) of the appropriate compounds with *n*-octanol at 25°C, and determining the final concentrations of the species in the aqueous phase spectrophotometrically: P = (concentration in octanol)/(concentration in aqueous layer), where the concentration in octanol was obtained by difference (13). All solution studies were carried out under N_2.

TABLE 1. XPS data for Ru(II) compounds and free ligands[a]

Atom	Compound[b]	Group	BE[c]	FWHM[c]
N	**1** *Ru'*(4-NO_2Im)$_2$	—NO_2	405.5 (405.35)	2.5 (2.6)
(1*s*)		N(3)	400.1 (399.7)	2.4 (2.6)
		N(1)	398.7 (398.1)	2.4 (2.5)
	8 *Ru'*(NMe-4-NO_2Im)$_2$	—NO_2	405.2 (404.9)	2.6 (2.4)
		N(3)	400.4 (399.8)	2.5 (2.4)
		N(1)	398.9 (397.9)	2.5 (2.4)
	10 *Ru'*(SR-2508)	—NO_2	404.6 (404.4)	2.4 (2.3)
	14 *Ru'*(NMe-4-NO_2Im)	—ONO	405.3 (404.9)	2.5 (2.4)
		N(3)	400.6 (399.8)	2.4 (2.3)
		N(1)	399.0 (397.9)	2.5 (2.3)
O	**2** $RuCl_2(tmso)_4$	—S(O)	530.9	3.6
(1*s*)	**3** *trans*-$RuBr_2(dmso)_4$	—S(O)Me_2	531.7	
	7 *Ru'*(4-NO_2Im)$_2$	—NO_2	531.9 (531.7)	3.6 (3.3)
		—S(O)	531.2	3.8
	8 *Ru'*(NMe-4-NO_2Im)$_2$	—NO_2	531.9 (531.9)	3.6 (3.8)
		—S(O)	531.2 (531.45)	3.8
	10 *Ru'*(SR-2508)	—NO_2	532.0 (530.4)	3.6 (3.5)
		—C=O	531.5	3.6
		—S(O)	531.2	3.8
		—OH	530.4	3.4
	11 *Ru'*(tmso)(CMNI)	—NO_2	532.0 (531.95)	3.5 (3.4)
		—S(O)	531.2	
	14 *Ru''*(NMe-4-NO_2Im)	—ONO	531.8 (530.7)	3.6 (3.5)
			530.9	
		—S(O)Me_2	531.7	
S	**2** $RuCl_2(tmso)_4$	—S(O)	165.1	2.7
($2p_{1/2,3/2}$)	**7** *Ru'*(4-NO_2Im)$_2$	—S(O)	165.1	2.9
	8 *Ru'*(NMe-4-NO_2Im)$_2$	—S(O)	165.2	2.9
	10 *Ru'*(SR-2508)	—S(O)	164.7	2.8
	12 $RuCl_2$(tmso)(RSU-3159)	—S(O)	165.1	
		—S	163.9 (163.0)	2.8 (2.7)
	14 *Ru''*(NMe-4-NO_2Im)	—S(O)	165.8	2.9

[a]XPS binding energies and peak widths given in eV; estimated maximum error ±0.15 eV; FWHM is peak width at half-maximum.

[b]*Ru'* and *Ru''* represent $RuCl_2(tmso)_2$ and $RuBr_2(dmso)_2$, respectively.

[c]The number in parentheses is the BE/FWHM for the corresponding atom in the free ligand; BE values for atoms are given in ref. 15.

Results and discussion

The complexes made and their structural types will be first summarized, the spectroscopic data and assignments being considered in later sections.

Complexes **4–6**, $RuCl_2(dmso)_2L_2$ (L = 2-NO_2Im, miso, and De-miso), like the analogue **1** (L = 4-NO_2Im) reported on previously (1), are synthesized from *cis*-$RuCl_2(dmso)_4$[4] by a net substitution of *cis* disposed sulfoxide ligands (one O- and one S-bonded), and have a *cis,cis,cis*-geometry with two S-bonded dmso ligands, as evidenced by the XPS, ^{1}H nmr, and ir data. The $RuCl_2(tmso)_4$, **2**, is a new complex but, unlike *cis*-$RuCl_2(dmso)_4$ (14), contains no O-bonded sulfoxide and is probably of *trans* geometry. The complexes of formulation $RuCl_2(tmso)_2L_2$, **7–9** (L = 4-NO_2Im, NMe-4-NO_2Im, and De-miso), $RuCl_2(tmso)_2$(SR-2508) **10**, $RuCl_2(tmso)_3$(CMNI) **11**, and $RuCl_2$(tmso)(RSU-3159) **12**, are synthesized from **2** by substitution of one to three of the S-bonded tmso ligands. Complexes **7–12** contain only S-bonded sulfoxides but the geometric arrangements of the total ligand sets are in general uncertain. The *trans*-$RuBr_2(dmso)_4$ complex[4] containing only S-bonded sulfoxides (11) provides routes into $RuBr_2(dmso)_2$-(4-NO_2Im)$_2$ **13**, and $RuBr_2(dmso)_2$(NMe-4-NO_2Im) **14**, these containing S-bonded sulfoxides only; **13** is a purely *trans* structure, while **14** contains a chelated imidazole (via the imidazole nitrogen and oxygen of the NO_2 group), *cis* sulfoxides and *trans* bromide ligands.

X-ray photoelectron spectroscopic data

Application of XPS to these Ru/sulfoxide/imidazole type complexes was described earlier (1), and has proved to be invaluable in that we have been frustratingly unsuccessful in attempts to grow crystals of sufficient quality for X-ray analysis. The XPS data for the N, O, and S atoms within complexes **7**, **8**, **10–12**, **14**, and $RuCl_2(tmso)_4$, and for some of the free ligands, are summarized in Table 1. The N assignments have been discussed previously (1), and in **7** and **8**, as for the dmso analogue of **7** (1), the coordination shifts for N(3) (400.1 vs. 399.70, and 400.4 vs. 399.8 eV) appear smaller than expected, perhaps because of π-donation from the low-spin Ru(II) centre. Chelation via the oxygen of the nitrito group of NMe-4-NO_2Im in **14** is evidenced by the doublet seen for the O 1*s* of the NO_2 group (531.8 and 530.9 eV), as well as perhaps by the greater shift to higher BE of N(3) (0.8 eV) compared to the case for **7** (0.4 eV) and **8** (0.6 eV); corresponding chelation data were found for the chloro analogue $RuCl_2(dmso)_2$(NMe-4-NO_2Im) (1) but it is interesting to note that **8**, $RuCl_2(tmso)_2$-

[4]NOTE ADDED IN PROOF: A recent paper (28) has described the previously unknown isomers, *trans*-$RuCl_2(dmso)_4$ and *cis*-$RuBr_2(dmso)_4$.

Can. J. Chem. Downloaded from www.nrcresearchpress.com by 41.223.56.140 on 09/07/12
For personal use only.

Can. J. Chem. Downloaded from www.nrcresearchpress.com by 41.223.56.140 on 09/07/12
For personal use only.

$(NMe\text{-}4\text{-}NO_2Im)_2$, the tmso analogue, contains two monodentate nitroimidazole ligands, the single O 1*s* BE of the NO_2-group (531.9) being close to that of the free ligand (531.7 eV). Why the more sterically demanding tmso ligand (vs. dmso) allows for a higher coordination number is not immediately clear. The dmso complex is thought to contain *trans*-sulfoxides and *cis*-chlorides, while the arrangement of the ligands within **8** is unknown (see below): *cis*-sulfoxides, each *trans* to a nitroimidazole ligand, with *trans*-chlorides could perhaps accommodate sterically the six monodentate ligands. The N and O data for the NO_2 group within **10** rule out chelation for the SR-2508 ligand and, together with the ^1H nmr data (see below), show five-coordinate geometry for this complex.

The XPS data distinguish nicely between O- and S-bonded sulfoxides in these types of complexes (1), and the appropriate O 1*s* data for $RuCl_2(tmso)_4$, **2**, and $RuBr_2(dmso)_4$, **3**, reveal only one type of sulfoxide (shown by ^1H nmr, and crystallographic data for **3** (11) to be S-bonded). The corresponding O 1*s* and S $2p_{1/2,3/2}$ data for **7**, **8**, **10**–**12**, and **14** indicate only S-bonded sulfoxides in all these species. The S $2p_{1/2,3/2}$ BE for **10** is 0.4–0.5 eV less than the values for **2**, **7**, and **8**, indicating a weaker interaction between the Ru and the sulfur atoms in **10**, which is consistent with axial tmso ligands in a trigonal bipyramidal geometry.

The BE for the S $2p_{1/2,3/2}$ in the thioether sulfur of RSU-3159 (163.0 eV) is increased by 0.9 eV within $RuCl_2(tmso)$ (RSU-3159) **12**, strongly implying coordination via this sulfur. The less sterically demanding dmso ligand (vs. tmso) gives rise to a $RuCl_2(dmso)_2$ (RSU-3159) complex (1). The RSU-3159 ligand is considered to be chelated via the sulfur and the nitrogen of the NMe group (see below).

Infrared and nuclear magnetic resonance data

Bonding through the S of a sulfoxide increases the ν_{SO} with respect to the free ligand value, this being 1050 and 950 cm^{-1} for dmso and tmso, respectively (16–18). The ir data for all the new complexes **2** and **4**–**14** (see Experimental section) show bands consistent with S-bonded sulfoxides. Bands seen at 1075, 1035, 952, and 875 cm^{-1} for $RuCl_2(tmso)_4$ must be due to ν_{ring} (17, 18), because the XPS and ^1H nmr data show the presence of only S-bonded tmso. The 1080 cm^{-1} ν_{SO} band found for **3** agrees with that reported previously (11).

All the complexes have ir bands at about 1520–1560 and at 1500–1550 cm^{-1}, attributable to asymmetric and symmetric ν_{NO_2}, respectively (19), the values in general being up to 24 cm^{-1} lower than the free ligand values. The single exception is found in **11**, $RuCl_2(tmso)_3(CMNI)$, where the ν_{NO_2} values are 6 cm^{-1} *higher* than the values for CMNI itself; this is the only complex that contains three sulfoxide ligands, including the earlier series of 4-nitroimidazole derivatives (1), and implies some enhanced π-donation from the Ru(II) to the CMNI ligand. The coordination shifts for **14** are at the high end, entirely consistent with chelation of the $NMe\text{-}4\text{-}NO_2Im$ ligand, consistent with the XPS data.

The coordination shifts in ν_{NO_2} for **10** are small and are consistent with no coordination via NO_2, and thus five-coordinate geometry as indicated by the XPS (and nmr) data. The ν_{NO_2} values for the bromo complexes **13** and **14** are very similar to those of the chloro analogues synthesized earlier (1). As noted in the earlier work (1), we have been unable to assign metal–halide stretches in the far-ir region, because of the many bands seen in the 400–250 cm^{-1} region; also, the bromo derivatives **13** and **14** have different geometrical arrangements of ligands than the "corresponding" chloro analogues (see below), and this makes comparisons of the ir spectra difficult.

Coordination through the sulfur of an alkyl sulfoxide typically deshields the α-protons of the sulfoxide by ~1–2 ppm, while the deshielding is only ~0.1 ppm for coordination via the oxygen (16). Table 2 summarizes the relevant ^1H nmr data. The methyl resonances of dmso, and the methylene resonances of tmso, appear at values corresponding to S-bonded sulfoxide only for all the complexes, the data complementing well the XPS data. Complexes **4**–**6** and **13** and **14** show the dmso protons some 0.8–1.1 ppm downfield from the free dmso resonance at δ 2.60. In D_2O or non-dried $CDCl_3$, **5** and **6** dissociate nitroimidazole ligand(s) (see later) and more complex multiplets for the methyl resonances are evident, but no free dmso is observed. The data for **3**, known to be of *trans* geometry with four S-bonded dmso ligands in the solid state (11), agree with those reported in the literature (10, 11). The ^1H nmr spectrum of free tmso in $CDCl_3$ shows three sets of multiplets centred at δ 2.60 (S—C—CH_2CH_2), 2.19 (S—CH_2), and 1.75 (S—CH_2) ppm with an integration ratio of 2:1:1, respectively, in agreement with literature values (18). On coordination to Ru(II), the two S—CH_2 resonances are shifted downfield by ~1.7–2.0 ppm, while the S—C—CH_2CH_2 resonance(s) move the other way by up to 0.3 ppm. For **2**, the 1:1:2 multiplets centred at δ 4.00, 3,42, and 2.30 ppm imply equivalent tmso ligands, and thus a *trans* configuration for this complex.

The presence of four major, equal intensity, partly resolved Me multiplets for **4**–**6** reveals inequivalent Me groups for each of two inequivalent dmso ligands, and only the low symmetry, all *cis*-structure, of 6-coordinate complexes gives such an nmr pattern (20). The data correspond to those reported earlier for the $RuCl_2(dmso)_2L_2$ systems where L = a $4\text{-}NO_2Im$ derivative (1). The Me data for the dibromo complex **13** are markedly different, showing two quartets centred at δ 3.70 and 3.59 ppm which is interpreted as inequivalent methyls for each of two equivalent dmso ligands; this requires an all *trans* geometry and, of note, the precursor **3** has such geometry. By corresponding arguments, the chelated, 6-coordinate complex **14** must have *cis*, inequivalent sulfoxides and *trans* bromides, which contrasts with the chloro analogue which has *trans*-sulfoxides and *cis*-chlorides (1).

The ^1H nmr spectra for **7**–**12** show five sets of multiplets for the CH_2 resonances of tmso, centred at the δ values listed in Table 2, in each case with an integration ratio of 2:1:1:2:2 on going from lower to higher field. These relative intensities suggest that the two protons of one of the S—CH_2 groups of the coordinated tmso ligand are magnetically inequivalent. This perhaps results from the fixed orientation of the S=O when the tmso ligand is coordinated, so that one of the S—CH_2 protons will be in the same "plane" as the O—S—C atoms and the other one will be out of the "plane". If this explanation is correct, one would expect to observe a similar effect by the other S—CH_2 groups, giving rise to four sets of S—CH_2 and two sets of S—C—CH_2—CH_2 multiplets with an integration ratio of 1:1:1:1:2:2. However, this is not observed; perhaps the coupling between one set of S—CH_2 protons is smaller and the multiplet signal overlaps to give the observed 2:1:1:2:2 integration ratio. Complexes **7**–**12** all give similar —CH_2— nmr patterns, and yet **7**–**9** and **11** are 6-coordinate containing two or three tmso ligands, **12** is 5-coordinate containing one tmso ligand, and **10** is 5-coordinate containing two tmso ligands: we consider it unwise to speculate on the relative ligand arrangements. Complex **7**, based on some aqueous solution chemistry,

TABLE 2. Selected ^{1}H nmr spectral data for the Ru(II) compounds and the free imidazole ligands[a]

Compound[b]	^{1}H nmr spectra H-4[c]	H-5[c]	CH_3(dmso)	CH_2(tmso)
2 $RuCl_2(tmso)_4$				2.30, 3.42, 4.00
3 *trans*-$RuBr_2(dmso)_4$			2.6, 3.35, 3.41 3.46, 3.57	
4 *Ru*(2-NO_2Im)$_2$	8.39 (8.37)	8.03 (7.99)	3.41, 3.46 3.50, 3.53	
5 *Ru*(miso)$_2$[d]	7.20 (7.19)	7.15 (7.11)	3.39, 3.48 3.50, 3.52	
6 *Ru*(De-miso)$_2$[e]	7.53 (7.45)	7.24 (7.19)	3.48, 3.53 3.61, 3.62	
9 *Ru'*(De-miso)$_2$[e]	7.48 (7.45)	7.38 (7.19)		2.20, 2.50, 3.12, 3.27, 3.08
10 *Ru'*(SR-2508)[f]	7.51 (7.45)	7.48 (7.24)		2.21, 2.51, 3.22, 3.31, 3.77

Compound[b]	^{1}H nmr spectra H-2[c]	H-5[c]	CH_3(dmso)	CH_2(tmso)
7 *Ru'*(4-NO_2Im)$_2$	8.92 (8.25)	8.21 (7.80)		2.20, 2.45, 3.15, 3.65, 4.00
8 *Ru'*(NMe-4-NO_2Im)$_2$[g]	7.91 (7.54)	8.25 (7.87)		2.23, 2.40, 3.45, 3.51, 4.00
11 *Ru'*(tmso)(CMNI)[g]	7.01 (7.00)			2.00, 2.13, 3.15, 3.35, 3.75
12 $RuCl_2$(tmso)(RSU-3159)[g]	7.73 (7.92)			2.21, 2.51, 3.21, 3.31, 3.75
13 *Ru''*(4-NO_2Im)$_2$	8.91 (8.25)	8.20 (7.80)	3.59, 3.70	
14 *Ru''*(NMe-4-NO_2Im)[g]	8.03 (7.54)	8.80 (7.87)	3.61, 3.65	

[a]δ in ppm with respect to TMS, in $CDCl_3$ at room temperature. In each case the integrations are consistent with the assignment. Resonances for the sulfoxide protons are multiplets, centred at the values shown; those for **13** are quartets; the imidazole protons appear as singlets.

[b]As in footnote *b* of Table 1, and *Ru* represents $RuCl_2$(dmso).

[c]Shifts in parentheses are for the free nitroimidazole ligand.

[d]Shifts for N—CH_2, CH_2—OCH_3, CH(OH), and —OCH_3 are at δ (ppm), 4.66 m, 4.42 m, 4.15 m, and 3.41 s, respectively, and are the same for the free miso ligand.

[e]Shifts for the N—CH_2, CH(OH), and CH_2OH are at δ (ppm) 4.39 m, 4.10 m, and 3.66 m ppm, respectively, and are the same for the free De-miso ligand.

[f]Shifts for the N—CH_2—C(O), —(O)CN(H)—CH_2 and CH_2OH are δ (ppm) 5.23 s, 3.66 t, and 3.39 t ppm, respectively, and are the same for the free SR-2508 ligand.

[g]Shifts for N—CH_3 δ (ppm): **8**, 3.91 (3.90)[c]; **11**, 3.56 (3.49)[c]; **12**, 3.62 (3.49)[c]; **14**, 3.95 (3.90).[c]

is, however, likely to be of the same all *cis* structure as the corresponding dmso analogue.

The relevant H-2, H-4, and H-5 resonances are, in every case except for **12**, slightly downfield compared with the free ligand values, similar to the situation in the 4-NO_2Im systems reported previously (1). With the chelated NMe-4-NO_2Im system, **14**, the effects are more marked, while the data for **10** (including footnote *f*) confirm no chelation by the SR-2508 ligand. In **12** there is an upfield shift for H-2, as well as a somewhat larger downfield shift (0.13 ppm) for the NMe protons; the data resemble those of the corresponding $RuCl_2$-$(dmso)_2$(RSU-3159) complex (1), and again are interpreted in terms of chelation via the S and nitrogen of NMe.

The $^{13}C(^1H)$ spectra for **13** and **14** are compatible with the corresponding ^{1}H nmr data: **13** has two ^{13}C shifts at δ 45.21 and 47.22 for the methyls of the two equivalent dmso ligands (as well as imidazole resonances at 112.35(C-2), 116.13(C-5), and 119.89(C-4)), while **14** has four peaks (δ 44.91, 45.16, 47.12, 47.58) for the inequivalent methyls (as well as imidazole resonances at 108.62(C-2), 112.39(C-5), 116.16(C-4), and 119.93(N-Me)). The small but significant differences in the imidazole carbon shifts for **13** and **14** compared to the chloro analogues (1) reflect (as do the ^{1}H nmr) differences in the geometrical isomers present (see above).

Aqueous solution chemistry

In water **4**, which contains the unsubstituted 2-NO_2Im ligand, does not dissociate a nitroimidazole, Cl^- or dmso, and the blue colour of the solution persists. When the substituted 2-nitroimidazole complexes **5** and **6** are dissolved in water, PBS, or water/PBS containing a 10-fold excess of Cl^- or dmso, the blue colour of the solutions disappears in about 5 min. The visible bands at 638 and 584 nm for complexes **5** and **6**, respectively, as observed in dry ethanol solution or in the solid state,

Can. J. Chem. Downloaded from www.nrcresearchpress.com by 41.223.56.140 on 09/07/12
For personal use only.

disappear. However, if the complexes are dissolved in water containing a 10-fold excess amount of the respective imidazole ligands, the colour of the solutions remains blue and the spectra are unchanged; the solutions are non-acidic and non-conducting and no Cl^- is liberated. These results together with the ^1H nmr data in D_2O indicate that the disappearance of the blue colour is due to the dissociation of the nitroimidazole ligand(s) and that the presence of the following aquation/anation equilibrium exists (L = miso, De-miso):

[1] $RuCl_2(dmso)_2L_2 + H_2O \rightarrow RuCl_2(dmso)_2(H_2O)_xL_y + xL$

Blue (**5**, **6**) Colourless ($x + y = 2$)

The different solution behaviour for **5** and **6** compared to **4** presumably reflects the hydrophilic nature of the hydroxy-containing substituents of the miso and De-miso systems which favours dissociation of the free ligands in the aqueous media. The aquation phenomenon (eq. [1]) is not observed for the tmso analogues **9** and **10**, and their aqueous solutions remain blue. Complexes **6** and **9** are analogous except for the sulfoxide ligands and the difference in aquation phenomenon may reflect the presence of different geometrical isomers (see above) or the more lipophilic tmso ligand in **9** (see below).

The aqueous solution behaviour of **7** follows closely that of the dmso analogue $RuCl_2(dmso)_2(4\text{-}NO_2Im)_2$ **1** (1): a molar conductivity of 108 $ohm^{-1}\,mol^{-1}\,cm^2$ results from loss of a chloride, and weak acidity results from a coordinated water ($pK_a = 4.40 \pm 0.10$, eq. [2]), while a second proton loss at higher pH ($pK_a = 9.01 \pm 0.10$) is attributed to loss of a pyrrolic-*N* hydrogen to form coordinated 4-nitroimidazolate.

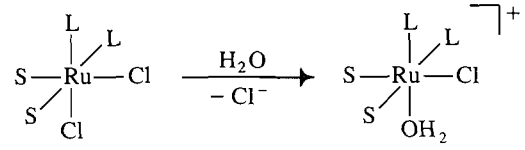
[2] $7 \xrightarrow[+H_2O]{-Cl^-} [RuCl(H_2O)(tmso)_2(4\text{-}NO_2Im)_2]^+$

$\xrightarrow{-H^+} RuCl(OH)(tmso)_2(4\text{-}NO_2Im)_2$

The pK_a values for the dmso analogue are 4.10 and 8.90 and the similarity in data suggests corresponding structures (all *cis*).

Aqueous solutions of **8**–**12** and **14** show no titratable protons are present at least up to pH 11 and, consistent with this, molar conductivity values measured within 10 min of dissolution are lower (18.0–30.0), showing little replacement of Cl^- by H_2O.

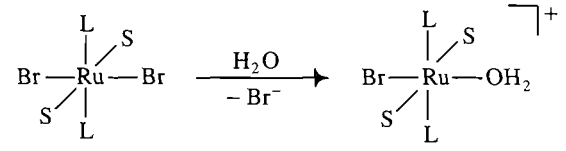
On dissolution in water **13**, $RuBr_2(dmso)_2(4\text{-}NO_2Im)_2$, instantly gives a molar conductivity of 118.7, corresponding to a 1:1 electrolyte formed by loss of a single Br^- (confirmed by $AgNO_3$ titration); however, the aquo derivative $[RuBr(H_2O)(dmso)_2(4\text{-}NO_2Im)_2]^+$, unlike the chloro analogues (e.g. [2] for both the tmso (**7**) and dmso (**1**) complexes) does not deprotonate at least up to pH 11. Thus this aquo(bromo) derivative has coordinated H_2O and imidazole ligands that are at least 10^7 and 10^2 times, respectively, less acidic than the corresponding ligands in $[RuCl(H_2O)(dmso)_2(4\text{-}NO_2Im)_2]^+$. The lower acidities are consistent with the presence of more basic bromide ligands, but a more important factor almost certainly arises because of the differences in the geometrical isomers present. The Cl^- loss from the all *cis* complex **1** (1) (and presumably **7**) is likely to be the one *trans* to the 4-NO_2Im (even though dmso has a strong *trans* effect (16)), because the other all *cis* $RuCl_2(dmso)_2L_2$ complexes with L = a substituted 4-NO_2Im (1) or a 2-NO_2Im (**4**–**6**) do not dissociate a Cl^-, i.e. the unsubstituted 4-NO_2Im is unique in labilizing the Cl^-:

[3] 

7, 15

(L = 4-NO_2Im, S = S-bonded tmso (**7**) or dmso (**1**))

For the all *trans* bromo complex **13**, bromide loss must occur according to eq. [4]:

[4] 

13

Now in terms of the pK_a values, for ligands *trans* to water, it has been argued that the higher the *trans* effect, the weaker the metal–oxygen bond and the stronger the oxygen–hydrogen bond, i.e. the weaker the acidity of the coordinated H_2O (21), this being based on data such as those for *cis*- and *trans*-$Pt(NH_3)_2(H_2O)_2^{2+}$ complexes (*cis*, $pK_a = 5.6$; *trans*, $pK_a = 4.3$). However, for the data: *trans*-$Pt(C_2H_4)(H_2O)Cl_2$ ($pK_a = 5$); *cis*-$Pt(NH_3)(H_2O)Cl_2$ ($pK_a \sim 7$), the correlation is clearly not valid because in terms of *trans* effects, $C_2H_4 \gg Cl^-$. Here, the strong π-acid properties of the C_2H_4 were invoked to account for stronger acidity of the water within the ethylene complex (21). The strong *trans* effect – weak acidity argument clearly does not hold for the aquo product of reaction [3] ($pK_a \sim 4$) vs. that of reaction [4] ($pK_a > 12$), because in the former the water is *trans* to 4-NO_2Im which is certain to have a stronger *trans* effect than Br^-. The stronger acidity could be rationalized in terms of the presence of the strong *trans* π-acceptor 4-NO_2Im.

Consistent with the aquation shown in eq. [4], the uv/vis spectrum of **13** in water is independent of pH (λ_{max} 342 nm, $\log \epsilon = 4.02$), this referring to the aquo species, while addition of Br^- regenerates **13** (λ_{max} 347 nm, $\log \epsilon = 4.13$). The uv/vis spectra of **7** and **15** (1) are both pH- and Cl^--dependent. All the new complexes show charge-transfer bands in the 310–500 nm region but they offer no insight into the coordination geometries.

Radiosensitization, toxicity, and related chemical properties

Table 3 lists reduction potentials, SER values, toxicity data, and partition coefficients (*P*) for the ligands, new complexes, and some of the $RuCl_2(dmso)_2L_n$ complexes (L = a 4-nitroimidazole, $n = 1$ or 2) described earlier (1). The techniques used have been given elsewhere (1–4, 12). Complexes **5** and **6** readily dissociate nitroimidazole ligand(s) (see above), but all the others listed are stable to nitroimidazole ligand loss within the 1 and 4 h periods used, respectively, for pre-incubation for the radiosensitizing experiments and for incubation during the toxicity experiments. The $E_{1/2}$, SER, and toxicity data refer to the aqueous solution species present, which is the same as the solid state formulations except for **5** and **6** (see eq. [1]), **7** and **1** (eqs. [2], [3]), and **13** (eq. [4]). The *P* values were measured at equilibrium conditions except for **5** and **6**, which were determined within 4 min of shaking the octanol/aqueous mixtures.

It is seen that the use of tmso, instead of dmso, increases the partition coefficient (lipophilicity) of the complexes. The neu-

Can. J. Chem. Downloaded from www.nrcresearchpress.com by 41.223.56.140 on 09/07/12
For personal use only.

TABLE 3. Reduction potentials, SER values, and PE data for the Ru(II) compounds and the free imidazole ligands[a]

Compound[b]	$E_{1/2}$[c]	SER	PE[d]	P[e]
1 *Ru*(4-NO_2Im)$_2$	−615 (−685)	1.6 (1.2)	0.10 (0.058)	0.42 (0.24)
Ru(NMe-4-NO_2Im)[f]	−500 (−535)	1.35 (1.2)	0.53 (0.49)	0.18 (0.16)
Ru(RSU-3159)[f]	−360 (−370)	1.3 (1.3)	0.16 (0.0027)	0.29 (0.26)
4 *Ru*(2-NO_2Im)$_2$	−435 (−445)	1.4 (1.3)	0.50 (0.003)	
5 *Ru*(miso)$_2$	−385 (−400)	1.4 (1.3)	0.77 (0.75)	0.12 (0.43)
6 *Ru*(De-miso)$_2$	−367 (−389)	1.4 (1.3)	0.14 (0.12)	0.04 (0.13)
7 *Ru'*(4-NO_2Im)$_2$	−605 (−685)	1.6 (1.2)	0.13 (0.058)	0.64 (0.24)
8 *Ru'*(NMe-4-NO_2Im)$_2$	−500 (−535)	1.4 (1.3)	0.53 (0.49)	0.20 (0.16)
9 *Ru'*(De-miso)$_2$	−355 (−389)	1.4 (1.3)	0.42 (0.11)	0.22 (0.13)
10 *Ru'*(SR-2508)[f]	−345 (−388)	1.5 (1.3)	0.099 (0.073)	0.21 (0.05)
11 *Ru'*(tmso)(CMNI)[g]	−490 (−517)	1.3 (1.2)	0.0007 (0.0004)	
12 $RuCl_2$(tmso)(RSU-3159)[f]	−345 (−370)	1.3 (1.2)	0.11 (0.0027)	
13 *Ru"*(4-NO_2Im)$_2$	−645 (−685)	1.25 (1.2)	0.32 (0.058)	0.07 (0.24)
14 *Ru"*(NMe-4-NO_2Im)[f]	−515 (−535)	1.4 (1.2)	0.62 (0.49)	0.14 (0.16)

[a]Ligand and complex concentrations used for the SER values were 400 and 200 μ*M*, respectively, unless stated otherwise. First five entries include $E_{1/2}$ and SER data from refs. 1–3; numbers in parentheses in each column refer to the free nitroimidazole ligand.
[b]As in footnote *b* of Table 2.
[c]Reduction potential, mV vs. SCE.
[d]Toxicity measured by the plating efficiency (PE) after 4 h of incubation at 37°C under hypoxia; a higher PE means lower toxicity, and vice versa.
[e]P = partition coefficient (see text).
[f]The ligand concentrations used for comparative data were 200 μ*M* because the complex contains only one nitroimidazole ligand per Ru; 100 μ*M* was used for **12** and the RSU-3159 ligand.
[g]The concentration used for the complex and CMNI (one ligand per Ru) was 50 μ*M* because of their high toxicity.

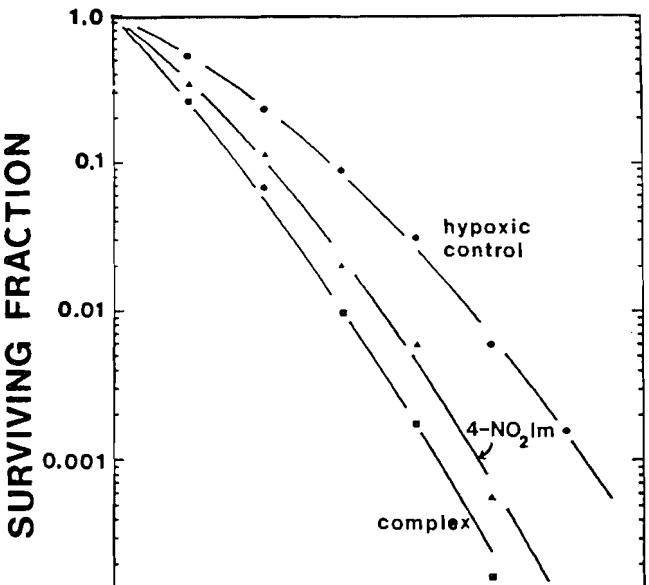


FIG. 2. Radiation response of hypoxic CHO cells treated with 200 μ*M* $RuCl_2(tmso)_2(4\text{-}NO_2Im)_2$, **7**, (■), and 400 μ*M* 4-NO_2Im (▲), compared with a control (●).

tral, aquation product $RuCl(OH)(tmso)_2(4\text{-}NO_2Im)_2$ from **7** has the highest P value (0.64) of all the complexes, while $RuCl(OH)(dmso)_2(4\text{-}NO_2Im)_2$ (from **1**) and **10** have P values (0.42 and 0.21, respectively) higher than the corresponding nitroimidazole ligands (P = 0.24 for 4-NO_2Im, and 0.05 for SR-2508). Moreover, it is noteworthy that **1**, **7**, and **10** have the highest SER values = 1.6, 1.6, and 1.5, respectively: these three complexes show the greatest improvement over the free ligand values (Table 3). The relevant data for **7** are shown in Fig. 2. No radiosensitizing enhancement was observed in hypoxic cells using dmso, tmso, $RuX_2(dmso)_4$ (X = Cl, Br), or $RuCl_2(tmso)_4$ at appropriate concentrations in control experiments, and there is no sensitization of oxic CHO cells to X-rays by any of the complexes or nitroimidazoles.

Coordinated nitroimidazole ligands have higher reduction potentials than the free ligands; that is, the ligand centres are more easily reduced when coordinated to metal, and this increase in reduction potential can be correlated with effectiveness of radiosensitizing ability within a given series of nitroimidazoles (1). The increased ligand reduction potential has been demonstrated for Pt(II) complexes (6, 22) and in our earlier Ru(II) work (1–3). This is again true for the new Ru(II) systems, and the change in potential on coordination of the unsubstituted 4-NO_2Im ligand (**1** and **7**) is significantly greater than for the other imidazole ligands. The absolute potential range does not appear critical in that **10**, an effective sensitizer, "operates" at a potential some 265 mV higher than **1** and **7**. The potential change for the bromide complex **13** (SER 1.25) is 30 mV less than for the chloride **1** (SER 1.6) and these data appear to fit the potential change: SER correlation, but there is certainly no such general correlation within the data of Table 3; indeed, it should be remembered that even within **13** and **7** the solution species present are in fact quite different (see eqs. [2]–[4]). Replacement of dmso by tmso increases the potential by 10–15 mV (**1** vs. **7**, **6** vs. **9**), while the comparable SER values are the same.

The hypoxic toxicity of the complexes toward CHO cells *in vitro*, measured as plating efficiency (PE) at a chosen time of drug treatment, is less than that of the corresponding free imidazole ligand (Table 3). The toxicity of some metal-free nitroheterocyclic compounds has been reported to increase with increasing electron affinity ($E_{1/2}$ value) (23, 24) but this is not

Can. J. Chem. Downloaded from www.nrcresearchpress.com by 41.223.56.140 on 09/07/12
For personal use only.

seen for the nitroimidazoles or Ru(II) complexes that we have used. For 4-nitroimidazoles, the toxicity:electron affinity trend was attributed to depletion of thiols (24); certain radiosensitizers are thought to act by binding free, non-protein sulfhydryl groups (NPSH) which normally have a protective effect in irradiated cells (25). Of the complexes listed, only **5** and **6** under hypoxic conditions deplete non-protein thiol levels (26) but this is presumed to result from the presence of the dissociated miso and De-miso ligands; these ligands, 4-NO_2Im, and SR-2508 (out of all the 2-NO_2- and 4-NO_2Im derivatives used), were the only free ligands found to deplete thiols (26). The enhancement of radiosensitization properties of nitroimidazoles on coordination to Ru does not result from increased depletion of NPSH.

None of the new complexes binds to DNA, as evidenced by their inability to inhibit the activity of certain enzymes (26); complex **1** had been shown previously by such an assay to bind to DNA (2, 3), but clearly this is not an essential factor for effective radiosensitization properties as both **7** and **10** (the former showing aqueous solution behaviour essentially identical to that of **1**) are equally effective.

Factors that could affect radiosensitizing ability were summarized in an earlier paper (1), and many of these are alluded to in this section on biological activities. The new findings reinforce the view that much remains to be done and that, even when attachment of nitroimidazoles to Ru (and Pt(5)) has been documented to improve radiosensitizer properties of the nitroimidazole, the "fine-tuning" of the systems remains thus far a very empirical approach. The extremely diverse coordination chemistry exhibited by the Ru/halide/sulfoxide/nitroimidazole systems even within minor variations in ligand sets has surprised us.

Preliminary *in vivo* experiments suggest that complexes **7** and **10** may have radiosensitizing properties in mouse tumours (27); of note, **10** $RuCl_2(tmso)_2$(SR-2508), which contains only a single nitroimidazole ligand, has one of the highest SER values of 1.5 (see Table 3).

Can. J. Chem. Downloaded from www.nrcresearchpress.com by 41.223.56.140 on 09/07/12
For personal use only.

Acknowledgements

The work was supported by the Natural Sciences and Engineering Research Council of Canada (operating grants to D.C.F. and B.R.J.), the Medical Research Council of Canada (operating grant to K.A.S.), and the British Columbia Cancer Foundation; P.K.L.C. held a UBC Graduate Fellowship. Johnson Matthey, Ltd. kindly loaned the Ru.

1. P. K. L. Chan, P. K. H. Chan, D. C. Frost, B. R. James, and K. A. Skov. Can. J. Chem. **66**, 117 (1988), and references therein.
2. P. K. L. Chan, K. A. Skov, B. R. James, and N. P. Farrell. Int. J. Radiat. Oncol. Biol. Phys. **12**, 1059 (1986).
3. P. K. L. Chan, K. A. Skov, and B. R. James. Int. J. Radiat. Biol. **52**, 49 (1987).
4. P. K. L. Chan, K. A. Skov, B. R. James, and N. P. Farrell. Chem. Biol. Interact. **59**, 247 (1986).
5. N. P. Farrell and K. A. Skov. J. Chem. Soc. Chem. Commun. 1043 (1987).
6. J. R. Bales, C. J. Coulson, D. W. Gilmour, M. A. Maxid, S. Neidle, R. Kurada, B. J. Peast, C. A. Ramsden, and P. J. Sadler. J. Chem. Soc. Chem. Commun. 432 (1983).
7. K. A. Skov, N. P. Farrell, T. Gomes de Carneiro, T. Jones, and F. W. B. Einstein. *In* Proceedings of the Seventh International Congress of Radiation Research. *Edited by* J. J. Broerse, G. W. Barendsen, H. B. Kal, and A. J. Van der Kogel. Martinus Nijhoff, 1983, Abstract B6-29.
8. R. Chibber, I. J. Stratford, I. Ahmed, A. B. Robbins, D. Goodgame, and B. Lee. Int. Radiat. Oncol. Biol. Phys. **10**, 1213 (1984).
9. B. A. Teicher, S. Rockwell, and F. B. Lee. Int. J. Radiat. Oncol. Biol. Phys. **11**, 937 (1985).
10. B. R. James, E. Ochiai, and G. L. Rempel. Inorg. Nucl. Chem. Lett. **7**, 781 (1971).
11. J. D. Oliver and D. P. Riley. Inorg. Chem. **23**, 156 (1984).
12. K. A. Skov, H. Adomat, D. C. Konway, and N. P. Farrell. Chem. Biol. Interact. **62**, 117 (1987).
13. T. Fujita, J. Iwasa, and C. Hansch. J. Am. Chem. Soc. **86**, 5175 (1964).
14. A. Mercer and J. Trotter. J. Chem. Soc. Dalton Trans. 2480 (1975).
15. T. A. Carlson. Photoelectron and Auger spectroscopy. Plenum Press, New York. 1975. p. 349.
16. J. A. Davies. Adv. Inorg. Chem. Radiochem. **24**, 115 (1981).
17. B. R. James and R. H. Morris. Can. J. Chem. **58**, 399 (1980).
18. F. D. Rochon, P. C. Kong, and L. Girard. Can. J. Chem. **64**, 1897 (1986).
19. K. Nakamoto. Infrared spectra of inorganic and coordination compounds. 2nd ed. John Wiley and Sons, Inc., New York. 1970. p. 160.
20. J. R. Barnes and R. J. Goodfellow. J. Chem. Res. Synop. 350 (1979); J. R. Barnes, P. L. Goggin, and R. J. Goodfellow. J. Chem. Res. Synop. 118 (1979).
21. F. Basolo and R. G. Pearson. Mechanisms of inorganic reaction; a study of metal complexes in solution. 2nd ed. John Wiley and Sons, Inc., New York. 1967, p. 367.
22. K. A. Skov, N. P. Farrell, and H. Adomat. Radiat. Res. **112**, 273 (1987).
23. G. E. Adams, I. J. Stratford, R. G. Wallace, P. Wardman, and M. E. Watts. J. Natl. Cancer Inst. **64**, 555 (1980).
24. I. J. Stratford, S. Hoe, G. E. Adams, C. Hardy, and C. Williamson. Int. J. Radiat. Biol. **43**, 31 (1983); H. Loman, S. Voogd, and J. Blok. Radiat. Res. **42**, 437 (1970).
25. R. A. McClelland, R. Panicucci, and A. M. Rauth. J. Am. Chem. Soc. **109**, 4308 (1987).
26. P. K. L. Chan. Ph.D. dissertation. University of British Columbia, Vancouver, B.C. 1988.
27. K. A. Skov, P. K. L. Chan, B. R. James, and N. P. Farrell. Canada Patent Application, Filed March 18, 1988.
28. E. Alessio, G. Mestroni, G. Nardin, W. M. Attia, M. Calligaris, G. Sava, and S. Zorzet. Inorg. Chem. **27**, 4099 (1988).

Vibrational spectral studies of solutions at elevated temperatures and pressures. 11. A Raman spectral study of aqueous iron(III) chloride solutions between 25 and 300°C

KATSUO MURATA,[1] DONALD E. IRISH,[2] AND GERALD E. TOOGOOD
Department of Chemistry, University of Waterloo, Waterloo, Ont., Canada N2L 3G1

Received August 31, 1988

KATSUO MURATA, DONALD E. IRISH, and GERALD E. TOOGOOD. Can. J. Chem. **67**, 517 (1989).

The Raman spectra of acidified aqueous iron(III) chloride solutions have been measured between 25 and 300°C. When Fe^{3+} concentrations are in the range 0.75 to 1.0 mol kg^{-1} and Cl^-/Fe^{3+} ratios, R, in the range 3 to 9.5, the dominant species at 25°C is *trans*-$[Fe(H_2O)_4Cl_2]^+$; at 300°C the sole iron-containing species is tetrahedral $FeCl_4^-$. Conversion of $[Fe(H_2O)_4Cl_2]^+$ into $FeCl_4^-$ appears not to involve intermediate iron species. In the presence of excess chloride the reaction $[Fe(H_2O)_4Cl_2]^+ + 2Cl^- \rightarrow FeCl_4^- + 4H_2O$ is presumed to occur; ΔH for this reaction has been estimated as $+65 \pm 8$ kJ mol^{-1}. In addition to increasing temperature, factors which favour $FeCl_4^-$ over other iron species include increasing acidity, increasing R, and decreasing dielectric constant.

Key words: high temperature aqueous solutions, iron(III) chloride, Raman spectroscopy.

KATSUO MURATA, DONALD E. IRISH et GERALD E. TOOGOOD. Can. J. Chem. **67**, 517 (1989).

Opérant à des températures allant de 25 à 300°C, on a mesuré les spectres Raman de solutions aqueuses acides de chlorure ferrique. A 25°C, à des concentrations de Fe^{3+} allant de 0,75 à 1,0 mol kg^{-1} et à des rapports de Cl^-/Fe^{3+} (R) allant de 3 à 9,5, l'espèce dominante est le $[Fe(H_2O)_4Cl_2]^+$-*trans*; à 300°C, la seule espèce contenant du fer est le $FeCl_4^-$ tétraédrique. La conversion du $[Fe(H_2O)_4Cl_2]^+$ en $FeCl_4^-$ ne semble pas impliquer d'espèces intermédiaires contenant du fer. En présence d'un excès d'ions chlorures, on suppose que le réaction $[Fe(H_2O)_4Cl_2]^+ + 2Cl^- \rightarrow FeCl_4^- + 4H_2O$; on a évalué que le ΔH de cette réaction est égal à $+65 \pm 8$ kJ mol^{-1}. En plus de l'augmentation de la température, les facteurs qui favorisent la formation du $FeCl_4^-$ par rapport aux autres espèces du fer sont les augmentations de l'acidité et de R et une diminution de la constante diélectrique.

Mots clés : solutions aqueuses à des températures élevées, chlorure ferrique, spectroscopie de Raman.

[Traduit par la revue]

Introduction

The nature and relative importance of species existing in aqueous solutions of ferric chloride have been studied by numerous investigators over many years using a variety of experimental techniques. Most of the work has involved studies at or close to room temperature, with the notable exception of some recent glassy state (−196°C) Raman work (1). Higher temperature investigations have been limited to the hydrated melt of $FeCl_3 \cdot 6H_2O$ (2, 3), at approximately 35–40°C, and to some aqueous solutions at 50°C (4). Because of the general interest in high temperature aqueous systems involving geochemically important elements, hydrometallurgy, corrosion of high temperature reactors, etc. (5), we have utilized Raman spectroscopic methods to study several such systems up to 300°C, with applied pressures up to 9 MPa to maintain the liquid phase (6, 7). We report here the results of a variable temperature investigation of several aqueous ferric chloride systems, between 25 and 300°C.

Although earlier workers have used Raman spectroscopy to study similar systems at room temperature (4, 8, 9) there is still disagreement concerning the interpretation of their results. Indeed such disagreements are not confined to Raman investigations. For example, various X-ray studies arrive at conflicting conclusions as to the major species present. A succinct summary of the major work through 1984 has appeared recently (10), and readers are referred to this paper for a discussion of the earlier work and possible reasons for the disagreements cited. It is clear that the nature of the species present, and their relative populations, stability constants, etc., are influenced to some degree by such variables as the concentration of $FeCl_3$, the Cl^-/Fe^{3+} ratio R, the pH, and the presence of other ions.

One particularly insidious problem is that of Fe(III) hydrolysis, a subject recently reviewed by Flynn (11). The slow formation, aging and agglomeration of hydrolytic polymers is one reason for some of the conflicting reports in the literature (12, 13). Signals due to hydrolysis products of general formula $[Fe(H_2O)_{6-n}(OH)_n]^{(3-n)+}$ occur in the Raman spectrum, as shown in Fig. 1, in the region 300–450 cm^{-1}. They clearly decrease in intensity with decreasing pH and are effectively absent in the most acidic solutions. For this reason, our variable temperature studies have been conducted in acid solutions which are sufficiently concentrated (5 *m* HCl or 5 *m* $HClO_4$) that hydrolysis is not observed.

Each of the systems we have studied over the 25–300°C temperature range had a fixed molality of iron (from $FeCl_3 \cdot 6H_2O$), acid (HCl or $HClO_4$), and of the internal Raman standard ($NaClO_4$ or $HClO_4$). Details are given in Table 1. We have used molalities because they are temperature-independent concentration units.

In separate studies, not reported in detail here, we have obtained the Raman spectra of numerous aqueous ferric solutions, at 25°C only, to provide background information for our high temperature work and to see whether advances in equipment (increased sensitivity) and data handling (more secure baseline subtractions and band fitting), coupled with the availability of recent XAFS and XANES results on species populations, enable a more definitive interpretation of such spectra than was possible in earlier studies (4, 8, 9). It is fair to say that, despite these advantages, we are not able to significantly improve on the quality of the spectra of Marsten and Bush (8), nor to offer major new definitive interpretations of the weaker signals in what are often very complicated spectra. As alluded

[1]Present address: Naruto University of Education, Takashima, Naruto-shi, Japan 772.

[2]To whom correspondence should be addressed.

Can. J. Chem. Downloaded from www.nrcresearchpress.com by 122.72.124.2 on 09/07/12
For personal use only.

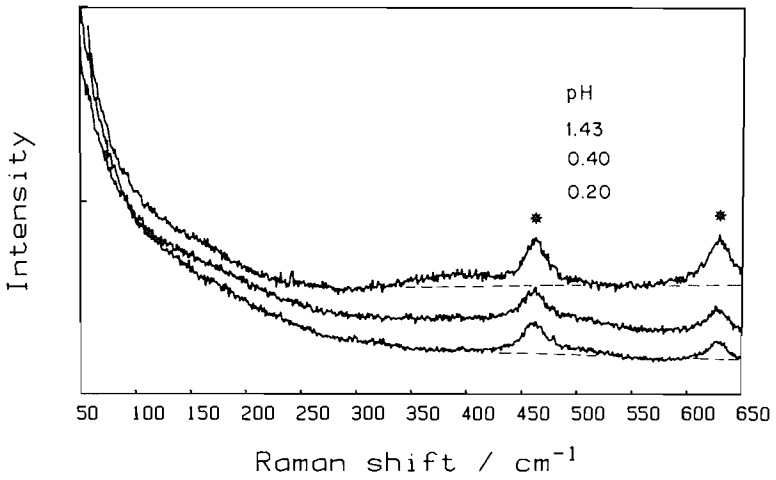


FIG. 1. Raman spectra of 0.67 *m* $Fe(ClO_4)_3$ at 25°C. pH has been adjusted with NaOH; lower spectrum: pH = 0.20; middle: pH = 0.40; upper: pH = 1.43. Bands of ClO_4^- are indicated with a star.

TABLE 1. Solution compositions

Solution	Composition				
	$m_{Fe^{3+}}$	m_{Cl^-}	m_{HCl}	m_{HClO_4}	R*
A	1.0	3.0	0.0	5.0	3.00
B	0.75	7.25	5.0	2.0	9.67
C	1.0	8.0	5.0	2.0	8.00
D	1.5	9.5	5.0	2.0	6.33
E	1.0	8.0	5.0	1.0†	8.00

*$R = m_{Cl^-}/m_{Fe^{3+}}$.
†1 *m* $NaClO_4$.

to in the preamble to the Results and discussion section, the problems of severe band overlapping and absence of standard spectra for many of the ferric species likely to be present are not easily overcome.

We will refer, where necessary, to these separate room temperature studies and comment upon those aspects of earlier Raman room temperature solution studies which can be corrected in the light of the recent X-ray and glassy state Raman work.

Experimental

Raman spectra were obtained using a digitally driven Jarrell-Ash 25-100 Spectrometer (1 m double Czerny-Turner monochromator), with an RCA 31034 photomultiplier and SSR model 1105/1120 photon counting system. Spectra were excited with the 647.1 nm line of a Coherent model 52 laser with a CR-500K krypton tube operating at 400 mW. Depolarization ratios were measured with a polaroid analyzer followed by an optical scrambler. Instrument control and data collection were performed with a Commodore Computer 2001 interfaced to the Spectrometer and to an HP 7470A plotter.

Resolution of overlapping lines was achieved with a BNDFT (Bandfit) program operating on an IBM 4341 computer (14). Raman spectra were recorded with a 3 cm^{-1} spectral slit width. The high temperature results were obtained using a furnace assembly described previously (15). Briefly, the apparatus provides controlled electrical heating of an insulated silver metal block within which the capillary Pyrex cell containing the sample is located. An applied pressure of 9 MPa was used to maintain the liquid phase. For room temperature runs samples were sealed in thin-walled capillary tubes held in a thermostatted copper block.

All solutions were prepared with Analar-Grade reagents. Iron(III) solutions were prepared from $FeCl_3 \cdot 6H_2O$ (BDH Chemicals) and $Fe(ClO_4)_3 \cdot xH_2O$ (Alfa Products) and standardized using gravimetric analysis (16). The water content of the Alfa compound was found to correspond to a formula $Fe(ClO_4)_3 \cdot 8H_2O$ — based on iron (16) and perchlorate (17) analyses. Acidity was controlled with HCl and $HClO_4$ (both Baker Analyzed Reagents) and measured by titration.

Results and discussion

Preamble

Notwithstanding the disagreements mentioned in the Introduction it seems clear that ferric chloride aqueous systems in which hydrolysis is prevented (i.e., low pH solutions) may contain one or more of the following species: $[Fe(H_2O)_6]^{3+}$ **[0]**,[3] $[Fe(H_2O)_5Cl]^{2+}$ **[I]**, $[Fe(H_2O)_4Cl_2]^+$ **[II]**, $[Fe(H_2O)_3Cl_3]$ **[III]**, and $[FeCl_4]^-$ **[IV]** — and it is probable that **III** and **I** are always minor contributors (1, 10, 18). Species with more than four chlorides per iron are not present in solution (though $[Fe(H_2O)Cl_5]^{2-}$ ions are known in some solids and their Raman spectra have been obtained (19, 20)), nor are polymeric species, despite earlier claims (4). It is possible for both **II** and **III** to have geometrical isomers and indeed both *cis* and *trans* forms of **II** have been identified by Mössbauer spectroscopy of *solids* (21). However, recent XANES work suggests only centrosymmetric species, apart from $FeCl_4^-$, as major iron-containing ingredients of aqueous ferric chloride solutions (10) so *cis* **II** and both *fac* and *mer* **III** are apparently unimportant, as are trigonal bipyramidal species such as $[Fe(H_2O)_2Cl_3]$ which have also been postulated earlier (8). However, stability constants have been calculated for each of the complexes (**I**–**IV**) (22, 23).

The Raman spectra of the limiting species **0** and **IV** have been unambiguously assigned, and the presence of either may be inferred by the appearance of bands at 510 cm^{-1} ($\nu_1(a_{1g})$ $[Fe(H_2O)_6]^{3+}$ polarized, broad, diffuse, Fig. 2) or 332 cm^{-1} ($\nu_1(a_1)$ $FeCl_4^-$ polarized, sharp, strong, Fig. 3). However, when these species occur in low concentrations relative to other iron-containing complexes such as **II**, their signals may be obscured by Fe—OH_2 or Fe—Cl stretches of the other species. Because the intermediate species, **I**, **II**, **III**, do not occur *alone* in solution, their spectra are not easily characterized. For example, in

[3]The symbols **0**, **I**, **II**, **III** and **IV** refer to the number of chloride ligands attached to the iron of the species listed.

Can. J. Chem. Downloaded from www.nrcresearchpress.com by 122.72.124.2 on 09/07/12
For personal use only.

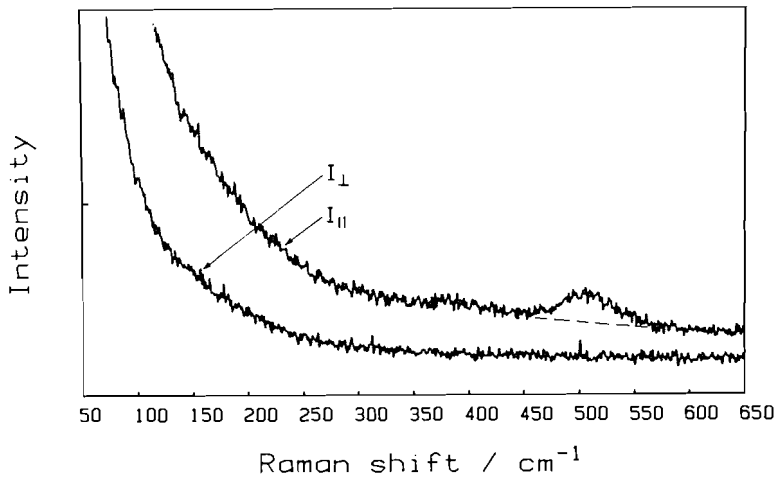


FIG. 2. Raman spectrum of 1.0 *m* $Fe(NO_3)_3$ at 25°C. Lower: $I_\perp$; upper: $I_\parallel$.

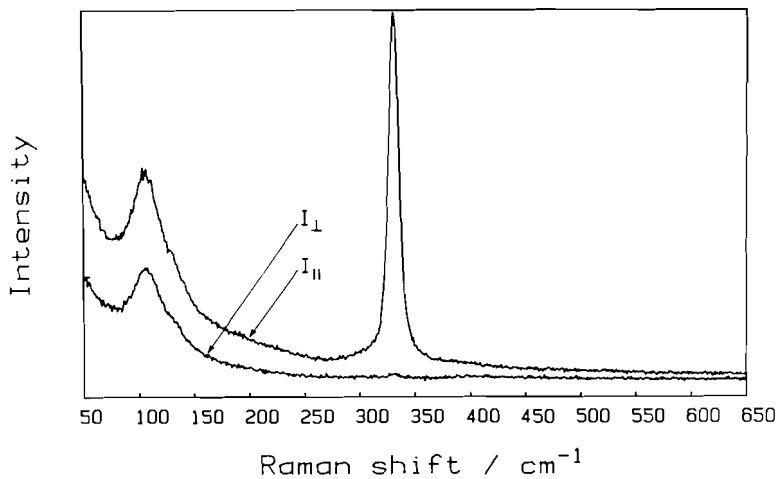


FIG. 3. Raman spectrum of 1.0 *m* $FeCl_3$ in concentrated HCl at 25°C. Lower: $I_\perp$; upper: $I_\parallel$.

Fig. 9*a*, which shows the effect of changing *R* (*vide infra*), for low *R* values the spectra clearly show the conversion of the hexaaquairon species (loss of 510 cm^{-1} shoulder) into a species characterized (for $R = 0.75$) by the ~316 cm^{-1} signal, via some intermediate(s) responsible for the asymmetry in the band envelope between 250–350 cm^{-1}, for $R = 0.16$ and 0.33. BNDFT analysis of these two spectra does not enable us to clearly identify the number and nature of the intermediate(s), although logically a sequence **0** → **I** → **II** is indicated (*vide infra*). It is true that *trans* **II** is a fairly common cation in $FeCl_3 \cdot nH_2O$ *solids* — and has been identified as such both by X-ray (24), and Mössbauer (21) investigations — and its Raman spectrum has been obtained (19). But the solution situation is different, even in the glassy state (−196°C), in respect of band positions (1) so it may not be possible to unambiguously assign all the signals due to **II** in any solution at room temperature.

We believe — on the basis of our study of the melted form of $FeCl_3 \cdot 6H_2O$, and by correlation with the recent XAFS and XANES work (2, 10) and glassy state Raman studies (1) — that we can assign the *strongest* signal of **II** in aqueous solution. It occurs at ~316 cm^{-1}. This is due to Fe—Cl stretches (ν_1, a_{1g}) of *trans*-$[Fe(H_2O)_4Cl_2]^+$. The position of other modes — stretches and deformations — may be speculated on (1, 4, 25) but such speculation is not useful here. Considering the apparent unimportance of **I** and **III** in most aqueous solutions, relative to some or all of the others, it is not surprising that spectroscopic evidence for them is uncertain. Due to band overlap, and weakness of signals from species present in small relative amounts, if it is not possible to unambiguously discern all possible Fe—OH_2 and Fe—Cl modes of **II**, this is doubly true for **I** and **III**. Bearing these facts in mind, we can discuss our results as follows.

Variable temperature results

It is clear from the spectra of each of the solutions A to E that at room temperature the dominant species is in all cases *trans*-$[Fe(H_2O)_4Cl_2]^+$, **II**, with its ~316 cm^{-1} band of much greater intensity than other signals. A typical baseline-corrected and resolved spectrum is shown in Fig. 4 in which the other major signal is that of the internal standard, ClO_4^-, at 462 cm^{-1} (ν_2).

The additional bands in the example, at approximately 420 cm^{-1} and in the 100–250 cm^{-1} region, are due to Fe—OH_2 stretches of **II** and to deformations of **II**, respectively. The exact band envelope and resolution of the low frequency region is uncertain to some extent because this is a very weak signal on the edge of the exciting line. It is not possible to draw firm

Can. J. Chem. Downloaded from www.nrcresearchpress.com by 122.72.124.2 on 09/07/12
For personal use only.

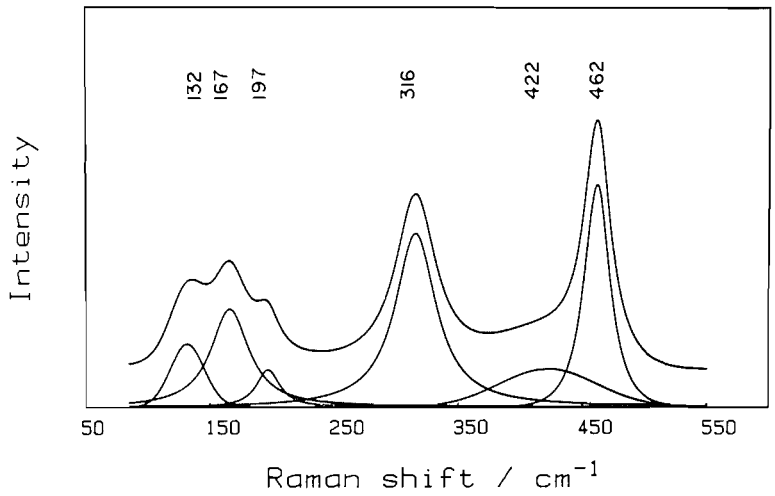


FIG. 4. Raman spectrum of 1.0 *m* $FeCl_3$ in 5 *m* $HClO_4$, solution A, at 25°C.

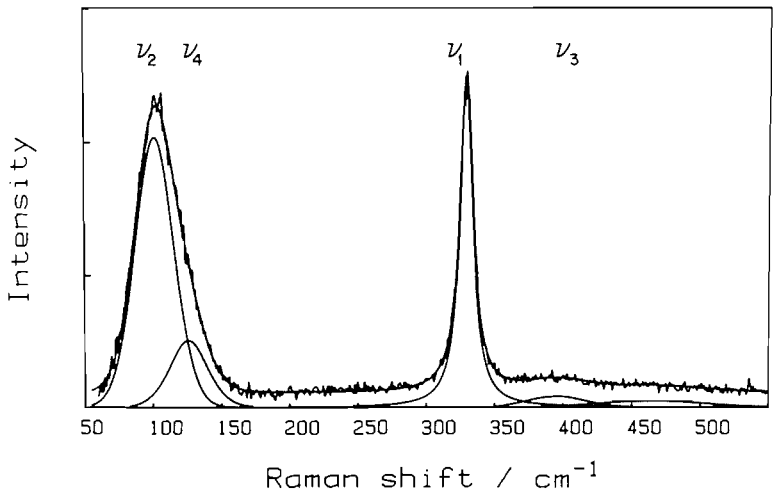


FIG. 5. The baseline-corrected and BNDFT-analyzed Raman spectrum of 1.0 *m* $FeCl_3$, 5 *m* HCl, 1 *m* $NaClO_4$, solution E, at 300°C and 9 MPa.

conclusions about all the components of the envelope. The ~167 cm^{-1} peak is a common feature whenever the ~316 cm^{-1} band is dominant.

For each of the systems studied the 300°C spectrum shows the characteristic four-line pattern $\nu_1(a_1)$ 332 cm^{-1}; $\nu_2(e)$ 107 cm^{-1}; $\nu_3(f_2)$ 395 cm^{-1}; $\nu_4(f_2)$ 132 cm^{-1} of tetrahedral $FeCl_4^-$ (26), which appears as the sole iron-containing species at that temperature. Figure 5 is a typical spectrum of this kind.

Spectra at intermediate temperatures in all cases contain either or both of **II** or **IV**, with no evidence for intervening species (Fig. 6). The threshold temperature at which the 332 cm^{-1} signal of **IV** becomes apparent varies depending on the composition of the solution.

From the variable temperature study of solutions A–E, and from the other room temperature studies, it is apparent that at least the following, in addition to higher temperatures, can affect the proportions of **IV** relative to other species. (*1*) Acidity: increasing acidity favours $FeCl_4^-$. In concentrated $HClO_4$, for example, essentially only **IV** exists, and a study at different molalities of $HClO_4$ (Fig. 7) shows the conversion from **II** to **IV** with increasing acid, at constant iron concentration, constant Cl^-/Fe^{3+}, *R*, and constant temperature. (*2*) *R* values: increasing *R* favours $FeCl_4^-$. Thus comparing the solution A and E results at, say, 100°C (Fig. 8) we see a larger contribution from **IV** in E ($R = 8$) than in A ($R = 3$), other things being equal. The combined affects of higher acidity and higher *R* are shown in Figs. 9*a* and 9*b* which include the spectra of solutions containing a constant iron concentration (0.67 *m* $Fe(ClO_4)_3$) and variable molalities of hydrochloric acid which provide *R* values ranging from 0.16 to 24. (*3*) Dielectric constant: it appears that lower solvent dielectric constants favour $FeCl_4^-$. As seen in Fig. 10, which shows spectra of $FeCl_3$ in various CH_3OH/H_2O ratio solutions, the proportion of **IV** is greater in the solution with the largest amount of alcohol. It should be noted that, even in this solution, water is present in large excess, relative to iron, so that it is not only the poor coordinating properties of methanol which contribute to this affect. The lower dielectric constant of water at elevated temperatures — at 200°C it is about the same as that of methanol at 25°C — may contribute to the increased proportion of **IV** with increasing temperature.

The increase in the proportion of $FeCl_4^-$ with temperature is analogous to that observed for $CoCl_4^{2-}$ (27) but is the reverse of the situation for $ZnBr_4^{2-}$ and $CdBr_4^{2-}$, where these species

Can. J. Chem. Downloaded from www.nrcresearchpress.com by 122.72.124.2 on 09/07/12
For personal use only.

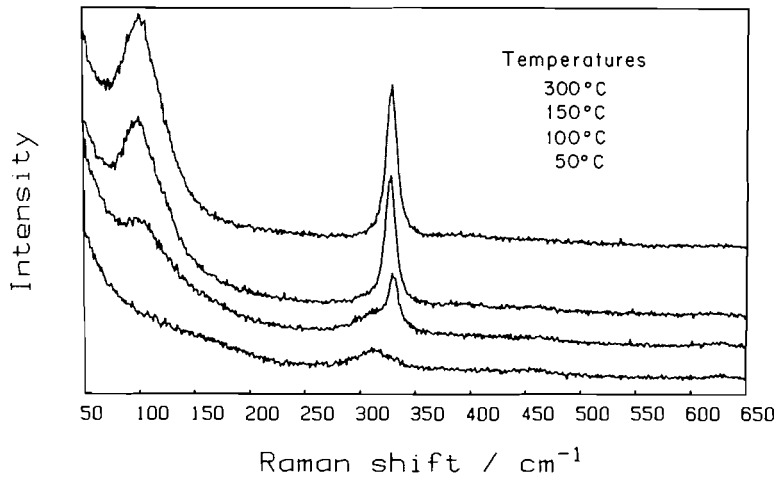


FIG. 6. Raman spectra of 1.0 *m* $FeCl_3$, 5 *m* HCl, 1 *m* $NaClO_4$, solution E, recorded at 50, 100, 150, and 300°C and 9 MPa.

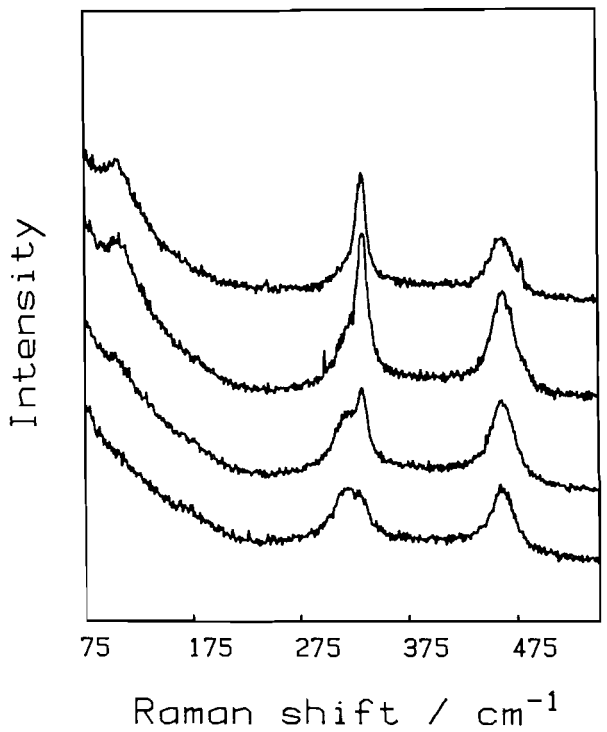


FIG. 7. Raman spectra of 1.0 *m* $FeCl_3$ with increasing molality of $HClO_4$ at 25°C. From bottom to top 8, 10, 12, and 14 *m* $HClO_4$.

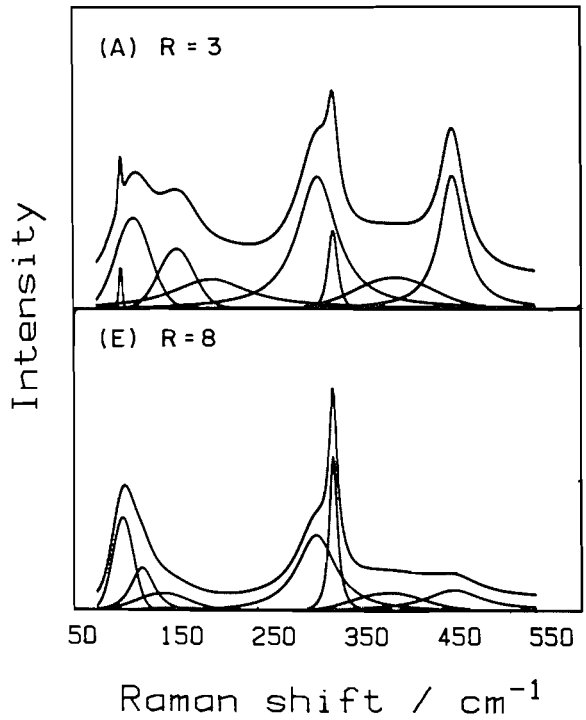


FIG. 8. Raman spectra of solutions A and E at 100°C.

are favored at low temperatures and their water-substituted complexes increase in importance with rising temperature (6, 7). Neither charge nor ligand field (LF) effects can be held solely responsible for these trends since Fe(III) (d^5 high spin), Zn(II), and Cd(II) (d^{10}) have zero LF stabilization energies in the geometries concerned, and the charge factors are the same for Co(II), Zn(II), and Cd(II).

The conversion of $[Fe(H_2O)_4Cl_2]^+$ into $FeCl_4^-$ in the solutions containing HCl (B–E) presumably occurs according to the equation:

[1] $[Fe(H_2O)_4Cl_2]^+ + 2Cl^- \rightarrow FeCl_4^- + 4H_2O$

since no evidence for other iron species (**0**, **I**, or **III**) is found. Solution A, on the other hand, has no extra chloride so such an equation cannot apply and a reaction such as:

[2] $2[Fe(H_2O)_4Cl_2]^+ \rightarrow FeCl_4^- + [Fe(H_2O)_6]^{3+} + 2H_2O$

must be occurring. However, there is no evidence for the hexaaquairon(III) cation (no 510 cm^{-1}, ν_1 signal). If it is present it should be 0.5 *m* in concentration according to [2] and ought to be weakly observable.

A feature of the $FeCl_4^-$ spectrum at elevated temperatures is the unexpectedly large intensity of the low frequency 102 cm^{-1} band, Fig. 5. The intensity of a deformation mode is normally much less than that of a stretching mode and is not expected to grow with a temperature increase. Possibly this phenomenon can be ascribed to a preferential hot band.

Another feature of considerable interest is the absence of intensity from the $\nu_2(e)$, 462 cm^{-1}, and $\nu_4(f_2)$, 625 cm^{-1} lines of ClO_4^-. In previous studies we have found that $HClO_4$ is stable to well above 150°C even for a composition as high as

Can. J. Chem. Downloaded from www.nrcresearchpress.com by 122.72.124.2 on 09/07/12
For personal use only.

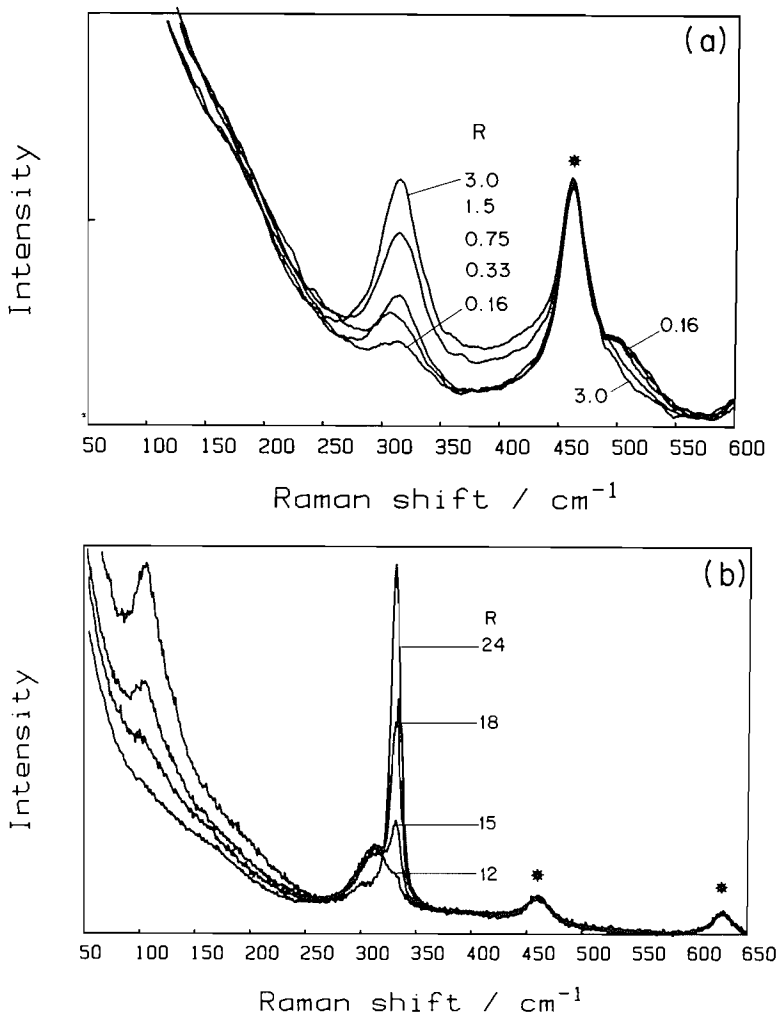


FIG. 9. (*a*) Raman spectra of 0.67 *m* $Fe(ClO_4)_3$ at 25°C with increasing *R*. At 315 cm^{-1} from bottom to top the *R* values are 0.16, 0.33, 0.75, 1.5, and 3.0. At 510 cm^{-1} the *R* values are reversed. Bands of ClO_4^- are indicated with a star. (*b*) Raman spectra of 0.67 *m* $Fe(ClO_4)_3$ at 25°C with increasing *R*. At 315 cm^{-1} from bottom to top the *R* values are 12, 15, 18, and 24. Bands of ClO_4^- are indicated with a star.

71 wt.% acid (28). In the presence of NH_4HSO_4 or Na_2SO_4 no decomposition was detected (29). However, the autocatalytic reaction

[3] $4H^+ + 4ClO_4^- \rightarrow 2H_2O + 2Cl_2 + 7O_2$

proceeds at measurable rates for 1.1–6.6 *m* $HClO_4$ in the range 295–332°C (30). Thus we did not anticipate that at the low concentrations used as an intensity standard ClO_4^- would be unstable. The evidence suggests otherwise.

In a separate experiment a sample with the composition 1.5 *m* $FeCl_3$, 5 *m* HCl, and 2 *m* $HClO_4$ was raised to 200°C and spectra were recorded at 200, 250, 300, 150, 100, and 75°C. At 300°C the 542 cm^{-1} band of aquated Cl_2 was detected; at 75°C it was much more intense and bubbles of gas were detected (cf. ref. 28). The 935 cm^{-1} band of ClO_4^- could still be seen. In another experiment with a sample of composition 1.5 *m* $FeCl_3$, 10 *m* HCl, and 5.0 *m* $HClO_4$ the temperature was raised and spectra were recorded at 100, 200, 250, and 100°C and the 935 cm^{-1} band of ClO_4^- was measured as a standard (twice at each temperature). The values for the integrated intensities were 1:0.73:0.64:1.02. Thus, although there was an apparent loss of intensity with increasing temperature, the intensity was reversibly recovered. The loss might be attributable to a change in refractive index (i.e., an optical effect) and not to a chemical decomposition in this case. However, we conclude from these and other experiments that the decomposition of ClO_4^-, as given by reaction [3], is apparently catalyzed in solutions containing iron(III).[4] Because of this decomposition, we have restricted a quantitative analysis based on relative integrated intensities to the temperature range 50 to 150°C.

We have obtained an approximate value for the apparent enthalpy change, ΔH, for reaction [1] from the observed population change with temperature. The strategy was to obtain a value for the molal scattering coefficient, J_{332}, of the 332 cm^{-1} band of $FeCl_4^-$ at 150°C, at which the conversion to $FeCl_4^-$ is essentially complete. This value was used to convert the intensities of the 332 cm^{-1} band to concentrations at temperatures of 50, 75, and 100°C:

[4] $m_{FeCl_4^-} = I^R_{332}/J_{332}$

The concentrations of other species were then obtained from the material balance expressions:

[4]It has been brought to our attention by a referee that Fe(III)-catalyzed decomposition of $HClO_4$ at 200°C has been reported previously (31).

Can. J. Chem. Downloaded from www.nrcresearchpress.com by 122.72.124.2 on 09/07/12
For personal use only.

TABLE 2. Species concentrations and equilibrium quotients for the given samples

Temperature (°C)	Molalities				Q_m	
	$FeCl_4^-$	$[Fe(H_2O)_4Cl_2]^+$	Cl^-	H_2O	Eq. [8] ($\times 10^4$)	Eq. [9] ($\times 10^{-2}$)
Solution B						
50	0.062	0.938	5.88	51.8	1.38	0.192
75	0.256	0.744	5.49	52.6	8.74	1.14
100	0.544	0.456	4.91	53.7	41.3	4.95
ΔH based on Q_m eq. [8]	67 ± 0.4 kJ mol^{-1}, $r = 0.9999$					
ΔH based on Q_m eq. [9]	64 ± 0.1 kJ mol^{-1}, $r = 0.9999$					
Solution C						
50	0.073	0.677	5.60	52.8	2.69	0.345
75	0.191	0.559	5.37	53.3	9.61	1.12
100	0.484	0.266	4.78	54.5	70.3	7.97
ΔH based on Q_m eq. [8]	64 ± 12 kJ mol^{-1}, $r = 0.9837$					
ΔH based on Q_m eq. [9]	62 ± 11 kJ mol^{-1}, $r = 0.9845$					
Solutions B and C (6 points)						
ΔH based on Q_m eq. [8]	66 ± 7 kJ mol^{-1}, $r = 0.9797$					
ΔH based on Q_m eq. [9]	63 ± 6 kJ mol^{-1}, $r = 0.9827$					

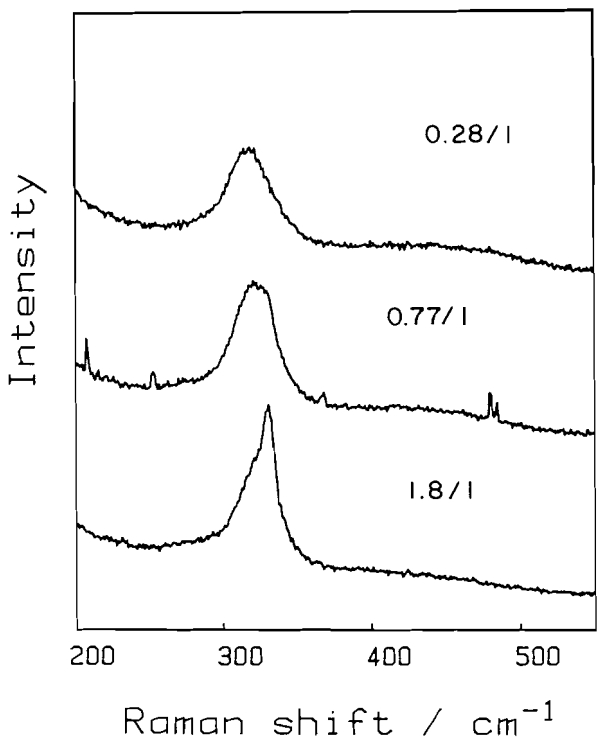


FIG. 10. Raman spectra in methanol/water mixtures with increasing CH_3OH/H_2O ratio. From top to bottom 0.28:1, 0.77:1, 1.8:1 mole ratios.

[5] $m_{[Fe(H_2O)_4Cl_2]^+} = m_{Fe(total)} - m_{FeCl_4^-}$

[6] $m_{Cl^-} = m_{Cl^-(total)} - 4m_{FeCl_4^-} - 2m_{[Fe(H_2O)_4Cl_2]^+}$

[7] $m_{H_2O} = 55.55 - 4m_{[Fe(H_2O)_4Cl_2]^+}$

The latter neglects hydration of chloride ion. From these equations it is possible to calculate the concentration quotient for process [1]:

[8] $$Q_m = \frac{m_{FeCl_4^-}(m_{H_2O})^4}{m_{[Fe(H_2O)_4Cl_2]^+}(m_{Cl^-})^2}$$

or, if one incorporates the water into the equilibrium quotient,

[9] $$Q_m = \frac{m_{FeCl_4^-}}{m_{[Fe(H_2O)_4Cl_2]^+}(m_{Cl^-})^2}$$

For the two solutions B, C (Table 1), at 150°C, the relative integrated intensities of the 332 cm^{-1} band were measured:

$$I^R_{332} = \frac{\text{Area of } 332 \text{ cm}^{-1} \text{ band}}{\text{Area of } 935 \text{ cm}^{-1} \text{ band}} m_{ClO_4^-}$$

The mean value of J_{332} was found to be 4.84 ± 0.13. Based on the insensitivity of J values of SO_4^{2-} and HSO_4^- to temperature over a greater range (29) this value was applied in eq. [4] for temperatures of 50, 75, and 100°C. The data are collected in Table 2.

ΔH was estimated from a fit to the van't Hoff equation

$$\left(\frac{\partial \ln K}{\partial T}\right)_p = \frac{\Delta H^0}{RT^2}$$

Activity coefficients are unknown and hence a rigorous treatment to obtain ΔH^0 from the temperature dependence of K is not possible. However, it has previously been shown that the slope obtained from a plot of $\ln Q_m$ versus T is almost parallel to the slope of $\ln K$ versus T for the HSO_4^-/SO_4^{2-} case (29). Thus we anticipate that an "apparent ΔH" value, within 30% of ΔH^0, is obtainable. The values of ΔH for the two compositions are collected in Table 2. A mean value of $+65 \pm 8$ kJ mol^{-1} is consistent with the data. For comparison ΔH for the analogous reaction of Co(II) has been reported as $+62$ kJ mol^{-1} by Fabes and Swaddle (27); and that for the reaction $[Fe(H_2O)_6]^{3+} + Cl^- \rightarrow [Fe(H_2O)_5Cl]^{2+} + H_2O$ as $+36$ kJ mol^{-1} (23).

Conclusions

When Fe^{3+} concentrations are in the range 0.75 to 1.0 mol kg^{-1}

Can. J. Chem. Downloaded from www.nrcresearchpress.com by 122.72.124.2 on 09/07/12
For personal use only.

and R values in the range 3 to 9.5, tetrahedral $FeCl_4^-$ is the dominant iron-containing complex in acidified aqueous solutions of "ferric chloride" above ≈200°C; at 300°C it is the sole chloroiron species. Octahedral *trans*-$[Fe(H_2O)_4Cl_2]^+$ is the major and only unambiguously identifiable complex in such solutions at room temperature. As the temperature is raised the octahedral complex is converted into the tetrahedral tetrachloroferrate(III) ion, apparently without the production of any other iron complexes. In the presence of excess chloride this conversion presumably occurs via the reaction [1] for which an approximate ΔH is calculated to be $+65 \pm 8$ kJ mol^{-1}.

The decomposition of the internal intensity standard, perchlorate, at elevated temperatures, especially in the presence of ions such as Fe(III) which apparently catalyze the reduction to Cl_2, presents a problem for Raman spectroscopists. This has been overcome to some extent by the use of trifluoromethanesulfonic acid (HTFMS), which has the additional advantage of being non-complexing (6, 7). Although ClO_4^- has usually been considered as not complexing with metal cations, especially in the presence of much stronger ligands such as Cl^-, several authors have reported that equilibrium constants change dramatically with changing perchlorate concentration in some cases (8, 32). However, HTFMS is also susceptible to metal ion catalyzed decomposition (31) at elevated temperatures so its suitability in a particular experiment must be considered carefully.

Acknowledgements

This work was supported by grants from the Natural Sciences and Engineering Research Council of Canada. Thanks are expressed to Miss J. Semmler for assistance and to J. T. Szymanski and D. Francis for helpful correspondence.

1. H. KANNO and J. HIRAISHI. J. Raman Spectrosc. **12**, 224 (1982).
2. K. MURATA and D. E. IRISH. Spectrochim. Acta, **44A**, 739 (1988).
3. M. MAGINI. J. Chem. Phys. **76**, 1111 (1982).
4. S. K. SHARMA. J. Chem. Phys. **60**, 1368 (1974).
5. H. L. BARNES. Geochemistry of hydrothermal ore deposits. 2nd ed. *Edited by* H. L. Barnes. Wiley, New York. 1979. p. 417.
6. M. M. YANG, D. A. CRERAR, and D. E. IRISH. J. Solution Chem. **17**, 751 (1988).
7. B. G. ANDERSON and D. E. IRISH. J. Solution Chem. **17**, 763 (1988).
8. A. L. MARSTON and S. F. BUSH. Appl. Spectrosc. **26**, 579 (1972).
9. S. K. SHARMA, V. N. SEHGAL, H. L. BAMI, and S. D. SHARMA. J. Inorg. Nucl. Chem. **37**, 2417 (1975).
10. M. J. APTED, G. A. WAYCHUNAS, and G. E. BROWN. Geochim. Cosmochim. Acta, **49**, 2081 (1985).
11. C. M. FLYNN, JR. Chem. Rev. **84**, 31 (1984).
12. R. J. KNIGHT and R. N. SYLVA. J. Inorg. Nucl. Chem. **37**, 779 (1975).
13. S. BALT. J. Inorg. Nucl. Chem. **29**, 2307 (1967).
14. (*a*) T. JARV, J. T. BULMER, and D. E. IRISH. J. Phys. Chem. **81**, 649 (1977); (*b*) K. MURATA and D. E. IRISH. Bunseki Kagaku, **36**, T72 (1987).
15. D. E. IRISH, T. JARV, and C. I. RATCLIFFE. Appl. Spectrosc. **36**, 137 (1982).
16. A. I. VOGEL. A textbook of quantitative inorganic analysis. Wiley, New York. 1961. p. 524.
17. D. J. GLOVER and J. M. ROSEN. Anal. Chem. **37**, 306 (1965).
18. K. ASAKURA, M. NOMURA, and H. KURODA. Bull. Chem. Soc. Jpn. **58**, 1543 (1985).
19. S. A. COTTON and J. F. GIBSON. J. Chem. Soc. (A), 1693 (1971).
20. S. K. SHARMA and D. K. PANDYA. J. Inorg. Nucl. Chem. **36**, 1165 (1974).
21. C. BORDELEAU and D. R. WILES. Inorg. Chim. Acta, **41**, 195 (1980).
22. J. BJERRUM and I. LUKES. Acta Chem. Scand. A**40**, 31 (1986).
23. J. F. ZEMAITIS, JR., D. M. CLARK, M. RAFAL, and N. C. SCRIVNER. Handbook of aqueous electrolyte thermodynamics. Am. Inst. Chem. Eng., New York. 1986. p. 425.
24. J. T. SZYMANSKI. Acta Crystallogr. B**35**, 1958 (1979).
25. H. KANNO and J. HIRAISHI. Chem. Phys. Lett. **72**, 541 (1980).
26. L. A. WOODWARD and M. J. TAYLOR. J. Chem. Soc. 4473 (1960).
27. T. W. SWADDLE and L. FABES. Can. J. Chem. **58**, 1418 (1980).
28. C. I. RATCLIFFE and D. E. IRISH. Can. J. Chem. **62**, 1134 (1984).
29. B. S. W. DAWSON, D. E. IRISH, and G. E. TOOGOOD. J. Phys. Chem. **90**, 334 (1986).
30. M. P. HENDERSON, V. I. MIASEK, and T. W. SWADDLE. Can. J. Chem. **49**, 317 (1971).
31. L. FABES and T. W. SWADDLE. Can. J. Chem. **53**, 3053 (1975).
32. J. K. ROWLEY and N. SUTIN. J. Phys. Chem. **74**, 2043 (1970).

Can. J. Chem. Downloaded from www.nrcresearchpress.com by 122.72.124.2 on 09/07/12
For personal use only.

A carbon-13 CP/MAS nuclear magnetic resonance study of several 1,4-disubstituted benzenes in the solid state

GLENN H. PENNER AND RODERICK E. WASYLISHEN[1]
Department of Chemistry, Dalhousie University, Halifax, N.S., Canada B3H 4J3

Received June 10, 1988

GLENN H. PENNER and RODERICK E. WASYLISHEN. Can. J. Chem. **67**, 525 (1989).

The carbon-13 chemical shifts of several 1,4-disubstituted benzenes in the solid state are reported. At least one of the substituents is unsymmetrical and in most cases this leads to different ^{13}C chemical shifts of C-2 and C-6 and in some cases to different shifts for C-3 and C-5. The ^{13}C chemical shifts observed in the solid state are compared with those measured in solution and, where possible, with those obtained in low temperature solution studies where internal rotation of the unsymmetrical substituent is slow on the ^{13}C chemical shift time scale. Agreement between the chemical shifts observed in the solid state and solution is excellent. The potential application of CP/MAS nuclear magnetic resonance in deducing the conformation of benzene derivatives with two unsymmetrical substituents is discussed.

Key words: carbon-13 CP/MAS NMR, ^{13}C NMR chemical shifts, substituent effects.

GLENN H. PENNER et RODERICK E. WASYLISHEN. Can. J. Chem. **67**, 525 (1989).

On a déterminé les déplacements chimiques du ^{13}C, à l'état solide, de plusieurs benzènes disubstitués en positions 1,4. Au moins un des substituants n'est pas symétrique et, dans la plupart des cas, ceci conduit à des déplacements chimiques du ^{13}C qui sont différents pour les carbones 2 et 6 et, dans quelques cas, à des déplacements chimiques différents pour les carbones 3 et 5. On a comparé les déplacements chimiques du ^{13}C qui ont été obtenus à l'état solide avec ceux qui ont été mesurés en solution et, lorsque cela s'est avéré possible, avec ceux obtenus au cours d'études en solution, à basse température, alors que la rotation interne du substituant qui n'est pas symétrique est lent par rapport à l'échelle de temps des déplacements chimiques du ^{13}C. L'accord entre les déplacements chimiques observés à l'état solide et en solution est excellent. On discute des possibilités d'utilisation de la résonance magnétique nucléaire CP/MAS pour déduire la conformation de dérivés du benzène portant deux substituants qui ne sont pas symétriques.

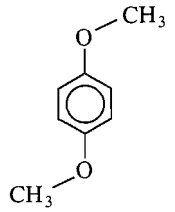
Mots clés : RMN CP/MAS du ^{13}C, déplacements chimiques du ^{13}C, effets des substituants.

[Traduit par la revue]

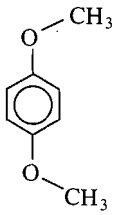
Can. J. Chem. Downloaded from www.nrcresearchpress.com by 122.72.124.2 on 09/07/12
For personal use only.

Introduction

It has been a decade since the first combined use of high-power proton decoupling, magic angle spinning (MAS), and cross-polarization (CP) in obtaining high resolution solid state nmr spectra (1). The application of these techniques has since become routine. Although these methods are said to produce "liquid-like" spectra, an important difference between liquid and CP/MAS solid state nmr spectra is that dynamic averaging due to internal rotation or inversion is often absent in the solid. There have been several examples of such "freezing" of internal rotation (2–14). A frequently cited example is 1,4-dimethoxybenzene (2, 3, 6, 15). In solution the four hydrogen-bearing ring carbon nuclei yield a single ^{13}C resonance due to rapid internal rotation of the methoxy substituents. The two possible "planar" structures in the solid state are **1***a* and **1***b*; X-ray crystallographic studies indicate that solid 1,4-dimethoxybenzene exists as **1***a* (16). The protonated ring carbons will experience two types of chemical environments and this is reflected in the ^{13}C CP/MAS spectrum, which indicates a shift difference between C-2 and C-6 (or C-5 and C-3) of 5.5 ppm.



1*a*

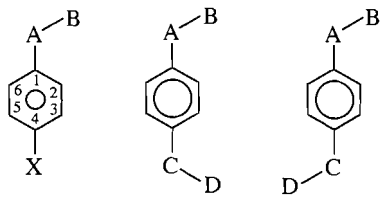


1*b*

Hays has warned that care should be taken in attributing observed shifts and splitting for a given carbon to changes in conformation, particularly if the X-ray structure is not available (14). Molecular packing may affect isotropic chemical shifts and splittings may also be due to the existence of non-congruent molecules in the unit cell. In recent years considerable experience has been gained in the analysis of high resolution solid state ^{13}C nmr spectra and, if appropriate caution is exercised, information about the molecular and crystal structure of moderately complex crystalline organic solids may be gleaned from the spectra.

Internal rotation in benzene derivatives has been extensively studied in solution. The dependence of both long-range spin–spin coupling (17) and chemical shifts (18) on the rotation of the side chain with respect to the ring is fairly well understood. The internal rotation of several unsymmetrical substituents attached to the benzene ring has been studied in solution by variable temperature dynamic nmr techniques (19). In the present study we examine the ^{13}C CP/MAS solid state spectra of several 1,4-disubstituted benzenes where one or both of the substituents are unsymmetrical (Fig. 1). The chemical shifts measured in the solid state are compared with those measured in solution at room temperature and, in some cases, at temperatures well below the coalescence temperature where internal rotation of an unsymmetrical substituent is slow. Diffraction data are available for some of the derivatives investigated and in such cases the chemical shifts are discussed in light of the known solid state structures. For molecules where the solid state structure is unavailable some effort is made to deduce the conformation of the side chain(s) from the ^{13}C chemical shifts observed in the solid state. The overall objective of this study is to report effects of unsymmetrical substituents on benzene ring carbon-13 chemical shifts and evaluate the utility of high resolution solid state nmr in deducing the conformation of 1,4-substituted benzenes in the solid state.

[1]Author to whom correspondence may be addressed.



a *b* *c*

FIG. 1. The general structures of 1,4-disubstituted benzenes studied. C-2 is taken to be *cis* to the A—B bond. The A, B, C, and D moieties may represent more than one atom; for example, in acetophenones B is the carbonyl oxygen and A is the C-CH_3 group. The X moiety represents a symmetric substituent e.g., NO_2, C≡N. The C—D bond may lie *cis* or *trans* to the A—B bond as shown by (*b*) and (*c*), respectively.

Experimental

Carbon-13 spectra of solid samples were obtained at 50.323 MHz on a Bruker MSL-200 using cross-polarization (CP), magic angle spinning (MAS), and high power decoupling. Contact and recycle times ranged from 1 to 5 ms and from 5 to 60 s respectively. MAS rates were 3.0–4.5 kHz. Aluminium oxide rotors of volume 0.35 cm^3 were used. Non-quaternary suppression (20) was occasionally used to aid in spectral assignment. Several samples required the use of the flipback (21) or TOSS (22) pulse sequences. Chemical shifts were referenced to external solid adamantane, which has shifts of 38.56 ppm (CH_2) and 29.50 ppm (*C*H) with respect to TMS (23). All spectra were recorded at ambient temperatures (20 ± 2°C). Errors in the chemical shifts relative to TMS are about ±0.3 ppm; however, errors in peak separations in any given spectrum are about ±0.1 ppm.

Solution carbon-13 spectra were obtained in acetone-d_6 solutions (0.2 g in 2.0 mL) at 90.81 MHz on a Nicolet 360 NB spectrometer with proton decoupling; chemical shifts were referenced to internal TMS.

All samples were commercially available with the exceptions of 4-methylformanilide (24), 4-(methylamino)acetophenone (25), and 1,4-di(methylthio)benzene (26).

Results and discussion

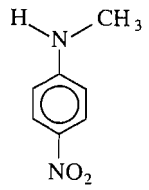
The ^{13}C chemical shifts of several solid 1,4-disubstituted benzenes measured using the CP/MAS nmr technique are presented in Table 1. All compounds studied contained at least one unsymmetrical substituent that is, in principle, capable of rendering C-2 and C-6 (as well as C-3 and C-5) nonequivalent (see Fig. 1). In solution, internal rotation of the unsymmetrical substituent is sufficiently rapid on the chemical shift time scale to cause chemical equivalence of C-2 and C-6 and of C-3 and C-5. Some of the compounds listed in Table 1 have also been studied in solution at low temperatures where internal rotation of one or both of the substituents is slow enough to render C-2 and C-6 (and possibly C-3 and C-5) nonequivalent.

With the exception of 4-nitrophenylformate, **12**, the heavy atoms of each compound are expected to reside in the plane (or nearly in the plane) of the benzene ring. This is based on crystal structures of these or related compounds.

(a) Molecules with one unsymmetrical substituent

(i) N-*Methylanilines*

The assignments of the ^{13}C resonances in the solid state were made largely on the basis of those in solution. As an example we briefly discuss the CP/MAS ^{13}C nmr spectrum of 4-nitro-*N*-methylaniline, **2**, shown in Fig. 2. First note that C-2 and C-6 are nonequivalent while separate resonances for C-3 and C-5 are not resolvable in the solid state. The magnitude of the chemical shift difference between C-2 and C-6, denoted $\Delta_{2,6} = \delta(C\text{-}2) - \delta(C\text{-}6)$, is −6.4 ppm in the solid state and is −6.5 ppm in solution at 210 K (27). On the basis of electron densities calculated using molecular orbital theory at the STO-3G level, earlier workers assigned $\delta(C\text{-}6) > \delta(C\text{-}2)$; thus $\Delta_{2,6}$ is negative (28). Based on the deviations from chemical shift additivity in 2-fluoro-*N*-methylaniline, where the *N*-methyl group is *trans* to the fluorine substituent (29), we also assign a negative value to $\Delta_{2,6}$ and a positive value to $\Delta_{3,5}$. These assignments are consistent with those expected for the "γ-substituent effect" as discussed by Olah and Donovan (30). Also, see ref. 18.



2

The second point to note is that all resonances that arise from carbon nuclei directly bonded to ^{14}N are broad or split into unsymmetrical doublets due to incomplete averaging of the $^{13}C-^{14}N$ dipolar interactions and the breakdown of the high field approximation (31).

The shift values for **2** in the solid state compare well with those observed in Freon solution at 210 K (27). Four $\Delta_{2,6}$ values for 4-X-*N*-methylanilines (X = F, H, Cl, NO_2) yield an average value of −6.2 ppm with a standard deviation of 0.2 ppm. The six available values of $\Delta_{3,5}$ (from low temperature solution work) range from 0.5 to 2.4 ppm (27).

(ii) Anisoles and thioanisoles

Internal rotation about the C_1—O and C_1—S bonds in anisoles and thioanisoles, respectively, has not been stopped by dynamic nmr techniques (32). X-ray diffraction studies of anisoles and thioanisoles unsubstituted in the 2 and 6 positions yield structures in which the O—CH_3 and S—CH_3 bonds are nearly in the plane of the benzene ring (33–37).

A negative value has previously been assigned to $\Delta_{2,6}$ in anisole derivatives on the basis of calculated electron densities (38). Examination of several *ortho*-substituted anisole derivatives confirms the negative value for $\Delta_{2,6}$ and indicates $\Delta_{3,5}$ is positive. Recent results (ref. 16, added in proof) also confirm our assignment. Together with the value reported here for 4-nitroanisole, **3**, a total of 17 $\Delta_{2,6}$ values, ranging from −2.9 to −9.2 ppm (ave. −6.5, std. dev. 2.0 ppm), are available for solid anisole derivatives (2, 8–10, 14, 38, 39). The large range in $\Delta_{2,6}$ may be due to varying compression of the methoxy group in different crystal environments. By comparison, the six $\Delta_{2,6}$ values available for *para*-substituted phenols only range from −1.6 to −2.7 ppm (12, 38) (ave. −2.1, std. dev. 0.4 ppm). The reduction in both magnitude and variation of $\Delta_{2,6}$ in the phenols is likely a result of the lack of a methyl group steric effect (18, 41, 42).

The largest reported value of $\Delta_{3,5}$ for a solid anisole derivative is +3.8 ppm (14). Several values of 0 ppm have been reported (10, 14, 38, 39). It is quite likely that most values are non-zero but simply unobservable due to large linewidths in the solid. As an example, a $\Delta_{3,5}$ value of 0 ppm was reported for the *para*-substituted carboxylic acid derivative of anisole (14) but a later investigation gave +0.8 ppm (38). No splitting of the *meta* ^{13}C resonance in solid phenols, with symmetric *para* substituents, has been reported.

The separation between the methyl and C-2 carbons is larger

Can. J. Chem. Downloaded from www.nrcresearchpress.com by 122.72.124.2 on 09/07/12
For personal use only.

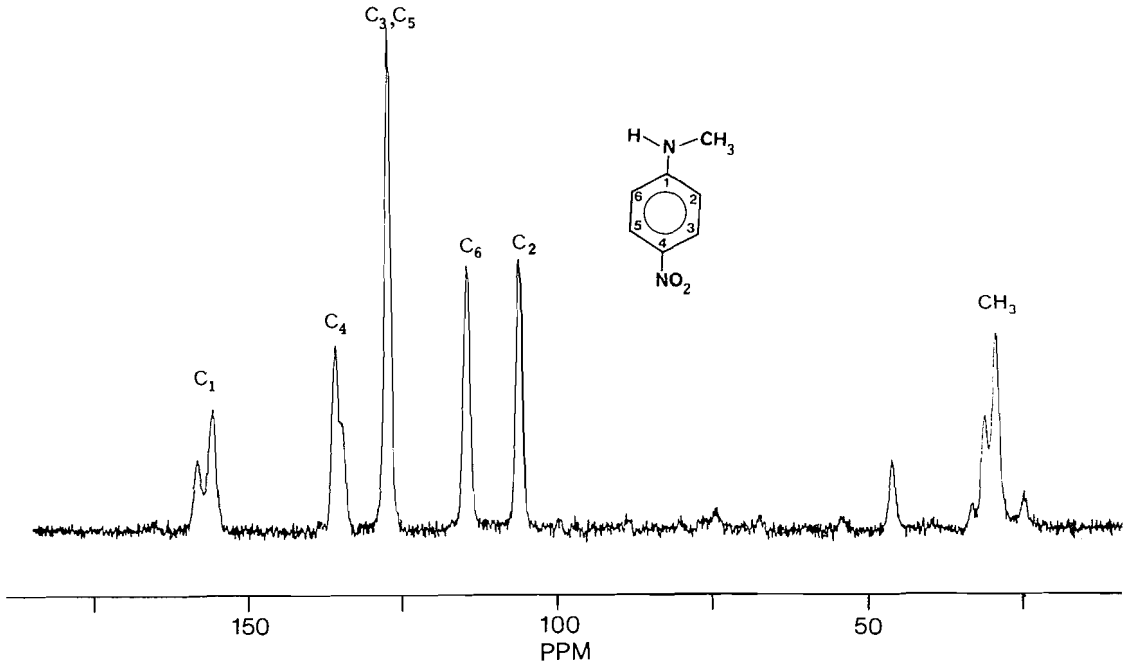


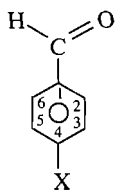
FIG. 2. The ^{13}C CP/MAS spectrum of solid 4-nitro-*N*-methylaniline **2**.

in thioanisoles than in anisoles, hence the steric contribution to $\Delta_{2,6}$ and the variation in $\Delta_{2,6}$ values are expected to be smaller. Values of $\Delta_{2,6}$ in solid thioanisoles are -3.9, -4.2, and -4.2 ppm for **4**, **5**, and **6**, respectively. The corresponding value in 4-methylmercaptobenzoic acid is -3.8 ppm.[2] Thus the average $\Delta_{2,6}$ value is -4.0 ppm with a range of only 0.2 ppm. We have assigned a negative value to $\Delta_{2,6}$ based on the sign deduced for the corresponding anisoles. Splitting of the *meta* ^{13}C resonances, $\Delta_{3,5}$, was not observed for **4** or **5**, where the *para* substituent is symmetric.

(iii) Benzaldehydes

In the solid state, benzaldehydes (43–48) and acetophenones (47–49) unhindered at the *ortho* positions are essentially planar, having angles, θ, between the carbonyl and phenyl ring planes less than 5°.

Based on low temperature solution ^{13}C spectra of 2-fluorobenzaldehyde, Drakenberg *et al.* have assigned δ(C-2) < δ(C-6) and δ(C-3) > δ(C-5) in *para*-substituted benzaldehydes (50, 51). These assignments are consistent with a negative value for $\Delta_{2,6}$ and a positive value for $\Delta_{3,5}$. The 12 values of $\Delta_{2,6}$ for *para*-substituted benzaldehydes, at low temperature in Freon solution, range from -7.6 to -9.0 ppm (ave. -8.4, std. dev. 0.5 ppm) (51). The value for 4-nitrobenzaldehyde, **7**, is -7.6 ppm (51); in the solid state a splitting of -6.7 ppm is observed. The CP/MAS spectrum of 4-dimethylaminobenzaldehyde, **8**, shows additional splittings (see Fig. 3) due to the



7 X = NO_2
8 X = $N(CH_3)_2$

[2]G. Penner and R. E. Wasylishen, unpublished results.

presence of two nonequivalent molecules within the crystallographic unit cell. Values of $\Delta_{2,6}$ and $\Delta_{3,5}$ may be partitioned between the nonequivalent molecules in two reasonable ways: first with values of -7.5 and $+5.3$ ppm and, alternatively, with -8.6 and $+4.2$ ppm, respectively.

Measured values of $\Delta_{3,5}$, in solution at low temperature, are generally about 0.5 ppm (0.4 ± 0.2 for 10 derivatives) with the exception of 2.7 ppm for 4-methoxybenzaldehyde (where the internal rotation of the methoxy substituent has not stopped) and 1.8 ppm for **8** (51). In the solid state, $\Delta_{3,5}$ is unobservable for **7** and has values ranging from 0.0 to 3.0 ppm for **8**, depending on assignment of the ^{13}C resonances of C-3 and C-5 in the nonequivalent molecules.

A recent ^{13}C CP/MAS study of an α-cyclodextrin complex of benzaldehyde at 193 K gave a $\Delta_{2,6}$ value of -7.8 ppm (52). The solution value at 150 K is -8.7 ppm (52).

(iv) Acetophenones

Low temperature nmr studies of six *para*-substituted acetophenones give $\Delta_{2,6}$ values ranging from -2.5 to -3.9 ppm and $\Delta_{3,5}$ values of 0 ppm (the exception, 4-OCH_3, has $\Delta_{3,5}$ = 2.1 ppm) (53). Following Drakenberg *et al.* (53) we assign negative and positive values to $\Delta_{2,6}$ and $\Delta_{3,5}$, respectively. With this assignment it can be seen that at low temperature in Freon solution the shift values of C-2 in the acetophenones are consistently about 1–2 ppm to low frequency of those in the corresponding benzaldehydes, whereas C-6 resonates about 3–5 ppm to low frequency. The substantial low frequency shift of C-6, with respect to the corresponding benzaldehyde, is consistent with the steric effect expected from a proximate methyl group (18, 41, 42).

The observed $\Delta_{2,6}$ values for **9** and **10** are -2.5 ppm and -4.8 ppm, respectively. The latter value is slightly higher than expected. The rotation of the acetyl group has not been stopped for either molecule by low temperature solution nmr. It is interesting to note that both molecules exhibit unexpectedly large $\Delta_{3,5}$ values. These are not due to non-congruence of molecules in the crystal (48, 49).

Can. J. Chem. Downloaded from www.nrcresearchpress.com by 122.72.124.2 on 09/07/12
For personal use only.

Can. J. Chem. Downloaded from www.nrcresearchpress.com by 122.72.124.2 on 09/07/12
For personal use only.

TABLE 1. Carbon-13 chemical shifts for several 1,4-disubstituted benzene derivatives in the solid state, in solution, and in solution at low temperatures[a]

Compound		C-1	C-2	C-6	C-3	C-5	C-4	Other			
4-Nitro-*N*-methylaniline **2**	Solid	156.8[d]	108.0	114.4	127.3		135.0[d]	CH_3	29.3[d]		
	Solution (218 K)[b]	156.0	107.9	114.4	127.7	126.4	136.3		29.9		
	Solution	156.1	113.3		126.8		137.8		29.2		
4-Nitroanisole **3**	Solid	165.5	109.9	117.8		125.5	141.5[d]	CH_3	56.6		
	Solution	165.7	115.1			126.5	142.3		56.6		
4-Nitrothioanisole **4**	Solid	149.6	123.1	127.0		123.9	142.7[d]	CH_3	15.7		
	Solution	150.6	126.0			124.5	145.6		14.6		
4-Cyanothioanisole **5**	Solid	146.5	124.6	128.8		131.9	—	CH_3	14.9	C≡N	107.6[d]
	Solution	147.1	126.3			132.9	119.5		14.4		108.2
1,4-(Dimethylthio)benzene **6**	Solid	135.4	125.8	130.0	130.0	125.8	135.4	CH_3	17.3		
	Solution	136.0	128.1		128.1		136.0		15.9		
4-Nitrobenzaldehyde **7**	Solid	139.7	126.9	133.6		124.2	150.0[d]	C=O	187.8		
	Solution (123 K)[c]	141.0	128.8	136.4	126.1	125.7	152.2		195.9		
	Solution	141.4	131.3		125.0		151.2		192.0		
4-Dimethylaminobenzaldehyde **8**	Solid[g]	(125.9	(129.7	(133.9	(112.4	(109.4	(153.3[d]	C=O	(190.6	CH_3	39.4[d]
		124.7)	128.6)	137.2)	112.4)	110.4)	153.3)		188.9)		39.4
	Solution (172 K)[c]	124.5	128.8	137.8	112.5	110.7	—		—		—
	Solution	126.2	132.1		111.8		155.2		189.9		40.0
4-Nitroacetophenone **9**	Solid	141.4	128.7	131.2	126.7	123.6	150.3[d]	C=O	197.4	CH_3	27.6
	Solution	142.5	130.3		124.5		151.2		197.0		27.1
4-Aminoacetophenone **10**	Solid	125.7	130.1	134.9	116.7	112.4	154.4[d]	C=O	197.9	CH_3	25.8
	Solution	127.1	131.3		113.7		154.0		195.4		25.9
4-Dimethylaminonitrosobenzene **11**	Solid	154.9[d]	111.0	141.8		111.0	164.2[d]	CH_3	39.9[d]		
	Solution (243 K)[e]	155.3	109.8	141.4	(110.3	110.5)	163.0		40.1		
4-Nitrophenylformate **12**	Solid	163.9	117.3		127.5		140.5[d]	C=O	—		
	Solution	164.2	116.4		126.7		141.5		206.8		

Can. J. Chem. Downloaded from www.nrcresearchpress.com by 122.72.124.2 on 09/07/12
For personal use only.

TABLE 1 (*concluded*)

Compound		C-1	C-2		C-6	C-3		C-5	C-4	Other					
4-Methylformanilide **13**	Solid	135.1[d]	120.8		118.0		130.4		135.1	C=O	167.1[d]	CH_3	22.3		
	Solution (*Z*)	136.8		120.1			130.0		133.8		159.7		20.8		
	Solution (*E*)	136.6		119.0			130.7		134.3		162.7		20.7		
Acetanilide **14**	Solid	141.0[d]	120.8		119.3		129.9		124.1	C=O	171.0[d]	CH_3	23.4		
	Solution	140.4		119.9			129.4		123.9		168.9		24.3		
4-Nitrobenzylcyanide **15**	Solid	137.7	(128.6		126.2)		123.2		148.1[d]	CH_2	22.5	C≡N	—		
	Solution	139.8		130.2			124.8		148.4		23.4		118.2		
4-Methylaminoacetophenone **16**	Solid	125.6		132.4		108.8		113.9	156.5[d]	C=O	198.2	CCH_3	26.4	NCH_3	28.5[d]
	Solution (153 K)[b]	125.0	129.9		131.6	107.8		112.5	153.8		—		25.5		28.8
		125.0	128.4		133.1	106.4		114.0	153.8		—		25.5		28.8
	Solution	126.5		131.2			111.3		154.6		195.7		25.9		28.8
4-Methoxyacetophenone **17**	Solid	130.8	129.0		133.7	110.0		117.8	163.7	C=O	197.7	CCH_3	26.8	OCH_3	58.2
	Solution (123 K)[f]	130.6	130.8		134.2	115.9		113.8	162.4		200.2		27.5		56.3
	Solution	131.2		131.2			114.4		164.3		206.0		26.4		55.8
4-Methoxyphenol **18**	Solid	149.2	117.1		118.0	112.1		119.4	153.7	CH_3	55.8				
	Solution	151.9		116.5			115.3		153.9		55.7				

[a]Chemical shifts in ppm with respect to external TMS. Numbers in parentheses may be interchanged.
[b]Reference 27.
[c]Reference 51.
[d]These lines are broad or asymmetric doublets due to incomplete averaging of the $^{13}C-^{14}N$ dipolar interaction by MAS; see ref. 31.
[e]See footnote 2.
[f]Reference 52.
[g]The carbon resonances appear to be further split, likely due to the presence of two inequivalent molecules per unit cell in the crystalline state.

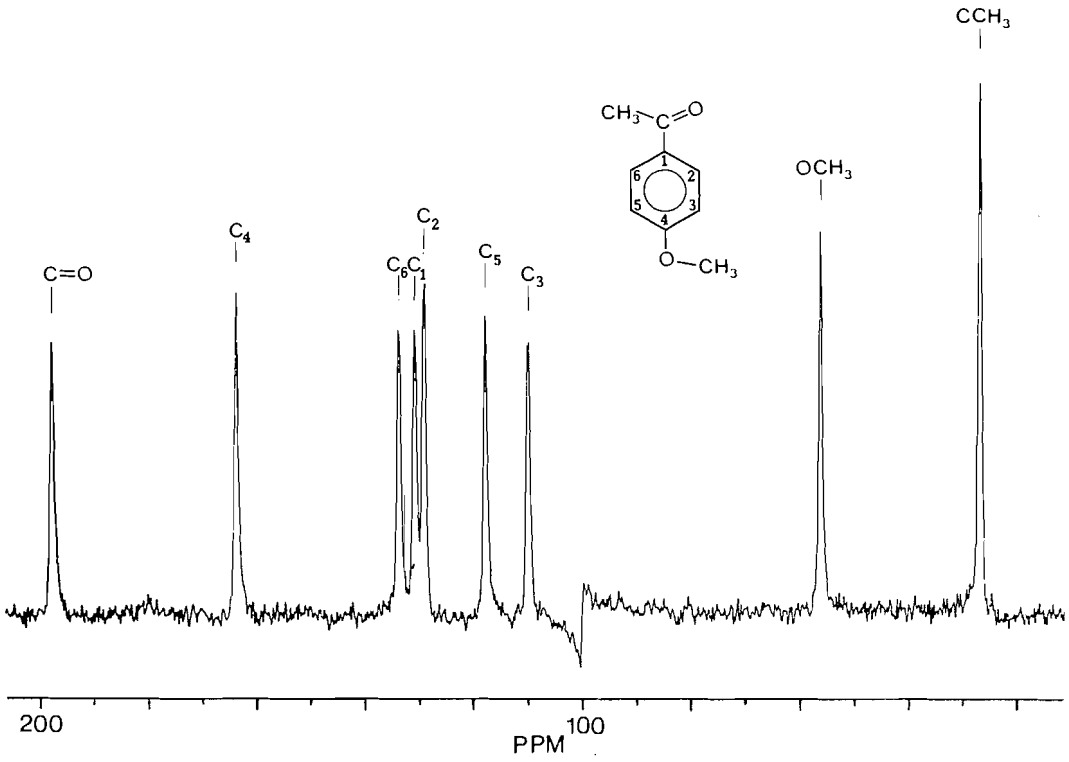
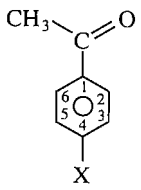


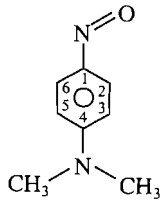
FIG. 3. The ^{13}C CP/MAS spectrum of solid 4-methoxyacetophenone **17** using the TOSS pulse sequence.



9 X = NO_2
10 X = NH_2

(v) Nitrosobenzenes

Nitrosobenzenes are unique in that they display the largest $\Delta_{2,6}$ value of any benzene derivative. In low temperature solutions $\Delta_{2,6}$ values for nitrosobenzene and *N*,*N*-dimethylaminonitrosobenzene, **11**, are −34.5 ppm (54) and −31.6 ppm (55), respectively. The CP/MAS spectrum of **11** yields −30.8 ppm.

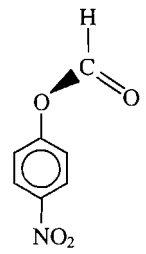


11

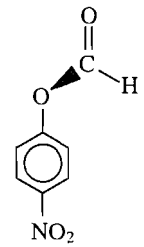
The negative sign of $\Delta_{2,6}$ is based on arguments by Lunazzi *et al.* (54), which are supported by electron density calculations.[2] The low temperature solution value for $\Delta_{3,5}$, 0.2 ppm, is not resolved in the CP/MAS spectrum of **11**.

(vi) Phenyl esters

As has already been mentioned, solid alkoxybenzenes unsubstituted in the *ortho* positions strongly prefer planar or nearly planar conformations. Replacement of the alkyl by an electron-withdrawing carbonyl moiety strongly reduces the conjugation between the ether oxygen and phenyl ring system. As a result, the preferred conformations of phenyl esters have θ values near 90°. This is in accord with the equivalence of the *ortho* ^{13}C resonances observed in solid 4-nitrophenylformate **12**. In the solid state **12** may exist in either the *Z* or *E* forms.



12*a* (*Z*)



12*b* (*E*)

Long-range couplings between the formate proton and ring protons (56) suggest that both forms exist in solution with the *Z* form predominating. Unfortunately, the $E \rightleftharpoons Z$ exchange has not been stopped in solution at low temperatures, hence the ^{13}C shifts of the two forms are not known and it is difficult to deduce the conformation of the formate group in **12** from the solid state CP/MAS spectrum. No crystal structures of phenyl formates unsubstituted in the *ortho* positions are available.

A recent ^{13}C CP/MAS spectrum of a phenylbenzoate derivative also reported identical shifts for C-2 and C-6 (8). An X-ray structure of this compound indicates that the phenyl and carbonyl planes are orthogonal (57).

(vii) Anilides

Internal rotation in amides has been studied extensively

Can. J. Chem. Downloaded from www.nrcresearchpress.com by 122.72.124.2 on 09/07/12
For personal use only.

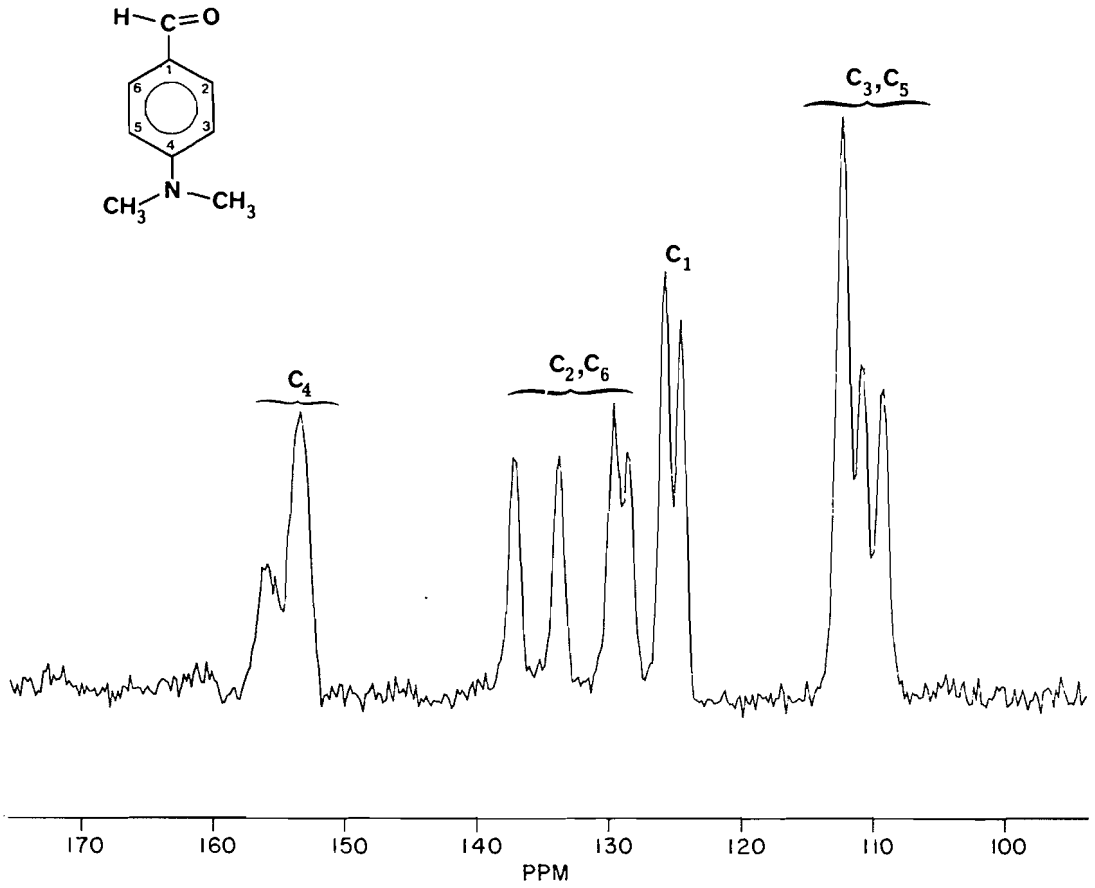


FIG. 4. The ^{13}C CP/MAS spectrum of the ring carbon-13 nuclei in 4-*N*,*N*-dimethylaminobenzaldehyde **8**.

by dynamic nmr techniques (58). In principle, two forms of internal rotation may occur in anilides: rotation about the N—C bond, which interconverts between *Z* and *E* isomers, and rotation about the C_1—N bond, which renders C-2 and C-6 (and C-3 and C-5) nonequivalent. The first form of internal rotation is slow, even at ambient temperatures (59). Low temperature nmr techniques have, as yet, failed to slow the second form of rotation to render C-2 and C-6 nonequivalent.

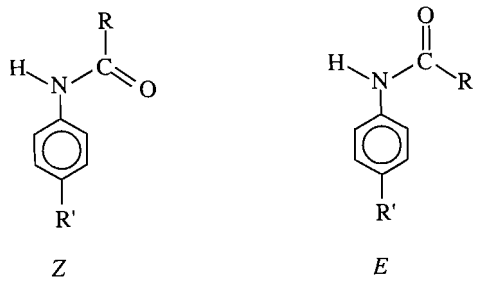
The ^{13}C CP/MAS spectrum of **13** shows a splitting of the *ortho* carbons, $\Delta_{2,6}$, of +2.8 ppm, implying that rotation about the C1—N bond is slow and that the molecule is effectively planar. In solution **13** exists in an approximate 1:2 ratio of *E*:*Z*. The differences in carbon-13 chemical shifts between *E* and *Z* isomers in solution are too small to make a definite assignment of structure in the solid state; however, on the basis of additivity effects (see discussion to follow) the *Z* form is favored. No crystal structures of formanilides are available.

Solid acetanilide, **14**, is in the planar *Z* form (60). The CP/MAS spectrum indicates that $\Delta_{2,6}$ is +1.5 ppm, consistent with a planar molecule in the solid.

In solution *o*-fluoroformanilide is expected to be in a conformation with the formyl group *trans* to the fluorine. The rotation of the formyl group is slow on the ^{13}C chemical shift time scale at room temperature and the *Z* and *E* forms exist in an approximately 2:1 ratio. The deviation of the *ortho* ^{13}C chemical shifts from additivity implies $\Delta_{2,6}$ values of +2.9 ppm and −0.3 ppm, respectively, for the *Z* and *E* forms in the absence of the fluorine substituent. The observed magnitude of 2.8 ppm for **13** is rather close to that predicted, considering that the additivity method probably has an uncertainty of as much as 0.5 ppm. It is on this agreement that we base the positive sign of $\Delta_{2,6}$ for **13** and **14**. The fact that the predicted and observed values of $\Delta_{2,6}$ are so much closer for the *Z* form than for the *E* form implies the former as the solid state conformation of 4-methylformanilide, **13**.

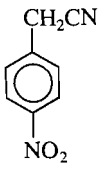
(viii) Benzylcyanides

In solution benzylcyanides unsubstituted in the *ortho* positions experience nearly free internal rotation (40). The ^{13}C CP/MAS spectrum of **15** yields a splitting, $\Delta_{2,6}$, of ±2.5 ppm. This suggests that solid **15** may be planar or nearly planar. As



Z *E*

13 R = H, R' = CH_3
14 R = CH_3, R' = H



15

Can. J. Chem. Downloaded from www.nrcresearchpress.com by 122.72.124.2 on 09/07/12
For personal use only.

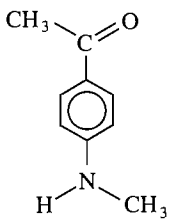
the splitting is not very large, the possibility of nonequivalence of C-2 and C-6 due to crystal packing forces certainly cannot be ruled out. The *ortho* ring carbon resonance in pentamethylbenzylcyanide ($\theta = 90°$) shows no such splittings (40).

(b) Derivatives with two different unsymmetrical substituents in the 1 and 4 positions

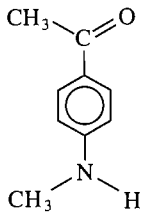
When two unsymmetrical substituents are *para* to each other, the observed splittings $\Delta_{2,6}$ and $\Delta_{3,5}$ depend on the $\Delta_{2,6}$ and $\Delta_{3,5}$ values associated with each individual substituent and on the relative orientation of the substituents. If the molecule has all heavy atoms in one plane, the two substituents may have a *cis* or *trans* configuration as shown in Figs. 1*b* and 1*c*, respectively.

(i) 4-N-Methylaminoacetophenone, ***16***

The influence of two unsymmetrical substituents, *para* to one another, on the ring carbon chemical shifts is nicely demonstrated by the low temperature solution spectrum of 4-methylaminoacetophenone **16** (27). In conformation **16***a* the contributions of the acetyl and *N*-methyl groups to $\Delta_{2,6}$ and $\Delta_{3,5}$ are of opposite sign and will tend to cancel. On the other hand, in **16***b* they will add, yielding larger $\Delta_{2,6}$ and $\Delta_{3,5}$ values. At



16*a*

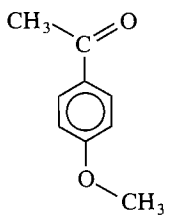


16*b*

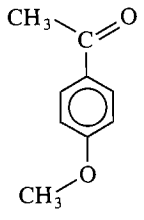
153 K in dimethyl ether solution internal rotation of both the *N*-methyl and acetyl groups is slow and two species **16***a* and **16***b*, of different stability, are present. We assign $\Delta_{2,6}$ and $\Delta_{3,5}$ magnitudes of 1.7 ppm and 6.2 ppm for **16***a* and 4.7 ppm and 7.6 ppm for **16***b*, respectively. The CP/MAS spectrum yields 0.6 ppm and 5.1 ppm, implying **16***a* as the solid state conformation.

(ii) 4-Methoxyacetophenone, ***17***

In Freon solution at 123 K, internal rotation of the acetyl group in **17** is slow, yielding $\Delta_{2,6}$ and $\Delta_{3,5}$ values of (−)3.4 ppm and (+)2.1 ppm, respectively (53). In solid **17** the



17*a*

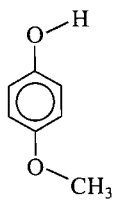


17*b*

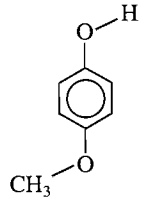
rotation of the methoxy group has also stopped and $\Delta_{2,6}$ and $\Delta_{3,5}$ are (−)4.7 and (−)7.8 ppm, respectively. That the rotation of the methoxy group has stopped is evident by the large increase in $\Delta_{3,5}$. The change in $\Delta_{2,6}$ may also be due to a contribution of the methoxy group. If this is so, the contributions of the acetyl and methoxy groups to $\Delta_{2,6}$ can only be additive if **17***b* is the conformation of 4-methoxyacetophenone in the solid state.

(iii) 4-Methoxyphenyl, ***18***

The magnitude of $\Delta_{2,6}$ in **18** is 0.9 ppm; this is smaller than the expected value (see Sect. *a.ii*). A possible explanation is that the OH and OCH_3 moieties are *cis* (**18***a*). In such a situation



18*a*

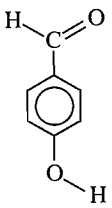


18*b*

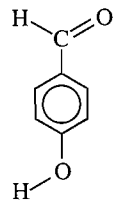
the contribution of the methoxy group to $\Delta_{2,6}$ is expected to be small and positive and that of the hydroxy group small and negative, thus diminishing the magnitude of $\Delta_{2,6}$. The value of $\Delta_{3,5}$ is (−)6.3 ppm, in the range expected for carbons *ortho* to a methoxy group. The hydroxy group is not expected to contribute to $\Delta_{3,5}$.

(iv) 4-Hydroxybenzaldehyde, ***19***

The values of $\Delta_{2,6}$ and $\Delta_{3,5}$ in solid 4-hydroxybenzaldehyde are (−)9.1 and (−)2.1 ppm (12). These values are consistent with those expected if there were no contribution of the formyl group towards $\Delta_{3,5}$ or of the hydroxyl group towards $\Delta_{2,6}$. Under such circumstances an assignment of conformation **19***a* or **19***b* to solid 4-hydroxybenzaldehyde cannot be made on the basis of $\Delta_{2,6}$ or $\Delta_{3,5}$. X-ray diffraction studies indicate that **19***a* is the conformation of 4-hydroxybenzaldehyde in the solid state (43).



19*a*



19*b*

Another possible interpretation of the ^{13}C CP/MAS spectrum of **19** is that $\Delta_{3,5}$ = (+)2.1 ppm. Such a value would be expected for conformation **19***a* if the contribution of the O=C—H group to $\Delta_{3,5}$ were in the range of +3.0–+4.0 ppm. This is larger than the expected contribution of about +0.5–+1.5 ppm, therefore it appears that neither the formyl nor hydroxyl group contributes significantly to $\Delta_{3,5}$ or $\Delta_{2,6}$, respectively.

Conclusions

The results presented in this paper show that, for a variety of benzene derivatives, ^{13}C chemical shifts in the solid state are usually within about 1 ppm of those in solution. In addition, splittings of the *ortho* and *meta* ring ^{13}C resonances are observed due to the rigid conformation of unsymmetric substituents. These splittings are in good agreement with those observed in solution at low temperatures where internal rotation of the unsymmetric substituents is slow. In some cases the splittings are large and provide a useful tool for determining the conformations of benzene derivatives in the solid state. This is particularly useful if structures from diffraction studies are unavailable.

Can. J. Chem. Downloaded from www.nrcresearchpress.com by 122.72.124.2 on 09/07/12
For personal use only.

In the present study we have presented a few examples where it is possible to suggest the solid state conformation of 1,4-disubstituted benzene derivatives with two unsymmetrical substituents. Unfortunately, in many cases, $\Delta_{2,6}$ and $\Delta_{3,5}$ for any given substituent vary too much to make the deductions with certainty. It is important to point out that it is only on the basis of $\Delta_{3,5}$ values that one can distinguish between the relative orientations (Fig. 1, *b* and *c*) of two unsymmetrical substituents in 1,4-disubstituted benzenes. Both *ortho*- and *meta*-disubstituted benzene derivatives with unsymmetrical substituents show more promise, in particular those where the two substituents are identical. Work on these is presently underway.

Acknowledgements

We wish to thank Dr. Michael S. McKinnon for obtaining a few preliminary CP/MAS spectra, Mr. Brian Millier and Mr. Ron Curtis for their assistance in maintaining the nmr spectrometers, and the Natural Sciences and Engineering Research Council of Canada (NSERC) for financial support. G.H.P. is grateful to Dalhousie University for the award of a Killam Postdoctoral Fellowship. Finally we wish to thank Professor Ted Schaefer for several of the compounds.

Can. J. Chem. Downloaded from www.nrcresearchpress.com by 122.72.124.2 on 09/07/12
For personal use only.

1. J. SCHAEFER and E. O. STEJSKAL. J. Am. Chem. Soc. **98**, 1031 (1976).
2. E. T. LIPPMAA, M. A. ALLA, T. J. PEHK, and G. ENGELHARDT. J. Am. Chem. Soc. **100**, 1929 (1978).
3. H. MIURA, T. TERAO, and A. SAIKA. J. Magn. Reson. **68**, 593 (1986).
4. J. SCHAEFER, E. O. STEJSKAL, and R. BUCHDAHL. Macromolecules, **10**, 384 (1977).
5. T. R. STEGER, E. O. STEJSKAL, R. A. MACKAY, B. R. STULTS, and J. SCHAEFER. Tetrahedron Lett. 295 (1979).
6. G. S. HARBISON, D. P. RALEIGH, J. HERZFELD, and R. G. GRIFFIN. J. Magn. Reson. **64**, 294 (1985).
7. G. E. BALIMANN, C. J. GROOMBRIDGE, R. K. HARRIS, K. J. PACKER, B. J. SAY, and S. F. TANNER. Philos. Trans. R. Soc. London, A: **299**, 643 (1981).
8. T. URYU and T. KATO. Chem. Lett. 211 (1987).
9. J. G. HEXEM. Ph.D. thesis, Univ. of Pennsylvania, 1982. p. 51.
10. M. A. WILSON, A. M. VASSALLA, M. I. BURGAR, P. J. COLLIN, B. W. SKELTON, and A. H. WHITE. J. Phys. Chem. **90**, 3944 (1986).
11. A. HÖHENER. Chem. Phys. Lett. **53**, 97 (1978).
12. F. IMASHIRO, S. MAEDA, T. TAKEGOSHI, T. TERAO, and A. SAIKA. Chem. Phys. Lett. **99**, 189 (1983).
13. A. M. CHIPPENDALE, A. MATHIA, R. K. HARRIS, K. J. PACKER, and B. J. SAY. J. Chem. Soc. Perkin Trans. 2, 1032 (1981).
14. G. R. HAYS. J. Chem. Soc. Perkin Trans, 1049 (1983).
15. M. MARICQ and J. S. WAUGH. Chem. Phys. Lett. **47**, 327 (1977).
16. C. M. CARTER, J. C. FACELLI, D. W. ALDERMAN, D. M. GRANT, N. K. DALLEY, and B. E. WILSON. J. Chem. Soc. Faraday Trans. 1, 3673 (1988).
17. W. J. E. PARR and T. SCHAEFER. Acc. Chem. Res. **13**, 400 (1980).
18. N. K. WILSON and J. B. STOTHERS. *In* Topics in stereochemistry. Vol. 8. *Edited by* E. L. Eliel and N. L. Allinger. John Wiley and Sons, New York. 1974. p. 1.
19. M. OKI. *In* Applications of dynamic NMR spectroscopy to organic chemistry methods of stereochemical analysis. Vol. 4. *Edited by* A. P. Marchand. VCH, Deerfield Beach, U.S.A. 1985.
20. S. J. OPELLA and M. H. FREY. J. Am. Chem. Soc. **101**, 5854 (1979).
21. J. TEGENFELDT and U. HAEBERLEN. J. Magn. Reson. **36**, 453 (1979).
22. W. T. DIXON. J. Chem. Phys. **77**, 1800 (1982).
23. W. L. EARL and D. L. VANDERHART. J. Magn. Reson. **48**, 35 (1982).
24. P. S. PREGOSIN. Ph.D. thesis, The City University of New York, 1970. p. 92.
25. R. A. W. JOHNSTONE, D. W. PAYLING, and C. THOMAS. J. Chem. Soc. (C), 2223 (1969).
26. J. D. BALEJA. Synth. Commun. **14**, 215 (1984).
27. L. LUNAZZI, C. MAGANNOLI, and D. MACCIANTELLI. J. Chem. Soc. Perkin Trans. 2, 1704 (1980).
28. L. LUNAZZI, C. MAGAGNOLI, M. GUERRA, and D. MACCIANTELLI. Tetrahedron Lett. 3031 (1979).
29. G. H. PENNER. M.Sc. thesis, University of Manitoba, 1984.
30. G. A. OLAH and D. J. DONOVAN. J. Org. Chem. **43**, 1743 (1978).
31. (*a*) A. NAITO, S. GANAPATHY, and C. A. MCDOWELL. J. Chem. Phys. **74**, 5395 (1981); (*b*) J. Magn. Reson. **48**, 367 (1982); (*c*) N. ZUMBILYADIS, P. M. HENRICHS, and R. H. YOUNG. J. Chem. Phys. **75**, 1603 (1981); (*d*) J. G. HEXEM, M. H. FREY, and S. J. OPELLA. J. Am. Chem. Soc. **103**, 224 (1981); (*e*) J. Chem. Phys. **77**, 3847 (1982); (*f*) J. BOHM, D. FENZKE, and H. PFEIFER. J. Magn. Reson. **55**, 197 (1983).
32. T. SCHAEFER, R. LAATIKAINEN, T. A. WILDMAN, J. PEELING, G. H. PENNER, J. BALEJA, and K. MARAT. Can. J. Chem. **62**, 1592 (1984).
33. (*a*) S. C. NYBURG and C. H. FAERMAN. J. Mol. Struct. **140**, 347 (1986); (*b*) P. A. KOLLMAN, K. N. HOUK, G. M. ANDERSON, and L. N. DOMELSMITH. J. Am. Chem. Soc. **101**, 2344 (1979), and references therein.
34. L. P. LUGER, E. RABIUS, E. KUTTER, and V. AUSTEL. Acta Crystallogr. Sect. C: Cryst. Struct. Commun. **C43**, 1937 (1987).
35. J. F. VOLLANO, R. O. DAY, D. N. RAN, V. CHANDRASEKHAR, and R. R. HOLMES. Inorg. Chem. **23**, 3153 (1984).
36. J. J. H. MCDOWELL. Acta Crystallogr. Sect. B: Struct. Crystallogr. Cryst. Chem. **31**, 2256 (1975).
37. O. I. WHARF and M. C. SIMARD. J. Organomet. Chem. **332**, 85 (1987).
38. H. SAITO, M. YOKOI, M. AIDA, M. KODAMA, T. ODA, and Y. SATO. Magn. Reson. Chem. **26**, 155 (1988).
39. A. M. CHIPPENDALE, R. S. AUJLA, R. K. HARRIS, K. J. PACKER, and S. PURSER. Magn. Reson. Chem. **24**, 81 (1986).
40. T. SCHAEFER and G. H. PENNER. Can. J. Chem. **64**, 2013 (1986).
41. H. DUDDECK. *In* Topics in stereochemistry. Vol. 16. *Edited by* E. L. Eliel, S. H. Wilen, and N. L. Allinger. John Wiley and Sons, New York. 1986. p. 219.
42. D. M. GRANT and B. V. CHENEY. J. Am. Chem. Soc. **89**, 5315 (1967).
43. F. IWASAKI. Acta Crystallogr. Sect. B: Struct. Crystallogr. Cryst. Chem. **33**, 1646 (1977).
44. R. CELIKEL, A. J. GEDDES, and B. SHELDRICK. Cryst. Struct. Commun. **7**, 683 (1978).
45. J. K. DATTAGUPTA and N. N. SAHA. Acta Crystallogr. Sect. B: Struct. Crystallogr. Cryst. Chem. **29**, 1228 (1973).
46. M. MASAO, S. KASHINO, F. IKEJIRI, T. OHNO, and K. TERANISHI. Acta Crystallogr. Sect. B: Struct. Crystallogr. Cryst. Chem. **32**, 857 (1976).
47. Y. TANIMOTO, H. KOBAYASHI, S. NAGAKURA, and Y. SAITO. Acta Crystallogr. Sect. B: Struct. Crystallogr. Cryst. Chem. **29**, 1822 (1973).
48. M. HAISA, S. KASHINO, T. YUASA, and K. AKIGONA. Acta Crystallogr. Sect. B: Struct. Crystallogr. Cryst. Chem. **32**, 1326 (1976).
49. J. K. S. KIM, E. R. BOYKO, and G. B. CARPENTER. Acta Crystallogr. Sect. B: Struct. Crystallogr. Cryst. Chem. **29**, 1141 (1973).
50. T. DRAKENBERG, R. JOST, and J. M. SOMMER. J. Chem. Soc. Perkin Trans. 2, 1683 (1975).

51. T. DRAKENBERG, J. M. SOMMER, and R. JOST. J. Chem. Soc. Perkin Trans. 2, 363 (1980).
52. J. A. RIPMEESTER. J. Inclusion Phenom. **6**, 31 (1988).
53. T. DRAKENBERG, J. M. SOMMER, and R. JOST. Org. Magn. Reson. **8**, 579 (1976).
54. L. LUNAZZI, D. MACCIANTELLI, and G. PLACUCCI. Tetrahedron Lett. **21**, 975 (1980).
55. Y. K. GRISHIN, N. M. SERYEYEV, O. A. SUBBOTIN, and Y. A. USTYNYUK. Mol. Phys. **25**, 297 (1973).
56. T. SCHAEFER, R. SEBASTIAN, and G. H. PENNER. Can. J. Chem. **66**, 1787 (1988).
57. U. BAUMEISTER, H. HARTUNG, and M. JASKOLSKI. Mol. Cryst. Liq. Cryst. **88**, 167 (1982).
58. (*a*) W. E. STEWART and T. H. SIDDALL. Chem. Rev. **70**, 517 (1970); (*b*) M. L. MARTIN, X. Y. SUN, and G. J. MARTIN. *In* Annual reports on NMR spectroscopy. Vol. 16. *Edited by* G. A. Webb. Academic Press, London. 1985. p. 187.
59. H. NAKANISHI and O. YAMAMOTO. Chem. Lett. 521 (1974).
60. C. J. BROWN. Acta Crystallogr. **21**, 442 (1966).

Can. J. Chem. Downloaded from www.nrcresearchpress.com by 122.72.124.2 on 09/07/12
For personal use only.

The vibrational spectra (100–1600 cm^{-1}) and scaled 3-21G *ab initio* harmonic force fields for 7-oxanorbornane and 7-thianorbornane

R. A. SHAW, N. IBRAHIM, AND H. WIESER[1]

The University of Calgary, Department of Chemistry, Calgary, Alta., Canada T2N 1N4

Received September 26, 1988

R. A. SHAW, N. IBRAHIM, and H. WIESER. Can. J. Chem. **67**, 535 (1989).

The vibrational spectra in the region of 1600–100 cm^{-1} are reported for 7-oxa- and 7-thianorbornane. *Ab initio* 3-21G harmonic force fields based on optimized structures determined previously at the same level of theory were calculated for both molecules. The vibrational spectra were assigned unambiguously and almost completely with the aid of the 3-21G force fields, scaled using ten factors previously optimized in an overlay refinement to fit assigned frequencies of norbornane, norbornene, and norbornadiene, and including two others, where appropriate, from dimethyl ether and thietane. Reoptimization of 12 scaling factors reproduced 60 assigned frequencies out of a total of 70 in the specified region with average errors of 7.4 and 4.9 cm^{-1}, respectively, for the two molecules. The final refinement changed the scaling factors transferred from norbornane generally by less than 1%.

Key words: 7-oxanorborane, 7-thianorborane, vibrational spectra, *ab initio* harmonic force field.

R. A. SHAW, N. IBRAHIM et H. WIESER. Can. J. Chem. **67**, 535 (1989).

On a déterminé les spectres vibrationnels de l'oxa-7 et du thia-7 norbornane dans la région de 1600 à 100 cm^{-1}. Pour chacune de ces molécules, on a effectué des calculs *ab initio* 3-21G de champs de force qui sont basés sur les structures optimisées déterminées antérieurement au même niveau de la théorie. On a fait une attribution non-ambiguë et pratiquement complète des spectres vibrationnels en se basant sur les champs de force 3-21G dont l'échelle a été déterminée à l'aide de dix facteurs optimisés antérieurement par un affinement des fréquences attribuées au norbornane, au norbornène et au norbornadiène et, lorsque c'était approprié, au méthoxyméthane et au thiéthane. Une réoptimisation de l'échelle de 12 facteurs a permis de reproduire 60 des 70 fréquences attribuées dans la région spécifiée; pour chacune des molécules, les erreurs moyennes sont respectivement de 7,4 et 4,9 cm^{-1}. L'affinement final n'a généralement modifié les facteurs de l'échelle du norbornane que par moins de 1%.

Mots clés : oxa-7 norborane, thia-7 norborane, spectres vibrationnels, *ab initio* de champs de force.

[Traduit par la revue]

Can. J. Chem. Downloaded from www.nrcresearchpress.com by 41.223.56.140 on 09/07/12
For personal use only.

Introduction

We have recently reported scaled *ab initio* force fields for norbornane, norbornene, and norbornadiene (1). These were derived by optimizing a set of 12 scaling factors to fit simultaneously the observed frequencies for all three molecules, with the assumption that analogous *ab initio* force constants were overestimated to the same extent for each compound. The validity of this assumption was verified by the excellent fit of calculated to observed frequencies (average error of 5.3 cm^{-1}), which further suggested that the derived factors might be appropriate for scaling the force fields of other related compounds.

In this report, we present the vibrational spectra of 7-oxabicyclo[2.2.1]heptane (7-oxanorbornane, 7-OXA) and 7-thiabicyclo[2.2.1]heptane (7-thianorbornane, 7-THIA; see Fig. 1). The 3-21G calculated force constants for each are scaled using the factors optimized for the norbornane–norbornene–norbornadiene set, and the spectra assigned on the basis of frequencies thus predicted.

The only previous work concerning the vibrational spectra of either molecule is that of Carlile *et al.* (2), who measured the far-infrared absorption spectrum of 7-OXA in the vapor phase. The transition energies for certain low frequency modes were also inferred from a microwave study (3), which in addition yielded certain structural data. Further structure information is available for both compounds from electron diffraction measurements (4, 5) and optimized STO-3G and 3-21G geometries (6).

Experimental and computational details

7-Oxabicyclo[2.2.1]heptane was purchased from Aldrich with a quoted purity of 98%, and used without further purification. 7-Thiabicyclo[3.2.1]heptane was prepared from the oxygen analog following a published procedure (7), and purified by sublimation to at least 99%.

The infrared absorption spectra were obtained with a Nicolet 8000 FT-IR spectrometer and the Raman on a Jarrell-Ash model 25-100 double grating monochromator interfaced to an IBM PC. The vapor phase infrared spectra (Figs. 2 and 3) were run using a Wilkes multipass cell, at a pathlength of about 18 m, and the spectra in solution (CCl_4 and CS_2) and of the neat liquid of 7-oxa in KBr cells of pathlength 0.1 and 0.015 mm, respectively (Figs. 4 and 5). Typically 400 scans were accumulated for the vapors and 1000 for the condensed phases. For the latter, closely spaced absorptions were resolved using the Fourier self-deconvolution (FSD) technique (8) with software supplied by Nicolet. The Raman spectra are presented in Figs. 6 and 7. Measured peak positions are summarized in Tables 1 and 2.

Cartesian force constants were evaluated for both molecules as numerical derivatives of the analytically calculated gradients at the optimized structures (6), using the 3-21G basis set with Gaussin 82 as implemented on the Cyber 205 supercomputer at the University of Calgary (9, 10). The force constants were then transformed to local symmetry coordinates (Table 3), chosen in accordance with those suggested by Pulay *et al.* (11) and defined analogously to those for the norbornane series (1). The local symmetry force constants were scaled according to $F_{ij} = (C_iC_j)^{1/2}K_{ij}$, were C_i and C_j denote the scaling factors for modes i and j, and F_{ij} and K_{ij} the scaled and unscaled *ab initio* force constants, respectively. For the least-squares refinement of the scaling factors, the observed frequency parameters λ_i were weighted by $(1/\lambda_i^{obs})^2$. Each refinement was allowed to continue until the calculated shifts were less than 0.0005 for all scaling factors.

Vibrational assignments and determination of force fields

The force fields for 7-OXA and 7-THIA were scaled initially using factors optimized to fit the observed frequencies for norbornane, norbornene, and norbornadiene (1), with additional factors for the C—O and C—S stretching coordinates

[1]To whom all correspondence should be addressed.

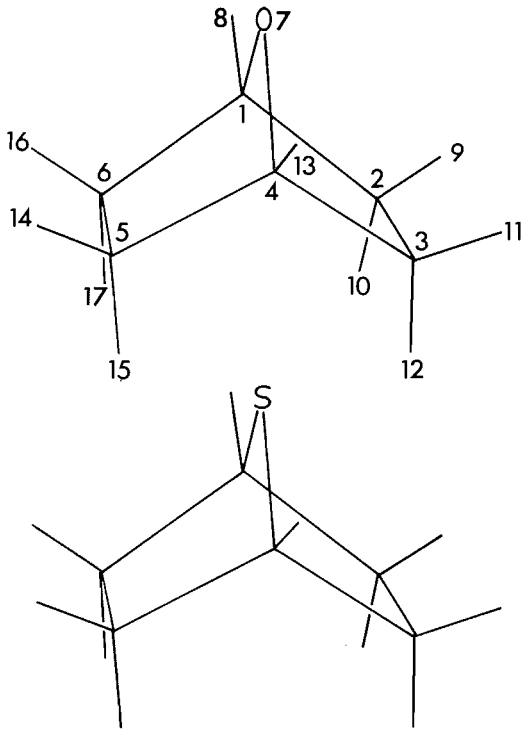


FIG. 1. Atom numbering for 7-oxanorbornane and 7-thianorbornane, used in defining the vibrational local symmetry coordinates in Table 3.

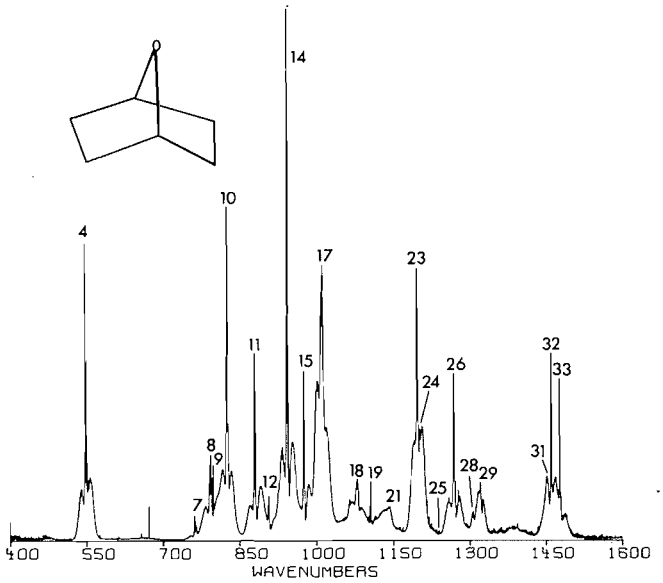


FIG. 2. Vapor phase infrared absorption spectrum of 7-oxanorbornane. Numbers identifying peaks correspond to "Peak no." in Tables 1 and 4.

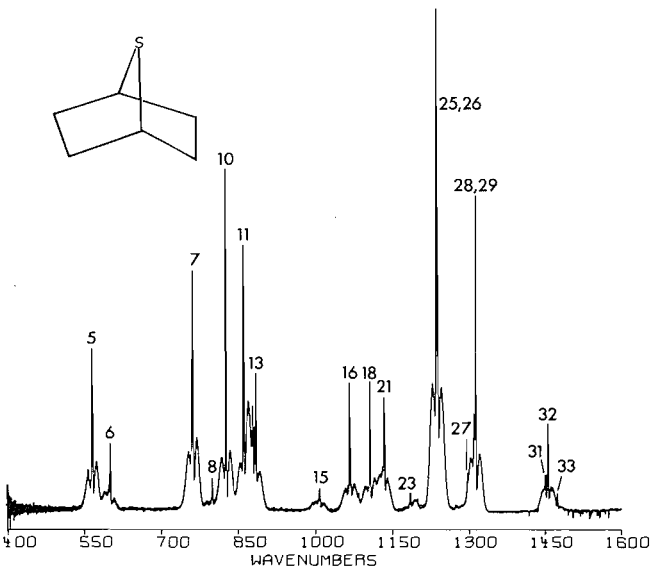


FIG. 3. Vapor phase infrared absorption spectrum of 7-thianorbornane. Numbers identifying peaks correspond to "Peak no." in Tables 2 and 5. Vapor pressure for region 1350–1600 cm^{-1} was reduced to about one seventh of that for the remainder of the spectrum.

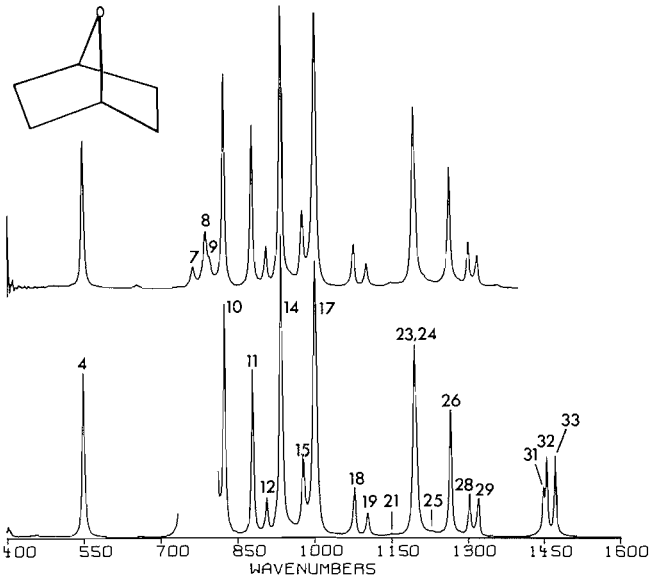


FIG. 4. Infrared absorption spectra of 7-oxanorbornane as the neat liquid (upper) and in CCl_4 solution (lower). Numbers identifying peaks correspond to "Peak no." in Tables 1 and 4.

transferred from previous studies of dimethylether (12) and thietane (13). The frequencies predicted on this basis are listed in Tables 4 and 5 under columns "(1)".

We have not attempted to assign the C—H stretches. The frequencies calculated for this region are therefore only approximate. The assignments proposed for the remaining transitions fall into three categories. First, there are those for which experimental evidence unambiguously confirms the correct symmetry species, i.e., polarized Raman lines for 7-OXA and 7-THIA, and three apparent B-contours in the vapor phase spectrum of the former. For all of these cases the assignment is confirmed by closely lying calculated frequencies of the correct symmetry. Second, there are a number of observed features whose assignment is completely unambiguous in light of the calculated positions. For example, for 7-OXA, the vapor phase band at 799.2 cm^{-1} is readily designated as ν_{44} (calcd. 795.6 cm^{-1}), and ν_{34} (calcd. 806.5 cm^{-1}) and ν_{11} (calcd. 816.3 cm^{-1}) as assigned previously at 793.6 cm^{-1} and 826.1 cm^{-1} (2). Similarly, all of the transitions predicted below about 650 cm^{-1} were readily located, as were the CH_2 scissoring modes.

Finally, in certain instances the vibrational assignments were not straightforward even in light of the calculated positions. These cases are discussed separately below.

Can. J. Chem. Downloaded from www.nrcresearchpress.com by 41.223.56.140 on 09/07/12
For personal use only.

Can. J. Chem. Downloaded from www.nrcresearchpress.com by 41.223.56.140 on 09/07/12
For personal use only.

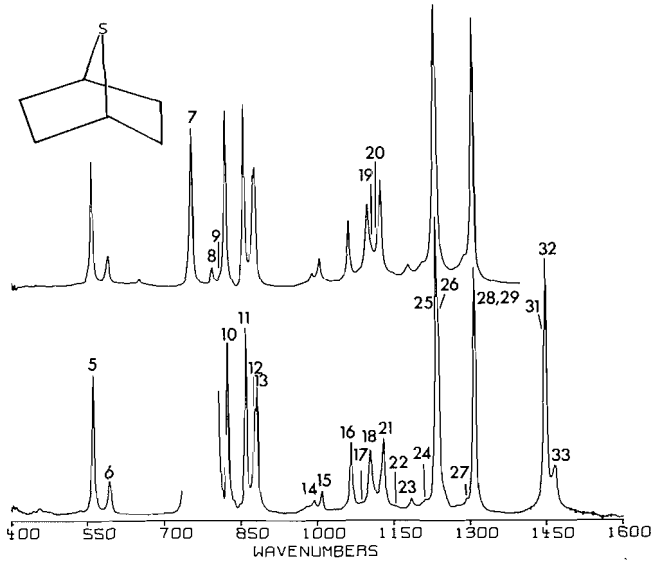


FIG. 5. Infrared absorption spectra of 7-thianorbornane in CS_2 (upper) and CCl_4 (lower) solutions. Numbers identifying peaks corresponds to "Peak no." in Tables 2 and 5.

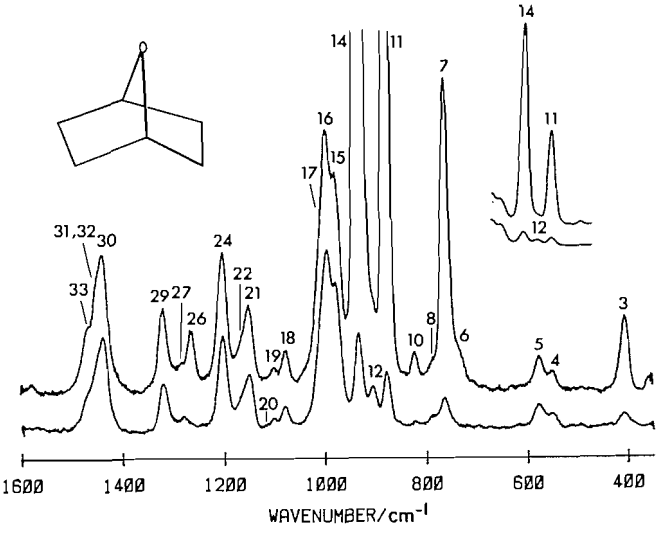


FIG. 6. Parallel (upper) and perpendicular (lower) polarized Raman spectra of liquid 7-oxanorbornane. Numbers identifying peaks correspond to "Peak no." in Tables 1 and 4.

7-Oxanorbornane

In the A_1 species ν_5 (calcd. 1334 cm^{-1}) is assigned to an infrared absorption observed at 1321.9 cm^{-1}, which we suspect to contain also the B_2 transition predicted at 1320 cm^{-1} (ν_{39}). Although they are not resolved in the condensed phase spectra, the unusual band contour suggests two overlapping absorptions (band no. 29 in Fig. 2). Both ν_7 (calcd. 1163 cm^{-1}) and ν_8 (calcd. 1025 cm^{-1}) are apparently weak or absent in the infrared absorption spectra, and are assigned to the Raman lines at 1164 and 997 cm^{-1} (peaks no. 22 and 16, respectively, in Fig. 6). Even in the absence of corroborative experimental evidence, such as infrared bandshapes or Raman polarization data, we believe that the calculated positions are sufficiently accurate and reliable to make these assignments with confidence. Two fundamentals namely ν_{30} (B_1) at 1193.8 cm^{-1} and ν_{40} (B_2) at 1199.6 cm^{-1} are predicted near the bands labelled 23 and 24 (Figs. 2 and 4). The dominant vapor phase absorption at lower

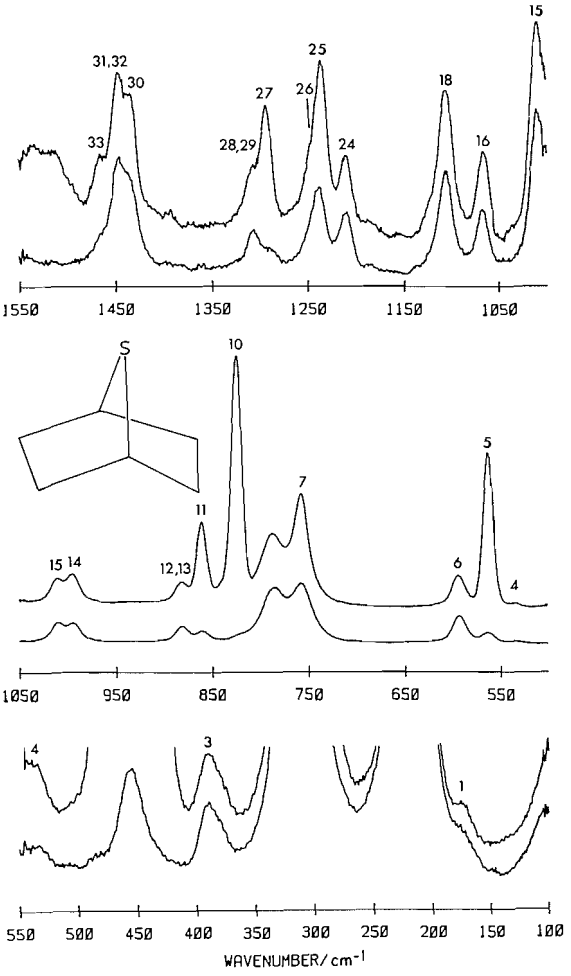


FIG. 7. Parallel (upper) and perpendicular (lower) polarized Raman spectra of 7-thianorbornane in CCl_4 solution. Peaks which are off scale in the 550–100 cm^{-1} region are CCl_4 lines. Numbers identifying peaks correspond to "Peak no." in Tables 2 and 5.

frequency (peak 23 at 1199.3 cm^{-1}) is assigned as the latter on the basis of its band contour which is very similar to that observed for the B_2 mode at 548.5 cm^{-1} (peak no. 4). The weaker feature on the high frequency side (1204.0 cm^{-1}) must then be the B_1 mode. The assignment of ν_{29} is based solely upon the predicted position at 1246 cm^{-1}, ascribing the status of a fundamental to the very weak infrared feature at 1240.8 cm^{-1} (peak 25 in Figs. 4 and 6). Such a low intensity is not entirely unexpected given that nature of the mode, which is primarily a CH_2 twist. Four of the eight A_2 modes below 1500 cm^{-1} were identified in the Raman spectrum. The others may be assumed to be a very low intensity and either absent or obscured by more prominent bands in all spectra.

7-Thianorbornane

Only six fundamentals fall into this category for 7-THIA. Two of these are predicted to lie very close to one another, namely ν_6 (A_1) at 1242.3 cm^{-1} and ν_{29} (B_1) at 1241.5 cm^{-1}. Two bands are clearly resolved upon Fourier self-deconvolution of the solution phase infrared spectrum at 1233.8 cm^{-1} and 1238.1 cm^{-1} (peaks nos. 25 and 26, Fig. 5). While the calculated frequencies suggest these should be assigned as B_1 and A_1, respectively, close inspection of the Raman spectrum over this region reveals that the lower frequency component of

TABLE 1. Observed infrared absorptions and Raman lines (in cm^{-1}) for 7-oxanorbornane

Peak no.[a]	Infrared		Raman[d]	Assignment
	Vapor[b]	Solution[c]		
1			148 w, dp	A_2
2	331.5[e]		333 w, dp	B_1
3	400.1[e]	405.5 vw	406 w, p	A_1
4	548.5	550.4 m	552 w, dp	B_2
5			577 w, dp	A_2
6			736 w, sh	
7	762.3	764.3 w	763 m, p	A_1
8	793.6 B	788.5 m	787 w, sh	B_1
9	799.2	796.8 w		B_2
10	826.1	824.0 s	822 w, p	A_1
11	882.3	879.6 s	879 s, p	A_1
12	908.9	907.5 w	906 w, dp	B_2
13		925.2 vw, dcn		
14	945.5	936.0 s	933 vs, p	A_1
15	977.8	977.5 m	978 m, dp	B_2
16			997 m	(A_1)
17	1013.6	1002.3 vs	1006 w, sh	B_1
18	1080.5 B	1078.6 w	1079 w, dp	B_1
19	1108.0	1103.0 w	1101 w	B_2
20			1121 vw	
21	1145	1149.0 vw	1151 m, dp	
22	1170.9		1164 w, sh	(A_1)
23	1199.3	1195.5 s, dcn		B_2
24	1204.0	1199.5 s, dcn	1203 m, dp	B_1
25	1240.8 B	1229.5 vvw		B_1
26	1270.5	1264.7 m	1265 m, p	A_1
27			1278 w, dp	A_2
28	1307 B	1302.0 w		B_1
29	1321.9	1319.5 w	1320 w, dp	A_1, B_2
30			1440 m, dp	A_2
31	1453.5	1449.6 w, dcn (CCl_4)	1450 m, dp	B_1
32	1461.2	1455.6 m, dcn (CCl_4)	1450 m, dp	B_2
33	1477.6	1472.5 m, dcn (CCl_4)	1466 w, sh, dp	A_1

[a]Corresponding to peaks labelled in Figs. 2, 4, and 6.
[b]Observed band contour is A, C, or A/C hybrid unless noted as B.
[c]CS_2 solution unless otherwise indicated. Abbreviations: s, m, w = strong, medium, weak; sh = shoulder; dcn denotes solution phase absorptions resolved by Fourier self-deconvolution.
[d]Neat liquid. Abbreviations: s, m, w = strong, medium, weak; sh = shoulder; p, dp = polarized, depolarized. Bands not designated as either p or dp are experimentally ambiguous in this respect.
[e]Vapor phase positions from ref. 2.

the feature at 1235 cm^{-1} (peak no. 25 in Fig. 7) is polarized. Since the residual feature in the perpendicular spectrum (peak no. 26) is shifted to higher frequency, we assign this band as B_1 and the polarized band as A_1. Similarly, two bands are predicted near 1320 cm^{-1}, namely ν_{28} (B_1) at 1322.8 cm^{-1} and ν_{39} (B_2) at 1317.4 cm^{-1}. The solution phase infrared band at 1313 cm^{-1} does resolve upon Fourier self-deconvolution to show a strong absorption at 1310.2 cm^{-1} and a weaker feature at 1307 cm^{-1} (peaks nos. 29 and 28 in Table 2 and Fig. 5). These are assigned to the B_1 and B_2 symmetry species so as to match the ordering calculated for these modes. Finally, ν_7 (A_1) and ν_{43} (B_2) are assigned to absorptions in the infrared spectra solely on the basis of their predicted positions (peaks 17 and 12, respectively, in Figs. 3 and 5).

Based upon these assignments, we had several options for further refining the scaling factors. One possibility was to reoptimize all scaling factors to fit the new assignments. There exists ample evidence, however, to suggest that the factors for coordinates in common with the norbornane series, i.e. those involving the six-membered ring, should be clearly transferable to the 7-OXA and 7-THIA derivatives. We deemed it preferable to identify and reoptimize only those factors which might be expected to deviate from the transferred values, holding all others fixed. Accordingly we refined initially only the scaling factors for the C—O and C—S stretches and the deformation of the C—O—C bridge of the oxygen compound. The latter obviously requires adjustment in view of the poor fit to ν_{45} of 7-OXA. The reoptimized factors for the C—O and C—S stretches and C—O—C bridge deformation are listed under "Rfnmt.1" in Table 6, and the corresponding calculated frequencies in Tables 4 and 5. In the final refinement, all scaling factors were floated to fit the assigned transitions ("Rfnmt.2" in Table 6, and "Calcd. positions (3)" in Tables 6 and 5). While we suspected that the data might not be sufficient to determine

Can. J. Chem. Downloaded from www.nrcresearchpress.com by 41.223.56.140 on 09/07/12
For personal use only.

TABLE 2. Observed infrared absorptions and Raman lines (in cm^{-1}) for 7-thianorbornane

Peak no.[a]	Infrared		Raman[d]	Assignment
	Vapor[b]	Solution[c]		
1			173 w	A_2
2			326 w (C_6H_6)	B_1
3			388 w	A_1
4			536 w	A_2
5	567.6	563.3 s	562 s, p	A_1
6	602.9	594.9 w	592 w, dp	B_1
7	762.7	758.5 s	756 m, p (C_6H_6)	A_1
8	800.4	798.7 w		B_2
9		813.3 w, sh, dcn		(B_1)
10	827.8	825.0 s	823 s, p	A_1
11	862.9	861.3 s	860 m, p	A_1
12		879.4 m		B_2
13	885.7	883.3 m	882 w, dp	B_1
14		995.1 w	994 w, p	A_1
15	1010.4	1009.9 w	1009 w, dp	B_2
16	1069.4	1067.2 m	1066 w, dp	B_1
17		1087.2 w, sh, dcn		(A_1)
18	1108.5	1103.9 m	1105 m, dp	B_2
19		1111 w, sh, dcn		
20		1126 w, sh, dcn		
21	1136.0	1130.1 m		B_1
22		1152 w, sh		
23	1187.3	1183.9 w		B_2
24		1211.6 w, sh, dcn	1209 w, dp	A_2
25	1240.3	1233.8 s	1235 m, p	A_1
26	1242.3	1238.1 s, sh, dcn	1237 m, dp	B_1
27	1298.1	1292.9 w, dcn	1292 m, p	A_1
28	(1311.7)	1307 m, sh, dcn		B_2
29	1315.6	1310.2 s, dcn	1307 w, dp	B_1
30			1434 m, dp	A_2
31	1451.8	1446.9 s (CCl_4)		B_1
32	1456.5	1450.5 vs (CCl_4)	1446 m, dp	B_2
33	1474.6	1468.4 w (CCl_4)	1464 w, p	A_1

[a]Corresponding to peaks labelled in Figs. 3, 5, and 7.

[b]Observed band contour is A, C, or A/C hybrid unless noted as B.

[c]CS_2 solution unless otherwise indicated. Abbreviations: s, m, w = strong, medium, weak; sh = shoulder; dcn denotes solution phase absorptions resolved by Fourier self-deconvolution.

[d]CCl_4 solution (Fig. 5), except for those bands obscured by CCl_4 emissions, which were measured in benzene (C_6H_6). Abbreviations: s, m, w = strong, medium, weak; sh = shoulder; p, dp = polarized, depolarized. Bands not designated as either p or dp are experimentally ambiguous in this respect.

Can. J. Chem. Downloaded from www.nrcresearchpress.com by 41.223.56.140 on 09/07/12
For personal use only.

reliable values for all 12 scaling factors, those for the six-membered ring coordinates adopted final values which differ generally by less than 1% of those transferred (Table 6).

The final scaled diagonal force constants for 7-OXA and 7-THIA are summarized and compared with those of norbornane in Table 7. Complete listings of all symmetry allowed force constants are available from the authors upon request.

Discussion

In the final analysis some apparent ambiguities remained, in particular for 7-OXA. For example, the optimized C—O stretching factor (0.839) is substantially lower than the value transferred from dimethyl ether (0.903). Because this relatively large change was unexpected, we carefully reexamined the assignments for those modes containing substantial contributions from the C—O stretching. In the A_1 species the transitions assigned as ν_9 and ν_{11} are both polarized in the Raman spectra, leaving little doubt that those assignments are correct. For the B_1 species ν_{32} is assigned to a very intense band in the infrared spectra, which exhibits an apparent B-contour in the vapor phase. Although we have not calculated theoretical infrared absorption intensities, and did not consider the experimental band intensities in deriving the proposed assignments, it emerged that the three strongest bands in the absorption spectra (nos. 10, 14, and 17) were assigned as C—O stretches (ν_9, ν_{11}, and ν_{32} respectively). These observations provide strong experimental evidence that all three assignments are correct. The discrepancy between the optimized scaling factors for the C—O stretches of 7-oxanorbornane and dimethyl ether thus reflects a non-uniform overestimation of the C—O stretching force constant, as calculated for different molecules using the 3-21G basis set. We have made a similar observation when deriving a scaled 3-21G force field for 2-methyloxetane, for which the optimized C—O stretching scaling factor is 0.851

TABLE 3. Local symmetry coordinate definitions for 7-oxanorbornane and 7-thianorbornane[a]

1	C—O(S) stretch	C(4)—O(S)	5 C—C stretch	C(3)—C(4)	
2		C(1)—O(S)	6	C(1)—C(2)	
3	C—C stretch	C(4)—C(5)	7	C(5)—C(6)	
4		C(1)—C(6)	8	C(2)—C(3)	
19	CH_2 scissor	C(5) 5α(14-5-15)	+ θ(4-5-6)		
20		C(6) 5α(16-6-17)	+ θ(5-6-1)		
21		C(2) 5α(9-2-10)	+ θ(1-2-3)		
22		C(3) 5α(11-3-12)	+ θ(2-3-4)		
23	CH_2 rock	C(5) β(14-5-4)	+ β(14-5-6)	− β(15-5-4)	− β(15-5-6)
24		C(6) β(16-6-1)	+ β(16-6-5)	− β(17-6-1)	− β(17-6-5)
25		C(2) β(9-2-1)	+ β(9-2-3)	− β(10-2-1)	− β(10-2-3)
26		C(3) β(11-3-4)	+ β(11-3-2)	− β(12-3-4)	− β(12-3-2)
27	CH_2 twist	C(5) β(14-5-4)	− β(14-5-6)	− β(15-5-4)	+ β(15-5-6)
28		C(6) β(16-6-1)	− β(16-6-5)	− β(17-6-1)	+ β(17-6-5)
29		C(2) β(9-2-1)	− β(9-2-3)	− β(10-2-1)	+ β(10-2-3)
30		C(3) β(11-3-4)	− β(11-3-2)	− β(12-3-4)	+ β(12-3-2)
31	CH_2 wag	C(5) −β(14-5-4)	+ β(14-5-6)	− β(15-5-4)	+ β(15-5-6)
32		C(6) −β(16-6-1)	+ β(16-6-5)	− β(17-6-1)	+ β(17-6-5)
33		C(2) −β(9-2-1)	+ β(9-2-3)	− β(10-2-1)	+ β(10-2-3)
34		C(3) −β(11-3-4)	+ β(11-3-2)	− β(12-3-4)	+ β(12-3-2)
35	C—H def. (i/p)	C(4) β(13-4-5)	− β(13-4-3)		
36		C(1) β(8-1-6)	− β(8-1-2)		
37	C—H def. (o/p)	C(4) 2β(13-4-7)	− β(13-4-5)	− β(13-4-3)	
38		C(1) 2β(8-1-7)	− β(8-1-6)	− β(8-1-2)	
39	ring def. (i/p) B_1	θ(3-4-5)	− θ(2-3-4)	+ θ(1-2-3)	
			− θ(6-1-2)	+ θ(5-6-1)	− θ(4-5-6)
40	A_1	2θ(3-4-5)	− θ(2-3-4)	− θ(1-2-3)	
			+ 2θ(6-1-2)	− θ(5-6-1)	− θ(4-5-6)
41	A_2	θ(2-3-4)	− θ(1-2-3)	+ θ(5-6-1)	− θ(4-5-6)
42	ring def. (o/p) B_1	τ(5-4-3-2)	− τ(4-3-2-1)	+ τ(3-2-1-6)	
			− τ(2-1-6-5)	+ τ(1-6-5-4)	− τ(6-5-4-3)
43	A_1	τ(5-4-3-2)	− τ(3-2-1-6)	+ τ(2-1-6-5)	− τ(6-5-4-3)
44	A_2	−τ(5-4-3-2)	+ 2τ(4-3-2-1)	− τ(3-2-1-6)	
			− τ(2-1-6-5)	+ 2τ(1-6-5-4)	− τ(6-5-4-3)
45	bridge def.	θ(7-4-5)	+ θ(7-1-6)	− θ(7-4-3)	− θ(7-1-2)

[a]Coordinate system recommended by Pulay *et al.* (11). Atom numbering is given in Fig. 1. C—H stretching coordinate nos. 9–18 are omitted. Abbreviations i/p and o/p designate displacements as "in-plane" or "out-of-plane" with respect to the six-membered ring.

Can. J. Chem. Downloaded from www.nrcresearchpress.com by 41.223.56.140 on 09/07/12
For personal use only.

(14). In view of the present results it is tempting to suggest some correlation between the optimized C—O stretching scaling factors and the C—O—C angles for the three molecules. Such an analogous correlation is not found for C—C stretching coordinates for which optimized factors were determined previously as 0.96, 0.95, and 1.013, respectively, for propane, cyclobutane, and 2-methyloxetane (12, 14).

For the C—S stretch, the optimized scaling factor for 7-thianorbornane is lower by 0.04 (1.005) than the value transferred from thietane (1.048) (13). The C—S stretching fundamentals ν_{12} and ν_{34}, both very pure modes, are well reproduced by the force field. The calculated splitting between these modes is governed in the usual fashion by the geometry through the **G** matrix, and the CS/CS interaction force constant in the **F** matrix. It might be suspected that neither the geometry nor the interaction constant are calculated particularly accurately with the small split-valence basis set, since it is generally understood that the 3-21G basis overestimates the C—S bond length, and no accurately known or accepted value for the CS/CS interaction constant is available for comparison. The fact that the C—S fundamentals for 7-thianorbornane and thietane are accurately reproduced with the present procedure demonstrates that despite the stated uncertainties the 3-21G calculated structures and scaled force fields are completely adequate for molecules which contain the C—S—C group, both as a guide to the vibrational assignments and as a means of reproducing the observed fundamental frequencies. While we had some concern initially whether *d* functions might be required on sulfur, we decided not to tailor the basis set to suit one specific molecule in the series, viz. 7-THIA, since in that case the transferability of the scaling factors from norbornane to 7-thianorbornane and from the latter to related molecules not necessarily containing sulfur atoms might be compromised, and a marginally better value for the C—S bond length would not affect the vibrational assignment.

The C—S—C bridge deformation, ν_{45} (B_2), cannot be identified with certainty for 7-thianorbornane. The predicted position is calculated by scaling the force field under the assumption, employed also for the norbornane series, that the bridge deformation force constant may be scaled by the same factor as the in-plane ring deformation modes. On this basis, ν_{45} is predicted to lie between ν_{13} and ν_{35}. Accordingly, the

TABLE 4. Observed and calculated frequencies (cm^{-1}) for 7-oxanorbornane

	ν	Observed[a]	Peak no.[b]	Calculated positions[c] (1)	(2)	(3)	Assignment[d]
A_1	1			3025.3			
	2			2994.9			
	3			2948.1			
	4	1477.6	33	1478.6	1478.6	1475.4	Scissor
	5	1321.9	29	1333.8	1332.1	1331.6	0.4 C—H bend (o/p) + 0.4 ring (o/p)
	6	1270.5	26	1259.4	1258.3	1251.9	0.4 wag + 0.2 twist
	7	1164 R	22	1162.6	1162.3	1161.2	0.5 twist + 0.4 C—H bend (o/p)
	8	997 R	16	1025.0	1025.2	1021.1	0.6 ring (o/p) + 0.3 wag
	9	945.5	14	961.8	947.5	951.1	0.7 C—O + 0.7 C—C (7, 8)
	10	882.3	11	872.4	872.5	874.5	0.3 C—C (7, 8) + 0.3 C—C (3, 4, 5, 6)
	11	826.1	10	818.4	803.9	806.6	0.5 C—O + 0.3 C—C (7, 8)
	12	762.3	7	757.1	755.8	757.4	0.5 C—C (3, 4, 5, 6) + 0.3 rock
	13	405.5 S	3	403.8	403.8	400.6	0.9 ring (i/p) + 0.5 ring (o/p)
A_2	14			2968.0			
	15			2933.0			
	16	1440 R	30	1443.4	1443.4	1440.0	Scissor
	17			1292.6	1292.6	1284.5	Wag
	18	1278 R	27	1281.3	1281.3	1279.0	0.6 C—H bend (i/p) + 0.3 C—C (3, 4, 5, 6)
	19			1208.0	1208.0	1203.1	Twist
	20			1013.0	1013.0	1013.5	0.3 rock + 0.3 C—H bend (i/p)
	21			933.3	933.3	932.4	0.4 C—C (3, 4, 5, 6) + 0.4 rock
	22	577 R	5	576.6	576.6	571.1	Ring (i/p)
	23	148 R	1	135.5	135.5	135.4	Ring (o/p)
B_1	24			3016.9			
	25			2973.6			
	26			2935.3			
	27	1453.6	31	1456.0	1455.9	1452.7	Scissor
	28	1307	28	1311.1	1311.1	1303.6	Wag
	29	1240.8	25	1245.6	1244.6	1243.2	0.6 twist + 0.3 C—H bend (o/p)
	30	1204.0	24	1193.8	1194.1	1194.9	0.4 C—H bend (o/p) + 0.3 twist
	31	1080	18	1104.4	1099.4	1100.4	0.5 rock + 0.2 C—H bend (o/p)
	32	1013.6	17	1050.8	1029.1	1026.1	0.6 C—O + 0.3 ring (i/p)
	33			825.4	822.5	825.6	C—C (3, 4, 5, 6)
	34	793.6	8	807.0	801.5	796.5	0.5 ring (i/p) + 0.2 C—O
	35	333 R	2	341.0	340.8	340.4	Ring (o/p)
B_2	36			2987.4			
	37			2945.0			
	38	1461.2	32	1462.3	1462.3	1459.2	Scissor
	39	1321.9	29	1320.0	1324.8	1320.5	C—H bend (i/p)
	40	1199.3	23	1199.6	1208.9	1203.9	Wag
	41	1108.0	19	1108.1	1110.2	1105.5	0.4 twist + 0.3 C—H bend (i/p)
	42	977.8	15	990.0	991.8	993.2	0.6 C—C (3, 4, 5, 6) + 0.4 twist
	43	908.9	12	891.1	892.8	897.1	C—C (7, 8)
	44	799.2	9	789.1	794.7	794.9	Rock
	45	548.5	4	502.7	548.2	548.6	Bridge (C—O—C) def.
	Ave. error in calc. frequencies/cm^{-1}			9.0	7.9	7.4	

[a]Vapor phase measurements unless designated as S (solution phase infrared) or R (Raman measurements of CCl_4 or C_6H_6 solution).

[b]Designates peaks labelled in Figs. 2, 4, and 6.

[c]Frequencies calculated for: (1) transferred scaling factors; (2) first refinement of selected scaling factors; (3) final refinement including all scaling factors. See Table 6 for values of scaling factors.

[d]Dominent elements of potential energy distribution matrix in full symmetry coordinates.

Can. J. Chem. Downloaded from www.nrcresearchpress.com by 41.223.56.140 on 09/07/12
For personal use only.

TABLE 5. Observed and calculated frequencies (cm^{-1}) for 7-thianorbornane

	ν	Observed[a]	Peak no.[b]	Calculated positions[c] (1)	(2)	(3)	Assignment[d]
A_1	1			3022.1			
	2			2984.2			
	3			2935.5			
	4	1474.6	33	1476.4	1476.4	1473.2	Scissor
	5	1298.1	27	1296.6	1296.8	1290.2	Wag
	6	1240.3	25	1242.3	1242.3	1237.5	Twist
	7	1087.2 S	17	1079.9	1079.8	1082.5	C—H bend (o/p)
	8	995.1 S	14	1001.3	1001.1	1003.0	0.5 C—C (7, 8) + 0.3 C—C (3, 4, 5, 6)
	9	862.9	11	860.7	860.4	861.1	0.5 ring (o/p) + 0.4 rock
	10	827.8	10	822.8	821.7	824.5	0.4 C—C (7, 8) + 0.2 C—C (3, 4, 5, 6)
	11	762.7	7	777.5	775.1	775.0	0.3 rock + 0.3 C—S + 0.3 ring (o/p)
	12	567.6	5	571.5	563.0	563.3	C—S
	13	388 R	3	396.8	396.4	394.0	0.7 ring (i/p) + 0.5 ring (o/p)
A_2	14			2962.6			
	15			2915.2			
	16	1434 R	30	1444.0	1444.0	1440.7	Scissor
	17			1304.8	1304.8	1296.3	Wag
	18			1256.7	1256.7	1254.2	0.6 C—H bend (i/p) + 0.4 C—C (3, 4, 5, 6)
	19	1209 R	24	1214.5	1214.5	1209.6	Twist
	20			1022.6	1022.6	1023.1	0.3 rock + 0.3 C—H bend (i/p)
	21			945.0	945.0	944.6	0.4 C—C (3, 4, 5, 6) + 0.4 rock
	22	536 R	4	537.8	527.8	532.6	Ring (i/p)
	23	173 R	1	172.8	172.8	172.6	Ring (o/p)
B_1	24			3017.8			
	25			2963.5			
	26			2921.0			
	27	1451.8	31	1455.2	1455.2	1451.9	Scissor
	28	1315.6	29	1322.8	1322.8	1315.0	Wag
	29	1242.3	26	1241.5	1241.2	1235.8	Twist
	30	1136.0	21	1142.8	1142.6	1144.5	0.5 rock + 0.3 C—H bend (o/p)
	31	1069.4	16	1066.3	1066.3	1066.5	0.5 C—H bend (o/p) + 0.3 rock
	32	885.7	13	894.7	893.0	891.2	0.4 ring (i/p) + 0.3 C—C (3, 4, 5, 6)
	33	813.3 S	9	815.6	815.2	814.9	0.5 C—C (3, 4, 5, 6) + 0.2 ring (i/p)
	34	602.9	6	611.9	602.0	602.0	C—S
	35	326 R	2	337.8	337.2	336.9	Ring (o/p)
B_2	36			2980.8			
	37			2928.9			
	38	1456.5	32	1461.3	1461.3	1458.1	Scissor
	39	1311.7	28	1317.4	1317.4	1311.7	0.5 C—H bend (i/p) + 0.4 wag
	40	1187.3	23	1187.9	1187.9	1183.8	0.5 wag + 0.3 twist
	41	1108.5	18	1121.0	1121.0	1115.8	0.4 C—H bend (i/p) + 0.3 twist
	42	1010.4	15	1026.8	1026.8	1029.4	0.6 C—C (3, 4, 5, 6) + 0.3 twist
	43	879.4	12	866.1	866.1	870.1	C—C (7, 8)
	44	800.4	8	792.7	792.7	792.6	Rock
	45	(379 R)		355.9	355.9	351.9	Bridge (C—S—C) def.
	Ave. error in calcd. frequencies/cm^{-1}			6.1	5.7	4.9	

[a]Vapor phase measurements unless designated as S (solution phase infrared) or R (Raman measurements of CCl_4 or C_6H_6 solution).

[b]Designates peaks labelled in Figs. 2, 4, and 6.

[c]Frequencies calculated for: (1) transferred scaling factors; (2) first refinement of selected scaling factors; (3) final refinement including all scaling factors. See Table 6 for values of scaling factors.

[d]Dominent elements of potential energy distribution matrix in full symmetry coordinates.

apparent shoulder to lower wavenumber on the Raman band, assigned as ν_{13} (peak no. 3, Fig. 7) is the only reasonable although uncertain choice.

The relatively high force constants for A_1 out-of-plane ring modes were initially quite unexpected (Table 7). For both 7-OXA and 7-THIA, as well as for norbornane, norbornene, and norbornadiene (1), the lowest A_1 transition corresponds primarily to the in-plane ring deformation (coordinate no. 40 in Table 3), whereas the out-of-plane mode is found to contribute to absorptions at higher frequencies, e.g. ν_8 (997 cm^{-1}) for

Can. J. Chem. Downloaded from www.nrcresearchpress.com by 41.223.56.140 on 09/07/12
For personal use only.

TABLE 6. Scaling factors for 3-21G force fields of 7-oxanorbornane and 7-thianorbornane

Force constant[a]	Value		
	Transferred[b]	Rfnmt. 1[c]	Rfnmt. 2[d]
1 C—C stretch	0.907	[0.907]	0.917 (15)
2 C—H stretch	[0.820]	[0.820]	[0.820]
3 CH_2 scissor	0.780	[0.780]	0.776 (09)
4 CH_2 rock	0.810	[0.810]	0.810 (18)
5 CH_2 wag	0.768	[0.768]	0.761 (16)
6 CH_2 twist	0.776	[0.776]	0.765 (15)
7 C—H def. (i/p)	0.780	[0.780]	0.774 (25)
8 C—H def. (o/p)	0.773	[0.773]	0.782 (23)
9 ring def. (i/p)	0.812	[0.812]	0.793 (16)
10 ring def. (o/p)	0.989	[0.989]	0.987 (19)
11 C—O stretch	0.903	0.839 (28)	0.845 (31)
12 C—S stretch	1.048	1.005 (29)	1.010 (31)
13 Bridge def. (7-OXA)	0.812	1.014 (42)	1.014 (44)

[a]See Table 3 for coordinate definitions.

[b]Scaling factors previously optimized to fit the observed frequencies of norbornane, norbornene, and norbornadiene (Calc. A, Table IX of Ref. 1), except those for the C—O and C—S stretches which were optimized for dimethyl ether (ref. 12) and thietane (ref. 13), respectively. Positions calculated with these factors are listed as calcd. 1 in Tables 4 and 5.

[c,d]Scaling factors after optimization to fit observed frequencies. Factors in square brackets were fixed in the refinements. Calculated positions are listed as calcd. 2 and calcd. 3, respectively, in Tables 4 and 5. Uncertainties in the best fitting scaling factors are given in parentheses.

7-OXA and ν_9 (863 cm^{-1}) for 7-THIA. The large force constants and high transition frequencies for the out-of-plane ring deformation may be rationalized by observing that although the coordinate (no. 43 in Table 3) is defined as a combination of ring torsions, the actual deformation involves considerable bending of the C—C—X angles. This motion, often termed the "butterfly" mode, is thus a hybrid of ring torsions and ring angle bends, and in fact appears in the vibrational spectra at frequencies characteristic of C—C—X bends.

Conclusions

The vibrational spectra for 7-oxa- and 7-thianorbornane are reported here for the first time. *Ab initio* 3-21G harmonic force fields were calculated for both molecules, based upon optimized geometries determined previously at the same level of theory (6). A total of 12 scaling factors, 10 of which were transferred from a previous study of the vibrational spectra of norbornane, norbornene, and norbornadiene (1), and one each from dimethyl ether (12) and thietane (13), proved sufficiently accurate to assign reliably 60 of the 70 vibrational modes in the region of 1600–100 cm^{-1}. Refinement of only three of the scaling factors, i.e. those from sources other than the norbornane set, reduced the average error of the calculated positions from 9.0 and 6.1 to 7.9 and 5.7 cm^{-1}, respectively, for 7-oxa- and 7-thianorbornane. Further refinement of the entire set of scaling factors to fit simultaneously the assigned transitions of both molecules further lowered the average error to 7.4 and 4.9

TABLE 7. Comparison of scaled diagonal force constants for norbornane, 7-oxanorbornane, and 7-thianorbornane[a]

Vibrational coordinate[b]	Norbornane[c]	7-OXA[d]		7-THIA[d]	
		1	2	1	2
C—X stretch (1-7)	4.651	5.074	5.098	3.200	3.216
C—C stretch (1-2)	3.948	3.974	4.018	3.986	4.030
C—C stretch (2-3)	4.415	4.617	4.668	4.147	4.193
CH_2 scissor	0.732	0.723	0.719	0.725	0.721
CH_2 rock	0.627	0.591	0.591	0.677	0.677
CH_2 twist	0.630	0.642	0.633	0.632	0.623
CH_2 wag	0.641	0.649	0.643	0.641	0.635
C—H def. (i/p)	0.563	0.543	0.539	0.545	0.541
C—H def. (o/p)	0.555	0.639	0.646	0.518	0.524
Ring def. (i/p) B_1	1.785	1.938	1.893	1.640	1.602
A_1	1.987	2.077	2.028	1.738	1.697
A_2	1.785	1.947	1.901	1.592	1.555
Ring def. (o/p) B_1	0.380	0.368	0.359	0.317	0.310
A_1	4.459	5.143	5.023	2.711	2.648
A_2	0.137	0.109	0.106	0.130	0.127
C—O—C/C—S—C def.	1.520	1.774	1.774	1.365	1.333

[a]Force constants in units of mdyn/A (stretch) or mdyn A/rad^2 (bends and torsions). Complete lists of all symmetry allowed force constants are available upon request from the authors.

[b]Refer to Fig. 1 for atom numbering, and Table 3 for coordinate definitions.

[c]Reference 1. The force constants listed here for norbornane are slightly different to those of Table X of ref. 1. This is because the scaling factors used here, and for the prediction of frequencies for 7-OXA and 7-THIA, are from Calc. A, Table IX of ref. 1, where separate ring torsional factors were refined for each of norbornane, norbornene, and norbornadiene. The force constants listed in Table X of ref. 1 were derived using the scaling factors optimized with the same scaling factor applied to all ring torsion modes ("Final refinement" of Table IX, Ref. 1). See also Table 6.

[d]Force constants listed under 1 and 2 are scaled using factors listed under "Rfnmt. 1" and "Rfnmt. 2", respectively, in Table 6.

Can. J. Chem. Downloaded from www.nrcresearchpress.com by 41.223.56.140 on 09/07/12
For personal use only.

cm^{-1}, respectively, the factors transferred from norbornane changing very little (generally by less than 1%). This further demonstrates the excellent transferability of scaling factors, optimized for closely related molecules, and suggests that the factors derived here to scale 3-21G force fields should be useful for accurately predicting the vibrational spectra of other derivatives of norbornane, norbornene, and norbornadiene.

Acknowledgements

R.A.S. gratefully acknowledges the award of a University of Calgary Postdoctoral Research Fellowship. This research was funded by an Operating Grant for the Natural Sciences and Engineering Research Council of Canada. The generous support by the Academic Computing Services and the Supercomputing Services of the University is greatly appreciated.

1. R. A. SHAW, C. CASTRO, R. DUTLER, A. RAUK, and H. WIESER. J. Chem. Phys. **89**, 716 (1988).
2. R. P. CARLILE, T. L. SMITHSON, and H. WIESER. J. Mol. Struct. **96**, 283 (1983).
3. R. A. CRESWELL. J. Mol. Spectrosc. **56**, 133 (1975).
4. K. OYANAGI, T. FUKUYAMA, K. KUCHITSU, R. K. BOHN, and S. LI. Bull. Chem. Soc. Jpn. **48**, 751 (1975).
5. T. FUKUYAMA, K. OYANAGI, and K. KUCHITSU. Bull. Chem. Soc. Jpn. **49**, 638 (1976).
6. C. CASTRO, R. DUTLER, A. RAUK, and H. WIESER. J. Mol. Struct. **152**, 241 (1987).
7. E. J. COREY and E. BLOCK. J. Org. Chem. **31**, 1663 (1966).
8. J. K. KAUPPINEN, D. J. MOFFATT, H. H. MANTSCH, and D. G. CAMERON. Appl. Spectrosc. **35**, 271 (1981); J. K. KAUPPINEN, D. J. MOFFATT, D. G. CAMERON, and H. H. MANTSCH. Appl. Opt. **20**, 1866 (1981).
9. J. S. BINKLEY, M. J. FRISCH, D. J. DEFREES, K. RAGHAVACHARI, R. A. WHITESIDE, H. B. SCHLEGEL, E. M. FLUDER, and J. A. POPLE. Department of Chemistry, Carnegie Mellon University, Pittsburgh, Pennsylvania, U.S.A.
10. A. RAUK and R. DUTLER. J. Comp. Chem. **8**, 324 (1987).
11. P. PULAY, G. FOGARASI, F. PANG, and J. E. BOGGS. J. Am. Chem. Soc. **101**, 2550 (1979).
12. R. A. SHAW, C. URSENBACH, A. RAUK, and H. WIESER. Can. J. Chem. **66**, 1318 (1988).
13. R. A. SHAW, C. CASTRO, N. IBRAHIM, and H. WIESER. J. Phys. Chem. **92**, 6528 (1988).
14. R. A. SHAW, N. IBRAHIM, and H. WIESER. J. Phys. Chem. In press.

Can. J. Chem. Downloaded from www.nrcresearchpress.com by 41.223.56.140 on 09/07/12
For personal use only.

The use of perchlorato(tetraphenylporphinato)manganese(III) as a reagent for the spectrophotometric determination of anions in nonaqueous solvents

A. Scott Hinman,[1] Karen McGarty, Clement Tang, and Brad J. Pavelich
Department of Chemistry, The University of Calgary, Calgary, Alta, Canada T2N 1N4
Received August 17, 1988

A. Scott Hinman, Karen McGarty, Clement Tang, and Brad J. Pavelich. Can. J. Chem. **67**, 545 (1989).

Perchlorato(tetraphenylporphinato)manganese(III) ($TPPMnClO_4$) is shown to be a useful reagent for the determination of a variety of anions in nonaqueous media. The analysis is based on the displacement of coordinated perchlorate by more strongly coordinating anions as monitored spectrophotometrically. The procedure is demonstrated for the determination of tetraalkylammonium salts of nitrate, nitrite, chloride, bromide, iodide, acetate, trifluoroacetate, cyanate, and thiocyanate in acetonitrile. Relative precisions and accuracies of the order of five parts per thousand are indicated.

Key words: perchlorato(tetraphenylporphinato)manganese(III), specrophotometric determination of anions, anions in nonaqueous media.

A. Scott Hinman, Karen McGarty, Clement Tang et Brad J. Pavelich. Can. J. Chem. **67**, 545 (1989).

On démontre que le perchlorato(tétraphénylporphinato)manganèse(III) ($TPPMnClO_4$) est un réactif utile pour déterminer divers anions dans des milieux non-aqueux. L'analyse est basée sur une détermination spectrophotométrique du déplacement du perchlorate par des anions qui se coordonnent plus fortement. On démontre l'utilité de la méthode par la détermination du nitrate, du nitrite, du chlorure, du bromure, de l'iodure, de l'acétate, du trifluoroacétate, du cyanate et du thiocyanate de tétraalkylammonium dans l'acétonitrile. On a évalué que les précisions et les exactitudes relatives sont de l'ordre de cinq parties par mille.

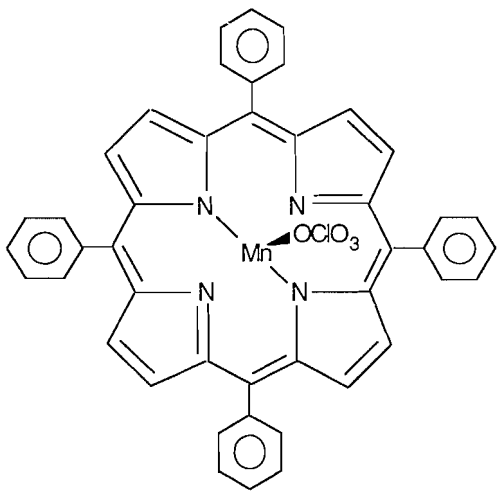
Mots clés : perchlorato(tétraphénylporphinato)manganèse(III), détermination spectrophotométrique des anions, anions dans des milieux non-aqueux.

[Traduit par la revue]

Can. J. Chem. Downloaded from www.nrcresearchpress.com by 41.223.56.140 on 09/07/12
For personal use only.

Introduction

In nonaqueous solvents, a great number of common anions can be solubilized through the use of large organic countercations. Tetraalkylammonium ions are probably the most frequently employed in this regard, and a great number of tetraalkylammonium salts are commercially available. Many such salts are either deliquescent, or extremely hygroscopic, and it can thus be difficult to prepare solutions with accurately known concentrations. In this paper, we report on the use of perchlorato(tetraphenylporphinato)manganese(III) ($TPPMnClO_4$, **I**) as a reagent for spectrophotometric assay of a number of anions in nonaqueous solvents.



I

[1]Author to whom correspondence should be addressed.

It has long been known that $TPPMn^+$ forms 5-coordinate complexes of the type TPPMnX with a great number of anions, and that the electronic spectrum of the complexes in noncoordinating solvents is sensitive to the identity of the anion X^- (1, 2). Six-coordinate complexes with two axially bound ligands are also known (2–5), but these are few in comparison to the number of 5-coordinate complexes identified. Perchlorate ion in $TPPMnClO_4$ has been shown by conductometric studies to remain coordinated to the central metal atom of the complex in noncoordinating solvents (2). Our studies indicate that it can be quantitatively replaced even by anions as normally poorly coordinating as nitrate, according to reaction [1].

[1] $TPPMnClO_4 + X^- \leftrightarrow TPPMnX + ClO_4^-$

We have exploited the large changes in the visible spectrum of the complex resulting from the metathesis to assay tetrabutylammonium salts (TBAX) of nitrate, nitrite, acetate, trifluoroacetate, thiocyanate, cyanate, bromide, and iodide, as well as tetraethylammonium chloride (TEACl), by spectrophotometric titration in toluene/acetonitrile solvent mixtures.

Experimental

Tetraalkylammonium salts

Tetra-*n*-butylammonium (TBA) salts of nitrate, nitrite, and cyanate were obtained from Fluka. TBABr was from Aldrich, and TBAI and TEACl (TEA = tetraethylammonium) were MCB reagents. These salts had all been utilized in previous unrelated experiments, and exposed to the atmosphere for varying periods of time (overnight in the case of TEACl). With the exception of TBABr, which was dried under vacuum at 70°C for a minimum of 4 h, no attempt was made to dry the salts, so the assays reported here should not be taken as an indication of the purity as obtained from the manufacturer.

$TBA(CF_3CO_2)$ was prepared by combining 5.36 g of CF_3CO_2H (Aldrich) with 32.3 g of TBAOH (40 wt% aq., Aldrich). The solution was extracted with five 40 mL portions of CH_2Cl_2 which had

TABLE 1. Visible absorption maxima (nm (log ϵ/L mol^{-1} cm^{-1})) of TPPMnX complexes in toluene

Complex	Absorption			
	Band VI	Band V	Band IV	Band III
TPPMn(ClO_4)[a]	389(4.83)	482(4.79)	570(4.08)	604(3.98)
TPPMnCl[b]	372(4.76)	476(5.08)	584(3.99)	620(4.06)
TPPMnBr[b]	379(4.84)	484(4.99)	590(3.92)	626(4.07)
TPPMnI[b]	387(4.85)	499(4.58)	612(3.78)	646(4.00)
TPPMn(NO_2)[c]	379(4.74)	475(4.95)	581(3.96)	618(4.00)
TPPMn(NO_3)[c]	383(4.73)	476(4.96)	574(4.02)	610(4.00)
TPPMn(SCN)[c]	384(4.71)	481(4.90)	582(3.91)	619(4.00)
TPPMn(OCN)[b]	373(4.73)	473(5.08)	582(3.97)	619(4.03)
TPPMn(CF_3CO_2)[b]	379(4.72)	473(5.10)	574(4.09)	609(4.01)
TPPMn(CH_3CO_2)[b]	375(4.67)	471(5.08)	576(4.03)	612(4.00)

[a]Concentration used for determination of molar absorptivities was determined by titration with standard TBABr.

[b]Wavelengths and molar absorptivities determined from solutions prepared from the solid complex assuming 100% purity.

[c]Wavelengths and molar absorptivities determined following addition of solid TBAX to a standard solution of $TPPMnClO_4$.

previously been shaken with basic alumina and filtered. The CH_2Cl_2 extracts were dried over anhydrous $MgSO_4$ (15 g). Removal of the CH_2Cl_2 under vacuum left an oily residue. This was dried in a vacuum oven at 95°C overnight. The salt was molten at this temperature but solidified on cooling. The resulting solid (13.9 g) had a slightly yellowish colour and an acrid odour, suggesting that some decomposition occurred during the drying process. The presence of $CF_3CO_2^-$ was indicated by a strong band at 1688 cm^{-1} in the ir spectrum in CH_2Cl_2. The salt is deliquescent.

TBA(CH_3CO_2) was prepared in a similar fashion to the $CF_3CO_2^-$ salt by combining 4.27 g of glacial acetic acid with 25.8 g of 40% aq. TBAOH. This was extracted with eight 50 to 60 mL portions of ethylacetate. The extracts were combined and dried over anhydrous $MgSO_4$ (30 g). White crystals were obtained on concentrating the solution. These were collected, washed with diethylether, and dried under vacuum at 60°C. The yield was 6.59 g. The presence of $CH_3CO_2^-$ was verified by a strong band at 1581 cm^{-1} in the infrared spectrum observed in CH_2Cl_2.

TBA(SCN) was prepared by combining equimolar quantities of $TBAClO_4$ (Fluka, 11.38 g dissolved in 40 mL absolute ethanol) and KSCN (3.23 g dissolved in 60 mL absolute ethanol). The resulting white precipitate ($KClO_4$) was removed by filtration. The ethanol was removed from the filtrate by vacuum distillation, leaving an oily residue which solidified on cooling to room temperature. This was dried in a vacuum oven at 85°C, leaving 9.5 g of product. The ir spectrum displays a strong band at 2056 cm^{-1} in CH_2Cl_2, confirming the presenence of the SCN^- anion.

TPPMnX complexes

All of the TPPMnX complexes listed in Table 1 were isolated in the solid state, with the exception of the nitrite complex for which no attempt was made. TPPMn(CH_3CO_2) served as the starting material for all of the complexes. This was prepared by refluxing 3.0 g of tetraphenylporphine ($TPPH_2$, Aldrich) with 2.1 g of Mn(CH_3CO_2)-2·4H_2O in glacial acetic acid (350 mL) for 3 to 4 h. The solution was concentrated to 150 mL by distillation. The crude product was precipitated by slow (overnight) dropwise addition of 500 mL of water. (Rapid addition of water should be avoided as this results in a colloidal suspension from which it is difficult to recover the product.) The solid product was collected by filtration and washed with water. Separation from unreacted $TPPH_2$ was accomplished by washing with methanol. $TPPH_2$ has no significant solubility in methanol, as evidenced by the lack of any observable absorbance of saturated solutions, and is left behind on the filter paper. After concentration of the methanol washings to 100 mL by distillation, 300 mL of water were added dropwise overnight to precipitate the product. This was recrystallized from glacial acetic acid containing 10 vol.% acetic anhydride, and dried in a vacuum oven overnight at 100°C. The ir spectrum observed in a cast prepared by evaporating a concentrated CH_2Cl_2 solution on a KCl window displays a strong broad absorbance at 1542 cm^{-1}, confirming the presence of acetate in the product.

TPPMnX, where $X^- = ClO_4^-$, I^-, Br^-, Cl^-, NO_3^-, or $CF_3CO_2^-$, were prepared by dissolving 100 to 200 mg of TPPMn(CH_3CO_2) in 150 ml of methanol. Two to three mL of a 1 *M* aq. solution of the appropriate acid HX were added, and the products were precipitated by slow overnight addition of 300 to 400 mL of water from a dropping funnel. These were collected by filtration and dried in a vacuum oven at 100°C. That the exchange reactions were successful was indicated by the absence of any band ascribable to acetate in ir spectra of the complexes observed as casts from CH_2Cl_2. Appropriate bands for the coordinated anions were present in ir spectra of the ClO_4^- (1131 cm^{-1}), $CF_3CO_2^-$ (1699 cm^{-1}), and NO_3^- (1285 cm^{-1}) complexes. We have not observed any shock sensitivity associated with $TPPMnClO_4$, consistent with previous workers (2) observations, but **since perchlorate salts pose potential explosion hazards, appropriate precautions should be observed in preparing or handling large quantities of this material**.

TPPMnX, where $X^- = OCN^-$ or SCN^-, were prepared from TPPMn(CH_3CO_2) similarly to the procedure described above, except that the solid potassium salts, KX, were employed rather than the acids, HX. These were dissolved in the methanol/porphyrin solution in 20-fold excess prior to precipitation of the porphyrin complex via addition of water, as above. Again, the ir spectra of the products showed no indication of acetate, but displayed appropriate bands for coordinated SCN^- (2028 cm^{-1}) or OCN^- (2168 cm^{-1}). All of the TPPMnX complexes isolated in the solid state gave visible spectra identical to those observed on titration of $TPPMnClO_4$ with the appropriate tetraalkylammonium salt, giving further confirmation of the identity of the coordinated anion.

Analyses

Stock $TPPMnClO_4$ solutions for the spectrophotometric titrations were prepared in toluene and filtered prior to standardization. Concentrations were 2.5 to 3.0 × 10^{-7} mole per g of solution, and were accurately determined by titration with standard TBABr solutions. Stock solutions of the tetraalkylammonium salts were prepared in CH_3CN. Concentrations of these solutions were 0.8 to 3.0 × 10^{-5} mole per g of solution. These solutions were used directly for the alternate analyses, but were diluted approximately 10-fold for spectrophotometric titrations.

Spectrophotometric titrations utilized a Cary model 16 uv-vis spectrophotometer. In all cases a 1 mm pathlength cylindrical quartz cell was utilized for absorbance measurements. This was fitted by means of a ground glass joint to the bottom of a 50 mL round bottom flask, which served as the titration vessel. After addition of a quantity of titrant, the cell/flask assembly was inverted several times to ensure complete mixing of the solutions before recording an absorbance measurement. In a typical experiment, *ca.* 10 g of the stock $TPPMnClO_4$ were delivered to the titration vessel from a polyethylene squeeze bottle. The exact quantity delivered was determined by weight loss of the squeeze bottle. Thirty mL of toluene and 2 mL of CH_3CN were then added to the titration vessel. This solution was then titrated with the tetraalkylammonium salt solution, monitoring the absorbance of the solution after each addition of titrant. The titrant was delivered from a polyethylene squeeze bottle fitted with a piece of fine bore HPLC tubing for delivery, and the quantities delivered were determined by weight loss.

Gravimetric determination of TBA as the tetraphenylboron (TPB) salt was employed for comparative assays of the $CH_3CO_2^-$, $CF_3CO_2^-$, NO_3^-, NO_2^-, and OCN^- salts. Typically, 10 g of the stock TBAX/CH_3CN solutions were combined with 30 mL of a 0.1 *M* aqueous acetate buffer solution. A 0.05 *M* aqueous solution of NaTPB (Fisher) was then added slowly from a buret to provide a 2-fold excess. The resulting solutions were warmed to *ca.* 50°C to promote coagulation of the precipitate. In some cases it was necessary to add an additional 1 to

Can. J. Chem. Downloaded from www.nrcresearchpress.com by 41.223.56.140 on 09/07/12
For personal use only.

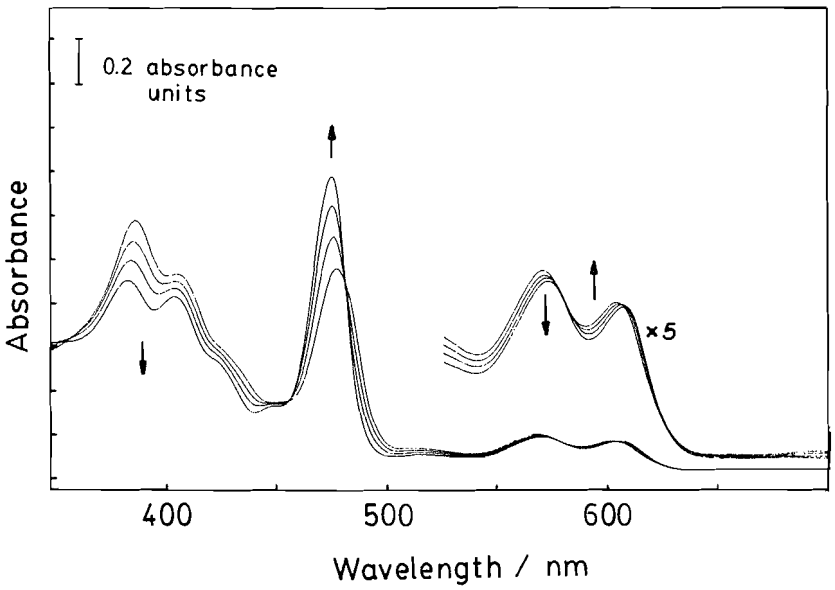


FIG. 1. Visible spectra observed during the titration of 1.4×10^{-4} *M* $TPPMnClO_4$ in toluene/5% acetonitrile with 3.4×10^{-3} *M* $TBANO_3$ in acetonitrile. Molar nitrate/porphyrin ratios increasing in the direction of the arrows were 0, 0.33, 0.65, and 1.17. The cell pathlength was 1 mm except for the spectra marked ×5, which employed a 5 mm pathlength.

Can. J. Chem. Downloaded from www.nrcresearchpress.com by 41.223.56.140 on 09/07/12
For personal use only.

2 g of $NaCH_3CO_2$ to bring about coagulation. The precipitates were collected on previously dried and tared Gooch crucibles, washed with aq. 0.1 *M* CH_3CO_2H, and dried overnight at 105°C. A similar procedure was employed for the gravimetric determination of Cl^- as AgCl in the TEACl solutions, except that aqueous $AgNO_3$ was employed as the precipitating agent.

Stock solutions of TBABr and TBAI were analyzed by potentiometric titration with standard $AgNO_3$. Aliquots (20 g) of the TBAX/CH_3CN solutions were titrated with standard 0.02 *M* $AgNO_3$ in $H_2O/CH_3CN/MeOH$ (10/20/70 vol%) delivered from a 50 mL buret. The potential difference of a Ag wire with respect to a commercial aq. SCE was monitored with a pH meter. The titrations gave the normal sigmoidal curves, and endpoints were determined by conventional means. It is well known that titrations of aq. I^- solutions with aq. Ag^+ frequently give rise to a hump on the rising portion of the sigmoidal titration curve due to the adsorption of I^- onto the colloidal AgI particles (6). This was not observed under our conditions.

The TBASCN/CH_3CN stock solution was analyzed by using it to titrate weighed quantities of $AgNO_3$ (*ca.* 100 mg) dissolved in *ca.* 20 mL of 0.1 *M* acetate buffer. The titrant was delivered from a squeeze bottle, and quantities determined by weight loss. The titrations were followed by measuring the potential difference of a Ag wire as measured with respect to a glass pH electrode.

Recovery of $TPPMnClO_4$

Because $TPPMnClO_4$ is not, to our knowledge, commercially available, it is desirable to be able to recover the reagent. This was conveniently accomplished by collecting all solutions from the spectrophotometric titrations, regardless of the anion, in an evaporating dish and allowing the solvent to evaporate in a fume hood. The $TPPMn^+$ was recovered in the perchlorate form by precipitation from a methanolic solution containing excess 1 *M* aq. $HClO_4$, as described above for the original preparation of the compound from TPPMn-(CH_3CO_2). A single precipitation appears to be adequate, although the procedure can be employed twice to ensure complete replacement of all other anions. The procedure provides 100% yield, as indicated by the absence of colour in the filtrate. In some instances, the methanol porphyrin solutions were first treated with $AgClO_4$ to remove halides, but this appeared to result in some decomposition of the porphyrin, resulting in lower yields.

Results and discussion

Spectra of the complexes

Table 1 indicates the major visible absorption bands and apparent molar absorptivities in reagent grade toluene of $TPPMn^+$ complexes of all the anions employed in this study. The Roman numeral designation of the bands is that originally employed by Boucher (1). The spectra are not significantly affected on addition of up to 10% acetonitrile. The spectrum of the perchlorate complex differs significantly from that of all other complexes investigated. Band V, in particular, differs significantly in wavelength and/or molar absorptivity for the TPPMnX complexes as compared to $TPPMnClO_4$, and can be used to monitor the conversion of $TPPMnClO_4$ to TPPMnX.

Figure 1 illustrates the spectral changes observed during the titration of $TPPMnClO_4$ with $TBANO_3$. The spectrum of the nitrate complex resembles that of the perchlorate complex more closely than any of the other anions involved in this study. Even so, it is evident from the figure that the visible spectrum provides a sensitive probe for following the formation of the nitrate complex.

Figure 2 illustrates the absorbance monitored at the wavelength of band V of the nitrate complex during a titration of $TPPMnClO_4$ with $TBANO_3$. Two linear regions are observed, intersecting at a nitrate to porphyrin molar ratio of unity. The first of these corresponds to increased absorbance due to the formation of the nitrate complex. The slightly negative slope in the second region results from dilution of the porphyrin complex on addition of titrant. Because the volume of the titrant added is small in comparison to the volume of the porphyrin solution, the dilution factor is small and can be considered constant throughout the titration.

The titration curve of Fig. 2 shows little, if any, curvature in the region of the equivalence point. The equilibrium constant associated with the titration reaction under the conditions employed is thus clearly large enough to be of analytical utility. Similar titration curves are obtained on monitoring the appropri-

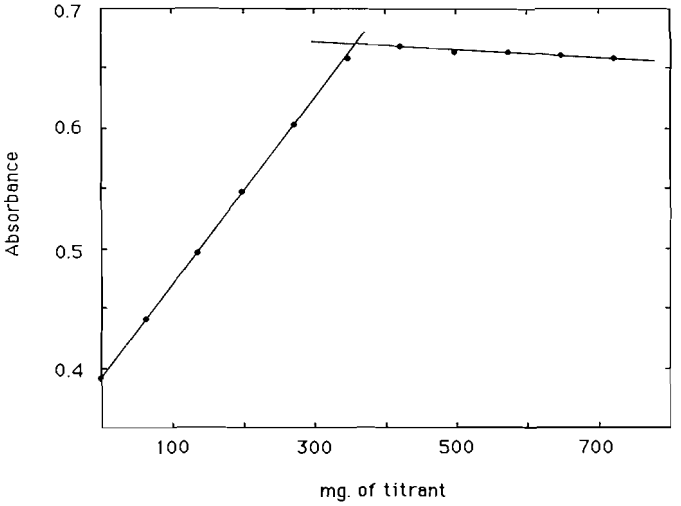


FIG. 2. Absorbance monitored at 476 nm during the titration of 2.3 mg of $TPPMnClO_4$ in 40 mL. of toluene/5% CH_3CN with $TBANO_3$ in CH_3CN (8.6×10^{-6} mol per g of solution). The pathlength was 1 mm.

ate band V absorbance when $TPPMnClO_4$ solutions are titrated with each of the anions listed in Table 1. It should be noted that during the early stages of most of the titrations employing band V, the wavelength will lie on the shoulder of the peak V absorbance for the perchlorate complex, rather than on a maximum. The absorbance will thus be quite sensitive to small variations in the wavelength. Measurements with the spectrometer set to a fixed wavelength throughout the titration are therefore preferable to those associated with spectral scans.

Most of the anions investigated show spectra more drastically different from that of the perchlorate complex than is apparent in Fig. 1 for titration of $TPPMnClO_4$ with nitrate. Figure 3 illustrates the spectral changes observed on titration of $TPPMnClO_4$ in toluene containing 5% acetonitrile with an acetonitrile solution of TBAI. It is apparent that, in this case, several wavelengths could be monitored to follow the complexation of I^- to the porphyrin. In particular, the $TPPMn^+$ complexes of I^-, Br^-, Cl^-, SCN^-, OCN^-, and NO_2^- all display band III absorbance at significantly higher wavelength than is observed for the perchlorate complex. These anions could thus readily be determined by monitoring the appropriate band III wavelength of the complex. Inspection of Table 1 reveals that, in general, the molar absorptivity associated with band III is lower by nearly an order of magnitude compared to that of band V. The availability of different wavelengths with different associated molar absorptivities is important in terms of providing versatility in choosing concentrations and/or optical pathlengths to be employed in the analytical procedure.

Analytical results

Table 2 illustrates replicate assays of some solid tetraalkylammonium salts as determined by the titration of $TPPMnClO_4$ in toluene/ 5% acetonitrile with acetonitrile solutions of the salt. The average values, $\bar{x}$, and standard deviations, σ_{n-1}, associated with these analyses are also included. TBABr is not included in the table as this salt served as a standard for determination of the porphyrin concentrations. In all cases the absorbance of band V of the complex was monitored and the endpoint was taken as the intersection of the two least squares lines obtained prior to and following the equivalence point. Although it is probable that a wide variety of solvents could be employed (see below), acetonitrile was specifically chosen as solvent for the salts since its miscibility with water allowed comparative assays to be obtained utilizing more conventional aqueous based methods. Results of these alternate assays are also included in Table 2.

In our hands, and following the procedures outlined in the Experimental section, titration of $TPPMnClO_4$ affords a relative precision generally better than 0.5% in assays of the various salts investigated. The only instance where a standard deviation better than this was not obtained was in the analysis of $TBANO_3$ solutions. While it is not clear that the somewhat greater standard deviation obtained in this case is significant, the spectrum of the nitrate complex does more closely resemble that of the perchlorate than most of the other anions. Also, nitrate is probably the most weakly coordinating anion investigated. It is possible that these factors are reflected in the precision.

It is evident in inspecting Table 2 that the results obtained by the spectrophotometric titrations, in general, agree within a few parts per thousand of those obtained by the alternate method of analysis, attesting to the general accuracy of the procedure. The exception is the trifluoroacetate case, where the spectrophotometric analysis afforded an average assay 1.4% higher than that indicated by gravimetric precipitation of the tetrabutylammonium counterion with tetraphenylboron. This difference does appear to be significant. Four different solutions of the trifluoroacetate were analyzed by both methods, and the spectrophotometric results were always higher by approximately 1.5% than the gravimetric results. There do not appear to be any problems inherent with the spectrophotometric procedure as applied to trifluoroacetate, however, as the spectra show several clearly defined isosbestic points during the titration, and plots of absorbance versus quantity of titrant show no departures from linearity or curvature in the endpoint region. As noted in the experimental section, some decomposition of this salt was indicated at the high temperatures employed to remove water, and this could be responsible for the apparent discrepancy in the analytical results. The presence of some trifluoroacetic acid formed via a Hoffman elimination reaction, for instance, would be anticipated to result in higher values for the spectrophotometric procedure since the cation, H^+, would not precipitate tetraphenylboron.

The list of anions determinable by this procedure probably goes beyond those included in the present study. Both azide (2) and cyanide (5) are known to form complexes with $TPPMn^+$ with spectra significantly different from that of the perchlorate complex, and these anions might well be determinable by this procedure.

Standardization of $TPPMnClO_4$

KBr disk infrared spectra of $TPPMnClO_4$ frequently display a broad absorbance near 3400 cm^{-1}, suggesting the presence of occluded water. This is lost only slowly with extended periods of drying in a vacuum oven at 105°C. For this reason it is necessary to standardize solutions of the porphyrin to be employed in analysis. Commercially available tetrabutylammonium bromide from Aldrich was found to be satisfactory for this purpose. After drying in vacuum at 70°C for 4 h, this salt afforded assays of 99.9, 100.1, and 100.2% by potentiometric titration with standard silver nitrate, and 99.8% by gravimetric precipitation of tetrabutylammonium ion with tetraphenylboron.

Titration with TBABr has indicated purities of greater than 99% for $TPPMnClO_4$ samples where these have been left in a vacuum oven at 105°C for 2 days or longer. Assays of 90 to 95%

Can. J. Chem. Downloaded from www.nrcresearchpress.com by 41.223.56.140 on 09/07/12
For personal use only.

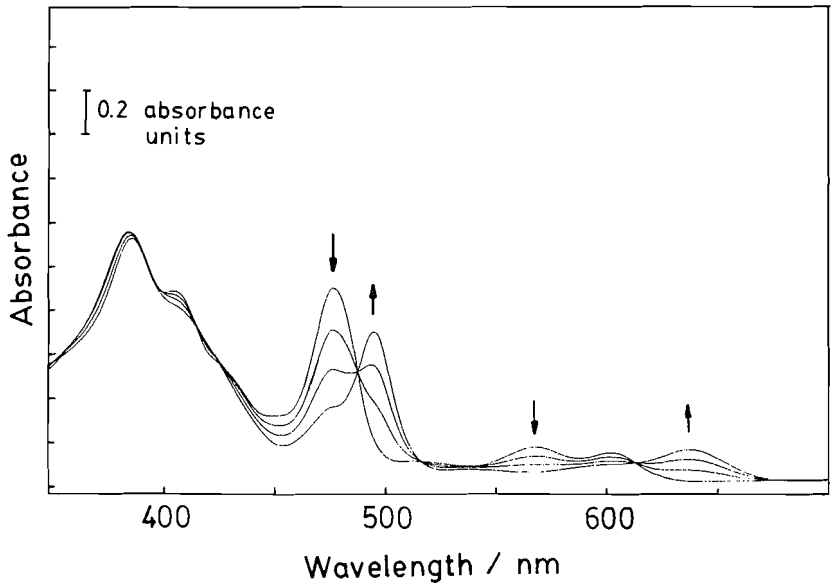


FIG. 3. Visible spectra observed during the titration of 1.4×10^{-4} *M* $TPPMnClO_4$ in toluene/5% acetonitrile with 3.7×10^{-3} *M* TBAI in acetonitrile. Molar iodide/porphyrin ratios increasing in the direction of the arrows were 0, 0.34, 0.67, and 1.26. The pathlength was 1 mm.

TABLE 2. Replicate analytical results from analyses[a] of tetraalkylammonium salts

Salt analyzed	$TPPMnClO_4$ spectrophotometric assays[b] ($\bar{x} \pm \sigma_{n-1}$)	Alternate assays[b]
$TBA(NO_3)$	99.5, 99.8, 98.5 (99.3 ± 0.7)	99.3, 99.2[c]
$TBA(NO_2)$	99.1, 99.7, 99.7 (99.5 ± 0.3)	99.3, 99.3[c]
$TBA(CH_3CO_2)$	84.7, 84.1, 84.4 (84.4 ± 0.3)	84.3, 84.7[c]
$TBA(CF_3CO_2)$	97.4, 97.4, 97.7 (97.5 ± 0.2)	95.9, 96.3[c]
TBA(OCN)	78.4, 78.8, 78.8 (78.7 ± 0.2)	78.8[c]
TBA(SCN)	98.3, 98.4, 97.6 (98.1 ± 0.4)	98.3, 98.4[d]
TBAI	99.9, 99.6, 100.2 (99.9 ± 0.3)	99.9, 100.2[d]
TEACl	71.0, 70.8, 71.0 (70.9 ± 0.1)	70.8, 70.6[e]

[a]$TPPMnClO_4$ solutions were standardized by titration with TBABr. The average of a minimum of four such standardizations was utilized in subsequent calculations.

[b]Assays are reported as percent TAAX (TAA = tetraalkylammonium ion) of the solid salt.

[c]Gravimetric precipitation of tetrabutylammonium ion with tetraphenylboron.

[d]Argentometric determination of the anion with potentiometric endpoint.

[e]Gravimetric precipitation of chloride with Ag^+.

are more common for samples which have been stored on the shelf for some time or have been subjected to shorter drying periods. This variability in the purity of the solid reagent does not affect its utility as an analytical reagent other than imposing the requirement of standardization. Once standardized, solutions of $TPPMnClO_4$ in toluene appear to be indefinitely stable when tightly sealed and stored in the dark. Identical standardizations by TBABr titration were obtained for the same solution 3 months apart.

Where lower precision is acceptable, it may be possible to use the initial absorbance of the $TPPMnClO_4$ solutions to determine their concentrations. We would caution, however, that the molar absorptivities of Table 1 were calculated from single absorbance measurements rather than Beer's law plots. The possibility of aggregration at higher concentrations, or dissociation of perchlorate at lower concentrations, should be ruled out before attempting to apply the simpler analytical procedure. Also, Kelly and Kadish have reported that the spectrum of $TPPMnClO_4$ is sensitive to solvent (2).

Solvents

It is clear that the choice of solvent, or solvents, is an important factor in the success of the analytical procedure. While titration of $TPPMnClO_4$ in toluene/5% acetonitrile with $TBANO_3$ in acetonitrile gives sharply defined endpoints, significant curvature in the endpoint region becomes apparent when similarly titrating porphyrin solutions in toluene containing 10% acetonitrile, and no endpoint is apparent at all for titrations of the porphyrin in acetonitrile alone. Titration of acetonitrile solutions of the porphyrin with chloride, on the other hand, gives rise to sharply defined endpoints with no apparent curvature near the equivalence point. Thus, while acetonitrile may effectively inhibit coordination of weakly coordinating anions such as nitrate, more strongly coordinating anions can still be analyzed in this more polar solvent. None of the anions could be determined by titration of methanol solutions of the porphyrin, but nitrate, trifluoroacetate, and chloride all gave well defined endpoints on titrating the porphyrin in 1,2-dichloroethane or dichloromethane.

While we have not conducted a complete investigation of the relative coordinating ability of the various anions employed in our work, or of the influence of various solvents, Kelly and Kadish (2) have reported on the coordination chemistry of a variety of TPPMnX compounds in twelve nonaqueous solvents, and their work should be consulted when considering analysis of anions in various solvents or solvent mixtures. In brief, they report that strongly bonding solvents coordinate to the porphyrin forming complexes of the type TPPMn(L)(X) and $TPPMnL_2^+$ (L = solvent). The extent to which these reactions occur depends on the particular anion involved, the donor number and dielectric constant of the solvent, and ionic strength. (The spectra of TPPMn(L)(X) complexes do not significantly differ from those of the TPPMnX complexes, so that coordination of a single solvent molecule should not preclude the observation of a sharply defined endpoint.)

Can. J. Chem. Downloaded from www.nrcresearchpress.com by 41.223.56.140 on 09/07/12
For personal use only.

Conclusions

$TPPMnClO_4$ serves as a convenient reagent for the spectrophotometric determination of a wide variety of anions under nonaqueous conditions. The anions can be determined in solution following dissolution of the solid salt, avoiding uncertainties in the solution concentrations associated with the weighing of very hygroscopic materials, or from the use of salts of uncertain composition. The reagent is readily prepared from commercially available materials, very little is required per analysis, and it can be conveniently recovered.

Acknowledgement

The authors gratefully acknowledge financial support from the Natural Sciences and Engineering Research Council of Canada.

1. L. J. Boucher. Coordination Chem. Rev. **7**, 289 (1972).
2. S. L. Kelly and K. M. Kadish. Inorg. Chem. **21**, 3631 (1982).
3. J. T. Landrum, K. Hatano, W. R. Scheidt, and C. H. Reed. J. Am. Chem. Soc. **102**, 6729 (1980).
4. B. B. Wayland, L. W. Olson, and Z. U. Siddiqui. J. Am. Chem. Soc. **98**, 94 (1976).
5. W. R. Scheidt, Y. J. Lee, W. Lauangdiloh, K. J. Haller, K. Anzai, and K. Hatano. Inorg. Chem. **22**, 1516 (1982).
6. J. J. Lingane. Anal. Chem. **26**, 622 (1954).

Can. J. Chem. Downloaded from www.nrcresearchpress.com by 41.223.56.140 on 09/07/12
For personal use only.

The structure of μ_4-oxo-hexa-μ-chloro-tetrakis{(dimethyl sulfoxide)copper(II)}. dimethyl sulfide[1]

SYDNEY BROWNSTEIN, NAM FONG HAN, ERIC GABE, AND FLORENCE LEE
Division of Chemistry, National Research Council of Canada, Ottawa, Ont., Canada K1A 0R9

Received May 24, 1988

SYDNEY BROWNSTEIN, NAM FONG HAN, ERIC GABE, and FLORENCE LEE. Can. J. Chem. **67**, 551 (1989).

μ_4-Oxo-hexa-μ-chloro-tetrakis{(dimethyl sulfoxide)copper(II)}·dimethyl sulfide, from the reaction of copper metal, dimethyl sulfoxide, and carbon tetrachloride crystallizes as orange crystals in the orthorhombic noncentrosymmetric space group $P2_12_12_1$ with a = 10.5820(20), b = 10.5710(20), and c = 28.255(5) Å and Z = 4. The chirality of the individual molecules is attributed to twists of the planes of the sulfur and carbon atoms of the dimethyl sulfoxide ligands relative to the oxygen–copper–oxygen axes.

Key words: crystal structure, copper cluster complex.

SYDNEY BROWNSTEIN, NAM FONG HAN, ERIC GABE et FLORENCE LEE. Can. J. Chem. **67**, 551 (1989).

Le μ_4-oxo-hexa-μ-chloro tétrakis(diméthylsulfoxyde) cuivre(II)·sulfure de diméthyle, obtenu par réaction du cuivre métallique, du diméthylsulfoxyde et du tétrachlorure de carbone, cristallise sous la forme de cristaux oranges dans le groupe d'espace orthorhombique non-centrosymétrique $P2_12_12_1$, avec a = 10,5820(20), b = 10,5710(20) et c = 28,255(5) Å et Z = 4. On attribue la chiralité des molécules individuelles à des croisements des plans des atomes de soufre et de carbone des ligands diméthylsulfoxydes par rapport aux axes oxygène–cuivre–oxygène.

Mots clés : structure cristalline, complexe de cluster de cuivre.

[Traduit par la revue]

Can. J. Chem. Downloaded from www.nrcresearchpress.com by 41.223.56.140 on 09/07/12
For personal use only.

Introduction

It has recently been reported that copper metal is dissolved at room temperature by a solution of dimethyl sulfoxide (DMSO) containing CCl_4 to yield dimethyl sulfide and $CuCl_2(DMSO)_2$ (1). No other copper-containing species were identified in this reaction. Similar results had been previously reported as part of a more extensive article (2). A considerably earlier publication (3) discussed the mechanism of the oxidation of Cu(I) chloride in DMSO–CCl_4 to yield Cu(II) along with carbon monoxide and carbon dioxide. These early workers made the point that all the Cu(I) is not oxidized to Cu(II) even with an excess of DMSO–CCl_4 but they were unable to identify the nature of the copper species. The crystal structure of $CuCl_2(DMSO)_2$ has been determined (4). We have been able to isolate in addition appreciable yields of μ_4-oxo-hexa-μ-chloro-tetrakis{(dimethyl sulfoxide)copper(II)}·dimethyl sulfide, **I**, from the reaction of copper metal, DMSO, and CCl_4.

I, without the solvated dimethyl sulfide, was first prepared from a refluxing mixture of $CuCl_2$ and CuO in methanol (5), and subsequently by decomposition of a phenoxo complex of Cu(II) (6). The crystal structure of $Cu_4Cl_6OL_4$, where L = diethyl sulfoxide, an analog of **I**, has been determined (7). The structures of many other $Cu_4Cl_6OL_4$ clusters have been solved but none of these has an inherent chirality (8–15). In the present article we will describe certain structural features of **I**.

Experimental

Chemicals

Copper powder (New Jersey Zinc Co.), cuprous chloride (Anachemia Chemicals), dimethyl sulfoxide (Baker Chemicals), carbon tetrachloride (Anachemia Chemicals), hexanes (BDH Chemicals), and absolute ethanol (des Alcohol de Commerce, Ltee.) were used as received.

Preparation of $Cu_4Cl_6O(DMSO)_4\cdot(CH_3)_2S$: Copper powder (0.635 g, 10 mmol) was stirred at room temperature in 20 mL of a 10:1 v/v solution of DMSO and CCl_4 until a homogeneous green solution was obtained. To this solution 20 mL absolute ethanol and 10 mL hexanes were added to give a green precipitate of $CuCl_2(DMSO)_2$ which was separated by filtration (mp 150–153°C, lit. 153–155 (16); ν_{S-O} 986 cm^{-1}, lit. 987 (16)). Orange crystals of **I** were obtained from the yellow–green filtrate by adding a further 20 mL of hexanes (or a 5:1 ratio of hexanes and CCl_4) and leaving the solution for a few hours at room temperature. In several preparative runs 0.2 to 0.7% CuCl was added to initiate dissolution of the copper powder (1). Isolated yields of 0.46 to 0.68 g of **I** were obtained. *Anal.* Calcd. for $Cu_4Cl_6O_5S_5C_{10}H_{30}$: C 14.00, H 3.52; found: C 14.48, H 3.51.

Microanalyses were performed by Mr. H. Seguin of the National Research Council of Canada. Infrared spectra were obtained on KBr pellets with a Perkin-Elmer 683 spectrometer.

X-ray diffraction intensities of a 0.25 × 0.10 × 0.03 mm crystal were collected at room temperature to $2\theta_{max}$ = 120° using a Picker diffractometer with graphite monochromatized CuK_α, radiation using the $\theta/2\theta$ scan technique with profile analysis (17). A total of 4675 unique reflections was collected in the octants $\pm h$, $\pm k$, and $\pm l$, of which 3883 reflections were considered significant with $I_{net} > 2.5\sigma(I_{net})$. In addition, 220 equivalent reflections were measured which yielded an agreement index of 0.031. Absorption corrections were made since μ = 104.6 cm^{-1}. The minimum and maximum transmission factors are 0.0497 and 0.4184. Cell parameters were obtained by least-squares refinement of the setting angles of 35 reflections with 2θ in the range 60–75° (CuK_α λ = 1.54056 Å). The structure was solved by direct methods and refined by full-matrix least-squares techniques. All calculations were performed using the NRCVAX program system (18). The final residuals are R_F 0.048 and R_W 0.057 for the significant data using unit weights, and R_F 0.063, R_W 0.070 for all reflections. An unbonded molecule of dimethyl sulfide was found for each copper cluster in the unit cell. All atoms were refined anisotropically except for the sulfur of the dimethyl sulfide molecule. This atom has a two-fold disorder with equal occupancy and therefore was refined isotropically.

The final atomic positional parameters and the mean of the principal axes of the thermal ellipsoids are listed in Table 1. The anisotropic temperature factors and the final structure factors are deposited as supplementary material.[2] The chirality parameter eta (19) refined to a

[1]NRCC No. 29870.

[2]A complete set of data may be purchased from the Depository of Unpublished Data, CISTI, National Research Council of Canada, Ottawa, Ont., Canada K1A 0S2.

TABLE 1. Atomic co-ordinates (esd's refer to the last digit printed)

Atom	x	y	z	B_{iso}
Cu 1	0.36724(20)	0.44016(23)	0.35547(7)	3.50(10)
Cu 2	0.15069(20)	0.63066(22)	0.33652(7)	3.32(9)
Cu 3	0.10685(20)	0.39658(23)	0.40084(7)	3.35(9)
Cu 4	0.27355(19)	0.61910(23)	0.43550(7)	3.23(9)
Cl 1	0.1306(4)	0.4853(4)	0.48007(12)	4.18(18)
Cl 2	0.1693(5)	0.7941(4)	0.39635(15)	4.82(19)
Cl 3	−0.0342(3)	0.4969(4)	0.34539(14)	4.11(17)
Cl 4	0.3208(4)	0.5654(5)	0.28748(13)	4.78(19)
Cl 5	0.2585(5)	0.2464(4)	0.37457(17)	5.00(21)
Cl 6	0.4836(3)	0.5482(4)	0.41931(14)	4.09(18)
S 1	0.6428(4)	0.3909(6)	0.33610(19)	5.69(24)
S 2	−0.0471(4)	0.8094(5)	0.30502(15)	4.65(20)
S 3	0.0095(4)	0.1839(4)	0.46083(15)	4.28(19)
S 4	0.2383(4)	0.7917(4)	0.51851(14)	3.66(17)
O 1	0.5070(11)	0.3507(14)	0.3274(4)	5.6(6)
O 2	0.0746(10)	0.7411(12)	0.2907(4)	4.5(5)
O 3	−0.0194(11)	0.2721(11)	0.4189(4)	4.4(5)
O 4	0.3309(10)	0.7163(10)	0.4888(3)	3.9(5)
O 5	0.2242(8)	0.5189(9)	0.3823(3)	2.6(4)
C 1	0.2810(20)	0.9531(17)	0.5071(7)	5.4(9)
C 2	0.3092(22)	0.7827(22)	0.5765(6)	6.9(11)
C 3	−0.1513(22)	0.7824(25)	0.2572(8)	7.6(13)
C 4	−0.0119(25)	0.9758(17)	0.2968(8)	6.4(12)
C 5	−0.0577(20)	0.0347(18)	0.4419(7)	5.9(10)
C 6	−0.1022(23)	0.2270(20)	0.5044(7)	6.2(10)
C 7	0.7237(21)	0.304(4)	0.2953(12)	13.7(22)
C 8	0.693 (3)	0.286(3)	0.3839(13)	12.7(23)
S 5	−0.0630(17)	0.0280(18)	0.8397(6)	8.1(4)
SS 5	−0.0722(17)	0.1015(18)	0.8487(6)	9.0(4)
C 9	−0.1991(15)	0.0349(18)	0.8486(6)	4.3(8)
C 10	0.013 (3)	0.058 (4)	0.8966(10)	10.8(20)

[a] B_{iso} is the mean of the principal axes of the thermal ellipsoid.

value of 1.19(14), confirming that the chirality of the structure is as reported in Table 1.

Results and discussion

It is not possible to derive **I** directly from $CuCl_2(DMSO)_2$ by a re-arrangement since the stoichiometry is different. It can therefore be concluded that the mechanism suggested for the dissolution of copper metal by CCl_4–DMSO (1) is not sufficient to explain all the observed products. The overall net equation [1] is

$$[1]\quad 2Cu + 2CuCl + 2{:}CCl_2 + 3(CH_3)_2SO \rightarrow Cu_4Cl_6O + 2CO + 3(CH_3)_2S$$

required for the formation of Cu_4Cl_6O, the kernel of **I**. The implication is that there must be a transfer of oxygen from DMSO directly to copper in some step of the reaction sequence, as well as oxygen transfer to dichlorocarbene which has been proposed as a reaction intermediate (1, 3).

The kernel of **I** is an oxygen surrounded tetrahedrally by four copper atoms. Each copper atom has a trigonal bipyramidal configuration with three equatorial chlorine atoms and two axial oxygen atoms. Therefore, the second nearest neighbours of the central oxygen atom are an octahedron of chlorines and the third nearest neighbours a tetrahedron of oxygens. This kernel structure is shown in Fig. 1 with the addition of the sulfur atoms of the co-ordinated DMSO molecules. A list of the bond distances and bond angles is presented in Table 2.

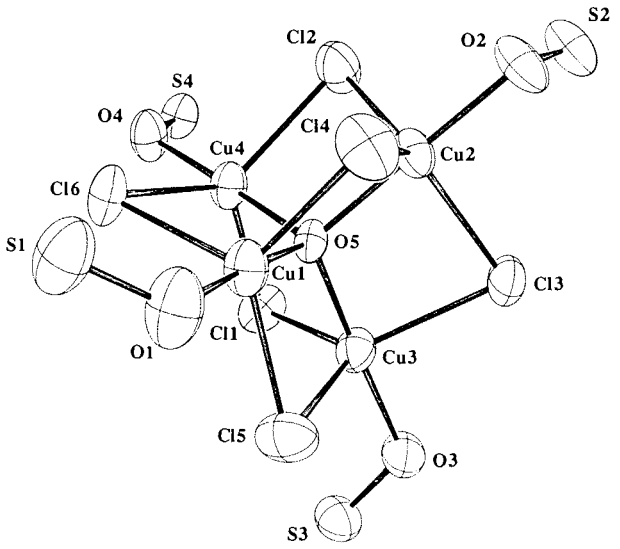


FIG. 1. The kernel structure of **I** with added sulfur atoms of the dimethyl sulfoxide ligands.

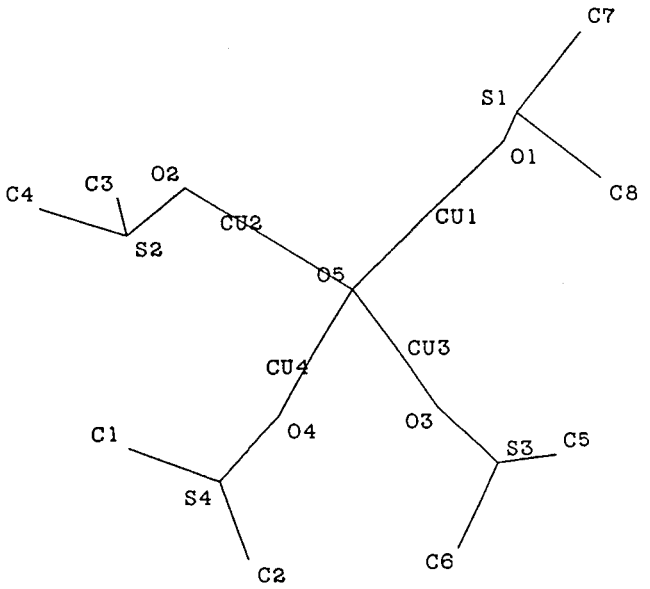


FIG. 2. A structure of **I** with the chlorine and dimethyl sulfide atoms deleted.

There is a slight, but significant distortion of the copper atoms from a perfect tetrahedral arrangement about the central oxygen with bond lengths varying from 1.868(10) to 1.917(9) Å and angles from 107.4(5) to 110.2(4)°. These results are very similar to those reported for the closely related molecule with diethyl sulfoxide as ligand (7). However, the DMSO oxygens of the third nearest neighbours have a smaller variation in the lengths of their bonds to copper (1.920(10) to 1.943(11) Å) and the bonds are significantly longer than for the diethyl sulfoxide analog (7). The copper–chlorine bond lengths range from 2.374(4) to 2.464(4) Å with a mean of 2.412 and an average deviation of 0.021 Å. These are similar to, but marginally longer than the bonds of the diethyl sulfoxide analog (7). A slight distortion from trigonal–bipyramidal geometry is observed in the equatorial plane of the copper atoms where the Cl—Cu—Cl bond angles vary between 113.5(2) and 125.2(2)° with a mean

Can. J. Chem. Downloaded from www.nrcresearchpress.com by 41.223.56.140 on 09/07/12
For personal use only.

TABLE 2. Bond distances and angles

Bond	Distance	Bond	Distance
Cu(1)—Cl(4)	2.384(5)	Cu(4)—O(5)	1.912(9)
Cu(1)—Cl(5)	2.411(5)	S(1)—O(1)	1.519(13)
Cu(1)—Cl(6)	2.464(4)	S(1)—C(7)	1.707(23)
Cu(1)—O(1)	1.927(12)	S(1)—C(8)	1.82(3)
Cu(1)—O(5)	1.886(9)	S(2)—O(2)	1.530(12)
Cu(2)—Cl(2)	2.425(5)	S(2)—C(3)	1.767(21)
Cu(2)—Cl(3)	2.427(4)	S(2)—C(4)	1.813(19)
Cu(2)—Cl(4)	2.374(4)	S(3)—O(3)	1.538(11)
Cu(2)—O(2)	1.920(10)	S(3)—C(5)	1.811(19)
Cu(2)—O(5)	1.917(9)	S(3)—C(6)	1.766(21)
Cu(3)—Cl(1)	2.440(4)	S(4)—O(4)	1.516(11)
Cu(3)—Cl(3)	2.410(4)	S(4)—C(1)	1.794(18)
Cu(3)—Cl(5)	2.376(5)	S(4)—C(2)	1.804(16)
Cu(3)—O(3)	1.943(11)		
Cu(3)—O(5)	1.868(10)	S(5)—C(9)	1.464(24)
Cu(4)—Cl(1)	2.424(5)	S(5)—C(10)	1.83(3)
Cu(4)—Cl(2)	2.421(5)	SS(5)—C(9)	1.516(24)
Cu(4)—Cl(6)	2.390(4)	SS(5)—C(10)	1.69(3)
Cu(4)—O(4)	1.922(10)		

Bonds	Angle	Bonds	Angle
Cl(4)—Cu(1)—Cl(5)	123.63(19)	Cl(6)—Cu(4)—O(5)	86.0(3)
Cl(4)—Cu(1)—Cl(6)	115.82(19)	O(4)—Cu(4)—O(5)	177.3(4)
Cl(4)—Cu(1)—O(1)	95.7(4)	Cu(3)—Cl(1)—Cu(4)	79.16(13)
Cl(4)—Cu(1)—O(5)	85.0(3)	Cu(2)—Cl(2)—Cu(4)	79.13(15)
Cl(5)—Cu(1)—Cl(6)	117.93(18)	Cu(2)—Cl(3)—Cu(3)	79.87(13)
Cl(5)—Cu(1)—O(1)	92.4(5)	Cu(1)—Cl(4)—Cu(2)	81.23(13)
Cl(5)—Cu(1)—O(5)	84.4(3)	Cu(1)—Cl(5)—Cu(3)	79.90(15)
Cl(6)—Cu(1)—O(1)	98.4(4)	Cu(1)—Cl(6)—Cu(4)	79.67(13)
Cl(6)—Cu(1)—O(5)	84.4(3)	O(1)—S(1)—C(7)	102.3(10)
O(1)—Cu(1)—O(5)	176.5(5)	O(1)—S(1)—C(8)	103.2(12)
Cl(2)—Cu(2)—Cl(3)	114.11(18)	C(7)—S(1)—C(8)	91.5(19)
Cl(2)—Cu(2)—Cl(4)	123.53(19)	O(2)—S(2)—C(3)	104.3(9)
Cl(2)—Cu(2)—O(2)	94.0(4)	O(2)—S(2)—C(4)	104.5(10)
Cl(2)—Cu(2)—O(5)	86.3(3)	C(3)—S(2)—C(4)	100.8(12)
Cl(3)—Cu(2)—Cl(4)	120.14(19)	O(3)—S(3)—C(5)	102.8(8)
Cl(3)—Cu(2)—O(2)	94.9(4)	O(3)—S(3)—C(6)	104.3(8)
Cl(3)—Cu(2)—O(5)	84.2(3)	C(5)—S(3)—C(6)	99.7(10)
Cl(4)—Cu(2)—O(2)	95.8(3)	O(4)—S(4)—C(1)	103.7(8)
Cl(4)—Cu(2)—O(5)	84.6(3)	O(4)—S(4)—C(2)	101.9(8)
O(2)—Cu(2)—O(5)	179.1(5)	C(1)—S(4)—C(2)	96.3(10)
Cl(1)—Cu(3)—Cl(3)	119.40(18)	Cu(1)—O(1)—S(1)	121.5(8)
Cl(1)—Cu(3)—Cl(5)	118.29(18)	Cu(2)—O(2)—S(2)	117.5(6)
Cl(1)—Cu(3)—O(3)	95.1(4)	Cu(3)—O(3)—S(3)	118.4(7)
Cl(1)—Cu(3)—O(5)	85.6(3)	Cu(4)—O(4)—S(4)	120.7(6)
Cl(3)—Cu(3)—Cl(5)	120.62(18)	Cu(1)—O(5)—Cu(2)	109.1(4)
Cl(3)—Cu(3)—O(3)	92.5(3)	Cu(1)—O(5)—Cu(3)	109.9(5)
Cl(3)—Cu(3)—O(5)	85.7(3)	Cu(1)—O(5)—Cu(4)	110.0(4)
Cl(5)—Cu(3)—O(3)	95.4(4)	Cu(2)—O(5)—Cu(3)	110.2(4)
Cl(5)—Cu(3)—O(5)	85.7(3)	Cu(2)—O(5)—Cu(4)	107.4(5)
O(3)—Cu(3)—O(5)	178.1(4)	Cu(3)—O(5)—Cu(4)	110.1(4)
Cl(1)—Cu(4)—Cl(2)	113.49(18)	C(9)—S(5)—C(10)	106.0(15)
Cl(1)—Cu(4)—Cl(6)	119.81(18)	C(9)—SS(5)—C(10)	110.5(16)
Cl(1)—Cu(4)—O(4)	95.8(4)		
Cl(1)—Cu(4)—O(5)	85.1(3)		
Cl(2)—Cu(4)—Cl(6)	125.17(19)		
Cl(2)—Cu(4)—O(4)	95.4(3)		
Cl(2)—Cu(4)—O(5)	86.5(3)		
Cl(6)—Cu(4)—O(4)	91.4(3)		

Can. J. Chem. Downloaded from www.nrcresearchpress.com by 41.223.56.140 on 09/07/12
For personal use only.

value of 119.3° and an average deviation of 2.8°. This is considerably less distortion than that found for the diethyl sulfoxide analog (7). The sulfur–oxygen bond lengths vary from 1.516(11) to 1.538(11) Å. There does not appear to be any correlation among the varying values for all the preceding bond lengths and angles.

A significant feature in the structure of **I** is the location of the sulfur–oxygen bonds with respect to the copper–chlorine bonds. Three of the bonds from oxygen to sulfur roughly bisect the angle between two of the chlorines attached to the appropriate copper and are trans to the third chlorine. Figure 1 clearly shows that the bond O2—S2 is between Cl 2 and Cl 3 and *trans* to Cl 4. The same spatial relationships hold for the bond O3—S3 with C15, C11, and C13 and for the bond O4—S4 with C11, C12, and C16. The fourth oxygen sulfur bond O1—S1 is parallel to the Cu4—C16 bond and directed away from C14 and C15. C7 and C8, which are attached to S1, have much larger thermal parameters than the carbon atoms of the other dimethyl sulfoxide ligands suggesting some disorder. The length of the S1—C7 bond at 1.707(23) Å is much shorter than the average value for the other S—C bonds at 1.80(2) Å. For the diethyl sulfoxide analog a methyl group on each of two ligands showed similar thermal disorders (7). The sulfur atom of the dimethyl sulfide of solvation may occupy either of two sites, S5 or SS5. There are no non-bonded atoms within 3.5 Å of this sulfur so the disorder is not readily explicable. A stick diagram of **I** is presented in Fig. 2 to identify the complete atom numbering scheme. In every case, the plane generated by the sulfur atom and two methyl carbon atoms of a dimethyl sulfoxide ligand is twisted from a perpendicular intersection with the corresponding oxygen–copper–O5 axis. It is this twist which gives the molecule its chirality in the solid state as required in $P2_12_12_1$.

1. Y. Tezuka, M. Miya, A. Hashimoto, and K. Imai. J. Chem. Soc. Chem. Commun. 1642 (1987).
2. S. N. Kurskov, I. N. Ivleva, I. P. Lavrent'er, O. S. Filipenko, and M. L. Khidekel. Izvest. Akad. Nauk SSSR, Ser. Khim. **7**, 1442 (1976).
3. R. R. Lavine, R. T. Iwamoto, and J. Kleinberg. J. Am. Chem. Soc. **88**, 4304 (1966).
4. R. D. Willet and K. Chang. Inorg. Chim. Acta, **4**, 447 (1970).
5. H. T. Dieck and H. P. Brehm. Chem. Ber. **102**, 3577 (1969).
6. B. Carr and J. F. Harrod. Can. J. Chem. **50**, 2792 (1972).
7. J. T. Guy, J. C. Cooper, R. D. Gilardi, J. L. Flippen-Anderson, and C. F. George. Inorg. Chem. **27**, 635 (1988).
8. J. A. Bertrand and J. A. Kelley. J. Am. Chem. Soc. **88**, 4746 (1966).
9. J. A. Bertrand. Inorg. Chem. **6**, 495 (1967).
10. T. Kilbourn and J. D. Dunitz. Inorg. Chim. Acta, **1**, 209 (1967).
11. J. A. Bertrand and J. A. Kelley. Inorg. Chem. **8**, 1982 (1969).
12. N. S. Gill and M. Sterns. Inorg. Chem. **9**, 1619 (1970).
13. M. R. Churchill, B. G. deBoer, and S. J. Mendak. Inorg. Chem. **14**, 2496 (1975).
14. R. C. Dickinson, F. T. Helm, W. A. Baker, T. D. Black, and W. H. Watson. Inorg. Chem. **16**, 1530 (1977).
15. M. R. Churchill and F. J. Rotella. Inorg. Chem. **18**, 853 (1979).
16. J. Selbin, W. E. Bull, and L. H. Holmes. J. Inorg. Nucl. Chem. **16**, 219 (1961).
17. D. F. Grant and E. J. Gabe. J. Appl. Crystallog. **11**, 114 (1978).
18. E. J. Gabe, F. L. Lee, and Y. LePage. Crystallographic computing 3: data collection, structure determination, proteins and databases. *Edited by* G. M. Sheldrick, C. Kruger, and R. Goddard. Clarendon Press, Oxford. 1985. p. 167.
19. D. Rogers. Acta Crystallogr. A**37**, 734 (1981).

Can. J. Chem. Downloaded from www.nrcresearchpress.com by 41.223.56.140 on 09/07/12
For personal use only.

Étude de l'annélation à partir de dérivés dibromomés-1,4 et -1,5 en présence de carbanions

P. CANONNE[1] ET J. PLAMONDON
Département de chimie, Université Laval, Québec (Qué.), Canada G1K 7P4

Reçu le 5 mai 1988

P. CANONNE et J. PLAMONDON. Can. J. Chem. **67**, 555 (1989).

Les dibromures primaires–secondaires ont été préparés à partir des diols correspondants et employés, avec des acides du carbone, pour la préparation de composés cycliques disubstitués-1,2. L'utilisation d'un acide du carbone non-symmétrique en présence de NaH dans le DME favorise une importante diastéréosélection conduisant à la formation de l'isomère *trans*. Les facteurs qui influencent la stéréosélectivité sont également proposés.

Mots clés: S_N2 intramoléculaire, décarboxylation, acides alkyl-2 cycloalcanecarboxyliques-1, acides alkyl-1 indanecarboxyliques-2.

P. CANONNE and J. PLAMONDON. Can. J. Chem. **67**, 555 (1989).

Primary–secondary dibromides have been prepared from the corresponding diols and used with carbon acids to prepare 1,2-disubstituted cyclic compounds. With unsymmetrical carbon acid in presence of NaH in DME, a high diastereoselection of the *trans* isomer is observed. Factors that affect the stereoselectivity are proposed.

Key words: intramolecular S_N2, decarboxylation, 2-alkylcycloalkanecarboxylic acids, 1-alkylindan-2-carboxylic acids.

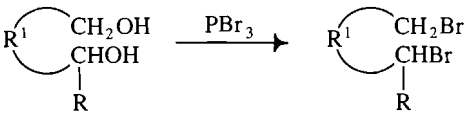
Can. J. Chem. Downloaded from www.nrcresearchpress.com by 41.223.56.140 on 09/07/12
For personal use only.

Les travaux de recherche de notre laboratoire ont été principalement axés sur l'élaboration de systèmes cycliques. Nous avons utilisé les réactifs de Grignard bisfonctionnels pour la synthèse des divers composés polycycliques et spiranniques fonctionnalisés (1). Récemment nous avons étudié la stéréochimie de la réaction de Grignard intramoléculaire (2), en utilisant les organodimagnésiens primaires–secondaires, et nous avons préparé stéréosélectivement des composés hydroxylés cycliques alkylés en position 2. En outre, l'introduction d'une fonction carboxylique nous a semblé d'un grand intérêt (3), surtout pour son aspect stéréochimique. Plus particulièrement, la synthèse des composés 1,2-disubstitués en séries cycloalcane et indane a attiré notre attention.

Dans cette perspective de développement de méthodologies intéressantes et rentables, nous nous sommes ainsi intéressés à la recherche des conditions opératoires permettant d'obtenir des acides alkylés en position 2. En effet, la littérature nous révèle que la formation la plus simple des acides méthyl-2 cyclohexanecarboxyliques-1 est basée sur la synthèse diénique (4), alors que celle des acides méthyl-2 cyclopentanecarboxyliques-1 (5) offre plusieurs possibilités mais paraît moins efficace. Par ailleurs, la synthèse des acides alkyl-2 cycloalcanecarboxyliques homologues ne semble pas être rapportée dans la littérature. Les méthodes de synthèse proposées pour la préparation des acides alkyl-1 indanecarboxyliques-2 sont encore moins satisfaisantes (6).

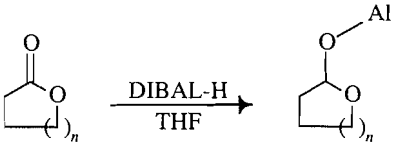
Pour ces raisons, il nous a semblé important de trouver une méthodologie générale et efficace pour la préparation de ces acides cycliques substitués en position 2 et de leurs dérivés. Nous avons alors entrepris d'examiner la réaction des dibromo-1,4 et -1,5 alcanes avec des acides du carbone, en fonction de la chaîne hydrocarbonée et de la grandeur du cycle.

Pour réaliser une telle étude, nous avons synthétisé (7) des dibromures primaires–secondaires (**21–34**) en se basant sur la transformation des diols correspondants (**3–11** à **16–19**) par le tribromure de phosphore (8) (éq. [1]).

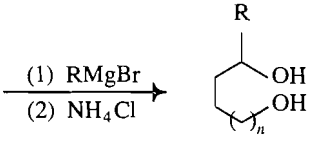
[1] 

I $R' = (CH_2)_2$; R = Me, **21**; R = Et, **22**; R = Pr, **23**; R = Bu, **24**; R = Ph, **25**
II $R' = (CH_2)_3$; R = Me, **26**; R = Et, **27**; R = Pr, **28**; R = Bu, **29**
III R' =  ; R = Me, **30**; R = Et, **31**; R = Pr, **32**; R = Ph, **33**; R = *i*Pr, **34**

Auparavant nous avons développé une méthode générale de préparation des alcanediols-1,4 et -1,5 en une seule étape en réduisant les lactones **1** et **2** par l'hydrure de diisobutylaluminium suivie de l'addition d'un réactif de Grignard à l'hémiacétal formé (éq. [2]). Les données spectroscopiques et les points d'ébullition sont en accord à ceux rapportés dans la littérature. (7*a–c*, 9).

[2] 

1, 2

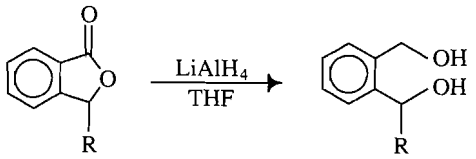


3–11

n = 1; **1** — I *n* = 1; R = Me, **3**; R = Et, **4**; R = Pr, **5**, R = Bu, **6**; R = Ph, **7**
n = 2; **2** — II *n* = 2; R = Me, **8**; R = Et, **9**; R = Pr, **10**, R = Bu, **11**

1. Auteur à qui adresser toute correspondance.

Les α-alkyl benzènediméthanols-1,2 (**16–19**) sont préparés selon une méthode que nous avons mis au point mettant en jeu soit les phtalides substitués correspondants par une simple réduction (éq. [3]), soit dans le cas de α-(méthyl-1 éthyl)-1 benzènedimethanol-1,2 (**20**), par l'action du bromure à isopropylmagnésium sur le phtalide (9). Ces résultats démontrent que notre méthode est de loin la plus générale pour la synthèse des dibromures non-symétriques aussi bien en série à chaîne ouverte que cyclique.

[3] 

12	R = Me	**16**
13	R = Et	**17**
14	R = Pr	**18**
15	R = Ph	**19**

Les dibromures, facilement accessibles par cette méthode, permettent de compléter une série homogène afin de cerner l'influence de la longueur de la chaîne sur la substitution nucléophile intramoléculaire, mettant en jeu un halogénure secondaire comme site réactionnel sensible à la réaction concurrente d'élimination.

Plusieurs nouvelles améliorations ont été proposées pour la réaction de substitution nucléophile, basées sur l'utilisation d'éthers en couronne (10) ou encore de sels d'ammonium quaternaires (11). Quelques essais préliminaires réalisés avec les dibromoalcanes primaires–secondaires n'ont montré aucun avantage appréciable au point de vue des rendements réactionnels mais, au contraire, augmenteraient le coût de revient opérationnel. Ainsi, nous avons retenu la méthode basée sur l'utilisation de l'hydrure de sodium dans le diméthoxy-1,2 éthane à la température ambiante, qui conduit avec des rendements satisfaisants aux composés désirés (**35–46**) et permet de minimiser les réactions secondaires lors de la cyclisation.

Les résultats obtenus sont présentés au tableau 1. De l'ensemble de ce travail, il ressort que la réaction d'élimination se manifeste seulement dans le cas des dihalogénures **26** et **29** qui ont fourni les composés d'annélation **40** et **41** avec des rendements plus faibles. Effectivement, la substitution nucléophile semble être légèrement empêchée en série cyclohexanique. Ainsi, les produits éthyléniques provenant de la réaction d'élimination intramoléculaire sont observés en faibles quantités. Il faut noter, cependant, que cette dernière est moins importante que lors de l'addition nucléophile intramoléculaire réalisée à l'aide des organomagnésiens (12).

On peut supposer que l'addition nucléophile sur le carbone du carbonyle est plus sensible à l'encombrement stérique, ou encore, que le transfert de l'hydrure par un mécanisme à six centres, dans le cas du cyclohexane, est particulièrement favorisé dans les réactions des organodimagnésiens.

Une deuxième analogie découle de cette recherche. Effectivement, quelques soient l'anion et le substrat secondaires, la formation des composés alkyl-2 cyclopentanedicarboxylate-1,1 de diéthyle (**35–39**) est très favorisée comme dans le cas des amines cycliques et autres composés hétérocycliques. Cette constatation rejoint notre première hypothèse concernant la formation des cyclopentanes. Les rendements moins élevés dans cette série ne sont attribuables qu'à une non-réaction, car le dibromure n'ayant las réagi a été récupéré.

La vitesse des réactions du dihalogénure benzylique **25** et des dihalogénures dibenzyliques (**30–34**) est loin supérieure à celle des alkyles, comme il fallait s'y attendre. Ceci s'explique facilement en tenant compte de la stabilisation électronique de l'état de transition conjugué et de la limitation des degrés de liberté de la chaîne. Ainsi, en présence de malonate de diéthyle dans NaH et DME, les dihalogénures dibenzyliques (**30–34**) ont conduit aisément à la formation des alkyl-1 indanedicarboxylate-2,2 de diéthyle correspondants (**42–46**).

En conclusion, le présent travail démontre que par double substitution nucléophile (attaque sur l'halogénure primaire suivie de l'attaque sur l'halogénure secondaire), la cyclisation s'effectue en une seule étape avec des bons rendements et semble être peu influencée par la nature du groupe alkyle situé sur le carbone secondaire, à l'exception du groupe phényle.

Les diesters ainsi obtenus (**35–39** et **42–46**) sont convertis en acides cyclopentanedicarboxyliques-1,1 (**47–51**) et en acides indanedicarboxyliques-2,2 (**52–56**) par hydrolyse en présence de KOH. La décarboxylation effectuée sous un léger vide, en absence de pyridine, fournit les acides (**57–63**) dont la spectroscopie de résonance magnétique nucléaire du proton révèle que l'isomère *trans* est légèrement favorisé. Ces acides diastéréoisomères sont dosés en se basant sur les signaux du proton en position 1 qui se présentent sous forme de deux multiplets bien séparés. En effet, lorsque le proton est *trans* par rapport au groupe alkyle, il résonne à ~2,80 ppm, et lorsqu'il est *cis*, il subit l'effet de blindage du groupe alkyle et, par conséquent, ce signal se situe à ~2,36 ppm. Ce même phénomène de blindage est constaté dans le cas d'esters méthyliques. Pour confirmer la précision du dosage nous avons également utilisé les signaux de groupe méthyle des esters méthyliques (**64–69**) obtenus par traitement des acides correspondants au diazométhane (tableau 2). La formation préférentielle de l'isomère *trans* observée peut facilement s'expliquer par le fait que le groupe alkyle dans la forme énolique prend la position équatoriale (13) et, par conséquent, la protonation s'effectue sélectivement du côté pseudoaxial.

Les résultats de la première partie du présent travail démontrent clairement que la méthode envisagée est générale, à ce qui a trait la réaction du malonate d'éthyle avec un grand nombre de dibromures-1,4 et -1,5 de structures fort variées. En outre, ils suggèrent de reprendre les travaux sur la phénylacetonitrile, précédemment décrits dans la littérature (14, 15), pour les raisons qui motivent notre recherche à savoir :

1. Améliorer l'efficacité de la réaction, en choisissant les conditions opératoires favorisant la réaction de substitution intramoléculaire et minimisant les réactions intermoléculaires en général et celles d'élimination intra- ou intermoléculaire en particulier. En effet, les rendements obtenus précédemment (14) étaient inférieurs à 60% lorsque le dihalogénure fut le dibromo-1,4 pentane, incluant le composé d'élimination difficilement séparable du composé cyclique, et de 30% dans le cas du dibromo-1,5 hexane (15).

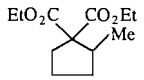
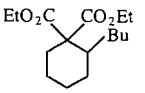
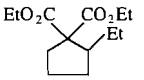
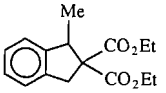
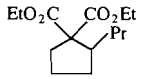
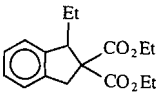
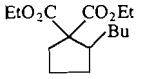
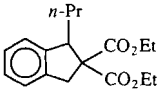
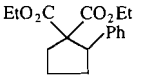
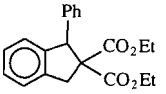
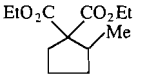
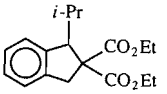
2. Améliorer la diastéréosélection, notamment lorsque les solvants utilisés sont peu dissociants.

3. Enfin, vérifier l'hypothèse précédemment émise à ce qui concerne la stéréosélectivité de la réaction de substitution nucléophile intramoléculaire en fonction de l'encombrement stérique de l'halogénure secondaire (15).

En premier lieu, nous avons vérifié si la nature du solvant ou de la base pouvait influencer la diastéréosélectivité. Pour ce faire, nous avons effectué la réaction de substitution nucléophile intramoléculaire du dibromo-1,4 pentane et du dibromo-

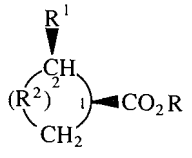
Can. J. Chem. Downloaded from www.nrcresearchpress.com by 41.223.56.140 on 09/07/12
For personal use only.

TABLEAU 1. Étude de la réaction de la substitution nucléophile intramoléculaire[a]

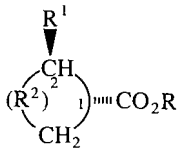
Dibromure	Diester cyclique		Rendement[b] (%)	Dibromure	Diester cyclique		Rendement[b] (%)
21		**35**	77	**29**		**41**	56
22		**36**	75	**30**		**42**	79
23		**37**	72	**31**		**43**	86
24		**38**	67	**32**		**44**	75
25		**39**	68	**33**		**45**	71
26		**40**	55	**34**		**46**	68

[a]Réactions effectuées dans DME en présence de NaH à la température ambiante.
[b]Les rendements sont évalués à partir des produits isolés par chromatographie sur colonne.

TABLEAU 2. Dosage des diastéréoisomères (*a* et *b*) des acides cycliques et de leurs dérivés esters méthyliques par résonance magnétique du proton



a



b

		Acide *cis*(*a*)				Ester *cis*(*a*)			Acide *trans*(*b*)				Ester *trans*(*b*)		
R^2	R^1	R = H	%	δH1	δC1	$R = CH_3$	%	δCH_3	R = H	%	δH1	δC1	R = Me	%	δCH_3
$(CH_2)_2$	Me	**57***a*	45	2,80	48,37	**64***a*	44	3,64	**57***b*	55	2,40	51,81	**64***b*	56	3,66
	Et	**58***a*	41	2,84	47,64	**65***a*	43	3,65	**58***b*	59	2,36	50,00	**65***b*	52	3,67
	Pr	**59***a*	49	2,86	47,75	**66***a*	47	3,65	**59***b*	51	2,35	50,37	**66***b*	53	3,67
	Bu	**60***a*	45	2,85	47,75	**67***a*	44	3,64	**60***b*	55	2,35	50,37	**67***b*	56	3,67
	Me	**61***a*	32	—	48,35	**68***a*	31	3,69	**61***b*	68	—	52,46	**68***b*	69	3,72
	Pr	**62***a*	32	—	49,10	**69***a*	39	3,61	**62***b*	68	—	49,50	**69***b*	61	3,63
	Ph	**63***a*	37	—	53,83	—	—	—	**63***b*	63	—	54,48	—	—	—

1,5 hexane avec le phénylacétonitrile dans différents milieux en utilisant, d'une part, les solvants et les bases mentionnés en littérature (13) et, d'autre part, en employant l'éther en couronne 18-C-6 afin de cerner si les facteurs précédemment mentionnés sont responsables de la diastéréosélection observée. L'addition de l'éther en couronne dans le milieu réactionnel à faible constante diélectrique, tel que le diméthoxy-1,2 éthane en présence de l'hydrure de potassium, devrait alors conduire à des résultats similaires à ceux obtenus dans le cas des solvants dissociants tels que le diméthylsulfoxyde, puisque l'éther en couronne permet de dissocier la paire d'ions en solution.

En effet, l'examen du tableau 3 ne montre aucune influence significative concernant la nature de la base dans divers solvants à faible constante diélectrique sur le déroulement stéréochimique de la réaction et vérifie les résultats précédemment décrits. Nous n'observons aucune variation importante de la distribution des diastéréoisomères concernant l'utilisation de l'éther en couronne 18-C-6. (La variation est de l'ordre de 5%.)

Dans un deuxième temps, nous avons entrepris une deuxième série de réaction sur le but d'étudier l'influence de la nature du groupe alkyle sur le contrôle stéréochimique de la réaction,

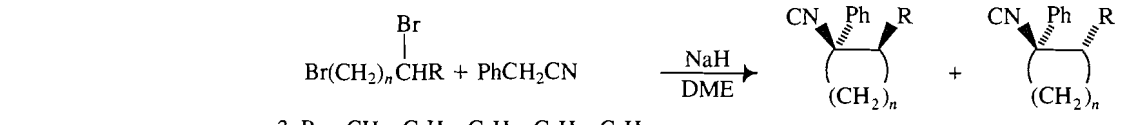
Can. J. Chem. Downloaded from www.nrcresearchpress.com by 41.223.56.140 on 09/07/12
For personal use only.

TABLEAU 3. Distribution des diastéréoisomères des réactions du dibromo-1,4 pentane et du dibromo-1,5 hexane sur le phénylacétonitrile en fonction du milieu réactionnel

Expérience	n	Base	Solvant	Méthyl-2 phényl-1 cycloalcanecarbonitrile-1 *cis* (%)[a]	*trans* (%)[a]
1	3	NaH	DME	18	82
2		KH	DME + 18-C-6	15	85
3		LDA	THF	13	87
4	4	NaH	DME	16	84
5		NaH	Benzène	11	89
6		KH	DME	14	86
7		KH	DME + 18-C-6	10	90

[a]Le dosage de diastéréoisomères a été réalisé par chromatographie en phase gazeuse et par rmn ^{1}H; les rendements réactionnels sont de 80%, sauf dans le cas de l'expérience 5.

TABLEAU 4. Distribution des diastéréoisomères des réactions de dibromo-1,4 et -1,5 alcanes avec le phénylacétonitrile



$n = 3$ R = CH_3, C_2H_5, C_3H_7, C_4H_9, C_6H_5
$n = 4$ R = CH_3, C_2H_5, C_3H_7, C_4H_9

a **70–74** *b* **75–78**

n	R	Rdt global[a] (%)	Alkyl-2 phényl-1 cycloalcanecarbonitrile-1 *cis* (%)[b]		*trans* (%)[b]	
3	Me	97	**70***a*	18	**70***b*	82
	Et	78	**71***a*	15	**71***b*	85
	Pr	86	**72***a*	7	**72***b*	93
	Bu	83	**73***a*	11	**73***b*	89
	Ph	91	**74***a*	90	**74***b*	10
4	Me	88	**75***a*	16	**75***b*	84
	Et	83	**76***a*	11	**76***b*	89
	Pr	70	**77***a*	13	**77***b*	87
	Bu	78	**78***a*	28	**78***b*	72

[a]Les rendements sont évalués à partir de produits isolés après chromatographie sur colonne.
[b]Le dosage des diastéréoisomères a été effectué par chromatographie en phase gazeuse et par rmn ^{1}H.

nous avons fait réagir le phénylacétonitrile avec divers dibromo-1,4 et -1,5 alcanes. Les résultats rassemblés au tableau 4 nous indiquent que la stéréochimie de la réaction de substitution nucléophile intramoléculaire est indépendante de la nature du substituant alkyle, contrairement à ce qui a été mentionné dans la littérature (15). Effectivement, quelque soit le dihalogénure utilisé, l'isomère *trans*-CN est majeur, sauf dans le cas du groupe phényle où l'isomère *cis*-CN est nettement favorisé. Nous pouvons également observer que les alkyl-2 phényl-1 cycloalcanecarbonitriles-1 (**62–70**) sont obtenus avec des rendements grandement améliorés (78–95%) aussi bien en série cyclopentanique que cyclohexanique.

En effet, les rendements moins élevés (30–60% selon le solvant) ainsi que la divergence de stéréosélectivité observée en fonction du dibromure chez les auteurs précédents (15) pourraient être attribuables, d'une part, à la faible dilution du milieu dans le DME et, d'autre part, à la température réactionnelle plus élevée. L'examen de leurs résultats montrent un écart beaucoup plus grand aussi bien dans les expériences avec le dibromo-1,4 pentane qu'avec le dibromo-1,4 hexane. Dans ce dernier cas les rendements n'étaient que de 30%.

Nos meilleurs résultats s'expliqueraient par le fait que nous avons opté pour un mode opératoire mettant en jeu des conditions plus douces qui optimisent le rendement global de la réaction (température ambiante, NaH et DME). Il est important de mentionner que nous avons réalisé ces réactions dans un milieu fortement dilué. Ainsi, le dibromure et l'anion ont été préalablement dissous dans les solvants réactionnels car la stéréochimie est influencée par l'homogénéité du milieu réactionnel.

Can. J. Chem. Downloaded from www.nrcresearchpress.com by 41.223.56.140 on 09/07/12
For personal use only.

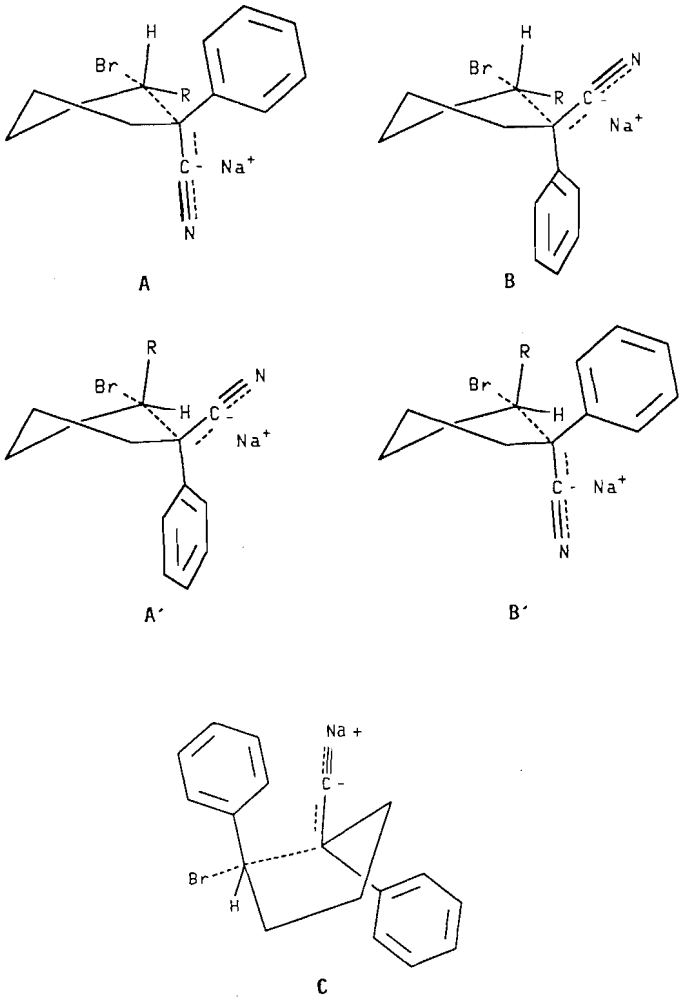


FIG. 1

De l'ensemble de ce travail il ressort que les réactions des dibromo-1,4 et -1,5 alcanes avec le malonate d'éthyle et le phénylacétonitrile conduisent aux composés cycliques correspondants avec des bons rendements quelle que soit la structure du groupe alkyle secondaire.

Il démontre, en outre, que la réaction du phénylacétonitrile est stéréosélective, en favorisant l'isomère *trans*, aussi quelle que soit la structure du groupe alkyle secondaire. L'examen des divers conformères présentés à la figure 1 indique que les A, A′ conduisent après cyclisation aux isomères *cis* alors que les conformères B, B′ conduisent aux isomères *trans* — composés majeurs.

Comme précédemment (14), nous retenons la délocalisation de la charge et la solvatation de l'anion nitrile. Par conséquent nous considérons que, dans tous les cas, le phényle, par son orientation, est moins volumineux que le groupe nitrile. L'état de transition B de la réaction de substitution nucléophile intramoléculaire est incontestablement plus favorisé aussi bien lorsque le groupe R est méthyle que lorsque le groupe R est éthyle, contrairement aux hypothèses précédemment émises (15). De même, en se basant sur les interactions entre atomes non liés, l'état de transition C est privilégié lors de la formation du composé **74***a*. En effet l'état de transition conduisant à l'isomère **74***b* présente un importante encombrement stérique.

La présente étude est surtout importante du point de vue synthétique, car les résultats obtenus nous ont permis d'envisager la synthèse de composés spiranniques intéressants du point de vue biologique.

Partie expérimentale

Les spectres de résonance magnétique nucléaire du proton ont été enregistrés sur les spectromètres 60 MHz Varian EM360A, 90 MHz Bruker HX-90 et 200 MHz Varian XL-200. Les spectres de résonance magnétique nucléaire du ^{13}C ont été déterminés à l'aide d'un appareil Bruker WP-80 (20,1 MHz) et Varian XL-200 multinoyaux (50,3 MHz). La plupart des spectres ont été enregistrés à partir de solutions de chloroforme deutérié et le tétraméthylsilane a été choisi comme standard interne. Les spectres dans le domaine de l'infrarouge ont été tracés à l'aide d'un spectromètre Beckmann (IR-4250). Quant aux spectres de masse, ils ont été effectués à l'aide d'un spectromètre Hewlett Packard 5992 GC/MS.

Les points de fusion, pris en tubes capillaires ouverts à l'aide d'un appareil Thomas–Hoover, ne sont pas corrigés. Les analyses chromatographiques sur couche-mince ont été réalisées sur des plaques de gel de silica 0,25 mm. Les séparations chromatographiques sur colonne ont été effectuées sur gel de silice Woelm (32–63 μm) pour colonne chromatographique « flash ».

Les analyses chromatographiques en phase gazeuse ont été réalisées à l'aide d'un chromatographe Varian 3700 muni d'une colonne de huit pieds 10% Dexsil 300 sur Chromosorb B et d'un détecteur à ionisation de flamme. Les spectres de masse précise ont été enregistrés au Centre régional de spectrométrie de masse à l'Université de Montréal.

Mode opératoire général de synthèse des cycloalcanedicarboxylates-1,1 et indanedicarboxylates-2,2 de diéthyle substitués en β (35–46)

À 0,033 mol d'hydrure de sodium en suspension dans 50 mL de diméthoxy-1,2 éthane (DME), est additionné 0,011 mol de malonate de diéthyle dilué dans 30 mL de DME, sous atmosphère d'azote. On laisse agiter 30 min à la température ambiante, ensuite on additionne goutte à goutte 0,01 mol du dibromure correspondant en solution dans 30 mL de DME. Une fois l'addition terminée, on maintient l'agitation durant 16 h à la même température, et si la réaction est incomplète, alors on porte à 60°C le mélange réactionnel, le temps nécessaire pour que la réaction soit complété. Dans le cas des dérivés d'indane, la réaction est complète après 8 h d'agitation à la température de la pièce. Après avoir refroidi le système à 0°C, on hydrolyse avec de l'acide chlorhydrique à 10%, jusqu'à un pH d'environ 4. On sépare les deux phases et on extrait la phase aqueuse à l'éther. Les extraits organiques sont séchés sur sulfate de magnésium, puis évaporés. On obtient une huile jaunâtre qu'on purifie par chromatographie flash sur gel de silice en utilisant un mélange acétate d'éthyle – éther de pétrole (35–60) comme éluant.

Méthyl-2 cyclopentanedicarboxylate-1,1 de diéthyle (35): Rdt, 77% (1,756 g). Liquide incolore; Eb (0,04 Torr; 1 Torr = 133.3 Pa) = 62°C (litt. (7*a*) Eb (17,5 Torr) 120–122°C); ir ν_{max} (film): 2960, 1720, 1450, 1365, 1250, 1170, 1090 cm^{-1}; rmn ^1H ($CDCl_3$) δ: 1,25 (6H, 2t), 1,30–1,95 (4H, m), 2,01 (1H, m, H-5), 2,43 (1H, m, H-5), 2,68 (1H, q, H-2), 4,18 (4H, m) ppm; rmn ^{13}C ($CDCl_3$) δ: 172,03, 170,89, 63,30, 60,50, 60,38, 40,20, 33,58, 33,17, 22,49, 16,10, 13,79, 13,67 ppm; sm *m/e*: 213 ($M^+ - CH_3$, 1%), 173 ($M^+ - C_4H_7$, 100%), 127 ($C_6H_7O_3$, 59%), 81 ($M^+ - 2CO_2Et$, 65%), 57 (C_4H_9, 59%).

Ethyl-2 cyclopentanedicarboxylate-1,1 de diéthyle (36): Rdt, 75% (1,977 g). Liquide incolore; Eb (0,02 Torr) = 74°C (litt. (7*a*) Eb (0,2 Torr) 81–82°C); ir ν_{max} (film): 2980, 2960, 2940, 1725, 1465, 1450, 1375, 1260, 1180 cm^{-1}; rmn ^1H ($CDCl_3$) δ: 0,93 (3H, t), 0,96–1,21 (2H, m), 1,25 (6H, t), 1,28–2,11 (5H, m), 2,44 (2H, m, H-2 et H-5), 4,17 (4H, m) ppm; rmn ^{13}C ($CDCl_3$) δ: 172,32, 171,26, 63,54, 60,86, 60,72, 48,04, 34,60, 30,47, 24,39, 22,95, 14,19, 14,12, 13,15 ppm; sm *m/e*: 173 ($M^+ - C_5H_9$, 63%), 127 ($C_6H_7O_3$, 30%), 95 ($M^+ - 2CO_2Et$, 100%), 67 (C_5H_7, 66%).

Propyl-2 cyclopentanedicarboxylate-1,1 de diéthyle (37): Rdt, 72% (2,224 g). Liquide incolore; Eb (0,017 Torr) = 73°C; ir ν_{max} (film):

Can. J. Chem. Downloaded from www.nrcresearchpress.com by 41.223.56.140 on 09/07/12
For personal use only.

Can. J. Chem. Downloaded from www.nrcresearchpress.com by 41.223.56.140 on 09/07/12
For personal use only.

2960, 2930, 1730, 1450, 1375, 1250, 1175 cm^{-1}; rmn ^1H ($CDCl_3$) δ: 0,87 (3H, t), 1,16 (6H, t), 1,02–1,50 (4H, m), 1,55–2,11 (5H, m), 2,49 (2H, m, H-2 et H-5α), 4,16 (4H, q) ppm; rmn ^{13}C ($CDCl_3$) δ: 172,83, 171,73, 63,80, 60,95, 60,80, 46,24, 34,68, 33,73, 31,02, 23,05, 21,73, 14,19 (3C) ppm; sm *m/e*: 256 (M^+, 1%), 173 ($M^+ - C_6H_{11}$, 100%), 127 ($C_6H_7O_3$, 41%), 109 ($M^+ - 2CO_2Et$, 57%), 67 (C_5H_7, 78%), 58 (C_3H_6O, 57%). *Anal.* calc. pour $C_{14}H_{24}O_4$: C 65,60, H 9,44; tr.: C 65,43, H 9,31.

*Butyl-2 cyclopentanedicarboxylate-1,1 de diéthyle (**38**)*: Rdt, 57% (1,539 g). Huile incolore; Eb (0,005 Torr) = 82°C; ir ν_{max} (film): 2960, 2940, 1730, 1470, 1450, 1375, 1255, 1205, 1175 cm^{-1}; rmn ^1H ($CDCl_3$) δ: 0,88 (3H, t), 1,25 (6H, t), 0,91–1,50 (6H, m), 1,50–1,68 (2H, m), 1,74–2,09 (3H, m), 2,33–2,59 (2H, m, H-2 et H-5α), 4,18 (4H, m) ppm; rmn ^{13}C ($CDCl_3$) δ: 172,26, 171,15, 63,32, 60,68, 60,54, 46,00, 34,34, 30,87, 30,69, 30,62, 22,81, 22,65, 14,00, 13,88 (2C) ppm; sm *m/e*: 270 (M^+, 1%), 173 ($M^+ - C_7H_{13}$, 100%), 127 ($C_6H_7O_3$, 44%), 123 ($M^+ - 2CO_2Et$, 35%), 81 ($M^+ - 2CO_2Et - (CH_2)_3$, 30%), 67 (C_5H_7, 37%). *Anal.* calc. pour $C_{15}H_{26}O_4$: C 66,33, H 9,69; tr.: C 66,61, H 9,70.

*Phényl-2 cyclopentanedicarboxylate-1,1 de diéthyle (**39**)*: Rdt, 68% (0,199 g). Huile incolore; ir ν_{max} (film): 3045, 3020, 2980, 2965, 2910, 2880, 1730, 1600, 1500, 1470, 1455, 1380, 1370, 1300, 1265, 1230, 1205, 1080, 1055, 1100, 1080, 1060, 1030, 750, 700 cm^{-1}; rmn ^1H ($CDCl_3$) δ: 0,76 (3H, 2d, $J_{A'X'}$ = 7.30 Hz, $CO_2CH_2CH_3$), 1,22 (3H, 2d, J_{AX} = 6,98 Hz, $CO_2CH_2CH_3$), 1,51–2,39 (6H, m), 2,69 (1H, m, H-2), 3,43 (1H, d de q, A'B'X', $J_{A'B'}$ = 10,79 Hz, $J_{A'X'}$ = 7,30 Hz, CO_2CHCH_3), 3,74 (1H, d de q, A'B'X', $J_{A'B'}$ = 10,79 Hz, $J_{A'X'}$ = 7,30 Hz, CO_2CHCH_3), 4,14 (1H, d de q, ABX, J_{AB} = 10,79 Hz, J_{AX} = 6,98 Hz, CO_2CHCH_3), 4,24 (1H, d de q, ABX, J_{AB} = 10,79 Hz, J_{AX} = 6,98 Hz, CO_2CHCH_3), 7,25 (5H, m) ppm; rmn ^{13}C ($CDCl_3$) δ: 172,32, 170,35, 140,88, 128,46 (2C), 127,59 (2C), 126,44, 65,44, 61,10, 60,63, 50,75, 35,00, 32,60, 24,21, 13,97, 13,35 ppm; sm *m/e*: 291 (M^+ + 1, 4%), 290 (M^+, 25%), 217 ($M^+ - CO_2Et$, 19%), 216 ($M^+ - CO_2Et$, 100%), 171 ($M^+ - CO_2Et - OEt$, 40%), 170 ($M^+ - CO_2Et - OEt$, 54%) 144 ($M^+ - 2CO_2Et$, 20%), 143 ($M^+ - 2CO_2Et$, 37%), 142 ($M^+ - 2CO_2Et$, 24%), 128 ($C_6H_8O_3$, 27%), 127 ($C_6H_7O_3$, 24%), 115 ($C_5H_7O_3$, 30%). Masse précise pour $C_{17}H_{22}O_4$: 290,1518; tr.: 290,1508.

*Méthyl-2 cyclohexanedicarboxylate-1,1 de diéthyle (**40**)*: Rdt, 55% (1,058 g). Liquide incolore; Eb (0,150 Torr) = 120°C (litt. (*7a*) Eb (0,25 Torr) 86–87°C); ir ν_{max} (film): 2980, 2930, 2875, 1730, 1470, 1450, 1390, 1370, 1200–1000 cm^{-1}; rmn ^1H ($CDCl_3$) δ: 1,00 (3H, d), 1,25 (6H, t), 1,29–2,00 (7H, m), 2,09 (1H, m, H-6), 2,31 (1H, m, H-2), 4,18 et 4,19 (4H, 2d) ppm; rmn ^{13}C ($CDCl_3$) δ: 171,78, 170,86, 60,76, 60,46, 58,34, 34,44, 29,77, 29,44, 22,51, 22,41, 16,53, 13,90 (2C) ppm; sm *m/e*: 243 (M^+ + 1, 1%), 242 (M^+, 3%), 173 ($M^+ - C_5H_9$, 81%), 169 ($M^+ - CO_2Et$, 17%), 168 ($M^+ - CO_2Et$, 15%), 160 (23%), 150 (21%), 141 (17%), 127 ($C_6H_7O_3$, 26%), 123 ($C_6H_3O_3$, 24%), 122 ($C_6H_2O_3$, 33%), 95 ($M^+ - 2CO_2$, Et, 100%), 81 (C_6H_9, 23%), 79 (C_6H_7 22%), 67 (C_5H_7, 39%), 55 (C_4H_7, 24%).

*Butyl-2 cyclohexanedicarboxylate-1,1 de diéthyle (**41**)*: Rdt, 56% (0,799 g). Liquide incolore; Eb (0,035 Torr) = 101°C; ir ν_{max} (film): 2975, 2955, 2930, 2860, 1735, 1465, 1440, 1375, 1200–1000 cm^{-1}; rmn ^1H ($CDCl_3$) δ: 0,87 (3H, t), 1,22 (6H, t), 1,26–1,63 (10H, m), 1,67–1,98 (5H, m), 4,15 (4H, q) ppm; rmn ^{13}C ($CDCl_3$) δ: 169,54 (2C), 60,76 (2C), 57,69, 51,46, 38,56, 30,07, 29,34, 28,66, 26,86, 26,35, 21,80, 13,72 (2C), 13,59 ppm; sm *m/e*: 193 (17%), 165 (18%), 160 (100%), 147 (18%), 133 (16%), 81 (C_6H_9, 20%), 73 (CO_2Et, 16%), 69 (C_5H_9, 18%), 55 (C_4H_7, 32%), 41 (C_3H_5, 17%). *Anal.* calc. pour $C_{16}H_{28}O_4$: C 67,57, H 9,92; tr.: C 67,38, H 9,85.

*Méthyl-1 indanedicarboxylate-2,2 de diéthyle (**42**)*: Rdt, 79% (1,974 g). Liquide incolore; Eb (0,038 Torr) = 110°C; ir ν_{max} (film): 3020, 2960, 2920, 2890, 2860, 1725, 1470, 1450, 1375, 1360, 1290, 1275, 1240, 1165, 1145, 1090, 1060, 1040, 750 cm^{-1}; rmn ^1H ($CDCl_3$) δ: 1,24 (3H, d), 1,22 et 1,25 (3H, 2d, $J_{A'X'}$ = 7,30 Hz, CO_2CHCH_3), 1,23 et 1,26 (3H, 2d, J_{AX} = 6,99 Hz, CO_2CHCH_3), 3,53 (2H, 2d, AB, J = 16,82 Hz, $\Delta\nu$ = 96,31 Hz, CH_2-3), 4,03 (1H, q, *CH*-1), 4,11–4,31 (4H, 4d de q, $CO_2CH_2CH_3$), 7,16 (4H, s) ppm; rmn ^{13}C ($CDCl_3$) δ: 171,32, 169,85, 145,49, 138,90, 126,68 (2C), 123,76, 122,95, 64,63, 60,90, 60,76, 44,66, 38,88, 16,12, 13,63 (2C) ppm; sm *m/e*: 277 (M^+ + 1, 1%), 276 (M^+, 8%), 203 ($M^+ - CO_2Et$, 15%), 202 ($M^+ - CO_2Et$, 43%), 143 ($M^+ - CO_2Et - CH_3CH_2O - CH_3$, 26%), 130 ($M^+ - 2CO_2Et$, 32%), 129 ($M^+ - 2CO_2Et$, 100%), 128 ($M^+ - 2CO_2Et$, 43%), 127 ($M^+ - 2CO_2Et$, 17%), 115 ($M^+ - 2CO_2Et - CH_3$, 57%). Masse précise pour $C_{16}H_{20}O_4$: 276,1362; tr.: 276,1371.

*Ethyl-1 indanedicarboxylate-2,2 de diéthyle (**43**)*: Rdt, 86% (1,751 g). Liquide incolore; Eb (0,022 Torr) = 119°C; ir ν_{max} (film): 3100, 3060, 3020, 2980, 2940, 2920, 1730, 1465, 1450, 1400, 1375, 1270, 1235, 1170, 1125, 1100, 1090, 1070, 950, 930, 880, 770, 750 cm^{-1}; rmn ^1H ($CDCl_3$) δ: 0,96 (3H, t), 1,17 et 1,19 (3H, 2d, $J_{A'X'}$ = 7,30 Hz, $CO_2CH_2CH_3$), 1,24 et 1,27 (3H, 2d, J_{AX} = 6,99 Hz, $CO_2CH_2CH_3$), 1,28–1,69 (2H, m), 3,56 (2H, 2d, AB, J = 16,51 Hz, $\Delta\nu$ = 104,71 Hz, CH_2-3), 3,81 (1H, m), 3,99–4,34 (4H, 4d, de q), 7,14 (4H, s) ppm; rmn ^{13}C ($CDCl_3$) δ: 171,37, 169,77, 144,12, 138,88, 126,79, 126,29, 124,64, 124,13, 65,41, 61,34, 61,21, 51,10, 38,94, 23,87, 14,08, 13,93, 11,70 ppm; sm *m/e*: 291 (M^+ + 1, 1%), 290 (M^+, 5%), 217 ($M^+ - CO_2Et$, 15%), 216 ($M^+ - CO_2Et$, 50%), 189 ($M^+ - CO_2Et - C_2H_4$, 10%), 171 ($M^+ - CO_2Et - CH_3CH_2O - H$, 9%), 144 ($M^+ - 2CO_2Et$, 20%), 143 ($M^+ - 2CO_2Et$, 100%), 142 ($M^+ - 2CO_2Et$, 25%), 129 ($M^+ - 2CO_2Et - CH_3$, 31%), 128 ($M^+ - 2CO_2Et - CH_3$, 37%), 127 ($M^+ - 2CO_2Et - CH_3$, 10%), 116 ($M^+ - 2CO_2Et - C_2H_4$, 12%), 115 ($M^+ - 2CO_2Et - C_2H_5$, 64%). Masse précise pour $C_{17}H_{22}O_4$: 290,1519; tr.: 290,1522.

*Propyl-1 indanedicarboxylate-2,2 de diéthyle (**44**)*: Rdt, 75% (1,487 g). Liquide incolore; Eb (0,012 Torr) = 120°C; ir ν_{max} (film): 3060, 2980, 2965, 2940, 1735, 1465, 1450, 1375, 1270, 1235, 1165, 1125, 1090, 1070, 750 cm^{-1}; rmn ^1H ($CDCl_3$) δ: 0,90 (3H, t), 1,16 et 1,19 (3H, 2d, $J_{A'X'}$ = 7,30 Hz, $CO_2CH_2CH_3$), 1,24 et 1,27 (3H, 2d, J_{AX} = 6,99 Hz, $CO_2CH_2CH_3$), 1,43 (4H, m), 3,56 (2H, 2d, AB, J = 16,51 Hz, $\Delta\nu$ = 104,08 Hz, CH_2-3), 3,89 (1H, m), 4,03–4,30 (4H, 4d de q), 7,13 (4H, s) ppm; rmn ^{13}C ($CDCl_3$) δ: 171,34, 169,77, 144,39, 138,84, 126,75, 126,35, 124,53, 124,12, 65,45, 61,38, 61,19, 49,40, 39,93, 33,11, 20,30, 14,17, 14,10, 13,95 ppm; sm *m/e*: 304 (M^+, 4%), 231 ($M^+ - CO_2Et$, 18%), 230 ($M^+ - CO_2Et$, 48%), 203 ($M^+ - CO_2Et - C_2H_4$, 11%), 185 ($M^+ - CO_2Et - CH_3CH_2O$, 10%), 158 ($M^+ - 2CO_2Et$, 13%), 157 ($M^+ - 2CO_2Et$, 62%), 156 ($M^+ - 2CO_2Et$, 70%), 143 ($M^+ - 2CO_2Et - CH_3$, 29%), 130 ($M^+ - 2CO_2Et - C_2H_4$, 13%), 129 ($M^+ - 2CO_2Et - C_2H_5$, 80%), 128 ($M^+ - 2CO_2Et - C_2H_5$, 33%), 127 ($M^+ - 2CO_2Et - C_2H_5$, 10%), 117 ($M^+ - 2CO_2Et - C_3H_5$, 19%), 116 ($M^+ - 2CO_2Et - C_3H_6$, 22%), 115 ($M^+ - 2CO_2Et - C_3H_7$, 100%). Masse précise pour $C_{18}H_{24}O_4$: 304,1675; tr.: 304,1682.

*Phényl-1 indanedicarboxylate-2,2 de diéthyle (**45**)*: Rdt, 71% (1,412 g). Cristaux blancs; F = 74,5–75,0°C; ir ν_{max} (KBr): 3075, 3040, 2990, 2940, 2910, 1730, 1500, 1490, 1455, 1370, 1310, 1255, 1200, 1090, 1065, 1055, 1040, 1020, 870, 750 cm^{-1}; rmn ^1H ($CDCl_3$) δ: 0,85 et 0,89 (3H, 2d, $J_{A'X'}$ = 7,30 Hz, $CO_2CH_2CH_3$), 1,24 et 1,26 (3H, 2d, J_{AX} = 6,98 Hz, CO_2CHCH_3), 3,50 (1H, d de q, A'B'X', $J_{A'B'}$ = 10,79 Hz, $J_{A'X'}$ = 7,30 Hz, CO_2CHCH_3), 3,71 (2H, 2d, AB, J = 16,38 Hz, $\Delta\nu$ = 135,45 Hz, CH_2-3), 3,78 (1H, d de q, A'B'X', $J_{A'B'}$ = 10,79 Hz, $J_{A'X'}$ = 7,30 Hz, CO_2CHCH_3), 4,16 (1H, d de q, ABX, J_{AB} = 10,79 Hz, J_{AX} = 6,98 Hz, CO_2CHCH_3), 4,27 (1H, d de q, ABX, J_{AB} = 10,79 Hz, J_{AX} = 6,98 Hz, CO_2CHCH_3), 5,36 (1H, s), 7,01–7,29 (9H, m) ppm; rmn ^{13}C ($CDCl_3$) δ: 171,55, 169,31, 143,67, 140,07, 139,91, 129,30 (2C), 127,91 (2C), 127,33, 127,19, 127,06, 125,15, 124,02, 66,27, 61,68, 61,18, 56,63, 39,86, 14,08, 13,59 ppm; sm *m/e*: 339 (M^+ + 1, 1%), 338 (M^+, 8%), 265 ($M^+ - CO_2Et$, 14%), 264 ($M^+ - CO_2Et$, 51%), 219 ($M^+ - CO_2Et - OCH_2CH_3$, 35%), 192 ($M^+ - 2CO_2Et$, 38%), 191 ($M^+ - 2CO_2Et$, 100%), 190 ($M^+ - 2CO_2Et$, 13%), 189 ($M^+ - 2CO_2Et$, 28%), 178 ($M^+ - 2CO_2Et - CH_2$, 18%), 165 ($M^+ - 2CO_2Et - C_2H_3$, 22%), 115 ($M^+ - 2CO_2Et - C_6H_5$, 30%), 89 (12%). Masse précise pour $C_{21}H_{22}O_4$: 338,1518; tr.: 338,1542.

*Isopropyl-1 indanedicarboxylate-2,2 de diéthyle (**46**)*: Rdt, 68% (1,687 g). Cristaux blancs; F = 55,5–56,5°C; ir ν_{max} (KBr): 3065, 3020, 2970, 2955, 2930, 2895, 2860, 1730, 1480, 1465, 1440, 1385,

Can. J. Chem. Downloaded from www.nrcresearchpress.com by 41.223.56.140 on 09/07/12
For personal use only.

1365, 1350, 1300, 1245, 1215, 1170, 1150, 1115, 1095, 1070, 1040, 1000, 905 cm^{-1}; rmn ^1H ($CDCl_3$) δ : 0,54 (3H, d), 1,10 (3H, d), 1,15 et 1,18 (3H, 2d, $J_{A'X'}$ = 7,30 Hz, $CO_2CH_2CH_3$), 1,26 et 1,30 (3H, 2d, J_{AX} = 6,98 Hz, $CO_2CH_2CH_3$), 2,01 (1H, sext.), 3,60 (2H, 2d, AB, J = 17,15 Hz, Δν = 127,10 Hz, CH_2-3), 3,96 (1H, large d), 4,03 (1H, d de q, A'B'X', $J_{A'B'}$ = 10,48 Hz, $J_{A'X'}$ = 7,30 Hz, CO_2CHCH_3), 4,15 (1H, d de q, A'B'X', $J_{A'B'}$ = 10,48 Hz, $J_{A'X'}$ = 7,30 Hz, CO_2CHCH_3), 4,18 (1H, d de q, ABX, J_{AB} = 10,48 Hz, J_{AX} = 6.98 Hz, CO_2CHCH_3, 4,32 (1H, d de q, ABX, J_{AB} = 10,48 Hz, J_{AX} = 6,98 Hz, CO_2CHCH_3), 7,15 (4H, s) ppm; rmn ^{13}C ($CDCl_3$) δ : 171,44, 169,59, 141,32 ,139,78, 126,70, 126,04, 125,22, 123,79, 65,07, 61,21, 61,07, 55,17, 39,86, 29,51, 22,47, 16,72, 13,90, 13,73 ppm; sm *m/e* : 305 (M^+ + 1, 1%), 304 (M^+, 7%), 231 (M^+ − CO_2Et, 17%), 230 (M^+ − CO_2Et, 64%), 215 (M^+ − CO_2Et − CH_3, 10%), 188 (M^+ − CO_2Et − C_3H_7, 20%), 161 (31%), 157 (M^+ − $2CO_2Et$, 57%), 156 (M^+ − $2CO_2Et$, 20%), 143 (M^+ − $2CO_2Et$ − CH_3, 24%), 142 (M^+ − $2CO_2Et$ − CH_3, 19%), 141 (M^+ − CO_2Et − CH_3, 13%), 129 (M^+ − $2CO_2Et$ − C_2H_5, 22%), 128 (M^+ − $2CO_2Et$ − C_2H_6, 23%), 117 (M^+ − $2CO_2Et$ − C_3H_5, 16%), 116 (M^+ − $2CO_2Et$ − C_3H_6, 23%), 115 (M^+ − $2CO_2Et$ − C_3H_7, 100%). Masse précise pour $C_{18}H_{24}O_4$: 304,1675; tr. : 304,1664.

*Mode opératoire général de synthèse des acides cyclopentanedicarboxyliques-1,1 et indanedicarboxyliques-2,2 substitués en β (**47–56**)*

On introduit 16,8 mmol de KOH dans 3 mL d'eau, puis 2,8 mmol de diester dissous dans 3 mL d'éthanol à 95%. On porte à reflux durant une nuit, puis on distille le solvant (distillation azéotropique), on refroidit le résidu, extrait à l'éther afin d'éliminer les produits neutres, puis on acidifie la phase aqueuse à pH 1. On sature la phase aqueuse en chlorure de sodium et extrait de nouveau à l'éther. Les extraits organiques sont lavés à l'eau salée, séchés sur sulfate de magnésium anhydre, filtrés et évaporés. Les diacides obtenus sont purifiés par recristallisation.

*Acide méthyl-2 cyclopentanedicarboxylique-1,1 (**47**)* : Rdt, 78% (4,263 g). Cristaux blancs; F = 171–173°C (litt. (*7a*) F = 173–175°C); ir ν_{max} (KBr) : 3500–2500, 1700, 1450, 1400, 1280, 1190, 910 cm^{-1}; rmn ^1H ($CDCl_3$ et DMSO) δ : 0,94 (3H, d), 1,25–1,98 (5H, m), 2,25 (1H, m, H-5α), 2,51 (1H, q), 12,25 (2H, 2COOH) ppm; rmn ^{13}C ($CDCl_3$ et DMSO) δ : 173,79, 172,57, 63,29, 39,50, 33,25, 33,11, 22,44, 16,70 ppm; sm *m/e* : 155 (M^+ + 1 − H_2O, 0,5%), 154 (M^+ − H_2O, 2%), 128 (M^+ − CO_2, 6%), 126 (M^+ − CO_2H, 27%), 117 (M^+ − C_4H_7, 100%), 113 (M^+ − CO_2 − CH_3, 45%), 99 ($C_4H_3O_3$, 61%), 81 (C_6H_9, 30%), 45 (CO_2H, 33%), 41 (C_3H_5, 24%).

*Acide éthyl-2 cyclopentadedicarboxylique-1,1 (**48**)* : Rtd, 80% (0,836 g). Cristaux blancs; F = 162°C (litt. (16) F = 158–160°C); ir ν_{max} (KBr) : 3500–2500, 1700, 1465, 1450, 1415, 1300, 1290, 1260, 1200, 1150, 930 cm^{-1}; rmn ^1H ($CDCl_3$ et DMSO) δ : 0,92 (3H, t), 1,00–1,24 (2H, q), 1,28–2,16 (5H, m), 2,29–2,46 (2H, m, H-2 et H-5α), 9,45 (2H, 2COOH) ppm; rmn ^{13}C ($CDCl_3$ et DMSO) δ : 176,36, 174,81, 62,52, 49,57, 34,58, 30,49, 23,99, 23,59, 12,99 ppm; sm *m/e* : 169 (M^+ + 1 − H_2O, 1%), 168 (M^+ − H_2O, 3%), 142 (M^+ − CO_2, 6%), 140 (M^+ − CO_2H, 41%), 117 (M^+ − C_5H_9, 100%), 113 (M^+ − CO_2 − C_2H_5, 86%), 99 ($C_4H_3O_3$, 63%), 95 (C_7H_{11}, 64%), 67 (C_5H_7, 67%), 55 (C_4H_7, 27%).

*Acide propyl-2 cyclopentanedicarboxylique-1,1 (**49**)* : Rdt, 77% (1,006 g). Cristaux blancs; F = 167°C (décarboxylation); ir ν_{max} (KBr) : 3500–2500, 1700, 1470, 1450, 1420, 1305, 1245, 1200, 935 cm^{-1}; rmn ^1H (DMSO) δ : 0,89 (3H, t), 1,09–1,76 (6H, m), 1,77–2,05 (2H, m), 2,12–2,50 (3H, m), 7,85 (2H, 2COOH) ppm; rmn ^{13}C (DMSO) δ : 176,52, 175,03, 62,58, 47,76, 34,47, 33,14, 30,78, 23,27, 21,57, 14,08 ppm; sm *m/e* : 183 (M^+ + 1 − H_2O, 1%), 182 (M^+ − H_2O, 5%), 156 (M^+ − CO_2, 5%), 154 (M^+ − CO_2H, 30%), 117 (M^+ − C_6H_{11}, 100%), 113 (M^+ − CO_2 − C_3H_7, 100%), 95 (C_7H_{11}, 42%), 81 (C_6H_9, 24%), 79 (C_6H_7, 25%), 67 (C_5H_7, 63%), 55 (C_4H_7, 25%). Masse précise pour $C_{10}H_{16}O_4$: 200,1049; tr. : 200,1064.

*Acide butyl-2 cyclopentanedicarboxylique-1,1 (**50**)* : Rtd, 66% (0,649 g). Cristaux blancs; F = 163°C (décarboxylation); ir ν_{max} (KBr) : 3500–2400, 1700, 1470, 1450, 1420, 1300, 1245, 1215, 1190, 925 cm^{-1}; rmn ^1H ($CDCl_3$ et DMSO) δ : 0,89 (3H, t), 1,14–2,16 (11H, m), 2,32–2,56 (2H, m, H-2 et H-5α), 7,73 (2H, 2COOH) ppm; rmn ^{13}C ($CDCl_3$ et DMSO) δ : 173,92, 172,72, 63,63, 46,73, 35,04, 31,76, 31,51, 31,36, 23,51, 23,43, 14,30 ppm; sm *m/e* : 197 (M^+ + 1 − H_2O, 3%), 196 (M^+ − H_2O, 18%), 178 (M^+ − $2H_2O$, 29%), 170 (M^+ − CO_2, 11%), 168 (M^+ − CO_2H, 39%), 150 ($C_{10}H_{14}O$, 29%), 139 ($C_9H_{15}O$, 30%), 126 (M^+ − CO_2H − C_3H_7, 25%), 117 (M^+ − C_7H_{13}, 99%), 113 (M^+ − CO_2 − C_4H_9, 100%), 99 ($C_4H_3O_3$, 59%), 95 (C_7H_{11}, 41%), 81 (C_6H_9, 28%), 79 (C_6H_7, 22%), 67 (C_5H_7, 52%), 55 (C_4H_7, 23%). Masse précise pour $C_{11}H_8O_4$: 214,1205; tr. : 214,1219.

*Acide phényl-2 cyclopentanedicarboxylique-1,1 (**51**)* : Rdt, 52% (0,055 g). Huile difficilement recristallisable; ir ν_{max} (film) : 3500–2600, 1705, 1600, 1470, 1450, 1300, 1250, 750, 700 cm^{-1}; rmn ^1H ($CDCl_3$) δ : 1,57–2,44 (6H, m), 2,74 (1H, m, H-2), 7,22 (5H, m) ppm. Masse précise pour $C_{13}H_{14}O$: 234,0892; tr. : 234,0907.

*Acide méthyl-1 indanedicarboxylique-2,2 (**52**)* : Rdt, 83% (0,598 g). Cristaux blancs; F = 144,5–145,5°C; ir ν_{max} (KBr) : 3500–2500, 2940, 1720, 1700, 1470, 1315, 1290, 1260, 1250 cm^{-1}; rmn ^1H ($CDCl_3$ et DMSO) δ : 1,29 (3H, d, J = 6,98 Hz, CH_3), 3,51 (2H, 2d, AB, J = 16,50 Hz, Δν = 74,70 Hz, CH_2-3), 3,96 (1H, q), 7,14 (4H, s), 9,12 (2H, 2COOH) ppm; rmn ^{13}C ($CDCl_3$ et DMSO) δ : 172,86, 171,26, 145,18, 138,74, 125,84 (2C), 123,13, 122,40, 63,88, 43,78, 38,20, 16,08 ppm; sm *m/e* : 221 (M^+ + 1, 1%), 220 (M^+, 5%), 176 (M^+ − CO_2, 9%), 174 (M^+ − CO_2H, 67%), 131 (M^+ − CO_2 − CO_2H, 26%), 130 (M^+ − $2CO_2H$, 84%), 129 (M^+ − $2CO_2H$, 100%), 128 (M^+ − $2CO_2H$, 54%), 127 (M^+ − $2CO_2H$, 25%), 116 (M^+ − $2CO_2H$ − CH_2, 29%), 115 (M^+ − CO_2H − CH_3, 97%), 91 (C_7H_7, 22%).

*Acide éthyl-1 indanedicarboxylique-2,2 (**53**)* : Rdt, 79% (0,515 g). Cristaux blancs; F = 169°C (décarboxylation); ir ν_{max} (KBr) : 3500–2300, 1710, 1475, 1465, 1450, 1310, 1285, 1260, 1250, 750 cm^{-1}; rmn ^1H ($CDCl_3$ et DMSO) δ : 0,98 (3H, t), 1,50 (1H, m), 1,75 (1H, m), 3,56 (2H, 2d, AB, J = 16,51 Hz, Δν = 74,05 Hz, CH_2-3), 3,77 (1H, m), 7,14 (4H, s), 8,38 (2H, s, 2COOH) ppm; rmn ^{13}C ($CDCl_3$ et DMSO) δ : 173,83, 172,06, 144,32, 139,48, 126,42, 125,90, 124,53, 124,00, 65,23, 51,13, 38,71, 23,76, 11,68 ppm; sm *m/e* : 235 (M^+ + 1, 1%), 234 (M^+, 4%), 190 (M^+ − CO_2, 4%), 189 (M^+ − CO_2H, 12%), 188 (M^+ − CO_2H, 46%), 161 (M^+ − CO_2H − C_2H_4, 20%), 144 (M^+ − $2CO_2H$, 13%), 143 (M^+ − $2CO_2H$, 65%), 129 (M^+ − $2CO_2H$ − CH_3, 40%), 128 (M^+ − $2CO_2H$ − CH_3, 32%), 117 (M^+ − $2CO_2H$ − C_2H_3, 20%), 116 (M^+ − $2CO_2$ − C_2H_4, 25%), 115 (M^+ − $2CO_2H$ − C_2H_5, 100%), 91 (C_7H_7, 13%).

*Acide propyl-1 indanedicarboxylique-2,2 (**54**)* : Rdt, 59% (0,537 g). Cristaux blancs; F = 170°C (décarboxylation); ir ν_{max} (KBr) : 3500–2400, 2970, 2940, 2920, 2870, 1750, 1700, 1600, 1490, 1465, 1415, 1300, 1280, 1240, 1190, 740 cm^{-1}; rmn ^1H ($CDCl_3$ et DMSO) δ : 0,90 (3H, t), 1,25–1,69 (4H, m), 3,56 (2H, 2d, AB, J = 16,51 Hz, Δν = 70,79 Hz, CH_2-3), 3,84 (1H, m), 7,15 (4H, s) ppm; rmn ^{13}C ($CDCl_3$ et DMSO) δ : 174,66, 172,72, 144,50, 139,43, 126,62, 126,13, 124,51, 124,15, 65,29, 49,86, 38,82, 33,03, 20,37, 14,19 ppm; sm *m/e* : 248 (M^+, 4%), 204 (M^+ − CO_2, 32%), 202 (M^+ − CO_2H, 30%), 174 (M^+ − CO_2H − C_2H_5, 22%), 161 (M^+ − CO_2H − C_3H_6, 20%), 143 (M^+ − $2CO_2H$ − CH_3, 25%), 129 (M^+ − $2CO_2H$ − C_2H_5, 36%), 128 (M^+ − $2CO_2H$ − C_2H_6, 43%), 117 (M^+ − $2CO_2H$ − C_3H_5, 34%), 116 (M^+ − $2CO_2H$ − C_3H_6, 23%), 115 (M^+ − $2CO_2H$ − C_3H_7, 100%). Masse précise pour $C_{14}H_{16}O_4$: 248, 1049; tr. : 248,1096.

*Acide phényl-1 indanedicarboxylique-2,2 (**55**)* : Rdt, 73% (0,315 g). Cristaux blancs; F = 169°C (décarboxylation); ir ν_{max} (KBr) : 3500–2400, 1700, 1475, 1450, 1310, 1280, 1260, 750 cm^{-1}; rmn ^1H ($CO(CD_3)_2$) δ : 3,74 (2H, 2d, AB, J = 16,85 Hz, Δν = 111,18 Hz, CH_2-3), 5,27 (1H, s, H-1), 6,98–7,40 (9H, massif) ppm; rmn ^{13}C ($CO(CD_3)_2$) δ : 174,12, 171,84, 151,08, 150,54, 139,71 (2C), 138,27 (2C), 137,64, 137,51, 137,38, 137,24, 135,31, 134,63, 66,97, 50,07, 38,82 ppm. Masse précise pour $C_{17}H_{14}O_4$: 282,0892; tr. : 282,0907.

*Acide isopropyl-1 indanedicarboxylique-2,2 (**56**)* : Rdt, 75% (0,438 g). Cristaux blancs; F = 170°C (décarboxylation); ir ν_{max} (KBr) : 3500–

Can. J. Chem. Downloaded from www.nrcresearchpress.com by 41.223.56.140 on 09/07/12
For personal use only.

2400, 2940, 2920, 2870, 1700, 1600, 1455, 1380, 1370, 1310, 1280, 1260, 1250, 750 cm^{-1}; rmn ^1H ($CDCl_3$ et DMSO) δ : 0,57 (3H, d), 1,14 (3H, d), 2,21 (1H, m), 3,60 (2H, 2d, AB, J = 16,82 Hz, $\Delta\nu$ = 100,17 Hz, CH_2-3), 3,94 (1H, d), 7,16 (4H, s), 8,88 (2H, s, 2COOH) ppm; rmn ^{13}C ($CDCl_3$ et DMSO) δ : 173,82, 171,68, 142,23, 141,05, 127,28, 126,52, 125,90, 124,46, 65,92, 55,61, 40,46, 30,05, 22,96, 17,08 ppm; sm *m/e* : 249 (M^+ + 1, 1%), 248 (M^+, 10%), 204 ($M^+ - CO_2$, 15%), 202 ($M^+ - CO_2H$, 29%), 162 ($M^+ - CO_2H - C_3H_5$, 14%), 161 ($M^+ - CO_2H - C_3H_6$, 77%), 160 ($M^+ - CO_2H - C_3H_7$, 29%), 143 ($M^+ - 2CO_2H - CH_3$, 36%), 128 ($M^+ - 2CO_2H - C_2H_6$, 19%), 117 ($M^+ - 2CO_2H - C_3H_5$, 41%), 116 ($M^+ - 2CO_2H - C_3H_6$, 40%), 115 ($M^+ - 2CO_2H - C_3H_7$, 100%). Masse précise pour $C_{14}H_{16}O_4$: 248,1049; tr. : 248,1062.

*Mode opératoire général de préparation des diastéréoisomères des acides alkyl-2 cyclopentanecarboxyliques-1 et alkyl-1 indanecarboxyliques-2 (**57**–**63**)*

Les acides alkyl-2 cycloalcanecarboxyliques-1 et alkyl-1 indanecarboxyliques-2 sont obtenus par simple décarboxylation thermique à partir des diacides correspondants. Ainsi, dans un montage de microdistillation, on porte 2–5 mmol de diacides à 170–180°C jusqu'à cessation du dégagement de dioxyde de carbone. Afin de s'assurer d'un meilleur rendement, on fait un léger vide pour compléter la réaction. L'acide est estérifié sans purification préalable.

*Acide méthyl-2 cyclopentanecarboxylique-1 (**57**a,b)*

La spectroscopie de rmn ^1H nous révèle que l'isomère *trans* (**57***b*) est majeur (55%); Rdt, 86% (0,158 g). Liquide; Eb (**57***b*) : (litt. (7*a*) Eb (8 Torr) 111°C); Eb (**57***a*) : (litt. (7*a*) Eb (23 Torr) 122–123°C); ir ν_{max} (film, mélange) : 3500–2500, 2960, 2930, 2875, 1705, 1460, 1450, 1420, 1250, 1240 cm^{-1}; rmn ^1H ($CDCl_3$, mélange) δ : 0,99 et 1,10 (3H, 2d, J = 6,96 Hz, CH_3 *cis* et *trans* COOH), 1,20–1,32 (7H, m), 2,40 et 2,80 (1H, 2m, H-1 *trans* et *cis* COOH), 11,78 (1H, COOH) ppm; rmn ^{13}C ($CDCl_3$, mélange) δ (**57***b*) : 183,12, 51,81, 39,47, 34,91, 30,01, 24,56, 19,59 ppm; δ (**57***a*) : 181,96, 48,37, 37,42, 33,71, 27,34, 23,72, 16,12 ppm.

*Acide éthyl-2 cyclopentanecarboxylique-1 (**58**a,b)*

La spectroscopie de rmn ^1H révèle que l'isomère *trans* (**58***b*) est majeur (59%); Rdt, 89% (0,225 g). Liquide; Eb (mélange) : (litt. (7*a*) Eb (11 Torr) 125°C); ir ν_{max} (film, mélange) : 3500–2500, 2960, 2930, 2875, 1705, 1460, 1450, 1420, 1380, 1290, 1250, 1230 cm^{-1}; rmn ^1H ($CDCl_3$, mélange) δ : 0,90 et 0,96 (3H, 2t, J = 7,33 Hz, CH_3 *trans* et *cis* COOH), 1,21–2,12 (9H, m), 2,36 et 2,84 (1H, 2m, H-1 *cis* et *trans* COOH), 12,08 (1H, s, COOH) ppm; rmn ^{13}C ($CDCl_3$, mélange) δ (**58***b*) : 183,65, 50,00, 46,20, 32,22, 30,36, 28,05, 24,94, 12,52 ppm; δ (**58***a*) : 182,45, 47,64, 45,73, 30,58, 28,30, 23,94, 23,76, 13,08 ppm.

*Acide propyl-2 cyclopentanecarboxylique-1 (**59**a,b)*

L'analyse de rmn ^1H révèle que l'isomère *trans* (**59***b*) est majeur (51%); Rdt, 99% (0,209 g). Huile; ir ν_{max} (film, mélange) : 3500–2500, 2960, 2940, 2875, 1705, 1470, 1450, 1420, 1290, 1240, 1220 cm^{-1}; rmn ^1H ($CDCl_3$, mélange) δ : 0,90 (3H, t), 1,16–2,11 (11H, m), 2,35 et 2,86 (1H, 2q, H-1, *trans* et *cis* COOH), 12,15 (1H, s, COOH) ppm; rmn ^{13}C ($CDCl_3$, mélange) δ (**59***b*) : 183,65, 50,37, 44,33, 37,69, 32,65, 30,32, 24,92, 21,44, 14,24 ppm; δ (**59***a*) : 182,49, 47,75, 43,58, 33,18, 30,89, 28,32, 23,79, 21,77, 14,24 ppm. Masse précise pour $C_9H_{16}O_2$: 156,1151; tr. : 156,1162.

*Acide butyl-2 cyclopentanecarboxylique-1 (**60**a,b)*

L'examen des spectres de rmn ^1H révèle que l'isomère *trans* (**60***b*) est majeur (55%); Rdt, 62% (0,142 g). Liquide; ir ν_{max} (film, mélange) : 3500–2500, 2960, 2930, 2875, 1705, 1460, 1450, 1420, 1250, 1230 cm^{-1}; rmn ^1H ($CDCl_3$, mélange) δ : 0,89 (3H, t), 1,12–2,12 (13H, m), 2,36 et 2,86 (1H, 2q, H-1, *trans* et *cis* COOH), 12,11 (1H, s, COOH) ppm; rmn ^{13}C ($CDCl_3$, mélange) δ (**60***b*) : 183,58, 50,37, 44,49, 35,09, 30,96, 30,88, 30,22, 24,92, 22,86, 14,06 ppm; δ (**60***a*) : 182,43, 47,75, 43,82, 32,67, 30,63, 30,43, 28,32, 23,79, 22,86, 14,06 ppm. Masse précise pour $C_{10}H_{18}O_2$: 170,1307; tr. : 170,1322.

*Acide méthyl-1 indanecarboxylique-2 (**61**a,b)*

En calculant le pourcentage des diastéréoisomères selon l'intégration des signaux du méthyle, on constate que l'isomère *trans* (**61***b*) est majeur (68%); Rdt, 83% (0,244 g). Huile; ir ν_{max} (film, mélange) : 3500–2500, 2935, 1700, 1450, 1250, 1230, 750 cm^{-1}; rmn ^1H ($CDCl_3$, mélange) δ : 1,22 et 1,40 (3H, 2d, J = 6,59 Hz, CH_3 *cis* et *trans* COOH), 2,78–3,09 (1H, m, H-2), 3,17–3,40 (2H, m, H-3), 3,44–3,49 (1H, m, H-1), 7,16 (4H, s), 9,12 (1H, COOH) ppm; rmn ^{13}C ($CDCl_3$, mélange) δ (**61***b*) : 178,57, 145,96, 140,70, 126,40 (2C), 123,91, 122,80, 52,46, 43,00, 35,05, 18,96 ppm; δ (**61***a*) : 177,26, 145,90, 140,48, 126,51 (2C), 124,20, 123,24, 48,35, 41,48, 32,87, 16,83 ppm. Masse précise pour $C_{11}H_{12}O_2$: 176,0838; tr. : 176,0857.

*Acide propyl-1 indanecarboxylique-2 (**62**a,b)*

La spectroscopie de rmn ^{13}C révèle que l'isomère *trans* (**62***b*) est majeur (68%); Rdt, 77% (0,052 g). Huile; ir ν_{max} (mélange) : 3400–2800, 3020, 2960, 2930, 1700, 1250, 750 cm^{-1}; rmn ^1H ($CDCl_3$, mélange) δ : 0,87 (3H, t), 1,20–2,65 (3H, m), 2,75 (1H, m), 2,92 (1H, m, H-2), 3,12–3,24 (2H, m, H-3), 3,25–3,58 (1H, m, H-1), 7,07 (4H, s), 12,13 (1H, COOH) ppm; rmn ^{13}C ($CDCl_3$, mélange) δ (**62***b*) : 182,45, 145,05, 140,76, 126,70 (2C), 124,48, 123,59, 49,50, 48,41, 35,51, 37,05, 20,08, 14,32 ppm; δ (**62***a*) : 180,32, 144,98, 141,03, 126,75 (2C), 126,02, 124,15, 49,10, 46,70, 33,25, 32,62, 20,28, 14,17 ppm. Masse précise pour $C_{13}H_{16}O_2$: 204,1151; tr. : 204,1158.

*Acide phényl-1 indanecarboxylique-2 (**63**a,b)*

La spectroscopie de rmn ^{13}C révèle que l'isomère *trans* (**63***b*) est majeur (63%); Rdt, 77% (0,0085 g). Huile; ir ν_{max} (mélange) : 3400–2400, 1700, 1475, 1250, 750 cm^{-1}; rmn ^1H ($CDCl_3$, mélange) δ : 3,05–3,38 (2H, m, H-3), 3,39–3,48 (1H, m, H-2), 4,74 (1H, m, H-1), 6,88–7,37 (9H, m) ppm; rmn ^{13}C ($CDCl_3$, mélange) δ (**63***b*) : 180,05, 144,65, 142,98, 140,96, 128,52, 127,37 (2C), 127,10 (2C), 126,90 (2C), 124,93, 124,09, 54,48, 53,83 ppm; δ (**63***a*) : 177,92, 144,60, 142,00, 140,05, 128,46, 128,33 (2C), 128,08 (2C), 126,95 (2C), 125,10, 124,48, 53,83, 50,19 ppm. Masse précise pour $C_{15}H_{15}O_2$: 238,0994; tr. : 238,1002.

*Mode opératiore général de préparation des diastéréoisomères des alkyl-2 cyclopentanecarboxylates-1 de méthyle et alkyl-1 indanecarboxylates-2 de méthyle (**64**–**69**)*

À une solution de 3 mmol d'acide alkyl-2 cyclopentanecarboxylique-1 ou alkyl-1 indanecarboxylique-2 dans 3 mL d'éther, à 0°C, est additionnée une solution éthérée de diazométhane à 70%. Après 1 h d'agitation à 0°C, le solvant est évaporé, et le produit est purifié par une filtration sur gel de silice.

*Méthyl-2 cyclopentanecarboxylate-1 de méthyle (**64**a,b)*

La spectroscopie de rmn ^1H nous révèle que l'isomère *trans* (**64***b*) est majeur (56%); Rdt, 85% (0,589 g). Huile; ir ν_{max} (film, mélange) : 2960, 1730, 1450, 1370, 1265, 1160, 1095 cm^{-1}; rmn ^1H ($CDCl_3$, mélange) δ : 0,89 et 1,05 (3H, 2d, J = 6,99 Hz et 6,35 Hz, CH_3 *cis* et *trans* CO_2CH_3); rmn ^{13}C ($CDCl_3$, mélange) δ (**64***b*) : 175,81, 51,35, 50,79, 38,96, 34,40, 29,61, 24,07, 19,10 ppm; δ (**64***a*) : 174,70, 50,39, 47,77, 37,05, 33,33, 27,12, 23,43, 15,75 ppm. *Anal.* calc. pour $C_8H_{14}O_2$: C 67,57, H 9,92; tr. : C 67,43, H 9,85.

*Ethyl-2 cyclopentanecarboxylate-1 de méthyle (**65**a,b)*

L'intégration des signaux des deux singulets du groupement ester méthylique en rmn ^1H nous indique que l'isomère *trans* (**65***b*) est majeur (57%); Rdt, 84% (0,165 g). Huile; ir ν_{max} (film, mélange) : 2955, 2920, 2860, 1730, 1460, 1430, 1375, 1255, 1165, 1150 cm^{-1}; rmn ^1H ($CDCl_3$, mélange) δ : 0,90 (3H, d de t), 1,09–2,14 (9H, m), 2,33 et 2,84 (1H, 2q, H-1, *trans* et *cis* CO_2Me), 3,65 et 3,67 (3H, 2s, CO_2CH_3, *cis* et *trans*) ppm; rmn ^{13}C ($CDCl_3$, mélange) δ (**65***b*) : 177,10, 51,46, 49,99, 46,17, 32,11, 30,41, 27,98, 24,74, 13,04 ppm; δ (**65***a*) : 175,83, 50,97, 47,46, 45,60, 30,67, 28,34, 24,07, 23,83, 12,52 ppm. *Anal.* calc. pour $C_9H_{16}O_2$: C 69,19, H 10,32; tr. : C 69,29, H 10,54.

*Propyl-2 cyclopentanecarboxylate-1 de méthyle (**66**a,b)*

La spectroscopie de rmn ^1H nous révèle, d'après l'intégration des signaux des esters méthyliques, que l'isomère *trans* (**66***b*) est majeur (53%); Rdt, 75% (0,146 g). Huile; ir ν_{max} (film, mélange) : 2955, 2920, 2855, 1730, 1460, 1430, 1375, 1255, 1170 cm^{-1}; rmn ^1H

Can. J. Chem. Downloaded from www.nrcresearchpress.com by 41.223.56.140 on 09/07/12
For personal use only.

($CDCl_3$, mélange) δ : 0,89 (3H, t), 1,07–2,17 (11H, m), 2,32 et 2,84 (1H, 2m, H-1, *trans* et *cis* CO_2Me), 3,65 et 3,67 (3H, 2s, CO_2CH_3, *cis* et *trans*) ppm; rmn ^{13}C ($CDCl_3$, mélange) δ (**66***b*) : 177,03, 51,89, 50,30, 44,24, 37,60, 32,51, 30,34, 24,74, 21,34, 14,23 ppm; δ (**66***a*) : 175,80, 50,93, 47,51, 43,48, 33,34, 30,96, 28,32, 23,85, 21,67, 14,23 ppm. *Anal.* calc. pour $C_{10}H_{18}O_2$: C 70,55, H 10,66; tr. : C 70,47, H 10,62.

*Butyl-2 cyclopentanecarboxylate-1 de méthyle (**67**a,b)*

La spectroscopie de rmn ^1H nous révèle que l'isomère *trans* (**67***b*) est majeur (56%); Rdt, 83% (0,131 g). Huile; ir ν_{max} (film, mélange) : 2940, 2920, 2855, 1730, 1465, 1450, 1375, 1255, 1185, 1150 cm^{-1}; rmn ^1H ($CDCl_3$, mélange) δ : 0,88 (3H, t), 1,27 (6H, massif), 1,40–2,18 (7H, m), 2,32 et 2,85 (1H, 2m, H-1, *trans* et *cis* CO_2Me), 3,65 et 3,67 (3H, 2s, CO_2CH_3, *cis* et *trans*) ppm; rmn ^{13}C ($CDCl_3$, mélange) δ (**67***b*) : 176,57, 51,35, 50,30, 44,40, 34,98, 31,02, 30,78, 30,38, 24,72, 22,79, 13,99 ppm; δ (**67***a*) : 175,76, 50,86, 47,50, 43,73, 32,53, 30,78, 30,31, 28,34, 23,81, 22,79, 13,99 ppm; sm *m/e* : 185 (M^+ + 1, 1%), 184 (M^+, 8%), 153 (M^+ − OCH_3, 19%), 152 (M^+ − OCH_3, 27%), 143 ($C_8H_{15}O_2$, 26%), 127 (M^+ − C_4H_9, 100%), 95 (C_7H_{11}, 15%), 87 ($C_4H_7O_2$, 56%), 67 (C_5H_7, 22%), 59 (CO_2CH_3, 14%), 55 (C_4H_7, 24%). *Anal.* calc. pour $C_{11}H_{20}O_2$: C 71,69, H 10,94; tr. : C 71,53, H 10,90.

*Méthyl-1 indanecarboxylate-2 de méthyle (**68**a,b)*

L'intégration des signaux des deux singulets du groupement ester méthylique nous indique que l'isomère *trans* (**68***b*) est majeur (69%); Rdt, 93% (0,247 g). Huile; ir ν_{max} (film, mélange) : 3075, 3030, 2960, 2930, 2870, 1735, 1470, 1450, 1375, 1250, 1225, 1215, 1190, 1165, 1020, 1000, 750 cm^{-1}; rmn ^1H ($CDCl_3$, mélange) δ : 1,10 et 1,39 (3H, 2d, J = 6,98 Hz, CH_3, *cis* et *trans* CO_2CH_3), 2,76–3,09 (1H, m, H-2), 3,14–3,44 (2H, m, H-3), 3,46–3,61 (1H, m, H-1), 3,69 et 3,72 (3H, 2s, CO_2CH_3, *cis* et *trans*), 7,07 (4H, s) ppm; rmn ^{13}C ($CDCl_3$, mélange) δ (**68***b*) : 175,02, 145,70, 140,50, 126,33 (2C), 123,82, 122,71, 52,33, 48,10, 42,93, 35,02, 18,77 ppm; δ (**68***a*) : 173,61, 145,21, 140,50, 126,42 (2C), 124,08, 123,11, 51,48, 48,10, 41,57, 32,83, 16,81 ppm; sm *m/e* : 190 (M^+, 3%), 175 (M^+ − CH_3, 11%), 131 (M^+ − CO_2CH_3, 26%), 129 (M^+ − CO_2CH_3, 29%), 116 (M^+ − CO_2CH_3 − CH_3, 12%), 115 (M^+ − CO_2CH_3 − CH_3, 23%), 91 (C_7H_7, 24%), 77 (C_6H_5, 11%), 66 (C_5H_6, 100%), 65 (C_5H_5, 21%). *Anal.* calc. pour $C_{12}H_{14}O_2$: C 75,76, H 7,42; tr. : C 75,47, H 7,75.

*Propyl-1 indanecarboxylate-2 de méthyle (**69**a,b)*

L'intégration des signaux des deux singulets du groupe méthoxycarbonyle nous indique que l'isomère *trans* (**69***b*) est majeur (61%); Rdt, 91% (0,053 g). Huile; ir ν_{max} (film, mélange) : 3080, 3030, 2960, 2880, 1735, 1480, 1460, 1435, 1365, 1225, 1190, 1165, 750 cm^{-1}; rmn ^1H ($CDCl_3$, mélange) δ : 0,86 (3H, t), 1,09–1,58 (3H, m), 1,75 (1H, m), 2,81–2,93 (1H, m, H-2), 3,08–3,34 (2H, m, H-3), 3,37–3,50 (1H, m, H-1), 3,61 et 3,63 (3H, 2s, CO_2CH_3, *trans* et *cis*), 7,70 (4H, s) ppm; rmn ^{13}C ($CDCl_3$, mélange) δ (**69***b*) : 175,86, 145,14, 140,90, 126,51 (2C), 124,42, 123,42, 51,72, 49,66, 48,31, 36,89, 35,71, 19,99, 14,28 ppm; δ (**69***a*) : 273,74, 145,09, 141,19, 126,61 (2C), 125,90, 124,02, 51,39, 48,93, 46,75, 33,62, 32,89, 20,23, 14,15 ppm; sm *m/e* : 219 (M^+ + 1, 2%), 218 (M^+, 9%), 159 (M^+ − CO_2CH_3, 16%), 158 (M^+ − CO_2CH_3, 32%), 157 (M^+ − CO_2CH_3, 12%), 131 (M^+ − CO_2CH_3 − C_2H_4, 36%), 130 (M^+ − CO_2CH_3 − C_2H_5, 28%), 129 (M^+ − CO_2CH_3 − C_2H_5, 47%), 117 (M^+ − CO_2CH_3 − C_3H_6, 30%), 116 (M^+ − CO_2CH_3, C_3H_7, 41%), 115 (M^+ − CO_2CH_3 − C_3H_7, 100%), 91 (C_7H_7, 37%), 89 (C_7H_5, 19%), 77 (C_6H_5, 47%), 65 (C_5H_5, 25%). *Anal.* calc. pour $C_{14}H_{18}O_2$: C 77,03, H 8,31; tr. : C 77,38, H 8,32.

*Mode opératoire général de préparation des diastéréoisomères des alkyl-2 phényl-1 cycloalcanecarbonitriles-1 (**70–78**)*

En suivant le même mode opératoire que celui des composés **35–46**, la réaction est complète après une agitation de 8 h à la température ambiante. Le produit est purifié par filtration sur gel de silice en utilisant un mélange acétate d'éthyle et éther de pétrole. Le pourcentage des diastéréoisomères est déterminé par chromatographie en phase gazeuse à l'aide d'une colonne Dexsil 300 et par spectroscopie de résonance magnétique nucléaire du proton.

*Méthyl-2 phényl-1 cyclopentanecarbonitrile-1 (**70**a,b)*

L'isomère *trans* (**70***b*) est majeur (82%); Rdt, 97% (1,792 g). Liquide incolore; Eb (0,05 Torr, mélange) = 82–83°C (litt. (14) Eb (2 Torr) 125–127°C); ir ν_{max} (film, mélange) : 3050, 3020, 2960, 2920, 2865, 2220, 1595, 1490, 1455, 1375, 750, 725, 690 cm^{-1}; rmn ^1H ($CDCl_3$, mélange) δ : 0,62 et 1,03 (3H, 2d, J = 6,35 Hz et 6,98 Hz, CH_3 *cis* et *trans* nitrile), 1,42 (1H, m), 2,01 (3H, m), 2,40 (2H, t), 2,59 (1H, q), 7,33 (5H, s) ppm; rmn ^{13}C ($CDCl_3$, mélange) δ (**70***b*) : 136,42, 128,07, 127,34 (2C), 126,96 (2C), 50,04, 45,35, 35,18, 31,37, 22,03, 15,26 ppm; δ (**70***a*) : 138,05, 128,44, 127,25 (2C), 125,53 (2C), 50,04, 46,28, 40,08, 31,90, 21,64, 14,43 ppm; sm *m/e*: 186 (M^+ + 1, 4%), 185 (M^+, 27%), 130 (C_9H_8N, 27%), 129 (C_9H_7N, 100%), 115 (C_8H_5N, 13%), 103 (C_7H_5N, 12%).

*Ethyl-2 phényl-1 cyclopentanecarbonitrile-1 (**71**a,b)*

L'isomère *trans* (**71***b*) est majeur (85%); Rdt, 78% (0,471 g). Liquide incolore; Eb (0,04 Torr, mélange) = 93°C; ir ν_{max} (film, mélange) : 3050, 3020, 2950, 2920, 2865, 2220, 1595, 1445, 1375, 1020, 750, 690 cm^{-1}; rmn ^1H ($CDCl_3$, mélange) δ : 0,65 (1H, m), 0,82 et 1,04 (3H, 2t, J = 7,30 Hz, CH_2CH_3, *cis* et *trans* CN), 1,25 (1H, m), 1,43 (1H, m), 1,60–2,28 (4H, m), 2,43 (2H, m), 7,34 (4H, s) ppm; rmn ^{13}C ($CDCl_3$, mélange) δ (**71***b*) : 137,08, 128,20, 127,44 (2C), 127,11 (2C), 53,28, 50,04, 37,18, 29,16, 23,32, 22,77, 12,57 ppm; δ (**71***a*) : 138,81, 128,60, 127,44 (2C), 125,77 (2C), 53,59, 50,04, 41,84, 29,85, 23,85, 22,08, 12,81 ppm. Masse précise pour $C_{14}H_{17}N$: 199,1362; tr. : 199,1360.

*Propyl-2 phényl-1 cyclopentanecarbonitrile-1 (**72**a,b)*

L'isomère *trans* (**72***b*) est majeur (93%); Rdt, 86% (0,898 g).

Propyl-2 phényl-1 cyclopentanecarbonitrile-1 r trans *(**72**b)*

Ce produit fut isolé par chromatographie sur gel de silice en utilisant AE:EP (5:95) comme éluant. Liquide incolore; Eb (0,032 Torr) = 101°C; ir ν_{max} (film) : 3050, 3020, 2950, 2920, 2870, 2220, 1595, 1460, 1375, 750, 690 cm^{-1}; rmn ^1H ($CDCl_3$) δ : 0,65 (1H, m), 0,76 (3H, t), 1,00–1,60 (3H, m), 2,00 (4H, m), 2,43 (3H, m), 7,33 (4H, s) ppm; rmn ^{13}C ($CDCl_3$) δ : 137,12, 128,19 (2C), 127,42, 127,13 (2C), 51,21, 50,00, 37,20, 32,32, 29,50, 22,79, 21,16, 14,02 ppm. Masse précise pour $C_{15}H_{19}N$: 213,1518; tr. : 213,1512.

*Butyl-2 phényl-1 cyclopentanecarbonitrile-1 (**73**a,b)*

L'isomère *trans* (**73***b*) est majeur (89%); Rdt, 83% (0,375 g). Liquide incolore; Eb (0,04 Torr, mélange) = 113°C; ir ν_{max} (film, mélange) : 3070, 3040, 2960, 2940, 2880, 2220, 1660, 1500, 1470, 1450, 1380, 1265, 760, 740, 700 cm^{-1}; rmn ^1H ($CDCl_3$, mélange) δ : 0,62 (1H, m), 0,71 (3H, t), 0,98–1,48 (6H, m), 1,85–2,05 (4H, m), 2,35 (2H, m), 7,27 (4H, s) ppm; rmn ^{13}C ($CDCl_3$, mélange) δ (**73***b*) : 137,20, 128,26 (2C), 127,51, 127,21 (2C), 51,39, 49,98, 37,17, 30,11, 29,78, 29,53, 22,74, 22,56, 13,81 ppm; δ (**73***a*) : 137,22, 128,67 (2C), 127,51, 125,54 (2C), 51,68, 49,98, 41,74, 32,87, 30,50, 30,40, 22,05, 21,99, 13,81 ppm; sm *m/e*: 228 (M^+ + 1, 1%), 227 (M^+, 2%), 129 (C_9H_7N, 13%), 121 ($C_8H_{11}N$, 27%), 119 (C_8H_9N, 88%), 117 (C_8H_7N, 100%), 84 (C_6H_{12}, 26%), 82 (C_6H_{10}, 38%). Masse précise pour $C_{16}H_{21}N$: 227,1675; tr. : 227,1660.

*Diphényl-1,2 cyclopentanecarbonitrile-1 (**74**a,b)*

L'isomère *trans* (**74***b*) est majeur (92%); Rdt, 91% (0,654 g). Cristaux blancs; F (mélange) = 51–56°C; ir ν_{max} (KBr, mélange) : 3200, 3090, 3070, 3040, 2960, 2880, 2240, 1600, 1495, 1450, 1260, 1195, 695 cm^{-1}; rmn ^1H ($CDCl_3$, mélange) δ : 2,00–2,75 (6H, m), 3,42 (1H, 2d, AB, J = 7,30 Hz, Δν = 8,06 Hz, H-2), 7,11 (2H, m), 7,24 (3H, m), 7,36 (5H, large s) ppm; rmn ^{13}C ($CDCl_3$, mélange) δ (**74***b*) : 137,71, 137,20 (2C), 128,54, 128,10 (2C),, 127,91, 127,62 (2C), 127,33, 126,05 (2C), 57,72, 55,37, 36,83, 28,50, 22,34 ppm; δ (**74***a*) : 137,71, 137,20 (2C), 128,54, 128,10 (2C), 127,91, 127,62 (2C), 127,33, 126,05 (2C), 58,00, 55,37, 41,03, 30,23, 22,12 ppm; sm *m/e*: 248 (M^+ + 1, 7%), 247 (M^+, 28%), 156 (M^+ − C_7H_7, 21%), 131 (C_9H_9N, 25%), 130 (C_9H_8N, 20%), 129 (C_9H_7N, 23%), 118 (C_8H_8N, 50%), 117 (C_8H_7N, 100%), 115 (C_8H_5N, 44%), 103 (C_7H_5N, 33%), 91 (C_7H_7, 48%), 77 (C_6H_5, 20%). Masse précise pour $C_{18}H_{17}N$: 247,1362; tr. : 247,1327.

Can. J. Chem. Downloaded from www.nrcresearchpress.com by 41.223.56.140 on 09/07/12
For personal use only.

*Méthyl-2 phényl-1 cyclohexanecarbonitrile-1 (75*a,b*)*

L'isomère *trans* (**75***b*) est majeur (84%); Rdt, 88% (1,742 g). Liquide incolore; Eb (105 Torr, mélange) = 105°C; ir ν_{max} (film, mélange): 3060, 3020, 2930, 2860, 2260, 2220, 1605, 1500, 1465, 1450, 1375, 920, 760, 740, 700 cm^{-1}; rmn ^1H ($CDCl_3$, mélange) δ: 0,62 et 0,79 (3H, 2d, J = 6,67 et 6,98 Hz, CH_3, *trans* et *cis*), 1,20–2,50 (9H, m), 7,33 (3H, m), 7,46 (2H, m) ppm; rmn ^{13}C ($CDCl_3$, mélange) δ (**75***b*): 140,61, 129,26 (2C), 128,07, 126,31 (2C), 51,87, 40,58, 39,86, 32,48, 26,12, 24,14, 18,25 ppm; δ (**75***a*): 140,61, 129,16 (2C), 128,07, 126,79 (2C), 51,87, 40,58, 38,86, 30,42, 27,26, 23,71, 13,55 ppm; sm *m/e*: 200 (M^+ + 1, 4%), 199 (M^+, 18%), 145 ($C_{10}H_{11}N$, 27%), 144 ($C_{10}H_{10}N$, 21%), 130 (C_9H_8N, 23%), 129 (C_9H_7,N, 100%), 115 (C_8H_5N, 19%). Masse précise pour $C_{14}H_{17}N$: 199,1362; tr.: 199,1357.

*Ethyl-2 phényl-1 cyclohexanecarbonitrile-1 (76*a,b*)*

L'isomère *trans* (**68***b*) est majeur (89%); Rdt, 83% (0,355 g).

Ethyl-2 phényl-1 cyclohexanecarbonitrile-1 r trans *(76)*: Ce produit fut isolé par chromatographie sur gel de silice en utilisant comme éluant AE:EP (3:97). Liquide incolore; ir ν_{max} (film): 3085, 3065, 3030, 2960, 2940, 2870, 2860, 2240, 1600, 1495, 1465, 1450, 1375, 750, 700 cm^{-1}; rmn ^1H ($CDCl_3$) δ: 0,68 (3H, t), 1,09 (2H, m), 1,31 (2H, m), 1,50–1,90 (5H, m), 1,95 (2H, m), 7,28 (3H, m), 7,40 (2H, m) ppm; rmn ^{13}C ($CDCl_3$) δ: 140,05, 128,72 (2C), 127,46, 125,77 (2C), 50,01, 46,44, 39,95, 27,97, 25,45, 24,36, 23,65, 11,47 ppm; sm *m/e*: 214 (M^+ + 1, 3%), 213 (M^+, 20%), 145 ($C_{10}H_{11}N$, 30%), 144 ($C_{10}H_{10}N$, 15%), 130 (C_9H_8N, 29%), 129 (C_9H_7N, 100%), 128 (C_9H_8N, 16%), 116 (C_8H_9N, 12%), 115 (C_8H_5N, 25%), 103 (C_8H_7, 19%), 102 (C_8H_6, 12%), 91 (C_7H_7, 11%), 77 (C_6H_5, 12%), 55 (C_4H_7, 13%). Masse précise pour $C_{15}H_{19}N$: 213,1518; tr.: 213,1509.

*Propyl-2 phényl-1 cyclohexanecarbonitrile-1 (77*a,b*)*

L'isomère *trans* (**69***b*) est majeur (87%); Rdt, 70% (0,317 g). Seul l'isomère *trans* fut isolé du mélange des diastéréoisomères par chromatographie sur gel de silice en utilisant AE:EP (5:95) comme éluant.

Propyl-2 phényl-1 cyclohexanecarbonitrile-1 r trans *(77b)*: Liquide incolore; ir ν_{max} (film): 3070, 3035, 2970, 2940, 2870, 2240, 1690, 1600, 1500, 1465, 1450, 1375, 760, 700 cm^{-1}; rmn ^1H ($CDCl_3$) δ: 0,71 (3H, t), 0,83–1,28 (6H, m), 1,31–1,61 (2H, m), 1,69–1,96 (5H, m), 1,96–2,20 (2H, m), 7,40 (5H, m) ppm; rmn ^{13}C ($CDCl_3$) δ: 140,05, 128,53 (2C), 127,30, 125,62 (2C), 50,97, 44,17, 40,02, 33,64, 28,60, 25,47, 23,65, 19,79, 13,79 ppm; sm *m/e*: 228 (M^+ + 1, 8%), 227 (M^+, 48%), 198 ($M^+ - C_2H_5$, 17%), 170 ($M^+ - C_4H_9$, 10%), 145 ($C_{10}H_{11}N$, 50%), 144 ($C_{10}H_{10}N$, 19%), 130 (C_9H_8N, 24%), 129 (C_9H_7N, 100%), 116 (C_8H_6N, 13%), 115 (C_8H_5N, 20%), 103 (C_8H_7, 12%), 77 (C_6H_5, 10%). Masse précise pour $C_{16}H_{21}N$: 227,1675; tr.: 227,1662.

*Butyl-2 phényl-1 cyclohexanecarbonitrile-1 (78*a,b*)*

L'isomère *trans* (**78***b*) est majeur (72%); Rdt, 78% (0,622 g). Huile visqueuse; ir ν_{max} (film, mélange): 3090, 3065, 3030, 2965, 2930, 2860, 2235, 1600, 1500, 1470, 1450, 1375, 755, 700 cm^{-1}; rmn ^1H ($CDCl_3$, mélange) δ: 0,73 (3H, t), 0,87–1,68 (8H, m), 1,68–2,00 (5H, m), 2,00–2,20 (2H, m), 7,34 (3H, m), 7,48 (2H, m) ppm; rmn ^{13}C ($CDCl_3$, **78***b*) δ: 139,36, 127,84 (2C), 126,60, 124,95 (2C), 50,32, 43,73, 39,26, 30,42, 28,21, 27,96, 24,79, 22,98, 21,63, 13,08 ppm; sm *m/e*: 243 (M^+ +, 2%), 242 (M^+ + 1, 7%), 241 (M^+, 49%), 212 ($M^+ - C_2H_5$, 29%), 198 ($M^+ - C_3H_7$, 18%), 145 ($C_{10}H_{11}N$, 44%), 144 ($C_{10}H_9N$, 14%), 130 (C_9H_8N, 32%), 129 (C_9H_7N, 100%), 128 (C_9H_6N, 22%), 116 (C_8H_9N, 20%), 115 (C_8H_8N, 31%), 103 (C_8H_7, 21%), 102 (C_8H_6, 1%), 91 (C_7H_7, 31%), 77 (C_6H_5, 10%). Masse précise pour $C_{17}H_{23}N$: 241,1832; tr.: 241,1825.

Remerciements

Nous remercions le Conseil de recherches en sciences naturelles et en génie du Canada et les Fonds pour la formation de chercheurs et l'aide à la recherche du Ministère de l'éducation du Québec, pour l'aide financière apportée sous forme de subventions et de bourse d'études (J.P.).

1. (*a*) P. Canonne, D. Bélanger, G. Lemay et G. B. Foscolos. J. Org. Chem. **46**, 3091 (1981); (*b*) P. Canonne, D. Bélanger et G. Lemay. J. Org. Chem. **47**, 3953 (1982).
2. (*a*) P. Canonne et M. Bernatchez. J. Org. Chem. **51**, 2147 (1986); (*b*) J. Org. Chem. **52**, 4025 (1987); (*c*) P. Canonne, R. Boulanger et M. Bernatchez. Tetrahedron Lett. **42**, 4997 (1987).
3. (*a*) Brevet de Belgique: BE 898,614 (Cl. CO7F), 02 mai 1984; Appl. 2, 121, 05 jan. 1984; Chem. Abstr. **101**, 177510w (1984); (*b*) D. Lednicer. The organic chemistry of drug synthesis. Vol. I. Wiley, New York. 1977. p. 276.
4. N. Green et M. Beroza. J. Org. Chem. **24**, 761 (1959).
5. (*a*) M. J. Jorgenson. J. Org. Chem. **34**, 1103 (1969); (*b*) M. J. Jorgenson et C. H. Heatchcook. J. Am. Chem. Soc. **87**, 5264 (1965).
6. (*a*) G. Singh, M. L. Purtkayastha, H. Ila et H. Junjappa. Chem. Soc. Perkin Trans. 1, 1289 (1985); (*b*) J. Vebrel, B. Laude et E. Cerutti. C.R. Hebd. Séances Acad. Sci. Ser. C, **286**, 87 (1987).
7. (*a*) M. Julia et M. Maumy. Bull. Soc. Chim. Fr. 2415 (1969); (*b*) R. D. Obolentsev et V. G. Bukharov. Khim. Seraorg. Soedin. Soderzh. Neftyakh Nefteprod. 9 (1957); Chem. Abstr. **55**, 25907g (1961); (*c*) J. MacMillan. J. Chem. Soc. 2203 (1959); (*d*) R. Paul. Bull. Soc. Chim. Fr. 311 (1935); (*e*) R. L. Hopkins, R. W. Higgens, H. J. Coleman, C. J. Thompson et H. T. Rall. U.S. Bur. Mines, Rep. Invest. No. 6970 (1967); Chem. Abstr. **68**, 95633z (1968); (*f*) G. Pifferi, R. Monguzzi et P. Consonni. Farm. Ed. Sci. **27**, 30 (1972); (*g*) P. Sanora, G. Cignarella, V. Anania, R. Siri et M. S. Desale. Farm. Ed. Sci. **40**, 777 (1985); (*h*) P. Canonne, J. Plamondon et M. Akssira. Tetrahedron, **44**, 2903 (1988).
8. N. Kornblum et J. Eicher. J. Am. Chem. Soc. **71**, 2259 (1949).
9. (*a*) E. Montaudon, J. Thépanier et R. Lalande. J. Heterocycl. Chem. **16**, 113 (1979); (*b*) K. Utimoto, K. Uchida, M. Yamaha et H. Nozaki. Tetrahedron, **33**, 1945 (1977); (*c*) K. Utimoto, K. Uchida et H. Nozaki. Tetrahedron Lett. **45**, 4527 (1973); (*d*) P. C. Lowen, L. P. Kakhubu et R. K. Brown. Can. J. Chem. **50**, 1502 (1972); (*e*) J. Buendia. Bull. Soc. Chim. Fr. 3598 (1966).
10. G. W. Gokel et H. D. Durst. Aldrichimica Acta, **9** (1976), et références citées.
11. (*a*) J. Dockx. Synthesis, 441 (1973); (*b*) E. V. Dehmlov. Angew. Chem. Int. Ed. Engl. **13**, 170 (1974).
12. P. Canonne, D. Bélanger et G. Lemay. Tetrahedron Lett. **22**, 4995 (1981).
13. E. C. Ashby et S. T. Laemmle. Chem. Rev. **75**, 521 (1975).
14. J. M. Fabre, B. Calas et L. Giral. Bull. Soc. Chim. Fr. 4285 (1972).
15. J. M. Fabre, B. Calas et L. Giral. Bull. Soc. Chim. Fr. 1473 (1974).
16. H. Pine et N. E. Hoffman. J. Am. Chem. Soc. **76**, 4417 (1954).

COMMUNICATION

Protium–deuterium exchange of 17-oxosparteine: Homoenolization of a lactam

NICK HENRY WERSTIUK, THOMAS HEMSCHEIDT, AND GEORGE TIMMINS
Department of Chemistry, McMaster University, Hamilton, Ont., Canada L8S 4M1

Received August 29, 1988

NICK HENRY WERSTIUK, THOMAS HEMSCHEIDT, and GEORGE TIMMINS. Can. J. Chem. **67**, 565 (1989).

The H–D exchange of 17-oxosparteine (**1***b*) has been studied under homoenolization conditions. We find that **1***b* undergoes H–D exchange at the bridgehead carbon C7 at 130°C, but forcing conditions (240°C) using the medium $(CD_3)_3COK/(CD_3)_3COD$ are required to induce exchange at C11, C15, and other sites. C15-H_a exchanges only marginally faster than C15-H_e, indicating that the β-lactam carbanion is stabilized primarily by the dipolar effect of the amide group.

Key words: protium–deuterium exchange, 17-oxosparteine, homoenolization.

NICK HENRY WERSTIUK, THOMAS HEMSCHEIDT et GEORGE TIMMINS. Can. J. Chem. **67**, 565 (1989).

Opérant dans des conditions d'homoénolisation, on a étudié l'échange H–D de l'oxo-17 spartéine (**1***b*). On a trouvé que, à 130°C, le composé **1***b* subit un échange H–D au niveau du carbone C7 de l'atome de pont; toutefois, on doit forcer les conditions et opérer à 240°C dans un milieu $(CD_3)_3COK/(CD_3)_3COD$, pour pouvoir induire des échanges dans les positions C11, C15 ainsi que sur d'autres sites. Les échanges du C15-H_a ne sont que marginalement plus rapides que ceux du C15-H_e; ces résultats indiquent que la stabilisation du carbanion de la β-lactame reflète principalement l'effet dipolaire du groupement amide.

Mots clés : échange protium–deutérium, oxo-17 spartéine, homoénolisation.

[Traduit par la revue]

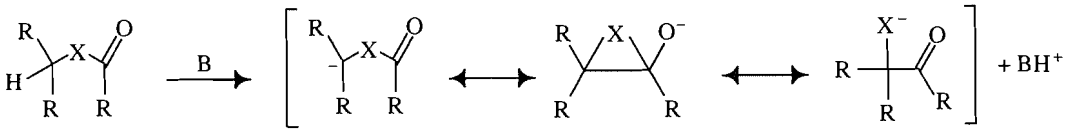
A wide variety of acyclic, monocyclic, and polycyclic ketones have been studied to detail the structural and stereoelectronic requirements for homoenolization (Scheme 1, X = C) of this class of compounds in $(CH_3)_3COK/(CH_3)_3COH(D)$ (1). However, there have been no reports of the homoenolization of amides (lactams), esters (lactones), or thioesters (thiolactones) in this medium even though carbanions can be generated α to nitrogen of amides or to sulfur of thioesters with LDA (2).

We set out to prepare sparteine (**1***a*) deuteriated at C8 in order to unambiguously assign the resonances for the axial and equatorial protons at this site, which was expected to be labelled by incorporation of cadaverine-3,3-d_2 (3). To this end, we undertook a study of the homoenolization of 17-oxosparteine (**1***b*) to establish whether deuterium could be incorporated at C8, β to the lactam carbonyl group. This 17-oxosparteine-8-d_n would be converted into **1***a*-8-d_n by LAH reduction (4). Furthermore, **1***b* also provides a unique opportunity to determine the relative rates of exchange at the other β sites (C6, C11, and C15) as well as at C7, the bridgehead carbon. This communication documents the first study of a lactam (amide) under homoenolization conditions.

At 130°C, **1***b* incorporates 0.73 of a deuterium atom (entry 1, Table 1). Analysis of the 125-MHz ^{13}C nmr spectra of **1***b*-$d_{0.73}$ and **1***a*-$d_{0.73}$ obtained by LAH reduction established that the deuterium is located at C7 (4). That exchange α to the carbonyl group is only 73% complete at 130°C is due to the unfavorable alignment of C7-H with the π-system of the carbonyl group (the dihedral angle is 23.6°) and to the fact that the enolate is generated at the bridgehead of a [3.3.1] system.

At 175°C, **1***b* incorporates 0.86 of the deuterium atom in 24 h (entry 2, Table 1). Its ^2H nmr spectrum showed that little deuterium is incorporated at sites other than C7. Consequently, **1***b* was reacted under more vigorous conditions. Since we showed previously that the medium $(CH_3)_3COK/(CH_3)_3COD$ is unstable (even at 185°C it decomposes slowly to isobutene and HOD), exchange reactions were carried out at 240°C in $(CD_3)_3COK/(CD_3)_3COD$ to avoid dilution of the deuterium pool and to increase the stability of the medium (5). Under these conditions (entries 3 and 4, Table 1), more deuterium is incorporated into **1***b*. Analysis of the high-field ^1H nmr and ^{13}C nmr spectra of **1***b*-d_n and **1***a*-d_n established that exchange at C7 was virtually complete; the signal for C7-H disappeared and the C7 resonance was replaced by ^2H-coupled ^{13}C satellites shifted upfield. That there was substantial H–D exchange at C15 was established by a marked decrease in the intensity of the C15 resonance of **1***a*-d_n. The ^2H spectra of **1***b*-$d_{1.73}$ and **1***b*-$d_{2.51}$ showed two additional strong signals at the chemical shifts of the axial (2.30 ppm) and equatorial (4.55 ppm) protons at C15 of **1***b* (6).

The ^2H nmr data show that the axial hydrogen at C15 undergoes H–D exchange marginally faster than the equatorial hydrogen (1.6:1) and that exchange at other sites occurs much



X = C, N, O, S

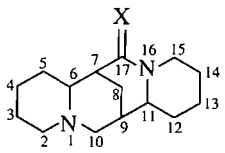
SCHEME 1

Can. J. Chem. Downloaded from www.nrcresearchpress.com by 41.223.56.140 on 09/07/12
For personal use only.

TABLE 1. H–D exchange of 17-oxosparteine

Entry	Conditions[a,b,c]	Deuterium atoms incorporated	Distribution[e]
1	0.049 g **1***b*, 130°C, 22 h $(CH_3)_3COK/(CH_3)_3COD$	0.73	C7(0.73)
2	0.024 g **1***b*, 175°C, 24 h $(CH_3)_3COK/(CH_3)_3COD$	0.86	C7(0.80), traces other
3	0.100 g **1***b*, 240°C, 48 h $(CD_3)_3COK/(CD_3)_3COD$	1.73	C7(0.84), C11(0.04), C15-D_a (0.48), C15-D_e (0.29), other (0.12)
4	0.114 g **1***b*, 240°C, 100 h $(CD_3)_3COK/(CD_3)_3COD$	2.51	C7(0.99), C11(0.07), C15-D_a (0.69), C15-D_e (0.50), other (0.25)

[a]The reactions were carried out in 2.5 mL of 1.2 M base.
[b]Recoveries of **1***b*-d_n were in the range of 70–80%.
[c]For temperatures below 150°C the variation was ±2°; for temperatures above 200°C, the variation was ±5°.
[d]Determined mass spectrometrically at low ionizing voltage.
[e]Determined by high-field ^1H, ^2H, and ^{13}C nmr spectroscopy.

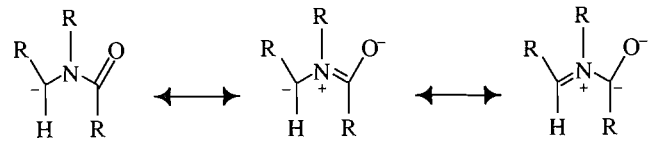


1

a, X = H_2

b, X = O

more slowly than at C7 and C15. The structure of **1***b*, optimized using the MM2 force field of MACROMODEL (7), is shown in Fig. 1. Ring D is a chair in keeping with an X-ray crystallographic structure determination (8). If homoconjugative stabilization of the incipient anion at C15 by the carbonyl group is important, a greater axial selectivity would be expected; while the dihedral angle between C15-H_a and the carbonyl group is 127.4°, C15-H_e is nearly in the plane (dihedral angle 9.5°) of the carbonyl group (Fig. 1). Axial selectivity would also be expected if the carbanion is resonance-stabilized as shown by the canonical forms **I**, **II**, and **III**. This resonance effect has



I **II** **III**

been invoked to account for the enhanced acidity of *N*-nitroso amines (9). That the diastereotopic hydrogens exchange at similar rates suggests that dipolar stabilization, through space and through bond, is the main mode of stabilization of this anion. This is in keeping with the results of computational studies carried out by Bach *et al.* on the anion derived from *N*-methyl formamide (10).

Although C11-H is adjacent to the lactam nitrogen as well, and its alignment (dihedral angle 132.9°) with the planar amide linkage (Fig. 1) is similar to C15-H_a, exchange at this site occurs

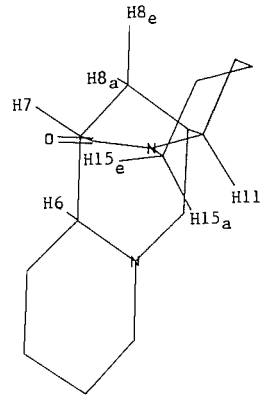


FIG. 1. MM2 optimized molecular structure of 17-oxosparteine (**1***b*).

much more slowly than exchange at C15, presumably because deprotonation yields a tertiary anion. This is also the case for C6. Four additional overlapping resonances ranging from 1.2 to 1.6 ppm and totaling 0.25 D (entry 4, Table 1) were present, but could not be assigned with certainty even though they fall in the region where the C8-H and C6-H resonances are expected (6). That exchange at C8 and C6 is slow relative to exchange at C15 is unexpected and is undoubtedly due to the fact that the electrophilicity of the carbonyl group is reduced by amide resonance. Studies on other sparteine derivatives are planned.

Even though **1***a*-8-d_n was not prepared, the C8 resonance of **1***a* was unambiguously assigned on the basis of the β-deuterium isotope shifts observed for the carbons β to C7 of **1***a*-7-$d_{0.73}$. Having assigned the C8 resonance, the C8-H resonances of **1***a* were then unambiguously assigned by carrying out a heteronuclear COSY experiment.

Acknowledgement

We thank the Natural Sciences and Engineering Research Council of Canada for financial support.

1. N. H. WERSTIUK. Tetrahedron, **39**, 205 (1983).
2. P. BEAK and R. FARNEY. J. Am. Chem. Soc. **95**, 4771 (1973).

Can. J. Chem. Downloaded from www.nrcresearchpress.com by 41.223.56.140 on 09/07/12
For personal use only.

3. T. HEMSCHEIDT and I. D. SPENSER. Can. J. Chem. **65**, 170 (1987).
4. W. M. GOLEBIEWSKI and I. D. SPENSER. Can. J. Chem. **63**, 716 (1985).
5. N. H. WERSTIUK and G. TIMMINS. Can. J. Chem. **63**, 526 (1985).
6. W. M. GOLEBIEWSKI. Magn. Reson. Chem. **24**, 105 (1986).
7. W. C. STILL. MACROMODEL. 1.5. Department of Chemistry, Columbia University, New York, NY.
8. A. KATRUSIAK, A. HOSER, E. GRESIAK, and Z. KALUSKI. Acta Crystallogr. Sect. B: Struct. Crystallogr. Cryst. Chem. **36**, 2442 (1980).
9. R. R. FRASER and L. K. NG. J. Am. Chem. Soc. **98**, 5895 (1976).
10. R. D. BACH, M. L. BRADEN, and G. J. WOLBER. J. Org. Chem. **48**, 1509 (1983).

Can. J. Chem. Downloaded from www.nrcresearchpress.com by 41.223.56.140 on 09/07/12
For personal use only.

On the regioselectivity of the condensation of stabilized phosphoylids with 3-substituted phthalic anhydrides

LIVAIN BREAU AND MARGARET M. KAYSER[1]

Department of Chemistry, University of New Brunswick, P.O. Box 5050, Saint John, N.B., Canada E2L 4L5

Received September 9, 1988

LIVAIN BREAU and MARGARET M. KAYSER. Can. J. Chem. **67**, 569 (1989).

Condensations of stabilized phosphorane **1** with 3-substituted phthalic anhydrides were investigated. The importance of various effects influencing regio- and stereoselectivity of these reactions is discussed. It is proposed that the oxygen atom on the substituents in position 3 can act as a Lewis base toward the electron-deficient phosphorus of the ylid. The resulting complexation stabilizes the transition state for the reaction at the *ortho* carbonyl group, thus offsetting the usual steric and "push" effects, which favour attack at the *meta* carbonyl function.

Key words: Wittig condensations, phthalic anhydrides, regioselectivity, stereoselectivity.

LIVAIN BREAU et MARGARET M. KAYSER. Can. J. Chem. **67**, 569 (1989).

On a examiné les condensations du phosphorane stabilisé **1** avec les anhydrides phtaliques substitués en position 3. On discute de l'importance de divers effets qui influencent la régio- et la stéréo-sélectivité de ces réactions. On suggère que l'atome d'oxygène présent sur les substituants en position 3 peut agir comme base de Lewis par rapport au phosphore électro-déficient de l'ylure. La complexation qui en découle stabilise l'état de transition conduisant à une réaction avec le groupement carbonyl en *ortho* et contre-balance les effets stériques et ceux qui proviennent d'une « poussée » qui favorisent généralement une attaque de la fonction carbonyle en *méta*.

Mots clés : condensations de Wittig, anhydrides phtaliques, régiosélectivité, stéréosélectivité.

[Traduit par la revue]

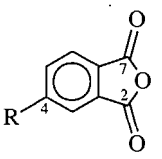
Can. J. Chem. Downloaded from www.nrcresearchpress.com by 41.223.56.140 on 09/07/12
For personal use only.

Introduction

Stabilized phosphoranes **1** react readily with phthalic anhydride (1). The condensation occurs under mild conditions, providing an excellent synthetic route to enol-lactones. The 4-substituted phthalic anhydrides show regioselectivity patterns that can be correlated with the electronic effects of the substituent. Thus, the electron-releasing groups such as $-NR_2$ or $-OCH_3$ promote reaction at the carbonyl-2, **2**, while the electron-withdrawing groups ($-NO_2$, -COOR) favour condensation at the carbonyl-7, **2** (2).

$Ph_3P{=}CHCOOCH_3$

1



2

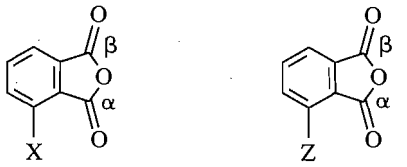
The fact that the reactions of certain phthalic anhydrides have been shown to be reversible (3) does not appear to interfere with a simple interpretation based on electronic effects. On the other hand, the 3-substituted phthalic anhydrides give results that cannot be simply explained (2). Particularly in the case of oxygen-containing substituents ($-OCH_3$, $-NO_2$, and -COOR), projections based on electronic and (or) steric effects appear to be of little value.

Our interest in regioselectivity control prompted us to investigate further the condensations of stabilized Wittig reagents with a number of 3-substituted phthalic anhydrides. The condensations of anhydrides with methyl- or ethyl-(triphenylphosphoranylidene) acetate **1** were carried out in refluxing dry THF under nitrogen. The appearance of the product(s) was monitored by gas chromatography. Proton nmr spectroscopy was found to be more suitable than gas chromatography for the determination of the product composition, since the retention times for the two *Z* or two *E* isomers were frequently very similar.

The isomers were separated on a centrifugally accelerated radial thin-layer chromatograph; their structures were established by proton nmr and isomerisation experiments. The results for a series of 3-substituted phthalides are shown in Table 1.

Results and discussion

According to FMO theory, nucleophilic addition to a carbonyl function is favoured at the carbon atom bearing the highest LUMO coefficient. The calculations for several 3-substituted phthalic anhydrides have shown that in alkyl-, hydroxyl-, methoxyl-, and halogen-substituted anhydrides the highest LUMO coefficient is located on the carbon atom of the *meta* carbonyl group, **3** (4). Hence, for these compounds the steric and electronic effects favour the reaction at the *meta* carbonyl function. When the substituent is electron withdrawing (-CN, $-NO_2$) the highest LUMO coefficient is located on the carbon atom of the *ortho* carbonyl group, **3** (4).



3

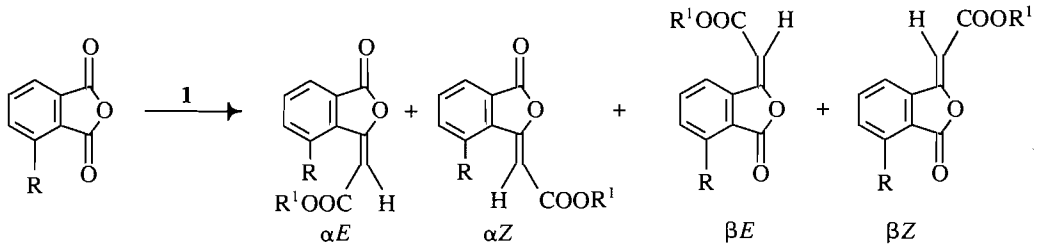
X = R, OH, halogens Z = CN, NO_2

From the steric viewpoint, the *meta* carbonyl group more remote from the substituent should be an easier target for the nucleophile in all cases.

Furthermore, the *ortho* carbonyl function is also deactivated vis-a-vis nucleophilic addition due to the repulsive van der Waals interaction with a substituent in position 3. Such an interaction causes a displacement of electrons from the oxygen to the carbon atom of the carbonyl function. The increased electronic density at the carbon atom lowers its electrophilicity, and consequently its reactivity towards nucleophiles. The above "push effect", related to the size of the substituent and not its electronic character, has been observed during ^{13}C and ^{17}O nmr studies of 3-substituted phthalic anhydrides (5).

[1]Author to whom correspondence may be addressed.

TABLE 1. Condensation of 3-substituted phthalic anhydrides with $Ph_3P{=}CHCOOCH_3$ **1**



Anhydride		Products				Total yield of lactonic product	Ratio	
R	No.	αE	αZ	βE	βZ	(%)	α:β	Reference
I	**3***a*	—	—	78	22	47	0:100[a]	
Br	**3***b*	—	—	95	5		0:100	2
Cl	**3***c*	—	5	43	52		5:95	2
F	**3***d*	21	23	38	18	78	44:56[a]	
CH_3	**3***e*	—	4	73	23		4.96	2
NH2	**3***f*	—	—	72	28	71	0:100[a]	
NMe_2	**3***g*	—	—	60	40		0:100	2
$COOCH_3$	**3***h*	—	40	60	—		40:60	2
OCH_3	**3***i*	7	50	29	14	76–82	57:43[a]	
OCH_2CH_3	**3***j*	7	36	11	46	80–83	43:57[a]	
NO_2	**3***k*	15	42	34	9	82	57:43[a]	

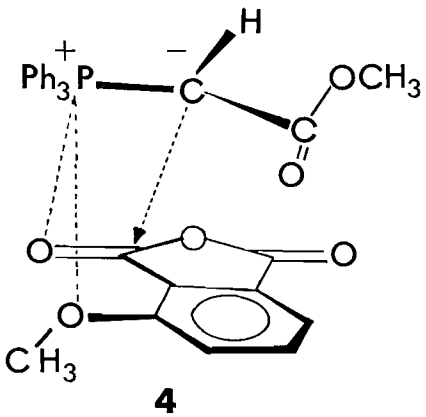
[a]The product ratio of the enol-lactones formed was established by proton nmr analysis of the crude reaction mixture, prior to the separation of individual enol-lactones.

The push-effect is, predictably, more important for bulkier groups such as I, Br, $N(CH_3)_3$, or NO_2 and is negligible for fluorine atoms.

In view of the above discussion, the results listed in Table 1 show an unexpectedly high proportion of the products resulting from the condensation at the *ortho* carbonyl group in phthalic anhydrides with the oxygen-bearing substituents in position 3.

Particularly intriguing are the results of the reactions with 3-methoxy, 3-ethoxy, and 3-nitrophthalic anhydrides. The methoxy and ethoxy substituents, by virtue of their electron-donating capacity as well as their steric influence, should exhibit regioselectivity similar to that observed in Cl- or Br-substituted phthalic anhydrides (6). The relatively important proportion of the reaction at the *ortho* carbonyl group suggests that effects other than those mentioned above are at work.

A possible explanation for the results obtained in the condensations with alkoxy-substituted phthalic anhydrides is that the reaction pathway for the ylid addition to the *ortho* carbonyl group is of lower energy than that leading to the condensation at the *meta* carbonyl group. We propose that the stabilization of the transition state lying along the preferred route is a result of a complexation between an oxygen atom of the substituent and a phosphorus atom of the ylid, **4**.



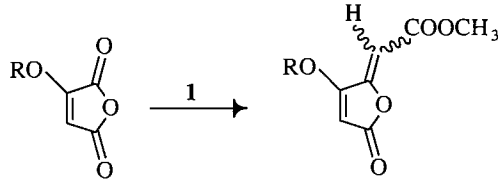
4

In view of the fact that interactions between bases such as -OR, -SR, -NR, and an electron-deficient phosphorus are well known (7–10), and lead to the formation of stable, sometimes isolable, hexacoordinated phosphorus complexes (11, 12), the transition state for an ylid addition should be stabilized when overlap between an accessible electron donor and the phosphorus atom can occur.

The highly regioselective condensations of alkoxy-substituted maleic anhydrides with stabilized phosphoranes, in which ylids add only to the carbonyl group adjacent to the alkoxy substituent (13), support the above hypothesis, **5**.

The amino substituents in position 3 (compounds **3***f* and **3***g*) do not manifest a similar stabilizing effect on the transition state. In aromatic amines the electrons of the lone pair on nitrogen are preferentially delocalized throughout the ring system, simultaneously deactivating the α-carbonyl function toward nucleophilic addition and diminishing the basicity of the amino group vis-a-vis an electron-deficient phosphorus of the ylid. As a result, the anticipated β-attack is in fact observed (Table 1).

In keeping with the above rationalization, the reactions of stabilized phosphoranes with 3-aminophthalic anhydrides are considerably slower than the condensations with alkoxy-



5

Can. J. Chem. Downloaded from www.nrcresearchpress.com by 41.223.56.140 on 09/07/12
For personal use only.

Can. J. Chem. Downloaded from www.nrcresearchpress.com by 41.223.56.140 on 09/07/12
For personal use only.

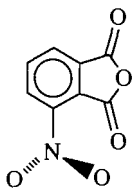
phthalic anhydrides. While the 3-aminophthalic anhydrides require prolonged reflux for the reaction to occur, the alkoxy analogues react rapidly at room temperature, and can be monitored by nmr.

In the course of several nmr experiments (^1H and ^{13}C) carried out for 3-methoxyphthalic anhydride at room temperature, as well as at low temperatures (−50 and −40°C), we were unable to detect any intermediates, even of a transient nature. The reaction proceeded smoothly to the products observed at termination. It may therefore be concluded that the rate-controlling step is irreversible and the reaction kinetically controlled.

A more exhaustive discussion of the studies of the mechanism of ylid reactions with cyclic anhydrides will be presented in a separate paper.

In the case of 3-NO_2 phthalic anhydrides, the selectivity for the *ortho* function could be associated with the electron-withdrawing effect of the substituent (4).

However, we should point out that the electron-withdrawing capacity of the NO_2 group is strongly reduced when it is rotated from coplanarity with the aromatic ring and, thus, the resonance effects suffer from "steric inhibition" (14). Recent experimental results suggest that the 3-nitro substituent in **6** assumes a

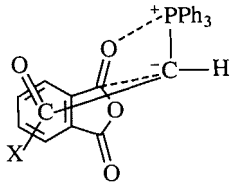


6

nonplanar conformation. From the study of the ^{17}O chemical shift–torsional angle relationship, it is estimated that the 3-nitro group is rotated 35° from the plane of the aromatic ring (15, 16). The MINDO/3 calculations (17) carried out on the model with nonplanar NO_2 show that the LUMO coefficient on the carbon of the *ortho* carbonyl group is only marginally larger than the LUMO coefficient on the carbon of the *meta* group **6**. The diminished electronic effects, coupled with the increased steric demand of the twisted NO_2 group and a strong push-effect, should promote the reaction at the more remote *meta* carbonyl function. Nevertheless almost 60% of the condensation takes place at the *ortho* carbonyl group (Table 1).

As in alkoxyphthalic anhydrides, a surprisingly high proportion of the sterically unfavourable enol-lactone may be due to the lower energy pathway leading to the condensation at the *ortho* carbonyl function. Here, partially negatively charged oxygen atoms of the NO_2 group are in an appropriate position for *p–d* overlap with the electron-deficient phosphorus atom of the ylid. This overlap should stabilize the transition state, and consequently facilitate the reaction at the *ortho* carbonyl group.

Finally, we should comment briefly on the stereochemistry of these reactions. The first Wittig reaction between phthalic anhydride and stabilized phosphorane **1** was described by Chopard *et al.* (1); the only product, an *E* isomer, was obtained in excellent yield. To account for the stereochemistry the authors proposed that the reaction proceeds through a transition state in which the -COOR group of the phosphorane is stacked in a plane parallel to the benzene ring, as shown in **7**. The π electrons of the carbonyl function interact with the relatively electron-deficient benzene ring of the phthalic anhydride. This explanation agrees reasonably well with our results, which



7

show that in the presence of an electron-withdrawing substituent on the aromatic ring the proportion of *E* isomer tends to be significant even in sterically unfavourable situations (see **3***d* and **3***k*, Table 1).

Conclusion

The results of the investigations discussed in this paper shed some light on the factors that control regioselectivity of phosphorane addition to 3-substituted phthalic anhydrides.

The combined steric, resonance, and push effects explain adequately the regioselectivity observed in the condensation of phosphorane with anhydrides **3***a*–**3***g*. The higher LUMO coefficient argument does not appear to be generally applicable in these reactions, judging by the relative lack of selectivity in the reaction with 3-fluorophthalic anhydride. This is probably due to the fact that certain condensations are under thermodynamic, while others are under kinetic, control.

The increased selectivity for the *ortho* carbonyl function in the reactions with anhydrides **3***h*–**3***k*, all bearing an oxygen-containing substituent, is best interpreted in terms of kinetic preference for the *ortho* function in these compounds. The complexation between the oxygen atom (from the 3-substituent) and an electron-deficient phosphorus stabilizes the "*ortho*" transition state **4** compared to that for the reaction at the *meta* carbonyl group, thus compensating somewhat for the unfavourable steric environment.

Recent studies of the mechanism of stabilized ylid reactions with aldehydes indicate that a transition state earlier than is generally believed may be involved in these condensations (18). The above conclusion agrees with our results suggesting that kinetic preference determines the regioselectivity of phosphorane addition to 3-alkoxy substituted phthalic anhydrides.

Experimental

Melting points were determined on a Fisher Scientific Co. hot-stage melting point apparatus and are uncorrected. Infrared spectra were obtained on a Perkin–Elmer 1420 ratio recording infrared spectrophotometer, either neat or with chloroform as solvent. Ultraviolet spectra were measured in methanol using a Varian Cary 219 spectrophotometer. The ^1H nmr and ^{13}C nmr spectra were recorded on a Varian EM 300L nmr spectrometer or on a Nicolet 360 spectrometer with $CDCl_3$ as solvent and $(CH_3)_4Si$ as internal standard. Mass spectra were recorded on a VG mass spectrometer with a DANI 7070 gas chromatograph. Gas chromatographic analyses were carried out with a Varian 3700 gas chromatograph, using a 50 cm × 1/8 in., 5% OV-101 on Chromosorb, G-HP 100/120 mesh column. Chromatographic separations were performed on a preparative, centrifugally accelerated, radial, thin-layer chromatograph (a Chromatotron model 7924T). tetrahydrofuran (THF) was dried over sodium metal and was distilled under nitrogen.

*General procedure for the reactions of $Ph_3P—CHCO_2CH_3$ **1** with phthalic anhydrides*

Molar equivalent amounts of an anhydride and methyl(triphenylphosphoranylidene) acetate **1** were dissolved in dry THF and the

Can. J. Chem. Downloaded from www.nrcresearchpress.com by 41.223.56.140 on 09/07/12
For personal use only.

solution was refluxed. The progress of the reaction was followed by gas chromatography and proton nmr. The crude products were separated on the Chromatotron. The isomeric lactones were identified by proton nmr, hydrogenation, and isomerization experiments.

Photochemical isomerization of enol-lactones

A pure sample of an enol-lactone was dissolved in cyclohexane and was placed in a petri dish surrounded by aluminum foil. The solution was immediately irradiated with an ultraviolet short wavelength lamp (254 nm), placed directly above the solution for a period of 15 min – 2 h. After evaporation of the solvent the residue was analyzed by proton nmr and gas chromatography.

The reaction of Ph_3P $CHCOOCH_3$ **1** *with 3-idiophthalic anhydrides* **3***a*

The reaction between 3-ideophthalic anhydride **3***a* (6) (0.50 g, 1.8 mmol) and the phosphorane **1** (0.60 g, 1.8 mmol) was completed in 5 h of reflux in THF. Proton nmr of the crude reaction mixture showed **3***aβE* and **3***aβZ* in the ratio 78:22. Chromatography, with petroleum ether/ether as elutant, gave (*E*)-3-methoxycarbonylmethylidene-7-iodophthalde **3***aβE*, 0.22 g (36%) (eluted first), crystallized from methanol as white crystals, mp 167–168°C: ir ($CHCl_3$) ν_{max}: 3120, 3010, 2960, 1790, 1715, 1655 cm^{-1}: proton nmr ($CDCl_3$) δ: 3.84 (s, 3H, $COOCH_3$), 6.16 (s, 1H, :CHCOOMe), 7.54 (t, J = 8.0 Hz, 1H), 8.12 (d, J = 8 Hz, 1H), 9.09 (d, J = 8 Hz, 1H); ms, *m/e*: 331 (M^+ + H, 100%), 330 (M^+, 58%), 299 (93%), 289 (17%), 203 (33%), 84 (41%), 83 (97%), and 75 (27%); and (*Z*)-3-methoxycarbonylmethylidene-7-iodophthalic **3***aβZ*, 60 mg (10%), which crystallized from methanol as white crystals, mp 213–215°C (dec.); ir ($CHCl_3$) ν_{max}: 2960, 1810, 1710, 1670 cm^{-1}; proton nmr ($CDCl_3$) δ: 3.82 (s, 3H, $COOCH_3$), 5.90 (s, 1H, :CHOOMe), 7.43 (t, J = 8 Hz, 1H), 7.74 (dd, J = 7.7 and 0.8 Hz, 1H, H4), 8.12 (dd, J = 7.7 and 0.8 Hz, 1H); ms, *m/e*: 331 (M^+ + H, 100%), 330 (53%), 299 (68%), 203 (96%), and 75 (13%). A solution of pure **3***aβZ* (25 mg) in cyclohexane was irradiated for 2 h to give a mixture of **3***aβE* and **3***aβZ* in the ratio of 22:78. Some polymeric material was also formed (proton nmr analysis).

The Wittig reaction with 3-fluorophthalic anhydride **3***d*

The 3-fluorophthalic anhydride **3***d* was synthesized as described in ref. 6. The reaction between 3-fluorophthalic anhydride **3***d* (1.00 g, 6.02 mmol) and the phosphorane **1** (2.02 g, 6.04 mmol) carried out according to the general procedure yields, after 15 min of stirring at room temperature, a white crystalline product, presumably the acyclic intermediates. These intermediates were converted into the corresponding enol-lactones upon 2 h reflux. Proton nmr analysis of the crude mixture showed that **3***dαE*, **3***dαZ*, **3***dβE*, and **3***dβZ* were present in the ratio of 21:23:38:18. Chromatography with petroleum ether/ether gave (*E*)-3-methoxycarbonylmethylidene-7-fluorophthalic **3***dβE* (eluted first) as white needles, mp 148.5–149°C; ir ($CHCl_3$) ν_{max}: 3040, 3020, 1800, 1720, 1655 cm^{-1}: proton nmr ($CDCl_3$) δ: 3.84 (s, 3H, OCH_3), 6.19 (s, 1H, :CHCOOMe), 7.35 (td, J = 8.2 and 0.3 Hz, 1H), 7.81 (td, J = 8.2 and 5 Hz, 1H), 8.93 (dd, J = 8.2 and 0.3 Hz, 1H); ms, *m/e*: 222 (M^+, 23%), 192 (12%), 191 (100%), 164 (9%), 107 (25%), 94 (14%), 69 (11%), and 28 (33%); (*E*)-3-methoxycarbonylmethylidene-4-fluorophthalic **3***dαE* (eluted second) as white crystals, mp 102–103°C; ir ($CHCl_3$) ν_{max}: 2960, 1730, 1670 cm^{-1}; proton nmr ($CDCl_3$) δ: 3.87 (s, 3H, OCH_3), 6.27 (s, 1H, :CHCOOMe), 7.44–7.84 (m, 3H); ms, *m/e*: 222 (M^+, 19%), 195 (11%), 192 (12%), and 191 (100%); (*Z*)-3-methoxycarbonylmethylidene-7-fluorophthalide **3***dβZ* (eluted third) as white crystals, mp 156–157°C; ir ($CHCl_3$) ν_{max}: 2960, 1810, 1715, 1675 cm^{-1}; proton nmr ($CDCl_3$) δ: 3.83 (s, 3H, OCH_3), 6.08 (d, J_{HF} = 0.77 Hz, 1H, :CHCOOMe), 7.36–7.82 (m, 3H); ms, *m/e*: 222 (M^+, 26%), 192 (15%), 191 (100%), 164 (11%), and 107 (33%); and (*Z*)-3-methoxycarbonylmethylidene-4-fluorophthalide **3***dαZ* (eluted last) as white crystals, mp 164–165°C; ir ($CHCl_3$) ν_{max}: 2960, 1805, 1710, 1675 cm^{-1}; proton nmr ($CDCl_3$) δ: 3.86 (s, 3H, OCH_3), 5.92 (s, 1H, :CHCOOMe), 7.25–7.89 (m, 3H); ms, *m/e*: 222 (M^+, 18%), 192 (11%), 191 (100%), 107 (26%), and 28 (78%). The fluorophthalide enol-lactones were obtained in an overall yield of 1.05 g (78%). The pure **3***dβE* (30 mg) in cyclohexane was isomerized to give **3***dβE*:**3***dβZ* 52:48 after 30 min and 36:64 after 1 h of irradiation. The pure **3***dαE* was isomerized to give **3***dαE*:**3***dαZ* 20:80 after 2 h of irradiation. In both cases a very small quantity of polymeric material was also formed.

The Wittig reaction with 3-aminophthalic anhydride **3**f

The reaction between 3-aminophthalic anhydride **3***f* (19) (0.5 g, 0.003 mmol) and the phosphorane **1** (1.0 g, 0.003 mmol) gave a mixture of two enol-lactones (0.4 g, 71%): **3***fβE* and **3***fβZ* in the ratio 72:28. Chromatography with petroleum ether/ether gave (*E*)-3-methoxycarbonylmethylidene-7-aminophthalide **3***fβE* (eluted first) as yellow-orange crystals, mp 145–150°C; ir ($CHCl_3$) ν_{max}: 3450, 3350, 2950, 1760, 1725 cm^{-1}; proton nmr ($CDCl_3$) δ: 3.78 (s, 3H, OCH_3), 5.32 (s, br, NH_2), 6.03 (s, 1H), 6.80 (d, 1H), 7.47 (t, 1H), 8.24 (d, 1H); and (*Z*)-3-methoxycarbonylmethylidene-7-aminophthalide **3***fβZ* (eluted second) as yellow crystals, mp 159–164°C; ir ($CHCl_3$) ν_{max}: 3450, 3350, 2950, 1775, 1725 cm^{-1}; proton nmr ($CDCl_3$) δ: 3.81 (s, 3H, OCH_3), 5.32 (s, br, NH_2), 5.78 (s, 1H), 6.77 (d, 1H), 6.95 (d, 1H), 7.42 (t, 1H). A solution of the mixture **3***fβE* and **3***fβZ* (72:28) in cyclohexane was irradiated for 1 h to give a mixture of **3***fβE* and **3***fβZ* in the ratio 30:0 (proton nmr analysis).

The Wittig reaction with 3-methoxyphthalic anhydride **3**i

The reaction between 3-methoxyphthalic anhydride **3***i* (20) (1.00 g, 5.62 mmol) and the phosphorane **1** (1.88 g, 5.62 mmol) was completed after 4 h of reflux in THF. Proton nmr analysis of the crude reaction mixture showed the **3***iαE*, **3***iαZ*, **3***iβE*, and **3***iβZ* in the ratio of 7:50:29:14. The observed regioselectivity, but not stereoselectivity, was consistent with the data reported in the literature (2). A characteristic resonance at δ 6.12 (s, 1H, :CHCOOMe), corresponding to the **3***iαE* isomer, has not been reported previously. This isomer was not isolated, as it isomerizes to α*Z* on chromatography.

The Wittig reaction with 3-ethoxphthalic anhydride **3**j

The reaction between 3-ethoxyphthalic anhydride **3***j* (20, 21) and phosphorane **1** was carried out as described for 3-methoxyphthalic anhydride **3***i*. Proton nmr of the crude mixture gave the distribution of the four enol lactones **3***jαE*, **3***jαZ*, **3***jβE*, and **3***jβZ* as 11:36:7:46. The irradiation experiment carried out on the mixture showed decrease of the vinylic proton signal of **3***jαE* and **3***jβE* and enrichment of the signals for **3***jαZ* and **3***jβZ*.

The Wittig reaction with 3-nitrophthalic anhydride **3**k

Using the general procedure, the reaction between 3-nitrophthalic anhydride **3***k* (3.00 g, 15.5 mmol) and the phosphorane **1** (5.19 g, 15.5 mmol) was completed in 8 h of reflux in THF. Proton nmr analysis of the crude reaction mixture showed that the **3***kαE*, **3***kαZ*, **3***kβE*, and **3***kβZ* were present in the ratio 15:42:34:9. Again the regioselectivity, but not the stereoselectivity, of the reaction was in agreement with the reaction carried out in $CHCl_3$ (2). The resonance at δ 6.30 (s, 1H, :CHCOOMe) for **3***kαE* has not been reported previously.

Acknowledgement

We thank the Natural Sciences and Engineering Research Council of Canada for support through research development grant no. 403 (M. M. Kayser) and a studentship award (L. Breau).

1. P. A. Chopard, R. F. Hudson, and R. J. G. Searle. Tetrahedron Lett. 2357 (1965).
2. A. Allahdad and D. W. Knight. J. Chem. Soc. Perkin Trans. **1**, 1855 (1982).
3. A. J. Speziale and D. E. Bissing. J. Am. Chem. Soc. **85**, 3878 (1963).
4. M. M. Kayser and O. Eisenstein. Can. J. Chem. **58**, 2457 (1981).
5. M. M. Kayser. Spectroscopy Lett. **21**, 831 (1988).
6. C. Soucy, D. Favreau, and M. M. Kayser. J. Org. Chem. **52**, 129 (1987).
7. M. Webster. Chem. Rev. **66**, 87 (1970).
8. I. K. Gregor. Chem. Ind. 385 (1965).

9. L. LUNAZZI and S. BROWNSTEIN. J. Magn. Reson. **1**, 119 (1969).
10. E. L. MUETTERTIES, T. A. BITHER, M. W. FARLOW, and D. COFFMAN. J. Inorg. Nucl. Chem. **16**, 52 (1960).
11. K. P. JOHN, R. SCHMUTZLER, and W. S. SHELDRICK. J. Chem. Soc. Dalton Trans. 1841 (1974); 2466 (1974).
12. D. ROBERT, H. A. GAWARD, and J. G. RIESS. Bull Soc. Chim. (France), 511 (1981).
13. M. M. KAYSER and L. BREAU. Tetrahedron Lett. **29**, 6203 (1988).
14. H. FOSTER and F. VOGTLE. Angew. Chem. Int. Ed. Engl. **16**, 429 (1977).
15. D. W. BOYKIN, A. BAUMSTARK, M. M. KAYSER, and C. SOUCY. Can. J. Chem. **65**, 1214 (1987).
16. P. BALAKRISHNAM and D. W. BOYKIN. J. Org. Chem. **50**, 3661 (1985).
17. M. BRAUN, R.VIETH, and G. MOLL. Chem. Ber. **118**, 1058 (1985).
18. E. VEDEJS, T. FLECK, and S. HARA. J. Org. Chem. **52**, 4637 (1987); E. VEDEJS and C. F. MARTH. J. Am. Chem. Soc. **110**, 3948 (1988).
19. E. L. ELIEL, A. W. BURGSTAHLER, D. E. RIVVARD, and L. HAEFELE. J. Am. Chem. Soc. **77**, 5092 (1955).
20. R. GREWE. Chem. Ber. **71**, 907 (1938).
21. K. WEYGAND, G. HILGETAG, and A. MARTINI (*Editors*). Weygand–Hilgetag preparative organic chemistry. Wiley Interscience, New York. 1972. p. 360.

Can. J. Chem. Downloaded from www.nrcresearchpress.com by 41.223.56.140 on 09/07/12
For personal use only.

Diels–Alder addition of the fumarate and acrylate of *S*-methyl lactate to α-hydroxy orthoquinodimethanes

JAMES L. CHARLTON,[1] GUY L. PLOURDE, KEVIN KOH, AND ANTHONY S. SECCO
Department of Chemistry, University of Manitoba, Winnipeg, Man., Canada R3T 2N2

Received September 16, 1988

JAMES L. CHARLTON, GUY L. PLOURDE, KEVIN KOH, and ANTHONY S. SECCO. Can. J. Chem. **67**, 574 (1989).

The cycloaddition of α-hydroxy orthoquinodimethane, generated photochemically from 2-methylbenzaldehyde, to the fumarate and acrylate of *S*-methyl lactate has been found to give a single diastereomer with high asymmetric induction (>95% de). This reaction provides a new and versatile synthetic route to substituted tetralins of high optical purity. A *trans* stereochemistry between the vicinal hydroxyl and carboxylactyl groups has been established for these cycloadducts. This is in contrast to previous work where *cis* stereochemistry has always been found for major cycloadducts of α-hydroxy *o*-QDMs. The high asymmetric induction, unusual diastereoselectivity, and the potential use of these reactions in asymmetric synthesis are discussed.

Key words: *o*-quinodimethanes, Diels–Alder, asymmetric, cycloaddition, induction, diastereoselective.

JAMES L. CHARLTON, GUY L. PLOURDE, KEVIN KOH et ANTHONY S. SECCO. Can. J. Chem. **67**, 574 (1989).

On a observé que la cycloaddition de l'α-hydroxy orthoquinodiméthane, obtenu d'une façon photochimique à partir du méthyl-2 benzaldéhyde, sur le fumarate et sur l'acrylate du lactate de *S*-méthyle conduit à un seul diastéréomère avec une induction asymétrique élevée (>95% de). Cette réaction s'avère être une route de synthèse nouvelle et versatile vers les tétralines substituées de pureté optique élevée. On a établi que les groupements hydroxyle et carboxylactyle vicinaux de ces cycloadduits sont de stéréochimie *trans*. Ce résultat est en opposition avec ceux obtenus au cours de travaux antérieurs alors qu'on a toujours obtenu une stéréochimie *cis* pour les cycloadduits principaux des α-hydroxy *o*-QDM. On discute de l'induction asymétrique élevée, de la diastéréosélectivité inhabituelle et des usages possibles de ces réactions en synthèses asymétriques.

Mots clés : *o*-quinodiméthanes, Diels–Alder, asymétrique, cycloaddition, induction, diastéréosélective.

[Traduit par la revue]

Introduction

Developing strategies towards the synthesis of enantiomerically pure compounds is one of the goals of modern organic chemistry and the study of asymmetric Diels–Alder reactions exemplifies the pursuit of this goal (1–5). The corresponding study of asymmetric Diels–Alder reactions of orthoquinodimethanes (*o*-QDMs) has received much less attention although *o*-QDMs have been extensively utilized as intermediates in non-asymmetric syntheses of chiral molecules (6). The addition of asymmetric control to the cycloaddition reactions of *o*-QDMs would provide a route to a large number of optically active compounds of interest. While a few examples of the intermolecular addition of chiral *o*-QDMs to achiral dienophiles have been published (6–9), only one example of a chiral dienophile reacting with an achiral *o*-QDM has been published (10). A possible reason for the lack of reports of asymmetric Diels–Alder reactions of *o*-QDMs is that high diastereoselectivity in such reactions is often achieved only in the presence of Lewis acid catalysts. Such catalysts are frequently incompatible with the conditions required to generate the transitory and very reactive *o*-QDMs.

Because of our interest in the use of *o*-QDMs in synthesis we have searched the literature to find chiral dienophiles that give high diastereoselectivity in Diels–Alder reactions in the absence of Lewis acid catalysts. Two of the more interesting candidates found were the acrylate and the fumarate of *S*-ethyl lactate (2, 11). At 0°C these dienophiles react with cyclopentadiene with diastereoselectivities of 80:20 and 95.5:4.5 respectively (*endo* adduct for addition of acrylate) (11). Because they have slightly less complex nmr spectra, we have chosen to study the reactions of the acrylate and fumarate of *S*-methyl lactate with *o*-QDMs. For ease of generation of the *o*-QDM we have chosen the photolysis of 2-methylbenzaldehyde (see Scheme 1).

[1]Author to whom correspondence may be addressed.

Although the α-hydroxy group on the *o*-QDM increases the number of potential diastereomeric products, it also allows one to determine the facial selectivity of the reaction with respect to the *o*-QDM as well as the dienophile.

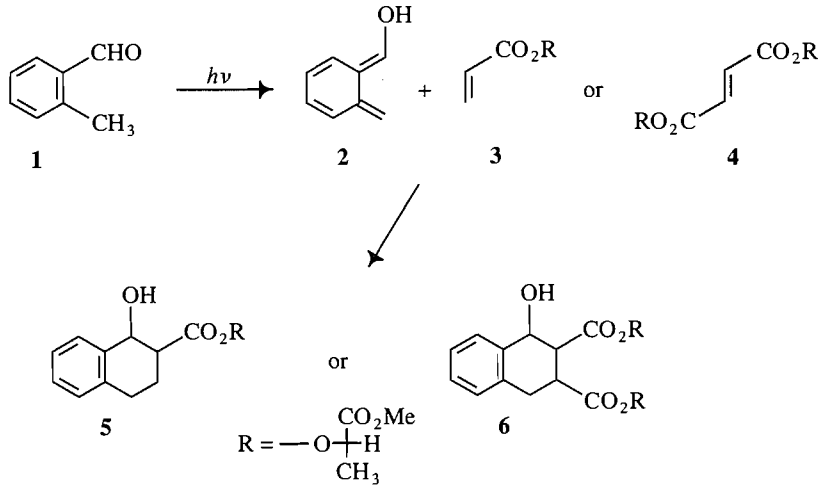
The photolysis of 2-methylbenzaldehyde is assumed to give the *E*-dienol (**2** in Scheme 1) (13–15) and, assuming that the cycloaddition is concerted, which appears to be true from previous studies (14), there are four possible approaches of the dienophile and the diene that can be classified as to their prochiral reacting faces as shown in Scheme 2 by modes **A–D**. (For an unsymmetrically substituted dienophile, there are four additional possible approaches and corresponding products with "*meta*" orientation. However, products with *meta* regiochemistry have not been observed previously (6, 12, 15), nor were they observed in this work.) In Scheme 2, the classification of the α-hydroxy carbon of the *o*-QDM is given first, followed by the classification of the face of the dienophile that will bond to that center.

The configurations of the respective cycloadducts resulting from the modes shown in Scheme 2 are shown in Scheme 3.

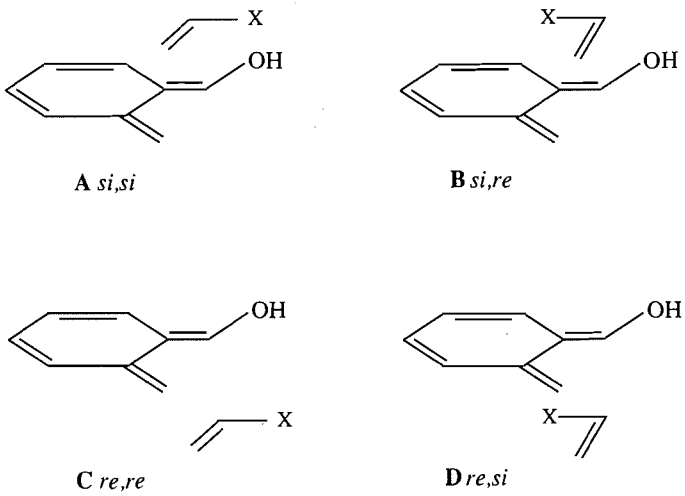
Previous work on *E*-α-hydroxy *o*-QDMs with achiral dienophiles such as dimethyl fumarate or methyl acrylate has shown that the major cycloadducts formed are **BB** or **DD**, having been formed via the *endo* transition states **B** or **D** shown in Scheme 2 (6, 15–18). The tendency towards *endo* transition states in Diels–Alder reactions (known as the Alder *endo* rule) has been explained on the basis of secondary orbital interactions between the electron-withdrawing group on the dienophile and carbon 2 of the diene (19). Solvent effects have shown that polar interactions between the diene and dienophile favor the *exo* transition states such as **A** and **C** (20). Transition states **A** and **C** and the resulting cycloadducts **AA** and **CC** are also thermodynamically more stable for steric reasons.

According to the most recent publication of Helmchen and co-workers, the most stable conformation of the fumarate of

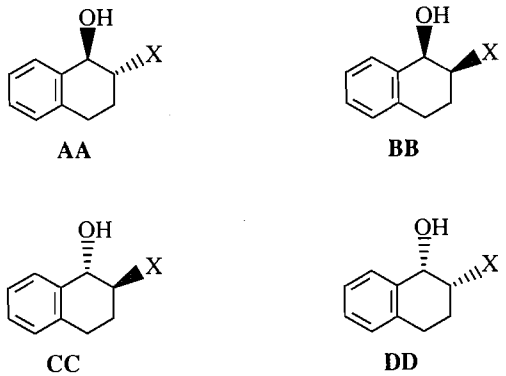
Can. J. Chem. Downloaded from www.nrcresearchpress.com by 41.223.56.140 on 09/07/12
For personal use only.



SCHEME 1



SCHEME 2. Reaction modes of *o*-QDM and dienophile classified according to their respective prochiral faces.



SCHEME 3

S-ethyl lactate is that shown in structure **7***a*, and addition of dienes to this dienophile occurs to the less hindered *re* (upper) face (11). Decreasing the polarity if the reaction medium increases the stereoselectivity for addition to the *re* face (11, 21). The reaction of the acrylate of *S*-ethyl lactate, **8***a*, with cyclopentadiene has been shown to yield primarily the *endo-re* cycloadduct as shown in **9** but the percentage of *exo* adduct increases with decreasing solvent polarity of the reaction medium as expected (20, 21).

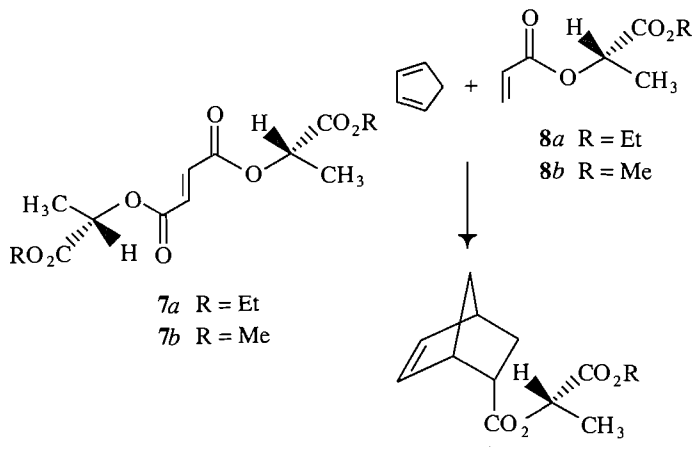
Based on the preceding work, we expected that the Diels–Alder cycloaddition between an α-hydroxy *o*-QDM and **8***b* would give a cycloadduct of configuration **BB** via transition state **B** and that the fumarate **7***b* would react analogously.

Results and discussion

2-Methylbenzaldehyde was prepared by reduction of *o*-toluic acid ($LiAlH_4$) and reoxidation to the aldehyde with chromic acid.

The fumarate and acrylate of *S*-methyl lactate (**7***a* and **8***b*) were prepared by heating the corresponding acid chlorides with the *S*-methyl lactate. Irradiations of benzene solutions of mixtures of the fumarate or acrylate and 2-methylbenzaldehyde were carried out under nitrogen using a 450-watt Hanovia medium pressure mercury lamp and a Pyrex filter (see Experimental for details).

Irradiation of 2-methylbenzaldehyde with an excess of the fumarate **7***b* gave a single crystalline cycloadduct, which was isolated by column chromatography in 55% yield. The nmr (300 MHz) of the crude irradiation product exhibited no signals consistent with the presence of other diastereomeric cycloadducts, indicating a de of >95%. The only other significant product was the maleate of *S*-methyl lactate, presumably formed via a photoisomerization of the starting fumarate. The



Can. J. Chem. Downloaded from www.nrcresearchpress.com by 41.223.56.140 on 09/07/12
For personal use only.

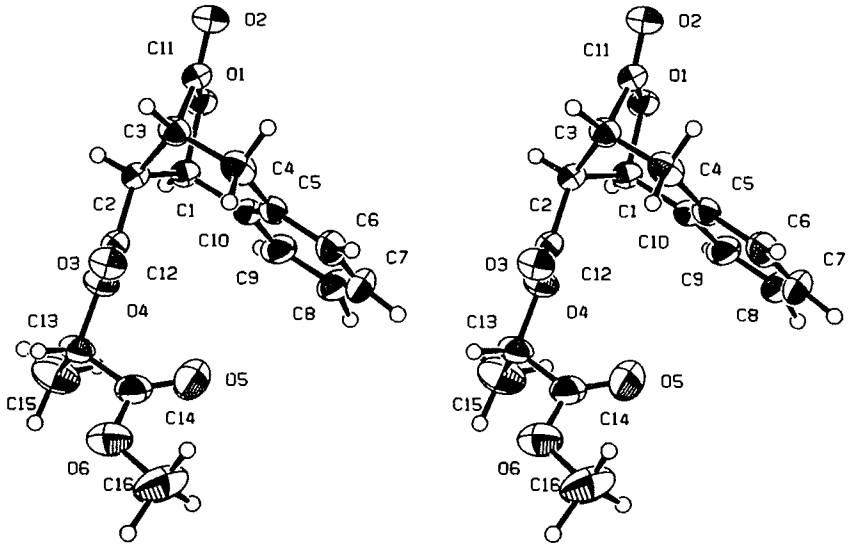
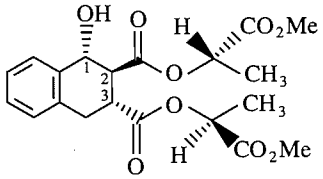


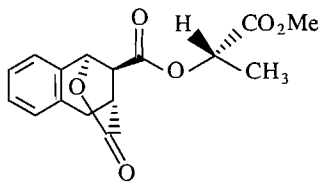
FIG. 1. Stereodiagram of the lactone, **11**; thermal ellipsoids at 50% probability level.

photoisomerization is probably sensitized by energy transfer from the excited 2-methylbenzaldehyde since irradiation of the fumarate in benzene alone gave only traces of the maleate isomer. The actual yield of the cycloadduct is much higher than the 55% isolated chromatographically, but we found it very difficult to separate the product from the maleate. The H-1 proton in the cycloadduct was clearly visible in the nmr, and a coupling constant ($J_{1,2}$) of 9.8 Hz suggested a *trans* disposition of the substituents on carbons 1 and 2. Similar compounds having a *cis* disposition of the 1 and 2 substituents have been found to exhibit a $J_{1,2}$ less than 5 Hz (17, 22). Although a *trans* 1,2 stereochemistry would mean that the cycloadduct would have formed via an unusual (see above) *exo* transition state (**A** or **C**), we tentatively assigned the cycloadduct structure **10**. The absolute stereochemistry shown in **10** is that which would arise from addition to the *re* face of the fumarate as expected.



10

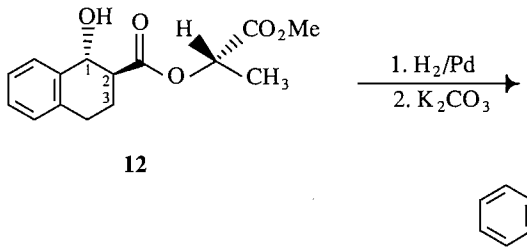
Treatment of the cycloadduct with toluenesulfonic acid in methylene chloride at room temperature for 3 days caused the elimination of one molecule of methyl lactate (determined by nmr), giving a product that appeared from ir to be a lactone (1788 cm^{-1}). The formation of a lactone between the 1-hydroxyl and the 3-carboxy group is not unreasonable and has been observed previously in a similar molecule (23). Thus the elimination product was assigned structure **11** shown below.



11

The lactone **11** fortunately produced crystals suitable for X-ray crystallography and we were therefore able to determine the relative stereochemistry of the chiral centers in **11** as shown in the ORTEP (24) drawing of **11** (Fig. 1). Since the absolute configuration of the lactate centers in **11** is known (*S*), the absolute configurations of the other centers could be assigned. In this way the absolute configuration of centers 2 and 3 in the cycloadduct was confirmed to be that shown in structure **10**. The relative stereochemistry of center 1 in **10** is based primarily on the nmr of **10** (see above) since inversion of this center could have occurred during the conversion of **10** to **11**.

Irradiation of 2-methylbenzaldehyde with an excess of acrylate **8***b* in a manner similar to that described above yielded only a single cycloadduct, which was purified by column chromatography (55% after chromatography). This adduct also exhibited a $J_{1,2}$ of 9.3 Hz, again indicative of a *trans* 1,2 stereochemistry. Based on our experience with the fumarate above, this acrylate adduct was assigned structure **12**. Nuclear



12

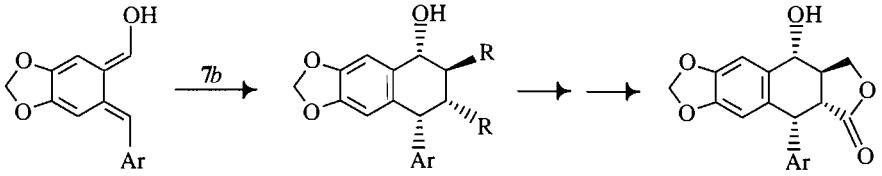
13

magnetic resonances of the crude cycloaddition product mixture did exhibit small signals, other that those due to **12**, which may be due to traces of other diastereomeric adducts. From integration we estimate that, as with the fumarate adduct, **12** is formed with a de of at least 95%. Hydrogenolysis and hydrolysis of **12** converted it to the known *S*-2-carboxy-1,2,3,4-tetrahydronaphthalene **13** ($[\alpha]_D$ −53° (lit. (25) $[\alpha_D]$ +55.5° for *R*)), confirming the assignment of the *S* configuration for center 2 and the absolute configuration of **12**.

Conclusions

From the results and discussion above we can conclude that

Can. J. Chem. Downloaded from www.nrcresearchpress.com by 41.223.56.140 on 09/07/12
For personal use only.



14

Ar = 3,4,5-trimethoxyphenyl; R = *S*-methyl lactylcarboxy

the cycloaddition of α-hydroxy *o*-QDM to the acrylate and fumarate of *S*-methyl lactate occurred between the *re* face of the dienophile and the *re* face of the *o*-QDM (mode **C** to give adduct type **CC**) (*exo* addition) with a diastereoselectivity of at least 95%. This is the first example of an intermolecular asymmetric cycloaddition to an *o*-QDM (giving a single enantiomer) that has high enough stereoselectivity to be truly synthetically useful (6). Based on earlier observations (see Introduction) we had expected addition by mode **B** to give adduct type **BB** (*re* face of the dienophile and *si* face of the *o*-QDM). The addition to the *re* face of the dienophile is as expected from earlier work of Helmchen and co-workers (2, 11, 21) and may be due to steric effects of the chiral auxiliary. The exclusive addition to the *re* face of the α-oxy center of the *o*-QDM (*exo* addition) is highly unusual and has not been observed previously for intermolecular cycloadditions of α-oxy *o*-QDMs except for those bearing an α′-phenyl group as well (17, 26). *Exo* addition to *o*-QDMs is common for intramolecular cycloadditions due to conformational preferences in the transition state (27). Perhaps hydrogen bonding between the α-hydroxy group of the *o*-QDM and the dienophiles used in this study make the subsequent addition more analogous to an intramolecular addition. Further studies of the mechanism underlying the diastereoselectivity and of the use of these highly selective reactions in asymmetric synthesis are in progress. We are particularly interested in whether addition of the fumarate **7** to an α-hydroxy-α′-aryl *o*-QDM will add with the same selectivity. If so, a very short asymmetric synthesis of podophyllotoxin **14** might be possible (28).

Experimental

The ^{1}H nmr spectra were recorded on a Bruker AM-300 instrument using tetramethylsylane as internal standard. The ir spectra were recorded on a Perkin Elmer 881 spectrometer. Merck Kieselgel 60 was used for all chromatography. Elemental analyses were performed by Guelph Chemical Laboratories Ltd., Guelph, Ontario, Canada. Exact mass/mass spectra were obtained on an Analytical VG 7070E-HF instrument. Melting points were measured on a hot stage instrument and are uncorrected. Optical rotations were recorded on a Rudolf Research Corporation Autopol III instrument.

Acrylate of S*-methyl lactate,* **8**b

A mixture of *S*-methyl lactate (4.42 g, 42.2 mmol), acryloyl chloride (11.53 g, 10.4 mL, 127 mmol, 3 equiv.), and 3 Å molecular sieves (9 g) in CCl_4 was heated to reflux under nitrogen for 4 days. The mixture was filtered, evaporated, and chromatographed (20% ethyl acetate/hexane) to give a colourless oil (5.83 g, 87%) that was >97% pure by nmr (300 MHz); $[\alpha]_D^{20}$–43.5° (*c* 0.433, $CHCl_3$); ir (CH_2Cl_2): 1768, 1740 cm^{-1}; ^{1}H nmr ($CDCl_3$) δ: 1.55 (d, 3H, $J_{1',2'}$ = 7.1), 3.76 (s, 3H), 5.16 (q, 1H, $J_{1,2}$ = 7.1), 5.88 (dd, 1H, $J_{2,2'}$ = 1.3, $J_{1,2}$ = 10.4), 6.20 (dd, 1H, $J_{1,2}$ = 10.4, $J_{1,2'}$ = 17.2), 6.46 (dd, 1H, $J_{2,2'}$ = 1.3, $J_{1,2'}$ = 17.2); mass spectrum *m/e* (rel. %) neohexane chemical ionization: 159 (12, *M* + 1), 127 (20), 71 (55), 55 (100); ammonia chemical ionization: 176 (10, *M* + 14), 159 (25, *M* + 1), 127 (20), 72 (17), 55 (100); electron impact: 114 (18), 99 (25), 55 (100).

Fumarate of S*-methyl lactate,* **7**b

A mixture of *S*-methyl lactate (5.44 g, 52.3 mmol) and fumaryl chloride (4.00 g, 26.1 mmol) was heated at 100°C for 20 h, dissolved in ethyl acetate, washed with aqueous $NaHCO_3$ (5%), dried ($MgSO_4$), and evaporated to give a yellow oil (7.58 g). The oil (1 g) was chromatographed (15% ethyl acetate/hexane) to give a colourless oil (0.62 g, 62% overall, >95% pure by 300 MHz nmr); $[\alpha]_D^{20}$–15.5° (*c* 0.32, $CHCl_3$); ir (CH_2Cl_2): 1733 cm^{-1}; ^{1}H nmr ($CDCl_3$) δ: 1.56 (d, 3H, *J* = 7.1, CH_3), 3.77 (s, 3H, OCH_3), 5.22 (q, 1H, *J* = 7.1), 6.97 (s, 2H); mass spectrum *m/e* (rel. %): 288 (10), 185 (65), 140 (20), 113 (23), 99 (20), 87 (100), 59 (31). *Exact Mass* calcd. for $C_{12}H_{16}O_8$: 288.0848; found 288.0845.

Cycloadduct of acrylate **8**b *and 2-methylbenzaldehyde,* **12**

A solution of 2-methylbenzaldehyde (133 mg, 1.1 mmol), acrylate **8***b* (0.228 g, 1.44 mmol, 1.3 equiv.), and hydroquinone (1 mg) in benzene (30 mL) was purged with nitrogen and irradiated with a Hanovia 450-watt medium pressure mercury lamp through a Pyrex filter from a distance of 10 cm for 17 h. The solvent was evaporated and the residue chromatographed (40% ethyl acetate/hexane) to give an oil (107 mg, 55%); $[\alpha]_D^{20}$=36.3° (*c*, 1.35, $CHCl_3$); ir (CH_2Cl_2): 3499, 1739 cm^{-1}; ^{1}H nmr ($CDCl_3$) δ: 1.55 (d, 3H, $J_{1',2'}$ = 7.1), 2.00 (m, 1H), 2.20 (m, 1H), 2.84 (m, 3H), 3.79 (s, 3H), 5.00 (d, 1H, $J_{1,2}$ = 9.3), 5.23 (q, 1H, $J_{1',2'}$ = 7.1), 7.20 (m, aromatics); mass spectrum *m/e* (rel. %): 278 (3), 173 (21), 156 (28), 146 (86), 129 (100). *Exact Mass* calcd. for $C_{15}H_{18}O_5$: 278.11543; found: 278.11534.

1,2,3,4-Tetrahydronaphthalene-2-carboxylate of S*-methyl lactate*

Cycloadduct **12** (146 mg, 0.525 mmol) and 5% palladium on charcoal (30 mg) in acetic acid (10 mL) were stirred under hydrogen (1 atom (101.3 kPa)) at 70°C for 3 days. The mixture was filtered, diluted with CH_2Cl_2 (40 mL), washed with water and 5% aqueous $NaHCO_3$, dried ($MgSO_4$), and evaporated to give a colourless oil (118 mg, 87%); $[\alpha]_D^{20}$–38.4° (*c*, 0.55, $CHCl_3$); ir (CH_2Cl_2): 1740 cm^{-1}; ^{1}H nmr ($CDCl_3$) δ: 1.50 (d, 3H, $J_{1',2'}$ = 7.1), 1.90 (m, 1H), 2.25 (m, 1H), 2.85 (m, 3H), 3.10 (m, 2H), 3.75 (s, 3H), 5.15 (q, 1H, $J_{1',2'}$ = 7.1), 7.10 (m, aromatics); mass spectrum *m/e* (rel. %): 262 (2), 137 (37), 130 (100), 129 (26), 115 (14). *Exact Mass* calcd. for $C_{13}H_{18}O_4$: 262.1205; found: 262.1201.

S*-(−)-1,2,3,4-tetrahydronaphthalene-2-carboxylic acid,* **13**

A solution of the methyl lactyl ester of **13** (118 mg, 0.45 mmol) and K_2CO_3 (200 mg) in methanol (15 mL) and water (2 mL) was refluxed for 4 h. Most of the methanol was evaporated, and the solution diluted with water and washed with CH_2Cl_2. The aqueous portion was then acidified with 10% HCl and extracted with CH_2Cl_2, dried ($MgSO_4$), and evaporated to give crystals (69 mg, 86%). Recrystallization from methylene chloride/hexane gave colourless needles; mp 98–100°C; $[\alpha]_D^{20}$–53° (*c*, 0.788, $CHCl_3$); ir (CH_2Cl_2): 1707 cm^{-1}; ^{1}H nmr ($CDCl_3$) δ: 1.90 (m, 1H), 2.25 (m, 1H), 2.85 (m, 3H), 3.05 (m, 2H), 7.12 (m, aromatics); mass spectrum *m/e* (rel. %): 177 (4), 176 (35), 131 (32), 130 (100), 115 (17), 104 (20). *Exact Mass* calcd. for $C_{11}H_{12}O_2$: 176.0837; found: 176.0843.

Cycloadduct of fumarate **7**b *and 2-methylbenzaldehyde,* **10**

A solution of 2-methylbenzaldehyde (96.7 mg, 0.81 mmol) and fumarate **7***b* (331.1 mg, 1.15 mmol, 1.42 equiv.) in benzene (30 mL) was flushed with nitrogen and irradiated for 6 h using a 450-watt

Can. J. Chem. Downloaded from www.nrcresearchpress.com by 41.223.56.140 on 09/07/12
For personal use only.

Can. J. Chem. Downloaded from www.nrcresearchpress.com by 41.223.56.140 on 09/07/12
For personal use only.

TABLE 1. Fractional atomic coordinates (esd's) and equivalent isotropic temperature factors, B_{eq} (Å^2) for the lactone **11**

Atom	x	y	z	B(eq)
O(1)	0.0418(2)	−0.02421(9)	0.2832(4)	3.9(1)
O(2)	0.0013(2)	−0.10465(8)	0.4570(5)	5.6(1)
O(3)	0.1658(2)	0.0813(1)	0.8769(4)	4.2(1)
O(4)	0.2168(2)	0.11781(8)	0.5578(4)	3.9(1)
O(5)	0.0331(3)	0.1931(2)	0.6896(9)	11.2(3)
O(6)	0.1684(3)	0.2296(1)	0.9224(5)	6.5(1)
C(1)	0.0705(3)	0.0345(1)	0.3495(5)	3.2(1)
C(2)	0.1435(3)	0.0248(1)	0.5585(5)	3.0(1)
C(3)	0.0553(3)	−0.0194(1)	0.6597(5)	3.7(1)
C(4)	−0.0716(3)	0.0073(1)	0.7336(6)	4.5(2)
C(5)	−0.1207(3)	0.0524(1)	0.5796(6)	3.8(1)
C(6)	−0.2337(3)	0.0816(2)	0.6263(9)	6.0(2)
C(7)	−0.2765(4)	0.1226(2)	0.483(1)	7.7(3)
C(8)	−0.2110(5)	0.1344(2)	0.295(1)	6.7(2)
C(9)	−0.0984(4)	0.1060(1)	0.2510(7)	4.9(2)
C(10)	−0.0536(3)	0.0651(1)	0.3920(5)	3.4(1)
C(11)	0.0299(3)	−0.0558(1)	0.4637(6)	4.0(1)
C(12)	0.1728(3)	0.0770(1)	0.6856(5)	3.0(1)
C(13)	0.2558(4)	0.1697(1)	0.6640(6)	4.4(2)
C(14)	0.1384(4)	0.1977(1)	0.7568(7)	5.2(2)
C(15)	0.3198(7)	0.2049(2)	0.492(1)	7.4(3)
C(16)	0.0614(7)	0.2592(2)	1.030(1)	9.2(4)

TABLE 2. Non-hydrogen atom bond lengths (esd's) in Å for the lactone **11**

Atoms	Length	Atoms	Length
O(1)—C(11)	1.350(4)	C(2)—C(3)	1.525(4)
O(1)—C(1)	1.477(3)	C(3)—C(11)	1.510(5)
O(2)—C(11)	1.194(4)	C(3)—C(4)	1.532(5)
O(3)—C(12)	1.192(3)	C(4)—C(5)	1.518(5)
O(4)—C(12)	1.330(3)	C(5)—C(10)	1.388(5)
O(4)—C(13)	1.450(4)	C(5)—C(6)	1.393(5)
O(5)—C(14)	1.175(5)	C(6)—C(7)	1.389(8)
O(6)—C(14)	1.311(5)	C(7)—C(8)	1.378(8)
O(6)—C(16)	1.473(6)	C(8)—C(9)	1.374(6)
C(1)—C(10)	1.502(4)	C(9)—C(10)	1.383(5)
C(1)—C(2)	1.518(4)	C(13)—C(14)	1.502(5)
C(2)—C(12)	1.494(4)	C(13)—C(15)	1.508(6)

Hanovia medium pressure mercury lamp through a Pyrex filter from a distance of 10 cm. The solvent was then evaporated *in vacuo* to give a colorless oil, which was chromatographed (10% ethyl acetate/hexane) to give a crystalline solid (180.6 mg, 55%) that was >95% pure (300 MHz nmr). Recrystallization from hexane gave colourless needles; mp 84.5–85.0°C; $[\alpha]_D^{20}$– 64° (*c* 0.74, $CHCl_3$); ir (CH_2Cl_2): 3471, 1743 cm^{-1}; ^{1}H nmr ($CDCl_3$) δ: 1.52 (d, 3H, *J* = 7.1, CH_3), 1.58 (d, 3H, *J* = 7.1, CH_3), 3.05 (m, 2H, H-2, H-4a), 3.27 (m, 2H, H-3, H-4b), 3.75 and 3.82 (s, 3H, OCH_3), 4.53 (br s, 1H, OH), 4.95 (d, 1H, *J* = 9.8, H-1), 5.13 (q, 1H, *J* = 7.1, H-1′), 5.31 (q, 1H, *J* = 7.1, H-1″), 7.11–7.27 (m, aromatics), 7.70 (d, 1H, *J* = 7.2, aromatics); mass spectrum *m/e* (rel. %): 408(2), 304(12), 276(17), 258(37), 201(34), 200(24), 173(35), 172(44), 171(19), 156(28), 155(100), 145(87), 129(78), 128(93), 127(24). *Exact Mass* calcd. for $C_{20}H_{24}O_9$: 408.1420; found: 408.1430. *Anal.* calcd. for $C_{20}H_{24}O_9$: C 58.80, H 5.93; found: C 58.81, H 5.70.

Lactone **11**

A solution of cycloadduct **10** (340 mg, 0.83 mmol) and *p*-toluenesulfonic acid (150 mg) in methylene chloride (40 mL) was stirred at room temperature for 3 days and then evaporated to give a semicrystalline solid. The product was chromatographed (25% ethyl acetate/hexane) to give a white crystalline solid (131 mg, 0.43 mmol, 52%), which was recrystallized from hexane and methylene chloride (traces) to afford white needles; mp 130.0–130.5°C; $[\alpha]_D^{20}$–22.0° (*c*, 1.18, $CHCl_3$); ir (CH_2Cl_2): 1747, 1788 cm^{-1}; ^{1}H nmr ($CDCl_3$) δ: 1.38 (d, 3H, *J* = 7.0, CH_3), 3.10 (d, 1H, *J* = 17.7, H-4a), 3.35 (m, 1H, H-3), 3.48 (dd, 1H, *J* = 5.2, 17.7, H-4b), 3.50 (s, 3H, OCH_3), 3.85 (t, 1H, *J* = 5.0, H-2), 4.95 (q, 1H, *J* = 7.0, H-1′), 5.48 (d, 1H, *J* = 5.0, H-1), 7.23 (m, aromatics); mass spectrum *m/e* (rel. %): 304 (16), 201 (19), 200 (34), 172 (10), 156 (18), 145 (17), 144 (25), 129 (68), 128 (100), 127 (16), 117 (11), 115 (12). *Exact Mass* calcd. for $C_{16}H_{16}O_6$: 304.0947; found: 304.0944. *Anal.* calcd. for $C_{16}H_{16}O_6$: C 63.14, H 5.30; found: C 62.96, H 5.51.

X-ray analysis

Crystals of the lactone **11** suitable for X-ray structure analysis were grown from a hexane/methylene chloride solution. The crystal chosen for data collection measured 0.20 mm × 0.15 mm × 0.06 mm and was mounted in a general orientation on a Rigaku AFC6S diffractometer. Unit cell parameters were obtained from the setting angles of 25 reflections in the range 36° < 2θ <51°; 1664 reflections were measured with graphite-monochromatized CuKα radiation ($2\theta_{max}$ = 150°); 1270 were considered observed with $I > 3\sigma(I)$. Standard reflections showed no change over the period of data collection. Lorentz and polarization corrections were applied, but correction for absorption was not warranted.

The structure was solved by direct methods and refined by full-matrix least-squares procedures using the TEXSAN system of computer programs (29). Final values for $R = \Sigma \| F_o | - | F_c \| / \Sigma | F_o |$ and $R_w = [\Sigma w(| F_o | - | F_c |)^2 / \Sigma w | F_o |^2]^{1/2}$ were 0.034 and 0.043, respectively, for 1270 observed data and 264 variables; for all 1664 data, $R = 0.063$ and $R_w = 0.045$. The goodness of fit was 1.43 with weights of $\sigma^{-2}(F_o)$, and the maximum shift in the final cycle of refinement was 0.18σ. The largest peak in the final difference map was 0.12 e Å^{-3}.

Non-hydrogen atom coordinates are given in Table 1 and selected bond lengths are given in Table 2. Hydrogen coordinates, complete lists of bond lengths and angles, temperature factors, and structure factors have been deposited as supplementary material.[2]

Crystal data:

$C_{16}H_{16}O_6$ *fw* = 304.30

Orthorhombic, $P2_12_12_1$, a = 10.387(2), b = 23.637(5), c = 6.195(1) Å, V = 1521.0(5) Å^3, Z = 4, ρ_c = 1.33 Mg m^{-3}, μ = 8.19 cm^{-1} (21°C; CuKα, λ = 1.54178 Å), $F(000)$ = 640.

Acknowledgments

We are grateful to the Natural Sciences and Engineering Research Council of Canada for financial support of this project. We are also indebted to Drs. James Trotter and Steven Rettig, Department of Chemistry, University of British Columbia, for allowing one of us (A.S.S.) to collect data and to solve and refine the structure on their X-ray diffraction and computing facilities.

1. D. A. EVANS, K. T. CHAPMAN, and J. BISAHA. J. Am. Chem. Soc. **110**, 1238 (1988), and references cited.
2. G. HELMCHEN, R. KARGE, and J. WEETMAN. *In* Modern synthetic

[2]Tables of supplementary data may be purchased from the Depository of Unpublished Data, CISTI, National Research Council of Canada, Ottawa, Ontario, Canada, K1A 0S2.

Hydrogen atom coordinates and tables of bond lengths and angles have also been deposited with the Cambridge Crystallographic Data Centre, and can be obtained on request from the Director, Cambridge Crystallographic Data Centre, University Chemical Laboratory, Lensfield Road, Cambridge CB2 1EW, U.K.

methods. Vol. 4. *Edited by* R Scheffold. Springer Verlag, New York. 1986. p. 261.
3. S. D. KAHN and W. J. HEHRE. J. Am. Chem. Soc. **109**, 663 (1987).
4. W. OPPOLZER. Angew. Chem. Int. Ed. Engl. **23**, 876 (1984).
5. O. DE LUCCHI, V. LUCCHINI, C. MARCHIORO, G. VALLE, and G. MODENA. J. Org. Chem. **51**, 1457 (1986), and references cited.
6. J. L. CHARLTON and M. M. ALAUDDIN. Tetrahedron, **43**, 2873 (1987), and references cited (1–13).
7. Y. ITO, Y. AMINO, M. NAKATSUKA, and T. SAEGUSA. J. Am. Chem. Soc. **105**, 1586 (1983).
8. J. L. CHARLTON. Can. J. Chem. **64**, 720 (1986).
9. J. L. CHARLTON and M. M. ALAUDDIN. J. Org. Chem. **51**, 3490 (1986).
10. R. W. FRANCK, T. V. JOHN, and K. OLEJNICZAK. J. Am. Chem. Soc. **104**, 1106 (1982).
11. H. HARTMANN, A. F. A. HADY, K. SARTOR, J. WEETMAN, and G. HELMCHEN. Angew. Chem. Int. Ed. Engl. **26**, 1143 (1987).
12. B. J. ARNOLD, P. G. SAMMES, and T. W. WALLACE. J. Chem. Soc. Perkin Trans. **1**, 409 (1974).
13. J. L. CHARLTON and KEVIN KOH. Tetrahedron Lett. **29**, 5595 (1988).
14. M. PFAU, S. COMBRISSON, J. E. ROWE, JR., and N. D. HEINDEL. Tetrahedron, **34**, 3459 (1978).
15. M. PFAU, J. E. ROWE, JR., and N. D. HEINDEL. Tetrahedron, **34**, 3469 (1978).
16. P. G. SAMMES. Tetrahedron, **32**, 405 (1976).
17. M. B. GLINSKI and T. DURST. Can. J. Chem. **61**, 573 (1983).
18. E. BLOCK and R. STEVENSON. J. Chem. Soc. Perkin Trans. **1**, 308 (1973).
19. I. FLEMING. *In* Frontier orbitals and organic chemical reactions. Wiley, New York. 1976. p. 106.
20. J. A. BERSON, Z. HAMLET, and W. A. MUELLER. J. Am. Chem. Soc. **84**, 297 (1962).
21. T. POLL, G. HELMCHEN, and B. BAUER. Tetrahedron Lett. **25**, 2191 (1984).
22. T. DURST, E. C. KOZMA, and J. L. CHARLTON. J. Org. Chem. **50**, 4829 (1985).
23. B. J. ARNOLD, S. M. MELLOWS, P. G. SAMMES, and T. W. WALLACE. J. Chem. Soc. Perkin Trans. **1**, 401 (1974).
24. C. K. JOHNSON. ORTEP II: Report ORNL-TM-306-5138, Oak Ridge National Laboratory, Oak Ridge, TN. 1976.
25. A. SCHOOFS, J. P. GUETTE, and A. HOREAU. Bull Chim. Soc. Fr. 1215 (1976).
26. J. L. CHARLTON, M. M. ALAUDDIN, and G. H. PENNER. Can. J. Chem. **64**, 793 (1986).
27. A. G. FALLIS. Can. J. Chem. **62**, 183 (1984).
28. D. I. MACDONALD and T. DURST. J. Org. Chem. **53**, 3663 (1988), and references cited.
29. TEXSAN: A structure-solving, refinement and analysis program library, Molecular Structure Corporation, College Stn., TX.

Can. J. Chem. Downloaded from www.nrcresearchpress.com by 41.223.56.140 on 09/07/12
For personal use only.

The chemistry of thujone. XIII.[1] Synthetic studies in the digitoxigenin series

JAMES P. KUTNEY,[2] KRYSTYNA PIOTROWSKA, JOHN SOMERVILLE, SHYH-PYNG HUANG, AND STEVEN J. RETTIG
Department of Chemistry, 2036 Main Mall, University of British Columbia, Vancouver, B.C., Canada V6T 1Y6
Received September 23, 1988

JAMES P. KUTNEY, KRYSTYNA PIOTROWSKA, JOHN SOMERVILLE, SHYH-PYNG HUANG, and STEVEN J. RETTIG. Can. J. Chem. **67**, 580 (1989).

The thujone-derived chiral synthon **1** is converted, via selenium chmistry, to the important cross-conjugated dienone **2** and the latter is then convertible to the unsaturated cardenolide analogue **3**, which through known methodology (**3** → **26** → **27** → **4**), completes a formal synthesis of digitoxigenin (**4**). Extensive studies to afford **2** from androstenedione (**5**) are also described and a new approach to elaborate the essential butenolide ring system, characteristic of the cardiac active steroids, is developed.

Key words: thujone, steroid synthesis, digitoxigenin.

JAMES P. KUTNEY, KRYSTYNA PIOTROWSKA, JOHN SOMERVILLE, SHYH-PYNG HUANG et STEVEN J. RETTIG. Can. J. Chem. **67**, 580 (1989).

En utilisant la chimie du sélénium, on a transformé le synthon chiral **1**, obtenu à partir de la thujone, en la diénone importante **2** à conjugaison croisée que l'on peut convertir en analogue cardénolide insaturé **3**; ce composé, par le biais d'une méthodologie connue (**3** → **26** → **27** → **4**), donne lieu à une synthèse formelle de la digitoxigénine (**4**). On décrit aussi les études poussées qui ont été effectuées pour obtenir le composé **2** à partir de l'androstènedione (**5**) et on a développé une nouvelle approche au système cyclique buténolide essentiel, caractéristique des stéroïdes actifs au niveau cardiaque.

Mots clés : thujone, synthèse des stéroïdes, digitoxigénine.

[Traduit par la revue]

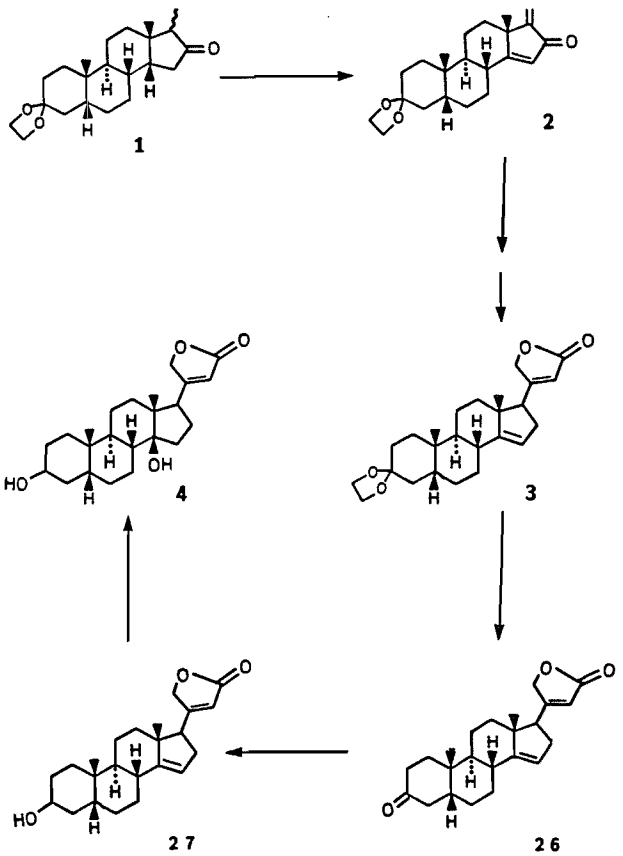
Can. J. Chem. Downloaded from www.nrcresearchpress.com by 41.223.56.140 on 09/07/12
For personal use only.

The cardiac active steroids are a well-known group of naturally occurring steroidal lactones of importance in the treatment of heart disease. One of the most commonly used cardiac active glycosides in medicine is digitoxin, isolated from *Digitalis purpurea* (Purple Foxglove) and the main constituent of the well-established heart drug, digitalis. This drug is responsible for one of the highest rates of drug-induced hospital admissions (2) since, to achieve the desired therapeutic effects, 60% of the lethal dose of the drug must be administered and, depending on the physical condition of the patient, the toxic dose can be much lower than anticipated (3). This latter effect is especially pronounced in the treatment of infants where the lethal dose can be much lower than the physician would estimate (4). As a result, there has been considerable incentive for medicinal chemists to synthesize analogues of the digitoxin system in the hope that an improved therapeutic index can be achieved.

Previous synthetic studies in various laboratories (5–17) have afforded synthetic routes to this series of compounds. In these studies, steroidal starting materials were employed and different routes to the butenolide ring system, characteristic of this family of natural products, were developed. We wish to present our studies involving thujone-derived chiral substrates as starting materials for the syntheses of compounds within this family.

Earlier studies in our laboratory (18, 19) revealed efficient routes to the chiral synthon **1** from thujone and we present herein the most recent results, in which **1** is converted into the appropriate building units for the digitoxigenin (**4**) series. The overall strategy of the synthetic program is summarized in Scheme 1.

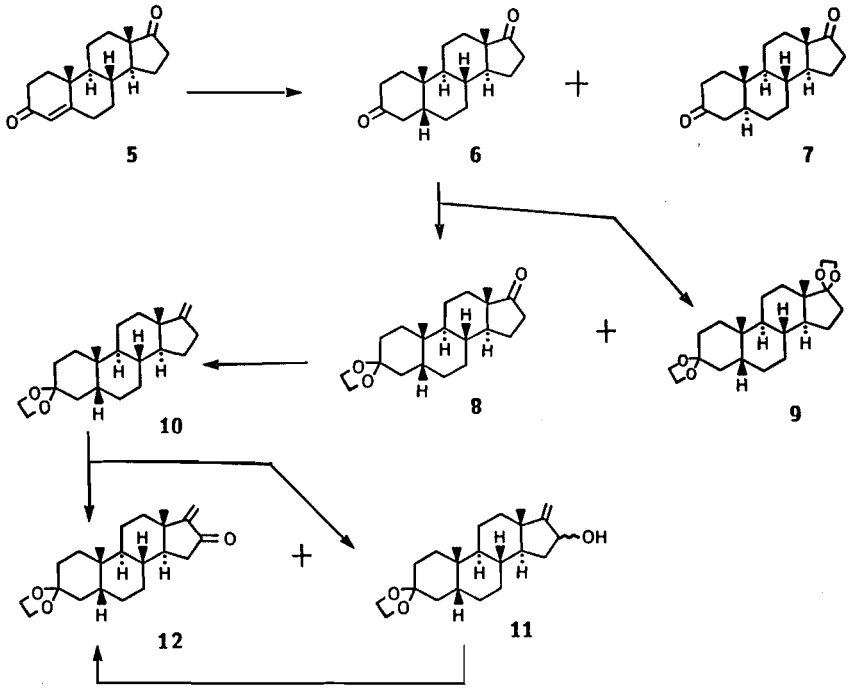
It is well established that one of the important synthetic requirements in deriving the cardiac active steroid system involves the introduction of the C14-α hydroxyl group. With the exception of one study (11) involving remote functionalization, the utilization of conventional steroid substrates, normally lacking this functionality, requires a number of synthetic steps



SCHEME 1

to introduce this functional group. The majority of the studies reported thus far depend on C14—C15 unsaturated steroids, derived from C17 functionalized steroids, which, in turn, via established chemistry, allow introduction of the C14 hydroxyl group. We felt that our thujone-derived steroid analogues, obtained earlier (18, 19), may be advantageous in affording a more direct route to such unsaturated steroid systems. For

[1]For Part XII, see ref. 1.
[2]Author to whom correspondence may be addressed.



SCHEME 2

example, the thujone-derived intermediates possessing a cyclopropyl ring attached to ring D of the steroid system would, after cyclopropyl ring opening and oxidative cleavage of the resulting unsaturated side chain (18), allow facile entry into 16-keto-17-methyl steroids as exemplified by **1** (Scheme 1). The carbonyl group allows efficient introduction of the required C14—C15 double bond while the C17 methyl group provides for subsequent attachment of the butenolide ring. With **1** on hand, the conversion **1** → **2** (Scheme 1) was considered in our initial phases of this program.

Selenium chemistry, as developed by Barton *et al.* (20), appeared well suited for the above conversion although private discussions with Barton revealed that five-membered ring carbonyl systems were not generally susceptible to dehydrogenation with benzeneseleninic anhydride. Neverthless, after considerable study with various reaction conditions, it was found that the desired dehydrogenation could be accomplished when a weak base (sodium bicarbonate) was employed. The dienone **2**, obtained in 42% overall yield, revealed the expected spectral characteristics (λ_{max} 249 nm; δ 5.23 (1H, s) and 5.97 (2H, s) for the olefinic protons).

It is noteworthy that the stereochemistry at C14 reflects the time and (or) yield in the above dehydrogenation reaction. The thujone-derived intermediate with the 14-β stereochemistry undergoes this reaction under milder conditions (42%, 20 h) while the corresponding 14-α isomer (**12**) (see later) converts to **2** only after 72 h (38%).

As the above thujone related chemistry was under study, a complementary route to **2** from the readily available steroid, androstenedione (**5**), was being developed. The latter study would allow comparisons of compounds prepared from these routes and thereby establish with certainty the total structure and absolute stereochemistry of **2**, as shown in Scheme 1. The overall sequence from **5** to **2** is summarized in Scheme 2.

Catalytic hydrogenation ($Pd/CaCO_3$) of **5** afforded a mixture of C5β (**6**) and C5α (**7**) isomers in an approximate ratio of 2:1 respectively and in excellent overall yield (95%). These isomers are conveniently separated by preparative hplc.

The desired A/B *cis* isomer (**6**) was treated with ethylene glycol and a catalytic amount of *p*-toluenesulfonic acid to provide the required C3 monoketal **8** as a major product (76%), and the latter, upon reaction under conventional Wittig olefination conditions, yielded the exocyclic olefin **10** (91%).

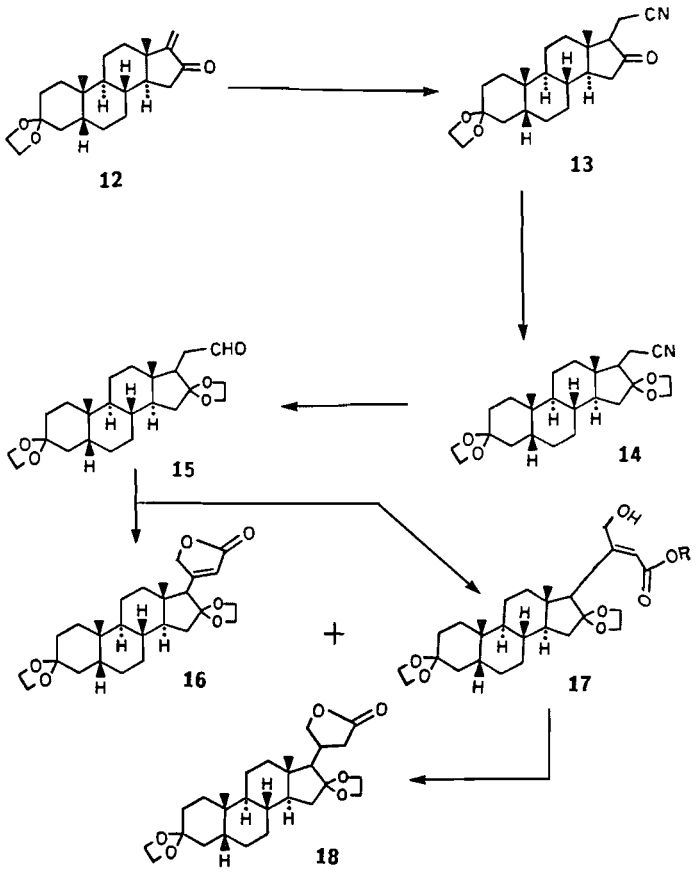
Allylic oxidation of **10** to a mixture of **11** and **12** followed essentially the procedure developed by Schmuff and Trost (21). The allylic alcohol **11** was the major product (75%) and facile separation from the ketone **12** could be achieved. However, for preparative purposes, the resulting mixture of **11** and **12** was subjected to treatment with oxalyl chloride and dimethyl sulfoxide to provide **12** in an overall yield of 82% from **10**. Dehydrogenation with benzeneseleninic anhydride afforded **2** (38%), identical in every respect with the product obtained earlier in the thujone sequence. As noted earlier, the conversion of **12** to **2** requires more drastic conditions (72 h vs. 20 h) than in the case of the corresponding C14-β isomer **1**. As we found later, an attractive alternative to the dehydrogenation reaction proved to be a method employed in the synthesis of the tricyclopentanoid (±)-coriolin (22). Thus, the enolate of the α,β-unsaturated ketone **12**, generated by treatment with lithium hexamethyldisilylamide in tetrahydrofuran at −40°C, was quenched with trimethylsilyl chloride to give the corresponding silyl-enol ether. Oxidation of this enol ether with 2,3-dichloro-5,6-dicyanoquinone resulted in the desired cross-conjugated dienone **2** in 84% yield.

The next phase of our synthetic program involved the development of appropriate chemistry for the elaboration of the required butenolide attached to ring D of the steroid skeleton. For this purpose, the conjugated ketone **12** was selected as starting material and the overall sequence is presented in Scheme 3.

Conjugate addition of cyanide proceeds smoothly to yield the cyano ketone **13** in 91% yield and the latter compound is

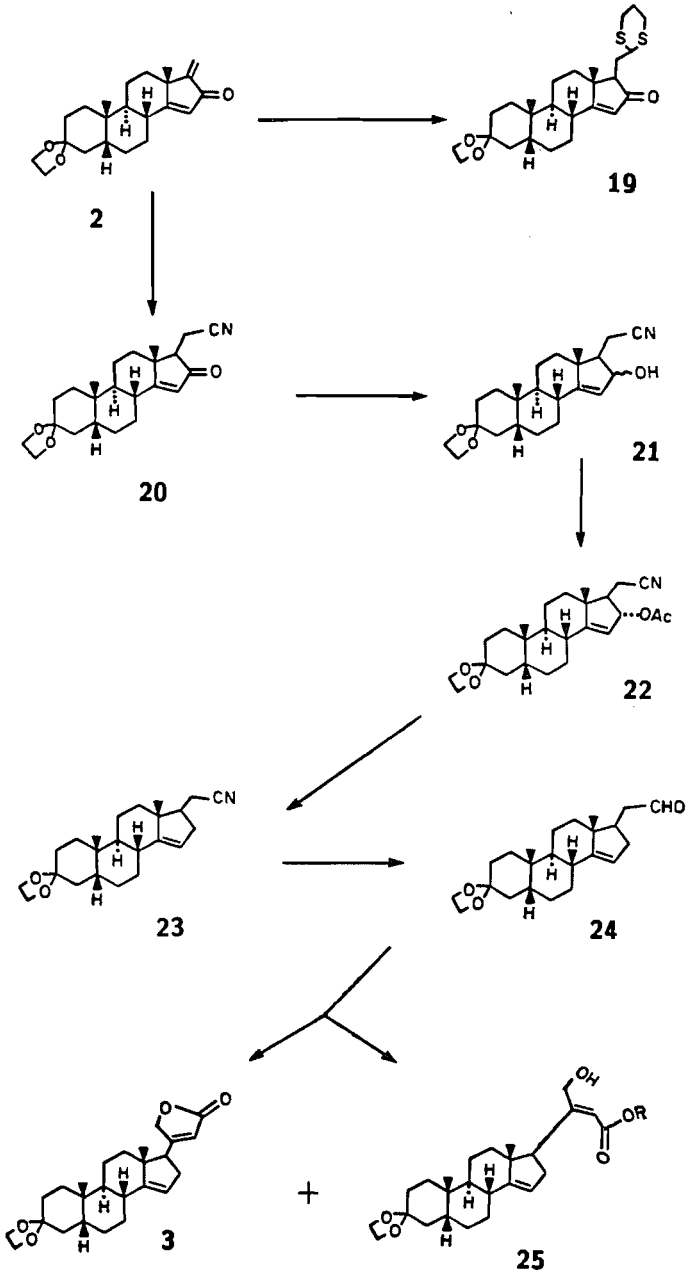
Can. J. Chem. Downloaded from www.nrcresearchpress.com by 41.223.56.140 on 09/07/12
For personal use only.

Can. J. Chem. Downloaded from www.nrcresearchpress.com by 41.223.56.140 on 09/07/12
For personal use only.



SCHEME 3

converted to the ketal **14** by conventional means. The proton and ^{13}C nmr spectra show that both compounds **13** and **14** are single isomers, rather than a mixture of C17 isomers as may be expected. To determine the configuration at C17, the nuclear Overhauser effect (nOe) was employed. Therefore, the nOe-difference experiment was performed for **13** and **14**. In the case of the cyano ketone **13**, irradiation at 0.75 ppm (C18 methyl group) resulted in the enhancement of a quartet at 2.17 ppm (assigned as one of the C20 proton signals). Similarly, in the case of the ketal derivative **14**, irradiation at 0.75 ppm (C18 methyl group) resulted in the enhancement of two quartets at 2.25 and 2.35 ppm (C20 hydrogens) but showed no effect on the C17 proton resonance. These results are consistent with the nitriles **13** and **14** having the desired C17-β configuration. DIBAL reduction of **14** afforded the important intermediate aldehyde **15** (79%). According to literature precedent, the conversion of the aldehyde function to the required butenolide ring system should be achieved. For example, Pettit *et al.*, in their extensive and elegant studies on syntheses of bufadienolides (23), established that steroidal ketones upon reaction with glyoxylic acid or its derivatives provide intermediates convertible to the desired lactones. Similarly Kreiser and Nazir (24) established that steroidal aldehydes undergo reaction with glyoxylic acid under acidic conditions (HCl or CH_3COOH, CH_3COONa) to afford the appropriate butenolide systems. Unfortunately, utilization of the latter conditions in the conversion **15** → **16** did not provide encouraging results and we turned our attention to the possibility of employing the stable methyl ester (25) in the condensation reaction with aldehyde **15**. Indeed reaction of **15** with potassium hydride and anhydrous menthyl



SCHEME 4

glyoxylate, followed by borohydride reduction, afforded a mixture of the desired butenolide **16** (17%) and the unsaturated hydroxyester **17** (24%, R = *l*-menthyl). The latter compound, on catalytic reduction to the saturated ester followed by alkaline hydrolysis and cyclization, affords the saturated lactone **18**, thereby potentially providing an additional source of the butenolide **16** via a dehydrogenation process.

Having established the above synthetic procedures with the more readily available ketone **12**, we turned our attention to studies with the cross-conjugated ketone **2**. Unfortunately the introduction of cyanide via conjugate addition employing the above-noted procedure afforded a complex mixture of products resulting from cyanide attack at both of the olefinic sites. However the Nagata procedure (26), in which diethylaluminum cyanide is involved, provided the desired cyano derivative **20** as a mixture of C17 isomers. This mixture was very difficult to separate, but after extensive chromatographic separations, it

Can. J. Chem. Downloaded from www.nrcresearchpress.com by 41.223.56.140 on 09/07/12
For personal use only.

was possible to obtain a pure sample of the major C17-β isomer (ratio of C17-β to C17-α is 2:1) for detailed nmr studies. The nOe difference experiments established the stereochemistry of the major product. Thus irradiation at 1.24 ppm (C18 methyl) resulted in enhancement (8%) of a quartet at 2.26 ppm, which is assigned to one of the C20 protons. The corresponding enhancement of the C17 proton signals (doublet of doublets) was only 4%, thereby suggesting a *trans* relationship between the C17 proton and the C18 methyl group.

Since the chromatographic purification of the major isomer **20** was very inefficient, we decided to perform the next two reactions employing the mixture of isomers. Thus, the cyano ketones were reduced with sodium borohydride, in the presence of cesium chloride (27), to a mixture of allylic alcohols (**21**). This mixture was again difficult to separate so it was treated directly with acetic anhydride, in the presence of dimethylaminopyridine (DMAP) in CH_2Cl_2, to produce a mixture of four acetates. The major acetate produced from cyanoketone **20** in 68% yield was separated from the mixture by column chromatography on TLC grade silica gel. The results of the nOe experiment suggested that the structure of the major acetate **22** was as shown in Scheme 4, since irradiation at 1.06 ppm (C18 protons) resulted in enhancement of a quartet at 2.47 ppm, assigned to one of the C20 protons, and enhancement of a broad doublet corresponding to the proton at C16. However, to establish definitely the structure of **22**, the compound was submitted for X-ray crystallography. The details of the X-ray studies are provided as an appendix.

In accord with our synthetic strategy, the next consideration was removal of the C16 substituent in **22**. This was achieved via nucleophilic displacement of the acetate group with hydride anion and involving palladium intermediates (28). For this purpose, the palladium complex of the acetate **22** was initially formed in a reaction with tetrakis(triphenyl phosphine) palladium(0) followed by addition of sodium borohydride to yield the desired derivative **23** in 79% yield.

Utilizing methodology employed for the conversion **15** → **16** + **17** (Scheme 3), the cyano derivative **23** was reduced with DIBAL and the resultant aldehyde **24** (81% yield) was reacted with potassium hydride followed by menthyl glyoxylate and sodium borohydride to produce a mixture of butenolide **3** and unsaturated *trans* ester **25** in 24 and 20% yield respectively.

The butenolide system **3** produced in the course of our synthesis can be easily transformed into digitoxigenin with the employment of well-known methods previously established in the chemistry of cardenolides (29). Thus, after deketalization to the known ketone **26**, reduction (**26** → **27**, Scheme 1) with iridium reagents (30), and subsequent hydroxylation of the C14—C15 double bond (30, 31), the final product digitoxigenin (**4**) is obtained.

It should be noted that another approach for elaboration of the butenolide ring system was considered, and employed the thioketal derivative **19**. For this purpose, **2** was reacted with the anion of 1,3-dithiane in the presence of HMPA (32) to afford a mixture (86% yield) of the C17 isomers (ratio 2:1, as established by nmr). Unfortunately the separation of these isomers proved extremely difficult and subsequent studies to remove the sulfur protecting group led to extensive decomposition. This approach was therefore abandoned.

Finally, it should be indicated that the above studies allow a rather versatile synthetic entry into cardenolide analogues with functionality in ring D. The latter series is not presently available from natural sources or alternative synthetic routes. For example, intermediates **16**, **18**, and **22** afford convenient routes into such analogues. We believe that the latter compounds will afford the opportunity for further structure–activity studies in the hope that lower toxicity within this family of compounds can be obtained. Such studies are being presently considered.

Experimental

Melting points were determined on a Reichert hot stage apparatus and are uncorrected. Ultraviolet spectra were recorded on a Cary 15 spectrometer in methanol solution. Infrared spectra were measured on Perkin Elmer 710 and 1710 (Fourier transform) spectrometers using chloroform as a solvent. The ^{1}Hmr spectra were recorded on Bruker WH-400 or Nicolet–Oxford H-270 instruments and the chemical shifts are in δ values. Deuteriochloroform was used as the solvent with TMS as internal standard. Low resolution mass spectra were determined on an AEI-MS-902 spectrometer. High resolution mass measurements were made on an AEI-MS-50. Optical rotations were measured on a Perkin Elmer 141 automatic polarimeter. Circular dichroism curves were recorded on a Jasco J-20 spectropolarimeter. Microanalyses were carried out by Mr. P. Borda, Microanalytical Laboratory, University of British Columbia. Column chromatography utilized Merck silica gel 60 G. Petroleum ether refers to the fraction with boiling range 30–60°C. The hplc chromatography was performed on a Waters LC-500 instrument.

17-Methylene-5β-androst-14-en-3,16-dione-3,3-ethylene ketal (2)

From 1[3]

A mixture of ketone **1** (80 mg, 0.23 mmol), sodium bicarbonate (50 mg), and benzeneselenic anhydride (208 mg, 0.58 mmol) in chlorobenzene (2 mL) was heated at 70°C with stirring for 20 h. The mixture was then evaporated and the oily residue dissolved in ethyl ether and filtered. Evaporation of the solvent and purification by preparative layer chromotography with ether – petroleum ether (1:1, v/v) yielded 34 mg (42.5%) of pure **2**; mp 146°C (hexane); $[\alpha]_D$ +221 ± 6° (*c* 0.2320, CH_2Cl_2); uv λ_{max} (EtOH): 249 nm (*c* = 2.32 × 10); ir ν_{max} (KBr): 1695 cm^{-1}; ^{1}Hmr δ: 1.07 (3H, s), 1.27 (3H, s), 1.3–2.05 (16H, m), 2.47 (1H, dt, *J* = 4, 10 Hz), 3.93 (4H, 2), 5.23 (1H, s), 5.97 (2H, s); ms *m/z*: 342 (M^+), 327, 125, 99. High resolution molecular weight determination calcd. for $C_{22}H_{30}O_3$: 342.2197; found: 342.2199. *Anal.* calcd. for $C_{22}H_{30}O_3$: C 77.21, H 8.83; found: C 77.16, H 8.59.

From 12, Method A

A mixture of enone **12** (344 mg, 1 mmol), sodium bicarbonate (250 mg), and benzeneselenic anhydride (360 mg, 1 mmol) in chlorobenzene (9 mL) was heated at 60°C with stirring for 72 h. The reaction mixture worked up and purified as above gave 131 mg (38%) of dienone **2**.

From 12, Method B

A solution of lithium hexamethyldisilylamide was prepared by adding 5.67 mL (9.07 mmol) of a solution of *n*-butyllithium (1.6 M, hexanes) to a solution of hexamethyldisilazane (3.34 mL, 15.1 mmol) in dry THF (15 mL) at −40°C (CH_3CN/CO_2 bath), and added to a solution of the α,β-unsaturated ketone **1** (2.60 g, 7.56 mmol) in dry THF (15 mL) under Ar atmosphere. After 15 min at −40°C, the reaction was quenched with an excess of TMSCl (4.8 mL, 38 mmol) and allowed to warm up to room temperature. The above solution was then added to a solution of 2,3-dicyano-4,5-dichlorobenzoquinone (2.06 g, 9.07 mmol) in CH_3CN (150 mL) at room temperature. After stirring for 1 h, the resulting black mixture was evaporated to dryness, redissolved in 200 mL ethyl acetate, and washed with NaOH (3×, 100 mL, 10% aqueous) and brine (2×, 100 mL). The organic layer was dried over $MgSO_4$, filtered, and concentrated *in vacuo* to yield a brown foam. This crude product was then purified on a short silica gel column using ethyl acetate – toluene (5:95, v/v) to yield 2.19 g (84%) of the cross-conjugate diene **2**.

Can. J. Chem. Downloaded from www.nrcresearchpress.com by 41.223.56.140 on 09/07/12
For personal use only.

5β-Androstane-3,17-dione (6)

A solution of androstenedione (**5**) (5.72 g, 20 mmol) in 2-propanol (500 mL) containing 10% $Pd/CaCO_3$ (500 mg) was stirred under H_2 for 5 h. The catalyst was removed by filtration through Celite and washed with hot 2-propanol (2 × 50 mL). The combined filtrate and washings were evaporated to leave a colourless oil. The reaction yielded a mixture of 5α and 5β isomers of androstanedione. The mixture was separated by hplc chromatography with ethyl acetate – petroleum ether (2:3, v/v) to yield 3.84 g (67%) of pure **6** and 1.60 g (28%) of pure **7**.

The physical properties of **6** are as follows: mp 131.0–132.5°C (ligroin); $[\alpha]_D$ 106.2 ± 2° (*c* 1.0165, $CHCl_3$); cd (MeCN, $c = 6.58 \times 10^{-3}$): 280 (+2.92); ir ν_{max}: 1725, 1705 cm^{-1}; ^{1}Hmr δ: 0.9 (3H, s), 1.06 (3H, s), 1.15–2.23 (16H, m), 2.32 (2H, dt, *J* = 6, 16 Hz), 2.47 (1H, dd, *J* = 8, 20 Hz), 2.68 (2H, t, *J* = 16 Hz); ms *m/z*: 288 (M^+), 273, 255. High resolution molecular weight determination calcd. for $C_{19}H_{28}O_2$: 288.2089; found: 288.2086. *Anal.* calcd. for $C_{19}H_{28}O_2$: C 79.12, H 9.79; found: C 78.86, H 9.80.

And for **7**: mp 133.5–134.0°C (ether/pentane); $[\alpha]_D$ 116 ± 2.5° (*c* 1.0266, $CHCl_3$); cd (MeCN, $c = 7.229 \times 10^{-3}$): 286 (+5.15); ir ν_{max} (KBr): 1725, 1705 cm^{-1}; ^{1}Hmr δ: 0.89 (3H, s), 1.05 (3H, s), 1.23–2.48 (22H, m); ms *m/z*: 288 (M^+), 270, 255. High resolution molecular weight determination calcd. for $C_{19}H_{28}O_2$: 288.2089; found: 288.2093. *Anal.* calcd. for $C_{19}H_{28}O_2$: C 79.12, H 9.79; found: C 78.96, H 9.69.

5β-Androstane-3,17-dione-3,3-ethylene ketal (8)

To a solution of **6** (4.3 g, 14.9 mmol) in benzene (200 mL) was added *p*-toluenesulfonic acid (50 mg) and ethylene glycol (0.923 g, 14.9 mmol). The mixture was heated under reflux with azeotropic removal of H_2O for 3 h. The mixture was cooled, diluted with petroleum ether, washed with $NaHCO_3$, dried ($MgSO_4$), and evaporated. The residue was chromatographed on silical gel with ether – petroleum ether (2:3, v/v) to give the desired product (**8**) (3.77 g, 76%) and diketal (**9**) (0.58 g, 10.3%) in addition to some unreacted starting diketone **6** (0.22 g, 5%).

The physical properties of **8** are as follows: mp 130.5–131.0°C; $[\alpha]_D$ +96 ± 4° (*c* 0.2035, EtOH); ir ν_{max}: 1725 cm^{-1}; ^{1}Hmr δ: 0.87 (3H, s), 0.99 (3H, s), 1.09–2.07 (20H, m), 2.1 (1H, t, *J* = 8 Hz), 2.45 (1H, dd, *J* = 8, 20 Hz), 3.94 (4H, s); ms *m/z*: 332 (M^+), 317, 276, 125, 99. High resolution molecular weight determination calcd. for $C_{21}H_{32}O_3$: 332.2350; found: 332.2350. *Anal.* calcd. for $C_{21}H_{32}O_3$: C 75.92, H 9.71; found: C 76.00, H 9.76.

The physical properties of **9** are as follows: mp 58.0–59.0°C (methanol); $[\alpha]_D$ −6.19 ± 0.7° (*c* 1.115, CH_2Cl_2); ^{1}Hmr δ: 0.85 (3H, s), 0.96 (3H, s), 1.00–2.10 (22H, m), 3.80–4.00 (8H, m); ms *m/z*: 376 (M^+), 125, 99. High resolution mass measurement calcd. for $C_{23}H_{36}O_3$: 376.2614; found: 376.2614. *Anal.* calcd. for $C_{23}H_{36}O_3$: C 73.47, H 9.65; found: C 73.75, H 9.16.

17-Methylene-5β-androstan-3-one-3,3-ethylene ketal (10)

To a bright yellow mixture of methyltriphenylphosphonium bromide (5.86 g, 16.4 mmol) and potassium *tert*-butoxide (1.76 g, 15.6 mmol) in THF (20 mL) was added ketone **8** (3.69 g, 11.1 mmol) in THF (100 mL). After refluxing for 5 h, the mixture was portioned between hexane (220 mL) and water (180 mL). The organic layer was washed with 50% MeOH (200 mL) and brine (200 mL), dried ($MgSO_4$), and evaporated *in vacuo*. Column chromatography of the crude product with 5% of ethyl ether in petroleum ether (v/v) yielded **10** (3.34 g, 91%) as a colorless oil; $[\alpha]_D$ +38.2° (*c* 0.2120, EtOH); ir ν_{max}: 1655 cm^{-1}; ^{1}Hmr δ: 0.77 (3H, s), 0.98 (3H, s), 1.0–2.53 (22H, m), 3.95 (4H, s), 4.61 (1H, br s), 4.63 (1H, br s); ms *m/z*: 330 (M^+), 315, 268, 125, 99. High resolution molecular weight determination calcd. for $C_{22}H_{34}O_2$: 330.2559; found: 330.259. *Anal.* calcd. for $C_{22}H_{32}O_2$: C 80.01, H 10.38; found: C 80.20, H 10.50.

16-Hydroxy-17-methylene-5β-androstane-3-one-3,3-ethylene acetal (11) and 17-methylene-5β-androstane-3,16-dione-3,3-ethylene ketal (12)

From 10

To a suspension of selenium dioxide (558 mg, 5 mmol) in methylene dichloride (25 mL) at room temperature was added a 70% solution of *tert*-butyl hyperoxide (1.93 mL, 1.82 g, 20 mmol). The mixture was stirred at room temperature for 1 h. The steroidal olefin **10** (3.30 g, 10 mmol) in methylene dichloride (55 mL) was then added and stirring was continued for 5 h. The reaction mixture was diluted with ethyl ether (500 mL) and washed with 10% sodium hydroxide (2 × 250 mL) and water, separated, dried ($MgSO_4$), and evaporated. Chromatographic separation of the reaction mixture with ether – petroleum ether (3.7 v/v) gave allylic alcohol **11** (2.59 g, 75%) and unsaturated ketone **12** (0.61 g, 18%).

The physical properties of **11** are as follows: mp 167–168°C (EtOH); $[\alpha]_D$ 2.4 ± 0.3° (*c* 2.852, CH_2Cl_2); ir ν_{max}: 3580 cm^{-1}; ^{1}Hmr δ: 0.77 (3H, s), 0.97 (3H, s), 1.06–1.91 (20H, m), 1.98 (1H, t, *J* = 12 Hz), 3.92 (4H, s), 4.63 (1H, br s), 4.83 (1H, d, *J* = 2 Hz), 5.03 (1H, d, *J* = 2 Hz); ms *m/z*: 346 (M^+), 328, 313, 125, 99. High resolution molecular weight determination calcd. for $C_{22}H_{34}O_3$: 346.2499; found: 346.2503. *Anal.* calcd. for $C_{22}H_{34}O_3$: C 76.37, H 9.91; found: C 76.31, H 9.88.

17-Methylene-5β-androstan-3,16-dione-3,3-ethylene ketal (12)

From 11

To a solution of oxalyl chloride (670 μL, 975 mg, 7.68 mmol) in methylene dichloride (15 mL) at −78°C was added a solution of dimethyl sulfoxide (1.7 mL, 1.2 g, 15.36 mmol) in methylene dichloride (5 mL) and the mixture stirred at −78°C for 5 min. A solution of allylic alcohol (**11**) (2.39 g, 6.9 mmol) in methylene chloride was then added to this mixture at −78°C. After stirring for 15 min, neat triethylamine (2.85 mL, 2.07 mmol) was added. The solution was allowed to warm to −20°C and held at this temperature for 3 h. The reaction mixture was diluted with chloroform (75 mL), washed with 10% hydrochloric acid, water, sodium bicarbonate, and again with water. After drying ($MgSO_4$), and removal of the solvent the product was purified by column chromatography to give pure **12** (2.04 g, 86%); mp 99.5–100°C (isopropanol); $[\alpha]_D$ −119 ± 0.3° (*c* 0.2771, EtOH); uv λ_{max}: 227 (3.66); ir ν_{max}: 1722 cm^{-1}; ^{1}Hmr δ: 0.95 (3H, s), 1.01 (3H, s), 1.09–2.07 (19H, m), 2.24 (1H, dd, *J* = 18, 8 Hz), 3.94 (4H, s), 5.0 (1H, d, *J* = 1 Hz), 5.79 (1H, d, *J* = 1 Hz); ms *m/z*: 344 (M^+), 329, 287, 195, 125, 99. High resolution molecular weight determination calcd. for $C_{22}H_{32}O_3$: 344.2351; found: 344.2351. *Anal.* calcd. for $C_{22}H_{32}O_3$: C 76.71, H 9.36; found: C 76.49, H 9.35.

17-Cyanomethyl-5β-androstan-3,16-dione-3,3-ethylene ketal (13)

A mixture of enone **12** (1.85 g, 5.4 mmol), dimethylformamide (85 mL), potassium cyanide (0.84 g, 12.5 mmol in 5.6 mL H_2O), and ammonium chloride (0.5 g, 9.4 mmol in 5.6 mL H_2O) was refluxed for 3 h, cooled, diluted with water, and extracted with ethyl acetate. The organic layer was washed with water, dried ($MgSO_4$), and evaporated. The crude product was purified on a short chromatography column with ether – petroleum ether (1:1, v/v), yielding pure cyano derivative **13** (1.82 g, 91.2%); mp 162–162.5°C (EtOH); $[\alpha]_D$ −126 ± 0.1° (*c* 1.3796, EtOH); ir ν_{max}: 2310, 1730 cm^{-1}, ^{1}Hmr δ: 0.77 (3H, s), 0.99 (3H, s), 1.12–1.95 (17H, m), 2.01 (1H, t, *J* = 12 Hz), 2.12–2.35 (4H, m), 2.72 (1H, dd, *J* = 18, 4 Hz), 3.94 (4H, s); ^{13}Cmr (75 MHz, $CDCl_3$) δ: 12.113 (C11), 13.158 (C18), 20.217 (C12), 22.879 (C19), 26.242 (C6), 29.886 (C1), 32.493 (C8), 33.678 (C2), 34.550 (C10), 35.477 (C4), 37.147 (C7), 37.404 (C20), 39.723 (C9), 40.4222 (C5), 41.776 (C13), 50.066 (C14), 58.773 (C17), 63.826 (C15), 63.885 and 64.016 (C3 ethyleneketal), 109.380 (C3), 118.434 (C21), 214.071 (C16); ms *m/z*: 371 (M^+), 356, 314, 125, 99. High resolution molecular weight determination calcd. for $C_{23}H_{33}O_3N$: 371.2460; found: 371.2460. *Anal.* calcd. for $C_{23}H_{33}O_3N$: C 74.36, H 8.95, N 3.77; found: C 74.24, H 9.02, N 3.99.

17-Cyanomethyl-5β-androstane-3,16-dione-3,3,16,16-diethylene diacetal (14)

To a solution of **13** (1.67 g, 4.5 mmol) in a mixture of toluene (100 mL) and benzene (100 mL) was added ethylene glycol (3.1 g, 50 mmol) and *p*-toluenesulfonic acid (50 mg). The mixture was refluxed with azeotropic removal of water for 48 h, then cooled, diluted with petroleum ether, washed with 10% sodium bicarbonate and water, dried ($MgSO_4$), and evaporated to dryness. The crude product was purified on a short column with ether – petroleum ether (1:1, v/v) to afford pure **14** (1.77 g, 94.5%); mp 149.0–149.5°C; $[\alpha]_{365}$ 21.4 ± 0.8°

Can. J. Chem. Downloaded from www.nrcresearchpress.com by 41.223.56.140 on 09/07/12
For personal use only.

(*c* 2.9192, CH_2Cl_2); ir ν_{max}: 2250 cm^{-1}, ^{1}Hmr δ: 0.77 (3H, s), 0.95 (3H, s), 1.00–2.20 (2H, m), 2.20–2.40 (2H, m), 3.75 (1H, q, *J* = 8 Hz), 3.94 (4H, s), 3.88–3.97 (2H, m), 4.0–4.06 (1H, m); ^{13}Cmr (75 MHz, $CDCl_3$) δ: 11.804 (C1), 12.753 (C18), 20.376 (C12), 23.062 (C19), 26.187 (C6), 26.518 (C7), 30.029 (C1), 33.991 (C2), 34.675 (C10), 34.798 (C8), 35.628 (C4), 37.775 (C15), 39.385 (C20), 39.893 (C9), 40.4729 (C5), 41.984 (C13), 51.953 (C14), 55.422 (C17), 63.456 (C16 ethyleneketal), 64.028 and 64.156 (C3 ethyleneketal), 65.266 (C16 ethyleneketal), 115.543 (C16), 109.716 (C3), 119.635 (C21); ms *m/z*: 415 (M^+), 375, 125, 99. High resolution molecular weight determination calcd. for $C_{25}H_{37}O_4N$: 415.2722; found: 415.2726. *Anal.* calcd. for $C_{25}H_{37}O_4N$: C 72.26, H 8.97, N 3.37; found: C 72.36, H 9.10, N 3.40.

20-Oxo-5β-pregnane-3,16-dione-3,3,16,16-diethylene ketal (15)

A solution of nitrile **14** (1.56 g, 3.5 mmol) in benzene (40 mL) was treated with a 1 M solution of diisobutylaluminum hydride in hexane solution (7.2 mL, 7.2 mmol) at room temperature. The mixture was stirred for 0.5 h, then quenched with saturated ammonium chloride solution and diluted with petroleum ether. The organic layer was washed with water, dried ($MgSO_4$), and evaporated to dryness. The product was purified on a chromatography column with ether – petroleum ether (2.3 /v) yielding pure **15** (1.25 g, 79.6%); mp 143–144°C; $[\alpha]_D$ −10.7° (*c* 0.01366,CCl_2H_2); ir ν_{max}: 1695 cm^{-1}; ^{1}Hmr δ: 0.74 (3H, s), 0.96 (3H, s), 1.03–1.92 (9H, m), 2.0 (1H, t, *J* = 12 Hz), 2.28 (1H, m), 2.45–2.53 (1H, m), 3.67–3.913 (4H, m), 3.93 (4H, s), 9.71 (1H, m); ms *m/z*: 418 (M^+), 403, 390, 128, 99. High resolution molecular weight determination calcd. for $C_{25}H_{38}O_5$: 418.2719; found: 418.2713. *Anal.* calcd. for $C_{25}H_{38}O_5$: C 71.74, H 9.15; found: C 71.92, H 9.27.

5β-Card-20(22)-enolide-3,16-dione-3,3,16,16-diethylene ketal (16) and R(−)-menthyl-21-hydroxy-3,3,16,16-diethylene-dioxy-24-nor-chol-20(22)-en-23-ate (17)

From ***15***

To a suspension of potassium hydride (244 mg of 22%, 122 mmol) in THF (6 mL) was added over 5 min at room temperature a solution of aldehyde **15** (418 mg, 1 mmol) in THF (6 mL). After hydrogen evolution had ceased, the turbid yellowish solution was stirred for another 15 min. Then freshly distilled anhydrous (*R*)-menthyl glyoxylate (318 mg, 1.5 mmol) in THF (2 mL) was added and the mixture was stirred for 1 h at room temperature. The reaction was quenched with H_2O (0.5 mL), diluted with 5 mL of MeOH, sodium borohydride (190 mg, 5 mmol) was added, and the mixture was stirred for 30 min. Excess of borohydride was decomposed with acetone. Then the reaction mixture was evaporated and partitioned between ethyl acetate (200 mL) and 1 M hydrochloric acid (200 mL). The organic layer was washed with water and sodium bicarbonate, dried ($MgSO_4$), and evaporated to give 970 mg of crude reaction product. Subsequent, careful separation on a chromatography column with ether – petroleum ether (2:3, v/v) yielded butenolide **16** (78 mg, 17.0%) and unsaturated hydroxyester **17** (147 mg, 24.0%).

The physical properties of **17** are as follows: mp 197–198°C (heptane); $[\alpha]_D$ 11.3 ± 0.7° (*c* 2.2629, CH_2Cl_2); ir ν_{max}: 3612, 1704 cm^{-1}; ^{1}Hmr δ: 0.75 (3H, d, *J* = 8 Hz), 0.85–0.98 (12H, m), 1.03–2.07 (30H, m), 2.28 (1H, t, *J* = 6 Hz), 3.72–3.95 (8H, m), 4.21 (1H, dd, *J* = 14, 8 Hz), 4.48 (1H, dd, *J* = 14, 8 Hz), 4.74 (1H, dt, *J* = 10, 2 Hz), 6.19 (1H, s); ms *m/z*: 614 (M^+), 552, 476, 125, 99. High resolution molecular weight determination calcd. for $C_{37}H_{58}O_7$: 614.4196; found: 614.4189. *Anal.* calcd. for $C_{37}H_{58}O_7$: C 72.32, H 9.15; found: C 72.12, H 9.38.

And for **16**: mp 94–95°C (EtOH); $[\alpha]_{365}$ (*c* 1.2505, EtOH); ir ν_{max}: 1782, 1747 cm^{-1}; ^{1}Hmr δ: 0.77 (3H, s), 0.98 (3H, s), 1.05–2.03 (20H, m), 3.64 (1H, s), 3.72–3.95 (4H, m), 3.93 (4H, s), 4.77 (2H, d, *J* = 2 Hz), 6.04 (1H, s); ms *m/z*: 458 (M^+), 414, 305, 125, 99. High resolution molecular weight determination calcd. for $C_{27}H_{38}O_6$: 458.2970; found: 458.2969. *Anal.* calcd. for $C_{27}H_{38}O_6$: C 70.74, H 8.30; found: C 70.98, H 8.49.

5β-Cardanolide-3,3,16,16-diethylene ketal (18)

A solution of **17** (100 mg, 0.16 mmol) in 2-propanol (20 mL) containing 10% $Pd/CaCO_3$ (30 mg) was stirred under H_2 for 2 h. The catalyst was removed by filtration and washed with hot propanol (10 mL). The combined filtrate and washings were evaporated. The crude reduction product was hydrolyzed in a mixture of 10% NaOH (50 mL) and ethanol (50 mL) for 10 min at reflux. Then the solution was diluted with water (50 mL) and, after evaporation of ethanol, neutralized (10% HCl) and extracted with ethyl acetate. The organic layer was washed with sodium bicarbonate, dried ($MgSO_4$), and evaporated *in vacuo*. The column chromatography with ether – petroleum ether (1:1, v/v) yielded pure **18** (47 mg, 62.5%); ir ν_{max}: 1772 cm^{-1}; ^{1}Hmr δ: 0.84 (3H, s), 0.95 (3H, s), 1.04–1.92 (2H, m), 1.98 (1H, t, *J* = 12 Hz), 2.35–2.55 (2H, m), 2.78–2.89 (1H, m), 3.75–3.95 (9H, m), 4.45 (1H, t, *J* = 6 Hz); ms *m/z*: 460 (M^+), 375, 305, 125, 99. High resolution molecular weight determination calcd. for $C_{27}H_{40}O_6$: 460.2829; found: 460.2827. *Anal.* calcd. for $C_{27}H_{40}O_6$: C 70.43, H 8.69; found: C 70.40, H 8.59.

20,20-(1′, 3′-Propylene)-dithio-5β-pregn-14-ene-3-one-3, 3-ethylene ketal (19)

To a solution of 1,3-dithiane (77 mg, 0.64 mmol) and HMPA (222 μL, 1.28 mmol) in THF (6 mL), *n*-BuLi in hexane (1.6 M, 0.42 mL, 0.67 mmol) was added and the mixture was stirred at −25°C for 2 h to form anion. Then cross-conjugated ketone **2** (219 mg, 0.64 mmol) in THF (7 mL) was added and the mixture was allowed to warm up slowly to room temperature and stirred for another hour. Quenching with aqueous ammonium chloride followed by extraction (methylene dichloride), evaporation, and chromatographic separation yielded pure dithio derivative **18** (159 mg, 86.1%) as a mixture of two 17-isomers (2:1 ratio). The separation of the isomers proved to be very difficult and only a small sample of the pure major isomer was isolated for the purpose of characterization; mp 186°C; ir ν_{max} ($CHCl_3$): 1700 cm^{-1}; uv λ_{max} (EtOH): 232 nm; ^{1}Hmr δ: 1.04 (3H, s), 1.09 (3H, s), 1.26–2.27 (10H, m), 2.43–2.51 (2H, m), 2.87 (4H, m), 3.94 (4H, s), 3.8 (1H, dd), 5.75 (1H, s); ms *m/z*: 462 (M^+), 343, 330, 216, 133, 125, 99. *Anal.* calcd. for $C_{26}H_{38}O_3S_2$: C 67.53, H 8.23; found: C 67.52, H 8.36.

17-Cyanomethyl-5-β-androstene-3,16-dione-3,3-ethylene ketal (20)

A solution of the diene **2** (443 mg, 130 mmol) in dry benzene (12 mL) was prepared at room temperature and to this was quickly added 1.30 mL (1.30 mmol) of a solution of diethylaluminum cyanide (1 M, toluene). Upon addition of the diethylaluminum cyanide the solution turned deep orange and quickly faded (in about 30 s) to a light orange color. After stirring for 30 min at room temperature, the reaction was quenched with NaOH (2 mL, 10% aqueous), which caused the orange color to disappear. This mixture was then diluted with ethyl acetate (100 mL) and washed with NaOH (2 × 50 mL, 10% aqueous), brine (2 × 50 mL), dried over $MgSO_4$, filtered, and concentrated *in vacuo* to yield a white foam. This crude product was purified on a short silica gel column using ethyl acetate – hexanes (1:4, v/v) to yield 360 mg (75%) of the unsaturated nitrile **20** as a mixture of C17 epimers. Gas–liquid chromatographic analysis of this mixture showed that the ratio of isomers was about 2:1. Repeated attempts to separate these isomers by column chromatography (hplc) was only partially successful. It was possible to enrich the mixture in the major isomer enough that the minor isomer could not be detected by ^{1}Hmr (but could be detected by capillary gas chromatography). The data given here are for this mixture.

The physical properties of the nitrile **20** are as follows: mp 54.0–55.0°C (hexanes); ir ν_{max}: (KBr): 2342, 1703, 1605 cm^{-1}; uv λ_{max}: 233 nm (9.64 × 10^3, ethanol); ^{1}Hmr δ: 1.05 (3H, s), 1.24 (3H, s), 0.83–2.35 (17H, m), 2.26 (1H, q, *J* = 18, 16 Hz, C20-H), 2.45 (1H, dd, *J* = 16.4 Hz, C17-H), 2.49 (1H, m, C8-H), 2.92 (1H, dd, *J* = 18.4 Hz, C20-H′), 3.93 (4H, s, C3 ketal), 5.80 (1H, s, C15-H); ms *m/z*: 369 (M^+), 125 ($C_7H_9O_2$), 99 ($C_5H_7O_2$). High resolution mass measurement for $C_{23}H_{31}O_3N$: 369.2292; found: 369.2298. *Anal.* calcd. for $C_{23}H_{31}O_3N$: C 74.79, H 8.40, N 3.79; found: C 74.40, H 8.86, N 3.58.

16-Hydroxy-17-cyanomethyl-5β-androstene-3-one-3,3-ethylene ketal (21)

The unsaturated cyanoketone **20** (mixture of C17 epimer, 1 g, 2.71 mmol) was dissolved in a 0.4 M solution (36 mL) of cerium

chloride hydrate in methanol. Then sodium borohydride (266 mg, 7 mmol) was added and the reaction was stirred at room temperature for 30 min. After evaporation of the solvent the residue was redissolved in ethyl acetate, washed with water, dried over $MgSO_4$, and evaporated again. Crude product (1.05 g) consisting of four isomeric allylic alkaloids was used in the next transformation without further purification.

A small sample of the major alcohol **21** was obtained after hplc separation; ir (neat) ν: 3600 (br), 2290; ^{1}Hmr δ: 0.98 (3H, s), 1.00 (3H, s), 1.24–2.11 (19H, m), 2.44 (1H, dd), 2.65 (1H, dd), 3.92 (4H, s), 4.46 (1H, m), 5.20 (1H, s); ms *m/z*: 371 (M^+), 353, 125, 99. *Anal.* calcd. for $C_{23}H_{33}NO_3$. C 74.36, H 8.95, N 3.77; found: C 74.10, H 8.87, N 3.90.

16-Acetoxy-17β-cyanomethyl-5β-androstene-3-one-3,3-ethylene ketal (22)

The crude mixture of the allylic alkaloids (**21** and isomers, 440 mg, 1.19 mol) was dissolved in methylene chloride (20 mL) and treated with acetic anhydride (380 μl, 1 mmol) in the presence of dimethylaminopyridine (146 mg, 1.2 mmol) at room temperature for 15 min. The reaction mixture was subsequently washed with 10% hydrochloric acid, water, and sodium bicarbonae, dried ($MgSO_4$), and evaporated to dryness. The column chromatography with ether – petroleum ether (3:7, v/v) of the crude product consisting of four isomeric allylic acetates yielded a pure major isomer **22** (255 mg, 68.1% from **17** cyanoketone; 54.2% from the mixture of **17**α and **17**β isomers); mp 158°C; ir ν_{max}: 2252, 1730 cm^{-1}; ^{1}Hmr δ: 0.98 (3H, s, C19), 1.06 (3H, s, C18), 1.26–2.14 (17H, m), 2.10 (3H, s, acetate), 2.2 (1H, m, C17), 2.47 (1H, dd, C20), 2.61 (1H, dd, C20), 3.92 (4H, s, ketal), 5.2 (1H, s, C15), 5.46 (1H, bd, C16); ms *m/z*: 413 (M^+), 370, 353, 338, 125, 99. *Anal.* calcd. for $C_{25}H_{35}NO_3$: C 72.64, H 8.47, 3.39; found: C 72.60, H 8.40, N 3.19.

17β-Cyanomethyl-4β-androstene-3-one-3,3-ethylene ketal (23)

A yellow solution of the acetate **22** (100 mg, 0.240 mmol) and tetrakis(triphenylphosphine) palladium (0) (9275 mg, 0.240 mmol) in 4 mL of THF was stirred at room temperature under an argon atmosphere. After 10–15 min, the mixture turned black, sodium borohydride (100 mg, 2.63 mmol) was added, and the stirring was continued until the starting material disappeared (tlc, 1–2 h). After the excess of sodium borohydride was decomposed with acetone, the reaction mixture was evaporated to dryness and purified on a short silica gel column with ether – petroleum ether (1:4, v/v) to yield 68 mg (79.1%) of cyano derivative **23**.

The physical properties of **23** are as follows: ir ν_{max}: 2248 cm^{-1}; ^{1}Hmr δ: 0.90 (3H, s, C18), 0.98 (3H, s, C19), 1.20–2.05 (18H, m), 2.165 (1H, m), 2.395 (2H, dd), 2.5 (1H, m), 3.94 (4H, s), 5.14 (1H, s); ms *m/z*: 355 (M^+), 340, 315, 298, 125, 99. High resolution mass measurement calcd. for $C_{23}H_{33}NO_2$: 355.2511; found: 355.2520.

20-Oxo-5β-pregn-14-ene-3-one-3,3-ethylene ketal (24)

A solution of nitrile **23** (355 mg, 1 mmol) in benzene (10 mL) was treated with a 1 M solution of diisobutylaluminum hydride in hexane solution (1.2 mL, 1.2 mmol) at room temperature. The mixture was stirred for 30 min, then quenched with saturated ammonium chloride solution and diluted with petroleum ether. The organic layer was washed with water, dried ($MgSO_4$), and evaporated to dryness. The chromatographic separation with ether – petroleum ether (3:7, v/v) yielded pure aldehyde **24** (290 mg, 81.0%); ir ν_{max}: 1719 cm^{-1}; ^{1}Hmr δ: 0.82 (3H, s, C18), 0.98 (3H, s, C19), 1.17–2.11 (1H, m), 2.27 (1H, m), 2.45 (2H, m), 2.56 (1H, m), 3.94 (4H, s), 5.18 (1H, s, C15), 9.8 (1H, 5); ms *m/z*: 358 (M^+), 330, 314, 125, 99. High resolution mass measurement calcd. for $C_{23}H_{34}O_3$: 358.2508; found: 358.2516.

5β-Card-14,20(22)-dienolide-3-one-3,3-ethylene ketal (23) and R *(−)-methyl-21-hydroxy-3,3-ethylenedioxy-24-nor-chol-14,20(22)-dien-23-153 (25)*

To a suspension of potassium hydride (50 mg of 30%, 0.36 mmol) in THF (2 mL), at room temperature, was slowly added a solution of aldehyde **24** (107 mg, 0.3 mmol) in THF (2 mL). After hydrogen evolution had ceased, the turbid yellow suspension was stirred for 20 min and the solution of freshly distilled anhydrous (*R*)-methylglyoxylate (95.4 mg, 0.45 mmol) in THF (2 mL) was added. The reaction was stirred for another hour at room temperature, then quenched with water (0.15 mL), diluted with methanol (1.5 ml), and treated with sodium borohydride (60 mg, 1.58 mmol). After 30 min of stirring the excess of sodium borohydride was decomposed with acetone. Then the reaction mixture was evaporated and partitioned between ethyl acetate (60 mL) and 10% hydrochloric acid (60 mL). The organic layer was washed with water and sodium bicarbonate, dried ($MgSO_4$), and evaporated to dryness. Separation of the crude product on a chromatography column with ether – petroleum ether (2:3, v/v) yielded butenolide **3** (29 mg, 24.4%) and hydroxyester **26** (33 mg, 19.9%).

The physical properties of **3** are as follows: ir ν_{max}: 1782, 1747, 1632 cm^{-1}; ^{1}Hmr δ: 0.81 (3H, s, C18), 0.97 (3H, s, C19), 1.23–2.11 (17H, m), 2.47 (2H, m, C16), 2.8 (1H, t, C17), 3.94 (4H, s, ketal), 4.77 (2H, dd, C2), 5.25 (1H, s, C15), 5.90 (1H, s, C22); ms *m/z*: 398 (M^+), 354, 125, 99. High resolution mass measurement calcd. for $C_{25}H_{34}O_4$: C 75.38, H 8.54; found: C 75.91, H 8.54.

And for the ester **25**: ir ν_{max}: 1690 cm^{-1}; ^{1}Hmr δ: 0.73–0.99 (15H, m), 1.23–2.22 (27H, m), 2.33 (2H, m, C16), 3.94 (4H, s, ketal), 4.25 (2H, t, C21), 4.29 (1H, s, OH), 4.71 (1H, dt), 5.17 (1H, s, C15), 6.17 (1H, s, C22); ms *m/z*: 554 (M^+), 536, 416, 398, 380, 354, 284, 125, 99. High resolution mass measurement calcd. for $C_{35}H_{54}O_5$: 554.3971; found: 554.3977. *Anal.* calcd. for $C_{35}H_{54}O_5$: C 75.77, H 9.81; found: C 75.70, H 9.62.

Acknowledgements

Financial aid from the Natural Sciences and Engineering Research Council of Canada is gratefully acknowledged. We also wish to thank the Upjohn Company, Kalamazoo, Michigan, for generous gifts of androstenedione.

1. A. Becalski, W. R. Cullen, M. D. Fryzuk, G. Herb, B. R. James, J. P. Kutney, K. Piotrowska, and D. Tapiolas. Can. J. Chem. **66**, 3108 (1988).
2. T. R. Watson, H. T. Andrew Cheung, and R. E. Thomas. Structure–activity studies in cardiac glycosides. *In* Natural Products and Drug Development, Alfred Benson Symposium 20. *Edited by* P. Krogsgaard-Larsen, S. Brogger Christensen, and H. Kofod. Munksgaard, Copenhagen. 1984.
3. D. Rohrer, D. Fullerton, A. From, and K. Ahmed. Functional receptor mapping for modified cardenolides: Use of the PROPFET system. *In* Computer Assisted Drug Design. ACS Symposium Series 112. American Chemical Society, Washington, DC 1979.
4. A. Osol (*Editor*). Remington's pharmaceutical sciences. 16th ed. Mack Publishing Company, Easton, PA. 1980. p. 795.
5. N. Danieli, Y. Mazur, and F. Sondheimer. J. Am. Chem. Soc. **84**, 875 (1962); Tetrahedron, **22**, 3189 (1966).
6. G. Boch, J. Capitaine, and C. R. Engle. Can. J. Chem. **46**, 733 (1968).
7. W. Fritsch, W. Haede, K. Radscheit, and H. Ruschig. Liebigs Ann. Chem. **721**, 168 (1969).
8. G. R. Pettit, L. E. Houghton, J. C. Knight, and F. Bruschweiler. J. Org. Chem. **35**, 2895 (1970).
9. U. Valcavi and S. Innocenti. Farm. Ed. Sci. **29**, 194 (1973).
10. E. Yoshii, T. Koizumi, H. Ikeshima, K. Ozaki, and I. Hayashi. Chem. Pharm. Bull. **23**, 462 (1975).
11. S. F. Donovan, M. A. Avery, and J. E. McMurry. Tetrahedron Lett. **35**, 3287 (1979), and references cited therein.
12. R. Marini-Bettolo, P. Flecker, T. Y. R. Tsai, and K. Wiesner. Can. J. Chem. **59**, 1403 (1981).
13. P. Welzel, H. Stein, and T. Milkova. Liebigs Ann. Chem. 2119 (1982).
14. M. M. Kabat, A. Kurek, and J. Wicha. J. Org. Chem. **48**, 4248 (1983).
15. H. Jin, T. Y. R. Tsai, and K. Wiesner. Can. J. Chem. **61**, 2442 (1983).

Can. J. Chem. Downloaded from www.nrcresearchpress.com by 41.223.56.140 on 09/07/12
For personal use only.

16. K. WIESNER, T. Y. R. TSAI, R. KUMAR, and H. SIVARAMAKRISHNAN. Helv. Chim. Acta, **67**, 1128 (1984).
17. J. WICHA and M. M. KABAT. J. Chem. Soc. Perkin Trans. **1**, 1601 (1985).
18. J. P. KUTNEY, P. GRICE, K. O. PASCOE, K. PIOTROWSKA, S. J. RETTIG, J. SZYKULA, and J. TROTTER. Helv. Chim. Acta, **66**, 1806 (1983).
19. J. P. KUTNEY, P. GRICE, K. PIOTROWSKA, S. J. RETTIG, J. SZYKULA, J. TROTTER, and L. V. CHU. Helv. Chim. Acta, **66**, 1820 (1983).
20. D. H. R. BARTON, D. J. LESTER, and S. V. LEY. J. Chem. Soc. Perkin Trans. **1**, 2209 (1980).
21. N. R. SCHMUFF and B. M. TROST. J. Org. Chem. **48**, 1404 (1983).
22. G. MEHTA, A. V. REDDY, A. N. MURTHY, and D. S. REDDY. J. Chem. Soc. Chem. Commun. 540 (1982).
23. G. R. PETTIT, B. GREEN, and G. L. DUNN. J. Org. Chem. **35**, 1367 (1970).
24. W. KREISER and M. NAZIR. Liebigs Ann. Chem. **755**, 12 (1972).
25. H. JURCZAK and A. ZAMOJSKI. Rocz. Chem. **44**, 2257 (1970).
26. W. NAGATA, M. YOSHIOKA, and M. MURAKAMI. J. Am. Chem. Soc. **94**, 4654 (1972).
27. J. L. LUCHE. J. Am. Chem. Soc. **100**, 2226 (1978).
28. R. O. HUTCHINS, K. LEARN, and R. P. FULTON. Tetrahedron Lett. **21**, 27 (1980).
29. R. H. ODE, G. R. PETTIT, and Y. KAMANO. *In* International review of science. Organic chemistry. Ser. 2. Vol. 8. Steroids. *Edited by* W. F. Johns. Butterworths, London. 1976. p. 145.
30. W. FRITSCH, W. HAEDE, K. RADSCHEIT, U. STACHE, and H. RUSCHIG. Liebigs Ann. Chem. 621 (1974).
31. C. R. ENGEL and G. BACH. Steroids, **3**, 593 (1964).
32. C. A. BROWN and A. YAMAICHI. J. Chem. Soc. Chem. Commun. 100 (1979).
33. International tables for X-ray crystallography. Vol. IV. Kynoch Press, Birmingham, AL. 1974. pp. 99–102 and 149.

Appendix

X-ray crystallographic analysis of the compound structure 22

A crystal bounded by the six faces (followed by the distances in mm between parallel faces): (0 0 1), 0.020, ±(0 1 −1), 0.30, (1 0 −1), 0.53 was mounted in a general orientation. Unit-cell parameters were refined by least squares on 2 sin θ/λ values for 25 reflections (2θ = 20–33°) measured on a diffractometer with Mo-$K\alpha$ radiation ($\lambda(K\alpha_1)$ = 0.70930, $\lambda(K\alpha_2)$ = 0.71359 Å). Crystal data at 22°C are as follows:

$C_{25}H_{35}NO_4$ f.w. = 413.56

Monoclinic, a = 6.526(1), b = 10.728(2), c = 17.011(2) Å, β = 94.867(8)°, V = 1137.5(3) Å^3, Z = 2, ρ_c = 1.207 Mg m^{-3}, $F(000)$ = 448, μ(Mo-$K\alpha$) = 0.75 cm^{-1}. Absent reflections: 0k0, k odd, space group $P2_1$.

Intensities were measured with graphite-monochromated Mo-$K\alpha$ radiation on an Enraf–Nonius CAD4-F diffractometer. An ω–2θ scan at 1.3–10.0° min^{-1} over a range of (0.85 + 0.35 tan θ) degrees in ω (extended by 25% on both sides for background measurement) was employed. Data were measured to 2θ = 55°. The intensities of 3 check reflections, measured every 3600 s throughout the data collection, showed only small (<4%) random variations. Of the 2351 independent reflections measured and processed,[3] 1033(43.9%) had intensities greater than or equal to 2σ(I) above background where σ^2(I) = S + 2B + (0.04(S–B))^2 with S = scan count and B = normalized background count.

Since the molecule is chiral the space group was assumed to be $P2_1$. The structure was solved by direct methods, all non-hydrogen atoms being positioned from an E-map. In the

[3]The computer programs used include locally written programs for data processing and locally modified versions of the following: ORFLS, full-matrix least squares, and ORFFE, function and errors, by W. R. Busing, K. O. Martin and H. A. Levy; FORDAP, Patterson and Fourier syntheses, by A. Zalkin; ORTEP II, illustrations, by C. K. Johnson.

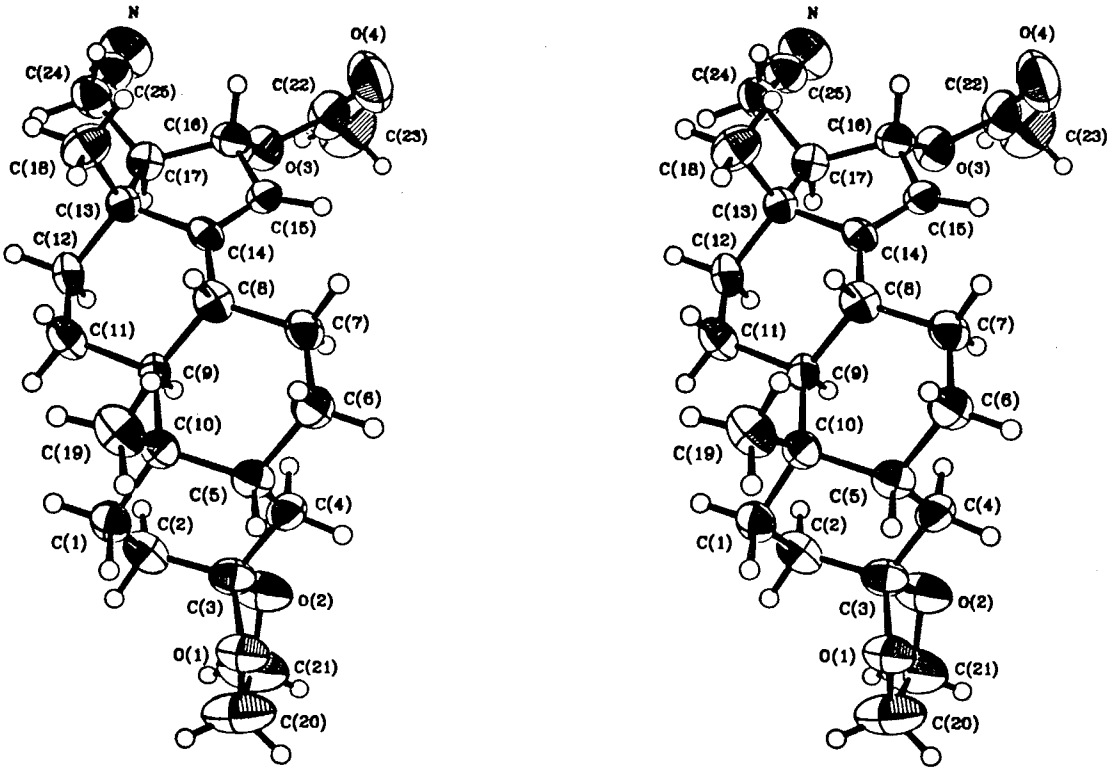
TABLE 1. Final positional (fractional × 10^4) and isotropic thermal parameters (U × 10^3 Å^2) with estimated standard deviations in parentheses

Atom	x	y	z	U_{eq}
O(1)	7687(7)	7306	10745(3)	57
O(2)	4912(8)	5964(6)	10541(3)	67
O(3)	3110(7)	2317(6)	6508(3)	56
O(4)	5397(12)	733(7)	6357(4)	103
N	−628(11)	2940(8)	4955(4)	84
C(1)	6843(10)	8182(8)	9053(4)	44
C(2)	5308(11)	7555(8)	9576(4)	49
C(3)	6417(11)	6668(8)	10136(4)	47
C(4)	7836(10)	5759(8)	9729(4)	45
C(5)	9324(9)	6407(8)	9196(3)	39
C(6)	10620(10)	5417(8)	8790(4)	47
C(7)	9261(9)	4669(8)	8174(4)	44
C(8)	8015(9)	5501(8)	7578(4)	39
C(9)	6749(9)	6539(7)	7967(3)	33
C(10)	8177(9)	7288(8)	8590(3)	38
C(11)	5529(10)	7335(8)	7329(4)	48
C(12)	3958(10)	6548(8)	6797(4)	45
C(13)	5041(10)	5474(8)	6395(4)	38
C(14)	6527(10)	4783(8)	6999(4)	33
C(15)	6334(10)	3560(7)	6922(4)	41
C(16)	4671(11)	3219(8)	6275(4)	44
C(17)	3443(10)	4434(8)	6110(4)	42
C(18)	6325(11)	5966(8)	5732(4)	59
C(19)	9798(10)	8093(8)	8192(4)	52
C(20)	6387(15)	7491(10)	11377(4)	95
C(21)	4574(15)	6586(10)	11230(5)	96
C(22)	3689(18)	1124(9)	6495(5)	70
C(23)	1830(17)	305(9)	6706(6)	114
C(24)	2380(11)	4580(8)	5278(4)	55
C(25)	674(13)	3658(9)	5094(5)	58

TABLE 2. Bond lengths (Å) with estimated standard deviations in parentheses

Bond	Length (Å)	Bond	Length (Å)
O(1)—C(3)	1.425(7)	C(8)—C(9)	1.548(8)
O(1)—C(20)	1.416(8)	C(8)—C(14)	1.507(8)
O(2)—C(3)	1.429(8)	C(9)—C(10)	1.551(8)
O(2)—C(21)	1.381(8)	C(9)—C(11)	1.532(8)
O(3)—C(16)	1.454(7)	C(10)—C(19)	1.532(8)
O(3)—C(22)	1.331(9)	C(11)—C(12)	1.533(8)
O(4)—C(22)	1.190(10)	C(12)—C(13)	1.527(8)
N—C(25)	1.131(8)	C(13)—C(14)	1.519(8)
C(1)—C(2)	1.520(9)	C(13)—C(17)	1.549(8)
C(1)—C(10)	1.533(8)	C(13)—C(18)	1.532(8)
C(2)—C(3)	1.478(9)	C(14)—C(15)	1.324(8)
C(3)—C(4)	1.524(9)	C(15)—C(16)	1.494(8)
C(4)—C(5)	1.522(8)	C(16)—C(17)	1.527(9)
C(5)—C(6)	1.535(8)	C(17)—C(24)	1.519(9)
C(5)—C(10)	1.532(8)	C(20)—C(21)	1.498(10)
C(6)—C(7)	1.522(8)	C(22)—C(23)	1.525(11)
C(7)—C(8)	1.516(8)	C(24)—C(25)	1.470(11)

Can. J. Chem. Downloaded from www.nrcresearchpress.com by 41.223.56.140 on 09/07/12
For personal use only.



Structure 22

TABLE 3. Bond angles (deg) with estimated standard deviations in parentheses

Bonds	Length (deg)	Bonds	Length (deg)
C(3)—O(1)—C(20)	107.4(6)	C(5)—C(10)—C(19)	110.8(5)
C(3)—O(2)—C(21)	108.0(5)	C(9)—C(10)—C(19)	110.8(5)
C(16)—O(3)—C(22)	116.5(6)	C(9)—C(11)—C(12)	111.6(5)
C(2)—C(1)—C(10)	115.0(5)	C(11)—C(12)—C(13)	113.2(5)
C(1)—C(2)—C(3)	112.2(6)	C(12)—C(13)—C(14)	109.5(5)
O(1)—C(3)—O(2)	104.7(5)	C(12)—C(13)—C(17)	112.6(5)
O(1)—C(3)—C(2)	111.2(6)	C(12)—C(13)—C(18)	110.5(6)
O(1)—C(3)—C(4)	109.1(6)	C(14)—C(13)—C(17)	101.7(5)
O(2)—C(3)—C(2)	111.0(6)	C(14)—C(13)—C(18)	109.7(5)
O(2)—C(3)—C(4)	108.3(6)	C(17)—C(13)—C(18)	112.5(5)
C(2)—C(3)—C(4)	112.3(6)	C(8)—C(14)—C(13)	120.1(5)
C(3)—C(4)—C(5)	112.8(6)	C(8)—C(14)—C(15)	128.1(6)
C(4)—C(5)—C(6)	109.0(6)	C(13)—C(14)—C(15)	111.8(6)
C(4)—C(5)—C(10)	114.1(5)	C(14)—C(15)—C(16)	111.6(6)
C(6)—C(5)—C(10)	111.1(5)	O(3)—C(16)—C(15)	113.8(5)
C(5)—C(6)—C(7)	112.9(5)	O(3)—C(16)—C(17)	106.2(5)
C(6)—C(7)—C(8)	112.1(5)	C(15)—C(16)—C(17)	103.6(5)
C(7)—C(8)—C(9)	113.0(5)	C(13)—C(17)—C(16)	104.8(5)
C(7)—C(8)—C(14)	112.9(5)	C(13)—C(17)—C(24)	116.0(5)
C(9)—C(8)—C(14)	109.7(5)	C(16)—C(17)—C(24)	115.7(5)
C(8)—C(9)—C(10)	112.3(5)	O(1)—C(20)—C(21)	104.9(6)
C(8)—C(9)—C(11)	109.9(5)	O(2)—C(21)—C(20)	106.7(6)
C(10)—C(9)—C(11)	114.7(5)	O(3)—C(22)—O(4)	126.3(9)
C(1)—C(10)—C(5)	106.6(5)	O(3)—C(22)—C(23)	109.6(9)
C(1)—C(10)—C(9)	111.6(5)	O(4)—C(22)—C(23)	124.0(8)
C(1)—C(10)—C(19)	106.5(5)	C(17)—C(24)—C(25)	112.4(6)
C(5)—C(10)—C(9)	110.5(5)	N—C(25)—C(24)	179.4(8)

Can. J. Chem. Downloaded from www.nrcresearchpress.com by 41.223.56.140 on 09/07/12
For personal use only.

TABLE 4. Intra-annular torsion angles (deg) with standard deviations in parentheses

Atoms	Angle (deg)
C(20)—O(1)—C(3)—O(2)	−28.5(8)
C(21)—O(2)—C(3)—O(1)	28.3(8)
C(3)—O(2)—C(21)—C(20)	−17.1(9)
O(1)—C(20)—C(21)—O(2)	−0.6(9)
C(3)—O(1)—C(20)—C(21)	18.1(9)
C(17)—C(13)—C(14)—C(15)	16.6(8)
C(13)—C(14)—C(15)—C(16)	−1.4(9)
C(14)—C(15)—C(16)—C(17)	−14.7(8)
C(15)—C(16)—C(17)—C(13)	24.1(6)
C(14)—C(13)—C(17)—C(16)	−24.4(6)
C(10)—C(1)—C(2)—C(3)	55.4(7)
C(1)—C(2)—C(3)—C(4)	−50.4(7)
C(2)—C(3)—C(4)—C(5)	50.0(8)
C(3)—C(4)—C(5)—C(10)	−53.1(7)
C(4)—C(5)—C(10)—C(1)	53.2(7)
C(2)—C(1)—C(10)—C(5)	−54.5(7)
C(10)—C(5)—C(6)—C(7)	−56.0(7)
C(5)—C(6)—C(7)—C(8)	53.0(7)
C(6)—C(7)—C(8)—C(9)	−50.3(7)
C(7)—C(8)—C(9)—C(10)	51.2(7)
C(8)—C(9)—C(10)—C(5)	−53.4(7)
C(6)—C(5)—C(10)—C(9)	55.5(7)
C(14)—C(8)—C(9)—C(11)	−52.8(7)
C(8)—C(9)—C(11)—C(12)	59.1(7)
C(9)—C(11)—C(12)—C(13)	−57.3(7)
C(11)—C(12)—C(13)—C(14)	47.3(7)
C(12)—C(13)—C(14)—C(8)	−45.5(8)
C(9)—C(8)—C(14)—C(13)	48.8(8)

final stages of refinement the non-hydrogen atoms were refined with anisotropic thermal parameters, and hydrogen atoms were fixed in idealized positions (methyl orientations based on observed positions, C(sp^2)–H = 0.97, C(cp^3)–H = 0.98 Å, $U_H \propto U_{\text{bonded atom}}$). The absolute configuration was based on the known configurations at atoms C(5), C(8), C(9), C(10), and C(13). Scattering factors for all atoms were taken from ref. 33. The weighting scheme $w = 1/\sigma^2(F)$, where $\sigma^2(F)$ is derived from the previously defined $\sigma^2(I)$, gave uniform average values of $w(|F_o| - |F_c|)^2$ over ranges of both $|F_o|$ and $\sin\theta/\lambda$ and was employed in the final stages of full-matrix refinement of 270 variables. Reflections with $I < 2\sigma(I)$ were not included in the refinement. Convergence was reached at $R = 0.047$ and $Rw = 0.041$ for 1033 reflections with $Ia \geqslant a2\theta(I)$. The function minimized was $\Sigma w(|F_o| - |F_c|)^2$, $R = \Sigma||F_o| - |F_c||/\Sigma|F_o|$ and $Rw = (\Sigma w(|F_o| - |F_c|)^2/\Sigma w|F_o|^2)^{1/2}$.

On the final cycle of refinement the mean and maximum parameter shifts corresponded to 0.01 and 0.21σ respectively. The mean error in an observation of unit weight was 1.406. A final difference map showed maximum fluctuations of −0.16 to +0.18 e Å^{-3}. The final position parameters for the non-hydrogen atoms appear in Table 1. Bond lengths, bond angles, and intra-annular torsion angles are given in Tables 2–4, respectively. Hydrogen atom parameters, anisotropic thermal parameters, torsion angles, and measured and calculated structure factors have been placed in the Depository of Unpublished Data.[4]

[4]Supplementary material mentioned in the text may be purchased from the Depository of Unpublished Data, CISTI, National Research Council of Canada, Ottawa, Ont., Canada K1A 0S2.

Can. J. Chem. Downloaded from www.nrcresearchpress.com by 41.223.56.140 on 09/07/12
For personal use only.

Basicity of substituted 2-phenyl-1,1,3,3-tetramethylguanidines and other bases in acetonitrile solvent

KENNETH T. LEFFEK,[1] PRZEMYSLAW PRUSZYNSKI, AND KOHILA THANAPAALASINGHAM
Department of Chemistry, Dalhousie University, Halifax, N.S., Canada B3H 4H6

Received August 15, 1988

KENNETH T. LEFFEK, PRZEMYSLAW PRUSZYNSKI, and KOHILA THANAPAALASINGHAM. Can. J. Chem. **67**, 590 (1989).

A series of 30 phenyl substituted derivatives of 2-phenyl-1,1,3,3-tetramethylguanidine was synthesized and the pK_a value of each was measured in acetonitrile using a conventional, general purpose glass electrode. The slope of the Hammett relationship, for the *para* and *meta* substituted compounds, $\rho = 2.18 \pm 0.16$, is significantly lower than $\rho = 2.85 \pm 0.06$ found for anilines in water, even though the phenyl ring is attached directly to the basic centre in both cases. The influence of electronic and steric effects on the basicity of the compounds is discussed. The solvent effect on the basicity is also discussed, by comparison of the pK_a values in acetonitrile and water. The mean value of $\Delta pK_a^{AN-H_2O} = 8.1 \pm 0.5$ is slightly higher than the value previously observed for ammonia and aliphatic amines, $\Delta pK_a^{AN-H_2O} = 7.5 \pm 0.3$. Additionally, the p$K_a$ values were measured for seven other cyclic bases, including 1,8-diazabicyclo[5.4.0]undec-7-ene (DBU) and 1,5-diazabicyclo[4.3.0]non-5-ene (DBN).

Key words: 2-phenyl-1,1,3,3-tetramethylguanidines, pK_a measurements.

KENNETH T. LEFFEK, PRZEMYSLAW PRUSZYNSKI et KOHILA THANAPAALASINGHAM. Can. J. Chem. **67**, 590 (1989).

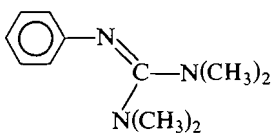
On a synthétisé une série de 30 phényl-2 tétraméthyl-1,1,3,3 guanidines substituées sur le noyau phényle et, utilisant une électrode de verre conventionnelle d'usage général, on a mesuré les valeurs de leur pK_a dans l'acétonitrile. La pente de la relation de Hammett, pour les composés substitués en *méta* et en *para*, $\rho = 2{,}18 \pm 0{,}16$, est beaucoup plus faible que la valeur de $\rho = 2{,}85 \pm 0{,}06$ qui a été observée pour les anilines dans l'eau, même si le noyau phényle est attaché directement au centre basique dans chacun des cas. On discute de l'influence des effets stériques et électroniques sur la basicité des composés. En se basant sur une comparaison des valeurs des pK_a dans l'acétonitrile et dans l'eau, on discute aussi de l'effet du solvant sur la basicité. La valeur moyenne du $\Delta pK_a^{AN-H_2O} = 8{,}1 \pm 0{,}5$ est légèrement supérieure à la valeur observée antérieurement pour l'ammoniac et les amines aliphatiques, $\Delta pK_a^{AN-H_2O} = 7{,}5 \pm 0{,}3$. De plus, on a mesuré les valeurs de pK_a de sept autres bases cycliques, dont le diaza-1,8 bicyclo[5.4.0]undécène (DBU) et le diaza-1,5 bicyclo[4.3.0]nonène-5 (DBN).

Mots clés : phényl-2 tétraméthyl-1,1,3,3 guanidines, mesures de pK_a.

[Traduit par la revue]

Introduction

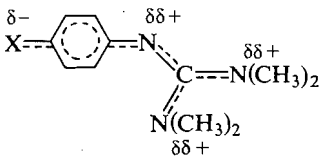
Derivatives of 2-phenyl-1,1,3,3-tetramethylguanidine (**1**) (PhTMG) represent a potentially useful group of strong bases within which smooth changes of basicity and (or) steric hindrance around the basic site may be achieved by substituting the phenyl ring with different groups.



1

Such series of bases are known in the case of weak bases, e.g., anilines or pyridines, and have been used in countless numbers of physicochemical studies. In the range of higher basicity the lack of such a family of closely related compounds has often forced the use of structurally different compounds, giving rise to difficulties in the interpretation of the experimental data. For studies concerned with proton transfer reactions from carbon acids such a series of strong bases is of special importance. Substitution at the *para* and *meta* positions allows the study of only electronic interactions with the reaction site. Thus the influence of base strength on the kinetics of the reaction under study can be isolated from steric factors. On the other hand, by changing the size of *ortho* substituents, the importance of steric factors can be evaluated.

PhTMG and its *para*-methyl substituted derivative (4-CH_3-PhTMG) were synthesized by Bredereck and Bredereck (1) by a condensation reaction of 1,1,3,3-tetramethylurea (TMU) with aniline and *p*-toluidine, respectively, in the presence of $POCl_3$. A number of other derivatives of PhTMG were later synthesized by Kessler and Leibfritz (2) and used for nmr studies of the mechanism of *syn–anti* isomerization. Interest in the basic properties of the derivatives of PhTMG in recent years resulted in the synthesis of further derivatives and pK_a measurements in ethanol–water (3) and water (4) solutions. Pruszynski (4) presented a fairly wide collection (17 compounds) of pK_a values in water and interpreted them in comparison with similarly substituted anilines. The unique ability of the $N{=}C[N(CH_3)_2]_2$ (TMG) group in a resonance interaction with electron-withdrawing substituents, like NO_2, was observed. This interaction was reflected in the need for a special σ value for NO_2. The slope of the Hammett plot for *meta* and *para* substituted derivatives of PhTMG, $\rho = 1.84 \pm 0.05$ (4), much lower than $\rho = 2.85 \pm 0.06$ found for anilines (5), was explained in terms of a resonance delocalization of the positive charge over all three nitrogens, resulting in an effective shift of the charge further from the phenyl ring and reducing the influence of substituents on the basicity. In other words, electron-withdrawing substituents reduce the density of the lone pair electrons of the nitrogen that is protonated, to a much lesser extent than in the case of the anilines. This is because the Π bond buffers this effect by shifting the partial positive charge towards the terminal 1 and 3 nitrogen atoms of the TMG group (**2**).



2

[1]Author to whom correspondence may be addressed.

Can. J. Chem. Downloaded from www.nrcresearchpress.com by 41.223.56.140 on 09/07/12
For personal use only.

TABLE 1. pK_a values for derivatives of PhTMG and other bases in water and acetonitrile

No.	Substituent	pK_a^{AN}	$pK_a^{H_2O}$[a]	$\Delta pK_a^{AN-H_2O}$	σ[b]
1.	H	20.6±0.1	12.18±0.02	8.4±0.1	0
2.	4-NO_2	17.82±0.07	9.78±0.09	8.0±0.1	1.26[c]
3.	4-CN	18.37±0.08	10.95±0.05*	7.42±0.09	1.00[c]
4.	4-CF_3	19.00±0.09	11.36±0.04*	7.6±0.1	0.74[c]
5.	4-Cl	19.68±0.10	11.70±0.02	8.0±0.1	0.24
6.	4-Br	19.6±0.1	11.60±0.10	8.0±0.1	0.22
7.	4-Me	20.9±0.1	12.37±0.01	8.5±0.1	−0.14
8.	4-OMe	21.0±0.1	12.57±0.03	8.4±0.1	−0.28
9.	3-CF_3	19.09±0.09	—	—	0.46
10.	3-Cl	19.30±0.09	11.47±0.09	7.8±0.2	0.37
11.	3-Me	20.8±0.1	12.25±0.04	8.5±0.1	−0.06
12.	3-OMe	20.4±0.1	11.96±0.04	8.4±0.1	0.11
13.	3,5-diCF_3	17.47±0.07	—	—	0.46+0.46
14.	2-CF_3	17.70±0.08	—	—	—
15.	2-Cl	18.80±0.09	11.2±0.1	7.6±0.1	0.67[d]
16.	2-Me	20.5±0.1	12.28±0.03	8.2±0.1	0.10[d]
17.	2-OMe	21.0±0.1	12.19±0.04	8.8±0.1	0[d]
18.	2,4-diCl	17.93±0.09	10.5±0.2	7.4±0.2	0.67d+0.24
19.	2,5-diCl	17.70±0.07	10.1±0.2	7.6±0.2	0.67d+0.37
20.	2,6-di-Me	20.5±0.1	12.3±0.1*	8.2±0.1	0.1+0.1[d]
21.	2,4-di-Me	21.0±0.1	12.50±0.03	8.5±0.1	0.1d+(−0.14)
22.	2,4-diOMe	21.6±0.1	12.54±0.04	9.1±0.1	0d+(−0.28)
23.	2-Et	20.2±0.1	—	—	0.05[d]
24.	2,6-di-Et	20.1±0.1	12.3±0.1*	7.8±0.1	0.05+0.05[d]
25.	2-iPr	20.1±0.1	12.5±0.2*	7.6±0.2	0.03[d]
26.	2,6-di-iPr	20.1±0.1	12.6±0.2*	7.5±0.2	0.03+0.03[d]
27.	2-OMe-4-NO_2	18.03±0.08	—	—	0d+1.26[c]
28.	2-Ph	19.8±0.1	—	—	0[d]
29.	3-TMG	21.7±0.1	—	—	—
30.	3-$TMGH^+$	18.80±0.09	—	—	—
31.	4-TMG	22.1±0.1	—	—	—
32.	4-$TMGH^+$	19.3±0.1	—	—	—
33.	DBU	23.9±0.1	—	—	—
34.	DBN	23.4±0.1			
35.	Thiomorpholine	16.60±0.06	9.00[e]	7.6	—
36.	1,2,3,4-Tetrahydroisoquinoline	17.25±0.07	9.41[e]	7.8	—
37.	*N*-Methylpiperidine	18.01±0.08	10.08[e]	7.9	—
38.	*N*-Methylpyrrolidine	18.42±0.08	10.46[e]	8.0	—
39.	*N*-Methylmorpholine	15.68±0.05	7.38[e]	8.3	—

[a]Values reported earlier (4) except those marked with *.
[b]σ values from ref. 11.
[c]The special σ values reported for anilines.
[d]The apparent σ_{ortho} values for anilines.
[e]From ref. 12.

The high basicity of the derivatives of PhTMG is a result of a resonance stabilization of the positive charge after protonation, the property typical for all guanidines. Electron-donating substituents on the phenyl ring stabilize the protonated form of the derivatives of PhTMG, but the sensitivity of these compounds to such stabilization is low because only a part of the positive charge is located next to phenyl ring, the rest being delocalized onto two bonds further away. These factors were used to explain the lower ρ value for 2-PhTMG than for anilines (4).

^{35}Cl nuclear quadropole resonance measurements for a series of five chloro substituted 2-PhTMG (6) proved the unusually effective electron-releasing action of the TMG group, and the sensitivity of this action towards the presence of *ortho* substituents. The origin of this sensitivity is steric in character and reflects the difficulty in achieving a planar structure in the presence of an *ortho* substituent.

With all of the above in mind, we decided to synthesize a further series of derivatives of PhTMG and to measure the pK_a values in acetonitrile solvent. Acetonitrile is the solvent of choice for many physical organic studies and the availability of pK_a values of a large series of bases in this solvent and in water will be of value in many future investigations. The method of measurement, potentiometric titration against a glass electrode, was designed to follow the exact procedure of Coetzee and Padmanabhan (7, 8) and Kolthoff and Chantooni (9, 10), to form a consistent series of data for basicity in acetonitrile.

Seven additional cyclic nitrogen bases were measured to further increase the range of structures available for physical organic investigations in acetonitrile.

Some further pK_a values in water, in addition to those reported earlier (4), were also measured using ultraviolet spectrophotometry.

Results and discussion

Table 1 presents the pK_a values measured in acetonitrile and water. The differences in pK_a of the bases in acetonitrile and

Can. J. Chem. Downloaded from www.nrcresearchpress.com by 41.223.56.140 on 09/07/12
For personal use only.

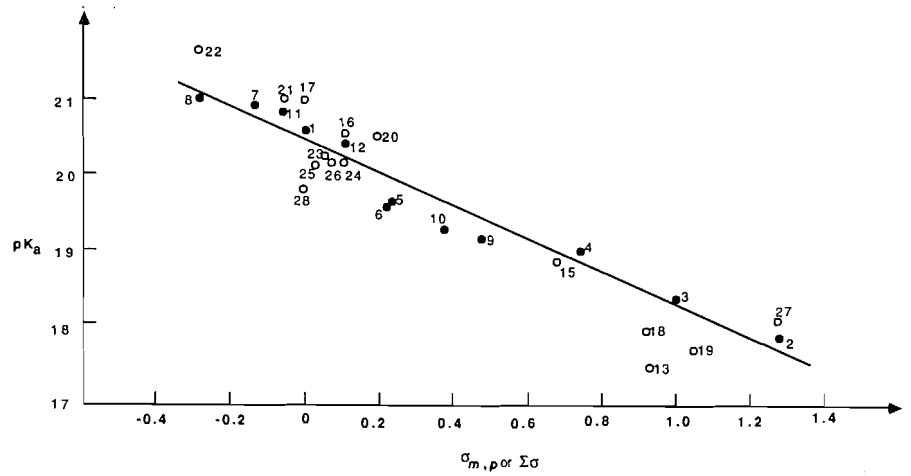


FIG. 1. Hammett relationship for the derivatives of PhTMG compounds. *meta* and *para* substituted compounds, filled circles; other derivatives, open circles. Compounds numbered as in Table 1.

water, $\Delta pK_a^{AN-H_2O}$, are also presented in this table together with the Hammett substituent constants, σ, where applicable.

The data in Table 1 show that all the compounds studied are stronger bases in acetonitrile than in water. Although the $\Delta pK_a^{AN-H_2O}$, value is fairly constant throughout the series of bases studied, the prediction of a pK_a in acetonitrile from the value in water cannot be done with an accuracy better than 0.5 pK_a units. For the PhTMG series the mean value of $\Delta pK_a^{AN-H_2O}$ is 8.1 ± 0.5 and for the five cyclic amines $\Delta pK_a^{AN-H_2O}$ is 7.9 ± 0.2. Both of these measurements are slightly higher than the value 7.5 ± 0.5 found by Coetzee and Padmanabhan (8) for the series of aliphatic amines, pyridine, some anilines, and diphenylguanidine.

Figure 1 shows the relationship of the measured pK_a^{AN} values against the Hammett substituent constant, σ, for all PhTMG bases.

The closed circles on the plot represent the *meta* and *para* monosubstituted compounds for which the slope ρ = 2.18 ± 0.16 was calculated. This value is significantly lower than ρ = 2.85 ± 0.06 (5) found for a series of anilines in water solvent, although both PhTMG and the anilines have nitrogen undergoing protonation bonded directly to phenyl ring. A lower than expected value of ρ = 1.84 ± 0.05 for the PhTMG series was also observed for the pK_a values in water (4). This means that there is a lower sensitivity of the density of the lone pair of electrons in the free base molecule, and (or) the stabilization of the protonated form, towards the presence of a substituent on the phenyl ring. This lower sensitivity is caused by the ability of the guanidinyl group to delocalize the positive charge over all three nitrogen atoms and thereby shift it further from the phenyl ring. As a result of such an action the electon-withdrawing substituents do not reduce the density of the lone pair electrons on the nitrogen at which protonation takes place to the extent that they do in the series of anilines. The pK_a values for *p*-di-(1,1,3,3-tetramethylguanidino)benzene and *m*-di-(1,1,3,3-tetramethylguanidino)benzene, 22.1 and 21.7 respectively, may be used to determine the substituent constants σ for the *meta* and *para* TMG substituent. If ρ and the intercept obtained from relationship for *meta* and *para* substituted compounds (Fig. 1) are used, these values are σ_m (TMG) = −0.6 and σ_p(TMG) = −0.80, in good agreement with values calculated from ^{35}Cl nqr measurements (6) (−0.62 and −0.88 respectively).

The open circles on Fig. 1 represent all disubstituted and *ortho* substituted derivatives of PhTMG. The σ values used in this relationship are given in Table 1. In the case of disubstituted compounds the sum of the substituent constants was used. Some of the points deviate from the general relation. The *ortho*-methoxy substituted bases, points 17, 22, and 27, show a pK_a higher than would be expected from the σ constant values (positive deviation). These compounds, 2-OMe, 2,4-diOMe, and 2-OMe-4NO_2 derivatives respectively, represent the case where intramolecular hydrogen bonding may occur in the protonated base. The positive deviations of about 0.5 pK_a unit correspond to stabilization due to such an effect of about 0.7 kcal mol^{-1}. Such an effect should also, according to other authors (8, 13), be reflected in an increased $\Delta pK_a^{AN-H_2O}$ value, which is the case of these bases (Table 1) and is discussed below.

Points 16(2-Me), 20(2,6-diMe), 21(2,4-diMe), which represent compounds with at least one methyl group in the position *ortho* to the TMG substituent, also show greater pK_a values than the general correlation predicts. This effect, observed previously for the 2-Me derivative in water (4), may be explained by a greater destabilization of the free base than its protonated form due to steric interactions, so that when the protonation takes place there is release of a steric strain. This effect is probably counterbalanced in the case of *ortho* substituents by the other effect, steric inhibition of solvation. This latter effect, according to Coetzee and Padmanabhan (8), operates in acetonitrile to a greater extent than in water and may be used to account for the pK_a values of the bases represented by points 23(2-iPr), 24(2,6-di-Et), 25(2-iPr), 26(2,6-di-iPr), 28(2-Ph). This negative contribution to the pK_a value is clearly dependent on the size of the *ortho* substituent, which gives additional support to the validity of such an explanation. Points 13, 18, 19 representing the 3,5-diCF_3, 2,4-diCl, and 2,5-diCl derivatives lie significantly lower than would be expected. This may be due to the inappropriateness of the standard σ values of these substituents in the reaction involving the very strong electron-releasing group, tetramethylguanidinyl. The values of σ_p and σ_m have been analyzed to consist of an inductive part (σ_I) and a resonance part (σ_R), as in eq. [1]:

$$[1] \quad \sigma = \sigma_I + \sigma_R$$

For σ_m the σ_R component is multiplied by a factor α less than unity (α = 0.33 has been used (14)). For the chloro substituents (σ_I = 0.47, σ_R = −0.23), because of the strongly electron-releasing nature of the TMG group, a reduction or elimination of

Can. J. Chem. Downloaded from www.nrcresearchpress.com by 41.223.56.140 on 09/07/12
For personal use only.

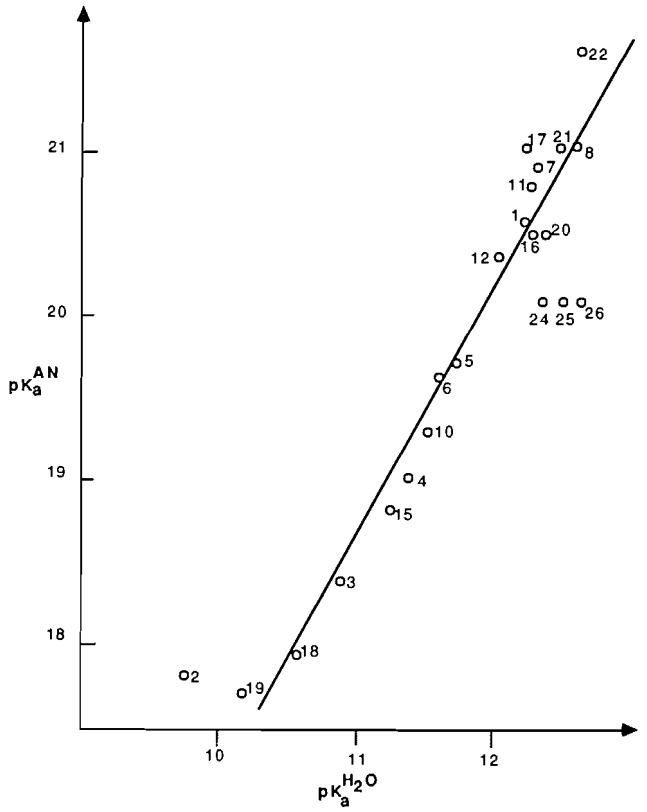


FIG. 2. The relation between pK_a in acetonitrile and in water for substituted derivatives of PhTMG.

the negative σ_R would enhance σ up to the limit 0.47 for σ_p and σ_m, which would move points 18 and 19 much closer to the correlation line. The 3,5-di-CF_3 compound (point 13) has a much smaller pK_a value than expected. This may be partially explained by assuming that the electron-withdrawing resonance effect ($\sigma_R = 0.11$) is increased by the electron-releasing TMG, which would again increase the value of σ_m by increasing α, possibly to a value 0.57 ($\sigma_I = 0.46$, $\sigma_R = 0.11$). The ^{19}F nmr measurements for the series of CF_3 substituted derivatives, listed in the experimental section, with the signals for *meta* derivatives presenting the largest upfield shift, seem to support this proposal.

Figure 2 presents the relationship between the pK_a values in water and in acetonitrile. If this relationship is assumed to be linear, the line drawn in Fig. 2 defines the regularity of the relationship. The slope of this line is not unity, therefore ΔpK_a is not constant throughout the series, reinforcing the conclusion that the pK_a of a base in a particular solvent can be only very roughly estimated from its pK_a in another solvent, within about half a pK_a unit at the best. Uncertainties of this magnitude are usually too large for meaningful discussion of kinetic or other data.

In addition to the fact that the slope of the line is greater than unity, certain points fall clearly off the line.

The position of points 17(2-OMe) and 22(2,4-diOMe) fall above the line, consistent with the postulated intramolecular hydrogen bonding in the protonated bases. This kind of interaction is more important in acetonitrile than in water (8, 13), giving additional stabilization of the protonated form in acetonitrile and as a consequence increasing the strength of the base. The points for sterically hindered bases, 24(2,6-di-Et), 25(2-iPr), 26(2,6-di-iPr), and to a lesser extent 20(2,6-di-Me) and 16(2-Me), show the pK_a^{AN} lower than would be expected from their values in water. This effect is a reflection of the steric inhibition of solvation, an effect more important in acetonitrile than in water (8, 13).

In the area of weaker bases, large positive deviations from the line are observed especially for the case of point 2 (4-NO_2). The strong resonance interaction of TMG and 4-NO_2 groups, which manifests itself for example in the λ_{max} of 398 nm in the free base compared to 380 for 4-nitroaniline, both measured in water, creates a substantial negative charge located on the oxygens of the NO_2 group. This gives rise to possible interactions by means of hydrogen bonding with water molecules, which stabilize the free base form reducing the strength of the base in water relative to that in acetonitrile. In the case of point 2 (4-NO_2) this effect corresponds to a difference of about 1–1.25 pK_a units or 1.3–1.6 kcal mol^{-1}.

The need for the empirical determination of pK_a values in each solvent for any meaningful discussions of kinetic data and the lack of extensive numerical values of pK_a in acetonitrile justify the presenting of results for some other bases in Table 1. The five unrelated cyclic bases show no systematic variation in $\Delta pK_a^{AN-H_2O}$ with structure, although the values range only from 7.6 to 8.3 pK_a units. Thus, despite the fact that $\Delta pK_a^{AN-H_2O}$ is fairly constant, it is not a reliable parameter for estimating undetermined pK_a values in any particular solvent, and should be used only when there is no alternative. One such case is found in the pK_a values for the strong amidine bases, DBU and DBN, which are of proven synthetic utility and are of interest also for synthetic organic chemists. These two bases are so strong that the direct measurements of their pK_a values in water are affected by the levelling effect of this solvent. This is true especially in the case of the stronger DBU base. Therefore, the pK_a of these bases in water may be estimated only from the measurements in other, less acidic solvents. Despite uncertainties of such estimates, the impossibility of direct measurements leaves no alternative. There is the pK_a value of 23.3 (10) in acetonitrile measured for 1,1,3,3-tetramethylguanidine (TMG), the base of almost the same strength as DBU. The corresponding values for this compound in water, $pK_a^{H_2O} = 13.6$ (15), and in 50% aqueous ethanol, pK_a = 13.3 (16), were reported. These data give the difference in pK_a values $\Delta pK_a^{AN-H_2O} = 9.7$. For DBN in 50% aqueous ethanol (16) pK_a = 13.5 was measured, which corresponds to the $pK_a^{H_2O} = 13.8$. If the measured value in acetonitrile $pK_a^{AN} = 23.4$ for DBN (Table 1) is used, a $\Delta pK_a^{AN-H_2O} = 9.6$ may be estimated. This value is in good agreement with the value previously calculated for TMG. The similar strength of the bases TMG, DBN, and DBU supports the use of $\Delta pK_a^{AN-H_2O} = 9.6$ for DBU, which together with the $pK_a^{AN} = 23.9$ (Table 1) give its $pK_a^{H_2O}$ as 14.3.

An alternative approach is to estimate the pK_a of DBU in water using phenyl substituted phenyltetramethylguanidines plotted in Fig. 2. A purely empirical approach to the plot in Fig. 2 requires points 2, 24, 25, 26 to be disregarded. The remaining points give a slope of 1.58 ± 0.08, different from what would be obtained by combining the ρ values for each solvent, because of different data values used. However, the slope 1.58, intercept 1.3 ± 1.0, represent the best empirical relationship for the calculation of the pK_a for DBU in water, which is (23.9 − 1.3)/1.58 = 14.3.

Experimental

2-Phenyl-1,1,3,3-tetramethylguanidines were synthesized by the method of Bredereck (1) with an additional extraction during the work-up that resulted in higher purity of the products (4). The solution of 0.1 mol of 1,1,3,3-tetramethylurea (Aldrich, dried over 4A

Can. J. Chem. Downloaded from www.nrcresearchpress.com by 41.223.56.140 on 09/07/12
For personal use only.

Can. J. Chem. Downloaded from www.nrcresearchpress.com by 41.223.56.140 on 09/07/12
For personal use only.

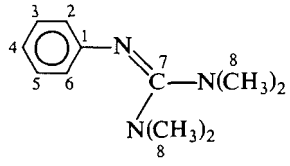
molecular sieve) in 100 mL of dry benzene was treated dropwise with 0.15 mol of $POCl_3$ in 20 mL of benzene. The reaction mixture was stirred overnight and a solution of 0.15 mol of the appropriate aniline was then added. The reaction mixture was refluxed for 7 h, after which the lower, oily phase was separated and water and 2 N NaOH solution were added to bring the pH to 8–9. An extraction with benzene performed at this pH removes the unreacted tetramethylurea and aniline. If performed carefully, the only component of the mixture present in the form of a salt in the water phase is the derivative of 2-phenyl-1,1,3,3-tetramethylguanidine. Thus by further raising the pH to about 14, followed by extraction with benzene, drying over anhydrous sodium sulphate, evaporation, and finally vacuum distillation, a pure sample of the base was obtained.

Thiomorpholine, 1,2,3,4-tetrahydroisoquinoline, *N*-methylpiperidine, *N*-methylpyrrolidine, *N*-methylmorpholine, DBN, and DBU were commercially available samples, which were dried over KOH.

The purity of all the bases was checked by means of gc–ms analysis using a Hewlett–Packard 5890 A/5970 MSD apparatus. All bases were dried and freshly distilled under vacuum on the day of measurements.

Commercial purity picric acid was recrystallized twice from acetone and dried at 80°C in a vacuum oven.

Picrates of the bases under study were prepared by dissolving 0.5–1 g of base in about 10 mL of absolute ethanol and titrating this solution with a saturated ethanol solution of picric acid using a glass electrode. The precipitate was dissolved by heating the suspension and the crystals were filtered after cooling. The second crystallization from ethanol was followed by drying in a vacuum desiccator. The spectra and other physical properties of many of the compounds were reported earlier (4). Several of the PhTMG derivatives used in these studies have not been reported in the literature before. The properties of these compounds are listed below. The melting points were measured using a Fisher–Johns melting point apparatus and are uncorrected. The ^1H, ^{13}C, and ^{19}F nmr spectra were obtained with TMS as the internal reference using a Nicolet 360 nmr spectrometer with Fourier transform, at the Atlantic Resonance Centre at Dalhousie University. The mass spectra were recorded on a modified Du Pont CEC model 21-104 mass spectometer at 70 eV. The ^{13}C nmr signals are reported in the sequence presented on the following structure, followed by signals for substituents on the phenyl ring:



2-(4′-Trifluoromethylphenyl)-1,1,3,3-tetramethylguanidine

Yield 55%; bp 142°C/5 Torr (1 Torr = 133.3 Pa); ^1H nmr δ: 6.72 (2H, d, 8.4 Hz), 7.42 (2H, d, 8.4 Hz), 2.71 (12H, s); ^{13}C nmr δ: 155.3, 121.7, 125.6, 123.3, 125.6, 121.7, 160.4, 39.3, CF_3 group 120.8 (q); ^{19}F nmr δ: −61.303; mass spectrum (rel. intensity, %): 259(42), 244(11), 215(100), 200(29). Picrate: mp 135–137°C.

2-(3′-Trifluoromethylphenyl)-1,1,3,3-tetramethylguanidine

Yield 70%, bp 120°C/3 Torr; ^1H nmr δ: 6.85 (1H, d, 8 Hz), 6.93 (1H, s), 703 (1H, d, 7.5 Hz), 726 (1H, t, 7.5 Hz), 2.68 (12H, s); ^{13}C nmr δ: 152.2, 117.6, 125.7, 115.5, 128.7, 124.4, 160.2, 39.1, CF_3 group 130(q); ^{19}F nmr δ: −62.848; mass spectrum (rel. intensity, %): 260.7(7), 259(43), 215(100), 201(25), 200(30). Picrate: mp 148–150°C.

2-(2′-Trifluoromethylphenyl)-1,1,3,3-tetramethylguanidine

Yield 40%; bp 135°C/4 Torr; mp 42–43°C; ^1H nmr δ: 6.54 (1H, d, 8 Hz), 6.83 (1H, t, 7.5 Hz), 7.28 (1H, t, 7.5 Hz), 7.48 (1H, d, 8 Hz), 2.68 (12H, s): ^{13}C nmr δ: 152.9, 123.4, 126.3, 118.7, 131.8, 123.0, 159.1, 39.5, CF_3 group 120.5(q); ^{19}F nmr δ: −61.303; mass spectrum (rel. intensity, %): 259(39), 216(18), 215(100), 200(22). Picrate: mp 135–137°C.

2-(3′,5′-Ditrifluoromethylphenyl)-1,1,3,3-tetramethylguanidine

Yield 75%; bp 199°C/5 Torr; mp 60.5–61°C, ^1H nmr δ: 7.08 (2H, s), 728 (1H, s), 2.74 (12H, s); ^{13}C nmr δ: 153.3, 121.0, 131.2, 112.4, 131.2, 121.0, 161.0, 39.6, CF_3 groups 131.7(q); ^{19}F nmr δ: −63.342; mass spectrum (rel. intensity, %): 327(25), 281(100), 267(24). Picrate: mp 187–189°C.

2-(2′-Ethylphenyl)-1,1,3,3-tetramethylguanidine

Yield 41%; bp 138.3°C; ^1H nmr δ: 7.11 (1H, d, 7.5 Hz), 7.02 (1H, t, 7.5 Hz), 6.81 (1H, t, 7.5 Hz), 6.48 (1H, d, 7.5 Hz), 2.65 (12H, s), 2.56 (2H, q, 7.5 Hz), 1.20 (3H, t, 7.5 Hz); ^{13}C nmr δ: 149.8, 134.7, 127.7, 120.0, 125.8, 121.1, 158.4, 39.4, ethyl group 13.5, 24.4; mass spectrum (rel. intensity, %): 219(20), 190(20), 175(21), 148(37). Picrate: mp 119–121°C.

2-(2′-Isopropylphenyl)-1,1,3,3-tetramethylguanidine

Yield 40%, bp 112°C/2 Torr; ^1H nmr δ: 6.43 (1H, d, 7 Hz), 6.82 (1H, t, 6.7 Hz), 6.95 (1H, t, 6.7 Hz), 7.15 (1H, d, 6.7 Hz), 3.23 (1H, septet, 7 Hz), 2.67 (12H, s), 120 (6H, d, 7 Hz); ^{13}C nmr δ: 148.8, 139.1, 125.4, 120.0, 125.0, 120.9, 157.9, 39.4, isopropyl group 23.0, 27.4; mass spectrum (rel. intensity, %): 232(22), 218(22), 190(67), 189(25), 162(38), 144(79). Picrate: mp 109–111°C.

2-(2′-Phenylphenyl)-1,1,3,3-tetramethylguanidine

Yield 60%, bp 199°C/5 Torr; ^1H nmr δ: 6.88–7.43 (9H, m), 2.36 (12H, s); ^{13}C nmr δ: 149.0, 132.4, 130.2, 120.3, 125.9, 124.1, 157.8, 38.5, phenyl substituent 127.4, 127.7, 128.5; mass spectrum (rel. intensity, %): 267(72), 266(20), 252(21), 223(100), 207(29), 196(48). Picrate: mp 131–132°C.

p-*Di-(1,1,3,3-tetramethylguanidyno)benzene*

Yield 60%; mp 153–154°C; ^1H nmr δ: 6.58 (4H, s), 2.66 (24H, broad signal at room temperature); ^{13}C nmr δ: 144.6, 121.8, 121.8, 144.6, 121.8, 121.8, 159.3, 39.3 (b); mass spectrum (rel. intensity, %): 305(22), 304(100), 289(31), 260(23), 233(32). Picrate: mp 276–280°C.

m-*Di-(1,1,3,3-tetramethylguanidyno)benzene*

Yield 70%; bp 198°C/4 Torr; mp 75–77°C; ^1H nmr δ: 6.12 (1H, s), 6.20 (2H, d, 7.8 Hz), 7.00 (1H, t, 7.8 Hz), 2.69 (24H, s); ^{13}C nmr δ: 152.3, 115.2, 152.3, 113.7, 128.3, 113.7, 159.4, 39.5; mass spectrum (rel. intensity, %): 305(20), 304(100), 303(20), 260(38), 233(21). Picrate: mp 253–255°C.

Tetramethylammonium perchlorate was prepared by titration of a 10% solution of tetraethylammonium hydroxide in water with perchloric acid using a glass electrode to just beyond the equivalence point. The salt was recrystallized twice from water and dried in a vacuum oven at 60°C.

Tetraethylammonium picrate was prepared by titration of a saturated aqueous solution of picric acid with a 10% solution of tetraethylammonium hydroxide in water using a glass electrode to just beyond the equivalence point. The solution was evaporated until crystallization occurred. This product was recrystallized once again from water, then from 90% ethanol, and finally it was dried in a vacuum over P_2O_5; mp 267–270°C (lit (17) mp 254–257°C).

Acetonitrile was prepared by the method of O'Donnell *et al.* (18), followed by fractional distillations from P_2O_5 and calcium hydride.

The potentiometric measurements were performed using the method described by Coetzee and Padmanabhan (7, 8). The H-type cell was constructed (Fig. 3) equipped with the thermostated water jacket (the temperature of the measurements was 25°C).

The side arm of an external reference electrode half-cell was dipped into the 0.1 M tetraethylammonium perchlorate solution. The reference electrode was a flowing junction silver – 0.01 M silver nitrate (in acetonitrile) half cell, as previously described by Kolthoff and Reddy (19). The middle compartment, closed on both sides with fine-porosity sintered glass disks, was filled with 0.1 M tetraethylammonium perchlorate solution in acetonitrile. The large, 20 mm i.d., compartment was filled with the buffer solution. The glass electrode (Corning, pH triple purpose Ag/AgCl, cat. no. 476022) was immersed in a way that allowed for tight closing and protection against moisture and

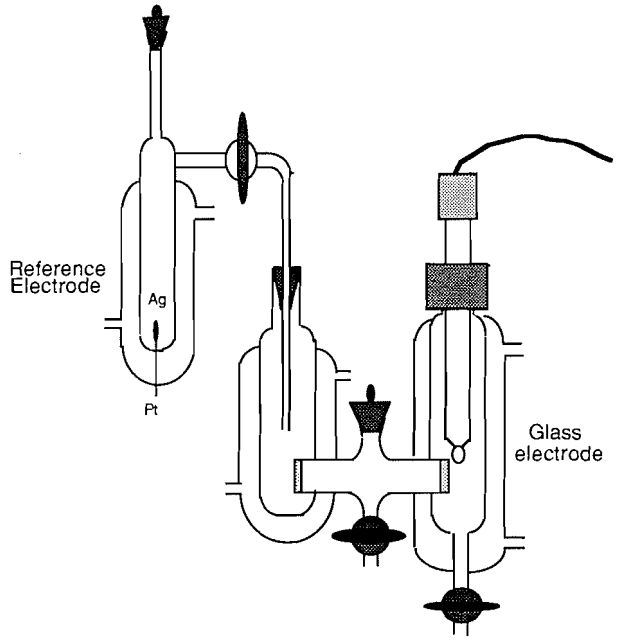


FIG. 3. The potentiometric cell for the pK_a measurements in acetonitrile.

carbon dioxide. The middle and glass electrode compartments were equipped with taps providing easy drainage after each set of measurements. When not in use the glass electrode was kept in water, and before each measurement it was washed with absolute ethanol, dried in a stream of dry nitrogen, and immersed for at least 2 h in acetonitrile. An Orion Research model 601A pH-meter was used. The glass electrode was calibrated in picric acid – tetraethylammonium picrate buffers. The theoretical justification for the use of above buffer system has been given previously (7). A $pK_a = 11.0$ for picric acid was used (9). The calibration was performed with five buffers of different ratios and was repeated several times during the course of the study. The agreement was such that the change in pK_a value was smaller than the calculated standards deviations when the results from different calibration curves were employed. The buffers of the bases for which the pK_a values were measured were prepared in such a way that the concentrations of tetraethylammonium perchlorate and picrate of the base under study were kept constant, both 5×10^{-4} M, and the concentration of the base was changed typically between 3×10^{-4} M and 4×10^{-3} M. Equilibrium was reached in about 5–10 min, and the readings of the emf were very stable (for at least half an hour). In the case of *p*-di-(1,1,3,3-tetramethylguanidino)benzene and *m*-di-(1,1,3,3-tetramethylguanidino)benzene, bases with two basic centres, both pK_a values (for di- and monovalent cations) were determined. The solution of monopicrate of both bases was prepared by dissolving an equimolar amount of dipicrate and free base. The dipicrate–monopicrate and monopicrate – free base buffers were used for the measurements of pK_{a1} and pK_{a2} respectively.

The pK_a value was calculated using eq. [2]:

$$[2] \quad pK_{a\ base} = pK_{a\ picric\ acid} + \log 0.89 + (C - E)/S$$

where $pK_{a\ picric\ acid} = 11.0$; C is the emf value for picric acid buffer of buffer ratio = 1; E is the emf value for base buffer of buffer ratio = 1; S is the slope of the relation, emf = $f(\log (c_{HPi}/c_{Pi^-}))$; 0.89 is the ratio of the activity coefficients for the monocharged and uncharged species at ionic strength 1×10^{-3} M as calculated by the "reduced" Debye–Hückel equation. The additional correction for the change of activity coefficients for mono and divalent cations was done in the case of both dipicrates. The mean value of slope from all measurements was $S = 59.1 \pm 1.8$ mV/pH unit.

The reproducibility of the results of Coetzee and Padmanabhan (8) was checked by repeating the pK_a measurements for piperidine. The value 18.92 ± 0.05 was reported by them and the value 19.06 ± 0.09 was found by us.

The pK_a values in water were measured spectrophotometrically using the procedure described previously (4). Fisher certified NaOH solutions were used. Measurements were done using a Cary 219 uv–vis spectrophotometer equipped with a thermostating device.

1. H. BREDERECK and K. BREDERECK. Chem. Ber. **94**, 2278 (1961).
2. H. KESSLER and D. LEIBFRITZ. Tetrahedron, **26**, 1805 (1970).
3. J. OSZCZAPOWICZ and J. OSEK. Pol. J. Chem. **57**, 93 (1983).
4. P. PRUSZYNSKI. Can. J. Chem. **65**, 626 (1987).
5. A. J. BIGGS and R. A. ROBINSON. J. Chem. Soc. 388 (1961).
6. B. NOGAJ and P. PRUSZYNSKI. Magn. Reson. Chem. **25**, 301 (1987).
7. J. F. COETZEE and G. R. PADMANABHAN. J. Phys. Chem. **66**, 1708 (1962).
8. J. F. COETZEE and G. R. PADMANABHAN. J. Am. Chem. Soc. **87**, 5005 (1965).
9. I. M. KOLTHOFF and M. K. CHANTOONI, JR. J. Am. Chem. Soc. **87**, 4428 (1965).
10. I. M. KOLTHOFF, M. K. CHANTOONI, JR., and S. BHOWMIK. J. Am. Chem. Soc. **90**, 23 (1968).
11. D. D. PERRIN, B. DEMPSEY, and E. P. SERJEANT. pK_a predictions for organic acids and bases. Chapman and Hall, London, New York. 1981. Appendix 1, 4, 5.
12. D. D. PERRIN. The dissociation constants for organic bases in aqueous solutions, Butterworths, London. 1965.
13. H. K. HALL, JR. J. Phys. Chem. **60**, 63 (1956).
14. O. EXNER. Collect. Czech. Chem. Commun. **31**, 65 (1966).
15. S. J. ANGYAL and W. K. WARBURTON. J. Chem. Soc. 2492 (1951).
16. D. H. R. BARTON, J. D. ELLIOTT, and S. D. GERO. J. Chem. Soc. Perkin. Trans. I, 2085 (1982).
17. A. UNMACK, E. BULLOCK, D. M. MURRAY-RUST, and SIR H. HATTLEY. Proc. R. Soc. London A:**132**, 427 (1931).
18. J. F. O'DONNELL, J. T. AYRES, and C. K. MANN. Anal. Chem. **37**, 1161 (1965).
19. I. M. KOLTHOFF and T. B. REDDY. Inorg. Chem. **1**, 189 (1962).

Can. J. Chem. Downloaded from www.nrcresearchpress.com by 41.223.56.140 on 09/07/12
For personal use only.

The binding of bilirubin by immobilized oligopeptides containing lysine

M. BOUVIER,[1] G. R. BROWN,[2] AND L. E. ST-PIERRE
Department of Chemistry, McGill University, Montreal, P.Q., Canada H3A 2K6

Received February 9, 1988[3]

M. BOUVIER, G. R. BROWN, and L. E. ST-PIERRE. Can. J. Chem. **67**, 596 (1989).

Peptides consisting of portions of the sequence Arg-$(Lys)_2$-$(Ser)_2$-Lys-$(Ala)_3$ have been immobilized onto a polyacrylamide support by solid phase peptide synthesis. Isotherms at 0°C for the adsorption of bilirubin from phosphate buffer by these peptide resins are highly dependent on pH, in the range 7.80–11.00, demonstrating the importance of ionic interactions. The adsorption behaviour of bilirubin-related tetrapyrroles shows that structural factors also influence the process. Peptide resins containing two or more residues of lysine have two binding sites on each pendant and are characterized by positive cooperativity, to a degree that is highly dependent on the number of residues. It is proposed that bilirubin molecules bound by lysine-containing pendants are stacked, the dimer state being stabilized by $\pi-\pi$ electron interactions, hydrogen bonds, and hydrophobic interactions. Site binding constants show that arginine-containing pendants manifest a stronger affinity for bilirubin.

Key words: bilirubin, adsorption, lysine, oligopeptides, cooperativity.

M. BOUVIER, G. R. BROWN et L. E. ST-PIERRE. Can. J. Chem. **67**, 596 (1989).

Des peptides consistant en différentes portions de la séquence Arg-$(Lys)_2$-$(Ser)_2$-Lys-$(Ala)_3$ ont été greffés, via la technique de synthèse en phase solide des peptides, à un support de polyacrylamide réticulé. Des isothermes caractérisant l'adsorption de la bilirubine en milieu tampon, à 0°C, par ces adsorbants sont dépendants du pH, dans l'intervalle 7,80–11,00, démontrant ainsi l'importance des interactions ioniques. L'adsorption de tétrapyrroles similaires à la molécule de bilirubine a démontré que des facteurs reliés à la structure du ligand influencent le processus d'association. Les adsorbants qui contiennent deux résidus de lysine ou plus ont deux sites d'adsorption par pendant et sont caractérisés par un mode d'adsorption à coopérativité positive, le degré duquel est dépendant du nombre de résidus de lysine dans la séquence. Il est proposé que les pendants contenant des résidus de lysine favorisent la dimérisation des molécules de bilirubine liées, le dimère étant stabilisé par des interactions $\pi-\pi$, des ponts hydrogènes et des interactions hydrophobiques. Des constantes d'association ont démontrées que les pendants qui contiennent des résidus d'arginine manifestent une grande affinité pour la bilirubine.

Mots clés : bilirubine, adsorption, lysine, oligopeptides, coopérativité.

Can. J. Chem. Downloaded from www.nrcresearchpress.com by 41.223.56.140 on 09/07/12
For personal use only.

Introduction

Bilirubin (Fig. 1) is the bile pigment known to produce a yellow coloration in the skin of neonates who show delayed development of the excretory functions. Under such circumstances the increased concentration of plasma bilirubin can result in serious physiological disorders (1). Attempts have been made to remove the toxic bile pigment by hemoperfusion using adsorbents such as cholestyramine, immobilized human serum albumin (HSA), and similar materials (2–5).

Previous reports from this laboratory have demonstrated that certain peptides immobilized on a cross-linked polymer support form efficient adsorbents for bilirubin (6–8). This paper describes the adsorption behaviour of adsorbents with pendants synthesized from amino acids, such as lysine and arginine, that have been shown previously to be of key importance for the adsorption of bilirubin (6–8) and have been reported to be involved in the binding of bilirubin by HSA (9–11). Residues of serine are also incorporated into the sequence. The adsorbents are designed to obtain a better understanding of the interactions between bilirubin and the peptide pendants. To this end, adsorption isotherms and corresponding Scatchard plots are obtained from which site binding constants are derived.

Experimental

Syntheses of peptide resins

The support used for synthesis of peptide resins was a copolymer of dimethylacrylamide and *N*-acryl-1,6-diaminohexane hydrochloride reticulated with bisacrylyl-1,2-diaminoethane (Polyamide Peptide Resin 1 from Chemical Dynamics Corp.). Potentiometric titration for the chloride using silver nitrate gave a substitution of 0.22 mmol/g. The amino acids were purchased as the L form of the Boc-α amino acids (Vega Biotechnologies) with the side-chain groups protected as follows: Lys (ε-2-chloro-benzyloxycarbonyl), Ser (*O*-benzyl), Arg (nitro). (Three-letter symbols are used for designations of the amino acids as recommended by the Joint Commission on Biochemical Nomenclature of IUPAC-IUB.) Syntheses were done using a Vega 250 synthesizer based on a previously published program (6). Activated amino acids in the form of symmetrical anhydrides were used in the coupling reactions. Coupling and deprotection procedures were monitored by the ninhydrin test (12). A spacer consisting of three alanine residues was introduced at the beginning of the sequence to separate the remaining amino acids from the support. Samples of the peptide resins were removed after each coupling step following the addition of the last residue of alanine. The protecting groups on the side chains of the amino acids were removed by treating the dried peptide resins with anhydrous hydrogen fluoride in the presence of anisole for 1 h at 0°C. The deprotected peptide resins were then washed with ether, dried, and stored in a desiccator.

Amino acid analyses

Peptide resins were hydrolyzed at 110°C for 48 h according to previously published procedures (8). Amino acid analyses were performed using a Varian 5500 Analyzer.

Adsorption experiments

A stock solution of bilirubin (Sigma Chemicals) was prepared daily by dissolving the pigment in a minimal amount of 0.10 M NaOH and adjusting the volume with degassed 0.050 M KH_2PO_4/NaOH buffer to give a final concentration of 10 mg/dL and a final pH of 7.80. Bilirubin was shown to be of high purity by thin-layer chromatography and by nmr studies (13), and was used without further purification.

Adsorption studies were performed with bilirubin solutions of different initial concentrations, prepared from the stock solution, with approximately 10 mg of adsorbent. The adsorption studies were done at 0°C, under a constant flow of nitrogen, using a specially designed flask (14). Prior to the adsorption experiments, the flask was routinely

[1]Present address: Health and Welfare Canada, Bureau of Radiation and Medical Devices, Environmental Health Center, Ottawa, Ont., Canada K1A 0L2.

[2]Author to whom correspondence may be addressed.

[3]Revision received November 7, 1988.

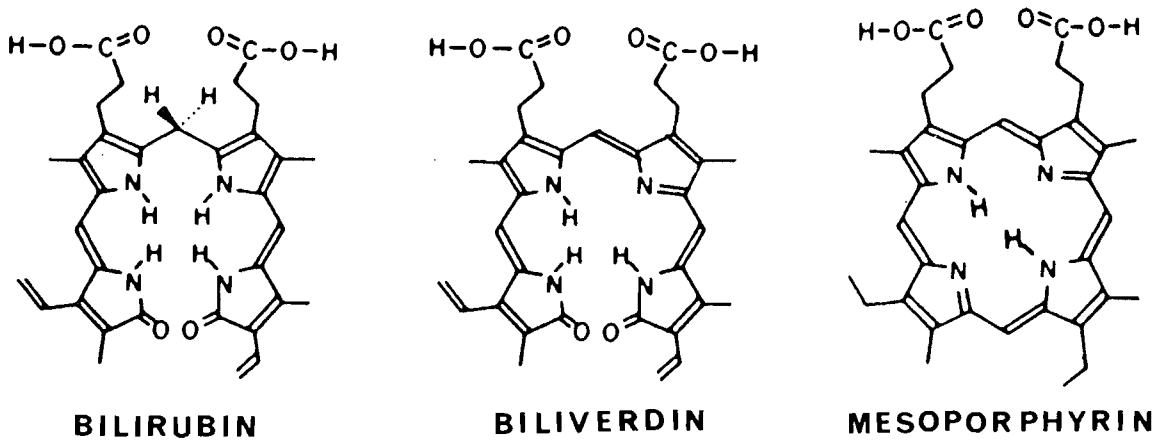


FIG. 1. Structures of bilirubin, biliverdin, and mesoporphyrin.

silanized and coated with bilirubin, by stirring in it a concentrated bilirubin solution, to minimize deposit of the pigment on the glass surface (14). The concentration change in the known volume was followed by measuring the absorbance of free bilirubin at the absorbance maximum, 438 nm, using a Beckman 25 spectrophotometer. Studies of the kinetics of adsorption were initially done to determine times required to achieve equilibrium for each adsorbent. All experiments were performed in the dark under a red light. Control experiments, without resin, showed minimal loss of bilirubin in the time allowed for these adsorption experiments.

Adsorption studies of biliverdin and mesoporphyrin (Porphyrin Products Inc.) by a selected adsorbent were done in a manner identical to that for the adsorption of bilirubin. In the concentration ranges used for adsorption, $(1.69–8.45) \times 10^{-5}$ M for biliverdin and $(1.51–5.82) \times 10^{-5}$ M for mesoporphyrin, the solutions obeyed Beer's law. Absorbance values for free biliverdin and mesoporphyrin were taken at 374 and 366 nm, respectively, corresponding to their absorbance maxima. The tetrapyrroles, as purchased, exhibited relatively high purity (85–90%), so that the compounds were used without further purification.

Results

Rationale

The completed peptide sequence designed to serve as an adsorbent for bilirubin is shown below:

Arg-Lys-Lys-Ser-Ser-Lys-$(Ala)_3$-support

Some of the characteristics of the selected amino acids are given in Table 1. Studies in this laboratory have demonstrated that the presence of the basic amino acids, arginine and lysine, results in materials with a high binding capacity and strong affinity for bilirubin (7, 8). Serine residues are incorporated into the sequence to provide the possibility of additional hydrogen bonding between the side-chain hydroxyl group and the hydrogen acceptor (two propionic acid groups and two lactam CO groups) or the hydrogen donor (four NH groups) on bilirubin. Although the acid form of bilirubin is known to have an intramolecularly hydrogen bonded structure (15, 16), it is not known to what extent these bonds are preserved in aqueous solution (17).

The order of attachment of the amino acids to the support is based on the following factors: A segment of the proposed sequence, -Lys-Ser-Ser-Lys-, forms a peptide with a symmetrical arrangement of amino acids. It is of interest to evaluate the ability of such a peptide to interact with bilirubin, which itself has high molecular symmetry (Fig. 1). It is noteworthy that a very similar peptide sequence is found in HSA between residues 189 and 194 (18).

TABLE 1. Characteristics of the amino acids immobilized onto the polyacrylamide support

Amino acids	Resin designation						Classification	Charge (pH 7.80)
	1	2	3	4	5	6		
$(Ala)_3$	↕	↕	↕	↕	↕	↕	Hydrophobic	
Lys	↕	↕	↕	↕	↕	↕	Basic	+
Ser		↕	↕	↕	↕	↕	Polar	
Ser			↕	↕	↕	↕	Polar	
Lys				↕	↕	↕	Basic	+
Lys					↕	↕	Basic	+
Arg						↕	Basic	+

Interestingly, both bovine and human serum albumins have a cluster of serine and lysine residues at the tips of loops no. 4 and no. 5. Residues located at the tips of loops represent, in accordance with Brown's model for the tertiary structure of albumin (19), sites with a high potential for binding bulky ligands like bilirubin. In particular, loop no. 4 has been mentioned as a potential location for the binding of bilirubin, as demonstrated from fragment studies (11, 20–23).

The single arginine residue at the end of the sequence forms, along with the adjacent lysines, a cluster of basic residues. Such a "nest" of basicity should be a very important factor for the adsorption of bilirubin, as suggested from previous results (7). Finally, the primary structure of the defined sequence is such that it carries a net overall positive charge of 4 + ; this represents an advantageous feature for the binding of a negatively charged molecule.

Based on the above rationale, the proposed sequence is expected to show many interesting features that justify the study of its properties for the adsorption of bilirubin.

Amino acid analyses

The results of the amino acid analyses are given in Table 2 as ratios based on the complete recovery of the three alanine residues of resin 1. They indicate coupling of the first lysine residue to 90% of the $(Ala)_3$ spacer units. Subsequently, no peptide chains fail to grow until resin 6, where there is an additional decrease of ratio to 0.7, indicating a further loss of 20%.

Adsorption isotherms and binding interactions

Studies of the kinetics of adsorption showed that 1–3 h are required for the adsorbents to reach adsorption equilibrium.

Can. J. Chem. Downloaded from www.nrcresearchpress.com by 41.223.56.140 on 09/07/12
For personal use only.

TABLE 2. Amino acid analysis results for each peptide resin describing the proposed sequence

^{6}Arg-^{5}Lys-^{4}Lys-^{3}Ser-^{2}Ser-^{1}Lys-(Ala)$_3$-support	
0.9—3.0–	Resin 1
0.9 ———	Resin 2
0.9 ———	Resin 3
0.9 ———	Resin 4
0.9 ———	Resin 5
0.7 ———	Resin 6

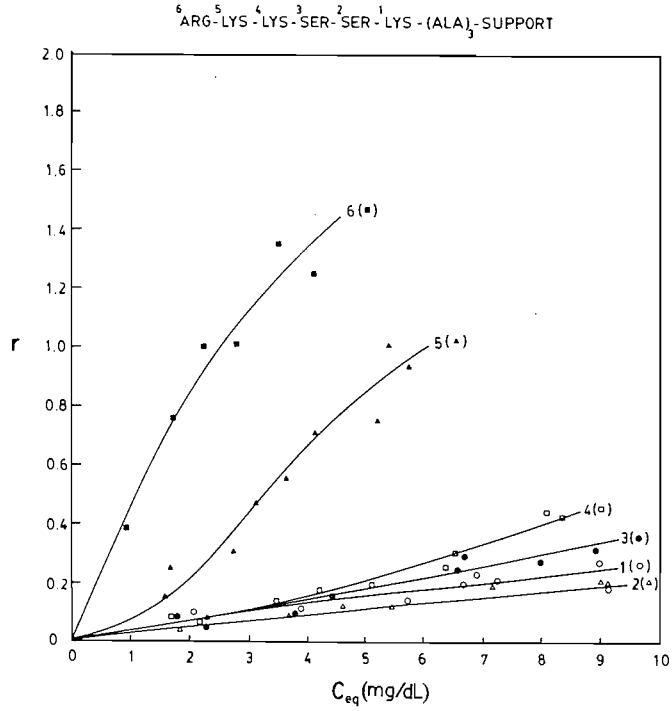


FIG. 2. Experimental adsorption isotherms, KH_2PO_4/NaOH (0.05 M), pH = 7.80, and 0°C.

Figure 2 presents the equilibrium isotherms, obtained at 0°C, for adsorbents with pendants composed of increasing portions of the proposed sequence. The parameters r and C_{eq} represent the equilibrium molar ratio of bound bilirubin per peptide pendant and the equilibrium concentration of free bilirubin (also $[A]_{eq}$, in M), respectively. The curves drawn through the experimental points are derived from a nonlinear iterative computer program from SAS (SAS Institute, 1982), using a method described previously (24). The adsorption data are estimated to have an associated uncertainty of ±5%.

A normalization process, based on the results of the amino acid analyses, was applied to the experimental adsorption isotherms in a manner described previously (8). The normalized isotherms (Fig. 3) describe the adsorption behaviour of adsorbents as though they were substituted at 100% by the indicated peptide sequence. Normalization causes some adjustments to the absolute values of r but the relative positions of the isotherms are unaffected. The adsorption isotherm corresponding to the polymer support is given in Fig. 3, for purposes of comparison, and shows minimal adsorption of bilirubin. Although the bilirubin solutions used for these studies are probably supersaturated, losses due to spurious nucleation by polymer therefore appear to be unimportant.

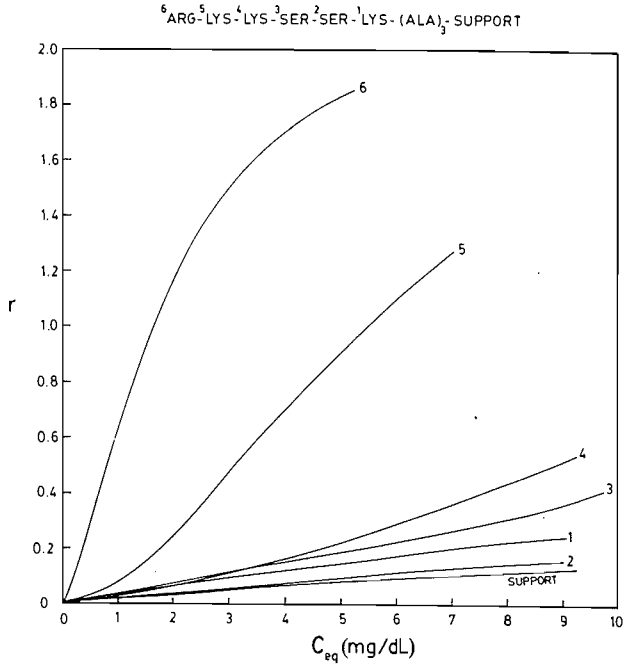


FIG. 3. Normalized adsorption isotherms.

As reported previously (7), the addition of the Lys-(Ala)$_3$-fragment to the polymer support, to form resin 1, results in an adsorbent with a binding capacity that is only slightly higher than that of the support (Fig. 3). This increment in capacity can be attributed to the presence of the lysine residue since the addition of three alanine residues has been shown previously to have minimal effect (7). A reverse trend, i.e., a decrease, occurs with the addition of a serine residue so that the binding capacity of the resulting adsorbent, resin 2, is similar, within experimental error, to that of the polymer support. The addition of this residue has slightly reduced the favorable contributions of the lysine residue to the adsorption process, possibly as a result of interactions, e.g., hydrogen bonds, between the lysine and serine residues.

An increase in binding capacity, above that of the isotherm corresponding to resin 1, results from the addition of a second serine residue to form resin 3. This suggests that the lysine residue, in particular, has become more available for interaction with bilirubin, possibly from a disruption of the interactions between the residues forming the sequence.

The trend towards moderate increase in binding capacity, especially at high adsorbate concentrations, is continued in the formation of resin 4 that includes a second residue of lysine. It is of interest to note that this isotherm is remarkably similar to that for the (Lys)$_2$-(Ala)$_3$-support resin (7). This points to a lack of involvement of the two serine residues in the binding process, a behaviour that was already manifested by resin 3. It should be noted that the isotherms corresponding to resins 3 and 4 demonstrate very low slopes at low adsorbate concentrations with continuously sharper increments in r, especially at high values of C_{eq}, and are quite different from those associated with regular "Langmuir" type adsorption. The shapes of the various adsorption isotherms will be considered in more detail later.

A considerable increase in binding capacity occurs as a result of the coupling of a third lysine residue to form resin 5. This large increase in capacity is thought to be related primarily to an increase in basicity although other factors, such as the length

Can. J. Chem. Downloaded from www.nrcresearchpress.com by 41.223.56.140 on 09/07/12
For personal use only.

of the resulting peptide sequence, should favorably influence binding of the adsorbate. The isotherm corresponding to resin 5 exhibits a sigmoidal shape, which resembles that for the binding of oxygen on hemoglobin (25).

Finally, the addition of an arginine residue completes the development of the sequence and results in a marked increase in binding capacity. This effect demonstrates the importance of arginine residues in the binding of bilirubin, as suggested by Jacobsen (9).

The adsorption results confirm some of the hypotheses presented initially in designing the sequence. Indeed, the addition of lysine and arginine residues affects the binding capacity in a manner that correlates with our previous results (6–8) and with evidence given in the literature regarding the participation of these amino acids in the binding of bilirubin by HSA (9–11). The clustering in the sequence of the basic residues produces a material with a high binding capacity for bilirubin. On the other hand, there is no indication that hydrogen bonds between the adsorbate and the OH groups on serine residues are of importance in the binding. The formation of resin 4, Lys-Ser-Ser-Lys-$(Ala)_3$-support, does not result in a large increase in binding capacity, relative to those of the previous sequences, indicating that the presence of the symmetrical unit has no special effect on the binding character of these pendants.

To verify the importance of ionic interactions in the binding process, adsorption studies were repeated at pH 10.85 using resin 5. At this pH the lysine residues should be mostly in a neutral form, based on the pK_a of the side chain of this residue being 10.58 (ref. 25, p. 90) and on the behaviour of polylysine at a similar pH (27). Changes in the ionic state of bilirubin in the pH range 7.80–10.85 are somewhat controversial. Some authors strongly hold that bilirubin exists as a monoanion in the pH range 6–9 and as a dianion above (28, 29), while others argue that bilirubin exists as a dianion even near neutrality (30). Assuming a change in the ionization state of bilirubin from monoanion to dianion, ionic interactions should be favored. However, Fig. 4 shows a considerable decrease in capacity at pH 10.85, in accordance with an adsorption mechanism involving ionic interactions. Changes in peptide conformations are expected to be a minor factor because of the limited development of secondary and tertiary structures for this relatively short sequence. Furthermore, the conformation of bilirubin can be assumed to play a minor role since X-ray analyses have shown that the bile pigment maintains a similar three-dimensional conformation regardless of its ionization state (31).

Based on the previous results, it is clear that ionic interactions are greatly influencing the binding between bilirubin and peptide pendants. However, it was of interest to determine if other factors were also contributing to the adsorption process. To this end, the binding behaviour of molecules that are chemically similar to bilirubin, but that bear some structural differences from it, were studied. The adsorbates selected for this purpose were biliverdin and mesoporphyrin. These compounds share many chemical features with bilirubin (Fig. 1), including the presence of two propionic carboxyl groups, but differ in that the inherent molecular flexibility is reduced. Indeed, biliverdin, in contrast to bilirubin, has a fully conjugated system since both pyrromethenone chromophores are connected by a methene bridge. This relatively small difference in the center of the molecule prevents free rotations within the molecule. Bilirubin and biliverdin, although shown in a cyclic conformation in Fig. 1 to emphasize basic chemical differences,

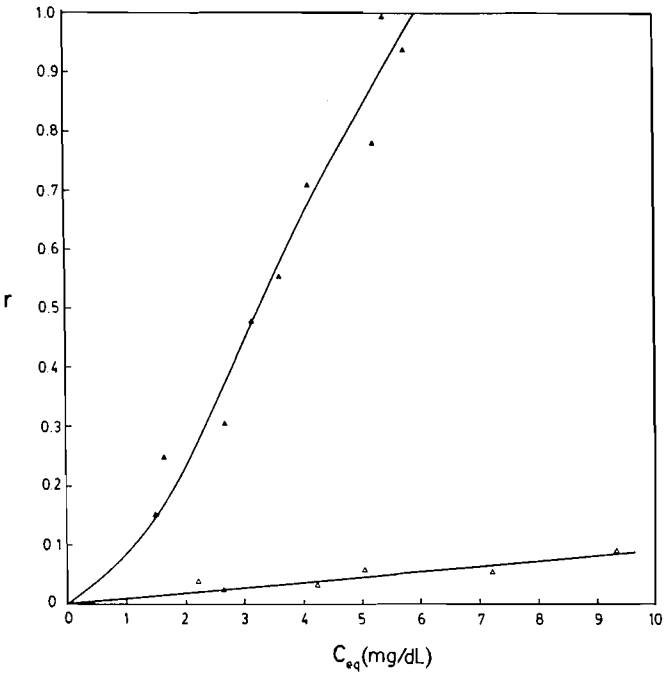


FIG. 4. Effect of pH on the adsorption of bilirubin by resin 5; ▲, pH = 7.80, KH_2PO_4/NaOH (0.05 M), 0°C; △, pH = 10.85, Na_2HPO_4/NaOH (0.05 M), 0°C.

are known to adopt "ridge-tile" and spiral configurations, respectively (16). On the other hand, mesoporphyrin is a conjugated, cyclic tetrapyrrole molecule with no possibility of internal rotation at the level of the ring system and hence is planar and rigid. Furthermore, whereas biliverdin and mesoporphyrin are dianions at pH 7.80, bilirubin is probably a monoanion (28, 29). This difference in the ionization state of the adsorbates should favor the adsorption of biliverdin and mesoporphyrin, assuming a binding process governed by ionic interactions.

The isotherms for the adsorption of these molecules by resin 6 (Fig. 5) show that it adsorbs considerably greater amounts of bilirubin than either biliverdin or mesoporphyrin, which suggests that binding cannot be rationalized solely on the basis of favorable ionic interactions. The observed differences are thought to reflect differences in the structural features of the adsorbates.

Therefore, although salt linkage interactions play a major role in the binding of bilirubin by the synthesized adsorbents, other factors are also involved. It is possible that the three-dimensional conformation of bilirubin is such that it confers a unique binding character to the molecule. Indeed, owing to an accentuated molecular flexibility compared to that of biliverdin and mesoporphyrin, bilirubin can adapt to the binding sites on the pendants in a manner such that well-fitted complexes can form. Since mesoporphyrin and biliverdin possess entirely different three-dimensional arrangements from that of bilirubin, the binding behaviour of these molecules reveals that the adsorption is also influenced by factors related to the structural features of the adsorbate.

Scatchard plots and binding constants

A quantitative assessment of the affinity of the peptide pendants for bilirubin is given by binding constants that can be derived from Scatchard plots. Resins 1 and 2 were found to

Can. J. Chem. Downloaded from www.nrcresearchpress.com by 41.223.56.140 on 09/07/12
For personal use only.

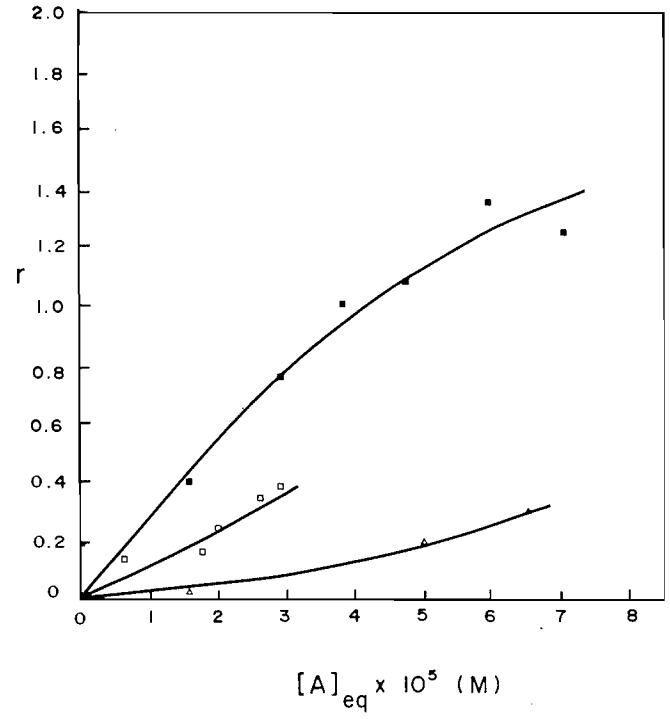


FIG. 5. Isotherms for the adsorption of tetrapyrroles by Arg-$(Lys)_2$-$(Ser)_2$-Lys-$(Ala)_3$-support, KH_2PO_4/NaOH (0.05 M), pH = 7.80, and 0°C. ■, bilirubin; △, biliverdin; □, mesoporphyrin.

have typical, linear Scatchard plots, as expected for adsorbents having only one binding site per pendant. The derived values of k (Table 3), as given by the Scatchard equation (32), are 2.1×10^3 and $1.2 \times 10^3\,M^{-1}$ for resins 1 and 2, respectively.

The Scatchard plots associated with the remaining peptide resins show concave downward curvature (Fig. 6), in a more or less developed manner, due to limitations that result from the low solubility of bilirubin. A maximum number of two moles of bound ligand per mole of pendant is assumed for these adsorbents, as demonstrated from a comparison of the size of the molecule of bilirubin relative to the length of the peptide pendants. Space filling molecular models indicate that steric factors would preclude the adsorption of additional ligands. The Scatchard plot associated with resin 6 strongly supports this assumption.

Downward curvature in a Scatchard plot reflects an adsorption process by which binding of the second molecule by the pendant occurs with a stronger affinity than that of the first, i.e., a second site binding constant larger than that of the first. This phenomenon is the manifestation of positive cooperativity between the binding sites, usually associated with an adsorption isotherm for which, as the adsorbate concentration increases, r rises slowly at low values, then increases sharply, and finally reaches saturation, i.e., a sigmoidal shape.

Site binding constants for these four peptide resins were derived graphically using a modified Scatchard equation described previously (24). It is based on a model that considers interactions between two initially *equivalent* binding sites on each pendant. The equations describing the binding model allow the derivation of site binding constants from Scatchard plots based on the following intercepts: $r/[A] = 2k_1$ (at $r = 0$) and $r/[A] = (k_1k_2)^{1/2}$ (at $r = 1$), where the parameters k_1 and k_2 represent first and second *site* binding constants. The ordinate intercepts of Figs. 6(A) and 6(B) are (1.8, 1.1, 1.8, and 30) $\times 10^3\,M^{-1}$ for resins 3, 4, 5, and 6, respectively. These values correspond to k_1 of (0.90, 0.55, 0.90, and 15) $\times 10^3\,M^{-1}$ (Table 3). The values of $r/[A]$ at half saturation are (2.2, 3.6, 11, and 37) $\times 10^3\,M^{-1}$ for resins 3, 4, 5, and 6, respectively, corresponding to k_2 values of (5.1, 23, 130, and 91) $\times 10^3\,M^{-1}$ (Table 3).

TABLE 3. Site equilibrium constants for the binding of bilirubin by peptide resins at 0°C

Bilirubin	Site binding constant $\times 10^{-3}$ (M^{-1}) k_1	k_2
1 -Lys-$(Ala)_3$-support	2.1	0
2 -Ser-	1.2	0
3 -Ser-	0.90	5.1
4 -Lys-	0.55	23
5 -Lys-	0.90	130
6 Arg-	15	91
Arg-$(Lys)_2$-$(Ser)_2$-Lys-$(Ala)_3$-support		
Biliverdin	0.065	630
Mesoporphyrin	5.1	27

Since k_2 is larger than k_1 for all four systems, the constants are consistent with positive cooperativity. If the binding sites are considered to be initially equivalent, the value of ξ, equal to k_2/k_1, can be thought of as a direct measure of the degree of cooperativity. The enhancement values for resins 3–6 are 6, 37, 141, and 6, respectively. There is a continuous increase in the value of ξ up to resin 5, but the addition of the arginine residue causes a marked decrease. Positive cooperativity for the binding of bilirubin by lysine-containing pendants has been observed in previously work (7, 33). Indeed, peptide resins such as $(Lys)_2$-$(Ala)_3$-support and $(Lys)_5$-$(Ala)_3$-support have enhancement values of 3 and 1500, respectively. Positive cooperativity has also been observed, but to a much lesser degree, for the binding of bilirubin by certain arginine-containing adsorbents (33). The $(Arg)_2$-$(Ala)_3$-support, $(Arg)_3$-$(Ala)_3$-support, and Arg-$(Ala)_3$-Arg-$(Ala)_3$-support adsorbents have enhancement values of 1.5, 1.1, and 1.7, respectively, whereas $(Arg)_5$-$(Ala)_3$-support has a value of ξ equal to 0.53. Such low values of ξ for arginine-containing pendants correlate well with the results of the present study and demonstrate that positive cooperativity is a characteristic of lysine-containing pendants and is considerably less evident for those with arginine.

Site binding constants for the adsorption of biliverdin and mesoporphyrin by resin 6 are also given in Table 3. It is of interest to note that values of k_2 larger than k_1 are also obtained for these systems.

Discussion

This study clearly demonstrates, by the effect of pH on the adsorption, the favorable interactions between oppositely charged species. The incorporation of the basic amino acids, arginine and lysine, into the pendants is generally accompanied by a considerable increase in the binding affinity (6–8) whereas the addition of the negatively charged glutamic acid markedly reduces it (8). These results are consistent with direct evidence for the interaction between the COO^- groups of bilirubin molecules and the NH_3^+ groups of L-lysyl-L-lysine from changes in nmr relaxation times (13). Thus, there is strong

Can. J. Chem. Downloaded from www.nrcresearchpress.com by 41.223.56.140 on 09/07/12
For personal use only.

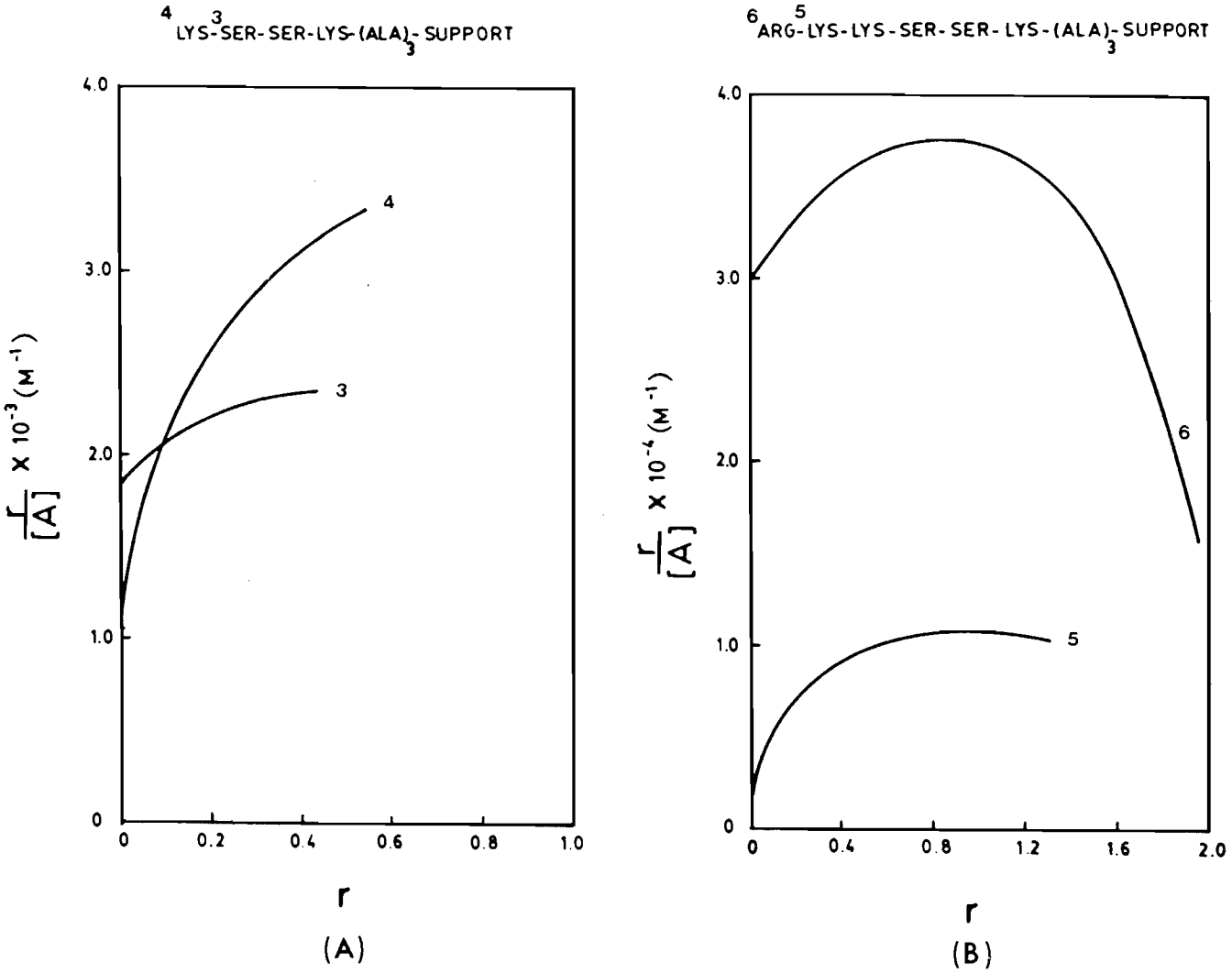


FIG. 6. Scatchard plots for resins 3–6.

experimental evidence to indicate that interactions based on salt linkages are the major driving force for the binding of bilirubin by immobilized peptides. However, the adsorption results for biliverdin and mesoporphyrin show that other factors, likely related to the structure of the adsorbate, also influence the process.

The positive cooperativity characterizing the adsorption behaviour of bilirubin by resins 3–6 suggests that specific interactions are involved between the bound ligands and the pendants. The binding of bilirubin molecules at or in the immediate neighborhood of lysine- and (or) arginine-containing pendants results in a partial neutralization of the negatively charged carboxylate groups. This should effectively decrease repulsions between the bound molecules and favor $\pi-\pi$ electron interactions between the conjugated systems, i.e., stacking of the bound ligands.

This model is based on the interactions of nucleotides or dyes with basic polypeptides at neutral pH. In aqueous solution, free nucleic acid bases and certain dye molecules manifest a pronounced tendency for stacking (34, 35). It is well documented (36–40) that the binding of these ligands by polylysine or polyarginine is characterized by positive cooperativity, i.e., the incoming ligands show a marked preference for binding to sites adjacent to those already occupied. This preference has been attributed to the effect of charge neutralization, upon addition of a positively charged polymer, on the tendency for negatively charged ligands to stack. Similarly, free bilirubin is also known to undergo dimerization and oligomerization in aqueous alkaline solutions (pH from about 8 to 12) (17, 41). The binding force responsible for the stability of the free dimer is thought to include $\pi-\pi$ electron interactions between the pyrromethenone chromophores (41), as well as hydrogen bonds (17).

Explanations for differences in the degree of positive cooperativity of the lysine- and arginine-containing pendants can be obtained from a consideration of the nature of the side-chain groups. Arginine has a bulky terminal guanidino group that provides some rigidity to the chain as well as delocalization of the charge. Consequently, $\pi-\pi$ electron interactions between the conjugated systems of bilirubin and the guanidino group are possible, as suggested by Wagner and Arav (38) for the binding of nucleotide bases by polyarginine. Thus, arginine-containing pendants should show a stronger binding affinity for bilirubin, i.e., the k_1 values are expected to be substantially larger than those for the lysine analogues. This is consistent with the data in Table 3 and with previous binding affinity results (8, 33) as well as with the more basic character of arginine. Thus, binding of the first bilirubin molecule by an arginine-containing pendant

Can. J. Chem. Downloaded from www.nrcresearchpress.com by 41.223.56.140 on 09/07/12
For personal use only.

can include highly favorable interactions that are not present in the lysine-containing pendants and can, to some extent, mask the positive cooperativity of the binding process. On the other hand, the accentuated molecular flexibility, minimal steric hindrance, and point-charge character of the lysine side chain represent features that should enhance the tendency for the bilirubin molecules to stack. It should be noted that favorable conformational changes in the peptide pendants, as a consequence of the binding of the first ligand, should also be considered as contributing to the phenomenon of positive cooperativity.

This explanation, which accounts for the observed positive cooperativity, is entirely consistent with the behaviour of free biliverdin and mesoporphyrin in aqueous solutions. Indeed, these molecules manifest a tendency for dimerization (42, 43) and it is therefore expected that they would exhibit a binding mode identical to that of bilirubin when adsorbed by lysine-containing pendants, if it is accepted that positive cooperativity is a reflection of the stacking tendency of the bound ligands. Furthermore, circular dichroism studies of the bilirubin–polylysine complex, at pH 11.00 (26), strongly support the presence of the bound dimers of bilirubin on the polypeptide.

Conclusions

The adsorption isotherms of these adsorbents have confirmed that the basic amino acids arginine and lysine are of major importance in the binding of bilirubin. This supports Jacobsen's proposal on the participation of these residues in the in vivo binding of bilirubin by the high-affinity site on HSA. The positive cooperativity characterizing the binding of bilirubin by lysine-containing pendants suggests a tendency of the bound molecules to dimerize on the immobilized pendants. This molecular mechanism is based on a consideration of the interactions thought to dominate the binding process, i.e., salt linkage interactions. Although the presence of an arginine residue in the sequence of a pendant reduces the degree of positive cooperativity, it causes an increased binding affinity consistent with the strongly basic character of this residue.

Finally, the adsorption results for the binding of biliverdin and mesoporphyrin show that a consideration of the chemical groups on the adsorbate, particularly the presence of carboxyl groups, is not a sufficient criterion to explain the binding data.

Acknowledgments

Financial support in the form of operating grants from the Natural Sciences and Engineering Research Council of Canada and the Province of Quebec (FCAR) is gratefully acknowledged. We would also like to express our appreciation to Dr. S.-D. Clas and Professor W. C. Galley of McGill University, for helpful discussions and suggestions.

1. P. Berthelot, Ph. Duvaldestin, and J. Fevery. Bilirubin. Vol. II. *Edited by* K. P. M. Heirwegh and S. B. Brown. CRC Press, Florida. 1982. pp. 173–214.
2. S. Sideman, L. Mor, J. M. Brandes, and S. Lupovitch. J. Biomed. Mater. Res. **17**, 91 (1983).
3. S. Sideman, L. Mor, and J. M. Brandes. Trans. Am. Soc. Artif. Intern. Organs, **25**, 497 (1979).
4. Y. Idezuki, M. Hamaguchi, S. Hamabe, H. Moriya, T. Nagashima, T. Watanabe, T. Sonada, K. Teramoto, T. Kikuchi, and H. Tanzawa. Trans. Am. Soc. Artif. Intern. Organs, **27**, 428 (1981).
5. B. F. Scharschmidt, P. H. Plotz, P. D. Berk, J. G. Waggoner, and J. Vergalla. J. Clin. Invest. **53**, 786 (1974).
6. D. S. Henning, G. A. Lajoie, G. R. Brown, L. E. St-Pierre, and S. St-Pierre. Int. J. Artif. Organs, **7**, 209 (1984).
7. D. S. Henning, G. R. Brown, and L. E. St-Pierre. Int. J. Artif. Organs, **9**, 33 (1986).
8. M. Bouvier, G. R. Brown, and L. E. St-Pierre. Can. J. Chem. **65**, 1927 (1987).
9. C. Jacobsen. Eur. J. Biochem. **27**, 513 (1972).
10. C. Jacobsen and J. Jacobsen. Biochem. J. **181**, 251 (1979).
11. C. Jacobsen. Biochem. J. **171**, 453 (1978).
12. E. Kaiser, R. L. Colescott, C. D. Bossinger, and P. I. Cook. Anal. Biochem. **34**, 595 (1970).
13. X. X. Zhu, G. R. Brown, and L. E. St-Pierre. Can. J. Spectrosc. **32**, 49 (1987).
14. D. S. Henning, G. R. Brown, and L. E. St-Pierre. Int. J. Artif. Organs, **5**, 373 (1982).
15. R. Bonnet, J. E. Davies, and M. B. Hursthouse. Nature, **262**, 326 (1976).
16. J. D. Ostrow. *In* Bile pigments and jaundice. *Edited by* J. D. Ostrow. Marcel Dekker Inc., New York. 1986. pp. 1–6.
17. R. Brodersen. CRC Crit. Rev. Clin. Lab. Sci. **11**, 305 (1980).
18. P. Q. Behrens, A. M. Spiekerman, and J. R. Brown. Fed. Proc. **34**, 591 (1975).
19. J. R. Brown and P. Shockley. Lipid–protein interactions. Vol. I. *Edited by* P. C. Jost and O. H. Griffith. John Wiley and Sons, New York. 1982. pp. 25–68.
20. N. Gitzelmann-Cumarasamy, C. C. Kuenzle, and K. J. Wilson. Experientia, **32**, 768 (1976).
21. M. J. Geisow and G. H. Beaven. Biochem. J. **163**, 477 (1977).
22. N. Gitzelmann-Cumarasamy and C. C. Kuenzle. Pediatr. Res. **10**, 876 (1976).
23. T. Sjodin, R. Hansson, and I. Sjoholm. Biochim. Biophys. Acta, **494**, 61 (1977).
24. W. C. Galley, M. Bouvier, S.-D. Clas, G. R. Brown, and L. E. St-Pierre. Biopolymers, **27**, 79 (1988).
25. A. L. Lehninger. Biochemistry. 1st ed. Worth Publishers, New York. 1970. p. 183.
26. M. Bouvier. Ph.D. thesis, McGill University (1988).
27. N. Greenfield and G. D. Fasman. Biochemistry, **8**, 4108 (1969).
28. J. D. Ostrow, L. Celic, and P. Mukerjee. J. Lipid Res. **29**, 335 (1988).
29. M. C. Carey and W. Spivak. *In* Bile pigments and jaundice. *Edited by* J. D. Ostrow. Marcel Dekker Inc., New York. 1986. pp. 81–132.
30. R. Brodersen. *In* Bile pigments and jaundice. *Edited by* J. D. Ostrow. Marcel Dekker Inc., New York. 1986. pp. 157–181.
31. D. A. Lightner, J.-S. Ma, and X.-X. Wu. Spectrosc. Lett. **19**, 311 (1986).
32. G. Scatchard. Ann. N.Y. Acad. Sci. **51**, 660 (1949).
33. S.-D. Clas, D. S. Henning, G. R. Brown, and L. E. St-Pierre. Biomater. Artif. Cells Artif. Organs. In press.
34. R. E. Ballard and C. H. Park. J. Chem. Soc. (A), 1340 (1970).
35. T. J. Gilligan III and G. Schwarz. Biophys. Chem. **4**, 55 (1976).
36. G. Schwarz and T. J. Gilligan III. Biochemistry, **16**, 2835 (1977).
37. K. G. Wagner. Eur. J. Biochem. **10**, 261 (1969).
38. K. G. Wagner and R. Arav. Biochemistry, **7**, 1771 (1968).
39. T. Takagishi, T. Ueno, N. Kuroki, S. Shima, and H. Sakai. J. Polym. Sci. Polym. Chem. Ed. **22**, 1281 (1984).
40. P. V. Scaria, M. Atreyi, and M. V. R. Rao. Biopolymers, **25**, 2349 (1986).
41. M. C. Carey and A. P. Koretsky. Biochemistry, **179**, 675 (1979).
42. R. R. Das, R. F. Pasternack, and R. A. Plane. J. Am. Chem. Soc. **92**, 3312 (1970).
43. R. F. Pasternack. Ann. N.Y. Acad. Sci. **206**, 614 (1973).

Can. J. Chem. Downloaded from www.nrcresearchpress.com by 41.223.56.140 on 09/07/12
For personal use only.

Electron affinities of substituted nitrobenzenes

S. CHOWDHURY, H. KISHI,[1] G. W. DILLOW, AND P. KEBARLE[2]
Department of Chemistry, University of Alberta, Edmonton, Alta., Canada T6G 2G2

Received May 17, 1988[3]

S. CHOWDHURY, H. KISHI, G. W. DILLOW, and P. KEBARLE. Can. J. Chem. **67**, 603 (1989).

The electron affinities of 14 substituted nitrobenzenes including nitrobiphenyls were determined by measurement of electron transfer equilibria [1] in the gas phase with a pulsed high pressure mass spectrometer: $A^- + B = A + B^-$ [1]. These data, when combined with previous determinations from this laboratory, lead to electron affinities for 35 substituted nitrobenzenes and provide a comprehensive data set for the examination of substituent effects. The data are used to derive Taft gas-phase substituent parameters. A qualitative discussion based on frontier orbital molecular theory examines the substituent effect on the benzene and nitrobenzene LUMOs. The lifetimes for electron autodetachment from excited nitrobenzene negative ions, $(A^-)^*$, studied earlier by Christophorou, are examined in light of the present electron affinity data.

Key words: electron affinities, substituent effects, frontier orbital treatment, electron autodetachment from nitrobenzene radical anions.

S. CHOWDHURY, H. KISHI, G. W. DILLOW et P. KEBARLE. Can. J. Chem. **67**, 603 (1989).

En se basant sur des mesures d'équilibre du transfert électronique [1] en phase gazeuse ($A^- + B = A + B^-$ [1]) effectuées à l'aide d'une spectromètre de masse pulsé à haute pression, on a déterminé les affinités électroniques de 14 nitrobenzènes substitués comprenant des nitrobiphényles. Lorsqu'on combine ces données avec des déterminations qui ont été faites antérieurement dans ce laboratoire, on obtient les affinités électroniques de 35 nitrobenzènes substitués qui forment un ensemble étendu de données qui permet d'évaluer les effets des substituants. On a utilisé ces données pour évaluer les paramètres de Taft des substituants, pour la phase gazeuse. Une discussion qualitative basée sur la théorie des orbitales moléculaires frontières permet d'examiner l'effet des substituants sur les OM basses vacantes du benzène et du nitrobenzène. Les temps de vie de l'auto-détachement électronique des ions négatifs de nitrobenzènes excités, $(A^-)^*$, étudiés antérieurement par Christophorou, ont été examinés à la lumière des nouvelles données sur l'affinité électronique.

Mots clés : affinités électroniques, effets des substituants, traitement des orbitales frontières, auto-détachement électronique des ions négatifs de nitrobenzène.

[Traduit par la revue]

Introduction

A large number of electron affinity (EA) determinations based on measurement of electron transfer equilibria [1] with a pulsed high pressure mass spectrometer (PHPMS) were reported recently from this laboratory (1) and have been summarized in a review article (2). The technique was shown to be highly suitable for the determination of EAs for many classes of compounds including nitro-, cyano-, and pentafluoro-substituted benzenes as well as quinones, dicarbonyl compounds, and polycyclic aromatics (1, 2).

[1] $A^- + B = A + B^-$

With the availability of extensive EA data on several series of substituted molecules, it has been possible to examine the effects of substituents on the stability of radical anions. Thermochemical data derived from the measurement of gas-phase equilibrium processes are best suited for the determination of intrinsic substituent effects in substituted series of ions since they are free of problems such as preferential solvation and ion-pairing, which may mask intrinsic substituent effects in solution. The determination of gas-phase acidities and basicities has been of central importance in recent studies of substituent effects (3). However, examination of substituent effects on gas-phase electron transfer equilibria is potentially equally as useful, but much less work has been done in this area.

In this paper we report new determinations of the EAs of 14 substituted nitrobenzenes that were measured by PHPMS. These data are combined with previous data from this laboratory (2) to give EAs for 35 substituted nitrobenzenes bearing the substituents H, NO_2, CHO, CH_3CO, CN, CF_3, C_6H_5, CH_3, F, Cl, Br, OCH_3, and NH_2. This extensive data set provides a good base for the examination of substituent effects on the stability of substituted nitrobenzene radical anions. Interest in this series of molecules was prompted in part by the availability of theoretical studies on substituent effects in substituted benzenes (4) and a few benzene radical anions (5).

In the earlier EA studies (1), a striking similarity between the substituent effects on the electron affinities of nitrobenzenes and the acidities of phenols was observed. This similarity was also reported earlier, by Fukuda and McIver (6). Since the electron affinities are generally related to the energy of the LUMO of the molecule, it seemed a challenge to uncover the factors responsible for the similarity with the acidity substituent effects.

Experimental

The measurements of electron transfer equilibria [1] were performed with a pulsed high pressure mass spectrometer (PHPMS), which has been described elsewhere (2, 7). The experimental procedures used were essentially the same as described previously (2, 7). Reaction mixtures in the ion source consisted of methane at 5 Torr pressure (1 Torr = 133.3 Pa) containing mTorr partial pressures of A and B, which were selected to ensure that electron transfer equilibrium was achieved within ~200 μs of initiation of the reactions by a 10-μs primary electron pulse. The ion intensities of A^- and B^-, $I(A^-)$ and $I(B^-)$, which were detected after equilibrium was reached, were inserted into equilibrium expression [2], enabling the equilibrium constant for reaction [1], K_1, to be calculated. The free energy change for reaction [1], ΔG_1^0, was calculated by inserting K_1 into eq. [3].

$$[2] \qquad K_1 = \frac{[B^-][A]}{[A^-][B]} = \frac{I(B^-)[A]}{I(A^-)[B]}$$

$$[3] \qquad \Delta G_1^0 = -RT \ln K_1$$

[1]Visiting scientist, Department of Industrial Chemistry, Oyama National College of Technology, Nakakuki Oyama-shi, Japan.

[2]Author to whom correspondence may be addressed.

[3]Revision received December 5, 1988.

Can. J. Chem. Downloaded from www.nrcresearchpress.com by 41.223.56.140 on 09/07/12
For personal use only.

Can. J. Chem. Downloaded from www.nrcresearchpress.com by 41.223.56.140 on 09/07/12
For personal use only.

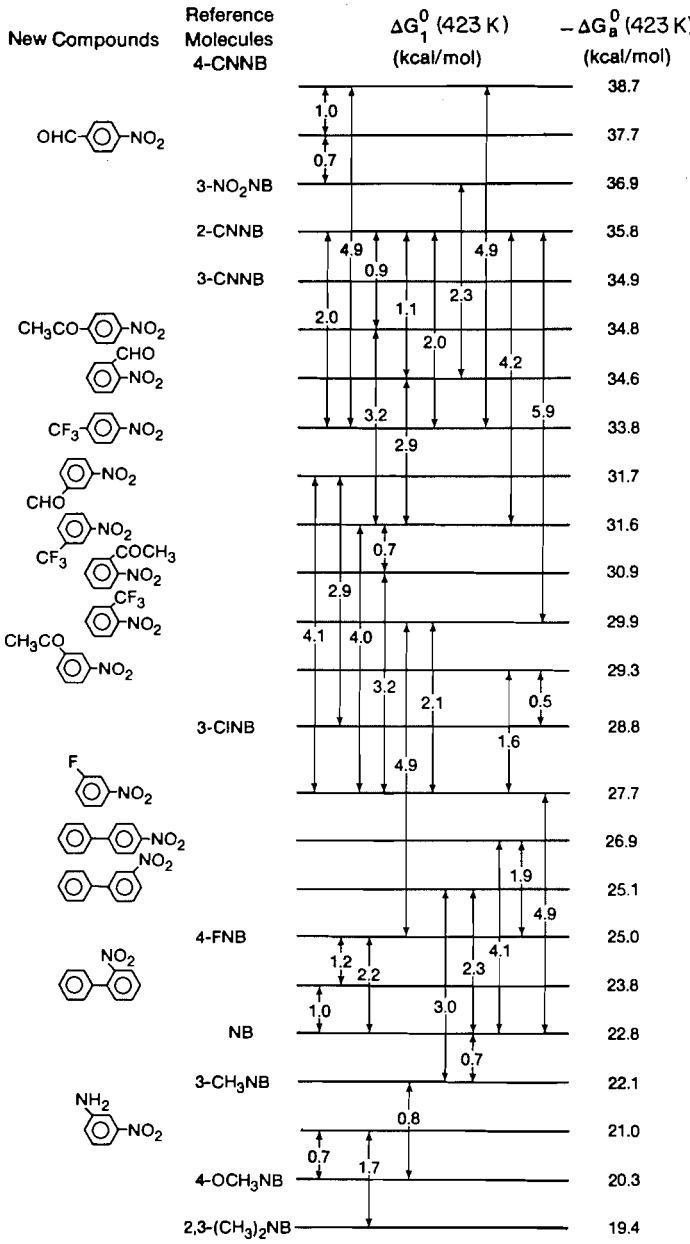


FIG. 1. Free energy changes, ΔG_1^0, for electron transfer reactions, $A^- + B = A + B^-$, measured at 423 K (NB = $C_6H_4NO_2$). The ΔG_a^0 values correspond to the free energy changes for the capture in the gas phase of a stationary electron: $e^- + A = A^-$. These were obtained from the ΔG_1^0 scale and the known ΔG_a^0 for the reference compounds (2).

A reaction temperature of 150°C (423 K) was used since intense adduct ions of the form AA^-, AB^-, and BB^- may be formed at lower temperatures while thermal electron detachment from the radical anions may occur at higher temperatures. In most of the measurements, A^- and B^- were by far the dominant ions. When side reactions were observed, measurements of K_1 were made only when the rates of the reactions removing A^- and B^- were much slower than the equilibration rate in equilibrium [1]. The [A]/[B] concentration ratio was varied by up to a factor of 10 to ensure that K_1 is independent of this ratio.

Results

The equilibrium constants for reaction [1], K_1, involving the 14 new nitrobenzenes and a series of reference compounds were measured as described in the experimental section. The ΔG_1^0 evaluated with eqs. [2] and [3] are shown in Fig. 1. Since the electron attachment free energy, $\Delta G_a^0(B)$, corresponding to the free energy for electron capture as shown in reaction [4], had been determined previously for the reference compounds (2), ΔG_a^0 could be evaluated for the new nitrobenzenes from the relative ΔG_1^0 values in Fig. 1. These ΔG_a^0 values are also shown in Fig. 1. The stationary electron convention (1*b*) was used in these evaluations.

TABLE 1. Thermochemical results for electron capture, reaction [4]

Compound	$-\Delta G_a^0$ (423 K) (kcal mol^{-1})	$-\Delta H_a^0$ (kcal mol^{-1})	= EA[a] (eV)
4-CHO·NB[c]	37.7	39.0	1.69
4-CH_3CO·NB	34.8	36.1	1.56
2-CHO·NB	34.6	35.9	1.56
4-CF_3·NB	33.8	34.6	1.50
3-CHO·NB	31.7	33.0	1.43
3-CF_3·NB	31.6	32.4	1.40
2-CH_3CO·NB	30.9	32.2	1.40
2-CF_3·NB	29.9	30.7	1.33
3-CH_3CO·NB	29.3	30.6	1.32
3-F·NB	27.7	28.5	1.23
4-C_6H_5·NB	26.9	27.7	1.20
3-C_6H_5·NB	25.1	25.9	1.12
2-C_6H_5·NB	23.8	24.6	1.07
3-NH_2·NB	21.0	21.8	0.95

[a] ΔH_a^0 obtained from ΔG_a^0 by subtracting 0.8 kcal mol^{-1} for all substituents except CHO, CH_3CO, and NO_2, for which 1.3 kcal mol^{-1} was subtracted. These values correspond to estimated $T\Delta S$ terms; see text.
[b] NB = $C_6H_4NO_2$.

[4] $\quad e^-_{(g)} + B_{(g)} = B^-_{(g)} \qquad \Delta G_4^0 = \Delta G_a^0$

The temperature dependence of K_1 was not determined in the present investigation. However, in a previous study (1*b*) the temperature dependence of K_1 was evaluated for a number of substituted nitrobenzenes, enabling ΔH_1^0 and ΔS_1^0 to be obtained from van't Hoff plots. Nitrobenzene was found to have $\Delta S_a^0 = -0.5$ cal deg^{-1} mol^{-1}. Many substituted nitrobenzenes had $\Delta S_a^0 \approx -2$ cal deg^{-1} mol^{-1}, while 1,4-dinitrobenzene had $\Delta S_a^0 = -4.5$ cal deg^{-1} mol^{-1}. The other two strong π-acceptor substituents, CHO and CH_3CO, caused similar entropy decreases. It is assumed that the negative ΔS_a^0 in 1,4-dinitrobenzene is due to stiffening of the C—N internal rotation and bending motions in the anion due to an increase in the C—N bond order as a result of the extra electron in the π-system (1*b*). Since the overall ΔS_a^0 values are small and the error in the ΔS_1^0 determinations is large (±2 eu), enthalpy values for electron capture by the new substituted nitrobenzenes, ΔH_a^0, were estimated by assuming that $\Delta S_a^0 = -2$ cal deg^{-1} mol^{-1} for all the compounds except the CHO, CH_3CO, and NO_2 substituted nitrobenzenes, for which $\Delta S_a^0 = -3$ cal deg^{-1} mol^{-1} was assumed. These ΔH_a^0 values are listed in Table 1. Since the data relate to 423 K, the corresponding $T\Delta S$ terms result in a difference between ΔG_a^0 and ΔH_a^0 of approximately 0.8 and 1.3 kcal mol^{-1} respectively.

Fukuda and McIver (6) have reported a ΔG_1^0 ladder involving several substituted nitrobenzenes, which was obtained by electron transfer equilibria measurements at much lower pressures ($\approx 10^{-6}$ Torr) with an ion cyclotron resonance (ICR) spectrometer. To facilitate a comparison of the ICR and PHPMS results, we have anchored the results of Fukuda and McIver to our primary reference compound, SO_2, for which a value of $\Delta G_a^0 = -26.1$ kcal mol^{-1} has been determined independently by a number of methods (1*a*, 1*b*). The ΔG_a^0 (ICR) obtained in

TABLE 2. Substituent coefficients determined by multiple regression fits of the substituted nitrobenzene $-\Delta G_a^0$ values to eq. [8]

Substituent type	Ring position	Substituent coefficients ρ_R	ρ_F	ρ_α	Coefficient of correlation
σ-Acceptor/π-acceptor	C-4	45.7±4.5	19.2±1.4	[a]	0.997
	C-3	15.1±3.0	17.5±1.0	[a]	0.997
	C-2	32.8±9.3	13.7±2.9	[a]	0.974
σ-Acceptor/π-donor	C-4	17.0±3.5	16.3±2.7	−1.5±2.0	0.987
	C-3	8.0±0.5	16.0±1.0	−0.2±0.3	0.999
	C-2	22.6±1.0	15.8±1.0	0.8±0.5	0.999

[a]Multiple regression analyses that included polarizability effects were performed for these substituents, but the calculated ρ_α values were small and did not improve the correlations significantly.

this manner, when compared with the ΔG_a^0 (PHPMS) from Fig. 1, were found to be in very good agreement, the differences being generally smaller than ±0.2 kcal mol^{-1}.

Discussion

Effect of substituents on the electron affinities of nitrobenzenes. Taft's resonance and field parameters

Most of the substituents used may be classified into two categories (4):

(*i*) σ-acceptor/π-acceptor substituents: NO_2, CHO, $COCH_3$, CN

(*ii*) σ-acceptor/π-donor substituents: F, Cl, Br, OCH_3, NH_2

It was noted in the earlier work on electron affinities (1*a*, 2, 6) that the substituent effect on the electron affinities of nitrobenzenes, i.e., the free energy change, eq. [5], was close to identical to the substituent effect on the gas-phase acidities of phenols, $\delta\Delta G^0_{PhOH}$, see eq. [6]. The correlation, which includes the latest data for the nitrobenzenes, is shown in Fig. 2.

[5] $$NO_2C_6H_5^- + NO_2C_6H_4X = NO_2C_6H_5 + NO_2C_6H_4X^- \qquad \delta\Delta G^0_{NB}$$

[6] $$C_6H_5O^- + XC_6H_4OH = C_6H_5OH + XC_6H_4O^- \qquad \delta\Delta G^0_{PhOH}$$

Taft *et al.* (3) have developed methods for the separation of the substituent effects, $\delta\Delta G^0$, into contributions due to resonance (R) and field-inductive effects (F). In early work (3*c*), the resonance R and field inductive term F were obtained from the experimental $\delta\Delta G^0$ values from measurements in solution and eqs. [7]. The assumptions in [7*b*] allow the separation into R and F to be obtained from the $\delta\Delta G_p^0$ and $\delta\Delta G_m^0$ of a single substituted series of compounds.

[7*a*] $$-\delta\Delta G_p^0 = R_p + F_p = \rho\sigma_p$$
$$-\delta\Delta G_m^0 = R_m + F_m = \rho\sigma_m$$

[7*b*] $$F_m \cong F_p \quad R_m = 0.2\,R_p \quad (\pi\text{-withdrawing substituents})$$
$$R_m = 0.6\,R_p \quad (\pi\text{-donating substituents})$$

The analysis could be greatly extended after $\delta\Delta G^0$ values from measurements of gas-phase proton transfer equilibria became available for many acid–base series. The separation of the σ and ρ values for substituents in a given position to the functional group was obtained (3*a*, *b*) with eq. [8], which includes also substituent polarizability (α) effects.

[8] $$-\delta\Delta G^0 = \rho_R\sigma_R + \rho_F\sigma_F + \rho_\alpha\sigma_\alpha$$

In eq. [8], $-\delta\Delta G^0$ is the relative free energy change for some chemical transformaion such as removal of a proton ($-\delta\Delta G^0$ = 0 kcal mol^{-1} for substituent -X); σ_R, σ_F and σ_α are system-independent substituent parameters that rank the resonance, field, and polarizability capacities, respectively, of the various substituents; ρ_R, ρ_F, and ρ_α are system-dependent coefficients that indicate the magnitude of the respective substituent effects on $-\delta\Delta G^0$ within a given family of molecules.

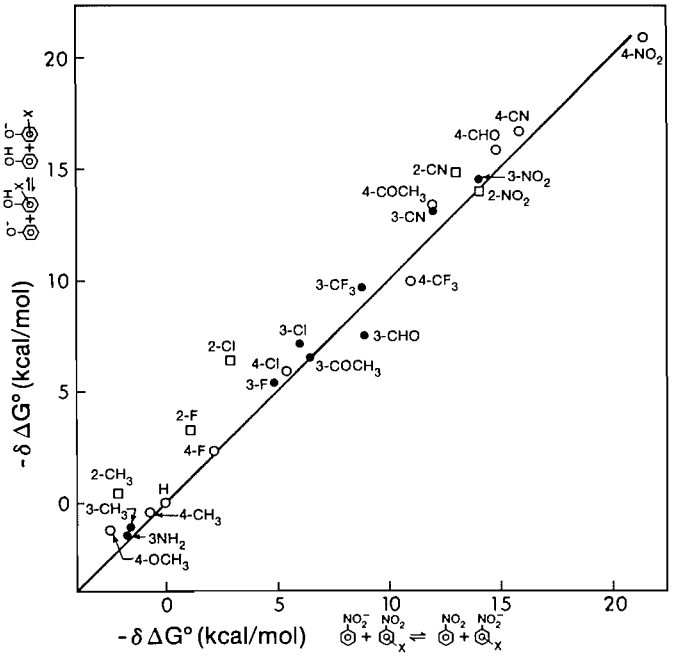


FIG. 2. Plot of $\delta\Delta G^0$ of gas phase acidities of substituted phenols, from refs. 12 and 13, versus $\delta\Delta G^0$ of electron attachment free energies for substituted nitrobenzenes.

In the present work, multiple regression analysis was used to correlate $-\delta\Delta G_a^0$ for electron capture by the substituted nitrobenzenes with the σ_R, σ_F, and σ_α values compiled by Taft *et al.* (3*b*). Table 2 lists the ρ_R, ρ_F, and ρ_α values determined by this procedure along with the coefficients of correlation for each fit. Generally, the high degree of correlation suggests that $-\delta\Delta G_a^0$ may be described very well by eq. [8]. This confirms that the influence of the substituents on the EA ($\approx -\delta\Delta G_a^0$) of the substituted nitrobenzenes may be accounted for well in terms of resonance and field effects, although the polarizability of the substituents also seems to play a small role with σ-acceptor/π-donor groups.

As expected from the closeness of the experimental $\delta\Delta G^0$ for the phenol acidities and the nitrobenzene electron attachment energies, the present ρ values (Table 2) are very similar to those obtained by Taft *et al.* (3) for the phenol acidities. Thus, for the

Can. J. Chem. Downloaded from www.nrcresearchpress.com by 41.223.56.140 on 09/07/12
For personal use only.

TABLE 3. Total effect ($\delta\Delta G^0_{NB}$) and field (F) and resonance (R) effect of substituent on the electron affinity of nitrobenzene[a]

Substituent[b]	$-\delta\Delta G^0_{NB}$	σ_R	R	σ_F	F	Substituent	$-\delta\Delta G^0_{NB}$	σ_R	R	σ_F	F
NH_2 4	—	0.52	−8.8	0.14	2.3	Br	6.2	−0.07[c]	−1.2	−0.45[c]	(7.3)
3	−1.8		−4.1		2.2		6.7		(−0.6)		(7.2)
2	—		−11.7		2.2		3.4		(−1.6)[c]		(7.1)
CH_3	−1.6	−0.08	−1.4	0.00	0.0	CF_3	11.0	0.07	3.2	0.44	8.4
	−0.7		−0.6		0.0		8.8		1.1		7.7
	−2.1		−1.8		0.0		7.1		2.3		6.0
OCH_3	−2.5	−0.42	−7.1	0.25	4.1	CH_3CO	12.0	0.17	7.7	0.26	5.0
	0.6		−3.4		4.0		6.5		2.6		4.5
	—		−9.5		3.9		8.1		5.6		3.6
C_6H_5	4.1	0.05[c]	(2.3)	0.08[c]	(1.5)	CHO	14.9	0.19	8.7	0.31	6.0
	2.3		(0.8)		(1.4)		8.9		2.7		5.4
	1.0		(1.6)		(1.1)		11.8		6.2		4.2
F	2.2	−0.25	−4.3	0.44	7.2	CN	15.9	0.10	4.6	0.6	11.5
	4.9		−2.0		7.0		12.0		1.5		10.5
	1.4		−5.6		6.9		13.0		3.3		8.2
Cl	5.4	−0.17	−3.0	0.45	7.3	NO_2	21.5	0.18	8.2	0.65	12.5
	6.0		−1.4		7.2		14.1		2.7		11.4
	2.9		−3.8		7.1		14.1		5.9		8.9

[a]$\delta\Delta G^0$ experimental results from Table 1 in kcal mol^{-1}; R and F values also in kcal mol^{-1}; σ_F and σ_R values from Taft (3*b*). Values for F and R that are shown without parentheses were obtained with Taft's σ values and ρ values shown in Table 2. Values for F and R shown in parentheses are for substituents for which σ are not available; these were obtained from σ_R and σ_F values calculated in this study.

[b]Values for substituents are shown in the order *para*, *meta*, *ortho*, i.e., positions 4, 3, 2.

[c]Calculated from eq. [8] using ρ_R and ρ_F values from Table 2.

Can. J. Chem. Downloaded from www.nrcresearchpress.com by 41.223.56.140 on 09/07/12
For personal use only.

σ-acceptor/π-acceptor substituents, in position 4, the ρ_R = 45.7 for nitrobenzenes vs. 49 for phenols (3*b*), and ρ_F = 19.2 for nitrobenzenes vs. 18.9 for phenols (3*b*).

The approximate contributions of resonance and field effects to $\delta\Delta G^0_a$ may be assessed for each substituted nitrobenzene by calculating $R = \rho_R\sigma_R$ and $F = \rho_F\sigma_F$ using the σ values compiled by Taft (3) and the ρ values determined in this study. Table 3 lists the R and F values obtained from this procedure along with the respective σ values used in this calculation and $\delta\Delta G^0_a$ for each substituted nitrobenzene. For the substituents phenyl and bromine, no σ values were available; the σ values shown in Table 3 for these substituents were calculated by inserting appropriate values of $\delta\Delta G^0_a$ and ρ from Table 3 into eq. [8] and solving the resultant simultaneous equations. Cross checks showed that the R and F terms obtained by eqs. [7] and [8] were very similar.

The magnitude of the R and F values for most of the substituents shown in Table 3 have been discussed previously in connection with acidities of phenols and other systems (3). All of these have involved even-electron, complete valence shell reactants. In the next section we discuss how the substituent effects on the electron affinities of benzenes can be related to those for the systems above.

MO and frontier orbital PMO

Taft's early separation of substituent effects into R and F contributions (3*c*) was inspired by valence bond concepts; however, the procedure itself was based entirely on experimental results. Later, when MO calculations could be executed for substituted benzenes (8) at the minimal STO-3G basis set level, it was found that changes in σ and π electron populations, based on Mulliken population analysis, conformed to the σ and π electron shifts expected from the F and R effects. More recent work (9, 10) has led to even closer confirmations. Also of interest is the fact that the energy changes ΔE for isodesmic reactions like [6] obtained from the total energies E of the reactants calculated with minimal STO-3G basis set were found to be close to the experimentally obtained ΔH values for the same reactions based on ion–molecule equilibria measurements (11–13).

A very useful qualitative extension of MO concepts occurred with the application of perturbation molecular orbital (PMO) theory to substituent effects (4). In this approach, the highest occupied or the lowest unoccupied orbitals (HOMO or LUMO) of the substituent ψ_j and of benzene, ψ_k, considered first as separate entities, interact to produce two new orbitals, one of lower and the other of higher energy. The new orbitals are substituted benzene orbitals.

The stabilization energy, SE, corresponding to the energy lowering of the new lower orbital relative to the lower of the two initial orbitals is given by eq. [9]:

$$[9] \qquad SE = \frac{C^2_{rj}C^2_{sk}\beta^2_{rs}}{\Delta E}$$

where C_{rj} and C_{sk} represent the coefficients of the atoms r in the orbital ψ_j and s in orbital ψ_k where atoms r and s are the interacting ones in the new orbital. $\beta_{r,s}$ is the resonance integral associated with these atoms and ΔE represents the energy separation between ψ_j and ψ_k. For a detailed account, see Pross and Radom (4*b*).

MO concepts are particularly well suited for discussion of the electron affinities of molecules, and the description that the extra electron enters the LUMO of the molecule and that the EA increases as the energy of the LUMO decreases is widely used. For this reason, the PMO framework outlined above appears particularly useful for the qualitative discussion of substituent effects on electron affinities.

The approximate energy levels of the π-withdrawing substituents' LUMOs, the π-donating substituents' HOMOs, and the

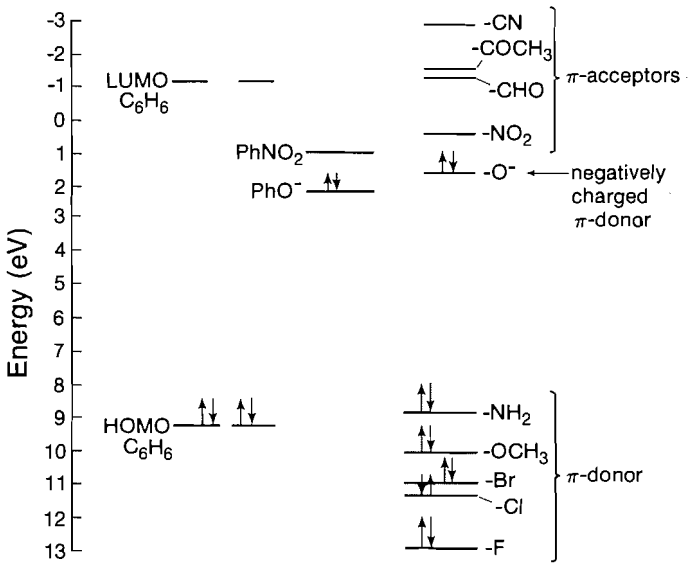


FIG. 3. Approximate orbital energies of HOMO and LUMO in benzene, the LUMO of π-acceptor groups, and the HOMO of π-donor groups. Also given are the LUMO of nitrobenzene ($PhNO_2$) and the HOMO of the phenoxide anion (PhO^-). For origin of data see text.

benzene LUMO and HOMO are given in Fig. 3. The energies of the LUMOs for the π-acceptor substituents were taken to be equal to the electron affinities of the corresponding substituted methanes determined by electron transmission spectroscopy (14) where the EA is negative or by PHPMS and other techniques for positive EA (2). The LUMOs of benzene are from ref. 14 while the energies of the HOMOs of benzene and the π-donating substituents were taken to be to the ionization potentials of benzene and the respective substituted methanes (15). Also shown in Fig. 3 are the energies of the HOMO of the phenoxide ion taken as the EA of phenoxide (17) and the HOMO of the π donor oxy substituent O^- taken as the EA of hydroxide (17). These orbitals will be of use in the subsequent discussion.

PMO. Single substitution of benzene with π acceptors

The qualitative frontier orbital scheme given in Fig. 4 shows the important interactions when the substituent is attached to benzene. The dominant interaction is the combination of the substituent LUMO (ψ_L) with one of the degenerate π* benzene LUMOS (ψ_3). These orbitals are close in energy (see Fig. 3) and the chosen benzene π* has high atomic orbital coefficients on the substitution site. The lower of the two resulting orbitals, ($\psi_{L'}$), interacts weakly with the energy distant HOMO of benzene (ψ_1); this slightly destabilizes $\psi_{L'}$ and stabilizes ψ_1 to produce ψ_{1a}. An additional factor that influences the orbital energies is the electrostatic effect of the substituent's electronegativity and dipole, which polarizes the electrons in benzene. Polarization of electrons towards the σ acceptor substituent "deshields" the nuclear charge and leads to stabilization of the orbitals of benzene and particularly those with high density near the substituent (4). Deshielding may be considered as the PMO counterpart of the σ-withdrawal field effect.

Taking nitro substitution as an example, the formation of the $\psi_{L'}$ LUMO for nitrobenzene leads to an increase of EA from -26.5 kcal mol^{-1} for benzene (14) to 23.0 kcal mol^{-1} in nitrobenzene (16). Hence, while electron capture into the π* LUMO produces only a temporary negative ion state in benzene, nitrobenzene forms a stable long-lived negative ion (16). Similarly strong interactions are expected for the other π-withdrawing substituents CHO, $COCH_3$, and CN, due to the closeness in energy between their LUMOs and that of benzene; see Fig. 3.

PMO single substitution of benzene with π donors

The interaction of π donor substituents like F and OH with benzene are also shown in Fig. 4. The main interaction is between the lone pair substituent HOMO (ψ_N) and the HOMO of benzene, since these two orbitals are close in energy, see Fig. 3. The resulting pair of occupied orbitals are designated as ψ_{1b} and $\psi_{N'}$. The higher of these ($\psi_{N'}$) engages in a weak secondary interaction with the distant in energy benzene LUMO (ψ_3), which slightly stabilizes $\psi_{N'}$ and destabilizes ψ_3 to produce ψ_{3b}. The benzene LUMO, ψ_4, which does not undergo any interaction, becomes the LUMO in these molecules. As discussed for π-acceptor substituents, the energy of that LUMO will be affected by deshielding due to the substituent's electronegativity. According to this scheme, the EA of benzenes substituted by π donors are not affected by π delocalization (resonance) and are thus close to the EA of benzene, but small EA increases are expected as a result of the deshielding (σ-withdrawing) effects of the substituents. These predictions are borne out by experimental results (14).

Of interest in connection with the similarity of the substituent effects on the electron affinities of nitrobenzenes and the acidities of phenols is the PMO scheme for substitution of benzene with the very strong π donor substituent, O^-. This substitution leads to formation of the phenoxy anion. The lone pair ψ_N orbital of the O^- lies very much higher than that of the neutral π donors, see Fig. 3. This results in a strong interaction with the close in energy ψ_3 LUMO of benzene, and is associated with extensive electron transfer from the substituent (O^-) to benzene. It will be seen in the next seciton that the similarities of the substituent effects on the phenol acidities and the nitrobenzene electron affinities can be traced to similarities of the LUMO of nitrobenzene and the HOMO of the phenoxide anion.

Double substitution, EA of substituted nitrobenzenes, and acidities of phenols

In much the same way as has been discussed for benzene, addition of a π-acceptor substituent to nitrobenzene leads to an interaction of the nitrobenzene LUMO, $\psi_{L'}$, with the LUMO of the substituent. Since the nitrobenzene LUMO is considerably lower than the benzene LUMO, the energy match with the substituent LUMO is not as good as was the case for benzene, see Fig. 3. Therefore the SE for nitrobenzene will be smaller relative to the SE for the same substituent on benzene. For example, CHO, a substituent that acts mostly by delocalization, increases the EA of benzene by ~36 kcal mol^{-1} (1*d*) but the EA of nitrobenzene by only 15 kcal mol^{-1}, see Table 3. The effect of a substituent like CN, which has a smaller delocalization term but a large deshielding (field) effect, is expected to decrease less from benzene to nitrobenzene and this is experimentally observed (1*d*). These changes cause a reversal of the substituent order: CHO > CN for benzene (1*d*), and CHO < CN for nitrobenzene, see Table 3.

In a previous experimental study (1*d*) of substituent effects by π-accepting substituents on the electron affinities of benzene, naphthalene, anthracene, and nitrobenzene, it was found that the above CHO, CN reversal proceeds gradually in the above order. It was also observed that the ρ values for a given strongly π-withdrawing substituent decreased in the same order, i.e.,

Can. J. Chem. Downloaded from www.nrcresearchpress.com by 41.223.56.140 on 09/07/12
For personal use only.

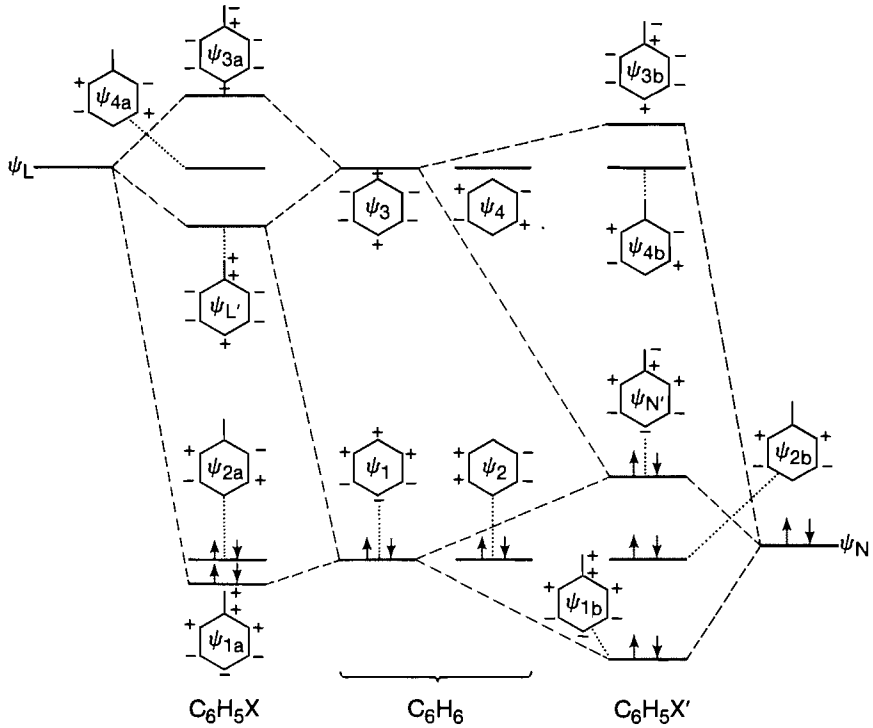


FIG. 4. Qualitative frontier orbital scheme showing interactions of benzene HOMO and LUMO with the LUMO of π-acceptor substituents and the lone pair HOMO of π-donor substituents.

benzene, naphthalene, anthracene, nitrobenzene. This order corresponds to increasing ΔE between the LUMO of the substituent and the LUMO of the above compounds (1*d*) and thus to a decrease of SE in the same order. The PMO scheme provides thus, in a very direct manner, a prediction of the concept: "The dependence of resonance effects of substituents on electron demand," investigated by Taft *et al.* (3*b*) in closed valence shell systems.

For the electron affinities of nitrobenzenes, the stabilizing effect of the substituent in different postions relative to the nitro group is experimentally observed to decrease in the order *para* > *ortho* > *meta*, see Tables 2 and 3. The orbital coefficients (C) for the nitrobenzene LUMO, obtained from *ab initio* calculations involving STO-3G basis sets (4*b*), are shown below.



According to eq. [9] the SE should follow the squares of these coefficients, C^2, and this predicts the experimentally observed order of decreasing ρ_R. On the basis of eq. [9] one would expect C^2 at each position to be proportional to ρ_R calculated for that position, see Table 2. An approximately linear relationship between C^2 and ρ_R for each position is evident, although ρ_a(*meta*) is larger than would be expected on the basis of C^2 at the *meta* position. The cause for this discrepancy is not clear. Possibly, π-electron changes in orbitals other than the frontier orbitals considered by eq. [9] could be responsible.

A comparison of the SE for the nitrobenzene LUMO and the phenoxide HOMO when interacting with the LUMO of a π-withdrawing substituent can be made on the basis of the orbital energies shown in Fig. 3 and the orbital coefficients shown above. The energies of the nitrobenzene and the phenoxide orbitals are seen to be relatively close. The carbon atom orbital coefficients are also fairly close. Therefore, similar substituent effects on the LUMOs of the substituted nitrobenzenes and HOMOs of the phenoxides are indicated by the PMO scheme. Since the electron affinities of the substituted nitrobenzenes follow the LUMOs and the acidities of the substituted phenols are largely determined by the stabilization of the substituted phenoxide ions, i.e., the energies of the phenoxide HOMOs, relatively similar substituent effects are predicted for these two systems by the PMO scheme.

The destabilizing effect of π-donor substituents on the electron affinity of nitrobenzene is due to the interaction of the HOMO of the substituent (ψ_N) with the LUMO of nitrobenzene ($\psi_{L'}$), see Figs. 3 and 4. The resulting lower energy orbital is fully occupied while the higher energy one becomes the LUMO of the substituted nitrobenzene. Since the interacting orbitals have fairly close energies, the interaction is expected to be significant and this is in accord with the substantial destabilization observed for the R terms of the π-donating substituents, see Table 3. The σ-withdrawing effect of the substituents leads to nuclear deshielding and stabilization of the substituted nitrobenzene LUMO, and therefore opposes the destabilizing π-donor effect.

The destabilizing effect due to π donation is expected to follow the squares of the nitrobenzene LUMO, i.e., *para* > *ortho* > *meta*. The order in Table 3 is *ortho* > *para* > *meta*. Generally Taft's scheme (3) is not used for the *ortho* position because of irregularities due to steric interference between the two groups and other factors. Possibly, in the present case, the *ortho* > *para* observation, Table 3, is due to an electrostatic repulsion, since both the NO_2 group and the substituent probably carry small partial negative charges in the negative ion. Since this repulsion is not accounted for in the ρ_F value, it appears in the destabilizing ρ_R.

Can. J. Chem. Downloaded from www.nrcresearchpress.com by 41.223.56.140 on 09/07/12
For personal use only.

Can. J. Chem. Downloaded from www.nrcresearchpress.com by 41.223.56.140 on 09/07/12
For personal use only.

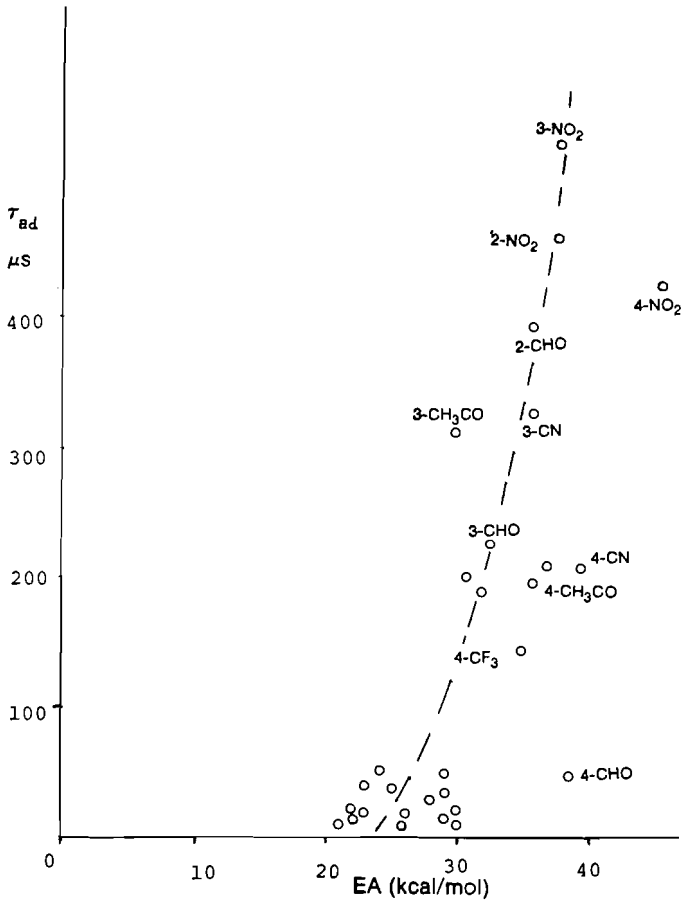


FIG. 5. Plot of autodetachment lifetimes τ_{ad} for $(A^-)^*$ formed by electron capture: $e + A = (A^-)^*$, Christophorou (16), versus electron affinities (actually $-\Delta G_a^0(NB)$) from present work. Due to high density of points only some points are identified. It will be noted that in general τ_{ad} increases with EA. For π-withdrawing substituents like CHO, CH_3CO, NO_2, the 4-substituted isomers have very much shorter lifetimes than the 3- and 2-substituted compounds.

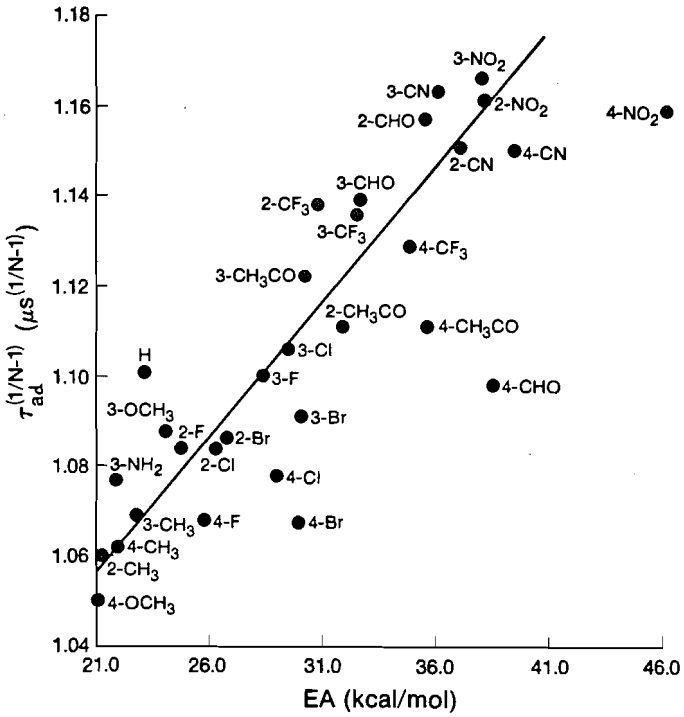


FIG. 6. Plot of $\tau^{1/(N-1)}$ versus electron affinities. Only rather poor correlation with straight line dependence predicted by eq. [13] is observed. The π-withdrawing substituents (CHO, CH_3CO, NO_2) in 4-position show largest deviations.

Stabilities and lifetimes of substituted nitrobenzenes after electron capture in the gas phase

Capture of (near) thermal electrons in the gas phase by molecules such as the nitrobenzenes is followed by eventual electron autodetachment in the absence of third body collisions. These processes are represented for molecule A in eq. [10]

$$[10] \quad e + A \underset{k_{ad}}{\overset{k_a}{\rightleftharpoons}} (A^-)^*$$

$$[11] \quad \tau_{ad} = 1/k_{ad}$$

$$[12] \quad \frac{k_a}{k_{ad}} = \frac{\rho(A^-)^*}{\rho(A)}$$

The autodetachment lifetime, τ_{ad}, is given by eq. [11], while eq. [12] gives the relationship between the rate constants for attachment and autodetachment and the density of the states for the ion $(A^-)^*$ and the neutral A (16). The τ_{ad} can be determined experimentally with time of flight or ICR mass spectrometers and a number of such values have been compiled by Christophorou (16). The τ_{ad} for substituted nitrobenzenes vary over a wide range, i.e., 10–530 μs. A plot of τ_{ad} from Christophorou versus the EA(NB) determined in this laboratory is shown in Fig. 5. The data show that τ_{ad} becomes of the order of a few μs around EA(NB) ≈ 20 kcal mol^{-1} and in geneal increases rapidly with increasing EA.

Christophorou (16) developed the very simple equation that gives a relationship between τ_{ad}, EA, and the number of normal vibrations N in the given NB. Details of the derivation can be found in Christophorou (16). Two important assumptions need to be mentioned: (*a*) the attachment rate constants, k_a, are assumed to be the same for all NB; (*b*) the internal energy in $(A^-)^*$ is assumed to be statistically distributed into all the vibrations *and* the vibrational frequencies, ν_i, of all vibrations are the same. Assumption (*a*) is probably correct if differences within a factor of 2 are neglected (16, 18), while (*b*) leads to the RRK form (19) of eq. [13].

$$[13] \quad \tau_{ad} \propto (EA(NB))^{N-1}$$

According to eq. [13], a plot of $\tau_{ad}^{1/(N-1)}$ vs. EA(NB) should lead to a straight line. At the time when Christophorou used the equation, the only source of EA(NB) where polarographic halfwave reduction potentials of the NB. These are expected to be linear with EA(NB) only if the solvation energies of the different NB^- are the same or if the solvation energies change but remain proportional to the EA(NB). Only a limited number of halfwave potentials obtained under identical conditions were available to Christophorou. The present EA(NB) plotted vs. $\tau_{ad}^{1/(N-1)}$ are shown in Fig. 6. Although a straight line can be drawn, the points are strongly scattered. The scatter is similar to that observed by Christophorou with the more limited polarographic data.

It is interesting to note that the largest deviations occur for the NB that are substituted in the *para* position by the strongly π-withdrawing substituents CHO, CH_3CO, and NO_2; see Fig. 6 and Table 3. These compounds have much shorter lifetimes relative to those expected on the basis of their electron affinities. As mentioned in the results section, the entropy changes for

electron capture by NB, i.e., ΔS_a^0(NB), were found to involve the largest loss of entropy for exactly these substituents.

The π-withdrawing substituents CHO, CH_3CO, and NO_2 increase their electron density and bond order in the radical anion due to π conjugation with the ring. This leads to stiffening of the C—CHO, C—$COCH_3$, and C—NO_2 internal rotations as well as stiffening of bending motions involving these substituents groups. It is exactly the soft modes, i.e., internal rotations and bending vibrations, that make the largest contributions to the density of states. The entropy losses indicate a large loss of density of states for the ions. Thus a treatment taking into account the actual contributions of the different vibrational modes to the density of the states of the molecule A and the ion A^-, particularly the loss of freedom in the above nitrobenzene anions, should provide a much better straight line correlation than that observed in Fig. 6.

Acknowledgement

P. K. thanks the Natural Sciences and Engineering Research Council of Canada for continuing financial support.

1. (*a*) E. P. GRIMSRUD, G. CALDWELL, S. CHOWDHURY, and P. KEBARLE. J. Am. Chem. Soc. **107**, 4627 (1985); (*b*) S. CHOWDHURY, T. HEINIS, E. P. GRIMSRUD, and P. KERBARLE. J. Phys. Chem. **90**, 2747 (1986); (*c*) S. CHOWDHURY, E. P. GRIMSRUD, T. HEINIS, and P. KEBARLE. J. Am. Chem. Soc. **108**, 3630 (1986); (*d*) S. CHOWDHURY, T. HEINIS, and P. KEBARLE. J. Am. Chem. Soc. **108**, 4662 (1986); (*e*) S. CHOWDHURY and P. KEBARLE. J. Am. Chem. Soc. **108**, 5453 (1986); (*f*) T. HEINIS, S. CHOWDHURY, S. L. SCOTT, and P. KEBARLE. J. Am. Chem. Soc. **110**, 400 (1988).
2. P. KEBARLE and S. CHOWDHURY. Chem. Rev. **87**, 513 (1987).
3. (*a*) R. W. TAFT and R. D. TOPSOM. Prog. Phys. Org. Chem. **16**, 1 (1987); (*b*) R. W. TAFT, J. L. M. ABBOUD, F. ANVIA, M. BERTHELOT, M. FUJIO, J.-F. GAL, A. D. HEADLEY, W. G. HENDERSON, I. KOPPEL, J. H. QIAN, M. MISHIMA, M. TAAGEPERA, and S. VEGI. J. Am. Chem. Soc. **110**, 1797 (1988); (*c*) R. W. TAFT and I. C. LEWIS. J. Am. Chem. Soc. **80**, 2436 (1958); **81**, 5343 (1959).
4. (*a*) A. PROSS, L. RADOM, and R. W. TAFT. J. Org. Chem. **45**, 818 (1980); (*b*) A. PROSS and L. RADOM. Prog. Phys. Org. Chem. **13**, 1 (1981).
5. A. J. BIRCH, A. L. HINDE, and L. RADOM. J. Am. Chem. Soc. **102**, 3370 (1980).
6. E. K. FUKUDA and R. T. MCIVER, JR. J. Phys. Chem. **87**, 2993 (1983); J. Am. Chem. Soc. **107**, 2291 (1985).
7. P. KEBARLE. *In* Techniques of chemistry, techniques for the study of ion–molecule reactions. *Edited by* W. H. Saunders and J. M. Farrar. Wiley, New York. 1988.
8. W. HEHRE, L. RADOM, and J. A. POPLE. J. Am. Chem. Soc. **94**, 1496 (1972).
9. (*a*) R. D. TOPSOM. Acc. Chem. Res. **16**, 292 (1983); (*b*) G. KEMISTER, A. PROSS, L. RADOM, and R. W. TAFT. J. Org. Chem. **45**, 1056 (1980); (*c*) R. D. TOPSOM. Prog. Phys. Org. Chem. **16**, 125 (1987).
10. R. W. TAFT. Prog. Phys. Org. Chem. **14**, 247 (1983).
11. P. KEBARLE. Ann. Rev. Phys. Chem. **28**, 445 (1977).
12. T. B. MCMAHON and P. KEBARLE. J. Am. Chem. Soc. **99**, 222 (1977).
13. (*a*) M. FUJIO, R. T. MCIVER, JR., and R. W. TAFT. J. Am. Chem. Soc. **103**, 4017 (1981); (*b*) L. RADOM. Chem. Commun. 403 (1974).
14. K. D. JORDON and P. D. BURROW. Acc. Chem. Res. **11**, 341 (1978).
15. J. L. FRANKLIN, J. G. DILLARD, H. M. ROSENSTOCK, J. T. HERRON, K. DRAXYL, and F. H. FIELD. Ionization potentials, appearance potentials, and heats of formation of gaseous positive ions. National Bureau of Standards (U.S.), NSRDS-NBS 26. 1969.
16. L. G. CHRISTOPHOROU. Adv. Electron. Electron Phys. **46**, 55 (1978).
17. S. L. LIAS, J. E. BARTMESS, J. L. LIEBMAN, J. L. HOLMES, R. D. LEVIN, and W. G. MALLARD. Gas phase ion and neutral thermochemistry. J. Phys. Chem. Ref. Data, Suppl. No. 1. **17** (1988).
18. F. C. FEHSENFELD, C. J. HOWAVER, and A. L. SCHMELTEKOPF. J. Chem. Phys. **63**, 2835 (1975); N. G. ADAMS, D. SMITH, A. A. VIGIANO, J. F. PAULSON, and M. J. HENCHMAN. J. Chem. Phys. **84**, 6728 (1986); D. C. CLARY and J. P. HENSHAW. Int. J. Mass Spectrom. Ion Processes, **80**, 31 (1987).
19. P. J. ROBINSON and K. A. HOLBROOK. Unimolecular reactions. Wiley (Interscience), New York. 1972.

Can. J. Chem. Downloaded from www.nrcresearchpress.com by 41.223.56.140 on 09/07/12
For personal use only.

Gas phase acidities of aliphatic carboxylic acids, based on measurements of proton transfer equilibria

GARY CALDWELL, RICHARD RENNEBOOG, AND PAUL KEBARLE[1]
Department of Chemistry, University of Alberta, Edmonton, Alta., Canada T6G 2G2

Received July 12, 1988

GARY CALDWELL, RICHARD RENNEBOOG, and PAUL KEBARLE. Can. J. Chem. **67**, 611 (1989).

Measurements of the gas phase proton transfer equilibrium [1]: AH + B^- = A^- + BH with a pulsed electron high pressure mass spectrometer (PHPMS) lead to ΔG^0_1 and ΔH^0_1 data. These relative acidities are converted to the absolute acidities [2]: AH = A^- + H^+ by calibration of the relative ΔG^0_1 and ΔH^0_1 scale to the known values for ΔG^0_1 and ΔH^0_1 of a reference compound (HCl). Earlier determinations that included 16 aliphatic AH are extended in the present work and provide data for 47 aliphatic carboxylic acids. These include halogen, OH, CH_3O, C_2H_5O, PhO, and NH_2 substituted acetic acids, and halogen substituted, unsaturated, and cyclic RCO_2H of higher carbon number. The effects of the various substituents on the gas phase acidity are briefly examined.

Key words: acidities in gas phase, proton transfer equilibria, ion–molecule equilibria, mass spectrometry.

GARY CALDWELL, RICHARD RENNEBOOG et PAUL KEBARLE. Can. J. Chem. **67**, 611 (1989).

En se basant sur des mesures de l'équilibre [1] de transfert de charge en phase gazeuse (AH + B^- = A^- + BH) réalisées à l'aide d'un spectromètre de masse à haute pression et à électrons pulsés (PHPMS), on a calculé les valeurs des ΔG^0_1 et ΔH^0_1. On a transformé ces acidités relatives en acidités absolues (AH = A^- + H^+ [2]) en calibrant l'échelle relative ΔG^0_1 et ΔH^0_1 par rapport aux valeurs de ΔG^0_1 et ΔH^0_1 connues pour un composé de référence (HCl). Dans le présent travail, on a étendu les déterminations antérieures qui incluaient 16 composés AH aliphatiques et l'on fournit des données pour 47 acides carboxyliques aliphatiques qui comprennent des acides acétiques portant des substituants halogène, OH, OCH_3, OC_2H_5 ou OPh ainsi que d'autres acides, contenant un plus grand nombre de carbones, qui sont substitués par des halogènes, insaturés ou cycliques. On discute brièvement des effets des divers substituants sur l'acidité en phase gazeuse.

Mots clés : acidités en phase gazeuse, mesures de l'équilibre de transfert de charge, équilibre ion–molécule, spectrométrie de masse.

[Traduit par la revue]

Introduction

Earlier determinations of the gas phase acidities of aliphatic and aromatic carboxylic acids (1–5) based on determination of the proton transfer equilibrium [1] with a pulsed electron high pressure mass spectrometer (PHPMS) (6) provided important first insights into the effects of substituents in the absence of solvent. Thus, for example, it was found (2) that for the halosubstituted acetic acids CH_2XCOOH, acidities increased in the gas phase in the order F, Cl, Br, which is the opposite of that found in aqueous solution. On the other hand, good linear correlations were obtained (4) between acidities in the gas phase and solution for benzoic acids substituted with a variety of substituents (linear free energy plots). Findings such as these, together with extensive measurements of equilibria (1) also with ion cyclotron resonance (ICR) mass spectrometers (7), have provided the required data for comprehensive investigations of substituent effects in the gas phase and solution (8).

[1] $AH + B^- = A^- + BH$

[2] $AH = A^- + H^+$

[3] $-RT \ln K = \Delta G^0$

The present work concentrates on aliphatic carboxylic acids RCO_2H. To obtain a fully consistent set of data, the 16 previously measured aliphatic acids RCO_2H were included in the present determinations. These acids, combined with the new compounds, lead to gas phase acidities for 47 RCO_2H. The resulting data provide information on alkyl group effects, halide substituent effects, and oxy (HO, MeO, EtO, PhO) substituent effects. The thermochemical data can be also used to obtain values for the electron affinities of the free radicals RCO_2, and bond dissociation energies RCOO—H.

In all gas phase acidity determinations (1–7, 9–11), one obtains the equilibrium constants K_1 from the experimental measurement of equilibrium [1] and evaluates $\Delta G^0_1 = -RT \ln K_1$. The ΔG^0_1 values are then combined into a scale of relative gas phase acidities. The relative values can be converted into an absolute scale for acid dissociation, ΔG^0_2, see eq. [2], by calibrating the scale of the ΔG^0_2 for one acid A_0H in the scale whose $\Delta G^0_2(A_0H^0)$ value is known from the literature, i.e., was determined by some other method. The number of determinations of acid dissociation energies of carboxylic acids, phenols, alcohols, nitrogen acids, and carbon acids obtained by this method cover more than 1000 compounds (11).

Experimental

Apparatus and method

The pulsed electron high pressure mass spectrometer (PHPMS) and method of measurements have been described in detail elsewhere (1–6). Only a brief outline and information specific to the present work will be given here.

Gas mixtures were prepared in a 5-L storage bulb that was part of the heated gas handling plant (6). The major (carrier) gas, methane, was at ~700 Torr (1 Torr = 133.3 Pa) while the reagents AH, BH, and NF_3 were in the Torr range. This gas mixture was allowed to flow in and out of the ion source – reaction chamber at a total pressure of ~4 Torr. Typical pressures in the ion source were: CH_4, 4 Torr, 30 mTorr of the weaker acid AH, a few mTorr BH, and 30 mTorr NF_3. A short 10–20 μs pulse of 2000-V electrons leads to ionization of the CH_4. The secondary electrons produced in this manner and slowed down by further collisions with CH_4 engage in dissociative electron capture, eq. [4*a*]. The strong base F^- deprotonates AH and BH, see eqs. [4*b*, *c*], and reactions of A^- and B^- with BH and AH lead to the proton transfer equilibrium [1].

[1]Author to whom correspondence may be addressed.

Can. J. Chem. Downloaded from www.nrcresearchpress.com by 41.223.56.140 on 09/07/12
For personal use only.

Can. J. Chem. Downloaded from www.nrcresearchpress.com by 41.223.56.140 on 09/07/12
For personal use only.

[4a] $e + NF_3 = F^- + NF_2$

[4b] $F^- + AH = FH + A^-$

[4c] $F^- + BH = FH + B^-$

The ion concentration changes with time are monitored through measurement of the intensities of the ions escaping through a slit from the ion source into the vacuum of a mass spectrometer (6).

The temperature of the ion source was 600 K for most equilibria measurements. At this temperature, the formation of adducts AHA^-, BHA^-, and BHB^- was relatively minor. The adducts, when present, were in equilibrium, see eq. [5], with the negative bases so that the simultaneous equilibrium [1] could still be measured.

[5] $A^- + HA \leftrightarrows AHA^-$

Thermal decomposition

The 4-L storage bulb in which the gas mixture spends approximately 1 h, is at 120°C, and the ion source, where the gas spends a few seconds, is at 327°C. These exposures to heat can lead to thermal decomposition of some of the acids. An auxiliary quadrupole mass spectrometer mounted in the vacuum chamber outside the ion source was used to monitor the neutral gases escaping through the ion source slits into the vacuum. The reported equilibria determination involve only acids that did not give indication of thermal decomposition. Decomposition was observed for malonic and succinic acids. For these acids the quadrupole detected significant amounts of CO_2. Furthermore, a large abundance of HCO_2^- ions originating from the high pressure ion source was also observed. These ions probably result from deprotonation of formic acid by F^-, where the formic acid is presumably formed by thermal decompostion of malonic and succinic acid. When measurements with $HSCH_2CO_2H$ were tried, the anion corresponding to the deprotonated acid could not be detected. We attribute this to thermal decomposition of the acid. Thermal decomposition of mercaptoacetic acid has been observed (12) at temperatures as low as 120°C. Decomposition of 4-acetylbutyric acid was also indicated by the present experiments.

Adsorption of acids on the wall

For certain acids, i.e., cyclohexane carboxylic acid, lactic acid, 1-adamantane acetic acid, and 1-adamantane carboxylic acid, it was observed that one had to maintain the flow from the storage bulb through the ion source for about 1 h, before consistent equilibrium [1] measurements could be obtained. The observations were consistent with a strong adsorption of these acids on the walls of the flow system and with the need for the establishment of a given wall coverage, before the partial pressure ratio of the acid in the ion source became equal to that expected on the basis of the gas mixture used.

Failed acidity measurements

Equilibrium [1] measurements involving several acids were not successful. The equilibrium quotient was not constant as the concentration [BH]/[AH] was changed. This was the case for $CNCH_2CO_2H$, $C_6H_5(CH_2)_3CO_2H$, $ClCH_2(CH_3)_2CCO_2H$, and $C_6H_5SCH_2CO_2H$. Attempted measurements involving the acids $(C_6H_5)_2CHCO_2H$, $(C_6H_5)_3CHCO_2H$, $C_6H_5C{\equiv}CCO_2H$, CCl_3CO_2H, $Br(CH_2)_2CO_2H$, and $I(CH_2)_2CO_2H$ were unsuccessful because the anion of these acids was not observed. Some of these acids probably have vapor pressures below 1 Torr at the 120°C storage bulb temperature; however, no serious attempts were made to establish the cause for the absence of the anion.

Chemicals

All samples were commercially available except $CF_3CH_2CO_2H$, for which sample we are indebted to Professor R. W. Taft. The following were purified by fractional distillation: acetic, propionic, valeric, isobutyric, pivalic, *n*-butyric, iso-valeric, and caproic acid. Dibromoacetic acid was sublimed and all other samples were used as is.

Results and discussion

(a) Relative acidities from proton transfer equilibria [1]

A typical measurement of the proton transfer equilibrium [1] is shown in Fig. 1. The two acids used were CH_2FCO_2H and $MeOCH_2CO_2H$ at a concentration ratio of 6. The figure shows the observed intensities of the two anions as a function of time after the electron pulse. The two ions are seen to rapidly reach equilibrium, which for the logarithmic plot used corresponds to a constant vertical distance between the two curves. The slow linear decrease is due to diffusion of the ions to the wall followed by discharge. The ion ratio observed is 3.6, which leads to a $\Delta G_1^0 = -3.7$ kcal mol^{-1} at 600 K, see eqs. [1] and [3].

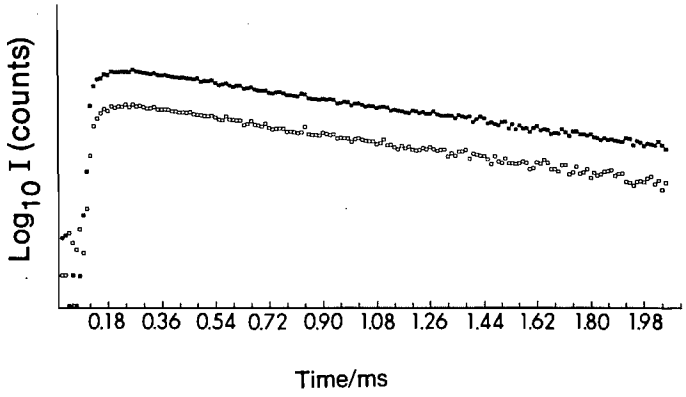


FIG. 1. Ion intensities observed after short (20 μs) electron pulse: $FCH_2CO_2^-$, $MeOCH_2CO_2^-$. Ions reach the proton transfer equilibrium [1] rapidly (200 μs). This is indicated by the constant ion ratio, which corresponds to constant vertical distance in the plot. The slow linear decrease of ion intensities is due to diffusion of ions to the wall. 5 Torr CH_4; pressure ratio, $CH_3OCH_2CO_2H/FCH_2CO_2H = 6$. Temperature 600 K.

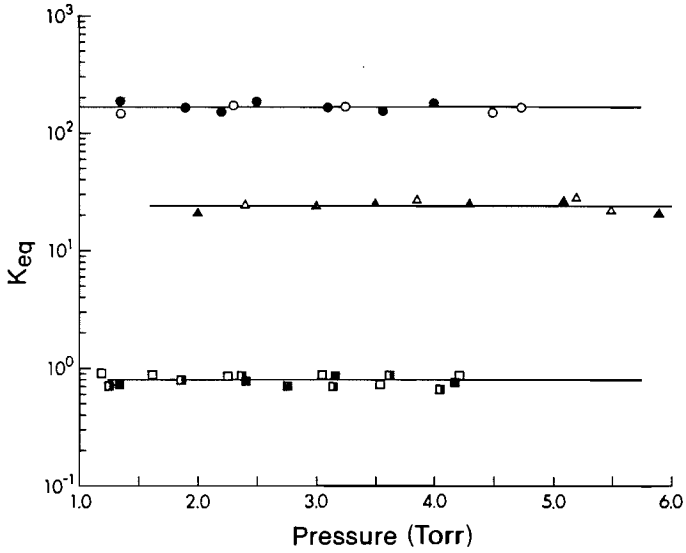


FIG. 2. Dependence of equilibrium constant K_1 for the proton transfer reaction [1]: $AH + B^- = A^- + BH$, on total ion source pressure (≈ bath gas CH_4 pressure) and on ratio of concentrations R = [BH]/[AH] in ion source. AH = $CH_3OCH_2CO_2H$, BH = CH_3CO_2H: R = 18 ●, R = 5 ○; AH = $CH_3OCH_2CO_2H$, BH = *t*-$BuCO_2H$: R = 2 ■, R = 5 □; AH = FCH_2CO_2H, BH = $CH_3OCH_2CO_2H$: R = 6 ▲, R = 2 △. Temperature 600 K.

Tests of the independence of the equilibrium constant K_1 on the reactant ratio and the total pressure are illustrated in Fig. 2.

The evaluated ΔG_1^0 at 600 K are shown in Fig. 3. The interconnecting data are combined in a scale that gives the

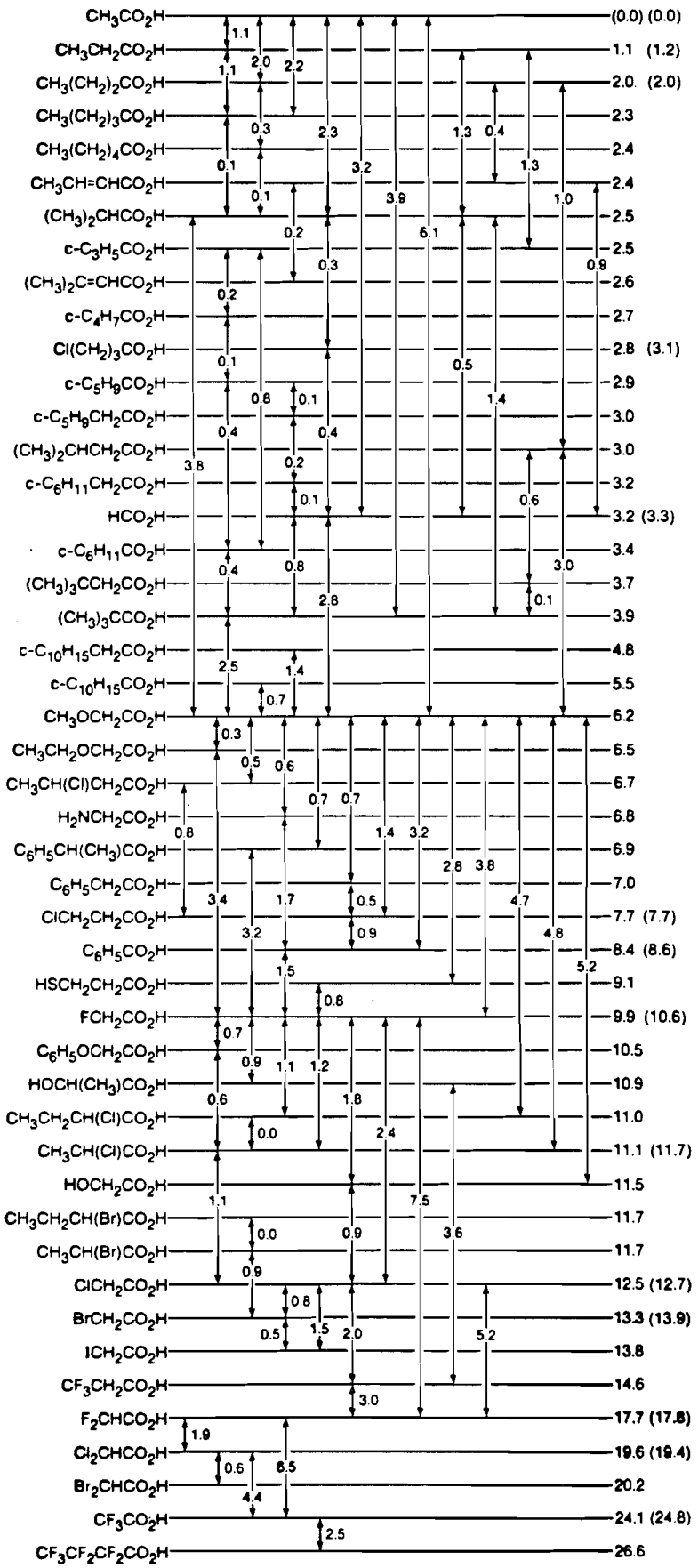


FIG. 3. Carboxylic acids acidity scale based on free energy changes ΔG_1^0 for proton transfer reaction [1]: AH + B^- = A^- + BH. Individual ΔG_1^0 values measured shown between double arrows. Acidities relative to acetic acid, i.e., ΔG_6^0 for reaction [6]: $CH_3CO_2H + B^- = CH_3CO_2^- +$ BH, shown in column to the right. Values given in parentheses are earlier data from Cumming and Kebarle (9). All values in kcal mol^{-1}, temperature 600 K; however, very similar values expected also for 300 K. *c*-$C_{10}H_{15}$ stands for 1-adamantyl. Acidity increases from top to bottom.

Can. J. Chem. Downloaded from www.nrcresearchpress.com by 41.223.56.140 on 09/07/12
For personal use only.

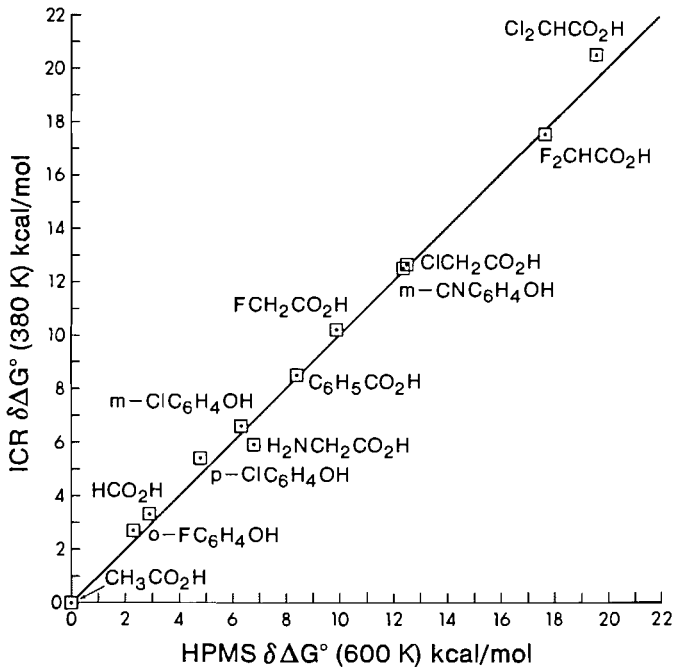


FIG. 4. Comparison of ΔG^0 values for proton transfer $CH_3CO_2H + B^- = CH_3CO_2^- + BH$, where BH are acids shown in figure. Solid line corresponds to slope = 1. The PHPMS data for 600 K, present work, and the ICR data for Bartmess and McIver (7) at ~380 K are very close, which means that the ΔS^0 changes are generally less than 2 cal deg^{-1} mol^{-1}. Largest deviation observed for $H_2NCH_2CO_2H$ is probably due to a larger ΔS due to intramolecular H bonding in anion, see Discussion, Sect. *j*.

acidities relative to that for the weakest acid CH_3CO_2H, i.e., the ΔG_6^0 value for reaction [6].

[6] $CH_3CO_2H + A^- = CH_3CO_2^- + AH$

There are many redundant thermodynamic cycles in Fig. 3, which illustrate that, in general, the data are consistent to ±0.2 kcal mol^{-1}. Data for those acids that were investigated previously in this laboratory and were included in the summary of Cumming and Kebarle (9) are also given in Fig. 3. For acids that are less acidic than FCH_2CO_2H, the agreement is within 0.3 kcal mol^{-1}. At FCH_2CO_2H and above, the present data become, on the average, lower by ~0.4 kcal mol^{-1}. Most of the acids in the earlier determinations (9) with acidity higher than FCH_2CO_2H were anchored to that acid. The present value for FCH_2CO_2H is 0.7 kcal mol^{-1} lower than the previous result. In the present determinations, see Fig. 3, there are five equilibria to acids with lower acidities that fix the value for FCH_2CO_2H while in the previous work there was only one. The present results for this acid and all higher acidity acids are more reliable.

(b) Entropy changes for proton transfer reactions [1]

As indicated in the experimental part, the available temperature range at which the proton transfer equilibria could be measured was restricted. A lower limit was set by excessive proton adduct formation (AHA^-, AHB^-, B_2H^-) and an upper limit by the thermal decomposition of the neutral acids. Therefore the temperature dependence of K_1 was determined only for one system of special interest, see Sect. *j* on cyclization of $HOCH_2CO_2^-$ due to intramolecular hydrogen bonding.

For the vast majority of acids only very small ΔS_1^0 changes are expected. Previous temperature determinations of proton transfer equilibria [1] led, via van't Hoff plots, to entropy changes ΔS_1^0 that were less than 2 cal deg^{-1} mol^{-1}. A summary of these measurements and procedures for estimating ΔS_1^0 on the basis of rotational symmetry number and estimated internal rotational changes is given in Cumming and Kebarle (9). For the present group of acids, see Fig. 3, little information on the internal motions of the acids and the anions is available and ΔS_1^0 estimates are in general difficult. The fact that the values are generally small can be illustrated by a comparison of ΔG_1^0 values determined by ICR (7, 10) at ~380 K and the present

TABLE 1. Absolute acid dissociation scale[a]

Acid	ΔG^0(300 K) (kcal mol^{-1})	ΔH^0 (kcal mol^{-1})
CH_3CO_2H	341.5	348.5
$CH_3CH_2CO_2H$	340.4	347.4
$CH_3(CH_2)_2CO_2H$	339.5	346.5
$CH_3(CH_2)_3CO_2H$	339.2	346.2
$CH_3(CH_2)_4CO_2H$	339.1	346.1
$CH_3CH{=}CHCO_2H$	339.1	346.1
$(CH_3)_2CHCO_2H$	339.0	346.0
c-$C_3H_5CO_2H$	339.0	346.0
$(CH_3)_2C{=}CHCO_2H$	338.9	345.9
c-$C_4H_7CO_2H$	338.8	345.8
$Cl(CH_2)_3CO_2H$	338.7	345.7
c-$C_5H_9CO_2H$	338.6	345.6
c-$C_5H_9CH_2CO_2H$	338.5	345.5
$(CH_3)_2CHCH_2CO_2H$	338.5	345.5
c-$C_6H_{11}CH_2CO_2H$	338.3	345.3
HCO_2H	338.3	345.3
c-$C_6H_{11}CO_2H$	338.1	345.1
$(CH_3)_3CCH_2CO_2H$	337.8	344.8
$(CH_3)_3CO_2H$	337.6	344.6
c-$C_{10}H_{15}CH_2CO_2H$[c]	336.7	343.7
c-$C_{10}H_{15}CO_2H$[c]	336.0	343.0
$CH_3OCH_2CO_2H$	335.3	342.3
$CH_3CH_2OCH_2H$	335.0	342.0
$CH_3CH(Cl)CH_2CO_2H$	334.8	341.8
$H_2NCH_2CO_2H$	334.7	341.7
$C_6H_5CH(CH_3)CO_2H$	334.6	341.6
$C_6H_5CH_2CO_2H$	334.5	341.5
$ClCH_2CH_2CO_2H$	333.8	340.8
$C_6H_5CO_2H$	333.1	340.1
$HSCH_2CH_2CO_2H$	332.4	339.4
FCH_2CO_2H	331.6	338.6
$C_6H_5OCH_2CO_2H$	331.0	338.0
$HOCH(CH_3)CO_2H$	330.6	337.6
$CH_3CH_2CH(Cl)CO_2H$	330.5	337.5
$CH_3CH(Cl)CO_2H$	330.4	337.4
$HOCH_2CO_2H$	327.8[b]	332.3[b]
$CH_3CH_2CH(Br)CO_2H$	329.8	336.8
$CH_3CH(Br)CO_2H$	329.8	336.8
$ClCH_2CO_2H$	329.0	336.0
$BrCH_2CO_2H$	328.2	335.2
ICH_2CO_2H	327.7	334.7
$CF_3CH_2CO_2H$	326.9	333.9
F_2CHCO_2H	323.8	330.8
Cl_2CHCO_2H	321.9	328.9
Br_2CHCO_2H	321.3	328.3
CF_3CO_2H	317.4	324.4
$CF_3CF_2CF_2CO_2H$	314.9	321.9

[a] ΔG_2^0 and ΔH_2^0 for acid dissociation: $AH = A^- + H^+$ in gas phase. Based on ΔG_6^0 values in Fig. 3 and $\Delta G_2^0(CH_3CO_2H)$ = 341.5 kcal mol^{-1}; $\Delta H_2^0(CH_3CO_2H)$ = 348.4 kcal mol^{-1} from previous work (9). ΔS_6^0 entropy changes assumed equal to zero, i.e., $\Delta G_6^0 = \Delta H_6^0$ except for $HOCO_2H$.

[b] ΔS change included, see Discussion, Sect. *j*.

[c] *c*-$C_{10}H_{15}$ stands for 1-adamantyl.

Can. J. Chem. Downloaded from www.nrcresearchpress.com by 41.223.56.140 on 09/07/12
For personal use only.

TABLE 2. Thermochemical data for RCO_2H acids

RCO_2H	ΔH_2^{0a}	$-\Delta H_{f298}^0(RCO_2H)^b$	$-\Delta H_{f298}^0(RCO_2^-)^c$	$DH(RCO_2H)^d$	$EA(RCO_2)^e$
HCO_2H	345.3	90.57±0.14	110.0	87.2±1.0	55.5
CH_3CO_2H	348.5	103.26±0.12	120.5	105.8±2	70.9
$EtCO_2H$	347.5	108.4 ±0.5	126.7	106.4±2	72.6
n-$PrCO_2H$	346.5	112.4 ±0.6	131.6	105.9±2	73.4
n-$BuCO_2H$	346.2	117.15±0.45	136.7	106[f]	~73.4
n-$PenCO_2H$	346.1	122.7 ±0.5	142.3	106[f]	~73.5
$C_6H_5CO_2H$	340.1	70.14±0.12	95.7	—	—
$H_2NCH_2CO_2H$	341.7	93.72±0.15	117.7	106[f]	~77.9
$ClCH_2CO_2H$	336.0	104.1 ±2.3	133.8	106[f]	~83.6

[a]All values in kcal mol^{-1}. ΔH_2^0 for the reaction: $RCO_2H \rightarrow RCO_2^- + H^+$, from Table 1.
[b]Cox and Pilcher (13).
[c]Calculated from eq. [9] where $\Delta H_{f298}^0(H^+)$ = 365.7 kcal mol^{-1} (11). Estimated error ±3 kcal mol^{-1}.
[d]Bond dissociation energies, Miller and Golden (16).
[e]Calculated from eq. [10] where $IP(H^0)$ = 313.6 kcal mol^{-1}.
[f]Estimated value.

determinations at 600 K. The data given in Fig. 4 show that only small deviations from the unity slope line are observed. Since the temperature difference is close to 220°, the less than 0.5 kcal mol^{-1} deviations from the unit slope line indicate ΔS_1 terms of less than 2 cal deg^{-1} mol^{-1}.

(c) Thermochemical data ΔG_2^0 and ΔH_2^0 for gas phase: $RCO_2H = RCO_2^- + H^+$

Evidence presented in Sect. *b* demonstrated that the ΔS_1^0 values are generally less than ±2 cal deg^{-1} mol^{-1}. Therefore the assumption in eq. [7] is justified. In the earlier work (9), the

[7] $\Delta G_1^0 = \Delta H_1^0$

acid dissociation energies for ΔH_2^0 and ΔG_2^0 at 300 K for acetic acid, see eq. [8], were obtained by calibrating the scale to the primary standard HCl.

[8] $\Delta H_2^0(CH_3CO_2H) = 348.5$ kcal mol^{-1}; $\Delta G_2^0(CH_3CO_2H) = 341.5$ kcal mol^{-1}

The same values, eq. [8], were adopted in the Ion–Thermochemistry compilation by Lias *et al.* (11).

Combining the values in Fig. 3 with the absolute acidity values in eq. [8] and using the assumption in eq. [7] we obtain the acidities $\Delta G_2^0(RCO_2H)$ and $\Delta H_2^0(RCO_2H)$ given in Table 1. These absolute values are believed accurate to ±2 kcal mol^{-1}.

(d) Heats of formation of RCO_2^- in the gas phase

When the heat of formation of the acid $HA_{(g)}$ is known, the $\Delta H_f(A^-_{(g)})$ can be evaluated by eq. [9], which follows from eq. [2]. The $\Delta H_f^0(RCO_2^-)$ evaluated with eq. [9] and $\Delta H_f(RCO_2H)$ from the literature (13) are given in Table 2 for nine acids. These data are only a sample of the $\Delta H_f(RCO_2^-)$ that can be obtained. Additional $\Delta H_f(RCO_2H)$ values can be found in compilations (14) and converted to $\Delta H_f(RCO_2^-)$ on the basis of ΔH_2 results in Table 1.

[9] $\Delta H_f(A^-) = \Delta H_2^0 - \Delta H_f(H^+) + \Delta H_f(HA)$

(e) Electron affinities of RCO_2 and bond energies RCOO—H

The acid dissociation enthalpy ΔH_2, the electron affinity EA(A), and the bond dissociation energy D(A—H) are related by eq. [10] where IE(H) is the ionization potential of the hydrogen atom. Thus, when D(RCOO—H) are available, $EA(RCO_2\cdot)$ can be evaluated (15), and vice versa, from the ΔH_2 data given in Table 1. Table 2 contains a sampling of $EA(RCO_2\cdot)$ evaluated from available D(RCOO—H) data, Miller and Golden (16). Unfortunately, the bond dissociation energies are not very reliable. Also no direct experimental determinations of $EA(RCO_2\cdot)$, which would have provided cross checks of the data, seem to be available.

TABLE 3. Comparison of alkyl group effect on acidity of RCO_2H and ROH[a]

R	$\delta\Delta G_{600K}$ (PHPMS)[b] RCO_2H	$\delta\Delta G_{380K}$ (ICR)[c] ROH
Me	0	0
Et	1.1	3.3
*n*Pr	2.0	4.5
*i*Pr	2.5	5.3
*n*Bu	2.3	5.3
*i*Bu	3.0	6.0
*t*Bu	3.7	6.0

[a]All values in kcal mol^{-1}. Positive values for $\delta\Delta G^0$ correspond to an increase of acidity from Me to R.
[b]Data from Table 1.
[c]Data from Bartmess and Scott (18) as quoted in Lias *et al.* (11).

[10] $\Delta H_2 = D(A—H) + IE(H) - EA(A\cdot)$

(f) Alkyl group effect on the acidity of RCO_2H

Methyl substitution on sp^2 hybridized carbon decreases the acidity, thus HCO_2H is 3.4 kcal mol^{-1} more acidic than CH_3CO_2H, see Fig. 3 and ref. 1. The methyl effect was first observed by Brauman and Blair (17), who found that the gas phase acidity of methylacetylene is lower than that of acetylene. A similar effect is observed for the phenols, where Me substitution in *m* and *p* positions leads to a (small) decrease of acidity (5, 8). From Fig. 3 one obtains the ΔG_6^0 data shown below for *n*-alkyl substitution of the aliphatic acids:

$MeCO_2H$	$EtCO_2H$	n-$PrCO_2H$	n-$BuCO_2H$	n-$PeCO_2H$	
0	1.1	2.0	2.3	2.4	(kcal mol^{-1})

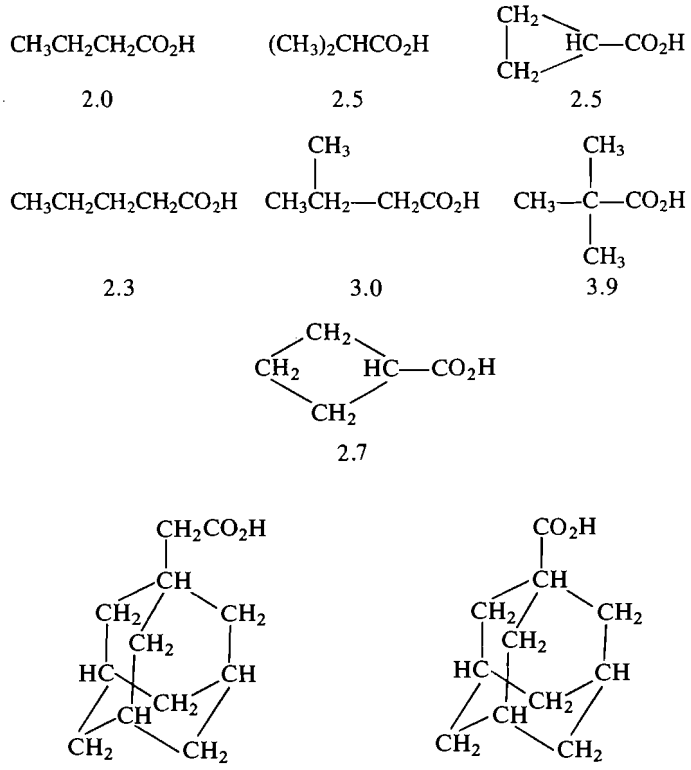
The acidity increase is relatively small and can be attributed to the stabilizing effect of the polarizability of the alkyl group on the negative ion. This stabilizing effect is somewhat larger than the destabilizing field-inductive effect and pseudo π donation.

Can. J. Chem. Downloaded from www.nrcresearchpress.com by 41.223.56.140 on 09/07/12
For personal use only.

Can. J. Chem. Downloaded from www.nrcresearchpress.com by 41.223.56.140 on 09/07/12
For personal use only.

The above order for alkyl substitution was observed also for the acidity of alcohols (7, 17) although a less complete series of compounds was involved. A comparison between effects of alkyl groups R in the acidity of RCO_2H and ROH is given in Table 3. The ROH data are due to Bartmess *et al.* (18) and are based on proton transfer equilibria measurements. The trends observed for RCO_2H and ROH are similar; however, for ROH the effect of increasing size of R or branching is seen to be roughly twice as large as that for RCO_2H. This is an expected result. In RCO_2^- the charge is delocalized onto two oxygens and the stabilization due to the polarizability of the alkyl group is smaller than for RO^- where the charge is mostly on the one oxygen atom.

Branched alkyl groups lead to a higher acidity than straight chain substituents. This is illustrated by the ΔG_6^0 values from Fig. 3 shown below:



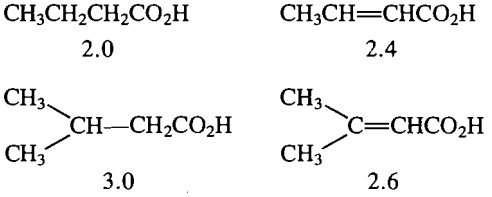
(ΔG_6^0 values in kcal mol^{-1})

It is interesting to note, in the C_4 series, that the t-C_4H_9 is of significantly higher acidity than the cyclic isomer. While the dominant conformations of the anions in the gas phase are not known, probably the tertiary compound leads to the closest distances of the alkyl carbons to the negative charge and thus maximizes the polarizability stabilization.

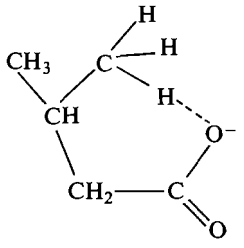
The strongest acid in the group shown above is 1-adamantyl carboxylic acid. Present in this case is the acidifying effect of the tertiary group and the additional polarizability due to the extensive carbon structure.

(g) Effect of π systems on the acidity of RCO_2H

Since π systems in R of RCO_2^- cannot directly conjugate with the CO_2^- group, relatively smaller stabilization is expected for this group in comparison to RO^- anions, where delocalization of the negative charge to the π system can occur. For example, the acidity difference between $MeCO_2H$ and $PhCO_2H$ is 8.4 kcal mol^{-1} (9), while that between MeOH and PhOH is 27.8 kcal mol^{-1} (5, 7). The dominant contributions to the acidifying effect of the phenyl group in $PhCO_2H$ should be the electron-withdrawing field-inductive effect and the polarizability. Of interest also is the comparison between acids that have one double bond and the corresponding alkanes RCO_2H:



The unsaturated crotonic acid is found to be 0.4 kcal mol^{-1} more acidic than butyric acid. This effect is expected due to the electron-withdrawing field-inductive effect of the vinyl group. Somewhat surprisingly, the β-methyl crotonic acid is found to be 0.4 kcal mol^- less acidic than the saturated 3-methyl butyric acid. It is conceivable that rotamers of the anion, see structure **I**, which correspond to intramolecular hydrogen bonded structures, contribute to the stabilization of the anion.



I

Convincing evidence for intramolecular hydrogen bonding stabilization is provided in Sect. *j* for the stronger hydrogen donor groups OH and NH_2, which lead to much stronger stabilization. The minor stabilization due to I, if real, is of course not restricted to that particular alkanoic anion but will occur with all acids RCO_2H where the alkane R contains a chain of at least 3 carbon atoms.

(h) Halide effects on acidity of RCO_2H

The effect of halide substituents on RCO_2H acids was examined in two earlier publications (2, 3). The new measurements are in good agreement with the older data. The availability of a larger number of compounds amplifies the previous findings. The introduction of a halide substituent is strongly acidifying. The effect decreases as the halide is removed farther away from the carboxy group, as illustrated by the ΔG_6^0 values for the chloride series below:

$CH_3CH_2CH_2CO_2H$	$CH_2ClCH_2CH_2CO_2H$	$CH_3CHClCH_2CO_2H$	$CH_3CH_2CHClCO_2H$	
2.0	2.8	6.7	11	kcal mol^{-1})

For single substituents the acidifying effect increases in the order F, Cl, Br, I. This is an order opposite to that observed in solution. The acidifying effect of the halide atom is due to the stabilization of the negative charge by the electron-withdrawing field-inductive effect and the polarizability of X. In the absence of solvent, the polarizability becomes very important and the increasing polarizability from F to I leads to the observed gas phase acidity increase. In the series X_2CHCO_2H, the introduction of the second X provides a somewhat smaller increase of acidity than the first. The effect of the second substituent decreases in the order F to Br. This result indicates that the effective decrease of negative charge on the CO_2^- oxygens due to the field effect of the X_2 substituents reduces the stabilizing effect of their polarizability. On this basis one might expect almost equal acidity in the CX_3CO_2H acids for X (F, Cl, Br). Unfortunately data for only CF_3CO_2H are available.

FCH_2CO_2H	$ClCH_2CO_2H$	$BrCH_2CO_2H$	ICH_2CO_2H	F_2CHCO_2H	Cl_2CHCO_2H	Br_2CHCO_2H	
9.9	12.5	13.3	13.8	17.7	19.6	20.2	(kcal mol^{-1})

Multiple fluorine substitution leads to large acidifying effects, thus CF_3CO_2H is 24 kcal mol^{-1} and $CF_3CF_2CF_2COOH$ 26.6 kcal mol^{-1} more acidic than CH_3CO_2H, see Fig. 3.

(i) Effect of oxy substituents on the acidity of RCO_2H

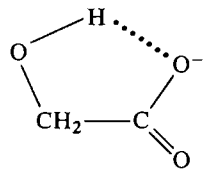
The oxy substituents HO, MeO, EtO, and PhO lead to relatively large increases of acidity, as shown by the data below, from Fig. 3.

$MeOCH_2CO_2H$	$EtOCH_2CO_2H$	$PhOCH_2CO_2H$	$HOCH_2CO_2H$	
6.2	6.5	10.5	11.5	(kcal mol^{-1})

The changes can be understood in terms of the field-inductive effect and polarizability for all groups except for OH. Evidently, for the OH substituent, additional stabilization of the anion must be present and this must be due to intramolecular hydrogen bonding.

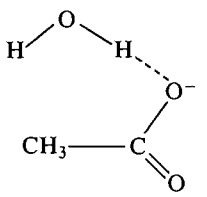
(j) Intramolecular hydrogen bonding in $HOCH_2CO_2^-$

The high acidity of $HOCH_2CO_2H$ relative to the MeO and EtO substituted acetic acids, observed in the preceding section, must be due to intramolecular hydrogen bonding. The cyclization induced by such bonding, see structure **II**, is expected to



$\Delta H_{cyc} \approx -10$ kcal mol^{-1}

II



$\Delta H \approx -17$ kcal mol^{-1}

III

lead to an entropy loss, which can be measured. Shown in Fig. 5 is a van't Hoff plot of the equilibrium constant K_{13} for the proton transfer reaction [13].

[13] $FCH_2CO_2^- + HOCH_2CO_2H = FCH_2CO_2H + HOCH_2CO_2^-$

The slope and intercept of the plot lead to $\Delta H^0_{13} = -6.3$ kcal mol^{-1}, $\Delta S^0_{13} = -7.5$ cal deg^{-1} mol^{-1}, and $\Delta G^0_{13}(600\ K) = -1.8$ kcal mol^{-1}.

Assuming that the entropy change for the proton transfer in eq. [13] would be negligible in the absence of cyclization, see Sect. *b*, the entire $\Delta S^0_{13} = -7.5$ cal deg^{-1} mol^{-1} can be attributed to the cyclization, i.e., $\Delta S^0_{cyc} \approx -7.5$ cal deg^{-1} mol^{-1}. The hydrogen bond energy, ΔH^0_{cyc}, can also be estimated assuming negligible entropy changes for proton transfer without cyclization. On adding $-\Delta H^0_{13} = 6.3$ kcal

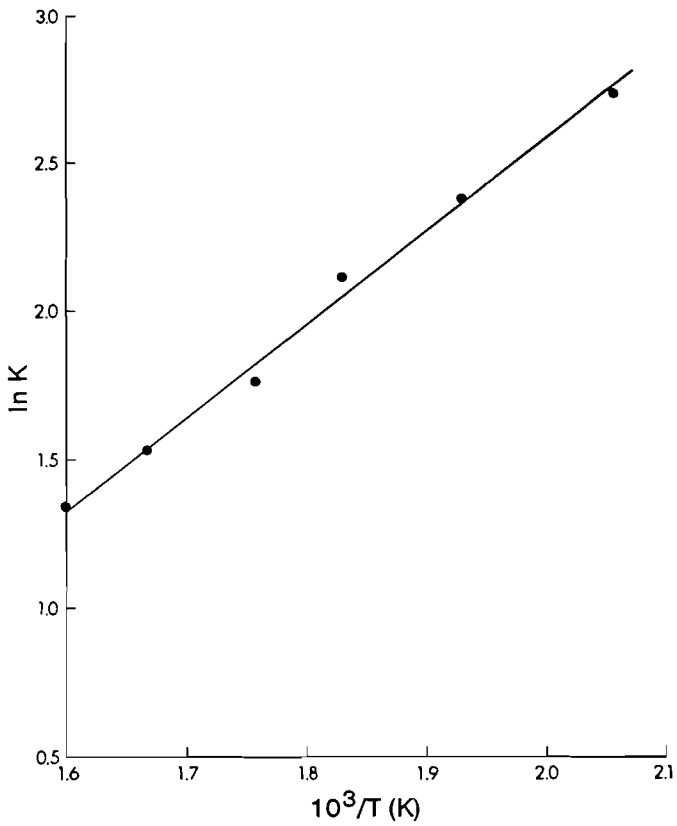


FIG. 5. van't Hoff plot of equilibrium constants K for proton transfer equilibrium: $FCH_2CO_2^- + HOCH_2CO_2H \rightleftharpoons FCH_2CO_2H + HOCH_2CO_2^-$.

mol^{-1} to $\Delta G^0_6(CH_2FCO_2H) = 9.9$ kcal mol^{-1}, from Fig. 3, one obtains $\Delta H^0_6(HOCH_2CO_2H) = 16.2$ kcal mol^{-1}, the estimated enthalpy change for proton transfer [6] involving the cyclized structure **II**. The enthalpy change ΔH^0_6 for the

Can. J. Chem. Downloaded from www.nrcresearchpress.com by 41.223.56.140 on 09/07/12
For personal use only.

uncyclized structure can be assumed to be the same as $\Delta G^0_6(CH_3OCH_2CO_2H) = 6.2$ kcal mol where it is assumed that in the absence of cyclization the acidifying effects of HO and CH_3O are the same. The cyclization enthalpy is, then, $-\Delta H_{cyc} = 16.2 - 6.2 = 10$ kcal mol^{-1}.

This is a reasonable value for the very strained hydrogen bond that is expected to occur in structure **II**. It can be compared with the H bond in structure **III**. This bond can be expected to be close to 17 kcal mol^{-1} on the basis of experimental measurements by Meot-Ner and Sieck (19) and a theoretical calculation by Jorgensen and co-workers (20), see structure 10c in Jorgensen. The bond in structure **II** is much weaker, mostly because it is very strained. Also, prior to the cyclization, the hydroxy group in $HOCH_2CO_2^-$ may be expected, due to the negative charge transfer from the carboxy group to the O atom, to be a slightly poorer hydrogen bond donor than the free HOH that leads to structure **III**.

The rather small $-\Delta S^0_{cyc} \approx 8$ cal deg^{-1} mol^{-1} indicates that structure **II** is quite loose at temperatures in the 300–600 K range.

Some cyclization may also be present in the anion of glycine, $NH_2CH_2CO_2^-$. Lock and McIver (21) have determined the gas phase acidity of glycine. If their free energy of proton transfer at 380 K, see Fig. 4, is combined with the present proton transfer value, see Figs. 3 and 4, at 600 K one obtains an estimate of $\Delta S^0_{cyc} \approx -4$ cal deg^{-1} mol^{-1}. This entropy loss is quite small and corresponds to the presence of hindered rotation rather than cyclization. It is known that NH is a much poorer hydrogen donor than OH. Therefore a much weaker H bond in the glycine anion is expected. The "cyclized" structure in this case is so loose that it allows hindered internal rotation around the C—C and the C—N bonds.

An even looser cyclized structure was suggested in Sect. *g*, involving CH groups as hydrogen donors and leading to a possible weak stabilization of unsubstituted alkane carboxyl anions.

Acknowledgement

This work was supported by the Natural Sciences and Engineering Research Council of Canada (NSERC).

1. R. YAMDAGNI and P. KEBARLE. J. Am. Chem. Soc. **95**, 4050 (1973).
2. K. HIRAOKA, R. YAMDAGNI, and P. KEBARLE. J. Am. Chem. Soc. **95**, 6833 (1973).
3. R. YAMDAGNI and P. KEBARLE. Can. J. Chem. **52**, 861 (1974).
4. R. YAMDAGNI, T. B. MCMAHON, and P. KEBARLE. J. Am. Chem. Soc. **96**, 4035 (1974).
5. T. B. MCMAHON and P. KEBARLE. J. Am. Chem. Soc. **99**, 2222 (1977).
6. P. KEBARLE. Techniques for the study of ion–molecule reactions. *In* Techniques of chemistry. *Edited by* W. H. Saunders and J. M. Farrar. Wiley Interscience, New York. 1988.
7. J. E. BARTMESS, J. A. SCOTT, and R. T. MCIVER, JR. J. Am. Chem. Soc. **101**, 6046 (1979).
8. R. W. TAFT. Prog. Phys. Org. Chem. **14**, 247 (1983).
9. J. B. CUMMING and P. KEBARLE. Can. J. Chem. **56**, 1 (1978).
10. J. E. BARTMESS and R. T. MCIVER, JR. *In* Gas phase ion chemistry. Vol. 2. *Edited by* M. T. Bowers. Academic Press, New York. 1979.
11. S. G. LIAS, J. E. BARTMESS, J. F. LIEBMAN, J. L. HOLMES, R. D. LEVIN, and W. G. MALLARD. J. Phys. Chem. Ref. Data, Suppl. No. 1. **17** (1988).
12. A. STRÖVEL and F. KRUMEY. Ber. Dtsch. Chem. Ges. B: **77**, 371 (1944).
13. J. D. COX and G. PILCHER. Thermochemistry of organic and organometallic compounds. Academic Press, New York. 1970.
14. J. B. PEDLEY, R. D. NAYLOR, and S. B. KIRBY. Thermochemical data of organic compounds. 2nd ed. Chapman and Hall, London. 1986.
15. R. YAMDAGNI and P. KEBARLE. Ber. Bunsen-Ges. Phys. Chem. **78**, 181 (1974).
16. D. F. MILLER and D. M. GOLDEN. Annu. Rev. Phys. Chem. **33**, 493 (1982).
17. J. I. BRAUMAN and L. K. BLAIR. J. Am. Chem. Soc. **93**, 4315 (1971).
18. J. E. BARTMESS, J. A. SCOTT, and R. T. MCIVER, JR. J. Am. Chem. Soc. **101**, 6047 (1979).
19. M. MEOT-NER (MAUTNER) and L. W. SIECK. J. Am. Chem. Soc. **110**, 3854 (1988).
20. J. GAO, D. S. GARNER, and W. L. JORGENSEN. J. Am. Chem. Soc. **108**, 4784 (1986).
21. M. J. LOCK and R. T. MCIVER, JR. J. Am. Chem. Soc. **105**, 4226 (1983).

Can. J. Chem. Downloaded from www.nrcresearchpress.com by 41.223.56.140 on 09/07/12
For personal use only.

Properties of a new one-dimensional semiconducting ternary compound: TEDA (triethylenediamine)·$I_{2.5}$·TCNQ

ANDRÉ D. BANDRAUK,[1] K. D. TRUONG, AND C. CARLONE

Groupe de recherche sur les semiconducteurs et diélectriques, Faculté des sciences, Université de Sherbrooke, Sherbrooke (Qué.), Canada J1K 2R1

Received October 5, 1988

ANDRÉ D. BANDRAUK, K. D. TRUONG, and C. CARLONE. Can. J. Chem. **67**, 619 (1989).

A new semiconducting ternary compound of stoichiometry TEDA·$I_{2.5}$·TCNQ is reported. The crystal is made up of linear chains of $TCNQ^{-1/2}$, nonlinear chains of I_3^-, and monodides of doubly charged triethylenediamines (TEDA). Half the TEDA's are hydrogen bonded to the TCNQ's and I_3^-. The conductivity measurements indicate semiconducting behaviour with two discontinuities in activation energy, one at high (330 K) and the other at low (160 K) temperatures. Resonance Raman spectra of the crystals manifest strong resonance enhancement of the iodide moieties. In particular, selective resonance excitation at 647 nm of nonsymmetric I_3^- is observed, thus indicating an increasing asymmetry of the I_3^- in the low temperature phase and suggesting coupling between the three species in this phase.

Key words: semiconductor, ternary compound, resonance Raman spectra, tetracyanoquinodimethane (TCNQ), tri-iodide (I_3).

ANDRÉ D. BANDRAUK, K. D. TRUONG et C. CARLONE. Can. J. Chem. **67**, 619 (1989).

On a préparé un nouveau composé ternaire semi-conducteur de stoechiométrie TEDA·$I_{2.5}$·TCNQ. Le cristal est formé de chaînes linéaires de $TCNQ^{-1/2}$, de chaînes non-linéaires de I_3^- et de monoiodures de triéthylènediamines, TEDA, doublement chargées. La moitié des TEDA sont liés par des ponts hydrogènes à des TCNQ et des I_3^-. Les mesures de conductivité indiquent que le comportement semi-conducteur est lié à deux discontinuités dans l'énergie d'activation, l'une à haute (330 K) et l'autre à basse température (160 K). Les spectres de résonance Raman présentent de forts renforcements de la résonance des portions iodures. En particulier, on observe une excitation sélective de la résonance non-symétrique du I_3^-, à 647 nm; cette propriété reflète une augmentation de l'asymétrie du I_3^- dans la phase à basse température et suggère que dans cette phase il existe un couplage entre les trois espèces.

Mots clés : semi-conducteur, composé ternaire, spectres de résonance Raman, TCNQ, I_3.

[Traduit par la revue]

Introduction

Many organic donors are known to form conducting charge transfer compounds with halide ions. One of the early organic metals, a perylene–iodine complex, exhibited various stoichiometries and conductivities (1, 2). Further research on a variety of organic conductors has led to the importance of obtaining segregated stacks, partial charge transfer, extensive π-overlap between adjacent molecules in the cation or anion columns (2), leading finally to the discovery of the ambient pressure low temperature organic superconductors $(TMTSF)_2ClO_4$ (3) and $(BEDT–TTF)_2I_3$ (4–6), the latter containing the I_3^- anion as a counterion.

Most organic conductors are formed from a single doner (D) and a single acceptor (A), albeit in different stoichiometries. One class of conductors involving iodine, tertiary amines, and TCNQ leads to ternary salts in which the iodine forms linear chains of I_3^- parallel to the conducting linear chains of TCNQ (tetracyanoquinodimethane), and the amine is hydrogen bonded to the $TCNQ^-$ anions. We suggested in previous work that these compounds should be more readily considered as alloys of $M^+I_3^-$ and $(M^+)_2(TCNQ_3)^{-2}$, giving the experimental composition $(M^+)_3I_3^-(TCNQ_3)^{-2}$, where M is the donor amine (7). In the course of our work on hydrogen bonding in these systems, we described a TCNQ complex with the di-tertiary amine triethylenediamine, $TEDA_2TCNQ_3$, which had the novel feature that linear chains of hydrogen-bonded TEDA's were now parallel to the linear chains of the TCNQ's (7, 8). This linear arrangement of the TEDA's was also found in two of its iodide salts, TEDA·I_3 and TEDA·$I_{3.4}$ (9). We have therefore tried to synthesize a ternary compound of TEDA, I, and TCNQ, obtaining a *new* compound of stoichiometry TEDA·$I_{2.5}$·TCNQ, unlike the previously known ternary compounds. We present here the structure, resonance Raman spectra, and other physical properties of this new compound.

One of the interesting aspects of the ternary compounds has been the question of the involvement of the iodine chain in the metal–semiconductor phase transition known to occur in these compounds at low temperatures. We were able to show, in previous work, by selective resonance Raman scattering (RRS) of I_3^- in single crystals of TMA (trimethylammonium·I·TCNQ, that the I_3^- anions are excellent probes of the phase transition (10). Thus the frequency, intensity, and linewidth of the ν_1 symmetric mode (115 cm^{-1}) of I_3^- were shown to have discontinuities at the phase transition, indicating a direct involvement of the ion chains, probably as a disorder–order transition within the iodine chain, and thus applying a commensurate potential of wavevector $2k_F$ on the TCNQ chains. Such external commensurate potentials due to counterions introduce pseudo Peierls gaps, with the consequence that the system becomes semiconducting (11–13).

We recently examined (14) the behaviour of I_3^- by similar RRS techniques on single crystals of the β-form of $(BEDT–TTF)_2I_3$, which is known to become superconducting at 7 K (4–6). Again we have found the I_3^- to be sensitive to the onset of a superlattice structure known to occur below 180 K in this compound (15). One motivation for our examining the new ternary compound reported here is that in both β-$(BEDT–TTF)_2I_3$ and TEDA·$I_{2.5}$·TCNQ one finds similar *nonlinear* (zigzag) chains of I_3^-, contrary to previous organic conductors, such as TMA·I·TCNQ (10, 16) and $DIPS\Phi_4I_{2.86}$ (13), where the I_3^- form *linear* chains.

[1]Author to whom correspondence may be addressed.

Can. J. Chem. Downloaded from www.nrcresearchpress.com by 41.223.56.140 on 09/07/12
For personal use only.

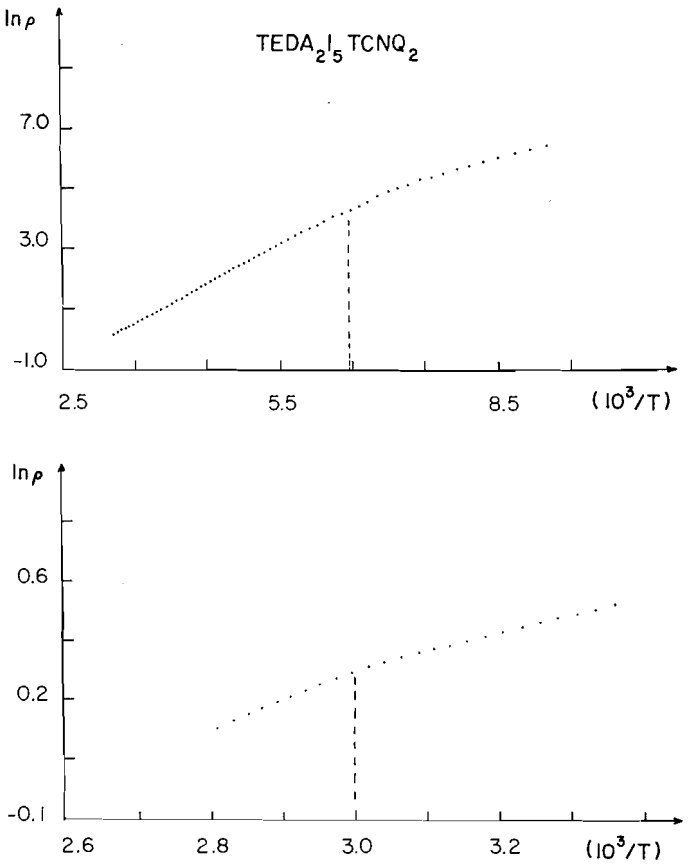


FIG. 1. Temperature variation of ln ρ vs. $10^3/T$ showing anomalies around 160 and 330 K.

Experimental

Preparation

TEDA·$I_{2.5}$·TCNQ was synthesized starting from $TEDA^{2+}(I^-)_2$ by oxidation with TCNQ in distilled methanol. The solvent factors formation of the triiodide ion. The final compound includes unoxidized I^- anions. Blue-black crystals are obtained from the solution. Chemical analysis confirms the reported stoichiometry (theoretical % in parentheses): C 34.47 (34.04), N 13.61 (13.20), H 2.95 (2.68), I 48.93 (50.0).

Conductivity

The electronic resistivity ρ (or conductivity $\sigma = \rho^{-1}$) is measured by a four-probe method along the long axis of the needlelike crystals. Room temperature conductivity is rather low, 0.651 $(\Omega\ m)^{-1}$. Anomalies are observed around 330 K and 160 K. A plot of ln ρ vs. $10^3/T$, Fig. 1, reveals that the anomalies are due to changes of activation energy E_c, if we apply the relation $\rho = \rho_0 \exp(E_c/RT)$. E_c is found to have a high temperature value (above 330 K) of 0.18 eV, a room temperature value of 0.1 eV, and a low temperature value (below 160 K) of 0.06 eV. Both transitions are gradual, unlike conductor–semiconductor transitions, which usually involve structural changes and accompanying discontinuities in $\rho(T)$ (11–13).

Electronic spectra

These were measured with a standard Cary 14 spectrometer. The spectra essentially resemble those of TEDA·CH_2Cl·$TCNQ_2$, a 1:2 complex (8). Thus maxima are found at 28 500, 17 000, 11 300, and 4000 cm^{-1}. The first two correspond to localized $TCNQ^-$ excitations, whereas the last two correspond to delocalized excitations, $A^-A^- \rightarrow A^{2-}A$, and $A^-A \rightarrow AA^-$, referred to usually as charge transfer bands (17). An I_3^- band, attributed to a $\sigma_g \rightarrow \sigma_u$ electronic transition (18) also is found to extend below 17 000 cm^{-1}. This I_3^- band will serve to selectively excite the ion in RRS.

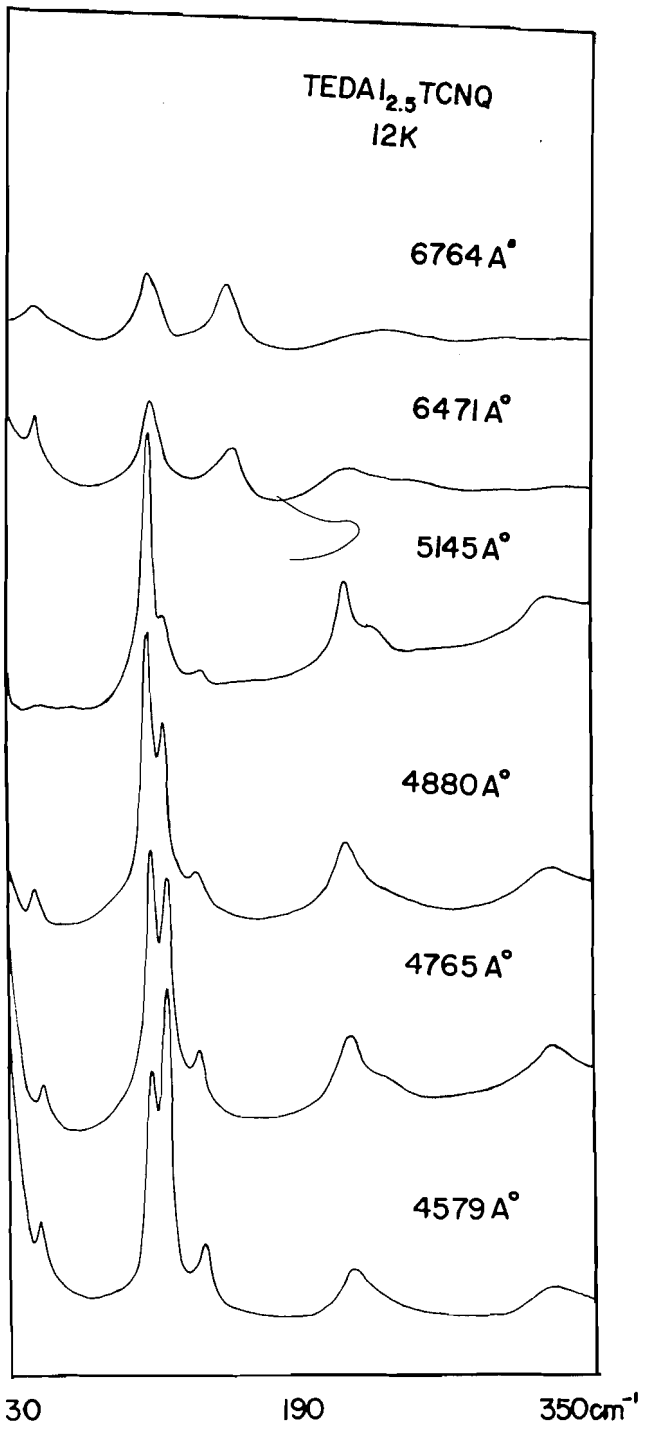


FIG. 2. Raman spectrum of a single crystal of TEDA·$I_{2.5}$·TCNQ at 12 K as a function of laser wavelength.

ESR spectrum

A rather large signal without hyperfine structure is observed ($g \sim 2.002$). The integrated intensity, I_n, increases with decreasing temperature, and follows a Curie-like law as in the $DEPD_2TCNQ_3$ complex (19). Plotting ln ($I_n \times T$) vs. $1/T$ gives a straight line, with a slope $-E_s/k$, from which one obtains the activation energy $E_T = 0.02$ eV. This small triplet activation energy was relatively constant as compared to the conduction activation energy E_c, Fig. 1, which manifests two sharp changes.

Raman spectra

The spectra were measured with argon ion and krypton lasers at low

Can. J. Chem. Downloaded from www.nrcresearchpress.com by 41.223.56.140 on 09/07/12
For personal use only.

Can. J. Chem. Downloaded from www.nrcresearchpress.com by 41.223.56.140 on 09/07/12
For personal use only.

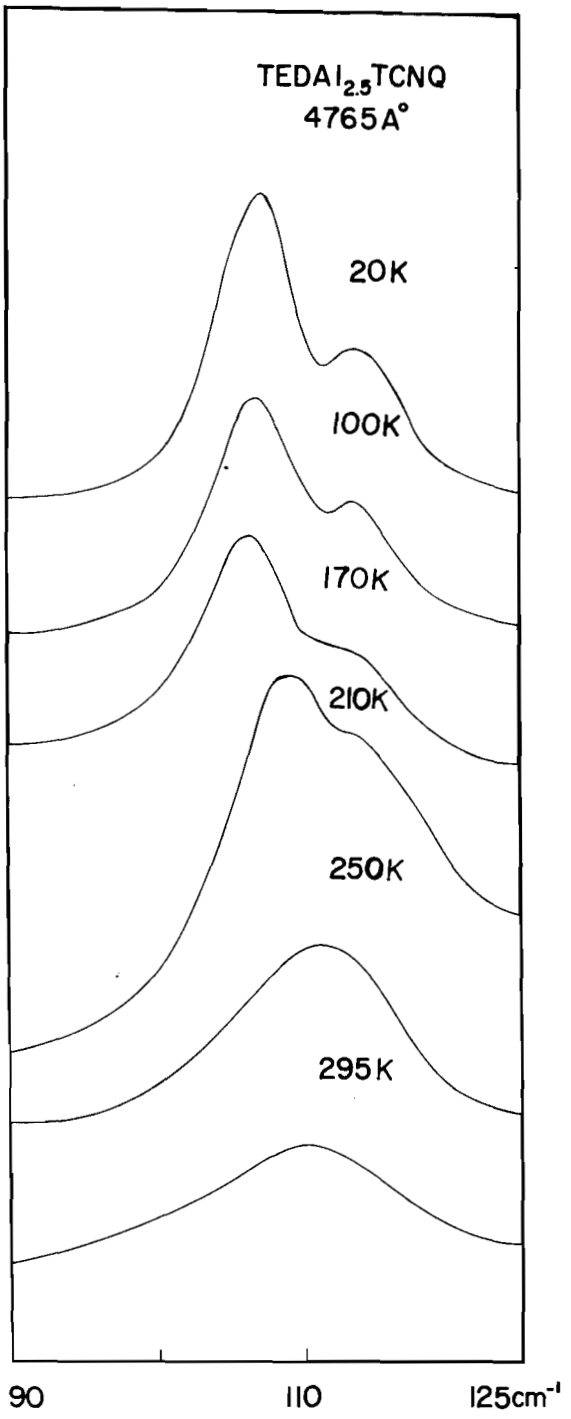


FIG. 3. Raman spectrum of a single crystal of TEDA·$I_{2.5}$·TCNQ as a function of temperature at 4765 Å laser wavelength excitation (power ≤ 5 mW).

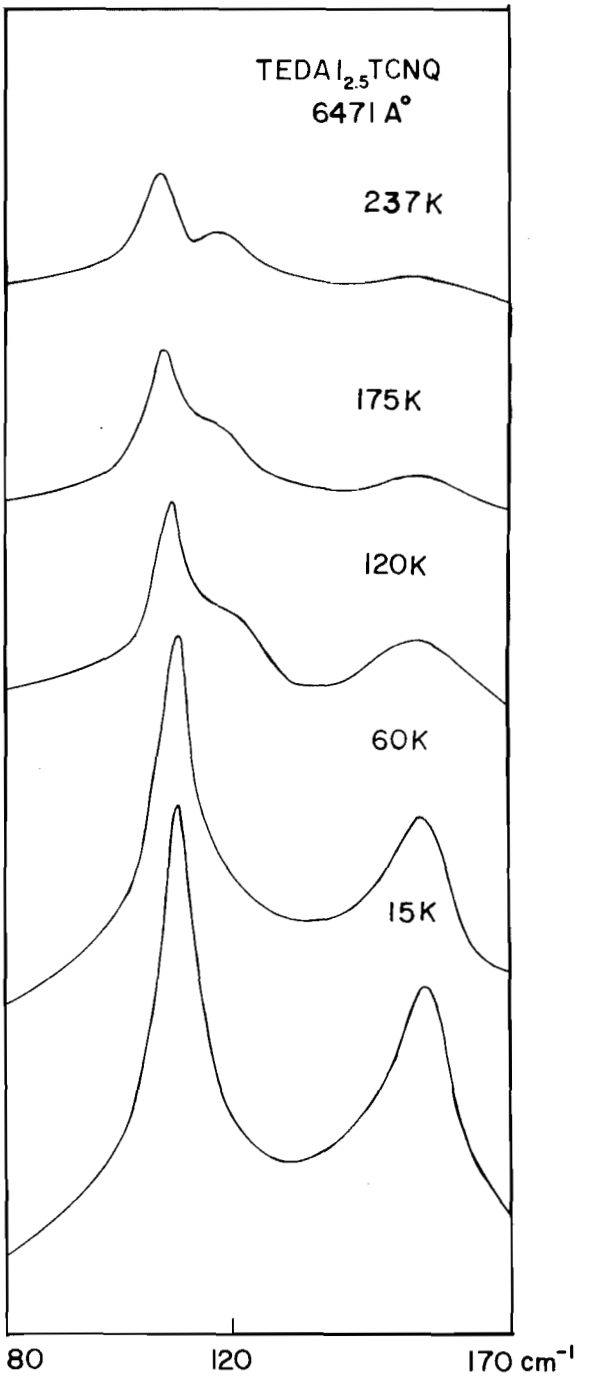


FIG. 4. Raman spectrum of a single crystal of TEDA·$I_{2.5}$·TCNQ as a function of temperature at 6471 Å laser wavelength excitation (power ≤ 5 mW).

powers, below 5 mwatts, to eliminate any surface heating and oxidation. Spectra were recorded with a perpendicular geometry, as in our previous work on single crystals of KTCNQ (20) and TMA·I·TCNQ (10). With high energy excitation (457.9, 488 nm), a large progression of overtones of the ν_1 symmetric mode of I_3^- as in TMA·I·TCNQ was observed. Lower energy excitation (647 nm) enhances nonsymmetric modes (see Fig. 2). The temperature dependence of these modes is illustrated in Figs. 3 and 4 and is discussed in the next sections with reference to the crystal structure.

Discussion

(a) Crystal structure

Preliminary X-ray results (21) show that there are two independent TCNQ molecules of similar geometry. The average bond distribution in each (Table 1) is consistent with the acquisition of a charge of 0.5 e (22). Average bond lengths in the TEDA ions are consistent with the assumed doubly protonated state (Table 1). Iodine is present as two isolated I^- ions and one I_3^- ion (Figs. 6 and 7). The latter is slightly nonlinear with different I—I distances (Table 1). The terminal I atom of the longer bond appears to be a proton acceptor. The

TABLE 1. Selected bond lengths and angles (see Fig. 5 for atom numbering) (ref. 21)

Bond	TCNQ(1)	TCNQ(2)
a	1.352 Å	1.353 Å
b	1.435	1.436
c	1.396	1.390
d	1.422	1.422
C—N	1.147	1.149
	TEDA	
C—C	1.520 Å	
C—N	1.586	
I(1)—I(2)	2.890 Å	
I(1)—I(3)	2.952	
I(2)—I(1)—I(3)	178.82°	

asymmetry and nonlinearity of the I_3^- ion have been discussed previously elsewhere (23).

The TCNQ molecules lie essentially normal to [101], and are arranged in staggered face-to-face stacks extended in this direction. The sequence is 1-2-2′-1′-1 etc. (Fig. 6). There are thus *three* types of nearest-neighbour interaction, with slightly different interplanar spacings (1–1′, 3.37 Å; 2–2′, 3.42 Å; 1–2, 3.29 Å). The modes of overlap are found to be all very similar, and are of the type commonly occurring in TCNQ complexes, with the double bond c (Fig. 5) lying over the centre of the ring of the adjacent molecule.

The I_3^- ions are arranged in zigzag chains parallel to, and lying between, adjacent TCNQ stacks (Fig. 6). The TCNQ–I_3^- complex thus fills a layer parallel to the x–z plane. Adjacent layers are separated by parallel layers of $TEDA^{2+}$ ions and I^- ions. The other TEDA ion donates a proton to one I^- ion, while its second proton appears to be *shared* by a terminal atom of the I_3^- ion and the CN groups of one TCNQ molecule. It appears that the latter interaction, by reducing charge mobility in the TCNQ stack, is one cause of the low conductivity of this compound (see next section). The TCNQ molecules that accept protons occur in *pairs* along the stack (i.e., TCNQ(1) and TCNQ(2), Fig. 6). The relation of this structural feature to the conductivity is discussed in the following section.

(b) Structure and semiconducting properties

The structure, as illustrated in Figs. 6 and 7 (the first gives a side view of the TCNQ columns whereas the second figure illustrates tentative N—H bonds), indicates a tetramerization of the TCNQ stacks with a weak dimerization within the stacks. The repetitive unit can be presented as 211′2′ with long 2–2′ distance (3.42 Å), short 1–2 distance (3.29 Å), and intermediate 1–1′ distances (3.37 Å). Such structure is typical of *spin-Peierls* systems (24, 25). The charge on each TCNQ is estimated to be close to 0.5 e. The total charge distribution per unit cell is $2TCNQ^{-1/2}$, $2TEDA^{2+}$, I_3^-, and $2I^-$, giving a net zero charge. From the X-ray structure and the stoichiometry it is clear that half of the TEDA's are oriented towards, and are therefore hydrogen bonded to, apparent TCNQ ions thus creating the short TCNQ(1)—TCNQ(2) distance of 3.29 Å. As a result of this distribution of the donors that have a repeat periodicity $4a$ (a = average distance between TCNQ's) (see Fig. 6), the anions create a donor modulating positive potential with wave vector $k_D = 2\pi/4a$ on the TCNQ's. The modulating potential due to the iodides is described to a first approximation by wave vector $k_I = 2\pi/2a$. Since for a half-charged uniform chain of TCNQ ions one has a Fermi level at $k_F = \pi/4a$, then a $2k_F$ Peierls instability should occur at $2k_F = 2\pi/4a$. Clearly the main influence of the counterions comes from the TEDA's that have periodicity $4a$; these are hydrogen bonded to the TCNQ's. These introduce a perturbation of wave vector $k_D = 2\pi/4a$, which will induce a gap, a Peierls "pseudo gap", at the Fermi surface. It is to be noticed that the cations on the left of the chain are displaced by the distance a with respect to the cations on the right, i.e., a phase difference $k_D a = \pi/2$. This phase shift does not cancel out the electrostatic potential on the next TCNQ molecule so that the counterion potential remains effective. We emphasize that in the TMTTF highly conducting complexes, the counterion potentials on each side of the organic chain are out of phase by π, thus reducing the counterion potential on the conducting chain (26, 27). In the present case the counterion potentials persist and can be expected to play a critical role in the conduction mechanism of the system. These are probably also responsible for the tetramerization observed, which results in a semiconductor with a gap of 0.1 eV at room temperature. We emphasize that, as a first approximation, the I_3^- should have no influence on the conducting properties since their periodicity is $2a$, i.e., a wavevector four times the Fermi vector $k_F = \pi/4a$.

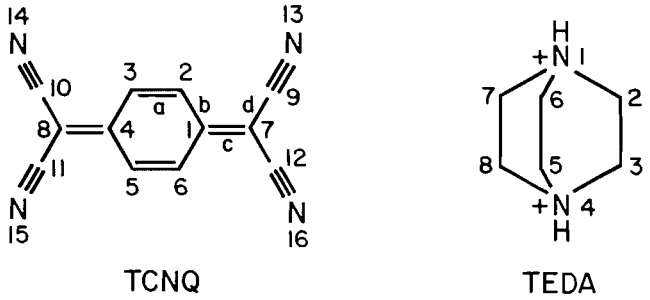


FIG. 5. Labelling of atoms reported in Table 1.

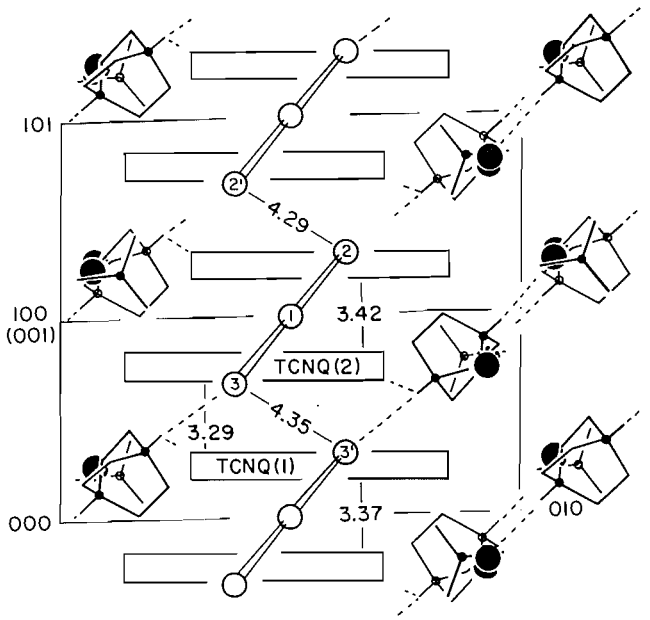


FIG. 6. Part of the structure viewed along [101]. Large circles are I atoms (shaded for I^-, open for I_3^-), small circles are N atoms. H atoms are omitted, except for the amino protons.

Can. J. Chem. Downloaded from www.nrcresearchpress.com by 41.223.56.140 on 09/07/12
For personal use only.

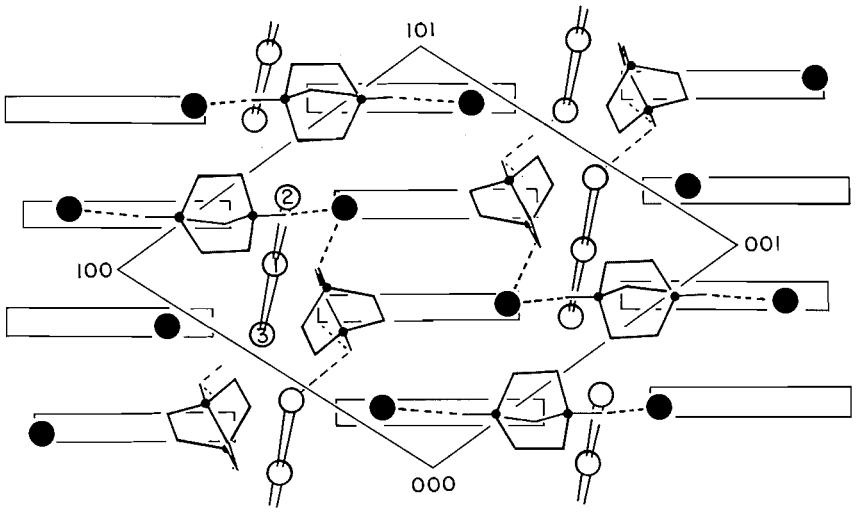


FIG. 7. The structure viewed along [101]. The TCNQ molecules are represented by rectangles.

This is similar to the case of the conductors $TTT_2 \cdot I_{3+\delta}$ as opposed to $DIPS\phi_4 \cdot I_{3(0.76)}$, where in the former the iodide periodicity is $4k_F$ and in the latter it is $2k_F$ with respect to the conducting bands (12). It is thus found that in the $TTT_2 \cdot I_{3+\delta}$ compound the conductivity is not altered by ordering of the iodides at low temperatures, whereas the iodide ordering induces the conductivity loss in $DIPS\phi_4 \cdot I_{3(0.76)}$ as in TMA·I·TCNQ due to $2k_F$ pseudo Peierls effects (13, 16).

Since in most of the known ternary TCNQ semiconducting compounds, $TCNQ^{-2/3}$ chains are parallel to linear chains of I_3^-, we have here a *novel* system with nonlinear chains of I_3^- parallel to chains of $TCNQ^{-1/2}$. Furthermore, in the previous ternary compounds such as TMA·I·TCNQ (16), it was the iodide chain that was shown to be involved in the metal–semiconductor transition known to occur at 160 K (10). This transition occurs in the latter because the iodine potential periodicity is equal to $2k_F$, k_F being the Fermi wavevector of the conduction electrons in the $TCNQ^{-2/3}$ chain. In the present case, the I_3^- seem to be spectators, whereas the hydrogen bonding of the TEDA donors regulates the semiconducting properties of the system by imposing a $2k_F$ modulating electrostatic potential on the conducting TCNQ chain and thus opening a gap at the Fermi level of the chain. The tetramerization evident in Fig. 6 is normally attributed to Peierls distortions as a result of charge or spin density wave formations (24). Intermolecular hydrogen bonding in the phenothiazine–TCNQ complex has recently been identified as the driving force for an observed structural modulation in that compound (28). In the present ternary compound we would seem to have both mechanisms operating, since it is clear that Peierls distortions and electrostatic (crystal) effects cannot be separated. In fact conductivity measurements were extended to high temperatures (400 K) to see if the reverse spin-Peierls transition (dimerization ↔ tetramerization) could be observed, as in $MEM \cdot TCNQ_2$ (24, 25). No change in conductivity or ESR spectrum was observed. A change in activation energy was observed at 330 K, with a quasidoubling of the activation energy occurring above that temperature (Fig. 1). This anomaly remains unexplainable as it did not show up in the RRS spectrum, as discussed in the following section. The doubling of the activation energy above 330 K with respect to its room temperature value is reminiscent of Q (quinolinium)·$TCNQ_2$, which essentially has the same activation energies as our compound but with the energy discontinuity occurring at about 400 K (17). This was considered to be an early example of an order–disorder semiconductor (29). The second discontinuity in activation occurs at ~160 K in $TEDA \cdot I_{2.5} \cdot TCNQ$. We will show in the next section that the iodide ions seem to be involved in this "pseudo" phase transition at this low temperature. We note that the terminal I atoms in the I_3^- anions are on the average at normal van der Waals contact distances, 4.3 Å, and are directed at a diagonal to the conducting chain. Similar conditions occur in the crystals of the superconductor β-$(BEDT\text{–}TTF)_2I_3$. For the latter compound, the angle between the I_3^- ion axis and the organic chain direction is 20° (15), while on our compound this angle is 39° (Fig. 6).

(c) Resonance Raman spectra

Figure 2 illustrates the resonance behaviour of different I_3^- vibrations at very low temperatures (12 K). At 676.4 nm excitation, three bands, 47, 100 and 152 cm^{-1}, are observed. These are usually attributed to bending, symmetric, and antisymmetric modes of I_3^- (30). At 457.9 nm excitation, the bending mode remains, whereas the $\nu_1 = 110\ cm^{-1}$ band is split in two vibrations at 107 and 115 cm^{-1}, thus reflecting the slight asymmetry in the bond lengths (Table 1). A new mode at 132 cm^{-1}, which could be an overtone (~ 47 + 107) cm^{-1}, and harmonics of the symmetric band (222, 327 cm^{-1}) also appear at this high energy excitation. The main resonant effect is the disappearance of the $\nu_1 = 115\ cm^{-1}$ mode and increasing intensity of the $\nu_2 = 152\ cm^{-1}$ mode as one goes from 457.9 to 676.4 nm excitation. Such a resonant effect confirms the antisymmetric character of the $\nu_2 = 152\ cm^{-1}$ mode, which is strongly coupled to the $\sigma_g \rightarrow \sigma_u$ electronic transition at ~600 nm of I_3^- (18). The 115 cm^{-1} mode, contrary to its 107 cm^{-1} partner, would seem to couple to high energy excitations, which is typical of symmetric modes of the iodide ion (19, 30).

Figures 3 and 4 illustrate in finer detail the structure of the I_3^- low frequency bands as a function of temperature for the two extreme excitations 476.5 and 647.1 nm, respectively. Thus in Fig. 3, at room temperature, one observes only a single ν_1 band at 476.5 nm excitation with a maximum at 110 cm^{-1}, typical of the I_3^- ν_1 symmetric mode. Around 200 K a splitting of the band into two components at 107 and 115 cm^{-1} begins to occur. The splitting of this band is accentuated as one lowers the temperature. A similar gradual splitting of the symmetric I_3^- mode has been observed upon lowering the temperature in β-(BEDT–

Can. J. Chem. Downloaded from www.nrcresearchpress.com by 41.223.56.140 on 09/07/12
For personal use only.

Can. J. Chem. Downloaded from www.nrcresearchpress.com by 41.223.56.140 on 09/07/12
For personal use only.

$TF)_2I_3$ and is attributed to a rearrangement of the donor molecule and the onset of a superstructure (14, 15) that is essential for superconductivity in that compound. In Fig. 4, the mode at 152 cm^{-1} attributed to the antisymmetric ν_2 vibration of I_3^- broadens and decreases considerably in intensity around the phase transition temperatures, 160 K, when it is resonant with the excitation wavelength 647.1 nm. The same resonant excitation of the ν_1 mode manifests an intensity nehaviour contrary to the 476.5 nm excitation (Fig. 3). At the lower energy excitation, the ν_1 mode is a single band below the phase transition, 160 K, and splits above that temperature. Contrary to the conductivity results, Fig. 1, the Raman spectra do not indicate a sharp transition but a rather gradual perturbation of the I_3^- ions beginning already above the transition temperature.

In our previous work on the ternary compound $TMA^+ \cdot I^{-1/3} \cdot TCNQ^{-2/3}$, we used the I_3^- symmetric vibration $\nu_1 = 115\ cm^{-1}$ as a probe to measure the involvement of the iodine chain in the conductor–insulator transition, which occurs at 160 K in that compound (10). No evidence was found of the antisymmetric $\nu_2 = 150\ cm^{-1}$ vibration in that compound and the ν_1 vibration underwent discontinuous intensity changes, but no splitting. In the present case, the ν_2 vibration is enhanced in intensity as one crosses the phase transition and the ν_1 mode splits in a continuous fashion around the transition temperature. Although the room temperature X-ray data suggest already a slight asymmetry in bond lengths of the I_3^- due to some weak hydrogen bonding to the TEDA's, Fig. 6 and Table 1, it is not clear why the ν_1 band splits above the phase transition for $\lambda = 647.1$ nm (Fig. 4) and below it for $\lambda = 476.5$ nm (Fig. 3). A possible explanation would be the presence of inequivalent TCNQ's, 2–2′ and 1–1′, resulting in different crystal effects for I_3 and I_3', Fig. 6.

Conclusion

As discussed in Sect. b, the periodicity of the iodides precludes any strong interaction of I_3^- with the TCNQ electronic bands. This would explain the gradual onset of perturbations in the I_3^- Raman spectra.

The TEDA periodicity, on the other hand, is expected to influence strongly the electronic properties of the compound via a $2k_F$ pseudo Peierls effect. These donors are, however, hydrogen bonded to both the I_3^-'s and to the TCNQ's (N(1)—I(3) = 3.76 Å; N(1)—N(16) = 2.98 Å, Figs. 5 and 6). Any rearrangement of the TEDA's should effect the activation energy as seen in the conductivity via the pseudo Peierls effect, Fig. 1. Simultaneously, such rearrangements would influence the I_3^- spectra via the H-bonding. The increase in the Raman intensity of the antisymmetric ν_2 I_3^- vibration below the phase transition is suggestive of increasing coupling between the three species around the phase temperature of 160 K. The anomalous intensity behaviour of the symmetric ν_1 doublet (Figs. 3 and 4) as one crosses the phase transition is complex and we offer no immediate explanation for this observation. Further temperature dependent X-ray work would be of help to elucidate the dynamics of this system and the coupling between the three species TCNQ, TEDA, and I_3^- at the phase temperature of 160 K indicated by the conductivity measurements.

Acknowledgments

We thank Dr. M. Aubin for use of low temperature conductivity equipment. This research was partly financed by the Research and Development Branch of the Department of National Defence under contract 8SD85-00313.

1. I. C. Kao, M. Jones and M. Labes. J. Chem. Soc. Chem. Commun. 329 (1979).
2. H. Meier. Organic semiconductors. Verlag Chemie, Berlin. 1974.
3. K. Bechgaard. Mol. Cryst. Liq. Cryst. **79**, 1 (1982).
4. E. B. Yakulshii, I. F. Schegolev, V. N. Laukhin, P. A. Kononvich, M. V. Kartsovnik, A. V. Zvarykina, and L. I. Buranov. JEPT Lett. **39**, 12 (1984).
5. H. Schwenk, C. Heidmann, F. Gross, E. Hess, K. Andres, D. Schweitzer, and H. J. Keller. Phys. Rev. B: Condens. Matter, **31**, 3138 (1985).
6. J. M. Williams, T. J. Emge, H. Wang, M. A. Benno, P. T. Copps, L. N. Hall, K. D. Carlson, and G. W. Crabtree. Inorg. Chem. **23**, 2558 (1984).
7. A. D. Bandrauk, K. Ishii, K. D. Truong, M. Aubin, and A. W. Hanson. J. Phys. Chem. **89**, 1478 (1985).
8. A. D. Bandrauk, K. D. Truong, C. Carlone, S. Jandl, and K. Ishii. J. Phys. Chem. **89**, 434 (1985).
9. A. D. Bandrauk, K. D. Truong, C. Carlone, and A. W. Hanson. J. Phys. Chem. **91**, 2063 (1987).
10. A. D. Bandrauk, K. D. Truong, C. Carlone, and S. Jandl. Chem. Phys. Lett. **95**, 78 (1983); J. Phys. **44**, (C-3), 1473 (1983).
11. P. Coppens. *In* Extended linear chain compounds. *Edited by* J. S. Miller. Plenum Press, New York. 1982. pp. 333–356.
12. P. Wu, T. Mori, T. Enoki, K. Imaeda, G. Saito, and H. Inokuchi. Bull. Chem. Soc. Jpn. **59**, 117 (1986).
13. P. A. Abouy, J. P. Pouget, and H. Strzelecka. Phys. Rev. B: Condens. Matter, **35**, 173 (1987).
14. A. D. Bandrauk, K. D. Truong, and C. Carlone. *In* Low dimensional materials. *Edited by* P. Delhaes and M. Drillon. NATO ASI Vol. B168. Plenum Press, New York. 1987. pp. 329–333.
15. P. W. Leung, T. J. Emge, M. A. Beno, H. Wang, J. Williams, V. Petricek, and P. Coppens. J. Am. Chem. Soc. **107**, 6184 (1985).
16. C. Coulon, S. Flandrois, P. Delhaes, C. Hawe, P. Dupuis. Phys. Rev. B: Condens. Matter, **23**, 2850 (1981).
17. N. Sakai, I. Shirotani, and S. Minomura. Bull Chem. Soc. Jpn. **45**, 3314 (1972).
18. E. Mullazi, I. Pollini, L. Piseri, and R. Tubino. Phys. Rev. B: Condens. Matter, **24**, 3355 (1981).
19. M. Ohmasa and M. Kinoshita. Bull. Chem. Soc. Jpn. **41**, 1998 (1968).
20. A. D. Bandrauk, K. D. Truong, and S. Jandl. Can. J. Chem. **60**, 1881 (1982).
21. A. W. Hanson. Observed and calculated structure factors of $TEDA_2\ I_5\ TCNQ_2$. To be published.
22. S. Flandrois and D. Classean. Acta Crystallogr. Sect. B: Struct. Crystallogr. Cryst. Chem. **33**, 2744 (1977).
23. J. Reinsik, S. Swen-Walstra, and T. Migchelsen. Acta Crystallogr. Sect. B: Struct. Crystallogr. Cryst. Chem. **28**, 1331 (1972).
24. S. Huizinga, J. Kommandeur, H. J. Jonkman, and C. Haas. Phys. Rev. B: Condens. Matter, **25**, 1717 (1982).
25. R. J. Visser, S. Costra, C. Vettier, and J. Voiron. Phys. Rev. B: Condens. Matter, **28**, 2074 (1983).
26. V. J. Emery, R. Bruinsma, and S. Barisic. Phys. Rev. Lett. **48**, 1039 (1982).
27. J. P. Pouget. *In* Low-dimensional conductors and superconductors. *Edited by* D. Jerome and L. Caron. NATO ASI Vol. B155. Plenum Press, New York. 1987. pp. 17–47.
28. H. Kobvayashi. Acta Crystallogr. Sect. B: Struct. Crystallogr. Cryst. Chem. **30**, 1010 (1974).
29. L. J. Alzevedo, W. G. Clark, E. O. McLean, and P. F. Seligman. Solid State Commun. **16**, 1267 (1975).
30. F. Inakagi, I. Harada, T. Shimanouchi, and M. Tasumi. Bull. Chem. Soc. Jpn. **45**, 3384 (1972).

Quantum chemical studies of alkyldinitrogen species implicated in nitrosamine carcinogenesis

MARTINE DEMEUNYNCK[1] and J. WILLIAM LOWN[2]
Department of Chemistry, University of Alberta, Edmonton, Alta., Canada T6G 2G2

AND

ANNE-MARIE SAPSE[2]
John Jay College of CUNY, New York, NY 10019, U.S.A. and Rockefeller University, New York, NY 10021, U.S.A.

Received June 30, 1988

MARTINE DEMEUNYNCK, J. WILLIAM LOWN, and ANNE-MARIE SAPSE. Can. J. Chem. **67**, 625 (1989).

Ab initio calculations (Hartree–Fock) at the level of 3-21G and 6-31G* as well as MP2/6-31G* have been performed on the carcinogen dimethylnitrosamine and its products of oxidative metabolism *E*- (and *Z*-) hydroxymethylmethylnitrosamines and certain ester conjugates. The *E*- and *Z*-hydroxymethylmethylnitrosamines are found to be close in energy and to be configurationally stable as is found experimentally. Alternative pathways are examined for the spontaneous decomposition of the primary metabolite in aqueous solution. Direct cleavage of *E*-hydroxymethylmethylnitrosamine to *Z*-methanediazohydroxide and formaldehyde is highly endothermic. Protonation of the NO group of the hydroxylated metabolite strongly stabilizes this species in contrast to nitrosoureas but in accord with experiment. Incorporation of water together with consideration of entropy effects satisfactorily accounts for the spontaneous exothermic decomposition of *E*-hydroxymethylmethylnitrosamine in aqueous media, as well as its relative stability in aprotic media. *Ab initio* calculations were also performed on selected nitrosoiminium ions which participate in the enzymatic activation and metabolism of certain dialkylnitrosamine carcinogens.

Key words: carcinogenesis, dimethylnitrosamine, *ab initio* calculations, nitrosoiminium ions.

MARTINE DEMEUNYNCK, J. WILLIAM LOWN et ANNE-MARIE SAPSE. Can. J. Chem. **67**, 625 (1989).

On a effectué des calculs *ab initio* (Hartree–Fock) aux niveaux 3-21G et 6-31G* ainsi que MP2/6-31G* sur la diméthylnitrosamine cancérigène et sur ses produits de métabolisme oxydant, les hydroxyméthylméthylnitrosamines-(*E*) et (*Z*), et sur certains de ses esters conjugués. On a trouvé que les hydroxyméthylméthylnitrosamines-(*E*) et (*Z*) sont proches d'un point de vue énergétique et que d'un point de vue de la configuration elles sont stables, comme on l'a trouvé expérimentalement. On a examiné d'autres voies qui permettraient une décomposition spontanée du métabolite primaire en solution aqueuse. Le clivage direct de l'hydroxyméthylméthylnitrosamine-(*E*) en hydroxydiazométhane-(*Z*) et en formaldéhyde est fortement endothermique. La protonation du groupement NO du métabolite hydroxylé stabilise beaucoup cette espèce par rapport aux nitrosourées; cette conclusion est en accord avec les données expérimentales. L'incorporation d'eau et de considérations d'effets d'entropie explique d'un façon satisfaisante la décomposition exothermique spontanée de l'hydroxyméthylméthylnitrosomine-(*E*) en solutions aqueuses ainsi que sa stabilité relative en milieux aprotiques. On a aussi effectué des calculs *ab initio* sur des ions nitrosoiminium choisis qui participent à l'activation enzymatique et au métabolisme de certaines dialkylnitrosamines cancérigènes.

Mots clés : carcinogenèse, diméthylnitrosamine, calculs *ab initio*, ions nitrosoiminium.

[Traduit par la revue]

Introduction

The current widespread interest in nitrosamines was spurred by the report of Magee and Barnes of their carcinogenicity (1–3). However, it has been established that, in most cases, nitrosamines are not carcinogenic in themselves but require enzymatic oxidative metabolism to convert them into a precursor of the ultimate carcinogen (3, 4). A considerable body of evidence indicates that damage to cellular DNA and proteins by electrophiles generated from these metabolites may be responsible for their characteristic biological effects (5–10). Certain DNA base lesions, particularly guanine O^6 alkylation (8), are apparently more critical in giving rise to cell transformation than others, e.g. N_7-alkylation (9). In order to provide a better understanding of structure – carcinogenic activity relationships, particularly as regards the site-selectivity of electrophile attack, the steps leading to the carcinogenic species must be considered. It has been demonstrated that, of the possible sites of enzymatic oxidation, hydroxylation at the positions α to the *N*-nitroso group ultimately produces the carcinogen (11). The resulting α-hydroxymethylnitrosamines have been suggested to lose formaldehyde readily to generate the primary alkylnitrosamine which tautomerizes to the alkanediazohydroxide (4*b–e*, 11). The latter being a powerful electrophile alkylates sensitive cellular nucleophiles, including DNA base sites (6–9).

The α-hydroxynitrosamines have until recently eluded direct isolation owing to their instability, and therefore information on the properties of these critical species is limited. Conjugates of these species, including esters, are more stable and may represent transportable forms of the latter which are subsequently subjected to esterase action close to the eventual site of alkylation (12, 13). The α-acetoxymethylalkylnitrosamines are especially pertinent since they have been shown to be potent carcinogens (14).

Accordingly, theoretical quantum chemical methods were used to investigate the parent dimethylnitrosamine **1** (Fig. 1), the isomeric *E*- and *Z*-hydroxymethylmethylnitrosamines **2** and **3** and their respective ester conjugates *E*- and *Z*-acetoxymethylmethylnitrosamines **5** and **6** and the results compared with experimental observations. The calculations were performed in order to obtain optimized geometries, energies, net atomic charges, and LUMO atomic contributions. A related object of study is the energetics of decomposition of the en-

[1]Present address: Laboratoire de Chimie Organique Biologique, Université des Sciences et Techniques de Lille, France.

[2]To whom correspondence should be addressed.

Can. J. Chem. Downloaded from www.nrcresearchpress.com by 41.223.56.140 on 09/07/12
For personal use only.

Can. J. Chem. Downloaded from www.nrcresearchpress.com by 41.223.56.140 on 09/07/12
For personal use only.

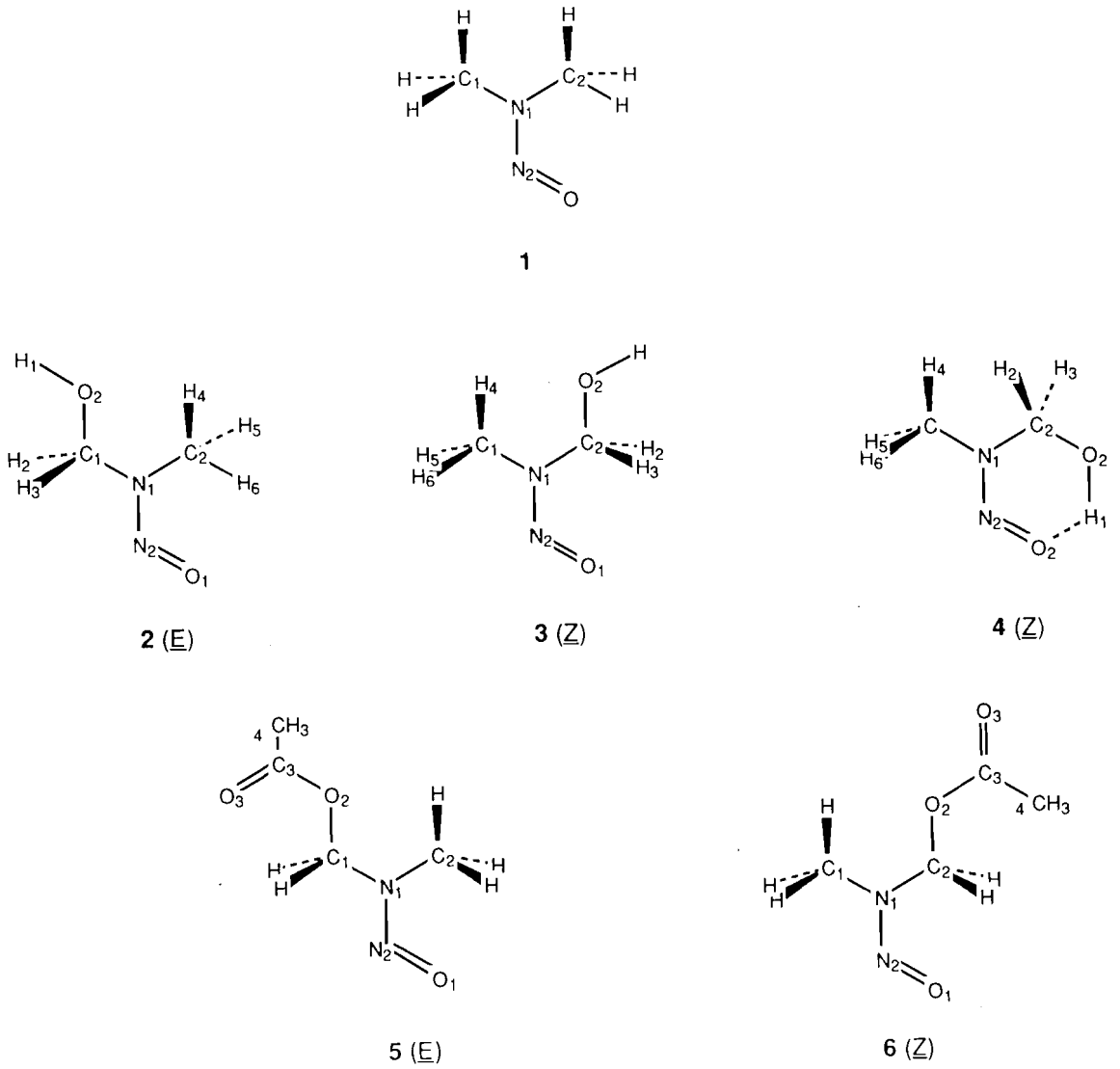


FIG. 1. Structures and numbering of dimethylnitrosamine, its metabolites and their conjugates.

zymatically selectively generated *E*-hydroxymethylmethylnitrosamine under physiological conditions into methylnitrosamine, methyldiazohydroxide, and formaldehyde, together with the pH dependence of the process.

Experimental evidence implicates nitrosoiminium ions in the enzymatic activation and metabolism of certain dialkylnitrosamine carcinogens (ref. 15*a*, *b*; for a review, see ref. 15*c*)[3]. Therefore, an additional objective was to elucidate the structure of such species together with their stabilities and other properties relevant to reactivity such as atomic charges and LUMO participation.

Methods

Self-consistent field (SCF) *ab initio* calculations were made, with full geometry optimization of the principal conformers, obtaining energies, net atomic charges, and LUMO atom contributions of dimethylnitrosamine, its metabolites and their conjugates. The *ab initio* calculations at the Hartree–Fock level were performed using the 3-21G and 6-31G* Gaussian basis set, as implemented in the Gaussian-80 program (16). The geometry optimization procedure is the Berny (gradient method) (17) and the Hessian matrices were examined in order to ensure that all the eigenvalues are positive and, as such, the stationary point is a true minimum. SCF calculations with split valence or larger basis sets are known usually to predict accurate geometries (16–19). The net atomic charges are calculated via the Mulliken Population Analysis. In certain cases the optimized geometries have been used to perform single point MP2/6-31G* calculations in order to estimate the correlation energies of the structures and to assess their influence on stabilities.

Results

Dimethylnitrosamine, E- and Z-hydroxymethylmethylnitrosamine

Dimethylnitrosamine **1** was investigated at Hartree-Fock level using the 3-21G basis set, and the *E*- and *Z*-hydroxymethylmethylnitrosamines **2** and **3** were examined with both 3-21G and 6-31G* basis sets (20). Examination of **3**

[3]The widespread significance of potentially reactive and toxic iminium species generated from the oxidative metabolism of xenobiotic N-alkylamino compounds has been recognized only relatively recently.

Can. J. Chem. Downloaded from www.nrcresearchpress.com by 41.223.56.140 on 09/07/12
For personal use only.

included consideration of the intramolecularly hydrogen bonded structure **4**. The reason for employing both basis sets for **2**, **3**, and **4** is that while geometries and net atomic charges are reliable with both basis sets, the energetics of chemical reactions (i.e. the decomposition of **2**, **3**, or **4**) are better described by the 6-31G* basis set (20).

The results of the optimization for **1–4** together with the energies are shown in Table 1 while Table 2 shows the net atomic charges and the LUMO atomic participation values. In dimethylnitrosamine, N_1 is, as expected, quite negative. N_2 is positive owing to the influence of the oxygen and there is no significant difference in the charges between C_1 and C_2, however C_2 participates more to the LUMO. It may be seen from Table 2 that the 6-31G* calculations predict shorter N_1N_2 bond lengths and shorter OH, CO, and N_2O_1 bond lengths than the 3-21G calculations. The N_1C_1 bonds are predicted to be longer by the 6-31G* basis set. Typical experimental lengths of such bonds fall between these values. The values of the interbond angles predicted by both basis sets are closely comparable. Both basis sets predict **3** to be somewhat more stable than **2**. However, the difference is small amounting to less than 1 kcal/mol.

The structure **4** is computationally a minimum in energy, but only a local minimum, higher by 6 kcal/mol than structure **3**. Loew *et al.* employing MNDO calculations also find structure **4** to be higher in energy (21). It therefore appears that **4** does not benefit significantly by intramolecular hydrogen bond formation. Indeed **4** is higher in energy than **3** by 4.7 kcal/mol at 3-21G level and by 6 kcal/mol at 6-31G* level. The charges and LUMO contributions are better predicted by the 6-31G* basis set (20) and are reported in Table 2. It is evident that, in structures **2–4**, the hydroxyl oxygen is much more negative than the nitroso oxygen (*vide infra*). The hydroxyl oxygen does not contribute to the LUMO in either case.

Ester conjugates of E- *and* Z-*hydroxymethylmethylnitrosamine*

The *E*- and *Z*-acetoxymethylmethylnitrosamines **5** and **6** were investigated at the Hartree–Fock level using the 3-21G basis set. The results of the geometry optimization for **5** and **6**, together with their energies are shown in Table 1. It is seen from Table 1 that **5** is somewhat more stable than **6**. This result is in agreement with experimental observations of Mochizuki *et al.* that the *E* structures are more stable than the *Z* isomers (22). Moreover, NMR evidence confirms that *E* and *Z* forms are configurationally stable and do not readily interconvert (22). The N_1N_2 bond length does not show any significant change from **1** to **5** or **6** and neither do the other bond lengths.

Stability of hydroxymethylmethylnitrosamine in aprotic media and decomposition in aqueous solution

Experimentally it is known that whereas *E*- and *Z*-hydroxymethylmethylnitrosamines have moderate stability in aprotic media, they decompose spontaneously to formaldehyde and methylnitrosamine or methanediazohydroxide, or its kinetic equivalent the methane diazonium ion (22). Possible alternative pathways were considered for this process and examined by quantum chemical methods. In the process for the protonated *E* isomer, which is formed preferentially in the enzymatic oxidation, the energies of different structures corresponding to a progressive stretching of the N_1C_1 bond were computed (Fig. 3). When the energy of the reactant is compared to that of the products the reaction appears to be endothermic. In fact, the differences in the energies of the protonated hydroxymethylmethylnitrosamine and its decomposition products (Fig. 2*a*, *b*) which exhibit much higher energies predict a highly endother-

TABLE 1. Optimized geometrical parameters and energies of structures **1–6** at 3-21G and 6-31G* levels (Å and degrees)

	1	**2**		**3**		**4**		**5**	**6**
Structural Parameter	3-21G	3-21G	6-31G*	3-21G	6-31G*	3-21G	6-31G*	3-21G	3-21G
N_1N_2	1.331	1.329	1.298	1.321	1.295	1.314	1.288	1.330	1.332
N_2O_1	1.240	1.239	1.194	1.248	1.199	1.258	1.204	1.238	1.242
N_1C_1	1.462	1.460	1.459	1.467	1.457	1.477	1.458	1.462	1.463
N_1C_2	1.462	1.462	1.456	1.459	1.457	1.488	1.493	1.463	1.457
C_1O_2	—	1.426	1.387	—	—	—	—	1.434	—
C_2O_2	—	—	—	1.428	1.392	1.413	1.376	—	1.436
O_2H_1	—	0.965	0.947	0.964	0.947	0.994	0.950	—	—
O_2C_3	—	—	—	—	—	—	—	1.367	1.367
O_3C_3	—	—	—	—	—	—	—	1.201	1.200
C_3C_4	—	—	—	—	—	—	—	1.496	1.503
$O_1N_2N_1$	111.4	114.8	115.6	113.7	115.8	119.3	120.7	114.6	114.4
$N_2N_1C_1$	115.7	114.1	113.2	117.7	117.1	113.0	114.8	119.1	118.4
$N_2N_1C_2$	118.8	120.1	122.0	117.4	118.7	127.1	113.3	112.1	118.6
$O_2C_1N_1$	—	106.9	106.7	—	—	—	—	121.1	—
$O_2C_2N_1$	—	—	—	106.9	106.4	114.8	114.8	—	106.3
Energy (au)	−261.4005	−335.8315	−337.7351	−335.8337	−337.7363	−335.8264	−337.7268	−486.7739	−486.7726

TABLE 2. Net atomic charges and LUMO atom participation for structures **1** (3-21G level) and **2**, **3**, and **4** (6-31G* level)

	Net atomic charges				LUMO (p_z)* atom orbital coefficient			
Atom	**1**	**2**	**3**	**4**	**1**	**2**	**3**	**4**
N_1	−0.589	−0.452	−0.450	−0.457	0.200	−0.236	−0.243	−0.257
					0.283	−0.285	−0.297	−0.317
N_2	0.293	0.286	0.298	0.323	−0.401	0.474	0.477	0.487
					−0.614	0.615	0.619	0.621
C_1	−0.315	0.253	−0.286	−0.296	—	−0.138	−0.272	−0.254
C_2	−0.330	−0.289	0.236	0.236	0.088	−0.270	−0.135	−0.151
					0.128			
O_1	−0.439	−0.463	−0.480	−0.504	0.301	−0.353	−0.347	−0.333
					0.461	−0.447	−0.443	−0.429
O_2	—	−0.746	−0.752	−0.768	—	—	—	—
H_1	—	0.452	0.459	0.491	—	—	—	—

*p_z is the orbital perpendicular to the plane of the molecule.

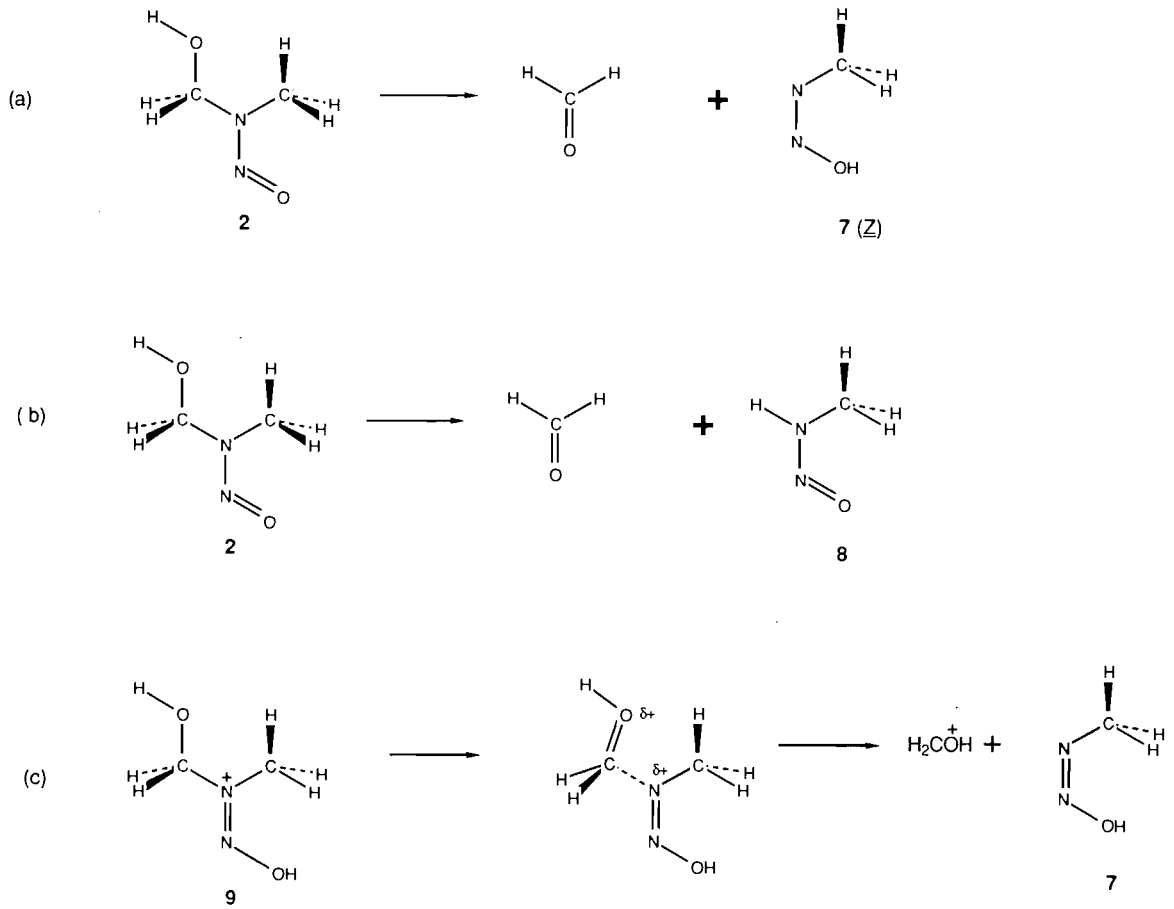


FIG. 2. Alternative hypothetical pathways of decomposition of *E*-hydroxymethylmethylnitrosamine.

mic reaction with ΔE = 42 kcal/mol. In addition, a transition state for this direct decomposition appears to be located at $N_1C_1 \simeq 3.0$ Å, corresponding to an energy of activation of 47 kcal/mol. These calculations, performed at Hartree–Fock level, do not include correlation energy. However, this reaction proceeds via the transfer of an electron pair and not via homolytic bond cleavage. Therefore neglect of the correlation energy should not affect the results significantly. Since, as we will show later this is *not* the proposed mechanism, MP2 calculations were not deemed necessary. Predictions of an endothermic reaction result whether one considers initial decomposition to formaldehyde and *Z*-methylnitrosamine **8** (Table 3, Fig. 2*b*) or to the more stable tautomer *Z*-methanediazohydroxide **7** (Fig. 2*a*).

The rationale for investigating the decomposition of the protonated species is the following.

We have previously demonstrated that the decomposition of other *N*-nitroso compounds (nitrosoureas) is greatly facilitated by the acquisition of a positive charge on the nitroso group, i.e.

Can. J. Chem. Downloaded from www.nrcresearchpress.com by 41.223.56.140 on 09/07/12
For personal use only.

TABLE 3. Optimized geometrical parameters and energies, net atomic charges, and LUMO atom contributions for *E* and *Z* methylnitrosamines[a]

Parameters			Net atomic charges (eu)			HOMO contribution		LUMO contribution	
Å or degree	*E*	*Z*	Atom	*E*	*Z*	*E*	*Z*	*E*	*Z*
N_1N_2	1.377	1.377	N_1[c]	−0.593	−0.593	0.389	0.390	−0.193	−0.202
						0.525	0.526	−0.302	−0.327
N_2O	1.235	1.235	N_2[c]	0.285	0.285	—	—	0.410	0.415
								0.627	0.635
N_1C_1	1.459	1.460	O[c]	−0.431	−0.431	−0.299	−0.294	−0.304	−0.308
						−0.371	−0.367	−0.468	−0.474
N_1H	1.002	0.994	C	−0.335	−0.335	−0.122	−0.112	−0.219	−0.125
						−0.090	−0.082	—	—
C_1H	1.081	1.081	H(N)	0.370	0.370	—	—	—	—
$<ON_2N_1$	114.5	113.8	H	~0.24	~0.24	—	—	—	—
$C_1N_1N_2$	118.7	120.6							
HN_1N_2	116.6	115.2							
HC_1N_1	109.9	109.6							
Energy (au)	−222.58215	−222.58695				−0.3958	−0.4006	0.1399	0.1447
		−223.86057[b]							

[a]Obtained by SCF 3-21G.
[b]Obtained by SCF 6-31G*.
[c]Contribution for HOMO and LUMO of p_z orbitals with axis orthogonal to the molecular plane.

by metal ion complexation or protonation (23). Accordingly, protonation of the NO group was considered as an alternative pathway in the case of nitrosamines (Fig. 2*c*). However, it may be seen from Table 4, which summarizes energies calculated at 6-31G* level, that protonation of the NO groups in **2** and **3** significantly stabilizes these species and as shown above this process is predicted to be highly unfavourable energetically. This result is in complete agreement with those of Mochizuki *et al.* who find that the rate of decomposition is much reduced in acidic media (22). Thus it appears that protonation stabilizes **2** and **3** in contrast to the nitrosoureas where, as we have shown, protonation or metal ion complexation of the nitroso group facilitates decomposition (23). This is illustrated in Fig. 3.

Therefore other mechanisms have to be examined. The difference in energy (endothermic process) between **2** and its decomposition products is ca. 7 kcal/mol. This energy difference is reduced if one takes into account the fact that formaldehyde is hydrated in aqueous solution. When the comparison is made between **2** plus a water molecule and the sum of energies of *Z*-methanediazohydroxide and hydrated formaldehyde as shown in Fig. 4, the energy difference reduces to 1.2 kcal/mol. Similar trends are observed if one considers *Z*-methylnitrosamine as a product. Thus at the 6-31G* level with *Z*-methylnitrosamine and formaldehyde as decomposition products an endothermic reaction is predicted with $\Delta H = 4.1$ kcal/mol. Incorporation of a water molecule in the transition state then predicts a slightly exothermic reaction with $\Delta H = -2.7$ kcal/mol.

Another factor to take into consideration is entropy as suggested by Loew *et al.* Indeed the $T\Delta S$ term in the free energy of the decomposition reaction as shown by Loew *et al.* (24) is about 12 kcal/mol. Thus the reaction becomes exothermic with $\Delta H \simeq -11$ kcal/mol. When correlation energy is taken into account, by performing MP2/6-31G* calculations on **2**, *Z*-methanediazohydroxide and formaldehyde, the results do not change substantially. Indeed, the energy of **2** is −338.6749 au while *Z*-methanediazohydroxide features an MP/G-31G* energy of −224.4879 au. Formaldehyde has an MP2/6-31G* energy of −114.1648 au. Therefore **2** is more stable by 14 kcal/mol. If the entropy term of 12 kcal/mol is taken into account, again the energy of the products becomes almost equal to that of the reactants. The MP2/6-31G* are single point calculations.

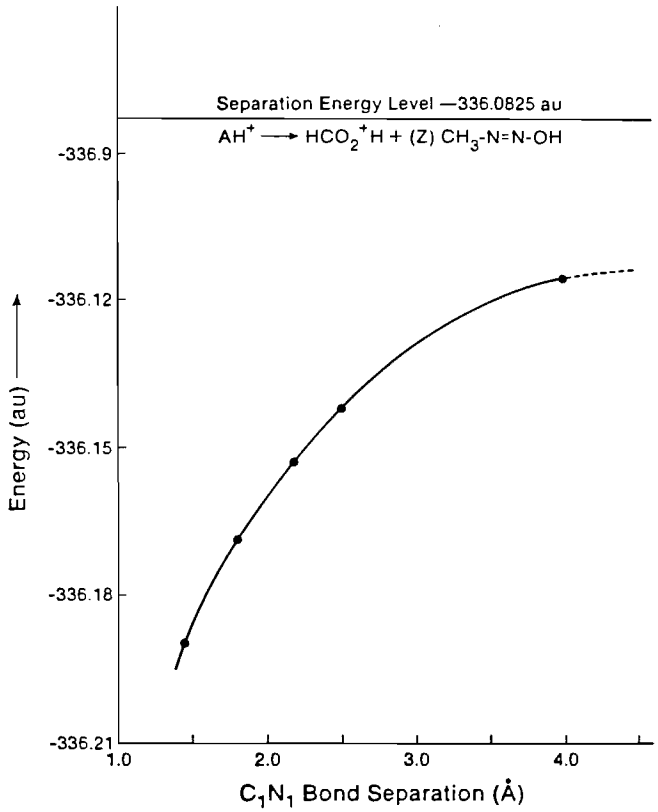


FIG. 3. Reaction pathway for decomposition of protonated *E*-hydroxymethylmethylnitrosamine **2** depicting rise in energy as a function of the C_1N_1 bond separation approaching the separation energy value.

The suggestion of the involvement of water in the facile

Can. J. Chem. Downloaded from www.nrcresearchpress.com by 41.223.56.140 on 09/07/12
For personal use only.

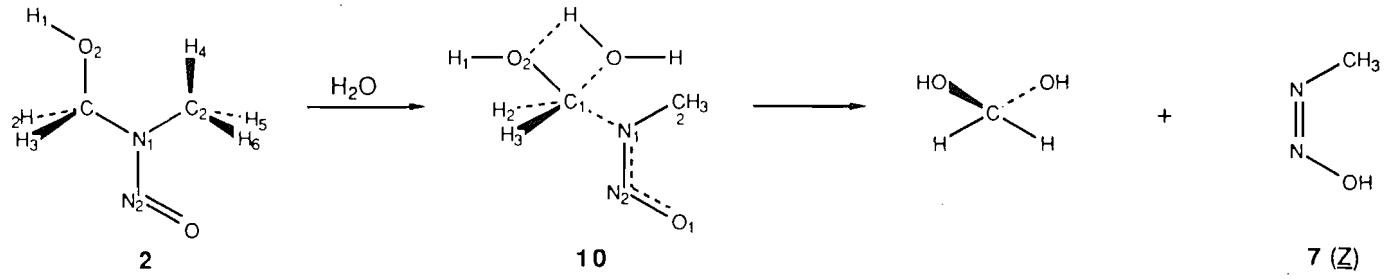


FIG. 4. Suggested pathway of decomposition of **2** in aqueous media featuring a transition state involving participation of a water molecule.

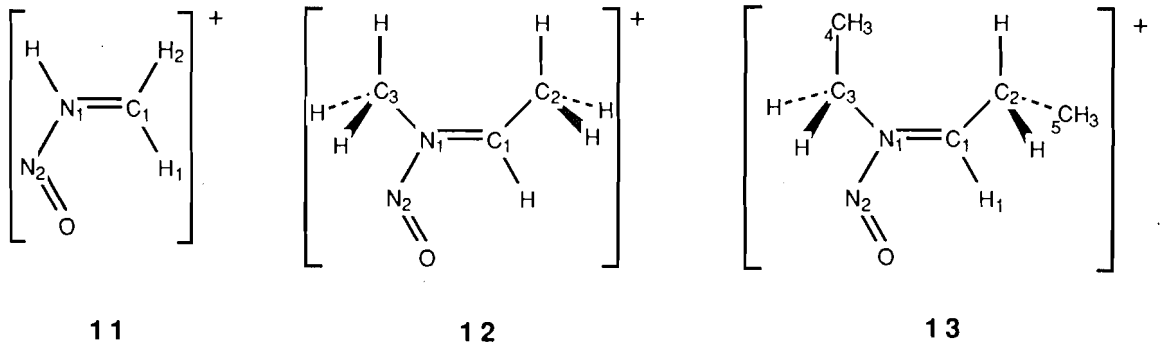


FIG. 5. Depiction of optimized geometries for parent nitrosoiminium ion and the corresponding 1,2-dimethyl and 1,2-diethyl species.

TABLE 4. Energies of hydroxymethylmethylnitrosamines **2** and **3** and their alternative decomposition products in aqueous media (at 6-31G* level)

Species	Energy (au)
2	−337.7351
2 H^+	−338.0821
3	−337.7363
3 H^+	−338.0816
E-Methanediazohydroxide	−223.8590
Z-Methanediazohydroxide	−223.8544
Z-Methylnitrosamine	−223.8606
HCHO	−113.8663
Protonated HCHO	−114.1564
HCHO hydrate	−189.8896
Z-Methanediazohydroxide + protonated HCHO	−338.0108

decomposition of hydroxymethylmethylnitrosamine **2** is in accord with the observations of Mochizaki *et al.* (22) who reported that, while **2** and **3** are relatively stable in aprotic solvents such as chloroform, decomposition is immediately initiated in aqueous media. Therefore, in order to investigate the possible incorporation of water, an appropriate transition state or intermediate **10** has been examined as shown in Fig. 4. The energy of this state, obtained with the 3-21G basis set, proved to be quite low. At a distance of 2.93 Å of the water oxygen to carbon C_1 and with one of the water hydrogens within hydrogen-bonding distance to O_2, this structure features an energy lower by 6 kcal/mol than the sum of the energies of **2** and a water molecule. This value is an approximation, due to superposition error and neglect of correlation energy. We estimated the magnitude of the superposition error as follows. Assuming that the 6-31G* basis set would provide less of a superposition error, we calculated the energy of hydroxymethylnitrosamine (replacing the CH_3 by H in structure **2**) and an approaching water molecule as in structure **10**. At 3-21G this structure is lower by 4 kcal/mol than the sum of hydroxymethylnitrosamine and water. At 6-31G* level, it is higher by ca. 8 kcal/mol. Therefore the superposition approximation can be estimated at about 12 kcal/mol. If structure **10** is then higher by only 6 kcal/mol than the reactants the reaction could still proceed readily when initiated by the incorporation of a water molcecule to C_1. Indeed, C_1 bears a net positive charge (as determined by Mulliken Population Analysis using the 6-31G* basis set, which is known to predict accurate atomic charges) so the oxygen of a water molecule would be attracted to it. When structure **4** is considered, a low energy hydration complex is also obtained.

Nitrosoiminium ions

Nitrosoiminium species have been proposed as intermediates in the nucleophilic displacement of ester conjugates of α-hydroxyalkylalkylnitrosamines (15). Additional experimental support for the existence of these species was obtained by the isolation of stable antimony hexachloride salts of the *Z*-nitrosoiminium ions (15*b*). No quantum chemical studies of these species have been reported hitherto. The nitrosoiminium ions **11**, **12**, and **13** (Fig. 5) were investigated using the 3-21G basis set to obtain optimized geometries, energies, net atomic charges, and LUMO participation of atoms. Table 5 summarizes the results on nitrosoiminium, 1,2-dimethylnitrosoiminium, and 1,2-diethylnitrosoiminium ions. In principle, these species could exist in *Z* or *E* forms. While the difference in energies between *E* and *Z* isomers is small (see Table 5), the geometry optimization calculations clearly show that the *Z*-configuration is preferred for these reactive ions with a coplanar geometry for the four atoms in the grouping $C{=}\overset{+}{N}{-}N{=}O$. Therefore, all the results on energies, atomic charges, and LUMO values presented pertain to the *Z* configurations. The rotational barrier around the NN bond is expected to be higher

Can. J. Chem. Downloaded from www.nrcresearchpress.com by 41.223.56.140 on 09/07/12
For personal use only.

Can. J. Chem. Downloaded from www.nrcresearchpress.com by 41.223.56.140 on 09/07/12
For personal use only.

TABLE 5. Optimized geometrical parameters, energies, net atomic charges, and coefficients of atomic orbitals in LUMO for *syn* (or *Z*) nitrosoiminium ions

Parameter (Å or degree)	Optimized geometries[a] 11	12	13
N_1N_2	1.658	1.582	1.586
N_1C_1	1.260	1.2679	1.270
N_2O	1.139	1.160	1.160
C_1H_1	1.074	1.078	1.082
C_2H	—	1.083	—
$C_1N_1N_2$	121.5	118.8	118.2
N_1N_2O	109.5	117.7	111.5
$C_1N_1H_1$	125.7	—	—
$H_1C_1N_1$	121.8	114.9	—
$H_2C_1N_2$	118.9	—	—
$C_1N_1N_2$	—	0	—
$C_1N_1C_3$	—	131.9	—
$C_2C_1N_1$	—	127.6	133.6
HC_2C_1	—	110.3	—
HC_3N_1	—	108.7	—
$C_5C_2C_1$	—	—	118.6
$C_3N_1C_1$	—	—	130.5
$C_4C_3N_1$	—	—	111.0
Energy (au)	−221.7179	−299.3857	−377.0194
	−221.7164[b]	−299.3841[b]	—
	Net atomic charges (eu)		
Atom	11	12	13
N_1	−0.644	−0.680	−0.682
N_2	0.585	0.494	0.501
C_1	0.090	0.333	0.354
C_2	—	−0.705	−0.625
C_3	—	−0.386	−0.542
C_4	—	—	−0.603
O	−0.193	−0.230	−0.245
H	0.463	0.357	—
H_1	0.368	—	—
H_2	0.353	—	—
CH_3	—	0.300	—
	Coefficients of atomic orbitals in LUMO[c]		
Atom	11	12	13
N_1	−0.1246	−0.1152[d]	0.1010[e]
	−0.2745	−0.2408	0.2198
C_1	0.2591	0.2722	−0.2579[e]
	0.4682	0.4855	−0.4628
N_2	−0.3157	−0.3030	0.3160[e]
	−0.4502	−0.4364	0.4565
			0.0964
O	0.2964	0.2866	−0.2935[e]
	0.4377	0.4244	−0.4384
C_3	—	—	−0.1014
Energy (au)	0.17801	0.15152	−0.14014

[a]Obtained by SCF 3-21G calculations.
[b]Energy for corresponding *anti* (or *E*) isomer.
[c]N_1C_1 antibonding, H_1N_2 bonding, N_2O antibonding.
[d]N_1C antibonding, N_1N_2 bonding, N_2O antibonding.
[e]N_1C_1 antibonding, N_1N_2 bonding, N_2O antibonding. LUMO atom orbital coefficients for N and O are the p_z orbital with axis orthogonal to the molecular plane.

than that for a single bond, owing to delocalization of the π electrons from the NO bond and NC bond into the NN bond. Indeed, this is the case in nitrosamines where the rotational barrier between **2** and **3**, calculated by setting the NO bond at 90° dihedral angle with the plane of $C_1N_1C_2$ and optimizing the other parameters of the molecule, with the 3-21G or 6-31G* basis sets, is ca. 32 kcal/mol. The value of 90° was chosen as the one which would completely break the overlap between the *p* orbitals of N_1, N_2, and O_1, by setting the N_2 and O_1 *p* orbitals perpendicular to those of N_1. In contrast, in nitrosoiminium ions a similar procedure (employing the 3-21G basis set) leads to values of 6.7 kcal/mol for **11**, 7.9 kcal/mol for **12**, and 8.3 kcal/mol for **13**. These much lower values are in agreement with the inordinate lengths of the NN bond in these species which are 1.658 Å, 1.582 Å, and 1.586 Å, respectively. These results suggest substantial contribution of the resonance form $H_2C{=}NH\ldots N{\equiv}\ddot{O}$. In support of this suggestion is the relatively low negative charge on the oxygen (−0.2 eu as compared to −0.44 eu in nitrosamines with both values calculated with the 3-21G basis set). The decreasing length of the NN bond in **12** and **13** is ascribed to stabilization of the nitrosoiminium ion by alkyl substitution.

Since these species are highly electrophilic it is conceivable that they may attack nucleophilic sites in DNA directly (6, 7, 25, 26). In this regard, the LUMO shows an antibonding character for the N_1C_1 bond and, therefore, breakage of this bond will be facilitated upon nucleophilic attack. This also implies that the attack will have a soft–soft character and, as such, attack might be expected at softer sites in the bases such as the O^6 of guanine (6, 7). The latter has been implicated as a carcinogenic lesion. In addition, the positive charge concentrated at C_1 will contribute to its chemoselectivity as an electrophile.

The 3-21G calculations are indicative of the properties of nitrosoiminium ions. However, calculations at higher level (6-31G* and MP2) are being performed in our group and will be reported in due course.

Discussion

Oxidative metabolism of nitrosamines can occur at the α, β or other positions relative to the *N*-nitroso function (4, 11). Several paths have been suggested for the oxidation process such as proton abstraction and subsequent oxidation of the carbanion (27). The data available do not distinguish between this possibility and that of homolytic cleavage. Other studies led to the suggestion of action by a complex of nitrosamine demethylase enzymes, several of which appear to be membrane bound (28). There is general agreement that, of the possible sites of oxidative metabolism, it is hydroxylation at the α positions that ultimately produces the carcinogenic electrophile from nitrosamine (4, 11). Michejda *et al.* (12) have presented evidence that enzymatic hydroxylation of dimethylnitrosamine occurs *anti* to the nitroso group and suggested that this reaction affords the more stable isomer. The present results indicating the configurational stability of the (*E*) and (*Z*) α-hydroxymethylmethylnitrosamine metabolites and the slightly greater stability of the latter suggests that the hydroxylation process may be kinetically controlled. However, the difference in stability between *E* and *Z* isomers is quite small. Our calculations refer to the gas phase. It is reasonable to suppose that in water the *E* isomer will be preferentially stabilized versus the *Z* isomer since its dipole moment is higher (4.4 vs. 3.6 D) as predicted from the 6-31G* basis set calculations.

The experimental ^{1}H-NMR studies confirm that the (*E*) and

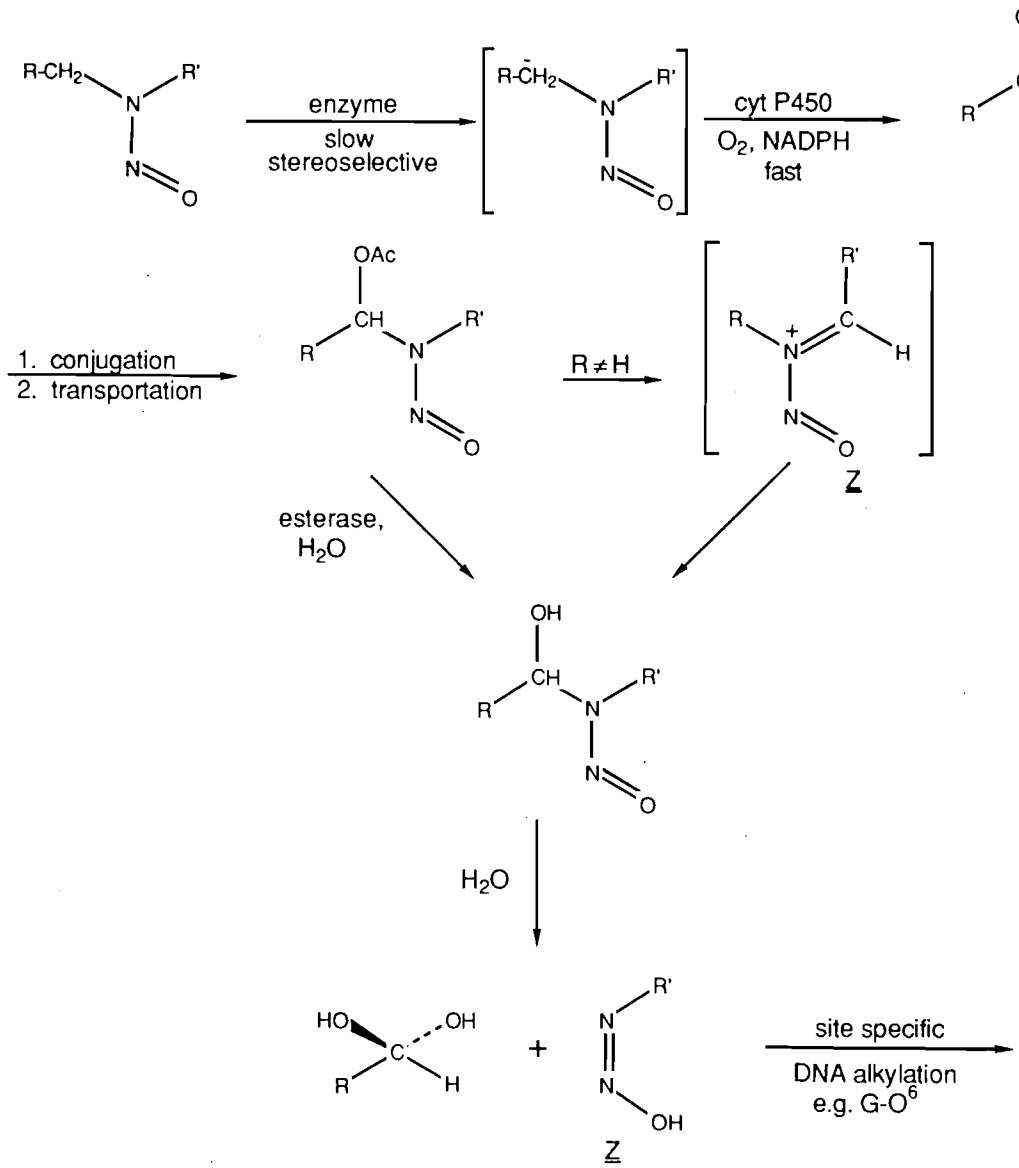


FIG. 6. Representation of metabolic fate of alkylnitrosamines with initial stereoselective and kinetically controlled enzymatic hydroxylation followed by conjugation of the resulting *E*-hydroxymethylalkylnitrosamine, transport, and esterase hydrolysis of the latter via competing pathways with water promoted stereospecific decomposition to afford *Z*-alkanediazohydroxide which, via HOMO–LUMO interaction, preferentially alkylates DNA bases including guanine-O^6.

(*Z*) ester conjugates are configurationally stable (22). As such the theoretical calculations are in agreement with the experimental observations which indicate *E* to be more stable than *Z* (15*a*, 22).

The instability of the hydroxymethylmethylnitrosamine towards decomposition to formaldehyde and *E*-methanediazohydroxide may be rationalized in terms of a combination of entropic factors and the contribution of hydration energies which predict a slightly exothermic process. This result is in contrast to the endothermic process predicted for either *E* or *Z* isomer when hydration is not taken into account. The theoretical treatment provides a rationale for the observed relative stability of *E*- and *Z*-hydroxymethylmethylnitrosamines in aprotic solvents contrasted with the spontaneous decomposition initiated by addition of water (22).

Results from solvolyses of substituted ester conjugates of hydroxyalkylnitrosamines are, by contrast, in accord with the intermediacy of nitrosoiminium species (15). The *ab initio* calculations on the latter indicate a preferred *Z* geometry but that the barrier to rotation about the NN bond is much lower than in the *N*-nitrosamine precursors.

A tentative overall scheme emerges for the fate of dialkylnitrosamines *in vivo*. This involves kinetically controlled *anti* enzymatic oxidation, conjugation to form the more stable ester derivatives, transportation of the latter to a sensitive cellular target, and esterase action to reform the reactive α-hydroxylated metabolite. The latter can be formed by two distinct pathways in the case of substituted ester conjugates as shown in Fig. 6.

The LUMO atom orbital coefficients summarized in Table 2 reveal that contributions of the methyl carbon in both *E*- and *Z*-hydroxymethylmethylnitrosamine isomers is small. This effect is carried over into the *Z*- and *E*-methanediazohydroxides where it assumes greater significance since these species are viewed as the ultimate electrophiles leading to carcinogenesis.

Can. J. Chem. Downloaded from www.nrcresearchpress.com by 41.223.56.140 on 09/07/12
For personal use only.

Calculations at the level of 6-31G* on methanediazohydroxides (25) showed that the LUMO contribution of the methyl carbon in the *E* isomer disappears almost entirely suggesting that attack of this species on guanine would occur, as is found experimentally, preferentially at the harder HOMO N_7 site. The *Z* isomer having a methyl carbon LUMO coefficient of the p_z orbital of 0.233 and therefore soft may permit attack at the softer HOMO O^6 site of guanine. Several lines of evidence suggest that the latter DNA lesion is carcinogenic (6–9).

Acknowledgements

This investigation was supported by grants (to J.W.L.) IRO1 CA21488-11 awarded by the National Cancer Institute, DHHS and A-2305 from NSERC; and (to A-M.S.) grant no 666275 from the City University of New York. The authors wish to thank the City University of New York for computer time and Drs. G. H. Loew and R. Rothchild for useful discussions.

1. P. N. MAGEE and J. M. BARNES. Adv. Cancer Res. **10**, 163 (1967).
2. P. N. MAGEE and J. M. BARNES. Brit. J. Cancer, **10**, 14 (1956).
3. P. N. MAGEE, R. MONTESARO, and R. PREUSSMAN. *In* Chemical carcinogenesis A.C.S. monograph 173. *Edited by* C. E. Searle, Am. Chem. Soc. D.C. 1970. pp. 491–625.
4. (*a*) H. R. DRUCKREY, R. PREUSSMAN, D. SCHMAHL, and M. MULLER. Naturwissenschaften, **48**, 134 (1961); (*b*) I. J. MIZRAHI and D. EMMELOT. Cancer Res. **22**, 339 (1962); (*c*) S. GRILLI and G. PRODI. Gann, **66**, 473 (1975); (*d*) H. DRUCKREY. Xenobiotics, **3**, 271 (1973); (*e*) B. G. LAKE, M. J. MINSKI, J. C. PHILLIPS, S. D. GANGOLLI, and A. G. LLOYD. Life Sci. **17**, 1599 (1976); (*f*) C. THOMPSON, D. PROVAN, and S. CLARK. Int. J. Quantum Chem. Quant. Biol. Symp. No. 4, 205 (1977).
5. G. P. MARGISON and P. J. O'CONNOR. *In* Chemical carcinogens and DNA. *Edited by* P. L. D. Grover. Vol. 1. CRC Press, Boca Raton. 1979. p. 111.
6. B. SINGER. *In* Molecular and cellular mechanisms of mutagenesis. *Edited by* J. Lemontt and R. M. Generoso. Plenum, New York. 1981.
7. B. SINGER. Nature (London), **264**, 333 (1976).
8. B. SINGER. J. Natl. Cancer Inst. **62**, 1329 (1979).
9. P. D. LAWLEY. *In* Chemical carcinogenesis. ACS Monograph **173**. *Edited by* C. E. Searle. Am. Chem. Soc. Washington, D.C., 1976. pp. 83–244.
10. P. N. MAGEE, J. W. NICHOLL, A. E. PEGG, and P. F. SWANN. Biochem. Soc. Trans. 3, 62 (1975).
11. C. BUTHNER and S. HUNIG. Chem. Ber. **104**, 1088 (1971).
12. C. J. MICHEJDA, M. B. KROEGER-KOEPPKE, S. R. KOEPPKE, and R. J. KUPPER. *In N*-Nitrosamines. ACS Symposium Series 101. *Edited by* J. P. Anselme. Am. Chem. Soc. Washington, D.C., 1979. p. 76.
13. (*a*) K. EITER, K. F. HEBENBROCK, and H. J. KABBE. Liebigs. Ann. Chem. **765**, 55 (1972); (*b*) M. WIESSLER. Angew. Chem. Intl. Ed. Engl. 742 (1974); (*c*) M. WIESSLER. Tetrahedron Lett. 2575 (1975); (*d*) J. E. BALDWIN, S. E. BRANZ, R. F. GOMEZ, P. L. KRAFT, A. J. SINSKEY, and S. R. TANNENBAUM. Tetrahedron Lett. 1923 (1978).
14. S. R. JOSHI, J. M. RICE, M. L. WENK, P. P. ROLLER, and L. K. KEEFER. J. Natl. Cancer Inst. **58**, 1531 (1977).
15. (*a*) M. MOCHIZUKI, T. ANJO, Y. WAKABAYASHI, T. SONE, and M. OKADA. Tetrahedron Lett. **21**, 1761 (1980); (*b*) M. WIESSLER. *In N*-Nitrosamines. Am. Chem. Soc. Symp. Ser. **101**. *Edited by* J. P. Anselme. Am. Chem. Soc. Washington, D.C. 1979. p. 57; (*c*) M. OVERTON, J. A. HICKMAN, M. D. THREADGILL, K. VAUGHAN, and A. GESCHER. Biochem. Pharmacol. **34**, 2055 (1985).
16. (*a*) J. S. BINKLEY, J. A. POPLE, and W. J. HEHRE. J. Am. Chem. Soc. **102**, 939 (1980); (*b*) J. S. BINKLEY, M. J. FRISCH, D. J. DEFREES, K. RAGHAVACHARI, R. A. WHITESIDE, H. B. SCHLEGEL, E. M. FLUDER, and J. A. POPLE. Gaussian 80, Carnegie-Mellon University, Pittsburgh, PA.
17. H. B. SCHLEGEL. J. Comput. Chem. **3**, 214 (1982).
18. W. J. HEHRE, R. F. STEWART, and J. A. POPLE. J. Chem. Phys **81**, 2657 (1969).
19. J. D. GODDARD. Can. J. Chem. **63**, 1910 (1985).
20. P. C. HARIHARAN and J. A. POPLE. Theoret. Chim. Acta, **28**, 213 (1973).
21. G. H. LOEW, M. T. POULSEN, D. SPANGLER, and E. KIRKJEAN. Int. J. Quantum Chem. Quant. Biol. Symp. **10**, 201 (1983).
22. M. MOCHIZUKI, T. ANGIO, and M. OKADA. Tetrahedron Lett. **21**, 3693 (1980).
23. A. M. SAPSE and E. B. ALLEN. Cancer Invest. **5**, 559 (1987).
24. M. POULSEN, D. SPANGLER, and G. H. LOEW. Mol. Toxic. **1**, 35 (1987).
25. J. W. LOWN, S. M. S. CHAUHAN, R. R. KOGANTY, and A. M. SAPSE. J. Am. Chem. Soc. **106**, 6401 (1984).
26. A. M. SAPSE, E. B. ALLEN, and J. W. LOWN. J. Am. Chem. Soc. **110**, 567, (1988).
27. L. K. KEEFER and C. H. FODOR. J. Am. Chem. Soc. **92**, 5748 (1970).
28. (*a*) M. B. KROEGER-KOEPPKE and C. J. MICHEJDA. Cancer Res. **38**, 2735 (1978); (*b*) B. LAKE, C. HEADING, J. PHILLIPS, S. GANGOLLI, and M. A. LLOYD. Biochem. Soc. Trans. **2**, 610 (1974).

Can. J. Chem. Downloaded from www.nrcresearchpress.com by 41.223.56.140 on 09/07/12
For personal use only.

Kinetics and mechanism of the oxidation of proline by periodate

ROSA PASCUAL,[1] MIGUEL A. HERRAEZ, AND EMILIO CALLE
Departamento de Química Física, Facultad de Química, Universidad de Salamanca, Salamanca, España

Received July 12, 1988

ROSA PASCUAL, MIGUEL A. HERRAEZ, and EMILIO CALLE. Can. J. Chem. **67**, 634 (1989).

The kinetics of oxidation of proline by periodate has been studied at pH 1.40–8.83 and 30.0°C. The reaction rate is first order in both periodate and amino acid, and the overall reaction follows second-order kinetics. There was no evidence for the formation of an appreciable amount of intermediate. The reaction rate is highest at pH 4–7 and the oxidation is catalysed by HPO_4^{2-} ions. The pH dependence of the reaction rate can be explained in terms of reaction of periodate monoanion and the protonated and dipolar forms of the amino acid. The mechanism proposed and the derived rate law are consistent with the observed kinetics. The rate constants obtained from the derived rate law are in agreement with the observed rate constants, thus justifying the rate law and the proposed mechanistic scheme.

Key words: oxidation of proline, oxidation by periodate.

ROSA PASCUAL, MIGUEL A. HERRAEZ et EMILIO CALLE. Can. J. Chem. **67**, 634 (1989).

Opérant à 30,0°C et à des pH allant de 1,40 à 8,83, on a étudié la cinétique de l'oxydation de la proline par le periodate. La vitesse de la réaction est du premier ordre tant en periodate qu'en acide aminé et la réaction globale est du deuxième ordre. On n'a trouvé aucune indication suggérant la formation de quantités appréciables d'intermédiaire. La vitesse réactionnelle est à son maximum à des pH allant de 4 à 7 et l'oxydation est catalysée par les ions HPO_4^{2-}. Pour expliquer la relation qui existe entre la vitesse de la réaction et le pH, on suggère que la réaction implique le monoanion du periodate et les formes protonées et dipolaires de l'acide aminé. Le méchanisme proposé et la loi de vitesse sont en accord avec les cinétiques observées. Les constantes de vitesse que l'on peut calculer à partir de la loi de vitesse sont en accord avec les constantes de vitesses qui ont été observées; cet accord justifie cette loi de vitesse et donc le schéma réactionnel proposé:

Mots clés : oxydation de la proline, oxydation par le periodate.

[Traduit par la revue]

Introduction

Periodate is a clean and relatively selective reagent for the oxidative cleavage of organic compounds containing α-hydroxy, -oxo, -amino, or -carboxyl groups. There is extensive literature on the kinetics of the periodic acid oxidation of glycols (1, 2) but the kinetics of the periodate oxidation of amino alcohols (3), dicarbonyl compounds (4), and amino acids (5), has received much less attention. Oxidation with periodate has been shown to cause denaturation of proteins and inactivation of enzymes and these findings have been interpreted on the basis of attack of periodate on essential amino acids. The importance of these reactions attracted our attention and mechanistic studies on periodic oxidations of amino acids were undertaken in our laboratory (6). In this paper, we report on the results obtained for the oxidation of proline by periodate. This amino acid is an essential constituent of some proteins, such as collagen.

Experimental

Materials

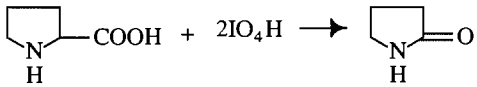
Proline was obtained from Sigma. All other reagents were Merck analytical grade. Doubly distilled water from alkaline permanganate was used to prepare all solutions. Chloroacetate, acetate, phosphate and borate buffers have been used to maintain constant pH. The ionic strength of the system was kept constant (0.20 *M*) by the addition of sodium perchlorate. Standard stock solutions of amino acid were freshly prepared by dissolving accurately weighed amino acid in buffer solution. Aqueous solution of periodate was standardized by iodometry (7) and preserved in brown bottles to prevent photochemical deterioration. Control experiments demonstrated that the short exposure of ultraviolet light at 310 nm used to take the readings did not cause significant decomposition of periodate.

Kinetic method

Reaction rates were measured by following the decrease of periodate concentration with time. A spectrophotometric procedure was used and the reactions were followed by measuring the absorbance at 310 nm of the unreacted periodate during the course of reaction at different time intervals as described in our previous paper (6). The runs were carried out in either a Pye-Unicam SP600 UV or a Shimazdu UV-240 spectrophotometer, with water-jacketted cell holders. Although the absorption maximum of periodate (8) is at 222 nm, this wavelength was not of practical use because of interfering absorption by other compounds in the reaction mixture. The molar absorptivities at 310 nm were obtained at all pH values used in the experiments. Reaction was followed in acid medium to ca. 80–90% conversion of the initial periodate concentration. Since the reaction becomes slow in basic medium, initial rates were determined in this pH range and the rates of duplicate runs were reproducible to ±10%.

Stoichiometry

Varying ratios of periodate to amino acid, keeping (periodate) > (amino acid) in all buffers, were allowed to stand until completion of the reaction. Estimation of residual oxidant (9) showed that 2 moles of periodate are consumed per mole of amino acid. Carbon dioxide and pyrrolid-2-one as the products of the reaction were detected (10). The reaction can be represented as:



$$+ CO_2 + H_2O + 2IO_3H$$

Results

The kinetics of oxidation of proline by periodate was investigated at several initial concentrations of the reactants in the pH range 1.40–8.83.

In acid medium at constant pH with the amino acid in excess, plots of log $(\text{periodate})_0/(\text{periodate})$ vs. time were linear,

[1]Author to whom correspondence should be addressed. Present address: Departamento de Didáctica de Matemática y Ciencias Experimentales, Escuela Universitaria E. G. B. Zamora, Zamora, España.

Printed in Canada / Imprimé au Canada

Can. J. Chem. Downloaded from www.nrcresearchpress.com by 41.223.56.140 on 09/07/12
For personal use only.

TABLE 1. Effect of reactant concentration on reaction rate*

		pH = 2.50		pH = 4.00	
10^3 (Per)$_0$ (M)	10^2 (AA)$_0$ (M)	$10^4\ k'_\psi$ (s^{-1})	$10^3\ k''_\psi$ ($L\,mol^{-1}\,s^{-1}$)	$10^4\ k'_\psi$ (s^{-1})	$10^3\ k''_\psi$ ($L\,mol^{-1}\,s^{-1}$)
11.0	8.00	4.10	5.84	5.16	6.43
10.0	8.00	4.01	5.70	5.17	6.98
9.00	8.00	4.05	5.69	5.23	7.25
8.00	8.00	4.23	5.75	5.20	7.15
7.00	8.00	4.00	5.81	5.17	6.85
6.00	8.00	4.06	5.76	5.29	7.32
5.00	8.00	4.29	5.83	5.23	6.87
11.5	22.9	13.6	5.85	17.1	7.51
11.5	20.1	11.7	5.90	14.1	7.10
11.5	17.2	9.53	5.72	11.7	6.96
11.5	13.8	7.62	5.78	9.26	6.92
11.5	11.5	6.55	5.84	7.53	6.80
11.5	8.52	4.94	5.70	5.54	6.97
11.5	5.50	3.56	5.77	3.61	6.78

*I = 0.200 M; t_C = 30.0°C.

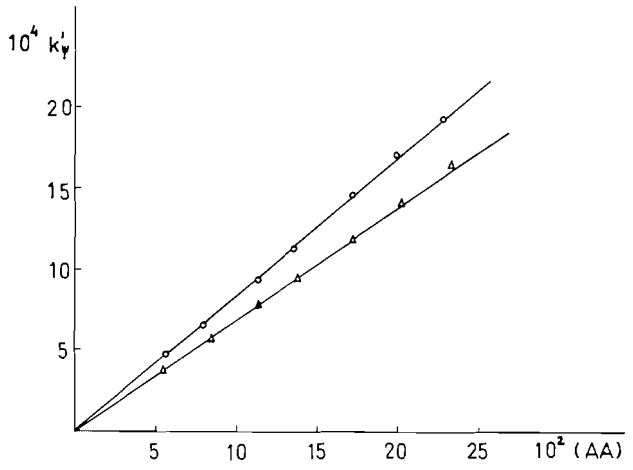


FIG. 1. Plot of k'_ψ vs. (AA); (Per) = 11.5 × 10^{-3} M; I = 0.200 M; t_C = 30.0°C; (○) pH = 4.94; (△) pH = 4.10.

indicating that the reaction is first-order in periodate concentration (Per). The pseudo first-order rate constants, k'_ψ, are given in Table 1. This was further confirmed by varying the periodate concentration, which did not show any change in the pseudo first-order rate constant (Table 1). The values of k'_ψ increase with amino acid concentration. Plots of log k'_ψ vs. log (amino acid)$_0$ are linear with a slope of unity, thus indicating a first-order dependence on the amino acid concentration (AA). Under these conditions the constancy of the second-order rate constants, k''_ψ was checked. Plots of k'_ψ against the amino acid concentration were linear (Fig. 1) with intercepts close to zero, and their slopes gave the second-order rate constants for the oxidation of amino acid.

In basic medium periodate was varied in the concentration range (10.0–5.00) × 10^{-3} M at fixed amino acid concentration (8.00 × 10^{-2} M). A plot of initial rates vs. (Per)$_0$ gave a straight line passing through the origin, indicating a first-order dependence on (Per). The pseudo first-order rate constant was obtained from the slope of the line (Table 2). The concentration of proline was varied in the range (23.0–5.00) × 10^{-2} M at constant initial periodate concentration (10.3 × 10^{-3} M). A plot of the initial rates vs. (AA)$_0$ gave a straight line passing through the origin, indicating a first-order dependence on (AA). The values of k''_ψ were obtained from the slopes of the lines (Table 2).

It was observed that pH changes have a marked effect on the rates of oxidation of the amino acid. The variation of the observed rate constants with pH is shown in Table 3. In this pH range the rate of oxidation in chloride, chloroacetate, acetate, and borate buffers at constant pH, is independent of the buffer concentration, but increased with increase in phosphate buffer concentration (Table 4). This acceleration is greater at pH 7.5 than at pH 6.5, suggesting that the reaction is subject to general base catalysis by HPO_4^{2-} ion. From the linear plots of the observed second-order constants against (HPO_4^{2-}) the value of k_B, the catalytic constant of HPO_4^{2-} was evaluated (Table 6).

In a separate set of experiments carried out in 1 M H_2SO_4, reaction mixtures with reactant concentrations as used in the kinetics were prepared. It was observed that no reaction occurred under these conditions.

Discussion

Amino acids exist as zwitterions in aqueous solution. The equilibria involved in acid and basic media are (11):

[1] $$^{+}H_2N\underset{AA^+}{\text{—R—}}COOH \overset{K_a}{\rightleftharpoons} H^+ + {}^{+}H_2N\underset{AA^{\pm}}{\text{—R—}}COO^- \overset{K_b}{\rightleftharpoons} HN\underset{AA^-}{\text{—R—}}COO^- + H^+$$

In aqueous periodate solutions, equilibria:

[2] $$H_5IO_6 \overset{K_1}{\rightleftharpoons} H_4IO_6^- + H^+$$

[3] $$H_4IO_6^- \overset{K_D}{\rightleftharpoons} IO_4^- + 2H_2O$$

[4] $$H_4IO_6^- \overset{K_2}{\rightleftharpoons} H_3IO_6^{2-} + H^+$$

[5] $$H_3IO_6^- \overset{K_3}{\rightleftharpoons} H_2IO_6^{3-} + H^+$$

Can. J. Chem. Downloaded from www.nrcresearchpress.com by 41.223.56.140 on 09/07/12
For personal use only.

TABLE 2. Initial rates, V_0, and rate constants of reaction*

(*a*) (AA) = 8.00×10^{-2} *M*						
10^3 (Per)/*M*	10.0	9.00	8.00	7.00	6.00	5.00
10^7 V_0/mol L^{-1} s^{-1}	19.1	17.8	15.0	13.9	12.0	9.40
$k'_\psi = 1.92 \times 10^{-4}$ s^{-1}						
(*b*) (Per) = 10.0×10^{-3} *M*						
10^2 (AA)/*M*	23.0	20.0	18.0	14.0	11.0	8.00	5.00
10^8 V_0/mol L^{-1} s^{-1}	58.6	51.8	45.6	36.2	28.8	20.2	12.4
$k''_\psi = 2.57 \times 10^{-3}$ L mol^{-1} s^{-1}						

*pH = 8.40; I = 0.200 *M*; t_C = 30.0°C

TABLE 3. Influence of pH on the rate constants

pH	10^3 k''_ψ (L mol^{-1} s^{-1})	pH	10^3 k''_ψ (L mol^{-1} s^{-1})
1.40	3.69	6.50	6.64
2.00	5.24	7.00	6.72
2.13	5.39	7.50	6.90
2.93	6.06	7.80	7.98
4.11	6.43	8.25	4.09
4.55	6.33	8.47	2.63
5.08	6.35	8.71	1.51
5.50	6.37	8.83	0.76
5.92	6.57		

*(Per) = 8.00×10^{-3} *M*; (AA) = 8.00×10^{-2} *M*; I = 0.200 *M*; t_C = 30.0°C.

have been detected (8) and several equilibrium constants determined.

The results suggest that the oxidation of proline by periodic acid involves multisteps. Since Δ^1-pyrroline has been reported to be formed during the course of reaction (10), for the purpose of the kinetic treatment, the following scheme can be proposed:

$$[6] \quad AA + Per \underset{k_-}{\overset{k}{\rightleftharpoons}} C_1$$

$$[7] \quad C_1 \xrightarrow{k_1} \Delta^1\text{-pyrroline} + CO_2 + HIO_3$$

$$[8] \quad \Delta^1\text{-pyrroline} + Per \underset{k_{-2}}{\overset{k_2}{\rightleftharpoons}} C_2$$

$$[9] \quad C_2 \xrightarrow{k_3} \text{pyrrolid-2-one} + HIO_3$$

We assume that the amino acid and periodate can reversibly form a complex (C_1) which decomposes to give the intermediates Δ^1-pyrroline, carbon dioxide, and iodate. Δ^1-pyrroline reacts with a second mole of periodate to give pyrrolid-2-one.

The observation of overall second-order kinetics under all conditions tested can be interpreted as an indication that there is no accumulation of a periodate – amino acid complex. We accept that the concentrations of C_1, Δ^1-pyrroline, and C_2 are low and that we can apply the steady-state approximation to them. In addition, if C_1 decomposes to products so rapidly that the rate of reaction is governed by the formation of C_1, i.e., $k_1 \gg k_-$, the kinetics expression for the reaction is:

$$[10] \quad -\frac{d(Per)}{dt} = k(AA)(Per)$$

This is in conformity with the orders in (AA) and (Per) as found experimentally.

To understand the process by which periodate oxidizes proline, it is necessary to know what species of periodate are active in this reaction. The pH dependence of the oxidation rate shown in Fig. 2, together with the pK values of Table 4, suggest that in the lower pH range (pH < 4) the oxidation of substrate must be brought about by the periodate monoanion (Per^-). Since in 1 *M* H_2SO_4 the reaction does not take place, we exclude the reaction of undissociated periodic acid (Per^0) with the protonated amino acid. It may be supposed that undissociated periodic acid does not react with the dipolar form of the amino acid either, or the probability of this reaction is low. Thus at pH < 4 we only consider reaction of periodate monoanion with the dipolar and protonated forms of amino acid, and the decline in rate constant around pH 4 as we get to higher acidities must be due to the decline in significance of the periodate monoanion in that region. Moreover, the reactivity of the protonated form of amino acid must not be high compared with that of the dipolar form. Then, moving to higher pH, where all amino acid is in the dipolar form, the decline in rate constant around pH 8 can only be due to the decline in the concentration of the reactive periodate species. This led us to consider that the reaction between the periodate dianion (Per^{2-}) and the dipolar amino acid is negligible and that the oxidation of substrate must be brought about by the periodate monoanion. In the pH range 4–8, where we must consider only reaction between dipolar amino acid and periodate monoanion, changes of rate constant are not expected and the increase in the rate in the pH range 6–8 can be attributed to the catalysis of the phosphate buffer.

In analyzing the variation of reaction rate with pH, we assume the effective reactants to be the monoanion ($H_4IO_6^- + IO_4^-$) of periodate and the protonated and dipolar ionic form of the amino acid. Thus, for the overall rate equation, we can write:

$$[11] \quad k'_\psi(Per)(AA) = k^0(Per^-)(AA^\pm) + k^+(Per^-)(AA^+)$$

where k^0 and k^+ represent the rate constants for reaction between periodate monoanion and zwitterion and protonated amino acid, respectively. Our kinetic treatment does not distinguish between the hydrated ($H_4IO_6^-$) and dehydrated (IO_4^-) forms of the periodate monoanion.

The total concentration of periodate (Per) and amino acid (AA) over the pH range studied are as follows:

$$[12] \quad (Per) = (Per^0) + (Per^-) + (Per^{2-})$$

$$[13] \quad (AA) = (AA^\pm) + (AA^+)$$

From dissociation equilibria [1]–[5] and eqs. [12] and [13], eq. [10] becomes:

$$[14] \quad -\frac{d(Per)}{dt} = k''_\psi(AA)(Per)$$

Can. J. Chem. Downloaded from www.nrcresearchpress.com by 41.223.56.140 on 09/07/12
For personal use only.

TABLE 4. Catalysis by phosphate buffer in the oxidation of proline

pH = 6.50			pH = 7.50		
10^2 ($H_2PO_4^-$) (M)	10^2 (HPO_4^{2-}) (M)	10^5 k'_ψ (s^{-1})	10^2 ($H_2PO_4^-$) (M)	10^2 (HPO_4^{2-}) (M)	10^5 k'_ψ (s^{-1})
0.740	0.420	53.1	0.100	0.608	54.8
1.48	0.840	57.9	0.200	1.22	55.2
2.22	1.26	62.3	0.300	1.82	59.0
2.96	1.68	65.3	0.500	3.04	64.9
3.70	2.10	69.1	0.700	4.25	69.2
5.18	2.94	76.4			

*(Per) = 8.00×10^{-3} M; (AA) = 8.00×10^{-2} M; I = 0.200 M; t_C = 30.0°C.

TABLE 5. Equilibrium constants

Parameter	Value	
	Periodic acid	Proline
K_1/(mol L^{-1})	4.78×10^{-2}	—
K_2/(mol L^{-1})	5.24×10^{-9}	—
K_D	30.3	—
K_a/(L mol^{-1})	—	1.02×10^{-2}
K_b/(mol L^{-1})	—	2.51×10^{-11}

TABLE 6. Reaction rate constants

Parameter	Value
10^3 k^0/(L mol^{-1} s^{-1})	6.13
10^3 k^+/(L mol^{-1} s^{-1})	7.00
10^2 k_B/(L^2 mol^{-2} s^{-1})	8.34

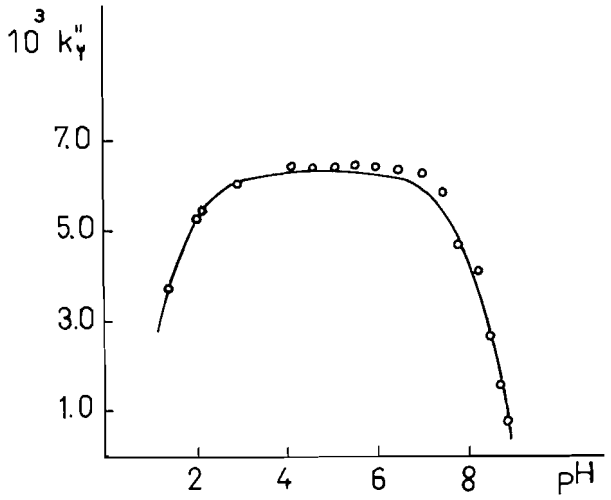


FIG. 2. Variation of the second-order rate constant with pH. The curve represents the dependence on pH calculated from eq. [15] and the points represent the observed rate constants (extrapolated to zero phosphate buffer concentration at pH 5.92–7.80). Experimental conditions in Table 3.

where

$$[15] \quad k''_\psi = \frac{k^0 K_1(H^+)}{(H^+)^2 + K_1(H^+) + K_1K_2}\frac{K_a}{(H^+) + K_a} + \frac{k^+ K_1(H^+)}{(H^+)^2 + K_1(H^+) + K_1K_2}\frac{(H^+)}{(H^+) + K_a}$$

To calculate the values of k^0 and k^+ in eq. [15], we will consider the various pH regions separately (Fig. 2). In treating the results we use values of K_1 and K_2, the apparent first and second dissociation constants of periodic acid (Table 5) expressed in terms of concentrations. They were determined for the ionic strength 0.200 M and 30.0°C from existing results (8).

At pH < 4 the term K_1K_2 is negligible if we compare it with $(H^+)^2$ and $K_1(H^+)$ and eq. [15] reduces to:

$$[16] \quad k''_\psi = \frac{k^0 K_1 K_a + k^+ K_1(H^+)}{(H^+)^2 + (H^+)(K_1 + K_a) + K_1K_a}$$

Using the values k''_ψ from Table 3 for pH < 4 and eq. [16] in the form:

$$[17] \quad k''_\psi f(H^+) = k^0 K_1 K_a + k^+ K_1(H^+)$$

where

$$[18] \quad f(H^+) = (H^+)^2 + (H^+)(K_1 + K_a) + K_1K_a$$

we obtain the values of k^0 and k^+ for the reaction. A plot of $k''_\psi f(H^+)$ vs. (H^+) gives a straight line. For the intercept and the slope of the line the values of 10^3k^0 = 5.85 L mol^{-1} s^{-1} and 10^3k^+ = 7.00 L mol^{-1} s^{-1} are obtained.

At pH 4.0–5.5 we consider all amino acid to be zwitterion. Under these conditions K_1K_2 and $(H^+)^2$ are insignificant compared to $K_1(H^+)$ and eq. [15] can be reduced to

$$[19] \quad k''_\psi = k^0$$

In this pH range k^0 equals k''_ψ and a constant value of k''_ψ would be expected, as found experimentally.

At pH > 5.5 where the amino acid is entirely zwitterion and $(H^+)^2$ is much lower than $K_1(H^+)$ and K_1K_2, eq. [15] reduces to:

$$[20] \quad k''_\psi = \frac{k^0(H^+)}{K_2 + (H^+)}$$

A plot of $k''_\psi(K_2 + (H^+))$ vs. (H^+) gives a straight line passing through the origin. From the slope of the line a value of 10^3k^0 = 6.40 L mol^{-1} s^{-1} was found. Since in the pH range 5.92–7.80, where phosphate buffer was used, a catalytic effect was observed, the values of k''_ψ used in the above plot were extrapolated to zero buffer concentration.

To verify rate law [15], we use it to calculate the rate constants as (H^+) varies with the constants in Table 6. The agreement between the k^0 value evaluated in neutral and basic media and those obtained from the acid region is reasonable, so

Can. J. Chem. Downloaded from www.nrcresearchpress.com by 41.223.56.140 on 09/07/12
For personal use only.

the mean values are used. The calculated values of k''_{ψ} are shown in Fig. 2 along with the experimental values.

In this treatment, it has been assumed that the reaction could be represented by a summation of bimolecular reactions, each involving one molecule of periodate monoanion and one molecule of amino acid either protonated or in the form of a zwitterion. The data agree with this assumption to within the experimental error.

To explain the general base catalysis we suggest that the intermediate C_1, in our reaction scheme, is cyclic, similar to that assumed to be formed between 1,2-diol, 1,2-diamines, or 1,2-aminoalcohols and periodate (2, 3) although their existence has not been demonstrated in many cases. It can be proposed, according to the treatment used by Buist *et al.* for pinacol oxidation (2*d*), that periodate monoanion and proline react reversibly to form an open-chain intermediate, C_1^*, which undergoes ring closure to a cyclic intermediate, C_1, which in turn decomposes rapidly to Δ^1-pyrroline. The general base catalysis can be attributed to the catalysis of the cyclization of the open-chain amino acid – periodate intermediate:

$$Per^- + AA^{\pm} \rightleftharpoons C_1^*$$

$$C_1^* + HPO_4^{2-} \rightleftharpoons C_1 + H_2PO_4^-$$

$$C_1 \rightarrow \Delta^1\text{-pyrroline}$$

It has been assumed that the formation of an open-chain intermediate is not general base catalysed, because this would require simultaneous reactions of amino acid, periodate, and catalyst, and such probability would be low. Since the breakdown of C_1 to products is intramolecular, the rate constant of this step is not dependent on base catalysis. The observation of general catalysis by phosphate at pH 6–8 indicates that the formation of cyclic intermediate C_1 is rate determining in this pH range. We have assumed that the formation of C_1 is rate determining over the entire pH range studied, but below pH 6 and above pH 8 where the rate is not affected by general catalysis an alternative explanation is that there is an equilibrium between C_1 and reactants and the decomposition of C_1 is rate determining. If the equilibrium constant is low, then second order kinetics will result. In both situations the rate constant is proportional to the concentration of the periodate monoanions and hence we can not discern between them.

1. (*a*) F. R. DUKE. J. Am. Chem. Soc. **69**, 3054 (1974); (*b*) F. R. DUKE and V. C. BULGRIN. J. Am. Chem. Soc. **76**, 3803 (1954).
2. (*a*) G. J. BUIST and C. A. BUNTON. J. Chem. Soc. 1406 (1954); 4580 (1957); J. Chem. Soc. (B) 2117 (1971); (*b*) G. J. BUIST, C. A. BUNTON, and J. H. MILES. J. Chem. Soc. 4567 (1957); 4575 (1957); 743 (1959); (*c*) S. SENENT, M. PÉREZ, and P. ESCUDERO. An. R. Soc. Esp. Fis. Quim. B**57**, 153 (1961); (*d*) G. J. BUIST, C. A. BUNTON, and J. LOMAS. J. Chem. Soc. (B) 1094 (1966); 1099 (1966); (*e*) G. J. BUIST and J. D. LEWIS. J. Chem. Soc. (B), 90 (1968); (*f*) G. J. BUIST, C. A. BUNTON, and W. C. P. HIPPERSON. J. Chem. Soc. (B) 2128 (1971).
3. (*a*) G. DAHLGREN and J. HODSON. J. Phys. Chem. **68**, 416 (1964); (*b*) G. DAHLGREN and E. RAND. J. Phys. Chem. **71**, 1955 (1967); (*c*) L. MAROS, I. MOLNÁR-PERL, E. SCHISSEL, and V. SZERDAHELYI. J. Chem. Soc. Perkin Trans. II, 39 (1980).
4. (*a*) V. SHINER and C. WASSMUTH. J. Am. Chem. Soc. **81**, 37 (1959); (*b*) G. DAHLGREN and K. REED. J. Am. Chem. Soc. **71**, 1380 (1967).
5. (*a*) SUSHILA and K. GROVER. J. Indian Chem. Soc. **54**, 1159 (1977); (*b*) M. PRASADA RAO, B. SETHURAM, and N. NAVANEETH RAO. J. Indian Chem. Soc. **57**, 149 (1980).
6. R. PASCUAL and M. A. HERRAEZ. Can. J. Chem. **63**, 2349 (1985).
7. D. SKOOG and D. WEST. Fundamentos de Química Analítica. Reverté, Barcelona. 1970.
8. C. CROUTHAMEL, H. MEEK, D. MARTIN, and C. BANKS. J. Am. Chem. Soc. **71**, 3031 (1949); C. CROUTHAMEL, A. HAYES, and D. MARTIN. J. Am. Chem. Soc. **73**, 82 (1951).
9. G. AVIGAD. Carbohyd. Res. **11**, 119 (1969).
10. P. D. BRAGG and L. HOUGH. J. Chem. Soc. 4050 (1958).
11. J. GREENSTEIN and M. WINITZ. Chemistry of the amino acids. John Wiley, Sons. Inc., New York. 1961.

Can. J. Chem. Downloaded from www.nrcresearchpress.com by 41.223.56.140 on 09/07/12
For personal use only.

Thiophenophane metal complexes. II. Preparation, structure, and properties of binuclear copper(II) complexes and of 2,5,9,12-tetrathia[13](2,5) thiophenophane. Evidence for *S*-coordinated thiophene[1]

C. Robert Lucas,[2] Shuang Liu, and Michael J. Newlands
Department of Chemistry, Memorial University of Newfoundland, St. John's, Nfld., Canada A1B 3X7
and
Jean-Pierre Charland and Eric J. Gabe
Division of Chemistry, National Research Council of Canada, Ottawa, Ont., Canada K1A 0R9

Received July 15, 1988

C. Robert Lucas, Shuang Liu, Michael J. Newlands, Jean-Pierre Charland, and Eric J. Gabe. Can. J. Chem. **67**, 639 (1989).

Preparations of the thiophenophane $C_{13}H_{20}S_5$, (L2), its binuclear copper(II) complex, $(CuCl_2 \cdot L2)_2$ and the related thiophenophane complex $(CuCl_2 \cdot L1)_2$ (L1 = $C_{10}H_{14}S_4$) are described. The ^{13}C and ^1H nmr spectra of L2 and the ir and electronic spectra of the complexes are reported. The molecular structures of L2, $(CuCl_2 \cdot L1)_2$, and $(CuCl_2 \cdot L2)_2$ have been determined. For L2: space group $P2_1/a$, a = 14.658(1), b = 5.9800(3), c = 19.772(2) Å, β = 111.00(1)°, Z = 4, R_f = 0.050, R_w = 0.046. For $(CuCl_2 \cdot L1)_2$: space group $Pbca$, a = 15.383(6), b = 11.409(3), c = 17.423(4) Å, Z = 4, R_f = 0.057, R_w = 0.036. For $(CuCl_2 \cdot L2)_2$: space group A_2/a, a = 12.616(1), b = 10.0542(6), c = 29.180(2) Å, β = 95.81(1)°, Z = 4, R_f = 0.055, R_w = 0.038. The complex $(CuCl_2 \cdot L1)_2$ has distorted octahedral coordination geometry about each copper. The copper atoms are linked by two bridging chlorines and each copper also bears one terminal chlorine, two thioether-sulfurs and a thiophene-sulfur. In contrast, $(CuCl_2 \cdot L2)_2$ does not involve coordination by thiophene-sulfur and the remaining coordination sphere has undergone distortion from square pyramidal towards trigonal bipyramidal. Differences in the electronic spectra are interpreted in terms of the structures of the complexes.

Key words: binuclear copper(II) thiophenophane complex.

C. Robert Lucas, Shuang Liu, Michael J. Newlands, Jean-Pierre Charland et Eric J. Gabe. Can. J. Chem. **67**, 639 (1989).

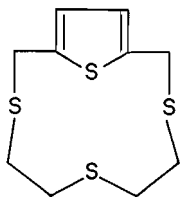
On décrit la préparation du thiophénophane $C_{13}H_{20}S_5$(L2), de son complexe binucléaire du cuivre(II), $(CuCl_2 \cdot L2)_2$, et du complexe apparenté [$(CuCl_2 \cdot L1)_2$ (L1 = $C_{10}H_{14}S_4$)] du thiophénophane. On a déterminé les spectres rmn du ^1H et du ^{13}C du L2 ainsi que les spectres ir et électroniques des complexes. On a déterminé les structures moléculaires du L2, du $(CuCl_2 \cdot L1)_2$ et $(CuCl_2 \cdot L2)_2$. Pour L2: groupe d'espace $P2_1a$, a = 14,658(1), b = 5,9800(3) et c = 19,772(2) Å, β = 111,00(1)°, Z = 4, R_f = 0,050 et R_w = 0,046. Pour $(CuCl_2 \cdot L1)_2$: groupe d'espace $Pbca$, a = 15,383(6), b = 11,409(3) et c = 17,423(4) Å, Z = 4, R_f = 0,057 et R_w = 0,036. Pour $(CuCl_2 \cdot L2)_2$: groupe d'espace A_2/a, a = 12,616(1), b = 10,0542(6) et c = 29,180(2) Å, β = 95,81(1)°, Z = 4, R_f = 0,055 et R_w = 0,038. Le complexe $(CuCl_2 \cdot L1)_2$ possède une géométrie de coordination octaédrique déformée autour de chaque cuivre. Les atomes de cuivre sont liés par deux chlores agissant comme ponts et chaque atome de cuivre porte aussi un chlore terminal, deux soufres de thioéthers et un soufre de thiophène. Par ailleurs, le $(CuCl_2 \cdot L2)_2$ n'implique par de coordination avec un soufre de thiophène et le reste de la sphère de coordination a subi une déformation de la pyramide carrée vers une bipyramide trigonale. On explique des différences dans les spectres électroniques en fonction des structures des complexes.

Mots clés : complexe binucléaire du cuivre(II) du thiophénophane.

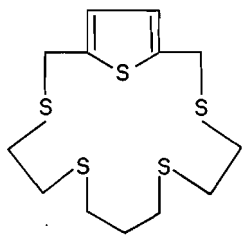
[Traduit par la revue]

Introduction

We have recently reported the preparation and some properties of the ligand, L1, and its copper(I) complex $[Cu(L1)_2]^+$ (1). As a continuation of that study, we now describe the synthesis of the thiophenophane, L2, which has a larger cavity and greater flexibility than L1, and of copper(II) complexes with L1 and L2. One of these, $(CuCl_2 \cdot L1)_2$ shows evidence of interaction between sulfur in the thiophene ring and the copper atom. Sulfur-bound thiophene complexes are rather rare although examples with iron (2), ruthenium (3), silver(I) (4), and copper(I) (5) are known. To our knowledge the present example is the first involving copper(II). Complexes of thiophene are of interest in the study of catalytic hydrodesulfurization of fossil fuels and in particular of coal (6).



L1



L2

Experimental

Commercially available reagents were obtained from the Aldrich Chemical Co. Inc. or from Morton Thiokol, Alfa Products Inc., and were used without further purification. We have previously described the preparation of L1 (1). Spectroscopic data were obtained using the following instruments: ir, Perkin Elmer Model 283; nmr, General Electric 300-NB; mass spectra, V.G. micromass 7070 HS. X-ray diffraction data were collected using an Enraf Nonius CAD-4 or a Picker ($(CuCl_2 \cdot L1)_2$) diffractometer. Analyses were performed by Canadian Microanalytical Service Ltd.

Preparative

(a) $C_{13}H_{20}S_5$ (ligand L2)

The 2,5-bis(chloromethyl)thiophene (8) used in this preparation

[1]NRCC No. 29871.
[2]To whom all correspondence should be addressed.

Can. J. Chem. Downloaded from www.nrcresearchpress.com by 41.223.56.140 on 09/07/12
For personal use only.

TABLE 1. Crystal data for L2, $(CuCl_2 \cdot L1)_2$, and $(CuCl_2 \cdot L2)_2$

Parameter	Value		
	L2	$(CuCl_2 \cdot L1)_2$	$(CuCl_2 \cdot L2)_2$
Empirical formula	$C_{13}H_{20}S_5$	$C_{20}H_{28}Cl_4Cu_2S_8$	$C_{26}H_{40}Cl_4Cu_2S_{10}$
Formula weight	336.60	793.82	942.11
Crystal dimensions, mm	$0.13 \times 0.30 \times 0.35$	$0.15 \times 0.20 \times 0.20$	$0.14 \times 0.12 \times 0.02$
Space group	Monoclinic, $P2_1/a$	Orthorhombic *Pbca*	Monoclinic, A_2/a
a, Å	14.658(1)[a]	15.383(6)[a]	12.616(1)[a]
b, Å	5.9800(3)	11.409(3)	10.0542(6)
c, Å	19.772(2)	17.423(4)	29.180(2)
β, deg	111.00(1)		95.81(1)
Z, (molecules/cell)	4	4	4
F(000), electrons	712.27	1607.82	1927.80
Vol, Å^3	1618.55	3057.82	3682.38
d_{calc}, g/cm^3	1.381	1.724	1.699
Linear absorption coefficient (μ) mm^{-1}	6.36	2.29	2.02
Radiation, Å	λ = 1.54056 ($CuK\alpha_1$)	λ = 0.70930 ($MoK\alpha_1$)	λ = 0.70930 ($MoK\alpha_1$)
2θ(max), deg	151.9	50.0	45.0
No. reflections measured	3816	5461	2797
No. unique reflections	3381	2713	2433
No. unique refl. $I_{net} > n\sigma(I_{net})$	2845(n = 3.0)	1322(n = 2.5)	1073(n = 3.0)
Last least sq. cycle calcd. with	38 atoms 244 parameters 2845 reflections	31 atoms 191 parameters 1322 reflections	41 atoms 191 parameters 1073 reflections
R_f (sig. refl.)	0.050[b]	0.057[b]	0.055[b]
R_w (sig. refl.)	0.046[c]	0.036[c]	0.038[c]
Goodness of fit (last cycle)	5.788[d]	2.520[d]	1.374[d]
R_f (all refl.)	0.057[b]	0.147[b]	0.145[b]
R_w (all refl.)	0.046[c]	0.039[c]	0.055[c]
Max. shift/σ	0.269	0.469	0.002
Last *D*-map:			
deepest hole, e/Å^3	−0.500	−0.880	−0.530
highest peak, e/Å^3	0.430	0.910	0.590
Sec. ext. coeff.	10.2(5)	0.05(2)	0.14(2)

[a]Throughout this work esd's are in parentheses and refer to the last digit printed.
[b]$R_f = \Sigma||F_o| - |F_c||/\Sigma|F_o|$.
[c]$R_w = [\Sigma w(|F_o| - |F_c|)^2/\Sigma(w|F_o|)^2]^{1/2}$ where $w = 1/\sigma^2 I$.
[d]Goodness of fit = $[\Sigma w(|F_o| - |F_c|)^2/(\text{No. of refl.} - \text{No. of parameters})]^{1/2}$.

must be purified or the overall yield of L2 will be low. Purification can be achieved by washing the crude brown liquid with saturated sodium carbonate solution and then water until the washings are neutral, drying over anhydrous $MgSO_4$, and recrystallizing from petroleum ether. Sodium (0.92 g, 40 mmol) was dissolved in commercial absolute ethanol (500 mL) under an atmosphere of dry nitrogen and 1,4,8,11-tetrathiaundecane (7) (4.57 g, 20 mmol) was added slowly. The mixture was refluxed for a further 10 min. To the refluxing mixture, a solution of purified 2,5-bis(chloromethyl)thiophene (3.62 g, 20 mmol) (8) was added dropwise with stirring over 8 h and the refluxing and stirring were continued for a further 4 h. Volatiles were removed on a rotary evaporator, the residue extracted with CH_2Cl_2, washed with water several times, dried over anhydrous $CaCl_2$, and taken to dryness. The yellow solid was recrystallized twice from benzene to give white needles. Melting point 128–129°C. Yield 3.2 g (47%). Mass spectrum: parent ion 336 $[C_{13}H_{20}S_5]^+$. Nuclear magnetic resonance ($CDCl_3$, ppm from TMS int. std., assignments from ^{13}C—^1H heteronuclear correlation and attached proton test, position identification from Fig. 1), ^{13}C: 142.6 Cl—C4, 125.7 C2—C3, 32.0 C7—C11, 31.6 C6—C12, 31.5 C9, 31.34 C8—C10, 31.27 C5—C13; ^1H: 6.78 (s, 2H) C2—C3, 3.90 (s, 4H) C5—C13, 2.67 (m, 4H) C6—C12, 2.57 (m, 4H), 2.46 (t, J = 7.52 Hz, 4H), C8—C10, 1.69 (m, 2H) C9.

(b) $(CuCl_2 \cdot L1)_2$

To a solution of $CuCl_2 \cdot 2H_2O$ (42.6 mg, 0.250 mmol) in acetonitrile (15 mL) was added a solution of ligand L1 (100 mg, 0.381 mmol) in CH_2Cl_2 (5 mL). The deep green solution was filtered and then allowed to evaporate gradually until dark green crystals formed. Yield 70 mg (71%), mp 132–135°C (dec). Infrared: (Nujol mull) 1430(m), 1412(m), 1349(w), 1292(m), 1252(sh), 1250(m), 1232(m), 1209(m), 1180(m), 1133(w), 1114(w), 1095(w), 1035(m), 1019(w), 1000(m), 940(vw), 928(w), 918(w), 872(m), 860(m), 845(m), 832(vs), 776(m), 740(vw), 719(w), 700(m), 690(s), 681(s), 674(m), 652(w), 635(w), 574(m), 482(m), 453(vw), 400(vw), 305(vs), 270(sh), 252(m), 244(s), 232(sh) cm^{-1}. *Anal.* calcd. for $C_{20}H_{28}Cl_4Cu_2S_8$: C 30.26, H 3.56; found: C 30.38, H 3.56.

(c) $(CuCl_2 \cdot L2)_2$

A procedure similar to that above was followed with $CuCl_2 \cdot 2H_2O$ (42.6 mg, 0.250 mmol) in tetrahydrofuran (10 mL) and ligand L2 (84.0 mg, 0.250 mmol) in the same solvent (5 mL). Yield of green crystals 95 mg (81%). Melting point 123–125°C (dec). Infrared: (Nujol mull) 1438(sh), 1410(s), 1390(s), 1345(m), 1300(m), 1255(sh), 1245(s), 1230(m), 1190(m), 1180(m), 1132(w), 1128(m), 1108(m), 1098(m), 1025(s), 960(w), 938(m), 860(m), 849(w), 830(w), 810(vs), 775(s),

Can. J. Chem. Downloaded from www.nrcresearchpress.com by 41.223.56.140 on 09/07/12
For personal use only.

745(w), 730(vs), 704(w), 689(s), 669(w), 659(w), 648(s), 580(m), 570(sh), 480(m), 460(sh), 420(vw), 400(w), 378(vw), 350(vw), 328(vw), 275(vs), 252(sh), 245(s), 220(vs). *Anal.* calcd. for $C_{26}H_{40}Cl_4Cu_2S_{10}$: C 33.15, H 4.28; found: C 33.05, H 4.26.

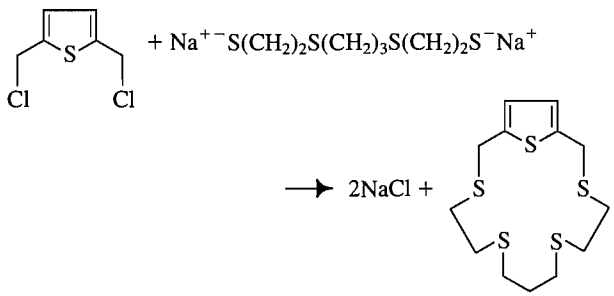
X-ray studies

A summary of crystal data for L2, $(CuCl_2 \cdot L1)_2$, and $(CuCl_2 \cdot L2)_2$ is in Table 1. The diffraction intensities were collected at 295 K using the $\theta/2\theta$ scan technique (ω scan mode for L2) with profile analysis (9) at a scan speed of 4°/min. Three standards were measured after every 100 reflections and no significant crystal decay was detected. Space groups were determined by systematic absences. Unit cell parameters in Table 1 were obtained by a least-squares refinement of the setting angles for 26 reflections ($88° \leq 2\theta \leq 117°$) for L2; 50 reflections ($40° \leq 2\theta \leq 50°$) for $(CuCl_2 \cdot L1)_2$ and 21 reflections ($7° \leq 2\theta \leq 23°$) for $(CuCl_2 \cdot L2)_2$. Lorentz and polarization factors were applied but no corrections were made for absorption.

The structures were solved with MULTAN (10) plus a difference Fourier map and refined by full matrix least-squares with counting statistics weights. H-atom positions were calculated but their parameters were not refined. All heavier atoms were refined anisotropically. All calculations were performed with the NRCVAX Crystal Structure programs (11). Scattering factors were taken from the International tables for X-ray crystallography (12). The final atomic positional parameters, the equivalent isotropic temperature factors and important bond lengths and angles are listed in Tables 2–7. Anisotropic thermal parameters, a full listing of bond lengths and bond angles and final structure factors are available as supplementary data.[3] Figures 1–4 show various views of the molecules and their atomic numbering schemes.

Results and discussion

Synthesis of L2 was carried out in 47% yield by a traditional high dilution S_N2 cyclization (equation [1]) similar to that which we reported earlier (1) for L1.

[1] 

As noted during preparation of L1, decreased yields of L2 also occur when impurities are present in the reagents (see Experimental).

The macrocyclic ligands L1 and L2 have constraints imposed upon the size and shape of their cavities and upon the orientations of non-bonding electron pairs of their thioether sulfur atoms. These constraints are a result of the rigidity of the thiophene sub-unit and its two adjacent methylene groups which limits the overall flexibility of the macrocyclic ring. For L1, the consequence is a ring cavity which although large enough to accommodate a first row transition metal such as copper, does not do so because the orientation of non-bonding electron pairs on the thioether-sulfurs is exocyclic and because approach to the cavity is hindered on both sides by hydrogen atoms. As a result, L1 acts as a bidentate ligand to Cu(I), forming $[Cu(L1)_2]ClO_4$ (1). In this report we examine the behaviour of L1 with Cu(II), in order to ascertain whether the chelating mode of bonding and other structural features of coordinated L1 are retained as the oxidation state of the central metal is changed. We then examine the effect on structural and spectroscopic properties of increased aliphatic chain length and flexibility and increased cavity size. As noted previously (1), the Cu(I) state is sufficiently stabilized by L1 that preparation of a Cu(II) complex can only be accomplished in solvents free from alcoholic or other easily oxidized components. Thus the Cu(II) complex of L1, $(CuCl_2 \cdot L1)_2$ was prepared in mixed acetonitrile–dichloromethane while that of L2, $(CuCl_2 \cdot L2)_2$, was obtained from tetrahydrofuran. The conformation of L1 in $(CuCl_2 \cdot L1)_2$ is essentially the same as that found in $[Cu(L1)_2]^+$ (1) and compared to uncomplexed L1, the main differences occur at S3 and C8 where inversions have taken place to orient the non-bonding electron pairs on S2 and S3 so that a chelate ring may form using these donor sites (Fig. 3).

Two views of L2 are shown in Figs. 1 and 2. The macrocycle's cavity is large (~4.8 × ~8.0 Å) but like L1, its cavity is inaccessible and unsuitable for complex formation, at least in the conformation of the free ligand. All electron pairs on thioether-sulfurs are exocyclic and the cavity is shielded on one side by hydrogens on C6, C9, and C12 and on the other by many hydrogens. As a result, complex formation (Fig. 4) occurs by conformational change within the flexible thioether chain so that the adjacent sulfurs, S2 and S3, may engage in chelation. The behaviour of L1 and L2 as ligands is therefore similar in spite of their differences in structure.

The complex, $(CuCl_2 \cdot L1)_2$ has two Cu(II) centres, the coordination geometry being the same at both. Each copper is surrounded by two chlorine-bridges to the other copper atom. One of these bridge-chlorines occupies a position on the tetragonal axis of a copper atom while the other bridge-chlorine occupies an equatorial site. The remaining three equatorial sites are occupied by a terminal chlorine and two adjacent sulfur atoms from L1. The molecule is centrosymmetric and thus the two terminal Cu—Cl bonds project on opposite sides of the

TABLE 2. Positional and thermal parameters and equivalent isotropic temperature factors for L2, $(C_{13}H_{20}S_5)$

Atom	x	y	z	B_{iso}[a]
S 1	0.07633(8)	0.21298(18)	0.74519(5)	4.17(5)
S 2	0.25153(8)	0.17413(20)	0.92579(5)	4.17(5)
S 3	0.45373(7)	0.70448(22)	0.90668(5)	4.54(5)
S 4	0.32435(8)	0.69458(21)	0.60298(5)	4.30(5)
S 5	0.09490(8)	0.17518(20)	0.56903(5)	4.38(5)
C 1	0.05531(25)	0.4106 (7)	0.67803(18)	3.03(16)
C 2	0.0789 (3)	0.6155 (7)	0.70677(20)	3.28(17)
C 3	0.1122 (3)	0.6154 (7)	0.78387(21)	3.41(19)
C 4	0.1138 (3)	0.4112 (7)	0.81266(19)	3.08(17)
C 5	0.1432 (4)	0.3495 (10)	0.89086(24)	4.10(23)
C 6	0.3380 (3)	0.3296 (8)	0.89814(21)	3.75(20)
C 7	0.3618 (3)	0.5565 (9)	0.93158(22)	3.88(21)
C 8	0.3820 (3)	0.8245 (8)	0.82024(21)	3.49(19)
C 9	0.3652 (3)	0.6820 (7)	0.75397(20)	3.30(18)
C10	0.3253 (3)	0.8209 (8)	0.68625(21)	3.48(18)
C11	0.2078 (3)	0.5524 (8)	0.56946(22)	3.88(21)
C12	0.2088 (3)	0.3281 (9)	0.60414(23)	3.69(20)
C13	0.0148 (3)	0.3491 (9)	0.59967(22)	3.94(20)

[a] B_{iso} is the mean of the principal axes of the thermal ellipsoid.

[3] A complete set of data may be purchased from the Depository of Unpublished Data, CISTI, National Research Council of Canada, Ottawa, Ont., Canada K1A 0S2.

Can. J. Chem. Downloaded from www.nrcresearchpress.com by 41.223.56.140 on 09/07/12
For personal use only.

Can. J. Chem. Downloaded from www.nrcresearchpress.com by 41.223.56.140 on 09/07/12
For personal use only.

TABLE 3. Selected bond lengths and angles in L2, ($C_{13}H_{20}S_5$)

Bond	Distance (Å)	Bonds	Angle (deg)
S(1) —C(1)	1.721(4)	C(1) —S(1)—C(4)	92.53(19)
S(1) —C(4)	1.721(4)	C(5) —S(2)—C(6)	101.54(23)
S(2) —C(5)	1.819(5)	C(7) —S(3)—C(8)	102.30(20)
S(2) —C(6)	1.808(5)	C(10)—S(4)—C(11)	103.18(21)
S(3) —C(7)	1.821(5)	C(12)—S(5)—C(13)	101.48(22)
S(3) —C(8)	1.804(4)	S(1) —C(1)—C(2)	110.6 (3)
S(4) —C(10)	1.807(4)	S(1) —C(1)—C(13)	121.7 (3)
S(4) —C(11)	1.808(5)	C(2) —C(1)—C(13)	127.6 (4)
S(5) —C(12)	1.809(5)	C(1) —C(2)—C(3)	113.0 (4)
S(5) —C(13)	1.827(5)	C(2) —C(3)—C(4)	113.6 (4)
C(1) —C(2)	1.343(6)	S(1) —C(4)—C(3)	110.2 (3)
C(1) —C(13)	1.493(5)	S(1) —C(4)—C(5)	121.7 (3)
C(2) —C(3)	1.424(5)	C(3) —C(4)—C(5)	128.1 (4)
C(3) —C(4)	1.344(6)	S(2) —C(5)—C(4)	115.1 (3)
C(4) —C(5)	1.495(6)	S(2) —C(6)—C(7)	114.2 (3)
C(6) —C(7)	1.495(7)	S(3) —C(7)—C(6)	113.5 (3)
C(8) —C(9)	1.508(6)	C(8) —C(9)—C(10)	110.6 (4)
C(9) —C(10)	1.504(6)	S(4) —C(10)—C(9)	117.0 (3)
C(11)—C(12)	1.504(7)	S(4) —C(11)—C(12)	113.5 (3)
		S(5) —C(12)—C(11)	114.8 (3)
		S(5) —C(13)—C(1)	114.9 (3)

TABLE 4. Positional parameters[a] and equivalent isotropic temperature factors for $(CuCl_2 \cdot L1)_2$

Atom	x	y	z	B_{iso}[b]
Cu	0.05832(8)	0.04194(13)	0.91950(8)	2.68(7)
Cl 1	0.00845(18)	−0.0797 (3)	0.82919(18)	3.44(15)
Cl 2	0.09116(17)	−0.1019 (3)	1.00917(17)	3.04(14)
S 1	0.23727(18)	0.0054 (3)	0.85331(15)	2.82(15)
S 2	0.13404(18)	0.1665 (3)	1.00348(17)	2.66(15)
S 3	0.03177(18)	0.2059 (3)	0.84044(17)	2.81(16)
S 4	0.20968(20)	0.1305 (3)	0.64717(17)	4.00(18)
C 1	0.2976 (6)	0.0615 (10)	0.7782 (6)	2.3 (5)
C 2	0.3514 (7)	0.1485 (11)	0.8032 (6)	3.0 (6)
C 3	0.3413 (7)	0.1734 (10)	0.8821 (6)	3.1 (6)
C 4	0.2808 (6)	0.1048 (10)	0.9176 (6)	2.5 (6)
C 5	0.2478 (8)	0.1151 (12)	0.9983 (6)	2.9 (7)
C 6	0.1372 (11)	0.3022 (15)	0.9523 (8)	3.9 (8)
C 7	0.0573 (11)	0.3235 (14)	0.9050 (8)	3.6 (8)
C 8	0.1207 (7)	0.2280 (11)	0.7711 (6)	2.5 (6)
C 9	0.1131 (7)	0.1336 (13)	0.7078 (6)	3.5 (7)
C10	0.2764 (8)	0.0212 (13)	0.6971 (6)	3.6 (7)

[a]Symmetry related atoms in the other half of the molecule have the parameters $-x, -y, 2 - z$.

[b]B_{iso} is the mean of the principal axes of the thermal ellipsoid.

Cu_2Cl_2 plane and the same is true for the macrocyclic ligands. All but one of the bond angles at Cu deviate less than 10° from ideal values with the largest deviation being 10.89° at Cl(1)—Cu—Cl(2′). Each copper atom lies 0.09 Å above the least-squares plane of its four nearest neighbours. The bridging Cu—Cl distances are 2.702(3) Å (axial) and 2.321(3) Å (equatorial) while the terminal Cu—Cl length is 2.234(3) Å. Angles at the chlorine bridgeheads are 86.87(10)° and the Cu—Cu distance is 3.464(7) Å. Corresponding distances and angles in the open chain chelate $(CuCl_2 \cdot BBTE)_2$ (13) (BBTE = $BuSCH_2CH_2SBu$) are 2.825(2) (axial), 2.266(2) (equatorial), 2.242(2) Å (terminal) while the chlorine bridgehead angle is 94.22(5)° and the Cu—Cu distance is 3.749(2) Å. The two complexes, $(CuCl_2 \cdot L1)_2$ and $(CuCl_2 \cdot BBTE)_2$, are superficially similar in the number and type of atoms bonded to copper but there are structural differences associated mainly with the Cu—Cu and Cu—Cl distances and associated angles. In fact, the structure of $(CuCl_2 \cdot L1)_2$ corresponds well to that of a fragment of cupric chloride consisting of two coppers and four chlorines from two adjacent bands in the band structure of anhydrous cupric chloride (14). In that structure, each copper is surrounded by four chlorines at 2.30 Å in a two-dimensional $(CuCl_2)_n$ band and by two more chlorines from adjacent bands at a distance of 2.95 Å to give a tetragonally distorted octahedral array. In $(CuCl_2 \cdot L1)_2$, the bridge angles at Cl are close to 90° as at the interband bridgehead in cupric chloride and the bridging equatorial Cu—Cl length is within 0.02 Å of the corresponding length in cupric chloride. The terminal Cu—Cl length of 2.23 Å is shorter than the 2.30 Å found in cupric chloride because the bond is terminal in $(CuCl_2 \cdot L1)_2$, not bridging as in cupric chloride. The axial Cu—Cl length of 2.70 Å in $(CuCl_2 \cdot L1)_2$ is significantly shorter than the 2.95 Å found in cupric chloride due to the absence of the *trans* influence of a second Cl on the tetragonal axis of $(CuCl_2 \cdot L1)_2$.

The Cu—S distances in $(CuCl_2 \cdot L1)_2$ are 2.349(3) and 2.358(3) Å compared to 2.308(2) and 2.369(2) in $(CuCl_2 \cdot BBTE)_2$ or 2.289–2.398 Å in $Cu^{II}([15]aneS_5)$ (15). Interestingly, the tetrahedral copper(I) complex ion $[Cu(L1)_2]^+$ also has Cu—S bond lengths in the range 2.301 to 2.392 Å which suggests that the Cu—S bond length is not very sensitive to oxidation state or coordination geometry unless, fortuitously, the two are having equal but opposite effects in this instance.

The thiophene-sulfur of L1 lies on the tetragonal axis of $(CuCl_2 \cdot L1)_2$ at a distance of 3.013(7) Å from copper. The covalent radius of divalent sulfur is 0.03 Å larger than that of chlorine (16) and following the analogy between the structures of anhydrous cupric chloride and $(CuCl_2 \cdot L1)_2$, the expected distance from copper to a coordinated thiophene-sulfur would be 2.98 Å. The observed distance is reasonably close to that predicted and significantly less than 3.20 Å which is the sum of the van der Waals radii (16). Shortening of the Cu—Cl(2)′ bond

TABLE 5. Selected bond lengths and angles in $(CuCl_2 \cdot L1)_2$

Bond	Distance (Å)	Bonds	Angle (deg)
Cu—Cl(1)	2.234(3)	C(7)—S(3)—C(8)	98.4 (7)
Cu—Cl(2)	2.321(3)	C(9)—S(4)—C(10)	101.2 (5)
Cu—Cl(2)′	2.702(3)	S(1)—C(1)—C(2)	110.7 (8)
Cu—S(1)	3.014(4)	S(1)—C(1)—C(10)	118.5 (9)
Cu—S(2)	2.349(3)	C(2)—C(1)—C(10)	130.3 (10)
Cu—S(3)	2.358(3)	C(1)—C(2)—C(3)	113.0 (10)
Cl(2)—Cu′	2.702(3)	C(2)—C(3)—C(4)	113.6 (10)
S(1)—C(1)	1.728(10)	S(1)—C(4)—C(3)	110.3 (8)
S(1)—C(4)	1.729(11)	S(1)—C(4)—C(5)	121.9 (9)
S(2)—C(5)	1.848(13)	C(3)—C(4)—C(5)	127.7 (10)
S(2)—C(6)	1.788(16)	S(2)—C(5)—C(4)	113.0 (7)
S(3)—C(7)	1.795(15)	S(2)—C(6)—C(7)	113.1 (11)
S(3)—C(8)	1.842(11)	S(3)—C(7)—C(6)	113.7 (11)
S(4)—C(9)	1.823(11)	S(3)—C(8)—C(9)	108.4 (8)
S(4)—C(10)	1.834(14)	S(4)—C(9)—C(8)	111.5 (8)
C(1)—C(2)	1.365(17)	S(4)—C(10)—C(1)	110.8 (9)
C(1)—C(10)	1.521(16)	Cl(1)—Cu—Cl(2)	96.29(12)
C(2)—C(3)	1.412(16)	Cl(1)—Cu—Cl(2)′	100.89(11)
C(3)—C(4)	1.365(16)	Cl(1)—Cu—S(2)	170.04(12)
C(6)—C(7)	1.499(23)	Cl(1)—Cu—S(3)	91.25(12)
C(8)—C(9)	1.547(18)	Cl(2)—Cu—Cl(2)′	93.13(10)
		Cl(2)—Cu—S(2)	84.29(12)
		Cl(2)—Cu—S(3)	172.46(12)
		Cl(2)′—Cu—S(2)	88.99(11)
		Cl(2)′—Cu—S(3)	85.45(10)
		S(2)—Cu—S(3)	88.28(12)
		Cu—Cl(2)—Cu′	86.87(10)
		C(1)—S(1)—C(4)	92.3 (5)
		Cu—S(2)—C(5)	104.3 (4)
		Cu—S(2)—C(6)	103.1 (5)
		C(5)—S(2)—C(6)	103.0 (7)
		Cu—S(3)—C(7)	100.9 (5)
		Cu—S(3)—C(8)	111.3 (4)
		Cu—S(1)—C(1)	136.8 (4)
		Cu—S(1)—C(4)	90.87(8)

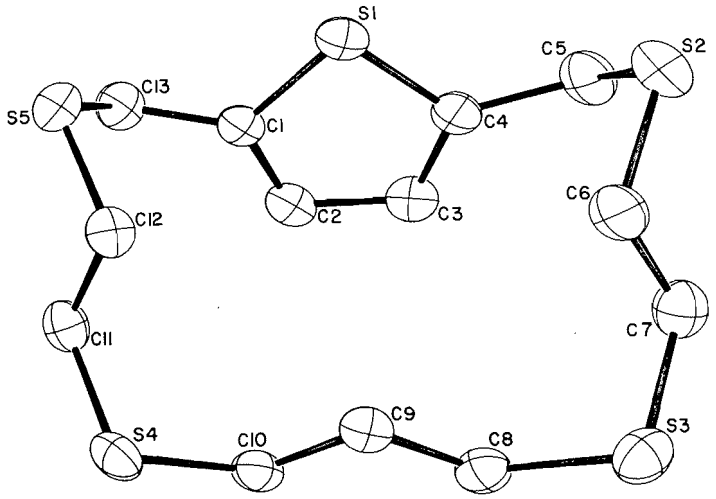


FIG. 1. ORTEP drawing of L2.

(2.702(3) Å) in $(CuCl_2 \cdot L1)_2$ compared to the corresponding bond (2.95 Å) in cupric chloride suggests a weaker *trans* influence by thiophene-sulfur than by a chlorine atom. Furthermore, in $(CuCl_2 \cdot L2)_2$ where the corresponding Cu—S distance is 3.307(9) Å, thiophene-sulfur is clearly too far away to be considered bonded to copper and the Cu—Cl distance *trans* to it is even shorter (2.661(4) Å). On these grounds, it seems reasonable to assume a bonding interaction between copper and thiophene-sulfur in $(CuCl_2 \cdot L1)_2$ and thus the coordination geometry of copper in $(CuCl_2 \cdot L1)_2$ is best regarded as distorted octahedral.

Thiophene does not usually form strong bonds through its

Can. J. Chem. Downloaded from www.nrcresearchpress.com by 41.223.56.140 on 09/07/12
For personal use only.

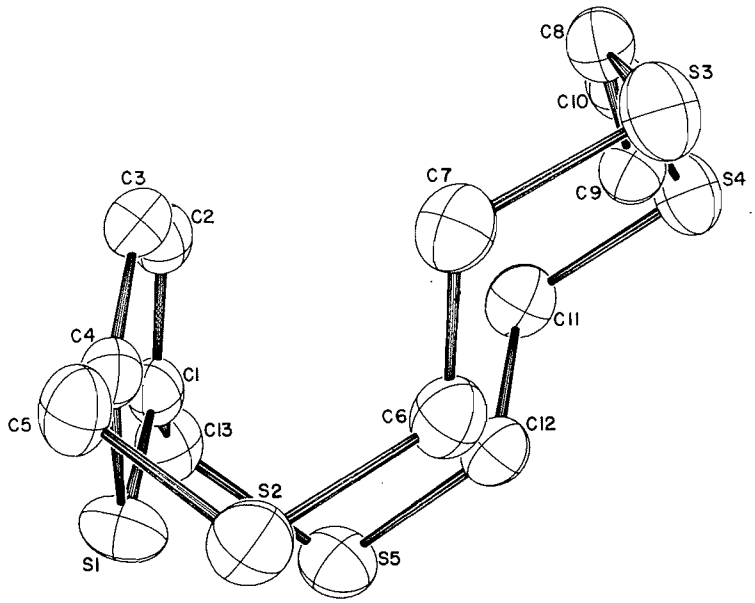


FIG. 2. ORTEP drawing of L2.

TABLE 6. Positional parameters[a] and equivalent isotropic temperature factors for $(CuCl_2 \cdot L2)_2$

Atom	x	y	z	B_{iso}[b]
Cu	0.06381(16)	0.32575(20)	0.20562(7)	2.23(10)
Cl 1	0.0297 (3)	0.5454 (4)	0.21313(13)	2.99(21)
Cl 2	−0.1056 (3)	0.2487 (4)	0.20692(13)	2.71(19)
S 1	0.0402 (4)	0.4592 (5)	0.10146(14)	3.25(22)
S 2	0.2414 (3)	0.3953 (4)	0.20332(13)	2.39(20)
S 3	0.1228 (3)	0.1401 (4)	0.16581(13)	2.14(19)
S 4	−0.0617 (4)	−0.1342 (5)	0.07808(18)	5.1 (3)
S 5	−0.1755 (4)	0.2799 (5)	0.05841(16)	4.9 (3)
C 1	0.0299 (13)	0.3679 (17)	0.0517 (5)	3.2 (9)
C 2	0.1250 (15)	0.3292 (18)	0.0416 (5)	3.5 (9)
C 3	0.2092 (14)	0.3694 (18)	0.0742 (6)	4.0 (10)
C 4	0.1783 (12)	0.4396 (16)	0.1104 (5)	2.3 (8)
C 5	0.2424 (11)	0.4952 (14)	0.1509 (5)	2.5 (8)
C 6	0.3147 (12)	0.2477 (17)	0.1888 (6)	3.7 (9)
C 7	0.2539 (12)	0.1228 (14)	0.1974 (5)	2.4 (8)
C 8	0.0607 (11)	−0.0138 (15)	0.1779 (4)	2.3 (8)
C 9	0.1016 (12)	−0.1298 (14)	0.1493 (6)	3.4 (9)
C10	0.0787 (14)	−0.1163 (17)	0.0991 (6)	4.2 (10)
C11	−0.1018 (16)	0.0240 (23)	0.0507 (6)	7.2 (14)
C12	−0.1126 (14)	0.1297 (21)	0.0842 (6)	5.4 (11)
C13	−0.0763 (13)	0.3432 (18)	0.0236 (5)	4.2 (9)

[a]Symmetry related atoms in the other half of the molecule have the parameters x, $0.5 - y$, $0.5 - z$.

[b]B_{iso} is the mean of the principal axes of the thermal ellipsoid.

sulfur atom to transition metals and there are very few structural reports with which $(CuCl_2 \cdot L1)_2$ may be compared. Recent studies of iron (2), silver (5), and copper(I) (4) thiophene complexes, however, suggest that a Cu—S (thiophene) bond length between 2.96 and 3.16 Å might be expected which compares favourably with the Cu—S distance we have observed. It should be noted, however, that the angles Cu—S(1)—C(1) and Cu—S(1)—C(4) are 136.8(4)° and 90.87(8)°, respectively, which reveal that the bonding between copper and thiophene is asymmetric and strained. Spectroscopic evidence (*vide infra*) supports our conclusion that the thiophene sulfur in $(CuCl_2 \cdot L1)_2$ is coordinated to copper.

For $(CuCl_2 \cdot L2)_2$, the coordination geometry is somewhat different. Additional atoms in the macrocycle make it possible for the thiophene-sulfur to lie further from copper in $(CuCl_2 \cdot L2)_2$ (3.307(9) Å) than in $(CuCl_2 \cdot L1)_2$ (3.013(7) Å) so that the geometry about each copper atom in $(CuCl_2 \cdot L2)_2$ is approximately square pyramidal. The reduced crowding near copper that results from the retreat of the thiophene-sulfur makes it possible for both S3 and Cl1 to swing down ~12° below the basal plane of an idealized square pyramid. The dimeric molecule is centrosymmetric and each copper atom lies 0.42 Å out of the least-squares plane defined by Cl1, Cl2′, and S3. If viewed as a trigonal bipyramid, the angles at copper between axial and equatorial positions deviate less than 10° from the ideal of 90° but the angles within the equatorial plane are the sites of great molecular distortion. They have values of 101.69(15)°, 102.01(15)°, and 153.12(17)° and it is readily apparent that the first two arise from ~12° distortion from the ideal value for a square pyramid. Thus, this structure is probably better regarded as a slightly distorted square pyramid than as a grossly distorted trigonal bipyramid. Apparently, the preferred geometry about copper(II) of this S_2Cl_3 ligand donor-set is trigonal bipyramidal but in the presence of coordination by thiophene-sulfur and the resulting steric crowding in $(CuCl_2 \cdot L1)_2$, a square pyramidal configuration is adopted. As crowding decreases upon changing to $(CuCl_2 \cdot L2)_2$, the square pyramidal structure begins to distort towards trigonal bipyramidal.

The Cu—S (thioether) distances in $(CuCl_2 \cdot L2)_2$ are 2.355(5) and 2.358(4) Å and Cu—Cl distances of 2.661(4) (bridging), 2.277(4) (bridging), and 2.265(4) Å (terminal) are similar to the corresponding distances in $(CuCl_2 \cdot L1)_2$. Angles at the chlorine bridgeheads are 90.94(14)° compared to 86.87(10)° in $(CuCl_2 \cdot L1)_2$ and the Cu—Cu distance is 3.530(4) Å compared to 3.464(7) Å in $(CuCl_2 \cdot L1)_2$.

Thus, the structures of $(CuCl_2 \cdot L1)_2$ and $(CuCl_2 \cdot L2)_2$ are superficially similar. Both resemble a fragment from the band structure of anhydrous cupric chloride to which S-donor ligands have been appended. In $(CuCl_2 \cdot L1)_2$ the coordination is distorted octahedral with one of the donor atoms being a thiophene-sulfur. The remaining S_2Cl_3 donor-set achieves a square pyramidal geometry with only slight distortion. In

Can. J. Chem. Downloaded from www.nrcresearchpress.com by 41.223.56.140 on 09/07/12
For personal use only.

TABLE 7. Selected bond lengths and angles in $(CuCl_2 \cdot L2)_2$

Bond	Distance (Å)	Bonds	Angle (deg)
Cu—Cl(1)	2.265(4)	Cl(1)—Cu—Cl(2)	98.17(16)
Cu—Cl(2)	2.277(4)	Cl(1)—Cu—Cl(2′)	101.69(15)
Cu—Cl(2)′	2.661(4)	Cl(1)—Cu—S(2)	84.50(16)
Cu—S(2)	2.355(5)	Cl(1)—Cu—S(3)	153.12(17)
Cu—S(3)	2.358(4)	Cl(2)—Cu—Cl(2′)	89.06(14)
Cl(2)—Cu′	2.661(4)	Cl(2)—Cu—S(2)	177.29(17)
S(1)—C(1)	1.711(17)	Cl(2)—Cu—S(3)	94.71(16)
S(1)—C(4)	1.747(15)	Cl(2′)—Cu—S(2)	90.80(14)
S(2)—C(5)	1.831(14)	Cl(2′)—Cu—S(3)	102.01(15)
S(2)—C(6)	1.821(17)	S(2)—Cu—S(3)	82.67(15)
S(3)—C(7)	1.819(15)	Cu—Cl(2)—Cu′	90.94(14)
S(3)—C(8)	1.785(15)	Cl(1)—S(1)—C(4)	93.2 (8)
S(4)—C(10)	1.825(18)	Cu—S(2)—C(5)	105.9 (5)
S(4)—C(11)	1.828(23)	Cu—S(2)—C(6)	105.8 (5)
S(5)—C(12)	1.832(20)	C(5)—S(2)—C(6)	101.8 (7)
S(5)—C(13)	1.807(16)	Cu—S(3)—C(7)	98.2 (5)
C(1)—C(2)	1.322(25)	Cu—S(3)—C(8)	115.0 (5)
C(1)—C(13)	1.519(22)	C(7)—S(3)—C(8)	102.3 (7)
C(2)—C(3)	1.41 (3)	C(10)—S(4)—C(11)	106.1 (9)
C(3)—C(4)	1.360(24)	C(12)—S(5)—C(13)	103.0 (8)
C(4)—C(5)	1.473(21)	S(1)—C(1)—C(2)	110.7 (12)
C(8)—C(9)	1.551(21)	S(1)—C(1)—C(13)	122.2 (13)
C(9)—C(10)	1.472(24)	C(2)—C(1)—C(13)	127.0 (15)
C(11)—C(12)	1.46 (3)	C(1)—C(2)—C(3)	113.9 (15)
		S(1)—C(4)—C(3)	107.6 (12)
		S(1)—C(4)—C(5)	122.4 (11)
		C(3)—C(4)—C(5)	130.0 (14)
		S(2)—C(5)—C(4)	114.4 (10)
		S(2)—C(6)—C(7)	111.2 (11)
		S(3)—C(7)—C(6)	106.8 (10)
		S(3)—C(8)—C(9)	111.7 (10)
		C(8)—C(9)—C(10)	115.0 (13)
		S(4)—C(10)—C(9)	114.3 (11)
		S(4)—C(11)—C(12)	112.3 (13)
		S(5)—C(12)—C(11)	113.0 (12)
		S(5)—C(13)—C(1)	112.1 (10)

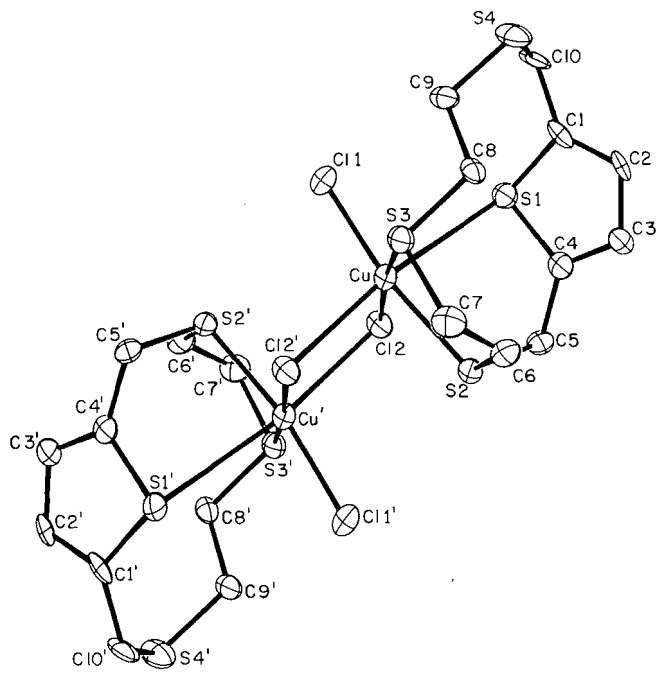


FIG. 3. ORTEP drawing of $(CuCl_2 \cdot L1)_2$.

$(CuCl_2 \cdot L2)_2$ the thiophene is not bonded and the S_2Cl_3 donor set has distorted ~12° from square pyramidal towards trigonal bipyramidal at the two basal sites S3 and Cl1.

The ir spectra of both complexes exhibit strong bands at ~300 and ~250 cm^{-1} that are absent from spectra of the free ligand and analogous copper(I) complexes (1). These bands are assigned to Cu—Cl vibrations. The double chlorine bridge in $[CuCl_3]_2^{2-}$ has ir-active Cu—Cl stretching modes at 236 and 193 cm^{-1} that are weaker and lower in energy than its terminal Cu—Cl stretches at 301 and 278 cm^{-1} (17). By comparison, the higher energy, more intense bands near 300 cm^{-1} in spectra of $(CuCl_2 \cdot L1)_2$ and $(CuCl_2 \cdot L2)_2$ are assigned to terminal Cu—Cl stretches and those near 250 cm^{-1} are also assigned to a Cu—Cl stretch but specific assignment to a terminal or bridge vibration is more problematical and has not been attempted.

Details of the electronic spectra are in Table 8 and are similar to those of the distorted square pyramidal CuS_2Cl_3 unit in $(CuCl_2 \cdot BBTE)_2$ (18). The lowest energy band in spectra of both $(CuCl_2 \cdot L1)_2$ and $(CuCl_2 \cdot L2)_2$ is an envelope of unresolved *d—d* transitions, no further absorptions being detected up to 2000 nm. Changes from a distorted CuS_3Cl_3 chromophore in $(CuCl_2 \cdot L1)_2$ towards distorted square pyramidal CuS_2Cl_3 in $(CuCl_2 \cdot BBTE)_2$ and $(CuCl_2 \cdot L2)_2$ have little effect on the energy of the charge transfer bands. They do, however, shift the maximum of the ligand field band envelope to longer wavelength. This shift is

Can. J. Chem. Downloaded from www.nrcresearchpress.com by 41.223.56.140 on 09/07/12
For personal use only.

TABLE 8. Electronic spectral results and assignments

Complex	λ_{max} in nanometers (ϵ) Solids	Solutions						Assignment
$(CuCl_2BBTE)_2$[a]	800[b]	750[c]	(460)					*d*—*d* envelope
	570(sh)							$\pi(S) \rightarrow d_{x^2-y^2}$
	448	449	(2740)					$\sigma(S) \rightarrow d_{x^2-y^2}$
	387	363	(6380)					$Cl \rightarrow d_{x^2-y^2}$
	292	272	(3830)					$Cl \rightarrow d_{x^2-y^2}$
	240							$Cl \rightarrow d_{x^2-y^2}$
	215							Thioether
$(CuCl_2 \cdot L1)_2$		730[e]	(120)	725[f]	(170)	725[c]	(100)	*d*—*d* envelope
	430[d]	450	(900)	430(sh)		450	(900)	$\sigma(S) \rightarrow d_{x^2-y^2}$
	360	360(sh)				360	(2700)	$Cl \rightarrow d_{x^2-y^2}$
		280(sh)				275(sh)		$Cl \rightarrow d_{x^2-y^2}$
		250	(7000)			250	(6700)	h
$(CuCl_2 \cdot L2)_2$		850[e]	(100)	750[f]	(130)	925[g]	(90)	*d*—*d* envelope
	450[d]	460	(900)	425(sh)		425	(300)	$\sigma(S) \rightarrow d_{x^2-y^2}$
	360	360(sh)				360(sh)		$Cl \rightarrow d_{x^2-y^2}$
		290(sh)						$Cl \rightarrow d_{x^2-y^2}$
		250	(7200)					h

[a]Reference 18.
[b]Nujol mull at 80 K.
[c]CH_2Cl_2.
[d]Nujol mull at 298 K.
[e]CH_3CN.
[f]CH_3NO_2.
[g]$HCON(CH_3)_2$.
[h]$Cl \rightarrow d_{x^2-y^2}$ + thiophene.

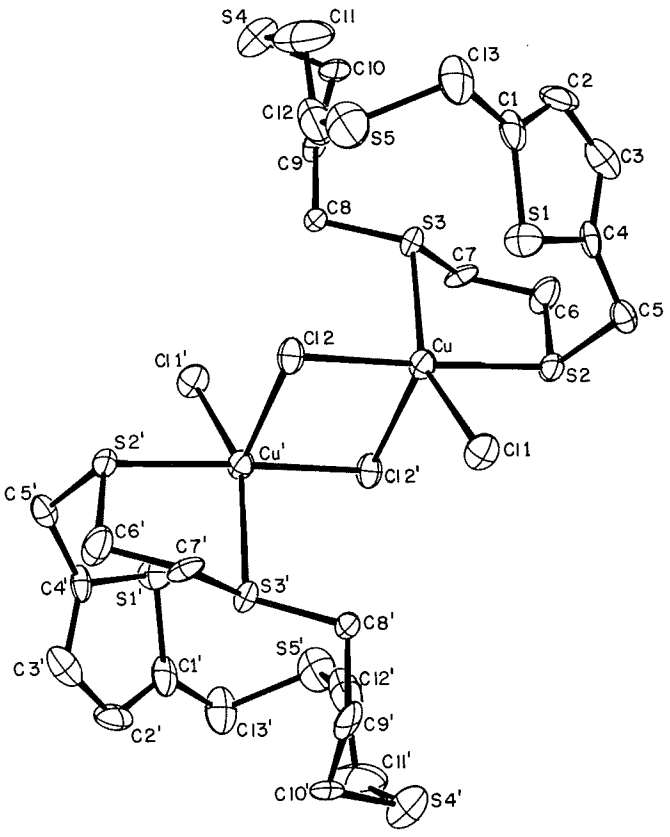


FIG. 4. ORTEP drawing of $(CuCl_2 \cdot L2)_2$.

probably due to changes in the relative intensities of the unresolved *d*—*d* transitions. That transition having the highest intensity has the longest wavelength in trigonal bipyramidal geometry but the opposite is true in square pyramidal or octahedral geometry (19). Spectra of $(CuCl_2 \cdot L1)_2$ are almost unaffected by changes in solvent in contrast to the noticeable effect of solvent on the ligand field band of $(CuCl_2 \cdot L2)_2$. Furthermore, the ligand field band of $(CuCl_2 \cdot L1)_2$ in all solvents used in this study is close to the energy of the corresponding band in the spectrum of $(CuCl_2 \cdot BBTE)_2$ recorded in the solid state or in the non-coordinating solvent CH_2Cl_2. These observations imply that solvent has little effect on the ligand field experienced by copper in $(CuCl_2 \cdot L1)_2$ but a significant effect upon that experienced by copper in $(CuCl_2 \cdot L2)_2$. Therefore, these spectral results support the conclusions concerning coordination of thiophene-sulfur obtained from our structural studies. Thus, in $(CuCl_2 \cdot L1)_2$, thiophene-sulfur occupies a coordination site on the copper atom in both the solid and in solution. In $(CuCl_2 \cdot L2)_2$, however, thiophene-sulfur is not coordinated to the metal in either the solid or in solution and solvent influence on the ligand field experienced by the metal is occurring presumably via the vacant octahedral site. In this regard, it may be noted that the shift in wavelength of the ligand field band of $(CuCl_2 \cdot L2)_2$ parallels the change in ligand field strength of the solvent. A strong absorption at 260 nm due to the thiophene portion of the organic ligand (thioether bands are expected at 194 and 215 nm) (20) obscures the highest energy Cl $\rightarrow d_{x^2-y^2}$ LMCT band which should appear in the same region (18).

Relationships between structure and redox properties of these compounds is a subject of our continuing studies.

Can. J. Chem. Downloaded from www.nrcresearchpress.com by 41.223.56.140 on 09/07/12
For personal use only.

Acknowledgements

Financial assistance in the form of a Hatcher Scholarship (L.S.) and an operating grant (C.R.L.) was provided by Memorial University. The cooperation of the Federal Department of Energy, Mines and Resources, Ottawa, upon whose diffractometer some of the X-ray data were collected is gratefully acknowledged.

1. C. R. LUCAS, LIU SHUANG, M. J. NEWLANDS, J. P. CHARLAND, and E. J. GABE. Can. J. Chem., **66**, 1506 (1988).
2. J. D. GOODRICH, P. N. NICKIAS, and J. P. SELEGUE. Inorg. Chem. **26**, 3424 (1987).
3. S. M. BUCKNOR, M. DRAGANJAC, T. B. RAUCHFUSS, C. J. RUFFING, W. C. FULTZ, and A. L. RHEINGOLD. J. Am. Chem. Soc. **106**, 5379 (1984).
4. A. L. SPEK, A. J. M. DUISENBERG, G. C. VAN STEIN, and G. VAN KOTEN. Acta. Crystallogr. C**41**, 374 (1985).
5. G. C. VAN STEIN, G. VAN KOTEN, K. VRIEZE, A. L. SPEK, E. A. KLOP, and C. BREVARD. Inorg. Chem. **24**, 1367 (1985).
6. G. D. GALPERN. *In* Chemistry of heterocyclic compounds. *Edited by* S. Gronowitz. Wiley, New York. 1985. Vol. 44. pp. 325–351.
7. K. TRAVIS and D. H. BUSCH. Inorg. Chem. **13**, 2591 (1974).
8. J. M. GRIFFING. J. Am. Chem. Soc. **70**, 3416 (1948).
9. D. F. GRANT and E. J. GABE. J. Appl. Crystallogr. **11**, 114 (1978).
10. G. GERMAIN, P. MAIN, and M. M. WOOLFSON. Acta Crystallogr. A**27**, 368 (1971).
11. E. J. GABE, F. L. LEE, and Y. LEPAGE. *In* Crystallographic computing 3. *Edited by* G. Sheldrick, C. Kruger, and R. Goddard. Clarendon Press, Oxford. 1985. p. 167.
12. International tables for X-ray crystallography. Vol IV. Kynoch Press, Birmingham, England. 1974. p. 99. Table 2.2B.
13. B. COHEN, C. C. OU, R. A. LALANCETTE, W. BOROWSKI, J. A. POTENZA, and H. J. SCHUGAR. Inorg. Chem. **18**, 217 (1979).
14. F. A. COTTON and G. WILKINSON. Advanced inorganic chemistry. 4th ed. Wiley, Toronto. 1980. p. 812.
15. P. W. R. CORFIELD, C. CECCARELLI, M. D. GLICK, I. W.-Y. MOY, L. A. OCHRYMOWYCZ, and D. B. RORABACHER. J. Am. Chem. Soc. **107**, 2399 (1985).
16. J. E. HUHEEY. Inorganic chemistry. 3rd ed. Harper and Row, New York. 1983. p. 258.
17. J. R. FERRARO. Low frequency vibrations of inorganic and coordination compounds. Plenum, New York. 1971. p. 175.
18. V. M. MISKOWSKI, J. A. THICH, R. SOLOMON, and H. S. SCHUGAR. J. Am. Chem. Soc. **98**, 8344 (1976).
19. A. B. P. LEVER. Inorganic electronic spectroscopy 2nd ed. Elsevier, Amsterdam. 1984. pp. 554–569.
20. A. I. SCOTT. Interpretation of the ultraviolet spectra of natural products. Pergamon Press, Oxford. 1964. p. 135.

Can. J. Chem. Downloaded from www.nrcresearchpress.com by 41.223.56.140 on 09/07/12
For personal use only.

Excess molar volumes, speeds of sound, and isentropic compressibilities of binary mixtures of furfural with some aliphatic alcohols

HOMENDRA NAOREM, NAND KISHORE, AND S. K. SURI[1]

Department of Chemistry, Indian Institute of Technology, Hauz Khas, New Delhi-110016, India

Received August 17, 1988

HOMENDRA NAOREM, NAND KISHORE, and S. K. SURI. Can. J. Chem. **67**, 648 (1989).

Excess molar volumes and isentropic compressibilities for the binary mixtures of furfural with methanol, ethanol, 1-propanol, 2-propanol, 1-butanol, and 2-butanol have been computed from the experimentally measured densities and sound speeds at 308.15 K over the entire composition range. All the systems studied exhibit contraction on mixing. The results have been discussed in terms of the specific interactions between the component molecules of the binary mixtures.

Key words: excess molar volumes, isentropic compressibilities, furfural, aliphatic alcohols, unlike reactions.

HOMENDRA NAOREM, NAND KISHORE et S. K. SURI. Can. J. Chem. **67**, 648 (1989).

Utilisant les densités et les vitesses du son mesurées expérimentalement, à 308,15 K, sur l'ensemble des compositions des mélanges, on a calculé les volumes molaires en excès ainsi que les compressibilités isentropiques des mélanges binaires du furfural avec le méthanol, l'éthanol, les propanols-1 et -2 et les butanols-1 et -2. Dans tous les systèmes étudiés, les mélanges provoquent une contraction. On discute des résultats en fonction d'interactions spécifiques entre les molécules qui composent les mélanges binaires.

Mots clés : volumes molaires en excès, compressibilités isentropiques, furfural, alcools aliphatiques, réactions dissemblables.

[Traduit par la revue]

Can. J. Chem. Downloaded from www.nrcresearchpress.com by 41.223.56.140 on 09/07/12
For personal use only.

1. Introduction

The thermodynamic properties of binary mixtures containing a self-associated component exhibit a significant deviation from ideality, arising not only from differences in molecular size but also from the changes in the hydrogen bonding between like and unlike molecules. As an extension to our studies on the thermodynamic properties of binary mixtures containing a self-associated component (1–3), the excess molar volumes, V^E, and the isentropic compressibilities, k_s, of binary mixtures of furfural with six aliphatic alcohols, namely, methanol, ethanol, 1-propanol, 2-propanol, 1-butanol, and 2-butanol have been determined at 308.15 K over the entire composition range and reported in this paper. These studies are aimed to provide information on the binary mixtures with a view to understanding the nature of interactions present in these mixtures.

2. Experimental

Analytical reagent grade samples of methanol, ethanol, 1-butanol and 2-butanol supplied by E. Merck and Laboratory reagent grade samples of 1-propanol and 2-propanol supplied by BDH were purified by following the standard established procedures (4). The sample of furfural was essentially the one used for our earlier studies (5). The liquids were stored in brown bottles and fractionally distilled immediately before use. The densities (ρ) and refractive indexes of the purified liquids agreed closely with the accepted literature values (4, 6).

The excess molar volumes of mixing have been calculated from the experimental density data. The solutions for the measurement of densities were prepared by weight and correction for buoyancy were applied. The details of experimental techniques for the preparation of solutions have been described elsewhere (7). The densities were measured using a vibrating tube flow densimeter (Model DMA 60/602 Anton Paar, Austria). Water from a thermostat was circulated through the densimeter module at a flow rate of 2–3 L min^{-1}. The temperature of the thermostat was maintained at ±0.01 K by using a precision temperature controller. The densimeter was calibrated with nitrogen gas and degassed ion exchanged water by using the densities of Kell (8). Duplicate densities of liquids and the liquid mixtures were reproducible to within 5×10^{-5} g cm^{-3}. An analysis of experimental uncertainties lead to the conclusion that the reported excess volumes of mixing are within ±0.008 cm^3 mol^{-1}.

TABLE 1. Values of the parameters in eq. [1] and standard deviation $\sigma(V^E)$

Furfural +	A_0	A_1	A_2	A_3	$\sigma(V^E)$
Methanol	−0.8247	−0.2498	0.1868	−0.0776	0.003
Ethanol	−0.7455	−0.2663	−0.0079	0.0329	0.002
1-Propanol	−0.6693	−0.3768	0.0369	0.1233	0.002
2-Propanol	−0.3100	−0.0408	0.1089	0.0489	0.002
1-Butanol	−0.5972	−0.2274	0.2008	0.1636	0.005
2-Butanol	−0.1351	−0.1193	0.0676	0.1650	0.004

The isentropic compressibilities were computed from the ultrasonic speeds of sound, u, using the relation:

$$k_s = (u^2\rho)^{-1}$$

The speeds of sound were measured using a single crystal interferometer (Model F-81, Mittal Enterprises, New Delhi, India) operating at a frequency of 2 MHz. The maximum error in the measurement of u was estimated to be around 0.15%. This renders the k_s values uncertain by ±2 T Pa^{-1}.

Results and discussion

The experimental data[2] on excess molar volumes were fitted to smoothing equation:

$$[1] \quad V^E/(cm^3\,mol^{-1}) = x(1-x)\sum_{i=0}^{n} A_i(2x-1)^i$$

Where x is the mole fraction of furfural in the mixture. The parameters A_i evaluated by the method of least squares (unweighted) are recorded in Table 1 along with the standard deviation $\sigma(V^E)$. Since the $\sigma(V^E)$ values in all the systems studied are less than the experimental uncertainty, the constants

[1]To whom all correspondence should be addressed.

[2]A complete set of data may be purchased from the Depository of Unpublished Data, CISTI, National Research Council of Canada, Ottawa, Ont., Canada K1A 0R6.

Printed in Canada / Imprimé au Canada

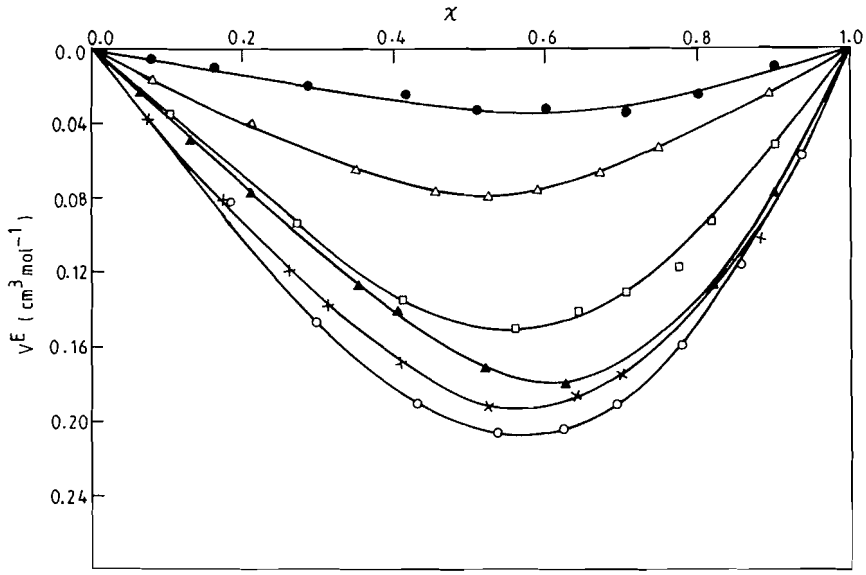


FIG. 1. Molar excess volumes, V^E, at 308.15 K for the binary mixtures of furfural with (○) methanol, (×) ethanol, (▲) 1-propanol, (△) 2-propanol, (□) 1-butanol, and (●) 2-butanol.

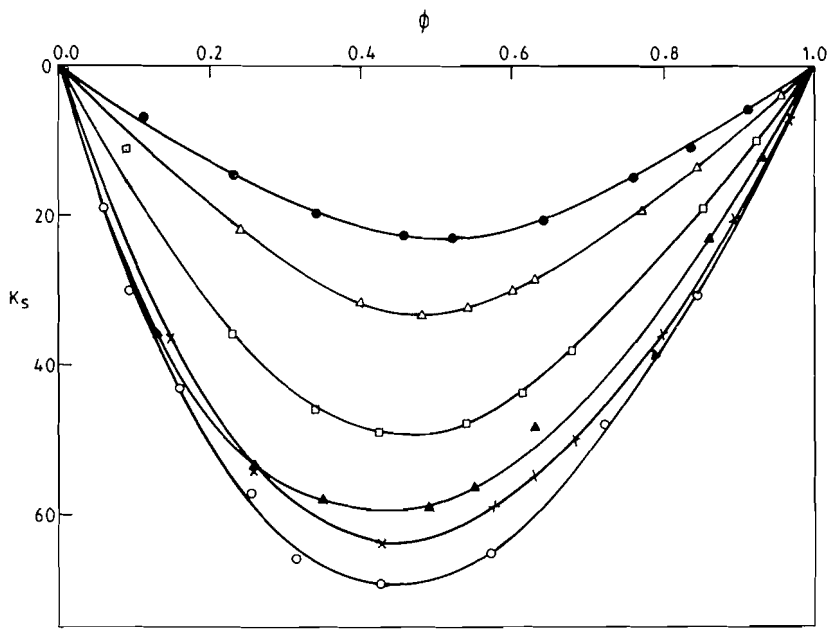


FIG. 2. Values of K_s against volume fraction of furfural for the binary mixtures of furfural with (○) methanol, (×) ethanol, (▲) 1-propanol, (△) 2-propanol, (□) 1-butanol, and (●) 2-butanol at 308.15 K.

of eq. [1] can be taken to represent experimental results. The graphical representation of the results are shown in Fig. 1.

The deviation in the isentropic compressibilities K_s of binary mixtures were computed from the experimentally determined isentropic compressibilities using the expression:

$$[2] \quad K_s = k_s - \phi k_{s,1} - (1 - \phi)k_{s,2}$$

where ϕ is the volume fraction of furfural in the binary mixtures, k_s, $k_{s,1}$ and $k_{s,2}$ are the isentropic compressibilities of the liquid mixture, furfural, and alcohols, respectively. The variation of K_s with the volume fraction of furfural in the binary mixtures are shown in Fig. 2. The K_s values thus obtained have been fitted to the polynomial:

$$[3] \quad K_s = \phi(1 - \phi)[B_0 + B_1(2\phi - 1) + B_2(2\phi - 1)^2 + B_3(2\phi - 1)^3]$$

The parameters B_0, B_1, B_2, and B_3 determined by the method of least squares (unweighted) are given in Table 2, along with the standard deviation $\sigma(K_s)$.

To the best of our knowledge there is no data available in the reported literature for the V^E and K_s of any of the binary mixtures under investigation to compare with our results.

It is observed from Fig. 1 that all the binary mixtures studied exhibit contraction on mixing over the entire composition range. The excess molar volumes at equimolar concentration, $V^E_{0.5}$ increases in the order: methanol < ethanol < 1-propanol

Can. J. Chem. Downloaded from www.nrcresearchpress.com by 41.223.56.140 on 09/07/12
For personal use only.

TABLE 2. Values of parameters of eq. [3] and standard deviation $\sigma(K_s)$

Furfural +	B_0	B_1	B_2	B_3	$\sigma(K_s)$
Methanol	−270	64	−24	13	2
Ethanol	−253	80	4	−87	2
1-Propanol	−231	54	41	53	3
2-Propanol	−134	85	89	−283	3
1-Butanol	−201	62	89	−103	1
2-Butanol	−93	3	30	−8	1

< 1-butanol < 2-propanol < 2-butanol. The large negative excess volume for the binary mixtures containing methanol (Fig. 1) indicate that the volumetric effects arising from the unlike interactions between furfural and methanol supercedes the positive contribution to V^E due to the structure breaking of the polymer aggregates of methanol. The self-associated polymer aggregates of higher alcohols are relatively easier to break and are associated with the relatively smaller volumetric effects. Also, the hydrogen bond energy between the hydroxyl group of the alcohol and the hydrogen acceptor oxygen of furfural and consequently the volumetric effects arising therefrom decrease with the increasing alkyl chain length of the alcohol. Experimentally determined V^E values (Fig. 1) reveal that the unlike interactions between the aliphatic alcohols and furfural are fairly strong and predominant to determine the solution behaviour of these binary mixtures. A comparison of V^E values for the binary mixtures of furfural + *n*-alkanols with data reported in literature for the binary mixtures of tetrahydrofuran + *n*-alkanols (3) reveals that the unlike interactions are very strong in the former case resulting in the formation of intermolecular "complexes" through hydrogen bonding. A relatively higher V^E for mixtures containing 2-propanol and 2-butanol as compared to those containing 1-propanol and 1-butanol, respectively, reflects on their weaker hydrogen-bonding interactions with furfural due to steric factors (3, 9). For these systems, the positive contribution to V^E arising from the easiness of breaking the intermolecular structure of branched chain alcohols is expected to be small and hence less significant.

It is observed from Fig. 2 that K_s values for all the mixtures studied are negative over the entire composition range and follow the order: methanol < ethanol < 1-propanol < 1-butanol < 2-propanol < 2-butanol. It is established that the presence of specific interactions between the component molecules in binary mixtures leads to a decrease in the free space whereby contributing to a positive deviation in speeds of sound and negative deviation in isentropic compressibilities (10). The K_s is expected to become increasingly negative as the strength of interactions between the unlike molecules increases. The observed K_s values corroborates the conclusions drawn from V^E studies.

1. S. K. SURI, R. C. MAHESHWARI, and P. L. YADAV. Indian J. Chem. **12**, 620 (1974).
2. S. K. SURI. Thermochim. Acta, **39**, 325 (1980).
3. B. CHAWLA and S. K. SURI. Thermochim. Acta, **41**, 147 (1980).
4. J. A. RIDDICK and W. B. BUNGER. Organic solvents 3rd ed. Wiley-Interscience, New York. 1970.
5. H. NAOREM and S. K. SURI. Can. J. Chem. **66**, 1295 (1988).
6. J. TIMMERMANS. Physico-chemical constants of pure organic compounds. Vol. II. Elsevier, Amsterdam. 1965.
7. R. C. MAHESHWARI, S. K. SURI, and V. S. TEWARI. J. Chem. Eng. Data, **24**, 237 (1979).
8. G. S. KELL. J. Chem. Eng. Data, **15**, 119 (1970).
9. G. NARAYANASWAMY, G. DHARMAJU, and G. K. RAMAN. J. Chem. Thermodyn. **13**, 327 (1981).
10. R. J. FORT and W. R. MOORE. Trans. Faraday Soc. **61**, 2102 (1965).

Can. J. Chem. Downloaded from www.nrcresearchpress.com by 41.223.56.140 on 09/07/12
For personal use only.

Carbohydrate metal ion complexes. Interaction of D-glucono-1,5-lactone with Zn(II), Cd(II), and Hg(II) ions in the solid and aqueous solution, studied by ^{13}C-NMR, FT-IR, and X-ray powder diffraction measurements

H. A. TAJMIR-RIAHI

Department of Chemistry, University of Laval, Quebec, P.Q., Canada G1K 7P4

Received August 12, 1988

H. A. TAJMIR-RIAHI. Can. J. Chem. **67**, 651 (1989).

D-Glucono-1,5-lactone interaction with zinc group metal ions has been studied in aqueous solution and solid salts of the type Zn(D-gluconate)$_2$.2H$_2$O, Cd(D-gluconate)$_2$ and Hg(D-gluconate)$_2$ have been isolated. These metal sugar salts were characterized by elemental analysis, ^{13}C-NMR, FT-IR spectroscopy, and X-ray powder diffraction measurements.

X-ray powder diffraction diagrams and other spectroscopic evidence showed that Zn(D-gluconate)$_2$.2H$_2$O is isomorphous with the structurally identified Mn(D-gluconate)$_2$.2H$_2$O, suggesting a similar metal–sugar binding mode, through a carboxylate oxygen atom (O-1) and an OH group of the two sugars anions as well as to two H$_2$O molecules, resulting in a six-coordinate Zn(II) ion. The Cd(II)- and Hg-D-gluconate salts are not similar and show dissimilarities to the Zn(II) compound. The Cd(II) ion binds to two D-gluconate anions possibly through the carboxylate O-1 and sugar O(2)—H, and O(3)—H groups of each anion, giving a six-coordinate Cd(II) ion. The Hg(II) ion is possibly four-coordinate, binding to two sugar anions via a carboxylate O-1 and O(2)—H groups of each D-gluconate anion. The zinc group metal–D-gluconate salts are aggregated through bridging sugar OCO$^-$ groups with sugar anion possibly having bent-chain conformation.

Key words: carbohydrate, metal ions, ^{13}C-NMR, FT-IR, X-ray powder diffraction.

H. A. TAJMIR-RIAHI. Can. J. Chem. **67**, 651 (1989).

Opérant en solutions aqueuses, on a étudié les interactions de la D-gluconolactone-1,5 avec les ions métalliques du groupe du zinc et on a isolé des sels solides du type Zn(D-gluconate)$_2$.2H$_2$O, Cd(D-gluconate)$_2$ et Hg(D-gluconate)$_2$. On a caractérisé ces sels métalliques des sucres en faisant appel à des analyses élémentaires, à la rmn du ^{13}C, à la spectroscopie ir par transformation de Fourier et par des mesures de diffraction des rayons-X sur des poudres.

Les diagrammes de diffraction des rayons-X sur des poudres et d'autres données spectroscopiques démontrent que le Zn(D-gluconate)$_2$.H$_2$O est isomorphe du Mn(D-gluconate)$_2$.H$_2$O dont la structure a été identifiée; ces résultats suggèrent que le mode de liaison métal–sucre est semblable, qu'il se produit par le biais d'un atome d'oxygène (O-1) du carboxylate et des groupements OH de deux anions de sucre ainsi que deux molécules de H$_2$O et qu'il conduit à la formaion d'un ion Zn(II) qui est hexa-coordonné. Les sels de Cd(II)– et Hg–D-gluconates ne sont pas semblables et ils présentent des dissymétries par rapport au composé Zn(II). L'ion de Cd(II) se lie à des anions de D-gluconate, possiblement par le biais de l'oxygène O-1 du carboxylate et des groupements O(2)—H et O(3)—H du sucre de chacun des anions, et il donne naissance à un ion Cd(II) qui est hexa-coordonné. Il est possible que l'ion Hg(II) soit tétra-coordonné par la liaison à deux anions de sucres par le biais des groupements O-1 d'un carboxylate et O(2)—H de chacun des anions de D-gluconate. Les sels métalliques du D-gluconate avec des métaux du groupe du zinc forment des agrégats à l'aide de groupements OCO$^-$ agissant comme ponts avec des anions de sucre qui existent peut-être dans des conformations de chaînes repliées.

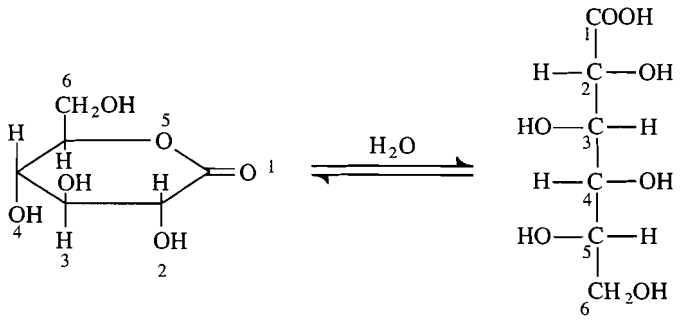
Mots clés : hydrate de carbone, ions métalliques, RMN du ^{13}C, FT-IR, diffraction des rayons-X.

[Traduit par la revue]

Introduction

On the basis of lanthanide-induced ^{1}H-NMR studies, Taga *et al.* (1) have demonstrated how the polyhydroxyl carboxylic acids containing α-carboxy, α-hydroxy, and β-hydroxy oxygen atoms such as glyceric acid, gluconic acid, and lactobionic acid can chelate the lanthanide(III) ions through O-1, O-2, and O-3 oxygen atoms. Similarly, the binding modes of lanthanide ions with D-galacturonic and D-glucuronic acids have been reported (2, 3). The chelating ability of several sugar moieties such as D-glucuronic acid, L-arabinose, D-fructose, and D-glucose with zinc group and alkaline earth metal ions has been reported (4–10). Recently, on the basis of ^{13}C-NMR, FT-IR spectroscopy, and X-ray powder diffraction measurements, we have shown (11) how the alkaline earth metal ions bind to D-gluconic acid (Scheme 1) through O-1, O-2, and O-3 oxygen atoms. Therefore, it is of interest to study the zinc group metal ion interaction with D-gluconic acid, both in the solid and in aqueous solution.

In the present work, we describe the synthesis and characterization of several complexes formed between D-gluconate anion and zinc group metal ions (zinc, cadmium, and mercury), both in the solid and in aqueous solution, using ^{13}C-NMR, FT-IR spectroscopy and X-ray powder diffraction measurements, that have not been reported elsewhere. Furthermore, comparisons were made between the spectroscopic properties of these metal–D-gluconate salts and those of the structurally known Mn(D-gluconate)$_2$.2H$_2$O (12), Pb(D-gluconate)$_2$ (13), and Mg(D-gluconate)$_2$.2H$_2$O (11), in order to detect the characteristic features of each structural type of compound synthesized for the zinc group metal cations and to establish a correlation be-



SCHEME 1

Can. J. Chem. Downloaded from www.nrcresearchpress.com by 41.223.56.140 on 09/07/12
For personal use only.

TABLE 1. ^{13}C-NMR chemical shifts (ppm) for D-glucono-1,5-lactone, D-gluconic acid, and their metal ion complexes in D_2O solution*

Compounds	Chemical shift					
	C-1	C-2	C-3	C-4	C-5	C-6
D-Glucono-1,5-lactone	175.20	82.24	73.50	72.00	67.95	60.80
D-Gluconic acid	176.40	73.25	72.30	71.95	71.50	63.50
Zn(D-gluconate)$_2$, $2H_2O$	178.80	73.67	72.93	71.87	71.47	63.37
Cd(D-gluconate)$_2$	179.10	73.95	72.95	71.83	71.65	63.47
Hg(D-gluconate)$_2$	177.90	74.45	72.50	71.89	71.50	63.49
Pb(D-gluconate)$_2$	180.50	75.40	72.99	71.99	71.77	63.40

*Using dioxane as the reference (67.40 ppm).

tween the spectral modifications and the binding sites used by D-gluconate anion.

Experimental

Materials and methods

D-Glucono-1,5-lactone was purchased from Aldrich Chemical Company and used as supplied. All other chemicals were reagent grade and were used without further purification.

Synthesis of the zinc group metal–D-gluconate complexes

A solution of zinc group metal carbonate (1 mmol) in H_2O (20 mL) was added to a hot solution of D-glucono-1,5-lactone (2 mmol) in H_2O (50 mL) and the mixture was heated up to 80°C till at the insoluble metal carbonate was dissolved. The solution was cooled down to room temperature and ethanol (75 mL) was added to precipitate the white compound. This was filtered off and washed with ethanol several times. *Anal.* calcd. for $Zn(C_6H_{11}O_7).2H_2O$: C 29.30, H 5.29, Zn 13.30; found: C 28.70, H 5.15, Zn 12.95. *Anal.* calcd. for $Cd(C_6H_{11}O_7)_2$: C 28.05, H 4.38, Cd 22.36; found: C 27.80, H 4.20, Cd 21.90. *Anal.* calcd. for $Hg(C_6H_{11}O_7)_2$: C 24.04, H 3.72, Hg 33.96; found: C 23.75, H 3.55, Hg 33.60. The zinc group metal–D-gluconate salts are soluble in hot water and not soluble in common organic solvents.

Physical measurements

The ^{13}C-NMR spectra were recorded on a Bruker WH-80 instrument in D_2O solution containing dioxane as reference. X-ray powder diffraction diagrams were recorded on a diffractometer Philips Pw 1011 with copper K_α radiation. The FT-IR spectra were recorded on a DIGILAB FTS-15C/D Fourier Transform infrared interferometer equipped with HgCdTe detector and KBr beam splitter. The spectra were taken as KBr pellets with resolution of 2 to 4 cm^{-1}.

Results and discussion

^{13}C-NMR spectra

The assignments of the ^{13}C-NMR chemical shifts of the free D-gluconic acid and D-glucono-1,5-lactone have been reported (14) and our results given in Table 1 are in good agreement with those reported in literature (14). Upon acid complexation, the free acid C-1 (carboxyl) chemical shift at 176.40 ppm showed major downfield shift at 178–179 ppm, the C-2 at 73.25 ppm was shifted to 73.7–74.5 ppm, and C-3 at 72.30 ppm also showed a small downfield shift at about 72.5–72.95 ppm, whereas the C-4, C-5, C-6 were almost unaffected by sugar complex formation (Table 1). The downfield shifts of the C-1 and C-2 chemical shifts are due to the participation of the sugar carboxylate oxygen atom and O(2)—H group in metal–D-gluconate bindings. Similar shifts were observed for the structurally known Pb(D-gluconate)$_2$ salt (Table 1), where metal–sugar bindings were found to be through carboxylate oxygen atom and O(2)—H hydroxyl group (13). Similar trends were also observed in the ^{13}C-NMR spectra of the alkaline earth metal–D-gluconate complexes, where metal–sugar binding via

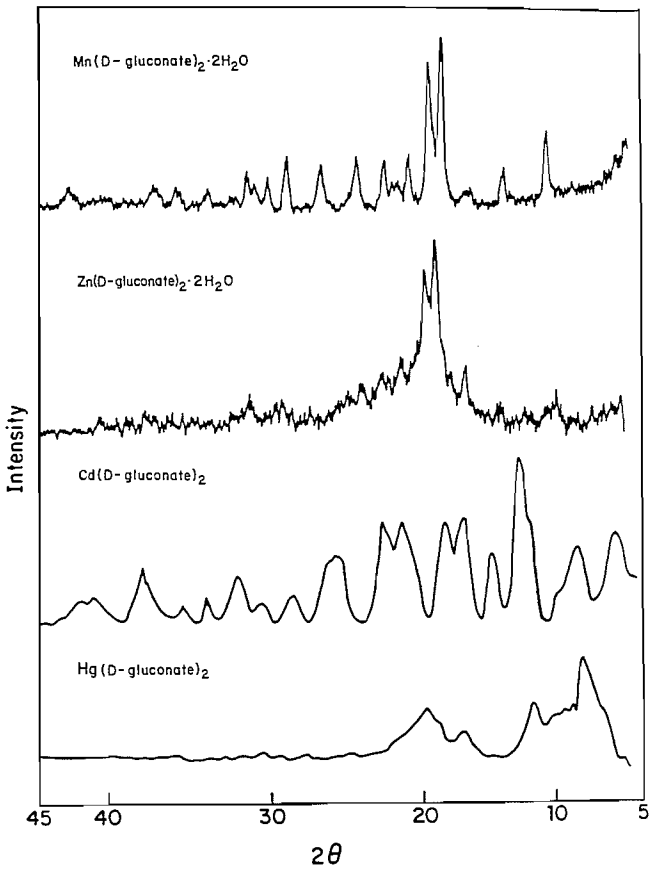


FIG. 1. X-ray powder diffraction patterns of the zinc group metal–D-gluconate complexes and the structurally known Mn(II)–D-gluconate salt.

O-1 and O-2 were suggested (11). It should be noted that although the structures of the zinc group metal–D-gluconate salts are different in the solid state (due to different coordination numbers and binding modes), their ^{13}C-NMR spectra are almost identical and this is indicative of similar structural behaviours of these metal–sugar complexes in aqueous solution.

X-Ray powder diffraction diagrams

The X-ray powder diffraction patterns of the zinc group metal–D-gluconate salts are compared with those of the structurally known Mn(D-gluconate)$_2$.$2H_2O$ in Fig. 1. It is evident that the X-ray powder pattern of the Zn(D-gluconate)$_2$.$2H_2O$ is almost similar to that of the known Mn(D-gluconate)$_2$.$2H_2O$ (particularly, the strongest features of both spectra) (Fig. 1). These suggest a similar coordination number and sugar binding mode, for the Zn(D-gluconate)$_2$.$2H_2O$ salt. On the other hand, the X-ray powder patterns of the Cd(II)– and Hg(II)–D-gluconate salts are dissimilar and they are different from those of the zinc and manganese complexes (Fig. 1). The observed dissimilarities are related to different sugar binding modes, in the Cd(II)– and Hg(II)–sugar salts. It might be possible that the binding of the D-gluconate anions in the Cd(D-gluconate)$_2$ occur through O-1, O-2, and O-3 of each sugar anion, resulting in a six-coordination around the cadmium ion, while in the Hg(D-gluconate)$_2$ salt, each sugar binding is via O-1 and O-2 oxygen atoms, with Hg(II) ion being four-coordinate. It should be noted that the poor quality of X-ray powder patterns of the Cd(II)– and Hg(II)–D-gluconate salts are related to the less crystallinity of these metal–sugar salts. However, several important features of each spectrum are comparable with those of the zinc– and manganese–D-gluconate complexes (Fig. 1).

Can. J. Chem. Downloaded from www.nrcresearchpress.com by 41.223.56.140 on 09/07/12
For personal use only.

Can. J. Chem. Downloaded from www.nrcresearchpress.com by 41.223.56.140 on 09/07/12
For personal use only.

FT-IR spectra

The FT-IR spectra of the zinc group metal–D-gluconate and D-glucono-1,5-lactone have been studied in the 3700–500 cm^{-1} region and comparisons were made with those of the corresponding structurally identified compounds Mn(D-gluconate)$_2$.2H$_2$O, Pb(D-gluconate), and Mg(D-gluconate)$_2$.2H$_2$O. The spectral analysis results are discussed below:

Sugar OH stretching vibrations and zinc group metal ion bindings

In the crystal structure of D-glucono-1,5-lactone, there are four distinct H-bonding systems (15) and based on the intermolecular O...O distances, the four strong and broad bands observed in the 3500–3200 cm^{-1} region in the IR spectrum of the free lactone are assigned as follows: A broad and strong band at 3462 cm^{-1} is assigned to the O(6)—H...O(2) with O...O = 2.882 Å, a broad and strong band at 3387 cm^{-1} is due to the O(4)—H...O(1) with O...O = 2.849 Å, a broad absorption band at 3277 cm^{-1} is attributed to the O(2)—H...O(3) with O...O = 2.720 Å and finally, a strong and broad band at 3225 cm^{-1} is assigned to the strongly hydrogen bonded O(3)—H...O(6) with O...O = 2.680 Å (Fig. 2).

Upon zinc group metal ions complex formation, the lactone OH stretching vibrations in the 3500–3200 cm^{-1} region showed shifting and broadening in the spectra of the Zn(II)–, Cd(II)–, and Hg(II)–D-gluconate salts (Fig. 2). The shifting and broadening of the sugar OH stretching vibrations, on complexation, are related to the participation of the sugar OH groups in metal–ligand bondings. Similar spectral changes were observed in the IR spectra of the structurally known Mn(D-gluconate)$_2$.2H$_2$O (Fig. 2), where metal–sugar bindings were found to be via sugar OH groups as well as carboxylate anions (12). It is interesting to note that the IR spectrum of the Mn(D-gluconate)$_2$.2H$_2$O, Mg(D-gluconate)$_2$.2H$_2$O, and Zn(D-gluconate)$_2$.2H$_2$O salts are almost identical (Fig. 2 and ref. 11). This is indicative of the similar coordination numbers (C.N. = 6) and sugar binding modes for the Zn(D-gluconate)$_2$.2H$_2$O salt. This is also consistent with X-ray powder diffraction patterns, which showed isomorphic features for the Zn(II)– and Mn(D-gluconate)$_2$.2H$_2$O compounds (Fig. 1). It should be noted that the major broadenings of sugar OH stretching vibrations, in the spectra of the zinc group metal–D-gluconate salts, are due to the presence of a strong H-bonding network between the sugar OH groups and H$_2$O molecules in the crystal structures of these metal–sugar salts, which is responsible for the stabilization of the solid structure and for holding the aggregate units together. Such a H-bonding system found in the crystal structure of the Mn(D-gluconate)$_2$.2H$_2$O salt in aggregated form (12).

A broad band with medium intensity at about 3150 cm^{-1}, in the spectra of the Zn(II)– and Mn(D-gluconate)$_2$.2H$_2$O, which is absent in the lactone spectrum and Cd(II)– or Hg(II)–D-gluconate salt, is attributed to the OH stretching vibration of the bonded H$_2$O molecules (Fig. 2). Similarly, a shoulder band at about 1640 cm^{-1} in the spectra of the Mn(II)– and Zn(D-gluconate)$_2$.2H$_2$O salts, which is not present in the uncomplexed sugar and other zinc group metal–D-gluconate compounds, is also assigned to the bending mode of the coordinated water molecule (Fig. 3).

Sugar carbonyl stretching vibration and zinc group metal ion bindings

The carbonyl stretching vibration of the D-glucono-1,5-lactone was observed as a strong band at 1728 cm^{-1} and exhibited splitting and shifting towards lower frequencies, in the spectra of the zinc group metal-D-gluconate complexes (Fig. 3). The

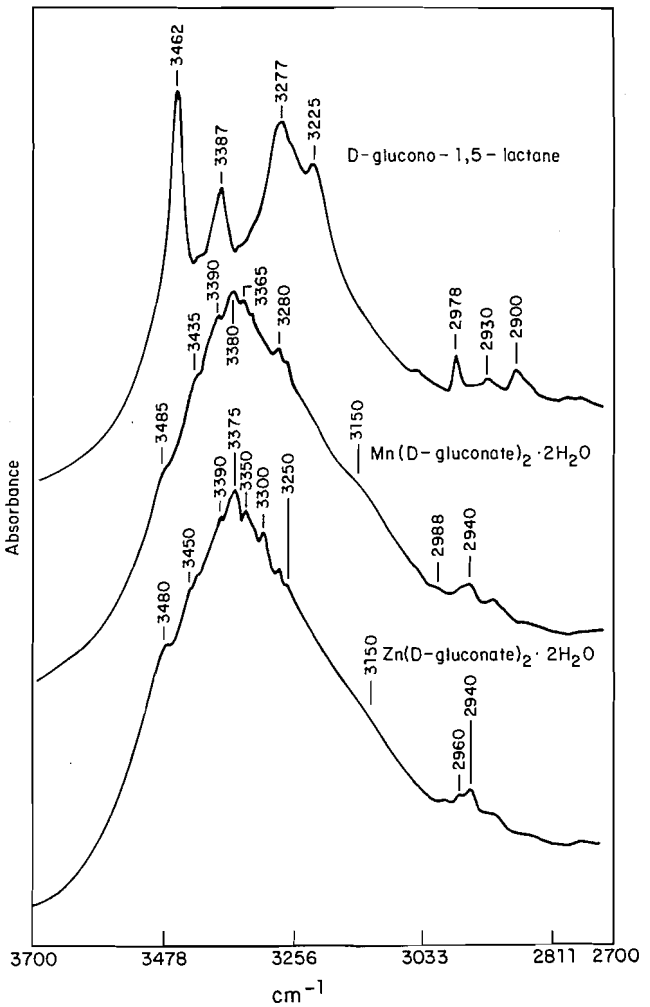


FIG. 2. FT-IR spectra of the free D-glucono-1,5-lactone and its metal ion salts in the region of 3700–2700 cm^{-1}.

two broad and strong bands at about 1600 and 1400 cm^{-1} observed in the spectra of these metal–sugar salts are assigned to the antisymmetric and symmetric carboxylate OCO^- stretching vibrations, respectively (16). The shifting and splitting of the carbonyl stretching vibration, upon lactone complexation, are due to the sugar ionization and participation of the OCO^- group in metal–sugar bindings. Similar shifting and splitting of the carbonyl group stretching frequency was observed in the spectra of the structurally known Mn(D-gluconate)$_2$.2H$_2$O (Fig. 3) and Pb(D-gluconate)$_2$ compounds (17), where direct metal–carboxylate coordination was observed (12, 13). It has been suggested that separation between the antisymmetric and symmetric OCO^- stretching vibrations is a measure of the unidentate, bidentate or bridging coordination of the carboxylate group, in a series of metal–carboxylate complexes (18). The separation of about 180–185 cm^{-1} of the two OCO^- components, observed in the IR spectra of the zinc group metal–D-gluconate compounds is indicative of the unidentate and bridging modes of OCO^- binding, in these metal–sugar complexes (Fig. 3). This is in agreement with the structural analysis of the Mn(D-gluconate)$_2$.2H$_2$O and Pb(D-gluconate)$_2$ salts, which contained unidentate and bridging metal–carboxylate bindings (12, 13). It should be noted that aggregation of these metal–sugar complexes occurs through carboxylate oxygen atoms.

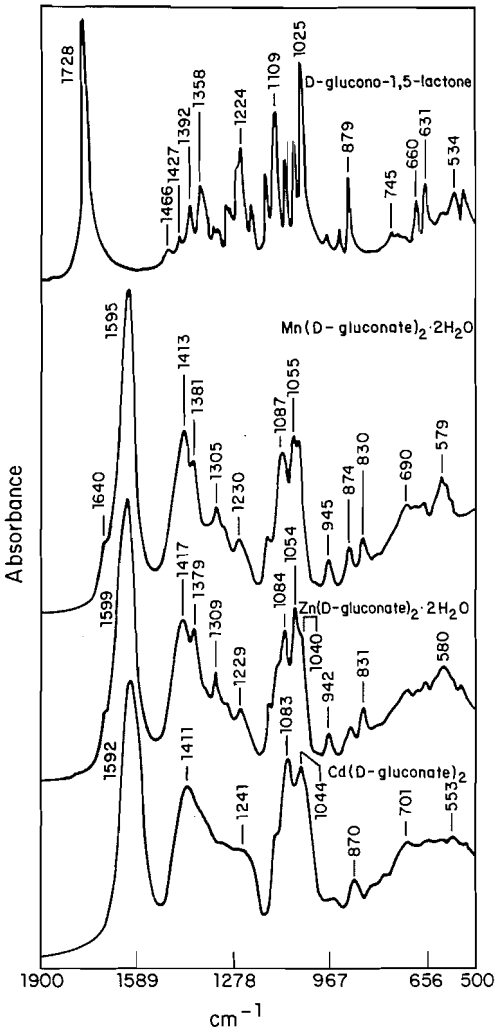


FIG. 3. FT-IR spectra of the free D-glucono-1,5-lactone and its metal ion salts in the region of 1900–500 cm^{-1}.

Sugar ring vibrational frequencies and zinc group metal ion interaction

The lactone ring CH_2, COH, and CCH bending modes (19, 20) at about 1460–1100 cm^{-1}, exhibited shifting and broadening, upon zinc group metal ion complex formation (Fig. 3). The observed spectral changes for the OH bending modes and sugar OH stretching vibrations in the region of 3500–3200 cm^{-1} together are the results of the metal–sugar binding via D-gluconate OH groups. Similar spectral modifications are observed in the sugar OH bending modes in the spectra of the known Mn–D-gluconate salt (Fig. 3), which contains Mn–sugar OH bindings as well as Mn—OCO^- interaction (12). The lactone ring C—O stretching vibrations (19, 20) appeared as several strong bands in the region of 1100–900 cm^{-1} and exhibited broadening and shifting, on sugar salt formation (Fig. 3). These observed spectral changes are the consequences of the metal–sugar OH bindings and the rearrangements of the sugar H-bonding system, upon acid ionization and metallation.

In conclusion, Zn((D-gluconate)$_2$.$2H_2O$ is similar in structure to that of the known Mn(D-gluconate)$_2$.$2H_2O$ (12) and Mg(D-gluconate)$_2$.$2H_2O$ (11) salts (having almost identical ^{13}C-NMR, FT-IR, and X-ray powder spectra), suggesting a similar six-coordination and binding mode (through each sugar anion carboxylate oxygen atom and an OH group as well as to two H_2O molecules) for the Zn(II) ion. The Cd(II) ion six-coordination could be completed by binding to two D-gluconate anions via O-1, O-2, and O-3 of each sugar anion. Similar binding modes through α-carboxy, α-hydroxy, and β-hydroxy oxygen atoms were found in the lanthanide(III)–D-gluconate complexes (1) and for the Ca(II), Sr(II), and Ba(II)–D-gluconate salts (11). The Hg(II) ion could be four-coordinate, binding to two sugar anions through O-1 and O-2 oxygen atoms of each acid anion, forming a five-membered ring chelation. The IR spectra and X-ray powder patterns of the Cd(II)– and Hg(II)–D-gluconate salts were different from those of the Zn(II)– and Mn(II)–sugar salts.

The marked spectral similarities of the zinc group metal–D-gluconate salts with those of the Mn(II)–, Pb(II)–, or alkaline earth metal–D-gluconate compounds suggest a similar aggregation for these metal–sugar complexes. Such aggregation can occur through a bridging carboxylate oxygen atoms or other sugar donor groups, which is consistent with the polymeric nature of the Mn(II)– or Pb(II)–D-gluconate salt, in the solid state, found through X-ray diffraction measurements (12, 13). In the structurally identified Mn(D-gluconate)$_2$.$2H_2O$ compound, the sugar anion has a bent-chain conformation (12) and on the basis of the similarities in their spectroscopic properties, one can suggest a similar bent-chain conformation, for the zinc group metal–D-gluconate salts.

1. T. TAGA, Y. KURODO, and M. OHASHI. Bull. Chem. Soc. Jpn. **51**, 2278 (1978).
2. K. ISUMI. Agr. Bio. Chem. **44**, 1623 (1980).
3. S. J. ANGYAL, D. GREEVES, and L. LITTLEMORE. Carbohydr. Res. **174**, 121 (1988).
4. H. A. TAJMIR-RIAHI. J. Inorg. Biochem. **26**, 23 (1986).
5. H. A. TAJMIR-RIAHI. J. Inorg. Biochem. **27**, 65 (1986).
6. H. A. TAJMIR-RIAHI. Carbohydr. Res. **172**, 1 (1988).
7. H. A. TAJMIR-RIAHI. Carbohydr. Res. **183**, 35 (1988).
8. H. A. TAJMIR-RIAHI. Carbohydr. Res. **122**, 241 (1983); J. Inorg. Biochem. **24**, 127 (1985).
9. H. A. TAJMIR-RIAHI. Carbohydr. Res. **127**, 1 (1984); J. Inorg. Biochem. **22**, 55 (1984); Biophys. Chem. **25**, 271 (1986).
10. H. A. TAJMIR-RIAHI. Carbohydr. Res. **172**, 327 (1988); Carbohydr. Res. In press; J. Inorg. Biochem. **27**, 123 (1986); Biophys. Chem. **23**, 223 (1986).
11. H. A. TAJMIR-RIAHI. Inorg. Chim. Acta, In press.
12. T. LIS. Acta Crystallogr. B**35**, 1699 (1979).
13. T. LIS. Acta Crystallogr. C**40**, 374 (1984).
14. K. BOCK and C. PEDERSEN. Adv. Carbohydr. Chem. Biochem. **41**, 27 (1983).
15. M. L. HACKERT and R. A. JACOBSON. Acta Crystallogr. **27**, 203 (1971).
16. H. A. TAJMIR-RIAHI. J. Inorg. Biochem. **27**, 205 (1986).
17. H. A. TAJMIR-RIAHI. Bull. Chem. Soc. Jpn. In press.
18. K. NAKAMOTO, Y. MORIMOTO, and A. E. MARTELL. J. Am. Chem. Soc. **80**, 4528 (1961).
19. M. HINENO. Carbohydr. Res. **56**, 219 (1977).
20. J. J. CAEL, J. L. KOENIG, and J. BLACKWELL. Carbohydr. Res. **32**, 79 (1974).

Can. J. Chem. Downloaded from www.nrcresearchpress.com by 41.223.56.140 on 09/07/12
For personal use only.

A spectroscopic study of the reaction of gold atoms with CO in a rotating cryostat: formation of a variety of gold carbonyls[1]

J. H. B. CHENIER, J. A. HOWARD,[2] H. A. JOLY,[3] B. MILE,[2] AND M. TOMIETTO
Division of Chemistry, National Research Council of Canada, Ottawa, Ont., Canada K1A 0R9

Received August 29, 1988

J. H. B. CHENIER, J. A. HOWARD, H. A. JOLY, B. MILE, and M. TOMIETTO. Can. J. Chem. **67**, 655 (1989).

Reaction of ^{197}Au atoms with CO has been studied in inert hydrocarbon matrices in a rotating cryostat at 77 K by EPR, FTIR, and UV/visible spectroscopy. $Au(CO)_2$ has been positively identified by FTIR spectroscopy and there is evidence for the formation of AuCO, a gold microcrystallite – CO complex and, upon annealing, $Au_2(CO)_4$. Electron paramagnetic resonance spectra are consistent with the formation of Au(CO) (OC) with the magnetic parameters: a_{13} = 325 MHz, a_{17} = 44 MHz, and g = 2.0014 and a gold microcrystallite – CO complex with g = 2.014. An intense broad absorption in the optical spectrum at 525 nm is assigned to $Au(CO)_2$ and a less intense narrow band at 320 nm is assigned to Au_nCO. There is no spectroscopic evidence for the formation of $Au(CO)_3$ in hydrocarbon matrices.

Key words: gold carbonyls, EPR, FTIR, UV/visible, matrix isolation.

J. H. B. CHENIER, J. A. HOWARD, H. A. JOLY, B. MILE et M. TOMIETTO. Can. J. Chem. **67**, 655 (1989).

Faisant appel aux spectroscopies rpe, UV/visible ainsi que IR par transformation de Fourier et opérant à 77 K, on a étudié la réaction des atomes du ^{197}Au avec le CO dans des matrices d'hydrocarbures inertes, dans un cryostat en rotation. Grâce à la spectroscopie IR par transformation de Fourier, on a pu identifier le $Au(CO)_2$ d'une façon positive et on a obtenu des indications relatives à la formation de AuCO, un complexe micro-cristallin d'or et de CO qui se transforme en $Au_2(CO)_4$ par recuisson. Les spectres rpe sont en accord avec la formation de Au(CO)(OC) dont les paramètres sont les suivants: a_{13} = 325 MHz, a_{17} = 44 MHz et q = 2,0014 et d'un complexe micro-cristallin d'or et de CO avec q = 2,014. On a attribué au $Au(CO)_2$ une bande d'absorption large et intense qui est observée à 525 nm du spectre optique alors qu'une bande fine et moins intense observée à 320 nm est attribuée au Au_nCO. On n'a décelé aucune indication spectroscopique suggérant la formation de $Au(CO)_3$ dans les matrices d'hydrocarbures.

Mots clés : carbonyles d'or, RPE, FTIR, UV/visible, isolement de la matrice.

[Traduit par la revue]

Introduction

Electron paramagnetic resonance (EPR) spectroscopic studies of the reaction of Cu and Ag atoms with CO in solid argon have confirmed the formation and structures of the unstable mononuclear mono- and tricarbonyls, CuCO, AgCO, $Cu(CO)_3$, and $Ag(CO)_3$ (1–4). The dicarbonyls $Cu(CO)_2$ and $Ag(CO)_2$ are also formed but they are EPR "silent" because they are linear molecules with a $^2\Pi$ electronic ground state (1, 3).

These reactions have also been performed in inert hydrocarbon matrices (5–10) and while CuCO and $Cu(CO)_3$ have the same structure in the two distinct types of matrix the silver di- and tricarbonyls can have two conformations in adamantane. Thus bent $Ag(CO)_2$ with the unpaired electron located essentially in the metal 5s orbital is EPR "visible" and $Ag(CO)_3$ can adopt a planar ($^2A_2''$) and a pyramidal ($^2A_1'$) conformation in the same adamantane matrix (9).

Reaction of Au atoms with CO has also been studied in rare gas matrices (11) by infrared spectroscopy and this coinage metal atom is different from Cu and Ag in that $Au(CO)_3$ is not formed but two isomers of the dicarbonyl are produced, one with two metal–carbon bonds, $Au(CO)_2$, and one with metal–carbon bond and one metal–oxygen bond, isocarbonyl(carbonyl)gold, Au(CO)(OC). EPR studies of the reaction of Au atoms with CO in argon (12) have confirmed the formation of AuCO but there was no evidence for isocarbonyl(carbonyl)gold.

Because of the interesting differences between reactions of CO with Cu and Ag and with Au in solid argon and CO with Ag in solid rare gas and inert hydrocarbon matrices we thought it worthwhile to study the reaction of CO with Au atoms in hydrocarbon matrices to determine whether the tricarbonyl can be formed under our experimental conditions and to confirm by EPR spectroscopy the formation of Au(CO)(OC). The results of this study are reported here.

Experimental

The rotating cryostat and furnace used to study the reactions of Au atoms with CO in inert hydrocarbon matrices have been described previously (13). Au was evaporated from a molybdenum pouch clamped between the electrodes of the furnace. EPR spectra were obtained on Varian E-4 and E-12 and Bruker ESP 300 instruments equipped with a Systron-Donner Model 6054 microwave frequency counter and a Bruker Model ER 035 proton magnetometer. Temperature control was achieved with an Oxford Instruments ESR 9 liquid helium cryostat and a cold nitrogen gas controller. The computing methods used to derive the magnetic parameters from the experimental spectra and to produce simulated spectra have already been discussed in previous papers (13, 14).

In situ IR spectra of deposits on the drum of the cryostat were obtained on a Mattson Sirius 100 FTIR spectrometer as described previously (14). They were recorded initially at 77 K and then at higher temperatures by warming up the deposits on the drum of the cryostat. If major changes in the spectrum occurred at high temperatures the cryostat was recooled to 77 K and the spectrum rerecorded at this temperature. Spectra were the average of 256 scans at 4 cm^{-1} resolution from 4000–400 cm^{-1}.

In situ UV/visible spectra were recorded with the aid of an Oriel pulsed light photometer. Light from the pulsed xenon lamp (10 Hz) monochrometer combination was directed with a silica fibre optic on to the deposit on the drum at an angle of 10° to the normal and the diffuse reflected beam was collected by another fibre optic along the normal and transmitted to a phase-locked photomultiplier detector. A reference spectrum was obtained by masking the lower half of the deposit so that only the top portion contained gold—CO species. A minicomputer with associated software was used to increment the wavelength output from the monochrometer, store the detector output at each wavelength

[1]NRCC No. 29939.
[2]To whom correspondence should be addressed.
[3]NSERC postdoctoral fellow, 1987–1988.

Can. J. Chem. Downloaded from www.nrcresearchpress.com by 41.223.56.140 on 09/07/12
For personal use only.

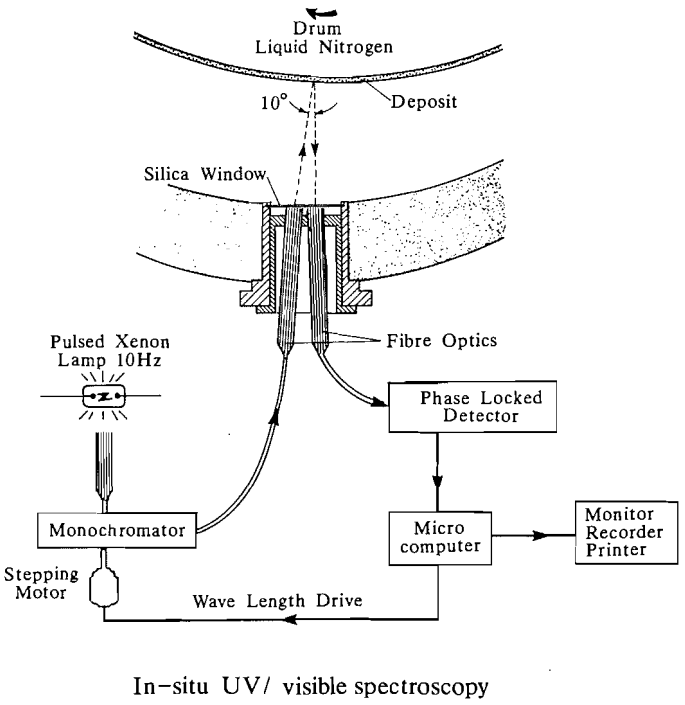


FIG. 1. Fibre optic plug for sample and reference UV/visible spectra.

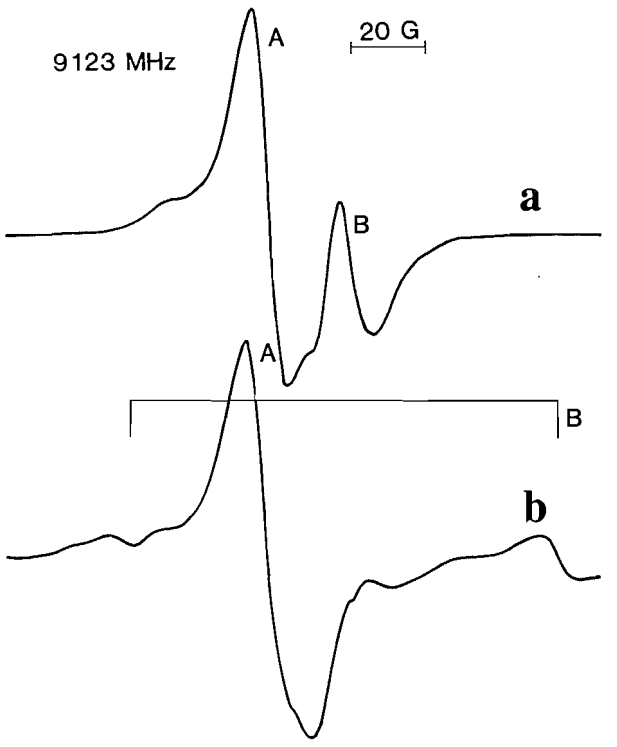


FIG. 2. EPR spectra of Au atoms and CO in adamantane at 77 K: (*a*) ^{12}CO and (*b*) ^{13}CO.

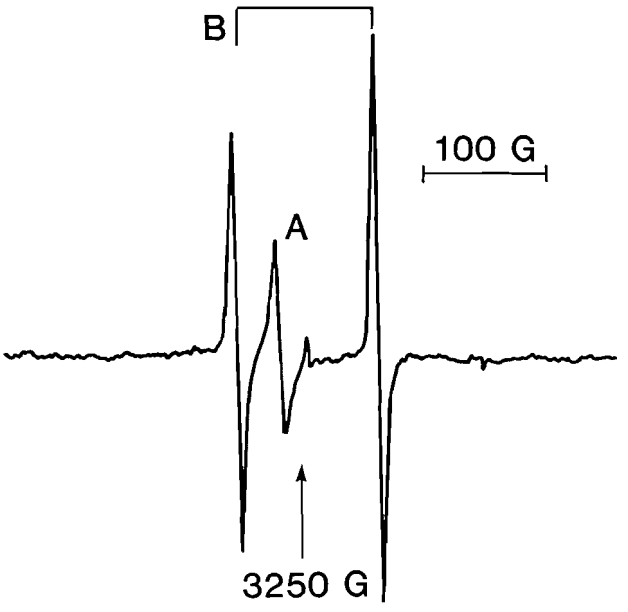


FIG. 3. EPR spectrum of Au atoms and ^{13}CO in adamantane at 250 K.

from the two halves of the deposit, and process the data so as to give an absorbance–wavelength curve. The cyrostat plug, mask, and fibre opticals are shown in Fig. 1.

Pure gold metal was kindly provided by Dr. C. M. Hurd (NRCC). Carbon monoxide (99.99%), ^{13}CO-enriched to 99.9 atom% in ^{13}C and $C^{17}O$-enriched to 36.8 atom% in ^{17}O were obtained from Matheson, Merck, Sharp, and Dohme Ltd., Montreal, and Prochem Isotopes, Summit, NJ, respectively. Adamantane was obtained from Aldrich.

Results

EPR

Au and CO (0.05 Torr) in adamantane at 77 K gave a red-colored deposit the EPR spectrum of which had three quartets from Au atoms isolated in three trapping sites (13) and the central feature shown in Fig. 2*a*. This part of the spectrum consists of two major resonances, a broad feature (A) centered at $g = 2.014$ and a line (B) at higher field with $g = 2.0014$. There was no evidence for a quartet with a Au hyperfine interaction (hfi) of *ca.* 1700 MHz similar to the quartet that has been assigned by Kasai and Jones (12) to monocarbonylgold, AuCO. When this reaction was performed with ^{13}CO the line at $g = 2.0140$ remained unchanged except for minor changes in lineshape, whereas the line centered at $g = 2.0014$ was replaced by two lines centered at the same g factor with a spacing of 325 MHz, indicating coupling with one carbon nucleus but no resolved Au hfi. The spectrum given by $Au/^{13}CO$ in adamantane is shown in Fig 2*b*.

Annealing experiments revealed that species A disappeared faster than species B until at 255 K the much sharper spectrum shown in Fig. 3 was obtained from Au and ^{13}CO.

Au and CO enriched in ^{17}O gave a spectrum similar to Fig. 2*a* at 100 K while annealing to 250 K revealed the presence of six satellite lines indicated by the stick diagram in Fig. 4. This sextet from one oxygen nucleus ($I = 5/2$) was centered at $g = 2.0014$ and is therefore associated with species B. Analysis of the ^{17}O-enriched spectrum gave $a_{17} = 44$ MHz.

FTIR

IR spectra given by Au atoms and ^{12}CO, ^{13}CO, and a 1:1 mixture of ^{12}CO and ^{13}CO in adamantane at 77 K in the CO stretching region are shown in Fig. 5. ^{12}CO gave two bands C and D at 2107 and 1943 cm^{-1} with relative intensities of 1:5.7, a weak band (E) at 2052 cm^{-1}, and a shoulder (F) to band D at 1930 cm^{-1}. Almost the same pattern of bands was obtained from $Au/^{13}CO$ with C at 2059 cm^{-1}, D at 1897.2 cm^{-1}, E at 2027 cm^{-1}, and F at 1885.6 cm^{-1}. Thus all the bands in the CO stretching region were shifted by ~45 cm^{-1} to lower frequency

Can. J. Chem. Downloaded from www.nrcresearchpress.com by 41.223.56.140 on 09/07/12
For personal use only.

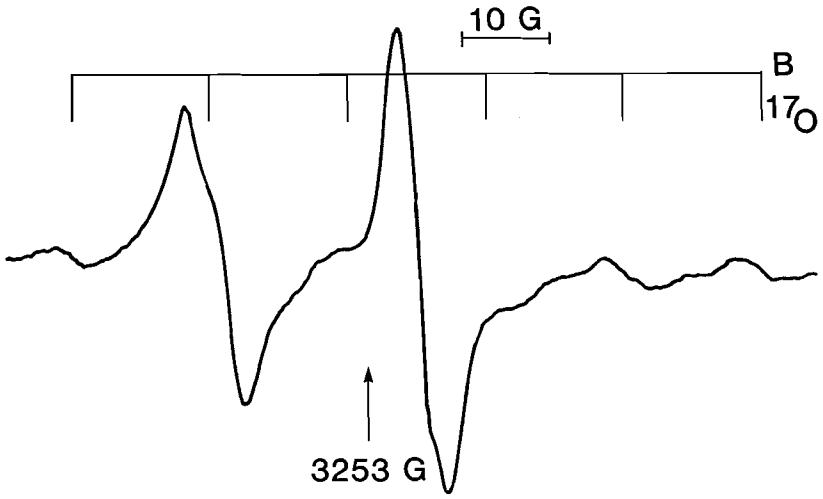


FIG. 4. EPR spectrum of Au atoms and CO enriched to 36.8 atom% in ^{17}O at 250 K.

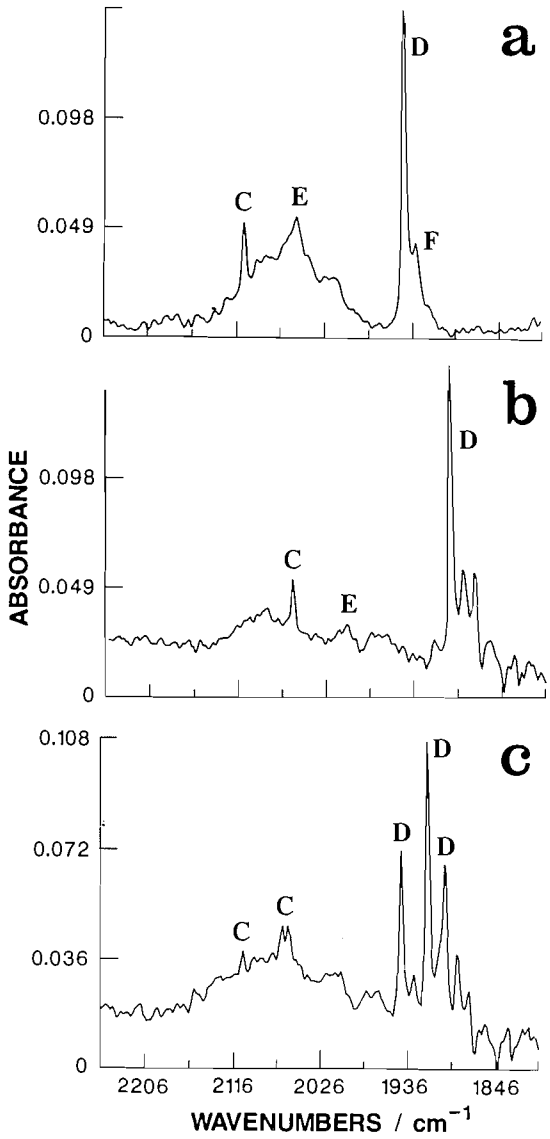


FIG. 5. FTIR spectra of Au and ^{12}CO (*a*), Au and ^{13}CO (*b*), and Au and 1:1 mixture of ^{12}CV and ^{13}CO (*c*).

in the Au/^{13}CO system and can be assigned to gold carbonyls. The spectrum from Au/^{12}CO/^{13}CO gave two bands C at 2106 and 2059 cm^{-1} and three bands D at 1943.5, 1916.5, and 1897.2 cm^{-1} with relative intensities of 1:2:1. Bands C and D are therefore assigned to gold carbonyls with one and two CO ligands, respectively. Bands E were too weak to detect in this mixed isotopes experiment.

Upon annealing Au/^{12}CO/adamantane to 104 K band E had disappeared and the intensity of band C had decreased by ~10% while band D remained unchanged. At 141 K band C had disappeared and band D had decreased by ~10% and a broad band (G) at 2072 cm^{-1} developed. At 200 K band G was the dominant band although band C was still evident. In the Au/^{13}CO system band G occurred at 2027 cm^{-1}. Infrared spectra of this system at 77, 141, 200 K are shown in Fig. 6.

UV/visible

Au atoms in adamantane gave a salmon pink deposit which exhibited a broad band centered at about 300 nm with a width-at-half-height of about 100 nm. There were, however, distinct broad adsorptions at 380, 345, and 320 nm and narrower adsorptions at 300, 290, 275, 265, and 250 nm (Fig. 7). This spectrum was similar to that of Au in rare gases and hydrocarbons (15) but was not as well resolved. The broad lower energy bands have been assigned to Au_2 and Au_3 while the higher energy bands are from Au atoms. The EPR spectrum of this deposit was dominated by the three quartets from Au atoms in three magnetically distinct trapping sites and a feature at $g = 2.008$ probably from a Au microcrystallite. There was no evidence for the spectrum of Au_3 (16), indicating that none of the bands in the optical spectrum were from this species. Au_2, on the other hand, is expected to be diamagnetic and would not influence the EPR spectrum.

Au atoms and CO in adamantane gave a deep red deposit at 77 K that exhibited the optical spectrum shown in Fig. 8*a*. Most of the features of the spectrum of Au/adamantane had disappeared except for a feature J at 250 nm. The broad intense band (H) and a narrow, less intense band I were new bands that appeared at 525 and 325 nm, respectively. Upon annealing to 132 K and 525 nm band decreased by ~20% and the 325 nm band by ~50% (Fig. 8*b*). At 200 K bands I and J were absent from the spectrum while band H was still evident, although down in intensity by a factor of about 3 (Fig. 8*c*) from the 77 K spectrum.

Can. J. Chem. Downloaded from www.nrcresearchpress.com by 41.223.56.140 on 09/07/12
For personal use only.

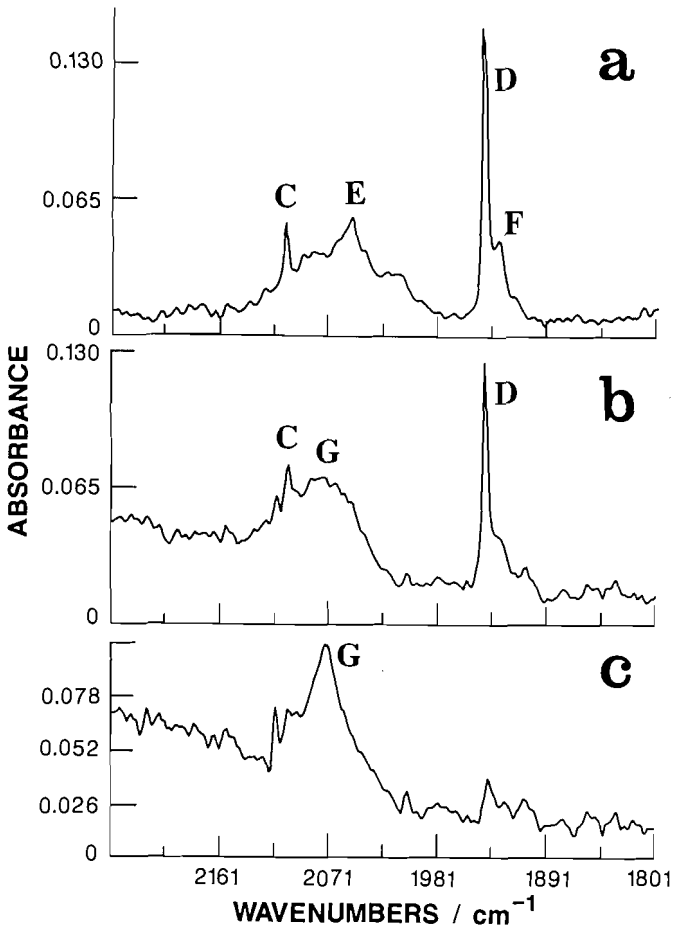


FIG. 6. FTIR spectra of Au and ^{12}CO at 77 K (*a*), 132 K (*b*), and 200 K (*c*).

Discussion

EPR spectral analysis

EPR spectra given by Au atoms and CO in adamantane reveal the presence of Au atoms and two paramagnetic species A and B with markedly different g factors but no features that can be unambiguously assigned to the mononuclear carbonyl AuCO and dicarbonyl $Au(CO)_2$; $Au(CO)_3$ is certainly not formed.

Species A. The only magnetic parameter that can be deduced for A is the g-value of 2.014, ^{197}Au, ^{13}C, and ^{17}O hyperfine interactions are all less than the linewidth of 10 MHz. The line shape is, however indicative of a conduction EPR spectrum and perhaps can be assigned to a gold microcrystallite with adsorbed CO molecules. The spin density at each Au nucleus and CO molecule is too low to give rise to a resolvable hyperfine interaction. The small g shift ($\Delta g = g - 2.0023 = 0.0117$) and the overall line shape with an asymmetry parameter (positive peak height/negative peak height) of ~1.5 indicates particles of 10^2–10^3 nm in size (17). We think that we are justified in suggesting adsorbed CO because this line is absent in Au/adamantane deposits in the absence of CO (13). Furthermore, CESR spectra of Au in pure gold slabs have $g = 2.11$ and broaden rapidly above 10 K (18).

Species B. The ^{13}C hfi of B (325 MHz) is similar to that of linear AuCO (12) but the absence of a Au hfi precludes this assignment. The ^{13}C and ^{17}O (44 MHz) hfi are remarkably similar to those of formyl, HCO, which is a bent σ radical with an HCO angle of ~110° (19) but we can again discount bent AuCO because it would have a Au hfi at least as large as the H hfi of HCO (a_H = 384 MHz). In the absence of a resolved Au hfi positive assignment of B is difficult. Two possible structures that warrant consideration are isocarbonylgold **1** and isocarbonyl (carbonyl) gold **2**.



1 **2**

Preliminary MO calculations indicate that linear isocarbonyl metal species with most of the unpaired spin on carbon have a significant unpaired spin population on oxygen but little unpaired spin population at the metal center which is consistent with structures **1** and **2**. In the absence of other evidence we favor **2** because under our experimental conditions higher carbonyls such as $Rh(CO)_4$ (20), $Al(CO)_2$ (21), and $Ga(CO)_2$ (14) are formed from metal atom – CO reactions in the rotating cryostat. We, therefore, very tentatively assign species B structure **2**. Why the Au atom and the Au atom alone among group 11 and 13 metals forms an isocarbonylcarbonyl is puzzling.

However, it should be noted that the ^{13}C hfi of B is also consistent with a second Au microcrystallite–CO complex with the spin density located mainly on one CO that is bent with respect to the Au—C bond. Examples are known where CO is angled with respect to the carbon–metal bond both in organometallic compounds (22) and on metal surfaces (23).

The magnetic parameters of the gold carbonyls formed from Au atoms and CO at cryogenic temperatures (<77 K) in rare gas and inert hydrocarbon matrices are summarized in Table 1.

FTIR spectral analysis

There is IR evidence for the production of at least five gold carbonyls from reaction of Au atoms with CO under our experimental conditions. Band D (1943 cm^{-1}) is assigned to the asymmetric stretching mode of linear ($D_{\infty h}$) dicarbonylgold, $Au(CO)_2$, because it is shifted by 45.8 cm^{-1} to lower frequency when ^{13}CO is used instead of ^{12}CO and only one triplet with relative band intensities of 1:2:1 is given by a 1:1 mixture of ^{12}CO and ^{13}CO with the centre band at 1917 cm^{-1} assigned to $Au(^{12}CO)$ (^{13}CO). Furthermore the frequency of the 1943 cm^{-1} band is similar to ν_{CO} = 1935.8 cm^{-1} of $Au(CO)_2$ produced by reaction of Au atoms with ^{12}CO in neon (11). The frequency of the CO stretching mode is significantly larger than ν_{CO} = 1842 cm^{-1} of $Cu(CO)_2$ (1) and ν_{CO} = 1842 cm^{-1} of $Ag(CO)_2$ (3) suggesting less p and/or d electron back donation from the metal-to-ligand antibonding orbitals. This is understandable since the 6p level is 1 eV further removed from the 2π^* orbital of CO.

Band E, which disappears quickly upon warm-up, has a frequency (2052 cm^{-1}) similar to ν_{CO} of AuCO in N_2, Ar, and Kr (11). Its instability is probably the reason why the EPR spectrum of linear AuCO is not observed in adamantane while it is readily detected at lower temperature in Ar (12). Again ν_{CO} of AuCO is higher than ν_{CO} of CuCO (2010 cm^{-1}) (1) and AgCO (1951 cm^{-1}) (3). The elusive $Au(CO)_3$ should have ν_{CO} ~ 2052 cm^{-1} if like $Cu(CO)_3$ and $Ag(CO)_3$ ν_{CO} is *ca.* 100 cm^{-1} higher than ν_{CO} of the dicarbonyl, but this assignment is unlikely because of our failure to detect the tricarbonyl by EPR, a more sensitive technique than FTIR.

Band G at 2072 cm^{-1} only appears upon annealing and is assigned to tetracarbonyldigold, $Au_2(CO)_4$, produced by dimerization of $Au(CO)_2$. This is because band G only appears as band D disappears and none of the other bands that disappear upon annealing are intense enough to contribute significantly to

Can. J. Chem. Downloaded from www.nrcresearchpress.com by 41.223.56.140 on 09/07/12
For personal use only.

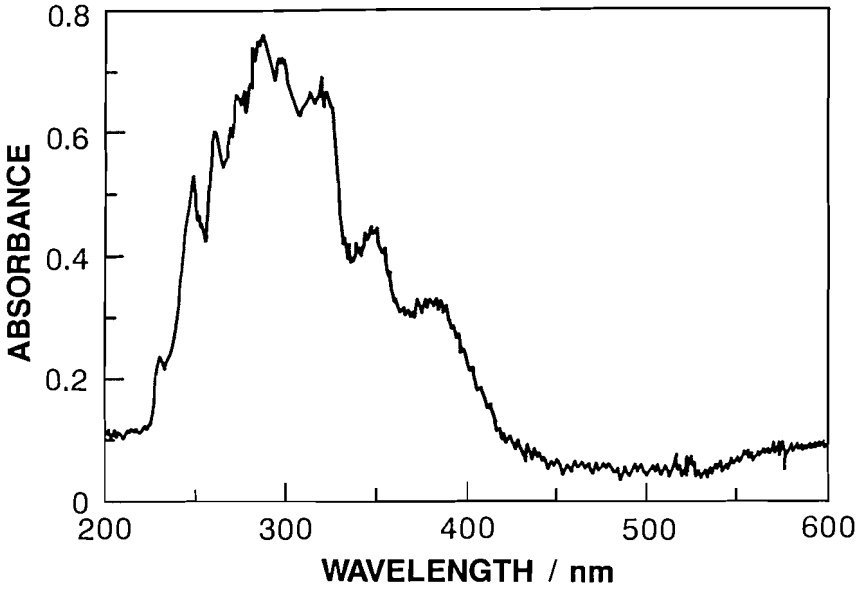


FIG. 7. Optical spectrum of Au atoms condensed on adamantane at 77 K.

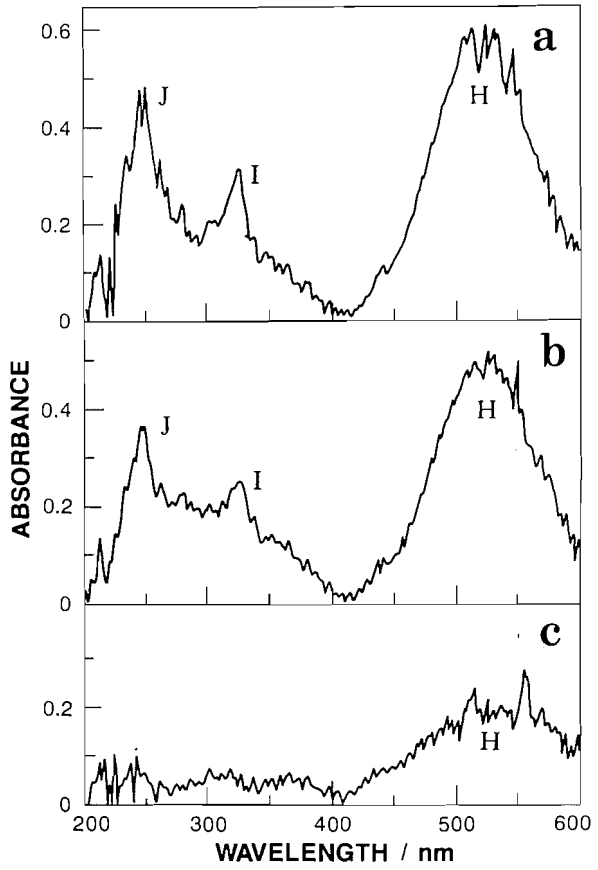


FIG. 8. Optical spectra of Au and ^{12}CO at 77 K (*a*), 132 K (*b*), and 200 K (*c*).

the intensity of band G. The frequency of this band is ~37 cm^{-1} higher than ν_{CO} of $Cu_2(CO)_6$ in adamantane (10).

ν_{CO} of band C (2107 cm^{-1}) is closer to ν_{CO} of trapped CO (2135 cm^{-1}) than ν_{CO} of $Cu_2(CO)_6$, Cu(CO), and $Cu(CO)_2$ (1) and is clearly not associated with a mono- or di-nuclear gold carbonyl. There does appear to be sound EPR evidence for a gold microcrystallite – CO complex and band C is therefore tentatively assigned to such a complex. This assignment is not unreasonable because Cu cluster monocarbonyls (Cu_2CO, Cu_3CO, and Cu_5CO) have ν_{CO} in the range 2116–2095 cm^{-1} (24) and CO adsorbed on polycrystalline gold has ν_{CO} = 2115 cm^{-1} (25). EPR and IR spectra assigned to this species decrease in intensity upon annealing perhaps because the CO is only weakly bound and is readily desorbed.

The high frequency shoulder F, ν_{CO} = 1930 cm^{-1}, to band D is difficult to assign. It could be from $Au(CO)_2$ in a second trapping site but it appears to be more intense from $Au/^{13}CO$ than from $Au/^{12}CO$. Unfortunately, the more intense band from $Au(^{12}CO)(^{13}CO)$ was not resolved so there is some doubt about this assignment. Alternatively, it could be from Au(CO) (OC) which in CO has ν_{CO} = 1927 cm^{-1} (11).

The infrared data of binary gold carbonyls formed from Au atoms and CO at cryogenic temperatures (< 77 K) in rare gas and inert hydrocarbon matrices are presented in Table 2.

UV/visible spectral analysis

Optical spectra are similar to those obtained by McIntosh and Ozin (11) for Au/CO in argon and CO which exhibit a main absorption at ~520 and ~538 nm, respectively, compared with a band maximum at 525 nm in adamantane. These bands have been assigned to the $^2\Pi_u \rightarrow {}^2\Pi_g$ electronic transition of $Au(CO)_2$ and Au(CO) (OC), respectively. Although we do not know the relative extinction coefficients of the various gold carbonyls IR spectra indicate that $Au(CO)_2$ is formed in the highest yields at 77 K. The 525 nm band is consequently assigned to the $^2\Pi_u \rightarrow {}^2\Pi_g$ electronic transition of $Au(CO)_2$, in agreement with the results in argon (11). There is some evidence for fine structure on this band and also on the corresponding band in McIntosh and Ozin's spectrum (11). It is probably associated with vibration of the Au—C bond at about 500 cm^{-1} but the poor resolution did not justify further analysis. The weak bands at 407 and 350 nm in Ar and CO that have been assigned to $^2\Pi_u \rightarrow 2\Sigma_g^+$ transitions of $Au(CO)_2$ and Au(CO) (OC) are not apparent in our spectra. The energy gap of ~6 eV between these levels in the quantitative molecular orbital energy level diagram

Can. J. Chem. Downloaded from www.nrcresearchpress.com by 41.223.56.140 on 09/07/12
For personal use only.

TABLE 1. Magnetic parameters of Au carbonyls isolated in inert matrices at low temperatures[a]

Species	Matrix	$a_{\parallel}$ (Au)	$a_{\perp}$ (Au)	$a_{\parallel}$ (13)	$a_{\perp}$ (13)	a_{17}	$g_{\parallel}$	$g_{\perp}$
AuCO	Ar	1742	1686	316	332		1.9791	1.9105
Au_nCO	Adamantane	<10					2.014	
B[c]	Adamantane	<10		325[b]		44[b]	2.0014[b]	

[a]Hyperfine interactions in MHz.
[b]Isotropic values.
[c]B is probably Au (CO) (OC) but could be Au_nCO with a bent CO ligand.

TABLE 2. Infrared absorptions of the products of reaction of Au atoms with CO in matrices at low temperatures

Species	Matrix	ν/cm^{-1}
AuCO	N_2	2060
	Ar	2039.4
	Kr	2040.5
	Xe	1985.5
	Adamantane	2052
Au $(CO)_2$	N_2	1927.7
	Ne	1928.6
	Ar	1923
	Kr	1917
	Xe	1909.9
	Adamantane	1943
Au (CO) (OC)	CO	1927.7[b]
		2072[c]
$Au_2 (CO)_4$	Adamantane	2072
$Au_x (CO)_y$	CO	~2200
	Adamantane	2104

[a]Two sites.
[b]AuC≡O.
[c]AuO≡C.

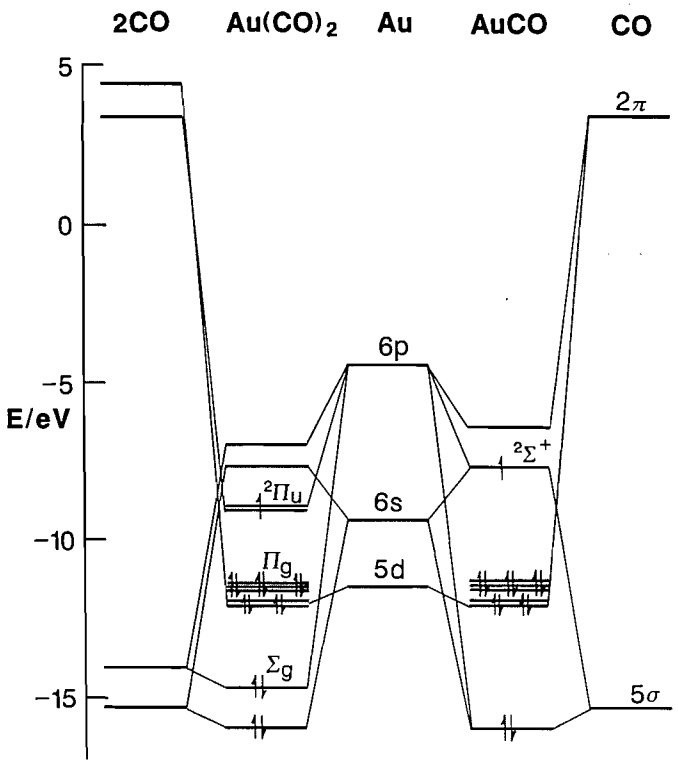


FIG. 9. Qualitative molecular orbital energy level scheme for $D_{\infty h}$ $Au(CO)_2$ and C_s AuCO.

of $Au(CO)_2$ (Fig. 9) and Au(CO) (OC) (11) is, however, not entirely consistent with transitions at 407 and 350 nm.

The band I at 325 nm in our spectra is not associated with $Au(CO)_2$ because it disappears at a faster rate than the 525 nm band upon warm-up and is tentatively assigned to a monocrystallite gold – CO complex. Band J at 250 nm is readily assigned to Au atoms because of the similarity with the bands at 246 and 253 nm from Au atoms in cyclohexane (15) and from the fact that the ESR spectrum of Au/CO/adamantane shows the presence of unreacted Au atoms. Interestingly a band at 285 nm observed in cyclohexane is absent in our spectrum.

Absence of $Au(CO)_3$

We have confirmed the conclusion drawn from lower temperature studies of the reaction of Au atoms with CO, that $Au(CO)_2$ is the highest carbonyl given by Au atoms and CO, unlike Cu and Ag which give 17 electron tricarbonyls. The non-formation of $Au(CO)_3$ compared with the facile production of the Cu and Ag congeners is at first sight puzzling but is probably associated with the higher ($6s$–$6p$) promotional energy in Au(4.63 eV) compared to Cu(3.8 eV) and Ag(3.86 eV), disfavoring sp^2 hybridization. The $6p$ level is also ~1 eV further removed from the antiboding $2\pi_z$* orbital of CO thus mitigating against stabilization by p–π back donation. The absence of $Au(CO)_3$ because of rapid dimerization to $Au_2(CO)_6$ can be discounted because of the absence of IR bands assignable to the dinuclear carbonyl in low temperature spectra.

Conclusions

Under our experimental conditions Au atoms react with CO to give principally dicarbonylgold and a gold microcrystallite – CO complex. The dinuclear carbonyl, $Au_2(CO)_4$, is only produced upon annealing and the 17 electron binary gold carbonyl $Au(CO)_3$ is absent. There is tentative IR evidence for the formation of AuCO but it is not confirmed by EPR spectroscopy. A major paramagnetic product with an unresolved Au hyperfine interaction but a large ^{13}C hfi of 325 MHz has magnetic parameters consistent with isocarbonyl(carbonyl)gold but we cannot completely discount a gold cluster – CO complex with a large spin density on a carbonyl with a C=O bond at an angle to the cluster surface. Neither structure has been confirmed by IR or UV/visible spectroscopy.

Acknowledgements

One of us (H.A.J.) thanks the Natural Sciences and Engineering Research Council of Canada for the award of a postdoctorate

Can. J. Chem. Downloaded from www.nrcresearchpress.com by 41.223.56.140 on 09/07/12
For personal use only.

fellowship. J.A.H. and B.M. are indebted to NATO for a travel award.

1. H. HUBER, E. P. KÜNDIG, M. MOSKOVITS, and G. A. OZIN. J. Am. Chem. Soc. **97**, 2097 (1975).
2. P. H. KASAI and P. M. JONES. J. Am. Chem. Soc. **107**, 813 (1985).
3. D. MCINTOSH and G. A. OZIN. J. Am. Chem. Soc. **98**, 3167 (1976).
4. P. H. KASAI and P. M. JONES. J. Phys. Chem. **89**, 1147 (1985).
5. J. A. HOWARD, B. MILE, J. R. MORTON, K. F. PRESTON, and R. SUTCLIFFE. Chem. Phys. Lett. **117**, 115 (1985).
6. C. A. HAMPSON, J. A. HOWARD, and B. MILE. J. Chem. Soc. Chem. Commun. 966 (1985).
7. J. A. HOWARD, B. MILE, J. R. MORTON, K. F. PRESTON, and R. SUTCLIFFE. J. Phys. Chem. **90**, 1033 (1986).
8. J. A. HOWARD, B. MILE, J. R. MORTON, and K. F. PRESTON. J. Phys. Chem. **90**, 2027 (1986).
9. J. H. B. CHENIER, C. A. HAMPSON, J. A. HOWARD, and B. MILE. J. Phys. Chem. **92**, 2745 (1988).
10. J. H. B. CHENIER, C. A. HAMPSON, J. A. HOWARD, and B. MILE. J. Phys. Chem. **93**, 114 (1989).
11. D. MCINTOSH and G. A. OZIN. Inorg. Chem. **16**, 51 (1977).
12. P. H. KASAI and P. M. JONES. J. Am. Chem. Soc. **107**, 6385 (1985).
13. A. J. BUCK, J. A. HOWARD, and B. MILE. J. Am. Chem. Soc. **105**, 3381 (1983).
14. J. A. HOWARD, R. SUTCLIFFE, C. A. HAMPSON, and B. MILE. J. Phys. Chem. **90**, 4268 (1986).
15. W. E. KLOTZBUCHER and G. A. OZIN. Inorg. Chem. **19**, 3767 (1980).
16. J. A. HOWARD, R. SUTCLIFFE, and B. MILE. J. Chem. Soc. Chem. Commun. 1449 (1983).
17. R. N. EDMONDS, M. R. HARRISON, and P. P. EDWARDS. Ann. Rep. Prog. Chem. Sect. C, **82**, 265 (1985).
18. P. MONOD and A. JANOSSY. J. Low Temp. Phys. **26**, 311 (1977).
19. F. J. ADRIAN, J. BOHANDY, and B. F. KIM. J. Chem. Phys. **85**, 2692 (1986).
20. M. HISTED, J. A. HOWARD, H. MORRIS, and B. MILE. Unpublished results.
21. J. H. B. CHENIER, C. A. HAMPSON, J. A. HOWARD, B. MILE, and R. SUTCLIFFE. J. Phys. Chem. **90**, 1524 (1986).
22. W. M. H. SACHLER and M. ICHIKAWA. J. Phys. Chem. **90**, 4752 (1986).
23. D. F. SCHRIVER. Adv. Chem. Ser. **152**, 1 (1981).
24. M. MOSKOVITS and J. E. HULSE. J. Phys. Chem. **81**, 2004, (1977).
25. P. HOLLINS and J. PRITCHARD. *In* Vibrational spectroscopy of adsorbed species. *Edited by* A. T. Bell and M. L. Hair. Am. Chem. Soc. Symp. Ser. Vol. 137, 1980. p. 51.

Can. J. Chem. Downloaded from www.nrcresearchpress.com by 41.223.56.140 on 09/07/12
For personal use only.

Synthesis, structural and magnetic properties of macrocyclic aza-amido binuclear copper(II) complexes[1]

SANAT K. MANDAL, LAURENCE K. THOMPSON,[2] AND MICHAEL J. NEWLANDS
Department of Chemistry, Memorial University of Newfoundland, St. John's, Nfld., Canada A1B 3X7
AMAL K. BISWAS, BIBHUTOSH ADHIKARY, AND KAMALAKSHA NAG[2]
Department of Inorganic Chemistry, Indian Association for the Cultivation of Science, Calcutta, India 70032
AND
ERIC J. GABE AND FLORENCE L. LEE
Division of Chemistry, National Research Council, Ottawa, Ont., Canada K1A 0R6

Received September 6, 1988

SANAT K. MANDAL, LAURENCE K. THOMPSON, MICHAEL J. NEWLANDS, AMAL K. BISWAS, BIBHUTOSH ADHIKARY, KAMALAKSHA NAG, ERIC J. GABE and FLORENCE L. LEE. Can. J. Chem. **67**, 662 (1989).

Binuclear, antiferromagnetically coupled, macrocyclic copper(II) complexes, $[Cu_2(C_{28}H_{32}N_4O_4)]\cdot H_2O$ (**II**) and $[Cu_2(C_{36}H_{32}N_4O_4)]\cdot CH_3CN\cdot H_2O$ (**III**), involving asymmetric ligands with two deprotonated amide, two azomethine nitrogen, and two phenoxide donors at the binuclear centre, have been synthesized and characterized by single-crystal X-ray diffraction and variable temperature magnetic studies. Complex **II** crystallizes in the monoclinic system, space group $P2_1/n$, with $a = 16.4854(9)$ Å, $b = 7.6005(13)$ Å, $c = 21.1617(11)$ Å, $\beta = 104.090(5)°$, $Z = 4$, $R_f = 0.068$ for 2062 significant reflections. The two copper(II) centres have square planar N_2O_2 donor sets with two phenoxide oxygen atoms bridging the copper centres with a copper–copper separation of 2.898(2) Å. A long copper–oxygen (amide) contact (2.808(10) Å) forms a weak dimer association. Complex **III** crystallizes in the triclinic system, space group $P\bar{1}$, with $a = 8.7771(9)$ Å, $b = 12.3983(16)$ Å, $c = 15.7299(16)$ Å, $\alpha = 85.003(11)°$, $\beta = 84.574(8)°$, $\gamma = 76.838(10)°$, $Z = 2$, $R_f = 0.041$ for 2966 significant reflections. The two copper(II) centres have distorted square-pyramidal geometry involving an N_2O_2 in plane donor set and two phenoxide oxygen bridges with a copper–copper separation of 3.018(1) Å. The fifth coordination site at each copper centre involves an amide oxygen from a neighbouring molecule (Cu(1)—O 2.371(4), Cu(2)—O 2.413(3) Å) in a staggered intermolecular array. Very strong antiferromagnetic exchange is observed in both cases ($-2J = 689 \pm 7$ cm^{-1} (**II**), $-2J = 816 \pm 8$ cm^{-1} (**III**)).

Key words: macrocycles, binuclear copper(II) complexes.

SANAT K. MANDAL, LAURENCE K. THOMPSON, MICHAEL J. NEWLANDS, AMAL K. BISWAS, BIBHUTOSH ADHIKARY, KAMALAKSHA NAG, ERIC J. GABE et FLORENCE L. LEE. Can. J. Chem. **67**, 662 (1989).

On a synthétisé les complexes macrocycliques, binucléaires et couplés d'une façon antiferromagnétique du cuivre(II), $[Cu_2(C_{28}H_{32}N_4O_4)]\cdot H_2O$ (**II**) et $[Cu_2(C_{36}H_{32}N_4O_4)]\cdot CH_3CN\cdot H_2O$ (**III**), impliquant des ligands asymétriques avec deux déprotonés, deux azotes d'azométhine et deux donneurs phénolates au centre binucléaires; on les a caractérisé par diffraction des rayons-X sur un cristal unique et par des études magnétiques à temperatures variables. Le complexe **II** cristallise dans le système monoclinique, groupe d'espace $P2_1/n$, avec $a = 16{,}4854(9)$, $b = 7{,}6005(13)$ et $c = 21{,}1617(11)$ Å, $\beta = 104{,}090(5)°$, $Z = 4$ et $R_f = 0{,}068$ pour 2062 réflexions significatives. Les deux centres de cuivre(II) comportent des ensembles de donneurs N_2O_2 plans carrés avec deux atomes d'oxygène du phénolate formant un pont entre les centres de cuivre séparés par une distance cuivre–cuivre de 2,898(2) Å. Un contact à longue distance entre le cuivre et l'oxygène (amide) (2,808(10) Å) forme une association dimère qui est faible. Le complexe **III** cristallise dans le système triclinique, groupe d'espace $P\bar{1}$, avec $a = 8{,}7771(9)$, $b = 12{,}3983(16)$ et $c = 15{,}7299(16)$ Å, $\alpha = 85{,}003(11)$, $\beta = 84{,}574(8)$, $\gamma = 76{,}838(10)^0$, $Z = 2$ et $R_f = 0{,}041$ pour 2966 réflexions significatives. Les deux centres de cuivre(II) possèdent une géométrie pyramide-carrée déformée impliquant un N_2O_2 dans l'ensemble de donneur plan et deux ponts formés par les oxygènes de phénolates avec une distance cuivre–cuivre de 3,018(1) Å. Le cinquième site de coordination de chaque centre de cuivre implique un oxygène d'amide d'une molécule adjacente (Cu(1)—O 2,371(4), Cu(2)—O 2,413(3) Å) dans un arrangement intermoléculaire décalé. Dans chacun des cas, on observe un échange antiferromagnétique très important ($-2J = 689 \pm 7$ cm^{-1} (**II**), $-2J = 816 \pm 8$ cm^{-1} (**III**)).

Mots clés : macrocycles, complexes binucléaires du cuivre(II).

[Traduit par la revue]

Introduction

In recent years metal complexes derived from macrocyclic ligands that possess dual ligand functions of saturated polyamine macrocycles and carboxamide moieties of oligopeptides have received considerable attention (1–14). The incorporation of a divalent 3*d* cation into the cavity of such diamidopolyamino macrocycles causes loss of two amido protons and the resulting neutral complexes attain considerable thermodynamic and kinetic stability that can be modulated by variation of ring size. Of particular interest are the copper(II) and nickel(II) complexes which undergo reversible one-electron oxidation at a moderately positive potential to produce corresponding stable complex species in the 3+ oxidation state. The implication that copper(III) might be involved in certain enzymatic processes (15–17), more especially in galactose oxidase, a two-electron oxidant that converts an alcohol to an aldehyde, has made these copper(III) macrocyclic systems attractive biomimetic models.

In contrast to the mononuclear macrocyclic systems considered above, Kida and co-workers (18) reported a neutral, binuclear copper(II) complex ((**I**), Fig. 1) containing two copper(II) centres bridged by two phenoxides and each bound to an azomethine and an amido nitrogen donor. The low room temperature magnetic moment observed for this compound (0.78 BM) indicates strong spin coupling between the copper centres. We have synthesized the neutral complexes **II** and **III** (Fig. 1),

[1]NRCC No. 29869.
[2]To whom correspondence should be addressed.

Printed in Canada / Imprimé au Canada

Can. J. Chem. Downloaded from www.nrcresearchpress.com by 41.223.56.140 on 09/07/12
For personal use only.

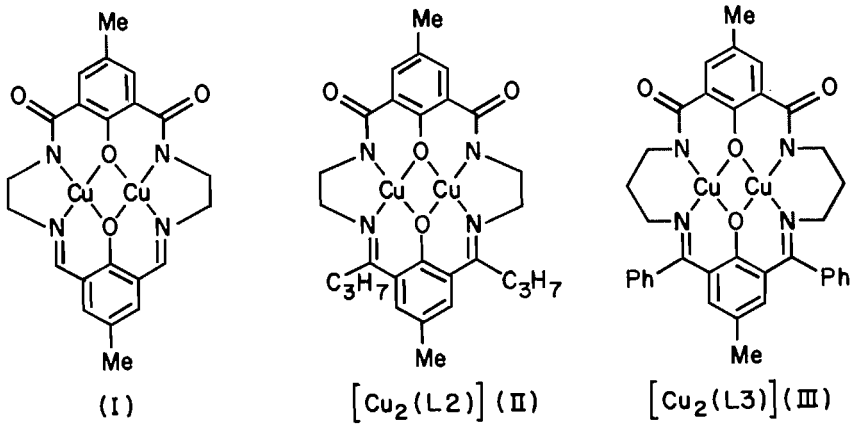


FIG. 1. Binuclear copper(II) aza-amido macrocyclic complexes.

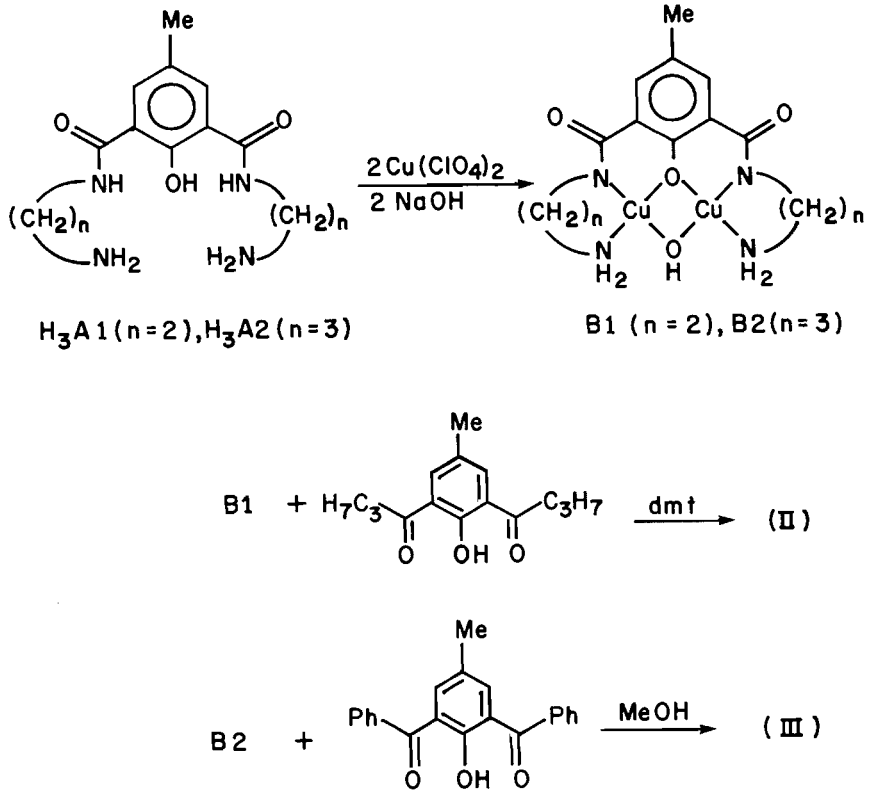


FIG. 2. Synthetic scheme for preparation of **II** and **III**.

which contain the same basic donor group arrangement as that found in **I**. Crystal structures are reported for **II** and **III** and a variable temperature magnetic study shows strong antiferromagnetic exchange in these complexes ($-2J = 689 \pm 7\ cm^{-1}$ (**II**), $-2J = 816 \pm 8\ cm^{-1}$ (**III**)).

Experimental

Synthesis of ligands and complexes

The following syntheses are outlined in the scheme given in Fig. 2.

$[Cu_2(L_2)]\cdot H_2O$ (II)

The intermediate complex B1 was synthesized as described previously (18). *Anal.* calcd. for $C_{13}H_{18}N_4O_4Cu_2\cdot 2H_2O$: C 34.14, H 4.85, N 12.25, Cu 13.89; found: C 34.05, H 4.75, N 12.30, Cu 13.75.

Complex B1 (0.45 g, 0.50 mmol) was suspended in *N,N*-dimethylformamide (dmf) (40 mL) and a solution (10 mL) of 1,3-dibutyryl-2-hydroxy-5-methylbenzene (19) (0.12 g, 0.50 mmol) in dmf was added. The reaction mixture was heated under reflux for 6 h in a nitrogen atmosphere. During this period complex B1 gradually dissolved and the resulting deep brown solution was filtered hot to remove any undissolved material. The solution was kept covered on a hot plate and on slow cooling brown crystals (**II**) deposited. These were collected by filtration, washed with methanol, and air dried. Yield 0.15 g. *Anal.* calcd. for $C_{28}H_{34}N_4O_5Cu_2$: C 53.03, H 5.37, N 8.84, Cu 20.06; found: C 53.00, H 5.44, N 8.91, Cu 20.45. Infrared (cm^{-1}): 3450(br), 1605(s), 1585(m), 1530(s), 1550(s). Ultraviolet (nm) (ε ($dm^3\ mol^{-1}\ cm^{-1}$)): 320(9675), 370(6825), 580(225) (spectrum run in dmso).

$[Cu_2(L_3)]$ (III)

This complex was prepared in a similar manner to **II** by reaction of the intermediate complex B2 (Fig. 2) with 1,3-dibenzoyl-2-hydroxy-5-methylbenzene (19) in methanol and obtained as green crystals. The

Can. J. Chem. Downloaded from www.nrcresearchpress.com by 41.223.56.140 on 09/07/12
For personal use only.

TABLE 1. Crystal data for **II** and **III**

Parameter	Value	
	II	**III**
Empirical formula	$C_{28}H_{20}N_4O_5Cu_2$	$C_{38}H_{32}N_5O_5Cu_2$
Formula weight	619.55	765.79
Crystal colour	Red–brown	Green
Crystal dimensions, mm	0.10×0.10×0.30	0.30×0.30×0.30
Space group	$P2_1/n$	$P\bar{1}$
a, Å	16.4854(9)[a]	8.777(19)
b, Å	7.6005(13)	12.3983(16)
c, Å	21.1617(11)	15.7299(16)
α, deg		85.003(11)
β, deg	104.090(5)	84.574(8)
γ, deg		76.838(10)
Z (molecules/cell)	4	2
$F(000)$ electrons	1319.69	743.83
Volume, Å^3	2571.73	1655.51
d_{calc}, Mg m^{-3}	1.600	1.536
Linear absolute coefficient; mm	0.170	0.133
Radiation (MoK_α), Å	λ=0.70930	λ=0.70930
2θ(max), deg	44.8	44.0
No. reflections measured	3400	8107
No. of unique reflections	3313	4311
No. unique reflections, $I_{net}>2.5\sigma(I_{net})$	2062	2966
Last least-squares	59 atoms	82 atoms
Calculated with	342 parameters	580 parameters
	2062 reflections	2966 reflections
R_f (single reflection)	0.068[b]	0.041[b]
R_w (single reflection)	0.041[c]	0.021[c]
Goodness of fit (last cycle)	4.006[d]	2.047[d]
R_f (all reflections)	0.110[b]	0.072[b]
R_w (all reflections)	0.042[c]	0.022[c]
Maximum shift/σ	0.008	0.329
Last D map:		
deepest hole, e/Å^3	−0.730	−0.380
highest peak, e/Å^3	0.660	0.560
Secondary extinction coefficient		0.113141[e]
σ		0.013065

[a]Throughout this paper, esd's are in parentheses and refer to the last digit printed.
[b]$R_f = \Sigma \mid F_o \mid - \mid F_c \mid / \Sigma \mid F_o \mid$
[c]$R_w = [\Sigma w(\mid F_o \mid - \mid F_c \mid)^2 / \Sigma (w \mid F_o \mid)^2]^{1/2}$, where $\omega = 1/\sigma^2 I$.
[d]Goodness of fit = $[\Sigma w(\mid F_o \mid - \mid F_c \mid)^2 /$(number of reflections − number of parameters)$]^{1/2}$.
[e]Reference 38.

complex was recrystallized from $MeCN/CHCl_3$. The intermediate diamine (H_3A2) was prepared in a similar manner to H_3A1, using 1,3-propanediamine and dimethyl-4-methyl-phenol-2,6-dicarboxylate (18) and was isolated as a pale yellow viscous oil on removal of excess diamine under vacuum. It was used, as before, without further purification. *Anal.* calcd. for $C_{36}H_{32}N_4O_4Cu_2$ (**III**): C 60.70, H 4.50, N 7.85, Cu 17.85; found: C 60.55, H 4.55, N 7.75, Cu 17.70. Infrared (cm^{-1}): 1610(s), 1575(s), 1540(s), 1535(s). Ultraviolet (nm) (ε (dm^3 mol^{-1} cm^{-1})): 325(14000), 370(8200), 580(190) (spectrum run in dmso).

The intermediate complex (B2) was obtained as blue–violet crystals and contained two additional ligand molecules, which are assumed either to be trapped in the crystal lattice or very weakly associated with the two copper centres. *Anal.* calcd. for $C_{45}H_{70}N_{12}O_{10}Cu_2$([$Cu_2$(A2)-(OH)]·2$H_3$A2): C 50.70, H 6.55, N 15.75, Cu 11.90; found: C 50.45, H 6.50, N 15.65, Cu 11.75. Details on this species will be published elsewhere.

C, H, N, Cu analyses were performed by the Australian Mineral Development Laboratories, Melbourne, and by Canadian Microanalytical Service, Vancouver. Infrared spectra were carried out as KBr pellets using a Beckman IR-20 and electronic spectra were recorded using a Pye-Unicam SP8-150 spectrometer. The sample of compound **III**, which was submitted for X-ray structural analysis, was prepared according to the procedures outlined above, but was shown to contain solvent of crystallization, [$Cu_2(L_3)$]·CH_3CN·H_2O(III)). X-ray diffraction data were collected using an Enraf Nonius CAD-4 diffractometer with graphite-monochromatised MoK_α radiation.

Magnetic measurements

Room temperature magnetic moments were measured with a PAR 150 vibrating sample magnetometer and variable temperature magnetic susceptibility data were obtained in the range 5–300 K (compounds **II** and **III**) using an Oxford Instruments superconducting Faraday magnetic susceptibility system with a Sartorius 4432 microbalance. A main solenoid field of 1.5 T and a gradient field of 10 T m^{-1} were employed.

X-ray crystallographic analysis of complexes II and III

Diffraction intensities were measured at 295 K using the ω scan technique at a scan speed of 4°/min. Three standards were measured after every 100 reflections and no significant crystal decay was detected. The space group of **II** was uniquely determined by systematic absences. Compound **III** was triclinic and its structure was solved and refined

Can. J. Chem. Downloaded from www.nrcresearchpress.com by 41.223.56.140 on 09/07/12
For personal use only.

successfully in the space group $P\bar{1}$. The unit cell parameters in Table 1 were obtained by a least-squares refinement for 38 reflections ($40° \leq 2\theta \leq 45°$) for $[Cu_2(L_2)]\cdot H_2O$ (**II**) and for 60 reflections ($40° \leq 2\theta \leq 45°$ for $[Cu_2(L_3)]\cdot CH_3CN\cdot H_2O$ (**III**). Lorentz and polarization factors were applied but no corrections were made for absorption.

The structures were solved by MULTAN (20) plus difference Fourier maps and refined by full-matrix least-squares with counting statistics weights. H-atom positions for **II** were calculated but their parameters were not refined. H-atoms for **III** were placed in calculated positions and allowed to refine. All heavier atoms (except for C14 and C25 in **II**) were refined anisotropically. All calculations were performed with the NRCVAX crystal structure programs (21). Scattering factors were taken from the International tables for X-ray crystallography (22). The final atomic positional parameters and equivalent isotropic temperature factors for **II** are listed in Table 2 and those for **III** in Table 3. Anisotropic thermal parameters (supplementary Tables 1 (**II**), 4 (**III**)), calculated hydrogen parameters (supplementary Table 3) and observed and calculated structure factors (supplementary Tables 2 (**II**), 6 (**III**)) are available as supplementary data.[3] Hydrogen atoms in **II** are given the U_{iso} value of the carbon atom to which they are attached, plus 0.01.

Results and discussion

Description of the structures of $[Cu_2(L_2)]\cdot H_2O$ (II) and $[Cu_2(L_3)]\cdot CH_3CN\cdot H_2O$ (III)

The molecular structure of complex **II** is illustrated in Fig. 3. Selected bond lengths and angles relevant to the copper coordination spheres and the ligand are given in Table 4 (a detailed listing of bond distances and angles for **II** is given in supplementary Table 6[3]). The structure consists of two essentially square-planar copper(II) centres bridged by two phenoxide oxygen atoms with one imino and one carboxamido nitrogen donor completing the CuN_2O_2 plane. The copper–copper separation is 2.898(2) Å and the oxygen bridge angles from the azomethine unit (Cu(1)—O(1)—Cu(2) 99.0(4)°) and from the carboxamido unit (Cu(1)—O(2)—Cu(2) 100.6(4)°) are slightly different. Azomethine linkages N(2)—C(11) and N(3)—C(22), (mean 1.246 Å), are essentially double bond in character, whereas the carboxamide C—N bond lengths (N(1)— C(8) 1.335(17), N(4)—C(28) 1.322(17) Å) have much more single bond character and do not differ significantly from the free peptide value (1.32 Å) (23). These values, however, contrast sharply with C—N bond lengths in a related macrocyclic dicopper(II) complex involving saturated azomethine groups (C—N 1.499(8) Å) (24). Cu—N bond lengths to the carboxamido nitrogen atoms (Cu(1)— N(4) 1.861(10) Å, Cu(2)—N(1) 1.865(10) Å) are marginally shorter than Cu—N bond lengths involving the azomethine nitrogen centres, but significantly shorter than in the related macrocyclic derivative with saturated azomethine centres (Cu—N 1.986(5) Å) (24).

Each copper square plane is somewhat distorted with fairly acute angles within the Cu_2O_2 ring (O(2)—Cu(1)—O(1) 79.8(3)°; O(2)—Cu(2)—O(1) 80.4(4)°). Copper atom Cu(2) coincides with the mean plane described by the donor set N(1)–N(2)—O(1)— O(2), while Cu(1) is displaced from the mean plane of the donor set O(1)—O(2)—N(3)—N(4) by 0.137 Å towards a carboxamide oxygen (O(3)) of a neighbouring molecule. In fact the molecules are arranged in pairs in the crystal lattice, related by a centre of symmetry, in such a way that the Cu(1)—O(3)′ interaction (2.808(10) Å) can be considered to be a very weak bonding contact. The coordination geometry around Cu(1) is therefore best described as a square pyramid with the weak axial interaction involving O(3)′. The basic binuclear centre itself is almost flat with displacements of individual donors from the mean N_2O_2 planes of <0.02 Å and an angle of 0.6° between the N_2O_2 mean planes themselves (least-squares plane data are given in supplementary Table 7[3]). The bridging oxygen atoms (O(2), O(3)) have virtually no pyramidal character with solid angles at O(1) and O(2) of 359.5 and 360.1°, respectively.

The molecular structure of complex **III** is shown in Fig. 4 and selected interatomic distances and angles relevant to the copper coordination spheres are given in Table 5 (a detailed listing of bond distances and angles for **III** is given in supplementary Table 8[3]). The two copper(II) centres are bound by four short equatorial contacts (CuN_2O_2) and somewhat longer contacts (Cu(1)—O(3)″ 2.371(4); Cu(2)—O(4)′ 2.413(9) Å) to carboxamide oxygen atoms from neighbouring molecular units in an arrangement that stacks the molecules in the ***b*** direction in the crystal lattice. Each copper(II) centre is thus best described as

TABLE 2. Final atomic positional parameters and equivalent isotropic Debye–Waller temperature factors (esd's) for $[Cu_2(L_2)]\cdot H_2O$ (**II**)

Atom	*x*	*y*	*z*	B_{iso}[a]
Cu 1	0.04593(10)	0.32383(26)	0.11443(7)	3.54(10)
Cu 2	−0.07976(10)	0.27268(25)	−0.00633(7)	3.18(10)
O 1	−0.0717(5)	0.3574(13)	0.0791(4)	3.7(5)
O 2	0.0367(5)	0.2553(13)	0.0274(4)	4.2(5)
O 3	−0.0257(5)	0.0183(13)	−0.1582(4)	4.7(6)
O 4	0.2930(5)	0.2612(13)	0.1259(4)	4.2(5)
O 5	0.0949(5)	0.0380(12)	0.2931(4)	5.2(6)
N 1	−0.0774(7)	0.1909(15)	−0.0890(4)	2.7(6)
N 2	−0.1968(6)	0.2939(15)	−0.0318(5)	2.9(6)
N 3	0.0455(7)	0.4262(15)	0.1959(5)	2.7(6)
N 4	0.1623(6)	0.3195(15)	0.1372(5)	3.0(6)
C 1	0.2222(9)	0.1047(17)	−0.0676(6)	3.4(8)
C 2	0.1369(10)	0.0940(18)	−0.0964(6)	3.0(8)
C 3	0.0717(8)	0.1396(18)	−0.0666(6)	2.7(8)
C 4	0.0954(8)	0.2054(18)	−0.0026(6)	2.8(8)
C 5	0.1817(9)	0.2167(19)	0.0310(6)	3.0(7)
C 6	0.2390(8)	0.1651(18)	−0.0030(7)	3.1(7)
C 7	0.2895(8)	0.0607(18)	−0.1023(6)	3.5(8)
C 8	−0.0153(9)	0.1101(19)	−0.1077(6)	2.8(8)
C 9	−0.1623(9)	0.1568(18)	−0.1270(6)	3.7(8)
C10	−0.2271(8)	0.2520(19)	−0.1019(6)	3.9(8)
C11	−0.2421(8)	0.3594(19)	0.0011(7)	3.4(8)
C12	−0.3394(10)	0.4140(20)	−0.0313(6)	4.9(10)
C13	−0.3975(10)	0.2621(21)	−0.0310(7)	6.7(11)
C14	−0.4887(9)	0.3370(18)	−0.0669(6)	4.9(4)
C15	−0.2154(8)	0.4000(18)	0.0741(6)	2.7(7)
C16	−0.2744(8)	0.4422(19)	0.1105(7)	3.4(8)
C17	−0.2572(9)	0.4879(18)	0.1742(6)	3.1(9)
C18	−0.1729(8)	0.5015(18)	0.2046(6)	3.0(8)
C19	−0.1077(9)	0.4623(18)	0.1756(6)	2.9(8)
C20	−0.1307(8)	0.4054(18)	0.1097(7)	2.7(8)
C21	−0.3243(8)	0.5265(18)	0.2108(6)	3.8(8)
C22	−0.0159(9)	0.4909(21)	0.2126(6)	3.7(9)
C23	−0.0046(8)	0.6259(20)	0.2748(7)	5.3(9)
C24	0.0008(8)	0.5266(25)	0.3352(8)	8.0(12)
C25	0.0068(8)	0.6700(19)	0.3903(6)	4.8(4)
C26	0.1296(8)	0.4650(19)	0.2302(6)	3.8(8)
C27	0.1925(8)	0.3567(19)	0.2058(6)	3.6(8)
C28	0.2154(8)	0.2703(19)	0.1028(6)	2.9(8)

[a] B_{iso} is the mean of the principal axes of the thermal ellipsoid.

[3]Tables of observed and calculated structure factor amplitudes, of temperature factors, of hydrogen parameters, of least-squares plane data and of detailed bond distances and angles for **II** and **III** may be obtained from the Depository of Unpublished Data, CISTI, National Research Council of Canada, Ottawa, Ont., Canada K1A 0S2.

Can. J. Chem. Downloaded from www.nrcresearchpress.com by 41.223.56.140 on 09/07/12
For personal use only.

TABLE 3. Final atomic positional parameters and equivalent isotropic Debye–Waller temperature factors (esd's) for $[Cu_2(L_3)]\cdot CH_3CN\cdot H_2O$ (**III**)

Atom	*x*	*y*	*z*	B_{iso}[a]
Cu 1	0.65954(8)	0.14460(5)	0.90730(4)	2.48(4)
Cu 2	0.85795(8)	−0.08134(5)	0.86944(4)	2.42(4)
O 1	0.7579(4)	0.0613(3)	0.80656(21)	2.48(19)
O 2	0.7555(4)	0.00677(25)	0.96121(21)	2.51(19)
O 3	1.1268(4)	−0.2220(3)	1.06750(20)	3.29(18)
O 4	0.3775(4)	0.1504(3)	1.13206(20)	3.18(19)
N 1	0.9206(5)	−0.1473(3)	0.7591(3)	2.96(24)
N 2	1.0082(4)	−0.1738(3)	0.9428(3)	2.20(21)
N 3	0.5007(4)	0.1812(3)	0.9998(3)	2.32(21)
N 4	0.5837(4)	0.2762(3)	0.8355(3)	2.20(22)
C 1	0.7115(6)	0.0804(4)	0.7295(3)	2.0(3)
C 2	0.6152(6)	0.1848(4)	0.7014(3)	2.3(3)
C 3	0.5683(6)	0.1997(4)	0.6187(4)	2.6(3)
C 4	0.6099(6)	0.1199(4)	0.5600(3)	2.6(3)
C 5	0.7039(7)	0.0203(4)	0.5875(4)	2.6(3)
C 6	0.7596(6)	−0.0034(4)	0.6688(3)	2.1(3)
C 7	0.5584(12)	0.1408(7)	0.4702(5)	4.4(4)
C 8	0.8649(6)	−0.1123(4)	0.6857(3)	2.1(3)
C 9	0.9084(6)	−0.1861(4)	0.6117(3)	2.4(3)
C10	1.0109(7)	−0.1641(5)	0.5442(4)	3.0(3)
C11	1.0449(8)	−0.2303(6)	0.4760(4)	4.0(4)
C12	0.9767(9)	−0.3184(6)	0.4750(5)	4.6(4)
C13	0.8764(8)	−0.3437(5)	0.5418(5)	4.3(4)
C14	0.8411(7)	−0.2768(5)	0.6113(4)	3.6(3)
C15	1.0292(9)	−0.2566(6)	0.7679(5)	5.1(4)
C16	1.1661(9)	−0.2481(7)	0.8109(5)	5.4(4)
C17	1.1456(7)	−0.2551(5)	0.9076(4)	3.4(3)
C18	1.0134(6)	−0.1658(4)	1.0256(3)	2.3(3)
C19	0.8808(6)	−0.0970(4)	1.0783(3)	2.1(3)
C20	0.8830(7)	−0.1155(4)	1.1665(4)	2.8(3)
C21	0.7662(7)	−0.0624(4)	1.2237(3)	2.9(3)
C22	0.6425(7)	0.0133(5)	1.1890(4)	2.9(3)
C23	0.6324(6)	0.0401(4)	1.1027(3)	2.0(3)
C24	0.7572(6)	−0.0163(4)	1.0455(3)	2.2(3)
C25	0.7757(11)	−0.0866(8)	1.3185(5)	5.2(5)
C26	0.4938(6)	0.1281(4)	1.0761(3)	2.4(3)
C27	0.3618(7)	0.2645(5)	0.9747(4)	3.2(3)
C28	0.3984(8)	0.3770(5)	0.9457(4)	3.8(4)
C29	0.5427(7)	0.3751(5)	0.8848(4)	2.9(3)
C30	0.5640(6)	0.2813(4)	0.7553(4)	2.3(3)
C31	0.5668(8)	0.4557(5)	0.6617(4)	4.1(3)
C32	0.4831(7)	0.3873(4)	0.7090(3)	2.5(3)
C33	0.2469(10)	0.5031(6)	0.6604(5)	5.3(5)
C34	0.3267(11)	0.5689(6)	0.6128(5)	5.8(5)
C35	0.4858(12)	0.5472(6)	0.6141(5)	6.1(5)
C36	0.3225(8)	0.4104(5)	0.7097(4)	3.9(4)
N 5	0.0769(18)	0.5919(13)	0.2525(7)	13.7(8)
C37	0.0788(18)	0.5670(12)	0.1835(9)	12.7(12)
C38	0.0578(15)	0.5372(9)	0.1005(6)	12.5(8)
H20	0.3537(7)	0.3522(4)	0.1935(3)	11.2(4)

[a] B_{iso} is the mean of the principal axes of the thermal ellipsoid.

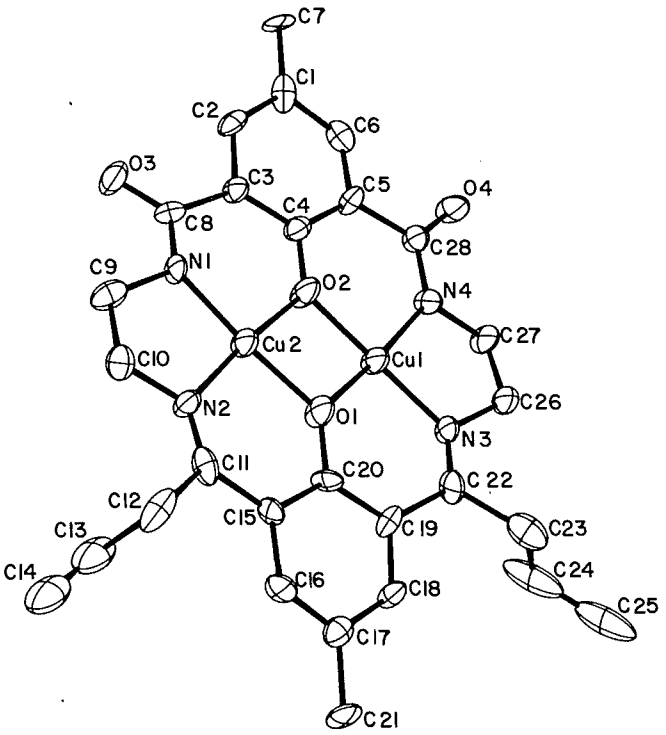


FIG. 3. Structural representation of $[Cu_2(L_2)]$ (**II**) with hydrogen atoms omitted (40% probability thermal ellipsoids).

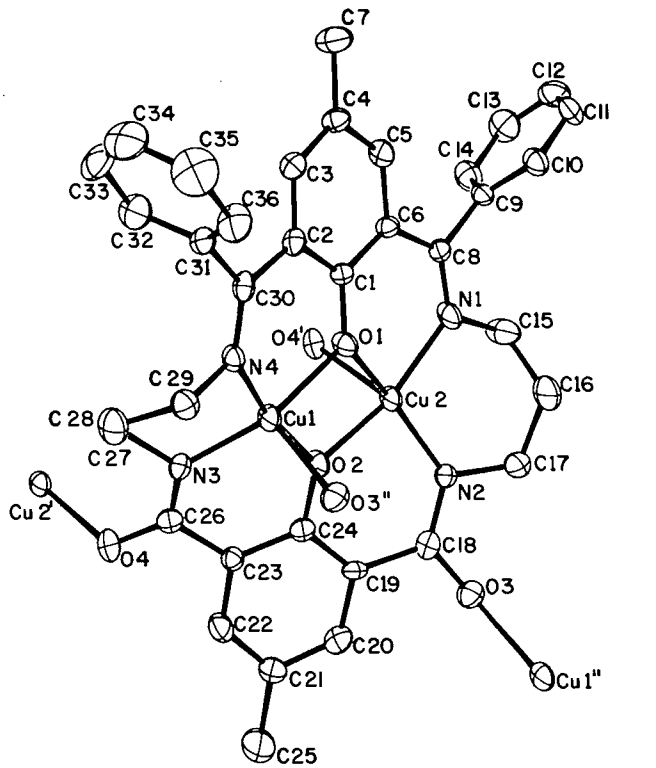


FIG. 4. Structural representation of $[Cu_2(L_3)]$ (**III**) with hydrogen atoms omitted (40% probability thermal ellipsoids).

having a five-coordinate, square-pyramidal structure. Copper–nitrogen distances in **III** are, in general, longer than those in **II**, which may be attributed, in part, to the presence of the $-(CH_2)_3-$ bridge, which creates a six-membered chelate ring. Once again Cu—N distances to the carboxamido nitrogen atoms are comparable with those associated with the azomethine centres, although Cu(2)—N(2) (1.937(4) Å) is significantly shorter than Cu(2)—N(1) (1.961(4) Å).

Some distortion occurs in the basal plane of the copper square-pyramids, with a marked compression of the O—Cu—O angles (O(1)—Cu(1)—O(2) 79.00(14); O(1)—Cu(2)—O(2) 77.90(13) Å), which are somewhat smaller than those found in **II**. Also both copper centres experience much more of a tetrahedral distortion of the equatorial donor set than is found in **II** (O(1)—Cu(1)— N(3) 153.63(16), O(2)—Cu(1)—N(4) 170.34(16)°; O(2)—Cu(2)—N(1) 165.41(16), O(1)—Cu(2)—

Can. J. Chem. Downloaded from www.nrcresearchpress.com by 41.223.56.140 on 09/07/12
For personal use only.

TABLE 4. Selected bond distances (Å) (esd's) and angles (deg) (esd's) for $[Cu_2(L_2)]\cdot H_2O$ (**II**)

Bond	Distance	Bond	Distance
Cu(1)—O(1)	1.918(8)	O(3)—C(8)	1.254(17)
Cu(1)—O(2)	1.885(8)	O(4)—C(28)	1.256(15)
Cu(1)—N(3)	1.893(10)	N(1)—C(8)	1.335(17)
Cu(1)—N(4)	1.861(10)	N(2)—C(11)	1.242(19)
Cu(2)—O(1)	1.893(8)	N(3)—C(22)	1.251(19)
Cu(2)—O(2)	1.883(8)	N(4)—C(28)	1.322(17)
Cu(2)—N(1)	1.865(10)	Cu(1)—Cu(2)	2.898(2)
Cu(2)—N(2)	1.879(10)	Cu(1)—Cu(2)′	3.946(3)
O(1)—C(20)	1.344(16)	Cu(1)—O(3)′	2.808(10)
O(2)—C(4)	1.334(15)		

Bonds	Angle	Bonds	Angle
O(1)—Cu(1)—O(2)	79.8(3)	O(2)—Cu(2)—N(1)	94.6(4)
O(1)—Cu(1)—N(3)	94.2(4)	O(2)—Cu(2)—N(2)	174.5(4)
O(1)—Cu(1)—N(4)	169.7(4)	N(1)—Cu(2)—N(2)	90.8(5)
O(2)—Cu(1)—N(3)	170.6(5)	Cu(1)—O(1)—Cu(2)	99.0(4)
O(2)—Cu(1)—N(4)	94.7(4)	Cu(1)—O(1)—C(20)	129.1(8)
N(3)—Cu(1)—N(4)	90.2(5)	Cu(2)—O(1)—C(20)	131.4(8)
O(1)—Cu(2)—O(2)	80.4(4)	Cu(1)—O(2)—Cu(2)	100.6(4)
O(1)—Cu(2)—N(1)	174.9(4)	Cu(1)—O(2)—C(4)	130.4(7)
O(1)—Cu(2)—N(2)	94.2(4)	Cu(2)—O(2)—C(4)	129.1(8)

TABLE 5. Selected bond distances (Å) (esd's) and angles (deg) (esd's) for $[Cu_2(L_3)]\cdot CH_3CN\cdot H_2O$ (**III**)

Bond	Distance	Bond	Distance
Cu(1)—O(1)	1.986(3)	O(3)—C(18)	1.279(6)
Cu(1)—O(2)	1.891(3)	O(4)—C(26)	1.279(6)
Cu(1)—N(3)	1.925(4)	N(1)—C(8)	1.298(7)
Cu(1)—N(4)	1.926(4)	N(2)—C(18)	1.322(7)
Cu(2)—O(1)	2.007(3)	N(3)—C(26)	1.322(7)
Cu(2)—O(2)	1.915(3)	N(4)—C(30)	1.283(7)
Cu(2)—N(1)	1.961(4)	Cu(1)—Cu(2)	3.018(1)
Cu(2)—N(2)	1.937(4)	Cu(1)—O(3)″	2.371(4)
O(1)—C(1)	1.300(6)	Cu(2)—O(4)′	2.413(3)
O(2)—C(24)	1.332(6)		

Bonds	Angle	Bonds	Angle
O(1)—Cu(1)—O(2)	79.00(14)	O(2)—Cu(2)—N(1)	165.41(16)
O(1)—Cu(1)—N(3)	153.63(16)	O(2)—Cu(2)—N(2)	92.51(15)
O(1)—Cu(1)—N(4)	91.63(15)	N(1)—Cu(2)—N(2)	102.06(17)
O(2)—Cu(1)—N(3)	94.18(15)	Cu(1)—O(1)—Cu(2)	98.18(15)
O(2)—Cu(1)—N(4)	170.34(16)	Cu(1)—O(1)—C(1)	125.6(3)
N(3)—Cu(1)—N(4)	95.29(17)	Cu(2)—O(1)—C(1)	130.5(3)
O(1)—Cu(2)—O(2)	77.90(13)	Cu(1)—O(2)—Cu(2)	104.91(16)
O(1)—Cu(2)—N(1)	89.01(15)	Cu(1)—O(2)—C(24)	125.2(3)
O(1)—Cu(2)—N(2)	154.46(15)	Cu(2)—O(2)—C(24)	129.7(3)

N(2) 154.46(15)°) which can be attributed in part to the flexibility imparted to the macrocyclic ligand by the six-membered chelate ring involving the N—$(CH_2)_3$—N moiety. Least-squares plane calculations show that for Cu(1) donors O(1) and N(3) are displaced by 0.190(4) and 0.236(5) Å, respectively, on one side of the N_2O_2 mean plane, whereas donors O(2) and N(4) are displaced by 0.189(4) and 0.262(5) Å, respectively, on the other side. A similar situation exists around Cu(2) (O(1) 0.209(4), N(2) 0.243(5), O(2) −0.206(4), N(1) −0.272(6) Å). Least-squares plane data are given in supplementary Table 9.[3]

The binuclear centre itself is somewhat bigger than that in **II** with a Cu(1)—Cu(2) separation of 3.0179(9) Å, longer average Cu—O bond lengths, and larger average Cu—O—Cu angles. The phenoxide bridge angles are quite different in this compound (Cu(1)—O(1)—Cu(2) 98.18(15)°, Cu(1)—O(2)—Cu(2) 104.91 (16)°), in contrast to **II**. The carboxamide C—O bond lengths are very slightly longer in this compound than in **II**,

Can. J. Chem. Downloaded from www.nrcresearchpress.com by 41.223.56.140 on 09/07/12
For personal use only.

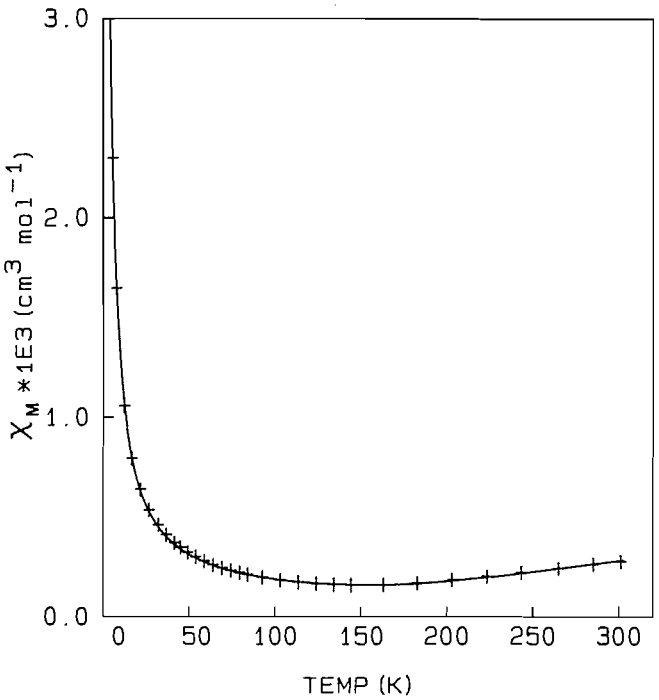


FIG. 5. Variable temperature magnetic susceptibility data for $[Cu_2(L_2)]\cdot H_2O$ (**II**). The solid line was calculated from eq. [1] with $g = 2.110 \pm 0.004$, $-2J = 689 \pm 7\,cm^{-1}$, $N\alpha = 120 \times 10^{-6}\,cm^3\,mol^{-1}$ complex, and $\rho = 0.030$ (3.0% paramagnetic impurity).

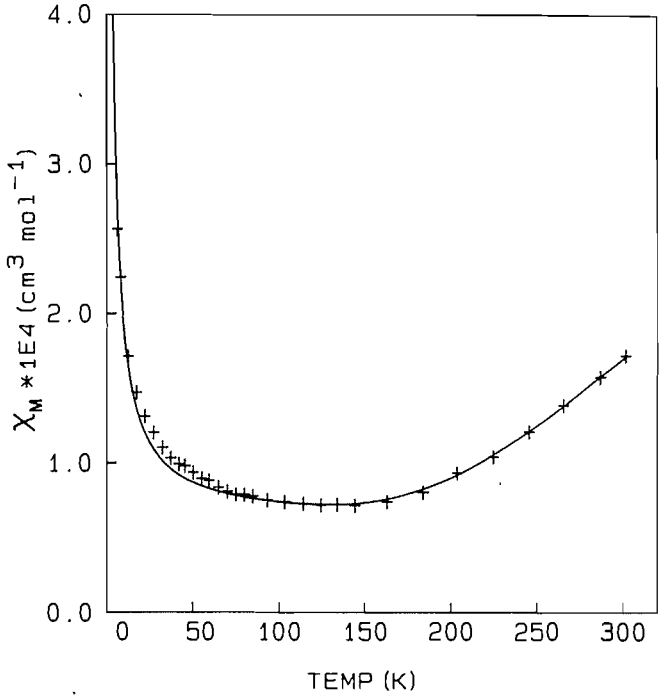


FIG. 6. Variable temperature magnetic susceptibility data for $[Cu_2(L_3)]\cdot CH_3CN\cdot H_2O$ (**III**). The solid line was calculated from eq. [1] with $g = 2.11 \pm 0.02$, $-2J = 816 \pm 8\,cm^{-1}$, $N\alpha = 120 \times 10^{-6}\,cm^3\,mol^{-1}$ complex, and $\rho = 0.00325$ (0.325% paramagnetic impurity).

indicating little change in the bonding character of this group as a result of the much more significant interaction of the carboxamide oxygens with the copper centres in adjacent molecules. Also, in contrast to the situation found in **II**, a significant pyramidal distortion exists at O(1) (solid angle 354.3°).

Magnetic properties

Room temperature magnetic moments for **II** and **III** are very low (0.52 (302 K), 0.72 (301 K) BM, respectively), indicative of strong antiferromagnetic coupling between the copper(II) centres. Variable temperature magnetic susceptibility measurements were performed on powdered samples of **II** and **III** in the temperature range 5–300 K. The results are summarized in Figs. 5 and 6, respectively. The shapes of the susceptibility plots reveal behaviour typical of strongly antiferromagnetically coupled binuclear compounds with the maximum of the susceptibility occurring at a temperature higher than 300 K. The susceptibility increase at low temperature is indicative of the presence of a small amount of monomeric paramagnetic impurity. The best-fit lines were calculated from the modified Van Vleck equation (25) for exchange-coupled pairs of copper(II) ions (eq. [1]):

$$[1]\quad \chi_M = \frac{N\beta^2 g^2}{3kT}\left[1 + \frac{1}{3}\exp(-2J/kT)\right]^{-1}(1-\rho) + \left[\frac{N\beta^2 g^2}{4kT}\right]\rho + N\alpha$$

In this expression $2J$ (in the spin Hamiltonian $H = 2Js_1 \cdot s_2$) is the singlet–triplet splitting or exchange integral and other symbols have their usual meaning and ρ represents the fraction of a possible magnetically dilute copper(II) impurity. The temperature-independent paramagnetism for a binuclear copper(II) complex, $N\alpha$, was taken as $120 \times 10^{-6}\,cm^3\,mol^{-1}$. The parameters giving the best fit were obtained by using a nonlinear regression analysis with ρ as a floating parameter. The exchange integral ($-2J$) for complex **II** was found to be $689 \pm 7\,cm^{-1}$ ($g = 2.110 \pm 0.004$, $\rho = 0.030$) and for complex **III** was found to be $816 \pm 8\,cm^{-1}$ ($g = 2.11 \pm 0.02$, $\rho = 0.00325$) indicating strong to very strong exchange between the copper(II) centres.

It is of interest to compare the magnetism of complexes **II** and **III** in the light of their structural data. The dominant structural feature, which is likely to influence the antiferromagnetic exchange between the copper centres the most, is the planar arrangement of oxygen bridges and the phenoxide bridge angle. It is well established that magnetic exchange in a series of dihydroxo-bridged binuclear copper(II) complexes, $[Cu_2B_2(OH)_2]^{2+}$ (B = bidentate nitrogen donor) varies as a function of hydroxide bridge angle (26). For a hydroxide bridge angle of, for example, 104°, $-2J$ was found to be $481\,cm^{-1}$. It may be noted than in complex **II**, for which $-2J = 689\,cm^{-1}$, the two phenoxo bridge angles are 99.0° and 100.6°, and for **III**, whose singlet–triplet energy separation is $816\,cm^{-1}$, the phenoxo bridge angles are 98.18° and 104.91°. These exchange integral values are significantly greater than those of dihydroxo-bridged copper(II) complexes having comparable bridge angles. Unfortunately magneto-structural data are not available for a related series of diphenoxo-bridged copper(II) complexes and so no comparable relationship has been established. However, in a number of dicopper(II) complexes with mixed phenoxo-hydroxo bridges, which are structurally and magnetically characterized (27–32), no obvious correlation emerged between $-2J$ and bridge angle values.

The average Cu—O—Cu bridge angle for **III** (101.55°) is slightly larger than that for **II** (99.80°), but one phenoxide oxygen in **III** (O1) has significant pyramidal character (solid

Can. J. Chem. Downloaded from www.nrcresearchpress.com by 41.223.56.140 on 09/07/12
For personal use only.

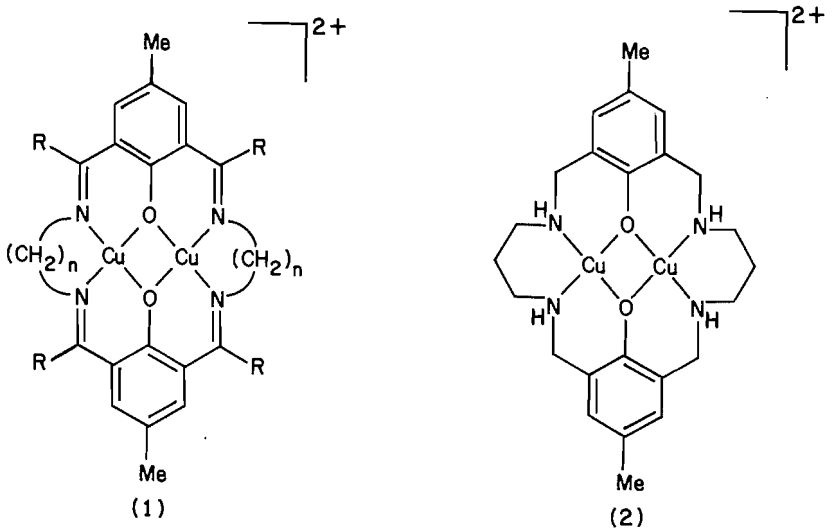


FIG. 7. (*1*) R = H, $n = 3$, $-2J = 850\ cm^{-1}$; R = H, $n = 4$, $-2J = 857\ cm^{-1}$; R = Me, $n = 3$, $-2J = 835\ cm^{-1}$; R = Pr, $n = 3$, $-2J = 806\ cm^{-1}$ (ref. 36). (*2*) $-2J = 824\ cm^{-1}$ (ref. 37).

angle 354.3°) and there are significant tetrahedral distortions in the CuN_2O_2 basal planes in this compound. Both of these effects might be expected to contribute to a reduced exchange in this system (33, 34). Pyramidal distortions in related phenoxo-bridged complexes (34) have been shown to lead to reduced antiferromagnetic exchange, but small distortions from planarity do not appear to influence exchange significantly (35). The large phenoxide bridge angle, Cu(1)—O(2)—Cu(2), of 104.9° in **III** might be considered to dominate the exchange situation for this compound, but considering the magnitude of the exchange ($-2J = 816\ cm^{-1}$) it seems reasonable to assume that both oxygen bridge groups contribute significantly to spin exchange. In comparing a variety of bisphenoxo-bridged macrocyclic dicopper(II) complexes of this sort (Fig. 7) it is evident that even major changes in the ligand itself, e.g. unsaturated versus saturated nitrogen donors and variable chelate ring sizes, do not have major effects on spin exchange (36, 37). Also for the butylene bridged complex $[Cu_2L(ClO_4)_2]$ (Fig. 7, 1, R = H, $n = 4$), which involves two pyramidally distorted oxygen bridges (solid angle 353.2°) and an oxygen bridge angle of 101.8°, very strong exchange is observed ($-2J = 857\ cm^{-1}$) (36) indicating the apparent insensitivity of the exchange towards pyramidal oxygen bridge distortions of this magnitude. Although distances within the amide framework are not really significantly different between the two compounds, quite major differences are observed in the bond distances within the $N_4O_2Cu_2$ framework (average Cu—N 1.875 Å, Cu—O 1.895 Å (**II**); average Cu—N 1.937 Å, Cu—O 1.950 Å (**III**)). This can be attributed, in part, to the "tight" binding arrangement generated by the ethylene bridge in **II** compared with the propylene bridge in **III**. On the basis of the shorter bond lengths within the magnetic framework ($d_{x^2-y^2}$) in **II**, a much larger exchange would have been expected.

In-plane Cu—O (bridge) distances, the degree of planarity of the copper magnetic orbitals and the slight pyramidal distortions at the oxygen bridge groups clearly do not account for the major differences in exchange between **II** and **III**. The only remaining structural feature of importance which could lead to a difference in exchange is the average phenoxide bridge angle, which differs by 1.75°. It is questionable whether such a small difference could be responsible for a difference in $-2J$ of $127\ cm^{-1}$. However, if the average oxygen bridge angles in **II** and **III** are substituted into the straight-line relationship observed for the dihydroxo-bridged species ($-2J = 74.53\phi - 7270\ cm^{-1}$; ϕ = hydroxide bridge angle) (26) a difference of $130\ cm^{-1}$ is obtained. It is perhaps unwise to attach much significance to the magnitude of the differences but to say that a 1.75° difference in phenoxide bridge angle could lead to a substantial difference in the exchange integral. It is clear that the situation concerning these macrocyclic complexes is much more complicated that that associated with the dihydroxo-bridged series and, until a larger selection of the macrocyclic systems is examined from a structural and magnetic standpoint, little can be said about magnetostructural trends.

Acknowledgements

We thank the Natural Sciences and Engineering Research Council of Canada (S.K.M., L.K.T.) and the CSIR, India (K.N., A.K.B.), for financial support for this study.

1. M. KODAMA and E. KIMURA. J. Chem. Soc. Dalton Trans. 325 (1979).
2. M. KODAMA and E. KIMURA. J. Chem. Soc. Dalton Trans. 694 (1981).
3. E. KIMURA, A. SAKONAKA, R. MACHIDA, and M. KODAMA. J. Am. Chem. Soc. **104**, 4255 (1982).
4. R. MACHIDA, E. KIMURA, and M. KODAMA. Inorg. Chem. **22**, 2055 (1983).
5. E. KIMURA, T. KOIKE, R. MACHIDA, R. NAGAI, and M. KODAMA. Inorg. Chem. **23**, 4181 (1984).
6. E. KIMURA, R. MACHIDA, and M. KODAMA. J. Am. Chem. Soc. **106**, 5497 (1984).
7. E. KIMURA. J. Coord. Chem. Sec. B, **15**, 1 (1986).
8. R. MACHIDA, E. KIMURA, and Y. KUSHI. Inorg. Chem. **25**, 3461 (1986).
9. E. KIMURA, M. YAMAOKA, M. MORIOKA, and T. KOIKE. Inorg. Chem. **25**, 3883 (1986).
10. L. FABBRIZZI and A. POGGI. J. Chem. Soc. Chem. Commun. 646 (1980).
11. A. BUTTAFAVA, L. FABBRIZZI, A. PERIOTTI, and B. SEGHI. J. Chem. Soc. Chem. Commun. 1166 (1982).
12. L. FABBRIZZI, F. FORLINI, A. PERIOTTI, and B. SEGHI. Inorg. Chem. **23**, 807 (1984).

Can. J. Chem. Downloaded from www.nrcresearchpress.com by 41.223.56.140 on 09/07/12
For personal use only.

13. A. BUTTAFAVA, L. FABBRIZZI, A. PERIOTTI, A. POGGI, and B. SEGHI. Inorg. Chem. **23**, 3917 (1984).
14. L. FABBRIZZI, TH. A. KADEN, A. PERIOTTI, B. SEGHI, and L. SIEGFRIED. Inorg. Chem. **25**, 321 (1986).
15. M. E. WINKLER and R. D. BEREMAN. J. Am. Chem. Soc. **102**, 6244 (1980).
16. D. W. MARGERUM. Pure Appl. Chem. **55**, 23 (1983).
17. J. M. JOHNSON, H. B. HALSHALL, and W. R. HEINEMAN. Biochemistry, **24**, 1579 (1985).
18. H. OKAWA, M. HONDA, and S. KIDA. Chem. Lett. 1027 (1972).
19. S. K. MANDAL and K. NAG. J. Chem. Soc. (Dalton), 2429 (1983).
20. G. GERMAIN, P. MAIN, and M. M. WOOLFSON. Acta Crystallogr. **A27**, 368 (1971).
21. E. J. GABE, F. L. LEE, and Y. PAGE. *In* Crystallographic computing III. *Edited by* G. M. Sheldrick and R. Goddard. Clarendon, Oxford, England. 1985. p. 167.
22. International tables for X-ray crystallography. Kynoch; Birmingham, England, 1974. Vol. IV. Table 2.2B. p. 99.
23. H. C. FREEMAN. Adv. Protein Chem. **22**, 257 (1967).
24. S. K. MANDAL, L. K. THOMPSON, K. NAG, J.-P. CHARLAND, and E. J. GABE. Inorg. Chem. **26**, 1391 (1987).
25. J. H. VAN VLECK. The theory of electric and magnetic susceptibilities. Oxford University Press, London. 1932. Chap. 9.
26. V. H. CRAWFORD, H. W. RICHARDSON, J. R. WASSON, D. J. HODGSON, and W. E. HATFIELD. Inorg. Chem. **15**, 2107 (1976).
27. J. J. GRZYBOWSKI, P. H. MERRELL, and F. L. URBACH. Inorg. Chem. **17**, 3078 (1978).
28. Y. NISHIDA, H. SHIMO, H. MAEHARA, and S. KIDA. J. Chem. Soc. Dalton Trans. 1945 (1985).
29. T. N. SORRELL, D. L. JAMESON, and C. J. O'CONNOR. Inorg. Chem. **23**, 190 (1984).
30. J. LOROSCH and W. HASSE. Inorg. Chim. Acta, **108**, 35 (1985).
31. G. D. FALLON, K. S. MURRAY, B. SPETHMANN, J. K. YANDELL, J. H. HODGKIN, and B. C. LOFT. J. Chem. Soc. Commun. 1561 (1984).
32. N. A. BAILEY, D. E. FENTON, J. LAY, P. B. ROBERTS, J.-M. LATOUR, and D. LIMOSIN. J. Chem. Soc. Dalton Trans. 2681 (1986).
33. D. J. HODGSON. Inorg. Chem. **15**, 3174 (1976).
34. W. MAZUREK, B. J. KENNEDY, K. S. MURRAY, M. J. O'CONNOR, J. R. RODGERS, M. R. SNOW, A. G. WEDD, and P. R. ZWACK. Inorg. Chem. **24**, 3258 (1985).
35. O. KAHN. Angew. Chem. Int. Ed. Engl. **24**, 834 (1986).
36. S. K. MANDAL and L. K. THOMPSON. Unpublished results.
37. S. K. MANDAL, L. K. THOMPSON, K. NAG, J.-P. CHARLAND, and E. J. GABE. Can. J. Chem. **65**, 2815 (1987).
38. A. C. LARSON. Crystallographic computing. Munksgaard, Copenhagen. 1970. p. 291.

Can. J. Chem. Downloaded from www.nrcresearchpress.com by 41.223.56.140 on 09/07/12
For personal use only.

Excess partial molar enthalpies of 2-butoxyethanol and water in 2-butoxyethanol–water mixtures

WILLIAM SIU[1] AND YOSHIKATA KOGA[2]

Department of Chemistry, The University of British Columbia, Vancouver, B.C., Canada V6T 1Y6

Received October 31, 1988

WILLIAM SIU and YOSHIKATA KOGA. Can. J. Chem. **67**, 671 (1989).

Excess partial molar enthalpies of 2-butoxyethanol (BE) and water, $H_m^E(i)$ (i = BE or H_2O), were measured from 25 to 35°C in the entire concentration range. The results indicated that there are three concentration regions bounded at about $x_B = 0.02$ and $x_B = 0.5$, x_B being the mole fraction of BE. In each region, the concentration and temperature dependence of $H_m^E(i)$ (i = BE or H_2O), is distinctively different from those in the other regions, and appears to support the following views: In the water-rich region, $x_B < 0.02$, BE molecules cause an enhancement in the structure of water, and this effect spans a long range via a structurally enhanced network of water. The solute–solute (BE–BE) interaction is repulsive and of a long range character in terms of enthalpy. As x_B increases, the repulsive solute–solute interaction becomes stronger sharply to the threshold value, $x_B \approx 0.017$, whereupon the mode of such mixing no longer becomes possible. In the intermediate range, $0.02 < x_B < 0.5$, a new scheme whereby BE molecules tend to associate is predominant. Two clathrate-like aggregates of the types $h[BE(H_2O)_k]$ with $k = 55$ and 4 may exist together with BE clusters $(BE)_n$. In the third region, $0.5 < x_B$, BE molecules are exactly in the same environment as in pure liquid, while water molecules are almost in the same environment as in pure water. The solution consists of BE and water clusters.

Key words: excess partial molar enthalpy, 2-butoxyethanol–water.

WILLIAM SIU et YOSHIKATA KOGA. Can. J. Chem. **67**, 671 (1989).

Opérant à des températures allant de 25 à 35°C et sur l'ensemble des concentrations, on a mesuré les enthalpies molaires partielles en excès du butoxy-2 éthanol (BE) et de l'eau, $H_m^E(i)$ (i = BE ou H_2O). Les résultats indiquent qu'il existe trois régions de concentrations dont les limites sont $x_B = 0{,}02$ et $x_B = 0{,}5$ (x_B correspond à la fraction molaire de BE). La relation qu'on peut observer dans une région entre $H_m^E(i)$ (i = BE ou H_2O) et la concentration ainsi que la température diffère beaucoup de celle que l'on peut dans les autres régions; cette observation supporte les hypothèses suivantes: dans la région riche en eau, $x_B < 0{,}02$, les molécules de BE provoquent une meilleure organisation de la structure de l'eau et cet effet s'étend à de grandes distances par le biais d'un réseau d'eau mieux organisé d'un point de vue structural. En termes d'enthalpie, l'interaction soluté–soluté (BE–BE) provoque des répulsions à longue distance. Avec une augmentation de x_B, les interactions de répulsions soluté–soluté deviennent beaucoup plus importantes, jusqu'à une valeur limite x_B d'environ 0,017 alors que ce mode de mélange n'est plus possible. Aux concentrations intermédiaires, $0{,}02 < x_B < 0{,}5$, un nouveau schéma dans lequel les molécules de BE tendent à s'associer devient prédominant. Deux agrégats ressemblant à des clathrates, du type $h[BE(H_2O)_k]$ avec $k = 55$ et 4, peuvent coexister avec des amas de $(BE)_n$. Dans la troisième région, $x_B > 0{,}5$, molécules de BE sont exactement dans le même environnement que dans le liquide pur alors que les molécules d'eau sont presque dans le même environnement que dans l'eau pure. La solution comporte des agrégats de BE et d'eau.

Mots clés : enthalpie molaire partielle en excès, butoxy-2 éthanol/eau.

[Traduit par la revue]

Introduction

In the previous papers from this laboratory (1–3), the measured values of excess *partial* molar enthalpies, $H_m^E(i)$ (i = TBA or H_2O), of tert-butanol (TBA) and water in the TBA–water mixtures were reported. The results have provided more direct information than hitherto available on the nature of the solute–solvent and solute–solute interactions, and hence provided more insight into the mode of molecular aggregation.

The present paper reports the directly measured values of excess *partial* molar enthalpies of BE and water, $H_m^E(BE)$ and $H_m^E(H_2O)$, in the BE–water mixtures from 25 to 35°C in the entire concentration range. This system has been studied extensively together with the TBA–water system, since anomalies in various physical properties are equally pronounced in the water-rich region (4–14). While the results of the recent light scattering (7, 9, 10) and ultrasonic relaxation measurements (8, 11, 13) have appeared to be consistent with the existence of molecular aggregates of the type $h[BE(H_2O)_k]$, with $k = 55$ and 4, there also exist some puzzling results. For example, the hydrodynamic radii calculated from the self-diffusion coefficient and viscosity were found to be about the same or even smaller than each molecular radius (12) in the concentration range where such molecular aggregates are believed to exist. On the other hand, there is an indication of the existence of a large cluster with hydrodynamic radius of about 1000 Å for $x_B < 0.02$ at room temperature (13, 14), although such existence may be sample-dependent (14), x_B being the mole fraction of BE.

The original purpose of this work was to obtain some information on the solute–solvent and the solute–solute interactions similar to that for the TBA–water system (1–3). It turned out that the concentration dependence of $H_m^E(BE)$ changes very drastically at $x_B \approx 0.017$. The plots of the derivative, $(\partial H_m^E(BE)/\partial x_B)_{N.T.P}$ (which is proportional to solute–solute interaction), exhibits a surprisingly similar shape of a heat capacity anomaly against temperature at a second order phase transition pertaining to a change in a bulk structure. This is relevant to the idea that there is a new type of phase transition in analogy to a surfactant solution (15).

Experimental

The specimen of 2-butoxyethanol used in this work was purchased from Aldrich, the same supplier as the samples used by Kato *et al.* (13) and Bender *et al.* (14). As will be discussed below, the existence of a species with a very large hydrodynamic radius of the order of 1000 Å

[1]Present address: Department of Pharmacology, The University of British Columbia.

[2]To whom correspondence should be addressed.

Can. J. Chem. Downloaded from www.nrcresearchpress.com by 41.223.56.140 on 09/07/12
For personal use only.

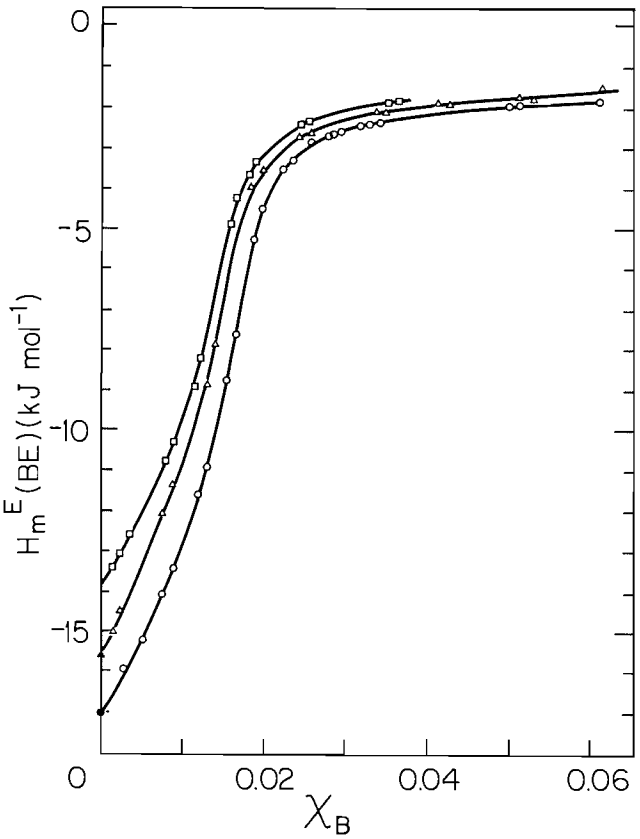


FIG. 1. The excess partial molar enthalpies of BE, H_m^E(BE), against mole fraction of BE, x_B. ○, 25°C; △, 30°C; □, 35°C; ●, ▲, refs. 17 and 18.

was observed in these two studies. An analytical gas chromatography indicated the purity to be better than 99.9%. This specimen was used without further purification.

The excess partial molar enthalpies were measured by means of an LKB Bromma precision calorimetry system. The buret method as described in a previous paper (2) was employed. The values of H_m^E(i) (i = BE or H_2O) were calculated as described previously (1–3, 16). The errors were estimated to be 1% with an upperbound error of ± 0.1 kJ mol^{-1} and a lower bound error of ± 0.03 kJ mol^{-1}. As pointed out previously, the buret method is not as accurate as the ampoule method (2).

Results and discussion

The measured values of H_m^E(i) (i = BE or H_2O) are listed in Table 1 and plotted in Figs. 1 and 2. In terms of their composition and temperature dependence, there are clearly three regions bounded at about $x_B = 0.02$ and $x_B = 0.5$. As shown in Fig. 1, the extrapolated values of H_m^E(BE) to $x_B = 0$ compare well with those available in literature (17, 18). For the entire concentration range, however, no data of H_m^E(i) (i = BE or H_2O) are available for direct comparison with the values from this work. Thus, the excess (integral) molar enthalpies, H_m^E, were calculated from the values of H_m^E(i), (i = BE and H_2O) read off the smooth curves drawn in Figs. 1 and 2. Such values are plotted in Fig. 3 together with the available literature values (19, 28). The comparison appears satisfactory.

If the values of the excess partial molar free energy, G_m^E(i), are available, those of the excess partial molar entropy, S_m^E(i), can be calculated. The values of S_m^E(i) and their concentration and temperature dependence together with those of H_m^E(i) would provide a deeper insight into the nature of the solution. The vapour pressures of eight mixtures of the BE–H_2O system were measured (20). The data were analysed by forcing a single analytic function for G_m^E for the entire concentration range, from which analytic expressions for G_m^E(i) (i = BE or H_2O) were given (20). However, the excess (integral) heats of dilution obtained from the temperature dependence of G_m^E did not fit well with the observed values (19) for $x_B > 0.2$. Moreover, the immiscibility gap calculated from the inflection points in G_m^E was wider in temperature and concentration than that observed. Therefore, such calculations for S_m^E(i) will have to be postponed until the vapour pressures are measured at very close intervals in concentration.

The solute–solvent interaction is given as the value of H_m^E(BE) at $x_B \approx 0.0$. As seen in Fig. 1, it is strongly exothermic. This result together with a large positive value of C_p^E(BE) at $x_B \approx 0.0$ (4) is consistent with the suggestion that the solute enhances the structure of the solvent water, as in the case of TBA–water solutions (1–3, 21–24).

Intuitively, the derivative of the partial molar enthalpy of BE with respect to the number of moles of BE is a measure of the solute–solute interaction. The formal connection between the two without invoking any model system, however, is not immediately obvious. To begin with, a formal separation of the internal energy of the system into solute–solvent and solute–solute interactions is a difficult task without relying on a model. If we have a model system, on the other hand, a relationship can be derived between the derivative, $(\partial H_m^E(\mathrm{BE})/\partial n_{\mathrm{BE}})_{n\mathrm{H_2O},T,P}$, and the solute–solute interaction defined within the scope of the model system. In the mean-field approximation, for example, it is elementary to show that the derivative is indeed proportional to the solute–solute interaction parameter defined in the mean-field approximation. Obviously, the mean-field approximation is far from the reality for the present system. In the absence of an appropriate model, we calculate the derivative graphically using the present data. Since H_m^E(BE) is an intensive variable, it follows that

$$[1]\quad N(\partial H_m^E(\mathrm{BE})/\partial n_{\mathrm{BE}})_{n_{\mathrm{H_2O}},T,P} = (1 - x_B)(\partial H_m^E(\mathrm{BE})/\partial x_B)_{N,T,P}$$

where $N = n_{\mathrm{BE}} + n_{\mathrm{H_2O}}$. The values of $(\partial H_m^E(\mathrm{BE})/\partial x_B)_{N,T,P}$ were evaluated as the tangents of the smooth curve drawn in Fig. 1, and the values of the right hand of eq. [1] are plotted in Fig. 4 for the range, $x_B < 0.04$. As is apparent from Fig. 4, the values of the solute–solute interaction are finite and positive in this concentration range, and do not appear to extrapolate smoothly to zero at $x_B = 0.0$. This indicates that the solute–solute interaction is repulsive and is of a very long (almost infinite) range. The ratio of the hydrogen bonds intact in water has been argued to be well above the percolation threshold (25). Namely, the hydrogen bond network spans over the entire bulk of water. If a BE molecule enhances the structure of such hydrogen bond network, the second BE molecule should feel the effect of structure enhancement even at an infinite distance via the hydrogen bond network. As the concentration of BE increases, the repulsive interaction becomes stronger sharply, as is apparent from Fig. 4, to a threshold, $x_B \approx 0.017$ at 25°C, beyond which such interaction diminishes sharply. In terms of the concentration dependence of $(1 - x_B)(\partial H_m^E(\mathrm{BE})/\partial x_B)$, the crossover from the water-rich region to the intermediate region is very drastic suggesting a kind of phase transition pertaining obviously not to a bulk structure but an intermediate scale structure. It is striking that the shape of the anomalies in Fig. 4 resembles that of the heat capacity vs. temperature for a second

Can. J. Chem. Downloaded from www.nrcresearchpress.com by 41.223.56.140 on 09/07/12
For personal use only.

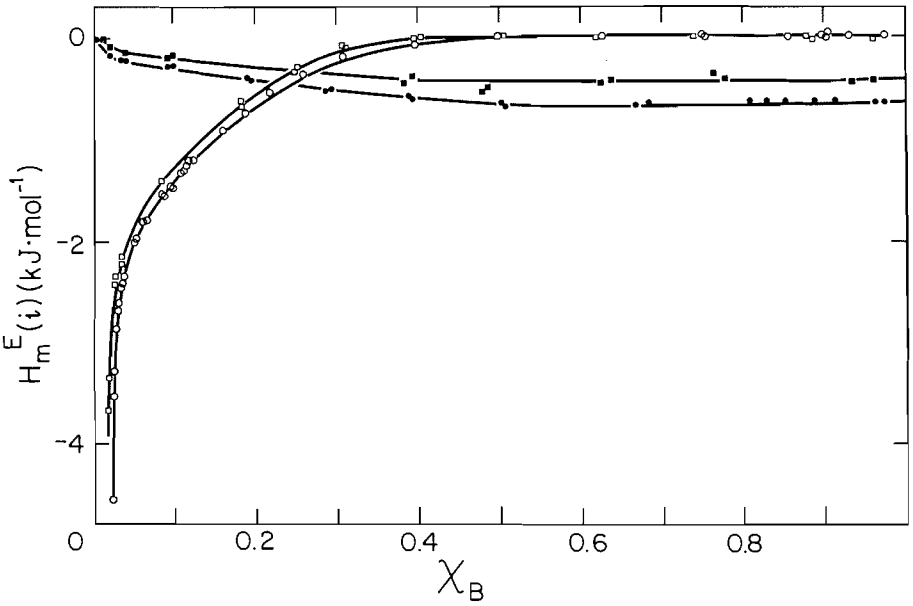


FIG. 2. The excess partial molar enthalpies of BE and water, $H_m^E(i)$ ((i = BE or H_2O)), against mole fraction of BE, x_B. ○, BE, 25°C; □, BE, 35°C; ●, H_2O, 25°C; ■, H_2O, 35°C.

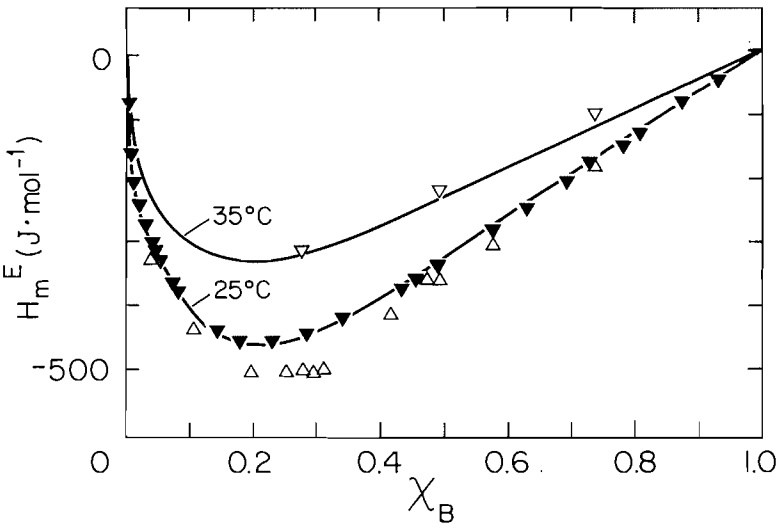


FIG. 3. The excess (integral) molar enthalpies, H_m^E, against mole fraction of BE, x_B. —, this work; ▼, 25°C (ref. 28); △, 20°C (ref. 19); ▽, 40°C, (ref. 19).

order (bulk) phase transition. A general relationship between the order of the transition and the shape of heat capacity anomalies has been explored (26, 27). It is worth noting that the same plots for the TBA–water system shows a smaller and much smoother hump (2) than the present case, resembling a heat capacity anomaly of a higher than the second order (bulk) phase transition (26, 27). Roux *et al.* (4, 15) have suggested a kind of phase transition in analogy to the formation of micellar aggregates of the surfactant solutions and drawn a phase boundary (4) from the peak position of the excess partial molar heat capacity, C_p^E(BE). Such a phase boundary is reproduced in Fig. 5, together with the positions of anomalies in the plots of Fig. 4. The recent ultrasonic relaxation (13) and light scattering measurements (14) showed that there is a boundary below which the hydrodynamic radii of diffusing species are very large, of the order of 1000 Å. These thresholds are also plotted in Fig. 5. While the sample-dependent feature in the light scattering measurements (14) needs to be clarified further, various techniques point to the existence of the "phase boundary" shown in Fig. 5, suggesting that there is a genuine change in the intermediate scale structure, or the mode of molecular aggregation across the boundary. It is important to note that the thermodynamic quantities which show anomalies at this phase boundary are related to the *third* derivative of the free energy; the partial molar heat capacity of the work by Roux *et al.* (4) is the derivative of the free energy with respect to temperature twice and concentration once, while the quantity expressed by eq. [1] of this work is that with respect to temperature once and concentration twice.

The mode of molecular aggregation that can be deduced from the present results is summarized as follows: In the water-rich region, below the boundary shown in Fig. 5, BE molecules

Can. J. Chem. Downloaded from www.nrcresearchpress.com by 41.223.56.140 on 09/07/12
For personal use only.

TABLE 1. The excess partial molar enthalpies of BE and H_2O

x_B	H_m^E(BE) (kJ mol^{-1})	x_B	H_m^E(BE) (kJ mol^{-1})
	Temperature = 25°C		
0.002583	−15.98	0.1092	−1.33
0.004961	−15.21	0.1107	−1.32
0.008809	−13.37	0.1169	−1.26
0.01176	−11.60	0.1185	−1.22
0.01275	−10.92	0.1219	−1.20
0.01519	−8.83	0.1236	−1.20
0.01629	−7.67	0.1624	−0.92
0.01858	−5.29	0.1887	−0.72
0.01975	−4.55	0.2212	−0.55
0.02205	−3.55	0.2628	−0.37
0.02321	−3.30	0.3091	−0.20
0.02559	−2.88	0.3116	−0.19
0.02824	−2.69	0.4006	−0.07
0.02943	−2.61	0.4027	−0.11
0.03175	−2.45	0.5024	+0.02
0.03299	−2.41	0.5047	+0.02
0.03418	−2.35	0.6240	−0.00
0.04993	−2.01	0.6264	+0.01
0.05136	−1.98	0.7457	+0.01
0.06148	−1.81	0.7475	+0.01
0.06279	−1.81	0.8564	−0.00
0.08362	−1.53	0.8575	+0.00
0.08515	−1.56	0.9015	−0.00
0.09585	−1.48	0.9022	−0.00
0.09744	−1.49	0.9358	−0.00
	Temperature = 30.0°C		
0.001095	−15.02	0.03496	−2.12
0.002106	−14.47	0.04163	−2.01
0.007599	−12.10	0.04294	−2.03
0.008835	−11.39	0.05160	−1.75
0.01301	−8.92	0.05290	−1.83
0.01414	−7.88	0.06172	−1.71
0.01863	−3.99	0.07167	−1.61
0.01972	−3.61	0.07306	−1.60
0.02458	−2.74	0.08180	−1.45
0.02575	−2.60	0.08333	−1.44
0.03392	−2.09		
	Temperature = 35.0°C		
0.001318	−13.37	0.08288	−1.43
0.002353	−13.08	0.1827	−0.64
0.003557	−12.62	0.1846	−0.66
0.007920	−10.74	0.3120	−0.09
0.008894	−10.31	0.3142	−0.11
0.01115	−8.95	0.4004	−0.02
0.01222	−8.26	0.4027	−0.01
0.01587	−4.85	0.5021	+0.01
0.01684	−4.21	0.5039	+0.01
0.01812	−3.67	0.6216	−0.00
0.01909	−3.36	0.6237	−0.03
0.02442	−2.42	0.7401	−0.00
0.02550	−2.34	0.7415	−0.00
0.03514	−1.95	0.8805	−0.00
0.03620	−1.89	0.8813	−0.01
0.08156	−1.42	0.9591	−0.03

TABLE 1 (*concluded*)

x_B	H_m^E(H_2O) (kJ mol^{-1})	x_B	H_m^E(H_2O) (kJ mol^{-1})
	Temperature = 25.0°C		
0.003952	−0.00	0.3901	−0.58
0.009807	−0.02	0.3948	−0.61
0.009898	−0.02	0.5038	−0.67
0.01959	−0.17	0.5115	−0.69
0.01978	−0.17	0.6708	−0.67
0.03935	−0.20	0.6842	−0.65
0.03971	−0.21	0.8082	−0.64
0.09784	−0.26	0.8282	−0.64
0.09875	−0.26	0.8509	−0.65
0.1948	−0.39	0.8896	−0.63
0.1968	−0.41	0.9131	−0.63
0.2910	−0.52	0.9640	−0.66
0.2955	−0.52	0.9798	−0.66
	Temperature = 35.0°C		
0.003900	−0.01	0.4805	−0.55
0.009930	−0.01	0.4822	−0.54
0.01987	−0.07	0.4886	−0.52
0.03965	−0.14	0.4891	−0.52
0.09825	−0.19	0.6291	−0.45
0.09920	−0.17	0.6398	−0.41
0.2530	−0.34	0.7655	−0.38
0.2559	−0.32	0.7812	−0.41
0.3874	−0.46	0.9389	−0.45
0.3931	−0.38	0.9604	−0.44

modify the hydrogen bond network of water. By so doing, they interact each other repulsively via the structurally enhanced network of the solvent. Thus the implication is that they avoid each other in this concentration range. Obviously, data of the excess partial molar entropy, or the excess partial molar free energy are required for a more definite conclusion in this regard. However, it is worthwhile to note that the Kirkwood–Buff parameter for the BE–BE pair is negative (10), and that the joint diffusion coefficient for the BE–BE pair is also negative (12) in this concentration range, suggesting mutual repulsion among BE molecules.

As the concentration of BE increases, the BE–BE repulsion becomes stronger until the concentration reaches that of the "phase boundary", at which this mode of mixing no longer becomes possible, and a new scheme becomes operative. The threshold concentration corresponds to the stoichiometric ratio, the number of water molecules over that of BE molecules, of about 55. Thus it appears that below this threshold a clathrate-like aggregate of the type $BE(H_2O)_k$ with a fixed value of 55 does not exist, but rather it is forced to form at and perhaps beyond the phase boundary.

In the intermediate region, beyond the phase boundary and up to about $x_B = 0.5$, a precursory situation of the phase separation that occurs above the critical solution temperature, 49.4°C (9), may be expected. Indeed, a Rayleigh and Raman scattering work suggested the existence of two kinds of clathrate-like species; $g[BE(H_2O)_{50}]$ and $h[BE(H_2O)_4]$, their compositions being the same as those of two phases into which the solution separates above 49.4°C. As apparent from Fig. 2, however, there is no singular behaviour in H_m^E(BE) at $x = 0.200$, where all the water molecules would be exhausted to form $h[BE(H_2O)_4]$.

Can. J. Chem. Downloaded from www.nrcresearchpress.com by 41.223.56.140 on 09/07/12
For personal use only.

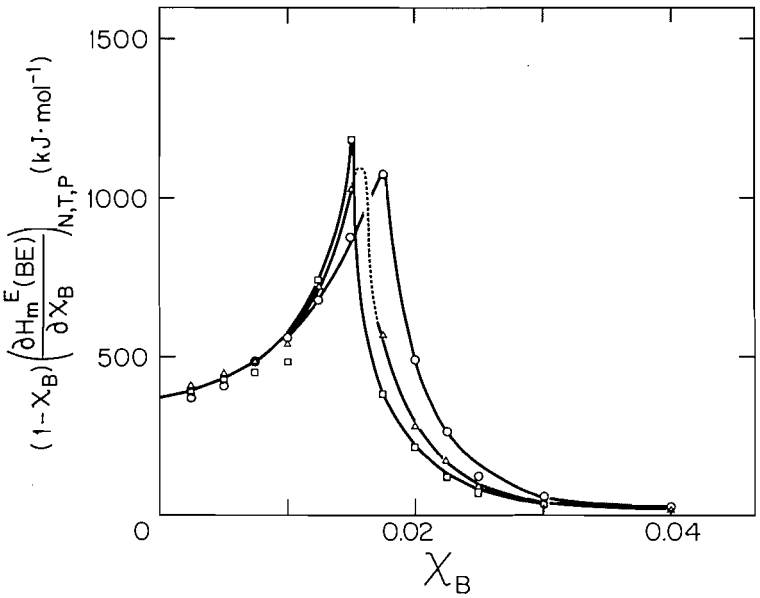


FIG. 4. The solute–solute interaction, $(1 - x_B)(\partial H_m^E(BE)/\partial x_B)_{N,T,P}$, against mole fraction x_B. ○, 25°C; △, 30°C; □, 35°C.

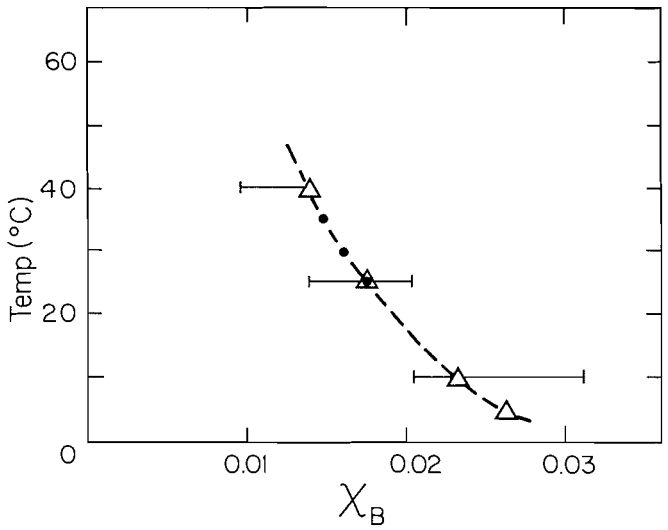


FIG. 5. The "phase diagram". ●, this work; △, ref. 4; ⊢⊣, ref. 14.

This may suggest that in this range the aggregates of BE have already started to mix in. The interpretation for the second mechanism of ultrasonic relaxation also pointed to the existence of BE clusters (13). The observations that the Kirkwood–Buff parameters (10) and the joint diffusion coefficients (12) for the BE–BE as well as the H_2O–H_2O pairs are highly positive support the notion of the formation of BE and H_2O aggregates already in this concentration range.

In the third concentration region, $x_B > 0.5$, it is striking that H_m^E(BE) is zero and $H_m^E(H_2O)$ is small, negative, and constant. These facts suggest that an additional BE molecule always settles in the environment which is exactly the same as that in pure liquid in terms of enthalpy. An additional H_2O molecule, on the other hand, finds itself in an environment very slightly more favourable than that in pure water. Such an environment stays the same all through this region. The following picture, though speculative, appears consistent with these findings: In this concentration range, the solution consists of clusters of BE and clusters of water. The enthalpy of the interfacial region between two kinds of clusters is slightly more exothermic for H_2O than in the inside of H_2O clusters, while for a BE molecule the inside of BE clusters is more exothermic than the interfacial region. Thus an additional BE molecule settles into the inside of BE clusters and an additional H_2O in the interfacial region of the two kinds of clusters. This presents an interesting question as to the size of such clusters, small enough not to be recognized as a bulk phase but large enough for the inside of the BE clusters to be the same as that of the bulk BE.

Acknowledgements

We would like to thank Dr. D. H. Dolphin for the use of the calorimeter. This research was supported by the Natural Sciences and Engineering Research Council of Canada.

1. Y. KOGA. Can. J. Chem. **64**, 206 (1986).
2. Y. KOGA. Can. J. Chem. **66**, 1187 (1988).
3. Y. KOGA. Can. J. Chem. **66**, 3171 (1988).
4. G. ROUX, G. PERRON, and J. E. DESNOYERS. J. Sol. Chem. **7**, 639 (1978).
5. S. HARADA, T. NAKAJIMA, T. KOMATSU, and T. NAKAGAWA. J. Sol. Chem. **7**, 463 (1978).
6. J. LARA and J. E. DESNOYERS. J. Sol. Chem. **10**, 465 (1981).
7. N. ITO, K. SAITO, T. KATO, and T. FUJIYAMA. Bull. Chem. Soc. Jpn. **54**, 991 (1981).
8. S. NISHIKAWA, M. TANAKA, and M. MASHIMA. J. Phys. Chem. **85**, 686 (1981).
9. N. ITO, T. FUJIYAMA, and Y. UDAGAWA. Bull. Chem. Soc. Jpn. **56**, 379 (1983).
10. T. KATO. J. Phys. Chem. **88**, 1248 (1984).
11. S. NISHIKAWA and K. KOTEGAWA. J. Phys. Chem. **89**, 2896 (1985).
12. T. KATO. J. Phys. Chem. **89**, 5750 (1985).
13. S. KATO, D. JOBE, N. P. RAO, C. H. HO, and R. E. VERRALL. J. Phys. Chem. **90**, 4167 (1986).
14. T. M. BENDER and R. PECORA. J. Phys. Chem. **92**, 1675 (1988).
15. R. ROUX, G. PERRON, and J. E. DESNOYERS. J. Phys. Chem. **82**, 966 (1978).

Can. J. Chem. Downloaded from www.nrcresearchpress.com by 41.223.56.140 on 09/07/12
For personal use only.

16. Y. KOGA. J. Chem. Thermodyn. **19**, 571 (1987).
17. K. KUSANO, J. SUURKUUSK, and I. WADSO. J. Chem. Thermodyn. **5**, 757 (1973).
18. S. CABANI, V. MOLLICA, and L. LEPORI. J. Chem. Soc. Faraday 1, **74**, 2667 (1978).
19. U. ONKEN. Z. Elektrochem. **63**, 321 (1959).
20. G. SCATCHARD and G. M. WILSON. J. Am. Chem. Soc. **86**, 133 (1964).
21. H. UEDAIRA and J. KIDA. Nippon Kagaku Kaishi, **1982**, 539 (1982).
22. T. M. BENDER and R. PECORA. J. Phys. Chem. **90**, 1700 (1986).
23. K. NAKANISHI, K. IKARI, S. OKAZAKI, and H. TOUHARA. J. Chem. Phys. **80**, 1656 (1984).
24. H. TANAKA, K. NAKANISHI, and H. TOUHARA. J. Chem. Phys. **81**, 4065 (1984).
25. H. E. STANLEY and J. TEIXEIRA. J. Chem. Phys. **73**, 3404 (1980).
26. Y. KOGA. Chem. Phys. Lett. **31**, 571 (1975).
27. Y. KOGA. Collect. Phenomen. **3**, 1 (1978).
28. M. I. DAVIS, M. C. MOLINA, and G. DOUHERET. Thermochim. Acta, **131**, 153 (1988).

Can. J. Chem. Downloaded from www.nrcresearchpress.com by 41.223.56.140 on 09/07/12
For personal use only.

Nitrogenous metabolites from the deep water sponge *Hexadella* sp.

SANDRA A. MORRIS AND RAYMOND J. ANDERSEN[1]

Departments of Chemistry and Oceanography, University of British Columbia, Vancouver, B.C., Canada V6T 1W5

Received September 23, 1988

SANDRA A. MORRIS and RAYMOND J. ANDERSEN. Can. J. Chem. **67**, 677 (1989).

The secondary metabolites of the sponge *Hexadella* sp., collected by SCUBA (−40 m) and manned submersible (−100 to −200 m) in Jervis Inlet, British Columbia, have been examined. The submersible-collected material contained only the previously reported compound topsentin B2 (**1**). Sponge material collected in shallower water via SCUBA contained hexadellins A (**2**) and B (**3**), two new dibromotyrosine derived metabolites. The structures of **2** and **3** were determined by spectroscopic analysis of the diacetyl derivatives **6** and **7**.

Key words: sponge, metabolite, *Hexadella*, nitrogenous.

SANDRA A. MORRIS et RAYMOND J. ANDERSEN. Can. J. Chem. **67**, 677 (1989).

On a étudié les métabolites secondaires d'éponges *Hexadella* sp., récoltées par plongée (−40 m) et par des submersibles habités (de −100 à −200 m) dans l'anse de Jervis, en Colombie britannique. Les éponges recueillies à l'aide des submersibles ne contiennent que de la topsentine B2 (**1**), un produit observé antérieurement. Les éponges recueillies dans des eaux moins profondes contiennent des hexadellines A (**2**) et B (**3**), deux nouveaux métabolites dérivés de la dibromotyrosine. On a déterminé les structures des composés **2** et **3** en se basant sur les données spectroscopiques de leurs dérivés acétyles, **6** et **7**.

Mots clés : éponge, métabolite, *Hexadella*, azoté.

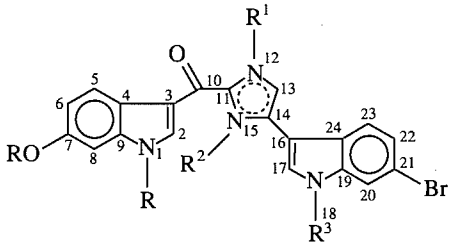
[Traduit par la revue]

Sponges are widely distributed in the world's oceans, occurring at all depths and latitudes. A large amount of work on SCUBA accessible species has shown that sponge secondary metabolism is spectacularly diverse, complex, and novel (1). Only a limited number of deep water species have been examined to date (2). It is already clear, however, that interesting chemistry is not restricted to species of sponges collected in shallow waters. What remains to be determined is the extent to which very deep water sponges will yield metabolites that are substantially different from those found in their shallow water relatives.

A recent opportunity to collect marine invertebrates with the manned submersible PICES IV has permitted us to investigate the secondary metabolites of the deep water sponge *Hexadella* sp. (3)[2] collected at Dark Cove and Agamemnon Channel in Jervis Inlet, B.C. We now wish to report that specimens of the sponge collected with PICES IV at −100 to −200 m contained only the previously reported metabolite topsentin B2 (**1**) (4),[2] while specimens of the same sponge collected with SCUBA at −40 m contained hexadellins A (**2**) and B (**3**), two new dibromotyrosine derived metabolites.

Hexadella sp. (Order Verongida, Family Aplysinidae (3)) is always found growing on the skeletons of dead hexactinellid glass sponges *Aphrocallistes vastus* and *Chonelasma calyx* at depths greater than −40 m. Freshly collected specimens of *Hexadella* sp. from both depths were immediately immersed in methanol. Contact with the methanol caused the *Hexadella* sp. tissue to undergo a rapid color change from bright sulfur yellow to dark purple that is characteristic of Verongiid sponges (5). Routine bioassays indicated significant cytotoxic (L1210) and antimicrobial activities (against *Staphylococcus aureus* and *Bacillus subtilus*) in the crude methanol extracts of *Hexadella* sp. from both depths.

Bioassay guided fractionation of the methanol extract of the PICES IV collected *Hexadella* sp., employing sequential application of Sephadex LH 20 (7:3 $MeOH/CH_2Cl_2$) and reverse phase high performance liquid (3:1 $MeOH/H_2O$) chromatographies, gave a pure biologically active molecule designated HEX I as the only detectable secondary metabolite. A parent ion doublet in the electron impact high resolution mass spectrum (EIHRMS) of **1**, having equal intensity peaks at m/z 420.0224 (ΔM, +0.2 mmu) and 422.0202 (ΔM, −0.1 mmu) daltons, was consistent with a molecular formula of $C_{20}H_{13}N_4O_2Br$. Both the ^1H and ^{13}C nmr spectra of **1** showed too many resonances for a molecule containing 20 carbon and 13 hydrogen atoms (see Experimental). We attributed the complexity in the nmr spectra of **1** to the existence of two tautomers. Treatment of HEX I (**1**) with dimethyl sulfate and potassium carbonate in refluxing acetone trapped the tautomers as a mixture of the trimethylated and tetramethylated derivatives **4** and **5**.



1 R = R^1 = R^3 = H
4 R = Me R^1 = Me R^3 = H
5 R = Me R^2 = Me R^3 = Me

TrimethylHEX I (**4**) showed parent ions (1:1) in the EIHRMS at m/z 462.0672 (ΔM, −1.8 mmu) and 464.0663 (ΔM, −0.7 mmu) daltons, appropriate for a molecular formula of $C_{23}H_{19}N_4O_2Br$, which contains three carbon and six hydrogen atoms more than the molecular formula of the parent compound. Resonances at δ 3.91 (s, 3H), 3.99 (s, 3H), and 4.16 (s, 3H) in the ^1H nmr spectrum of **4** confirmed that the new atoms had been added as three methyl groups. Proton nmr double resonance and nOe (Fig. 1) experiments suggested the presence of a 1-methyl-3-alkyl-6-methoxyindole fragment in **4**. A series of mass spectral fragments at m/z 188 ($C_{11}H_{10}O_2$), 174 ($C_{10}H_8O_2$), and 145 (C_9H_8O) daltons confirmed the existence of the indole

[1]Author to whom correspondence may be addressed.

[2]The sponge specimens were identified by Dr. W. Austin. Voucher samples are deposited at U.B.C.

Can. J. Chem. Downloaded from www.nrcresearchpress.com by 41.223.56.140 on 09/07/12
For personal use only.

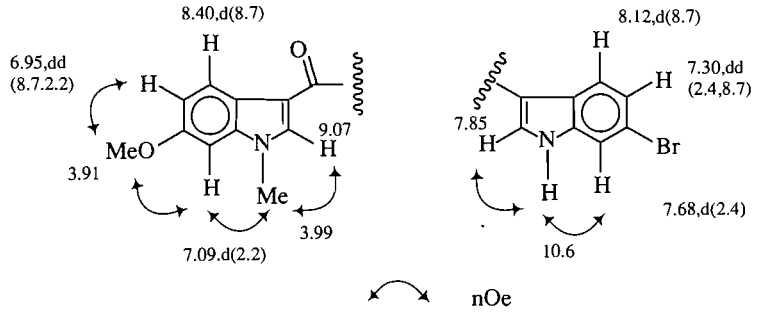


FIG. 1.

fragment and also revealed that the C3 substituent was a carbonyl. Further nOe (Fig. 1) and decoupling experiments identified a second set of proton resonances that could be assigned to a 3-alkyl-6-bromoindole fragment by comparison with published ^{1}H nmr chemical shifts for molecules containing this substructure (2*c*, 6). The remaining atoms ($C_4H_4N_2$) and unaccounted for spectral features (^{1}H nmr δ 7.65 (s, 1H), 4.16 (s, 3H); ^{13}C nmr δ 121.8 (CH), 136.7 (C), 138.8 (C), 36.5 (CH_3)) of **4** could readily be assigned to a 2,4-disubstituted-*N*-methylimidazole moiety. A series of nOe experiments (Fig. 2) unambiguously located the 1-methyl-3-keto-6-methoxyindole, 6-bromoindole, and methyl substituents on the imidazole ring as shown in **4**. HETCOR, COSY, and a series of SINEPT experiments were in complete agreement with the proposed structure **4** for trimethylHEX I. With the structure of trimethylHEX I (**4**) in hand, it was a routine exercise to assign structures to tetramethylHEX I (**5**) and the parent metabolite HEX I (**1**).

Shortly after we had determined the structure of **1**, Bartik *et al.* (4*a*) reported the isolation of the same compound, which they named topsentin B2, from the shallow water Mediterranean sponge *Topsentia genetrix* collected off the coast of France. We subsequently learned that topsentin B2 had also been isolated from a deep water Caribbean sponge (4*b*).

The crude methanol extract of the SCUBA collected *Hexadella* sp. (−40 m) was evaporated *in vacuo* to give an oily residue that was suspended in water and sequentially extracted with hexane and chloroform. Separation of the chloroform soluble materials by Sephadex LH 20 chromatography (3:1 MeOH/CH_2Cl_2) gave an antimicrobial green/yellow fraction containing mainly hexadellins A (**2**) and B (**3**) as indicated by ^{1}H nmr analysis. Acetylation of the material in this fraction with acetic anhydride and pyridine gave a crude acetylated mixture that was fractionated via silica gel flash (gradient: 4:1 hexane/EtOAc to 4:1 EtOAc/MeOH) and normal phase high performance liquid (95:5 EtOAc/MeOH) chromatographies to give pure samples of diacetylhexadellin A (**6**) and diacetylhexadellin B (**7**). There was no detectable topsentin B2 (**1**) in the methanol extracts of the SCUBA collected samples (−40 m) of *Hexadella* sp.

Diacetylhexadellin A (**6**) failed to show a molecular ion in either the electron impact or chemical ionization mass spectra. The molecular formula of $C_{25}H_{27}Br_4N_3O_7$ for **6** was therefore obtained by summing the atoms present in a number of fragments that were readily identified from the ^{1}H and ^{13}C nmr spectra (Tables 1 and 2).

The ^{1}H nmr resonances observed at δ 3.76 (s, 3H, OMe), 5.85 (s, H1), 6.32 (s, H5), 3.09 (d, J = 18 Hz, H7), 3.46 (d, J = 18 Hz, H7′), and 2.15 (s, OAc) in the spectrum of **6** could be assigned to a spirocyclohexadienyldihydroisoxazole

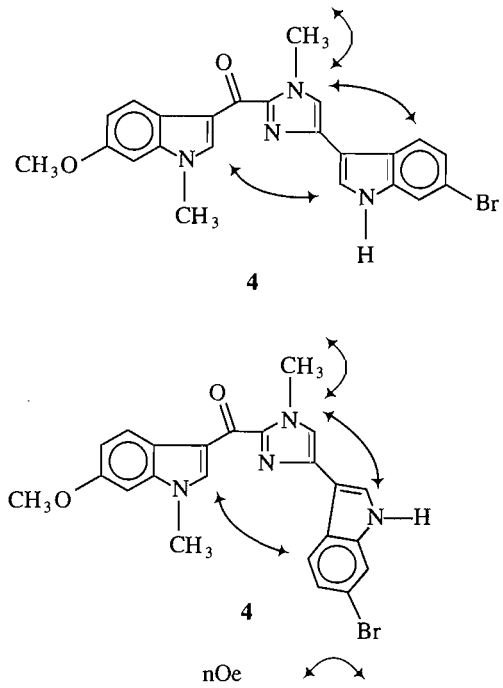


FIG. 2.

fragment **A** by comparison with published chemical shifts for diacetylaerothionin (**8**) (7) and tetraacetylfistularin-3 (**9**) (8) (Table 1). A second set of resonances at δ 7.17 (bt, J = 6 Hz, H10), 3.71 (dt, J = 5.2, 6.0 Hz, H11,11′), 2.11 (tt, J = 5.6, 6.2 Hz, H12,12′), 4.09 (t, J = 5.6 Hz, H13,13′), 7.35 (s, H16,16′), 2.75 (t, J = 7.2 Hz, H18,18′), 3.47 (dt, J = 5.2, 7.2 Hz, H19,19′), and 5.58 (bt, J = 6 Hz, H20) in the ^{1}H nmr spectrum of **6** could be assigned to fragment **B** by comparing their chemical shifts (Table 1) with published values for the identical fragment found in diacetylpsammaplysin-A (**10**) (7). Double resonance, COSY, and nOe ^{1}H nmr experiments verified the structure of fragment **B**. A final methyl singlet at δ 1.98 was assigned to an acetamide. Having identified all the substructures of diacetylhexadellin A (**6**), it only remained to determine which of the terminal nitrogen atoms (N10 or N20) in fragment **B** was attached to the acetyl residue and which was attached to the carbonyl functionality in fragment **A**.

Examination of the NH chemical shifts in a series of model compounds such as diacetylpsammaplysin A (**10**) (7) and diacetylfistularin-3 (**9**) (8) (Table 1) revealed that a proton on a nitrogen attached to fragment **A** would have a chemical shift in the range of δ 6.60–7.30, while a proton on a nitrogen that was acetylated would have a chemical shift in the range of

Can. J. Chem. Downloaded from www.nrcresearchpress.com by 41.223.56.140 on 09/07/12
For personal use only.

TABLE 1. Proton nmr assignments for diacetylhexadellins A (**6**) and B (**7**), diacetylaerothionin (**8**) (6), acetylfistularin-3 (**9**) (7), and diacetylpsammaplysin A (**10**) (6). All spectra were recorded in $CDCl_3$. Chemical shifts are reported in ppm from internal TMS

Proton	6	7	8	9	10
1	5.85, s	5.84, s	5.83, s	5.86, s	6.40, s
5	6.32, s	6.32, s	6.28, s	6.33, s	7.05, s
7	3.09, d(18)	3.08, d(18)	3.06, d(18.5)	3.08, d(18)	3.02, d(15.9)
	3.46, d(18)	3.44, d(18)	3.41, d(18.5)	3.06, d(18)	
				3.45, d(18)	3.23, d(15.9)
				3.47, d(18)	
10	7.17, bt(6)	6.10, bt(4)	6.67, bt	7.07, d(6.5)	7.16, bt(6.2)
11	3.71, dt(5.2, 6)	3.56, dt(4, 6)	—	3.80, m	3.72, dt(6.2, 7.3)
				3.96, m	
12	2.11, tt(5.6, 6.2)	2.07, tt(6, 5.2)	—	5.27, m	2.11, tt(6.2, 7.3)
13	4.09, t(6)	4.09, t(5.2)	—	4.14, dd	4.08, t(5.6)
				4.21, dd	
16	7.35, s	7.39, s	—	7.50, s	7.35, s
18	2.75, t(7.2)	2.81, t(7.6)	—	5.75, dd	2.75, t(7)
19	3.47, dt(5.2, 7.2)	3.58, dt(5.6, 7.6)	—	3.57, m	3.46, dt(5.5, 7)
				3.70, m	
20	5.58, bt(6)	6.65, bt(5.6)	—	6.82, bt(6)	5.60, bt(5.5)
OMe	3.76, s	3.78, s	3.75, s	3.77, s	3.67, s
				3.78, s	
NHAc	1.98, s	2.01, s	—	1.98, s	
OAc	2.15, s	2.15, s	2.13, s	2.14, s	2.22, s

TABLE 2. Carbon-13 nmr assignments for diacetylhexadellin A (**6**), diacetylhexadellin B (**7**), diacetylaerothionin (**8**) (6), and diacetylpsammaplysin A (**10**) (6). All spectra were recorded in $CDCl_3$

Carbon	6[a]	7	8	10
1	73.2(CH)	73.1	73.2	77.1
2	121.7(C)	122.1	121.9	121.8
3	149.7(C)	149.7	149.9	149.2
4	107.8(C)	107.8	107.8	105.9
5	130.5(CH)	130.2	130.6	145.5
6	89.7(C)	89.9	89.8	102.3
7	40.1(CH_2)	39.9	40.0	37.8
8	153.6(C)	153.5	154.0	153.9
9	158.6(C)	158.6	158.8	157.5
11	37.3(CH_2)	37.7	39.0	37.4
12	29.3(CH_2)	29.4	26.7	29.2
13	71.2(CH_2)	72.1	—	71.2
14	151.2(C)	151.5	—	151.4
15,15′	118.1(C)	118.2	—	118.2
16,16′	132.8(CH)	132.8	—	133.0
17	137.9(C)	137.2	—	138.2
18	34.5(CH_2)	34.4	—	34.5
19	60.2(CH_2)	40.4	—	40.4
OMe	60.2(CH_3)	60.3	60.2	59.2
OAc	169.3(C)	169.4	169.6	168.1
OAc	20.8(CH_3)	20.8	20.7	21.0
NAc	170.1(C)	170.0	—	170.4
NAc	23.4(CH_3)	23.6	—	23.1

[a]Proton attachments determined via APT.

δ 5.5–6.1. Since H10 in **6** had a chemical shift of δ 7.17 and H20 had a chemical shift of δ 5.58 it was possible to conclude that fragment **A** was attached to N10 and the acetyl group was attached to N20 of fragment **B** as shown. The nonacetylated parent molecule hexadellin A therefore had structure **2**.

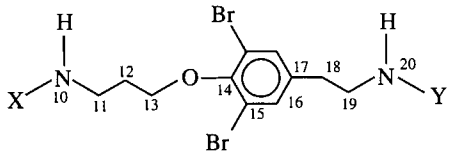
Diacetylhexadellin B (**7**), like diacetylhexadellin A (**6**), failed to show molecular ions in either the EI or CI mass spectra so its molecular formula of $C_{25}H_{27}Br_4N_3O_7$ was also obtained by summing the atoms present in fragments that could be clearly identified from nmr experiments. The nmr data for **7** were nearly identical to those of **6** (Tables 1 and 2), allowing the almost immediate recognition of fragments **A** and **B** as well as an N-acetyl in **7**. Once again, double resonance and COSY experiments confirmed the structures of the proposed fragments. A difference in the chemical shifts of NH10 (δ 6.10 in **7**: δ 7.17 in **6**) and NH20 (δ 6.65 in **7**: δ 5.58 in **6**) in **6** and **7** indicated that fragment **A** was attached to N20 and the acetyl group to N10 in **7** as shown. The structure of the parent metabolite hexadellin B therefore must be **3**.

Our studies of the chemistry of *Hexadella* sp. have shown that the sponge apparently has different secondary metabolite contents at the extremes of its depth distribution. The new dibromotyrosine derived compounds hexadellin A (**2**) and B (**3**) isolated from the SCUBA collected material are typical metabolites of Verongiid sponges. The absence of dibromotyrosine derived metabolites and the presence of topsentin B2 (**1**) in the PICES IV collected material is unexpected and difficult to reconcile within the framework of our current knowledge about chemical taxonomy of the porifera (5). There is no precedent for a sponge having different chemistry at different depths, and tryptophan derived metabolites such as topsentin B2 (**1**) are unknown from Verongiid sponges.

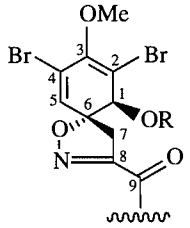
One obvious explanation would be that the PICES IV collected material was simply incorrectly identified. However, the deep sponges were found growing on the dead remains of glass sponges, they underwent the color change characteristic of the Verongidae, and to an experienced sponge taxonomist[2] they appeared identical to the shallower sponges by both visual inspection and microscopic examination. Therefore, we feel confident that both collections were *Hexadella* sp.

Perhaps the most likely explanation for our observations

Can. J. Chem. Downloaded from www.nrcresearchpress.com by 41.223.56.140 on 09/07/12
For personal use only.

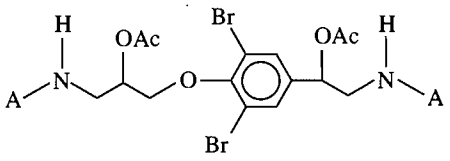


B

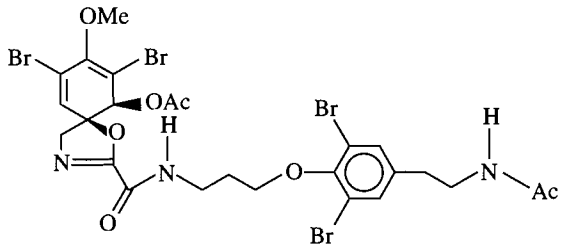


A

2 X = A, R = Y = H
3 Y = A, R = X = H
6 X = A, R = Y = CH_3CO-
7 Y = A, R = X = CH_3CO-
8 ANH$CH_2CH_2CH_2CH_2$NHA, R = CH_3CO-



9



10

is that *Hexadella* sp. contains dibromotyrosine derived metabolites (i.e., **2** and **3**) at −40 m and that it contains neither these metabolites nor topsentin B2 (**1**) at −100 to −200 m. The discovery of topsentin B2 (**1**) in the deep water collection could be explained by the presence of a small undetected amount of a second sponge, probably a *Topsentia* species (4), buried in the glass sponge skeleton. Unfortunately, due to suspension of the submersible program, we have not been able to re-collect deep water specimens of *Hexadella* sp. and consequently we have been unable to adequately resolve this issue.

Experimental

The nmr spectra were recorded on Varian XL 300 and Bruker WH 400 spectrometers. Tetramethylsilane was used as an internal standard. Low resolution mass spectra were recorded on an AEI MS 902 spectrometer and high resolution mass spectra were recorded on an AEI MS 50 spectrometer. Infrared spectra were recorded on a Perkin–Elmer 1600 Fourier Transform spectrometer. Merck silica gel 230–400 mesh was used for flash chromatography and a Whatman Magnum-9 Partisil-10 column was used for preparative hplc. Sephadex LH 20 was used for molecular exclusion chromatography.

Collection

Hexadella sp. was collected at Dark Cove, Jervis Inlet, in November, 1986, using the manned submersible PICES IV (−110 to −200 m) and at Agamemnon Channel in October, 1987, using SCUBA (−40 m).

*Isolation of HEX I (Topsentin B2) **1***

The PICES IV collected sponge (500 g, wet wt.) was immersed in methanol immediately after collection. Concentration of the methanol extract *in vacuo* yielded 6 g of crude residue. A 400-mg portion of the crude residue was chromatographed on a Sephadex LH 20 column prepared and eluted with methanol/dichloromethane (7:3). Fractions containing **1** were further purified via reverse phase hplc (methanol/water; 3:1) to give 71 mg (1.8% of crude residue) of **1**.

*HEX I (Topsentin B2) **1***: yellow/green oil (2:1 mixture of tautomers); uv (MeOH): 286 nm (ε 17 000), 382 nm (ε 15 500); ir (film): 3300 (br), 1702, 1524, 1158, 868 cm^{-1}; ^1H nmr (acetone-d_6), major tautomer, δ: 6.87 (dd, J = 8.7, 2.2 Hz, H6), 7.02 (d, J = 2.2 Hz, H8), 7.27 (dd, J = 8.6, 1.5 Hz, H22), 7.68 (d, J = 1.5 Hz, H20), 7.72 (d, J = 2.1 Hz, H13), 7.86 (d, J = 2.5 Hz, H17), 8.09 (s, OH), 8.22 (d, J = 8.6 Hz, H23), 8.32 (d, J = 8.7 Hz, H5), 9.43 (s, H2), 10.59 (bs, H18), 10.90 (bs, H15), and 12.20 (bs, H1); minor tautomer, δ: 6.84 (dd, J = 8.7, 2.2 Hz, H6), 6.99 (d, J = 2.2 Hz, H8), 7.33 (dd, J = 8.6, 1.5 Hz, H22), 7.61 (d, J = 1.5 Hz, H20), 7.73 (d, J = 1.5 Hz, H13), 7.87 (d, J = 2.6 Hz, H17), 7.92 (d, J = 8.6 Hz, H23), 8.09 (s, OH), 8.29 (d, J = 8.7 Hz, H5), 9.22 (s, H2), 10.80 (bs, H18), 10.90 (bs, H12), 12.20 (bs, H1); EIMS (formula, rel. intensity): 422/420 (M^+, 23), 289/287 ($C_{12}H_7N_3OBr$, 5), 263/261 ($C_{11}H_8N_3Br$, 4), 160 ($C_9H_6NO_2$, 44), 133 (C_8H_8NO, 100); HREIMS, $C_{20}H_{13}BrN_4O_2$, M^+: 422.0203/420.0222 (ΔM, −0.6 mmu/+0.2 mmu).

*Methylation of **1***: 40 mg of **1** (0.09 mmol) was refluxed overnight under N_2 together with 35 μL (0.4 mmol) of dimethyl sulfate and 66 mg (0.5 mmol) of potassium carbonate in 15 mL of freshly distilled acetone. Removal of excess reagents and solvent *in vacuo* gave an oily residue that was purified via reverse phase preparatory tlc (eluent: MeOH/CH_3CN/H_2O (82:10:8) to give 11 mg of pure **4** (R_f 0.52) and 3 mg of pure **5** (R_f 0.44).

*TrimethylHEX I (**4**)*: yellow/green oil; ir (film): 3134, 1706, 1593, 1520, 1250, 1072, 926, 836 cm^{-1}; ^1H nmr (acetone-d_6) δ: 3.91 (s, H25), 3.99 (s, H26), 4.16 (s, H27), 6.95 (dd, J = 8.7, 2.2 Hz, H6), 7.09 (d, J = 2.4 Hz, H8), 7.30 (dd, J = 8.7, 2.4 Hz, H22), 7.65 (s, H13), 7.68 (d, J = 2.4 Hz, H20), 7.85 (s, H17), 8.12 (d, J = 8.7 Hz, H23), 8.40 (d, J = 8.7 Hz, H5), 9.07 (s, H2), 10.60 (bs, H18); ^{13}C nmr (acetone-d_6) δ: 33.9(q), 36.5(q), 55.9(q), 94.2(d), 111.7(s), 112.3(d), 115.1(s), 115.2(d), 115.3(s), 121.8(d), 122.4(s), 122.6(d), 123.2(d), 123.6(d), 123.8(d), 125.1(s), 136.7(s), 138.4(s), 138.8(s), 140.5(d), 143.8(s), 157.9(s), 178.4(s); EIMS (formula, rel. intensity): 464/462 (M^+, 96), 275/273 ($C_{12}H_{10}BrN_3$, 1), 188 ($C_{11}H_{10}NO_2$, 100), 174 ($C_{10}H_8NO_2$, 7), 145 (C_9H_7NO, 20); HREIMS, $C_{23}H_{19}BrN_4O_2$: 464.0670/462.0690 (ΔM, +0.7/−1.8 mmu).

*TetramethylHEX I (**5**)*: yellow-green oil; ir (film): 1709, 1595, 1522, 1076, 843 cm^{-1}; ^1H nmr (acetone-d_6) δ: 3.90 (s, H25), 3.96 (s, H28), 3.99 (s, H26), 4.04 (s, H27), 6.93 (dd, J = 8.6, 2.4 Hz, H6), 7.08 (d, J = 2.4 Hz, H8), 7.26 (s, H17), 7.31 (dd, J = 8.7, 2.5 Hz, H22), 7.59 (d, J = 8.7 Hz, H23), 7.63 (s, H13), 7.77 (d, J = 2.5 Hz, H20), 8.39 (d, J = 8.6 Hz, H5), 8.90 (s, H2); HREIMS, $C_{24}H_{21}BrN_4O_2$: 478.0813/476.0828 (ΔM, −1.3/+0.2 mmu).

Isolation of hexadellins A and B

The SCUBA collected *Hexadella* sp. (800 g, wet wt.) (Agamemnon Channel −40 m) was immediately immersed in methanol. Evaporation of the methanol *in vacuo* gave a residue that was suspended in water and sequentially extracted with hexane (2 × 1L) and chloroform (2 × 1L). The combined chloroform extracts were concentrated and

Can. J. Chem. Downloaded from www.nrcresearchpress.com by 41.223.56.140 on 09/07/12
For personal use only.

chromatographed on Sephadex LH 20 ($MeOH/CH_2Cl_2$ 3:1) to give a number of antibacterial fractions containing a mixture of **2** and **3** (74 mg). The material in these fractions was acetylated with acetic anhydride/pyridine (room temperature, 24 h) to give a crude mixture of **6** and **7**. The acetylated derivatives were purified via gradient silica gel column chromatography (EtOAc/hexane 4:1 to EtOAc/MeOH 4:1) and normal phase hplc (EtOAc/MeOH 95:5) to give pure diacetylhexadellin A (**6**) (30 mg) and pure diacetylhexadellin B (**7**) (19 mg).

Diacetylhexadellin A (6): pale yellow oil; ir (film): 3338, 2928, 1752, 1656, 1544, 1215, 737 cm^{-1}; ^1H nmr, see Table 1; ^{13}C nmr, see Table 2; HREIMS, $C_{23}H_{25}{}^{79}Br_3{}^{81}BrN_3O_5$ ($M^+ - C_2H_2O_2$): 740.8505 (ΔM, −0.1 mmu); EIMS (rel. intensity): 739/741/743/745/747 (0.5), 418/420/422 (0.5:1.0:0.5), 407/405/409 (1:2:1), 359/361/363 (12:24:12), 303/305/307 (18:36:18), 276/278/280 (50:100:50).

Diacetylhexadellin B (7): pale yellow oil; ir (film): 3305, 2936, 1758, 1657, 1543, 1216, 772, 737 cm^{-1}; ^1H nmr, see Table 1; ^{13}C nmr, see Table 2; EIHRMS, $C_{23}H_{25}O_5N_3{}^{79}Br_2{}^{81}Br_2$ ($M^+ - C_2H_2O_2$): 742.8490 (ΔM, +0.4 mmu); EIMS (rel. intensity): 755/757/759/761/763 ($M^+ - C_2H_2O$, <0.5), 739/741/743/745/747 ($M^+ - C_2H_2O_2$, <0.5), 638/640/642/644/646 (<0.5), 303/305/307 (50:100:50), 276/278/280 (7:14:7).

Acknowledgements

Financial support was provided by grants from NSERC and the National Cancer Institute of Canada to R.J.A. S.A.M. was supported by an NSERC Postgraduate Fellowship. The authors wish to thank M. LeBlanc, W. Austin, and the crew of PICES IV for assistance with the collection of *Hexadella* sp.

1. D. J. Faulkner. Nat. Prod. Rep. **4**, 539 (1987), and references therein.
2. (*a*) B. J. Burreson and P. J. Scheuer. J. Chem. Soc. Chem. Commun. 1035 (1974); (*b*) B. J. Burreson, C. Christophersen, and P. J. Scheuer. J. Am. Chem. Soc. **97**, 210 (1975); (*c*) S. Kohmoto, Y. Kashman, O. J. McConnell, K. L. Rinehart, A. Wright, and F. Koehn. J. Org. Chem. **53**, 3116 (1988); (*d*) G. P. Gunawardana, S. Kohmoto, S. P. Gunasekera, O. J. McConnell, and F. E. Koehn. J. Am. Chem. Soc. **110**, 4856 (1988); (*e*) A. E. Wright, S. A. Pompani, O. J. McConnell, S. Komoto, and P. J. McCarthy. J. Nat. Prod. **50**, 976 (1987); (*f*) S. Komoto, O. J. McConnell, A. Wright, and S. Cross. Chem. Lett. 1687 (1987); (*g*) S. Komoto, O. J. McConnell, A. Wright, F. Koehn, W. Thompson, M. Lui, and K. M. Snader. J. Nat. Prod. **50**, 336 (1987).
3. (*a*) W. C. Austin. An annotated checklist of marine invertebrates in the cold temperate Northeast Pacific. Kyotan Marine Laboratory, Cowichan Bay, B.C., 1985; (*b*) E. N. Kozloff. Marine invertebrates of the Pacific Northwest. University of Washington Press, Seattle, WA. 1987.
4. (*a*) K. Bartik, J. C. Braekman, D. Daloze, C. Stoller, J. Huysecom, G. Vandevyver, and R. Ottinger. Can. J. Chem. **65**, 2118 (1987); (*b*) S. Tsujii, K. L. Rinehart, S. P. Gunasekera, Y. Kashman, S. S. Cross, M. S. Lui, S. A. Pompani, and M. C. Diaz. J. Org. Chem. **53**, 5446 (1988).
5. P. R. Bergquist and R. J. Wells. *In* Marine natural products—chemical and biological perspectives. Vol. V. *Edited by* P. J. Scheuer. Academic Press, New York, NY. 1983. Chap. 1.
6. R. J. Andersen and R. J. Stonard. Can. J. Chem. **57**, 2325 (1979).
7. M. Rotem, S. Carmely, and Y. Kashman. Tetrahedron, **39**, 667 (1983).
8. Y. Gopichand and F. J. Schmitz. Tetrahedron Lett. 3921 (1979).

Can. J. Chem. Downloaded from www.nrcresearchpress.com by 41.223.56.140 on 09/07/12
For personal use only.

Kadsulignan A and B, two novel lignans from *Kadsura coccinea*

JIA-SEN LIU,[1] LIANG LI, AND HAN-GANG YU
Shanghai Institute of Materia Medica, Academia Sinica, 319 Yueyang Rd., Shanghai 200031, China

Received September 20, 1988

JIA-SEN LIU, LIANG LI, and HAN-GANG YU. Can. J. Chem. **67**, 682 (1989).

Two novel lignans, kadsulignan A (**1**) and B (**2**), were isolated from the seeds of *Kadsura coccinea*. Their structures were elucidated by 2D ^1H–^{13}C COSY, 2D ^1H–^{13}C long-range COSY experiments, and chemical transformation to a known compound (**5**) using $AlCl_2H$.

Key words: isolation and structures, kadsulignan A, kadsulignan B, *Kadsura coccinea*.

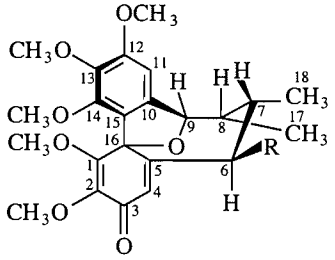
JIA-SEN LIU, LIANG LI et HAN-GANG YU. Can. J. Chem. **67**, 682 (1989).

On a isolé deux nouveaux lignanes, les kadsulignanes A (**1**) et B (**2**), à partir des graines de la *Kadsura coccinea*. On a déterminé leurs structures en soumettant le composé connu **5** à un transformation chimique à l'aide de $AlCl_2H$ et en faisant appel à des expériences de COSY en 2D de ^1H–^{13}C et de ^1H–^{13}C à longue distance.

Mots clés : isolation et structures, kadsulignane A, kadsulignane B, *Kadsura coccinea*.

[Traduit par la revue]

In our continuing studies on the chemistry of *Schisandraceae* plants (1), 13 new lignan compounds were isolated from the seeds of *Kadsura coccinea* (Lem.) A.C.Sm., collected in Rongshui county of Guangxi, China. Two of the new lignans, named kadsulignan A (**1**) and B (**2**), possess a novel spiro-dienone structure. In the present paper we report the isolation and structural elucidation of these two novel lignans.



1 R = H **2** R = $OCOCH_3$

Kadsulignan A (**1**) is a yellow gum, $C_{23}H_{28}O_7$, the spectra of which display different features in comparison with those of dibenzocyclooctadiene lignans commonly found in this family of plants. Its ultraviolet (uv) spectrum shows maxima at 212, 240, 283, and 301 nm. The infrared (ir) spectrum (1662, 1650 cm^{-1}) and ^{13}C nmr spectrum (δ 183.7) reveal the presence of a α,β,α′,β′-dienone moiety and two oxygenated carbons, a tertiary sp^3 carbon (δ 89.6), and a quaternary sp^3 carbon (δ 87.1). Analysis of 2D ^1H–^{13}C COSY and 2D ^1H–^{13}C long-range COSY spectra (Fig. 1) allowed us to establish the connectivity between carbon-13 nuclei and hydrogens via $^2J_{CH}$ and $^3J_{CH}$, and showed that the same oxygen connects both of the tertiary (C-9) and quaternary (C-16) sp^3 carbons forming a spiro ring. Thus, structure **1** is proposed for kadsulignan A.

A further confirmation of the structure assignment of **1** and determination of its absolute stereochemistry were provided by chemical transformation. Treatment of **1** with dichloroaluminum hydride (2) cleaved the spiro-oxy bridge and gave the common dibenzocyclooctadiene lignans, compounds **3** and **4**. Then, methylation of the latter (**4**) afforded a known compound, deangeloyl schisantherin F dimethyl ether (**5**) (3). Since the absolute configurations of **5** are known, the absolute configurations of **1** are unambiguously assigned as 7*R*, 8*R*, 9*R*, and 16*S*.

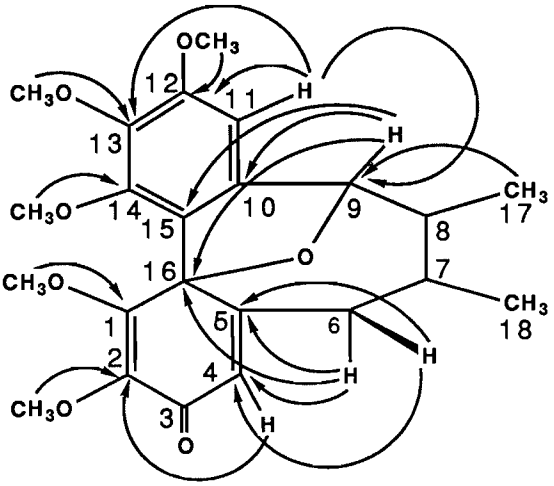
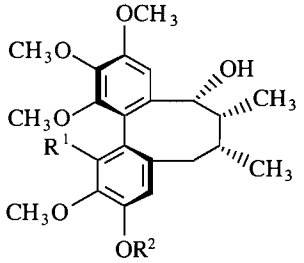


FIG. 1. ^1H–^{13}C long range shift correlation via $^2J_{CH}$ and $^3J_{CH}$ in kadsulignan A (**1**).

Kadsulignan B (**2**) is also a yellow gum, $C_{25}H_{30}O_9$, and shows a similar uv spectrum to that of **1**. Its ir spectrum (1740 cm^{-1}), ^1H nmr (δ 2.04, 3H, s and δ 5.79, 1H, d) and ^{13}C nmr (δ 169.6, 15.9, and 73.4) spectra display the presence of an acetoxyl in the molecule. Comparison of ^1H and ^{13}C nmr data (Tables 1, 2) of **1** and **2** indicates that compounds **1** and **2** differ by an acetoxyl substituent at C-6 of **2**. The coupling



3 $R^1 = R^2 = H$
4 $R^1 = OCH_3$ $R^2 = H$
5 $R^1 = OCH_3$ $R^2 = CH_3$

[1]Author to whom correspondence may be addressed.

Can. J. Chem. Downloaded from www.nrcresearchpress.com by 41.223.56.140 on 09/07/12
For personal use only.

TABLE 1. The ^{1}H nmr data* of kadsulignan A (**1**) and B (**2**)

Compound	H-4 (d)	H-11 (s)	H-6$_\beta$ (d)	H-6$_\alpha$ (ddd or dd)	H-7 (m)	H-8 (m)	H-9 (s)	Me-7 (d)	Me-8 (d)	OMe (s)	OAc (s)
1	5.86 (2.2)	6.42	2.07 (17.0)	2.72 (17.0/10.0/2.2)	1.38	1.76	5.35	0.82 (6.9)	1.13 (6.9)	3.73, 3.74 3.78, 3.85 3.96	
2	5.84 (2.2)	6.43		5.79 (9.9/2.2)	1.58	1.82	5.34	0.80 (7.0)	1.22 (7.0)	3.71, 3.72 3.76, 3.83 3.96	2.04

*δ, ppm, in $CDCl_3$ (400 MHz); *J*, Hz, in parentheses; the assignments are based on selective decoupling and nOe experiments.

TABLE 2. The ^{13}C nmr data* of kadsulignan A (**1**) and B (**2**)

Carbon (multiplicity)	Compound **1**	Compound **2**
1(s)	157.1	155.9
2(s)	137.8	138.0
3(s)	183.7	184.0
4(d)	122.1	122.7
5(s)	158.8	157.8
6	37.2(t)	73.4(d)
7(d)	28.8	34.7
8(d)	45.2	44.8
9(d)	89.6	89.4
10(s)	138.4	139.6
11(d)	99.3	99.3
12(s)	155.3	155.8
13(s)	141.5	141.9
14(s)	147.6	148.2
15(s)	122.6	122.7
16(s)	87.1	86.0
17(q)	11.0	12.8
18(q)	20.0	20.4
OMe-12(q)	55.8	56.3
OMe(q)	59.7	60.4(2)
	59.9(2)	60.7
	60.1	60.8
Ac		15.9(q, Me) 169.6(s, CO)

*δ, ppm in $CDCl_3$ (25.2 MHz); the assignments are based on DEPT spectra, 2D ^{1}H–^{13}C COSY and 2D ^{1}H–^{13}C long-range COSY experiments.

constants between H-6 and H-7 ($J = 9.9$ Hz) and between H-6 and H-4 ($J = 2.2$ Hz) indicate that H-6 should have an α configuration. Examination of a molecular model of **2** shows a dihedral angle close to 90° between the C_6—H and C_4—H bonds, and a dihedral angle close to 180° between the C_6—H and C_7—H bonds, consistent with the assignment. Therefore, we propose that kadsulignan B (**2**) is 6β-acetoxyl kadsulignan A.

Further support for the structure of **2** was obtained by nOe measurement of **2**. On irradiation of Me-8 (δ 1.22), H-6 (δ 5.79) and H-9 (δ 5.34) show 10.2 and 9.0% nOe enhancements respectively, indicating a *cis* relationship between H-6, H-9, and Me-8 of **2**. These results also indicate a boat conformation of the cyclooctene ring and a chair conformation of the cycloheptoxide ring, since a chair conformation of the cyclooctene ring with a boat conformation of the cycloheptoxide ring cannot accommodate the nOe result between H-6 and Me-8. Furthermore, the consistent ^{1}H nmr data between **1** and **2** (Table 1) show a similar conformation in **1** and **2**. The absolute configurations of **2** are assigned as 6*R*, 7*S*, 8*R*, 9*R*, and 16*S* based on the similarity of the circular dichroism (cd) curves of **2** to that of **1**.

Experimental

Melting points were determined on a Kofler hot stage apparatus and are uncorrected. The following instruments were used for the spectra described here: uv, Pye Unicam SP1800; ir, Perkin–Elmer 599B; ^{1}H nmr and nOe experiments, Bruker AM-400 (400 MHz); ^{13}C nmr, 2D ^{1}H–^{13}C COSY, and 2D ^{1}H–^{13}C long-range COSY experiments, Bruker AC-100 (25.18 MHz for ^{13}C nmr, 100 MHz for ^{1}H nmr); hrms, Varian MAT-711; cd, Jasco J-500A; optional rotations, Jasco DIP-181. Silica gel for column chromatography was manufactured in the Qingdao Haiyang Chemical Factory.

Extraction and preliminary separation

The crude alcoholic extract of the seeds of *Kadsura coccinea* (Lem.) A.C.Sm. was suspended in water and extracted with ether. The ether extract was chromatographed on a silica gel column (100–200 mesh) eluting, in turn, with petroleum ether – benzene (1:1), benzene, benzene – ethyl acetate (10:1, 4:1, and 2:1). The fractions eluted with petroleum ether – benzene (1:1) and the early fractions of benzene were combined and designated Part A. Similarly, the late fractions of benzene and fractions eluted by benzene – ethyl acetate (10:1) were combined as Part B; fractions eluted by benzene – ethyl acetate (4:1) were combined as Part C; and fractions eluted with benzene – ethyl acetate (2:1) were combined as Part D.

Kadsulignan A (1)

Part B was chromatographed on a silica gel column (200–300 mesh) eluting with petroleum ether – acetone (10:1). The middle fractions were subjected to chromatography again on a silica gel column (200–300 mesh) using petroleum ether – diethyl ether (6:1) as an eluent. Crude kadsulignan A was found in the early fractions. It was purified by preparative tlc (petroleum ether – diethyl ether (6:1)) to give 350 mg (0.0049%) of **1** as a yellow gum; $[\alpha]_D$ +100.89° (*c* 0.0451, acetone); uv (MeOH) λ_{max} (log ε): 212(4.68), 240(4.28), 283(3.71), 301(3.59) nm; ir (KBr) ν_{max}: 1662, 1650, 1610, 1470 cm^{-1}; ^{1}H nmr and ^{13}C nmr, see Tables 1 and 2; hrms *m/z*: 416.1849 (M^+, 100%, calcd. for $C_{23}H_{28}O_7$: 416.1835), 401.1563 ($M - CH_3$, 12.1%), 385.1676 ($M - OCH_3$, 9.6%), 331.1148 ($C_{18}H_{19}O_6$, 32.7%), 301.1043 ($C_{17}H_{17}O_5$, 28.3%); cd (MeOH) Δε (nm): +5.60(239), −1.30(258), +2.60(281), +4.60(304), −0.45(356).

Kadsulignan B (2)

Part C was chromatographed on a silica gel column (200–300 mesh) eluting with petroleum ether – diethyl ether (5:1 and 2:1). The late fractions eluted by petroleum ether – diethyl ether (5:1) and the early fractions of petroleum ether – diethyl ether (2:1) were combined and

Can. J. Chem. Downloaded from www.nrcresearchpress.com by 41.223.56.140 on 09/07/12
For personal use only.

chromatographed again on the silica gel column using the same eluent. The late fractions of petroleum ether – diethyl ether (5:1) gave **2**, 59 mg (0.00082%) as a yellow gum, $[\alpha]_D$ +97.03° (*c* 0.0133, acetone); uv (MeOH) λ_{max} (log ε): 213(4.75), 240(4.32), 284(3.72), 305(3.63) nm; ir (KBr) ν_{max}: 1740, 1735, 1655, 1610 cm^{-1}; ^1H and ^{13}C nmr, see Tables 1 and 2; ms *m/z*: 474 (M^+), 414 (M − CH_3COOH), 389, 347; cd (MeOH) Δε (nm): +8.50(235), −1.50(259), +1.80(279), +3.20(303), −1.10(349).

*Reduction products (**3** and **4**) of **1***

Kadsulignan A (**1**, 40 mg) dissolved in diethyl ether and cooled to 0°C was reacted for 5 min at 0°C with an ethereal solution of dichloroaluminum hydride (freshly prepared from aluminum chloride (100 mg) and lithium aluminum hydride (10 mg) (2)). The reaction mixture was treated with water (10 mL) and extracted with diethyl ether. The concentrated ether extract was separated by preparative tlc (solvent: petroleum ether – acetone (3:1)), affording a major product **3**, 20 mg, and a minor product **4**, 4 mg.

The structure of compound **3**, mp 203–205°C, is based on the following spectral data: ir (KBr) ν_{max}: 3550–3385, 1585, 1510 cm^{-1}; ^1H nmr (400 MHz, $CDCl_3$) δ: 0.95(3H, d, *J* = 7.6, Me-7), 1.18(3H, d, *J* = 7.1, Me-8), 1.95(1H, m, H-7), 2.08 (1H, m, H-8), 2.60(2H, m, H-6), 3.45, 3.86, 3.87, 3.88(3H each, s, OCH_3 × 4), 4.62(1H, s, H-9), 5.64(1H, s, OH), 6.38, 6.84, 6.86(1H each, s, Ar-H × 3); cd (MeOH) Δε (nm): +43.00(218), −28.40(236), −23.50(252), −4.25(292).

For compound **4** the spectral data are as follows: ^1H nmr (400 MHz, $CDCl_3$) δ: 0.92(3H, d, *J* = 7.4, Me-7), 1.18(3H, d, *J* = 7.3, Me-8), 1.92(1H, m, H-7), 2.07(1H, m, H-8), 2.59(2H, m, H-6), 3.57, 3.64, 3.86, 3.87, 3.93(3H each, s, OCH_3 × 5), 4.71(1H, s, H-9), 5.77(1H, s, OH), 6.38(1H, s, H-11), 6.67(1H, s, H-4); ms *m/z*: 418 (M^+), 400 (M − H_2O), 388, 223.

*Deangeloyl schisantherin F dimethyl ether (**5**)*

Compound **4** (4 mg) was methylated with an ethereal solution of diazomethane. Work-up in the usual way gave compound **5**, 3 mg, mp 162–163°C (from MeOH); ir (KBr) ν_{max}: 3520, 1590, 1580 cm^{-1}; ^1H nmr (400 MHz, $CDCl_3$) δ: 0.92(3H, d, *J* = 7.5, Me-7), 1.18(3H, d, *J* = 7.2, Me-8), 1.92(1H, m, H-7), 2.08(1H, m, H-8), 2.61(2H, m, H-6), 3.60, 3.67, 3.85(3H each, s, OCH_3 × 3), 3.87(9H, s, OCH_3 × 3), 4.64(1H, s, H-9), 6.37(1H, s, H-11), 6.56(1H, s, H-4); ms *m/z*: 432 (M^+), 414 M − H_2O), 376, 225, 209, 182. Comparison of the ir spectra and mixture melting points shows that it is identical with authentic compound **5** derived from schisantherin F (3).

Acknowledgements

Support for this research was provided by the National Natural Science Foundation of China. The authors are grateful to Professor Yu-Hu Liu, Huanan Institute of Botany, Academia Sinica, China, for the botanical identification of materials investigated, and also to Dr. Lois Browne, University of Alberta, Canada, for reviewing the manuscript of this paper.

1. Jia-Sen Liu. Youji Huaxue, 316 (1987), and references cited therein.
2. J. H. Brewster, H. O. Bayer, and S. F. Osman. J. Org. Chem. **29**, 110 (1964).
3. Jia-Sen Liu and Yu-Ting Ma. Huaxue Xuebao, **46**, 460 (1988).

Can. J. Chem. Downloaded from www.nrcresearchpress.com by 41.223.56.140 on 09/07/12
For personal use only.

Gas phase ligand substitution reactions in fast atom bombardment mass spectrometry: effects of ligand base strength and choice of matrix liquid in substitution reactions of difluoroborn cations

K. BALASANMUGAM, J. S. HARTMAN,[1] J. M. MILLER,[1] AND Z. YUAN
Department of Chemistry, Brock University, St. Catharines, Ont., Canada L2S 3A1

Received October 14, 1988

K. BALASANMUGAM, J. S. HARTMAN, J. M. MILLER, and Z. YUAN. Can. J. Chem. **67**, 685 (1989).

Strongly basic amidine and guanidine ligands displace weaker-base ligands such as pyridine from $D_2BF_2^+$ complexes in the gas phase in Fast Atom Bombardment mass spectrometry. The choice of protic vs. aprotic matrix liquid inhibits or promotes gas phase ligand substitution reactions.

Key words: ligand substitution, difluoroboron cations, FABMS.

K. BALASANMUGAM, J. S. HARTMAN, J. M. MILLER et Z. YUAN. Can. J. Chem. **67**, 685 (1989).

Dans des spectromètres de masse par bombardement avec des atomes rapides, les ligands fortement basiques, comme l'amidine et la guanidine, déplacent les ligands de bases plus faibles, comme la pyridine, des complexes $D_2BF_2^+$. Le choix de matrices protiques vs. aprotiques inhibe ou favorise les réactions de substitution des ligands en phase gazeuse.

Mots clés : substitution de ligands, cations difluorobores, FABMS.

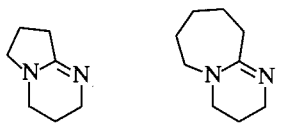
[Traduit par la revue]

Can. J. Chem. Downloaded from www.nrcresearchpress.com by 41.223.56.140 on 09/07/12
For personal use only.

Introduction

Fast atom bombardment mass spectrometry (FAB) has become an important technique for the characterization of cationic compounds (1–4). However, recent work by several research groups has demonstrated that significant ion–molecule reactions can take place in the gas phase (5–8). We have shown, using a dual target FAB probe tip made by dividing a wider FAB probe target, that ligands such as crown ethers react with gas phase species containing alkali metal ions, giving alkali metal ion – crown ether complexes (8); in this system most of the complex ions detected by FAB are apparently produced by gas phase reaction. Reinterpretation of FAB results, and re-thinking of how closely FAB spectra correspond to composition of the samples being analysed, is therefore a high priority.

We now report dual target FAB studies of gas phase ligand substitution in fluoroboron cations $[D_2BF_2]^+$, which have previously been characterized by FAB and other methods (9). Especially stable fluoroboron cations have been shown to form when the donors D are the strongly basic amidine ligands 1,5-diazabicyclo[4.3.0]non-5-ene (DBN) and 1,8-diazabicyclo[5.4.0]undec-7-ene (DBU) (10).



DBN DBU

Experimental

FAB mass spectra were obtained on a Kratos (AEI) MS 30 mass spectrometer, retrofitted (11) with a Kratos FAB source in beam 1 and interfaced to a Kratos DS 55 data system. Argon was used as the bombarding gas with atom gun (Ion Tech) energies of 8 kV and a gun current of approximately 1 mA. Ions were accelerated to 4 kV, with a repeller potential on the FAB tip on the order of 20 V. The source pressure was typically 10^{-5} Torr for normal FAB operation and the pressure rose to (1–5) $\times$ 10^{-4} Torr when the volatile bases were introduced. (This measurement was made in the pumping line just outside the source housing, but unlike an EI source, the FAB source is of an open design, and the measured pressure may be within a half order of that in the source proper, though much lower than the high pressure region jsut above the sample surface.) The system was operated at room temperature at a resolving power of 1000. The divided FAB probes (Fig. 1) are 4.3 mm in diameter and are cut in half by a 3 mm deep and 0.6 mm wide slot so that different samples can be placed on either half without being mixed (8). To obtain FAB spectra, fluoroboron cations (9, 10) were dissolved in a matrix (15 mg/mL), either 3-nitrobenzyl alcohol (NBA) and tetramethylene sulfone (SUL), and placed on the "A" half of the probe tip which is closer to the ion optics (8). These probe tips are similar to those used by Munster *et al.* (7). Different ligands without any matrix liquid were deposited on the "B" half of the divided FAB probe. Each spectrum is an average of eight to ten scans.

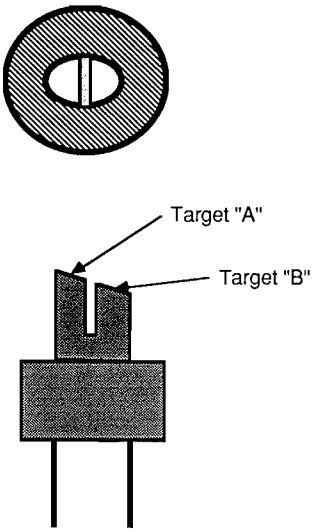


FIG. 1. MS30 divided FAB probe tip.

Use of NBA as matrix liquid allowed many scans to be collected before degradation of the sample, while normally only four to seven scans could be obtained using SUL. Considerable adjustment of experimental conditions was necessary in order to match vaporization rates from the "A" and "B" halves of the probe tip and optimize the formation of ions containing components from both halves.

The possibility of spattering of material from one half of the probe tip to the other during a run was excluded by collecting the samples from each half of the probe tip after a run, and obtaining their FAB

[1]To whom correspondence should be addressed.

Can. J. Chem. Downloaded from www.nrcresearchpress.com by 41.223.56.140 on 09/07/12
For personal use only.

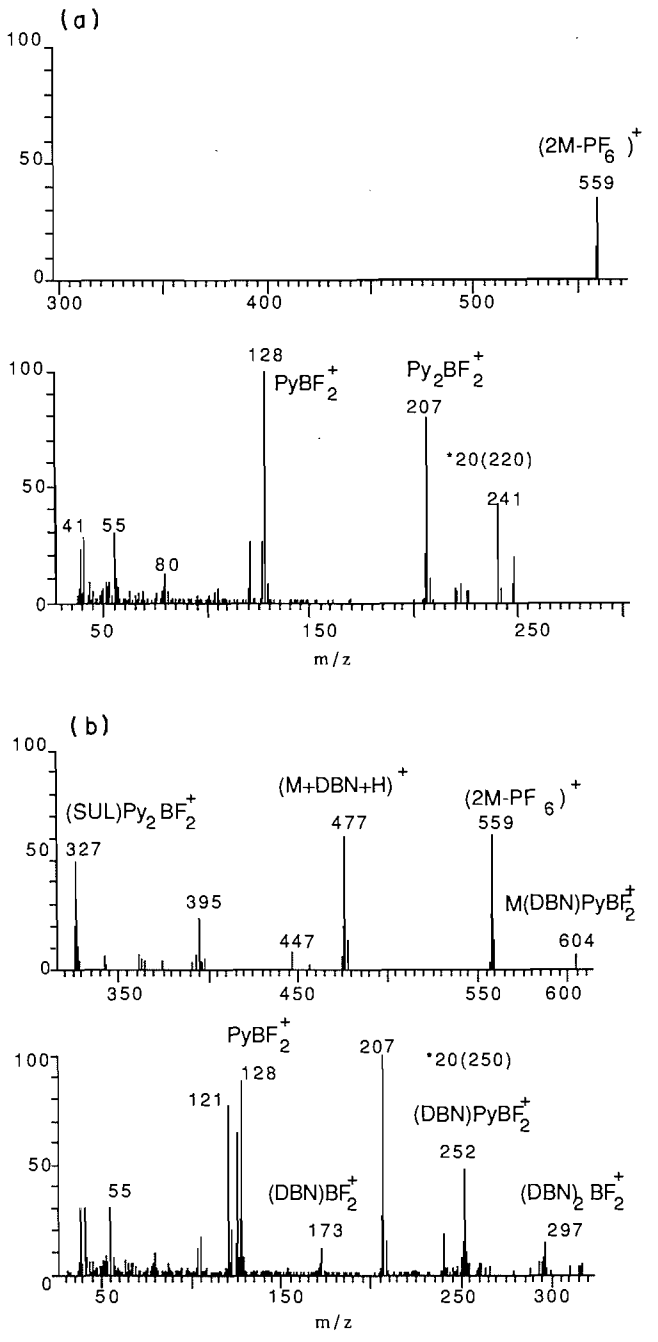


FIG. 2. (*a*) Positive ion FAB spectrum of $[py_2BF_2][PF_6]$ in SUL matrix, (*b*) positive ion FAB spectrum of $[py_2BF_2][PF_6]$ in SUL matrix on target "A" in the presence of neat DBN on target "B".

spectra separately, or simple cleaning off one side and examining the spectrum obtained from the other side. These spectra were clean, with no evidence of cross-contamination, when samples were relatively non-volatile. However, the possibility of adsorption of a volatile material from the gas phase into the liquid matrix, followed by sputtering back into vacuum cannot be ruled out for very volatile samples.

The ligands pyridine (py), quinuclidine (Q), 1,5-diazabicyclo-[4.3.0]non-5-ene (DBN), 1,1,3,3-tetramethylguanidine (TMG), and 15-crown-5 (15C5) were purchased from the Aldrich Chemical Company and used without further purification. 1,8-Diazabicyclo-[5.4.0]undec-7-ene (DBU) was a gift from Air Products and Chemicals Incorporated, and was distilled at a pressure of 20 Torr, the fraction distilling at 130–134°C being used.

Since gas phase basicities are available only for some of the ligands, and for those available the trends are in the same order as the aqueous solution values, we use the latter in our discussion.

Results and discussion

The positive ion FAB spectrum of $[py_2BF_2]^+.[PF_6]^-$ in SUL matrix liquid is shown in Fig. 2*a*. Similar spectra were obtained using either NBA or SUL as matrix liquid, except for differences in minor solvated-cation peaks. This spectrum is typical of FAB spectra of fluoroboron cations (9, 10): the parent cation peak at $m/z = 207$ is prominent, as are peaks corresponding to $pyBF_2^+$ and $(py + H)^+$. In addition, a cluster ion is present at $m/z = 559$, corresponding to $[(py_2BF_2)_2PF_6]^+$, i.e., $[2M - PF_6]^+$. Note that peaks of m/z greater than 220 in Fig. 2*a*, and 250 in Fig. 2*b*, have been amplified by a factor of twenty. Figure 2*b* was obtained using the dual target FAB probe tip, with SUL as the matrix liquid for $py_2BF_2^+$ on "A" and neat DBN on "B". All of the ions of Fig. 2*a* are still detected, and in addition there is a major peak corresponding to $(DBN + H)^+$, and lower-intensity peaks corresponding to $py(DBN)BF_2^+$, $(DBN)_2BF_2^+$, and $(DBN)BF_2^+$, as well as new cluster ion peaks (Table 1). Since DBN and $py_2BF_2^+$ can mix only in the gas phase (see Experimental), the DBN-containing fluoroboron cations must be produced by gas phase substitution reactions.

Except for $(DBN + H)^+$, the intensities of the additional peaks of Fig. 2*b* are very low when the matrix liquid for $py_2BF_2^+$ is NBA rather than SUL. We attribute this to gas phase protonation of the basic ligand by $(NBA + H)^+$ ions produced by the primary ionization process, so that the ligand is no longer able to react with the $py_2BF_2^+$ cation.

Tables 1–3 summarize the results obtained with the series of difluoroboron cation salts $[(py)_n(Q)_{2-n}BF_2]^+.[PF_6]^-$ (n = 2–0) on the "A" side of the dual probe tip, and a number of free ligands on the "B" side. The matrix-liquid peaks $(SUL + H)^+$ and $(2SUL + H)^+$ are omitted from the tables. In each case the difluoroboron salt side "A" of the dual target FAB probe tip was preferentially irradiated with the fast atom beam as a result of the geometry of the FAB retrofit and the source ion optics. In the reverse experiment in which the free ligand was placed on "A" and fluoroboron cation salt dissolved in a matrix on "B", no boron-containing species were detected, the spectrum consisting of peaks from the ligand itself.

Quinuclidine and pyridine were also used as free ligands on the "B" side, but no peaks attributable to boron-containing ions with these ligands could be detected. Pyridine is the least basic of the ligands studied (pK_b = 8.77), and may well be insufficiently basic to displace quinuclidine from $Q_2BF_2^+$ and $pyQBF_2^+$. However, pyridine is also very volatile and probably volatilized too quickly from the probe tip. Quinuclidine (pK_b = 2.9) is far more basic than pyridine, but its low volatility may have prevented our detecting mixed products.

A number of trends are evident from the data in the tables. The peak arising from the parent difluoroboron cation is always a major peak, except for the anomaly of $py_2BF_2^+$ with DBU (Table 1). The protonated-incoming-ligand peak (e.g., $(DBN + H)^+$) is always a major peak, the proton-donor source when SUL rather than NBA is the matrix liquid presumably being radiation-damaged matrix. The quinuclidine radical cation peak is major when starting from $Q_2BF_2^+$ but is not detected at all when starting from $pyQBF_2^+$, consistent with preferential loss of py from this complex ion. Displacements to give other four-coordinate cations occur most readily from $py_2BF_2^+$ (compare Table 1 with Tables 2 and 3). The greater ease of

TABLE 1. Positive ion FAB mass spectra of $[Py_2BF_2]^+PF_6^-$ on "A" with various ligands on "B"

Ligand on "B"	Primary sequence ions	Intensity	Ligand-only ions	Intensity	Cluster ions[a]	Intensity
DBN	$Py_2BF_2^+$	100	$(DBN + H)^+$	63.9	$(2M - PF_6)^+$	3.1
	$Py(DBN)BF_2^+$	2.4			$[M + (DBN)Py(BF_2)]$	0.3
	$(DBN)_2BF_2^+$	0.7			[M + DBN + H]	3.0
	$(DBN)BF_2^+$	11.4			$[Py_2(SUL)BF_2]^+$	2.4
	$PyBF_2^+$	88.1				
DBU	$Py_2BF_2^+$	1.2	$(DBU + H)^+$	100		
	$Py(DBU)BF_2^+$	1.7				
	$(DBU)_2BF_2^+$	0.6				
	$DBUBF_2^+$	9.0				
	$PyBF_2^+$	—				
TMG	$Py_2BF_2^+$	26.0	$(TMG + H)^+$	100	(M + TMG + H)	0.1
	$Py(TMG)BF_2^+$	—				
	$(TMG)_2BF_2^+$	4.0				
	$TMGBF_2^+$	22.4				
	$PyBF_2^+$	44.4				
15C5	$PyBF_2^+$	100	$(15C5 + H)^+$	3.6	$(2M - PF_6)^+$	0.3
	$Py(15C5)BF_2^+$	0.1				
	$(15C5)_2BF_2^+$	—				
	$[(15C5)BF_2^+$	0.4				
	$PyBF_2^+$	74.1				

[a]$M = [Py_2BF_2]^+PF_6^-$.

TABLE 2. Positive ion FAB mass spectra of $[PyQBF_2]^+PF_6^-$ on "A" with various ligands on "B"

Ligand "B"	Primary sequence ions	Intensity	Ligand-only ions	Intensity	Cluster ions[a]	Intensity
DBN	$PyQBF_2^+$	94.3	$(DBN + H)^+$	98.7	$(2M - PF_6)^+$	4.9
	$Py(DBN)BF_2^+$	—			$(M + DBN + H)^+$	2.0
	$Q(DBN)BF_2^+$	—				
	$(DBN)_2BF_2^+$	—				
	$(DBN)BF_2^+$	21.5				
	QBF_2^+	100				
	$PyBF_2^+$	—				
DBU	$PyQBF_2^+$	53.8	$(DBU + H)^+$	100	$(2M - PF_6)^+$	1.8
	$Py(DBU)BF_2^+$	—			$(M + DBU + H)^+$	
	$Q(DBU)BF_2^+$	—				
	$(DBU)_2BF_2^+$	1.6				
	$(DBU)BF_2^+$	11.0				
	$PyBF_2^+$	—				
	QBF_2^+	77.8				
TMG	$Py(Q)BF_2^+$	55.5	$(TMG + H)^+$	100		
	$Py(TMG)BF_2^+$	—				
	$Q(TMG)BF_2^+$	—				
	$(TMG)_2BF_2^+$	—				
	$(TMG)BF_2^+$	4.9				
	$PyBF_2^+$	17.7				
	QBF_2^+	66.3				
15C5	$Py(Q)BF_2^+$	100	$(15C5 + H)^+$	35.6	$(2M - PF_6)^+$	1.8
	$(15C5)PyBF_2^+$	—			$[(PyQ(15C5)BF_2)]^+$	0.5
	$(15C5)QBF_2^+$	0.7				
	$(15C5)_2BF_2^+$	—				
	$(15C5)BF_2^+$	0.6				
	$PyBF_2^+$	9.5				
	QBF_2^+	39.4				

[a]$M = [PyQBF_2]^+PF_6^-$.

Can. J. Chem. Downloaded from www.nrcresearchpress.com by 41.223.56.140 on 09/07/12
For personal use only.

TABLE 3. Positive ion FAB mass spectra of $[Q_2BF_2]^+PF_6^-$ on "A" with various ligands on "B"

Ligand "B"	Primary sequence ions	Intensity	Ligand-only ions	Intensity	Cluster ions[a]	Intensity
DBN	$Q_2BF_2^+$	32.4	$(DBN + H)^+$	74.1		
	$Q(DBN)BF_2^+$	—	$Q^{+\cdot}$	36.7		
	$(DBN)_2BF_2^+$	—				
	$(DBN)BF_2^+$	9.0				
	QBF_2^+	100.				
DBU	$Q_2BF_2^+$	25.6	$(DBU + H)^+$	100	$(2M - PF_6)^+$	0.3
	$Q(DBU)BF_2^+$	—	$Q^{+\cdot}$	30.0	$(M + DBU + H)^+$	0.4
	$(DBU)_2BF_2^+$	—				
	$(DBU)BF_2^+$	0.9				
	QBF_2^+	23.0				
TMG	$Q_2BF_2^+$	50.4	$(TMG + H)^+$	8.9	$(2M - PF_6)^+$	1.0
	$Q(TMG)BF_2^+$	—	$Q^{+\cdot}$	33.6	$(M + Q)^{+\cdot}$	0.2
	$(TMG)_2BF_2^+$	0.2				
	$(TMG)BF_2^+$	2.2				
	QBF_2^+	100.				
15C5	$Q_2BF_2^+$	100.	$(15C5 + H)^+$	43.3	$(2M - PF_6)^+$	2.1
	$Q(15C5)BF_2^+$	2.5	$Q^{+\cdot}$	33.9		
	$(15C5)_2BF_2^+$	—				
	$(15C5)BF_2^+$	5.2				
	QBF_2^+	55.0				

[a]$M = [Q_2BF_2]^+PF_6^-$.

displacement is consistent with pyridine's weaker basicity. In most cases starting from $pyQBF_2^+$ and $Q_2BF_2^+$, the substituted four-coordinate cations have not been detected. In all cases except $pyQBF_2^+$ with 15C5, the peak of the substituted three-coordinate cation ($DBN.BF_2^+$, etc.) is by far the largest peak arising from a species which incorporates both boron and the substituting ligand. In the $pyQBF_2^+$ systems (Table 2), the QBF_2^+ peak is always much more intense than the $pyBF_2^+$ peak, again consistent with pyridine's weaker basicity and greater ease of displacement.

The extent of the gas phase reactions summarized in Tables 1–3 can be rationalized by the volatilities and basicities of the ligand used. DBN, DBU, and TMG are all strong bases, with pK_b's in the 0.4 to 1.1 range (12), and all three are of intermediate volatility: sufficient to provide adequate vapour pressure, but low enough to be long-lasting. The volatility of 15C5 is intermediate between quinuclidine and the DBN, DBU, and TMG group, so gas phase concentrations are lower. Basicities would also be lower; hence the low relative intensities of 15C5-containing ions.

Cluster ion peaks have fairly low relative intensities which vary considerably from system to system, and the causes of the variations are not obvious. However, it is clear from the intensities of the $(M + \text{ligand} + H)^+$ peaks, which can approach the intensity of the $(2M - PF_6)^+$ peaks, that the clusters need not originate in the matrix liquid, but frequently form in the gas phase. The greatest intensities are consistently seen with DBN as ligand and with $py_2BF_2^+$ and $pyQBF_2^+$, and it is difficult to rationalize the absence of cluster peaks with the same ligand and $Q_2BF_2^+$. We have previously observed weak cluster peaks $(2M - Br)^+$ from $Q_2BF_2^+.Br^-$ (9).

Conclusion

Gas phase displacement reactions are a complication in FAB that can make interpretation more difficult, especially if complex mixtures are being analysed. Displacement reactions by basic ligands that may be present in such mixtures can be minimized by choice of a slightly acidic matrix liquid such as NBA.

Acknowledgements

We thank Mel Farquharson for preparing $py_2BF_2^+$ and $Q_2BF_2^+$, Tim Jones for technical assistance and maintenance of the mass spectrometer system, Air Products and Chemicals Inc. for a gift of DBU, and the Natural Sciences and Engineering Research Council of Canada for financial support.

1. K. BALASANMUGAM, S. K. VISWANADHAM, D. M. HERCULES, R. J. COTTER, D. HELLER, A. BENNINGHOVEN, W. SICHTERMAN, V. ANDERS, T. KEOUGH, R. D. MCFARLANE, and C. J. MCNEAL. Appl. Spectrosc. **41**, 821 (1987).
2. J. M. MILLER, K. BALASANMUGAM, J. NYE, G. B. DEACON, and N. C. THOMAS. Inorg. Chem. **26**, 560 (1987).
3. E. TOLUN and J. F. J. TODD. Org. Mass Spectrom. **23**, 98 (1988).
4. K. J. KROHA and K. L. BUSCH. Org. Mass Spectrom. **21**, 507 (1986).
5. J. A. SUNNER, R. KULATUNGA, and P. KEBARLE. Anal. Chem. **58**, 1312 (1986).
6. J. A. SUNNER, A. MORALES, and P. KEBARLE. Anal. Chem. **60**, 98 (1988).
7. H. MUNSTER, F. THEOBALD, H. BUDZIKIEWICZ, and E. SCHRODER. Int. J. Mass Spectrom. Ion Process, **79**, 73 (1987).
8. J. M. MILLER, K. BALASANMUGAM, and A. FULCHER. Org. Mass Spectrom. In press.
9. M. J. FARQUHARSON and J. S. HARTMAN. J. Chem. Soc. Chem. Commun. 256 (1984); M. J. FARQUHARSON. M.Sc. thesis. Brock University. 1985; M. J. FARQUHARSON and J. S. HARTMAN. To be published.
10. J. S. HARTMAN and Z. YUAN. Third Chemical Congress of North America, Toronto, June 5–10, 1988; Z. YUAN. M.Sc. thesis. Brock University. 1988; J. S. HARTMAN and Z. YUAN. To be published.
11. J. M. MILLER and A. FULCHER. Can. J. Chem. **63**, 208 (1985).
12. D. H. R. BARTON, J. D. ELLIOTT, and S. D. GERO. J. Chem. Soc. Perkin Trans. 1, 2085 (1982); I. HERNECZ. Adv. Heterocycl. Chem. **42**, 84 (1987); G. J. DURANT. Chem. Soc. Rev. **14**, 375 (1985); W. REPPE. Justus Liebigs Ann. Chem. **596**, 210 (1967).

Can. J. Chem. Downloaded from www.nrcresearchpress.com by 41.223.56.140 on 09/07/12
For personal use only.

Radical ions in photochemistry. 21. The photosensitized (electron transfer) tautomerization of alkenes; the phenyl alkene system[1]

DONALD R. ARNOLD[2] AND SHELLEY A. MINES
Department of Chemistry, Dalhousie University, Halifax, N.S., Canada B3H 4J3

Received September 28, 1988

DONALD R. ARNOLD and SHELLEY A. MINES. Can. J. Chem. **67**, 689 (1989).

Alkenes, conjugated with a phenyl group, can be converted to nonconjugated tautomers by sensitized (electron transfer) irradiation. For example, irradiation of an acetonitrile solution of the conjugated alkene 1-phenylpropene, the electron accepting photosensitizer 1,4-dicyanobenzene, the cosensitizer biphenyl, and the base 2,4,6-trimethylpyridine gave the nonconjugated tautomer 3-phenylpropene in good yield. Similarly, 2-methyl-1-phenylpropene gave 2-methyl-3-phenylpropene, and 1-phenyl-1-butene gave *E*- and *Z*-1-phenyl-2-butene. The reaction also works well with cyclic alkenes. For example, 1-phenylcyclohexene gave 3-phenylcyclohexene, and 1-(phenylmethylene)cyclohexane gave 1-(phenylmethyl)cyclohexene. The proposed mechanism involves the initial formation of the alkene radical cation and the sensitizer radical anion, induced by irradiation of the sensitizer and mediated by the cosensitizer. Deprotonation of the radical cation assisted by the base gives the ambident radical, which is then reduced to the anion by the sensitizer radical anion. Protonation of the ambident anion at the benzylic position completes the sequence. Reprotonation at the original position is an energy wasting step. Tautomerization is driven toward the isomer with the higher oxidation potential, which is, in the cases studied, the *less* thermodynamically stable isomer. The regioselectivity of the deprotonation step is dependent upon the conformation of the allylic carbon–hydrogen bond. The tautomerization of 2-methyl-1-phenylbutene gave both 2-phenylmethyl-1-butene and 2-methyl-1-phenyl-2-butene (*E* and *Z* isomers), while 2,3-dimethyl-1-phenylbutene gave only 3-methyl-2-phenylmethyl-1-butene. In the latter case, steric interaction of the methyls on the isopropyl group prevents effective overlap of the tertiary carbon–hydrogen bond with the singly occupied molecular orbital, thus inhibiting deprotonation from this site.

Key words: photosensitized, electron transfer, alkene, tautomerization, radical cation.

DONALD R. ARNOLD et SHELLEY A. MINES. Can. J. Chem. **67**, 689 (1989).

Sous l'influence d'une irradiation sensibilisée (transfert d'électron), on peut transformer des alcènes conjugués avec un groupement phényle en tautomères qui ne le sont pas. Par exemple, l'irradiation du phényl-1 propène, un alcène conjugué, en solution dans l'acétonitrile, en présence de dicyano-1,4 benzène agissant comme photo-sensibilisateur acceptant des électrons, de biphényle agissant comme cosensibilisateur et de triméthyl-2,4,6 pyridine agissant comme base, fournit de phényl-3 propène, le tautomère qui n'est pas conjuguée, avec un bon rendement. De la même manière, le méthyl-2 phényl-1 propène fournit du méthyl-2 phényl-3 propène alors que le phényl-1 butène-1 conduit à un mélange des phényl-1 butènes-2-(*E*) et -(*Z*). La réaction donne aussi de bons résultats avec les alcènes cycliques. Par exemple, le phényl-1 cyclohexène fournit du phényl-3 cyclohexène alors que le (phénylméthylène)-1 cyclohexane conduit au (phénylméthyl)-1 cyclohexene. Le mécanisme proposé implique la formation initiale du cation radical de l'alcène et l'anion radical du sensibilisateur qui est induite par l'irradiation du sensibilisateur avec la médiation du cosensibilisateur. La déprotonation du cation radical sous l'influence de la base fournit le radical ambivalent qui est alors réduit en anion par l'anion radical du sensibilisateur. La protonation de la position benzylique de l'anion ambivalent complète la séquence. La reprotonation dans la position originale est une étape qui fait perdre de l'énergie. La tautomérisation est orientée vers l'isomère possédant le potentiel d'oxydation le plus élevé; dans les cas étudiés, il s'agit de l'isomère qui est le *moins* stable d'un point de vue thermodynamique. La régiosélectivité de l'étape de déprotonation dépend de la conformation de la liaison allylique carbone–hydrogène. Le méthyl-2 phényl-1 butène fournit les deux tautomères, phénylméthyl-2 butène-1 ainsi que méthyl-2 phényl-1 butène-2 (isomères *E* ainsi que *Z*) alors que le diméthyl-2,3 phényl-1 butène ne fournit que le méthyl-3 phénylméthyl-2 butène-2. Dans ce dernier cas, l'interaction stérique des groupements méthyles de l'isopropyle empêche le recouvrement efficace de la liaison tertiaire carbone – hydrogène avec l'orbitale moléculaire occupée par un seul électron; la déprotonation de ce site est ainsi inhibée.

Mots clés : photo-sensibilisé, transfert d'électron, alcène, tautomérisation, cation radical.

[Traduit par la revue]

Introduction

Tautomerization of alkenes, by either acid or base catalysis, is an old and relatively well-understood process (3). The composition of the equilibrium mixture is a direct reflection of the relative thermodynamic stability of the isomers. Alkenes substituted with electron-donating groups (e.g., alkyl) or with groups that interact by conjugation (e.g., aryl) are generally more stable than the alternative tautomer(s). Archetypical of the conjugated aryl substituted alkenes is 1-phenylpropene (**1**). Equilibration favors **1** over the nonconjugated tautomer, 3-phenylpropene (**2**), by several orders of magnitude (4).

The conjugated tautomers are frequently more readily available than the nonconjugated isomers. Many synthetic procedures for the preparation of alkenes, including those which involve an elimination by the E1 mechanism, are limited to the preparation of the most stable of the possible isomers. While there are procedures for the specific preparation of the less stable tautomers, a general method for the tautomerization of conjugated alkenes to nonconjugated isomers would be synthetically useful.

We have reported a general photochemical method for the tautomerization of 1,1-diphenyl substituted alkenes to nonconjugated isomers (2). The mechanism proposed for this process involves the initial formation of the alkene radical cation and the sensitizer radical anion, induced by irradiation of the sensitizer and mediated by the cosensitizer. Deprotonation of the radical cation, assisted by the base, gives the ambident

[1]Preceding publications in these series are refs. 1 and 2.
[2]Author to whom correspondence may be addressed.

Can. J. Chem. Downloaded from www.nrcresearchpress.com by 41.223.56.140 on 09/07/12
For personal use only.

TABLE 1. The photosensitized (electron transfer) tautomerization of phenyl alkenes[a]

Reaction	Starting alkene	Product (yield)[b]
1	1-Phenylpropene (**1**)[c]	3-Phenylpropene (**2**) (41%)
2	2-Methyl-1-phenylpropene (**3**)	2-Methyl-3-phenylpropene (**4**) (90%)
3	1-Phenyl-1-butene (**5**)[d]	1-Phenyl-2-butene (**6**) (65%)[e]
4	2-Methyl-1-phenylbutene (**7**)[f]	2-Phenylmethyl-1-butene (**8**) (40%); 2-Methyl-1-phenyl-2-butene (**9**) (12%)[g]
5	2,3-Dimethyl-1-phenylbutene (**10**)[h]	3-Methyl-2-phenylmethyl-1-butene (**11**) (65%)
6	1-Phenylcyclohexene (**13**)	3-Phenylcyclohexene (**14**) (86%)
7	1-(Phenylmethylene)cyclohexane (**15**)	1-(Phenylmethyl)cyclohexene (**16**) (41%)

[a]A solution in acetonitrile of 2,4,6-trimethylpyridine, 1,4-dicyanobenzene, biphenyl, and the starting alkene was irradiated at 10°C with a 1-kW medium-pressure Hg vapor lamp until reaction was essentially complete.
[b]Yields were determined by quantitative gas chromatography with a flame-ionization detector (gc/fid).
[c]Starting with the *E* isomer (93%). Configurational isomerization was more rapid than tautomerization; the photostationary state was ca. 1:1 *Z*:*E*.
[d]Starting with the *E* isomer (99%). Configurational isomerization was more rapid than tautomerization; the photostationary state was ca. 1:4 *Z*:*E*.
[e]The ratio of *Z* to *E* isomers was 1:4.
[f]Starting with a mixture of the *Z* and *E* isomers (6:4). The photostationary state was ca. 1:1.
[g]The ratio of *Z* to *E* isomers was 3:1.
[h]Starting with a mixture of the *Z* and *E* isomers. The photostationary state was ca. 5:1 *Z*:*E*.

Can. J. Chem. Downloaded from www.nrcresearchpress.com by 41.223.56.140 on 09/07/12
For personal use only.

radical, which is then reduced to the anion by the sensitizer radical anion. Protonation of the ambident anion at the bis-benzylic position completes the sequence.

Only minor modification of the reported procedure was required to extend this method to the tautomerization of the monophenyl analogues. The results provide further insight into the mechanism of the reaction, which knowledge helps to define the scope and limitations of the process.

Results

The starting materials, conjugated phenyl alkenes, were known compounds prepared by classical methods (dehydration of the alcohol prepared by the Grignard reaction, or by the Wittig reaction). Spectral analysis, in particular ^{1}H nmr spectroscopy, confirmed the structural assignments.

The photosensitized (electron transfer) tautomerization reaction involves a simple, convenient procedure. A solution of the conjugated alkene in acetonitrile, with 1,4-dicyanobenzene as electron-accepting sensitizer, biphenyl as a cosensitizer, and collidine (2,4,6-trimethylpyridine) as base, was irradiated through Pyrex with a medium-pressure mercury vapor lamp. Progress of the reaction was followed by gas chromatography (gc/fid). Irradiation was continued until the reaction was complete, when column chromatography of the crude photolysate gave the tautomer, usually in excellent yield. The electron-accepting sensitizer, the cosensitizer, and the base were largely recovered. The results are summarized in Table 1.

The tautomerization does not require the cosensitizer. However, the yield of tautomer and the efficiency of the reaction were improved when biphenyl was added to the irradiation mixture. The yields reported in Table 1 are from cosensitized reactions.

In the previous study involving tautomerization of 1,1-diphenyl alkenes, lutidine (2,6-dimethylpyridine) was used as the base (2). Collidine was found to be more effective than lutidine for these reactions involving monophenyl alkenes.

The yields reported in Table 1 were determined by quantitative gas chromatography using a flame ionization detector (gc/fid). The isolated yield of some of the more volatile tautomers was lower than that reported in the table due to evaporation of the product along with the solvent following the chromatographic separation.

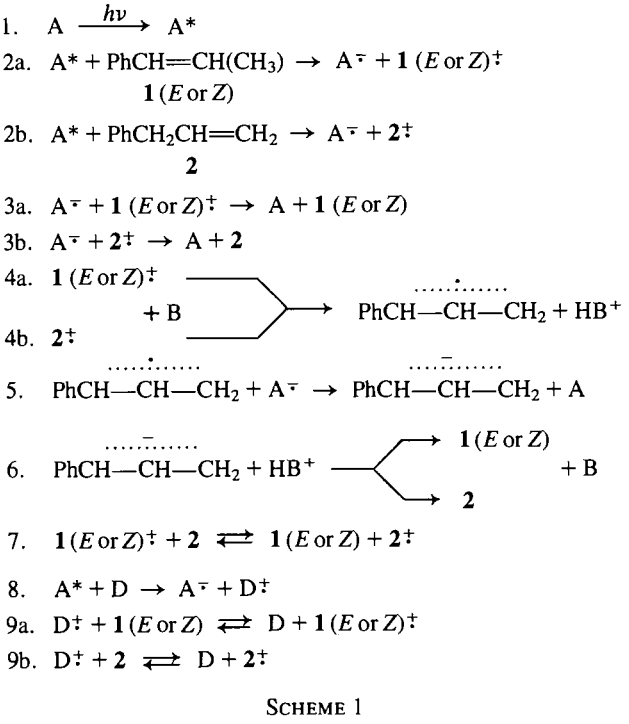
TABLE 2. Oxidation potentials of the phenyl alkenes studied[a]

Phenyl alkene	$E^{ox}_{1/2}$ (V)[b]
(*E*)-1-Phenylpropene (**1**)	1.73
3-Phenylpropene (**2**)	2.26
2-Methyl-1-phenylpropene (**3**)	1.60
2-Methyl-3-phenylpropene (**4**)	2.24
(*E*)-1-Phenyl-1-butene (**5**)	1.67
3-Methyl-2-phenylmethyl-1-butene (**11**)	2.25
1-Phenylcyclohexene (**13**)	1.61
3-Phenylcyclohexene (**14**)	2.13
1-(Phenylmethylene)cyclohexane (**15**)	1.62
1-(Phenylmethyl)cyclohexene (**16**)	1.95

[a]Oxidation potentials measured at a platinum electrode relative to a saturated calomel electrode (SCE) using tetraethylammonium perchlorate (0.1 M TEAP) as electrolyte in acetonitrile.
[b]The anodic wave was not reversible; the half-wave potential was taken as 0.03 V before the peak potential (6).

Structural assignments for the products were unambiguously established on the basis of spectral analysis (^{1}H and ^{13}C nmr) and comparison with literature data when it was available. The nonconjugated alkene **11** was a new compound. The gross structures were easily assigned. The configuration of the isomeric 1-phenyl-2-butenes (**6**, *E* and *Z*) and 2-methyl-1-phenyl-2-butenes (**9**, *E* and *Z*) was assigned on the basis of the magnitude of the coupling between the carbon of the allylic methyl group and the vicinal vinyl proton in the ^{13}C nmr spectrum. This carbon–proton coupling follows the same trend as the analogous *cis–trans* proton–proton coupling; that is, the allylic carbon – vinyl proton coupling constant is greater for the *trans* than for the *cis* orientation (5).

The oxidation potentials of the alkenes were determined by cyclic voltammetry. Pure samples of the alkenes were obtained



SCHEME 1

by preparative gas chromatography prior to analysis. The shape of the voltammogram was indicative of an irreversible oxidation. The oxidation potential was estimated as 0.03 V before the peak potential (6). These data are summarized in Table 2.

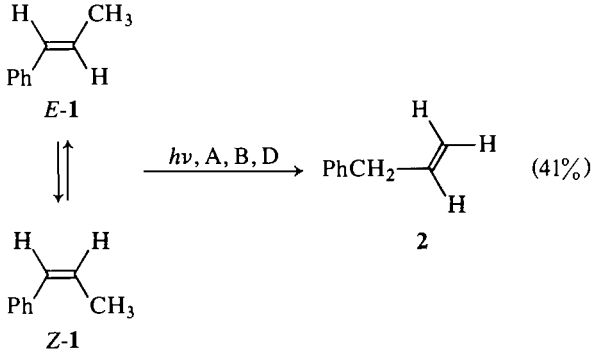
Discussion

Several very different types of reaction can result from the irradiation of a solution of a given cyanoaromatic compound and an alkene. These include, in addition to tautomerization of the alkene (2): configurational isomerization (*E*–*Z*) of the alkene (7); cyclodimerization of the alkene, forming either cyclobutane or, in the case of conjugated alkenes, cyclohexene dimers (8, 9); cycloaddition of the alkene to the aromatic ring at the 1,2-, 1,4-, or 2,4-position (10), or at the cyano group (11); addition of nucleophile to the alkene radical cation followed either by addition of the resulting radical to the cyanoaromatic radical anion to give the substituted dihydroaromatic (12), or by substitution of the resulting radical for the cyano substituent on the ring (the photo-NOCAS reaction) (1*a*, 13); substitution of the allylic radical for the cyano substituent on the aromatic ring (14); and, *anti*-Markovnikov addition of hydroxylic solvent to the alkene with the cyanoaromatic acting as a photosensitizer (15). The problem of understanding this complex behaviour is exacerbated by the fact that some of these products may be formed by more than one mechanism. Nevertheless, it is frequently possible to obtain a good yield of a single product and to explain (if not predict) why a particular reaction dominates.

The ultimate result of the irradiation of a given pair of reactants depends upon the relative rates of several competing processes. The ability to predict this reactivity will require an understanding of how reactant structure and irradiation conditions influence these rates.

The proposed mechanism for the tautomerization reaction is shown in abbreviated form in Scheme 1, using Reaction 1 as an example. Consideration of the factors that influence the rate of each step provides a basis for predicting when to expect this reaction.

Reaction 1



A = 1,4-dicyanobenzene
B = collidine
D = biphenyl

Steps 1–7 are involved when the reaction is brought about by irradiation of the electron-accepting sensitizer (A = 1,4-dicyanobenzene) in the absence of an added donor that serves as a cosensitizer (D = biphenyl). Steps 8 and 9 occur in preference to step 2 when a cosensitizer has been added to the irradiation mixture.

The long wavelength ultraviolet absorption spectrum of 1,4-dicyanobenzene extends beyond 280 nm. This is about the short wavelength limit of the transmission of Pyrex glass. The alkenes are transparent in this region, so the first step in the reaction scheme is excitation of the electron acceptor.

The second step involves electron transfer from the alkene to the singlet excited state of 1,4-dicyanobenzene. The likelihood of this process is accurately predicted by the Weller equation (eq. [1]) (16), using the singlet energy and reduction potential of 1,4-dicyanobenzene and the oxidation potential of the alkene.

[1] ΔG (kcal mol^{-1}) =
$$23.06[E_{ox}(D)\text{-}E_{red}(A)\text{-}e/\varepsilon\alpha]\text{-}E_{o,o}(\text{kcal mol}^{-1})$$

The excited singlet state of 1,4-dicyanobenzene will accept an electron, at the diffusion controlled rate, from any donor with an oxidation potential less than ca. 2.4 V.[3] All of the phenyl conjugated alkenes have an oxidation potential significantly less than this. In fact, the oxidation potentials of the nonconjugated tautomers are also below this limit. Clearly, the exclusive formation of the nonconjugated tautomer cannot be explained on the basis of the relative rates of the alternative electron transfer processes. Steps 2a and 2b should both be diffusion controlled.

There are several distinct stages involved during the electron transfer process (step 2): sequential formation of an encounter complex, an exciplex, a radical cation – radical anion pair, and finally, there may be degrees of solvent separated radical ions. The rates of progression through these stages of increasing charge separation are dependent upon the polarity of the solvent. Since the degree of charge separation has an influence on the ultimate product, product formation is also a function of solvent.

[3]The reduction potential of 1,4-dicyanobenzene is −1.66 V, the singlet energy is 97.6 kcal mol^{-1} (17), and the oxidation potential of the aryl conjugated alkenes is ca. 1.7 V (Table 2). The Coulombic attraction within the radical ion pair, the last term in the brackets, is relatively small (1.29 kcal mol^{-1}) in acetonitrile solution. The rate of the electron transfer process becomes diffusion limited when $\Delta G < -3$ kcal mol^{-1} (16). All of the potentials cited here are in reference to the saturated calomel electrode (SCE).

Can. J. Chem. Downloaded from www.nrcresearchpress.com by 41.223.56.140 on 09/07/12
For personal use only.

Can. J. Chem. Downloaded from www.nrcresearchpress.com by 41.223.56.140 on 09/07/12
For personal use only.

In nonpolar solvents, deactivation of the exciplex is relatively slow; as a result, the lifetime of the exciplex may be sufficient for reaction to compete with deactivation. Reaction at the exciplex stage generally leads to the formation of cycloaddition products (10, 11). Exciplex deactivation is more rapid in polar solvent, therefore the cycloaddition reaction can be inhibited by carrying out the irradiation in polar solvent (e.g., acetonitrile).

The tautomerization reaction requires formation of the alkene radical cation and is therefore favored in polar solvent. The rate constant for the solvent separation of some radical ion pairs, similar to those involved here (step 2), and in acetonitrile solution, is ca. 5×10^8 s^{-1} (18).

Alkene radical cations are susceptible to attack by nucleophiles. If methanol were used as solvent, the product could be the methyl ether having the *anti*-Markovnikov regiochemistry (15). Irradiation of 1-phenylcyclohexene (**13**) in acetonitrile–methanol (3:1) gives a good yield of the *anti*-Markovnikov adducts, *E*- and *Z*-1-methoxy-2-phenylcyclohexane (Reaction 8) (15*c*). There was no evidence for formation of the tautomer under these conditions. When this reaction was carried out using methanol -OD, only one deuterium atom was incorporated in the ether product, at the benzylic 2-position. There was no evidence for exchange of proton(s) at the allylic position in unreacted alkene. In acetonitrile–methanol, nucleophilic addition of methanol to the alkene radical cation competes favorably with deprotonation. Acetonitrile is a polar, relatively non-nucleophilic solvent suitable for the tautomerization reaction. The added base must also be non-nucleophilic.

Step 3, the back electron transfer process from the radical anion of the electron acceptor to the alkene radical cation, is one of the most important energy wasting steps. The rate of this process in closely related systems has been determined and the main factor affecting the rate has been identified (19). Back electron transfer becomes slower with increasing exothermicity, as indicated by the sum of the reduction potential of the acceptor (E_{red}(A)) and the oxidation potential of the donor (E_{ox}(D)), eq. [2].

$$[2] \quad \Delta G_{-3} = E_{red}(A) - E_{ox}(D)$$

That is, the rate falls in the Marcus "inverted region" (20). For example, back electron transfer from the radical anion of 9,10-dicyanoanthracene to the radical cation of biphenyl is exothermic by 2.9 eV ($\Delta G = -67$ kcal mol^{-1}) and the rate constant is ca. 1.0×10^8 s^{-1}, competitive with diffusive separation (19). Step 3a is even more exothermic ($\Delta G = -75$ kcal mol^{-1}), so the lifetime of the radical ion pair is long enough to allow solvent separation.

The relative rates of steps 3a and 3b could conceivably play a role in determining the final ratio of tautomers. However, the oxidation potential of the nonconjugated tautomer is significantly greater than that of the conjugated alkene, hence step 3b must be even slower than step 3a. The product ratio cannot be explained on this basis.

The detailed mechanism of step 3 has been studied by the technique of photochemically induced dynamic nuclear polarization (photo-CIDNP) (7*a*). When the energy of the radical ion pair is greater than the triplet energy of one of the components of the pair, back electron transfer within the triplet radical ion pair will give the triplet of that component with the lower triplet energy. The energy (eq. [2]) stored within the radical ion pair in step 3a (75 kcal mol^{-1}) is greater than the triplet energy of both the electron acceptor (1,4-dicyanobenzene, 70.1 kcal mol^{-1} (17)) and of the donor (phenyl conjugated alkenes, ca. 50 kcal mol^{-1} (7*a*)). Hence the triplet donor, which has the lower triplet energy, is preferentially produced.

The intersystem crossing process from the π,π^* triplet of the alkene will yield both configurations (*E* and *Z*) of the ground state. This process may account for the relatively efficient configurational isomerization of the starting conjugated alkene. There was no evidence in these photo-CIDNP studies for tautomerization of the conjugated alkene (7*a*).

Another mechanism for the configurational isomerization, involving a radical-ion chain process, has been identified. In fact, the photosensitized (electron transfer) isomerization of **1** to an *E*:*Z* mixture (1:1), under conditions very similar to those used here, was studied by Pac and co-workers (7*d*). The reaction conditions were identical to those used here *except that no base was added to the irradiation mixture*. The proposed mechanism involves formation of a π-complex between the radical cation of the cosensitizer and the alkene. The development of partial positive charge and (or) spin density on the alkene component of the π-complex may decrease the bond order of the double bond, thus lowering the barrier for isomerization. If π-complex formation were reversible, the isomerization would occur by a chain mechanism with the cosensitizer radical cation serving as a catalyst. There was no mention of tautomerization of **1** in this report (7*d*). The significant difference between this reported configurational isomerization reaction and the tautomerization reaction reported here can be attributed to the presence of base.

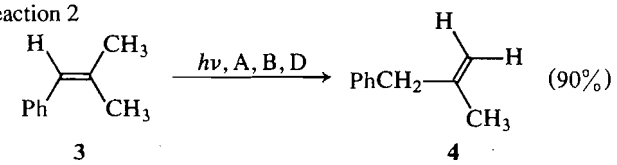
We have confirmed Pac's observation (7*d*): irradiation of an acetonitrile solution of **1**, 1,4-dicyanobenzene, and biphenyl leads to *cis–trans* isomerization; however, no tautomerization is observed in the absence of added base. We take this to mean that step 4, the deprotonation of the alkene radical cation, requires base. In fact, the strength of the base is important. This effect was observed previously in the case of the 1,1-diphenyl alkene tautomerization (2). While tautomerization of the diphenyl alkenes was catalyzed by pyridine ($pK_a = 12.3$ (21)), the reaction was significantly more efficient when the stronger base lutidine ($pK_a = 15.4$) was used. Now we find that for the tautomerization of these monophenyl alkenes, the even stronger base collidine ($pK_a = 16.8$) is significantly more effective than lutidine, and pyridine is almost ineffective.

An estimate of the acidity of the alkene radical cation, toward deprotonation at the allylic position, can be obtained from analysis of the thermochemical cycle based upon the oxidation potential of the alkene and the allylic carbon–hydrogen bond dissociation energy (22). For compounds with very similar standard oxidation potentials, a difference in their respective bond dissociation free energies of 2.5 kcal mol^{-1} corresponds to a difference of ca. 2 pK_a units in the acidity of the respective radical cations. Conversely, for compounds with very similar bond dissociation free energies, a difference in the standard oxidation potentials of 0.1 V corresponds to a difference of ca. 2 pK_a units in the acidity of the radical cations.

As an example we may compare the radical cation of **1** with that of toluene. The resonance stabilization energy of the 1-phenylpropenyl radical is 5.4 kcal mol^{-1} greater than that of the benzyl radical (23). However, the resulting increase in acidity of the radical cation of **1** is more than compensated for by the lower oxidation potential of **1**, 0.25 V less than that of toluene. The estimated pK_a of the radical cation of **1** is ca. −12 compared to −13 for the radical cation of toluene.

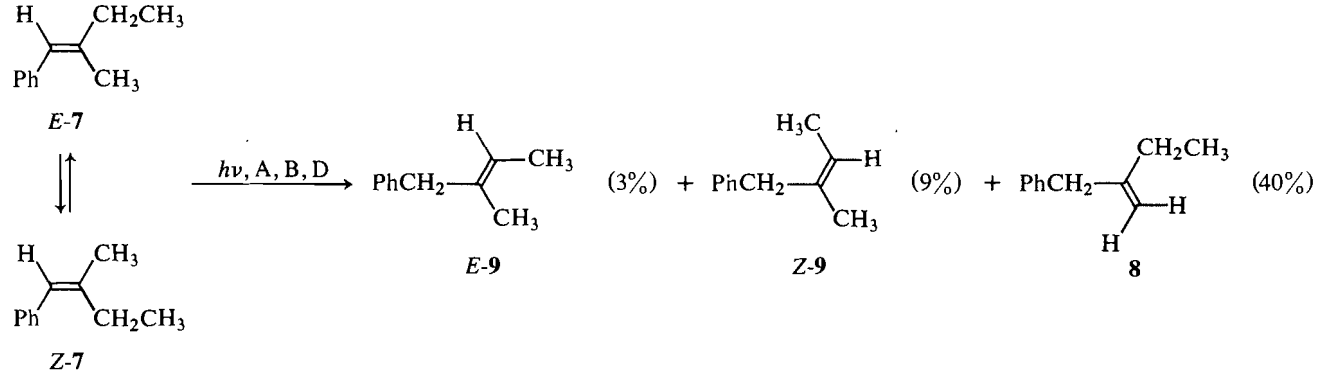
The bond dissociation free energy of the allylic, benzylic carbon–hydrogen bond in **2** is even less than the allylic carbon–

Reaction 2



3 4

Reaction 4



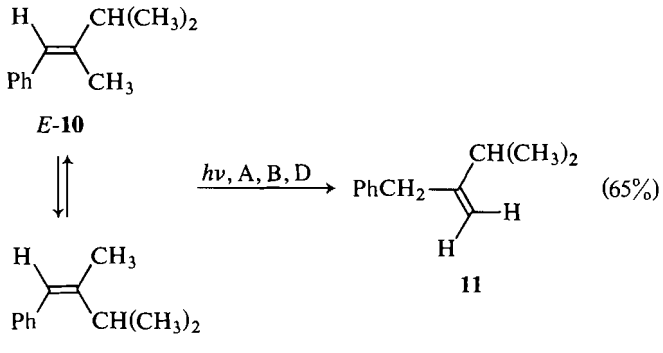
A = 1,4-dicyanobenzene
B = collidine
D = biphenyl

hydrogen bond in **1**, and the oxidation potential of **2** is greater than that of **1**; hence the thermodynamic acidity of the radical cation of **2** must be significantly greater than that of **1**. Step 4b is more exothermic than step 4a; preferential formation of **2** obviously cannot result from thermodynamic inhibition of the deprotonation process. In fact, from these thermodynamic considerations, it is not clear that deprotonation should require an added base. Acetonitrile (pK_a ca. −11) could conceivably serve as a base for such strong acids.

There is, however, no reason to expect that the rate of deprotonation will be rapid (i.e., diffusion limited), even for such an exothermic process. Other factors influence the kinetics of the deprotonation. Analysis of the product(s) resulting from the tautomerization of the series 2-methyl-1-phenylpropene (**3**), 2-methyl-1-phenylbutene (**7**), and 2,3-dimethyl-1-phenylbutene (**10**) provides evidence that the conformation of the allylic carbon–hydrogen bond, relative to the singly occupied molecular orbital (SOMO), has an influence on the kinetics of the deprotonation process.

Tautomerization of **3** gives an excellent yield of 2-methyl-3-phenylpropene (**4**) (Reaction 2), which indicates there is no impediment to deprotonation from a primary allylic position. Deprotonation from the radical cation of **7** can occur from either a primary or a secondary allylic position. Formation of the secondary allylic radical is favored on the basis of thermodynamics since the carbon–hydrogen bond strength is less. In fact, the nature of the observed products indicates that both radicals are formed (Reaction 4). The difference in bond strength is even greater for the carbon–hydrogen bonds in the two allylic positions of **10**, primary vs. tertiary; yet in this case only the terminal alkene is formed (Reaction 5). Deprotonation from the primary position is apparently favored. The rate of deprotonation from alternative allylic positions of the alkene radical cation does not follow the order of thermodynamic acidity.

Reaction 5



11

A = 1,4-dicyanobenzene
B = collidine
D = biphenyl

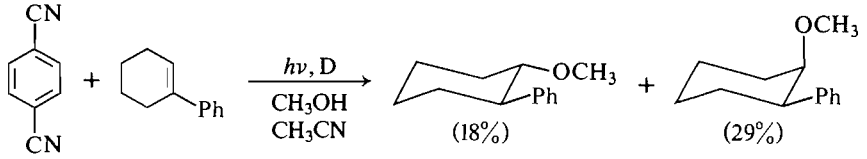
The profound increase in acidity of the allylic proton of the alkene radical cation requires overlap of the allylic carbon–hydrogen bond with the SOMO. In the likely event that the preferred conformation of the radical cation of **10** places the methyl groups of the isopropyl group in the staggered orientation, the tertiary allylic carbon–hydrogen bond is held orthogonal to the SOMO, and deprotonation will be slow. Alternatively, an allylic carbon–hydrogen bond of the freely rotating methyl group can overlap with the SOMO and deprotonation is uninhibited. This type of stereoelectronic effect, controlling the reactivity of radical cations, has been observed before (2, 24).

The relative rates of steps 4a and 4b could influence the ratio of tautomers. Before discussing the conformational overlap of the allylic carbon–hydrogen bond with the SOMO of the radical cation of **2**, it is necessary to define the "site" of the SOMO. Consideration of the oxidation potentials of the separated, noninteracting, moieties would suggest that the SOMO is largely associated with the phenyl ring. The oxidation potential of toluene, $E^{ox}_{1/2} = 2.0$ V (25*a*), is significantly lower than that of propene, $E^{ox}_{1/2} = 3.1$ V (25*b*). The measured oxidation potential of **2**, $E^{ox}_{1/2} = 2.26$ V (Table 2), is close to that of toluene. It therefore seems likely that the SOMO of **2** is largely associated with the benzyl moiety.

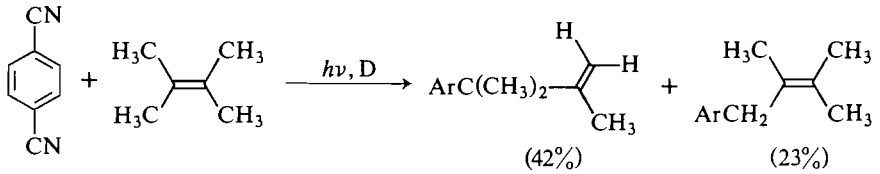
The preferred conformation of the radical cation should allow overlap of the benzylic carbon–hydrogen bond with the SOMO. However, significant reorganization is required at the transition

Can. J. Chem. Downloaded from www.nrcresearchpress.com by 41.223.56.140 on 09/07/12
For personal use only.

Reaction 8 (ref. *c*)



Reaction 9 (ref. 13)



D = biphenyl
Ar = 4-cyanophenyl

state for deprotonation, to bring both the phenyl and the vinyl groups into conjugation with the incipient radical. This may be a factor controlling the ratio of tautomers in some cases.[4]

Step 5 represents the reduction of the allylic radical by the sensitizer radical anion. This step will impose a limitation on the tautomerization reaction in general. The reduction potential of the electron-accepting sensitizer must be negative enough to reduce the allylic radical; otherwise, competing reactions will occur. The reduction potentials of the allylic radicals involved here are not known, but for the related diphenylmethyl radical $E^{red}_{1/2}$ is -1.14 V and that of the benzyl radical is -1.45 V (26). The reduction potential of 1,4-dicyanobenzene is -1.66 V; hence it is reasonable to suggest that step 5 is exothermic for these diphenyl and phenyl substituted allylic radicals.

Such is not the case for alkyl substituted allylic radicals; the reactivity of 2,3-dimethyl-2-butene is illustrative. Irradiation of an acetonitrile solution of 1,4-dicyanobenzene and 2,3-dimethyl-2-butene initially follows the same course, steps 1–4. However, the reduction potential available in the anion radical of 1,4-dicyanobenzene is insufficient to reduce the allylic radical (step 5) in this case. Instead, the allylic radical adds to the *ipso* position of the anion radical. Loss of cyanide ion then completes the sequence, forming the substitution product (Reaction 9) (13). Cyclohexene and 1-methylcyclohexene gave similar allylic radical substitution products. Here, again, the reduction potential of the allylic radical is not known, but alkyl groups increase (make more negative) the reduction potential of radicals. For example, the reduction potential of the *tert*-butyl radical is less than -2 V and $E^{red}_{1/2}$ of the cumyl radical is -1.73 V (26). It seems likely that the radical anion of 1,4-dicyanobenzene cannot reduce a *tert*-allylic radical.

Step 5, as shown, represents a bimolecular process involving two relatively reactive species that would normally be present in very low concentration. It seems likely that, during the course of the irradiation, processes such as coupling and disproportion initially consume the more reactive radical. Eventually the concentration of the radical anion increases to the point where step 5 can compete with the other reactions of the radical. This is an example of a reaction controlled by "internal suppression of fast modes" (27).

Step 6 in Scheme 1, protonation of the ambident anion, completes the sequence. The competition for reprotonation at the two ends of the ambident anion will affect the efficiency of the tautomerization reaction, but not the position of the equilibrium. A thorough study probing the effects that influence the position of protonation and the configurational stability of allylic anions have been reported (*4b*). The allylic anion from *E*-1-phenylpropene, when protonated, gives *E*-1-phenylpropene two to four times faster than 3-phenylpropene. Configurational isomerization of the allylic anion is slow.

Step 7 involves the equilibration of the radical cation of the conjugated and nonconjugated alkenes. Much of the control over the ratio of tautomers, in the cases reported here, can be attributed to this step. Equilibration will favor formation of that radical cation with the lower oxidation potential. In the first approximation, if the equilibrium follows the Nernst equation (eq. [3]) the radical cation of the conjugated alkene **1** will be favored over that of the nonconjugated alkene **2**, by ca. 10^9.

$$[3] \quad \ln[(\mathbf{1})(\mathbf{2}^{\cdot+})/(\mathbf{1}^{\cdot+})(\mathbf{2})] = F[E^{ox}_{1/2}(\mathbf{2}) - E^{ox}_{1/2}(\mathbf{1})]/RT$$

Although the tautomerization reaction occurs upon irradiation in the absence of an additional donor (D), the efficiency of the reaction is improved upon cosensitization. That is, the irradiation time required to complete the reaction is reduced and the yield of product is increased when biphenyl is added to the irradiation mixture.

The long wavelength ultraviolet adsorption of biphenyl does not extend much beyond 290 nm; 1,4-dicyanobenzene is still absorbing most of the light. In fact, the singlet energy of 1,4-dicyanobenzene (97.6 kcal mol^{-1}) and biphenyl (95.9 kcal mol^{-1} (28)) are similar. Substituting the oxidation potential ($E^{ox}_{1/2} = 1.80$ V) and singlet energy of biphenyl, and the reduction potential of 1,4-dicyanobenzene, in the Weller equation (eq. [1]) gives $\Delta G = -17.43$ kcal mol^{-1}. The electron transfer process (Scheme 1, step 8) should be diffusion controlled. The back electron transfer energy wasting process is exothermic by 3.5 V (eq. [2]) in this case, so diffusive separation of the radical ion pair should be competitive.

The secondary electron transfer process (Scheme 1, step 9) involves oxidation of the alkene by the radical cation of the cosensitizer. In the most simple terms, this process would give

[4]Stereoelectronic effects are known to affect the rate of ionization of the neutral alkene to form the allylic carbanion. However, the second-order rate constant for the ionization of **1** (1×10^{-7} L mol^{-1} s^{-1}) is significantly slower than for **2** (4×10^{-5} L mol^{-1} s^{-1}) in potassium *tert*-butoxide – *tert*-butyl alcohol at 25°C (*4b*).

Can. J. Chem. Downloaded from www.nrcresearchpress.com by 41.223.56.140 on 09/07/12
For personal use only.

an equilibrium mixture of the radical cations controlled by the relative oxidation potentials of biphenyl and the alkenes. Since the oxidation potential of biphenyl falls between the oxidation potential of the conjugated and nonconjugated alkenes, formation of the radical cation of the conjugated alkene should be favored. This may be an important factor influencing the ratio of products. In fact, while biphenyl should serve as a cosensitizer for the formation of the radical cation of **1**, the sensitized formation of the radical cation of **2** should be quenched by biphenyl. However, there is evidence for complex formation involving the biphenyl and alkene radical cation, so factors other than oxidation potential may be important in influencing the relative rates of these processes (Scheme 1, steps 9a and 9b) (*1a*, *7d*, 29).

Conclusions

Several of the conditions necessary for the photosensitized (electron transfer) tautomerization reaction have now been identified.

1. The photosensitizer must be chosen so that the electron transfer process from the conjugated alkene, or from the cosensitizer if one is used, to the photosensitizer is exothermic. This choice can be guided by the use of the Weller equation (eq. [1]). Electron transfer can be expected to be diffusion controlled if ΔG is negative by 3 or more kcal mol^{-1}.
2. The oxidation potential of the cosensitizer must be greater than that of the conjugated alkene.
3. Reaction requires a polar, non-nucleophilic solvent.
4. Reaction requires a non-nucleophilic base. The strength of the base depends upon the structure of the alkene. Collidine is a strong enough base for the tautomerization of monophenyl alkenes.
5. The reduction potential of the photosensitizer must be great enough to reduce the allylic radical formed upon deprotonation of the radical cation of the alkene. The reduction potential of 1,4-dicyanobenzene (−1.66 V) is sufficient to reduce the phenyl substituted allylic radical.
6. Tautomerization is driven toward the tautomer with the higher oxidation potential.
7. Competitive deprotonation from alternative allylic positions is influenced be a stereoelectronic effect. The preferred conformation of the radical cation must allow favorable overlap of the allylic carbon–hydrogen bond with the SOMO, for deprotonation to occur.

These conditions, which must be considered necessary but not sufficient for tautomerization, will be helpful in ultimately determining the scope and limitations of the reaction. It is already clear that the reaction will have some synthetic utility. The reaction works well for diphenyl and monophenyl conjugated alkenes. How general and how useful the reaction will be remains to be established.

Experimental

General Information

The ^1H and ^{13}C nmr spectra were recorded on a Nicolet 360 NB nmr spectrometer coupled to an Oxford Instruments superconducting magnet and a Nicolet 192 kword data acquisition system, and are reported in parts per million to high frequency from TMS. Coupling constants are reported as absolute values; the signs of the couplings were not determined. Infrared spectra (ir) were recorded on an air-purged Perkin–Elmer 180 grating infrared spectrometer and are reported in wavenumbers relative to the 1601.4 cm^{-1} absorption of polystyrene. Mass spectra (ms) were recorded on a Hewlett–Packard 5970 series mass selective detector and are reported as m/z (relative intensity). The melting points were determined using a Cybron Corporation Thermolyne melting point apparatus and are uncorrected.

Product analyses were determined by gas chromatography (gc) using either a Hewlett–Packard (HP) 5890 gc, fitted with a 5% phenyl methyl silicone fused silica WCOT column (25 m × 0.20 mm, 0.33-μm film thickness), coupled to a HP 5970 mass selective detector (ms), or a Hewlett–Packard 5890 gc, fitted with a DB-1701 or DB-225 fused silica WCOT column (30 m × 0.25 mm, 0.25-μm film thickness), with a flame ionization detector (fid). The digital signal from the fid was transmitted to a HP 3392A integrator and the data were acquired by software developed at the Department of Chemistry, Dalhousie University, using a Commodore PC-II.

Compounds that were obtained as liquids were purified prior to analysis by preparative gas chromatography using a Varian Aerograph 90-P and a 3/8 in. × 6 ft aluminum column packed with 10% SE-30 on Chromosorb W 60/80 NAW, or a 3/8 in. × 10 ft aluminum column packed with 10% DEGS on Chromosorb W 60/80 NAW. Preparative medium-pressure liquid chromatography (mplc) was carried out using a 2.5 cm × 1 m column packed with TLC grades silica gel (without binder) (Merck) at 15 psi (helium) (1 psi = 6.9 kPa). The chromatograms were developed with hexanes and the eluant was monitored–collected by a uv spectrometer-fraction collector.

Materials

Solvents were fractionally distilled. Acetonitrile (Fisher ACS grade) was distilled successively from sodium hydride and phosphorus pentoxide, and was then passed through a column of basic alumina, refluxed over calcium hydride for 24 h (under a nitrogen atmosphere), and fractionally distilled. The 1,4-dicyanobenzene (Aldrich) was purified by treatment with Norite in methylene chloride, followed by sublimation and recrystallization from 95% ethanol. Biphenyl (Aldrich) was recrystallized from methanol. Collidine (BDH) was purified by distillation. Tetraethylammonium perchlorate (TEAP) (Aldrich) was recrystallized (three times) from 95% ethanol and dried in a vacuum oven (12 h, 80°C, 10 Torr; 1 Torr = 133.3 Pa) before use.

Irradiations

An acetonitrile solution of the alkene (0.2 M), the electron accepting photosensitizer (1,4-dicyanobenzene) (0.15 M), the cosensitizer (biphenyl) (0.12 M), and the base (2,4,6-trimethylpyridine) (0.4 M) was flushed with dry nitrogen and sealed in a Pyrex tube (2 cm i.d.). The irradiation vessel was placed ca. 2.5 cm from a CGE 1-kW medium-pressure mercury vapor lamp contained in a water cooled quartz immersion well. The temperature was maintained at 10°C. The photolysate was separated by medium-pressure liquid chromatography (mplc) on a silica gel column, taking ca. 10-mL fractions. For quantitative studies, the progress of the reaction and the ratio of products were followed by gc/fid. Peak areas were calibrated relative to an inert internal standard (cyclododecane).

Cyclic voltammetric measurements

Oxidation potentials were obtained by cyclic voltammetry using an apparatus similar to that previously described (30). The working electrode was a platinum sphere (1 mm diameter), while the counter electrode was a platinum wire. The reference electrode was a saturated calomel electrode (SCE), which was connected to the solution by a Luggin capillary. The electrolyte was TEAP (0.1 M) and the solvent was acetonitrile. Substrate concentrations were typically 0.005 M. The anodic wave was not reversible; the half-wave potential was taken as 0.03 V before the anodic peak potential (6).

Preparation and characterization of starting materials

E-*1-Phenylpropene* (*1*)

This alkene (*E*/*Z*, 95:5) was purchased from Aldrich Chemical Co. The ^1H nmr of the *E* isomer (361.1 MHz, $CDCl_3$) δ: 7.31–7.11 (m, 5H, aromatic), 6.35 (dd, 1H, H1, ^4J(H1, H3)= 1.4 Hz, ^3J(H1, H2)= 14.5 Hz), 6.18 (dq, 1H, H2, ^3J(H2, H1)= 14.5 Hz, ^3J(H2, H3)= 5.1 Hz), 1.83 (dd, 3H, H3, ^3J(H3, H1) = 1.4 Hz, ^3J(H3, H2) = 5.1 Hz); ^{13}C nmr of the *E* isomer (90.1 MHz, $CDCl_3$) δ: 137.8, 130.9, 128.3, 126.6, 125.7, 125.4, 18.3; ms (HP) m/z: M^+ 118 (80), 117 (100), 115 (49), 91 (52); $E^{ox}_{1/2}$ 1.73 V (SCE).

Can. J. Chem. Downloaded from www.nrcresearchpress.com by 41.223.56.140 on 09/07/12
For personal use only.

Can. J. Chem. Downloaded from www.nrcresearchpress.com by 41.223.56.140 on 09/07/12
For personal use only.

*2-Methyl-1-phenylpropene (**3**)*

The Grignard reaction, starting with isobutyraldehyde and phenylmagnesium bromide, gave the crude alcohol in excellent yield (97%). Dehydration of the alcohol, by the copper(II) triflate catalyzed procedure (31), gave the alkene **3**, which was purified by column chromatography with silica gel and hexanes as the eluent. Pure alkene 3 was isolated in 73% yield; ^{1}H nmr (361.1 MHz, $CDCl_3$) δ: 7.32–7.14 (m, 5H, aromatic), 6.27 (brs, 1H, H1), 1.90 (d, 3H, H3, ^4J(H3, H1)= 0.8 Hz), 1.86 (d, 3H, H2, ^4J(H2, H1)= 1.0 Hz) (these experimental values are in agreement with literature values (32)); ^{13}C nmr (90.1 MHz, $CDCl_3$) δ: 138.5, 135.3, 128.6, 127.9, 125.6, 125.0, 26.8, 19.3; ms (HP) *m/s*: M^+ 132 (77), 131 (20), 117 (100), 115 (51), 91 (45); $E^{ox}_{1/2}$ 1.60 V (SCE).

*1-Phenylbutene (**5**) (E- and Z-)*

A solution of butyraldehyde (10.9 g, 0.15 mol) in diethyl ether was added dropwise to phenylmagnesium bromide (0.18 mol, prepared by adding 28.4 g of bromobenzene to 4.4 g of magnesium turnings) in ether at 0°C. After 24 h the reaction was quenched by addition to an iced solution of saturated NH_4Cl (200 mL). The aqueous layer was extracted with ether and the combined ether layers were washed with saturated NaCl and distilled water to remove inorganic impurities. The ethereal layer was then dried over magnesium sulphate, filtered, and evaporated. The crude alcohol (21.9 g, 0.145 mol), obtained in 96% yield, was purified by column chromatography over silica gel using hexanes as the eluent. The pure alcohol (18.2 g, 0.12 mol) was obtained in good yield (83%).

The pure alcohol (4.14 g, 27.6 mmol) was added to $Cu(Otf)_2$ (copper(II) triflate) (0.82 g, 2.76 mmol) and heated to reflux (ca. 100°C) for 27 h (31). The mixture was cooled, water was added, and the alkene was extracted with ether. The combined ether layers were washed with saturated NaCl and distilled water to remove the inorganic impurities. The solution was then dried over magnesium sulphate and the solvent was evaporated. The resulting alkene was purified by column chromatography over silica gel, eluting with hexanes. The pure alkene, a mixture of *E*- and *Z*-**5** (99:1) (2.41 g, 0.018 mol), was obtained in 67% yield based upon reacted alcohol.

For the *E* isomer: ^{1}H nmr (361.1 MHz, $CDCl_3$) δ: 7.35–7.15 (m, 5H, aromatic), 6.37 (d, 1H, H1, ^3J(H1, H2)= 15.9 Hz), 6.25 (dt, 1H, H2, ^3J(H2, H1)= 15.9 Hz, ^3J(H2, H3)= 6.3 Hz), 2.23 (dq, 2H, H3, ^3J(H3, H2)= 6.3 Hz, ^3J(H3, H4)= 7.4 Hz), 1.08 (t, 3H, H4, ^3J(H4, H3)= 7.4 Hz) (these values compare well with literature values (33)); ^{13}C nmr (90.1 MHz, $CDCl_3$) δ: 138.4, 132.6, 128.8, 128.4, 126.7, 125.9, 26.1, 13.7; ms (HP) *m/s*: M^+ 132 (39), 117 (100), 116 (13), 115 (48), 91 (39); $E^{ox}_{1/2}$ = 1.67 V (SCE).

*2-Methyl-1-phenylbutene (**7**) (E- and Z-)*

Starting with triphenylbenzylphosphonium bromide and 2-butanone, the Wittig procedure gave the alkene, which was purified by distillation under vacuum (5×10^{-2} Torr (1 Torr = 133.3 Pa); ca. 40°C). Pure alkene **7** (*E*- and *Z*-) (3:2) was obtained in 80% yield.

For the *E* isomer: ^{1}H nmr (361.1 MHz, $CDCl_3$) δ: 7.33–7.15 (m, 5H, aromatic), 6.27 (brs, 1H, H1), 2.18 (q, 2H, H3-*E*, ^3J(H3, H4)= 7.5 Hz), 1.86 (d, 3H, H2-*E*, ^4J(H2, H1)= 1.2 Hz), 1.12 (t, 3H, H4-*E*, ^3J(H4, H3)= 7.5 Hz) (these values are in good agreement with those reported (34)); ^{13}C nmr (90.1 MHz, $CDCl_3$) δ: 123.5, 33.4, 17.7, 12.7; ms (HP) *m/z*: M^+ 146 (100), 131 (82), 115 (64), 91 (52).

For the *Z* isomer: ^{1}H nmr (361.1 MHz, $CDCl_3$) δ: 7.33–7.15 (m, 5H, aromatic), 6.27 (brs, 1H, H1), 2.23 (q, 2H, H3-*Z*, ^3J(H3, H4)= 7.5 Hz), 1.88 (d, 3H, H2-*Z*, ^4J(H2, H1)= 1.4 Hz), 1.01 (t, 3H, H4-*Z*, ^3J(H4, H3)= 7.5 Hz; ^{13}C nmr (90.1 MHz, $CDCl_3$) δ: 124.8, 25.5, 23.6, 12.9; ms (HP) *m/z*: M^+ 146 (100), 131 (75), 115 (52), 91 (40).

*2,3-Dimethyl-1-phenylbutene (**10**) (E- and Z-)*

This alkene was prepared by the Wittig reaction, starting with triphenylbenzylphosphonium bromide and 3-methyl-2-butanone, using a procedure similar to that described above. The pure alkene was obtained by vacuum distillation in 57% yield (35).

For the *E* isomer: ^{1}H nmr (361.1 MHz, $CDCl_3$) δ: 7.30–7.12 (m, 5H, aromatic), 6.26 (brs, 1H, H1-*E*), 2.40 (qn, 1H, H3-*E*, ^3J(H3, H4)= 6.8 Hz), 1.80 (d, 3H, H2-*E*, ^4J(H2, H1)= 1.3 Hz), 1.08 (d, 6H, H4-*E*, ^3J(H4, H3) = 6.9 Hz; ^{13}C nmr (90.1 MHz, $CDCl_3$) δ: 122.7, 37.7, 21.4, 15.1; ms (HP) *m/z*: M^+ 160 (74), 145 (100), 117 (81), 115 (5), 105 (29), 91 (78).

For the *Z* isomer: ^{1}H nmr (361.1 MHz, $CDCl_3$) δ: 7.33–7.15 (m, 5H, aromatic), 6.18 (brs, 1H, H1-*Z*), 3.03 (qn, 1H, H3-*Z*, ^3J(H3, H4)= 6.8 Hz), 1.77 (d, 3H, H2-*Z*, ^4J(H2, H1)= 1.5 Hz), 1.01 (d, 6H, H4-*Z*, ^3J(H4, H3) = 6.8 Hz); ^{13}C nmr (90.1 MHz, $CDCl_3$) δ: 124.3, 28.8, 21.0, 18.2; ms (HP) *m/z*: M^+ 160 (48), 145 (100), 117 (48), 115 (38), 91 (51).

*1-Phenylcyclohexene (**13**)*

This alkene was purchased from Aldrich Chemical Co.; ir (neat) ν, cm^{-1}: 3040 (m), 2942 (s), 1610 (m), 1585 (w), 1503 (s), 1455 (s), 762 (s), 743 (s), 697 (s); uv (hexanes) λ_{max}: 246 nm (ε 9000); ^{1}H nmr (361.1 MHz, $CDCl_3$) δ: 7.36–7.16 (m, 5H, aromatic), 6.10–6.08 (m, 1H, H2), 2.40–2.35 (m, 2H), 2.20–2.15 (m, 2H), 1.77–1.72 (m, 2H), 1.66–1.60 (m, 2H); ^{13}C nmr (90.1 MHz, $CDCl_3$) δ: 142.6, 136.6, 128.7, 128.1, 126.5, 124.9, 124.7, 27.4, 25.9, 23.1, 22.2; ms (HP) *m/z*: M^+ 158 (39), 143 (50), 130 (77), 129 (100), 115 (77), 91 (39); $E^{ox}_{1/2}$ 1.16 V (SCE).

*1-(Phenylmethylene)cyclohexane (**15**)*

To a round-bottom flask (500 mL, N_2 atmosphere), fitted with a reflux condenser, was added sodium hydride (2.30 g, 0.050 mol) (50% suspension in oil). Pentane (20 mL) was added to dissolve the oil and then the supernatant was carefully decanted. Dimethylsulfoxide (20 mL) was added to the flask and the mixture was stirred until the evolution of hydrogen was complete (ca. 1/2 h). Triphenylbenzylphosphonium bromide (20.0 g, 0.050 mol) was slowly added to the reaction mixture in portions, with stiring between each addition. The mixture turned a bright orange colour and was left to stir for 1/2 h. Cyclohexanone (9.50 g, 0.110 mol) was added in excess to the reaction mixture and then refluxed at ca. 75°C for 3 h. The reaction was quenched by addition to water (250 mL) and the mixture was extracted with pentanes. The organic layer was washed with water, dried over $MgSO_4$, filtered, and the solvent was evaporated. The crude product (9.74 g, 0.057 mol) was distilled under vacuum (5×10^{-2} Torr) at ca. 56°C and pure alkene **15** was obtained (6.75 g, 0.059 mol) in 80% overall yield; ^{1}H nmr (361.1 MHz, $CDCl_3$) δ: 7.31–7.14 (m, 5H, aromatic), 6.22 (s, 1H), 2.36 (t, 2H, ^3J=5.6 Hz), 2.25 (t, 2H, ^3J=5.6 Hz), 1.66–1.52 (m, 6H) (in good agreement with reported values (32)); ^{13}C nmr (90.1 MHz, $CDCl_3$) δ: 143.4, 138.3, 128.9, 128.1, 127.9, 125.7, 121.9, 37.7, 29.4, 28.6, 27.9, 26.7; ms (HP) *m/z*: M^+ 172 (65), 143 (13), 129 (60), 115 (50), 104 (77), 91 (81), 81 (100); $E^{ox}_{1/2}$ 1.62 V (SCE).

Isolation and characterization of product alkenes

*3-Phenylpropene (**2**)*

Irradiation of a solution of *E*-1-phenylpropene (**1**), under the conditions described above, gave 3-phenylpropene (**2**) in 41% yield at 94% conversion. The unreacted 1-phenylpropene was a 1:1 mixture of the *E* and *Z* isomers. When a solution of **2** was irradiated under these conditions, no **1** was detected.

The structure of this alkene (**2**) was firmly established by direct comparison with an authentic sample obtained from Aldrich Chemical Co.; ir (neat) ν, cm^{-1}: 3045 (s), 2920 (m), 1650 (m), 1613 (m), 1505 (s), 1463 (s), 1441 (m), 1000 (s), 926 (s), 742 (s), 701 (s); uv (hexanes) λ_{max}: 253, 260 nm (ε 9000); ^{1}H nmr (361.1 MHz, $CDCl_3$) δ: 7.28–7.11 (m, 5H, aromatic), 5.99–5.90 (m, 1H, H2, ^3J(H2, H3)= 6.6 Hz), 5.09–5.03 (m, 2H, H1A, H1B), 3.36 (d, 2H, H3, ^3J(H3, H2)= 6.6 Hz); ^{13}C nmr (90.1 MHz, $CDCl_3$) δ: 140.0, 137.3, 128.4, 128.3, 125.9, 115.6, 40.1; ms (HP) *m/z*: M^+ 118 (62), 117 (100), 115 (41), 91 (46); $E^{ox}_{1/2}$ 2.26 V (SCE).

*2-Methyl-3-phenylpropene (**4**)*

Irradiation of 2-methyl-1-phenylpropene (**3**) under these conditions gave 2-methyl-3-phenylpropene (**4**) in 90% yield. The spectral data, obtained on a pure sample isolated from the irradiation mixture, are in good agreement with those reported (36); ir (neat) ν, cm^{-1}: 3048 (m), 2990 (s), 2939 (s), 1660 (w), 1508 (s), 1465 (s), 1386 (m), 1088 (w), 895 (s), 741 (s), 702 (s); uv (cyclohexane) λ_{max}: 259 nm (ε 500); ^{1}H

nmr (361.1 MHz, $CDCl_3$) δ: 7.32–7.14 (m, 5H, aromatic), 4.80 (d, 2H, H1, ^2J= 0.7 Hz), 3.31 (s, 2H, H3), 1.67 (s, 3H, H2); ^{13}C nmr (90.1 MHz, $CDCl_3$) δ: 145.1, 139.7, 128.9, 128.2, 126.0, 111.9, 44.7, 22.1; ms (HP) *m/z*: M^+ 132 (65), 117 (100), 115 (41), 91 (65), 65 (28); $E^{ox}_{1/2}$ 2.24 V (SCE).

*1-Phenyl-2-butene (**6**) (E- and Z-)*

These alkenes were formed upon irradiation of *E*-1-phenyl-1-butene (**5**). When the reaction was 98% complete, the combined yield of *E*- and *Z*-1-phenyl-2-butene was 65% and the *E*:*Z* ratio was 4:1. The ratio of the *E*:*Z* isomers of unreacted starting material (**5**) was also 4:1.

These alkenes have been described (37) and the ^1H nmr spectrum of the products isolated from the irradiation mixture is in good agreement with the reported spectra.

For the *E* isomer: ^1H nmr (361.1 MHz, $CDCl_3$) δ: 7.30–7.16 (m, 5H, aromatic), 5.60–5.52 (m, 2H, H2-*E*, H3-*E*), 3.30 (d, 2H, H1-*E*, ^3J(H1-*E*, H2-*E*)= 6.3 Hz), 1.68 (d, 3H, H4-*E*, ^3J(H4-*E*, H3-*E*)= 6.0 Hz); ^{13}C nmr (90.1 MHz, $CDCl_3$) δ: 124.8, 39.1, 17.9; ms (HP) *m/z*: M^+ 132 (50), 117 (100), 115 (92), 91 (48), 65 (39).

For the *Z*-isomer: ^1H nmr (361.1 MHz, $CDCl_3$) δ: 7.30–7.16 (m, 5H, aromatic), 5.60–5.52 (m, 2H, H2-*Z*, H3-*Z*), 3.40 (d, 2H, H1-*Z*, ^3J(H1-*Z*, H2-*Z*)= 5.1 Hz), 1.72 (d, 3H, H4-*Z*, ^3J(H4-*Z*, H3-*Z*)= 4.9 Hz); ^{13}C nmr (90.1 MHz, $CDCl_3$) δ: 125.8, 33.1, 12.9; ms (HP) *m/z*: M^+ 132 (32), 117 (100), 115 (75), 91 (36), 65 (25).

*Irradiation of 2-methyl-1-phenylbutene (**7**)*

Irradiation of a solution of a mixture of the *E*- and *Z*-2-methyl-1-phenylbutene (**7**) (*E*:*Z*, 6:4) isomers led to formation of all three tautomers, *E*- and *Z*-2-methyl-1-phenyl-2-butene (**9**), and 2-phenylmethyl-1-butene (**8**), in a combined yield of 50%. The ratio of products, *E*-**9**:*Z*-**9**:**8**, was 1:2:11. At the beginning of the irradiation the ratio of the isomeric starting alkenes (2-methyl-1-phenylbutene), *E*-**7** to *Z*-**7**, was 2:1; after 90% conversion, the ratio was 1:1.

The structural assignments were made on the basis of the good agreement between the spectral data obtained on pure samples of the products isolated from the irradiation mixture and those reported (38).

*2-Phenylmethyl-1-butene (**8**)*: ^1H nmr (361.1 MHz, $CDCl_3$) δ: 7.27–7.15 (m, 5H, aromatic), 4.82 (brs, 1H, H1), 4.73 (brs, 1H, H1), 3.35 (s, 2H, H2), 1.97 (q, 2H, H3, ^3J(H3, H4)= 7.4 Hz), 1.54 (t, 3H, H4, ^3J(H4, H3)= 7.4 Hz); ^{13}C nmr (90.1 MHz, $CDCl_3$) δ: 109.8, 43.2, 28.2, 23.3; ms (HP) *m/z*: M^+ 146 (27), 131 (27), 117 (100), 115 (32), 91 (66).

E-*2-Methyl-1-phenyl-2-butene* (E-**9**): ^1H nmr (361.1 MHz, $CDCl_3$) δ: 7.27–7.15 (m, 5H, aromatic), 5.39 (qt, 1H, H3-*E*), 3.37 (brs, 2H, H1-*E*), 1.72 (dd, 3H, H4-*E*), 1.62–1.60 (m, 3H, H2-*E*); ^{13}C nmr (90.1 MHz, $CDCl_3$) δ: 120.4, 37.5, 15.5, 13.7; ms (HP) *m/z*: M^+ 146 (51), 131 (100), 117 (18), 115 (18), 91 (70).

Z-*2-Methyl-1-phenyl-2-butene* (Z-**9**): ^1H nmr (361.1 MHz, $CDCl_3$) δ: 7.27–7.15 (m, 5H, aromatic), 5.31 (qt, 1H, H3-*Z*), 3.27 (brs, 2H, H1-*Z*), 1.62–1.60 (m, 3H, H4-*Z*), 1.52 (t, 3H, H2-*Z*); ^{13}C nmr (90.1 MHz, $CDCl_3$) δ: 125.8, 46.2, 13.5, 12.2; ms (HP) *m/z*: M^+ 146 (34), 131 (100), 117 (17), 115 (17), 91 (68).

*3-Methyl-2-phenylmethyl-1-butene (**11**)*

Irradiation of a solution of 2,3-dimethyl-1-phenylbutene (a mixture of the isomers *E*-**10** and *Z*-**10** in the ratio of 4:5), under the above conditions, resulted in the formation of 2-phenylmethyl-3-methylbutene (**11**) in 65% yield; the other possible tautomer, 2,3-dimethyl-1-phenyl-2-butene (**12**) was not detected. At 98% conversion the ratio of *E*-**10** to *Z*-**10** was 1:8. The structural assignment for **11** rests on an analysis of the spectral data observed for the pure product isolated from the irradiation mixture; ir (neat) ν, cm^{-1}: 3042 (w), 2980 (s), 2890 (w), 1654 (w), 1613 (w), 1508 (m), 1465 (m), 1389 (w), 1373 (w), 1085 (w), 896 (s), 701 (s); ^1H nmr (361.1 MHz, $CDCl_3$) δ: 7.30–7.14 (m, 5H, aromatic), 4.85 (s, 1H, H1), 4.62 (s, 1H, H1), 3.37 (s, 2H, H2), 2.20 (qn, 1H, H3, ^3J(H3, H4)= 6.8 Hz), 1.03 (d, 6H, H4, ^3J(H4, H3)= 6.8 Hz); ^{13}C nmr (90.1 MHz, $CDCl_3$) δ: 155.2, 140.1, 129.1, 128.2, 125.9, 109.0, 41.6, 33.0, 21.9; ms (HP) *m/z*: M^+ 160 (49), 145 (100), 117 (62), 115 (52), 104 (22), 91 (36); $E^{ox}_{1/2}$ 2.25 V (SCE).

*3-Phenylcyclohexene (**14**)*

Irradiation of 1-phenylcyclohexene (**13**), under the conditions described above, gave 3-phenylcyclohexene (**14**) in 86% yield. Spectral data, obtained on a sample isolated from the irradiation mixture, were in good agreement with those reported (39); ir ν, cm^{-1} (neat): 3038 (m), 2942 (s), 1611 (m), 1502 (s), 1461 (s), 1085 (w), 758 (s), 701 (s); uv (hexanes) λ_{max}: 247 nm (ε 9000); ^1H nmr (361.1 MHz, $CDCl_3$) δ: 7.36–7.15 (m, 5H, aromatic), 5.91–5.85 (m, 1H), 5.74–5.69 (m, 1H), 3.41–3.37 (m, 1H), 2.11–1.50 (m, 6H); ^{13}C nmr (90.1 MHz, $CDCl_3$) δ: 146.2, 130.1, 128.3, 128.2, 127.7, 125.9, 125.5, 41.9, 32.6, 25.0, 21.2; ms (HP) *m/z*: M^+ 158 (96), 130 (85), 129 (100), 128 (50), 115 (82), 91 (47); $E^{ox}_{1/2}$ 2.13 V (SCE).

*1-(Phenylmethyl)cyclohexene (**16**)*

This alkene was obtained, in 41% yield, from the irradiation of 1-(phenylmethylene)cyclohexane (**15**). Comparison of spectral data obtained on a sample isolated from the irradiation mixture with those reported (40) established the structure; uv (hexane) λ_{max}: 248 nm (ε 500); ^1H nmr (361.1 MHz, $CDCl_3$) δ: 7.29–7.16 (m, 5H, aromatic), 5.46 (brs, 1H), 3.24 (brs, 2H), 2.02–2.00 (m, 2H), 1.85 (brs, 2H), 1.61–1.51 (m, 4H); ^{13}C nmr (90.1 MHz, $CDCl_3$) δ: 140.4, 137.2, 128.9, 128.1, 125.8, 122.9, 44.7, 28.0, 25.3, 22.9, 22.4; ms (HP) *m/z*: M^+ 172 (53), 129 (35), 104 (18), 91 (55), 81 (100); $E^{ox}_{1/2}$ 1.95 V (SCE).

Acknowledgments

This work was supported by grants from the Natural Sciences and Engineering Research Council of Canada and from the Petroleum Research Fund administered by the American Chemical Society. We thank Dr. D. L. Hooper at the Atlantic Regional Magnetic Resonance Centre at Dalhousie University for the high-field nmr spectra and for help in the preparation of the manuscript.

1. (*a*) D. R. Arnold and M. S. Snow. Can. J. Chem. **66**, 3012 (1988); (*b*) D. R. Arnold, B. J. Fahie, L. J. Lamont, J. Wierzchowski, and K. M. Young. Can. J. Chem. **65**, 2734 (1987).
2. D. R. Arnold and S. A. Mines. Can. J. Chem. **65**, 2312 (1987).
3. (*a*) C. K. Ingold. Structure and mechanism in organic chemistry. Cornell University Press, Ithaca, NY. 1953. Chap. 10; (*b*) D. J. Cram. Fundamentals of carbanion chemistry. Academic Press, New York, NY. 1965. Chap. 5.
4. (*a*) A. G. Catchpole, E. D. Hughes, and C. K. Ingold. J. Chem. Soc. 8 (1948); (*b*) S. W. Ela and D. J. Cram. J. Am. Chem. Soc. **88**, 5791 (1966).
5. J. L. Marshall. Carbon–carbon and carbon–proton NMR coupling: Application to organic stereochemistry and conformational analysis. Verlag Chemie International, Deerfield Beach, FL. 1983.
6. R. S. Nicholson and I. Shain. Anal. Chem. **36**, 706 (1964).
7. (*a*) H. D. Roth and M. L. Manion-Schilling. J. Am. Chem. Soc. **101**, 1898 (1979); (*b*) W. Hub, U. Kluter, S. Schneider, F. Dorr, J. D. Oxman, and F. D. Lewis. J. Phys. Chem. **88**, 2308 (1984); (*c*) F. D. Lewis, J. R. Petisce, J. D. Oxman, and M. J. Nepras. J. Am. Chem. Soc. **107**, 203 (1985); (*d*) T. Majima, C. Pac, and H. Sakurai. Chem. Lett. 1133 (1979).
8. (*a*) S. Kuwata, Y. Shigemitsu, and Y. Odaira. J. Org. Chem. **38**, 3803 (1973); (*b*) T. R. Evans, R. Wake, and O. Jaenicke. *In* The exciplex. *Edited by* M. Gordon and W. R. Ware. Academic Press, New York, NY. 1975. p. 345; (*c*) T. Majima, C. Pac, A. Nakasone, and H. Sakurai. J. Am. Chem. Soc. **103**, 4499 (1981); (*d*) R. A. Pabon, D. J. Bellville, and N. L. Bauld. J. Am. Chem. Soc. **106**, 2730 (1984).
9. (*a*) R. A. Neunteufel and D. R. Arnold. J. Am. Chem. Soc. **95**, 4080 (1973); (*b*) S. L. Mattes and S. Farid. J. Am. Chem. Soc. **108**, 7356 (1986); (*c*) C. R. Jones, B. J. Allman, A. Mooring, and B. Spahic. J. Am. Chem. Soc. **105**, 652 (1983);

Can. J. Chem. Downloaded from www.nrcresearchpress.com by 41.223.56.140 on 09/07/12
For personal use only.

(*d*) G. C. CALHOUN and G. B. SCHUSTER. J. Am. Chem. Soc. **106**, 6870 (1984).
10. (*a*) J. G. ATKINSON, D. E. AYER, G. BUCHI, and E. W. ROBB. J. Am. Chem. Soc. **85**, 2257 (1963); (*b*) T. S. CANTRELL. J. Am. Chem. Soc. **94**, 5929 (1972); (*c*) M. G. B. DREW, A. GILBERT, P. HEATH, A. J. MITCHELL, and P. W. RODWELL. J. Chem. Soc. Chem. Commun. 750 (1983); (*d*) N. C. YANG and K. SRINIVASAN. J. Am. Chem. Soc. **97**, 5006 (1975); (*e*) E. M. OSSELTON and J. CORNELISSE. Tetrahedron Lett. **26**, 527 (1985).
11. (*a*) N. C. YANG, B. KIM, W. CHIANG, and T. HAMADA. J. Chem. Soc. Chem. Commun. 729 (1976); (*b*) T. S. CANTRELL. J. Org. Chem. **42**, 4238 (1977).
12. (*a*) F. D. LEWIS and R. J. DEVOE. Tetrahedron, **38**, 1069 (1982); (*b*) F. D. LEWIS, R. J. DEVOE, and D. B. MACBLANE. J. Org. Chem. **47**, 1392 (1982); (*c*) J. J. MCCULLOUGH, R. C. MILLER, and W.-S. WU. Can. J. Chem. **55**, 2909 (1977).
13. R. M. BORG, D. R. ARNOLD, and T. S. CAMERON. Can. J. Chem. **62**, 1785 (1984).
14. (*a*) D. R. ARNOLD, P. C. WONG, A. J. MAROULIS, and T. S. CAMERON. Pure Appl. Chem. **52**, 2609 (1980).
15. (*a*) R. A. NEUNTEUFEL and D. R. ARNOLD. J. Am. Chem. Soc. **95**, 4080 (1973); (*b*) A. J. MAROULIS, Y. SHIGEMITSU, and D. R. ARNOLD. J. Am. Chem. Soc. **100**, 535 (1978); (*c*) Y. SHIGEMITSU and D. R. ARNOLD. J. Chem. Soc. Chem. Commun. 407 (1975); (*d*) P. G. GASSMAN and K. J. BOTTORFF. Tetrahedron Lett. **28**, 5449 (1954).
16. (*a*) D. REHM and A. WELLER. Isr. J. Chem. **8**, 259 (1970); (*b*) Ber. Bunsen-ges. Phys. Chem. **73**, 834 (1969).
17. D. R. ARNOLD and A. J. MAROULIS. J. Am. Chem. Soc. **98**, 5931 (1976).
18. (*a*) S. L. MATTES and S. FARID. Org. Photochem. **6**, 233 (1983); (*b*) J. Am. Chem. Soc. **104**, 1454 (1982); (*c*) J. Am. Chem. Soc. **108**, 7356 (1986); (*d*) A. WELLER. Z. Phys. Chem. **69**, 183 (1970).
19. I. R. GOULD, D. EGE, S. L. MATTES, and S. FARID. J. Am. Chem. Soc. **109**, 3794 (1987).
20. (*a*) R. A. MARCUS. J. Chem. Phys. **24**, 966 (1956); (*b*) Annu. Rev. Phys. Chem. **15**, 155 (1964).
21. C. J. SCHLESENER, C. AMATORE, and J. K. KOCHI. J. Am. Chem. Soc. **106**, 7472 (1984).
22. A. M. P. NICHOLAS and D. R. ARNOLD. Can. J. Chem. **60**, 2165 (1982).
23. D. A. ROBAUGH and S. E. STEIN. J. Am. Chem. Soc. **108**, 3224 (1986).
24. (*a*) F. D. LEWIS. Acc. Chem. Res. **19**, 401 (1986); (*b*) T. SHONE and Y. MATSUMURA. J. Org. Chem. **35**, 4157 (1970); (*c*) P. J. WAGNER, R. J. TRUMAN, A. E. PUCHALSKI, and R. WAKE. J. Am. Chem. Soc. **108**, 7727 (1986); (*d*) L. M. TOLBERT and R. K. KHANNA. J. Am. Chem. Soc. **109**, 3477 (1987).
25. (*a*) E. S. PYSH and N. C. YANG. J. Am. Chem. Soc. **85**, 2124 (1963); (*b*) M. FLEISCHMANN and D. PLETCHER. Tetrahedron Lett. **60**, 6255 (1968).
26. D. D. M. WAYNER, D. J. MCPHEE, and D. GRILLER. J. Am. Chem. Soc. **110**, 132 (1988).
27. (*a*) J. Y. LAN and G. B. SCHUSTER. Tetrahedron Lett. **27**, 4261 (1986); (*b*) H. FISCHER. J. Am. Chem. Soc. **108**, 3925 (1986).
28. R. O. LOUTFY and R. O. LOUTFY. Can. J. Chem. **54**, 1454 (1976).
29. (*a*) A. TERAHARA, H. OHYA-NISHIGUCHI, N. HIROTA, and A. OKU. J. Phys. Chem. **90**, 1564 (1986); (*b*) O. W. HOWARTH and G. K. FRAENKEL. J. Chem. Phys. **52**, 6258 (1970); (*c*) T. BALLY, K. ROTH, and R. STRAUB. J. Am. Chem. Soc. **110**, 1639 (1988).
30. A. OKAMOTO, M. S. SNOW, and D. R. ARNOLD. Tetrahedron, **42**, 6175 (1986).
31. K. LAALI, R. J. GERZINA, C. M. FLANIK, C. M. GERIC, and A. M. DOMBROSKI. Helv. Chim. Acta, **70**, 706 (1987).
32. I. HOPPE and U. SCHOLLKOPF. Liebigs. Ann. Chem. **2**, 219 (1979).
33. E. J. PANEK, B. L. NEFF, and M. G. PANEK. J. Am. Chem. Soc. **97**, 3996 (1975).
34. L. HEVESI, J. B. NAGY, A. KRIEF, and E. G. DEROUANE. Org. Magn. Reson. **10**, 14 (1977).
35. J. G. DUBOUDIN and B. JOUSSEAUME. J. Organomet. Chem. **162**, 209 (1978).
36. U. VOGELI and W. VON PHILIPSBORN. Org. Magn. Reson. **7**, 617 (1975).
37. S. WAZONEKS, B. J. STUDNICHA, and A. R. ZIGMAN. J. Org. Chem. **34**, 1316 (1969).
38. J. KLEIN, A. MEDLIK-BALAN, A. Y. MEYER, and M. CHOREV. Tetrahedron, **32**, 1839 (1976).
39. K. MURATO, T. YATSUNAMI, and S. IWASAKI. Helv. Chim. Acta, **63**, 588 (1980).
40. E. WENKERT and T. W. FERREIRA. Organometallics, **1**, 1670 (1982).

Can. J. Chem. Downloaded from www.nrcresearchpress.com by 41.223.56.140 on 09/07/12
For personal use only.

Oxidation of allyl and benzyl ethers by 2,3-dichloro-5,6-dicyanobenzoquinone (DDQ)

E. LEE-RUFF AND F. J. ABLENAS
Department of Chemistry, York University, North York, Ont., Canada M3J 1P3

Received April 4, 1988[1]

E. LEE-RUFF and F. J. ABLENAS. Can. J. Chem. **67**, 699 (1989).

Benzylic and allylic ethers are oxidized by 2,3-dichloro-5,6-dicyanobenzoquinone (DDQ) to give the corresponding carbonyl containing compounds (aldehydes and ketones) and alcohols. The reaction proceeds readily with ethers bearing activating groups. Primary ethers are further oxidized with excess DDQ giving the corresponding esters. Mechanisms for these processes are proposed, based on nuclear magnetic resonance and stoichiometric analyses.

Key words: dehydrogenation, allylic and benzylic ethers.

E. LEE-RUFF et F. J. ABLENAS. Can. J. Chem. **67**, 699 (1989).

L'oxydation d'éthers benzyliques et allyliques par la dichloro-2,3 dicyano-5,6 benzoquinone (DDQ) fournit les composés carbonylés correspondants (aldéhydes et cétones) ainsi que les alcools. La réaction se produit facilement avec les éthers portant des groupements activants. Sous l'influence d'un excès de DDQ, les éthers primaires subissent une oxydation plus poussée conduisant aux esters correspondants. En se basant sur les spectres en résonance magnétique nucléaire et sur des analyses stoechiométriques, on propose des mécanismes pour ces processus.

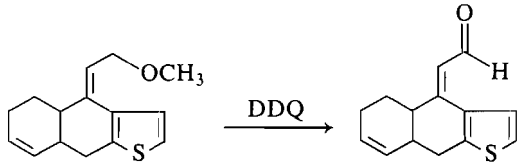
Mots clés : déhydrogenation, éthers benzyliques et allyliques.

[Traduit par la revue]

Can. J. Chem. Downloaded from www.nrcresearchpress.com by 41.223.56.140 on 09/07/12
For personal use only.

Introduction

The use of 2,3-dichloro-5,6-dicyanobenzoquinone (DDQ) (1, 2) in the dehydrogenation of annelated cyclohexanes to give polycyclic benzenoid derivatives is the method of choice principally because of the relatively mild conditions compared to other dehydrogenation agents. The oxidation proceeds by a mechanism thought to involve initial hydride abstraction (1*b*, *c*) to generate a stabilized benzylic or allylic cation, followed by loss of a proton and concomitant formation of reduced 2,3-dichloro-5,6-dicyanohydroquinone, which usually precipitates out of solution in nonpolar solvents. Evidence for such an ionic mechanism has been obtained from trapping of the intermediate carbocations with nucleophilic solvents such as water (3) and methanol (4). In our investigations on the preparation of polynuclear aromatic hydrocarbons incorporating thiophene rings (5) we observed that, upon attempted dehydrogenation of the tetrahydro naphthothiophene **1** with DDQ, the only product formed was the unsaturated aldehyde **2**. Although oxidations of allylic alcohols with DDQ have been observed (6, 7), the conversion of **1** and **2** by DDQ represents formally a demethanation reaction that to our knowledge is unprecedented in quinone chemistry. Recently Yonemitsu and co-workers (8, 9) have shown that the 4-methoxybenzyl group can be used as a protecting group for hydroxy functions with selective deprotection taking place in the presence of DDQ and water. However, no mechanistic details were provided in these studies. To investigate the scope and limitation of this unusual oxidation we carried out a systematic study of the DDQ reaction with representative benzylic and allylic ethers.



1 **2**

[1]Revision received December 14, 1988.

Results and discussion

In addition to the allyl methyl ether **1** used in the study, the following allylic and benzylic ethers were investigated: benzyl methyl ether (**3**), benzyl ethyl ether (**4**), *trans*-cinnamyl methyl ether (**5***a*), *trans*-cinnamyl benzoate (**5***b*), *trans*-cinnamyl benzyl ether (**5***c*), *trans*-cinnamyl trityl ether (**5***d*), 1,1-phenylmethoxyethane (**6**), methyl 4-methoxy-2-butenoate (**7**), thiophenoxymethyl methyl ether (**8**), 1,2-phenylmethoxyethane (**9**), *p*-nitrobenzyl methyl ether (**10**), and 3-methoxycyclohexene (**11**). The reactions were carried out in toluene solution heated to reflux or in carbon tetrachloride at room temperature. The details of individual reactions are tabulated in Table 1. All of the products were compared with known compounds. Although these reactions formally represent oxidative dealkylations, the alkyl group is transformed to its alcohol in the products as seen from the reactions of **5***b–d*. Although the presence of methanol could be confirmed by nmr spectroscopy from the reactions of the methyl ethers, its isolation was difficult due to losses in the work-up procedures. It is noteworthy that the oxidations proceed with allyl and benzyl ethers that do not possess electron-withdrawing groups, as can be seen from the absence of oxidation products in the cases of **7** and **10**.

Furthermore, the inertness of **7**, **9**, and **10** to oxidation suggests that the initial hydride abstraction and formation of a carbocation is rate determining. To shed some light on the mechanism and establish the fate of the methyl group during the oxidation of the methyl allyl/benzyl ethers with DDQ we carried out a systematic nmr investigation of ether **5***a*, which was found to be most reactive in this series and gave smooth conversion at room temperature.

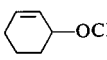
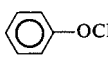
The ^{1}H nmr spectrum of a $CCl_4/CDCl_3$ solution containing *trans*-cinnamyl methyl ether (20 mM) and DDQ (20 mM) was observed at room temperature. The spectrum after 1 h showed a small amount of cinnamaldehyde (17%) in addition to signals corresponding to an acetal **13**. The presence of cinnamaldehyde was significantly diminished upon the addition of ground and freshly activated 4 Å molecular sieves.

The assignment of the mixed acetal was based on the splitting pattern of the acetal and vinylic protons at 5.8 (J=5.8 Hz)

TABLE 1. Results of DDQ oxidation of allyl/benzyl methyl ethers

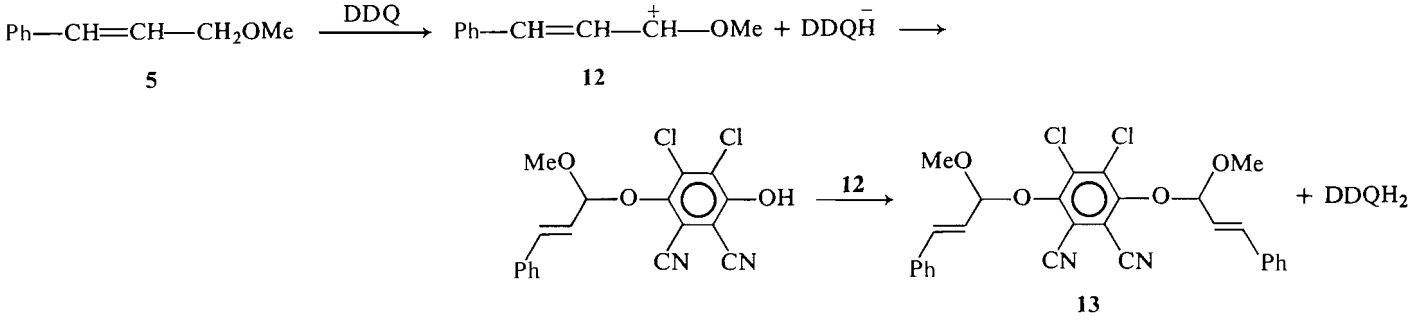
$$Z\text{—}CH_2\text{—}OCH_3 \xrightarrow[(2)\ H_2O]{(1)\ DDQ/PhMe,\ \Delta} Z\text{—}CHO$$

Z = aryl or vinyl substituent

Ether	Reaction conditions	Product (yield)
1	Reflux, 2 h	**2** (52)[a]
Ph—CH_2OCH_3 (**3**)	Reflux, 5 h	Ph—CHO (75)[e,f]
Ph—CH_2—O—CH_2CH_3 (**4**)	Reflux, 5 h	Ph—CHO (37)[b]
t—Ph—CH=CH_2OCH_3 (**5***a*)	CCl_4/r.t./3 h	*t*—Ph—CH=CH—CHO (85)[c,e,f]
t—Ph—CH=CH—CH_2OCH_3 (**5***a*)	Chloranil/PhMe/reflux, 4 h	*t*—Ph—CH=CH—CHO (54)[c]
t—Ph—CH=CH—CH_2OCPh (**5***b*)	CCl_4/r.t./3 h	Cinnamaldehyde (61)[e,f] + $PhCO_2H$ (72)[e,f]
t—Ph—CH=CH—CH_2OCH_2Ph (**5***c*)	CCl_4/r.t./3 h	Cinnamaldehyde (68) + $PhCH_2OH$ (53)[e,f]
t—Ph—CH=CH—$CH_2OC(Ph)_3$ (**5***d*)	CCl_4/r.t./3 h	Cinnamaldehyde (69) + $(Ph)_3COH$ (87)[e,f,g]
Ph·$CH(CH_3)OCH_3$ (**6**)	Reflux, 22 h	Ph—CO—CH_3 (58)[d,e,f]
Ph·$CH(CH_3)OCH_3$ (**6**)	1,4—Dioxan/reflux, 5 h	N.R.
$MeOCH_2CH$=$CHCO_2Me$ (**7**)	Reflux, 20 h	N.R.
Ph—S—CH_2OCH_3 (**8**)	Reflux, 22 h	N.R.
Ph—CH_2CH_2—OCH_3 (**9**)	Reflux, 5 h	N.R.
p—NO_2—C_6H_4—CH_2OCH_3 (**10**)	Reflux, 3 h	N.R.
 (**11**)	Reflux, 3 h	 (50)[c]

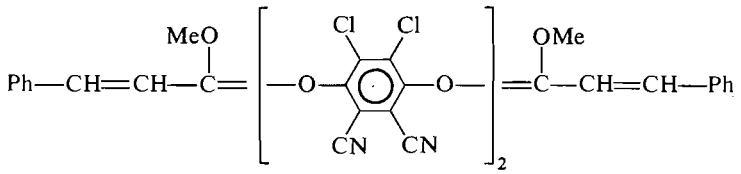
[a]Structure tentatively assigned on the basis of ir, nmr, and mass spectral data.
[b]Product aldehyde isolated as bisulfite addition compound.
[c]Yield estimated by ^{1}H nmr spectroscopy after aqueous work-up.
[d]Conversion was 77% based on unreacted starting material.
[e]Product identified by comparison of ^{1}H nmr and ir spectra with those of an authentic sample.
[f]Product identified by tlc comparison to authentic standard.
[g]Recrystallized product had mp identical with that reported in the literature.

Can. J. Chem. Downloaded from www.nrcresearchpress.com by 41.223.56.140 on 09/07/12
For personal use only.

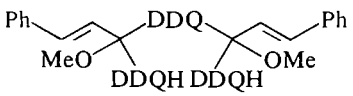


SCHEME 1

(H—C—O), 6.1, and 6.7 ppm respectively, and comparison of these with acetal **14** prepared independently. The methoxy protons of **13** appeared as a pair of singlets at 3.35 and 3.40 ppm. The relative integration of the methoxyl to acetal proton signals was approximately 3:1. Comparison of the spectral data of the reaction mixture with authentic **14** rules out the presence of the dimethyl acetal **14**. Furthermore, only one half of the expected reduced $DDQH_2$ precipitated from solution at this point in time, although the reduction product $DDQH_2$ is insoluble in carbon tetrachloride. This observation, along with the formation of a major product containing an acetal proton as seen by ^{1}H nmr, suggests that one half equivalent of DDQ is covalently bound to the oxidized substrate. Attempted isolation and purification of acetal **13** by chromatography led to its hydrolysis to *trans*-cinnamaldehyde and $DDQH_2$ (~½ equiv.). Increasing the initial concentration of DDQ to 1.8 equivalents (36 mM) resulted in the formation of methyl *trans*-cinnamate in addition to cinnamaldehyde. (This ester was also obtained in 12% yield as a by-product from the oxidation of the ether **5***a* with 1.1 equivalents of DDQ.) Following this reaction mixture by ^{1}H nmr spectroscopy, we observed another transient with peaks at 3.24 ppm (OCH_3) and an AB pattern at 5.9 and 6.9 ppm. This



15



16

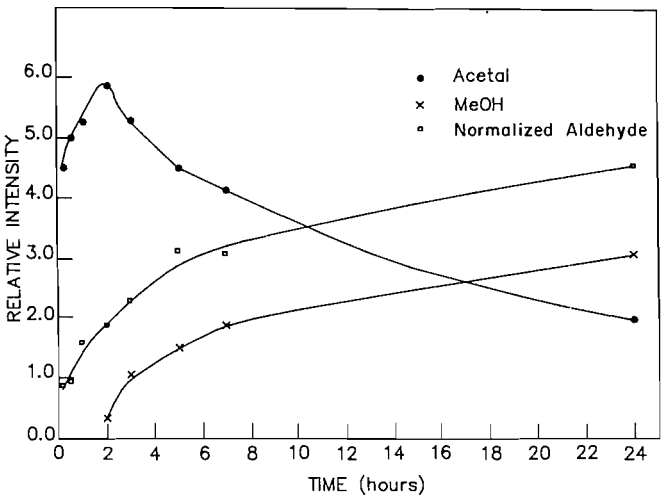


FIG. 1. Reaction profile for DDQ/ether **5***a* = 1:1 equiv.

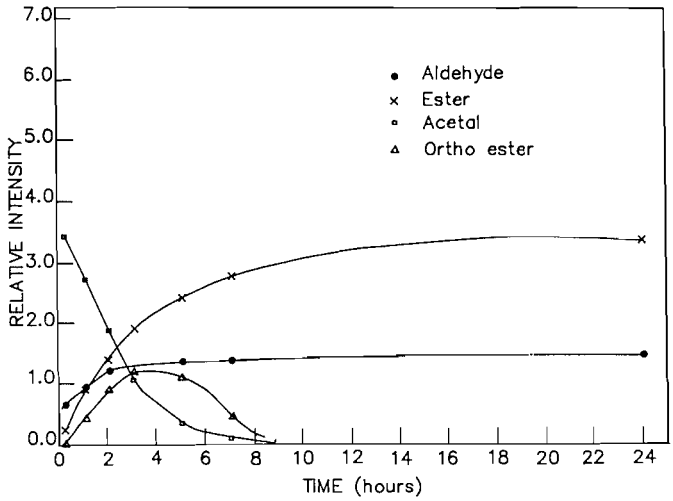


FIG. 2. Reaction profile for DDQ/ether **5***a* = 1.8:1 equiv.

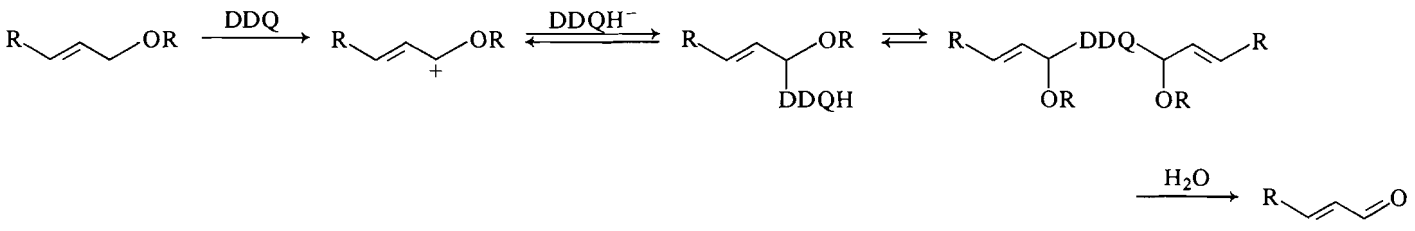
transient has been tentatively assigned the structure of the ortho ester **15**. No signal associated with an acetal proton was observed in this case. The relative integration of the methoxy signal (3.43) to the vinyl signal (AB 5.9 ppm or 6.9 ppm) was approximately 3;1. These data do not preclude structures such as **16** as the transient species although the OH signals associated with **16** were not discernible in the ^{1}H nmr spectrum.

This transient upon prolonged reaction (and, ostensibly, hydrolysis) gave methyl cinnamate. Kinetic profiles based on nmr time-resolved spectra of the reaction mixtures containing 1:1 and 1.8:1 molar ratios of DDQ and ether **5** are shown in Figs. 1 and 2 respectively. It can be seen in Fig. 1 that the concentration of the acetal **13** peaks at about 2 h and then decreases with accompanying increase in formation of both methanol and cinnamaldehyde. In Fig. 2 the concentration of acetal **13** peaks earlier and decreases more rapidly than in Fig. 1. At the same time the transient associated with the ortho ester **15** gradually increases and peaks at 3.5 h before diminishing while the aldehyde and ester concentrations level off. These observations point to two intermediates from which the aldehyde and ester are formed. The nmr spectroscopic evidence suggests that the acetal **13** and the ortho esters **15** or **16** may be precursors to cinnamaldehyde and methyl cinnamate respectively. It is clear from the spectral data that cinnamaldehyde is not oxidized by DDQ to methyl cinnamate, but DDQ is oxidizing the acetal **13** to an ortho ester. The minor amount of cinnamaldehyde formed initially is attributed to the presence of adventitious water, which could be minimized by the addition of activated molecular sieves. This is demonstrated when the addition of D_2O to the reaction mixture results in hydrolysis of the acetal **13** to cinnamaldehyde in a separate nmr experiment. The data suggest that the oxidation of allylic/benzylic ethers by DDQ proceeds by initial and rate-determining hydride abstraction of the α-carbon (Scheme 2). This is seen from the relative reactivities of ethers possessing electron-donating and -withdrawing R substituents. Electron-deficient electrophilic R groups will deactivate this process as is seen in the inertness of ethers **7** and **10**, although the lack of reactivity of **8** is somewhat surprising. Given the failure of the reaction to occur in dioxan, it may be that the formation of a π-complex between DDQ and the Lewis base renders DDQ inactive as a dehydrogenating reagent. Furthermore, the stabilization of the resultant cation is crucial, as is observed in the unreactive nature of ether **9**. Thus oxidation of allylic or benzylic ethers by DDQ is possible, provided that no electrophilic substituent is prpesent in the conjugated chromophore and no available β-hydrogen is present. In the latter case dehydrogenation results as the dominant process, as is observed for ether **11**.

These results suggest that DDQ can be used as an alternative method for the deprotection of benzyl ethers under neutral conditions as was also shown by Yonemitsu (8, 9). Furthermore, the benzyl methyl ether function can be used as a "masked" aryl carboxaldehyde in which the methoxymethyl substituent would activate the aryl ring system and direct electrophilic substitution with a regiochemistry different from the formyl group.

These results also indicate that electron-rich allyl alcohols or

Can. J. Chem. Downloaded from www.nrcresearchpress.com by 41.223.56.140 on 09/07/12
For personal use only.



SCHEME 2

unsaturated aldehydes (via acetals) can be oxidized to aldehydes and esters with DDQ, without the competing degradative oxidation that is frequently a complication with the use of chromium-(VI) reagents.

Experimental

The ^{1}H nmr spectra were recorded in $CDCl_3$ or CCl_4 solution with TMS as an internal reference on a Bruker AM-300 nmr spectrometer. Infrared spectra were recorded neat on NaCl discs on a Unicam SP1000 instrument, low resolution mass spectra were obtained on a VG Micromass 16F instrument, and high resolution mass spectra were obtained on a VG ZAB-E instrument.

Anhydrous $CDCl_3$ and CCl_4 were obtained by storing these over molecular sieves for 48 h. Toluene was dried over sodium metal. Cinnamyl methyl ether (**5**) was prepared from cinnamyl alcohol (10).

General procedure for DDQ oxidations

In a typical run cinnamyl methyl ether **5***a* (157.4 mg; 1.06 mmol) and DDQ (244.5 mg, 1.08 equiv.) were dissolved in dry toluene (20 mL) and refluxed for 1.5 h. The resulting slurry was cooled, $DDQH_2$ filtered out, and the solvent removed to afford an oil, which was flash chromatographed (silica gel, dichloromethane) to afford methyl cinnamate (20.0 mg, 12%) followed by cinnamaldehyde (112.0 mg, 80%).

(8a-H-4,4a,7,8-Tetrahydronaphtho[2,3-b]thien-9-ylidene)-acetaldehyde (2)

The methyl ether **1** (62.7 mg; 0.255 mmol) was dissolved in dry toluene (50 mL) with DDQ (127.8 mg, 2.2 equiv.) and the solution refluxed 2 h. The solution was cooled, concentrated, and flash chromatographed (silica gel, dichloromethane) to afford the aldehyde as the only product, **2** (30.6 mg, 52%); ir ν_{NaCl}:1680 (C=O) cm^{-1}; ^{1}H nmr δ:10.20, d(J = 6.0 Hz), CHO; 7.24, d(J = 5.2 Hz), H2; 7.13, d(J = 5.2 Hz), H1; 6.32, d(J = 6.0 Hz), Hα; 5.75–5.95, m, H5,6; 3.65, d(J = 7.5 Hz), 1H; 3.13, dd(J = 7.5,1.0 Hz), 1H; 2.60–2.80, m, 2H; 2.15–2.80, m, 2H; 1.65–2.00, m, 2H; ppm; ms m/z : 230(100), 201(84).

Nuclear magnetic resonance analysis of DDQ: ether 5a mixtures

The ether **5***a* and DDQ were mixed together in dry carbon tetrachloride to afford a 40 mM solution, which was diluted to 20 mM with deuteriochloroform. The ^{1}H nmr spectra were recorded at 23°C. The relative concentrations of the aldehyde, ester, methanol, acetal **13**, and ortho ester **15** were based on the height of the peaks (relative to $CHCl_3$) at δ 9.72, 3.81, 3.48, 3.36, and 3.24 ppm, respectively.

Cinnamaldehyde dimethyl acetal

This compound was prepared by the general procedure involving 2,2-dimethoxypropane (11) and had a bp identical to the known dimethyl acetal (12); ^{1}H nmr δ: 7.26–7.43, m, 5H; 6.73, d(J = 16.1 Hz), Hα; 6.15, dd(J = 16.1, 4.9 Hz), Hβ; 4.96, d(J = 4.9 Hz), Hγ; 3.38, s, OCH_3.

Preparation of cinnamyl trityl ether 5d (Z-3-phenyl-1-triphenylmethoxy-2-propene)

Cinnamyl alcohol (0.69 mL, 5.36 mmol) was dissolved in dry dichloromethane (10 mL) with trityl chloride (1.50 g, 1.0 equiv.) and lutidine (0.62 mL, 1.0 equiv.). The solution was stirred for 4 days, the solvent removed, and the residue recrystallized from petroleum ether-:toluene (5:1, 10 mL) to afford the trityl ether (1.04 g, 52%); mp (pet. ether) 126.5–127°C; ir ν_{CHCl_3}: 2985, 1587, 1480, 1439 cm^{-1}; ^{1}H nmr δ: 7.2–7.6 m, 20H; 6.70, d(J = 15.9 Hz), Hα; 6.20, dt (J = 15.9, 5.0 Hz), Hβ; 3.79, d(J = 5.0 Hz), CH_2; ppm; ms m/z: 244(35), 243(100, Ph_3C^+), 183(17), 149(18). *Anal.* calcd. for $C_{28}H_{24}O$: C 89.31, H 6.44; found: C 89.49, H 6.78.

Acknowledgements

We would like to thank NSERC and the Ontario Ministry of the Environment, Air Resources Branch, for their generous financial support of this project.

1. (*a*) H. BECKER. *In* The chemistry of quinonoid compounds. Part 1. *Edited by* S. Patai. Wiley, New York. 1974. p. 335; (*b*) P. P. FU and R. G. HARVEY. Chem. Rev. **78**, 317 (1978); (*c*) E. A. BRAUDE, L. M. JACKMAN, and R. P. LINSTEAD. J. Chem. Soc. 3548 (1954).
2. A. B. TURNER. *In* Synthetic reagents. Vol. 4. *Edited by* J. S. Pizey. Wiley, New York. 1977. p. 193.
3. H. LEE and R. G. HARVEY. J. Org. Chem. **48**, 749 (1983).
4. C. CORTEZ, K. B. SUKUMARAN, and R. G. HARVEY. J. Org. Chem. **44**, 4265 (1979).
5. E. LEE-RUFF and F. J. ALBENAS. Can. J. Chem. **65**, 1663 (1987).
6. A. BOWERS, P. G. HOLTON, E. NECOECHEA, and F. A. KINCL. J. Chem. Soc. 4057 (1961).
7. J. W. FINDLAY and A. B. TURNER. Chem. Ind. (London), 158 (1970).
8. Y. OIKAWA, T. YOSHIOKA, and O. YONEMITSU. Tetrahedron Lett. 885 (1982).
9. N. NAKAJIMA, T. HAMADA, T. TANAKA, Y. OIKAWA, and O. YONEMITSU. J. Am. Chem. Soc. **108**, 4645 (1986).
10. H. BEAUFOUR. Bull. Soc. Chim. Fr. **11**, 648 (1904).
11. H. E. BAUMGARTEN (*Editor*). Organic syntheses. Vol. V. John Wiley & Sons, New York. 1973. p. 292.
12. Beilsteins Handbuch der Organischen Chemie. B VII. Edwards Brothers Inc., Ann Arbor, MI. 1943. p. 643.

Can. J. Chem. Downloaded from www.nrcresearchpress.com by 41.223.56.140 on 09/07/12
For personal use only.

Structure of the lipopolysaccharide O-antigen of *Actinobacillus (Haemophilus) pleuropneumoniae* serotype 6 (ATCC 33590)[1]

ELEONORA ALTMAN, JEAN-ROBERT BRISSON, AND MALCOLM B. PERRY[2]
Division of Biological Sciences, National Research Council, Ottawa, Ont., Canada K1A 0R6

Received October 11, 1988

ELEONORA ALTMAN, JEAN-ROBERT BRISSON, and MALCOLM B. PERRY. Can. J. Chem. **67**, 703 (1989).

One- and two-dimensional high resolution ^1H and ^{13}C nuclear magnetic resonance spectroscopy at 500 MHz and 125 MHz together with methylation and partial hydrolytic degradation methods were used to determine the structure of the antigenic O-polysaccharide produced by *Actinobacillus (Haemophilus) pleuropneumoniae* serotype 6 (ATCC 33590). The O-polysaccharide was shown to be a high molecular weight unbranched linear polymer of repeating pentasaccharide units having the structure: →3)-α-D-Glc*p*-(1→2)-β-D-Gal*f*-(1→6)-α-D-Glc*p*-(1→6)-β-D-Glc*p*-(1→3)-β-D-Gal*f*-(1→.

Key words: *Actinobacillus pleuropneumoniae*, lipopolysaccharide, O-antigen, nuclear magnetic resonance.

ELEONORA ALTMAN, JEAN-ROBERT BRISSON et MALCOLM B. PERRY. Can. J. Chem. **67**, 703 (1989).

On a fait appel à la résonance magnétique nucléaire mono- et bi-dimensionnelle du ^1H et du ^{13}C, à 125 et à 500 MHz, ainsi qu'à des méthodes de méthylation et de dégradation par hydrolyse partielle pour déterminer la structure du polysaccharide antigénique qui est produit par l'*Actinobacillus (Haemophilus) pleuropneumoniae* du sérotype 6 (ATCC 33590). On a démontré que le O-polysaccharide est un polymère linéaire, de haut poids moléculaire et sans ramifications, formé d'unités d'un pentasaccharide possédant la structure suivante : →3)-α-D-Glc*p*-(1→2)-β-D-Gal*f*-(1→6)-α-D-Glc*p*-(1→6)-β-D-Glc*p*-(1→3)-β-D-Gal*f*-(1→.

Mots clés : *Actinobacillus pleuropneumoniae*, lipopolysaccharide, O-antigène, résonance magnétique nucléaire.

[Traduit par la revue]

Can. J. Chem. Downloaded from www.nrcresearchpress.com by 41.223.56.140 on 09/07/12
For personal use only.

Introduction

Actinobacillus (Haemophilus) pleuropneumoniae is an important primary bacterial pathogen causing contagious pleuropneumonia in pigs. The organism is encapsulated and 10 serotypes based on the structurally different polysaccharide capsular antigens have been identified (1–3). Two further serotypes of as yet undetermined antigenic structure have recently been added (4).

The lipopolysaccharides (endotoxin) associated with *A. pleuropneumoniae* strains have been implicated in the pathogenesis of porcine pleuropneumonia (5). Our structural studies of the antigens of the different serotypes of *A. pleuropneumoniae* have revealed the association of a unique lipopolysaccharide with each serotype, the differences residing in the structure of their respective O-polysaccharide components (6–9).

This paper records the structural analysis of the O-polysaccharide component of the lipopolysaccharide produced by *A. pleuropneumoniae* serotype 6 and relates its structure and observed serological cross reactivity (10) with that of the lipopolysaccharide produced by *A. pleuropneumoniae* serotype 3.

Experimental

Production of O-polysaccharide

Actinobacillus pleuropneumoniae serotype 6 (ATCC 33590) was grown in Bacto PPLO broth (yield 3 g wet weight/L) and the lipopolysaccharide isolated by the phenol extraction procedure as previously described (8). A solution of LPS (0.2 g) in aqueous 2% acetic acid (100 mL) was kept at 100°C for 2 h, the precipitated lipid A was removed by low speed centrifugation, and the O-polysaccharide was recovered by Sephadex G-50 gel filtration as previously described (8).

Analytical methods

Quantitative methods for glycose analysis and glc and glc–ms methods used were the same as previously described (8). Samples (0.5 mg) of oligo- and polysaccharides were hydrolyzed in sealed glass tubes with 10 M hydrochloric acid (1 mL) for 15 min at 90°C, or with 2 M hydrochloric acid (1 mL) for 17 h at 100°C, followed by concentration to dryness. Glycoses were determined by glc of their alditol acetate derivatives (11) using *myo*-inositol as an internal standard. The configuration of glycoses was established by capillary glc of their acetylated (−)-2-butyl glycosides (12). Lipids were identified by glc–ms of their methyl esters derived by sealed-tube methanolysis of samples (1 mg) with 3% methanolic HCl for 4 h at 100°C. Thin-layer chromatography was performed on silica gel (Merck) with 1-propanol – concentrated ammonia – water (6:3:1). Gel filtration was performed on columns on Sephadex G-50 (2 × 100 cm) or Bio-Gel P-2 (1.6 × 100 cm) (200–400 mesh) (Bio-Rad Labs). SDS-PAGE and methylation analyses were made under the same previously reported conditions (8).

Partial hydrolysis

A solution of the O-polysaccharide (18.6 mg) in cold aqueous 48% hydrofluoric acid (1 mL) was kept for 96 h at 4°C, then concentrated to dryness in high vacuum over NaOH. The residue was neutralized with aqueous 5% ammonium hydroxide and lyophilized. The products were fractionated by gel filtration on a column of Bio-Gel P-2.

Nuclear magnetic resonance spectroscopy

Proton-decoupled ^{13}C nmr spectra (125 MHz) were recorded at 24°C for a 25-kHz spectral width, using a $\pi/2$ pulse and a 32K data set on a Bruker AM 500 spectrometer. Chemical shifts are expressed relative to internal acetone (1%, 31.07 ppm). The ^1H nmr spectra (500 MHz) were recorded at 24°C using a spectral width of 2.5 kHz, a $\pi/2$ pulse, and a 16K data set for a digital resolution of 0.3 Hz/point. Chemical shifts are expressed relative to internal acetone (0.1%, 2.225 ppm) and coupling constants are reported in Hz. A sample of purified O-polysaccharide was passed through Chelex-100 (Bio-Rad) resin (3 mL) and then exchanged twice with D_2O (99.8%). Spectra were recorded on solutions (25 mg/mL, pD 9.0) in 99.8% D_2O (5-mm-diameter tubes).

Proton homonuclear-correlated 2D-nmr experiments COSY (13) and relay COSY (14) were performed at 24°C, using the standard software provided by Bruker (DISNMR). Quadrature detection in both dimensions was employed in the COSY experiments. The initial (t_1, t_2) matrices of 512 × 2048 data points were zero-filled to 1024 × 2048 data points to provide digital resolution of 1 Hz/point in both domains. Resolution enhancement in both domains was done by non-shifted sine bell function prior to Fourier transformation. Magnitude spectra, symmetrized about the diagonal, were used to represent the data. The number of transients per FID was 8 for the COSY experiment. The nOe experiments were performed in the difference mode with sequential

[1]Issued as N.R.C.C. No. 29942.

[2]Author to whom correspondence may be addressed.

TABLE 1. The glc–ms of the products of methylation analysis of the O-chain of *A. pleuropneumoniae* serotype 6 and its degradation products

Derivative	T_{GM}[a]	Molar ratio			
		O-LPS[b]	Oligosaccharide		
			A1	*B1*	*C1*
2-*O*-Acetyl-1,3,4,5,6-penta-*O*-methyl-D-galactitol-1-*d*	0.71	—	—	—	0.5
3-*O*-Acetyl-1,2,4,5,6-penta-*O*-methyl-D-galactitol-1-*d*	0.78	—	0.5	0.5	—
1,5-Di-*O*-acetyl-2,3,4,6-tetra-*O*-methyl-D-glucitol-1-*d*	1.00	—	1.0	1.0	1.0
1,3,4-Tri-*O*-acetyl-2,5,6-tri-*O*-methyl-D-galactitol-1-*d*	1.35	2.0	—	—	—
1,3,5-Tri-*O*-acetyl-2,4,6-tri-*O*-methyl-D-galactitol-1-*d*	1.35		—	—	—
1,2,4-Tri-*O*-acetyl-3,5,6-tri-*O*-methyl-D-galactitol-1-*d*	1.41	0.8	0.3	—	—
1,5,6-Tri-*O*-acetyl-2,3,4,-tri-*O*-methyl-D-glucitol-1-*d*	1.43	2.0	0.9	1.1	—

[a]Retention time of the derived alditol acetate relative to that of 1,5-di-*O*-acetyl-2,3,4,6-tetra-*O*-methylglucitol-1-*d*; glc capillary column fused silica OV17, 200°C (2 min) to 240°C at 1°C/min.
[b]O-polysaccharide.

irradiation of each line in a multiplet (15, 16). The total irradiation time was 400 ms. A heteronuclear ^{13}C–^{1}H shift correlation experiment was done on a Bruker AM 500 spectrometer using the CHORTLE (carbon–hydrogen correlations from one-dimensional polarization transfer spectra by least-squares analysis) techniques (17). The experiment was done at 24°C on a solution (15 mg/mL) of the O-polysaccharide in D_2O. Four proton evolution times of 0.24, 1.0, 2.4, and 3.2 ms were used with 4000 transients/FID.

Results and discussion

Extraction of *Actinobacillus pleuropneumoniae* serotype 6 cells (185 g, wet weight) by a modified lysozyme phenol–water procedure (18), followed by purification of the LPS by repeated ultracentrifugation, afforded an aqueous-phase LPS (924 mg) and a phenol-phase soluble LPS (328 mg). Both LPS preparations gave identical separation patterns on SDS-PAGE analysis (19), indicative of S-type LPS (20). However, the phenol-phase soluble LPS contained less O-chain polysaccharide (8.6%) than the aqueous phase LPS and was not examined further. Fission of the aqueous-phase soluble LPS (233 mg) with hot dilute acetic acid gave an insoluble lipid A (21 mg). Gel filtration of the water-soluble products on Sephadex G-50 afforded an O-chain polysaccharide (K_{av} 0.03, 46 mg), a core oligosaccharide (K_{av} 0.63, 24 mg), and a low-molecular-weight fraction (K_{av} 0.83, 26 mg), containing 3-deoxy-2-octulosonate.

The O-polysaccharide was contaminated by a minor quantity of previously characterized capsular polysaccharide, which was a contaminant of the LPS preparation due to its coprecipitation in the preparative ultracentrifugation. Purification of the O-chain was achieved by ion-exchange chromatography on DEAE-Sephacel; the O-polysaccharide was eluted at the void volume, whereas the capsular polysaccharide (21) was eluted with ≈0.1 M sodium chloride.

The purified O-polysaccharide was readily soluble in water and had $[\alpha]_D$ +30° (*c* 0.75, water) (*Anal.* found: C 41.38, H 5.99, N 0.90, ash 2.5%). On the basis of pc and glc of the derived alditol acetates and the acetylated derivatives of their (−)-2-butyl glycosides, the O-polysaccharide was found to be composed of D-glucose and D-galactose in the molar ratio ≈ 3:2. The ^{1}H nmr spectrum (500 MHz, 24°C) of the O-chain polysaccharide contained five signals for anomeric protons at δ 5.26 (d, 1H, $J_{1,2}$ 0.8 Hz), 5.16 (d, 1H, $J_{1,2}$ 1.6 Hz), 5.05 (d, 1H, $J_{1,2}$ 3.7 Hz), 4.95 (d, 1H, $J_{1,2}$ 3.7 Hz), and 4.67 ppm (d, 1H, $J_{1,2}$ 7.9 Hz). Consistent with these results, the ^{13}C nmr spectrum (125 MHz, 24°C) contained signals for anomeric carbons at δ 109.6, 107.0, 103.1, 98.9, and 98.8 ppm. The methylated and hydrolyzed O-chain afforded a product that, after reduction ($NaBD_4$) and acetylation, gave glc–ms results (Table 1) that indicated that the O-chain of *A. pleuropneumoniae* serotype 6 is composed of linear pentasaccharide repeating units containing →3)-D-Gal*f*-(1→,→3)-D-Glc*p*-(1→,2→)-D-Gal*f*-(1→, and →6)-D-Glc*p*-(1→ (1:1:1:2) residues. The methylation data showed that two D-galactose residues were furanoid, a conclusion substantiated by the observed characteristic signals for anomeric carbons at δ 109.6 and 107.0 ppm in the ^{13}C nmr spectrum, and two signals at δ 5.26 and 5.16 ppm in the anomeric region of the ^{1}H nmr spectrum of the O-polysaccharide. Both ^{1}H nmr and ^{13}C nmr spectra of the O-chain showed a close similarity to the spectra of the O-chain of the LPS *A. pleuropneumoniae* serotype 3, which is composed of a repeating pentasaccharide unit containing two galactofuranosyl residues (8). However, as expected from the composition and methylation analyses, the O-chain of *A. pleuropneumoniae* serotype 6 contains a second 1,6-linked glucopyranosyl residue instead of a 1,6-linked galactopyranosyl residue, present in the O-chain of *A. pleuropneumoniae* serotype 3 (8).

Assignments of the proton resonances were made from COSY (13) (Fig. 1) and relayed COSY (14) experiments. The residues in the O-chain polysaccharide were arbitrarily labelled a–e according to the decreased order of the chemical shifts of the H-1 resonances. Following the cross-peaks, the majority of the proton resonances were readily assigned (Table 2). The heteronuclear shift-correlated experiment (CHORTLE (17)) enabled unambiguous assignments of all the carbon resonances in the repeating unit of the O-polysaccharide (Table 3). Comparison of the ^{1}H and ^{13}C nmr spectra of the *A. pleuropneumoniae* serotype 3 (8) and serotype 6 O-chains (Tables 2 and 3) shows a striking similarity in the chemical shifts with the exception of the resonances of unit **d** (6-linked α-D-glucopyranosyl). These spectral features suggest that the linear sequence found for the *A. pleuropneumoniae* serotype 3 O-polysaccharide was maintained in the O-chain of the *A. pleuropneumoniae* serotype 6.

Since all proton resonances were assigned it was possible to determine the monosaccharide sequence by one-dimensional nOe difference experiments (15, 16). Irradiation of each anomeric resonance gave an intraresidue nOe, which provided linkage information (Fig. 2) and established the linkage sequence **a**→**c**→**b**→**d**→**e**→. In the case of unit **e**, saturation of

Can. J. Chem. Downloaded from www.nrcresearchpress.com by 41.223.56.140 on 09/07/12
For personal use only.

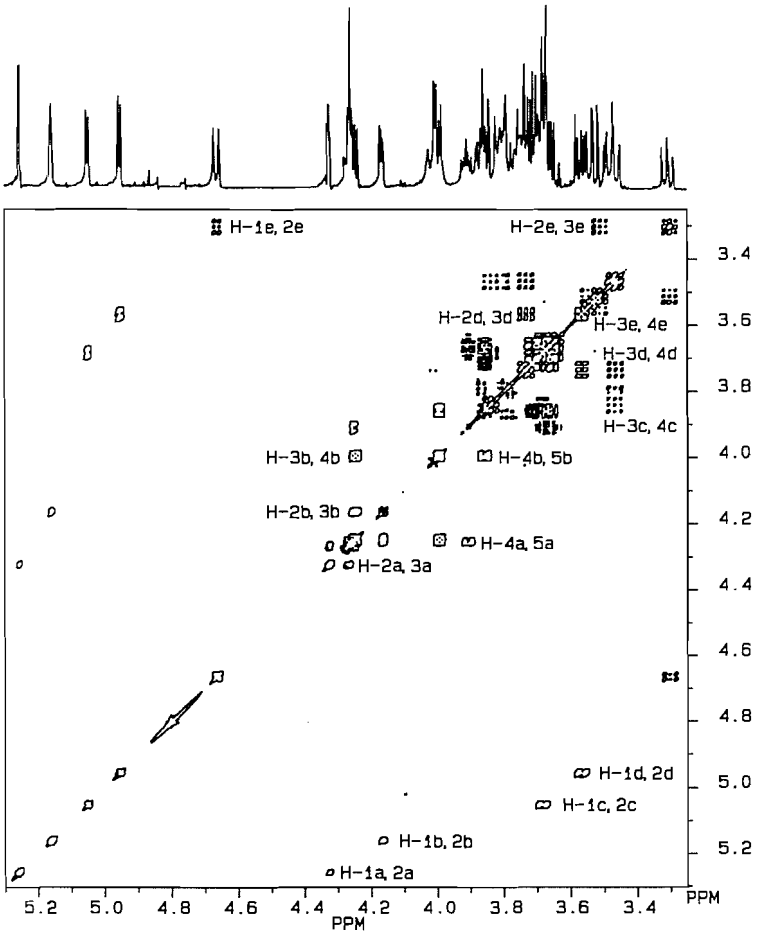


FIG. 1. COSY contour plot of the complete ^{1}H nmr spectrum (5.30–3.25 ppm) of *A. pleuropneumoniae* serotype 6 O-polysaccharide recorded at 24°C. The 1-D spectrum is displayed along the F_2 axis.

TABLE 2. ^{1}H chemical shifts[a] for the O-chain polysaccharide of *Actinobacillus pleuropneumoniae* serotype 6

Proton	Unit **a** →3)-β-D-Gal*f*-(1→	Unit **b** →2)-β-D-Gal*f*-(1→	Unit **c** →3)-α-D-Glc*p*-(1→	Unit **d** →6)-α-D-Glc*p*-(1→	Unit **e** →6)-β-D-Glc*p*-(1→
H-1	5.256 (0.8)[b]	5.160 (1.6)	5.051 (3.7)	4.954 (3.7)	4.665 (7.9)
H-2	4.33	4.17	3.68	3.57	3.30
H-3	4.27	4.24	3.84	3.75	3.51
H-4	4.26	4.00	3.47	3.47	3.57
H-5	3.91	3.85	3.80	3.80	3.68
H-6	3.69	3.71	3.87	3.75	3.74
H-6′	3.66	3.67	3.78	4.02	4.00

[a]In ppm measured at 24°C in D_2O with acetone 0.1% as the internal reference (2.225 ppm).
[b]$J_{1,2}$ in hertz.

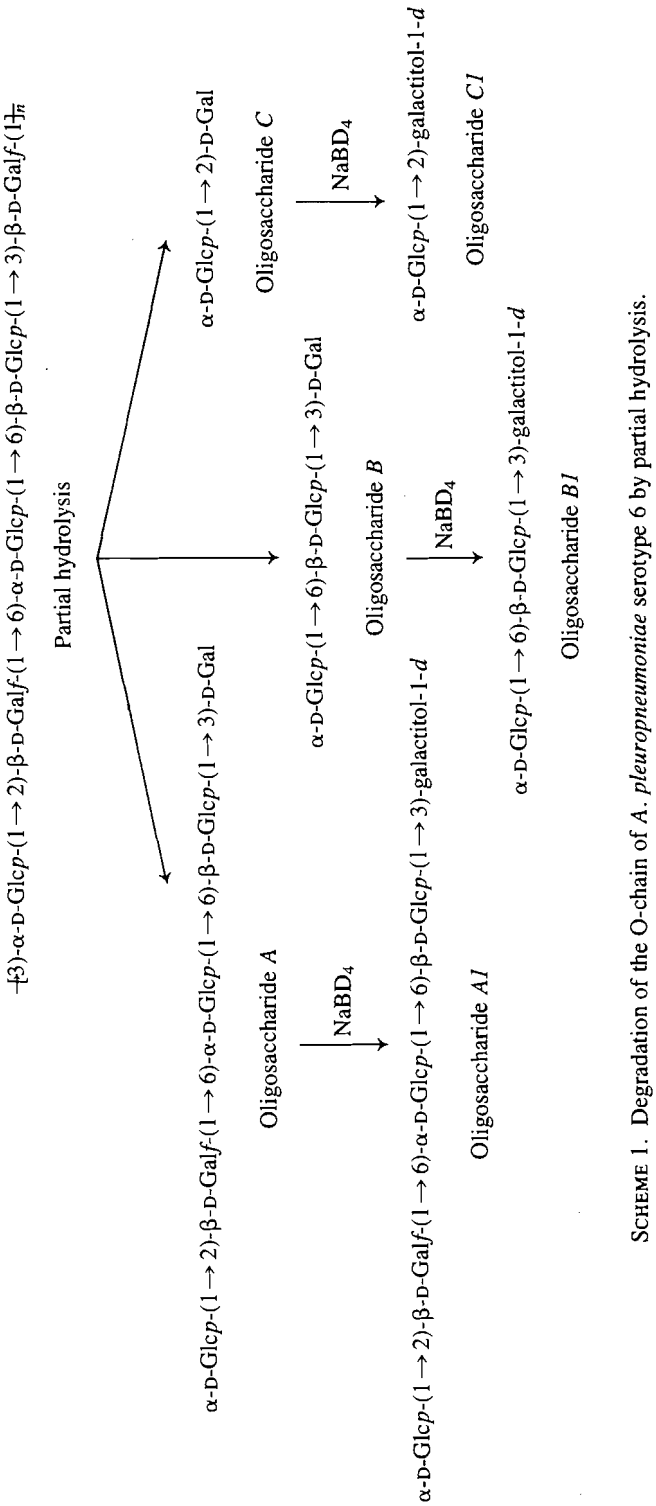
TABLE 3. ^{13}C chemical shifts[a] of the O-chain polysaccharide[b] from *Actinobacillus pleuropneumoniae* serotype 6 at 27°C

Carbon atom	Unit **a** →3)-β-D-Gal*f*-(1→	Unit **b** →2)-β-D-Gal*f*-(1→	Unit **c** →3)-α-D-Glc*p*-(1→	Unit **d** →6)-α-D-Glc*p*-(1→	Unit **e** →6)-β-D-Glc*p*-(1→
C-1	109.6	107.0	98.9	98.8	103.1
C-2	80.5	87.4	72.0	72.3	73.8
C-3	85.9	76.1	80.3	73.9	76.6
C-4	83.1	82.8	68.7	70.4	70.1
C-5	71.3	71.2	73.1	71.6	75.2
C-6	63.9	63.7	61.4	67.1	66.2

[a]In ppm from internal acetaone (1%, 31.07 ppm).
[b]Assignments confirmed by CHORTLE experiment.

Can. J. Chem. Downloaded from www.nrcresearchpress.com by 41.223.56.140 on 09/07/12
For personal use only.

Can. J. Chem. Downloaded from www.nrcresearchpress.com by 41.223.56.140 on 09/07/12
For personal use only.



SCHEME 1. Degradation of the O-chain of *A. pleuropneumoniae* serotype 6 by partial hydrolysis.

the H-1**e** resonance (Fig. 2E) produced intraresidue nOe's to both H-2**a** and H-3**a**; however, the methylation and ^{13}C nmr data required that the unit **e** was linked 1,3 to a β-D-galactofuranosyl residue, unit **a**.

Further proof of the proposed structure was obtained from partial hydrolysis of the O-chain with aqueous 48% hydrofluoric acid, followed by gel filtration on Bio-Gel P-2, which afforded oligosaccharides *A*, *B*, and *C* (Scheme 1). Oligosaccharide *C* (K_{av} 0.80) had $[\alpha]_D$ +108.5° (*c* 0.19, water) and gave a single spot in tlc (R_f 0.31). Reduction of *C* with $NaBD_4$ afforded oligosaccharide *C1*, which, on hydrolysis and glc–ms of the derived alditol acetates, was shown to contain D-glucose and galactitol-1-*d* in the molar ratio 1:1; nmr data: ^1H (500 MHz, 24°C), δ: 5.47 (d, 0.3H, $J_{1,2}$ 3.6 Hz, H-1α), 5.38 (d, 0.7H, $J_{1,2}$ 3.9 Hz, H-1′), 5.10 (d, 0.3H, $J_{1,2}$ 3.8 Hz, H-1′), 4.74 (d, 0.7H, $J_{1,2}$ 8.4 Hz, H-1β) ppm; ^{13}C (125 MHz, 27°C), δ: 98.8 (0.6C), 97.5 (0.4C), 97.1 (0.6C), and 90.5 (0.4C) ppm. The glc–ms of methylated *C1* (Table 1, column IV) in conjunction with the ^1H and ^{13}C nmr data indicated *C* to be α-D-Glc*p*-(1→2)-D-Gal.

Oligosaccharide *B* (K_{av} 0.67) had $[\alpha]_D$ +52.3° (*c* 0.24, water) and gave a single spot on tlc (R_f 0.15). Reduction of *B* with $NaBD_4$ gave oligosaccharide *B1*, which, by glc–ms of the derived alditol acetates, was shown to be a trisaccharide composed of D-glucose and galactitol-1-*d* in the molar ratio 2:1; nmr data: ^1H (500 MHz, 24°C), δ: 5.28 (d, 0.3H, $J_{1,2}$ 3.5 Hz, H-1α), 4.96 (d, 1H, $J_{1,2}$ 3.9 Hz), 4.71 (d, 1H, $J_{1,2}$ 7.7 Hz), 4.63 (d, 0.7H, $J_{1,2}$ 7.9 Hz, H-1β) ppm; ^{13}C (125 MHz, 27°C), δ: 104.7 (1C), 98.8 (1C), 97.1 (0.6C), 93.0 (0.4C) ppm. The glc–ms analysis of methylated *B1* (Table 1) together with the ^1H and ^{13}C nmr data indicated *B* to be α-D-Glc*p*-(1→6)-β-D-Glc*p*-(1→3)-D-Gal.

Oligosaccharide *A* (K_{av} 0.43) had $[\alpha]_D$ +37.9° (*c* 0.33, water) and gave a single spot of tlc (R_f 0.07). Reduction of *A* with $NaBD_4$ gave oligosaccharide *A1*, which, by glc–ms of the derived alditol acetates, was shown to be a pentasaccharide composed of D-glucose, D-galactose, and galactitol-1-*d* in the molar ratio 3:1:1; nmr data: ^1H (500 MHz, 24°C), δ: 5.28 (d, 0.3H, $J_{1,2}$ 3.3 Hz, H-1α), 5.15 (d, 1H, $J_{1,2}$ <2 Hz), 5.06 (d, 1H, $J_{1,2}$ 3.8 Hz), 4.95 (d, 1H, $J_{1,2}$ 3.8 Hz), 4.71 (d, 1H, $J_{1,2}$ 8.1 Hz), 4.63 (d, 0.7H, $J_{1,2}$ 7.9 Hz, H-1β) ppm; ^{13}C (50 MHz, 24°C), δ: 107.0 (1C), 104.7 (1C), 98.9 (1C), 98.7 (1C), 97.0 (0.7 C), 93.0 (0.3C) ppm. The glc–ms analysis of methylated *A1* (Table 1) indicated that the D-glucopyranosyl unit formed the nonreducing end of the pentasaccharide and that the D-galactose residue formed the reducing end. The prior structural identification of *B* and *C* now permits the sequence of the pentasaccharide *A* to be established as

α-D-Glc*p*-(1→2)-β-D-Gal*f*-(1→6)-α-D-Glc*p*-(1→6)-β-D-Glc*p*-(1→3)-D-Gal

The combined chemical and nmr evidence permits the structure of the O-antigen chain to be established as the linear repeating pentasaccharide unit:

→3)-α-D-Glc*p*-(1→2)-β-D-Gal*f*(1→6)-α-D-Glc*p*-(1→6)-β-D-Glc*p*-(1→3)-β-D-Gal*f*-(1→$_n$

Structural similarity between O-antigenic chains of *A. pleuropneumoniae* serotype 3 (8) and serotype 6 could account for a serological cross-reactivity between serotypes 3 and 6 (10).

Core oligosaccharide

The core oligosaccharide obtained from the aqueous-phase LPS had $[\alpha]_D$ +66° (*c* 0.55, water) and was composed of D-glucose, D-galactose, D-*glycero*-D-*manno*-heptose, and L-*glycero*-D-*manno*-heptose in the molar ratio 1.1:1.0:0.6:1.0.

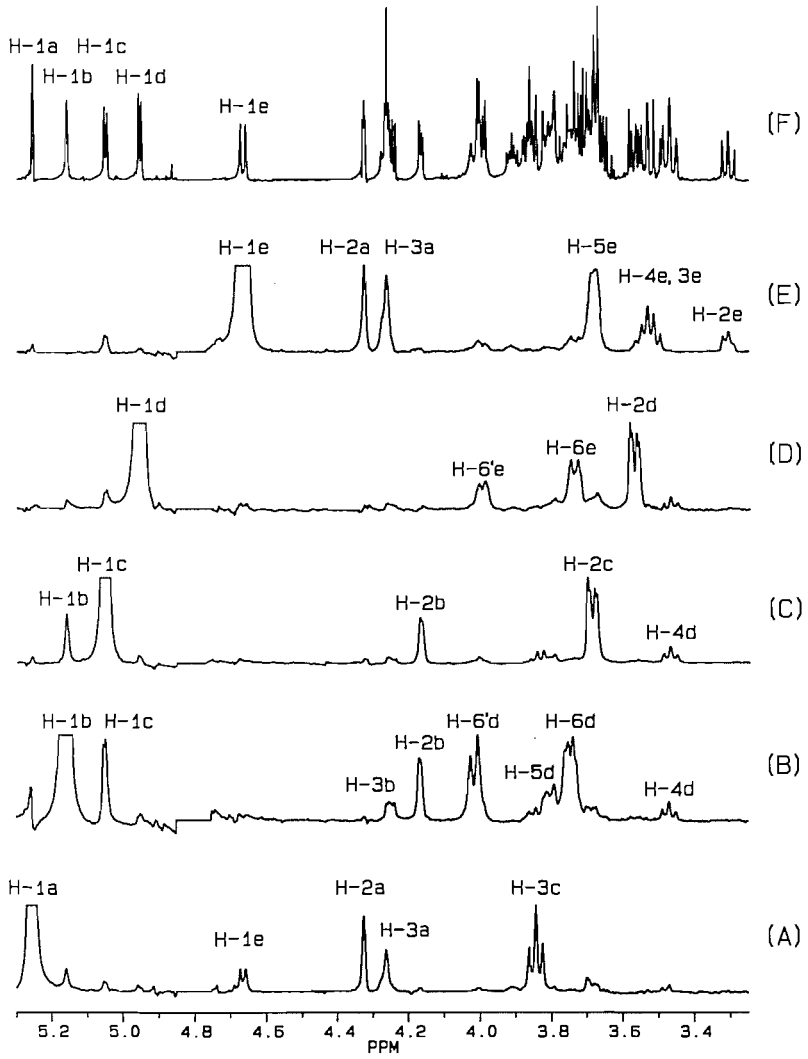


FIG. 2. The nOe difference ^{1}H nmr spectra for the *A. pleuropneumoniae* serotype 6 O-polysaccharide on saturation of the resonances: (A) H-1**a**, (B) H-1**b**, (C) H-1**c**, (D) H-1**d**, (E) H-1**e**, and (F) an off-resonance control spectrum, measured at 24°C.

Lipid A

Methanolysis of lipid A followed by glc–ms (programme C) showed the lipid A of the aqueous-phase LPS to be composed of the following fatty acids: 3-hydroxydodecanoic acid (1.2%), *n*-tetradecanoic acid (39.7%), *cis*-9-tetradecenoic acid (2.4%), 3-hydroxytetradecanoic acid (55.6%), and *n*-hexadecanoic acid (1.1%).

Acknowledgements

We thank Mr. F. P. Cooper for the glc–ms and Mr. D. W. Griffith for the large-scale production of cells.

1. A. GUNNARSSON, E. L. BIBERSTEIN, and B. HURRELL. Am. J. Vet. Res. **38**, 1111 (1977).
2. S. ROSENDAL and D. A. BOYD. J. Clin. Microbiol. **16**, 840 (1982).
3. R. NIELSEN and P. J. O'CONNOR. Acta Vet. Scand. **25**, 96 (1984).
4. R. NIELSEN. Acta Vet. Scand. **27**, 453 (1987).
5. H. HANI, H. KONIG, J. NICOLET, and E. SCHOLL. Schweiz. Arch. Tierheilkd. **115**, 191 (1973).
6. E. ALTMAN, J.-R. BRISSON, and M. B. PERRY. Biochem. Cell Biol. **64**, 1317 (1986).
7. E. ALTMAN, J.-R. BRISSON, and M. B. PERRY. Biochem. Cell Biol. **65**, 876 (1987).
8. E. ALTMAN, J.-R. BRISSON, and M. B. PERRY. Carbohydr. Res. **179**, 245 (1988).
9. E. ALTMAN, M. B. PERRY, and J.-R. BRISSON. Carbohydr. Res. In press.
10. K. R. MITTAL, R. HIGGINS, and S. LARIVIERE. J. Clin. Microbiol. **26**, 985 (1988).
11. S. W. GUNNER, J. K. N. JONES, and M. B. PERRY. Can. J. Chem. **39**, 1892 (1961).
12. K. LEONTEIN, B. LINDBERG, and J. LONNGREN. Carbohydr. Res. **62**, 359 (1978).
13. A. BAX, R. FREEMAN, and G. MORRIS. J. Magn. Reson. **42**, 164 (1981).
14. A. BAX and G. DROBNY. J. Magn. Reson. **61**, 306 (1985).
15. D. NEUHAUS. J. Magn. Reson. **53**, 109 (1983).
16. M. KINNS and J. K. M. SANDERS. J. Magn. Reson. **56**, 518 (1984).
17. G. A. PEARSON. J. Magn. Reson. **64**, 487 (1985).
18. K. G. JOHNSON and M. B. PERRY. Can. J. Microbiol. **22**, 29 (1976).
19. G. M. TSAI and C. E. FRASCH. Anal. Biochem. **119**, 115 (1982).
20. M. B. PERRY and L. A. BABIUK. Can. J. Biochem. **62**, 108 (1984).
21. E. ALTMAN, J.-R. BRISSON, and M. B. PERRY. Carbohydr. Res. **183**, 321 (1988).

Can. J. Chem. Downloaded from www.nrcresearchpress.com by 41.223.56.140 on 09/07/12
For personal use only.

Behaviour of 2′-*O*-*p*-toluenesulfonyl uridine towards excess of a Grignard reagent

ANNIE GROUILLER AND HASSAN ESSADIQ

Université Lyon 1. École supérieure de chimie industrielle de Lyon, Laboratoire de chimie organique II, 43 Boulevard du 11 Novembre 1918, 69622 Villeurbanne, France

Received July 18, 1988

ANNIE GROUILLER and HASSAN ESSADIQ. Can. J. Chem. **67**, 708 (1989).

Two C-methylated base nucleosides were obtained when 2′-*O*-tosyl-5′-*O*-trityluridine was reacted with 30 equivalents of methylmagnesium iodide.

Key words: nucleoside, Grignard reaction, *C*-methyl pyrimidinone, anhydro derivative, arabinofuranosyl.

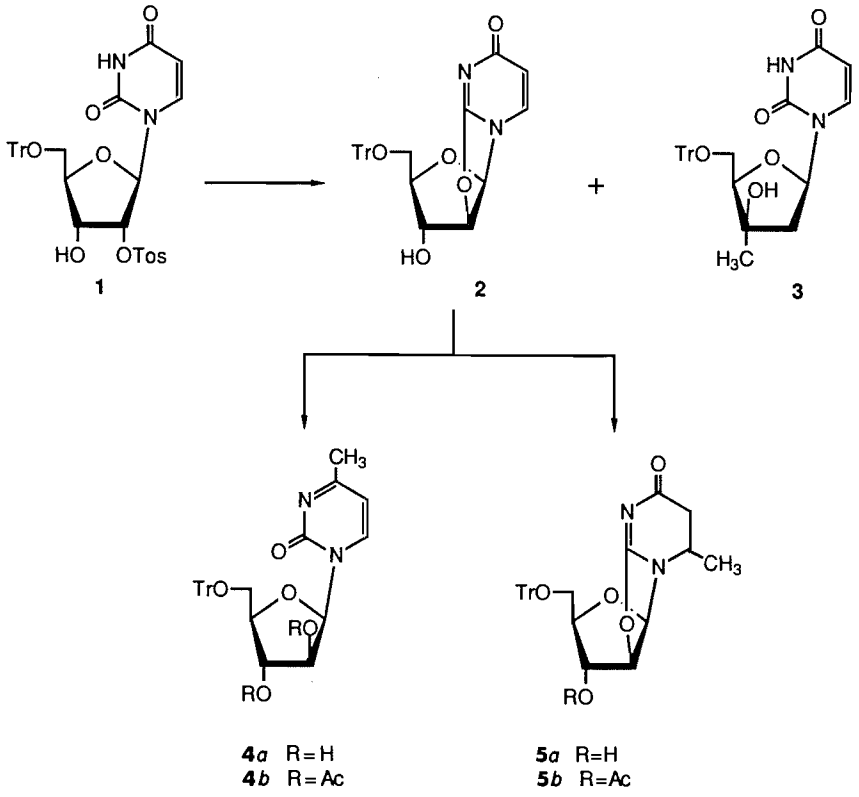
ANNIE GROUILLER et HASSAN ESSADIQ. Can. J. Chem. **67**, 708 (1989).

La réaction d'un excès d'iodure de méthylmagnésium avec la *O*-tosyl-2′ *O*-trityl-5′ uridine conduit à la formation de deux nucléosides C-méthylés sur la base.

Mots clés : nucléoside, réaction de Grignard, pyrimidinone *C*-methylée, dérivé anhydro, arabinofuranosyl.

Previous studies (1, 2) have shown that the Grignard reactions of 2′-*O*-tosyl-5′-*O*-trityluridine (**1**) with 7 and 15 equivalents of methylmagnesium iodide afford, respectively, either the anhydro nucleoside **2** or the branched-chain deoxy-sugar nucleoside **3**. This paper[1] now reports the results obtained when **1** was reacted with 30 equivalents of the same Grignard reagent under the conditions previously described (1) for the preparation of **3**.

Besides the deoxy nucleoside **3** formed in 17% yield, a mixture of two products **4***a* and **5***a* in 1:1 ratio was obtained in 42% yield. The latter two compounds were characterized after their separation, which was made possible only at the level of their peracetylated derivatives **4***b* and **5***b*. Their structures were deduced using various spectrometric techniques (UV, ^{1}H and ^{13}C NMR, mass). The mechanism proposed for the formation of these C-methylated base arabinofuranosyl nucleosides involves, respectively, a 1,2 or 1,4 nucleophilic addition to the C=C—C=O system of the presumed intermediate, anhydronucleoside **2**. To verify this suggestion, the same reaction was applied to 5′-*O*-trityl-2,2′-anhydro-1-β-D-arabinofuranosyluracil (**2**) prepared from 5′-*O*-trityluridine via its 2′,3′-carbonate according to Ogilvie and Iwacha (4). The same mixture was obtained, consisting of a similar ratio of **4***a*:**5***a*, in 77% yield.



[1]This work is a part of the thesis of H. Essadiq (3).

Printed in Canada / Imprimé au Canada

Can. J. Chem. Downloaded from www.nrcresearchpress.com by 41.223.56.140 on 09/07/12
For personal use only.

This result provides a direct synthesis of the methylpyrimidinone nucleosides studied for their biological interest, some years ago, by two teams (5, 6).

Experimental

General methods

Melting points were determined on an Electrothermal apparatus. ^1H and ^{13}C NMR spectra were recorded on a Cameca spectrometer at 350 MHz and a Bruker spectrometer at 50.32 MHz. The proton chemical shifts (δ) are given relative to Me_4Si (δ=0). IR spectra were recorded on a Beckman Acculab 4 spectrophotometer and UV spectra on a Beckman DU 8 spectrophotometer. Mass spectra were obtained on a ZAB HF mass spectrometer (FAB^+ source). TLC was performed using silica gel 60 F_{254} aluminum sheets and short column chromatography (7) on silica gel 60 G.

Procedure for Grignard reaction

To a stirred solution at 0°C, containing 2′-*O*-tosyl-5′-*O*-trityluridine (**1**) (1.20 g, 1.85 mmol) in anhydrous tetrahydrofuran (60 mL) a solution of methylmagnesium iodide (30 equiv.) in diethylether (40 mL) was added under a nitrogen atmosphere over a period of 0.5 h. The reaction mixture was then stirred at room temperature over a period of 1.5 h, subsequently heated at 65°C for 0.5 h, cooled to ice-bath temperature, and finally treated with 10% aqueous ammonium chloride (13 mL). The organic layer was separated, dried, and concentrated under high vacuum at a temperature less than 35°C. The residue was chromatographed on a silica gel column using 2% ethanol/chloroform mixture. Elution of the more polar compound afforded the Grignard reaction product **3** (152 mg, 17%). Continued elution with the same solvent afforded the mixture of **4***a* and **5***a* (370 mg, 42%).

Peracetylation of the compounds **4**a *and* **5**a

Acetic anhydride (0.20 mL) was added to a stirred solution of the foregoing mixture in pyridine (10 mL) at room temperature. After 4 h, the reaction mixture was diluted with ice-water, poured into aqueous sodium hydrogen carbonate (5% w/v), and extracted with chloroform. The organic layer was dried and concentrated. The crude crystalline product was chromatographed on a silica gel column, eluting first with dichloromethane and then with 1% ethanol–chloroform mixture to give a clean separation of **4***b* (90 mg, 42%) and **5***b* (83 mg, 42%).

*1-(2,3-DiO-acetyl-5-O-triphenylmethyl-β-D-arabinofuranosyl)-4-methyl-2-pyrimidinone (***4***b)*

Melting point 170–172°C; R_f 0.80 (15% methanol–chloroform): UV λ_{max}: 305 nm (at pH 4.7 and 12): IR ν_{KBr}: 3060, 1750, 1680, and 1650 cm^{-1}; ^1H nmr ($CDCl_3$) δ: 1.77 and 2.10 (2s, 6H, MeCO), 2.35 (s, 3H, MeCN), 3.55–3.45 (m, 2H, H-5′ and H-5′′), 4.22 (t, 1H, H-4′), 5.35–5.20 (m, 1H, H-3′), 5.60–5.50 (m, 1H, H-2′), 6.05 (d, 1H, $J_{5,6}$ = 7.0 Hz, H-5), 6.30 (d, 1H, $J_{1',2'}$ = 4.0 Hz, H-1′), 7.60–7.20 (m, 15H, trityl), 7.80 (d, 1H, H-6); ms (FAB^+), *Exact Mass* calcd. for $C_{33}H_{33}N_2O_7$ $(M + H)^+$: 569, 2288; found: 569, 2316.

*3′-O-Acetyl-5,6-dihydro-6-methyl-5′-O-triphenylmethyl-2,2′-anhydro-1-β-D-arabinofuranosyluracil (***5***b)*

Melting point 164–165°C; R_f 0.70 (15% methanol–chloroform): UV λ_{max}: 302 (pH 7), 301 (pH 4), and 303 nm (pH 12): IR ν_{KBr}: 3060, 1750, and 1580 cm^{-1}; ^1H nmr ($CDCl_3$) δ: 1.31 (d, 3H, $J_{Me,6}$ = 5.5 Hz, Me), 2.13 (s, 3H, MeCO), 2.22 (dd, 1H, $J_{5a,6}$ = 9.9 Hz, $J_{5a,5b}$ = 19.0, H-5a), 2.27 (dd, 1H, $J_{5b,6}$ = 7.4 Hz, H-5b), 3.05 (dd, 1H, $J_{5',5''}$ = 11.5 Hz, H-5′); 3.12 (dd, 1H, H-5″), 3.65–3.54 (m, 1H,H-6), 4.41 (t, 1H, $J_{4',5'}$ = 6.6 Hz, H-4′), 5.13 (d, 1H, H-2′), 5.35 (s, 1H, H-3′), 5.89 (d, 1H, $J_{1',2'}$ = 6.6 Hz, H-1′), 7.45–7.20 (m, 15H, trityl); ^{13}C nmr δ: 17.9 (Me-6), 20.7 (Me-acetyl), 37.2 (C-5), 45.3 (C-6), 63.3 (C-59), 77.2 (C-4′), 84.5 (C-2′), 84.9 (C-1′), 87.0 (quaternary C-trityl), 88.9 (C-3′), 127.2, 128.4, and 129.2 (C-Ar), 143.0 (quaternary C-Ar), 164.9 (C-2), 169.1 (C-4), 177.1 (CO-acetyl); ms (FAB^+), *Exact Mass* calcd. for $C_{31}H_{31}N_2O_6$ $(M + H)^+$: 527, 2182; found: 527, 2211.

1. A. GROUILLER, H. ESSADIQ, H. PACHECO, S. JUNTUNEN, and J. CHATTOPADHYAYA. Angew. Chem. Int. Ed. Engl. **24**, 52 (1985).
2. L. H. KOOLE, H. M. MOODY, H. M. BUCK, A. GROUILLER, H. ESSADIQ, J. M. VIAL, and J. CHATTOPADHYAYA. Recl. Trav. Chim. Pays-Bas, **107**, 343 (1988).
3. H. ESSADIQ. Dissertation No. 87 ISAL 0011, Institut national des sciences appliquées de Lyon (1987).
4. K. K. OGILVIE and D. IWACHA. Can. J. Chem. **47**, 495 (1969).
5. R. S. KLEIN, I. WEMPEN, K. A. WATANABE, and J. J. FOX. J. Org. Chem. **35**, 2330 (1970).
6. R. W. BALD and A. HOLY. Collect. Czech. Chem. Commun. **36**, 3657 (1971).
7. B. J. HUNT and W. RIGBY. Chem. Ind. (London), 1868 (1967).

Can. J. Chem. Downloaded from www.nrcresearchpress.com by 41.223.56.140 on 09/07/12
For personal use only.

An acidity scale, $[H^+]^{h\nu}$, for proton quenching of excited states in aqueous perchloric acid

J. A. PINCOCK[1] AND P. R. REDDEN
Department of Chemistry, Dalhousie University, Halifax, N.S., Canada B3H 4J3

Received September 12, 1988

J. A. PINCOCK and P. R. REDDEN. Can. J. Chem. **67**, 710 (1989).

An acidity scale for excited state protonation kinetics in aqueous perchloric acid has been developed using 1-cyanonaphthalene as a fluorescent indicator. A comparison of the quenching rate constants obtained using this scale is made with both the more general excess acidity function, X, and the transition state activity coefficient approach. A variety of chromophores were studied including 1- and 2-cyanonaphthalenes, 1- and 2-methoxynaphthalenes, benzyl alcohols, toluenes, benzonitriles, and 2-vinylnaphthalene.

Key words: acidity scale, proton fluorescence quenching.

J. A. PINCOCK et P. R. REDDEN. Can. J. Chem. **67**, 710 (1989).

Utilisant le cyano-1 naphtalène comme indicateur fluorescent, on a mis au point une échelle d'acidité pour la cinétique de protonation des états excités dans l'acide perchlorique aqueux. On a établi une comparaison entre les constantes de vitesse de piégeage obtenues avec cette échelle et celles obtenues avec la fonction plus générale d'acidité en excès, X, ainsi qu'avec l'approache basée sur le coefficient d'activité de l'état de transition. On a examiné une variété de chromophores, y compris les cyano-1 et -2 naphtalènes, les méthoxy-1 et -2 naphtalènes, des alcools benzyliques, des toluènes, des benzonitriles et le vinyl-2 naphtalène.

Mots clés : échelle d'acidité, piégeage de la fluorescence par le proton.

[Traduit par la revue]

Introduction

Recently, we described a procedure for establishing an acidity scale, $[H^+]^{h\nu}$, that proved to be a useful way of analyzing data for proton quenching of the fluorescence of excited states of aromatic substrates (1, 2). Thus, the modified Stern–Volmer expression, eq. [1], can be used to obtain linear plots even in quite concentrated acidic solutions where the concentration of the quenching protons is no longer a measure of their activity. Only a single indicator, 1-cyanonaphthalene, was required to obtain $[H^+]^{h\nu}$.

$$[1] \quad I^0/I = 1 + K_{SV}[H^+]^{h\nu}$$

$$[2] \quad [H^+]^{h\nu} = k_q^I\tau^{0I}/K_{SV}^I(a_{H^+}f_{S1}^I/f_{\neq}^I)$$

An analysis of this equation by current acidity function – activity coefficient approaches revealed that $[H^+]^{h\nu}$ can be expressed as in eq. [2], where a_{H^+} is the activity of the proton relative to a standard state of infinite dilution,[2] $f_{S_1}^I$ and $f_{\neq}^I$ are the activity coefficients for the excited singlet state of the indicator and for the transition state for protonation of that excited state respectively, k_q^I, τ^{0I}, and K_{SV}^I are the quenching rate constant, the lifetime of the excited state, and the empirical Stern–Volmer slope for the indicator 1-cyanonaphthalene, respectively. If a substrate gives a linear Stern–Volmer plot versus this function with a slope K_{SV}, then eq. [3] applies, where f_{S_1} and $f_{\neq}$ are similar activity coefficients but now for the substrate of interest. It is obvious that the Stern–Volmer slope can only be used to obtain $k_q\tau^0$ if the activity coefficient term in parentheses equals unity.

$$[3] \quad K_{SV} = k_q\tau^0\cdot(K_{SV}^I/k_q^I\tau^{0I})\cdot(f_{S1}/f_{\neq}\cdot f_{\neq}^I/f_{S_1}^I)$$

In our previous paper (2) we made the assumption that this might be true and, therefore, discussed the k_q values as if they were correct. The reactions involved are rapid, exothermic protonations with very low activation barriers (ref. 3, *vide infra*) so that the transition state for protonation may be early and have a structure and solvation very similar to that of the excited state itself. We suggested that the necessary cancellation occurs because $f_S/f_{\neq} \sim 1$ for the substrates examined. These results were obtained in a medium consisting of 20% ethanol: 80% aqueous sulfuric acid, which made it impossible to test this assumption because the required activity coefficient data cannot be obtained.

In this paper, we report results for the fluorescence quenching of the substrates **1–19** in aqueous perchloric acid. The results allow a comparison between the $[H^+]^{h\nu}$ method and the established ground-state methods: excess acidity (4) and transition-state activity coefficients (5).

TABLE 1. Fluorescence quenching values in aqueous perchloric acid for compounds **1–4**

	I^0/I^b			
$[H^+]^a$	**1**	**2**	**3**	**4**
0.065	1.08	1.03	1.03	1.09
0.103	1.13	1.07	1.06	1.13
0.205	1.30	1.15	1.06	1.22
0.297	1.43	1.27	1.13	1.25
0.398	1.63	1.33	1.20	1.32
0.490	1.80	1.57	1.32	1.44
0.982	3.22	2.50	1.87	2.07
1.43	5.30	4.03	2.70	3.21
1.92	9.32	6.27	4.31	4.95
2.41	13.9	9.52	6.41	7.73
2.93	22.9	15.5	9.79	12.0
3.29	29.0	22.0	13.2	16.1
3.67	38.8	27.3	16.9	20.9
3.96	48.7	34.8	22.9	28.7
4.38	69.5	49.1	32.6	41.2
4.87	103	70.4	46.3	61.6
5.21	125	86.3	57.0	77.8

[a]Determined by titration.
[b]I^0 refers to the fluorescence intensity in water.

[1]Author to whom correspondence may be addressed.

[2]This is not really a single-ion activity but refers to the activity of the acid as a proton source relative to a standard state of infinite dilution of that acid in the solvent.

Can. J. Chem. Downloaded from www.nrcresearchpress.com by 41.223.56.140 on 09/07/12
For personal use only.

TABLE 2. Fluorescence quenching values in aqueous perchloric acid for compounds **5–10**

	I^0/I^b					
$[H^+]^a$	**5**	**6**	**7**	**8**	**9**	**10**
0.065	2.42	2.58	2.12	—	—	—
0.103	3.53	4.22	3.08	—	—	—
0.205	6.44	9.55	5.68	—	1.06	1.06
0.297	8.75	12.9	8.15	—	1.11	1.09
0.398	11.9	17.5	10.7	1.05	1.14	1.12
0.490	14.6	23.1	13.0	1.05	1.18	1.15
0.982	30.7	46.0	25.9	1.10	1.49	1.33
1.43	48.0	73.7	40.7	1.20	1.87	1.57
1.92	70.0		56.7	1.31	2.56	1.97
2.41			76.0	1.47	3.60	2.38
2.93			80.9	1.72	4.77	3.42
3.29				2.07	5.06	3.76
3.67				2.39	7.47	4.99
3.96				2.76	9.37	6.25
4.38				3.54	12.5	7.82
4.87				4.99	18.0	11.0
5.21				5.84	21.8	14.6

[a]Determined by titration.
[b]I^0 refers to the fluorescence intensity in water.

TABLE 3. Fluorescence quenching values in aqueous perchloride acid for compounds **11–14**

	I^0/I^b			
$[H^+]^a$	**11**	**12**	**13**	**14**
0.065	—	—	1.07	1.59
0.103	—	—	1.11	2.02
0.205	—	—	1.26	3.22
0.297	1.03	1.03	1.32	4.69
0.398	1.06	1.06	1.44	6.03
0.490	1.13	1.10	1.62	7.57
0.982	1.25	1.12	2.36	15.2
1.43	1.43	1.26	3.36	24.2
1.92	1.70	1.47	4.91	37.7
2.41	2.12	1.74	6.47	51.8
2.93	2.74	2.14	8.94	68.0
3.29	3.40	2.55	11.4	84.4
3.67	4.09	2.91	13.9	96.6
3.96	4.84	3.47	16.6	
4.38	6.17	4.50	21.4	
4.87	9.11	6.11	30.3	
5.21	11.2	7.44	34.5	

[a]Determined by titration.
[b]I^0 refers to the fluorescence intensity in water.

TABLE 4. Fluorescence quenching values in aqueous perchloric acid for compounds **15–19**

	I^0/I^b				
$[H^+]^a$	**15**	**16**	**17**	**18**	**19**
0.065	—	—	—	—	—
0.103	—	—	—	—	—
0.205	—	—	—	—	—
0.297	—	—	—	—	—
0.398	—	—	—	—	—
0.490	1.05	1.22	1.03	—	—
0.982	1.11	1.55	1.13	—	—
1.43	1.25	2.13	1.38	1.09	—
1.92	1.50	3.08	1.67	1.13	—
2.41	1.81	4.46	2.15	1.27	1.11
2.93	2.21	6.80	2.85	1.41	1.15
3.29	2.50	8.75	3.75	1.61	1.27
3.67	3.09	11.4	4.62	1.83	1.34
3.96	3.62	15.1	5.98	2.09	1.42
4.38	5.00	21.5	8.43	2.79	1.81
4.87	7.29	33.2	13.6	4.14	2.55
5.21	9.72	41.5	18.1	5.32	2.98

[a]Determined by titration.
[b]I^0 refers to the fluorescence intensity in water.

Results

Fluorescence quenching data at 25.0°C as a function of acidity in aqueous perchloric acid are reported in Table 1 (**1–4**), Table 2 (**5–10**), Table 3 (**11–14**), and Table 4 (**15–19**). In addition, fluorescence quenching data for **1** as a function of temperature at 35, 45, and 55°C were obtained. Compounds **1–15** have previously been described (2). Compounds **16–19** are available from the Aldrich Chemical Company.

Discussion

As stated in the Introduction, the objective of this study was to examine the proton quenching of excited state fluorescence in an aqueous acidic medium where current ground-state acidity function approaches have been extensively examined. Aqueous sulfuric acid was not chosen because of the possibility of sulfonation of some of the reactive aromatic substrates. Moreover, sulfuric acid is dibasic and not completely ionized at high acidities (6). Since excited state protonation reactions have recently been shown (7, 8) to display general acid behaviour, the complication of having several sources of protons present seemed undesirable. Several preliminary experiments with aqueous hydrochloric acid revealed that excited-state quenching by the halide ion was occurring for substrates like 1-cyanonaph-

Can. J. Chem. Downloaded from www.nrcresearchpress.com by 41.223.56.140 on 09/07/12
For personal use only.

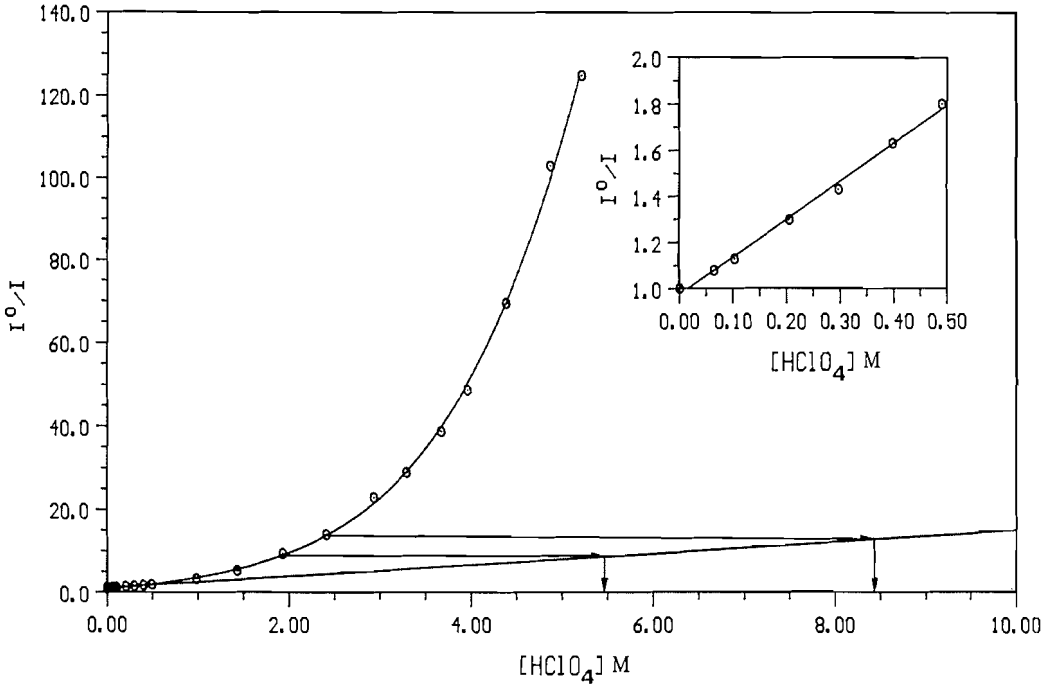
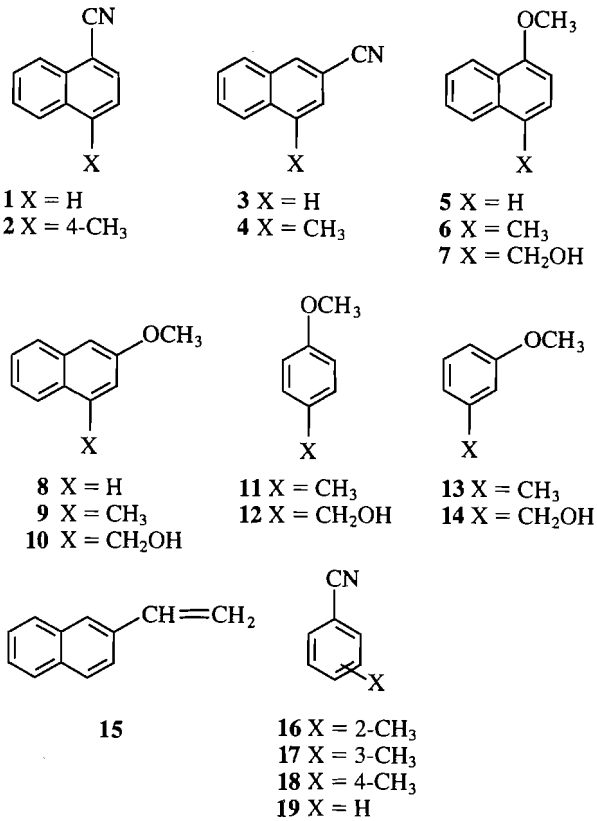


FIG. 1. Fluorescence quenching of 1-cyanonaphthalene in aqueous perchloride acid. The inset shows the results in dilute acid solutions.



1 X = H
2 X = 4-CH_3

3 X = H
4 X = CH_3

5 X = H
6 X = CH_3
7 X = CH_2OH

8 X = H
9 X = CH_3
10 X = CH_2OH

11 X = CH_3
12 X = CH_2OH

13 X = CH_3
14 X = CH_2OH

15

16 X = 2-CH_3
17 X = 3-CH_3
18 X = 4-CH_3
19 X = H

thalene with electron-withdrawing groups. This type of quenching has been well documented and is known to occur by electron transfer from the halide ion to the neutral aromatic (9). Aqueous perchloric acid therefore proved to be the best choice since it is monobasic, completely ionized at all concentrations, and is unreactive.

Evaluation of $[H^+]^{h\nu}$ in aqueous perchloric acid

The fluorescence quenching data for **1** are plotted versus titratable proton concentration in Fig. 1. The inset shows the expanded region up to 0.6 M in acidity as determined by titration. The least-squares slope of this line is 1.53 M^{-1} and obviously the normal Stern–Volmer relationship, $I^0/I = 1 + k_q\tau^0[H^+]$ is valid up to this point. As outlined previously (1, 2) extrapolation of this line into the high acidity region followed by a horizontal projection from the quenching curve gives values of $[H^+]^{h\nu}$. This is shown pictorially in Fig. 1. These values are listed in Table 5 along with values for h_0 (10), h_c (11), log a_{H^+} (12), and X (6) obtained by interpolation of plots of literature data for each of these functions versus perchloric acid concentration.

Plots of I^0/I values for 1-cyanonaphthalene and 3-methoxy-1-methylnaphthalene versus h_0 and h_c are shown in Fig. 2. Clearly, these plots are unsuitable for obtaining slopes and the related k_q values. The "correct" slopes from the X method (*vide infra*) are shown as solid lines on the figure and the curves tend to converge to that slope at low acidities. Both acidity functions overcorrect at high acidities and h_c is worse than h_0 in that respect. However, h_c undercorrects at low acidities. Interestingly, although h_0 is derived from protonation of amines and h_c for aromatic hydrocarbons, neither function correlates the excited state protonations; 1-cyanonaphthalene probably protonates on nitrogen and 3-methoxy-1-methylnaphthalene probably on the ring (1, 2).

Evaluation of k_q values using $[H^+]^{h\nu}$

Plots of I^0/I versus $[H^+]^{h\nu}$ gave good straight lines for **1**, **4**, **8–12**, and **15–19**. Two assumptions are now required to obtain k_q values. The first is that the activity coefficient term in parentheses of eq. [3] is unity. The second is that, for aqueous perchloric acid, $[H^+]$, for the titratable protons, equals C_{H^+}, the concentration of free protons in the solution so that $K^I_{SV}/k^I_q\tau^{0I}$ equals unity. Values of $k_q\tau^0 = k_{SV}$ along with correlation coefficients of the Stern–Volmer plots are given in Table 6. For substrates that are quenched at low enough acidities so that the acidity function treatment is unnecessary, plots of I^0/I versus $[H^+]$ were also nicely linear; $k_q\tau^0$ values and

Can. J. Chem. Downloaded from www.nrcresearchpress.com by 41.223.56.140 on 09/07/12
For personal use only.

TABLE 5. Various acidity function values in aqueous perchloric acid

$[HClO_4]^a$	$[H^+]^{h\nu}$	$h_0{}^b$	$-H_0{}^c$	$h_c{}^d$	$-H_c{}^e$	log $a_{H_3O^+}{}^f$	X^g
0.065	0.065						0.010
0.103	0.103						0.025
0.205	0.205						0.045
0.297	0.297						0.055
0.398	0.398						0.075
0.490	0.490	0.96	−0.02	1.00	0	−0.05	0.10
0.982	1.45	2.19	0.34	2.95	0.47	0.55	0.20
1.43	2.85	3.98	0.60	7.94	0.90	1.09	0.35
1.93	5.44	6.92	0.84	25.1	1.40	1.60	0.47
2.42	8.43	12.0	1.08	63.1	1.80	2.09	0.65
2.93	14.3	21.9	1.34	158	2.20	2.64	0.85
3.29	18.3	31.6	1.50	224	2.35	3.00	1.03
3.67	24.7	47.9	1.68	631	2.80	3.34	1.17
3.96	31.2	66.1	1.82	1000	3.00	3.60	1.30
4.38	44.8	100	2.00	1780	3.25	4.05	1.50
4.87	66.7	166	2.22	7940	3.90	4.60	1.73
5.21	81.0	251	2.40	19950	4.30	5.02	1.90

[a]Determined by titration.
[b]$h_0 = 10^{-H_0}$.
[c]From ref. 10.
[d]$h_c = 10^{-h_c}$.
[e]From ref. 11.
[f]From ref. 12.
[g]From ref. 6.

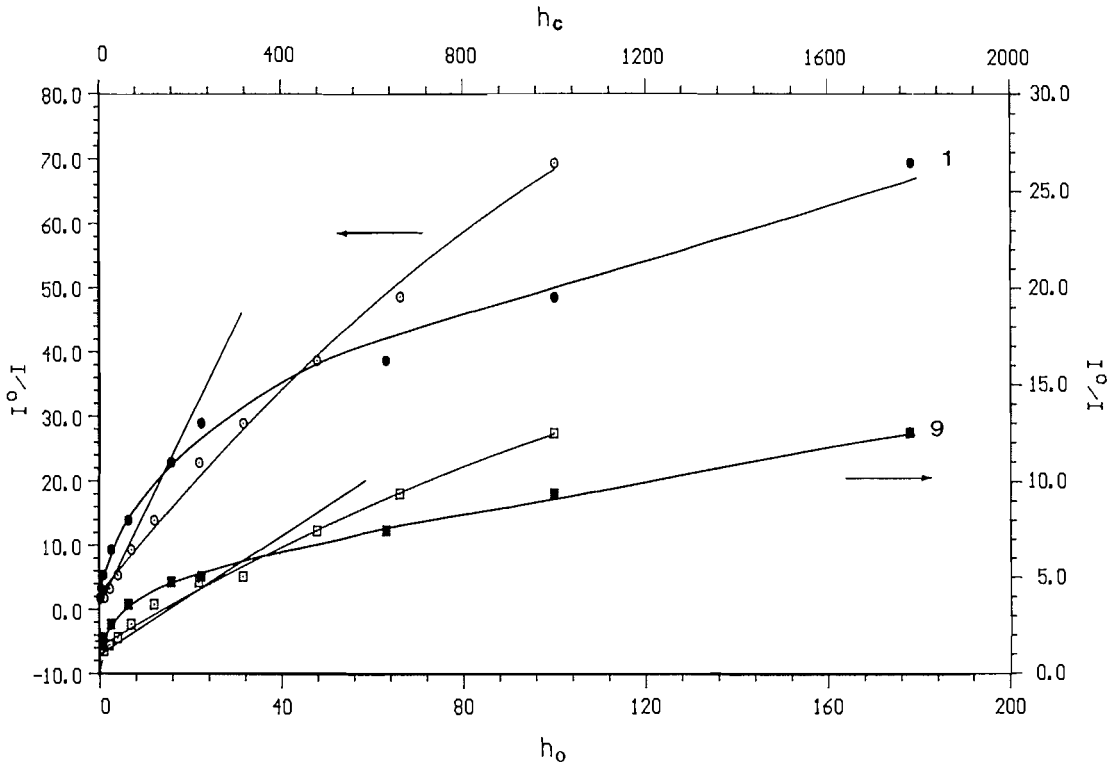


FIG. 2. Fluorescence quenching data for 1-cyanonaphthalene versus h_0 (⊙) and h_c (●), and for 3-methoxy-1-methylnaphthalene versus h_0 (⊡) and h_c (■). The straight lines are the Stern–Volmer slopes by the X method.

correlation coefficients for **5**, **6**, **7**, **13**, and **14** are listed in Table 6. For all compounds, measurement of τ^0 in water by nanosecond single-photon counting allows for the determination of k_q values (Table 6).

As was discussed previously (2), complications due to static quenching should become apparent when k_q values exceed $10^9\,M^{-1}\,s^{-1}$ and when proton concentrations exceed 1 M. Normally, static quenching will lead to upward curvature of Stern–Volmer fluorescence intensity plots because the observed fluoresence intensity is lower than one would expect based on a rate resulting from a process requiring diffusion through the medium. However, when data for substrates like **5**, **6**, **7**, **13**, and **14** are obtained in the higher acidity region, plots versus $[H^+]^{h\nu}$) show downward curvature. The probable reason for this is that

Can. J. Chem. Downloaded from www.nrcresearchpress.com by 41.223.56.140 on 09/07/12
For personal use only.

TABLE 6. Singlet lifetimes and Stern–Volmer results using $[H^+]^{h\nu}$, excess acidity, X, and TSAC approaches

Compound	$\tau^{0\,a}$ (ns)	$[H^+]^{h\nu}$ ($k_q\tau^0$)	$[H^+]^{h\nu\,b}$ ($10^{-7}k_q$)	X^c ($10^{-7}k_q$)	TSAC^d ($10^{-7}k_q$)	$H_2SO_4{}^e$ ($10^{-7}k_q$)
1	6.5	—	24	23 (0.68,0.97)	23	13
2	5.1	1.05 (0.999)	21	25 (0.63,0.98)	22	11
3	12.7	0.691 (0.999)	5.44	4.70 (0.72,0.96)	3.89	4.52
4	12.3	0.929 (0.998)	7.55	7.00 (0.68,0.99)	6.76	5.97
5	11.4	28.5 (0.999)	250	226 (0.32,0.98)	281	190
6	13.9	47.0 (0.996)	338	287 (0.32,0.98)	525	400
7	11.9	26.8 (0.999)	225	196 (0.20,0.99)	263	210
8	10.3	0.0595 (0.999)	0.577	0.843 (0.54,0.99)	1.00	1.06
9	12.1	0.255 (0.999)	2.10	3.15 (0.56,0.98)	2.82	2.87
10	10.6	0.159 (0.994)	1.50	2.51 (0.51,0.99)	2.88	3.10
11	5.1	0.123 (0.998)	2.4	4.0 (0.51,0.99)	6.6	5.2
12	4.4	0.078 (0.999)	1.8	2.7 (0.52,0.99)	4.1	2.8
13	5.7	1.23 (0.98)	22	21 (0.40,0.99)	24	23
14	4.1	14.0 (0.997)	340	320 (0.26,0.96)	370	310
15	59.7	0.102 (0.988)	0.171	0.174 (0.64,0.98)	0.158	0.240
16	7.1	0.50 (0.997)	7.0	6.5 (0.68,0.99)	5.6	—
17	7.0	0.20 (0.985)	2.9	1.5 (0.83,0.94)	0.83	—
18	9.1	0.053 (0.978)	0.58	0.24 (0.87,0.92)	0.25	—
19	3.7	0.027 (0.979)	0.72	0.32 (0.79,0.98)	0.43	—

[a]Determined by single photon counting.
[b]Determined from the least-squares slope of I^0/I versus $[H^+]^{h\nu}$ in perchloride acid.
[c]Determined from the least-squares intercept of eq. [5]. Values in parentheses are the slope or $m^{\neq}m^*$ (see text) and the correlation coefficient, respectively.
[d]Determined from the extrapolation of eq. [7] to zero molarity.
[e]The values are those obtained in 20% ethanol: 80% aqueous sulfuric acid of ref. 2.

an acidity function is proportional to a_{H^+}, which is increasing rapidly as an acid becomes more concentrated. Static quenching is determined by the concentration, and not by the activity of the protons. Thus, as the quenching becomes more and more dominated by the value of C_{H^+} the points will begin to fall below the line defined by $[H^+]^{h\nu}$.

Evaluation of k_q *values using excess acidity,* X

As has been demonstrated by Cox (4), the excess acidity method is a reliable technique for the investigation of reaction mechanisms in concentrated acidic media. Its application to various ground-state kinetic schemes has been discussed in detail (13). The closest analogy to the reactions discussed here would be rate-determining proton transfer to the substrate with subsequent reactions of SH^+ being fast, i.e., the A-S_E2 mechanism, eq. [4], where log k_ψ is the observed pseudo first-order rate constant, C_{H^+} the concentration of protons, which is equal to the titratable concentration for perchloric acid, $m^{\neq}$ is a slope parameter for the kinetics of protonation, m^* is a slope parameter for equilibrium protonation relative to the excess acidity, X, and k_0 is the desired medium-independent rate constant. Application of these ideas to Stern–Volmer fluorescence quenching gives eq. [5]. Plots of the left-hand side of eq. [4] versus X (Table 5) should give a straight line of slope $m^{\neq}m^*$ and intercept of log k_q. Examples for compounds **1**, **8**, and **11** are shown in Fig. 3. Values of $m^{\neq}m^*$, k_q, and correlation coefficients are listed in Table 6. Although the excess acidity method was used to determine the correct k_q values they should be used with caution since at very low X values the plots deviate markedly from linearity. A similar effect was previously

Can. J. Chem. Downloaded from www.nrcresearchpress.com by 41.223.56.140 on 09/07/12
For personal use only.

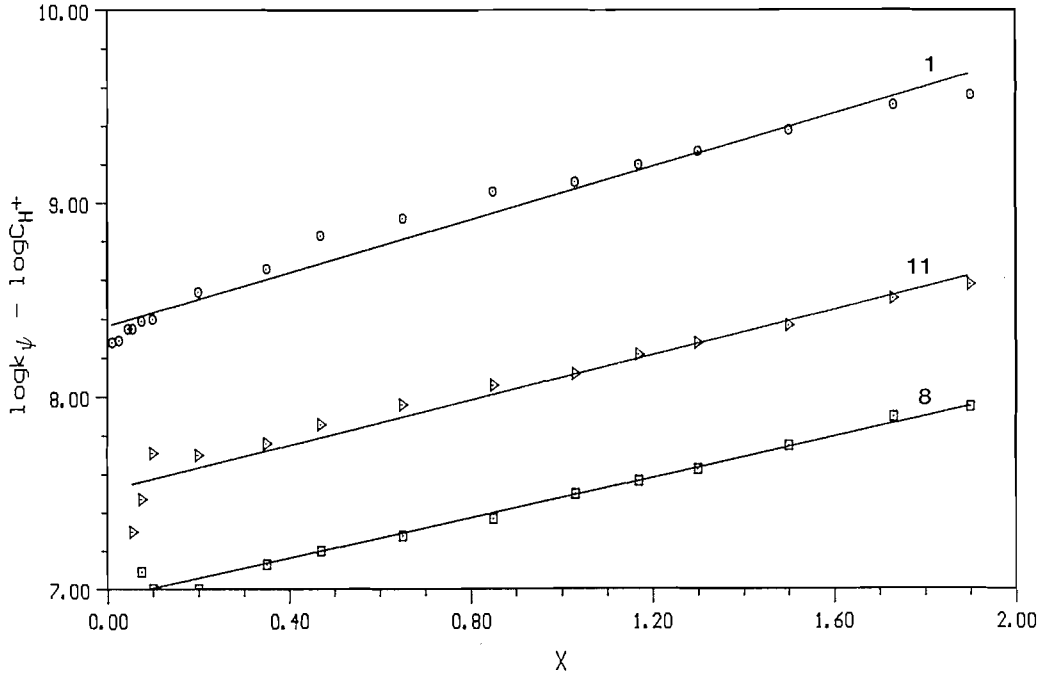


FIG. 3. Plots of eq. [4], the X method, for 1-cyanonaphthalene, **1**, 4-methoxytoluene, **11**, and 1-methylnaphthalene, **8**.

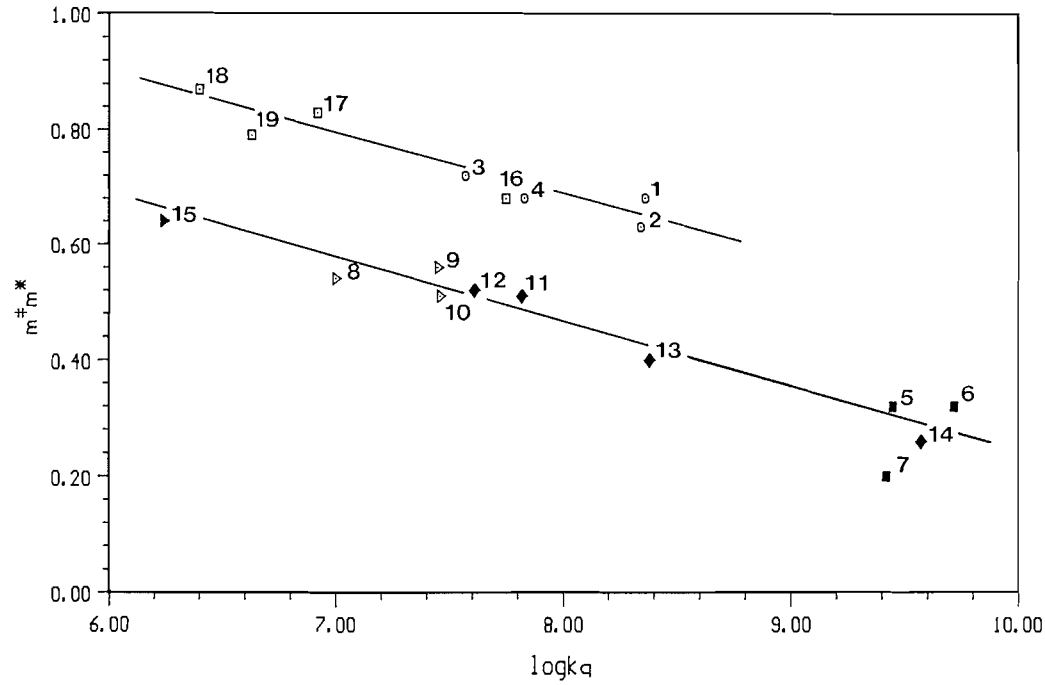


FIG. 4. Plots of $m^{\neq}m^*$ versus log k_q. (⊙) are for cyanonaphthalenes, (⊡) for cyanobenzenes, (■) for 1-methylnaphthalenes, (▷) for 2-methoxynaphthalenes, ◆ for methoxybenzenes, and ▶ for 2-vinylnaphthalene.

observed (2) where log $C_{H^+} + H_0$ (14) was used to approximate X in 20% ethanol: 80% aqueous sulfuric acid. Since in both treatments the intercept gives k_q, the scatter will affect the intercept and hence k_q.

[4] $$\log k_\psi - \log C_{H^+} = m^{\neq}m^*X + \log k_0$$

[5] $$\log\{(I^0/I - 1)/\tau^0\} - \log C_{H^+} = m^{\neq}m^*X + \log k_q$$

As has been discussed, the slopes of the excess acidity plots are a composite of $m^{\neq}m^*$ where m^* is a slope parameter for the equilibrium protonation and $m^{\neq}$ is a slope parameter for the kinetics of protonations. For ground-state reactions, this composite can be separated into the individual components since independent estimates of m^* are often available. Interpretation of $m^{\neq}$ then gives useful mechanistic information (6). This slope parameter is identical to the term, α, which has been defined by Kresge *et al.* (15) and is interpretable as the degree of proton transfer at the transition state. For excited-state protonations

Can. J. Chem. Downloaded from www.nrcresearchpress.com by 41.223.56.140 on 09/07/12
For personal use only.

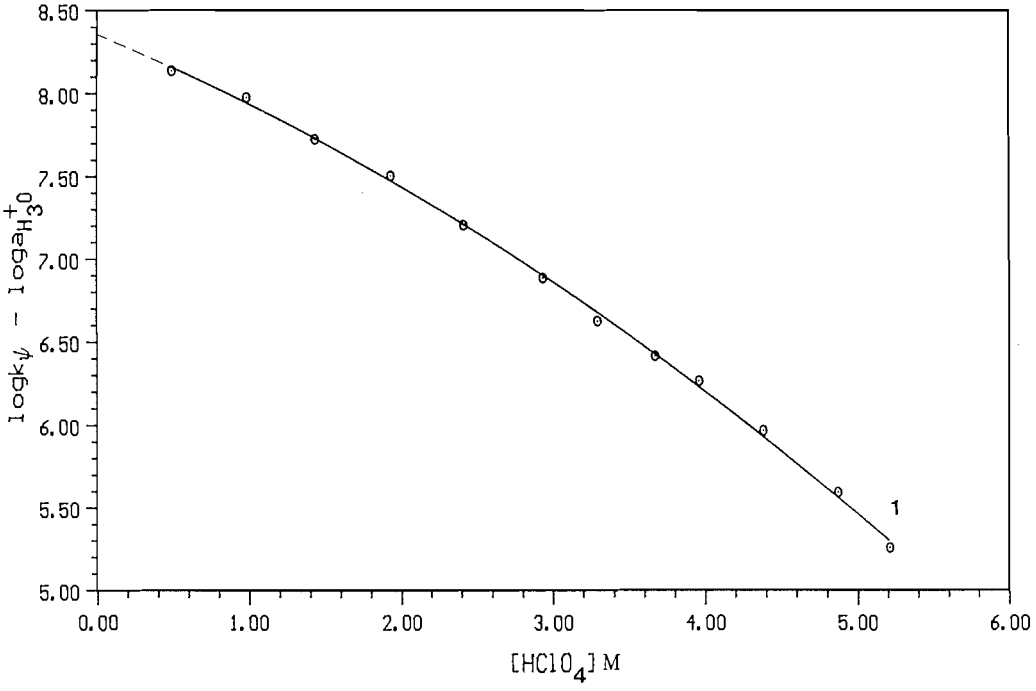


FIG. 5. Plot of eq. [7], the TSAC method, for 1-cyanonaphthalene, **1**.

separation is impossible since values of m^* for equilibrium protonation are not available. However, there are trends in the composites themselves. This is shown in Fig. 4 where $m^{\neq}m^*$ is plotted versus log k_q. The results seem to define two lines of the same slope, one line for the methoxy derivatives and one for the cyano derivatives. The negative slope indicates that the more reactive compounds have lower $m^{\neq}m^*$ values. Until more results are available, any interpretation of this trend would be quite speculative.

Evaluation of k_q *values using the transition-state activity coefficient method (TSAC)*

This approach for studying the mechanisms of reactions in concentrated acidic media avoids the difficulties inherent in acidity function methods (5). Activities and activity coefficients are used directly since values are now available for both aqueous perchloric and sulfuric acid. For a mechanism involving rate-determining protonation the desired expression for ground-state reactions is eq. [6] where $a^*_{H_3O^+}$, Table 5, is the activity of the hydronium ion (the asterisk refers to the fact that these are experimentally inaccessible single-ion activities and are therefore expressed relative to a standard reference ion, tetraethylammonium (16), and f_S and $f^*_{S_{\neq}}$ are the activity coefficients for the substrate and its transition state for rate-determining protonation, respectively. Application of these ideas to Stern–Volmer fluorescence quenching gives eq. [7] where now f_{S_1} and $f^*_{\neq}$ are activity coefficients for the excited singlet state and its transition state for protonation, respectively. Plots of the left-hand side of eq. [7] versus any function of the acidity are smooth and monotonic. An example for compound **1** is given in Fig. 5. Extrapolation of these plots to zero acidity gives log k_q since $f_{S_1}/f^*_{\neq}$ should approach unity at this standard state. Values of log k_q obtained by this method are included in Table 6 as well.

[6] $\log a^*_{H_3O^+} - \log k_\psi = \log(f^*_{S_{\neq}}/f_S) - \log k_0$

[7] $\log\{(I^0/I - 1)/\tau^0\} - \log a^*_{H_3O^+} = \log k_q + \log(f_{S_1}/f^*_{\neq})$

For ground-state reactions, once k_0 is known log $f_{S_{\neq}}$ can be determined since log f_S values can be measured experimentally. These TSAC values, as a function of acidity, have been shown (5) to give useful information about the structure of the transition state and hence details about the reaction mechanism that would not have been available otherwise. For the excited-state Stern–Volmer approach, f_{S_1} values are not experimentally available. However, values of $\log(f_{S_1}/f^*_{\neq})$ can be calculated. Plots for compounds **1**, **8**, and **11** are shown in Fig. 6. All other plots are very similar to those shown with the range of $\log(f_{S_1}/f^*_{\neq})$ at 5.2 M $HClO_4$ being only from 3.06 to 3.64. It is satisfying to notice that these plots extrapolate to zero at zero acidity as required. In the Introduction of this paper, the assumption that the values of $f_{S_1}/f^*_{\neq}$ might approximate unity (or log $f_{S_1}/f^*_{\neq}$ approach zero) independent of the acidity was discussed. Clearly, this is not true since $f_{S_1}/f^*_{\neq}$ values vary from unity at zero acid concentration to almost 10^4 at 5.2 M perchloride acid.

Therefore, although qualitative information about activity coefficients can be obtained from the TSAC approach, the k_q values obtained should again be used with caution since they are obtained by extrapolation to the intercept of a nonlinear function. Of greater consequence is the problem outlined in eq. [3]. The Stern–Volmer slopes obtained by the $[H^+]^{h\nu}$ method do not give $k_q\tau^0$ directly but are altered by the product between this ratio of activity coefficients for the substrate of interest and the reciprocal of this ratio for the indicator, 1-cyanonaphthalene, as shown in eq. [3]. Not surprisingly, since the plots of Fig. 6 are nearly superimposable for all substrates, the cancellation works reasonably well. More quantitatively, calculation of these products of ratios can be made and plots for compounds **2**, **3**, **4**, **5**, **8**, **10**, **13**, and **14** are shown in Fig. 7. Despite the rather large experimental error in calculating these values it is apparent that above 1.0 M perchloric acid, where the acidity function approach is required, these plots are relatively flat. Thus, the $[H^+]^{h\nu}$ method will give straight lines in general.

Can. J. Chem. Downloaded from www.nrcresearchpress.com by 41.223.56.140 on 09/07/12
For personal use only.

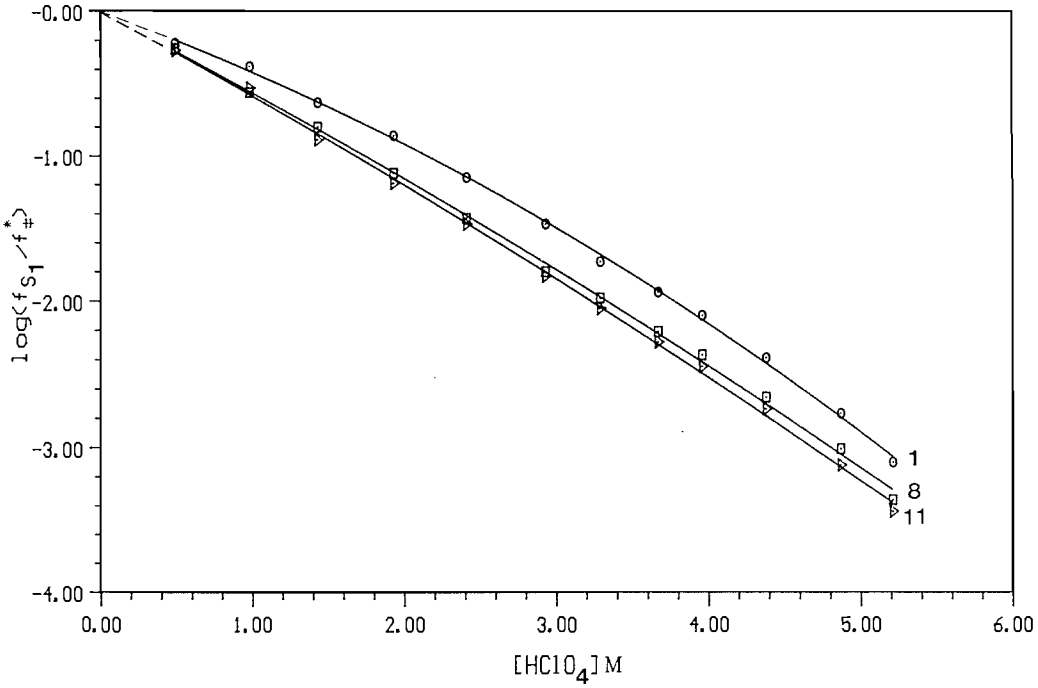


FIG. 6. Plots of $\log(f_{S_1}/f_{\neq}^{*})$ versus $[HClO_4]$ for 1-cyanonaphthalene, **1**, 4-methoxytoluene, **11**, and 2-methoxynaphthalene, **8**.

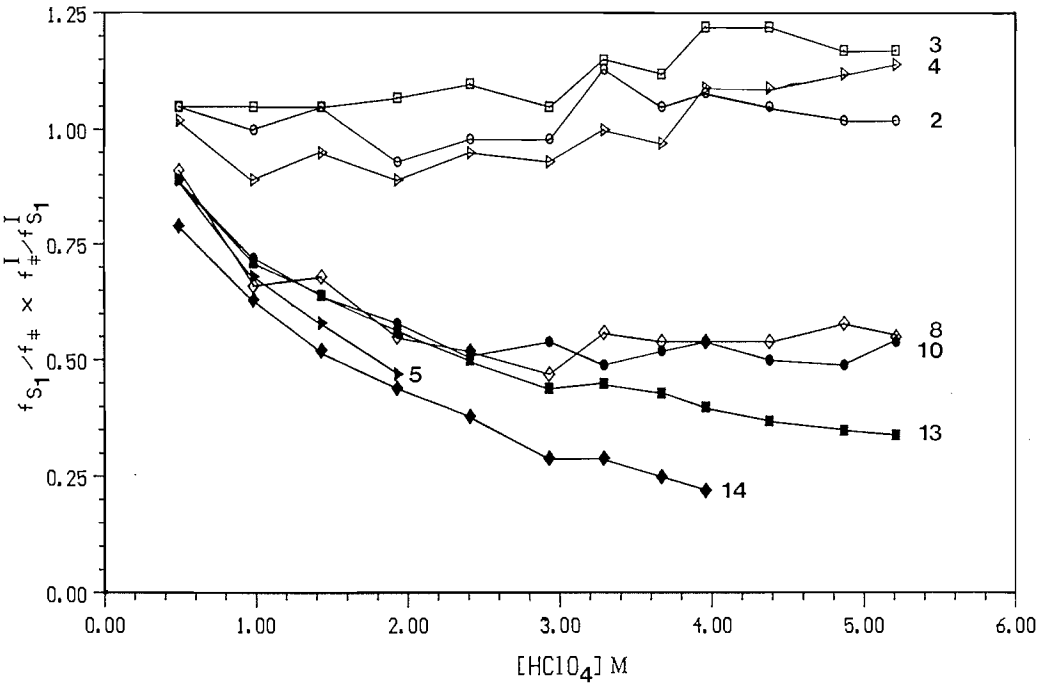


FIG. 7. Plots of $f_{S_1}/f_{\neq} \times f_{\neq}^{I}/f_{S_1}^{I}$ versus $[HClO_4]$.

For the cyanonaphthalene derivatives, the $(f_{S_1}/f_{\neq}^{*})(f_{\neq}^{*I}/f_{S_1}^{I})$ values are close to unity, as expected for compounds that are structurally related to the indicator. For a compound such as 2-methoxynaphthalene, the values average around 0.6 so that the $[H^+]^{h\nu}$ method will give a rate constant that is too small by that factor (see Table 6). Since these ratios are around unity or less for all compounds studied, the k_q values obtained by the $[H^+]^{h\nu}$ method are usually somewhat lower than the correct values. Although this seems like a criticism of the method, examination of the values in Table 6 reveals that the $[H^+]^{h\nu}$ method does remarkedly well at determining photochemical quenching constants since these deviations are relatively small.

The Arrhenius plot of the quenching rate constant, k_q, for **1** versus $1/T$ is shown in Fig. 8. The activation energy obtained is only 1.6 kcal/mol, which is similar to but larger than the value of 0.5 kcal/mol reported for **5** (3). As mentioned in the Introduction, this is consistent with the idea that these reactions are rapid, exothermic protonations indicating that the transition

Can. J. Chem. Downloaded from www.nrcresearchpress.com by 41.223.56.140 on 09/07/12
For personal use only.

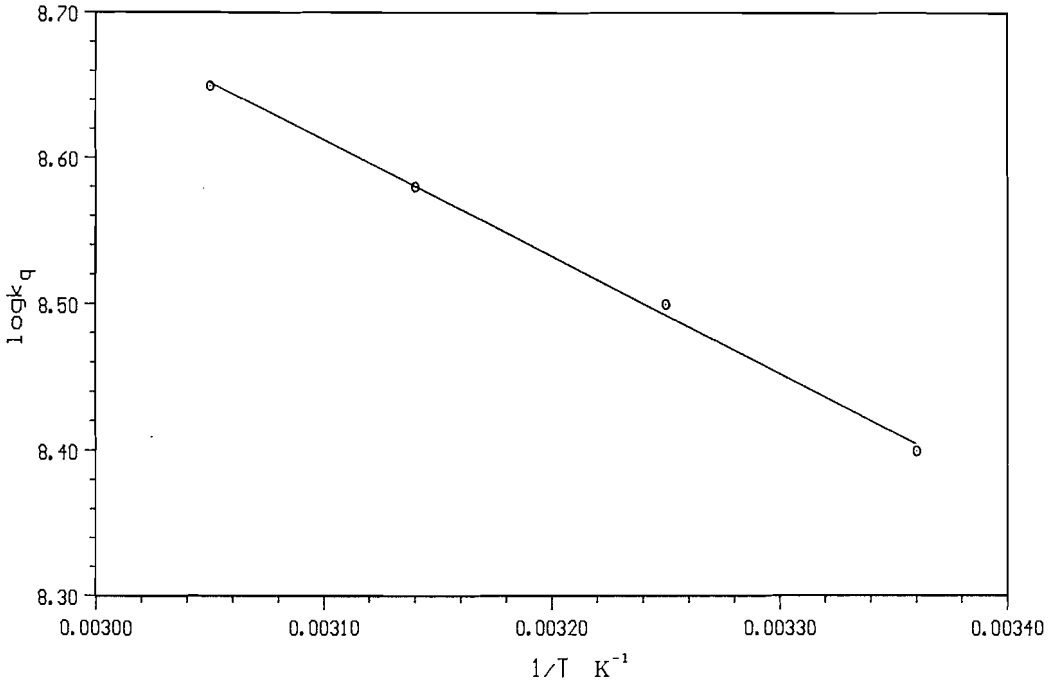


FIG. 8. Arrhenius plot for 1-cyanonaphthalene.

state is early. In fact, the rate constant for quenching of **5** is approaching diffusion so that the measured activation energy might be largely a reflection of decreased viscosity with increased temperature. For 1-cyanonaphthalene, however, the rate constant for quenching is almost two orders of magnitude below the diffusional rate so that the measured activation energy reflects a real kinetic barrier. Since no emission is seen from the conjugate acid of any of these excited-state bases, the question of whether these protonations are diabatic or adiabatic followed by rapid internal conversion cannot be answered. Of course, once in the ground state these conjugate acids will deprotonate rapidly.

Analysis of quenching rate constants

For the most part the k_q values obtained in perchloric acid are in good agreement with the values obtained for the same compounds in 20% ethanol: 80% aqueous sulfuric acid media (2). The relative order of quenching of the naphthalene compounds is the same as before so a discussion is not required here. The results for the cyanobenzenes are new and there does appear to be a small substituent effect. Both 2- and 3-methylcyanobanzene are quenched at a faster rate than unsubstituted cyanobenzene, which is in turn quenched slightly faster than 4-methylcyanobenzene. This is as predicted by excited-state electron density distribution as estimated by HMO calculations, i.e., the "*meta* effect" (17, 18). It was previously suggested by gas phase results that cyanobenzene in the excited state protonates in the nitrile functional group (19). Recent *ab initio* MO calculations on the excited states of simple nitriles suggest that protonation on either carbon or nitrogen would be favourable.[3] Our observation of a small *meta* effect is suggestive of nitrogen protonation since that puts the positive charge on the carbon and allows interaction of this charge with the substituents.

[3]K. Yates and M. K. Boyd. Unpublished results.

Summary

The results presented here along with the previous discussion (2) suggest that developing an acidity scale for protonation of excited states via quenching of fluorescence is a valid procedure. The quenching rate constants obtained are in good agreement with the values obtained from more traditional methods, i.e., excess acidity and the TSAC approaches. Although each of the three methods has pitfalls for determination of k_q, the fact that all three methods give approximately the same value suggests that each method is quite reliable. The great advantage of the $[H^+]^{h\nu}$ method is that the scale can be generated very quickly and very easily in any solvent system and at any temperature. In contrast, a great many years and much labour have gone into devising and developing the excess acidity function. As long as there is recognition of the activity coefficient problem, the $[H^+]^{h\nu}$ method should prove very useful in giving k_q values that were previously unobtainable. Moreover, in the past solvent systems have been chosen on the basis of whether there was an associated excess acidity function or at least a ground-state acidity function. This is no longer necessary.

Experimental

Perchloric acid, 70%, was used directly as supplied by Fisher Scientific, without further purification. The molarities of the aqueous perchloric acid solutions were determined by titration with NaOH and are given in Tables 1–5.

All fluorescence values were measured using a Perkin–Elmer MPF-66 spectrofluorimeter whose sample holder was maintained at 25.0 ± 0.1°C. Solutions of substrates were prepared to have an approximate concentration of 10^{-4} M by pipetting 3 mL of the aqueous perchloric acid into a fluorescent cuvette designed to be attached to a vacuum line, and then adding 5 μL of a stock solution of the substrate. A blank solution containing water and 5 μL of the substrate was also prepared. The intensity ratio, I^0/I, was obtained by measuring the emission of the blank over the emission in the acidic solutions. Five readings of each sample were taken and the values reported are averages.

Can. J. Chem. Downloaded from www.nrcresearchpress.com by 41.223.56.140 on 09/07/12
For personal use only.

All singlet lifetimes were determined by single photon counting using a PRA instrument.

Substrates **1–15** have previously been described (2); **16–19** are commercially available from Aldrich and were vacuum distilled prior to use.

Acknowledgements

This work was supported by a grant from NSERC of Canada and a Dalhousie University Faculty of Graduate Studies Award (including a Walter C. Summer Fellowship) to P.R.

1. W. Brandon, A. L. Pincock, J. P. Pincock, P. R. Redden, and C. Schmbey. J. Am. Chem. Soc. **109**, 2181 (1987).
2. J. A. Pincock and P. R. Redden. Can. J. Chem. **67**, 227 (1989).
3. H. Shizuka and J. Tobita. J. Am. Chem. Soc. **104**, 6919 (1972).
4. R. A. Cox. Acc. Chem. Res. **20**, 27 (1987).
5. K. Yates and T. A. Modro. Acc. Chem. Res. **11**, 190 (1978).
6. R. A. Cox and K. Yates. J. Am. Chem. Soc. **100**, 3861 (1978).
7. P. Wan and K. Yates. J. Org. Chem. **48**, 869 (1983).
8. J. McEwan and K. Yates. J. Am. Chem. Soc. **109**, 5800 (1987).
9. H. Shizuka, M. Nakamura, and T. Morita. J. Am. Chem. Soc. **84**, 989 (1980).
10. K. Yates and H. Wai. J. Am. Chem. Soc. **86**, 5408 (1964).
11. M. T. Reagan. J. Am. Chem. Soc. **91**, 5506 (1969).
12. T. A. Modro, K. Yates, and J. Janata. J. Am. Chem. Soc. **97**, 1492 (1975).
13. R. A. Cox and K. Yates. Can. J. Chem. **57**, 2944 (1979).
14. C. Capobianco, F. Magno, and G. Scorrano. J. Org. Chem. **44**, 1654 (1979).
15. A. J. Kresge, R. A. More O'Ferrall, L. E. Hakka, and V. P. Vitullo. J. Chem. Soc. Chem. Commun. **46**, (1965).
16. K. Yates and R. A. McClelland. Prog. Phys. Org. Chem. Interscience. **11**, 323 (1974).
17. H. E. Zimmerman and V. R. Sandel. J. Am. Chem. Soc. **85**, 915 (1963).
18. H. E. Zimmerman and V. R. Sandel. J. Am. Chem. Soc. **85**, 922 (1963).
19. B. S. Freiser, R. L. Woodin, and J. L. Beauchamp. . J. Am. Chem. Soc. **97**, 6893 (1975).

Can. J. Chem. Downloaded from www.nrcresearchpress.com by 41.223.56.140 on 09/07/12
For personal use only.

Sulfonation reactions of β-carbolines[1]

M. C. CARMONA GUZMÁN, M. BALÓN ALMEIDA,[2] J. HIDALGO TOLEDO, AND M. A. MUÑOZ PEREZ
Departamento de Química Física, Facultad de Farmacia, Universidad de Sevilla, 41012 Sevilla, Spain

AND

M. LOPEZ POVEDA
Departamento de Química Inorgánica, Instituto de Ciencias de los Materiales, Universidad de Sevilla – C.S.I.C., 41012 Sevilla, Spain

Received August 15, 1988

M. C. CARMONA GUZMÁN, M. BALÓN ALMEIDA, J. HIDALGO TOLEDO, M. A. MUÑOZ PEREZ, and M. LOPEZ POVEDA. Can. J. Chem. **67**, 720 (1989).

The homogeneous sulfonations of β-carboline derivatives norharmane **2**, harmane **3**, harmine **4**, harmol **5**, *N*,*N'*-dimethylharmane **6**, and harmaline **7** have been studied in 80–90% w/w sulfuric acid solutions at 25°C. Ultraviolet–visible and ^{13}C nuclear magnetic resonance spectra and chemical analysis of the reaction mixtures show that for all the substrates studied only C-6 sulfonated products are obtained. The sulfonation reactions of the benzene unsubstituted substrates **2**, **3**, and **6** and the partially aromatic substrate **7** proceed by direct electrophilic attack of the $H_3SO_4^+$ cation on the benzene ring of the β-carboline skeleton. Sulfonation of **4** and **5** at the lower sulfuric acid concentrations is effected by the $H_3SO_4^+$ entity. With increasing sulfuric acid concentration there is a gradual changeover of the sulfonating entity from $H_3SO_4^+$ to $H_2S_2O_7$. The different mechanisms of sulfonation are discussed.

Key words: β-carbolines, sulfonation, kinetics.

M. C. CARMONA GUZMÁN, M. BALÓN ALMEIDA, J. HIDALGO TOLEDO, M. A. MUÑOZ PEREZ et M. LOPEZ POVEDA. Can. J. Chem. **67**, 720 (1989).

Opérant à 25°C, dans des solutions à 80–90% P/P d'acide sulfurique, on a étudié les sulfonations homogènes des dérivés de la β-carboline que sont le norharmane (**2**), l'harmane (**3**), l'harmine (**4**), l'harmol (**5**), le *N*,*N'*-diméthylharmane (**6**) et l'harmaline (**7**). Les spectres ultraviolet–visible et résonance magnétique nucléaire du ^{13}C et les analyses chimiques des mélanges réactionnels montrent que tous les substrats étudiés ne fournissent que les produits substitués en C-6. Les réactions de sulfonation des substrats qui ne sont pas substitués sur le noyau benzénique (**2**, **3** et **6**) ou qui ne sont que partiellement aromatiques (**7**) se produisent par une attaque électrophile directe du cation $H_3SO_4^+$ sur le noyau benzénique du squelette de la β-carboline. La sulfonation des composés **4** et **5** aux concentrations les plus faibles d'acide sulfurique se produisent sous l'effet de l'entité $H_3SO_4^+$. Avec une augmentation de la concentration d'acide sulfurique, il se produit un changement graduel de l'entité responsable de la sulfonation, de $H_3SO_4^+$ à $H_2S_2O_7$. On discute des divers mécanismes de sulfonation.

Mots clés : β-carbolines, sulfonation, cinétique.

[Traduit par la revue]

Introduction

During a recent study of the prototropic equilibria of some β-carboline alkaloids (1–3) it was observed that, unlike other β-carboline derivatives, solutions of fully and partially aromatic compounds were very unstable in highly concentrated sulfuric acid solutions. Apparently these compounds are easily sulfonated in these media (4). This behaviour is noteworthy because related compounds such as pyridine, indole, and carbazole are insensitive towards sulfonation in concentrated sulfuric acid solutions. Sulfonation of the latter compounds requires more powerful sulfonating agents and more vigorous conditions of reaction (5). However, in spite of the synthetic and theoretical interest of this kind of process, relatively little is known concerning this and other electrophilic substitution reactions of β-carboline derivatives (6).

In fact, nitration and sulfonation reactions of some β-carbolines have been only qualitatively studied to establish the position of substitution, and there is still no clear evidence about the structure of the reaction products. While nitration of β-carboline **2** with concentrated nitric acid yields 6-nitronorharmane (7), nitration of **3** gave two mononitro derivatives (8). The higher melting isomer was shown to be 6-nitroharmane and the lower melting isomer was presumed to be the 8-nitro derivative, although this was not established. More recently (9, 10), it was reported that nitration of **4** gives the 6-nitro derivative, but in the nitration of **7** the nitro group was present at C-8.

The sulfonation of **4** gave a compound that was initially formulated as an N_{ind}-sulfonic acid (4). However, Kermack *et al.* (11) found that *N*,*N'*-dimethylharminium chloride, in which N-substitution was no longer possible, was also sulfonated to give a compound that they formulated as the 6-sulfonated derivative. They rejected their earlier tentative suggestion (4) that N-sulfonation of **4** had occurred and postulated that sulfonation of the benzene ring had taken place.

On the other hand, in a recent study on the prototropic equilibria of some Harmala alkaloids (12) in highly concentrated sulfuric acid solutions, the authors established that after the protonation of the pyridinic nitrogen of the β-carboline ring, a second protonation on carbon took place. According to the authors, the blue shift of the fluorescence maxima in solutions of H_0 close to -7 was the result of C-6 protonation with the formation of a positive charge on the pyrrolic nitrogen atom. The possibility of a sulfonation process was not even mentioned.

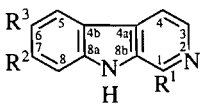
Recently, evidence of sulfonation instead of protonation of **3** in highly concentrated sulfuric acid solutions has been presented

[1]The β-carboline ring is named systematically as 9*H*-pyrido[3,4-*b*]-indole; trivial names of β-carboline derivatives will be used throughout.

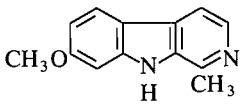
[2]Author to whom correspondence may be addressed.

Printed in Canada / Imprimé au Canada

Can. J. Chem. Downloaded from www.nrcresearchpress.com by 41.223.56.140 on 09/07/12
For personal use only.

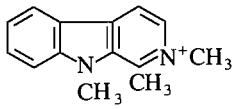


1 Norharmane-6-sulfonic acid
$R^1 = R^2 = H$; $R^3 = HSO_3$

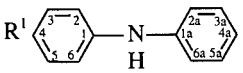


7 Harmaline

2 Norharmane $R^1 = R^2 = R^3 = H$
3 Harmane $R^1 = CH_3$; $R^2 = R^3 = H$
4 Harmine $R^1 = CH_3$; $R^2 = OCH_3$; $R^3 = H$
5 Harmol $R^1 = CH_3$; $R^2 = OH$; $R^3 = H$



6 *N,N'*-dimethylharmane cation



8 Diphenylamine R' = H
9 Diphenylamine sulfonic acid R' = HSO_3

SCHEME 1

(13). We have now extended this work to other β-carboline derivatives to obtain quantitative data on these kinetically controlled sulfonation processes and to definitively establish the structure of the sulfonated products.

Experimental

Norharman-6-sulfonic acid **1**, norharmane **2**, harmane **3**, harmine **4**, harmol **5**, harmaline **7**, diphenylamine **8**, and diphenylaminesulfonic acid **9** were purchased from Aldrich Chemie. All these materials were of the best available commercial quality and were used without further purification. R.A. sulfuric acid was purchased from Merck. *N,N'*-Dimethylharmane **6** sulfate was synthesized by known procedures (14).

The ^{13}C nmr spectra were run at 50.2 MHz on a Varian XL-200 spectrometer. The spectra of the free bases were recorded in DMSO-d_6 as the solvent, the internal lock, and the internal standard. In sulfuric acid solutions, benzene was used as an external standard (coaxial tube). The assignments were made with the aid of the Frequency Off-resonance Decoupling Spectra (SFORD) and the ^{13}C nmr data of the alkaloids were taken from the literature (15–18). Also, to confirm the structural assignments of the sulfonated products the spectra of three model compounds **1**, **8**, and **9** were recorded in sulfuric acid solutions and DMSO.

Kinetic runs were made in the thermostated cell compartment of a Perkin Elmer Lambda-5 spectrophotometer. The temperature in the cell was fixed at 25.0 ± 0.1°C. The sulfonation reactions were carried out in a very large excess of sulfuric acid, so that the concentration of this reagent remained essentially constant during the reaction. The pseudo-first-order rate constants, k_{obs}, were obtained by a non-linear least-squares fitting of the absorbance–time data to eq. [1]:

$$[1] \quad A_t = A_\infty + (A_0 - A_\infty)\cdot\exp(-k_{obs}\cdot t)$$

where A_0, A_∞, and k_{obs} were taken as floating parameters. Excellent agreement between experimental and calculated A_t values was always obtained for more than 3–4 half-lives. Rate constants in duplicate runs were reproducible to within better than 5%.

Results and discussion

Isolation and identification of sulfonated products

The stability of alkaloid solutions in sulfuric acid was monitored by uv–visible spectrometry. Spectra did not show much change from 0.1 M to 14–16 M (70–80% w/w) sulfuric acid solutions. In media of higher sulfuric acid concentrations, time dependent changes of the spectra were evident. These changes were irreversible and their rates depended upon sulfuric acid concentration. The spectral characteristics of these solutions after complete substrate conversion are collected in Table 1. It is noteworthy that these spectra are completely similar to those reported by M. Krishnamurthy and S. K. Droga (12) for the C-6 protonated dications of the respective β-carbolines.

Precipitation by dilution from concentrated sulfuric acid solutions of **2** and **3** yielded products whose elemental analysis and mass spectrometry were in agreement with the formulae $C_{11}H_8N_2SO_3\cdot H_2O$ and $C_{12}H_{10}N_2SO_3\cdot 2H_2O$ (13), respectively. Furthermore, the uv–visible spectrum of **2s** was fully superimposable with that of **1** obtained in a weakly acidic solution of methanol.

The structure of the sulfonated products was determined by ^{13}C nmr spectral analysis of the concentrated sulfuric acid solutions of the alkaloids after complete substrate conversion (Tables 2 and 3). Sulfonation occurs on the benzene ring of the β-carboline skeleton for all the compounds and only one sulfonated derivative was obtained. The main evidence for sulfonation on carbon is supported by the replacement of a strong doublet in the nondecoupled ^{13}C nmr spectra of the substrates by a small singlet upon acidification in 90% w/w H_2SO_4.

The sulfonation site was established by comparison with the ^{13}C nmr spectra of the substrates in DMSO and in concentrated sulfuric acid solutions. The assignments of the ^{13}C resonances of the alkaloids in DMSO were aided by the literature data (15–18). As there are no data on the ^{13}C chemical shifts of these alkaloids in concentrated sulfuric acid solutions, the following procedure was used to assign the ^{13}C signals in these media; as is known (19, 20), the β-carboline alkaloids are very easily protonated on their pyridinic nitrogen atom (pK_a values ranged between 7 and 10). The effect of this protonation was studied by recording the ^{13}C nmr spectra of four selected compounds **2**, **3**, **4**, and **7** in weak sulfuric acid solutions (~0.1 M). The influence of sulfonation on ^{13}C chemical shifts was analyzed by comparison with the spectra of the model compounds **1**, **8**, and **9** obtained in concentrated sulfuric acid solutions.

This comparative analysis of the ^{13}C nmr spectra allowed us to establish C-6 as the only position of sulfonation for all the substrates studied in 80–90% w/w sulfuric acid solutions and at room temperature. This carbon atom, as previously stated, is the most reactive center for other electrophilic substitution reactions of β-carbolines (6, 9, 10).

Kinetics and mechanisms of sulfonation reactions

It is well known that electrophilic aromatic sulfonations usually proceed by an S_E2 mechanism involving a σ-complex as an intermediate state (21, 22). The electrophilic attacking species and, therefore, the detailed reaction mechanism varies with the nature of the sulfonating reagent and the experimental conditions (23, 24). To obtain this information in the reactions under study, we have tried a correlation between the observed rate constants (Table 4) and the activities of the sulfonating entities previously established to be more reactive in aqueous sulfuric acid solutions of characteristics similar to those used in this work, viz. $H_3SO_4^+$ and $H_2S_2O_7$ (24).

As can be seen, the plots of log k_{obs} vs. log $a_{H_2S_2O_7}$ (Fig. 1) or log $a_{H_3SO_4^+}$ (Fig. 2) for the unsubstituted benzene substrates **2**, **3**, and **6** are straight lines over the whole range of sulfuric acid activities studied (85–90% w/w). The slopes of these plots are 0.72 and 1.07 for **2**, 0.75 and 1.10 for **3**, and 0.72 and 1.07 for **6**

Can. J. Chem. Downloaded from www.nrcresearchpress.com by 41.223.56.140 on 09/07/12
For personal use only.

TABLE 1. Ultraviolet–visible spectral characteristics of protonated β-carbolines[a] and **6** in 50% w/w sulfuric acid, and of their sulfonated products[b] in 95% w/w sulfuric acid

Compound	λ_{max}, nm (log ε)
2p	372.0 (3.58), 302.6 (4.14), 248.6 (4.36)
2s	364.8 (3.68), 298.8 (4.07), 250.8 (4.64), 200.4 (4.21)
3p	364.8 (3.65), 297.4 (4.12), 246.2 (4.51), 204.1 (4.28)
3s	359.2 (3.76), 297.8 (4.13), 250.6 (4.71), 201.4 (4.20)
4p	361.4 (3.94), 319.8 (4.26), 246.0 (4.51), 204.1 (4.33)
4s	359.2 (3.98), 318.6 (4.28), 313.2 (4.19), 254.8 (4.65), 203.2 (4.32)
5p	360.0 (3.84), 319.4 (4.23), 246.2 (4.50), 203.8 (4.31)
6	367.1 (3.50), 304.0 (4.06), 248.6 (4.27), 204.4 (4.14)
6s	361.6 (3.53), 300.2 (3.97), 251.8 (4.50), 202.0 (4.01)
7p	376.0 (4.36), 256.0 (3.89), 213.6 (4.36), 203.8 (4.38)
7s	375.6 (4.36), 279.6 (4.01), 223.1 (4.36), 213.4 (4.39)

[a]Named with the number of the free base and the letter **p**.
[b]Named with the letter **s**.

TABLE 2. The ^{13}C nmr shifts[a] of selected β-carbolines and model compounds and their monocations in DMSO-d_6 and weakly concentrated sulfuric acid solutions, respectively

Carbon	**2**	**2p**	**3**[b]	**3p**[b]	**4**	**4p**	**7**	**7p**	**8**	**8p**	**9**	**9p**
1	142.3	138.6	142.3	138.6	142.0	137.4	162.1	165.2	143.7	135.4	144.3	142.5
1a											143.0	134.8
2									117.0	122.6	117.6	123.9
2a											115.1	122.7
3	137.6	128.7	137.6	128.7	137.6	128.8	41.6	41.6	129.4	130.5	127.1	128.1
3a											129.5	130.6
4	112.6	116.6	112.6	116.6	111.9	114.7	17.3	19.1	119.9	130.5	138.7	138.5
4a	127.1	133.7	127.1	133.7	127.1	133.4	126.6	125.8			120.5	130.6
4b	121.3	119.8	121.3	119.8	114.8	115.1	114.4	118.9				
5	121.7	121.7	121.7	121.7	122.5	124.8	121.7	123.2				
6	119.2	121.4	119.2	121.4	109.1	112.7	109.3	114.2				
7	127.8	131.8	127.8	131.8	160.1	162.8	157.7	160.8				
8	112.0	113.2	112.0	113.2	94.6	94.5	90.7	93.8				
8a	140.5	143.2	140.5	143.2	134.5	145.6	136.8	142.6				
8b	134.7	131.6	134.7	131.6	131.2	132.3	126.6	124.4				
OCH_3					56.9	56.0	55.7	55.7				

[a]Chemical shifts are expressed in δ units relative to Me_4Si.
[b]From ref. 13.

TABLE 3. The ^{13}C nmr shifts of sulfonated β-carbolines and model compounds in 95% w/w sulfuric acid

Carbon	**1s, 2s**[a]	**3s**	**6s**	**4s**	**5s**	**7s**	**8**	**9**
1	129.9	140.7	142.5	138.2	140.0	167.4	134.7	140.0
1a								133.7
2							122.1	124.4
2a								122.3
3	130.7	131.0	136.7	130.3	131.7	42.6	130.8	129.6
3a								131.5
4	114.8	117.3	117.4	115.1	115.7	18.6	130.6	138.3
4a	135.7	135.7	137.0	134.7	134.8	129.1		131.1
4b	119.3	120.5	120.6	113.0	114.5	117.6		
5	124.6	125.1	125.0	126.9		126.3		
6	128.9(s)	129.8(s)	129.6(s)	119.3(s)	119.8(s)	120.2(s)		
7	126.9	130.0	129.6	159.7	155.8	157.2		
8	118.6	115.4	115.3	95.6		95.6		
8a	146.6	146.5	146.6	148.4	142.9	145.3		
8b	135.1	134.6	133.2	134.3	134.3	126.8		
OCH_3				56.9		56.8		

[a]These spectra were fully superimposable.

Can. J. Chem. Downloaded from www.nrcresearchpress.com by 41.223.56.140 on 09/07/12
For personal use only.

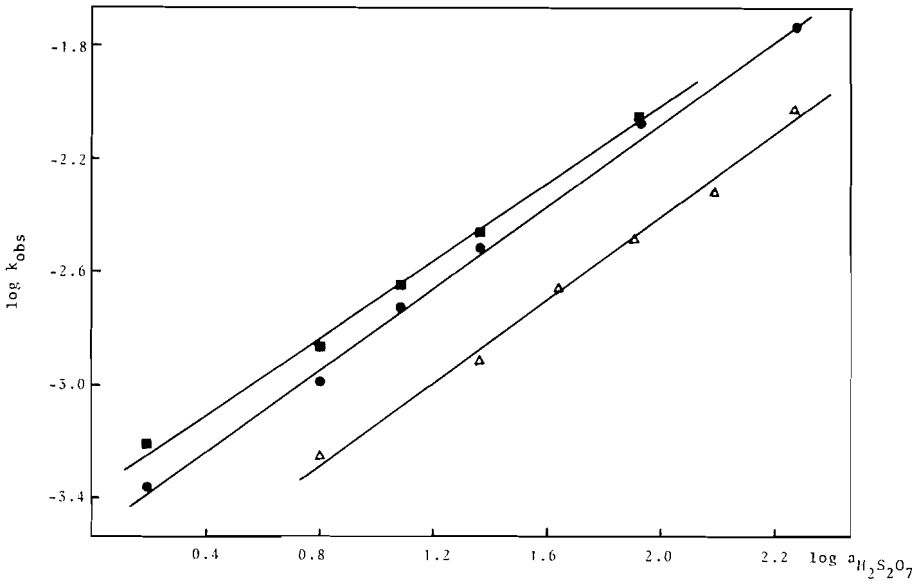


FIG. 1. Correlation of log k_{obs} of the sulfonation of **2** (△), **3** (●), and **6** (■) with log $a_{H_2S_2O_7}$.

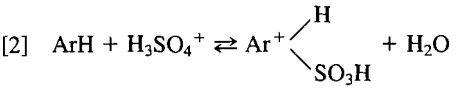
TABLE 4. First-order rate constants ($k_{obs} \times 10^4$ s^{-1}) for the homogeneous sulfonation of β-carbolines in concentrated sulfuric acid[a]

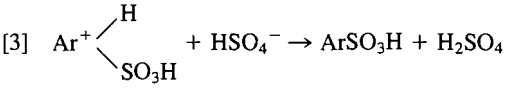
H_2SO_4 (% w/w)	2	3	4	5	6	7
81.8	—	—	3.31	—	—	12.6
82.5	—	—	4.40	5.81	—	20.6
83.3	—	—	6.62	—	—	27.3
84.1	—	4.64	—	10.5	6.78	36.9
84.9	—	—	—	22.4	—	55.3
85.7	6.1	10.5	18.8	34.8	14.4	65.9
86.4	—	20.0	33.4	63.4	24.3	—
87.1	12.9	32.8	58.4	100.0	35.5	—
87.8	24.1	—	113.3	—	—	—
88.5	35.2	94.9	—	—	95.2	—
89.2	50.4	—	—	—	—	—
90.0	101.4	201.8	—	—	—	—

[a]Substrate concentration usually (4–8) $\times 10^{-5}$ M.

respectively. These slopes are very similar to those observed for the sulfonation of other aromatic hydrocarbons, such as mono and dialkylbenzenes, for which the rates of sulfonation are also more nearly proportional to the activity of $H_3SO_4^+$ than to the activity of $H_2S_2O_7$ (25). Considering these slopes and the interpretation of the results for the alkylbenzenes (25, 26), we proposed on the basis of the unit slope criterion that sulfonation of compounds **2**, **3**, and **6** in 85–90% w/w sulfuric acid is effected by the species $H_3SO_4^+$.

On the other hand, it is interesting to consider that, as in the case of aniline (27), the sulfonations of these compounds could proceed via the formation of an N-sulfonated derivative intermediate, which rearranges further to give the final product. The fact that **6**, for which N-substitution is no longer possible, is also sulfonated in a similar way to **3**, rules out this possibility. Therefore, it can be concluded that sulfonation of **2**, **3**, and **6** in 85–90% w/w sulfuric acid at 25°C must occur by direct electrophilic attack of the $H_3SO_4^+$ species on the C-6 position of the benzene ring of the β-carboline, according to the following mechanism:





with reaction [2] as the rate-limiting step.

The correlations of log k_{obs} with log $a_{H_3SO_4^+}$ and log $a_{H_2S_2O_7}$ for **4** and **5** are shown in Figs. 3 and 4, respectively. Each of the graphs has two linear parts below and above 85% w/w sulfuric acid. The slopes of the graphs log k_{obs} vs. log $a_{H_3SO_4^+}$ are 0.73 and 1.39 for **4** and 0.77 and 1.19 for **5**. The corresponding slopes of the similar graphs for $a_{H_2S_2O_7}$ are 0.50 and 0.93 for **4** and 0.48 and 0.80 for **5**. Similar behaviour and differences in slopes between the two types of graphs have already been observed for such other aromatic substrates as anisole and phenol (28).

The main difference between this group of alkaloids and the one discussed before is the presence of an OR substituent (R = H or CH_3) on their benzene rings. In the case of the similarly substituted aromatic substrates anisole and phenol, it has been claimed that protonation of the OR group gave rise to smaller values of the slopes than those observed for the nonsubstituted substrates (28). In our case, the only cationic species present in solution are those protonated on the pyridinic nitrogen and they are the majority species in the sulfuric acid range studied. The protonation of the OR group does not apparently occur. Thus, O-protonation should induce a downfield shift of the OCH_3 lines (29). As can be seen in Table 2, the ^{13}C chemical shifts of the OCH_3 groups of **4** and **5** essentially do not change on passing from DMSO to highly concentrated sulfuric acid solutions.

The protonation of the OR group of these β-carbolines seems to occur at higher acid concentrations than those used in the present study. Recently it has been observed that the fluorescence maxima of **4**, **5**, and **7** suffered a blue shift in solutions of H_0 close to −10, although no changes were observed in their absorption spectra (12). The authors have argued that these shifts were presumably due to the protonation

Can. J. Chem. Downloaded from www.nrcresearchpress.com by 41.223.56.140 on 09/07/12
For personal use only.

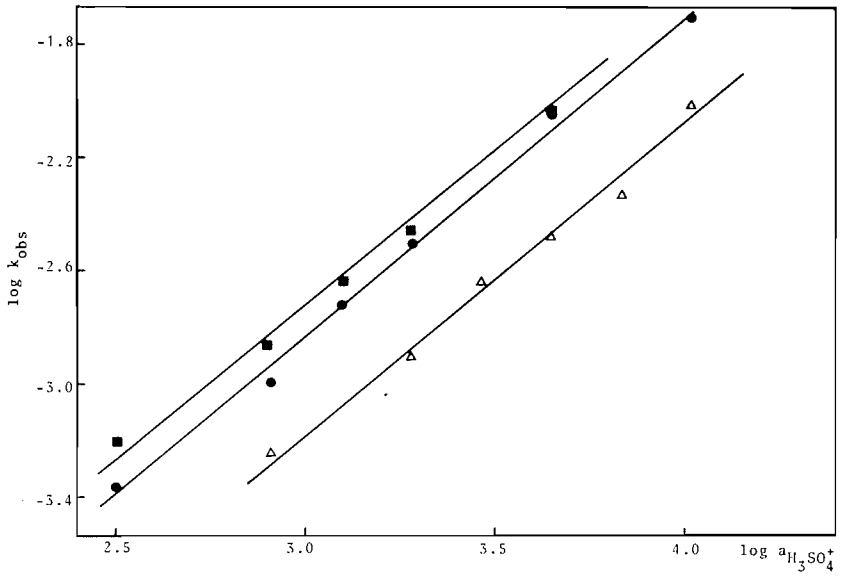


FIG. 2. Correlation of log k_{obs} of the sulfonation of **2** (△), **3** (●), and **6** (■) with log $a_{H_3SO_4^+}$.

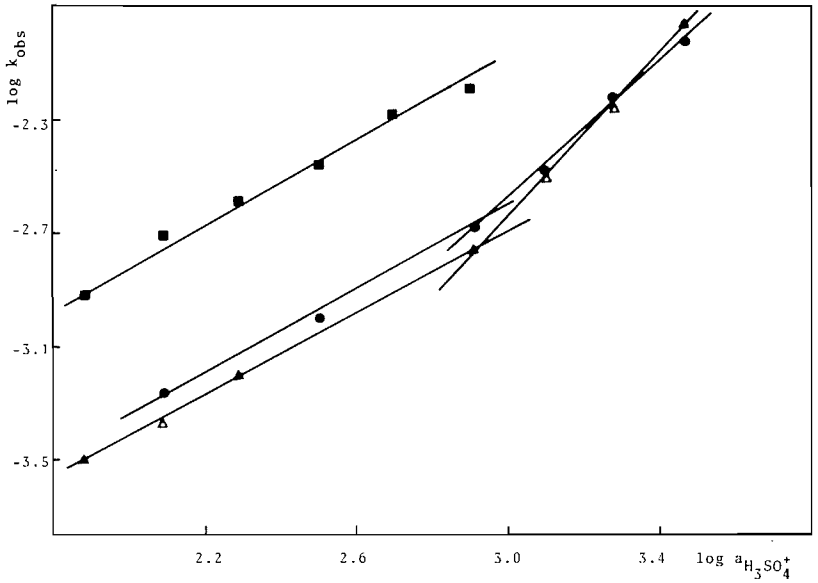


FIG. 3. Correlation of log k_{obs} of the sulfonation of **4** (△), **5** (●), and **7** (■) with log $a_{H_3SO_4^+}$.

of the OR group, since in the case of **3**, where no phenolic oxygen is present, this shift was not observed.

Then, in the sulfuric acid range used in the present work, the sulfonation of **4** and **5** will proceed predominantly via the monoprotonated substrates. Considering the slopes of the log k_{obs} vs. log $a_{H_3SO_4^+}$ and log $a_{H_2S_2O_7}$ and the interpretation of the results of other similar aromatic substrates (28), we propose that sulfonation at the lower sulfuric acid concentrations is effected by the species $H_3SO_4^+$ according to the sequence [2]–[3]. With increasing sulfuric acid concentration there is a changeover in the sulfonating entity from $H_3SO_4^+$ to $H_2S_2O_7$, with the latter species effecting the sulfonation according to the sequence [4]–[3].

$$[4]\quad ArH + H_2S_2O_7 \rightleftarrows Ar^+\begin{matrix}H\\ \diagup\\ \diagdown\\ SO_3H\end{matrix} + HSO_4^-$$

The constancy of the product obtained indicates that the substitution position is the same for both sulfonation mechanisms. This fact has already been observed in the sulfonation reactions of anisole and phenol (28).

The graphs of log k_{obs} vs. log $a_{H_3SO_4^+}$ and log $a_{H_2S_2O_7}$ for the partially aromatic compound **7** (Figs. 3 and 4) are linear with slopes of 0.69 and 0.46 respectively. Therefore, under these conditions sulfonation of **7** will be effected by the species $H_3SO_4^+$ according to the sequence [2]–[3]. It is to be noted

Can. J. Chem. Downloaded from www.nrcresearchpress.com by 41.223.56.140 on 09/07/12
For personal use only.

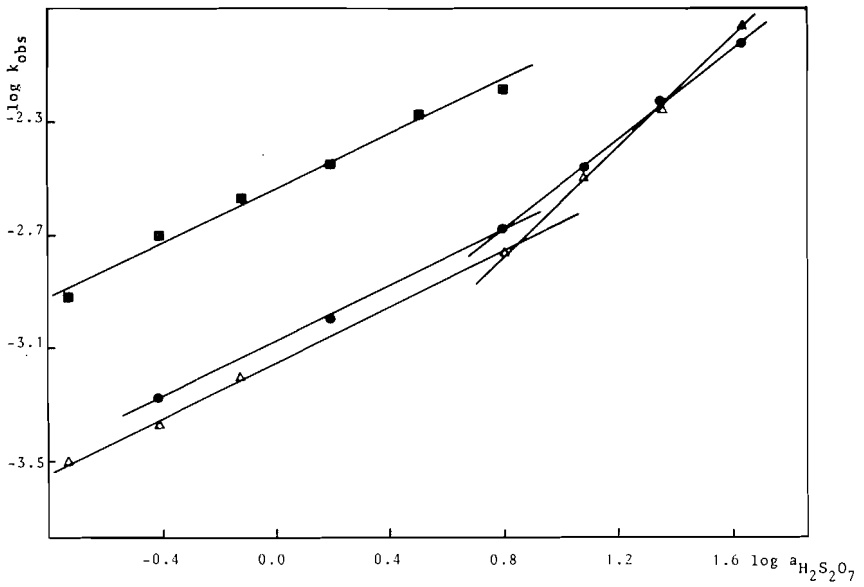


FIG. 4. Correlation of log k_{obs} of the sulfonation of **4** (△), **5** (●), and **7** (■) with log $a_{H_2S_2O_7}$.

that, while **4** and **5** show a similar behaviour, **7** appears to be far more reactive than the fully aromatic substrates. This can be explained by taking into account the different delocalization of the positive charge of the monocations on the benzene ring of the β-carbolines. The greater the aromaticity, the greater the delocalization by resonance of the positive charge will be. Thus the partially aromatic substrate **7** will be more reactive towards electrophilic substitutions than the fully aromatic ones.

The differences, previously mentioned in the Introduction, among sulfonation reactions of β-carbolines and other related compounds can be rationalized in a similar way. Thus, in the range of sulfuric acid concentration used in the present work, indole and carbazole are fully protonated on carbon (30) and nitrogen (31) respectively. This process disrupts the aromaticity of these compounds and the positive charge of the resulting indoleninium and anilinium cations strongly deactivates their benzene ring upon electrophilic substitution reactions. This is also the case of tetrahydro-β-carboline derivatives, which, as typical indoles, protonate on carbon (1) and, therefore, are not easily sulfonated. On the contrary, the pyridinic protonation of β-carbolines does not disrupt the aromaticity and their benzene rings are deactivated in less extension towards electrophilic substitution. Moreover, as our experimental results indicate, the concentration of sulfonating electrophiles, in the sulfuric acid range used, is sufficient to favour the kinetically controlled process over the thermodynamically controlled second protonation previously suggested (12).

Finally, the different reactivity of the unsubstituted benzene and substituted benzene β-carbolines can be qualitatively explained on the basis of substituent effects. The OR-substituted substrates are activated with respect to the non-OR-substituted owing to the electron-releasing effects of the OR substituents.

Acknowledgements

We acknowledge financial support from the Dirección General de Investigación Científica y Técnica (PB86-0236).

1. M. BALÓN, C. CARMONA-GUZMÁN, and D. GONZALEZ. Tetrahedron, **41**, 4703 (1985).
2. J. HIDALGO, M. BALÓN, M. A. MUÑOZ, and C. CARMONA. Tetrahedron, **42**, 1497 (1986).
3. M. A. MUÑOZ, C. CARMONA-GUZMÁN, J. HIDALGO TOLEDO, and M. BALÓN ALMEIDA. J. Chem. Soc. Perkin Trans. 2, 1573 (1986).
4. W. H. PERKIN and R. ROBINSON. J. Chem. Soc. **115**, 933 (1919).
5. ALAN R. KATRITZKY. Handbook of heterocyclic chemistry. Pergamon Press, Oxford. 1985.
6. R. A. ABRAMOVITCH and I. D. SPENCER. Adv. Heterocycl. Chem. **3**, 79 (1964).
7. I. C. TUNG. Chem. Abstr. **55**, 22314 (1961).
8. H. R. SNYDER, S. M. PARMETER, and L. KATZ. J. Am. Chem. Soc. **70**, 222 (1948).
9. S. SIDDIQUI, V. V. AHMAD, M. A. KHAN, and S. ISMAIL. Z. Naturforsch. B: Anorg. Chem. Org. Chem. **28**, 486 (1973).
10. S. SIDDIQUI and S. I. HAMMED. Pakistan J. Sci. Ind. Res. **18**(6), 247 (1975).
11. W. O. KERMACK, W. H. PERKIN, and R. ROBINSON. J. Chem. Soc. **121**, 1872 (1922).
12. M. KRISHNAMURTHY and S. K. DROGA. J. Chem. Soc. Perkin Trans. 2, 1247 (1986).
13. M. A. MUÑOZ PEREZ, M. BALÓN ALMEIDA, C. CARMONA GUZMÁN, J. HIDALGO TOLEDO, and M. LOPEZ POVEDA. Heterocycles, **27**, 2067 (1988).
14. B. T. HO, W. M. MCISAAC, K. E. WALKER, and V. ESTEVEZ. J. Pharm. Sci. **57**, 274 (1968).
15. C. A. COUNE, L. J. G. AUGENOT, and J. DENOËL. Phytochemistry, **19**, 2009 (1980).
16. D. H. WELTI. Magn. Reson. Chem. **23**, 872 (1985).
17. C. SZÁNTAY, G. TOTH, E. MÁRRÁNYOS, G. THALER, and H. DUDDECK. J. Chem. Soc. Perkin Trans. 2, 537 (1988).
18. R. VERPOORTE, T. A. VAN BEEK, R. L. M. RIEGMAN, P. J. HYLANDS, and N. G. BISSET. Org. Magn. Reson. **22**, 328 (1984).
19. K. T. DOUGLAS, R. K. SHARMA, J. F. WALMSLEY, and R. C. HIDER. Mol. Pharmacol. **33**, 614 (1983).
20. A. MAESTRE, M. BALÓN, M. A. MUÑOZ, P. P. TEJEDA, J. HIDALGO, and M. SANCHEZ. An. R. Acad. Farm. **50**, 105 (1984).
21. H. ZOLLINGER. Advances in physical organic chemistry. Vol. 2. *Edited by* V. Gold. Academic Press, London. 1964.
22. J. MARCH. Advanced organic chemistry: reactions, mechanisms, and structure. 2nd ed. McGraw–Hill, Tokyo. 1977.
23. H. CERFONTAIN. Mechanistic aspects in aromatic sulfonation and desulfonation. Interscience Publishers, New York. 1968.

Can. J. Chem. Downloaded from www.nrcresearchpress.com by 41.223.56.140 on 09/07/12
For personal use only.

24. H. CERFONTAIN and C. W. F. KORT. Int. J. Sulfur Chem. Part C: **6**, 123 (1971).
25. C. W. F. KORT and H. CERFONTAIN. Recl. Trav. Chim. Pay-Bas, **87**, 24 (1968).
26. K. LAMMERTSMA, C. J. VERLAAN, and H. CERFONTAIN. J. Chem. Soc. Perkin Trans. 2, 719 (1978).
27. P. K. MAARSEN and H. CERFONTAIN. J. Chem. Soc. Perkin Trans. 2, 1008 (1977).
28. H. CERFONTAIN, H. LAMBRECHTS, Z. R. H. SCHAASBERG-NIENHUIS, R. G. COOMBES, PATTADJIEORGIOU, and G. P. TUCKER. J. Chem. Soc. Perkin Trans. 2, 659 (1985).
29. D. TOUITI, R. JOST, and J. SOMMER. J. Chem. Soc. Perkin Trans. 2, 1793 (1986).
30. R. L. HINMAN and E. B. WHIPPLE. J. Am. Chem. Soc. **84**, 2534 (1962).
31. H. J. CHEN, L. E. HAKKA, R. L. HINMAN, A. J. KRESGE, and E. B. WHIPPLE. J. Am. Chem. Soc. **93**, 5102 (1971).

Can. J. Chem. Downloaded from www.nrcresearchpress.com by 41.223.56.140 on 09/07/12
For personal use only.

Apparent molar volume and adiabatic compressibility studies of aqueous solutions of some drug compounds at 25°C

MOHAMMAD IQBAL and R. E. VERRALL[1]

Department of Chemistry, University of Saskatchewan, Saskatoon, Sask., Canada S7N 0W0

Received August 5, 1988

MOHAMMAD IQBAL and R. E. VERRALL. Can. J. Chem. **67**, 727 (1989).

Apparent molar adiabatic compressibilities and volumes of aqueous solutions of the following drugs (sodium salicylate, methyl orange, L-tryptophan, phenol, and the hydrochloride salts of propranalol, procaine, pilocarpene, and ephedrine) have been calculated from high precision density and sound velocity measurements at 25°C. These drugs are considered important in several biochemical phenomena such as anomalous protein binding, anesthesia, or unique structure–activity relationship and this study is part of a comprehensive investigation of drug–protein interactions in biological systems. The data are qualitatively interpreted in terms of solute–solvent and solute–solute interactions. Some plausible modes of drug hydration are discussed with particular reference to the structure of the drug molecules. The adiabatic compressibility shows a strong correlation with the hydrational behaviour of the solute molecule and appears to be sensitive to the structural features of the solute, such as shape, size, branching, and presence of aromatic rings. It is argued that these aspects are important in terms of considering the geometrical fit of the solute into the ordered form of the aqueous solvent surrounding these solutes.

Key words: apparent molar adiabatic compressibilities, apparent molar volumes, hydration of drugs.

MOHAMMAD IQBAL et R. E. VERRALL. Can. J. Chem. **67**, 727 (1989).

Utilisant des mesures de haute précision de la densité ainsi que de la vitesse du son, à 25°C, on a calculé les volumes et les compressibilités molaires apparentes de solutions aqueuses des drogues suivantes: salicylate de méthyle, orange de méthyle, L-tryptophane, phénol ainsi que les chlorhydrates de la propanolamine, de la procaïne, du pilocarpène et de l'éphédrine. Ces drogues sont souvent considérées comme importantes dans plusieurs phénomènes biochimiques tels que la liaison anormale des protéines, l'anesthésie ou une relation structure–activité particulière; cette étude a été réalisée dans le cadre d'un examen général des interactions drogues–protéines dans des systèmes biologiques. Qualitativement, on interprète ces données en fonction d'interactions soluté–solvant et soluté–soluté. On discute de quelques modes plausibles pour l'hydratation des drogues et en particulier la structure des drogues. Il existe une importante corrélation entre les compressibilités adiabatiques et les possibilités d'hydratation des molécules en solution vis-à-vis de l'hydratation; de plus, elles semblent être sensibles aux caractéristiques structurales du soluté, comme la forme, la grosseur, les ramifications et la présence de noyaux aromatiques. On suggère que ces aspects sont importants lorsqu'on veut insérer ces solutés dans la forme ordonnée du solvant aqueux qui entoure ces solutés.

Mots clés : compressibilités adiabatiques molaires apparentes, volumes molaires apparentes, hydratation des drogues.

[Traduit par la revue]

Introduction

Drug–macromolecular interactions are an important phenomenon in physiological media, such as blood, membranes, intra- and extracellular fluids. The processes of drug transport, protein-binding, anesthesia are but a few examples where drug and biomacromolecules appear to interact in an important and vitally significant manner. The mechanisms of these molecular processes, however, are not clearly understood. Because of the complexities associated with the structure of biomacromolecules, or with the interpretation of their data, it is generally difficult to carry out direct studies of the physiological media. Consequently, it is imperative that one first investigate the properties of each component in an aqueous medium before beginning studies of the more complex systems.

One of the well recognized approaches to the study of molecular interactions in fluids is the use of thermodynamic methods. Thermodynamic properties are generally convenient parameters for interpreting solute–solvent and solute–solute interactions in the solution phase. Fundamental properties such as enthalpy, entropy, and Gibbs energy represent the macroscopic state of the system as an average of numerous microscopic states at a given temperature and pressure. An interpretation of these macroscopic properties in terms of molecular phenomena is generally difficult. Sometimes, higher derivatives of these properties can be interpreted more effectively in terms of molecular interactions. For example, the partial molar volume, the pressure derivative of partial molar Gibbs energy, is a useful parameter for interpreting solute–solvent interactions. Various concepts regarding molecular processes in solutions, electrostriction (1), hydrophobic hydration (2), micellization (3), and cosphere overlap during solute–solute interactions (4, 5), to a large extent have been derived and interpreted from the partial molar volume data of many compounds. The compressibility property, which is the second derivative of the Gibbs energy, also is a sensitive indicator of molecular interactions and can provide useful information about these phenomena, particularly in cases where partial molar volume data alone fail to provide an unequivocal interpretation of the interactions.

It has been shown that perceptible thermodynamic changes are associated with the processes of drug–protein binding (6–15), anesthesia (16–18), etc. In the case of protein binding, anomalous behavior has been noted with respect to certain drugs (19–24). For example, Scatchard plots with positive slopes are observed which signify a decrease in the amount of bound drug as the concentration of protein is increased. This type of binding appears to involve unusual and complex mechanisms. Despite various explanations of the phenomenon, viz., cooperativity or drug-induced protein aggregation (22–24), the role of these drugs remains uncertain and there is a need to further investigate the molecular interactions between proteins and certain specific drugs.

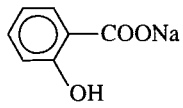
Volumetric changes in drug-containing membranes have been implicated in the phenomenon of anesthesia (16–18). According to the concept of critical volume (16, 17), the anesthetic drug causes an expansion in the bilayer system up to a critical volume level, resulting in a diminution of nerve conduc-

[1]To whom correspondence should be addressed.

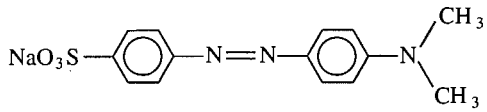
Can. J. Chem. Downloaded from www.nrcresearchpress.com by 41.223.56.140 on 09/07/12
For personal use only.

Can. J. Chem. Downloaded from www.nrcresearchpress.com by 41.223.56.140 on 09/07/12
For personal use only.

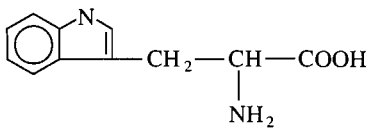
Sodium salicylate (NaSl)



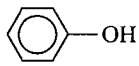
Methyl orange (MeOr)



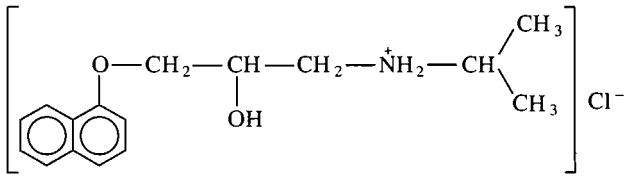
L-Tryptophan (Trp)



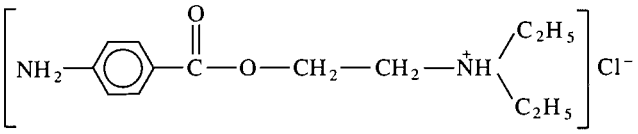
Phenol (PhOH)



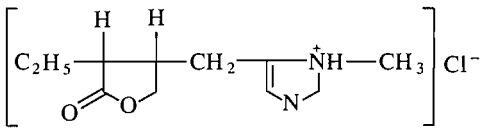
Propranalol HCl (PrHCl)



Procaine HCl (PcHCl)



Pilocarpene HCl (PlHCl)



Ephedrine HCl (EpHCl)

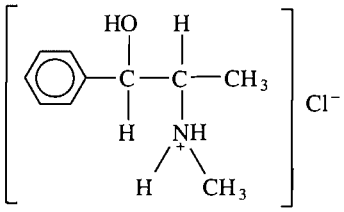


FIG 1. Drugs used in this study and their molecular structures.

tion. The importance of the volumetric behavior of the anesthetic agent is clearly identified in this concept and it appears certain that a definite mechanism will be difficult to establish without a better understanding of the volumetric behaviour of the drugs involved.

As part of the longer term objective to investigate thermodynamic aspects of biochemical processes involving such drug–macromolecular interactions, we report the results of determinations of apparent molar adiabatic compressibilities and volumes of eight drugs in aqueous solution at 25°C. The drugs studied are: (*i*) sodium salicylate (NaSl): an analgesic that binds with plasma proteins (19); (*ii*) methyl orange (MeOr): a dye that binds with proteins (19); (*iii*) L-tryptophan (L-Trp): an amino acid that binds with proteins (19); (*iv*) phenol (PhOH): a molecule that binds to serum proteins (7, 8, 25); (*v*) propranalol HCl (PrHCl): a β-adrenergic blocking agent that binds with proteins (19); (*vi*) procaine HCl (PcHCl): an anesthetic (26) agent; (*vii*) pilocarpene HCl (PlHCl): a muscle and gland stimulant of unique molecular structure that acts through membranes (26); (*viii*) ephedrine HCl (EpHCl): a drug that stimulates the central nervous system by acting through membranes (26). The molecular structures of these drugs are shown in Fig. 1.

The rationale for choosing these drugs for study is based primarily on their role in various pharmacological phenomena as discussed above.

Experimental

Materials

All drugs were recrystallised from commercial samples of reasonably high purity. Their source and the purification procedures followed are given below: (*i*) Sodium salicylate (Sigma, lot No. 32F-012B) was recrystallised twice from an ethanol–water mixture (15:1, v/v), and

dried under vacuum in a pistol dryer over boiling water. (*ii*) Methyl orange (BDH, lot No. 788569) was recrystallised twice from hot water, then washed with cold ethanol followed by diethyl ether. It was dried under vacuum in a pistol dryer over boiling water. (*iii*) L-tryptophan (Sigma, lot No. 63F-0321) was recrystallised twice from a water–ethanol mixture (ca. 1:1, v/v) washed with anhydrous diethyl ether, and dried at room temperature under vacuum over P_2O_5. (*iv*) Phenol (Analar BDH, lot No. 0605270) was recrystallised from 75% (w/w) solution in water by cooling to 11°C. The crystallised material was centrifuged, rinsed with cold water (0–2°C) saturated with phenol, and dried at room temperature. (*v*) Propranalol HCl (Sigma, lot No. 81F-0306) was recrystallised twice from absolute ethanol, dried under vacuum at room temperature over P_2O_5, and stored at 0–5°C. (*vi*) Procaine HCl (Sigma, lot No. 80F-0020) was recrystallised twice from absolute ethanol and dried under vacuum in a pistol dryer over a boiling mixture of ethylene glycol – water (3:7 v/v). (*vii*) Pilocarpene HCl (McArthur Chemical Co. lot No. K12433417) was recrystallised twice from absolute ethanol and dried as in the case of PcHCl over a boiling mixture of ethylene glycol – water (3:2 v/v). (*viii*) Ephedrine HCl (Sigma, lot No. 121F-0223) was recrystallised twice from absolute ethanol and dried as in the case of PcHCl over boiling ethylene glycol.

The purity of the drug compounds was checked by comparing the observed melting points with those reported in the literature. In all cases, excellent agreement was found between the observed and reported values.

Water used in these experiments was distilled and deionized by using a Millipore Super-Q system and was degassed before use. All solutions used for thermodynamic measurement were prepared on a weight basis.

Apparatus and procedure

Apparent molar volumes (ϕ_v) of the drugs were calculated using the following relation

$$[1] \qquad \phi_v = \frac{M}{d} + \frac{1000(d_0-d)}{mdd_0}$$

where M is the relative molar mass of the solute, m is the molality of the solution, and d and d_0 are the densities of solution and solvent, respectively. Densities of the aqueous drug solutions were measured at 25°C using a high precision digital densimeter (Model 02D Sodev Inc.) experimental details of which are described elsewhere (27). Thermostating of the densimeter was maintained by a closed-loop Sodev Temperature Controller which maintained the temperature constant to better than ±0.001°C. The absolute temperature of the solution in the cavity was obtained by using a tissue implantation thermistor calibrated against a Pt resistance thermometer (Leeds and Northrup). Temperatures were found to be accurate to within ±0.01°C. The instrument was calibrated with water (28), dry nitrogen (density calculated from the ideal gas equation), and NaCl solution (29) using density data from the literature. In order to minimize errors instrument calibration was performed prior to each series of measurements. The density of each solution was obtained relative to that of the solvent which was measured immediately before and after measuring the solution density. The precision in the density data are better than ±2.0 ppm.

Compressibility can be measured under either isothermal or adiabatic conditions. The former is difficult to obtain experimentally with high accuracy for dense fluids. On the other hand, the adiabatic compressibility is more complex to interpret but is relatively easy to measure with high accuracy. It is calculated from sound velocity and density data. The isothermal compressibility can be estimated from the adiabatic analogue if the coefficient of thermal expansion, α, heat capacity at constant pressure, C_p, and density of the solution are known (1).

Ultrasonic velocities were measured as previously described (30). The following equation was used to calculate the sound speed, u, in ms^{-1}.

$$[2] \qquad u = \ell f(1 + \alpha t)/(7 - t_d f)$$

where ℓ is the sonic path length in meters, f is the frequency in hertz, t is the temperature of the solution in degrees Celsius, α is the coefficient of thermal expansion of the probe metal, and t_d is the electrical delay time in seconds. Values of ℓ, α, and t_d are supplied by the manufacturer, but ℓ and t_d can be determined independently. The original glass vessel supplied with the instrument was replaced by a cell having a smaller volume (70 mL) fitted with a thermostating arrangement and a suitable lid for transferring material to and from the cell whenever required. The temperature was controlled by a closed-loop temperature controller (Sodev Inc. Canada), capable of maintaining the temperature constant to better than ±0.001°C. The velocimeter was calibrated by obtaining values of ℓ and t_d using previously reported sonic velocity data for water (31) and aqueous NaCl solutions (32). In the case of NaCl, the data were statistically analysed and regression constants were obtained as a function of concentration. In order to minimize errors, instrument calibration was performed prior to each series of measurements. The precision in the sound velocity was found to be better than ±0.02 ms^{-1}.

Adiabatic compressibility coefficients, β, in units of Pa^{-1} were derived from the relation

$$[3] \qquad \beta = 1/u^2 d$$

where d is the solution density in kg m^{-3}. The apparent molar adiabatic compressibility (ϕ_k) of liquid solutions was calculated from the relation

$$[4] \qquad \phi_k = \frac{1000}{md_0}(\beta - \beta_0) + \phi_v \beta$$

where m is the molality of the solution, M is the relative molar mass of the solute, d is the density of the solution, d_0 is the density of the solvent, and β_0 and β are the compressibility coefficients of the solvent and solution, respectively.

Results

Apparent molar volume

ϕ_v data for all compounds in aqueous solution were calculated using eq. [1]. Experimental ϕ_v data for all the systems studied are found in the supplementary material.[2] Apparent molar volume data for the hydrochloride salts and phenol were checked for possible changes arising from the proton ionisation reaction (33, 34).

$$[5] \qquad BH^+ + H_2O \rightleftarrows B + H_3O^+$$

where BH^+ and B represent the protonated and unprotonated form of the compound, respectively. The volume correction can be either calculated or can be eliminated by studying the solutions in sufficiently acidic medium (in order to suppress these reactions). In the former case, the corrected value, ϕ_v(corr) is related to the observed value, ϕv(obs), through the following relation

$$[6] \qquad \phi_v(corr) = \phi_v(obs) - \gamma \Delta \bar{V}^0$$

where $\Delta \bar{V}^0$ is the change in volume for eq. [5] and γ is the degree of dissociation. In the present cases it can be calculated from the following relation

$$[7] \qquad \gamma = -K + (K^2 + 4Km_0)^{1/2}/2m_0$$

where K is the ionisation constant for eq. [5] and can be obtained from pK data and m_0 is the initial concentration of the solute. $\Delta \bar{V}^0$ can be calculated from the corresponding volumes of the individual species involved in eq. [5], e.g.,

$$[8] \qquad \Delta \bar{V}^0 = \bar{V}^0(B) + \bar{V}^0(H_3O^+) - \bar{V}^0(BH^+) - \bar{V}^0(H_2O)$$

[2]A complete set of tables of apparent molar volume, apparent molar compressibility, sound velocity, and density data for these systems may be purchased from the Depository of Unpublished Data, CISTI, National Research Council of Canada, Ottawa, Ont., Canada K1A 0S2.

Can. J. Chem. Downloaded from www.nrcresearchpress.com by 41.223.56.140 on 09/07/12
For personal use only.

Can. J. Chem. Downloaded from www.nrcresearchpress.com by 41.223.56.140 on 09/07/12
For personal use only.

where $\bar{V}^0(H_2O)$ is taken from the density of the pure solvent and $\bar{V}^0(B)$ is generally obtained from experimental data. In the absence of experimental data, however, it can be approximated through the use of simple additivity rules. $\bar{V}^0(BH^+)$ can also be estimated through such additivity methods, e.g.,

[9] $\bar{V}^0(B) = \bar{V}^0(BHCl) - \bar{V}^0(HCl)$

[10] $\bar{V}^0(BH^+) = \bar{V}^0(BHCl) - \bar{V}^0(Cl^-)$

The magnitude of the correction to the volume arising from the ionisation process, eventually, depends on the value of γ. In the case of the compounds studied in this work, it was found that, due to the high pK values of the bases (35, 36), values of γ were found to be sufficiently small so that the net correction to experimental ϕ_v values was negligible and within the experimental error. The observed volumetric data were thus taken as the true data for the hydrochloride salts. A similar assessment was obtained in the case of phenol, which is known to undergo slight proton ionisation in aqueous medium. Corrections due to other possible reactions (disproportionation, etc.) were not considered since the degree to which these reactions occur is believed to be much smaller than that of the proton ionisation.

ϕ_v data for hydrochlorides, sodium salicylate, and methyl orange were treated as a function of the square root of concentration, to take into account their electrolyte character. They were fitted to the following equation

[11] $\phi_v = \phi_v^0 + S_v m^{1/2}$

The use of empirical slopes rather than theoretical slopes for the electrolyte compounds may lead to different infinite dilution data but in the present cases the differences lie within the uncertainty of the extrapolated values obtained from the empirical relation, eq. [11].

Data for the remaining compounds, viz., phenol and L-tryptophan were fitted to the relation

[12] $\phi_v = \phi_v^0 + S_v m$

Table 1 contains the values of the coefficients obtained for these fits. The limiting values of the apparent molar volumes were taken as the partial molar volumes, $\bar{V}^0$, of the respective compounds at infinite dilution. Figure 2 shows graphs of the concentration dependence of ϕ_v for all the drugs studied.

With one exception, a linear relation between the apparent molar volumes and the independent variable, either molality or $m^{1/2}$, is seen to hold throughout the entire concentration range studied. Propranalol hydrochloride shows (Fig. 2) a linear dependence at low concentrations (below 0.0625 m), only. Above this concentration values of ϕ_v begin to rise rather sharply. The coefficients $\bar{V}^0$ and S_v for PrHCl were obtained by fitting the data in the linear region only.

Efforts were made to minimise personal error and possible experimental artifacts by carefully controlling experimental procedures. Systematic errors were analysed separately and were found to be significant at lower solute concentrations. However, errors in apparent molar volumes arising from uncertainty in concentration were, generally, not a limiting factor. Uncertainties associated with the density were found to be more important. The maximum estimated error in ϕ_v derived from the error analysis treatment was $\pm 1.00 \times 10^{-6}$ m^3 mol^{-1} at 0.002 m, the lowest limit of concentration used in this study.

Apparent molar adiabatic compressibility

ϕ_k values of drug compounds were calculated using eq. [4]. Density, sound velocity, and ϕ_k data for all systems are found in the supplementary material.[2] ϕ_k data for the hydrochloride salts and phenol were analyzed for possible changes arising from the proton ionisation reaction (33, 34). The correction to ϕ_k due to this reaction was found to be within the experimental error.

ϕ_k data for hydrochloride salts, sodium salicylate, and methyl

TABLE 1. Volumetric data for drugs: values of $\bar{V}^0$ and S_v at 25°C

Compound	$\bar{V}^{0a}$	S_v^b
NaSl	93.40	1.20
	0.02[d]	0.04
MeOr	227.58	−11.12
	0.14	0.89
Trp	144.24	0.59[c]
	0.02	0.45
PhOH	85.20	−0.64[c]
	0.01	0.02
PrHCl	245.14	0.86
	0.06	0.40
PcHCl	225.84	−1.61
	0.03	0.10
PlHCl	193.34	−1.05
	0.03	0.10
EpHCl	168.79	0.29
	0.02	0.11

[a]Expressed in units of $10^6 \times$ m^3 mol^{-1}.
[b]Expressed in units of $10^6 \times$ m^3 mol$^{-3/2}$ kg$^{1/2}$.
[c]Expressed in units of $10^6 \times$ m^3 mol^{-2} kg.
[d]Numbers represent standard deviations obtained from weighted least-squares fit of the data.

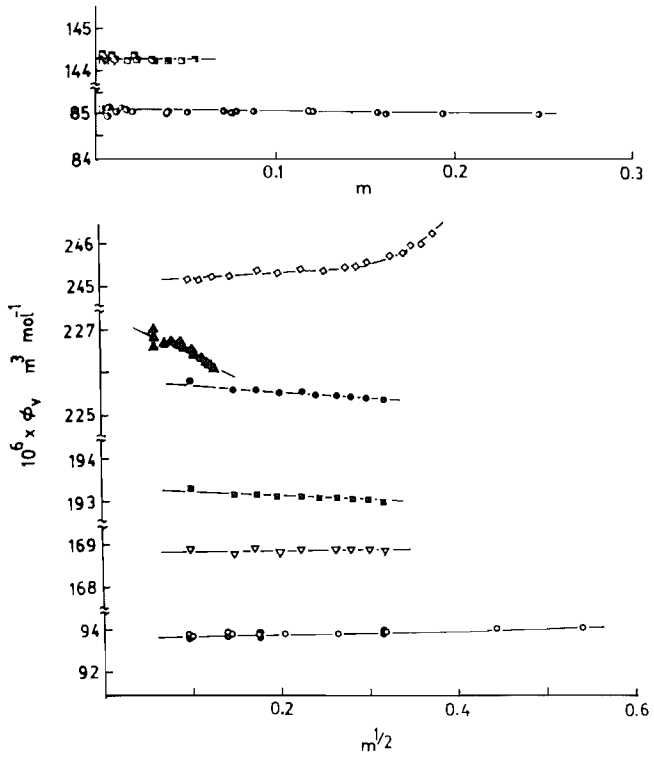


FIG. 2. ϕ_v vs. concentration (m or $m^{1/2}$) plots for -○- NaSl, -▲- MeOr, -□- Trp, -◑- PhOh, -◇- PrHCl, -●- PcHCl, -■- PlHCl, -▽- EpHCl.

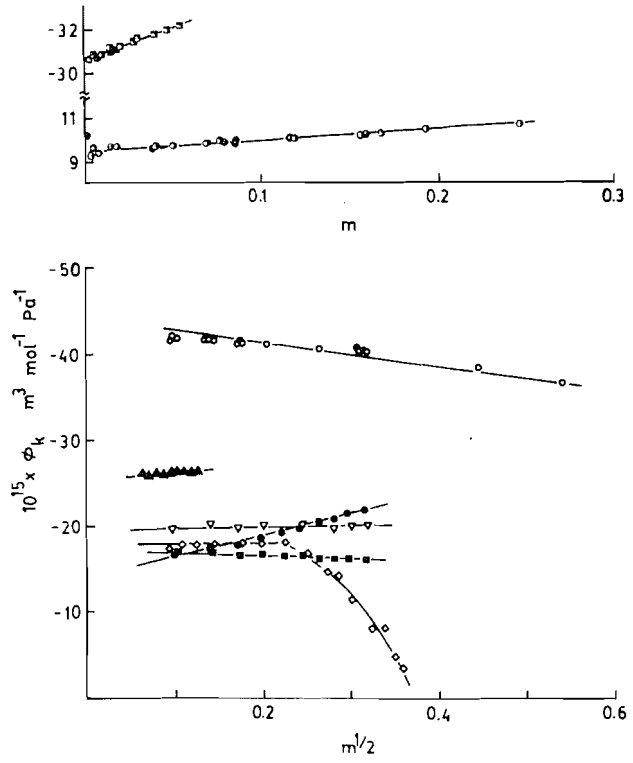


FIG. 3. ϕ_k vs. concentration (m or $m^{1/2}$) plots for -○- NaSl, -▲- MeOR, -□- Trp, -◑- PhOH, -◇- PrHCl, -●- PcHCl, -■- PlHCl, -▽- EpHCl.

TABLE 2. Compressibility data for drugs: values of $\bar{K}^0$ and S_k at 25°C

Compound	$\bar{K}^{0a}$	S_k^b
NaSl	−45.59	17.06
	0.30[d]	0.57
MeOr	−25.67	6.09
	0.17	1.11
Trp	−30.64	−29.49[c]
	0.02	0.51
PhOH	+9.63	4.76[c]
	0.01	0.11
PrHCl	−18.85	9.08
	0.68	5.48
PcHCl	−13.07	−27.75
	0.03	1.10
PlHCl	−17.41	4.31
	0.03	0.17
EpHCl	−19.73	1.10
	0.27	0.98

[a]Expressed in units of $10^{15} \times$ m^3 mol^{-1} Pa^{-1}.
[b]Expressed in units of $10^{15} \times$ m^3 mol$^{-3/2}$ Pa^{-1} kg$^{1/2}$.
[c]Expressed in units of $10^{15} \times$ m^3 mol^{-2} Pa^{-1} kg.
[d]Numbers represent standard deviations obtained from weighted least squares fit of the data.

orange were treated as a function of the square root of concentration, to take into account their ionic nature. They were fitted to the following equation

[13] $\phi_k = \phi_k^0 + S_k m^{1/2}$

Data for phenol and L-tryptophan were treated as a direct function of concentration and were fitted to the following equation

[14] $\phi_k = \phi_k^0 + S_k m$

The infinite dilution value, ϕ_k^0, of the apparent molar adiabatic compressibility is equal to the partial molar adiabatic compressibility, $\bar{K}^0$. Figure 3 shows graphs of the concentration dependence of ϕ_k for the systems studied and values of ϕ_k and S_k are shown in Table 2.

A linear relation between the apparent molar adiabatic compressibilities and the independent variable, either molality or $m^{1/2}$, is seen to hold throughout the entire concentration range studied, with one exception. Propranalol hydrochloride shows a linear dependence at low concentrations (below 0.0625 m), only. Above this concentration ϕ_k appears to increase rather sharply, the change being more pronounced than in the case of ϕ_v. The coefficients $\bar{K}^0$ and S_k for PrHCl were obtained by fitting the data within the linear region only.

Errors in ϕ_k data were estimated and it was found that, due to the observed uncertainties in density (2 ppm) and in sound velocity (1 ppm), the overall magnitude of the uncertainty at 0.002 m, the lower limit of concentration studied, was $\pm 1.0 \times 10^{-15}$ m^3 mol^{-1} Pa^{-1}.

Discussion

The partial molar volumes and adiabatic compressibilities at infinite dilution of these compounds can be described in terms of two primary contributions, i.e., constitutive and hydrational.

[15] $\bar{M}^0 = \bar{M}_c^0 + \bar{M}_h^0$

where $\bar{M}^0$ is the partial molar property at infinite dilution, $\bar{M}_c^0$ is the constitutive component, composed of the sum of atomic and group contributions, and $\bar{M}_h^0$ is the hydrational component. The latter is believed to be more significant in terms of interpreting solute–solvent interactions.

In the case of volume studies, $\bar{V}_h^0$ can be obtained from $\bar{V}^0$ and $\bar{V}_c^0$ values. $\bar{V}_c^0$ data may be estimated either from the crystallographic volumes or by using an additivity scheme for atomic or group (van der Waals) volumes. No crystallographic data were available for these compounds. Furthermore, the use of additivity schemes generally was found to be too unrealistic, and, consequently, no further estimation of $\bar{V}_h^0$ was attempted. Assuming that the molecular skeleton of these solutes is practically incompressible, the $\bar{K}_c^0$ component of the partial molar compressibility can be considered to be negligible. Therefore, to a good approximation, the observed compressibility can be taken as the compressibility of hydration, $\bar{K}_h^0$.

Most of the drug compounds studied in this work are ionic in nature. Extrathermodynamic assumptions can be applied to obtain relative measures of partial molar ionic volumes and compressibilities at infinite dilution. This procedure provides for a qualitative comparison of ion–solvent interaction for different ions. For sodium and hydrochloride salts, literature values of $\bar{V}^0$ and $\bar{K}^0$ for Na^+ and Cl^- ions were employed in some cases to estimate the respective thermodynamic values for their counter ions.

The concentration dependence of the volume and compressibility properties in aqueous medium were interpreted in terms of the cosphere overlap model (4, 5), the characteristics of the

Can. J. Chem. Downloaded from www.nrcresearchpress.com by 41.223.56.140 on 09/07/12
For personal use only.

Can. J. Chem. Downloaded from www.nrcresearchpress.com by 41.223.56.140 on 09/07/12
For personal use only.

cospheres being dependent upon the drug structure, size, shape, and hydrophobicity. The results are discussed below in more detail for the volume and compressibility studies. A brief description of the behaviour and use of the drug compounds in physiological systems is included with the discussion of the volume results. The volume and compressibility results are discussed separately to focus better on variations in these properties within the series of compounds. In general, it has been found that the compressibility results provide better insight into the hydration phenomena of these compounds.

Apparent molar volume

Sodium salicylate

The use of NaSl as a drug is largely based on its analgesic and antipyretic properties, much like aspirin (26, 36–39). Salicylates are found to exhibit protein-binding properties (19, 22, 24) and Scatchard plots having positive slopes have been reported (22, 24) for salicylate – serum albumin systems. Salicylates are also found to impair the binding of the drug diflunisal to plasma protein by displacing it from the primary binding sites (40).

While the Na^+ ion is believed to cause electrostriction in water, the hydration of the salicylate ion is not clearly understood. Various studies of benzene and its derivatives in water have led to conflicting interpretations with respect to their hydration behaviour. Shahidi (41) has described benzene solvation in terms of extensive hydrophobic hydration in aqueous medium. Contrary to this explanation, Masterton (42) and Hepler (43) have indicated that the aromatic ring causes little influence on water structure, presumably due to the counterbalancing effects arising from its hydrophobic and structure breaking character. The structure-breaking effect is due to a poor fit of the planar ring into the tetrahedral structure of water. The data reported here support the view presented by Masterton and Hepler. However, the effect of substituents and the negative charge on the salicylate ion may disturb this apparent balance such that a weaker hydration of the anion can be expected as a result of the diffuse charge and the potential for hydrogen bond formation between water and phenolic OH. An overall constriction in the solution volume possibly may occur.

A value of $\bar{V}^0$ for NaSl was calculated from group volume data obtained from the literature and compared to the experimental value obtained in this study. Values of 85.92×10^{-6} m^3 mol^{-1} for PhCOONa (41) (Ph = phenyl group) and 3.63×10^{-6} m^3 mol^{-1} for phenolic OH (41) give a calculated $\bar{V}^0$ of 89.55×10^{-6} m^3 mol^{-1} for NaSl, 3.85×10^{-6} m^3 mol^{-1} smaller than the experimental value. The difference may be due to interactions between the adjacent substituents on the ring that, otherwise, are not taken into account in the additivity scheme.

The concentration dependence of the apparent molar volume is given by the S_v value which is 1.20×10^{-6} m^3 $mol^{-3/2}$ $kg^{1/2}$. This is smaller than the Debye–Hückel limiting law slope value (1.868×10^{-6} m^3 $mol^{-3/2}$ $kg^{1/2}$), for 1:1 electrolytes in water at 25°C (1). However, a direct comparison of the S_v data of this work with the Debye–Hückel coefficient is not appropriate since the lower range of concentration used in this study is well above the range of the limiting law region.

Methyl orange

This dye is known to bind to proteins. Its medicinal value is due to its germicidal action and selective staining capability on certain tissues and skin (26, 36–38). It is one of the drugs that exhibit positive Scatchard plots (22, 23). ϕ_v data for this compound were obtained at very low concentrations in water because its poor solubility precluded determination of apparent molar volumes at concentrations above 0.016 *m*. The data, consequently, have substantial scatter and larger standard deviations in calculated parameters than for the other compounds. $\bar{V}^0$ of the anion was estimated from the measured value of $\bar{V}^0$(MeOR) (227.58×10^{-6} m^3 mol^{-1}) and the literature value of $\bar{V}^0(Na^+)$ (-6.61×10^{-6} m^3 mol^{-1}) (44) to give a value of 234.19×10^{-6} m^3 mol^{-1}.

The negative value of S_v (cf. Table 1) is presumably due to the hydrophobicity of this molecule. The solute–solute interactions in such cases are believed to occur by means of constructive overlap of cospheres (5).

L-*Tryptophan*

This essential amino acid has been widely investigated in protein-binding studies (19–24, 45). Scatchard plots having positive slopes have been reported for L-tryptophan binding with serum albumins (22, 23). L-tryptophan in its zwitterionic form is believed to be extensively hydrated in aqueous medium. Some previous studies have reported volumetric data for D- and DL-tryptophan. Millero *et al.* (46) reported a value of $\bar{V}^0$ for D-tryptophan of $(143.91 \pm 0.14) \times 10^{-6}$ m^3 mol^{-1} while Cohn and Edsall (47), and Mishra and Ahluwalia (48) have reported $\bar{V}^0$ values for DL-tryptophan of 144.1 and $(143.8 \pm 0.2) \times 10^{-6}$ m^3 mol^{-1}, respectively. The value of $\bar{V}^0$ for L-tryptophan reported here compares well with these data. Differences due to subtle stereo-specific interactions, however, cannot be discerned.

The values of S_v for tryptophan reported in the literature differ markedly from one study to another. The value reported by Millero *et al.* (46) for D-tryptophan is $(0.233 \pm 0.14) \times 10^{-6}$ m^3 mol^{-2} kg while that reported by Mishra and Ahluwalia (48), for the DL-isomer is $(5 \pm 19) \times 10^{-6}$ m^3 mol^{-2} kg. The value of $(0.59 \pm 0.45) \times 10^{-6}$ m^3 mol^{-2} kg reported here for L-tryptophan differs from both, although it lies within the range of the two.

Phenol

Phenol and its derivatives are well known for their antibacterial action. There are many reports of phenol binding with proteins. Breuer (7, 8) has measured volume changes associated with the binding of phenol with keratin. Normal binding of phenol with serum albumin is indicated from Scatchard plots (25). Shahidi (41) has reported partial molar volume studies of phenol and has given a value of $\bar{V}^0$ of $(84.90 \pm 0.03) \times 10^{-6}$ m^3 mol^{-1}. The value of $(85.20 \pm 0.01) \times 10^{-6}$ m^3 mol^{-1} reported here compares well with it.

The molecular solvation of phenol in water is expected not to be too dissimilar from that of benzene. The effect of OH substitution on the benzene ring, in terms of hydrational changes, is difficult to predict from the partial molar volume data.

Propranalol HCl

Propranalol hydrochloride is used as a β-adrenergic blocking agent (35–38). It is well known as a suppressor of heart rate and contractility and can be used in cardiac failures resulting from arrhythmia. The D-isomer is a better antiarrhythmic but is found to be nearly devoid of β-adrenergic blocking activity. The compound studied in this work was the DL-isomer.

Values of $\bar{V}^0$ of PrHCl in this work are derived from extrapolation of ϕ_v data below 0.0625 *m*. Above this concentration, apparent molar volumes tend to rise quite sharply. This rise can be interpreted as due to the onset of molecular aggregation (49). The overall hydrational picture of this molecule is difficult to

predict. Its molecular structure (Fig. 1) shows a naphthalene ring attached to a hydrocarbon chain with an intervening amino group and two hydrogen bonding sites. The effect of charge on the amino nitrogen appears to be dissipated because of its delocalisation over the extended structure, leaving the cation with little electrostatic character. The aggregation above 0.0625 *m*, in effect, implies an overall hydrophobic nature of the molecule. The presumed aggregation may be described as due either to the stacking of aromatic rings (50) or micellization promoted by the hydrophobic chain of the molecule.

Procaine HCl

It is the least toxic and most widely used anesthetic drug in a variety of conditions where nerve blockage is desired (35–38). No data, however, are available to test the critical volume hypothesis.

The hydrational picture of the PcHCl molecule is difficult to establish with certainty because of its complex structure. Figure 1 shows the structure of the molecule as having several polar sites dispersed among hydrophobic regions. The polarity of these sites, however, appears to be diminished by the hydrophobicity of the remaining structure. An aromatic ring, two intervening methylenes and a branched hydrocarbon portion of the molecule seem to impart an overall hydrophobic character to the molecule. A negative value of S_v, presumably, is indicative of this hydrophobicity and thus suggestive of a molecular hydration similar to that associated with typical hydrophobic solutes. The presence of the aromatic ring is expected to perturb the hydration layer stretching around the extended structure of the molecule. It may be argued that solute–solute interactions, in this case, can occur via overlap of hydration spheres engulfing the branched chain terminus of the molecule.

Pilocarpene HCl

This drug is known for its direct action on cells and is used as a stimulant for muscles and gland cells (35–38). It shares many of the properties of acetylcholine.

Like PrHCl and PcHCl, its structure is complex so that its hydration behavior is difficult to predict from partial molar volume data alone. A small negative value of S_v (Table 1) may be interpreted as showing the compound to be slightly hydrophobic in character. It appears that there is a near balance between hydration of the polar and hydrophobic parts of the molecules leading to the observed small net hydrophobicity.

Ephedrine HCl

This drug is a strong stimulant of the central nervous system that penetrates membranes and the brain better than other drugs of similar function (35–38). It is used to prevent a variety of allergic syndromes, to act as a respiratory stimulant and as an antidote to morphine and other barbiturates.

The present volumetric data indicate solution behaviour similar to that seen in the case of pilocarpene HCl. However, the net result of the opposing ionic and hydrophobic effects in the structure of ephedrine HCl appears to indicate marginal dependence of the volume on the ionic effect, as shown by the slightly positive value of S_v (Table 1).

Apparent molar compressibility

It is well established that solutes causing electrostriction lead to a decrease in the compressibility of the solution (51, 52). This is reflected by the negative values of $\bar{K}^0$ of electrolyte solutions. Hydrophobic solutes often show negative compressibilities, as well, due to the ordering that is induced by them in the water structure (3, 51). The compressibility of hydrogen bonded structures, however, varies depending on the nature of the H-bonds involved (51).

TABLE 3. Ionic compressibilities of the drug compounds

Ion	$\bar{K}^0 \times 10^{15}$ ($m^3\ mol^{-1}\ Pa^{-1}$)
Salicylate	−12.09
$MeOr^-$	+7.83
PrH^+	−1.85
PcH^+	+3.93
PlH^+	−0.41
EpH^+	−2.73

Data reported here indicate that all the compounds studied in this work, except phenol, have negative compressibilities, which range from $(-13$ to $-46) \times 10^{-15}$ $m^3\ mol^{-1}\ Pa^{-1}$. $\bar{K}^0$ of phenol is $+9.53 \times 10^{-15}$ $m^3\ mol^{-1}\ Pa^{-1}$ which may be a result of combined effects of the aromatic ring and of the hydrogen bonding between phenolic OH and water molecules. The poor fit of the aromatic ring (42, 43) as well as the possibility of flexible H-bond formation appear to be responsible for causing a more compressible environment in the aqueous medium. The negative values of compressibilities for the remaining compounds indicate an overall constriction in the solution volumes, caused by varying degrees of electrostriction or hydrophobic hydration.

Individual ionic compressibilities were calculated for the ionic drugs, using values of $\bar{K}^0(Na^+)$ (46) $= -33.5 \times 10^{-15}$ $m^3\ mol^{-1}\ Pa^{-1}$ and $\bar{K}^0(Cl^-)$ (46) $= -17 \times 10^{-15}$ $m^3\ mol^{-1}\ Pa^{-1}$. Values of the counterion compressibilities were obtained by subtracting these values from the experimental data and are shown in Table 3. The results show that the counterions have a relatively larger compressibility than the smaller Na^+ and Cl^- ions. Also, they appear to show the existence of a correlation between compressibility and the size of the counterion or the structural complexity (e.g., branching or ring structure). It can be argued that as the size of the ion increases or its structure becomes more complex, it becomes increasingly difficult for the solute to be accommodated in the ordered aqueous medium. Consequently, it appears to cause a greater degree of disorder in the solvent. The compressibility of such disordered structures is expected to be higher than the ordered structures, such as those accompanying electrostriction or hydrophobic hydration. For example, the salicylate ion, being the smallest in size among these ions, has the lowest value of $\bar{K}^0$(ion). The anion of methyl orange appears to be the largest in size due to the presence of two aromatic rings joined in an extended structure. This is likely to create greater structural disorder in the aqueous environment. As well, a similar effect appears to be present in the hydrochloride salts. For example, EpH^+ is the smallest ion and has the lowest compressibility whereas PcH^+, a larger ion, has the greatest ionic compressibility.

The concentration dependence of the apparent adiabatic compressibility, S_k (Table 2), is seen to vary considerably among these solutes. While the values of S_v (Table 1) are generally positive for ionic solutes and tend to decrease as the hydrophobic character of the solute increases, there does not appear to be a strong correlation between values of S_k and such qualitative

Can. J. Chem. Downloaded from www.nrcresearchpress.com by 41.223.56.140 on 09/07/12
For personal use only.

features of the solutes. In the case of simple model compounds S_k and S_v data follow the same trend, however, in the case of these somewhat amphiphilic solutes the solute–solute interactions, as monitored by the compressibility property, appear to depend on the net hydration effect in an unpredictable manner.

Millero *et al.* (46) have reported a value of $\bar{K}^0$ for D-tryptophan of -30.24×10^{-15} m^3 mol^{-1} Pa^{-1} and an S_k value of -41.10×10^{-15} m^3 mol^{-2} kg Pa^{-1}. The values of these parameters for L-tryptophan in this work are -30.64×10^{-15} m^3 mol^{-1} Pa^{-1} and -29.49×10^{-15} m^3 mol^{-2} kg Pa^{-1}, respectively. The reasons for the large difference in S_k values are difficult to ascertain. It is to be noted that the low solubility of this compound is a factor which restricts the determination of thermodynamic properties to very low concentrations, below 0.01 *m*. Consequently, a larger scatter in ϕ_k values is obtained. The process of deriving the infinite dilution value ($\bar{K}^0$) and the interaction parameter (S_k) is strongly dependent on the type of data treatment used. It is likely that different methods of statistical analysis may produce different values of $\bar{K}^0$ and S_k parameters. Values of $\bar{K}^0$ reported herein were obtained using a weighted least squares fit, whereas Millero *et al.* (46) have reported an unweighted least-squares treatment of their data. Stereoisomerism may give rise to some of this difference but it is difficult to ascertain from these results.

In the case of PrHCl, the change in ϕ_k with increasing concentration, above 0.0625 *m*, is much more pronounced than was observed in the case of ϕ_v. This change is believed to be due to the onset of aggregation similar to micellization, an observation supported by the ϕ_v results and ultrasonic relaxation studies (49).

Conclusion

Apparent molar volume data of the drugs studied in this work show solution behaviour consistent with the general rules governing the behaviour of electrolytic, non-polar, and amphiphilic solutes in water. The S_v data appear to depend upon the net polar or hydrophobic character of the solute. Propranalol hydrochloride shows a marked increase in ϕ_v values above 0.06 *m* and this suggests possible aggregation of the drug in aqueous medium. The calculated values of individual ionic compressibilities show that a rough correlation exists between the observed compressibility and factors such as size of the ion, structural complexity (e.g., branching or ring structures), etc. The larger size or the greater structural intricacy of the ion appears to perturb an otherwise compact and homogeneous hydration shell around the solute species. The results also can be viewed in terms of the geometrical fit of the solute species in an ordered solvent. It can be argued that as the size of the ion increases or its structure becomes more complex, it is increasingly difficult to accommodate the solute in an ordered solvent environment.

Acknowledgement

Financial support from the Natural Sciences and Engineering Research Council of Canada is gratefully acknowledged.

1. H. S. Harned and B. B. Owen. The physical chemistry of electrolyte solutions. Reinhold, New York. 1943. Chap. 8.
2. C. Tanford. Hydrophobic effect: formation of micelles and biological membranes. 2nd ed. Wiley-Interscience, New York. 1980.
3. E. Vikingstad. Aggregation process in solutions. *Edited by* E. Wyn-Jones and J. Gormally. Elsevier, Amsterdam. 1983. pp. 100–117.
4. R. W. Gurney. Ionic processes in solutions. McGraw Hill, New York. 1954.
5. J. E. Desnoyers, M. Arel, G. Perron, and C. Jolicoeur. J. Phys. Chem. **73**, 3347 (1969).
6. R. Lumry and S. Rajender. Biopolymers, **9**, 1125 (1970).
7. M. M. Breuer. J. Phys. Chem. **68**, 2074 (1964).
8. M. M. Breuer. J. Phys. Chem. **68**, 2081 (1964).
9. L. M. Krausz. J. Am. Chem. Soc. **92**, 3168 (1970).
10. J. Rasper and W. Kauzmann. J. Am. Chem. Soc. **84**, 1771 (1962).
11. W. Kauzmann, A. Bodanszky, and J. Rasper. J. Am. Chem. Soc. **84**, 1777 (1962).
12. S. Katz, M. E. Shan, S. Chillag, and J. E. Miller. J. Biol. Chem. **247**, 5228 (1972).
13. S. Katz, J. K. Crissman, and L. C. Roberson. J. Biol. Chem. **249**, 7892 (1974).
14. S. Katz, R. G. Shinaberry, E. L. Heck, and W. Squire. Biochemistry, **19**, 3805 (1980).
15. G. Ogunmula, W. Kauzmann, and A. Zipp. Proc. Natl. Acad. Sci. USA. **73**, 4271 (1976).
16. L. J. Mullins. Chem. Rev. **45**, 289 (1954).
17. S. Roth. Ann. Rev. Pharmacol. Toxicol. **19**, 1959 (1979).
18. N. P. Franks and W. R. Leib. Nature, **292**, 248 (1981).
19. J. Judis. J. Pharm. Sci. **66**, 802 (1977).
20. J. Judis. J. Pharm. Sci. **69**, 885 (1980).
21. D. Shen and M. Gibaldi. J. Pharm. Sci. **63**, 1698 (1974).
22. C. J. Bowmer and E. W. Lindup. J. Pharm. Sci. **67**, 1193 (1978).
23. C. J. Bowmer and E. W. Lindup. Biochem. Pharmacol. **22**, 937 (1978).
24. S. W. Boobies and C. F. Chignell. Biochem. Pharmacol. **28**, 751 (1979).
25. J. Judis. J. Pharm. Sci. **71**, 1145 (1982).
26. C. O. Wilson, O. Gisvold, and R. Doerge. (*Editors*). Text book of organic medicinal and pharmaceutical chemistry. J. Lippincot & Co., Philadelphia. 1977.
27. P. Picker, E. Tremblay, and C. Jolicoeur. J. Soln. Chem. **3**, 377 (1974).
28. G. S. Kell. J. Chem. Eng. Data, **20**, 97 (1975).
29. F. Vaslow. J. Phys. Chem. **70**, 2286 (1966).
30. M. Alauddin, N. P. Rao, and R. E. Verrall. J. Phys. Chem. **92**, 1301 (1988).
31. A. Del Grosso and C. W. Mader. J. Acoust. Soc. Am. **52**, 1442 (1972).
32. M. Sakurai, T. Nakajima, T. Komatsu, and T. Nakagawa. Chem. Lett. Chem. Soc. Jpn. 971 (1975).
33. S. Cabani, V. Mollica, L. Lepori, and S. T. Lobo. J. Phys. Chem. **81**, 982 (1977).
34. F. Shahidi and P. G. Farrell. J. Soln. Chem. **7**, 549 (1978).
35. A. N. Martin, J. Swarbrick, J. Cammarta, and K. Chun. Physical pharmacy. Lea and Febiger, Philadelphia. 1969.
36. Remington's pharmaceutical sciences. 14th ed. Mack, Easton, PA. 1970.
37. Merck manual of diagnosis and therapy. 12th ed. Merck Sharp and Dohm, Rahway, NJ. 1972.
38. C. Davidson. *In* Fundamentals of drug metabolism and drug disposition. *Edited by* B. N. Ladu, H. G. Mandell, and E. L. Way. The Williams and Wilkins Co. Baltimore. USA. 1971.
39. M. C. Meyer and D. E. Guttman. J. Pharm. Sci. **57**, 895 (1968).
40. R. Verbeeck, A. Bod, A. Buntix and P. J. De Schepper. Biochem. Pharmacol. **29**, 571 (1980).
41. F. Shahidi. J. Chem. Soc. Faraday Trans. I, **77**, 1511 (1981).
42. W. L. Masterton. J. Chem. Phys. **22**, 1830 (1954).
43. L. G. Hepler. Can. J. Chem. **47**, 4613 (1969).
44. F. J. Millero. Chem. Rev. **71**, 147 (1971).
45. N. P. Sollenne, H.-L. Wu, and G. E. Means. Arch. Biochem. Biophys. **207**, 264 (1981).

Can. J. Chem. Downloaded from www.nrcresearchpress.com by 41.223.56.140 on 09/07/12
For personal use only.

46. F. J. MILLERO, A. LO SURDO, and C. SHIN. J. Phys. Chem. **82**, 784 (1978).
47. E. J. COHN and J. T. EDSALL. Proteins, amino acids and peptides. Hafner, New York. 1965. Chap. 7, Chap. 16.
48. A. K. MISHRA and J. C. AHLUWALIA. J. Phys. Chem. **88**, 963 (1984).
49. D. CAUSON, J. GETTIN, J. GORMALLY, R. GREENWOOD, N. NATARAJAN, and E. WYN-JONES. J. Chem. Soc. Faraday Trans. I, **77**, 143 (1981).
50. H. HØILAND, A. SKAUGE, and I. STOKKELAND. J. Phys. Chem. **88**, 6350 (1984).
51. B. E. CONWAY and R. E. VERRALL. J. Phys. Chem. **70**, 3952 (1966).
52. K. GEKKO and H. NOGUCHI. J. Phys. Chem. **83**, 2706 (1979).

Can. J. Chem. Downloaded from www.nrcresearchpress.com by 41.223.56.140 on 09/07/12
For personal use only.

Kinetics of oxidation of Cu(I) complexes of cysteine and penicillamine: nature of intermediates and reactants at pH 10.0

STEPHEN P. MEZYK AND DAVID A. ARMSTRONG
Department of Chemistry, University of Calgary, Calgary, Alta., Canada T2N 1N4

Received August 15, 1988

STEPHEN P. MEZYK and DAVID A. ARMSTRONG. Can. J. Chem. **67**, 736 (1989).

The Cu(I).L_2 complex with cysteine ligands at total Cu(I) concentrations of 10–30 μM was shown to be oxidised by cysteinyl radicals ($RS^{\cdot}$) with a diffusion-controlled rate constant $k_{11a} = 1.8 \times 10^9\ M^{-1}\ s^{-1}$. The corresponding reaction with the cysteine disulphide anion ($RS^{\cdot}$—SR^-) proceeded at a slower rate, $k_{11b} = 2.7 \times 10^8\ M^{-1}\ s^{-1}$. At higher Cu(I) concentrations, a slow and a fast component of absorption growth was observed. The slow component rate was independent of Cu(I) concentration, but it became more intense as the Cu(I) concentration rose. The yields and kinetic data were shown to be consistent with the presence of an equilibrium between the Cu(I).L_2 species and a second Cu(I) complex, $Cu(I)_2.L_3$, with an equilibrium constant of $K_1 = 162$.

[1] $$2Cu(I).L_2 \underset{}{\overset{K_1}{\rightleftharpoons}} Cu(I)_2.L_3 + L$$

This finding is consistent with the earlier work of Bagiyan *et al.* The rate constant of the oxidation of $Cu(I)_2.L_3$ by the cysteinyl radical was $k_{12} = 1.0 \times 10^9\ M^{-1}\ s^{-1}$. Similar results were obtained with penicillamine, except the rate constants and equilibrium constant were smaller, ($k_{11a} = 4.5 \times 10^8\ M^{-1}\ s^{-1}$, $k_{11b} < 2 \times 10^8\ M^{-1}\ s^{-1}$, $k_{12} = 5.5 \times 10^8\ M^{-1}\ s^{-1}$ and $K_1 = 113$). This was attributed to the presence of the β-methyl groups in penicillamine, which exert a large steric effect.

The ultraviolet spectra of the long-lived products, which are stable on a millisecond timescale, was consistent with a Cu(II).L_2 structure with a square planar geometry. The oxidation of the $Cu(I)_2.L_3$ species proceeded via intermediates, which relaxed to the final product spectra with rate constants of $k_{13b} = 2.6$ and $1.1 \times 10^4\ s^{-1}$ for cysteine and penicillamine, respectively. Comparison of the spectra of the intermediates with published data showed that they were consistent with the presence of a bridging thiolate ligand between Cu(I) and Cu(II).

Key words: oxidation, copper, mixed valence, cysteine, penicillamine, complexation.

STEPHEN P. MEZYK et DAVID A. ARMSTRONG. Can. J. Chem. **67**, 736 (1989).

On a montré que, à des concentrations totales de Cu(I) allant de 10 à 30 μM, les complexes Cu(I).L_2 portant des ligands cystéines sont oxydés par les radicaux cystéinyles ($RS^{\cdot}$) avec une constante de vitesse $k_{11a} = 1{,}8 \times 10^9\ M^{-1}\ s^{-1}$ qui est contrôlée par la diffusion. La réaction correspondante avec l'anion disulfure de la cystéine ($RS^{\cdot}$—SR^-) se produit à une vitesse plus lente, $k_{11b} = 2{,}7 \times 10^8\ M^{-1}\ s^{-1}$. A des concentrations de Cu(I) plus élevées, on a observé une composante lente et une autre qui est rapide pour la croissante de l'absorption. La composante lente est indépendante de la concentration du Cu(I) et elle devient plus intense avec une augmentation de la concentration du Cu(I). On a démontré que les rendements et les données cinétiques sont en accord avec la présence d'un équilibre entre le Cu(I).L_2 et un second complexe de Cu(I), $Cu(I)_2.L_3$, avec une constante d'équilibre de 162.

[1] $$2Cu(I).L_2 \underset{}{\overset{K_1}{\rightleftharpoons}} Cu(I)_2.L_3 + L$$

Cette observation est en accord avec le travail antérieur de Bagiyan et de ses collaborateurs. La constante de vitesse pour l'oxydation du $Cu(I)_2.L_3$ par le radical cystéinyle est $k_{12} = 1{,}0 \times 10^9\ M^{-1}\ s^{-1}$. On a obtenu des résultats semblables avec la pénicillamine, excepté que les constantes de vitesse et d'équilibre sont plus faibles ($k_{11a} = 4{,}5 \times 10^8\ M^{-1}\ s^{-1}$, $k_{11b} < 2 \times 10^8\ M^{-1}\ s^{-1}$, $k_{12} = 5{,}5 \times 10^8\ M^{-1}\ s^{-1}$ et $K_1 = 113$). On attribue cet abaissement à la présence, dans la pénicillamine, de groupements méthyles en β qui exercent un effet stérique important.

Les spectres uv des produits de longue vie, qui sont stables à l'échelle de la milliseconde, sont en accord avec une structure Cu(II).L_2 avec une géométrie plan carré. L'oxydation des espèces $Cu(I)_2.L_3$ procède par le biais d'intermédiaires qui se relaxent en spectres du produit final avec des constantes de vitesse respectives de $K_{13b} = 2{,}6$ et $1{,}1 \times 10^4\ s^{-1}$ pour la cystéine et la pénicillamine. Une comparaison des spectres des intermédiaires avec les données rapportées dans la littérature a permis de montrer qu'ils sont en accord avec la présence d'un ligand thiolate agissant comme pont entre le Cu(II) et le Cu(II).

Mots clés : oxydation, cuivre, valences mixtes, cystéine, pénicillamine, complexation.

[Traduit par la revue]

Introduction

The strong binding between mercaptide and copper ions has been a subject of interest for many years (1). During the past two decades, several studies of the stoichiometry and dissociation constants of both the copper(I) (2, 3) and copper(II) (4–6) complexes have been made, and some spectroscopic (6, 7) and crystallographic (8, 9) evidence relating to their structural features has been reported. The diversity of structures and redox states of the complexes is very intriguing, and interest has been further stimulated by the resemblance between some of the simple mercaptide complexes and the copper–sulphur centres, which occur in important redox-active proteins (3, 7, 9). Particular attention has been paid to 1,2-amino thiol compounds, since these can become bidentate ligands when the nitrogen atoms are deprotonated (2–6).

This paper describes an investigation of the redox reactions of copper(I) complexed with cysteine and penicillamine in aqueous solution. At strongly alkaline pH these two amino acids have the structures $^-SCH_2C(NH_2)HCO_2^-$ and $^-SC(CH_3)_2C(NH_2)HCO_2^-$, respectively.

The extensive studies of aqueous Cu(I) systems by Bagiyan and co-workers (2) have shown that there is a strong tendency

Can. J. Chem. Downloaded from www.nrcresearchpress.com by 41.223.56.140 on 09/07/12
For personal use only.

to form polynuclear complexes of stoichiometry $(Cu.L)_n$ and $(Cu_2.L_3)_m$ at Cu(I) concentrations above 10^{-4} *M*. The proportions of the two forms and the degree of polymerisation depend on the [Cu(I)]:[L] ratio, the absolute Cu(I) concentration and the structure of L. Mononuclear species dominate, however, as [L] is raised and [Cu(I)] reduced. Thus for 0.01 *M* cysteamine ($^-SCH_2CH_2NH_2$) with 10^{-4} *M* total Cu(I) at pH 8.5, 30% of the copper was found to be in the polynuclear form. The remainder was identified as $Cu(I).L_2$ and $Cu(I)_2.L_3$ with the magnitude of the equilibrium constant K_1

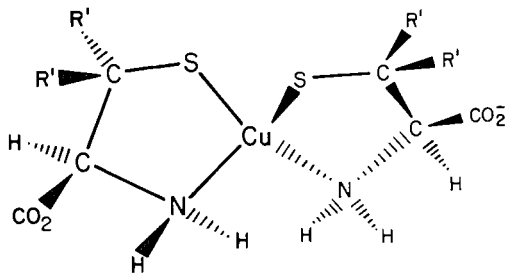
[1] $2Cu(I).L_2 \rightleftharpoons Cu(I)_2.L_3 + L$

estimated to be 2.2×10^3. When the Cu(I) concentration was confined to less than 10^{-5} *M*, their spectroscopic studies of the mononuclear complex gave $K_2 = 2 \times 10^{-3}$ and $K_3 = 1.6 \times 10^{-11}$.

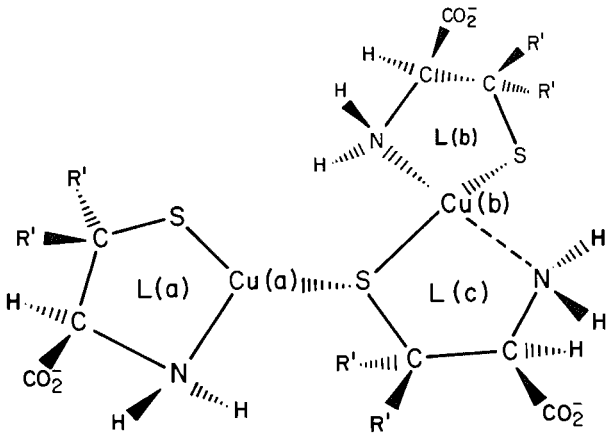
[2] $Cu(I).L_2 \rightleftharpoons Cu(I).L + L$

[3] $Cu(I).L \rightleftharpoons Cu(I) + L$

For cysteine and penicillamine, K_1 and K_2 were not reported, but K_3 was found to be 4.2×10^{-12} and 3.0×10^{-12} for the two thiols, respectively. Acid–base titrimetry showed that the NH_2 lone pairs were involved in complexation at alkaline pH with the thiolate group being the more strongly bound site of these bidentate ligands. Since the normal geometry of Cu(I) complexes is tetrahedral (10, 11), one would anticipate the following structures for the $Cu(I).L_2$ and $Cu(I)_2.L_3$ species:



I



II

(R' = H for Cysteine, CH_3 for penicillamine)

with the accommodation of the S to N distance of the 1,2-amino thiol possibly requiring some degree of distortion of the tetrahedron.

As in the case of Cu(I) complexes, the first thiolate ligand is bonded very strongly to Cu(II). However, spectrophotometric titrations have shown that the preferred stoichiometry of Cu(II) complexes with cysteine and penicillamine in alkaline solution is $Cu(II).L_2$ (4–6) and the tendency to form polynuclear complexes is less strong. The structures for these complexes are square planar, with the possibility of *cis* and *trans* forms (6).

An earlier investigation (12) demonstrated that one or more intermediates, with lifetimes in the region of 10^{-4} s, occurred in the one-electron oxidation of $Cu(I).(Cl^-)_x.L_y$ complexes, with L = cysteine and penicillamine, to $Cu(II).L_2$. The primary purpose of this work was to determine whether similar species occurred when there was no chloride ion in the system, and only species I and II were present. As in the previous study, the thiyl radicals ($RS^{\cdot}$) of cysteine and penicillamine, which have $E_{RS^{\cdot}/RS^-} = 0.80$ V (13), were used as the one-electron oxidants. The choice of these species was dictated by the fact that the free RS^- ligand concentration must be kept in the region of 10^{-2} *M* to establish the desired equilibria [1] and [2]. Other one-electron oxidants, such as $^{\cdot}N_3$ and $^{\cdot}ClO_2$, would therefore interact with it and not react directly with the Cu(I) complexes.

The thiyl radicals were produced through the following well-established radiation initiated reactions (14):

[4] $4.2H_2O \longrightarrow 2.7e^-_{(aq)} + 0.5H^{\cdot} + 2.8^{\cdot}OH + 2.7H^+_{(aq)} + 0.5H_2 + 0.7H_2O_2$

[5] $e^-_{(aq)} + N_2O + H_2O \rightarrow OH^- + {}^{\cdot}OH + N_2$

[6] $^{\cdot}OH$ (or $^{\cdot}H$) + $RSH \rightarrow H_2O$ (or H_2) + $RS^{\cdot}$

Solute concentrations were adjusted so that [5] and [6] were the only significant reactions of $e^-_{(aq)}$, $^{\cdot}OH$, and $^{\cdot}H$, and reaction of the thiyl radicals with copper species was then observed on a ~1 μs or longer time scale by using the technique of pulse radiolysis (14).

Quantitative information relating to the uv spectrum of $Cu(II).L_2$ was also obtained in this study for the case of L = penicillamine. Here the steric hindrance caused by the two methyl groups of the β-carbon atom substantially reduces the rate of reaction [7]

[7] $2Cu(II).L_2 + 2RSH \rightleftharpoons 2Cu(I).L_x + RSSR + 2H^+ + (4 - 2x)L$

Can. J. Chem. Downloaded from www.nrcresearchpress.com by 41.223.56.140 on 09/07/12
For personal use only.

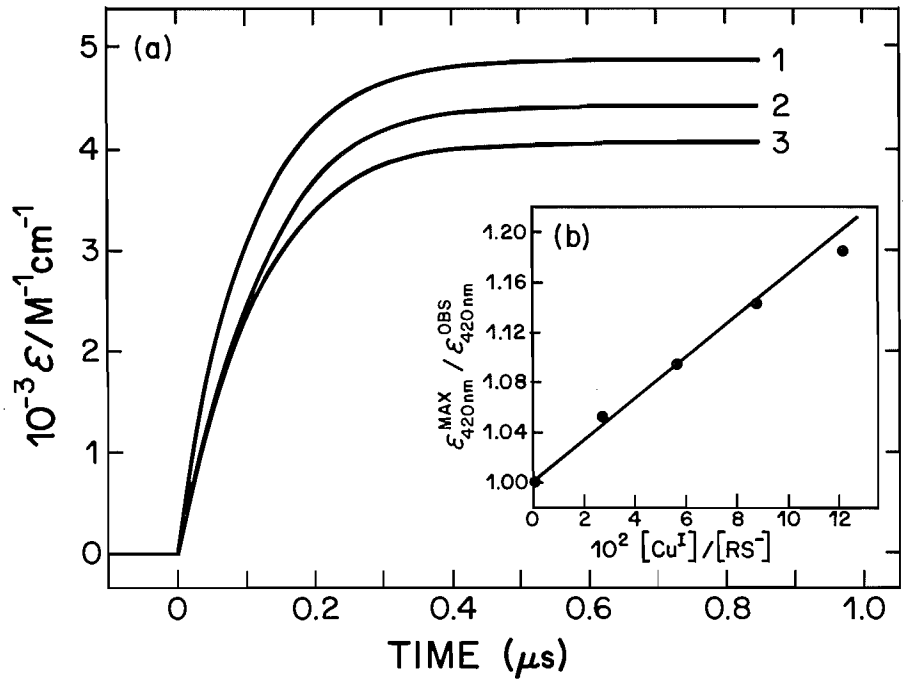


FIG. 1. (*a*) The change in the absorption intensity observed at 420 nm in 10^{-2} *M* CysSH solutions with (*1*) [Cu(I)] = 0, (*2*) [Cu(I)] = 4.0×10^{-4} *M*, (*3*) [Cu(I)] = 8.0×10^{-4} *M*. (*b*) The competition plot analysis for Cu(I)/10^{-2} *M* CysSH showing the fitted slope, k_{10} = $1.5 \times 10^9\ M^{-1}\ s^{-1}$ in comparison with the experimental data.

a process which is thermodynamically favoured and occurs quite rapidly for unhindered thiols (6, 15, 16).

Experimental

Pulse radiolysis experiments were performed using the 1.5 MeV Van de Graaff accelerator at the University of Calgary, and the 8 MeV linear accelerator at the Notre Dame Radiation Laboratory. Details for the facilities, the pulse radiolytic methods, and the dosimetry measurements for both systems have been previously described (17, 18). The dose used throughout these experiments was in the range of 4–6 Gray per pulse.

The D-penicillamine free base (99.5%) and L-cysteine (99.5%) were purchased from Sigma Chemical Company. Cuprous and cupric chloride (99.9%) were obtained from Fisher Scientific Company. Other chemicals were the purest available from standard suppliers. All were used as received.

Solutions were prepared from triply distilled, or Millipore Milli-Q water and were buffered using 20 m*M* borax. The pH was adjusted to 10.0 using NaOH and measured with an Orion 811 pH meter, calibrated against Orion reference buffers. All solutions were made by adding the N_2O degassed RSH/buffer solutions to the directly weighed copper chlorides. Unless otherwise stated, the total thiol concentrations used in these experiments were 1.0×10^{-2} *M* cysteine and 1.5×10^{-2} *M* penicillamine. All experiments were performed at 23 ± 2°C and an ionic strength of 0.05.

Radical yields, which are needed for each system where extinction coefficients are to be calculated were determined by using the formula (19):

$$[8] \qquad g_{R^\cdot} = 5.2 + 3.0\left\{\frac{(k[RSH]/\lambda)^{1/2}}{1 + (k[RSH]/\lambda)^{1/2}}\right\}$$

Here $g_{R^\cdot}$ is the yield of radical production (molecules per 100 eV), k is the rate constant for the reaction of $^\cdot$OH with RSH, [RSH] is the concentration of the protonated thiol in the system, and λ is the track recombination coefficient which is equal to $4.7 \times 10^8\ s^{-1}$.

For solutes where the $^\cdot$H atom also reacted to produce a radical, an additional term of +0.55 is added to account for the $^\cdot$H atom contribution (14). Rate constants for the reaction of various solutes with $^\cdot$OH were as follows: penicillamine $k = 5.9 \times 10^9\ M^{-1}\ s^{-1}$ cysteine, $k = 1.8 \pm 0.1 \times 10^{10}\ M^{-1}\ s^{-1}$ (20). The yields obtained for $g_{PenS^\cdot}$ and $g_{CysS^\cdot}$ at pH = 10 were 6.2 ([PenSH] = 2.4×10^{-3} *M*) and 6.5 ([CysSH] = 3.0×10^{-3} *M*), respectively.

Results

1. Oxidation of Cu(I)/CysSH complexes

Overall spectral changes

In the presence of thiolate ions the thiol radical forms disulphide anions ($RS^\cdot$—SR^-), as shown in equilibrium [9]

$$[9] \qquad RS^\cdot + RS^- \underset{k_{-9}}{\overset{k_9}{\rightleftharpoons}} RS^\cdot\text{—}SR^-$$

The magnitude of K_9 for cysteine was determined under our conditions of ionic strength at pH 10 to be 366 ± 27 (21). The absorption of $RS^\cdot$—SR^- is much stronger than that of $RS^\cdot$, and the absorption maximum is shifted: $\epsilon_{RS^\cdot} = 140\ M^{-1}\ cm^{-1}$ at $\lambda_{max} = 340$ nm, and $\epsilon_{RS^\cdot\text{—}SR^-} = 7600\ M^{-1}\ cm^{-1}$ at $\lambda_{max} = 420$ nm (22). Hence in the absence of Cu(I), the absorbance at 420 nm grows very rapidly after the pulse, until equilibrium [9] is established. In the presence of Cu(I) complexes, this growth is still observable (see Fig. 1*a*), but the maximum absorbance at 420 nm is smaller, due to the competition for $RS^\cdot$ between RS^- and the Cu(I) complex in reactions [9] and [10].

$$[10] \qquad RS^\cdot + (\text{Cu(I) complex}) \xrightarrow{k_{10}} \text{products}$$

This competition was not analytically solvable, due to the presence of the back reaction [−9] and the fact that $RS^\cdot$—SR^- also reacts with Cu(I) complexes (see below). However, an approximate analysis by means of the competition kinetics plot shown in Fig. 1*b* indicated that k_{10} was in the range $1–2 \times 10^9\ M^{-1}\ s^{-1}$. The ratio of ϵ^{max}_{420}, the maximum absorbance of $RS^\cdot$—SR^- per initial $RS^\cdot$, calculated from K_9 and [RS^-] and assuming no other reactants, to ϵ^{obs}_{420} has been plotted against

Can. J. Chem. Downloaded from www.nrcresearchpress.com by 41.223.56.140 on 09/07/12
For personal use only.

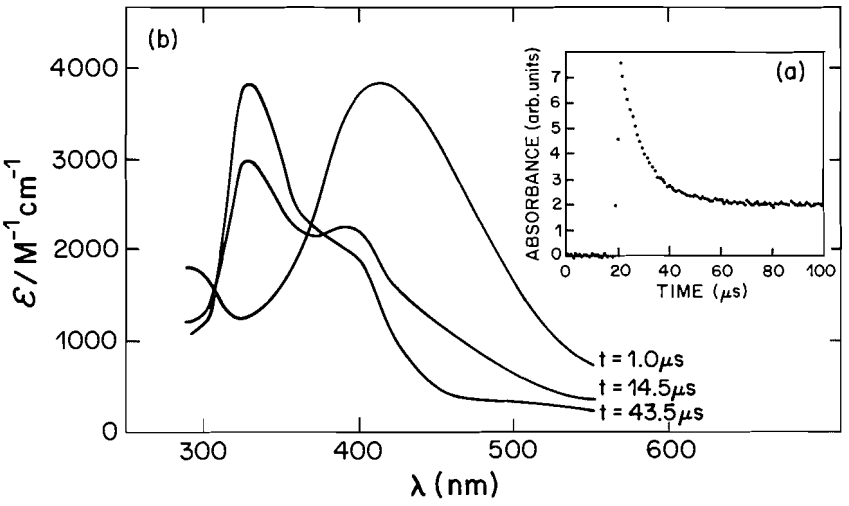


FIG. 2. (*a*) The absorbance growth and decay of a 10^{-3} *M* Cu(I) and 10^{-2} *M* CysSH solution, observed at 420 nm on a 100 μs timescale. (*b*) The time evolution of the spectrum of the same solution on the same timescale.

[Cu(I)]/[RS$^-$] and the slope is an approximate measure of k_{10}/k_9. The value of k_9 used, (9.6×10^8 M^{-1} s^{-1}), was measured under the actual pH and ionic strength conditions, and corrections were made for the proportion of RS$^-$ bound in the copper complexes.

Figure 2*a* shows a trace of the dependence of the absorbance at 420 nm for a 10^{-3} *M* Cu(I) solution over a much longer timescale. It is evident that the absorbance due to the RS$^{\cdot}$—SR$^-$ radical decays beyond the maximum, and this is attributed to the continuing oxidation of Cu(I) complexes via reactions [−9], [10], and other processes (see below). The analysis which follows is based on the assumption that reactions [9] and [−9] are sufficiently rapid that equilibrium [9] was maintained during the decay, and all data were consistent with this.

The time evolution of the spectrum in Fig. 2*b* shows that the initial broad absorbance, centered at 420 nm, disappears to give a more structured absorbance with a peak at 335 nm. This product absorbance extends out to 600 nm, but has a very small extinction coefficient at wavelengths above 470 nm. At 470 nm, there is a large RS$^{\cdot}$—SR$^-$ absorbance ($\epsilon = 6600$ M^{-1} cm^{-1}), no absorbance due to the RS$^{\cdot}$ radical and only a small contribution due to the product. Thus all kinetic measurements of RS$^{\cdot}$—SR$^-$ decay were done at this wavelength.

Kinetics of the 340 nm growth

To follow the kinetics of the growth, observed at 340 nm, it was necessary to subtract the absorbance of the sulphur radical species at this wavelength from the total absorbance. This contribution can be calculated from the absorbance at 470 nm and the ratio of the absorbance of the sulphur species at 470 nm and 340 nm, obtained from an identical experiment with no Cu(I). It was in fact demonstrated, from the intensities at 1.0 μs, that more than 95% of the initial absorbance at 340 nm was due to sulphur radical species.

An example of the corrected growth at 340 nm as a function of time is shown in Fig. 3. This cannot be fitted with a single first order growth plot. There are two distinct processes, one being fast and the other much slower. When the Cu(I) concentration was varied over the range (2.0–10.0) $\times 10^{-4}$ *M*, the total absorbance per unit dose and the spectrum at long times remained constant. However, the proportion of absorbance due to the fast and the slow processes changed, the amount of the slower component becoming more important at higher Cu(I) concentrations. The rate of the fast component also became faster, while there was no visible effect on the rate of the slow component. The latter was fitted by a first order rate constant, k_s, with a value of $(2.6 \pm 0.1) \times 10^4$ s^{-1}.

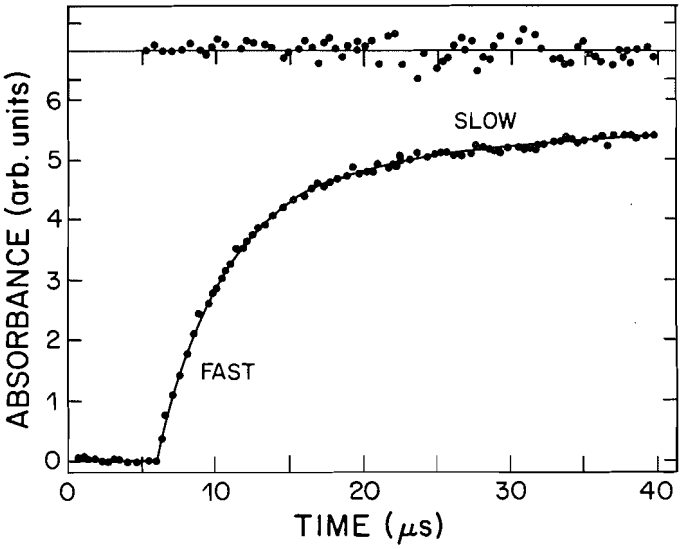


FIG. 3. Example of the growth kinetics seen at 340 nm for 10^{-3} *M* Cu(I) solution in 10^{-2} *M* CysSH. The solid line and residuals plotted on an arbitrary scale at the top of the diagram show the agreement obtained on fitting the sum of two first order growths to this data.

The 340 nm absorption growth was found to be fitted excellently by the sum of two exponentials (see fitted line and residuals in Fig. 3):

$$F = A[1 - \exp(-k_f t)] + B[1 - \exp(-k_s t)]$$

The two parameters, *A* and *B*, were related to the proportions of the fast and slow components. These two variables, and the fast growth rate constant, k_f, were obtained iteratively by a non-linear χ^2 minimisation routine (23) on an IBM PC, with the k_s rate constant being fixed at its measured value. This was done for all Cu(I) concentrations. The subtraction of the sulphur radical absorbance at 340 nm before the fitting of the 340 nm peak growth was found to be very important. When this was not

Can. J. Chem. Downloaded from www.nrcresearchpress.com by 41.223.56.140 on 09/07/12
For personal use only.

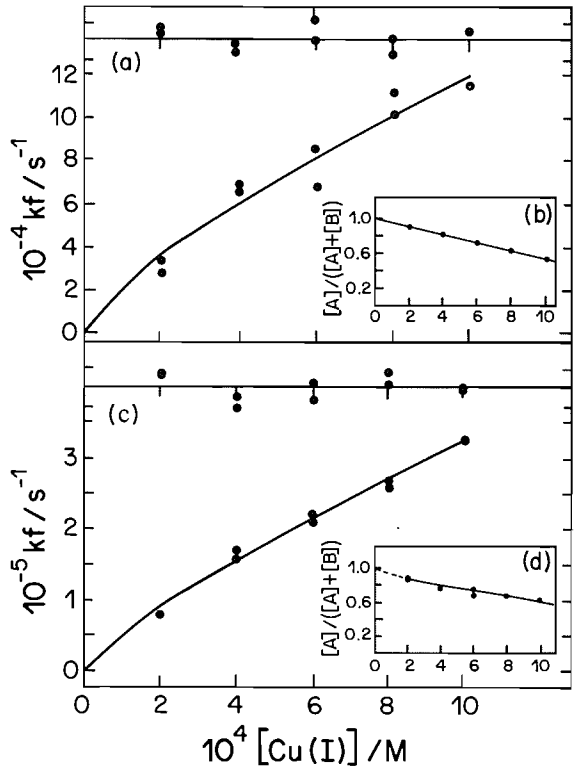


FIG. 4. (*a*) The Cu(I) concentration dependence of the fitted k_f rate constants for Cu(I)/10^{-2} *M* CysSH solutions. The solid line and residuals plot show the agreement of the experimental data and the values predicted using the appropriate equilibrium and rate constants from Table 1. (*b*) The Cu(I) concentration dependence of the ratio of the fast growth component intensity to the total intensity under the same conditions. (*c*) and (*d*) As for (*a*) and (*b*), respectively, but for Cu(I)/1.5 × 10^{-2} *M* PenSH solutions.

done, good fits could not be obtained, and the fast component rate constants were in error by up to 75%. The k_f rate constants obtained by this technique for a fixed total cysteine concentration of 10^{-2} *M* are shown in Fig. 4*a*, as a function of the total Cu(I) concentration. The ratio of the intensity of the fast process to the total intensity, over the same Cu(I) range, is shown in Fig. 4*b*.

The proportion of the fast component of the growth in Fig. 4*b* is seen to increase towards unity as the Cu(I) concentration falls. This feature suggests that the slow component is due to the presence of different Cu(I) species at higher concentrations. As stated in the Introduction, species **I** should dominate at low Cu concentrations, while species **II** should become important as the Cu concentration and the ratio of Cu to sulphydryl is raised. Thus it appears that the slow growth component has to be attributed to reactions with species **II**.

In the previous work of Bagiyan *et al.* (2) it was found that only a single Cu(I) species was formed when a Cu(I):sulphydryl ratio of less than 5 × 10^{-3} was used. In the data of Fig. 4, that ratio was (1.3–6.7) × 10^{-2}. Thus two or more Cu(I) species could have been present, which would explain the effects observed when the Cu(I) concentration was increased. Experiments to determine whether a slow growth component could be seen from species **I** were therefore performed, using Cu(I):cysteine ratios of (6–13) × 10^{-4}. Under these conditions Cu(I).L_2 would be the only initial species, and the oxidation processes should be

TABLE 1. Summary of equilibrium and rate constants*

Parameter	Value	
	Cu(I)/CysSH	Cu(I)/PenSH
K_1	162 ± 23	113 ± 14
K_9/M^{-1}	366 ± 27	16 ± 1
$k_{11a}/M^{-1}\,s^{-1}$	1.8 ± 0.1 × 10^9	4.5 ± 0.5 × 10^8
$k_{11b}/M^{-1}\,s^{-1}$	2.7 ± 0.1 × 10^8	< 2 × 10^8
$k_{12}/M^{-1}\,s^{-1}$	1.0 ± 0.3 × 10^9	5.5 ± 0.3 × 10^8
k_{13b}/s^{-1}	2.6 ± 0.1 × 10^4	1.1 ± 0.1 × 10^4

*Standard deviations were derived from the fitting procedures described in the text. Temperature, 296 ± 2 K: ionic strength, 0.05; and pH, 10.0.

[11*a*] $RS^{\cdot} + Cu(I).L_2 \xrightarrow{k_{11a}} RS^- + Cu(II).L_2$

and/or

[11*b*] $RS^{\cdot}—SR^- + Cu(I).L_2 \xrightarrow{k_{11b}} 2RS^- + Cu(II).L_2$

Writing $\theta = K_9[RS^-]$, a kinetic analysis shows

$$k_f = \{k_{11a} + k_{11b}\theta\}[Cu(I).L_2](1 + \theta)^{-1}$$

Thus a plot of $(1 + \theta)k_f$ versus θ, which can be varied by changing the total RSH concentration, should give a straight line of intercept k_{11a}[Cu(I).L_2] and slope k_{11b}[Cu(I).L_2]. This is shown for 20 μM Cu(I).L_2 in Fig. 5*a*, from which one finds $k_{11a} = 1.8 \times 10^9\,M^{-1}\,s^{-1}$ and $k_{11b} = 2.7 \times 10^8\,M^{-1}\,s^{-1}$.

Further experiments over the [Cu(I).L_2] range 10–30 μ*M* with a CysSH concentration of 10^{-2} *M* established that the growth at 340 nm could be fitted excellently by using single first order kinetics. Another important point was that the pseudo first order rate constants for the 340 nm growths and the 470 nm decays were identical. The overall second order rate constant for the combined oxidation by $RS^{\cdot}$ and $RS^{\cdot}—SR^-$ was found from the slope of a plot of the pseudo first order constants versus [Cu(I).L_2] to be 4.6 × $10^8\,M^{-1}\,s^{-1}$. This corresponds to $\{k_{11a} + k_{11b}\theta\}(1 + \theta)^{-1}$ and is in good agreement with k_{11a} and k_{11b} above.

Returning to the higher Cu(I) concentrations, where species **II** is present, one must also consider the oxidation reactions:

[12*a*] $RS^{\cdot} + Cu(I)_2.L_3 \rightarrow RS^- + Cu(I).Cu(II).L_3$

[12*b*] $RS^{\cdot}—SR^- + Cu(I)_2.L_3 \rightarrow 2RS^- + Cu(I).Cu(II).L_3$

However, due to the greater steric hindrance expected in species **II** and the small value of k_{11b} relative to k_{11a}, it was assumed that k_{12b} would be negligibly small.

Because of the higher affinity of Cu(II) for the bidentate ligands (24), the mixed product of reaction [12*a*] would not be expected to be stable under our conditions. Thus the slow process could be explained by reactions [13*a*] and [13*b*], which involve the addition of a fourth ligand, followed by a dissociative rearrangement.

[13*a*] $Cu(I).Cu(II).L_3 + L \rightarrow Cu(I).Cu(II).L_4$

[13*b*] $Cu(I).Cu(II).L_4 \rightarrow Cu(I).L_2 + Cu(II).L_2$

There is an alternative reaction pathway, in which the oxidising $RS^{\cdot}$ radical would add to the complex upon Cu(I) oxidation to form the species Cu(I).Cu(II).L_4 directly:

[12*c*] $RS^{\cdot} + Cu(I)_2.L_3 \rightarrow Cu(I).Cu(II).L_4$

Can. J. Chem. Downloaded from www.nrcresearchpress.com by 41.223.56.140 on 09/07/12
For personal use only.

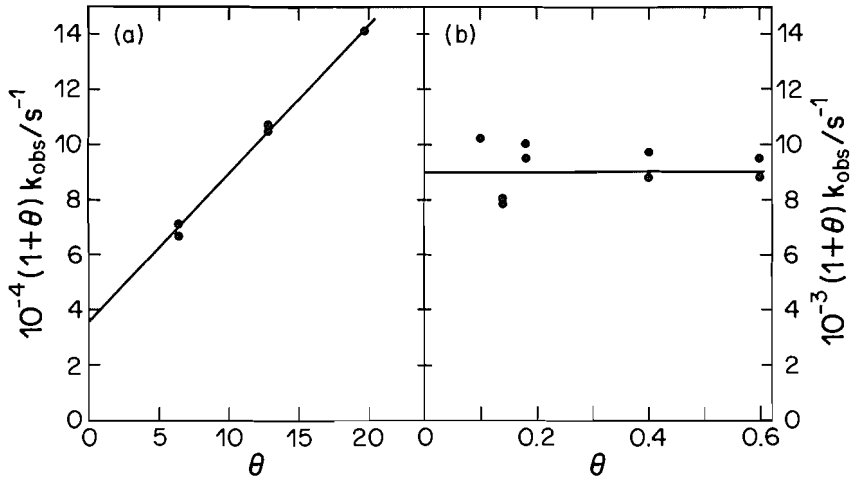
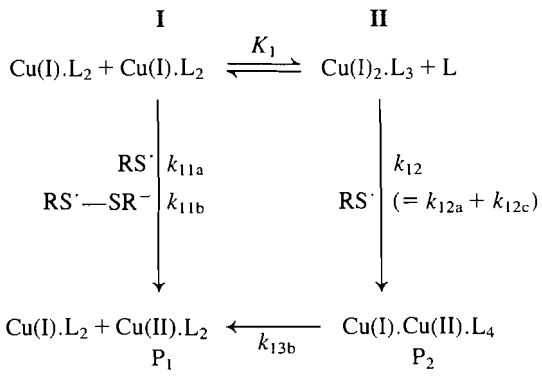


FIG. 5. (*a*) The determination of the rate constants k_{11a} and k_{11b} for 20 μ*M* Cu(I)/CysSH solutions. (*b*) As for (*a*) but for 20 μ*M* Cu(I)/PenSH solutions.

However, as the RS^- concentration is high, reaction [13*a*] would be rapid, and the slow process, k_s, would mainly reflect the ligand rearrangement (reaction [13*b*]). This was confirmed in experiments where the RS^- concentration was varied over the range 4.6×10^{-3} *M* to 3.0×10^{-2} *M* with no change in the slow step reaction rate constant being observed. Since it was not possible to distinguish between these two formation pathways, only a single Cu(I).Cu(II) intermediate, with four co-ordinating ligands, was used in the reaction mechanism. In schematic form, this is given by:



SCHEME 1

From this mechanism, the first order rate constant for the fast growth seen at 340 nm, which is assumed to result from the direct oxidation, is given by

$$[14] \quad (1 + \theta)k_f = (k_{11a} + k_{11b}\theta)[\mathbf{I}] + k_{12}[\mathbf{II}] = k_{11}^*[\mathbf{I}] + k_{12}[\mathbf{II}]$$

From equilibrium [1], (with constant K_1) and the mass balance equation [15],

$$[15] \quad [\mathbf{I}] + 2[\mathbf{II}] = [Cu]$$

we can write the values of [**I**] and [**II**] in terms of K_1:

$$[16] \quad k_f = k_{11}^*\left\{\frac{([RS^-]^2 + 8K_1[Cu][RS^-])^{1/2} - [RS^-]}{4K_1}\right\} + k_{12}\left\{\frac{(4K_1[Cu] + [RS^-]) - ([RS^-]^2 - 8K_1[Cu][RS^-])^{1/2}}{8K_1}\right\}$$

This expression was fitted to the total Cu(I) concentration dependence of the measured k_f values for a total CysSH concentration of 10^{-2} *M*. The RS^- concentration available for reaction [9] was corrected for the amount of thiol bound in the Cu(I) complexes by subtracting a value of $1.7 \times$ [Cu(I)] from the initial RS^- concentration. This was an "averaged" value, because the amount of complexed thiol depended on the relative concentrations of the species present. If all the Cu(I) were in the species **I** form, then the correction would be $2 \times$ [Cu(I)], and, if there were only species **II** present, it would be $1.5 \times$ [Cu(II)]. Knowing this and the value of k_{11}^*, a non-linear fitting routine (algorithms and programs taken from ref. 23) was used to determine the best values for K_1 and k_{12}. The values, which have been included in Table 1, were $K_1 = 162$ and $k_{12} = 1.0 \times 10^9\ M^{-1}\ s^{-1}$. Varying the RS^- concentration correction ratio from 1.5 to 2.0 had no effect on k_{12a} and gave only a 3% change in the equilibrium constant. This uncertainty was small in comparison to the standard deviations in K_1 and k_{12a}, which were derived from the fitting procedure and are shown in Table 1. The solid line in Fig. 4*a* shows the values of k_f predicted from the determined k_{11}^*, k_{12}, and K_1 values. The agreement with the experimental points is good.

At the higher Cu(I) concentrations, changing the RS^- (or L) concentrations affects the ratio of species **I** and **II**, as well as the values of θ. Values of k_f predicted from the parameters in Table 1 and eq. [14] for total [RSH] of 6, 10, 20, and 40 m*M* were 19, 14, 11, and $10 \times 10^4\ s^{-1}$, respectively. The good agreement with the observed values of 19, 13, 11, and $9 \times 10^4\ s^{-1}$ substantiates the stoichiometry of equilibrium [1].

The spectrum of the intermediate

The spectrum of the intermediate complex Cu(I).Cu(II).L_4 can now be determined. This was done most accurately from the 1.0×10^{-3} *M* Cu(I)/1.0×10^{-2} *M* Cys solution as it gave the highest concentration of species **II**. The unresolved spectrum at 43.5 μs is shown in Fig. 2*b*. At this time the absorbance observed at 470 nm had reached a limiting value, and thus the $RS^{\cdot}$—SR^- radical decay was judged to be complete. It was assumed that the Cu(I).L_2 and Cu(I)$_2$.L_3 concentrations did not change significantly from their initial equilibrium values on the radical reaction timescale. As the total change in the concentrations of the two Cu(I) species is very small, at worst 3.8 and 1.0% (assuming total reaction of the initial $RS^{\cdot}$

Can. J. Chem. Downloaded from www.nrcresearchpress.com by 41.223.56.140 on 09/07/12
For personal use only.

Can. J. Chem. Downloaded from www.nrcresearchpress.com by 41.223.56.140 on 09/07/12
For personal use only.

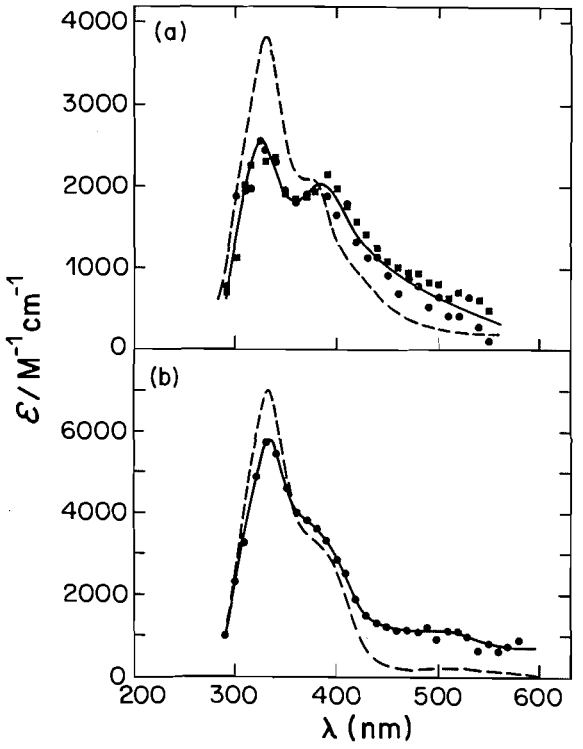


FIG. 6. (*a*) Comparison of the cysteine P_2 intermediate spectrum with the 500 μs final product spectrum (---) in a 10^{-3} *M* Cu(I)/10^{-2} *M* CysSH solution. (●) Determination of intermediate spectrum from data at t = 29.0 μs. (■) Determination from t = 43.5 μs. (*b*) Comparison of the penicillamine P_2 intermediate spectrum (●) determined from data at 43 μs in a 10^{-3} *M* Cu(I)/1.5×10^{-2} *M* PenSH solution with the spectrum of Cu(II).L_2 of penicillamine taken on a Cary 219 spectrophotometer (---).

radical concentration, 4.8 μ*M*, with species **I** (1.26×10^{-4} *M*) or species **II** (4.37×10^{-4} *M*) respectively), this appears reasonable.

A Runge–Kutta differential equation-solving program (23) was then used to calculate the time dependence of the concentration of all the species in these reactions until the time, 43.5 μs, had been reached. At this time, the concentrations of the final (P_1) and intermediate (P_2) products, relative to the initial RS· concentration, were 0.786 and 0.208, respectively. The unreacted sulphur radicals accounted for the small remaining fraction.

The spectrum of the P_2 intermediate is given by

$$\epsilon_{P_2} = \frac{\epsilon_{43.5\,\mu s} - 0.786\epsilon_{P_1}}{0.208}$$

and is shown in Fig. 6*a*, in comparison to the 500 μs spectrum where the spectrum was essentially stable. The intermediate spectrum is structured, and shows two distinct peaks at low wavelengths (326 nm, ϵ = 2480 M^{-1} cm^{-1} and 390 nm, ϵ = 1980 M^{-1} cm^{-1}) and an absorbance tailing into the visible.

The reliability of this method for determining intermediate spectra was checked by repeating the calculation at 29.0 μs. Under the same initial conditions, the P_1 and P_2 fractions were 0.680 and 0.298, respectively, with 0.02 remaining in the RS·/RS·—SR$^-$ form. In this instance, the remaining radical fraction had a significant absorbance, which also had to be subtracted from the intermediate spectrum. This calculated spectrum is also shown in Fig. 6*a*. Although there was some scatter at the higher wavelengths, the agreement between the two determinations confirms the validity of the results obtained.

Kinetics of the 470 nm decay

Further evidence supporting the proposed reaction mechanism can be obtained from the RS·—SR$^-$ absorbance decay observed at 470 nm. The absorbance at any time t, $A_{470,t}$, is given by:

$$A_{470,t} = \epsilon_{RS\cdot\text{—}SR^-}[RS\cdot\text{—}SR^-] + \epsilon_{P_2}[P_2]$$

This expression can now be solved explicitly, in terms of known parameters. Since we are observing the decay of the RS·—SR$^-$ radical,

$$[RS\cdot\text{—}SR^-] = K_9[SR^-][RS\cdot] \quad \text{from [9]}$$
$$= \theta[RS\cdot]$$

Therefore

$$\frac{d[RS\cdot\text{—}SR^-]}{dt} = \frac{d\theta[RS\cdot]}{dt} = \theta\frac{d[RS\cdot]}{dt}$$

and

$$(1 + \theta)\frac{d[RS\cdot]}{dt} = \{k_1^*[\mathbf{I}] + k_{12}[\mathbf{II}]\}[RS\cdot]$$

giving

[17] $$[RS\cdot] = [RS\cdot]_0[\exp(-k_f t)]$$
and $$[RS\cdot\text{—}SR^-] = \theta[RS\cdot]_0[\exp(-k_f t)]$$

The rate expression for the P_2 species is:

$$\frac{d[P_2]}{dt} = k_{12}[\mathbf{II}][RS\cdot] - k_{13b}[P_2]$$

i.e.

$$\frac{d[P_2]}{dt} + k_{13b}[P_2] = k_{12}[\mathbf{II}][RS\cdot]_0[\exp(-k_f t)]$$

and on integration this yields:

[18] $$[P_2] = \frac{k_{12}[\mathbf{II}][RS\cdot]_0}{(k_f - k_{13b})}\{[\exp - k_{13b}t] - [\exp(-k_f t)]\}$$

Thus the absorbance at 470 nm is given by:

[19] $$A_{470,t} = \left\{\epsilon_{RS\cdot\text{—}SR^-}\theta[RS]_0 - \frac{\epsilon_{P_2}k_{12}[\mathbf{II}][RS\cdot]_0}{(k_f - k_{13b})}\right\}\{\exp(-k_f t)\} + \left\{\frac{\epsilon_{P_2}k_{12}[\mathbf{II}][RS\cdot]_0}{(k_f - k_{13b})}\right\}\{\exp(-k_{13b}t)\}$$

This analysis shows that the decay seen at 470 nm is composed of two exponential decays, with rate constants the same as those calculated from the 340 nm growth data, i.e.

[20] $$A_{470,t} = A'[\exp(-k_f t)] + B'[\exp(-k_s t)]$$

When these rate constants were substituted into eq. [20], it was found that the 470 nm decays fitted well over the entire range of Cu(I) concentrations used.

When allowance is made for the small absorbance due to the Cu(II) product, and the decay rate constants are fixed at the values determined from the 340 nm data, the parameters A' and B' can be calculated. In terms of extinction coefficients one has:

$$B' = \frac{\epsilon_{P_2}k_{12}[\mathbf{II}]}{(k_f - k_{13b})}[RS\cdot]_0$$

This enables ϵ_{P_2} at 470 nm to be determined. The value obtained

Can. J. Chem. Downloaded from www.nrcresearchpress.com by 41.223.56.140 on 09/07/12
For personal use only.

by this method for the 10^{-3} *M* Cu(I) solution was $\epsilon_{P_2} = 780 \pm 100\ M^{-1}\,cm^{-1}$, which agrees very well with the value of $\epsilon_{P_2} = 850\ M^{-1}\,cm^{-1}$ from the calculated spectrum.

The rate constants, and the other values for this system, have been summarized in Table 1.

II. Cu(I)/PenSH oxidation

Similar oxidation experiments were also performed for the aminothiol 2,2-dimethyl cysteine (penicillamine). The major difference between these two thiols was in the magnitude of their K_9 values, the measured value for PenSH being only 16 ± 1 (21). The large value for cysteine ($K_9 = 366 \pm 27$) meant that most of the radicals in the irradiated solution existed in the dimer form $RS^{\cdot}—SR^{-}$ (74% at 1.0×10^{-2} *M* thiol). Because of this and the small value of k_{11b}, reaction [−9] would have been an important process in the Cu(I) oxidation. In contrast the lower K_9 for penicillamine meant that almost all the radicals were in the $RS^{\cdot}$ form (84% at 1.5×10^{-2} *M* thiol), and hence reaction [−9] would have little role in the oxidation.

The Cu(II).L_2 spectrum of PenSH taken on a Cary 219 spectrophotometer was found to be structured, with a peak at 330 nm, and very little absorbance above 470 nm (see Fig. 6*b*). For consistency, the wavelengths 340 nm and 470 nm were again used for kinetic measurements. The decay at 470 nm again showed a limiting baseline and its intensity was larger than for cysteine.

The subtraction of the 470 nm time profile from the kinetic data at 340 nm was also important for this system. After subtraction the 340 nm absorbance was again shown to consist of a fast and a slow growth process. Over the Cu(I) range studied, $(2–10) \times 10^{-4}$ *M*), the slow growth rate constant was $= 1.1 \pm 0.1 \times 10^4\ s^{-1}$, and independent of Cu(I) concentration.

Using the determined k_s value, the fast growths at 340 nm and the proportions of the fast and slow processes were determined as for cysteine, and are shown in Figs. 4*c* and 4*d*. Due to the smaller values of θ the k_f rate constants obtained are much faster than those for cysteine (cf. Fig. 4*a*). Also the dependence of the k_f values on Cu(I) concentration was more linear for penicillamine than for cysteine.

As the 340 nm data in penicillamine exhibited the same kinetic characteristics as seen for cysteine, the same reaction mechanism was assumed to apply in this system. In experiments conducted at very low Cu(I) concentrations (10–30 μ*M*) the 340 nm absorbance was excellently fitted by single first order growth kinetics, confirming that the slow component reaction was again due to radical reaction with the dimer Cu(I) complex, species **II**. The pseudo first order growth rate constants at 340 nm were also identical to the decay rate constants at 470 nm.

The rate of oxidation of Cu(I).L_2 was determined from the dependence of $(1 + \theta)k_f$ on θ shown in Fig. 5*b* for 20 μ*M* Cu(I).L_2 and varying the [PenSH]. Because of the smaller value of K_9, the accessible range of θ was limited to 0.1 to 0.6. Over that range the experimental data exhibited no dependence on θ, within the scatter of data points, from which one can show that $k_{11b} < 2 \times 10^8\ M^{-1}\ s^{-1}$. The intercept leads to $k_{11a} = (4.5 \pm 0.5) \times 10^8\ M^{-1}\ s^{-1}$, which is significantly smaller than for cysteine (cf. $(1.8 \pm 0.1) \times 10^9\ M^{-1}\ s^{-1}$). The same value was obtained from a plot of the pseudo first order rate constants for 340 nm growth and 470 nm decay vs. [Cu(I)] for values below 30 μM.

The K_1 and k_{12} values were determined by applying eq. [16] to the k_f data of Fig. 4*c*. In this instance, the thiolate ion concentration correction was given by $(1.50 \times 10^{-2} - 1.7 \times$ [Cu(I)]) *M*, and the best fit values were $K_1 = 113$ and $k_{12} = (5.5 \pm 0.3) \times 10^8\ M^{-1}\ s^{-1}$.

The spectrum of the intermediate was determined from the 1.0×10^{-3} *M* Cu(I)/1.5×10^{-2} *M* penicillamine solution, as before, and is seen in Fig. 6*b*. Once again, we can confirm the extinction coefficient at 470 nm obtained from the Runge Kutta simulation, $1200\ M^{-1}\,cm^{-1}$, by looking at the kinetic 470 nm decays. Fitting the two known rate constants, and determining the *B'* parameter, gives ϵ_{P_2} as $1100 \pm 200\ M^{-1}\,cm^{-1}$, which is in very good agreement with the other value.

The kinetic parameters are shown in comparison to the Cu(I)/CysSH data in Table 1.

Discussion

1. Characterisation of Cu(I) species

The fact that the 340 nm growth and 470 nm $RS^{\cdot}—SR^{-}$ decays for both amino thiols were fitted by a single kinetic process for total Cu(I) concentrations of 10–30 μ*M* is consistent with the presence of one type of Cu(I) complex. The observation of a long-lived intermediate, which became increasingly important at higher Cu(I) concentrations (see Figs. 4*b* and 4*d*), and the fact that the fast growth became non-linear in total [Cu(I)] represents unequivocal evidence for the presence of additional Cu(I) species with different kinetics of oxidation by $RS^{\cdot}$ and $RS^{\cdot}—SR^{-}$ radicals.

In the preceeding section the data for cysteine and penicillamine have been shown to be consistent with parameters in Table 1 for species **I** and **II**, which exist in an equilibrium as proposed by Bagiyan *et al.* (2). The characterisation of Cu(I)–thiolate complexes by titrimetry and ultraviolet spectroscopy, which have previously been used (2, 3), is a difficult and involved process. Thus independent evidence from the present kinetic observations for two of the copper species proposed by Bagiyan *et al.* is a very significant contribution. The larger polynuclear complexes proposed by them are not required to explain the present data for pH 10 up to 10^{-3} *M* [Cu(I)]. However, they may be present in small concentrations.

Bagiyan *et al.* did not report K_1 for penicillamine or cysteine. Their value for cysteamine is somewhat larger (2000) than those in Table 1. However, that may be caused by a reduction in the stability of Cu(I)$_2$.L_3, as this complex bears a −4 charge for penicillamine and cysteine, as opposed to −1 for cysteamine.

2. The long-lived products of reaction

As shown by the dashed line in Fig. 6*b*, the spectrum of Cu(II).L_2 for L = PenSH, taken on a Cary 219 spectrophotometer, consisted of two unresolved peaks centered at 370 nm, and an absorbance tail extending from 440 to 600 nm. These features are typical of a thermally equilibrated square planar Cu(II) with thiolate ligands (4, 5). The strong peaks are attributed to $RS^{-}(\sigma) \rightarrow$ Cu(II)(*d*) charge transfer transitions, while the tail probably contains bands due to $RS^{-}(\pi) \rightarrow$ Cu(II)(*d*) and Cu(II)($d \rightarrow d$) transitions (7). The Cu(I) species used here do not absorb significantly above 300 nm (2).

The systematic studies of Bosnich and co-workers (7) have shown that distortion from the square planar geometry causes significant changes in the absorption spectrum. For example, for a tetrahedral geometry, which is expected for the initial Cu(I) thiolate environment, the $RS^{-}(\sigma) \rightarrow$ Cu(II)(*d*) bands are red-shifted to the 400 to 500 nm range. In the present systems, the dominant feature of the spectra of all long-lived products at 500 μs was the strong unresolved double peak at 370 nm, confirming that on that time scale the main product was

Can. J. Chem. Downloaded from www.nrcresearchpress.com by 41.223.56.140 on 09/07/12
For personal use only.

$Cu(II).L_2$ with the thiolate ligands close to their equilibrium square planar configurations. This has been illustrated in Fig. 6*a* for cysteine, the 500 μs product spectrum of which is shown by the dashed line.

Similar conclusions relating to the nature of the long-lived products were reached in ref. 12. The present study has concentrated on establishing the mechanism of reaction and the origin of the slow growth component of the 340–380 nm absorbance in the absence of chloride ion, which nucleates the formation of Cu(I)–Cu(II) mixed valence clusters (8, 9). Further work will be required to determine whether Cl^- affects the mechanism of oxidation.

3. Oxidation of $Cu(I).L_2$

The kinetic analysis for the 10–30 μM Cu(I) solutions showed the 340 nm growths and the 470 nm radical decays to be identical. This means that the initial product of oxidation of species **I** by $RS^\cdot$ and $RS^\cdot$—SR^- must rearrange from the Cu(I) geometry (see structure **I**) to the square planar configuration of Cu(II) on a time scale of $\sim 10^{-5}$ s or less. Also any Cu(I).L.$RS^\cdot$—SR^- complex, formed by the addition of $RS^\cdot$ to an RS^- ligand, must be similarly short lived. When allowance is made for ionic strength and the charges of the $RS^\cdot$ and $Cu(I).L_2$ reactants (−1 and −3, respectively), it is evident that reaction [11*a*] for cysteine is a diffusion controlled process with an interaction distance of about 0.6 nm.[1] The negative free energy of reaction is significant ($E^0_{RS^\cdot/RS^-} = 0.8$ V (13), $E^0_{Cu(II)/(Cu)(I)} \sim 0.2$ V (footnote 2)) and the process may occur via an outer sphere mechanism. With penicillamine the free energy change will be similar, but the β-methyl groups in both the $RS^\cdot$ and the copper bound ligand will create steric effects, which would restrict the approach of $RS^\cdot$ to the S—Cu—S centres. This appears to reduce the value of k_{11a} by a factor of about 4 (see Table 1).

The present experiments appear to be the first in which rates of oxidation of a metal centre by $RS^\cdot$ and $RS^\cdot$—SR^- have been separately delineated. The driving force for reaction [11*b*] is about 0.2 V lower than that of [11*a*], since $E^0_{RS^\cdot—SR^-/2RS^-}$ (0.6 V (13)) is smaller than $E^0_{RS^\cdot/RS^-}$. However, due to the presence of the second R group, $RS^\cdot$—SR^- is much larger than $RS^\cdot$ and this should exert a steric effect, which could also reduce the rate of reaction [11*b*]. For cysteine the value of k_{11b} is about six fold less than k_{11a}, but still significant.

4. Oxidation of $Cu(I)_2.L_3$

As in the case of $Cu(I).L_2$, the rate constant for oxidation of $Cu(I)_2.L_3$ by $RS^\cdot$ in the cysteine system was effectively diffusion controlled. The rate for the penicillamine system was a factor of two slower, which again can be attributed to steric effects caused by the presence of β-methyl groups. The smaller value of k_{13b} for penicillamine (see Table 1) shows that they also hinder the dissociation/rearrangement of the $Cu(I).Cu(II).L_4$ intermediate.

A consideration of molecular models of $Cu(I)_2.L_3$ showed that structures which yielded optimal ligand interactions did not provide identical geometries of the two Cu(I) atoms. Furthermore, the Cu site with the greatest number of ligand interactions was (obviously) the least accessible to $RS^\cdot$ or $RS^\cdot$—SR^-, and at the same time, the one able to afford the greatest stabilisation of the excess positive charge, following oxidation of the S—Cu—S—Cu—S system. The Cu(b) site in structure **II** (see Introduction) illustrates these points. This structure was drawn to maximise the Cu(I)–L interactions and minimise steric and coulombic repulsions.

Formation of the intermediate in reaction [12*a*] should lead immediately to localisation of excess positive charge at the Cu(b) site.[3] A Cu(II) geometry close to square planar could subsequently be achieved by a simple rotation of L(b). The result is a Cu(I)–Cu(II) mixed valence compound with a bridging thiolate ligand, and it is of interest to compare the spectra of the present intermediates with those of two systems of this type, which have been reported in the literature.

The mercaptosuccinic acid complexes are of stoichiometry [Cu(I)—RS^-]$_4$Cu(II) (26). Those of the bidentate 1,2-amino-thiols-2,2 dimethyl-β-mercaptoethylamine and penicillamine, which are also stable in solution, have been shown by crystallographic examinations to form $(Cu(I))_8(Cu(II)_6(^-SC(Me)_2CH(R)NH_2)_{12}$ networks around a Cl^- core (8, 9, 27). Every thiolate is coordinated to two of the eight Cu(I) ions, and also to a Cu(II). The Cu(II) ions are in square planar configuration with overall S_2N_2 coordination by two amino thiols. Both systems have absorption maxima at 520 nm. These are attributed to charge transfer transitions from the Cu(I)-complexed RS^- electrons to Cu(II)(d), and have absorbance coefficients per RS^- of $\sim 1000\ M^{-1}\ cm^{-1}$ (9, 15, 27). Neither system has any non-Cu(I)-coordinated RS^- and there are therefore no strong absorbances of the kind seem here at 340–380 nm.

The main characteristics of the P_2 spectra in Fig. 6 can now be explained. The spectrum for penicillamine in Fig. 6(*b*) shows clear evidence of a shoulder at 520 nm, which is more intense than the d → d bands of the $Cu(II)L_2$ product (dashed line) and is of the intensity expected for a [Cu(I)RS^-] → Cu(II)(d) transition. The data for cysteine are more scattered, but also exhibit significant absorbance at 520 nm. At the same time, for both ligands, the absorbances in the 340–380 nm region are diminished from those of $Cu(II).L_2$, as would be expected since only one non-Cu(I)-coordinated thiolate is now present per Cu(II).

More specific characteristics, such as the quantitative features and differences between the spectra for the cysteine and penicillamine ligands, cannot be accounted for until more precise structural information is obtained. However, the steric hindrance of the methyl groups in penicillamine may cause a preference for different orientations of the complexes. Also, it is conceivable that with cysteine there is significant addition of $RS^\cdot$ radicals at Cu(a) (see structure **II**) in reaction [12*c*], which could lead to a Cu(II) coordination that is not S_2N_2 square planar. This would account for the greater distortion of the 340–380 nm bands seen in P_2 of Fig. 6*a*.

Acknowledgements

The authors gratefully acknowledge the use of the LINAC facilities of the Notre Dame Radiation Laboratory supported by the U.S. Department of Energy, and the kind co-operation of the director and other members of the staff. They are also indebted to Drs. A. McAuley and P. S. Surdhar for helpful discussions and to Dr. P. S. Surdhar for technical assistance. Financial support was provided by the Natural Sciences and Engineering Research Council of Canada.

[1]This calculation was based on a sum of diffusion coefficients equal to $1.6 \times 10^{-9}\ m^2\ s^{-1}$.

[2]This is for the Cl^- complex, which should resemble the complexes used here more closely than the purely aquated species (25).

[3]Note that, if Cu(b) were in a *cis* transformation and both L(b) and L(c) provided S atoms bridging Cu(I) and Cu(II), the 370 nm peaks should be absent.

1. I. M. KOLTOFF and W. STRICKS. J. Am. Chem. Soc. **73**, 1723 (1951).
2. (*a*) G. A. BAGIYAN, A. K. VALEEV, I. K. KOROLEVA, and N. V. SOROKA. Russ. J. Inorg. Chem. **28**, 1143 (1983); *Transl. from* Zh. Neorg. Khim. **28**, 2016 (1983); (*b*) G. A. BAGIYAN, I. K. KOROLEVA, and N. V. SOROKA. Russ. J. Inorg. Chem. **23**, 232 (1978); *Transl. from* Zh. Neorg. Khim. **23**, 416 (1978); Russ. J. Inorg. Chem. **23**, 1337 (1978); *Transl. from* Zh. Neorg. Khim. **23**, 2422 (1978).
3. V. VORTISCH, P. KRONECK, and P. HEMMERICH. J. Am. Chem. Soc. **98**, 2821 (1976).
4. D. CAVALLINI, C. DE MARCO, S. DUPRE, and G. ROTILIO. Arch. Biochem. Biophys. **130**, 354 (1969).
5. E. W. WILSON and R. B. MARTIN. Arch. Biochem. Biophys. **142**, 445 (1971).
6. F. J. DAVIS, B. C. GILBERT, and R. O. C. NORMAN. J. Chem. Soc. Perkin Trans. 2, 1763 (1983).
7. A. R. AMUNDSEN, J. WHELAN, and B. BOSNICH. J. Am. Chem. Soc. **99**, 6730 (1977); J. M. DOWNES, J. WHELAN, and B. BOSNICH. Inorg. Chem. **20**, 1081 (1981).
8. P. J. M. W. L. BIRKER and H. C. FREEMAN. J. Chem. Soc. Chem. Commun. 312 (1976).
9. P. J. M. W. L. BIRKER and H. C. FREEMAN. J. Am. Chem. Soc. **99**, 6890 (1977).
10. F. A. COTTON and G. WILKINSON. Advanced inorganic chemistry. 3rd ed. Interscience Publishers, New York. 1972. p. 906.
11. H. C. FREEMAN. Adv. Protein Chem. **22**, 257 (1967).
12. A-D. LEU and D. A. ARMSTRONG. J. Phys. Chem. **90**, 1449 (1986).
13. P. S. SURDHAR and D. A. ARMSTRONG. J. Phys. Chem. **91**, 6532 (1987).
14. I. G. DRAGANIĆ and Z. D. DRAGANIĆ. The radiation chemistry of water. Academic Press, New York. 1971.
15. A. G. LAPPIN and A. J. MCAULEY. J. Chem. Soc. Dalton Trans. 1606 (1978).
16. G. D. STEVENS and R. A. HOLWENDA. Inorg. Chem. **23**, 2777 (1984).
17. A. J. ELLIOT, F. WILKINSON, and D. A. ARMSTRONG. Int. J. Radiat. Biol. **38**, 1 (1980).
18. E. JANATA and R. H. SCHULER. J. Phys. Chem. **86**, 2078 (1982).
19. R. H. SCHULER, A. L. HARTZELL, and B. BEHAR. J. Phys. Chem. **85**, 192 (1981).
20. Selected specific rates of reactions of transients from water in aqueous solution. III. Hydroxyl radical, perhydroxyl radical and their radical ions. NSRDS-NBS 59. 1977.
21. S. P. MEZYK and D. A. ARMSTRONG. To be published.
22. J. E. PACKER. The chemistry of the thiol group. Part 2. *Edited by* S. Patai. Wiley, London. 1974; G. G. JAYSON, D. A. STERLING, and A. J. SWALLOW. Int. J. Radiat. Biol. **19**, 143 (1971).
23. C. F. GERALD. Applied numerical analysis. 2nd ed. Addison-Wesley, London. 1978.
24. M. FRIEDMAN. The chemistry and biochemistry of the sulfhydryl group in amino acids, peptides and proteins. Pergamon Press, New York. 1973.
25. J. ALBERY. Electrode kinetics. Claredon, Oxford. 1975. p. 141.
26. I. M. KLOTZ, G. H. CZERLINSKI, and H. A. FIESS. J. Am. Chem. Soc. **80**, 2920 (1958).
27. H. J. SCHUGAR, C. OU, J. A. THICH, J. A. POTENZA, R. A. LALANCETTE, and W. FINEY. J. Am. Chem. Soc. **98**, 3047 (1976).

Can. J. Chem. Downloaded from www.nrcresearchpress.com by 41.223.56.140 on 09/07/12
For personal use only.

Coordination compounds of indium. Part 45. Indium(I) derivatives of aromatic diols

HASSAN E. MABROUK AND DENNIS G. TUCK
Department of Chemistry and Biochemistry, University of Windsor, Windsor, Ont., Canada N9B 3P4

Received August 18, 1988

HASSAN E. MABROUK and DENNIS G. TUCK. Can. J. Chem. **67**, 746 (1989).

The electrochemical oxidation of anodic indium in acetonitrile solutions of the aromatic diols $R(OH)_2$ (= 1,2-dihydroxybenzene; 2,3-dihydroxynaphthalene; 2,2′-dihydroxybiphenyl; 1,2-dihydroxytetrabromobenzene) yields the new compounds In[OR(OH)]. These unusual indium(I) species can be oxidized by iodine to $In^{III}I_2[OR(OH)]$, and by the *ortho*-quinone $Br_4C_6O_2$ to $In^{III}[OR(OH)](O_2C_6Br_4)$. The hydroxy–oxo ligand can be deprotonated by Et_3N to give the salts $Et_3NH[In(O_2R)]$. The nature of these reactions, and the structure of the initial products, are confirmed by infrared and ^1H nmr spectroscopy.

Key words: indium, electrochemistry, oxidation, aromatic diols.

HASSAN E. MABROUK et DENNIS G. TUCK. Can. J. Chem. **67**, 746 (1989).

L'oxydation electrochimique de l'indium anodique, dans des solutions d'acétonitrile des diols aromatiques $R(OH)_2$, (= dihydroxy-1,2 benzène; dihydroxy-2,3 naphtalène; dihydroxy-2,2′ biphényl; dihydroxy-1,2 tétrabromobenzène), fournit de nouveaux composés In[OR(OH)]. Sous l'influence de l'iode, ces espèces inusitées de l'indium(I) peuvent être oxydées en $In^{III}I_2[OR(OH)]$ alors que sous l'influence de l'*ortho*-quinone $Br_4C_6O_2$ il y a formation de $In^{III}[OR(OH)](O_2C_6Br_4)$. Le ligand hydroxy-oxo peut être déprotoné par la base Et_3N pour donner les sols $Et_3NH[In(O_2R)]$. En se basant sur les specroscopies infrarouge et rmn du ^1H, on a confirmé la nature de ces réactions ainsi que la structure des produits initiaux.

Mots clés : indium, électrochimie, oxydation, diols aromatiques.

[Traduit par la revue]

Can. J. Chem. Downloaded from www.nrcresearchpress.com by 41.223.56.140 on 09/07/12
For personal use only.

The coordination chemistry of indium(I) received little or no attention for many years, largely no doubt because of the lack of suitable synthetic materials. Relatively few simple salts have been described, and the four monohalides, together with the oxide In_2O and sulphide In_2S, are the only known binary compounds. These substances are not very satisfactory as the starting point of synthetic work, but the situation was improved significantly by the discovery that the chloride, bromide, and iodide form solutions, stable at low temperatures, in mixtures of aromatic solvents and neutral donors (1). The oxidative addition reactions of indium(I) halides in such media have been investigated (2–6). Cyclopentadienylindium(I), InCp, is also a useful compound synthetically, since it is soluble in a number of organic solvents, and it is relevant to the present work to note that the reaction of InCp with β-ketoenolates such as 4,4,4-trifluoro-1-(thiene-2′-yl)butane-1, 3-dionate (ttaH) in ether/benzene mixtures gave the extremely hygroscopic indium(I) derivatives (e.g., In(tta)), and analogous derivatives of other bidentate chelating monoanionic ligands were also obtained by the metathetical reaction $InCp + HL \rightarrow InL + C_5H_6$ (7).

We have now found that the electrochemical oxidation of anodic indium in non-aqueous solutions of aromatic diols $R(OH)_2$ (= 1,2-dihydroxybenzene; 2,3-dihydroxynaphthalene; 2,2′-dihydroxybiphenyl; 1,2-dihydroxytetrabromobenzene) gives rise to the unusual indium(I) compounds In[OR(OH)], which are derivatives of the corresponding oxophenolate anions. These compounds undergo oxidative addition reactions with I_2 to give $In^{(III)}I_2[OR(OH)]$, and with the substituted *ortho*-quinone $Br_4C_6O_2$ in the presence of 2,2′-bipyridine (bpy) to form the corresponding $In[OR(OH)](O_2C_6Br_4)bpy$.

Experimental section

General

Indium metal (Alfa, m4N) was beaten into a thin sheet 1 × 1 cm^2 to form the anode of the cell. Acetonitrile, diethyl ether, and benzene were dried and distilled before use, and stored over drying agents. All other substances including the aromatic diols listed above, tetrabromo-*o*-quinone, and 2,2′-bipyridine (Aldrich), were used as supplied.

Infrared spectra were run as KBr discs on a Nicolet 5DX spectrometer, and ^1H nmr spectra were recorded on a Bruker W-80 instrument. Conductivity measurements were performed with a YSI Model 31 conductivity bridge and a conventional cell calibrated with 0.1 mol L^{-1} aqueous KNO_3 solution.

Indium analysis was by atomic absorption spectrophotometry, using an IL-250 instrument, and halogen analysis by Volhard titration. Carbon, hydrogen, and nitrogen microanalyses were by the Guelph Chemical Laboratories Ltd.

Electrochemical techniques

The preparative electrochemistry followed the techniques described elsewhere (8–10). The cell consisted of a 100 mL tall-form beaker containing an acetonitrile solution of the parent dihydroxy compound, with a platinum wire cathode and the sacrificial indium anode immersed in the liquid via a platinum wire lead. The high applied voltage required to drive the ions through the low conductivity solution phase was supplied by a Coutant LQ 50/50 power supply. All preparative work was carried out under dry nitrogen. The solution composition, electrochemical conditions, and yields are given in Table 1.

A typical experiment involved the electrochemical oxidation of indium metal in a solution of CH_3CN (50 mL) containing Et_4NClO_4 (ca. 20 mg) and 1,2-$C_6H_4(OH)_2$ (0.19 g). As the electrolysis proceeded, hydrogen gas evolved at the cathode, and a white product formed at the anode. This material gradually deposited in the cell, and at the end of the experiment was collected by filtration, washed with acetonitrile (5 mL) and then diethyl ether (5 mL), and dried *in vacuo*. The colourless solid was identified as In[OC_6H_4(OH)-1,2], 2-hydroxyphenolato indium(I). Essentially identical procedures were used to prepare and isolate the corresponding In^I[OR(OH)] compounds (R = $C_{10}H_6$, $C_{12}H_8$, C_6Br_4), which were characterized by elemental analysis (Table 2), and by infrared and ^1H nmr spectroscopy.

Preparation of $[In(O_2R)]^-$ anionic complexes

(*i*) Et_3N (0.2 mL, 0.15 g, 1.43 mmol) was added to In[OC_6(OH)-1,2] (0.30 g, 1.33 mmol) suspended in acetonitrile (20 mL), and the reaction mixture stirred for 4 h at room temperature. At the end of this period, the white product was collected, washed with 5 mL acetonitrile, and dried *in vacuo*. The product (0.37 g, 86% yield) was identified as $Et_3NH[In(O_2C_6H_4$-1,2)]. The molar conductivity of a millimolar solution in dimethylsulphoxide (dmso) was 46 ohm^{-1} mol^{-1} cm^2.

(*ii*) To In[$OC_{10}H_6$(OH)-2,3] (0.40 g, 1.46 mmol) was added Et_3N

TABLE 1. Experimental conditions for the direct electrochemical synthesis of $In^{I}[OR(OH)]$ compounds

Diol[a]	Solution composition[b] $R(OH)_2$ (g)	Initial voltage[c] (V)	Time of electrolysis (h)	Metal dissolved (mg)	% Yield[d]	E_F[e]	Product
$C_6H_4(OH)_2$	0.19	40	2	190	92	1.01	$In[OC_6H_4(OH)$-1,2]
$C_{10}H_6(OH)_2$	0.26	10	2	190	100	1.00	$In[OC_{10}H_6(OH)$-2,3]
$C_{12}H_8(OH)_2$	0.34	10	2	190	77	1.00	$In[OC_{12}H_8(OH)$-2,2′]
$C_6Br_4(OH)_2$	0.74	10	2	195	88	1.03	$In[OC_6Br_4(OH)]$

[a]$C_6H_4(OH)_2$ = 1,2-dihydroxybenzene; $C_{10}H_6(OH)_2$ = 2,3-dihydroxynaphthalene; $C_{12}H_8(OH)_2$ = 2,2′-dihydroxybiphenyl; $C_6Br_4(OH)_2$ = 1,2-dihydroxytetrabromobenzene.
[b]In 50 mL acetonitrile containing 20 mg Et_4NClO_4.
[c]All experiments run at 20 mA.
[d]Based on quantity of metal dissolved.
[e]Defined as mole metal dissolved per Faraday of charge.

(0.25 mL, 1.81 mmol) in tetrahydrofuran (thf) (20 mL). After 4 h stirring, the white solid was collected, washed with thf, and dried *in vacuo*. The product (0.49 g, 80% yield) was identified as $Et_3NH[In(O_2C_{10}H_6$-2,3)]. The molar conductivity of a millimolar solution in dmso was 51 ohm^{-1} mol^{-1} cm^2.

Reaction of In[OR(OH)] with I_2

(*i*) $In[OC_6H_4(OH)$-1,2] (0.25 g, 1.0 mmol) was added to a solution of I_2 (0.25 g, 1.0 mmol as I_2) in petroleum ether (20 mL) with stirring under nitrogen, and the mixture stirred for 4 h. During this time, the purple colour of iodine discharged and a gray–blue solid formed; this was collected, washed with petroleum ether (5 mL), and dried *in vacuo*. The deep blue product (0.45 g, 94% yield) was identified as $I_2In[OC_6H_4(OH)$-1,2].

(*ii*) Solid $In[OC_{10}H_6(OH)$-2,3] (0.28 g, 1.02 mmol) was added gradually to a solution of I_2 (0.26 g, 1.02 mmol) in thf (10 mL). The suspension of $In[OC_{10}H_6(OH)$-2,3] dissolved immediately and a pale yellow–brown solution formed. This was stirred for 4 h, after which the solution was filtered to remove impurities, and the filtrate evaporated *in vacuo* to give a deep brown solid (0.52 g, 97% yield), identified as $InI_2[OC_{10}H_6(OH)]$. Similar reactions involving other In[OR(OH)] compounds gave the corresponding products in yields of 87% or better.

Reaction of In[OR(OH)] with o-$Br_4C_6O_2$

(*i*) $In[OC_6H_4(OH)]$ (0.16 g, 0.73 mol) was added to CH_3CN (20 mL) containing bpy (0.12 g, 0.73 mmol). After a period of stirring (1 h), *o*-$Br_4C_6O_2$ (0.31 g, 0.73 mmol) in the same solvent was added, causing an immediate change in the colour of the solution to green. After 4 h stirring, the solid, which by then had become deep green in colour, was collected, washed, and dried *in vacuo*. The product is the bpy complex of the oxidative adduct, $In[OC_6H_4(OH)$-1,2]$(O_2C_6Br_4$-1,2).bpy; yield 0.53 g, 91%.

(*ii*) A solution of *o*-$Br_4C_6O_2$ (0.59 g, 1.38 mmol) in diethyl ether (20 mL) was added to $In[OC_{10}H_6(OH)$-2,3] (0.38 g, 1.38 mmol) in the same solvent. The red solution changed colour to green. The mixture was stirred for 4 h, by which time a brown solid had formed; bpy (0.22 g, 1.41 mmol) was then added, at which point a yellow product immediately formed. After a further 2 h period of stirring, the yellow product was collected, washed with diethyl ether, and dried *in vacuo*. The product is $In[OC_{10}H_4(OH)$-2,3]$(O_2Br_4C_6$-1,2).bpy; yield 1.02 g 86%. Analogous oxidative addition processes were also identified when the derivatives of other 1,2-diols were treated with *o*-$Br_4C_6O_2$ in the presence of bpy.

Unsuccessful reactions

(*i*) Methyl iodide (0.09 mL, 1.45 mmol) was added to a suspension of $In[OC_6H_4(OH)]$ (0.30 g, 1.34 mmol) in acetonitrile (20 mL) at room temperature. The mixture was stirred for 24 h, after which time the solid was collected, washed with acetonitrile, and dried *in vacuo*. The material recovered at the end of this period was identified as the unchanged In[OR(OH)] (0.30 g).

TABLE 2. Analytical results for In[OR(OH)] compounds and related products

Compound	Colour	In % found (calcd)
$In[OC_6H_4(OH)$-1,2][a]	Colourless	50.9 (51.3)
$In[OC_{10}H_6(OH)$-2,3][b]	Pale yellow	42.1 (42.0)
$In[OC_{12}H_8(OH)$-2,2′]	Pale yellow	38.6 (38.3)
$In[OC_6Br_4(OH)]$	Colourless	21.2 (21.4)
$Et_3NH[InO_2C_6H_4$-1,2]	Colourless	35.7 (35.4)
$Et_3NH[InO_2C_{10}H_6$-2,3]	Colourless	30.9 (30.7)
$In[OC_6H_4(OH)](O_2C_6Br_4)$.bpy[c]	Green	14.1 (14.3)
$In[OC_{10}H_6(OH)](O_2C_6Br_4)$.bpy[d]	Yellow	13.3 (13.5)
$In[OC_{12}H_8(OH)](O_2C_6Br_4)$.bpy	Yellow–green	13.3 (13.1)
$In[OC_6Br_4(OH)](O_2C_6Br_4)$.bpy	Deep yellow	10.5 (10.3)

Compound	Colour	In % found (calcd)	Halogen % found (calcd)
$I_2In[OC_6H_4(OH)$-1,2]	Deep blue	24.2 (24.1)	53.1 (53.1)
$I_2In[OC_{10}H_6(OH)$-2,3]	Brown	21.7 (21.8)	48.3 (48.1)
$I_2In[OC_{12}H_8(OH)$-2,2′]	Green	20.9 (20.8)	45.7 (45.8)
$I_2In[OC_6Br_4(OH)]$	Greenish	14.4 (14.5)	

[a]Found C 31.9, H 1.92; calcd. C 32.1, H 2.23.
[b]Found C 44.1, H 2.18; calcd. C 43.8, H 2.55.
[c]Found C 33.7, H 1.63, N 3.88; calcd. C 32.9, H 1.62, N 3.49.
[d]Found C 37.1, H 1.19, N 2.91; calcd. C 36.6, H 1.64, N 3.27.

(*ii*) Ethyl bromide (0.1 mL, 1.34 mmol) in acetonitrile (20 mL) was added to a suspension of 0.30 g (1.34 mmol) of $In[OC_6H_4(OH)]$ in the same solvent. The mixture was stirred with refluxing for about 4 h; after this time, the solid was collected, washed with acetonitrile, and dried *in vacuo*, and identified as the original In[OR(OH)] (0.30 g).

Results and discussion

Preparation of $In^{I}[OR(OH)]$ compounds

The anodic oxidation of indium in the presence of aromatic 1,2-diols is a simple and efficient route to a series of novel indium(I) compounds which have not been previously reported, although the use of electrochemical synthesis to produce metal derivatives of catecholates and similar aromatic diolates has been described elsewhere. In the case of zinc and cadmium (11), the products were the homopolymeric $M(O_2R)$ compounds, while with tin, the analogous tin(II) derivatives were obtained (10). This latter group of compounds was shown to undergo oxidation by iodine or tetrahalogeno-*o*-quinones to give the appropriate tin(IV) species, reactions which obviously parallel

Can. J. Chem. Downloaded from www.nrcresearchpress.com by 41.223.56.140 on 09/07/12
For personal use only.

Can. J. Chem. Downloaded from www.nrcresearchpress.com by 41.223.56.140 on 09/07/12
For personal use only.

to those described above for In[OR(OH)]. In the present work, as in the previous studies, the electrochemical synthesis is simple and efficient, and although the experiments were conducted on a relatively small scale, there is little difficulty in producing larger quantities of product either by using larger cells or by running several cells in series.

The electrochemical efficiency, defined as moles of metal dissolved per Faraday of charge, is 1.01 ± 0.01 mol F^{-1} for the synthesis of all the In[OR(OH)] compounds reported here (see Table 1). This E_F value, together with the evolution of hydrogen gas at the cathode, at its simplest implies the formation of a singly charged anion $[(HO)RO]^-$ at the cathode. This would migrate to the anode to form the product, according to the reaction sequence:

Cathode

[1] $R(OH)_2 + e \rightarrow [(HO)RO]^- + (1/2)H_2\,(g)$

Anode

[2] $[(HO)RO]^- + In \rightarrow In[OR(OH)] + e$

We should note that in previous papers (10, 11) a possible alternative mechanism was also proposed, based on the formation of RO_2^{2-} anions at the cathode, and in this case the anode reaction would be

[3] $RO_2^{2-} + 2In \rightarrow In_2(O_2R) + 2e$

followed by the electronless process

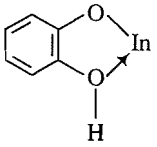
[4] $In_2(O_2R) + R(OH)_2 \rightarrow 2In[OR(OH)]$

This problem will be the subject of a future study.

As noted in the Introduction, there is little previous work against which this electrochemical preparative route can be compared. An analogous thallium compound $Tl[OC_{12}H_8(OH)]$, derived from 2,2′-dihydroxybiphenyl, was prepared some years ago by Brady and Hughes (12) by reacting thallium(I) acetate with the parent diol in basic aqueous ethanol; treatment with KOH yielded $Tl_2(O_2C_{12}H_8)$. With Et_2TlOH, reaction with this same diol gave $Et_2Tl[OC_{12}H_8(OH)]$, and in this compound, as in $Tl[OC_{12}H_8(OH)]$, the hydroxy group was assumed to be acting as part of a chelating ligand, although no spectroscopic evidence was of course available at the time. Compounds with such oxo-hydroxy ligands are unusual, and present a number of interesting structural problems for future investigation.

Reactions of In[OR(OH)] compounds

The oxo-hydroxy derivatives of aromatic diols are novel and interesting substances, partly because they represent the first known 2-dihydroxyphenolatoindium(I) compounds (and analogues), and equally because they show typical indium(I) chemistry. The compounds are unstable in air, changing colour to green–gray or gray with a few hours. They do not melt below ~300°C, and are insoluble in acetonitrile, tetrhydrofuran, pyridine, but soluble in dimethylsulphoxide at room temperature, and in these properties they closely resemble the tin(II) derivatives of the same aromatic diols. The solubilities suggest crosslinking to give a homopolymer in the solid state, with solvation then being responsible for the solubility in dimethylsulphoxide. The exact mode of this cross-linking cannot be identified at this point. Given that the simplest representation of In[OR(OH)] is

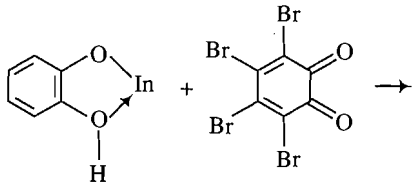


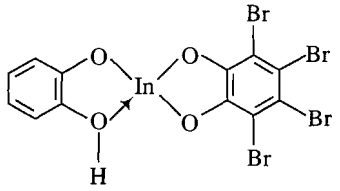
the homopolymer may simply involve O → In donation to give chains similar to those recently identified in the solid state of $In(SeC_6H_5)_3$ (13). Additionally, or alternatively, the hydrogen atom of the hydroxy group may hydrogen-bond to the oxo-oxygen of the ligand of a neighbouring molecule, and the lone pair of the indium atom may also be involved in lattice stabilization.

The presence of the hydroxy group in the various $RO(OH)^-$ ligands has been confirmed spectroscopically (see below) but direct chemical evidence was also obtained by deprotonation with Et_3N to give the corresponding salt $Et_3NH[InO_2R]$, shown to be a 1:1 electrolyte in dimethylsulphoxide (c.f. conductivities of 46–51 ohm^{-1} cm^2, compared with standard range of 50–70 ohm^{-1} mol^{-1} cm^2 established for such salts in this solvent (14)). The anions of these salts are isoelectronic with the tin(II) derivatives of aromatic diols discussed elsewhere (10).

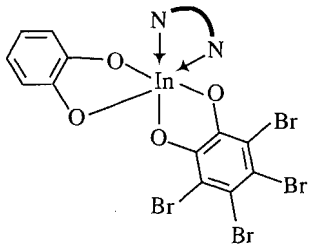
We have shown previously that indium(I) compounds are readily oxidized, and the present compounds confirm this generality. The reaction of $In^I[OR(OH)]$ with iodine gives $In^{III}I_2[OR(OH)]$, which formally results from the oxidative insertion of indium(I) into the I—I bond; analogous reactions are known for CpIn (15), InX (16), and InX_2^- (17). Similarly, when In[OR(OH)] reacts with the *ortho*-quinone *o*-$Br_4C_6O_2$ in the presence of the bidentate ligand 2,2′-bipyridine, the final product is a six-coordinate indium(III) complex. The first process is clearly that of oxidative addition

[5]





and this reaction is exactly analogous to those of InX (6), SnX_2 (18), and tin(II) catecholates (10). The details of such oxidations are discussed elsewhere, and it is sufficient to note here that the product is an indium(III) derivative with two dioxoligands, one being the tetrabromocatecholato ligand, and the other the oxo-hydroxy ligand formed in the original electrochemical synthesis. This oxidation process is followed by coordination by the neutral bidentate ligand to give the six-coordinate complex



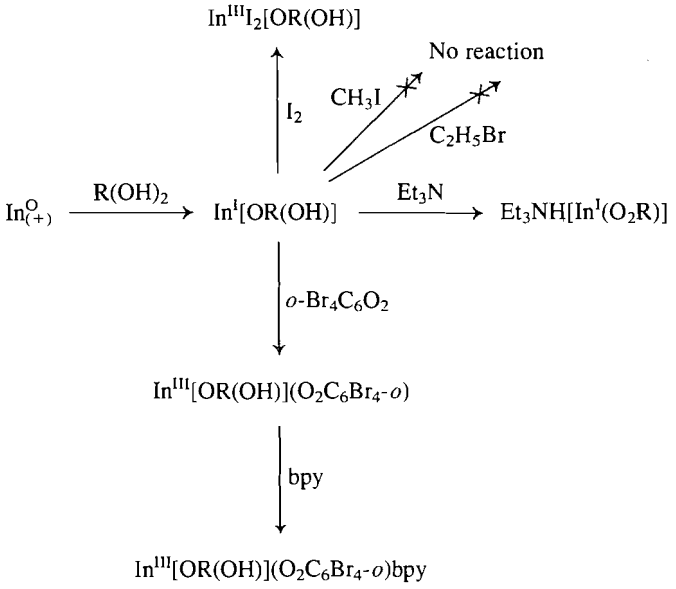
typical of indium(III) chemistry. The oxidative addition reaction of InX (X = Cl,Br) with *o*-$X_4C_6O_2$ (Y = Cl,Br) in the presence of neutral bidentate ligands such as bpy, phen, or tmen (= L) has been shown to yield diolato-indium(III) derivatives of the type $InX(O_2C_6Y_4).L$ (6).

The reactions identified at this point for these In[OR(OH)]

TABLE 3. ^{1}H nmr spectra for In[OR(OH)] compounds and derivatives

Compound	Solvent	Chemical shifts[a] Aromatic	Other
1,2-$C_6H_4(OH)_2$	d_6-acetone	6.8 (m)	7.7 (br) OH
In[OC_6H_4(OH)-1,2]	d_6-dmso	6.5–7.1 (m)	6.1 (br) OH
2,3-$C_{10}H_6(OH)_2$	d_6-dmso	6.8–7.7 (m)	9.3 (br) OH
In[$OC_{10}H_6$(OH)-2,3]	d_6-dmso	6.5–7.3 (m)	9.5 (br) OH
2,2′$C_{12}H_8(OH)_2$]	d_6-acetone	6.8–7.3 (m)	5.9 (br) OH
In[$OC_{12}H_8$(OH)-2,2′]	d_6-dmso	6.8–7.1 (m)	6.3 (br) OH
$Et_3NH[InO_2C_6H_4$-1,2]	CD_3CN	6.57–6.63 (br)	4.95 (br) NH 3.04 (q) CH_2 1.14 (t) CH_3
$Et_3NH[InO_2C_{10}H_6$-2,3]	d_6-dmso	6.6–7.3 (m)	3.73 (br) NH 2.82 (q) CH_2 1.05 (t) CH_3

[a]In ppm from Me_4Si; br = broad, t = triplet, q = quartet, m = multiplet.



SCHEME 1

species are summarized in Scheme 1. No reaction was observed with either CH_3I or C_2H_5Br, although oxidative addition reactions between alkyl halides and indium(I) compounds have been observed (19–21), and this may be because the polymeric nature of the solid In[OR(OH)] resists attack under the mild conditions used in the present work.

Spectroscopic results

The infrared spectra of all the In[OR(OH)] compounds studied showed the presence of ν(O—H) of the anion, observed as broad absorptions in the 3200–3400 cm^{-1} region. The ν(C—O) mode, observed between 1280 and 1230 cm^{-1} in the parent diols, occurs at 1254 (R = $O_2C_6H_4$-1,2), 1257 (R = $O_2C_{10}H_6$-2,3), 1222 (R = $O_2C_6Br_4$-1,2), and 1249 and 1212 cm^{-1} (R = $O_2C_{12}H_8$), respectively. The adducts with bpy showed the characteristic infrared spectrum of the complexed ligand.

For the products of the reaction of In[OR(OH)] with *o*-$Br_4C_6O_2$, the most important observation is that ν(C=O) of the *ortho*-quinone at ~1700 cm^{-1} is absent in every case in the product, being replaced by bands at 1430 and 1240 cm^{-1}, assigned as ν(C—O). Similar results were observed in the $Sn(O_2R)$/*o*-$Br_4C_6O_2$ (10), SnX_2/*o*-$Br_4C_6O_2$ (18), and InX/*o*-$Br_4C_6O_2$ (6) systems. In the infrared spectrum of $Et_3NH[In(O_2C_6H_4)]$, multiplet absorptions between 2490 and 2780 cm^{-1} are identified as ν(N—H^+), and ν(C—H) occurs at 2842 and 2931 cm^{-1}, in agreement with the earlier work of Chenon and Sandorfy (22).

The ^{1}H nmr spectra of a number of In[OR(OH)] compounds and their derivatives are presented in Table 3. The important feature of the nmr spectra of In[OR(OH)] in d_6-dmso is the presence of broad signals at 6.1, 9.5, and 6.3 ppm (R = C_6H_4, $C_{10}H_6$, and $C_{12}H_8$) which are assigned to the hydrogen of the hydroxy group of the ligand. This hydrogen is removed in the reaction of In[OR(OH)] with Et_3N to form $Et_3NH[InO_2R]$ (R = C_6H_4, $C_{10}H_6$), and the spectrum changes accordingly; the broad signals at 4.95 and 3.73 ppm were assigned to the hydrogen of the Et_3NH^+ cation in CD_3CN and d_6-dmso, respectively. The remaining features are also consistent with the presence of the Et_3NH^+ cation.

In general, the spectroscopic results confirm the proposed reaction Scheme.

Acknowledgments

This work was supported by Operating Grants (to D.G.T.) from the Natural Sciences and Engineering Council of Canada. H.E.M. thanks the Ministry of Education of the Arab Republic of Egypt for financial support.

1. C. PEPPE, D. G. TUCK, and L. VICTORIANO. J. Chem. Soc. Dalton Trans. 2165 (1982).
2. C. PEPPE and D. G. TUCK. Can. J. Chem. **62**, 2793 (1984).
3. C. PEPPE and D. G. TUCK. Can. J. Chem. **62**, 2798 (1984).
4. M. A. KHAN, C. PEPPE, and D. G. TUCK. Organometallics, **5**, 525 (1986).
5. T. A. ANNAN and D. G. TUCK. J. Organomet. Chem. **325**, 83 (1987).
6. T. A. ANNAN and D. G. TUCK. Can. J. Chem. **66**, 2935 (1988).
7. J. J. HABEEB and D. G. TUCK. J. Chem. Soc. Dalton Trans. 1815 (1975).
8. J. J. HABEEB and D. G. TUCK. Inorg. Synth. **19**, 257 (1979).
9. C. OLDHAM and D. G. TUCK. J. Chem. Educ. **59**, 420 (1982).
10. H. E. MABROUK and D. G. TUCK. J. Chem. Soc. Dalton Trans. In press.
11. H. E. MABROUK, D. G. TUCK, and M. A. KHAN. Inorg. Chim. Acta, **129**, 75 (1987).
12. O. L. BRADY and E. D. HUGHES. J. Chem. Soc. 1227 (1933).

Can. J. Chem. Downloaded from www.nrcresearchpress.com by 41.223.56.140 on 09/07/12
For personal use only.

13. T. A. ANNAN, R. CHADHA, R. KUMAR, H. E. MABROUK, and D. G. TUCK. Polyhedron. In press.
14. W. J. GEARY. Coord. Chem. Rev. **7**, 81 (1971).
15. J. G. CONTRERAS and D. G. TUCK. J. Organomet. Chem. **66**, 405 (1974).
16. B. H. FREELAND and D. G. TUCK. Inorg. Chem. **15**, 475 (1976).
17. J. E. DRAKE, J. L. HENCHER, L. N. KHASROU, D. G. TUCK, and L. VICTORIANO. Inorg. Chem. **19**, 34 (1986).
18. T. A. ANNAN, R. K. CHADHA, D. G. TUCK, and K. D. WATSON. Can. J. Chem. **65**, 2670 (1987).
19. (*a*) L. WATERWORTH and I. J. WORRALL. Chem. Commun. 569 (1971); (*b*) M. J. S. GYNANE and I. J. WORRALL. Inorg. Nucl. Chem. Lett. **8**, 547 (1972); (*c*) M. J. S. GYNANE, L. G. WATERWORTH, and I. J. WORRALL. J. Organomet. Chem. **43**, 257 (1972).
20. J. S. POLAND and D. G. TUCK. J. Organomet. Chem. **42**, 315 (1972).
21. J. H. GREEN, R. KUMAR, N. SEUDEAL, and D. G. TUCK. Inorg. Chem. **28**, 123 (1989).
22. B. CHENON and C. SANDORFY. Can. J. Chem. **36**, 1181 (1958).

Can. J. Chem. Downloaded from www.nrcresearchpress.com by 41.223.56.140 on 09/07/12
For personal use only.

The synthesis, characterization, and some reactions of phosphonium thiolates and selenolates: the X-ray crystal structure of tetraphenylphosphonium 2,4,6-trimethylbenzenethiolate

JOANNE M. BALL, P. MICHAEL BOORMAN,[1] JAMES F. FAIT, A. SCOTT HINMAN, AND PENELOPE J. LUNDMARK
Department of Chemistry, University of Calgary, Calgary, Alta., Canada T2N 1N4

Received August 19, 1988

JOANNE M. BALL, P. MICHAEL BOORMAN, JAMES F. FAIT, A. SCOTT HINMAN, and PENELOPE J. LUNDMARK. Can. J. Chem. **67**, 751 (1989).

Synthetic methods for the preparation of $PPh_4[SAr]$, PPN[SAr], and $PPh_4[SeAr]$ (Ar = aryl; PPN = bis(triphenylphosphine)iminium) salts are described, and ^1H NMR, infrared, and ^{77}Se NMR spectroscopic characterization is given. The X-ray crystal structure of $[PPh_4][Smes]$ (mes = 2,4,6-trimethylbenzene) was carried out: space group $P\bar{1}$, a = 9.946(3) Å, b = 10.100(2) Å, c = 14.874(3) Å, α = 70.19(2)°, β = 69.13(2)°, γ = 82.54(2)°, Z = 2, R = 0.100, R_w = 0.074. The structure establishes the ionic nature of this compound in the solid state, and conductance measurements in acetonitrile are consistent with 1:1 electrolyte behaviour. It is shown, however, that solutions of the thiolates are quite sensitive to hydrolysis to the thiol, and also the strong nucleophilicity of the thiolate and selenolate anions enables them to react with halocarbon solvents. The selenolate solutions are extremely sensitive to oxidation to the diselenide, which limited their study. Cyclic voltammetry on selected thiolate salts shows that impurities quickly develop even in acetonitrile solvent, but comparisons with the voltammograms of thiols and disulphides confirm the assignment of an irreversible oxidation wave at ca. −0.3 V (vs. $Ag/AgNO_3$, 0.01 *M*) to the process: $2SR^- \rightarrow R_2S_2 + 2e^-$. The potential at which this reaction occurs is related to the degree of substitution of the phenyl ring of the SAr^- ion.

Key words: phosphonium thiolates, phosphonium selenolates, tetraphenylphosphonium 2,4,6-trimethylbenzene thiolate.

JOANNE M. BALL, P. MICHAEL BOORMAN, JAMES F. FAIT, A. SCOTT HINMAN et PENELOPE J. LUNDMARK. Can. J. Chem. **67**, 751 (1989).

On décrit des méthodes de synthèse pour la préparation des sels $PPh_4[SAr]$, PPN[SAr] et $PPh_4[SeAr]$ (Ar = aryl; PPN = bis(triphénylphosphine)iminium) et on présente les données des spectroscopies infrarouge ainsi que RMN du ^1H et du ^{77}Se. On a déterminé la structure cristalline du sel $[PPh_4][Smes]$ à l'aide de la diffraction des rayons-X : groupe d'espace $P\bar{1}$, a = 9,946(3), b = 10,100(2) et c = 14,874(3) Å, α = 70,19(2), β = 69,13(2), γ = 82,54(2)°, Z = 2, R = 0,100 et R_w = 0,074. La structure a permis d'établir la nature ionique de ce composés à l'état solide et des mesure de conductance dans l'acétonitrile sont en accord avec le comportement d'un électrolyte 1:1. Toutefois, on démontre que les solutions des thiolates sont très sensibles à une hydrolyse en thiol et que le caractère nucléophile marqué des anions thiolate et sélénolate leur permet de réagir avec les halogénures de carbone qui agissent comme solvant. Les solutions de sélénolates sont extrêmement sensibles aux oxydations en disélénures et cette particularité a limité leur étude. La voltamétric cyclique sur des sels choisis de thiolate a permis de montrer que des impuretés se forment rapidement, même dans l'acétonitrile; toutefois, des comparaisons avec les voltamogrammes de thiols et de disulfures ont permis de confirmer l'attribution d'une vague d'oxydation irréversible, à environ −0.3 V (vs. $Ag/AgNO_3$, 0,01 *M*), au processus: $2SR \rightarrow R_2S_2 + 2e^-$. Le potentiel caractéristique de cette réaction est relié au degré de substitution du noyau phényle de l'ion SAr^-.

Mots clés : thiolates de phosphonium, sélénolates de phosphonium, thiolate triméthyl-2,4,6 benzène de tétraphénylphosphonium.

[Traduit par la revue]

Introduction

The recent publication of three reviews (1–3) on metal thiolate complexes is an indication of the high current interest in this area of chemistry. The subject has been of ongoing interest in our laboratory with particular emphasis on the preparation of tungsten and molybdenum thiolate complexes (4). During this work, we had occasion to examine the use of simple quaternary thiolate salts as synthetic reagents, following reports by several workers on their ability to displace both neutral and anionic ligands (5–10). Such compounds would complement the more commonly used reagents such as the alkali metal thiolates, thiol/Et_3N, and the trialkylsilyl- and trialkyltin-thiolates, as a means of forming metal–thiolate bonds.

The very recent publication (11) of an application of quaternary ammonium thiolates as initiators for the polymerization of *n*-butyl acrylate suggests that the possible uses of simple thiolate salts may be much wider than merely in the synthesis of metal complexes. We therefore undertook a literature search on the synthesis and characterization of both thiolates and selenolates, to establish what evidence there is for the existence of pure compounds which can be truly formulated as $[R_4X]^+[ER]^-$, (where X = N, P; E = S, Se, Te).

The first report of the preparation of a phosphonium thiolate which we could find was by Liesk, Schulz, and Klar in 1975 (12). These workers found that alkali metal benzenechalcogenolates could be prepared by reduction of the dichalcogenides in liquid ammonia. By adding PPh_4Cl to solutions of the alkali salts in liquid ammonia and recrystallizing the products from ethanol/THF compounds were prepared which analysed as $PPh_4[EPh]$. No further characterization was reported, and in the light of other literature which demonstrates the feasibility of P(V) compounds of this type existing as 5-coordinate phosphoranes rather than simple salts (13) some ambiguity was left by this report.

More recent work on the synthesis of thiolato metal complexes has involved tetraalkylammonium thiolates, but in many instances these salts have been generated *in situ*, and not been isolated. A notable exception to this can be found in a paper by McDonald and co-workers who, after utilizing the *in situ* method in much of their work reported the successful isolation of $[NEt_4][SPh]$ and $[NEt_4][S(benzyl)]$ in 1987 (6). Characterization was again restricted to elemental analysis, but cyclic

[1]To whom correspondence should be addressed.

Can. J. Chem. Downloaded from www.nrcresearchpress.com by 41.223.56.140 on 09/07/12
For personal use only.

Can. J. Chem. Downloaded from www.nrcresearchpress.com by 41.223.56.140 on 09/07/12
For personal use only.

voltammetry was performed on a series of tetraethylammonium thiolate salts by Wedd and co-workers (14). In total there appeared to be no spectroscopic data on these compounds and certainly no X-ray crystallographic structural evidence to justify formulation of these compounds as ionic species.

We report here the synthesis of several aryl thiolate and aryl selenolate salts,[2] their spectroscopic and solution properties, and the X-ray crystal structure of one of these salts, tetraphenylphosphonium 2,4,6-trimethylbenzene thiolate, **1**. This compound, with its proven structure, is then used as the reference point for characterization of the other salts. Since the alkylthiolates are too unstable to handle, we restricted this study to arylthiolates and selenolates but with ring substituents chosen to give convenient ^{1}H NMR labels and a range of chemical behaviour.

Finally we report the cyclic voltammetry of several of the compounds and compare these data with those reported by Wedd and co-workers (14).

Experimental

General procedures

Because of the extreme sensitivity of the chalcogenolate salts to moisture and/or oxygen all solvents were rigorously dried and deoxygenated prior to use, by standard literature methods. The chloride salts used as starting materials for all syntheses, PPh_4Cl and PPNCl(PPN = bis(triphenylphosphineiminium)), were obtained from Aldrich, and were dried by heating to 80°C under vacuum for 24 h. All materials were handled using glovebox and double manifold techniques.

Spectra and physical measurements

Nuclear magnetic resonance spectra were recorded using a Bruker ACE 200 spectrometer (^{1}H and ^{13}C) and a Bruker ACE 400 spectrometer (^{77}Se). Infrared spectra were recorded as Nujol mulls on a Nicolet 5DX FTIR or a Perkin Elmer 467 spectrometer. Conductance measurements were made in acetonitrile solution at varying concentrations using a closed glass cell and a YSI Model 35 conductance bridge.

Synthesis

All the salts were synthesised by essentially the same method, namely, by reacting the sodium thiolate (or selenolate) with $PPh_4^+Cl^-$ (or PPN^+Cl^-) in acetonitrile. The synthesis of the sodium salts was specific to each case, however. In a typical synthesis, tetraphenylphosphonium *para*-tolylthiolate was prepared as follows. *p*-Tolythiol was reacted, in a slight excess, with sodium in methanol. After removal of the methanol the sodium salt was washed with ether, and dried in vacuum at 80°C for 24 h. Approximately 2 g of this salt was then reacted in a 1.2:1.0 molar excess with PPh_4Cl (4 g) in a Schlenk tube with dry MeCN (ca. 50 mL) as the solvent. The resulting slurry was stirred for ca. 72 h, after which the solids were removed by filtration, leaving a solution of (mainly) the desired product. This solution was evaporated to dryness under vacuum leaving the crude product which was then redissolved in acetonitrile, and ether was added until a fine, crystalline solid began to form. The solution was then cooled to 5°C and left for 24 h, after which the product was filtered off, rinsed with ether, and dried in vacuum. (Yield, 85%, based on the limiting reagent, PPh_4Cl.) This procedure had to be modified to prepare 2,4,6-triisopropylbenzenethiolate (Stip) in that the reaction of the thiol with sodium was carried out in 1,2-dimethoxyethane, rather than in methanol. This solvent was also more satisfactory for the preparation of the sodium mesitylthiolate salt.

The selenolate salts can be prepared from the analogous reaction of sodium selenolate with the phosphonium chloride, using acetonitrile as the solvent. However, the sodium salts are most conveniently prepared by reduction of the appropriate diselenide with sodium in THF. In many instances it is necessary to prepare the diselenides from an aryl halide, since few are available commercially. This can be achieved by making the aryl Grignard reagent in THF, reacting it with elemental selenium and hydrolysing the ArSeMgBr so formed to yield the selenol. This product is immediately oxidized in alkaline solution to give the desired product. The synthesis follows a procedure published by Sharpless and Young (15).

The ease of handling the phosphonium and PPN thiolates and selenolates varies considerably from case to case. These salts are in some instances low melting (e.g. Ph_4P[Stip]), and hence difficult to purify and work with. On the other hand, Ph_4P(Smes), **1**, can be obtained as well-formed crystals, and this enabled us to obtain an X-ray crystal structure of this compound (see below). Some were found to crystallize with solvent in the lattice, and the lability of this solvent led to difficulty in obtaining reproducible analytical data. An added problem is the ease of oxidation of the salts to produce the disulfide (or diselenide), and also the hydrolysis of the thiolate to yield free thiol in solution. Hence we found that, having verified the existence and nature of these salts it was most convenient to use ^{1}H NMR spectroscopy to monitor the purity of new members of the series, and new batches of the salts.

Anal calcd. for $[P(C_6H_5)_4][SC_7H_7]$: C 80.49, H 5.88; found (M.H.W.): C 76.02, H 5.36.

Anal calcd. for $[P(C_6H_5)_4][SC_9H_{11}]$: C 81.60, H 6.11; found (M.H.W.): C 78.15, H, 6.24.

Anal. calcd. for $[(C_6H_5)_3P]_2NSC_7H_7$: C 78.03, H 5.63, N 2.13, S 4.84; found (Canadian Microanalytical Services): C 72.53, H 5.32, N 2.12, S 5.11.

Previously, Liesk and co-workers have reported very good analyses for the compounds $[PPh_4][EPh]$ (E = S, Se, Te), and McDonald and co-workers also reported C and H analyses on a sample of Et_4NSPh, but in no case were we able to obtain such good agreement on samples sent by mail to commercial analysts. We ascribe these poor analyses to the instability of the salts as noted above, and were unable to obtain microanalytical services "in house".

Infrared spectra

In general the IR spectra of these salts were uninformative since the presence of phenyl rings in both the anion and the cation (in most instances) dominates the spectra. However, we report them as part of the complete characterization, making comments only on unique bands associated with the anion. Spectra of closely related species (e.g. PPh_4Cl, PhEEPh) are given for comparative purposes. Spectra (2000–250 cm^{-1}) were recorded as Nujol mulls unless otherwise stated, and peaks in the Nujol regions (1380, 1460 cm^{-1}) have been included in the listings in cases where they cannot be distinguished from absorptions due to the compounds under study.

$[PPh_4]$[Sptol]: 1575, m; 1440, s, br; 1370, vs; 1335, sh; 1308, m; 1205, m; 1180, m; 1160, sh; 1100, s; 1050, m; 1030, w; 1010, w; 990, m; 975, m; 850, w; 813, m; 800, sh; 760, s, br; 720, vs; 688, s; 670, m, sh; 550, m, sh; 515, vs; 445, w.

$[PPh_4]$[Smes]: 1575, m; 1450, s, br; 1365, s; 1335, sh; 1308, m; 1183, m; 1160, sh; 1100, s; 1050, m; 997, m; 970, m; 860, m; 775, m; 765, m; 725, vs; 700, m, sh; 692, s; 610, w; 591, w; 515, vs; 450, w.

$[PPh_4]$[Stip]: 1580, m; 1440, s, br; 1370, s; 1335, m, sh; 1305, m; 1295, m, sh; 1190, m; 1160, m; 1040, m, br; 1000, m; 970, m; 940, w; 880, m; 760, m; 722, s; 690, m; 650, w; 620, w; 515, s; 450, w.

tip_2S_2: 1600, m; 1560, w; 1450, s, br; 1375, s; 1360, m, sh; 1310, w; 1260, w; 940, w; 880, w; 725, m; 530, w.

ptolSH: 1890, w; 1590, w; 1560, w; 1490, s; 1465, s, sh; 1460, s; 1395, m; 1375, s; 1300, m; 1212, m; 1185, m; 1120, m; 1080, m; 1050, w; 1020, m; 970, w; 850, w; 815, s; 810, s; 730, w; 530, m; 490, s; 480, s.

[PPN][Sptol]: 1580, m; 1430–1460, s, br; 1370*, s; 1310, m, sh; 1290, m, br; 1255, m, br; 1180, m; 1155, m; 1100, m, br; 1080, m; 1020, m; 1000, m; 975, m; 810, s; 800, m, sh; 765, s, sh; 720, s; 692, s; 670, w; 600, w; 540, s; 520, s; 495, s; 440, w; 395, m; 385, w; 330, w.

[PPN]Cl (in KBr): 1580, m; 1470, m; 1435, s, sh; 1430, s; 1310, m;

[2]Throughout this paper the following abbreviations will be used: 2,4,6-trimethylbenzenethiolate, (mesitylthiolate) = (Smes); 2,4,6-triisopropylbenzenethiolate = (Stip); 4-methylbenzenethiolate, (paratolythiolate) = (Sptol); analogous abbreviations for selenolates.

Can. J. Chem. Downloaded from www.nrcresearchpress.com by 41.223.56.140 on 09/07/12
For personal use only.

1290, m, br; 1255, m, br; 1225, s; 1180, m; 1100, s, br; 1020, m; 998, m; 810, m; 800, m; 755, s, sh; 740, s; 730, s; 698, s; 548, s; 530, s; 505, s; 465, w; 440, w; 390, w; 340, w.

[PPh_4][SePh]: 2940, s, br; 1590, w; 1320, w; 1200, m; 1175, w, sh; 1100, s, br; 1040, w; 1010, m; 960, sh; 870, m; 780, s; 765, s; 740, vs; 710, s; 610, w; 530, vs, br.

PhSeSePh: 1260, m; 1080, m, sh; 1040, m br; 850, m sp; 800, m; 720, w.

PPh_4Cl: 1575, m; 1478, s; 1430, s; 1308, m; 1185, w; 1158, w; 1100, s; 1025, vw; 990, ms; 810 w; 758, s; 720, s; 685, s; 515, s, br; 438, w.

[PPh_4][Semes]: 2870, vs, br.(Nujol + n(C-H)); 1595, w; 1340, w; 1200, s; 1120, s; 1040, m; 1008, m; 860, m sp; 765, m sp; 740, vs; 710, s; 550, vs; 460, m.

mesSeSemes: 1570, m; 1435, s; 1065, m; 1030, m sp; 1005, m sp; 910, w; 750, vs; 700, vs; 680, m; 465, s.

The most useful aspect of these spectra, as far as the identification of the products is concerned, is the presence of bands characteristic of multiply substituted aromatic rings in the spectra of the *p*-tolyl and 2,4,6-trialkylbenzenethiolate salts. These can be used as an indication of the completion of the metathesis reaction of PPh_4Cl with the sodium thiolates. Since this is a heterogeneous reaction such an indicator of its progress can be of assistance. Most characteristic of the multiply substituted rings are bands in the region 800–880 cm^{-1}, which are associated with aromatic C—H bending modes. In the spectra of PPh_4S(*p*-tol) and the parent thiol there are bands at 813 and 815 cm^{-1}, respectively. In the more highly substituted rings these vibrations occur at higher wavenumbers, namely at 860 cm^{-1} in both the Smes and Semes salts of the tetraphenylphosphonium cation, and at 880 cm^{-1} for PPh_4[Stip]. Unfortunately these vibrations also occur, with very little change in frequency, in the spectra of the thiols and the disulfides (or diselenides). Since these are the major possible contaminants of the salts this limits the usefulness of the IR spectra as indicators of product purity.

X-ray structural determination of Ph_4P(Smes), 1

Data collection

A suitable transparent, block-shaped crystal was wedged into a Lindemann glass capillary, and mounted on an Enraf-Nonius CAD4 diffractometer. The triclinic unit cell parameters and their standard deviations were derived from the setting angles of 24 reflections in the range $6.32° < \theta < 12.11°$. Reduced cell calculations did not indicate any higher metric symmetry. The space group was determined to be $P\bar{1}$ on the basis of the strongly centric distribution of E values, and the choice was supported by the successful solution of the structure in this space group. Crystal and instrumental instability were monitored through the measurement of three standard reflections every 0.5 h of X-ray exposure time; there were no indications of crystal decomposition. The net intensities of the data were corrected for Lorentz and polarization effects. Variance, $\sigma^2(I)$, was calculated based on counting statistics and instrumental instability as estimated from the standard reflections. Crystal data and experimental details of the structure determination are given in Table 1.

Structure solution

The mesityl ring of the anion and much of the tetraphenylphosphonium cation were located in an E map with phases derived from symbolic addition using the program SIMPEL(16). The remaining non-hydrogen atoms were located in difference Fourier maps. All non-hydrogen atoms were refined anisotropically, with hydrogens refined with independent isotropic temperature factors. Convergence was reached at $R = 0.100$. The final values of the refined positional parameters are presented in Table 2.[3] Neutral atom scattering factors were used with anomalous dispersion corrections applied (17). All calculations were carried out on a VAX 11/780 computer at the University of Calgary using the program package XTAL2.2 (16).

TABLE 1. Experimental data for tetraphenylphosphonium 2,4,6-trimethylbenzenethiolate

Formula	$C_{33}H_{32}PS$
Cell dimensions a	9.946(3) Å
b	10.100(2) Å
c	14.874(3) Å
α	70.19(2)°
β	69.13(2)°
γ	82.54(2)°
Space Group	$P\bar{1}$
D_c	1.240 g cm^{-3}
Crystal dimensions	0.09 × 0.49 × 0.17 mm
λ	0.71069 Å Mo Kα graphite monochromato
$\sin\theta/\lambda_{max}$	0.594 $Å^{-1}$
Range h	0 to 11
k	−11 to 11
l	−15 to 17
Total reflections	6315
Unique reflections	4604
Observed reflections	3086 $I \geq 3\sigma(I)$
Number of parameters refined	440
$R = \left[\frac{\Sigma(\lvert\lvert F_o\rvert - \lvert F_c\rvert\rvert)}{\Sigma\lvert F_o\rvert}\right] =$	0.100
$R_w = \left[\frac{\Sigma(\lvert\lvert F_o\rvert - \lvert F_c\rvert\rvert)w}{\Sigma\lvert F_o\rvert w}\right] =$	0.074
$S = \left[\frac{\Sigma(\lvert\lvert F_o\rvert - \lvert F_c\rvert\rvert)w}{(m-n)}\right]^{1/2} =$	0.852
$w = 1/\sigma(F)^2$	

Electrochemistry

Electrochemical experiments were carried out in a dry box, under an argon atmosphere. The solvent was acetonitrile containing 0.1 *M* tetra-*n*-butylammonium perchlorate (TBAP) as supporting electrolyte. Acetonitrile was purified as noted above. TBAP (Fluka) was recrystallised from isopropanol/water (70:30, vol:vol) and dried for 24 h in a vacuum oven at 100°C before use. The electrochemical cell and the instrumentation are described in detail in ref. 18. The working electrode was a platinum wire, positioned concentrically within the coils of a Pt wire helix, which served as the counter electrode. The reference electrode was a silver wire immersed in CH_3CN/0.01 *M* $AgNO_3$/0.1 *M* TBAP. Two fine glass frits and a Luggin capillary positioned within 2 mm of the working electrode surface separated the working and reference electrode compartments. Solutions were prepared in the dry box utilizing previously degassed CH_3CN. Argon was bubbled through the solutions immediately after preparation to ensure complete removal of any traces of residual oxygen.

Results and discussion

Structure of tetraphenylphosphonium 2,4,6-trimethylbenzenethiolate 1

The conclusive identification of the series of compounds as salts of general formula $[Cation]^+[ER]^-$, (E = S, Se) is based on the successful determination of the X-ray crystal structure of [PPh_4][Smes], **1**. The anion of **1** is shown in Fig. 1, with a stereo

[3]Tables of observed and calculated structure factor amplitudes, of hydrogen positions, thermal parameters, and a comprehensive list of bond lengths and bond angles may be purchased from the Depository of Unpublished Data, CISTI, National Research Council of Canada, Ottawa, Ont., Canada K1A 0S2.

TABLE 2. Refined coordinates and equivalent isotropic temperature factors for the non-hydrogen atoms

Atom	X	Y	Z	1000 U_{eq}
P(1)	0.8195(1)	0.5886(2)	0.2082(1)	36.0
S(2)	0.4930(2)	1.1368(2)	0.2498(1)	60.4
C(1)	0.3617(5)	1.0046(5)	0.3014(4)	39.8
C(2)	0.3499(5)	0.9215(6)	0.2448(4)	37.5
C(3)	0.2450(6)	0.8174(6)	0.2874(5)	38.0
C(4)	0.1473(6)	0.7944(5)	0.3839(5)	42.2
C(5)	0.1599(6)	0.8759(6)	0.4400(5)	42.7
C(6)	0.2627(5)	0.9783(6)	0.4012(4)	38.4
C(7)	0.4512(7)	0.9414(8)	0.1376(4)	48.8
C(8)	0.0286(8)	0.6877(8)	0.4268(7)	58.7
C(9)	0.2702(9)	1.0641(8)	0.4654(6)	60.7
C(11)	0.7240(5)	0.6140(5)	0.3288(4)	30.5
C(12)	0.7341(6)	0.5157(6)	0.4175(4)	34.8
C(13)	0.6657(6)	0.5415(7)	0.5085(4)	41.5
C(14)	0.5846(6)	0.6635(6)	0.5131(5)	44.1
C(15)	0.5741(6)	0.7594(7)	0.4253(5)	44.5
C(16)	0.6412(6)	0.7352(6)	0.3332(5)	43.5
C(21)	0.8974(6)	0.4157(5)	0.2280(4)	35.3
C(22)	1.0292(6)	0.3929(7)	0.2419(4)	43.7
C(23)	1.0864(7)	0.2589(7)	0.2639(4)	52.7
C(24)	1.0137(8)	0.1495(8)	0.2702(5)	55.0
C(25)	0.8815(8)	0.1699(7)	0.2580(5)	60.4
C(26)	0.8221(7)	0.3030(6)	0.2365(4)	46.0
C(31)	0.9636(5)	0.7111(6)	0.1346(4)	36.7
C(32)	1.0690(7)	0.6883(8)	0.0493(5)	53.9
C(33)	1.1750(7)	0.7861(9)	−0.0097(5)	61.8
C(34)	1.1806(8)	0.9038(9)	0.0146(6)	72.3
C(35)	1.0793(7)	0.9272(7)	0.0991(5)	59.4
C(36)	0.9703(6)	0.8320(6)	0.1591(5)	47.2
C(41)	0.6983(5)	0.6096(5)	0.1403(4)	35.2
C(42)	0.7387(7)	0.6777(6)	0.0367(5)	45.2
C(43)	0.6436(9)	0.6899(7)	−0.0144(6)	61.7
C(44)	0.5092(9)	0.6313(7)	0.0383(6)	68.4
C(45)	0.4677(8)	0.5636(7)	0.1400(6)	60.6
C(46)	0.5618(6)	0.5534(6)	0.1904(5)	45.9

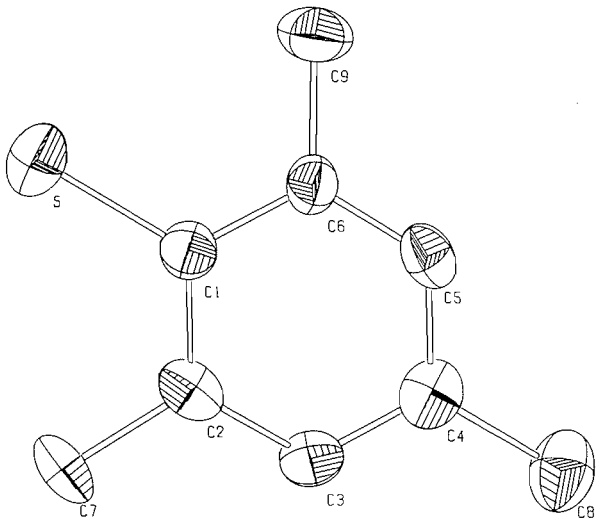


FIG. 1. ORTEP drawing of the 2,4,6-trimethylbenzenethiolate anion showing the numbering scheme; 50% thermal ellipsoids are drawn, hydrogens are omitted for clarity.

packing diagram in Fig. 2. The key feature of the structure can be seen from the packing diagram, namely that there are no close contacts between the thiolate sulfur, S, and any other atoms, and especially that it is not coordinated to the phosphorus to give a phosphorane, in this crystal at least. The calculated separation of S and P is 6.149(3) Å. Hence further experiments were designed to show that the solution and spectroscopic properties of **1** were consistent with this formulation, and that the other members of the series had similar properties, and hence analogous structures.

The bond lengths and bond angles within the anion (Table 3) are within the ranges expected; the S—C(1) distance is 1.767(6) Å, and the S—C(1)—C(2) and S—C(1)—C(6) angles are 121.7(4) and 121.2(5), respectively. The sum of the angles subtended at C(1) is 360°, confirming its planarity. At the centre of the phosphonium cation the C—P—C bond angles are all close to 109°, and again verify that no coordination of the sulfur of the anion to the P atom is occurring. The packing of the cations is such that layers of phenyl groups occur in the *ab* plane, and at $z = 0.5$ a layer of alternating phenyl rings from the anion and the cation is observed. It appears that the anions help to bind the layers of cations together.

Solution properties and NMR spectra

As mentioned in the Experimental section, the instability of the thiolate and selenolate salts presented a significant problem in handling them, particularly in solution. However, those members of the series which crystallized from solution to give solids with reasonably high melting points could be kept under a dry nitrogen atmosphere for periods of weeks without decomposition. The most useful method of characterization was the ^1H NMR spectrum. Pertinent data are given in Table 4.

The ^{77}Se spectra of selected samples were obtained, and compared with literature values of related compounds. For PhSeSePh a δ of 481 ppm (in $CDCl_3$ solution, D_2O lock; ref. Me_2Se, 0 ppm, KSeCN, −330 ppm) which is consistent with the literature value (19) while in mesSeSemes the chemical shift is 391 ppm. The sample of PPh_4[SePh], whose ^1H spectrum is uninformative at 200 MHz, showed a peak at relatively high field in CH_3CN solution, viz. −601 ppm, thus making it very useful as a diagnostic technique to identify the anion. The spectrum showed no resonance at 481 ppm, indicating no measurable oxidation of the sample to Ph_2Se_2.

Conductance measurements

To demonstrate that the salts are indeed dissociated in the preferred solvent, acetonitrile, conductance measurements were made over a concentration range of 10^{-2}–10^{-4} *M* (25°C). Interpolated values at 10^{-3} *M*, commonly cited to establish 1:1 electrolyte behaviour, were as follows:

PPh_4[Smes], 112; PPh_4[tipt], 80; PPN[S(ptol)], 100; PPh_4[SePh], 186; PPh_4Br, 148; PPh_4Cl, 170; PhSeSePh, 2.2; $ohm^{-1}\ cm^2\ mol^{-1}$. (Literature values for 1:1 electrolytes, 10^{-3} *M*, 25°C: 120–160 $ohm^{-1}\ cm^2\ mol^{-1}$ (20).)

These data clearly establish that the thiolate and selenolate salts exist as 1:1 electrolytes in acetonitrile. As expected they show increasing association at higher molarities, reflected in lower conductance values. The predicted dependence of the Λ_M values on the anion size, and consequently on the mobility, is consistent with these data. The conductance measurements were also found to be very sensitive to sample oxidation in the dilute solutions, and for this reason data were recorded on freshly prepared solutions, in a stoppered conductance cell. Even under these circumstances the conductance values diminished over a period of 1 h. Some specific salts (e.g. PPh_4[Sptol]) were so sensitive that even the data obtained as described here showed

Can. J. Chem. Downloaded from www.nrcresearchpress.com by 41.223.56.140 on 09/07/12
For personal use only.

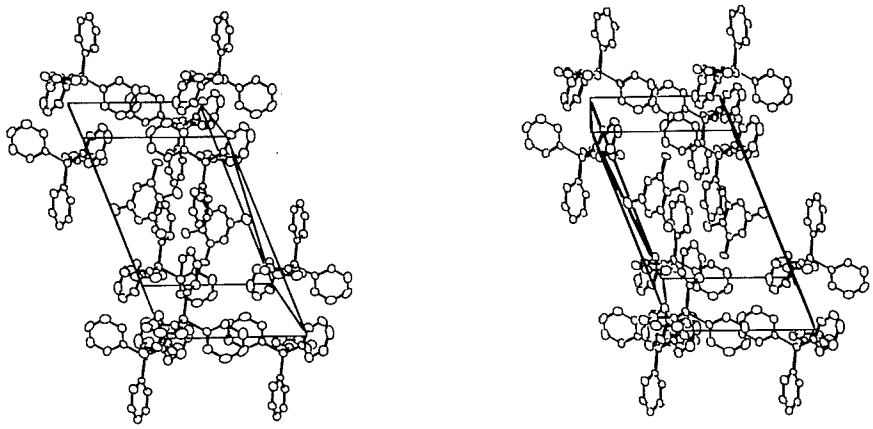


FIG. 2. Stereoscopic view of the contents of the unit cell of tetraphenylphosphonium 2,4,6-trimethylbenzenethiolate, showing only the non-hydrogen atoms which are drawn at the 50% probability level.

Can. J. Chem. Downloaded from www.nrcresearchpress.com by 41.223.56.140 on 09/07/12
For personal use only.

that the solution had already undergone partial oxidation and/or hydrolysis.

Electrochemical behaviour

The solution properties of the thiolate salts were next examined by cyclic voltammetry in acetonitrile solution. Previous work by Wedd and co-workers on tetraethylammonium thiolates (14) had established that an oxidation peak occurs in the region −0.5 to −0.2 V relative to the $Ag|AgNO_3$ (0.1 *M*) electrode Figure 3 shows the cyclic voltammogram for a 0.001 *M* solution of [PPN][Sptol] in acetonitrile. There are three peaks, labelled A, B, and C. In accordance with the results of Wedd, and the observations discussed below, the anodic peak A is assigned as the oxidation of thiolate to disulphide, as per the equation:

$$2SR^- \rightarrow 2RSSR + 2e^- \qquad E_p = -0.34 \text{ V}$$

The cathodic peak C is observed only following anodic sweeps into the region of peak A, indicating it is due to reduction of a product of the thiolate oxidation. That this product is the disulphide was confirmed in cyclic voltammetric studies of a solution of *p*-tolyldisulfide, which underwent reduction at potentials identical to that of peak C in Fig. 3. This reduction process was irreversible, but led to the appearance, on subsequent anodic scans, of a peak occurring at identical potentials to A for oxidation of the thiolate. Thus, peak C is assigned as reduction of the disulfide to the thiolate according to:

$$RSSR + 2e^- \rightarrow 2RS^- \qquad E_p = -2.24 \text{ V}$$

Also apparent in Fig. 3 is a second anodic peak, labelled B, at +0.17 V. This only occurs in solutions which have been standing for some time and is not related to any species generated by electrochemical processes. This peak was not reported by other workers (14), but we observed it in all solutions of thiolate after a period of time. We ascribe this peak to an oxidation process involving an unidentified decomposition product of thiolate. The intensity of peak B grows over a period of time under open circuit conditions, while peak A, due to oxidation of the thiolate, decreases. Peak A is completely absent in solutions left standing under argon for more than an hour. Peak B is not evident in the voltammetry of the disulfide, and thus does not appear to be related to any process involving this species.

Cyclic voltammetry of a solution of *p*-tolylthiol was undertaken in order to investigate the possibility that the unassigned peak B might involve this species. No process at potentials comparable to peak B was evident. Consistent with the results of Wedd (14), reduction of the thiol gave rise to an irreversible cathodic peak at −2.05 V, 190 mV positive of that observed for reduction of the disulfide. Subsequent anodic scans following this reduction displayed an anodic peak at −0.34 V, coincident with peak A observed for thiolate oxidation. These observations are again consistent with Wedd's interpretation of the thiol reduction occurring according to:

$$RSH + 1e^- \rightarrow RS^- + \tfrac{1}{2} H_2 \qquad E_p = -2.05 \text{ V}$$

Anodic scans of the *p*-tolylthiol solution revealed an irreversible anodic peak at +0.74 V. This was followed on subsequent cathodic scans by the appearance of a new cathodic peak coincident with that observed for reduction of the disulfide. The

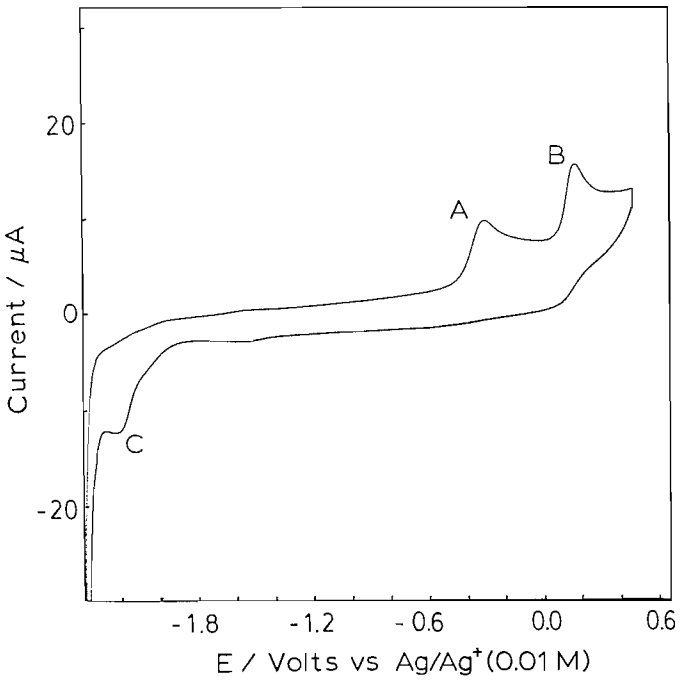


FIG. 3. Continuous sweep cyclic voltammetry of [PPN][Sptol] (0.001 *M*) in CH_3CN using $[N(n\text{-}Bu)_4][ClO_4]$ as supporting electrolyte. The solution had been allowed to stand ca. 20 min prior to initiating the cycling.

TABLE 3. Table of bond lengths and angles involving the non-hydrogen atoms

Bond		Length (Å)	Bonds			Angle (deg)
P	C(11)	1.795(5)	C(2)	C(1)	C(6)	117.1(5)
P	C(21)	1.789(5)	S	C(1)	C(2)	121.7(4)
P	C(31)	1.791(5)	S	C(1)	C(6)	121.2(5)
P	C(41)	1.781(7)	C(12)	C(11)	C(16)	119.5(5)
S	C(1)	1.767(6)	P	C(11)	C(12)	120.8(4)
C(1)	C(2)	1.42(1)	P	C(11)	C(16)	119.7(4)
C(1)	C(6)	1.415(7)	C(11)	C(12)	C(13)	119.5(5)
C(2)	C(3)	1.399(8)	C(12)	C(13)	C(14)	121.2(5)
C(2)	C(7)	1.513(7)	C(13)	C(14)	C(15)	118.9(6)
C(3)	C(4)	1.377(8)	C(14)	C(15)	C(16)	120.8(6)
C(4)	C(5)	1.40(1)	C(11)	C(16)	C(15)	120.0(5)
C(4)	C(8)	1.51(1)	C(1)	C(2)	C(3)	120.6(5)
C(5)	C(6)	1.378(8)	C(1)	C(2)	C(7)	121.0(5)
C(6)	C(9)	1.52(1)	C(3)	C(2)	C(7)	118.4(6)
C(11)	C(12)	1.385(7)	C(22)	C(21)	C(26)	119.8(5)
C(11)	C(16)	1.391(8)	P	C(21)	C(22)	119.4(5)
C(12)	C(13)	1.378(9)	P	C(21)	C(26)	120.7(5)
C(13)	C(14)	1.391(9)	C(21)	C(22)	C(23)	120.2(7)
C(14)	C(15)	1.368(9)	C(22)	C(23)	C(24)	119.8(7)
C(15)	C(16)	1.38(1)	C(23)	C(24)	C(25)	120.8(7)
C(21)	C(22)	1.376(9)	C(24)	C(25)	C(26)	120.2(8)
C(21)	C(26)	1.39(1)	C(21)	C(26)	C(25)	119.2(7)
C(22)	C(23)	1.377(9)	C(2)	C(3)	C(4)	121.9(7)
C(23)	C(24)	1.36(1)	C(32)	C(31)	C(36)	119.2(5)
C(24)	C(25)	1.37(1)	P	C(31)	C(32)	119.5(5)
C(25)	C(26)	1.377(9)	P	C(31)	C(36)	121.3(4)
C(31)	C(32)	1.396(8)	C(31)	C(32)	C(33)	119.2(8)
C(31)	C(36)	1.40(1)	C(32)	C(33)	C(34)	121.2(7)
C(32)	C(33)	1.37(1)	C(33)	C(34)	C(35)	120.6(7)
C(33)	C(34)	1.37(1)	C(34)	C(35)	C(36)	119.6(8)
C(34)	C(35)	1.37(1)	C(31)	C(36)	C(35)	120.1(6)
C(35)	C(36)	1.377(9)	C(3)	C(4)	C(5)	117.3(5)
C(41)	C(42)	1.387(8)	C(3)	C(4)	C(8)	121.5(7)
C(41)	C(46)	1.383(8)	C(5)	C(4)	C(8)	121.2(6)
C(42)	C(43)	1.38(1)	C(42)	C(41)	C(46)	118.4(7)
C(43)	C(44)	1.38(1)	P	C(41)	C(42)	121.5(5)
C(44)	C(45)	1.36(1)	P	C(41)	C(46)	120.0(5)
C(45)	C(46)	1.37(1)	C(41)	C(42)	C(43)	120.3(6)
			C(42)	C(43)	C(44)	119.3(7)
			C(43)	C(44)	C(45)	121.3(9)
			C(44)	C(45)	C(46)	119.1(7)
			C(41)	C(46)	C(45)	121.5(6)
			C(4)	C(5)	C(6)	122.5(5)
			C(1)	C(6)	C(5)	120.5(6)
			C(1)	C(6)	C(9)	119.4(5)
			C(5)	C(6)	C(9)	120.0(5)
			C(11)	P	C(21)	109.2(2)
			C(11)	P	C(31)	111.4(3)
			C(11)	P	C(41)	109.5(3)
			C(21)	P	C(31)	107.3(2)
			C(21)	P	C(41)	110.1(3)
			C(31)	P	C(41)	109.4(2)

thiol oxidation thus appears to follow:

$$2\,RSH^- \rightarrow RSSR + 2H^+ + 2e^- \qquad E_p = +0.74\ V$$

Since none of the processes discussed is reversible, changes in sweep rate result in changes to the peak potentials. All the results described here were obtained using a sweep rate of 100 mV s^{-1}.

The results obtained for a series of thiolate salts are collected in Table 5, and compared with those of Wedd and co-workers (14). For the *p*-tolyl compounds common to both studies there is close agreement in the results and their interpretation, with the exception of the oxidation wave for the thiol. We did not experience the same problem that Wedd and co-workers reported, namely, a very low current density for this wave lending uncertainty to its identification. On the contrary we observed a readily identified peak at +0.74 V, very similar to the other two thiols in our study. The data for PPh_4[Smes] and PPh_4[Stip] are very similar to those reported (14) for the $[SPh]^-$ and $[Sptol]^-$ salts, except that once again we were unable to leave the solutions for any period of time without the appearance

Can. J. Chem. Downloaded from www.nrcresearchpress.com by 41.223.56.140 on 09/07/12
For personal use only.

TABLE 4. ^{1}H NMR spectra of representative thiolate and selenolate salts and related compounds (in CD_3CN solution; ref. CHD_2CN, δ 1.93)

Compound	Chemical shift	Integration	Assignment
PPh_4[Sptol]	7.70–7.30 (m)	20 H	PPh_4 cation
	7.10 (d)	2 H	*ortho*-H, ptol
	7.67 (d)	2 H	*meta*-H, ptol
	2.12 (s)	3 H	CH_3 of ptol
ptolSH	7.64 (d)	2 H	*ortho*-H, ptol
	7.58 (d)	2 H	*meta*-H, ptol
	2.26 (s)	3 H	CH_3 of ptol
PPh_4[Smes]	7.70–7.30 (m)	20 H	PPh_4 cation
	6.83 (s)	2 H	*meta*-H, mes
	2.37 (s)	6 H	*ortho*-CH_3, mes
	2.34 (s)	3 H	*para*-CH_3, mes
mesSH	7.04 (s)	2 H	*meta*-H, mes
	2.60 (s)	6 H	*ortho*-CH_3, mes
	2.56 (s)	3 H	*para*-CH_3, mes
PPh_4[Stip]	7.70–7.30 (m)	20 H	PPh_4 cation
	6.98 (s)	2 H	*meta*-H, tipt
	3.56 (sept.)	2 H	*ortho*-$CH(CH_3)_2$
	2.80 (sept.)	1 H	*para*-$CH(CH_3)_2$
	1.18 (d)	6 H	*ortho*-$CH(CH_3)_2$
	1.14 (d)	3 H	*para*-$CH(CH_3)_2$
tipSH	7.04 (s)	2 H	*meta*-H, tipt
	4.15 (sept.)	2 H	*ortho*-$CH(CH_3)_2$
	2.89 (sept.)	1 H	*para*-$CH(CH_3)_2$
	1.22 (d)	6 H	*ortho*-$CH(CH_3)_2$
	1.18 (d)	3 H	*para*-$CH(CH_3)_2$
PPh_4[Semes]	7.70–7.40 (m)	20 H	PPh_4 cation
	6.68 (s)	2 H	*meta*-H, mes
	2.30 (s)	6 H	*ortho*-CH_3
	2.25 (s)	3 H	*para*-CH_3
mesSeSemes	6.87 (s)	2 H	*meta*-H, mes
	2.24 (s)	6 H	*ortho*-CH_3
	2.20 (s)	3 H	*para*-CH_3

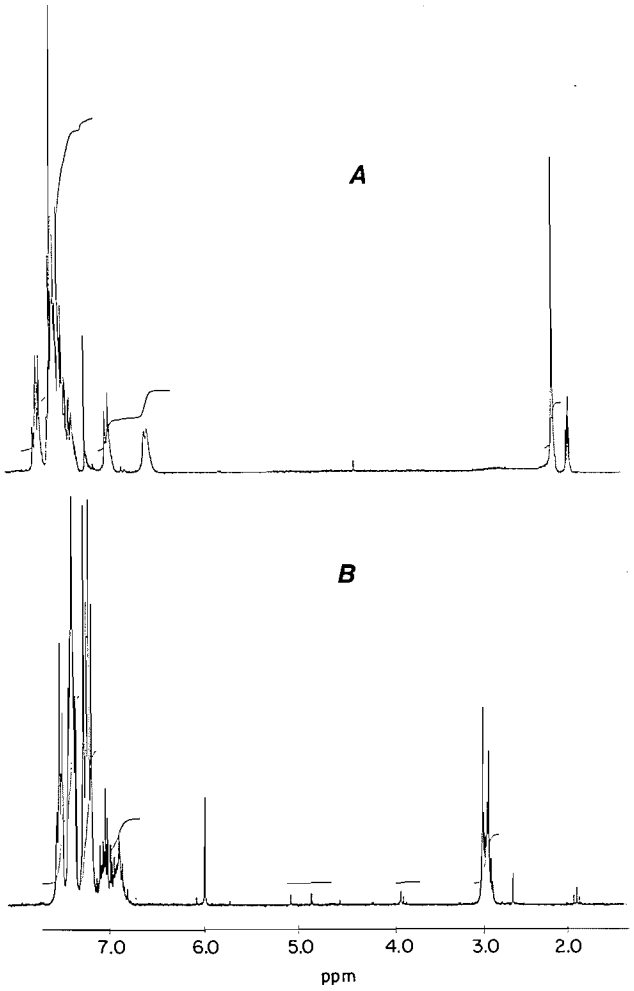


FIG. 4. ^{1}H NMR OF [PPh_4][Sptol] in (*A*) CD_3CN, (*B*) $C_2D_2Cl_4$ showing the reactivity of the thiolate anion with chlorocarbon solvents.

of the wave B. This was present at −0.04 and −0.02 V, respectively, even in freshly prepared solutions, and this peak grew to be predominant after extended periods of time spent under open circuit conditions.

The positions of the peaks for thiolate oxidation show a trend, indicating that oxidation becomes easier as the degree of substitution of the phenyl ring of the thiolate anion increases. The electron donating effect of the alkyl substituents may thus be more important in determining the ease of oxidation of the thiolates to the disulfides than steric crowding around the sulfur atom. On the basis of steric arguments alone, it might be anticipated that $Smes^-$ and $Stip^-$ would be the most resistant to oxidation, which is the opposite of what is actually observed in the electrochemical studies.

Reactions of thiolate salts

The potential uses of the phosphonium chalcogenolates in synthetic coordination chemistry are limited by the highly nucleophilic nature of the naked anions. Although at first sight

TABLE 5. Cyclic voltammetric data for phosphonium arylthiolates and related species

Process for the assigned waves	Peak potentials (V)				
	This work[a]			Data from ref. 14[b]	
	Sptol	Smes	Stipt	Sptol	SPh
$HSR \rightarrow RSSR + 2H^+ + 2e^-$	+0.74	+0.74	+0.76	1.06	0.66
$2SR^- \rightarrow RSSR + 2e^-$	−0.34	−0.44	−0.45	−0.33	−0.25
$2e^- + RSSR \rightarrow 2RS^-$	−2.20	−2.28	−2.32	−2.16	−2.14

[a]Data referenced to Ag|$AgNO_3$ (0.01 *M*).
[b]Original data referenced to Ag|$AgNO_3$ (0.1 *M*), and corrected to be comparable with the present study.

Can. J. Chem. Downloaded from www.nrcresearchpress.com by 41.223.56.140 on 09/07/12
For personal use only.

this may seem attractive in terms of ligand replacement reactions it imposes a severe constraint on the selection of solvent. Chlorocarbon solvents, a popular choice for many syntheses, are likely to react with ER^-, with the displacement of chloride. The ^1H NMR spectra of PPh_4[Sptol] in CD_3CN (*A*) and in $C_2D_2Cl_4$ (*B*) are shown in Fig. 3. The resonance for the CH_3 protons of the tolyl group is a clean singlet in acetonitrile whereas it appears as a complex multiplet in the chlorocarbon. Further experiments showed that the salts are rapidly degraded in dichloromethane and hence this useful solvent is inappropriate for preparing and handling thiolate or selenolate salts. This compares with the report of Shaver and co-workers (21) who reacted NaSH with a metal complex in CH_2Cl_2 and unexpectedly prepared a complex of the chelating ligand $CH_2S_2^{2-}$.

The other major difficulty we encountered in handling the salts, even in an apparently inert solvent, was that the solutions are extremely sensitive to oxidation and in the case of the thiolate, to hydrolysis. Fortunately the ^1H NMR spectra of the alkyl-substituted aryl thiolates or selenolates provide a convenient method of checking for the degree of decomposition of the salts. Hence any problems with reagent decomposition can be identified.

Given these constraints it is still possible to use the salts for many synthetic purposes and some of these will be described later.

Acknowledgements

The authors thank the Natural Sciences and Engineering Council of Canada for financial support (to P.M.B., J.M.B., and A.S.H. and for an Infrastructure Grant to assist the X-ray Structure Service), and Dr. K. A. Kerr for the use of the diffractometer. The assistance of Allen Apblett in obtaining ^{77}Se spectra, and helpful discussions with Dr. M. E. Peach are gratefully acknowledged.

1. J. R. DILWORTH. Studies in inorganic chemistry. Vol. 5. "Sulfur". *Edited by* A. Muller and B. Krebs. Elsevier Science Publishers, Amsterdam. 1984. pp. 141–165.
2. P. J. BLOWER and J. R. DILWORTH. Coord. Chem. Rev. **76**, 121 (1987).
3. I. G. DANCE. Polyhedron, **5**, 1037 (1986).
4. V. D. PATEL, P. M. BOORMAN, K. A. KERR, and K. J. MOYNIHAN. Inorg. Chem. **21**, 1383 (1982); P. M. BOORMAN, J. M. BALL, K. J. MOYNIHAN, V. D. PATEL, and J. F. RICHARDSON. Can. J. Chem. **61**, 2809 (1983); J. M. BALL, P. M. BOORMAN, and J. F. RICHARDSON. Inorg. Chem. **25**, 3325 (1986).
5. S. G. ROSENFIELD, W. H. ARMSTRONG, and P. K. MASHARAK. Inorg. Chem. **25**, 3014 (1986).
6. L. D. ROSENHEIM, W. E. NEWTON, and J. W. MCDONALD. Inorg. Chem. **26**, 1695 (1987).
7. I. L. ABRAHAMS and C. D. GARNER. J. Chem. Soc. Dalton Trans. 1577 (1987).
8. C. D. GARNER, J. K. NICHOLSON, and W. CLEGG. Inorg. Chem. **23**, 2148 (1984).
9. P. J. BLOWER, J. R. DILWORTH, J. P. HUTCHINSON, and J. A. ZUBIETA. J. Chem. Soc. Dalton Trans. 1577 (1987).
10. S. G. ROSENFIELD, H. P. BERENDS, L. GELMINI, D. W. STEPHAN, and P. K. MASCHARAK. Inorg. Chem. **26**, 2792 (1987).
11. M. T. REETZ and R. OSTAREK. J. Chem. Soc. Chem. Commun. 213 (1988).
12. V. J. LIESK, P. SCHULZ, and G. KLAR. Z. Anorg. Allg. Chem. **435**, 98 (1977).
13. J. H. CLARK and D. J. MACQUARRIE. J. Chem. Soc. Chem. Commun. 229 (1988).
14. J. R. BRADBURY, A. F. MASTERS, A. C. MCDONELL, A. A. BRUNETTE, A. M. BOND, and A. G. WEDD. J. Am. Chem. Soc. **103**, 1959 (1981).
15. K. B. SHARPLESS and M. W. YOUNG. J. Org. Chem. **40**, 948 (1975).
16. S. R. HALL and J. M. STEWART. (*Editors*). XTAL2.2 User's Manual. Universities of Western Australia and Maryland.
17. International tables for crystallography. Vol. IV. Kynoch Press, Birmingham, England, 1974.
18. A. S. HINMAN, B. J. PAVELICH, A. E. KONDO, and S. PONS. J. Electroanal. Chem. **234**, 149 (1987).
19. J. D. ODOM, W. H. DAWSON, and P. D. ELLIS. J. Am. Chem. Soc. **101**, 5815 (1979).
20. W. J. GEARY. Coord. Chem. Rev. **7**, 81 (1971).
21. A. SHAVER, R. D. LAI, P. D. BIRD, and W. WICKRAMASINGHE. Can. J. Chem. **63**, 2555 (1985).

Can. J. Chem. Downloaded from www.nrcresearchpress.com by 41.223.56.140 on 09/07/12
For personal use only.

Étude chimique et cinétique de l'oxydation homogène en phase gazeuse d'alcanes légers. I. Isobutane

BERNARD VOGIN,[1] FRANÇOIS BARONNET[2] ET GÉRARD SCACCHI

Département de chimie physique des réactions, Unité associée n° 328 du Centre national de la recherche scientifique, Institut national polytechnique de Lorraine – École nationale supérieure des industries chimiques, 1, rue Grandville, B.P. 451, 54001 Nancy CEDEX, France

Reçu le 9 juin 1988

BERNARD VOGIN, FRANÇOIS BARONNET et GÉRARD SCACCHI. Can. J. Chem. **67**, 759 (1989).

Une mise au point bibliographique sur l'oxydation en phase gazeuse homogène des alcanes légers montre que, malgré un nombre substantiel de travaux, il subsiste, y compris dans le cas de l'isobutane, une liste importante de problèmes non résolus, rendant aléatoire l'écriture d'un schéma réactionnel. Afin de disposer de données expérimentales plus sûres, nous avons entrepris une étude de l'oxydation homogène de l'isobutane en appareillage statique classique à 310 et 340°C, à pression subatmosphérique. Le but principal de cette étude était de mettre en évidence les produits primaires principaux de la réaction. Pour interpréter ces observations, un mécanisme radicalaire en chaînes s'appuyant sur les produits primaires et sur l'évaluation des constantes de vitesse de réactions élémentaires par les méthodes de la Cinétique Thermochimique est proposé. Les différents processus élémentaires sont discutés et comparés aux observations expérimentales. Il est possible de mettre en évidence deux chemins réactionnels prépondérants, l'un conduisant à la formation d'isobutène et l'autre à la formation d'oxyde d'isobutène. Les conclusions du présent travail et les perspectives en découlant sont également précisées.

Mots clés : oxydation, cinétique chimique, méchanisme de réaction, isobutane.

BERNARD VOGIN, FRANÇOIS BARONNET, and GÉRARD SCACCHI. Can. J. Chem. **67**, 759 (1989).

A literature survey on the homogeneous gas-phase oxidation of light alkanes shows that despite a rather high number of papers there are still, even in the case of isobutane, an important number of unresolved questions, which makes the writing of a reaction scheme rather difficult. To obtain more reliable experimental data, we have studied the homogeneous gas-phase oxidation of isobutane in a conventional static system, at 310 and 340°C and subatmospheric pressure. This investigation is chiefly aimed at identifying and measuring the major primary products of the reaction. A chain radical scheme based on the primary products and on estimation of the rate constants of the elementary steps by the methods of Thermochemical Kinetics is put forward to interpret our experimental results. Two major reaction routes appear, one corresponding to the formation of isobutene and the other to the formation of isobutene oxide. The conclusions of the present investigation and suggestions for further developments are also mentioned.

Key words: oxidation, chemical kinetics, reaction mechanism, isobutane.

I. Introduction. Généralités sur l'oxydation des alcanes légers : cas de l'isobutane

I.1. Mise au point bibliographique

Malgré de nombreux travaux et la publication d'un certain nombre de mises au point dont celles de Baker et Yorke (1), Pollard (2) et Benson (3, 4), le mécanisme de l'oxydation homogène de substances organiques, y compris des alcanes, est loin d'être totalement élucidé et des aspects que l'on peut considérer comme fondamentaux ne sont pas encore résolus. Sans aller jusqu'à tenter d'interpréter des phénomènes tels que les flammes froides ou les inflammations de 2ème stade, la simple oxydation lente des hydrocarbures pose encore des problèmes même au niveau des processus élémentaires constituant le mécanisme.

D'après les auteurs qui se sont intéressés à ces réactions, deux types de mécanismes ont été proposés pour rendre compte des résultats observés :

(*i*) Certains travaux soulignent la prépondérance de l'isomérisation des radicaux alcoylperoxy qui avait été plus spécialement développée par Fish (5). Cette interprétation peut être représentée par le mécanisme symbolique ci-dessous où RH représente l'alcane de départ, R· le radical alcoyle qui en dérive par arrachement d'hydrogène, RO_2· le radical alcoylperoxy formé à partir de R· par addition de O_2 et ·QOOH le radical isomérisé issu de RO_2· par transfert interne d'hydrogène :

[1] $RH + O_2 \rightarrow R\cdot + HO_2\cdot$

[2] et [−2] $R\cdot + O_2 \rightleftarrows RO_2\cdot$

[3] et [−3] $RO_2\cdot \rightleftarrows \cdot QOOH$

[4] $\cdot QOOH \rightarrow$ produit + $OH\cdot$ ou $HO_2\cdot$

La facilité d'isomérisation de RO_2· en ·QOOH dépend de la taille du cycle constituant l'état de transition; le cycle à six centres est favorisé en raison de la très faible énergie de tension. Il convient également de noter que la réversibilité du processus [2] semble limiter ce mécanisme à des températures relativement basses, inférieures à des valeurs de l'ordre de 300–350°C selon la littérature.

(*ii*) À plus haute température, entre 300 et 500°C, les résultats expérimentaux publiés paraissent suggérer que l'alcane se transforme essentiellement en l'alcène conjugué. Pour expliquer ces observations, Knox (6) a proposé une théorie dite théorie oléfinique. L'alcène apparaîtrait essentiellement lors du processus suivant :

[5] $R\cdot + O_2 \rightarrow$ alcène + $HO_2\cdot$

et l'oxydation de l'alcène contribuerait pour une part appréciable à la formation de produits oxygénés. Toujours d'après Knox, les produits mineurs seraient formés de façon hétérogène à partir des radicaux alcoylperoxy. Les processus suivants peuvent donc être écrits :

[5] $R\cdot + O_2 \rightarrow$ alcène + $HO_2\cdot$

[6] $RH + HO_2\cdot \rightarrow R\cdot + H_2O_2$

[2] $R\cdot + O_2 \rightleftarrows RO_2\cdot$

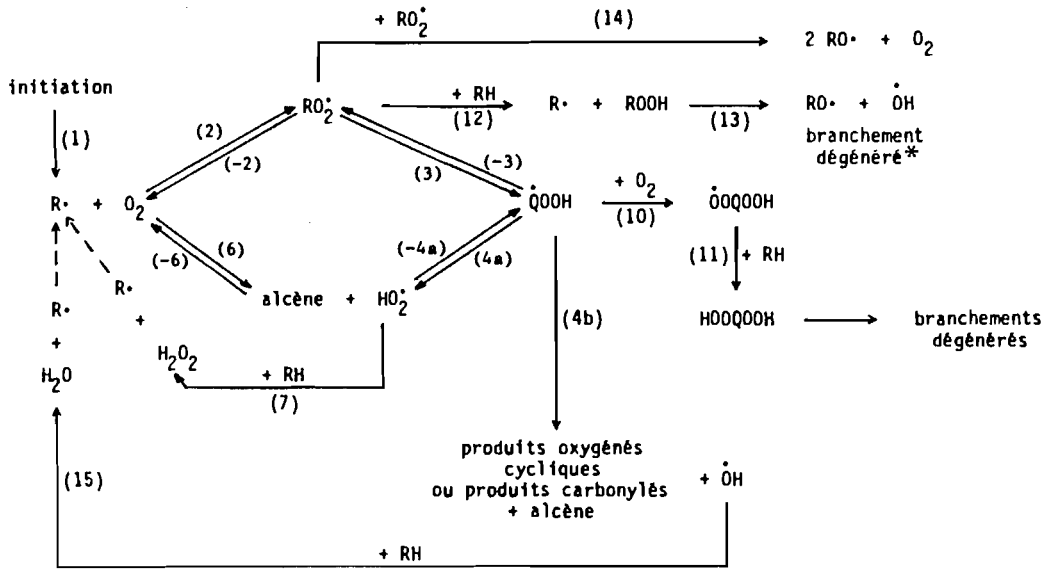
[7] $RO_2\cdot \xrightarrow{\text{paroi}}$ produits mineurs

1. Nouvelle adresse : Rhône-Poulenc, Usine de Chalampé, 68490 Ottmarsheim, France.

2. Auteur à qui adresser toute correspondance.

Printed in Canada / Imprimé au Canada

Can. J. Chem. Downloaded from www.nrcresearchpress.com by 41.223.56.140 on 09/07/12
For personal use only.



* Un branchement dégénéré correspond à la formation de radicaux libres à partir d'une espèce intermédiaire élaborée elle-même par les étapes de propagation, engendrant ainsi de nouvelles chaînes réactionnelles.

FIG. 1. Schéma mécanistique généralisé de l'oxydation des alcanes d'après la mise au point de Fish (5).

Knox (7) suggère qu'en début de réaction, c'est $HO_2\cdot$, radical sélectif et relativement peu réactif, qui arrache l'atome d'hydrogène à l'alcane et que, par la suite, il est remplacé par $OH\cdot$, radical réactif et peu sélectif. Ceci pose donc le problème du mécanisme pouvant convertir $HO_2\cdot$ en $OH\cdot$. Sans anticiper sur la suite de cette présentation, ce mécanisme pose aussi la question de la réactivité de $HO_2\cdot$ qui est en fait très limitée; il paraît difficile d'imaginer que ce radical puisse arracher un atome H à une molécule d'alcane avec une vitesse suffisante pour conduire à des phénomènes tels que les flammes froides ou les inflammations spontanées qui sont des phénomènes à la fois cinétiques et thermiques.

En accord avec le point de vue de Knox, confirmé par des travaux sur l'oxydation d'alcanes en C_6, hexane (8) et méthyl-2 pentane (9), la théorie oléfinique est censée s'appliquer surtout aux alcanes légers (C_2–C_4); dans le cas d'hexanes, on observe relativement peu d'alcène conjugué et une gamme assez large de produits oxygénés. Fish (5) a tenté de concilier les deux types de mécanismes en un schéma unique puisque le radical $RO_2\cdot$ est présent dans la théorie oléfinique de Knox comme dans les mécanismes faisant intervenir son isomérisation.

Le mécanisme généralisé que l'on peut proposer compte-tenu de la mise au point de Fish est présenté figure 1.

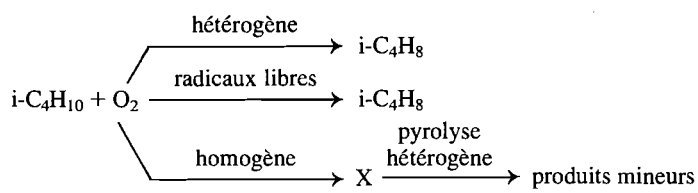
Si un tel schéma généralisé constitue une approche intéressante, il n'est cependant pas applicable directement à un alcane particulier car il n'est qu'un mécanisme formel.

Ceci nous conduit donc, avant de développer une étude expérimentale, à faire le point sur les travaux déjà publiés sur l'oxydation de l'isobutane. Il est à noter qu'il y a relativement peu de publications fondamentales susceptibles d'apporter des précisions sur les points soulevés précédemment.

En effet, la majeure partie des articles sur la réaction d'oxydation des alcanes légers concerne les réactions *catalytiques* qui ont des applications industrielles plus directes que la réaction non-catalytique alcane + oxygène. De plus, il faut mettre de côté, sans les rejeter, les articles concernant cette fois l'oxydation non-catalytique mais qui commentent les résultats de manipulations effectuées à un trop fort avancement de la réaction. Dans ce cas il devient très difficile de distinguer les produits primaires des produits secondaires et l'écriture des mécanismes réactionnels s'en ressent, en ce sens que l'auteur bénéficie alors d'une liberté plus grande, mais qui ne lui est pas toujours permise. Les articles concernant les flammes froides sont également à tenir à l'écart car les manipulations auxquelles ils font référence ne correspondent pas non plus aux conditions expérimentales que nous nous sommes fixées.

Semenov (10) et Sawerysyn et Lucquin (11) suggèrent que la réaction est entièrement hétérogène dans les tout premiers instants, puis devient homogène une fois la réaction autocatalytique stabilisée. Nous rappellerons pour mémoire que Zeelenberg et Bickel (12) ont proposé une réaction totalement homogène, dans laquelle tous les produits sont formés par des réactions d'isomérisation et de décomposition des radicaux alcoylperoxy au cours desquelles les chaînes sont propagées par les radicaux $\cdot OH$, $HO_2\cdot$ et $RO_2\cdot$.

Un mécanisme global de réaction est schématisé par Irvine et Knox dans le cadre d'une étude du rôle de la surface dans l'oxydation d'alcanes de C_2 à C_4 entre 300 et 480°C (13) :



Irvine et Knox ont étudié l'oxydation compétitive de mélanges binaires et ternaires d'éthane, propane et isobutane dans des réacteurs traités et non traités. Leurs résultats les conduisent à faire apparaître trois chemins réactionnels symbolisés ci-dessus dans le cas de mélanges contenant de l'isobutane : (*i*) une voie purement hétérogène, négligeable, pour l'éthane et le propane mais plus importante dans le cas de l'isobutane et susceptible de

Can. J. Chem. Downloaded from www.nrcresearchpress.com by 41.223.56.140 on 09/07/12
For personal use only.

Can. J. Chem. Downloaded from www.nrcresearchpress.com by 41.223.56.140 on 09/07/12
For personal use only.

provenir, d'après ces auteurs, de l'adsorption de cet alcane à la surface; (*ii*) une voie homogène, avec propagation radicalaire conduisant à la formation de l'alcène conjugué; (*iii*) une voie «mixte» conduisant à la formation homogène d'un produit intermédiaire X de nature non précisée, dont la pyrolyse hétérogène rendrait compte de produits mineurs.

Il ne semble pas que cette interprétation et cette spécificité de l'isobutane aient été confirmées par d'autres auteurs.

Parmi les travaux que nous avons relevés sur l'isobutane, une première publication en 1973 de Barnard et Handscombe (14) semblait assez prometteuse, compte-tenu, en particulier, des objectifs fixés par les auteurs : réaction isotherme et à très faible avancement. Ils annonçaient également un article plus détaillé sur l'oxydation de l'isobutane, qui est paru en 1977. Leurs auteurs, Barnard et Brench (15), se sont en fait rapidement écartés de l'étude de la réaction isotherme à faible avancement pour s'intéresser aux phénomènes non-isothermes (flammes froides, ...). Ils ont cependant présenté un mécanisme interprétant la formation d'un bon nombre de produits identifiés et dosés, mais certains processus qui y conduisent sont peu réalistes en termes de mécanismes ou de cinétique.

Cette étude bibliographique nous conduit à penser qu'il n'existe pas d'étude expérimentale publiée répondant de façon satisfaisante aux objectifs. Son élargissement aux cas du propane et du *n*-butane conduit à la même conclusion (16).

Le choix de l'isobutane pour cette première étude expérimentale reposait sur les considérations suivantes :

(*i*) Les études de Barnard (14, 15) constituent une première approche qui pouvait servir de base à une étude plus détaillée.

(*ii*) La molécule d'isobutane possède un hydrogène tertiaire, donc plus mobile, sur lequel pourraient s'effectuer préférentiellement les arrachements d'atomes d'hydrogène. On peut donc espérer, par cette orientation de la réactivité, une certaine simplification (dans le cas du propane, les atomes d'hydrogène portés par le carbone central sont secondaires; la différence de mobilité de ces atomes par rapport aux atomes primaires des groupements terminaux est moins marquée).

(*iii*) Des recherches sur l'oxydation de l'isobutane paraissaient bien intégrées à des travaux déjà en cours au laboratoire, une osmose entre différents sujets assurant une meilleure progression des résultats. Cette étude ne constituait qu'un moyen d'approche des réactions d'oxydation homogène et, dans la seconde phase de ce travail, nous nous intéresserons à des hydrocarbures tels que le propane ou le *n*-butane étant donné qu'ils sont produits en larges quantités par l'industrie pétrochimique et que, de ce fait, leur valorisation présente un important intérêt économique.

I.2. Homogénéité de la réaction

Dans le cas de l'isobutane comme dans celui des autres alcanes légers se pose le problème de l'homogénéité de la réaction et de l'influence des parois. De ce point de vue, les résultats publiés sont plutôt contradictoires et nous avons déjà mentionné dans ce qui précède des travaux faisant appel à certains processus hétérogènes. Il apparaît, compte tenu des travaux publiés dans ce domaine, que les hautes températures ont tendance à favoriser le mécanisme homogène, ce qui paraît logique si l'on considère des résultats antérieurs obtenus au laboratoire sur des réactions de pyrolyse et que l'hétérogénéité du mécanisme diminue également lorsque la masse moléculaire de l'alcane augmente, ce qui paraît plus difficile à interpréter. Selon certains auteurs, c'est la formation de l'alcène conjugué qui contribue pour une large part à l'hétérogénéité de la réaction (17) alors que d'autres ont constaté que la formation des produits oxygénés intermédiaires était sensible aux effets de parois du réacteur (18, 19). Le comportement homogène ou hétérogène dépendrait alors de la compétition entre différents processus concurrents.

Il est à noter cependant que certains auteurs (dont Knox *et al.*) présentent la part hétérogène comme indépendante de la part homogène (13). D'autres auteurs ont recherché des corrélations entre hétérogénéité et structure. C'est ainsi que pour Atherton *et al.* (17), la part hétérogène serait d'autant plus importante que l'isomérisation du radical alcoylperoxy par un cycle à six centres et arrachement d'un atome d'hydrogène secondaire ou tertiaire est empêchée. Ceci expliquerait alors pourquoi les alcanes légers s'oxyderaient selon un mécanisme dont la part hétérogène est importante.

Les différents points mentionnés dans ce qui précède montrent la quasi-impossibilité d'aboutir à des conclusions sûres. Pour y arriver, il paraît nécessaire d'entreprendre des essais systématiques de différents réacteurs variant tant par leur rapport surface sur volume que par la nature des parois.

Faute d'une telle étude, d'ailleurs de mise en oeuvre longue et délicate, il est difficile d'estimer l'importance des effets hétérogènes. Ceux-ci se manifestent d'abord au niveau des problèmes de reproductibilité des expériences, point dont nous reparlerons plus loin.

Du point de vue mécanisme réactionnel et contrairement à l'opinion d'un certain nombre d'auteurs, il semble que les effets de parois soient à attribuer aux radicaux OH· plutôt qu'aux radicaux HO_2· (20), ce qui paraît qualitativement en accord avec les résultats expérimentaux obtenus dans notre laboratoire, en particulier dans le cas du méthyl *tert*-butyl éther (MTBE), relativement peu sensible aux effets de parois dans le cas de la réaction d'oxydation (21).

Ces quelques rappels soulignent non seulement l'imprécision des données expérimentales mais aussi leur insuffisance. Ils corroborent l'opinion de Benson et Nangia (4) qui soulignent qu'un nombre appréciable de problèmes ne sont pas encore résolus. Parmi ces problèmes figurent la nature des porteurs de chaînes, HO_2· ne paraissant pas suffisamment réactif, l'origine du coefficient négatif de température, les réactions des radicaux HO_2· et RO_2· entre eux (par exemple, la dismutation $2RO_2\cdot \rightarrow 2RO\cdot + O_2$), les processus d'amorçage (la réaction $RH + O_2 \rightarrow R\cdot + HO_2\cdot$ paraissant trop lente, même à 300°C) et les processus d'isomérisation.

Toutes ces incertitudes nous ont donc paru justifier une nouvelle étude expérimentale dans le cas de l'isobutane, sans pour autant prétendre résoudre toutes les questions soulevées précédemment en une étude de durée limitée.

II. Étude expérimentale de l'oxydation de l'isobutane

II.1. Appareillage et analyses

L'oxydation de l'isobutane est étudiée à pression sub-atmosphérique, généralement avec des mélanges équimoléculaires isobutane/O_2, vers des pressions totales de 125 Torr (1 Torr = 133.3 Pa), dans le domaine de température 300–350°C. Les réacteurs statiques de verre Pyrex ont un volume intérieur voisin de 250 cm^3. Le réacteur est chauffé par un dispositif à faible inertie, constitué de deux coquilles formées de spires jointives de fil chauffant «Thermocoax» isolé électriquement, l'ensemble étant équipé d'une régulation appropriée reliée à un thermocouple placé sous les spires.

L'isobutane et l'oxygène prémélangés sont introduits dans le réacteur à l'instant $t = 0$ et, pour déterminer la composition au temps t, les gaz sont détendus et trempés à l'ambiante et prélevés dans des ampoules en U permettant une insertion facile dans les circuits de gaz vecteur de chromatographes.

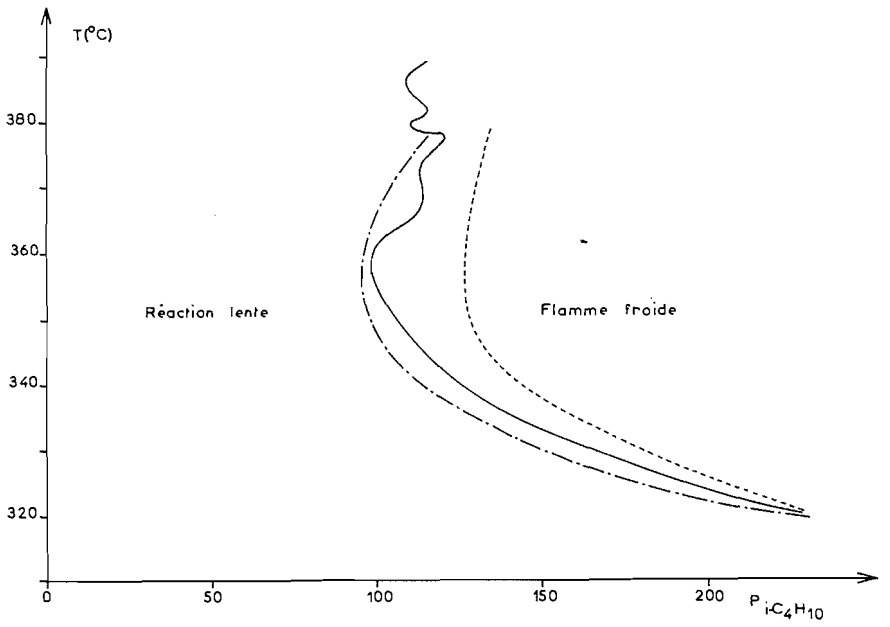


FIG. 2. Diagramme pression – température de l'oxydation de l'isobutane. Mélange équimolaire isobutane–oxygène. Réacteur sphérique en verre Pyrex d'un volume de 250 cm^3. (—) mélange binaire isobutane–oxygène; (- - -) mélange ternaire isobutane–oxygène–azote, P_{totale} = 600 Torr; (- - - -) mélange ternaire isobutane–oxygène–hélium, P_{totale} = 600 Torr.

Les hydrocarbures sont dosés sur une colonne de Durapak (phényl isocyanate greffé sur Porasil), les produits oxygénés sur une colonne de Carbowax 20 M, O_2 et CO sur une colonne de tamis moléculaire, CO_2 et l'eau sur une colonne de Porapak Q. Le formaldéhyde est dosé par colorimétrie, l'eau oxygénée et les peroxydes par une méthode utilisant la chimiluminescence que nous avons adaptée aux conditions de cette étude (22).

II.2. Diagramme pression–température

Ce diagramme a été étudié en utilisant un réacteur muni d'un thermocouple fin (0,08 mm de diamètre) situé en son centre afin de déterminer les conditions expérimentales correspondant à la réaction lente. La limite réaction lente – flammes froides a été déterminée point par point, par encadrement; elle est représentée sur la figure 2.

Bien que légèrement déplacée par rapport à des limites analogues publiées dans la littérature, la limite obtenue expérimentalement paraît compatible avec d'autres travaux publiés (cf. par ex., réf. 17). Les écarts peuvent être attribués à des conditions expérimentales quelque peu différentes (forme et volume du réacteur, rapport i-C_4H_{10}/O_2...).

Afin d'observer qualitativement l'effet que provoque la dilution par des gaz inertes, nous avons ajouté de l'azote puis de l'hélium pour travailler à une pression totale de 600 Torr en conservant le rapport i-C_4H_{10}/O_2 voisin de 1. L'azote a peu d'influence; il déplace simplement la limite réaction lente – flammes froides vers des pressions un peu plus basses.

L'hélium présente au contraire la particularité de déplacer la limite réaction lente – flammes froides vers des pressions plus élevées; toutes choses égales par ailleurs, une addition d'hélium transforme une flamme froide en réaction lente. Une telle observation avait déjà été faite par J. Wilson (23) dans le cas du méthyl-2 pentane. Ce phénomène est dû aux propriétés thermiques de l'hélium, plus spécifiquement à sa conductivité thermique, et ceci confirme, si besoin en était, la nature cinétique *et* thermique des flammes froides.

À la suite de ces premiers essais, nous avons choisi pour notre étude les conditions expérimentales suivantes : rapport i-C_4H_{10}/O_2 = 1; pression initiale de mélange, 125 Torr; température de réaction variant de 310 à 340°C.

II.3. Reproductibilité des expériences. Effets de parois

Compte-tenu des résultats mentionnés par d'autres auteurs, nous nous attendions à des difficultés expérimentales liées aux effets de parois, se traduisant en particulier par une certaine irreproductibilité des expériences.

Nous avons d'abord utilisé un réacteur sphérique de Pyrex, vide, de volume intérieur 250 cm^3 et de rapport surface sur volume (s/v) voisin de 0,8 cm^{-1}, sans traitement préalable. Une seconde série d'essais a été effectuée dans ce même réacteur, mais après traitement des parois selon la méthode que nous mentionnerons plus loin.

Les conditions expérimentales de la réaction ont été fixées de manière à obtenir environ 2% de l'isobutane transformé en isobutène pour un temps de réaction de 6 min, la pression initiale de mélange équimoléculaire isobutane–oxygène étant 125 Torr et la température du réacteur 330°C.

La réaction a été suivie en dosant l'isobutène formé et ces essais ont confirmé nos craintes concernant la reproductibilité, la variation étant de l'ordre de 10% autour d'une valeur moyenne.

Nous avons alors tenté de «conditionner» le réacteur en faisant précéder l'expérience proprement dite d'une première manipulation non retenue, de façon à ce que le réacteur ait toujours subi les mêmes opérations avant d'être utilisé pour l'expérience de référence. Cette technique de «conditionnement» conduit à une atténuation relative des variations mais la reproductibilité paraît encore insuffisante pour des études cinétiques. Le vieillissement du réacteur («seasoning») par des expériences répétées ne semble pas conduire à une limitation de ces irreproductibilités. C'est pourquoi nous avons essayé un traitement des parois de ce même réacteur.

Nous avons préféré ne pas utiliser de traitements ou de recouvrements ayant a priori des effets cinétiques importants comme KCl. Par ailleurs, les traitements ou recouvrements envisagés doivent être stables en présence d'oxygène et à des températures pouvant atteindre 400°C. Ceci excluait donc des recouvrements par des résines ou des dérivés halogénés (24) ou par des matériaux riches en carbone provenant de pyrolyses de composés halogénés (25); ce dernier type de traitement s'était révélé efficace dans l'étude de la pyrolyse du MTBE, réaction qui s'était révélée très sensible aux effets de parois (26).

Compte-tenu de ces remarques, nous avons choisi la méthode proposée par Marshall et coll. (27) consistant en un traitement à la soude 10 M puis à l'acide nitrique 10 N et rinçage à l'eau distillée. On constate d'abord que la réaction est accélérée par rapport à la cinétique avant traitement par un rapport voisin de 2, toutes autres conditions égales par ailleurs. Ceci souligne l'importance des effets hétérogènes évoqués précédemment, même en réacteur vide.

Can. J. Chem. Downloaded from www.nrcresearchpress.com by 41.223.56.140 on 09/07/12
For personal use only.

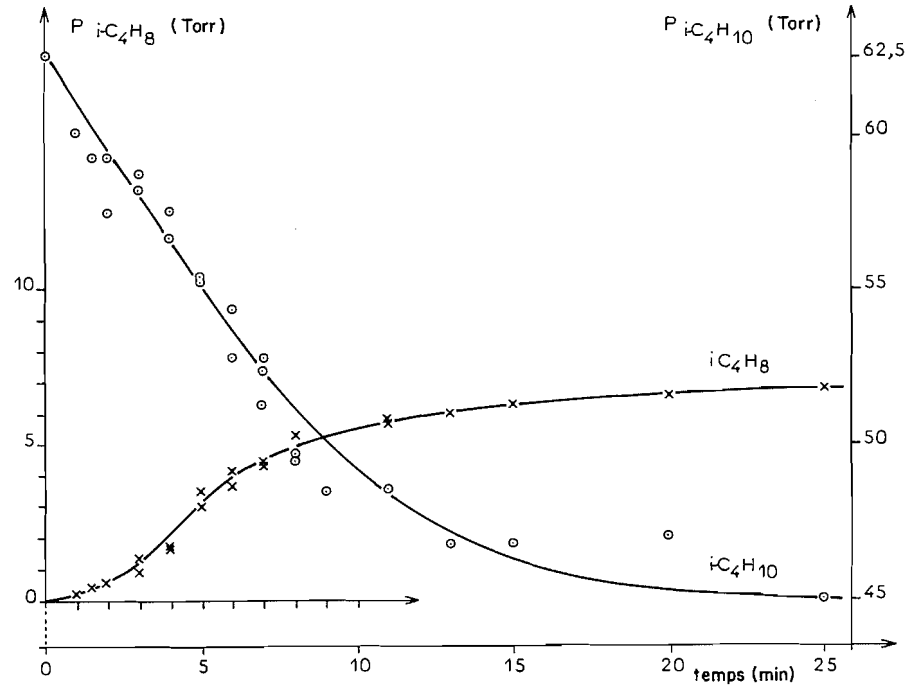


FIG. 3. Courbes de consommation de l'isobutane et de formation de l'isobutène. Pression initiale du mélange équimoléculaire isobutane–oxygène : 125 Torr. Température de réaction : 340°C.

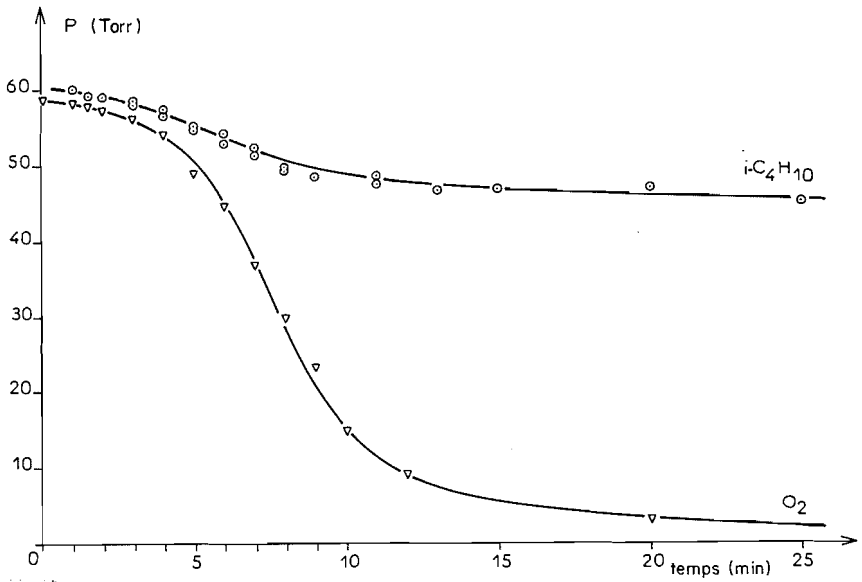


FIG. 4. Oxydation de l'isobutane à fort avancement : courbes de consommation des réactifs. Pression initiale du mélange équimoléculaire isobutane–oxygène : 125 Torr. Température de réaction : 340°C.

La dispersion des résultats est encore sensible mais nous l'avons jugée tolérable, en particulier pour une étude préliminaire visant d'abord à établir les bilans-matière de la réaction.

II.4 Étude préliminaire de la réaction. Bilans matière

Cette étude préliminaire a été effectuée à 340°C, à une pression de 125 Torr de mélange équimoléculaire isobutane–oxygène. Nous avons d'abord dosé l'isobutane consommé et l'isobutène formé; les résultats obtenus sont représentés figure 3. Il apparaît que le rapport isobutène formé sur isobutane consommé est sensiblement inférieur à 80%, en désaccord avec un certain nombre de travaux sur l'oxydation d'alcanes légers; les valeurs calculées à partir des points expérimentaux non lissés varient entre 20 et 45%.

Nos premiers résultats suggèrent qu'une quantité importante d'isobutane se transforme en produits autres que l'isobutène, directement ou via l'isobutène qui serait alors consommé en partie par des réactions secondaires.

Sur la figure 4 nous avons comparé la consommation d'isobutane et la consommation d'oxygène. Cette dernière présente la forme en S classique obtenue dans les réactions d'oxydation.

Il apparaît donc très rapidement une consommation beaucoup plus importante de l'oxygène qui tend à devenir pratiquement totale alors que seulement 30% de l'isobutane initial est consommé. Ceci explique qu'après être passé par un maximum, la vitesse de la réaction diminue à la suite du manque d'oxygène, ce qui est en accord avec l'allure sigmoïdale des courbes de production d'isobutène et de consommation d'isobutane. Il convient également de noter que les proportions d'isobutane et d'oxygène correspondent à un mélange riche par

Can. J. Chem. Downloaded from www.nrcresearchpress.com by 41.223.56.140 on 09/07/12
For personal use only.

TABLEAU 1. Bilan sur les éléments carbone, oxygène et hydrogène lors de l'oxydation de l'isobutane à 340°C (125 Torr de mélange équimoléculaire)

Temps de réaction (min)	2	3	4	5	6	7	8	10	11	15
Taux de conversion (%)	3,44	6,64	9,15	15,7	21,9	25,0	26,1	27,8	28,8	30,5
Bilan en carbone (%)	100,2	99,4	102,1	100,0	97,9	98,5	100,4	104,4	104,8	105,1
Bilan en oxygène (%)	101,6	100,0	97,1	97,2	91,8	85,0	83,9	80,4	80,0	79,6
Bilan en hydrogène (%)	99,7	99,8	102,4	101,9	101,4	99,5	102,5	105,2	103,8	103,1

rapport à l'équation stoechiométrique de combustion totale. L'équation stoechiométrique : i-C_4H_{10} + O_2 = i-C_4H_8 + H_2O_2 ne permettrait donc pas de représenter l'essentiel de la réaction.

Ces premiers résultats paraissent suggérer également qu'il se forme de substantielles quantités de produits oxygénés, ce qui nous a conduits à identifier les produits formés et à déterminer leur nature primaire ou secondaire.

Les produits suivants ont été identifiés et dosés : hydrocarbures : à côté de l'isobutène, méthane, éthylène et propène; produits oxygénés : formaldéhyde, acétaldéhyde, propionaldéhyde, isobutyraldéhyde et acétone, oxydes d'isobutène et de propylène, CO, CO_2, H_2O.

Ces résultats ont permis d'établir des bilans de matière sur les trois éléments carbone, oxygène et hydrogène. Les premières déterminations ont fait apparaître des anomalies, en particulier un écart entre la pression mesurée en fin de réaction et la somme des pressions partielles des produits dosés. Ces anomalies ont été rapidement attribuées à un dosage erroné (par défaut) de l'eau, en raison de sa condensation dans différentes parties de l'appareillage, y compris les tubulures et l'ampoule de prélèvement. Les différentes parties concernées ont été chauffées par un cordon chauffant vers 70°C, ce qui a nettement amélioré les bilans (tableau 1).

Ces bilans comportent des incertitudes et des irreproductibilités qui se traduisent par certaines valeurs supérieures à 100% mais, globalement, l'examen de ces bilans conduit à penser que nous n'avons pas manqué de produits importants lors de cette étude expérimentale. La fiabilité de notre étude paraissant ainsi établie, il nous a été possible d'aborder l'étude de l'oxydation à faible avancement, de manière à déterminer les produits primaires de la réaction, donnée importante pour l'établissement d'un mécanisme réactionnel.

II.5. Étude de l'oxydation à faible avancement

Pour réaliser cette étude, nous avons réduit la température de réaction de 30°C, l'avancement à 5 min passant de 15,7% à 340°C à 0,65% à 310°C, toujours pour une pression initiale de 125 Torr de mélange équimoléculaire. Cet abaissement de température devrait également limiter ou éviter certaines réactions secondaires car l'isobutène, alcène conjugué, paraît être plus réactif que l'isobutane.

La gamme de produits obtenus est la même que celle reportée précédemment; les courbes de formation de produits sont regroupées sur la figure 5 mais, pour en faciliter la lecture, nous n'avons pas reporté les points expérimentaux.

Cependant les courbes représentées ne permettent pas de distinguer facilement entre les produits primaires et les produits non primaires, en raison de l'allure auto-accélérée des courbes de formation.

Pour tenter de faire la différence entre produits primaires et produits non primaires, nous avons calculé le rapport de la quantité de chacun des produits dosés (sauf l'eau et les peroxydes) à leur somme pour les différents temps de séjour explorés. Ces rapports, extrapolés à l'instant initial (avancement nul), permettent de déterminer le pourcentage du produit considéré à l'instant initial par rapport à la somme des produits dosés. Si l'extrapolation donne une valeur nulle le produit est secondaire.

Les résultats de cette étude figurent dans le tableau 2 où nous avons reporté les valeurs déterminées à l'instant initial et observées à un temps de séjour de 5 min. L'isobutène est effectivement le produit principal. Ces résultats nous permettent de penser que l'oxyde de propylène et le monoxyde de carbone ne sont pas primaires ainsi vraisemblablement que l'éthylène et le méthane; la détermination se révèle plus délicate pour le formaldéhyde et l'acétaldéhyde. Les autres produits peuvent être considérés comme primaires.

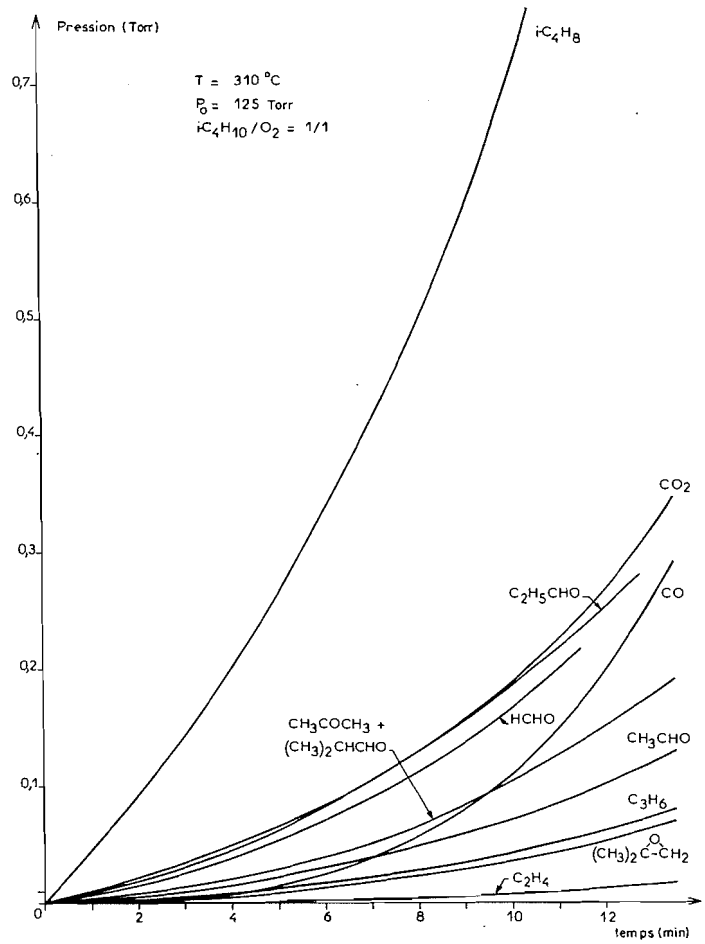


FIG. 5. Oxydation de l'isobutane à faible avancement : courbes de formation des produits. Pression initiale du mélange équimoléculaire isobutane–oxygène : 125 Torr. Température de réaction : 310°C.

Notons que les valeurs du tableau sont surestimées puisque l'eau, produit formé en relativement grandes quantités, n'est pas comptabilisée dans ces calculs en raison de l'imprécision du dosage. Pour fixer les idées, à 5 min il y a des quantités presque doubles (1,85 fois) d'eau par rapport à celles d'isobutène.

La principale difficulté qui apparaît à la lecture de ce tableau est la valeur obtenue pour le dioxyde de carbone qu'on attendrait comme produit non primaire. Malgré des investigations complémentaires, nous n'avons pas pu lever cette ambiguïté. Il convient de noter cependant que CO_2 doit être dosé sur un chromatographe muni d'un détecteur à conductibilité thermique (thermistances), méthode nettement moins sensible que l'ionisation de flamme (F.I.D.). L'appareil utilisé dans cette série, de conception relativement ancienne (F6.3 Perkin–Elmer) et donc de sensibilité limitée, peut être pour une part à l'origine d'erreurs appréciables.

Can. J. Chem. Downloaded from www.nrcresearchpress.com by 41.223.56.140 on 09/07/12
For personal use only.

Can. J. Chem. Downloaded from www.nrcresearchpress.com by 41.223.56.140 on 09/07/12
For personal use only.

TABLEAU 2. Répartition des produits dosés à 5 min et extrapolation à l'instant initial (T = 310°C, 125 Torr de mélange équimoléculaire)

Produit	% Molaire à $t = 0$	% Molaire à $t = 5$ min
CH_4	0	0
C_2H_4	0,1 ≃ 0	0,2
C_3H_6	2,35	2,4
i-C_4H_8	56,7	49,2
HCHO	?	10,1
CH_3CHO	≃0	4,2
C_2H_5CHO	10,4	11,8
i-C_3H_7CHO + CH_3COCH_3	4,9	5,5
Oxyde de propène	0	<0,1
Oxyde d'isobutène	2,0	1,7
CO	0	2,7
CO_2	[13,2]	12,2
Total		100

Malgré ces quelques difficultés, nous pensons ainsi avoir obtenu suffisamment de données expérimentales pour aborder l'aspect mécanistique.

III. Détermination du mécanisme de la réaction et commentaires

III.1. Détermination du mécanisme

Le mécanisme réactionnel est déterminé en s'appuyant sur les résultats expérimentaux précédents, en particulier les produits primaires, pour écrire les processus élémentaires auxquels peuvent donner lieu les différentes espèces radicalaires présentes dans le système. Ce que nous cherchons à écrire, ce sont des processus élémentaires vrais et non des réactions globales, compatibles avec les principes de la cinétique (réversibilité microscopique, moindre changement de structure, etc...) et avec les connaissances actuelles en chimie radicalaire et en thermochimie. Les processus écrits tiennent compte également des schémas proposés antérieurement par d'autres auteurs (Fish et Knox en particulier) pour rendre compte des oxydations d'alcanes.

L'écriture de ce mécanisme réactionnel peut être obtenue de manière systématique en analysant les diverses catégories de processus élémentaires pouvant intervenir, compte-tenu de la nature des radicaux dérivés de la molécule d'isobutane.

Compte-tenu de la plus faible énergie de dissociation de liaison entre un carbone et un H tertiaire (qu'entre un carbone et un H primaire), il est logique d'admettre que le radical *tert*-butyle t-$C_4H_9\cdot$ sera prépondérant devant le radical isobutyle i-$C_4H_9\cdot$ lors de l'amorçage primaire de la réaction.

On considère ensuite l'addition réversible de l'oxygène sur les radicaux alcoyles R· dérivés de la molécule d'isobutane RH par arrachement d'un atome d'hydrogène ($R^1\cdot$, t-$C_4H_9\cdot$ et $R^2\cdot$, i-$C_4H_9\cdot$)

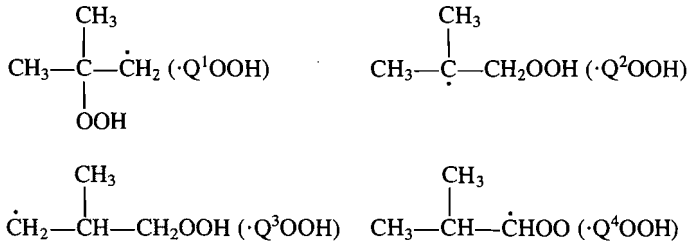
$$R\cdot + O_2 \rightleftarrows RO_2\cdot$$

Cette réaction conduit à la formation de radicaux alcoylperoxy $RO_2\cdot$, *tert*-butylperoxy $R^1O_2\cdot$ et isobutylperoxy $R^2O_2\cdot$.

En accord avec les schémas retenus par Fish, ces radicaux alcoylperoxy, ici sous deux formes isomères $R^1O_2\cdot$ et $R^2O_2\cdot$, peuvent s'isomériser par transfert d'hydrogène interne en radicaux hydroperoxyalcoyle ·QOOH

$$RO_2\cdot \rightleftarrows \cdot QOOH$$

Compte-tenu de la structure des radicaux alcoylperoxy et des isomérisations internes possibles, il est possible théoriquement d'obtenir ainsi quatre formes de radicaux hydroperoxy alcoyle :

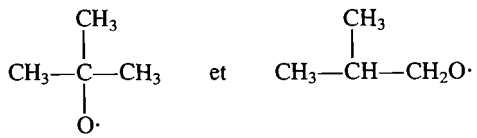


Cependant la formation de $\cdot Q^4OOH$ suppose le passage par un état de transition constitué par un cycle à quatre centres, donc nécessitant une énergie d'activation élevée, en raison de la tension du cycle. Les calculs montrent, en accord avec cette observation, que la concentration des radicaux $\cdot Q^4OOH$ peut être considérée comme négligeable par rapport à celle des autres radicaux isomérisés provenant de $R^2O_2\cdot$.

Nous postulons, en accord avec le mécanisme de Fish, que certains produits primaires proviennent également de la décomposition des radicaux alkoxy, que l'on peut supposer être dérivés des radicaux $RO_2\cdot$ par des réactions de dismutation.

Il est certain que l'écriture de *tous* les processus élémentaires possibles conduirait à un mécanisme global particulièrement complexe qui ne serait que d'une aide très limitée à l'interprétation de nos résultats expérimentaux. Pour simplifier ce schéma réactionnel et surtout déterminer les réactions élémentaires *essentielles* susceptibles de rendre compte des caractéristiques observées, il faudrait disposer des constantes de vitesse de tous les processus élémentaires pouvant être écrits. Les données expérimentales étant généralement limitées dans le cas des réactions d'oxydation, très peu de ces constantes sont disponibles.

Compte-tenu de ce manque de données, nous avons jugé préférable d'utiliser une méthode semi-empirique d'estimation des constantes de vitesse des processus élémentaires figurant

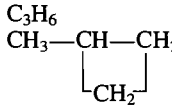
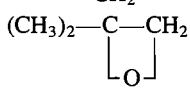
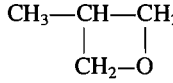
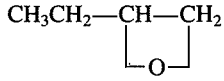
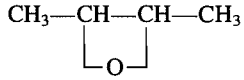


dans les schémas réactionnels, méthode qui a également l'avantage de fournir des données homogènes, même si leur précision est limitée. Il serait fastidieux de développer ici les calculs correspondants ou même d'exposer les principes de la méthode utilisée. Rappelons que ces méthodes ont été développées par Benson et co-auteurs sous le nom de «Cinétique Thermochimique». Elles ont été détaillées par S. W. Benson dans l'ouvrage intitulé «Thermochemical kinetics—Methods for the estimation of thermochemical data and rate parameters», dont la seconde édition est parue en 1976 (28). L'application plus spécifique de ces méthodes aux réactions d'oxydation et de combustion a fait l'objet d'une mise au point par Golden (29). Rappelons seulement que ces méthodes nécessitent d'abord l'estimation des données thermochimiques (ΔH_f^0, S^0, C_p^0) par des méthodes d'additivité de groupes ou en tenant compte des paramètres structuraux de l'espèce considérée, molécule ou radical.

Dans le cas présent, tous les calculs de ΔH_f^0 et S^0 sont faits

Can. J. Chem. Downloaded from www.nrcresearchpress.com by 41.223.56.140 on 09/07/12
For personal use only.

TABLEAU 3. Grandeurs thermodynamiques (ΔH_f^0 et S^0) pour les espèces intervenant dans le mécanisme proposé d'oxydation de l'isobutane (calcul à 300 K)

	Espèce	$\Delta H^0_{f_{300\,K}}$ (kcal·mol^{-1})	$S^0_{300\,K}$ (cal·mol^{-1}·K^{-1} : ue)
	i-C_4H_{10}	−32,5	70,4
$R^1\cdot$	t-$\dot{C}_4H_9$	7,4[a]	74,8
$R^2\cdot$	i-$\dot{C}_4H_9$	13,4[b]	74,7
$R^1OO\cdot$	t-$C_4H_9OO\cdot$	−22,5[c]	83,1
$R^2OO\cdot$	i-$C_4H_9OO\cdot$	−15,7[c]	88,4
$\dot{Q}^1OOH$	$HOOC(CH_3)_2\dot{C}H_2$	−12,1[b]	91,8
$\dot{Q}^2OOH$	$(CH_3)_2\dot{C}CH_2OOH$	−11,3[a]	97,0
$\dot{Q}^3OOH$	$HOOCH_2CH(CH_3)\dot{C}H_2$	−5,3[b]	96,3
$\dot{Q}^4OOH$	$(CH_3)_2CH\dot{C}HOOH$	−11,8[d]	95,1
$R^1O\cdot$	t-$C_4H_9O\cdot$	−23,2[e]	75,0
$R^2O\cdot$	i-$C_4H_9O\cdot$	−16,4[e]	80,2
	$\cdot CH_2OOH$	15,0[f]	69,0
	$HO_2^{\cdot}$	3,0[g]	54,4[g]
	$\dot{O}H$	9,4[h]	43,9[h]
	$\dot{C}H_3$	34,3[h]	54,4[h]
	$H\cdot$	52,1[h]	27,4[h]
	i-C_4H_8	−3,8	70,0
	C_3H_6	4,7	63,8
		5,6	67,1
		−31,4	71,8
		−25,8	72,1
		−26,7	75,6
		−31,1	73,6
	HCHO	−26,0[g]	52,3[g]
	$CH_3—CH_2—CHO$	−44,5	72,7
	$(CH_3)_2—CH—CHO$	−51,2	79,3
	$CH_3—CO—CH_3$	−51,6	70,0
	$CH_3—CO—CH_2—CH_3$	−56,9	81,0
	$CH_2=C(CH_3)OOH$	−15,7[i]	83,9[i]
	$CH_3—CH=CHOOH$	−15,7[i]	83,9[i]
	$CH_2=CH—CH_2OOH$	−12,5	84,0

[a]Calculé avec DH^0 (t-C_4H_9 − H) = 92,0 kcal·mol^{-1} (28).
[b]Calculé avec DH^0 (RCH_2 − H) = 98,0 kcal·mol^{-1} (28).
[c]Calculé avec DH^0 (ROO − H) = 87,6 kcal·mol^{-1} (30).
[d]Calculé avec DH^0 (RCH(OOH) − H) = 91,5 kcal·mol^{-1} (31) et d'après réf. 21.
[e]Calculé avec DH^0 (RO − H) = 104,0 kcal·mol^{-1} (28).
[f]Calculé avec DH^0 ($HOOCH_2$ − H) = 98,0 kcal·mol^{-1} (31).
[g]Référence 21.
[h]Référence 28.
[i]Calculé par la méthode d'additivité de liaisons.

à 300 K; ils seront utilisés à 583 K sans correction en raison du nombre important de valeurs de C_p^0 non tabulées. Les variations en fonction de la température sont relativement faibles et il faut noter que les corrections sur ΔH^0 et S^0 se compensent lors du calcul de ΔG^0. Les résultats de ces calculs sont donnés tableau 3.

Compte-tenu de la relation entre les grandeurs thermodynamiques ΔH^0, ΔS^0 et la constante d'équilibre K:

$$-RT \log K = \Delta H^0 - T\Delta S^0$$

la connaissance de ΔH^0, de ΔS^0 et de la constante de vitesse de la réaction directe k_d ou inverse k_i conduit à la valeur de l'autre ce qui suppose, en l'absence de données expérimentales, des approximations raisonnables obtenues par des analogies avec des réactions voisines.

Les résultats de l'estimation des grandeurs cinétiques sont donnés dans le tableau 4.

Dans ce tableau, nous donnons les valeurs du facteur préexponentiel A, de l'énergie d'activation E et de la constante k calculée à 583 K (unités : L, mol, s).

TABLEAU 4. Paramètres cinétiques calculés pour les différents processus élémentaires proposés dans le mécanisme d'oxydation de l'isobutane (A, E et constante calculée à 583 K)

Réactions	A	E (kcal·mol^{-1})	k (s^{-1}) (à 583 K)
(2.1)	$10^{9,5}$ L·mol^{-1}·s^{-1}	0	$k(O_2) = 5,4\cdot10^6$ (28)
(−2.1)	$10^{16,22}$ s^{-1}	30,0	$1,1\cdot10^5$
(2.2)	$10^{9,5}$ L·mol^{-1}·s^{-1}	0	$k(O_2) = 5,4\cdot10^6$ (28)
(−2.2)	$10^{15,05}$ s^{-1}	27,9	$4,6\cdot10^4$
(3.1)	$10^{13,70}$ s^{-1}	26,3	$8,3\cdot10^3$
(−3.1)	$10^{11,83}$ s^{-1}	15,9	$8,0\cdot10^5$
(3.2)	$10^{12,75}$ s^{-1}	20,3	$1,6\cdot10^5$
(−3.2)	$10^{10,89}$ s^{-1}	15,9	$9,3\cdot10^4$
(3.3)	$10^{12,78}$ s^{-1}	21,0	$9,0\cdot10^4$
(−3.3)	$10^{11,06}$ s^{-1}	10,6	$1,3\cdot10^7$
(3.4)	$10^{13,82}$ s^{-1}	43,0	$6,4\cdot10^{-3}$
(−3.4)	$10^{12,36}$ s^{-1}	39,1	$6,3\cdot10^{-3}$
(4.1)	$10^{14,35}$ s^{-1}	16,1	$2,3\cdot10^8$
(−4.1)	$10^{9,38}$ s^{-1}	6,0	$1,4\cdot10^7$
(4.2)	$10^{12,76}$ s^{-1}	18,0	$1,1\cdot10^6$
(4.3)	$10^{14,13}$ s^{-1}	15,3	$2,7\cdot10^8$
(−4.3)	$10^{10,29}$ s^{-1}	6,0	$1,1\cdot10^8$
(4.4)	$10^{12,76}$ s^{-1}	18,0	$1,1\cdot10^6$
(4.5)	$10^{12,00}$ s^{-1}	16,8	$5,5\cdot10^5$
(4.6)	$10^{14,26}$ s^{-1}	30,8	$6,1\cdot10^2$
(4.7)	[10^{11} s^{-1}]	[5]	[$1,4\cdot10^9$]
(4.8)	$10^{14,33}$ s^{-1}	37,5	2,3
(4.9)			≃0
(4.10)			≃0
(4.11)	$10^{14,20}$ s^{-1}	33,3	62
(4.12)			≃0
(4.13)	$10^{13,61}$ s^{-1}	39,2	0,1
(4.14)			≃0
(5.1)	$10^{14,76}$ s^{-1}	7,9	$6,6\cdot10^{11}$
(5.2)	$10^{14,70}$ s^{-1}	9,5	$1,5\cdot10^{11}$
(5.3)			—
(5.4)	$10^{13,89}$ s^{-1}	18,6	$9,2\cdot10^6$
(6)	$10^{9,54}$ L·mol^{-1}·s^{-1}	7,66	$k(O_2) = 8,3\cdot10^3$ (32)
(10)	$10^{9,5}$ L·mol^{-1}·s^{-1}	0	$k(O_2) = 5,4\cdot10^6$ (28)
(12)	10^9 L·mol^{-1}·s^{-1}	19,4[a]	k(RH) = 0,1 (32)
		17,1[b]	k(RH) = 0,74
		14,4[c]	k(RH) = 7,4
(14)	$10^{9,5\pm0,5}$ L·mol^{-1}·s^{-1}	0	$3,2\cdot10^9$ L·mol^{-1}·s^{-1} (32)
Parois			≃0,5 (17)

[a]Pour l'arrachement d'un atome H primaire.
[b]Pour l'arrachement d'un atome H secondaire.
[c]Pour l'arrachement d'un atome H tertiaire.

L'ensemble des processus élémentaires retenus, compte-tenu des commentaires précédents, ainsi que les constantes de vitesse calculées à 583 K sont donnés dans les tableaux 5 et 6, le premier à partir du radical *tert*-butyle, le second à partir du radical isobutyle.

Des calculs ont pu ainsi être développés à partir des schémas mécanistiques proposés dans ces deux tableaux et en tenant compte des valeurs numériques des constantes de vitesse. Il a été possible par exemple d'estimer les rapports des concentrations des différents radicaux ·QOOH. À partir de ces calculs, nous avons pu établir que ·Q^1OOH, ·Q^2OOH et ·Q^3OOH sont présents en des concentrations d'ordres de grandeur voisins alors que celle de ·Q^4OOH peut être considérée comme négligeable. Compte-tenu de ces calculs, des comparaisons ont pu être établies avec les résultats expérimentaux. En effet, disposant d'une estimation des constantes de vitesse des processus de décomposition des radicaux ·QOOH, il devient possible de déterminer les rapports théoriques des vitesses initiales de formation des produits primaires et de les confronter aux résultats expérimentaux tout au moins en ce qui concerne les produits primaires ne provenant pas de la dismutation éventuelle des radicaux RO_2·.

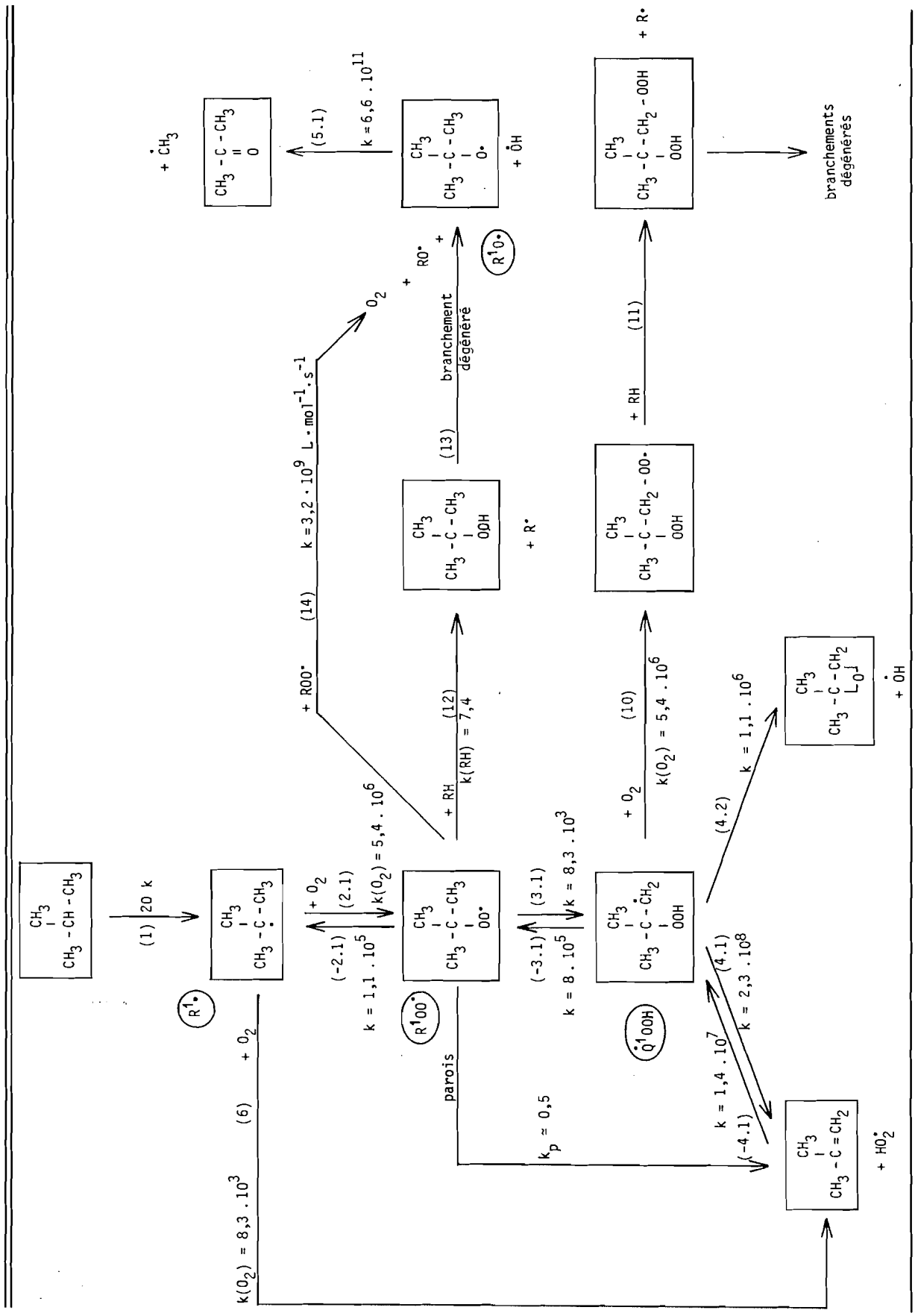
III.2. Commentaires sur le mécanisme proposé

Il serait fastidieux de discuter ici chaque chemin réactionnel en le comparant avec les formations de produits observées expérimentalement. Une comparaison détaillée de cette nature a été faite dans un mémoire de thèse (16). Il est à noter qu'à ce stade de notre travail nous n'avons pas ajusté les paramètres cinétiques obtenus par les méthodes de Benson à nos résultats expérimentaux. Comme nous l'avons déjà mentionné, ces méthodes ne visent qu'à donner une valeur approximative des

Can. J. Chem. Downloaded from www.nrcresearchpress.com by 41.223.56.140 on 09/07/12
For personal use only.

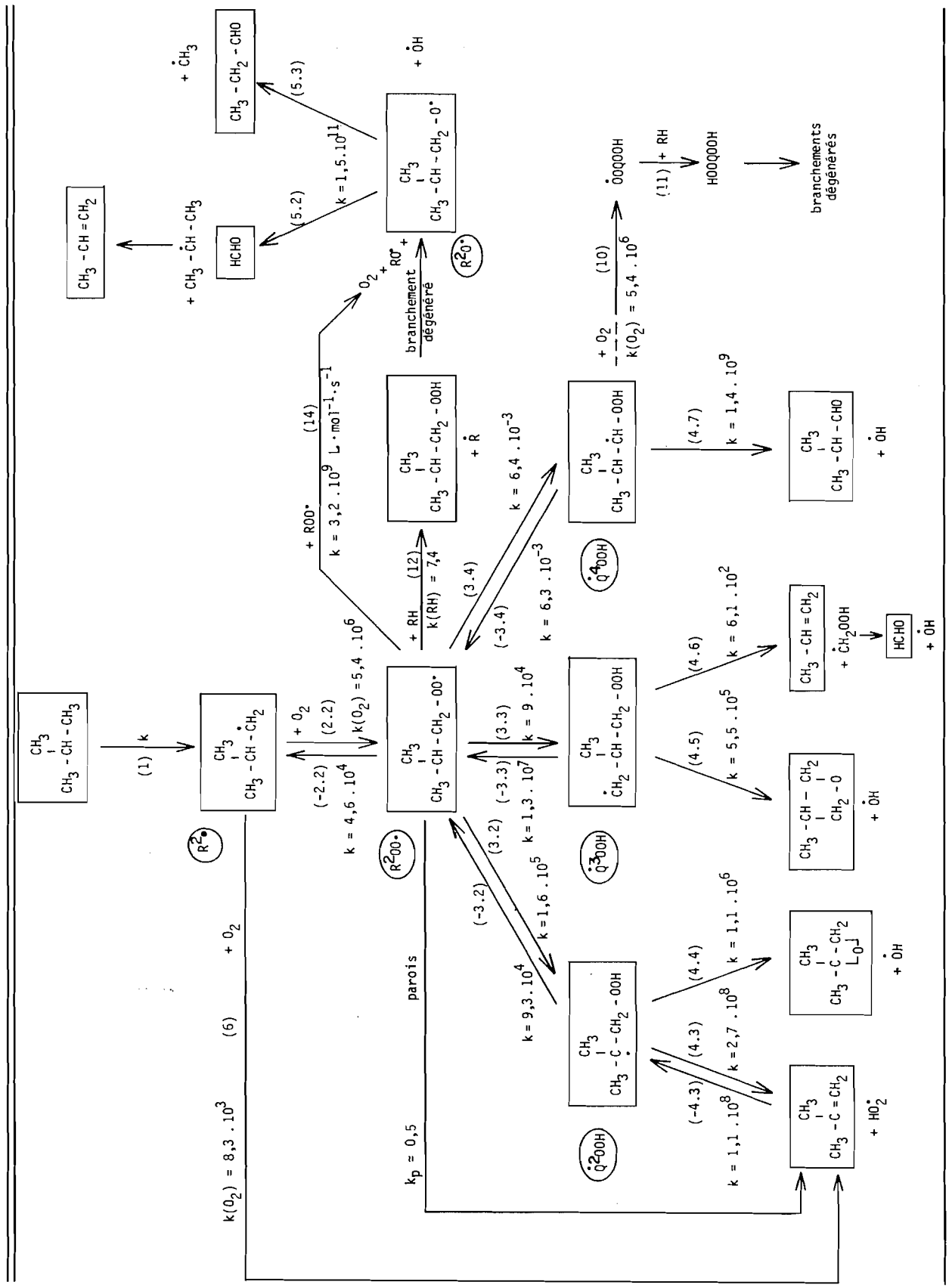
Can. J. Chem. Downloaded from www.nrcresearchpress.com by 41.223.56.140 on 09/07/12
For personal use only.

TABLEAU 5. Mécanisme d'oxydation de l'isobutane (processus élémentaires issus du radical $t\text{-}C_4H_9^{\cdot}$)



Can. J. Chem. Downloaded from www.nrcresearchpress.com by 41.223.56.140 on 09/07/12
For personal use only.

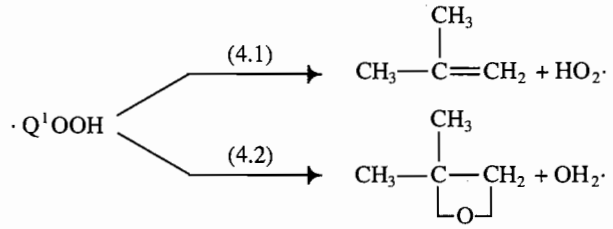
TABLEAU 6. Mécanisme d'oxydation de l'isobutane (processus élémentaires issus du radical i-$C_4H_9^{\cdot}$).



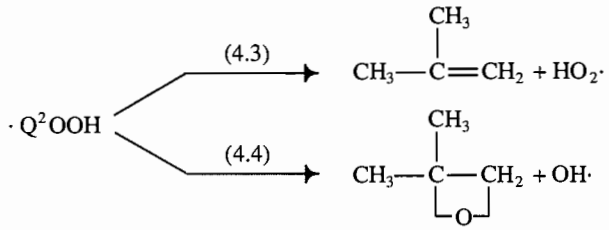
constantes de vitesse et un écart d'une puissance de 10 demeure tout à fait acceptable.

Pour fixer les idées, traitons d'abord le cas du couple isobutène – oxyde d'isobutène (désigné dans certains calculs par i-Butox). Ces deux produits sont issus parallèlement de deux voies (se reporter aux tableaux 5 et 6 pour la nomenclature) :

(*i*) à partir du radical $\cdot Q^1OOH$:



(*ii*) à partir du radical $\cdot Q^2OOH$:



Le calcul du rapport des vitesses de formation des deux espèces s'écrit alors :

$$\frac{v_{\text{i-C}_4\text{H}_8}}{v_{\text{i-Butox}}} = \frac{k_{4.1}(\cdot Q^1OOH) + k_{4.3}(\cdot Q^2OOH)}{k_{4.2}(\cdot Q^1OOH) + k_{4.4}(\cdot Q^2OOH)}$$

Compte-tenu de l'évaluation des concentrations relatives des radicaux et de l'estimation des constantes de vitesse, ce rapport peut être estimé à 220 dans nos conditions expérimentales.

Expérimentalement, le rapport des pourcentages initiaux des deux produits conduit à :

$$\frac{\%\ \text{i-C}_4\text{H}_8}{\%\ \text{i-Butox}} = \frac{56.7}{2} \simeq 28$$

Si l'on se reporte aux remarques précédentes sur l'estimation des constantes de vitesse, la concordance peut être considérée comme correcte.

D'autres remarques peuvent être faites à partir du mécanisme proposé. Dans nos conditions expérimentales, le processus oléfinique direct :

$$R\cdot + O_2 \rightarrow \text{i-C}_4\text{H}_8 + HO_2\cdot$$

apparaît relativement peu important, de l'ordre de 1,5% par rapport à la formation issue de l'isomérisation de $RO_2\cdot$ (via $\cdot QOOH$). La formation directe d'oléfines aux parois apparaît négligeable (de l'ordre de 10^{-2}%), en accord avec le point de vue de Walker (32).

La comparaison entre la formation théorique de propène et nos observations expérimentales montre des difficultés au niveau du processus (4.6); il paraît nécessaire d'envisager un autre processus de formation via (5.2) selon une suggestion de Barnard et Brench (15).

La formation de certains produits carbonylés, dont le propionaldéhyde suscite également quelques difficultés au niveau de la comparaison entre formations estimées à partir du schéma réactionnel et résultats expérimentaux. En effet, il paraît logique d'attribuer la formation de ces produits à la décomposition de radicaux alcoxy, eux-mêmes pouvant être attribués à la dismutation de deux radicaux alcoylperoxy :

$$2RO_2\cdot \rightarrow 2RO\cdot + O_2$$

si l'on veut être en accord avec la nature primaire de ces produits. En réalité, ces produits carbonylés pourraient être pour une part de nature secondaire mais avoir une allure pseudo-primaire, s'ils sont formés à partir de produits primaires suffisamment réactifs et en quantités relativement importantes (oléfines par exemple).

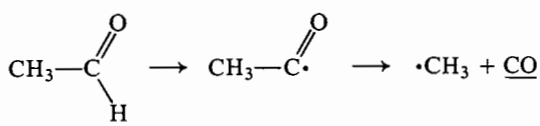
En ce qui concerne les hydroperoxydes, une comparaison entre résultats expérimentaux et prévisions déduites du mécanisme est assez difficile à réaliser. Elle nécessiterait d'abord davantage de précision au niveau expérimental par la réalisation d'un dosage permettant de différencier les peracides, l'eau oxygénée et les peroxydes organiques. Savaya (33) et Hoare et coll. (34) utilisent une méthode par iodométrie proposée par Cullis et Newitt (35) permettant cette distinction mais, en raison des relativement faibles avancements de nos réactions, les méthodes de dosage par iodométrie classique avaient déjà échoué. Néanmoins le rapport calculé de la formation globale d'hydroperoxyde à celle de l'oxyde d'isobutène paraît acceptable par rapport aux observations expérimentales.

Il serait intéressant de disposer de davantage de données quantitatives concernant l'eau. Il convient de remarquer que son dosage, dans nos conditions opératoires, est généralement difficile pour deux raisons :

(*i*) il est relativement difficile de prélever quantitativement l'eau formée d'un appareillage statique en Pyrex, en raison des phénomènes d'absorption sur les parois des lignes de transfert et des ampoules d'échantillonnage. Les quantités dosées sont très sensibles à la température de ces éléments et comme nous l'avons mentionné précédemment, nous avons dû utiliser des cordons chauffants pour obtenir des mesures paraissant satisfaisantes.

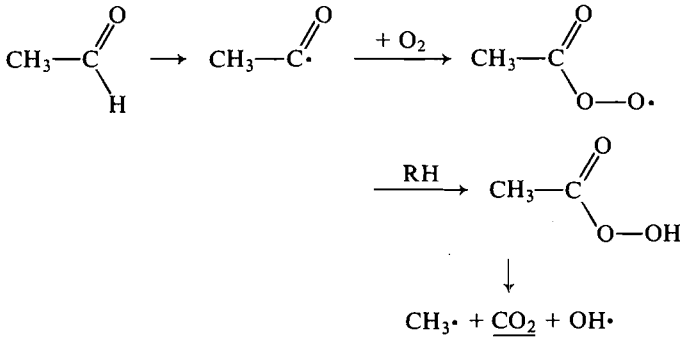
(*ii*) Les analyses chromatographiques sont elles-mêmes délicates, surtout pour de faibles quantités. Rappelons que l'eau a été dosée sur colonne de Porapak Q, longueur 1 m, température 39°C, gaz porteur H_2 et détection par thermistances.

Si la nature non primaire du monoxyde de carbone ne pose pas de problème, il paraît difficile de préciser un mécanisme sûr rendant compte de sa formation. Un des schémas les plus raisonnables, mais non vérifié expérimentalement, expliquerait sa formation par l'intermédiaire d'aldéhydes :



En revanche, la nature apparemment primaire de CO_2 semble très paradoxale, surtout si l'on tient compte du fait que le monoxyde de carbone est non primaire. À ce stade de nos recherches, nous ne pouvons pas donner de solution par un mécanisme réactionnel. Comme nous l'avons signalé, la sensibilité limitée de nos méthodes chromatographiques peut être, en partie au moins, à l'origine de cette apparente anomalie. Ici encore, la source de dioxyde de carbone pourrait être pseudo-primaire, c'est-à-dire passer par l'intermédiaire de produits réactifs formés primairement. L'oxydation d'un aldéhyde conduisant à un peracide correspond à ce type de schéma mais, ici encore, il ne s'agit que d'hypothèses :

Can. J. Chem. Downloaded from www.nrcresearchpress.com by 41.223.56.140 on 09/07/12
For personal use only.



Cette hypothèse, ainsi que la précédente sur la formation de CO, souligne le rôle très important des aldéhydes dans les schémas d'oxydation.

L'examen des différents produits fait donc apparaître encore un certain nombre de difficultés ou de schémas détaillés non encore résolus. Cependant, le but poursuivi dans le cadre du présent travail n'était pas de donner une interprétation précise et sûre de tous les produits formés, y compris en faibles quantités, mais plutôt de proposer un schéma général de l'oxydation d'alcanes légers.

IV. Discussion et conclusion

Un nombre substantiel de processus élémentaires figurant dans le mécanisme a fait l'objet de discussions et commentaires dans ce qui précède. Nous nous bornerons ici à reprendre certains problèmes plus généraux.

Le problème essentiel qui se pose dans l'interprétation mécanistique est la nature des porteurs de chaînes. Si le radical hydroperoxyle paraît être formé de manière prépondérante dans les premiers instants de la réaction, les caractéristiques de celles-ci, dont en particulier la nature des produits formés, paraissent suggérer que le radical hydroxyle OH·, réactif et non sélectif, joue un rôle essentiel dans le schéma réactionnel. C'est par la réactivité de OH· que l'on interprète un certain nombre de phénomènes dans les réactions non isothermes, dont les flammes froides et les inflammations de 2ème stade (cf. par ex., les références 36, 37).

À partir du schéma réactionnel précédent, nous pouvons estimer le rapport des concentrations initiales de $HO_2\cdot$ et de OH· en calculant le rapport des vitesses initiales de formation. Dans nos conditions expérimentales :

$$\frac{V_{HO_2\cdot}}{V_{OH\cdot}} \simeq 60$$

Initialement, ce qui paraît d'ailleurs logique compte-tenu du schéma réactionnel, il y aurait un large excès de radicaux hydroperoxyle par rapport aux radicaux hydroxyle, mais ceci n'est pas incompatible avec un rôle prédominant des radicaux OH·, ceux-ci étant beaucoup plus réactifs que $HO_2\cdot$. Si nous comparons l'arrachement d'un hydrogène tertiaire par ces deux radicaux :

$$HO_2\cdot + RH \rightarrow H_2O_2 + R\cdot \qquad k = 4{,}3 \times 10^3\ L\cdot mol^{-1}\cdot s^{-1}$$

$$OH\cdot + RH \rightarrow H_2O + R\cdot \qquad k = 1{,}3 \times 10^9\ L\cdot mol^{-1}\cdot s^{-1}$$

d'après les données de Walker (32), les valeurs numériques étant calculées dans nos conditions expérimentales (310°C).

Le seuil de concentration élevé des radicaux $HO_2\cdot$ compense en partie leur faible réactivité mais les réactions auxquelles ils peuvent donner lieu ne sont pas encore complètement élucidées (4). En dehors de l'arrachement d'hydrogène relativement difficile (cf. valeur précédente de la constante) et d'une éventuelle destruction hétérogène à la paroi, deux radicaux hydroperoxyle peuvent donner lieu à une dismutation :

$$HO_2\cdot + HO_2\cdot \rightarrow H_2O_2 + O_2 \qquad k = 10^{9,3}\ L\cdot mol^{-1}\cdot s^{-1}$$

l'eau oxygénée donnant lieu à des réactions de branchement, surtout à relativement haute température (400–500°C).

Il faut remarquer que les réactions impliquant l'alcane de départ RH (réactions de métathèse ou de transfert d'hydrogène) sont très vraisemblablement rapidement remplacées par des processus analogues impliquant un (ou des) produit(s) possédant un atome d'hydrogène mobile comme l'ont déjà remarqué plusieurs auteurs (4) (36). Ces produits à hydrogène mobile peuvent en particulier être des aldéhydes.

Compte-tenu des schémas écrits précédemment et du rôle du radical OH·, il paraît logique d'observer l'accumulation de quantités substantielles d'eau. On s'attendrait aussi à d'appréciables quantités d'eau oxygénée, compte-tenu du seuil élevé de concentration des radicaux $HO_2\cdot$ et de la relativement basse température de réaction (310–340°C) pour laquelle l'eau oxygénée est encore stable. Or les dosages globaux de peroxydes, incluant l'eau oxygénée, conduisent à des valeurs basses.

Il faut cependant remarquer que les difficultés soulignées pour le dosage de l'eau se retrouvent pour l'eau oxygénée et que les méthodes de dosage de H_2O_2 sont vraisemblablement moins sensibles que l'analyse de l'eau par chromatographie en phase gazeuse. Le rôle des différents processus écrits pour le radical hydroperoxyle paraît assez difficile à quantifier; la faible réactivité de $HO_2\cdot$, la décomposition des peroxydes organiques et la destruction de $HO_2\cdot$ aux parois peuvent rendre compte, pour une part au moins, des faibles concentrations observées.

En conclusion, l'étude précédente montre qu'aux environs de 300°C, le mécanisme global d'oxydation de l'isobutane rendant compte des caractéristiques essentielles de la réaction peut être représenté par un schéma très simple faisant intervenir deux chaînes réactionnelles prépondérantes, l'une conduisant à l'alcène conjugué et l'autre à l'oxyde de l'alcène, en accord avec l'étude expérimentale et avec les constantes de vitesse des processus élémentaires déterminées par les méthodes de la Cinétique Thermochimique.

Si la présente étude n'a pas permis de répondre à tous les problèmes posés par le mécanisme d'oxydation des alcanes, tels que ceux mis en évidence par des auteurs comme Benson (4), elle a permis de proposer un schéma de principe cohérent, en accord satisfaisant avec les constantes de vitesse estimées et avec les résultats expérimentaux.

Il est certain qu'une preuve plus complète de la validité d'un mécanisme réactionnel, apportant de plus des éléments de réponse à des questions restant posées, serait la modélisation de la réaction, permettant en particulier de reproduire les courbes de formation des divers produits en fonction du temps, à partir du mécanisme réactionnel et en utilisant des valeurs ajustées des constantes de vitesse des processus élémentaires. Par addition d'une équation thermique, une telle modélisation pourrait même conduire à reproduire les phénomènes non-isothermes.

Il nous paraît cependant, en tenant compte des connaissances actuellement acquises, que nous ne disposons pas encore de tous les éléments nécessaires pour mener à bien une telle modélisation; il serait utile de disposer d'éléments plus complets,

Can. J. Chem. Downloaded from www.nrcresearchpress.com by 41.223.56.140 on 09/07/12
For personal use only.

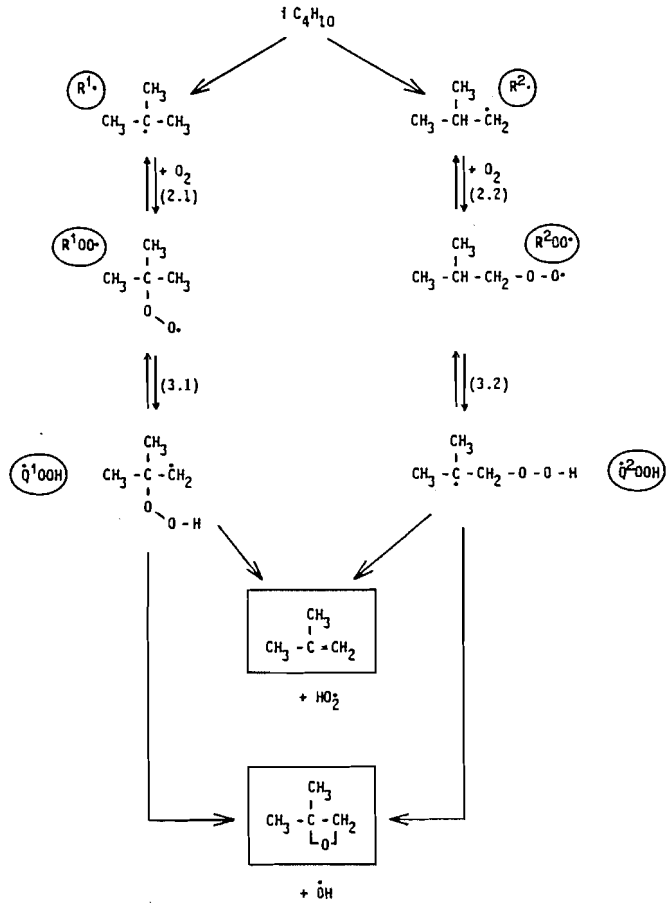


FIG. 6. Représentation schématique du mécanisme d'oxydation de l'isobutane.

par exemple sur l'amorçage de la réaction (nature des agents de branchement dégénéré), sur la terminaison de la réaction, sur certaines constantes de vitesse de processus élémentaires et vraisemblablement de méthodes numériques plus performantes. Les premiers essais que nous avons tentés dans cette voie sur l'exemple du propane[3] ont montré la complexité de cette tâche, qui cependant est susceptible d'apporter d'utiles précisions sur le mécanisme. Le travail que nous avons présenté dans ce mémoire nous paraît constituer une étape intermédiaire très importante, voire essentielle, dans la réalisation d'une modélisation complète.

Nous pensons vérifier les premières conclusions de la présente étude et le degré envisageable de généralisation du schéma proposé sur un second exemple qui sera le propane (38).

Remerciements

Les auteurs remercient la Société Rhône-Poulenc pour l'aide matérielle apportée sous la forme d'une bourse de thèse (B.V.) lors de la réalisation de ce travail.

1. R. R. BAKER et D. A. YORKE. J. Chem. Educ. **49**, 351 (1972).
2. R. T. POLLARD. *Dans* Comprehensive chemical kinetics. Vol. 17. *Éditeurs*: C. H. Bamford et C. F. H. Tipper. Elsevier, Amsterdam. 1977. p. 249.
3. S. W. BENSON. *Dans* The mechanisms of pyrolysis, oxidation and burning of organic materials. *Éditeur* : L. A. Wall. NBS Publication, U.S. Government Printing Office, Washington, DC. 1972. p. 121.
4. S. W. BENSON et P. S. NANGIA. Acc. Chem. Res. **12**, 223 (1979).
5. A. FISH. Adv. Chem. Ser. **76**, 69 (1968).
6. J. H. KNOX. *Dans* Photochemistry and reaction kinetics. *Éditeurs*: P. G. Ashmore, T. M. Sugden et F. S. Dainton. Cambridge University Press, Cambridge. 1967. p. 250.
7. J. H. KNOX. Combust. Flame, **9**, 297 (1965).
8. C. F. CULLIS, A. FISH, M. SAEED et D. L. TRIMM. Proc. R. Soc. London, A: **289**, 402 (1966).
9. A. FISH. Proc. R. Soc. London, A: **298**, 204 (1967).
10. N. N. SEMENOV. *Dans* Photochemistry and reaction kinetics. *Éditeurs*: P. G. Ashmore, T. M. Sugden et F. S. Dainton. Cambridge University Press, Cambridge. 1967. p. 229.
11. J. P. SAWERYSYN et M. LUCQUIN. Bull. Soc. Chim. Fr. 18 (1977).
12. A. P. ZEELENBERG et A. F. BICKEL. J. Chem. Soc. 4014 (1960).
13. G. W. IRVINE et J. H. KNOX. *Dans* Mechanisms of hydrocarbon reactions. *Éditeurs*: F. Marta et D. Kallo. Akadémiai Kiadó, Budapest. 1975. p. 733.
14. J. A. BARNARD et R. D. HANDSCOMBE. *Dans* Combustion Institute European Symposium 1973. *Éditeur*: F. J. Weinberg. Academic Press Inc., Londres. 1973. p. 82.
15. J. A. BARNARD et A. W. BRENCH. Combust. Sci. Technol. **15**, 243 (1977).
16. B. VOGIN. Thèse de Docteur-Ingénieur, INPL, Nancy, France. 1984.
17. J. G. ATHERTON, A. J. BROWN, G. A. LUCKETT et R. T. POLLARD. 14th Symp. (Int.) on Combustion. The Combustion Institute, Pittsburgh, PA. 1973. p. 513.
18. J. HAY, J. H. KNOX et J. M. C. TURNER. 10th Symp. (Int.) on Combustion, The Combustion Institute, Pittsburgh, PA. 1965. p. 331.
19. C. G. KINNEAR et J. H. KNOX. 13th Symp. (Int.) on Combustion, The Combustion Institute, Pittsburgh, PA. 1971. p. 209.
20. C. J. HOWARD. 6th Int. Symposium on Gas Kinetics, Southampton. 14–17 juillet 1980.
21. J. C. BROCARD, F. BARONNET et H. E. O'NEAL. Combust. Flame, **52**, 25 (1983).
22. B. VOGIN, F. BARONNET et J. C. ANDRE. Anal. Chim. Acta, **142**, 293 (1982).
23. J. WILSON. Thèse présentée à la City University de Londres. 1970.
24. R. B. BADACHHAPE, P. KAMARCHIK, A. P. CONROY, G. P. GLASS et J. L. MARGRAVE. Int. J. Chem. Kinet. **8**, 23 (1973).
25. N. J. DALY et C. J. WENTRUP. Aust. J. Chem. **21**, 1535 (1968).
26. J. C. BROCARD et F. BARONNET. J. Chim. Phys. **84**, 19 (1987).
27. A. SEPEHRAD, R. M. MARSHALL et J. H. PURNELL. Int. J. Chem. Kinet. **9**, 411 (1979).
28. S. W. BENSON. Thermochemical kinetics. 2e éd. John Wiley, New York. 1976.
29. D. M. GOLDEN. 14th Symp. (Int.) on Combustion, The Combustion Institute, Pittsburgh, PA. 1973. p. 121.
30. M. WEISSMAN, L. G. S. SHUM, S. P. MENEGHEN et S. W. BENSON. J. Phys. Chem. **85**, 2863 (1981).
31. D. F. MACMILLEN et D. M. GOLDEN. Annu. Rev. Phys. Chem. **33**, 493 (1982).
32. R. W. WALKER. React. Kinet. **1**, 161 (1975).
33. Z. F. SAVAYA. Ph.D. thesis, Dundee University. 1982.
34. J. W. FALCONER, D. E. HOARE et Z. F. SAVAYA. 2nd Int. Specialists' Meeting of the Combustion Institute on Oxidation, Technical University, Budapest (Hongrie), 18–22 août 1982.
35. C. F. CULLIS et E. J. NEWITT. Proc. R. Soc. London, A: **237**, 530 (1956).
36. M. P. HALSTEAD, L. J. KIRSCH, A. PROTHERO et C. P. QUINN. Proc. R. Soc. London, A: **346**, 515 (1975).
37. R. A. COX et J. A. COLE. Combust. Flame, **60**, 109 (1985).
38. B. VOGIN, F. BARONNET et G. SCACCHI. Oxid. Commun. Soumis.

3. M. H. Ametrano et G. Scacchi. Résultats non encore publiés.

Can. J. Chem. Downloaded from www.nrcresearchpress.com by 41.223.56.140 on 09/07/12
For personal use only.

Novel sesquiterpenoids from the fairy ring fungus, *Marasmius oreades*

WILLIAM A. AYER[1] AND PETER A. CRAW
Department of Chemistry, University of Alberta, Edmonton, Alta., Canada T6G 2G2

AND

THOMAS J. STOUT AND JON CLARDY
Department of Chemistry, Baker Laboratory, Cornell University, Ithaca, NY 14853, U.S.A.

Received December 5, 1988

WILLIAM A. AYER, PETER A. CRAW, THOMAS J. STOUT, and JON CLARDY. Can. J. Chem. **67**, 773 (1989).

The structures of four new drimane-type sesquiterpenes **1–4** produced in liquid cultures of the fairy ring fungus, *Marasmius oreades*, have been determined by a combination of chemical and spectroscopic methods. The structure assigned to one of these sesquiterpenes (**1**) has been confirmed by an X-ray crystallographic study. An unprecedented feature of all four sesquiterpenes is the biosynthetic elaboration of C8–C12 and C15 of the drimane skeleton to a dioxabicyclooctane moiety. In addition, two of the sesquiterpenes possess an uncommon α orientation of the hydroxyl groups at C3.

Key words: sesquiterpenes, fungal metabolites, drimanes, fairy ring mushroom, crystal structure.

WILLIAM A. AYER, PETER A. CRAW, THOMAS J. STOUT et JON CLARDY. Can. J. Chem. **67**, 773 (1989).

Faisant appel à une combinaison de méthodes chimiques et spectroscopiques, on a déterminé les structures de quatre nouveaux sesquiterpènes (**1–4**) du type drimane qui sont produits dans des cultures liquides de champignons mousserons, *Marasmius oreades*. La structure attribuée au sesquiterpène **1** a été confirmée par une étude effectuée à l'aide de la diffraction des rayons-X. Ces quatre sesquiterpènes possèdent une caractéristique nouvelle, l'élaboration biosynthétique des carbones C8–C12 et C15 du squelette du drimane en une portion dioxabicyclooctane. De plus, les groupements hydroxyles présents en position C3 de deux des sesquiterpènes se trouvent dans la configuration α qui est inhabituelle.

Mots clés : sesquiterpènes, métabolites des champignons, drimanes, champignons mousserons, structure du cristal.

[Traduit par la revue]

Introduction

Fairy rings (witches' rings) in turf grasses are found throughout the world and can be caused by a variety of Basidiomycete fungi (1, 2). In Western Canada the fungus most commonly associated with fairy rings is *Marasmius oreades* (Bolt.:Fr.)Fr. (3). The fairy rings result from the apical growth habit of fungal hyphae and increase in diameter by about 15–30 cm per year. On the prairies there are some rings, with diameters over one kilometer, that are several centuries old (2).

The mature rings of *Marasmius oreades* are conspicuous because they often occur in lawns, golf courses, playing fields, and parks, disfiguring the turf. These rings have an inner and outer zone of stimulated grass growth and a zone of dead grass in the middle attributed to the dense mycelium interfering with the penetration of water. There are also reports that the fungus produces hydrogen cyanide and other cyanogenic compounds (4), with the suggestion that these kill the grass and at the same time restrict the growth of other soil microorganisms that are notably scarce in the soil of fairy rings of *Marasmius oreades*. Very little is known about the chemistry of *Marasmius oreades*, which we felt was surprising in view of the resistance of this fungus to currently available fungicides. We therefore decided to undertake an investigation of the metabolites produced by *Marasmius oreades* in the hope of better understanding the factors that may be responsible for the distinctive and disfiguring zones associated with fairy rings of this fungus.

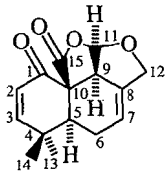
Results and discussion

Marasmius oreades was grown in still culture on a medium of potato dextrose broth containing yeast extract. After 8 weeks the broth was separated from the mycelium and extracted with ethyl acetate. Flash chromatography of this extract then led to the isolation of the four new sesquiterpenes anhydromarasmone (**1**), marasmone (**2**), isomarasmone (**3**), and dihydromarasmone (**4**). It was apparent from a comparison of ^1H and ^{13}C nuclear magnetic resonance (nmr) spectra that each of the four new sesquiterpenes possesses the same dioxabicyclooctane moiety fused with ring B in a drimane-type skeleton. Thus, the ^1H nmr spectrum of each compound displays an acetal doublet (J 4.3–4.5 Hz) in the range δ 5.98–6.44 (H11), which is coupled to a broad singlet between δ 3.30 and 3.68 (H9). The varying positions of these signals reflect changes in the position and oxidation state of substituents in ring A of each compound. The signal of H9 is in each case coupled to a vinyl hydrogen signal in the region δ 5.94–6.00 (H7), which in turn is coupled to two allylic dihydrofuran hydrogen multiplets from δ 4.48 to 4.61 (H12), and a multiplet due to two allylic hydrogens within the range δ 2.18–2.50 (H6). Coupling between the H6 multiplet and a doublet of doublets due to H5 (δ 2.36–2.49) can be demonstrated in all but the spectrum of isomarasmone (**3**) where the signal of H5 is obscured within the multiplet due to H6. In the ^{13}C nmr spectra of the four new sesquiterpenes the positions of the signals due to C6 (δ 24.0–25.4), C7 (δ 124.0–126.3), C8 (δ 131.3–133.5), C9 (δ 47.9–49.5), C11 (δ 103.9–106.0), and C12 (δ 72.2–73.6) show little variation within the quoted ranges of chemical shifts, whereas the difference in the ring A substituents is reflected more clearly in the positions of the signals due to C5 (δ 34.0–42.0), C10 (δ 55.7–64.8), and C15 (δ 169.5–176.3). The location of the substituents in ring A of the four different compounds was determined as described below for the individual compounds.

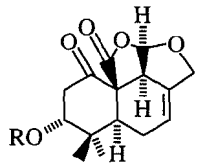
Anhydromarasmone (**1**) was obtained as prisms, mp 194–196°C, and is the least polar sesquiterpene eluted by flash chromatography of the ethyl acetate extract of the culture broth. High resolution mass spectrometry (hrms) and chemical ionization mass spectrometry (cims) indicate a molecular formula of $C_{15}H_{16}O_4$. The Fourier transform infrared (Ftir) spectrum displays characteristic lactone (1760 cm^{-1}) and α,β-unsaturated

[1]Author to whom correspondence may be addressed.

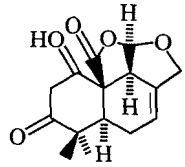
Can. J. Chem. Downloaded from www.nrcresearchpress.com by 41.223.56.140 on 09/07/12
For personal use only.



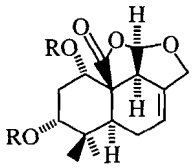
1



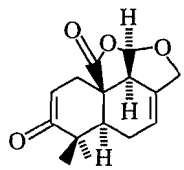
2, R = H
8, R = Ac



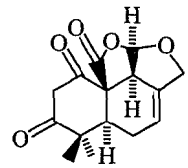
3



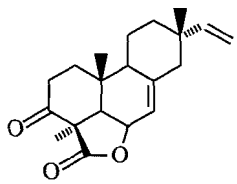
4, R = H
9, R = Ac



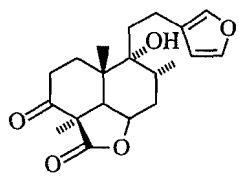
5



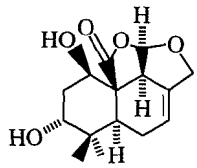
10



6



7

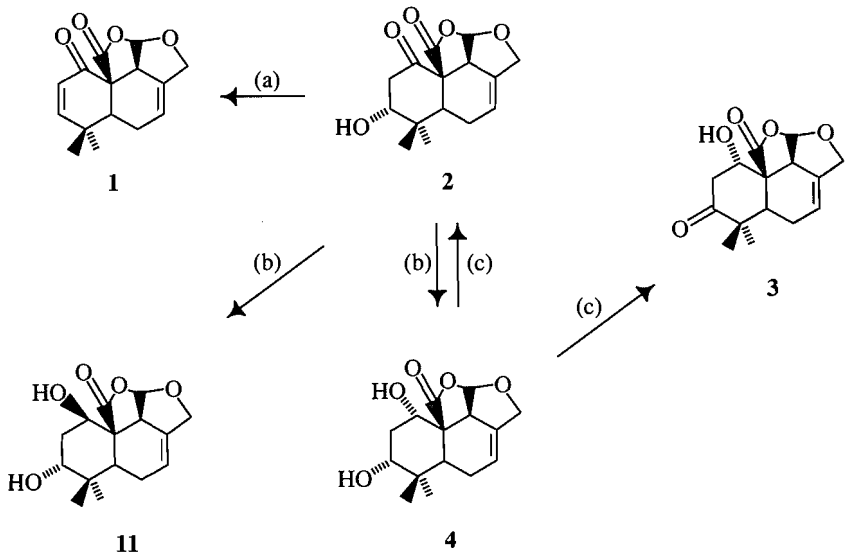


11

ketone (1663 cm^{-1}) absorptions (5). The presence of an α,β-unsaturated ketone is also apparent from a maximum in the ultraviolet (uv) spectrum at 235 nm, doublets in the ^1H nmr spectrum at δ 6.01 (*J* 10.2 Hz) and δ 6.87 (*J* 10.2 Hz), and methine carbons in the ^{13}C nmr spectrum at δ 125.6 (C2) and δ 162.7 (C3). The remaining signals in the ^1H and ^{13}C nmr spectra are in accord with the structure assigned to anhydromarasmone (**1**), but equally well may be accounted for by the isomeric structure **5**. However, two features of the nmr spectra strongly favor structure **1**. First, the signals of the lactone (δ 169.7) and the α,β-unsaturated ketone (δ 193.6) carbonyl carbons occur significantly upfield (ca. 8–10 ppm) of the positions normally associated with either of these classes of carbon signals. Upfield shifts of similar magnitude have, however, been reported for the lactone and saturated ketone carbonyl signals of momilactone A (**6**) (δ 174.3 and δ 205.0 respectively) (6) and the ballotinone derivative **7** (δ 174.8 and δ 207.1 respectively) (7). These upfield shifts are possibly due to an interaction between the dipoles of the lactone and ketone carbonyl groups causing a mutual shielding of the carbonyl carbons. Such a dipole–dipole interaction may be responsible for the uncharacteristic upfield positions of the lactone and conjugated carbonyl signals in the spectrum of anhydromarasmone (**1**), but is not consistent with the isomeric structure **5**. The second and perhaps more conclusive feature that is inconsistent with **5** is the presence of large nuclear Overhauser enhancements (nOe) of the β-hydrogen doublet (δ 6.87) of the α,β-unsaturated ketone (10.2% and 11.2%) when either of the C4 methyl singlets (δ 1.23 and δ 1.48 respectively) are irradiated. These nOe enhancements can only be accounted for if the β-hydrogen of the α,β-unsaturated ketone is located adjacent to the two methyl groups at C4 as in the structure assigned to anhydromarasmone (**1**). A large nOe (8.3%) from only the methyl singlet at δ 1.48 (H13) to a doublet of doublets at δ 2.37 (H5) is consistent with the assignment of the methyl singlets in the ^1H nmr spectrum of **1**. Significant negative nOe effects are observed from H3 to H2 (−3.5% and −2.8%) when either of the methyl singlets (δ 1.23 and δ 1.48 respectively) is irradiated. As the structures of the other three sesquiterpenes from *Marasmius oreades* reported in this paper can be correlated with anhydromarasmone (**1**) (Scheme 1), the structure of **1** was confirmed by an X-ray crystallographic study. A computer generated perspective drawing of the final X-ray model of anhydromarasmone is given in Fig. 1. The enantiomer illustrated was not determined by the X-ray experiment but was selected arbitrarily. The structure contains few surprises. The two six-membered rings are roughly planar, that is, C1–C4 and C6–C9 are planar while C5 is above and C10 is below this plane. Both of the six-membered rings are in the half-chair conformation. The two five-membered rings are both in the *C*2 or skew conformation with the approximate twofold axes running from O3 through the C9—C10 bond and from O2 through the C9—C8 bond.

Marasmone (**2**) is the corresponding β-ketol of anhydromarasmone (**1**). Compound **2** was obtained as an oil that resisted all attempts to induce crystallization. The molecular ion was not detected in the hrms of this compound, but cims confirmed a molecular weight of 278 corresponding to a formula of $C_{15}H_{18}O_5$. As in the mass spectrum of anhydromarasmone (**1**), an abundant ion arising from loss of CO_2 (*m/z* 234) is observed in the spectrum of **2**. The Ftir spectrum displays the expected hydroxyl (3490 cm^{-1}) and ketone (1716 cm^{-1}) carbonyl absorptions. The ^1H nmr spectrum differs most notably from that of anhydromarasmone (**1**) by the replacement of the signals of the α,β-unsaturated ketone by two geminally coupled doublets of doublets at δ 2.50 (*J* 14.0, 4.4 Hz, H2α) and δ 3.17 (*J* 14.5, 2.3 Hz, H2β), which are both vicinally coupled to a doublet of doublets at δ 3.95 (*J* 3.8, 2.4 Hz, H3). The two small coupling constants for the H3 signal support an α orientation of the C3-hydroxyl (assuming a chair conformation of ring A), but equally well might correspond to a β-hydroxyl at C3 if ring A

Can. J. Chem. Downloaded from www.nrcresearchpress.com by 41.223.56.140 on 09/07/12
For personal use only.



SCHEME 1. (a) $(CH_3CO)_2O$, pyridine, rt, 8 h; (b) $NaBH_4$, CH_3OH, rt, 10 min; (c) PDC, CH_2Cl_2, rt, 8 h.

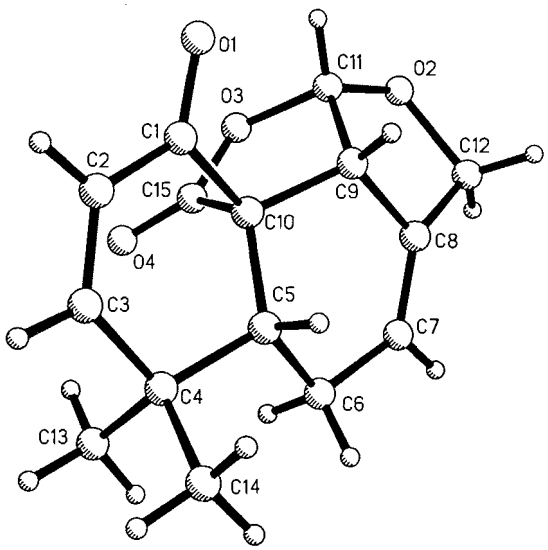


FIG. 1. A computer generated perspective drawing of the final X-ray model of anhydromarasmone.

adopts a boat conformation. Unfortunately, extensive nOe experiments (Table 1) failed to provide any information that would allow the stereochemistry of the C3-hydroxyl to be assigned, although the presence of large nOe effects from both of the methyl groups at C4 to H3 (8% and 13%) did at least support the regiochemistry of the β-ketol in ring A of marasmone (**2**). The regiochemistry of **2** was also confirmed when attempted acetylation gave a good yield of anhydromarasmone (**1**) instead of the corresponding acetate **8**. The stereochemistry at C3 of **2** was determined by chemical correlation with another of the sesquiterpenes isolated from *Marasmius oreades* (see below). Somewhat surprisingly, attempted dehydration of marasmone (**2**) to anhydromarasmone (**1**) failed with either catalytic or larger amounts of *p*-toluenesulfonic acid in benzene. Even after refluxing for several hours very little of the β-ketol appeared (tlc) to have been consumed in the reaction. The regiochemistry of the β-ketol in **2** is further supported by the positions of the lactone (δ 169.5) and ketone (δ 203.9) carbonyl signals in the

TABLE 1. Nuclear Overhauser enhancements in the ^1H nmr spectrum of marasmone (**2**)

Saturated signal (δ)	Observed enhancements (δ)
1.07 (13-CH_3)	2.28–2.36 (H6, 5%), 2.50 (H2α, 13%), 3.95 (H3, 8%)
1.40 (14-CH_3)	2.28–2.36 (H6, 10%), 3.17 (H2β, 6%), 3.95 (H3, 10%)
3.38 (H9)	6.16 (H11, 16%)
3.95 (H3)	2.50 (H2α, 5%), 3.17 (H2β, 5%)

^{13}C nmr spectrum. These signals are significantly upfield (ca. 8–10 ppm) of the more usual positions of isolated lactone and ketone carbonyl signals and, as in the case of anhydromarasmone (**1**), support a 1,3-disposition of these carbons in marasmone (**2**). It appears that the positions of lactone and ketone carbonyl signals in the ^{13}C nmr are useful for predicting the location of a ketone in ring A of related decalin type terpenes that contain a lactone carbonyl at either C13, C14, or C15.

Isomarasmone (**3**) was obtained as prisms, mp 247–250°C, which, unlike marasmone (**2**), did display a molecular ion in the hrms corresponding to a molecular formula of $C_{15}H_{18}O_5$. The mass spectra of **2** and **3** also differ in that the abundant ion at m/z 234 in the spectrum of **3** ($C_{13}H_{14}O_4$) arises from loss of elements of vinyl alcohol (presumably from C1, C2) rather than CO_2. In the Ftir spectrum of **3** strong absorptions are seen for the lactone (1755 cm^{-1}) and ketone (1699 cm^{-1}) carbonyl groups. The signals of the β-ketol moiety in the ^1H nmr spectrum of **3** occur as two geminally coupled doublets of doublets at δ 2.49 (*J* 14.2, 4.3 Hz, H2α) and δ 3.31 (*J* 14.3, 2.1 Hz, H2β), which are vicinally coupled to a doublet of doublets at δ 4.35 (*J* 4.0, 2.1 Hz, H1). The small coupling constants of the latter signal, like those of H3 in the spectrum of **2**, support either an α or β orientation for the β-ketol hydroxyl depending on the conformation adopted by ring A. The positions of the lactone (δ 176.3) and ketone (δ 215.6) carbonyl signals in the ^{13}C nmr spectrum of **3** indicate the lack of a dipole–dipole interaction between the carbonyl groups and support the regiochemistry assigned to the β-ketol functionality of isomarasmone (**3**).

Can. J. Chem. Downloaded from www.nrcresearchpress.com by 41.223.56.140 on 09/07/12
For personal use only.

Can. J. Chem. Downloaded from www.nrcresearchpress.com by 41.223.56.140 on 09/07/12
For personal use only.

TABLE 2. Nuclear Overhauser enhancements in the ^{1}H nmr spectrum of isomarasmone (**3**)

Saturated signal (δ)	Observed enhancements (δ)
1.11 (13-CH_3)	2.28–2.36 (H6, 6%), 3.81 (H3, 6%)
1.26 (14-CH_3)	2.17 (H2, 2%), 2.28–2.36 (H6, 2%), 3.81 (H3, 9%)
2.17 (H2)	1.26 (14-CH_3, 2%), 3.81 (H3, 13%), 3.88 (H1, 13%)
3.68 (H9)	2.28–2.36 (H6, 2%), 5.97 (H11, 14%)
3.81 (H3)	1.11 (13-CH_3, 1%), 1.26 (14-CH_3, 2%), 2.17 (H2, 4%)
3.88 (H1)	2.17 (H2, 3%), 3.68 (H9, 3%), 5.97 (H11, 11%)

The stereochemistries of the C3-hydroxyl in marasmone (**2**) and the C1-hydroxyl in isomarasmone (**3**) were secured by chemical correlation with dihydromarasmone (**4**), which is the fourth sesquiterpene we obtained from chromatography of the broth extract of *Marasmius oreades*. Dihydromarasmone (**4**) crystallizes as irregular prisms, mp 164–165°C, which displayed an abundant ion (*m/z* 280) in the hrms corresponding to a molecular formula of $C_{15}H_{20}O_5$. The base peak in the hrms at *m/z* 200 arises from loss of CO_2 and two molecules of water (fragment ions at *m/z* 262, 236, 218). The presence of two hydroxyl groups was also indicated by a strong absorption at 3394 cm^{-1} in the Ftir spectrum and methine signals at δ 68.8 (C1) and δ 78.5 (C3) in the ^{13}C nmr spectrum, while the presence of a lactone group was confirmed by a carbonyl absorption at 1768 cm^{-1} in the Ftir spectrum and a signal at δ 174.4 in the ^{13}C nmr spectrum. The signals due to H1, H3, and H9 (δ 3.88, 3.81, 3.68) were assigned in the following manner. Irradiation of the broad singlet at δ 3.68 collapsed the acetal doublet at δ 5.97 (H11) to a singlet, confirming the assignment of the signal due to H9. Of the two remaining signals, that at δ 3.88 must be due to H1 since saturation of this signal results in a large nOe enhancement of the acetal doublet (H11) and a small nOe enhancement of the H9 signal (Table 2). Finally, the signal at δ 3.81 must be that of H3 since large nOe enhancements of this signal are observed when either of the C4-methyl singlets at δ 1.11 and δ 1.26 are irradiated. The signals of H1 (br ddd, *J* 8.0, 3.0, 3.0 Hz) and H3 (dd, *J* 3.0, 3.0 Hz) are equally coupled to an apparent two-proton triplet at δ 2.17 (*J* 3.0 Hz), which is in fact two coincident doublets of doublets (*J* 3.0, 3.0 Hz, H2α, H2β). Irradiation of the signal of either H1 or H3 simplifies the signal for the C2 hydrogens to a doublet (*J* 3.0 Hz). The additional coupling observed in the signal of H1 (*J* 8.0 Hz) is to a doublet at δ 4.93 (*J* 8.8 Hz), which we have assigned to the C1-hydroxyl hydrogen. The second hydroxyl hydrogen (C3-OH) occurs as a broad singlet at δ 2.40.

The equivalent small coupling between the hydrogens at C2 and those at C1 and C3 indicated that the two hydroxyl groups in dihydromarasmone (**4**) have the same orientation and are either both α-axial if ring A exists in a chair conformation, or β if ring A exists in a twist conformation. To distinguish between the two possible orientations of the hydroxyl groups, the ^{1}H nmr spectrum was recorded in solutions of 1% and 5% v/v deuteropyridine in deuterochloroform containing tetramethylsilane. The most significant changes observed for the spectrum in 1% C_5D_5N–$CDCl_3$ were the broad singlet at δ 2.40 (C3-OH) shifted to δ 4.11, the doublet at δ 4.93 (C1-OH) shifted to δ 5.50, and the doublet of doublets at δ 2.36 (*J* 11.5, 7.0 Hz, H5) shifted to δ 2.41. In the spectrum recorded in 5% C_5D_5N–$CDCl_3$ the C3-OH signal now occurred at δ 5.80, the C1-OH signal at δ 6.18, and the H5 signal had shifted to δ 2.46. There were also small shifts (<0.05 ppm) of the signals of H1, H3, and H9 in both spectra. The large shifts of the hydroxyl signals indicate hydrogen bonding between the hydroxyls and the deuteropyridine, which also results in the observed deshielding of H5 (8). Accordingly, the two hydroxyls in dihydromarasmone (**4**) must have an α orientation. Dihydromarasmone (**4**) was also characterized as the corresponding diacetate **9** for which the signals of H1, H2, and H3 in the ^{1}H nmr spectrum occur as an identical doublet of doublets (*J* 3.0, 3.0 Hz) at δ 5.25 and δ 4.80, while the signal of H2 occurs as a similar doublet of doublets at δ 2.20.

Having established the stereochemistry of dihydromarasmone (**4**) at C1 and C3, the stereochemistry of the hydroxyl groups in marasmone (**2**) and isomarasmone (**3**) could now be confirmed. Thus, oxidation of dihydromarasmone (**4**) with one equivalent of pyridinium dichromate in dichloromethane gave a low yield of a mixture of marasmone (**2**) and isomarasmone (**3**) and establishes that the hydroxyl groups in both β-ketols are α oriented. None of the diketone **10** was isolated from the oxidation of dihydromarasmone (**4**). Furthermore, sodium borohydride reduction of marasmone (**2**) to dihydromarasmone (**4**) also supports the stereochemistry assigned to **2**.[2] The reduction of marasmone (**2**) also gave the 1β,3α-diol **11**, which crystallized as fine needles, mp 235–237°C. The differences between the spectra of **4** and **11** are consistent with these two compounds being epimeric at C1. Thus, hydrogen bonding to the C1-hydroxyl shifts the lactone carbonyl absorption in the Ftir spectrum of **11** to 1750 cm^{-1} (cf. 1768 cm^{-1} in the spectrum of **4**). In addition, the difference in C1 stereochemistry results in upfield shifts of the signals of H2α, H5, and H9 in the ^{1}H nmr spectrum of the 1β,3α-diol **11**, and downfield shifts of the signals of H1 and H11. The coupling constant of 12.5 Hz between the signals of H1 and H2β is consistent with an *anti* relationship of these hydrogens. The 1β,3α-diol **11** was not isolated from the extracts of the cultures of *Marasmius oreades*.

Investigations are currently in progress to determine the possible relationship between the physiology of fairy rings of *Marasmius oreades* and the metabolites produced in our liquid cultures of this fungus. One possibility is that the sesquiterpenes reported in this paper or related sesquiterpenes produced by the fungus may function as plant growth regulators. Preliminary tests also indicate that the sesquiterpenes from *Marasmius oreades* may possess some antibiotic activity. We are currently reexamining the extracts of liquid cultures of *Marasmius oreades* in the search for further novel sesquiterpenes.

Experimental

General

High resolution electron impact mass spectra (hreims) were recorded on an AEI MS-50 mass spectrometer. Unless diagnostically significant, only those peaks with an intensity of <20% of the base peak are recorded. Chemical ionization mass spectra (cims) were obtained using an AEI-MS-12 mass spectrometer with ammonia as the reagent gas. The data were processed using DS-55 software and a Nova-4 computer. Fourier transform infrared (Ftir) spectra were recorded on a Nicolet 7199 FTIR interferometer. Nuclear magnetic resonance (nmr) spectra (^{1}H and ^{13}C) were obtained on Bruker WH-300, WM-360, or WH-400 spectrometers with either Aspect 2000 or Aspect 3000 computer systems. ^{1}H chemical shifts and coupling con-

[2]The reduction of isomarasmone (**3**) was not examined as only small amounts of this compound were isolated from the broth extract.

Can. J. Chem. Downloaded from www.nrcresearchpress.com by 41.223.56.140 on 09/07/12
For personal use only.

stants are reported as if they are first order. Tetramethylsilane was used as an internal standard. Ultraviolet (uv) spectra were obtained on a Hewlett Packard 8450A Diode Array spectrophotometer and optical rotations in a Perkin Elmer 241 polarimeter. Circular dichroism (cd) spectra were recorded on a Jasco Optical Rotatory Dispersion SS-20-2 recorder. Melting points are uncorrected and were determined on a Thomas model 40 melting point apparatus. E. Merck silica gel 60 (230–400 mesh) was used for flash chromatography. Preparative thin-layer chromatography (ptlc) was performed on E. Merck precoated 20 × 20 glass plates of silica gel 60 F-254. Analytical thin-layer chromatography (tlc) was carried out on cut sections of E. Merck precoated aluminium sheets of silica gel 60 F-254. Ultraviolet active materials were detected by visualization under a uv lamp (254 nm). The tlc plates were then dipped in a solution of phosphomolybdic acid for several seconds, and the spots were visualized by gentle heating over a hot plate. All solvents were distilled prior to use. Skellysolve B refers to Skelly Oil Company light petroleum, bp 62–70°C.

Growth of Marasmius oreades *on potato dextrose yeast broth and isolation of metabolites*

Slant tubes of *Marasmius oreades* (strain Mo 17) were obtained from Dr. K. Mallett, Northern Forest Research Institute, Edmonton, and a specimen sample of the fungus was deposited with the University of Alberta Microherbarium, Edmonton (register number UAMH 5750). Slant cultures of the fungus were maintained on potato dextrose agar (PDA) at 4°C. A PDA plate was inoculated with the fungus and incubated at 25°C for approximately 4 weeks and then the contents of the plate were aseptically transferred to a sterile blender and blended with 200 mL of distilled water to give a mycelial suspension. Ten 2.8-L Fernbach flasks each containing 1 L of potato dextrose broth (PBD) plus yeast medium (20 g PDB (Difco), 0.4 g yeast extract (Difco), 1 L water) were inoculated with ca. 20 mL of a mycelial suspension of the fungus (see above) and the still cultures were kept at room temperature (20–25°C) for 8 weeks.

The mycelium was separated by filtration through cheesecloth, then air-dried for 72 h and ground to a coarse powder (70.2 g). The filtered broth was concentrated to 0.5 L at reduced pressure (waterbath 40–45°C) and then filtered through Celite. The Celite was washed with 100 mL water, and methanol (20 mL) and sodium chloride (20 g) were added to the combined filtrates, which were then continuously extracted with 1.5 L refluxing ethyl acetate for 18 h. Evaporation at reduced pressure gave a brown foam (3.96 g), which was adsorbed onto silica gel (20 g) and then loaded onto a column of silica gel (150 g) that had been packed using dichloromethane. Fractions of 25 mL were collected eluting successively with 1% (fractions 1–20), 2% (fractions 21–40), and 4% (fractions 41–84) methanol–dichloromethane. Each fraction was examined by analytical tlc (5% methanol–dichloromethane) and fractions with similar mixtures of components were combined and subjected to further chromatography.

Fractions 33–45 (9.4 mg) were combined and chromatographed on a column of silica gel (20% ethyl acetate – Skellysolve B) to give anhydromarasmone (**1**, 4.9 mg). Fractions 46–49 (148 mg) were combined and chromatographed on a column of silica gel (33% ethyl acetate – Skellysolve B) to give, successively, further anhydromarasmone (**1**, 2.3 mg), marasmone (**2**, 19.7 mg), isomarasmone (**3**, 1.5 mg), and dihydromarasmone (**4**, 13.6 mg).

[4a*S*-(4aα,8a*S**,10aα,10bα)]-2,4,4a,5,10a,10b-Hexahydro-5,5-dimethyl-8*H*,9*H*-benzo[*e*]furo[2,3,4-*cd*]isobenzofuran-8,9-dione (anhydromarasmone) **1** crystallized from dichloromethane – Skellysolve B as prisms, mp 194–196°C; $[\alpha]_D^{24}$ −59.8° (*c* 0.40, CH_3OH); cd (*c* 3.46 mM, CH_3OH) 24°C: $[\theta]_{345}$ −1600, $[\theta]_{333}$ −1900, $[\theta]_{250}$ −8800; tlc: R_f 0.68 (66% ethyl acetate – Skellysolve B), 0.91 (5% methanol–dichloromethane); uv (CH_3OH) λ_{max} (log ε): 215 (sh, 3.49), 235 (3.54), 245 (sh, 3.52), 331 (3.0) nm; Ftir ($CHCl_3$ cast): 1760 (s, lactone C=O), 1663 (s, conj. ketone C=O) cm^{-1}; ^1H nmr ($CDCl_3$) δ: 1.23 (3H, s, H13), 1.48 (3H, s, H14), 2.37 (1H, dd, *J* = 11.5, 6.0 Hz, H5), 2.43 (2H, m, H6), 3.30 (1H, m, H9), 4.48 (1H, ddd, *J* = 10.5, 1, 1 Hz, H12), 4.56 (1H, dddd, *J* = 10.5, 1, 1, 1 Hz, H12), 6.00 (1H, m, H7), 6.01 (1H, d, *J* = 10.2 Hz, H2) 6.44 (1H, d, *J* = 4.3 Hz, H11), 6.87 (1H, d, *J* = 10.2 Hz, H3); ^{13}C nmr ($CDCl_3$) δ: 23.9 (C14), 24.8 (C6), 30.9 (C13), 35.6 (C4), 42.0 (C5), 49.5 (C9), 59.9 (C10), 72.2 (C12), 106.0 (C11), 124.0 (C7), 125.6 (C2), 131.3 (C8), 162.7 (C3), 169.7 (C15), 193.6 (C1); hreims (probe 180°C), *m/z* calcd. for $C_{15}H_{16}O_4$ (M^+): 260.1048; found: 260.1047 (2), 216 ($M^+ - CO_2$, 56), 201 (31), 187 (27), 120 (100), 96 (32), 91 (29); cims, *m/z*: 278 (M^+ + 18, 100).

[4a*S*-(4aα,6α,8a*S**,10aα,10bα)]-2,4,4a,5,6,7,10a,10b-Octahydro-5,5-dimethyl-8*H*,9*H*-benzo[*e*]furo[2,3,4-*cd*]isobenzofuran-8,9-dione (marasmone) **2** was obtained as a clear foam that could not be induced to crystallize; $[\alpha]_D^{24}$ +74.6° (*c* 1.44, CH_3OH); tlc: R_f 0.62 (66% ethyl acetate – Skellysolve B), 0.51 (5% methanol–dichloromethane); Ftir ($CHCl_3$ cast): 3490 (br, OH), 1768 (s, lactone C=O), 1716 (s, ketone C=O) cm^{-1}; ^1H nmr ($CDCl_3$) δ: 1.07 (3H, s, H13), 1.40 (3H, s, H14), 1.75 (1H, br s, OH), 2.18–2.30 (1H, m, H6), 2.36–2.44 (1H, m, H6), 2.49 (1H, dd, *J* = 12.0, 5.0 Hz, H5), 2.50 (1H, dd, *J* = 14.0, 4.4 Hz, H2α), 3.17 (1H, dd, *J* = 14.5, 2.3 Hz, H2β), 3.38 (1H, m, H9), 3.95 (1H, dd, *J* = 3.8, 2.4 Hz, H3), 4.52 (1H, ddd, *J* = 10.7, 1, 1 Hz, H12), 4.61 (1H, dddd, *J* = 10.7, 1, 1, 1 Hz, H12), 5.97 (1H, m, H7), 6.16 (1H, d, *J* = 4.3 Hz, H11); ^{13}C nmr ($CDCl_3$) δ: 21.7 (C14), 24.7 (C6), 26.7 (C13), 37.2 (C4), 41.5 (C5), 44.0 (C2), 48.6 (C9), 64.8 (C10), 72.2 (C12), 79.3 (C3), 105.6 (C11), 126.3 (C7), 131.4 (C8), 169.5 (C15), 203.9 (C1); hreims (probe 100°C), *m/z* calcd. for $C_{14}H_{18}O_3$ ($M^+ - CO_2$): 234.1256; found: 234.1251 (91), 216 ($M^+ - CO_2 - H_2O$, 14), 162 (33), 161 (100), 120 (27), 119 (35), 91 (61), 77 (29), 65 (41); cims, *m/z*: 296 (M^+ + 18, 100).

[4a*S*-(4aα,8α,8a*S**,10aα,10bα)]-2,4,4a,5,7,8,10a,10b-Octahydro-5,5-dimethyl-6*H*,9*H*-benzo[*e*]furo[2,3,4-*cd*]isobenzofuran-6,9-dione (isomarasmone) **3** crystallized from chloroform as prisms, mp 247–250°C; tlc: R_f 0.46 (66% ethyl acetate – Skellysolve B); Ftir (KBr disc): 3435 (br, OH), 1755 (s, lactone C=O), 1699 (s, ketone C=O) cm^{-1}; ^1H nmr ($CDCl_3$) δ: 1.17 (3H, s, H13), 1.42 (3H, s, H14), 2.28–2.50 (3H, m, H5, H6), 2.49 (1H, dd, *J* = 14.2, 4.3 Hz, H2α), 3.31 (1H, dd, *J* = 14.3, 2.1 Hz, H2β), 3.60 (1H, m, H9), 4.35 (1H, dd, *J* = 4.0, 2.1 Hz, H1), 4.53 (1H, ddd, *J* = 11.0, 1, 1 Hz, H12), 4.58 (1H, dddd, *J* = 11.0, 1, 1, 1 Hz, H12), 6.00 (1H, m, H7), 6.02 (1H, d, *J* = 4.5 Hz, H11); ^{13}C nmr (CD_3OD) δ: 22.6 (C14), 24.8 (C13), 25.4 (C6), 30.8 (C4), 40.7 (C5), 43.7 (C2), 47.9 (C9), 56.6 (C10), 70.1 (C1), 73.6 (C12), 105.9 (C11), 126.3 (C7), 133.5 (C8), 176.3 (C15), 215.6 (C3); hreims (probe 200°C), *m/z* calcd. for $C_{15}H_{18}O_5$ (M^+): 278.1154; found: 278.1149 (9), 234 ($M^+ - CO_2$, 87), 216 ($M^+ - CO_2 - H_2O$, 15), 163 (21), 162 (86), 147 (29), 146 (22), 145 (81), 120 (78), 119 (61), 117 (42), 115 (28), 105 (25), 95 (26), 93 (28), 91 (100), 86 (27), 79 (28), 77 (49), 70 (77), 67 (22), 65 (26), 53 (21).

[4a*S*-(4aα,6α,8α,8a*S**,10aα,10bα)]-4,4a,5,6,7,8,10a,10b-Octahydro-6,8-dihydroxy-5,5-dimethylbenzo[*e*]furo[2,3,4-*cd*]isobenzofuran-9(2*H*)-one (dihydromarasmone) **4** crystallized from ethyl acetate – dichloromethane – Skellysolve B as prisms, mp 164–165°C; $[\alpha]_D^{24}$ +28.0° (*c* 0.50, CH_3OH); tlc: R_f 0.45 (66% ethyl acetate – Skellysolve B); Ftir ($CHCl_3$ cast): 3394 (br, OH), 1768 (s, lactone C=O) cm^{-1}; ^1H nmr ($CDCl_3$) δ: 1.11 (3H, s, H13), 1.26 (3H, s, H14), 2.17 (2H, dd, *J* = 3.0, 3.0 Hz, H2), 2.28–2.36 (2H, m, H6), 2.36 (1H, dd, *J* = 11.5, 7.0 Hz, H5), 2.40 (1H, br s, 3-OH), 3.68 (1H, m, H9), 3.81 (1H, dd, *J* = 3.0, 3.0 Hz, H3), 3.88 (1H, br ddd, *J* = 8.0, 3.0, 3.0 Hz, H1), 4.48 (1H, ddd, *J* = 10.7, 1, 1 Hz, H12), 4.56 (1H, dddd, *J* = 11.0, 1, 1, 1 Hz, H12), 4.93 (1H, d, *J* = 8.8 Hz, 1-OH), 5.94 (1H, m, H7), 5.98 (1H, d, *J* = 4.3 Hz, H11); ^{13}C nmr ($CDCl_3$) δ: 21.9 (C14), 24.0 (C6), 27.5 (C13), 29.7 (C2), 34.0 (C5), 37.1 (C4), 48.2 (C9), 55.7 (C10), 68.8 (C1), 72.7 (C12), 78.5 (C3), 103.9 (C11), 125.0 (C7), 132.3 (C8), 174.4 (C15); hreims (probe 100°C), *m/z* calcd. for $C_{15}H_{20}O_5$ (M^+): 280.1311; found: 280.1310 (24), 262 ($M^+ - H_2O$, 21), 236 ($M^+ - CO_2$, 14), 218 ($M^+ - CO_2 - H_2O$, 28), 217 (33), 200 ($M^+ - CO_2 - 2H_2O$, 100), 185 (35), 155 (39), 135 (29), 121 (21), 120 (27), 119 (40), 117 (35), 105 (23), 93 (25), 91 (64), 71 (21), 77 (31), 72 (39).

Single crystal X-ray diffraction analysis of anhydromarasmone (1)

Compound **1** crystallized as rough cubes suitable for X-ray diffraction analysis. A crystal approximately 0.5 mm on an edge was attached to a glass fiber with epoxy cement. Preliminary X-ray photographs

showed orthohombic symmetry and lattice constants of $a = 8.542$ (1), $b = 14.132$ (3), $c = 10.436$ (2) Å. Systematic absences, a calculated density (1.37 g/cm^3), and the optical activity were uniquely accommodated in space group $P2_12_12_1$ with one molecule of composition $C_{15}H_{16}O_4$ forming the asymmetric unit. All unique diffraction maxima with $2\theta \leq 112°$ were collected on a computer controlled four-circle diffractometer with Cu Kα radiation (1.54178 Å) and 1° ω-scans. Of the 1251 reflections surveyed, 1224 (98%) were judged observed ($|F| \geq 4\sigma(F)$) and used in subsequent calculations. No corrections were made for absorption or decomposition. The structure was solved relatively easily using the direct methods procedure in SHELXTL-PLUS. Full-matrix least-squares refinements with anisotropic heavy atoms and fixed isotropic hydrogens riding on the heavy atoms have converged to a conventional crystallographic residual of 0.0535 for the observed data. Crystallographic parameters have been deposited as archival data.[3]

Reduction of marasmone (2)

Sodium borohydride (1.0 mg) was added to a solution of compound **2** (5.4 mg) in methanol (0.5 mL) and the mixture was stirred at room temperature for 10 min, then 1 M hydrochloric acid (0.1 mL) was added. Evaporation gave an oil, which was chromatographed on silica gel. Elution with 50% ethyl acetate – Skellysolve B gave dihydromarasmone (**4**, 1.7 mg), which crystallized from dichloromethane – ethyl acetate – Skellysolve B as prisms, mp 163–165°C (correct ^{1}H nmr spectrum). Further elution with 66% ethyl acetate – Skellysolve B gave [4a*S*-(4aα,6α,8β,8a*S**,10aα,10bα)]-4,4a,5,6,7,8,10a,10b-octahydro-6,8-dihydroxy-5,5-dimethylbenzo[*e*]furo[2,3,4-*cd*]isobenzofuran-9(2*H*)-one, **11** (2.0 mg), which crystallized from dichloromethane – ethyl acetate – Skellysolve B as thin needles, mp 235–237°C; $[\alpha]_D^{24}$ −21.4° (*c* 0.22, CH_3OH); tlc: R_f 0.40 (66% ethyl acetate – Skellysolve B); Ftir ($CHCl_3$ cast): 3450 (br, OH), 1750 (s, lactone C=O) cm^{-1}; ^{1}H nmr ($CDCl_3$) δ: 1.04 (3H, s, H13), 1.25 (3H, s, H14), 1.72 (2H, br s, OH), 1.92 (1H, ddd, J = 13.1, 4.1, 4.1 Hz, H2α), 2.16–2.25 (1H, m, H6β), 2.19 (1H, dd, J = 12.0, 5.2 Hz, H5), 2.20 (1H, ddd, J = 13.0, 12.5, 2.0 Hz, H2β), 2.22–2.27 (1H, m, H6α), 3.04 (1H, m, H9), 3.72 (1H, dd, J = 3.9, 2.0 Hz, H3), 4.29 (1H, br ddd, J = 12.2, 4.8, 4.8 Hz, H1), 4.42 (1H, ddd, J = 10.5, 1, 1 Hz, H12β), 4.50 (1H, dddd, J = 10.5, 1, 1, 1 Hz, H12α), 5.98 (1H, m, H7), 6.17 (1H, d, J = 4.5 Hz, H11); ^{13}C nmr ($CDCl_3$) δ: 22.1 (C14), 24.1 (C6), 27.3 (C13), 35.2 (C2), 36.9 (C4), 38.7 (C5), 52.6 (C9), 55.7 (C10), 71.4 (C1), 72.0 (C12), 77.2 (C3), 105.1 (C11), 126.2 (C7), 131.7 (C8), 173.9 (C15); hreims (probe 150°C), m/z calcd. for $C_{14}H_{20}O_3$ ($M^+ - CO_2$): 236.1413; found: 236.1406 (2), 218 ($M^+ - CO_2 - H_2O$, 9), 190 (70), 175 (48), 172 (28), 157 (53), 147 (22), 143 (21), 135 (25), 132 (22), 131 (24), 129 (30), 121 (22), 119 (41), 118 (30), 117 (57), 116 (51), 105 (53), 104 (23), 96 (24), 95 (24), 93 (41), 92 (30), 91 (100), 83 (24), 81 (33), 79 (41), 77 (48), 74 (76), 73 (20), 71 (31), 70 (24), 69 (60), 67 (37), 65 (22), 60 (23), 57 (61), 56 (64), 55 (70), 53 (28); cims, m/z: 298 ($M^+ + 18$, 100).

Oxidation of dihydromarasmone (4)

Pyridinium dichromate (15 mg, 0.04 mmol) was added to a solution of compound **4** (10.3 mg, 0.037 mmol) in dichloromethane (2 mL) and the resulting suspension was stirred at room temperature for 2 h. Ether (5 mL) was added and the precipitated chromium complexes were removed by filtration through a short column of silica gel. The column was washed with ether and the combined filtrates were evaporated to give an oil (5.3 mg), which was chromatographed on silica gel. Elution with 33% ethyl acetate – Skellysolve B gave successively marasmone (**2**, 1.4 mg, correct ^{1}H nmr spectrum), and isomarasmone (**3**, 0.7 mg, correct ^{1}H nmr spectrum).

Acetylation of dihydromarasmone (4)

A solution of **4** (3.8 mg) and acetic anhydride (0.01 mL) in pyridine (0.025 mL) was allowed to stand at room temperature for 18 h, then benzene (2 mL) was added and the solution evaporated to dryness. Column chromatography of the resulting solid, eluting with 25% ethyl acetate – Skellysolve B, gave [4a*S*-(4aα,6α,8α,8a*S**,10aα,10bα)]-4,4a,5,6,7,8,10a,10b-octahydro-6,8-diacetyloxy-5,5-dimethylbenzo[*e*]furo[2,3,4-*cd*]isobenzofuran-9(2*H*)-one, **9** (4.6 mg), which crystallized from dichloromethane – Skellysolve B as fine needles, subl. 265–266°C; tlc: R_f 0.24 (33% ethyl acetate – Skellysolve B); ^{1}H nmr ($CDCl_3$) δ: 1.03 (3H, s, H13), 1.33 (3H, s, H14), 2.07 (3H, s, OAc), 2.14 (3H, s, OAc), 2.20 (2H, dd, J = 3.0, 3.0 Hz, H2), 2.30–2.38 (2H, m, H6), 2.44 (1H, dd, J = 11.2, 6.2 Hz, H5), 3.10 (1H, m, H9), 4.51 (1H, ddd, J = 11.5, 1.5, 1.5 Hz, H12), 4.56 (1H, dddd, J = 11.2, 1.5, 1.5, 1.5 Hz, H12), 4.80 (1H, dd, J = 3.0, 3.0 Hz, H3), 5.25 (1H, dd, J = 3.0, 3.0 Hz, H1), 5.95 (1H, d, J = 4.2 Hz, H11), 5.98 (1H, m, H7); ^{13}C nmr ($CDCl_3$) δ: 21.1, 21.2, 22.1, 24.0, 26.8, 27.3, 35.6, 35.9, 48.4, 53.1, 67.5, 72.5, 76.2, 104.0, 125.6, 131.1, 169.6, 170.2, 172.5.

Attempted acetylation of marasmone (2)

A solution of compound **2** (5.0 mg) in acetic anhydride (0.05 mL) and pyridine (0.05 mL) was allowed to stand at room temperature for 8 h, then benzene (4 mL) was added and the mixture evaporated to dryness. Column chromatography of the resulting pale brown solid, eluting with 20% ethyl acetate – Skellysolve B, gave anhydromarasmone (**1**, 4.0 mg, correct ^{1}H nmr spectrum), which crystallized from dichloromethane – Skellysolve B as prisms, mp 193–194°C.

[3]These tables may be purchased from the Depository of Unpublished Data, CISTI, National Research Council of Canada, Ottawa, Ont., Canada K1A 0S2. Tables of atomic coordinates, bond lengths, and angles have also been deposited with the Cambridge Crystallographic Data Centre, and can be obtained on request from The Director, Cambridge Crystallographic Data Centre, University Chemical Laboratory, Lensfield Road, Cambridge CB2 1EW, U.K.

Acknowledgements

The financial support of the Natural Sciences and Engineering Council of Canada and the National Institutes of Health (CA 24487) is gratefully acknowledged. We also thank Dr. K. I. Mallett, Northern Forest Research Institute, Edmonton, for bringing this problem to our attention, and for cultures of *Marasmius oreades*, and Mrs. Anna Szenthe for maintaining and growing the cultures.

1. H. B. Couch. Diseases of turfgrasses. 2nd ed. R. E. Krieger Publishing Co., Huntington, NY. 1973.
2. J. D. Smith. Plant Dis. **64**, 348 (1980).
3. K. I. Mallett and L. M. Harrison. Can. J. Bot. **66**, 1111 (1988).
4. J. A. Traquair and W. E. McKeen. Can. J. Plant Pathol. **8**, 59 (1986).
5. K. Nakanishi and P. H. Solomon. Infrared absorption spectroscopy. Holden-Day, Inc., Oakland, CA. 1977. pp. 38–44.
6. T. Kato, C. Kabuto, N. Sasaki, M. Tsunagawa, H. Aizawa, K. Fujita, Y. Kato, and Y. Kitahara. Tetrahedron Lett. 3861 (1973).
7. G. Savona, F. Piozzi, J. R. Hanson, and M. Siverns. J. Chem. Soc. Perkin Trans. **1**, 1607 (1976).
8. P. V. Demarco, E. Farkas, D. Dodrell, B. L. Mylari, and E. Wenkert. J. Am. Chem. Soc. **90**, 5480 (1968).

Can. J. Chem. Downloaded from www.nrcresearchpress.com by 41.223.56.140 on 09/07/12
For personal use only.

The synthesis, separation, and crystal and molecular structures of the three bisphenols, an ethanol solvate of one of them, and of a minor by-product, 6,6′,7,7′-tetrachloro-8,8′-methylenebis(4*H*-benzo-1,3-dioxin), prepared by condensation of formaldehyde with 3,4-dichlorophenol

GEORGE FERGUSON,[1] ROBERT MCCRINDLE,[1] AND ALAN JAMES MCALEES
Department of Chemistry and Biochemistry, University of Guelph, Guelph, Ont., Canada N1G 2W1

Received September 6, 1988

GEORGE FERGUSON, ROBERT MCCRINDLE, and ALAN JAMES MCALEES. Can. J. Chem. **67**, 779 (1989).

Samples of all three of the expected bisphenols, 4,4′,5,5′-tetrachloro-2,2′-methylenebisphenol (**1**) and the 3,4,4′,5′- (**2**) and 3,3′,4,4′-tetrachloro (**3**) isomers, and of a minor by-product, 5,5′,6,6′-tetrachloro-8,8′-methylenebis(4*H*-benzo-1,3-dioxin) (**4**), have been isolated from the mixture formed by acid-catalyzed condensation of 3,4-dichlorophenol with one half of a molar equivalent of formaldehyde. In addition, the structures and solid state conformations of all four compounds, and of an ethanol solvate of **1**, have been revealed by X-ray crystallographic studies. The three bisphenols (**1**, **2**, **3**) all crystallize in space group $P\bar{1}$, as centrosymmetric hydrogen-bonded dimers, while the solvate, **1·EtOH**, although it also belongs to space group $P\bar{1}$, forms relatively open infinite bands of hydrogen-bonded molecules. Crystals of **4** belong to space group *Fdd*2 and the molecules have twofold crystallographic symmetry.

Key words: X-ray crystallography, bisphenols, tetrachloro-2,2′-methylenebisphenols, tetachloro-8,8′-methylenebis(4*H*-benzo-1,3-dioxin).

GEORGE FERGUSON, ROBERT MCCRINDLE et ALAN JAMES MCALEES. Can. J. Chem. **67**, 779 (1989).

La condensation acido-catalysée du dichloro-3,4 phénol avec un demi équivalent molaire de formaldéhyde conduit à un mélange à partir duquel on a pu isoler les trois bisphénols attendus, les tétrachloro-4,4′,5,5′ (**1**), -3,4,4′,5′ (**2**) et -3,3′,4,4′ (**3**) méthylène-2,2′ bisphénols, ainsi qu'un sous-produit mineur, la tétrachloro-5,5,6,6′ méthylène-8,8′ bis(4*H*-benzodioxinne-1,3) (**4**). De plus, faisant appel à la diffraction des rayons-X, on a déterminé les structures ainsi que les conformations à l'état solide de chacun de ces quatre composés. Les trois bisphénols (**1**, **2** et **3**) cristallisent dans le groupe d'espace $P\bar{1}$, sous la forme de dimères centrosymétriques reliés par des liaisons hydrogènes; par ailleurs, le composé **1** sous une forme solvatée, **1·EtOH**, appartient au même groupe d'espace mais il forme des bandes infinies relativement ouvertes de molécules liées par des ponts hydrogènes. Les cristaux de composé **4** appartiennent au groupe d'espace *Fdd*2 et les molécules possèdent une symétrie cristallographique binaire.

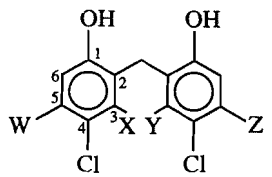
Mots clés : diffraction des rayons-X, bisphénols, tétrachloro méthylène-2,2 bisphénols, tétrachloro méthylène-8,8′ bis(4*H*-benzodioxinne-1,3).

[Traduit par la revue]

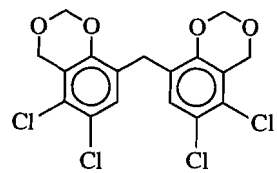
Can. J. Chem. Downloaded from www.nrcresearchpress.com by 41.223.56.140 on 09/07/12
For personal use only.

In the course of a synthetic project, we required a sample of 2,2′-methylene-4,4′,5,5′-tetrachlorobisphenol **1**. This was reported (1) as the major product isolated from the mixture formed by acid-catalyzed condensation of 3,4-dichlorophenol with one half of a molar equivalent of formaldehyde. Formation of the isomers **2** and **3** was also claimed. A more recent paper (2) assigned structure **2** to the major product by chemical interconversions. We have repeated this reaction under similar conditions and have confirmed the latter assignment. In addition, we have been able to isolate and characterize the other two isomers and an additional, minor, product.

The solid product obtained by work-up of the phenol–formaldehyde reaction mixture gave an ^{1}H nmr spectrum that clearly indicates the presence of all three expected bisphenols, **1**–**3**. In particular, the resonances arising from the methylene bridges are well resolved (even at 60 MHz) and were assignable using the spectra of the pure components, thus allowing an estimation of the relative proportions of the isomers (ca. 9:4:2 for **2**:**1**:**3**). Other non-aromatic resonances of relatively minor intensity are present, the most prominent of these being a pair of singlets arising from the by-product **4**. The subsequent separation of these products by fractional crystallization was readily monitored by ^{1}H nmr spectroscopy. Thus, crystallization of the reaction mixture from toluene gave a relatively pure sample of **2**. Crystallization of the residue from toluene, or cyclohexane, *containing a small amount of ethanol, or*



1 W = Z = Cl, X = Y = H
2 W = Y = Cl, X = Z = H
3 W = Z = H, X = Y = Cl



4

methanol, gave a fraction containing mainly the originally desired isomer **1** as its mono-alcohol solvate. Although **1** did not crystallize readily from the mixture in the absence of alcohol, the crystalline solvate could be recrystallized from toluene alone to give unsolvated material. After separation of bisphenol **1** from the reaction mixture, a further crop of crystals was recovered by crystallization from toluene. This fraction contained comparable quantities of the major product **2** and of the minor isomer **3**. Crystallization of this mixture from a small

[1]Authors to whom correspondence may be addressed.

TABLE 1. Crystallographic data

Parameter	Compound 1	2	3	1·EtOH	4
Formula	$C_{13}H_8Cl_4O_2$	$C_{13}H_8Cl_4O_2$	$C_{13}H_8Cl_4O_2$	$C_{13}H_8Cl_4O_2 \cdot C_2H_6O$	$C_{17}H_{12}Cl_4O_4$
Molar mass	338.02	338.02	338.02	384.09	422.1
Crystal system	Triclinic	Triclinic	Triclinic	Triclinic	Orthorhombic
Space group	$P\bar{1}$	$P\bar{1}$	$P\bar{1}$	$P\bar{1}$	$Fdd2$
a (Å)	11.344(2)	8.975(2)	7.334(2)	8.295(1)	23.925(4)
b (Å)	12.103(2)	9.707(1)	9.756(2)	9.021(2)	33.316(7)
c (Å)	10.356(2)	8.581(1)	9.842(2)	12.229(3)	4.243(1)
α (°)	78.77(1)	100.12(1)	82.61(2)	77.45(2)	90
β (°)	94.94(1)	108.89(1)	73.78(2)	101.33(2)	90
γ (°)	101.69(1)	69.24(2)	80.59(2)	74.84(1)	90
V (Å^3)	1364.1(6)	659.8(3)	664.6(4)	830.4(4)	3382(2)
Z	4	2	2	2	8
ρ_c (g/mL)	1.65	1.70	1.69	1.54	1.66
$F(000)$	680	340	340	392	1712
Radiation	Mo	Mo	Mo	Mo	Mo
μ (cm^{-1})	8.6	8.9	8.9	7.2	7.2
Crystal dimensions	0.20 × 0.25 × 0.50	0.30 × 0.36 × 0.40	0.10 × 0.30 × 0.30	0.13 × 0.38 × 0.50	0.20 × 0.20 × 0.35
Scan type	ω–2θ	ω–2θ	ω–2θ	ω–2θ	ω–2θ
Scan range (deg. in ω)	0.60 + 0.35 tan θ	0.60 + 0.35 tan θ	0.60 + 0.35 tan θ	0.60 + 0.35 tan θ	0.60 + 0.35 tan θ
Data collected	6076	3138	2990	3723	1137
Max 2θ (deg)	54	54	54	54	54
Unique reflections	5931	3053	2911	3623	1054
Reflections with $I > 3\sigma(I)$	3091	2600	2020	2425	868
Number of variables	360	181	180	212	114
R	0.037	0.030	0.039	0.038	0.028
Rw	0.046	0.047	0.053	0.047	0.041
$S = (\Sigma w\Delta^2/(m-n))^{1/2}$	1.34	2.13	1.19	1.53	1.19
Max Δ/σ	0.01	<0.005	<0.06	0.04	<0.005
Residual electron density (e/Å^3)	0.19	0.32	0.31	0.27	0.20
p in $w = 1/[\sigma^2F + pF_o^2]$	0.045	0.030	0.070	0.040	0.055
Extinction correction g	2×10^{-9}	2×10^{-6}	—	2×10^{-6}	2×10^{-7}

volume of methanol yielded a substantially pure sample of **3**. Yet a further crop of crystals was obtained from the residues of the original mixture by crystallization from methanol. This proved to consist largely of the non-phenolic by-product **4**, which was purified by recrystallization from chloroform.

The structures of the three bisphenols, **1–3**, were assigned on the basis of the ^{1}H nmr spectra and were confirmed by X-ray cyrstallography. The ^{1}H nmr spectrum of the by-product **4** at 60 MHz contains only four singlets. Assuming that the singlet at highest field arises from a bridging methylene and therefore represents two protons, a structure such as **4** (or the other possible symmetrical isomer) appeared to be a likely candidate. A mass spectrum of this compound showed *inter alia* the appropriate molecular ion pattern in addition to prominent $M - 60$ peaks corresponding to the loss of two mols of formaldehyde. A proton 2D COSY nmr plot for this product revealed that each aromatic proton has small couplings of similar magnitude both to the bridging methylene and to a benzylic methylene of a dioxin ring. Thus, unfortunately, the relative sizes of these couplings could not be used as a basis for the assignment of structure to the compound. Earlier reports (3) indicate that *ortho* and *para* benzylic coupling constants are frequently similar in magnitude. That this product has structure **4** was revealed by an X-ray crystallographic study of a single crystal. Perhaps surprisingly, in view of the extensive literature on phenol–formaldehyde condensation, there is apparently only a single report (4) of a product with an analogous structure, 6,6′-dinitro-8,8′-methylenebis(4*H*-benzo-1,3-dioxin). In the present reaction, **4** may be produced in preference to the other isomers because of steric factors (see following section). However, ^{1}H nmr spectra of residues from crystallization of the bisphenols show small peaks that can possibly be attributed to other benzo-1,3-dioxin-containing species.

As noted above, the key to recovering the required bisphenol **1** from the product mixture was the presence of a *small* proportion of methanol or ethanol in the crystallizing medium. Interestingly, when pure samples of each of the three isomers, **1–3**, were recrystallized in the presence of alcohol, only **1** gave an alcohol solvate. Since this solvent was readily lost from the crystals on standing at room temperature and solvent-free crystals could be obtained by crystallizing **1** from toluene alone, it was initially surmised that the alcohol molecules were loosely trapped in voids in the crystal lattice; our X-ray analysis of **1·EtOH**, however, shows that the compound has a quite different crystal structure and solid state conformation from those found for **1**, **2**, and **3**.

Crystal structures of 1, 2, 3, and 1·EtOH

Crystal data and refinement details for these four compounds are given in Table 1, fractional coordinates are in Table 2, and

Can. J. Chem. Downloaded from www.nrcresearchpress.com by 41.223.56.140 on 09/07/12
For personal use only.

Can. J. Chem. Downloaded from www.nrcresearchpress.com by 41.223.56.140 on 09/07/12
For personal use only.

TABLE 2. Positional and thermal parameters and esd's

(a) Compound **1**, the 4,4′,5,5′-tetrachloro isomer

Atom	*x*	*y*	*z*	*B* (Å^2)
Cl14A	0.59982(9)	0.26788(8)	−0.56184(9)	5.64
Cl15A	0.75947(8)	0.50023(9)	−0.5039(1)	5.53
Cl24A	0.32463(9)	−0.13596(8)	0.0078(1)	6.24
Cl25A	0.4159(1)	−0.05301(9)	0.2779(1)	6.54
O11A	0.4525(2)	0.4957(2)	−0.1706(2)	5.03
O21A	0.3907(2)	0.3469(2)	0.0539(2)	4.65
CA	0.3123(3)	0.2857(3)	−0.2058(3)	3.87
C11A	0.4930(3)	0.4439(3)	−0.2615(3)	3.64
C12A	0.4237(3)	0.3406(3)	−0.2821(3)	3.24
C13A	0.4596(3)	0.2891(2)	−0.3759(3)	3.44
C14A	0.5614(3)	0.3362(3)	−0.4442(3)	3.58
C15A	0.6303(3)	0.4383(3)	−0.4192(3)	3.86
C16A	0.5955(3)	0.4924(3)	−0.3283(3)	3.98
C21A	0.3761(3)	0.2349(2)	0.0376(3)	3.34
C22A	0.3371(3)	0.2021(3)	−0.0822(3)	3.29
C23A	0.3238(3)	0.0861(3)	−0.0874(3)	3.66
C24A	0.3469(3)	0.0072(3)	0.0217(3)	3.94
C25A	0.3848(3)	0.0426(3)	0.1391(3)	3.92
C26A	0.3996(3)	0.1566(3)	0.1468(3)	4.00
Cl14B	0.2075(1)	0.19813(9)	−0.62479(9)	6.20
Cl15B	0.23983(9)	−0.04093(9)	−0.4518(1)	6.56
Cl24B	0.1209(1)	0.65304(8)	−0.2582(1)	5.96
Cl25B	0.21936(9)	0.56468(8)	0.03194(9)	5.57
O11B	−0.0763(2)	0.0085(2)	−0.1597(2)	4.68
O21B	−0.0027(2)	0.1708(2)	−0.0076(2)	4.77
CB	−0.0885(3)	0.2334(3)	−0.2849(3)	4.03
C11B	−0.0045(3)	0.0517(3)	−0.2653(3)	3.62
C12B	−0.0126(3)	0.1615(3)	−0.3325(3)	3.39
C13B	0.0547(3)	0.2035(3)	−0.4428(3)	3.79
C14B	0.1290(3)	0.1413(3)	−0.4832(3)	3.98
C15B	0.1402(3)	0.0355(3)	−0.4107(3)	4.20
C16B	0.0719(3)	−0.0103(3)	−0.3029(3)	3.96
C21B	0.0251(3)	0.2816(3)	−0.0722(3)	3.51
C22B	−0.0147(3)	0.3164(3)	−0.2024(3)	3.51
C23B	0.0183(3)	0.4324(3)	−0.2553(3)	3.98
C24B	0.0868(3)	0.5095(3)	−0.1853(3)	3.88
C25B	0.1275(3)	0.4716(3)	−0.0588(3)	3.85
C26B	0.0958(3)	0.3581(3)	−0.0021(3)	3.73
HO11A	0.487(3)	0.550(2)	−0.164(3)	4.2(7)*
HO21A	0.397(2)	0.396(2)	−0.008(3)	4.2(7)*
HO11B	−0.061(3)	−0.054(2)	−0.126(3)	4.8(7)*
HO21B	−0.041(3)	0.121(3)	−0.045(3)	7(1)*

(b) Compound **2**, the 3,4,4′,5′-tetrachloro isomer

Atom	*x*	*y*	*z*	*B* (Å^2)
Cl14	−0.10427(5)	0.72821(4)	0.14857(6)	3.94
Cl15	−0.38365(5)	0.61458(5)	−0.11166(6)	4.51
Cl23	0.41245(5)	0.35807(5)	0.61504(6)	4.53
Cl24	0.75788(5)	0.23189(7)	0.54340(7)	5.17
O11	−0.1000(1)	0.1237(1)	0.1556(1)	3.77
O21	0.2293(1)	−0.0127(1)	0.1546(2)	4.02
C1	0.1464(2)	0.2181(2)	0.4038(2)	3.07
C11	−0.1085(2)	0.2686(2)	0.1545(2)	2.90
C12	0.0128(2)	0.3170(2)	0.2746(2)	2.79
C13	0.0104(2)	0.4607(2)	0.2701(2)	2.93
C14	−0.1092(2)	0.5518(2)	0.1513(2)	2.92
C15	−0.2310(2)	0.5015(2)	0.0357(2)	3.00
C16	−0.2307(2)	0.3593(2)	0.0366(2)	3.19
C21	0.3476(2)	0.0509(2)	0.2490(2)	2.96
C22	0.3145(2)	0.1619(2)	0.3720(2)	2.75
C23	0.4430(2)	0.2185(2)	0.4614(2)	2.98
C24	0.5966(2)	0.1651(2)	0.4288(2)	3.29
C25	0.6232(2)	0.0549(2)	0.3065(2)	3.46
C26	0.4996(2)	−0.0029(2)	0.2162(2)	3.46
HO11	−0.154(2)	0.113(2)	0.091(2)	5.6(5)*
HO21	0.142(2)	0.017(2)	0.177(2)	4.0(4)*

(c) Compound **3**, the 3,3′,4,4′-tetrachloro isomer

Atom	*x*	*y*	*z*	*B* (Å^2)
Cl13	0.61398(9)	−0.43439(7)	−0.39966(6)	4.04
Cl14	0.2294(1)	−0.52166(8)	−0.20839(9)	5.35
Cl23	1.0085(1)	−0.29730(7)	−0.59461(7)	4.24
Cl24	0.9248(1)	−0.0579(1)	−0.81983(7)	5.64
O11	0.6506(3)	−0.1688(2)	−0.0030(2)	4.11
O21	0.6097(3)	0.0297(2)	−0.2182(2)	3.95
C1	0.8119(3)	−0.2460(2)	−0.2793(2)	2.95
C11	0.5485(4)	−0.2518(3)	−0.0483(2)	3.44
C12	0.6253(3)	−0.2919(2)	−0.1856(2)	2.86
C13	0.5235(3)	−0.3769(2)	−0.2324(2)	3.05
C14	0.3520(4)	−0.4164(3)	−0.1472(3)	3.52
C15	0.2805(4)	−0.3723(3)	−0.0123(3)	4.36
C16	0.3784(4)	−0.2910(3)	0.0377(3)	4.15
C21	0.6857(3)	0.0004(2)	−0.3573(2)	2.98
C22	0.7858(3)	−0.1294(2)	−0.3933(2)	2.68
C23	0.8641(3)	−0.1450(2)	−0.5388(2)	3.09
C24	0.8322(3)	−0.0387(3)	−0.6398(3)	3.58
C25	0.7266(4)	0.0871(3)	−0.5987(3)	3.92
C26	0.6546(3)	0.1071(3)	−0.4578(3)	3.60
HO11	0.599(5)	−0.151(3)	0.081(3)	7.1(9)*
HO21	0.655(4)	−0.025(3)	−0.167(3)	5.2(7)*

(d) Compound **1·EtOH**

Atom	*x*	*y*	*z*	*B* (Å^2)
Cl14	0.5832(1)	0.19174(9)	−0.05358(6)	5.63
Cl15	0.90071(9)	0.3271(1)	−0.03067(5)	5.64
Cl24	0.89909(9)	−0.15638(8)	0.56718(6)	4.53
Cl25	0.76731(9)	−0.07461(8)	0.77969(6)	4.46
O11	0.7416(2)	0.4957(2)	0.3136(1)	3.41
O21	0.3376(2)	0.4372(2)	0.4913(1)	3.07
C1	0.4509(3)	0.3889(3)	0.2986(2)	2.95
C11	0.7061(3)	0.4272(3)	0.2263(2)	2.69
C12	0.5631(3)	0.3718(3)	0.2162(2)	2.72
C13	0.5281(3)	0.3022(3)	0.1280(2)	3.27
C14	0.6307(3)	0.2856(3)	0.0522(2)	3.46
C15	0.7709(3)	0.3423(3)	0.0635(2)	3.44
C16	0.8080(3)	0.4132(3)	0.1502(2)	3.29
C21	0.4693(3)	0.2980(2)	0.5125(2)	2.48
C22	0.5299(3)	0.2674(2)	0.4180(2)	2.45
C23	0.6608(3)	0.1257(3)	0.4382(2)	2.85
C24	0.7329(3)	0.0181(3)	0.5476(2)	2.87
C25	0.6737(3)	0.0524(3)	0.6401(2)	2.91
C26	0.5406(3)	0.1925(3)	0.6224(2)	2.87
OE	0.0166(2)	0.5875(2)	0.3219(2)	4.94
CE1	0.0264(3)	0.7449(3)	0.2998(2)	4.55
CE2	−0.1398(4)	0.8592(4)	0.2275(4)	6.8
HO11	0.822(2)	0.526(2)	0.312(2)	3.1(5)*
HO21	0.326(3)	0.453(3)	0.552(2)	3.5(5)*
HOE1	0.095(3)	0.533(3)	0.363(2)	5.3(7)*

TABLE 2 (*concluded*)

(e) Compound **4**, the methylenebis(benzodioxin)

Atom	*x*	*y*	*z*	*B* (Å^2)
Cl14	0.03218(3)	0.13502(2)	0.0†	5.23
Cl15	0.15128(3)	0.10313(2)	−0.2102(3)	5.05
C1	0.0	0.0	0.5865(10)	3.26
C11	0.0887(1)	0.01228(7)	0.2824(8)	2.89
C12	0.0376(1)	0.02630(7)	0.3879(7)	2.92
C13	0.0218(1)	0.06482(7)	0.3007(8)	3.20
C14	0.0556(1)	0.08795(7)	0.1141(8)	3.31
C15	0.1072(1)	0.07390(8)	0.0172(8)	3.31
C16	0.1252(1)	0.03568(8)	0.1042(7)	3.21
C17	0.1822(1)	0.0200(1)	0.0178(10)	4.38
O18	0.19332(8)	−0.01672(7)	0.1793(7)	5.01
C19	0.1477(1)	−0.04169(9)	0.1720(9)	4.45
O20	0.10332(7)	−0.02641(5)	0.3622(5)	3.75

†The *z*-coordinate of Cl14 was fixed to define the origin

*Starred atoms were refined isotropically. Anisotropically refined atoms are given in the form of the isotropic equivalent thermal parameters defined as: $4/3(a^2B_{11} + b^2B_{22} + c^2B_{33} + ab\cos\gamma B_{12} + ac\cos\beta B_{13} + bc\cos\alpha B_{23})$.

principal dimensions are summarized in Table 3. Compounds **1**, **2**, and **3** crystallize as centrosymmetric hydrogen-bonded dimers as shown in Fig. 1; in each molecule there is also an O—H···O intramolecular hydrogen bond. The crystal packing in **1**, **2**, and **3** results in centrosymmetric eight-membered [(O-H)$_4$] rings formed by pairs of intra- and inter-molecular O—H···O hydrogen bonds, with O—H···O 2.705(2)–2.796(2) Å; geometrical details are summarized in Table 2. The intramolecular hydrogen bonds are achieved by appropriate rotation of the phenyl rings about the central C—CH$_2$—C moiety to bring the O—H groups into suitable juxtaposition. The conformational angles, which precisely describe the conformation of each molecule, are given in Table 4 and illustrate that achieving an intramolecular O···O separation of 2.7–2.8 Å can be realized with a considerable range of phenyl ring orientations, the different orientations presumably serving to minimize intramolecular repulsions between adjacent phenyl rings, as well as intermolecular packing effects. The role of these intermolecular packing forces can be seen in compound **1** (Table 3) where there are two independent molecules in the asymmetric unit with similar overall geometry but whose conformational angles ϕ_1 and ϕ_2 differ by 4° and 10° respectively.

The crystal structure of **1·EtOH** (Figs. 2 and 3) proved to be entirely different from those of **1**, **2**, and **3**. The ethanol molecules link pairs of molecules of **1** to form centrosymmetric 12-membered [(O-H)$_6$] rings in which the ethanol acts as both an acceptor and a donor in O—H···O hydrogen bond formation. This involvement with ethanol totally changes the orientation of the phenyl rings about the central C—CH$_2$—C moiety from those found in the unsolvated species and results in the formation of centrosymmetric dimers with 16-membered rings, an intermolecular O—H···O distance of 2.743(2) Å, and no intramolecular hydrogen bond. This leads to the development of relatively open infinite bands of hydrogen-bonded molecules as shown in Fig. 3.

As mentioned above, crystals of **1·EtOH** lose solvent on standing in air, becoming opaque and powdery on the surface. This can be easily envisaged upon examination of the structure of **1·EtOH** (Fig. 3); loss of ethanol will totally disrupt the crystal lattice. However, despite the marked structural differences between **1** and **1·EtOH**, they have identical melting

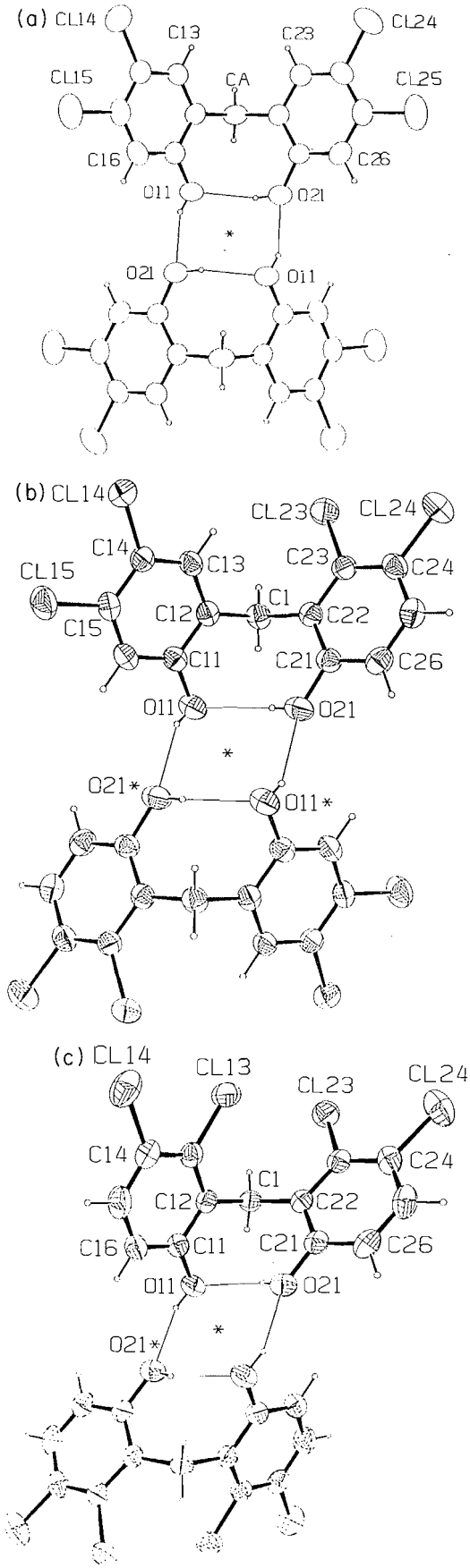


FIG. 1. Views of the centrosymmetric dimer structures, showing the atom numbering schemes. (a) One of the two independent dimers of molecule **1**; (b) molecule **2**; (c) molecule **3**. Ellipsoids are at the 50% level (except for hydrogen atoms, which are shown as spheres of an arbitrary size).

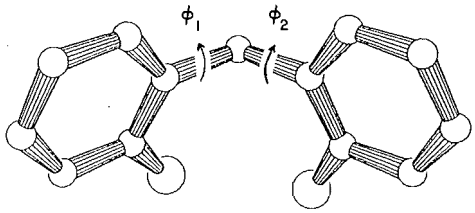
Can. J. Chem. Downloaded from www.nrcresearchpress.com by 41.223.56.140 on 09/07/12
For personal use only.

TABLE 3. Summary of principal dimensions

	1*a*	1*b*	2	3	1·EtOH	4
Mean C—Cl	1.728(3)	1.731(3)	1.731(2)	1.730(2)	1.731(3)	1.731(3)
Mean C—OH	1.378(4)	1.370(4)	1.380(2)	1.375(3)	1.367(3)	—
Mean C_{sp^3}—C_{sp^2}	1.514(4)	1.516(4)	1.511(2)	1.521(3)	1.514(3)	1.513(3)
Mean aromatic C—C	1.377(4)	1.380(4)	1.385(2)	1.383(4)	1.384(3)	1.386(4)
C_{sp^2}—C_{sp^3}—C_{sp^2}	113.3(3)	112.3(3)	113.5(1)	114.1(2)	114.0(2)	112.3(3)
O···O (intra-)	2.698(3)	2.711(3)	2.780(2)	2.728(2)	*	
O···O (inter-)	2.721(3)	2.752(3)	2.733(2)	2.796(2)	2.743(2)	
Mean O—H	0.75(3)	0.82(3)	0.72(2)	0.81(3)	0.80(3)	
O—H···O (intra)	163(3)	160(4)	159(2)	155(3)	*	
O—H···O (inter)	150(3)	159(3)	152(2)	148(3)	171(2)	

*There are no intramolecular O—H...O bonds in **1·EtOH**. The hydrogen bond dimensions involving ethanol are O(EtOH)···O(11) (at $-1+x, y, z$), 2.615(3) Å; O(EtOH)···O(21), 2.818(2) Å; O(EtOH)—H, 0.72(2) Å; O(11)—H···O(EtOH) (at $1+x, y, z$), 175(2)°; O(EtOH)—H···O(21), 163(3)° (see Fig. 3).

TABLE 4. Conformational details



Compound	1		2	3	1·EtOH	4
ϕ_1*	−2.3	−6.7	−15.8	−13.4	+12.9	+1.8†
ϕ_2	+3.8	+14.1	+14.8	+29.0	−69.9	+1.8†

*ϕ_1 and ϕ_2 are the rotation angles (as shown above) by which the molecules differ from a theoretical model in which the plane of each phenyl ring is normal to the C_{sp^2}—C_{sp^3}—C_{sp^2} plane with the O—H groups proximal. Positive ϕ values rotate the phenolic oxygen towards the centre of the diagram, negative values rotate the oxygen away from the centre. The standard deviation in torsion angles is between 0.3° and 0.4°.

†Because **4** has twofold crystallographic symmetry the rotation angles ϕ_1 and ϕ_2 have the same magnitude and sign. The oxygens at C11 are distal.

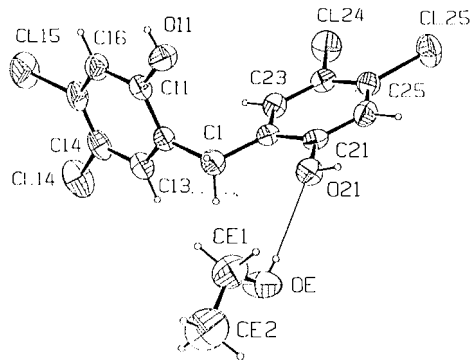


FIG. 2. A view of the asymmetric unit of **1·EtOH**, with our numbering scheme. Ellipsoids are at the 50% level (except for hydrogen atoms, which are shown as spheres of an arbitrary size).

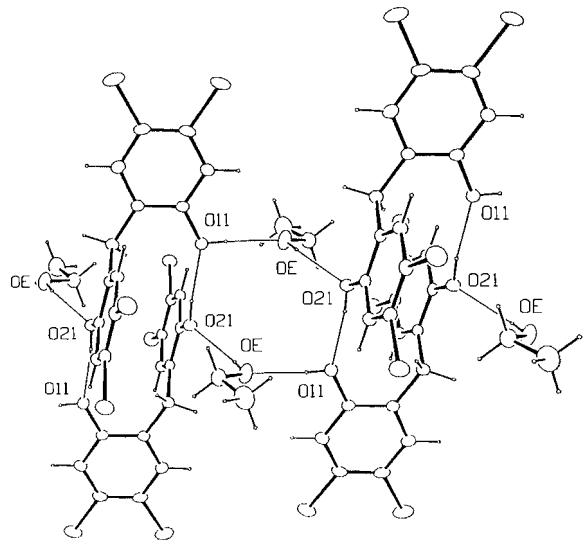


FIG. 3. The hydrogen bonding arrangement in **1·EtOH**. Non-hydrogen atoms are shown as open ellipsoids at the 20% probability level. Hydrogen atoms are shown as spheres of an arbitrary size.

points. Upon loss of ethanol, the intermolecular hydrogen bonds linking molecules of **1** may very well be retained, and reorganization, with loss of overall crystallinity to yield the intramolecular hydrogen bonded structure found for pure **1**, may proceed only as the temperature approaches the melting point.

The failure of compounds **2** and **3** to form ethanol or methanol solvates is probably associated with their inability to adopt a conformation similar to that found in **1·EtOH** because the bulky 3-chloro substituent would cause severe intramolecular overcrowding with the adjacent phenyl ring.

The molecular dimensions summarized for these four structures in Table 2 are unexceptional and are in accord with accepted values. No obvious effect of intramolecular overcrowding was anticipated in **1** and none was found. In **2**, with the 3,4,4′,5′-tetrachloro substitution, there are no untoward bond angles, and conformational angles ϕ (Table 3) are not much larger than were found for **1**. In the 4,4′,5,5′-tetrachloro isomer, the adoption of conformational angles similar to those found in **1** and **2** would have led to impossibly short intra-ring Cl···Cl contacts, which are overcome by one of the rings rotating further about the exocyclic C—C bond while still retaining the intramolecular O—H···O hydrogen bond.

The structures of five additional 2,2′-methylenebisphenols have been reported (5*a–e*). None of these displays the association into centrosymmetric dimers found for **1**, **2**, and **3**, presumably because all five have bulky substituents in the 6 and 6′ positions. In four of these compounds (5*a–d*) the two hydroxyl groups are proximal and form an intramolecular hydrogen bond, although in one case (5*d*) it is relatively weak. The fifth compound (5*e*) has its two hydroxyl groups distal.

Can. J. Chem. Downloaded from www.nrcresearchpress.com by 41.223.56.140 on 09/07/12
For personal use only.

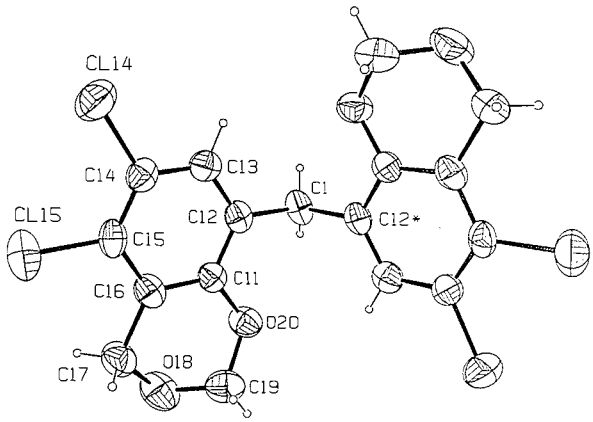


FIG. 4. A view of the molecule **4**, with our numbering scheme. Ellipsoids are at the 50% level (except for hydrogen atoms, which are shown as spheres of an arbitrary size). The twofold crystallographic axis passes through C1.

Crystal structure of 4

Crystal data and refinement details for **4** are given in Table 1, fractional coordinates in Table 2, and principal dimensions are summarized in Table 3. In the crystal, **4** has twofold crystallographic symmetry as illustrated in Fig. 4, the conformation of the molecules being close to the idealized structure depicted in Table 4 but with the phenol-derived oxygens distal. Conformations with these oxygens proximal would be subject to severe steric interactions. The preferred formation of **4** rather than the analogous methylenebis(benzodioxin) isomers derivable from bisphenols **2** and **3** may result because these isomers would have one or two severe chlorine...oxygen interactions if they were to adopt a conformation similar to that found for **4**.

The molecular dimensions for the dioxin ring of **4** (Table 3) are in good agreement with those reported for other benzodioxins (for leading references see ref. 6). This ring has a puckered conformation, with the deviations of C17, O18, C19, O20 from the aromatic ring plane being −0.10, −0.33, +0.47, +0.07 Å respectively. Interestingly, the C—O bond lengths C17—O18 and C19—O20 are identical (1.426(4) Å), while C19—O18 is significantly shorter (1.373(4) Å).

Experimental

Melting points were determined on a Kofler hot-stage apparatus and are uncorrected. The ^{1}H nmr spectra were run on a Varian EM360 spectrometer using $CDCl_3$–CD_3OD (5:1; v,v) as solvent (internal TMS standard) for the bisphenols and $CDCl_3$ for **4**. We thank Wellington Environmental Consultants, Guelph, for the electron impact mass spectrum of **4**.

Reaction of 3,4-dichlorophenol with formaldehyde

The procedure used was similar to that reported (2). A mixture of 3,4-dichlorophenol (20 g), paraformaldehyde (1.9 g), water (5 mL), concentrated sulfuric acid (20 mL), and dichloromethane (50 mL) was stirred at ambient temperature for 18 h. The resulting mixture was partitioned between water (100 mL) and dichloromethane (75 mL additional) and the aqueous layer was washed with dichloromethane (2 × 25 mL). The combined organic layers were evaporated *in vacuo* and the residue subjected to steam distillation to remove traces of unreacted dichlorophenol. A ^{1}H nmr spectrum (in CD_3CN) of the residue remaining after drying *in vacuo* revealed the presence of mainly **1**, **2**, and **3** in a ratio of ca. 4:9:2. This material was crystallized from toluene (100 mL) to give fraction A (7.5 g), which was largely (^{1}H nmr) **2**. Recrystallization from toluene gave pure **2**, mp 200–202°C; δ: 4.04 (s, 2H, CH_2), 6.72 (d, 1H, J = 10 Hz), 6.92 (s, 1H), 7.03 (d, 1H, J = 10 Hz), and 7.25 (s, 1H). The mother liquors from fraction A were evaporated *in vacuo* and the residue allowed to crystallize from toluene–ethanol (40 mL:2 mL) to give fraction B (4.5 g), which consisted largely of **1**, mp 175–177°C (ex toluene), mp 176–177°C (ex methanol – carbon tetrachloride), and mp 170–176°C (ex ethanol–cyclohexane); δ: 3.75 (s, 2H, CH_2), 6.88 (s, 2H), and 7.15 (s, 2H). The last two samples contained (^{1}H nmr) 1 mol of alcohol. The residue, after separation of fraction B, was dissolved in toluene (25 mL) to give crystalline fraction C (1.3 g), the major component of which was **3** along with a substantial amount of **2**. Recrystallization of this material from methanol (2 mL) gave substantially pure **3** (0.34 g), mp 220–226°C (after recrystallization from ethanol–hexane); δ: 4.25 (s, 2H, CH_2), 6.56 (d, 2H, J = 10 Hz), and 7.09 (d, 2H, J = 10 Hz). The residues remaining after recovery of crop C were dissolved in hot methanol and yielded, upon cooling, fraction D (0.43 g), which was essentially pure **4**, mp 198–202°C (upon recrystallization from chloroform); δ: 3.80 (s, 2H, bridging CH_2), 4.86 (s, 4H, OCH_2C), 5.23 (s, 4H, OCH_2O), and 7.07 (s, 2H).

X-ray crystallography

Crystallographic data for **1**, **1·EtOH**, **2**, **3**, and **4** are given in Table 1. As crystals of **1·EtOH** lose solvent on standing in air, a freshly prepared crystal of **1·EtOH** was selected and quickly coated with epoxy cement for the X-ray diffraction experiment. This procedure proved very satisfactory. In each case, the cell dimensions and crystal orientation matrix were determined on a CAD-4 diffractometer by a least-squares treatment of the setting angles of 25 reflections in the range $10° < \theta < 20°$. Intensity data were collected using graphite monochromatized Mo-Kα radiation. Intensities of three reflections measured as standards every two hours of exposure time showed no evidence of decay. Data were corrected for Lorentz and polarization factors. The data for **2** were also corrected for absorption (but this had a negligible effect on the molecular geometry, the dimensions changing by less than 1σ between the absorption-corrected and non-absorption-corrected data sets). The structures were solved with the aid of MULTAN (7). Refinement was by full-matrix least-squares calculations minimizing $\Sigma w\Delta^2$ initially with isotropic and then with anisotropic thermal parameters; in the final rounds (except for **3**) an extinction correction was also refined (Table 1). At intermediate stages in the refinements, difference maps showed maxima in the anticipated locations of all hydrogens. In subsequent refinement cycles, the hydrogens bonded to oxygen were allowed to refine with isotropic motion and all other hydrogen atoms were positioned on geometrical grounds (C—H, 0.95 Å; B_{iso} = 5 Å^2) and included (as riding atoms) in the structure factor calculations. Final difference maps were devoid of significant features. Scattering factor data and anomalous dispersion corrections (for non-hydrogen atoms) were from International Tables for X-ray Crystallography (8) and all calculations were performed on a PDP11/73 computer using SDP-Plus (9). Atomic coordinates are listed in Table 2 and details of molecular geometry conformation in Tables 3 and 4. Tables of all bond lengths and angles, calculated hydrogen coordinates, mean-plane data, anisotropic thermal parameters, and structure factors for **1**, **1·EtOH**, **2**, **3**, and **4** have been placed in the Depository of Unpublished Data.[2]

Acknowledgements

We thank Dr. Margaret H. Hunt for assistance with the ORTEP plots and NSERC for financial support (to G. Ferguson and R. McCrindle).

1. J. R. GEIGY A.-G. Brit. Patent No. 722590, Jan. 26, 1955; Chem. Abstr. **50**, 5756b (1956).

[2]These tables may be purchased from the Depository of Unpublished Data, CISTI, National Research Council of Canada, Ottawa, Ont., Canada K1A 0S2.

Calculated hydrogen coordinates and bond lengths and angles for these structures have also been deposited with the Cambridge Crystallographic Data Centre, and can be obtained on request from The Director, Cambridge Crystallographic Data Centre, University Chemical Laboratory, Lensfield Road, Cambridge CB2 1EW, U.K.

Can. J. Chem. Downloaded from www.nrcresearchpress.com by 41.223.56.140 on 09/07/12
For personal use only.

2. W. S. GUMP and G. R. WALTER. J. Soc. Cosmet. Chemists, **15**, 717 (1964).
3. L. M. JACKMAN and S. STERNHELL. Applications of nuclear magnetic resonance spectroscopy in organic chemistry, 2nd ed. Pergamon Press, Oxford. 1969. p. 330.
4. F. D. CHATTAWAY and R. M. GOEPP. J. Chem. Soc. 699 (1933).
5. (*a*) S. RANTSORDAS and M. PERRIN. Acta Crystallogr. Sect. B: Struct. Crystallogr. Cryst. Chem. **38**, 1871 (1982); (*b*) S. RANTSORDAS, M. PERRIN, A. THOZET, and S. LECOCQ. Acta Crystallogr. Sect. B: Struct. Crystallogr. Cryst. Chem. **37**, 1253 (1981); (*c*) L. A. CHETKINA, V. E. ZAVODNIK, V. K. BELSKII, I. G. ARZAMANOVA, M. I. NAIMAN, and YA. A. GURVICH. Zh. Strukt. Khim. **25**, 109 (1984); (*d*) S. RANTSORDAS, M. PERRIN, and A. THOZET. Acta Crystallogr. Sect. B: Struct. Crystallogr. Cryst. Chem. **34**, 1198 (1978); (*e*) L. A. CHETKINA, V. E. ZAVODNIK, V. K. BELSKII, I. G. ARZAMANOVA, and YA. A. GURVICH. Zh. Strukt. Khim. **27**, 114 (1986).
6. A. IRVING and H. M. N. H. IRVING. J. Crystallogr. Spectrosc. Res. **17**, 271 (1987).
7. P. MAIN, S. J. FISKE, S. HULL, L. LESSINGER, G. GERMAIN, J.-P. DECLERCQ, and M. M. WOOLFSON. MULTAN 80: a system of computer programs for the solution of crystal structures from X-ray diffraction data. Universities of York and Louvain. 1980.
8. D. T. CROMER. International tables for X-ray crystallography. Vol. IV. The Kynoch Press, Birmingham, England. 1974. Table 2.3.1.
9. SDP-Plus. B. A. Frenz and Associates Inc., College Station, Texas, and Enraf–Nonius, Delft, The Netherlands. 1983.

Can. J. Chem. Downloaded from www.nrcresearchpress.com by 41.223.56.140 on 09/07/12
For personal use only.

Étude cinétique de la N-chloration de la diméthylamine et de la diéthylamine en phase aqueuse

DENISE MATTE,[1] BERNARD SOLASTIOUK, ANDRÉ MERLIN ET XAVIER DEGLISE[2]

Université de Nancy I, Laboratoire de photochimie appliquée (Unité associée au Centre national de la recherche scientifique, n° 328), B. P. 239, 54506 Vandoeuvre les Nancy CEDEX, France

Reçu le 27 juin 1988

DENISE MATTE, BERNARD SOLASTIOUK, ANDRÉ MERLIN et XAVIER DEGLISE. Can. J. Chem. **67**, 786 (1989).

Nous présentons une étude des mécanismes et déterminons les constantes de vitesse des N-chlorations de la diméthylamine et de la diéthylamine en milieu aqueux, tant par l'acide hypochloreux et les ions hypochlorites (milieu neutre et basique), que le chlore moléculaire dissous (milieu acide). Les énergies d'activation des processus mis en cause ont été déterminées. Ces cinétiques rapides ont été étudiées sur spectrophotomètre à écoulement bloqué. En milieu neutre et basique, deux processus sont susceptibles de rendre compte des résultats expérimentaux.

$$R_2NH + ClOH \xrightarrow{k_1} \text{produits}$$

$$R_2NH_2^+ + ClO^- \xrightarrow{k_2} \text{produits}$$

Ces processus sont indiscernables du point de vue cinétique; ceci est dû au fait de l'existence d'un équilibre rapide entre les deux groupes de réactifs. En milieu acide, la chloration s'effectue par l'action du dichlore (Cl_2) sur l'amine non protonée; cette cinétique est limitée par la diffusion des réactifs.

$$R_2NH + Cl_2 \xrightarrow{k_{Cl_2}} R_2NCl + H^+ + Cl^-$$

Les valeurs numériques des constantes de vitesse pour chaque amine sont

$$R = CH_3 : k_1 = (1{,}2 \times 10^{11}) \exp(-17600/RT)\ M^{-1}\ s^{-1}$$
$$k_{Cl_2} = (3{,}3 \times 10^{10}) \exp(-7500/RT)\ M^{-1}\ s^{-1}$$

$$R = CH_3CH_2 : k_1 = 2{,}3\ 10^{10} \exp(-15000/RT)\ M^{-1}\ s^{-1}$$
$$k_{Cl_2} = 9{,}4\ 10^8\ M^{-1}\ s^{-1} \text{ (à 298 K)}$$

Mots clés : cinétique, N-chloration, amines, phase aqueuse.

DENISE MATTE, BERNARD SOLASTIOUK, ANDRÉ MERLIN, and XAVIER DEGLISE. Can. J. Chem. **67**, 786 (1989).

A complete kinetic study of the N-chlorination, in aqueous medium, of dimethylamine and diethylamine by a stopflow spectrophotometric method is presented. In neutral or basic medium our experimental results can be interpreted by two kinetically indistinguishable mechanisms; the reactions between protonated amine ($R_2NH_2^+$) and hypochlorite ion (ClO^-) and the reaction between R_2NH and hypochlorous acid (ClOH) are equivalent because of the fast equilibrium of proton exchange existing between the two groups of possible reactants ($R_2NH + ClOH \leftrightarrows ClO^- + R_2NH_2^+$). In acid medium, in the presence of chloride ions, we observed a reaction by aqueous chlorine (Cl_2) on the amine ($Cl_2 + R_2NH \rightarrow$ chloramine).

Key words: kinetics, N-chlorination, amines, aqueous medium.

Introduction

En milieu aqueux, les amines aliphatiques réagissent, comme l'ammoniac, avec le chlore dissous pour former des chloramines. Les cinétiques de chloration de ces amines ont été souvent suivies (2, 3) par des techniques peu adaptées à la rapidité de ces réactions et dans des domaines étroits de variation des paramètres (pH, température ...).

Grâce à la spectrophotométrie à écoulement bloqué, nous avons pu étendre cette étude à toute la gamme de pH couverte par les solutions aqueuses et déterminer l'influence de la température.

Techniques expérimentales

En milieu basique nous avons suivi la consommation de chlore à 290 nm au maximum d'absorption de l'ion ClO^-. En milieu acide il est par contre possible d'observer l'apparition de la chloramine, celle-ci absorbant seule à 270 nm. Dans tous les cas, la concentration en amine étant en large excès par rapport à celle du chlore, nous mesurons donc une constante de vitesse expérimentale du pseudo premier ordre (k_{exp}), pente de la droite $\ln(A - A_\infty)$ en fonction du temps (A est la densité optique de la solution à un instant donné).

Résultats expérimentaux et interprétation

Chloration par ClOH et ClO^-

Influence des concentrations (ordres de réaction)

Diméthylamine et diéthylamine réagissent de façon similaire avec le chlore en solution. Les figures 1 et 2 montrent pour la diméthylamine une variation linéaire de la constante de vitesse de réaction en fonction des concentrations globales de chacun des réactifs. Pour les deux molécules, dans toutes les conditions de pH, la cinétique de réaction est du second ordre, c'est à dire d'ordre un par rapport à chacun des réactifs *amine* et *chlore*.

Influence du pH et de la force ionique

En milieu neutre ou basique une solution de chlore ne contient que deux espèces prédominantes: les ions hypochlorites et l'acide hypochloreux. De la même manière, l'amine existe en solution sous formes protonée ou non, ceci selon les équilibres ci-dessous :

1. Adresse actuelle : Département de génie chimique, Université Laval, Québec (Qué.), Canada G1K 7P4.

2. Auteur à qui adresser toute correspondance.

Printed in Canada / Imprimé au Canada

Can. J. Chem. Downloaded from www.nrcresearchpress.com by 41.223.56.140 on 09/07/12
For personal use only.

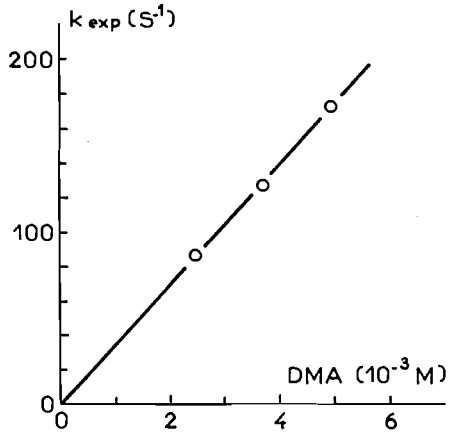


FIG. 1. Influence de la concentration en amine. T = 298 K; pH = 9,25; $Cl_t = 2{,}5 \times 10^{-4}$ M; force ionique $I = 0{,}071 \pm 0{,}003$ M; k_{exp} : pente de la droite $\ln(A - A_\infty)$ en fonction du temps.

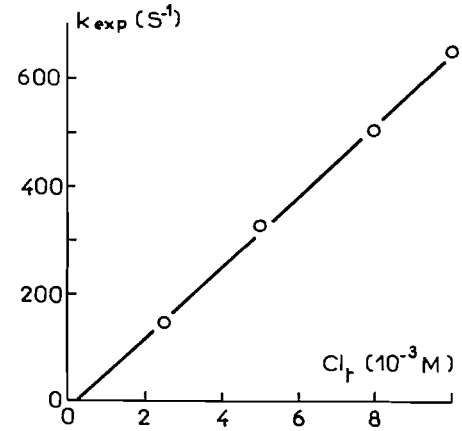


FIG. 2. Influence de la concentration en chlore. T = 298 K; pH = 4,45; $DMA_t = 7{,}5 \times 10^{-3}$ M; force ionique $I = 0{,}135 \pm 0{,}004$ M; k_{exp} : pente de la droite $\ln(A - A_\infty)$ en fonction du temps.

[I] $HOCl \leftrightarrows ClO^- + H^+$ $\quad pK_I = 7{,}54$ à 298 K (4)

[II] $R_2NH_2^+ \leftrightarrows R_2NH + H^+$ $\quad R = CH_3$, $pK_{II} = 10{,}73$ à 298 K; $R = CH_2CH_3$, $pK_{II} = 11{,}00$ à 298 K (5)

Ces équilibres sont rapides devant la cinétique de chloration; nous pouvons donc envisager quatre processus différents susceptibles de limiter la vitesse globale de réaction, compte tenu de la constatation expérimentale d'un ordre un par rapport à chacun des réactifs :

P1 : $R_2NH + ClOH \xrightarrow{k_1}$ produits

P2 : $R_2NH_2^+ + ClO^- \xrightarrow{k_2}$ produits

P3 : $R_2NH + ClO^- \xrightarrow{k_3}$ produits

P4 : $R_2NH_2^+ + ClOH \xrightarrow{k_4}$ produits

Afin de relier constante de vitesse expérimentale et constante de vitesse absolue calculée à partir de la théorie de l'état de transition, nous utilisons les relations suivantes :

$$[1] \qquad K_I = \frac{(ClO^-)(H^+)}{(ClOH)}$$

$$[2] \qquad K_{II} = \frac{(R_2NH)(H^+)}{(R_2NH_2^+)}$$

$$[3] \qquad Cl_t = [ClO^-] + [ClOH]$$

$$[4] \qquad Am_t = [R_2NH_2^+] + [R_2NH]$$

Am_t et Cl_t représentent les concentrations courantes globales des réactifs; les activités des espèces s'expriment à partir de leurs concentrations et des coefficients d'activité γ :

$$[5] \qquad (X) = \gamma_X[X]$$

La constante de vitesse expérimentale calculée à partir de la relation

$$[6] \qquad V = k_{exp}Cl_tAm_t$$

s'exprime à l'aide des relations [1]–[5] selon que l'on envisage les differents processus :

$$k_{exp}^{P1} = \frac{k_1^0 K_{II}}{\gamma_1^{\neq}}\left[\frac{(H^+)\gamma_{R_2NH}\gamma_{ClOH}\gamma_{R_2NH_2}\gamma_{ClO^-}}{[K_I\gamma_{ClOH}+(H^+)\gamma_{ClO^-}][K_{II}\gamma_{R_2NH_2}+(H^+)\gamma_{R_2NH}]}\right]$$

$$k_{exp}^{P2} = \frac{k_2^0 K_I}{\gamma_2^{\neq}}\left[\frac{(H^+)\gamma_{R_2NH}\gamma_{ClOH}\gamma_{R_2NH_2}\gamma_{ClO^-}}{[K_I\gamma_{ClOH}+(H^+)\gamma_{ClO^-}][K_{II}\gamma_{R_2NH_2}+(H^+)\gamma_{R_2NH}]}\right]$$

$$k_{exp}^{P3} = \frac{k_3^0 K_I K_{II}}{\gamma_3^{\neq}}\left[\frac{\gamma_{R_2NH}\gamma_{ClOH}\gamma_{R_2NH_2}\gamma_{ClO^-}}{[K_I\gamma_{ClOH}+(H^+)\gamma_{ClO^-}][K_{II}\gamma_{R_2NH_2}+(H^+)\gamma_{R_2NH}]}\right]$$

$$k_{exp}^{P4} = \frac{k_4^0}{\gamma_4^{\neq}}\left[\frac{(H^+)^2\gamma_{R_2NH}\gamma_{ClOH}\gamma_{R_2NH_2}\gamma_{ClO^-}}{[K_I\gamma_{ClOH}+(H^+)\gamma_{ClO^-}][K_{II}\gamma_{R_2NH_2}+(H^+)\gamma_{R_2NH}]}\right]$$

Les figures 3a et 3b représentent ces fonctions sur le domaine de pH de l'eau (pour des paramètres arbitraires). Il apparaît clairement que si les processus P3 et P4 sont facilement discernables par une simple étude de l'influence du pH sur la constante de vitesse expérimentale, il n'en est pas de même pour les processus P1 et P2 pour lesquels les variations théoriques de la constante de vitesse sont strictement identiques tant du point de vue du pH que de celui des coefficients d'activité (donc de tout paramètre, comme la force ionique par exemple, agissant sur ces coefficients).

Sur la figure 4 où nous avons porté, pour la diéthylamine, le logarithme népérien de k_{exp} en fonction du pH, nous obtenons une courbe avec maximum correspondent aux cas P1 ou P2.

Pour le vérifier (figure 5) nous avons porté $\ln(k_{exp})$ en fonction de $\ln(W)$ avec :

$$W = \left[\frac{(H^+)\gamma_{R_2NH}\gamma_{ClOH}\gamma_{R_2NH_2}\gamma_{ClO^-}}{[K_I\gamma_{ClOH} + (H^+)\gamma_{ClO^-}][K_{II}\gamma_{R_2NH_2}+(H^+)\gamma_{R_2NH}]}\right]$$

et an admettant une forme approchée par la loi limite de Debye–Hückel pour les coefficients d'activité des espèces ioniques :

$$\gamma_{R_2NH} = \gamma_{ClOH} = 1 \qquad \gamma = \gamma_{R_2NH_2} = \gamma_{ClO^-} = 10^{-0{,}5\sqrt{I}}$$

$$W = \left[\frac{(H^+)\gamma^2}{[K_I + (H^+)\gamma][K_{II}\gamma + (H^+)]}\right]$$

Pour chaque amine, nous avons obtenu une droite dont l'ordonnée à l'origine peut représenter indifféremment $\ln(k_1^0K_{II})$ ou $\ln(k_2^0K_I)$ ou même la somme des deux valeurs si les deux processus sont possibles et de vitesse équivalente.

Ce problème, remarqué pour les N-chlorations de la méthylamine et de la diméthylamine par Morris et Weil (1), est

Can. J. Chem. Downloaded from www.nrcresearchpress.com by 41.223.56.140 on 09/07/12
For personal use only.

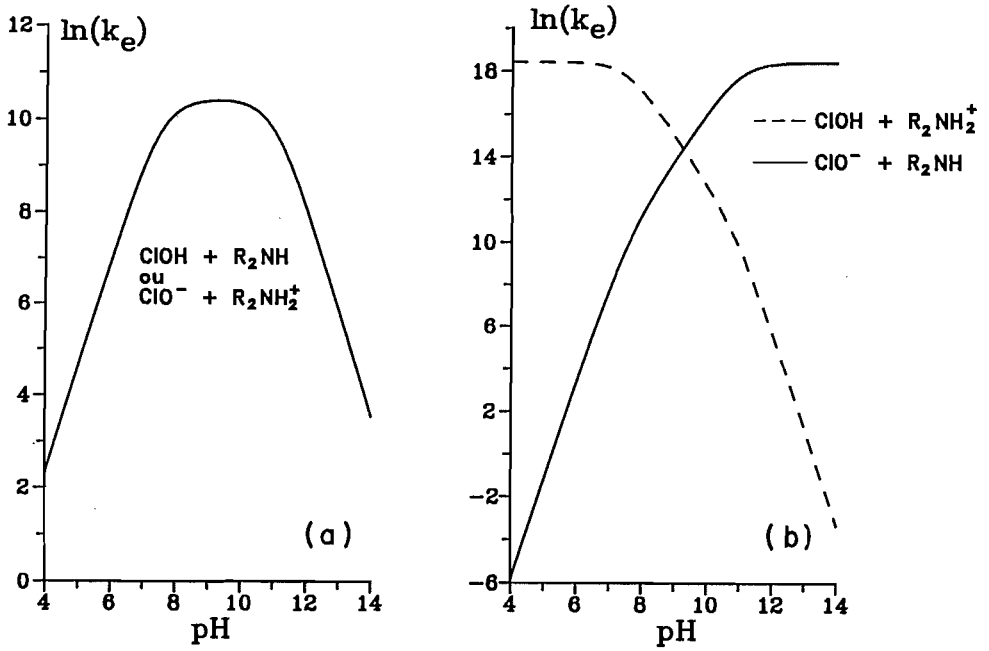


FIG. 3. Variation théoriques de la constante de vitesse expérimentale avec le pH selon le mécanisme envisagé entre acides et bases faibles en solution aqueuse.

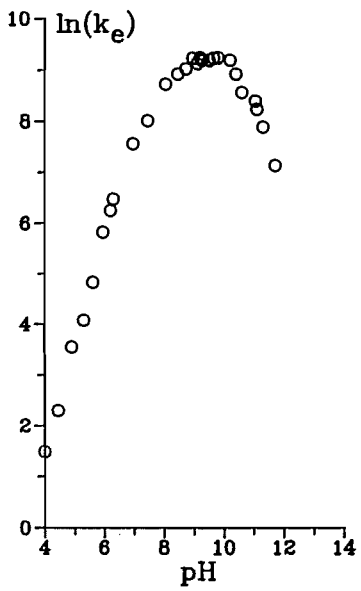


FIG. 4. Logarithme népérien de la constante de vitesse expérimentale de chloration de la diéthylamine en fonction du pH. $T = 298$ K; $DEA_t = 5 \times 10^{-3}$ M; $Cl_t = 5 \times 10^{-4}$ M; force ionique $I = 0{,}10 \pm 0{,}03$ M.

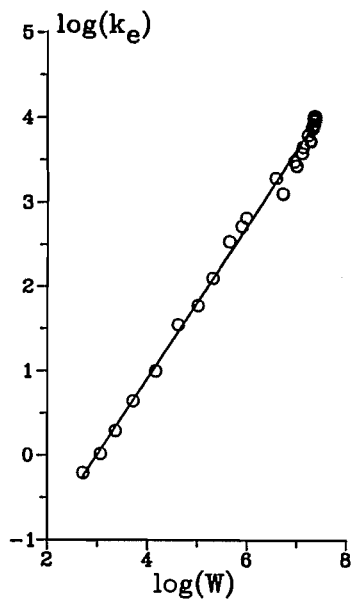


FIG. 5. Logarithme népérien de la constante de vitesse expérimentale de chloration de la diéthylamine en fonction de ln(W)

$$W = \frac{(H^+)^2}{[K_I + (H^+)][K_{II} + (H^+)]}$$

(pente = 0,9; coefficient de corrélation = 0,9895).

strictement analogue à celui analysé par Pearson et Frost (6) à propos de la conversion cyanate d'ammonium en urée en milieu aqueux. Nous observons là aussi deux processus entre acides et bases faibles conjugués, qui rendent compte des données expérimentales

$$NH_4^+ + CNO^- \rightarrow (NH_2)_2CO$$

ou

$$NH_3 + HCNO \rightarrow (NH_2)_2CO$$

Dans un tel cas chaque série de point expérimentaux conduit à deux valeurs possibles des constantes de vitesse selon que l'on fait l'hypothèse de l'un ou l'autre des processus.

Influence de la température

En milieu acide (pH = 3,35), à concentration suffisamment faible en ions chlorures pour que la chloration par le chlore moléculaire n'intervienne pas, les expressions de k_{exp} se simplifient pour les processus P1 et P2 :

Can. J. Chem. Downloaded from www.nrcresearchpress.com by 41.223.56.140 on 09/07/12
For personal use only.

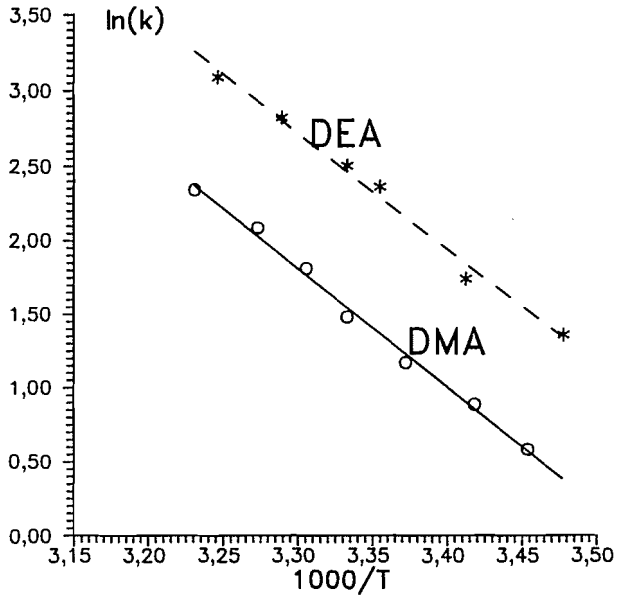


FIG. 6. Énergie d'activation globale. Diéthylamine : $\ln(k_{exp}) = -8100/T + 28{,}39$ (coeff. corr. = 0,9576); E_a = 67 kJ mol^{-1}. Diéthylamine : $\ln(k_{exp}) = -7800/T + 28{,}40$ (coeff. corr. = 0,9807); E_a = 65 kJ mol^{-1}.

$$k_{exp}^{P1} = k_1^0 K_{II}\left[\frac{\gamma_{ClOH}\gamma_{R_2NH_2}}{(H^+)\gamma_1^{\neq}}\right] \qquad k_{exp}^{P2} = k_2^0 K_I\left[\frac{\gamma_{ClOH}\gamma_{R_2NH_2}}{(H^+)\gamma_2^{\neq}}\right]$$

Soit avec les notations déjà utilisées précédemment :

$$k_{exp}^{P1} = k_1^0 K_{II}\left[\frac{\gamma}{(H^+)}\right] \qquad k_{exp}^{P2} = k_2^0 K_I\left[\frac{\gamma}{(H^+)}\right]$$

Pour chaque amine, les points $\ln(k_{exp})$ versus $1/T$ sont portés par une droite dont la pente représente les énergies d'activation globales, soit 67,1 kJ mol^{-1} pour la DMA et 64,7 kJ mol^{-1} pour la DEA (figure 6).

Dans ces conditions de pH, les énergies d'activations des processus se déduisent de la valeur de l'énergie d'activation globale à partir des relations :

$$\ln(k_{exp}) = \frac{-E_a}{RT} + C = \frac{-E_1 - \Delta H_{II}^0}{RT} + C$$

soit $E_1 = E_a - \Delta H_{II}^0$

ou

$$\ln(k_{exp}) = \frac{-E_a}{RT} + C = \frac{-E_2 - \Delta H_I^0}{RT} + C$$

soit $E_2 = E_a - \Delta H_I^0$

Avec ΔH_I^0 = 16,3 kJ mol^{-1} (4), $\Delta H_{II(DMA)}^0$ = 49,5 kJ mol^{-1} (7) et $\Delta H_{II(DEA)}^0$ = 49,7 kJ mol^{-1} (8), les énergies d'activations des processus prennent les valeurs pour le processus ionique $E_{2(DMA)}$ = 50,8 kJ mol^{-1}, $E_{2(DEA)}$ = 48,4 kJ mol^{-1} et pour le processus moléculaire $E_{1(DMA)}$ = 17,6 kJ mol^{-1}, $E_{1(DEA)}$ = 15 kJ mol^{-1}.

Chloration par Cl_2

En milieu acide, en présence de chlorures, nous observons (figure 7) une accélération de la réaction par rapport à celle due à ClO^- ou ClOH. Cet écart aux valeurs théoriquement attendues apparait dés que la concentration de Cl_2 n'est plus négligeable.

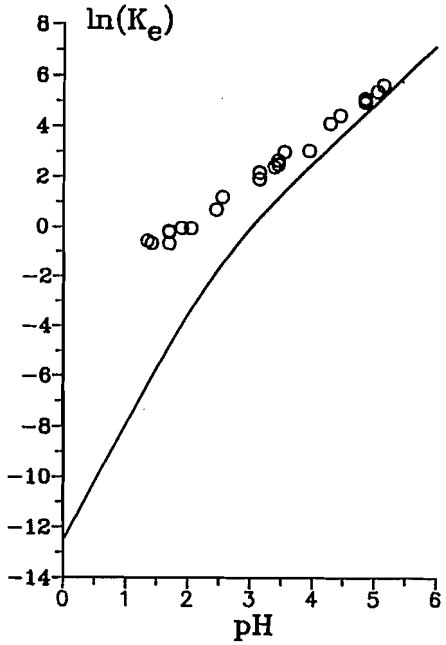


FIG. 7. Chloration par Cl_2. Logarithme népérien de la constante de vitesse expérimentale de chloration de la diéthylamine en fonction du pH. T = 298 K; $DMA_t = 7{,}5 \times 10^{-3}$ M; $Cl_t = 8 \times 10^{-4}$ M; $[Cl^-]$ = 0,2 M (en trait plein courbe théorique pour une chloration par ClOH ou ClO^- uniquement).

Dans ces conditions il faut tenir compte de deux équilibres supplémentaires.

[III] $Cl_2 + H_2O \leftrightarrows ClOH + H^+ + Cl^-$ $\quad pK_{III} = 3{,}4$ à 298 K (9)

[IV] $Cl_2 + Cl^- \leftrightarrows Cl_3^-$ $\quad pK_{IV} = 0{,}74$ à 298 K (10)

Quelques essais à pH constant et à concentration variable d'ions chlorures nous ont permis de vérifier que la chloration engage le chlore moléculaire Cl_2 et non Cl_3^-. De plus, la persistance de la décroissance de la vitesse avec le pH permet d'affirmer que la chloration se fait sur l'amine non protonée pourtant espèce très minoritaire aux pH acides.

Nous avons donc, aux pH où Cl_2 et ClOH coexistent, une vitesse globale qui s'exprime par une double contribution due à la chloration par les deux espèces :

$$V = k_{Cl_2}[Cl_2][R_2NH] + k_1[ClOH][R_2NH]$$

En milieu acide le bilan en chlore libre total devient :

[7] $\quad Cl_t = [Cl_2] + [ClOH] + [Cl_3^-]$

avec pour expression des concentrations de ClOH et Cl_2

$$[ClOH] = \left[\frac{K_{III}}{K_{III} + K_{IV}[Cl^-]^2\gamma(H^+) + [Cl^-]\gamma(H^+)}\right] Cl_t$$

$$[Cl_2] = \left[\frac{[Cl^-]\gamma(H^+)}{K_{III} + K_{IV}[Cl^-]^2\gamma(H^+) + [Cl^-]\gamma(H^+)}\right] Cl_t$$

Pour l'amine en milieu acide nous avons : $[R_2NH_2^+] \neq Am_t$ D'où l'expression simplifiée de la concentration de R_2NH :

$$[R_2NH] = K_{II}\frac{\gamma}{(H^+)} Am_t$$

À partir de ces relations et celle de la vitesse [6] nous obtenons

Can. J. Chem. Downloaded from www.nrcresearchpress.com by 41.223.56.140 on 09/07/12
For personal use only.

Can. J. Chem. Downloaded from www.nrcresearchpress.com by 41.223.56.140 on 09/07/12
For personal use only.

TABLEAU 1. Résultats numériques à 298 K

Réactions	k^0 ($M^{-1}\,s^{-1}$)	E (kJ mol^{-1})	$\Delta H^{\neq}$ (kJ mol^{-1})	$\Delta S^{\neq}$ (J $K^{-1}\,mol^{-1}$)
$(CH_3)_2NH + HOCl \rightarrow (CH_3)_2NCl + H_2O$	$9{,}8 \times 10^7$	17,6	15,1	−41
$(CH_3)_2NH + Cl_2 \rightarrow (CH_3)_2NCl + H^+ + Cl^-$	$1{,}6 \times 10^9$	7,5	5,5	−50,2
$(C_2H_5)_2NH + HOCl \rightarrow (C_2H_5)_2NCl + H_2O$	$5{,}3 \times 10^7$	15,0	12,5	−54
$(C_2H_5)_2NH + Cl_2 \rightarrow (C_2H_5)_2NCl + H^+ + Cl^-$	$9{,}4 \times 10^8$	—	—	—

pour valeur de la constante expérimentale de réaction :

$$k_{exp} = \left(\frac{k_{Cl_2}[Cl^-]\gamma(H^+) + k_1K_{III}}{K_{III} + K_{IV}[Cl^-]^2\gamma(H^+) + [Cl^-]\gamma(H^+)}\right)\frac{K_{II}\gamma}{(H^+)}$$

Pour

$$X = \frac{(H^+)\gamma[Cl^-]}{K_{III} + K_{IV}[Cl^-]^2(H^+)\gamma + (H^+)\gamma[Cl^-]}$$

et

$$Y = \frac{k_{exp}(H^+)}{K_{II}\gamma} - \frac{k_1K_{III}}{K_{III} + K_{IV}[Cl^-]^2(H^+)\gamma + (H^+)\gamma[Cl^-]}$$

nous avons, à partir de nos résultats expérimentaux, obtenu une droite $Y = f(X)$ dont la pente est une mesure de k_{Cl_2} égale à $1{,}6 \times 10^9\,M^{-1}\,s^{-1}$ pour la diméthylamine et $9{,}4 \times 10^8\,M^{-1}\,s^{-1}$ pour la diéthylamine à 298 K (figure 8).

Pour la DMA nous avons déterminé une énergie d'activation de 7,5 kJ mol^{-1}.

Les résultats numériques sont resumés dans le tableau 1.

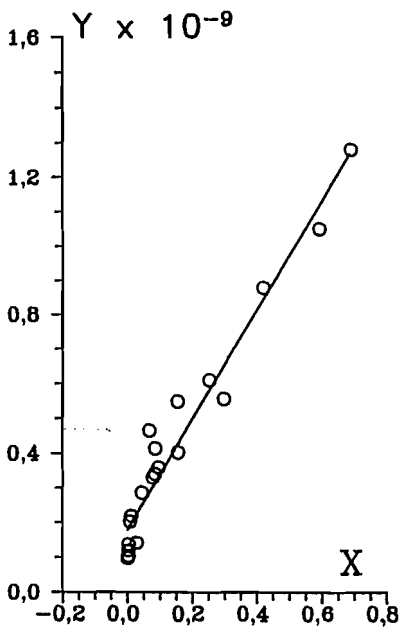


FIG. 8. Détermination de k_{Cl_2} pour la diméthylamine.

$$X = \frac{(H^+)\gamma[Cl^-]}{K_{III} + K_{IV}[Cl^-]^2(H^+)\gamma + (H^+)\gamma[Cl^-]}$$

et

$$Y = \frac{k_{exp}(H^+)}{K_{II}\gamma} - \frac{k_1K_{III}}{K_{III} + K_{IV}[Cl^-]^2(H^+)\gamma + (H^+)\gamma[Cl^-]}$$

Pente = $k_{Cl_2} = 1{,}1 \times 10^9\,M^{-1}\,s^{-1}$ (coefficient de corrélation = 0,9895).

Conclusions

Pour les deux amines la chloration par Cl_2 se fait par réaction de R_2NH et Cl_2. Ces cinétiques sont limitées par la diffusion ce qui est général pour les N-chlorations par Cl_2 en milieu aqueux (11).

Par analogie il semblerait raisonnable d'admettre un mécanisme similaire entre ClOH et R_2NH.

Ces deux mécanismes se conçoivent facilement par une attaque nucléophile de l'amine sur un chlore :

$$R_2\bar{N}H + Cl\text{—}Cl \rightarrow R_2NClH^+ + Cl^- \rightarrow R_2NCl + Cl^- + H^+$$

$$R_2\bar{N}H + Cl\text{—}OH \rightarrow R_2NClH^+ + OH^- \rightarrow R_2NCl + H_2O$$

Toutefois l'expérience ne permet pas d'exclure une réaction de type ionique entre ClO^- et $R_2NH_2^+$.

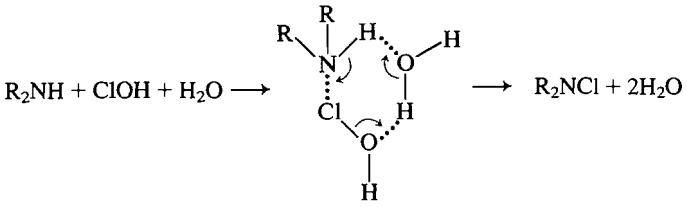
Si l'on admet que le mécanisme de chloration moléculaire est le plus probable, les valeurs faibles des énergies d'activations liées à celui-ci (17,6 et 15 kJ mol^{-1}) sont proches des paramètres d'activation d'une cinétique limitée par la diffusion.

En fait pour les deux amines le facteur 10 entre les valeurs de k_1 et k_{Cl_2}, et le facteur 2 entre les énergies d'activation incitent à penser que la cinétique de chloration par ClOH n'est que partiellement limitée par la diffusion. En effet les valeurs proches des coefficients de diffusion de ClOH et Cl_2 dans l'eau ($D_{Cl_2} = 1{,}83\,m^2\,s^{-1}$ et $D_{ClOH} = 1{,}28\,m^2\,s^{-1}$ à 298 K (12)) ne peuvent expliquer, dans l'hypothèse de cinétiques limitées par la diffusion, cet écart entre les valeurs des constantes de vitesse.

À partir de la valeur du coefficient de diffusion de la DEA($0{,}97\,m^2\,s^{-1}$ (13)), nous obtenons dans les conditions de Smoluchovski ($k_d = 4\pi\rho_0(D_A + D_B)$, avec $\rho_0 = 10^{10}$ m), les valeurs théoriques $k_d^{Cl_2} = 2{,}1 \times 10^9\,M^{-1}\,s^{-1}$ et $k_d^{ClOH} = 1{,}6 \times 10^9\,M^{-1}\,s^{-1}$ à comparer aux valeurs expérimentales, $k_{Cl_2} = 9{,}4 \times 10^8$ et $k_1 = 5{,}3 \times 10^7\,M^{-1}\,s^{-1}$. Il apparait que pour le chlore moléculaire les valeurs sont du même ordre de grandeur, ce qui confirme un régime diffusionnel alors que pour l'acide hypochloreux, si nous admettons une situation intermédiaire, nous calculons à partir de la relation :

$$k_1 = \frac{k_1^x}{(1 + k_1^x/k_d)}$$

une valeur de k_1^x (constante de vitesse réelle du processus) de $5{,}7 \times 10^7\,M^{-1}\,s^{-1}$ soit une valeur très proche de k_1. L'influence de la diffusion apparait donc faible pour un tel processus. Par contre, le proposition (1) d'une participation d'une molécule d'eau au mécanisme avec formation d'un intermédiaire stabilisé par liaison hydrogéne :



permet d'expliquer la faiblesse relative des énergies d'activation et des constantes de vitesse par rapport à l'hypothèse d'un processus bimoléculaire simple.

1. J. C. Morris et I. Weil. J. Am. Chem. Soc. **71**, 1664 (1949).
2. C. R. Edmont et F. G. Soper. J. Chem. Soc. 2942 (1949).
3. A. G. Friend, Ph.D. thesis, Harvard University. 1954.
4. J. C. Morris. J. Phys. Chem. **70**, 3798 (1966).
5. R. T. Morrison et R. N. Boyd. Organic chemistry. 3e éd. Allyn and Bacon Inc., Boston, MA. 1973.
6. R. G. Pearson et A. A. Frost. Kinetics and mechanism. The ammonium cyanate – urea conversion. John Wiley & Sons, Inc., New York, London. 1962. Chap. 12, part B.
7. D. H. Everett et W. F. K. Wynne-Jones. Trans Faraday Soc. **37**, 373 (1941).
8. G. Dienis et P. Adomenas. Zh. Fiz. Khim. **44**, 2070 (1970).
9. R. E. Connick et Y. T. Chia. J. Am. Chem. Soc. **81**, 1280 (1959).
10. M. Eigen et K. Kustin. J. Am. Chem. Soc. **84**, 1355 (1962).
11. D. Matte. Thèse de doctorat, Université de Nancy I. 1986.
12. M. S. Chao. J. Electrochem. Soc. **115**, 1172 (1968).
13. J. B. Lewis. J. Appl. Chem. (London), **5**, 228 (1955).

Can. J. Chem. Downloaded from www.nrcresearchpress.com by 41.223.56.140 on 09/07/12
For personal use only.

Medium isotope effect for isobutyrophenone in aqueous solution. Solvent isotope effects on carbonyl group hydration

J. R. KEEFFE[1] AND A. J. KRESGE[2]

Department of Chemistry, University of Toronto, Toronto, Ont., Canada M5S 1A1

Received December 12, 1988

J. R. KEEFFE and A. J. KRESGE. Can. J. Chem. **67**, 792 (1989).

A medium solvent isotope effect of $\Phi = 0.827 \pm 0.013$ was determined for transfer of isobutyrophenone from H_2O to D_2O. This result, in conjunction with the average solvent isotope effect on hydration of a number of carbonyl compounds, leads to $\phi = 0.987 \pm 0.009$ as the fractionation factor for the hydroxyl group hydrogens of the hydration reactions' *gem*-diol products, which is consistent with the expectation that fractionation factors for uncharged hydroxyl groups should be unity.

Key words: isobutyrophenone, fractionation factors, solvent isotope effects, deuterium oxide.

J. R. KEEFFE et A. J. KRESGE. Can. J. Chem. **67**, 792 (1989).

Pour le transfert de l'isobutyrophénone du H_2O au D_2O, on a déterminé que l'effet isotopique du solvant est $\Phi = 0{,}827 \pm 0{,}013$. Ce résultat, utilisé de concert avec la valeur moyenne de l'effet isotopique du solvant sur l'hydratation d'un certain nombre de composés carbonylés conduit à une valeur de $\phi = 0{,}987 \pm 0{,}009$ pour le facteur de fractionnement des hydrogènes des groupements hydroxyles des produits *gem*-diols obtenus par réaction d'hydratation; ce résultat est en accord avec la valeur de 1 à laquelle on s'attend pour le facteur de fractionnement de groupement hydroxyles qui ne sont pas chargés.

Mots clés : isobutyrophénone, facteurs de fractionnement, effets isotopiques du solvant, oxyde de deutérium.

[Traduit par la revue]

Fractionation factor theory (for recent reviews, see ref. 1) expresses solvent isotope effects on equilibria as the product of fractionation factors[3] for all exchangeable hydrogens in the reactants, ϕ_i^R, divided by a like product for all exchangeable hydrogens in the products, ϕ_j^P, eq. [1].

$$[1] \quad K_{H_2O}/K_{D_2O} = \Pi_i\phi_i^R/\Pi_j\phi_j^P$$

Application of this formalism at its simplest level to the hydration of carbonyl compounds in aqueous solution, eq. [2],[4]

$$[2] \quad \text{>C=O} + L_2O \underset{}{\overset{K}{\rightleftharpoons}} \text{>C(OL)(OL)}$$

leads to an expression, eq. [3], containing only the fractionation factor for the hydroxyl group hydrogen of the *gem*-diol product, ϕ_{ROL}, and that fractionation factor can thus be evaluated directly from this solvent isotope effect. When that is done using the average value of eight separate determinations of this isotope effect (2), $K_{H_2O}/K_{D_2O} = 0.849 \pm 0.009$, the result $\phi_{ROL} = 1.085 \pm 0.006$ is obtained (3).

$$[3] \quad K_{H_2O}/K_{D_2O} = 1/\phi_{ROL}^2$$

It is generally believed, however, that fractionation factors for the hydrogens of uncharged hydroxyl groups should be unity (1, 3), and it is not readily apparent why *gem*-diols would be different. The simple expression of eq. [3] cannot of course accommodate a *gem*-diol fractionation factor of unity and a solvent isotope effect different from unity, but the expression could be modified by introducing additional terms. In particular, fractionation factors might be added to allow for medium isotope effects (4). Such effects are generally produced by small differences between the water molecules of bulk solvent and those directly involved in solvating the dissolved species; the individual fractionation factors of these solvating sites are usually not very different from unity, but because several water molecules are generally involved, the aggregate effect can be appreciable. A medium isotope effect of this kind would appear to be especially likely for the carbonyl compound substrate of the present hydration reaction (eq. [2]), inasmuch as carbonyl groups are strongly dipolar. The modification of eq. [3] that this would require is shown as eq. [4],

$$[4] \quad K_{H_2O}/K_{D_2O} = \Phi_C/\phi_{ROL}^2$$

in which Φ_C is the medium isotope effect for transferring the carbonyl compound from H_2O to D_2O.[5]

To determine whether or not this is so, we have measured the medium isotope effect for a simple carbonyl compound. We chose isobutyrophenone for this purpose because it has a strong ultraviolet chromophore that facilitates accurate concentration measurements, and also because we have an interest in this molecule from the point of view of its keto–enol equilibrium (5). We determined the medium isotope effect in two independent ways: (1) by measuring the ratio of the solubilities of isobutyrophenone in H_2O and D_2O, and (2) by measuring the ratio of its partition coefficients between hexane and H_2O and hexane and D_2O.

Experimental

Solubilities

Saturated solutions of isobutyrophenone in H_2O and D_2O were prepared by adding 3.0-μL quantities of ketone to cuvettes containing 3.0-mL volumes of each solvent and shaking the mixtures mechanically for 3 h. The presence of haziness in each mixture indicated that the amount of ketone supplied was more than enough to achieve saturation. These mixtures were allowed to stand at room temperature (23–24°C) in the dark for 10 days, to ensure that all undissolved ketone had ample

[1]Permanent address: Department of Chemistry, San Francisco State University, 1600 Holloway Avenue, San Francisco, CA 94132, U.S.A.

[2]Author to whom correspondence may be addressed.

[3]A fractionation factor for a given site is equal to the D:H ratio at that site divided by the D:H ratio of some reference; for phenomena occurring in aqueous solution, the reference is usually taken to be the solvent, and the fractionation factor of water hydrogens is then unity.

[4]L = D or H.

[5]Following the recommendation of ref. 4, we use the symbol Φ for medium isotope effects and retain φ for individual fractionation factors.

Can. J. Chem. Downloaded from www.nrcresearchpress.com by 41.223.56.140 on 09/07/12
For personal use only.

opportunity to float to the top. Absorbance measurements at $\lambda = 300$ nm were made during this time; these remained constant over the final three days. The ratio of these final absorbances gives the medium isotope effect $\Phi_C = 0.852$. Use of the extinction coefficient $\varepsilon_{300} = 285$ M^{-1} cm^{-1} also provides a saturation solubility of 4.4×10^{-3} M for isobutyrophenone in H_2O solution.

Partition coefficients

Solutions of isobutyrophenone in H_2O and D_2O that were ca. three-quarters saturated were prepared and their absorbances were measured at $\lambda = 300$ and 310 nm. Nine-millilitre aliquots of these solutions were then shaken with 1.00-mL portions of hexane and the resulting mixtures were allowed to stand for 5 h to ensure complete phase separation. Absorbance measurements of the aqueous portions were made during this time at $\lambda = 300$ and 310 nm; these remained constant over the final hour. Medium isotope effects were calculated using the relationship $\Phi_C = (A_0)_{H_2O}(A_0-A)_{D_2O}/(A_0)_{D_2O}(A_0-A)_{H_2O}$, in which A_0 and A are the absorbances measured before and after extraction respectively. The measurements at $\lambda = 300$ nm give $\Phi_C = 0.819$ and those at $\lambda = 310$ nm, $\Phi_C = 0.809$. These experiments also provide a partition coefficient of 3.4×10^{-3} for isobutyrophenone between hexane and H_2O.

Results and discussion

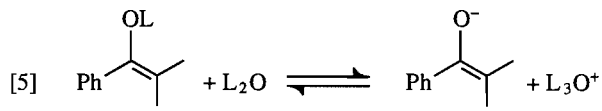
The three determinations of the medium isotope effect for isobutyrophenone made here are in good agreement with one another. Their average value is $\Phi_C = 0.827 \pm 0.013$.

This is a reasonable result. Carbonyl groups of simple aldehydes and ketones will be solvated in aqueous solution principally through their negatively charged oxygen atoms, inasmuch as this end of the carbonyl group dipole is more accessible to solvent molecules than is the positively charged carbon atom. These solvent molecules, moreover, will be linked to the carbonyl oxygen atom through hydrogen bonds, and hydrogen bonding is known to loosen the bonds involved and lead to lowered isotopic fractionation factors (6); water molecules solvating the hydroxide ion, for example, have $\phi = 0.7$ (1, 4, 7).

It is likely that in the present case this hydrogen bonding involves two water molecules, one bound to each of the unshared electron pairs of the carbonyl oxygen atom. The aggregate medium isotope effect is then equal to the fractionation factor for these hydrogen-bonding hydrogens raised to the second power, and the value of this fractionation factor may thus be calculated as $\phi = \sqrt{\Phi_C} = 0.0909 \pm 0.007$.

Use of the presently determined medium isotope effect in conjunction with the isotope effect on carbonyl compound hydration, $K_{H_2O}/K_{D_2O} = 0.849$ (2), leads, via eq. [4], to $\phi_{ROL} = 0.987 \pm 0.009$. This result is hardly different from unity, and that is nicely consistent with the fact that this value refers to an uncharged hydroxyl group for which a unit fractionation factor would be expected.

If a unit value of ϕ_{ROL} may be assumed to apply to the hydroxyl groups of enols as well, then the value of Φ_C determined here can be used together with the recently measured solvent isotope effect on the acid ionization of isobutyrophenone enol, eq. [5],



[5]

$(K_a^E)_{H_2O}/(K_a^E)_{D_2O} = 5.88 \pm 0.32$ (5*b*), to estimate the medium isotope effect for isobutyrophenone enolate ion, Φ_{E^-}. The fractionation factor theory expression for this acid ionization isotope effect is given by eq. [6],

$$[6] \quad (K_a^E)_{H_2O}/(K_a^E)_{D_2O} = \phi_{ROL}/(\Phi_E \cdot \ell^3)$$

in which ℓ is the fractionation factor for the hydronium ion whose value is 0.69 (1, 4); use of this plus $\phi_{ROL} = 1.00$ then leads to $\Phi_{E^-} = 0.52 \pm 0.03$. To the best of our knowledge, this is the first medium isotope effect ever reported for the enolate ion of a monofunctional carbonyl compound; it is a sensible value in that medium isotope effects for anions are expected to be less than unity (1, 4, 7). On the expectation that this isotope effect, like the medium isotope effect for the hydroxide ion, is produced by three hydrogen-bonded water molecules each attached to one unshared electron pair of the enolate oxygen atom, $\phi = (\Phi_{E^-})^{1/3} = 0.80 \pm 0.02$ may be calculated as the fractionation factor for the hydrogen-bonding hydrogens; this is consistent with $\phi = 0.7$ for the hydrogen-bonding hydrogens of the water molecules solvating the hydroxide ion (1, 4, 7).

Acknowledgements

We are grateful to the Natural Sciences and Engineering Research Council of Canada and the Donors of the Petroleum Research Fund, administered by the American Chemical Society, for financial support of this work.

1. F. J. ALVAREZ and R. L. SCHOWEN. *In* Isotopes in organic chemistry. Vol. 7. *Edited by* E. Buncel and C. C. Lee. Elsevier, New York. 1987. Chap. 1; A. J. KRESGE, R. A. MORE O'FERRALL, AND M. F. POWELL. *In* Isotopes in organic chemistry. Vol. 7. *Edited by* E. Buncel and C. C. Lee. Elsevier, New York. 1987. Chap. 4.
2. L. C. GRUEN and P. T. MCTIGUE. J. Chem. Soc. 5217 (1963); G. E. LIENHARD AND W. P. JENCKS. J. Am. Chem. Soc. **88**, 3982 (1966); J. L. KURZ. J. Am. Chem. Soc. **89**, 3524 (1967); T. J. BURKEY and R. C. FAHEY. J. Am. Chem. Soc. **105**, 868 (1983).
3. R. BONE and R. WOLFENDEN. J. Am. Chem. Soc. **107**, 4772 (1985).
4. W. J. ALBERY. *In* Proton transfer reactions. *Edited by* E. F. Caldin and V. Gold. Chapman and Hall, London. 1975. Chap. 9.
5. (*a*) P. PRUSZYNSKI, Y. CHIANG, A. J. KRESGE, N. P. SCHEPP, and P. A. WALSH. J. Phys. Chem. **90**, 3760 (1986); (*b*) Y. CHIANG, A. J. KRESGE, and P. A. WALSH. Z. Naturforsch. In press.
6. M. M. KREEVOY and T. M. LIANG. J. Am. Chem. Soc. **102**, 3315 (1980).
7. V. GOLD and S. GRIST. J. Chem. Soc. Perkin Trans. 2, 89 (1972).

Can. J. Chem. Downloaded from www.nrcresearchpress.com by 41.223.56.140 on 09/07/12
For personal use only.

Efficient synthesis of *exo*- and *endo*-brevicomin from a single precursor

SOWMIANARAYANAN RAMASWAMY AND ALLAN C. OEHLSCHLAGER[1]
Department of Chemistry, Simon Fraser University, Burnaby, B.C., Canada V5A 1S6

Received October 12, 1989

SOWMIANARAYANAN RAMASWAMY and ALLAN C. OEHLSCHLAGER. Can. J. Chem. **67**, 794 (1989).

Diastereoselective reduction of 2-propionyl-6-methyl-3,4-dihydropyran and its ring opened derivatives, followed by acidic work-up, gives mixtures rich (>9:1) of either *exo*- or *endo*-brevicomin.

Key words: *exo*- and *endo*-brevicomin, diastereoselective ketone reduction.

SOWMIANARAYANAN RAMASWAMY et ALLAN C. OEHLSCHLAGER. Can. J. Chem. **67**, 794 (1989).

La réduction diastéréosélective du propionyl-2 méthyl-6 dihydro-3,4 pyranne et de ses dérivés en chaîne ouverte, suivie d'une extraction en milieu acide, conduit à des mélanges riches (>9:1) soit en *exo*- ou en *endo*-brévicomine.

Mots clés : *exo*- et *endo*-brévicomine, réduction diastéréosélective des cétones.

[Traduit par la revue]

Can. J. Chem. Downloaded from www.nrcresearchpress.com by 41.223.56.140 on 09/07/12
For personal use only.

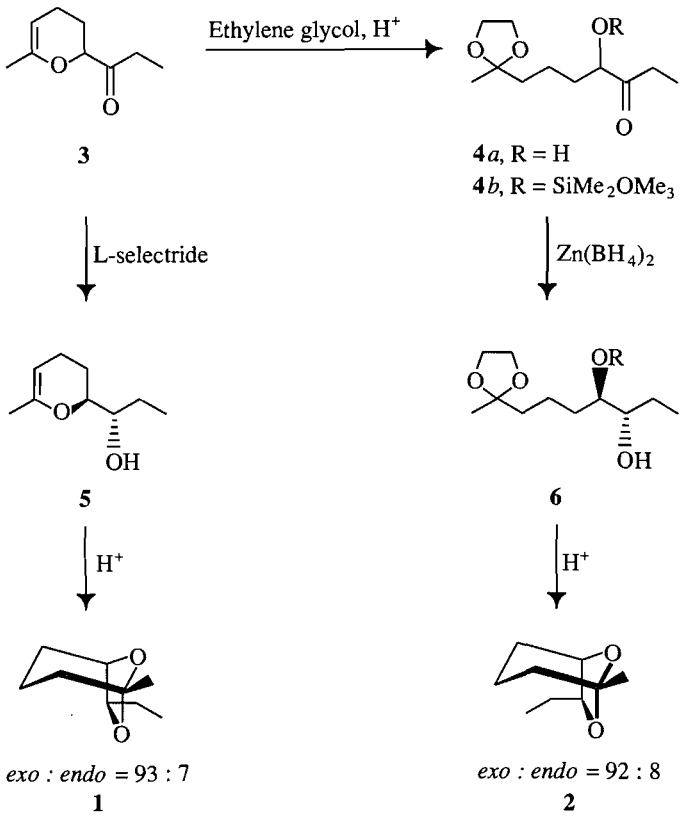
Introduction

We recently reported (1) an investigation of chelation and non-chelation controlled organometallic addition to acrolein dimer as a route to the economically important bicyclic ketals *exo*-brevicomin **1** and *endo*-brevicomin, **2**.[2] Although diastereoselectivity of organometallic addition was quite high, the approach was beset by the difficult vinyl metalation. The present investigation was undertaken to develop an efficient route to racemic **1** and **2** from a single inexpensive intermediate. We have achieved highly diastereoselective chemical reduction of **3** (2) and its acyclic analogs **4***a* and **4***b*. The dihydroxyketones (**5** and **6**) generated in each case readily cyclize in acid to mixtures of alkylated 2,6-dioxabicyclo[3.2.1]octanes (**1** and **2**).

Results and discussion

threo-Selective chemical chemical reduction of **3**, **4***a*, or **4***b* is required to produce **1**. *threo*-Selective reduction of α- and β-oxy-carbonyl compounds is usually achieved by delivery of a hydride from the least hindered side of the carbonyl in the presence of a reagent capable of enhancing the dipolar repulsion between the carbonyl and the α-oxy function but devoid of bidentate chelating ability (non-chelation control). The *erythro*-selective chemical reduction required to produce **2** is usually achieved through use of a Lewis acid capable of coordination of both the carbonyl and α-oxy function followed by hydride delivery from the less hindered side (chelation control) (for an excellent discussion, see ref. 3). Selectride^R reagents effect *threo*-selective reductions while, owing to its superior chelating ability, zinc borohydride is the efficient reagent for *erythro*-selective reductions (4–8).

We found the reductions of **3** and its acyclic derivatives, **4***a* and **4***b*, with several hydride reducing agents are highly diastereoselective (Table 1). The stereochemical course of these reductions was followed by conversion of intermediates **5** and **6** to **1** and **2**, respectively. As previously reported (9), reduction of **3** with $NaBH_4$ in methanol did not show useful selectivity (Table 1, entry 1). Use of either lithium tetrahydridoaluminate or diisobutylaluminum hydride in the reduction of **3** gave similar low diastereoselectivity (entries 2 and 3). Addition of $CeCl_3$ as a chelating agent unexpectedly gave an increased proportion of *threo* product **1** in the reduction of **3** by $NaBH_4$ (entry 4). Neither **4***a* nor **4***b* underwent diastereoselective reduction with $NaBH_4$ (entries 5 and 6). Reduction of **3** with potassium tri(*sec*-butyl)borohydride (10*a*) (K-Selectride^R, entry 7) gave an increased proportion of *threo* product **1**, which was not significantly increased upon addition of BF_3 (entry 8). Reduction of **4***a* or **4***b* with K-Selectride^R offered no advantage in production of **1** (entries 9 and 10). The highest proportion of *threo* product (93:7) from reduction of **3** was achieved using lithium tri(*sec*-butyl)borohydride (10*b*) (Li-Selectride^R, entries 11 and 12). This reducing agent was also the most *threo* selective in reductions of **4***a* (entry 13) and **4***b* (entry 14). The lower yields obtained with BF_3 (entries 8 and 12) may be attributed to competing Lewis acid catalyzed polymerization of the substrates.



SCHEME 1

[1]Author to whom correspondence may be addressed.

[2]For other syntheses of these pheromones see references cited in ref. 1.

TABLE 1. Hydride reduction of **3**, **4***a*, and **4***b*

Entry	Substrate	Hydride donor	Lewis acid	**1**/**2**[a]	Yield(%)[b]
1	**3**	$NaBH_4$	None	55/45	78[c]
2	**3**	$LiAlH_4$	None	55/45	88[c]
3	**3**	Dibal-H	None	67/33	92[c]
4	**3**	$NaBH_4$	$CeCl_3$	70/30	58
5	**4***a*	$NaBH_4$	None	53/47	71
6	**4***b*	$NaBH_4$	None	48/52	71
7	**3**	K-selec	None	79/21	94
8	**3**	K-selec	BF_3	82/18	41
9	**4***a*	K-selec	None	71/29	92
10	**4***b*	K-selec	None	80/20	100
11	**3**	L-selec	None	93/7	88[c]
12	**3**	L-selec	BF_3	93/7	44
13	**4***a*	L-selec	None	89/11	82
14	**4***b*	L-selec	None	86/14	85
15	**3**	$Zn(BH_4)_2$	None	27/73	91[c]
16	**3**	K-selec	$ZnCl_2$	74/26	93
17	**3**	L-selec	$ZnCl_2$	80/20	80
18	**4***a*	$Zn(BH_4)_2$	None	8/92	93[c]
19	**4***b*	$Zn(BH_4)_2$	None	22/78	92
20	**3**	K-selec	$MgBr_2$	21/79	85
21	**3**	L-selec	$MgBr_2$	89/11	82
22	**4***a*	K-selec	$MgBr_2$	48/52	93
23	**4***b*	K-selec	$MgBr_2$	22/78	82

[a]Estimated by gas chromatographic analysis (please see Experimental).
[b]Unless otherwise specified, yields determined by gas chromatographic analysis (please see Experimental).
[c]Isolated yields.

Chelation controlled reduction of **3** with zinc borohydride (10*c*) afforded a *threo*:*erythro* ratio of 27:73 (entry 15). Use of K- or Li-Selectride^R with $ZnCl_2$ (entries 16 and 17, respectively) did not dramatically improve *erythro* selectivity. We reasoned that *erythro* selectivity would be increased if the α-oxygen were more available for complexation. Indeed, when **4***a* was reduced with zinc borohydride *erythro* selectivity improved significantly (entry 18).

Addition of $MgBr_2$–Et_2O effected a dramatic alteration of the stereochemical outcome of reduction of **3** by Li-Selectride^R (compare entries 7 and 20) but had little effect in the case of Li-Selectride^R (compare entries 11 and 21). In the former reaction KBr precipitates from the reaction, giving a reducing agent most probably coordinated with magnesium. Lewis acid mediated reversal of selectivity was not observed when $ZnCl_2$ was added to Li-Selectride^R reduction of **3** (compare entries 11 and 17). No improvements of selectivity were observed when **4***a* and **4***b* were reduced with Li-Selectride^R in the presence of $MgBr_2$–Et_2O (compare entries 9, 10, 22, and 23).

Experimental

The nmr spectra were recorded using Bruker WM400 and SY100 spectrometers. Infrared spectra were recorded of neat films between NaCl plates on a Perkin Elmer 599B spectrophotometer. Low resolution mass spectra were recorded on an in-house Hewlett–Packard 5985B GC/MS/DS system operating at 70 eV. Gas chromatographic analysis utilized a Hewlett–Packard 5880A operated with a J + W fused silica DB-1 capillary column (15 m × 0.25 mm), a flame ionization detector, and linear oven temperature programs initiated at 60°C (Program 1) or 100°C (Program 2) and increased at 5°C/min to 200°C. Elemental analyses were performed at the microanalytical laboratory of the Department of Biological Sciences, Simon Fraser University, on a Perkin Elmer Model 240 elemental analyzer.

Chromatography sovents were distilled before use. Tetrahydrofuran (THF) was distilled from sodium benzophenone ketyl immediately prior to use. All reactions involving air or moisture sensitive reagents were performed under an argon atmosphere.

*Preparation of 2-propionyl-6-methyl-2,3-dihydro-4*H*-pyran,* ***3***

Fractional distillation of 200 g of an aged (6 months) sample of methyl vinyl ketone afforded 88 g (44%) of methyl vinyl ketone dimer: bp 65–70°C (20 Torr; 1 Torr = 133.3 Pa), lit. (11) bp 68°C (13 Torr); ir (film): 1720 and 1684 cm^{-1}; ^1H nmr ($CDCl_3$) δ: 1.83 (d, J = 1.0 Hz, 3H), 1.95 (m, 4H), 2.22 (s, 3H), 4.25 (m, 1H), 4.50 (bs, 1H).

The *N*-cyclohexyl imine of methyl vinyl ketone dimer was prepared according to the procedure of Chaquin *et al.* (2); ir (film): 1685 and 1668 cm^{-1}. This compound was treated sequentially with ethylmagnesium bromide in ether and iodomethane to give **3** in 75% overall yield from methyl vinyl ketone dimer; bp, Kugelrohr, 40°C (0.25 Torr), lit. (2) bp 83°C (14 Torr).

Preparation of **4**a

A mixture of 0.79 g (5.13 mmol) of **3**, 0.31 g (5 mmol) of ethylene glycol, and ca. 5 mg of oxalic acid monohydrate was kept stirred at 25°C for 48 h. The reaction mixture was chromatographed on 25 g of neutral activity grade 3 alumina using 10–30% ether in hexanes (v/v, gradient) to afford 0.931 g (84%) of **4***a* as a colorless, thermally unstable oil that cyclized to **3** slowly upon standing and rapidly upon attempted distillation. The oil was therefore used immediately following chromatography; ir (film): 3450, 1715 cm^{-1}; ^1H nmr ($CDCl_3$) δ: 1.027 (t, J = 7.3 Hz, 3H), 1.20 (t, J = 7.2 Hz, 2H), 1.38 (s, 3H), 1.4–2.05 (m, 4H), 2.60 (m, 2H), 3.50 (m, 4H), 3.72 (br t, 1H), 4.08 (dd, J = 11.7, 3 Hz, 1H). Low resolution CIMS (isobutane) m/e: 217 ($M + H^+$). *Anal.* calcd. for $C_{11}H_{20}O_4$: C 61.09, H 9.32; found: C 61.02, H 9.25.

Preparation of **4**b

To a solution of 0.532 g (2.0 mmol) of **4***a* and 0.33 g (2.2 mmol) of *tert*-butyldimethylchlorosilane in 2.0 mL of dichloromethane were added 0.164 g (2.08 mmol) of pyridine and ca. 5 mg of DMAP and the reaction mixture was kept stirred at 25°C for 3 h. The reaction mixture was then diluted with 50 mL of ether and washed successively with 2 × 10 mL of 0.05 M KH_2PO_4 and 10 mL of H_2O, dried ($MgSO_4$), and solvents removed *in vacuo*. The residue, upon chromatography on 25 g of neutral activity grade 3 alumina using 10–30% ether in hexane (v/v, gradient) to afford 0.535 g (81%) of **4***b* as a colorless oil, was also thermally unstable and therefore must be stored in the fridge and used within a few days of purification; ir (film): 1720, 1052 cm^{-1}; ^1H nmr ($CDCl_3$) δ: 0.054 (s, 6H), 0.88 (s, 9H), 1.03 (t, J = 7 Hz, 3H), 1.36 (s, 3H), 1.2–2.0 (m, 6H), 2.61 (q, J = 7 Hz, 2H), 3.52 (m, 2H), 3.75 (m, 2H), 4.23 (dd, J = 11.7, 2.5 Hz, 1H). *Anal.* calcd. for $C_{17}H_{34}O_4Si$: C 61.77, H 10.37; found: C 61.71, H 10.16.

General procedure for hydride reduction of ***3***, **4**a, *and* **4**b

In the case of reduction by $NaBH_4$ the reaction was conducted at 0°C in methanol. All other reductions were conducted in dry THF. Thus, typically, the substrate (~0.5 mmol) was dissolved in 2 mL of dry THF and maintained under an atmosphere of argon. The solution was cooled to −78°C and the accompanying salt, if any (2 equivalents), was added. Next, a twofold excess of hydride reagent was added and the reaction was allowed to stir for 1 h at −78°C, then warmed slowly to room temperature. Excess hydride was quenched by addition of a proton source. In the case of $LiAlH_4$ reductions, reaction mixtures were treated with aqueous 5 M NaOH until aluminum salts precipitated. In the case of Dibal-H reductions, reaction mixtures were treated with methanol to achieve precipitation of aluminum salts. The salts were filtered and washed with ether. The aqueous portion of each reaction was extracted with 3 × 10 mL of ether. The combined ether extracts and washings were treated with 2 mL of 2 M H_2SO_4 if this was not already part of the work-up. The ether phase was separated and dried over anhydrous $MgSO_4$ and, where isolation was pursued, these ether extracts were concentrated *in vacuo* to give mixtures of *exo*- and *endo*-brevicomin in the yields and ratios reported in Table 1. Where isolation was not pursued, yields were estimated by capillary gas

Can. J. Chem. Downloaded from www.nrcresearchpress.com by 41.223.56.140 on 09/07/12
For personal use only.

chromatographic analyses of the ether extracts to which a known amount of *n*-dodecane internal standard had been added prior to treatment with aqueous 2 M H_2SO_4 and extraction with ether.

Acknowledgements

This work was funded by a Natural Sciences and Engineering Research Council Strategic Grant (Biotechnology) and an Operating Grant to A.C.O.

1. S. M. SINGH and A. C. OEHLSCHLAGER. Can. J. Chem. **66**, 209 (1988).
2. P. CHAQUIN, J.-P. MORIZUR, and J. KOSSANYI. J. Am. Chem. Soc. **99**, 903 (1977).
3. M. NÓGRÁDI. Stereoselective synthesis. VCH Publishers, New York. 1986. pp. 131–148.
4. K. SUZUKI, M. SHIMAZAKI, and G.-I. TSUCHIHASHI. Tetrahedron Lett. 6233 (1986).
5. K. MEAD and T.L. MACDONALD. J. Org. Chem. **50**, 422 (1985).
6. F. SATO, O. TAKAHASHI, T. KATO, and Y. KOBAYASHI. J. Chem. Soc. Chem. Commun. 1638 (1985).
7. M. LARCHEVEQUE and J. LALANDE. J. Chem. Soc. Chem. Commun. 83 (1985).
8. T. NAKATA, T. TANAKA, and T. OISHI. Tetrahedron Lett. 2653 (1983).
9. K. B. LIPKOWITZ, S. SCARPONE, B. P. MUNDY, and W. G. BORNMANN. J. Org. Chem. **44**, 486 (1979).
10. (*a*) C. A. BROWN. J. Am. Chem. Soc. **95**, 4100 (1973); (*b*) H. C. BROWN and S. KRISHNAMURTHY. J. Am. Chem. Soc. **94**, 7159 (1972); (*c*) W. G. GENSLER, F. A. JOHNSON, and A. D. B. SLOAN. J. Am. Chem. Soc. **82**, 6074 (1960).
11. K. ALDER, H. OFFERMANNS, and E. RUDEN. Chem. Ber. **74**, 905 (1941).

Can. J. Chem. Downloaded from www.nrcresearchpress.com by 41.223.56.140 on 09/07/12
For personal use only.

Synthesis and fast atom bombardment mass spectrometry of the coordination complexes of the ligand 5,5,7,12,12,14-hexamethyl-1,4,8,11-tetraazacyclotetradecane

CINDY LEE MACLAURIN, JACK MARTIN MILLER,[1] AND MARY FRANCES RICHARDSON
Department of Chemistry, Brock University, St. Catharines, Ont., Canada L2S 3A1

Received September 19, 1988

CINDY LEE MACLAURIN, JACK MARTIN MILLER, and MARY FRANCES RICHARDSON. Can. J. Chem. **67**, 797 (1989).

Metal complexes containing the ligand 5,5,7,12,12,14-hexamethyl-1,4,8,11-tetraazatetradecane were synthesized and characterized using electron impact (EI) and fast atom bombardment (FAB). The FAB mass spectra were obtained in positive and negative ion mode. FAB in the positive ion mode proved to be the most successful technique for the identification of these compounds. The majority of the FAB spectra obtained were structurally informative, although not all showed molecular (M^+) or quasimolecular ($[M + H]^+$) ions. The fragmentations observed were characteristic of the ligands and the metal, and were interpreted based on the chemical and spectroscopic properties of these compounds.

Key words: FAB mass spectroscopy, tetraazacyclotetradecane complexes.

CINDY LEE MACLAURIN, JACK MARTIN MILLER et MARY FRANCES RICHARDSON. Can. J. Chem. **67**, 797 (1989).

On a synthétisé des complexes métalliques contenant le ligand hexaméthyl-5,5,7,12,12,14 tétraaza-1,4,8,11 décane et on les a caractérisés par spectrométrie de masse sous impact électronique (IE) et par bombardement avec des atomes rapides (FAB). On a déterminé les spectres de masse par FAB tant dans le mode positif que négatif. La technique des spectres de masse par FAB dans le mode positif s'avère la plus utile pour l'identification de ces composés. Même si les spectres obtenus par cette technique ne présentaient pas tous des ions moléculaires (M^+) ou quasimoléculaires ($[M + H]^+$), la majorité d'entre eux s'est avérée utile pour la détermination des structures. Les fragmentations observées étaient caractéristiques des ligands et du métal et on les a interprétées en se basant sur les propriétés chimiques et spectroscopiques de ces composés.

Mots clés : spectrométrie de masse par FAB, complexes de tétraazacyclotétradécane.

[Traduit par la revue]

Introduction

Fast Atom Bombardment (FAB) mass spectrometry was introduced by Barber in 1981, and has become a popular ionization technique (1). The sample is dissolved in a matrix liquid (which resulted in long-lived spectra compared to solid samples (2)) and is energized by neutral atom bombardment (in the keV energy range). Sputtered ions characteristic of the sample are produced. Some common matrices are glycerol, sulfolane, thioglycerol, and nitrophenyloctylether and 3-nitrobenzyl alcohol.

Mass spectroscopic analysis of non-volatile, thermally labile inorganic complexes has generally proved so difficult that in the past mass spectroscopy has not been a common tool of the inorganic chemist. FAB makes it possible to obtain mass spectra of organometallic, coordination, and ionic compounds that could not be analyzed previously (3, 4).

Cerny *et al.* found that FAB fragments could be useful in predicting the solution chemistry of some neutral, 1+, and 2+ cationic transition metal coordination complexes (5). They obtained both parent ion information and fragments for the 1+ complexes and generalized that monodentate ligands are lost in preference to bidentate ligands. If redox processes occur, then the spectrum is complicated with many fragment peaks, most of these fragments being formed by the reduction of a higher oxidation state to a lower one. In those compounds in which metal reduction is disfavored, simple ligand loss occurred. Further, the solution chemistry of the complex was paralleled by FAB fragmentation.

Johnstone studied crown ether complexes of metallic cations using FAB (6, 7). Molecular ions of the type $[\text{crown} + M^{n+} + A^{(n-1)-}]^+$ (where A is the anion) were observed. Competitive reactions showed that the order of preference for complex formation with 18-crown-6 in Group 1 is K > Cs > Na, which reflects the trends found in solution. This trend is different for each crown ether investigated. It was suggested that this method could be used to rapidly analyze trace metals as low as 10^{-10} *M*. Johnstone also proposed a method by which stability constants could be measured (6). In another FAB–MS study (8), $[HgCl_2(18\text{-crown-}6)]$ gave a cluster of peaks centered at *m/z* 501, corresponding to the $[HgCl(18\text{-crown-}6)]^+$ ion. This shows that the mercury ion remains associated with the crown ligand despite the weak mercury-to-oxygen bonds. Finally, FAB–MS has been used to determine the nature of mixed-ligand magnesium complexes (9); oligomeric species were identified in which the mixed ligand content was retained.

We chose to study the metal complexes of the macrocyclic ligand 5,5,7,12,12,14-hexamethyl-1,4,8,11-tetraazacyclotetradecane, in order to determine the usefulness of FAB–MS in studying the chemistry of macrocyclic complexes. The ligand has two isomers, designated teta (the meso isomer) and tetb (the racemic isomer). We use the symbol L throughout this paper to represent this ligand generally, and the symbols teta and tetb when referring to a specific isomer.

Experimental

Mass spectra were obtained using a Kratos MS-30 double beam, double focusing mass spectrometer, retrofitted with a Kratos FAB source in beam 1. A resolution of 1000 and an accelerating voltage of 4 kV were used. Scan rates of 10 s/decade and 30 s/decade were used.

EI samples were introduced by a heated solids probe (beam 2) with an ionization voltage of 70 eV. The source temperature was varied between 180 and 220°C.

The samples for FAB were introduced on a stainless steel probe. The atom gun (Ion Tech) was operated at a voltage of 6–8 keV, at a source pressure of 10^{-5} Torr and a gun-current of 1–2 mA. All data collection and computation were done with a Kratos DS-55 data system with Brock modified software, including the programs BMASROS and BMASABD used for computation of isotopic multiplets and deconvolution of overlapping multiplets. Positive and negative FAB ion spectra were obtained, using Xe as the primary atom beam.

Infrared spectra were recorded on an Analect FX-6260 FTIR

[1]Author to whom correspondence should be addressed.

Can. J. Chem. Downloaded from www.nrcresearchpress.com by 41.223.56.140 on 09/07/12
For personal use only.

TABLE 1. Analytical data for complexes of L

Formula		Metal	C	H	N
$Hg_2Cl_4(C_{16}H_{36}N_4)$	% Found	48.07	23.43	4.50	—
	% Calculated	48.48	23.22	4.38	—
$CdCl_2(C_{16}H_{36}N_4)$	% Found	25.21	38.04	7.09	—
	% Calculated	24.03	41.09	7.76	—
$PtCl_4(C_{16}H_{38}N_4)$	% Found	—	30.70	6.07	8.93
	% Calculated	—	30.85	6.10	8.99
$ZnCl_2(C_{16}H_{36}N_4), H_2O$	% Found	—	43.16	8.41	12.45
	% Calculated	—	43.79	8.65	12.76
$NiCl_2(C_{16}H_{36}N_4), 3H_2O$	% Found	—	40.99	8.51	11.91
	% Calculated	—	41.05	9.04	11.97
$CuCl_2(C_{16}H_{36}N_4), H_2O$	% Found	—	44.13	8.68	13.18
	% Calculated	—	43.93	8.23	12.82

spectrometer. The shift in ν(N—H) was used to determine if complexation had occurred. All IR samples were prepared as KBr pellets. Elemental analysis were done by Galbraith Laboratories Inc., and Guelph Chemical Laboratories Ltd.

The macrocyclic ligand was obtained from the Parish Chemical Co., and Strem Chemicals Inc. The Parish chemical is a mixture of teta and tetb isomers and will be referred to as L. The chemical obtained from Strem has only the teta isomer present, and will be referred to as teta. One of the Strem lots was contaminated with Cl, probably due to teta.2HCl.

(1) Cobalt complexes: Co(teta)$CoCl_4$ was prepared according to the basic procedure of Endicott and co-workers (11). The remaining cobalt complexes $[Co(teta)(NO_2)(OH)]ClO_4.H_2O$, $[Co(teta)(NO_2)_2]$-$ClO_4.(1/2)H_2O$, $[Co(teta)ClN_3]ClO_4.H_2O$, $[Co(teta)Cl_2]Cl.4H_2O$, $[Co(teta)(CN)_2]ClO_4.H_2O$, $[Co(teta)(SCN)_2]SCN.H_2O$, $[Co(L)Cl_2]ClO_4$ (where L is a mixture of teta and tetb) were synthesized by the methods of Whimp and Curtis (12).

(2) $CdCl_2(L)$: 0.40 g of cadmium chloride was dissolved in 10 mL of warm distilled water and allowed to cool. A stoichiometric amount of the ligand was dissolved in 10 mL of 1-butanol and cooled. The ligand solution was then layered on top of the cadmium solution in a separatory funnel and allowed to stand for 48 h. A large quantity of precipitate formed at the interface. A small amount of precipitate had formed in the aqueous layer and this was drawn off. The precipitate from the interface was filtered, washed with 10 mL of cold 1-butanol, and allowed to air dry.

(3) $ZnCl_2(teta).H_2O$: 0.14 g of $ZnCl_2$ was dissolved in 5 mL of ethanol, and 0.23 g of the teta ligand in another 5 mL of ethanol. Both solutions were filtered and then combined. The resulting solution clouded and a white precipitate formed. The product was recrystallized using ethanol as the solvent.

(4) $NiCl_2(teta).3H_2O$: this complex has been prepared by Ito and Toriumi (13), but our method was different, being similar to that used for the zinc complex. Both the teta and $NiCl_2.6H_2O$ were dissolved in hot 1:1 ethanol/water and combined. The characteristic orange crystals of the low-spin $[Ni(teta)]Cl_2.3H_2O$ complex were obtained. The product turned mauve at approximately 160–165°C which represents a conversion of this product to the high-spin Ni complex (13).

(5) $CuCl_2(teta).H_2O$: 0.43 g of teta was dissolved in 10 mL of absolute ethanol. A stoichiometric amount of cupric chloride was dissolved in 5 mL of absolute ethanol and added to the teta solution. The combined solution was heated for 15 min, and filtered. After 24 h a blue precipitate formed and was filtered and recrystallized from hot ethanol.

$[Ag(teta)(ONO_2)_2]$, $[Mn(teta)Cl_2]Cl.3H_2O$, and $CuL(ClO_4)_2$ were prepared by literature methods (14–16). The $(HgCl_2)_2$(tetb) had been prepared previously (10). Elemental analysis data are provided in Table 1.

The FAB samples were prepared by adding approximately 0.1 g of the complex to 0.05 mL of the matrix liquid. The following matrices were used in an attempt to produce suitable spectra: nitrophenyloctylether (NPOE), di-*t*-amylphenol (DAP), Nujol, glycerol, thioglycerol, glycerol in sulfolane, sulfolane, polyethyleneglycol (PEG), glycerol/DMF, glycerol/water, 18-crown-6(10% tetraglyme), and 3-nitrobenzylalcohol (NBA). To increase the amount dissolved and thus to improve the quality of spectra, samples were left in the matrix for 12–24 h, which greatly improved the quality of the spectra obtained. Heating the sample slightly also improved the results.

Obtaining mass spectra for a number of the cobalt complexes proved to be difficult so a doping technique was employed. The sample (0.1 g) was dissolved in glycerol and then 0.05 mL of a 0.1 *M* NH_4Cl was added to provide doping anions. However, the chloride anion did not produce useful results for cobalt compounds that contained nitrite, so for these compounds 0.1 *M* $NaNO_2$ was used.

The method of sample preparation of Zhang and Liang (17) was used on a number of the more intractable complexes. The sample is dissolved in a suitable solvent and 2 μL of this solution is transferred to the surface of the liquid matrix on the probe tip using a microsyringe. The probe is then inserted into the vacuum lock, where the solvent is evaporated. After 1–2 min the probe is inserted into the ionization chamber.

Results and discussion

A. Electron impact ionization

Previous mass spectral studies of the ligand and its complexes have been concerned with molecular weight determination only (18, 19). The spectra of teta or tetb show the parent ion peak at m/z 284, with a peak at m/z 269 corresponding to the loss of one methyl group (18). Our own results are no better. Spectra could not be obtained for many complexes: those spectra obtained were short lived (one or two scans). The inability to obtain spectra using electron impact is believed to result from the involatility and thermal lability of these compounds, in agreement with Busch's work on iron complexes of the L ligand which showed only low m/z values due to the decomposition of the complex (19).

Molecular ions were not observed even when usable EI spectra were obtained. Spectra contained peaks due only to the decomposition of the complex. The EI spectra of the dinitro and dichloro cobalt complexes had in common uninterpretable peaks at m/z 333, 315, 301, and 287, as well as peaks due to the decomposition of the ligand. It should be noted that the cobalt complexes of $[Co(teta)ClNO_3]ClO_4$ and $[Co(teta)(OH)$-$(NO_2)]ClO_4$ also gave similar spectra, but barely above the detection threshold. The Ag, Mn, and Cd compounds had peaks

Can. J. Chem. Downloaded from www.nrcresearchpress.com by 41.223.56.140 on 09/07/12
For personal use only.

TABLE 2. Major peaks in the FAB negative ion spectra of the $Me_6[14]aneN_4$ complexes

$Co(teta)(CoCl_4)$			$[Co(L)Cl_2]ClO_4$			$[Cu(L)](ClO_4)_2$			$CdCl_2(L)$		
Fragment	m/z	% (TIC)	Fragment	m/z	% (TIC)	Fragment	m/z	% (TIC)	Fragment	m/z	% (TIC)
Cl^-	35	(68.5)	Cl^-	35	(30.5)	Cl^-	35	(24.1)	$CdCl_2^-$	184	(18.8)
$CoCl_2^-$	129	(4.6)	ClO_4^-	99	(50.1)	ClO_4^-	99	(44.5)	$CdCl_3^-$	219	(45.2)
$CoCl_3^-$	164	(5.2)				$Cu(ClO_4)Cl^-$	199	(2.1)			
						$Cu(ClO_4)(ClO_3)^-$	247	(0.9)			
						$Cu(ClO_4)_2^-$	263	(4.9)			

due only to the decomposition of the ligand, teta. The mercury complex had peaks corresponding to Hg^+ and $HgCl_2^+$, as well as ligand decomposition peaks. The $CuL(ClO_4)_2$ spectrum had peaks due to the presence of $[CuL]^+$ and $[CuLClO_4]^+$, however, these peaks were of extremely low intensity. The $Ni(teta)Cl_2$ complex showed a peak due to $[Ni(teta)]^+$. The fragmentation pattern of the nickel complex is similar to the cobalt complexes, as it has the same peaks present in the 300–350 range as the cobalt complexes. The fragmentation products from the ligand are easily observed in all the EI spectra of the complexes as well as the ligand itself.

B. Negative ion FAB

Negative ion FAB was attempted for about one third of the complexes. The results were rather unproductive in terms of providing molecular ions or fragment ions containing the ligand. The complexes for which negative ion FAB results were obtained were $Co(teta)CoCl_4$, $[CoLCl_2]ClO_4$, $Cu(L)(ClO_4)_2$, and $CdCl_2(L)$. The major fragments are shown in Table 2. Results could not be obtained either for the $(HgCl_2)_2(tetb)$ or the $Ni(teta)Cl_2$ complexes.

In the $[CoLCl_2]ClO_4$ spectrum, the base peak was the perchlorate ion, followed in intensity by the peak due to the chloride ion with the remaining peaks of low intensity. The most intense peak in the $Co(L)CoCl_4$ spectrum corresponded to the chloride ion, with other peaks due to $[CoCl_2]^-$ and $[CoCl_3]^-$ ions.

The $[Cu(L)](ClO_4)_2$ spectrum was remarkably similar to the $[Co(L)Cl_2]ClO_4$ in that the anion with the greatest intensity was the perchlorate. The second most intense peak was due to the chloride ion, most likely resulting from the perchlorate species. A reasonably intense cluster of peaks was obtained around mass m/z 263, which corresponded in isotope pattern to $[Cu(ClO_4)_2]^-$. Peaks at m/z 247 and 199 corresponded to $[Cu(ClO_4)(ClO_3)]^-$ and $[CuCl(ClO_4)]^-$. Thus the perchlorate ion decomposes under FAB conditions to produce chloride ion, consistent with the reducing nature of the matrix under FAB conditions.

The loss of the counter ion ClO_4^- in the $[Co(L)Cl_2]ClO_4$ spectrum was expected in terms of what has been found by other workers (5, 18, 20). The chloride and the perchlorate anions had been used in a study by Cohen *et al.* (20). As with our present work, Cohen *et al.* found that no negative ions of any analytical significance were observed.

C. Positive ion FAB mass spectra

Figures 1 and 2 show the EI and FAB mass spectra of the ligand. The FAB spectrum is cleaner, and the total ion current (TIC) is an order of magnitude higher than in the EI spectrum. Furthermore, the highest-intensity peak in the FAB spectrum is the protonated molecular ion at m/z 285 (21% TIC), whereas the molecular ion is only 1.9% of the TIC in the EI spectrum.

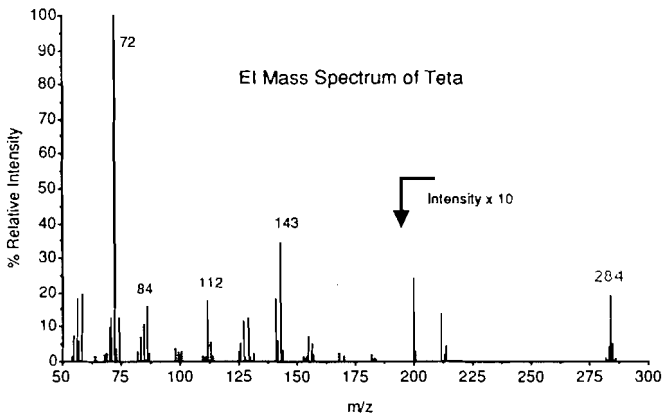


FIG. 1. EI mass spectrum of teta.

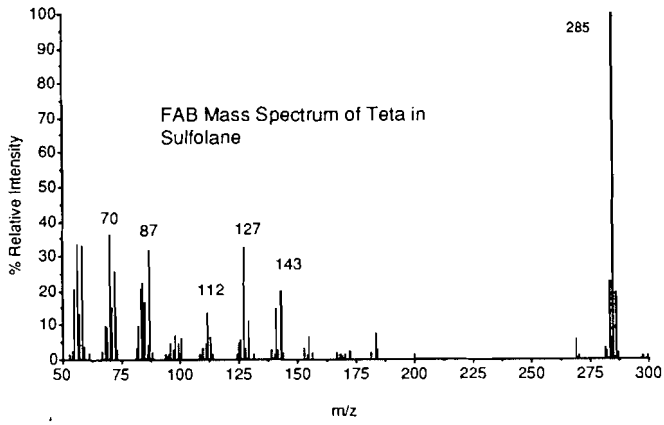


FIG. 2. FAB mass spectrum of teta in sulfolane.

(a) Studies on the cobalt complexes

Figure 3 illustrates the positive ion FAB spectra of a typical cobalt(III) compound. The matrix used was monothioglycerol, which gives a significantly more intense spectrum than that in glycerol. The principal positive ions result from the cation $[C^+]$, the subsequent loss of the anionic ligands (accompanied by reduction of the metal) followed by Co(III) loss, and the formation of ions originating from the teta ligand.

The $teta^+$ and the $[Co(teta)]^+$ species are common to all the positive ion spectra of the cobalt compounds. These observed ion clusters are complicated because of successive loss of hydrogen via ion/molecule or matrix/molecule reactions.

The spectrum of the uncomplexed ligand also had peaks due to addition and subtraction of hydrogens. The quasimolecular ion at m/z 285 was very intense, and the peaks due to hydrogen loss were of minor intensity. In the cobalt spectra the quasimolecular ion associated with the teta species is weak and the

Can. J. Chem. Downloaded from www.nrcresearchpress.com by 41.223.56.140 on 09/07/12
For personal use only.

TABLE 3. Comparison of the ion intensities in the FAB mass spectra of the $[Co(teta)Cl_2]Cl$ and $[Co(L)Cl_2]ClO_4$ complexes

	Ion intensities[a]			
	$[Co(teta)Cl_2]Cl$		$[Co(L)Cl_2]ClO_4$	
Ions observed	Glycerol	Thioglycerol	Glycerol[b]	Thioglycerol
C^+	22.3	50.8	2.2	27.1
$(C - Cl)^+$	30.0	24.1	45.2	44.5
$(C - 2Cl)^+$	45.2	23.1	45.2	28.4
$(C - 2Cl - Co)^+$	2.6	0.2	7.5	0.0

[a]Ion intensities are a percentage of the teta-containing species. Isotope cluster peak intensities of the same elemental composition are summed and included with the parent species. Peaks due to deprotonation of an elemental cluster are also summed and included with the parent peak.
[b]$C^+ = Co(teta)Cl_2^+$.

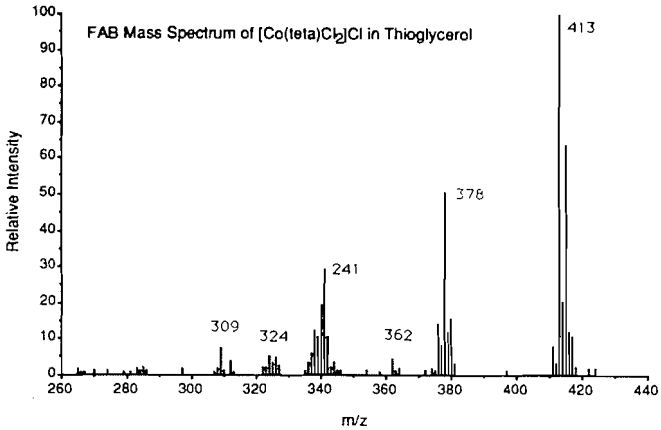


FIG. 3. FAB mass spectrum of the cobalt teta chloride complex.

surrounding peaks are more intense. The explanation for the observed dehydrogenation of these species will be discussed later.

For the cobalt(III) cationic complexes which have perchlorate as the counter ion, a peak is observed corresponding to $[Co(II)(L)ClO_4]^+$. This is interesting since the perchlorate ion is often used where an anion unlikely to coordinate is required, although if no other donor is present to compete with the perchlorate, it can behave as a donor (21). The intensity of this species is low in all the cobalt perchlorate complexes. Further there is a great difference in the intensities of the peaks that are obtained in the spectra of $[Co(L)Cl_2]ClO_4$ and $[Co(teta)Cl_2]Cl$ (Table 3), and the clusters of peaks due to dehydrogenation of the $[Co(L)]^+$ or $[Co(teta)]^+$ ions have very different patterns in the two spectra. One possible explanation for these differences is that the outer sphere ion affects the spectrum, although this is contrary to results obtained by other authors (20); it is also possible that $[Co(L)Cl_2]ClO_4$ is actually a mixture of the teta and tetb complexes, or is even just the tetb complex. This has implications for the structures of the complexes since teta prefers to coordinate in a planar fashion to give a *trans*-octahedral complex, whereas the most stable tetb coordination occurs when tetb folds and a *cis*-octahedral complex is produced (22).

Good quality spectra were obtained for the $[Co(teta)(CN)_2]ClO_4$ and the $[Co(teta)(SCN)_2]SCN$ complexes in both glycerol and thioglycerol.

Molecular cations or molecular ions could not be obtained for a number of the cobalt complexes. The $Co(teta)CoCl_4$ spectrum proved to be very difficult to analyze, and a molecular ion could not be obtained. The ions that were observed were similar to $[CoLCl_2]ClO_4$ or $[Co(teta)Cl_2]Cl$ complexes. Peaks were observed at masses which corresponded to $[Co(teta)Cl_2]^+$, $[Co(teta)Cl]^+$, $[Co(teta)]^+$, and $teta^+$. The blue $(Co(teta))(CoCl_4)$ turned pink upon dissolving in most of the matrices used, indicating destruction of the deep blue $CoCl_4^{2-}$ ion.

It was also difficult to obtain spectra of $[Co(teta)(NO_2)(OH)]ClO_4.H_2O$ and $[Co(teta)(NO_2)_2]ClO_4.(1/2)H_2O$ due to low solubility, and the ions that were observed were of low intensity. Even the doping method using NH_4Cl and $NaNO_2$ did not produce worthwhile results. The C^+ molecular ion was not obtained for the $[Co(teta)(NO_2)(OH)]ClO_4$ complex, nor was a peak observed for the $[Co(teta)(OH)]^+$ species even in a thioglycerol matrix. The cation molecular ion peak was obtained in both glycerol and thioglycerol matrices for the dinitro complex, as well as the peak created by the loss of one NO_2 group. The intensities of these species were low, particularly in glycerol.

$[Co(teta)ClN_3]ClO_4$ did not produce a C^+ parent ion. The azide was not observed in any of the peaks present in the spectrum. This is not an uncommon observation, as previous EI work done with inorganic azides had shown that these compounds show a distinct preference for N_3^- loss (23). The major peaks were $[Co(teta)]^+$ and the $[Co(teta)Cl]^+$. Other peaks included the $[Co(teta)Cl_2]^+$ and the $[Co(teta)ClO_4]^+$ ions. $[Co(teta)Cl_2]^+$ might be due to perchlorate decomposition.

(b) Studies on the complexes of metals other than cobalt

For the remaining metal complexes, the matrix did not have a great effect on the spectrum observed, as the spectra appeared the same in both glycerol and thioglycerol.

Spectra of the complexes $Ag(teta)(ONO_2)_2$ and $(HgCl_2)_2(tetb)$ proved to be extremely difficult to obtain. Both the silver and the mercury complex showed ligand-related peaks with a wide variety of matrices. The di-mercury complex gave spectra when the coprecipitation technique was employed. Methanol was the solvent used to dissolve the complex and glycerol was the matrix layered on the probe tip. The peaks at m/z 485, m/z 521, and m/z 593 were identified as the $[Hg(tetb)]^+$, $[Hg(tetb)Cl]^+$, and $[Hg(tetb)Cl_3]^+$ species, respectively.

$[Mn(teta)Cl_2]Cl.3H_2O$, $CdLCl_2$, and $Zn(teta)Cl_2.H_2O$ had the $(\mathbf{M}(teta)Cl)^+$ as the most intense peak in the spectrum (where **M** represents the metal, since M represents the molecular ion). The cluster due to the $[\mathbf{M}(teta)Cl]^+$ represented more

Can. J. Chem. Downloaded from www.nrcresearchpress.com by 41.223.56.140 on 09/07/12
For personal use only.

TABLE 4. The observed ion intensities in the positive ion FAB mass spectra of the L metal complexes of Cd, Zn, and Mn in glycerol and thioglycerol

$CdCl_2(L)$			$Zn(teta)Cl_2.H_2O$			$[Mn(teta)Cl_2]Cl.3H_2O$		
Fragment	m/z	% (TIC)	Fragment	m/z	% (TIC)	Fragment	m/z	% (TIC)
Thioglycerol matrix								
teta + H	285	(4.9)	teta + H	285	(2.3)	teta + H	285	(4.3)
Cd(teta)Cl	433	(14.9)	Zn(teta) − H	347	(0.9)	Mn(teta)Cl	375	(35.3)
			Zn(teta)Cl	383	(35.5)			
Glycerol matrix								
teta + H	285	(3.3)	teta + H	285	(1.3)	teta + H	285	(1.4)
Cd(teta)Cl	433	(35.7)	Zn(teta) − H	347	(1.1)	Mn(teta)Cl	375	(32.8)
			Zn(teta)Cl	383	(35.0)			
			$(Zn(teta))_2Cl_3$	805	(0.4)			

Can. J. Chem. Downloaded from www.nrcresearchpress.com by 41.223.56.140 on 09/07/12
For personal use only.

than 35% of the TIC for these complexes in glycerol. This was also true of the Mn and Zn complexes in a thioglycerol matrix; however, the cluster was reduced to 15% for the Cd complex using thioglycerol. The only other peak of significant intensity in the spectra of the Cd and Mn complexes was the teta or L peak. The zinc complex had a peak corresponding to the $[Zn(teta) - H]^+$ species as well as the $[teta + H]^+$ species. The spectrum of $Zn(teta)Cl_2$ in glycerol also has a cluster at m/z 805 which corresponded in isotope pattern to the species $[(Zn(teta))_2Cl_3]^+$. It should be noted that these peaks are of minor intensity in comparison to the $[\mathbf{M}(teta)Cl]^+$ peak which overwhelms the spectra. Table 4 gives the intensities of the peaks obtained in the spectra of the Zn, Cd, and Mn complexes. The appearance of the $[\mathbf{M}(teta)Cl]^+$ ion as the highest-mass peak is normal for chlorinated compounds, which usually exhibit much stronger $[M - Cl]^+$ peaks than $[M]^+$ peaks (8, 9). This is to be contrasted with the Cu and Ni complexes which do not give strong $[\mathbf{M}(teta)Cl]^+$ peaks, possibly because the chloride is not coordinated, or only weakly coordinated in these complexes.

The spectra of $Cu(L)(ClO_4)_2$ and the $Cu(teta)Cl_2$ are similar. The species common to these compounds included $teta^+$, $[Cu(teta)]^+$, and $[Cu(teta)X]^+$, where X is the anion, either ClO_4^- or Cl^-. The spectrum of $Cu(teta)Cl_2$ in thioglycerol has a peak at m/z 800 which corresponds to $[(Cu(teta))_2Cl_3 - H]^+$, as well as the other common peaks.

The $Cu(teta)(ClO_4)_2$ spectrum includes a cluster of peaks due to the $[Cu(teta)Cl]^+$ species. This cluster is believed to be a result of ClO_4^- decomposition and is more predominant in thio-matrices. This is consistent with the results obtained in the negative ion FAB mass spectrum of this complex, as ions were observed which were formed as a result of the decomposition of perchlorate (Table 2). The $[\mathbf{M}(teta)Cl]^+$ ion has been observed before in cobalt complexes containing no coordinated chloride, but having perchlorate as the outersphere anion.

There is a strong correspondence between the copper complexes and the nickel complex in terms of the species obtained in the FAB spectra. The nickel complex has peaks due to $teta^+$, $[Ni(teta)]^+$, and $[Ni(teta)Cl]^+$. A peak also appears at m/z 423 whose identity is unknown; it may result from some type of matrix interaction. As in the mercury and silver complexes the protonated ligand peak at m/z 285 is the most intense peak in this spectrum.

TABLE 5. The data from the deconvolution calculation of the complex $[Co(teta)(SCN)_2]SCN$, the % composition of the dehydrogenated fragments

Fragment	% Composition[a]
Co(teta)	4.9
Co(teta)-H	26.6
Co(teta)-2H	12.0
Co(teta)-3H	22.7
Co(teta)-4H	5.4
Co(teta)-5H	15.2
Co(teta)-6H	11.1
Co(teta)-7H	1.4
Co(teta)-8H	0.4

[a]NOTE: Species with less than 1% composition are not statistically valid but are known to exist on a chemical basis.

(c) Dehydrogenation

It is common in the teta complexes to observe successive dehydrogenations of the main fragment ions. A good example is the $[Co(teta)]^+$ ion which loses up to eight hydrogens. Least squares analysis of the peak cluster associated with this ion gave the percentages of the various dehydrogenated species; Table 5 shows the results for $[Co(teta)(SCN)_2]SCN$. Five other cobalt complexes were also examined in this way. In each instance, the percent composition obtained for each fragment was comparable, confirming that the spectra are reproducible. The results for $[Co(teta)(SCN)_2]SCN$ complex in glycerol and thioglycerol are also very similar. Further, the teta complexes of Cu and Ni also display dehydrogenation of the $[\mathbf{M}(teta)]^+$ species with dehydrogenation occurring one step at a time. Hydrogen loss occurs independently of the matrix, indicating that it is not due to a specific matrix/ion reaction.

The extent of dehydrogenation is dependent on the presumed oxidation state of the metal in the fragment. For example, $[Cu(teta)Cl]^+$ and $[Ni(teta)Cl]^+$, which contain metal ions in the 2+ oxidation state, show a small amount of dehydrogenation, but this is minor compared to that observed for $[Cu(teta)]^+$ and $[Ni(teta)]^+$. Similarly, $[Co(teta)Cl_2]^+$ shows no dehydrogenation, but it is extensive in $[Co(teta)]^+$ and $[Co(teta)Cl]^+$.

These dehydrogenations are consistent with the fact that

TABLE 6. Comparison of C^+ and $(C - X)^+$ for the series of cobalt complexes $[Co(teta)X_2]Y$ in glycerol and thioglycerol

Complex	C^+	$(C-X)^+$	$C^+/(C-X)^+$
Matrix: glycerol			
$[Co(teta)Cl_2]ClO_4$	2.2	45.2	1/21
$[Co(teta)(SCN)_2]SCN$	1.2	17.6	1/15
$[Co(teta)(NO_2)_2]ClO_4$	1.9	5.6	1/3
$[Co(teta)(CN)_2]ClO_4$	3.1	6.3	1/2
Matrix: thioglycerol			
$[Co(teta)Cl_2]ClO_4$	27.1	44.5	0.6/1
$[Co(teta)(SCN)_2]SCN$	18.0	22.7	0.8/1
$[Co(teta)(NO_2)_2]ClO_4$	9.5	3.2	3/1
$[Co(teta)(CN)_2]ClO_4$	53.3	2.7	20/1

oxidative dehydrogenation is a useful synthetic technique for new macrocyclic complexes (24). The ease of oxidation is metal–ion dependent, and the proposed mechanisms involve higher oxidation states of the metal (24–26). The aliphatic rings become unsaturated as a result of the dehydrogenation (26, 27).

Our data suggest that an essential requirement for dehydrogenation in the FAB–MS is that the metal ion be in an easily oxidized oxidation state. This is consistent with the first step of the oxidative dehydrogenation mechanism, which is a $1\text{-}e^-$ oxidation of the metal (26). The overall mechanism for the production of dehydrogenated species probably involves the following processes: reduction of the parent complex during the ionization step, consistent with the fact that reduction is commonly observed in FAB spectra (5, 28); loss of one or more anionic ligands to produce a singly charged species; and rapid successive loss of hydrogens by oxidative dehydrogenation.

The solution chemistry of these complexes in the 1+ oxidation state has no parallel to the reaction observed in FAB–MS. Dehydrogenation of the 1+ oxidation state has not been observed in the electrochemistry of these complexes (29, 30). It has been noted by Busch that the overall oxidation–reduction behaviour of the macrocyclic metal complexes is a function of the degree and type of ligand unsaturation (30).

In the Cu(I) complexes it is necessary to have some degree of unsaturation in the ligand in order for Cu(I) macrocyclic complexes to exist in solution. It has been published that this behaviour is related to σ and π bonding features of the Cu(I) macrocycle (31). It is possible if unsaturation exists for Cu(I) to transfer electron density to low energy antibonding orbitals of the ligand through a π mechanism (32), and as a result stabilize the Cu(I) complex.

Similar arguments would apply to the Ni(I) and Co(I) complexes. As mentioned, the FAB spectra of the nickel and cobalt complexes show extensive dehydrogenation for fragments in which the metal is formally in the 1+ oxidation state, (and the 1+ and 2+ state for cobalt).

The case for oxidative dehydrogenation is strengthened by the results obtained in oxidizing matrices containing nitro groups such as NBA. $[Co(teta)(CN)_2]ClO_4$ and $[Cu(teta)](ClO_4)_2$ showed increased dehydrogenation of the $[\mathbf{M}(teta)]^+$ cations. Thus the oxidizing matrix may help to facilitate the oxidation of the metal, the initial step in the dehydrogenation mechanism (26).

(d) π-Acidity

We also hoped that FAB would mimic the solution chemistry of these complexes. The complexes $[Co(teta)X_2]Y$ (Y = SCN or ClO_4 and X = NO_2, SCN, CN, and Cl) were studied to see if a π-acidity trend might be discovered by FAB. Two different matrices were used for the study, glycerol and thioglycerol. In the glycerol matrix, the $[C - X]^+$ species had a more intense peak than the C^+ species. In thioglycerol, the opposite trend was observed. This type of effect is not uncommon and may be explained in terms of the reducing potential of the matrix. Pelzer investigated the oxidation–reduction chemistry of glycerol solutions under ion (SIMS) or atom (FAB) bombardment. A reduction process occurred in glycerol for both inorganics and organics (33). The reduction process occurring in glycerol solutions could be governed by a simple redox equilibrium between hydrogen atoms produced in glycerol by bombardment and the oxidized species present in solution. Meili and Seibl also investigated matrix effects in the FAB analysis of cobalamines (34). They concluded that if any metal-containing system appears to give as the highest mass ion in FAB a species corresponding to the reduction of the metal, then a slightly oxidizing matrix is advisable.

In glycerol, $[C - X]^+$ is more intense than C^+. The process involves reduction of the Co(III) center to Co(II) accompanied by the formation of an X radical; this process is favoured over X dissociation. Since glycerol enhances reduction (35), according to Meili a slightly oxidizing matrix should produce the opposite effect, i.e. increase the C^+ cation concentration. This is in fact what is observed in thioglycerol: the C^+ peak is more intense than the $[C - X]^+$ peak. Thus, the thioglycerol is sufficiently oxidizing to produce the desired molecular ion. It is clearly important that the matrix be kept constant in comparing trends among complexes. Table 6 shows the intensity of the C^+ and the $[C - X]^+$ species for the complexes of interest in both glycerol and thioglycerol. Previous workers have used a ratio of $C^+/[C - X]^+$ when making comparisons in spectra of similar complexes (36), where C^+ is the cation and $[C - X]^+$ represents the cation minus an axial ligand.

In both matrices, the trend observed is that of $CN^- > NO_2^- > SCN^- > Cl^-$ in terms of the relative intensity of the parent ion versus loss of the axial ligand. This is a familiar trend in terms of the ability of the ligand to split the *d* orbitals.

Conclusions

Molecular weights, or more correctly, cationic weights, were obtained in the majority of the spectra. There were exceptions such as the nitrite-containing cobalt complexes and the complexes containing two metal ions. The problem in producing quality spectra for these complexes was their insolubility, a prerequisite for obtaining a good spectrum being sufficient solubility in the matrix.

In those complexes which yielded good spectra, the ion with the greatest intensity at high m/z could be attributed to the complex. Peaks did occur at high m/z values which could not be attributed to the complex, but these were usually of low intensity. The cobalt complexes gave spectra containing the intact cation $[Co(teta)X_2]^+$, and the fragments from this cation. These complexes did not have ions corresponding to the (cation + anion) in positive ion FAB. Information concerning the anion could be easily obtained using negative FAB–MS. However, care had to be exercised in the interpretation of the spectra containing perchlorates, since perchlorates were both reduced and sometimes coordinated under FAB conditions.

The metal(II) complexes have the $[\mathbf{M}(teta)X]^+$ ion as the highest mass cluster in the spectrum. No other peaks could

Can. J. Chem. Downloaded from www.nrcresearchpress.com by 41.223.56.140 on 09/07/12
For personal use only.

be identified at higher m/z values. Although this provides information concerning the metal and the anion present, it would not allow for the complete identification of the complex. The oxidation state of the metal would still be lacking for a total determination.

The information obtained through a comparison of peak heights allowed for the determination of the chemical reactivity of the complexes. A π-acidity trend was determined through a comparison of the C^+ and $[C - X]^+$ peaks which paralleled known solution behaviour.

Acknowledgements

We wish to thank the Natural Sciences and Engineering Research Council of Canada for operating grant support (J.M.M. and M.F.R.), the Government of Ontario for scholarship support (C.L.M.), and NSERC, The Shaver Foundation, The Bickell Foundation, and the Joseph E. DeFees Grant of the Research Corporation for equipment support.

1. M. Barber, R. S. Bordoli, R. D. Sedgwick, and A. N. Tyler. J. Chem. Soc. Chem. Commun. 325 (1981).
2. M. Barber, R. S. Bordoli, E. J. Elliott, R. P. Sedgwick, and A. N. Tyler. Anal. Chem. **54**, 645A (1982).
3. J. M. Miller. Fast atom bombardment mass spectrometry and related techniques. *In* Advances in inorganic chemistry and radiochemistry. *Edited by* H. J. Emeleus and A. G. Sharp. Academic Press, New York. 1984. p. 28.
4. M. I. Bruce and M. J. Liddell. Appl. Organomet. Chem. **1**, 191 (1987).
5. R. L. Cerny, B. P. Sullivan, M. M. Bursey, and T. J. Meyer. Anal. Chem. **55**, 1954 (1983); R. L. Cerny, B. P. Sullivan, M. M. Bursey, and T. J. Meyer. Inorg. Chem. **24**, 397 (1985).
6. R. A. W. Johnstone and M. E. Rose. J. Chem. Soc. Chem. Commun. 1268 (1983).
7. R. A. W. Johnstone and I. A. S. Lewis. Int. J. Mass Spectrom. Ion Phys. **46**, 451 (1983).
8. C. R. Paige and M. F. Richardson. Can. J. Chem. **62**, 332 (1985).
9. P. R. Ashton, D. E. Fenton, R. N. Prasad, M. Jindal, and M. Jain. Inorg. Chim. Acta, **146**, 99 (1984).
10. M. R. Burke and M. F. Richardson. Inorg. Chim. Acta, **69**, 29 (1983).
11. D. P. Rillema, J. F. Endicott, and E. Papaconstaninou. Inorg. Chem. **10**, 1739 (1971).
12. P. O. Whimp and N. F. Curtis. J. Chem. Soc. A, 867 (1966).
13. T. Ito and K. Toriumi. Acta Crystallogr. B**37**, 88 (1981).
14. K. B. Mertes. Inorg. Chem. **17**, 49 (1978).
15. P. S. Bryan and J. C. Dabrowiak. Inorg. Chem. **14**, 296 (1975).
16. N. F. Curtis. J. Chem. Soc. 2644 (1964).
17. M.-Y. Zhang and X.-Y. Liang. Anal. Chem. **56**, 2288 (1984).
18. B. E. Douglas. Inorg. Synth. **18**, 12 (1978).
19. J. C. Dabrowiak, P. H. Merrell, and D. H. Busch. Inorg. Chem. **11**, 1979 (1972).
20. A. I. Cohen, K. A. Glaven, and J. F. Kronauge. Biomed. Mass Spectrom. **10**, 287 (1983).
21. F. A. Cotton and G. Wilkinson. Advanced inorganic chemistry. 4th ed. John Wiley and Sons, Inc., New York. 1980. pp. 174, 560.
22. P. O. Whimp, M. F. Bailey, and N. F. Curtis. J. Chem. Soc. A, 1956 (1970).
23. J. M. Miller and T. R. B. Jones. The chemistry of functional groups. Part 1. *Edited by* Saul Pati and Zvi Rappoport. John Wiley and Sons, Great Britain. 1983. p. 96.
24. C. J. Hipp, L. F. Lindoy, and D. H. Busch. Inorg. Chem. **11**, 1988 (1972).
25. G. M. Brown, T. R. Weaver, F. R. Keene, and T. J. Meyer. Inorg. Chem. **15**, 190 (1976).
26. J. F. Endicott and B. Durham. *In* Coordination chemistry of macrocyclic compounds. *Edited by* G. A. Melson. Plenum, New York. 1979. p. 431.
27. E. K. Barefield and M. T. Mocella. J. Am. Chem. Soc. **97**, 4238 (1975).
28. G. Bojesen. Org. Mass Spectrom. **20**, 413 (1985).
29. J. Vasilevskis and D. C. Olson. Inorg. Chem. **10**, 1228 (1971).
30. F. V. Lovecchio, E. Gore, and D. H. Busch. J. Am. Chem. Soc. **96**, 3109 (1974).
31. L. Fabbrizzi, A. Lari, and A. Poggi. Inorg. Chem. **21**, 2083 (1982).
32. L. Fabbrizzi and A. Poggi. J. Chem. Soc. Dalton Trans. 2191 (1983).
33. G. Pelzer, E. DePauw, D. V. Dung, and J. Marien. J. Phys. Chem. **88**, 5065 (1984).
34. J. Meili and J. Seibl. 31st Annu. Conf. Mass Spec. (ASMS) Boston. May, 1983.
35. B. Sundqvist, P. Roepstorff, J. Fohlman, A. Hedin, P. Hakansson, I. Kamensky, M. Lindberg, M. Salehpour, and G. Sawe. Science, **226**, 696 (1984).
36. J. Miller. J. Organomet. Chem. **249**, 299 (1983).

Can. J. Chem. Downloaded from www.nrcresearchpress.com by 41.223.56.140 on 09/07/12
For personal use only.

Dielectric relaxation of acetyl- and benzoyl-acetones

R. K. KHANNA[1] AND ABHA BHATNAGAR
Microwave Laboratory, Physics Department, Government College, Ajmer-305 001, Rajasthan, India

Received May 26, 1988[2]

R. K. KHANNA and ABHA BHATNAGAR. Can. J. Chem. **67**, 804 (1989).

Dielectric absorption measurements are reported at radio and microwave frequencies (at six different wavelengths) for acetylacetone and benzoylacetone solutions in benzene, in a temperature range 25–60°C. Analysis of dielectric data in terms of Cole–Cole arc plots and multiple relaxation processes reveals that, at higher temperatures, overall molecular relaxation is the dominant relaxation mechanism in these β-diketones. The observed relaxation times, distribution parameters, and dipole moments are in reasonable agreement with the few data reported for some temperatures, in the literature. The activation energy parameters are also evaluated assuming dielectric relaxation to be a rate process. Molar polarization vs. weight fraction (concentration) plots show anomalous behaviour for acetylacetone.

Key words: dielectric properties, dielectric losses, relaxation times, dipole moment, dielectric absorption and dispersion, microwave measurements.

R. K. KHANNA et ABHA BHATNAGAR. Can. J. Chem. **67**, 804 (1989).

Opérant à des températures allant de 25 à 60°C et à six longueurs d'onde couvrant des fréquences radio et micro-ondes, on a mesuré les absorptions diélectriques des acétyl- et benzoyl-acétones en solution dans le benzène. Une analyse des données diélectriques en fonction d'une courbe de Cole–Cole et des processus de relaxations multiples révèle que, à des températures plus élevées, la relaxation moléculaire globale est le mécanisme de relaxation prédominant dans ces β-dicétones. Les valeurs observées pour le temps de relaxation, le paramètre de distribution et le moment dipolaire sont en bon accord avec les quelques données disponibles dans la littérature, pour quelques températures. En faisant l'hypothèse que la relaxation diélectrique est un processus impliquant une vitesse, on en a aussi évalué les paramètres d'activation. Dans le cas de l'acétyl acétone, les courbes de polarisation molaire en fonction de la fraction molaire exprimée en poids (concentration) présentent des anomalies.

Mots clés : propriétés diélectriques, pertes diélectriques, temps de relaxation, moment dipolaire, absorption et dispersion diélectrique, mesures micro-ondes.

[Traduit par la revue]

Introduction

Dielectric relaxation measurements can be profitably used, apart from NMR and IR absorption, to study inter- and intramolecular hydrogen bonding. These studies in solutions containing electron donor molecules can reveal valuable information, such as complex formation, extent of hydrogen bonding, and, in general, molecular motion (1–4). β-Diketones are known to form an intramolecular hydrogen bond and have been found to exist predominantly in enolic form in dilute solution. Relatively few studies have been carried out on the dielectric behaviour of β-diketones, especially acetylacetone and benzoylacetone. The excess value of the dielectric constant of binary mixtures of acetylacetone with carbon tetrachloride and tetrachloroethylene at 383.15 K has been studied by Jain *et al.* (5). Dielectric permittivity and loss measurements have been reported by Gupta *et al.* (6) for benzoylacetone and *p*-substituted benzoylacetone at a single frequency in the microwave region and at a single temperature of 40°C. Similar types of dielectric measurements have also been reported by Purohit *et al.* (7) on some β-diketones, but again at a single temperature of 35°C. In general there appear to be few, and limited, investigations on these molecules. For an accurate collection of relaxation data, dielectric measurements must be carried out at different frequencies (at least three) so as to have an even distribution of points in the Cole–Cole plot and a point at high frequency (8). Hence in the present paper dielectric measurements on β-diketone solutions in benzene are presented in the extended high frequency region (up to 67.7 GHz) and at temperatures ranging from 25 to 60°C.

Experimental

Measurements of dielectric constant (ε') and dielectric loss (ε'') were made on β-diketones in benzene solution at five different concentrations (weight fraction from 0.010 to 0.035) at 1000 MHz, 8.8 GHz, 30.5 GHz, and 67.7 GHz using four different experimental arrangements. Transmission line methods were used for the 1000-MHz, 8.8-GHz, and 30.5-GHz (plunger technique) measurements, and a free space interferometric technique was used for the 67.7-GHz measurements. The details of the apparatus and technique have been described previously (9–11). The estimated accuracy of dielectric constant and dielectric loss is 1% and 3% for the transmission line methods, and 0.5% and 1% for the free space method. In addition, the static dielectric constant was measured at 10 kHz using a dipolemeter bridge, and the value of ε_∞ from the refractive index (n) in the optical region (sodium light) was determined using an Abbé refractometer. The temperature of the solution under study was maintained within ±1°C by circulating water around the dielectric cell from a temperature controlled bath.

Analysis of data

For dilute solutions of polar solutes in a nonpolar solvent, the dielectric constant (ε') and dielectric loss (ε'') are proportional to solute concentration expressed as weight fractions (W_2) of the solute, i.e.,

$$\begin{aligned} \varepsilon' &= \varepsilon_1' + a' W_2 \\ \varepsilon'' &= a'' W_2 \\ \varepsilon_0 &= \varepsilon_{01} + a_0 W_2 \\ \varepsilon_\infty &= \varepsilon_{\infty 1} + a_\infty W_2 \end{aligned} \qquad [1]$$

The measured values of ε', ε'', ε_0, and ε_∞ for different solutions were fed into the computer as a function of ω and, from the straight line best-fit program, the coefficients a', a'', a_0, and

[1]Author to whom correspondence may be addressed.
[2]Revision received December 16, 1988.

Can. J. Chem. Downloaded from www.nrcresearchpress.com by 41.223.56.140 on 09/07/12
For personal use only.

TABLE 1. Values of slope parameters a_0, a', a'', and a_∞ for β-diketones at different temepratures and at different frequencies

Frequency	25°C		30°C		40°C		50°C		60°C	
Acetylacetone	$a_0 = 10.40$ $a_\infty = 0.20$		$a_0 = 10.10$ $a_\infty = 0.18$		$a_0 = 9.66$ $a_\infty = 0.16$		$a_0 = 9.35$ $a_\infty = 0.15$		$a_0 = 7.04$ $a_\infty = 0.14$	
1000 MHz	10.00	0.55	9.87	0.52	9.30	0.45	9.00	0.44	8.85	0.41
8.8 GHz	8.35	2.20	8.30	2.10	7.8	2.10	7.65	2.05	7.55	1.90
30.5 GHz	4.50	3.30	4.40	3.15	4.20	3.00	3.75	2.90	3.45	2.80
67.7 GHz	2.85	2.65	2.65	2.60	2.55	2.10	2.10	2.20	1.80	2.11
Benzoylacetone	$a_0 = 7.95$ $a_\infty = 0.35$		$a_0 = 7.78$ $a_\infty = 0.28$		$a_0 = 7.86$ $a_\infty = 0.26$		$a_0 = 6.51$ $a_\infty = 0.25$		$a_0 = 6.50$ $a_\infty = 0.20$	
1000 MHz	7.40	0.80	7.30	0.75	6.65	0.80	6.12	0.75	6.10	0.70
8.8 GHz	4.70	2.40	4.60	2.40	4.10	2.35	3.90	2.22	3.85	2.22
30.5 GHz	1.80	1.70	1.68	1.68	1.58	1.72	1.40	1.60	0.90	1.31
67.7 GHz	1.19	1.20	1.00	1.15	0.89	1.10	0.80	1.00	0.61	0.90

a_∞ were obtained. The values of these slope parameters for acetylacetone and benzoylacetone at different frequencies and temperatures are presented in Table 1. The most probable relaxation time (τ_0) and distribution parameter (α) were obtained at different temperatures by fitting the data to Cole–Cole plots represented by the equation:

$$[2] \quad \frac{(a' - ja'') - a_\infty}{a_0 - a_\infty} = \frac{1}{(1 + j\omega\tau_0)^{1-\alpha}}$$

Typical Cole–Cole plots for acetylacetone in benzene solution at different temperatures (25°C, 30°C, 40°C, 50°C, and 60°C) are shown in Fig. 1. The values of α and mean relaxation time (τ_0) are presented in Table 2. The equation for evaluating the dipole moment by Higasi's method (12) is

$$[3] \quad \mu = B(a_0 - a_\infty)^{1/2}$$

where

$$B = \frac{1}{2(\varepsilon_1 + 2)}\left[\frac{27M_2kT}{\pi N d_1}\right]^{1/2}$$

M_2 is the molecular weight of the solute, k is the Boltzman constant, d_1 is the density of the solvent, ε_1 is the dielectric constant of the solvent, and N is the Avogadro number. Calculated values of the dipole moment at different temperatures are given in Table 3. The dielectric data were also analysed in terms of overall and group rotation of the molecules. Double relaxation analysis was carried out using Bergmann's equations, which were further simplified by Bhattacharya *et al.* (13) for a straightforward calculation. Bergmann's equations are

$$[4] \quad \frac{a' - a_\infty}{a_0 - a_\infty} = A = \frac{g_1}{1 + \omega^2\tau_1^2} + \frac{g_2}{1 + \omega^2\tau_2^2}$$

$$[5] \quad \frac{a''}{a_0 - a_\infty} = B = \frac{g_1\omega\tau_1}{1 + \omega^2\tau_1^2} + \frac{g_2\omega\tau_2}{1 + \omega^2\tau_2^2}$$

and

$$g_1 + g_2 = 1$$

The simplified relation is

$$[6] \quad \frac{1 - A}{B\omega} = (\tau_1 + \tau_2) - \frac{A\omega}{B}\tau_1\tau_2$$

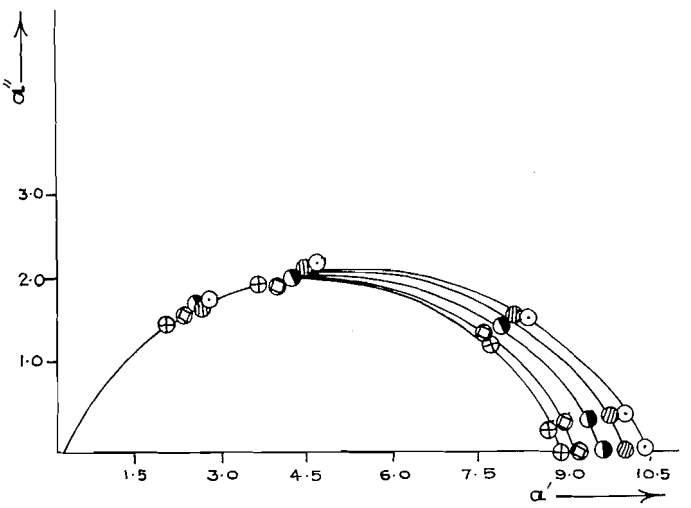


FIG. 1. Cole–Cole plots for acetylacetone in benzene solution at different temperatures: ⊙ 25°C; ◍ 30°C; ◑ 40°C; ⊘ 50°C; ⊕ 60°C.

This linear equation was solved and τ_1 and τ_2 were evaluated for different g_1 and g_2 values. The consolidated results are given in Table 4.

Results and discussion

For both the β-diketones, i.e., acetylacetone and benzoylacetone, fairly smooth depressed semicircular arc plots could be drawn between slope parameters a' and a''. Examination of the results in Table 2 shows a fairly large value of the distribution parameter (α) for both the β-diketones, while Crossley (14) found very small values for the distribution parameter for some aliphatic ketones in cyclohexane. The value of α is found to decrease with increasing temperature. This may be due to greater uniformity in the energy barrier at higher temperature, hindering molecular relaxation processes. The significant value of the distribution parameter for β-diketones indicates the presence of more than one mechanism contributing to the dielectric relaxation. The Cole–Cole plots also reveal a notable difference between ε_∞ and n^2, which further suggests the presence of an additional high frequency internal mode of vibration. A similar observation for many polar liquids has been reported and discussed by many workers (15). Data from

Can. J. Chem. Downloaded from www.nrcresearchpress.com by 41.223.56.140 on 09/07/12
For personal use only.

TABLE 2. Values of the distribution parameter (α) and mean relaxation time (τ_0) obtained from Cole–Cole plots for two β-diketones in benzene at different temperatures

Temperature (°C)	Acetylacetone		Benzoylacetone	
	Distribution parameter (α)	Relaxation time ($\tau_0 \times 10^{12}$ s)	Distribution parameter (α)	Relaxation time ($\tau_0 \times 10^{12}$ s)
25	0.27	5.46	0.25	14.50
30	0.25	5.22	0.23	14.53
40	0.24	5.18	0.20	14.23
50	0.22	4.92	0.18	14.17
60	0.20	4.85	0.16	13.49

TABLE 3. Values of dipole moment for β-diketones in benzene obtained by different methods at different temperatures

Temperature (°C)	Acetylacetone		Benzoylacetone	
	Higasi μ (D)	Guggenheim μ (D)	Higasi μ (D)	Guggenheim μ (D)
25	3.04	2.92	3.40	3.34
30	3.03	2.90	3.35	3.23
40	3.02	2.76	3.24	3.21
50	3.01	2.75	3.22	3.20
60	3.00	2.72	3.20	3.18

Table 2 also show that the mean relaxation time (τ_0) for benzoylacetone is very large (about three times) compared to acetylacetone. This may be partly due to large molecular size and partly because of a hindrance to free rotation expected to arise from intramolecular hydrogen bonding. Such intramolecular hydrogen bonding and its effect on the dielectric relaxation mechanism of the molecules has been reported by Antony *et al.* (16) for the case of phenols. For both β-diketones, the value of the mean relaxation time (τ_0) decreases with a rise in temperature, which is normal behaviour for a polar solute in a nonpolar solvent.

Double relaxation analysis by Bhattacharya's method (13) led to values of relaxation time τ_1 of 14.1 and 26.8 ps at 30°C for acetylacetone and benzoylacetone, respectively. The value of τ_1 for acetylacetone is found to be very large compared to the only literature value (7) known to the authors (8 ps at 35°C). For the benzoylacetone no such values are available in the literature. τ_1 exhibits the temperature variation to be expected for overall molecular rotation. Again, the value of τ_2 for acetylacetone (3.8 ps at 30°C) is found to be large compared to the literature value of 0.7 ps at 35°C (7). The τ_2 value shows relatively little dependence on temperature (Table 4), as may be expected for an intramolecular process. The large value of τ_2 indicates intramolecular hydrogen bonding, hindering the free group rotation in these molecules. For both the β-diketones the value of weight factors g_1 compares well with g_2 at low temperatures ($g_1 = 0.44$ at 25°C) while at higher temperatures $g_1 \gg g_2$ ($g_1 = 0.69$ and 0.74 at 60°C for acetylacetone and benzoylacetone, respectively). The increasing value of g_1 with temperature indicates that overall molecular rotation is becoming more prominent at higher temperature. The tendency of τ_2 to become less important at higher temperature suggests that this need not result from the intramolecular segment rotation, which will be more prominent at higher temperature, but may result from an intramolecular cooperative relaxation mechanism, so that the reorientation of one segment triggers many other reorientations and consequently the rotating group does not relax independently.

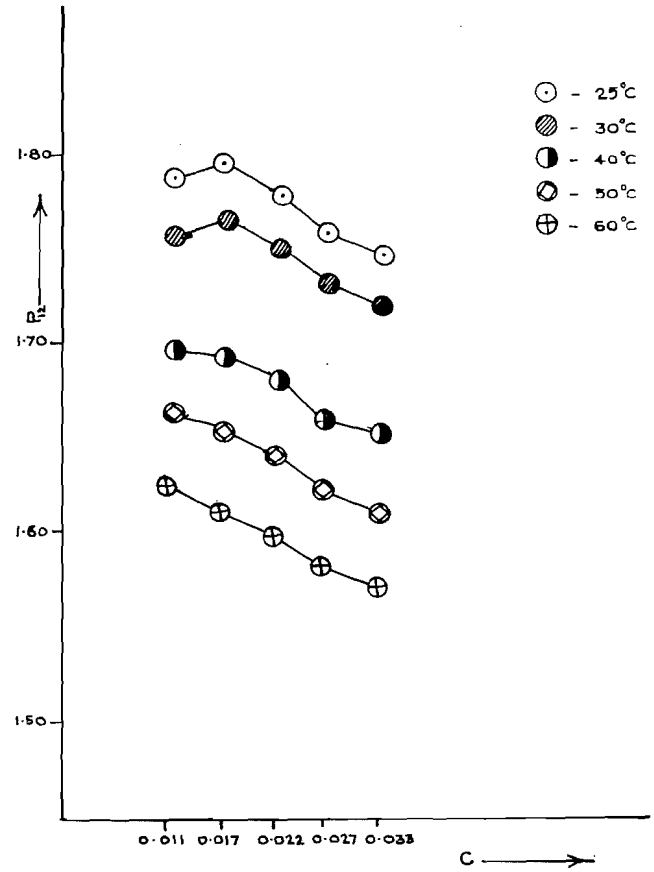


FIG. 2. Plot of log ($\tau_0 T$) vs. $1/T$ for acetylacetone and benzoylacetone.

Dipole moments of these molecules have been determined in dilute solution in benzene using Guggenheim's method at RF frequency and Higasi's method at microwave frequencies. The dipole moment values at different temperatures are listed in Table 3. Dipole moment values obtained by Guggenheim's method are found to be small compared to those obtained by Higasi's method, at all temperatures, which may be due to the difference in the square of the refractive index and dielectric constant of solution. Present values of the dipole moment for acetylacetone and benzoylacetone, i.e., 3.03 D and 3.35 D respectively at 30°C, by Higasi's method, compare well with

Can. J. Chem. Downloaded from www.nrcresearchpress.com by 41.223.56.140 on 09/07/12
For personal use only.

TABLE 4. Values of relaxation time for overall rotation (τ_1), group rotation (τ_2), and weight factors (g_1) for β-diketones in benzene at different temperatures

Temperature (°C)	Acetylacetone			Benzoylacetone		
	Relaxation time		Weight factor	Relaxation time		Weight factor
	$\tau_1 \times 10^{12}$ (s)	$\tau_2 \times 10^{12}$ (s)	g_1	$\tau_1 \times 10^{12}$ (s)	$\tau_2 \times 10^{12}$ (s)	g_1
25	15.0	5.0	0.44	28.0	8.0	0.46
30	14.1	3.8	0.52	26.8	6.2	0.54
40	10.0	2.3	0.56	24.8	5.5	0.60
50	9.8	2.0	0.61	23.8	4.6	0.66
60	8.1	0.7	0.69	22.0	3.8	0.74

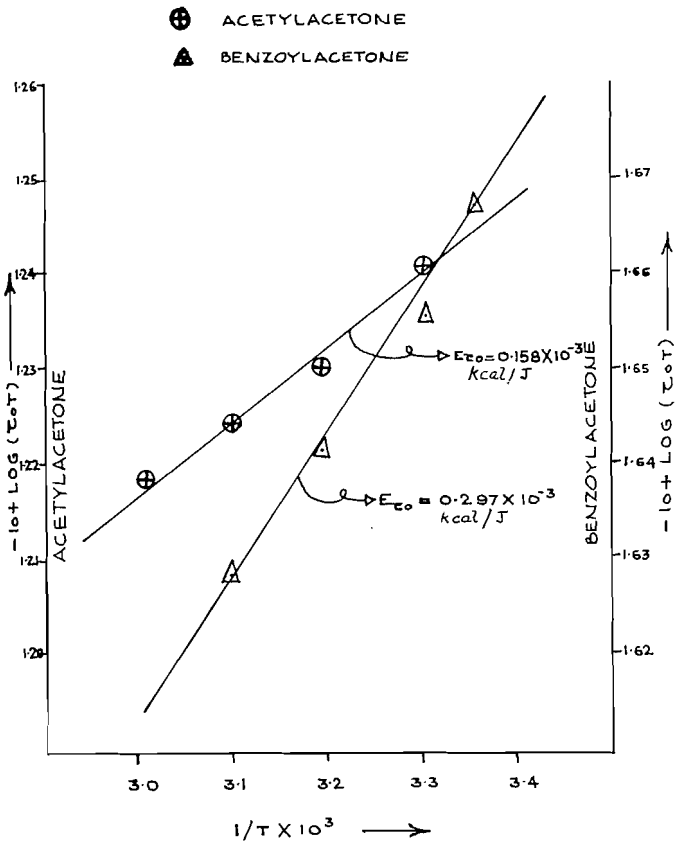


FIG. 3. Molar polarization (P_{12}) vs. concentration in wt. fraction (c) plot for acetylacetone in benzene at different temepratures.

the reported (7) values (3.00 D and 3.34 D respectively at 35°C). These values are found to be high compared to values reported by Gupta *et al.* (6) for benzoylacetone (2.68 D at 40°C). The dipole moments were also calculated theoretically by combining vectorially the group moments (17, 18), assuming the enolic form for both acetylacetone and benzoylacetone in benzene solution. The calculated value of the dipole moment for acetylacetone is 2.98 D and for benzoylacetone is 2.62 D, which are small compared to experimental results. Small deviations in these values from the experimental results may be due to neglect of hydrogen bonding and the mesomeric effect (6) in the theoretical calculations.

From the temperature variation of relaxation times (τ_0), the free energy of activation for the molecular relaxation mechanism is evaluated for both β-diketones using the Eyring equation (19), assuming it to be a rate process.

$$[10] \quad \ln(\tau_0 T) = \ln(h/k) + (E_{\tau_0}/R)T^{-1}$$

where h is Plank's constant, k the Boltzman constant, T the absolute temperature, R the gas constant, and E_{τ_0} the free energy of activation. When $\log(\tau_0 T)$ were plotted against $1/T$ for different diketones, a good linear relationship within experimental error was observed. Figure 2 gives such a linear plot along with the values of activation energy for both acetylacetone ($E_{\tau_0} = 0.158 \times 10^{-3}$ kcal/J) and benzoylacetone ($E_{\tau_0} = 0.297 \times 10^{-3}$ kcal/J) in benzene solution.

The molar polarization vs. weight fraction (concentration) curves for acetylacetone at different temperatures show anomalous behaviour (Fig. 3). In place of the decrease with increasing concentrations usually observed for an unassociated solute in nonpolar solvent, these curves show maxima and minima for acetylacetone while for benzoylacetone this anomalous behaviour is not observed. The anomalous behaviour for acetylacetone was also found to be less predominant at higher temperatures. These observations indicate complex formation and the presence of hydrogen bonding. IR absorption studies reported earlier (20) also show a similar type of behaviour for these compounds.

Acknowledgements

The authors would like to express their sincere thanks to Prof. J. Sobhandri, Physics Department, IIT Madras, and Dr. M. L. Sisodia, Physics Department, University of Rajasthan, Jaipur, for permitting the authors to use some of their apparatus for these measurements and for useful discussions. The authors are grateful to the Principal Government College, Ajmer, for providing the facilities for this work. Thanks are also due to Principal, Regional College of Education, Ajmer, for the permission to use their computer for data analyses.

1. G. WILLIAMS. Chem. Rev. **7**, 89 (1978).
2. M. A. MAZID, M. A. ENAVETULLAH, and S. WALKER. J. Chem. Soc. Faraday Trans. 2, **77**, 1143 (1931).
3. M. W. EVANS, G. J. EVANS, W. T. COFFEY, and P. DRIGOLINE. Molecular dynamics and theory of broad band spectroscopy. Wiley/Interscience, New York. 1982.
4. V. I. GAIOUL and Y. P. KALMYKOV. J. Mol. Liq. **34**, 1 (1987).
5. V. S. DHARAM JAIN, R. K. WADI, and B. S. SAINI. Ind. J. Chem. Soc. A, 488 (1979).
6. P. C. GUPTA, M. L. ARRAWATIA, and M. L. SISODIA. Ind. J. Pure Appl. Phys. **16**, 934 (1978).

Can. J. Chem. Downloaded from www.nrcresearchpress.com by 41.223.56.140 on 09/07/12
For personal use only.

7. H. C. PUROHIT, S. KUMAR, and A. D. VYAS. Z. Naturforsch. A: Phys. Phys. Chem. Kosmophys. **32**, 684 (1977).
8. D. FARMER and S. WALKER. Tetrahedron, **22**, 111 (1966).
9. R. K. KHANNA and J. SOBHANDRI. J. Phys. D: **5**, 1453 (1972).
10. R. K. KHANNA and J. SOBHANDRI. Ind. J. Pure Appl. Phys. **12**, 268 (1974).
11. M. JEYARAJ and J. SOBHANDRI. Can. J. Phys. **59**, 1698 (1988).
12. K. HIGASI. Denaki Kenkyusho Ino, **4**, 231 (1952).
13. J. BHATTACHARYA, A. HASAN, S. B. ROY, and G. S. KASTHA. J. Phys. Soc. Jpn. **28**, 284 (1970).
14. J. CROSSLEY. J. Chem. Phys. **56**, 2549 (1972).
15. N. E. HILL. Proc. R. Phys. Soc. **82**, 723 (1963).
16. A. A. ANTONY, F. K. FONG, and C. P. SMYTH. J. Phys. Chem. **68**, 2035 (1964).
17. C. P. SMYTH. Dielectric behaviour and structure. McGraw Hill, London. 1955.
18. V. I. MINKIN, O. A. OSIPOV, and Y. A. ZHADANOV. Dipole moments in organic chemistry. *Translated by* B. J. Hazard. Plenum Press, London. 1970. Chap. III.
19. E. EYRING, S. GLASSTON, and K. J. LAIDLER. The theory of rate processes. McGraw Hill, New York. 1941. p. 477.
20. S. BRATOZ, D. HADZI, and G. ROSSMY. Trans. Faraday Soc. **54**, 464 (1956).

Can. J. Chem. Downloaded from www.nrcresearchpress.com by 41.223.56.140 on 09/07/12
For personal use only.

Solubility of nonpolar gases in 2-methylcyclohexanone between 273.15 and 303.15 K at 101.32 kPa partial pressure of gas

MARIA ASUNCION GALLARDO, MARIA DEL CARMEN LOPEZ, JOSE SANTIAGO URIETA,[1] AND CELSO GUTIERREZ LOSA
Química Física, Facultad de Ciencias, Universidad de Zaragoza, 50009-Zaragoza, Spain

Received July 22, 1988

MARIA ASUNCION GALLARDO, MARIA DEL CARMEN LOPEZ, JOSE SANTIAGO URIETA, and CELSO GUTIERREZ LOSA. Can. J. Chem. **67**, 809 (1989).

Solubility measurements of several nonpolar gases (He, Ne, Ar, Kr, Xe, H_2, D_2, N_2, CH_4, C_2H_4, C_2H_6, CF_4, SF_6, and CO_2) in 2-methylcyclohexanone at 273.15–303.15 K and a partial pressure of gas of 101.32 kPa are reported. Thermodynamic functions (Gibbs energy, enthalpy, and entropy) for the solution process at 298.15 K and 101.32 kPa partial pressure of gas are evaluated. Use is made of the Scaled Particle Theory applied to gas solubility for determining Lennard-Jones (6, 12) pair-potential parameters and temperature dependence of the effective hard-sphere diameter of the solvent. The values that this theory predicts for the solution thermodynamic functions are also calculated.

Key words: 2-methylcyclohexanone, gas solubility, thermodynamic functions of solution, Henry coefficient, scaled particle theory.

MARIA ASUNCION GALLARDO, MARIA DEL CARMEN LOPEZ, JOSE SANTIAGO URIETA et CELSO GUTIERREZ LOSA. Can. J. Chem. **67**, 809 (1989).

Opérant à des températures allant de 273,15 à 303,15 K et à des pressions partielles de gaz de 101,32 kPa, on a effectué des mesures de solubilité de plusieurs gaz non polaires (He, Ne, Ar, Kr, Xe, H_2, D_2, N_2, CH_4, C_2H_4, C_2H_6, CF_4, SF_6 et CO_2) dans la méthyl-2 cyclohexanone. On a évalué les fonctions thermodynamiques (énergie de Gibbs, enthalpie et entropie) des processus de solution à 298,15 K et à une pression partielle de gaz de 101,32 kPa. On a appliqué la théorie de la particule scalaire à la solubilité des gaz pour déterminer les paires de paramètres de potentiel de Lennard-Jones (6, 12) et la relation entre la température et le diamètre effectif de la sphère dure du solvant. On a aussi calculé les valeurs que cette théorie permet de prédire pour les fonctions thermodynamiques de solution.

Mots clés : méthyl-2 cyclohexanone, solubilité de gaz, fonctions thermodynamiques de solution, coéfficient de Henry, théorie de la particule scalaire.

[Traduit par la revue]

Introduction

In a previous paper in this same journal we presented the solubility measurements of some nonpolar gases in cyclohexanone (1). In the present work we are interested in studying the influence of the presence of methyl groups in the molecule on both solubility and thermodynamic functions, and on intermolecular interactions between the solvent molecules. We started to do so by choosing 2-methylcyclohexanone as solvent for our experiments. The Scaled Particle Theory (SPT) as applied by Pierotti to gas solubility (2) assumes a Lennard-Jones (6, 12) potential well for the interactions between molecules, and allowed us to determine the corresponding interaction parameters for 2-methylcyclohexanone. Thermodynamic functions for the solution process are also reported.

Experimental

Equipment and the procedure used for solubility measurements have been described in detail elsewhere (3, 4); the volume of gas dissolved in a known (by calibration of the solution vessel) mass of solvent at constant pressure and temperature is determined and, assuming ideality of the gas phase, the mole fraction of the solute in the liquid phase, x_2, is calculated. The apparatus is lodged in a thermostatic air bath, the temperature of which is controlled within ±0.2 K. The temperature of the solution vessel is controlled within ±0.05 K. The precision in the mole fraction x_2 is estimated to be ±0.7%, except for gases with low solubility (He and Ne) for which it is approximately ±2.0%. For CO_2, both dry gas and a slightly different procedure were used (see ref. 4), and mole fraction x_2 was calculated taking into account the nonideality of the gas by introducing the CO_2 gas virial coefficient (5).

By means of different empirical approaches (6, 7) the virial coefficients for the solvent and the mixture were estimated, and from them the mole fractions for C_2H_4, C_2H_6, and SF_6, taking into account the nonideality of the gas phase. Such estimates led to mole fractions 1%, 1.4%, and 2% higher, respectively, than when ideality is assumed. One must bear in mind that this is simply a reckoning of the error, because the lack of experimental data for 2-methylcyclohexanone and the gas mixtures studied meant that most of the values for the necessary properties and parameters (even the critical data for the solvent) were merely estimates.

Gases were from Sociedad Española del Oxígeno, except Ne and CF_4, which were from Baker, and their mole-percentage purities were as follows: He 99.995, Ne 99.9, Ar 99.9990, Kr 99.95, Xe 99.995, H_2 99.99, D_2 99.4, N_2 99.998, CH_4 99.95, C_2H_4 99.90, C_2H_6 99.0, CF_4 99, SF_6 99.5, and CO_2 99.998.

2-Methylcyclohexanone was a Merck product (better than 98%) and its purity was checked by refractive index measurements (experimental n_D (293.15 K) = 1.44766; lit. (8) n_D = 1.4483) and by glc (2-methylcyclohexanone: 98.1%). The main impurity, in a proportion of 0.6%, was found to be cyclohexanone, which has similar solubilities (differences of 25% on average). Solvent vapour pressures were determined in our laboratory in the working temperature range, and fit the equation

$$[1] \quad \ln (p/\text{kPa}) = -5552.37\,(T/\text{K})^{-1} + 18.046$$

The densities of 2-methylcyclohexanone were taken from the literature (9).

Results and discussion

Table 1 shows the experimental equilibrium mole fraction of gas, x_2, in 2-methylcyclohexanone at temperatures ranging from 273.15 to 303.15 K and at a partial pressure of gas of 101.32 kPa. The results for x_2 (101.32 kPa, T) were fitted by a least-squares routine to an equation of the form

$$[2] \quad -\ln x_2 = A_0 + A_1 T^{-1}$$

over the given temperature range. Table 1 also contains the

[1]Author to whom correspondence may be addressed.

Printed in Canada / Imprimé au Canada

Can. J. Chem. Downloaded from www.nrcresearchpress.com by 41.223.56.140 on 09/07/12
For personal use only.

Can. J. Chem. Downloaded from www.nrcresearchpress.com by 41.223.56.140 on 09/07/12
For personal use only.

TABLE 1. Experimental solubility of gases ($x_2 \cdot 10^4$) in 2-methylcyclohexanone at 101.32 kPa partial pressure of gas between 273.15 and 303.15 K, values of the coefficients A_1 of eq. [2], and standard deviations as defined by eq. [3]

	T (K)							
Gas	273.15	283.15	293.15	298.15	303.15	A_0	A_1	σ
He	0.688	0.781	0.896	0.950	1.02	5.6256	1082.84	0.0071
Ne	0.968	1.08	1.21	1.29	1.37	5.7553	954.13	0.0081
Ar	9.73	9.69	9.72	9.68	9.70	6.9694	−9.17	0.0021
Kr	34.5	32.4	30.7	29.9	29.1	7.3755	−465.66	0.0005
Xe	176	154	135.0	127.0	119.7	7.9460	−1067.39	0.0011
H_2	2.31	2.51	2.72	2.80	2.89	6.0866	624.03	0.0031
D_2	2.45	2.64	2.82	2.92	3.00	6.2649	559.61	0.0016
N_2	4.59	4.74	4.94	5.03	5.10	6.6028	296.46	0.0028
CH_4	24.1	22.9	21.9	21.5	21.1	7.3759	−367.62	0.0002
C_2H_4	188	164	140.7	131.5	122.8	8.3232	−1190.24	0.0068
C_2H_6	204	175	150	140.1	130.9	8.4036	−1233.29	0.0032
CF_4	5.60	5.61	5.63	5.67	5.69	7.3332	42.72	0.0021
SF_6	31.9	29.2	27.1	26.3	25.2	8.0784	−635.96	0.0029
CO_2	272	221	185	166	153	9.4330	−1592.35	0.0061

fitting coefficients A_0 and A_1, and the standard deviation σ,

[3] $\sigma^2 = \Sigma[\ln x_{2,i} - (A_0 + A_1 T_i^{-1})]^2/(n-2)$

No literature data were found for any of the systems studied.

The changes in partial molar Gibbs free energy, $\Delta G^0_{m,2}$, partial molar enthalpy, $\Delta H^0_{m,2}$, partial molar entropy, $\Delta S^0_{m,2}$, for the solution process (10–12)

[4] Y(gas, 101.32 kPa, T)
$\rightarrow$ Y(P, T, $x_2 = 1$ but infinite dilute solution behaviour)

and Hildebrand entropy, ΔS_H (10–12) for

[5] Y(gas, 101.32 kPa, T) $\rightarrow$ Y($p_2 = 101.32$ kPa, T, x_2 but infinite dilute solution behaviour)

were evaluated from the fitting coefficients A_0 and A_1 in eq. [2], using our experimental results. Table 2 shows the values obtained for $\Delta G^0_{m,2}$, $\Delta H^0_{m,2}$, $\Delta S^0_{m,2}$, and ΔS_H at 298.15 K.

SPT applied by Pierotti (2, 13, 14) to the gas solution process can be used as a method for predicting Henry coefficients when Lennard-Jones (6, 12) pair-potential parameters for both solute and solvent are known, and can also be used in a reverse way for calculating Lennard-Jones (6, 12) pair-potential parameters of the solvent when experimental solubility data are provided and the corresponding parameters for the gases are known (1, 2, 4, 12–22).

Readers are referred to other papers for a detailed description of SPT for gases (2, 13–17, 23). According to this theory, solution can be thought of as a two-step process, the first consisting of the creation of a cavity in the solvent large enough to accommodate the solute molecule, and the second consisting of the introduction into the cavity of a solute molecule that interacts with the solvent. For the thermodynamic functions associated with the solution process the following expressions are obtained (2, 13–16, 23):

[6] $\Delta G^0_{m,2} = -RT \ln K_H = G_c + G_i + RT \ln (RT/v_1^0)$

[7] $\Delta H^0_{m,2} = [\partial(\Delta G^0_{m,2}/T)/\partial(1/T)]_p = H_c + H_i - RT + \alpha_p RT^2$

[8] $T\Delta S^0_{m,2} = H_c - RT + \alpha_p RT^2 - G_c - RT \ln (RT/v_1^0)$

TABLE 2. Experimental values for partial molar Gibbs energy, $\Delta G^0_{m,2}$, partial molar enthalpy, $\Delta H^0_{m,2}$, partial molar entropy, $\Delta S^0_{m,2}$, and partial molar Hildebrand entropy, ΔS_H, of dissolution of gases in 2-methylcyclohexanone at 298.15 K and 101.32 kPa partial pressure of gas

Gas	$\Delta G^0_{m,2}$ (kJ mol^{-1})	$\Delta H^0_{m,2}$ (kJ mol^{-1})	$\Delta S^0_{m,2}$ (kJ K^{-1} mol^{-1})	ΔS_H (kJ K^{-1} mol^{-1})
He	22.95	9.0	−0.047	0.030
Ne	22.20	7.9	−0.048	0.027
Ar	17.20	−0.08	−0.058	0.000
Kr	14.41	−3.87	−0.061	−0.013
Xe	10.82	−8.87	−0.066	−0.030
H_2	20.28	5.19	−0.051	0.017
D_2	20.18	4.65	−0.052	0.016
N_2	18.83	2.46	−0.055	0.008
CH_4	15.23	−3.06	−0.061	−0.010
C_2H_4	10.74	−9.9	−0.069	−0.033
C_2H_6	10.58	−10.3	−0.070	−0.034
CF_4	18.53	0.36	−0.061	0.001
SF_6	14.74	−5.29	−0.067	−0.018
CO_2	10.14	−13.2	−0.078	−0.044

where R is the gas constant, T the absolute temperature, $K_H = p_2/x_2$ is the Henry's law constant, p_2 being the partial pressure of gas and x_2 the gas mole fraction in the solution, v_1^0 is the molar volume of the pure solvent, and α_p is the thermal expansion coefficient of the solvent; the subscripts 1 and 2 refer to the solvent and the solute respectively, and c and i refer to the cavity formation and interaction steps respectively.

For the cavity formation contribution to the free energy, use is made of SPT developed by Reiss *et al.* (24) and, for the interaction, a Lennard-Jones (6, 12) potential corrected with a term for the dipole-induced dipole interaction.

By means of eq. [6] Lennard-Jones (6, 12) pair-potential parameters for the solvent can be determined. The necessary properties for gases were taken from the literature (15) and the dipole moment of the solvent was estimated, from dielectric permittivity measurements, to be 2.93 D. The value found for the effective hard-sphere diameter of 2-methylcyclohexanone

TABLE 3. Thermodynamic functions, $\Delta G^0_{m,2}$, $\Delta H^0_{m,2}$, and $\Delta S^0_{m,2}$, for the dissolution of gases in 2-methylcyclohexanone at 298.15 K and 101.32 kPa partial pressure of gas calculated according to SPT for gases

Gas	$\Delta G^0_{m,2}$ (kJ mol^{-1})	$\Delta H^0_{m,2}$ ($l_1 = 0$) (kJ mol^{-1})	$\Delta H^0_{m,2}$ ($l_1 \neq 0$) (kJ mol^{-1})	$\Delta S^0_{m,2}$ ($l_1 = 0$) (kJ K^{-1} mol^{-1})	$\Delta S^0_{m,2}$ ($l_1 \neq 0$) (kJ K^{-1} mol^{-1})
He	22.12	4.7	9.4	−0.043	−0.046
Ne	19.45	1.9	7.1	−0.042	−0.047
Ar	15.64	−2.14	4.88	−0.036	−0.058
Kr	13.86	−4.02	3.89	−0.033	−0.062
Xe	11.84	−6.16	2.82	−0.030	−0.067
H_2	20.27	2.72	8.06	−0.041	−0.051
D_2	20.10	2.55	7.89	−0.041	−0.052
N_2	18.23	0.34	8.36	−0.033	−0.055
CH_4	14.51	−3.39	4.63	−0.033	−0.062
C_2H_4	11.42	−6.62	2.77	−0.029	−0.071
C_2H_6	11.36	−6.79	3.84	−0.025	−0.071
CF_4	18.33	0.08	11.90	−0.022	−0.061
SF_6	15.18	−3.36	12.47	−0.009	−0.068
CO_2	13.01	−4.97	3.93	−0.031	−0.080

at 298.15 K was $\sigma_1 = 5.988 \times 10^{-10}$ m and for the energy parameter was $\varepsilon_1/k = 627$ K.

Comparison of these values with those obtained for cyclohexanone ($\sigma_1 = 5.651 \times 10^{-10}$ m, $\varepsilon_1/k = 584$ K) (1) shows an increase of both the distance and the energy parameters when a methyl group is introduced. The same behaviour was found for cyclohexane and methylcyclohexane (15, 25).

The linear coefficient of expansion of the effective hard-sphere diameter of the solvent (17), $l_1 = (1/a_1)(\partial a_1/\partial T)_P$, at 298.15 K was evaluated both by the method proposed by Pierotti (26) from solubility data of rare gases at several temperatures, $l_1 = -1.80 \times 10^{-4}$ K^{-1}, and by the method more recently suggested by Cosgrove and Walkley (23), from enthalpy solution data, $l_1 = -1.66 \times 10^{-4}$ K^{-1}. Agreement between the two values is good and similar to that obtained with other solvents (1, 23).

Once σ_1, ε_1/k, and l_1 are known, solubility and thermodynamic functions for the solution process predicted by the theory can be calculated with eqs. [6]–[8] together with the corresponding expressions for G_c, G_i, H_i, and H_c (2, 13–16, 23). Table 3 includes these theoretical values. $\Delta H^0_{m,2}$ and $\Delta S^0_{m,2}$ were calculated with $H_i = G_i$ as assumed by SPT and either using $l_1 = -1.66 \times 10^{-4}$ K^{-1} or using $l_1 = 0$. The same pattern of agreement between experimental and calculated values of $\Delta H^0_{m,2}$ and $\Delta S^0_{m,2}$ is obtained for 2-methylcyclohexanone and for cyclohexanone (1). For a further discussion on the enthalpy and entropy values predicted by SPT, the different methods of calculating them, and their agreement with experimental values, see the paper by Cosgrove and Walkley (23) and our previous paper on cyclohexanone (1).

Acknowledgements

The authors are grateful to the Comisión Asesora de Investigación Científica y Técnica (Project Number 1788/82) for financial assistance.

1. M. A. GALLARDO, J. M. MELENDO, J. S. URIETA, and C. GUTIERREZ LOSA. Can. J. Chem. **65**, 2198 (1987).
2. R. A. PIEROTTI. J. Phys. Chem. **69**, 281 (1965).
3. J. CARNICER, F. GIBANEL, J. S. URIETA, and C. GUTIERREZ LOSA. Rev. Acad. Cienc. (Zaragoza), **34**, 115 (1979).
4. M. A. GALLARDO, J. S. URIETA, and C. GUTIERREZ LOSA. J. Chim. Phys. **80**, 621 (1983).
5. J. H. DYMOND and E. B. SMITH. The virial coefficients of pure gases and mixtures. Oxford University Press, Oxford. 1980.
6. E. WILHELM. Pure Appl. Chem. **57**, 303 (1985).
7. R. C. REID, J. M. PRAUSNITZ, and B. E. POLING. The properties of gases and liquids. 4th ed. McGraw-Hill Book Company, New York, NY. 1987.
8. R. C. WEAST (*Editor*). CRC handbook of chemistry and physics. 59th ed. The chemical Rubber Co., Cleveland, OH. 1978–1979.
9. J. TIMMERMANS. Physico-chemical constants of pure organic compounds. Vol. I. Elsevier Publishing Company, New York, NY. 1965.
10. H. L. CLEVER and R. BATTINO. *In* Weissberger: Techniques of chemistry. Vol. 8. Part 1. M. R. J. Dack, Wiley–Interscience, New York, NY. 1975.
11. E. WILHELM and R. BATTINO. Chem. Rev. **73**, 1 (1973).
12. E. WILHELM, R. BATTINO, and R. J. WILCOCK. Chem. Rev. **77**, 219 (1977).
13. R. A. PIEROTTI. J. Phys. Chem. **67**, 1840 (1963).
14. R. A. PIEROTTI. Chem. Rev. **76**, 717 (1976).
15. E. WILHELM and R. BATTINO. J. Chem. Phys. **55**, 4012 (1971).
16. E. WILHELM and R. BATTINO. J. Chem. Thermodyn. **3**, 379 (1971).
17. E. WILHELM. J. Chem. Phys. **58**, 3558 (1973).
18. T. R. RETTICH, Y. P. HANDA, R. BATTINO, and E. WILHELM. J. Phys. Chem. **85**, 3230 (1981).
19. T. R. RETTICH, R. BATTINO, and E. WILHELM. Ber. Bunsen-ges. Phys. Chem. **86**, 1128 (1982).
20. T. R. RETTICH, R. BATTINO, and E. WILHELM. J. Solution Chem. **13**, 335 (1984).
21. T. TOMINAGA, R. BATTINO, H. K. GOROWARA, R. D. DIXON, and E. WILHELM. J. Chem. Eng. Data, **31**, 175 (1986).
22. F. GIBANEL, J. S. URIETA, and C. GUTIERREZ LOSA. J. Chim. Phys. **78**, 171 (1981).
23. B. A. COSGROVE and J. WALKLEY. Can. J. Chem. **60**, 1896 (1982).
24. H. REISS, H. L. FRISCH, and J. L. LEBOWITZ. J. Chem. Phys. **31**, 369 (1959).
25. S. GOLDMAN. J. Phys. Chem. **80**, 1697 (1976).
26. R. A. PIEROTTI. J. Phys. Chem. **71**, 2366 (1967).

Can. J. Chem. Downloaded from www.nrcresearchpress.com by 41.223.56.140 on 09/07/12
For personal use only.

Protium–deuterium exchange of benzo-substituted heterocycles in neutral D_2O at elevated temperatures

NICK HENRY WERSTIUK AND CHEN JU[1]

Department of Chemistry, McMaster University, Hamilton, Ont., Canada L8S 4M1

Received September 14, 1988

N. H. WERSTIUK and CHEN JU. Can. J. Chem. **67**, 812 (1989).

H–D exchange of 2-methylbenzofuran (**1**), 2-methylindole (**2**), 2-methylbenzimidazole (**3**), 2-methylbenzothiazole (**4**), and 2-methylbenzoxazole (**5**) has been studied in neutral D_2O at elevated temperatures. While **1**, **2**, **3**, and **4** can be specifically labelled and **4** can be perlabelled at 255°C, **5** undergoes facile hydrolysis in D_2O at 115°C to 2-acetamidophenol (**8**) with the incorporation of deuterium into the methyl group.

Key words: H–D exchange, heterocycles, D_2O, elevated temperatures.

N. H. WERSTIUK et CHEN JU. Can. J. Chem. **67**, 812 (1989).

Opérant à des températures élevées, dans du D_2O neutre, on a étudié les réactions d'échange H–D du méthyl-2 benzofuranne (**1**), du méthyl-2 indole (**2**), du méthyl-2 benzimidazole (**3**), du méthyl-2 benzothiazole (**4**) et du méthyl-2 benzoxazole (**5**). Les composés **1**, **2**, **3**, et **4** peuvent être marqués d'une façon spécifique et on peut perdeutérer le composé **4** en opérant à 255°C; par ailleurs, le composé **5** subit une hydrolyse facile, dans le D_2O à 115°C, qui conduit à la formation de l'acétamido-2 phénol (**8**) avec une incorporation de deutérium dans le groupement méthyle.

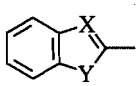
Mots clés : échange H–D, hétérocycles, D_2O, températures élevées.

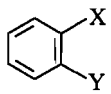
[Traduit par la revue]

Introduction

As an extension of our research on the hydrogen-isotope exchange of aromatic compounds in neutral D_2O at elevated temperatures, we undertook a study of the H–D exchange of the benzo-substituted five-membered-ring heterocycles 2-methylbenzofuran (**1**), 2-methylindole (**2**), 2-methylbenzimidazole (**3**), 2-methylbenzothiazole (**4**), and 2-methylbenzoxazole (**5**). This work, along with our other studies (1–4), begins to detail the scope and limitations of this methodology, which may be generally useful for hydrogen isotope labelling of heterocycles. To obtain mechanistic information, 2-acetamidophenol (**8**), 2-aminophenol (**9**), phenol, and aniline were studied as well.

This publication documents the results of our study, which establishes that **1**, **2**, **3**, **4**, **5**, **9**, phenol, and aniline can be labelled with deuterium in good yield.





1 X = C, Y = O
2 X = C, Y = NH
3 X = N, Y = NH
4 X = N, Y = S
5 X = N, Y = O

6 X = NHAc, Y = NH_2
7 X = SH, Y = NHAc
8 X = OH, Y = NHAc
9 X = OH, Y = NH_2

Results and discussion

H–D exchange of 2-methylbenzofuran (1)

As shown in Table 1 (entry 1), C3-H and the hydrogens of the methyl group of **1** undergo H–D exchange at 185°C. Exchange at these sites can occur via two mechanisms: by electrophilic substitution (Scheme 1) or by ring opening to 1-(2-hydroxyphenyl)-2-propanone, which undergoes exchange, then cyclizes to **1**-d_n (Scheme 2). that the aromatic ring of **1** does not undergo H–D exchange at 185°C while phenol incorporates deuterium at temperatures as low as 130°C (entries 5 and 6, Table 2) establishes that H–D exchange of the furan ring occurs by electrophilic substitution and not by the mechanism shown in Scheme 2; if a statistical factor is included, exchange at C3 is approximately three times as fast as exchange of the methyl. It is noteworthy that **1** does not undergo ring opening at 185°C.

H–D exchange of 2-methylindole (2)

As shown in Table 1 (entry 2) **2** undergoes H–D exchange faster than **1**. The relative stabilities of the cations derived from **1** and **2** (the cation derived from **2** is expected to be more stable than the cation derived from **1**) may play a role in determining the exchange rates. That C3-H of **2** exchanges approximately five times faster than the methyl, relative to **1** in which the relative rates are 3:1, is in accord with the fact that indole exhibits a higher resonance energy than benzofuran (5); the selectivity for deprotonation from C3 of **2** is higher than from C3 of **1**.

H–D exchange of 2-methylbenzimidazole (3)

From entries 3–6 of Table 1 it is seen that the methyl group of **3** undergoes exchange at a lower temperature than the methyls of **1** and **2**. The mechanism shown in Scheme 3 accounts for the enhanced reactivity of **3**, which is in accord with the observation that the methyl groups of 2- and 4-methylpyridine undergo H–D exchange readily in D_2O at elevated temperatures (1). The higher basicity of **3** results in a higher concentration of the cationic species in this case than the imidazolinium ion in the case of **1** and **2**. Furthermore, the hydroxide ion concentration is higher as well. At higher temperatures, the aromatic ring undergoes H–D exchange by electrophilic substitution (entries 5 and 6, Table 1). This result illustrates the advantage of carrying out exchange reactions in neutral D_2O. Since the D_3O^+ and OD^- concentrations are equal, acid- and base-catalyzed processes occur without exclusion of one or the other. The expected orientation of deuteronation by the —N=C and —NH— groups accounts for the similar rates of exchange at C4, C5, C6, and C7 of the aromatic ring. That aniline undergoes exchange in D_2O at 250°C with *ortho* and *para* selectivity (entry 7, Table 2) provides support for this proposal.

Hydrolysis of **3** to 2-aminoacetanilide (**6**) via a tetrahedral

[1]Visiting Scholar, 1986–1988, Xian Modern Chemistry Institute, People's Republic of China.

Can. J. Chem. Downloaded from www.nrcresearchpress.com by 41.223.56.140 on 09/07/12
For personal use only.

TABLE 1. Protium–deuterium exchange of benzo-substituted heterocycles in neutral D_2O

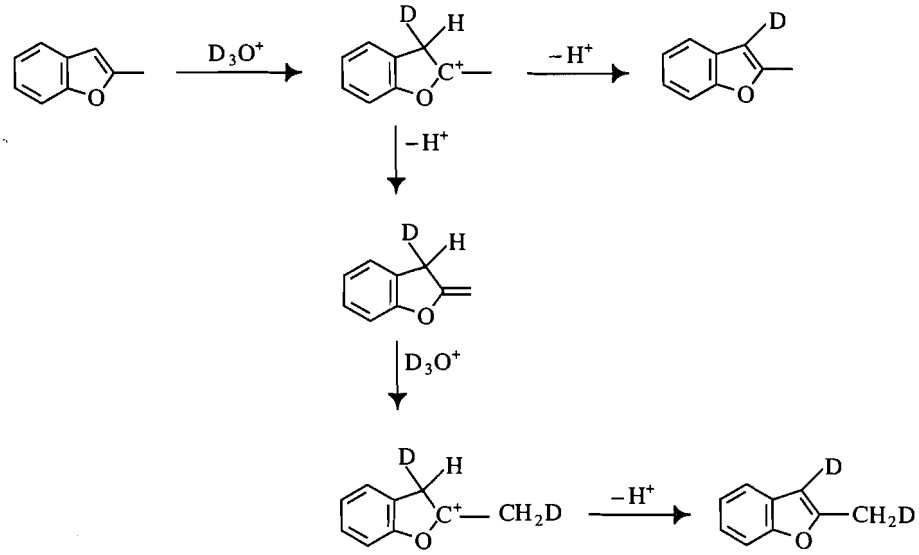
Entry	Substrate[a]	Conditions[b]	Percent exchange[c] C3	C4	C5	C6	C7	Me	D atoms incorporated[d]
1	**1**	185°C, 24 h	14	Trace	Trace	Trace	Trace	13	0.65
2	**2**	185°C, 24 h	50		[e]	[e]	[e]	30	1.88
3	**3**	145°C, 47 h						98	3.01
4		190°C, 24 h						98	2.97
5		230°C, 24 h		10	10	10	10	94	3.04
6		255°C, 48 h		18	15	15	18	84	3.20
7	**4**	145°C, 47 h						34	1.08
8		190°C, 24 h						63	1.99
9		230°C, 24 h		21	23	14	32	98	3.89
10		255°C, 48 h		97	97	91	98	98	6.81
11	**5**	115°C, 24 h						17	0.49[f]

[a]The yields of all the reactions were over 80%.
[b]For temperatures below 150°C the variation was ±2°; for temperatures above 200°C the variation was ±5°.
[c]Incorporations of >94% correspond to equilibration with the deuterium pool.
[d]Determined mass spectrometrically at low ionizing voltage.
[e]The ^{1}Hmr peaks overlap; approximately 0.5D is incorporated into the aromatic ring.
[f]The product is **8**.

TABLE 2. Protium–deuterium exchange of phenols and aniline in neutral D_2O

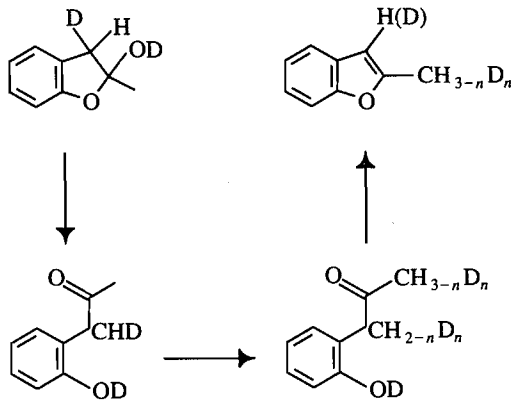
Entry	Substrate[a]	Conditions[b]	Percent exchange[c] C2	C3	C4	C5	C6	Me	D atoms incorporated[e]
1	**8**	115°C, 20 h	—	—	—	—	—		0.06
2	**9**	115°C, 24 h		4	23	0	80		1.07
3		130°C, 70 h		71	98	71	98		3.42
4		165°C, 24 h		88	98	88	98		3.76
5	Phenol	130°C, 70 h	18[d]	3	22[d]	3	18[d]		0.64
6		165°C, 24 h	[d]	3	[d]	3	[d]		1.57
7	Aniline	250°C, 25 h	47	3	64	3	47		1.66

[a]The yields of all reactions were over 80%.
[b]For temperatures below 150°C the variation was ±2°, and above 200°C, ±5°.
[c]Incorporations of >94% correspond to equilibration with the deuterium pool.
[d]The ^{1}Hmr peaks overlap.
[e]Determined mass spectrometrically at low ionizing voltage.



SCHEME 1

Can. J. Chem. Downloaded from www.nrcresearchpress.com by 41.223.56.140 on 09/07/12
For personal use only.



SCHEME 2

intermediate is a possibility as well. That **6** is not a product of the reaction is in keeping with the fact that Morgan and Turner have shown that **6** cyclizes to **3** in aqueous solution in the pH range 2–12.25 (6). On the basis of their study, the rate constant for cyclization of **6** at pH 7 at 50°C is 1.7×10^{-8} s^{-1}. We estimate that the rate constant for cyclization in D_2O at 145°C is in the range 10^{-3}–10^{-4} s^{-1}. That **6** is not a product establishes that cyclization is faster than hydrolysis of the amide under the conditions of the exchange reaction. In fact, imidazole **3** is very resistant to hydrolysis and yields only small amounts of *o*-phenylene diamine in strongly alkaline solutions of pH > 12.25 (6).

H–D exchange of 2-methylbenzothiazole (4)

As seen from the data in entries 7–10 (Table 1), **4** also undergoes H–D exchange of the methyl group and the aromatic ring. That the methyl group does not exchange as fast as the methyl of **3** is likely due to the fact that **4** is not as basic as **3** and consequently the equilibrium concentration of the benzothiazolinium ion is lower than the concentration of the benzoimidazolinium ion derived from **3**. It is remarkable that **4** can be perlabelled in excellent yield using only D_2O at 255°C.

As in the case of **3**, hydrolysis of **4** is a possibility as well. In this case 2-acetamidothiophenol (**7**) and 2-aminothiophenyl acetate can be formed. Studies by Collings and Morgan on the partial hydrolysis of *N*,*S*-diacyl-2-aminothiophenols in 1 N alcoholic KOH established that 2-acetamidothiophenols cyclize quantitatively to benzothiazoles. In fact, **7** cyclizes spontaneously to **4** on standing in the absence of hydroxide ion (7). Studies by Tee *et al.* (8) on the reversible ring opening of quaternary thiazolium ions established that the thiazolium ions are the stable species in the pH range 4.5–9. If **4** ring opens, the products recyclize to **4** faster than they hydrolyze. That exchange *ortho* and *para* to the sulfur is slightly faster than exchange at other sites is perhaps an indication that ring opening of **4** to **7** does occur. This thiophenol then undergoes H–D exchange via elctrophilic substitution, perhaps via deuteronation of the thiophenolate, and then cyclizes.

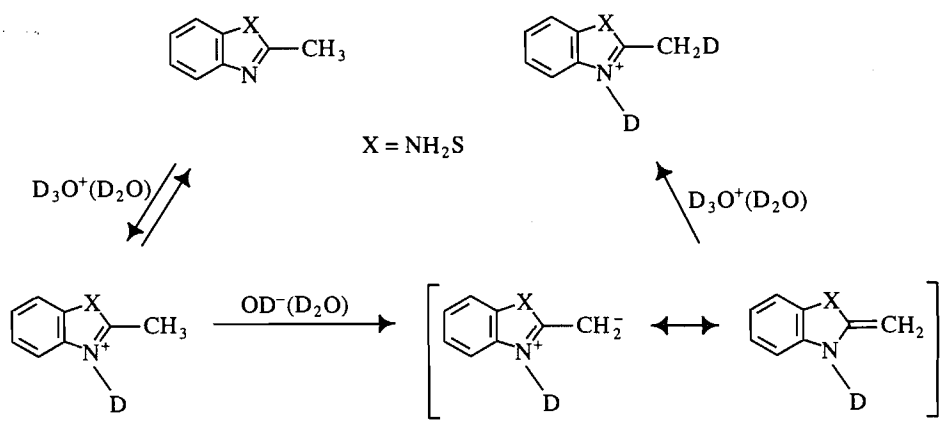
H–D exchange of 2-methylbenzoxazole (5)

In D_2O at 115°C, **5** hydrolyzes to 2-acetamidophenol (**8**), which incorporates 0.49 atoms of deuterium (entry 11, Table 1). Analysis of **8** by ^{1}Hmr, ^{2}Hmr, and mass spectroscopy established that within the limits of detection the deuterium is located in the methyl group. When **8** is heated in D_2O at 115° (entry 1, Table 2), it does not undergo deuterium exchange. At higher temperatures **8** hydrolyzes to 2-aminophenol (9) and acetic acid. To ensure that exchange of the methyl of **8** is not catalyzed by **9**, **8** was heated in D_2O in the presence of **9**. No detectable deuterium was incorporated into the methyl group, but **9** underwent facile exchange. Additional experiments (entries 2–4, Table 2) established that **9** can be selectively labelled *ortho* and *para* to the hydroxyl group or perlabelled. This result suggests that **9** undergoes H–D exchange by deuteronation of the phenolate anion. These experiments also establish that **5** hydrolyzes faster than the methyl group undergoes H–D exchange and that **8** does not cyclize to **5**.

In principle, the hemi-orthoamide derived from **5** can ring open in two ways to yield either **8** or 2-aminophenyl acetate. In fact, imidates generally give a mixture of two products with aminoesters being the kinetic products (9). That **8** is the only detectable product at 115°C is in keeping with the results of studies carried out by Morgan and co-workers (10) in the pH range 2–5. The ease with which **5** hydrolyzes contrasts with the stability of **3** and **4**. These researchers propose that the hemi-orthoamide decomposes via the zwitterionic form in the pH range 2–5. This proposal is consistent with the fact that **8** is the only product of the reaction; the stability of the phenolate anion leaving group overrides any stereoelectronic effects (9).

Conclusions

This study establishes that benzo-substituted heterocycles can be specifically labelled or perlabelled in good yield by heating the compounds in neutral D_2O at elevated temperatures. It



SCHEME 3

Can. J. Chem. Downloaded from www.nrcresearchpress.com by 41.223.56.140 on 09/07/12
For personal use only.

should be possible to prepare corresponding tritiated compounds simply by using tritiated water of the appropriate specific activity.

Experimental

The reagents (95–98% purity) were obtained from Aldrich Chemical Co. and were used without further purification.

Proton and deuterium magnetic resonance spectra were recorded on Bruker AM 500 (^{1}H 500-MHz, ^{2}H 76.8-MHz), WM 250 (^{1}H 250-MHz, ^{2}H 38.4-MHz), and Varian EM 390 spectrometers. Carbon tetrachloride was used as nmr solvent for **1** and **2** and acetone was used for **3**, **4**, **5**, **8**, and **9**. Deuterium assays were performed on a VG Micromass 7070 mass spectrometer at low ionization voltage (12–15 eV) and expressed as atoms of deuterium per molecule in excess of natural abundance deuterium. All samples that contained OH, SH, or NH groups were back-exchanged in H_2O before analysis.

In a typical exchange reaction, substrate (0.20 g) was added to D_2O (5 mL) in a 5/8-in. medium-walled glass tube. The mixture was degassed via three freeze–pump–thaw cycles, placed in a 600-mL Parr pressure vessel that contained water to equalize pressure, and heated at the desired temperature for an appropriate period. The deuteriated compounds were isolated by extraction with ether or by filtration.

Acknowledgement

We thank the Natural Sciences and Engineering Research Council of Canada for financial support.

1. N. H. Werstiuk and G. Timmins. Can. J. Chem. **59**, 1022 (1981).
2. N. H. Werstiuk and G. Timmins. Can. J. Chem. **59**, 3038 (1981).
3. N. H. Werstiuk. Isotopes in physical and biomedical sciences. Vol. 1. Labelled compounds (Part A). *Edited by* J. R. Jones and E. Buncel. Elsevier, Amsterdam. 1987. pp. 122–155.
4. N. H. Werstiuk and Chen Ju. Can. J. Chem. **67**, 5 (1989).
5. B. A. Hess, L. J. Schaad, and G. W. Holyoke. Tetrahedron, **28**, 3657 (1972).
6. K. J. Morgan and A. M. Turner. Tetrahedron, **25**, 915 (1969).
7. A. J. Collings and K. J. Morgan. Tetrahedron, 2167 (1964).
8. O. S. Tee, G. D. Spiropoulos, R. S. McDonald, V. D. Geldart, and D. Moore. J. Org. Chem. **51**, 215 (1986).
9. P. Deslongchamps. Stereoelectronic effects in organic chemistry. Pergamon Press, Oxford. 1983. Chap. 4.
10. P. F. Jackson, K. J. Morgan, and A. M. Turner. J. Chem. Soc. Perkin Trans. 2, 1582 (1972).

Can. J. Chem. Downloaded from www.nrcresearchpress.com by 41.223.56.140 on 09/07/12
For personal use only.

A very short synthesis of 3-methoxyestra-1,3,5,8,14-pentaen-17-one

D. JEAN BURNELL[1] AND YONG-JIN WU

Department of Chemistry, Memorial University of Newfoundland, St. John's, Nfld., Canada A1B 3X7

Received September 7, 1988

D. JEAN BURNELL and YONG-JIN WU. Can. J. Chem. **67**, 816 (1989).

3-Methoxyestra-1,3,5,8,14-pentaen-17-one (**4**) was prepared from 6-methoxy-1-tetralone (**8**) by an efficient two-pot procedure in which the D ring was generated by the Lewis acid catalysed reaction of 1,2-bis(trimethylsiloxy)cyclobutene (**5**) with an appropriate ketal (**10**).

Key words: steroid, estrone, annellation.

D. JEAN BURNELL et YONG-JIN WU. Can. J. Chem. **67**, 816 (1989).

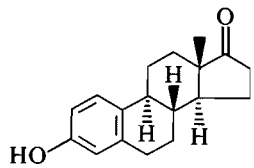
On a préparé la méthoxy-3 estrapentaène-1,3,5,8,14 one-17 (**4**) à partir de la méthoxy-6 tétralone-1 (**8**) en faisant appel à une méthode efficace en deux étapes dans lesquelles le cycle D est généré par la réaction, catalysée par un acide de Lewis, du bis(triméthylsiloxy)-1,2 cyclobutène (**5**) avec un cétal approprié (**10**).

Mots clés : stéroïde, estrone, annelation.

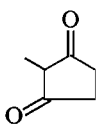
[Traduit par la revue]

Introduction

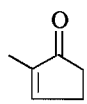
Considerable effort has gone into the total synthesis of estrone (**1**) and the other physiologically active aromatic steroids (1). In many, if not most, syntheses the D ring of the steroid has been derived from either 2-methyl-1,3-cyclopentanedione (**2**) or 2-methyl-2-cyclopenten-1-one (**3**). This paper



1



2

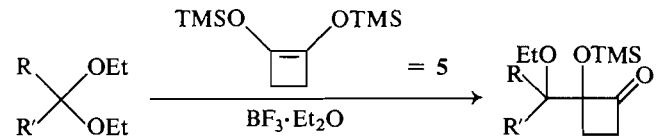


3

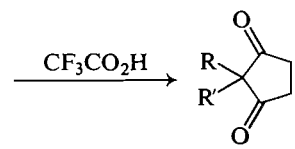
describes a very expedient, alternative route to the steroidal diene **4**, which is the key intermediate in the Torgov estrone synthesis (2) as well as in a number of more recent approaches (3). In our synthesis neither **2** nor **3** is used as the D ring precursor: this route serves to illustrate further the considerable synthetic utility of 1,2-bis(trimethylsiloxy)cyclobutene (**5**)[2] for the formation of a five-membered ring.

Results and discussion

Kuwajima and co-workers (5) demonstrated that under Lewis acid catalysis a dimethyl or diethyl ketal reacts with 1,2-bis(trimethylsiloxy)cyclobutene (**5**) to provide the cyclobutanone **6**, which can be rearranged in the presence of trifluoroacetic acid (TFA) to yield ultimately a 2,2-disubstituted 1,3-cyclopentanedione moiety **7**. In the course of our recent synthesis of isokhusimone (6)[3] we showed that this annellation procedure is viable with cyclic ketals, and, more importantly, that prolonged



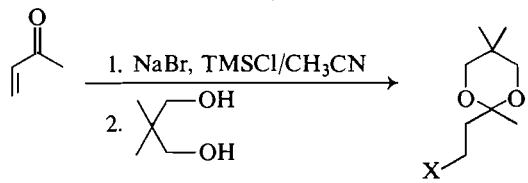
6



7

treatment of a ketal with **5** and a large excess of boron trifluoride etherate provides a superior yield of the cyclopentanedione **7** *directly*. Thus, our strategy for the synthesis of **4** was simply to add a ketal-containing synthon to 6-methoxy-1-tetralone (**8**), then to build a 1,3-cyclopentanedione D ring moiety, which might spontaneously cyclize to **4** in the acidic medium.

The ketal **9** was prepared from 3-buten-2-one by a procedure derived from that of Larson and co-workers (8).[4] Whereas we expected only the bromo-ketal **9***a*, we found that it was always accompanied by a lesser amount of the chloro-ketal **9***b*.[5]



9*a* X = Br
9*b* X = Cl

[1]Author to whom correspondence may be addressed.

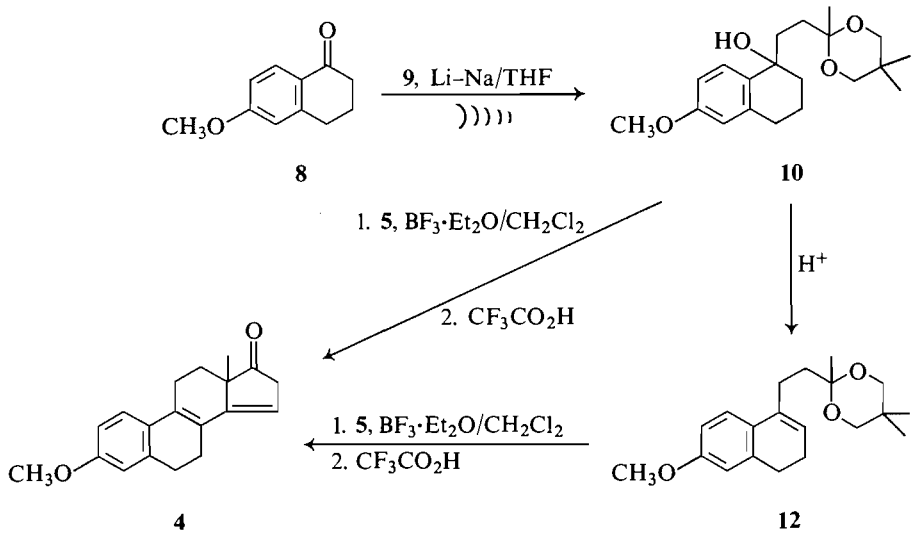
[2]Acyloin coupling of diethyl succinate and trapping with chlorotrimethylsilane affords **5** in multigram quantities (4).

[3]Other syntheses that have employed this reaction are given in ref. 7.

[4]These workers prepared iodo-ketals and iodo-acetals derived from ethanediol and 1,3-propanediol. We prefer the bromo-ketal derived from 2,2-dimethyl-1,3-propanediol because it is more easily separated from the corresponding bromo-ketone by vacuum distillation, and it can be stored in a freezer for several months.

[5]Larson and co-workers (8*b*) reported that in a reaction to prepare a bromo-acetal the product was contaminated with 40% of an unidentified impurity. We suggest this was the corresponding chloro-acetal.

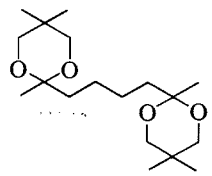
Can. J. Chem. Downloaded from www.nrcresearchpress.com by 41.223.56.140 on 09/07/12
For personal use only.



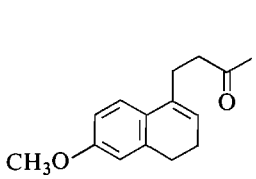
8 10 4 12

Attempts to separate these by vacuum distillation proved to be unnecessary. Reaction of the mixture of halo-ketals **9** with magnesium turnings or lithium metal was extremely sluggish even with ultrasonic irradiation. However, addition of THF solutions of **8** and an excess of **9** to lithium containing a small amount of sodium, followed by ultrasonic irradiation (9) for 4 h, provided the desired Barbier reaction product **10** in a yield of 76% accompanied by 19% recovered **8** and a small amount of the diketal **11**. (Increasing the initial amount of **9** did not increase the yield of **10**.) Dehydration of **10** occurred readily. From a sample of **10** that had been stored at room temperature for a week we recovered 64% of **10**, 30% of the unsaturated compound **12**, and 2% of the unsaturated ketone **13** by flash chromatography. The 2-D nmr spectra, i.e., COSY and ^1H–^{13}C correlation, of **12** left no doubt as to the position of the double bond in this molecule. A benzene solution of **10** was heated with a small amount of pyridinium *para*-toluenesulfonate (PPTS) and 2,2-dimethyl-1,3-propanediol to provide **12** in a yield of 96%.

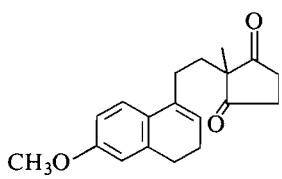
Compound **12** was treated with four equivalents of **5** and 15 equivalents of boron trifluoride etherate at −78°C (6). The crude product was subjected to gc–ms analysis, which revealed that D ring annellation had occurred giving the diketone **14**,



11



13



14

but it was clear that cyclization of the C ring had not taken place. Longer reaction times and more boron trifluoride etherate resulted in some destruction of **14** but still no C ring cyclization. However, addition of TFA to a solution of crude **14** at room temperature provided **4** (91%) as a pale brown powder. Furthermore, it is not surprising that direct treatment of the alcohol-ketal **10** with **5** and boron trifluoride etherate followed by TFA also gave **4** in an excellent yield. We have witnessed considerable destruction of **4** during its rigorous purification by flash chromatography.[6] Therefore this reaction was repeated with anthracene as an internal standard, which allowed us to calculate (from gc–ms data) an actual chemical yield of 83% for the one-pot conversion of **10** to **4**. Thus, we have demonstrated that the important estrone precursor 3-methoxyestra-1,3,5,8,14-pentaen-17-one (**4**) can be produced in good yield from 6-methoxy-1-tetralone (**8**) by an efficient two-pot procedure using **5** to generate the D ring.

Experimental

Melting points (mp) were determined on a Fisher–Johns apparatus and are uncorrected. Infrared (ir) spectra were recorded on a Perkin Elmer 283 spectrophotometer. Nuclear magnetic resonance (nmr) spectra were obtained in $CDCl_3$ solution on a General Electric GE 300-NB (300-MHz) instrument. Signal multiplicities in the ^{13}C nmr data were determined from APT spectra; ^1H and ^{13}C signal assignments were aided by COSY and heteronuclear-correlation 2-D spectra. A Hewlett–Packard system (5890 gas chromatograph coupled to a 5970 mass selective detector) equipped with a Hewlett–Packard 12.5-m fused silica capillary column with cross-linked dimethylsilicone as the liquid phase was used for gc–ms analyses. Except where noted, both the low and the high resolution mass spectral data were obtained on a V.G. Micromass 7070HS instrument.

*2-(2-Bromoethyl)-2,5,5-trimethyl-1,3-dioxane (**9**a)*

3-Buten-2-one (8.1 mL, 0.10 mol) was added to a stirred suspension of sodium bromide (15.4 g, 0.15 mol) in anhydrous acetonitrile (250 mL) under an atmosphere of dry nitrogen, then chlorotrimethylsilane (19.0 mL, 0.15 mol) was introduced by syringe over a period of 5 min. Stirring was continued at room temperature overnight. 2,2-Dimethyl-1,3-propanediol (15.6 g, 0.15 mol) was added, and the mixture was stirred for a further 4 h. The mixture was poured into a flask containing petroleum ether (300 mL) and 8% aqueous Na_2CO_3 (100 mL), then stirred thoroughly and transferred to a separatory funnel: *three* layers were clearly evident. The lowest (aqueous) layer was removed, and 5% aqueous sodium thiosulfate (100 mL) was added: only two layers were visible. The organic layer was washed

[6]It is better to hydrogenate **4** using Torgov's procedure (2) before flash chromatography. In this way we obtained a 69% overall yield of pure 3-methoxyestra-1,3,5,8-tetraen-17-one from **10**.

Can. J. Chem. Downloaded from www.nrcresearchpress.com by 41.223.56.140 on 09/07/12
For personal use only.

Can. J. Chem. Downloaded from www.nrcresearchpress.com by 41.223.56.140 on 09/07/12
For personal use only.

with water (2 × 100 mL), saturated NaCl (150 mL), then dried over anhydrous $MgSO_4$. The solution was concentrated by rotary evaporation, and the residue was distilled under vacuum to provide 12.2 g (58%) of a mixture of **9***a* and **9***b* (the corresponding chloro compound) in a ratio of 77:23, respectively (by gc–ms), as a colorless liquid, bp 63–64°C/0.1 Torr (1 Torr = 133.3 Pa). For **9***a*, ^{1}H nmr δ: 0.855 (3H, s) and 1.032 (3H, s) C-5 methyls, 1.385 (3H, s, C-2 methyl), 2.279 (2H, m, -C*H*$_2$CH$_2$Br), 3.406 (2H, d, *J* = 11.4 Hz, -C*H*$_2$O-), 3.525 (2H, m, -C*H*$_2$Br), 3.581 (2H, d, *J* = 11.4 Hz, -C*H*$_2$O-); ^{13}C nmr δ: 20.0 (C-2 methyl), 22.4 and 22.8 (C-5 methyls), 27.0 (-*C*H$_2$Br), 29.8 (C-5), 42.9 (-*C*H$_2$CH$_2$Br), 70.4 (2C, C-4 and C-6), 98.4 (C-2); ms (from gc–ms) *m/z* (%): 223 (21, M$^+$), 221 (20, M$^+$), 153 (11), 151 (10), 137 (11), 135 (10), 129 (71), 107 (10), 69 (44), 56 (43), 55 (15), 43 (100), and 41 (51). For **9***b*, ^{1}H nmr as for **9***a* except δ: 1.396 (3H, s, C-2 methyl), 2.190 (2H, m, -C*H*$_2$CH$_2$Cl), 3.685 (2H, m, -C*H*$_2$Cl); ^{13}C nmr as for **9***a* except δ: 39.5 (-*C*H$_2$Cl), 42.3 (-*C*H$_2$CH$_2$Cl), 97.8 (C-2); ms (from gc–ms) *m/z* (%): 179 (10, M$^+$), 177 (35, M$^+$), 129 (54), 109 (9), 107 (23), 93 (7), 91 (21), 69 (50), 56 (54), 55 (23), 43 (100), and 41 (41).

Alcohol-ketal ***10***

A flask containing lithium metal (60.5 mg, 8.72 mmol) and sodium metal (4 mg) under vacuum was heated with a heat gun to alloy the metals. The flask was cooled and an atmosphere of dry nitrogen was introduced. Dry THF (50 mL, distilled from potassium) was added, followed by **8** (227.5 mg, 1.29 mmol) in dry THF (20 mL) and **9** (mixture of **9***a* and **9***b*, 1.80 mL, 9.77 mmol). The flask was placed in an ultrasonic cleaning bath (Branson) and irradiated at room temperature for 4 h. After concentration of the mixture by rotary evaporation, ether (30 mL) and saturated aqueous NH_4Cl (30 mL) were added. The aqueous layer was reextracted with ether (4 × 20 mL). The combined organic layers were washed with saturated NaCl (30 mL), dried over anhydrous $MgSO_4$, and the solvent was removed by rotary evaporation. Flash chromatography of the residue (3% acetone in petroleum ether) provided 326.1 mg (76%) of **10**, 42.0 mg (19%) of recovered **8**, and 30.1 mg of the diketal **11**. For **10**,[7] ir (film) ν_{max}: 3460 (br) and 1610 cm^{-1}; ^{1}H nmr δ: 0.887 (3H, s) and 1.026 (3H, s) dioxane's C-5 methyls, 1.371 (3H, s, C-18*H*$_3$), 1.6–2.05 (8H, br m), 2.20 (1H, s, -O*H*, disappears with D$_2$O shake), 2.75 (2H, m, C-6*H*$_2$), 3.433 (2H, d, *J* = 11.5 Hz, -C*H*$_2$O-), 3.559 (2H, d, *J* = 11.5 Hz, -C*H*$_2$O-), 3.780 (3H, s, -OC*H*$_3$), 6.590 (1H, d, *J* = 2.5 Hz, C-4*H*), 6.775 (1H, dd, *J* = 2.5, 8.7 Hz, C-2*H*), 7.482 (1H, d, *J* = 8.7 Hz, C-1*H*); ^{13}C nmr δ: 19.7 (C-7), 20.4 (C-18), 22.4 and 22.7 (dioxane's C-5 methyls), 29.7 (dioxane's C-5), 30.1 (C-6), 32.4, 35.6, and 35.9 (C-8, C-11, and C-12), 55.0 (-O*C*H$_3$), 70.1 (2C, -*C*H$_2$O-), 71.4 (C-9), 98.8 (C-13), 112.4 (C-2), 112.8 (C-4), 127.6 (C-1), 134.8 and 138.0 (C-5 and C-10), 158.1 (C-3); ms *m/z* (%): (no M$^+$), 316 (5, M$^+$ − H$_2$O), 175 (13), 174 (68), 172 (17), 129 (14), 85 (65), and 83 (100). For **11**: mp 69–70°C; ^{1}H nmr δ: 0.906 (6H, s) and 0.999 (6H, s) dioxanes' C-5 methyls, 1.353 (6H, s, dioxanes' C-2 methyls), 1.422 (4H, m) and 1.711 (4H, m) methylenes, 3.444 (4H, d, *J* = 11.3 Hz) and 3.530 (4H, d, *J* = 11.3 Hz) -C*H*$_2$O- signals; ^{13}C nmr δ: 20.4 (dioxanes' C-2 methyls), 22.5 and 22.7 (dioxanes' C-5 methyls), 23.6 (methylenes β to dioxanes), 29.9 (dioxanes' C-5), 37.7 (methylenes α to dioxanes), 70.2 (-*C*H$_2$O-), 98.9 (dioxanes' C-2); ms *m/z* (%): (no M$^+$), 299 (17, M$^+$ − 15), 213 (7), 129 (100), 125 (27), 84 (16), 81 (29), 71 (19), 69 (77), 56 (31), 43 (100), and 41 (57).

Unsaturated ketal ***12***

Approximately 8 mg of PPTS was added to a solution of **10** (105.6 mg, 0.32 mmol) and 2,2-dimethyl-1,3-propanediol (99 mg, 0.95 mmol) in benzene. After heating at reflux overnight (Dean–Stark), the solvent was evaporated and the residue was purified by flash chromatography (2% acetone in petroleum ether) to provide pure **12**[7] (95.4 mg, 96%), which crystallized in the freezer, mp 46–47°C; ir (film) ν_{max}: 1610, 1500, and 1255 cm^{-1}; ^{1}H nmr δ: 0.920 (3H, s) and 1.029 (3H, s) dioxane's C-5 methyls, 1.909 (2H, m, C-12*H*$_2$), 2.218 (2H, m, C-7*H*$_2$), 2.557 (2H, m, C-11*H*$_2$), 2.707 (2H, t, *J* = 7.9 Hz, C-6*H*$_2$), 3.473 (2H, d, *J* = 11.3 Hz, -C*H*$_2$O-), 3.573 (2H, d, *J* = 11.3 Hz, -C*H*$_2$O-), 3.793 (3H, s, -OC*H*$_3$), 5.759 (1H, t, *J* = 4.5 Hz, C-8*H*), 6.708 (1H, apparent s, C-4*H*), 6.723 (1H, partially overlapped, C-2*H*), 7.223 (1H, distorted d, C-1*H*); ^{13}C nmr δ: 20.7 (C-18), 22.5 and 22.8 (dioxane's C-5 methyls), 23.0 (C-7), 26.5 (C-11), 28.9 (C-6), 29.9 (dioxane's C-5), 36.9 (C-12), 55.2 (-O*C*H$_3$), 70.4 (2C, -*C*H$_2$O-), 98.9 (C-13), 110.8 and 113.7 (C-2 and C-4), 122.0 (C-8), 123.8 (C-1), 128.1 (C-9), 136.0 and 138.5 (C-5 and C-10), 158.2 (C-3); ms *m/z* (%): 316 (5, M$^+$), 301 (3), 230 (5), 199 (5), 187 (17), 174 (82), 172 (29), 129 (81), 83 (20), 69 (55), and 43 (100). When this procedure was carried out for 3 h in the absence of the diol, flash chromatography provided **12** (81%) and **13**[7] (6%): ir (film) ν_{max}: 1715, 1610, 1500, and 1255 cm^{-1}; ^{1}H nmr δ: 2.140 (3H, s, C-18*H*$_3$), 2.16–2.25 (2H) and 2.62–2.73 (6H) methylenes, 3.790 (3H, s, -OC*H*$_3$), 5.719 (1H, t, *J* = 4.5 Hz, C-8*H*), 6.71 (2H, m, C-2*H* and C-4*H*), 7.129 (1H, apparent d, *J* = 8.7 Hz, C-1*H*); ^{13}C nmr δ: 23.0, 26.7, 28.8, 30.1, 42.6, 55.2, 110.8, 113.9, 122.8, 123.5, 127.4, 134.8, 138.6, 158.4, and 208.6; ms *m/z* (%): 230 (8, M$^+$), 187 (8), 172 (22), 125 (12), 111 (17), 107 (10), 97 (13), and 43 (100). *Exact Mass* calcd. for $C_{15}H_{18}O_2$: 230.1306; found: 230.1310.

3-Methoxyestra-1,3,5,8,14-pentaen-17-one ***4***

With isolation of pure ***4***

A solution of **10** (271.2 mg, 0.81 mmol) in anhydrous dichloromethane (30 mL) under an atmosphere of dry nitrogen was cooled to −78°C before 1.50 mL of boron trifluoride etherate was added. A solution of **5** (0.86 mL, 3.24 mmol) in dichloromethane (10 mL) was added slowly. The mixture was stirred overnight as it was allowed to reach room temperature. Trifluoroacetic acid (TFA) (3 mL) was added and the mixture was stirred for a further 4 h. The organic solution was washed with saturated $NaHCO_3$, water, and saturated NaCl, then dried over anhydrous $MgSO_4$ and rotary evaporated to give **4** (226.8 mg, 91%) as a pale brown powder, mp 106–110°C. Flash chromatography (2% acetone in petroleum ether) provided a very pure fraction (100.4 mg, 44%) as colorless crystals, mp 110–110.5°C (mixture mp 110–110.5°C with similarly purified **4** synthesized by Torgov's method (2)); ir (Nujol) ν_{max}: 1740 and 1610 cm^{-1}; ^{1}H nmr δ: 1.132 (3H, s, C-18*H*$_3$), 1.590 (1H, m) and 2.034 (1H, br dt, *J* = 3.6, 12.9 Hz) C-12*H*$_2$, 2.300 (1H, m) and 2.55–2.67 (3H, m) C-7*H*$_2$ and C-11*H*$_2$, 2.794 (2H, t, *J* = 7.8 Hz, C-6*H*$_2$), 2.926 (1H, dd, *J* = 2.8, 23.4 Hz) and 3.309 (1H, br d, *J* = 23.4 Hz) C-16*H*$_2$, 3.804 (3H, s, -OC*H*$_3$), 5.853 (1H, br t, $W_{1/2}$ = 6 Hz, C-15*H*), 6.724 (1H, apparent s, C-4*H*), 6.739 (1H, partially overlapped, C-2*H*), 7.243 (1H, d, *J* = 8.2 Hz, C-1*H*); ^{13}C nmr δ: 20.5 (C-18), 22.6 and 22.9 (C-7 and C-11), 27.2 (C-12), 28.3 (C-6), 41.8 (C-16), 48.9 (C-13), 55.1 (-O*C*H$_3$), 111.0 and 113.5 (C-2 and C-4), 114.6 (C-15), 124.0 (C-1), 125.2, 128.5, 129.7, 138.0, and 146.8 (olefinic and aromatic), 158.5 (C-3), 220.0 (C-17); ms *m/z* (%): 280 (64, M$^+$), 252 (100), 237 (34), 223 (11), 178 (10), and 165 (16). A chemical yield of 83% was calculated by gc–ms analysis of a reaction involving **10** admixed with anthracene. Reactions starting with **12** gave **4** in very similar yields. The gc–ms analysis of reaction mixtures prior to the addition of TFA showed the mixtures to be composed very predominantly of **14**: ms (from gc–ms) *m/z* (%): 298 (50, M$^+$), 280 (8), 241 (18), 240 (17), 228 (100), 227 (52), 171 (23), 165 (22), 153 (23), 141 (22), 128 (26), 115 (30), and 43 (58).

With hydrogenation of crude ***4***

Alcohol-ketal **10** (304.5 mg, 0.910 mmol) with **5** (0.73 mL) and boron trifluoride etherate (1.68 mL) provided crude **4** after addition of TFA following the procedure above. This was dissolved in toluene (30 mL) and 90 mg of 5% Pd–$CaCO_3$ was added (2*a*). The reaction was maintained under 1 atmosphere (101.3 kPa) of H_2 until 24 mL of H_2 was taken up. The catalyst was removed and the filtrate was concentrated by rotary evaporation. Flash chromatography (2% acetone in petroleum ether) afforded 178.5 mg (69%) of *3-methoxyestra-1,3,5,8-tetraen-17-one* as colorless crystals, mp 117–118°C (lit. (2*a*) mp 120–121°C), which were identical spectroscopically with material

[7]Carbons are identified by steroid numbering.

prepared by reduction of the **4** that had been synthesized by Torgov's method (2), mixture mp 117–118°C.

Acknowledgements

We thank Dr. Ž. Stojanac of the University of New Brunswick for a generous sample of **4** synthesized by Torgov's method. We are grateful to Dr. C. R. Jablonski and Messrs. A. Earle and R. Sammynaiken for 300-MHz nmr spectra, and to Dr. B. Gregory and Miss M. Baggs for mass spectra. The Natural Sciences and Engineering Research Council of Canada and the Memorial University of Newfoundland provided financial support.

1. A. A. AKHREM and Y. A. TITOV. Total steroid synthesis. Plenum Press, New York. 1970; R. T. BLICKENSTAFF, A. C. GHOSH, and G. C. WOLF. Total synthesis of steroids. Academic Press, New York. 1974; G. QUINKERT and H. STARK. Angew. Chem. Int. Ed. Engl. **22**, 637 (1983); D. TAUB. *In* The total synthesis of natural products. Vol. 2. *Edited by* J. ApSimon. John Wiley & Sons, New York. 1973. pp. 641–725; D. TAUB. *In* The total synthesis of natural products. Vol. 6. *Edited by* J. ApSimon. John Wiley & Sons, New York. 1984. pp. 1–49. For recent estrone syntheses see: J. H. HUTCHINSON and T. MONEY. Can. J. Chem. **65**, 1 (1987), and references therein; D. F. TABER, K. RAMAN, and M. D. GAUL. J. Org. Chem. **52**, 28 (1987).
2. (*a*) S. N. ANANCHENKO and I. V. TORGOV. Tetrahedron Lett. 1553 (1963); (*b*) A. V. ZAKHARYCHEV, S. N. ANANCHENKO, and I. V. TORGOV. Steroids, **4**, 31 (1964); (*c*) A. V. ZAKHARYCHEV, I. HORA, S. N. ANANCHENKO, and I. V. TORGOV. Tetrahedron Lett. 3585 (1966).
3. E. D. STERNBERG and K. P. C. VOLLHARDT. J. Org. Chem. **49**, 1574 (1984); A. R. DANIEWSKI and T. KOWALCZYK-PRZEWŁOKA. J. Org. Chem. **50**, 2976 (1985); N. S. NARASIMHAN and P. A. PATIL. Tetrahedron Lett. **27**, 5133 (1986); N. S. NARASIMHAN and N. M. SUNDER. Tetrahedron Lett. **29**, 2985 (1988).
4. J. J. BLOOMFIELD and J. M. NELKE. Org. Synth. **57**, 1 (1977).
5. J. SHIMADA, K. HASHIMOTO, B. H. KIM, E. NAKAMURA, and I. KUWAJIMA. J. Am. Chem. Soc. **106**, 1759 (1984); E. NAKAMURA and I. KUWAJIMA. Org. Synth. **65**, 17 (1987).
6. Y.-J. WU and D. J. BURNELL. Tetrahedron Lett. **29**, 4369 (1988).
7. W. K. ANDERSON and G. E. LEE. J. Org. Chem. **45**, 501 (1980); W. K. ANDERSON and G. E. LEE. Synth. Commun. **10**, 351 (1980); W. OPPOLZER and R. D. WYLIE. Helv. Chim. Acta, **63**, 1198 (1980); K. A. PARKER, K. A. KOZISKI, and G. BREAULT. Tetrahedron Lett. **26**, 2181 (1985).
8. (*a*) G. L. LARSON and R. KLESSE. J. Org. Chem. **50**, 3627 (1985); (*b*) Y.-S. LEE, L. DEL VALLE, and G. L. LARSON. Synth. Commun. **17**, 385 (1987).
9. J.-L. LUCHE and J.-C. DAMIANO. J. Am. Chem. Soc. **102**, 7926 (1980).

Can. J. Chem. Downloaded from www.nrcresearchpress.com by 41.223.56.140 on 09/07/12
For personal use only.

Potential functions for the inner branches of diatomic potential curves

JOEL TELLINGHUISEN
Department of Chemistry, Vanderbilt University, Nashville, TN 37235, U.S.A.

Received August 31, 1988

JOEL TELLINGHUISEN. Can. J. Chem. **67**, 820 (1989).

The performance of simple three-parameter potential functions in predicting the inner branches of known diatomic potentials is tested for 35 diatomic molecular states. The Varshni III potential outperforms the Morse and Rydberg functions when the spectroscopic R_e, ω_e, and $\mathcal{D}_e$ values are used to define the potential parameters, but all three functions perform comparably well when R_e, ω_e, and $\omega_e x_e$ are used. In the latter case the 35 potentials show an average absolute value of about 0.6% for the *maximum* relative error.

Key words: diatomic molecules, potential energy curves.

JOEL TELLINGHUISEN. Can. J. Chem. **67**, 820 (1989).

On a testé la performance de fonctions de potentiel simples à trois paramètres à prédire les potentiels diatomiques connus des branches internes de 35 états moléculaires diatomiques. Lorsqu'on utilise les valeurs spectroscopiques R_e, ω_e et $\mathcal{D}_e$ pour définir les paramètres de potentiel, le potentiel de Varshni III donne de meilleures performances que les fonctions de Morse et de Rydberg; par ailleurs, si on utilise les valeurs R_e, ω_e et $\omega_e x_e$, les trois fonctions donnent des bonnes performances. Dans ce dernier cas, pour les 35 potentiels, la valeur absolue moyenne de l'erreur relative *maximale* est d'environ 0,6%.

Mots clés : molécules diatomiques, courbes d'énergie potentielle.

[Traduit par la revue]

Potential energy curves are all-important in diatomic spectroscopy, and there are well-established methods for determining them from experimental data. The Rydberg–Kelin–Rees (RKR) method yields the classical turning points as functions of the energy via a semiclassical direct inversion process requiring as input the vibrational energy G_v and rotational constant B_v, both being functions of the vibrational quantum number v (1). The validity of the RKR potential is then of course limited to the range of v spanned by the data, although judicious extrapolations can be used somewhat beyond this range with fair reliability. For most applications, RKR potentials are fully trustworthy; however, in precision work, and especially for molecules of small reduced mass, it may be necessary to correct the RKR potential for the semiclassical errors inherent in it. For this task, too, there are established methods (2, 3).

Sometimes one can obtain a fairly complete analysis of the vibrational structure in an electronic spectrum but little or no information about the rotational constants. This is particularly true for emission spectra of heavy diatomics, where the rotational structure may be very congested. Since the vibrational information is sufficient to determine the RKR *width* of the potential, in such cases one can still obtain a fair approximation of the potential in question – provided one can somehow "guess" one branch of the potential.

Perhaps the simplest approach to this problem is to use the workhorse of diatomic potentials, the Morse function, to fix the needed "half potential." Several years ago Henderson and I (4) examined a number of fairly well-known potentials with the goal of answering the question: How well does the Morse function approximate the inner or repulsive branch of the potential? Because the inner branches of potentials rapidly become very steep with increasing energy, it is more appropriate to assess errors in R as a function of energy than vice versa. We found that the Morse curve does surprisingly well, often producing errors of less than 0.01 Å all the way to the dissociation limit.

Recently Varshni (5) has extended these comparisons to two other easily used closed-form potentials – the Rydberg potential (6) and a potential devised earlier by Varshni (7). His conclusion was that the Varshni potential (Varshni III) is the best performer of the three. While the additional comparisons constitute a useful exercise, Varshni's computational procedure has unfairly tilted the scales against the other two functions in the comparisons of his Table 2.

All three of the functions examined by Varshni are three-parameter functions. For such it is customary to use the experimental internuclear distance R_e, vibrational frequency ω_e, and dissociation energy $\mathcal{D}_e$ to fix the three parameters. In fact, if one is interested in the whole potential, this is the only choice that makes sense, since these three quantities are needed to properly locate the potential on the R-axis and give it the correct curvature near the minimum and the correct asymptotic energy. However, if one is interested in only the *inner* branch of the potential, one can use in place of $\mathcal{D}_e$ some other experimental quantity; the obvious choices are the vibrational anharmonicity $\omega_e x_e$ and the vibration–rotation coupling constant α_e. In our comparisons, Henderson and I found that Morse repulsive branches defined by R_e, ω_e, and $\omega_e x_e$ gave appreciably better agreement with known RKR potentials than curves defined by R_e, ω_e, and $\mathcal{D}_e$. Varshni has considered only the latter definition in his comparisons.

I have repeated Varshni's comparisons using both $\mathcal{D}_e$ and $\omega_e x_e$ alternately to define the three parameters needed for each potential function. For the Morse function and the Rydberg function, the use of $\omega_e x_e$ is straightforward, since the equations relating $\omega_e x_e$ to $\mathcal{D}_e$ are simple (7, 8). (Of course, one cannot use $\omega_e x_e$ in those very rare cases where it is negative, as in the alkali hydrides.) For the Varshni III function, the relations among ω_e, $\omega_e x_e$, $\mathcal{D}_e$, and R_e are more complex; and it is necessary to solve numerically for the quantity Δ in the expression relating $\omega_e x_e$ to the equilibrium rotational constant B_e and Δ (7, 8). This, however, is also easily accomplished using any good root finder, e.g. Newton's method. (There are exceptions such as $H_2(X)$, where there is no physical root to this equation.)

In my comparisons I have used the 25 molecular states considered in ref. 4, updated in accord with more recent data, plus 10 more states included in a recent study of reduced potentials (9). These 35 potentials have considerable overlap with the set used by Varshni; however, I have not included the hydrides and the interhalogens (except ICl) in my set. Many of the members

Can. J. Chem. Downloaded from www.nrcresearchpress.com by 41.223.56.140 on 09/07/12
For personal use only.

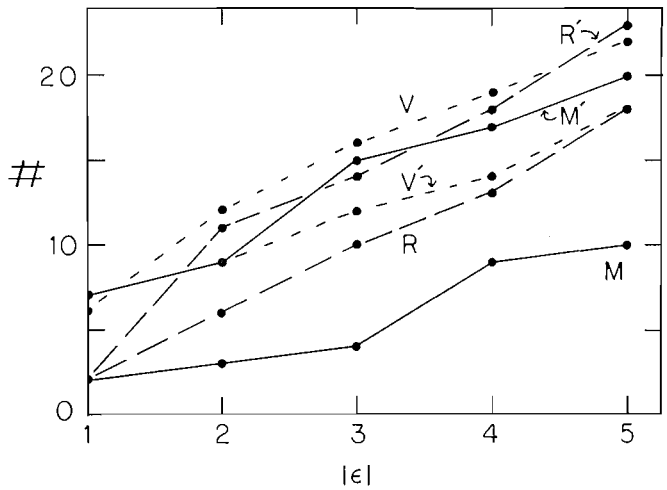


FIG. 1. Comparison of six potential forms in reproducing inner branches of known diatomic potentials. The quantity ϵ on the abscissa is defined as 1000 times the maximum relative error, $[R(\text{calc}) - R(\text{known})]/R_e$. (The maximum relative error usually occurs at the highest energy.) The quantity on the ordinate is the number of cases where the error is less than the value on the abscissa. M, R, and V refer to the Morse, Rydberg, and Varshni III functions, respectively. Primes indicate potentials determined by R_e, ω_e, and $\omega_e x_e$, while unprimed labels refer to use of $\mathcal{D}_e$ in place of $\omega_e x_e$.

of these two groups are experimentally known to less than 50% of their well depths; and in such cases it is inappropriate to extend the RKR potentials to 75–95% of well depth for the purpose of such comparisons, as Varshni has done (e.g. his Table 2).

Figure 1 gives a semiquantitative picture of the performance of these potential functions for the 35 known potentials tested here. In terms of the quantities displayed in this figure, a good performance is exemplified by a rapid rise at small $|\epsilon|$; however, from the cumulative nature of the plotted quantity, all curves must rise eventually to the total number of cases considered (here 35). The Varshni curve based on $\mathcal{D}_e$ is the best performer over much of the displayed range of $|\epsilon|$; but the $\omega_e x_e$-based Morse and Rydberg functions perform about as well, and the $\omega_e x_e$-based Varshni function is only slightly poorer. In fact, only the $\mathcal{D}_e$-based Morse function is noticeably poorer than the others over the full range of this diaplay.

Some further comparisons are given in Table 1, from which it can be seen that all three $\omega_e x_e$-based potentials show smaller average absolute values and smaller rms values of the maximum relative errors than the $\mathcal{D}_e$-based functions. It is interesting to note that all six functions show *positive* average error, which means that they are systematically too "hard." However, for the V′ potential, the systematic error is noticeably smaller than for the other five.

The comparisons of Table 1 are strongly influenced by the results for the alkali–metal dimers, for which the errors are noticeably larger for all six functions. When the 7 potentials in this group are excluded, I obtain the values given in parentheses, from which it can be seen that the V, M′, and R′ functions are comparably "good" in columns 2 and 3. From the standpoint of systematic errors, the V potential is now the best.

Henderson and I also examined the ability of the Morse potential to predict α_e, and I have repeated this check for all six forms. With double counting in cases where the calculated values are very close, the tally of best predictions is: V′(15), V(10), M′(10), R′(3), M(2), R(1). Since the Rydberg α_e value is almost always sandwiched between the other two (in each group of three), the Rydberg potential is at a disadvantage in this particular test.

TABLE 1. Average maximum error, average absolute maximum error, and rms maximum error for six functions used on 35 (28)[a] molecular states; quantities as defined in Fig. 1

Potential	$\langle\epsilon\rangle$	$\langle\|\epsilon\|\rangle$	rms ϵ
M	8.3(5.0)	9.7(6.2)	12.7(7.1)
R	5.2(2.4)	7.9(4.8)	10.6(5.8)
V	3.3(−0.2)	6.6(3.9)	9.7(5.3)
M′	3.8(2.2)	5.8(4.0)	7.8(5.2)
R′	2.6(1.1)	5.5(3.9)	7.3(5.0)
V′	0.2(−2.2)	5.8(4.8)	7.4(6.1)

[a]Values in parentheses obtained when 7 alkali-metal dimer potentials are excluded.

Varshni (5) reported a large error for NaAr(X), in discord with results of Henderson and myself (4). The correct experimental potential to use in this case is the modified Morse curve reported in eq. [8] of the original paper (10); since the rotational constants B_v were determined only for $v = 0$ and 1, and RKR calculation is inappropriate.

Schwartz and Le Roy (11) have criticized the use of the Morse function to approximate the repulsive branch on the grounds that the Morse function cannot accommodate higher-order semiclassical corrections to the potential. However, the cases where such an approximation is needed are "ignorance" situations where the rotational constants are not known. In the face of the uncertainties that this lack of information entails, higher-order semiclassical corrections pale to insignificance.

In summary, the repulsive branches of diatomic potentials are remarkably simple, permitting surprisingly reliable prediction from closed-form potentials based on equilibrium spectroscopic constants. Although the Varshni III function outperforms the Morse and Rydberg functions when R_e, ω_e, and $\mathcal{D}_e$ are used to define the potentials, the latter two functions perform comparably well when R_e, ω_e, and $\omega_e x_e$ are used. It seems likely that other potential forms will be found to perform similarly well. However, in cases where chemically analogous potentials are known experimentally, the use of reduced potentials may be preferable to these closed-form potential functions (4, 9).

1. J. TELLINGHUISEN. J. Mol. Spectrosc. **44**, 194 (1972).
2. W. M. KOSMAN and J. HINZE. J. Mol. Spectrosc. **56**, 93 (1975).
3. C. R. VIDAL and H. SCHEINGRABER. J. Mol. Spectrosc. **65**, 46 (1977).
4. J. TELLINGHUISEN and S. D. HENDERSON. Chem. Phys. Lett. **91**, 447 (1982).
5. Y. P. VARSHNI. Can. J. Chem. **66**, 763 (1988).
6. R. RYDBERG. Z. Phys. **73**, 376 (1931).
7. Y. P. VARSHNI. Rev. Mod. Phys. **29**, 664 (1957).
8. D. STEELE, E. R. LIPPINCOTT, and J. T. VANDERSLICE. Rev. Mod. Phys. **34**, 239 (1962).
9. J. TELLINGHUISEN, S. D. HENDERSON, D. AUSTIN, K. P. LAWLEY, and R. J. DONOVAN. Phys. Rev. A. **39**, 925 (1989).
10. J. TELLINGHUISEN, A. RAGONE, M. S. KIM, D. J. AUERBACH, R. E. SMALLEY, L. WHARTON, and D. H. LEVY. J. Chem. Phys. **71**, 1283 (1979).
11. C. SCHWARTZ and R. J. LE ROY. J. Chem. Phys. **81**, 3996 (1984).

Can. J. Chem. Downloaded from www.nrcresearchpress.com by 41.223.56.140 on 09/07/12
For personal use only.

The effect of temperature and salinity on the Setschenow parameters of naphthalene in seawater

GERARDO GOLD[1] AND SILVIO RODRIGUEZ
Department of Chemistry, University of the Pacific, Stockton, CA 95211, U.S.A.

Received April 12, 1988[2]

G. GOLD and S. RODRIGUEZ. Can. J. Chem. **67**, 822 (1989).

Solubility measurements of naphthalene in seawater of different salinities have been determined by the Generator Column Method in the 276.6 K to 316.8 K temperature range. The Gibbs free energy, enthalpy, and entropy of solution were evaluated at 298 K by means of the Clarke and Glew equation. The temperature dependence of the Setschenow parameters for naphthalene in seawater has been studied and compared with the values calculated using current models for the salting-out of nonpolar molecules. The Surface Tension Approach gives the best correlation with experimental values.

Key words: Setschenow parameters, solubility of naphthalene in seawater.

G. GOLD et S. RODRIGUEZ. Can. J. Chem. **67**, 822 (1989).

Opérant à des températures allant de 276,6 à 316,8 K et faisant appel à la méthode de la colonne génératrice, on a mesuré la solubilité du naphtalène dans de l'eau de mer de salinités diverses. Utilisant l'équation de Clarke et Glew, on a évalué l'énergie libre de Gibbs, l'enthalpie et l'entropie de solution. On a étudié la relation qui existe entre la température et les paramètres de Setschenow du naphtalène dans l'eau et on l'a comparée avec les valeurs calculées en utilisant les modèles actuels pour le salage des molécules non polaires. L'approche de la tension superficielle donne la meilleure corrélation avec les valeurs expérimentales.

Mots clés : les paramèters de Setschenow, la solubilité du naphtalène dans de l'eau de mer.

[Traduit par la revue]

Introduction

Although considerable progress has been made in research concerning identification and distribution of contaminants in the ocean, little is known about fundamental properties such as the effect of salinity, temperature, and pressure on the aqueous solubility of contaminant molecules. Of these compounds, polycyclic aromatic hydrocarbons (PAH) are particularly important because of their wide distribution in the environment and the carcinogenic character of some of them. A number of review articles have been published about the incidence and consequences of their presence in aquatic systems (1, 2). Solubilities of polycyclic aromatic hydrocarbons in seawater have been reported at 298 K for naphthalene (3, 4), biphenyl and phenanthrene (4), acenaphthene and pyrene (5). More recently Whitehouse has reported the aqueous solubility of phenanthrene, anthracene, 1,2-benzanthracene, and benzo(*a*)pyrene at temperatures ranging from 276.8 to 298.4 K and salinities ranging from 0 to 36.7% (6), and the abnormal solubility behaviour of some aromatic hydrocarbons in seawater (7). Estimates of the aqueous solubilities of organic hydrophobic molecules have been obtained from molecular parameters and activity coefficients (8). The presence of an electrolyte changes the activity coefficient of a dissolved nonelectrolyte and its solubility. For many electrolyte–nonelectrolyte systems the experimental results can be described by the empirical Setschenow equation

$$[1] \quad \log (S^0/S) = k_s C_s$$

where S^0 and S are the solubilities of the electrolyte in pure water and in an aqueous electrolyte solution, respectively; C_s is the concentration of the non-electrolyte, and k_s is the salting constant, also known as the Setschenow constant. Given that the aqueous solubilities of PAH are low, and self interaction terms may be considered negligible, the Setschenow constants can be identified with the true salting-out coefficients of the electrolytes. Many different models have been proposed to predict the magnitude of k_s for any given pair of electrolyte–nonelectrolyte cosolutes. It is the objective of the present work to determine the Setschenow parameters of naphthalene, the simplest PAH, in seawater of different salinities, in the temperature range 276.6 to 316.8 K. For the ideally dilute solution of the hydrocarbon, the thermodynamic parameters ΔG^0, ΔH^0, and $\Delta C_p{}^0$ for the solution process are then determined using the Clarke and Glew equation. Also, Setschenow constants have been calculated, as a function of temperature, using the different models for nonelectrolyte salting currently available.

Experimental

Naphthalene was zone refined (James Hinton, Valparaiso, FL), and methylene chloride was spectro quality (Aldrich, Gold Label). These reagents were used as received, without further purification. Natural seawater was IASOP (Institute of Oceanographic Sciences, Surrey, England) standard seawater, which is used as a salinity standard and therefore is provided with a very accurate value of its salt content. Prior to use, this water was irradiated with ultraviolet light from a medium-pressure mercury vapour lamp. Artificial seawater was prepared according to Lyman and Fleming (9).

The solubility of naphthalene in seawater, in the range from 276.6 to 316 K in temperature and 0 to 35 parts per thousand (ppt) in salinity was measured using a modified version of the Generator Column Method developed at the U.S. National Bureau of Standards (8, 10, 11). With this method it is possible to minimize the problems commonly associated with the so-called "shake-flask" method, such as supersaturation of the solution, adsorption of the solute onto the walls of the container, and interference from other compounds. Typically, naphthalene was deposited onto 60–80 mesh glass beads (Alltech Associates) by adding 20 g of the beads to 200 mL of a 0.1% w/w solution of the hydrocarbon in methylene chloride, and then evaporating the solvent in a rotary evaporator. A 60 × 0.6 cm polypropylene tube was then filled with the dry beads and placed inside a one meter water jacket connected to a thermoregulated circulator (Lauda model B-1). Each new column was conditioned by pumping distilled water at 50°C using a Bodine NSI-34RH pump. After equilibrium was reached, water or seawater at the

[1]Present address: Centro de Investigacion y de Estudios Avanzados del IPN-Unidad Merida, A.P. 73 Cordemex C. P. 97310, Merida, Yucatan, Mexico.

[2]Revision received January 9, 1989.

Printed in Canada / Imprimé au Canada

Can. J. Chem. Downloaded from www.nrcresearchpress.com by 41.223.56.140 on 09/07/12
For personal use only.

Can. J. Chem. Downloaded from www.nrcresearchpress.com by 41.223.56.140 on 09/07/12
For personal use only.

TABLE 1. Solubility of naphthalene in water and seawater between 276.6 and 316.8 K; the values in parentheses are the estimated experimental errors

T/K	$S \times 10^4$/(mol/kg)	Mole fraction $\times 10^6$
Water		
316.8	5.38 (0.07)	9.79 (0.19)
307.8	3.78 (0.05)	6.85 (0.13)
298.0	2.59 (0.05)	4.67 (0.11)
286.6	1.68 (0.02)	3.03 (0.06)
276.6	1.18 (0.02)	2.12 (0.06)
Seawater, $m = 0.2679$		
316.8	4.55 (0.05)	8.23 (0.13)
307.8	3.23 (0.05)	5.82 (0.13)
298.0	2.20 (0.04)	3.96 (0.11)
286.4	1.41 (0.02)	2.53 (0.06)
276.6	1.00 (0.02)	1.79 (0.05)
Seawater, $m = 0.3587$		
316.8	4.32 (0.07)	7.80 (0.18)
307.8	3.05 (0.05)	5.48 (0.12)
298.0	2.10 (0.04)	3.77 (0.11)
286.4	1.34 (0.02)	2.41 (0.05)
276.6	0.981 (0.01)	1.70 (0.03)
Seawater, $m = 0.5329$		
316.8	3.92 (0.05)	7.06 (0.13)
307.8	2.80 (0.05)	5.03 (0.12)
298.0	1.91 (0.03)	3.43 (0.06)
286.4	1.23 (0.02)	2.20 (0.06)
276.6	0.854 (0.01)	1.52 (0.03)

appropriate temperature was pumped through the column. The Generator Column technique was modified by eliminating the extraction of the saturated solution, and measuring the absorbance of the column effluent directly (12). The concentrations of naphthalene in the effluent were calculated from the absorbance at 276 nm and the extinction coefficient at that wavelength (3). All absorption spectra were recorded with a Cary 219 double beam uv–vis spectrophotometer with a nominal slit of 0.5 nm. The temperature was monitored with a digital thermometer (Bailey model BAT-12). Seawater with salinities less than 35 ppt were prepared by gravimetric dilution of the standard seawater with distilled deionized water.

Results

The solubilities of naphthalene in seawater, as a function of both temperature and salt content, are listed in Table 1. The electrolyte concentration in seawater was calculated by taking advantage of the fact that the proportion between the major constituents of seawater is constant and independent of the salinity. Results obtained with natural seawater are indistinguishable from those obtained with artificial seawater. Absorbances were corrected for temperature induced volume changes using the one-atmosphere equation of state for seawater given by Wang and Millero (13)

$$[2] \quad V_{sw} = 1.000027/(1.0 + \rho_t 10^{-3})$$

where V_{sw} is the specific volume of seawater, and ρ_t is given by

$$[3] \quad \rho_t = A_t + B_t\rho_0 + C_t\rho_0^2 + \ldots$$

where ρ_0 is a function of salinity and the coefficients A_t, B_t, C_t, ... are a function of the temperature. The corrected solubility values were then converted to the mole fraction scale. The solubility of naphthalene in pure water at 298 K reported here, 4.67×10^{-6} agrees very well with the values given recently by other authors: 4.48×10^{-6} (11) and 4.32×10^{-6} (14).

TABLE 2. Setschenow parameters for the salting-out of naphthalene in seawater as a function of temperature; σ is the standard deviation and r is the correlation coefficient

T/K	k_s/(kg/mol)	$\sigma \times 10^4$	r^2
316.8	0.267 (0.007)	0.012	0.9988
307.8	0.254 (0.009)	0.150	0.9969
298.0	0.252 (0.007)	0.067	0.9993
286.4	0.262 (0.014)	0.270	0.9947
276.6	0.270 (0.003)	0.012	0.9998

Solubilities were fitted to the Setschenow equation using least-squares. The resulting Setschenow parameters, and their uncertainties, as a function of temperature are given in Table 2. The uncertainty in the values for the slope and the correlation coefficient were calculated using standard statistical techniques. Our value for the salting-out constant of naphthalene in seawater at 298 K, 0.252 kg/mol, compares very well with the value of 0.256 kg/mol given by Gordon and Thorne (3) and is lower than the value of 0.303 kg/mol reported by Eganhouse and Calder (4). In order to calculate the thermodynamic functions for the process

$$\text{naphthalene (solid)} \Leftrightarrow \text{naphthalene (aqueous)}$$

the corrected solubilities were fitted to the Clarke and Glew equation

$$[4] \quad R \ln X = -\Delta G_\theta^0/\theta + \Delta H_\theta^0(1/\theta - 1/T) + \Delta C_{p\theta}^0 [\theta/T - 1 + \ln (T/\theta)]$$

where θ is a reference temperature, and the other symbols have their usual thermodynamic meaning. This equation does not assume the heat capacity change to be zero, and has the advantage that the adjustable coefficients are not mutually correlated (11, 15, 16). The thermodynamic functions are given in Table 3 for the process of solution of naphthalene in water and seawater. Values calculated from the data reported by May *et al.* (11) are included for comparison.

Discussion

The enthalpy of solution of hydrocarbons in water can be considered to be the result of four contributions: (*a*) the lattice enthalpy of the hydrocarbon, (*b*) an enthalpy of solvation which is negative because of a more ordered structure of the solvent around the hydrocarbon molecules in solution, (*c*) a positive enthalpy of cavity formation, which is the energy required to make a hole in the solvent for the dissolved hydrocarbon, and (*d*) an enthalpy of hydrocarbon–solvent interaction that is usually considered to be negative, and includes all the remaining solvent–solute interactions. From the results in Table 3 it can be seen that ΔH^0 of solution for naphthalene is the same for water and seawater, and the more positive value for the Gibbs free energy of solution of naphthalene in seawater, as compared to the value in pure water, can be ascribed to an entirely entropic contribution. This is usually interpreted as the predominance of water structure formation, promoted by the hydrocarbon, over the destruction of the structure induced by the electrolytes.

Many different models have been proposed to predict the magnitude of the salting-out coefficient for any given pair of electrolyte–nonelectrolyte cosolutes. In general, these models can be divided into three categories: electrostatic, statistical mechanical, and thermodynamic. Electrostatic equations usually predict k_s values that are very similar for all 1:1 electrolytes,

TABLE 3. Thermodynamic functions for the process solid naphthalene – aqueous naphthalene

Solvent	ΔG^0/(kJ/mol)	ΔH^0/(kJ/mol)	$T\Delta S^0$/(kJ/mol)	ΔC^0_p/(kJ/mol K)
Water	30.41 (0.019)	28.4 (0.1)	−2.01	0.26 (0.02)
Water[a]	30.55 (0.032)	28.6 (1.3)	−1.95	0.31 (0.17)
Seawater	31.16 (0.014)	28.4 (0.09)	−2.76	0.19 (0.02)

[a]Calculated from the experimental data of May *et al.* (11).

and in many cases fail to predict salting-in (17). Having proved unsatisfactory, electrostatic theories have received minor attention in the literature. Statistical mechanical models consider the dissolution process of a solute in a liquid as a two step process: (*1*) the creation of a cavity in the solvent, large enough to accommodate the solute, and (2) the introduction of a solute molecule into the cavity (18). At present, the best approach to calculate the free energy changes associated with these processes is the Scaled Particle Theory (SPT) (19, 20). In this theory, a fluid is considered to be formed by a system of spherical molecules obeying a pairwise additive potential into which an additional molecule, obeying the same potential, is introduced by the procedure of distance scaling. Pierotti (21, 22) applied the SPT to the solubility of gases in real liquids, and calculated the molecular parameters of water that are needed in the calculations. Shoor and Gubbins (23) applied Pierotti's results to the solubility of gases in concentrated electrolyte solutions, finding an expression for k_s. Pierotti's SPT assumes solutions to consist of hard-core spherical molecules in which solvent molecules are uniformly distributed around each molecule of solute. Masterton and Lee (24) obtained a general expression for k_s

$$[5] \quad k_s = k_\alpha + k_\beta + k_\gamma$$

where k_α is the contribution from the free energy of cavity formation, k_β is the term containing the solute–cavity interaction, and k_γ is a statistical term that becomes negligible for slightly soluble hydrocarbons. The term k_α always leads to salting-out. It is proportional to the molecular diameter of the solute and inversely proportional to the temperature. The term k_β always leads to salting-in and it decreases with increasing temperature. Masterton (25) derived an equation for salting-out in seawater in the 273 to 313 K temperature range. His equations for k_s are expressed in terms of ionic strength I_w, therefore, in order to apply the SPT to our results, the values of solubility from Table 2 were recalculated according to the equation

$$[6] \quad I_w = 0.01994S/(1 - S/1000)$$

where S is the salinity in parts per thousand (13). The calculation of k_s requires the knowledge of the Lennard–Jones parameters for the solute. These parameters were calculated using two different approaches. The first approach uses an empirical relationship between the critical properties of the compound and the Lennard–Jones parameters (26, 27). The critical constants for naphthalene were taken from the compilations by Kudchaker *et al.* (28) and Dreisbach (29). Using this method, the work function was calculated to be 394.1 K and the intermolecular distance as 6.89 Å. The value of k_s at 298 K calculated using these parameters is 0.546 kg/mol which is three times higher than the experimental result of 0.186 kg/mol, expressed in terms of ionic strength. In the second approach, the work function was calculated using the Mavroyannis–Stephen equation (24)

$$[7] \quad \epsilon/k = 2.28 \times 10^{-8} (\alpha^{3/2} E^{1/2} \delta^6)$$

where α is the molecular polarizability, E is the total number of electrons, and δ is the intermolecular distance. The molecular polarizability of naphthalene, 17.48×10^{-24} cm^3, was taken from the compilation by Miller and Savchik (30) and the intermolecular distance 6.58 Å was taken to be equal to the crystallographic diameter (29) which was calculated from the bond lengths and angles determined from X-ray diffraction data by Ponomarev *et al.* (31) and Sellers and Boggs (32). The calculated value for the work function is 169.3 K, and the calculated salting-out constant is 0.333 kg/mol, which is about two times greater than the experimental value of 0.186 kg/mol.

Although pairwise additivity seems unlikely in aqueous solution, the experimental values of the salting coefficients of simple gases in seawater are in reasonable agreement with the values calculated from the SPT (25). However, for large nonpolar solutes, the assumption of random distribution of molecules is more difficult to justify and cavity terms in seawater cannot be accurately evaluated. Moreover, the assumption that the molecules in solution have a hard-core leads to the problem of the selection of the correct diameter. Thermodynamic functions for cavity formation are very sensitive to the solvent molecular diameter. A change of only 0.1 Å in the diameter of water produces an almost 30% change in the free energy of the cavity (20).

The disagreement between experiment and theory can also be partially attributed to the magnitude of the calculated ion–solute interactions (24). Given that in this case the calculated value of the salting-out constant is higher than the experimental one, this seems to indicate that we have underestimated the effect of the interaction between the naphthalene and the surrounding ions.

Thermodynamic models were developed in their original form by McDevit and Long (33), and are based on the Tamman, Tait, and Gibson equation for electrolyte solutions (13) which assumes that the properties of an aqueous electrolyte solution are the same as those of pure water under an additional pressure, P_e, exerted by the electrolyte. This pressure is the result of an electrostriction in which the coulombic field of the ions interact with the water dipoles, thus compressing the solvent in their immediate neighborhood. McDevit and Long (33) assumed that the only significant interaction in the process of dissolving a nonelectrolyte is the work necessary to create a cavity in the solvent, without considering any solute–cavity interactions. For very low concentrations of both salt and nonelectrolyte they found

$$[8] \quad k_s = V_i^0 (V_s - V_s^0)/2.3B_0RT$$

where V_s and V_s^0 are the "liquid" volume and partial molar volume of the salt respectively; B_0 is the isothermal compressibility of water; V_i^0 is the partial molar volume of the nonelectrolyte, R and T have their usual meaning. An equivalent expression for k_s is

Can. J. Chem. Downloaded from www.nrcresearchpress.com by 41.223.56.140 on 09/07/12
For personal use only.

Can. J. Chem. Downloaded from www.nrcresearchpress.com by 41.223.56.140 on 09/07/12
For personal use only.

[9] $k_s = \lim V_i^0/2.3RTdP_e/dC_s$

where C_s is the electrolyte concentration. This equation contains explicitly the pressure exerted by the electrolyte, P_e, instead of the "liquid" volume of the salt, V_s^0, which is not clearly defined. Equations [8] and [9] correctly predict the relative change of k_s for different salts, and are in good quantitative agreement for small molecules such as O_2, H_2, and the noble gases (34). However, for larger nonelectrolytes such as benzene or naphthalene the estimated values of k_s are off by a factor of two or three. This is probably due to the neglect of nonzero distance of closest approach. The effective pressure, P_e, exerted by sea salt was calculated from

[10] $B^pV^p = 0.4343X_l(0.135\ V_w)/(B_t + P_e + P)$

where B^p is the isothermal compressibility at pressure P, V^p, and V_w are the volume of the solution at pressure P and the volume of pure water at atmospheric pressure, X_l is the number of grams of water per gram of solution, and B_t refers to the pressure exerted by pure water. The values of B^p and V^p for seawater in the salinity and temperature ranges of this work were calculated from the high pressure equation of state given by Millero *et al.* (35). The calculated value for k_s at 298 K is 0.836 kg/mol, which is about three times greater than the experimental value.

Recently, Aveyard (36) used a different approach assuming that the nonideal work of transferring a nonelectrolyte solute from water to a salt solution depends not on P_e but on the change of the surface tension of the aqueous solution when the salt is added. He assumed that the surface tension of a microscopic cavity is the same as the macroscopic value and the solute–solvent interactions are the same in water and in the aqueous electrolyte solution. For a 1:1 electrolyte Aveyard found

[11] $k_s = 3.86\ V_w^{1/3}\ V_i^{2/3}\ \Phi_s$

where Φ_s is the osmotic coefficient for a one molal solution and the volumes are given in m^3/mol. In this case, the osmotic coefficients for seawater were calculated from the equation given by Millero (37)

[12] $1 - \Phi_s = 2.303A^{1/2}(\xi/3) + BI + CI^{3/2} + DI^2 + \ldots.$

where I is the ionic strength of the solution and $A, B, C, D, \xi\ldots.$ are temperature-dependent parameters. The calculated value of k_s for naphthalene in seawater at 298 K using the Aveyard approach gives a value of 0.267 kg/mol, which is in good agreement with the experimental value of 0.252 kg/mol.

Figure 1 shows the experimental and calculated values of k_s using the TTG and ST models for naphthalene in seawater as a function of temperature. It has been pointed out that the prediction of the temperature dependence of the Setschenow parameters is a more stringent test of the models available than the prediction of k_s at a single temperature (36). As shown in this figure, Aveyard's surface tension method predicts the correct sign and order of magnitude for the temperature coefficient of the salting constant while the TTG model shows a strong temperature dependence that is not consistent with the experimental data.

By assuming that in the presence of an electrolyte the water in an aqueous solution behaves as if it was subjected to an additional pressure, the TTG model has the advantage of making no assumptions about the distribution of molecules and ions in solution or about the explicit mathematical characterization of their interactions. Nevertheless, in many cases, this approach predicts Setschenow parameters that are high by a factor of two and three (33, 36, 38).

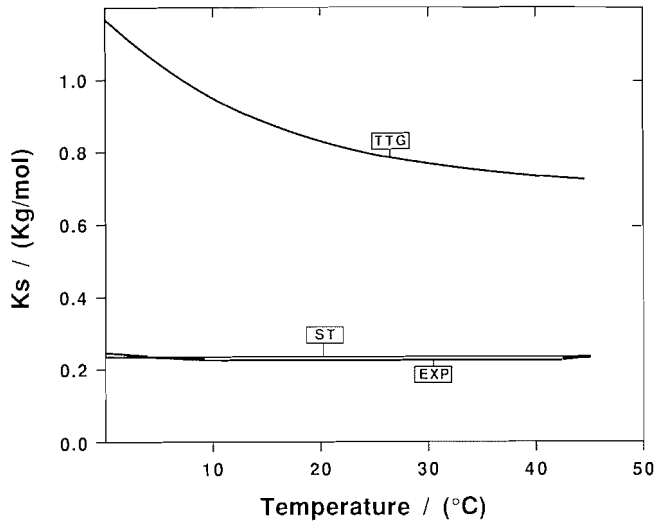


FIG. 1. Experimental and calculated values of k_s for naphthalene in seawater as a function of temperature. EXP, experimental values. TTG, values calculated by the Tamman, Tait, and Gibson model. ST, values calculated using the Surface Tension approach.

Whether the agreement we found between our experimental values and the Surface Tension approach is fortuitous or an indication of the validity of the model, it is evident that more experimental results and more theoretical work are needed in order to predict the behaviour of nonelectrolytes in aqueous electrolyte solutions.

1. J. FUTOMA, S. R. SMITH, T. E. SMITH, and J. TANAKA. Polycyclic aromatic hydrocarbons in water systems. CRC Press. 1981.
2. J. W. FARRINGTON and J. WESTALL. *In* The role of the oceans as a waste disposal option. *Edited by* G. Kullenberg. D. Reidel. 1986.
3. J. E. GORDON and R. L. THORNE. J. Phys. Chem. **71**, 4390 (1967).
4. R. P. EGANHOUSE and J. A. CALDER. Geochim. Cosmochim. Acta, **37**, 2459 (1973).
5. S. S. ROSSI and W. H. THOMAS. Environ. Sci. Technol. **15**, 715 (1981).
6. B. G. WHITEHOUSE. Mar. Chem. **14**, 319 (1984).
7. B. G. WHITEHOUSE. Mar. Chem. **17**, 277 (1985).
8. S. P. WASIK, M. M. MILLER, Y. B. TEWARI, W. E. MAY, W. J. SONNEFELD, H. DEVOE, and W. H. ZOLLER. Res. Rev. **85**, 29 (1983).
9. J. LYMAN and R. H. FLEMING. J. Mar. Res. **3**, 134 (1940).
10. H. DEVOE, M. M. MILLER, and S. P. WASIK. J. Res. Natl. Bur. Stands. **86**, 361 (1981).
11. W. E. MAY, S. P. WASIK, M. M. MILLER, Y. B. TEWARI, J. M. BROWN-THOMAS, and R. N. GOLDBERG. J. Chem. Eng. Data, **28**, 197 (1983).
12. R. A. VELAPOLDI, P. A. WHITE, W. E. MAY, and K. R. EBERHARDT. Anal. Chem. **55**, 1896 (1983).
13. J. V. LEYENDEKKERS. Thermodynamics of seawater. Marcel Dekker Inc. 1976.
14. D. BENNETT and W. J. CANADY. J. Am. Chem. Soc. **106**, 910 (1984).
15. E. C. CLARKE and D. N. GLEW. Trans. Faraday Soc. **62**, 539 (1966).
16. M. J. BLANDAMER, J. BURGESS, R. E. ROBERTSON, and J. M. W. SCOTT. Chem. Rev. **82**, 259 (1982).
17. J. E. GORDON. The organic chemistry of electrolyte solutions. Wiley-Interscience, New York. 1975.

18. H. L. CLEVER and R. BATTINO. Solutions and solubilities, techniques of chemistry series, Vol. 8. Part I. *Edited by* M. R. J. Dack. Wiley, New York. 1975.
19. R. A. PIEROTTI. J. Phys. Chem. **67**, 1840 (1963).
20. N. MOREL-DESROSIER and J. P. MOREL. Can. J. Chem. **59**, 1 (1981).
21. R. A. PIEROTTI. J. Phys. Chem. **69**, 281 (1965).
22. R. A. PIEROTTI. Chem. Rev. **76**, 717 (1976).
23. S. K. SHOOR and K. E. GUBBINS. J. Phys. Chem. **73**, 498 (1969).
24. W. L. MASTERTON and T. P. LEE. J. Phys. Chem. **74**, 1776 (1970).
25. W. L. MASTERTON. J. Solution Chem. **4**, 523 (1975).
26. L. I. STIEL and G. THODOS. J. Chem. Eng. Data, **7**, 234 (1962).
27. L. SEN TEE, S. GOTOH, and W. E. STEWART. Ind. Chem. Fundam. **5**, 356 (1966).
28. A. P. KUDCHAKER, S. A. KUDCHAKER, and R. C. WILHOIT. Naphthalene, API Monograph Series, API Publication. 707 (1978).
29. R. R. DREISBACH. Physical properties of chemical compounds. Adv. Chem. Ser. 15, American Chemical Society (1955).
30. K. J. MILLER and J. A. SAVCHIK. J. Am. Chem. Soc. **101**, 7206 (1979).
31. V. I. PONOMAREV, O. S. FILIPENKO, and L. O. ATOVMAN. Sov. Phys. Crystallogr. **21**, 215 (1976).
32. H. SELLERS and J. E. BOGGS. J. Mol. Struc. **74**, 137 (1981).
33. W. F. MCDEVIT and F. A. LONG. J. Am. Chem. Soc. **74**, 1773 (1952).
34. F. A. LONG and W. F. MCDEVIT. Chem. Rev. **51**, 119 (1952).
35. F. J. MILLERO, C.-T. CHEN, A. BRADSHAW, and K. SCHLEICHER. Deep-Sea Res. **27**, 255 (1980).
36. R. AVEYARD. Can. J. Chem. **60**, 1317 (1982).
37. F. J. MILLERO and W. H. LEUNG. Am. J. Sci. **276**, 1035 (1976).
38. R. F. CROSS. J. Phys. Chem. **79**, 1822 (1975).

Can. J. Chem. Downloaded from www.nrcresearchpress.com by 41.223.56.140 on 09/07/12
For personal use only.

A positive $^6J(H,CHO)$ in some *meta* derivatives of benzaldehyde. A simple model

TED SCHAEFER AND CRAIG S. TAKEUCHI
Department of Chemistry, University of Manitoba, Winnipeg, Man., Canada R3T 2N2

Received November 7, 1988

TED SCHAEFER and CRAIG S. TAKEUCHI. Can. J. Chem. **67**, 827 (1989).

^6J(H,CHO), the long-range coupling constant between the aldehydic and *para* protons in benzaldehyde, has not been detected, possibly because the $\sigma-\pi$ interaction giving rise to a negative coupling is intrinsically rather small and because the internal barrier to rotation about the C_{sp^2}—C_{sp^2} bond is large. However, ^6J(H,CHO) in some *meta* substituted derivatives is actually positive and as large as 0.09 Hz in 3,5-difluorobenzaldehyde; the barrier to internal rotation in this molecule is some 4 kJ/mol lower than in the parent molecule. The magnitude of ^6J(H,CHO) in these derivatives correlates well with $\sigma_{R,ST}$ values, a recent set of substituent constants derived from ^{13}C nuclear magnetic resonance chemical shifts of the β carbon in styrene derivatives. It is hypothesized that the substituents with negative $\sigma_{R,ST}$ values stabilize an ionic valence bond structure that has a positive ^6J(H,CHO). A brief discussion of ^4J(H,CHO) in some of these molecules is also presented.

Key words: NMR, spin coupling NMR, benzaldehyde.

TED SCHAEFER et CRAIG S. TAKEUCHI. Can. J. Chem. **67**, 827 (1989).

La constante de couplage à longue distance, ^6J(H,CHO), entre les protons aldéhydique et en *para* du benzaldéhyde n'a pas été détectée, probablement parce que l'interaction $\sigma-\pi$ qui donnerait lieu à un couplage négatif est intrinsèquement plutôt faible et parce que la barrière interne à la rotation autour de la liaison C_{sp^2}—C_{sp^2} est grande. Toutefois, le couplage ^6J(H,CHO) observé dans quelques dérivés substitués en *méta* est de fait positif; dans le cas du difluoro-3,5 benzaldéhyde, il est même de 0,09 Hz alors que la barrière interne à la rotation dans cette molécule est 4 kJ/mol plus faible que celle observée dans la molécule de base. Il existe une bonne corrélation entre l'amplitude du couplage ^6J(H,CHO) dans ces dérivés et les valeurs $\sigma_{R,ST}$, un ensemble de constantes de substituants qui a été établi à partir des déplacements chimiques observés dans les spectres en résonance magnétique nucléaire du ^{13}C pour le carbone β de dérivés du styrène. On fait l'hypothèse que les substituants avec des valeurs négatives de $\sigma_{R,ST}$ stabilisent une structure de liaison de valence ionique possédant une valeur de ^6J(H,CHO) qui est positive. On présente aussi une brève discussion des ^4J(H,CHO) dans quelques-unes de ces molécules.

Mots clés : RMN, couplage du spin, benzaldéhyde.

[Traduit par la revue]

Introduction

Positive long-range spin–spin coupling constants between *para* ring protons and α protons in the side chain of benzene derivatives are not expected. For example, $^6J(H,CH_3)$ in toluene is negative because it is a $\sigma-\pi$ coupling constant whose sign is proportional to the product of the negative hyperfine interaction, Q^H_{CH}, at the *para* C—H bond and the positive hyperfine interaction, Q^H_{CCH}, between the α C—H bond and the π electrons (1, 2). The latter interaction is proportional to $\sin^2\theta$, where θ is the angle by which the C—H bond of the methyl group twists out of the benzene plane. A ^6J(H,CH) as small in magnitude as 0.04 Hz and negative in sign is known for a highly hindered toluene derivative in which the C—H bond containing the coupled proton is strongly confined to the aromatic plane (unpublished work in this laboratory). Because of its simple conformational behaviour, ^6J(H,CH) has proved informative about side-chain orientations and about internal rotational potentials in benzene derivatives, particularly for those to which classical methods are not easily applicable (3–5). Again, ^6J(H,SH) in thiophenol derivatives (6) or, for example, $^6J(H,^{13}C)$ in derivatives of benzyl cyanide-8-^{13}C (7) have the signs expected of a $\sigma-\pi$ spin–spin coupling mechanism.

In benzaldehyde, $^6J(H,CHO) \equiv {}^6J$ has not been measured. Indeed, it must be very small (see Fig. 1, where the linewidth at half-height of the aldehyde proton peaks is about 0.02_5 Hz) and probably not more than about 0.01 Hz in magnitude. As the aldehyde group twists about the C_{sp^2}—C_{sp^2} bond the usual $\sigma-\pi$ coupling mechanism should give rise to a negative ^6J. As discussed recently (8), ^6J in 2,6-dichlorobenzaldehyde is −0.14 Hz and, in conjunction with molecular calculations, implies an unusually small magnitude of $^6J_{90}$, the coupling constant when the C—H bond of the side chain lies in a plane perpendicular to that of the benzene moiety. Thus, $^6J_{90}$ in toluene is −1.20 Hz (2) whereas it appears (8) to be only −0.3 Hz in benzaldehyde. The standard INDO MO FPT computations (9) agree closely with the experimental result for toluene, including the $\sin^2\theta$ dependence of ^6J (1), but calculate $^6J_{90}$ as −0.8 Hz in benzaldehyde (10). For rather subtle reasons, not understood (but see a suggestive discussion of $^6J(H,^{13}C)$ for acetophenone-β-^{13}C (8)), the carbonyl group hinders the transfer of nuclear spin state information via a $\sigma-\pi$ mechanism.

If $^6J_{90}$ in benzaldehyde is only 0.3 Hz in magnitude, then the assumption that the barrier (11) of 32.2 kJ/mol in dimethyl ether solution is twofold (12) implies a $\langle\sin^2\theta\rangle$ of about 0.04 at 300 K and hence a ^6J of $-0.3\langle\sin^2\theta\rangle$ or −0.01 Hz. Consequently, the unmeasurably small ^6J in benzaldehyde is rationalized.

Here we report on small positive ^6J values in some *meta* derivatives of benzaldehyde and interpret them in terms of an ionic valence bond structure; their correlation with a new set of substituent constants is also discussed.

Results and discussion

Some *meta* substituents should decrease the rotational barrier of the C_{sp^2}—C_{sp^2} bond (13) and perhaps give rise to an observable, negative ^6J in the appropriate benzaldehyde derivatives. For example, STO-3G MO computations on benzaldehyde (12) and ours on 3,5-difluorobenzaldehyde imply a decrease of 1.6 kJ/mol in the latter. Because the barrier to internal rotation in benzaldehyde is so large, however, these computations suggest that $\langle\sin^2\theta\rangle$ in the 3,5-difluoro derivative will increase by less than 10% and hence no observable ^6J would arise, it being estimated above as −0.01 Hz. Of course, an experimental

Can. J. Chem. Downloaded from www.nrcresearchpress.com by 41.223.56.140 on 09/07/12
For personal use only.

Can. J. Chem. Downloaded from www.nrcresearchpress.com by 41.223.56.140 on 09/07/12
For personal use only.

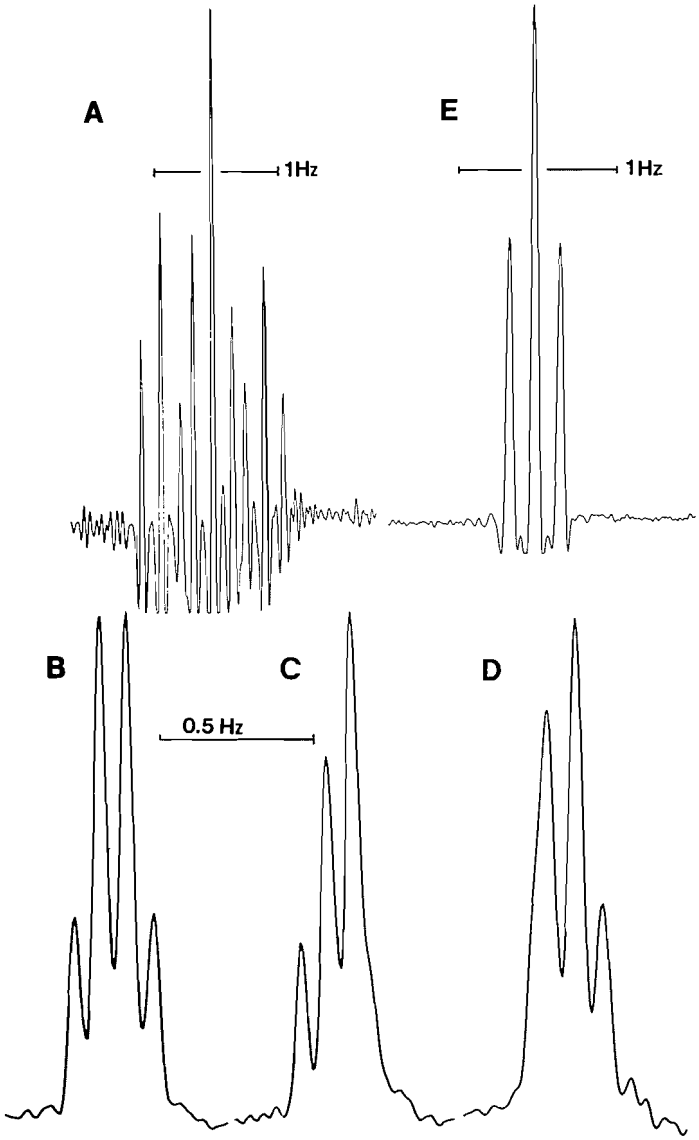


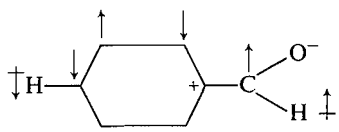
FIG. 1. In A the aldehydic ^1H nmr spectrum is shown for a 4.0 mol% solution of benzaldehyde in acetone-d_6 at a probe temperature of 300 K and 300 MHz. The digital resolution is 0.006 Hz. Severe resolution enhancement, LB −0.2 and GB 0.5, is employed in an attempt to detect ^6J(H,CHO). The linewidth is 0.02_5 Hz. The triplet of triplets arises from a ^5J(H,CHO) of 0.430(1) Hz and a ^4J(H,CHO) of −0.161(1) Hz (Table 1). In B the aldehydic ^1H nmr spectrum appears for a 3.9 mol% solution of 3,5-dimethoxybenzaldehyde. ^4J and ^6J are nearly equal in magnitude, causing the quartet structure. In C the *ortho* protons are being decoupled for one spin state of the *para* proton. Therefore one "triplet" within the spectrum collapses onto one peak of the remaining "triplet" (the couplings are not exactly the same so that these statements are only approximate, but sufficient for the purpose). In this experiment the *ortho* proton peaks at low frequency are irradiated. The triplet at low frequency of the aldehydic proton spectrum collapses. Hence ^6J(H,CHO)/^4J(H-2,H-4) > 0. ^4J(H-2,H-4) is known to be positive. These results were confirmed by further double resonance experiments. In D the *para* proton is being decoupled for a given spin state combination of the *ortho* protons, that is, the *para* proton peaks at lowest frequency are being irradiated. The irradiation intensity is not quite high enough for a clean result. Nevertheless, the two peaks at highest frequency in the aldehydic proton region are nearly collapsed into one another. Hence ^4J(H,CHO)/^4J(H-2,H-4) < 0. This result was confirmed by other experiments and also for a solution in CS_2. In E the ^1H nmr spectrum of the aldehydic proton is shown for a 6 mol% solution of 3,5-dimethylbenzaldehyde in acetone-d_6 at 300 MHz and 300 K. Again, no evidence for ^6J(H,CHO) appears. The linewidth at half-heights is about 0.04 Hz, perhaps because of very small residual coupling to the six methyl protons (the acquisition time was 41 s). Considerable resolution enhancement has caused distortions of peak intensities.

barrier height is to be preferred. For 3,5-difluorobenzaldehyde in dimethyl ether solution, an ^{19}F DNMR experiment (see below) gave $\Delta G^{\ddagger}$ as 28.0 ± 0.4 kJ/mol at 144 ± 2 K. For a twofold barrier $\langle \sin^2 \theta \rangle$ at 300 K is then 0.048 on the assumption that $\Delta S^{\ddagger}$ is negligible and that $\Delta H^{\ddagger}$ is roughly the same as V_2. Hence a ^6J of -0.01_5 Hz might exist by the above hypotheses.

In fact, for 3,5-difluorobenzaldehyde in CS_2 or acetone-d_6 solutions at 300 K, ^6J is +0.086(3) Hz. Furthermore, ^6J is +0.078(6) Hz for the 3,5-dimethoxy derivative in the same solvents and is +0.051(2) Hz for 3,5-dichlorobenzaldehyde. Analysis of the ^1H and ^{19}F nmr spectra of 3-fluorobenzaldehyde in these solvents gave ^6J as 0.047(2) Hz, while good iterative fits to the ^1H nmr spectra of 3-methoxybenzaldehyde in CS_2 and acetone-d_6 solutions could only be obtained with ^6J as +0.043(4) Hz. By way of contrast, ^6J in 3,5-dimethylbenzaldehyde is not detectable under the linewidth conditions for the aldehyde group (Fig. 1) and is probably <0.02 Hz. Similar remarks apply to the 3,5-dinitro and 3,5-bis(trifluoromethyl) derivatives, although linewidth conditions were less favourable; no evidence for significant magnitudes of ^6J was found.

A simple model

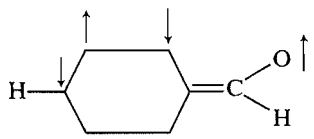
The positive sign of ^6J can be rationalized in terms of an ionic valence bond structure similar to that first proposed in connection with the transmission of electron spin density in nickel(II) aminotroponeiminates (14). In structure **1**, the usual



1

negative hyperfine interaction, Q_{CH}, at the site of the *para* C—H bond leads to a preferred parallel arrangement of the proton (crossed arrow) and the π electron. The ionic structure at the carbonyl group then ensures an antiparallel arrangement of the two protons in question and therefore a positive ^6J.

It appears that in benzaldehyde itself the contributing structure, **1**, is either not important enough to lead to a measurable positive ^6J or the hyperconjugative contribution, described above as negative and proportional to $\langle \sin^2 \theta \rangle$, happens to cancel the positive component. Another possibility involves the conjugative structure, **2**, which contributes to a



2

negative ^6J. This structure is contraindicated by ^6J(F,CHO) in 4-fluorobenzaldehyde being −0.44 Hz (8). Because Q_{CF} is positive, the ionic structure, **1**, is clearly predominant. Furthermore, the π electron donor, fluorine, must increase the

Can. J. Chem. Downloaded from www.nrcresearchpress.com by 41.223.56.140 on 09/07/12
For personal use only.

contribution of the ionic structure; Q_{CF} is only about twice as large in magnitude as Q_{CH} and yet ^6J(F,CHO) is sizeable. It is also probably true that the mobile bond order of the exocyclic C_{sp^2}—C_{sp^2} bond increases in the presence of the *para* fluorine substituent, thereby causing an increase in the internal rotational barrier (15). However, the ionic structure must also increase in importance if the magnitude of ^6J(F,CHO) is to be understood.

With these considerations in mind, the ^6J values above indicate that *meta* fluorine or methoxy substituents also stabilize ionic structures at the carbonyl site, that residual π electron donation to a *meta* site is most pronounced for these substituents, and that it is roughly additive for two *meta* substituents. A nonzero π electron donation (resonance effect) for *meta* substituents is apparently somewhat problematical in the theory of substituent effects.

It is therefore of interest that a recent and novel analysis of substituent effects (16), based on ^{13}C nmr chemical shifts for the β-carbon in styrene derivatives (17), deduces so-called standard resonance substituent constants, $\sigma_{R,ST}$, whose values for the *meta* substituents of interest here are −0.30(F), −0.29(OCH_3), −0.18(Cl), −0.04(CH_3), 0.01(CF_3), and −0.05(NO_2). According to the authors (16), these nonzero values are a conceptual problem. Nevertheless, their values can rationalize the present ^6J values.

With the assumption that the *meta* substituent effects are additive, as suggested by the values of ^6J, a linear regression yields $^6J/\text{Hz} = 0.007 - 0.127\Sigma\sigma_{R,ST}$ with a correlation coefficient of 0.992 (5 points). The mean deviation between the numbers given by this equation and those measured is 0.002 Hz. The predicted ^6J values for the CH_3, CF_3, and NO_2 substituents, not included in the correlation, are 0.017, 0.004, and 0.020 Hz and are certainly compatible with the experimental linewidths of the aldehyde proton peaks for these compounds.

Other considerations

In terms of structures **1** and **2** the present correlation implies a stabilization of the ionic structure by those *meta* substituents with negative $\sigma_{R,ST}$ values (π donation). Yet, the usual interpretation has it that π donation will increase the mobile bond order of the C_{sp^2}—C_{sp^2} bond and lead to an increase in the internal barrier to rotation of the aldehyde group. Actually, the barrier in 3,5-difluorobenzaldehyde is lower than in benzaldehyde. Furthermore, the STO-3G MO calculations, although agreeing qualitatively with the barrier changes, find only an insignificant increase in the C_{sp^2}—C_{sp^2} length, 0.002 Å, for the difluoro derivative in the planar conformation. It does seem that the common interpretation of changes in barriers caused by *para* substituents, namely, that, as appropriate, their presence increases or decreases the mobile bond order of the exocyclic bond in question, cannot easily be applied to *meta* substitution. Indeed, some *ab initio* molecular orbital computations (18) on *meta* substituted phenols provide examples in which, although a decrease in the internal barrier is computed, the mobile bond order of the C—O bond is higher than in the parent molecule.

Standard INDO MO FPT computations on benzaldehyde find ^6J as −0.29 Hz for the planar molecule (10). The origin of such a sign and magnitude has been examined in some detail for styrene and its analogs (19). One important factor is the p_z spin density at the ipso carbon atom. Another is that the p_z orbital on the oxygen atom (by analogy to the discussion for styrene (19)) increases the spin polarizability of the p_z orbital on the α carbon atom. Indeed, when the p_z orbital on oxygen is removed from the coupling interaction by the PRMO (20) procedure, ^6J is computed as +0.007 Hz, in fortuitous agreement with the correlation above. Similar calculations on 3,5-difluorobenzaldehyde change ^6J from −0.36 to −0.03 Hz. Because structure **1**, unlike **2**, does not place spin density in the p_z orbital of oxygen, the computations are probably compatible with the present interpretation of the positive ^6J, particularly if the negative charge on oxygen in **1** reduces its ability to influence the spin polarizability of a p_z orbital on the neighbouring carbon atom.

Evidence that *meta* substituents do not significantly alter the double bond character of the exocyclic C_{sp^2}—C_{sp^2} bond comes from ^1J(C,C) ≡ ^1J for the carbonyl group (21). For example, a *para* methoxy substituent causes an increase of 2.5 Hz in ^1J, in line with an increased double bond character caused by π donation. A *meta* methoxy group does not change ^1J to within experimental error (21). In fact, ^1J is the same in benzaldehyde and in its 3-fluoro, 3-CF_3, and 3,5-di CF_3 derivatives (21). These data are therefore compatible with the assumptions inherent in the simple model of ^6J above.

Remarks on ^{4}J(H,CHO) ≡ ^{4}J and ^{5}J(H,CHO) ≡ ^{5}J

^4J is −0.15 Hz in benzaldehyde in CS_2 solution (see below). Computations (22) suggest that ^4J is a composite of positive σ electron and negative π electron contributions. It is interesting that ^4J remains very near this value in 3,5-dimethylbenzaldehyde, becomes −0.08 Hz in the 3,5-dimethoxy derivative, −0.05 Hz in the 3,5-dichloro, and is not detected in the 3,5-difluoro derivative. Furthermore, a precise analysis of the ^1H and ^{19}F nmr spectra of 3-fluorobenzaldehyde as a dilute solution in CS_2 yields ^4J(H-6,CHO) as −0.14 Hz whereas ^4J(H-2,CHO) is apparently not present. ^5J(H,CHO) in this molecule shows that the two conformers are presented in effectively equal proportions. All these data are consistent with the hypothesis that an electronegative substituent at the *meta* position causes an increase in the positive σ component of ^4J involving the neighbouring *ortho* C—H bond, thereby cancelling the negative π electron component; a polarization of the σ electron framework occurs at C-2 in a 3-X derivative. ^4J was not detected in the 3,5-dinitro and 3,5-di CF_3 derivatives but linewidth problems do not allow the statement that ^4J is insignificant in magnitude for these compounds.

The ^1H nmr spectrum of the aldehyde proton for 3,5-dimethylbenzaldehyde in Fig. 1E implies that ^5J in benzaldehyde must be very nearly a pure σ electron coupling constant.

Experimental

The 3,5-di X-benzaldehydes were commercial (X = OCH_3, F, Cl) or were prepared from the corresponding benzyl alcohols (X = CH_3, CF_3, NO_2). Aldrich was the source of all compounds not synthesized, as it was for the benzyl alcohols.

Samples for nmr spectral work were prepared as 2–4 mol% solutions in CS_2/C_6D_{12}/TMS/C_6F_6 and in acetone-d_6/TMS/C_6F_6 solvent mixtures. The solutions were transferred to 5 mm o.d. nmr sample tubes and were then degassed by the freeze–pump–thaw procedure; flame-sealing completed the sample preparation.

The ^1H nmr and ^{19}F nmr spectra were accumulated on a Bruker AM300 nmr spectrometer at a probe temperature of 300 K, by methods previously described (23). The $^{19}F\{^1H\}$ spectra at low temperatures were also obtained on the AM300 system by standard methods. Homonuclear partial decoupling experiments (24), meant to ascertain the signs of ^6J(H,CHO) and ^4J(H,CHO), were also performed. Figure 1 gives an example of such experiments.

The ^1H and ^{19}F nmr spectra were analyzed with the locally modified computer program NUMARIT (25). The ^1H nmr spectral parameters of benzaldehyde are found in Table 1 (see ref. 26 for an early analysis).

TABLE 1. The ^{1}H nmr spectral parameters for benzaldehyde at 300 K

Parameter	Value		Parameter	Value	
ν(CHO)	2976.706(2)[a,c]	3017.474(1)[b]	$^5J_{25}$	0.624(1)[a]	0.635[b](1)
$\nu_2 = \nu_6$	2329.902(1)[d]	2379.589(1)	^4J(H,CHO)	−0.152(2)	−0.161(1)
$\nu_3 = \nu_5$	2234.130(1)	2281.263(1)	^5J(H,CHO)	0.431(2)	0.430(1)
ν_4	2259.766(2)	2310.558(1)	^6J(H,CHO)	−0.018(2)[e]	−0.013[e](1)
$^3J_{23}$	7.695(2)	7.718(1)	Calculated transitions	164	162
$^3J_{34}$	7.443(2)	7.468(1)	Assigned transitions	160	157
$^4J_{24}$	1.333(2)	1.322(1)	Peaks observed	110	118
$^4J_{26}$	1.738(2)	1.766(1)	Largest difference	0.026	0.017
$^4J_{35}$	1.236(2)	1.239(1)	Root-mean-square deviation	0.009	0.005

[a]As a 4.0 mol% solution in CS_2 containing also 10 mol% C_6D_{12} and 0.5 mol% TMS.
[b]As a 4.0 mol% solution in acetone-d_6 containing also 0.5 mol% TMS.
[c]In Hz at 300.135$_2$ MHz to high frequency of internal TMS.
[d]Numbers in parentheses are the standard deviations in the NUMARIT analysis.
[e]No direct evidence exists for this number in the spectrum.

^4J(H,CHO) and ^6J(H,CHO) values for the *meta* derivatives have been quoted and used above. Full spectral analytical results, usually in two solvents, are available to the interested reader.

The coupling constants for benzaldehyde are larger in acetone-d_6 than in CS_2 solution in some instances. It is a common experience in this laboratory with polar benzene derivatives and is unlikely to be an artefact of the analysis. On the other hand, the values of ^6J(H,CHO) in Table 1 may well be an artefact because no direct evidence exists in the spectra for a finite value of this coupling constant. Again, with a digital resolution of 0.006 Hz, this conclusion is probably correct to about 0.01 Hz.

The ^{19}F{^{1}H} spectra of 3,5-difluorobenzaldehyde at low temperatures in dimethyl ether solution are very similar to those reported and displayed (27) for 4-bromo-2,6-difluoro-*N*-methylaniline. They were treated in the same way. In brief, the ^{19}F doublet coalesced at 144 ± 1 K, the linewidth at coalescence was 93 ± 5 Hz (conservative error estimate), and hence (28) $\Delta G^{\ddagger}$ is 28.0 ± 0.5 kJ/mol. The reference peak has a linewidth of 2.8 ± 0.4 Hz, yielding the estimate above. The total width at half-height at coalescence is the sum of the static splitting (slow rotation) and the natural width (29).

Acknowledgments

We thank Dr. G. H. Penner for the STO 3G MO computations on 3,5-difluorobenzaldehyde, Dr. R. Laatikainen for the restricted INDO computations on benzaldehyde, Mr. K. Marat for help with the ^{19}F DNMR experiments, and Mr. R. Sebastian for the datum on 3-methoxybenzaldehyde. The work was aided by financial assistance from the Natural Sciences and Engineering Research Council of Canada. A referee is thanked for helpful suggestions.

1. R. WASYLISHEN and T. SCHAEFER. Can. J. Chem. **50**, 1852 (1972), and references therein.
2. T. SCHAEFER, R. SEBASTIAN, and G. H. PENNER. Can. J. Chem. **63**, 2597 (1985).
3. W. J. E. PARR and T. SCHAEFER. Acc. Chem. Res. **13**, 400 (1980).
4. G. H. PENNER. Can. J. Chem. **65**, 538 (1987).
5. G. H. PENNER, T. SCHAEFER, R. SEBASTIAN, and S. WOLFE. Can. J. Chem. **65**, 1845 (1987).
6. T. SCHAEFER, J. D. BALEJA, and G. H. PENNER. Can. J. Chem. **63**, 2471 (1985), and references therein.
7. T. SCHAEFER and G. H. PENNER. Can. J. Chem. **64**, 2013 (1986).
8. T. SCHAEFER, J. PEELING, G. H. PENNER, A. LEMIRE, and R. LAATIKAINEN. Can. J. Chem. **64**, 1859 (1986).
9. J. A. POPLE, J. W. MCIVER, JR., and N. S. OSTLUND. J. Chem. Phys. **49**, 2960, 2965 (1968).
10. R. WASYLISHEN and T. SCHAEFER. Can. J. Chem. **49**, 3216 (1971).
11. L. LUNAZZI, D. MACCIENTELLI, and A. BOICELLI. Tetrahedron Lett. 1205 (1975).
12. G. H. PENNER, P. GEORGE, and C. W. BOCK. J. Mol. Struct. (Theochem), **152**, 201 (1987).
13. T. DRAKENBERG, R. JOST, and J. M. SOMMER. J. Chem. Soc. Perkin Trans. 2, 1682 (1975).
14. D. R. EATON, A. D. JOSEY, and R. E. BENSON. J. Am. Chem. Soc. **89**, 4040 (1967).
15. T. DRAKENBERG, J. SOMMER, and R. JOST. J. Chem. Soc. Perkin Trans. 2, 363 (1980).
16. G. F. FADHIL and M. GODFREY. J. Chem. Soc. Perkin Trans. 2, 133 (1988).
17. W. F. REYNOLDS, A. GOMES, A. MARON, D. W. MACINTYRE, R. G. MAUNDER, A. TANIN, H. E. WONG, G. K. HAMER, and I. R. PEAT. Can. J. Chem. **61**, 2367 (1983).
18. A. PROSS and L. RADOM. Prog. Phys. Org. Chem. **13**, 1 (1981).
19. R. LAATIKAINEN and E. KOLEHMAINEN. J. Magn. Reson. **65**, 89 (1985).
20. A. R. ENGELMANN, R. H. CONTRERAS, and J. C. FACELLI. Theor. Chim. Acta (Berlin), **59**, 17 (1981).
21. V. V. KRISHNAMURTHY, G. K. S. PRAKASH, P. S. IYER, and G. A. OLAH. J. Am. Chem. Soc. **106**, 7068 (1984).
22. I. R. PEAT and W. F. REYNOLDS. Can. J. Chem. **52**, 2403 (1974).
23. T. SCHAEFER, J. PEELING, and R. SEBASTIAN. Can. J. Chem. **63**, 3219 (1985).
24. J. P. MAHER and D. F. EVANS. Proc. Chem. Soc. London, 208 (1961).
25. J. S. MARTIN, A. R. QUIRT, and K. E. WORVILL. The NMR program library. Daresbury Laboratory, Daresbury, U.K.
26. R. J. KOSTELNIK, M. P. WILLIAMSON, D. E. WISNOSKY, and S. M. CASTELLANO. Can. J. Chem. **47**, 3313 (1969).
27. T. SCHAEFER, G. H. PENNER, K. MARAT, and R. SEBASTIAN. Can. J. Chem. **62**, 2686 (1984).
28. J. SANDSTRÖM. Dynamic NMR spectroscopy. Academic Press, New York. 1982. p. 96.
29. G. BINSCH and H. KESSLER. Angew. Chem. Int. Ed. Engl. **19**, 411 (1980).

Can. J. Chem. Downloaded from www.nrcresearchpress.com by 41.223.56.140 on 09/07/12
For personal use only.

Solution and solid phase chemical synthesis of arabinonucleotides

MASAD JOSÉ DAMHA,[1] NASSIM USMAN,[2] AND KELVIN KENNETH OGILVIE[3]
Department of Chemistry, McGill University, Montreal, P.Q., Canada H3A 2K6

Received August 29, 1988

MASAD JOSÉ DAMHA, NASSIM USMAN, and KELVIN KENNETH OGILVIE. Can. J. Chem. **67**, 831 (1989).

A fast and convenient procedure for the chemical synthesis of arabinonucleotides, which eliminates the multistep protection of the arabinonucleoside building blocks, is described. The results of these studies were successfully applied to the automated chemical synthesis of the hexanucleotide 5′-aU$_p$aA$_p$aU$_p$aA$_p$aU$_p$aA-3′. Both solution and solid phase phosphite triester procedures are described.

Key words: arabinonucleotides, arabinophosphoramidites, automated chemical synthesis, protected arabinonucleosides.

MASAD JOSÉ DAMHA, NASSIM USMAN et KELVIN KENNETH OGILVIE. Can. J. Chem. **67**, 831 (1989).

Une méthode générale et rapide a été developpée pour la synthèse chimique d'arabinonucléotides en solution et sur support solide. La méthode a été appliquée à la synthèse automatisée de l'hexanucleotide 5′-aU$_p$aA$_p$aU$_p$aA$_p$aU$_p$aA-3′.

Mots clés : arabinonucléotides, arabinophosphoramidites, synthèse chimique automatisée, arabinonucléosides protégés.

Can. J. Chem. Downloaded from www.nrcresearchpress.com by 41.223.56.140 on 09/07/12
For personal use only.

Introduction

Arabinonucleosides, analogues of naturally occurring nucleosides, have been shown to possess a wide range of biological activities including antiviral and antitumor properties (1, 2). Unfortunately, the cytotoxicity, enzymic modification, and relative insolubility of these analogues (e.g., 9-β-D-arabinofuranosyladenine, aA) limit their utility for systemic administration. Some of these problems have been bypassed by chemically modifying the sugar or base moieties of these molecules (3). A different approach, which might be envisaged to improve the biological action and solubility of arabinonucleosides, is their incorporation into a nucleotide chain (4, 5). In addition to possible resistance to enzymic modifications and cleavage of the phosphodiester linkage, arabinonucleotides are expected to possess an inherent stability comparable to that of deoxyribonucleic acids (DNA). The unfavourable (*trans*) orientation of the 2′-hydroxyl function in arabinonucleotides prevents 2′-hydroxyl assisted cleavage of the vicinal 3′–5′ phosphodiester linkage (4).

The chemical synthesis of arabinonucleic acids (ANA, **1**), like that of ribonucleic acids (RNA), is difficult due to the presence of the 2′-hydroxyl function. The selective protection of the 2′-hydroxyl group is generally difficult due to its orientation towards the hindered β face of the arabinofuranosyl sugar. In the original work by Wechter (4), the 2′- and 3′-hydroxyls were left unprotected during nucleotide coupling steps, resulting in a mixture of 2′–5′- and 3′–5′-linked dinucleoside monophosphates. Smrt and Sorm (6) reported the incorporation of arabinouridine (aU) and arabinocytidine (aC) as the terminal 3′-end nucleoside of two trinucleotide diphosphates. Syntheses of aU-containing nucleotides were presented by Nagyvary and Provenzale (7), Ogilvie and Iwacha (8), and Schramm (9) but these procedures are limited to nucleosides that possess a C-2 keto function (pyrimidines) as they require formation of an O^2,2′-anhydro intermediate. Chattopadhyaya and co-workers (10) described the regiospecific, stepwise synthesis of the 3′–5′-linked nucleotides aA$_p$aA and aA$_p$aA$_p$aA but protection of the nucleoside monomers required numerous steps. Our laboratory has previously described the use of 2′-*O*-silyl-protected ribonucleosides as building blocks for the synthesis of ribonucleotides (11, 12). The successful use of the *tert*-butyldimethylsilyl group (TBDMS) in providing a rapid method for protecting the 2′-hydroxyl in ribonucleosides suggested that the same approach should be investigated in the arabinonucleoside area. Indeed, 5′-*O*-monomethoxytrityl 2′-*O*-TBDMS arabinonucleosides have been successfully prepared (13) and incorporated into nucleotide chains (5). In this report we describe a more practical and efficient procedure for the preparation of arabinonucleotide fragments. This method minimizes the protection of the arabinonucleoside units and affords 3′–5′-linked arabinonucleotide oligomers in good yields. A preliminary report of some of these results has appeared (14).

Results and discussion

Preparation of arabinonucleoside phosphoramidites

The key reagents used for the synthesis of arabinonucleotides were the nucleoside 3′-phosphoramidite derivatives **3***a* and **3***b*, which were easily prepared, in good yields, in a manner analogous to the preparation of ribonucleoside 3′-phosphoramidites (12*b*). Thus, *N*,*N*-diisopropyl-β-cyanoethylphosphonamidic chloride (1.1 equiv.) selectively reacted with the 5′-tritylated arabinonucleosides **2***a* and **2***b* (1.0 equiv.) at 0°C (2 h) to afford the corresponding 3′-phosphoramidites **3***a* and **3***b* in 90 and 60% yields, respectively (Scheme 1). The 2′,3′-*O*-bisphosphoramidites **5***a* and **5***b* were also isolated in ca. 5% yield and were easily separated from the desired 3′-*O*-phosphoramidites by silica gel chromatography. The arabinouridine 2′-*O*-phosphoramidite **4***a* was formed in ca. 3–5% yield (^{31}P NMR) and was separated from the 3′-*O*-phosphoramidite isomer **3***a* by repeated purifications on a silica gel column. The arabinoadenosine 2′-*O*-phosphoramidite **4***b* could not be detected. These results clearly indicate the marked difference in the steric environments of the 2′- and 3′-hydroxyl functions of arabinonucleosides.

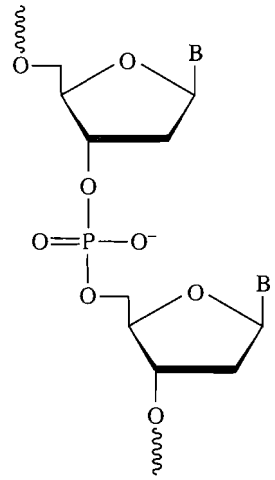
Solution phase synthesis of arabinonucleotides

To evaluate the arabinonucleoside 3′-*O*-phosphoramidites as building blocks for arabinonucleotide synthesis, **3***a* (1.0 equiv.) was activated with tetrazole (4 equiv.) in THF in the presence of 2′,3′-*O*-diacetylarabinouridine (**6***a*, 1.3 equiv.). After 30 min at 20°C, the resulting 3′,5′ dinucleoside phosphite

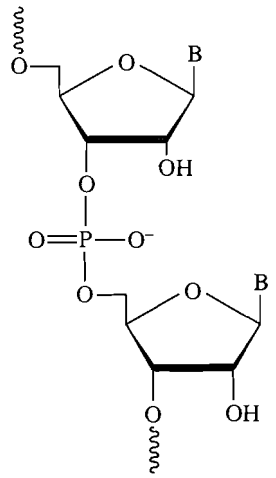
[1]Present address: J. Tuzo Wilson Research Laboratories, Department of Chemistry, University of Toronto, Erindale College, Mississauga, Ont., Canada L5L 1C6.

[2]Present address: Department of Biology, 16-739, Massachusetts Institute of Technology, Cambridge, MA 02139, U.S.A.

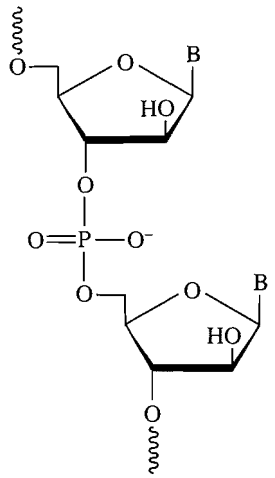
[3]Author to whom correspondence may be addressed. Present address: Vice-President (Academic), Acadia University, Wolfville, N.S., Canada B0P 1X0.



DNA



RNA



ANA, **1**

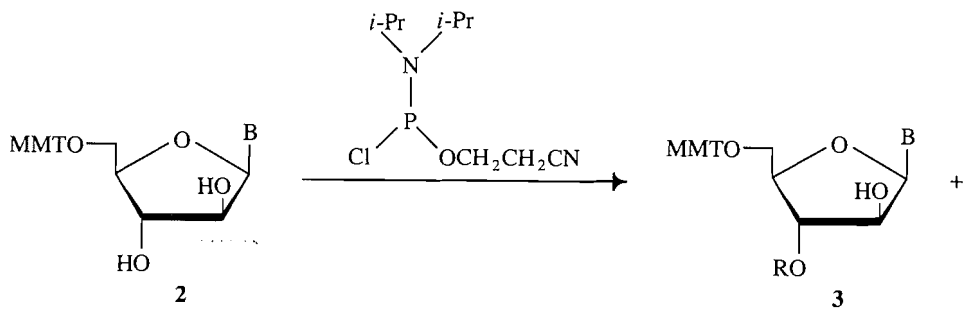
triester intermediate **7***a* was reacted *in situ* with a mixture of acetic anhydride/4-dimethylaminopyridine/collidine (5.0/0.5/7.0 equiv.) for 30 min to block the 2′-hydroxyl position. Upon completion of the capping reaction, an excess of an aqueous iodine solution was added to oxidize the fully protected phosphite intermediate (Scheme 2). Thus, activation of the nucleoside 3′-phosphoramidite with tetrazole, acetylation of the 2′-hydroxyl, and iodine oxidation were all carried out sequentially without intermediate product isolation. The work-up of the condensation reaction involved removal of excess iodine using an aqueous sodium bisulfite solution followed by purification of the product by silica gel chromatography. This procedure resulted in the isolation of phosphotriester aU_paU (**8***a*) in 78% yield based on the 3′-phosphoramidite **3***a*. The reaction of the adenosine 3′-phosphoramidite **3***b*, nucleoside **6***b*, and tetrazole by this condensation procedure gave the dinucleoside phosphotriester aA_paA (**8***b*) in 60% yield.

It is worth noting that, unlike ribonucleoside phosphite triesters (15), the phosphite triester linkage of aU_paU (**7***a*) and aA_paA (**7***b*) does not undergo 2′-hydroxyl assisted cleavage, because of the unfavourable (*trans*) orientation of the 2′-hydroxyl group.

During the coupling step one may envisage the possibility of the formation of branches at the unprotected 2′-hydroxyl of phosphite intermediates aUpaU (**7***a*) and aApaA (**7***b*). However, branched trinucleotides did not form under the condensation conditions. It appears that the ratio of nucleoside amidite **3** to nucleoside **6** employed in these couplings (1:1.3), as well as the steric hindrance of the 2′-hydroxyl group, disfavour this side reaction. Chain branching does occur in solid phase syntheses where the ratio of phosphoramidites to solid-support-bound arabinonucleoside reaches 20:1 (*vide infra*).

Solid phase synthesis of arabinonucleotides

The use of a solid phase approach eliminates the need for purification of the protected nucleotides, allows the rapid

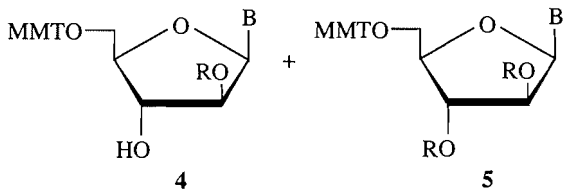


2

a, B = U
b, B = A^{Bz}

R = $P(OCH_2CH_2CN)NiPr_2$

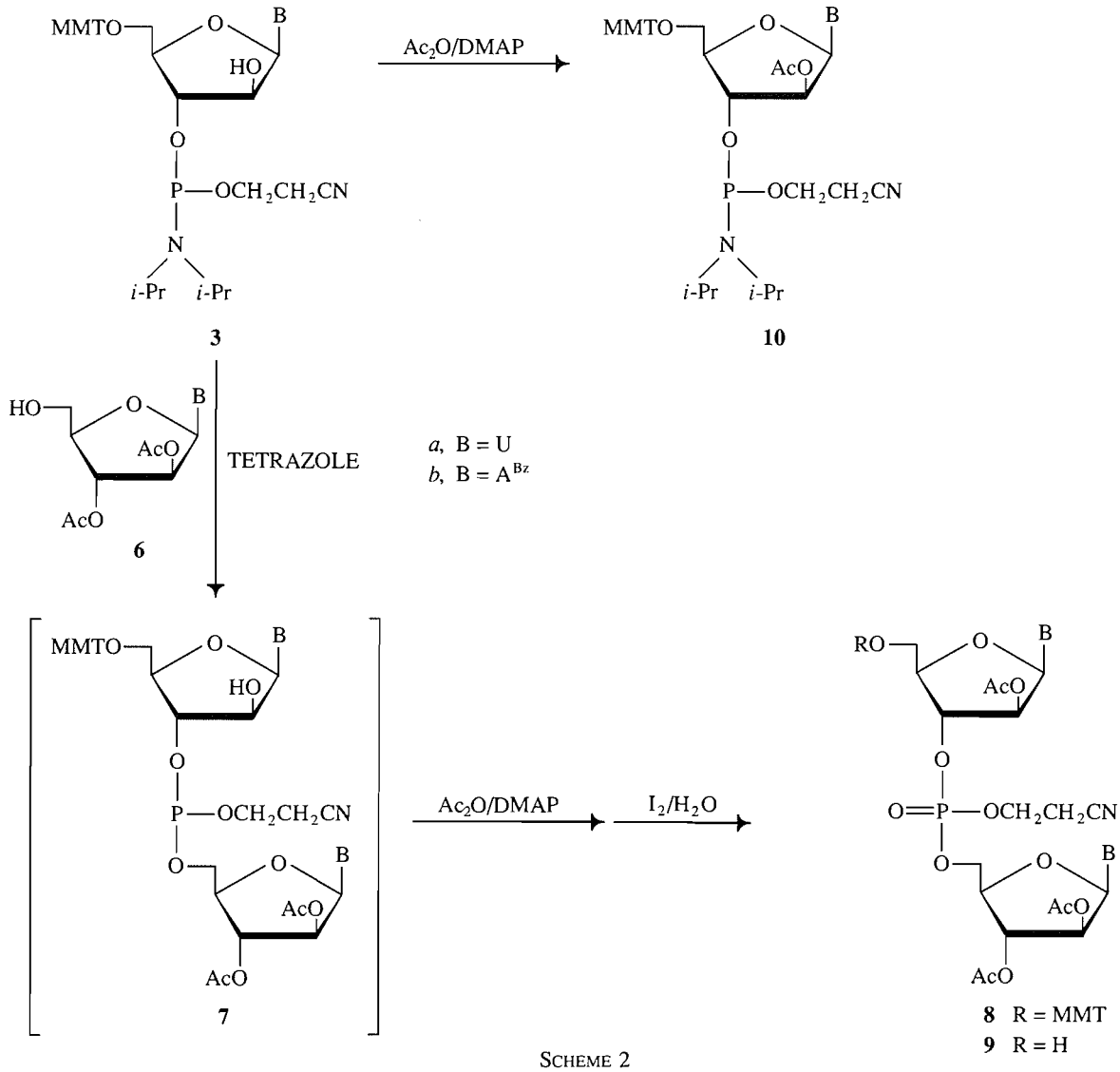
3



4 **5**

SCHEME 1

Can. J. Chem. Downloaded from www.nrcresearchpress.com by 41.223.56.140 on 09/07/12
For personal use only.



SCHEME 2

synthesis of long sequences, and reduces the amount of (expensive) nucleoside 3′-phosphoramidite needed. Because our methodology employs the same synthetic strategy currently used for the solid phase synthesis of DNA and RNA chains, the preparation of ANA oligomers was attempted on a DNA/RNA synthesizer (12*b*).

Preparation of solid supports

To carry out the solid phase syntheses it was first necessary to prepare a suitable solid support, which avoided the preparation of a derivative of the arabinonucleosides. Thus, a support bearing a carboxylic acid would be most suitable as the carboxyl moiety could simply be esterified with one of the hydroxyl groups of compound **2**. Four different supports were evaluated: aminopropyl controlled pore glass (CPG), long chain alkylamine (LCAA) CPG, carboxyl CPG, and aminopropylsuccinylated Vydac TP silica gel. In the case of the two amino derivatized CPG supports a succinyl linker was attached according to the literature procedure (16), which resulted in supports bearing a terminal carboxylic acid. All four supports were then treated with compound **2** and DCC followed by *p*-nitrophenol (to esterify any remaining carboxyl groups). Finally, piperidine was added to convert the *p*-nitrophenyl esters to amides. None of the three CPG supports gave satisfactory results. The aminopropylsuccinylated Vydac TP silica gel gave loadings of 20–25 μmol g^{-1}. Therefore all solid phase syntheses were performed on the silica gel support (Fig. 1).

Solid phase synthesis

The first syntheses performed were those of the trimer of aU using 60- and 300-s recycle times in the cycle shown in Table 1. At the end of each coupling cycle any unreacted 5′- and all of the 2′-hydroxyls of the newly added nucleoside were acetylated using an Ac_2O solution. The average coupling yields obtained, determined by trityl cation analysis, were 94 and 115%, respectively. The coupling yield higher than 100% obtained in the latter synthesis indicated that a side reaction (i.e., chain branching) was occurring at the unprotected 2′-hydroxyl group. The formation of side products was confirmed by polyacrylamide gel electrophoresis (Fig. 2) and HPLC analyses (data not shown) of the crude products after complete deprotection. Consistent with the formation of branches during the coupling step is the observation that the amount of side product increases with increasing coupling time (Fig. 2).

To eliminate chain branching two approaches were taken. The first was to decrease the coupling time, to favour only the reaction of the amidite at the less hindered 5′-OH, and the

Can. J. Chem. Downloaded from www.nrcresearchpress.com by 41.223.56.140 on 09/07/12
For personal use only.

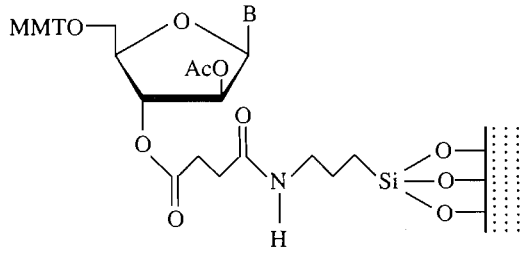


FIG. 1. Arabinonucleoside-derivatized silica gel.

TABLE 1. Synthesis cycle for the synthesis of arabinonucleotides[a]

Step	Reagent	Time (s)
1	Acetonitrile	30
2	5% TCA/DCE	90
3	Acetonitrile	60
4	0.05 M Amidite + 0.17 M tetrazole/acetonitrile	15
5	Recycle	15–885
6	0.25 M Ac_2O/DMAP/collidine/THF	60
7	0.1 M I_2 THF/pyridine H_2O: 7/2/1	30
8	Acetonitrile	50
9	0.25 M Ac_2O/DMAP/collidine/THF	30

[a]TCA = trichloroacetic acid; DCE = dichloroethane; DMAP = 4-dimethylaminopyridine.

second was to use the amidites bearing 2′-OAc protection (**10***a* and **10***b*). In each case the sequences were deprotected (*vide infra*) and analyzed by gel electrophoresis and HPLC.

In the first approach, coupling times of 30 and 60 s were used in the synthesis of dimers and trimers of both aA and aU. The use of the 30-s recycle resulted in almost the complete elimination of the branching reactions (Fig. 2); however, the stepwise coupling yields were low, only ca. 75%. The use of a 60-s recycle suppressed the branching somewhat compared to the 300-s recycle (Fig. 2); however, there was still an unacceptable amount of branching and the average coupling yields were ca. 90%. The use of a 900-s recycle time did not increase the amount of branching relative to the 300-s recycle time; therefore it appears there is a saturating level of branching occurring at approximately 300 s.

In the second approach, compounds **10***a* and **10***b* were used, in which no branching may occur due to the presence of the 2′-OAc protecting group. These derivatives were prepared in high yields by the reaction of their corresponding 2′-hydroxyl amidites **3***a* and **3***b* with an Ac_2O/4-dimethylaminopyridine/EtN*i*Pr_2/THF solution at room temperature. A trimer of aU was prepared with compound **10***a* using a 300-s recycle time, and an average coupling yield of 96% was obtained. The isolated material after deprotection appeared as one well-defined band and, as expected, the branching reaction was entirely eliminated (Fig. 2).

From these experiments it appeared that the best approach was to use a 30-s recycle time with amidites **3** (method 1) or the 2′-OAc protected amidites **10** and a 300-s recycle time (method 2). As a test, the synthesis of 5′-aU$_p$aA$_p$aU$_p$aA$_p$aU$_p$aA-3′ was performed using the two methods. In the case of method 1 an average coupling yield of 86% was obtained and in the case of method 2, 98.5%. The overall yields following deprotection were consistent with what would be expected from the average coupling yields, 39 A_{260} units for method 1 and 57 A_{260} units for method 2. Gel electrophoresis analysis indicated some small amount of branching in the case of method 1 (data not shown). The branching reaction appeared to occur early in the synthesis (at the dimer or trimer level).

Deprotection and isolation of arabinonucleotides

All nucleotides (5′-hydroxyl free) were fully deprotected in a single treatment with 15 M aqueous ammonia in ethanol at 20°C (sequences containing aU) or 50°C (sequences containing aA) for 16 h. The crude products aU$_p$aU and aA$_p$aA (solution phase synthesis) were passed through a column of Dowex Na^+ ion exchange resin and subsequently purified by size exclusion chromatography (Sephadex G-25) and cellulose TLC. The hexanucleotide 5′-aU$_p$aA$_p$aU$_p$aA$_p$aU$_p$aA-3′ was purified by electrophoresis on a preparative polyacrylamide gel and desalted on a Sephadex G-25 column.

Characterization of arabinonucleoside phosphoramidites and arabinonucleotides

Arabinonucleoside phosphoramidites

Because the phosphoramidite derivatives represent a new class of protected arabinonucleosides it was necessary to characterize the products in detail. The chromatographic and spectroscopic properties of the phosphoramidite derivatives are presented in Table 2. The NMR data show that there is, as expected, only one pair of diastereomeric signals in the ^{31}P NMR spectra of **3** and **10**, thereby establishing the isomeric purity of these compounds.

The isomeric uridine 3′- and 2′-phosphoramidites **3***a* and **4***a* were characterized by conversion to the acetylated derivatives **10***a* and **11**, respectively. The same compounds **10***a* and **11** were prepared from the known 5′-MMT-2′- and 5′-MMT-3′-TBDMS-arabinouridine (5, 13) as shown in Scheme 3.

The position of the phosphoramidite moiety of the adenosine phosphoramidite **3***b* was established by ^{13}C NMR. In the ^{13}C spectrum of **3***b* (one diastereoisomer, Fig. 3) the C4′, C3′, and C2′ resonances are coupled to ^{31}P while that of C1′ is not. The presence of the phosphoramidite group causes shielding and deshielding of the arabinose carbon resonances relative to the corresponding signals in **2***b*, the effect being more pronounced for the carbon directly attached to the phosphoramidite group (C3′).

Protected nucleotides

The chromatographic and spectral properties of the fully protected (**8***a*, **8***b*) and 5′-unprotected (**9***a*, **9***b*) nucleotides are summarized in Table 2. The UV and ^{31}P NMR spectra are in complete agreement with the proposed structures.

Free nucleotides

The physical (UV, ^1H, ^{13}C, and ^{31}P NMR, and R_f values) properties of aU$_p$aU and aA$_p$aA (solution phase synthesis) are presented in Table 3. The ^1H and ^{13}C NMR base resonances clearly indicated the composite nature of the deprotected products. The ^1H NMR spectrum of aA$_p$aA was identical to that reported by Doornbos *et al.* (17).

As found by Wechter (4), the fully deprotected arabinonucleotides were stable to alkaline treatment (0.1 N KOH, 37°C, 16 h, HPLC analysis), conditions that degrade ribonucleotide chains. Furthermore, they were completely degraded by spleen phosphodiesterase (2′–5′-linked arabinonucleotides are not hydrolyzed by this enzyme) and snake venom phosphodiesterase to the corresponding monomer components (HPLC

Can. J. Chem. Downloaded from www.nrcresearchpress.com by 41.223.56.140 on 09/07/12
For personal use only.

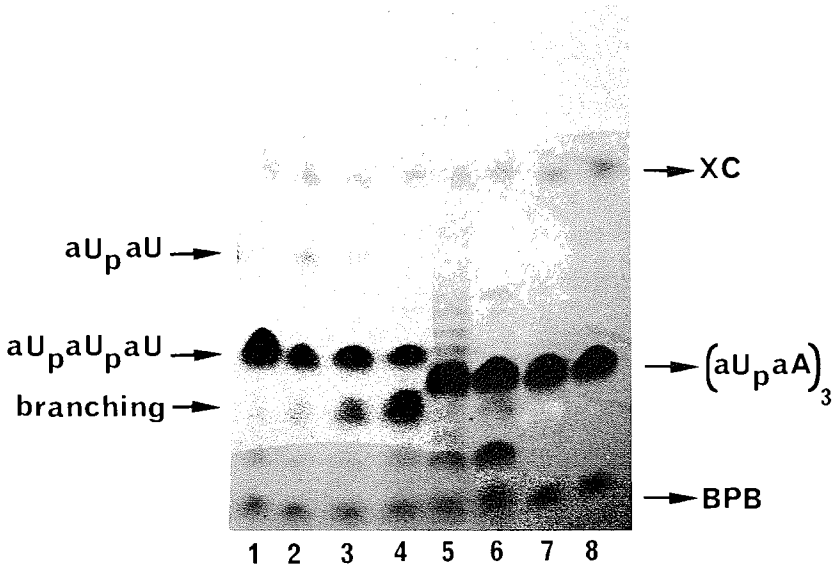


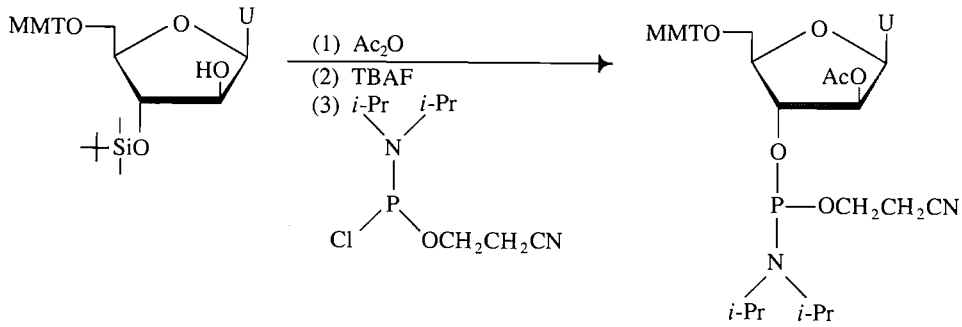
FIG. 2. Gel electrophoresis (24% polyacrylamide/7 M urea) of fully deprotected arabinonucleotides. Lanes: **1**, aU_paU_paU prepared with the 2′-OAc amidite **10***a* using a 300-s recycle time; **2**, **3**, **4**, aU_paU_paU prepared with the 2′-hydroxyl amidite **3***a* using, respectively, recycle times of 30, 60, and 300 s; **5**, crude 5′-$aU_paA_paU_paA_paU_paA$-3′ (method 1); **6**, crude 5′-$aU_paA_paU_paA_paU_paA$-3′ (method 2); **7**, pure 5′-$aU_paA_paU_paA_paU_paA$-3′ (method 1); **8**, pure 5′-$aU_paA_paU_paA_paU_paA$-3′ (method 2). All samples were loaded with xylene cyanol (XC) and bromophenol blue (BPB).

TABLE 2. Physical properties of arabinonucleoside phosphoramidites and protected arabinonucleotides

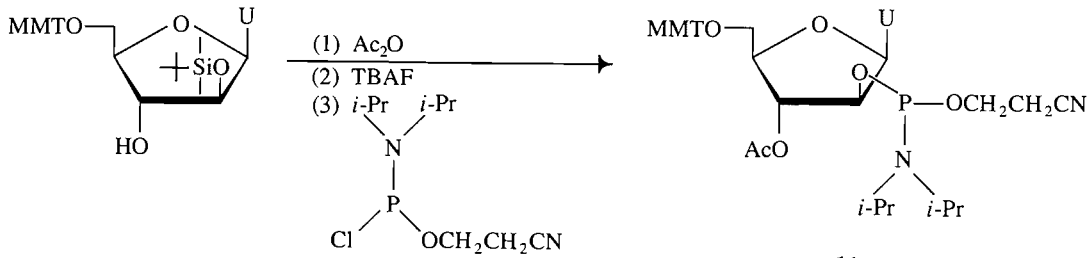
Compound	UV (EtOH) λ_{max} (λ_{min})	^{31}P NMR ($CDCl_3$, 121.5 MHz)	R_f
MMT_{aU_p}, **3***a*	232,260 (227,248)	150.7,150.0	(0.58,0.51)[a]
MMT_{aU^p}, **4***a*	232,260 (227,248)	151.9,151.2	(0.75,0.68)[a]
$MMT_{aU^\beta_p}$, **5***a*	232,262 (229,249)	151.9,150.9 151.7,149.8 151.6,150.8 151.7,150.1	(0.73,0.65,0.60)[b] (0.83,0.74)[a]
$MMT_{aU^{OAc}_p}$, **10***a*	234,262 (228,250)	151.7,151.4	(0.41,0.29)[b]
$MMT_{aU^\beta_{OAc}}$, **11**	234,264 (227,249)	152.7,152.3	(0.47,0.29)[b]
MMT_{aA_p}, **3***b*	232,282 (229,254)	150.3,150.8	(0.70,0.63)[a]
$MMT_{aA^\beta_p}$, **5***b*	234,282 (227,256)	151.6,150.6 151.3,150.1 151.0,149.8 150.9,150.6	(0.81,0.64,0.48)[b] (0.80,0.73)[a]
$MMT_{aA^{OAc}_p}$, **10***b*	232,280 (227,254)	151.8,151.6	(0.68,0.56)[b]
MMT_{aU_paU}, **8***a*	236,260 (229,246)	−2.2, −2.5	0.30,[c] 0.21[d]
HO_{aU_paU}, **9***a*	260 (232)	−1.8[f]	0.04,[c] 0.70[e]
MMT_{aA_paA}, **8***b*	234,282 (220,254)	−2.2, −2.3	(0.35, 0.29)[c] 0.08[d]
HO_{aA_paA}, **9***b*	234,282 (226,250)	−1.7, −1.8	0.06,[c] 0.67[e]

[a] EtOH/EtOAc/$CHCl_3$ 5:50:45.
[b] Ether/CH_2Cl_2 1:1.
[c] MeOH/$CHCl_3$ 5:95.
[d] EtOAc.
[e] THF.
[f] DMSO-d_6.

Can. J. Chem. Downloaded from www.nrcresearchpress.com by 41.223.56.140 on 09/07/12
For personal use only.



10*a*



11

SCHEME 3

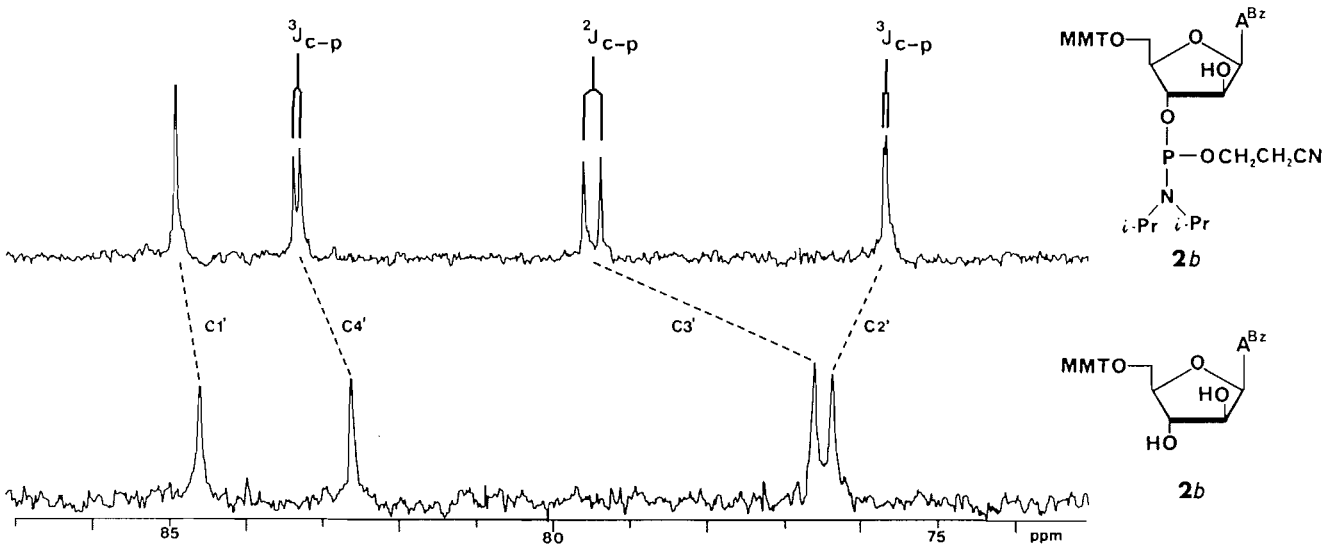


FIG. 3. ^{13}C NMR (DEPT, 75.4 MHz) spectra of arabinoadenosine phosphoramidite **3***b* (one diastereoisomer) and arabinonucleoside **2***b* in $CDCl_3$.

analysis). This established the integrity of the 3′–5′-phosphodiester linkages.

Conclusions

The procedure described in this study permits the rapid and efficient synthesis of 3′–5′-linked arabinonucleotides with a minimum effort involved in the protection of the monomer units. This represents the first general procedure for direct conversion of arabinonucleosides to phosphoramidite derivatives, and these can be immediately incorporated into nucleotide chains. This feature, along with the facile removal of the protecting groups, makes this an attractive and efficient procedure.

Experimental

All general procedures and techniques including chromatography, UV, NMR, enzyme assays, condensation and deprotection procedures, gel electrophoresis analyses, and general reagents are as previously described (15, 12*b*). Solid phase syntheses were performed according to ref. 12.

High performance liquid chromatography (HPLC) analyses were carried out on a Spectra-Physics SP8000 HPLC equipped with a 254 nm UV detector and a chromatography data system under the following conditions: reverse phase 4.6 × 250 mm Whatman Partisil ODS-2 column (10-μm particles, Chromatographic Specialities); mobile phase, solvent A: 0.02 M KH_2PO_4 (pH = 5.5, adjusted with KOH), solvent B: methanol, gradient 0–50% solvent B in 30 min;

Can. J. Chem. Downloaded from www.nrcresearchpress.com by 41.223.56.140 on 09/07/12
For personal use only.

TABLE 3. Physical properties of free aU_paU and aA_paA

Nucleotide	^{1}H NMR (300 MHz)[a] 1′	8(6)	2(5)	^{31}P NMR[a] (121.5 MHz)	UV (EtOH) λ_{max} (λ_{min})	R_f
aU_paU	6.18 6.11	7.80 7.77	5.84 5.80	−0.42	262(233)	0.51,[b] 0.19[c]
aA_paA	6.21 6.10	8.23 8.15	7.95 7.93	−0.49	260(231)	0.45,[b] 0.09[c]

Nucleotide		^{13}C NMR (75.4 MHz)[a] 1′	2′	3′	4′	5′	2(5)	8(6)
aU_paU	aU	87.6	77.0	82.1	86.2	63.5	145.7	103.7
	$_p$aU	88.6	78.2	76.9	83.6	66.8	145.6	103.6
aA_paA	aA	85.4	76.3	83.0	86.9	63.9	155.1	143.9
	$_p$aA	86.9	78.3	76.3	82.8	66.7	154.9	143.6

[a] D_2O; pD = 7–8; concentration, 5–10 mM.
[b] *n*-Propanol:aq. NH_3(15 M):H_2O, 55:10:35.
[c] Isopropanol:aq. NH_3(15 M):H_2O, 70:10:20.

flow rate 2 mL/min; temperature 30°C. About one A_{260} unit (in 10 μL buffer) of crude nucleotide was injected in the HPLC column per run.

An A_{260} unit is the amount of material that will produce an absorbance of 1.0 at 260 nm, when dissolved in 1 mL of solvent, in a 1-cm cell.

Synthesis of arabinonucleosides

Derivatives **2**a *and* **2**b

The synthesis of compound **2***b* has been described (15). Compound **2***a* was prepared in 89% yield according to the procedure developed by Ogilvie *et al.* (13).

*2′,3′-*O*-Diacetylarabinouridine (***6***a)*

To a THF (15 mL) solution of 5′-*O*-monomethoxytritylarabinouridine (**2***a*) (1.9 mmol, 1.0 g), 4-dimethylaminopyridine (0.8 mmol, 98 mg), and 2,4,6-collidine (8.0 mmol, 1.1 mL), was added acetic anhydride (8.0 mmol, 750 μL) at room temperature. After stirring for 1 h, the solution was diluted with CH_2Cl_2 (75 mL) and washed with 5% $NaHCO_3$ solution (50 mL). The organic layer was dried (anhydrous Na_2SO_4) and evaporated under reduced pressure to give a gum. The monomethoxytrityl group was removed by treatment of the crude product with 80% acetic acid (40 mL) at 90°C. After 15 min, ethanol was added (50 mL) and the solvents removed under vacuum. The residue was diluted with CH_2Cl_2 (5 mL) and added to a stirred hexane solution (100 mL). The resulting precipitate was filtered and dried under vacuum to obtain derivative **6***a* as a white powder. The product crystallized (94% yield, 613 mg) from CH_2Cl_2 or CH_2Cl_2/hexanes (3:1), mp 164–165°C; TLC (methanol/$CHCl_3$, 5:95): R_f 0.24; UV (95% EtOH/H_2O): λ_{max} 262 nm, λ_{min} 232 nm; ^{1}H NMR ($CDCl_3$, 200 MHz) δ: 8.94 (b, 1, NH), 7.63 (d, 1, H6), 6.27 (d, $J_{H1'-H2'}$ = 4.8 Hz, 1, H1′), 5.73 (d, 1, H5), 2.13 (s, 3, $COCH_3$), 2.01 (s, 3, $COCH_3$).

N^6*-Benzoyl-2′,3′-*O*-diacetylarabinoadenosine (***6***b)*

Compound **6***b* was prepared from N^6-benzoyl-5′-*O*-monomethoxytritylarabinoadenosine (**2***b*) (2.0 mmol, 1.3 g) as described for the preparation of compound **6***a*. The product was isolated on silica gel column chromatography using ethanol/ethyl acetate/CH_2Cl_2 1:50:49 as solvent. The yield of **6***b* was 78% yield (708 mg). A faster moving product identified as N^6-acetyl-N^6-benzoyl-2′,3′-di-*O*-acetylarabinoadenosine was also isolated in 13% yield (127 mg). **6***b*, TLC (methanol/$CHCl_3$ 5:95): R_f 0.26; (ethanol/ether/CH_2Cl_2 3:71:26): R_f 0.08; (ethanol/ethyl acetate/$CHCl_3$ 5:50:45): R_f 0.11; UV (95% EtOH/H_2O): λ_{max} 236, 282 nm, λ_{min} 230, 248 nm; ^{1}H NMR ($CDCl_3$, 200 MHz) δ: 9.34 (b, 1, NH), 8.78 (s, 1, H8), 8.27 (s, 1, H2), 6.58 (d, $J_{H1'-H2'}$ = 4.6 Hz, 1, H1′), 2.12 (s, 3, $COCH_3$), 1.71 (s, 3, $COCH_3$). Physical properties of N^6-acetyl-N^6-benzoyl-2′,3′-di-*O*-acetylarabinoadenosine: TLC (methanol/$CHCl_3$ 5:95): R_f 0.34; (ethanol/ether/CH_2Cl_2 3:71:26): R_f 0.19; (ethanol/ethyl acetate/$CHCl_3$ 5:50:45): R_f 0.38; UV (95% EtOH/H_2O): λ_{max} 250, 274 nm, λ_{min} 231, 263 nm; ^{1}H NMR ($CDCl_3$, 200 MHz) δ: 8.71 (s, 1, H8), 8.28 (s, 1, H2), 6.55 (d, $J_{H1'-H2'}$ = 5.3 Hz, H1′), 2.60 (s, 3, $COCH_3$), 2.13 (s, 3, $COCH_3$), 1.59 (s, 3, $COCH_3$).

Synthesis of arabinonucleoside phosphoramidites

*5′-*O*-Monomethoxytritylarabinouridine-3′-*O*-N,N-diisopropyl-β-cyanoethylphosphoramidite (***3***a)*

To a stirred THF (18 mL) of derivative **2***a* (6.0 mmol, 3.1 g) and diisopropylethylamine (21.8 mmol, 3.8 mL) was added dropwise, over 15 min, *N*,*N*-diisopropyl-β-cyanoethylphosphonamidic chloride (6.3 mmol, 1.34 mL) at 0°C. The reaction was then stirred for 2 h at room temperature. Ethyl acetate (100 mL, prewashed with 5% $NaHCO_3$) was added and the solution washed with saturated brine solution (3 × 100 mL). The organic phase was dried (anhydrous Na_2SO_4) and the solvent removed under vacuum to yield the crude product as a white foam. The crude product was purified (twice) by silica gel chromatography by elution with CH_2Cl_2/hexane/triethylamine, gradient: 50:45:5 to 50:40:10. After evaporation of the pooled fractions the product was coevaporated, first with 95% ethanol to remove traces of triethylamine, and then with ether to provide the product as a white foam. The purification was repeated until **3***a* was isomerically pure (^{31}P NMR). Derivative **3***a* was obtained in 90% yield (3.8 g). A faster moving product identified as 5′-*O*-monomethoxytritylarabinouridine-2′,3′-*O*-di-*N*,*N*-diisopropyl-β-cyanoethylphosphoramidite (**5***a*) was also isolated in ca. 5% yield. The chromatographic and spectroscopic properties of **3***a*, **4***a*, and **5***a* are presented in Table 2. *Anal.* calcd. for $C_{38}H_{45}N_4O_8P \cdot 1/2H_2O$: C 62.88, H 6.39, N 7.72; found: C 62.33, H 6.37, N 7.92.

N^6*-Benzoyl-5′-*O*-monomethoxytritylarabinoadenosine-3′-*O*-N,N-diisopropyl-β-cyanoethylphosphoramidite (***3***b)*

Compound **2***b* (3.0 mmol, 1.9 g) and *N*,*N*-diisopropyl-β-cyanoethylphosphonamidic chloride (3.2 mmol, 672 μL) were reacted according to the method described for the preparation of compound **3***a*. The products were separated on silica gel column chromatography using CH_2Cl_2/hexane/triethylamine 50:45:5 as solvent. The 3′-phosphoramidite and 2′,3′-bisphosphoramidite derivatives **3***b* and **5***b* were

Can. J. Chem. Downloaded from www.nrcresearchpress.com by 41.223.56.140 on 09/07/12
For personal use only.

obtained in 66% (1.65 g) and 11% (335 mg) yields, respectively. The physical properties of these derivatives are presented in Table 2. *Anal.* calcd. for **3***b*, $C_{46}H_{50}N_7O_7P \cdot H_2O$: C 64.10, H 6.08, N 11.38; found: C 64.30, H 6.15, N 11.45.

*5′-O-Monomethoxytritylarabinouridine-2′-O-acetyl-3′-O-N,N-diisopropyl-β-cyanoethylphosphoramidite (**10**a)*

From derivative **3**a: To a THF (4 mL) solution of compound **3***a* (0.5 mmol, 358 mg), 4-dimethylaminopyridine (0.2 mmol, 25 mg), and diisopropylethylamine (4.0 mmol, 0.7 mL) was added dropwise, over 1 min, acetic anhydride (2.0 mmol, 187 μL) at room temperature. After stirring for 45 min, ethyl acetate (prewashed with 5% $NaHCO_3$) was added and the solution washed with saturated brine solution (5 × 100 mL). The organic phase was dried (anhydrous Na_2SO_4) and the solvent removed under vacuum to yield derivative **10***a* as a white foam in 95% yield (360 mg). The purity of this material judged by TLC and ^{31}P NMR was greater than 95%. The physical properties of this compound are presented in Table 2.

From 5′-O-monomethoxytrityl-3′-O-tert-butyldimethylsilylarabinouridine: (*a*) 5′-*O*-MMT-2′-*O*-acetylarabinouridine. To a THF (1.5 mL) solution of 5′-*O*-monomethoxytrityl-3′-*O*-*tert*-butyldimethylsilylarabinouridine (13) (0.23 mmol, 145 mg), 4-dimethylaminopyridine (0.07 mmol, 8 mg), and 2,4,6-collidine (0.92 mmol, 130 μL) was added acetic anhydride (0.92 mmol, 86 μL) at room temperature. After stirring for 1 h, the crude product was diluted with CH_2Cl_2 and the solution washed with saturated brine solution (50 mL) followed by water (50 mL). The organic phase was dried (anhydrous Na_2SO_4) and the solvent removed under vacuum to yield an oil. Analysis of this product by TLC showed complete conversion of the starting material (TLC: methanol/CH_2Cl_2 5:95, R_f 0.58) to a faster moving product (TLC: methanol/CH_2Cl_2 5:95, R_f 0.68). The 3′-silyl group was removed by treatment of the crude product with 1 M TBAF/THF (1.2 mmol, 1.2 mL) at room temperature. After 15 min, water was added (1 mL) and the product extracted with CH_2Cl_2 (50 mL). The organic phase was dried (anhydrous Na_2SO_4) and the solvent removed under vacuum to yield an oil. The crude product was diluted with CH_2Cl_2 (5 mL) and added to a stirred hexane solution (100 mL). The resulting precipitate was filtered and dried under vacuum to obtain 5′-MMT-2′-*O*-acetylarabinouridine in quantitative yield (155 mg); TLC (methanol/CH_2Cl_2 5:95): R_f 0.49; UV (95% EtOH/H_2O): λ_{max} 234, 262 nm, λ_{min} 227, 251 nm; ^1H NMR ($CDCl_3$, 200 MHz) δ: 6.30 (d, $J_{H1'-H2'}$ = 5.7 Hz, 1, H1′), 1.98 (s, 3, $COCH_3$).

(*b*) 5′-*O*-MMT-2′-*O*-acetyl-3′-*O*-phosphoramidite **10***a*. To a stirred THF (0.6 mL) solution of 5′-*O*-MMT-2′-*O*-acetylarabinouridine (0.20 mmol, 110 mg) and diisopropylethylamine (0.84 mmol, 144 μL) was added *N,N*-diisopropyl-β-cyanoethylphosphonamidic chloride (0.24 mmol, 51 μL) at room temperature. After stirring for 2 h, ethyl acetate (prewashed with 5% $NaHCO_3$) was added and the mixture was worked up and purified as for **3***a*. Chromatographic solvent: CH_2Cl_2/hexane/triethylamine; gradient: 50:45:5. The pure product was obtained as a white foam in 50% yield (75 mg). The chromatographic and spectral properties of this derivative are presented in Table 2.

*5′-O-Monomethoxytritylarabinouridine-3′-O-acetyl-2′-O-N,N-diisopropyl-β-cyanoethylphosphoramidite (**11**)*

Derivative **11** was prepared and purified as for **10***a* from 5′-*O*-MMT-3′-*O*-TBDMS-arabinouridine (13) (*vide supra*). Physical properties of the intermediate, 5′-*O*-MMT-3′-*O*-acetylarabinouridine: TLC (methanol/$CHCl_3$ 5:95): R_f = 0.27; UV (95% EtOH/H_2O): λ_{max} 234, 264 nm, λ_{min} 230, 252 nm; ^1H NMR ($CDCl_3$, 200 MHz) δ: 6.10 (d, $J_{H1'-H2'}$ = 4.3 Hz, 1, H1′), 2.08 (s, 3, $COCH_3$).

The chromatographic and spectral properties of **11** are presented in Table 2.

*N^6-Benzoyl-5′-O-monomethoxytritylarabinoadenosine-2′-O-acetyl-3′-O-N,N-diisopropyl-β-cyanoethylphosphoramidite (**10**b)*

To a THF (4 mL) solution of compound **3***b* (0.5 mmol, 422 mg), 4-dimethylaminopyridine (0.2 mmol, 25 mg), and diisopropylethylamine (4.0 mmol, 0.7 mL) was added dropwise, over 1 min, acetic anhydride (2.0 mmol, 187 μL) at room temperature. After stirring for 1 h, ethyl acetate (prewashed with 5% $NaHCO_3$) was added and the solution washed with saturated brine solution (5 × 100 mL). The organic phase was dried (anhydrous Na_2SO_4) and the solvent removed under vacuum to yield the crude product as a white foam. The crude product was purified by silica gel chromatography by elution with CH_2Cl_2/hexane/triethylamine 40:55:5. After evaporation of the pooled fractions the product was coevaporated, first with 95% ethanol to remove traces of triethylamine, and then with ether to provide the product as a white foam. Derivative **10***b* was isolated in 75% yield (332 mg). The physical and chromatographic properties of **10***b* are presented in Table 2. A faster moving product identified as N^6-acetyl-N^6-benzoyl-5′-*O*-monomethoxytritylarabinoadenosine-2′-*O*-acetyl-3′-*O*-*N,N*-diisopropyl-β-cyanoethylphosphoramidite was also isolated in 25% yield (116 mg); TLC (ether/CH_2Cl_2 1:1): R_f 0.83, 0.76; UV (95% EtOH/H_2O): λ_{max} 231, 271 nm, λ_{min} 227, 261 nm; ^1H NMR ($CDCl_3$, 400 MHz) δ: 8.65 (s, 1, H8), 8.63 (s, 1, H8), 8.18 (s, 1, H2), 8.16 (s, 1, H2), 6.60 (d, $J_{H1'-H2'}$ = 4.2 Hz, 1, H1′), 6.59 (d, $J_{H1'-H2'}$ = 4.2 Hz, 1, H1′), 2.59 (s, 6, $COCH_3$), 1.66 (s, 3, $COCH_3$), 1.62 (s, 3, $COCH_3$); ^{13}P NMR ($CDCl_3$, 121.5 MHz) δ: 152.0, 151.9.

Solution phase synthesis of arabinonucleotides

*Dinucleotides aU_paU (**8**a) and aU_paU (**9**a)*

To a sealed vial containing **3***a* (0.50 mmol, 359 mg), **6***a* (0.67 mmol, 219 mg), and tetrazole (2.0 mmol, 140 mg) was added THF (3.0 mL) and the solution stirred at room temperature for 45 min. At this point a mixture of 4-dimethylaminopyridine (0.26 mmol, 33 mg) and 2,4,6-collidine (3.6 mmol, 0.5 mL) in THF (2.7 mL) was added and, after 15 min, the phosphite triester intermediate aU_paU (**7***a*) was oxidized to the phosphate with an aqueous iodine solution (0.1 M in THF/water 3:1.5, excess, 5 min). The reaction mixture was diluted with CH_2Cl_2 (75 mL) and washed with an aqueous sodium bisulfite solution (2–5 mL of 5% sodium bisulfite in 200 mL water). The organic phase was washed with saturated brine (2 × 100 mL), dried (anhydrous Na_2SO_4), and evaporated under reduced pressure to yield a foam. The crude product was purified by silica gel chromatography by elution with ethanol/ethyl acetate/$CHCl_3$, gradient: 5:50:45 to 10:50:40. The pure product **8***a* was obtained in 78% yield (392 mg) and its physical properties are presented in Table 2.

It should be noted that 5′,3′,2′-*O*-triacetylarabinouridine is obtained as by-product and is easily separated during the purification step; TLC (ethanol/ethyl acetate/$CHCl_3$ 5:50:45): R_f 0.63; UV (95% EtOH/H_2O): λ_{max} 231 nm, λ_{min} 262 nm.

The monomethoxytrityl group was removed by treatment of **8***a* (0.43 mmol, 430 mg) with 80% acetic acid (10 mL) at 90°C for 15 min. At the end of this period, ethanol was added and the resulting solution was evaporated under reduced pressure to give an oil. This material was diluted with CH_2Cl_2 (5 mL) and added to a stirred hexane solution (100 mL). The resulting precipitate was filtered and dried under vacuum to obtain the 5′-deprotected dinucleotide **9***a* as a white powder in 80% yield (249 mg). The physical properties of this derivative are presented in Table 2. *Anal.* calcd. for $C_{27}H_{32}N_5O_{17}P$: C 44.45, H 4.42, N 9.60; found: C 44.32, H 4.48, N 9.13.

*Dinucleotides aA_paA (**8**b) and aA_paA (**9**b)*

Compounds **3***b* (0.61 mmol, 518 mg) and **6***b* (0.67 mmol, 373 mg) were coupled in the presence of tetrazole in dry THF as described for the preparation of **8***a*. The product **8***b* was purified as for **8***a*. The yield of **8***b* was 60% (453 mg) and its physical properties are presented in Table 2. It should be noted that N^6-benzoyl-5′,3′,2′-*O*-triacetylarabinoadenosine is obtained as by-product and is easily separated during the purification step (TLC, ethanol/ethyl acetate/$CHCl_3$ 5:50:45; R_f 0.51). *Anal.* calcd. for **8***b*, $C_{63}H_{58}N_{11}O_{16}P \cdot 3/2H_2O$: C 58.97, H 4.79, N 12.00; found: C 59.00, H 4.92, N 11.30.

Compound **8***b* (0.25 mmol, 330 mg) was detritylated and purified (silica gel column, methanol/$CHCl_3$: gradient 3–10% methanol) in a similar way as described for the preparation of compound **9***a* to give compound **9***b* (181 mg, 74%). The physical properties of this derivative are presented in Table 2.

Can. J. Chem. Downloaded from www.nrcresearchpress.com by 41.223.56.140 on 09/07/12
For personal use only.

Can. J. Chem. Downloaded from www.nrcresearchpress.com by 41.223.56.140 on 09/07/12
For personal use only.

Solid phase synthesis of arabinonucleotides

Preparation of Vydac TP silica gel supports

In a 50-mL round bottomed flask under argon, **2***a* (129 mg, 0.25 mmol) or **2***b* (161 mg, 0.25 mmol) was shaken with aminopropylsuccinylated Vydac TP silica gel (1.0 g) (16), 4-dimethylaminopyridine (25 mg, 0.20 mmol), and dicyclohexylcarbodiimide (2.06 g, 10 mmol) in anhydrous pyridine (9 mL) for 5 days. To the slurry was added *p*-nitrophenol (70 mg, 0.50 mmol) and the reaction shaken for 16 h. The support was filtered on a sintered glass funnel (M) and washed with pyridine (2 × 5 mL) and THF (2 × 5 mL). The support was then transferred to a 50-mL round bottomed flask and treated with 0.25 M Ac_2O/2,4,6-collidine/4-dimethylaminopyridine in THF (20 mL) for 18 h. The support was filtered and washed with THF. The support was then treated in a 50-mL round bottomed flask with piperidine (20 mL) for 18 h. The silica support was filtered and successively washed with acetone, EtOH, MeOH, and Et_2O. The support was dried overnight in a MeOH drying pistol. Loadings of 20.6 μmol g^{-1} and 25.3 μmol g^{-1} for the aA and aU supports respectively were obtained. Loadings were determined by detritylation of 5.0-mg samples with 5% trichloroacetic acid/dichloroethane solution (extinction coefficient used for the MMT cation = 56 $\mu mol^{-1} cm^{-1}$ mL).

Solid phase synthesis

Approximately 100 mg of derivatized solid support was used in each synthesis (ref. 12*b* for details). In each synthesis either amidite **3** or **12** was used with the cycle shown in Table 1. The time of recycle was varied (30, 60, 300, and 900 s) to examine the branching reaction when amidites **3***a* and **3***b* were used. In the case of amidites **10***a* and **10***b* a 5-min recycle time was used.

Deprotection and isolation of arabinonucleotides

*Deprotection of aU_paU (**9**a)*

This derivative (25 μmol, 18 mg) was fully deprotected in a single step by treatment with aqueous ammonia (15 M) in ethanol (3 mL: 1 mL) at room temperature for 16 h. At the end of this period, the ammonia was evaporated in a Speed-Vac concentrator to yield a white foam. This material was diluted with water (1 mL) and passed slowly through a column of Dowex Na^+ ion exchange resin and the eluant (40 mL) lyophilized. The residue was diluted with water (1 mL) and applied to a column packed with preswollen Sephadex G-25 size exclusion gel. The fractions containing the nucleotide were lyophilized to give 396 A_{260} units of aU_paU (87% yield, ca. 12 mg). The chromatographic and spectral properties of aU_paU are summarized in Table 3.

aU_paU was enzymatically degraded to aU by a mixture of snake venom and alkaline phosphatase. Degradation of aU_paU with spleen phosphodiesterase resulted in the formation of aU3′p and aU in a 1:1 ratio.

*Deprotection of aA_paA (**9**b)*

Compound **9***b* (25 μmol, 25 mg) was deprotected as for aU_paU **9***a*. The following conditions were used: (*a*) 15 M ammonium hydroxide/ethanol (3 mL: 1 mL), 55°C, 18 h; (*b*) ion exchange chromatography (Dowex Na^+, 90 mL water as eluant); (*c*) cellulose TLC (solvent F); (*d*) size exclusion (Sephadex G-25, water as eluant). A 32% yield (216 A_{260} units) of aA_paA was obtained. The chromatographic and spectral properties of aA_paA are presented in Table 3.

aA_paA was enzymatically degraded to aA by a mixture of snake venom and alkaline phosphatase. Degradation of aA_paA with spleen phosphodiesterase resulted in the formation of aA3′p and aA in a 1:1 ratio.

Deprotection of 5′-$aU_paA_paU_paA_paU_paA$-3′ (methods 1 and 2)

Silica gel (50 mg) bearing the protected sequences was placed in a sterile 5-mL polypropylene test tube to which was added aqueous ammonia (15 M) in ethanol (3:1, 3 mL) and the tube sealed with a septum (the septum was taped to the tube using commonly available electrical tape). The tube was placed in a thermostated oil bath at 55°C for 18 h to effect the concomitant decyanoethylation, removal of the sequence from the support, and the removal of the exocyclic amino benzoyl protecting groups. After cooling the tube in an EtOH/Dry Ice bath, the washings were removed with a sterile silanized pipette and placed in a sterile 15-mL test tube. The support was further washed with aqueous ammonia (15 M) in ethanol (3:1, 4 × 2 mL). The combined washings were frozen in an EtOH/Dry Ice bath and evaporated in a Speed-Vac evaporator overnight. The residue was extracted with sterile H_2O (5 × 1 mL) to yield 57 and 39 A_{260} units of 5′-$aU_paA_paU_paA_paU_paA$-3′, methods 1 and 2, respectively. Each sequence isolated from methods 1 and 2 (20 A_{260} units each) was loaded into 15 cm wide slots on a 1.5 mm × 20 cm × 20 cm 24% polyacrylamide gel for purification. The gels were visualized by UV shadowing and the desired bands cut out. The gel pieces were cut into small pieces and extracted by soaking in 0.05 M NH_4OAc, pH 7.0, at room temperature (16 h). The resulting supernatants were applied to a Sephadex G-25 column packed and run in 0.05 M NH_4OAc, pH 7.0 (12*b*). A final desalting step was carried out on Waters C18-SepPak cartridges. The final yields were 3.6 and 4.7 A_{260} units for the hexamers prepared by methods 1 and 2, respectively; UV (H_2O): λ_{max}, 262. All sequences were stored as 1 A_{260} units/10 μL aqueous solutions. Analytical gels were run with 0.5 A_{260} units of the sequence.

Acknowledgements

We gratefully acknowledge financial support from the Natural Sciences and Engineering Research Council of Canada and the FCAR program of Quebec. M.J.D. and N.U. acknowledge, respectively, a Dalbir-Bindra fellowship from the Graduate Faculty of McGill University and the award of post-graduate scholarship funds by NSERC.

1. J. L. Rideout, D. W. Henry, and L. M. Beacham III (*Editors*). Nucleosides, nucleotides, and their biological activity. Academic Press, New York. 1983, and references cited therein.
2. R. S. K. Young and G. A. Fischer. Biochem. Biophys. Res. Commun. **32**, 23 (1968).
3. R. Vince, S. Daluge, H. Lee, W. M. Shannon, G. Arnett, T. W. Schafer, T. L. Nagabhushan, P. Reichert, and H. Tsai. Science, **221**, 1405 (1983).
4. W. J. Wechter. J. Med. Chem. **10**, 762 (1967).
5. D. P. C. McGee. M.Sc. thesis, McGill University, Montreal, Canada (1981).
6. (*a*) J. Smrt and F. Sorm. Biochim. Biophys. Acta, **138**, 210 (1967); (*b*) Collect. Czech. Chem. Commun. **32**, 3169 (1967).
7. (*a*) R. G. Provenzale and J. Nagyvary. Biochemistry, **9**, 1744 (1970); (*b*) J. Nagyvary and G. Provenzale. Biochemistry, **8**, 4769 (1969).
8. K. K. Ogilvie and D. Iwacha. Can. J. Chem. Chem. **48**, 862 (1970).
9. G. Schramm. Angew. Chem. Int. Ed. Engl. **6**, 460 (1967).
10. C. Gioeli, J. B. Chattopadhyaya, A. F. Drake, and B. Oberg. Chem. Scr. **19**, 13 (1982).
11. (*a*) K. K. Ogilvie, A. L. Schifman, and C. L. Penney. Can. J. Chem. **57**, 2230 (1979); (*b*) K. K. Ogilvie, S. L. Beaucage, A. L. Schifman, N. Y. Theriault, and K. L. Sadana. Can. J. Chem. **56**, 2768 (1978).
12. (*a*) R. T. Pon and K. K. Ogilvie. Nucleosides Nucleotides, **3**, 485 (1984); (*b*) N. Usman, K. K. Ogilvie, M.-Y. Jiang, and R. J. Cedergren. J. Am. Chem. Soc. **109**, 7845 (1987).
13. K. K. Ogilvie, D. P. C. McGee, S. M. Boisvert, G. H. Hakimelahi, and Z. A. Proba. Can. J. Chem. **61**, 1204 (1983).
14. M. J. Damha, N. Usman, and K. K. Ogilvie. Tetrahedron Lett. **28**, 1633 (1987).
15. M. J. Damha and K. K. Ogilvie. J. Org. Chem. **53**, 3710 (1988).
16. (*a*) P. Tundo and P. Venturello. J. Am. Chem. Soc. **101**, 6607 (1979); (*b*) R. L. Kaas and J. L. Kardos. Polym. Eng. Sci. **11**, 11 (1971); (*c*) R. E. Majors and M. J. Hopper. J. Chromatogr. Sci. **12**, 767 (1974); (*d*) R. Schwarzenbach. J. Chromatogr. **117**, 206 (1976).
17. J. Doornbos, J. L. Barascut, H. Lazrek, J. L. Imbach, J. van Westrenen, G. M. Visser, J. H. van Boom, and C. Altona. Nucleic Acids Res. **11**, 4583 (1983).

Model compounds of aromatic nylons. 3. The conformation of the 4T Nylon, poly(tetramethylene terephthalamide), using X-ray diffraction, solid-state ^{13}C nmr spectroscopy and ir spectroscopy

JOSÉE BRISSON, JOHANNE GAGNÉ, AND FRANÇOIS BRISSE

Département de Chimie, Université de Montréal, C.P. 6128, Succ. A, Montréal (Qué.), Canada H3C 3J7

Received November 21, 1988

JOSÉE BRISSON, JOHANNE GAGNÉ, and FRANÇOIS BRISSE. Can. J. Chem. **67**, 840 (1989).

Three model compounds of poly(tetramethylene terephthalamide) or 4T Nylon have been synthesized and characterized using single crystal X-ray diffractometry, infrared spectroscopy, and ^{13}C CP/MAS nmr spectroscopy. The model compounds are the *para*-substituted *N,N'*-tetramethylene dibenzamides, where the substituents are the —OMe, —*t*Bu, —CN, and —CH_3 groups. The crystal structure determinations reveal three distinct conformations for the CO—NH—$(CH_2)_4$—NH—CO sequence of atoms. The conformation is all *trans* for OMe, *tgttt*$^-$*t* for the *t*Bu substituent, and *tsttts*$^-$*t* for the CN substituent (*t* = *trans* ≃ 180°, $g^{\pm}$ = *gauche* ≃ ±60°, and $s^{\pm}$ = *skew* ≃ ±120°). In all three derivatives, the dihedral angle between the aromatic ring and the amide plane is around 30°. The OMe and *t*Bu *para*-substituted molecules are interconnected by nearly linear hydrogen bonds of normal N...O distances. However, for the CN derivative the N...O distance is exceptionally short, 2.402(4) Å. On the basis of its infrared and solid state nmr spectra, it is proposed that *N,N'*-tetramethylene di-*para*-methyl benzamide has a crystal structure comparable to that of its unsubstituted analog. The methylenic sequence of the parent polyamide, 4T Nylon, has the *tgtttg*$^-$*t* conformation. Furthermore, the polyamide chains form sheets within which the chains, parallel to one another, are connected through hydrogen bonds.

Key words: polyamide, crystal structure, solid-state nmr.

JOSÉE BRISSON, JOHANNE GAGNÉ et FRANÇOIS BRISSE. Can. J. Chem. **67**, 840 (1989).

On a synthétisé trois composés modèles du poly(tétraméthylène téréphtalamide) (Nylon 4T) et on les a caractérisés par diffraction des rayons-X sur un cristal unique, par spectroscopie infrarouge ainsi que par rmn du ^{13}C en mode CP/MAS. Les composés modèles sont des *N,N'*-tétraméthylène dibenzamides substitués en position *para* par des groupements —OMe, —*tert*-butyle, —CN ou —CH_3. Les déterminations des structures ont permis d'identifier trois conformations distinctes pour la séquence d'atomes CO—NH—$(CH_2)_4$—NH—CO. On observe la conformation complètement *trans* avec le substituant OMe, la conformation *tgtttg*$^-$*t* avec le substituant *tert*-butyle et la conformation *tsttts*$^-$*t* avec le substituant CN (*t* = *trans* ≃ 180°, $g^{\pm}$ = *gauche* ≃ ±60° et $s^{\pm}$ = *skew* ≃ ±120°). Dans les trois dérivés, l'angle dièdre entre le plan du noyau aromatique et celui de l'amide est d'environ 30°. Les molécules substituées par des groupements OMe ou *tert*-butyle sont reliées par des liaisons hydrogènes linéaires dont les distances N...O sont normales. Toutefois, dans le cas du dérivé portant un substituant CN, la distance N...O est exceptionnellement courte, 2,402(4) Å. En se basant sur ses spectres ir et de rmn à l'état solide, on suggère que la structure cristalline du *N,N'*-tétraméthylène di-*p*-méthyl benzamide doit être comparable à celle de son analogue qui n'est pas substitué. Dans le polyamide de base, le Nylon 4T, la conformation de la séquence méthylénique est *tgtttg*$^-$*t*. De plus, les chaînes de polyamide forment des couches à l'intérieur desquelles les chaînes, parallèles les unes aux autres, sont reliées par des liaisons hydrogènes.

Mots clés : polyamide, structure cristalline, rmn état solide.

[Traduit par la revue]

Introduction

Recently we have studied the crystalline phase of various polyesters such as poly(oligomethylene terephthalates) (1–3), or poly(1,4-*trans*-cyclohexanediyldimethylenesuccinate) (4). We have also undertaken to establish the structure of the series of aromatic Nylons or *n*T Nylons which are in some ways related to the above-mentioned poly(oligomethylene terephthalates). However, the *n*T Nylons cannot be easily obtained in an oriented form, hence the X-ray diffraction patterns or films of fibers are not of a very high quality. Therefore, we have sought to gain information on the polymer's structure through other means.

Structural data were obtained from single crystal determinations of a series of related model compounds chosen for their similarity with the chemical repeat of the parent polymer. The crystal structures of the series of *N,N'*-oligomethylene dibenzamides, abbreviated *n*DBN where *n* is the number of methylene units, have been reported previously (5–10).

In the present paper, *para*-substituted *N,N'*-tetramethylene dibenzamides are studied with cyano, methyl, methoxy, and *tert*-butyl groups as substituents. These compounds are abbreviated *n*DBN-*p*-X where X is CN, Me, OMe, or *t*Bu. It is hoped that this study will bring a new understanding of the factors governing the conformation of 4T Nylon.

Infrared spectroscopy, which was used in the study of the *n*DBN, was also used in the study of this new series. We hoped to confirm our previous findings as well as to gain structural information on certain model compounds for which no single crystals suitable for X-ray diffraction have yet been obtained.

A solid state CP/MAS ^{13}C nmr study of the model compounds was also undertaken in order to correlate the chemical shifts of the methylenic carbons with the conformation of the aliphatic segments as obtained by X-ray diffraction. Our aim was to use the γ-*gauche* effect on the chemical shifts in order to deduce the conformation of the aliphatic chain of polymers and model compounds. It has been shown that the γ-*gauche* effect and the molecular packing interactions both affect to different degrees the chemical shift and we hoped to be able to quantify the factors influencing the chemical shift.

A comparison of specific absorption frequencies and ^{13}C nmr chemical shifts of the model compounds will provide structural information on those model compounds for which no single crystals are available.

Finally, we will propose a structure for the crystalline phase

Can. J. Chem. Downloaded from www.nrcresearchpress.com by 41.223.56.140 on 09/07/12
For personal use only.

TABLE 1. Crystal data

Parameter	Value		
	p-OMe	*p*-*t*Bu	*p*-CN
Composition	$C_{20}H_{24}N_2O_4$	$C_{26}H_{36}N_2O_2$	$C_{20}H_{18}N_4O_2$
MW	356.43	408.59	346.39
$F(000)$	760	444	364
Crystal system	Monoclinic	Monoclinic	Monoclinic
Space group	$C2/c$	$P2_1/c$	$P2_1/c$
a, Å	41.320(8)	9.602(2)	11.593(2)
b	5.089(1)	14.234(2)	5.008(1)
c	8.417(2)	9.832(2)	16.954(2)
β, deg	90.70(2)	111.33(2)	113.65(1)
V, Å^3	1769.7	1251.7	901.7
d_o, g cm^{-3}	1.29	1.03	1.22
d_c	1.337	1.084	1.275
Z	4	2	2
μ, mm^{-1}	0.724	0.500	0.653
Crystal size, mm	0.29 × 0.17 × 0.04	0.29 × 0.29 × 0.11	0.35 × 0.20 × 0.02

of 4T Nylon that is coherent with the set of information and correlations deduced from model compounds.

Experimental

Spectroscopy

^{13}C CP/MAS nmr spectra were recorded on a Bruker CXP200 200 MHz at a frequency of 50.3 MHz. For all compounds a 1 ms contact time was used with a 10 s delay between sequences. An average number of 700 contacts was used.

Infrared spectra were recorded on a FTIR Nicolet 7199 using a HeNe class II laser. The number of scans accumulated was on the average 200, with a resolution of 2 cm^{-1} resolution. The samples were ground with KBr.

X-ray diffraction

Well-developed crystals suitable for X-ray diffractometry were obtained by slow evaporation of solutions of 4DBN-*p*-OMe and 4DBN-*p*-*t*Bu in a 50:50 mixture of isopropanol and water while 4DBN-*p*-CN was dissolved in DMSO. The unit cell dimensions were calculated from 25 reflections accurately centered on the Nonius CAD-4 diffractometer. The space groups were established from photographic investigation combined with an analysis of the intensity data. The densities were measured by the flotation method using $ZnCl_2$ aqueous solutions. The crystal data of interest are presented in Table 1. Integrated intensities were collected on the Enraf-Nonius CAD-4 diffractometer in the $\omega/2\theta$ scan mode using graphite monochromatized CuK$\bar{\alpha}$ radiation, λ(CuK$\bar{\alpha}$) = 1.54178 Å, and a scan width calculated by the relation $\Delta\omega = (1.00 + 0.14 \tan\theta)°$. The stabilities of the crystals were monitored by measuring every hour the intensities of seven reference reflections. The X-ray scattering factors used were those of Cromer and Mann (11) for all non-hydrogen atoms. The X-ray scattering factor for H atoms were those of Stewart, Davidson, and Simpson (12).

All structures were solved by direct-methods using the MULTAN80 or SHELX programs.[1] In all cases, the H atoms were found on difference Fourier syntheses. The H atoms were included in the refinement with isotropic temperature factors while all the non-hydrogen atoms were treated anisotropically. In the case of 4DBN-*p*-*t*Bu, the *t*Bu group was found to be disordered over two sites, each with an occupancy factor of 50%. The full-matrix least-squares refinement of the atomic coordinates using anisotropic temperature factors for nonhydrogen atoms and isotropic thermal parameters for H atoms, proceeded smoothly. The various criteria indicating the correctness of the structures are given in Table 2.

[1]The programs used here are modified versions of NRC-2, data reduction; NRC-3, absorption correction; NRC-10, bond distances and angles; NRC-22, mean planes (13); FORDAP, Fourier and Patterson maps; MULTAN80, multisolution program (14); SHELX program (15); NUCLS, least-squares refinement (16); ORTEP, stereoviews (17).

Results and discussion

Crystal structures

The final atomic coordinates and their standard deviations are presented in Tables 3*a*, *b*, and *c*.[2] The atomic numbering is shown in Fig. 1 and the various molecular structures are presented, as stereopairs in Fig. 2. The final bond distances and angles are compared in Table 4. There is no unusual feature among the bond distances and angles in the benzamide groups. Each six-membered ring is planar within experimental errors and so are the amide groups of atoms [C(1), C(7), N(1), O(1)]. The dihedral angles between the above two planes are very similar having values of 27.3, 27.3, and 33.7° for the *p*-OMe, *p*-*t*Bu, and *p*-CN derivatives, respectively. This compares well with the value of 30.0° reported for 4DBN (6) and is in the range of 19.0 to 34.1° observed for other *n*DBN's (9, 10).

The tetramethylene sequence

The bond distances, bond angles, and torsion angles of the —NH—$(CH_2)_4$—NH— sequence of atoms are compared in Table 5 to the corresponding quantities in 4DBN. In all four molecules there is a crystallographic center of symmetry at the mid-point of the central CH_2—CH_2 bond so that all symmetrically related (τ, τ', ϕ_1, ϕ_1') torsion angles have the same numerical value but are of opposite signs. The three torsion angles (ϕ_1, ϕ_2, ϕ_1') that define the conformation of the —NH—$(CH_2)_4$—NH— sequence are all *trans*. In other words, the atoms of the methylenic sequence are coplanar in all three compounds. What distinguishes most a compound from another is the torsion angle τ = C(7)—N(1)—C(8)—C(9). It has the values of 169.5(3) and 173.4(3)° for 4DBN and 4DBN-*p*-OMe, respectively, while τ is 79.8(2)° for 4DBN-*p*-*t*Bu and −120.0(4)° for 4DBN-*p*-CN.

[2]Structure factor tables, H atom coordinates, anisotropic thermal parameters, and the assignments of the infrared spectra may be purchased from the Depository of Unpublished Data, CISTI, National Research Council of Canada, Ottawa, Ont., Canada K1A 0S2.

Can. J. Chem. Downloaded from www.nrcresearchpress.com by 41.223.56.140 on 09/07/12
For personal use only.

TABLE 2. Data collection and refinement

Parameter		Value		
		p-OMe	*p*-*t*Bu	*p*-CN
Radiation		CuKα	CuKα	CuKα
$2\theta_{max}$, deg		140.0	140.0	140.0
Octants measured	*h*	0,50	0,11	0,14
	k	0,6	0,17	0,6
	l	−10,10	−11,11	−20,20
Number of measured reflections		1697	2363	1700
Acceptance level, $\sigma(I)$		1.96	1.96	1.96
Number of observed reflections		1301	1723	1081
Largest fluctuations of reference reflections, %		0.80	1.17	1.69
$R = \Sigma\|\|F_o\| - \|F_c\|\|/\Sigma\|F_o\|$		0.051	0.056	0.058
$R_w = [\Sigma w(\|F_o\| - \|F_c\|)^2/\Sigma wF_o^2]^{1/2}$		0.048	0.044	0.039
$S = [\Sigma w(\|F_o\| - \|F_c\|)^2/(m - n)]^{1/2}$		3.14	3.35	2.10
Residual fluctuation in electron density map, e Å^{-3}		−0.14, 0.08	−0.18, 0.12	−0.21, 0.18
Average Δ/σ ratio at the end of the refinement		0.14	0.12	0.09

In this respect, 4DBN-*p*-*t*Bu resembles 2DBN, $\tau = 91.5(3)°$, 5DBN, $\tau = 71.3(2)°$ and $\tau' = 90.2(3)°$ or one end of 7DBN, $\tau = 91.6(4)°$. On the other hand, 4DBN-*p*-CN may be compared to 3DBN, $\tau = -140.3(3)°$, and to the other extremity of 7DBN, $\tau' = -105.0(4)°$.

Hydrogen bonding

The distances and angles describing the hydrogen bonding scheme are compared in Table 6. In an earlier work on *n*DBN's, the N...O distances were found in the range 2.838(2) to 3.012(3) Å while the N—H...O and N...O—C angles were within 147–168° and 125.5–166°, respectively. The corresponding quantities fall within the above limits for 4DBN-*p*-OMe and 4DBN-*p*-*t*Bu. The H bonds in all three compounds are nearly linear. However, in the case of 4DBN-*p*-CN, the N...O distance is remarkably short, 2.402(4) Å. For both 4DBN-*p*-OMe and 4DBN-*p*-CN, each molecule forms two H bonds with each of two molecules. This association results in the formation of a ribbon extending in the *b* direction.

Each 4DBN-*p*-*t*Bu molecule is H-bonded to four distinct molecules, thus forming a three-dimensional network similar to that observed for 2DBN (5). The various packing modes are shown as stereopairs in Fig. 3*a*, *b*, *c*.

Infrared spectroscopy

The assignments of the absorption bands of the infrared spectra of the various models have been deposited.

Although there is no obvious correlation between specific absorption frequencies and the conformation of the aliphatic chains, some other features of the ir spectra are useful diagnostics in identifying the type of hydrogen bonding present and assigning values to the τ torsion angles.

(1) The amide II band

It has been found that the frequency of the amide II band was dependent upon the type of hydrogen bonding in the structure. This observation is confirmed here. All the *n*DBN's which form extended ribbons through H-bonding between adjacent molecules have a strong ir absorption at around 1535 cm^{-1}. In the case of 4DBN-*p*-OMe the absorption is observed at

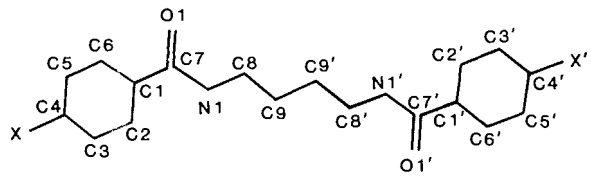


FIG. 1. Schematic representation of the molecules and atomic numbering.

1534 cm^{-1} in agreement with the observed one-dimensional ribbon-like structure (Fig. 3*a*).

The amide II band in 4DBN-*p*-*t*Bu is a doublet at 1555–1551 cm^{-1}. This value compares very well to that of 1562 cm^{-1} reported for 2DBN a molecule whose packing is identical to that of 4DBN-*p*-*t*Bu (Fig. 3*b*). In this arrangement each molecule forms one H bond with four distinct molecules (5) as opposed to the ribbon-like packing of 4DBN and 4DBN-*p*-*t*Bu where each molecule forms two H-bonds with each of two different molecules. In the case of 4DBN-*p*-CN, the amide II band is observed split at 1542–1559 cm^{-1}. Normally, one would expect an absorption band at ~1535 cm^{-1} since the hydrogen-bonded 4DBN-*p*-CN molecules form extended ribbons (Fig. 3*c*). However, the CN group is strongly electroattractive and this affects the frequency of the amide II band. It is this characteristic of the CN group which is also responsible for the extremely short N...O bond. Its length of 2.402(4) Å is significantly shorter than in the other *n*DBN's for which it is observed in the range of 2.8 to 3.0 Å.

(2) The amide V band

In a previous study (9) of non-substituted model compounds of the *n*T Nylons, it was proposed that the τ torsion angle was related to the position of the absorption of the amide V band. For $\tau \simeq 180°$, the absorption was observed in the lower frequencies, in the range 642–652 cm^{-1} while for $\tau \simeq 90°$, the absorption was shifted to the 664–675 cm^{-1} range. Since for 4DBN-*p*-OMe, the absorption of the amide V band is at 642 cm^{-1}, one may conclude that τ is near 180°. This is in good agreement with the observed τ value of 173.4(2)°. On the other hand, in the solid

Can. J. Chem. Downloaded from www.nrcresearchpress.com by 41.223.56.140 on 09/07/12
For personal use only.

Can. J. Chem. Downloaded from www.nrcresearchpress.com by 41.223.56.140 on 09/07/12
For personal use only.

TABLE 3

(*a*) Fractional atomic coordinates ($\times 10^5$) and U_{eq} ($\times 10^4$) for 4DBN-*p*-OMe, $U_{eq} = \frac{1}{3}\sum_i\sum_j U_{ij} a_i^* a_j^* \boldsymbol{a}_i \cdot \boldsymbol{a}_j$

Atom	*X*	*Y*	*Z*	U_{eq}
O(1)	42558(4)	59343(35)	19217(26)	489
O(2)	28921(4)	19954(41)	40821(23)	469
N(1)	43399(6)	16830(47)	13632(33)	397
C(1)	38306(6)	29958(51)	25120(30)	300
C(2)	36513(6)	8844(54)	19558(34)	351
C(3)	33354(7)	4883(54)	24342(34)	357
C(4)	32011(6)	21827(55)	35233(32)	345
C(5)	33822(7)	42639(57)	41258(35)	382
C(6)	36913(7)	46626(54)	36111(33)	347
C(7)	41598(6)	36300(55)	19333(34)	357
C(8)	46559(7)	22256(59)	6967(44)	427
C(9)	48316(7)	−2776(62)	3027(43)	399
C(10)	27007(8)	−1498(76)	35253(50)	542

(*b*) Fractional atomic coordinates ($\times 10^4$) and U_{eq} ($\times 10^4$) for 4DBN-*p*-CN, $U_{eq} = \frac{1}{3}\sum_i\sum_j U_{ij} a_i^* a_j^* \boldsymbol{a}_i \cdot \boldsymbol{a}_j$

Atom	*X*	*Y*	*Z*	U_{eq}
O(1)	3397(2)	9517(4)	472(2)	633
N(1)	2862(2)	5194(6)	397(2)	530
N(2)	9851(2)	4468(7)	3237(2)	881
C(1)	5025(2)	6422(6)	1207(2)	387
C(2)	5339(3)	4366(7)	1795(2)	509
C(3)	6587(3)	3882(7)	2329(2)	564
C(4)	7526(3)	5412(7)	2250(2)	486
C(5)	7223(3)	7449(8)	1657(2)	589
C(6)	5974(3)	7967(7)	1148(2)	544
C(7)	3688(3)	7167(7)	658(2)	419
C(8)	1522(3)	5634(10)	−147(3)	652
C(9)	696(3)	4723(10)	270(3)	594
C(10)	8833(3)	4878(8)	2800(2)	623

(*c*) Fractional atomic coordinates ($\times 10^5$) and U_{eq} ($\times 10^4$) for 4DBN-*p*-*t*Bu, $U_{eq} = \frac{1}{3}\sum_i\sum_j U_{ij} a_i^* a_j^* \boldsymbol{a}_i \cdot \boldsymbol{a}_j$

Atom	*X*	*Y*	*Z*	U_{eq}
O(1)	44954(17)	27377(9)	78934(13)	907
N(1)	47096(18)	28366(10)	102269(15)	698
C(1)	33907(21)	15093(12)	88110(17)	607
C(2)	35778(23)	9097(13)	99630(19)	717
C(3)	27961(25)	766(14)	97540(21)	776
C(4)	17763(22)	−1992(13)	84062(20)	675
C(5)	16023(25)	4224(15)	72709(21)	878
C(6)	23924(25)	12477(14)	74565(20)	840
C(7)	42346(22)	23992(13)	89419(18)	671
C(8)	55468(24)	36980(14)	104677(20)	770
C(9)	45567(24)	45572(13)	98862(24)	817
C(10)	9128(23)	−11126(14)	81655(22)	804
C(11)*	18869(88)	−19554(48)	85584(88)	1205
C(12)	−2324(96)	−11162(53)	89862(91)	1315
C(13)	−1697(84)	−13358(48)	65268(72)	1080
C(14)	−6946(39)	−9006(26)	74763(42)	1154
C(15)	14282(46)	−17190(25)	71393(42)	1220
C(16)	12835(47)	−16510(24)	95931(42)	1230

*Atoms C(11) to C(16) have half occupancy.

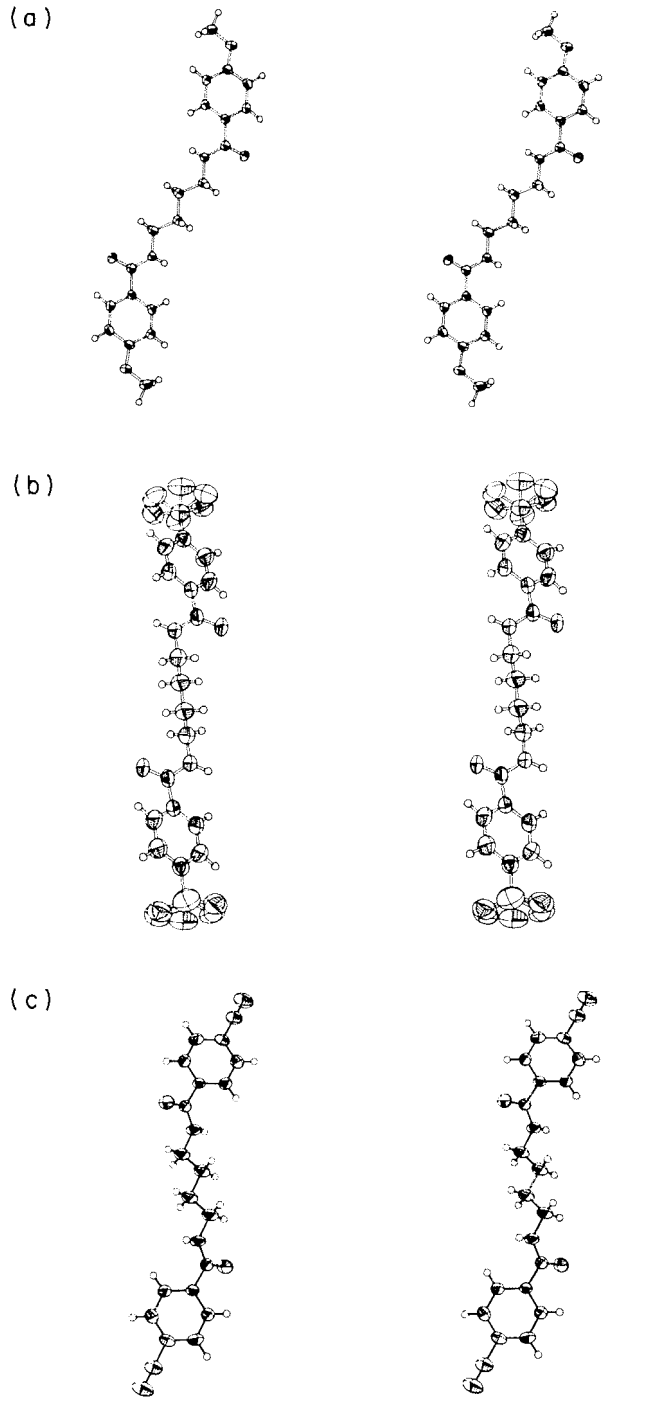


FIG. 2. Stereopairs showing the molecular conformation of (*a*) 4DBN-*p*-OMe, (*b*) 4DBN-*p*-*t*Bu, and (*c*) 4DBN-*p*-CN.

state 4DBN-*p*-*t*Bu and 4DBN-*p*-CN have τ values of 79.8(2)° and −120(4)°, respectively. The corresponding amide V frequencies should be in the 664–675 cm^{-1} range but are observed at 697 (4DBN-*p*-*t*Bu) or 690 cm^{-1} (4DBN-*p*-CN).

*(3) In the case of 4DBN-*p-*Me*, the amide II band observed at 1537 cm^{-1} points to a ribbon-like type of packing as observed for 4DBN. The amide V band is recorded at 657–662 cm^{-1}. We are unable to decide on the value of τ, since the amide V band falls in between the two above defined ranges for the τ torsion angle of 180 or 90°.

TABLE 4. Comparison of bond distances (Å), bond angles (deg), and torsion angles (deg) and their esd's

Parameter	Value			
	4DBN (6)	*p*-OMe	*p*-*t*Bu	*p*-CN
Distances				
C(1)—C(2)	1.383(3)	1.384(4)	1.377(2)	1.377(5)
C(2)—C(3)	1.387(4)	1.385(4)	1.378(3)	1.386(5)
C(3)—C(4)	1.366(4)	1.380(4)	1.387(3)	1.381(5)
C(4)—C(5)	1.375(3)	1.389(4)	1.386(3)	1.375(5)
C(5)—C(6)	1.372(3)	1.369(4)	1.374(3)	1.381(5)
C(6)—C(1)	1.382(3)	1.385(4)	1.379(2)	1.382(5)
C(4)—X	—	1.369(3)	1.514(3)	1.450(5)
C(1)—C(7)	1.497(3)	1.486(4)	1.483(3)	1.500(4)
C(7)—O(1)	1.238(2)	1.238(3)	1.243(2)	1.230(4)
C(7)—N(1)	1.334(2)	1.332(4)	1.331(2)	1.323(4)
Bond angles				
C(1)—C(2)—C(3)	119.7(2)	121.1(3)	120.6(2)	120.4(3)
C(2)—C(3)—C(4)	120.9(2)	119.4(3)	122.9(2)	119.8(3)
C(3)—C(4)—C(5)	119.3(2)	120.0(2)	115.2(2)	120.2(3)
C(4)—C(5)—C(6)	120.3(2)	119.9(2)	122.7(2)	119.5(3)
C(5)—C(6)—C(1)	120.7(2)	121.2(2)	121.0(2)	121.0(3)
C(6)—C(1)—C(2)	119.3(2)	118.4(2)	117.6(2)	119.0(3)
C(7)—C(1)—C(2)	122.6(2)	123.1(2)	123.6(2)	122.8(3)
C(7)—C(1)—C(6)	118.4(2)	118.4(2)	118.7(2)	118.0(3)
O(1)—C(7)—N(1)	121.6(2)	121.4(2)	120.2(2)	122.8(3)
O(1)—C(7)—C(1)	120.5(2)	120.2(2)	121.8(2)	120.4(3)
N(1)—C(7)—C(1)	117.7(2)	118.3(2)	118.0(2)	116.8(3)
C(7)—N(1)—C(8)	121.4(2)	120.4(2)	122.2(2)	122.6(3)
C(3)—C(4)—X	—	124.7(2)	123.3(2)	119.8(3)
C(5)—C(4)—X	—	115.4(2)	121.6(2)	120.1(3)
Torsion angles				
C(2)—C(1)—C(7)—O(1)	148.7(2)	150.2(3)	152.1(2)	144.8(3)
C(2)—C(1)—C(7)—N(1)	−31.3(3)	−26.6(4)	−28.2(3)	−34.8(5)
C(6)—C(1)—C(7)—O(1)	−28.5(2)	−26.9(4)	−25.9(3)	−31.7(5)
C(6)—C(1)—C(7)—N(1)	151.5(3)	156.2(3)	153.8(2)	148.7(3)
C(2)—C(3)—C(4)—X	—	179.9(2)	180.0(2)	−179.1(3)
C(6)—C(5)—C(4)—X	—	−178.3(2)	−178.8(2)	−178.9(3)

Solid-state ^{13}C nmr spectroscopy

The spectra of the model compounds studied appear in Fig. 4*A*. Since all the model compounds have a crystallographic center of symmetry at the mid-point of the aliphatic chain, only one peak is observed for each of the two symmetrically related carbon atoms. It is observed that, in most cases, C(7) of the amide group and C(8) of the aliphatic chain, which are both attached to the nitrogen atom, have doubled peaks. This is caused by the quadrupole moment of the nitrogen atom, which is not averaged out entirely by the rotation of the sample. It is also noted that the carbon signals of the methyl and *tert*-butyl groups are much more intense than those of the other carbon atoms. This is a common feature due to the rapid rotation of these specific groups in the solid state (Table 7).

(a) Chemical shift of atom C(9)

As can be seen in Fig. 4*Ba*, the chemical shift of the C(9) atom may be affected by the γ-*gauche* effect of the τ and ϕ_1' torsion angles. In their study of model compounds of 4GT, Grenier–Loustalot and Bocelli (18) reported that the γ-*gauche* effect related to a change of the torsion angle O—C(8)—C(9)—C(8′) from *trans* to *gauche* is of the order of −3 ppm. Their torsion angle is similar to our φ (and φ′) torsion angle. However, in all the *n*T Nylon model compounds whose structures have been established, the φ torsion angle is always *trans*. Thus there should not be any γ-*gauche* effect on the C(9) atom due to φ.

On the other hand, the torsion angle τ is *trans* for 4DBN and 4DBN-*p*-OMe whereas it has the values of 79.8(2) and −120.0(4)° for 4DBN-*p*-*t*Bu and 4DBN-*p*-CN, respectively (Table 5). A change of τ from ≈180° to ≈100° results in a γ-*gauche* effect of +1.8 ppm, since the chemical shifts for 4DBN and 4DBN-*p*-OMe are 27.3 and 27.6 ppm, respectively, whereas they are 29.1 and 29.4 ppm for 4DBN-*p*-*t*Bu and 4DBN-*p*-CN. In this case, the effect is towards low fields. However, it is normally found to be towards high fields as in the case of alkanes for which it has been observed in solution (19). This has been explained as resulting from a steric interaction between two methylenes in δ position from one another. In the present case, the methylene group C(9) is brought very close to the carbonyl group when τ is near 90° (Fig. 4*c*). This causes the methylene to be in the vicinity of the electron cloud circulating

Can. J. Chem. Downloaded from www.nrcresearchpress.com by 41.223.56.140 on 09/07/12
For personal use only.

TABLE 5. Comparison of bond distances (Å), bond angles (deg), and torsion angles (deg) and their esd's in the aliphatic sequence of the 4T Nylon model compounds; dihedral angles (deg) and equivalent fiber repeats (Å)

Parameter	Value			
	4DBN (6)	*p*-OMe	*p*-*t*Bu	*p*-CN
Distances				
N(1)—C(8)	1.459(3)	1.454(4)	1.438(3)	1.471(5)
C(8)—C(9)	1.505(3)	1.505(4)	1.527(3)	1.474(6)
C(9)—C(9′)	1.513(3)	1.515(4)	1.490(3)	1.528(4)
Angles				
N(1)—C(8)—C(9)	111.8(2)	111.2(3)	112.7(2)	112.3(4)
C(8)—C(9)—C(9′)	112.0(2)	111.3(3)	111.9(2)	112.9(3)
Torsion angles				
ω = C(1)—C(7)—N(1)—C(8)	178.6(3)	176.4(2)	179.5(2)	−179.8(3)
τ = C(7)—N(1)—C(8)—C(9)	169.5(3)	173.4(2)	79.8(2)	−120.0(4)
ϕ_1 = N(1)—C(8)—C(9)—C(9′)	−178.4(3)	−176.7(2)	−178.7(2)	177.5(4)
ϕ_2 = C(8)—C(9)—C(9′)—C(8′)	180	180	180	180
Dihedral angles				
Phenyl/amide	30.0	27.3	27.3	33.7
Amide/methylene plane	15.5	2.4	0.7	0.5
Equivalent fiber repeat	13.590	13.598	13.112	13.368

TABLE 6. Characteristics of the hydrogen bonds in the 4DBN derivatives

Parameter	Value			
	4DBN (6)	*p*-OMe	*p*-*t*Bu	*p*-CN
N(1)—H(N1), Å	0.87(2)	0.82(3)	0.91(2)	0.78(3)
N(1)...O(1*)	2.999(4)	2.984(3)	2.815(2)	2.402(4)
H(N1)...O(1*)	2.13(2)	2.18(3)	1.94(2)	2.13(3)
N—H...O*, deg	165(2)	166(3)	162(2)	169(3)
N...O*—C*	166.5(2)	166.9(4)	139.6(1)	168.7(2)

TABLE 7. Chemical shifts (δ, ppm) of 4T Nylon and its model compounds

Atom	Chemical shift					
	4DBN	4DBN-*p*-OMe	4DBN-*p*-CN	4DBN-*p*-*t*Bu	4DBN-*p*-Me	4T Nylon
C(9)	27.3	27.6	29.4	29.1	27.2	27.1
C(8)	44.0	45.2	41.1	41.6	44.5	43.2
	42.6	43.6	39.8		42.8	40.4
C(1)	135.4	129.4	138.2	125.3	133.3	
C(6)	130.3	134.0	130.1	132.7	130.5	
C(5)	128.0	110.6	132.1	154.3	137.8	137.4
C(4)	129.4	159.3	120.4	128.4	129.8	to
C(3)	128.0	116.3	132.1	125.3	129.8	126.8
C(2)	128.8	129.4	128.8	128.4	128.8	
C(7)	169.8	169.0	167.5	169.3	169.6	168.2
	168.2	167.2	165.9		168.0	
CH_3	—	55.2	—	32.4	22.9	—
C≡N	—	—	114.9	—	—	—
C—$(CH_3)_3$	—	—	—	35.0	—	—

Can. J. Chem. Downloaded from www.nrcresearchpress.com by 41.223.56.140 on 09/07/12
For personal use only.

Can. J. Chem. Downloaded from www.nrcresearchpress.com by 41.223.56.140 on 09/07/12
For personal use only.

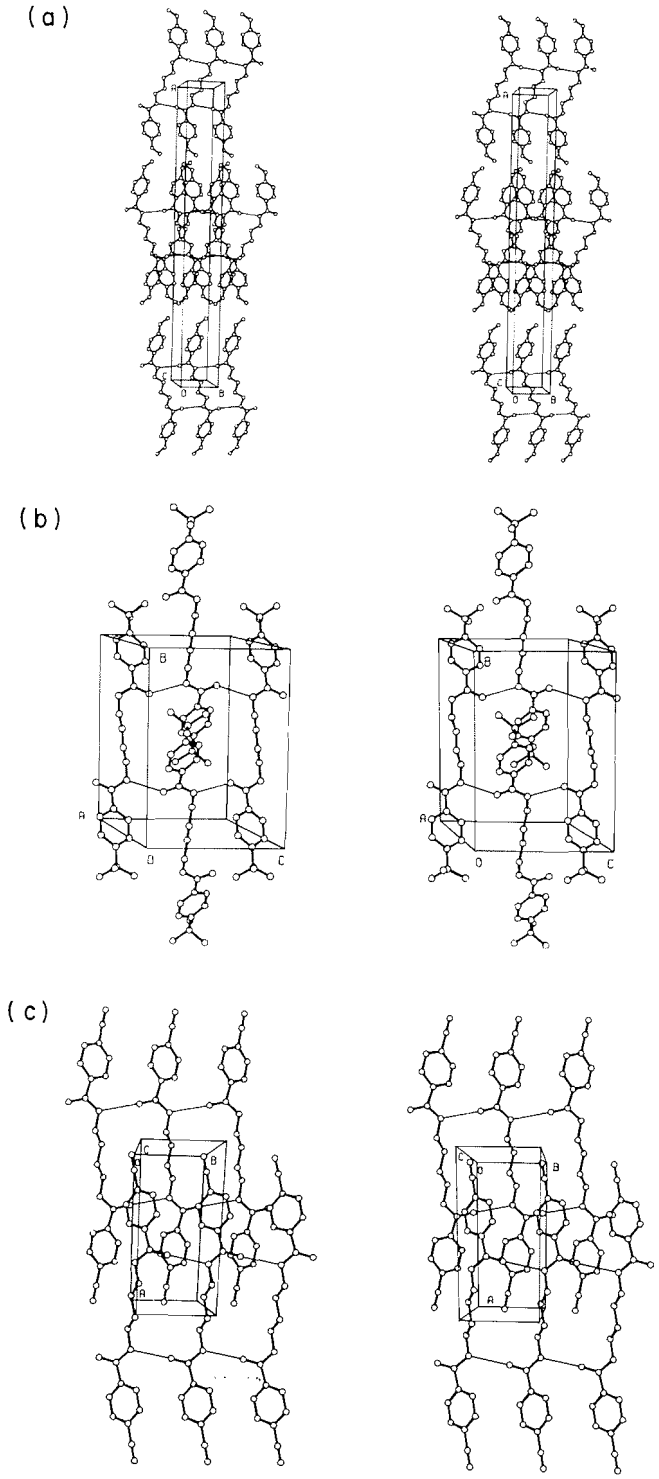


FIG. 3. Packing of the molecules. (*a*) 4DBN-*p*-OMe, (*b*) 4DBN-*p*-*t*Bu, and (*c*) 4DBN-*p*-CN.

about the amide group and could explain the deshielding γ-*gauche* effect of the τ torsion angle on the C(9) methylene group.

(b) Chemical shift of atom C(8)

The chemical shift of this atom should be affected by the γ-*gauche* effect related to the ω and ϕ_2 torsion angles. Both these angles are close to 180° in all the structures analyzed here. Consequently, if the γ-*gauche* effect were the sole factor involved, it would be expected that the chemical shift of the C(8) would remain constant. Nevertheless, the mean chemical shift of the split peak varies significantly. For 4DBN and 4DBN-*p*-OMe, it is observed at 43.3 and 44.4 ppm, but for 4DBN-*p*-CN and 4DBN-*p*-*t*Bu it is observed at 40.4 and 41.6 ppm, respectively. Since the difference is approximately 3 ppm, it can hardly be attributed to the inaccuracy of the measurements. This observation is interpreted as a molecular packing interaction effect. In a previous study of polypropylene a chemical shift difference of about 1 ppm was attributed to van der Waals interactions (20). Similarly, chemical shift differences of approximately 1 ppm have been observed between the orthorhombic and triclinic forms of polyethylene which have also been attributed to differences in intermolecular interactions (21). In the case of *n*T Nylons and of their model compounds, we must also take into account possible interactions between the electron cloud surrounding the benzamido group and the aliphatic and amide sections of neighbouring molecules.

The packing modes of 4DBN (Fig. 4*Da*) and 4DBN-*p*-OMe (Fig. 3*a*) are comparable. The molecules, assembled in ribbons, are placed in such a way that the atoms of the amide group and the aliphatic chain are far from the aromatic rings of neighbouring molecules. However, in the case of 4DBN-*p*-CN and 4DBN-*p*-*t*Bu (Fig. 3*b*,*c*), although the molecular packings differ greatly, both molecules have in common the fact that the C(7)—N—C(8) section of one molecule is facing the aromatic moiety of neighbouring molecules. It is proposed that the observed difference of +3 ppm could be due to the position of the C(8) atom in relation to the aromatic rings of adjacent molecules. This effect has been quantified in solution state and has been calculated (22) by the relation:

$$\Delta\delta(\text{ppm}) = \mu(1 - 3\cos^2\Phi)r^3$$

where μ is the equivalent dipole, Φ is the angle between the dipole axis and the atom (in degrees), and *r* is the distance (in Å) between the center of the aromatic ring and atom C(8).

In the case of 4DBN-*p*-CN where $\Phi = 15°$ and $r = 3.8$ Å, we estimated a value of $\Delta\delta$ of -1.8 ppm for this interaction using a value of μ of 27.0 (23). This compares relatively well with the observed value of $\Delta\delta$ of -2.9 ppm relative to 4DBN, since the van der Waals interactions account for the difference of 1.1 ppm observed between 4DBN-*p*-OMe and 4DBN.

(c) Chemical shift of atom C(7)

The chemical shift of atom C(7) is influenced by the value of the τ torsion angle as well as by the molecular packing, as was the case for atom C(8). However, the chemical shift is also influenced by the substitution of the aromatic ring. These combined factors make the interpretation of the chemical shifts of atom C(7) difficult.

On Fig. 4*Bc*, one can see that the chemical shift of C(7) should be influenced by the γ-*gauche* effect due to the τ torsion angle. The interchain interactions should be of the same order of magnitude as for the C(8) and N atoms. Since the γ-*gauche* effect and the interchain interactions are of similar values but of opposite signs, it is expected that the chemical shifts of C(7) should be roughly the same for the four model compounds. We observe a mean value for the doublets ranging from 168.1 ppm for 4DBN-*p*-OMe to 169.3 ppm for 4DBN-*p*-*t*Bu. However, in the case of 4DBN-*p*-CN, this mean value is of 166.7 ppm. The strongly electron-withdrawing capability of the cyano substituent, may account, in part, for the shielding of C(7).

Because of this additional factor involved in the case of the chemical shift of C(7), care should be taken when comparing the

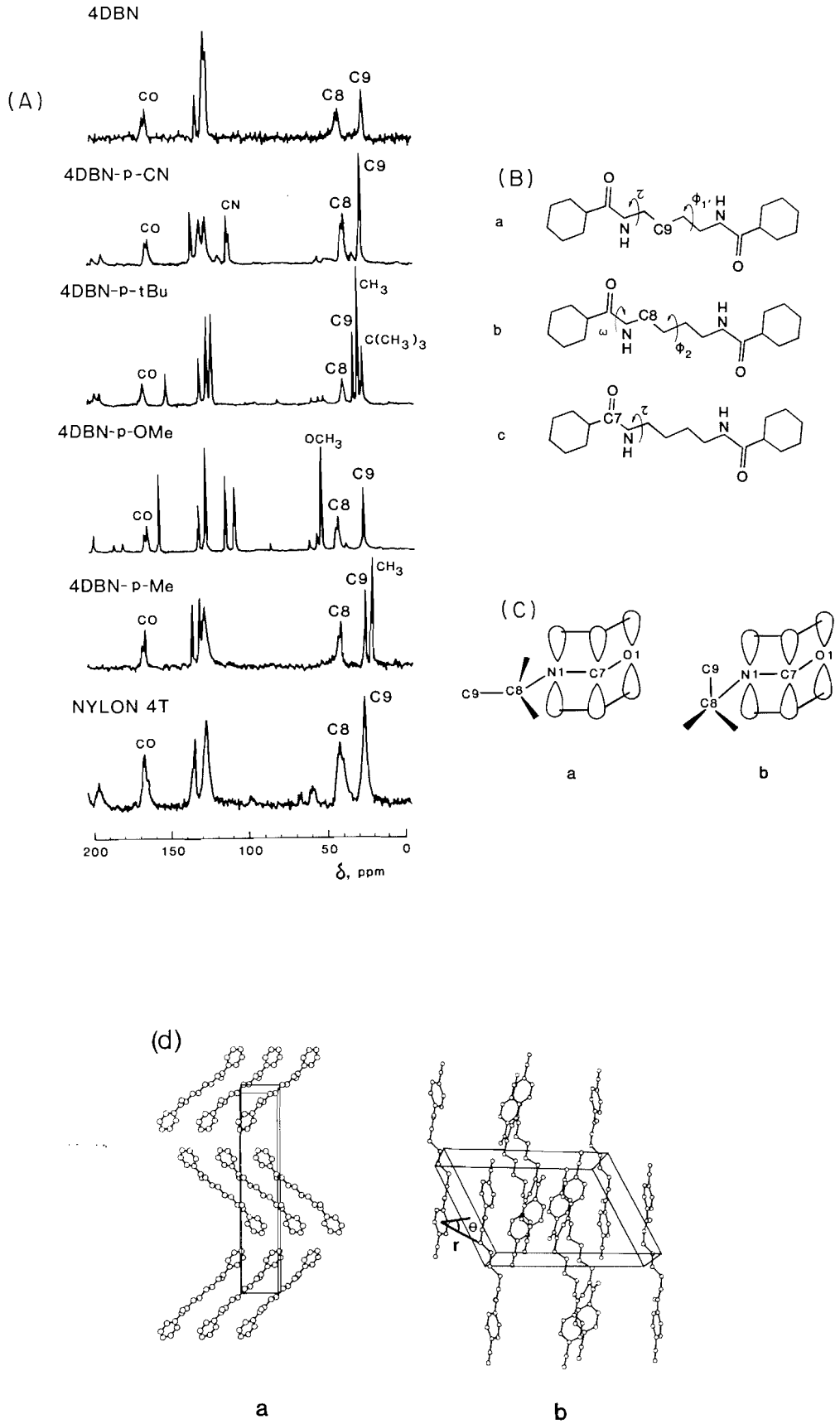


FIG. 4. (*A*) CP/MAS ^{13}C nmr spectra of 4T Nylon and its model compounds. The unidentified peaks in the 120–160 ppm region are due to the aromatic carbon atoms. (*B*) γ-*gauche* effect: (*a*) on C(9), (*b*) on C(8), (*c*) on C(7). (*C*) Relative disposition of the atoms involved in the τ torsion angle: (*a*) $\tau = 180°$, (*b*) $\tau = 90°$. (*D*) Comparison of the molecular packing of (*a*) 4DBN and (*b*) 4DBN-*p*-CN. Note the aromatic ring – methylenic chain interaction in the latter.

Can. J. Chem. Downloaded from www.nrcresearchpress.com by 41.223.56.140 on 09/07/12
For personal use only.

CP/MAS spectra of polymers to those of model compounds which have weakly interacting substituents, such as H, Me, or *t*Bu.

The structure of 4DBN-p-Me

The study of the model compounds whose structures are known has shown that: (*1*) the chemical shift of atom C(9) can be related directly to the torsion angle τ. This γ-*gauche* effect is of +2 to +3 ppm when $\tau \approx 90°$. It might also be affected by the ϕ_1' torsion angle, but this has not been quantified. It is assumed, on the basis of the study of Grenier–Loustalot and Bocelli (18) on related esters, that this effect should be approximately −3 ppm. (*2*) The chemical shift of atom C(8) is influenced by two main factors: the γ-*gauche* effect related to ϕ_2, which should be approximately −2 ppm, and the interchain interactions, more specifically the interaction of the electron cloud of the aromatic ring with C(8), which depends on the packing of the molecules.

Using this information, we should be able to determine the conformation, and possibly the type of interactions resulting from the packing mode.

The number of peaks observed for 4DBN-*p*-Me corresponds to an asymmetric unit composed of half a molecule, which implies a symmetry element in the middle of the aliphatic chain (most probably a center of symmetry as in all the model structures solved previously). Thus ϕ_2 should be near 180° and the chemical shift of C(8) should not be affected by the γ-*gauche* effect. Its mean value (43.7 ppm) is in the same range as observed for 4DBN and 4DBN-*p*-OMe, therefore corresponding to τ and ϕ_1' torsion angles in *trans* conformations. However, it must be noted that the combination of $\tau \approx 90°$ and $\phi_1' \approx 60°$ would lead to a similar chemical shift, and this hypothesis cannot be ruled out at this point.

Finally, since the substituent is not strongly electron withdrawing or donating, we can use the C(7) chemical shift. We have already established that there is no notable aromatic interaction with C(8)—N—C(7). The sole remaining effect on C(7) is the γ-*gauche* effect of τ. The mean chemical shift of this atom is 168.8 ppm, which compares well with that of 4DBN which was 169.0 ppm. This argument supports the hypothesis of τ and ϕ_1' in *trans* conformation. In conclusion 4DBN-*p*-Me has a structure similar to that of 4DBN. This is supported in part by the analysis of its infrared spectra.

Extension to the parent polyamide, 4T Nylon

The fiber diffraction pattern of 4T Nylon reveals a limited number of diffraction spots to a d_{min} value of 1.90 Å. The strongest reflections, which are well resolved, appear on the equator. There are, however, enough diffraction spots on the meridian and the upper levels to evaluate the value of the fiber repeat, p_0 = 13.2(1) Å. In this study of model compounds of 4T Nylon as well as in (10) it has been observed that ϵ, the dihedral angle between the amide group of atoms, [C(1), C(7), N(1), O(1)], and the benzene ring is always very near ±30°. The fiber repeat calculated for a chain of 4T Nylon constructed using average values of the bond distances and angles, taken from the above described model compounds, and with ϵ = 30 or −30° has a value of 13.5 Å. As it can be observed in Table 5, the ω, ϕ_1, and ϕ_2 torsion angles in the model compounds always assume values near 180°. The τ torsion angle, however, is the most flexible since it has values of about 80, 120, or 180°. The same behavior of the torsion angles has been noted for other *n*DBN's (10). Thus we have chosen to calculate the fiber repeat, p_c, as τ was varied from −180 to 180°. In this manner (Fig. 5)

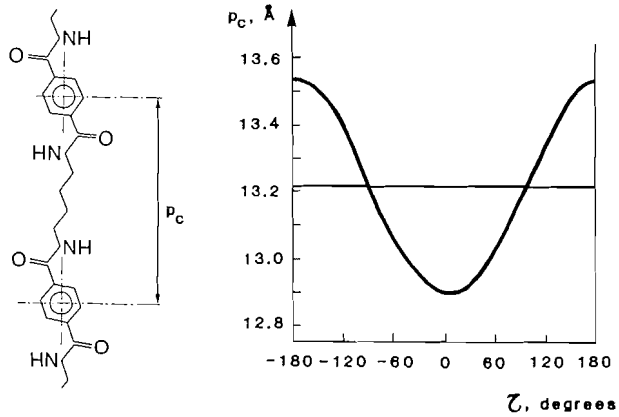


FIG. 5. Variation of p_c vs. τ for ϵ = 30°. The horizontal line corresponds to the experimental value, p_0 = 13.2 Å, of the fiber repeat.

when τ takes the values of 90° or −90°, the observed and calculated fiber repeats are perfectly matched. We conclude that the 4T Nylon structure has the conformation *tgtttg*$^-$*t*. It is indeed very reassuring that $\tau = \pm 90°$ is a very common occurrence among the *n*DBN's (10).

It is also of interest to note that the amide V band of the infrared spectra of both 4T Nylon and 4DBN-*p*-*t*Bu is observed at 700 and 697 cm^{-1}, respectively, and that the conformation of the model compound is *tgtttg*$^-$*t*, the same as that proposed here for the polyamide.

The frequency of the amide II band of 4T Nylon at 1545 cm^{-1} indicates that the polyamide chains are connected through H bonds so as to form sheets where the chains, parallel to one another, extend in one direction while they are "cross-linked" by H bonds in the perpendicular direction.

Conclusions

This series of model compounds of 4T Nylon has led to very promising conclusions. We have observed, using X-ray diffraction, that the τ torsion angle may take a value near 90°. We have also verified that the interpretation of the ir spectra of an earlier study of model compounds (10) is in agreement with the observations on *para*-substituted compounds. Finally, we have quantified two important factors affecting the chemical shift of these model compounds; the γ-*gauche* effect related to the τ torsion angle and the presence of a 2 to 3 ppm shift which is attributed to a specific interchain interaction between an aromatic ring and the C(7)—N(1)—C(8) group of atoms from a neighbouring molecule. This information, combined with that of the literature, led us to propose a structure for 4DBN-*p*-Me whose structure is not presently known.

The solid-state ^{13}C CP/MAS nmr spectroscopy is being used more and more for obtaining conformational information on the crystalline phase of various polymers. However, it must still be used with circumspection, especially in the case where aromatic rings are present. We have shown that in such cases, interchain interactions can be responsible for chemical shifts comparable in size to the γ-*gauche* interactions. This can significantly complicate the analysis of the spectra. The analysis of spectra of model compounds should enable us to quantify such effects and to use the conformation information from such a study for predicting that of polymers of unknown crystal structures.

The proposed conformation, *tgtttg*$^-$*t*, for 4T Nylon is in agreement with that obtained by infrared spectroscopy and is consistent with the X-ray data.

Can. J. Chem. Downloaded from www.nrcresearchpress.com by 41.223.56.140 on 09/07/12
For personal use only.

Acknowledgements

Financial support of this research by the Natural Sciences and Engineering Research Council of Canada and the Fonds FCAR of the Province of Québec is gratefully acknowledged. We are thankful to Mr. M.-J. Olivier for the X-ray data collections. We also wish to acknowledge M. G. Taylor and R. H. Marchessault of the Xerox Research Centre of Canada Ltd. for letting us use their solid-state nmr facility.

1. S. POULIN-DANDURAND, S. PÉREZ, J.-F. REVOL, and F. BRISSE. Polymer, 419 (1979).
2. A. PALMER, S. POULIN-DANDURAND, and F. BRISSE. Can. J. Chem. **63**, 3079 (1985).
3. F. BRISSE, A. PALMER, B. MOSS, D. DORSET, W. A. ROUGHEAD, and D. P. MILLER. Eur. Pol. J. **20**, 791 (1984).
4. F. BRISSE, B. RÉMILLARD, and H. CHANZY. Macromolecules, **17**, 1980 (1984).
5. A. PALMER and F. BRISSE. Acta Crystallogr. Sect. B, **36**, 1447 (1980).
6. S. HARKEMA, R. J. GAYMANS, and G. J. VAN HUMMEL. Acta Crystallogr. Sect. B, **36**, 3182 (1980).
7. C. PINEAULT and F. BRISSE. Acta Crystallogr. Sect. C, **39**, 1437 (1983).
8. J. BRISSON and F. BRISSE. Acta Crystallogr. Sect. B, **38**, 2662 (1982).
9. J. BRISSON and F. BRISSE. Macromolecules, **19**, 2632 (1986).
10. J. BRISSON and F. BRISSE. Can. J. Chem. **63**, 3390 (1985).
11. D. T. CROMER and J. B. MANN. Acta Crystallogr. Sect. A, **24**, 321 (1968).
12. R. F. STEWART, E. R. DAVIDSON, and W. T. SIMPSON. J. Chem. Phys. **42**, 3175 (1965).
13. F. R. AHMED, S. R. HALL, M. E. PIPPY, and C. P. HUBER. J. Appl. Crystallogr. **6**, 309 (1973). Accession Nos. 133–147.
14. P. MAIN, S. J. FISKE, S. E. HALL, L. LESSINGER, G. GERMAIN, J. DECLERCQ, and M. M. WOOLFSON. MULTAN80. A system of computer programs for the automatic solution of crystal structures from X-ray diffraction data. Universities of York, England, and Louvain, Belgium. 1980.
15. G. M. SHELDRICK. SHELX. Program for crystal structure determination. University of Cambridge, England. 1976.
16. R. J. DOEDENS and J. A. IBERS. Inorg. Chem. **6**, 204 (1967).
17. C. K. JOHNSON. ORTEP. Report ORNL-3794. Oak Ridge National Laboratory, TN. 1965.
18. M.-F. GRENIER-LOUSTALOT and G. BOCELLI. Eur. Pol. J. **20**, 957 (1984).
19. G. C. LEVY. Topics in ^{13}C nmr spectroscopy. Vol. VI. John Wiley, New York. 1974. pp. 54–69.
20. L. W. JELINSKY. CHEMTECH, **16**, 186 (1986).
21. I. ANDO, T. SORITA, T. YAMANOHE, T. KOMOTO, H. SATO, K. DEGUSHI, and M. IMANARI. Makromol. Chem. Rapid Commun. **6**, 349 (1985).
22. R. J. ABRAHAM and P. LOFTUS. Proton and ^{13}C nmr spectroscopy. Heyden, London. 1980. p. 20.

Can. J. Chem. Downloaded from www.nrcresearchpress.com by 41.223.56.140 on 09/07/12
For personal use only.

Effect of precipitation inhibitors on calcium phosphate scale formation

ZAHID AMJAD

The BFGoodrich Company, Specialty Polymers and Chemicals Division, Avon Lake Technical Center, Avon Lake, OH 44012, U.S.A.

Received July 12, 1988

ZAHID AMJAD. Can. J. Chem. **67**, 850 (1989).

The highly reproducible pH-stat technique was used to study the influence of various types of inhibitors on the precipitation of calcium phosphate from solution. Three types of inhibitors were evaluated: (*1*) homo- and copolymers of acrylic acid, (*2*) polyphosphate and phosphonates, and (*3*) polycarboxylic acids. Experimental variables studied included pH, temperature, and inhibitor dosage all of which were found to greatly affect the precipitation of calcium phosphate. The role of polyacrylic acid molecular weight is addressed. Comparative data for the various types of inhibitors is discussed.

Key words: precipitation inhibitors, calcium phosphate scale formation.

ZAHID AMJAD. Can. J. Chem. **67**, 850 (1989).

On a utilisé la très reproductible technique du "pH-stat" pour étudier l'influence de divers types d'inhibiteurs sur la précipitation du phosphate de calcium à partir de solutions. On a évalué trois types d'inhibiteurs: (*1*) des homo- et des co-polymères de l'acide acrylique, (*2*) du polyphosphate et des phosphonates et (*3*) des acides polycarboxyliques. On a étudié l'influence des variables expérimentales suivantes: le pH, la température et la concentration des inhibiteurs; on a trouvé que tous ces facteurs avaient une grande influence sur la précipitation du phosphate de calcium. On a aussi examiné le rôle du poids moléculaire de l'acide polyacrylique. On discute de données comparatives concernant les divers types d'inhibiteurs.

Mots clés : inhibiteurs de précipitation, formation des écailles du phosphate de calcium.

[Traduit par la revue]

Can. J. Chem. Downloaded from www.nrcresearchpress.com by 41.223.56.140 on 09/07/12
For personal use only.

Introduction

Formation of mineral scales on equipment surfaces is a problem in many areas such as industrial water systems, secondary oil recovery utilizing water flooding techniques, desalination, and clothing washing machines. Precipitation of mineral salts such as calcium carbonate results in incrustation on clothes washed with hard water. Among the problems caused by scale deposits are obstruction of fluid flow, impedence of heat transfer, wear of metal parts, localized corrosion attack, and unscheduled equipment shutdown. The scales consist primarily of carbonates, sulfates, hydroxides, phosphates, and silicates of alkaline earth metals, particularly calcium and magnesium. The problem of scale formation is intensified at higher temperatures because of the peculiar inverse temperature – solubility characteristics of these minerals in water.

In addition to scaling problems, cooling water systems and boilers constructed of carbon steel also experience corrosion problems caused by the presence of dissolved oxygen. In the past, this corrosion problem was combated using chromate compounds. More recently, polyphosphate/orthophosphate compounds have been replacing chromates because of the toxicity problems associated with chromates. However, the use of phosphate compounds adds to scale formation of highly insoluble calcium phosphate.

Recently, the problem of calcium orthophosphate scaling in industrial water system has become increasingly important (1–3). Higher orthophosphate levels are being encountered in cooling waters due to increased water reuse, use of low quality make-up water such as waste water treatment plant effluent and the use of organic phosphonate scale and corrosion inhibitors which are degraded to orthophosphate. The increased orthophosphate levels, combined with alkaline operating conditions can lead to the formation of highly insoluble calcium phosphate scale deposits which are normally attributed to hydroxyapatite ($Ca_5(PO_4)OH$,HAP). In cooling water systems, however, it is not the HAP which is initially formed, but instead a precursor phase is obtained which is widely known as amorphous calcium phosphate.

The influence of trace amounts of polyphosphates and phosphonates on the precipitation of calcium phosphate has been the subject of numerous investigations. Results of previous studies have shown that hydroxyethane 1,1-diphosphonic acid, HEDP, is an effective inhibitor when added to barium sulfate (4), calcium fluoride (5), calcium carbonate (6), and calcium oxalate (7). However, with more soluble calcium sulfate dihydrate, this inhibitor appeared to have only a slight effect on the growth kinetics (8). Varsanik (9) reported that among various phosphonates studied in laboratory and pilot plant experiments, HEDP was the most effective inhibitor for limiting calcium phosphate scale formation. However, system pH had a dramatic effect upon inhibitor effectiveness. At neutral pH values, the performance of aminotri(methylene phosphonic acid), AMP, was comparable to that of HEDP.

The effect of trace amounts of polymeric scale inhibitors on both the rate of precipitation and crystal modification of scale forming minerals has been the subject of numerous investigations (10–12). McCartney and Alexander (10) showed that polymers containing carboxyl groups such as carboxymethyl cellulose, aliginic acid, polymethacrylic acid, and polyacrylic acid (PAA) were particularly effective as $CaSO_4 \cdot 2H_2O$ crystal growth inhibitors. Electrophoretic studies (11) suggest that the inhibitory effect of polyelectrolytes such as PAA (11), is due to the adsorption of the molecules on the surfaces of calcium sulfate crystals. Amjad (12), in a recent study on the influence of polyacrylic acids (PAAs) in controlling $CaSO_4 \cdot 2H_2O$ scale formation on heat transfer surfaces, reported that the molecular weight (mol wt) plays an important role on the inhibitory effect of PAAs on $CaSO_4 \cdot 2H_2O$ (gypsum) crystal growth from aqueous solution.

The work discussed in this paper focuses on the precipitation of calcium phosphate in the presence of PAAs of varying molecular weights over a range of temperature, pH, and polymer concentration using a pH-stat technique. The influence of functional groups originating from the monomers, other than carboxylic acid attached to the polymer backbone, on the inhibiting activity of the polymers has also been investigated.

TABLE 1. Inhibitors tested

Description	Acronym
Polymers	
Acrylic Acid (AA) homopolymers	PAA
AA/methacrylic acid (MAA) copolymer	AA/MAA
AA/carbitol acrylate (E)	AA/E
Polyphosphate and phosphonates	
Sodium pyrophosphate	PP
Aminotri (methylene phosphonic acid)	AMP
Hydroxyethane 1,1-diphosphonic acid	HEDP
Polycarboxylic acids	
Benzene hexacarboxylic acid or mellitic acid	MA
1,3,5-Benzene tricarboxylic acid (trimesic acid)	TMA
Citric acid	CA

For quantitative comparison, precipitation studies were also performed in the presence of polyphosphates, phosphonates, and polycarboxylic acids (e.g., citric acid, benzene hexacarboxylic acids, etc.). Table 1 identifies the inhibitors used in this study. As shown, the inhibitors vary appreciably in terms of both the functional group and the molecular weight. The purpose of this study was to quantify the effectiveness of these inhibitors and provide an explanation for the mechanism of inhibition of calcium phosphate precipitation in aqueous systems.

Experimental

Grade A glassware and reagent grade chemicals were used. Stock solutions of calcium chloride and disodium hydrogen phosphate were prepared using distilled water, filtered through 0.22 micron filter paper (Millipore Corp.) and analyzed for calcium and phosphate as described previously (9). Sodium pyrophosphate (PP) and citric acid (CA) were prepared from reagent grade chemicals. The AMP and HEDP used in this study were provided by The Monsanto Company. The polymeric inhibitors used were selected from commercial and experimental materials supplied by The BFGoodrich Company, Specialty Polymers and Chemicals Division. Polymer solutions were prepared on a dry weight basis. The desired concentrations were obtained by dilution.

Subsaturated calcium phosphate solutions were prepared in a double-walled glass cell maintained at constant temperature by adding stock solutions of calcium chloride and disodium hydrogen phosphate to the distilled water to attain initial calcium and orthophosphate concentrations of 140 and 9.0 parts per million (ppm), respectively. Spontaneous precipitation was induced by raising the pH of this acidic solution with 0.10 *M* NaOH. The pH of the solution was maintained at a constant value (±0.01) using a Metrohm pH stat (pH meter Model 632, dosimat Model 655, impulsomat Model 616, Brinkmann Instruments, Westbury, NY). Hydrogen ion measurements were made with a combination electrode equilibrated at the required temperature. The electrode was calibrated before and checked after each experiment using NBS standard buffer solutions. The solutions were continuously stirred with a Teflon-coated stirring bar at ~400 revolutions per minute. Experiments involving inhibitors were performed by adding the inhibitor to the subsaturated calcium phosphate solution before inducing spontaneous precipitation. Precipitation of calcium phosphate in this supersaturated solution was monitored by analyzing aliquots of the filtered (0.22 micron filter paper) solution for phosphate by spectrophotometric method (9).

Percent inhibition attained was then calculated using the following equation:

$$[1] \quad \% \text{ Inhibition} = \frac{(PO_4)_{exp} - (PO_4)_{final}}{(PO_4)_{initial} - (PO_4)_{final}} \times 100$$

where

$(PO_4)_{exp}$ = concentration of phosphate in the filtrate in presence of the inhibitor at known time

$(PO_4)_{final}$ = concentration of phosphate in filtrate in absence of the inhibitor at 20 h

$(PO_4)_{initial}$ = concentration of phosphate ion at the beginning of the experiment

Results and discussion

The initial conditions used and the results of typical precipitation experiments made in the presence of inhibitors are summarized in Table 2. The experiments reported here had good reproducibility (±6% or better). Initiation of precipitation by foreign particles, which are always present, does not seem likely, since the experiments were reproducible. Furthermore, the experiments were repeated after having filtered the solutions prior to mixing through 0.1 micron membrane filters without any change in the observed results. However, the possibility of heterogeneous nucleation on the walls of the glass vessels used cannot be precluded, although experiments were conducted in two different experimental set-ups.

Effect of concentration of polyacrylic acid

Results of precipitation experiments made in the presence of varying concentrations (5–50 ppm) of polyacrylic acid (PAA-1, mol wt 2 100), are summarized in Table 2 and shown in Fig. 1. It can be seen (Fig. 1) that the precipitation reaction in the presence of 15 ppm of PAA-1 is reduced by ~50% compared to that in the absence of PAA-1. Figure 1 further indicates that an increase in polymer concentration results in an increase in inhibition value and at 50 ppm of polymer concentration, the precipitation of calcium phosphate was completely inhibited (>95% inhibition) for at least 20 h.

Effect of polyacrylic acid molecular weight

Recently the influence of PAAs as antiscalants for controlling scale formation in industrial water systems has attracted the attention of several investigators. It has been shown that one of the factors determining the effectiveness of PAA is its mol wt (12–14). Based upon the results for similar mol wt polyelectrolytes, Smith and Alexander (15) reported that PAA was more effective than polymethacrylic acid in inhibiting the precipitation of calcium sulfate from supersaturated solutions. Furthermore, growth inhibition results for series of experiments with styrene/maleic anhydride copolymers suggest an optimum effectiveness at a mol wt of 1 600.

Precipitation experiments made in the presence of PAAs of varying mol wt (2 100 – 60 000) are summarized in Table 2. Figure 2 shows precipitation curves in the presence of 10 ppm of various PAAs. The curves in Fig. 2 show that at constant temperature and polymer concentration, the phosphate inhibition value increases with decreasing mol wt, reaches a maximum at a mol wt about 2 100, and thereafter decreases with decreasing mol wt (2 100 to 800). It is interesting to note that Amjad and Masler (14) in their study on the evaluation of PAAs (mol wt 800 – 12 000) as $CaSO_4 \cdot 2H_2O$ crystal growth inhibitors showed optimum performance with an ~2 000 mol wt PAA. Similarily, Amjad (12) in a recent study on the influence of PAA in controlling gypsum ($CaSO_4 \cdot 2H_2O$) scale formation on heat transfer surfaces, reported that the molecular weight of PAA plays an important role in the inhibition of $CaSO_4 \cdot 2H_2O$ crystal growth from aqueous solution. The amount of gypsum scale formed on heat exchanger surface was found to be higher

Can. J. Chem. Downloaded from www.nrcresearchpress.com by 41.223.56.140 on 09/07/12
For personal use only.

TABLE 2. Phosphate inhibition data in the presence of inhibitors*

Expt. No.	Inhibitor	Concentration (ppm)	Temperature (°C)	Residual phosphate concentration (ppm) at 1 h	5 h	20 h	% Inhibition at 20 h
2	none	0	50	0.16	0.06	0.05	0
3	none	0	50	0.18	0.07	0.05	0
5	PAA-1	5	50	1.92	1.32	1.02	11
4	PAA-1	10	50	2.48	1.86	1.62	18
6	PAA-1	15	50	6.82	5.52	4.45	49
7	PAA-1	15	50	6.75	5.45	4.67	52
8	PAA-1	20	50	8.22	7.45	7.29	81
10	PAA-1	50	50	8.86	8.72	8.65	96
9	PAA-2	10	50	1.67	1.52	1.06	11
12	PAA-2	15	50	1.98	1.66	1.26	14
11	PAA-2	20	50	3.91	2.76	1.94	21
14	PAA-3	10	50	2.84	1.72	0.72	8
15	PAA-3	20	50	4.55	3.91	2.43	27
16	PAA-4	10	50	1.91	1.63	0.49	5
17	PAA-5	10	50	1.02	0.50	0.09	1
19	PAA-6	10	50	0.75	0.34	0.06	0
22	AA/E	10	50	8.22	7.93	7.49	83
29	AA/MAA	10	50	2.63	1.75	1.35	15
30	none	0	40	2.43	0.34	0.04	0
31	PAA-1	10	40	5.98	5.45	4.38	48
32	PAA-2	5	40	1.81	1.64	1.38	15
33	PAA-2	10	40	5.98	4.47	2.67	29
36	PAA-2	15	40	5.72	5.16	4.72	52
35	PAA-3	10	40	6.15	4.73	3.06	34
34	PAA-4	10	40	2.02	1.75	1.39	16
37	PAA-5	10	40	2.02	1.75	0.72	8
38	none	0	30	5.15	3.64	0.22	0
39	PAA-1	5	30	6.78	5.92	4.63	50
40	PAA-1	10	30	7.89	7.55	6.75	74
42	PAA-2	10	30	7.85	7.17	4.91	54
41	PAA-2	15	30	9.26	9.21	8.83	98
44	PAA-3	10	30	6.22	5.45	5.15	56
43	PAA-4	10	30	3.88	3.73	2.88	32
45	PAA-5	10	30	2.06	1.80	0.75	9

*See Table 1 for inhibitor acronyms. Note: the number following PAA- refers to the PAA's mol wt as follows: 1 = 2 100; 2 = 5 100; 3 = 800; 4 = 10 000; 5 = 26 000; 6 = 60 000. Experimental conditions: calcium = 140 ppm, phosphate = 9.0 ppm, pH = 8.50.

in the case of a high (240 000) mol wt PAA than that obtained on the presence of 2 100 mol wt PAA.

The phenomenon of a markedly decreasing PAA effectiveness with increasing mol wt as observed in the present study may be due to several factors including different rates and degrees of adsorption/desorption of PAA molecules on the precipitating calcium phosphate particles. Other factors such as coiling/uncoiling of the polymer molecule and the type of end groups in the polymer could also influence the adsorption processes. Adsorption studies are currently underway in our laboratories to better understand the role of PAA mol wt in inhibiting the precipitation of sparingly soluble salts from aqueous solutions.

Effect of polymer composition

The effect of polymer composition at a constant concentration of 10 ppm was studied using the pH-stat technique. The results are summarized in Table 2 and illustrated in Fig. 3. As shown in Fig. 3, the copolymer of acrylic acid/methacrylic acid (AA:MAA) shows better performance than PAA-4. For example, % inhibition values obtained for AA:MAA and PAA-4 are 5 and 15, respectively (expts. 29, 16). The slight performance increase observed for AA:MAA over PAA-4 may be attributed to the presence of additional methyl groups attached to carbon atoms between carboxylate carrying carbon atoms.

The next polymer in order of increasing inhibitor effectiveness is a copolymer of acrylic acid and an acrylate ester (carbitol acrylate) or AA/E. Compared with PAA, the acrylic acid segments for AA/E are partially substituted by a carbitol acrylate group. The carboxylic acid group concentration and thus the anionic charge density are significantly lower than PAA-4. The effectiveness of AA/E as calcium phosphate inhibitor (Table 2, expt. 22) is surprisingly better than PAA-4, suggesting that the carbitol acrylate group is more effective in improving the inhibitory activity of AA/E than the corresponding carboxyl group in PAA-4. Phosphate inhibition data (Table 2, expts. 16, 29, 22) indicate the following order of polymer effectiveness:

$$\text{AA/E} > > \text{AA/MAA} > \text{PAA}$$

Effect of temperature

The results on the effect of temperature on the inhibition of

Can. J. Chem. Downloaded from www.nrcresearchpress.com by 41.223.56.140 on 09/07/12
For personal use only.

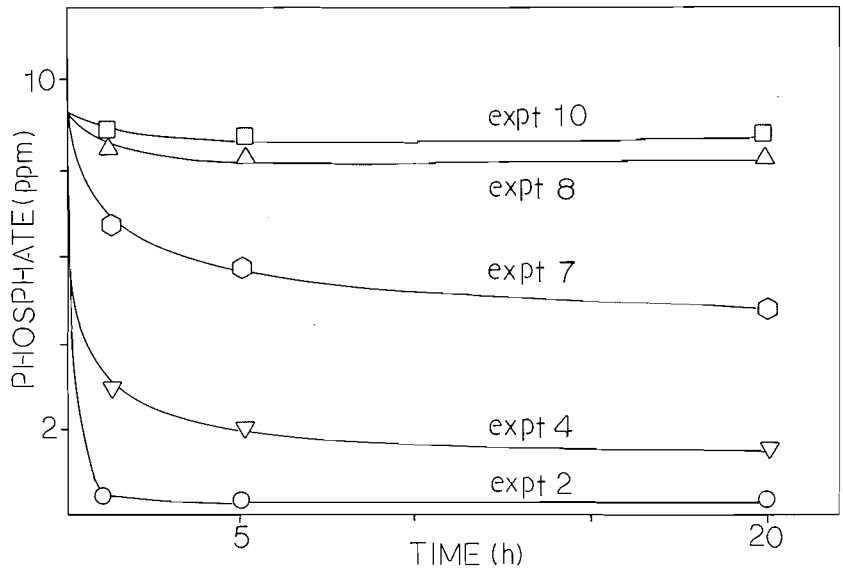


FIG. 1. Plots of phosphate concentration as a function of time at 50°C in the presence of PAA-1 of varying concentrations (ppm): (○) 0; (▽) 10; (⬡) 15; (△) 20; (□) 50.

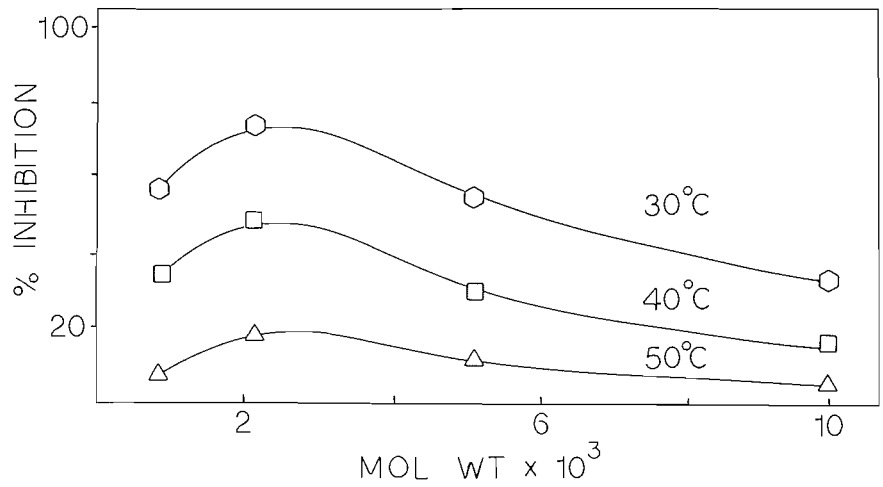


FIG. 2. Relationships of % inhibition with polyacrylic acid molecular weight for calcium phosphate inhibition at temperatures from 30–50°C.

calcium phosphate precipitation in the presence of PAAs are shown in Table 2. It can be seen (Table 2) that as the temperature is raised, there is a concomitant marked decrease in the phosphate inhibition. At a given calcium phosphate and PAA concentration, the relationship between the temperature and the phosphate inhibition can roughly be expressed quantitatively by an empirical equation:

$$[2] \quad \% \text{ Inhibition} = a(1/T) + b$$

where T is the absolute temperature; a and b are constants. The linear plots of % inhibition against $1/T$ for PAA-1 and PAA-2 are illustrated in Fig. 4.

Effect of solution pH

The influence of pH on the performance of several phosphonic acids as $CaSO_4 \cdot 2H_2O$ crystal growth inhibitors has been studied by seeded growth technique (16). Results of this study show that an increase in the pH of the crystal growth medium over a pH 4 to 9 range brings about an improvement in inhibitor performance that runs parallel to the phosphonic acid titration curve.

For polymeric inhibitors, such as polyacrylic acid and acrylic acid based copolymers, the degree of protonation should, just as phosphonate inhibitors, be considered in explaining their action. Unfortunately, their acid dissociation constants are not available. It can nevertheless be expected that the affinity of polymeric molecules towards the crystal surface should also be influenced by the solution pH due to the dissociation of carboxylic acid group.

The effect of the solution pH on the precipitation of calcium phosphate in the presence of 10 ppm of PAA-1 and AA/C polymers was studied using the spontaneous precipitation technique. Results are summarized in Table 3. Figure 5 compares phosphate inhibition values for PAA-1 and AA/E at pH 7.5, 8.0, and 9.0. As shown in Fig. 5, at pH 7.5, both polymers (Table 3, expts. 53, 55) exhibit excellent performance (>90% inhibition). However, at pH 8.5, AA/E shows 85% inhibition vs. 30% obtained for PAA-1 (Table 3, expts. 60, 61). Data presented in Table 3 also shows that increasing the solution pH to 9.0 does not significantly affect the performance of AA/E whereas a marked performance decrease occurs for PAA-1 (Table 3, expts. 62, 66).

Can. J. Chem. Downloaded from www.nrcresearchpress.com by 41.223.56.140 on 09/07/12
For personal use only.

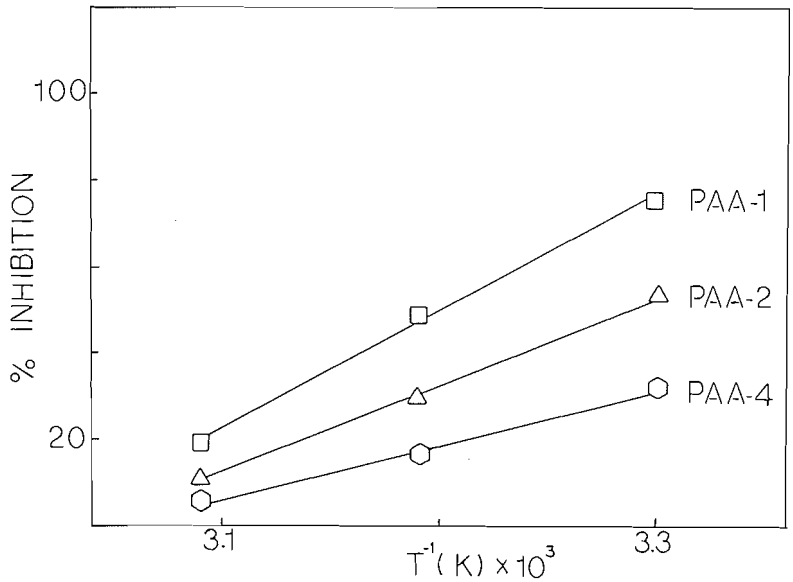


FIG. 3. Plots of % inhibition as a function of 1/T for PAA-1, PAA-2, and PAA-4.

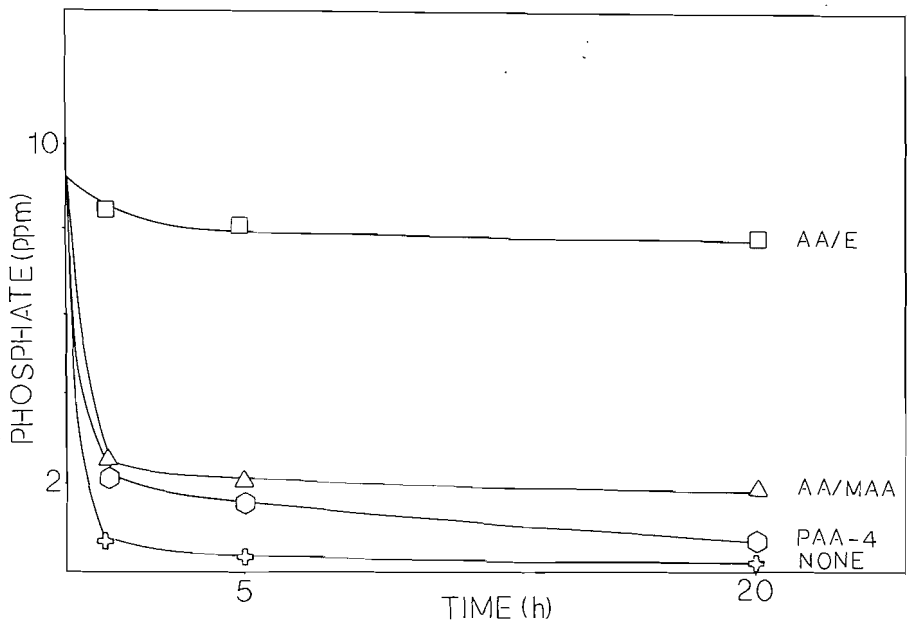


FIG. 4. Plots of phosphate concentration as a function of time at 50°C in the presence of 10 ppm of PAA-4, AA/MAA, and AA/E.

It is interesting to note that in the seeded growth study of $CaSO_4 \cdot 2H_2O$ in the presence of PAA, the inhibitory effect of PAA was found to increase with increasing solution pH (17). This is inconsistent with the results obtained in the present study. The observed difference in PAA performance for two different sparingly soluble salts as a function of solution pH may be explained in terms of differences in solubility values of calcium phosphate and calcium sulfate salts (i.e. an increase in solution pH results in an increased supersaturation in the case of calcium phosphate, whereas pH does not significantly affect the calcium sulfate supersaturation).

Effect of polyphosphate, phosphonate, benzene polycarboxylic acid, and citric acid

The inhibiting properties of condensed phosphates of both the meta- and polyphosphate types have been extensively studied in relation to scale formation and biological calcification processes. In the former case it has been shown that sodium pyrophosphate is an effective growth inhibitor when added to $CaCO_3$ (6) and $BaSO_4$ (18) systems. In biological calcification processes, pyrophosphate ion has been found to be an effective crystal growth inhibitor for calcium phosphate (19) and calcium oxalate (7) systems. A surface adsorption mechanism has been found useful in describing the effect of pyrophosphate in many of these systems.

Precipitation experiments made in the presence of pyrophosphate (PP) are summarized in Table 4. It can be seen (Table 4, expt. 47) that at 10 ppm, PP exhibits a smaller inhibiting effect compared to PAA-1 (Table 2, expt. 40). For example, % phosphate inhibition values obtained for PP and PAA-1 are 28 and 74, respectively. It is interesting to note that PP, which exhibits strong inhibitory effect for calcium oxalate (7), barium

Can. J. Chem. Downloaded from www.nrcresearchpress.com by 41.223.56.140 on 09/07/12
For personal use only.

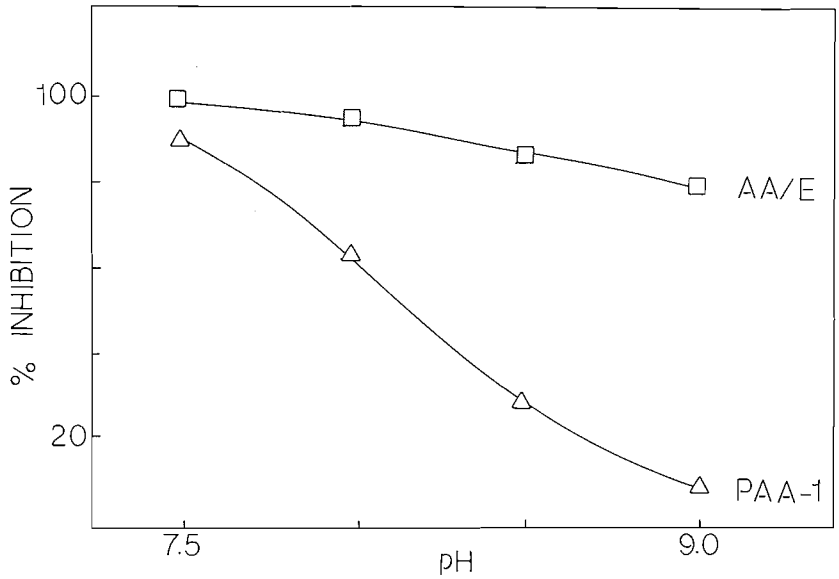


FIG. 5. The effect of solution pH on the inhibition of calcium phosphate at 50°C in the presence of 10 ppm of PAA-1 and AA/E polymers.

TABLE 3. Phosphate inhibition data in the presence of inhibitors: effect of solution p*H**

Expt.	Inhibitor	pH	% Phosphate inhibition at 20 hr
53	PAA-1	7.5	91
55	AA/E	7.5	99
56	PAA-1	8.0	62
58	AA/E	8.0	96
60	PAA-1	8.5	30
61	AA/E	8.5	85
62	PAA-1	9.0	10
66	AA/E	9.0	80

*Experimental conditions: calcium = 140 ppm, phosphate = 9.0 ppm, inhibitor = 10 ppm, 50°C.

TABLE 4. Phosphate inhibition data in the presence of inhibitors*

Expt. No.	Inhibitor	Residual phosphate concentration (ppm) at 1 h	5 h	20 h	% Inhibition at 20 h
47	PP	3.41	2.99	2.58	28
49	HEDP	4.02	3.75	3.16	33
48	AMP	5.17	4.29	3.65	40
52	MA	4.66	4.31	3.85	41
51	TMA	2.02	1.60	0.45	5
50	CA	4.72	2.09	0.27	1

*See Table 1 for acronyms. Experimental conditions: calcium = 140 ppm, phosphate = 9.0 ppm, pH = 8.50, 30°C, inhibitor = 10 ppm.

sulfate (18), and calcium carbonate (6) systems, only has moderate inhibitory effect on calcium phosphate precipitation.

Organophosphonates such as HEDP have been found to markedly inhibit the crystallization of calcium carbonate (6), calcium oxalate (20) and barium sulfate (18). Inhibition data summarized in Table 4 show that AMP is a better inhibitor than HEDP. For example, % inhibition values obtained at 10 ppm inhibitor concentration, 30°C, and at 20 h for AMP and HEDP are 40 and 33, respectively. It is noteworthy that for HAP crystal growth in the presence of polyphosphates and phosphonates (19), the relative order of effectiveness reported was:

$$\text{HEDP} > \text{AMP} > \text{PP}$$

The above order of inhibitor effectiveness is inconsistent with the results obtained in the present study (expts. 47, 48, 49). It should be noted that for dicalcium phosphate dihydrate, (DCPD), seeded growth on DCPD seed crystals (21) in the presence of PP and phosphonates, the order of effectiveness suggested was:

$$\text{AMP} > \text{HEDP} > \text{PP}$$

The differences observed in the order of phosphonates effectiveness for HAP, DCPD, and this investigation, may be due to several factors including different rates of adsorption/desorption of inhibitors on different types of substrates.

Results summarized in Table 4 for the inhibitory effect of benzene hexacarboxylic acid (mellitic acid, MA) show that compared to PAA, MA is a moderately effective calcium phosphate inhibitor. However, under similar experimental conditions, MA exhibits a much greater effectiveness compared to citric acid (CA) but is significantly less effective than PAA-1. For example, % inhibition values obtained at 30°C for 10 ppm concentration of PAA-1, MA, trimesic acid, and CA are 74, 41, 5, and 1, respectively. These results are consistent with those reported by Coffey (22) which indicate that the best inhibitors for barium sulfate precipitation were those that imparted the most negative electrophoretic mobility to the barium sulfate particles. Similar observations have been reported in recent seeded growth studies on the effect of polycarboxylic acid on the crystal growth of calcium carbonate (23), dicalcium dihydrogen phosphate (24), and hydroxyapatite (25) from aqueous solutions.

Mechanism of inhibitor action

The results discussed above show that trace quantities of certain inhibitors markedly reduce the precipitation of calcium phosphate. The influence of these inhibitors on precipitation reaction may be explained in terms of three effects, (*a*) direct

Can. J. Chem. Downloaded from www.nrcresearchpress.com by 41.223.56.140 on 09/07/12
For personal use only.

complexation of inhibitor with crystal lattice ions in solution; (*b*) adsorption of inhibitor on the crystal surface either generally or at the active growth sites; (*c*) inhibitor may change the ionic strength of the solution and hence the effective solubility of the calcium phosphate.

Under the experimental conditions employed in the present investigation, the marked reduction in calcium phosphate precipitation must be attributed to surface adsorption factor rather than the calcium–inhibitor complex formation or the concomitant increase in ionic strength of the supersaturated solution in the presence of inhibitors.

If the action of the inhibitor, which stabilizes supersaturated solutions of calcium phosphate, is to be adsorbed on the crystal embryos and prevent their growth, the question arises why the nuclei do not go on forming until all the stabilizing material (i.e. inhibitor) has been used up, since the formation of nuclei involves a negligible change in the concentration of the solution. There are two possible reasons for this. Nucleation may take place only on a limited number of "stray nuclei", or it may be that the inhibitors stop development of the nuclei below the critical size and they redisperse, forcing the inhibitor to interact with other embryos. An adsorption mechanism is also indicated in many systems by an appreciable habit modification of crystals grown in the presence of impurities (12).

Summary

In the present work it has been shown that low levels of both polymeric and non-polymeric type inhibitors can significantly inhibit the precipitation of calcium phosphate from aqueous solution. The results on the performance of PAAs of varying molecular weight (800 to 60 000) suggest that optimum effectiveness for PAAs occurs at a mol wt ~2 000. The results of the present study also suggest that the inhibition of calcium phosphate precipitation strongly depends upon the concentration of polymer, solution pH, and polymer composition. In addition, it has also been shown that the presence of pyrophosphate, phosphonates, and mellitic acid at low concentrations can significantly inhibit calcium phosphate precipitation. A mechanism based upon surface adsorption has been proposed to explain the influence of inhibitors on calcium phosphate precipitation.

Acknowledgements

The author expresses his thanks to Mr. J. Hooley and Mr. R. Whalen for technical assistance; Dr. W. F. Masler for polymer synthesis, Mr. R. W. Zuhl for valuable comments, and The BFGoodrich Company, Specialty Polymers & Chemicals Division, for permission to publish this work.

1. G. H. NANCOLLAS. Corrosion/82 Paper No. 20. National Association of Corrosion Engineers, Houston, TX. 1982.
2. W. J. BEER and J. F. ERTEL. Corrosion/85, Paper No. 125. National Association of Corrosion Engineers, Houston, TX. 1986.
3. R. ZUHL, Z. AMJAD, and W. F. MASLER. J. Cooling Tower Institute, **8**, 41 (1987).
4. S. T. LIU and G. H. NANCOLLAS. J. Colloid Interface Sci. **52**, 582 (1975).
5. L. SHYU. Ph.D. Thesis, State University of New York at Buffalo, New York. 1982.
6. M. M. REDDY and G. H. NANCOLLAS. Desalination, **12**, 61 (1973).
7. E. N. RIZKALLA and M. M. MOAWAD. J. Chem. Soc. Faraday Trans. **80**, 1617 (1984).
8. S. T. LIU and G. H. NANCOLLAS. J. Colloid Interface Sci. **44**, 422 (1973).
9. R. G. VARSANIK. Mater. Perform. **14**, 16 (1975).
10. E. R. MCCARTNEY and A. E. ALEXANDER. J. Colloid Sci. **13**, 383 (1958).
11. C. H. NESTLER. J. Colloid Interface Sci. **26**, 10 (1968).
12. Z. AMJAD. J. Colloid Interface Sci. **123**, 523 (1988).
13. P. FLESHER, E. L. STREETFIELD, A. S. PEARCE, and O. D. HYDES. 3rd Int. Symp. Fresh Water Sea **1**, 493 (1970).
14. Z. AMJAD and W. F. MASLER. Corrosion/85, Paper No. 357, National Association of Corrosion Engineers, Houston, TX. 1985.
15. B. R. SMITH and A. E. ALEXANDER. J. Colloid Interface Sci. **34**, 81 (1970).
16. D. W. GRIFFITHS, S. D. ROBERTS, and S. T. LIU. Int. Symp. Oilfield Geothermal Chem. Society of Petroleum Engineers. 1979. Paper 7861.
17. Z. AMJAD. Corrosion/88, Paper No. 421. National Association of Corrosion Engineers, Houston, Tx. 1988.
18. E. N. RIZKALA. J. Chem. Soc. Faraday Trans. **79**, 1857 (1983).
19. Z. AMJAD. Langmuir, **3**, 1063 (1987).
20. G. L. GARDNER. J. Phys. Chem. **82**, 864 (1978).
21. Z. AMJAD. Can. J. Chem. **66**, 2181 (1988).
22. M. D. COFFEY. Paper No. SPE 5302, Inter. Symp. Oilfield, Soc. Pet. Eng. Dallas, 1975.
23. Z. AMJAD. Langmuir, **3**, 224 (1987).
24. Z. AMJAD. J. Colloid Interface Sci. **117**, 98 (1987).
25. Z. AMJAD. *In* Adsorption on and surface chemistry of hydroxyapatite. *Edited by* D. N. Misra. Plenum Press, New York. 1984.

Can. J. Chem. Downloaded from www.nrcresearchpress.com by 41.223.56.140 on 09/07/12
For personal use only.

Hydrogen isotope exchange between D_2 and H_2O catalyzed by platinum plate

SHIN-ICHI MIYAMOTO, TETSUO SAKKA, AND MATAE IWASAKI
Institute of Atomic Energy, Kyoto University, Uji, Kyoto 611, Japan

Received May 26, 1988

SHIN-ICHI MIYAMOTO, TETSUO SAKKA, and MATAE IWASAKI. Can. J. Chem. **67**, 857 (1989).

The reaction rate of hydrogen isotope exchange between D_2 and H_2O catalyzed by platinum plate is studied. The exchange reaction is described with the kinetic model which is the modification of that for the exchange reaction catalyzed by alumina-supported platinum catalyst. For the comparison of experimental results with this model relative amount of the number of sites for hydrogen adsorption was estimated from the initial rate of hydrogen isotope exchange between H_2 and D_2 on the same surface. The results show that the kinetic model is applicable for the plate catalyst if the number of the sites for hydrogen absorption, which is very sensitive to the surface state of the catalyst, was estimated not from the macroscopic surface area but from our scheme.

Key words: hydrogen isotope exchange reaction, platinum plate as catalyst.

SHIN-ICHI MIYAMOTO, TETSUO SAKKA et MATAE IWASAKI. Can. J. Chem. **67**, 857 (1989).

On a étudié la vitesse de la réaction d'échange isotopique entre le D_2 et le H_2O, catalysée par une plaque de platine. On peut décrire la réaction d'échange grâce à un modèle cinétique qui est une modification de celui proposé pour la réaction d'échange catalysée par un catalyseur de platine supporté par de l'alumine. Pour faire une comparaison des données expérimentales avec ce modèle, on a évalué la quantité relative de sites pour l'adsorption d'hydrogène à partir de la vitesse initiale de l'échange des isotopes de l'hydrogène (H_2 et D_2) sur la même surface. Les résultats démontrent que le modèle cinétique peut être appliquer au catalyseur en plaque si on évalue le nombre de sites pour l'adsorption de l'hydrogène en se basant sur notre schéma et non pas sur la superficie de la surface macroscopique.

Mots clés : réaction d'échange des isotopes de l'hydrogène, plaque de platine comme catalyseur.

[Traduit par la revue]

I. Introduction

Catalytic behavior of platinum for hydrogen isotope exchange reaction between hydrogen and water in gas phase has been investigated by several researchers (1–7) and some related studies have been reported (8, 9). Most of the researches, however, are confined to the investigations on the supported catalyst or the powder catalyst, which are often used in practical processes. In those systems catalytic behaviors of platinum itself become ambiguous, because the effect of support and the effect of particle sizes and shapes are not negligible (1, 2). The catalytic activity of the platinum surface itself remains unclear in these investigations.

The aim of the present study is to determine the catalytic activity of the surface of a platinum plate for the hydrogen isotope exchange between H_2O gas and D_2 gas and to clarify the reaction mechanism.

Previous works (10–12) revealed that the factors for surface activity, such as microscopic roughness and contamination by oxygen, influence the catalytic reaction on platinum. It is shown that the kinetic phenomena, such as sticking rate of hydrogen or H_2/D_2 exchange reaction rate, are enhanced by the microscopic surface roughness, such as steps or kinks, in the investigation of the surface of single crystal platinum (10).

Pretreatment conditions of catalyst play an important role in the catalytic activity (12). In our experiments the obtained data varied considerably among runs performed under the same experimental conditions. This result indicates that the surface activity of the platinum plate used differs from one run to another, and it is not easy to control the surface activity by the pretreatment made in this study. We then tried to evaluate the surface activity by relative intensity of the number of the sites for the hydrogen absorption, which was estimated by measuring the exchange rate between H_2 and D_2. The evaluation of the surface activity was done before each run for the exchange reaction between D_2 and H_2O. Using these evaluated values of surface activity, we could obtain reasonable kinetic relationships for the isotope exchange between D_2 and H_2O without it being affected by the initial surface state of the platinum plate used in each run.

In Section II, the experimental procedure and experimental results are described. In Section III the model for the hydrogen exchange reaction on the surface of the platinum plate is described. The method of the estimation of the surface state and the examination of the model are also described. In Section IV, the model was examined and some parameters are obtained. Furthermore, some comments on the experimental results and on the model are described, and a comparison between supported catalyst and platinum plate catalyst is made.

II. Experimental procedure and results

The rate of the hydrogen isotope exchange between H_2O and D_2 on a platinum plate at high temperature is determined by the analysis of D_2, HD, and H_2 in a sample container using a quadrapole mass spectrometer, Nichiden Anelva model AQA-100MPX.

The apparatus used is illustrated in Fig. 1. The whole manifold of the apparatus was made of Pyrex glass, and vacuum gauge heads were isolated from the sample gas by glass cocks. As a blank test, the occurrence of the exchange reaction in the whole apparatus was examined. This test shows that no reaction occurs without the platinum plate.

Polycrystalline platinum plate (99.99% in purity, 32.0 cm^2 macroscopic surface area, obtained from Fukuda Kinzoku Hakufun Ltd.) was used. Contamination of the surface of the plate was removed by boiling in concentrated nitric acid for 20 min. The plate was set in a reaction chamber made of silica glass tubing. The volume of the chamber was 310 cm^3.

The whole system was baked at 200°C for 7 h. The base pressure of the reaction chamber was 10^{-4} Pa. The base pressure of the quadrapole mass spectrometer became 3×10^{-6} Pa by differential evacuation.

D_2 gas, 99.5% in purity, containing H_2 as main impurity was

Printed in Canada / Imprimé au Canada

Can. J. Chem. Downloaded from www.nrcresearchpress.com by 41.223.56.140 on 09/07/12
For personal use only.

Can. J. Chem. Downloaded from www.nrcresearchpress.com by 41.223.56.140 on 09/07/12
For personal use only.

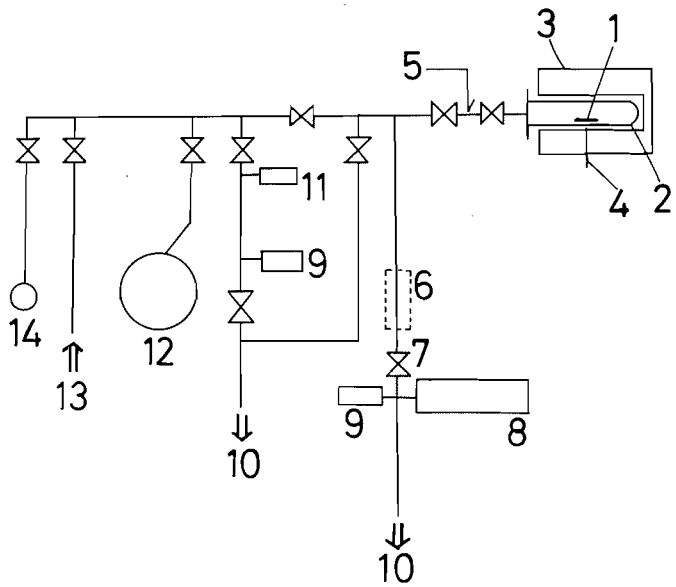


FIG. 1. Experimental setup for the measurement of the rate of hydrogen isotope exchange between D_2 and H_2O catalyzed by platinum plate. The numbers in the figure correspond to the following components: *1*, platinum plate; *2*, reaction chamber; *3*, electric furnace; *4*, chromel–alumel thermocouple; *5*, sampling room; *6*, liquid-N_2 trap; *7*, leak valve; *8*, mass spectrometer; *9*, ion gauge; *10*, diffusion pump; *11*, Pirani gauge; *12*, Macleod gauge; *13*, D_2; *14*, H_2O.

introduced to the apparatus to a given pressure. The pressure was measured with a Macleod pressure gauge. The evacuation of water sample vessel was made after freezing its water by liquid nitrogen. The pressure of the water vapor was measured with a Pirani gauge.

Finally, the gases in the apparatus other than that in the reaction chamber were evacuated. The reaction chamber was heated with an electric furnace, and its temperature was controlled with a temperature regulator with chromel–alumel thermocouple attached to the outside of the silica glass tube just below the inserted platinum plate. The heating of the reaction chamber was completed within 1 min and the time at which the temperature became the set temperature was taken as the starting time of the reaction.

During the reaction, sample gas was collected intermittently into a sampling room (Fig. 1). After water vapor was removed from sample gas with a cold trap at liquid nitrogen temperature, the residual sample gas was introduced through a variable leak valve into the quadrapole mass spectrometer, and the ratio of D_2 to whole hydrogen gas was determined. The removal of water vapor was necessary to avoid its attack on an ion source filament.

By repeating this procedure, time dependence of the isotopic ratio of the hydrogen gas was obtained. Figure 2 shows the time dependence of the fraction of D_2 during the exchange reaction. The initial concentrations of D_2 and H_2O were both 5.38×10^{-1} mol/m^3 (this corresponds to 10.0 Torr at room temperature) and the reaction temperature was 773 K. Blank tests for reaction chamber show that silica glass is a suitable material for the reaction chamber, because it has no catalytic activity, but alumina is found to be unsuitable.

The experiments were carried out specifically at the early stage of the reaction. An example is shown in Fig. 3. In this run the initial concentrations of D_2 and H_2O were both 5.38×10^{-2} mol/m^3 and the temperature was 443 K. From the series

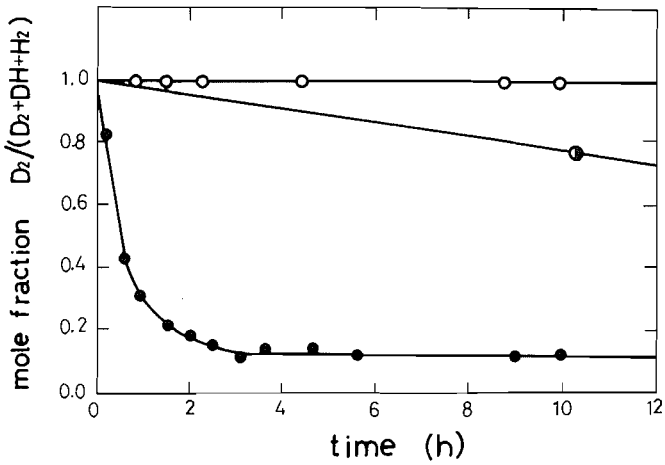


FIG. 2. Decrease in D_2 fraction by the exchange reaction between D_2 and H_2O in the alumina reaction chamber without platinum plate (half-filled circle), the silica reaction chamber without platinum plate (open circle), and the silica reaction chamber with platinum plate (filled circle) at 773 K. The initial concentrations of D_2 and H_2O were both 5.38×10^{-1} mol/m^3, which corresponds to a pressure of 10 Torr each.

of figures, of which an example is illustrated in Fig. 3, the initial rates of the exchange reaction were determined.

As will be mentioned in Section III, the number of the sites for hydrogen adsorption should be estimated before each run of the exchange reaction between D_2 and H_2O. The estimation was made through determining the initial rate of hydrogen isotope exchange between H_2 and D_2 before each run. The experimental procedure was similar to that of the reaction between D_2 and H_2O.

III. Kinetics of the exchange reaction

A. Kinetics of D_2/H_2O exchange reaction

The kinetic model for the reaction on the alumina-supported platinum catalyst proposed by Rolston and Goodale (1) is modified for the reaction on the platinum plate. The model contains five steps: the adsorption of a water molecule and the dissociative adsorption of a hydrogen molecule on the platinum surface, exchange reaction on the surface, the desorption of a water molecule and of a hydrogen molecule from the surface. It is assumed that the third step, i.e., the exchange reaction on the surface is rate controlling, and the other steps are in equilibrium. The early stage reaction process is as follows:

$$[1] \quad D_2(g) + 2S_1 \rightleftarrows 2D_{ads} \qquad K_1 = T_D^2/C_{D_2}[S_1]^2$$

$$[2] \quad H_2O(g) + S_2 \rightleftarrows H_2O_{ads} \qquad K_2 = T_{H_2O}/C_{H_2O}[S_2]$$

$$[3] \quad H_2O_{ads} + D_{ads} \xrightarrow{2k_3} HDO_{ads} + H_{ads}$$

$$[4] \quad D_{ads} + H_{ads} \rightleftarrows HD(g) + 2S_1 \qquad K_4 = C_{HD}[S_1]^2/T_D T_H$$

$$[5] \quad HDO_{ads} \rightleftarrows HDO(g) + S_2 \qquad K_5 = C_{HDO}[S_2]/T_{HDO}$$

where S_1 is the site for adsorption of dissociated hydrogen on the surface of platinum plate; S_2 is the site for physical adsorption of water; D_{ads} and H_{ads} are dissociatively adsorbed D and H, respectively; H_2O_{ads} is a physically adsorbed water molecule; K_1, K_2, K_3, and K_4 are equilibrium constants of reactions [1], [2], [3], and [4], respectively; $2k_3$ is a rate constant of the reaction [3]; C_{H_2O}, C_{HDO}, C_{D_2}, and C_{HD} are the concentrations of $H_2O(g)$, $HD(g)$, $D_2(g)$, and $HD(g)$, respectively; T_D, T_H, T_{H_2O}, and T_{HDO} are the number of D atoms, H atoms, H_2O

molecules, and HDO molecules adsorbed on the surface, respectively; and $[S_1]$ and $[S_2]$ are the number of the vacant sites on the platinum plate available for the adsorption of hydrogen atoms and water molecules, respectively. The symbol (g) means gaseous molecules. We have the following relations between the numbers of adsorbed species and the numbers of vacant sites,

$$[6] \quad [S_1]_0 = [S_1] + T_H + T_D$$

$$[7] \quad [S_2]_0 = [S_2] + T_{H_2O} + T_{HDO} + T_{D_2O}$$

where $[S_1]_0$ and $[S_2]_0$ are the overall number of the sites for the adsorption of hydrogen atoms and that for the adsorption of water molecules, respectively. We neglected the exchange reaction between the produced species, such as HDO or HD, because of their small concentration at the early stage of the reaction.

The rate of hydrogen isotope exchange between D_2 and H_2O is written as

$$[8] \quad v = -d[D_2]/dt = k_3 T_D T_{H_2O}$$

The initial rate of the reaction is

$$[9] \quad v_0 = (-d[D_2]/dt)_{t=0} = (k_3 T_D T_{H_2O})_{t=0}$$

Substituting eqs. [1] and [2] into eq. [9], we get

$$[10] \quad v_0 = k_3 K_1^{1/2} K_2 C_{D_2}^{1/2} C_{H_2O} [S_1][S_2]$$

Using eqs. [6], [1], and [4], we get

$$[11] \quad [S_1] = [S_1]_0 [1 + K_1^{1/2} C_{D_2}^{1/2} + C_{HD}/K_1^{1/2} K_4 C_{D_2}^{1/2}]^{-1}$$

and, using eqs. [7], [2], and [5], we get

$$[12] \quad [S_2] = \{[S_2]_0 - T_{D_2O}\}[1 + K_2 C_{H_2O} + C_{HDO}/K_5]^{-1}$$

Substituting eqs. [11] and [12] into eq. [10] and using the fact that at the early stage of the reaction,

$$C_{HD} = C_{HDO} = 0$$

and

$$T_{D_2O} = 0$$

we obtain

$$[13] \quad v_0 = a[S_1]_0$$

$$a \equiv k_3 K_1^{1/2} K_2 [S_2]_0 C_{D_2}^{1/2} C_{H_2O} / [1 + (K_1 C_{D_2})^{1/2}][1 + K_2 C_{H_2O}]$$

Notice that a depends on the temperature and concentrations of the reacting gases, and $[S_1]_0$ depends on the surface state of the platinum plate. Because the number of sites for the physical adsorption of water, $[S_2]_0$, is supposed to be independent of the surface state, a is independent of the surface state of the platinum plate.

B. Correction of $[S_1]_0$

For the evaluation of $[S_1]_0$ in eq. [13], we used the reaction of hydrogen isotope exchange between D_2 and H_2. Two mechanisms of this reaction are well-known: Rideal type (13) and Bonhoeffer–Farkas type (14). At high temperature the reaction proceeds in the former mechanism (15):

$$[14] \quad H_2(g) + 2S_1 \rightleftarrows 2H_{ads} \qquad K_{14} = T_H^2/C_{H_2}[S_1]^2$$

$$[15] \quad D_2(g) + 2S_1 \rightleftarrows 2D_{ads} \qquad K_{15} = T_D^2/C_{D_2}[S_1]^2$$

$$[16] \quad H_{ads} + D_{ads} \xrightarrow{k_{16}} HD(g) + 2S_1$$

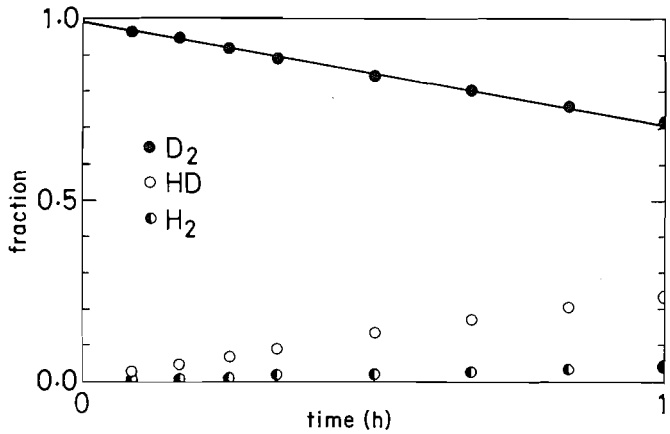


FIG. 3. An example of the figures for the determination of the initial rate of the reaction between D_2 and H_2O. In this run the initial concentrations of D_2 and H_2O were both 5.38×10^{-2} mol/m^3, which corresponds to 1 Torr each, and the temperature was 443 K.

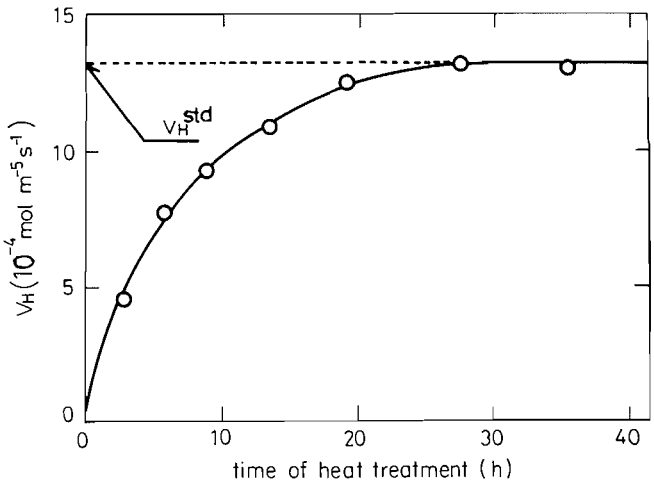


FIG. 4. Time of the heat treatment of the catalyst in hydrogen atmosphere (8.07 mol/m^3) at 973 K vs. the initial rate of exchange reaction between H_2 and D_2 at 373 K. The initial concentrations of H_2 and D_2 were both 2.69×10^{-2} mol/m^3. Using the chamber volume the unit mol/m^3 s can be converted to 3.1×10^{-4} mol/m^2 s, which is the unit of reaction rate on a unit surface.

where K_{14} and K_{15} are equilibrium constants for reactions [14] and [15], respectively, C_{H_2} is a concentration of H_2(g), and k_{16} is the rate constant for reaction [16]. We get the relation $K_{14} = K_{15} = K_1$ by neglecting the isotope effect. From eqs. [6], [14], and [15], the initial rate for reaction [16] is

$$[17] \quad v_H = k_{16} T_H T_D = b[S_1]_0^2$$

$$[18] \quad b \equiv k_{16} K_1 C_{H_2}^{1/2} C_{D_2}^{1/2} / [1 + (K_1 C_{H_2})^{1/2} + (K_1 C_{D_2})^{1/2}]^2$$

Notice that b depends on the temperature and concentration of hydrogen and deuterium gases and $[S_1]_0$ depends on the surface state of the platinum plate, as mentioned in Section IIIA.

Our experiments show that the initial rate seems to saturate by pretreatment of heating in hydrogen gas for 25 h (Fig. 4). The measurement of the saturation level seems to be reproducible within a few percent, because the measured saturation levels for v_H after treatment for 27.5 h and 35 h show good agreement. We regard the number of sites at this saturated stage as the

Can. J. Chem. Downloaded from www.nrcresearchpress.com by 41.223.56.140 on 09/07/12
For personal use only.

Can. J. Chem. Downloaded from www.nrcresearchpress.com by 41.223.56.140 on 09/07/12
For personal use only.

standard number of sites, $[S_1]_0^{std}$. The experiments suggest that the catalytic activity will change delicately and that we must carefully estimate the activity of the platinum plate surface. Relative amount of the number of sites for hydrogen adsorption may be good measure for the estimation of catalytic activity of the platinum plate surface. We, therefore, estimated it by determining the initial rate, v_H, of hydrogen isotope exchange between D_2 and H_2 before each run.

From eq. [17] the initial rate of hydrogen isotope exchange between H_2 and D_2 at this stage is

$$[19] \quad v_H^{std} = b([S_1]_0^{std})^2$$

The initial rate v_H was evaluated at the same condition as that made for obtaining v_H^{std} in Fig. 4, i.e., $C_{D_2} = C_{H_2} = 2.69 \times 10^{-2}$ mol/m^3 and $T = 373$ K. Then, from eqs. [17] and [19] the number of the sites, $[S_1]_0$, is written as follows,

$$[20] \quad [S_1]_0 = [S_1]_0^{std}(v_H/v_H^{std})^{1/2}$$

From eqs. [13] and [20] the corrected initial reaction rate for hydrogen isotope exchange between D_2 and H_2O,

$$[21] \quad v_0^{cor} \equiv v_0(v_H^{std}/v_H)^{1/2}$$

is written as

$$[22] \quad v_0^{cor} = a[S_1]_0^{std}$$

Notice that v_0^{cor} can be determined experimentally using eq. [21], and that $[S_1]_0^{std}$ is independent of the surface state of the platinum plate.

C. Examination of the model

When the initial concentration of hydrogen is fixed at a value of $C^0_{D_2}$, the following relation between the initial rate and the water concentration is obtained from eqs. [22] and [13]:

$$[23] \quad 1/v_0^{cor} = (1/k_{app})(1/C_{H_2O}) + K_2/k_{app}$$

$$k_{app} \equiv k_3K_1^{1/2}K_2[S_2]_0[S_1]_0^{std}C^0_{D_2}{}^{1/2}/[1 + (K_1C^0_{D_2})^{1/2}]$$

$$= \text{constant}$$

The value of $1/v_0^{cor}$ plotted against $1/C_{H_2O}$ is expected to be linear.

Similarly, in the case that the initial concentration of water vapor is fixed at a value of $C^0_{H_2O}$, the following relation is obtained from eqs. [22] and [13].

$$[24] \quad 1/v_0^{cor} = (1/k'_{app})(1/C_{D_2}{}^{1/2}) + K_1^{1/2}/k'_{app}$$

$$k'_{app} \equiv k_3K_1^{1/2}K_2[S_2]_0[S_1]_0^{std}C^0_{H_2O}/(1 + K_2C^0_{H_2O})$$

In this case, $1/v_0^{cor}$ plotted against $1/C_{D_2}{}^{1/2}$ is expected to be linear.

IV. Results and discussion

In Fig. 5 the corrected initial reaction rates measured under the condition of a constant temperature, $T = 423$ K, and a constant water-vapor concentration, 2.69×10^{-2} mol/m^3, are plotted against the concentration of D_2. In Fig. 6 the corrected initial reaction rates are plotted against the various concentrations of water vapor. The measurement is performed under the condition that the initial concentration of D_2 is 5.37×10^{-8} mol/cm^3 and the temperatures are 463 K, 443 K, and 423 K. In these figures, each plot does not deviate from a certain curve. Our scheme of the correction of the initial rate by estimating the relative intensity of the number of sites for the adsorption of dissociated hydrogen seems to be satisfactory.

Plots of $1/v_0^{cor}$ against $1/C_{D_2}{}^{1/2}$ and $1/v_0^{cor}$ against $1/C_{H_2O}$ are described in Figs. 7 and 8, respectively. These plots show

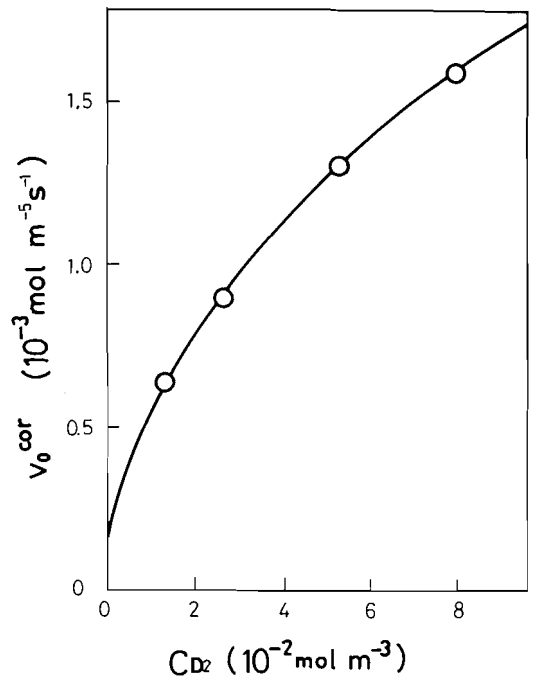


FIG. 5. The plots of corrected initial rates of the reaction against the concentration of D_2. The concentration of H_2O is 2.69×10^{-2} mol/m^3. The temperature was 423 K.

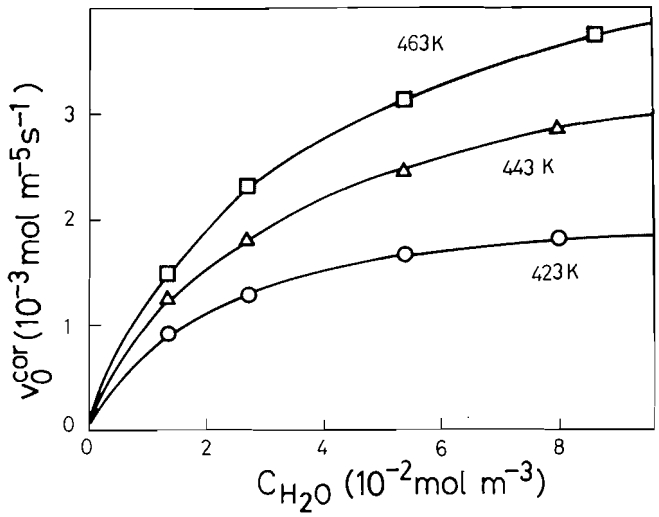


FIG. 6. The plots of corrected initial rates of reaction against the concentration of H_2O. The concentration of D_2 is 5.37×10^{-2} mol/m^3.

linearity, as predicted by eqs. [24] and [23]. The model seems to be successful in explaining the exchange reaction on the platinum plate surface.

The present study revealed that the relative number of sites for the adsorption of hydrogen atom which is obtained from the model calculation based on the exchange reaction between H_2O and D_2 can be simulated by that between H_2 and D_2. In the experiment the reproducibility of uncorrected experimental results for the initial rate of the hydrogen isotope exchange between H_2O and D_2 is not satisfactory. This seems to originate in the variation of the number of sites as a consequence of some delicate differences in the treatment of the platinum plate.

There seems to be two factors affecting the uncertainty of the number of sites for hydrogen adsorption. One is the reconstruction of surface atoms by heating or by other treatments, the

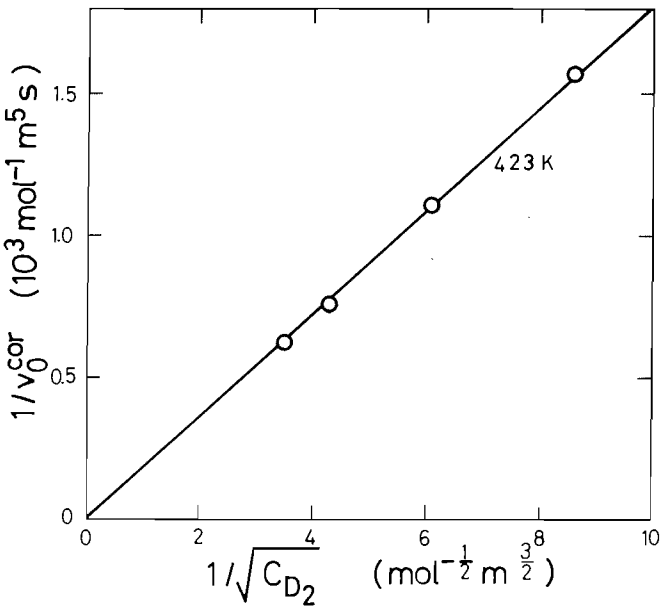


FIG. 7. The plot of $1/v_0^{cor}$ against $1/C^0{}_{D_2}{}^{1/2}$ for an examination of the model.

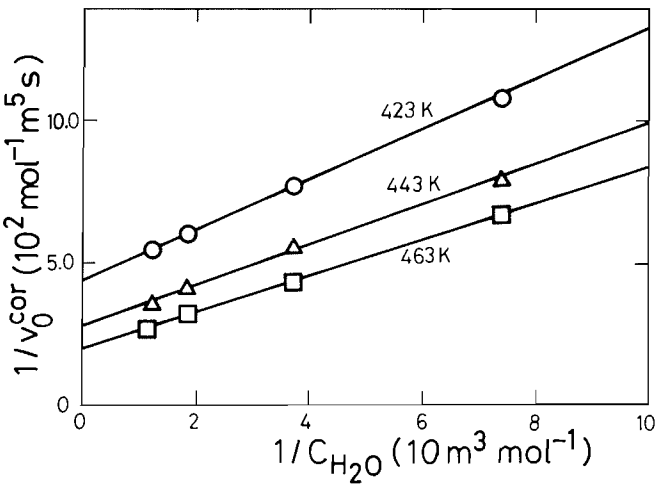


FIG. 8. The plot of $1/v_0^{cor}$ against $1/C^0{}_{H_2O}$ for an examination of the model.

possibility of which was pointed out by Nishiyama *et al.* (11). It is also pointed out by Somorjai (16) and Salmeron *et al.* (17) that the steps on the surface of single-crystal platinum will promote the reaction. The other is the site blocking by oxygen adsorbed on the surface. It has been found by Chon *et al.* (18) that the heat of hydrogen adsorption on platinum black depends considerably upon the concentration of surface oxygen.

In our experiments the effect of oxygen seems to be larger. Auger electron spectroscopy and X-ray photoemission spectroscopy have shown that the surface contamination by carbon can be removed by the heat treatment in concentrated nitric acid but oxygen cannot be removed completely. On platinum surface there seems to be two kinds of adsorbed oxygen: weakly adsorbed oxygen and strongly adsorbed oxygen at step sites (19). The adsorbed oxygen which can be titrated by hydrogen at the standard temperature (18) may be the former one. The fact that the platinum plate used in our study needed high temperature and long time to reduce (Fig. 4) suggests that the blocking of sites for hydrogen adsorption should be due to the strongly adsorbed oxygen. It may be interesting to investigate, in detail, the effect of the adsorbed oxygen upon the number of sites for hydrogen adsorption.

The reaction mechanism of the hydrogen exchange between D_2 and H_2O on a platinum powder catalyst or on a supported platinum catalyst has been investigated by several researchers. According to Rolston and Goodale (1), the rate of hydrogen isotope exchange between water and hydrogen on the alumina-supported platinum catalyst has explained by the five elementary reactions similar to those in this paper, except that alumina plays an important role in the adsorption of water in their case. Besides these reactions, it is proposed that the support plays an important role in the exchange reaction between the adsorped species (4). In this paper, we clarified, however, that the rate of hydrogen isotope exchange between D_2 and H_2O on the surface of platinum plate can be described fairly well by assuming physical adsorption of water vapor on platinum plate itself.

There are two major conclusions in the present study. One is that the relative number of the sites for hydrogen adsorption which is obtained from the model calculation based on the exchange reaction between H_2O and D_2 can be simulated by that between H_2 and D_2. The other is that the experimental results of the exchange reaction between H_2O and D_2 are successfully explained by the model in which the step of hydrogen exchange between H_2O adsorbed physically and D_2 adsorbed dissociatively on the platinum surface is rate controlling.

Acknowledgments

We would like to thank Mr. Koukichi Hotta for his assistance in experiments and Professor Ichiro Fujiwara (Otemon Gakuin University) and Dr. Nobutsugu Imanishi (Faculty of Engineering, Kyoto University) for their valuable discussions. The measurements of AES, XPS owes the kindness of Dr. Hidekazu Touhara (Faculty of Engineering, Kyoto University).

1. J. H. ROLSTON and J. W. GOODALE. Can. J. Chem. **50**, 1900 (1972).
2. N. H. SAGERT and R. M. L. POUTEAU. Can. J. Chem. **51**, 4031 (1973).
3. N. H. SAGERT and R. M. L. POUTEAU. Can. J. Chem. **49**, 3411 (1971).
4. N. H. SAGERT and R. M. L. POUTEAU. Can. J. Chem. **50**, 3686 (1972).
5. N. H. SAGERT and R. M. L. POUTEAU. Can. J. Chem. **52**, 2960 (1974).
6. I. IIDA, J. KATO, and K. TAMARU. Bull. Chem. Soc. Jpn. **49**, 3433 (1976).
7. E. HALLABA and E. M. ABDEL-WAHAB. Z. Anorg. Allg. Chem. **388**, 169 (1972).
8. R. A. DALLA BETTA and M. BOUDART. J. Chem. Soc. Faraday Trans. I, **72**, 1723 (1976).
9. C. M. GREENLIEF, S. AKHTER, and J. M. WHITE. J. Phys. Chem. **90**, 4080 (1986).
10. K. CHRISTMANN and G. ERTL. Surf. Sci. **60**, 365 (1976).
11. S. NISHIYAMA, S. MATSUURA, H. MORITA, S. TSURUYA, and M. MASAI. Appl. Catal. **15**, 185 (1985).
12. J. B. BUTT. Appl. Catal. **15**, 161 (1985).
13. E. K. RIDEAL. Proc. Cambridge Philos. Soc. **35**, 130 (1939).
14. K. F. BONHOEFFER and A. FARKAS. Z. Phys. Chem. (B) **12**, 231 (1930).
15. A. OZAKI. Isotopic studies of heterogeneous catalysis, Kodansha, Tokyo. 1977. p. 11.
16. G. A. SOMORJAI. Acc. Chem. Res. **9**, 248 (1976).
17. M. SALMERON, R. J. GALE, and G. A. SOMORJAI. J. Chem. Phys. **67**, 5324 (1977).
18. H. CHON, R. A. FISHER, and J. G. ASTON. J. Am. Chem. Soc. **82**, 1055 (1960).
19. G. E. GDOWSKI and R. J. MADIX. Surf. Sci. **119**, 184 (1982).

Can. J. Chem. Downloaded from www.nrcresearchpress.com by 41.223.56.140 on 09/07/12
For personal use only.

Methanation on exfoliated and supported MoS_2

GUENTER A. SCHOLZ[1] AND S. ROY MORRISON
Energy Research Institute, Simon Fraser University, Burnaby, B.C., Canada V5A 1S6

Received November 14, 1988

GUENTER A. SCHOLZ and S. ROY MORRISON. Can. J. Chem. **67**, 862 (1989).

The methanation reaction on MoS_2 exfoliated to a thickness of a few layers or less and adsorbed onto alumina is found to be very small. However, by calcining and resulfiding the exfoliated MoS_2 catalysts, greatly improved performance is achieved that is at least equal to the commercial catalysts based on ammonium heptamolybdate. The creation of molybdenum oxysulfide surface species therefore appears to be a necessary step toward producing significant methanation rates with exfoliated and supported MoS_2. The methanation products are almost exclusively CO_2 and CH_4, their mole ratios near unity, with otherwise only very much smaller amounts of longer chain hydrocarbons. The activation energy for methanation is generally observed to be near 100 kJ/mol, with the overall reaction being first order in the carbon monoxide concentration and third order in the hydrogen concentration. In contrast to the transition-metal catalysts, no water could be detected in the reaction products of the molybdenum based catalyst.

Key words: methanation reaction on MoS_2, exfoliated and supported MoS_2 as catalyst.

GUENTER A. SCHOLZ et S. ROY MORRISON. Can. J. Chem. **67**, 862 (1989).

On a trouvé que la réaction de méthanation, réalisée sur du MoS_2 affouillé jusqu'à une épaisseur maximale de quelques épaisseurs et adsorbé sur de l'alumine, est faible. Toutefois, si on procède à une calcination et à une resulfuration des catalyseurs de MoS_2 affouillé, on obtient des meilleures performances qui sont au moins équivalentes à celles obtenues avec des catalyseurs commerciaux basés sur l'heptamolybdate d'ammonium. Il semble donc que la création à la surface d'espèces oxysulfure de molybdène soit une étape nécessaire lorsqu'on veut obtenir des vitesses de méthanation significatives avec du MoS_2 affouillé et déposé sur un support. Les produits de méthanation sont presqu'exclusivement le CO_2 et le CH_4 accompagnés de faibles quantités d'hydrocarbures en longues chaînes. On observe généralement que l'énergie d'activation de la méthanation est d'environ 100 kJ/mol et que la réaction globale est du premier ordre en monoxyde de carbone et du troisième ordre en hydrogène. Par opposition avec ce qui est observé avec les catalyseurs de métaux de transition, on n'a pas pu détecter d'eau dans les produits de réaction obtenus à l'aide du catalyseur basé sur le molybdène.

Mots clés : réaction de méthanation sur MoS_2, MoS_2 affouillé et déposé sur un support comme catalyseur.

[Traduit par la revue]

1.0. Introduction

In attempts to convert syngas to hydrocarbon fuels, transition-metal catalysts (e.g. nickel, cobalt, etc.) have been used (1, 2). These catalysts, however, all suffer severe drawbacks because of deactivation caused by sulphur poisoning and/or build-up of carbon residues. The large scale removal of sulphur and nitrogen from a variety of petroleum feedstocks is presently accomplished with catalysts having mainly Ni—MoS_2 or Co—MoS_2 as the active components. Therefore, the search for a sulphur-tolerant methanation catalyst has recently also focussed attention on MoS_2 and to a lesser extent WS_2 (3–6). Commercial MoS_2 based catalysts are typically prepared by impregnating alumina powder with aqueous ammonium heptamolybdate $[(NH_4)_6Mo_7O_{24}\cdot 6H_2O]$ solutions followed by drying, calcining at about 800 K, and finally by sulfiding with a mixture of H_2S (typically 10%) in H_2 at about 700 K.

In studying the physical properties of layered dichalcogenides in this laboratory, it has become possible to exfoliate and subsequently separate these layer compounds along their basal planes (7, 8). The resulting crystallites are usually only a few layers thick and, recently, monolayers of the dichalcogenide sandwiches in suspension have also been produced (8). These layers are typically about 6 Å thick. If exfoliation is carried out in the presence of alumina powder, these monolayers can be made to deposit on the aluminum oxide by carefully controlling the pH of the suspension. Furthermore, promoters can be conveniently precipitated onto the dichalcogenide layers while they are still in suspension.

In this work we present a comparison between the methanation ability of MoS_2 based catalysts (*i*) derived from the above-mentioned exfoliation technique, (*ii*) those further treated by calcining and resulfiding, and (*iii*) a commercial MoS_2 catalyst. The reaction stoichiometry and the reaction order are also considered since the behaviour of MoS_2 is found to be different from those of well known transition metal catalysts like nickel.

2.0. Experimental methods

2.1. Apparatus

Quantitative analysis of feed and product gases is done in a standard way with a Varian model 6000 gas chromatograph in conjunction with a Vista 401 controller using a series-bypass arrangement (Fig. 1). A built-in nickel catalyst will allow the use of FID with its much higher sensitivity for detecting CO and CO_2. However, the presence of some sulfides in the reaction products, which will poison the nickel catalyst, is found to be unavoidable. Therefore these two gases are monitored via TCD. Feed gases are Matheson's UHP (99.999%) H_2 and Matheson grade (99.9%) CO. Whereas the former is used without further purification, the latter is first passed over copper shavings at about 500 K to decompose the nickel carbonyl that is found to be present.

Methanation is carried out at 1 atm in a continuous-flow manner in a quartz reaction tube in a single pass rather than a circulation system so that potential interference from reaction products (e.g. H_2O) will be minimized. The 12 mm i.d. reaction tube is heated with an external cylindrical heater and its temperature monitored with a chromel/alumel thermocouple. Feed and product gases can be diverted to a 0.25 mL sampling loop for quantitative analysis by the gas chromatograph.

2.2. Sample preparation

The general recipe for preparing the exfoliated catalyst, i.e. supporting the exfoliated MoS_2 layers on alumina, is described in detail

[1]Present address: Guelph–Waterloo Program for Graduate Work in Physics, Physics Department, University of Waterloo, Waterloo, Ontario, Canada N2L 3G1.

Can. J. Chem. Downloaded from www.nrcresearchpress.com by 41.223.56.140 on 09/07/12
For personal use only.

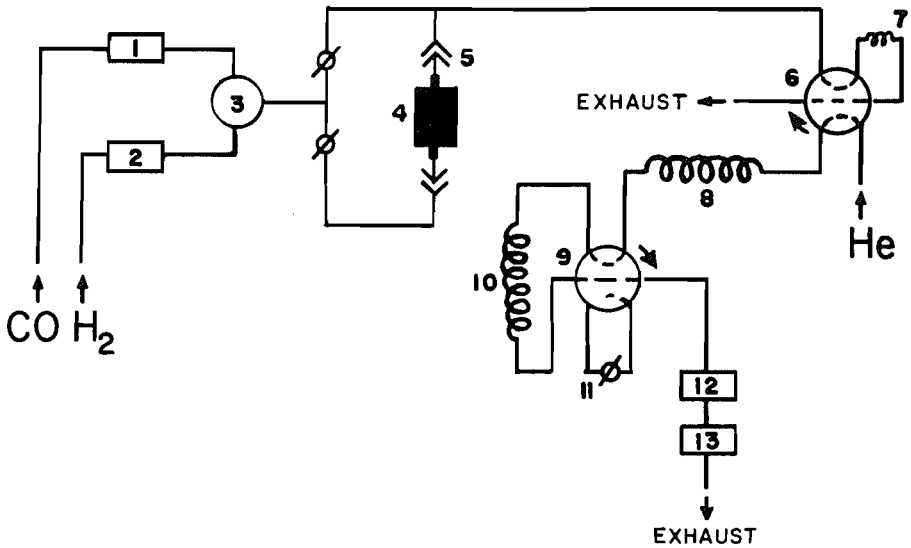


FIG. 1. Schematic of the experimental arrangement: flow meters (*1*, *2*); mixing chamber (*3*); furnace (*4*); o-ring joints (*5*); 6-way sampling valves (*6*, *9*); 1/4 mL sample loop (*7*); 4′ × 1/8″ Poropak T (*8*); 13′ × 1/8″ molecular sieve 13 × (*10*); restriction valve (*11*); TCD (*12*); FID (*13*).

in ref. 8 and involves the intercalation of lithium into powdered MoS_2 followed by immersion in water. The Li/H_2O reaction generates hydrogen which "blows" the crystallites apart into, at times, single 6.2 Å thick layers. In neutral or slightly basic pH these layers will then precipitate onto alumina without first flocculating. One would therefore expect that with an increasing MoS_2 to alumina concentration the alumina should eventually become covered with, but not exceed, one layer of MoS_2. This was experimentally confirmed in that MoS_2 suspensions cleared when the surface area (BET) of these layers is less than that of alumina, and the suspensions did not clear when the layers surface area is greater. In practice, the former occurs at concentrations of less than about 2 wt% MoS_2, and the latter at concentrations greater than about 5 wt% MoS_2. The alumina powder is obtained from Alfa Chemicals and is about 1 μm in diameter. The alumina does not appear to be porous since its BET surface area is found to be only about 5 m^2/g. The MoS_2 powder for exfoliation came from Materials Research Corp. The crystallites are from 5 to 10 μm in diameter with a surface area (BET) of about 6 m^2/g. The thickness of the MoS_2 layers deposited on the alumina is estimated by measuring the broadening of the initial (00.2) diffraction line while the layers are still in suspension.

A summary for the preparation of a series of MoS_2 based catalysts is given below. Some commercially available ammonium heptamolybdate catalysts and untreated MoS_2 are also included in order to provide reference points for the methanation ability of our exfoliated catalysts.

A: a 5 wt% mixture of MoS_2 crystallites from Materials Research Corp. and alumina; the MoS_2 crystallites are about 5 to 10 μm in diameter and BET measurements on those yield a surface area of about 6 m^2/g.

B1,B2: respectively 5% and 0.5% exfoliated MoS_2 supported on alumina; line broadening suggests that in each case the MoS_2 is about 4 layers thick.

$B2_s$: B2 sulfided at 700 K with 6 vol% H_2S in H_2 for about 12 h.

$B1_{cs}$: B1 calcined in air at 800 K for about 3 h and then resulfided with 6 vol% H_2S in H_2 at 700 K for about 1/2 h.

C: 1% exfoliated MoS_2 on alumina; some (*hk*.0) but no (00.*l*) lines are observed and indicate the presence of monolayers.

C_{cs}: C calcined in air at 800 K for about 3 h and then resulfided with 6 vol% H_2S in H_2 at 700 K for about 1/2 h.

D1,D2: 5 wt% MoS_2 on alumina; a pseudo-commercial type of catalyst prepared by impregnating alumina with an ammonium heptamolybdate solution followed by calcining in air at 800 K for about 3 h and then sulfiding with 6 vol% H_2S in H_2 at 700 K also for about 3 h.

$D2_e$: D2 subjected to the exfoliation procedure.

F: a hydrosulfurization Ni—Mo/Al catalyst (Harshaw catalyst HT 500) containing 15.5 wt% MoO_3 and 3.5 wt% NiO on alumina. The alumina has a BET surface area of 200 m^2/g.

F_s: F sulfided for about 12 h with 6 vol% H_2S in H_2 at 700 K.

The amount of catalyst in the reaction tube is near 6 g in all cases and results in a bed depth of about 4 cm. Pretreatment of the samples consisted of drying under vacuum at about 650 K for 1 day. Because the BET surface area for all the catalysts prepared by us is quite constant near 6 m^2/g, the methane yields are normalized to per gram MoS_2.

3.0. Results and discussion

The production of methane and CO_2 is given in Table 1 for a 3:1 mixture of H_2 and CO at 650 K and a total flow rate of 20 mL/min. The yields correspond to steady state conditions after several hours. The CO consumed is always less than about 1 vol%.

Primary reactions of interest are

[1] $2CO + 2H_2 \rightarrow CH_4 + CO_2$

[2] $CO + 3H_2 \rightarrow CH_4 + H_2O$

and possibly also the water-gas shift reaction

[3] $CO + H_2O \rightarrow H_2 + CO_2$

To establish a basis for comparison, in (3.1) we will first give a short discussion of the methanation rate and net reaction observed for untreated MoS_2 powder (A) and the commercial type of moly catalysts derived from impregnating alumina with an ammonium heptamolybdate solution (F, F_s, D1, D2). Then in (3.2) results for the exfoliated and supported MoS_2 catalysts (B1, B2, $B2_s$, C) are discussed. Finally in (3.3) we discuss the orders of magnitude improvement found in the methanation rates of the exfoliated catalysts subsequent to their calcining and resulfiding treatment ($B1_{cs}$, C_{cs}).

3.1. As-received MoS_2 (A) exhibited poor performance and had a negligible methane yield when normalized to either the unit area or weight of the catalyst (Table 1). A relatively large amount of CO_2 is produced ($[CH_4]/[CO_2] \equiv R$ is small) and may in part be related to the removal of active sites because of the accumulation of either carbidic or graphitic carbon on the catalyst surface ($2CO \rightarrow C + CO_2$).

A commercial hydrodesulphurization catalyst from Harshaw

Can. J. Chem. Downloaded from www.nrcresearchpress.com by 41.223.56.140 on 09/07/12
For personal use only.

TABLE 1. Catalyst performance at 650 K, 1 atm and a space velocity[a] of 250 h^{-1}

Sample[b]	wt% MoS_2	BET (m^2/g)	$[CH_4]^c$ $\left(\frac{\mu mol}{min\ g}\right)$	R^d	E_a (kJ/mol)	Comments
A	5.0	5.1	0.01	0.03	92 ± 10	Dispersed MoS_2 physically mixed with alumina
B1	5.0	5.7	<0.2	0.1	40 ± 5	Exfoliated MoS_2 (about 4 layers thick) deposited on Al_2O_3. $B2_s$ is sulfided B2 exposed to 6 vol% H_2S in H_2
$B2,B2_s$	0.5	5.7	0.2	0.02	44 ± 5	
C	1.0	5.7	<0.2	0.1	—	Monolayers of exfoliated MoS_2 deposited on Al_2O_3
D1	5.0	6.7	17	0.9	100 ± 6	Similar catalysts prepared from $(NH_4)_6Mo_7O_{24}.6H_2O$ and presulfided. Samples give extremes in methanation rates
D2	5.0	6.8	33	1.1	96 ± 5	
F	0	225	139 (>500)[e]	3.3	116 ± 10	NiO–MoO_3/Al (Harshaw HT-500) the only catalyst to produce observable amounts of H_2O
$D2_e$	5.0	6.1	1.0	0.3	96 ± 7	D2 subjected to exfoliation procedure
F_s	15.5	200	14	1.1	108 ± 7	F presulfided. Ni is poisoned so no more H_2O is observed
$B1_{cs}$	5.0	7.2	6.7	0.7	90 ± 7	B1 calcined and presulfided
C_{cs}	1.0	—	16	0.5	96 ± 10	C calcined and presulfided

[a]5 mL/min and 15 mL/min of H_2 and CO, respectively.
[b]About 6 g of catalyst.
[c]Normalized to per g MoS_2.
[d]Mole ratio of methane to carbon dioxide yield.
[e]Normalized to per g Ni.

(F) contains 3.5 wt% nickel oxide and 15.5% MoO_3 and following the reduction of nickel oxide has by far the largest methane yield and is also the only catalyst in this study to produce water as a methanation product. After sulfiding F to produce F_s, water production cannot be detected via gas chromatography and the methane and CO_2 yields decrease. Whereas the methane yield decreases by an order of magnitude from 139 to 14 μmol/min g, the CO_2 production decreases somewhat less so that R shifts near unity and the net reaction of eq. [1] appears to satisfactorily explain the products and yields observed. The lower activity of F_s and the change in reaction products is of course quite expected since the two major effects of sulfiding is the poisoning of the catalytically very active elemental nickel and the sulfiding of MoO_3. Consequently, the smaller catalytic activity of F_s can now be primarily attributed to supported molybdenum sulfide or oxysulfide species. Arrhenius plots for the two catalysts yield activation energies for methanation which are surprisingly similar (i.e. 116 ± 10 kJ/mol for F and 108 ± 7 kJ/mol for F_s; Fig. 2), in view of the differences in the active materials and reaction products.

Results for the heptamolybdate based catalysts prepared by us are summarized for D1 and D2 whose methane yield of 17 μmol/min g and 33 μmol/min g respectively, illustrate the largest spread in the observed rates. These methanation rates and the reaction products of methane and carbon dioxide with a mole ratio near unity are in general agreement with studies on heptamolybdate catalysts by Hou and Wise (6). However, the activation energies which we find to be 100 ± 6 kJ/mol and 96 ± 5 kJ/mol, respectively, are at variance with the 31 kJ/mol reported by them.

3.2. From a large number of supported catalysts prepared by the exfoliation technique, typical results for a few of these samples (i.e. B1, B2, C) are given in Table 1. Compared to the ammonium heptamolybdate based catalysts (D1, D2, F_s) the exfoliated and supported catalysts have quite disappointing methane yields of about 0.2 μmol/min g or less. Although the rates do generally increase by about one order of magnitude compared to as-received MoS_2 (A), they are still consistently more than two orders of magnitude below those of the heptamolybdate based catalysts. The order of magnitude increase in the methanation rates between the exfoliated and as-received MoS_2 catalysts may actually be the result of the latter breaking up into smaller fragments, resulting in an increased edge area, following the exfoliation procedure. Exfoliated catalysts also demonstrate a low R, in common with A, so that an accumulation of carbidic or graphitic carbon on their surfaces again appears very likely. The activation energy for methanation for the exfoliated catalysts is found to be surprisingly low at 40 ± 5 kJ/mol and 44 ± 5 kJ/mol (Fig. 2) and may well be related to the exfoliation process. To probe whether or not the small methanation rates and low activation energies are the result of a poor molybdenum/sulphur stoichiometry caused by exfoliation, B2 was sulfided at 700 K for 12 h ($B2_s$). The behaviour of $B2_s$ proved indistinguishable from B2 so that it would appear that the sulphur defect composition is not at fault. Further evidence that the exfoliation procedure may be detrimental is observed by subjecting the heptamolybdate based catalyst D2 to an exfoliation procedure ($D2_e$). Even though the activation energy for $D2_e$ remains unchanged at 96 kJ/mol, the methane yield decreases from 33 to 1.0 μmol/min g and the R value

Can. J. Chem. Downloaded from www.nrcresearchpress.com by 41.223.56.140 on 09/07/12
For personal use only.

Can. J. Chem. Downloaded from www.nrcresearchpress.com by 41.223.56.140 on 09/07/12
For personal use only.

decreases from near unity to 0.3. These rather disappointing results for our exfoliated catalysts clearly demonstrate that our exfoliation technique is either detrimental to the catalytically active sites, or is still incomplete with respect to a critical preparative step which will "activate" potential catalytic sites.

3.3. Evidence has been presented by other researchers (9–11) that the presence of molybdenum oxysulfide surface species having strong interactions with the alumina substrate may be critically important to the development of catalytically active sites for methanation. The correct environment for methanation may therefore not be produced when we simply adsorb monolayers of exfoliated MoS_2 onto alumina. In an attempt to produce an oxysulfide surface species, a number of the exfoliated MoS_2 samples are subjected to a calcining and resulfiding procedure. Calcining should promote the presence of oxysulfide surface species and establish strong interactions between these species and the alumina substrate. Subsequent to calcining, the samples are sulfided for about 1/2 h even though this vigorous reaction appears to last only a few minutes if judged by the water produced from the reduction of the oxides. The prolonged sulfiding will, however, help in reducing any lattice oxygen possibly introduced during calcining. The complete absence of oxygen is important because during the rate studies below, it will avoid ambiguities such as the formation of water in a parallel reaction. Typical results chosen from a number of calcined and resulfided samples are given in Table 1 for samples $B1_{cs}$ and C_{cs} derived from catalysts B1 and C, respectively. The dramatic increase in their methanation rates clearly establishes that calcining and resulfiding is very beneficial.[2] As with the previous MoS_2 based catalysts, there is no water observed in the methanation products. Along with the increased methanation ability, it is also interesting to note that R has moved nearer to unity and that the activation energies have increased, from 40 kJ/mol for B1 to 90 kJ/mol for $B1_{cs}$. It is therefore clear that new catalytic sites must have been activated by the calcining and resulfiding process.

An investigation of the reaction order for methanation using the calcined and resulfided catalysts is presented in Figs. 3 and 4 for C_{cs} at 670 K. Measurements are made in the usual manner using a three component gas mixture (CO, H_2, and He) by holding one of the reactants fixed and varying the other while using He as the diluent to keep the net flow rate constant. Small rate changes caused by temperature drifts in the furnace ($< \pm 4$ K) are corrected by using the already determined activation energy for C_{cs}. As mentioned earlier, because the total conversion of CO is less than 1% the reactor is in the differential mode. These rate measurements suggest that methanation is first order in the carbon monoxide concentration (Fig. 3) and third order in the hydrogen concentration (Fig. 4), i.e.

$$[4] \quad (d/dt)[CH_4] = -k[CO][H_2]^3$$

It may be of note that while the reaction products are in agreement with eq. [1], the reaction orders are in agreement with the stoichiometric coefficients of eq. [2]. The latter agreement is very likely fortuitous and, if anything, points to a relatively complex reaction mechanism for methanation. However, considering that MoS_2 does have some propensity (13) for the water-gas shift reaction (eq. [3]), and considering that the net reaction of eqs. [2] and [3] is that of eq. [1], it may be true that methanation on MoS_2 and, for example, nickel are similar in that an intermediate step in the methanation reaction on MoS_2 also produces water (eq. [2]). The fact that no water is observed in the reaction products could be accounted for by assuming a subsequent rapid water-gas shift reaction on the part of MoS_2. Some support for this hypothesis comes from the unexpectedly similar activation energies found for F (i.e. elemental nickel) and most of our other MoS_2 based catalysts, even though water is observed in the reaction products only for the former but never for the latter catalysts.

[2]Further studies have been done to investigate the effects of promoters in addition to calcining (12).

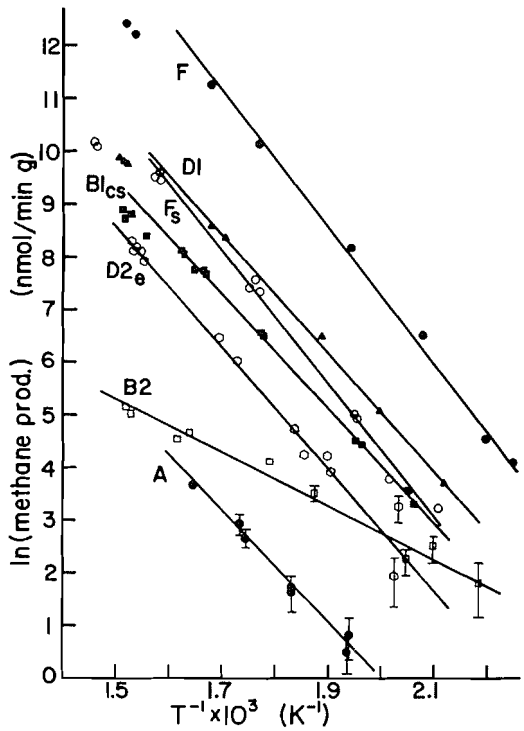


FIG. 2. Arrhenius plots for some of the catalysts listed in Table 1. The highest temperature methanation rates tend to level off and were therefore not included when determining the slope. H_2 and CO flow rates are 5 mL/min and 15 mL/min, respectively, with a resulting space velocity of about 250 h^{-1}.

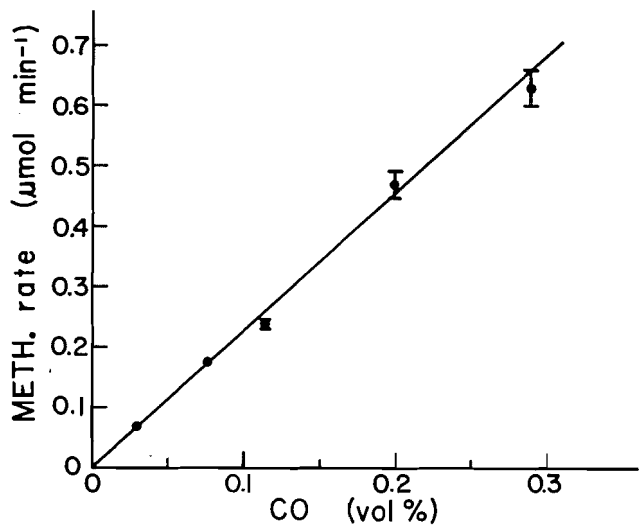


FIG. 3. Changes in the methanation rate with carbon monoxide concentration for sample C_{cs} at 670 K and 1 atm. The hydrogen concentration is 50 vol% and the space velocity is about 500 h^{-1}.

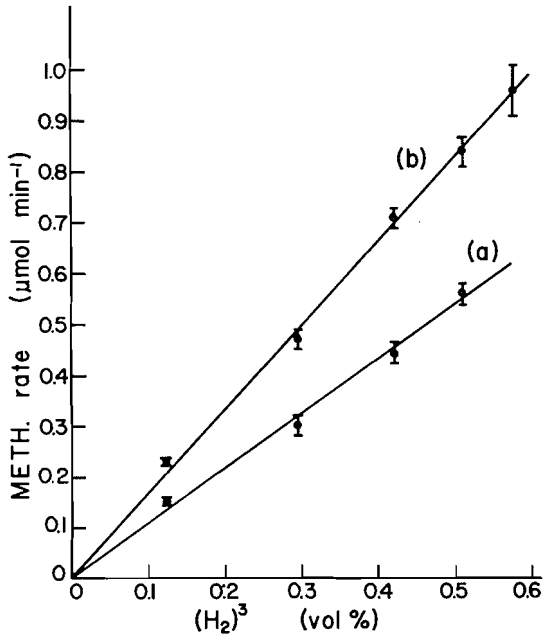


FIG. 4. Changes in the methanation rate with the cube of the hydrogen concentration for sample C_{cs} at 670 K and 1 atm. The carbon monoxide concentration is 17 vol% and the space velocity is about 375 h^{-1}. Data in (*a*) corresponds to initial rates and in (*b*) after methanation has continued for about 2 days. Although the methanation rate increases somewhat with time, the reaction order remains the same.

The rate equation for methanation determined by Hou and Wise (6) for a molysulfide catalyst is different from ours (eq. [4]). This is in part expected because they added small quantities of H_2S to the $CO/H_2/He$ feed gas in an attempt to control the sulphur defect composition of the catalyst. Strictly speaking, these rate equations are therefore not comparable. Nevertheless, it is interesting to make some limited comparisons. They find

$$[5] \quad (d/dt)[CH_4] = \frac{-k_1[H_2S]^{1/2}[CO][H_2]^{1/2}}{1 + \gamma[CO_2]}$$

The rate dependence on H_2S and CO_2 is not tested for by us. However, without any H_2S in the feed gas we observe relatively constant methanation rates over a period of days that are similar (when normalized to wt% Mo loading) to those reported by Hou and Wise. For example, Fig. 4*b* actually indicates a slight improvement in the catalysts methanation rates while it is continuously on-line for over 2 days. Therefore, we do not find the presence of H_2S in the feed gas to be a necessary condition for methanation as is implied by eq. [5]. The $[CO_2]$ dependence in eq. [5] is not a point of major difference since our use of a single pass reactor that has less than 1% conversion of CO guarantees the term $\gamma[CO_2] \ll 1$. Since we both find methanation to be first order in the CO concentration, the other major difference between the two rate equations appears to be with respect to the reaction order for H_2. A possible explanation for this might be related to pore diffusion limitations. Whereas we deposit "sheets" of MoS_2, onto a low (5 m^2/g) surface area alumina, they impregnate a high (320 m^2/g) surface area alumina, which is very likely porous, with a heptamolybdate solution. While in the former case the MoS_2 layers will "wrap" themselves around the alumina particles, in the latter case the heptamolybdate ions are free to disperse, in particular, into the pores of the alumina particles. Pore diffusion limitations could therefore become of concern and result in the apparently lower reaction orders along with the decreased activation energies observed.

Although not specifically mentioned previously, all of the MoS_2 catalysts discussed do produce small amounts of the longer chain hydrocarbons whose concentration decreases rapidly as their carbon number increases. To be more specific, at 650 K the calcined and resulfided catalysts produce ethane and propane at rates which are typically a few percent and a few permill, respectively, of the methane rate. The largest molecules detected are *i*- and *n*-pentane. Unsaturated hydrocarbons are generally not found, except in a few cases where the catalyst has a low methane yield. For those catalysts a few permill, with respect to the methane concentration, of ethylene is typically observed. The catalysts with low methane yields generally also produce proportionately higher concentrations of the longer hydrocarbons.

4.0. Conclusion

We have shown that methanation rates comparable to the ammonium heptamolybdate based catalysts can be obtained with exfoliated and separated MoS_2 layers adsorbed onto alumina after they are calcined. Since this procedure is known to result in molybdenum oxysulfide surface species, these species therefore appear to be necessary for methanation to proceed at substantial rates. Methanation is observed to be first order in the carbon monoxide concentration and third order in the hydrogen concentration. The reaction products are primarily methane and carbon dioxide at a 1:1 ratio and unlike corresponding transition-metal catalyst like nickel, water is not observed. The activation energy for methanation is near 100 kJ/mol. The overall reaction products and their concentrations are in general agreement with results by Hou and Wise; however, we find differences in the rate law and can not confirm their relatively low activation energy.

Acknowledgements

The authors are grateful for the support of this research by the Natural Sciences and Engineering Research Council of Canada, and to Mr. P. Joensen for preparing the catalyst samples.

1. A. T. BELL. Catal. Rev. **23**, 203 (1981).
2. C. H. BARTHOLOMEW, P. K. AGRAWAL, and J. R. KATZER. Adv. Catal. **31**, 135 (1982).
3. M. SAITO and R. B. ANDERSON. J. Catal. **63**, 438 (1980).
4. R. R. CHIANELLI. Catal. Rev. Sci. Eng. **26**, 361 (1984).
5. H. TOPSOE and B. S. CLAUSEN. Catal. Rev. Sci. Eng. **26**, 395 (1984).
6. P. HOU and H. WISE. J. Catal. **93**, 409 (1984).
7. C. LIU, O. SINGH, P. JOENSEN, A. E. CURZON, and R. F. FRINDT. Thin Solid Films, **113**, 165 (1984).
8. P. JOENSEN, R. F. FRINDT, and S. R. MORRISON. Mater. Res. Bull. **21**, 4 (1986).
9. N. GIORDANO, J. C. J. BART, A. VOGHI, A. CASTELLAN, and G. MARTINOTTI. J. Catal. **36**, 81 (1975).
10. P. ARNOLDY, J. A. M. VAN DEN HEIJKANT, G. D. DE BOK, and J. A. MOULIJN. J. Catal. **92**, 35 (1985).
11. H. TOPSOE, B. S. CLAUSEN, R. CANDIA, C. WIVEL, and S. MORUP. J. Catal. **68**, 433 (1981); **68**, 553 (1981).
12. B. MIREMADI and S. R. MORRISON. J. Catal. In press.
13. P. HOU, D. MEEKER, and H. WISE. J. Catal. **80**, 280 (1982).

Can. J. Chem. Downloaded from www.nrcresearchpress.com by 41.223.56.140 on 09/07/12
For personal use only.

Thermal diffusion of aqueous alcohols

ASHIS KUMAR MUKHERJEE
Department of Chemistry, Presidency College, Calcutta-700 073, India
AND
S. K. SANYAL[1]
Department of Agricultural Chemistry and Soil Science, Bidhan Chandra Krishi Viswavidyalaya, Kalyani-741 235, West Bengal, India

Received June 10, 1988[2]

ASHIS KUMAR MUKHERJEE and S. K. SANYAL. Can. J. Chem. **67**, 867 (1989).

The thermal diffusion of aqueous solutions of methanol, ethanol, propan-1-ol, butan-1-ol, ethan-1,2-diol, and propan-1,2-diol contained in the pores of a sintered glass disc (of porosity G4) has been studied. The Soret coefficient (σ) and the heat of transport ($\hat{Q}$) values are reported in the temperature range of 25–40°C. The heat capacities of transport are ascertained at 30°C from the temperature coefficient of heat of transport values. The results are explained on the basis of changes in local entropy in the solvent (water), arising out of solute–solvent interactions. Correlations of the observed experimental values with certain relevant thermodynamic parameters, taken from the literature, have also been sought, with encouraging results.

Key words: thermal diffusion, heat of transport, entropy of hydration.

ASHIS KUMAR MUKHERJEE et S. K. SANYAL. Can. J. Chem. **67**, 867 (1989).

On a étudié la diffusion thermique de solutions aqueuses de méthanol d'éthanol, de propanol-1, de butanol-1, d'éthanediol-1,2 et de propanediol-1,2 contenus dans les pores d'un disque en verre frité (de porosité G4). On rapporte les valeurs des coefficients de Soret (σ) et des chaleurs de transport ($\hat{Q}$) pour l'intervalle de température allant de 25 à 40°C. En se basant sur le coefficient de température des valeurs des chaleurs de transport à 30°C, on a déterminé les capacités calorifiques de transport. On explique les résultats en se basant sur des changements d'entropie locale dans le solvant (eau) qui résultent d'interactions soluté–solvant. On a aussi recherché, avec des résultats encourageants, des corrélations entre les valeurs experimentales observées et certains paramètres thermodynamiques appropriés relevés dans la littérature.

Mots clés : diffusion thermique, chaleur de transport, entropie d'hydratation.

[Traduit par la revue]

Can. J. Chem. Downloaded from www.nrcresearchpress.com by 41.223.56.140 on 09/07/12
For personal use only.

Introduction

Even though there have been many studies on thermal diffusion of electrolytes (1–5), relatively less attention seems to have been paid to the thermal diffusion of non-electrolytes. The present communication describes experiments on thermal diffusion of aqueous solutions of alcohols, contained in the pores of a coarse G4 glass diaphragm. The diffusion cell used has been described earlier (6).

Theoretical

A solution-filled pore in a highly porous non-isothermal diaphragm (e.g., a sintered G4 glass disc) may be considered to be equivalent to a porous Soret cell free from flow caused by external stirring. Thus, the relations used for thermal diffusion in a binary system (7) (and for a solvent-fixed reference frame) can be adopted in the present case with the supposition that the chemical potential of the component i(μ_i) just within the diaphragm at each of its surfaces is the same as that in the adjacent layer of free solution outside the diaphragm (8, 9). The latter holds true for the assumed equilibrium across each surface of the glass disc used in the present case, and the heat of transport of solute ($\hat{Q}$) for a solvent-fixed reference frame is given (10) by

$$[1] \quad \hat{Q} = RT^2\sigma\left(1+\frac{\mathrm{d}\ln\gamma}{\mathrm{d}\ln m}\right)_T$$

where σ is the Soret coefficient, obtained as

$$[2] \quad \sigma = -\left(\frac{\mathrm{d}\ln m}{\mathrm{d}T}\right)_{st} = -\frac{1}{\bar{m}}\left(\frac{\Delta m}{\Delta T}\right)_{st}$$

$\bar{m}$ being the mean molal concentration, γ the mean activity coefficient on the molality scale, and T the mean (absolute) temperature. Δm refers to the concentration difference between the cold and warm sides of the diaphragm at the steady state (denoted by the subscript "st" in eq. [2]), the solution in each half-cell being kept thoroughly mixed by means of magnetic stirrers (6). The thermodynamic factor

$$\left(1+\frac{\mathrm{d}\ln\gamma}{\mathrm{d}\ln m}\right)_T$$

is often given a symbol "B". The above relation, eq. [1], relating $\hat{Q}$ to σ, assumes the validity of Onsager's Reciprocity Relations between the cross-effect phenomenological (L) coefficients.

Experimental

The cell

The thermodiffusive cell used is the same as that described earlier (6). It consists of two compartments, holding the non-isothermal diaphragm sandwiched in between, and having several arrangements to monitor *in situ* concentration changes and temperatures. The details have already been reported (6).

Materials and method

The alcohols used were of high purity grade and their solutions were prepared in double distilled (deaerated) water of conductivity less than 0.5 μmho cm^{-1}. The initial concentration of each solution studied was 0.1 m.

The experimental method followed was similar to the one described in our earlier paper (6). On applying a thermal gradient across the diaphragm, the temperatures were monitored by the thermocouples, and any solvent flow was ascertained by noting the rate of development of a pressure difference between the glass capillary tubes emerging from the top and the bottom half-cells. Such solvent flow, however,

[1]Author to whom correspondence may be addressed.
[2]Revision received December 13, 1988.

TABLE 1. Experimental parameters for the solutions studied

Solution (0.1 *m*)	*T* (K)	*B*	$10^3\sigma$ (deg^{-1})	$\hat{Q}$ (J mol^{-1})	$\left(\frac{d\hat{Q}}{dT}\right)_{30°C}$ (J mol^{-1} deg^{-1})	$\hat{C}_{30°C}$ (J mol^{-1} deg^{-1})
Methanol	298	0.990	2.95 (±0.02)	2156 (±14.6)		
	303	0.990	2.41 (±0.04)	1821 (±30.2)	−50.0 (±4.2)	−56.0
	308	0.990	2.14 (±0.03)	1671 (±23.4)		
	313	0.990	2.01 (±0.03)	1621 (±24.3)		
Ethanol	298	0.990	5.01 (±0.06)	3662 (±43.9)		
	303	0.990	4.59 (±0.07)	3469 (±52.9)	−47.6 (±1.8)	−59.0
	308	0.990	4.10 (±0.10)	3201 (±78.1)		
	313	0.990	3.66 (±0.04)	2951 (±32.3)		
Propan-1-ol	298	0.970	6.96 (±0.14)	4985 (±100.3)		
	303	0.970	6.21 (±0.02)	4598 (±14.8)	−80.0 (±2.9)	−95.2
	308	0.970	5.50 (±0.08)	4208 (±61.2)		
	313	0.970	4.70 (±0.04)	3713 (±31.6)		
Butan-1-ol	298	0.945	8.03 (±0.04)	5603 (±27.9)		
	303	0.945	6.98 (±0.11)	5035 (±79.3)	−104.3 (±2.1)	−120.9
	308	0.945	6.12 (±0.03)	4561 (±22.4)		
	313	0.945	5.27 (±0.06)	4056 (±46.2)		
Ethan-1,2-diol*	298	—	4.22 (±0.01)	3116 (±7.4)		
	303	—	4.06 (±0.05)	3099 (±38.2)	−9.2 (±1.1)	−19.4
	308	—	3.82 (±0.09)	3013 (±71.0)		
	313	—	3.64 (±0.03)	2965 (±24.4)		
Propan-1,2-diol*	298	—	6.60 (±0.01)	4873 (±7.4)		
	303	—	6.25 (±0.11)	4771 (±84.0)	−40.0 (±4.1)	−55.7
	308	—	5.76 (±0.10)	4543 (±78.9)		
	313	—	5.21 (±0.09)	4244 (±73.3)		

*As stated in the results section, the variation of activity coefficient with mean molality for these diols was neglected and, therefore, the value of the thermodynamic factor (*B*) was taken to be unity, at each temperature of study, for calculating $\hat{Q}$ from the corresponding experimental value of σ.

Can. J. Chem. Downloaded from www.nrcresearchpress.com by 41.223.56.140 on 09/07/12
For personal use only.

TABLE 2. Data at 25°C

Solution (0.1 *m*)	$\hat{Q}$ (J mol^{-1})	$\hat{S}$ (J mol^{-1} deg^{-1})	$\bar{V}$ (mL mol^{-1})	$-\Delta S_n^0$ (J mol^{-1} deg^{-1})
Methanol	2156	7.23	38.7	139.7
Ethanol	3662	12.29	55.0	166.5
Propan-1-ol	4985	16.73	73.3	185.4
Butan-1-ol	5603	18.80	85.0	197.1
Ethan-1,2-diol	3116	10.45	55.6	—
Propan-1,2-diol	4873	16.35	72.9	—

turned out to be negligible[3] after making proper correction for unequal thermal expansions in the two compartments (6).

At the steady state, suitable aliquots were withdrawn from each compartment, and the concentration difference was determined by using a Brice–Phoenix differential refractometer. The latter was previously calibrated with a number of standard pairs of solutions of each solute, having known concentration differences.

A number of tests, as described earlier (6), were applied to ensure a satisfactory operation of the cell, thereby obtaining reliable experimental data.

Results and discussion

The results are incorporated in Tables 1 and 2. The errors in the determination of σ and the heat of transport ($\hat{Q}$) are calculated as standard deviations and shown in parentheses below each value.

The values of the thermodynamic factor

$$\left(1+\frac{d\ln\gamma}{d\ln m}\right)$$

at 25°C are calculated from the appropriate activity or osmotic coefficient data available in the literature (11*a*, *b*) and are assumed constant over the experimental temperature range. In some cases (e.g., for diols), owing to unavailability of such appropriate activity or osmotic coefficient data, the variations of the latter with mean molality over the concentration range used in the present study were neglected, and the value of the thermodynamic factor (B) was thus taken to be unity. The latter appears to be a reasonably satisfactory approximation for these moderately dilute non-electrolyte solutions. The temperature variations of B have also been neglected.

Positive $\hat{Q}$ corresponds to the promotion of "local" structure (10) of water, i.e., it finds an interpretation in terms of local ordering (i.e., loss of entropy) of water adjacent to the solute molecules in dilute solutions. The gradual increase of $\hat{Q}$ from methanol to butan-1-ol (Table 1) may be ascribed to the gradually increasing hydrophobic chain length of the alcohols, which causes a lowering of entropy of neighbouring water molecules because of hydrophobic hydration effects (12–14). Introduction of a hydroxyl group, on the other hand, is seen to cause a lowering of $\hat{Q}$, e.g., from ethanol to ethanediol and from propan-1-ol to propan-1,2-diol (Table 1). This agrees well with earlier observations reported in the literature (15) and is attributed to the ability of hydroxyl groups to take part in hydrogen bonding with neighbouring water molecules, thereby increasing their entropy, and also to transmit the cluster-disruptive perturbations from solvent molecules lying outside the cluster regions formed around these largely hydrophobic solutes (10).

[3]In fact, such minute volume flow contributes not more than 0.1% towards the observed Δm values at the steady state, and the attendant error in ignoring such volume flow is thus considered negligible.

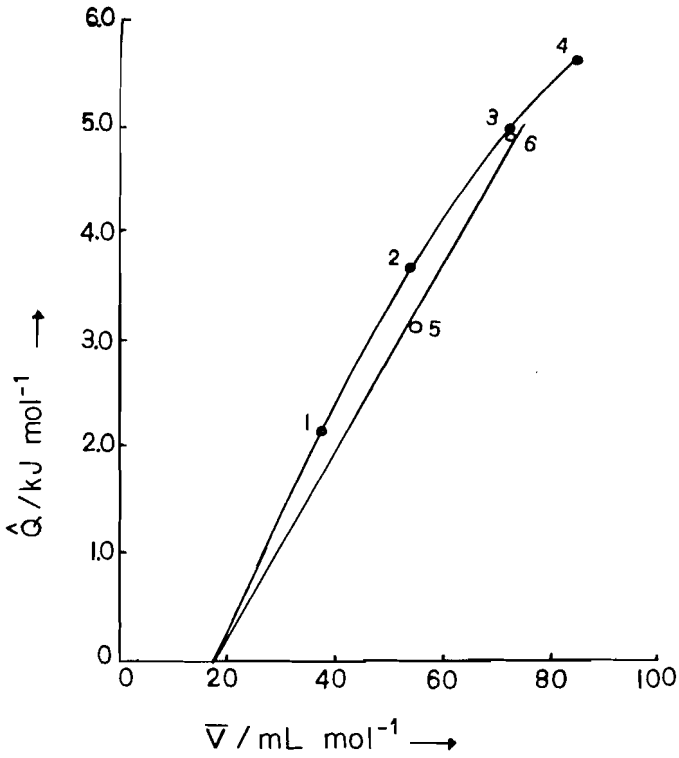


FIG. 1. Correlation between heats of transport and partial molal volumes of the solutes methanol (1), ethanol (2), propan-1-ol (3), butan-1-ol (4), ethan-1,2-diol (5), propan-1,2-diol (6), at 25°C.

The temperature dependence of $\hat{Q}$ has been described in terms of the corresponding heat capacities of transport (at 30°C) of the various non-electrolytes studied. The heat capacity of transport ($\hat{C}$) is given (10) by

$$[3]\quad \hat{C}=\left(\frac{d\hat{Q}}{dT}\right)-\frac{\hat{Q}}{T}$$

The appropriate $d\hat{Q}/dT$ values (at T = 30°C), noted from the slope of $\hat{Q}$ vs. T (and given in Table 2), as well as the corresponding $\hat{C}$ values, are both seen to be negative and may be attributed to the higher thermal energy of water molecules, especially in the bulk, as the mean temperature is raised; the latter renders structure promotion in water by the alcohols more difficult. Further, the trend to gradually increasing negative magnitudes of $\hat{C}$ with increase in chain length of the monohydric alcohols, and also a sharp fall in $\hat{C}$ for the diols (Table 2), fit in with the line of argument presented above.

It is of interest to plot the $\hat{Q}$ values (at 25°C) for the alcohols studied against the corresponding partial molal volumes. A nearly linear correlation is obtained for both the monohydric alcohols and diols (Fig. 1). This implies that the positive $\hat{Q}$ of

Can. J. Chem. Downloaded from www.nrcresearchpress.com by 41.223.56.140 on 09/07/12
For personal use only.

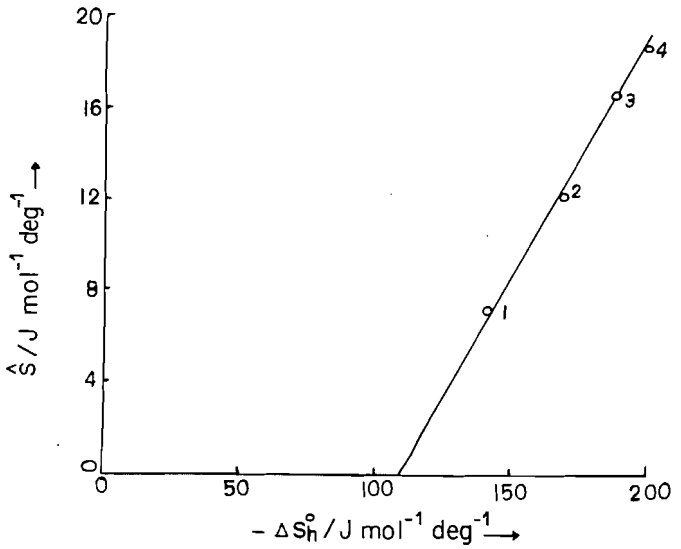


FIG. 2. Correlation between entropy of transport and standard entropy of hydration of the solutes methanol (1), ethanol (2), propan-1-ol (3), butan-1-ol (4), at 25°C.

these alcohols can be accounted for in terms of the enhanced degree of hydrogen bonding between the water molecules in the layer of water in the neighbourhood of the hydrocarbon chain. This, in turn, is a function of the size of the cavity in the aqueous solution required to accommodate the solute molecule, and thus it is not surprising that $\hat{Q}$ is related to the corresponding partial molal volumes.

A plot (Fig. 2) of the entropy of transport ($\hat{S} = \hat{Q}/T$) at 25°C of the aqueous alcohols against the corresponding standard entropies of hydration, $-\Delta S_h^0$ (quoted in Table 2), is given for those compounds for which the latter data are available from the literature (16). On the assumption of ideal gas behaviour for the vapours of the solute, such hydration entropy gives a measure of total solute–solvent interactions in dilute solutions.

Indeed, these negative hydration entropies originally led Frank and Evans (17) to postulate the "iceberg" formation through the water structure-enforcing character of the hydrocarbon chains of alcohols and other similar solutes in aqueous solutions.

It is in this context that the linear correlation between $\hat{S}$ and $-\Delta S_h^0$ (Fig. 2) is satisfactory, and is taken to highlight the importance of local interactions (i.e., of the hydrophobic hydration effects referred to above) in determining the net $\hat{Q}$ or $\hat{S}$ for diffusional transport through the given non-isothermal diaphragm.

The intercepts on the x-axes of Figs. 1 and 2 (for $\hat{Q} = \hat{S} = 0$) are seen to be rather close to the molar volume (18.05 mL) and the standard entropy of vaporization (118.7 J mol^{-1} K^{-1}) of pure water at 25°C and 1 atm pressure (101.3 kpa), respectively (for which $\hat{Q}_w = 0$). This indeed is interesting and serves to increase confidence in the present experimental results.

1. (*a*) D. J. TREVOY and H. G. DRICKAMER. J. Chem. Phys. **17**, 1120 (1949); (*b*) R. L. SAXTON, E. L. DOUGHERTY, and H. G. DRICKAMER. J. Chem. Phys. **22**, 1166 (1954); (*c*) W. M. RUTHERFORD, E. L. DOUGHERTY, and H. G. DRICKAMER. J. Chem. Phys. **22**, 1289 (1954); (*d*) W. M. RUTHERFORD and H. G. DRICKAMER. J. Chem. Phys. **22**, 1157 (1954).
2. K. F. ALEXANDER. Z. Phys. Chem. (Leipzig), **197**, 233 (1951).
3. F. BELLUCCI, M. BOBIK, E. DRIOLI, F. S. GAETA, D. G. MITA, and G. ORLANDO. Can. J. Chem. Eng. **56**, 698 (1978).
4. F. BELLUCCI, E. DRIOLI, F. G. SUMMA, F. S. GAETA, D. G. MITA, and N. PAGLIUCA. J. Chem. Soc. Faraday Trans. 2, **75**, 247 (1979).
5. S. K. SANYAL and A. K. MUKHERJEE. Can. J. Chem. **66**, 435 (1988).
6. A. K. MUKERJEE and S. K. SANYAL. Can. J. Chem. **64**, 717 (1986).
7. J. N. AGAR. *In* The structure of electrolyte solutions. *Edited by* W. J. Hamer. Wiley, New York, NY. 1959. Chap. 13. p. 200.
8. A. KATCHALSKY and P. F. CURRAN. Non-equilibrium thermodynamics in biophysics. Vol. 112. Harvard University, Cambridge, MA. 1965. p. 185.
9. J. G. KIRKWOOD. *In* Ion transport across membranes. *Edited by* H. T. Clark. Academic Press, New York, NY. 1954. p. 119.
10. J. N. AGAR. Adv. Electrochem. Electrochem. Eng. **3**, 31 (1963).
11. (*a*) J. A. V. BUTLER, D. W. THOMSON, and W. H. MACLENNAN. J. Chem. Soc. 674 (1933); (*b*) H. J. E. DOBSON. J. Chem. Soc. **127**, 2866 (1925).
12. G. H. HAGGIS, J. B. HASTED, and T. J. BUCHANAN. J. Chem. Phys. **20**, 1452 (1952).
13. D. B. DAHLBERG. J. Phys. Chem. **76**, 2045 (1972).
14. S. K. SANYAL. Chem. Educ. (New Delhi), **1**(2), 14 (1984).
15. M. KENNERLEY, H. J. V. TYRRELL, and M. ZAMAN. J. Chem. Soc. 1041 (1966).
16. F. FRANKS. *In* Water—A comprehensive treatise. Vol. 2. *Edited by* F. Franks. Plenum Press, New York, London. 1972. p. 340.
17. H. S. FRANK and M. W. EVANS. J. Chem. Phys. **13**, 507 (1945).

Can. J. Chem. Downloaded from www.nrcresearchpress.com by 41.223.56.140 on 09/07/12
For personal use only.

The chemistry of the chromotropic acid method for the analysis of formaldehyde

PARIS E. GEORGHIOU[1] AND CHI KEUNG (JIMMY) HO

Department of Chemistry, Memorial University of Newfoundland, St. John's, Nfld., Canada A1B 3X7

Received October 14, 1988

PARIS E. GEORGHIOU and CHI KEUNG (JIMMY) HO. Can. J. Chem. **67**, 871 (1989).

Formaldehyde is present in the indoor air of many industrial and non-industrial environments. The procedure for its analysis which is commonly employed in North America is a NIOSH recommended one that uses chromotropic acid and concentrated sulphuric acid. The nature of the purple chromogen that is produced in the analytical procedure has not been fully understood until now. Using ^{1}H and ^{13}C nuclear magnetic resonance spectroscopic techniques and calibration line studies, evidence has been obtained to support the hypothesis that the chromogen has a mono-cationic dibenzoxanthylium structure and not a *para,para*-quinoidal one that is commonly cited.

Key words: Formaldehyde, formaldehyde analysis, chromotropic acid, chromogen, dibenzoxanthylium cation.

PARIS E. GEORGHIOU et CHI KEUNG (JIMMY) HO. Can. J. Chem. **67**, 871 (1989).

Le formaldéhyde est présent dans l'air ambiant de nombreux environnements industriels et non-industriels. La méthode communément utilisée en Amérique du nord pour en faire l'analyse est une méthode recommandée par NIOSH et elle est basée sur l'utilisation de l'acide chromotropique et de l'acide sulfurique concentré. Jusqu'à maintenant, on n'a pas encore bien compris quelle est la nature du chromogène violacé qui se produit au cours de cette procédure. Faisant appel à la rmn du ^{1}H et du ^{13}C ainsi qu'à des études de calibrations linéaires, on a obtenu des données suggérant que le chromogène possède une structure dibenzoxanthylium mono-cationique et non pas une structure de type quinonoïde-*para,para* comme il a souvent été proposé.

Mots clés : formaldéhyde, analyse du formaldéhyde, acide chromotropique, chromogène, cation dibenzoanthylium.

[Traduit par la revue]

Can. J. Chem. Downloaded from www.nrcresearchpress.com by 41.223.56.140 on 09/07/12
For personal use only.

Introduction

Since its discovery in 1859 by Butlerov (1) formaldehyde has become one of the most important and widely used industrial chemicals. In recent years the presence of significant amounts of formaldehyde in domestic indoor air has been recognized. This has been a result of formaldehyde being released from a variety of sources including plywood, particleboard (2) and urea–formaldehyde foam insulation (U.F.F.I.) (3). Formaldehyde in air can be analysed by several different chemically-based procedures in which a chromogen is produced with formaldehyde-specific reagents. In North America one of the most widely used chromogen-forming reagent with formaldehyde is chromotropic acid **1** (4,5-dihydroxy-2,7-napthalenedisulphonic acid) which is used in the method recommended by the National Institute for Occupational Safety and Health (NIOSH), Method P&CAM 125 (4).

The use of chromotropic acid as a formaldehyde-specific reagent was first described by Eegriwe in 1937 (5). The nature of the chromogen and its formation by the reaction of chromotropic acid with formaldehyde has never been unambiguously proven. The most often-quoted structure (4–8) for the chromogen formed between chromotropic acid and formaldehyde has been the *para,para*-quinoidal adduct (**2**). No direct proof of this structure has ever been presented. It is based on an analogy with the reaction of formaldehyde with aromatic compounds in the LeRosen test (6). Chromotropic acid is known to form a large number of compounds with diazotised derivatives of aromatic compounds. In all of these cases, the structures presented (for which very little direct proof has been advanced) have diazo groups undergoing substitution in the position *ortho* to both the hydroxyl and sulphonic acid groups. An example is provided by Sulfonazo III (**3**) (9). The strongest evidence presented in support of its formula is that it is consistent with its chemical properties.

An alternative structure for the chromogen from the reaction of **1** and formaldehyde that has been proposed by Kamel and Wizinger (10) but which appears to have been ignored in the recent literature and for which there are only three brief citations (11–13) is **4**. This mono-cationic dibenzoxanthylium structure was proposed by analogy with the product obtained **5** when J-acid **6** (7-amino-4-hydroxy-2-naphthalenesulphonic acid) reacts with formaldehyde in concentrated sulphuric acid. Carbon, hydrogen, and sulphur analyses were consistent with the proposed structure **5** but no other direct evidence was presented. The analogous chromotropic acid – formaldehyde adduct **4** could not be isolated from the reaction mixture, since it was found to be much more water soluble than **5** thus precluding similar elemental analysis.

The work described in this paper was aimed at understanding the chemistry and establishing the structure of the chromotropic acid – formaldehyde chromogen. A better understanding of the chemistry of the reaction between chromotropic acid and formaldehyde could potentially lead to a modification of the method to avoid the use of concentrated sulphuric acid.

Experimental

^{1}H NMR spectra were recorded with the following instruments at the designated frequencies: Varian Anaspect EM 360 at 60 MHz, Bruker WP-80 at 80 MHz, and GE GN-300NB at 300 MHz. ^{13}C NMR spectra were recorded with the Bruker WP-80 at 20.1 MHz, and/or the GE GN-300NB at 75.47 MHz. The solvent used was either deuterium oxide or water as noted in the experimental details. Ultraviolet and visible spectra were determined on a Unicam SP800 Ultraviolet spectrophotometer. Calibration lines were determined with a Perkin–Elmer Hitachi–Coleman 139 grating single-beam spectrophotometer. Infrared spectra were recorded on a Perkin–Elmer 1320 infrared spectrophotometer using KBr disks.

Sephadex LH-20 purchased from Pharmacia Fine Chemicals was used for the gel permeation chromatography. Merck silica gel was used for preparative-layer chromatography using 20 × 20 cm plates of 0.75 mm thickness.

*Purification of 4,5-dihydroxy-2,7-naphthalenedisulphonic acid disodium salt (**1**)*

Purified **1** was obtained by dissolving, with heating, in 100 mL of water 20 g of 98% reagent purchased from Sigma Chemical Co.

[1]Author to whom correspondence may be addressed.

Can. J. Chem. Downloaded from www.nrcresearchpress.com by 41.223.56.140 on 09/07/12
For personal use only.

A saturated solution of sodium chloride was added to the chromotropic acid solution until a precipitate formed. The precipitate was recrystallized from water to afford a near-colourless product: ^{1}H NMR (D_2O) δ ppm: 7.20 (d, J = 2 Hz, 1H, Ar—H), 7.92 (d, J = 2 Hz, 1H, Ar—H); ^{13}C NMR (D_2O) δ ppm (for assignments see ref. 14): 106.44 (C-3, C-6), 116.18 (C-10), 118.12 (C-1, C-8), 134.64 (C-9), 141.36 (C-2, C-7), 153.76 (C-4, C-5); uv (H_2O) λ_{max} absorbances: 316, 332, 346 nm; ir (KBr) ν_{max}: 3 500 cm^{-1} (Ar*O*—*H*), 1 200 cm^{-1} (S=O).

In-situ ^{1}H NMR studies of the reaction with 1:2 and 1:1 molar ratios of formaldehyde and ***1***

In 15 mL of deionized organic-free water 1.0 g of **1** was treated with either 1.0 or 2.0 mL of aqueous 1.32 *M* methanol-free formaldehyde and the mixture refluxed. One-mL aliquots were removed periodically and were evaporated to dryness. The residues were each redissolved in 0.3 mL of D_2O and their 60 MHz NMR spectra were recorded.

Preparation of adduct ***9***

The 1:1 chromotropic acid – formaldehyde adduct was prepared exactly in the same way as described below for **12** except that equimolar amounts of **1** and formaldehyde were used. The resulting cherry-red reaction mixture was chromatographed on Sephadex LH-20 in the same manner as for **12**. Only one major component was isolated, and its spectral properties was consistent with the structure **9**: ^{1}H NMR (D_2O) δ ppm: 8.10 (s, C_1- and C_8-protons); ^{13}C NMR (D_2O) δ ppm: 26.94 (C-11, methylene bridge carbon), 117.48 (C-10), 119.28 (C-3 and C-6), 120.01 (C-1 and C-8), 130.45 (C-9), 140.03 (C-2 and C-7), 151.52 (C-4 and C-5); uv (H_2O) λ_{max} absorbances: 320, 337, 353 nm.

Preparation of adduct ***12***

To a solution of 876 mg (2.04 mmol) of purified **1** in 10.0 mL of deionized organic-free water was added 0.87 mL (1.1 mmol) of aqueous 1.32 *M* methanol-free formaldehyde solution. The reaction mixture was heated and maintained at gentle refluxing while the formaldehyde solution was added dropwise over 40 min. After completion of the addition the mixture was refluxed for a further 20 min. The reaction mixture was cooled and concentrated to approximately 6 mL on a rotatory evaporator. This concentrate was fractionated on a 2.0 cm × 25 cm open glass column packed with 20 g Sephadex LH-20 gel in water. The eluting solvent used was deionized organic-free water at a flow rate of 2 mL/min. Approximately thirty 10-mL fractions were collected. Those fractions having similar uv–visible absorbances were combined and evaporated to dryness. Two components were isolated and characterized. Fractions 10–12 contained 235 mg (27%) of a product whose ir, uv–vis, and ^{1}H NMR spectra, and R_f on paper chromatography were identical to those of **1**. Fractions 13–16 contained 475 mg (55%) of **12**: ^{1}H NMR (D_2O) δ ppm: 5.03 (s, methylene protons), 7.00 (d, J = 2 Hz, 1H, C_3—H), 7.83 (d, J = 2 Hz, 1H, C_1—H); 8.17 (s, 1H, C_8—H); ^{13}C NMR (D_2O) δ ppm: 26.73 (C-11, methylene bridge carbon), 106.96 (C-6), 117.26 (C-10), 118.08 (C-8), 118.96 (C-3), 120.35 (C-1), 132.94 (C-9), 140.98 (C-2 and C-7), 152.21 (C-5), 153.65 (C-4); uv (H_2O) λ_{max} absorbances: 320, 337, 353 nm; ir (KBr) λ_{max}: 3 500 cm^{-1} (Ar*O*—*H*), 1 200 cm^{-1} (S=O).

Preparation of ***13****, the tetra-acetate of adduct* ***12***

In 0.033 mL of 6.1 *M* aqueous sodium hydroxide solution was dissolved 37 mg (5.0×10^{-5} mol) of adduct **12**. The mixture was cooled to 0°C and 0.019 mL (2.0×10^{-4} mol) of acetic anhydride was added with stirring. The resultant pale reddish solution was stirred with cooling for 5 min. The sodium acetate produced in the reaction was removed by precipitating it as insoluble silver acetate with an aqueous solution of silver nitrate. After the insoluble silver acetate was filtered off the filtrate was concentrated down to approximately 0.6 mL and fractionated on a 10 cm × 1 cm open-glass column packed with approximately 0.7 g of Sephadex LH-20 gel in water. The eluate was collected as thirty 0.5-mL fractions which were examined by uv–vis spectroscopy. Those fractions having similar absorbances were combined and evaporated to dryness. Seven milligrams of a product whose spectral properties were consistent with the structure **13** was obtained: ^{1}H NMR (D_2O) δ ppm: 1.97 (s, 6H), 2.08 (s, 6H), 5.13 (s, methylene protons, 2H), 7.63 (d, J = 2 Hz, 2H, C_3—H), 8.47 (d, J = 2 Hz, 2H, C_1—H); 8.73 (s, 2H, C_8—H); uv (H_2O) λ_{max} absorbances: 319, 334, 356 nm.

Calibration line determinations

(*a*). Modified NIOSH procedure. The basic NIOSH procedure was followed for the determination of calibration lines for standard formaldehyde solutions with the following modifications (15): The standard formaldehyde solutions and the aqueous chromotropic acid solutions were freshly prepared on each day that calibration lines were determined. Purified **1** was used to prepare 5% aqueous solutions in deionized organic-free water. A 1.00 L stock solution containing 4.470 g of sodium formaldehyde bisulphite was used. The standard formaldehyde solutions were prepared from a solution whose formaldehyde concentration was 10 μg/mL prepared from the stock solution. Seven standard solutions were prepared by pipetting 0.00, 0.50, 1.0, 2.0, 3.0, 4.5, and 6.0 mL of the 10 μg/mL solution into 25-mL volumetric flasks. These were made up to 25 mL with the appropriate amounts of deionized organic-free water. These solutions correspond to aqueous formaldehyde concentrations of 0.00, 0.20, 0.40, 0.80, 1.2, 1.8 and 2.4 μg/mL, respectively.

Two-mL aliquots of each of the seven standard solutions were pipetted into separate clean 25-mL glass culture tubes. To each of these solutions 300 μL of aqueous 5% chromotropic acid solution was added and thoroughly mixed by vortexing. Three mL of concentrated sulphuric acid (96%) was added to each tube cautiously in order to avoid spattering. The mixtures were thoroughly vortexed. The tubes were sealed with Parafilm and were capped loosely with Teflon-lined screw caps and were placed in a boiling water bath for 1 h. The tubes were cooled to room temperature and were again thoroughly mixed with a vortex to prevent layering prior to the removal of samples for spectrophotometric determinations. Absorbances were measured at 580 nm using 1.0 cm optical glass cells. The spectrophotometer was zeroed against analytical blanks. The analytical blanks corresponding to a 0.00 μg/mL formaldehyde solution consisted of 2.00 mL deionized organic-free water, 300 μL of aqueous 5% chromotropic acid solution, and 3.00 mL of concentrated sulphuric acid (96%). The analytical blanks were treated in an identical manner as the solutions which contained formaldehyde.

(*b*). Effect of different concentrations of sulphuric acid. The procedures described above in (*a*) were employed with the following modifications:

(*i*) 10.2 *M* solutions. Seven standard solutions were prepared by pipetting 0.0, 0.90, 1.8, 3.6, 5.4, 8.0, and 10.7 mL of the 10 μg/mL solution into 25-mL volumetric flasks. These were made up to 25 mL with the appropriate amounts of deionized organic-free water. These solutions correspond to aqueous formaldehyde concentrations of 0.00, 0.36, 0.71, 1.4, 2.1, 3.2, and 4.3 μg/mL, respectively. After treatment of the standard solutions, a calibration line slope of 0.21 AU/(μg/mL) was obtained.

(*ii*) 4.10 *M* solutions. The exact procedures described above in (*a*) were employed except that aqueous sulphuric acid (38%) was used. No colour could be formed after treatment of these solutions.

(*iii*) Reconstituted 4.10 *M* solutions. Two-mL aliquots of the chromogen-containing solutions obtained in (*i*) which are 10.2 *M* in sulphuric acid were removed and each was diluted with 3.0 mL deionized organic-free water. The mixtures were thoroughly mixed by vortexing. The resulting solutions correspond to formaldehyde concentrations of 0.00, 0.14, 0.29, 0.57, 0.89, 1.3, 1.7 μg/mL, respectively. No additional heating was conducted on these solutions. A calibration line slope of 0.21 AU/(μg/mL) was obtained.

(*iv*) Reconstituted 10.2 *M* solutions. To each of the solutions from (*ii*) which are 4.10 *M* in sulphuric acid, was added 4.15 mL of concentrated (96%) sulphuric acid. The mixtures were thoroughly mixed by vortexing. The resulting solutions correspond to formaldehyde concentrations of 0.00, 0.20, 0.40, 0.80, 1.2, 1.8, 2.4 μg/mL, respectively. A calibration line slope of 0.20 AU/(μg/mL) was obtained after heating for 1.0 h.

(*c*) Calibration line determination using adduct **12**. A 500 mL stock

aqueous solution containing 38.6 mg of a sample of **12** was prepared in a volumetric flask. The molar mass of **12** was assumed to be 740 g/mol and the equivalent formaldehyde concentration of the stock solution was calculated to be 3.12 μg/mL. Six standard diluted solutions containing the equivalent formaldehyde concentrations of 0.00, 0.20, 0.40, 0.80, 1.2, and 1.6 μg/mL, respectively, were prepared by appropriate dilutions of the stock solution with deionized organic-free water. Two-mL aliquots of each of these solutions were pipetted into separate 25-mL glass culture tubes. A duplicate set of these six solutions was also prepared. To each culture tube in the first set was added 300 μL of deionized organic-free water and the solutions thoroughly mixed by vortexing. Three mL of concentrated sulphuric acid (96%) was cautiously added to each tube and the mixtures thoroughly vortexed. To each culture tube of the second set was added 300 μL of aqueous 5% chromotropic acid solution and the solutions thoroughly mixed by vortexing. Three mL of concentrated sulphuric acid (96%) was cautiously added to each tube and all subsequent operations were conducted as described previously above in (*a*). A control set of six standard formaldehyde solutions was prepared exactly as described in (*a*) except that the highest formaldehyde concentration was 1.8 μg/mL. The calibration line slopes measured were 0.096 AU/(μg/mL) for the first set of solutions prepared from **12** which did not contain the added 5% aqueous chromotropic acid solution: 0.23 AU/(μg/mL) for the second set of solutions prepared from **12** which did contain the added 5% aqueous chromotropic acid solution; and 0.23 AU/(μg/mL) for the control set of solutions which were prepared from sodium formaldehyde bisulphite.

Results and discussion

The formation of the *para,para*-quinoidal adduct **2**, the alternative *ortho,ortho*-quinoidal adduct **7**, and/or the *ortho,para*-quinoidal adduct **8** can all be envisioned to be formed by pathways similar to those known for the condensation of formaldehyde and phenol (16).

Nuclear magnetic resonance spectroscopy appeared to be the best method for determining the exact position on **1** where condensation of formaldehyde occurs. Both the ^{1}H and ^{13}C NMR spectra of **1** were first unambiguously defined (14). During the course of these assignments, a regioselective hydrogen–deuterium exchange of the 7.20 ppm ^{1}H NMR signal was observed. The corresponding ^{13}C NMR spectrum revealed that the intensity of the signal at 106.44 ppm due to C-3 and C-6 was diminished by over 90%, all other signals remaining unchanged. Thus the C-3 (and C-6) position of **1** was the most reactive for the deuterium exchange. If the reactivity of **1** towards deuterium oxide is assumed to be similar to that towards formaldehyde, the fact that only this regioselective hydrogen–deuterium exchange occurs suggested that the chromotropic acid – formaldehyde adduct is the *ortho,ortho*-product and not **2**, or **8**. In principle, the analytical reaction could be monitored directly by NMR. These solutions, however, contain large excesses (240 – 3 000-fold) of **1** relative to formaldehyde, thereby precluding the use of even a high-resolution NMR instrument. Experiments were therefore conducted with larger concentrations of reagents which would permit direct monitoring in a 60 MHz NMR spectrometer. Molar ratios of formaldehyde to **1** of only 1:1 and 1:2 were employed.

The reactions at either molar ratio in the presence of catalytic amounts of sulphuric acid were found to be too rapid to monitor. A typical series of the low-field region of the spectra obtained when only water was used without any sulphuric acid, is presented in Fig. 1. Figure 1*b* taken after 0.5 h shows that new signals appeared in the aromatic region at 8.25 and 7.86 ppm and that there were changes in the chemical shifts and line shapes of the signals of **1**. In addition, a new signal appeared at

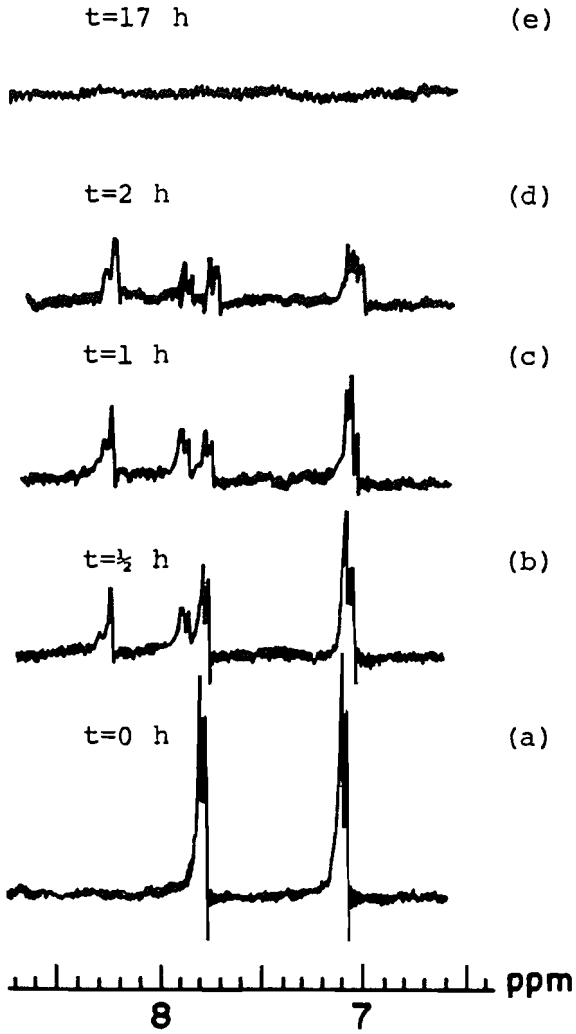


FIG. 1. Time series of nuclear magnetic resonance spectra of 1:2 molar ratio of chromotropic acid to formaldehyde in deuterium oxide.

5.40 ppm (not shown) presumably due to methylene protons. After 1.0 h the lowest field signals consisted of two singlets, a smaller one at approximately 8.30 ppm, and the larger one at 8.25 ppm. The two doublets at 7.90 and 7.80 ppm had similar coupling constants, J = 2 Hz. The signals centered at 7.10 ppm consisted of two overlapping doublets, of similar intensities and coupling constants, J = 2 Hz. No major significant changes were evident in the spectra recorded after 2.0 h up to 4.0 h. After refluxing for 17 h, however, all the aromatic region signals apparently disappeared. The high viscosity of the resulting solution, however, could account for this last observation.

When the 1:1 molar ratio of formaldehyde to **1** (or when a large excess of formaldehyde was used) was reacted and followed as above, a different series of NMR spectra was obtained. Typical low-field spectra are shown as Fig. 2. Figure 2*d* shows a spectrum recorded at 1.0 h which indicated that **1** had nearly all been consumed as the signals originally centered at 7.15 ppm had all but disappeared. The lowest field signals consisted of two singlets, as noted previously except that now the lower field singlet was the larger of the two. In addition, a methylene peak centered at 5.60 ppm (not shown) was observed. After 4.0 h all the aromatic region signals had disappeared except for a sharp singlet at 8.20 ppm. The signal due to the methylene protons was still present, but shifted

Can. J. Chem. Downloaded from www.nrcresearchpress.com by 41.223.56.140 on 09/07/12
For personal use only.

Can. J. Chem. Downloaded from www.nrcresearchpress.com by 41.223.56.140 on 09/07/12
For personal use only.

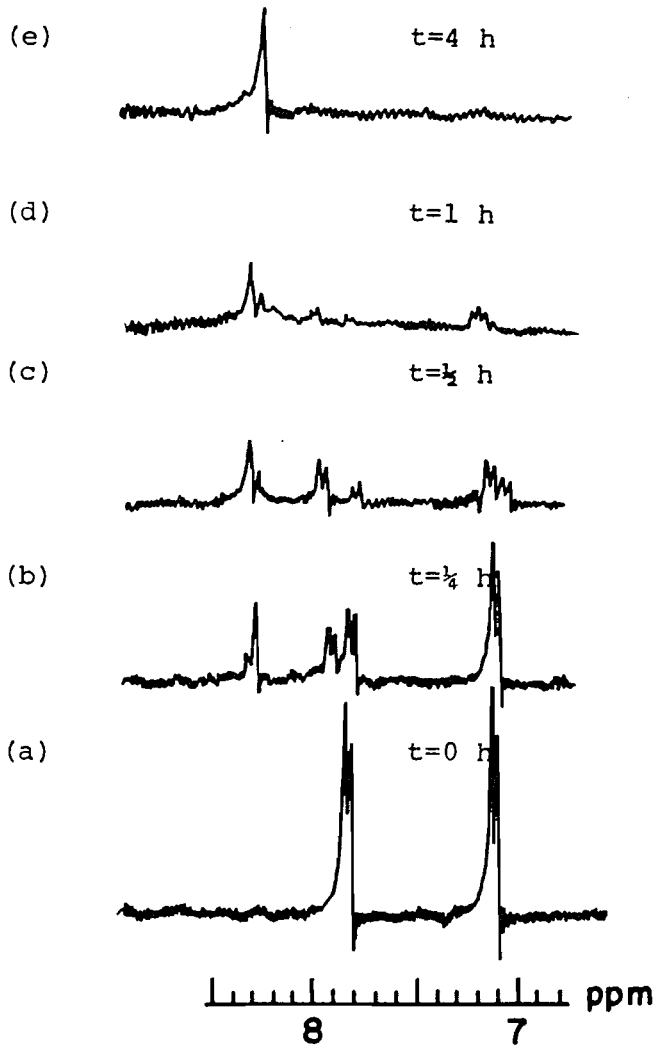
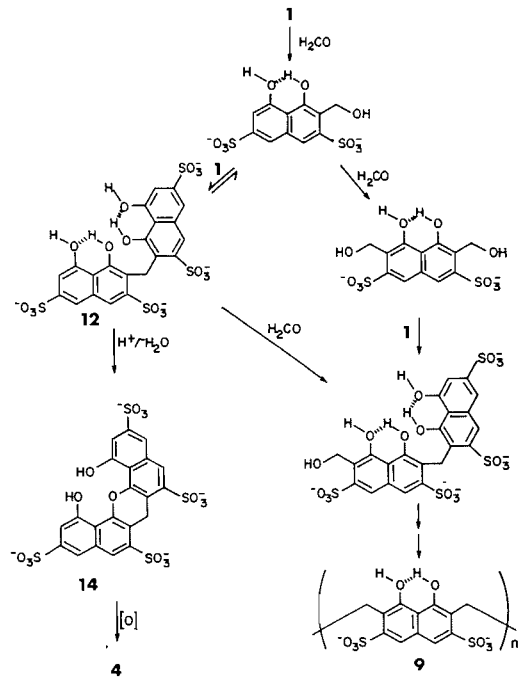


FIG. 2. Time series of nuclear magnetic resonance spectra of 1:1 molar ratio of chromotropic acid to formaldehyde in deuterium oxide.

to 4.90 ppm (not shown). It therefore appeared that cleaner reaction mixtures were being formed when the 1:1 conditions were employed. All attempts at separating the components of the reaction mixtures obtained under either sets of conditions using several different standard techniques, proved to be futile as were attempts to crystallize the product(s).

The proton-decoupled ^{13}C NMR spectrum of the crude product obtained from the 1:1 conditions showed only 7 signals. This spectrum indicated that the signal due to C-3 (and C-6) in chromotropic acid was the most affected with its chemical shift changing from 106.44 ppm in **1** to 119.28 ppm in the reaction product. The additional signal at 26.94 ppm was presumably due to a methylene carbon (17). The simplicity of the spectrum suggested that a highly symmetrical product was formed. In the 300 MHz ^1H NMR spectrum only a singlet in the aromatic region at 8.10 ppm and a singlet at 4.85 ppm was observed. This suggested that the crude product obtained was a linear polymer of formaldehyde and **1**, linked in the *ortho,ortho* positions as shown in structure **9**. The two-dimensional $^1H-^{13}C$ chemical shift correlation (18) spectrum and the attached-proton test (18) (APT) of **9** was consistent with the assigned structure.

To compare spectra with those obtained in the in-situ experiments, the mono- and dibromo derivatives **10**, **11** were



SCHEME 1

synthesized (19, 20). The ^1H NMR spectrum of **10** was similar to that of **9** but that of **11** was more revealing, showing one singlet and two doublets in the aromatic region. Its two-dimensional $^1H-^{13}C$ chemical shift correlation spectrum and the APT were also consistent with the assigned structure (14). The NMR spectra of **11** provided essential information for interpretation of the spectra obtained earlier in the in-situ experiments. These indicated that a monosubstituted chromotropic acid – formaldehyde adduct was likely being formed in the earlier stages of the reaction. Subsequently, the adduct was being converted in the presence of excess formaldehyde into the disubstituted *ortho–ortho* linear polymer **9**. Other intermediate adducts as outlined in Scheme 1 could also be formed. The in-situ spectra also indicated that after 1.0 h the optimal amounts of mono-substituted adduct could be obtained when using the 1:2 molar ratio conditions. Unreacted **1** itself was always present.

The reaction could be terminated after approximately 1.0 h by rapidly evporating the solvent and any unreacted formaldehyde under high vacuum. Some of the components of these mixtures were separated by gel permeation chromatography (21) using Sephadex LH-20. The major components that could be identified were **1** (25–30%) and a new compound **12** (55–60%). The two-dimensional $^1H-^{13}C$ chemical shift correlation spectrum and the APT of **12** was consistent with the proposed structure except that the ^{13}C NMR spectrum consisted of only ten discernable carbon signals when eleven carbon signals were predicted. Peak height comparisons in ^{13}C NMR spectra are generally unreliable (18) nevertheless, for the series of compounds that were described above, the peak heights of the ^{13}C signals due to C-4 and C-5 (those carbon atoms which are attached to the hydroxyl groups) were clearly very similar to those of the ^{13}C signal of C-2 and C-7 (those carbon atoms which are attached to the sulphonic acid groups). In the spectra of **12**, however, the combined peak heights of the carbon signals at 153.65 and 152.21 ppm assigned to C-4 and C-5 in **12** were approximately only one-half of the peak height of the signal at 140.98 ppm. This latter signal whose chemical shift is

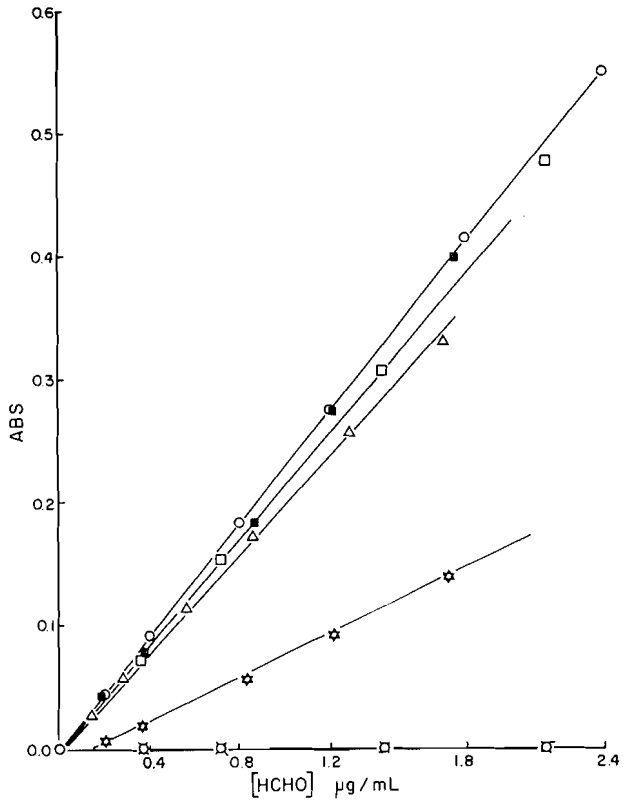


FIG. 3. Calibration lines for chromotropic acid and standard formaldehyde solutions with varying sulphuric acid concentrations; and for standard solutions derived from the adduct **12**, with concentrated sulphuric acid. □, 10.2 *M* H_2SO_4 solutions, slope = 0.21; △, 10.2 *M* H_2SO_4 solutions diluted to 4.10 *M*, slope = 0.20; ⊠, 4.10 *M* H_2SO_4 solutions, slope = 0; ○, 4.10 *M* H_2SO_4 solutions increased to 10.2 *M*, slope = 0.23; ✡, adduct **12** only, slope = 0.096; ■, adduct **12** + chromotropic acid, slope = 0.23.

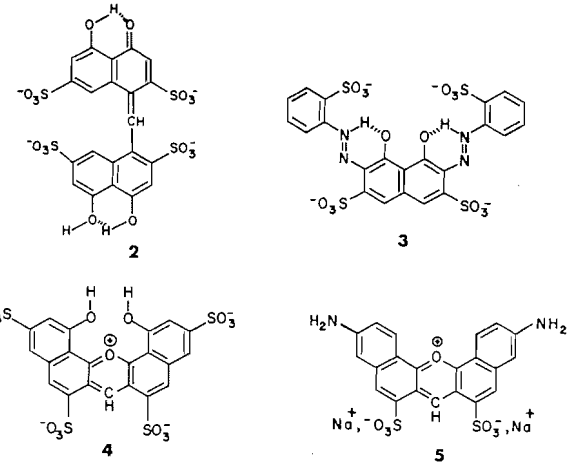
consistent with the shifts associated with C-2 and C-7 in **1** and its derivatives described above, was therefore assigned to *both* carbon atoms C-2 and C-7 in **12**. Acetylation of **12** afforded a tetra-acetoxy compound **13** whose ^1H NMR spectrum was similar to that of **12** but which in addition showed clearly two different types of acetate methyl groups. These experiments provided additional strong evidence that reaction of formaldehyde occurs at C-3 (or C-6) of **1**.

The purple chromogen could also be produced using concentrated hydrochloric acid, concentrated perchloric acid, and 85% phosphoric acid but not with glacial acetic acid. Calibration lines were determined for each of the above acids in the usual way using standard formaldehyde and 5% aqueous solutions of **1**. Concentrated sulphuric acid (96%), however, was found to give the highest calibration line slope (0.23 AU/(μg/mL)). Since sulphuric acid appeared to be the optimal acid to use, the effect of using different acidic concentrations was examined. Concentrated (96%) or diluted sulphuric acid (38%) were then compared, affording solutions which were 10.2 *M* and 4.10 *M* in sulphuric acid, respectively. After heating, only the former solutions developed the purple chromogen. The purple solutions were diluted by the addition of water in proportions such that the sulphuric acid concentrations were reduced to 4.10 *M*. The calibration line slopes derived from these diluted solutions were equivalent to those obtained before the dilution. Thus the chromogen formed originally with concentrated sulphuric acid could still exist in the 4.10 *M* sulphuric acid solutions. When concentrated sulphuric acid was added to the original 4.10 *M* sulphuric acid solutions the calibration line slopes of these reconstituted solutions were identical to the previously obtained slopes within experimental error implying that the chromogen formation was therefore not simply pH-dependent alone. These results are shown in Fig. 3.

Using chromatographically-pure **12** several attempts to isolate and characterize the polar chromogen were unsuccessful, due to its very high water solubility. The only compounds that could be recovered consistently were **1** and unreacted **12**. Nuclear magnetic resonance experiments revealed that **12** could decompose in aqueous solution to regenerate **1**. An experiment to show inferrentially that **12** was the precursor of **4** via **14** was then undertaken. An aqueous 1.04×10^{-4} *M* solution of **13** was prepared and from this solution, five aqueous solutions were prepared by appropriate dilution. One mole of formaldehyde per mole of the adduct **12** was assumed to be present, and the five solutions which were prepared had formaldehyde equivalent concentrations in the range normally employed in the analytical calibration line determinations. Two-mL aliquots of these solutions were treated with 300 μL of deionized organic-free water and 3.0 mL of concentrated sulphuric acid in a manner exactly analogous to the NIOSH procedures. As a control, the usual standard formaldehyde calibration line was also determined. The slopes were found to be different: 0.23 AU/(μg/mL) for the control solutions, and 0.096 AU/(μg/mL) for those prepared from the adduct.

The analytical solutions normally contain a large excess of **1** over the formaldehyde that is being determined. A true comparison between the absorbances measured from the solutions derived from **12** could only be made if the 300 μL of 5% aqueous **1** was also present. Therefore, replicate sets of the five solutions prepared previously from the aqueous solution of **12** were prepared and each solution was treated as before except that each now contained 300 μL of 5% aqueous **1** instead of only the 300 μL amount of water. The calibration lines were again determined in the usual way. The slopes now obtained were found to be identical to those of the controls. Typical results are included in Fig. 3. From these slopes the absorptivity for the chromogen was calculated to be $1.8 \times 10^4\ M^{-1}\ cm^{-1}$ which is two- to four-fold greater than those values reported previously (22).

All of the evidence presented above is consistent with a mono-cationic dibenzoxanthylium structure for the chromogen and not the *para,para*-quinoidal one that is commonly cited. The experimental data suggests that the first step in the



Can. J. Chem. Downloaded from www.nrcresearchpress.com by 41.223.56.140 on 09/07/12
For personal use only.

analytical reaction is the reversible formation of an adduct such as **12**. The second step involves the dehydration by a strong acid to form the dibenzoxanthene-type compound **14**. The oxidation of such a compound once formed should be facile since it can produce the mono-cationic dibenzoxanthylium species **4** which is planar and contains 22 π electrons, and satisfies the Huckel $(4n + 2)$ rule for aromaticity. The calibration line observations provided additional evidence that an equilibrium reaction exists in which the excess **1** shifts the equilibrium favourably toward the direction of the optimal chromogen formation. Scheme 1 shows a likely mechanism for the reaction.

Conclusions

The site of the reaction of formaldehyde with chromotropic acid in aqueous or aqueous acidic conditions most likely occurs on the carbon atom which is *ortho-* to both the hydroxyl and sulphonic acid groups. An adduct containing a methylene bridge formed by the coupling of a single molecule of formaldehyde between two molecules of chromotropic acid could be isolated and characterized by ^{1}H and ^{13}C NMR spectroscopy. Attempts at crystallization of this adduct were unsuccessful, however, the adduct has been shown to undergo a retro-addition equilibrium in aqueous solution. Using calibration line studies, with a large excess of chromotropic acid, the adduct was shown to be a precursor of the same chromogen that is observed in the NIOSH analytical method. Its formation is not simply a function of pH alone. It is hypothesised that a dehydration step is first required to produce a dibenzoxanthene-type compound which then undergoes facile oxidation to produce the corresponding mono-cationic dibenzoxanthylium structure. The mono-cation is planar and obeys the Huckel $(4n + 2)$ rule for aromaticity.

Finally, the often-quoted *para,para*-quinoidal structure for the chromogen appears to be very unlikely and concentrated sulphuric acid appears to be the optimal acid to use in the method. Therefore, simple modifications to the procedure would not seem to be feasible in light of the understanding of the reaction gained during this study.

Acknowledgements

The authors wish to thank Dr. C. J. Jablonski and Mr. A. Earle for their invaluable advice and recording of all the high resolution proton and carbon-13 nuclear magnetic resonance spectra. We also thank the Department of Chemistry, Memorial University of Newfoundland, for its financial support to C.K.H.

1. A. Butlerov. Ann. **111**, 242 (1859).
2. B. Meyer, B. A. K. Andrews, and R. M. Reinhardt (*Editors*). Formaldehyde release from wood products. Am. Chem. Soc. Symp. Ser. Vol. 316. Am. Chem. Soc. Washington, DC. 1986.
3. P. E. Georghiou, D. Snow, and D. T. Williams. Environment Int. **9**, 279 (1983).
4. M. Katz (*Editor*). Methods of air sampling and analysis. 2nd ed. American Public Health Association Intersociety Committee, American Public Health Association, Washington, DC. 1977. pp. 300–307.
5. E. Eegriwe. Z. Anal. Chem. **110**, 22 (1937).
6. F. Feigl. Spot tests in organic analysis. 7th ed. Elsevier Publishing Co., Amsterdam. 1966. pp. 434–438.
7. E. L. R. Krug and W. E. Hirt. Anal. Chem. **49**, 1865 (1977).
8. B. A. K. Andrews and R. M. Reinhardt. *In* Formaldehyde, analytical chemistry and toxicology. *Edited by* V. Turoski. Am. Chem. Soc. Adv. Chem. Ser. Vol. 210. Am. Chem. Soc. Washington, DC. 1985. p. 88.
9. B. Budesinsky. *In* Chelates in analytical chemistry. Vol. 2. *Edited by* H. A. Flaschka and A. J. Barnard. Marcel Dekker Inc., New York. 1969.
10. M. Kamel and R. Wizinger. Helv. Chim. Acta. **79**, 594 (1960).
11. A. S. Olansky and S. N. Deming. Anal. Chim. Acta, **83**, 241 (1976).
12. C. W. Lee, Y. S. Fung, and K. W. Fung. Analyst, **107**, 30 (1982).
13. E. Sawicki, T. R. Hauser, and S. McPherson. Anal. Chem. **34**, 1460 (1962).
14. C. K. Ho. M.Sc. thesis. Memorial University of Newfoundland, St. John's, Nfld. 1987.
15. R. R. Miksch. Formaldehyde in air. A revised NIOSH procedure. Lawrence Berkeley Laboratory Report, Lawrence Berkeley Laboratory, Berkeley, CA. 1980.
16. K. P. C. Vollhardt. Organic chemistry. W. H. Freeman & Co., New York. 1987. pp. 1115, 1116.
17. R. A. Pethrick and B. Thomson. Brit. Polymer J. **18**, 380 (1986).
18. J. K. M. Saunders and B. K. Hunter. Modern NMR spectroscopy. A guide for chemists. Oxford University Press, Oxford. 1987.
19. J. Maslowska and J. Duda. Chem. Anal. **23**, 805 (1978).
20. V. I. Kuznetsov and N. N. Basargin. Zh. Obsch. Khim. **35**, 879 (1965).
21. R. L. Reeves, R. S. Kaiser, and K. T. Finley. J. Chromatogr. **47**, 217 (1970).
22. J. A. Alfheim and C. H. Langford. Anal. Chem. **57**, 861 (1985).

Can. J. Chem. Downloaded from www.nrcresearchpress.com by 41.223.56.140 on 09/07/12
For personal use only.

Structure of the capsular polysaccharide antigen of type IV group B *Streptococcus*[1]

JOSE L. DI FABIO,[2] FRANCIS MICHON,[2] JEAN-ROBERT BRISSON, AND HAROLD J. JENNINGS[3]
Division of Biological Sciences, National Research Council of Canada, Ottawa, Ont., Canada K1A 0R6

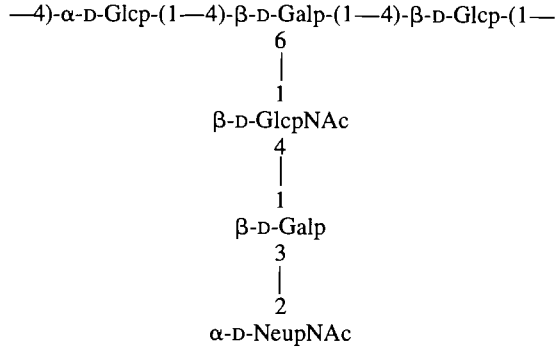
AND

MICHAEL R. WESSELS, VICENTE-JAVIER BENEDÍ, AND DENNIS L. KASPER
Channing Laboratory, Department of Medicine, Brigham and Women's Hospital and Division of Infectious Diseases, Beth Israel Hospital, Harvard Medical School, Boston, MA 02115, U.S.A.

Received October 20, 1988

JOSE L. DI FABIO, FRANCIS MICHON, JEAN-ROBERT BRISSON, HAROLD J. JENNINGS, MICHAEL R. WESSELS, VICENTE-JAVIER BENEDÍ, and DENNIS L. KASPER. Can. J. Chem. **67**, 877 (1989).

The native polysaccharide antigen isolated from type IV group B *Streptococcus* contains D-galactose, D-glucose, 2-acetamido-2-deoxy-D-glucose, and sialic acid in the molar ratio 2:2:1:1 and is composed of the following repeating unit:

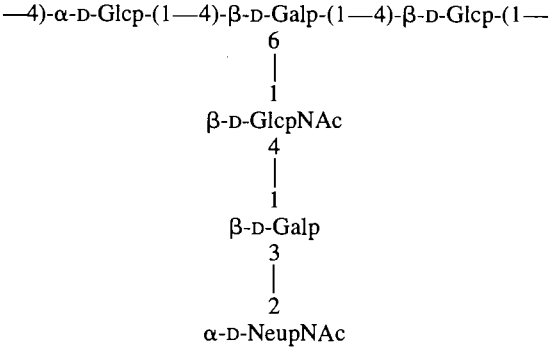


The structural analysis of this antigen was based on results obtained from methylation analysis, partial hydrolysis, nitrous acid deamination, and nuclear magnetic resonance spectroscopic techniques.

Key words: capsular polysaccharide, high resolution NMR spectroscopy, group B *Streptococcus*, polysaccharide structure, polysaccharide degradation.

JOSE L. DI FABIO, FRANCIS MICHON, JEAN-ROBERT BRISSON, HAROLD J. JENNINGS, MICHAEL R. WESSELS, VICENTE-JAVIER BENEDÍ et DENNIS L. KASPER. Can. J. Chem. **67**, 877 (1989).

Le polysaccharide naturel de l'antigène extrait du *Streptococcus* du type IV du groupe B contient du D-galactose, du D-glucose, de l'acétamido-2 désoxy-2 D-glucose et de l'acide sialique dans un rapport molaire de 2 : 2 : 1 : 1 et il est composé de l'unité de base suivante :



L'analyse de la structure de cet antigène est basée sur les résultats obtenus à l'aide de techniques de méthylation, d'hydrolyses partielles, de désaminations nitreuses et de spectroscopie en résonance magnétique nucléaire.

Mots clés : polysaccharide capsulaire, spectroscopie RMN de haute résolution, groupe B *Streptococcus*, structure du polysaccharide, dégradation du polysaccharide.

[Traduit par la revue]

Introduction

Group B *Streptococcus* (GBS) is a major cause of neonatal sepsis and meningitis. In early immunological studies, Lancefield characterized the type-specific polysaccharide antigens of GBS (1–3), which were isolated by hot hydrochloric acid extraction of the whole organisms (2, 3). While still retaining type-specificity, these acid extracted antigens are structurally and, in most cases, immunologically incomplete. They form the lower molecular weight core structures of their respective native antigens, which all contain additional terminal sialic acid residues (4–8). The structures of the types Ia, Ib, II, and III capsular polysaccharides have been elucidated (9–11), and the important role of sialic acid in the pathogenicity of GBS (12)

[1]NRCC No. 29974.

[2]Supported by IAF Biochem Int., des Prairies Blvd., Laval, P.Q., Canada H7V 1B7.

[3]Author to whom correspondence may be addressed.

Can. J. Chem. Downloaded from www.nrcresearchpress.com by 41.223.56.140 on 09/07/12
For personal use only.

Can. J. Chem. Downloaded from www.nrcresearchpress.com by 41.223.56.140 on 09/07/12
For personal use only.

TABLE 1. Sugar analysis of the native type IV GBS capsular polysaccharide and derived polysaccharides

Glycoses[a]	Molar ratio		
	Native	Core	Backbone
D-Glucose	1.81 (2)[b]	1.87 (2)	1.88 (2)
D-Galactose	2.02(2)	1.96 (2)	1.00 (1)
2-Acetamido-2-deoxy-D-glucose[c]	1.00 (1)	1.00 (1)	ND[e]
NANA[d]	0.93 (1)	ND	ND

[a]Analyzed as alditol acetates.
[b]Nearest integer ratios in parentheses.
[c]Measured as peracetylated 2,5-anhydromannitol.
[d]Analyzed by quantitative colorimetric method (18).
[e]ND: not detected.

and in the unique formation of conformational determinants critical to the immunogenicity of many of the GBS polysaccharides has been defined (13–15).

While the majority of the GBS isolates from human neonatal infections bear one of the above four major capsular types (Ia, Ib, II, and III), a number of previously non-typable GBS isolates have recently been identified as belonging to an antigenically distinct group, type IV (16). This serogroup is also based on a capsular antigen and its isolation, purification, and immunochemical characterization have been previously described (17). We now report the structural elucidation of the type IV GBS polysaccharide.

Results and discussion

The type IV GBS capsular polysaccharide had $[\alpha]_D$ + 9.0 (*c* 0.3, in water) and contained D-glucose, D-galactose, 2-acetamido-2-deoxy-D-glucose, and *N*-acetylneuraminic acid in the molar ratio of 2:2:1:1 (Table 1). The configuration of the glycoses was established by the characteristic retention times of their acetylated (-)-2-butanol glycosides (22) on capillary glc. Methylation analysis (Table 2) indicated that the type IV polysaccharide was composed of a branched hexasaccharide repeating unit, the branch point being a β-D-galactopyranosyl residue linked at O-4 and O-6. The presence of a fully methylated sialic acid derivative is indicative of a terminal sialic acid residue, and this is consistent with the known neuraminidase sensitivity of the sialic acid residues of the type IV polysaccharide (17). The other sugar residues present in the repeating unit are two glucopyranoses, both linked through O-4, a galactopyranose residue linked through O-3, and a 2-acetamido-2-deoxy-glucopyranosyl residue linked through O-4. The ^{1}H nmr spectrum (500 MHz at 27°C and 37°C) of the native type IV GBS polysaccharide indicated the presence of five anomeric signals (Table 3), only one of them corresponding to an α-D-linked hexopyranosyl residue, and two signals of equal intensity at 2.07 and 2.03 ppm corresponding to the respective *N*-acetyl groups of the 2-acetamido-2-deoxy-D-glucopyranose and *N*-acetylneuraminic acid residues in the repeating unit. A quartet at 2.75 ppm and a triplet at 1.81 ppm are similar in chemical shift to the respective signals associated with the equatorial and axial H-3 protons of an α-linked sialic acid residue. These results together with the ^{13}C nmr spectrum (125 MHz at 37°C) shown in Fig. 1, which exhibited six anomeric signals at 104.15, 103.48, 103.16, 101.56, 100.69, and 100.35 ppm, confirm that the type IV polysaccharide is composed of a hexasaccharide repeating unit.

TABLE 2. Methylation analysis of the native and modified type IV GBS polysaccharides

Methylated glycose derivatives[a]	Retention times[b]	Molar ratios[d]		
		Native	Core	Backbone
2,3,4,6-Tetra-*O*-methyl-D-galactose	1.00	–	1.2	–
2,3,6-Tri-*O*-methyl-D-galactose	1.27	–	–	1.0
2,3,6-Tri-*O*-methyl-D-glucose	1.29	2.1	2.3	1.8
2,4,6-Tri-*O*-methyl-D-galactose	1.34	1.0	–	–
2,3-Di-*O*-methyl-D-galactose	1.82	1.1	1.0	–
3,6-Di-*O*-methyl-*N*-methyl-*N*-acetyl-D-glucosamine	3.14	0.6	0.7	–
4,7,8,9-Tetra-*O*-methyl-*N*-methyl-*N*-acetyl-D-neuraminic acid[c]		+	–	–

[a]As the methylated alditol acetates.
[b]Retention times of the alditol acetates relative to 1,5-di-*O*-acetyl-2,3,4,6-tetra-*O*-methylgalactitol.
[c]Identified as the methyl ester methyl glycoside.
[d]+, slight non-quantitative response; –, not detected.

TABLE 3. Chemical shifts[a] (δ) and coupling constants[b] ($^3J_{1,2}$) of anomeric proton signals in the ^{1}H spectra of the native capsular polysaccharide and derived polysaccharides of the Type IV GBS

Glycosyl residue	Polysaccharide		
	Native	Core	Backbone
a	4.967 (brs)	4.967 (brs)	4.915 (3.5 Hz)
b	4.480 (brd)	4.471 (brd)	4.506 (7.6 Hz)
c	4.547 (brd)	4.563 (7.3 Hz)	4.560 (7.8 Hz)
d	4.611 (7.3 Hz)	4.621 (7.3 Hz)	—
e	4.547 (7.6 Hz)	4.471 (7.7 Hz)	—

[a]Measured at 37°C in D_2O with acetone as internal reference (δ = 2.225 ppm).
[b]In parentheses, Hz = hertz; brs = broad singlet; brd = broad doublet.

Following mild acid treatment of the native type IV polysaccharide, another polysaccharide called the core polysaccharide was obtained and had $[\alpha]_D$ + 17.0 (*c* 0.4, in water). Sugar analysis (Table 1) indicated only the loss of the sialic acid from the native polysaccharide, and this was confirmed by the absence of the aforementioned charactistic H-3a and H-3e of sialic acid in the ^{1}H nmr spectrum of the core polysaccharide. Methylation of the core polysaccharide (Table 2) shows that the 2,4,6-tri-*O*-methyl-galactose derivative of the native polysaccharide is replaced by a new 2,3,4,6-tetra-*O*-methyl-galactose derivative; thus in the native polysaccharide sialic acid must be α-(2–3)-linked to a galactose residue. Traces of a 3,4,6-tri-*O*-methylglucosamine derivative were detected in the methylation analysis of the core polysaccharide that could have originated from the partial removal, due to the mild acid treatment, of the terminal galactopyranosyl residues from O-4 of the 2-

TABLE 4. ^{1}H chemical shifts[a] of the backbone polysaccharide of type IV GBS

Residue	Protons						
	H-1	H-2	H-3	H-4	H-5	H-6	H-6′
a —4)-α-D-Glcp-(1—	4.915	3.59	3.86	3.69	4.26	3.83	3.92
b —4)-β-D-Galp-(1—	4.506	3.57	3.76	4.02	3.85	nd[b]	nd
c —4)-β-D-Glcp-(1—	4.560	3.36	3.66	3.70	nd	nd	nd

[a]Measured at 37°C in D_2O, assignments made from data obtained by homonuclear 2D shift correlated (H,H) COSY with one- and two-step relays.
[b]nd, not determined.

acetamido-2-deoxy-D-glucopyranose residues. The ^{1}H nmr spectrum (500 MHz at 37°C) of the core polysaccharide exhibited five anomeric signals (Table 3), with only one of them undergoing a considerable displacement in comparison with the equivalent signals of the native type IV polysaccharide. This particular signal at 4.547 and 4.471 ppm in the spectra of the native and core polysaccharides, respectively, can be assigned to the β-D-galactopyranosyl residue in the side chain of each of the polysaccharides.

Following removal of the *N*-acetyl groups of the native type IV polysaccharide by base treatment, the *N*-deacetylated polysaccharide was deaminated with nitrous acid. A new polymeric material was again obtained, which is henceforth referred to as the backbone polysaccharide. It had $[\alpha]_D$ + 39.0 (*c* 0.4, in water) and was composed of D-glucose and D-galactose in the molar ratio of 2:1 (Table 1). Methylation analysis of the backbone polysaccharide (Table 2) indicated that it had a linear structure in which all the glycose residues were linked through O-4. The ^{1}H nmr (500 MHz at 37°C) spectrum of the backbone polysaccharide exhibited three anomeric signals and the coupling constant ($^3J_{1,2}$ = 3.5 Hz) of one of them indicated that the backbone still retained the only α-D-linked glycose reside in the native type IV polysaccharide. This sugar was identified by further ^{1}H nmr analysis. Based on 2-D COSY and relay COSY experiments it was possible to assign most of the signals in the ^{1}H nmr spectrum of the backbone polysaccharide (Table 4). The signal at 4.915 ppm was assigned to one of the two glucopyranosyl residues, which could then be identified as the glycose residue having the α-D configuration (Table 3).

The remaining information required to reconstruct the repeating unit of the type IV polysaccharide was the sequence of the glycose residues in the backbone. This was ascertained from the ^{1}H nmr nOe data and is depicted in Fig. 2. Following assignment of the proton signals of the backbone polysaccharide, the anomeric signals of its component sugars were selectively irradiated and the observed nOe's are listed in Table 5. Irradiation of H1(a) gave enhancements on H2(a), H4(b), H5(b), and H6(b), indicating that the glucopyranose residue (a) is in the α-D configuration and linked to the β-D-galactopyranose residue (b) through O-4. Irradiation of H1(b) gave enhancements on H2(b), H3(b), H4(b), H5(b), and H4(c), thus confirming the β-D configuration of (b) and confirming that (b) is linked to the remaining β-D-glucopyranose residue (c) through O-4. The configuration of (c) and the fact that it is also

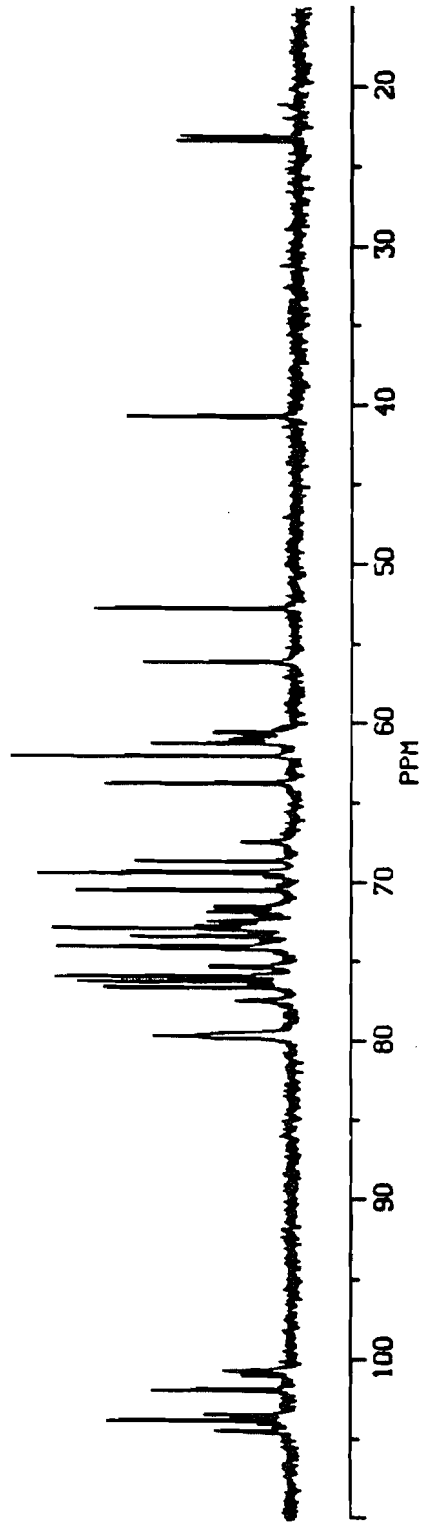


FIG. 1. The ^{13}C nmr spectrum of the native type IV GBS capsular polysaccharide.

Can. J. Chem. Downloaded from www.nrcresearchpress.com by 41.223.56.140 on 09/07/12
For personal use only.

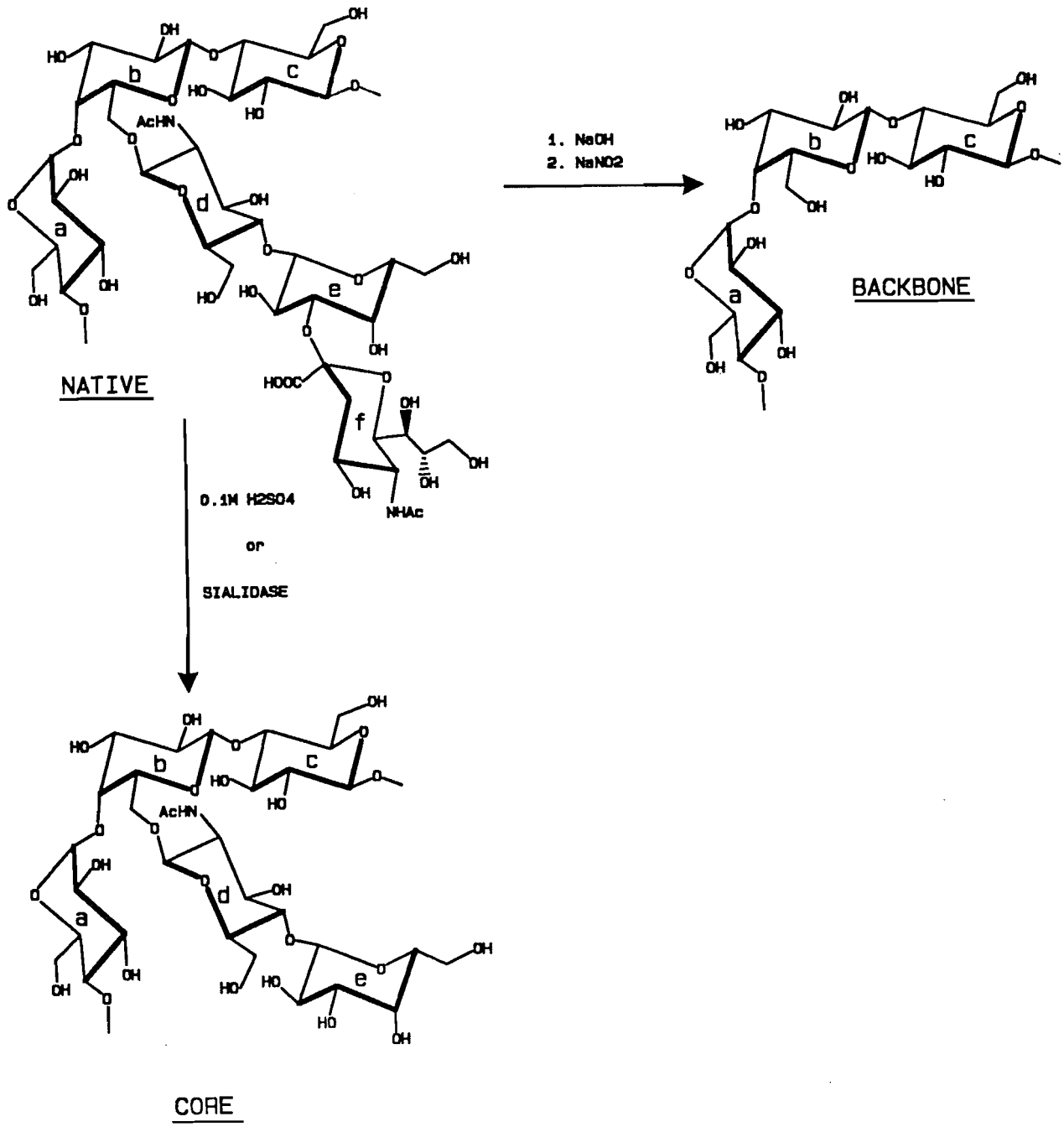


FIG. 2. Structure of the backbone and the core polysaccharide obtained by chemical and enzymatic degradations of the native antigen.

linked to O-4 of (a) was also confirmed by enhancements obtained on H2(c), H3(c), and H4(a) by irradiating H1(c).

Knowing the structure and sequence of the backbone polysaccharide, the structure of the core polysaccharide (Fig. 2) can easily be reconstructed from its glycose (Table 1), methylation (Table 2), and ^{1}H nmr (Table 3) analysis. It is obviously related to the backbone by the addition of a β-D-Galp-(1–4)-β-D-GlcpNAc branch (residues (e) and (d)) to O-6 of residue (b) of the backbone and this structure is consistent with the backbone being formed by deamination of the native polysaccharide (Fig. 2). Finally, glycose (Table 1) and methylation (Table 2) analysis of the native type IV polysaccharide indicate that it can be constructed from the core polysaccharide by the simple addition of α-linked sialic acid (f) to O-3 of its terminal β-D-galactopyranose residues (e). Thus the repeating unit of the type IV GBS polysaccharide is as depicted in Fig. 2.

The ^{13}C nmr spectrum of the type IV polysaccharide is shown in Fig. 1 and it is interesting to observe that some of the signals are sharper and hence more intense than others. This result can be explained in terms of the molecular dynamics of the polysaccharide, where the branches of the polysaccharide are much more flexible than its more rigid backbone. This was ascertained by the fact that the more intense signals, usually associated with the more flexible part of the polysaccharide (25), could all be readily assigned to the carbons in the branch consisting of residues (f), (e), and (d) (Fig. 2) as the signals had

Can. J. Chem. Downloaded from www.nrcresearchpress.com by 41.223.56.140 on 09/07/12
For personal use only.

TABLE 5. Nuclear Overhauser enhancements for the backbone polysaccharide of Type IV GBS

Proton saturated	Observed negative nOe[a]	
	Same residue	Other residues
H-1a	H-2a (4)	H-4b (5) H-5b (11) H-6b (8)
H-1b	H-2b (6) H-3b (12) H-4b (3) H-5b (4)	H-4c (9)
H-1c	H-2c (1) H-3c (6)	H-4a (14)

[a]Values in parentheses are percentage enhancements.

virtually identical chemical shifts to the corresponding signals previously assigned (26) to the free trisaccharide α-NeupNAc-(2–3)-β-D-Galp-(1–4)-β-D-GlcpNAc.

Comparison of the structure of the type IV polysaccharide with those of the other GBS polysaccharides (9–11) indicates that they are all constructed from the same glycose constituents, and all have extensive structural and sequence homology. All have terminal sialic acid linked to O-3 of β-D-galactopyranose, the closest structural homologue to the type IV polysaccharide being the type Ia polysaccharide (9). Both polysaccharides have identical trisaccharide branches and a common backbone disaccharide sequence. However, despite this extensive structural homology the type IV polysaccharide remains antigenically distinct (17). This is due in large part to the fact that the regions of structural homology in the types Ia and IV polysaccharides, and also in all the other GBS polysaccharides, are also present in human and animal tissues (14). For example, the terminal trisaccharide, α-NeupNAc-(2–3)-β-D-Galp-(1–4)-β-D-GlcpNAc, has been identified in fetuin (27, 28), M and N blood group substances (29), and human erythrocytes (30). Therefore because they are self antigens, the formation of antibodies to these structures common to the GBS polysaccharides is normally suppressed.

Another phenomenon associated with the GBS polysaccharides is that their sialic acid residues play a major role in controlling the conformations of the epitopes of the types Ia, II, and III polysaccharides (13–15). In contrast, it would appear that the type IV polysaccharide (17) resembles more that of type Ib (7, 8) in which this conformational dependence was not detected.

Experimenal

Materials

Type IV GBS strain 3139, Czechoslovak National Collection of Type Cultures (CNCTC), was kindly provided by Dr. J. Jélinková, Institute of Hygiene and Epidemiology, Prague. The growth of the organism and the isolation and purification of the capsular polysaccharide have been previously described (17).

Analytical methods

Sialic acid was determined by the method of Aminoff (18). Solutions were concentrated below 50°C under diminished pressure in a rotatory evaporator. Gel filtration was done on columns of Sephadex G-100 (2.0×80 cm), Sephadex G-50 (2.0×80 cm), and Sephadex G-15 (2.0×40 cm) (Pharmacia Fine Chemicals) at 20°C using PBS buffer (0.01 M sodium phosphate, 0.15 M sodium chloride, pH 7.0) and (or) pyridinium acetate buffer (0.05 M, pH 4.5) as the eluants.

Instrumental methods

Optical rotations were determined on a Perkin–Elmer 243 instrument with 1-dm semimicro cells at 23±1°C.

Gas–liquid chromatography (glc) was performed on a Hewlett–Packard model 5830A instrument equipped with a flame ionization detector and a model 3380A electronic integrator. The following conditions were used with a capillary column (0.32 mm×25 m) of 007 bonded phase, fused silica OV-17 (Quadrex Corp.). Program A for alditol acetates: from 180°C to 240°C at 4°C/min; program B for methylated alditol acetates: from 200°C to 240°C at 1°C/min; and program C for methylated sialic acid derivatives: isothermal at 230°C. Combined gas–liquid chromatography – mass spectrometry (glc–ms) was carried out on a Hewlett–Packard 5985B instrument using the above capillary column and employing programs A, B, and C as described above and an ionization potential of 70 eV.

The ^{13}C nmr spectra were obtained with the samples in 5 mm diameter tubes at 27°C and 37°C, with a Bruker AM500 spectrometer operating at 125 MHz, in the pulsed Fourier transform mode with complete proton decoupling. The ^{1}H nmr spectra were recorded at 27°C and 37°C with a Bruker AM200 spectrometer operating at 200 MHz or a Bruker AM500 spectrometer operating at 500 MHz, in the pulsed Fourier transform mode. The chemical shifts (δ) are quoted relative to the CH_3 signal of internal acetone at 2.225 ppm for ^{1}H and 31.07 ppm for ^{13}C. Coupling constants are expressed in hertz.

Proton homonuclear shift correlated 2-D nmr experiments, COSY (19) and related COSY (20), were performed by using the standard pulse sequences provided by Bruker (DISB87). Quadrature detection in both dimensions was employed. The initial (t_1, t_2) matrices of 256×1024 data points were zero filled to 512×2048 points, providing 1.6 Hz/point digital resolution in the second domain. Resolution enhancement in both dimensions was done by the unshifted sine bell window function prior to Fourier transformation. Magnitude spectra symmetrized about the diagonal were used to represent data.

Heteronuclear shift correlation spectroscopy was performed by the CHORTLE technique (21). A total of 4000 scans for each of the five proton evolution times of 0.16, 0.40, 1.0, 2.4, and 3.2 ms was collected and data were processed to give a table of data correlating ^{1}H and ^{13}C chemical shifts.

Glycose analysis

Polysaccharide samples (0.5–1.0 mg) were hydrolyzed with 0.25 M sulfuric acid at 100°C for 16 h. The hydrolysate was neutralized with barium carbonate, filtered, and evaporated to dryness. The residue in water (0.6 mL) was then treated with 33% acetic acid (1 mL) and 5% sodium nitrite (1 mL) for 1 h at room temperature. The solution was deionized with Dowex 50 (h^+) ion-exchange resin and lyophilized, and the residue was analyzed by glc–ms (Program A) after conversion of the glycoses into their alditol acetates. The configuration of the glycoses was established by capillary glc of their acetylated (−)-2-butyl glycosides according to the method of Leontein *et al.* (22).

Methylation analysis

Samples (1.0–2.0 mg) were methylated using sodium methylsulfinylmethanide and methyl iodide in dimethylsulfoxide according to the Hakomori procedure (23). The products were purified with C18 Sep-Pak cartridges (Waters Associates). Methylated products were hydrolyzed with 0.5 M trifluoroacetic acid at 100°C for 16 h. After evaporation the hydrolyzates were reduced with sodium borodeuteride followed by acetylation, and examined by glc–ms (Program B). The methylated sialic acid was identified by glc–ms (Program C) as the methyl ester methyl glycoside obtained by methanolysis of the permethylated polysaccharide.

Preparation of the core polysaccharide

Purified capsular polysaccharide was treated with 0.1 M sulfuric acid at 80°C for 60 min. The solution was diluted, applied to a small column of AG3-X4A (acetate form) resin, eluted with water, and

Can. J. Chem. Downloaded from www.nrcresearchpress.com by 41.223.56.140 on 09/07/12
For personal use only.

freeze-dried. The solid was dissolved in pyridinium acetate buffer and applied to a small Sephadex G-15 column. The material eluting in the void volume corresponded to the core polysaccharide.

N-Deacetylation and deamination of the capsular polysaccharide

The capsular polysaccharide (20 mg) was dissolved in 2 M NaOH (3 mL) and sodium borohydride (50 mg) was added. The solution was heated at 100°C for 5 h. After neutralization with acetic acid, the solution was dialyzed and freeze-dried. The *N*-deacetylated capsular polysaccharide was then deaminated essentially by the method of Dmitriev *et al.* (24). The *N*-deacetylated material was dissolved in water (1.2 mL) and, following the addition of 33% aqueous acetic acid (2.0 mL), the solution was treated with 5% aqueous sodium nitrite (3.0 mL) for 1.5 h at room temperature. The reaction mixture was passed through Dowex 50 (H^+) ion-exchange resin, evaporated to dryness, and applied to a small Sephadex G-50 gel permeation column eluted with pyridinium acetate buffer. The void volume was collected.

Acknowledgement

We thank Fred Cooper for the glc–ms measurements.

1. R. C. LANCEFIELD. J. Exp. Med. **57**, 571 (1933).
2. R. C. LANCEFIELD. J. Exp. Med. **59**, 441 (1934).
3. R. C. LANCEFIELD. J. Exp. Med. **67**, 25 (1938).
4. R. C. LANCEFIELD and E. H. FREIMER. J. Hyg. **64**, 191 (1966).
5. H. RUSSELL and N. L. NORCROSS. J. Immunol. **109**, 90 (1972).
6. J. A. KANE and W. W. KARAKAWA. Infect. Immun. **19**, 983 (1978).
7. J. Y. TAI and E. C. GOTSCHLICH. J. Exp. Med. **149**, 58 (1979).
8. D. L. KASPER, C. J. BAKER, R. S. BALTIMORE, J. H. CRABB, G. SCHIFFMAN, and H. J. JENNINGS. J. Exp. Med. **149**, 327 (1979).
9. H. J. JENNINGS, E. KATZENELLENBOGEN, C. LUGOWSKI, and D. L. KASPER. Biochemistry, **22**, 1258 (1983).
10. H. J. JENNINGS, K-G. ROSSEL, E. KATZENELLENBOGEN, and D. L. KASPER. J. Biol. Chem. **258**, 1793 (1983).
11. M. R. WESSELS, V. POZSGAY, D. L. KASPER, and H. J. JENNINGS. J. Biol. Chem. **262**, 8262 (1987).
12. M. S. EDWARDS, D. L. KASPER, H. J. JENNINGS, C. J. BAKER, and A. NICHOLSON-WELLER. J. Immunol. **128**, 1278 (1982).
13. H. J. JENNINGS, C. LUGOWSKI, and D. L. KASPER. Biochemistry, **20**, 4511 (1981).
14. H. J. JENNINGS, E. KATZENELLENBOGEN, C. LUGOWSKI, F. MICHON, R. ROY, and D. L. KASPER. Pure Appl. Chem. **56**, 893 (1984).
15. R. E. SCHIFFERLE, H. J. JENNINGS, M. R. WESSELS, E. KATZENELLENBOGEN, R. ROY, and D. L. KASPER. J. Immunol. **135**, 4164 (1985).
16. J. JÉLINKOVÁ and J. MOTLOVÁ. J. Clin. Microbiol. **21**, 361 (1985).
17. M. R. WESSELS, V-J, BENEDÍ, H. J. JENNINGS, F. MICHON, J. L. DI FABIO, and D. L. KASPER. Infect. Immun. **57**, 1089 (1989).
18. D. AMINOFF. Biochem. J. **81**, 384 (1961).
19. A. BAX and R. FREEMAN. J. Magn. Reson. **44**, 542 (1981).
20. A. BAX and G. DROBNY. J. Magn. Reson. **61**, 306 (1985).
21. G. A. PEARSON. J. Magn. Reson. **64**, 487 (1985).
22. K. LEONTEIN, B. LINDBERG, and J. LONNGREN. Carbohydr. Res. **62**, 359 (1978).
23. S. HAKOMORI. J. Biochem. (Tokyo), **55**, 205 (1964).
24. B. A. DMITRIEV, L. V. BACKINOWSKY, V. L. LVOV, N. K. KOTCHETKOV, and I. L. HOFFMAN. Eur. J. Biochem. **50**, 539 (1975).
25. M. VIGNON, F. MICHON, J. P. JOSELEAU, and K. BOCK. Macromolecules, **16**, 835 (1983).
26. L. O. SILLERUD, J. H. PRESTEGARD, R. K. YU, D. E. SCHAFER, and W. H. KONIGSBERG. Biochemistry, **17**, 2619 (1978).
27. J. U. BAEZIGER and D. FIETE. J. Biol. Chem. **254**, 789 (1979).
28. B. NILSSON, N. E. NORDEN, and S. SVENSSON. J. Biol. Chem. **254**, 4545 (1979).
29. J. E. SADLER, J. C. PAULSON, and R. L. HILL. J. Biol. Chem. **254**, 2112 (1979).
30. K. WATANABE, M. POWELL, and S.-I. HAKOMORI. J. Biol. Chem. **253**, 8962 (1978).

Can. J. Chem. Downloaded from www.nrcresearchpress.com by 41.223.56.140 on 09/07/12
For personal use only.

Coordinatively unsaturated binuclear clusters of rhodium. The reactivity of $[\{Pr^i_2P(CH_2)_nPPr^i_2\}Rh]_2(\mu\text{-}H)_2$ (n = 2, 3, and 4) with dihydrogen, and their use in the catalytic hydrogenation of olefins

MICHAEL D. FRYZUK[1] AND WARREN E. PIERS

Department of Chemistry, University of British Columbia, 2036 Main Mall, Vancouver, B.C., Canada V6T 1Y6

AND

FREDERICK W. B. EINSTEIN[1] AND TERRY JONES[2]

Department of Chemistry, Simon Fraser University, Burnaby, B.C., Canada V5S 2N2

Received July 4, 1988

MICHAEL D. FRYZUK, WARREN E. PIERS, FREDERICK W. B. EINSTEIN, and TERRY JONES. Can. J. Chem. **67**, 883 (1989).

The coordinatively unsaturated binuclear rhodium hydrides $[\{Pr^i_2P(CH_2)_nPPr^i_2\}Rh]_2(\mu\text{-}H)_2$ (n = 2: **1***b*; n = 3: **1***c*; n = 4: **1***d*) react rapidly with dihydrogen to yield the fluxional binuclear tetrahydrides $[\{Pr^i_2P(CH_2)_nPPr^i_2\}RhH](\mu\text{-}H)_3[Rh\{Pr^i_2P(CH_2)_nPPr^i_2\}]$ **2***b*–*d* (n = 2–4). The dihydride **1***b* was structurally characterized by single crystal X-ray diffraction. While the tetrahydrides **2***b* and **2***c* were found to be stable only in solution in the presence of excess dihydrogen, **2***d* was stable in the solid state. Three separate exchange processes were characterized for **2***b*–*d* via ^1H and $^{31}P\{^1H\}$ NMR spectroscopy: intermolecular exchange with free dihydrogen, and two intramolecular processes exchanging the four hydride ligands. The geometry about the rhodium centres in the limiting structures involved in these processes is affected by the chelate ring size of the ancillary diphosphine ligand. A "rocking" process observed at low temperatures for each of these tetrahydrides has a $\Delta G^{\ddagger}$ of $<$7.0(5) kcal/mol, 8.6(5) kcal/mol, and 11.5(5) kcal/mol for **2***b*, **2***c*, and **2***d*, respectively. The dihydrides **1***b* and **1***c* were found to catalyze the hydrogenation of 1-hexene. Turnover numbers of 850–950 h^{-1} and 700 h^{-1} were observed for **1***b* and **1***c*, respectively, along with isomerization side reactions. Catalyst concentration studies on the hydrogenation of styrene using **1***c* as the catalyst precursor revealed a decrease in turnover frequency with increasing total metal concentration, suggesting that the active catalyst is a mononuclear species. Chemical evidence suggests that a pathway involving binuclear intermediates is also available, but that in the **1***c* system at least, a pathway utilizing mononuclear species as intermediates predominates.

Key words: binuclear rhodium hydrides, homogeneous catalysis.

MICHAEL D. FRYZUK, WARREN E. PIERS, FREDERICK W. B. EINSTEIN et TERRY JONES. Can. J. Chem. **67**, 883 (1989).

Les hydrures de rhodium binucléaires et insaturés par coordination $[\{Pr^i_2P(CH_2)_nPPr^i_2\}Rh]_2(\mu\text{-}H)_2$ (n = 2 : **1***b*; n = 3 : **1***c*; n = 4 : **1***d*) réagissent rapidement avec le dihydrogène pour fournir les tétrahydrures binucléaires de fluxion $[\{Pr^i_2P(CH_2)_nPPr^i_2\}RhH]_2(\mu\text{-}H)_3[Rh\{Pr^i_2P(CH_2)_nPPr^i_2\}]$ **2***b*–*d* (n = 2–4). On a caractérisé la structure du dihydrure **1***b* à l'aide de la diffraction des rayons-X. Les tétrahydrures **2***b* et **2***c* ne sont stables qu'en solution, en présence de dihydrogène; par ailleurs, le composé **2***d* est stable à l'état solide. En se basant sur la rmn du ^1H et du $^{31}P\{^1H\}$, on a pu caractériser trois processus différents d'échanges : un échange intermoléculaire avec le dihydrogène libre et deux processus intramoléculaires permettant l'échange des quatre ligands. Dans les structures limites impliquées dans ces processus, la géométrie autour des centres de rhodium est influencée par la grandeur du cycle chélate du ligand diphosphine ancillaire. Les $\Delta G^{\ddagger}$ du processus de «balancement» observé à basses températures pour chacun de ces tétrahydrures sont respectivement de $<$7,0(5), 8,6(5) et 11,5(5) kcal/mol pour les composés **2***b*, **2***c* et **2***d*. On a trouvé que les dihydrures **1***b* et **1***c* catalysent l'hydrogénation de l'hexène-1. On a trouvé que les activités des composés **1***b* et **1***c* sont respectivement de 850 à 900 et 700 heure^{-1} et qu'elles sont accompagnées de réactions d'isomérisations secondaires. Des études de concentration de catalyseur sur l'hydrogénation du styrène utilisant le composé **1***c* comme précurseur du catalyseur ont permis de mettre en évidence qu'une augmentation de la concentration totale du métal est accompagnée d'une diminution de l'activité; ces résultats suggèrent que le catalyseur actif est une espèce mononucléaire. Des données de nature chimique suggèrent qu'une voie réactionnelle impliquant des intermédiaires binucléaires est aussi disponible; toutefois, au moins avec le système **1***c*, la voie réactionnelle utilisant l'espèce mononucléaire comme intermédiaire prédomine.

Mots clés : hydrures de rhodium binucléaires, catalyse homogène.

[Traduit par la revue]

Introduction

Polynuclear transition metal complexes with coordinative unsaturation associated with one or more metal centres have been an attractive target in synthetic inorganic chemistry (1). Activation of small molecules, whether stoichiometrically or catalytically, requires that the substrate molecule be able to access a metal centre in the cluster. In the triosmium cluster series, the advent of the "lightly stabilized" complexes $Os_3(CO)_{10}L_2$ (L = cyclooctene, acetonitrile (2); L_2 = 1,3-cyclohexadiene (3)) greatly expanded the range of substrates for activation by simply making the metal centres more accessible as compared (4) to the parent cluster $Os_3(CO)_{12}$. The related dihydride $Os_3(\mu\text{-}H)_2(CO)_{10}$ (5), unsaturated by virtue of the bridging hydrides of the $Os_2(\mu\text{-}H)_2$ part of the cluster, has also been extremely important in developing the chemistry of osmium clusters (6).

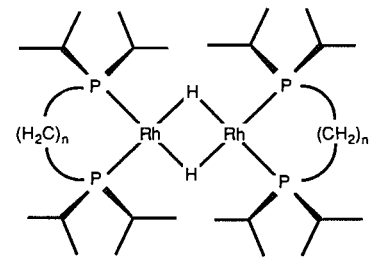
The carbonyl-free family of polynuclear rhodium hydrides of the general formula $[L_2Rh]_n(\mu\text{-}H)_n$ (n = 2, 3, or 4, depending on the steric bulk of L) are inherently unsaturated. For example, the binuclear complexes of the formula $[L_2Rh]_2(\mu\text{-}H)_2$ are 28 electron systems; by comparison, coordinatively saturated binuclear clusters such as $Fe_2(CO)_9$ and $M_2(CO)_{10}$ (M = Mn and Re) are 34 electron species. The unsaturation of these rhodium hydride clusters is reflected by their high reactivity with a range of small molecules such as dihydrogen (7), alkenes

[1]To whom correspondence may be addressed.

[2]NSERC Postgraduate Scholar (1984–1988).

[3]Revision received December 23, 1988.

Can. J. Chem. Downloaded from www.nrcresearchpress.com by 41.223.56.140 on 09/07/12
For personal use only.



b n = 2 [(dippe)Rh]$_2$(μ-H)$_2$

c n = 3 [(dippp)Rh]$_2$(μ-H)$_2$

d n = 4 [(dippb)Rh]$_2$(μ-H)$_2$

1

(8), alkynes (9), dienes (10), imines (11), isonitriles (12), and carbon monoxide (13). In addition, these unsaturated clusters are active as catalyst precursors for the hydrogenation of alkenes and alkynes (7, 9).

The most intensely studied members of this family of rhodium hydride clusters are the binuclear derivatives. The complex [{(Pr^{i}O)$_3$P}$_2$Rh]$_2$(μ-H)$_2$, **1***a*, was the first derivative in this class to be reported (14) and it has provided the underpinning for the understanding of both the stoichiometric and catalytic reactivities of these 28 electron clusters. Modification of these systems by the use of chelating bidentate phosphines and phosphinites has provided complexes with enhanced reactivity as compared to **1***a* above (15). Thus complexes of the formula [{Pr$^i{}_2$P(CH$_2$)$_n$PPr$^i{}_2$}Rh]$_2$(μ-H)$_2$ (n = 2: **1***b*; n = 3: **1***c*; n = 4: **1***d*) react with dihydrogen, olefins and other unsaturated substrates under exceedingly mild conditions.

These particular bidentate ligands all have isopropyl substituents on the phosphorus donors separated by two, three, and four methylene units. The substituents are large enough to generate the binuclear structure (16) but do allow access to the unsaturated Rh$_2$(μ-H)$_2$ core by a variety of substrate molecules. However, it is the chelate ring size that dramatically affects the reactivity patterns of these hydride dimers. In this paper, we examine the addition of dihydrogen to these binuclear 28 electron complexes (**1***b*–**1***d*). Also presented is a discussion of the possible pathways for these systems to hydrogenate olefins in the catalytic mode.

Experimental

General

All manipulations were performed under prepurified dinitrogen in a Vacuum Atmospheres HE-553-2 glovebox equipped with a MO-40-2H purifier, or in standard Schlenk-type glassware. The description "reactor bomb" refers to a cylindrical, thick-walled Pyrex vessel equipped with a 5 mm Kontes needle valve and a ground glass joint for attachment to a vacuum line. Larger bombs have 10 mm Kontes valves.

Hydrated rhodium trichloride was obtained from Johnson–Matthey and used as received. The syntheses of (η^3-C$_3$H$_5$)Rh(COD) (COD = 1,5-cyclooctadiene) (7) and the binuclear complex [{Pr$^i{}_2$P(CH$_2$)$_2$-PPr$^i{}_2$}Rh]$_2$(μ-H)$_2$, [(dippe)Rh]$_2$(μ-H)$_2$, **1***b* (8) were as reported previously. Literature preparations were used to generate the bidentate ligands, Pr$^i{}_2$PCH$_2$CH$_2$CH$_2$PPr$^i{}_2$, dippp (17) and Pr$^i{}_2$PCH$_2$CH$_2$PPr$^i{}_2$, dippe (8).

Toluene and diethylether were purified by distillation from sodium-benzophenone ketyl under argon. Tetrahydrofuran (THF) and hexanes were predried by refluxing over calcium hydride followed by distillation from sodium-benzophenone ketyl under argon.

Melting points were determined on a Mel-Temp apparatus in sealed capillaries under nitrogen, and are uncorrected. Carbon, hydrogen, and halogen analyses were performed by Mr. P. Borda of this department. ^{1}H NMR spectral measurements were carried out on one of the following instruments: Varian XL-300, Bruker WP-80, or a Bruker WH-400. (All ^{1}H{^{31}P} NMR spectra were obtained on the Bruker WH-400.) ^{31}P{^{1}H} NMR measurements were carried out at 121.421 MHz on the Varian XL-300, using trimethylphosphite as an external standard (141.0 ppm). ^{13}C{^{1}H} spectra were run at 75.429 MHz, also on the Varian instrument, using internal solvent peaks as a reference (C$_6$D$_6$, 128.0 ppm). NMR solvents C$_6$D$_6$ and C$_7$D$_8$ were bought from MSD Isotopes, and dried over activated 3 Å molecular sieves and vacuum transferred, while d_8-THF was dried over sodium-benzophenone ketyl, and stored under dry nitrogen. Simulated NMR spectra were obtained using the program UBCPANIC.

The 1,4-dibromobutane used in the preparation of 1,4-bis(diisopropylphosphino)butane (dippb) was obtained from the Aldrich Chemical Co. and distilled under argon prior to use. The substrates 1-hexene and styrene (99%) were also obtained from Aldrich. 1-Hexene was dried for 8 h over activated 3 Å molecular sieves, vacuum transferred into a storage vessel, and degassed thoroughly via three freeze–pump–thaw cycles. It was then passed through neutral alumina and stored under N_2 in a glove box. Styrene was distilled under argon just prior to use.

Hydrogen gas used in the hydrogenation of 1-hexene was purified by passing through a glass tower (4″ in diameter) packed with MnO (bottom layer) and 4 Å molecular sieves separated by a plug of glass wool and a layer of glass beads. The towers were made by packing with 200 g $MnCO_3$ and 1700 mL Vermiculite (mixed) followed by the molecular sieves. Activation was accomplished by passing H_2 gas through the tower while heating at about 200°C until the brown colour of the $MnCO_3$ had turned the characteristic green of MnO. Heating was effected by passing current through a wire wrapped around the tower in spirals separated by about 1″ (18). Hydrogen gas used for the kinetic measurements on the hydrogenation of styrene was purified by passing through an Englehard Deoxo hydrogen purifier, attached to the hydrogen cylinder.

Analysis of hexenes and hexane in the hydrogenation of 1-hexene was done by gas chromatography on a Varian 6000 instrument equipped with FID detectors and a 20% tri-*o*-cresylphosphate on 60/80 chromosorb-P column (20′ × 1/8″ SS) operating at 50°C. UV/VIS spectral measurements were performed on a Perkin Elmer 552A UV/VIS spectrometer.

*Structure determination of [(dippe)Rh]$_2$(μ-H)$_2$ (**1**b).* A deep red crystal (0.12 × 0.16 × 0.24 mm) was mounted in a Lindemann glass capillary. Precession and Weissenberg photographs were used to obtain approximate unit cell dimensions and to assign the space group as $P1$ or $P\bar{1}$ (subsequent structure solution uniquely defined the space group as $P\bar{1}$). Accurate cell dimensions (Table 1) were determined by least-squares refinement of the diffractometer angles of 34 independent reflections (2θ = 35.0 − 42.8°; Mo-K$_{\alpha 1}$ = 0.70926 Å) chosen from a variety of points in reciprocal space. Data were collected, at 293 K, using a Picker FACS-I four-circle diffractometer with a graphite monochromator and a scintillation counter with pulse height discrimination. The take-off angle was 3° and symmetrical θ–2θ scans (2° min^{-1}) of (1.3 + 0.692 tan θ)° were used. Stationary crystal stationary counter counts of 10% of the scan time were formed on each reflection and the intensity and its associated error determined by the method of Grant and Gabe (19). Measurement of two standards every 70 reflections showed no significant variation in intensity.

Intensities were measured for 6213 independent reflections of which 5170 were classed observed ($I \geq 2.3\sigma(I)$). Lorentz, polarization, and absorption corrections were made (transmission coefficients varied from 0.719–0.804).

The structure was solved by Patterson and Fourier methods. The Patterson shows there to be three Rh atoms in the asymmetric unit, two of which are contained within a single dimeric molecule and the third which when considered with its symmetry equivalent (1) fives rise to a second dimeric molecule; thus there are six "C$_{14}$H$_{33}$P$_2$Rh" units per unit cell. Subsequent Difference-Fourier syntheses revealed the positions of all non-hydrogen atoms. The atoms C(61) and C(611) were found to be disordered; C(61A) and C(611A) take up one orientation while C(61B) and C(611B) take up a second with the axis along P(6)...C(612) acting as a pivot between the two arrangements. (Occupancies of 0.5 were derived for each arrangement.) Subsequent Difference-maps revealed the positions of most of the hydrogen atoms, and the positions of those not located were calculable (apart from those hydrogen atoms associated with the disordered isopropyl group).

Can. J. Chem. Downloaded from www.nrcresearchpress.com by 41.223.56.140 on 09/07/12
For personal use only.

Can. J. Chem. Downloaded from www.nrcresearchpress.com by 41.223.56.140 on 09/07/12
For personal use only.

TABLE 1. Crystal data for $C_{28}H_{66}P_4Rh_2$ (**1***b*)

a, Å	10.660(2)
b, Å	11.703(2)
c, Å	23.952(8)
α, deg	94.21(2)
β, deg	95.98(2)
γ, deg	113.10(1)
U, Å^3	2712.54
Space group	$P\bar{1}$
Mr (dimer)	732.54
μ, cm^{-1}	10.88
ρ_{obsd}[a], g mL^{-1}	1.34
ρ_{calcd}, g mL^{-1}	1.346
Final R_1[b]	0.027
Final R_2[c]	0.028

[a]Flotation in a mixture.
[b]$R_1 = \Sigma||F_o| - |F_c||/\Sigma|F_o|$.
[c]$R_2 = [\Sigma w(|F_o| - |F_c|)^2/\Sigma w|F_o|^2]^{1/2}$.

Later stages of refinement required that the asymmetric unit be treated in two portions, viz. molecule **1**[a] and molecule **2** (see Table 2).

Alternate block-diagonal least-squares refinement of the coordinates of all non-hydrogen atoms and the majority of hydrogen atoms[b] of each molecule, with variable anisotropic temperature factors for all non-hydrogen atoms (apart from C(61A) and C(61B)) and fixed isotropic temperature factors for hydrogen atoms ($B_{iso} \propto B_{iso}$(parent carbon)) gave final agreement factors of $R_1 = 0.027$ and $R_2 = 0.028$. The final difference-map was essentially clean. Unit weights were applied. Atomic scattering factors together with anomalous dispersion terms were taken from International tables for X-ray crystallography (20). Final positional and B_{iso} thermal parameters are given in Table 2. The computer programs used here are those belonging to "The PDP-8e crystal structure system" (21).

The synthesis of $Pr^i_2P(CH_2)_4PPr^i_2$ *(dippb).* The procedure used was identical to that used for the ligand $Pr^i_2P(CH_2)_3PPr^i_2$, dippp (17). Starting with 2.22 g (0.018 mol) of $LiPPr^i_2$ and 1.05 mL (1.90 g, 0.009 mol) $Br(CH_2)_4Br$, 1.98 g (77%) of dippb was obtained. Bp: 100–102°C (0.1 mm Hg). ^{1}H NMR (C_6H_6, ppm): 1.65, $CH_2(CH_2)_2CH_2$ (br m, 4H); 1.59, $CH(CH_3)_2$ (d of sp, 4H, ^3J_H = 7.6 Hz, ^2J_P = 2.8 Hz); 1.32, $CH_2(CH_2)_2CH_2$ (br m, 4H); 1.02, 1.06, $CH(CH_3)_2$ (overlapping dd, 24H, ^3J_P = 12.9, 13.3 Hz). $^{31}P\{^1H\}$ NMR (C_6D_6, referenced to external $P(OMe)_3$ at +141.0 ppm): 2.41 (s).

Synthesis of $[(dippp)Rh]_2(\mu\text{-}H)_2$, **1***c*. To a solution of $(\eta^3\text{-}C_3H_5)$Rh-(COD) (1.00 g, 3.97 mmol) in toluene (25 mL) was added a solution of the ligand dippp (1.09 g, 3.97 mmol) in toluene (10 mL), yielding a golden yellow solution of $(\eta^3\text{-}C_3H_5)$Rh(dippp). (This compound may be isolated as yellow crystals through recrystallization from toluene/hexanes in 92% yield; see below for spectral data.) Toluene and 1,5-cyclooctadiene were removed under reduced pressure, and the yellow residues were redissolved in toluene (25 mL), and the solution was transferred to a large reactor bomb equipped with a magnetic stirring bar. The solution was degassed on a vacuum line, cooled to −196°C, and was pressurized with dihydrogen to 1 atm. The reactor was sealed and was allowed to warm to room temperature. Efficient stirring was continued for 1 day, after which the reaction vessel was repressurized with H_2 at −196°C. After a further day of stirring at room temperature, the excess of dihydrogen and the solvent were removed, leaving a black–green solid from which 1.32 g (88.0%) of **1***c* could be obtained after three recrystallizations from toluene/hexanes. Melting point 226°C. ^{1}H NMR (C_6D_6, ppm): $CH(CH_3)_2$, 1.83 (d of sp, ^2J_P = 2.2 Hz, ^3J_H = 6.9 Hz); $CH(CH_3)_2$, 1.59, 1.22 (dd, ^3J_P = 12.1 Hz); $CH_2CH_2CH_2$, 0.97 (m); Rh—H—Rh, −6.65 (br m, $^1J_{Rh}$ = 35.2 Hz). $^{31}P\{^1H\}$ NMR (C_6D_6, ppm referenced to $P(OCH_3)_3$ at 141.0): 50.3 (d, $^1J_{Rh}$ = 161.0 Hz). *Anal.* calcd. for $C_{15}H_{35}P_2Rh$: C 47.37, H 9.28; found: C 47.49, H 9.21. The deuterated analogue of **1***c*, d_2-**1***c*, was prepared in a procedure analogous to that employed for preparing the dippe dideuteride d_2-**1***b* (8). Spectroscopic data for

TABLE 2. Final atomic parameters[a] for $C_{28}H_{66}P_4Rh_2$ (**1***b*)

(*a*) Molecule **1**

Atom	*x*	*y*	*z*	B_{iso}[b]
Rh(1)	0.03157(4)	0.11134(3)	0.02749(2)	3.65(2)
P(1)	0.2175(1)	0.2795(1)	0.05795(5)	3.46(6)
P(2)	−0.0801(1)	0.2180(1)	0.05873(6)	3.88(6)
C(11)	0.3307(8)	0.2723(7)	0.1193(3)	9.1(5)
C(111)	0.4592(7)	0.3880(7)	0.1405(3)	7.6(4)
C(112)	0.2933(10)	0.1719(9)	0.1463(4)	12.4(7)
C(12)	0.3357(6)	0.3495(6)	0.0076(2)	5.7(3)
C(121)	0.4066(11)	0.2667(9)	−0.104(5)	15.5(8)
C(122)	0.2578(10)	0.3729(12)	−0.0427(4)	15.5(8)
C(13)	0.1771(7)	0.4089(6)	0.0844(4)	10.0(5)
C(21)	−0.2088(6)	0.2360(5)	0.0055(3)	6.0(3)
C(211)	−0.1409(9)	0.2843(7)	−0.0461(3)	9.9(5)
C(212)	−0.3327(7)	0.1132(7)	−0.0115(3)	8.7(5)
C(22)	−0.1821(7)	0.1629(6)	0.1166(3)	6.9(4)
C(221)	−0.1009(10)	0.1319(11)	0.1625(4)	15.4(7)
C(222)	−0.2495(8)	0.2474(8)	0.1384(3)	10.2(5)
C(23)	0.0345(6)	0.3820(5)	0.0853(3)	6.3(3)
H(1)	0.117(5)	0.034(5)	−0.004(2)	7.2(14)

(*b*) Molecule **2**

Atom[c]	*x*	*y*	*z*	B_{iso}
Rh(2)	0.38074(4)	0.08035(3)	0.37807(2)	3.04(2)
Rh(3)	0.30589(4)	−0.13720(3)	0.31657(2)	3.01(2)
P(3)	0.5695(1)	0.2497(1)	0.40346(5)	3.35(6)
P(4)	0.2739(1)	0.1922(1)	0.40870(6)	4.27(7)
P(5)	0.1111(1)	−0.2881(1)	0.27721(5)	3.42(6)
P(6)	0.4030(1)	−0.2312(1)	0.26505(6)	4.11(6)
C(31)	0.6819(5)	0.3098(5)	0.3490(2)	4.4(3)
C(311)	0.7524(7)	0.2251(6)	0.3329(3)	7.0(4)
C(312)	0.5984(7)	0.3238(7)	0.2959(3)	8.1(4)
C(32)	0.6949(6)	0.2430(5)	0.4624(2)	5.0(3)
C(321)	0.8235(6)	0.3643(6)	0.4792(3)	6.2(4)
C(322)	0.6242(7)	0.1994(8)	0.5129(3)	8.4(5)
C(33)	0.5346(6)	0.3863(5)	0.4279(3)	6.3(3)
C(41)	0.1462(6)	0.2122(6)	0.3556(3)	6.5(3)
C(411)	0.0236(7)	0.0910(7)	0.3363(4)	9.4(5)
C(412)	0.2167(9)	0.2662(9)	0.3057(4)	11.2(6)
C(42)	0.1654(8)	0.1346(7)	0.4646(3)	8.7(4)
C(421)	0.2348(9)	0.0898(11)	0.5092(4)	14.7(7)
C(422)	0.1023(10)	0.2226(9)	0.4876(4)	12.4(6)
C(43)	0.3919(7)	0.3535(6)	0.4378(3)	8.6(4)
C(51)	0.0086(5)	−0.3957(5)	0.3242(2)	4.2(3)
C(511)	−0.0387(7)	−0.3265(6)	0.3677(3)	6.4(3)
C(512)	0.0924(7)	−0.4592(6)	0.3537(3)	6.8(4)
C(52)	−0.200(6)	−0.2416(6)	0.2390(2)	5.5(3)
C(521)	0.0461(8)	−0.1464(7)	0.2007(3)	8.8(5)
C(522)	−0.1483(7)	−0.3518(7)	0.2075(3)	8.1(4)
C(53)	0.1347(6)	−0.3956(5)	0.22270(2)	5.0(3)
C(61A)	0.4339(11)	−0.1755(1)	0.1948(4)	4.7(2)
C(61B)	0.5026(12)	−0.1287(11)	0.2114(5)	5.8(3)
C(611A)	0.4961(15)	−0.0305(11)	0.2041(6)	7.7(8)
C(611B)	0.4196(19)	−0.0681(17)	0.1829(6)	11.4(12)
C(612)	0.5370(9)	−0.2153(8)	0.1656(3)	10.8(5)
C(62)	0.5478(6)	−0.2644(5)	0.2977(3)	5.9(3)
C(621)	0.5963(8)	−0.3306(7)	0.3494(3)	8.9(5)
C(622)	0.6768(7)	−0.1456(7)	0.3150(3)	8.4(4)
C(63)	0.2785(6)	−0.3900(6)	0.2334(3)	6.5(3)
H(2)	0.464(4)	−0.005(4)	0.353(2)	4.0(10)
H(3)	0.239(5)	−0.059(4)	0.360(2)	5.0(11)

[a]Remaining hydrogen coordinates have been deposited.
[b]$B_{iso} = 8\pi^2[(U_{11}^2 + U_{22}^2 + U_{33}^2/3)]^{1/2}$.
[c]The atoms C(61) and C(611) were found to be disordered (see text).

Can. J. Chem. Downloaded from www.nrcresearchpress.com by 41.223.56.140 on 09/07/12
For personal use only.

(η^3-C_3H_5)Rh(dippp): ^{1}H NMR (C_6D_6, ppm): H_{cent}, 4.86 (m, $^3J_{H_{syn}}$ = 7.0 Hz, $^3J_{H_{anti}}$ = 12.8 Hz, $^2J_{Rh}$ = 2.0 Hz); H_{syn}, 3.65 (d); H_{anti}, 2.19 (dd, J_P = 4.8 Hz); C*H*(CH_3)$_2$, 1.92 (br sp, ^3J_H = 7.0 Hz), 1.81 (br sp, ^3J_H = 7.0 Hz); CH(C*H*$_3$)$_2$, 1.20 (dd, ^3J_P = 14.4 Hz), 1.10 (two overlapping dd, ^3J_P = 12.9, 13.6 Hz), 1.01 (dd, ^3J_P = 12.8 Hz); $CH_2CH_2CH_2$, ~1.8, 1.2 (resonances obscured by other peaks). ^{31}P{^{1}H} NMR (C_6D_6, ppm referenced to $P(OCH_3)_3$ at 141.0): 42.9 (d, $^1J_{Rh}$ = 188.0 Hz). *Anal.* calcd. for $C_{18}H_{39}P_2Rh$: C 51.42, H 9.35; found: C 51.22, H 9.33.

*The synthesis of [(dippb)Rh]$_2$(μ-H)$_3$(H), 2*d. To a solution of (η^3-C_3H_5)Rh(COD) (0.356 g, 1.4 mmol) in toluene (5 mL) was added dropwise a solution of dippb (0.409 g, 1.4 mmol) in toluene (5 mL) with stirring. A rapid deepening of the orange colour of the solution signified that the reaction was instantaneous. The toluene was removed under reduced pressure, and the residue pumped under high vacuum to remove as much COD as possible. The residue was then redissolved in toluene (25 mL) and the resulting solution placed in a 250 mL thick-walled reactor bomb, degassed, cooled to −196°C, and exposed to 1 atm of purified dihydrogen. The reactor was sealed at this temperature and allowed to warm to room temperature. After 3 days of efficient stirring the yellow–orange to dark yellow–green colour change was complete, and the excess dihydrogen and toluene were pumped off. The dark green–brown residue was recrystallized from toluene/hexanes (1:3) at −20°C, yielding 2–3 crops of black–green plates of **2***d* (0.407 g, 73% from (η^3-C_3H_5)Rh(COD)). ^{1}H NMR (C_7H_8, ppm): ^{31}P{^{1}H} NMR (C_7D_8, referenced to external $P(OMe)_3$ at +141.0 ppm). *Anal.* calcd. for $C_{32}H_{76}P_4Rh_2$: C 48.61, H 9.69; found: C 48.49, H 9.80.

The intermediate complex (η^3-C_3H_5)Rh(dippb) may also be isolated via recrystallization from toluene/hexanes as yellow crystals in 79% yield. ^{1}H NMR (C_6H_6, ppm): 4.80, H_c (tt, $^3J_{H_a}$ = 11.6 Hz, $^3J_{H_s}$ = 7.0 Hz); 3.44, H_s (dd, $^3J_{H_a}$ = 1.1 Hz); 2.10, H_a (ddd, J_P = 5.1 Hz); 1.92, C*H*(CH_3)$_2$ (d of sp, ^3J_H = 7.0–7.4 Hz; ^2J_P ≈ 2.6 Hz); 1.45–1.85, C*H*(CH_3)$_2$, (CH_2)$_4$ (overlapping multiplets); 1.18, 1.06, 1.05, 0.98, CH(C*H*$_3$)$_2$ (overlapping dd, ^3J_P = 13.0–13.4 Hz).

*The synthesis of [(dippb)Rh]$_2$(μ-H)$_2$, 1*d. The generation and observation of **1***d* was carried out in an NMR tube. A solution of **2***d* was dissolved in C_6D_6 and placed in a sealable 5 mm NMR tube. The tube was fitted to a 180° needle valve adapter and the whole assembly attached to a vacuum line. After degassing, about 1.1 equiv. of 1-hexene were vacuum transferred into the tube and the tube was sealed with a torch. ^{1}H NMR spectra recorded immediately after the tube had warmed to room temperature showed the presence of hexane and **1***d* in nearly quantitative yield. ^{1}H NMR (C_6H_6, ppm): ^{31}P{^{1}H} NMR (C_7D_8, referenced to external $P(OMe)_3$ at +141.0 ppm): 59.8 (d, J_{Rh} = 166.2 Hz).

The reactions of [{Pr$^i_2$P(CH$_2$)$_n$PPr$^i_2$}Rh]$_2$(μ-H)$_2$ (n = 2 and 3) with dihydrogen. An appropriate amount of [(dippe)Rh]$_2$(μ-H)$_2$, **1***b*, or [(dippp)Rh]$_2$(μ-H)$_2$, **1***c* (25–30 mg) were dissolved in C_7D_8, and the solution loaded into a sealable 5 mm NMR tube. The tube was fitted with a 180° needle valve adapter, and the assembly attached to a vacuum line with access to purified dihydrogen. The sample was degassed, and H_2 was admitted to nearly 1 atm pressure. Reaction with dihydrogen was immediate as indicated by a rapid deep green to brown colour change. To ensure an excess of dihydrogen in the sample, it was cooled to −196°C before sealing with a torch. ^{31}P{^{1}H} NMR spectroscopic data obtained are discussed in the text. ^{1}H NMR (hydride region of **1***b*, −80°C, C_7H_8, ppm): −7.05, $2H_b$ (d of br m, J_P = 122.1 Hz, J_{Rh} = 20.6 Hz); −13.17, H_t/$H_{b'}$ (br m). Further cooling to −95°C results in nearly complete coalescence of this high field signal. ^{1}H NMR (hydride region of **1***c*, −90°C, C_7H_8, ppm): −2.35, $2H_b$ (d of br m, J_P = 116 Hz, J_{Rh} = 19.2 Hz); −5.50, $H_{b'}$ (br m); −11.15, H_t (br m).

Crossover experiment

The hydrogenation of 1-hexene with a mixture of [(dippe)Rh]$_2$(μ-H)$_2$ (1b) and [(dippp)Rh]$_2$(μ-H)$_2$ (1c). A toluene solution (10 mL) of **1***b* (0.080 g) and **1***c* (0.075 g) was loaded into a small thick-walled reactor bomb. After degassing, 5.0 mL of 1-hexene was syringed into the bomb under a strong flow of dihydrogen. The hydrogenation was allowed to proceed to completion by stirring overnight under an atmosphere of H_2. The volatiles were then removed and the residues examined by ^{31}P{^{1}H} NMR. The only peaks observed were the doublets characteristic of **1***b* and **1***c*.

Synthesis of the mixed dimer [(dippe)Rh](μ-H)$_2$[Rh(dippp)]. A mixture of (dippe)Rh(C_3H_5) (generated from 0.150 g Rh(COD)(C_3H_5) and 0.156 g dippe) and (dippp)Rh(C_3H_5) (generated from 0.150 g Rh(COD)(C_3H_5) and 0.164 g dippp) was dissolved in 25 mL of toluene and loaded into a 250 mL thick-walled reactor bomb. The solution was degassed and cooled to −196°C; H_2 was admitted to 1 atm of pressure. After a 2–3 day period of efficient stirring, excess dihydrogen and toluene were removed under reduced pressure. The residues were redissolved in hexanes (30 mL) and filtered through a pad of celite. Concentration of the filtrate to 10–15 mL, followed by cooling to −20°C resulted in isolation of a crop of red–black crystals (0.217 g, 49% on mass balance). Analysis by ^{31}P{^{1}H} NMR spectroscopy revealed the presence of **1***b* and **1***c* (approximately 10% in total) as well as signals expected for the AA′MM′XY spin system in the mixed dimer. ^{31}P{^{1}H} NMR (C_6D_6, referenced to external $P(OMe)_3$ at +141.0 ppm): 103.7, *P*(CH_2)$_2$*P* (d of m, J_{Rh} = 157.3); 52.7, *P*(CH_2)$_3$*P* (d of m, J_{Rh} = 150.9 Hz).

The hydrogenation of 1-hexene with [(dippe)Rh]$_2$(μ-H)$_2$ (1b) and [(dippp)Rh]$_2$(μ-H)$_2$ (1c). A 250 mL thick-walled glass bomb equipped with an efficient magnetic stir bar was charged with catalyst precursor (**1***b* or **1***c*, 0.050 g) and purified 1-hexene (10.00 g, substrate:catalyst, 1700–1800:1). **1***b* reacted immediately with the substrate, producing an orange solution, whereas **1***c* was unreactive and the intense green colour of the dihydrides was maintained. The bomb was then attached to a vacuum line with access to purified H_2 and the solution degassed thoroughly via three freeze–pump–thaw cycles. When the solution had warmed to room temperature (22–23°C), hydrogen was admitted to 1 atm. Samples were periodically removed through the bomb's Teflon needle valve port using an argon and hydrogen flushed syringe. The volatiles were vacuum transferred away from the catalyst, and analyzed by gas chromatography. Identification of the peaks in the GC trace was carried out by "spiking" with the pure materials (Aldrich).

Kinetic measurements. Kinetic measurements on the hydrogenation of styrene by **1***b* were made by following the uptake of H_2 at constant pressure. The apparatus was identical to that described by James and co-workers (22). Samples for each run were prepared from varying amounts (0.5–4.0 mL) of a stock solution of **1***b* (0.048 g in 25 mL toluene, 1.58×10^{-2} *M*). The total volume of each sample was made up to 4.0 mL with toluene. Higher concentrations of catalyst were attained by dissolving accurately weighed amounts of **1***b* (0.016, 0.024 g) in 4.0 mL of toluene. Styrene was then added (0.55 mL; substrate: catalyst ratios ranged from ≈150–3800), and the reaction vessel assemblage attached to the constant pressure uptake apparatus. The sample solution was degassed with two freeze–pump–thaw cycles, and then allowed to thermally equilibrate in an oil bath thermostatted to 30°C. Once equilibrated, shaking was begun, and H_2 admitted to 1 atm of pressure. After a brief (2 min) induction period, gas uptake was monitored by measuring the difference in levels of a liquid of negligible vapour pressure in a capilliary manometer thermostatted together with a gas burette at 25°C. Admission of H_2 to the system through a needle valve maintained a constant pressure by raising the mercury level in a calibrated tube of the burette. A travelling microscope was used to follow the change in height of this mercury column. Runs were typically allowed to go for 4–5 turnovers. The sole product in the reaction was ethylbenzene.

Results and discussion

The crystal and molecular structure of [{Pr$^i_2$P(CH$_2$)$_2$PPr$^i_2$}-Rh]$_2$(μ-H)$_2$ (1b)

A single crystal X-ray analysis of [(dippe)Rh]$_2$(μ-H)$_2$, **1***b*, was performed to establish the structural parameters of this

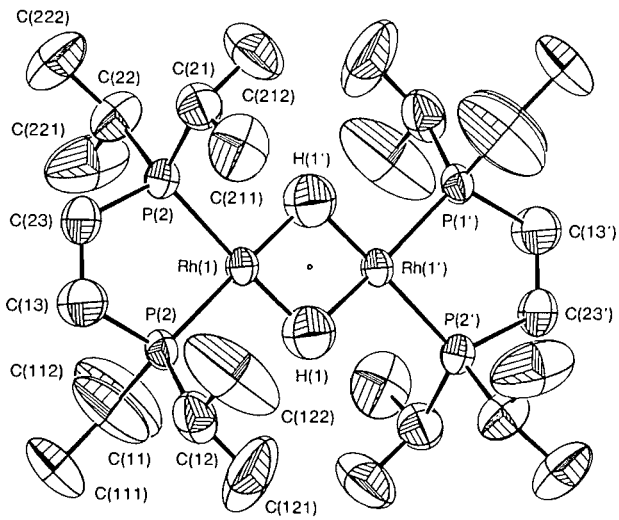


FIG. 1. ORTEP diagram of the dihydride $[(dippe)Rh]_2(\mu\text{-}H)_2$, **1***b*.

central compound in our ongoing research on the reactivity of polynuclear unsaturated clusters, Figure 1 shows the molecular structure of **1***b* along with the atom numbering scheme, and Tables 1, 2, and 3 give the crystal data, final atomic parameters, and selected bond parameters, respectively, for this compound. The structure was found to have two crystallographically separate molecules in the crystal lattice. The unit cell consisted of two dimers of molecule **1**, and one of molecule **2**.

Bond distances and angles were all within expected ranges. In particular, the Rh—Rh distances of 2.629(1) Å (molecule **1**) and 2.6266(8) Å (molecule **2**) are only slightly shorter to that found for the dimer $[\{Pr^i O)_3P\}_2Rh]_2(\mu\text{-}H)_2$, **1***a*, at 2.647 Å (23). The P—Rh—P bond angles of 85.7° are about 10° less than those found for **1***a* (94.7°) and that expected for **1***c*.[4] This small P—Rh—P angle of the dippe hydride **1***b* has the effect of "pulling back" the isopropyl groups on the phosphorus atoms, and thus exposing the $Rh_2(\mu\text{-}H)_2$ core of this molecule to a greater extent than other members of the dihydride family. While the metal centres of **1***b* still experience some steric crowding, we have observed that the dippe hydride dimer has heightened reactivity when compared to its more sterically crowded analogs, the dippp dimer **1***c* and the dippb dimer **1***d* (*vide infra*).

The reaction of $[\{Pr^i{}_2P(CH_2)_nPPr^i{}_2\}Rh]_2(\mu\text{-}H)_2$ (n = 2, 3, *and 4) with dihydrogen*

The effect of chelate ring size is apparent in the synthesis of these binuclear complexes. The standard procedure involves the reaction of the mononuclear rhodium allyl complexes $(\eta^3\text{-}C_3H_5)Rh\{Pr^i{}_2P(CH_2)_nPPr^i{}_2\}$ where n = 2 and 3, with dihydrogen to generate, respectively, the binuclear rhodium *dihydride* complexes $[(dippe)Rh]_2(\mu\text{-}H)_2$ (**1***b*) and $[(dippp)\text{-}Rh]_2(\mu\text{-}H)_2$ (**1***c*) upon workup. However, the analogous reaction of the corresponding allyl complex containing the bidentate phosphine ligand 1,4-bis(diisopropylphosphino)butane (dippb) generates the binuclear *tetrahydride* $[(dippb)Rh]_2(H)_4$ (**2***d*) under the same conditions. Further experiments established that the binuclear dihydrides **1***b* and **1***c* add one molecule of dihydrogen to generate the respective tetrahydrides **2***b* and **2***c*, but these latter tetrahydrides are unstable and lose H_2 upon removal of excess H_2. Although the dippb tetrahydride **2***d* is stable even under vacuum, we were able to synthesize the corresponding dihydride **1***d* by reaction of **2***d* with 1 equiv. (or a slight excess) of 1-hexene. This is summarized in Scheme 1. By comparison, the binuclear dihydride containing the monodentate triisopropylphosphite ligands $[\{(Pr^iO)_3P\}_2Rh]_2(\mu\text{-}H)_2$, **1***a*, also adds H_2 to generate an unstable tetrahydride $[\{(Pr^iO)_3\text{-}P\}_2Rh]_2(H)_4$, **2***a*.

All of the binuclear tetrahydrides **2***a*–**2***d* exhibit fluxional behaviour as evidenced by variable temperature ^1H and $^{31}P\{^1H\}$ NMR spectroscopy. Although the fluxional processes appear qualitatively similar, there are some important differences that depend on the particular ancillary ligand. At room temperature, solutions under H_2 of the two tetrahydrides **2***c* and **2***d*, having six- and seven-membered chelate rings, respectively, show a broad peak in the hydride region of the ^1H NMR spectrum indicative of both fast exchange of the hydrides with themselves and with free H_2 dissolved in solution. As the temperature is lowered to −20°C, the latter process effectively stops and the self exchange slows to give a doublet of broad multiplets for two equivalent bridging hydrides and a broad singlet for two terminal hydrides. As the temperature is lowered further (−80°C), the singlet for the two terminal hydrides broadens and coalesces to give two different broad singlets assignable to one bridging hydride and one terminal hydride. This pattern and temperature behaviour are nearly identical to that reported for **2***a*. Thus the structure in the slow exchange limit is consistent with the formulation $[P_2RhH](\mu\text{-}H)_3[RhP_2]$, that is, a Rh(III) centre with a terminal hydride and a Rh(I) centre separated by three bridging hydrides; at slightly higher temperatures (−80°C to −20°C), one of the bridging hydride ligands exchanges with the terminal hydride to give an averaged, excited state structure formulated as $[P_2RhH_2](\mu\text{-}H)_2[RhP_2]$. The $^{31}P\{^1H\}$ NMR of the dippp tetrahydride **2***c* at various temperatures (Fig. 2) provides clear evidence for the stereochemical arrangement about each metal centre as a function of temperature. At room temperature, two doublets were observed at 61.6 ($^1J_{Rh—P}$ = 167.3 Hz) and 67.6 ($^1J_{Rh—P}$ = 105.8 Hz) ppm (at higher temperatures these signals collapsed into one doublet).[5] The magnitudes of the $^1J_{Rh—P}$ coupling constants are consistent with a Rh(I)/Rh(III) formulation for the dimer (22). As the temperature is lowered, the doublet due to the phosphorus nuclei coupled to the Rh(I) centre coalesces and reemerges at −100°C as two doublets of doublets (an ABX spin system). A stereochemical arrangement for the ground state structure consistent with the low temperature limit is an octahedral Rh(III) centre, coupled with a trigonal bipyramidal geometry at the Rh(I) centre. As H_t and $H_{b'}$ equilibrate via the rocking motion depicted in Scheme 2, the two phosphorus nuclei on the rhodium(I) centre undergo axial/equatorial exchange, while the other two phosphorus atoms remain equivalent at all times.

Although the trigonal bipyramidal geometry would undoubtedly be highly distorted from the ideal, the square pyramidal geometry would not give rise to two inequivalent phosphorus nuclei on the Rh(I) centre in the low temperature limit. The excited state structure is therefore likely tetrahedral at the Rh(I) centre in **2***c*, although the spectra do not rule out a square planar geometry. The activation free energy (26) for this "rocking"

[4]The bite angle for the dippp ligand (8*b*), as well as other six membered chelate ligands (21*b*), is in the range 93–96°C. See, for example, ref. 24.

[5]It has been found empirically (22*b*) and calculated theoretically (22*c*) that the magnitude of $^1J_{Rh—P}$ is about 50% larger for complexes with a formal oxidation state of I than for those with an oxidation state of III (25).

Can. J. Chem. Downloaded from www.nrcresearchpress.com by 41.223.56.140 on 09/07/12
For personal use only.

TABLE 3. Selected bond parameters for $C_{28}H_{66}P_4Rh_2$ (**1***b*)

(*a*) Molecule **1**

Bond	Length	Bond	Length
Rh(1)—P(1)	2.182(1)	P(2)—C(21)	1.859(6)
Rh(1)—P(2)	2.180(1)	P(2)—C(22)	1.849(6)
Rh(1)—H(1)	1.70(5)	P(2)—C(23)	1.843(5)
Rh(1)—H(1′)	1.81(5)	P(1)—C(11)	1.831(6)
C(13)—C(23)	1.428(9)	P(1)—C(12)	1.835(6)
Rh(1)—Rh(1′)	2.629(1)	P(1)—C(13)	1.819(6)

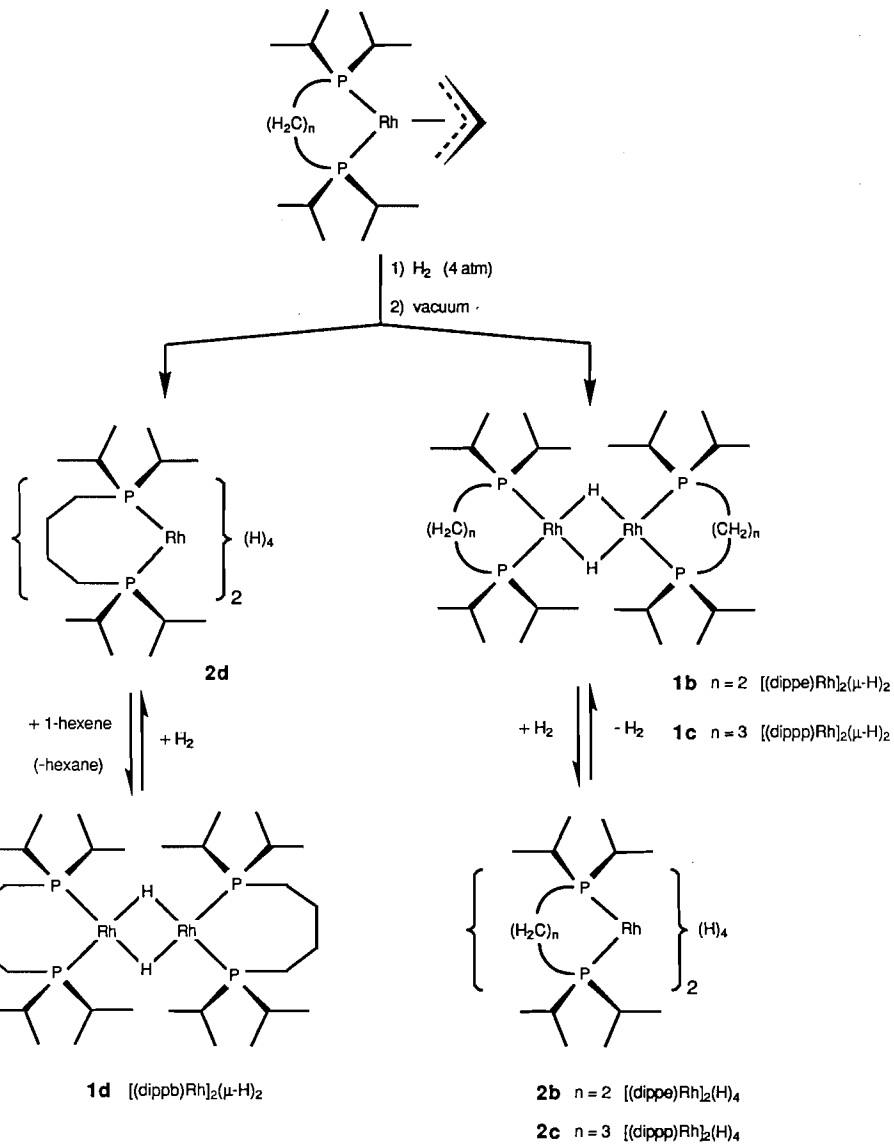
Bonds	Angle	Bonds	Angle
P(1)—Rh(1)—P(2)	85.75(5)	Rh(1)—P(1)—C(13)	111.8(2)
P(1)—Rh(1)—H(1)	94(2)	C(11)—P(1)—C(12)	103.9(3)
P(1)—Rh(1)—H(1′)	176(2)	C(11)—P(1)—C(13)	100.8(4)
P(2)—Rh(1)—H(1)	174(2)	C(12)—P(1)—C(13)	102.4(3)
P(2)—Rh(1)—H(1′)	97(2)	Rh(1)—P(2)—C(21)	115.8(2)
H(1)—Rh(1)—H(1′)	83(2)	Rh(1)—P(2)—C(22)	118.5(2)
Rh(1)—H(1)—Rh(1′)	97(2)	Rh(1)—P(2)—C(23)	112.4(2)
Rh(1)—P(1)—C(11)	117.3(2)	C(21)—P(2)—C(22)	101.8(3)
Rh(1)—P(1)—C(12)	118.4(2)	C(21)—P(2)—C(23)	102.3(3)
		C(22)—P(2)—C(23)	104.1(3)

(*b*) Molecule **2**

Bond	Length	Bond	Length
Rh(2)—P(3)	2.187(1)	Rh(3)—P(5)	2.188(1)
Rh(2)—P(4)	2.180(1)	Rh(3)—P(6)	2.183(1)
Rh(2)—H(2)	1.68(4)	Rh(3)—H(2)	1.86(4)
Rh(2)—H(3)	1.72(4)	Rh(3)—H(3)	1.72(4)
P(3)—C(31)	1.853(5)	P(5)—C(51)	1.853(5)
P(3)—C(32)	1.868(5)	P(5)—C(52)	1.867(5)
P(3)—C(33)	1.847(5)	P(5)—C(53)	1.852(5)
P(4)—C(41)	1.859(6)	P(6)—C(61A)	1.864(11)
P(4)—C(42)	1.851(7)	P(6)—C(61B)	1.931(12)
P(4)—C(43)	1.841(6)	P(6)—C(62)	1.846(6)
		P(6)—C(63)	1.854(6)
C(33)—C(43)	1.465(9)	C(53)—C(63)	1.501(8)
Rh(2)—Rh(3)	2.6266(8)		

Bonds	Angle	Bonds	Angle
P(3)—Rh(2)—P(4)	85.76(5)	P(5)—Rh(3)—P(6)	85.49(5)
P(3)—Rh(2)—H(2)	94(1)	P(5)—Rh(3)—H(2)	176(1)
P(3)—Rh(2)—H(3)	176(1)	P(5)—Rh(3)—H(3)	98(1)
P(4)—Rh(2)—H(2)	179(1)	P(6)—Rh(3)—H(2)	99(1)
P(4)—Rh(2)—H(3)	97(1)	P(6)—Rh(3)—H(3)	176(1)
H(2)—Rh(2)—H(3)	83(2)	H(2)—Rh(3)—H(3)	78(2)
Rh(2)—P(3)—C(31)	117.7(2)	Rh(3)—P(5)—C(51)	117.0(0)
Rh(2)—P(3)—C(32)	116.7(2)	Rh(3)—P(5)—C(52)	117.1(2)
Rh(2)—P(3)—C(33)	112.5(2)	Rh(3)—P(5)—C(53)	112.7(2)
C(31)—P(4)—C(32)	101.7(3)	C(51)—P(5)—C(52)	102.0(3)
C(31)—P(4)—C(33)	102.4(3)	C(51)—P(5)—C(53)	103.0(3)
C(32)—P(4)—C(33)	104.0(3)	C(52)—P(5)—C(53)	103.0(1)
Rh(2)—P(4)—C(41)	116.2(2)	Rh(3)—P(6)—C(61A)	115.1(3)
Rh(2)—P(4)—C(42)	117.5(2)	Rh(3)—P(6)—C(61B)	112.5(4)
Rh(2)—P(4)—C(43)	112.9(2)	Rh(3)—P(6)—C(62)	120.2(2)
		Rh(3)—P(6)—C(63)	111.3(2)
C(41)—P(4)—C(42)	99.9(3)	C(61A)—P(6)—C(62)	111.2(4)
C(41)—P(4)—C(43)	104.1(3)	C(61A)—P(6)—C(63)	93.2(4)
C(42)—P(4)—C(43)	104.4(4)	C(61B)—P(6)—C(62)	96.1(4)
		C(61B)—P(6)—C(63)	114.2(4)
		C(62)—P(6)—C(63)	101.5(3)
Rh(2)—H(2)—Rh(3)	96(2)	Rh(2)—H(3)—Rh(3)	99(2)

Can. J. Chem. Downloaded from www.nrcresearchpress.com by 41.223.56.140 on 09/07/12
For personal use only.



SCHEME 1

process which equilibrates the two rhodium(I) phosphorus nuclei is about 8.6(5) kcal mol^{-1}, which is near the value of 9 kcal mol^{-1} reported for **2***a* (7). The $^{31}P\{^1H\}$ NMR spectra of **2***d* are qualitatively identical to those of **2***c* as a set, but are broadened and complicated by the fact that the chemical shifts for the two equivalent rhodium(III) phosphorus atoms and the downfield resonance for one of the rhodium(I) phosphorus nuclei are very nearly coincident in the low temperature limiting spectrum. Nonetheless, it is apparent that the two sets of spectra are analogous, and that the same geometries may be invoked for **2***d* as for **2***c*. The activation energy for this low temperature ("rocking") process for the larger chelate ring size dimer is about 11.5(5) kcal mol^{-1}.

As mentioned above, the tetrahydride $[\{(Pr^iO)_3P\}_2Rh]_2(H)_4$, **2***a*, behaves similarly as a function of temperature; however, a different proposal to explain this exchange process has been given based on the isolation and structure of the moderately stable related tetrahydride complex $[\{(Me_2N)_3P\}_2RhH_2](\mu\text{-}H)_2[Rh\{P(NMe_2)_3\}_2]$, **2***e* (23), since it was shown to have the structure **2***e* shown.

The molecule consists of an octahedral rhodium(III) centre and a square planar rhodium(I) centre joined by two bridging hydrides. In this tetrahydride, the phosphorus nuclei on the rhodium(III) centre are *trans* disposed across the $H_2Rh(\mu\text{-}H)_2RhP_2$ plane. Thus it was suggested that exchange of the terminal hydride with the one unique bridging hydride occurred via an excited state structure similar to **2***e*. The fact that chelating phosphines with four or fewer methylene units cannot span *trans* coordination sites precludes this type of excited state geometry for the systems reported here.

The effect of the ancillary ligand is again evident when the binuclear complex of the five-membered chelate ring diphosphine dippe is considered. The tetrahydride **2***b* presents a qualitatively different set of $^{31}P\{^1H\}$ NMR spectra (Fig. 3), characterized by two doublets which, rather than undergoing coalescence and decoalescence, show a marked dependance of chemical shift as a function of the temperature.

This is the spectral behaviour expected if the rhodium(I) centre in the structures in Scheme 2 were now square pyramidal (ground state) and square planar (excited state) in geometry

Can. J. Chem. Downloaded from www.nrcresearchpress.com by 41.223.56.140 on 09/07/12
For personal use only.

Can. J. Chem. Downloaded from www.nrcresearchpress.com by 41.223.56.140 on 09/07/12
For personal use only.

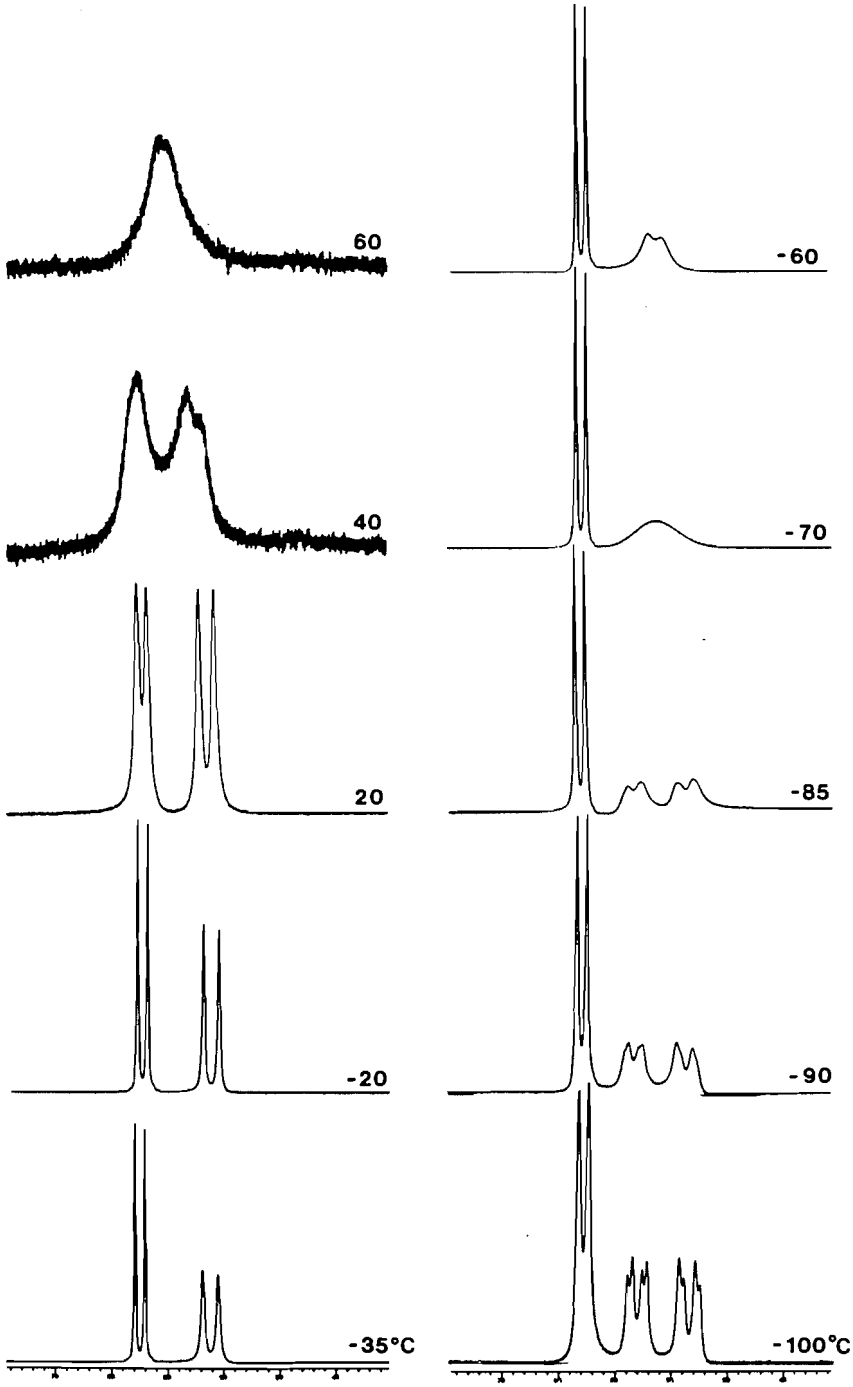
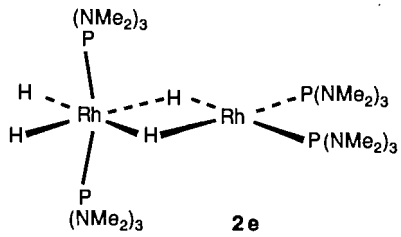


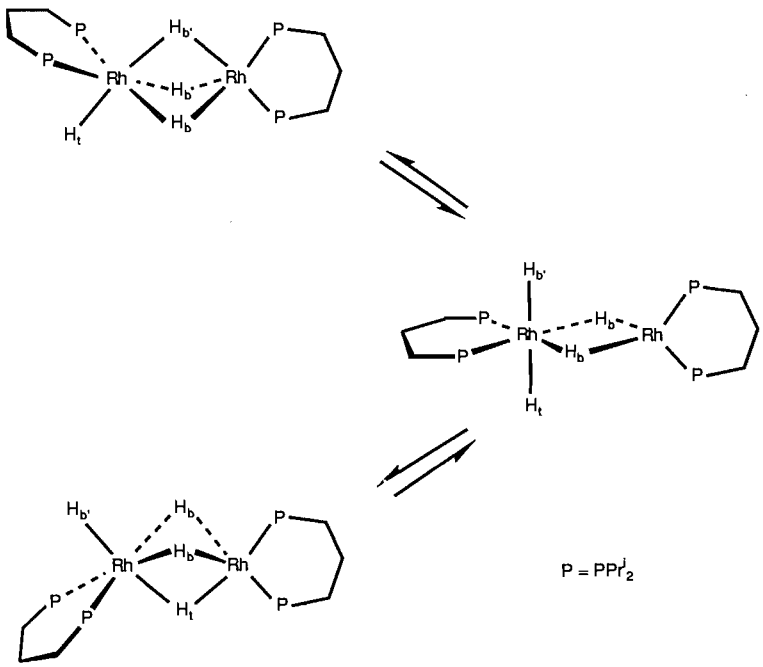
FIG. 2. $^{31}P\{^1H\}$ NMR spectra of the tetrahydride $[(dippp)Rh]_2(H)_4$, **2***c*, at various temperatures.



2e

(Scheme 3). In this process, the two phosphorus nuclei on each rhodium centre remain pairwise equivalent, but due to the structural changes involved, the chemical shifts of the two doublets change with temperature. This is consistent with the ^1H NMR spectra as well wherein the same low temperature limit observed for the dippp and dippb tetrahydrides, **2***c* and **2***d*, is not attained, that is, the terminal hydride signal only broadens as the temperature is lowered (to −95°C).

This observed dependance of the geometry about the rhodium(I) centre on the chelate ring size of the diphosphine ligand may be rationalized partially on the basis of steric arguments. On going from the square pyramidal to the trigonal bipyramidal geometry in the low temperature limit (ground state), steric interactions between the isopropyl groups of the opposing diphosphine ligands are relieved. Similarly, these interactions may be lessened by decreasing the bite angle of the chelating ligand which results in a "pulling back" of the isopropyl groups on phosphorus. Evidently, the contraction of bite angle by about



SCHEME 2

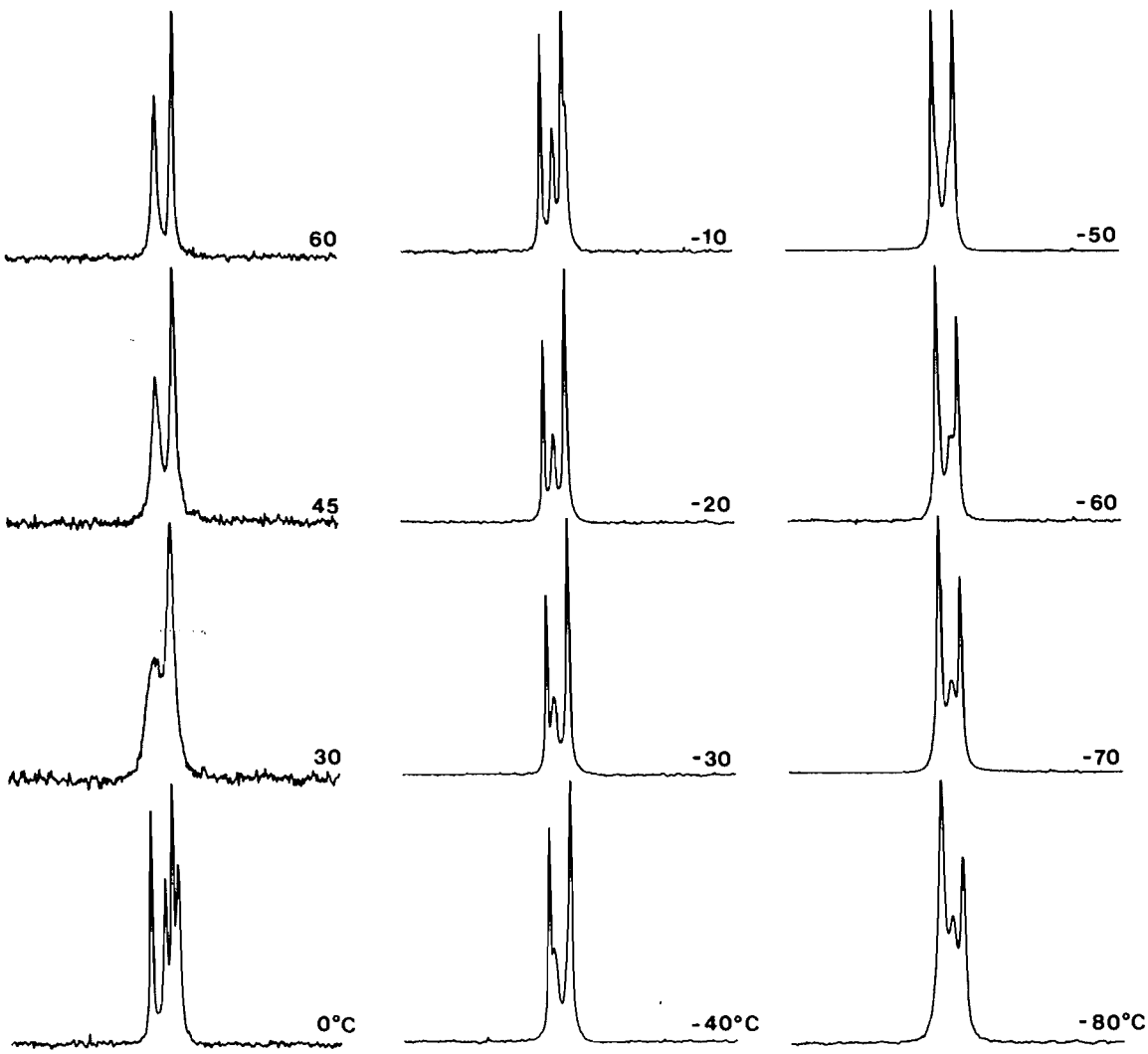
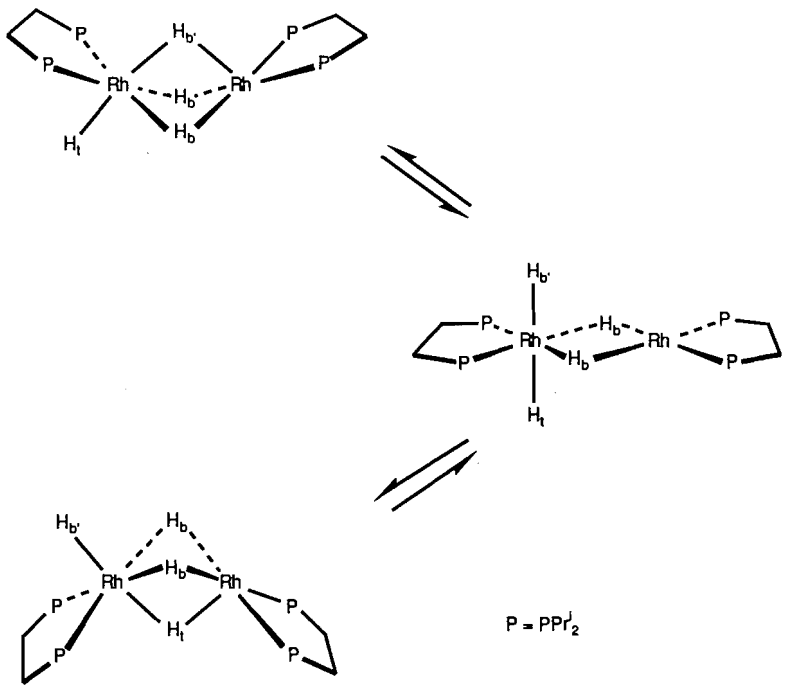


FIG. 3. $^{31}P\{^1H\}$ NMR spectra of the tetrahydride $[(dippe)Rh]_2(H)_4$, **2***b*, at various temperatures.

Can. J. Chem. Downloaded from www.nrcresearchpress.com by 41.223.56.140 on 09/07/12
For personal use only.



SCHEME 3

TABLE 4. Hydrogenation and isomerization rates[a] for the hydrogenation of 1-hexene by **1***a* and **1***b*[b]

Catalyst	Loss of 1-hexene	Products			Internal olefin hydrogenation	
		Hexane	*t*-2-Hexene	*c*-2-Hexene	*t*-2-Hexene	*c*-2-Hexene
1*b*	2600	850–950	13–1700	750–1100	520	240
1*c*	2100	280	1150	700	210	170

[a]All rates are given as the turnover frequencies in h^{-1}.
[b]Hydrogenation reactions carried out at 1 atm pressure of H_2, and 23–25°C.

10° (*vide supra*) was enough to render the change from square pyramidal to trigonal bipyramidal unnecessary for the dippe tetrahydride **2***b*. In **2***c* and **2***d* however, this change in geometry is required to stagger the isopropyl groups and relieve the steric tension. The chelate ring size also affects the activation energy for the exchange of the terminal hydride and the unique bridging hydride ligands: for the seven-membered dippb system, $\Delta G^{\ddagger} = 11.5(5)$ kcal mol^{-1}; for the six-membered dippp system, $\Delta G^{\ddagger} = 8.6(5)$ kcal mol^{-1}; and for the five-membered dippe ligand, $\Delta G^{\ddagger} = <7.0(5)$ kcal mol^{-1} (estimated).

*The hydrogenation of 1-hexene using [{Pr$^i_2$P(CH$_2$)$_n$PPr$^i_2$}-Rh]$_2$(μ-H)$_2$ (**1**b: n = 2; **1**c: n = 3) as catalyst precursors*

The activity of the dimer containing triisopropylphosphite ligands, **1***a*, towards the hydrogenation of olefins (7) lead us to explore the ability of the dippe dimer **1***b* and the dippp dimer **1***c* to bring about this transformation. Neither proved to be more active than **1***a* in this capacity, but we were also interested in probing the reaction mechanistically in some detail.

The dimer **1***b* was found to be a reasonably efficient catalyst precursor for the hydrogenation of 1-hexene at ambient temperature and pressure. With a substrate/catalyst ratio arbitrarily set at about 1700, hexane was generated with a turnover rate of about 850–950 h^{-1} (Table 4). Rapid olefin isomerization steps also occurred, with production of *cis*- and *trans*-2-hexene along with hexane. The catalyst hydrogenated the terminal olefin selectively until it was used up, and then began to hydrogenate the internal olefins, producing hexane at a slightly lower turnover frequency of about 700 h^{-1}.

The dippp dimer **1***c* was also active as a catalyst precursor for this reaction, but was significantly slower under the same conditions. Turnover rates are shown in Table 4. In this reaction, some evidence for the build-up of 3-hexenes was also observed. Notably, while relative rates of isomerization were higher for **1***c*, the overall rate of hexane production was steady, probably reflecting similar rates in the hydrogenation of terminal and internal olefins, or selective hydrogenation of internal olefins only.

A cursory study of the dippb tetrahydride **2***d* showed that its activity was not significantly different from that of the dippp dimer **1***c* and it was therefore not studied in any detail.

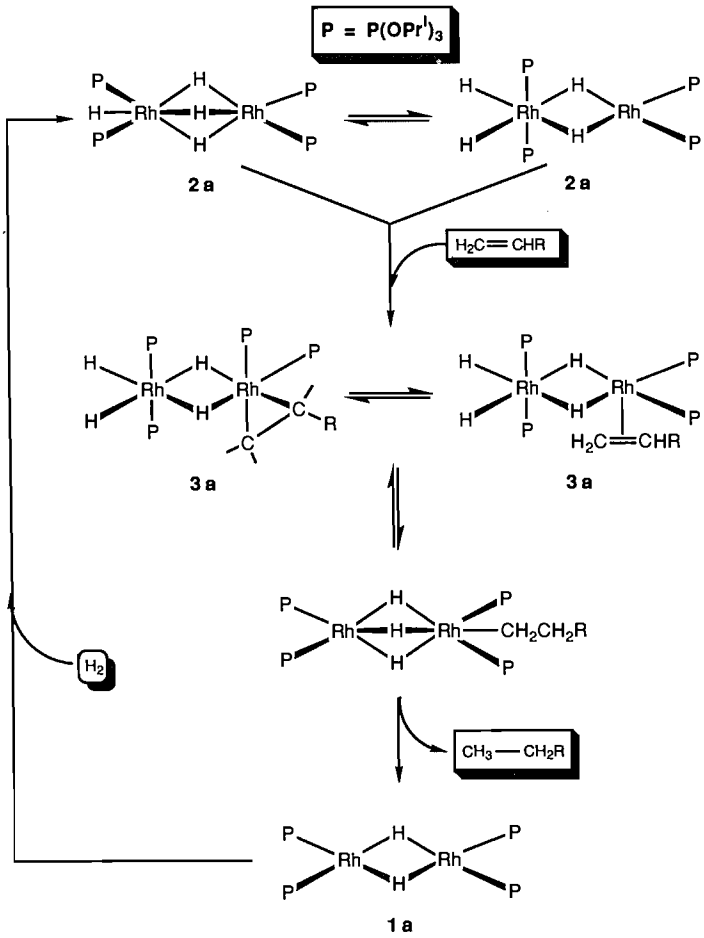
Mechanistic studies

Chemical evidence abounds for a mechanistic pathway for hydrogenation which involves solely binuclear intermediates. The early work on the use of [{(Pr^{i}O)$_3$P}$_2$Rh]$_2$(μ-H)$_2$, **1***a*, as a catalyst precursor for the hydrogenation of olefins provided the first such mechanistic proposal as shown in Scheme 4 (7).

The reaction of this dihydride **1***a* with H_2 leads to the

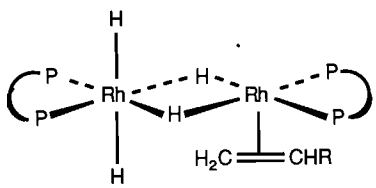
Can. J. Chem. Downloaded from www.nrcresearchpress.com by 41.223.56.140 on 09/07/12
For personal use only.

Can. J. Chem. Downloaded from www.nrcresearchpress.com by 41.223.56.140 on 09/07/12
For personal use only.



SCHEME 4

tetrahydride **2***a* which adds 1 equiv. of alkene to the coordinatively unsaturated Rh(I) centre to produce **3** (in the geometry suggested by the isolation of **2***e*); a subsequent migratory insertion and reductive elimination regenerates the dimer **1***a* and produces alkane. This proposal was based on the observation of a fast dehydrogenation of the tetrahydride **2***a* by the stoichiometric addition of an alkene. In our systems, we have also observed this same dehydrogenation reaction, in fact, it is the pathway for the synthesis of the dippb dihydride **1***d* starting from the stable tetrahydride **2***d*. A modification of the catalytic cycle shown in Scheme 4 to take into account the use of chelating bidentate ligands that cannot span *trans* coordination sites requires that the binuclear alkene–tetrahydride intermediate **3'** have a structure as shown.



3'

Further chemical evidence for a binuclear hydrogenation cycle exists in a crossover experiment. When a mixture of equal amounts of **1***b* and **1***c* was used to hydrogenate a large excess of 1-hexene, the mixed dimer [(dippe)Rh](μ-H)$_2$[Rh(dippp)], expected should fragmentation/aggregation occur, was not detected after workup. This observation does not totally eliminate the possibility of crossover, but does show that (within the detection limits of $^{31}P\{^1H\}$ NMR) crossover is minimal.

This chemical evidence certainly suggests that a pathway exists which contains only binuclear intermediates. It does not, however, totally eliminate the possibility that fragmentation occurs to yield a highly reactive mononuclear species which may (or may not) be responsible for the majority of the catalysis observed. This is a long standing problem encountered in cluster catalysis (28, 29), and chemical evidence alone does not provide sufficient grounds to state firmly that catalysis by the cluster is the major mechanistic pathway in the reaction. In order to determine this with confidence it is necessary to carry out kinetic analysis on the reaction, and even then it is sometimes difficult to reach meaningful conclusions.

One of the kinetic criteria arguing for cluster catalysis is an increase in turnover frequency upon increasing catalyst concentration (29). Catalyst concentration studies were carried out using varying amounts of the dippp dimer **1***c* as the catalyst precursor. Styrene was used as the substrate to eliminate isomerization side reactions, and the dihydrogen uptake was monitored as a function of time at 30°C. A plot of the rate of dihydrogen uptake (mol s^{-1} L^{-1}) vs. the concentration of **1***c*, should be linear if no fragmentation occurs. In the plot in Fig. 4, it is clear that this is not a linear relationship, and in fact, is better represented by the plot in Fig. 5 that actually shows the reaction to be half order in the concentration of the dippp dimer **1***c*.

When the turnover frequency (TF = mole substrate consumed per mole catalyst precursor per unit time) is plotted vs. catalyst concentration (Fig. 6), it is clear that the TF decreases with increasing [**1***c*]. This is diagnostic and provides clear kinetic evidence that, in this system, fragmentation occurs such that the majority of the actual catalysis is performed by small amounts of a highly reactive mononuclear fragment.

Unfortunately, similar kinetic analysis of the reaction involving the dippe dimer **1***b* was hampered by this compound's extreme sensitivity to minor amounts of oxygen and water unavoidably included under the conditions employed. (The scatter apparent in Figs. 4–6 was likely due to this factor as well, particularly at low catalyst concentrations, but **1***c* was generally more well-behaved under the monitoring conditions.) Thus, it cannot be similarly concluded that mononuclear fragments carry out the majority of catalysis in the reaction utilizing **1***b* as a catalyst precursor. Indeed, the chemical evidence suggests that the pathway involving binuclear intermediates is the major one in the **1***b* catalyzed reaction, since we observe no crossover in the hydrogenation with a mixture of **1***b* and **1***c*. This is the expected result if only *one* of **1***b* or **1***c* were fragmenting under the hydrogenation conditions, and since **1***c* does fragment, by process of elimination, **1***b* cannot.

Based on both sets of evidence (chemical and kinetic) we propose that both binuclear and mononuclear pathways exist for the hydrogenation of alkenes by the dippp dimer **1***c* as shown in Scheme 5.

Attempts to detect fragmentation of the tetrahydride **2***c* in the absence of substrate alkenes by deviation from Beer–Lambert behaviour especially at low concentration were unsuccessful; plots of absorbance vs. [**2***c*] were linear for concentrations spanning a range of 0.14 m*M* to 0.0012 m*M*. Thus it can be concluded that the mononuclear pathway for hydrogenation is kinetically much more efficient than the binuclear one since mononuclear fragments have not yet been spectroscopically detected.

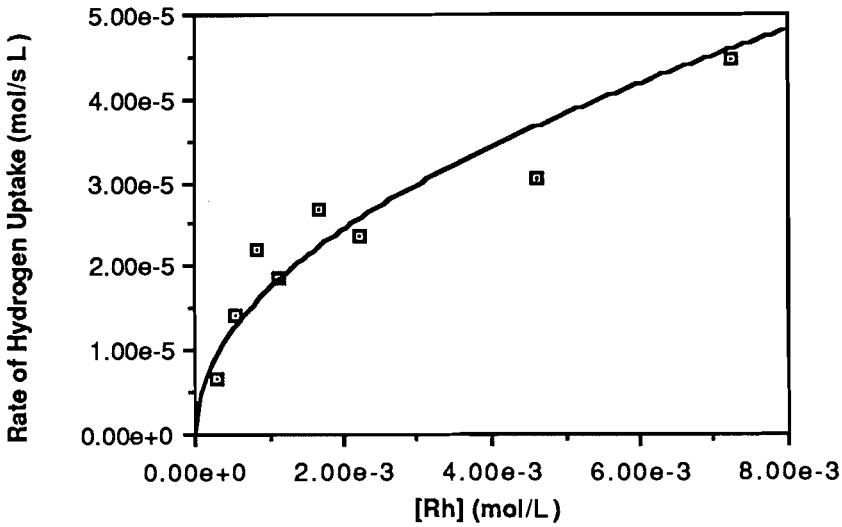


FIG. 4. Plot of the rate of hydrogen uptake vs. the catalyst concentration in the hydrogenation of styrene using $[(dippp)Rh]_2(\mu\text{-}H)_2$, **1***c*, as catalyst precursor.

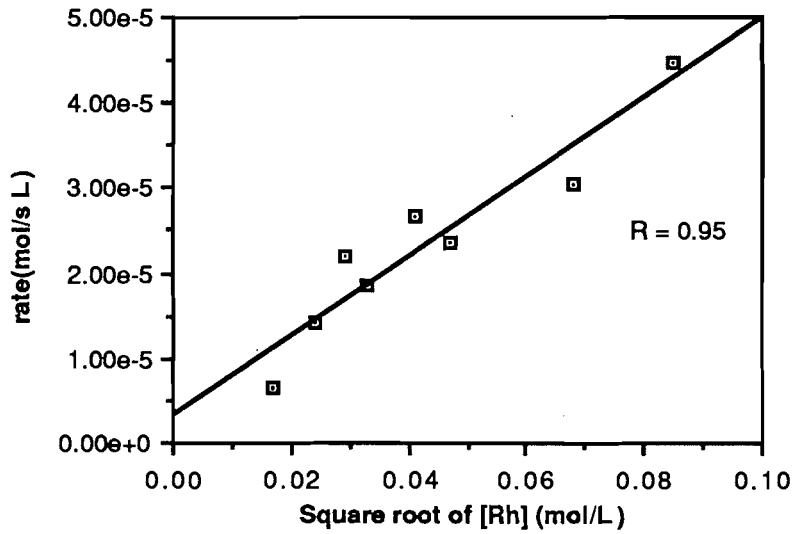


FIG. 5. Plot of the rate of hydrogen uptake vs. the square root of catalyst concentration in the hydrogenation of styrene using $[(dippp)Rh]_2(\mu\text{-}H)_2$, **1***c*, as catalyst precursor.

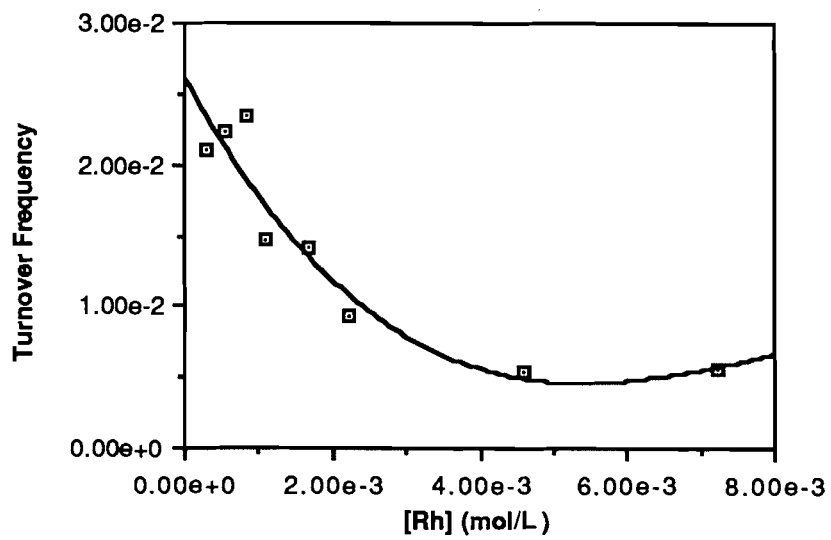
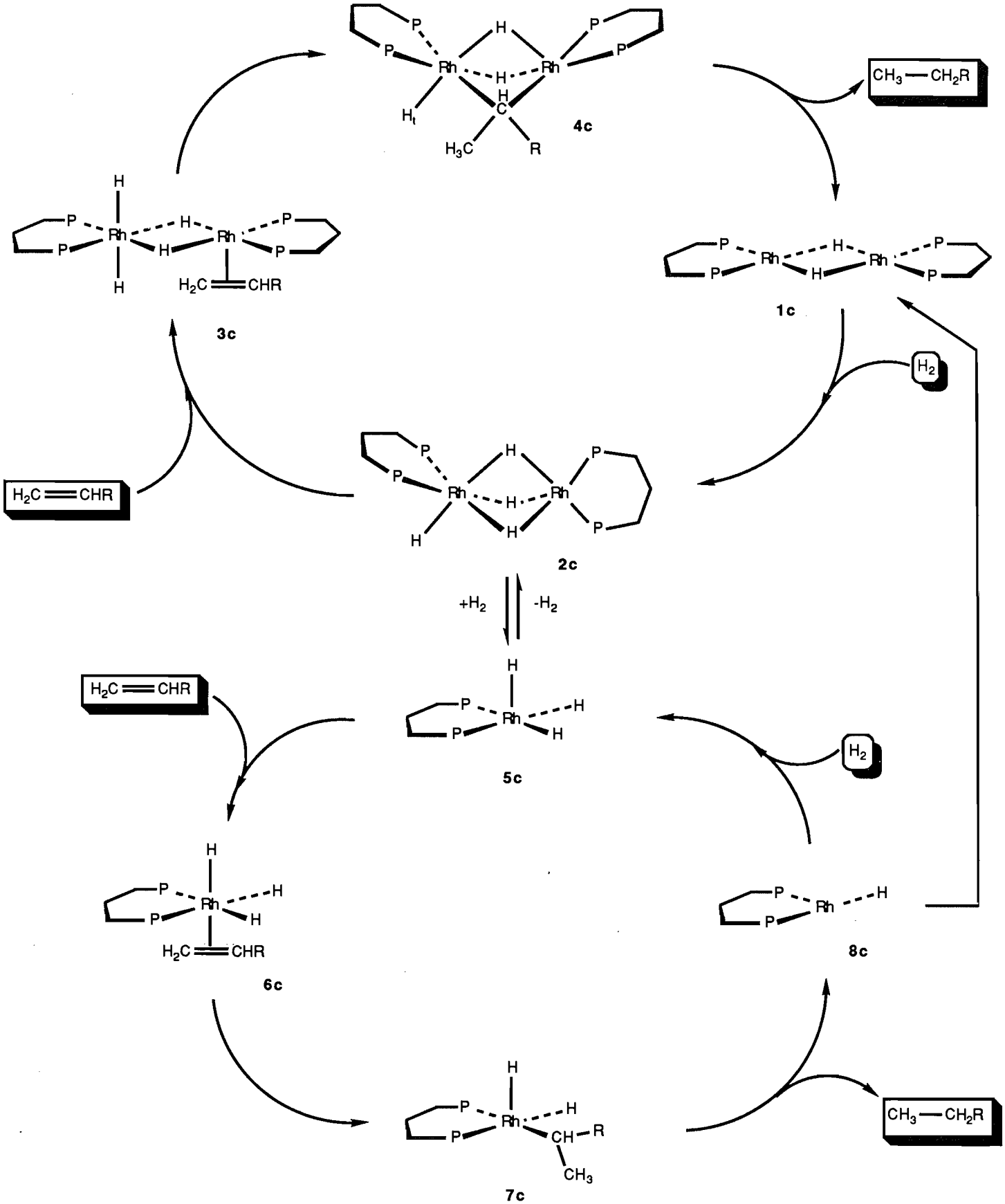


FIG. 6. Plot of turnover frequency vs. catalyst concentration in the hydrogenation of styrene using $[(dippp)Rh]_2(\mu\text{-}H)_2$, **1***c*, as catalyst precursor.

Can. J. Chem. Downloaded from www.nrcresearchpress.com by 41.223.56.140 on 09/07/12
For personal use only.



SCHEME 5

Can. J. Chem. Downloaded from www.nrcresearchpress.com by 41.223.56.140 on 09/07/12
For personal use only.

A number of features of the proposed binuclear cycle (top in Scheme 5) are different than those given in Scheme 4 (7, 28). As already mentioned, the olefin complex **3***c* has *trans* terminal hydrides on the Rh(III) centre. The migratory insertion step to form the alkyl complex **4***c* is also in contrast to that in Scheme 4; to account for the substantial and rapid olefin isomerization, a bridging, *secondary* alkyl ligand in **4***c* is invoked. Although speculative, the bridging alkyl (30) is in line with other proposals that involve dehydrogenation of the dihydride dimers **1***b* and **1***c* by olefins and dienes (10*c*). In addition, the alkyl must be secondary at some point to explain the olefin isomerization; how this occurs is not explicitly detailed, but would obviously involve a β-elimination back to **3***c* but with an *internal* olefin coordinated to the Rh(I) centre. Reductive elimination from **4***c* generates the product alkane and the dihydride **1***c*.

The bifurcation to the mononuclear cycle (bottom Scheme 5) is proposed to occur at the tetrahydride species **2***c*. Rather than bind the olefin, the tetrahydride can fragment under dihydrogen to generate the mononuclear trihydride **5***c*. This coordinatively unsaturated fragment undergoes the usual olefin binding, migratory insertion, and reductive elimination to produce olefin and the 14-electron, monohydride **8***c*. The mononuclear cycle can continue by oxidative addition of H_2 to **8***c* to regenerate **5***c*, or the monohydride monomer **8***c* can dimerize to **1***c* and thus gain entrance back into the binuclear regime.

A possible reason for the fragmentation pathway in the dippp dimer **1***c* system is again the increased steric crowding about the metal centres as compared to the dippe dimer **1***b*. The observed differences in the geometries about the rhodium(I) centre in the ground state structures of the tetrahydrides may stymie the alkene binding by **2***c*, and lead to fragmentation, while with **2***b*, the binding of the alkene is facilitated. It thus appears that contact between the catalyst and the substrate is significantly hindered in the pathway invoking dimeric intermediates for the larger chelate ring system, and that when such contact is made, fragmentation is induced and the mononuclear regime dominates. Other fragmentation points in the binuclear cycle are of course possible; for example, the dihydride **1***c* could generate **8***c* spontaneously. However, the proposal that it is the binding of the substrate to the tetrahydride that induces fragmentation is more compelling, in our opinion.

Acknowledgements

Financial support for this research was provided by NSERC (operating grants to M.D.F. and F.W.B.E., and a postgraduate scholarship to W.E.P.) and ESSO Canada Limited (operating grant to M.D.F.). We are especially grateful to Johnson Matthey for the loan of $RhCl_3$.

1. (*a*) E. L. MUETTERTIES. Chem. Eng. News, **60**, 28 (1982); (*b*) E. L. MUETTERTIES. Bull. Soc. Chim. Belg. **84**, 959 (1975); (*c*) E. L. MUETTERTIES. Science, **196**, 839 (1977).
2. J. R. SHAPLEY and M. TACHIKAWA. J. Organomet. Chem. **124**, C19 (1977).
3. E. G. BRYAN, B. F. G. JOHNSON, and J. LEWIS. J. Chem. Soc. Dalton Trans. 1328 (1977).
4. A. J. DEEMING. *In* Transition metal clusters. *Edited by* B. F. G. Johnson. Wiley, Chichester. 1980. p. 391.
5. S. A. R. KNOX, J. W. KOEPKE, M. A. ANDREWS, and H. D. KAESZ. J. Am. Chem. Soc. **97**, 3942 (1975).
6. A. J. DEEMING. Adv. Organomet. Chem. **26**, 1 (1986).
7. E. L. MUETTERTIES and A. J. SIVAK. J. Am. Chem. Soc. **101**, 4878 (1979).
8. M. D. FRYZUK, F. W. B. EINSTEIN, and T. JONES. Organometallics, **3**, 185 (1984).
9. R. R. BURCH, A. J. SHUSTERMAN, E. L. MUETTERTIES, R. G. TELLER, and J. M. WILLIAMS. J. Am. Chem. Soc. **105**, 3546 (1983).
10. (*a*) M. D. FRYZUK, F. W. B. EINSTEIN, and T. JONES. J. Chem. Soc. Chem. Commun. 1556 (1984); (*b*) M. D. FRYZUK, W. E. PIERS, and S. J. RETTIG. J. Am. Chem. Soc. **107**, 8057 (1985); (*c*) M. D. FRYZUK and W. E. PIERS. Polyhedron, **7**, 1001 (1988).
11. M. D. FRYZUK and W. E. PIERS. Organometallics, **7**, 2062 (1988).
12. S. T. MCKENNA, E. L. MUETTERTIES, and R. A. ANDERSEN. Organometallics, **5**, 2233 (1986).
13. R. R. BURCH, E. L. MUETTERTIES, A. J. SHULTZ, E. G. GEBERT, and J. M. WILLIAMS. J. Am. Chem. Soc. **103**, 5517 (1981).
14. A. J. SIVAK, E. L. MUETTERTIES, V. W. DAY, M. F. FREDRICH, G. S. REDDY, and W. R. PRETZER. J. Am. Chem. Soc. **99**, 8091 (1977).
15. M. D. FRYZUK. Can. J. Chem. **61**, 1347 (1983).
16. M. D. FRYZUK. Organometallics, **1**, 408 (1982).
17. K. TANI, E. TANIGAWA, Y. TATSUBO, and S. OTSUKA. J. Organomet. Chem. **279**, 87 (1985).
18. D. F. SHRIVER. The manipulation of air-sensitive compounds. McGraw-Hill, New York. 1969. p. 199.
19. D. F. GRANT and E. J. GABE. J. Appl. Crystallogr. **11**, 114 (1977).
20. International tables for X-ray crystallography. Vol. IV. Kynoch Press, Birmingham, England.
21. E. J. GABE, A. C. LARSON, F. L. LEE, and Y. WANG. The NRC PDP-8e crystal structure system. Chemistry Division, NRC, Ottawa, Ont. 1979.
22. (*a*) B. R. JAMES and D. MAHAJAN. Isr. J. Chem. **15**, 214 (1977); (*b*) B. R. JAMES and G. L. REMPEL. Discuss. Faraday Soc. **46**, 48 (1968); (*c*) B. R. JAMES and G. L. REMPEL. Can. J. Chem. **44**, 233 (1966).
23. R. G. TELLER, J. M. WILLIAMS, T. F. KOETZLE, R. R. BURCH, R. M. GAVIN, and E. L. MUETTERTIES. Inorg. Chem. **20**, 1806 (1981).
24. B. R. JAMES, D. MAHAYAN, G. M. WILLIAMS, and S. J. RETTIG. Organometallics, **2**, 1452 (1983).
25. D. W. MEEK and T. J. MAZANEC. Acc. Chem. Res. **14**, 266 (1981); J. F. NIXON and A. PIDCOCK. Ann. Rev. NMR Spectrosc. **2**, 345 (1969).
26. M. D. FRYZUK, S. J. RETTIG, A. WESTERHAUS, and H. D. WILLIAMS. Inorg. Chem. **24**, 4316 (1985).
27. E. L. MUETTERTIES, R. R. BURCH, E. B. MEIER, and V. W. DAY. J. Am. Chem. Soc. **104**, 2661 (1982).
28. E. L. MUETTERTIES and M. J. KRAUSE. Angew. Chem. Int. Eng. Ed. **22**, 135 (1983).
29. R. M. LAINE. J. Mol. Catal. **14**, 137 (1982).
30. J. HOLTON, M. F. LAPPERT, R. PEARCE, and P. I. W. YARROW. Chem. Rev. **83**, 135 (1983).

Can. J. Chem. Downloaded from www.nrcresearchpress.com by 41.223.56.140 on 09/07/12
For personal use only.

Detection at the picogram level of bis(cyclopentadienyl)ruthenium by gas chromatography – flame photometry[1]

XUN-YUN SUN AND WALTER A. AUE[2]
Department of Chemistry, Dalhousie University, Halifax, N.S., Canada B3H 4J3

Received November 2, 1988

XUN-YUN SUN and WALTER A. AUE. Can. J. Chem. **67**, 897 (1989).

Ruthenocene — bis(cyclopentadienyl)ruthenium — can be determined with surprisingly high sensitivity and selectivity by gas chromatography – flame photometry. The detector's response relies mainly on an unidentified emission system (RuH?) with major peaks at 484 and 528 nm, while some familiar atomic lines show up as well. Without interference filter, the minimum detectable amount of ruthenocene, at S/N = 2, is approximately 2 pg (or 2×10^{-13} g/s or 1×10^{-15} mol/s), the elemental selectivity ruthenium/carbon 4×10^5, and the linear range $1 : 4 \times 10^4$. These calibration characteristics place ruthenium among the strongest luminescing and best performing species in the flame photometric detector. In fact, under conditions optimized for ruthenocene, ruthenium responds stronger than other FPD-active atoms (Sn, P, Cr, S, B). Fortunately, quenching effects are very weak: for instance, it takes about 1600 ppm (v/v) of methane in the detector to reduce the ruthenocene peak height by 50%.

Key words: ruthenocene, gas chromatography, flame photometric detector, ruthenium hydride.

XUN-YUN SUN et WALTER A. AUE. Can. J. Chem. **67**, 897 (1989).

Utilisant la chromatographie en phase gazeuse couplée à la photométrie à flamme, on peut déterminer le ruthénocène — le bis(cyclopentadiényl)ruthénium — avec une grande sensibilité et une grande sélectivité. La réponse du détecteur dépend principalement d'un système d'émission qui n'a pas été identifié (RuH?), qui possède des pics importants à 484 et à 528 nm et dans lequel on remarque la présence de quelques raies atomiques familières. Sans faire appel à un filtre d'interférence, la quantité minimale de ruthénocène que l'on peut détecter, à S/N = 2, est approximativement 2 pg (ou 2×10^{-13} g/s ou 1×10^{-15} mol/s), la sélectivité élémentaire ruthénium/carbone est de 4×10^5 et la plage linéaire est $1 : 4 \times 10^4$. Sur la base de ces caractéristiques de calibration, le ruthénium s'avère être l'espèce possédant la plus forte luminescence et celle qui donne les meilleurs résultats dans un détecteur de photométrie à flamme. En fait, utilisant les conditions optimisées pour le ruthénocène, le ruthénium répond mieux que les autres atomes actifs avec cette méthode (Sn, P, Cr, S, B). Heureusement, les effets de piégeage sont très faibles : par exemple, il faut avoir 1600 ppm (v/v) de méthane dans le détecteur pour réduire la hauteur du pic du ruthénocène par 50%.

Mots clés : ruthénocène, chromatographie gazeuse, détecteur de photométrie à flamme, hydrure de ruthénium.

[Traduit par la revue]

Introduction

Recently we wanted to determine ruthenocene — bis(cyclopentadienyl)ruthenium — with high sensitivity and selectivity. This simple metallocene — as well as other, related ruthenium structures — is of interest in a variety of areas, e.g. in catalysis. The fact that ruthenocene is volatile and stable suggests the use of gas chromatography. Ruthenocene has been subjected to this technique before (1, 2); however, no conventional gas chromatographic detector is known to be selective to ruthenium.

The microwave-excited atmospheric pressure helium plasma has been used on ruthenocene (and many other organometallics) eluted from a capillary column. Spectrophotometric monitoring of the 240.3 nm Ru^+ line yielded a minimum detectable amount of 7.8 pg/s, an elemental selectivity against carbon of 1.34×10^5, and a linear range of 10^3 (3). Beyond capillary GC-MED, any of a number of "hyphenated" techniques (GC-MS, GC-ICP, GC-ETV-AS, GC-ICP-MS, etc.) could be used for a fairly sensitive and selective determination of ruthenocene. However, for reasons of simplicity, ruggedness, quantitative accuracy, and cost, a typical GC detector seemed preferable.

Among the common GC detectors, the flame photometric (FPD) stands out as a possible candidate. Although the FPD is generally used for compounds of sulfur (via S_2*) and phosphorus (via HPO*), it can respond to other hetero-atoms as well. Listed in order of decreasing sensitivity — and spanning a range of minimum detectable amounts from 5×10^{-18} to 4×10^{-13} mol/s — the elements to which the FPD has proven sufficiently sensitive to be of analytical interest are Sn, Ge, P, Cr, S, As, Se, B, Fe, and Te (4). An extensive literature review of the FPD — and other GC detectors — has recently become available (5).

The above list of responsive elements reveals no easily discernable pattern, and we known of no reports on the FPD's behaviour vis-a-vis ruthenium or any of the platinum metals.

Experimental

A Shimadzu GC-4BMPF gas chromatograph with dual-channel FPD was used with a 100 × 0.3 cm i.d. column, packed with 5% OV-101 on Chromosorb W, purged by 22 mL/min of nitrogen, and heated to 155°C. (Under these conditions ruthenocene elutes 2 min after injection.) The temperature of the injection port was 180°C, as was that of the detector base. A simple *RC* filter ($R = 10\,k\Omega$, $C = 200\,\mu F$) was inserted between the electrometer and strip chart recorder. For *analytical* purposes, the detector was usually operated under the optimized conditions of 300 mL/min hydrogen, 80 mL/min air, an additional 20 mL/min nitrogen (added to the air supply), and without the conventional quartz chimney and interference filter. Under these conditions, the only spectral discrimination was that inherent in the Hamamatsu R-268 photomultiplier tube (bialkali, 300 to 650 nm, maximum at 420 nm).

The same tube was used for *spectral* purposes in conjunction with a Jarrel-Ash 82-415 quarter-meter scanning spectrophotometer with a 1180 lines/mm grating of 500 nm blaze. To suppress any background (there was little), "spectra" were obtained by repeatedly injecting ruthenocene while manually advancing the wavelength drive.

Quenching experiments were conducted by adding methane to the hydrogen supply via an exponential dilution flask; or, for constant levels, via a very fine metering dual valve (Nupro).

The visual detection of ruthenium luminescence was carried out after

[1]Part of doctoral thesis requirements of first author.
[2]To whom correspondence should be addressed.

Can. J. Chem. Downloaded from www.nrcresearchpress.com by 41.223.56.140 on 09/07/12
For personal use only.

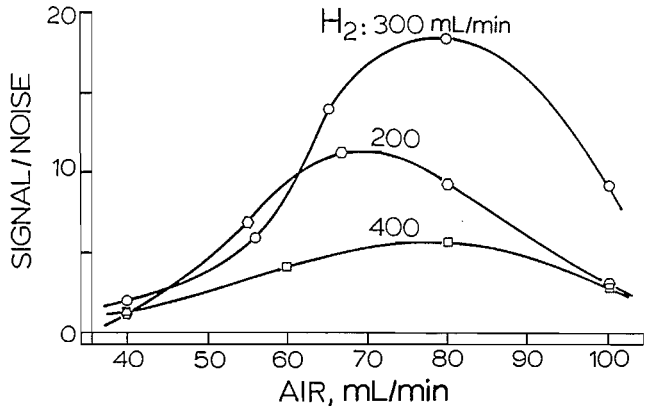


FIG. 1. Examples of optimization curves. Other conditions as given in the Experimental section. Amount ruthenocene injected: 20 pg.

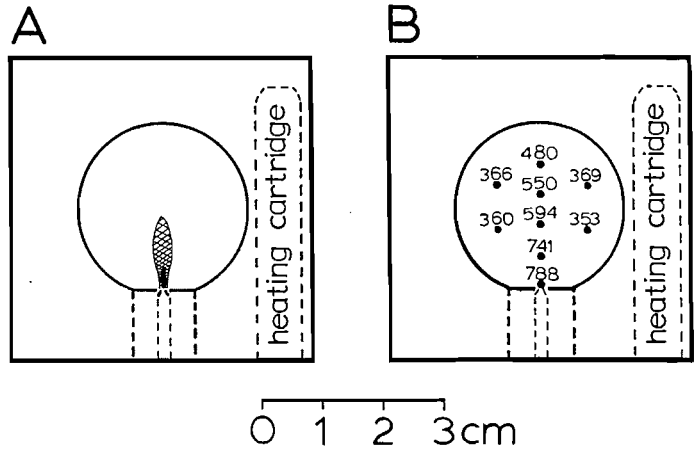


FIG. 2. *A*: Approximate visual flame shapes for optimized flow and a ca. 1 μg ruthenocene peak (hatched) vs. the baseline state (dark). *B*: Approximate thermocouple temperatures for optimized flow (calibration curve # 1 in Fig. 5).

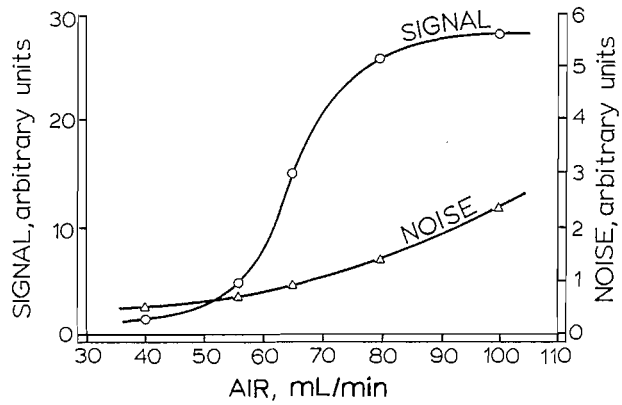


FIG. 3. Separate contributions of signal and noise. Similar to Fig. 1. Hydrogen flow 300 mL/min.

adapting the eyesight of one of us (X.Y.S.) to a darkened lab for about half an hour. The temperature at various positions in the FPD was estimated with a 0.2 mm diameter fine-wire iron–constantan thermocouple connected to a simple amplifier (Omega OMNI-AMP II-A). (Iron–constantan thermocouples made of 0.4 mm diameter wires and/or dipped into phosphoric acid prior to use gave essentially the same readings.)

Results and discussion

The variation of detector gas flow rates in Fig. 1 shows that the highest signal/noise ratios are obtained around 300 mL/min of hydrogen and 80 mL/min of air (with "noise" defined as the peak-to-peak baseline fluctuation). The hydrogen flow rate is quite high (c.f. ref. 5), but it should be noted that the flame gas volume in the detector is also somewhat larger than usual, owing to the removal of the protective (and constrictive) traditional quartz chimney. Removing the chimney produces a significantly larger signal/noise ratio (for *ruthenocene*, not necessarily for other FPD-active elements such as sulfur).

Visual observation of the ruthenocene peak was possible: The slim luminescence, green with an upper bluish tinge, appeared strongest in the flame itself, diminished gradually above it, and vanished about halfway up the viewing area — without ever significantly spreading out to the sides. (The term "flame" refers here to the minute region where a very weak glow can be visually observed under *no-analyte* conditions.) Thus the visible luminescence did by no means fill the total accessible volume — as, for instance, low concentrations of sulfur would have done.

The region where the luminescence appeared — as well as other detector regions — were measured with a fine-wire thermocouple. The temperature was obviously highest right in the central flame area (788°C) and decreased from there to values around 600°C at the upper end of the observable luminescence. The introduction of saturation amounts of ruthenocene showed no effect on the thermocouple temperature; the introduction of part-per-thousand levels of methane (see later) produced only a very minor decrease.

Although such temperature measurements are notoriously unreliable, particularly in diffusion flames, it is obvious that the system is fairly low in thermal energy. For comparison: the maximum theoretical temperature of the hydrogen-air flame is 2115°C, the highest measured values range from 2000 to 2050°C (6). The excess of hydrogen, with its very high thermal conductivity, does help to depress the temperature. Note that 300 mL of hydrogen would need 750 mL of air for a stoichiometric mixture, while the optimum flow of air is not much more than one tenth of that. Figure 2 provides an approximate drawing of the visually observable flame shapes with and without analyte, as well as a few selected thermocouple temperatures measured at flow-optimized conditions.

In the context of excitation mechanisms, it is interesting to know whether and to what extent emission rises with increasing air flow (temperature). Figure 1 displays only the signal/noise ratio and, while this criterion is of paramount importance in an analytical setting, the signal per se is of more interest in a spectral context. Figure 3 shows that the signal itself does not rise much anymore beyond the region where S/N reaches its maximum (in several cases involving other elements, both signal and noise kept right on rising with increasing air flow rates). This fact, as well as the relatively low temperature and the surprisingly high sensitivity, all point to a chemiluminescent process.

Using the optimum flow rates, the spectrum of the luminescence was determined. It is shown in Fig. 4. The emissions in the 350 to 400 nm range agree with the atomic Ru lines most prominently found, and most often used, in atomic spectroscopy (7). They are all transitions to the ground state (a^5F_5) from $z^5G_6^0$ (349.9 nm), $z^5F_5^0$ (372.8), and $z^5D_4^0$ (379.9) (8). The 349.9 nm line is the most energetic one found (3.55 eV, 342 kJ/mol). Finding an atomic line at this low a temperature

Can. J. Chem. Downloaded from www.nrcresearchpress.com by 41.223.56.140 on 09/07/12
For personal use only.

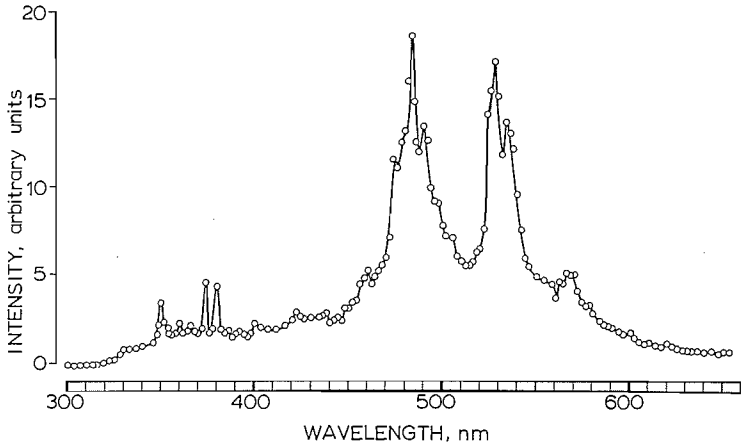


FIG. 4. "Spectrum" obtained by repeatedly injecting 500 ng ruthenocene and measuring its peak height. Slits: 0.5 mm.

Can. J. Chem. Downloaded from www.nrcresearchpress.com by 41.223.56.140 on 09/07/12
For personal use only.

may seem unusual in the context of conventional atomic spectroscopy. However, the flame photometric detector — particularly, one assumes, because of its hydrogen-rich environment — is low in thermal but high in chemical energy. The fact that *atomic* emission is seen points to a chemical excitation process: If the process were purely thermal, it would be hard to explain why it is that many other hetero-elements do not respond at all (or, in a few cases, do not respond with commensurate strength).

The atomic lines in the 350 to 400 nm region constitute, however, only a minor part of the observed total light intensity. The larger part of the spectrum consists of two similarly shaped, complex structures, whose dominant, sharp emissions are centered at approximately 484 and 528 nm. Our search of the literature failed to locate that system (or systems). It should be noted that the peak width of the 484 and 528 nm bands as shown in Fig. 4 is likely not natural but determined by the 0.5 mm slit width (1.7 nm bandpath). We suggest that these major emissions originate from a di (or perhaps tri) atomic system. Based on their relatively open and sharp structure, and on the chemical environment whence they originate, we further suggest that they might be due to the (so far unknown but theoretically investigated (9)) ruthenium hydride. Additional, indirect support for the likelihood of RuH being the emitter comes from the great similarity of the measured spectral features with those of FeH (we are indebted to Professor John Coxon for pointing this out to us). The iron hydride emits complex bands in the blue from 486 to 497 (strongest band at 493.2257 nm) and in the green from 528 to 536 nm (strongest band at 533.6044 nm), in a King-type furnace at ca. 2600 K and 400 Torr of H_2, as well as in the sun and particular in sunspots (10). However, it should be added that, in the FPD, ruthenocene's congener ferrocene shows spectral features other than the FeH bands in the relevant wavelength region (11).

Again, it is quite likely that the driving process is chemiluminescent in nature. The wavelength 484 nm corresponds to 2.56 eV or 248 kJ/mol. Note that the ruthenocene molecule is unusually stable: Its enthalpy of formation $\Delta H_f^{298} = -782$ kJ/mol and its decomposition temperature is 610°C (12). Its break-up might involve fairly selective reactions with hydrogen atoms or other radicals (as contrasted with the general, complex pyrolysis/combustion schemes commonly associated with flames). Note that only about 10% of the hydrogen (and an unknown but perhaps small percentage of ruthenocene) is *oxi*dized, that the maximum temperature measured is below 790°C (and below 590°C at only slightly less efficient conditions, *vide infra*), and that the residence time in the hottest parts of the detector is extremely short (about a tenth of a millisecond if the "flame" volume — marked dark in Fig. 2 — is assumed to be 3 mm^3).

The calibration curves shown in Fig. 5 tally six for the analyte ruthenocene and two for the hydrocarbon standard dodecane. The unconventional showing of *six* calibration curves for a single compound is used here to point out important detector characteristics, appraise various optimization strategies, and assess the magnitude of quenching effects. Since noise levels vary among the different conditions at which these calibration curves were obtained (*vide infra*), the results are plotted as signal/noise ratios: these allow a better appreciation of potential analytical utility than conventional (signal-only) measurements.

The analytically "best" calibration curve — i.e. #1, the one farthest to the left — is obtained without interference filter and quartz chimney, and at the optimized conditions noted in the Experimental section. The minimum detectable amount of ruthenocene, as defined by a signal/noise ratio of two, is 2.2×10^{-12} g. On a peak with a base width of 20 s ($2\sigma = 10$s), 2.2 pg translates to 2.2×10^{-13} g/s or 0.95×10^{-15} mol/s. (To compare: For the two most prominent analyte heteroatoms in the FPD, phosphorus and sulfur, Dressler reports a literature range of minimum detectable mass flow rates of 1×10^{-13} to 2×10^{-12} g P/s and 2×10^{-12} to 5×10^{-11} g S/s (5) — corresponding to 3×10^{-15} to 6×10^{-14} mol P/s and 6×10^{-14} to 2×10^{-12} mol S/s.)

The selectivity against dodecane, on an (atom Ru/atom C) basis — and measured at the same conditions as the "best" ruthenocene calibration curve — is 4.2×10^5. The calibration is linear over a range of 1 to 4×10^4. (Note that, for the abstract, most of these data have been rounded off to an overall more reasonable single significant digit.)

The next best calibration curve (#2) is obtained at similar conditions, except that the additional 20 mL/min flow of nitrogen (piped into the detector's air supply) was shut off. We have not investigated the reason for this difference in response.

The next calibration curve (#3) uses a significantly smaller amount of air (50 instead of 80 mL/min). Despite the fact that the temperature measured (583°C at the bottom to ca. 420°C in the upper regions of the luminescence) is now considerably lower, the detector performance is only slightly diminished. That fact is worth mentioning (*a*) in the spectral context of earlier speculation on chemical vs. thermal excitation, and (*b*) in the analytical context of ruthenocene having to be determined

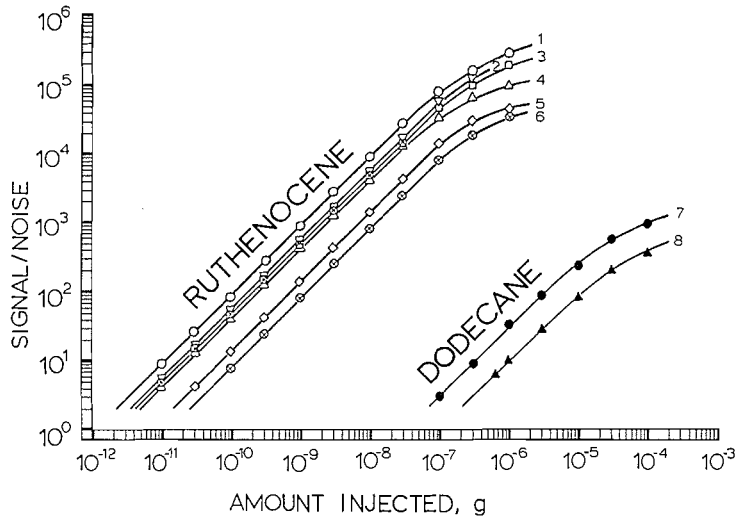


FIG. 5. Calibration curves for ruthenocene and dodecane at different conditions. See text for explanation. ○ (*1*) ruthenocene response optimized for maximum S/N ratio; ▽ (*2*) as (*1*), but no nitrogen added to detector gases; □ (*3*) as (*1*), but air flow = 50 mL/min; △ (*4*) as (*1*), but 526 nm interference filter present; ◇ (*5*) as (*1*), but quartz chimney present; ⊗ (*6*) as (*1*), but ca. 1600 ppm methane present in total detector gases; ● (*7*) dodecane response at conditions of (*1*); ▲ (*8*) dodecane response at conditions of (*4*).

in conjunction with other organometallic compounds, which may require different flame temperatures and/or compositions.

The next calibration curve (#4) is obtained at optimum conditions (like # 1), but with a 526 nm interference filter of at least 75% maximum transmission and at most 6 nm bandpass at half-height (the specifications of a typical FPD "phosphorus filter" that came as part of the original Shimadzu FPD package). Such a filter — or one for 484 nm, depending on the particular case — could be used for spectral discrimination, depending on the spectral characteristics of the sample matrix. Not surprisingly, the selectivity against dodecane is now at a higher level, i.e. at 7.4×10^5.

(The reader may in fact be surprised how *small* an improvement in selectivity the interference filter has brought about. The "dodecane" spectrum can not be procured by our spectrophotometer under these conditions; the maximum luminescence is too weak. It may be that the very strong 516 nm, 0,0 bandhead of the Swan bands, $C_2(d^3\Pi_g \rightarrow a^3\Pi_u)$, is the culprit, particularly since the filter, at a nominal 526 nm, does not quite match the peak at 528 nm.)

The next ruthenocene calibration curve (#5) simply shows what happens when the original Shimadzu quartz chimney is being put back in: The S/N value drops to one sixth of optimum. Again, the reason for this effect is unknown.

The last ruthenocene calibration curve (#6) employs optimum conditions (like # 1), but with ca. 1600 ppm CH_4 (as an example of a quencher) added to the detector gases. This large amount of methane reduces the ruthenocene peak by about one half. The calibration curve, however, shifts to the right by one full decade — owing to the effect of a drastic rise in baseline (background luminescence) on noise in the S/N measurement. Still, it remains linear.

There is good reason for running a "quenched" calibration curve: It is not unusual in FPD practice that other organic material should co-elute with the compound of interest and quench its response — be the former a chromatographic solute of the same rate of migration, or the continuously eluting twin scourges of column bleed and carrier gas contamination. This type of interference can present a major problem at the low-temperature of the FPD — as it does, for instance, in the well-known case of hydrocarbons quenching the response of sulfur compounds.

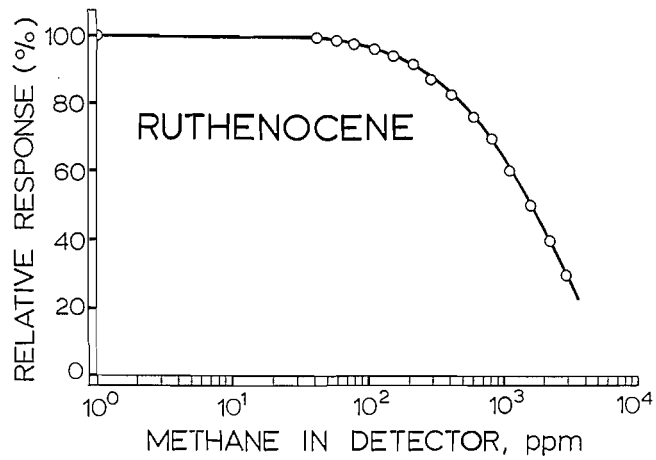


FIG. 6. Response of 3 ng ruthenocene at optimized conditions, but with varying concentrations of methane added to the hydrogen supply via an exponential dilution flask.

Figure 6 shows one of a series of experiments that use methane as a quencher and are designed to clarify the magnitude of the expected interference. (Note: methane is added to the hydrogen supply line which, in turn, joins the column effluent *prior* to reaching the flame.) It takes about 500 ppm (v/v) of methane to reduce the peak height of ruthenocene by a mere 20%. As mentioned before, to reduce the peak to one half of its former size requires about 1600 ppm CH_4.

Furthermore, the concentration of methane is calculated here on the *total* volume of detector gases (ca. 422 mL/min), not just on the nitrogen flow through the column. These 1600 ppm would correspond to about 3.1 volume percent, or 7.1×10^{-6} g/s, or 4.5×10^{-7} mol/s, of methane in the 22 mL/min of nitrogen carrier gas. That means that it takes a column flow of methane 3.6×10^6 and 4.5×10^7 times larger — on a weight and on a molar basis, respectively — than that of ruthenocene at its (quenched) minimum detectable limit, to reduce the ruthenocene peak by 50%.

Can. J. Chem. Downloaded from www.nrcresearchpress.com by 41.223.56.140 on 09/07/12
For personal use only.

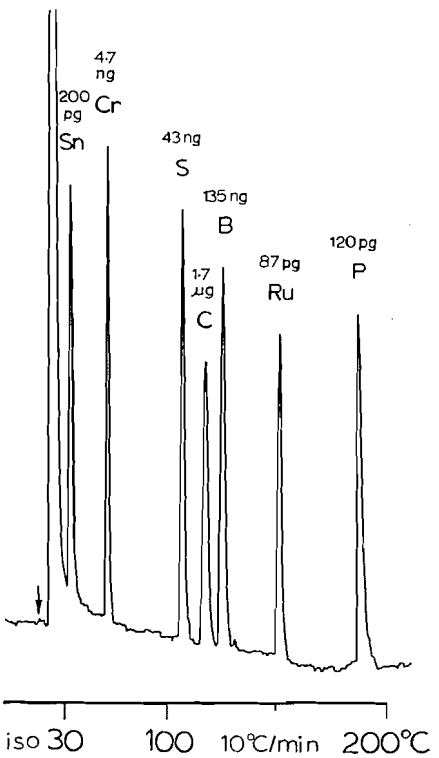


FIG. 7. Temperature-programmed chromatography. Amounts injected (in order of elution): 0.30 ng tetramethyltin, 20 ng chromium hexacarbonyl, 120 ng di-*t*-butyldisulfide, 2.0 µg dodecane, 180 ng *o*-carborane, 0.20 ng ruthenocene, 1.0 ng tri-*n*-butylphosphate. Flows in mL/min: hydrogen 300, air 80, carrier nitrogen 25, additional nitrogen 23. Detector and injector temperature 200°C.

Thus, if the quencher behaves similar to methane and is being continuously introduced (as are column bleed, carrier contamination, etc.), the quenching effect should be unobservably small in most practical cases. If the quencher behaves similar to methane but comes in the form of a peak of equal retention time, it will increase rather than decrease the ruthenocene peak at all quencher concentrations but those way beyond linear range. This can be easily visualized by comparing the dodecane response shown in Fig. 5, with the methane-quenched ruthenocene response shown in Fig. 6.

Prompted by one of the reviewers of this manuscript, we are pleased to add a chromatogram showing ruthenocene in the company of other hetero-organics. The detector gas flows are roughly optimized according to the ruthenium signal/noise ratio, hence the responses of other elements are depressed to varying extents, but the conditions are *not* optimal for obtaining the largest possible selectivity for ruthenium vis-a-vis one or more of these other elements. Further selectivity can be achieved by adjusting flow conditions and using various interference filters; however, such optimization is most effectively performed only after particulars of the sample matrix are known. For obtaining Fig. 7, no optical discrimination is used, and selectivity is reflected by the amounts of analytes necessary to produce peaks of similar height. The elemental responses, under these conditions and normalized to ruthenium on an atomic basis, are roughly Ru 1, Sn 0.6, P 0.3, Cr 1×10^{-2}, S 9×10^{-4}, B 8×10^{-5}, and C 5×10^{-6}. Note that the response of sulfur, as usual, is approximately quadratic and that tributylphosphate also exhibits minor non-linearity due to some premature decomposition. Note further that these response ratios are intended for determination of ruthenocene in the presence of other hetero-analytes: they should not be confused with a general FPD sensitivity ranking (for which each element is measured at its own, optimized conditions).

Acknowledgements

This research was supported by NSERC operating grant A-9604. For part of his time on the project, one of us (X.Y.S.) was supported as a Visiting Scholar by the People's Republic of China. We are thankful to Professor John Coxon for his well reasoned review and constructive critique of this manuscript, and to Mr. Wayne LeMoine for his prompt and efficient electronic assistance.

1. A. N. NESSMEYANOV, L. P. YURYEVA, M. S. KOTSCHETKOWA, and S. W. VITT. Bull. Acad. Sci. U.S.S.R. Div. Chem. Sci. 1966. pp. 530–532; as cited in G. Guiochon and C. Pommier. Gas chromatography in inorganics and organometallics. Ann Arbor Science, Ann Arbor. 1973. p. 195.
2. P. C. UDEN, D. E. HENDERSON, F. P. DISANZO, R. J. LLOYD, and T. TETU. J. Chromatogr. **196**, 403 (1980); as cited in P. C. UDEN. Gas chromatography of inorganic compounds, organometallics, and metal complexes. *In* Inorganic chromatographic analysis. *Edited by* J. C. MacDonald. Wiley Interscience, Toronto. 1985. p. 264.
3. S. A. ESTES, P. C. UDEN, and R. M. BARNES. Anal. Chem. **53**, 1829 (1981).
4. C. G. FLINN and W. A. AUE. Can. J. Spectrosc. **25**, 141 (1980).
5. M. DRESSLER. Selective gas chromatographic detectors. J. Chrom. Library, Vol. 36, Elsevier, Amsterdam. 1986.
6. R. N. KNISELEY. Flames for atomic absorption and emission spectrometry. *In* Flame emission and atomic absorption spectrometry. Vol. 1. *Edited by* J. A. Dean and T. C. Rains. Marcel Dekker, New York. 1969. p. 191.
7. M. L. PARSONS and P. M. MCELFRESH. Flame spectroscopy: atlas of spectral lines. IFI/Plenum, New York. 1971. p. 62.
8. Gmelins Handbuch der anorganischen Chemie. 8th ed. Vol. 63. Ruthenium (Ergaenzungsband), Verlag Chemie, Weinheim/Bergstrasse. 1970.
9. J. R. PLATT. J. Chem. Phys. **18**, 932 (1950).
10. P. K. CARROLL and P. MCCORMACK. Astrophys. J. **177**, L33 (1972).
11. X.-Y. SUN and W. A. AUE. J. Chromatogr. **467**, 75 (1989).
12. E. O. FISCHER and H. GRUBERT. Chem. Ber. **92**, 2302 (1959).

Can. J. Chem. Downloaded from www.nrcresearchpress.com by 41.223.56.140 on 09/07/12
For personal use only.

Carbodithioato derivatives of weak nitrogenous nucleophiles. I. Electronic structure and ground state properties of Ni(II) amide *N*-carbodithioates

C. C. HADJIKOSTAS, G. A. KATSOULOS, M. P. SIGALAS, AND C. A. TSIPIS
Department of General and Inorganic Chemistry, Aristotle University, Thessaloniki 540 06, Greece

Received October 14, 1988

C. C. HADJIKOSTAS, G. A. KATSOULOS, M. P. SIGALAS, and C. A. TSIPIS. Can. J. Chem. **67**, 902 (1989).

Nickel(II) complexes of the general type $[Ni(S_2CN(COR')R)_2]$ have been synthesized by the reaction of the appropriate Ni(II) *N*-alkyldithiocarbamate with acetic anhydride or benzoyl chloride in the presence of triethylamine. The complexes obtained were identified and characterized by elemental analyses, conductivity measurements, and ir and electronic spectra. It was concluded that the bonding mode of the dithiocarbamato ligands to the metal ion is not altered by the acylation reaction, the chromophore remaining square-planar NiS_4. Moreover, EHMO-SCCC calculations have been used in the analysis of electronic structure, and related properties of the novel compounds. From the calculated molecular orbital description of the complexes and the frontier molecular orbital approach of chemical reactivity, plausible mechanisms of their formation reactions have been deduced.

Key words: Ni(II) amide *N*-carbodithioates, *N*-alkyldithiocarbamates, dithiocarbimates, electrophilic substitution reactions, EHMO-SCCC calculations.

C. C. HADJIKOSTAS, G. A. KATSOULOS, M. P. SIGALAS et C. A. TSIPIS. Can. J. Chem. **67**, 902 (1989).

On a synthétisé des complexes du Ni(II), du type général $[Ni(S_2CN(COR')R)_2]$, en faisant réagir les *N*-alkyldithiocarbamates de Ni(II) appropriés avec de l'anhydride acétique ou de chlorure de benzoyle, en présence de triéthylamine. On a identifié et caractérisé les complexes à l'aide d'analyses élémentaires, de mesures de conductivité et de spectres ir et électroniques. On en a conclu que le mode de liaison des ligands dithiocarbamato avec les ions métalliques n'est pas modifié par la réaction d'acylation; le chromophore demeure le NiS_4 plan carré. De plus, on a utilisé des calculs EHMO-SCCC pour faire l'analyse de la structure électronique ainsi que des propriétés apparentées des nouveaux composés. En se basant sur la description par orbitales moléculaires des complexes ainsi que sur l'approche par orbitales moléculaires frontières de la réactivité chimique, on propose divers mécanismes qui peuvent éventuellement expliquer leurs réactions de formation.

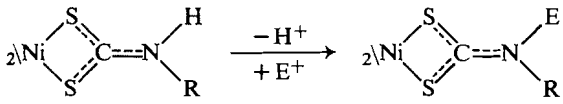
Mots clés : Amide de *N*-carbodithionates de Ni(II), *N*-alkyldithiocarbamates, dithiocarbamates, réactions de substitutions électrophiles, calculs EHMO-SCCC.

[Traduit par la revue]

Introduction

Since it was first demonstrated that dithiocarbamates, with an electron-withdrawing group and a proton on the nitrogen atom, may lose the proton to form dithiocarbimates (1, 2), there have been many studies in our laboratory concerning the reactions of Lewis bases, such as phosphines and amines, with square-planar d^8 bis(*N*-monosubstituted-dithiocarbamato)metal(II) complexes (3–9). In particular, our studies have shown (5) that reacting platinum(II) and palladium(II) *N*-alkyldithiocarbamates, $[M(S_2CNHR)_2]$, with excess tertiary phosphine, they easily afford neutral dithiocarbimato complexes, $[M(S_2C{=}NR)(PR'_3)_2]$, via a deprotonation reaction on the coordinated bidentate dithio-ligand. In this respect, the chemical behaviour of the *N*-alkyldithiocarbamato ligands is similar to that of the isoelectronic xanthates, which easily undergo dealkylation reactions (10). Moreover, the *N*-alkyldithiocarbamates of nickel triad metals, when treated with amines (e.g. NH_3) afford (6, 8) in most cases the corresponding dithiocarbimate complex anions, $[M(S_2C{=}NR)]^{2-}$. The mechanism of these reactions has been fully investigated by EH MO-SCCC quantum chemical calculations based on the frontier molecular orbital interactions which are the main factor controlling the nucleophilic substitution reactions under consideration (9). An interesting perspective of these theoretical investigations is that, for the dithiocarbimato complex, its HOMO is mainly localized on the nitrogen atom, and hence this atom should be the nucleophilic center of the complex in reactions with electrophiles. Actually, this prediction has been experimentally verified (5, 6, 8), since the dithiocarbimato complexes react with the electrophile H^+, affording the protonated products on the nitrogen atom, namely, the corresponding dithiocarbamato complexes.

Taking advantage of this labile to electrophilic attack nitrogen atom it seems reasonable to react the dithiocarbimato complexes with a variety of electrophiles (E^+), in order to prepare new classes of dithiocarbamates, according to the scheme:



The gain of such a work is that selecting electrophiles with strong electron-withdrawing groups the synthesis of carbodithioato derivatives of weak nitrogenous nucleophiles can be achieved. The direct preparation of such ligands by the reaction of the corresponding amine with carbon disulfide in alkaline media is difficult even impossible to afford, although some examples concerning the formation of *N*-formyl and *N*-methyl *N*-formyl dithiocarbamates have already been published (11–15). However, no reports on their corresponding complexes have been found by us to date. Consequently, in this paper we present our results on the synthesis and characterization of some novel nickel(II) amide *N*-carbodithioates of the general formulae $[Ni(S_2CNHR)(S_2CN(COR')R)]$ and $[Ni(S_2CN(COR')R)_2]$. Furthermore, we have utilized the EHMO-SCCC method, in relation to the frontier molecular orbital theory of chemical reactivity, to investigate the acylation reactions of nickel(II) dithiocarbamates. Particular emphasis has also been placed upon the interpretation of the observed electronic properties of these compounds with respect to their highly delocalized covalent bonding.

Printed in Canada / Imprimé au Canada

Can. J. Chem. Downloaded from www.nrcresearchpress.com by 41.223.56.140 on 09/07/12
For personal use only.

Can. J. Chem. Downloaded from www.nrcresearchpress.com by 41.223.56.140 on 09/07/12
For personal use only.

Experimental

Physical measurements

Infrared spectra were recorded in the 4000–250 cm^{-1} region on a Perkin-Elmer 467 spectrophotometer using KBr pellets or Nujol mulls. Electronic spectra were obtained on a Cary 17DX spectrophotometer using freshly prepared chloroform solutions at 25°C. Magnetic susceptibility measurements in solid state were done by the Faraday technique using $Hg[Co(SCN)_4]$ as the calibrant. Conductivity measurements were done on a WTW conductivity bridge using 10^{-3} *M* solutions in chloroform. Molecular weights were determined using a Perkin-Elmer molecular weight apparatus Model 115 in $CHCl_3$ solutions. Melting points were determined with a Büchi apparatus and are uncorrected. The elemental analysis of carbon, nitrogen, and hydrogen was performed on a Perkin-Elmer 240B Elemental Analyzer. Nickel was determined according to published methods (16).

Starting materials

All solvents were of reagent grade and were used without further purification in synthetic work. The bis(*N*-alkyldithiocarbamato)nickel(II) complexes were obtained from the reaction between nickel chloride and the appropriate ammonium dithiocarbamate in dimethylsulfoxide (DMSO) solution (17). The ammonium *N*-alkyldithiocarbamates were prepared and recrystallised as previously reported (8). All the other reagents were obtained commercially.

Preparation of the complexes

The (*N*-alkyldithiocarbamato)(*N*-alkyl *N*-acetyldithiocarbamato)-nickel(II) complexes, $[Ni(S_2CNHR)(S_2CN(COMe)R)]$ (R = Me, Et, Bu^i, Bz), were prepared according to the following synthetic route: A solution of 1 mmol of the appropriate $[Ni(S_2CNHR)_2]$ in 20 cm^3 of acetone was treated with 1 mmol of triethylamine and 1 mmol of acetic anhydride and the mixture was left for 1 h at room temperature under continuous magnetic stirring. In the resulted solution a solid material was formed, which on addition of 100 cm^3 of water, was quantitatively separated. The precipitate was filtered off, washed several times with water, and dried over $CaCl_2$ under vacuum. Recrystallization was carried out by dissolving the complex in acetone–chloroform (1:1) and reprecipitating with water. The yields in this procedure were about 70%.

The bis(*N*-alkyl *N*-acetyldithiocarbamato)nickel(II) complexes, $[Ni(S_2CN(COMe)R)_2]$ (R = Me, Et, Bu^i, Bz, Ph, *p*-MePh, *p*-ClPh), were prepared as follows: 1 mmol of the appropriate $[Ni(S_2CNHR)_2]$ was dissolved in 20 cm^3 of acetone and treated with 2 mmol of triethylamine and 2 mmol of acetic anhydride. The resulting clear solution was left at room temperature under continuous magnetic stirring. After a period of 1 h a reddish precipitate was formed and the precipitation was completed by addition of 100 cm^3 of water. The solid material was filtered off, washed with acetone, and dried under vacuum. Purification was achieved by dissolving the solid in chloroform and reprecipitating with ethanol (yield: 75%).

The bis(*N*-alkyl *N*-benzoyldithiocarbamato)nickel(II) complexes, $[Ni(S_2CN(COPh)R)_2]$ (R = Me, Ph), were prepared according to the following method: A solution of 1 mmol of the appropriate $[Ni(S_2CNHR)_2]$ in 20 cm^3 of acetone was treated with 2 mmol of triethylamine and 2 mmol of benzoyl chloride. The reaction mixture was stirred for 1 h at room temperature. During this period a microcrystalline solid was formed which on addition of 100 cm^3 of water was quantitatively separated. The precipitate was filtered off, washed several times with water, and dried over $CaCl_2$ under vacuum. Recrystallization was carried out by dissolving the complex in acetone and reprecipitating with water. The yields in this procedure were about 70%.

Calculations

All calculations were performed in the framework of the extended Hückel LCAO-MO method (18–20) with self-consistent charge and configuration (EHMO-SCCC) by using the FORTICON-8 computer program (21). In these iterative calculations the so-called "weighted H_{ij} formula" for the off-diagonal matrix elements (H_{ij}) was used in order to reduce the intriguing phenomenon of counterintuitive orbital mixing (COM) common in calculations of transition-metal complexes (22). Moreover, a Madelung energy correction (21, 23, 24) was applied to the diagonal matrix elements, H_{ii}. The value of 1.65 was used for the parameter *K*, as this value was found by a series of calculations to give the best agreement between the experimental and theoretical frequencies of the electronic transitions of the complexes studied, as well as over a wide range of dithio-complexes (9, 25). Orbital exponents, valence state ionization energies (VSIE), and parameters of the polyonymic charge dependence of the VSIES for all the basis AO's were those previously used (21, 25–30).

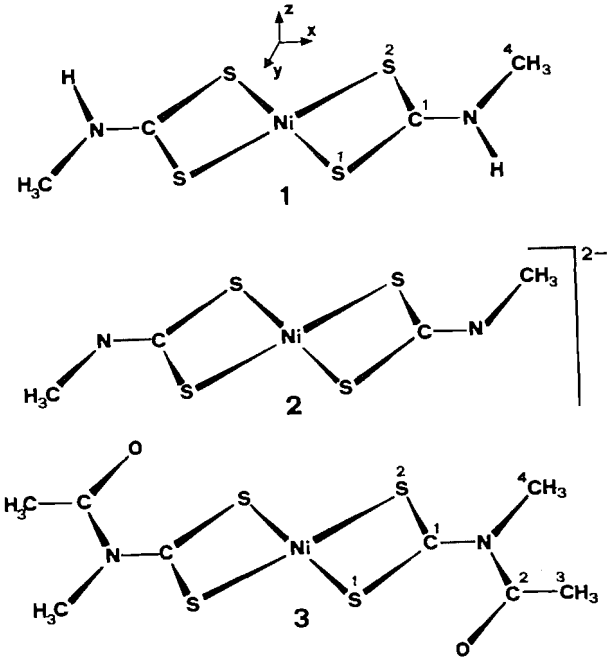


FIG. 1. Molecular geometries of the compounds studied along with the coordinate system used.

The geometries of the $[Ni(S_2CNHMe)_2]$ and $[Ni(S_2CN(COMe)Bz)_2]$ complexes were taken from already published X-ray crystal data (31, 32). In the case of $[Ni(S_2C{=}NBz)_2]^{2-}$ complex, structure parameters for the $(S_2C{=}NBz)^{2-}$ moiety were taken from the X-ray crystal data of the $[Pt(S_2C{=}NBz)(PEt_3)_2]$ complex (33), whereas optimization was carried out for the NiS_4 chromophore. For the sake of simplicity, as well as to avoid very large basis sets, the Bz substituents were replaced by methyl groups, the bond length value of C—H being 1.01 Å. The molecular geometries of the compounds studied along with the coordinate system used are displayed in Fig. 1.

Results and discussion

Reaction of acetone solutions of bis(*N*-alkyldithiocarbamato)nickel(II) complexes, $[Ni(S_2CNHR)_2]$, with acetic anhydride or benzoyl chloride in the presence of triethylamine (1:2:2 molar ratios) rapidly gave clear solutions from which solid compounds of stoichiometry $[Ni(S_2CN(COR')R)_2]$ (R' = Me, Ph) were isolated by precipitation with water. Similarly, the mixed-ligand $[Ni(S_2CNHR)(S_2CN(COMe)R)]$ complexes were prepared by the action of acetic anhydride and triethylamine on $[Ni(S_2CNHR)_2]$ in a 1:1:1 molar ratio. The above formulations have been further corroborated on the basis of spectral properties of these compounds. These novel complexes

TABLE 1. Analytical data for the new complexes

Compound†	Melting point (°C)	Analysis (%)* C	N	H	Ni	Molecular weight
[Ni(S_2CNHMe)(S_2CN(COMe)Me)]	153–155d‡	22.90 (23.02)	8.86 (8.94)	3.30 (3.22)	18.65 (18.75)	330 (313.1)
[Ni(S_2CNHEt)(S_2CN(COMe)Et)]	105–107d	28.40 (28.16)	7.98 (8.21)	3.97 (4.14)	17.36 (17.21)	360 (341.2)
[Ni(S_2CNHBu^i)(S_2CN(COMe)Bu^i)]	110–112d	36.14 (36.28)	7.00 (7.05)	5.42 (5.58)	14.86 (14.78)	430 (397.3)
[Ni(S_2CNHBz)(S_2CN(COMe)Bz)]	175–177d	46.66 (46.46)	6.03 (6.02)	4.03 (3.89)	12.59 (12.62)	470 (456.3)
[Ni(S_2CN(COMe)Me)$_2$]	157–159d	26.83 (27.06)	7.80 (7.89)	3.35 (3.41)	16.60 (16.53)	350 (355.2)
[Ni(S_2CN(COMe)Et)$_2$]	125–127d	31.12 (31.34)	7.22 (7.31)	4.15 (4.21)	15.28 (15.32)	390 (383.2)
[Ni(S_2CN(COMe)Bu^i)$_2$]	152–154d	38.36 (38.28)	6.42 (6.38)	5.38 (5.51)	13.70 (13.36)	440 (439.3)
[Ni(S_2CN(COMe)Bz)$_2$]	170–172d	47.18 (47.35)	5.36 (5.52)	4.09 (3.97)	11.48 (11.57)	520 (507.4)
[Ni(S_2CN(COMe)Ph)$_2$]	190–192d	45.16 (45.11)	5.68 (5.84)	3.44 (3.36)	12.32 (12.25)	490 (479.3)
[Ni(S_2CN(COMe)*p*-MePh)$_2$]	206–208d	47.51 (47.35)	5.64 (5.52)	4.06 (3.97)	11.63 (11.57)	510 (507.4)
[Ni(S_2CN(COMe)*p*-ClPh)$_2$]	173–175d	39.29 (39.44)	5.27 (5.11)	2.55 (2.57)	10.79 (10.71)	560 (548.2)
[Ni(S_2CN(COPh)Me)$_2$]	169–171d	45.33 (45.11)	5.67 (5.84)	3.42 (3.36)	12.13 (12.25)	490 (479.3)
[Ni(S_2CN(COPh)Ph)$_2$]	148–150d	55.56 (55.73)	4.53 (4.64)	3.33 (3.34)	9.80 (9.73)	610 (603.4)

*Figures in parentheses are the calculated values.
†Abbreviations used throughout: Me = methyl, Et = ethyl, Bu^i = *i*-butyl, Ph = phenyl, Bz = benzyl, *p*-MePh = *p*-methylphenyl, *p*-ClPh = *p*-chlorophenyl.
‡d = decomposition.

TABLE 2. The most relevant ir frequencies (cm^{-1}) of the investigated compounds and their assignments (KBr discs)*

Compound	ν(N—H)	ν(C=O)	ν(C=N)	ν(CSS)	ν(M—S)
[Ni(S_2CNHMe)(S_2CN(COMe)Me)]	3280s	1720s	1543vs	992s	392m
[Ni(S_2CNHEt)(S_2CN(COMe)Et)]	3280m	1705vs	1530m	995m	394w
[Ni(S_2CNHBu^i)(S_2CN(COMe)Bu^i)]	3250m	1712vs	1470m	976vs	395w
[Ni(S_2CNHBz)(S_2CN(COMe)Bz)]	3220m	1693vs	1538s	997s	398w
[Ni(S_2CN(COMe)Me)$_2$]		1713vs	1453m	994vs	397m
[Ni(S_2CN(COMe)Et)$_2$]		1705vs	1532m	995w	393m
[Ni(S_2CN(COMe)Bu^i)$_2$]		1709vs	1468m	973vs	400w
[Ni(S_2CN(COMe)Bz)$_2$]		1720vs	1497s	984s	396m
[Ni(S_2CN(COMe)Ph)$_2$]		1724vs	1590m	1001s	384m
[Ni(S_2CN(COMe)*p*-MePh)$_2$]		1727s	1510vs	1004s	395w
[Ni(S_2CN(COMe)*p*-ClPh)$_2$]		1725m	1480s	1004s	394m
[Ni(S_2CN(COPh)Me)$_2$]		1688vs	1448m	980m	390m
[Ni(S_2CN(COPh)Ph)$_2$]		1713s	1490s	1003m	384m

*vs = very strong, s = strong, m = medium, w = weak.

are probably some of the first examples in the pure chemistry of the dithiocarbamato ligands which may be considered as derivatives of secondary amides. Until recently, as far as we know, only the [S_2CN(HCO)H]$^-$ and [S_2CN(HCO)CH_3]$^-$ ligands had been reported (14, 15). Moreover, the formation of [S_2CN(HCS)H]$^-$ and [S_2CN(HCS)CH_3]$^-$ ligands by the reaction of thioformamide with carbon disulfide in the presence of hydroxides had also been reported (12, 13). It should be noted, however, that all our efforts to prepare the corresponding free ligands according to the procedure described by Gattow and Gerner (14, 15) were unsuccessful, leading to unstable, easily oxidized species.

All the complexes are microcrystalline red–brown solids, quite stable both in solid and solution state. They are soluble in most of the common organic solvents, such as chloroform, acetone, and methylene chloride, but insoluble in ethanol, diethyl ether, carbon tetrachloride, and water. The low values of the molar conductivity in chloroform indicate the non-electrolyte character of the complexes, whereas their monomeric nature was established by osmometric molecular weight measurements in chloroform. Moreover, they are diamagnetic, as would be expected for d^8 species. Data from elemental analyses, decomposition temperatures, and molecular weights of the new compounds are given in Table 1.

Infrared spectra

The frequencies (cm^{-1}) of the most relevant absorption bands in the ir spectra of the studied compounds and their tentative assignments are presented in Table 2. The spectra of the mixed-ligand [Ni(S_2CNHR)(S_2CN(COMe)R)] complexes show one broad band in the 3300–3200 cm^{-1} region due to the N—H stretching frequency (34). In contrast, no such band appears in the spectra of the [Ni(S_2CN(COR′)R)$_2$] complexes, as a consequence of abstraction of the hydrogen atom in the S_2CNHR system and its substitution by a COR′ group. Moreover, the strong band found between 1730–1680 cm^{-1} in all the complexes was assigned to the C=O stretch, thereby indicating the acylation of the *N*-alkyldithiocarbamato ligands. The ν(C=N) and ν(CSS) stretching frequencies fall in the range 1590–1460 and 1010–970 cm^{-1}, respectively (35, 36).

Can. J. Chem. Downloaded from www.nrcresearchpress.com by 41.223.56.140 on 09/07/12
For personal use only.

Can. J. Chem. Downloaded from www.nrcresearchpress.com by 41.223.56.140 on 09/07/12
For personal use only.

TABLE 3. Transitions and assignments in the electronic spectrum of the $[Ni(S_2CN(COMe)Bz)_2]$ complex

Observed bands kK (log ϵ_{mol})	Assignment	Calcd kK	General classification
16.2sh (2.41)	$^1B_{1g}{}^+ \leftarrow {}^1A_g$	16.2	$M(d) \leftarrow M(d)$
18.3sh (3.06)	$24a_u \leftarrow 21a_g$	17.2	$L(\pi^*) \leftarrow M(d)$
	$^1B_{3g} \leftarrow {}^1A_g$	17.5	$M(d) \leftarrow M(d)$
21.2 (3.81)	$^1B_{1g}{}^- \leftarrow {}^1A_g$	19.3	$M(d) \leftarrow M(d)$
	$25a_u \leftarrow 26a_g$	21.6	$L(\pi^*) \leftarrow M(d)$
	$25a_u \leftarrow 25a_g$	22.6	$L(\pi^*) \leftarrow M(d)$
	$^1B_{2g} \leftarrow {}^1A_g$	22.6	$M(d) \leftarrow M(d)$
26.1sh (3.51)	$25a_u \leftarrow 23a_g$	23.6	$L(\pi^*) \leftarrow M(d)$
	$25a_g \leftarrow 19a_u$	25.4	$M(d) \leftarrow L(\pi)$
	$25a_u \leftarrow 21a_g$	27.7	$L(\pi^*) \leftarrow M(d)$
30.3 (4.57)	$28a_g \leftarrow 17a_u$	28.1	$L(\pi^*) \leftarrow L(\pi)$
	$25a_u \leftarrow 20a_g$	28.6	$L(\pi^*) \leftarrow L(\pi)$
	$30a_g \leftarrow 19a_u$	28.6	$L(\pi^*) \leftarrow L(\pi)$
	$29a_g \leftarrow 18a_u$	29.8	$M(d) \leftarrow L(\pi)$
	$29a_g \leftarrow 17a_u$	32.9	$M(d) \leftarrow L(\pi)$
38.1 (4.53)	$34a_g \leftarrow 23a_u$	35.8	$L(\pi^*) \leftarrow L(\pi)$
	$30a_g \leftarrow 17a_u$	36.1	$L(\pi^*) \leftarrow L(\pi)$
	$25a_u \leftarrow 16a_g$	36.1	$L(\pi^*) \leftarrow L(\pi)$
	$35a_g \leftarrow 23a_u$	38.1	$L(\pi^*) \leftarrow L(\pi)$
	$34a_g \leftarrow 21a_u$	39.1	$L(\pi^*) \leftarrow L(\pi)$
	$28a_g \leftarrow 14a_u$	40.0	$L(\pi^*) \leftarrow L(\pi)$
	$31a_u \leftarrow 27a_g$	40.0	$L(\pi^*) \leftarrow L(\pi)$
	$28a_u \leftarrow 20a_g$	40.3	$L(\pi^*) \leftarrow L(\pi)$
	$35a_g \leftarrow 21a_u$	41.4	$L(\pi^*) \leftarrow L(\pi)$

The presence of only one strong band in the region where ν(CSS) lies strongly supports chelation of the dithiocarbamates, a doublet being expected in the region $1000 \pm 70\ cm^{-1}$ in the unchelated dithiocarbamates (37). However, the spectra did not show any peaks that could be ascribed to unidentate dithiocarbamato ligand or to thiuram disulfide (38). The bidentate bonding mode of the dithio ligands was further established by the analysis of the position of the ν(C=N) band. This band undergoes a blue shift in all the dithiocarbamato complexes, while for unidentate coordination this stretching would be shifted towards lower wavenumbers or remain unchanged at the value of the free dithiocarbamate ammonium salt (38). Finally, single peaks have been observed in the range 400–380 cm^{-1}, which are likely to be due to metal–sulphur modes according to the observed values for the dithiocarbamates of the nickel triad metals.

The ir data, the diamagnetic nature of the complexes under investigation and their stoichiometry allowed us to suggest a square-planar configuration. This conclusion is consistent with an X-ray crystal structure determination (32) of one derivative of this series, namely the $[Ni(S_2CN(COMe)Bz)_2]$.

Electronic spectra

The electronic spectra of the studied compounds are complicated, exhibiting a number of overlapping intense bands in the ultraviolet and visible region. This complicated nature of the spectra prevents any simple classification and rationalization in terms of the ligand-field model. This is a general problem encountered in any ligand-field interpretation of the electronic spectra of many nickel(II) dithiocarbamates (17). Therefore, an attempt was made to interpret the electronic spectra of the complexes under investigation by means of EHMO-SCCC quantum-chemical calculations on a representative member of the series, namely $[Ni(S_2CN(COMe)Bz)_2]$. The electronic

TABLE 4. Electronic spectral data of the new compounds for chloroform solutions

Compound	Observed bands, kK (log ϵ_{mol})					
	Band I $L(\pi^*) \leftarrow L(\pi)$	Band II $L(\pi^*) \leftarrow L(\pi)$ $M(d) \leftarrow L(\pi)$	Band III $L(\pi^*) \leftarrow M(d)$	Band IV $L(\pi^*) \leftarrow M(d)$	Band V $M(d) \leftarrow M(d)$ $L(\pi^*) \leftarrow M(d)$	Band VI $M(d) \leftarrow M(d)$
$[Ni(S_2CNHMe)(S_2CN(COMe)Me)]$	40.4 (4.98)	31.3 (4.76)	26.3sh* (3.50)	21.6 (3.59)	18.5sh (2.76)	15.5sh (1.87)
$[Ni(S_2CNHEt)(S_2CN(COMe)Et)]$	38.5 (4.54)	30.6 (4.61)	26.1sh (3.52)	21.4 (3.83)	18.4sh (2.99)	
$[Ni(S_2CNHBu^t)(S_2CN(COMe)Bu^t)]$	38.2 (4.54)	30.5 (4.54)	26.3sh (3.55)	21.3 (3.86)	18.5sh (3.35)	
$[Ni(S_2CNHBz)(S_2CN(COMe)Bz)]$	39.5 (4.47)	30.5 (4.61)	26.1sh (3.54)	21.0 (3.70)	18.3sh (2.88)	15.4sh (1.95)
$[Ni(S_2CN(COMe)Me)_2]$	38.5 (4.67)	30.6 (4.68)	26.7sh (3.62)	21.5 (3.90)	18.8sh (3.20)	
$[Ni(S_2CN(COMe)Et)_2]$	38.3 (4.64)	30.5 (4.69)	26.3sh (3.63)	21.3 (3.92)	18.6sh (3.23)	
$[Ni(S_2CN(COMe)Bu^t)_2]$	37.9 (4.72)	30.6 (4.69)	26.1sh (3.62)	21.3 (3.95)	18.6sh (3.25)	
$[Ni(S_2CN(COMe)Bz)_2]$	38.1 (4.53)	30.3 (4.57)	26.1sh (3.51)	21.2 (3.81)	18.3sh (3.06)	16.2sh (2.41)
$[Ni(S_2CN(COMe)Ph)_2]$	38.2 (4.43)	30.0 (4.51)	25.4sh (3.63)	21.2 (3.78)	18.4sh (3.16)	16.4sh (2.75)
$[Ni(S_2CN(COMe)p\text{-}MePh)_2]$	38.4 (4.69)	30.0 (4.74)	25.6sh (3.66)	20.3 (3.85)	18.4sh (3.34)	16.5sh (2.92)
$[Ni(S_2CN(COMe)p\text{-}ClPh)_2]$	38.4 (4.49)	29.9 (4.52)	24.8sh (3.67)	20.5 (3.79)	18.3sh (3.14)	16.5sh (2.73)
$[Ni(S_2CN(COPh)Me)_2]$	38.2 (4.62)	30.2 (4.58)	26.0sh (3.60)	21.3 (3.81)	18.5sh (3.20)	
$[Ni(S_2CN(COPh)Ph)_2]$	38.3 (4.28)	30.0 (4.24)	25.5sh (3.26)	20.8 (3.42)	18.3sh (2.86)	15.6sh (2.04)

*sh = shoulder.

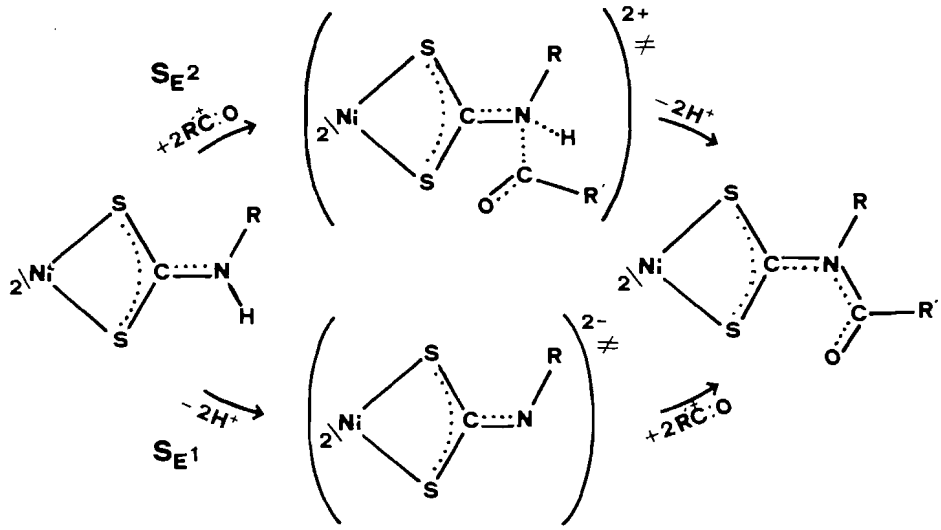


FIG. 2. Possible reaction mechanisms for the acylation of the nickel(II) dithiocarbamates.

excitation energies of the latter complex are compared with the experimental peak positions of the corresponding absorption spectrum in Table 3. Assignments were made by associating the observed bands with the transitions they most nearly match in energy. The resulting assignments of the bands were also invoked for the rest of the complexes (Table 4), whose spectra closely resemble to that of $[Ni(S_2CN(COMe)Bz)_2]$.

Furthermore, for a more precise characterization of the LF part of the spectrum the calculated one electron LF transitions were corrected for electronic repulsions (39), according to the following equations:

$$E(^1B_{1g}{}^a \leftarrow {}^1A_g) = E(xy) - E(z^2) - (4B + C)$$
$$E(^1B_{3g} \leftarrow {}^1A_g) = E(xy) - E(xz) - (3B + C)$$
$$E(^1B_{1b}{}^b \leftarrow {}^1A_g) = E(xy) - E(x^2 - y^2) - C$$
$$E(^1B_{2g} \leftarrow {}^1A_g) = E(xy) - E(yz) - (3B + C)$$

The values of the nephelauxetic parameters B and C were those found from a full AOM-CI description of the spectrum of $[Ni(S_2CNEt_2)_2]$ complex (17), and are equal to 0.28 and 1.28 kK, respectively. It must be noted also that we have considered the NiS_4 chromophore as belonging to the D_{2h} point group.

As can be seen from Table 3, the low intensity bands VI and V are assigned to the $^1B_{1b}{}^a \leftarrow {}^1A_g$ and $^1B_{3g} \leftarrow {}^1A_g$ LF excitations with a remarkably good agreement between calculated and experimentally observed energies. For the latter band a mixing with one $L(\pi^*) \leftarrow M(d)$ type excitation cannot be excluded, particularly when this band has high intensity. The other two expected LF transitions for the quadratic NiS_4 chromophore were impossible to observe, since the intense CT bands are extended up to the ligand-field part of the spectra, obscuring the weaker d–d transitions. The bands IV and III, in the region 21–27 kK, include all the calculated excitations of the $L(\pi^*) \leftarrow M(d)$ type and are reasonably assigned to MLCT transitions, in accordance with the results of previously published electronic spectral data on nickel(II) dithiocarbamato complexes (17, 40). Band II at ca. 30 kK can be assigned as a mixture of LMCT and L–L transitions, according to the calculated excitations. This fact is quite in line with the contradictory assignments (17, 40, 41) of that band in nickel(II) dithiocarbamates. Finally, band I includes all the $L(\pi^*) \leftarrow L(\pi)$ excitations and can be characterized as an intraligand L–L band.

Frontier orbital approach of chemical reactivity

In order to gain more information about the reaction of Ni(II) *N*-alkyldithiocarbamates with acetic anhydride or benzoyl chloride in the presence of triethylamine, EHMO-SCCC calculations were carried out. The experimentally verified (5, 6, 8) electrophilic substitution on the nitrogen atom of the coordinated dithiocarbamato ligand may proceed via either a unimolecular (S_E1) or a bimolecular (S_E2) mechanisms both depicted schematically in Fig. 2. It should be also noted that in the latter case the electrophile $(RC{=}O)^+$ attacks the parent dithiocarbamato complex, $[Ni(S_2CNHR)_2]$, whereas in the case of the S_E1 mechanism the deprotonated dianionic form, $[Ni(S_2C{=}NR)_2]^{2-}$, is likely to be attacked. This anion is formed during the nucleophilic substitution reaction of the Ni(II) *N*-alkyldithiocarbamates with amine nucleophiles (1, 2), in a manner analogous to the deprotonation reactions of the Pt(II) dithiocarbamates with phosphines (5, 9). Hence, the $[Ni(S_2CNHBz)_2]$ and $[Ni(S_2C{=}NBz)_2]^{2-}$ complexes were selected for the calculations, their corresponding electronic structures being depicted schematically in Fig. 3.

In terms of the frontier molecular orbital theory of chemical reactivity the aforesaid electrophilic substitution reaction requires high lying occupied MO's localized on nitrogen atoms for both the $[Ni(S_2CNHBz)_2]$ and/or $[Ni(S_2C{=}NBz)_2]^{2-}$ molecular species. However, in the case of the former complex, such MO's are the $2b_g$, and $4a_u$ π-MO's found in low energies, whereas the corresponding σ-MO's have much lower energies. Thus, energetically any interaction of these MO's with the unoccupied MO's of the electrophilic reagent is not possible. Furthermore, the net charge on the nitrogen atoms ($q_N = -0.22$) as compared with that on the sulphur atoms ($q_S = -0.30$) shows that such an interaction is not electrostatically favoured as well. However, in the case of the $[Ni(S_2C{=}NBz)_2]^{2-}$ complex the picture is quite different. Thus, beside the arising of the whole MO band in higher energies, MO's localized mainly on the nitrogen atoms, such as $4a_u$, $9b_u$, $13a_g$, and $4b_g$ were found near the HOMO's. Therefore these MO's, been of σ- and π-type, should interact with MO's of the electrophile. These frontier MO's interactions are demonstrated schematically in Fig. 4. It should be also noted that the deprotonation of the $[Ni(S_2CNHBz)_2]$ complex leads to an increasing of the net charge on the nitrogen atoms ($q_N = -0.55$; $q_S = -0.52$) showing that this reaction path is also electrostatically favoured. In conclusion, from the molecular orbital point of view, it

Can. J. Chem. Downloaded from www.nrcresearchpress.com by 41.223.56.140 on 09/07/12
For personal use only.

Can. J. Chem. Downloaded from www.nrcresearchpress.com by 41.223.56.140 on 09/07/12
For personal use only.

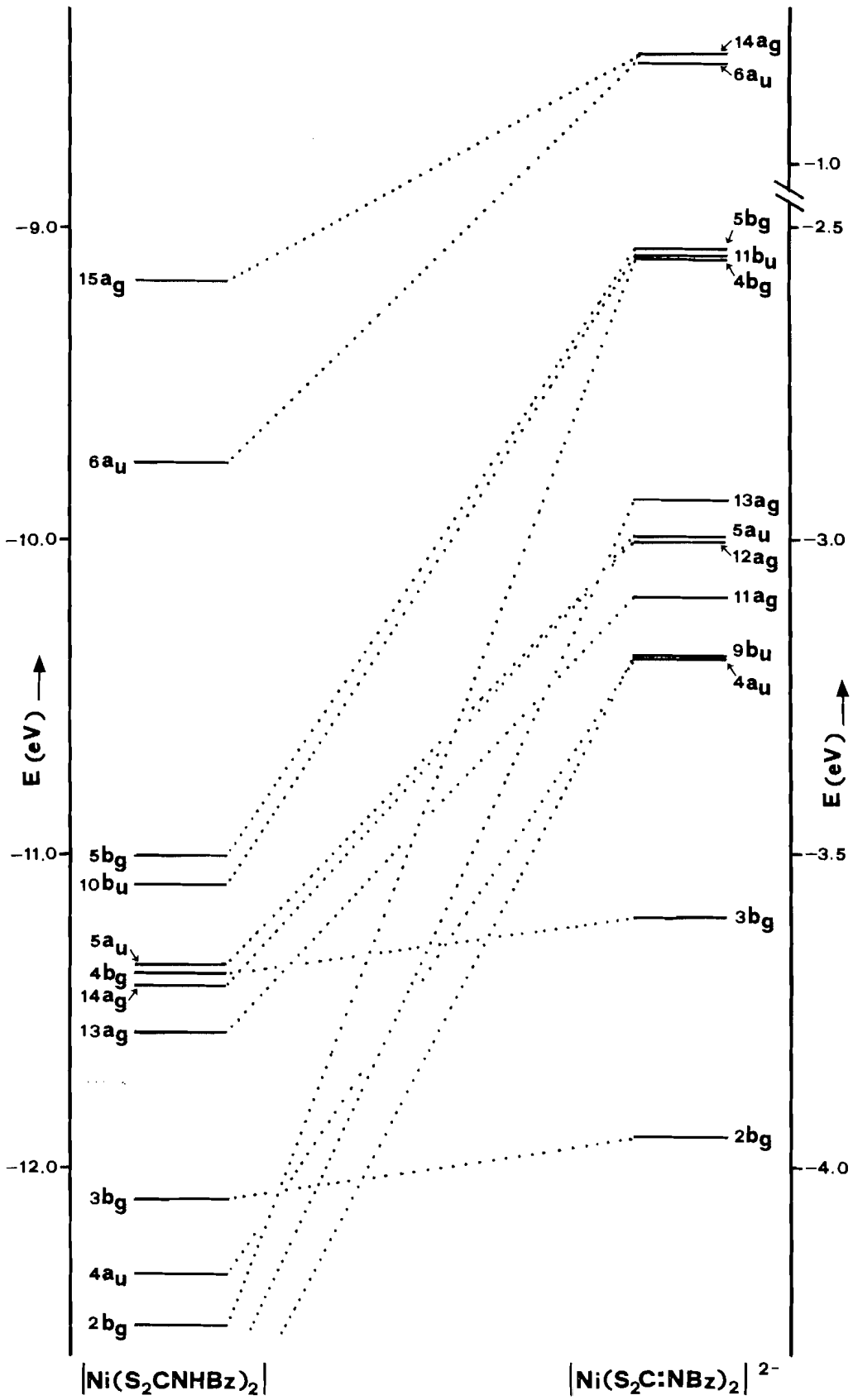


FIG. 3. Electronic structure of the $[Ni(S_2CNHBz)_2]$ and $[Ni(S_2C{=}NBz)_2]^{2-}$ complexes in their diamagnetic singlet ground state.

Can. J. Chem. Downloaded from www.nrcresearchpress.com by 41.223.56.140 on 09/07/12
For personal use only.

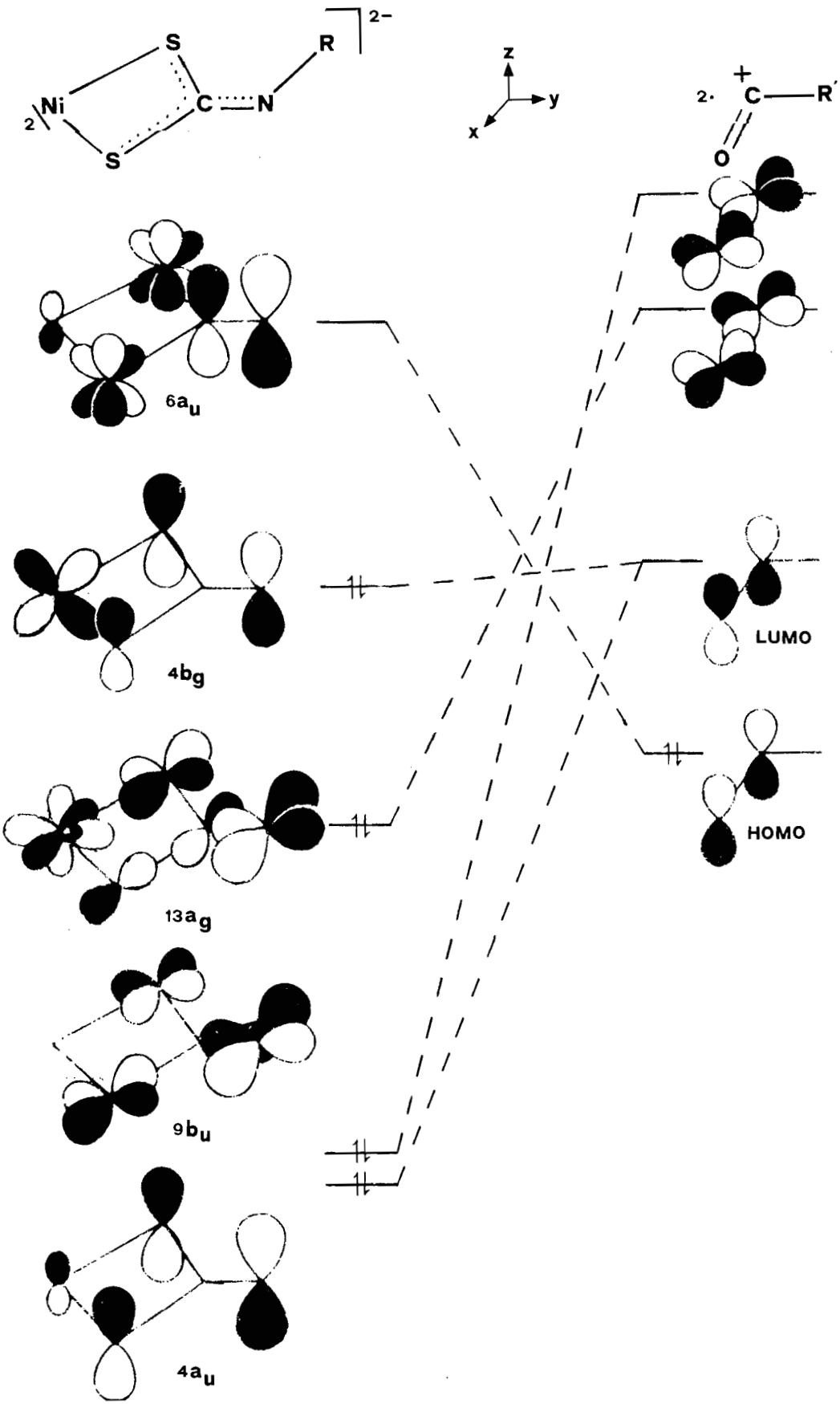


FIG. 4. Frontier MO interactions between the $[Ni(S_2C{=}NR)_2]^{2-}$ complex and the $[RC{=}O]^+$ electrophile.

TABLE 5. Atomic net charges, orbital populations, and two-center energy terms calculated for the $[Ni(S_2CN(COMe)Bz)_2]$ and $[Ni(S_2CNHBz)_2]$ complexes

Atom*	Net charge	Bond	Overlap population	Energy, eV
Ni	0.434 (0.443)†	Ni—S_1	0.420 (0.416)	−8.918 (−8.701)
S_1	−0.293 (−0.309)	Ni—S_2	0.410 (0.412)	−8.693 (−8.619)
S_2	−0.203 (−0.297)	C_1—S_1	1.074 (1.023)	−25.983 (−24.293)
C_1	0.294 (0.304)	C_1—S_2	1.077 (1.019)	−25.818 (−24.137)
N	−0.268 (−0.222)	C_1—N	0.892 (0.955)	−25.234 (−26.708)
C_2	0.632	N—C_2	0.830	−23.245
O	−0.631	N—C_4	0.646 (0.669)	−17.764 (−18.255)
C_3	−0.024	C_2—O	1.003	−27.467
C_4	0.208 (0.304)	C_2—C_3	0.813	−21.532

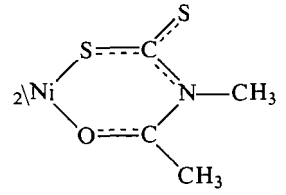
*Atomic numbering as in Fig. 1.
†Values in parentheses are the corresponding values for the parent $[Ni(S_2CNHBz)_2]$ complex, **1**.

seems that the acylation reaction of the bis(*N*-alkyldithiocarbamato)nickel(II) complexes in the presence of triethylamine proceeds via an S_E1 mechanism, involving as a transition state the deprotonated $[Ni(S_2C{=}NR)_2]^{2-}$ complexes.

Moreover, in an attempt to investigate the possibility of an alternative coordination of the new ligands through the S and O ligating atoms, we have performed EHMO-SCCC calculations on the model compound **4**, in both D_{2h} (square planar) and T_d (tetrahedral) coordination microsymmetry. The total energies (in 10^3 kcal mol^{-1}) of these model compounds compared with that of complex **3** are as follows:

$$\mathbf{3}(D_{2h}): -39.987 < \mathbf{4}(D_{2h}): -39.891 < \mathbf{4}(T_d): -39.659$$

Thus any O- and S-coordination should be excluded for the compounds under study in accordance with the X-ray structure found for the $[Ni(S_2CN(COMe)Bz)_2]$ complex (32). This conclusion is consistent with the two-center energy terms and overlap population data for the coordination bonds of the complex under investigation listed in Table 5. For comparison reasons the corresponding results for the parent $[Ni(S_2CNHBz)_2]$ complex are also included.



4

1. J. P. FACKLER JR. and D. COUCOUVANIS. J. Am. Chem. Soc. **88**, 3913 (1966).
2. D. COUCOUVANIS and J. P. FACKLER JR. Inorg. Chem. **6**, 2047 (1967).
3. G. A. KATSOULOS, G. E. MANOUSSAKIS, and C. A. TSIPIS. Inorg. Chim. Acta, **30**, L295 (1978).
4. G. A. KATSOULOS, G. E. MANOUSSAKIS, and C. A. TSIPIS. Polyhedron, **3**, 735 (1984).
5. G. A. KATSOULOS and C. A. TSIPIS. Inorg. Chim. Acta, **84**, 89 (1984).
6. C. A. TSIPIS, I. J. MELEZIADIS, D. P. KESSISSOGLOU, and G. A. KATSOULOS. Inorg. Chim. Acta, **90**, L19 (1984).
7. C. A. TSIPIS, D. P. KESSISSOGLOU, and G. A. KATSOULOS. Chim. Chron. **14**, 195 (1985).
8. C. C. HADJIKOSTAS, G. A. KATSOULOS, and S. A. SHAKHATREH. Inorg. Chim. Acta, **133**, 129 (1987).
9. E. G. BAKALBASSIS, G. A. KATSOULOS, and C. A. TSIPIS. Inorg. Chem. **26**, 3151 (1987).
10. J. M. C. ALISON and T. A. STEPHENSON. J. Chem. Soc. Dalton, 254 (1973).
11. G. GATTOW and B. STURM. Z. Anorg. Allg. Chem. **461**, 125 (1980).
12. G. GATTOW and R. GERNER. Z. Anorg. Allg. Chem. **524**, 122 (1985).
13. G. GATTOW and R. GERNER. Z. Anorg. Allg. Chem. **528**, 157 (1985).
14. R. GERNER and G. GATTOW. Z. Anorg. Allg. Chem. **522**, 145 (1985).
15. R. GERNER and G. GATTOW. Z. Anorg. Allg. Chem. **526**, 122 (1985).
16. A. VOGEL. Quantitative inorganic analysis. Longmans, London. 1964.
17. C. C. HADJIKOSTAS. Ph.D. Thesis, University of Thessaloniki. 1986.
18. C. J. BALLHAUSEN and H. B. GRAY. Inorg. Chem. **1**, 111 (1962).
19. R. HOFFMANN. J. Chem. Phys. **39**, 1397 (1963).
20. A. VISTE and H. B. GRAY. Inorg. Chem. **3**, 1113 (1964).
21. J. HOWELL, A. ROSSI, D. WALLACE, K. HARAKI, and R. HOFFMANN. Forticon 8. Q.C.P.E. No. 344, Indiana University.
22. J. H. AMMETER, H. B. BURGI, J. C. THIBEAULT, and R. HOFFMANN. J. Am. Chem. Soc. **100**, 3686 (1978).
23. K. OHNO. Theoret. Chim. Acta, **86**, 1463 (1964).
24. G. KLOPMAN. J. Am. Chem. Soc. **86**, 4550 (1964).
25. M. P. SIGALAS and C. A. TSIPIS. Inorg. Chem. **25**, 1875 (1986).
26. C. J. BALLHAUSEN and H. B. GRAY. Molecular orbital theory, W. A. Benjamin, New York. 1964.
27. C. J. BURNS. Chem. Phys. **41**, 1521 (1964).
28. J. W. RICHARDSON, W. C. NIEUWPOORT, R. R. POWELL, and W. F. EDGELL. J. Chem. Phys. **36**, 1057 (1962).
29. J. W. RICHARDSON, R. R. POWELL, and W. C. NIEUWPOORT. J. Chem. Phys. **38**, 796 (1963).
30. E. CLEMENTI and D. RAIMONDI. J. Chem. Phys. **38**, 286 (1963).
31. P. W. G. NEWMAN and A. H. WHITE. J. Chem. Soc. Dalton, 1460 (1972).
32. P. C. CHRISTIDIS. Acta Crystallogr. C**42**, 781 (1986).
33. R. SCHIERL, U. NAGEL, and W. BECK. Z. Naturforsch, **39**B, 649 (1984).
34. K. J. RAO and M. L. VENKATARAGHA. Can. J. Chem. **39**, 1757 (1961).
35. D. A. BROWN, W. K. GLASS, and M. A. BURKE. Spectrochim. Acta, **32**A, 137 (1976).
36. B. B. KAUL and K. B. PANDEYA. J. Inorg. Nucl. Chem. **40**, 229 (1978).
37. F. BONATI and R. UGO. J. Organomet. Chem. **10**, 257 (1967).
38. C. O'CONNER, J. D. GILBERT, and G. WILKINSON. J. Chem. Soc. A, 84 (1969).
39. S. SUGANO, Y. TANABE, and H. KAMIMURA. Multiplets of transition metal ions in crystals. Academic Press, New York. 1970.
40. R. DINGLE. Inorg. Chem. **10**, 1141 (1971).
41. K. J. CAVELL, R. J. MAGEE, and J. O. HILL. Inorg. Nucl. Chem. **41**, 1281 (1979).

Can. J. Chem. Downloaded from www.nrcresearchpress.com by 41.223.56.140 on 09/07/12
For personal use only.

Continuous flow fast atom bombardment mass spectrometry of mononucleotides and their metal complexes

M. J. BERTRAND,[1] V. BENHAM, R. ST-LOUIS, AND M. J. EVANS

Department of Chemistry, University of Montreal, P.O. Box 6128, Station A, Montreal, P.Q., Canada H3C 3J7

Received September 7, 1988

M. J. BERTRAND, V. BENHAM, R. ST-LOUIS, and M. J. EVANS. Can. J. Chem. **67**, 910 (1989).

The mass spectra of mononucleotides and their metal adducts Na, K, Mg, Ca, Ni, Co, Cu, and Zn of guanosine 5′-monophosphate (5′-GMP) as well as H, Na, and Mg of adenosine 5′-monophosphate (5′-AMP) and H and Ni of inosine 5′-monophosphate (5′-IMP) have been obtained in low concentrations of matrix in water using continuous-flow fast atom bombardment. The results indicate that this technique is suitable for the analysis of these complexes in aqueous media and yields spectra that are highly characteristic of the compounds analyzed. Parent-molecular ions and structurally significant fragment ions are observed for all compounds studied and the different binding sites for the metal on the nucleotides can be isolated from the fragment ions. Experimental parameters influencing the quality of the spectra such as flow rate, matrix concentration, matrix nature, and analyte concentration have been studied and optimized. For the thirteen compounds studied, it appears that continuous-flow FAB is superior to conventional FAB and that good quality spectra can be obtained with as little as 0.5% of added matrix thus minimizing spectral interferences.

Key words: continuous flow FAB, FAB MS, mass spectrometry, nucleotides, metal-nucleotides.

M. J. BERTRAND, V. BENHAM, R. ST-LOUIS et M. J. EVANS. Can. J. Chem. **67**, 910 (1989).

Utilisant la technique du bombardement par atomes rapides en flux continu, on a déterminé les spectres de masse de mononucléotides et de leurs adduits métalliques (les sels de Na, K, Mg, Ca, Ni, Co, Cu et Zn de la monophosphate-5′ guanosine (5′-GMP), les adduits du H, Na et Mg de la monophosphate-5′ adénosine (5′-AMP) ainsi que les adduits H et Ni de la monophosphate-5′ inosine (5′-IMP)) présents à de faibles concentrations dans des matrices d'eau. Les résultats obtenus indiquent que cette technique est appropriée pour l'analyse de ces complexes dans des milieux aqueux et qu'elle fournit des spectres très caractéristiques des composés analysés. Pour chacun des composés étudiés, on a observé les ions moléculaires parents ainsi que des ions correspondants à des fragments importants du point de vue de la structure; en se basant sur les ions de ces fragments, on peut identifier les divers sites de liaison du métal sur les nucléotides. On a étudié et optimisé les paramètres expérimentaux qui influencent la qualité des spectres, comme la vitesse d'écoulement, la concentration matricielle, la nature de la matrice et la concentration du produit à analyser. Pour les treize composés étudiés, il semble que cette méthode soit supérieure à la méthode FAB conventionnelle et que l'on puisse obtenir des spectres de bonne qualité avec une addition minimale de 0,5% de la matrice; on minimise ainsi les interférences spectrales.

Mots clès: FAB à debit-continu, FAB MS, spectrométrie de masse, nucléotides, adduits metallique.

[Traduit par la revue]

Introduction

In life sciences, tremendous importance is attributed to nucleosides, nucleotides, and their metal adducts. Metals and their complexes are known to play a crucial role in various biological systems. Alkaline and alkaline earth metals play the role of charge carriers and activators for several enzymes. The transition metal ions are efficient in blocking active sites of metallo-enzymes in redox and oxygenation reactions. Accordingly, the structural characterization of nucleic acid derivatives and their metal adducts in biological media should pave the way for a better understanding of their behavior in different micro-organism environments.

The first applications of mass spectrometry in the characterization of nucleotides and nucleosides were reported by Biemann and McCloskey who demonstrated the use of electron ionization in the structure elucidation of the so-called low volatility nucleosides (1). They used free nucleosides and sublimed them directly in the ionizing electron beam to produce mass spectra. Further accomplishments involve the analysis of chemically modified nucleosides (2) and nucleotides (3), the sequencing of deoxyribonucleotides (4), and the use of chemical ionization, field desorption, thermospray, and other desorption–ionization techniques (5–10) for the analysis of these polar compounds. Since the introduction of fast atom bombardment (FAB) (11, 12), a desorption–ionization technique that allows the analysis of polar, thermally labile and involatile compounds, a number of publications dealing with its application to the analysis of nucleotides, nucleosides, and their derivatives have appeared in the literature (13–20).

Although FAB is known to be a relatively simple and versatile technique, its application to the analysis of nucleotides, nucleosides, and their metal adducts is often limited because of the lack of solubility and/or chemical stability of these compounds in the commonly used matrices. Furthermore, the use of liquid matrices such as glycerol and diethanolamine can modify the structures of the metal adducts and often create strong spectral interferences in the mass spectra of complexes of relatively low molecular weights. Recently, a technique known as continuous-flow FAB or dynamic FAB has been introduced (21, 22) and it appears promising for the analysis of nucleotides, nucleosides, and their metal adducts, since it allows the analysis to be conducted in aqueous media containing relatively low concentrations of added matrix. Under these conditions, it becomes possible to vary matrix conditions to increase solubility and chemical stability and consequently spectral interferences can be reduced substantially (23).

The present work reports a feasibility study on the use of continuous-flow FAB for the characterization of nucleotides and their metal adducts in aqueous media. The purine mononucleotides, Na_2-5′-GMP, H_2-5′-AMP, and H_2-5′-IMP (see Fig. 1) and some of their metal adducts with alkaline, alkaline earth, and transition metals (Na, Mg, Ca, Ni, Co, Cu, Zn) have been studied and their mass spectra have been obtained in water using a home-made continuous-flow probe. Most of the compounds studied in this work give complexes of the type $M_2L \cdot nH_2O$ and $M'L \cdot nH_2O$ where M = Na, K; M′ = alkaline earths and transi-

[1]To whom correspondence should be addressed.

Can. J. Chem. Downloaded from www.nrcresearchpress.com by 41.223.56.140 on 09/07/12
For personal use only.

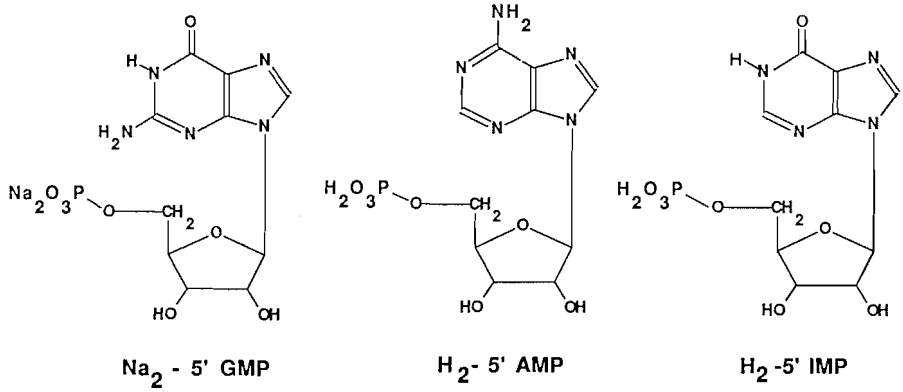


FIG. 1. Structures of the mono-nucleotides Na_2-5′-GMP, H_2-5′-AMP, and H_2-5′-IMP.

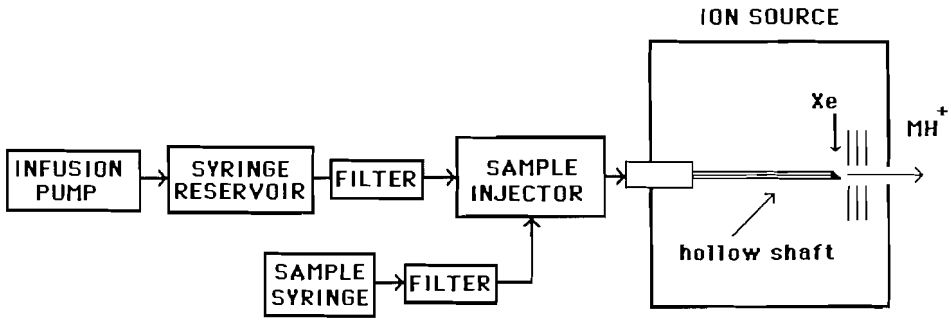


FIG. 2. Schematic diagram of the continuous-flow system.

tion metals; and L = guanosine 5′-monophosphate (5′-GMP), adenosine 5′-monophosphate (5′-AMP) and inosine 5′-monophosphate (5′-IMP) (24, 25). In the solid phase, the alkaline and transition metals are normally bound to N(7) and indirectly interact with phosphate groups through a hydrogen bonding network (26–30). The effect of several experimental parameters that have an influence on the quality of the mass spectra recorded under dynamic FAB conditions such as pH, matrix concentration, matrix basicity, and analyte concentration have also been studied.

Experimental

Continuous-flow probe

The block diagram of the continuous-flow probe, which is similar in design to a commercially available continuous-flow probe (22), and sample delivery system that have been built and used in this study is shown in Fig. 2. The constant and continuous flow of the mobile phase, contained in a syringe reservoir, is provided by a suitable infusion pump (Harvard Apparatus Inc.) normally operated at 3–5 μL/min. The pump is connected to an adjustable probe (capped with an angled brass tip through which a 0.35 mm hole is drilled) via a Rheodyne (Model 7125) injector for samples of 5 μL and larger volumes or a Rheodyne (Model 7520) injector for submicroliter volumes. The probe is constructed from a stainless steel hollow shaft through which an electrically isolated 1.5 m long (0.08 mm id, 0.3 mm od) fused silica capillary is centered coaxially and fixed to the brass tip. The other end of the capillary is connected to the Rheodyne injection valve. The hollow shaft is continuously evacuated through a 3 mm hole in the side of the brass tip. All injections, as well as the mobile phase, are continuously filtered by appropriate line filters (see Fig. 2). In this project, the samples were dissolved in the mobile phase before they were injected.

Mass spectrometry

All mass spectral analyses presented in this study were conducted on a Kratos MS-50TC triple analyzer mass spectrometer arranged in a C-shaped geometry (EBE). The instrument was equipped with a standard Kratos FAB source operated at 8 kV and a post-acceleration detector. The xenon (Matheson 99.9%) atom beam was generated by an Iontech B-11NF saddle-field gun mounted on the FAB source and had a kinetic energy of 6 keV. Data acquisition and treatment were done using a Kratos DS-90 system and the spectra presented were obtained by averaging 6–8 scans.

Chemicals

The nucleotides H_2-5′-IMP, H_2-5′-AMP as well as Na-5′-AMP (6.8% sodium content), Na_2-5′-GMP, and K_2-5′-GMP were obtained from Sigma Chemical Company (St. Louis, MO, U.S.A.) and were used without further purification. The alkaline earth complexes Ca-5′-GMP, Mg-5′-GMP, and Mg-5′-AMP together with the transition metal complexes Ni-5′-GMP, Co-5′-GMP, Cu-5′-GMP, Zn-5′-GMP, and Ni-5′-IMP, were all prepared according to established methods (ref. 29 and references therein – ref. 31). The mobile phases used were HPLC grade water, glycerol, diethanolamine, triethanolamine, and mixtures thereof.

Results and Discussion

In spite of numerous attempts, little or no success was achieved in recording the conventional FAB spectra of a number of mononucleotides and their metal adducts presented in this work. The partial solubility and chemical instability of the compounds in commonly used FAB matrices are some of the reasons attributed to the poor results. In the case of metal adducts, the pH of the matrix and the nature of the matrix are quite important to the stability of the complexes. Some polar matrices can interact strongly with nucleotide metal adducts and compete with the nucleotides for the metal ion, thus changing the nature and chemical structure of the molecules to be studied. However, the use of a technique such as continuous-flow FAB

Can. J. Chem. Downloaded from www.nrcresearchpress.com by 41.223.56.140 on 09/07/12
For personal use only.

Can. J. Chem. Downloaded from www.nrcresearchpress.com by 41.223.56.140 on 09/07/12
For personal use only.

should eliminate several of the drawbacks described above since a water solution of variable pH can be used for the analysis, and the amount of support matrix added to water for ionization to occur can be very small. Under these experimental conditions, it should be possible to reduce the background in the spectra and to study the nature of the metal adducts of nucleotides that exist in aqueous media.

The positive ion spectra of the nucleotides Na_2-5′-GMP and Ni-5′-GMP obtained using continuous-flow FAB and conventional FAB are shown in Fig. 3. Comparison of the spectrum of Na_2-5′-GMP obtained with conventional FAB (Fig. 3*a*) by dissolving the compound in glycerol with that obtained from a 0.01 *M* aqueous solution at pH 5.9 containing 0.5% of glycerol using the continuous-flow system reveals that a much higher S/N ratio is obtained under dynamic conditions. Even if the ions (M − Na + 2H), (M + H), and (M + Na) at *m/z* 386, 408, and 430 are observed in both spectra, the spectrum recorded using water clearly shows the presence of ions (M + 2Na − H) and (M + G+ H) at *m/z* 452 and 500 that are lost in the background under conventional FAB. As another example, the spectrum of Ni-5′-GMP obtained from a 0.01 *M* aqueous solution at pH 3.5 containing 0.5% of thioglycerol using continuous-flow FAB (Fig. 3*c*) can be compared with that obtained using conventional FAB by dissolving the compound in thioglycerol (Fig. 3*d*). It can readily be observed from the spectra that ions which are characteristic of the metal adduct are present under continuous-flow conditions whereas under conventional FAB, the ions present are mostly formed from thioglycerol. The spectrum obtained under dynamic conditions (Fig. 3*c*) shows parent-molecular ions (M + H) and (M + T + H) at *m/z* 420 and 528 and fragment ions (RP + Ni + $2H_2O$ + H), (B + H), and S at *m/z* 306, 151, and 133 that are characteristic of the compound under study. In the above assignments RP, B, and S refer to the ribose-phosphate, the base, and the sugar moiety, respectively. Furthermore, it can be seen that interference from the matrix ions is very small (*m/z* 109), indicating the preferred ionization of the analyte. The spectrum recorded using conventional FAB does not show ions that are characteristic of the metal adduct. The intense ions that are present are mostly formed from thioglycerol and the only two ionic species containing Ni are (T + Ni + H) and (2T + Ni − H) at *m/z* 165 and 273 and these ions do not contain structural information. Thus, for the examples shown, the continuous-flow system is clearly advantageous.

In order to confirm the potential of the continuous-flow mode for the analysis of nucleotides and their metal adducts in aqueous solutions, a series of metal complexes and nucleotides have been analyzed. The positive ion spectra of the transition metal complexes Zn-5′-GMP, Cu-5′-GMP, Co-5′-GMP, and Ni-5′-GMP have been obtained from 0.01 *M* aqueous solutions (pH = 2–3.5) containing 0.5% of glycerol and are shown in Fig. 4. It can be seen that in all cases parent-molecular ions and characteristic fragments are observed. The parent-molecular ions (M + H) for Zn, Cu, Co, and Ni are present at *m/z* 426, 425, 421, and 420, respectively. Intense fragment ions of the type (RP + M′ + $2H_2O$ + H), (B + 2H), and (S), where M′ = metal are also observed. The (B + 2H) and (S) ions usually appear at *m/z* 152 and 133 whereas the (RP + M′ + $2H_2O$ + H) fragments are observed at *m/z* 312, 311, 307, and 306 for Zn, Cu, Co, and Ni, respectively. The fragment ions observed are of special interest because they include the different binding sites on the molecules such as the base, the sugar, and the phosphate moieties. The transition metals are usually bonded to N(7) in the solid state and interact indirectly with the phosphate moiety via the hydrogen bonding network (26–30). In water and under FAB bombardment, ions of the type (RP + M′ + $2H_2O$ + H) are intense, indicating that a metal–phosphate interaction is favored in the fragmentation. These results can be interpreted with the view that in the reaction of *cis*-diaminediaquoplatinum-(II) with disodium 5′-uridine phosphate in solution, it has been observed using vibrational spectroscopy that Pt atoms are temporarily bound to the phosphate group (31). The presence of (B + 2H) ions in the spectra is also consistent with the assumption that the metals interact strongly with the phosphate group in the ionic state. Thus the use of continuous-flow FAB not only yields mass spectra that are characteristic of the complexes but furthermore they may provide a tool by which the metal nucleotide interaction in water can be studied. Considerations related to the identification of the binding site of the metal from the spectra will be discussed furtheron.

The positive ion spectra of H_2-5′-AMP, Na-5′-AMP, Mg-5′-AMP, and H_2-5′-IMP were also recorded using aqueous solutions and continuous-flow FAB and are shown in Fig. 5. The spectra were obtained from 0.01 *M* aqueous solutions containing 0.5% of glycerol. As seen from Fig. 5*a* and *d*, both H_2-5′-AMP and H_2-5′-IMP give relatively simple spectra with parent-molecular ions (M + H) at *m/z* 348 and 349 and fragment ions (B + 2H) at 136 and 137 which are common in the spectra of nucleotides and nucleosides. The spectrum obtained for Na-5′-AMP (Fig. 5*b*) is characteristic of the compound and different from the spectrum of H_2-5′-AMP showing parent-molecular ions (M + H), (M + Na), and (M + 2Na − H) at *m/z* 370, 392, and 414. Fragment ions that are characteristic of the base are observed at *m/z* 136 and 164 and they correspond to (B + 2H) and (B + 30). The spectrum of Mg-5′-AMP shown in Fig. 5*c* has features that are indicative of the structure of this metal adduct. The parent-molecular ion (M + H) is present at *m/z* 370 and fragment ions corresponding to the base and the sugar moieties (B + 2H), (B + 44), and (S) are seen at *m/z* 136, 178, and 133. It is interesting to note that the ion at 133 corresponding to the sugar moiety is essentially present when a divalent cation is present (Cu, Ni, Co, Mg...). In this spectrum, contrary to the metal adducts of transition metals where the (RP + $2H_2O$ + H + M′) ion was intense, this type of ion is not observed for Mg but instead the fragment ions (Mg + 2B) and (Mg + BH) are observed at *m/z* 159 and 292. This may imply that with Mg the preferred site of interaction in the ionic state is the base and not the phosphate moiety as is the case for the transition metals. The magnesium complex was soluble at pH ~ 2 contrary to H_2-5′-IMP, H_2-5′-AMP, and Na-5′-AMP that were soluble at pH ~ 6.

Although most compounds yield acceptable spectra in the positive ion mode, it was not possible to obtain significant positive spectra for the compounds Mg-5′-GMP, Ca-5′-GPM, and Ni-5′-IMP and consequently these compounds were analyzed in the negative ion mode. The spectra obtained for Mg-5′-GMP (pH = 2, 0.5% glycerol) Ca-5′-GMP (pH = 2, 1% diethanolamine), and Ni-5′IMP (pH = 11, 0.5% triethanolamine) are shown in Fig. 6. In all three cases, parent-molecular ions $(M - H)^-$ are observed at *m/z* 384, 400, and 404. The common fragment ions that are present in the three spectra are B^- and $H_2PO_4^-$ at *m/z* 135 or 150 and 97. However, the spectrum of the magnesium complex differs from the two others because it exhibits ions at *m/z* 323 and 209 that can be attributed to (2B + Mg − H) and (Mg + B + $2H_2O$ − H). The latter is equivalent to the (RP + M′ + $2H_2O$ + H) ion observed for the transition metals but the ribose-phosphate moiety has been

Can. J. Chem. Downloaded from www.nrcresearchpress.com by 41.223.56.140 on 09/07/12
For personal use only.

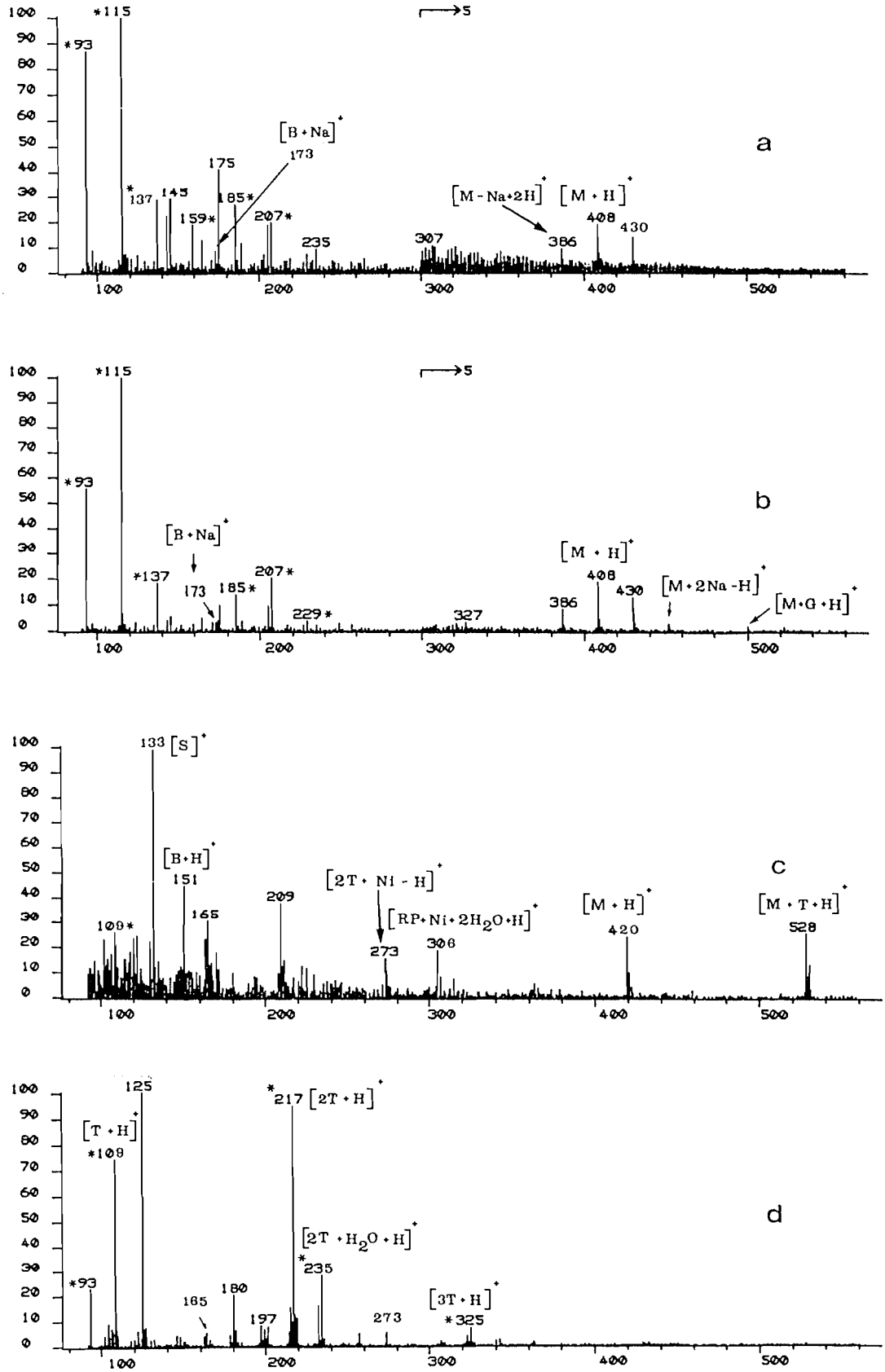


FIG. 3. Positive ion spectra of (*a*) Na_2-5′-GMP, in glycerol conventional FAB, (*b*) 10^{-2} *M* aqueous Na_2-5′-GMP, pH 5.9, 0.5% glycerol continuous flow, (*c*) 10^{-2} aqueous Ni-5′-GMP, pH 3.5, 0.5% thioglycerol continuous flow, and (*d*) Ni-5′-GMP, in thioglycerol conventional FAB are used to identify matrix adducts with protons on the metals. T is thioglycerol.

Can. J. Chem. Downloaded from www.nrcresearchpress.com by 41.223.56.140 on 09/07/12
For personal use only.

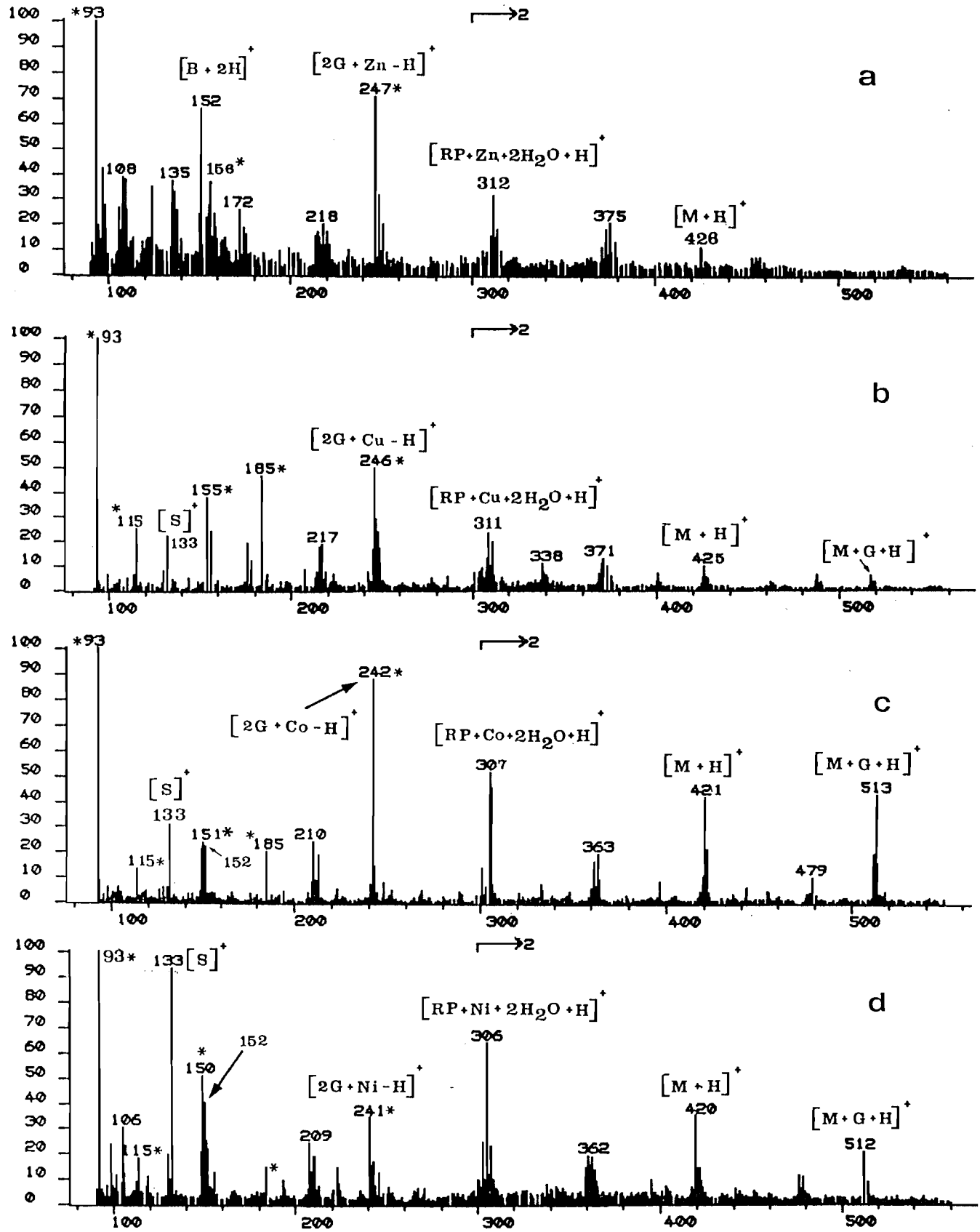


FIG. 4. Positive ion continuous flow FAB spectra of (*a*) 10^{-2} *M* Zn-5′-GMP, (*b*) 10^{-2} *M* Cu-5′-GMP, (*c*) 10^{-2} *M* Co-5′-GMP, and (*d*) 10^{-2} *M* Ni-5′-GMP, at pH 2–3.5 with 0.5% glycerol. B, G, RP, and S represent the base, glycerol, ribophosphate, and the sugar, respectively.

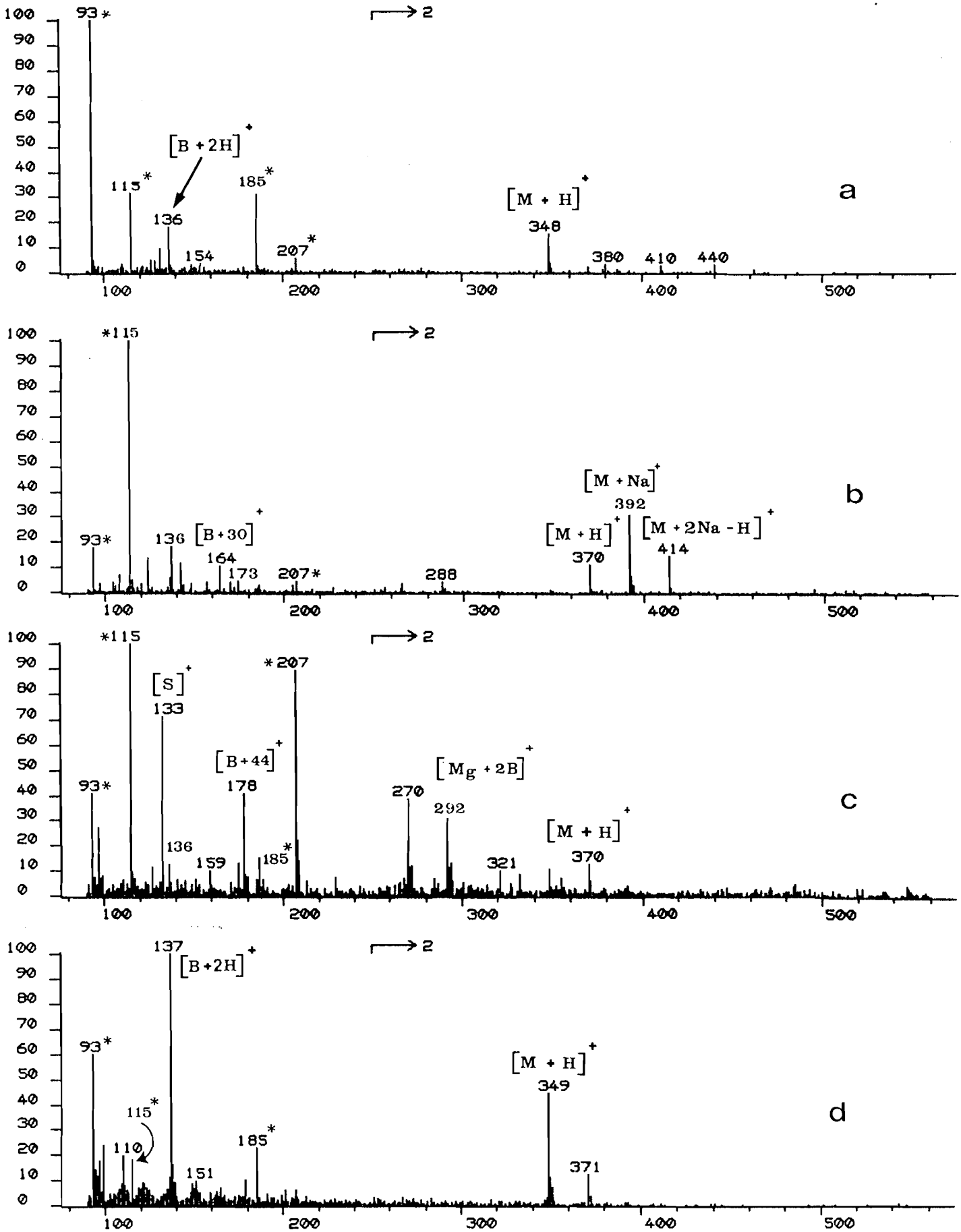


FIG. 5. Positive ion continuous-flow FAB spectra of 10^{-2} *M* aqueous solution with 0.5% glycerol of (*a*) H_2-5′-AMP, pH ~ 6, (*b*) Na-5′-AMP, pH = 6, (*c*) Mg-5′-GMP, pH ~ 2, and (*d*) H_2−IMP, pH ~ 6.

Can. J. Chem. Downloaded from www.nrcresearchpress.com by 41.223.56.140 on 09/07/12
For personal use only.

Can. J. Chem. Downloaded from www.nrcresearchpress.com by 41.223.56.140 on 09/07/12
For personal use only.

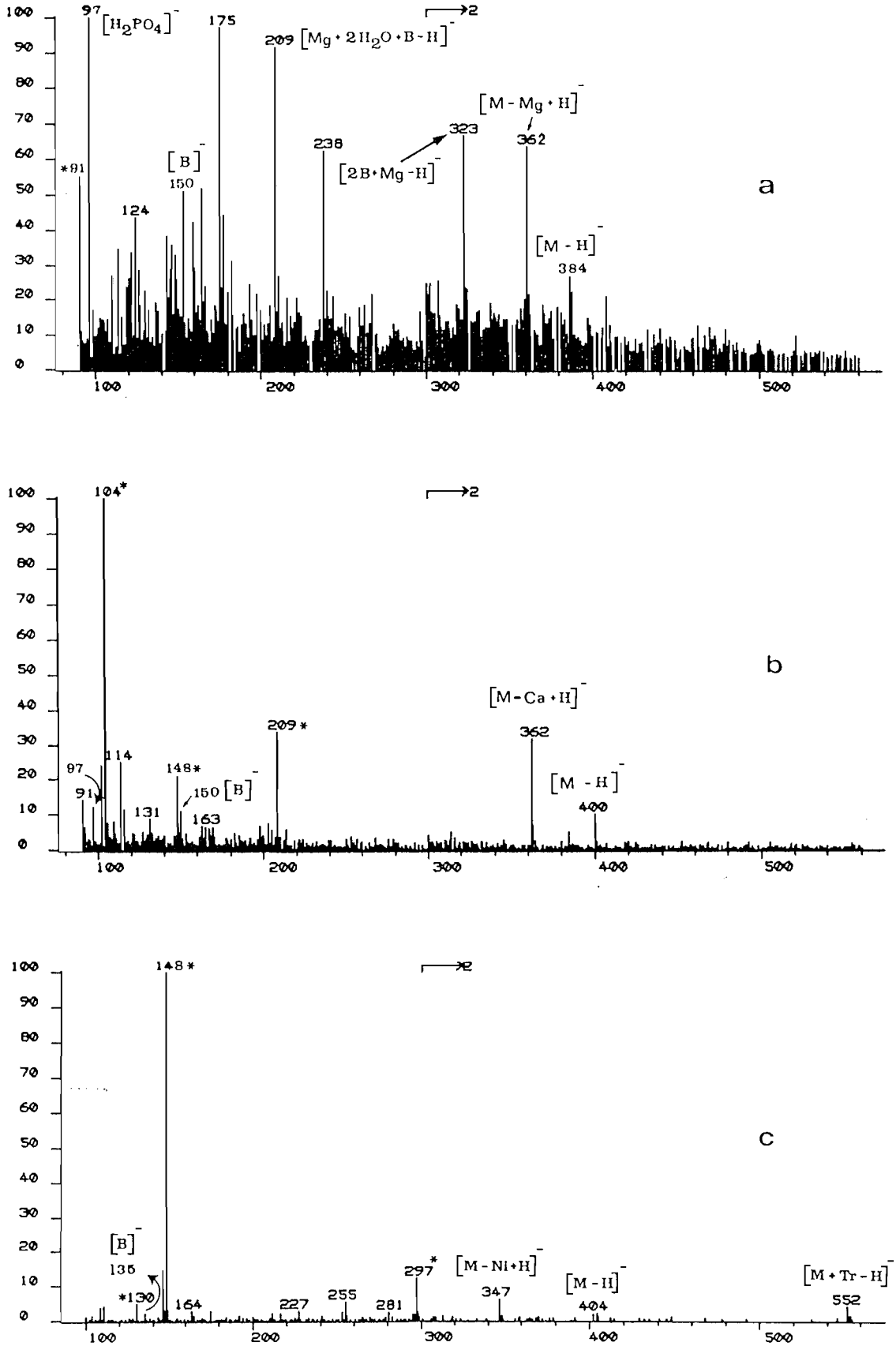


FIG. 6. Negative ion continuous-flow FAB spectra of 10^{-2} *M* aqueous solutions of (*a*) Mg-5′-GMP, 0.5% glycerol, pH = 2, (*b*) Ca-5′-GMP, 1% diethanolamine, pH = 2, and (*c*) Ni-5′-IMP, pH = 11, in 0.5% triethanolamine. Tr is triethanolamine.

TABLE 1. Significant ions observed in the mass spectra of nucleotides and metal adducts analyzed by continuous-flow FAB

	Intensity						
	$[M + H]^+$	$[M - H]^-$	$[B + 2H]^+$	$[B^-]$	$[RP + \ddot{M} + 2H_2O + H]^+$	$[\ddot{M} + 2B]$	$[S]^+$
Na_2-5′-GMP	408(18)	406(13)	—	150(19)	—	—	—
K_2-5′-GMP	440(15)	—	—	—	—	—	—
Mg-5′-GMP[a]	—	384(27)		150(51)		323(68)	—
Ca-5′-GMP[a]	—	400(11)		150(12)		—	—
Ni-5′-GMP	420(38)	418(86)	152(42)	150(27)	306(67)	—	133(100)
Co-5′-GMP	421(44)	419(49)	152(23)	150(13)	307(53)	—	133(35)
Cu-5′-GMP	425(11)	423(24)	—	150(18)	311(47)	—	133(20)
Zn-5′-GMP	426(11)	—	152(69)	—	312(33)	—	—
H_2-5′-AMP	348(5)	346(17)	136(8)	134(38)	—	—	—
Na-5′-AMP	370(11)	368(23)	136(18)	134(47)	—	—	—
Mg-5′-AMP	370(13)	368(65)	136(12)	134(92)	—	292(35)	133(70)
H_2-5′-IMP	349(13)	347(67)	137(45)	135(21)	—	—	—
Ni-5′-IMP[a]	—	404(5)	137(7)	135(2)	—	—	—

[a]The spectrum recorded in the positive ion mode was not reproducible.

Can. J. Chem. Downloaded from www.nrcresearchpress.com by 41.223.56.140 on 09/07/12
For personal use only.

replaced by the base moiety indicating that Mg possibly has a preferred interaction with the base moiety as observed previously for Mg-5′-AMP. If the results reflect the binding site of the metal in solution (see later) these findings differ from published results in which Mg was found to be bonded to the phosphate moiety in solutions having a pH lower than 5 (32).

The results that have been obtained for the analysis of thirteen nucleotides and metal adducts using continuous-flow FAB in the positive and negative ion modes are summarized in Table 1. The ions that are most significant and common to most compounds are given and the numbers in parentheses refer to their relative intensities in the spectra. It can be seen that most compounds yield a spectrum in both negative and positive ion modes and that ions which are specific to each part of the molecules are present, allowing structure assignment. In several cases, ions are present to isolate the possible binding sites and the nature of the metal is seen to have an important influence on the fragmentation of the molecule.

During the evaluation of the continuous-flow probe, several parameters were found to have an influence on the quality of the results and those are (*i*) flow rate, (*ii*) solute concentration, (*iii*) droplet size and shape, (*iv*) matrix concentration, and (*v*) the nature of the matrix.

Flow rate

To obtain a stable operation, it is important that the evaporation rate of the mobile phase from the probe surface be in constant equilibrium with the pumping speed of the mass spectrometer and this is to a large extent controlled by the adoption of an optimum flow rate. In this work the flow rates used were in the vicinity of 3–5 μL/min. Lower and higher flow rates resulted in freezing within the end of the capillary tip, and spattering of the liquid surface, respectively. Both these conditions lead to considerable instability in the ion current.

Solute concentration

The range of solute concentrations that can be used is limited at the higher end by the possibility of blocking the capillary with precipitation or crystallization of the sample in the capillary or at the probe surface and at the lower end by the sensitivity of the method for a particular compound. In this study, it was found that good signal-to-noise ratio and stable operation could be achieved routinely using 0.01 *M* solutions. However, reasonable spectra could be achieved with concentrations as low as 10^{-5} *M* for some nucleotides.

Matrix concentration

Since the main objective of this project was to explore the nature of the metal adducts of nucleotides in aqueous media, considerable effort was made to use the lowest possible added matrix concentration. Correspondingly, the majority of the samples were analyzed with 0.5% of added matrix in water. Smaller amounts lead to the inhibition of ionization of the analyte or freezing of the water at the probe tip. Caprioli *et al.* have used up to 25% of glycerol and thioglycerol (22) but under these conditions contamination of the spectrum at lower masses by ions generated by the matrix is substantial and not acceptable for the compounds studied in this work.

Nature of the matrix

In FAB mass spectrometry, solute, and matrix are in constant competition in scavenging the available protons and this to a large extent depends on their acidic properties (33, 34). The outcome of such a competition will have a determining effect on the intensities of the fragments observed in both the positive and negative ion modes. Since the amount of added matrix was relatively small (0.5%) in our experiments, a short study was conducted to evaluate the extent of the influence of the acidic properties of the matrix. Aqueous solutions of Na_2-5′-GMP containing 0.5% of thioglycerol, glycerol, diethanolamine, and triethanolamine were analyzed in the positive and negative ion modes and the variation of the signal-to-noise ratio was evaluated by measuring the ratios of the intensities of the parent-molecular ions to the base peak of the matrix. The negative ion spectra obtained with glycerol, diethanolamine, and triethanolamine are shown in Fig. 7 and the variations of S/N are given in Table 2. It is seen from the spectra that as the nature of the added matrix is changed, the features of the spectra remain essentially the same but that the intensities vary. The results shown in Table 2 indicate that the nature of the added matrix even at low-concentrations has a definite effect on the quality of the spectra. For positive ion spectra the more acidic matrices such as thioglycerol and glycerol yield better results whereas for negative ion spectra it is preferable to use an

Can. J. Chem. Downloaded from www.nrcresearchpress.com by 41.223.56.140 on 09/07/12
For personal use only.

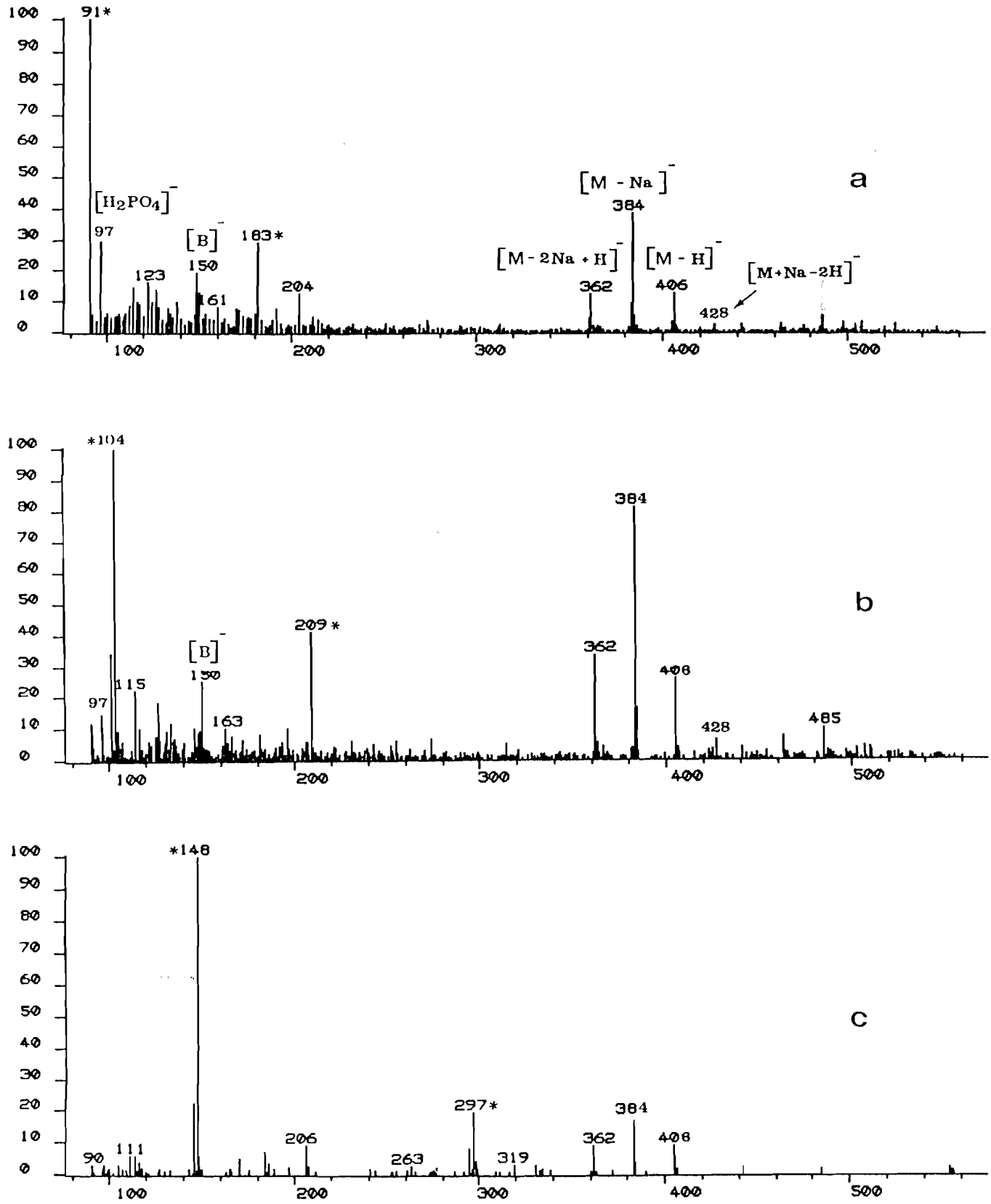


FIG. 7. Negative ion continuous-flow FAB spectra of 10^{-2} *M* aqueous solution Na_2-5′-GMP in (*a*) 0.5% glycerol, (*b*) 0.5% diethanolamine, and (*c*) 0.5% triethanolamine.

TABLE 2. Matrix effect on parent-molecular ion intensities

Matrix	$\frac{[M + H]^+ + [M + Na]^+}{[Matrix + H]^+}$	$\frac{[M - H]^- + [M - Na]^-}{[Matrix - H]^-}$
Thioglycerol	2.3	0.14
Glycerol	0.9	0.52
Triethanolamine	0.05	0.27
Diethanolamine	—	1.1

alkaline matrix such as diethanolamine. However, under the conditions of continuous-flow FAB contrary to conventional FAB, the solubility of the analyte does not depend on the added matrix but mostly on the pH of the aqueous solution which is advantageous.

Conclusion

On the basis of the results obtained in our mass spectrometric investigation of mononucleotides and their metal adducts using continuous-flow fast atom bombardment it can be concluded that this approach is better suited than conventional FAB to analyze these compounds. Under the dynamic conditions used it appears that not only a higher signal-to-noise, reducing the background interferences, is obtained, but the spectra recorded are more reliable and reproducible. The nature of the matrix that is present in small concentration has an effect on the intensities of the parent-molecular ions but contrary to conventional FAB the solubility does not depend greatly on the added matrix. The solubility of the analyte can be augmented by varying the pH, which is an advantageous feature. The mass spectra that have been obtained using the continuous-flow approach are very characteristic of the structure of the compounds analyzed since parent-molecular ions are present and fragment ions corresponding to the base, the sugar and the phosphate are dependent on the nature of the metal in metal adducts. It thus appears that the continuous-flow approach can be useful for characterizing the structures of nucleotides, nucleosides, and their derivations directly from aqueous media.

Finally, an important question arises from the results that have been obtained and it relates to the possibility to elucidate the positions of the binding of the metal to the nucleotide from the mass spectral data. It is doubtful that a definite answer can be given from the preliminary experiments that have been conducted in this study. Since the primary objective of the work was to obtain the mass spectra of metal adduct of nucleotides, the project was not designed to answer such a question. Furthermore, since our knowledge of all the aspects involved in the production of a FAB spectrum and the phenomena of chemical reactions that can be induced by high energy particles is still incomplete (35), it is difficult to accurately predict the relation between observations made on fragments and structures that can exist in the liquid solution. However, there are some elements in the spectra of the metal adducts that indicate a definite relation between the spectrum obtained and the nature of the divalent ions. For example, the presence of an intense ions at *m/z* 133 corresponding to the sugar moiety is observed whenever a divalent cation is present in the adduct. The mass spectra of Ni, Ca, Co, and Zn complexes exhibit similar features whereas the magnesium adducts differ from them both in the positive and negative ion mode indicating that this behavior is probably structure related. Thus, although the information gathered in this work is not sufficient to answer the important question on the binding site, it is sufficient to warrant further investigation on well-characterized systems to verify if the binding sites can be determined by this technique.

Acknowledgement

The authors are grateful to the Natural Sciences and Engineering Research Council of Canada and to "Fonds FCAR", Government of Quebec, for financial assistance. Professor T. Theophanides is also acknowledged for his helpful comments on this work.

1. K. BIEMANN and J. A. MCCLOSKEY. J. Am. Chem. Sci. **84**, 2005 (1962).
2. H. A. HOWLETT, M. W. JOHNSON, A. R. TRIM, J. EAGLES, and R. SELF. Anal. Biochem. **39**, 429 (1971).
3. C. J. MCNEAL, K. K. OGILVIE, N. Y. THERIAULT, and M. J. NAMER. J. Am. Chem. Soc. **104**, 972 (1982); **104**, 976 (1982); **104**, 982 (1982).
4. L. GROTJAHN, R. FRANK, and H. BLOKER. Nucl. Acids Res. **10**, 4671 (1982).
5. M. S. WILSON and J. A. MCCLOSKEY. J. Am. Chem. Soc. **97**, 3436 (1975).
6. W. ENS, K. G. STANDING, B. T. CHAIT, and F. H. FIELD. Anal. Chem. **53**, 1241 (1981).
7. H. BUDZIKIEWICZ and M. LINSCHIED. Biomed. Mass Spectrom. **4**, 103 (1977).
8. C. R. BLAKLEY, J. J. CARMODY, and M. L. VESTAL. J. Am. Chem. Soc. **102**, 5931 (1980).
9. G. W. WOOD. Tetrahedron, **38**, 1125 (1982).
10. H. R. SCHULTEN. Int. J. Mass Spectrom. Ion Phys. **32**, 97 (1979).
11. M. BARBER, R. S. BORDOLI, R. D. SEDWICK, and A. N. TYLER. J. Chem. Soc. Chem. Commun. 325 (1981).
12. M. BARBER, R. S. BORDOLI, R. D. SEDWICK, and A. N. TYLER. Nature, 293 (1981).
13. H. MOSER and G. W. WOOD. 35th ASMS Conference on Mass Spectrometry and Allied Topics, May 24–29, Denver Co., 882 (1987).
14. D. L. SLOWIKOWSKI and K. H. SCHRAM. Nucleosides and Nucleotides, **4**, 309 (1985) and **4**, 347 (1985).
15. H. M. SCHIEBEL, P. SCHULZE, W. D. STOHRER, D. LEIBFRITZ, B. JASTORFF, and K. H. MAURER. Biomed. Mass Spectrom. **12**, 170 (1985).
16. J. EAGLES, C. JAVANAUD, and R. SELF. Biomed. Mass Spectrom. **11**, 41 (1984).
17. G. BREWER and C. M. GRISHAM. Biomed. Mass Spectrom. **11**, 400 (1984).
18. D. H. WILLIAMS, C. BRADLEY, G. BOJESEN, S. SENTIKARN, and L. E. C. TAYLOR. J. Am. Chem. Soc. **103**, 5700 (1981).
19. C. FENSELAU, V. T. YU, R. J. COTTER, G. HANSEN, D. HELLER, T. CHEN, and O. M. CALVIN. Spectrosc. Int. J. **1**, 145 (1982).
20. H. MOSER and G. W. WOOD. Biomed. Enn. Mass Spectrom. **15**, 547 (1988).

Can. J. Chem. Downloaded from www.nrcresearchpress.com by 41.223.56.140 on 09/07/12
For personal use only.

21. Y. ITO, T. TAKEUCHI, D. ISHI, and M. J. GOTO. J. Chromatogr. **346**, 161 (1985).
22. R. M. CAPRIOLI, T. FAN, and J. S. COTTRELL. Anal. Chem. **58**, 2949 (1986).
23. J. S. M. DE WIT, L. J. DETERDING, M. A. MOSELEY, and K. B. TOMER. Rap. Comm. Mass Spectrom. **2**, 100 (1988).
24. K. AOKI. J. Cryst. Soc. Jpn. **23**, 309 (1981).
25. A. D. COLLINS, P. DE MEESTER, D. M. GOODGAME, and A. C. SKAPSK. Biochim. Biophys. Acta, **402**, 1 (1975).
26. M. OGAWA and T. SAKAGUCHI. Chem. Pharm. Bull. **20**, 190 (1972).
27. M. OGAWA and T. SAKAGUCHI. Yakugaki Zaashi. **91**, 750 (1971); **92**, 1166 (1972).
28. M. OGAWA. Yakugaki Zaashi, **91**, 618 (1971).
29. M. OGAWA and T. SAKAGUCHI. Yakugaki Zaashi, **19**, 1650 (1971).
30. HELMUT SIEGEL. Metal ions in biological systems. Vol. 8. John Wiley and Sons. 1979.
31. V. BENHAM, I. S. BUTLER, K. OKAMOTO, and T. THEOPHANIDES. Inorg. Chim. Acta. In press.
32. H. A. Tajmir-Riahi and T. THEOPHANIDES. Can. J. Chem. **61**, 1813 (1983).
33. G. PUZO and J. C. PROME. Org. Mass Spectrom. **19**, 448 (1984).
34. J. A. SUNNER, R. K. TUNGA, and P. KEBARLE. Anal. Chem. **58**, 1312 (1986).
35. C. DASS and D. M. DESIDERIO. Anal. Chem. **60**, 2723 (1988).

Can. J. Chem. Downloaded from www.nrcresearchpress.com by 41.223.56.140 on 09/07/12
For personal use only.

Surface electrochemistry of the oxidation of glycine at Pt

DANIEL G. MARANGONI, RICHARD S. SMITH, AND SHARON G. ROSCOE[1]
Chemistry Department, Acadia University, Wolfville, N.S., Canada B0P 1X0

Received September 21, 1988

DANIEL G. MARANGONI, RICHARD S. SMITH, and SHARON G. ROSCOE. Can. J. Chem. **67**, 921 (1989).

The electrochemical oxidation of glycine at a Pt electrode was investigated in aqueous solutions at pH 1 and 13 using steady-state current–potential measurements, cyclic voltammetry, and open circuit potential decay. The capacitance behaviour and the high Tafel slopes suggest the production of free radicals at the surface of the electrode accompanied by a second reaction involving loss of CO_2 which is the rate determining step. In the electro-oxidation of glycine, it appears that the adsorbed intermediate species is either hydrolyzed anodically to formaldehyde and ammonia, or is oxidized to a carbonium ion which is subsequently hydrolyzed to formaldehyde and ammonia in solution. This behaviour differs from the dimerization process typical of the radical reactions associated with the Kolbe mechanism.

Key words: glycine, amino acid, electrochemical oxidation, surface electrochemistry, Kolbe mechanism.

DANIEL G. MARANGONI, RICHARD S. SMITH et SHARON G. ROSCOE. Can. J. Chem. **67**, 921 (1989).

Faisant appel à des mesures de potentiel du courant à l'état stationnaire, à la voltamétrie cyclique et à la dégénérescence du potentiel en circuit ouvert et opérant en solutions aqueuses, à des pH de 1 et de 13, on a étudié l'oxydation électrochimique de la glycine, au niveau d'une électrode de Pt. Le comportement de la capacitance et les courbes de Tafel élevées suggèrent qu'il y a une production de radicaux libres à la surface de l'électrode et que celle-ci est accompagnée d'une deuxième réaction, impliquant une perte de CO_2, qui détermine la vitesse de la réaction. Dans l'électro-oxydation de la glycine, il semble que l'espèce intermédiaire adsorbée est soit hydrolysée à l'anode en formaldéhyde et en ammoniac soit oxydée en un carbocation qui est subséquemment hydrolysé en formaldéhyde et en ammoniac, en solution. Ce comportement diffère du processus de dimérisation typique des réactions radicaliques associées au mécanisme de la réaction de Kolbe.

Mots clés : glycine, acide aminé, oxydation électrochimique, électrochimie de surface, mécanisme de la réaction de Kolbe.
[Traduit par la revue]

Can. J. Chem. Downloaded from www.nrcresearchpress.com by 41.223.56.140 on 09/07/12
For personal use only.

Introduction

Several investigations of the electro-oxidation of α-amino acids were reported in the early 1930's (1–5). Fichter and Schmid (1) concluded from product analysis, that the electrolytic oxidation of α-amino acids in sulfuric acid solution produces the next lower aldehyde in the first step of the oxidation. However, Takayama (2, 3) found that oxidation at a PbO_2 anode resulted in a facile further oxidation of the aldehyde by the following:

$$RCH(NH_2)COOH \xrightarrow{[o]} RCHO + NH_3 + CO_2$$

$$RCHO \xrightarrow{[o]} RCOOH$$

Fichter and Kuhn (2) and Takayama (5) reported the formation of ammonia, formaldehyde, formic acid, carbon dioxide, and methyl, dimethyl, and trimethyl amines as products from the electrolytic oxidation of glycine. Plochl (6) has suggested that the amines probably resulted from the interaction of formaldehyde and ammonia. Takayama concluded that, from the experimental results, the first stage of the oxidation of amino acids is the aldehyde formation and that the other products either result from further oxidation (formation of carboxylic acids) or the chemical interaction of one product with another. He also concluded that the general reaction above best represents the course of the electrolytic oxidation of an α-amino acid.

The present research has been undertaken to investigate the kinetics, mechanisms, and surface effects of the electrochemical oxidation of glycine at the Pt electrode. Steady-state current–potential measurements, cyclic voltammetry, and open circuit potential decay have been used to study 0.45 *M* aqueous solutions of glycine at pH 1 and pH 13 in order to characterize these reactions with a fully protonated and fully unprotonated reactant, respectively. Anodic reactions in aqueous solutions at the Pt electrode are complicated by the electrocatalytic surface oxide film which develops on the anode metal surface. Thus, electrocatalysis occurs for such reactions as O_2 (7, 8), Cl_2 (9–13), N_2 (from N_3^-) (14–17) evolution, and the Kolbe reaction (18). Generally, in anodic reactions in aqueous media, the electrode may be considered "demetallized" (19) by its oxide film. Thus, the present work examines the influence of surface oxidation on the kinetics of anodic oxidation of glycine on well defined states of the Pt surface oxide film.

Experimental

(a) Methods

Steady-state polarization measurements were made on solutions of the amino acid at a pH of 1 and 13. A Wenking potentiostat (Fast Rise Model 6288RS) was used to control the potential of the working electrode, and the current and potential measurements were read from Keithley autoranging multimeters (model 175 and model 195), respectively. Polarization lines were determined by holding for 10 s per current-density point, at 10 mV intervals of potential. Data analysis and graphics were carried out using both the Cyber 830 and Commodore PC-10 computers.

Corrections for uncompensated solution resistance ("*iR*" drop corrections) were made to the Tafel plots. These "*iR*" corrections were determined using a mercury-wetted vacuum relay to give a clean fast break in the circuit, and the rapid potential drop was recorded on a digital storage Tektronics oscilloscope (model 5440). Potential decay transients were determined in the same manner following steady-state potentiostatic polarization. Analysis of the potential–time data was accomplished using a Commodore PC-10 computer with the Asystant data processing software.

Cyclic voltammograms were obtained using the potentiostat and a function generator (Hokuto Denko Ltd, Model HB-111) to produce a repeating triangular potential function. The potential, read directly from the working and the reference electrodes, and the current, measured by the potential across a variable resistor placed in the counter electrode circuit, were connected to a Hewlett-Packard X-Y recorder (model HP 489-5093) to give the potential–current profile.

[1]To whom correspondence should be addressed.

Can. J. Chem. Downloaded from www.nrcresearchpress.com by 41.223.56.140 on 09/07/12
For personal use only.

(b) Solutions

Solutions of glycine were prepared from 99+% purity, gold label reagent (Aldrich Chemical Company) using conductivity water (Nanopure water, resistivity = 18.3 megohm cm^{-1}) which had been distilled from acid potassium permanganate to remove organic impurities. Sulfuric acid solutions were prepared from Aristar grade 98% purity reagent (BDH Chemicals Limited), while sodium hydroxide solutions were prepared from the standardized Aldrich Acculute concentrate. All solutions were prepared to a concentration of 0.45 *M* in amino acid.

(c) Electrochemical cell and electrodes

Three compartment, all glass cells, provided with glass-sleeved stopcocks as two of the compartments, were used. A specially designed gas-tight cell having a small volume was used for analysis of electrogenerated gaseous products by means of gas chromatography. Johnson Matthey and Mallory high-purity grade Pt wires were degreased by refluxing in acetone, sealed in soft glass, and electrochemically cleaned by potential cycling in 1 *M* sulfuric acid, and stored in 98% H_2SO_4. The reference electrodes used were saturated calomel electrodes made according to a standard procedure (19). Their potentials were checked frequently against a standard hydrogen electrode and compared with the literature value (20). The saturated calomel electrodes were found to be reproducible to within ±1 mV.

(d) Product analysis

A Perkin-Elmer model 226 gas chromatograph fitted with a flame ionization detector was used to detect products from electrolysed solutions of glycine at pH 1 and pH 13. The 2.5 m by 0.6 cm copper column, packed with Chromosorb 103, was maintained at 140°C. This column packing is selective for nitrogen-containing compounds, aldehydes, and some lower molecular weight alcohols. In addition, formaldehyde was quantitatively determined from electrolysed solutions of glycine maintained at carefully controlled anodic potentials, using the pentane-2,4-dione colorimetric method (21). Carbon dioxide was detected by passing the evolved gases through a saturated BaOH solution. Ammonia was determined by the Kjeldahl method (22).

Results

Tafel plots derived from the steady-state polarization experiments for each of the systems studied are shown in Figs. 1 and 2, and the numerical values for the Tafel slopes determined by least-squares analysis are presented in Table 1. The Tafel slopes for both systems are significantly higher than those normally observed for oxygen evolution in aqueous solution (i.e. $2.3(2RT/F) = 120$ mV) (23). In Fig. 2, the Tafel plots for the amino acid under acidic conditions (pH 1) showed a long linear Tafel region with a slope which was twice those observed for oxygen evolution. In a 1 *M* sulfuric acid solution, in the absence of amino acid, oxygen evolution occurs at 1.36 V, E_{SCE}. This difference in the Tafel behaviour may be attributed to the barrier layer effect observed by Conway and Dzeiciuch (24) where the oxygen evolution reaction is suppressed because of a dipole barrier due to the presence of adsorbed species on the surface of the electrode.

A different effect is observed under alkaline conditions. There is a distinct inflection observed in the Tafel slopes (Fig. 1). This is similar to that observed in the Kolbe reaction of acetate ion in aqueous solution (18) and again appears at the same potential where oxygen evolution would occur in a 1 *M* sodium hydroxide solution (i.e. 1.10 V, E_{SCE}). Thus it appears, as in the Kolbe mechanism, that the oxygen evolution reaction is suppressed by the amino acid anion. Glycine shows an unusually high Tafel slope over this potential region. The value of 363 mV corresponds to a Tafel slope of $3(2.3(2RT/F))$. It is also interesting that below the inflection region the slope is the same as those observed under acidic conditions.

Cyclic voltammograms for glycine in both alkaline and acidic solutions are shown in Figs. 3 and 4. Table 2 shows the numerical values for the charge Q_0 associated with the formation of oxide, the charge Q_r due to the reduction of the surface oxide, and the ratio Q_0/Q_r. A comparison may also be made of the charge from the oxidation process with that of the reduction process in a sulfuric acid or sodium hydroxide solution.

The results from Table 2 show that the charge Q_r due to the reduction of the oxide is very much smaller than Q_0 in all cases, suggesting that there are species other than the normal oxide adsorbed on the surface of the electrode which are not removed during the oxide reduction process. The ratio of Q_r for oxide reduction to Q_r (=210 μC cm^{-2}) for hydrogen reduction is also significant. For a sulfuric acid solution in the absence of amino acids this ratio is about 2.5 (18). For amino acids at pH 1, the ratio is about 2.1, whereas an even smaller ratio of ca. 1.0 is observed in solutions of pH 13. This indicates that adsorption by amino acids occurs at platinum causing a reduction in the

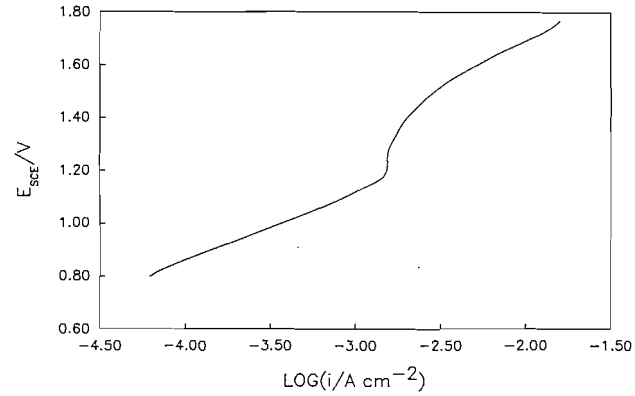


FIG. 1. Tafel behaviour of 0.45 *M* glycine in NaOH (pH 13) at the Pt electrode.

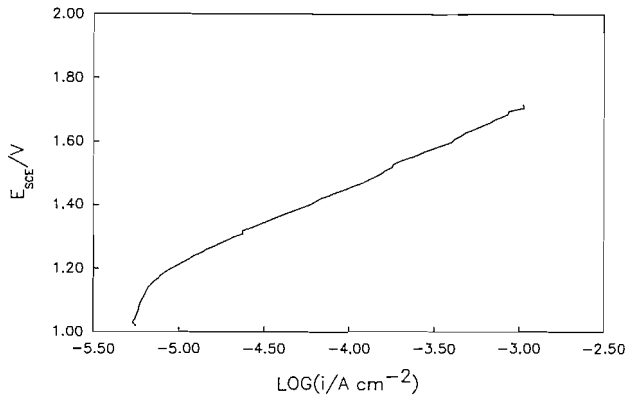


FIG. 2. Tafel behaviour of 0.45 *M* glycine in H_2SO_4 (pH 1) at the Pt electrode.

TABLE 1. Experimental Tafel parameters for the electro-oxidation of glycine (0.45 *M*) in acidic and alkaline solutions

pH	Potential range (E_{SCE} (V))	Tafel slope *b* (mV)
13.0	(0.900–1.100)	239
13.0	(1.480–1.700)	363
1.0	(1.280–1.680)	237

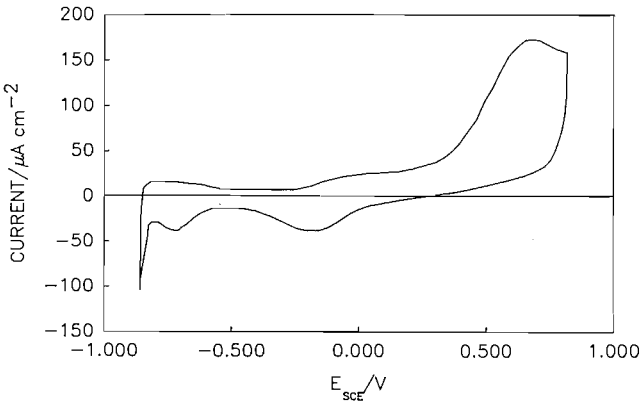


FIG. 3. Cyclic-voltammogram of 0.45 *M* glycine in NaOH (pH 13) at the Pt electrode.

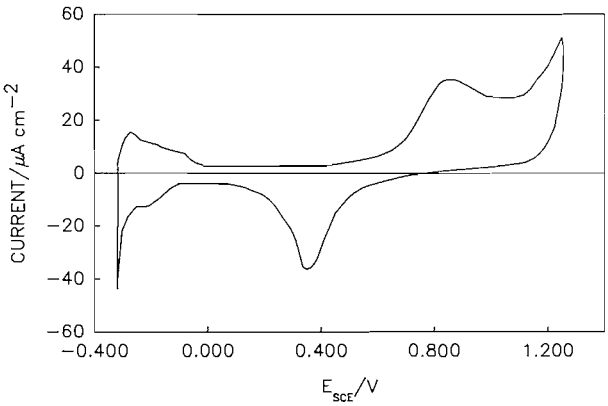


FIG. 4. Cyclic-voltammogram of 0.45 *M* glycine in H_2SO_4 (pH 1) at the Pt electrode.

TABLE 2. Evaluation of the charge and surface coverage of the cyclic voltammograms of glycine (0.45 *M*) at a platinum electrode

pH	Potential range (E_{SCE} (V))	Q_0 ($\mu C\,cm^{-2}$)	Q_r ($\mu C\,cm^{-2}$)	Q_0/Q_r
13.0	(−0.854–0.816)	2136	223	9.58
1.0	(−0.317–1.220)	1315	451	2.92

normal oxide growth due to a blocking effect by the bulkier molecules with an even stronger adsorption and diminished oxide formation occurring in the basic solutions. This is also consistent with the larger Q_0/Q_r for anodic oxidation and reduction in the basic compared with the acidic solutions. In the aqueous acid solution (Fig. 4) a blocking effect by glycine of the submonolayer film of upd (underpotential deposition) OH species occurs similar to the blocking effect of Cl^- ions adsorbed at Pt electrodes during anodic Cl_2 evolution from an aqueous solution (25–29).

Open circuit potential decay curves for glycine in basic and acidic solutions are shown in Figs. 5 and 7. Plots of potential versus log $(-dV/dt)$ were obtained from a curve-fitting routine on the potential versus time data. Multiple correlation coefficients were determined using the *F*-test. In all cases, the fit was better than 99.99%. The pseudo-capacitance (C_ϕ) was then evaluated as a function of potential (Figs. 6 and 8) (30).

These graphs indicate a rapid decrease in capacitance in the basic solution at the lower potentials to a capacitance of about

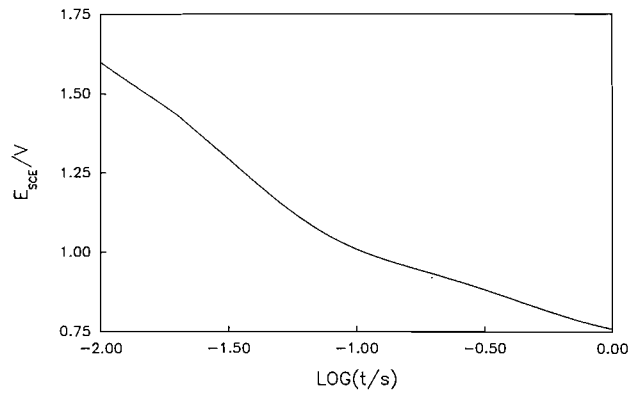


FIG. 5. Open-circuit potential decay of 0.45 *M* glycine (pH 13) at the Pt electrode.

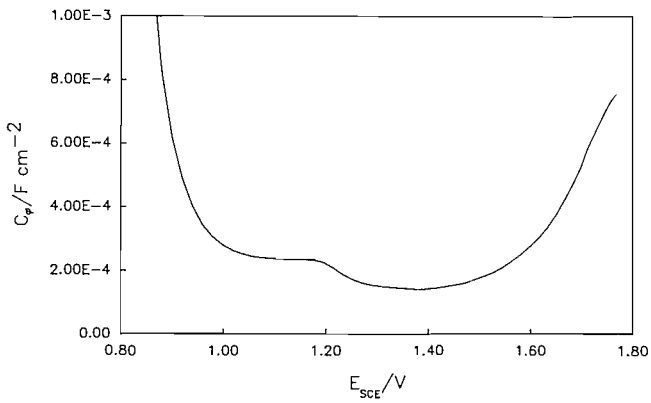


FIG. 6. Capacitance behaviour at anodic potentials of 0.45 *M* glycine (pH 13) at the Pt electrode.

250 $\mu F\,cm^{-2}$ (Fig. 5). An inflection in the capacitance is observed at potentials coincident with the inflection in the Tafel plot (Fig. 1). The capacitance decreases to a minimum of about 100 $\mu F\,cm^{-2}$ before increasing again at higher potentials, indicating that the initial coverage of adsorbed species on the electrode surface is rapidly diminished as the Faradaic process proceeds. This decrease in surface coverage corresponds to a mechanism where the initial or electron discharge step is slow, followed by fast consecutive reactions which reduce the surface coverage (31). The inflection regions in the capacitance and the Tafel plots suggest a change in the mechanism of the reaction associated with surface coverage of adsorbed species.

The potential decay curve in the acidic solution shows three linear regions with very small changes in slope (Fig. 7). These correspond to very slight inflections observed in the Tafel slope (Fig. 2). However, the plots of C_ϕ versus potential (Fig. 8) show a similar rapid decrease in capacitance followed by an increase to ca. 600 $\mu F\,cm^{-2}$ at a potential of 1.47 V. This behaviour is similar to the inflection region observed in the alkaline solution.

Qualitative analysis of the products obtained from the electrolysis of glycine agreed with those found by Fichter and co-workers (1, 2) and Takayama (3–5). The electrolysis was carried out at high current densities under controlled potentials of 2.2 V in the acidic solution and 1.8 V in the basic solution. The products identified by gas chromatographic analysis were formaldehyde and methyl and trimethyl amine in acidic solution and formaldehyde and methyl amine in the basic solution. Carbon dioxide and ammonia were also detected as products of the electrolysis. A quantitative analysis of the formaldehyde

Can. J. Chem. Downloaded from www.nrcresearchpress.com by 41.223.56.140 on 09/07/12
For personal use only.

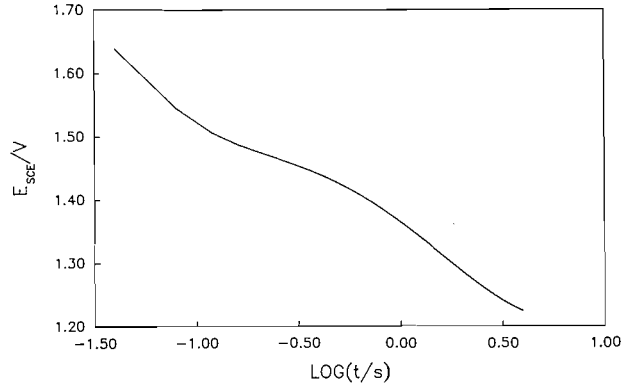


FIG. 7. Open-circuit potential decay of 0.45 *M* glycine (pH 1) at the Pt electrode.

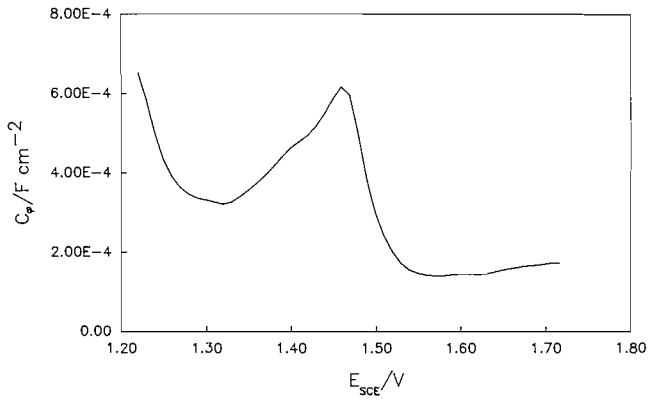


FIG. 8. Capacitance behaviour at anodic potentials of 0.45 *M* glycine (pH 1) at the Pt electrode.

formed after electrolyzing the basic solution at an anodic potential of 1.32 V, E_{SCE} using the pentane-2,4-dione colorimetric method (21) indicated an 85–90% yield. From the same experiments, analysis of ammonia using the Kjeldahl method (22) indicated ca. 83% yield. When the electrolysis was carried out at the anodic potential of 1.06 V, E_{SCE}, which is just below the inflection region, the yield of formaldehyde dropped to 60% and ammonia to ca. 55%.

Discussion

Analysis of the products of the electro-oxidation of glycine shows that formaldehyde is the main product in both basic and acidic conditions. Ammonia and carbon dioxide were also detected as products of this reaction in agreement with Fichter (1, 2). These products suggest a dissociative, adsorptive type of mechanism, with the overall reaction for the basic solution

$$CH_2(NH_2)COO^- + OH^- \rightarrow CH_2O + NH_3 + CO_2 + 2e$$

The thermodynamic potential for the basic glycine solution was calculated to be 1.33 V, E_{SCE} using the standard free energies of formation (20). A similar calculation for the acidic solution gave a value of 1.17 V, E_{SCE}. These correspond to the observed inflection regions discussed previously which are also coincident with the potentials for oxygen evolution, which suggests that oxygen evolution is suppressed by the amino acid oxidation process in a manner similar to that observed for the Kolbe reaction (24). The overall reaction must, however, be written in terms of elementary electrochemical steps because it has become well established in electrodics that it is not energetically favourable for two electrons to tunnel simultaneously between the solution and the metal surface (32). Elementary steps using single electron transfer are therefore preferred.

TABLE 3. Theoretical Tafel slopes calculated on the basis of each of the steps being rate-determining for the mechanism proposed for the electro-oxidation of glycine at Pt

RDS	Theoretical Tafel slope	Calculated Tafel slope (mV)	r_2/r_1
Step I	$2.3(2RT/F)$	120	—
Step II	$2.3(2RT/F)(r_1/(r_1 - r_2))$	180	0.33
		240	0.50
		360	0.66
Step III	$2.3(2RT/F)(r_1/(r_1 + r_2))$	90	0.33
		80	0.50
		72	0.66

The production of CO_2 in the alkaline solution may be explained by a series of steps similar to the initial two steps in the Kolbe reaction (18),

$$CH_2(NH_2)COO^- \rightarrow CH_2(NH_2)COO(M) + e$$
$$CH_2(NH_2)COO(M) \rightarrow NH_2CH_2(M) + CO_2$$

This series of steps could lead to formaldehyde and ammonia by either of two routes, a hydrolysis reaction of the adsorbed radical accompanied by an electron transfer at the surface of the electrode,

$$NH_2CH_2(M) + OH^- \rightarrow NH_3 + CH_2O + e$$

or with the formation of a carbonium ion by electron transfer (18, 33) followed by subsequent hydrolysis in solution to give ammonia and formaldehyde:

$$NH_2CH_2(M) \rightarrow NH_2CH_2^+ + e$$
$$NH_2CH_2^+ + OH^- \rightarrow NH_3 + CH_2O$$

The corresponding mechanism for the acidic solution would be

$$CH_2(NH_3^+)COOH \rightarrow CH_2(NH_3^+)COO(M) + H^+ + e$$
$$CH_2(NH_3^+)COO(M) \rightarrow (NH_3^+)CH_2(M) + CO_2$$

followed by:

$$(NH_3^+)CH_2(M) + H_2O \rightarrow NH_4^+ + CH_2O + H^+ + e$$

A carbonium ion mechanism in the acidic solution, however, is rather unlikely due to the formation of a positive charge on adjacent atoms:

$$(NH_3^+)CH_2(M) \rightarrow (NH_3^+)CH_2^+ + e$$
$$(NH_3^+)CH_2^+ + H_2O \rightarrow NH_4^+ + CH_2O + H^+$$

In order to verify these mechanisms it is necessary to compare the experimentally determined Tafel slopes with those derived from theoretical considerations (34–36). The Tafel slope is calculated separately for each possible rate determining step (Table 3).

Considering step I of the mechanisms to be rate determining, the following rate expression is obtained:

$$i_1 = zFk_1(1 - \theta_{G\cdot})C_{G+}\exp\{-(\Delta G_1^{\neq} - \beta VF + \beta r_1\theta)/RT\}$$

where the subscript G· refers to the radical species on the electrode surface, G+ the amino acid species in the bulk solution, θ the fractional surface coverage, and β the symmetry factor, which will be considered for these calculations to be equal to

Can. J. Chem. Downloaded from www.nrcresearchpress.com by 41.223.56.140 on 09/07/12
For personal use only.

Can. J. Chem. Downloaded from www.nrcresearchpress.com by 41.223.56.140 on 09/07/12
For personal use only.

0.5, which is the value expected for most reactions (18). The possibility of very low values for β due to a barrier-layer discharge process will be discussed later. The r term is introduced in the above equation to allow for variation in the heat of adsorption with coverage.

The experimental Tafel slopes may be compared with those calculated from the rate expressions. For the case where step I is rate controlling the derivative is:

$$dV/d \log i_1 = 2.3(2RT/F)$$

If step II of the mechanisms were rate determining, the rate equation would rearrange as follows:

$$\ln i_2 = \ln zFk_2 + \ln (1 - \theta_{G1\cdot}) + \ln \theta_{G\cdot} - (\Delta G_2^{\neq} - \beta r_1\theta + (1 - \beta)r_2\theta)/RT$$

where G· refers to the initially adsorbed radical in step I and G_1· refers to the adsorbed radical after rearrangement occurs. Now if step II was rate controlling and step I was in quasi-equilibrium, and with $\beta = 0.5$, the equation may be written as

$$\ln i_2 = \ln zFk_2 + \ln (1 - \theta_{G1\cdot}) + \ln (\theta_{G\cdot}) - [\Delta G_2^{\neq} + (VF/2r_1)(r_2 - r_1)]/RT$$

Rearranging and differentiating gives

$$dV/d \ln i_2 = (2RT/F)[r_1/(r_1 - r_2)]$$

If step III of the mechanisms were rate determining

$$\ln i_3 = \ln zFk_3 + \ln \theta_{G1\cdot} - (\Delta G_3^{\neq} - \beta VF - \beta r_2\theta)/RT$$

Substituting in terms of θ and differentiating gives

$$dV/d \ln i_3 = (2RT/F)[r_1/(r_1 + r_2)]$$

The Tafel slopes obtained have factors designated as r related to the heats of adsorption. Under Temkin conditions, that is conditions of intermediate coverage, the r values become important, whereas under Langmuir conditions, either $\theta \cong 0$ or $\theta \cong 1$, these effects need not be considered. Under Temkin conditions, values must be assigned to r_1 and r_2. The high Tafel slopes may be explained by taking r_1 to be 1.5 to 2 times greater than r_2, and the Tafel slopes calculated in this way for each of the possible steps considered to be rate controlling are given in Table 3. From these results and a comparison with the Tafel slopes observed experimentally (Table 1), a mechanism consistent with step II as the rate-determining step is proposed.

For the alkaline solution of glycine, the experimental Tafel slope was 239 mV over the potential range 0.90 to 1.10 V, which is below the inflection region. This would correspond to $r_2/r_1 = 0.5$ where r_1 and r_2 represent the heats of adsorption of $CH_2(NH_2)COO\cdot$ and $NH_2CH_2\cdot$, respectively. At the inflection point, the Tafel slope increased abruptly to 363 mV which would correspond to $r_2/r_1 = 0.66$. The capacitance decreased abruptly at this point indicating a smaller surface coverage. At very high potentials the capacitance gradually increased due to the growth of thicker films of adsorbed species.

In the acidic solution of glycine, the Tafel slope of 237 mV again corresponds to a value of $r_2/r_1 = 0.5$ where r_1 and r_2 are now $CH_2(NH_3^+)COO\cdot$ and $(NH_3^+)CH_2\cdot$. An inflection region is not observed in the Tafel slope, although the capacitance behaviour shows an increase in surface coverage which maximizes and then drops as in the alkaline solution.

Similar Tafel relationships were obtained for the reaction of formate ion in 100% formic acid (36) and trifluoroacetate in 100% trifluoroacetic acid (24). The reaction mechanisms were treated in terms of a Temkin isotherm. In the case of the trifluoroacetate reaction, the value of r_1 for adsorption of the bulky polar $CF_3COO\cdot$ was considered to be greater than that for the smaller $CF_3\cdot$ groups.

If the mechanism involving formation of carbonium ions for step III proceeds as follows,

$$NH_2CH_2(M) \rightarrow NH_2CH_2^+ + e$$

followed by hydrolysis in solution to give ammonia and formaldehyde, a similar analysis for this step III as the rate-determining step results in the same theoretical Tafel slope as that obtained previously for step III (Table 3). Thus, although the mechanism may proceed via a carbonium ion intermediate formed in solution, it is not the rate-determining step for the process.

Another possibility which may be considered is the formation of the carbonium ion during the decarboxylation step, step II, although generally carbonium ion formation is considered to occur in a step following decarboxylation (18, 33).

$$CH_2(NH_2)COO(M) \rightarrow CO_2 + NH_2CH_2^+ + e$$

However, if this were the rate-determining step, the derivative would be

$$dV/d \log i_1 = 2.3(RT/2\beta F)$$

which gives a value of 60 mV for the Tafel slope if $\beta = 0.5$, which is too low a value compared to that observed experimentally.

High Tafel slopes observed in anodic oxidations of this type have also been interpreted by a change in the effective symmetry factor due to the formation of a thin moderately conducting dipole barrier-layer film of adsorbed species on the electrode (18, 24, 36). This may cause the effective symmetry factor to be less than 0.5. In order to explain the high Tafel slopes observed, the β values would have to be as low as 0.25 and 0.17 for the lower and upper Tafel slopes, respectively. However, there is evidence for strong adsorption of species as shown by the blocking of the upd OH species and the large anodic charge in the cyclic voltammograms. The capacitance behaviour shows a rapid decrease in surface coverage with increasing potential at the onset of the Faradaic process, which gives further evidence for the second step following adsorption being the rate determining step, followed by fast consecutive reactions (31). As even higher potentials are reached, the capacitance again begins to increase due to the strongly adsorbed intermediate species on the surface of the electrode. Therefore, although a barrier-layer film and consequently a modified β value may be used to explain the high Tafel slopes, there is evidence that a changing surface coverage due to adsorbed species may account for these results. It is of interest that a more normal vaue of β is actually observed for the acetate Kolbe reaction in completely anhydrous solution (18). Recently, the results of several studies of the Kolbe electrosynthesis under a variety of conditions have been attributed to the surface adsorption of radicals (37–39).

In conclusion, the mechanism of electrolytic oxidation of glycine at a platinum electrode, in both basic and acidic solution, may be accounted for by a radical mechanism for the first two steps similar to that observed for the Kolbe reaction with the loss of carbon dioxide, the second step in the mechanism being rate-determining. However, rather than the dimerization typical of those radical reactions associated with the Kolbe mechanism, it appears that the adsorbed intermediate species is either hydrolyzed anodically in these aqueous solutions to formaldehyde and ammonia, or is possibly further

oxidized to a carbonium ion which is subsequently hydrolyzed to ammonia and formaldehyde in solution.

1. F. FICHTER and M. SCHMID. Helv. Chim. Acta, **3**, 704 (1920).
2. F. FICHTER and F. KUHN. Helv. Chim. Acta, **7**, 164 (1924).
3. Y. TAKAYAMA. Bull. Chem. Soc. Jpn. **12**, 342 (1924).
4. Y. TAKAYAMA. Bull. Chem. Soc. Jpn. **8**, 213 (1933).
5. Y. TAKAYAMA. Bull. Chem. Soc. Jpn. **12**, 338 (1937).
6. PLOCHE. Ber. **21**, 2117 (1888).
7. D. DAMJANOVIC. *In* Modern aspects of electrochemistry. Vol. 5. *Edited by* J. O'M. Bockris and B. E. Conway. Plenum, New York. 1969. p. 369.
8. A. DAMJANOVIC, L. S. R. YEH, and J. F. WOLF. J. Electrochem. Soc. **127**, 784 (1980); **127**, 1951 (1980); **122**, 471 (1975).
9. E. L. LITTAUER and L. L. SHRIER. Electrochim. Acta, **11**, 527 (1966).
10. B. E. CONWAY and D. M. NOVAK. J. Chem. Soc. Faraday Trans. I, **75**, 2454 (1979).
11. B. E. CONWAY and D. M. NOVAK. J. Electroanal. Chem. **99**, 133 (1979).
12. B. E. CONWAY and J. MOZOTA. J. Chem. Soc. Faraday Trans. I, **78**, 1717 (1982).
13. S. G. ROSCOE and B. E. CONWAY. J. Electroanal. Chem. **224**, 163 (1987).
14. H. P. STOUT. Trans. Faraday Soc. **41**, 64 (1945).
15. L. KRISHTALIK and G. E. TITOVA. Elektrokhimiya, **4**, 285 (1968).
16. S. G. ROSCOE and B. E. CONWAY. J. Chem. Soc. Chem. Commun. 900 (1988).
17. S. G. ROSCOE and B. E. CONWAY. J. Electroanal. Chem. **249**, 217 (1988).
18. A. K. VIJH and B. E. CONWAY. Chem. Rev. **67**, 623 (1967).
19. Polariter Instructions Manual, Radiometer Company.
20. R. C. WEAST (*Editor*). CRC handbook of chemistry and physics. 64th ed. The Chemical Rubber Company, Cleveland. 1983.
21. S. C. CHURMS (*Editor*). CRC handbook of chromatography, carbohydrates. Vol. I. CRC Press, Inc., FL. 1982. p. 182.
22. I. M. KOLTOFF and E. B. SANDELL. Textbook of quantitative inorganic analysis. 3rd ed. MacMillan Co., New York. 1963. p. 538.
23. M. TARASEVICH, A. SADKOWSKI, and E. YEAGER. *In* Comprehensive treatise on electrochemistry. *Edited by* B. E. Conway *et al.* Plenum Press, New York. 1983. pp. 301–397.
24. B. E. CONWAY and M. DZIECIUCH. Can. J. Chem. **41**, 38 (1963).
25. A. K. N. REDDY, M. A. GENSHAW, and J. O'M. BOCKRIS. J. CHEM. PHYS. **48**, 671 (1968).
26. J. L. ORD and F. C. HO. J. Electrochem. Soc. **118**, 46 (1971).
27. R. PARSONS and W. VISSCHER. J. Electroanal. Chem. **36**, 329 (1972).
28. J. W. SCHULTZE and K. J. VETTER. J. Electroanal. Chem. **34**, 131, 141 (1972).
29. D. M. NOVAK and B. E. CONWAY. J. Chem. Soc. Faraday Trans. I, **77**, 2341 (1981).
30. B. E. CONWAY, L. BAI, and D. F. TESSIER. J. Electroanal. Chem. **161**, 39 (1984).
31. B. V. TILAK, C. G. RADER, and B. E. CONWAY. Electrochem. Acta, **22**, 1167 (1976).
32. J. O'M. BOCKRIS and A. K. N. REDDY. Modern electrochemistry. 1st ed. Vol. 2, Plenum Press. 1970. p. 1082.
33. J. H. P. UTLEY. *In* Techniques of electroorganic synthesis, Part I. *Edited by* N. L. Weinberg. Wiley, New York. 1974, pp. 793–906.
34. B. E. CONWAY and P. L. BOURGAULT. Can. J. Chem. **37**, 292 (1959).
35. J. O'M. BOCKRIS. J. Chem. Phys. **24**, 817 (1956).
36. B. E. CONWAY and M. DZIECIUCH. Can. J. Chem. **41**, 21 (1963).
37. Y. B. VASSILIEV, V. S. BAGOTZKY, E. P. KOVSMAN, V. A. GRINBERG, L. S. KANEVSKY, and V. R. POLISHCHYUK. Electrochem. Acta, **27**, 919 (1982).
38. R. M. CERVINO, W. E. TRIACA, and A. J. ARVIA. J. Electroanal. Chem. **172**, 255 (1984).
39. B. KRAEUTLER, C. D. JAEGER, and A. J. BARD. J. Am. Chem. Soc. **100**, 4903, 1978.

Can. J. Chem. Downloaded from www.nrcresearchpress.com by 41.223.56.140 on 09/07/12
For personal use only.

A laser flash photolysis study of the behaviour of polyfluorophenyl ketones in solution[1]

D. R. BOATE, L. J. JOHNSTON, AND J. C. SCAIANO
Division of Chemistry, National Research Council of Canada, Ottawa, Ont., Canada K1A 0R6

Received August 19, 1988

D. R. BOATE, L. J. JOHNSTON, and J. C. SCAIANO. Can. J. Chem. **67**, 927 (1989).

Decafluorobenzophenone triplets, which have a triplet energy very close to that of benzophenone, are much more reactive than benzophenone in quenching reactions that involve hydrogen transfer and/or charge transfer. An excellent correlation has been observed between the rate constants for charge transfer quenching and the oxidation potential of the substrate. In the case of 2-propanol, where the reactivity can be fully accounted for by hydrogen transfer, decafluorobenzophenone is 35 times more reactive than benzophenone. Pentafluorobenzophenone shows intermediate behaviour.

Key words: laser photolysis, benzophenones, triplet states, charge transfer, photoreduction.

D. R. BOATE, L. J. JOHNSTON et J. C. SCAIANO. Can. J. Chem. **67**, 927 (1989).

Les triplets de la décafluorobenzophénone, dont l'énergie du triplet est très proche de celle de la benzophénone, sont beaucoup plus réactifs que la benzophénone dans les réactions de piégeage impliquant un transfert d'hydrogène et/ou un transfert de charge. On a observé une excellente corrélation entre les constantes de vitesse de piégeage du transfert de charge et le potentiel d'oxydation des substrats. Dans le cas du propanol-2, où on peut expliquer complètement la réactivité à l'aide d'un transfert d'hydrogène, la décafluorobenzophénone est 35 fois plus réactive que la benzophénone. Le comportement de la pentafluorobenzophénone est intermédiaire entre les deux.

Mots clés : photolyse du laser, benzophénones, états du triplet, transfert de charge, photoréduction.

[Traduit par la revue]

Can. J. Chem. Downloaded from www.nrcresearchpress.com by 41.223.56.140 on 09/07/12
For personal use only.

Introduction

The photochemical and photophysical properties of benzophenone have been studied extensively and are rather well understood (1–5). Benzophenone (as do many other aromatic ketones) undergoes intersystem crossing rapidly and efficiently to populate its lowest triplet state, which is responsible for most of its photochemistry (1). Typical reactions of this triplet state include electronic energy transfer to suitable acceptors, charge transfer reactions where the ketone can behave as an electron donor or acceptor, addition to unsaturated systems, and hydrogen abstraction. This last process has been the subject of extensive studies, and the radical-like properties of the benzophenone triplet have been long recognized (5). Conventional and laser flash photolysis have been widely employed in the study of triplet benzophenone reactivity (3). By contrast, very little is known about the reactivity of the corresponding triplet states of polyfluorinated phenyl ketones (6–11), although the short triplet lifetime of decafluoro and pentafluorobenzophenone in cyclopentane as a reactive solvent has been reported previously (11).

In this paper we report the results of a laser flash photolysis study of the photochemistry of decafluorobenzophenone. A comparison is made with pentafluorobenzophenone and pentafluoroacetophenone.

Experimental

Materials

Decafluorobenzophenone (DFB) (Aldrich) was sublimed and benzophenone (BP) and phenol were recrystallized from ethanol and hexane, respectively. Pentafluorobenzophenone (PFB), pentafluoroacetophenone (PFA) (Aldrich), Aberchrome-540 (Aberchromics Ltd., Cardiff, U.K.), and the solvents (acetonitrile and carbon tetrachloride, spectroscopic grade) were used as received. All triplet quenchers were used as received except 1,3-cyclohexadiene (1,3-CHD) which was vacuum distilled before use in order to eliminate polymeric impurities.

General techniques

Ultraviolet–visible spectra were recorded on a HP-8451-A diode array spectrometer. Phosphorescence spectra were recorded on a Perkin-Elmer LS-5 spectrofluorimeter.

Cyclic voltammetry[2] of DFB in acetonitrile (containing 0.1 *M* tetraethylammonium perchlorate as supporting electrolyte) at a platinum disk electrode with a scan rate of 50 mV s^{-1} afforded a cathodic peak potential of −1.21 V vs. SCE.

Laser flash photolysis

The laser flash photolysis facility has been described in detail elsewhere (12). A Molectron UV-24 nitrogen laser (337 nm, ~8 ns pulses, ≦10 mJ/pulse) or a Lumonics TE-860-2 excimer laser with a Xe/HCl gas mixture (308 nm, ~5 ns pulses, ≦20 kJ/pulse) was used for excitation. All quenching studies were carried out on static samples of either DFB, PFB, or PFA (typically 10^{-2} *M*) in either acetonitrile or carbon tetrachloride with 3 × 7 mm^2 quartz cells.

The extinction coefficients for benzophenone ketyl radical (BPH) and DFB triplet in acetonitrile were measured using Aberchrome-540 actinometry (13). All experiments were performed using a flow system with 3 × 7 mm^2 quartz cells, with the same cell being used for both the actinometer and the sample. Solutions of BP (ca. 10^{-3} *M*) in ACN with 1,4-cyclohexadiene (ca. 10^{-2} *M*) or of DFB in acetonitrile and of Aberchrome-540 (ca. 10^{-4} *M*) in toluene were prepared with matched optical densities (typically 0.3 for a 3 mm optical path) at the laser wavelength (337 nm). The optical density at 494 nm following the pulse for Aberchrome was measured as a function of the laser intensity, which was adjusted with a set of calibrated neutral-density filters (evaporated metal on quartz plates). The optical densities for the samples were then measured at the corresponding transient absorption maxima, again as a function of the laser intensity.

In the case of the DFB ketyl radical (DFBH) it is straightforward to obtain the product ($\Phi_K\epsilon_{516}$) of its yield of formation (Φ_K) and its extinction coefficient (ϵ_{516}) at 516 nm (not λ_{max}) using the Aberchrome-540 technique described above. However, separating these two values requires at least one additional piece of information. To obtain this we have employed a competitive method based on the reactions of triplet BP and DFB with phenol to estimate ϵ_{516} for DFBH. This method is described in some detail in the Results section. The method requires the knowledge of ratios of extinction coefficients for each of the radicals at its own maximum and at the maximum for the other species with which it may overlap. Independent spectra of BPH,

[1]NRCC No. 30033.

[2]The measurement was performed by D. Wayner, N.R.C., Canada.

TABLE 1. Ratios of extinction coefficients utilized in the study of decafluorobenzophenone ketyl radical

Radical	Symbol[a]	ϵ_x/ϵ_y
$(C_6F_5)_2\dot{C}OH$	$\epsilon_{400}/\epsilon_{516}$	0.17
$(C_6H_5)_2\dot{C}OH$	$\epsilon_{400}/\epsilon_{540}$	0.09
$C_6H_5O\cdot$	$\epsilon_{516}/\epsilon_{400}$	0.226
$C_6H_5O\cdot$	$\epsilon_{540}/\epsilon_{400}$	0.248

[a]The subscripts identify the wavelengths at which the ratio was determined.

TABLE 2. Phosphorescence data and triplet energies at 77 K

Substrate	Media[a]	$\lambda_{0,0}$[b]	E_T[c]	Reference
BP	MCH	418	68.4	7
BP	EPA	413	69.3	7
DFB	MCH	424	67.4	This work
DFB	EPA	410	69.7	This work
PFB	MCH	417	68.6	This work
PFA	MCH	415	68.9	This work
Acetophenone	EPA	386	74.1	15
Acetophenone	MCH	388	73.7	15

[a]MCH = methylcyclohexane; EPA = ether:isopentane:ethanol, 5:5:2.
[b]In nm.
[c]In kcal mol^{-1}.

DFBH, and phenoxyl radicals were obtained as follows: (*a*) BPH by reaction of triplet BP with 1,4-cyclohexadiene (10^{-2} *M*) in acetonitrile; (*b*) DFBH by reaction of triplet DFB with 0.3 *M* cyclohexane in acetonitrile; and (*c*) phenoxyl by reaction of *tert*-butoxyl (from 0.2 *M* peroxide) with 0.2 *M* phenol in acetonitrile. The relevant ratios of extinction coefficients are given in Table 1.

An independent determination of the BP–DFB ketyl radical (BPH–DFBH) optical density ratio was performed in static 3 × 7 mm^2 quartz cells. Solutions of BP (ca. 10^{-3} *M*) and DFB (ca. 10^{-2} *M*) with 1,4-cyclohexadiene (ca. 10^{-2} *M*) in acetonitrile were prepared with matched optical densities at the laser wavelength. The transient optical densities were measured at 540 and 516 nm for BPH and DFBH radicals, respectively. Due to the presence of overlapping triplet ketone at the monitoring wavelength, the optical densities for both ketyl radicals were corrected by extrapolation to the time of laser excitation.

All samples except for Aberchrome-540 were deaerated with a stream of nitrogen.

Results

Phosphorescence

The 77 K phosphorescence of the various ketones examined was recorded in methylcyclohexane, and occasionally in EPA. They all show the band structure which is characteristic of n,π* triplet states (ref. 1, chap. 5). Table 2 summarizes the triplet energies derived from the 0,0 bands in the emission spectra. Quite clearly, fluorine substitution does not have any dramatic effect on the triplet energy. These triplets are known to show short phosphorescence lifetimes, in accordance with their n,π* character (7).

Figure 1 shows a comparison of the phosphorescence spectra from DFB in an EPA glass at 77 K and in acetonitrile solution at room temperature. Some of the resolution is lost at room temperature and a small shift is noted between these two solvents. The broadness and the small shift observed in the room temperature spectrum (obtained with an OMA detector) was

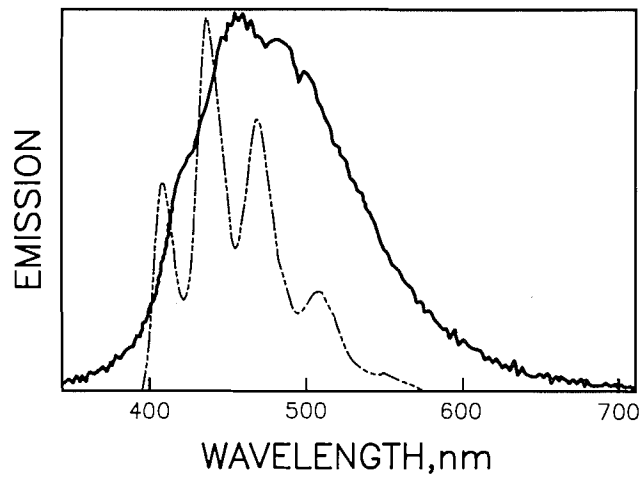


FIG. 1. Phosphorescence spectra for DFB obtained 400 ns after 337 nm excitation of 8 × 10^{-2} *M* DFB in acetonitrile at 293 K (—) and in an EPA glass at 77 K (· · – · ·).

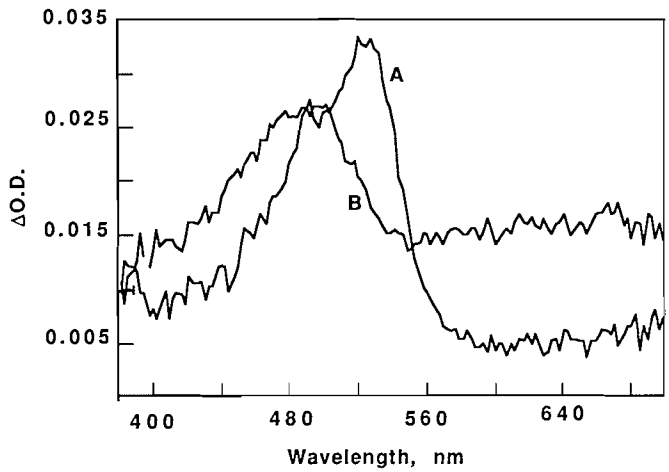


FIG. 2. Transient absorption spectra for triplet DFB (*B*) obtained by laser excitation of 9.4 × 10^{-3} *M* DFB in acetonitrile, and for its ketyl radical (DFBH) for a similar sample but containing 0.6 *M* cyclohexane (*A*). Both spectra recorded 500 ns after 337 nm excitation.

verified upon repeating the measurement (not shown) under more dilute conditions (1 × 10^{-3} *M*), with the same spectrometer as that used to obtain the 77 K spectrum.

The phosphorescence yields at 77 K have been reported to be 0.21 (in perfluorodimethylcyclohexane (8)) and 0.74 (in isooctane (16)) for DFB and BP, respectively. Intersystem crossing quantum yields are 1.0 for both ketones (8, 16).

Transient absorption spectra

The high reactivity of triplet DFB (*vide infra*) makes the selection of inert solvents rather limited. We have found that acetonitrile and carbon tetrachloride are reasonable choices, since triplet lifetimes in excess of 10 μs could be easily achieved at room temperature in these solvents. Figure 2 shows the transient absorption spectra obtained at room temperature for DFB triplet and its ketyl radical (*vide infra*). Figure 3 shows triplet spectra for BP, PFB, and PFA. Fluorine substitution leads to a blue shift in the spectra; this appears reasonable, since promoting an electron should be more difficult in the electron-deficient polyfluorinated ketones. The spectrum for triplet DFB is considerably broader than that from BP.

Can. J. Chem. Downloaded from www.nrcresearchpress.com by 41.223.56.140 on 09/07/12
For personal use only.

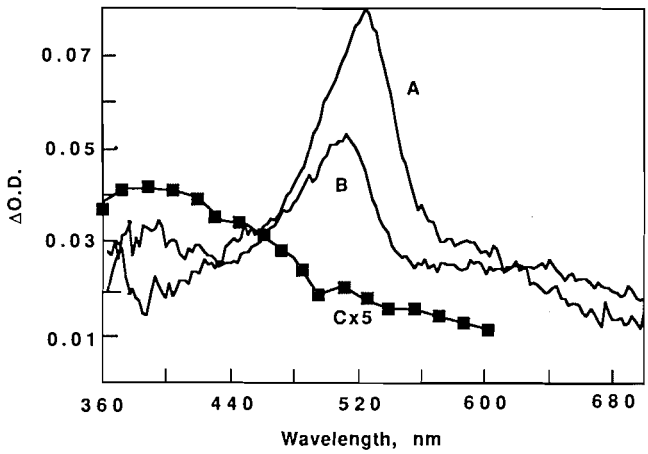


FIG. 3. Triplet–triplet absorption spectra for 7.3×10^{-3} *M* BP (*A*), 2.4×10^{-2} *M* PFB (*B*), and 3.2×10^{-2} *M* PFA (*C*) in acetonitrile. The delays after 337 nm excitation are 500, 500, and 200 ns for spectra *A*, *B*, and *C*, respectively. The ΔOD scale in spectrum (*C*) has been expanded 5 times.

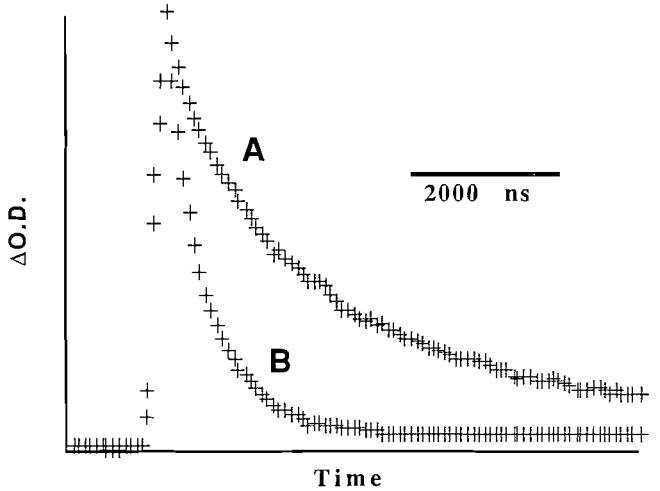


FIG. 4. Experimental decay traces for triplet DFB in the absence of quencher (*A*) at 610 nm, where only the triplet absorbs and in the presence of 6.0×10^{-3} *M* *tert*-butylbenzene (*B*), recorded at 516 nm, where both triplet and ketyl radical absorb. Note that *B* has virtually no residual absorption after triplet decay.

The triplet spectra in carbon tetrachloride (not shown) were very similar to those obtained in acetonitrile.

Kinetics of triplet quenching by various substrates

The experimental rate constants for triplet decay (k_{exptl}) were obtained by monitoring the transient absorption due to the carbonyl triplet at 600 nm for the three benzophenones, and at 400 nm for PFA. It is clear from the spectra in Figs. 2 and 3 that 600 nm is considerably removed from the triplet absorption maxima for BP, PFB, and DFB. However, at $\lambda \geqq 600$ nm the ratio of extinction coefficients for the carbonyl triplet and the corresponding ketyl radical is large (usually >10) thus making measurements of triplet decay rates more accurate. Figure 4 shows representative traces obtained in carbon tetrachloride in the absence and presence of *tert*-butylbenzene, one of the quenchers examined in this study. Each trace yields a value of k_{exptl} from a single exponential treatment of the decay data. The bimolecular rate constants, k_q, for the reaction of the triplet with quencher Q were determined by measuring k_{exptl} for different concentrations of Q and plotting according to eq. [1],

$$[1] \quad k_{exptl} = k_0 + k_q[Q]$$

where k_0 (i.e. τ_T^{-1}) is the first order rate constant for triplet decay in the absence of quencher and incorporates radiationless decay, emission, and possibly interactions with the solvent. As is frequently the case in laser flash work, the decays in the absence of quencher tend to incorporate second order contributions resulting from triplet–triplet annihilation. For this reason our quenching plots normally do not include a point at [Q] = 0. Some representative examples are shown in Fig. 5. Table 3 summarizes the rate constants obtained for DFB in this work, along with some literature values for benzophenone. Table 4 summarizes a few representative values for PFB and PFA.

Several of the quenchers used are excellent hydrogen donors (e.g. 2-propanol, cyclohexane, 1,4-cyclohexadiene, phenol). In all these cases the corresponding ketyl radical was readily detectable following triplet decay. For example, DFB in acetonitrile reacts with cyclohexane with a rate constant of $4.3 \times 10^7\ M^{-1}\ s^{-1}$. Figure 2 illustrates the observed shift in λ_{max} from 491 nm (triplet) to 526 nm (ketyl radical) when cyclohexane (0.60 *M*) is added to a solution of DFB in ACN.

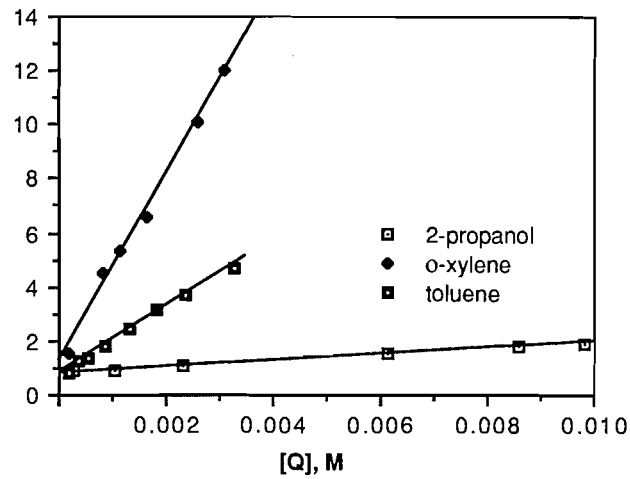


FIG. 5. Representative quenching plots for DFB triplet in acetonitrile.

With the exception of phenol, most of the aromatic quenchers listed in Tables 3 and 4 did not yield substantial amounts of ketyl radical. These results indicate that charge transfer quenching of the triplet is an important process for these ketones. In order to establish to what extent hydrogen abstraction competes with charge transfer when such a competition is possible (e.g. toluene), we measured the extinction coefficients of triplet DFB and of the ketyl radical $(C_6F_5)_2\dot{C}OH$. With these data it is possible to estimate the yields of ketyl radical formation. The experiments are presented in the following section.

Extinction coefficients and photoreduction yields for DFB

Reactions [2] and [3] illustrate the competition that would normally be responsible for the quenching rate constants of Table 3.

$$[2] \quad (C_6F_5)_2CO^* + RH \xrightarrow{k_2} (C_6F_5)_2\dot{C}OH + R\cdot$$

$$[3] \quad (C_6F_5)_2CO^* + RH \xrightarrow{k_3} \text{other quenching reactions}$$

The efficiency of ketyl radical formation will be given by:

Can. J. Chem. Downloaded from www.nrcresearchpress.com by 41.223.56.140 on 09/07/12
For personal use only.

TABLE 3. Kinetic parameters[a] at 20°C for DFB and BP triplet quenching

Quencher	DFB k_q(ACN)	DFB k_q(CCl_4)	BP k_q(ACN)	Reference
1,3-Cyclohexadiene	867 ± 131	411 ± 28		
Phenol	594 ± 81		8	17
Durene	545 ± 67	324 ± 36		
Anisole	443 ± 72	374 ± 19	0.039	18
1,4-Cyclohexadiene	383 ± 41	304 ± 24	29[b]	19
o-Xylene	350 ± 34	279 ± 33	0.025[c]	20
Toluene	124 ± 60	95.7 ± 15	0.041	21
t-Butylbenzene	26.0 ± 1.9	23.5 ± 1.2		
Benzene	14.3 ± 1.4	7.8 ± 0.8	0.0027	21
2-Propanol	11.3 ± 1.3	7.7 ± 1.0	0.32	22
Chlorobenzene	7.8 ± 0.9	4.6 ± 0.3		
Fluorobenzene	5.8 ± 0.8	4.3 ± 0.3		
Cyclohexane	4.3 ± 0.4	4.0 ± 0.5	0.075	21
Triethylamine		489 ± 58	380	23

[a]In units of $10^7\ M^{-1}\ s^{-1}$, errors are $\pm 2\sigma$.
[b]In benzene.
[c]For *p*-xylene.

TABLE 4. Kinetic parameters at 20°C for PFB and PFA triplet quenching[a]

Quencher	PFB k_q(CCl_4)[b]	PFA k_q(CCl_4)
1,4-Cyclohexadiene	253 ± 10	15.0 ± 1.5
Anisole	102 ± 6	≪1
Cyclohexane	1.3 ± 0.2	
Cyclopentane	1.3 ± 0.2	
2-Propanol	1.7 ± 0.5	
Benzene	0.28 ± 0.01	
Durene	(337 ± 27)[c]	

[a]Errors are $\pm 2\sigma$.
[b]In units of $10^7\ M^{-1}\ s^{-1}$.
[c]In acetonitrile.

$$[4]\quad \psi_K = \frac{k_2}{k_2 + k_3}$$

that is, ψ_K is the fraction of quenching events that lead to ketyl radical generation. If the only important mode of decay of the triplet state is by interaction with RH, then ψ_K is identical to the quantum yield for ketyl radical formation, Φ_K. Triplet DFB is sufficiently reactive than there are many cases where this criterion is met.

There are several transient actinometry techniques with which it is straightforward to determine values of $\Phi_K\epsilon_K$, the product of the quantum yield times the extinction coefficient of the transient at the monitoring wavelength. For example, for $Ph_2\dot{C}OH$ we employed the Aberchrome-540 technique (13) to obtain $\epsilon_{540} = 3000\ M^{-1}\ cm^{-1}$ in acetonitrile using 1,4-cyclohexadiene (for which $\Phi_K = 0.94$ (19)) as a hydrogen donor. In the case of $(C_6F_5)_2\dot{C}OH$, for which the values of Φ_K are not known in any solvent, separating the two values requires an approach where one of them can be measured independently, for at least one hydrogen donor. In order to achieve this, we have compared the reaction of BP and DFB with phenol, and have employed the 400 nm signals from phenoxyl radicals to compare the ketyl signals in both systems. Reactions [5] and [6] illustrate the chemistry in these systems.

$$[5]\quad Ph_2CO^* + PhOH \rightarrow PhO\cdot + Ph_2\dot{C}OH$$

$$[6]\quad (C_6F_5)_2CO^* + PhOH \rightarrow PhO\cdot + (C_6F_5)_2\dot{C}OH$$

While there is some overlap between the spectrum of PhO· and the spectra of the two ketyl radicals, this is sufficiently small that it can be readily taken into account (Table 1).

At each of the monitoring wavelengths the absorption in a ketone–phenol system is the sum of contributions from phenoxyl and ketyl radicals which can be readily separated with the coefficients given in Table 1. Since reactions [5] and [6] have a 1-to-1 stoichiometry, the initial concentrations of phenoxyl and the corresponding ketyl radical should be identical. Thus, the ratio of ketyl-to-phenoxyl optical densities is directly proportional to the extinction coefficient for the ketyl radical. Since the value for $Ph_2\dot{C}OH$ is known (*vide supra*) this analysis leads to a value for $(C_6F_5)_2\dot{C}OH$ of $1580\ M^{-1}\ s^{-1}$ at 516 nm. Combining this analysis with the measured triplet signals it is possible to obtain ψ_K values for phenol or other substrates. These are summarized in Table 5. For phenol $\psi_K = 0.66$.

A check of the estimated values of ψ_K can readily be made by comparing the measured values for the BP–DFB ketyl extinction coefficients and experimental optical densities according to:

$$[7]\quad \frac{OD_{BPH}^{540}}{OD_{DFBH}^{516}} = \frac{\epsilon_{BPH}^{540}}{\epsilon_{DFBH}^{516}} \cdot \frac{\psi_K^{BPH}}{\psi_K^{DFBH}}$$

Using values of 0.94 (19) and 0.65 for the efficiencies of ketyl formation for BP and DFB (with 1,4-cyclohexadiene) we obtained a calculated value of 2.7 which should be compared with an experimental value of 2.3 for the left term in eq. [7].

As part of these measurements we also determined an extinction coefficient for triplet DFB at 516 nm of $\epsilon_{516} = 2200\ M^{-1}\ cm^{-1}$.

Discussion

It is noteworthy that in all the examples examined (see Table 3) the triplet state of DFB is quenched faster than triplet BP, with PFB showing intermediate behaviour (Table 4). Only

Can. J. Chem. Downloaded from www.nrcresearchpress.com by 41.223.56.140 on 09/07/12
For personal use only.

Can. J. Chem. Downloaded from www.nrcresearchpress.com by 41.223.56.140 on 09/07/12
For personal use only.

in the case of 1,3-cyclohexadiene, which is a near-diffusion controlled quencher for numerous carbonyl compounds (24), are the rate constants for the various substrates comparable. The triplet energy for 1,3-cyclohexadiene is 52.3 kcal/mol (25), much lower than that for the carbonyl compounds studied in this work (see Table 2). The main mode of quenching by 1,3-cyclohexadiene must, therefore, be energy transfer. For the remaining aromatic compounds typical triplet energies are in the 80–85 kcal/mol range (25); i.e. too high for energy transfer to be an important quenching mode. The predominant mode of quenching for phenol, cyclohexane, 2-propanol, and 1,4-cyclohexadiene is hydrogen abstraction, as indicated by the ketyl yields of Table 5. These results are consistent with the efficient photoreduction which has been observed for DFB in cyclohexane ($\Phi = 0.41$ for ketone disappearance (8)). The products in this system are derived from combination and aromatic substitution of the cyclohexyl and ketyl radicals. Efficient photoreduction has also been reported in 2-propanol (9).

Since the triplet energies for both BP and the fluorinated systems are essentially the same (ca. 69 kcal/mol), the large differences in the quenching rate constants must be a direct consequence of the presence of multiple fluorine substituents in DFB and PFB. Dedinas and Regan have also reported large differences in the quenching rate constants for triplet BP and DFB by cyclohexane and benzene under conditions of lamp irradiation (8). Their values of rate constants for DFB are 7.5×10^6 and 1.6×10^8 M^{-1} s^{-1} for cyclohexane and benzene, respectively. The differences with our values (see Table 3) are likely a reflection of errors introduced by the fact that the triplet lifetimes (needed for the Stern–Volmer analysis) were not determined in the same work. Since the laser photolysis technique does not depend on assumptions of this type, this error is not incorporated in our values. The large differences in rate constants between BP and DFB were attributed to the increased inductive effect due to the fluorine substituents, which increase the degree of charge polarization of the $^3n,\pi^*$ state in the polyfluorinated ketones.

Wagner *et al.* have also observed increased rates of photoreduction in the case of α,α,α-trifluoroacetophenone (AF_3) as compared to acetophenone (26), although it should be noted that for AF_3 the lowest triplet state has π,π^* character with a close by n,π^* level, so that these results may not be directly comparable to those for DFB. In spite of these differences, substituent effects in AF_3 also demonstrate enhanced reactivity induced by electron-withdrawing groups which are in line with DFB if an appropriate allowance is made for the difference in reduction potentials (20). Wagner, Truman, and Scaiano also reported increased reactivity of substituted benzophenones towards cyclopentane when electron-withdrawing substituents are employed (11). For example, 4-carboxymethylbenzophenone is 50% more reactive than benzophenone, in spite of a decrease in triplet energy upon substitution (11).

Anisole is one of the aromatic substrates for which it is possible to compare the reactivities of the various ketones. The data in Tables 3 and 4 lead to relative reactivities of 9600:2600:1 for DFB, PFB, and BP, respectively. For comparison, Wagner and Leavitt report that AF_3 is typically 35 times more reactive than BP towards aromatic substrates (26). Rate enhancements in excess of 1000 are not uncommon between BP and DFB (Table 3) in the case of aromatic substrates.

We find that the rate constants for quenching by aromatic substrates correlate well with the energy requirements for electron transfer (Table 6). Figure 6 shows the corresponding plot; for aromatics only, the slope is −2.21 and the correlation coefficient is 0.91. From Fig. 6 it can be seen that both phenol and 2-propanol do not fit well in the plot. However, for these substrates two parallel processes appear to occur; i.e. reactive and unreactive processes take place. The reactive path involves hydrogen transfer which occurs with the yields indicated in Table 5. When the rate constant for phenol is corrected for this reactive path the point fits very well within the same plot (Fig. 6); this would suggest that hydrogen abstraction and charge transfer are parallel paths, as opposed to a possible charge transfer process that could lead to reactive or unreactive quenching. Since for 2-propanol the reaction is all hydrogen abstraction, the corrected point in this case falls below the line in Fig. 6 and must be considered only as an upper limit.

In the case of toluene no correction has been introduced, since the fraction of hydrogen abstraction (Table 5) is too small to make a significant difference in Fig. 6. The efficiency of the process (0.09) is in reasonable agreement with the reported quantum yield of ketone disappearance in toluene of 0.055 (8). Note that the solvents are different for these two measurements.

For 2-propanol we have only been able to estimate an upper limit for the rate constant for charge transfer interactions, since the efficiency data (Table 5) suggest that hydrogen abstraction

TABLE 5. Efficiencies of ketyl radical formation in the reactions of decafluorobenzophenone in acetonitrile[a]

Substrate	ψ_K
Phenol	0.66
1,4-Cyclohexadiene	0.65
Toluene	0.09
2-Propanol	1.07
Cyclohexane	0.83
Cyclopentane	0.71

[a]An error of ±15% is estimated for the efficiency for phenol; the errors for the other quenchers will be slightly higher.

TABLE 6. Ionization and oxidation potentials for the various DFB triplet quenchers

No.	Quencher	I.P.[a] (eV)	E^0_{ox}[b] (V)	ΔE^0_{ox}[c] (V)	log k_q[d]
1	2-Propanol	10.10	3.38(3.0)[e]	4.21	8.05
2	Benzene	9.25	2.71(2.62)[f]	3.82	8.16
3	Fluorobenzene	9.22	2.69	3.89	7.76
4	Chlorobenzene	9.12	2.61	3.81	7.89
5	*t*-Butylbenzene	8.83	2.39	3.59	8.41
6	Toluene	8.81	2.37(2.25)[f]	3.45	9.09
7	*o*-Xylene	8.56	2.18(2.16)[f]	3.36	9.54
8	Phenol	8.50	2.13	3.33	9.77
9	Anisole	8.39	2.04(1.80)[g]	3.00	9.65
10	Durene	8.05	1.78(1.79)[f]	2.99	9.74

[a]From ref. 14.
[b]From $E^0_{ox} = 0.78 \times$ I.P. $- 4.50$ (from ref. 32); potentials are against S.C.E. Values in parentheses are experimental values.
[c]$\Delta E^0_{ox} = E^0_{ox}$(quencher) $- E^0_{red}$(DFB); the experimental E^0_{ox} value was used when available.
[d]In acetonitrile.
[e]Reference 30.
[f]Reference 27.
[g]Reference 31.

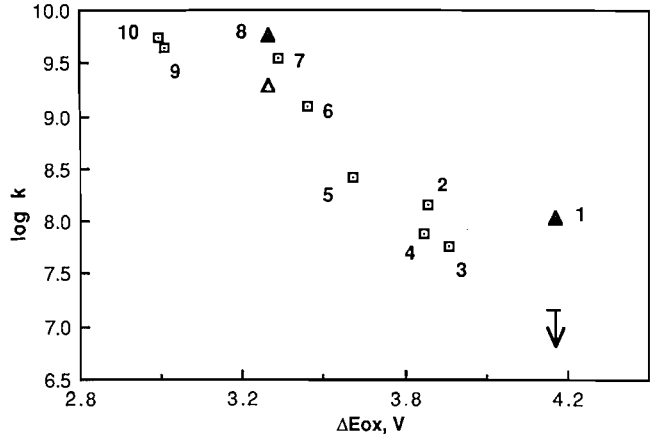


FIG. 6. Correlation between the oxidation potentials of the quenchers and the rate constants for quenching (see Table 6 for data and identifying numbers). The triangles correspond to uncorrected (▲) and corrected (△) data using the yields in Table 5 (see text).

is the only significant reaction path. The fact that the measured efficiency somewhat exceeds one may in fact be significant, since reaction [8] may partially contribute to the yield measured. The process is well established for benzophenone (3) and is likely to be even more efficient for DFB.

[8] $(CH_3)_2\dot{C}OH + (C_6F_5)_2C{=}O \rightleftharpoons (CH_3)_2CO + (C_6F_5)_2\dot{C}OH$

A comparison of the rate constants for quenching of triplet DFB in acetonitrile and in carbon tetrachloride (Table 3) reveals only a small polar solvent effect. Others have noted similar results for charge-transfer quenching of benzophenone and various phenyl alkyl ketones (23, 28, 29). This is usually taken as an indication that only partial charge transfer takes place.

In summary, the spectroscopy of decafluorobenzophenone (triplet absorption and phosphorescence) is very similar to that for benzophenone, although the triplet reactivities of these two ketones are quite different. Decafluorobenzophenone shows enhanced reactivity in hydrogen abstraction and charge transfer processes; for the latter the rate constants correlate well with the oxidation potentials of the quenchers.

Acknowledgements

Thanks are due to Mr. S. E. Sugamori for technical assistance.

1. N. J. TURRO. Modern molecular photochemistry. Benjamin-Cummings, Menlo Park. 1978.
2. J. A. BELL and H. LINSCHITZ. J. Am. Chem. Soc. **85**, 528 (1963); H. TSUBORUMA, N. YAMAMOTO, and S. TANAKA. Chem. Phys. Lett. **1**, 309 (1967); T. S. GODFREY, J. W. HILPERN, and G. PORTER. Chem. Phys. Lett. **1**, 496 (1967).
3. J. D. COYLE. Introduction to organic photochemistry. Wiley, Chichester. 1986. p. 117.
4. J. C. SCAIANO. J. Photochem. **2**, 81 (1973/4).
5. A. PADWA. Tetrahedron Lett. 3465 (1964); C. WALLING and M. J. GIBIAN. J. Am. Chem. Soc. **87**, 3361 (1965).
6. N. FILIPESCU, J. P. PINION, and F. L. MIN. J. Chem. Soc. Chem. Commun. 1413 (1970).
7. J. SIMPSON and H. OFFEN. J. Chem. Phys. **55**, 4832 (1971).
8. J. DEDINAS and T. H. REGAN. J. Phys. Chem. **76**, 3926 (1972).
9. J. DEDINAS. J. Am. Chem. Soc. **95**, 7172 (1973).
10. S. S. TIBILOV and V. L. ERMOLAEV. Opt. Spektrosk. **36**, 1227 (1974).
11. P. J. WAGNER, R. J. TRUMAN, and J. C. SCAIANO. J. Am. Chem. Soc. **107**, 7093 (1985).
12. J. C. SCAIANO. J. Am. Chem. Soc. **102**, 7747 (1980).
13. V. WINGTGENS, L. J. JOHNSTON, and J. C. SCAIANO. J. Am. Chem. Soc. **110**, 511 (1988).
14. R. D. LEVIN and S. G. LIAS. Ionization potential and appearance potential measurements 1971–81. U.S. Government Printing Office, Washington. 1982. NSRDS-NBS 71.
15. I. CARMICHAEL and G. L. HUG. *In* Handbook of organic photochemistry. Vol. 1. *Edited by* J. C. Scaiano. CRC Press, Boca Raton. In press. Chap. 16.
16. W. D. K. CLARKE, A. D. LITT, and C. STEEL. J. Am. Chem. Soc. **91**, 5413 (1969).
17. P. K. DAS, M. V. ENCINAS, and J. C. SCAIANO. J. Am. Chem. Soc. **103**, 4154 (1981).
18. P. K. DAS and K. BOBROWSKI. J. Chem. Soc. Faraday Trans. II, **77**, 1009 (1981).
19. M. V. ENCINAS and J. C. SCAIANO. J. Am. Chem. Soc. **103**, 6393 (1981).
20. P. J. WAGNER, R. J. TRUMAN, A. E. PUCHALSKI, and R. WAKE. J. Am. Chem. Soc. **108**, 7727 (1986).
21. L. GIERING, M. BERGER, and C. STEEL. J. Am. Chem. Soc. **96**, 953 (1974).
22. J. C. SCAIANO, A. F. BECKNELL, and R. D. SMALL. J. Photochem. Photobiol. A (Chem.), **44**, 99 (1988).
23. A. A. GORMAN, C. T. PAREKH, M. A. J. RODGERS, and P. G. SMITH. J. Photochem. **9**, 11 (1978).
24. E. A. LISSI and M. V. ENCINAS. *In* Handbook of organic photochemistry. Vol. 2. *Edited by* J. C. Scaiano. CRC Press, Boca Raton. In press. Chap. 7.
25. S. L. MUROV. Handbook of photochemistry. Marcel Dekker, New York. 1973.
26. P. J. WAGNER and R. A. LEAVITT. J. Am. Chem. Soc. **95**, 3669 (1973).
27. J. O. HOWELL, J. M. GONCALVES, C. AMATORE, L. KLASINC, R. M. WIGHTMAN, and J. K. KOCHI. J. Am. Chem. Soc. **106**, 3968 (1984).
28. J. B. GUTTENPLAN and S. G. COHEN. J. Am. Chem. Soc. **94**, 4040 (1972).
29. P. J. WAGNER and A. E. KEMPPAINEN. J. Am. Chem. Soc. **91**, 3085 (1969).
30. A. J. BARD and H. LUND. Encyclopedia of electrochemistry of the elements, organic section. Vol. XI. Marcel Dekker, New York. 1978.
31. T. HAMADA, A. NISHIDA, and O. YONEMITSU. J. Am. Chem. Soc. **108**, 141 (1986).
32. L. EBERSON. *In* Advances in physical organic chemistry. Vol. 18. Academic Press, New York. 1982. p. 79.

Can. J. Chem. Downloaded from www.nrcresearchpress.com by 41.223.56.140 on 09/07/12
For personal use only.

Structural studies of organoboron compounds. XXXIII.[1] 4,4-Dimethyl-2,2-diphenyl-1,3-dioxa-4-azonia-2-boratacyclohexane and 3,3-dimethyl-2-phenoxy-2-phenyl-1-oxa-3-azonia-2-boratacyclopentane

ECKARDT EBELING and WOLFGANG KLIEGEL
Institut für Pharmazeutische Chemie, der Technischen Universität Braunschweig, Beethovenstraße 55, 3300 Braunschweig, Bundesrepublik Deutschland

AND

STEVEN J. RETTIG and JAMES TROTTER
Department of Chemistry, University of British Columbia, 2036 Main Mall, Vancouver, B.C., Canada V6T 1Y6

Received October 31, 1988

ECKARDT EBELING, WOLFGANG KLIEGEL, STEVEN J. RETTIG, and JAMES TROTTER. Can. J. Chem. **67**, 933 (1989).

Details of the syntheses, physical properties, and crystal structures of the title compounds are reported. Crystals of 4,4-dimethyl-2,2-diphenyl-1,3-dioxa-4-azonia-2-boratacyclohexane, **3**, are monoclinic, a = 6.512(1), b = 15.765(2), c = 14.342(4) Å, β = 93.170(7)°, Z = 4, space group Pn, and those of 3,3-dimethyl-2-phenoxy-2-phenyl-1-oxa-3-azonia-2-boratacyclopentane, **4**, are orthorhombic, a = 13.5829(8), b = 16.940(1), c = 6.3181(4) Å, Z = 4, space group $P2_12_12$. Both structures were solved by direct methods and were refined by full-matrix least-squares procedures to R = 0.034 and 0.034 for 1974 and 1478 reflections with $I \geq 3\sigma(I)$, respectively. The molecular structures are discussed in terms of the thermally-induced 1,2-migration of B-substituents by which **3** is converted to **4**.

Key words: crystal structures, boron compounds, organoboron compounds.

ECKARDT EBELING, WOLFGANG KLIEGEL, STEVEN J. RETTIG et JAMES TROTTER. Can. J. Chem. **67**, 933 (1989).

On rapporte les détails relatifs à la synthèse, aux propriétés physiques et aux structures cristallines des composés mentionnés dans le titre. Les cristaux du diméthyl-4,4 diphényl-2,2 dioxa-1,3 azonia-4 borata-2 cyclohexane, **3**, sont monocliniques, avec a = 6,512(1), b = 15,765(2) et c = 14,342(4) Å, β = 93,170(7)°, Z = 4 et groupe d'espace Pn; ceux du diméthyl-3,3 phénoxy-2 phényl-2 oxo-1 azonia-3 borata-2 cyclopentane, **4**, sont orthorhombiques, avec a = 13,5829(8), b = 16,940(1) et c = 6,3181(4) Å, Z = 4 et groupe d'espace $P2_12_12$. On a résolu les deux structures par des méthodes directes et on les a affinées par la méthode des moindres carrés (matrice entière) jusqu'à des valeurs respectives de R de 0,034 et 0,034 pour 1974 et 1478 réflexions avec $I \geq 3\sigma(I)$. On discute des structures moléculaires en fonction de migrations-1,2 des substituants-B, induites d'une façon thermique et qui conduisent à la conversion de **3** en **4**.

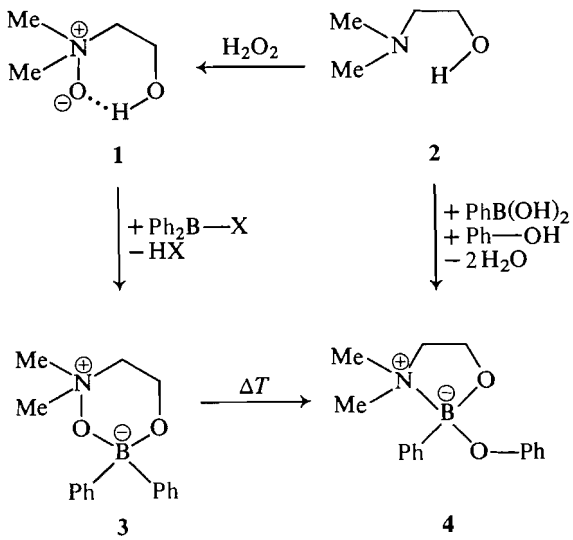
Mots clés : structures cristallines, composés du bore, composés du organobore.

[Traduit par la revue]

Introduction

2-Dimethylaminoethanol N-oxide **1** has been found to possess an intramolecular hydrogen bond both in solution and in the solid state (1). These findings are consistent with the fact that the bridge-bonded proton in **1** can be replaced by the diphenylborenium ion (Ph_2B^+) in a reaction leading to the diphenylboron chelate **3** (2). Diarylboron chelates of this type rearrange upon heating, undergoing an intramolecular redox reaction during which the N-oxide is deoxygenated and the diarylborinic acid component is oxidized to a monoarylboronic acid (2, 3). In this thermally-induced rearrangement, the six-membered chelate **3** is converted to the five-membered ring compound **4**, formulated with an assumed intramolecular N→B coordination analogous to similar five-membered boron chelates of 2-aminoalcohols (4–6). The supposed ring contraction from **3** to **4**, an exothermic reaction with ΔH about −200 kJ mol^{-1} (7), does not only change the steric conditions but also increases the number of electron-rich donating non-carbon ligands at the boron centre.

Compound **3** can be considered as an example of an isolable intermediate in the oxidation reaction between trialkylaminoxides and organylboranes (8). This type of reaction belongs to a general class of organoborate anion rearrangements involving a 1,2-migration of B-substituents (9). The intramolecular mechanism of the 1,2-shift within the initially formed N-oxide borane adduct as the transient species appears to be established by stereochemical experiments which show retention of configuration (10) as well as by product analyses of variously substituted adducts of the type **3** (3) and by oxidation experiments with trimethylamine N-oxide and several organylboranes (11). From these experiments it has been established that the sites of cleavage and recombination for the migrating alkyl or aryl group are identical. The intermediacy of the N-oxide borane adduct has been postulated generally (9, 12) and is well proven



1 **2** **3** **4**

[1]Previous paper in this series: ref. 19.

Can. J. Chem. Downloaded from www.nrcresearchpress.com by 41.223.56.140 on 09/07/12
For personal use only.

TABLE 1. Crystallographic data[a]

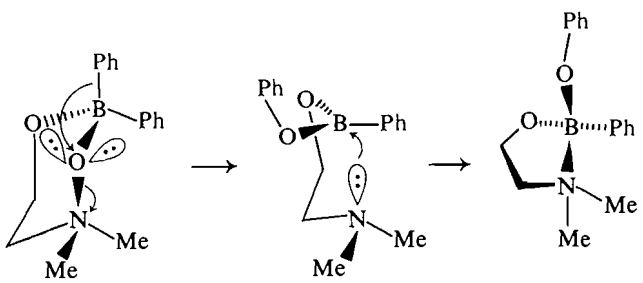
Compound	**3**	**4**
Formula	$C_{16}H_{20}BNO_2$	$C_{16}H_{20}BNO_2$
fw	269.15	269.15
Crystal system	Monoclinic	Orthorhombic
Space group	*Pn*	$P2_12_12$
a (Å)	6.512(1)	13.5829(8)
b (Å)	15.765(2)	16.940(1)
c (Å)	14.342(4)	6.3181(4)
β (deg)	93.170(7)	—
V (Å^3)	1470.1(4)	1453.8(2)
Z	4	4
ρ_c (g/cm^3)	1.216	1.230
F(000)	576	576
μ(Mo-K$_\alpha$) (cm^{-1})	0.73	0.74
Crystal dimensions (mm)	0.25 × 0.40 × 0.40	0.38 × 0.38 × 0.55
Scan type	$\omega - 2\theta$	$\omega - 2\theta$
Scan range (deg in ω)	0.80 + 0.35 tan θ	0.75 + 0.35 tan θ
Scan speed (deg/min)	0.8–6.7	1.1–10.0
Data collected	$+h, +k, \pm l$	$+h, +k, +l$
$2\theta_{max}$ (deg)	55	55
Crystal decay	Negligible	Negligible
Unique reflections	3376	1932
Reflections with $I \geq 3\sigma(I)$	1974	1478
Number of variables	399	261
R	0.034	0.034
R_w	0.036	0.040
S	1.585	1.783
Mean Δ/σ (final cycle)	0.001	0.009
Max Δ/σ (final cycle)	0.006	0.11
Residual density (e/Å^3)	−0.16 to +0.15	−0.19 to +0.17

[a]Temperature 294 K, Enraf-Nonius CAD4-F diffractometer, Mo-K$_\alpha$ radiation ($\lambda_{K_{\alpha1}} = 0.70930$, $\lambda_{K_{\alpha2}} = 0.71359$ Å), graphite monochromator, takeoff angle 2.7°, aperture (2.0 + tan θ) × 4.0 mm at a distance of 173 mm from the crystal, scan range extended by 25% on both sides for background measurement, $\sigma^2(I) = C + 2B + [0.04(C - B)]^2$ (C = scan count, B = normalized background count), function minimized: $\Sigma w(|F_o| - |F_c|)^2$ where $w = 1/\sigma^2(F)$, $R = \Sigma \| F_o| - |F_c\| / \Sigma |F_o|$, $R_w = (\Sigma w(|F_o| - |F_c|)^2 / \Sigma w|F_o|^2)^{1/2}$, $S = (\Sigma w(|F_o| - |F_c|)^2/(m - n))^{1/2}$. Values given for R, R_w, and S are based on those reflections with $I \geq 3\sigma(I)$.

Can. J. Chem. Downloaded from www.nrcresearchpress.com by 41.223.56.140 on 09/07/12
For personal use only.

by stable cyclic adducts like **3** that can be transformed into the products (like **4**) of the 1,2-migration (2, 3).

Following a proposed model (11) in which the trialkylamine group leaves antiperiplanar to the migrating group during the oxidation process, the conformational requirements are represented approximately by the formulations **3'** and **4'**. In order to assess the degree of accordance with this model and to obtain precise molecular dimensions in the solid state, especially since the transformations **3**→**4** can be performed as a solid state reaction (2, 3), X-ray crystallographic analyses of both compounds have been undertaken.



3' **4'**

Compound **3** also represents a six-membered homolog of the cyclic *B*,*N*-betaine **5**, the structure of which has been determined (13), and is isomeric with the symmetrical diphenylboron chelate **6** (14) which has also been structurally characterized. **3** and **6** are examples of isomeric cyclic *B*,*N*-betaines of the same ring size that have different relative locations of the ionic centres. Compound **3** can be prepared by the known (2) synthetic pathway **2**→**1**→**3**. The rearrangement product **4** is moisture-sensitive and tends to incorporate up to one mole of water, probably by insertion into the N→B bond. To avoid this problem the synthesis can be achieved by the condensation of 2-dimethylaminoethanol **2** with phenylboronic acid and phenol in benzene or toluene solvent under anhydrous conditions (2). This method was chosen for the preparation of water-free crystals of **4**.

Experimental

4,4-Dimethyl-2,2-diphenyl-1,3-dioxa-4-azonia-2-boratacyclohexane, 3

This compound was prepared as described previously (2). Crystals suitable for X-ray analysis were obtained by recrystallization from acetonitrile/acetone. Melting point (corr.) 156°C. ^{1}H nmr (90 MHz, d_6-DMSO/TMS): δ (ppm) = 3.19 (s, NMe_2), 3.48 (t, J = 5 Hz, N—CH_2C), 3.98 (t, J = 5 Hz, O—CH_2C), 6.9–7.5 (m, BPh_2).

3,3-Dimethyl-2-phenoxy-2-phenyl-1-oxa-3-azonia-2-boratacyclopentane, 4

2-Dimethylaminoethanol (0.89 g, 10 mmol), phenylboronic acid (1.22 g, 10 mmol), and phenol (0.94 g, 10 mmol) were refluxed in toluene (50 mL, dried over Na before use) for 30 min, water being continuously removed using a Dean–Stark trap. The resulting clear solution is slowly cooled (stepwise over a 12 h period) down to room temperature. The formation of colorless crystals yields 1.4 g (52%) of

Can. J. Chem. Downloaded from www.nrcresearchpress.com by 41.223.56.140 on 09/07/12
For personal use only.

4. Melting point 184°C; lit. (2) 190–192°C. ^{1}H nmr (90 MHz, d_6-DMSO/TMS): δ (ppm) = 2.32 (s, NMe_2), 2.63 (t, J = 6 Hz, N—CH_2C), 3.59 (t, J = 6 Hz, O—CH_2C), 6.6–8.0 (m, BPh and OPh); (90 MHz, $CDCl_3$/TMS): 2.50 (s, NMe_2), 3.09 (m, N—CH_2C), 3.99 (t, J = 6 Hz, O—CH_2C), 6.7–8.2 (m, BPh and OPh).

X-ray crystallographic analyses of ***3*** *and* ***4***

Crystallographic data for the two compounds are presented in Table 1. Unit-cell parameters were refined by least-squares on 2 sin θ/λ values for 25 reflections (2θ = 30–41° for **3** and 34–50° for **4**) measured with Mo-$K\alpha$ radiation. The intensities of three standard reflections, measured each hour of X-ray exposure time, showed only small random variations in each case (<4%). Data were corrected[2] for Lp but not for absorption in view of the low values of μ. The systematic absences for **3** ($h0\ell$, $h+\ell$ odd) allow space groups Pn or $P2/n$, the former being suggested by the E-statistics. The structure analysis of **3** was initiated (and successfully completed) in the non-centrosymmetric space group Pn. Both structures were solved by direct methods, the coordinates of the non-hydrogen atoms being determined from E-maps. Non-hydrogen atoms were refined with anisotropic thermal parameters. For **3**, hydrogen atoms were fixed in idealized positions (C(sp^2)—H = 0.97, C(sp^3)—H = 0.98 Å) and their isotropic thermal parameters varied, and for **4** hydrogen atom coordinates and thermal parameters were refined. Neutral atom scattering factors of ref. 15 were used. Final positional and anisotropic thermal parameters appear in Tables 2 and 7,[3] respectively. Measured and calculated structure factors have been placed in the Depository of Unpublished Data.[3]

The thermal motion in both structures has been analysed in terms of the TLS model (16). The rms errors in the temperature factors σU_{ij} (derived from the least-squares analyses) are 0.0019 and 0.0011 Å^2 for **3** and **4**, respectively. The structural subunits PhB and the six-membered ring plus all substituent atoms were separately analysed for each of the two crystallographically independent molecules of **3** (rms ΔU_{ij} = 0.0015–0.0031 Å^2) and for **4** the subunits PhO, PhB, and the five-membered ring plus substituent atoms were similarly treated (rms ΔU_{ij} = 0.0015–0.0029 Å^2). The appropriate bond distances have been corrected for libration (16, 17), using shape parameters q^2 of 0.08 for all atoms involved. Corrected bond lengths appear in Table 3 along with the uncorrected values; bond angles appear in Table 4 and intra-annular torsion angles in Table 5. Hydrogen atom parameters (Table 6), bond lengths and angles involving hydrogen and a complete listing of torsion angles (Tables 8–10) have been deposited.[3]

Results and discussion

The structure analysis of **3** confirms the presence of the expected six-membered chelate ring system (Fig. 1). Any open-chain intermolecular association between the N-oxide and diphenylborinate sites of the molecule can therefore be excluded from consideration. Osmometric determination of the molecular mass of this type of chelate are ambiguous (3), probably as a result of the dissociation process. Mass spectra show the presence of the peak due to the monomeric parent ion, but this peak may also be due to the rearranged product **4** which gives a nearly identical fragmentation pattern.

The crystal structure of **3** (Fig. 2) consists of discrete

[2]The computer programs used include locally written programs for data processing and locally modified versions of the following: MULTAN 80, multisolution program by P. Main, S. J. Fiske, S.E. Hull, L. Lessinger, G. Germain, J. P. Declercq, and M. M. Woolfson; BMFIT, best molecular fit, by S. C. Nyburg; AGNOST, absorption corrections, by J. A. Ibers; ORFLS, full-matrix least-squares, and ORFFE, function and errors, by W. R. Busing, K. O. Martin and H. A. Levy; FORDAP, Patterson and Fourier syntheses, by A. Zalkin; ORTEP II, illustrations, by C. K. Johnson.

[3]Supplementary material mentioned in the text may be purchased from the Depository of Unpublished Data, CISTI, National Research Council of Canada, Ottawa, Ont., Canada K1A 0S2.

TABLE 2. Final positional (fractional × 10^4) and isotropic thermal parameters ($U \times 10^3$ Å^2) with estimated standard deviations in parentheses

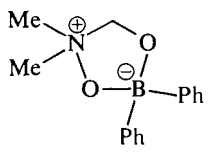
Atom	x	y	z	U_{eq}
		3		
O(1)	6006	4662(1)	1270	37
O(2)	2437(5)	5198(1)	1118(2)	44
N	6546(5)	5106(2)	448(2)	38
C(1)	3020(6)	5722(3)	385(3)	52
C(2)	4613(7)	5283(2)	−155(2)	52
C(3)	7669(6)	5901(2)	688(3)	44
C(4)	7892(7)	4516(3)	−37(3)	58
C(5)	4751(6)	5800(2)	2468(2)	34
C(6)	3262(6)	6391(2)	2679(3)	43
C(7)	3658(8)	7060(2)	3298(3)	56
C(8)	5577(8)	7152(2)	3725(3)	58
C(9)	7113(7)	6584(2)	3542(3)	52
C(10)	6696(6)	5910(2)	2931(2)	42
C(11)	3530(6)	4177(2)	2401(2)	37
C(12)	1552(7)	3854(2)	2371(3)	52
C(13)	1032(7)	3139(3)	2871(3)	65
C(14)	2512(10)	2724(2)	3421(3)	67
C(15)	4490(8)	3033(2)	3477(3)	59
C(16)	4984(7)	3745(2)	2980(3)	46
B	4162(7)	4989(3)	1802(3)	37
O(1′)	−420(5)	603(1)	4025(2)	36
O(2′)	3076(5)	79(1)	3763(2)	41
N′	−1185(5)	290(2)	3136(2)	38
C(1′)	2273(7)	−305(3)	2931(3)	52
C(2′)	554(7)	219(3)	2500(2)	52
C(3′)	−2306(6)	−521(2)	3232(3)	48
C(4′)	−2680(7)	952(2)	2781(3)	53
C(5′)	1067(6)	−695(2)	5005(2)	36
C(6′)	2562(6)	−1320(2)	5118(3)	47
C(7′)	2226(8)	−2080(2)	5579(3)	64
C(8′)	350(9)	−2240(2)	5938(3)	65
C(9′)	−1150(7)	−1625(3)	5860(3)	57
C(10′)	−798(6)	−871(2)	5410(3)	46
C(11′)	2389(6)	905(2)	5211(2)	33
C(12′)	4462(6)	1133(2)	5323(3)	42
C(13′)	5134(6)	1749(2)	5965(3)	51
C(14′)	3767(7)	2156(2)	6501(3)	50
C(15′)	1695(7)	1954(2)	6404(3)	47
C(16′)	1042(6)	1332(2)	5771(3)	41
B′	1560(6)	188(2)	4474(3)	33
		4		
O(1)	9710(1)	1250(1)	4958(2)	43
O(2)	10230(1)	1382(1)	1264(2)	42
N	8600(1)	1757(1)	2366(3)	37
C(1)	8918(2)	699(1)	4762(5)	53
C(2)	8359(2)	909(1)	2757(5)	47
C(3)	8415(2)	1984(2)	134(5)	54
C(4)	8002(2)	2265(2)	3794(6)	50
C(5)	11193(1)	1190(1)	1080(3)	35
C(6)	11864(2)	1230(1)	2739(4)	38
C(7)	12836(2)	1017(1)	2408(5)	45
C(8)	13146(2)	761(1)	436(5)	51
C(9)	12478(2)	716(1)	−1188(5)	51
C(10)	11506(2)	929(1)	−893(4)	44
C(11)	10190(1)	2619(1)	3619(3)	34
C(12)	10166(2)	2942(1)	5645(4)	43
C(13)	10478(2)	3706(1)	6042(4)	51
C(14)	10834(2)	4167(1)	4427(5)	55
C(15)	10890(2)	3853(2)	2408(5)	58
C(16)	10577(2)	3092(1)	2018(4)	47
B	9783(2)	1747(1)	3118(3)	33

TABLE 3. Bond lengths (Å) with estimated standard deviations in parentheses

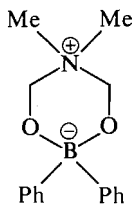
Bond	Length		Bond	Length	
	Uncorr.	Corr.		Uncorr.	Corr.
			3		
O(1)—N	1.432(3)	1.434	O(1′)—N′	1.430(3)	1.433
O(1)—B	1.547(4)	1.552	O(1′)—B′	1.554(4)	1.558
O(2)—C(1)	1.405(4)	1.408	O(2′)—C(1′)	1.412(4)	1.415
O(2)—B	1.487(4)	1.493	O(2′)—B′	1.468(4)	1.473
N —C(2)	1.513(4)	1.520	N′ —C(2′)	1.497(4)	1.502
N —C(3)	1.482(4)	1.486	N′ —C(3′)	1.483(4)	1.487
N —C(4)	1.477(5)	1.481	N′ —C(4′)	1.496(4)	1.500
C(1)—C(2)	1.497(6)	1.502	C(1′)—C(2′)	1.497(5)	1.500
C(5)—C(6)	1.390(5)	1.398	C(5′)—C(6′)	1.388(5)	1.398
C(5)—C(10)	1.408(5)	1.414	C(5′)—C(10′)	1.403(5)	1.410
C(5)—B	1.629(5)	1.633	C(5′)—B′	1.626(5)	1.631
C(6)—C(7)	1.393(5)	1.398	C(6′)—C(7′)	1.392(5)	1.397
C(7)—C(8)	1.368(6)	1.375	C(7′)—C(8′)	1.375(6)	1.382
C(8)—C(9)	1.379(6)	1.386	C(8′)—C(9′)	1.376(6)	1.385
C(9)—C(10)	1.395(5)	1.399	C(9′)—C(10′)	1.379(5)	1.384
C(11)—C(12)	1.383(5)	1.393	C(11′)—C(12′)	1.397(5)	1.406
C(11)—C(16)	1.400(5)	1.409	C(11′)—C(16′)	1.394(5)	1.401
C(11)—B	1.609(5)	1.613	C(11′)—B′	1.620(4)	1.624
C(12)—C(13)	1.389(5)	1.393	C(12′)—C(13′)	1.392(5)	1.395
C(13)—C(14)	1.375(6)	1.383	C(13′)—C(14′)	1.368(5)	1.375
C(14)—C(15)	1.375(7)	1.386	C(14′)—C(15′)	1.385(6)	1.395
C(15)—C(16)	1.378(5)	1.383	C(15′)—C(16′)	1.387(5)	1.390
			4		
O(1)—C(1)	1.428(3)	1.432	C(6)—C(7)	1.384(3)	1.391
O(1)—B	1.439(3)	1.446	C(7)—C(8)	1.385(4)	1.393
O(2)—C(5)	1.353(2)	1.357	C(8)—C(9)	1.372(4)	1.379
O(2)—B	1.457(3)	1.464	C(9)—C(10)	1.382(3)	1.388
N —C(2)	1.494(3)	1.500	C(11)—C(12)	1.392(3)	1.401
N —C(3)	1.483(3)	1.490	C(11)—C(16)	1.394(3)	1.403
N —C(4)	1.489(3)	1.495	C(11)—B	1.608(3)	1.613
N —B	1.676(3)	1.682	C(12)—C(13)	1.386(3)	1.390
C(1)—C(2)	1.519(4)	1.526	C(13)—C(14)	1.373(4)	1.382
C(5)—C(6)	1.391(3)	1.399	C(14)—C(15)	1.385(5)	1.393
C(5)—C(10)	1.389(3)	1.397	C(15)—C(16)	1.379(4)	1.383

monomeric molecules, the shortest intermolecular distances between non-hydrogen atoms being O(2′)···C(3′)(1 + x,y,z) = 3.282(4) Å, O(2)···C(3)(x −1,y,z) = 3.322(4) Å, and C(3)···C(8′)(1/2 + x, 1 − y,z−1/2) = 3.341(5) Å. The two shortest of these contacts may represent weak C—H···O hydrogen bonds linking the molecules into ribbons extending along the a axis (C(3)—H(3a)···O(2), H···O = 2.44 and 2.40 Å, C—H···O = 150° and 149°, for the unprimed and primed molecules, respectively.)

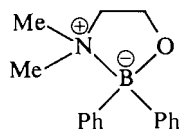
The two independent molecules of **3** have almost identical geometries, with slightly-distorted chair conformations (Table 5) for the six-membered chelate rings, similar to that observed for the isomeric compound **6** (18). The B—C bond distances involving the axial phenyl groups are longer than those involving the equatorial phenyl groups by an average of 0.014 Å in **3**, comparable to a corresponding difference of 0.020 Å in **6**. Bond length differences of this type have also been noted for (pseudo)-axial and (pseudo)-equatorial *B*-phenyl groups in seven- (19) and eight-membered (20) chelates of the type "Ph_2BO_2" and also between the corresponding B—C bond distances in compound **8** (21). Comparable but smaller differences between B—C distances have been noted for the diphenylboron chelates of acetylacetone (22), salicylaldehyde (23), and trishydroxymethylated phenylphosphine (24).



5

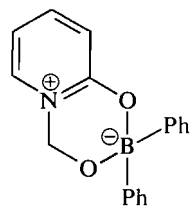


6

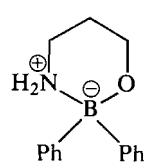


7

The significant differences between the O—B bond lengths in **3** are as expected. In general, the O—B distance involving the *N*-oxide oxygen atom is longer than that involving an alcoholate or phenolate oxygen atom within the same molecule, as in **5** (13) and other diphenylboron chelates with an *N*-oxide ligand (refs. 19, 25, 26, and references therein). The mean C—B/mean



8



9

Can. J. Chem. Downloaded from www.nrcresearchpress.com by 41.223.56.140 on 09/07/12
For personal use only.

TABLE 4. Bond angles (deg) with estimated standard deviations in parentheses

Bonds	Angle (deg)	Bonds	Angle (deg)
	3		
N —O(1)—B	118.4(2)	N′ —O(1′)—B′	117.6(2)
C(1)—O(2)—B	113.5(2)	C(1′)—O(2′)—B′	113.9(2)
O(1)—N —C(2)	109.0(2)	O(1′)—N′ —C(2′)	109.4(2)
O(1)—N —C(3)	111.3(2)	O(1′)—N′ —C(3′)	111.3(2)
O(1)—N —C(4)	105.0(2)	O(1′)—N′ —C(4′)	104.5(2)
C(2)—N —C(3)	111.2(3)	C(2′)—N —C(3′)	112.6(3)
C(2)—N —C(4)	110.1(3)	C(2′)—N —C(4′)	110.2(3)
C(3)—N —C(4)	110.1(3)	C(3′)—N —C(4′)	108.6(3)
O(2)—C(1)—C(2)	109.8(3)	O(2′)—C(1′)—C(2′)	110.3(3)
N —C(2)—C(1)	111.6(3)	N′ —C(2′)—C(1′)	111.3(3)
C(6)—C(5)—C(10)	115.8(3)	C(6′)—C(5′)—C(10′)	115.4(3)
C(6)—C(5)—B	120.6(3)	C(6′)—C(5′)—B′	120.5(3)
C(10)—C(5)—B	123.3(3)	C(10′)—C(5′)—B′	124.1(3)
C(5)—C(6)—C(7)	122.6(4)	C(5′)—C(6′)—C(7′)	122.6(4)
C(6)—C(7)—C(8)	119.8(4)	C(6′)—C(7′)—C(8′)	120.1(4)
C(7)—C(8)—C(9)	120.0(3)	C(7′)—C(8′)—C(9′)	118.8(3)
C(8)—C(9)—C(10)	119.8(4)	C(8′)—C(9′)—C(10′)	120.6(3)
C(5)—C(10)—C(9)	121.9(3)	C(5′)—C(10′)—C(9′)	122.4(3)
C(12)—C(11)—C(16)	116.0(3)	C(12′)—C(11′)—C(16′)	116.4(3)
C(12)—C(11)—B	122.8(3)	C(12′)—C(11′)—B′	122.6(3)
C(16)—C(11)—B	121.3(3)	C(16′)—C(11′)—B′	121.0(3)
C(11)—C(12)—C(13)	122.4(4)	C(11′)—C(12′)—C(13′)	121.4(3)
C(12)—C(13)—C(14)	119.9(4)	C(12′)—C(13′)—C(14′)	120.6(3)
C(13)—C(14)—C(15)	119.4(3)	C(13′)—C(14′)—C(15′)	119.7(3)
C(14)—C(15)—C(16)	120.1(4)	C(14′)—C(15′)—C(16′)	119.3(3)
C(11)—C(16)—C(15)	122.2(3)	C(11′)—C(16′)—C(15′)	122.5(3)
O(1)—B —O(2)	109.1(2)	O(1′)—B′ —O(2′)	109.6(2)
O(1)—B —C(5)	112.7(3)	O(1′)—B′ —C(5′)	111.9(3)
O(1)—B —C(11)	103.1(3)	O(1′)—B′ —C(11′)	102.4(2)
O(2)—B —C(5)	111.0(3)	O(2′)—B′ —C(5′)	112.5(3)
O(2)—B —C(11)	108.8(3)	O(2′)—B′ —C(11′)	108.8(3)
C(5)—B —C(11)	111.7(2)	C(5′)—B′ —C(11′)	111.0(2)
	4		
C(1)—O(1)—B	111.4(2)	C(8)—C(9)—C(10)	121.1(3)
C(5)—O(2)—B	125.0(2)	C(5)—C(10)—C(9)	119.8(2)
C(2)—N —C(3)	111.7(2)	C(12)—C(11)—C(16)	116.8(2)
C(2)—N —C(4)	109.6(2)	C(12)—C(11)—B	122.2(2)
C(2)—N —B	98.9(2)	C(16)—C(11)—B	121.0(2)
C(3)—N —C(4)	109.5(2)	C(11)—C(12)—C(13)	121.8(2)
C(3)—N —B	115.8(2)	C(12)—C(13)—C(14)	120.3(2)
C(4)—N —B	110.9(2)	C(13)—C(14)—C(15)	119.0(2)
O(1)—C(1)—C(2)	107.3(2)	C(14)—C(15)—C(16)	120.5(3)
N —C(2)—C(1)	104.6(2)	C(11)—C(16)—C(15)	121.6(2)
O(2)—C(5)—C(6)	123.8(2)	O(1)—B —O(2)	115.5(2)
O(2)—C(5)—C(10)	116.7(2)	O(1)—B —N	99.7(2)
C(6)—C(5)—C(10)	119.4(2)	O(1)—B —C(11)	113.7(2)
C(5)—C(6)—C(7)	119.9(2)	O(2)—B —N	100.1(2)
C(6)—C(7)—C(8)	120.5(2)	O(2)—B —C(11)	113.9(2)
C(7)—C(8)—C(9)	119.3(2)	N —B —C(11)	112.1(2)

O—B bond length ratios for the two independent molecules of **3**, 1.066 and 1.074, are similar to the corresponding value of 1.069 for compound **6** (18). These values represent a relatively strong overall bonding of the *O,O*-chelating ligand to the diphenylboron moiety when compared with the values of 1.039–1.088 (average 1.058) observed for other "Ph_2BO_2" compounds containing six-membered chelate rings (ref. 27 and references therein).

The chemical differences between the isomeric compounds **3** and **6** give rise to significant structural differences. All of the N—C bond lengths in **3** are shorter by about 0.02 Å than the corresponding distances in **6** (18). The C—O bonds[4] in **5** (1.378(9) Å) and **6** (average 1.374 Å), derived from inserted formaldehyde, are shorter than the C(1)—O bond in **3** (average 1.412 Å) which is chemically similar to those found in other boron chelates with hydroxyalkyl ligands displaying normal C—O single bond distances (refs. 4–6, 20 and references therein); cf. compounds **7** and **9** (6). The N—O bond in **3** (average

[4]Libration corrected bond lengths (esd's assumed equal to those of the uncorrected values) are employed in the discussion and are, in general, compared with other corrected distances.

Can. J. Chem. Downloaded from www.nrcresearchpress.com by 41.223.56.140 on 09/07/12
For personal use only.

Can. J. Chem. Downloaded from www.nrcresearchpress.com by 41.223.56.140 on 09/07/12
For personal use only.

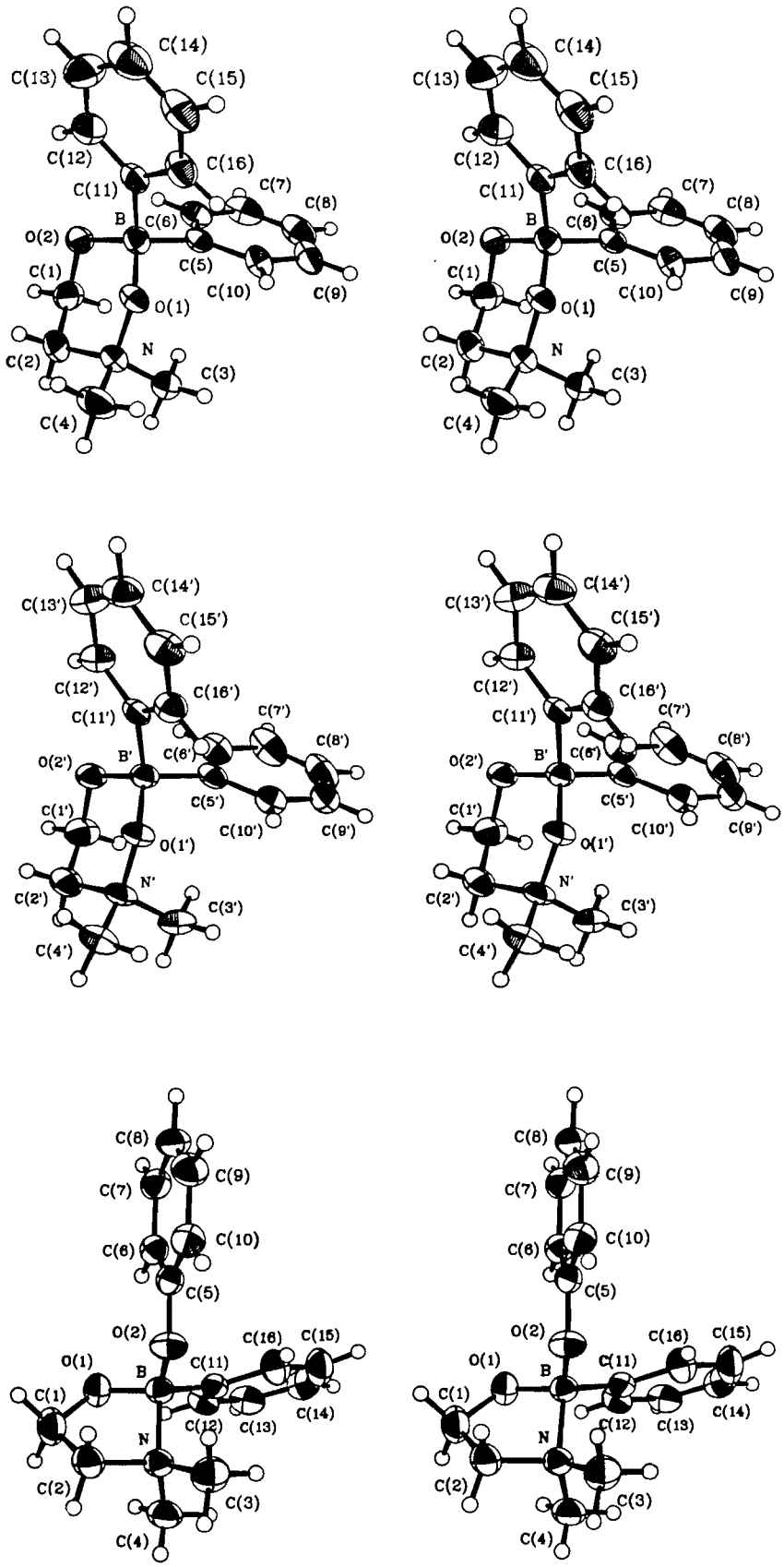


Fig. 1. Stereoscopic views of the two independent molecules of **3** (top and middle) and **4** (bottom); 50% probability thermal ellipsoids are shown for the non-hydrogen atoms.

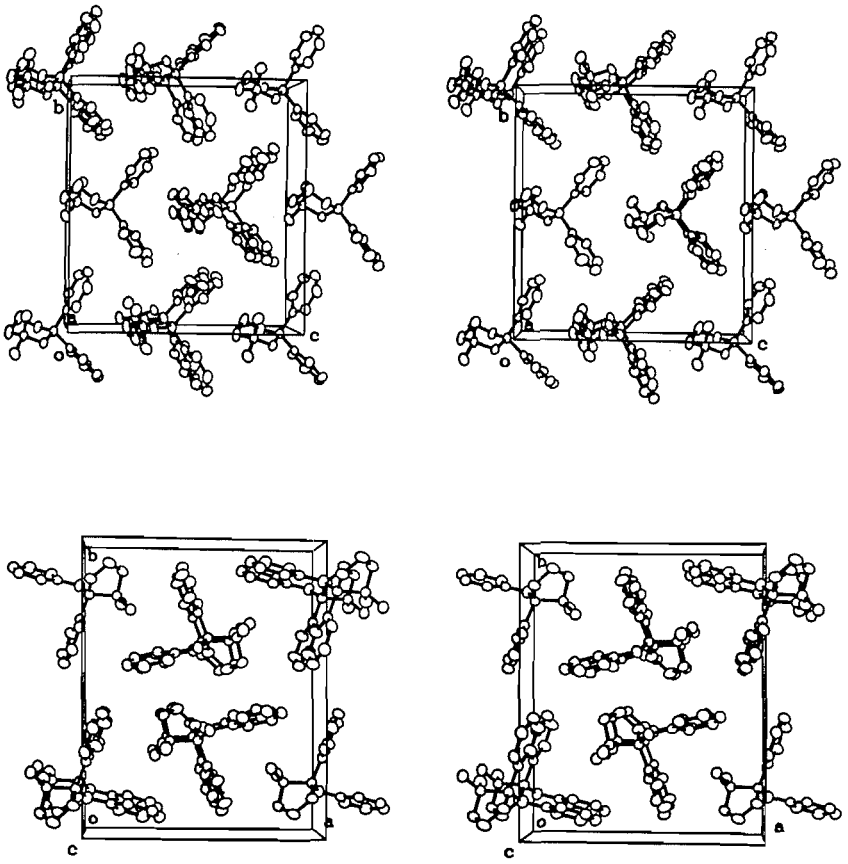


FIG. 2. Stereoscopic views of the packing arrangements of **3** (top) and **4** (bottom).

TABLE 5. Intra-annular torsion angles (deg) standard deviations in parentheses

Atoms	Value (deg)
3	
B —O(1)—N —C(2)	−45.8(3)
O(1)—N —C(2)—C(1)	53.0(3)
O(2)—C(1)—C(2)—N	−62.1(4)
B —O(2)—C(1)—C(2)	61.2(4)
C(1)—O(2)—B —O(1)	−50.4(4)
N —O(1)—B —O(2)	44.1(4)
B′—O(1′)—N′ —C(2′)	−46.9(3)
O(1′)—N′—C(2′)—C(1′)	54.2(4)
O(2′)—C(1′)—C(2′)—N′	−61.6(4)
B′ —O(2′)—C(1′)—C(2′)	59.6(4)
C(1′)—O(2′)—B′ —O(1′)	−49.0(3)
N′ —O(1′)—B′ —O(2′)	43.9(3)
4	
B —O(1)—C(1)—C(2)	−6.7(3)
O(1)—C(1)—C(2)—N	−22.6(3)
B —N —C(2)—C(1)	37.6(2)
C(2)—N —B —O(1)	−40.8(2)
C(1)—O(1)—B —N	29.2(2)

1.434 Å) is longer than that in the free ligand **1** (1.38 and 1.41 Å for intra- and intermolecular hydrogen-bonded *N*-oxide groups, respectively). Five-membered diphenylboron chelates with *N*-oxide ligands like **5** (13, 25) have shorter N—O bonds than **3**: 1.409 Å for **5** (13) and 1.410 Å for a substituted derivative (25). The ligand bite in **3**, mean O(1)···O(2) = 2.471 Å, is smaller than the corresponding distance of 2.53 Å in the hydrogen-bridged free ligand **1** (1).

The crystal structure of the rearrangement product **4** (Fig. 2) consists of molecules separated by normal van der Waals distances, the shortest intermolecular contact between non-hydrogen atoms being C(14)···C(14) ($2 - x$, $1 - y$, $-z$) = 3.618(5) Å. The *N*-oxide group of **3** has been cleaved during its thermal rearrangement to **4**, the N···O(2) distance being 2.406(2) Å in the product. The exocyclic N—B—O(2) angle (100.10(15)°) is relatively small, the corresponding C—B—O angle in the diphenylboron chelate **7** (6) (involving the pseudo-axial *B*-phenyl group) being 109.7°. The overall geometry of **4** is quite similar to that of **7** although there appears to be less intramolecular steric strain in the former. The C(1)—O(1) bond in **4** (1.432 Å) is longer than the corresponding bond in **7** (1.418 Å), and the B—O(1) bond in **4** is shorter (1.446 Å) than that in **7** (1.476 Å). The N—B bond in **4** (1.682 Å), like that in **7** (1.691 Å), is longer than the N—B bonds in *N*-substituted "boroxazolidines" (4, 5) and other sterically less hindered boron chelates of aminoalcohols such as **9** (6).

The bond lengths involving the boron atom in **4** all lie within the ranges previously observed for compounds of the type "PhBN(sp^3)O_2" (ref. 28 and references therein). The sum of bond lengths at boron, 6.205 Å, is fairly small for a compound of this type (6.191–6.297, mean 6.23 Å), consistent with relatively low overall strain about the boron atom (28).

The thermally induced 1,2-migration of one *B*-phenyl substituent to the *N*-oxide oxygen atom can be assumed to involve an approach of C(11) to O(1), if the migrating group is approaching antiperiplanar to the leaving trialkylamine group (**3′**→**4′**). The

Can. J. Chem. Downloaded from www.nrcresearchpress.com by 41.223.56.140 on 09/07/12
For personal use only.

C(11)—B—O(1) angle (average 102.8°) involving the equatorial phenyl group of **3** is considerably smaller than the C(5)—B—O(1) angle (average 112.4°) involving the axial *B*-phenyl substituent. The average C(11)···O(1) and C(5)···O(1) distances in **3** are 2.474 and 2.641 Å, respectively. Thus relatively small changes have to occur during the reaction. The rearrangement of **3** seems to be sterically "conditioned" by fortuitous relative positioning of both the migrating and leaving groups, as well as bonds and lone pairs involved in the transformation. It is possible that the long N—O bond in **3** (see above) is involved in facilitating the pending 1,2-shift, thus the structure of **3** may be interpreted as an example of a "frozen" intermediate in the progress of the oxidation of organylboranes with *N*-oxides. The best molecular fit between compounds **3** and **4** is good ($\Sigma\Delta^2$ = 13.2 Å^2 for all 20 non-hydrogen atoms) and the molecular volumes differ by only 1.1%. These data are consistent with a unimolecular process in a topochemically-allowed solid state reaction, and, considering the similarity of the unit-cell parameters, suggest the possibility of a single-crystal to single-crystal transformation. However, a comparison of the packing diagrams for **3** and **4** (Fig. 2) leads to the conclusion that too great a rearrangement of the lattice is required for such a topotactic reaction (involving these particular crystal forms) to occur.

Acknowledgments

We thank the Natural Sciences and Engineering Research Council of Canada and the Fonds der Chemischen Industrie, Frankfurt am Main, for financial support and the University of British Columbia Computing Centre for assistance.

1. E. R. Maia, A. Péguy, and S. Pérez. Can. J. Chem. **62**, 6 (1984).
2. W. Kliegel. Liebigs Ann. Chem. **763**, 61 (1972).
3. W. Kliegel and E. Ahlenstiel. J. Organomet. Chem. **277**, 173 (1984).
4. S. J. Rettig and J. Trotter. Can. J. Chem. **51**, 1288 (1973); **54**, 3130 (1976).
5. S. J. Rettig and J. Trotter. Acta Crystallogr. Sect. B, **30**, 2139 (1974).
6. S. J. Rettig and J. Trotter. Can. J. Chem. **61**, 2334 (1983).
7. W. Kliegel, S. Sarge, H. K. Cammanga, S. J. Rettig, and J. Trotter. *In* Reactivity of solids. Materials science monographs. Vol. 28 A and B. *Edited by* P. Barret and L. C. Dufor. Amsterdam. 1985. p. 725.
8. R. Köster and Y. Morita. Angew. Chem. **78**, 589 (1966); Liebigs Ann. Chem. **704**, 70 (1967).
9. (*a*) P. I. Paetzold and H. Grundke. Synthesis, 635 (1973); (*b*) D. S. Matteson. Organometallic reaction mechanisms of the nontransition elements. New York. 1974. p. 154; (*c*) E. Negishi. J. Chem. Ed. **52**, 159 (1975); J. Organomet. Chem. **108**, 281 (1976); (*d*) A. Pelter. *In* Rearrangements in ground and excited states. Vol. 2. *Edited by* P. de Mayo. New York. 1980. p. 95.
10. A. G. Davies and B. P. Roberts. J. Chem. Soc. Sect. C, 1474 (1968).
11. J. A. Soderquist and M. R. Najafi. J. Org. Chem. **51**, 1330 (1986).
12. W. Kliegel. Organomet. Rev. Sect. A, **8**, 153 (1972).
13. S. J. Rettig, J. Trotter, and W. Kliegel. Can. J. Chem. **52**, 2531 (1974).
14. W. Kliegel. Angew. Chem. **80**, 614 (1968).
15. International tables for X-ray crystallography. Vol. IV. Kynoch press, Birmingham. 1974. pp. 99–102 and 149.
16. V. Schomaker and K. N. Trueblood. Acta Crystallogr. Sect. B, **24**, 63 (1968).
17. D. W. J. Cruickshank. Acta Crystallogr. **9**, 747 (1956); **9**, 754 (1956); **14**, 896 (1961).
18. W. Kliegel, S. J. Rettig, and J. Trotter. Can. J. Chem. **66**, 377 (1988).
19. W. Kliegel, M. Tajerbashi, S. J. Rettig, and J. Trotter. Can. J. Chem. **66**, 2621 (1988).
20. W. Kliegel, S. J. Rettig, and J. Trotter. Can. J. Chem. **66**, 1091 (1988).
21. W. Kliegel, H.-W. Motzkus, D. Nanninga, S. J. Rettig, and J. Trotter. Can. J. Chem. **64**, 507 (1986).
22. S. J. Rettig and J. Trotter. Can. J. Chem. **60**, 2957 (1982).
23. S. J. Rettig and J. Trotter. Can. J. Chem. **54**, 1168 (1976).
24. B. A. Arbuzov, O. A. Erastov, G. N. Nikonov, A. A. Espenbetov, A. I. Yanovskii, and Yu. T. Struchkov. Izv. Akad. Nauk. SSSR, Ser. Khim. 1545 (1981); Bull. Acad. Sci. USSR, Div. Chem. Sci. 1243 (1981).
25. W. Kliegel, H.-W. Motzkus, S. J. Rettig, and J. Trotter. Can. J. Chem. **62**, 838 (1984).
26. W. Kliegel, U. Lauterbach, S. J. Rettig, and J. Trotter. Can. J. Chem. **65**, 1457 (1987).
27. W. R. Cullen, S. J. Rettig, J. Trotter, and E. B. Wickenheiser. Can. J. Chem. **66**, 2007 (1988).
28. H. Amt, W. Kliegel, S. J. Rettig, and J. Trotter. Can. J. Chem. **66**, 1117 (1988).

Can. J. Chem. Downloaded from www.nrcresearchpress.com by 41.223.56.140 on 09/07/12
For personal use only.

Vibrational spectroscopic studies of the phase transition behavior in solid cyclohexene

JULIAN HAINES and D. F. R. GILSON[1]

Department of Chemistry, McGill University, 801 Sherbrooke St. W., Montreal, Que., Canada H3A 2K6

Received December 5, 1988

JULIAN HAINES and D. F. R. GILSON. Can. J. Chem. **67**, 941 (1989).

The vibrational spectra (FT-ir and Raman) of cyclohexene have been examined as functions of temperature. The phase transition behavior is complex and highly dependent upon the thermal treatment of the sample. Spectra of the stable low temperature form (phase II) are quite different from those of the other phases, and suggest that the crystal has either C_i or C_{2h} symmetry with two molecules per primitive unit cell. The asymmetric line shapes of the internal vibrational bands and the presence of broad peaks in the low frequency region of the Raman spectra of the high temperature phase indicate that the molecules undergo anisotropic rotation. The frequency of the ring inversion mode is highly phase dependent.

Key words: cyclohexene, FT-ir, Raman, phase transition.

JULIAN HAINES et D. F. R. GILSON. Can. J. Chem. **67**, 941 (1989).

On a déterminé les spectres de vibration (ir-FT et Raman) du cyclohexène en fonction de la température. Le comportement à la transition de phase est complexe et dépend beaucoup du traitement thermique de l'échantillon. Les spectres de la phase II (forme stable à basse température) sont très différents de ceux des autres phases et ils suggèrent que la symétrie du cristal est soit C_i ou C_{2h} avec deux molécules par cellule unitaire. Les formes asymétriques des raies des bandes de vibration interne ainsi que la présence de pics larges dans la région de basse fréquence des spectres Raman de la phase de température élevée indiquent que les molécules subissent une rotation anisotrope. La fréquence du mode d'inversion du cycle dépend beaucoup de la phase.

Mots clés : cyclohexène, ir-FT, Raman, transition de phase.

[Traduit par la revue]

Introduction

Organic molecular crystals, particularly pseudo-spherical cage hydrocarbons such as adamantane, often possess an order–disorder phase transition in the solid state (1). The high temperature phase is usually face-centered cubic and melts with a low entropy of fusion (less than 21 J K^{-1} mol^{-1}). The low temperature crystal structures are seldom known, but, in principle, it is possible to analyze the splittings that occur in the vibrational spectra when the crystal symmetry changes at the transition and to determine the number of molecules per unit cell and to identify possible space groups (2). These phase transitions are not limited to rigid compounds and have been observed in monocyclic compounds such as cyclohexane, and in the present study, we have examined the temperature dependence of the FT-ir and Raman spectra of the analogous compound cyclohexene. The existence of a transition in this compound has been known for many years (3, 4). Adiabatic calorimetric studies showed that a single transition occurred at 139 K, with an entropy of transition of 30.7 J K^{-1} mol^{-1}, which is much larger than the entropy of fusion of 19.4 J K^{-1} mol^{-1} at 170 K, indicating that the high temperature phase is disordered. A more recent and extensive dta and adiabatic calorimetric study by Haida and co-workers (5, 6) has shown that the behavior is more complicated and involves metastable and "glassy crystalline" states, depending on the rate of cooling and the thermal history of the sample. When cooled slowly, the high temperature phase, phase I, transforms reversibly to a metastable phase III at 112 K. Upon rapid cooling a "glassy crystal" is formed, termed phase gI, which when heated undergoes a series of overlapping transitions some of which are exothermic; gI→I→III→I→II →I→liquid at 92 K, 100 K, 115 K, 120 K, 140 K, and 170 K, respectively. The stable low temperature phase II is formed irreversibly from phase I at 120 K and could be cooled to 61 K. Phase III was also found to form a glassy crystal if cooled below 83 K. This unusual sequence of transitions was explained by Haida and co-workers using a Gibbs free energy schematic diagram.

Molecular motion is commonly observed to occur in the high temperature phases of these materials (7). El Saffar and co-workers (8) have examined the nmr second moment and spin–lattice relaxation time for cyclohexene as functions of temperature. The phase transition behavior described in this study is in agreement with that subsequently observed by Haida and co-workers for rapidly cooled samples. A decrease in second moment was observed between 100 and 110 K and attributed to rotation of the cyclohexene molecule around an axis perpendicular to the four co-planar carbon atoms. A sudden increase in second moment was observed at 110 K when the stable low temperature phase was formed irreversibly, then at 139 K, the transition to phase I occurred, with a reduction in second moment due to the above mentioned rotation in conjunction with ring inversion. Upon cooling a transition was observed at 129 K with the ring inversion process persisting down to 115 K.

The vibrational spectrum of cyclohexene has been studied previously (9), but no results on the solid phases have been reported. A study of the vibrational spectra of solid cyclohexene enables more information to be obtained on the phase transition behavior and the different solid forms.

Experimental

Cyclohexene (Aldrich Chemical Co., Purity 99%) was distilled under reduced pressure before use.

Raman spectra were recorded on a Instruments S.A. spectrometer with a Jobin-Yvon Ramanor U-1000 1.0 m double monochromator. A Spectra Physics model 164, 5 W (all lines) argon-ion laser (514.5 nm line, approximately 200 mW at the sample) was used for excitation. The resolution was typically 1 or 2 cm^{-1}. Infrared spectra (2 cm^{-1} resolution) were acquired on a Analect AQS-18 FT-ir spectrometer equipped with a triglycine sulfate (TGS) detector. The infrared spectra were measured on samples sprayed on a potassium bromide window and annealed at a temperature just below the melting point. The Raman spectra were obtained by cooling liquid samples in sealed glass capillary tubes, which were mounted on to the cold finger of a cryostat using indium foil as a conducting junction. The sample temperature was

[1]Author to whom correspondence should be addressed.

Can. J. Chem. Downloaded from www.nrcresearchpress.com by 41.223.56.140 on 09/07/12
For personal use only.

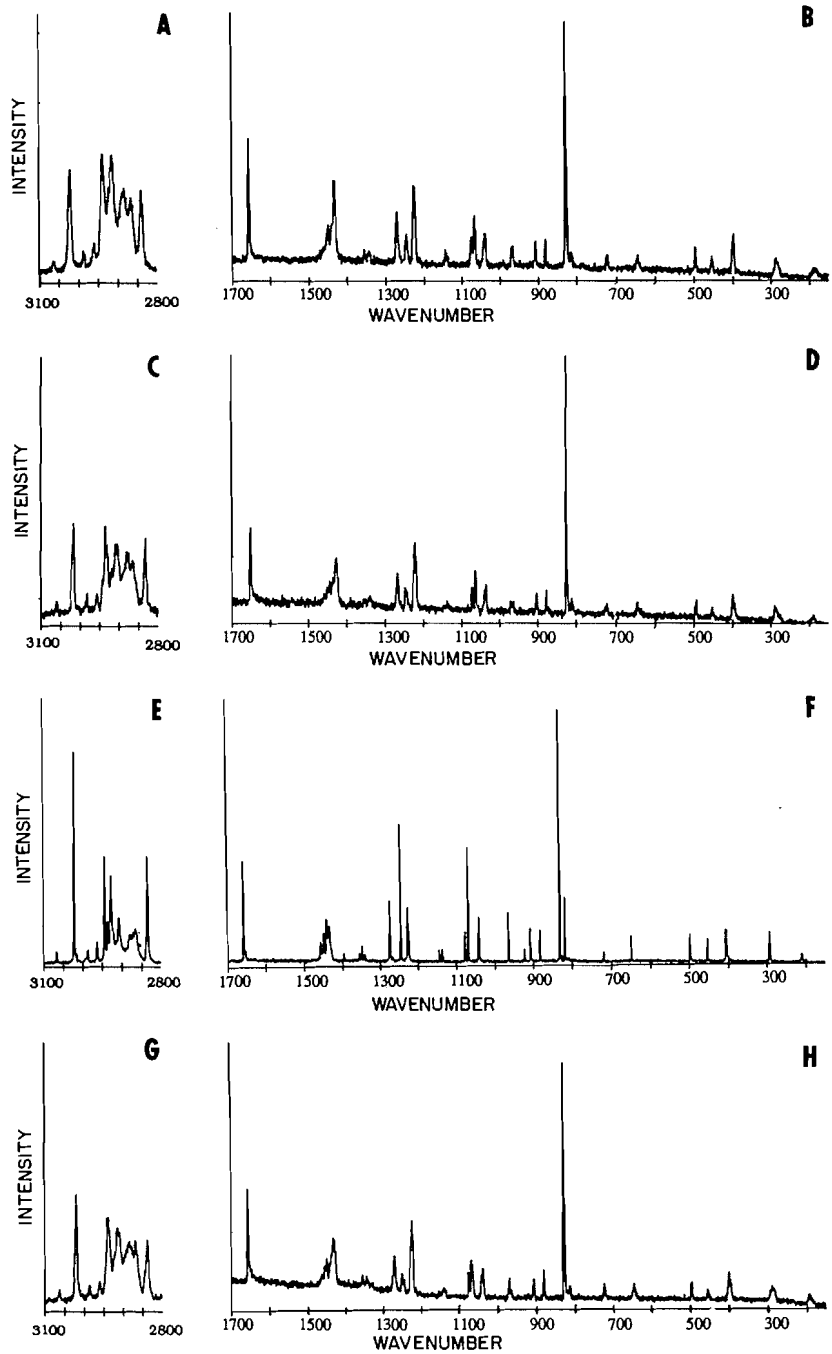


FIG. 1. Comparison of the Raman spectrum of cyclohexene: *A*,*B*, phase I at 149 K; *C*,*D*, phase III at 72 K; *E*,*F*, phase II at 61 K; and *G*,*H*, phase gI at 58 K (not to scale).

controlled, for both FT-ir and Raman spectra, with a Cryodyne Cryocooler Model 21 cryostat (Cryogenics Technology Inc.) and measured using a silicon-diode temperature sensor attached to a Cryophysics Model 4025 controller. The sample temperature remained essentially constant (±0.5 K).

Results and discussion

Raman spectra were obtained for both the metastable phase III and the glassy phase gI, as well as those of the stable phases I and II, Figs. 1 and 2, but, due to cooling rate limitations, infrared spectra could only be obtained for phases I and III, Fig. 3. The spectroscopic results conform to the dta and calorimetric results of Haida and co-workers (5, 6), and to the nmr results of El Saffar *et al.* (8). Upon slow cooling, many of the infrared and Raman bands of phase I were found to split into doublets at the transition to phase III, but remained quite broad. For example, ν_{39} and ν_{40}, at 718 and 641 cm^{-1} in the infrared spectrum of phase I, both split into two components, Table 1. This splitting could be due to the presence of two conformers related by the ring inversion mode. Rapid cooling of phase I, leading to the formation of the glassy crystalline phase gI, gave spectra that were very similar to those of phase III. The most noticeable differences were observed for the low frequency Raman region and in the intensity distribution between the peaks of the dou-

Can. J. Chem. Downloaded from www.nrcresearchpress.com by 41.223.56.140 on 09/07/12
For personal use only.

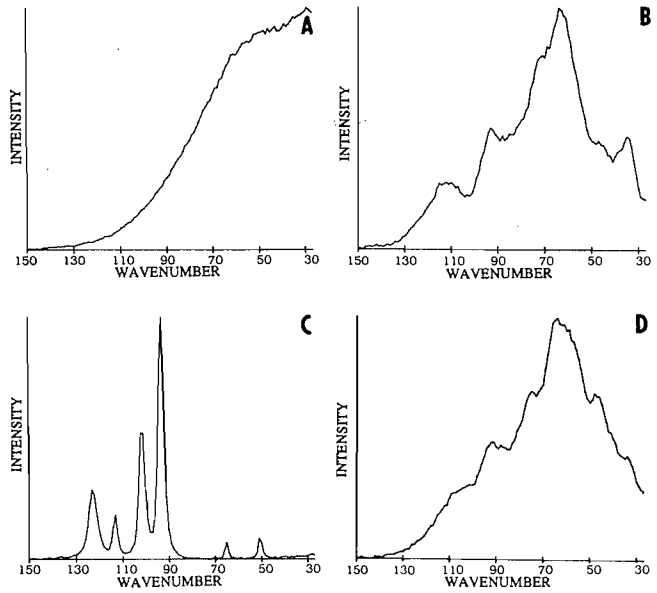


FIG. 2. Comparison of the low frequency Raman spectrum of cyclohexene: *A*, phase I at 149 K; *B*, phase III at 58 K; *C*, phase II at 61 K; and *D*, phase gI at 58 K (not to scale).

blets arising from the splittings of the internal modes, but the broad bands present in the spectra of both phases indicate that a significant degree of disorder was still present. In the low temperature stable phase II the lines in the Raman spectra were very much sharper than those in any other phase, and with some increases in relative intensities, notably for the C—H stretching region, and for ν_{11}, ν_{15} and the combination $\nu_{40} + \nu_{42}$ at 1244, 1068, and 818 cm^{-1}, respectively. These latter vibrations correspond to the CH_2 wag, the CH_2 twist and a combination of the CH wag and the ring inversion modes.

The external modes, as seen in the low frequency Raman region, Fig. 4, provide spectra which are quite characteristic of the type and behavior of each solid phase. For instance, the two overlapping broad bands in the spectrum of phase I persisted under slow cooling conditions down to 96 K, indicating that a considerable degree of motion is still present in phase III, well below the phase transition temperature. A similar conclusion was drawn on the basis of the wide line nmr results (8). At 96 K, a sudden change occurred to at least seven broad and overlapping bands. Upon heating the glassy phase (produced by rapid cooling), the transition to phase III and the subsequent transition to phase I were easily observable. The spectrum of phase I obtained by this path was identical to that obtained by cooling the liquid phase. At approximately 120 K, a sudden transformation to phase II occurred and the lattice region spectrum changed from two broad bands in phase I to six narrow bands, indicating the formation of the ordered phase. Thus the spectral evidence confirms the sequence of transitions reported by Haida *et al.* (5, 6). The temperature dependence of the lattice mode frequencies is shown in Fig. 4.

The possible site symmetries for cyclohexene, which belongs to the C_2 molecular point group, are C_1 and C_2. The presence of six external modes in the Raman spectrum of phase II, indicates that there are at least two molecules per unit cell. The absence of splitting in the Raman spectrum restricts the unit cell symmetry

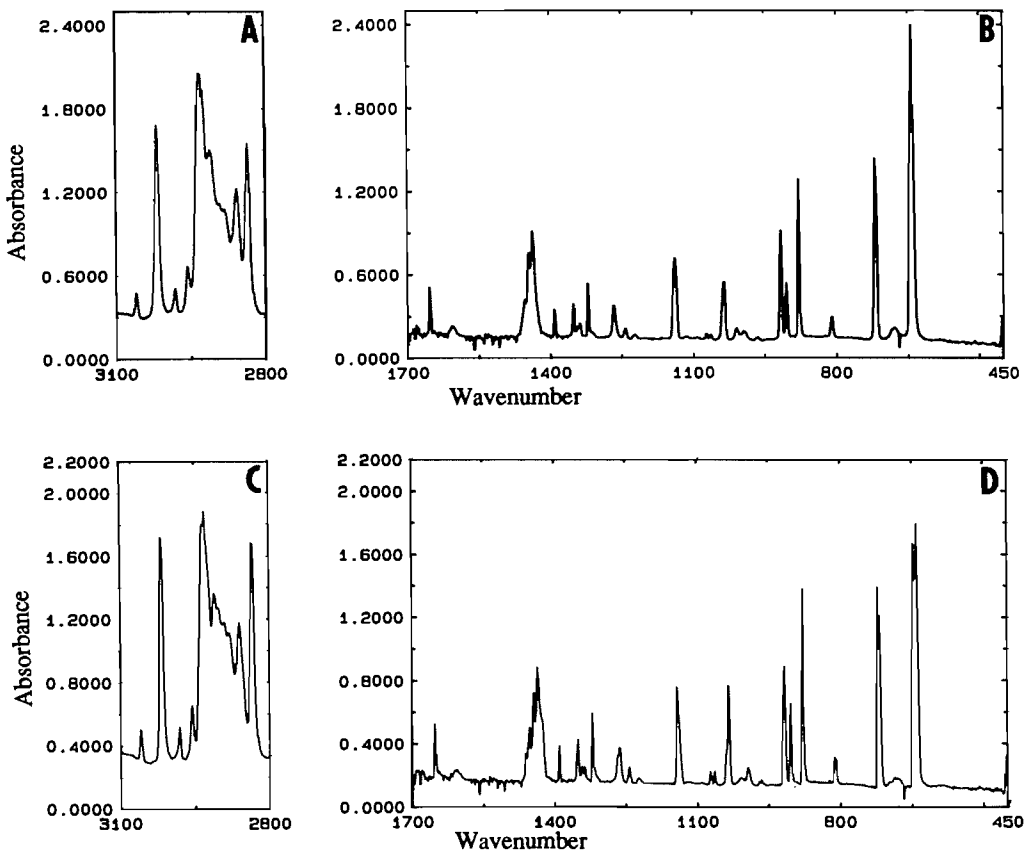


FIG. 3. Comparison of the FT-ir spectrum of cyclohexene: *A*,*B*, phase I at 121 K; and *C*,*D*, phase III at 56 K.

Can. J. Chem. Downloaded from www.nrcresearchpress.com by 41.223.56.140 on 09/07/12
For personal use only.

Can. J. Chem. Downloaded from www.nrcresearchpress.com by 41.223.56.140 on 09/07/12
For personal use only.

TABLE 1. Vibrational data (cm^{-1}) for cyclohexene

Raman				FT-ir		
Phase gI (58 K)	Phase II (61 K)	Phase III (72 K)	Phase I (149 K)	Phase III (48 K)	Phase I (145 K)	Assignment[a]
3062w	3065w	3062w	3063w	3060m	3061m	ν_{23}
3019s	3020s	3020s	3021s	3017s	3019s	ν_1
2988sh		2988sh				
2985w	2987w	2985w	2986w	2982m	2982m	
2961sh						
2959w	2962w	2959w	2960w	2956w	2958w	ν_{24}
2937s	2943s	2937s	2937s	2933vs	2930vs	ν_2
	2935m					ν_{25}
2918sh	2926s	2924sh		2920s		ν_3
2913m		2912s		2910sh		
2902sh	2905m			2905sh		
				2991sh	2893sh	
2883m	2880m	2883m	2884m	2882s	2884s	ν_{26}
2867m	2870m	2869m	2866m	2861s	2858s	ν_4
2864sh	2864m					
2837m	2833s	2836s	2839m	2834vs	2836s	ν_5
1655s	1657s	1654s	1655s	1655m	1653m	ν_6
1455w	1458mw	1460w		1463mw	1461m	ν_7
				1457m	1454m	
				1454m		
1450w	1448m	1448w	1449w	1444m	1445m	ν_{28}
1440m	1441m	1440m		1440ms	1442s	ν_{29}
1434sh				1436sh	1435s	ν_8
1430m	1434m	1430m	1432s	1432sh		
					1393sh	
	1394vw	1393vw		1390w	1390w	$\nu_{12} + \nu_{42}$
				1387sh		
1355vw	1354vw	1354vw	1354vw	1352w	1353w	ν_9
1344vw	1346vw	1342vw	1342vw	1343vw		ν_{10}
	1340vw			1337vw	1337vw	ν_{30}
				1321m	1321m	ν_{31}
1270w	1274w	1270w	1269w	1264w	1265w	ν_{32}
1250w		1248w			1249sh	ν_{11}
1245w	1244s	1244w	1245m	1244w	1242w	
1224m	1226m	1224m	1225m	1225vw	1225vw	ν_{12}
1141vw	1143vw	1141vw	1141vw	1143m	1137m	ν_{13}
1135vw	1135vw	1135vw				ν_{34}
1075mw	1077mw	1076mw	1075mw	1074vw	1072vw	ν_{14}
1070m	1068s	1066m	1066m	1066w	1062w	ν_{15}
1067m		1064m				
1042m	1041m	1043m	1040m	1039sh	1038ms	ν_{35}
1039m		1040m		1035ms		
970vw	964vw	970vw	967vw	971vw	960vw	ν_{16}
966vw		965sh		966vw		
921vw	922vw			917s	916s	ν_{37}
907w	907w	906w	906w	904s	903m	ν_{17}
880m	882m	881m	881m	879s	878s	ν_{38}
878sh						
828vvs	830vvs	830vvs	828vvs	824vvw		ν_{18}
826sh		826sh				
814w	818m	815w	813w	812w	808w	$\nu_{40} + \nu_{42}$
				809w		
724w	716w	724w	722w	722s	718s	ν_{39}
				718s		
646w	647m	648w	644w	648w	641w	ν_{40}
				641w		
496w	496m	498w	495w			ν_{20}
		496w				
455w	451w	456w	454w	452m	455m	ν_{41}
400w	403m	401w	397m			ν_{21}

TABLE 1. (*Continued*)

Raman				FT-ir		
Phase gI (58 K)	Phase II (61 K)	Phase III (72 K)	Phase I (149 K)	Phase III (48 K)	Phase I (145 K)	Assignment[a]
290w	290w	291w	285w			ν_{22}
193vw	208vw	192vw	185vw			ν_{42}
	122m					
	133w					
102sh	101m	109w				
91m	93s	90m				Inter-
75m	64w	79sh	44s,br			molecular
63s	50w	71s				vibrations
47m		61s				
34m		45m				
		34w				

[a]Following ref. 9.

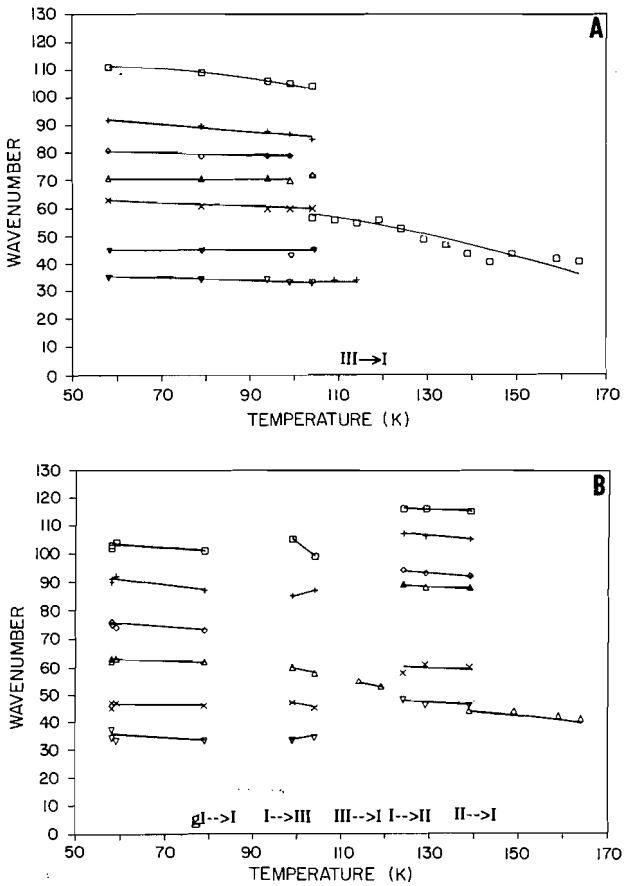
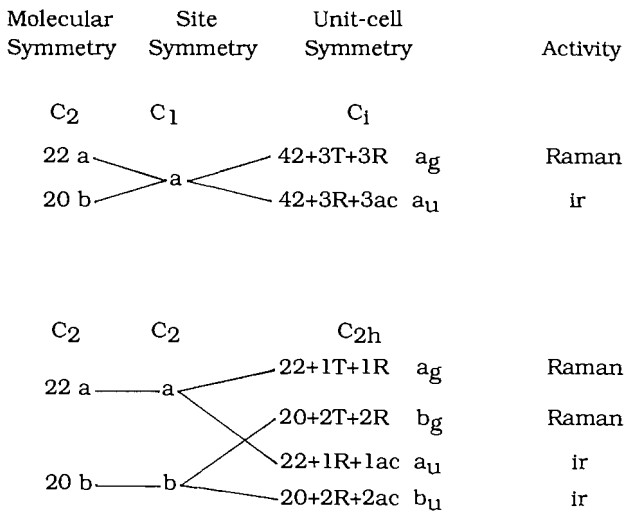


FIG. 4. Temperature dependence of the low frequency Raman spectrum of cyclohexene: *A* for a slowly cooled sample and *B* for a rapidly cooled sample.



note: T=translation, R=rotation and ac=acoustic.

FIG. 5. Correlation diagrams for cyclohexene phase II.

to doubly occupied centrosymmetric groups under the triclinic or monoclinic system, whereby each internal mode, which is both ir- and Raman-active under the C_2 molecular point group, is split into one infrared and one Raman active component. Based on the above, a symmetry of C_i or C_{2h} with two molecules per primitive unit cell is proposed for this crystal (Fig. 5).

It is interesting to note that while most of the internal modes showed only small shifts in frequency at the various phase transitions, the transition from phase II to I produced the most pronounced changes. In most cases the shift was less than 5 cm^{-1}. The ring inversion mode, however, was strongly affected and was observed in the Raman spectrum at 185 cm^{-1} in the liquid and in phase I, at 193 cm^{-1} and 192 cm^{-1} in phases gI and III, respectively, and at 208 cm^{-1} in phase II. This band was found not to shift with temperature in phase I and the liquid, and only shifted 2 cm^{-1} from 62 K to 130 K in phase II. The shifts that occur at the phase transformations indicate that the crystal structure has a significant effect on the ring inversion process. Intermolecular forces, which are distance dependent, affect the barrier to ring inversion, therefore an increase in the frequency of the ring inversion mode is indicative of a crystal of higher density due to closer packing. This is in agreement with the arguments of Haida and co-workers (5, 6), who concluded, based on residual entropy arguments, that the energy difference between conformers in phase gI is less than in phase gIII, with the energy difference in phase II, which has no residual entropy, being so high that the lattice is rigid below the phase transition. The residual entropy in phase gI was found to be greater than

Can. J. Chem. Downloaded from www.nrcresearchpress.com by 41.223.56.140 on 09/07/12
For personal use only.

that of phase gIII by about R ln 3, therefore the possibility of a three-fold disordering process, such as the distribution of the double bond about an axis passing through the center of the ring, could be considered. The total residual entropy of phase gI is about R ln 4, which is consistent with a four-fold disordering process. The vibrational spectra of these two glassy crystals are so similar that it is difficult to draw any conclusions on the relative degree of disorder. Both crystals are disordered and hence their spectra contain broad bands which partially obscure any splitting that might be present.

The broad bands in the low frequency Raman spectra of the high temperature phase of cyclohexene are characteristic of molecules that are undergoing anisotropic reorientation (10). In addition, the lineshapes of the internal modes are asymmetric with visible shoulders in many cases. These features are similar to those found in the spectra of the high temperature phases of cyclopentene (11), furan (12), and thiophene (13, 14), for which reorientation about an axis perpendicular to the ring was confirmed by nmr experiments (15–17). The nmr experiments (8) on cyclohexene also indicate the same motion is present along with ring inversion. A similarity is also noticed between the entropies of fusion of the four compounds, which are close to or greater than the upper limit of 2.5R which Timmermans (18) set for what he termed "plastic crystals". It should be noted that the high temperature phases of furan and thiophene are orthorhombic in contrast to the majority of "plastic crystals" which have cubic or hexagonal structures. The similarity between these two compounds and cyclopentene and cyclohexene could be due to the fact that, in the latter, the ring puckering only involves a portion of the ring as opposed to the situation in cyclobutane, cyclopentane and cyclohexane where the whole ring is affected and, consequently, a much greater degree of disorder is present in the high temperature phases.

Acknowledgements

This research was supported by grants from NSERC (Canada). J.H. acknowledges the award of a scholarship from NSERC.

1. N. G. Parsonage and L. A. K. Staveley. Disorder in crystals. Clarendon, Oxford. 1978.
2. W. G. Fateley, F. R. Dollish, N. T. McDevitt and F. F. Bentley. Infrared and Raman selection rules for molecular and lattice vibrations: the correlation method. Wiley-Interscience, New York. 1972.
3. G. S. Parks and H. M. Huffman. J. Am. Chem. Soc. **52**, 4381 (1930).
4. H. M. Huffman, M. Eaton, and G. D. Oliver. J. Am. Chem. Soc. **70**, 2911 (1948).
5. O. Haida, H. Suga, and S. Seki. Chem. Lett. 79 (1973).
6. O. Haida, H. Suga, and S. Seki. Bull. Chem. Soc. Jpn. **50**, 802 (1977).
7. N. Boden. The plastically crystalline state. *Edited by* J. N. Sherwood. Wiley-Interscience, Chichester. 1970. Chap. 5.
8. Z. M. El Saffar, R. G. Eades, and J. P. Llewellyn. J. Chem. Phys. **50**, 3462 (1969).
9. N. Neto, C. Di Lauro, E. Castellucci, and S. Califano. Spectrochim. Acta, **23**a, 1763 (1967).
10. S. S. Bukalov and L. A. Leites. Proc. Int. Conf. Raman Spectrosc. **8**, 611 (1982).
11. J. Haines and D. F. R. Gilson. J. Phys. Chem. **93**, 20 (1989).
12. L. Colombo and D. Kirin. Mol. Cryst. Liq. Cryst. **59**, 85 (1980).
13. P. R. Salvi, M. G. Migliorini, and G. Sbrana. Mol. Cryst. Liq. Cryst. **35**, 239 (1976).
14. D. Andre, A. Dworkin, P. Figuine, A. H. Fuchs, and H. Szwarc. J. Phys. Chem. Solids, **46**, 505 (1985).
15. I. J. Lawrenson and F. A. Rushworth. Proc. Phys. Soc. **72**, 791 (1958).
16. F. Fried. C. R. Hebd. Seanc. Acad. Sci. Paris, **262**C, 1497 (1966).
17. J. E. Anderson. Mol. Cryst. Liq. Cryst. **11**, 343 (1970).
18. J. Timmermans. J. Phys. Chem. Solids, **18**, 1 (1961).

Can. J. Chem. Downloaded from www.nrcresearchpress.com by 41.223.56.140 on 09/07/12
For personal use only.

Cryptowolinol et cryptowolidine, nouveaux alcaloïdes de type dibenzopyrrocoline

MICHEL LEBŒUF, ANDRÉ CAVÉ[1] ET ANISSA RANAIVO

Laboratoire de pharmacognosie, Unité associée n° 496 du Centre national de la recherche scientifique, Faculté de pharmacie, 92296 Châtenay-Malabry CEDEX, France

ET

HENRI MOSKOWITZ

Laboratoire de chimie organique, Unité associée n° 496 du Centre national de la recherche scientifique, Faculté de pharmacie, 92296 Châtenay-Malabry CEDEX, France

Reçu le 23 septembre 1988

MICHEL LEBŒUF, ANDRÉ CAVÉ, ANISSA RANAIVO et HENRI MOSKOWITZ. Can. J. Chem. **67**, 947 (1989).

Au cours de l'étude de deux Lauracées néocalédoniennes, *Cryptocarya phyllostemon* et *Cryptocarya oubatchensis*, quatre alcaloïdes quaternaires à squelette dibenzopyrrocoline ont été isolés. Deux d'entre eux ont été identifiés à la cryptowoline et à la cryptaustoline, les deux seuls produits naturels de ce type structural connus jusqu'alors. Les deux autres, nommés cryptowolinol et cryptowolidine, sont nouveaux; leur structure a été déterminée et la synthèse de la cryptowolidine a été réalisée. La structure du cryptowolinol est originale par la présence inhabituelle d'un hydroxyle alcoolique sur le carbone benzylique, et sa possible origine biogénétique est discutée.

Mots clés : *Cryptocarya*, Lauraceae, alcaloïdes dibenzopyrrocolines.

MICHEL LEBŒUF, ANDRÉ CAVÉ, ANISSA RANAIVO, and HENRI MOSKOWITZ. Can. J. Chem. **67**, 947 (1989).

Four quaternary dibenzopyrrocoline alkaloids were isolated from the Neocaledonian Lauraceae *Cryptocarya phyllostemon* and *C. oubatchensis*. Two of them were identified as cryptowoline and cryptaustoline, the only natural representatives of this structural type known up to now. The other two are new products and have been named cryptowolinol and cryptowolidine; their structures were elucidated, and synthesis of cryptowolidine was perfomed. An original feature of cryptowolinol is the unusual presence of an alcoholic hydroxyl on the benzylic carbon; its putative biogenetic origin is discussed.

Key words: *Cryptocarya*, Lauraceae, dibenzopyrrocoline alkaloids.

Introduction

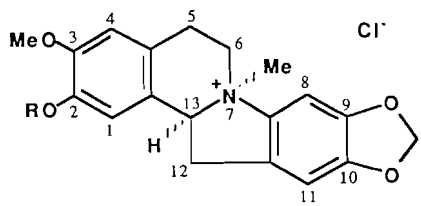
Parmi les très nombreux alcaloïdes isoquinoléiques ou biogénétiquement apparentés actuellement connus, deux seulement, la cryptowoline et la cryptaustoline, possèdent un squelette de type dibenzopyrrocoline ou indolo[2,1-*a*]isoquinoléine (1). Depuis leur découverte il y a plus de 35 ans dans une Lauracée australienne, *Cryptocarya bowiei* (Hook.) Druce (2, 3), leur présence n'a jamais été de nouveau signalée dans une quelconque espèce végétale.

Au cours d'un travail d'ensemble portant sur le contenu alcaloïdique d'une dizaine d'espèces de *Cryptocarya* originaires d'Australie, des Nouvelles-Hébrides et de Nouvelle-Calédonie, l'étude de deux de ces dernières, *C. phyllostemon* Kost. et *C. oubatchensis* Schlechter, a permis d'isoler quatre alcaloïdes quaternaires à noyau dibenzopyrrocoline. Deux d'entre eux, présents respectivement dans *C. phyllostemon* et dans *C. oubatchensis*, ont été identifiés à la cryptowoline et à la cryptaustoline. Les deux autres, qui sont nouveaux, ont été nommés cryptowolinol et cryptowolidine; ils ont été isolés, le premier à partir des deux espèces étudiées, le second seulement à partir de *C. phyllostemon*.

L'extraction de ces alcaloïdes quaternaires a été réalisée de façon classique. La détermination structurale de ces différents produits, ainsi que la synthèse de l'un d'entre eux, la cryptowolidine, font l'objet du présent mémoire.

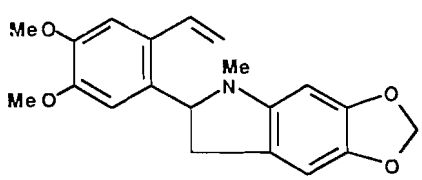
Résultats et discussion

L'alcaloïde quaternaire **1**, de formule brute $C_{19}H_{20}O_4N^+$, a été isolé sous forme de chlorure. Son appartenance au groupe des dibenzopyrrocolines est déduite de l'examen de son spectre de masse. Le pic moléculaire, à *m/z* 326, n'a qu'une faible intensité en ionisation chimique et est totalement absent en impact électronique; mais, sur ce dernier, toutes les fragmentations classiques des dibenzopyrrocolines quaternaires sont observées (4) et elles indiquent que l'alcaloïde **1** est substitué en 9 et 10 par un méthylènedioxyle et que le cycle A porte un méthoxyle et un hydroxyle phénolique dont les positions exactes, en 2 et en 3, restent à déterminer. La localisation des substitutions oxygénées sur le noyau est confirmée par comparaison du dérivé O-méthylé **2**, obtenu par action du diazométhane sur **1**, avec un échantillon de O-méthyl cryptowoline. Le spectre de RMN ^1H de **1** (Tableau 1) est en accord avec les données précédentes, mais il ne permet pas de placer avec certitude les substituants en 2 et 3. Une étude des effets nucléaires Overhauser (ENO) observés sur le spectre de **1**, enregistré dans CD_3OD à 500 MHz, a conduit sans ambiguïté à attribuer à cet alcaloïde la structure de la cryptowoline dans



1 : R = H : Cryptowoline

2 : R = Me



3

[1]Auteur à qui adresser toute correspondance.

Printed in Canada / Imprimé au Canada

Can. J. Chem. Downloaded from www.nrcresearchpress.com by 41.223.56.140 on 09/07/12
For personal use only.

Can. J. Chem. Downloaded from www.nrcresearchpress.com by 41.223.56.140 on 09/07/12
For personal use only.

TABLEAU 1. Résonance magnétique nucléaire (δ pm, J Hz) de ^{1}H de la cryptowoline **1**, de la cryptaustoline **4**, du cryptowolinol **5** et de la cryptowolidine **7**

Proton	**1**[a]	**1**[b]	**4**[c]	**5**[b]	**7**[a]	**7**[b]
H-1	6,91	6,76	6,75	6,83	6,91	6,91
H-4	6,91	6,86	6,85	6,91	6,80	6,72
H-8	7,81	7,37	7,18	7,41	7,66	7,38
H-11	7,15	6,96	6,90	7,11	7,13	6,96
H-12α		3,20*		—		3,21*
H-12β		3,76*		5,41(d, J = 6)		3,84*
H-13	5,41(t, J = 8)	5,28(t, J = 9)		5,16(d, J = 6)	5,36(t, J = 8)	5,32(t, J = 9)
N^+CH_3	3,56	3,54	3,53	3,50	3,53	3,54
OCH_3-2	—	—	—	—	3,81	3,88
OCH_3-3	3,81	3,87	3,85**	3,89	—	—
OCH_3-9	—	—	3,88**	—	—	—
OCH_3-10	—	—	3,93**	—	—	—
OCH_2O-9,10	6,25	6,11(d, J = 1,5) 6,13(d, J = 1,5)	—	6,16(d, J = 1,5) 6,18(d, J = 1,5)	6,25	6,11(d, J = 1) 6,13(d, J = 1)

[a]Dans DMSO-d_6 à 60 MHz.
[b]Dans CD_3OD à 500 MHz.
[c]Dans CD_3OD à 60 MHz.
*: dd, J = 10 Hz, J' = 2 Hz; **: valeurs non attribuées.

TABLEAU 2. Résonance magnétique nucléaire (δ ppm) de ^{13}C de la cryptowoline **1** et du cryptowolinol **5** (CD_3OD, 25,2 MHz)

Carbone	**1**	**5**	Carbone	**1**	**5**
C-1	106,9	107,0	C-10	149,8	149,5
C-2	142,7	142,8	C-11	114,1[a]	114,4[d]
C-3	147,9	147,2	C-11a	121,0[b]	122,5[e]
C-4	112,4[a]	112,1[d]	C-12	37,6	72,4
C4a	123,0[b]	119,0[e]	C-13	76,3	79,7
C-5	25,1	25,2	C-13a	127,8	130,4
C-6	60,0	64,2	OMe-3	56,5	56,3
C-7a	151,8[c]	151,5	N^+Me-7	50,1	48,3
C-8	99,7	99,4	OCH_2O	104,4	104,5
C-9	150,3[c]	151,5			

[a,b,c,d,e]Valeurs interchangeables.

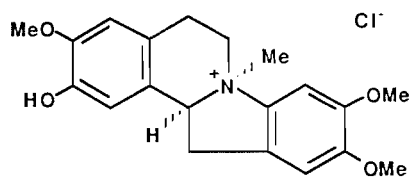
laquelle l'hydroxyle est en 2 et le méthoxyle en 3. Enfin, les spectres de RMN ^{13}C des dibenzopyrrocolines quaternaires n'ayant pas encore été décrits, celui du chlorure de cryptowoline a été enregistré; les attributions ont été faites (Tableau 2) par comparaison aux données publiées d'une part pour d'autres alcaloïdes isoquinoléiques (5, 6), d'autre part pour une dibenzopyrrocoline tertiaire synthétique tétraméthoxylée en 2, 3, 9 et 10 (7).

La cryptowoline isolée ici de *C. phyllostemon* possède la même configuration 13-*S* que celle précédemment extraite de *C. bowiei* (pouvoir rotatoire négatif, même effet Cotton négatif à 242 nm sur le spectre de dichroïsme circulaire); quant à la configuration de l'atome d'azote quaternaire, elle a été établie récemment comme étant 7-*R* (8).

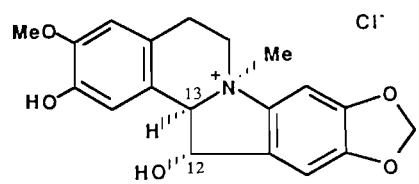
Lors de la préparation de la O-méthyl cryptowoline **2**, il a été constaté que la réaction de méthylation de la cryptowoline **1** par le diazométhane en solution éthérée était particulièrement laborieuse et nécessitait, pour être complète, un temps de contact supérieur à 1 semaine. Nous avons également tenté de méthyler la cryptowoline par action de l'iodure de méthyle dans la potasse méthanolique, selon une technique déjà utilisée dans le cas d'autres alcaloïdes quaternaires phénoliques (9). Cependant, il n'a pas été obtenu dans ces conditions le dérivé **2** espéré, mais le produit vinylique **3** formé par O-méthylation et élimination spontanée de Hofmann. Sa structure a été déduite de son spectre de RMN ^{1}H qui présente en particulier les signaux caractéristiques du N-méthyle tertiaire (singulet à 2,55 ppm) et de la chaîne vinylique (trois doublets dédoublés à 5,23, 5,56 et 6,86 ppm, avec des couplages respectivement *gem* et *cis*, *gem* et *trans*, *cis* et *trans*).

La dibenzopyrrocoline quaternaire **4**, $C_{20}H_{24}O_4N^+$, a comme la précédente été isolée sous forme de chlorure. Elle a été facilement identifiée à la cryptaustoline par examen de ses spectres de masse et de RMN ^{1}H (Tableau 1) et comparaison à ceux de la cryptowoline **1** dont elle ne diffère que par la présence en 9,10 de deux méthoxyles au lieu du groupe méthylènedioxy. Le placement de l'hydroxyle phénolique en 2 et du méthoxyle en 3 résulte de la similitude des déplacements chimiques des protons aromatiques en 1 et 4 observés pour ces deux alcaloïdes.

Les deux autres dibenzopyrrocolines quaternaires isolées au cours de ce travail sont nouvelles. La première, nommée cryptowolinol, **5**, $C_{19}H_{20}O_5N^+$, cristallise sous forme de chlorure. Son spectre UV est comparable à celui des alcaloïdes précé-



4 : Cryptaustoline



5 : Cryptowolinol

Can. J. Chem. Downloaded from www.nrcresearchpress.com by 41.223.56.140 on 09/07/12
For personal use only.

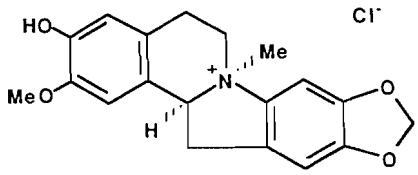
dents. Un déplacement bathochrome observé en milieu alcalin révèle la présence d'une fonction phénolique, ce qui est confirmé par l'existence d'un singulet de trois protons à 2,28 ppm sur le spectre de RMN ^1H du dérivé acétylé **6**; mais on observe également sur ce spectre la présence d'un autre singulet de trois protons, à 1,75 ppm, attribuable à un O-acétyle alcoolique. Sur le spectre de masse du cryptowolinol en ionisation chimique, le pic moléculaire n'a qu'une faible intensité (2%) et se trouve à m/z 342, soit à 16 u.m.a. de plus que pour la cryptowoline **1**, ce qui confirme la présence d'une fonction alcool supplémentaire. Les fragmentations observées sur le spectre de masse de **5** en impact électronique sont en accord avec celles des dibenzopyrrocolines portant un méthylènedioxyle en 9,10 ainsi qu'un méthoxyle et un hydroxyle phénolique sur le cycle A (4).

Le cryptowolinol est donc une dibenzopyrrocoline quaternaire du même type que la cryptowoline et portant une fonction alcool secondaire. Pour des raisons biogénétiques, cet hydroxyle alcoolique ne peut être qu'en position 5 ou 12; c'est l'interprétation du spectre de RMN ^1H, enregistré à 500 MHz dans CD_3OD (Tableau 1), qui a permis de trancher en faveur de cette seconde hypothèse. En effet, ce spectre comporte, outre les signaux provenant du N-méthyle quaternaire, du méthoxyle, du méthylènedioxyle et des quatre protons aromatiques, deux doublets de un proton chacun, à 5,16 et 5,41 ppm, $J = 6$ Hz, qui ne peuvent être attribués respectivement qu'au proton en 13 et à celui en 12, ce dernier étant géminé à la fonction alcool secondaire.

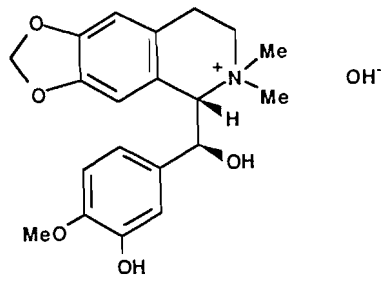
À ce stade, deux structures planes isomères peuvent être proposées pour le cryptowolinol, selon la position de l'hydroxyle phénolique et du méthoxyle en 2 et 3 sur le cycle A. L'étude des effets nucléaires Overhauser a permis d'attribuer au cryptowolinol la structure **5**. L'irradiation du doublet à 5,16 ppm (H en 13) provoque une augmentation d'intensité d'une part du singulet à 3,50 ppm (N-méthyle quaternaire), d'autre part du singulet à 6,83 ppm qui est de ce fait attribué au proton aromatique en 1. L'irradiation du doublet à 5,41 ppm (H en 12) entraîne un accroissement de l'intensité du singulet précédent, mais aussi du singulet à 7,11 ppm qui correspond donc au proton aromatique en 11. D'autre part, en irradiant le troisième singulet de proton aromatique situé à 7,41 ppm, on observe un effet sur le signal à 3,50 ppm du N-méthyle, ce qui permet de placer en 8 ce proton; il s'agit du proton aromatique le plus déblindé, ce qui est logique car il subit l'influence du N-méthyle quaternaire. Le dernier singulet d'un proton, à 6,91 ppm, est donc celui du proton en 4; ceci est confirmé par le fait qu'en l'irradiant on augmente l'intensité du multiplet à 3,10 ppm du CH_2-5; cette même irradiation augmente également l'intensité du singulet à 3,89 ppm du méthoxyle qui, par conséquent, se trouve en position 3.

Le spectre de RMN ^{13}C du cryptowolinol a été enregistré et les attributions ont été faites (Tableau 2) par comparaison à celles de la cryptowoline **1**. La présence de l'hydroxyle alcoolique se traduit par un fort déblindage (35 ppm) du C-12 qui résonne ici à 72,4 ppm, et les carbones 11a et 13, situés en *ortho*, sont faiblement déblindés. Les autres valeurs sont très voisines de celles observées pour la cryptowoline.

Le cryptowolinol **5** est donc une hydroxy-12 cryptowoline dont il reste à établir la configuration absolue. Sa courbe de DC est tout à fait semblable à celle de la cryptowoline et en particulier elle présente, comme elle, un effet Cotton négatif à 244 nm. Ces deux alcaloïdes ont donc la même configuration au niveau du C-13. La stéréochimie en 12 peut être déduite de la valeur



7 : Cryptowolidine



15

($J = 6$ Hz) de la constante de couplage observée en RMN ^1H pour les doublets des protons en 12 et en 13, qui indique un couplage de type axial-équatorial. L'examen du modèle Dreiding du cryptowolinol montre qu'une telle situation est observée lorsque l'hydroxyle en 12 est en dessous du plan moyen, du même côté que le proton en 13; dans ces conditions, le proton en 12 occupe une position pseudo-équatoriale au dessus du plan moyen de la molécule. La configuration absolue proposée pour le cryptowolinol **5** est donc 12-*S*, 13-*R*.

La dernière dibenzopyrrocoline quaternaire isolée, sous forme de chlorure, au cours de ce travail est également nouvelle et a été nommée cryptowolidine. De formule brute $C_{19}H_{20}O_4N^+$, cet alcaloïde **7** est un isomère de la cryptowoline **1** et l'examen de ses données spectrales révèle la très grande parenté des deux produits. En particulier, son spectre de masse est, aux intensités des pics près, pratiquement identique à celui de la cryptowoline, indiquant ainsi que le cycle D porte un méthylènedioxyle en 9,10 et le cycle A un hydroxyle phénolique et un méthoxyle. Il est donc logique de penser que dans la cryptowolidine le phénol est en 3 et le méthoxyle en 2; cette hypothèse a été confirmée par une étude ENO réalisée dans CD_3OD à 500 MHz. L'irradiation du triplet à 5,32 ppm (H en 13) entraîne une augmentation de l'intensité du singulet du proton aromatique résonnant à 6,91 ppm; il s'agit donc du proton en 1. Ce même singulet est également affecté par irradiation du signal à 3,88 ppm du méthoxyle, qui se trouve donc bien en position 2. Les autres signaux du spectre de RMN peuvent alors être attribués sans difficulté (Tableau 1), en particulier celui du proton aromatique en 4 à 6,72 ppm. On constate ainsi qu'en passant de la cryptowoline **1** à la cryptowolidine **7**, le proton en 1 est déblindé de 6,76 à 6,91 ppm, tandis que celui en 4 est blindé de 6,86 à 6,72 ppm; ces déplacements sont tout à fait logiques compte-tenu de la structure de ces deux alcaloïdes.

Ne disposant que d'une très faible quantité de cryptowolidine, nous avons réalisé la synthèse de cet alcaloïde, pour confirmer la structure proposée et pouvoir envisager son triage pharmacologique. Plusieurs méthodes de synthèse du noyau dibenzopyrrocoline ont été décrites (1); parmi elles, nous avons choisi la cyclisation d'une benzyltétrahydroisoquinoléine halogénée convenablement substituée, en la dibenzopyrrocoline correspondante, par l'intermédiaire d'un benzyne obtenu par

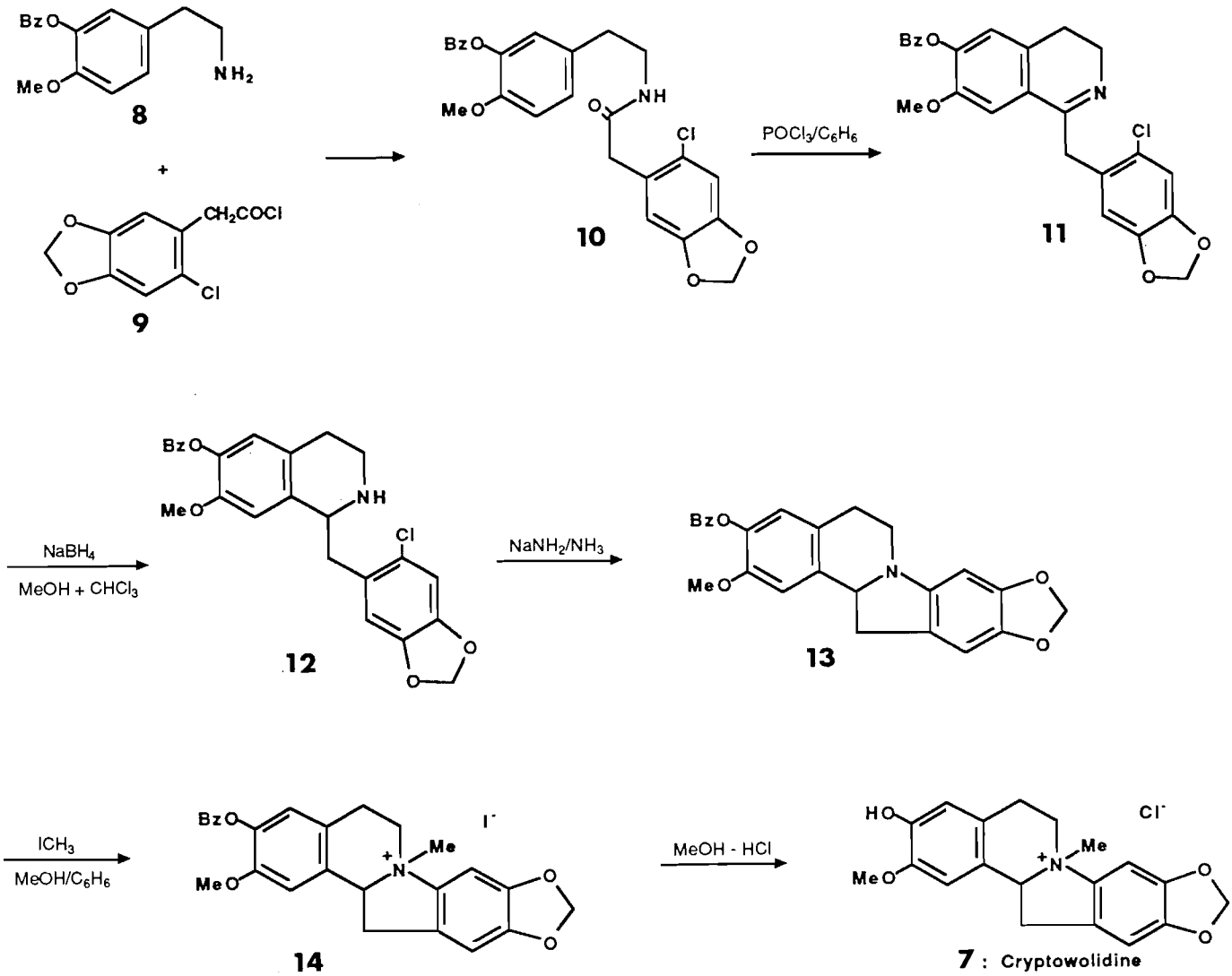


SCHÉMA 1: Synthèse de la cryptowolidine.

réaction de l'amidure de sodium dans l'ammoniac liquide (10, 11). Les étapes de la synthèse de la cryptowolidine sont représentées sur le schéma 1.

Les matières premières utilisées sont la benzyloxy-3 méthoxy-4 β-phényléthylamine **8** et le chlorure de l'acide chloro-2 homopipéronylique **9**; ces deux produits ont été préparés de façon classique, le premier (12, 13) en trois étapes à partir de l'isovanilline, le second (14, 15) en six étapes à partir du pipéronal. La condensation des deux dérivés **8** et **9** conduit à l'amide **10**. Une cyclisation de Bischler–Napieralski, réalisée sur cet amide par action de l'oxychlorure de phosphore dans le benzène à reflux, fournit la (chloro-2′ pipéronyl)-1 benzyloxy-6 méthoxy-7 dihydro-3,4 isoquinoléine **11**, dont la réduction par le borohydrure de sodium livre la benzyltétrahydroisoquinoléine correspondante **12**. La première de ces trois étapes se fait avec un rendement de l'ordre de 70% et les deux autres avec un rendement supérieur à 90%. Traitée par l'amidure de sodium dans l'ammoniac liquide selon la technique décrite par Kametani et Ogasawara (10), la benzyltétrahydroisoquinoléine chlorée **12** subit une cyclisation conduisant à la dibenzopyrrocoline tertiaire **13** qui, très instable comme cela a été déjà observé pour un produit du même type, n'est obtenue pure qu'avec un faible rendement (29%). La N-méthylation de l'amine tertiaire **13** est réalisée par action de l'iodure de méthyle à température ambiante. Enfin, la libération de la fonction phénolique de l'ammonium quaternaire **14** par débenzylation est effectuée par chauffage au bain-marie de sa solution dans un mélange méthanol – acide chlorhydrique. Chacune de ces deux dernières étapes se fait avec un rendement de 75% et on obtient ainsi le chlorure de cryptowolidine racémique, correspondant au produit naturel **7** par son R_f en CCM, ses spectres IR, UV, de masse et de RMN ^1H.

Ainsi, au cours de ce travail portant sur deux espèces néocalédoniennes de *Cryptocarya*, les deux seuls alcaloïdes à squelette dibenzopyrrocoline jusqu'alors connus, la cryptowoline et la cryptaustoline, ont été trouvés pour la seconde fois et deux autres dibenzopyrrocolines quaternaires non encore décrites, le cryptowolinol et la cryptowolidine, ont été isolées. C'est le cryptowolinol **5** qui, par la présence inhabituelle d'un hydroxyle alcoolique sur le carbone benzylique C-12, présente le plus d'originalité. D'un point de vue biogénétique, il est couramment admis, bien que non encore expérimentalement prouvé, que le squelette dibenzopyrrocoline a pour précurseur une benzyltétrahydroisoquinoléine telle que la laudanosoline qui, après oxydation du cycle benzylique, subirait une cyclisation intramoléculaire entre l'atome d'azote et le carbone-2′;

Can. J. Chem. Downloaded from www.nrcresearchpress.com by 41.223.56.140 on 09/07/12
For personal use only.

Can. J. Chem. Downloaded from www.nrcresearchpress.com by 41.223.56.140 on 09/07/12
For personal use only.

cette hypothèse biogénétique a d'ailleurs été mise à profit pour réaliser des synthèses biomimétiques des dibenzopyrrocolines par couplage oxydatif enzymatique de la laudanosoline (16). Dans le cas du cryptowolinol, on peut s'interroger sur son mode de formation in vivo et plus précisément sur le moment de l'hydroxylation en 12 du squelette. Deux hypothèses peuvent être envisagées : ou bien l'hydroxylation est tardive et ne se produit qu'après formation du noyau dibenzopyrrocoline; ou bien cette hydroxylation est précoce et elle concerne alors une *N*-benzyltétrahydroisoquinoléine qui, après hydroxylation de son carbone benzylique C-α, subit la cyclisation en dibenzopyrrocoline. Ces considérations biogénétiques incitent à rapprocher la structure du cryptowolinol **5** de celle de la phyllocryptonine **15**, également présente dans la même espèce *Cryptocarya phyllostemon* (17); la phyllocryptonine est la première benzyltétrahydroisoquinoléine quaternaire naturelle hydroxylée sur son carbone-α. Il est possible, par conséquent, qu'un analogue proche de la phyllocryptonine puisse conduire in vivo au cryptowolinol.

Partie expérimentale

Points de fusion déterminés un tube capillaire à l'aide d'un appareil Tottoli. Pouvoirs rotatoires mesurés à l'aide d'un polarimètre Schmidt–Haensch, type Polatronic I, à la longueur d'onde de la raie D du sodium. Spectres enregistrés sur les appareils suivants : IR, Perkin–Elmer type 257; UV, Unicam SP 1800; DC, Auto-dichrograph Mark V; SM, VG Micromass 70; RMN ^{1}H, Varian T 60 à 60 MHz ou Bruker à 500 MHz; RMN ^{13}C, Varian CFT 20 à 25,2 MHz.

Matériel végétal

L'échantillon de *Cryptocarya phyllostemon* étudié est constitué d'écorces de tiges récoltées en Nouvelle-Calédonie sur les pentes du Mont Dzumac en Novembre 1977; des échantillons d'herbier sont conservés sous la référence PC NC 219 à l'Herbarium de l'ORSTOM à Nouméa.

L'échantillon de *Cryptocarya oubatchensis* consiste en feuilles et écorces de tronc récoltées en Nouvelle Calédonie, à Haute-Tchamba, en juillet 1979; l'échantillon d'herbier (référence Sévenet-Pusset 1901) est déposé au Museum National d'Histoire Naturelle de Paris.

Extraction et isolement des alcaloïdes

Les écorces de tiges broyées (600 g) de *Cryptocarya phyllostemon*, après un dégraissage par l'éther de pétrole en appareil de Soxhlet, sont épuisées dans un lixiviateur par de l'éthanol à 80%. L'extrait, concentré, est repris par une solution aqueuse d'acide citrique à 2%. La phase aqueuse, alcalinisée par NH_4OH, est extraite par $CHCl_3$. L'évaporation de la phase organique fournit un résidu constitué d'alcaloïdes non quaternaires. La phase aqueuse précédente, qui présente encore une réaction de Mayer positive, est acidifiée à pH 1 par HCl concentré et les bases quaternaires sont précipitées par addition de réactif de Mayer concentré. Les iodomercurates ainsi obtenus (84 g) représentent une teneur en bases quaternaires de 4,5%. Une partie (12 g) de ces iodomercurates est solubilisée dans 10 mL d'un mélange Me_2CO–MeOH–H_2O (6:2:1, v/v), et est transformée en chlorures par passage sur une colonne de résine Amberlite IRA 400 en phase Cl^-; 5,1 g de chlorures sont ainsi obtenus. Ils sont dissous dans un mélange $CHCl_3$–MeOH–NH_4OH (70:30:8, v/v) et chromatographiés, en utilisant le même système de solvants, sur une colonne de 200 g de Kieselgel 60 H (Merck 7736). On isole ainsi successivement, après purification par cristallisation ou par chromatographie préparative sur couche mince de gel de silice, cinq bases quaternaires parmi lesquelles la cryptowoline **1** (0,32 g, rdt 0,30% exprimé par rapport au poids de plante sèche), le cryptowolinol **5** (0,81 g, rdt 0,75%) et la crytowolidine **7** (0,09 g, rdt 0,07%). L'isolement et la structure des autres alcaloïdes seront décrits ailleurs (18).

Les alcaloïdes quaternaires de *Cryptocarya oubatchensis* ont été isolés par une méthodologie identique. La teneur en bases quaternaires est de 2,71% dans les écorces de tiges et de 0,77% dans les feuilles. Deux bases quaternaires ont été isolées à partir des écorces de tiges, la crystaustoline **4** (0,07 g, rdt 0,02%) et le cryptowolinol **5** (5,1 g, rdt 1,52%), et une seule à partir des feuilles, le cryptowolinol **5** (1,22 g, rdt 0,30%).

*(−)-Cryptowoline, **1***

$C_{19}H_{20}O_4N^+$ = 326,36. Obtenue cristallisée sous forme de chlorure; *F* 188–190°C ($CHCl_3$); $[\alpha]_D$ −200 (EtOH, *c* = 1); UV, λ_{max} (EtOH) : 210 (log ε 4,59), 222 (log ε 4,03) (épaule), 292 (log ε 3,83); EtOH + NaOH: 212, 240 (épaule), 298; DC (MeOH) : $\Delta\varepsilon_{212}$ −5,9, $\Delta\varepsilon_{225}$ −1,82, $\Delta\varepsilon_{242}$ −3,6, $\Delta\varepsilon_{270}$ 0, $\Delta\varepsilon_{282}$ +0,2, $\Delta\varepsilon_{290}$ 0, $\Delta\varepsilon_{300}$ −0,4, $\Delta\varepsilon_{340}$ 0; SM (ic, NH_3), *m/z* (%) : 326 (M^+, 9); SM (ie), *m/z* (%) : 311 (41), 310 (60), 309 (100), 294 (75), 280 (8), 278 (3), 266 (28), 250 (3); RMN ^{1}H : voir tableau 1; RMN ^{13}C : voir tableau 2.

*O-Méthyl cryptowoline, **2***

Cryptowoline **1** (50 mg), en solution dans 12,5 mL de méthanol, est traitée par 12,5 mL de diazométhane en solution éthérée. Après 1 mois de contact, le solvant est évaporé à sec. *O*-Méthyl cryptowoline **2** (25 mg) est obtenue parfaitement pure après CCM préparative sur silice 60F 254 ($CHCl_3$–MeOH 90 : 10 v/v, vapeurs d'ammoniac). Le produit obtenu est identique à un témoin de *O*-méthyl cryptowoline synthétique. $C_{20}H_{22}O_4N^+$; RMN ^{1}H, $CDCl_3$, 60 MHz, δ : 3,66 (3H, N^+-Me), 3,87 et 3,90 (2 × 3H, OMe-2 et OMe-3), 6,10 (2H, OCH_2O-9,10), 6,76 et 6,81 (2 × 1H, H-1 et H-4), 6,88 (1H, H-11), 7,47 (1H, H-8).

*O-Méthyl cryptowoline méthine, **3***

Cryptowoline **1** (26,5 mg) est dissoute dans 1 mL de potasse méthanolique 0,5 N, puis additionnée de 1 mL de CH_3I. Le mélange est chauffé à reflux pendant 1 h. Après évaporation à sec du solvant, le résidu est extrait par $CHCl_3$. Les solutions chloroformiques évaporées laissent un résidu (14,5 mg) du dérivé vinylique **3** identifié par son spectre de RMN; RMN ^{1}H, $CDCl_3$ 60 MHz, δ : 2,55 (s, 3H, N-CH_3), 3,88 et 3,91 (2s, 2 × 3H, OMe-2 et OMe-3), 5,23 (dd, J_{gem} = 2 Hz, J_{cis} = 11 Hz, 1H, CH-C*H*$_2$), 5,56 (dd, J_{gem} = 2 Hz, J_{trans} = 18 Hz, 1H, CH-C*H*$_2$), 5,86 (s, 2H, OCH_2O-9,10), 6,86 (dd, J_{cis} = 11 Hz, J_{trans} = 18 Hz, 1H, C*H*=CH_2), 6,21, 6,61, 7,01, 7,31 (4s, 4 × 1H, H aromatiques).

*(−)-Cryptaustoline, **4***

$C_{20}H_{24}O_4N^+$ = 342,40. Obtenue à l'état amorphe sous forme de chlorure; $[\alpha]_D$ −150 (EtOH, *c* = 0,45); UV, λ_{max} (EtOH) : 216 (log ε 4,72), 222 (log ε 4,21) (épaule), 288 (log ε 4,03); EtOH + NaOH : 222, 244 (épaule), 296; SM (ic, NH_3), *m/z* (%) : 342 (M^+, 4), 328 (77), 327 (100); SM (ie), *m/z* (%) : 328 (17), 327 (81), 326 (42), 325 (100), 313 (20), 312 (10), 311 (15), 310 (17), 296 (13), 294 (5), 282 (4), 266 (4); RMN ^{1}H : voir tableau 1.

*(−)-Cryptowolinol, **5***

$C_{19}H_{20}O_5N^+$ = 342,36. Obtenu cristallisé de l'acétone sous forme de chlorure; *F* 218–220°C; $[\alpha]_D$ −152 (EtOH, *c* = 1); UV, λ_{max} (EtOH) : 211 (log ε 4,60), 224 (log ε 3,91) (épaule), 230 (log ε 3,90), 293 (log ε 3,89); EtOH + NaOH : 223, 243 (épaule), 298; DC (MeOH) : $\Delta\varepsilon_{215}$ −5,6, $\Delta\varepsilon_{230}$ −2,1, $\Delta\varepsilon_{244}$ −5,2, $\Delta\varepsilon_{281}$ 0, $\Delta\varepsilon_{299}$ −0,5, $\Delta\varepsilon_{342}$ 0; SM (ic, NH_3), *m/z* (%) : 342 (M^+, 2), 310 (100), 309 (74); SM (ie), *m/z* (%) : 341 (6), 327 (1), 325 (2), 324 (9), 323 (38), 321 (16), 310 (21), 309 (100), 308 (16), 295 (15), 294 (73), 280 (10), 266 (30), 250 (6); RMN ^{1}H : voir tableau 1; RMN ^{13}C : voir tableau 2.

*O,O-Diacétyl cryptowolinol, **6***

Préparé à partir de **5** (Ac_2O/Pyr); IR, ν_{max} (KBr) : 1760 cm^{-1}; RMN ^{1}H, CD_3OD, 60 MHz, δ : 1,75 (s, 3H, OAc-12), 2,28 (s, 3H, OAc-2), 3,68 (s, 3H, N^+-Me), 3,88 (s, 3H, OMe-3), 5,68 (d, *J* = 6 Hz, 1H, H-13), 6,16 (s, 2H, OCH_2O-9,10), 6,66 (d, *J* = 6Hz, 1H, H-12), 7,06 (s, 2H, 2 protons aromatiques), 7,11 et 7,53 (2s, 2 × 1H, 2 protons aromatiques).

*(−)-Cryptowolidine, **7***

$C_{19}H_{20}O_4N^+$ = 326,36. Obtenue à l'état amorphe sous forme de chlorure; $[\alpha]_D$ négatif (EtOH); UV, λ_{max} (EtOH) : 212 (log ε 4,48), 225 (log ε 4,04) (épaule), 290 (log ε 3,86); EtOH + NaOH : 219, 240 (épaule), 298; SM (ic, NH_3), *m/z* (%) : 326 (M^+, 6), 312 (100), 311 (14); SM (ie), *m/z* (%): 326 (M^+, 1), 311 (45), 310 (63), 309 (100), 294 (2), 266 (2); RMN ^{1}H : voir tableau 1.

Can. J. Chem. Downloaded from www.nrcresearchpress.com by 41.223.56.140 on 09/07/12
For personal use only.

Synthèse de la cryptowolidine, 7

N-(Benzyloxy-3 méthoxy-4 phényléthyl)-chloro-2' homopipéronyl-amide, 10

L'acide chloro-2 homopipéronylique (5g; 0,022 mol), 5 mL de C_6H_6 anhydre et 6,4 mL de $SOCl_2$ sont chauffés à reflux pendant 2 h. Le benzène et l'excès de $SOCl_2$ sont évaporés sous pression réduite. Le résidu, constitué par le chlorure d'acide **9**, est dissous dans 5 mL d'éther anhydre et ajouté goutte à goutte sous agitation à une solution de 18 g (0,07 mol) de benzyloxy-3 méthoxy-4 β-phényléthylamine **8** dans 650 mL d'éther. Il se forme un précipité blanc qui est recueilli et lavé par de l'éther. On l'agite ensuite pendant 15 min dans de l'eau chaude (50°C) qui dissout le chlorure d'amine. L'amide **10** est alors recueilli par filtration, lavé à l'eau et séché. On obtient 7,6 g de produit brut qui est purifié par chromatographie sur colonne (silice 60 H, élution par $CHCl_3$–MeOH 98 : 2 v/v) et cristallisation dans $CHCl_3$. On isole ainsi 7,1 g de l'amide **10** pur en fins cristaux blancs (rendement 68%). $C_{25}H_{24}O_5NCl$; *F* 178–179°C; RMN ^1H, $CDCl_3$, 60 MHz, δ : 3,48 (s, 2H, CH_2-CO), 3,83 (s, 3H, OMe), 5,06 (s, 2H, OCH_2-φ), 5,91 (s, 2H, OCH_2O), 6,63–6,76 et 7,30–7,40 (2 massifs de m, 2 × 5H, 10H aromatiques).

(Chloro-2' méthylènedioxy-4',5' benzyl)-1 benzyloxy-6 méthoxy-7 dihydro-3,4 isoquinoléine, 11

Un mélange de 4,2 g (9,6 mmol) de l'amide **10**, 25 mL de C_6H_6 et 8,5 mL de $POCl_3$ est porté à reflux pendant 1 h 30. La solution devient brun clair. En refroidissant, un solide jaune pâle précipite. Filtré, lavé par C_6H_6, ce produit est dissous dans une solution hydro-méthanolique chaude. La solution est alcalinisée par NaOH 10%. Par refroidissement, l'imine **11** cristallise et l'on isole 3,97 g de produit pur en CCM (rendement 99%). $C_{25}H_{22}O_4NCl$; *F* 147–148°C; RMN ^1H, $CDCl_3$, 60 MHz, δ : 2,62 (t, *J* = 7,5 Hz, 2H, CH_2-4), 3,70 (t, *J* = 7,5 Hz, 2H, CH_2-3), 3,83 (s, 3H, OMe-7), 4,10 (s large, 2H, CH_2-α), 5,16 (s, 2H, OCH_2-φ), 5,90 (s, 2H, OCH_2O-4',5'), 6,71 et 6,80 (2s, 2 × 1H, H-5 et H-8), 6,86 (s, 1H, H-6'), 7,01 (s, 1H, H-3'), 7,40 (s large, 5H, $OCH_2C_6H_5$).

(Chloro-2' méthylènedioxy-4',5' benzyl)-1 benzyloxy-6 méthoxy-7 tétrahydro-1,2,3,4 isoquinoléine, 12

L'imine **11** étant peu soluble dans le méthanol, sa réduction est effectuée dans un mélange de MeOH et de $CHCl_3$. On dissout 3,66 g de **11** (8,4 mmol) dans 450 mL du mélange $CHCl_3$–MeOH 3 : 7 v/v. On ajoute 850 mg de $NaBH_4$ (22,5 mmol) petit à petit en agitant à température ambiante pendant 30 min, puis le mélange est chauffé à reflux pendant 30 min. Après refroidissement, le milieu réactionnel est alcalinisé par NH_4OH 10% (pH = 9). Le solvant est évaporé et le résidu est extrait par $CHCl_3$. L'extrait chloroformique, lavé, séché sur Na_2SO_4 et évaporé à sec, abandonne un résidu pur en CCM de 3,34 g de l'amine **12** (rendement 91%). $C_{25}H_{24}O_4NCl$; RMN ^1H, $CDCl_3$, 60 MHz, δ : 2,56–3,46 (m, 6H, CH_2-3, CH_2-4 et CH_2-α), 3,78 (s, 3H, OMe-7), 5,06 (s, 2H, OCH_2-φ), 5,75 (s, 2H, OCH_2O-4',5'), 6,60 et 6,68 (2s, 2 × 1H, H-5 et H-8), 6,70 (s, 1H, H-6'), 6,80 (s, 1H, H-3'), 7,28–7,36 (m, 5H, $OCH_2C_6H_5$).

Méthoxy-2 benzyloxy-3 méthylènedioxy-9,10 tétrahydro-5,6,7,13 dibenzo[b,g]pyrrocoline, 13

Une solution d'amidure de sodium dans l'ammoniac liquide anhydre est préparée à partir de 7 g de Na, 250 mL de NH_3 liquide et une pointe de spatule de nitrate de fer. À cette solution de $NaNH_2$ est ajoutée sous agitation vigoureuse une solution de 3,2 g de l'amine chlorée **12** (7,3 mmol) dans 25 mL de THF anhydre. L'agitation est maintenue 3 h. NH_4Cl (16 g) est alors ajouté par petites fractions et on laisse l'ammoniac s'évaporer pendant la nuit. Le résidu est repris par 70 mL d'eau glacée et on extrait par $CHCl_3$. La solution chloroformique, lavée à l'eau, séchée sur K_2CO_3 et évaporée, livre 3,16 g du produit cyclisé **13**, impur en CCM. Connaissant l'instabilité de ce type de produit (19), sa purification est réalisée par une simple filtration rapide sur colonne (silice 60 H, élution par $CHCl_3$). On obtient ainsi 835 mg de la dibenzopyrrocoline **13** pure (rendement 29%). $C_{25}H_{23}O_4N$; RMN ^1H, $CDCl_3$, 60 MHz, δ : 2,98–3,70 (m, 6H, CH_2-5, CH_2-6 et CH_2-12), 3,83 (s, 3H, OCH_3-2), 5,01 (s, 2H, OCH_2-φ), 5,76 (s, 2H, OCH_2O-9,10), 6,23, 6,48, 6,56, 6,63 (4s, 4 × 1H, H-4, H-1, H-11, H-8), 7,33 (s large, 5H, $OCH_2C_6H_5$).

Méthoxy-2 benzyloxy-3 méthyl-7 méthylènedioxy-9,10 tétrahydro-5,6,7,13 dibenzo [b,g]pyrrocoline, 14

En raison de l'instabilité de l'amine **13**, celle-ci est méthylée aussitôt après sa purification. On dissout 320 mg (0,8 mmol) de **13** dans MeOH additionné de C_6H_6 pour améliorer la solubilité. À cette solution est ajouté 5 mL de CH_3I et le mélange bien bouché est laissé à température ambiante pendant 1 nuit. Le solvant est alors évaporé, abandonnant un résidu de 420 mg de **14** impur. Après chromatographie sur colonne (silice 60 H, élution par $CHCl_3$–MeOH 95 : 5 v/v), on isole 365 mg de l'iodure de dibenzopyrrocolinium **14** (rendement 75%). $C_{26}H_{26}O_4N^+,I^-$; SM (ie), *m/z* (%) : 401 (M^+ − 142, 61), 400 (15), 310 (16), 309 (7), 308 (15), 279 (10), 278 (17). *Anal.* calc. % : C 57,45, H 4,79, N 2,58; tr.% : C 57,32, H 4,60, N 2,45.

Méthoxy-2 hydroxy-3 méthyl-7 méthylènedioxy-9,10 tétrahydro-5,6,7,13 dibenzo[b,g]pyrrocoline, 7: (±)-cryptowolidine

On dissout 150 mg de **14** dans un mélange de 5 mL de MeOH et de 3 mL de HCl et la solution est chauffée au bain-marie pendant 10 min. Le résidu (115 mg) obtenu par évaporation à sec est purifié par chromatographie sur colonne (silice 60 H, élution par $CHCl_3$–MeOH 85:15 v/v); 75 mg de chlorure de cryptowolidine racémique pur **7** est obtenu (rendement 75%). Ce produit est identique au produit naturel (co-CCM, SM, RMN ^1H, IR, UV).

Remerciements

Les auteurs expriment leur gratitude aux Docteurs T. Sévenet et J. Pusset (CNRS, Noumea) et P. Cabalion (Centre ORSTOM, Noumea) pour la récolte du matériel végétal. Ils remercient les Professeurs W. C. Taylor (Université de Sydney) et T. Kametani (Université de Tohoku) pour l'envoi d'échantillons de *O*-méthylcryptowoline et de cryptowoline, ainsi que les Docteurs D. Davoust (Université P. et M. Curie, Paris), J. Mahuteau (Faculté de Pharmacie de Châtenay-Malabry) et T. Bécue (S.A.M.M., Faculté de Pharmacie de Châtenay-Malabry) pour l'enregistrement des spectres de RMN et de masse.

1. I. Elliott. Dibenzopyrrocoline alkaloids. *Dans* The alkaloids. Vol. 31. *Éditeur* : A. Brossi. Academic Press, New York. 1987.
2. J. Ewing, G. K. Hugues, E. Ritchie et W. C. Taylor. Nature (London), **169**, 618 (1952).
3. J. Ewing, G. K. Hugues, E. Ritchie et W. C. Taylor. Aust. J. Chem. **6**, 78 (1953).
4. T. Kametani et K. Ogasawara. Chem. Pharm. Bull. **16**, 1498 (1968).
5. M. Shamma et D. M. Hindenlang. Carbon-13 NMR shift assignments of amines and alkaloids. Plenum Press, New York. 1979.
6. A. J. Marsaioli, E. A. Ruvéda et F. De A. M. Reis. Phytochemistry, **17**, 1655 (1978).
7. C. P. Mak et A. Brossi. Heterocycles, **12**, 1413 (1979).
8. S. Takano, S. Satoh, Y. Oshima et K. Ogasawara. Heterocycles, **26**, 1487 (1987).
9. E. Sanchez et J. Comin. Tetrahedron Lett. 1139 (1967).
10. T. Kametani et K. Ogasawara. J. Chem. Soc. (C), 2208 (1967).
11. F. Benington et R. D. Morin. J. Org. Chem. **32**, 1050 (1967).
12. R. Robinson et S. Sugasawa. J. Chem. Soc. 3163 (1931).
13. Fou-Tian et Dou-Bian. J. Pharm. Soc. Jpn. **58**, 783 (1938).
14. H. Weil. Beilstein, **43**, 2605 (1910).
15. R. G. Naik et T. S. Wheeler. J. Chem. Soc. 1780 (1938).
16. A. Brossi, A. Ramel, J. O'Brien et S. Teitel. Chem. Pharm. Bull. **21**, 1839 (1973).
17. I. R. C. Bick, W. Sinchai, T. Sévenet, A. Ranaivo, M. Nieto et A. Cavé. Planta Med. **39**, 205 (1980).
18. A. Cavé, M. Lebœuf, H. Moskowitz, A. Ranaivo, I. R. C. Bick, W. Sinchai, M. Nieto, T. Sévenet et P. Cabalion. Aust. J. Chem. Soumis.
19. T. Kametani, A. Ujiie, K. Takahashi, T. Nakano, T. Suzuki et K. Fukumoto. Chem. Pharm. Bull. **21**, 766 (1973).

Compressibilités de l'eau et du benzène dans tout le domaine de miscibilité du système eau + 2-propanol + benzène

DANIEL HÉTU[1]
Institut national de la recherche scientifique – Énergie, Varennes (Qué.), Canada J0L 2P0

ET

JAIME LARA[2] ET JACQUES E. DESNOYERS[3]
Département de chimie, Université de Sherbrooke, Sherbrooke (Qué.), Canada J1K 2R1

Reçu le 5 juillet 1988[4]

DANIEL HÉTU, JAIME LARA et JACQUES E. DESNOYERS. Can. J. Chem. **67**, 953 (1989).

Les vitesses du son ont été mesurées de façon à couvrir tout le domaine de miscibilité du système eau + 2-propanol + benzène. Les compressibilités isentropiques molaires apparentes du benzène et de l'eau ont été calculées à partir de ces données. Les compressibilités molaires apparentes du benzène et de l'eau présentent respectivement de grandes variations dans les régions riches en eau et en benzène, alors que les variations deviennent plus régulières dans la région intermédiaire. Ces résultats suggèrent qu'il se produit, aux deux extrémités du diagramme de phase, des micro-transitions analogues à la formation de micelles et de micelles inverses. L'absence de transition dans la région intermédiaire est, quant à elle, conforme au modèle bi-continu de microémulsion. Plus d'attention a été portée à la région riche en eau, où les compressibilités de transfert du benzène à dilution infinie, de l'eau aux mélanges eau + 2-propanol, ont été simulées à l'aide du modèle de Roux et coll. Cette simulation tend à confirmer que l'alcool et le benzène forment des agrégats mixtes.

Mots clés : compressibilité, système ternaire, microémulsion, eau, benzène, 2-propanol.

DANIEL HÉTU, JAIME LARA, and JACQUES E. DESNOYERS. Can. J. Chem. **67**, 953 (1989).

Sound velocities have been measured over the whole miscibility domain of the water + 2-propanol + benzene system. The apparent molar isentropic compressibilities of benzene and water were calculated from these data. The apparent molar compressibilities of benzene and water present large changes in the water-rich and benzene-rich regions, respectively, whereas the changes are smooth in the intermediate region. These results suggest that microtransitions similar to the formation of micelles and inverse micelles occur at the two ends of the phase diagram. The regularity of the intermediate region is consistent with a bicontinuous model of microemulsions. For the water-rich region, the compressibilities of transfer of benzene at infinite dilution, from water to water + 2-propanol mixtures, were simulated with the model of Roux and co-workers. This simulation tends to confirm that the alcohol and the benzene form mixed aggregates.

Key words: compressibility, ternary system, microemulsion, water, benzene, 2-propanol.

Introduction

Les alcools ont longtemps été reconnus comme des agents secondaires aidant à stabiliser les microémulsions. Toutefois, depuis quelques années, le rôle des alcools dans la formation et la stabilisation des microémulsions a fait l'objet de nombreuses études (1–4). Il a ainsi été démontré qu'un alcool pouvait en fait solubiliser à lui seul d'importantes quantités d'huile dans l'eau (5–7) et que les systèmes ainsi formés présentaient des propriétés physiques typiques des microémulsions (8, 9).

De curcroît, il y a maintenant de plus en plus de preuves démontrant l'existence de micro-phases dans les simples mélanges eau–alcool (10, 11). Leurs propriétés, en particulier leurs propriétés thermodynamiques, ressemblent aussi à plusieurs égards à celles des solutions micellaires (12). D'ailleurs, afin d'expliquer les propriétés thermodynamiques des systèmes eau–alcool, Roux et Desnoyers (13) ont récemment proposé un modèle très semblable à un modèle de micellisation.

Ces dernières années, la présente équipe s'est grandement impliquée dans l'étude du comportement d'additifs dans les systèmes micellaires. Une étude précédente a révélé que les volumes et les capacités calorifiques molaires apparentes du benzène, dans tout le domaine de miscibilité du système eau + 2-propanol + benzène (14), sont très semblables à ceux du toluène dans le système toluène + eau + *n*-butanol + dodécylsulfate de sodium. Ce dernier système est reconnu pour former des microémulsions (15). Les importantes transitions observées dans les régions riches en eau et en benzène du système eau + 2-propanol + benzène ont donc été expliquées par la formation de micro-agrégats du genre micelles et micelles inverses. Une autre étude des fonctions thermodynamiques de transfert du benzène, de l'eau aux mélanges eau + 2-propanol (16), a montré que ces fonctions présentaient de grandes similitudes avec les fonctions de transfert de certains solutés hydrophobes aux systèmes micellaires (17, 18), ce qui soutient l'idée que les alcools peuvent former des agrégats mixtes avec un soluté hydrophobe.

Compte tenu que la plupart des études thermodynamiques visant à comprendre l'effet d'un soluté hydrophobe sur un système micellaire ont été effectuées en utilisant l'approche des fonctions de transfert du soluté hydrophobe, de l'eau aux mélanges tensioactif, un modèle d'équilibre chimique permettant de simuler ces fonctions a été proposé (19–21). Ce modèle a été appliqué avec succès aux volumes et aux capacités de transfert du benzène (21) et d'alcools (19, 20), les paramètres thermodynamiques extraits à l'aide de ces simulations étant, lorsque la comparaison était possible, en excellent accord avec ceux obtenus à partir d'autres modèles théoriques semblables. Le modèle a aussi été appliqué aux volumes, aux enthalpies et aux

---

1. Présente adresse : Université de Moncton, Centre Universitaire de Shippegan, Shippegan, N.B., Canada E0B 2P0.

2. Présente adresse : Institut de recherche en santé et sécurité au travail, 505 boul. de Maisonneuve Ouest, Montréal (Qué.), Canada H3A 3C2.

3. La correspondance doit être adressée à cet auteur, Institut national de la recherche scientifique, C.P. 7500, Ste-Foy (Qué.), Canada G1V 4C7.

4. Révision reçue le 18 janvier 1989.

Can. J. Chem. Downloaded from www.nrcresearchpress.com by 41.223.56.140 on 09/07/12
For personal use only.

Can. J. Chem. Downloaded from www.nrcresearchpress.com by 41.223.56.140 on 09/07/12
For personal use only.

capacités calorifiques de transfert du benzène aux solutions aqueuses d'alcools (19), mais aucune simulation de compressibilités n'a à ce jour été publiée.

Afin de compléter l'étude du système eau + 2-propanol + benzène, les compressibilités de l'eau et du benzène dans tout le domaine de miscibilité sont présentées ici. L'analyse qualitative des résultats de cette démarche est appuyée par la simulation théorique des compressibilités de transfert du benzène à dilution infinie de l'eau aux mélanges eau + 2-propanol.

Conditions expérimentales

Les compressibilités isentropiques β_S, en bar^{-1}, ont été obtenues à partir des vitesses du son μ, en m s^{-1}, en utilisant la relation suivante :

$$[1] \quad \beta_S = 100/\mu^2 d$$

où d représente la densité des solutions en g cm^{-3}. Les mesures de vitesses du son ont été effectuées avec un vélocimètre Nusonic (Mapco, modèle 6105) basé sur la méthode du «sing around» (22, 23). Les vitesses du son ont été obtenues à partir des fréquences f avec la relation :

$$[2] \quad \mu = A(1 + \alpha t)/(7/f - 10^{-6}B)$$

où A et B sont des constantes de la cellule, α le coefficient d'expansion thermique de la cellule et t, la température en °C. les valeurs de A et B ont été obtenues par calibration de la cellule avec de l'eau, en utilisant les données de Del Grosso et Mader (24). Lors des mesures, la température a été maintenue à 25.00 ± 0.01°C à l'aide d'un bain à circulation SODEV et vérifiée avec un thermomètre à quartz Hewlett–Packard. Les densités ont été mesurées à l'aide d'un densimètre à écoulement SODEV, ou obtenues par interpolation à partir des données de l'étude antérieure sur les volumes du système benzène + 2-propanol + eau (14).

Les compressibilités isentropiques molaires apparentes ϕ_{KS} du composant 3, soit l'eau (W) ou le benzène (B), ont été obtenues en prenant, selon le cas, le mélange binaire eau + 2-propanol (W + P) ou 2-propanol + benzène (P + B) comme solvant de référence, le calcul se faisant à l'aide de l'équation :

$$[3] \quad \phi_{KS} = \beta_S\phi_v + (X_1M_1 + X_2M_2)(\beta_S - \beta_{S,0})/X_3d_0$$

où ϕ_V est le volume molaire apparent du soluté 3 dans le solvant mixte de densité d_0; X, la fraction molaire; M, la masse molaire; β_S et $\beta_{S,0}$ représentant respectivement les coefficients de compressibilité des systèmes ternaires et binaires. Les indices 1 et 2 réfèrent respectivement à W et P ou à P et B.

Comme ce fut le cas pour les volumes et les capacités calorifiques (14), les solutions ont été préparées gravimétriquement de façon à couvrir tout le domaine de miscibilité. La cellule était d'abord remplie avec un mélange binaire W + P ou P + B initial et le troisième constituant, W ou B, était ajouté par quantités pesées, directement dans la cellule, jusqu'à pleine capacité.

L'eau utilisée pour la préparation des solutions ainsi que comme solvant de référence a été distillée, déionisée (Continental deionized water system), filtrée sur filtre millipore 0.22 μm type GS et dégazée. Sa conductivité était en tout temps inférieure à 5×10^{-6} cm^{-1} Ω^{-1}. Le 2-propanol (Fisher Scientific) était de qualité Certifié ACS. Il a été gardé sur tamis moléculaire 4A (Davidson Chemicals) pour être filtré sur filtre millipore 0.22 μm juste avant son utilisation. Le benzène (Fisher Scientific) a subi le même traitement que le 2-propanol, mais était de qualité spectro-analysé.

Résultats

Toutes les données originales pour les compressibilités isentropiques molaires apparentes de B ($\phi_{KS,B}$) et de W ($\phi_{KS,W}$) dans tout le domaine de miscibilité du système W + P + B sont données sous forme de tableaux condensés.[5] Sont aussi incluses

5. On peut acheter ces tableaux en s'adressant au Dépôt des données non publiées, ICIST, Conseil national de recherches du Canada, Ottawa (Ontario), Canada K1A 0S2.

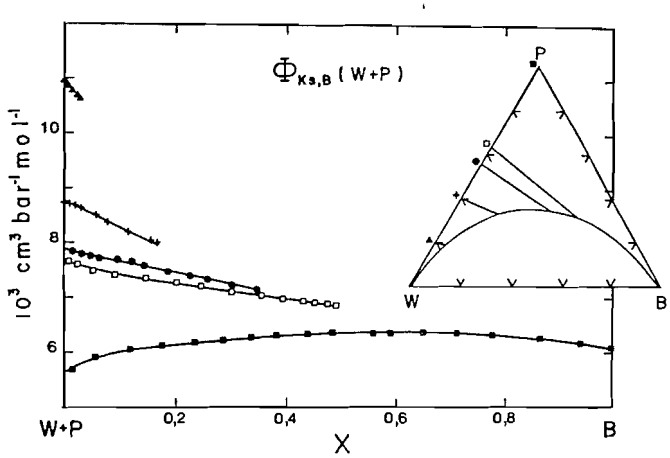


FIG. 1. Compressibilités isentropiques molaires apparentes du benzène dans le système ternaire eau–2-propanol–benzène en fonction de la concentration de benzène, à 25°C.

les données pour B à dilution infinie dans les mélanges W + P, dont les résultats ont déjà été publiés graphiquement (16). Les données de densité nécessaires pour le calcul des compressibilités sont disponibles ailleurs (14).

Les valeurs de $\phi_{KS,B}$ ont été portées en graphique en fonction de X_B à la figure 1, où les valeurs limites $\phi^0_{KS,B}$ (W + P) délimitent la fonction standard de B à dilution infinie ($X_B \rightarrow 0$) dans les mélanges W + P. Les trajets suivis dans le domaine de miscibilité sont montrés sur le diagramme de phase en surimpression, les concentrations des mélanges binaires W + P initiaux étant X_P = 1,00, 0,63, 0,56, 0,40 et 0,20. Pour ces concentrations, la solubilité de B est, relativement à la sensibilité des appareils, assez élevée pour permettre des mesures raisonnables. Compte tenu de la grande volatilité du benzène et de la difficulté à manipuler les solutions, la limitation de la précision des mesures provient donc essentiellement de la détermination de la concentration de B. Ainsi, en admettant une incertitude d'environ 1% sur X_B, l'erreur sur les valeurs de compressibilités de la figure 1 serait généralement de 1×10^{-5} cm^3 bar^{-1} mol^{-1}. L'erreur peut toutefois atteindre jusqu'à 0.2×10^{-3} cm^3 bar^{-1} mol^{-1} aux faibles concentrations de B. C'est par exemple le cas pour la détermination directe de la fonction standard de B à dilution infinie en fonction de X_P (16), où la concentration de B a été maintenue aussi faible que possible de façon à rendre l'effet de concentration de B négligeable, et où la solubilité de B à $X_P < 0,1$ devient particulièrement limitée. Compte tenu de la grandeur des changements observés, la précision des mesures est néanmoins largement suffisante.

Pour avoir un profil global du comportement du système étudié dans tout le domaine de miscibilité, les données de la figure 1 sont présentées sur un graphique tridimensionnel permettant de mettre les propriétés en relation avec le diagramme de phase. Ce type de graphique pour les propriétés apparentes de B est présenté à la figure 2. Dans ce diagramme, les valeurs de $\phi^0_{KS,B}$ (W + P) se retrouvent sur le plan gauche, les compressibilités molaires apparentes de B dans P, $\phi_{KS,B}$ (P), sur le plan de droite, la ligne pointillée de l'axe W + B représentant les compressibilités de B à la limite de la zone de miscibilité. Les lignes pâles allant de l'axe W + P vers B pur correspondent, comme à la figure 1, aux trajets suivis dans le domaine de miscibilité.

En général, les tendances observées pour les valeurs de compressibilités de la figure 2 ressemblent grandement à celles des volumes (14). Ainsi, dans la région riche en eau, les valeurs de $\phi_{KS,B}$ changent d'une façon très marquée avec X_P et X_B, attei-

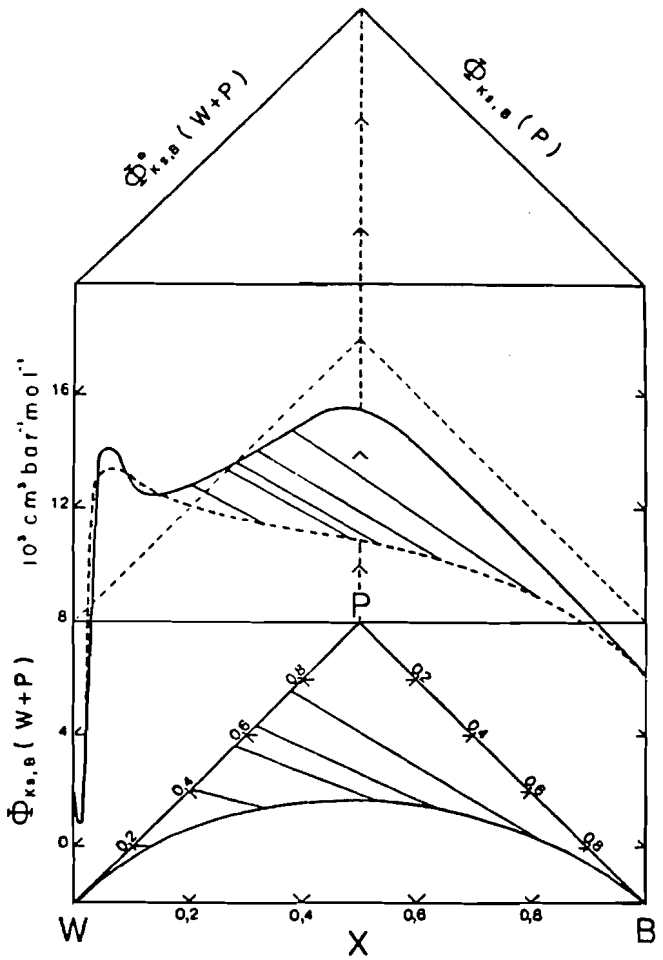


FIG. 2. Compressibilités isentropiques molaires apparentes du benzène sur toute la zone de miscibilité du système eau–2-propanol–benzène, à 25°C.

gnant un minimum aux environs de $X_P = 0{,}03$ et un maximum, particulièrement important lorsque X_B tend vers zéro, autour de $X_P = 0{,}05$. Il semble aussi exister une diminution accentuée des valeurs dans la région riche en P, mais les changements se font généralement plus réguliers dans la partie centrale du diagramme. Ainsi, sur l'axe W + B, soit le long de la limite de la zone de miscibilité, les valeurs tendent simplement vers la valeur de B pur, alors que sur l'axe B + P, les compressibilités changent presque idéalement, de la valeur standard à dilution infinie dans P pur, à la valeur molaire de B pur.

Dans la région riche en B, les valeurs de $\phi_{KS,B}$ sont peu sensibles aux changements, car les interactions sont imputées à un très grand nombre de molécules. Pour investiguer les changements structuraux de la région non-aqueuse, ce sont donc les compressibilités de l'eau, présente en petite quantité, qui sont examinées. Les résultats en fonction de la concentration d'eau, ainsi que les trajets suivis pour des mélanges initiaux P + B de concentrations $X_B = 0$, 0,09, 0,43 et 0,76 sont présentés à la figure 3.

Afin d'avoir un profil global de comportement dans tout le domaine de miscibilité, les $\phi_{KS,W}$ de la figure 3 ont, comme les $\phi_{KS,B}$, été reportés sur un diagramme en trois dimensions présenté à la figure 4. Comme dans le cas des volumes et des capacités calorifiques (14), les changements de l'axe W + P sont, comparativement aux $\phi_{KS,B}$, grandement amoindris, la seule variation d'importance se trouvant dans la région riche en

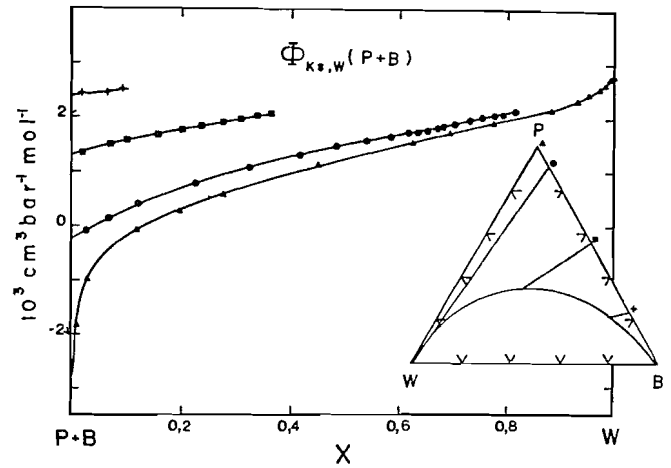


FIG. 3. Compressibilités isentropiques de l'eau dans le système ternaire eau–2-propanol–benzène en fonction de la concentration de l'eau, à 25°C.

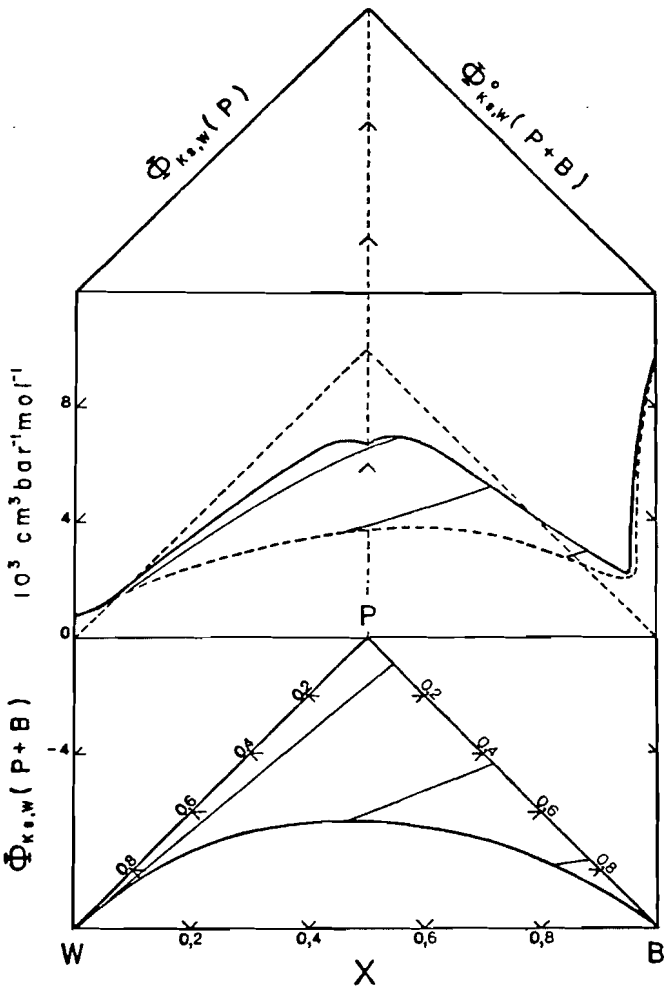


FIG. 4. Compressibilités isentropiques molaires apparentes de l'eau sur toute la zone de miscibilité du système eau–2-propanol–benzène, à 25°C.

B. Il est toutefois à noter qu'il existe encore ici une diminution accentuée des valeurs dans la région riche en P.

Discussion

En règle générale, le comportement des compressibilités mène aux mêmes conclusions que les volumes et les capacités calorifiques (14), à savoir qu'il existe d'importantes transitions

Can. J. Chem. Downloaded from www.nrcresearchpress.com by 41.223.56.140 on 09/07/12
For personal use only.

Can. J. Chem. Downloaded from www.nrcresearchpress.com by 41.223.56.140 on 09/07/12
For personal use only.

dans les régions riches en W et en B, correspondant respectivement à la formation d'agrégats de type huile dans l'eau et eau dans l'huile. De plus, en accord avec le modèle bi-continu de Scriven (25), la régularité des changements dans le reste du domaine de miscibilité tend à démontrer qu'il y a coexistence de ces deux types d'agrégats et non un changement abrupt d'une forme à l'autre à une composition donnée.

À la figure 2, il est visible que, dans les mélanges B + P, le benzène se comporte à peu près idéalement. La présence de traces d'eau dans ces mélanges aurait donc comme effet d'orienter les molécules de P, par établissement de liens hydrogène entre l'eau et les groupements −OH de P, de façon à en promouvoir l'association. Il en résulterait la formation d'agrégats de type eau dans l'huile, ce dont témoigne le signe inversé de la transition des $\phi_{KS,W}$ (P + B) de la région riche en B, figure 4, comparativement au $\phi_{KS,B}$ (W + P) de la région riche en eau, figure 2. La promotion de la structure de P par l'eau se confirme de plus par l'analyse des compressibilités de l'eau dans les mélanges binaires W + P de la région riche en alcool, dont la courbe est présentée à la figure 3. Bien que plutôt faible à la figure 2, où il n'y a qu'une légère accentuation dans la variation des valeurs de $\phi_{KS,B}$, l'accentuation dans les valeurs de $\phi_{KS,W}$ de la région riche en P est très évidente et résulte certainement de la formation d'ilots plus structurés de P au coeur du solvant. Cette interprétation est en conformité avec l'idée d'agrégats inverses, où les groupements −OH des alcools seraient orientés vers les molécules d'eau se trouvant alors enfermées au coeur de ces agrégats.

L'axe W + P de la figure 2 est celui qui est le plus affecté par les transitions. Aussi, afin d'analyser les transitions de la région riche en eau, les compressibilités de transfert standard de B de l'eau mélanges W + P, $\Delta K^0_{S,B}$ (W→W + P), ont, comme les volumes (21), été simulées à l'aide du modèle de Roux et coll. (19, 20). Ce modèle a été prévu pour décrire le comportement d'un soluté hydrophobe peu soluble dans l'eau, lorsqu'il est transféré de l'eau aux solutions aqueuses d'un tensioactif nonionique. Ceci permet ainsi de vérifier si le P a un comportement associatif analogue à celui des tensioactifs.

Selon ce modèle, l'allure générale des courbes de fonctions de transfert peut s'expliquer par trois principales contributions : (1) les interactions hydrophobes par paire entre les monomères du soluté transféré et ceux du tensioactif; (2) le partage du soluté transféré entre l'eau et les micelles du tensioactif; (3) le déplacement d'équilibre du tensioactif, induit par l'action du soluté transféré. Dans le cas des propriétés dérivées secondes de l'enthalpie libre, comme la compressibilité, la courbe est généralement plus complexe et une quatrième contribution, dite de relaxation et dépendant de la propriété dérivée première, doit aussi être considérée. Ainsi, la courbe des compressibilités de transfert peut être reproduite à partir de l'équation suivante :

$$[4]\quad \Delta K_3(\mathrm{W}\rightarrow \mathrm{W}+2) = 2\alpha\beta B_{K,AB} m_2 + (m_2/m_3)(\alpha_0-\alpha)(K_{A'}-K_A) + (1-\beta)(K_{B'}-K_B) - (m_2/m_3)\times\left(\frac{\partial\alpha_0}{\partial P}-\frac{\partial\alpha}{\partial P}\right)(V_{A'}-V_A) + (V_{B'}-V_B)\frac{\partial\beta}{\partial P}$$

Dans cette équation, m_2 et m_3 sont respectivement les molalités du soluté principal et du soluté transféré, $B_{K,AB}$ est la pente d'interaction hydrophobe par paire entre les monomères A du soluté 2 et B du soluté 3, P étant la pression. $K_{A'}$ et $K_{B'}$ représentent respectivement les compressibilités molaires des solutés 2 et 3 dans les micelles ou agrégates, K_A et K_B les compressibilités molaires dans la phase aqueuse, alors que $V_{A'}$, $V_{B'}$, V_A et V_B symbolisent les volumes molaires des différentes espèces. Finalement α et β sont les fractions de monomères des solutés 2 et 3 restant dans la phase aqueuse, le 0 en indice indiquant les valeurs pour les systèmes binaires des solutés dans l'eau. Les valeurs de α et β sont obtenues en résolvant, par itération, les deux équations suivantes conditionnant l'équilibre

$$[5]\quad -(1/n)\ln K_M = \ln \alpha m_2 - (1/n)\ln[(1-\alpha)m_2/n] + X_{B'}$$

$$[6]\quad -\ln K_D = \ln(\beta m_3/X_{B'}) + X_{B'} - 1$$

Dans ces équations, K_M représente la constante d'équilibre du processus d'aggrégation du soluté 2, K_D la constante de distribution du soluté 3 entre l'eau et les micelles ou agrégats, n le nombre d'agrégation, R la constante des gaz parfaits, T la température en Kelvin et $X_{B'}$ la fraction molaire du soluté 3 dans les agrégats, définie comme :

$$[7]\quad X_{B'} = \frac{(1-\beta)m_3}{(1-\beta)m_3 + (1-\alpha)m_2}$$

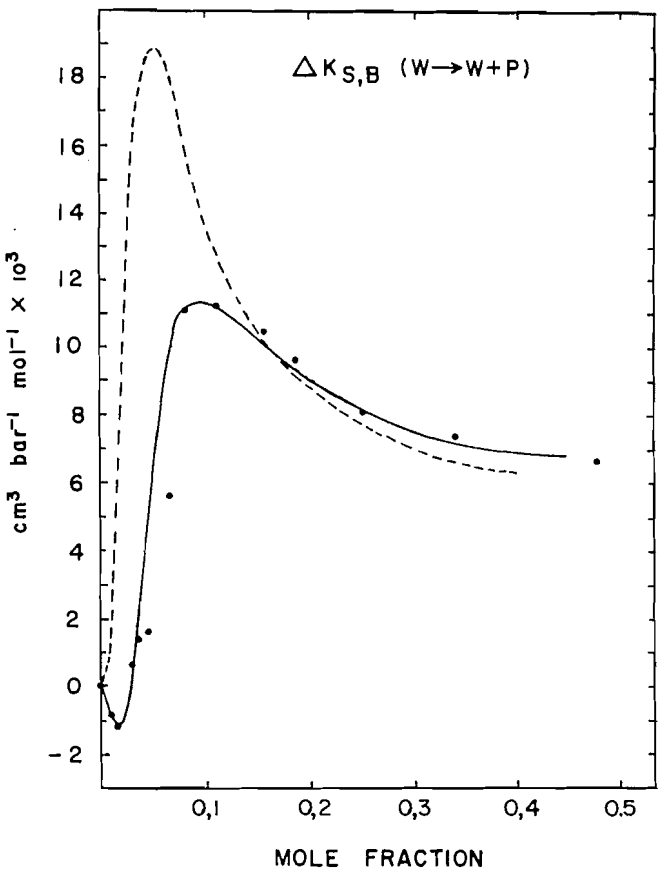


FIG. 5. Simulations des compressibilités isentropiques de transfert du benzène à dilution infinie, de l'eau aux mélanges eau–2-propanol, à 25°C. (---) simulation idéale; (—) simulation ajustée.

Les points expérimentaux et les simulations sont présentés à la figure 5. Les valeurs expérimentales de $\Delta K_{S,B}$ (W→W + P) ont été calculées en soustrayant systématiquement la valeur du $\phi^0_{KS,B}$ (W) de B à dilution infinie dans l'eau, soit (1,9 ± 0,2) × 10^{-3} cm^3 bar^{-1} mol^{-1}, des valeurs de la fonction standard de B à dilution infinie dans les mélanges W + P. Les simulations, représentées par la ligne pleine et la ligne pointillée, ont été effectuées à partir des paramètres du tableau 1, où leur prove-

TABLEAU 1. Paramètres utilisés pour les simulations des compressibilités isentropiques de transfert du benzène, de l'eau aux mélanges eau–2-propanol, à 25°C

Paramètres	Simulation idéale	Simulation ajustée
$\Delta K^{M}_{S,P}$ cm^3 bar^{-1} mol^{-1}	7.09×10^{-3}[a]	7.09×10^{-3}[a]
ΔV^{M}_{P} cm^3 mol^{-1}	3.88[b]	3.88[b]
m_I (cmc) mol kg^{-1}	4[c]	4[c]
n	4[c]	4[c]
$B_{K,AA}$ cm^3 kg bar^{-1} mol^{-2}	0	-0.31×10^{-3}[a]
$\Delta K^{M}_{S,B}$ cm^3 bar^{-1} mol^{-1}	4.20×10^{-3}[d]	4.25×10^{-3}
ΔV^{M}_{B} cm^3 mol^{-1}	6.45[e]	6.45[e]
K_D	43.3[f]	4.4
$B_{K,AB}$ cm^3 kg bar^{-1} mol^{-2}	0	-1.54×10^{-3}[g]
m_3 mol kg^{-1}	0.02	0.02

[a]Référence 26.
[b]Référence 27.
[c]Calculé en appliquant le modèle de Roux et coll. (28) sur les données expérimentales de Hétu (29).
[d]Référence 30.
[e]Référence 19.
[f]Référence 14.
[g]Évalué graphiquement à partir des données expérimentales (30).

nance est indiquée. Il faudrait toutefois préciser que la molalité à l'inflexion m_I et le nombre d'agrégation n du système binaire W + P ont été obtenus en simulant la courbe des volumes molaires apparents du P dans l'eau à l'aide du modèle de micellisation de Roux et coll. (28), pour les systèmes binaires eau–tensioactif, considérant que l'alcool a un comportement associatif similaire à celui d'un tensioactif. La valeur de 4 obtenue pour m_I correspond bien à ce qui est observé expérimentalement. Il faudrait cependant considérer que le nombre d'agrégation de 4 obtenu n'a qu'une signification qualitative montrant que le P n'a tendance à former que de très petits agrégats, probablement très labiles. Compte tenu du nombre d'agrégation de 10 obtenu par Quirion[6] pour le butoxy-2 éthanol, utilisant plusieurs techniques, la valeur de 4 pour le P semble néanmoins très réaliste, d'autant plus que la tendance montre que des alcools plus petits comme l'éthanol et le méthanol présenteraient des nombres d'agrégation très voisin de zéro.

La ligne pointillée représente la simulation idéale obtenue en négligeant les interactions hydrophobes par paire et en assumant que le benzène se partage, entre la phase aqueuse et les micelles, comme il le ferait entre l'eau et une phase pure de benzène. Cette simulation implique donc que la constante de distribution K_D est simplement évaluée par l'inverse de la solubilité S de B dans l'eau, alors que la compressibilité molaire de B dans les agrégats, $K_{S,B'}$, est simplement donnée par la compressibilité molaire de B pur, $K^{*}_{S,B}$. Cette simulation prédit bien l'allure générale de la courbe. Toutefois, comme le démontre son pauvre accord quantitatif avec les données expérimentales, la solution ne se comporte visiblement pas d'une façon aussi idéale que ne l'impliquent ces approximations. Aussi, afin de rendre cette analyse plus quantitative, la constante de distribution K_D et la fonction de micellisation de B $\Delta K^{M}_{S,B}$ ont été ajustées de façon à tenir compte des diverses sources secondaires de non-idéalité du processus d'agrégation. De plus, la pente initiale tenant compte des interactions hydrophobes par paire dans la phase aqueuse a été considérée, celle-ci ayant été évaluée par régression linéaire des points expérimentaux de la partie linéaire de la région diluée. La simulation obtenue, qui est représentée à la figure 5 par la ligne en trait plein, est quantitativement en accord avec les données expérimentales.

Au tableau 1, la valeur obtenue pour le $\Delta K^{M}_{S,B}$ ajusté, soit la variation entre la compressibilité de B dans les agrégats et sa compressibilité dans l'eau, est sensiblement la même que la valeur idéale. Par contre, la valeur ajustée de K_D, 4,4, est environ 10 fois plus faible que l'inverse de la solubilité, ce qui confirme bien la faible valeur de 1,8 obtenue par la simulation des volumes (21). Bien que de nature semi-quantitative, ces résultats tendent néanmoins à démontrer que le B se retrouve essentiellement dans un milieu très semblable à une phase pure de B, mais que ce milieu lui est beaucoup moins accessible qu'une phase pure. Comme l'ont démontré Abuin et Lissi (31), lorsque la fraction molaire du soluté intra-micellaire $X_{B'}$ atteint 0,5, les valeurs de K_D chutent abruptement pour tendre vers une nouvelle valeur. Ainsi, compte tenu du faible nombre d'agrégation moyen de P rapporté au tableau 1, $X_{B'}$ tendrait rapidement vers 0,5, les agrégats se saturant rapidement et restreignant ainsi l'accès à des molécules supplémentaires. Il y aurait donc formation de micro-phases de B stabilisées par quelques molécules de P, où les molécules de B seraient en grande partie en contact avec d'autres molécules de B et isolées de l'eau par les molécules de P, ce qui est caractéristique des microémulsions (32).

Conclusion

L'analyse des compressibilités isentropiques molaires apparentes de B et de W dans tout le domaine de miscibilité du système W + P + B tend, à l'instar des volumes et des capacités calorifiques, à démontrer l'existence d'agrégats mixtes de B et de P de type huile dans l'eau dans la région riche en eau du diagramme de phase et de type eau dans l'huile dans la région riche en B, le passage d'une forme à l'autre se faisant graduellement, conformément à un modèle bi-continu de microémulsion. Cette analyse est appuyée par le fait que les compressibilités de transfert de B, de l'eau aux solutions aqueuses de P, peuvent être simulées à l'aide d'un modèle destiné aux transferts de solutés hydrophobes dans les systèmes micellaires, les paramètres obtenus montrant que les agrégats formés présentent des caractéristiques de microémulsions.

Remerciements

Nous sommes reconnaissants au Fonds pour la formation de chercheurs et l'aide à la recherche et au Conseil de recherches en sciences naturelles et en génie du Canada pour l'aide financière apportée à ce projet.

1. L. M. PRINCE (*Éditeur*). Microemulsions: Theory and practice. Academic Press, New York. 1977.
2. K. L. MITTAL (*Éditeur*). Micellization solubilization and microemulsion. Plenum Press, New York. 1976.
3. I. D. ROBB. Microemulsions. Plenum Press, New York. 1982.
4. J. F. SCAMEHORN (*Éditeur*). Phenomena in mixed surfactant systems: ACS Symposium Ser. n° 311 (1986).
5. A. L. VOROB'EVE et M. KH. KARAPET'YANTS. Russ. J. Phys. Chem. **40**, 1619 (1966); **41**, 602 (1967); **41**, 1061 (1967).
6. N. P. FEDOSEEVA, V. M. KUCHUMOVA, L. A. KOCHANOVA et E. D. SHCHUKIN. Russ. J. Colloid Sci. **39**, 1055 (1977).
7. C.-U. HERRMANN, U. WÜRZ et M. KAHLWEIT. Ber. Bunsen-ges. Phys. Chem. **82**, 560 (1978).
8. G. D. SMITH, C. E. DONOLAN et R. E. BARDEN. J. Colloid Interface Sci. **60**, 488 (1977).
9. B. A. KEISER, D. VARLE, R. E. BARDEN et S. L. HOLT. J. Phys. Chem. **83**, 1276 (1977).
10. N. ITO, K. SAITO, T. KATO et T. FUJIYAMA. Bull. Chem. Soc. Jpn. **54**, 991 (1981).
11. F. FRANKS et J. E. DESNOYERS. *Dans* Water Science Reviews.

6. F. Quirion. Manuscrit en préparation.

Can. J. Chem. Downloaded from www.nrcresearchpress.com by 41.223.56.140 on 09/07/12
For personal use only.

Vol. 1. *Editeur* : F. Franks. Cambridge Univ. Press, Londres. 1985. p. 171.
12. J. E. DESNOYERS, G. PERRON et A. H. ROUX. *Dans* Surfactant solutions: New methods of investigations. *Éditeur* : R. Zana. M. Dekker Inc., New York. 1987.
13. A. H. ROUX et J. E. DESNOYERS. Proc. Indian Chem. Soc. **98**, 435 (1987).
14. J. LARA, G. PERRON et J. E. DESNOYERS. J. Phys. Chem. **85**, 1600 (1981).
15. A. ROUX, G. ROUX-DESGRANGES, J. P. GROLIER et A. VIALLARD. J. Colloid Interface Sci. **84**, 250 (1981); **84**, 536 (1981).
16. J. LARA, L. AVÉDIKIAN, G. PERRON et J. E. DESNOYERS. J. Solution Chem. **10**, 301 (1981).
17. J. E. DESNOYERS, D. HÉTU ET G. PERRON. J. Solution Chem. **12**, 427 (1983).
18. G. PERRON, R. DELISI, I. DAVIDSON, S. GÉNÉREUX et J. E. DESNOYERS. J. Colloid Interface Sci. **79**, 432 (1981).
19. A. H. ROUX, D. HÉTU, G. PERRON et J. E. DESNOYERS. J. Solution Chem. **13**, 1 (1984).
20. D. HÉTU, A. H. ROUX et J. E. DESNOYERS. J. Solution Chem. **16**, 529 (1987).
21. D. HÉTU, A. H. ROUX et J. E. DESNOYERS. J. Colloid Interface Sci. **122**, 418 (1988).
22. R. GARNSEY, R. MAHONEY et T. A. LITOVITZ. J. Chem. Phys. **64**, 2073 (1964).
23. I. DAVIDSON, G. PERRON et J. E. DESNOYERS. Can. J. Chem. **59**, 2212 (1981).
24. V. A. DEL GROSSO et C. W. MADER. J. Acoust. Soc. **52**, 1442 (1972).
25. L. E. SCRIVEN. *Dans* Micellization solubilization and microemulsion. Vol. 2. *Éditeur* : K. L. Mittal. Plenum Press, New York. 1976. p. 877.
26. J. LARA et J. E. DESNOYERS. J. Solution Chem. **10**, 465 (1981).
27. G. ROUX, D. ROBERTS, G. PERRON et J. E. DESNOYERS. J. Solution Chem. **9**, 629 (1980).
28. J. E. DESNOYERS, G. CARON, R. DELISI, D. ROBERTS, A. ROUX et G. PERRON. J. Phys. Chem. **87**, 1397 (1983).
29. D. HÉTU. Mémoire de maîtrise, Sherbrooke (1982).
30. J. LARA. Thèse de doctorat, Sherbrooke (1981).
31. E. B. ABUIN et E. A. LISSI. J. Colloid Interface Sci. **95**, 198 (1983).
32. G. CARON et J. E. DESNOYERS. J. Colloid Interface Sci. **119**, 141 (1987).

Can. J. Chem. Downloaded from www.nrcresearchpress.com by 41.223.56.140 on 09/07/12
For personal use only.

Complexes binaires et ternaires du cuivre(II) avec la 1-canavanine et la 1-arginine examinés par potentiométrie, spectrophotométrie visible et dichroïsme circulaire

ABDALLAH ALBOURINE, MICHELLE PETIT-RAMEL ET GERMAINE THOMAS-DAVID
Laboratoire de chimie analytique II, Université Claude Bernard, Lyon I, 43 Boulevard du 11-Novembre-1918, 69622 Villeurbanne CEDEX, France

ET

JEAN-JACQUES VALLON
Laboratoire de chimie analytique III, Université Claude Bernard, Faculté de Pharmacie, 8 Avenue Rockefeller, 69373 Lyon CEDEX 2, France

Reçu le 17 octobre 1988

ABDALLAH ALBOURINE, MICHELLE PETIT-RAMEL, GERMAINE THOMAS-DAVID et JEAN-JACQUES VALLON. Can. J. Chem. **67**, 959 (1989).

Les constantes de protonation de la 1-canavanine (Can) et de son analogue structural, la 1-arginine (Arg) ont été calculées à 25°C et à force ionique $\mu = 0{,}1$ ($NaNO_3$). Dans les mêmes conditions, les constantes de stabilité des complexes binaires et ternaires formés avec le cuivre(II) ont été déterminées par potentiométrie, complétée par des mesures spectrophotométriques et de dichroïsme circulaire dans le domaine du visible. Cette étude comparative de ces deux aminoacides a permis de mettre en évidence une différence d'ordre de protonation des trois groupements fonctionnels (carboxylique, aminé et guanidyle) qui se traduit par une différence de mode de complexation avec le cuivre(II) situé dans un état de coordinence octaédrique : l'arginine se comporte comme un ligand bidenté (type glycine) alors que la canavanine se comporte comme un ligand tridenté.

Mots clés : 1-arginine, 1-canavanine, dichroïsme circulaire, coordination ternaire du cuivre, potentiométrie.

ABDALLAH ALBOURINE, MICHELLE PETIT-RAMEL, GERMAINE THOMAS-DAVID, and JEAN-JACQUES VALLON. Can. J. Chem. **67**, 959 (1989).

The protonation constants of 1-canavanine (Can) and its structural analogue 1-arginine (Arg) have been calculated at 25°C and at ionic strength $\mu = 0.1$ ($NaNO_3$). Under the same conditions, the stability constants of the binary and ternary complexes with Cu(II) have been determined by potentiometry, spectrophotometry, and by circular dichroïsm in the visible region. A comparative study of these two amino acids allows us to differentiate the order of protonation of the three functional groups (carboxylic, amino, and guanidyl), mainly by the different modes of complexation with copper(II), which is found in an octahedral coordination: arginine behaves like a bidentate ligand (glycine type) whereas canavanine behaves like a tridentate ligand.

Key words: 1-arginine, 1-canavanine, circular dichroïsm, copper ternary coordination, potentiometry.

Can. J. Chem. Downloaded from www.nrcresearchpress.com by 41.223.56.140 on 09/07/12
For personal use only.

Introduction

La qualité biologique des protéines varie avec leur teneur en acides aminés essentiels. Si les protéines animales représentent le «haut de gamme» dans cette échelle de valeur, il ne faut pas moins négliger l'apport important que constituent les protéines végétales rencontrées dans la plupart des noix, légumes et racines comestibles. Que ce soit pour l'alimentation de l'homme (soja) ou celle de l'animal (luzerne), l'utilisation des protéines végétales tend à s'amplifier au fil des années et dans ce contexte nous nous sommes intéressés à un amino acide de soja et de luzerne (alfalfa), la 1-canavanine.

La 1-canavanine ou acide amino-2 (guanidinoxy)-4 butyrique, analogue structural de la 1-arginine (figure 1a) a été isolée en 1929 à partir de farine de «jack bean» (*Canavalia ensiformis*) par T. Tomiyama et coll. (1).

Bien que la détection de la 1-canavanine dans diverses plantes alfalfa, soja trèfle... ait intéressé de nombreux auteurs (2–4), très peu d'études fondamentales relatives à ses modes de protonation et de chélation ont été abordées (5, 6). Ceci semble d'autant plus anormal que sa ressemblance structurale avec la 1-arginine, aminoacide bien connu des chimistes de coordination, lui confère une certaine toxicité liée à deux mécanismes : inhibition des enzymes du métabolisme de l'arginine et dénaturation des propriétés fonctionnelles des protéines où elle se trouve incorporée (3, 7). Ceci justifie l'intérêt du contrôle de qualité qui devrait permettre de vérifier l'absence de la canavanine dans les protéines végétales destinées à l'alimentation humaine ou animale.

Dans le but de mettre en évidence les caractéristiques particulières de la 1-canavanine ligand, et de ses complexes avec le cuivre, nous procéderons à une étude potentiométrique complétée par des mesures d'absorbance et de dichroïsme circulaire dans le domaine du visible.

Pour chacune des techniques utilisées, nous nous attacherons à établir une comparaison avec le comportement de la 1-arginine et à dégager les paramètres caractéristiques utilisables pour une détection ultérieure. En outre, dans le cas où les deux ligands seraient extraits simultanément il nous a semblé particulièrement souhaitable de compléter cette étude par l'examen du complexe mixte ternaire qui pourrait se former avec le métal choisi à titre d'exemple.

Nous définirons par β_{pqrs} la constante de stabilité globale d'une espèce complexe de formule générale : $M_pH_qL_rL'_s$ où M représente l'atome métallique central, H l'atome d'hydrogène, L et L′ les deux ligands susceptibles de complexer le métal. Cette formule est régie par l'équilibre :

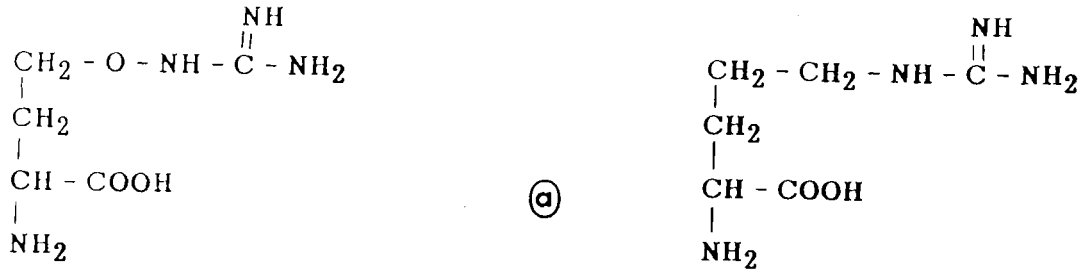
$$pM + qH + rL + sL' \rightleftarrows M_pH_qL_rL'_s$$

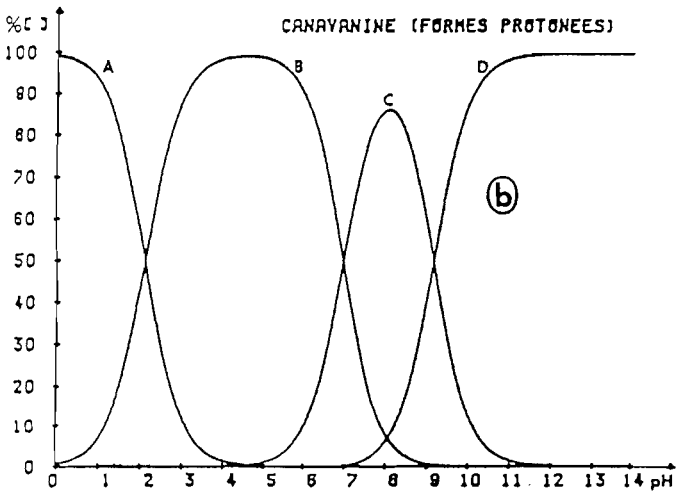
$$[1] \quad \beta_{pqrs} = \frac{[M_pH_qL_rL'_s]}{[M]^p[H]^q[L]^r[L']^s}$$

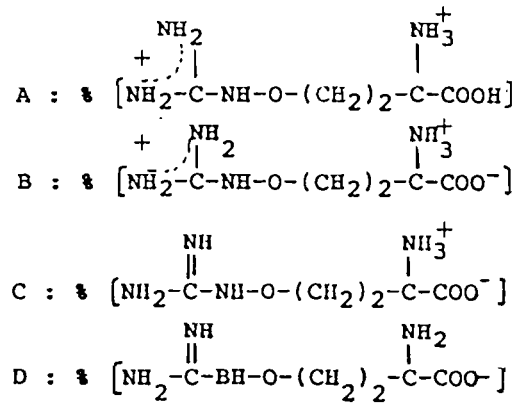
Lors de la neutralisation nous pourrons définir le nombre moyen de protons neutralisables par mole de ligand :

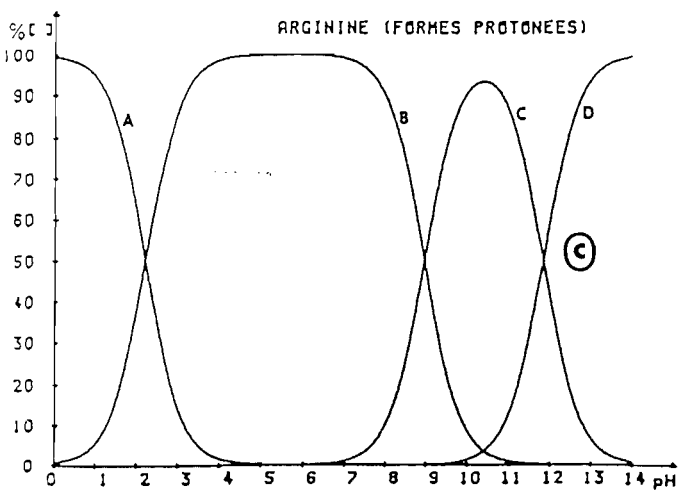
1. Auteur à qui adresser toute correspondance.

Printed in Canada / Imprimé au Canada









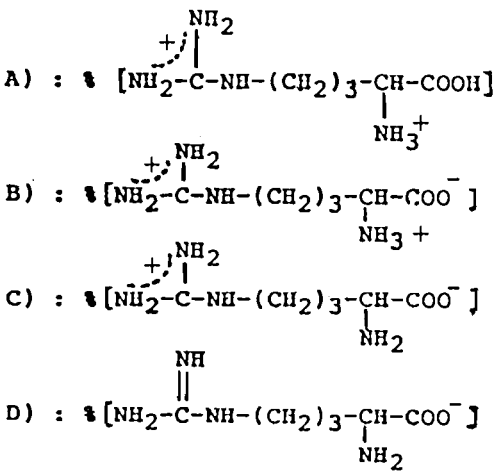


FIG. 1. (a) Formules développées de la 1-canavanine et de la 1-arginine. (b) Répartition des formes protonées de la 1-canavanine. (c) Répartition des formes protonées de la 1-arginine.

Can. J. Chem. Downloaded from www.nrcresearchpress.com by 41.223.56.140 on 09/07/12
For personal use only.

TABLEAU 1. Constantes des stabilités des complexes cuivriques avec la l-canavanine et la l-arginine; t = 25°C et μ = 0,1 ($NaNO_3$)

	$pqrs$	log β_{pqrs}	log K	Domaine de formation	Références 6	8	15
		l-Canavanine					
$-NH_2$	0110	9,16 (0,01)*	9,16		9,22		
$-NH-\overset{\overset{NH}{\|}}{C}-NH_2$	0210	16,14 (0,01)	6,98		7,01		
-COOH	0310	18,29 (0,01)	2,15		2,35		
		l-Arginine					
$-NH-\overset{\overset{NH}{\|}}{C}-NH_2$	0101	11,58 (0,02)	11,58				11,50
$-NH_2$	0201	20,83 (0,02)	8,98			8,92	9,35
-COOH	0301	23,05 (0,02)	2,22			2,02	
Cu–Can	1010	8,85 (0,07)	8,85	pH 3,5–9			
$Cu(Can)_2$	1020	14,16 (0,07)	5,30	pH 6–10			
Cu–Arg	1001	7,44 (0,01)	7,44	pH 2–7,5		7,49	7,93
$Cu(Arg)_2$	1002	13,83 (0,01)	6,39	pH 3,5–10		6,10	6,64
Cu–Can–Arg	1011	14,30 (0,08)		pH 5,5–10			

*Écart-type correspondant aux constantes.

$$[2] \quad \bar{q} = \frac{C_H - [H] - [OH]}{C_L}$$

où C_L est la concentration du ligand; [H] et [OH] sont respectivement les concentrations en H^+ et OH^- à l'équilibre; C_H est la concentration en protons telle que $C_H = qC_L - B$; B est la concentration de l'hydroxyde ajouté.

En ce qui concerne l'étude spectroscopique, la mesure d'une grandeur additive quelconque X, variable au cours de la chélation, prend en compte les contributions secondaires dues au métal et aux autres espèces libres du coordinat.

$$[3] \quad X = l(\sum_0^n X_n[ML_n] + \sum_0^p X'_p[H_pL])$$

où l est la longueur de la cuve, X_n et X_p sont respectivement les facteurs intensifs des complexes ML_n et des différentes formes du coordinat L associé, suivant sa basicité, à p protons.

Les méthodes utilisées, absorption lumineuse et dichroïsme circulaire, permettent d'éliminer partiellement ou totalement certaines contributions parasites. La mesure de l'absorption lumineuse dans le visible d'un complexe coloré permet d'annuler l'absorbance molaire du coordinat libre n'absorbant que dans l'ultra-violet (amino acide); seul subsiste le terme relatif au métal x_0[M] d'accès facile. Plus intéressant est le dichroïsme circulaire pour lequel x_0[M] inactif est nul et qui donne accès à une mesure directe de la formation du complexe.

Résultats

1. Protonation

Au regard du nombre important de travaux concernant l'arginine, il faut souligner que les quelques travaux recensés dans la littérature laissent encore très ouvert le champ des investigations fondamentales sur l'étude du ligand canavanine. Dès 1935, Tomiyama (5) avait donné des valeurs très approchées des constantes apparentes de dissociation de la canavanine sulfatée. Beaucoup plus tard, en 1981, Boyar et Marsh (6) ont recalculé ces paramètres à partir des valeurs expérimentales de Tomiyama. Cette démarche ne nous paraissant pas satisfaisante, nous avons repris ces déterminations sur la l-canavanine sulfatée d'une part et la l-canavanine «free base» d'autre part.

La transformée de la courbe de neutralisation conduit aux valeurs moyennes ($\bar{q}$) de protons neutralisables par mole de ligand. Pour les deux qualités de ligand, cette valeur tend vers 3. Ceci est en bonne concordance avec l'examen des formules précédentes qui font ressortir trois groupements fonctionnels susceptibles d'être protonés. Après affinement de 160 couples de valeurs ($\bar{q}$, pH) répartis sur plusieurs concentrations (canavanine sulfatée : 2×10^{-3} M, 10^{-3} M; canavanine free base : 2×10^{-3} M et 10^{-3} M), les constantes de protonation sont rassemblées dans le tableau 1, les courbes de répartition de chaque forme protonée apparaissent sur la figure 1b.

L'ordre de protonation est bien connu pour la l-arginine (8) et concerne successivement les groupements carboxylique, aminé et guanidyle. Alors que pour la l-canavanine, si la dissociation du groupement aminé NH_3^+/NH_2 reste situé à pH 9, le groupement guanidyle semble se déprotoner vers pH 7 en accord avec les conclusions de Boyar et Marsh (6).

2. Complexation binaire : cuivre–canavanine et cuivre–arginine

A. Mesures potentiométriques

Pour chaque système cuivre–canavanine et cuivre–arginine, deux rapports des concentrations ont été étudiés : ligand : métal = $1,92 \times 10^{-3}$ M : $7,68 \times 10^{-4}$ M d'une part et $1,92 \times 10^{-3}$ M : $4,05 \times 10^{-4}$ M d'autre part. Le tableau 1 donne les constantes de stabilité des complexes successifs ML et ML_2 par affinement des valeurs expérimentales issues des deux premières constantes de protonation dans le cas de l'arginine (le cuivre étant généralement complexé dès pH 9) et des trois constantes de protonation dans le cas de la canavanine, puisque les trois groupements se déprotonent dans le domaine de complexation du cuivre. Nous obtenons les courbes de répartition représentées sur les figures 2a et 2b.

Can. J. Chem. Downloaded from www.nrcresearchpress.com by 41.223.56.140 on 09/07/12
For personal use only.

Can. J. Chem. Downloaded from www.nrcresearchpress.com by 41.223.56.140 on 09/07/12
For personal use only.

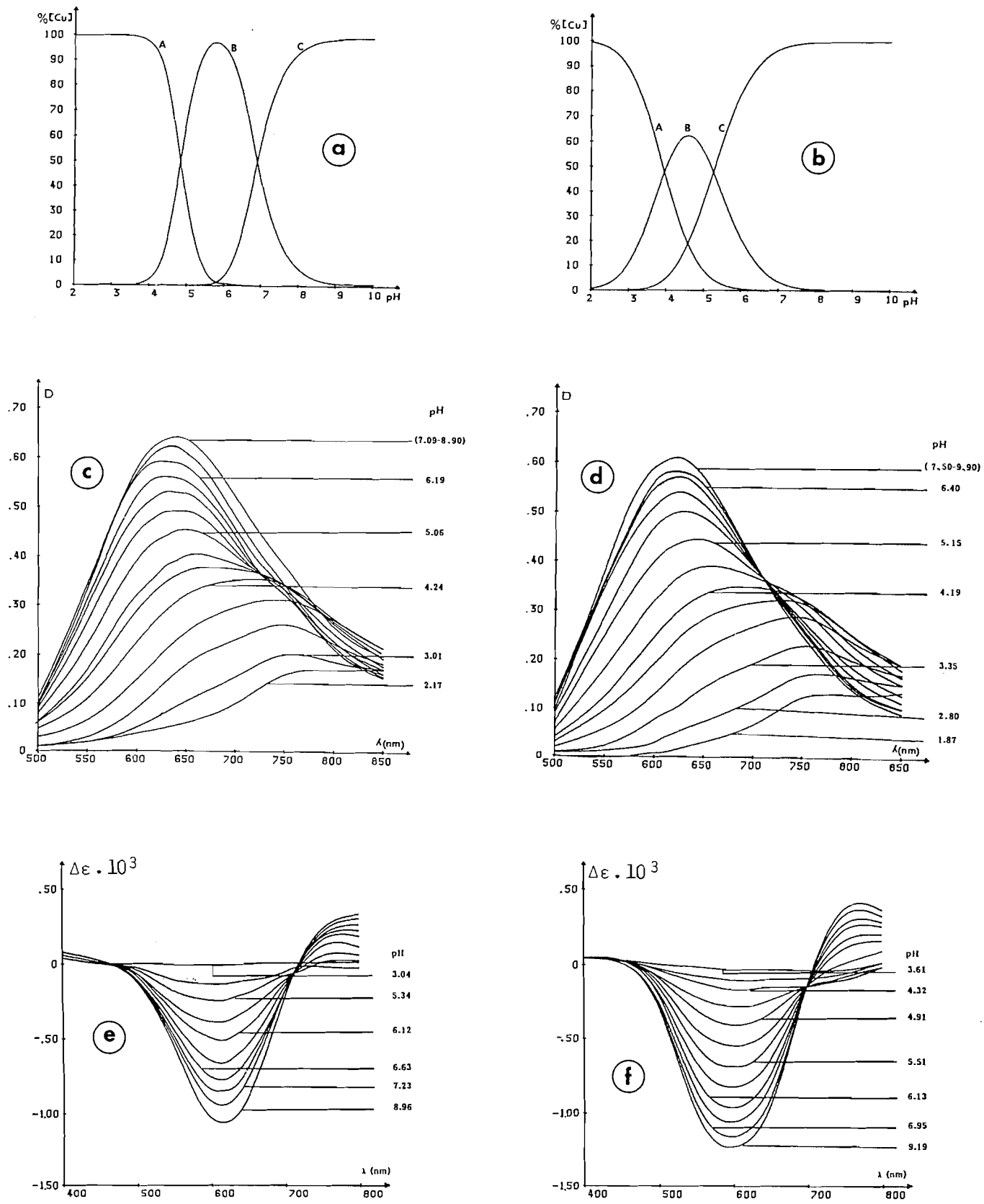


FIG. 2. (a) Répartition des complexes de la l-canavanine avec le cuivre(II) rapport 2,5 : 1; A : Cu^{2+}; B : Cu–Can; C : $Cu(Can)_2$. (b) Répartition des complexes de la l-arginine avec le cuivre(II) rapport 2,5 : 1; A : Cu^{2+}; B : Cu–Arg; C : $Cu(Arg)_2$. (c) Faisceau des spectres d'absorption lumineuse du système l-canavanine ($1{,}25 \times 10^{-2}$ M) – cuivre(II) ($5{,}05 \times 10^{-3}$ M). (d) Faisceau des spectres d'absorption lumineuse du système l-arginine ($1{,}25 \times 10^{-2}$ M) – cuivre(II) ($5{,}05 \times 10^{-3}$ M). (e) Faisceau des spectres dichroïques du système l-canavanine ($2{,}5 \times 10^{-3}$ M) – cuivre(II) ($1{,}01 \times 10^{-3}$ M). (f) Faisceau des spectres dichroïques du système l-arginine (5×10^{-3} M) – cuivre(II) ($2{,}02 \times 10^{-3}$ M).

TABLEAU 2. Facteurs intensifs spectrophotométriques et dichroïques des complexes cuivriques avec la 1-canavanine et la 1-arginine

	Spectrophotométrie		Dichroïsme circulaire	
	λ (nm) de mesure	ε	λ (nm)	$\lvert\Delta\varepsilon\rvert$
Cu–Can	640	60,4 (1,0)*	616	−0,105 (0,001)*
$Cu(Can)_2$	640	63,4 (0,5)	616	−0,212 (0,001)
Cu–Arg	620	45,7 (5,0)	595	−0,003 (0,001)
$Cu(Arg)_2$	620	60,4 (0,5)	595	−0,123 (0,001)
Cu–Can–Arg	632	63,0 (1,0)	604	−0,194 (0,002)

*Écart-type correspondant aux facteurs intensifs.

B. Mesures spectroscopiques

Pour une solution $5{,}05 \times 10^{-3}$ M en cuivre(II) et $1{,}25 \times 10^{-3}$ M en canavanine sulfatée, nous faisons varier le pH entre 2,1 et 8,9 en enregistrant chaque fois le spectre d'absorption dans un domaine de longueur d'onde compris entre 500 et 800 nm. Le faisceau de spectres représenté sur la figure 2c montre la formation graduelle des complexes ML et ML_2 (tableau 1) avec l'accroissement du pH, le complexe ML_2, plus stable, provoquant un déplacement hypsochromique d'environ 120 nm par rapport au cuivre.

De pH 2 à pH 4, seule l'espèce ML est formée et présente une faible absorbance.

Au voisinage de pH 4,5, un point isobestique apparaît à 720 nm, ce qui confirme l'existence de deux complexes en équilibre absorbant identiquement à cette longueur d'onde. Au delà de pH 8,9 nous n'observons aucune modification des spectres; le complexe ML_2 est entièrement formé et présente pour la canavanine un maximum d'absorption à 640 nm.

En ce qui concerne le système cuivre–arginine nous pouvons citer l'étude partielle faite par Phan *et al.* (8); dans un souci d'homogénéité il nous a semblé utile de refaire et compléter ces mesures dans les conditions expérimentales utilisées pour la canavanine.

Le maximum d'absorption du complexe ML_2 pour l'arginine est situé à 620 nm et le point isobestique à 710 nm (figure 2d), ce qui concorde avec les résultats de Phan *et al.* (8).

Pour ces deux maxima : 640 nm pour la canavanine et 620 nm pour l'arginine, l'expression [4] reliant l'absorbance totale à l'absorbance molaire de chaque contribution permet de calculer par affinement les facteurs intensifs de chaque complexe (tableau 2).

$$[4] \quad X = l(\sum_{0}^{n} X_n[ML_n])$$

Les solutions étudiées par dichroïsme circulaire contiennent $2{,}5 \times 10^{-3}$ M en 1-canavanine et $1{,}01 \times 10^{-3}$ M en cuivre(II) d'une part et 5×10^{-3} M en 1-arginine et $2{,}02 \times 10^{-3}$ M en cuivre(II) d'autre part, soit un rapport ligand : métal = 2,5. Le domaine d'étude en longueur d'onde est de 400 à 800 nm (figures 2e et 2f). Nous observons deux faisceaux de spectres comparables à ceux obtenus par spectrophotométrie. Ils correspondent à la réponse directe des complexes métalliques ML et ML_2 (tableau 1) puisque le cuivre non complexé ne possède pas de dichroïsme circulaire.

Un extremum négatif apparaît à 616 nm pour la 1-canavanine alors que pour la 1-arginine, il est situé à 595 nm.

La figure 3e représente la variation du dichroïsme circulaire molaire $\lvert\Delta\varepsilon\rvert$, en fonction du pH.

En fin de complexation l'intensité dichroïque molaire du système cuivre(II)–1-canavanine est nettement supérieure à celle du système cuivre(II)–1-arginine. Le dichroïsme circulaire molaire de chaque forme complexée est représenté dans le tableau 2 et conduit à deux remarques :

(*i*) Comme ceci a déjà été montré dans le cas d'autres ligands (9), l'effet Cotton correspondant aux espèces ML est nettement inférieur à celui des espèces ML_2; l'intensité dichroïque croît notamment avec le nombre de cycles de chélation et par là-même, avec le degré de coordination du complexe.

(*ii*) D'autre part, la comparaison des dichroïsmes circulaires molaires de chaque espèce ML ($\lvert\Delta\varepsilon\rvert_{Cu-Can} = -0{,}105$ trente fois supérieur à $\lvert\Delta\varepsilon\rvert_{Cu-Arg} = -0{,}003$) laisse prévoir deux modes de coordination différents liés aux nombres de cycles (figures 4a et 4b).

3. Complexation ternaire : cuivre–canavanine–arginine

A. Mesures potentiométriques

Plusieurs rapports ont été étudiés pour le système cuivre : canavanine : arginine, 1 : 1 : 1, 1 : 2 : 2, 1 : 2 : 1 et 1 : 1 : 2. Une valeur approchée de la constante de stabilité du complexe mixte ternaire est donnée par l'expression [5] :

$$[5] \quad \log X_{11} = 2 \log \beta_{1011} - (\log \beta_{1020} + \log \beta_{1002})$$

où β_{1011} : constante globale du complexe Cu–Can–Arg; β_{1020} : constante globale du complexe $Cu(Can)_2$; β_{1002} : constante globale du complexe $Cu(Arg)_2$; $\log X_{11}$: renforcement de stabilité par chélation mixte (10). Pour les amino acides, $\log X_{11}$ est généralement voisin de 0,2 d'où $\beta_{1011} = 1{,}2 \times 10^{14}$. Cette valeur est affinée de la même manière que pour les systèmes simples et nous avons : $\beta_{1011} = 2{,}00 \times 10^{14}$ soit $\log \beta_{1011} = 14{,}30$.

Le renforcement de stabilité apparaît nettement puisque $\log \beta_{1011}$ est supérieur à $\log \beta_{1020}$ et $\log \beta_{1002}$. La répartition des espèces est donnée pour les rapports les plus favorables à l'obtention du complexe mixte : Cu : Can : Arg = 1 : 1 : 1 (figure 3a) et 1 : 2 : 2 (figure 3b).

B. Mesures spectroscopiques

L'examen des spectres d'absorption visible correspondant au rapport Cu : Can : Arg = 1 : 2 : 2 (figure 3c) permet de localiser un maximum d'absorption à 632 nm, soit une valeur intermédiaire entre les deux maxima des complexes simples : 640 nm pour $Cu(Can)_2$ et 620 nm pour $Cu(Arg)_2$. En accord avec les observations de Mecca et coll. (11) et Petit-Ramel et Pâris (12) on peut avancer que ce maximum correspond bien au complexe mixte Cu–Can–Arg dont l'absorbance molaire est donnée dans le tableau 2.

Sur la figure 3d est représenté le spectre dichroïque du complexe mixte rapport Cu : Can : Arg = 1 : 1 : 1 (B) à pH = 9,65 avec un maximum d'absorption dichroïque à 604 nm ainsi que les spectres des complexes simples : cuivre–1-canavanine

Can. J. Chem. Downloaded from www.nrcresearchpress.com by 41.223.56.140 on 09/07/12
For personal use only.

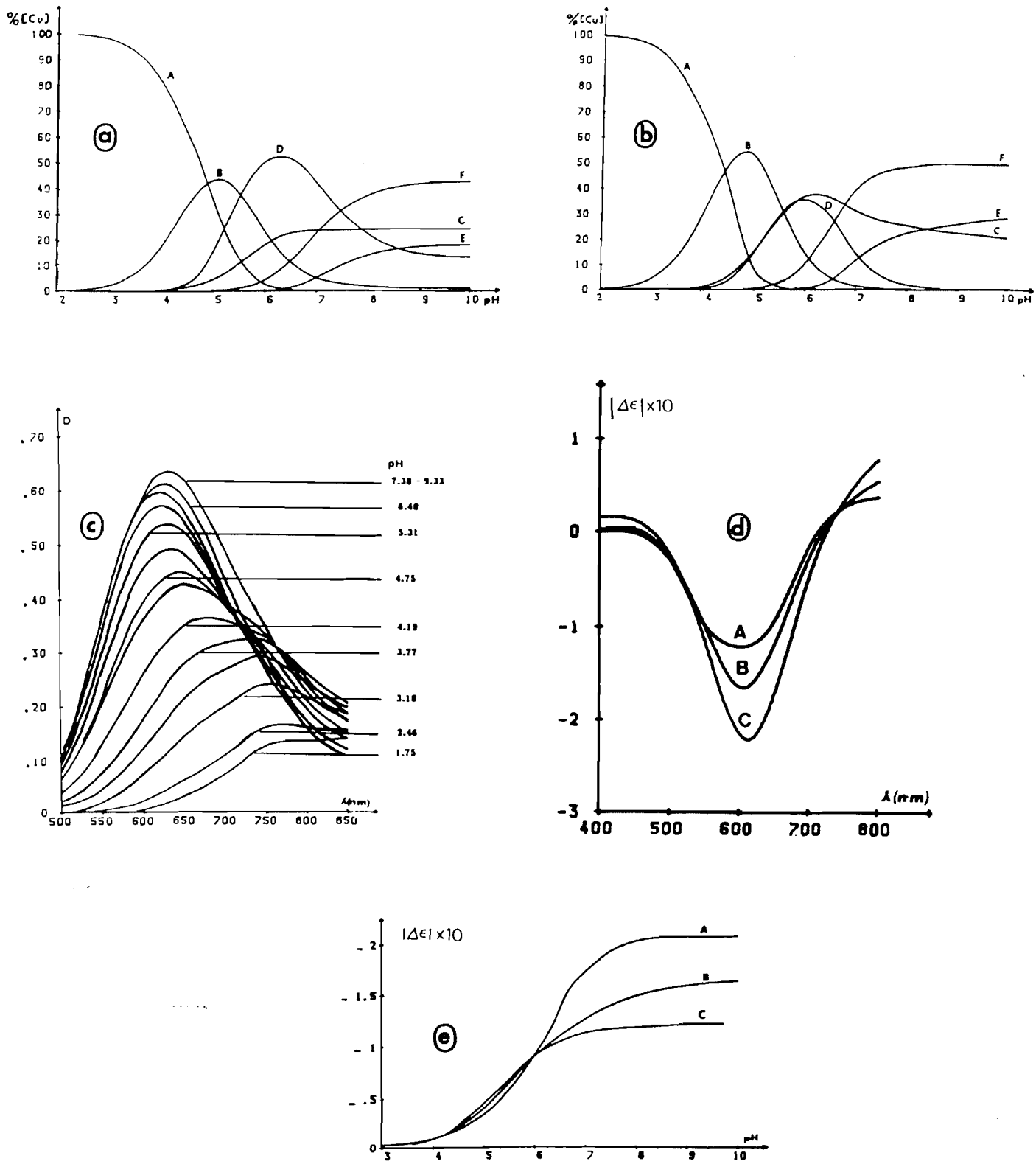


FIG. 3. (a) Répartition des complexes mixtes Cu–Can–Arg rapport 1 : 1 : 1. (b) Répartition des complexes mixtes Cu–Can–Arg rapport 1 : 2 : 2. A : Cu^{2+}; B : Cu–Arg; C : $Cu(Arg)_2$; D : Cu–Can; E : $Cu(Can)_2$; F : Cu–Can–Arg. (c) Faisceau des spectres d'absorption lumineuse du système 1-canavanine ($9{,}99 \times 10^{-3}$ M) – l-arginine ($9{,}98 \times 10^{-3}$ M) – cuivre(II) ($5{,}05 \times 10^{-3}$ M). (d) Dichroïsme circulaire molaire du complexe mixte Cu–Can–Arg à pH 9,72 (B) avec les deux simples correspondant $Cu(Arg)_2$ à pH 9,65 (A) et $Cu(Can)_2$ à pH 9,70 (C). (e) Dichroïsme circulaire molaire en fonction du pH : A : système 1-canavanine–cuivre(II) à 616 nm. B : système 1-canavanine–l-arginine–cuivre(II) (courbe calculée à 604 nm à l'aide des $\Delta\varepsilon$). C : système 1-arginine–cuivre(II) à 595 nm.

Can. J. Chem. Downloaded from www.nrcresearchpress.com by 41.223.56.140 on 09/07/12
For personal use only.

Can. J. Chem. Downloaded from www.nrcresearchpress.com by 41.223.56.140 on 09/07/12
For personal use only.

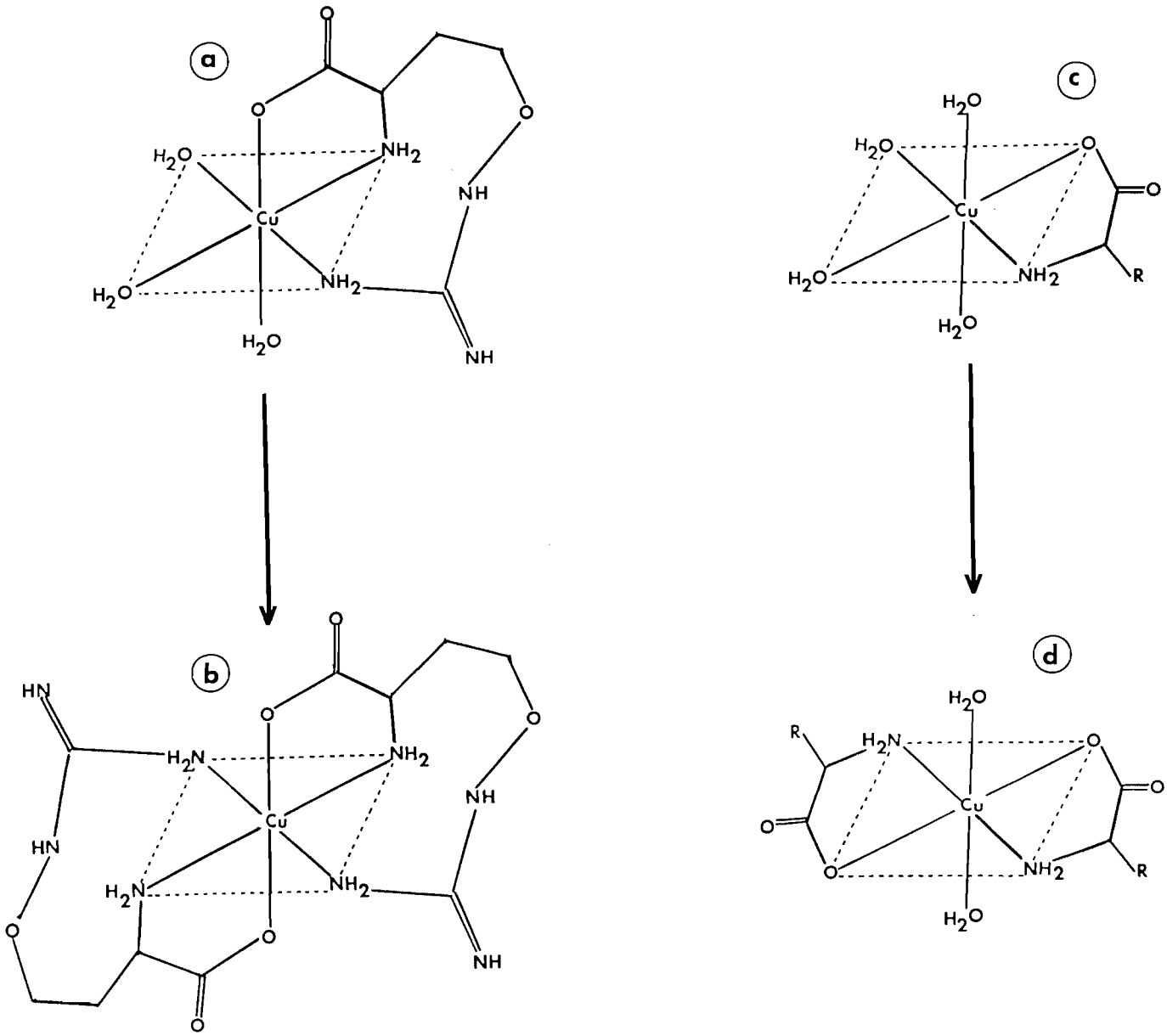


FIG. 4. Mode de complexation des systèmes 1-canavanine–cuivre(II) et 1-arginine–cuivre(II); R = $(CH_2)_3$—NH—C(=NH)—NH_2. (a) Cu–Can; (b) $Cu(Can)_2$; (c) Cu–Arg; (d) $Cu(Arg)_2$.

(C) à pH = 9,70 et cuivre–1-arginine (A) à pH = 9,72 dont les maxima sont respectivement 616 nm et 595 nm.

Comme dans le cas des mesures spectrophotométriques le maximum d'absorption dichroïque du complexe mixte Cu–Can–Arg prend une valeur intermédiaire entre les deux maxima des complexes simples correspondants. Pour ces valeurs de pH, nous sommes en présence de quatre types de complexes pour lesquels nous avons déterminé les $|\Delta\varepsilon|$ molaires à 604 nm : Cu–Can, 13%, $|\Delta\varepsilon|_{604} = 0{,}085$, $Cu(Can)_2$, 18%, $|\Delta\varepsilon|_{604} = -0{,}210$, $Cu(Arg)_2$, 24,5%, $|\Delta\varepsilon| = -0{,}122$ et Cu–Can–Arg, 44,5%. Il est donc aisé d'obtenir la valeur correspondant à l'espèce mixte (tableau 2).

Discussion

L'étude potentiométrique préalable de la 1-canavanine et de la 1-arginine a mis en évidence une différence notable au niveau de l'ordre de déprotonation des groupements guanidyle et aminé. Dans le cas de la canavanine, le groupement guanidyle se déprotone en effet avant le groupement aminé ($pK = 6{,}98$), alors que pour l'arginine, il se déprotone bien au-delà ($pK = 11{,}85$). La conséquence directe de ce phénomène se traduit par des modes de complexation différents (figure 4) vis à vis du cuivre(II) dans le domaine de pH considéré ($2 < pH < 10$). La 1-arginine se comporte comme un coordinat bidenté (type glycine), sans déprotonation du groupement guanidyle. La 1-canavanine, au contraire, se comporte comme un coordinat tridenté (type histidine) puisque le groupement guanidyle se déprotone.

La spectrophotométrie et surtout le dichroïsme circulaire illustrent encore cette différence dans le mode de chélation. La densité optique varie en effet comme la «force de covalence» de la liaison métal–coordinat (13), liée au nombre de cycles

de chélation. La comparaison des absorbances molaires, plus tranchée pour les espèces ML, met en évidence une covalence plus importante pour la 1-canavanine que pour la 1-arginine. Ce phénomène apparaît encore plus nettement avec le dichroïsme circulaire : lors de la complexation, il existe avec les amino acides un effet vicinal dû à la modification d'activité optique du ligand. L'effet Cotton correspondant dépend principalement de la mobilité conformationnelle du ligand et augmente avec le nombre de cycles de chélation (14). Nos observations recoupent parfaitement ces conclusions dans la mesure où le dichroïsme circulaire des formes complexées ML (un cycle de chélation) est toujours inférieur à celui des complexes ML_2 (deux cycles de chélation). De même le dichroïsme circulaire des complexes ML et ML_2 de la 1-arginine, bidentée (respectivement un et deux cycles de chélation) est toujours inférieur à celui des espèces ML et ML_2 formées avec la 1-canavanine tridentée (respectivement deux et quatre cycles de chélation).

En ce qui concerne la chélation mixte ternaire du cuivre(II) avec ces deux amino acides, l'étude potentiométrique, illustrée par les courbes de répartition des figures 3a et 3b montre bien l'existence d'un complexe mixte Cu–Can–Arg qui se forme majoritairement (environ 50% pour le rapport 1 : 2 : 2) au détriment des deux complexes simples $Cu(Can)_2$ et $Cu(Arg)_2$ et nous avons l'équilibre suivant

$$Cu(Can)_2 + Cu(Arg)_2 \rightleftarrows 2Cu\text{–}Can\text{–}Arg$$

Dans ce cas, la spectrophotométrie et surtout le dichroïsme circulaire présentent des maxima d'absorption dont les longueurs d'onde sont intermédiaires par rapport à celles des deux complexes binaires. Ceci confirme encore une fois les résultats obtenus par potentiométrie.

Nous avons signalé dans l'introduction que la détection de la canavanine dans les produits naturels et possible par CLHP. Les premières mesures que nous avons effectuées à l'aide de cette technique s'avèrent encourageantes notamment après extractions multiples. Mais le protocole de mesure CLHP nécessite un intermédiaire dérivé d'orthophtaldialdehyde/ethanethiol peu stable, qui peut avoir une incidence sur la reproductibilité des mesures. D'autre part les premiers spectres de dichroïsme circulaire que nous avons enregistrés sur l'extrait naturel complexé par le cuivre(II), concordent parfaitement avec les spectres dichroïques de canavanine–cuivre étudiés précédemment.

Dans un premier temps, une détection rapide peut donc être effectuée directement sur l'extrait.

L'utilisation conjointe de la CLHP et du dichroïsme circulaire devrait se traduire par une amélioration sensible de la détection de la canavanine dans les produits naturels.

Partie expérimentale

Matériel

Nous disposons d'une chaîne de mesures étalonnée avec précision :

électrode de verre | solution thermostatée | KCl saturé | électrode calomel

Le jeu d'électrodes est relié à un potentiomètre ISIS 20000 Tacussel et les mesures sont effectuées sur des solutions aqueuses thermostatées à 25 ± 0,1°C et sous atmosphère d'azote. La force ionique de chaque solution est maintenue constante à l'aide d'une solution de $NaNO_3$ 0,1 M.

Les spectres d'absorption sont tracés à l'aide d'un spectrophotomètre Varian 634 et les spectres dichroïques à l'aide du dichrographe Jobin-Yvon Mark IV. Les cuves Hellma sont en quartz et ont un trajet optique de 1 cm pour l'absorption et de 5 cm pour le dichroïsme circulaire dans le domaine du visible.

Réactifs

La canavanine utilisée est sous deux formes : 1-canavanine sulfatée (Sigma) et 1-canavanine free base (Sigma). L'arginine est sous forme free base (Sigma). Ces amino acides sont conservés constamment à basse température.

Le sel métallique est introduit sous forme de nitrate de cuivre(II) : $Cu(NO_3)_2,3H_2O$ (Prolabo) dissous dans de l'eau distillée et dont le titre est déterminé par un dosage complexométrique à l'EDTA préalablement dosé à l'aide d'une solution titrisol de zinc(II).

1. M. KITAGAWA et T. TOMIYAMA. J. Biochem. (Tokyo), **11**, 265 (1929).
2. L. E. WEISSBERGER et M. K. ARMSTRONG. J. Chromatogr. Sci. **22**, 438 (1984).
3. S. NATELSON. J. Agric. Food Chem. **33**, 413 (1985).
4. K. H. FISCHER et H. D. BELITZ. Z. Lebensm. Unters. Forsch. **162**, 227 (1976).
5. T. TOMIYAMA. J. Biol. Chem. **111**, 45 (1935).
6. A. BOYAR et R. E. MARSH. J. Am. Chem. Soc. **104**, 1995 (1982).
7. A. E. KAMMER et D. L. DAHLMAN. J. Exp. Biol. **75**, 123 (1978).
8. C. V. PHAN, L. TOSI et A. GARNIER. J. Inorg. Nucl. Chem. **37**, 2385 (1975).
9. M. M. PETIT-RAMEL et M. PÂRIS. *Dans* Analytical chemistry. Essays in memory of A. Ringbom. *Editeur* : E. Wanninn. Pergamon Press, Oxford. 1977.
10. R. P. MARTIN, M. M. PETIT-RAMEL et J. P. SCHARFF. Metal ions in biological systems. Vol. 22. Helmut Sigel, New York. 1974.
11. K. M. WELLMAN, T. C. MECCA, W. MUNGALL et C. R. HARE. J. Am. Chem. Soc. **89**, 3645 (1967).
12. M. M. PETIT-RAMEL et R. PÂRIS. Bull. Soc. Chim. Fr. **9**, 3070 (1969).
13. J. E. CROOKS. The spectrum in chemistry. Academic Press, London. 1978.
14. G. SNATZKE (*Éditeur*). Optical rotatory dispersion and circular dichroïsm in organic chemistry. London. 1967.
15. E. R. CLARKE et A. E. MARTELL. J. Inorg. Nucl. Chem. **32**, 911 (1970).

Can. J. Chem. Downloaded from www.nrcresearchpress.com by 41.223.56.140 on 09/07/12
For personal use only.

Time-resolved nanosecond and picosecond absorption studies of excited-state properties of 1-thiobenzoylnaphthalene[1]

R. MINTO,[2] A. SAMANTA, and P. K. DAS[3]
Radiation Laboratory, University of Notre Dame, Notre Dame, IN 46556, U.S.A.

Received December 29, 1988

R. MINTO, A. SAMANTA, and P. K. DAS. Can. J. Chem. **67**, 967 (1989).

1-Thiobenzoylnaphthalene (TBN), known for its pericyclization reaction from the lowest excited singlet state (S_1), has been subjected to nanosecond and picosecond laser flash photolysis studies. The two major transients observed in the course of nanosecond laser pulse excitation are (*i*) the short-lived triplet characterized by two absorption maxima (400–410 and 740–750 nm) and submicrosecond intrinsic lifetimes (80–130 ns) and (*ii*) a relatively long-lived species (λ_{max} = 520 nm and τ = 220–240 ns). Various triplet-related photophysical data of TBN, including self-quenching and bimolecular quenching rate constants, have been determined. The existence of a photochemical path from S_1 manifests itself in low intersystem crossing quantum yields, particularly in the polar/hydrogen-bonding solvent, methanol. From the build-up of the triplet under picosecond excitation into S_1, the lifetime of the latter is estimated to be $\leq$50 ps (in benzene). The fast intrinsic decay of TBN triplet is attributable to facile intra- and intermolecular photochemistry. The 520 nm transient species could not be definitively assigned, except that it is neither a triplet nor a triplet-derived product and that it arises via photochemistry from S_1.

Key words: laser flash photolysis, triplet, transients, absorption maxima, lifetimes, quenching rate constants, photochemistry, 1-thiobenzoylnaphthalenes.

R. MINTO, A. SAMANTA et P. K. DAS. Can. J. Chem. **67**, 967 (1989).

Le thiobenzoyl-1 naphtalène (TBN), bien connu pour sa réaction de péricyclisation à partir de l'état singulet excité le plus bas (S_1), a été soumis à des études de photolyses flash au laser à la nanoseconde et à la picoseconde. Les deux intermédiaires majeurs observés au cours de l'excitation pulsée au laser à la nanoseconde sont: (*i*) le triplet de courte vie caractérisé par deux maxima d'absorption (400–410 et 740–750 nm) et des temps de vie intrinsèques inférieurs à la microseconde (80–130 ns) et (*ii*) une espèce dont la vie est relativement longue (λ_{max} = 520 nm et τ = 220–240 ns). On a déterminé diverses données photochimiques reliées à l'état triplet du TBN, dont les constantes de vitesse d'auto-piégeage et de piégeage bimoléculaire. L'existence d'une voie photochimique à partir de l'état S_1 se manifeste par des rendements quantiques faibles pour le passage entre les systèmes, particulièrement dans le méthanol, un solvant polaire pouvant former des liaisons hydrogènes. En se basant sur l'accumulation de l'état triplet dans des conditions d'excitation de l'état S_1 au niveau de la picoseconde, on peut évaluer le temps de vie de ce dernier à $\leq$50 ps (dans le benzène). On attribue la dégénérescence intrinsèque rapide du triplet du TBN à une photochimie intra- et inter-moléculaire facile. On n'a pas pu déterminer d'une façon définitive la nature des espèces intermédiaires à 520 nm; on peut toutefois affirmer qu'il ne s'agit ni d'un produit triplet ni d'un produit dérivé d'un triplet et qu'il se forme d'une façon photochimique à partir de l'état S_1.

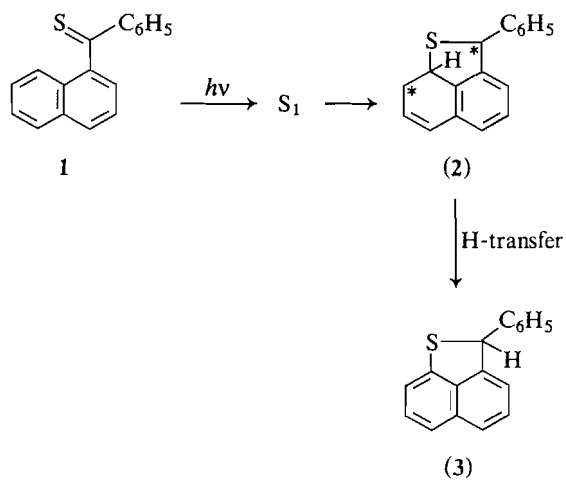
Mots clés : photolyses flash au laser, triplet, intermédiaires, maxima d'absorption, temps, constantes de vitesse de piégeage, photochimie, thiobenzoyl-1 naphtalène.

[Traduit par la revue]

Introduction

The photochemistry and photophysics associated with the lowest triplet (T_1) and the second excited singlet (S_2) states of thiocarbonyl compounds have received considerable attention in recent years (3–7). The T_1 states in thioketones are invariably assigned to be of (n,π^*) character. At millimolar concentrations of substrates in fluid solutions at room temperature, the triplets decay with lifetimes in the submicrosecond time domain; the major part of the shortening of T_1 lifetimes arises from diffusion-controlled self-quenching (5–17). On the other hand, the S_2 states originate from $\pi \rightarrow \pi^*$ transitions and are characterized by subnanosecond lifetimes (18–21). For a given thioketone, both S_2 and T_1 states have usually been implicated in biomolecular interactions of physical and chemical consequences.

In continuation of our interest in time-resolved behaviors of aliphatic and aromatic thione triplets as observable by nanosecond laser flash photolysis (10–16), we have carried out a study of 1-thiobenzoylnaphthalene (TBN, **1**). Discovered by de Mayo and co-workers (22), an interesting photochemical reaction of this thioketone as well as similar polycyclic aromatic thiones containing a free peri position is the photocyclization leading to thiophene derivatives. This is shown in Scheme 1. In contrast to the majority of thione photoreactions which take place from S_2 or T_1 states, de Mayo *et al.* (22) have shown that



SCHEME 1

[1]The research described herein was supported by the Office of the Basic Energy Sciences, Department of Energy (U.S.). This is Document No. NDRL-3151 from the Notre Dame Radiation Laboratory.

[2]Visiting undergraduate research student from the University of Waterloo, Waterloo, Ont., Canada.

[3]Present address: 347 PL, Phillips Research Center, Bartlesville, OK 74004, U.S.A.

Can. J. Chem. Downloaded from www.nrcresearchpress.com by 41.223.56.140 on 09/07/12
For personal use only.

TABLE 1. Spectral and photophysical data of 1-thiobenzoylnaphthalene in various solvents at 295 K

Solvent	$\lambda_{max}^{abs\ a}$ (nm)	$\epsilon_{max}^{abs\ b}$ (M^{-1} cm^{-1})	$\lambda_{max}^{T\ c}$ (nm)	$\epsilon_{max}^{T\ d}$ ($10^3\ M^{-1}$ cm^{-1})	$\phi^{T\ d}$	$\tau_0^{T\ b}$ (ns)	$k_{SQ}^{T\ e}$ ($10^9\ M^{-1}$ s^{-1})
Cyclohexane	220	5.6×10^4	405	4.0	0.7	132	4.8
	316	1.4×10^4	740				
	370	2.8×10^3					
	620	1.3×10^2					
Benzene	319	1.3×10^4	410	3.5	0.7	86	4.0
	378	2.5×10^3	750				
	610	1.3×10^2					
Methanol	219	6.0×10^4	405	4.7	0.4	78	7.5
	374	1.3×10^4	740				
	318	2.6×10^3					
	602	1.4×10^2					

[a] ±2 mm.
[b] ±10%.
[c] ±5 nm.
[d] ±20%; λ_{ex} = 532 nm.
[e] ±15%.

the photocyclization in the case of **1** occurs from the lowest excited singlet state (S_1) of (n,π*) character. Furthermore, they suggested the involvement of a dipolar intermediate (**2**) in the course of the cyclization process. The main objective of the present laser flash photolysis study of TBN was to shed light on the mechanism of this interesting S_1-mediated pericyclization reaction. Furthermore, TBN provided us with an example of aromatic thiones with a substantially low triplet energy (E_T = 39 kcal mol^{-1}). It was of interest to examine in detail various triplet-related properties of TBN in the context of those of related aromatic thiocarbonyl systems studied earlier (10–16).

Experimental

1-Thiobenzoylnaphthalene (TBN), prepared by a literature procedure (23), was obtained as a gift from Dr. V. Ramamurthy. It was recrystallized from toluene. The solvents used in spectroscopy and kinetics studies were all of spectral grades. The sources and methods of purification of reagents are given in earlier papers (10–16) from the Radiation Laboratory. For removal of oxygen from solutions, high-purity argon was bubbled through them.

The steady-state absorption and emission spectra were recorded in a Cary 219 spectrophotometer (1 nm bandpass) and an SLM spectrofluorimeter (24), respectively. In the latter instrument, a right-angle geometry was used for the excitation and observation of emission. The phosphorescence spectra at 77 K were obtained from solutions taken in 3 mm × 3 mm square quartz cells immersed in liquid nitrogen contained in a finger Dewar. A red-sensitive photomultiplier tube (Hamamatsu R928) enabled emission spectral measurements at long wavelengths (≤850 nm).

For nanosecond laser flash photolysis, use was made of the following two pulsed laser sources: Molectron UV-400 nitrogen (337.1 nm, ~8 ns, 2–3 mJ/pulse), and Quanta-Ray DCR-1 Nd:YAG coupled with Quanta-Ray PDL-1 dye (355, 532, and 640 nm, ~6 ns, 5–50 mJ/pulse). The laser intensities were attenuated in accordance with the ground-state absorbance of the thioketone solutions at a given laser excitation wavelength. The details of kinetic spectrophotometers, data collection systems, and experimental procedures are available elsewhere (10–16, 24, 25).

The picosecond laser flash photolysis was carried out in a system from Quantel. The laser excitation wavelengths were 355 and 532 nm (pulse width ~18 ps). The apparatus has been described in a recent paper (26).

Results

(a) *Absorption and emission spectra*

Millimolar solutions of TBN in cyclohexane, benzene, and methanol are bluish in appearance and are characterized by four well-defined absorption band systems in the spectral region 200–700 nm. The absorption spectra in cyclohexane are shown in Fig. 1 (parts *A*, *A'*, and *A''*). The lowest-energy band system at 500–700 nm is weak in intensity (ϵ_{max} = 130–140 M^{-1} cm^{-1}), and undergoes a blue shift on going from cyclohexane (or benzene) to methanol. This band system is characteristic of thiocarbonyl compounds in general and is assignable to the lowest-lying excited singlet state (S_1) of (n,π*) origin. The next higher-lying singlet state (S_2) has its absorption maxima at 370–378 nm; calculated from the peak locations, the energy gap between S_1 and S_2 for TBN in cyclohexane is 10 898 cm^{-1}. Table 1 summarizes the wavelength maxima and extinction coefficient data of TBN in various solvents.

At room temperature, cyclohexane solutions of TBN show a weak emission at 400–550 nm (see Fig. 1*B*). The location of this emission suggests that it originates from the S_2 state (see Fig. 1). This is not uncommon; by virtue of large S_1–S_2 gaps (azulene-like), many thioketones exhibit moderately intense S_2 emissions, particularly in solvents that do not strongly interact with the S_2 state (e.g., perfluoroalkanes) (18–20). In benzene and methanol, the S_2-emission from TBN becomes too weak to be discerned under steady-state excitation in our setup; its presence, however, becomes noticeable under laser pulse excitation.

The phosphorescence spectra of TBN in 3-methylpentane glass at 77 K were measured and were found to occupy the spectral region >700 nm (see Fig. 1*C*). From the portion of the spectra we were able to monitor at 700–850 nm, two component bands are evident. The spacing between them is 1 270 cm^{-1}. The triplet energy (E_T) is estimated to be 39 kcal mol^{-1}. It should be noted that most of our data concerning absorption and phosphorescence spectra of TBN are in reasonable agreement with those reported by Cox *et al.* (22).

(b) *Nanosecond laser flash photolysis*

TBN was subjected to detailed nanosecond laser flash photol-

Can. J. Chem. Downloaded from www.nrcresearchpress.com by 41.223.56.140 on 09/07/12
For personal use only.

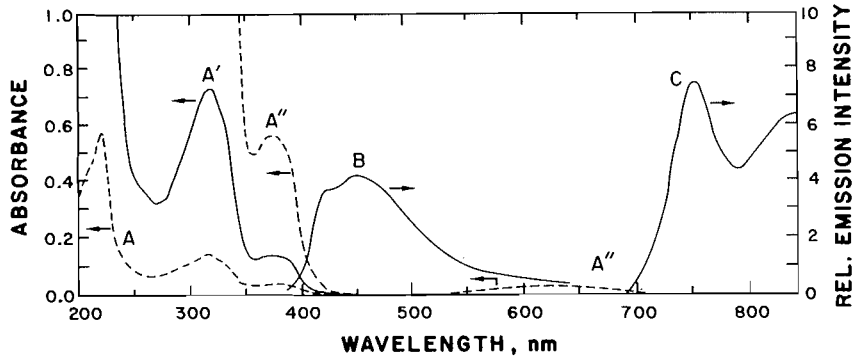


FIG. 1. Absorption (A, A', and A''), S_2-fluorescence (B), and phosphorescence (C) spectra of TBN. Solvents: cyclohexane for A, A', A'', and B, and 3-methylpentane for C. Temperatures: 295 K for A, A', A'', and B, and 77 K for C. Bandpass: 1 nm for the absorption spectra and 16 nm for both excitation and emission monochromators used for fluorescence and phosphorescence spectra. The absorption spectra A, A', and A'' were measured with 1.0, 0.25, and 0.050 nM TBN in cells of 2 mm pathlength.

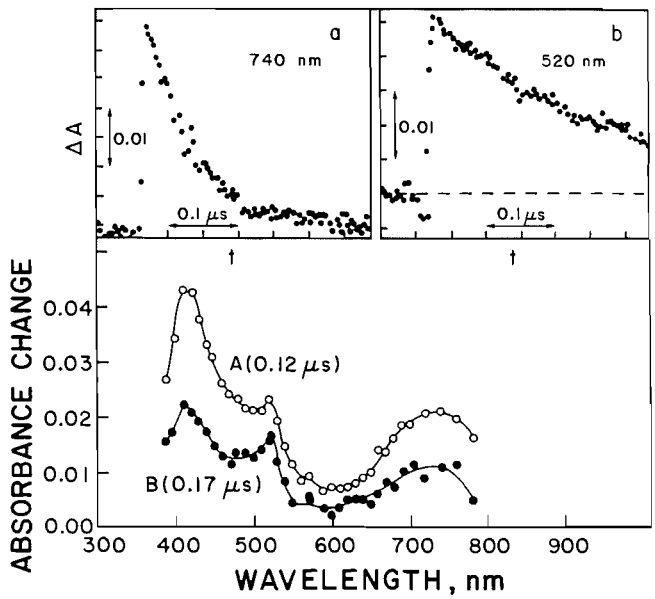


FIG. 2. Transient absorption spectra observed at (A) 0.12 and (B) 0.17 μs following 355 nm laser pulse excitation of 0.5 mM TBN in benzene. Insets: a representative kinetic traces for transient absorption decay at (a) 740 and (b) 520 nm.

ysis studies using 337.1, 355, 532, and 640 nm as laser excitation wavelengths. In the course of the pulse photoexcitation, we observed a short-lived transient species characterized by submicrosecond lifetimes and absorption spectra consisting of two maxima at 400–410 and 730–740 nm. In addition, the formation of a second species with slightly longer lifetimes and absorption maxima at 520 nm was noted. The transient spectra and representative decay traces in benzene are shown in Fig. 2. The efficient quenching of the first transient by oxygen, nitroxy radicals, ferrocene, and azulene, as well as the fact that its quenching by *all-trans*-1,6-diphenyl-1,3,5-hexatriene (DPH) led to the formation of DPH triplet, strongly suggested a triplet assignment for it. Furthermore, as expected for a thioketone triplet, this transient was quenched by TBN ground state with bimolecular rate constants in the limit of diffusion control. By following procedures described in earlier papers (12–16), we determined the triplet-related photophysical data, namely, triplet–triplet extinction coefficients (ϵ_{max}^T), intrinsic triplet lifetimes (τ_0^T), triplet yields (ϕ^T), and self-quenching rate constants (k_{SQ}^T). These data are presented in Table 1.

The bimolecular rate constants (k_q^T) for the quenching of TBN triplet in benzene by various quenchers (Q) were determined from the slopes of the linear plots of observed, pseudo-first-order rate constants (k_{obs}) vs. [Q]. These are given in Table 2. For comparison, in the same table, the corresponding data for 4,4'-dimethoxythiobenzophenone (DMTBP) and xanthione (XT) are also quoted from our previous work (10).

The effect of TBN triplet quenching by oxygen in benzene was examined in terms of singlet oxygen ($^1O_2^*$, $^1\Delta_g$) generation. In particular, the efficiency (ϕ_Δ^T) of $^1O_2^*$ production in the course of the quenching was measured under 640 nm laser pulse excitation. DMTBP was used as the reference ($\phi^T = 1$, $\phi_\Delta^T = 1$) (10) and $^1O_2^*$ was monitored via its reaction with 1,3-diphenylisobenzofuran (DPBF) leading to the bleaching of the ground state absorption of the latter. A series of benzene solutions of TBN and DMTBP, optically matched at 640 nm and containing DPBF at 0.04 mM and oxygen at varying concentrations (1.91–9.12 mM), were flash-photolyzed in 2 mm cells and the negative absorbance changes (ΔA_D^∞) due to DPBF depletion were monitored at 425 nm following the completion of the bleaching process (over ~100 μs). The double reciprocal plots of $1/\Delta A_D^\infty$ vs. $1/[O_2]$, shown in Fig. 3, were reasonably linear. If the thioketone triplets were the only photosensitizers for $^1O_2^*$ under the conditions of our experiments, the intercept-to-slope ratios of these plots were expected to give the corresponding ($k_q^T\tau_T$) values. Based on Figs. 3A and B, we obtained intercept-to-slope ratios of 150 and 170 M^{-1} for TBN and DMTBP, respectively. These results, combined with the triplet lifetimes (τ_T) of 38 and 55 ns as observed in the solutions of TBN and DMTBP respectively (under deoxygenated conditions), gave $k_{O_2}^T$ as 3.9×10^9 and 3.1×10^9 M^{-1} s^{-1}, respectively. These values are in close agreement with $k_{O_2}^T$'s measured via direct triplet quenching by O_2 (3.3×10^9 and 3.7×10^9 M^{-1} s^{-1}, respectively). Thus, the triplets are established to be the primary photosensitizing species leading to singlet oxygen. From the comparison of the reciprocals of the intercepts of the plots for the two thioketones in Fig. 3, the product ($\phi^T \cdot \phi_\Delta^T$) for TBN is estimated to be 0.8 ± 0.2. Since ϕ^T of TBN in benzene is 0.7 ± 0.1, this result indicates that the efficiency of $^1O_2^*$ sensitization by TBN triplet is essentially quantitative.

The behavior of the second transient with absorption maximum at 520 nm (see Fig. 2) was examined in various solvents. In benzene, its quenching by oxygen (≤9.1 mM) ferrocene (≤5.0 mM) and ground-state TBN (≤5.0 mM) was negligible. This ruled out the assignment of the transient as a triplet.

Can. J. Chem. Downloaded from www.nrcresearchpress.com by 41.223.56.140 on 09/07/12
For personal use only.

TABLE 2. Bimolecular rate constants for the quenching of 1-thiobenzoylnaphthalene (TBN), 4,4'-dimethoxythiobenzophene (DMTBP), and xanthione (XT) triplets in benzene at 295 K

Quencher	Maximum concentration used (m*M*)	$k_q^{T\,a}$ ($10^9\ M^{-1}\ s^{-1}$) TBN	DMTBP	XT
Oxygen	5.5	3.3	3.7	2.8
Di-*tert*-butylnitroxide	7.6	3.1	1.4	3.0
2,5-Dimethyl-2,4-hexadiene	87.5	0.23	0.27	1.4
Azulene	4.0	3.6	4.6	8.2
Ferrocene	5.1	5.6	6.7	9.8

[a] ±15%. The data for DMTBP and XT are taken from ref. 10.

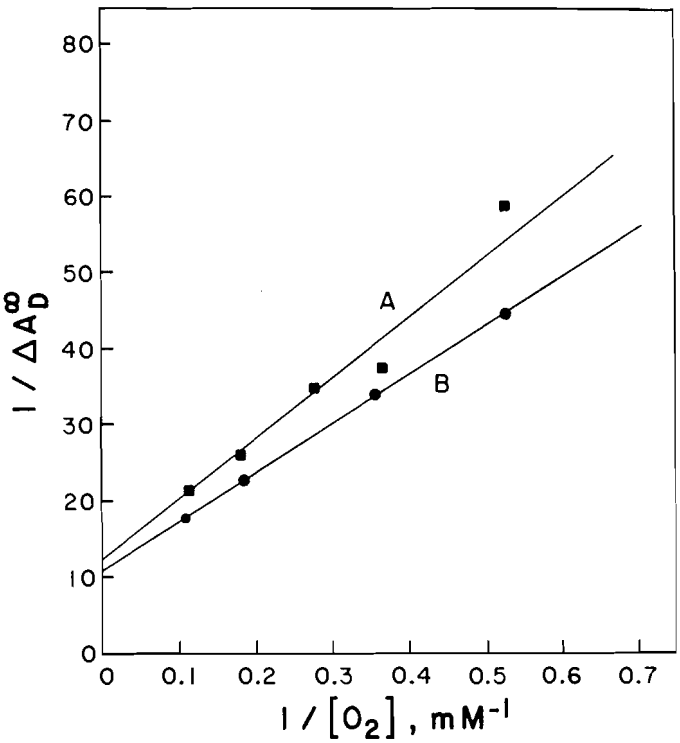


FIG. 3. Double reciprocal plots of $1/\Delta A_D^\infty$ vs. $1/[O_2]$ for (*A*) TBN and (*B*) DMTBP in benzene. ΔA_D^∞ is the absorbance change due to DPBF depletion, monitored at 425 nm, as a result of the reaction of DPBF with $^1O_2$* (see text).

Furthermore, the quenching of TBN triplet by oxygen and ferrocene did not cause a proportionate reduction in the yield of the 520 nm transient, suggesting that the latter was not a triplet-mediated product. The lifetime and relative yield of the 520 nm transient, measured in four different solvents (Table 3), were essentially independent of the nature of the solvent. Also, in methanol, it was found to be nonquenchable by perchloric acid (added up to 0.12 *M*).

Practically no residual absorption was observed following the decay of TBN triplet and the 520 nm transient in benzene, methanol, or cyclohexane. Thus, intermediate **2** (Scheme 1), if formed in high yields, could not possibly be a species with strong absorption in the visible and a lifetime longer than a microsecond.

(*c*) *Picosecond transient absorption studies*

In order to shed light on S_1 and S_2 lifetimes, benzene solutions

TABLE 3. Lifetimes and relative yields of 520 nm transient in various solvents (λ_{ex} = 337.1 nm)

Solvent	τ, ns[a]	Relative yield[b]
Benzene	230	1.0 (1.0)
Cyclohexane	220	1.1 (0.8)
Acetonitrile	230	0.9 (0.8)
Methanol	220	0.9 (0.8)

[a] ±10%.

[b] Measured in solutions (otpically matched at laser excitation wavelength) from end-of-pulse transient absorbance changes at 520 nm. The numbers in the parentheses are from 532 nm laser excitation, and those not parenthesized are from 337.1 nm excitation. ±20%.

of TBN were excited by 18 ps laser pulses at 355 and 532 nm. Note that while the latter wavelength corresponds to excitation into the S_1 band system, the former leads to absorption into the higher-energy side of S_2 band system and possibly lower vibronic levels of S_3 (see Fig. 1). Within 50–100 ps of the excitation at both wavelengths, transient absorption spectra were noted at 400–660 nm; these were comparable to those of the triplet observed in the course of nanosecond flash photolyses. Note that the short wavelength portion of the spectra (near 400 nm) in picosecond measurements was unreliable because of the low intensity of the probe light. Since the formation of the triplet was essentially complete within ~50 ps of the excitation at both wavelengths, lifetimes ≤50 ps could be associated with both S_1 and S_2 excited states of TBN in benzene. No additional prominent absorption that could be attributed to intermediate **2** (Scheme 1) was apparent in the picosecond time scale.

Discussion

(*a*) *Assignment of observed transients*

The triplet assignment for the major species with absorption maxima at ~405 and 745 nm is straightforward on the basis of its quenching behavior (see the Results section) and needs no further elaboration. In this connection, mention may be made of the laser flash photolytic observation by Cox *et al.* (22) of TBN triplet monitored at 550 nm (λ_{ex} = 353 nm). For 0.89 m*M* TBN in cyclohexane, they measured a triplet decay rate of 1.41×10^7 s^{-1}. Based on our τ_T and k_{SQ}^T data in cyclohexane (Table 1), we calculate a value of 1.3×10^7 s^{-1} for the triplet decay under the given conditions. The agreement between the data from the two

Can. J. Chem. Downloaded from www.nrcresearchpress.com by 41.223.56.140 on 09/07/12
For personal use only.

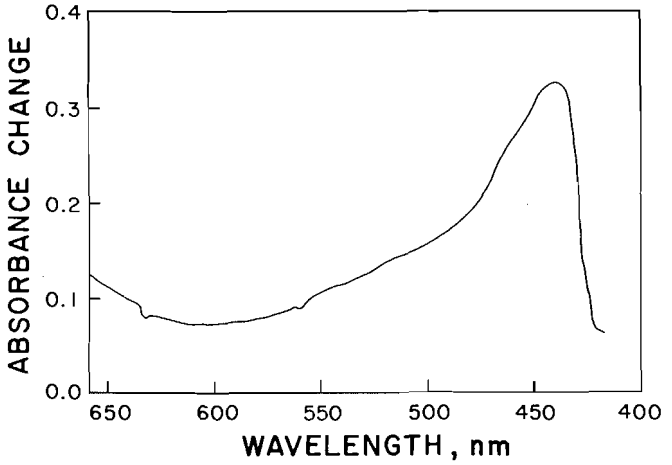


FIG. 4. Transient absorption spectrum at 50 ps following ~18 ps laser pulse excitation (532 nm) of TBN in benzene.

laboratories is satisfactory. Furthermore, in benzene, Cox *et al.* (22) measured a unimolecular triplet decay rate of $(1.0 \pm 0.1) \times 10^7$ s^{-1} and a triplet self-quenching rate constant (k_{SQ}^T) of 1.8×10^9 M^{-1} s^{-1}. While the former value is not very different from the one determined in the present work, the latter is lower (Table 1). It should be noted that as evident from the triplet absorption spectrum (Fig. 2), the monitoring wavelength of 550 nm used in ref. 22 is well removed from either of the maxima.

In view of the observed photochemistry of TBN (Scheme 1), it is tempting to assign the second transient (λ_{max} = 520 nm, Fig. 2) as the S_1-mediated photointermediate **2**. However, several experimental observations do not conform to this assignment. First, the 520 nm transient is not quenched by acids; this goes against its dipolar character (as tentatively proposed for **2** by Cox *et al.* (22)). Second, the yield of this species is not affected by the polarity of solvents (Table 3). On the contrary, the quantum yield of the photocyclization (Scheme 1) has been shown to increase on going from nonpolar to polar solvents (namely, by factors of 2 to 2.5 on going from benzene to acetonitrile and 4:1 acetonitrile:acetic-acid mixture) (22). Third, although the relatively sharp band at 520 nm is detected at an early stage following nanosecond pulse excitation into S_1 (e.g., by laser pulses at 532 nm), it is not discernible in the picosecond absorption spectra in the course of picosecond excitation at the same wavelength (Fig. 4). This rules out the 520 nm species as an S_1-derived product as primary as the triplet.

At the current level of our understanding, it is not possible to give a definitive identification for the 520 nm species, except that it arises via photochemistry from S_1.

(b) Triplet state behaviors. Comparison with other aromatic thiones

In terms of diffusion-limited self-quenching, submicrosecond triplet lifetimes, high triplet yields (in nonpolar solvents), quantitative singlet oxygen sensitization by triplet, and efficient bimolecular quenching by various quenchers, TBN triplet exhibits general similarities to aromatic and aliphatic thiocarbonyl triplets studied earlier (10–16). However, a few significant differences are also noticeable. These are discussed below.

The triplet yields of TBN, obtained by photoexcitation into S_1, are considerably less than unity. This is particularly true for the polar/H-bonding solvent, methanol, in which ϕ_T is only 0.4. Such a low ϕ_T has not been observed for any of the aromatic thiones previously studied (10, 11, 16). It seems logical to attribute the low ϕ_T to photochemistry, especially, the path described in Scheme 1. However, the quantum yields of the photocyclization have been measured (22) to be low ($(1.2–3.0) \times 10^{-3}$) in various solvents. If the photocyclization is the only photoreaction responsible for loss of quanta from S_1, then the ring opening of the intermediate **2** leading to the ground state has to be highly efficient (as proposed by Cox *et al.* (22)).

The intrinsic triplet lifetimes (τ_0^T) of TBN are much shorter than those of related aromatic thiones. In view of the fact that the solvents used are of "reactive" nature (e.g., relative to perfluoroalkanes) (9), part of the lifetime shortening is attributable to intermolecular quenching, namely, hydrogen transfer or charge transfer interactions with solvents. Since these interactions are also operative for other arylthiones in the given solvents, additional factor(s) should be sought in the case of TBN. One such factor would be the lower T_1–S_0 energy gap for TBN enhancing the related nonradiative process. However, it has been recently shown (9) that the energy gap law manifests itself in the case of thiones in terms of an increase in k_{nr} to the extent of $(4–6) \times 10^4$ s^{-1} on going from 4*H*-pyran-4-thione (E_T = 49.3 kcal mol^{-1}) to 4*H*-1-benzopyran-4-thione (E_T = 46.2) to xanthione (E_T = 43.3) in perfluoro-1,3-dimethylcyclohexane. Such a small change alone cannot account for the large decrease in τ_0^T from 1.4 μs for DMTBP (E_T = 41.1 kcal mol^{-1}) to 0.086 μs for TBN (E_T = 39 kcal mol^{-1}) in benzene. It is feasible that the intramolecular photochemistry as shown in Scheme 1 is also operative from T_1 (rendering it short-lived), although the contribution of the triplet pathway to the overall photochemistry may be negligible because of efficient reversion to the ground state in the subsequent steps.

The effect of the lowering of E_T is generally evident in the trend of the bimolecular rate constants for triplet quenching (Table 2) for XT (E_T = 43.3 kcal mol^{-1}), DMTBP (E_T = 41.1 kcal mol^{-1}), and TBN (E_T = 39 kcal mol^{-1}). Interestingly, in spite of the isoenergetic nature of the energy transfer, the quenching of TBN triplet by azulene (E_T ~40 kcal mol^{-1}) and ferrocene (E_T ~39–41 kcal mol^{-1}) is diffusion-limited. Of particular note is the fact that on going from XT to TBN, the rate constant for quenching by the nitroxide radical remains unchanged. Energy transfer quenching (1) is out of the question in the case of the low-energy TBN triplet. The unusually efficient quenching by the stable radical in this case is attributable to electron exchange (2) with the thiocarbonyl *S* atom enhancing intersystem crossing in the encounter complex.

Acknowledgement

We are grateful to Dr. V. Ramamurthy for the generous gift of 1-thiobenzoylnaphthalene and for helpful discussions.

1. V. A. KUZMIN and A. S. TATIKOLOV. Chem. Phys. Lett. **51**, 45 (1977); **53**, 606 (1978).
2. O. L. J. GIJZEMAN, F. KAUFMAN, and G. PORTER. J. Chem. Soc. Faraday Trans. 2, **69**, 727 (1973).
3. P. DE MAYO. Acc. Chem. Res. **9**, 52 (1976).
4. N. J. TURRO, V. RAMAMURTHY, W. CHERRY, and W. FARNETH. Chem. Rev. **78**, 125 (1978).
5. R. P. STEER. Rev. Chem. Intermed. **4**, (1981).
6. V. RAMAMURTHY. Org. Photochem. **7**, 231 (1985).
7. A. SAFARZADEH-AMIRI, D. A. CONDIRSTON, R. E. VERRALL, and R. P. STEER. Chem. Phys. Lett. **77**, 99 (1981).
8. A. SAFARZADEH-AMIRI, R. E. VERRALL, and R. P. STEER. Can. J. Chem. **61**, 894 (1983).
9. R. P. STEER and V. RAMAMURTHY. Acc. Chem. Res. **21**, 380 (1988).
10. C. V. KUMAR, L. QIN, and P. K. DAS. J. Chem. Soc. Faraday Trans. 2, **80**, 783 (1984).

Can. J. Chem. Downloaded from www.nrcresearchpress.com by 41.223.56.140 on 09/07/12
For personal use only.

11. C. V. KUMAR, H. F. DAVIS, and P. K. DAS. Chem. Phys. Lett. **109**, 184 (1984).
12. K. BHATTACHARYYA, C. V. KUMAR, P. K. DAS, V. JAYASREE, and V. RAMAMURTHY. J. Chem. Soc. Faraday Trans. 1, **81**, 1383 (1985).
13. K. BHATTACHARYYA, P. K. DAS, V. RAMAMURTHY, V. PUSHKARA RAO. J. Chem. Soc. Faraday Trans. 1, **82**, 135 (1986).
14. K. BHATTACHARYYA, B. N. RAO, P. K. DAS, and V. RAMAMURTHY. J. Photochem. **32**, 331 (1986).
15. K. BHATTACHARYYA, S. SHARAT, V. RAMAMURTHY, and P. K. DAS. J. Photochem. **35**, 299 (1986).
16. K. BHATTACHARYYA, V. RAMAMURTHY, and P. K. DAS. J. Phys. Chem. **91**, 5626 (1987).
17. U. BRÜHLMANN and J. K. HUBER. Chem. Phys. Lett. **54**, 606 (1978).
18. A. MACIEJEWSKI and R. P. STEER. Chem. Phys. Lett. **100**, 540 (1983).
19. A. MACIEJEWSKI and R. P. STEER. J. Am. Chem. Soc. **105**, 6738 (1983).
20. A. MACIEJEWSKI and R. P. STEER. J. Photochem. **24**, 303 (1984).
21. A. MACIEJEWSKI, D. R. DEMMER, D. R. JAMES, A. SAFARZADEH-AMIRI, R. E. VERRALL, and R. P. STEER. J. Am. Chem. Soc. **107**, 2831 (1985).
22. A. COX, D. R. KEMP, R. LAPOUYADE, P. DE MAYO, J. JOUSSOT-DUBIEN, and R. BONNEAU. Can. J. Chem. **53**, 2386 (1975).
23. J. C. D. BRAND and J. R. DAVIDSON. J. Chem. Soc. **15** (1976).
24. S. K. CHATTOPADHYAY, P. K. DAS, and G. L. HUG. J. Am. Chem. Soc. **104**, 4507 (1982).
25. V. NAGARAJAN and R. W. FESSENDEN. J. Phys. Chem. **89**, 2330 (1985).
26. T. EBBESEN. Rev. Sci. Instru. **59**, 1307 (1988).

Can. J. Chem. Downloaded from www.nrcresearchpress.com by 41.223.56.140 on 09/07/12
For personal use only.

Complexation binaire et ternaire des ions Cu(II), Hg(II) et Pt(II) par la D-valine et une série d'homologues de l'uracile

RAOUL M'BOUNGOU, MICHELLE PETIT-RAMEL[1] ET GERMAINE THOMAS-DAVID
Laboratoire de chimie analytique II, Université Claude Bernard, Lyon I, 43 Boulevard du 11-Novembre-1918, 69622 Villeurbanne CEDEX, France

ET

GÉRARD PERICHET ET BERNARD POUYET
Laboratoire de Photochimie, Université Claude Bernard, Lyon I, 43 Boulevard du 11-Novembre-1918, 69622 Villeurbanne CEDEX, France

Reçu le 17 octobre 1988

RAOUL M'BOUNGOU, MICHELLE PETIT-RAMEL, GERMAINE THOMAS-DAVID, GÉRARD PERICHET et BERNARD POUYET. Can. J. Chem. **67**, 973 (1989).

Les constantes de protonation de l'uracile (UR), de la cytosine (CY) et de la D-valine (VA) ont été calculées à 25°C et à force ionique $\mu = 0{,}1$ ($NaNO_3$). Dans les mêmes conditions, les constantes de stabilité des complexes simples formés avec le Cu(II), le Hg(II) et le Pt(II) ainsi que celles des complexes mixtes formés entre un acide aminé, la D-valine et une série d'homologues de l'uracile : thymine, thymidine, acide orotique et cytosine avec les mêmes ions métalliques ont été déterminées par protométrie. En ce qui concerne les complexes mixtes, nous avons développé et testé une nouvelle méthode simple d'estimation de leurs constantes de stabilité.

Mots clés : coordination du Cu(II), du Hg(II) et du Pt(II), coordination ternaire, homologues de l'uracile, D-valine, méthodes protométriques.

RAOUL M'BOUNGOU, MICHELLE PETIT-RAMEL, GERMAINE THOMAS-DAVID, GÉRARD PERICHET, and BERNARD POUYET. Can. J. Chem. **67**, 973 (1989).

The protonation constants of uracil (UR), cytosine (CY), and D-valine (VA) have been calculated at 25°C and at ionic strength $\mu = 0.1$ ($NaNO_3$). In a first step the stability constants of their Cu(II), Hg(II) and Pt(II) simple complexes were determined. In a second step the mixed complexation of several uracil homologues as thymine, thymidine, orotic acid and cytosine was also investigated under the same conditions by protometric methods. Concerning the mixed complexes, a new simple method of estimating their stability constants has been developed and verified.

Key words: Cu(II), Hg(II), Pt(II) coordination, ternary coordination, uracil homologues, D-valine, protometric methods.

Introduction

Ce travail est dans le prolongement direct d'un précédent mémoire (1) concernant les interactions du Cu(II), du Hg(II) et du Pt(II) avec les formes monomère et dimère de la thymine, de la thymidine et de l'acide orotique.

Depuis les travaux de Rosenberg *et al.* (2, 3), le cis-dichlorodiamineplatine(II) ou cis-platine est utilisé en chimiothérapie pour ses propriétés antitumorales bien connues, mais sa faible solubilité dans l'eau et sa toxicité vis à vis du rein limitent son utilisation dans certains traitements anticancéreux (4–6). Par contre, les nombreuses combinaisons de substitution des groupes aminés ou des groupes chlorés par des amino-acides (7), des amines (8), des amino-acides et amines (9–14), des molécules d'eau (2, 8, 15), des acides alcools (16) ou des diacides (17) ont permis d'obtenir des produits à la fois plus solubles et moins toxiques. Enfin la découverte des complexes bleus des dérivés de la purine et la pyrimidine, les «platin-blues», solubles dans l'eau, peu toxiques, élargit notablement le domaine d'application des composés du platine(II) (15, 18–24). Dans ce but, nous avons étudié les complexes binaires du platine(II) avec la D-valine (figure 1a), l'uracile (figure 1b) et la cytosine (figure 1c) ainsi que les espèces ternaires obtenues avec la D-valine d'une part, la thymine (figure 1d), la thymidine (figure 1e), l'acide orotique (figure 1f), l'uracile, la cytosine d'autre part.

En outre, d'un point de vue purement structural, il est utile de comparer les complexes binaires et ternaires du Pt(II) avec, d'une part ceux du Hg(II), en liaison avec une réponse photochimique possible (25), et d'autre part ceux du Cu(II), qui demeure un métal de référence intéressant dans la complexation des amino-acides.

Nous rappelons brièvement le protocole développé dans les mémoires précédents (1, 26) pour la mise en évidence des espèces protonées puis des espèces complexes simples $M_pH_qL_r$, ainsi que le calcul de leurs constantes de stabilité β_{pqr} :

(*i*) examen des courbes de formation $\bar{n} = f(pL)$ où n représente le nombre moyen de ligands L déprotonés fixés par métal.

(*ii*) affinement par minimisation d'écart-type sur les points expérimentaux et calculés, des transformées de courbes de titration, $\bar{q} = f(pH)$, rendues linéaires où q est le nombre de protons neutralisables par mole de ligand.

En ce qui concerne l'affinement des espèces complexes mixtes, la difficulté essentielle réside dans une appréciation convenable de la valeur initiale de la constante de stabilité (27–29*a*). Nous avons développé et testé sur une dizaine d'exemples une nouvelle méthode simple d'estimation de la constante du mixte. Soit une espèce complexe mixte de formule générale $M_pH_qL_1L_2$ où M représente l'atome métallique central, H l'atome d'hydrogène, L_1 et L_2 les deux ligands, dont la formation est régie par l'équilibre :

$$[1] \quad pM + qH + L_1 + L_2 \rightleftarrows M_pH_qL_1L_2$$

avec q le nombre global des protons neutralisables tel que :

$$[2] \quad q = q_1 + q_2$$

1. Auteur à qui adresser toute correspondance.

Printed in Canada / Imprimé au Canada

Can. J. Chem. Downloaded from www.nrcresearchpress.com by 41.223.56.140 on 09/07/12
For personal use only.

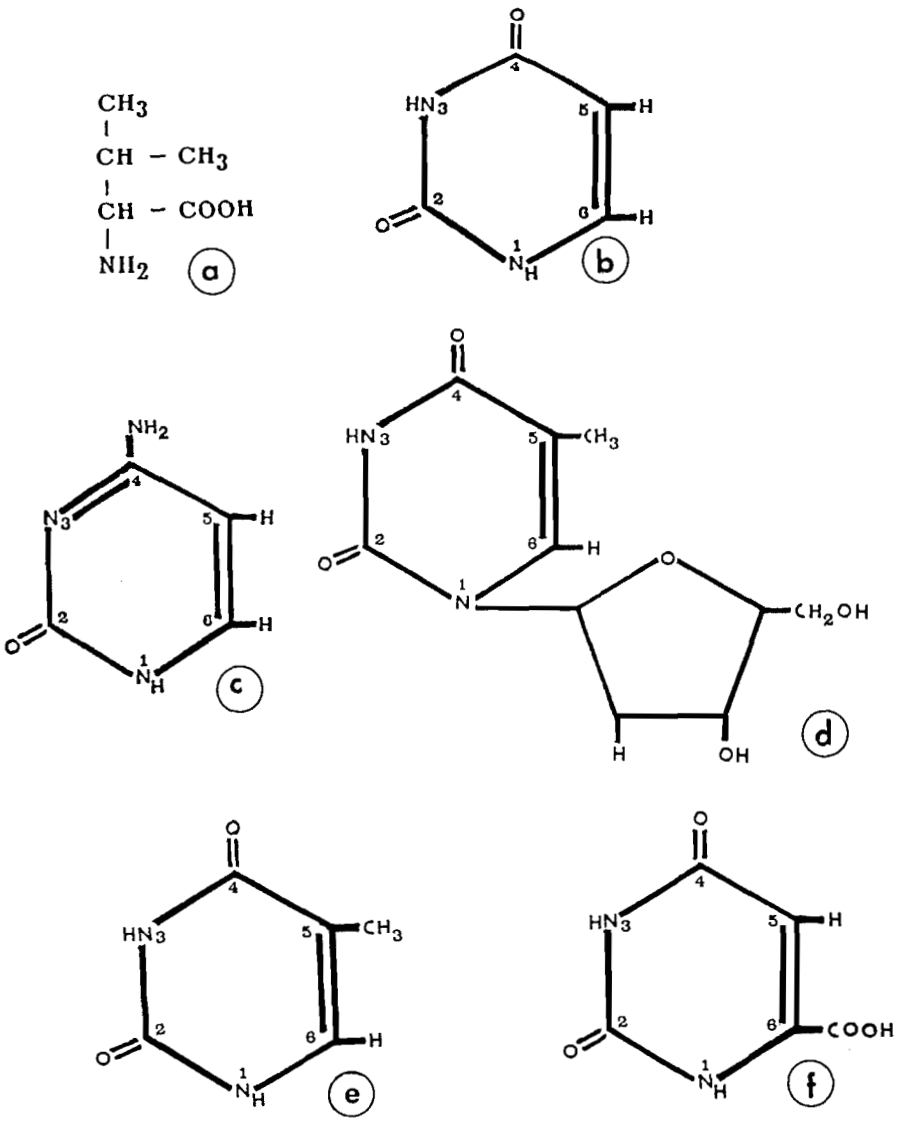


FIG. 1. (a) D-Valine, (b) uracile, (c) cytosine, (d) thymidine, (e) thymine, (f) acide orotique.

q_1 et q_2 sont respectivement le nombre de protons neutralisables du ligand L_1 et du ligand L_2.

En considérant l'ensemble des deux ligands L_1 et L_2 de concentration totale respective C_{L_1} et C_{L_2} dans l'espèce mixte comme un seul ligand L, nous avons, si C_L est la concentration totale en ligand L :

$$[3] \quad C_L = C_{L_1} + C_{L_2}$$

Dans ces conditions, l'équilibre [1] devient par analogie avec un complexe binaire :

$$[4] \quad pM + qH + L \rightleftarrows M_pH_qL$$

Pour $p = 1$, en faisant abstraction des espèces hydroxydées et protonées, nous pouvons calculer un degré de formation défini par Bjerrum :

$$[5] \quad \bar{n} = \frac{[ML]}{C_M}$$

où [ML] est la concentration de l'espèce mixte sous la forme ML; C_M est la concentration en métal telle que :

$$[6] \quad C_M = [M] + [ML]$$

La concentration en ligand total est définie par :

$$[7] \quad C_L = \sum_1^q [H_qL] + [ML] + [L]$$

Alors

$$[8] \quad [ML] = C_L - [L] - \sum_1^q [H_qL]$$

où

$$[9] \quad \sum_1^q [H_qL] = \sum_1^q [H]^q[L]\beta'_{q1}$$

avec β'_{q1}, le paramètre de stabilité protonique relatif au ligand global L, tel que :

$$[10] \quad \beta'_{q1} = \beta_{q10} + \beta_{q01}$$

où β_{q10} et β_{q01} représentent respectivement les constantes de stabilité protonique du premier et du second ligand. L'expression [5] devient en combinant les relations [8] et [9] :

$$[11] \quad \bar{n} = \frac{C_L - [L] - \sum_1^q [H]^q[L]\beta'_{q1}}{C_M}$$

La courbe de formation du système ternaire est donc obtenue en représentant graphiquement $\bar{n} = f(p[L])$.

D'autre part, nous pouvons relier graphiquement le paramètre de formation du mixte β'_{101} et ce même degré de formation

Can. J. Chem. Downloaded from www.nrcresearchpress.com by 41.223.56.140 on 09/07/12
For personal use only.

TABLEAU 1. Constantes de formation des complexes simples; t = 25°C; μ = 0,1 ($NaNO_3$)

Espèces	pqr	log β_{pqr}	Domaine de formation	Références						
				1	29	30	32	37	43	45
H(VA)	011	9,64 (0,02)*				9,62				
H_2^+(VA)	021	11,85 (0,02)				11,97				
$[Cu(VA)]^+$	101	7,98 (0,01)	pH 3–10		8,06					
$[Cu(VA)_2]$	102	14,96 (0,01)	pH 4,5–10		14,78					
$[Hg(VA)]^+$	101	3,46 (0,03)	pH 7,25–12							
$[Hg(VA)_2]$	102	6,83 (0,03)	pH 8,5–12							
cis-$[Pt(VA)(NH_3)_2]^+$	101	6,61 (0,01)	pH 3,5–12							
cis-$[Pt(VA)_2(NH_3)_2]$	102	11,24 (0,01)	pH 6–12							
H(UR)	011	9,29 (0,02)					8,8	9,46	9,5	9,29
$[Cu(UR)]^+$	101	4,97 (0,04)	pH 5–12				5,6	6,14		6,04
$[Cu(UR)_2]$	102	10,06 (0,04)	pH 6–12					11,42		11,23
$[Hg(UR)]^+$	101	8,10 (0,01)	pH 2–7							
$[Hg(UR)_2]$	102	14,96 (0,01)	pH 4–12							
cis-$[Pt(UR)(H_2O)(NH_3)_2]^+$	101	6,27 (0,01)	pH 4–12							
cis-$[Pt(UR)_2(NH_3)_2]$	102	10,96 (0,01)	pH 5,75–12							
H(CY)	011	10,67 (0,02)					10		12,2	
H_2^+(CY)	021	15,28 (0,02)					14,2		16,65	
$[Cu(CY)]^+$	101	6,49 (0,04)	pH 5,5–9							
$[Cu(CY)_2]$	102	13,24 (0,04)	pH 6–12							
$[Hg(CY)]^+$	101	7,85 (0,02)	pH 4,5–9,5							
$[Hg(CY)_2]$	102	14,12 (0,02)	pH 6–12							
cis-$[Pt(CY)(H_2O)(NH_3)_2]^+$	101	7,93 (0,03)	pH 4,5–12							
cis-$[Pt(CY)_2(NH_3)_2]$	102	13,89 (0,03)	pH 6–12							
H(TY)	011			9,78						
cis-$[Pt(TY)(H_2O)(NH_3)_2]^+$	101	6,73 (0,01)	pH 4–10							
cis-$[Pt(TY)_2(NH_3)_2]$	102	11,93 (0,01)	pH 6–12							

*Écarts-types correspondants aux constantes.

en combinant les expressions [5] et [6].

$$[12] \quad \bar{n} = \frac{[L]\beta'_{101}}{1 + [L]\beta'_{101}}$$

Il est clair qu'il existe une relation entre la courbe de formation et la constante de stabilité de «l'espèce ternaire» ML. Sans entrer dans les développements mathématiques de Bjerrum, nous utiliserons une méthode approchée pour déterminer la constante de stabilité du mixte β'_{101}, ou mieux β_{1011}, d'après l'équilibre [1] en traçant sur la même figure les courbes de formation relatives aux systèmes binaires ML_1 et ML_2 et au système ternaire ML_1L_2. Nous distinguons les cas suivants :

(a) Les courbes de formation des systèmes ML_1L_2 et ML_1 (ou ML_2) sont confondues pour toutes les valeurs de $\bar{n}$: il n'y a pas formation d'espèce mixte.

(b) Les courbes de formation des systèmes ML_1L_2 et ML_1 (ou ML_2) sont confondues pour chaque valeur de $\bar{n}$ comprise entre 0 et 1 ou pour toutes les valeurs de $\bar{n}$ supérieures ou égales à 1,5, ou encore ne sont pas confondues quel que soit $\bar{n}$: la valeur de β_{1011} est estimée comme pour le cas d'un simple MA_2 (avec $\beta_{1011} = K_1 \cdot K_2$).

(c) Les courbes de formation des systèmes ML_1L_2 et ML_1 (ou ML_2) sont confondues pour toutes les valeurs de $\bar{n}$ supérieures ou égales à 1 : la valeur de β_{1011} est estimée pour $\bar{n} = 0,5$.

La constante du mixte étant ainsi estimée, elle est affinée à l'aide d'un programme basic développé dans notre laboratoire.

Résultats

Les valeurs définitives des constantes affinées par la méthode de «pit mapping» sont rassemblées dans les tableaux 1 et 2.

1. Systèmes binaires

1. D-Valine H_2^+(VA)

Bien que la D-valine ait déjà été étudiée (29, 30), nous avons recalculé ses constantes de protonation ainsi que les constantes de stabilité des complexes du cuivre pour donner le maximum d'homogénéité à nos résultats (figure 2).

(a) Interactions avec le cuivre. Les deux chélates $[Cu(VA)]^+$ et $[Cu(VA)_2]$ répondent aux équilibres connus :

$$Cu^{2+} + H_2^+(VA) \rightleftarrows [Cu(VA)]^+ + 2H^+$$

$$Cu^{2+} + 2H_2^+(VA) \rightleftarrows [Cu(VA)_2] + 4H^+$$

(b) Interactions avec le mercure. Les interactions D-valine–mercure n'ont pas donné lieu, à notre connaissance à une évaluation précise de la constante de stabilité des complexes obtenus. Pour notre part, le traitement des données potentiométriques relatives à ce système fait apparaître deux espèces complexes $[Hg(VA)]^+$ et $[Hg(VA)_2]$ correspondant aux équilibres :

$$Hg^{2+} + H_2^+(VA) \rightleftarrows [Hg(VA)]^+ + 2H^+$$

$$Hg^{2+} + 2H_2^+(VA) \rightleftarrows [Hg(VA)_2] + 4H^+$$

(c) Interactions avec le platine. Si l'état solide et particulièrement l'étude cristallographique des complexes platine–valine ont retenu l'attention des chercheurs (9, 14), les interactions en solution ne semblent pas avoir été étudiées systématiquement. Cela tient sans doute à la transformation préalable obligée du cis-platine dans lequel il est nécessaire de libérer une ou deux positions de coordination en substituant les groupements chlorures. En solution dans l'eau, le cis-platine donne lieu aux

Can. J. Chem. Downloaded from www.nrcresearchpress.com by 41.223.56.140 on 09/07/12
For personal use only.

réactions d'hydrolyse suivantes (15) :

$$\text{cis-}[PtCl_2(NH_3)_2] + H_2O \rightleftarrows \text{cis-}[PtCl(H_2O)(NH_3)_2]^+ + Cl^-$$

$$\text{cis-}[PtCl(H_2O)(NH_3)_2]^+ + H_2O \rightleftarrows \text{cis-}[Pt(H_2O)_2(NH_3)_2]^{2+} + Cl^-$$

Nous avons identifié deux espèces complexes cis-$[Pt(VA)(NH_3)_2]^+$ et cis-$[Pt(VA)_2(NH_3)_2]$ répondant aux équilibres :

$$\text{cis-}[Pt(H_2O)_2(NH_3)_2]^{2+} + H_2{}^+(VA) \rightleftarrows \text{cis-}[Pt(VA)(NH_3)_2]^+ + 2H^+ + 2H_2O$$

$$\text{cis-}[Pt(H_2O)_2(NH_3)_2]^{2+} + 2H_2{}^+(VA) \rightleftarrows \text{cis-}[Pt(VA)_2(NH_3)_2] + 4H^+ + 2H_2O$$

Il a été montré (12, 31) que dans le cas de la plupart des amino-acides, l'espèce ML, cis-$[Pt(VA)(NH_3)_2]^+$ présente un cycle de chélation, le platine étant lié par les groupements carboxylique et aminé. Pour la seconde espèce ML_2, cis-$[Pt(VA)_2(NH_3)_2]$, le cycle de chélation disparaît et le complexe présente deux liaisons Pt – groupement aminé de l'amino-acide (8–13, 31).

2. Uracile H(UR), cytosine $H_2{}^+(CY)$ et thymidine H(TY)

En ce qui concerne la thymidine, les constantes de protonation ainsi que les constantes de stabilité des complexes du cuivre et mercure ont déjà été publiées dans un mémoire précédent (1). Nous ne donnerons que les équilibres relatifs aux complexes du platine.

(a) Protonation. Bien qu'il y ait dans chaque molécule d'uracile deux possibilités d'échange relatives aux hydrogènes portés par les fonctions amines N1 et N3, seule la déprotonation N3 (32, 33) est observable dans le domaine de pH envisagé (tableau 1).

En ce qui concerne la cytosine, la forme cationique $H_2{}^+(CY)$ prédomine en milieu acide et la protonation de l'atome d'azote N3 (34–36) induit préférentiellement la fixation d'ions métalliques. Comme l'indique la majorité des références bibliographiques (33, 37–40), les valeurs de la constante d'acidité de l'hydrogène lié à l'azote N3 sont homogènes. Par contre, la disparité des valeurs collectées pour la constante d'acidité relative à la déprotonation N1 (32, 41–44) nécessite un calcul complet et précis bien que cette position ne soit pas un site de coordination privilégié.

(b) Interactions avec le cuivre. L'existence de deux complexes d'uracile $[Cu(UR)]^+$ et $[Cu(UR)_2]$ a été signalée par Taqui Khan *et al.* (32, 37, 45*a*). Bien que Tan et Beck aient identifié uniquement l'espèce $[Cu(UR)]^+$ (46), nous avons aisément mis en évidence deux espèces successives $[Cu(UR)]^+$ et $[Cu(UR)_2]$ répondant aux équilibres :

$$Cu^{2+} + H(UR) \rightleftarrows [Cu(UR)]^+ + H^+$$

$$Cu^{2+} + 2H(UR) \rightleftarrows [Cu(UR)_2] + 2H^+$$

Dans ce cas, il y a coordination par l'intermédiaire de l'azote N3 (46, 47).

Pour la cytosine, nous avons identifié les complexes successifs $[Cu(CY)]^+$ et $[Cu(CY)_2]$ selon les équilibres de formation :

$$Cu^{2+} + H_2{}^+(CY) \rightleftarrows [Cu(CY)]^+ + 2H^+$$

$$Cu^{2+} + 2H_2{}^+(CY) \rightleftarrows [Cu(CY)_2] + 4H^+$$

Ces espèces complexes obtenues sous forme cristalline (47, 48) chélatent le métal par l'azote N3 et l'oxygène adjacent O2 afin de respecter la coordinence quadrangulaire plane du cuivre.

(c) Interactions avec le mercure. Les quelques données bibliographiques relatives aux complexes du système mercure–uracile concernent surtout l'état solide (49–51) et ponctuellement la détermination de la stabilité de l'espèce $[HgCl_2(UR)]$ qui relève de la complexation ternaire avec les ions chlorures peu labiles (52). Plus directement, le cas de complexation binaire que nous étudions en utilisant le nitrate mercurique, $Hg(NO_3)_2$, porte sur la formation de deux espèces complexes $[Hg(UR)]^+$ et $[Hg(UR)_2]$ répondant aux équilibres :

$$Hg^{2+} + H(UR) \rightleftarrows [Hg(UR)]^+ + H^+$$

$$Hg^{2+} + 2H(UR) \rightleftarrows [Hg(UR)_2] + 2H^+$$

La cytosine est comme nous l'avons annoncé précédemment un diacide faible protoné en N3 et N1. Ferreira *et al.* (53) ont montré l'existence de l'espèce $[Hg(CY)_2]$; ceci procède d'une démarche incomplète puisque seule la déprotonation en N3 a été considérée. En ce qui nous concerne, la prise en compte des deux déprotonations conduit aux équilibres suivants :

$$Hg^{2+} + H_2{}^+(CY) \rightleftarrows [Hg(CY)]^+ + 2H^+$$

$$Hg^{2+} + 2H_2{}^+(CY) \rightleftarrows [Hg(CY)_2] + 4H^+$$

Pour les deux ligands envisagés, les complexes du mercure présentent une géométrie linéaire (53); il y a coordination par l'intermédiaire de l'azote N3, site de liaison préférentiel (30, 36*b*).

(d) Interactions avec le platine. Comme dans le cas de la valine, plusieurs auteurs (18–20, 22, 23, 54–61) ont préparé les complexes platinés de l'uracile, de la cytosine et ses dérivés sous forme cristalline, leur stabilité en solution demeurant inconnue. Les complexes cis-$[Pt(UR)(H_2O)(NH_3)_2]^+$, cis-$[Pt(UR)_2(NH_3)_2]$, cis-$[Pt(CY)(H_2O)(NH_3)_2]^+$ et cis-$[Pt(CY)_2(NH_3)_2]$, dont nous avons montré l'existence, répondent aux équilibres :

$$\text{cis-}[Pt(H_2O)_2(NH_3)_2]^{2+} + H(UR) \rightleftarrows \text{cis-}[Pt(UR)(H_2O)(NH_3)_2]^+ + H^+ + H_2O$$

$$\text{cis-}[Pt(H_2O)_2(NH_3)_2]^{2+} + 2H(UR) \rightleftarrows \text{cis-}[Pt(UR)_2(NH_3)_2] + 2H^+ + 2H_2O$$

$$\text{cis-}[Pt(H_2O)_2(NH_3)_2]^{2+} + H_2{}^+(CY) \rightleftarrows \text{cis-}[Pt(CY)(H_2O)(NH_3)_2]^+ + 2H^+ + H_2O$$

$$\text{cis-}[Pt(H_2O)_2(NH_3)_2]^{2+} + 2H_2{}^+(CY) \rightleftarrows \text{cis-}[Pt(CY)_2(NH_3)_2] + 4H^+ + 2H_2O$$

La thymidine ne réagit pas directement avec le cis-platine (62, 63). Nous avons donc procédé, comme dans le cas de la valine, à la substitution des chlorures par des molécules d'eau et obtenu les espèces successives suivantes :

$$\text{cis-}[Pt(H_2O)_2(NH_3)_2]^{2+} + H(TY) \rightleftarrows \text{cis-}[Pt(TY)(H_2O)(NH_3)_2]^+ + H^+ + H_2O$$

$$\text{cis-}[Pt(H_2O)_2(NH_3)_2]^{2+} + 2H(TY) \rightleftarrows \text{cis-}[Pt(TY)_2(NH_3)_2] + 2H^+ + 2H_2O$$

II. Systèmes ternaires

Dans un premier temps, nous calculons la valeur approchée de la constante de stabilité de l'espèce ternaire par la méthode d'estimation décrite en introduction. L'affinement des constantes de stabilité du complexe ternaire MLL′ converge ainsi aisément et conduit aux courbes de répartition de l'ensemble des espèces (figures 3 et 4).

Seuls le cuivre et le platine donnent naissance à des espèces ternaires. Le mercure provoque une précipitation immédiate de la solution contenant les deux ligands quels que soient les rapports envisagés.

Can. J. Chem. Downloaded from www.nrcresearchpress.com by 41.223.56.140 on 09/07/12
For personal use only.

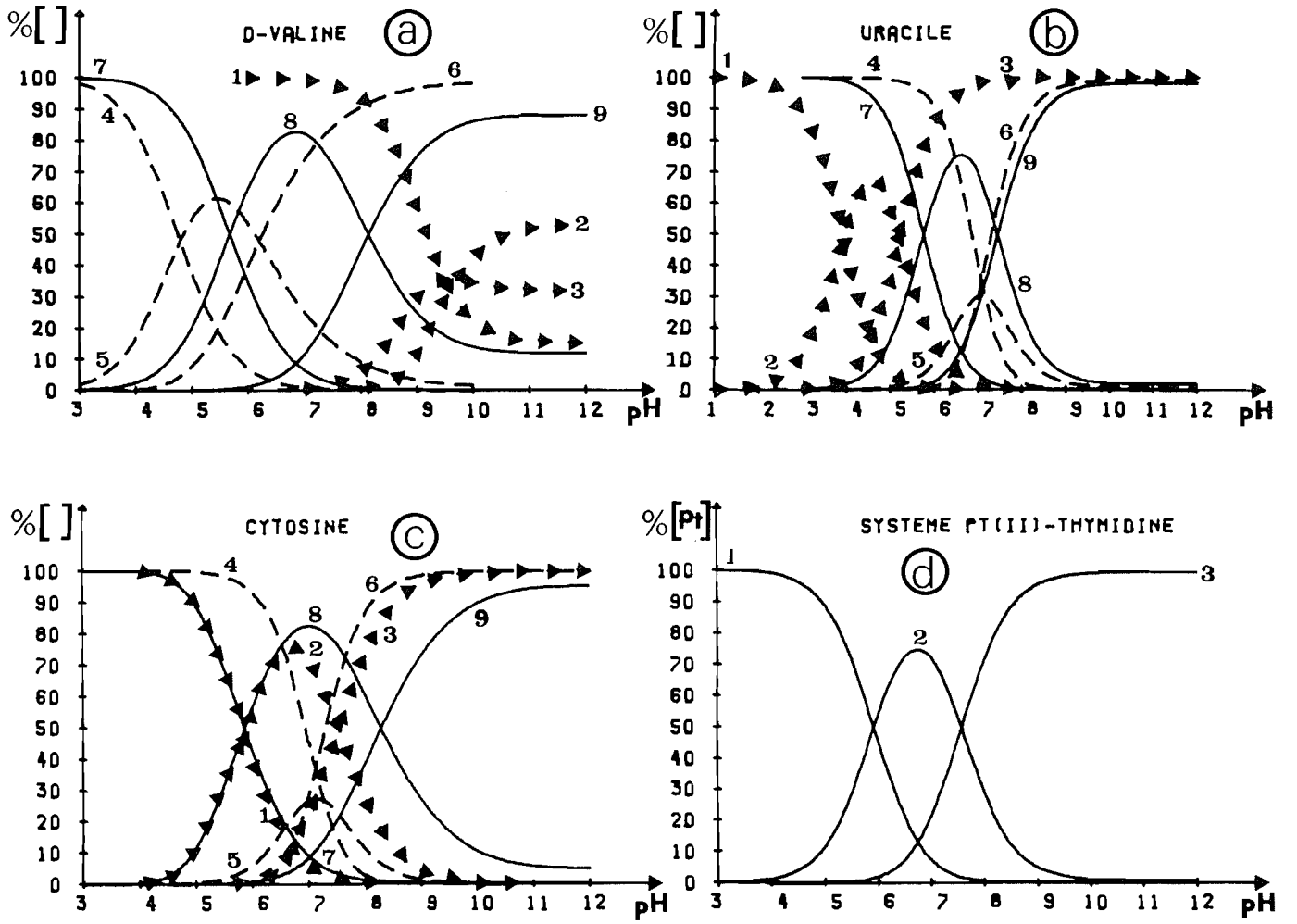


FIG. 2. (a) D-Valine : (▲▲) $[H_2^+ VA] = 10^{-3}$ M; $[Hg^{2+}] = 2 \times 10^{-4}$ M; (--) $[H_2^+ VA] = 10^{-3}$ M; $[Cu^{2+}] = 5 \times 10^{-4}$ M; (—) $[H_2^+ VA] = 3 \times 10^{-3}$ M; $[Pt^{2+}] = 1{,}5 \times 10^{-3}$ M. 1, Hg^{2+}; 2, $[Hg(VA)]^+$; 3, $[Hg(VA)_2]$; 4, Cu^{2+}; 5, $[Cu(VA)]^+$; 6, $[Cu(VA)_2]$; 7, cis-$[Pt(H_2O)_2(NH_3)_2]^{2+}$; 8, cis-$[Pt(VA)(NH_3)_2]^+$; 9, cis-$[Pt(VA)_2(NH_3)_2]$.

(b) Uracile : (▲▲) $[HUR] = 2 \times 10^{-3}$ M; $[Hg^{2+}] = 2{,}667 \times 10^{-4}$ M; (--) $[HUR] = 2 \times 10^{-3}$ M; $[Cu^{2+}] = 5 \times 10^{-4}$ M; (—) $[HUR] = 2 \times 10^{-3}$ M; $[Pt^{2+}] = 4 \times 10^{-4}$ M. 1, Hg^{2+}; 2, $[Hg(UR)]^+$; 3, $[Hg(UR)_2]$; 4, Cu^{2+}; 5, $[Cu(UR)]^+$; 6, $[Cu(UR)_2]$; 7, cis-$[Pt(H_2O)_2(NH_3)_2]^{2+}$; 8, cis-$[Pt(UR)(H_2O)(NH_3)_2]^+$; 9, cis-$[Pt(UR)_2(NH_3)_2]$.

(c) Cytosine : (▲▲) $[H_2^+ CY] = 10^{-3}$ M; $[Hg^{2+}] = 2{,}027 \times 10^{-4}$ M; (--) $[H_2^+ CY] = 10^{-3}$ M; $[Cu^{2+}] = 1{,}99 \times 10^{-4}$ M; (—) $[H_2^+ CY] = 10^{-3}$ M; $[Pt^{2+}] = 5 \times 10^{-4}$ M. 1, Hg^{2+}; 2, $[Hg(CY)]^+$; 3, $[Hg(CY)_2]$; 4, Cu^{2+}; 5, $[Cu(CY)]^+$; 6, $[Cu(CY)_2]$; 7, cis-$[Pt(H_2O)_2(NH_3)_2]^{2+}$; 8, cis-$[Pt(CY)(H_2O)(NH_3)_2]^+$; 9, cis-$[Pt(CY)_2(NH_3)_2]$.

(d) Thymidine : (—) $[HTY] = 2 \times 10^{-3}$ M; $[Pt^{2+}] = 4 \times 10^{-4}$ M; 1, cis-$[Pt(H_2O)_2(NH_3)_2]^{2+}$; 2, cis-$[Pt(TY)(H_2O)(NH_3)_2]^+$; 3, cis-$[Pt(TY)_2(NH_3)_2]$.

1. Complexation ternaire avec le cuivre

Récemment, les systèmes cuivre–histidine–cytosine (40) et cuivre–glycine–thymine (64) ont été étudiés. Pour notre part, nous avons identifié les espèces suivantes (figure 3) : [Cu(VA)(TM)], [Cu(VA)(TY)], $[Cu(VA)(OM)]^+$, [Cu(VA)(UR)] et [Cu(VA)(CY)].

2. Complexation ternaire avec le platine

Seul, B. Lippert (61) a signalé l'existence des complexes mixtes du cis-platine par combinaison deux à deux des quatre principales bases de l'ADN (adénine, cytosine, guanine et thymine). La complexation ternaire entre un acide aminé d'une part, et une quelconque de ces bases, n'a par contre jamais été abordée à notre connaissance. Notre choix s'est donc porté sur la D-valine entrant dans la préparation de différents produits anticancéreux et les homologues de l'uracile étudiés précédemment.

Comme pour les systèmes binaires, l'ion platine est sous forme cis-$[Pt(H_2O)_2(NH_3)_2]^{2+}$ et conduit à la formation d'espèces ternaires que l'on pourrait qualifier en terme limite «d'espèces quaternaires» (figure 4), cis-[Pt(VA)(TM)$(NH_3)_2$], cis-[Pt(VA)(TY)$(NH_3)_2$], cis-$[Pt(VA)(OM)(NH_3)_2]^+$, cis-[Pt(VA)(UR)$(NH_3)_2$] et cis-[Pt(VA)(CY)$(NH_3)_2$].

Conclusion

Les tableaux 1 et 2 regroupent tous les résultats obtenus. Les répartitions des différentes espèces simples et mixtes sont consignées dans les figures 2, 3 et 4. Cette étude de stabilité appelle plusieurs remarques.

1. Complexation binaire

D-Valine

Les complexes simples de la D-valine avec le cuivre(II) sont des chélates (29, 30), tandis que ceux du platine(II) sont de deux types : chélate (figure 5a) dans des composés de formule ML

Can. J. Chem. Downloaded from www.nrcresearchpress.com by 41.223.56.140 on 09/07/12
For personal use only.

Can. J. Chem. Downloaded from www.nrcresearchpress.com by 41.223.56.140 on 09/07/12
For personal use only.

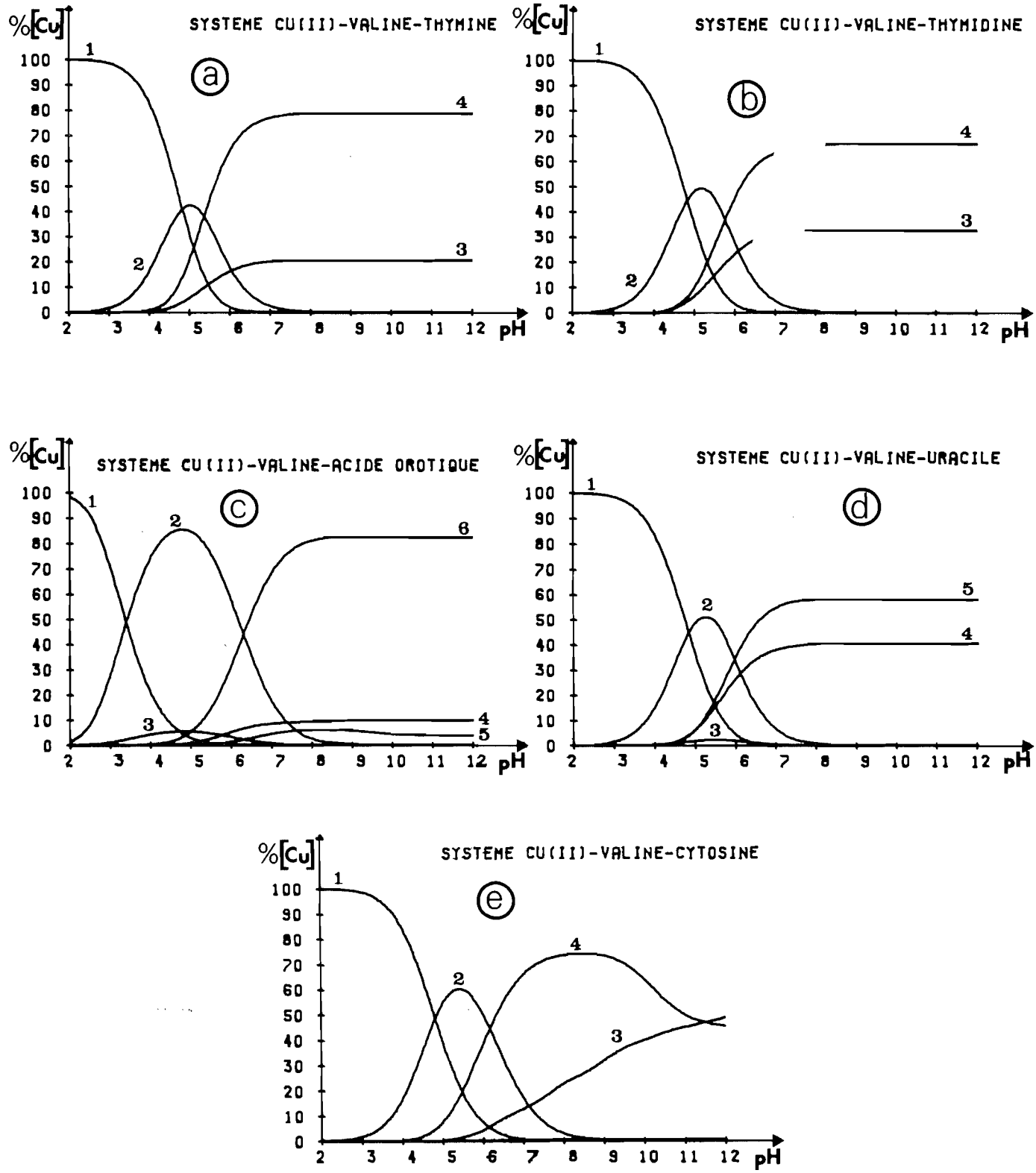


FIG. 3. (a) Système Cu(II)–valine–thymine : $[H_2^+ VA] = 10^{-3}$ M; [HTM] = 10^{-3} M; $[Cu^{2+}] = 5{,}022 \times 10^{-4}$ M. 1, Cu^{2+}; 2, $[Cu(VA)]^+$; 3, $[Cu(VA)_2]$; 4, [Cu(VA)(TM)].

(b) Système Cu(II)–valine–thymidine : $[H_2^+ VA] = 10^{-3}$ M; [HTY] = 10^{-3} M; $[Cu^{2+}] = 5 \times 10^{-4}$ M. 1, Cu^{2+}; 2, $[Cu(VA)]^+$; 3, $[Cu(VA)_2]$; 4, [Cu(VA)(TY)].

(c) Système Cu(II)–valine – acide orotique : $[H_2^+ VA] = 10^{-3}$ M; $[H_2OM] = 10^{-3}$ M; $[Cu^{2+}] = 5 \times 10^{-4}$ M. 1, Cu^{2+}; 2, $[Cu(OM)]^+$; 3, [Cu(VA)]; 4, $[Cu(OM)_2]^{2-}$; 5, $[Cu(VA)_2]$; 6, $[Cu(VA)(OM)]^+$.

(d) Système Cu(II)–valine–uracile : $[H_2^+ VA] = 10^{-3}$ M; [HUR] = 10^{-3} M; $[Cu^{2+}] = 5 \times 10^{-4}$ M. 1, Cu^{2+}; 2, $[Cu(VA)]^+$; 3, $[Cu(UR)]^+$; 4, $[Cu(VA)_2]$; 5, [Cu(VA)(UR)].

(e) Système Cu(II)–valine–cytosine : $[H_2^+ VA] = 10^{-3}$ M; $[H_2^+ CY] = 10^{-3}$ M; $[Cu^{2+}] = 5 \times 10^{-4}$ M. 1, Cu^{2+}; 2, $[Cu(VA)]^+$; 3, [Cu(VA)(CY)]; 4, $[Cu(VA)_2]$.

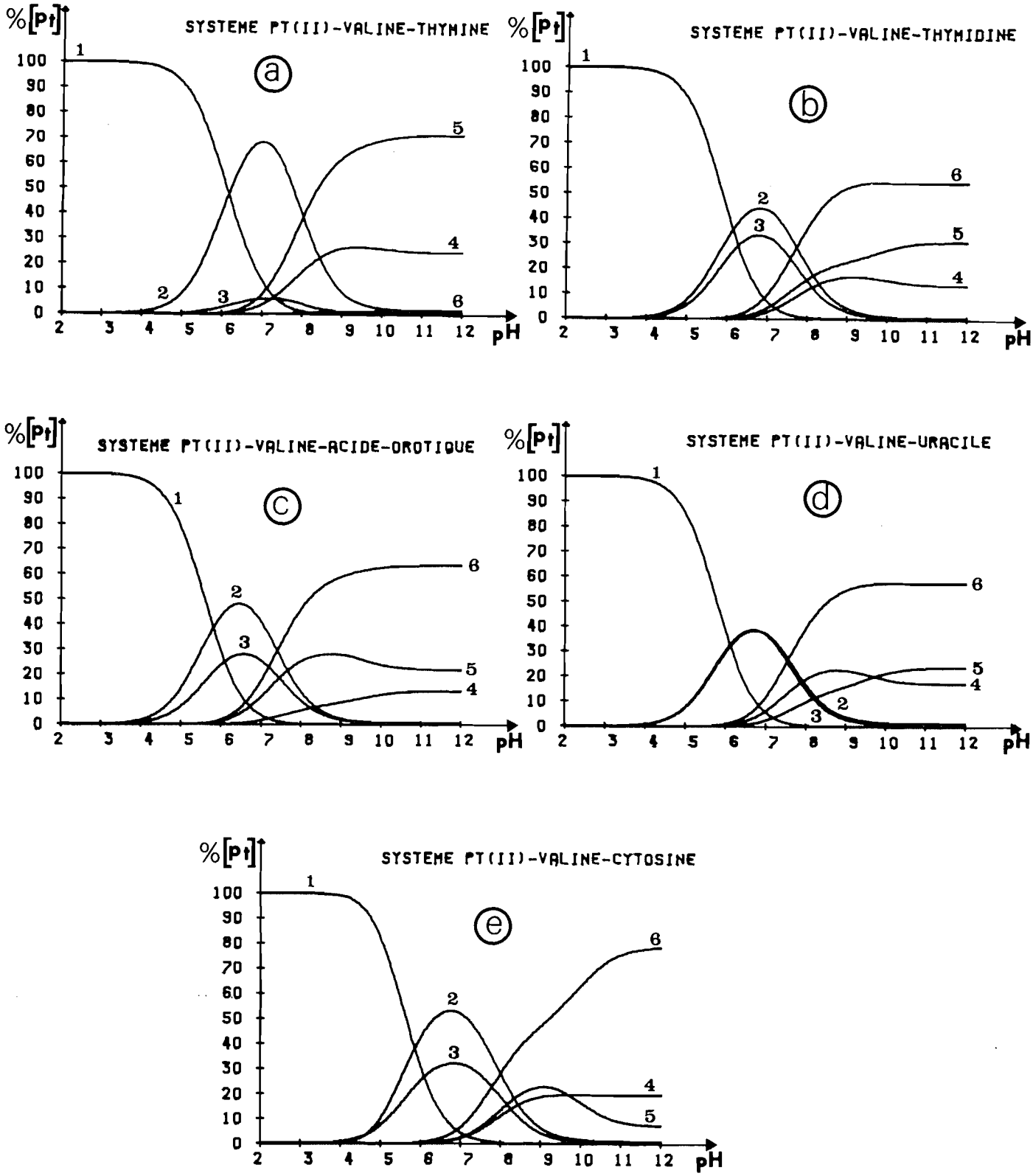


FIG. 4. (a) Système Pt(II)–valine–thymine : $[H_2^+ VA] = 10^{-3}$ M; $[HTM] = 10^{-3}$ M; $[Pt^{2+}] = 5 \times 10^{-4}$ M. 1, cis-$[Pt(H_2O)_2(NH_3)_2]^{2+}$; 2, cis-$[Pt(VA)(NH_3)_2]^+$; 3, cis-$[Pt(TM)(H_2O)(NH_3)_2]^+$; 4, cis-$[Pt(VA)_2(NH_3)_2]$; 5, cis-$[Pt(VA)(TM)(NH_3)_2]$; 6, cis-$[Pt(TM)_2(NH_3)_2]$.
(b) Système Pt(II)–valine–thymidine : $[H_2^+ VA] = 10^{-3}$ M; $[HTY] = 10^{-3}$ M; $[Pt^{2+}] = 5 \times 10^{-4}$ M. 1, cis-$[Pt(H_2O)_2(NH_3)_2]^{2+}$; 2, cis-$[Pt(VA)(NH_3)_2]^+$; 3, cis-$[Pt(TY)(H_2O)(NH_3)_2]^+$; 4, cis-$[Pt(VA)_2(NH_3)_2]$; 5, cis-$[Pt(TY)_2(NH_3)_2]$; 6, cis-$[Pt(VA)(TY)(NH_3)_2]$.
(c) Système Pt(II)–valine – acide orotique : $[H_2^+ VA] = 10^{-3}$ M; $[H_2OM] = 10^{-3}$ M; $[Pt^{2+}] = 5 \times 10^{-4}$ M. 1, cis-$[Pt(H_2O)_2(NH_3)_2]^{2+}$; 2, cis-$[Pt(OM)(NH_3)_2]$; 3, cis-$[Pt(VA)(NH_3)_2]^+$; 4, cis-$[Pt(VA)_2(NH_3)_2]$; 5, cis-$[Pt(OM)_2(NH_3)_2]^{2-}$; 6, cis-$[Pt(VA)(OM)(NH_3)_2]^+$.
(d) Système Pt(II)–valine–uracile : $[H_2^+ VA] = 10^{-3}$ M; $[HUR] = 10^{-3}$ M; $[Pt^{2+}] = 5 \times 10^{-4}$ M. 1, cis-$[Pt(H_2O)_2(NH_3)_2]^{2+}$; 2, cis-$[Pt(UR)(H_2O)(NH_3)_2]^+$; 3, cis-$[Pt(VA)(NH_3)_2]^+$; 4, cis-$[Pt(UR)_2(NH_3)_2]$; 5, cis-$[Pt(VA)_2(NH_3)_2]$; 6, cis-$[Pt(VA)(UR)(NH_3)_2]$.
(e) Système Pt(II)–valine–cytosine : $[H_2^+ VA] = 10^{-3}$ M; $[H_2^+ CY] = 10^{-3}$ M; $[Pt^{2+}] = 5 \times 10^{-4}$ M. 1, cis-$[Pt(H_2O)(NH_3)_2]^{2+}$; 2, cis-$[Pt(CY)(H_2O)(NH_3)_2]^+$; 3, cis-$[Pt(VA)(NH_3)_2]^+$; 4, cis-$[Pt(VA)(CY)(NH_3)_2]$; 5, cis-$[Pt(VA)_2(NH_3)_2]$; 6, cis-$[Pt(CY)_2(NH_3)_2]$.

Can. J. Chem. Downloaded from www.nrcresearchpress.com by 41.223.56.140 on 09/07/12
For personal use only.

TABLEAU 2. Constantes de formation des complexes mixtes $t = 25°C$; $\mu = 0,1$ ($NaNO_3$)

Espèces	$pqrr'$	log $\beta_{pqrr'}$	log $\chi_{pqrr'}$	Domaine de formation
[Cu(VA)(TM)]	1011	15,51 (0,04)*	3,215	pH 5,75–12
[Cu(VA)(TY)]	1011	15,23 (0,01)	3,95	pH 4,5–12
$[Cu(VA)(OM)]^+$	1011	15,56 (0,01)	2,023	pH 4,5–12
[Cu(VA)(UR)]	1011	14,40 (0,01)	3,78	pH 4,5–12
[Cu(VA)(CY)]	1011	14,66 (0,03)	1,12	pH 5,5–12
cis-$[Pt(VA)(TM)(NH_3)_2]$	1011	11,50 (0,01)	2,05	pH 6,5–12
cis-$[Pt(VA)(TY)(NH_3)_2]$	1011	12,01 (0,02)	0,85	pH 6,25–12
cis-$[Pt(VA)(OM)(NH_3)_2]^+$	1011	11,99 (0,04)	1,15	pH 6–12
cis-$[Pt(VA)(UR)(NH_3)_2]$	1011	11,56 (0,01)	0,92	pH 6–12
cis-$[Pt(VA)(CY)(NH_3)_2]$	1011	12,33 (0,01)	−0,47	pH 7–12

*Écarts-types correspondants aux constantes.

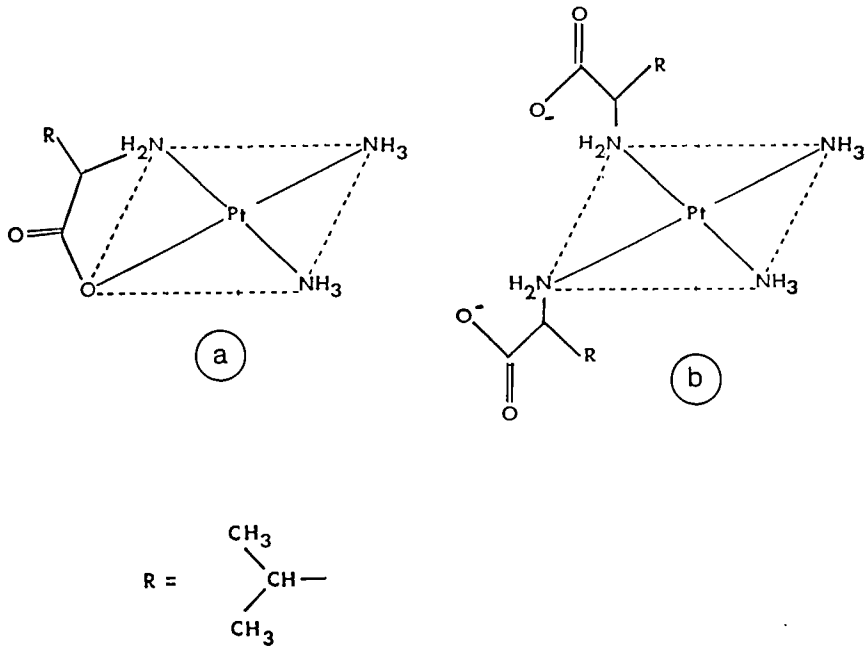


FIG. 5. (a) Espèce ML. (b) Espèce ML_2.

(12, 31) ou complexe non chélaté (figure 5b) dans lequel la liaison métal–ligand passe par l'azote du groupement amino de l'acide aminé, comme l'ont montré les études de certains autres (8–11, 13, 31) pour les complexes de formule ML_2. Ceci nous incite à penser que les sites de liaisons dans les complexes de mercure avec la D-valine sont les mêmes que ceux de l'espèce ML_2 du platine(II) avec la D-valine.

Uracile

Dans le domaine de pH envisagé ($2 < pH < 12$), l'uracile est monodentate. Le site de complexation avec le platine et le cuivre est N3 (21, 32, 45, 46, 65), quelquefois N1, avec possibilité de conversion entre les deux sites (22, 53); la liaison platine–N1 serait alors plus stable en milieu acide que la liaison platine–N3. Les complexes dont nous avons montré l'existence se forment dans la zone de pH où se produit la déprotonation de l'hydrogène lié à N3, ce qui laisse prévoir, dans ce cas, une complexation préférentielle avec l'azote N3. Ceci a été confirmé par Flynn *et al.* (21) par la non formation de platin-blue en utilisant un homologue de l'uracile auparavant substitué en position N3.

Cytosine

La cytosine et ses dérivés sont soit des coordinats monodentates dont le site de liaison est N3 (58, 59, 62, 67, 68) et parfois l'azote du groupement amino déprotoné porté par le carbone C4 (66, 69), soit des ligands bidentates dans certains chélates du platine, du mercure et du cuivre. Dans ce dernier cas, il y a chélation des ions métalliques par l'azote N3 et l'oxygène O2 (46*b*–48, 63, 70–72), ou par l'azote N3 et le groupement amino déprotoné porté par C4 (57, 60, 67). Cependant les études de RMN sur les complexes de la cytidine (nucléoside de la cytosine) avec le mercure et le platine (73, 74) ont montré que le site de liaison est N3 tout en excluant la possibilité de fixation d'ions métalliques sur l'azote du groupement amino. Nos complexes appartiennent simultanément à ces deux modes de complexation dans lesquels la cytosine est monodentate vis à vis du mercure et du platine dans les espèces ML et ML_2 (le site de liaison étant l'azote N3), bidentate pour le cuivre dans les chélates de formule ML et ML_2 avec chélation du cuivre par l'oxygène O2 et l'azote N3.

Thymidine

Comme nous l'avons déjà montré pour la thymine (1), l'ion

Can. J. Chem. Downloaded from www.nrcresearchpress.com by 41.223.56.140 on 09/07/12
For personal use only.

hydraté cis-$[Pt(H_2O)_2(NH_3)_2]^{2+}$ a une bonne réactivité vis à vis de la thymidine (nucléoside de la thymine) et le site de liaison évident reste l'atome d'azote N3 (65).

2. Complexation ternaire

La bonne et rapide convergence des processus d'affinement relatifs à toutes nos espèces ternaires confirme bien la validité de la méthode d'estimation exposée.

Au cours de cette étude, nous constatons que la plupart des espèces mixtes sont plus stables que les espèces complexes simples et à l'aide des valeurs obtenues, nous avons pu vérifier la règle bien connue de renforcement de stabilité ionique résultant de la dissymétrie de la chélation mixte (28, 75).

Considérons l'équilibre $ML_2 + ML'_2 \rightleftarrows 2MLL'$; nous pouvons définir sa constante χ_{1011} par la relation :

$$\log \chi_{1011} = 2 \log \beta_{1011} - (\log \beta_{1020} + \log \beta_{1002})$$

Toutes les valeurs de $\log \chi_{1011}$ sont consignées dans le tableau 2. Ce renforcement ne s'est pas vérifié dans le cas du mixte cis-$[Pt(VA)(CY)(NH_3)_2]$ pour lequel la valeur de la constante de stabilité de l'espèce simple cis-$[Pt(CY)_2(NH_3)_2]$ ($\log \beta_{1011} = 13{,}89$) est plus élevée que celle de l'espèce mixte, cis-$[Pt(VA)(CY)(NH_3)_2]$ ($\log \beta_{1011} = 12{,}33$) pour les mêmes rapports de concentration. Ceci se traduit dans les courbes de répartition par un faible pourcentage de l'espèce mixte comparé aux espèces simples (figure 4e).

Complexes mixtes du cuivre. Dans ces espèces, la D-valine, la cytosine et l'acide orotique sont des coordinats bidentates tandis que les autres ligands sont monodentates (1, 29, 30, 46*b*, 47, 48).

Complexes mixtes du platine. Il a été montré que dans les espèces mixtes du cis-platine avec le tertiobutylamine et certains amino-acides, le groupement carboxylique de ces derniers ne participe pas à la liaison; ils sont monodentates (9–11). Il en est de même des complexes ternaires que nous avons étudiés dans lesquels la D-valine n'est liée que par le groupement amine : le platine est alors entouré uniquement d'atomes d'azote. Cette configuration lui confère l'ensemble de ses propriétés antitumorales.

Cette étude permet de mettre en évidence les deux modes de complexation, monodentate et bidentate, de la valine et de la cytosine selon le métal envisagé.

Partie expérimentale

Une chaîne de mesure, convenablement étalonnée, permet de mesurer le pH dans un large domaine ($2 < pH < 12$) :

électrode de verre | solution thermostatée | NaCl saturé | électrode au calomel

Le jeu d'électrodes est relié à un potentiomètre ISIS 20 000 Tacussel et les mesures sont effectuées sur des solutions aqueuses thermostatées à 25 ± 0,1°C et sous atmosphère d'azote. La force ionique de chaque solution est maintenue constante à l'aide d'une solution de $NaNO_3$ 0,1 M.

Sels métalliques

Les sels de cuivre et de mercure sont préparés par dissolution de $Cu(NO_3)_2,3H_2O$ et $Hg(NO_3)_2,H_2O$ Prolabo dans l'eau déminéralisée et dosés par complexométrie à l'EDTA notamment à l'aide d'une électrode réversible aux ions Hg^{2+} couplée à une électrode de référence au sulfate mercureux pour le mercure.

La solution de cis-$[Pt(H_2O)_2(NH_3)_2]^{2+}$ est préparée à partir de cis-$[PtCl_2(NH_3)_2]$ R. Bellon par substitution stoechiométrique des ions Cl^- effectuée à l'aide d'une solution titrée de nitrate d'argent (16, 20, 65). Une triple centrifugation du chlorure d'argent permet de garantir la reproductibilité de l'échange qui n'affecte en rien la liaison Pt—N (76).

Coordinats

La D-valine, la thymine, la thymidine, l'acide orotique, la cytosine et l'uracile proviennent respectivement des laboratoires Chemische Fabrik, Merck, Boehringer Mannhein GMBH, Sigma Chemical Company, Janssen Chimica et Merck.

Pour chaque système nous avons suivi la titration par la soude Prolabo 0,2 N, des solutions correspondant à deux rapports de concentration ligand : ion métallique (~2 et ~5) pour les systèmes simples et ligand 1 : ligand 2 : ion métallique (~1 : 1 : 1 et ~2 : 2 : 1) pour les systèmes mixtes, soit environ 100 points expérimentaux.

Remerciements

Nous remercions vivement les laboratoires Roger Bellon, 159 avenue du Roule, 92200 Neuilly sur Seine, de nous avoir fourni gracieusement le cis-$[PtCl_2(NH_3)_2]$.

1. R. M'Boungou, M. Petit-Ramel, G. Thomas-David, G. Perichet et B. Pouyet. Can. J. Chem. **65**, 1479 (1987).
2. B. Rosenberg, L. Van Camp et Th. Krigas. Nature, **205**, 698 (1965).
3. B. Rosenberg. Cancer Chemother. Rep. Part 1, **59**, 589 (1975).
4. J. L. Butour. Thèse Doctorat d'Etat, Toulouse. 1980.
5. B. Rosenberg. Biochimie, **60**, 859 (1978).
6. S. E. Sherman, D. Gibson, A. H. J. Wang et S. J. Lippard. Science, **230**, 412 (1985).
7. A. J. Charlson et W. A. Shorland. Inorg. Chim. Acta, **93**, L67 (1984).
8. R. Wilkinson, P. J. Cox, M. Jones et K. R. Harrap. Biochimie, **60**, 851 (1978).
9. A. Pasini et E. Bersanetti. Inorg. Chim. Acta, **107**, 259 (1985).
10. A. Colombo, R. di Gioia, A. Pasini, T. Dasdia et F. Zunino. Inorg. Chim. Acta, **125**, L1 (1986).
11. E. Bersanetti, A. Pasini, G. Pezzoni, G. Pratesi, G. Savi, R. Supino et F. Zunino. Inorg. Chim. Acta, **93**, 167 (1984).
12. L. Kumar, N. R. Kandasamy, T. S. Srivastava, A. J. Amonkar, M. K. Adwankar et M. P. Chitnis. J. Inorg. Biochem. **23**, 1 (1985).
13. L. Kumar, N. R. Kandasamy et T. S. Srivastava. Inorg. Chim. Acta, **67**, 139 (1982).
14. R. Mital, K. S. Ray, T. S. Srivastava et R. K. Bhattacharya. J. Inorg. Biochem. **27**, 133 (1986).
15. S. J. Lippard. Science, **218**, 1075 (1982).
16. H. A. Tajmir-Riahi. Biophys. Chem. **27**, 243 (1987).
17. M. J. Cleare, P. C. Hydes, B. W. Malerbi et D. M. Watkins. Biochimie, **60**, 835 (1978).
18. A. A. Zaki, C. A. McAuliffe, M. E. Friedman, W. E. Hill et H. H. Kohl. Inorg. Chim. Acta, **69**, 93 (1983).
19. M. Seul, H. Neubacher et W. Lohmann. Z. Naturforsch. B: Anorg. Chem. Org. Chem. **36B**, 272 (1981).
20. J. K. Barton, S. A. Best, S. J. Lippard et R. A. Walton. J. Am. Chem. Soc. **100**, 1385 (1978).
21. Ch. M. Flynn, Jr., T. S. Viswanathan et B. Martin. J. Inorg. Nucl. Chem. **39**, 437 (1977).
22. R. Faggiani, B. Lippert et C. J. L. Lock. Inorg. Chem. **19**, 295 (1980).
23. J. P. Davidson, P. J. Faber, R. G. Fischer, Jr., S. Mansy, H. J. Peresie, B. Rosenberg et L. Vancamp. Cancer Chemother. Rep. Part 1, **59**, 287 (1975).
24. L. S. Hollis et S. J. Lippard. J. Am. Chem. Soc. **103**, 1230 (1981).
25. G. Perichet, P. Meallier, B. Pouyet, M. Petit-Ramel et G. Thomas-David. J. Photochem. **29**, 375 (1985).
26. M. M. Petit-Ramel, G. Thomas-David, G. Perichet et B. Pouyet. Can. J. Chem. **62**, 22 (1984).
27. R. P. Martin et R. A. Pâris. Bull. Soc. Chim. Fr. (*a*) 1600 (1963); (*b*) 80 (1964); (*c*) 3170 (1964).
28. J. P. Scharff et M. R. Pâris. Bull. Soc. Chim. Fr. **5**, 1782 (1967).
29. M. M. Petit-Ramel et M. R. Pâris. Bull. Soc. Chim. Fr. (*a*) **7**, 2791 (1968); (*b*) **9**, 3070 (1969).

Can. J. Chem. Downloaded from www.nrcresearchpress.com by 41.223.56.140 on 09/07/12
For personal use only.

30. M. M. PETIT-RAMEL et M. R. PÂRIS. Bull. Soc. Chim. Fr. **4**, 1359 (1967).
31. L. E. ERICKSON, J. W. MCDONALD, J. K. HOWIE et R. P. CLOW. J. Am. Chem. Soc. **90**, 6371 (1968).
32. M. M. TAQUI KHAN et C. R. KRISHNAMOORTHY. J. Inorg. Nucl. Chem. **36**, 711 (1974).
33. A. M. FISKIN et M. BEER. Biochemistry, **4**, 1289 (1965).
34. N. PADMAYA, S. RAMAKUMAR et M. A. VISWAMITRA. Acta Crystallogr. Sect. C: Cryst. Struct. Commun. **43**, 2157 (1987).
35. O. JARDETZKY, P. PAPPAS et N. G. WADE. J. Am. Chem. Soc. **85**, 1657 (1963).
36. (*a*) S. M. WANG et N. C. LI. J. Am. Chem. Soc. **88**, 4592 (1966); (*b*) S. MANSY, T. E. WOOD, J. C. SPROWLES et R. S. TOBIAS. J. Am. Chem. Soc. **96**, 1762 (1974).
37. M. M. TAQUI KHAN, S. SATYANARAYANA, M. S. JYOTY et CH. A. LINCOLN. Indian J. Chem. Sect. A: **22**, 357 (1983).
38. P. R. REDDY et B. M. REDDY. Polyhedron, **12**, 1947 (1986).
39. I. WEMPEN, R. DUSCHINSKY, L. KAPLAN et J. J. FOX. J. Am. Chem. Soc. **83**, 4755 (1961).
40. M. M. TAQUI KHAN et S. SATYANARAYANA. Indian J. Chem. Sect. A: **22**, 584 (1983).
41. T. UEDA et J. J. FOX. J. Am. Chem. Soc. **85**, 4024 (1963).
42. C. PARKANYI, D. BOUIN, D. C. SHIEH, S. TUNBRANT, J. J. AARON et A. TINE. J. Chim. Phys. **81**, 3099 (1984).
43. D. SHUGAR et J. J. FOX. Biochim. Biophys. Acta, **9**, 199 (1952).
44. D. GNINGUE et J. J. AARON. Talanta, **32**, 183 (1985).
45. M. M. TAQUI KHAN et S. SATYANARAYANA. Indian J. Chem. Sect. A: (*a*) **20**, 814 (1981); (*b*) **21**, 913 (1982).
46. (*a*) Y. L. TAN et A. BECK. Biochim. Biophys. Acta, **299**, 500 (1973); (*b*) H. PEZZANO et F. PODO. Chem. Rev. **80**, 366 (1980).
47. J. A. CARRABINE et M. SUNDARALINGAM. J. Chem. Soc. Chem. Commun. 746 (1968).
48. M. SUNDARALINGAM et J. A. CARRABINE. J. Mol. Biol. **61**, 287 (1971).
49. S. MANSY et R. S. TOBIAS. Inorg. Chem. **14**, 287 (1975).
50. J. A. CARRABINE et M. SUNDARALINGAM. Biochemistry, **10**, 292 (1971).
51. M. GOODGAME et D. A. JAKUBOVIC. Coord. Chem. Rev. **79**, 97 (1987).
52. B. S. SEKHON. J. Indian Chem. Soc. **64**, 308 (1987).
53. R. FERREIRA, E. BEN-ZVI, T. YAMANE, J. VASILEVSKIS et N. DAVIDSON. Adv. Chem. Coord. Compd. 457 (1961).
54. B. LIPPERT. Inorg. Chem. **20**, 4326 (1981).
55. B. LIPPERT, C. J. L. LOCK et R. A. SPERANZINI. Inorg. Chem. **20**, 335 (1981).
56. C. J. L. LOCK, R. A. SPERANZINI et J. POWELL. Can. J. Chem. **54**, 53 (1976).
57. R. BEYERLE-PFNUR, H. SCHÖLLHORN, U. THEWALT et B. LIPPERT. J. Chem. Soc. Chem. Commun. 1510 (1985).
58. B. LIPPERT, C. J. L. LOCK et R. A. SPERANZINI. Inorg. Chem. **20**, 808 (1981).
59. P. C. KONG et T. THEOPHANIDES. Inorg. Chem. **13**, 1981 (1974).
60. R. FAGGIANI, B. LIPPERT, C. J. L. LOCK et R. A. SPERANZINI. J. Am. Chem. Soc. **103**, 1111 (1981).
61. B. LIPPERT. Biochimie, **60**, 1041 (1978).
62. G. Y. H. CHU, R. E. DUNCAN et S. TOBIAS. Inorg. Chem. **16**, 2625 (1977).
63. S. NANSY, B. ROSENBERG et A. J. THOMSON. J. Am. Chem. Soc. **95**, 1633 (1973).
64. Y. D. FRIDMAN, Z. M. PULATOVA et M. G. LEVINA. Koord. Khim. **7**, 73 (1981).
65. M. C. LIM et R. B. MARTIN. J. Inorg. Nucl. Chem. **38**, 1915 (1976).
66. C. M. MIKULSKI, C. J. LEE, T. B. TRAN et N. M. KARAYANNIS. Inorg. Chim. Acta, **136**, L13 (1987).
67. L. PRIZANT, R. RIVEST et A. L. BEAUCHAMP. Can. J. Chem. **59**, 2290 (1981).
68. K. SAITO, R. TERASHIMA, T. SAKAKI et K. TOMITA. Biochem. Biophys. Res. Commun. **61**, 83 (1974).
69. S. MANSY, J. P. FRICK et R. S. TOBIAS. Biochim. Biophys. Acta, **378**, 319 (1975).
70. T. J. KISTENMACHER, D. J. SZALDA et L. G. MARZILLI. Acta Crystallogr. Sect. B: Struct. Crystallogr. Cryst. Chem. **31**, 2416 (1975).
71. D. J. SZALDA, L. G. MARZILLI et T. J. KISTENMACHER. Inorg. Chem. **14**, 2076 (1975).
72. M. AUTHIER-MARTIN et A. L. BEAUCHAMP. Can. J. Chem. **55**, 1213 (1977).
73. J. DEHAND et J. JORDANOV. J. Chem. Soc. Dalton Trans. 1588 (1977).
74. L. S. KAN et N. C. LI. J. Am. Chem. Soc. **92**, 4823 (1970).
75. R. P. MARTIN, M. M. PETIT-RAMEL et J. P. SCHARFF. Metal Ions Biol. Syst. **2**, 1 (1974).
76. S. E. LIVINGSTONE. Comprehensive inorganic chemistry. Vol. 3. Pergamon Press, Oxford. 1975.

Can. J. Chem. Downloaded from www.nrcresearchpress.com by 41.223.56.140 on 09/07/12
For personal use only.

New trends in differential scanning calorimetry

H. TACHOIRE
Laboratoire de Thermochimie, Université de Provence, F-13331 Marseille CEDEX 03, France

AND

V. TORRA
Departament de Fisica, Universitat de les Illes Balears, E-07071 Palma de Mallorca, Spain

Received January 26, 1989

This paper is dedicated to the memory of Professor James A. Morrison

H. TACHOIRE and V. TORRA. Can. J. Chem. **67**, 983 (1989).

Recent applications of differential scanning calorimetry in the study of solid–solid transformations are presented. The importance of the deconvolution of the thermograms and of the modelling of the calorimetric equipment is stressed.

Investigations of the phase transformations of the martensitic type in shape-memory alloys have made clear the influence of thermomechanical treatment of the material and have evaluated the influence of defects on the dynamics of transformation. A combination of calorimetric and acoustical observations has demonstrated irreversibilities, even in the so-called thermoelastic transitions.

Key words: martensitic transformation, differential scanning calorimetry, entropy production, thermomechanical treatments, acoustic emission.

H. TACHOIRE et V. TORRA. Can. J. Chem. **67**, 983 (1989).

On présente de récentes applications de l'analyse calorimétrique différentielle dans l'étude des transformations solide–solide. L'importance de la modélisation des instruments et de la déconvolution de leur réponse est clairement mise en évidence.

Une étude des transformations de phase de type martensitique dans les alliages à mémoire de forme permet de montrer l'influence d'un traitement thermomécanique du matériau et celle des défauts sur la dynamique de la transformation. Le couplage d'observations calorimétriques et acoustiques prouve l'existence d'irréversibilités même au cours de transformations réputées thermoélastiques.

Mots clés : transformation martensitique, analyse calorimétrique différentielle, production d'entropie, traitements thermomécaniques, émission acoustique.

Can. J. Chem. Downloaded from www.nrcresearchpress.com by 41.223.56.140 on 09/07/12
For personal use only.

Introduction

Calorimetric equipment with thermal fluxmeters are stable instruments. Equipped with semiconductor elements, they possess a high sensitivity (about 400 mV W^{-1} at ambient temperature). The response of these instruments contains the energy production of the phenomena studied, deformed by the inertia of the apparatus. The techniques of acquisition and processing of data allow compensation for this inertia. In certain cases, it is possible to link to the calorimeter other techniques of measurement and/or observation leading to the simultaneous determination of several parameters and hence to a better understanding of the phenomenon under study (1).

In our application, we observed a change in the dynamics of the instrumental response during the course of manipulation. Therefore, for solid–solid transitions, it is necessary to model the instrumental response and to reconstitute the true evolution of heat, thermogenesis $P(t)$, using appropriate algorithms such as inverse filtering.

Knowledge of the thermogenesis of the process allows either the development of phenomenological interpretations or the modelling of processes which develop within the laboratory cell.

In this paper, we describe the application of techniques developed for the study of the dynamics of a martensitic-type transformation induced by a programmed temperature change in shape-memory alloys. Using thermomechanical treatments, it is possible to describe the influence of the initial state of the samples and of the subsequent development of defects, surface polishing, cycling effects, ... on the transformation process (2).

Calorimeters and heat-transfer equations

A system of N first order differential equations allows the description of experimental equipment having a classical laboratory cell (Fig. 1 top) or in which a sample under investigation is in contact with thermocouples (Fig. 1, middle section). When this is the case, one adopts a model with localised constants composed of N thermal capacities. This approach is obviously only valid for linear experimental systems. The conditions of linearity are always checked in the normal region of use of the heat conduction calorimeters (constant mass and temperature).

In the case where the thermal evolution $P(t)$ occurs in a single capacity, the system of N linear equations takes the following form, since the calorimetric response $s(t)$ (the amplitude of the thermogram) is proportional to the temperature differences (3),

$$[1]\quad P(t) + a(\mathrm{d}P(t)/\mathrm{d}t) + \ldots + m(\mathrm{d}^M P(t)/\mathrm{d}t^M) = A(\mathrm{d}^N s(t)/\mathrm{d}t^N) + B(\mathrm{d}^{N-1} s(t)/\mathrm{d}t^{N-1}) + \ldots \quad (\text{with } M < N)$$

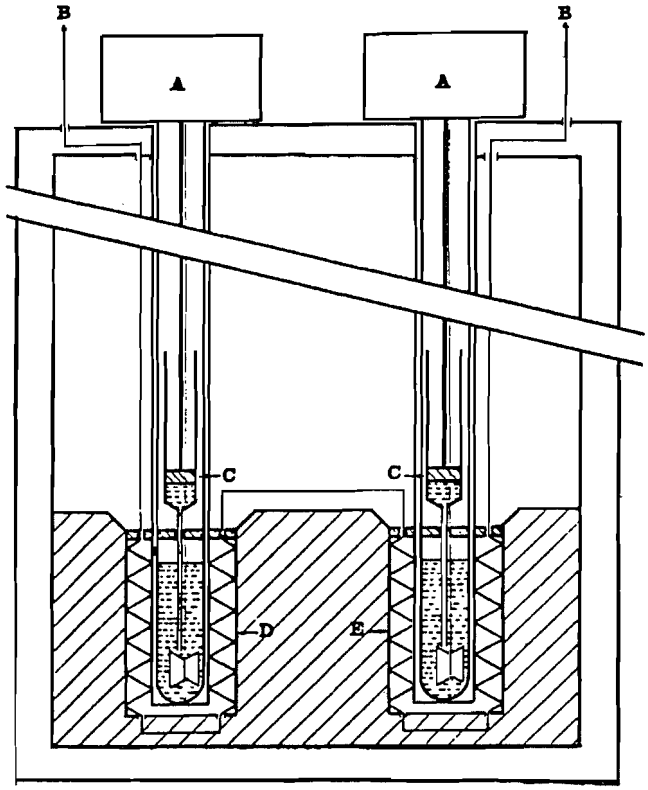
When the temperature of these systems changes slowly with time, the coefficients of the preceding equation also change. It is possible to extend the application of this formalism and to obtain the thermogenesis, $P(t)$, of the phenomena from experimental thermograms using appropriate calibration.

In this simple case, in which temperature T is a function of time t (4), one obtains

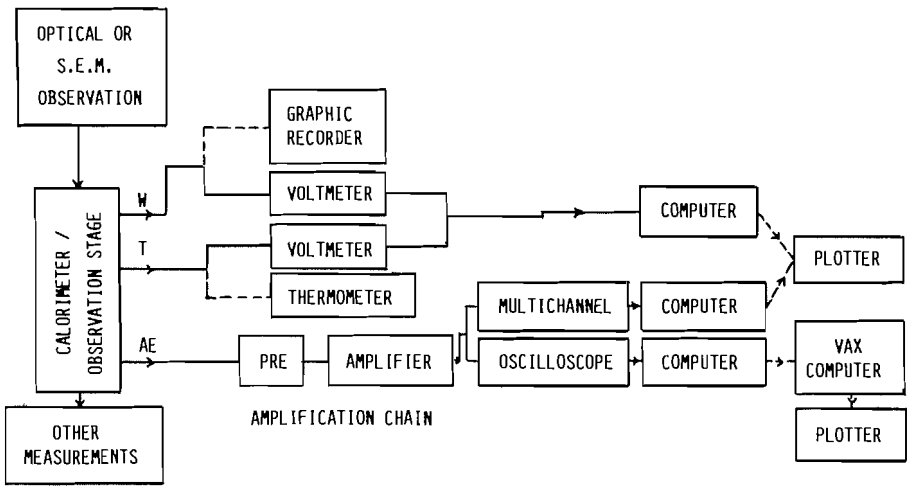
$$[2]\quad \text{Energy}\Big\}_{t_1}^{t_2} = \int_{t_1}^{t_2} \{s(t)/S(T)\}\mathrm{d}t$$

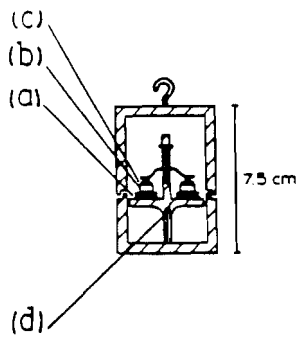
Printed in Canada / Imprimé au Canada

Can. J. Chem. Downloaded from www.nrcresearchpress.com by 41.223.56.140 on 09/07/12
For personal use only.



CALORIMETRIC AND ACOUSTIC SET-UP





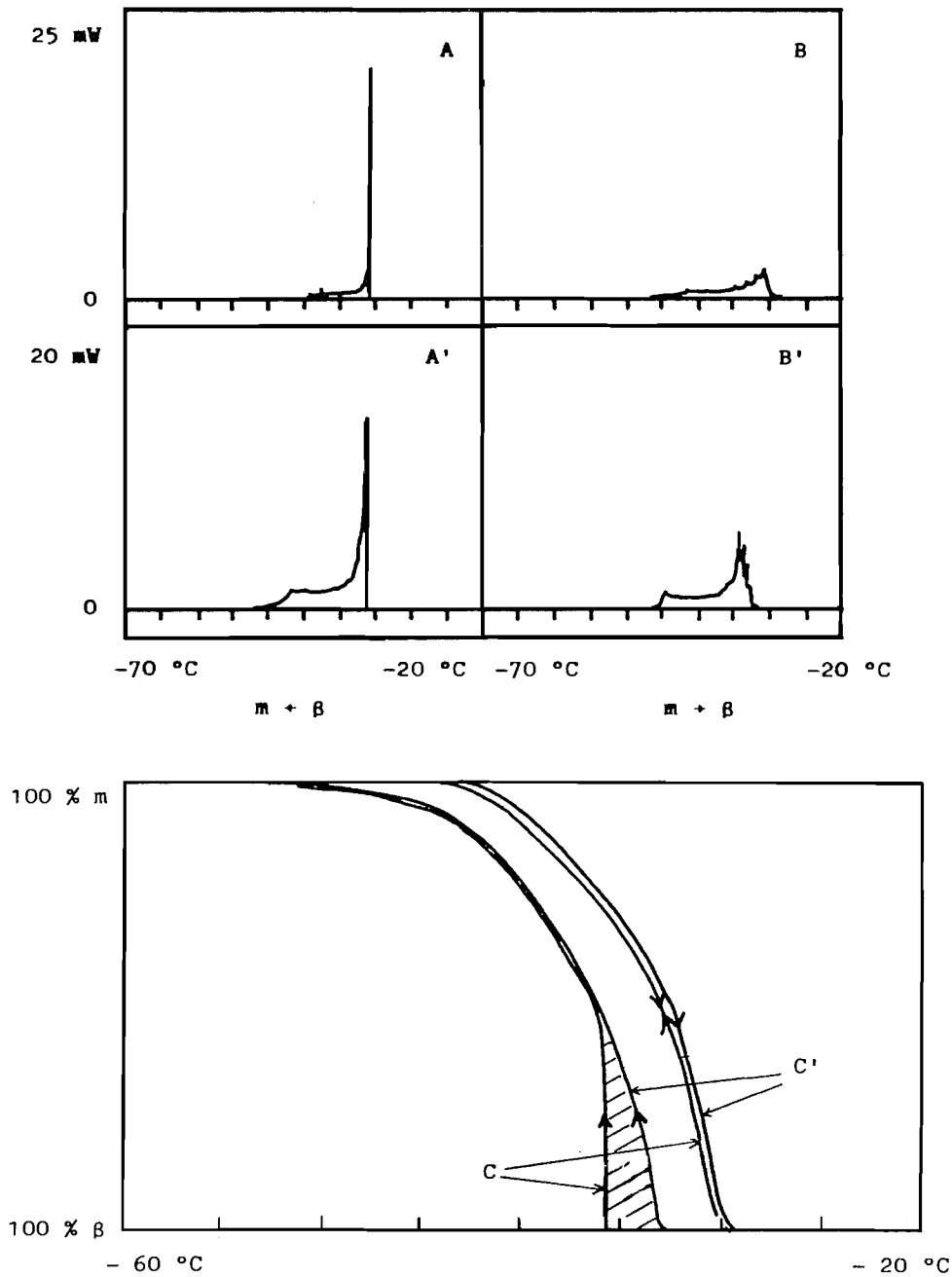


FIG. 2. Influence of centres for nucleation on a transformation of the type phase β → martensite in an alloy Cu 74.4 wt.% – Al 7.41% – Zn 18.18%. Graphs *A*, *B*, *C* refer to the first thermal cycle, graphs *A'*, *B'*, *C'* refer to the second thermal cycle. Graphs *C* and *C'* represent the hysteresis of each cycle and are obtained by integration of the thermogenesis from graphs *A* and *B*, and *A'* and *B'*. The hachured area corresponds to the nucleation process related to the first cycle.

FIG. 1. (*Top*) Vertical cross-section of a differential heat-conduction calorimeter. Diagram to show the principle of the calorimetric system for measuring heats of mixing or heats of dilution (1). *A*, stirrer and mixing system; *B*, to amplifier; *C*, syringe; *D*, measurement cell; *E*, reference cell. Equipment designed for the simultaneous experiments in thermosonimetry and calorimetry (1), (2). (*Middle*) Data processing scheme. (*Bottom*) Calorimetric system: *a*, thermoelectric sensor; *b*, sample and reference material; *c*, piezoelectric sensor; *d*, thermometric sensor.

The thermobatteries (Melcor FC 0.6-66-05L) consist of an ensemble of thermoelectric couples made from two elements of semiconductor (bismuth telluride) placed between two square ceramic plates (11.2 × 11.2 mm) separated 2.4 mm. Their temperature range is limited to between −150 and +110°C, which results in the same limitation for the temperatures at which the calorimeter can operate.

The acoustic emission transducers are pill-shaped piezolectric crystals PHILIPS PXE5 (ϕ 5 mm, different thicknesses from 0.5 mm to 2 mm). Their resonance frequency centres around 500 kHz.

Using this configuration and detectors, the main features of the calorimeter are its high sensitivity, between 100 and 360 mV W^{-1} in the whole temperature range, and a first time constant $\tau_1 \approx 12$ s.

Can. J. Chem. Downloaded from www.nrcresearchpress.com by 41.223.56.140 on 09/07/12
For personal use only.

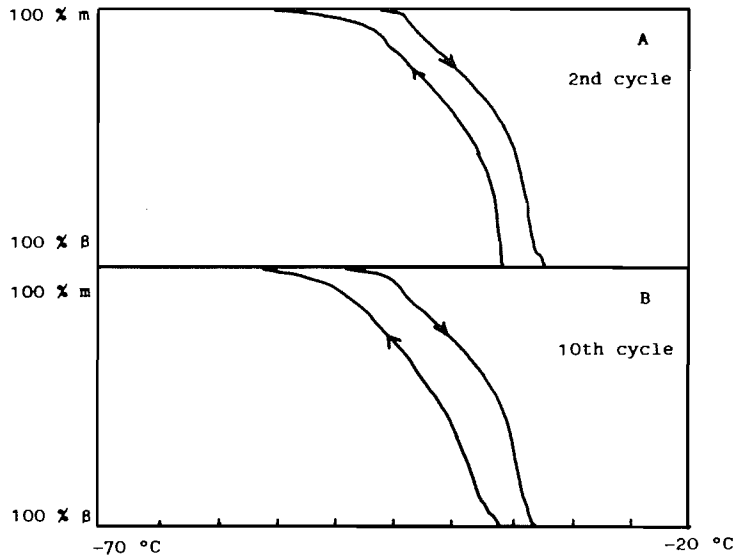


FIG. 3. Change of the hysteresis of the transformations with the number of thermal cycles applied to a sample identical in composition to that of Fig. 2. Graph *A*, 2nd cycle; graph *B*, 10th cycle.

The sensitivity $S(T)$ is obtained by fitting to the experimental values S_1, S_2, ... corresponding to temperatures T_1, T_2, ...

When the mass of the contents of the experimental cell changes with time (as in calorimetric titration) there are corresponding changes in the coefficients of eq. [1]. In modelling these variable systems by comparing the predictions of the models with the experimental results, routines can be established which allow the determination of the instantaneous power associated with a continuous mixing or dilution process (3, 5–7).

In both cases, the inverse filtering permits the compensation of the influence of the most important time constants of the calorimetric equipment (6, 7).

Description of martensitic-type transformations in shape-memory alloys

The properties of these materials make them interesting. They adapt to the conditions imposed on them with several interesting effects (one and two shape-memory effects, pseudo-elasticity, rubber effect, etc). These effects are accompanied by the production of martensitic variants corresponding to the external stress. Alloys of this type include the titanium–nickel system (Nitinol) and copper alloys. The copper–aluminium–zinc and copper–aluminium–nickel alloys are easier to fabricate and produce than the titanium–nickel alloy and their cost is only about 1% of the latter.

There is much current interest in the study of the fundamental properties of these materials with the aim of delaying their ageing, that is, minimising the change in their properties (8).

From calorimetric studies (1, 6, 9), thermograms are obtained which are representative of the complete transformation and these can be used to show how the transformation is influenced by the properties of the material and the treatment imposed upon it. Our experimental results clearly show a change in the transformation depending on the state of the surface (whether or not it favours nucleation) (Fig. 2), the number of thermal cycles (Fig. 3), and the concentration of defects resulting, for example, from quenching in water. Such quenching promotes the appearance of microtransformations at a temperature about 20 K over the normal transformation (10).

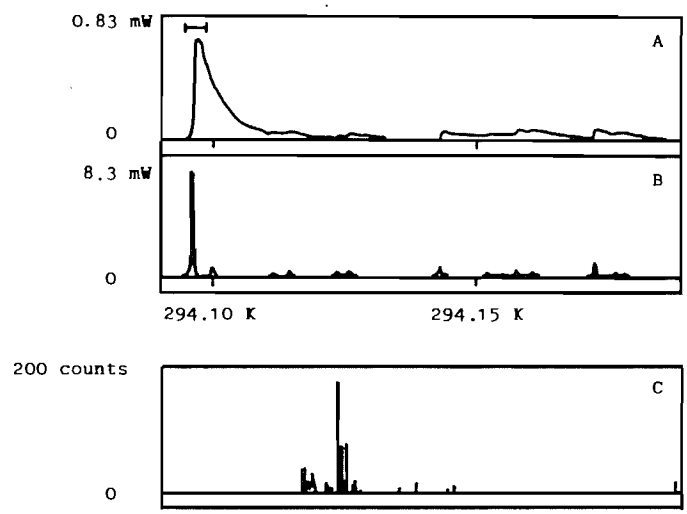


FIG. 4. Transformation of the type martensite → phase β experienced by an alloy Cu, 81.2 wt.% – Al, 11.8% – Mn, 6.8% – Fe, 0.2%. *A*, experimental thermogram; *B*, thermogenesis obtained by deconvolution of the preceding graph; *C*, acoustic emission obtained in the window indicated on graph *A*. Graph shows the ringdown counts as a function of time. (The ringdown counting gives the number of times that the acoustic emission signal crosses a preselected threshold voltage).

Figure 2 relates to changes observed in a sample of the copper–aluminium–zinc alloy (Cu 74.41 wt.% – Al 7.41% – Zn 18.8%). The transformation, phase β → martensite has been studied calorimetrically over the temperature range −20°C to −70°C and the inverse transformation from −70°C to −20°C. The initial sample (about 450 mg) is electrolytically polished before being subjected to the first thermal cycle to which the graphs A, B, and C correspond. Graphs A′, B′, and C′ relate to the second cycle applied to the sample.

In the initial sample, there are very few centres for nucleation and hence the "explosive" nature of the first transformation, phase β → martensite (graph A) is justified. In the second transformation, this characteristic is largely attenuated by the

Can. J. Chem. Downloaded from www.nrcresearchpress.com by 41.223.56.140 on 09/07/12
For personal use only.

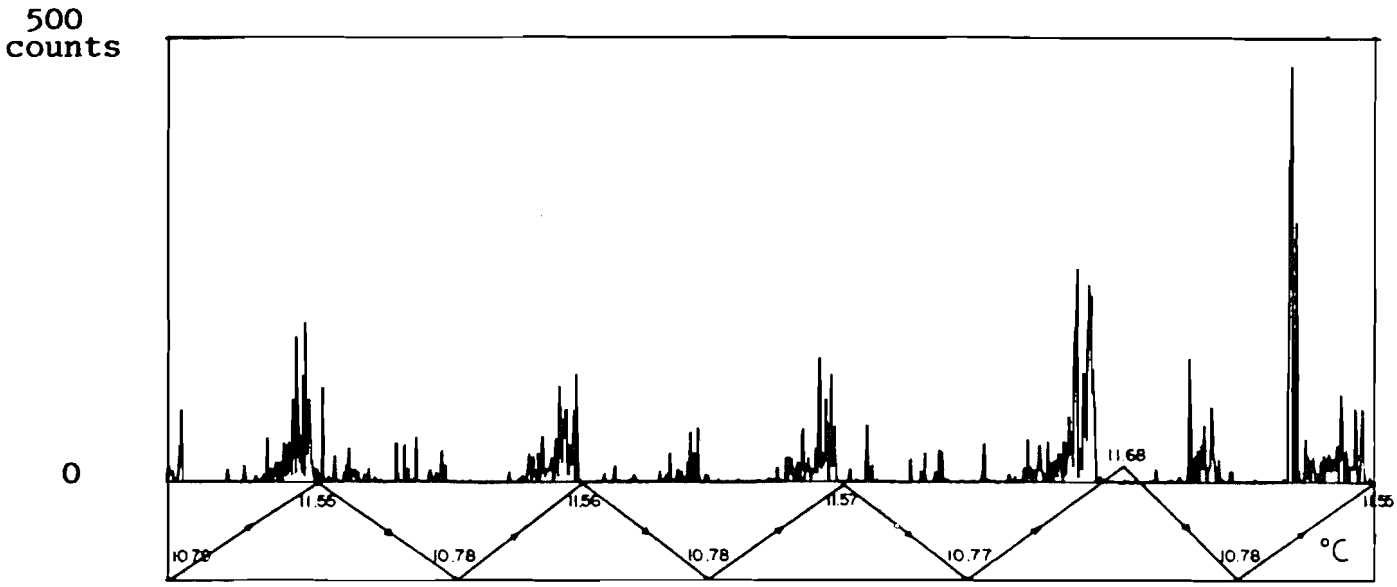


FIG. 5. Change of acoustic emission during thermal cycling for a sample (about 450 mg) of alloy Cu, 68.5 at.% – Al, 16.6% – Zn, 14.9% not subjected to stress. Note the very small changes at the extreme temperatures of the cycle (cycling controlled to about ± 0.01 K).

presence of centres for nucleation created during the first thermal cycle (graph A′).

Figure 3 concerns the same type of sample and shows changes in the hysteresis of the transformation with the number of thermal cycles applied to the material. A broadening of the width of the hysteresis cycle is observed. This is due to a progressive increase in the number of defects promoted by the successive thermal cycles, the transformations gradually becoming more and more complex with increasing number of cycles.

The study of the hysteresis cycles thus provides complementary information since their form is influenced by the characteristics of the material: their breadth is related to the influence of friction, their temperature-dependent extension indicates the existence and importance of the interactions between the variants of martensite. The area of the cycle in temperature–entropy diagram indicates, on the other hand, the importance of the energy losses caused by the thermal cycling associated to the motion of interfaces; the increase of area indicates the increase of friction as a result of defects developed during the cycle.

The thermograms obtained show the complexity of the dynamics of the transformations. This complexity is confirmed by the simultaneous study of the acoustic emission and/or by optical observations (11). In particular, acoustic emission shows evidence of the fine structure of the transformations which from calorimetry appear to be instantaneous and thus elementary.

Figure 4 relates to the inverse transformation martensite → phase β experienced by a sample (about 450 mg) of the alloy Cu 81.2 wt.%, Al 11.8%, Mn 6.8%, Fe 0.2%. The programmed temperature change was very slow (0.01 K min^{-1}). Graph A represents the raw thermogram; graph B is the thermogenesis obtained by deconvolution of the preceding thermogram in the same temperature region; graph C is the acoustic emission (the ringdown histogram versus time) observed in the window, the position and length of which are indicated on graph A. This figure clearly shows that the simultaneous study of acoustic emission describes the fine structure of events which might

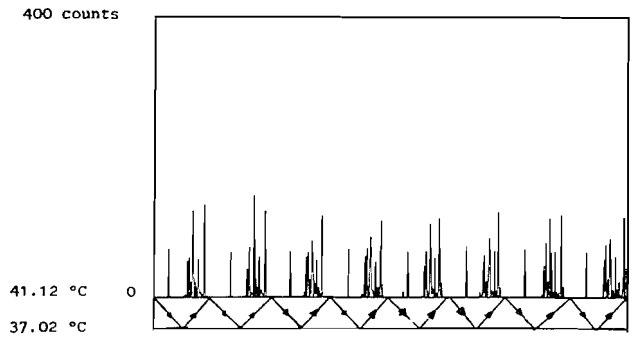


FIG. 6. Change of acoustic emission during thermal cycling in the presence of an external stress for a sample of identical composition to that of Fig. 5.

be assimilated into the elementary transformation or internal stresses reorganization.

When studying the "elementary" transformations in a limited temperature region (less than 5 K for example), a stochastic uncontrolled change of acoustic emission is again observed as seen in Fig. 5. This figure shows the change in acoustic emission observed in the course of several successive thermal cycles applied to a sample of the alloy Cu 68.5 atm.%, Al 16.6%, Zn 14.9%. The stochastic nature of the transformations is apparent in this sample which is not subjected to any stress. The transformation is such that the sum of the internal stresses is minimised. It is therefore evident that there are several orientations of the variants of martensite, that is, several orientations of the independent domains of martensite. These are the parts of the crystal which are transformed by internal adaptation of internal stresses and the local temperature differences induced by (dT/dt) effects.

On the other hand, when the material is subjected to mechanical stress, a completely reproducible process is observed even when measured by acoustic emission. The mechanical stress produces a favoured axis of transformation which results in the appearance of a simple variant of martensite (12). Since the number of degrees of freedom of the material is reduced, a

Can. J. Chem. Downloaded from www.nrcresearchpress.com by 41.223.56.140 on 09/07/12
For personal use only.

Can. J. Chem. Downloaded from www.nrcresearchpress.com by 41.223.56.140 on 09/07/12
For personal use only.

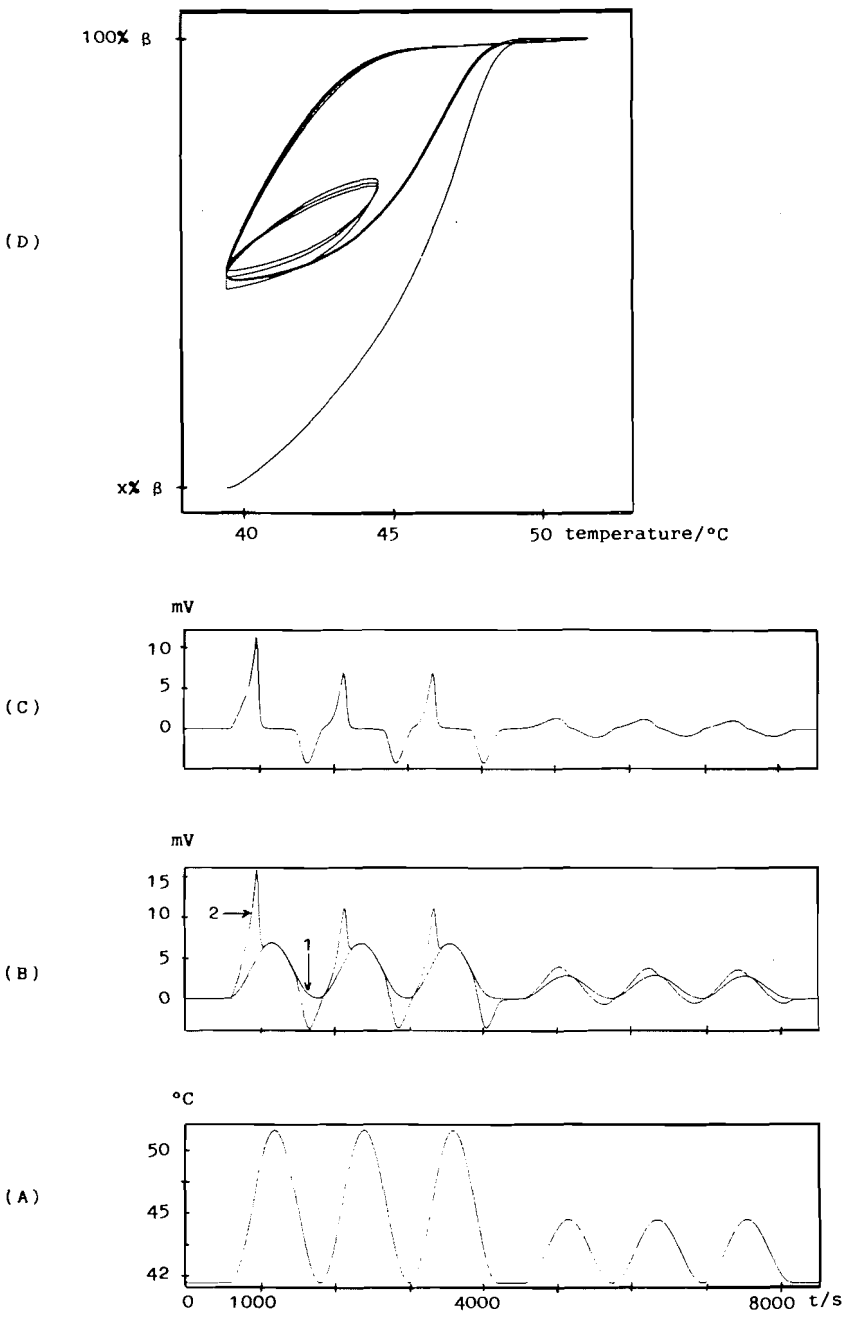


FIG. 7. Partial hysteresis cycle associated with a transformation of the type phase β → martensite experienced by a shape-memory alloy (Cu, 76.99 wt.% – Al, 8.24% – Zn, 14.77%). (*A*): Temperature change of a calorimetric block containing the samples. (*B*): (*1*), Base line of the calorimetric equipment determined in a temperature region where all the material is in its β phase; (*2*), raw thermogram. (*C*) Thermogram obtained after "subtraction" of the base line *1* from thermogram *2*. (*D*) Partial hysteresis cycles obtained by integration of graph *C*.

temperature control of about ±0.01 K is seen to be sufficient for this system.

Figure 6 emphasises the reproducibility of the acoustic emission observed during a thermal cycle (controlled to about ±0.01 K) applied to a sample subjected to mechanical stress. The transformation is favoured by the presence of the external stress and a single variant of martensite is produced. The peaks observed in the acoustic emission with the aid of a multichannel oscilloscope are identical.

These results show that the existence of instantaneous elementary transformations is not indicative of changes in the material. As a parameter of change, one is therefore inclined to use the global entropy increase uniquely associated with the instantaneous process (burst process) and its change during thermal cycling.

The basis of the calculation is the implication that the burst processes produce locally, within the sample, a temperature increase associated with the phase change. The heat conduction in the material and that towards the external thermostat produce an increase in the global entropy, $\Delta S_u(T)$, such that

$$[3] \quad \Delta S_u(T) = \Sigma \Delta S_i = \Sigma Q_i \{(1/T) + (1/(T_m - T))\} \ln (T/T_m)$$

Q_i represents the quantity of heat produced at the time of the elementary transformation, T_m is the temperature of the

region i immediately after the preceding loss, and T is the initial temperature of the material. ΔS_u represents the increase in entropy of the universe associated to temperature internal gradients.

We have also studied the entropy production associated with successive thermal cycles experienced by a sample of a copper–aluminium–zinc alloy of similar composition to that of the material described in Fig. 2. This electrolytically polished sample initially contained few defects since it had been air quenched.

The study of successive cycles (between 280 and 230 K) showed a pronounced tendency for a decrease of entropy production as seen from Table 1.

This entropy production was associated with an increase in the number of defects developed in the course of each cycle. Positron absorption (13) and transmission electron microscopy (14) show evidence for this phenomenon. The observed transformations were less of the burst-like type and more "spreaded" in this temperature region.

The identification and deconvolution techniques allowed the samples to be subjected to a very sophisticated temperature programme whilst at the same time studying the resultant changes in the partial hysteresis cycles. Figure 7 shows the power of the technique developed: graph A represents the temperature change to which the calorimetric block containing the sample under investigation (shape-memory alloy Cu 76.99 wt.% – Al 8.24% – Zn 14.77%) was subjected. This change, which was numerically displayed, had a reproducibility (from one cycle to another) greater than one-hundredth of a degree. Graph B shows the base line of the calorimetric equipment (determined within a temperature region where all the material was in its β phase) and the raw thermogram. Graph C represents the thermogram after "subtraction" of the base line. An excellent signal/noise ratio was obtained after filtering-out the effects of fluctuation of the Peltier current produced by the temperature-controlling system (noise 1 μV).

Total and partial investigation of graph C allows the automatic recording of the global and partial hysteresis curves experienced by the shape-memory alloy, cycles which are of fundamental interest for the macroscopic characterisation of the material (graph D). These cycles define the instantaneous state of the alloy which is of interest both for practical applications and for simulation of its behaviour (15).

The detailed observation of the displacement of an interface caused by temperature change showed evidence of the existence of an intrinsic hysteresis cycle (of width of about 0.5 K) and of the effects of pinings and unpinnings of the interface which (in the case of unpinnings) produced acoustic emission (15–18).

Figure 8 concerns the free displacement of an interface under the influence of temperature as given by optical observation (video). The position of the interface was measured to ±1 μm. The global hysteresis represented by the figure corresponds to a total displacement of 60 μm.

A similar study showed that this cycle possessed several components, including an intrinsic component probably associated with the shuffling of atoms. Interactions with the surface and/or precipitates as well as other interactions with network defects (frictions and observable pinnings) may also occur (15, 18).

Examination of the partial cycle observed even at the centre of the transformation region shows that the reproducibility was satisfactory when the temperature was correctly programmed.

TABLE 1. Entropy production associated with successive thermal cycles

Thermal cycle	Entropy production/(J K^{-1} kg^{-1})
1	0.320
2	0.182
3	0.156
4	0.147

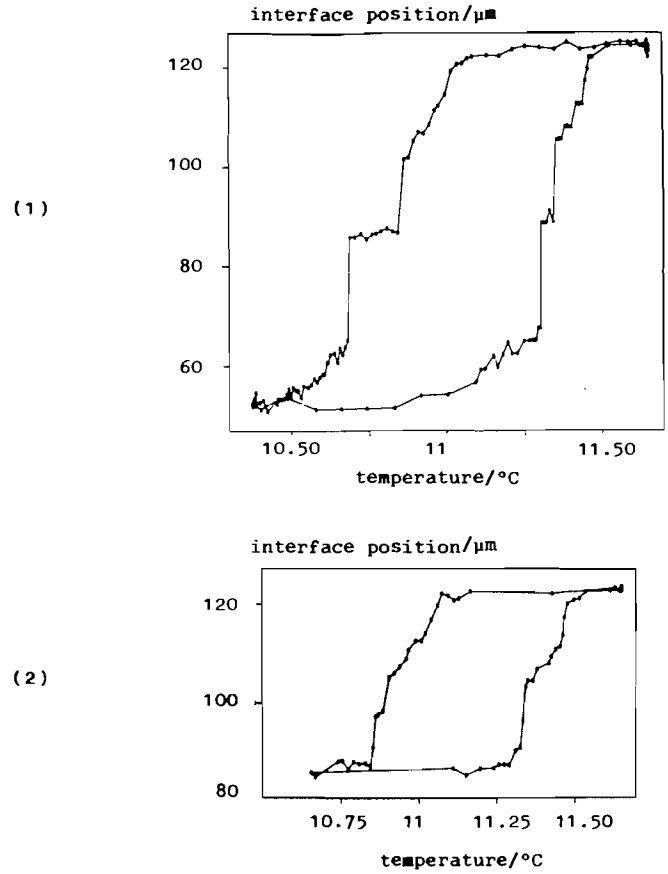


FIG. 8. Transformation of the type β-phase → martensite experienced, in the absence of strain, by a shape-memory alloy (Cu, 76.99 wt.% – Al, 8.24% – Zn, 14.77%). Displacement of an interface under the influence of temperature.

Maximum temperature rate of the sample 8.55 mK s^{-1}.

Hysteresis cycles corresponding to the displacement of an interface (position located optically to ±1 μm). Partial cycle 2 shows the existence of an intrinsic cycle.

The width of a macroscopic hysteresis cycle greatly exceeded that of an intrinsic cycle of a so-called "thermoelastic" material. There are probably interactions between the various variants, frictions, coupling between the interfaces and stabilization effects of β and martensite phases (19) which are responsible for this width (about 3 K).

Conclusions

The modelling of calorimetric equipment (variable or invariant) allows for the establishment of algorithms for the deconvolution of the thermograms and the determination of the dynamic energy (thermogenesis) of the phenomenon under investigation. Our studies have entailed an increase of the area of application and of the degree of resolution of differential scanning calorimeters.

Can. J. Chem. Downloaded from www.nrcresearchpress.com by 41.223.56.140 on 09/07/12
For personal use only.

In the study of phase transformations of the martensitic type, a calorimetric study makes clear the influence of thermomechanical treatment of the material and allows the evaluation of the influence of defects on the dynamics of transformation.

By combining calorimetric and acoustical observations, the change in the dynamics of the transformations demonstrates the existence of irreversibilities even in the so-called thermoelastic transitions (transitions produced in limited temperature regions).

When the materials are subjected to mechanical stresses and when the temperature is rigorously controlled, these irreversibilities do not induce any structural changes in these materials. On the other hand, during spontaneous transformation, changes in the medium may be characterized by the production of entropy as inferred from the calorimetric results.

Acknowledgements

The authors thank the authorities responsible for the link between the Universities of Balearic Islands and Aix-Marseilles I (University of Provence) and for program CAICyt 3562-83. They express their gratitude to their colleagues at the Marseilles and Palma laboratories and also to R. Rapacioli for the fruitful discussions about the martensitic transformations and for his generous gift of a large number of samples of shape-memory alloys.

1. H. TACHOIRE, J. L. MACQUERON, and V. TORRA. Thermochemistry and its applications to chemical and biological systems. Vol. 119. *Edited by* M. A. Ribeiro da Silva. NATO AS1 Series, Series C, Reidel Publishing Co., Dordrecht. 1984. pp. 77–126; Thermochim. Acta, **105**, 333 (1986).
2. G. PADIN, R. RAPACIOLI, J. ORTÍN, and V. TORRA. Proceedings of the 2nd International Seminar on Shape-memory Alloys. University of Palma, Spain. 1985.
3. H. TACHOIRE and V. TORRA. Thermochim. Acta, **110**, 171 (1987).
4. J. ORTÍN, V. TORRA, and H. TACHOIRE. Thermochim. Acta. **121**, 333 (1987).
5. J. R. RODRIGUEZ, C. REY, V. PEREZ-VILLAR, J. P. DUBÈS, V. TORRA, and H. TACHOIRE. Thermochim. Acta, **75**, 51 (1984); E. CESARI, V. TORRA, J. L. MACQUERON, J. P. DUBÈS, R. KÉCHAVARZ, and H. TACHOIRE. Thermochim. Acta, **79**, 23 (1984).
6. H. TACHOIRE, J. L. MACQUERON, and V. TORRA. Thermochim. Acta, **105**, 333 (1986); E. BOITARD, J. P. DUBÈS, R. KÉCHAVARZ, and H. TACHOIRE. Thermochim. Acta, **116**, 1 (1987); **116**, 21 (1987).
7. J. NAVARRO, E. CESARI, V. TORRA, J. L. MACQUERON, R. PROST, J. P. DUBÈS, and H. TACHOIRE. Bull. Soc. Chim. I, 54 (1982).
8. Proceedings of the 1st International Seminar on Shape-memory Alloys, University of Palma, Spain. 1984; Proceedings of the 2nd International Seminar on Shape-memory Alloys, University of Palma, Spain. 1985.
9. C. SEGUI. Ph.D. Thesis. University of Balearic Islands, Spain. 1987.
10. C. PICORNELL. Ph.D. Thesis. University of Balearic Islands, Spain. 1987.
11. F. C. LOVEY, E. CESARI, V. TORRA, and J. M. GUILEMANY. Mater. Lett. **5**, 159 (1987); F. C. LOVEY, J. ORTÍN, and V. TORRA. Phys. Lett. A**121**, 352 (1987).
12. A. AMENGUAL, L. MAÑOSA, F. MARCO, C. PICORNELL, S. SEGUI, and V. TORRA. Thermochim. Acta, **116**, 195 (1987).
13. J. VAN HUMBEECK, D. SEEGERS, and L. DELAEY. Scr. Metall. **19**, 477 (1985); D. SEEGERS, J. VAN HUMBECK, and L. DELAEY. Ann. Phys. **736**, 179 (1985).
14. M. SADE, F. C. LOVEY, and M. AHLERS. Proceedings ICOMAT 86, Nara, Japan. *Edited by* The Japan Institute of Metals. 1987. p. 934; M. SADE, A. URIBARI, and F. C. LOVEY. Philos. Mag. A**55**, 445 (1987).
15. A. AMENGUAL, F. GARCIAS, F. MARCO, C. SEGUI, and V. TORRA. Acta Metall. **36**, 2329 (1988).
16. P. A. LINDGARD and O. G. MOURITSEN. Phys. Rev. Lett. **57**, 2458 (1986).
17. P. E. CLADIS, W. VAN SAARLOOS, P. L. FINN, and A. R. KORTAN. Phys. Rev. Lett. **58**, 222 (1987).
18. F. C. LOVEY, J. ORTÍN, and V. TORRA. Phys. Lett. A**121**, 352 (1987).
19. A. AMENGUAL, F. C. LOVEY, and V. TORRA. Unpublished results.

Can. J. Chem. Downloaded from www.nrcresearchpress.com by 41.223.56.140 on 09/07/12
For personal use only.

Substituent effects at silicon in cations SiX^+, $HSiX^{+\cdot}$, and H_2SiX^+, and in radicals $H_2SiX^{+\cdot}$

A. C. HOPKINSON
Department of Chemistry, York University, Downsview, Ont., Canada M3J 1P3

AND

M. H. LIEN
Department of Chemistry, National Chung-Hsing University, Taichung, Taiwan 400

Received November 15, 1988

A. C. HOPKINSON and M. H. LIEN. Can. J. Chem. **67**, 991 (1989).

Ab initio molecular orbital calculations at the 6-31G* level have been used to optimise structures for ions SiX^+, $HSiX^{+\cdot}$, and H_2SiX^+, and for neutrals HSiX (singlets), $H_2SiX^\cdot$, and H_3SiX, where X is H, CH_3, NH_2, OH, F, CN, and NC. Single point calculations at the MP4(SDTQ)/6-31G* level were used to calculate substituent stabilisation energies.

The amino group is the strongest π-donor and also is the most stabilising group in the cations, the silylenes, and the silyl radicals. Stabilisation is greatest in ions SiX^+. Ions $HSiX^{+\cdot}$ and H_2SiX^+ are stabilised by similar but smaller amounts, although CN and NC are destabilising in these ions. Substituent stabilisation energies in radicals $H_2SiX^\cdot$ are almost zero. There is a linear relationship between the stabilisation energies of ions H_2SiX^+ and the ionisation potentials of radicals $H_2SiX^\cdot$, but a similar plot correlating stabilisation energies for ions $HSiX^{+\cdot}$ with the ionisation potential of HSiX (singlet) shows considerable scatter.

Key words: silications, silyl radicals, stabilisation energies.

A. C. HOPKINSON et M. H. LIEN. Can. J. Chem. **67**, 991 (1989).

On a utilisé des calculs d'orbitales moléculaires ab initio au niveau 6-31G* pour optimiser les structures des ions SiX^+, $HSiX^{+\cdot}$ et H_2SiX^+ ainsi que des composés neutres HSiX (singulets), $H_2SiX^\cdot$ et H_3SiX dans lesquels X est égal à H, CH_3, NH_2, OH, F, CN ainsi que NC. Afin de calculer les énergies de stabilisation des substituants, on a utilisé des calculs au niveau MP4(SDTQ)/6-31G*.

Le groupement amino est le meilleur donneur π; il est le plus stabilisant des cations et des radicaux silyle et silylènes. Sa stabilisation est maximale dans les ions SiX^+. Les ions $HSiX^{+\cdot}$ et H_2SiX^+ sont stabilisés de la même manière, mais un peu moins; toutefois, dans ces ions, les groupements CN et NC sont déstabilisants. Les énergies de stabilisation des substituants dans les radicaux $H_2SiX^\cdot$ sont pratiquement égales à zéro. Il existe une relation linéaire entre les énergies de stabilisation des ions H_2SiX^+ et les potentiels d'ionisation des radicaux $H_2SiX^\cdot$; dans le cas de la courbe équivalente reliant les énergies de stabilisation des ions $HSiX^{+\cdot}$ avec le potentiel d'ionisation du HSiX (singulet), on note toutefois une dispersion importante.

Mots clés : des cations et des radicaux silyle, les énergies de stabilisation des substituants.

[Traduit par la revue]

Carbenium ions are common intermediates in organic reactions and many are sufficiently stable to be long-lived in strong acid solutions. Silicon is more electropositive than carbon and carries a positive charge more easily, but silicenium ions R_3Si^+ have proved to be elusive species in solution and only recently has there been good experimental evidence for their existence (1–4). Silicenium ions are more commonly observed in the gas phase (5–8) and in this phase carbenium ions abstract hydride or alkyl anions from silanes to form silicenium ions (8). Also *ab initio* molecular orbital calculations have shown that carbenium ions with a silyl or trimethylsilyl group in the α-position undergo a 1,2-shift of hydrogen or methyl, with little or no barrier, to form the lower energy silicenium ions (4, 9). Clearly then, in the absence of solvent, silicenium ions are thermodynamically more stable than the isomeric carbenium ions.

π-Donation from an α-substituent is strongly stabilising in carbenium ions (10–14), but less so in silicenium ions (15, 16). The decreased stabilisation in silicenium ions is attributed to the higher intrinsic ability of silicon to carry a positive charge and to the poor overlap between the π-donating 2*p*-orbital on nitrogen and oxygen with the vacant 3*p*-orbital on silicon (15, 16). Better overlap with silicon can be achieved by using donor elements from the second row, but PH_2 is less effective at stabilising silicenium ions than NH_2, and this has been attributed to the higher energy required to take the pyramidal PH_2 group into the more planar conformation required for π-donation. Some unsaturated molecules containing silicon are known e.g.

$$\rangle Si{=}C\langle \ (17),\quad \rangle Si{=}O\ (18, 19),\quad \text{and}\quad \rangle Si{=}Si\langle \ (20, 21)$$

but, in general, compounds with multiple bonds to silicon are very reactive and rarely encountered in the laboratory. Several such molecules are, however, either known or predicted to exist in interstellar space. SiO and SiS are believed to be present in interstellar space. SiO and SiS are believed to be present in interstellar clouds (22, 23) and lines in the spectrum from interstellar space have been tentatively assigned to HSiN (24) and $HSiC_2$ (25). *Ab initio* molecular orbital calculations cast doubt upon the existence of these last two structures. The $HSiC_2$ radical was assigned to be $^2\Sigma$ whereas theory shows the ground state to be $^2\Pi$ (26), and radical HSiN is at least 55 kcal/mol above the isomeric HNSi (27–31). Also the latter molecule is expected to be formed easily from Si^+ (^2P) and NH_3, both of which are abundant in interstellar clouds, followed by proton transfer from $SiNH_2^+$, possibly to NH_3 (31). The reactions of Si^+ with a variety of small molecules have been shown to form several ions SiX^+ (5, 32, 33).

Previously, we have compared the role of substituents in carbocations and carbenes with formally different amounts of electron deficiency at carbon (13). In all these species NH_2, the most potent π-donor, has the largest stabilising effect, while the CN group, normally both σ- and π-electron withdrawing, functions as a π-donor but is destabilising in carbocations and weakly stabilising in carbenes. For the smallest cations CX^+, it is not possible to draw a reasonable resonance structure in

Can. J. Chem. Downloaded from www.nrcresearchpress.com by 41.223.56.140 on 09/07/12
For personal use only.

TABLE 1. Symmetries, HF/6-31G*, zero-point and MP4/6-31G*//HF/6-31G* energies for SiX^+, $HSiX^{+\bullet}$, $HSiX^+$, $H_2SiX^\bullet$, and H_3SiX

Molecule	Point group	HF/6-31G* [a]	ZPE [b]	MP4/6-31G*//HF/6-31G* [a]
SiH^+	$C_{\infty v}$	−289.13646	3.4	−289.20787
$SiH_2^{+\bullet}$	C_{2v}	−289.70983	8.4	−289.77369
SiH_3^+	D_{3h}	−290.32891	15.1	−290.41057
$SiH_3^\bullet$	C_{3v}	−290.60612	14.4	−290.69575
SiH_4	T_d	−291.22513	21.0	−291.33129
H_3CSi^+	C_{3v}	−328.21235	22.9	−328.43266
$H_3CSiH^{+\bullet}$	C_s	−328.78048	28.4	−328.99328
$H_3CSiH_2^+$	C_s	−329.39833	34.6	−329.62816
$H_3CSiH_2^\bullet$	C_s	−329.65181	34.5	−329.88779
H_3CSiH_3	C_{3v}	−330.27241	40.9	−330.52461
H_2NSi^+	C_{2v}	−344.26126	16.6	−344.51276
$H_2NSiH^{+\bullet}$	C_s	−344.81804	22.6	−345.06209
$H_2NSiH_2^+$	C_{2v}	−345.43913	29.1	−345.70066
$H_2NSiH_2^\bullet$	C_s	−345.66304	27.3	−345.92577
H_2NSiH_3	C_s	−346.28394	33.8	−346.56068
$HOSi^+$	$C_{\infty v}$	−364.10509	8.7	−364.36678
$HOSiH^{+\bullet}$	C_s	−364.63973	13.6	−364.89284
$HOSiH_2^+$	C_s	−365.25793	20.3	−365.52620
$HOSiH_2^\bullet$	C_1	−365.50554	19.1	−365.77471
$HOSiH_3$	C_s	−366.13039	25.9	−366.41588
FSi^+	$C_{\infty v}$	−388.08850	1.6	−388.33954
$FSiH^{+\bullet}$	C_s	−388.62409	5.9	−388.86523
$FSiH_2^+$	C_{2v}	−389.24401	12.7	−389.50137
$FSiH_2^\bullet$	C_s	−389.52283	12.0	−389.78159
$FSiH_3$	C_{3v}	−390.14839	18.6	−390.42286
$NCSi^+$	$C_{\infty v}$	−380.87024	5.2	−381.23685
$NCSiH^{+\bullet}$	C_1	−381.43213	8.9	−381.78385
$NCSiH_2^+$	C_{2v}	−382.05166	16.3	−382.42591
$NCSiH_2^\bullet$	C_s	−382.35509	15.7	−382.72993
$NCSiH_3$	C_{3v}	−382.97440	22.5	−383.36713
$CNSi^+$	$C_{\infty v}$	−380.90769	4.9	−381.25354
$CNSiH^{+\bullet}$	C_1	−381.45322	9.5	−381.79153
$CNSiH_2^+$	C_{2v}	−382.07251	16.0	−382.42761
$CNSiH_2^\bullet$	C_s	−382.35303	15.6	−382.71833
$CNSiH_3$	C_{3v}	−382.97508	22.1	−383.35639

[a]Total energies in hartrees.
[b]Zero-point energies in kcal mol^{-1}.

Can. J. Chem. Downloaded from www.nrcresearchpress.com by 41.223.56.140 on 09/07/12
For personal use only.

which the carbon atom has a complete octet and these ions then have the largest positive charges on carbon and have the largest

$$:\overset{+}{C}—X \leftrightarrow :C{=}X^+$$

substituent stabilisation energies. Radical cations $CHX^{+\bullet}$ (again formally lacking an octet in any resonance structure) and methyl cations CH_2X^+ have smaller, but similar, stabilisation energies. Singlet carbenes, like carbocations, formally have a vacant *p*-orbital and are strongly stabilised by π-donors. Singlet carbene substituent stabilisation energies, then, are similar to those of methyl cations and are much larger than those of triplet carbenes (34–36).

In silicenium ions (4, 15, 16) and silylenes (30, 37) π-donating α-substituents are stabilising, but less so than in their carbon analogues. Here we extend the study of substituent effects in silacations to ions which are of current interest in interstellar chemistry, ions SiX^+ and $SiHX^{+\bullet}$ which are formally more electron-deficient at silicon than the silicenium ions SiH_2X^+. We have also re-examined the silicenium ions SiH_2X^+ at the same high level of theory (MP4SDTQ/6-31G*) as used in the recent work on silylenes (30). Finally, in order to calculate ionisation energies, we have also included calculations on the silyl radicals $SiH_2X^\bullet$. The unsubstituted SiH_n and SiH_n^+ (where *n* takes values from 1 to 4) have previously been studied at the 6-21G level of theory (38).

Computational methods

All molecular geometries were fully optimised with the 6-31G* basis set (39) initially using the Monstergauss program (40). The Gaussian 82 program (41) was used to construct the force constant matrix and all structures were shown to be at minima (i.e. no negative eigenvalues). Singlet spin states were calculated by using closed-shell spin-restricted Hartree–Fock theory (RHF) (42) and doublets were calculated with spin-unrestricted theory (UHF) (43). Post-Hartree–Fock calculations were performed at the fourth-order Møller–Plesset level (44) (MP4SDTQ) on the structures previously optimised at the 6-31G* level (such calculations are denoted by MP4/6-31G*//HF/6-31G*).

Can. J. Chem. Downloaded from www.nrcresearchpress.com by 41.223.56.140 on 09/07/12
For personal use only.

Results and discussion

(a) Structures

The HF/6-31G* and post-Hartree–Fock energies for all the monosubstituted silicon-containing molecules are listed in Table 1. The structural parameters of greatest interest, the Si—X bond lengths and the angles HSiX are reported in Table 2, along with the net-charges on the silicon atom and, in the planar cations and the silylenes, the populations of the formally vacant 3*p*-orbital on silicon. The triplet states are higher in energy than the singlets (41) and only the singlets are included in Table 2.

Several structural features are worthy of comment. The ions have Si—X bond lengths which are dependent only on X and not on the coordination number of silicon, i.e. the bond lengths of SiX^+, $HSiX^{+\cdot}$, and H_2SiX^+ are almost identical, regardless of the extent of electron-deficiency at silicon. Similarly in the neutrals HSiX (singlets), $H_2SiX^{\cdot}$, and H_3SiX, the Si—X distances are almost identical, but are longer than in the cations. Comparing ions with the neutrals from which they are generated by ionisation, then in the parent system the bond length of $SiH_3^{\cdot}$ is only 0.022 Å longer than that of SiH_3^+, but the differences are considerably larger when X is a π-donor. For example, in $H_2SiX^{\cdot}$ when X is NH_2 and NC the Si—N bond lengths are both 0.095 Å longer than in H_2SiX^+, while the more unsaturated system $HSiNC^{+\cdot}$ has an Si—N bond length 0.112 Å shorter than in singlet HSiNC.

Ionisation of $H_2SiX^{\cdot}$ and HSiX (singlet) formally replaces Si with Si^+ and the Mulliken population analysis shows that more than half the positive charge is added to the silicon. This increases the electronegativity of the silicon and results in the Si—H bonds being shorter in the cations. The β-linkages in the substituent (heteroatom-H, or C—H) are the least affected by ionisation and these all increase slightly except when X is CN.

(b) Stabilisation energies

The effect of the substituent X in the silacations relative to that in silanes can be assessed from the isodesmic bond-separation reactions in eqs. [1]–[3].

[1] $SiX^+ + SiH_4 \rightarrow SiH^+ + H_3SiX$

[2] $HSiX^{+\cdot} + SiH_4 \rightarrow SiH_2^{+\cdot} + H_3SiX$

[3] $H_2SiX^+ + SiH_4 \rightarrow SiH_3^+ + H_3SiX$

Equation [3] can be modified for silyl radicals by replacing the superscript positive sign by an electron dot. A positive energy difference for these reactions indicates that the substituent is more stabilising in the cation (or radical) than in the silane (where interactions are assumed to be minimal). The stabilisation energies for SiX^+, $HSiX^{+\cdot}$, H_2SiX^+, HSiX (singlet), and $H_2SiX^{\cdot}$ are given in Table 3, along with those for the identically substituted carbon analogues.

Several trends emerge from the stabilisation energies of the silacations. In cations SiX^+ all substituents are stabilising and the stabilisation energies are considerably larger than in $HSiX^{+\cdot}$ and H_2SiX^+. As with the analogous carbocations the stabilisation energies of the latter two ions are almost identical.

The ability of substituents to stabilise silacations follows the order $NH_2 > OH > CH_3 > F > NC > CN$. Fluorine is strongly stabilising in SiF^+, but has little effect in $HSiF^{+\cdot}$ and H_2SiF^+. Isocyano is somewhat less stabilising in $SiNC^+$ and is weakly destabilising in $HSiNC^{+\cdot}$ and in H_2SiNC^+. The cyano group is only weakly stabilising in $SiCN^+$ and is strongly destabilising in $HSiCN^{+\cdot}$ and H_2SiCN^+. For substituents with a lone pair of π-symmetry there is a rough correlation between the stabilisation energy and the amount of π-donation. For a given substituent X the Si—X distance is almost the same in all ions and the amount of π-donation from substituent to Si^+ is also the same. The amino group is the strongest π-donor and even the cyano group, normally a π-acceptor in neutral molecules, also functions as a weak π-donor in the cations. The order of

TABLE 2. Structural parameters and charge distributions

Species	Si—X[a]	H—Si—X[b]	Net charge on Si	Valence π-density on Si
SiH^+	1.492	—	1.054	
$SiH_2^{+\cdot}$	1.466	119.8	0.932	
SiH_2	1.509	93.3	0.325	
SiH_3^+	1.454	120.0	0.932	
$SiH_3^{\cdot}$	1.476	51.2[c]	0.348	
SiH_4	1.475	109.5	0.545	
H_3CSi^+	1.835	—	1.058	0.070
$H_3CSiH^{+\cdot}$	1.852	120.0	0.973	0.067
H_3CSiH	1.914	95.6	0.447	0.034
$H_3CSiH_2^+$	1.837	121.6	0.999	0.070
$H_3CSiH_2^{\cdot}$	1.895	50.7[c]	0.478	
H_3CSiH_3	1.888	110.7	0.683	
H_2NSi^+	1.646	—	1.054	0.318
$H_2NSiH^{+\cdot}$	1.638	117.2	1.003	0.314
H_2NSiH	1.706	95.5	0.450	0.233
$H_2NSiH_2^+$	1.634	118.2	1.015	0.314
$H_2NSiH_2^{\cdot}$	1.729	56.3[c,d]	0.574	
H_2NSiH_3	1.724	115.5[e], 108.2	0.832	
$HOSi^+$	1.533	—	1.181	0.200
$HOSiH^{+\cdot}$	1.563	114.1	1.147	0.208
$HOSiH$	1.651	96.1	0.556	0.163
$HOSiH_2^+$	1.561	120.7[f], 115.2[g],	1.171	0.211
$HOSiH_2^{\cdot}$	1.651	51.0[c]	0.677	
$HOSiH_3$	1.648	106.8[h] 111.4	0.897	
FSi^+	1.533	—	1.380	0.141
$FSiH^{+\cdot}$	1.537	115.8	1.334	0.141
$FSiH$	1.603	97.4	0.717	0.111
$FSiH_2^+$	1.535	116.4	1.326	0.141
$FSiH_2^{\cdot}$	1.599	55.5[c]	0.796	
$FSiH_3$	1.594	108.8	0.987	
$NCSi^+$	1.822	—	1.153	0.082
$NCSiH^{+\cdot}$	1.784	118.2	1.028	0.093
$NCSiH$	1.891	92.4	0.521	0.044
$NCSiH_2^+$	1.789	117.9	0.998	0.094
$NCSiH_2^{\cdot}$	1.852	54.1[c]	0.499	
$NCSiH_3$	1.866	107.5	0.657	
$CNSi^+$	1.654	—	1.142	0.144
$CNSiH^{+\cdot}$	1.647	117.0	1.068	0.166
$CNSiH$	1.759	94.7	0.588	0.087
$CNSiH_2^+$	1.645	118.0	1.080	0.155
$CNSiH_2^{\cdot}$	1.740	55.6[c]	0.624	
$CNSiH_3$	1.742	108.1	0.803	

[a]Bond lengths in Angstroms.
[b]Bond angles in degrees.
[c]In radicals $SiH_2X^{\cdot}$ angle between SiX bond and plane defined by SiH_2.
[d]Preferred conformation has C_s symmetry with lone pair and unpaired electron antiperiplanar $\angle SiNH_2$ is 28°.
[e]Hydrogen in symmetry plane, *gauche* to hydrogens on NH_2.
[f]*cis* to hydroxy hydrogen.
[g]*trans* to hydroxy hydrogen.
[h]Hydrogen antiperiplanar to hydrogen of OH group.

TABLE 3. Stabilisation energies (kcal mol^{-1})

Species	Silicon-containing compounds at MP4/6-31G*//6-31G* level including ZPE					
	CH_3	NH_2	OH	F	CN	NC
SiX^+	20.2	47.0	46.2	24.6	4.0	12.6
$HSiX^{+\bullet}$	16.4	35.6	21.4	0.1	−13.3	−4.5
H_2SiX^+	15.6	37.0	19.3	−0.4	−12.6	−4.8
HSiX(singlet)[a]	0.7(0.7)	21.9(22.3)	14.7(15.0)	9.3(9.3)	4.6	7.4
$H_2SiX^\bullet$	0.9	2.1	−1.5	−1.7	0.9	0.2
	Carbon analogues at CISD/6-31G*//6-31G* level[b]					
CX^+	65.0	126.6	123.1	82.0	−5.4[c]	61.3[c]
$HCX^{+\bullet}$	42.3	101.5	72.5	27.6	−11.5[c]	22.4[c]
H_2CX^+	36.0	98.8	64.7	23.9	−12.8[c]	15.3[c]
HCX(singlet)	12.2	61.6	51.2	32.9	8.3[c]	21.3[c]
$H_2CX^\bullet$[d]	3.3	9.6	6.2	2.3	11.7	—

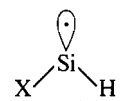
[a]Numbers in parentheses are at the MP4/6-31G*//HF/3-21G* level from ref. 41.
[b]Reference 13.
[c]At HF/6-31G* level.
[d]HF/4-31G level calculations from ref. 50.

π-donation is $NH_2 > OH > F \approx NC > CH_3 > CN$ i.e. substituents formally carrying lone pairs are better π-donors than groups which delocalise through unsaturated bonds or hyperconjugation. Clearly then the amount of π-donation is a poor indicator of the methyl group's ability to stabilise silacations.

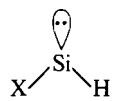
In the carbocations CH_nX^+ for a given X the C—X bond length increases with n and, somewhat surprisingly, the amount of π-donation to C^+ also increases (13). The donor orbitals have better overlap with the vacant 2p-orbital on carbon than with the 3p-orbital on silicon and consequently all the substituents are better π-donors in CH_nX^+ than in SiH_nX^+.

Stabilisation energies again roughly follow the amount of π-donation and are much larger for carbocations than for silacations. The cyano group is somewhat anomalous; in the carbocations it is a strong π-donor but is destabilising, while in $SiCN^+$ it is a weak π-donor, but also weakly stabilising.

Both the radical cations $HSiX^{+\bullet}$, **1**, and the singlet silylenes HSiX, **2**, are, in principle, stabilised by the same mechanism, π-donation to the vacant 3p-orbital in silicon.



1



2

There is larger π-donation in the more electron-deficient silacations and for potent donors NH_2 and OH π-stabilisation dominates and the cation stabilisation is larger than that of the silylenes. When X is a weaker π-donor and a stronger σ-withdrawing group (X = F, CN, and NC) then the singlet silylene is weakly stabilised but in the cations σ-withdrawal dominates and the result is destabilisation.

(c) Ionisation energies and stabilisation energies

The following thermochemical cycle has been used to relate the stabilisation energies of cations (SE^+) with the ionisation potentials of the radicals (45).

$$H_2SiX^+ + SiH_4 \xrightarrow{SE^+} H_3SiX + SiH_3^+$$
$$\downarrow -I_{H_2SiX_2^\bullet} \qquad \uparrow I_{SiH_3^\bullet}$$
$$XSiH_2^\bullet + SiH_4 \xrightarrow{SE^\bullet} H_3SiX + SiH_3^\bullet$$

Formally the stabilisation of the cation is given by eq. [4].

$$[4]\quad SE^+ = SE^\bullet + I_{SiH_3^\bullet} - I_{H_2SiX^\bullet}$$

From Table 3 the stabilisation energies of the radicals ($SE^\bullet$) are small, varying from 2.1 kcal mol^{-1} for NH_2 to −1.7 kcal mol^{-1} for F. If $SE^\bullet$ is taken to be zero then SE^+ is linearly related to the ionisation potential of $H_2SiX^\bullet$. Ionisation potentials were calculated at the MP4/6-31G*//HF/6-31G* level of theory by taking the difference in energy between $H_2SiX^\bullet$ and H_2SiX^+ (including zero-point energy). Further improvement in theory should favour the radical and the ionisation potentials may therefore be slightly too small. However, any error is likely to be common to all ionisation potentials and the plot of stabilisation versus ionisation potential shows a good linear correlation (Fig. 1).

The ionisation potentials of the radicals can also be estimated by using the orbital energies of the highest occupied molecular orbitals (Koopmans' theorem). This more approximate method does not allow for the increased binding in the cation and leads to an overestimation of the ionisation potential. Nevertheless, a plot of the stabilisation energies of SiH_2X^+ against the HOMO of the radicals $SiH_2X^\bullet$ produces a linear plot (Fig. 1), but with more scatter.

Silylenes are ground state singlets and a plot of stabilisation energies of $HSiX^{+\bullet}$ versus the ionisation potential of HSiX (determined by taking the difference between the energies of HSiX and $HSiX^{+\bullet}$) shows considerable scatter (Fig. 2(*a*)). The two points which deviate furthest from the line are for the methyl and hydrogen (parent) substituted ions, i.e., the stabilisation energies of both these ions are too small. The largest positive deviation is for the amino-substituted ion. Hydrogen is not a π-donor and the methyl group is the weakest π-donor, while the amino group is the strongest donor. The ability of the substituent to function as a π-donor, then, dictates whether the stabilisation energy for a substituent will fall above or below the line in Fig. 2(*a*).

The scatter in Fig. 2(a) arises from the stabilisation energy of the singlet. For the same type of thermochemical cycle as used above, but involving the radical cation and silylene, $SE^{+\bullet}$, is given by equation 5.

$$[5]\quad SE^{+\bullet} = SE(\text{silylene}) + I_{SiH_2} - I_{HSiX}$$

A plot of $SE^{+\bullet}$ against I_{HSiX} will be linear only if the

Can. J. Chem. Downloaded from www.nrcresearchpress.com by 41.223.56.140 on 09/07/12
For personal use only.

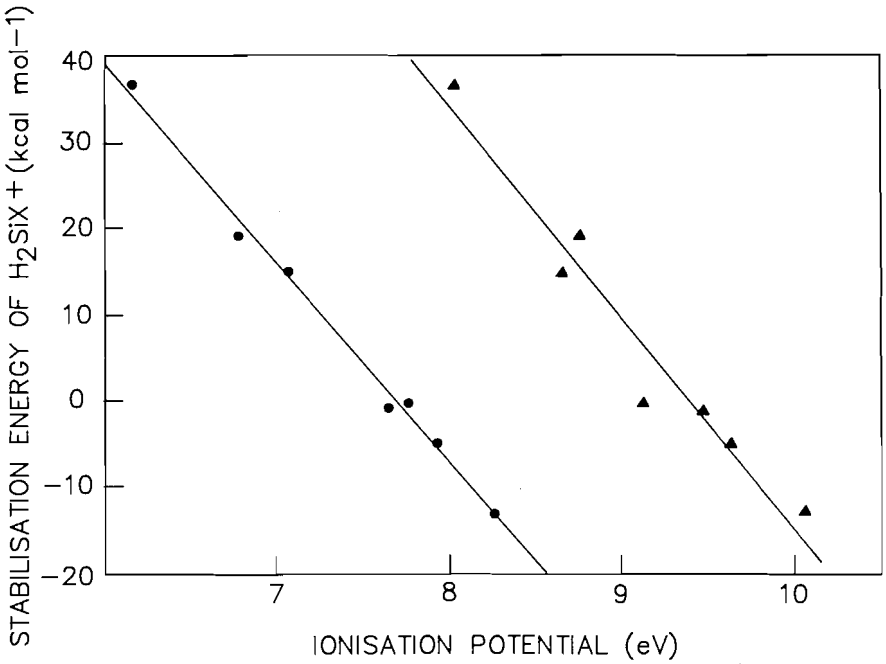


FIG. 1. Plot of stabilisation energies for ions H_2SiX^+ against the ionisation potential of the radicals $H_2SiX^{\cdot}$; ● indicates ionisation potential taken from ($E_{H_2SiX^{\cdot}} - E_{H_2SiX^+}$); ▲ indicates energy of radical HOMO.

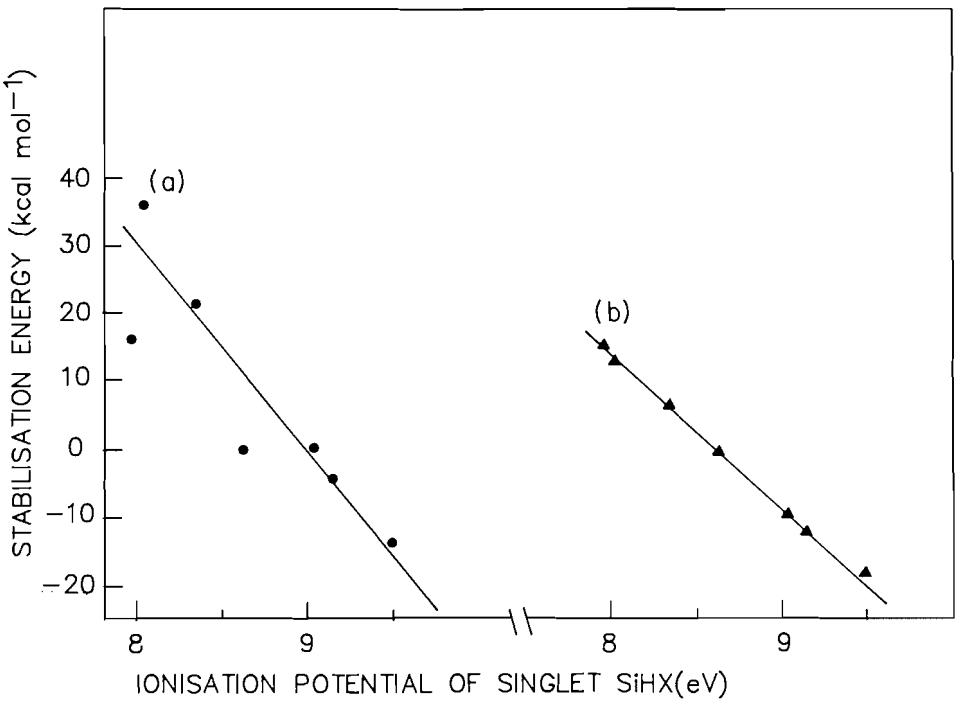


FIG. 2. (*a*) Plot of stabilisation energies for ions $HSiX^{+\cdot}$ against the ionisation potential of singlet silylenes HSiX; (*b*) plot of difference in stabilisation energies of cations $HSiX^{+\cdot}$ and singlet silylenes HSiX against ionisation potentials of silylenes.

stabilisation energy of the silylene is constant. In Table 3 the stabilisation energies of silylenes are shown to vary, from 14.7 kcal mol^{-1} for NH_2 to zero for H, and hence there is considerable scatter in Fig. 2(*a*). However, a plot of [$SE^{+\cdot}$ − SE(silylene)] against I_{HSiX} should be linear and this is found to be the case (Fig. 2(*b*)).

$$\begin{array}{ccc} HSiX^{+\cdot} + SiH_4 & \xrightarrow{SE^{+\cdot}} & H_3SiX + SiH_2^{+\cdot} \\ \Big\downarrow -I_{HSiX} & & \Big\uparrow I_{SiH_2} \\ HSiX + SiH_4 & \xrightarrow{SE(silylene)} & H_3SiX + SiH_2 \end{array}$$

(d) Proton affinities of silylenes and carbenes

The proton affinity of a silylene is the negative of the enthalpy of the reaction described in eq. [6]. At the MP4/6-31G* level of theory, including zero-point energies, the proton affinity of the parent singlet silylene (X = H) is 193.9 kcal mol^{-1}.

[6] $HSiX + H^+ \rightarrow H_2SiX^+$

Can. J. Chem. Downloaded from www.nrcresearchpress.com by 41.223.56.140 on 09/07/12
For personal use only.

TABLE 4. Proton affinities (kcal mol^{-1}) of singlet silylenes and singlet carbenes

X	Silylenes HF/6-31G*	Silylenes MP4/6-31G* + ZPE	Carbenes HF/6-31G*
H	206.5	193.9	224.6
CH_3	220.7	208.9	244.3
NH_2	220.5	209.0	256.5
OH	210.7	198.4	234.0
F	195.9	184.1	212.7
CN	187.1	176.8	203.8
NC	197.6	181.8	219.0

In singlet silylenes the bond angle at silicon is close to 90°, indicating that the bonds have mainly *p*-orbital character with the lone pair having a high percentage *s*-character (30). Protonation of singlet silylenes to generate a trigonal geometry at the silicon atom then involves promotion of these 3*s* electrons into a bonding pair. In contrast, the bond angles in singlet carbenes are somewhat larger and the lone pair has more *p*-character. Protonation of singlet carbene then is more exothermic than protonation of silylene (by 18 kcal mol^{-1} at the 6-31G* level).

Stabilisation by π-delocalisation is important in singlet silylenes but is larger in the product of the protonation reaction, the silicenium ions. When X is CH_3, NH_2, and OH the proton affinities of silylenes are larger than that of the parent (Table 4). Conversely, silylenes which contain substituents that are destabilising in silicenium ions (X = F, CN, and NC) have lower proton affinities than SiH_2. The proton affinities of singlet carbenes show a very similar substituent dependence to that found in the silylenes (13).

(e) Relative energies of cyanides and isocyanides

Organonitriles are generally lower in energy than the isomeric isonitriles (46). However, the isonitrile group is a better π-donor than cyano and in α-X-substituted carbocations, the isocyano-substituted carbocations are lower in energy. When CN and NC are attached to silicon the effect is less pronounced but somewhat similar. In five neutral species, SiX$^{\bullet}$ (47), HSiX (singlet), HSiX (triplet), $H_2SiX^{\bullet}$, and H_3SiX the cyano-substituted molecules have the lower energy (Table 5), but the differences are smaller than in the carbon analogues. When adjacent to Si^+ the isocyano group acts as a π-donor, resulting in a shortening of the Si—N bond and a slight lengthening of N—C. These structural changes are consistent with appreciable contribution from valence bond structure **3***b*.

$$H_nSi^{+}—N^{+}\equiv C^{-} \longrightarrow H_nSi=N^{+}=C$$

3*a* **3***b*

A similarly situated cyano group is a much weaker π-donor and the net-result is that isocyano-substituted silacations are lower in energy than the isomeric cyano-substituted ions. The difference is most pronounced in the most unsaturated ion, SiX^+ and smallest in H_2SiX^+.

Inclusion of correlation energy consistently favours cyano-substituted molecules and ions over the isomeric isocyanides. This appears to be a general phenomenon as it has previously (47–49) been observed for SiCN/SiNC, HCN/HNC, LiCN/LiNC, BCN/BNC, CH_3CN/CH_3NC, and NH_2CN/NH_2NC.

TABLE 5. Relative energies[a] of RCN and RNC[b]

Species		6-31G*	MP4/6-31G*
Silicon-containing molecules			
Neutrals	$SiX^{\bullet}$	−2.4[c]	2.2[c]
	$H_2SiX^{\bullet}$	1.2	7.2
	H_3SiX	−0.8	6.3
	HSiX (singlet)	−2.9	3.6
	HSiX (triplet)[d]	4.0	8.7
Cations	SiX^+	−23.8	−10.7
	$HSiX^{+\bullet}$	−12.6	−4.2
	H_2SiX^+	−13.2	−1.2
Carbon-containing molecules			
Neutrals[e]	H_3CX	20.8	
	HCX (singlet)	7.9	
	HCX (triplet)	18.9	
Cations[e]	CX^+	−45.9	−30.4[f]
	$HCX^{+\bullet}$	−13.0	
	H_2CX^+	−7.3	

[a]Energy in kcal mol^{-1}.
[b]A positive energy difference indicates the cyanide is lower in energy.
[c]Reference 47.
[d]Does not contain ZPE.
[e]Reference 13, does not contain ZPE.
[f]CISD/DZ//HF/DZ (M. H. Lien and A. C. Hopkinson, unpublished work).

Conclusions

Substituent stabilisation energies in silacations are largest in ions SiX^+, and smaller but similar in $SiHX^{+\bullet}$ and SiH_2X^+. Substituents have little or no effect in radicals. The substituent dependence of silacations and silaradicals, then, is very similar to that of the carbon analogues, although the effects at silicon are smaller in magnitude. For cations SiH_2X^+ and $SiHX^{+\bullet}$ the stabilisation energies are linearly related to the ionisation potentials of $SiH_2X^{\bullet}$ and SiHX, respectively. A similar relationship has recently been reported for the methyl cations CH_2X^+.

Using standard heats of formation for the hydride transfer reaction in eq. [7] (X = H) ΔH^0_{298} is 57 kcal mol^{-1}, indicating

[7] $CH_3X + SiH_2X^+ \rightarrow SiH_4 + CH_2X^+$

that the parent silyl cation intrinsically supports the positive charge more easily than the methyl cation. However, substituents overlap more effectively with orbitals on carbon and all the substituents are more stabilising, or less destabilising, in the carbocations CH_nX^+ than in the silacations SiH_nX^+. In all the cations, π-donation to the vacant *p*-orbital at the cation centre has the strongest stabilising effect and the amino group is the most effective donor. Stabilisation at carbon by the amino group is so strong that for eq. [7] when X is NH_2 the calculated ΔE^0_0 is −36 kcal mol^{-1} (at the 6-31G* level), i.e., the intrinsic ability of silicon to support a positive charge relative to carbon has been more than overcome by the stabilisation endowed by the amino group.

Acknowledgement

We thank the Natural Sciences and Engineering Research Council of Canada for financial support.

1. L. R. ROBINSON, G. T. BURNS, and T. J. BARTON. J. Am. Chem. Soc. **107**, 3935 (1985).

Can. J. Chem. Downloaded from www.nrcresearchpress.com by 41.223.56.140 on 09/07/12
For personal use only.

2. J. B. LAMBERT and W. J. SCHULZ JR. J. Am. Chem. Soc. **105**, 1671 (1983); J. B. LAMBERT, J. A. MCCONNELL, and W. J. SHULTZ JR. J. Am. Chem. Soc. **108**, 2482 (1986); J. B. LAMBERT, W. J. SCHULTZ JR., J. A. MCCONNELL, and W. SCHILF. J. Am. Chem. Soc. **110**, 2201 (1988); J. B. LAMBERT and W. SCHILF. J. Am. Chem. Soc. **110**, 6364 (1988); J. B. LAMBERT, J. A. MCCONNELL, W. SCHILF, and W. J. SCHULZ JR. J. Chem. Soc. Chem. Commun. 455 (1988).
3. C. EABORN, P. D. LICKISS, S. T. NAJIM, and M. N. ROMANELLI. J. Chem. Soc. Chem. Commun. 1754 (1985).
4. Y. APELOIG and A. STANGER. J. Am. Chem. Soc. **109**, 272 (1987).
5. J. R. KRAUSE and F. W. LAMPE. J. Phys. Chem. **81**, 281 (1977).
6. G. W. GOODLOE, E. R. AUSTIN, and F. W. LAMPE. J. Am. Chem. Soc. **101**, 3472 (1979).
7. G. W. GOODLOE and F. W. LAMPE. J. Am. Chem. Soc. **101**, 5649 (1979).
8. M. K. MURPHY and J. L. BEAUCHAMP. J. Am. Chem. Soc. **99**, 2085 (1977).
9. A. C. HOPKINSON and M. H. LIEN. J. Org. Chem. **46**, 998 (1981).
10. R. W. TAFT, R. H. MARTIN, and F. W. LAMPE. J. Am. Chem. Soc. **87**, 2490 (1965).
11. Y. APELOIG, P. v. R. SCHLEYER, and J. A. POPLE. J. Am. Chem. Soc. **99**, 1291 (1977).
12. M. H. LIEN and A. C. HOPKINSON. J. Mol. Struct. (Theochem). **121**, 1 (1985).
13. A. C. HOPKINSON and M. H. LIEN. Can. J. Chem. **63**, 3582 (1985).
14. C. F. RODRIQUEZ and A. C. HOPKINSON. J. Mol. Struct. (Theochem). **152**, 55 (1987).
15. Y. APELOIG and P. v. R. SCHLEYER. Tetrahedron Lett. **17**, 4647 (1977).
16. Y. APELOIG, S. A. GODESKI, and D. J. HEACOCK. Tetrahedron Lett. **22**, 3297 (1981).
17. A. G. BROOK, S. C. NYBURG, F. ABDESAKEN, B. GUTEKUNST, G. GUTEKUNST, R. K. M. R. KALLURY, Y. C. POON, Y. M. CHANG, and W. WONG-NG. J. Am. Chem. Soc. **104**, 5667 (1982).
18. C. M. GOLINO, R. D. BUSH, and L. H. SOMMER. J. Am. Chem. Soc. **97**, 7371 (1975).
19. R. WITHALL and L. ANDREWS. J. Am. Chem. Soc. **107**, 2567 (1985).
20. Y. S. CHEN and P. P. GASPAR. Organometallics, **1**, 1410 (1982).
21. H. MATSUMOTO, T. ARAI, H. WATANABE, and Y. NAGAI. J. Chem. Soc. Chem. Commun. 724 (1984).
22. T. J. MILLAR. Astrophys. Space Sci. (Reidel), **72**, 509 (1980).
23. G. BERTHIER, F. PANZAT, and Y. Q. TAO. Astron. Astrophys. **135**, L1 (1984).
24. F. J. LOVAS. Astrophys. J. **193**, 265 (1974).
25. M. GUELIN, J. CERNICHARO, C. KAHONE, and J. GOMEZ-GONZALEZ. Astron. Astrophys. **157**, L17 (1986).
26. A. LARGO-CABRERIZO and J. FLORES. Chem. Phys. Lett. **147**, 90 (1988).
27. R. PREUSS, R. J. BUENKER, and S. PEYERIMHOFF. J. Mol. Struct. **49**, 171 (1978).
28. H. W. KROTO, J. N. MURRELL, A. AL-DERZI, and M. F. GUEST. Astrophys. J. **219**, 886 (1978).
29. F. F. ROELANDT, D. F. VAN DER VONDEL, and G. P. VAN DER KELEN. J. Mol. Struct. **54**, 221 (1979).
30. B. T. LUKE, J. A. POPLE, M. B. KROGH-JESPERSEN, Y. APELOIG, M. KARNI, J. CHANDRASEKHAR, and P. v. R. SCHLEYER. J. Am. Chem. Soc. **108**, 270 (1986).
31. S. WLODEK, C. F. RODRIQUEZ, M. H. LIEN, A. C. HOPKINSON, and D. K. BOHME. Chem. Phys. Lett. **143**, 385 (1988).
32. S. WLODEK, A. FOX, and D. K. BOHME. J. Am. Chem. Soc. **109**, 6663 (1987).
33. A. FOX, S. WLODEK, A. C. HOPKINSON, M. H. LIEN, M. SYLVAIN, C. F. RODRIQUEZ, and D. K. BOHME. J. Phys. Chem. **93**, 1549 (1989).
34. N. C. BAIRD and K. F. TAYLOR. J. Am. Chem. Soc. **100**, 1333 (1978).
35. D. FELLER, W. T. BORDEN, and E. R. DAVIDSON. Chem. Phys. Lett. **71**, 22 (1980).
36. P. H. MUELLER, N. G. RONDAN, K. N. HOUK, J. F. HARRISON, D. HOOPER, B. H. WILLEN, and J. F. LIEBMAN. J. Am. Chem. Soc. **103**, 5049 (1981).
37. W. J. HEHRE, L. RADOM, P. v. R. SCHLEYER, and J. A. POPLE. Ab Initio molecular orbital theory. John Wiley and Sons, New York. 1986. p. 352.
38. D. POWER, P. BRINT, and T. SPALDING. J. Mol. Struct. (Theochem). **108**, 81 (1984).
39. P. C. HARIHARAN and J. A. POPLE. Theor. Chim. Acta, **28**, 213 (1973); M. M. FRANCL, W. J. PIETRO, W. J. HEHRE, J. S. BINKLEY, M. S. GORDON, D. J. DEFREES, and J. A. POPLE. J. Chem. Phys. **77**, 3654 (1982).
40. M. R. PETERSON and R. A. POIRIER. Monstergauss. University of Toronto, Toronto, Ontario. 1980.
41. J. S. BINKLEY, M. J. FRISCH, K. RAGHAVACHARI, D. J. DEFREES, H. B. SCHLEGEL, R. WHITESIDE, E. FLUDER, R. SEEGER, and J. A. POPLE. Gaussian 82. Release A Carnegie-Mellon University, Pittsburgh.
42. C. C. J. ROOTHAAN. Rev. Mod. Phys. **23**, 69 (1951).
43. J. A. POPLE and R. K. NESBET. J. Chem. Phys. **22**, 571 (1954).
44. R. KRISHNAN and J. A. POPLE. Int. J. Quantum Chem. **14**, 91 (1978); R. KRISHNAN, M. J. FRISCH, and J. A. POPLE. J. Chem. Phys. **72**, 4244 (1980).
45. J. C. WHITE, R. J. CAVE, and E. R. DAVIDSON. J. Am. Chem. Soc. **110**, 6308 (1988).
46. M. H. LIEN and A. C. HOPKINSON. Int. J. Quant. Chem. **27**, 1 (1985).
47. A. LARGO-CABRERIZO. Chem. Phys. Lett. **147**, 95 (1988).
48. L. T. REDMAN, G. D. PURVIS, and R. J. BARTLETT. J. Chem. Phys. **69**, 5386 (1978); J. Chem. Phys. **72**, 986 (1980).
49. M. A. VINCENT and C. E. DYKSTRA. J. Chem. Phys. **73**, 3838 (1980).
50. G. LEROY. *In* Computational theoretical organic chemistry. *Edited by* I. G. Csizmadia and R. Daudel. D. Reidel Publishing Company. 1981. pp. 253–334.

Can. J. Chem. Downloaded from www.nrcresearchpress.com by 41.223.56.140 on 09/07/12
For personal use only.

The biosynthesis of ephedrine

GUNNAR GRUE-SØRENSEN[1] AND IAN D. SPENSER[2]
Department of Chemistry, McMaster University, Hamilton, Ont., Canada L8S 4M1

Received November 28, 1988

GUNNAR GRUE-SØRENSEN and IAN D. SPENSER. Can. J. Chem. **67**, 998 (1989).

It is shown by ^{13}C nuclear magnetic resonance spectroscopy that the labelled C_2 fragment of [2,3-$^{13}C_2$]pyruvic acid is transferred intact into the C-methyl group and the adjacent carbon atom of the Ephedra alkaloids, norephedrine, ephedrine, norpseudoephedrine, and pseudoephedrine, in growing plants of *Ephedra gerardiana*. This finding serves to identify pyruvate as the elusive precursor of the aliphatic C_2 terminus of the skeleton of the alkaloids. In earlier experiments with ^{14}C-labelled substrates, label from [3-^{14}C]pyruvic acid was incorporated mainly, but not exclusively, into the C-methyl group of ephedrine, and label from [2-^{14}C]pyruvate was incorporated similarly into the carbon atom adjacent to the C-methyl group. A C_6–C_1 unit related to benzaldehyde or benzoic acid has long been known to generate the benzylic fragment of the carbon skeleton of the Ephedra alkaloids. It is likely that the carbon skeleton of ephedrine is generated from pyruvate and either benzaldehyde or benzoic acid, by a reaction analogous to the formation of acetoin or diacetyl from pyruvate and acetaldehyde or acetic acid, respectively.

Key words: biosynthesis of ephedrine, Ephedra alkaloids, ^{13}C NMR spectra, ephedrine, biosynthesis of pyruvic acid, incorporation into ephedrine ^{13}C NMR spectra.

GUNNAR GRUE-SØRENSEN et IAN D. SPENSER. Can. J. Chem. **67**, 998 (1989).

Utilisant la résonance magnétique nucléaire du ^{13}C, on a démontré que, dans les plants d'*Ephedra gerardiana* en croissance, le fragment en C_2 de l'acide pyruvique-[$^{13}C_2$-2,3] est transféré tel quel au groupement C-méthyle et à l'atome de carbone adjacent de la norépédrine, de l'éphédrine de la norpseudoéphédrine et de la pseudoéphédrine, des alcaloïdes de l'Ephedra. Sur la base de ces résultats, on peut identifier le pyruvate comme le précurseur de la portion aliphatique en C_2 du squelette des alcaloïdes. Dans des expériences antérieures réalisées à l'aide de substrats marqués au ^{14}C, le marqueur provenant de l'acide pyruvique-[^{14}C-3] avait été incorporé principalement, mais pas exclusivement, dans le groupement C-méthyle de l'éphédrine alors que le marqueur du pyruvate-[^{14}C-2] s'était lui aussi incorporé dans l'atome de carbone adjacent au groupement C-méthyle. Ou sait depuis longtemps que l'unité C_6–C_1 reliée au benzaldéhyde ou à l'acide benzoique génère le fragment benzylique du squelette de carbone des alcaloïdes de l'Ephedra. Il est probable que le squelette carboné de l'éphédrine est généré, à partir du pyruvate et du benzaldéhyde ou de l'acide benzoique, par une réaction analogue à celle conduisant à la formation de l'acétoine ou du diacétyle à partir du pyruvate et respectivement de l'acétaldéhyde ou de l'acide acétique.

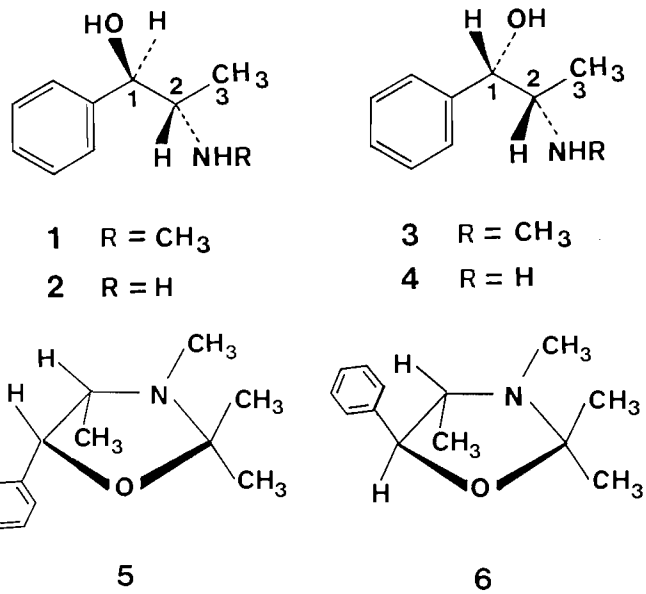
Mots clés : biosynthèse de l'éphédrine, alcaloïdes de l'Ephedra, RMN du ^{13}C, éphédrine, biosynthèse de l'acide pyruvique, incorporation dans les spectra RMN du ^{13}C de l'éphédrine.

[Traduit par la revue]

Introduction

(−)-Ephedrine (**1**) is the active principle of the herb "Ma Huang," which has been used in Chinese medicine for centuries (1). The compound has received much attention by pharmacologists because of its action on the central nervous system (2), but despite its simple chemical structure the biosynthetic origin of its carbon skeleton is still not established. In plants of the genus *Ephedra* (−)-ephedrine is usually found together with (−)-norephedrine (**2**), (+)-pseudoephedrine (**3**), and (+)-norpseudoephedrine (**4**) (1, 3), and it is likely that the phenylpropanoid skeleton of these four alkaloids is derived from common precursors. *Catha edulis*, a plant of an unrelated genus, which is used as a stimulant in many parts of the Middle East (4), contains (+)-norpseudoephedrine (**4**). It was shown some 30 years ago (5) that, in this plant, radioactivity from the benzylic carbon atom of phenylalanine was transferred into the benzylic carbon atom of (+)-norpseudoephedrine (**4**), and that, in *E. distachya*, the N-methyl group of **1** is derived from the S-methyl group of methionine (6).

It was originally thought that the aminophenylpropanoid system of ephedrine was derived directly from phenylalanine (7) or by reaction of a phenylalanine-derived phenethylamine with a formate-derived one-carbon unit (8–10). These views had to be abandoned when it was found (11, 12) that label from [2-^{14}C]phenylalanine did not enter ephedrine, and that label from [2,3-^{14}C]phenylalanine was found solely at the benzylic carbon atom, C-1, of ephedrine (from [3-^{14}C]phenylalanine) but not at C-2, the site predicted for entry of label from [2-^{14}C]phenylalanine. It thus became evident that phenylalanine supplies neither the intact phenylpropanoid system of the alkaloids, nor a C_6–C_2 moiety, but merely a C_6–C_1 unit. Benzoic



[1]Present address: Leo Pharmaceutical Products, DK-2750 Ballerup, Denmark.

[2]Author to whom correspondence may be addressed.

Can. J. Chem. Downloaded from www.nrcresearchpress.com by 41.223.56.140 on 09/07/12
For personal use only.

Can. J. Chem. Downloaded from www.nrcresearchpress.com by 41.223.56.140 on 09/07/12
For personal use only.

acid and benzaldehyde, whose side-chain carbon atom enters the benzylic carbon atom of ephedrine (11, 12), are presumably intermediates on the route from phenylalanine into the C_6–C_1 unit of the alkaloids.

The origin of the C_2 unit, C-2,-3, of ephedrine remained unknown. None of a wide range of ^{14}C-labelled substrates ([2-^{14}C]glycine (12), [U-^{14}C]alanine (12), [U-^{14}C]serine (12), [U-^{14}C]aspartic acid (12), [2-^{14}C]propanoic acid (12), [^{14}C]formic acid (8, 12), [6-^{14}C]glucose (12)) delivered radioactivity preferentially into this unit.

We have investigated the origin of this C_2 unit. Experiments with ^{14}C-labelled substrates did not lead to unequivocal results. It was only with the advent of high field ^{13}C nmr spectroscopy that definitive proof emerged that the nonbenzylic C_2 unit of the Ephedra alkaloids is derived intact from pyruvic acid.[3]

Methods and results

Specifically ^{14}C-labelled samples of serine (in admixture with [ring-^{3}H]phenylalanine), of pyruvic acid, and of acetic acid were administered to *Ephedra gerardiana* and *E. distachya* plants by infusion into their stems through cotton wicks or by external application (Table 1, Expts. 1–8). Extraction of the plants yielded a mixture of the diastereomeric alkaloids, (−)-ephedrine ((1*R*,2*S*)-2-methylamino-1-phenylpropan-1-ol) (**1**) and (+)-pseudoephedrine ((1*S*,2*S*)-2-methylamino-1-phenylpropan-1-ol) (**3**). Separation was achieved by conversion into the corresponding acetonides, (4*S*,5*R*)-2,2,3,4-tetramethyl-5-phenyloxazolidine (**5**) and (4*S*,5*S*)-2,2,3,4-tetramethyl-5-phenyloxazolidine (**6**), which were separated by liquid chromatography and reconverted into the alkaloids by acid hydrolysis.

The *Ephedra* species used were *E. distachya* (Expts. 1–6) and *E. gerardiana sikkimensis* (Expts. 7–9). The early experiments (Expts. 1–6), with mature plants, were performed in the greenhouse at McMaster University. Radioactive tracers, dissolved in glass distilled water, were administered by the wick method and were kept in contact with the plants for 4–5 days before harvesting (see Table 1). For the more recent experiments (Expts. 7–9) small plants were used, which were grown from one year old cuttings, obtained from The Geographic Garden, Kolding, Denmark. In these experiments a solution of the tracers was painted onto the growing aerial parts of the plants over a period of 3–5 days. The plants were in contact with the tracer for a total of 7–8 days before being harvested (see Table 1). Only the aerial parts of the plants were extracted.

The procedures for the isolation of the alkaloids varied to some extent from experiment to experiment. In Expts. 1–3 the plant material was dried (50°C, 1 week) before extraction with methanol, whereas in Expts. 4–9 the fresh plant material was extracted immediately with methanol. In Expts. 1–8 a Soxhlet apparatus was used for the extraction and in Experiment 9 methanol was percolated through a column containing the plant material until extraction was complete.

In Expts. 1–6 the methanolic extracts were evaporated *in vacuo*, whereas in Expts. 7–9 the methanolic extracts were acidified with hydrochloric acid before evaporation of solvent.

After the usual work-up, with acid/base partitioning between water and ether, the crude alkaloids were purified in several ways.

In Expts. 1–3 the Ephedra bases were treated with acetone/silica gel (14) to convert ephedrine (**1**) and pseudoephedrine (**3**) into their acetonides **5** and **6**, respectively. Facile separation of **5** and **6** by liquid chromatography followed by acidic demasking gave ephedrine and pseudoephedrine as their hydrochlorides (see Table 2). The radioactive (−)-ephedrine was further purified by recrystallization after addition of unlabelled (−)-ephedrine hydrochloride. In Expts. 4–8 addition of radioinactive (−)-ephedrine hydrochloride to the crude mixture of alkaloid hydrochlorides, followed by repeated recrystallization, gave radiochemically pure (−)-ephedrine hydrochloride. In Expts. 2 and 3 (−)-ephedrine hydrochloride was converted to (−)-ephedrine sulfate via the free base.

It is apparent from Table 2 that both the amount of isolated (−)-ephedrine as well as the relative amounts of (−)-ephedrine and (+)-pseudoephedrine isolated from individual experiments varied from experiment to experiment. Whether this reflects a natural variation or is a consequence of different work-up procedures is not known, but some loss of (−)-ephedrine during standard isolation procedures has been observed (15). In most cases (−)-ephedrine was the more abundant alkaloid. The amount of either alkaloid isolated was too small for the chemical manipulation required to determine the distribution of radioactivity. Carrier dilution was thus essential to obtain enough material for a complete degradation. Since, of the two alkaloids, (−)-ephedrine invariably had the higher specific activity, this compound was chosen for carrier dilution and degration.

Even so, the carrier dilution that was required to obtain sufficient material for determination of the sites of labelling within an alkaloid sample was such that the degradation experiments had to be performed with samples whose specific radioactivity (cpm per mg above background) was close to the limits of detectability. As a result, the confidence limits of the values for the molar specific activity (dpm per mmol) of the individual degradation products were unusually wide.

The distribution of label within (−)-ephedrine derived from radioactive precursors (Expts. 1–8) was determined by a degradation sequence (Schemes 1 and 2) that permitted individual assay of activity at C-1, C-2, C-3, N-methyl, and at the phenyl group. Dehydration with 50% (v/v) sulfuric acid[4] at 110°C gave, within 15 min, a mixture of ephedrine and pseudoephedrine (ca. 1:1 by ^{1}H nmr) (Scheme 1) that on standing 24 h was converted almost quantitatively into methylamine, isolated by conversion into the *N*-phthaloyl derivative (**9**), and 1-phenyl-2-propanone (**7**), which was recovered as the semicarbazone (**8**) in unexpectedly poor yield.

Chromic acid oxidation of 1-phenyl-2-propanone (**7**), or of ephedrine (**1**) itself (12), gave a mixture of benzoic acid and acetic acid. A portion of this mixture was converted into a mixture of the corresponding 1-acylaminonaphthalenes (**10**, **11**), which were then separated by liquid chromatography. Another portion of the mixture of benzoic and acetic acids was reacted with azide in concentrated sulfuric acid (8) at 25°C for 3 h to give aniline (isolated as its hydrochloride) (aromatic C-atoms), or at 100°C for 2 h to give methylamine (C-3) (isolated as *N*-methylphthalimide (**9**)). The degradation sequence is shown in Scheme 2.

The sample of (−)-ephedrine obtained from plants that had been fed with a mixture of L-[3-^{14}C]serine and L-[ring-2,6-^{3}H]phenylalanine (Expt. 1) showed a much higher incorpora-

[3]An account of the conclusive experiment has appeared (13).

[4]More concentrated sulfuric acid (e.g., 85% (v/v)) (cf. ref. 8) led to sulfonation in the *para* position of the aromatic nucleus, as shown by the appearance of an AB system in the aromatic region of the ^{1}H nmr spectrum of the reaction mixture.

Can. J. Chem. Downloaded from www.nrcresearchpress.com by 41.223.56.140 on 09/07/12
For personal use only.

TABLE 1. Administration of tracers to *Ephedra distachya L.* and *E. gerardiana sikkimensis*

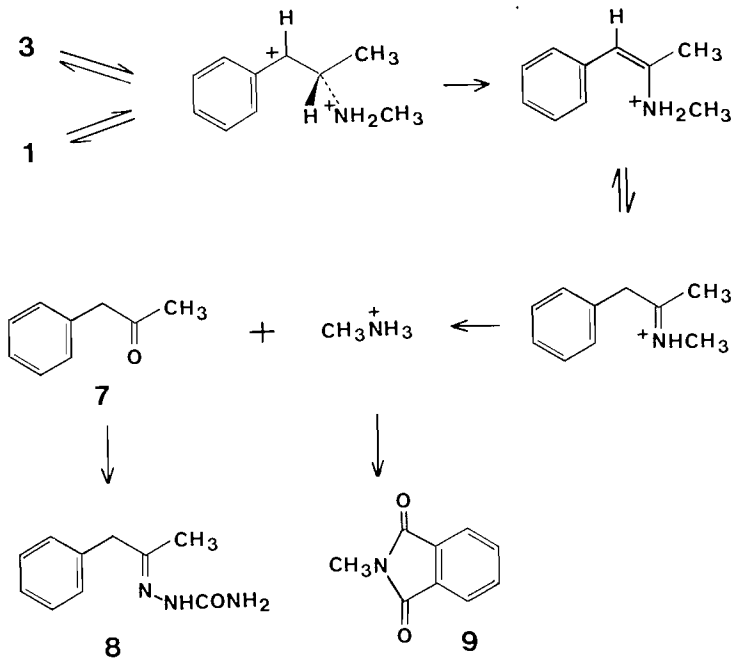
Expt. no.	Date	Precursor	Nominal total activity (mCi)	Nominal specific activity (mCi/mmol)	*Ephedra*	Tracer application method	Tracer administered over ...	... followed by water for	Weight of aerial parts of plant material (g)	
									Fresh wt.	Dry wt.
1	June 1978	L-[ring-2,6-^{3}H]Phenylalanine[a] } [d,e]	1.0	54×10^{3}	*distachya* L.	Wick	1 day	3 days	56	20
		L-[3-^{14}C]Serine[a] } [d,e]	0.1	56						
2	Sept 1978	Sodium [2-^{14}C]pyruvate[b,e]	0.1	6.5	*distachya* L.	Wick	1 day	4 days	191	73
3	Sept 1978	Sodium [3-^{14}C]pyruvate[b,e]	0.1	18.4	*distachya* L.	Wick	1 day	4 days	169	63
4	Sept 1979	Sodium [1-^{14}C]acetate[a,f]	0.25	57.2	*distachya* L.	Wick	1 day	4 days	80	—
5	Sept 1979	Sodium [2-^{14}C]pyruvate[b,f]	0.25	7.7	*distachya* L.	Wick	1 day	4 days	84	—
6	Sept 1979	Sodium [3-^{14}C]pyruvate[b,f]	0.25	21.0	*distachya* L.	Wick	1 day	4 days	102	—
7	July 1982	Sodium [2-^{14}C]pyruvate[b]	0.15	15.2	*gerardiana sikkimensis*	Painting	3 days	5 days	60	—
8	July 1982	Sodium [3-^{14}C]pyruvate[b]	0.15	19.0	*gerardiana sikkimensis*	Painting	3 days	5 days	68	—
9	Sept 1987	Sodium [2,3-$^{13}C_2$]pyruvate[c]	—	—	*gerardiana sikkimensis*	Painting	5 days	2 days	66	—

[a]Radiochemical Centre, Amersham, England.
[b]New England Nuclear, Boston, Mass., U.S.A.
[c]Merck, Sharp and Dohme, Point-Claire, P.Q., Canada.
[d]Measured $^{3}H/^{14}C$ ratio of the mixture, 13:1.
[e]In 10 ml glass distilled water.
[f]In 20 mL glass distilled water. Three days before administration of the tracer solution, a solution containing 0.6 mg thiamin chloride hydrochloride and 11 mg sodium benzoate in 20 mL glass distilled water was administered to the plants. The pH was adjusted to pH 7 with dilute sodium hydroxide solution.

TABLE 2. Incorporation of labelled precursors into *Ephedra* alkaloids

Expt. no.	Precursor	Yield[a] (mg) 1	3	2	4	Specific activity (dpm/mmol) ($\times 10^{-4}$)	$^3H/^{14}C$	Total incorporation[b] (%)	Specific incorporation[c] (%)
	L-[ring-2,6-^{3}H]Phenylalanine[a]					^{3}H: 2.1		8.5×10^{-5}	1.8×10^{-8}
1		18					3.0		
	L-[3-^{14}C]Serine[a]					^{14}C: 0.7		2.8×10^{-4}	5.6×10^{-6}
			3			—			
2	Sodium [2-^{14}C]pyruvate	15				0.8		2.7×10^{-4}	5.5×10^{-5}
			18			—			
3	Sodium [3-^{14}C]pyruvate	47				2.0		2.1×10^{-3}	4.9×10^{-5}
			19			—			
4	Sodium [1-^{14}C]acetate	9				0.1		8.1×10^{-6}	7.9×10^{-7}
5	Sodium [2-^{14}C]pyruvate	6				1.5		8.1×10^{-5}	8.8×10^{-5}
6	Sodium [3-^{14}C]pyruvate	41				0.3		1.1×10^{-4}	6.4×10^{-6}
7	Sodium [2-^{14}C]pyruvate	87				10.8		1.4×10^{-2}	3.2×10^{-4}
8	Sodium [3-^{14}C]pyruvate	127				13.5		2.6×10^{-2}	3.2×10^{-4}
9	Sodium [2,3-$^{13}C_2$]pyruvate	20[d]						7.1×10^{-3}	3.2×10^{-1}
			31[d]					7.6×10^{-3}	2.2×10^{-1}
				2[d]				3.0×10^{-3}	1.4
					6[d]			7.0×10^{-3}	1.0

[a]Alkaloid hydrochlorides.
[b]100 × (total activity within product/total activity within substrate) (Expts. 1–8); 100 × (g-atom ^{13}C within product/g-atom ^{13}C within substrate) (Expt. 9).
[c]100 × (specific activity of product/specific activity of substrate) (Expts. 1–8); 100 × (at.% ^{13}C above natural abundance within product/at.% ^{13}C above natural abundance within substrate) (Expt. 9) (see Table 6).
[d]Calculated from the ^{13}C nmr spectrum of the alkaloid mixture.



SCHEME 1

tion of ^{14}C than of ^{3}H (Table 2). Both the benzoic acid and the acetic acid obtained on degradation contained ^{14}C (Table 3), but more than half of the ^{14}C was located within the N-methyl group (ephedrine minus (benzoic plus acetic acid)). Tritium was confined to the benzoic acid (Table 4).

The sample of (−)-ephedrine from the experiment with [1-^{14}C]acetic acid (Expt. 4) was essentially inactive (Table 2).

The results of the degradation of the samples of ephedrine obtained from the experiments with [2-^{14}C]- and [3-^{14}C]pyruvic acid (Expts. 2, 3, 5–8) are summarized in Table 3. In each case, the acetic acid obtained by degradation, representing the C-methyl group of (−)-ephedrine and the adjacent carbon atom, contained between one and two thirds of the activity of the intact ephedrine, the N-methyl group contained ca. one tenth, and the C_6–C_1 unit accounted for a significant portion ranging from one quarter to more than one half of the total activity.

The distribution of the activity within the acetate differed in the experiments with [3-^{14}C]- and those with [2-^{14}C]pyruvic

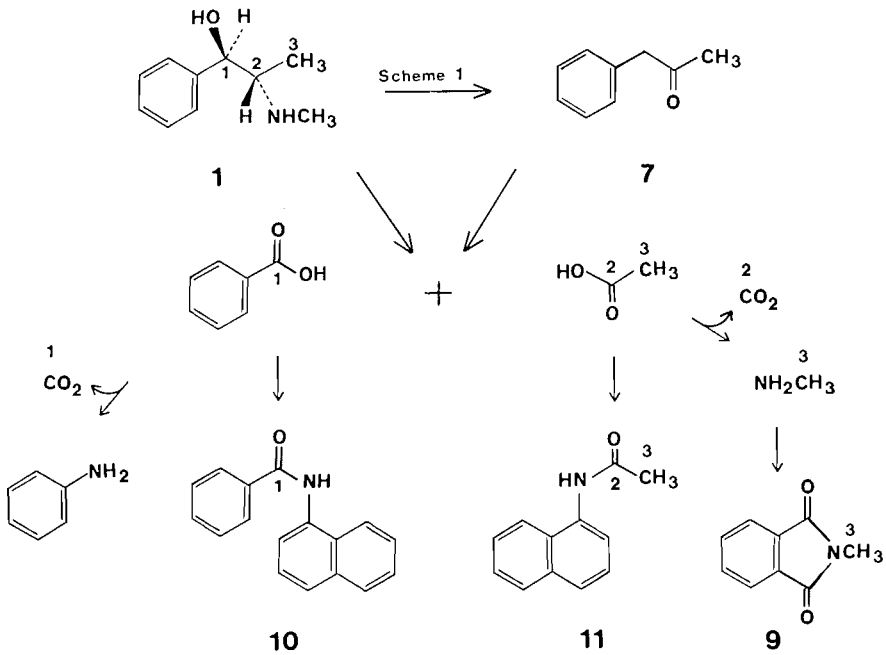
Can. J. Chem. Downloaded from www.nrcresearchpress.com by 41.223.56.140 on 09/07/12
For personal use only.

Can. J. Chem. Downloaded from www.nrcresearchpress.com by 41.223.56.140 on 09/07/12
For personal use only.

Table 3. Incorporation of ^{14}C into ephedrine

Expt. no.	Precursor	Specific activity[a,b] (relative specific activity)[c,d]							
		Ephedrine HCl[a]	Ephedrine sulfate[b]	*N*-Methyl-phthalimide[a]	1-Phenyl-2-propanone semicarbazone[a]	1-Benzamido-naphthalene[a]	1-Acetamido-naphthalene[a]	*N*-Methyl-phthalimide[a]	Aniline HCl[a]
1	L-[3-^{14}C]Serine	3.4 (100±12)				0.7 (22±13)	0.3 (8±9)		
2	Sodium [2-^{14}C]pyruvate	2.5 (100±4)	2.4 (97±9)	0.3 (11±8)		1.1 (44±29)	1.2 (49±8)	0.2 (6±9)	
5	Sodium [2-^{14}C]pyruvate	0.9 (100±5)				0.2 (21±9)	0.6 (63±6)	0.1 (10±8)	
7	Sodium [2-^{14}C]pyruvate	12.8 (100±2)		1.4 (11±2)		7.7 (60±2)	3.2 (25±2)	1.0 (8±2)	6.7 (52±2)
3	Sodium [3-^{14}C]pyruvate		8.6 (100±2)	0.7 (8±1)	5.7 (67±4)	2.0 (23±3)	4.6 (55±2)	3.5 (41±2)	
6	Sodium [3-^{14}C]pyruvate	1.3 (100±6)				0.8 (57±8)	0.8 (58±12)	0.6 (44±19)	
8	Sodium [3-^{14}C]pyruvate	17.3 (100±2)		2.0 (12±2)		9.4 (54±2)	6.5 (38±2)	4.0 (23±2)	7.0 (40±2)
	C-atoms of ephedrine:	All	All	N-CH_3	All except N-CH_3	Aromatic, C-1	C-2, C-3	C-3	Aromatic

[a]Specific activity (dpm/mmol) × 10^{-3}.
[b]Specific activity (dpm/mmol) × 0.5 × 10^{-3}.
[c]Relative specific activity (per cent) (ephedrine HCl or ephedrine sulfate = 100%).
[d]Confidence limits shown are standard deviation of the mean.



SCHEME 2

acid. In the former case (Expts. 3, 6, and 8) the greater part of the activity (approximately three quarters) was recovered in *N*-methylphthalimide representing the C-methyl group of (−)-ephedrine. In the latter case (Expts. 2, 5, and 7) the greater part of the activity (approximately three quarters) was located in the carboxyl group of acetate, i.e., within the carbon of (−)-ephedrine adjacent to the C-methyl group.

The distribution of label within the four Ephedra bases **1**–**4**, derived from plants to which [2,3-$^{13}C_2$]pyruvic acid had been administered (Expt. 9), was determined by ^{13}C nmr.

To facilitate the analysis of the ^{13}C nmr spectrum of the mixture of ^{13}C-enriched alkaloid hydrochlorides, the individual natural abundance ^{13}C nmr spectra of the four compounds were determined under similar conditions (Table 5). Spectra of three of the compounds had previously been reported and assigned (16–18).[5]

The ^{13}C nmr spectrum of the mixture of alkaloid hydrochlorides from plants to which sodium [2,3-$^{13}C_2$]pyruvate had been administered (Expt. 9) (see Fig. 1 and Table 2) shows that the sample consists of pseudoephedrine (**3**), ephedrine (**1**), norpseudoephedrine (**4**), and norephedrine (**2**), in the molar ratio 52:35:10:3 (based on the peak integrals of the central lines of the C-methyl signals). The C-methyl signal (C-3) of each of the four alkaloids consists of a central line (δ 12.49 (**1**), 14.39 (**3**), 15.24 (**2**), and 17.36 (**4**) ppm) straddled by a doublet (J = 37 Hz). A similar pattern is discernible in each of the signals due to C-2 (δ 54.95 (**2**), 55.51 (**4**), 62.61 (**3**), and 62.69 (**1**) ppm). The benzylic carbon atoms (C-1) (δ 74.16 (**1**), 75.69 (**2**), 76.81 (**3**), and 77.55 (**4**) ppm) and the phenyl carbon atoms (δ 128–142 ppm) give signals that appear as singlets. The relative intensity of all singlet signals was identical with that in the spectra of authentic non-labelled alkaloids. This indicates that all detectable ^{13}C enrichment in the nmr spectrum of the four alkaloids from Expt. 9 originates from intact $^{13}C_2$ units. The average specific incorporation of C-2,3 of sodium [2,3-$^{13}C_2$]pyruvate into norephedrine (**2**), norpseudoephedrine (**4**), ephedrine (**1**), and pseudoephedrine (**3**) was 1.4, 1.0, 0.32, and 0.22%, respectively (see Table 6).

Discussion

It was shown by Leete (5) and by Shibata and his students (11, 12) that the benzylic fragment of the carbon skeleton of the Ephedra alkaloids originates from a C_6–C_1 unit derived from phenylalanine. In plant cuttings, radioactivity from DL-[3-^{14}C]phenylalanine entered C-1 and no other sites of (+)-norpseudoephedrine (5) and of (−)-ephedrine (11, 12), and label from DL-[ring-^{3}H]phenylalanine entered the benzylic fragment of (−)-ephedrine (11, 12). Label from DL-[2-^{14}C]phenylalanine was not incorporated (11, 12).

Similarly, label from [3-^{14}C]cinnamic acid, from [carboxyl-^{14}C]benzoic acid, and from [carbonyl-^{14}C]benzaldehyde also entered C-1 of (−)-ephedrine (11, 12). Thus, it is likely that a C_6–C_1 unit related to benzaldehyde or benzoic acid and derived from L-phenylalanine by the phenylalanine ammonia lyase route (22) is the direct precursor of the benzylic fragment of the Ephedra alkaloids (see Scheme 3).

The search for the source of the remaining C_2-unit of the alkaloid skeleton had so far proved fruitless. Less than one third of the total activity within the samples of (−)-ephedrine derived

[5]The assignment of two signals (C-2′,6′ and C-3′,5′) in the spectra has not been settled (cf., refs. 16–18). Assignment is now made on the basis of the following considerations:

Comparison of the chemical shifts of the signals in the spectrum of benzyl alcohol (19) with those of the substituted benzyl alcohols, **1**–**4**, permits the prediction that the signals due to C-2′,6′ be 1–2 ppm upfield from those due to C-3′,5′. The observed chemical shift differences between C-2′,6′ and C-3′,5′ are (**1**) 2.73, (**2**) 2.51, (**3**) 2.00, and (**4**) 2.12 ppm (see Table 5). Secondly, the magnitude of two-, three-, and four-bond carbon–proton coupling constants in monosubstituted benzenes permits a distinction to be made between C-2′,6′ and C-3′,5′ (20, 21). It is predicted that, for C-2′,6′, the numerical values of two of the carbon–proton coupling constants ($J_{2',3'}$ and $J_{2',5'}$) would be <2 Hz and two ($J_{2',4'}$ and $J_{2',6'}$) would be 4.5–8 Hz. For C-3′,5′, the numerical values of three of the carbon–proton coupling constants ($J_{3',2'}$,$J_{3',4'}$, and $J_{3',6'}$) are predicted to be <2 Hz and one ($J_{3',5'}$) to be 7–9 Hz.

The assignments shown in Table 5 are the only ones consistent with these predictions.

Can. J. Chem. Downloaded from www.nrcresearchpress.com by 41.223.56.140 on 09/07/12
For personal use only.

TABLE 4. Incorporation of ^3H into ephedrine

Expt. no.	Precursor	Specific activity[a] (relative specific activity)[b] Ephedrine HCl	1-Benzamidonaphthalene	1-Acetamidonaphthalene
1	L-[ring-2,6-^{3}H]Phenylalanine	10.2 (100±7)	9.0 (88±9)	0.0 (0±5)
	H-atoms of ephedrine:	All	Aromatic	At C-3

[a]Specific activity (dpm/mmol) × 10^{-3}.
[b]Relative specific activity (per cent) (ephedrine HCl = 100%).

TABLE 5. The ^{13}C nmr chemical shifts[a] of *Ephedra* alkaloids[b]

	C-1′	C-2′,6′	C-3′,5′	C-4′	C-1	C-2	C-3	N–CH_3
Ephedrine (**1**) HCl	141.21	128.85	131.58	131.17	74.15	62.68	12.49	33.53
Norephedrine (**2**) HCl	141.09	129.10	131.61	131.36	75.68	54.90	15.24	—
Pseudoephedrine (**3**) HCl	141.97	129.83	131.83	131.83	76.81	62.60	14.39	32.49
Norpseudoephedrine (**4**) HCl	142.07	129.65	131.77	131.68	77.55	55.50	17.36	—

[a]Relative to sodium 2,2,3,3-tetradeuterio-3-(trimethylsilyl)propionate (δ 0.00 pm).
[b]Fifty milligrams alkaloid HCl in D_2O (0.6 mL).

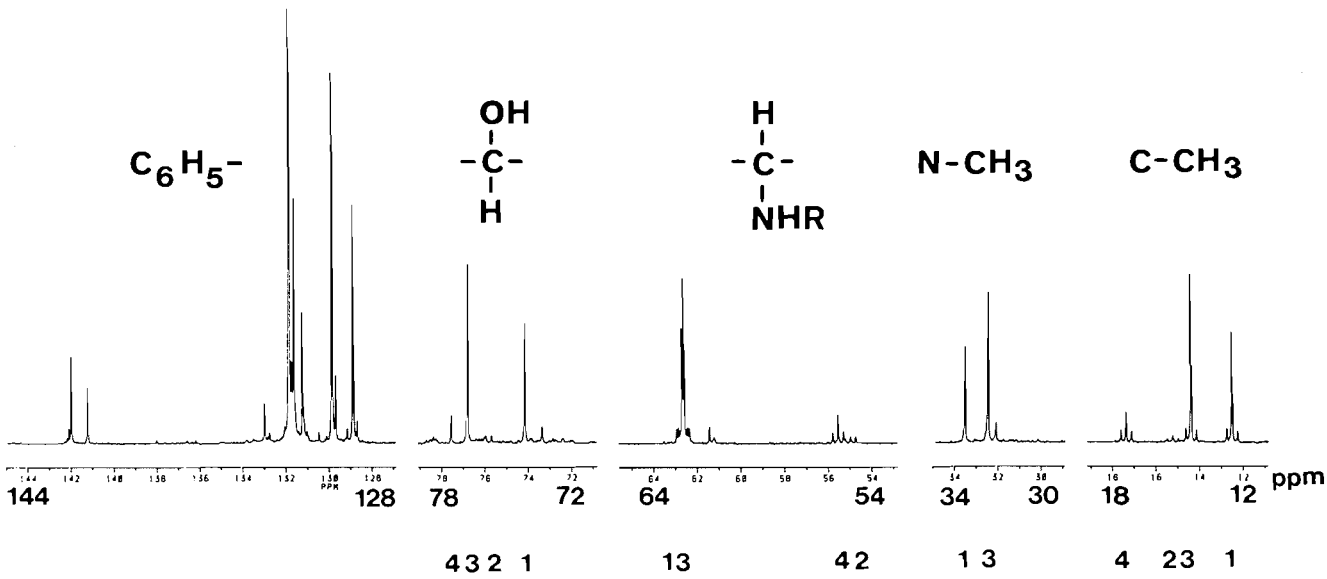


FIG. 1. Proton noise decoupled ^{13}C nmr spectrum (75.47 MHz, 5000 transients) of alkaloid hydrochlorides (57 mg in 0.6 mL D_2O) obtained from plants of *Ephedra gerardiana* after administration of sodium [2,3-$^{13}C_2$]pyruvate. The spectrum was recorded on a Bruker AC 300 spectrometer under standard conditions, with sodium 2,2,3,3-tetradeuterio-3-(trimethylsilyl)propionate (δ 0.00 ppm) as internal reference. The numbers below the δ (ppm) scale show assignments of the signals to the four compounds **1**–**4**.

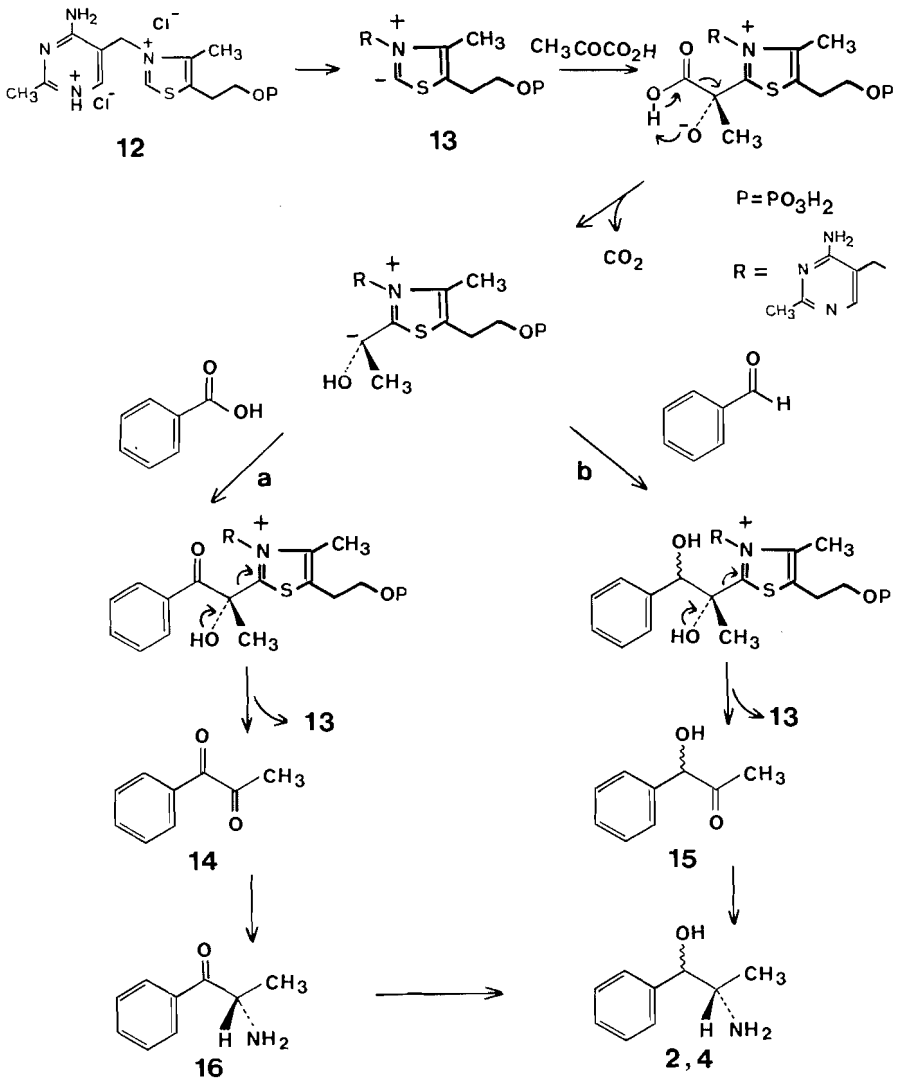
from a variety of radioactive substrates was present within this unit; 70% or more of the label was distributed over the rest of the molecule.

The multicarbon substrates that delivered the highest fraction (ca. 25%) of the total activity of ephedrine into the C_2 unit were D-[6-^{14}C]glucose, and L-[U-^{14}C]aspartic acid and L-[U-^{14}C]alanine, two amino acids closely related to the tricarboxylic acid cycle. But in each case at least an equal fraction of label entered the C_6–C_1 unit and twice as much was incorporated into the N-methyl group (12).

[2-^{14}C]Glycine and L-[U-^{14}C]serine delivered ca. 75% of activity into the N-methyl group, 20% into the benzylic fragment, and only ca. 5% into the C_2 unit (12). This distribution of label was maintained (see Tables 2 and 3) when L-[3-^{14}C]serine was administered in the presence of L-[ring-^{3}H]phenylalanine ($^3H/^{14}C$ ratio 13:1) (Expt. 1). Even though the ephedrine that was isolated showed a $^3H/^{14}C$ ratio 3:1, indicating that ^{14}C (i.e., serine) had been incorporated almost four times as efficiently as ^3H (i.e., phenylalanine), the presence of phenylalanine had not caused a redirection of ^{14}C from the C_6–C_1 into the C_2 unit.

Evidently, in all the above experiments metabolic fragmenta-

Can. J. Chem. Downloaded from www.nrcresearchpress.com by 41.223.56.140 on 09/07/12
For personal use only.



SCHEME 3

TABLE 6. Incorporation of sodium [2,3-$^{13}C_2$]pyruvate into *Ephedra* alkaloids; ^{13}C nmr analysis (Expt. 9)

	1	2	3	4
R(C-2)[a]	0.31	1.5	0.22	0.9
R(C-3)[a]	0.26	1.0	0.17	0.9
Average specific incorporation:[b]	0.32%	1.4%	0.22%	1.0%

[a]*R*(C-*n*) = ^{13}C nmr doublet area of C-*n*/^{13}C nmr singlet area of C-*n*.

[b]Average specific incorporation of ^{13}C from sodium [2,3-$^{13}C_2$]pyruvate into C-2 and C-3 of the *Ephedra* alkaloids = (E_E/E_P) × 100%, where E_E = average enrichment above natural abundance (at.% ^{13}C) at C-2 and C-3 = [(*R*(C-2) + *R*(C-3))/2] × 1.1% and E_P = average at.% ^{13}C at C-2 and C-3 of sodium [2,3-$^{13}C_2$]pyruvate = 99%.

tion of the precursors had occurred prior to incorporation of label into the alkaloid. Glycine and serine are known to participate in one-carbon metabolism (23). Another one-carbon donor, [^{14}C]formic acid (9, 12), supplied 50% of the total activity into the N-methyl group and ca. 20% into the phenyl nucleus. In this instance the C_2 unit contained 30% of the total activity. Most of this activity was present in the C-methyl group (9).

The scrambling of label and, in particular, the predominant presence of label in the N-methyl group that was observed in every one of the above experiments points to rapid metabolic turnover in the course of the feeding experiments. The distribution of label observed in these experiments tended to obscure rather than to illuminate the origin of the C_2 fragment.

Since the carbon skeleton of the Ephedra bases does not appear to be derived directly from an amino acid, it is likely that the nitrogen atom is introduced at a late stage of biosynthesis. Indeed, the stereospecific transfer of the amino group of L-glutamic acid into (±)-1-hydroxy-1-phenyl-2-propanone (**15**), to yield a mixture of (−)-norephedrine (**2**) as the major and (+)-norpseudoephedrine (**4**) as the minor product, is catalyzed by transaminases that have been obtained from several plant species (24). The same enzyme system catalyzes the reverse reaction, converting (−)-norephedrine into (−)-1-hydroxy-1-phenyl-2-propanone.

The latter compound has been reported to be the major product when yeast (*Saccharomyces cerevisiae*) is incubated with benzaldehyde (25–35) in the presence of fermentable sugars (25, 27, 30, 33–35), pyruvic acid (25, 29, 31, 32), or acetyl phosphate (31). The relative amounts of (*S*)- and (*R*)-1-hydroxy-1-phenyl-2-propanone that are formed are determined by the stereoselectivity of this reaction.

The reaction is catalyzed by "α-carboxylase" (E.C. 4.1.1.1,

Can. J. Chem. Downloaded from www.nrcresearchpress.com by 41.223.56.140 on 09/07/12
For personal use only.

Can. J. Chem. Downloaded from www.nrcresearchpress.com by 41.223.56.140 on 09/07/12
For personal use only.

2-oxo acid carboxylyase, pyruvate decarboxylase), and requires thiamin as a cofactor (31, 32). The course of the reaction (Scheme 3) is evidently analogous to that of the carboxylase-catalyzed formation of acetoin from acetaldehyde and pyruvate (36–38).

If the carbon skeleton of the Ephedra alkaloids were generated in Ephedra plants by a reaction analogous to the formation of 1-hydroxy-1-phenyl-2-propanone in yeast, the stereoselectivity of the process would ultimately determine the relative amounts of (1*R*) alkaloids ((−)-norephedrine (**2**) and (−)-ephedrine (**1**)) and (1*S*) alkaloids ((+)-norpseudoephedrine (**4**) and (+)-pseudoephedrine (**3**)) present in the plants.

The primary objective of this investigation was to test whether, in analogy with the condensation reaction that takes place in yeast, the C_2 unit of the Ephedra alkaloids is derived from pyruvate.

Samples of sodium [2-^{14}C]pyruvate (Expts. 2, 5, 7) and sodium [3-^{14}C]pyruvate (Expts. 3, 6, 8) were administered to plants of two different Ephedra species by two different methods, under various conditions (Table 1). In some cases (Expts. 5, 6) thiamin and sodium benzoate were administered 3 days before the solution containing the pyruvate was applied, in an attempt to enhance the condensation reaction (thiamin) and to suppress incorporation of label into the benzylic fragment of the alkaloid (benzoic acid). The yield of ephedrine, the per cent incorporation, and the specific incorporation of radioactivity into the alkaloid (Table 2) as well as the distribution of label over the three fragments, N-methyl, C_6–C_1, and C_2, within the alkaloid (Table 3) varied from experiment to experiment and no consistent pattern was evident. As in the earlier experiments, label was heavily scrambled over the three fragments, indicating rapid metabolic turnover of pyruvate (Table 3).

Even though label from [2-^{14}C]- and [3-^{14}C]pyruvate did not necessarily enter the C_2 unit predominantly, the distribution of activity within this C_2 unit showed a strong trend (Table 3): In each of the three experiments with [3-^{14}C]pyruvate most of the label (ca. 75%) within the C_2 unit was located at the C-methyl group (C-3) of ephedrine (recovered as methylamine by Schmidt degradation of the Kuhn–Roth acetate), whereas in each of the three experiments with [2-^{14}C]pyruvate most of the label (ca. 75%) within the C_2 unit was located at the adjacent carbon atom, C-2 (Kuhn–Roth acetate minus Schmidt methylamine). Even though this distribution of label tends to be in accord with that expected if pyruvate were the source of the C_2 unit (Scheme 3), these results could not be regarded as conclusive evidence in support of the proposition that the C_2 unit was generated from an acetyl unit derived from pyruvate by decarboxylation.

Incorporation of radioactivity into ephedrine from acetate itself (Expt. 4) was too low to attempt the chemical degradation required to determine the distribution of label. This was not altogether surprising. The kinases required to convert acetate into its biologically active species, acetyl CoA or acetyl phosphate, are absent from many biological systems. The conversion of pyruvate into acetyl CoA, on the other hand, takes place in most living species. Thus, for example, pyruvate served as the direct precursor of the non-tyrosine derived C_2 unit of anhalonidine and pellotine, alkaloids of the peyote cactus (39), whereas acetate was incorporated only indirectly, with scrambling of label (40). In yeast, acetate did not serve as a precursor of the nonbenzylic C_2 unit of 1-hydroxy-1-phenyl-2-propanone, whereas acetyl phosphate or pyruvate did (31). Even so, in the present instance the experiments with ^{14}C-labelled samples of pyruvate (Expts. 2, 3, 5–8), while indicative, were inconclusive, since label from these substrates was not confined to the predicted sites.

Conclusive evidence was obtained, almost 10 years after our first experiments with ^{14}C-labelled precursors, by means of an experiment with [2,3-$^{13}C_2$]pyruvic acid. The distribution of label within the four alkaloids, **1**–**4**, derived from this precursor in *E. gerardiana sikkimensis*, is evident from the high field ^{13}C nmr spectrum of the mixture of alkaloid hydrochlorides (Fig. 1). The signals due to the C-methyl group and the adjacent carbon atom of each of the four alkaloids show satellites, due to ^{13}C–^{13}C coupling, a clear demonstration of the incorporation of the intact $^{13}CH_3$–^{13}CO unit of the precursor into each of the four alkaloids. A full interpretation of the spectrum has appeared (13).

The question arises why the experiments with [^{14}C]pyruvate gave results that were inconclusive whereas the experiment with [$^{13}C_2$]pyruvate gave an unequivocal result, even though the sensitivity of detecting ^{14}C within the product[6] is approximately 3 orders of magnitude greater than that of detecting ^{13}C (cf. ref. 41).[7]

It is probable that it is this sensitivity which permitted the detection of radioactivity in all parts of the ephedrine molecule, when [^{14}C]pyruvate served as the substrate, indicating rapid metabolic turnover of pyruvate. There is no reason to think that in the experiment with [$^{13}C_2$]pyruvate a similar rapid turnover did not also occur. But since such turnover would have led to enrichment at all carbon atoms of ephedrine, leading to a small increase in the height of every peak in the ^{13}C nmr spectrum of the product, these increases were not detectable.

What was detectable were the satellites due to intact transfer

---

[6]Radioactivity of carrier free ^{14}C-labelled precursor: Specific activity = ca. 62 mCi per mmol, i.e., ca. 1.4×10^{11} disintegrations per minute per mmol, i.e., ca. 1.2×10^{11} counts per minute per mmol, when radioactivity is assayed in a modern liquid scintillation counter at ca. 90% efficiency. Radioactivity of a product of MW 200 (say), determined on a weighed sample of 0.1 mg (say) to be 50 counts per minute above background (say). Specific activity of product is 1.0×10^5 counts per minute per mmol, i.e., 1.1×10^5 disintegrations per minute per mmol. Thus a dilution of radioactivity of six orders of magnitude is detectable.

[7]To detect, in unequivocal fashion, incorporation of ^{13}C from a singly ^{13}C-labelled substrate, the peak height of the ^{13}C nmr signal due to the enriched carbon atom of the product must show an enhancement of at least 20–30% over that of the corresponding signal of a sample containing only natural abundance ^{13}C. This enhancement, which corresponds to an incorporation of 0.2–0.3% ^{13}C above natural abundance (1.1%), must be determined relative to the peak height of signals due to unenriched carbon atoms in the sample containing the enriched carbon.

Thus the maximum permissible dilution of ^{13}C of a precursor containing 100% ^{13}C at a single position, en route to a biosynthetic product, is less than three orders of magnitude.

If the ^{13}C-labelled substrate is enriched in ^{13}C at a pair of contiguous carbon atoms, i.e., the substrate is "bond-labelled", and if this enriched C_2 unit is transferred intact into a product, detection of incorporation no longer depends on observing the increase in peak height of a single signal in the ^{13}C nmr spectrum, but on the appearance of signal satellites due to ^{13}C–^{13}C coupling. The use of such bond-labelled substrates thus permits much greater dilution of the administered precursor.

The limit of detection of these satellites depends less on the per cent incorporation of ^{13}C than on the field strength of the spectrometer and the quality of the probe used in recording the spectrum. The field strength controls the signal dispersion while the quality of the probe determines the signal-to-noise ratio of the spectrum, for a given amount of sample.

Can. J. Chem. Downloaded from www.nrcresearchpress.com by 41.223.56.140 on 09/07/12
For personal use only.

of pairs of contiguous carbon atoms from substrate into each of the products.

Thus the less sensitive tracer technique provided an unequivocal result whereas the more sensitive technique gave information that was not readily interpretable.

A further difference between the experiments with ^{14}C and ^{13}C-labelled pyruvate is the enhanced specific incorporation of label into the alkaloids in the latter case (Expt. 9) (10^3-fold) compared to that in the ^{14}C-pyruvate experiments (Expts. 7, 8), in the same *Ephedra* species (Table 1). This may be related to the fact that, whereas in the ^{14}C experiments (Expts. 7, 8) only tracer amounts of sodium pyruvate (ca. 1 mg) were administered, in the ^{13}C experiment (Expt. 9) a massive dose of substrate (500 mg) was applied.

The final question that must be raised concerns the status of 1-hydroxy-1-phenyl-2-propanone (**15**) in the biosynthesis of the Ephedra alkaloids. Attempts to trap this compound in the plant extracts from our tracer experiments, or to demonstrate specific incorporation into ephedrine, of label from ^{14}C-labelled samples of 1-hydroxy-1-phenyl-2-propanone by means of feeding experiments with *E. distachya*,[8] did not meet with success.

There is thus no experimental evidence supporting the intermediacy of this compound in ephedrine biosynthesis. The supposition that it is implicated is based entirely on chemical analogy (28, 33, 35).

A closely related compound, (*S*)-(−)-2-amino-1-phenyl-1-propanone ((−)-cathinone) (**16**) is a major constituent of *Catha edulis* Forsk., where it occurs together with (+)-norpseudoephedrine (**4**) and (−)-norephedrine (**2**) (42, 43). It is, of course, possible that (−)-cathinone (**16**) is derived from (+)-norpseudoephedrine or (−)-norephedrine by enzymic dehydrogenation. However, it is also conceivable that (−)-cathinone might, in fact, serve as the substrate for stereospecific enzymic reduction and represent the precursor of (+)-norpseudoephedrine and of (−)-norephedrine (42). If so, the compound from which the alkaloids are derived would not be 1-hydroxy-1-phenyl-2-propanol (**15**) but 1-phenyl-1,2-propandione (**14**).

This compound, which has been detected in *Catha edulis* (42), in turn would be generated in the presence of thiamin by the carboxylase-catalyzed reaction of pyruvate with benzoic acid (rather than with benzaldehyde) (Scheme 3), analogous to the carboxylase-catalyzed formation of butan-2,3-dione (diacetyl) (44, 45).

Such a biosynthetic sequence would be consistent with the apparent lack of participation of 1-hydroxy-1-phenyl-2-propanone in ephedrine biosynthesis. It would also explain the observation that benzoic acid as well as benzaldehyde serves as the precursor of the C_6–C_1 unit of the Ephedra alkaloids (12). Whereas the biological oxidation of benzaldehyde to benzoic acid is likely to be a facile process (46), the reverse reaction, reduction of benzoic acid to benzaldehyde, does not appear to have been observed in higher plants (46).

Experiments are in hand to examine the possible intermediacy of 1-hydroxy-1-phenyl-2-propanone (**15**), 1-phenyl-1,2-propandione (**14**), and cathinone (**16**) in the biosynthesis of the Ephedra alkaloids.

Experimental

Labelled compounds

The labelled compounds employed in the nine feeding experiments were obtained from commercial suppliers (see Table 1).

[8]K. Yamasaki. Personal communication.

Tracer experiments

Administration of labelled compounds to Ephedra distachya *L. and* E. gerardiana sikkimensis

Experiments 1–6

Stocks of *Ephedra distachya* L. were obtained from Hillier Nurseries, Winchester, England. The plants were propagated in the greenhouse at approximately 24°C. Large stocks were split in the spring. Labelled compounds were administered to actively growing plants by the wick method. The plants were kept in contact with tracer for 4–5 days. Alkaloids were isolated from the plants as described below.

Experiments 7–9

Plants of *E. gerardiana sikkimensis* were propagated in a greenhouse at 25–30°C for 1 year, from cuttings obtained from The Geographic Garden, Kolding, Denmark. Labelled compounds were administered in an aqueous solution of Tween 80 (1% w/v). This solution (1.0 mL per day) was applied to the light green shoots with a fine paint brush. After administration of tracer the plants were painted with 1.0 mL of water per day (see Table 1). In Experiment 9 a total of 500 mg sodium [2,3-$^{13}C_2$]pyruvate (99 at.% ^{13}C per position) was administered over 5 days.

Details of the feeding experiments are summarized in Table 1.

Isolation of ephedrine and pseudoephedrine

Extraction of the alkaloid mixture

Expts. 1–3: The aerial parts of the plants were cut into pieces (approximately 1 cm long) and dried at 50°C for 1 week. The weight loss was 60–65%. The dry plant material was finely ground in a blender and extracted with methanol in a Soxhlet extractor until the extract was no longer coloured (ca. 8 h). Expts. 4–8: The fresh aerial parts of the plants were ground in a blender and extracted with methanol in a Soxhlet apparatus. Experiment 9: The fresh aerial parts of the plants were ground in a blender and extracted with methanol at 20°C. In each case the extraction of the alkaloids was considered complete when chlorophyll had been completely extracted from the plant material.

In Expts. 1–6, the extract was then concentrated *in vacuo*, sulfuric acid (0.1 M, 70 mL) was added to the oily residue, the mixture was extracted with ether (4 × 35 mL), and the ether extract discarded. The aqueous phase was basified to pH 10 with solid potassium carbonate and then extracted with ether (5 × 30 mL). In Expts. 7–9, the methanol extracts were acidified with hydrochloric acid (4 M, 3 mL) before concentration *in vacuo*. Hydrochloric acid (0.1 M, 50 mL) was added to the residue and the aqueous mixture was washed with ether (4 × 50 mL), basified with potassium carbonate, and extracted with ether (4 × 50 mL).

In Expts. 1–3, the ether extract was dried (anhydrous sodium sulfate) and concentrated *in vacuo* to yield an oily residue that contained the crude alkaloids, which were then separated via the acetonides (*vide infra*). In Expts. 4–9, the ether extracts were extracted with hydrochloric acid (1 M, 2 × 5 mL) and the aqueous phase was evaporated to dryness *in vacuo* to yield a mixture of crude alkaloid hydrochlorides. In Expts. 4–8, radioinactive (−)-ephedrine hydrochloride (60–220 mg) was then added as carrier and the product was recrystallized from ethanol/ether, mp 217°C (lit. (12) mp 220°C). In Expt. 9 the 75.5-MHz ^{13}C nmr spectrum (see Fig. 1) of the mixture of alkaloid hydrochlorides (57 mg) showed that the sample consisted of the hydrochlorides of pseudoephedrine (**3**), ephedrine (**1**), norpseudoephedrine (**4**), and norephedrine (**2**) in the molar ratio 52:35:10:3 (see Table 2). An analysis of the ^{13}C nmr spectrum is presented in Tables 5 and 6.

Separation of ephedrine and pseudoephedrine via their acetonides ***5*** *and* ***6*** *(Expts. 1–3)*

The residue containing the crude alkaloids was dissolved in acetone (50 mL). Silica gel 60 (60–200 mesh, 700 mg) and a few boiling chips were added, the mixture was refluxed 20 h, filtered, and concentrated *in vacuo* (14). The oily residue was dissolved in a mixture of ethyl acetate (2.5 mL) and petroleum ether (bp 30–60°) (2.5 mL), and residual solid was removed by centrifugation. The supernatant liquid was applied to a column (Merck Silica Gel 60, prepacked, size B) and eluted with a mixture of ethyl acetate and petroleum ether (bp 30–60°C) (1:1 v/v). The ultraviolet absorption of the effluent was monitored continuously at 254 nm. The fractions containing the two products, (4*S*,5*R*)-2,2,3,4-

Can. J. Chem. Downloaded from www.nrcresearchpress.com by 41.223.56.140 on 09/07/12
For personal use only.

tetramethyl-5-phenyloxazolidine (i.e., (−)-ephedrine acetonide (**5**)) and (4*S*,5*S*)-2,2,3,4-tetramethyl-5-phenyloxazolidine (i.e., (+)-pseudoephedrine acetonide (**6**)) were collected separately (tlc (ethyl acetate:petroleum ether (bp 30–60°C) 1:1, v/v): R_f 0.6 and 0.5, respectively) and concentrated *in vacuo*.

Each acetonide was hydrolyzed without further purification. Each residue was dissolved in ethanol (1 mL) and hydrochloric acid (0.25 M, 1 mL), and the solution kept 1.5 h at 70°C. Each solution was evaporated *in vacuo*, the residue was dried over P_2O_5, an inactive sample of (−)-ephedrine hydrochloride or (+)-pseudoephedrine hydrochloride, respectively, was added as carrier, and the products were recrystallized from ethanol/ether: (−)-ephedrine hydrochloride, mp 217°C (lit. (12) mp 220°C: (47*a*) mp 218°C; (+)-pseudoephedrine hydrochloride, mp 180–181°C (lit. (48) mp 179–181°C; (47*a*) mp 182–182.5°C).

(−)-Ephedrine sulfate

A sample of (−)-ephedrine hydrochloride (50 mg) was dissolved in water (3 mL), solid potassium carbonate was added (to pH 10), and the solution was continuously extracted with ether (20 h). Ether was evaporated and sulfuric acid (0.1 M) was added dropwise to the residue (to pH 4). The solution was concentrated and the solid residue recrystallized (water/ethanol/ether) to give (−)-ephedrine sulfate (44 mg, 0.10 mmol, 83%); mp 259°C (lit. (48) mp 257°C).

Determination of radioactivity

Radioactivity was assayed by liquid scintillation counting (Mark 1 liquid scintillation computer, Model 6860, Nuclear Chicago (Expts. 1–6) or Beckman LS 9000 liquid scintillation system (Expts. 7, 8). Activity due to ^3H and ^{14}C was determined simultaneously, by external standardization counting with ^{133}Ba.

Samples (0.5–1.0 mg) were dissolved in ethanol or water, and the solution dispersed in Aquasol (New England Nuclear). The incorporation of the radioactive precursors into the alkaloids (Expts. 1–8) is summarized in Table 2.

Degradation of labelled ephedrine

The radioactively labelled samples of ephedrine (Expts. 1–8) were degraded by the reactions outlined below. The purity of all labelled samples was checked by thin-layer chromatography and melting point determination. All samples were recrystallized to constant specific activity. The molar specific activities of the samples of ephedrine and its degradation products, obtained from individual tracer experiments, are summarized in Tables 3 and 4. Confidence limits shown in Tables 3 and 4 are standard deviation from the mean.

Carbon atoms 1–3 and the aromatic carbon atoms as 1-phenyl-2-propanone semicarbazone

(−)-Ephedrine sulfate (27 mg, 0.06 mmol) or an equivalent quantity of the hydrochloride was dissolved in sulfuric acid (50% (v/v), 0.5 mL), and kept 24 h in a sealed flask at 110°C. Water (1 mL) was added and the mixture was extracted with ether (3 × 1 mL). The ether extract was washed with water (2 × 1 mL) and concentrated in a stream of nitrogen. The residue was dissolved in a solution of potassium acetate (20 mg, 0.20 mmol) in ethanol (0.5 mL). A solution of semicarbazide hydrochloride (20 mg, 0.18 mmol) in water (0.5 mL) was added, the mixture was heated 1 min on a steam bath, solvent was removed *in vacuo*, and the residue was sublimed at 140°C and 0.027 Torr. The sublimate was applied to a column (Merck Silica Gel 60 prepacked, size A), which was eluted with ethanol. The fraction containing *1-phenyl-2-propanone semicarbazone* (detected by continuous monitoring of the effluent at 254 nm) (tlc (ethanol) R_f 0.7) was concentrated *in vacuo*. Yield 3 mg (0.02 mmol, 25%); mp 181°C (from ethanol) (lit. (49) mp 177°C).

This degradation of ephedrine to 1-phenyl-2-propanone was a modification of an established method (8).

The N-methyl group of ephedrine as N-methylphthalimide

(−)-Ephedrine sulfate (71 mg, 0.16 mmol) or an equivalent quantity of the hydrochloride was dissolved in sulfuric acid (50% (v/v), 1 mL) and kept 24 h in a sealed flask at 110°C. The flask was cooled and a solution of potassium carbonate (2.0 g) in water (6 mL) was added. The mixture was heated until 4 mL distillate had been trapped in hydrochloric acid (1 M, 0.5 mL). The acidified distillate was concentrated to dryness *in vacuo*. The crystalline residue of methylamine hydrochloride was redissolved in water (0.5 mL), the solution was basified with solid sodium carbonate (to pH 9), and *N*-carboethoxyphthalimide (62 mg, 0.28 mmol) was added. The reaction mixture was stirred until precipitation of N-*methylphthalimide* was complete (15 min). The product was sublimited at 70°C and 0.025 Torr and recrystallized (methanol/water). Yield 11 mg (0.07 mmol, 44%), mp 133°C (lit. (47*b*) mp 133–134°C; (50) mp 134°C)).

Carbon atoms 2 and 3 as acetic acid and carbon atom 1 and the aromatic carbons as benzoic acid (isolated as 1-acylaminonaphthalenes)[9] (12)

(−)-Ephedrine hydrochloride (50 mg, 0.25 mmol) was dissolved in a solution of chromium trioxide (750 mg, 7.5 mmol) in concentrated sulfuric acid (0.7 mL) and water (10 mL). The mixture was distilled, with simultaneous addition of water to maintain constant volume, until 50 mL distillate had been collected. The distillate was neutralized with dilute sodium hydroxide and the solution was divided in two portions in a ratio of 1:3. Both portions were concentrated to dryness *in vacuo*. The larger portion was kept for a Schmidt degradation of benzoic acid and acetic acid (*vide infra*).

The smaller portion was dissolved in water (2 mL) and 1-naphthylamine hydrochloride (53 mg, 0.34 mmol) and *N*-ethyl-*N'*-[3-(dimethylamino)propyl]carbodiimide hydrochloride (170 mg, 0.89 mmol) were added and the solution stirred for 1 h. Hydrochloric acid (1 M, 1 mL) was then added and the mixture was extracted with ether (3 × 3 mL). The ether extracts were dried (sodium sulfate) and evaporated to dryness *in vacuo* and the residue was chromatographed on silica gel 40 (70–230 mesh, 15 g) with ether as eluent. The fractions containing 1-benzamidonaphthalene and 1-acetamidonaphthalene were collected (tlc (ether) R_f 0.8 and 0.4, respectively) and evaporated, and the products were recrystallized. 1-Benzamidonaphthalene, yield 5 mg (0.02 mmol, 32%), mp 162–163°C, after sublimation at 135°C and 0.025 Torr, and recrystallization from benzene/hexane (lit. (47*c*) mp 162°C; (52) mp 157–159°C). 1-Acetamidonaphthalene, yield 7 mg (0.04 mmol, 61%), mp 158–159°C, after sublimation at 95°C and 0.025 Torr, and recrystallization from benzene/hexane (lit. (47*c*) mp 160°C; (53) mp 159–160°C).

The C-methyl group of ephedrine (C-3) as methylamine (isolated as N-methylphthalimide) and the aromatic carbon atoms as aniline hydrochloride

The solid residue containing the sodium salts of benzoic acid and acetic acid obtained from the major portion of the distillate from the chromic acid oxidation, which had been kept for a Schmidt degradation (*vide supra*), was dissolved in concentrated sulfuric acid (1.8 mL). Sodium azide (120 mg, 1.85 mmol) was added. When a homogeneous solution was obtained the mixture was divided into two equal portions.

One portion was kept 3 h at 25°C. The mixture was added to water (8 mL) and solid sodium hydrogen carbonate was added, to pH 8. The mixture was extracted with ether (3 × 3 mL) and the extracts were dried (sodium sulfate). Hydrochloric acid (1 M, 0.5 mL) was added and the mixture was concentrated to dryness *in vacuo*. Recrystallization from ethanol/ether gave aniline hydrochloride: 3 mg (0.02 mmol, 34%), mp 194°C (lit. (54) mp 198°C).

[9]These simple compounds do not appear to have a unique name assigned to them: IUPAC nomenclature rules (51) permit any one of four alternative names: (*i*) IUPAC rule C-824-1: *N*-1-naphthalenylacetamide and -benzamide. This is the nomenclature used in Chem. Abstr. (registry numbers 575-36-0 and 634-42-4, respectively). (*ii*) IUPAC rule C-824-2: 1-acetyl- and 1-benzoylaminonaphthalene or, since the name 1-naphthylamine is permissible for 1-aminonaphthalene (see rule C-812), acetyl- and benzoyl-1-naphthylamine. These are the names found in the Dictionary of Organic Compounds (47*c*). (*iii*) IUPAC rule C-824-3: 1-acetamido- and 1-benzamidonaphthalene. Furthermore, IUPAC rule C-823-1 refers to either (*ii*) or (*iii*), but not to (*i*). So much for uniformity of chemical nomenclature.

The second portion was heated on a steam bath for 2 h. After cooling, the mixture was added to water (10 mL). Solid sodium hydroxide was then added to pH 13. The mixture was heated until 5 mL distillate had been collected in hydrochloric acid (1 M, 2 mL). The acidified distillate was concentrated to dryness *in vacuo* and the solid residue of methylamine hydrochloride was converted to *N*-methylphthalimide, as described above. Yield: 5 mg (0.03 mmol, 47%).

Acknowledgements

We are grateful to Thelma Leech, Greenhouse Supervisor, McMaster University, for providing facilities for this work, to N. J. Bollerup, The Geographic Garden, Kolding, Denmark, for a gift of *Ephedra* plants and help with their propagation, and to N. Rastrup Andersen, Leo Pharmaceutical Products, for recording and assigning[5] the ^{13}C nmr spectra. This investigation was supported by a grant from the Natural Sciences and Engineering Research Council of Canada.

1. L. RETI. *In* The alkaloids. Vol. 3. *Edited by* R. H. F. Manske and H. L. Holmes. Academic Press, New York. 1953. p. 339.
2. N. WEINER. *In* The pharmacological basis of therapeutics. 7th ed. *Edited by* A. G. Gilman, L. S. Goodman, T. W. Rall, and F. Murad. Macmillan, New York. 1985. p. 145.
3. T. A. HENRY. The plant alkaloids. 4th ed. J. & A. Churchill, London. 1949. pp. 634–648.
4. J. H. JAFFE. *In* The pharmacological basis of therapeutics. 6th ed. *Edited by* A. G. Gilman, L. S. Goodman, and A. Gilman. MacMillan, New York. 1980. p. 535.
5. E. LEETE. Chem. Ind. (London). 1088 (1958).
6. S. SHIBATA, I. IMASEKI, AND M. YAMAZAKI. Chem. Pharm. Bull. **5**, 71 (1957).
7. S. SHIBATA and I. IMASEKI. Chem. Pharm. Bull. **4**, 277 (1956).
8. S. SHIBATA, I. IMASEKI, and M. YAMAZAKI. Chem. Pharm. Bull. **5**, 594 (1957).
9. I. IMASEKI, S. SHIBATA, and M. YAMAZAKI. Chem. Ind. (London), 1625 (1958).
10. S. SHIBATA, I. IMASEKI, and M. YAMAZAKI. Chem. Pharm. Bull. **7**, 449 (1959).
11. K. YAMASAKI, U. SANKAWA, and S. SHIBATA. Tetrahedron Lett. 4099 (1969).
12. K. YAMASAKI, T. TAMAKI, S. UZAWA, U. SANKAWA, and S. SHIBATA. Phytochemistry, **12**, 2877 (1973).
13. G. GRUE-SØRENSEN and I. D. SPENSER. J. Am. Chem. Soc. **110**, 3714 (1988).
14. K. YAMASAKI, K. FUJITA, M. SAKAMOTO, K. OKADA, M. YOSHIDA, and O. TANAKA. Chem. Pharm. Bull. **22**, 2898 (1974).
15. A. H. BECKETT, G. R. JONES, and D. A. HOLLINGSBEE. J. Pharm. Pharmacol. **30**, 15 (1978).
16. L. F. JOHNSON and W. C. JANKOWSKI. Carbon-13 nmr spectra. Wiley, New York. 1972. Spectrum 355.
17. K. YAMASAKI and K. FUJITA. Chem. Pharm. Bull. **27**, 43 (1979).
18. A. PATRA, A. K. MITRA, and A. K. MUKHOPADHYAY. J. Indian Chem. Soc. **56**, 1245 (1979).
19. E. PRETSCH, T. CLERC, J. SEIBL, and W. SIMON. Tabellen zur Strukturaufklärung organischer Verbindungen mit spectroskopischen Methoden. 3rd ed. Springer Verlag, Berlin. 1986. p. C120.
20. P. E. HANSEN. Prog. Nucl. Magn. Reson. Spectrosc. **14**, 175 (1981).
21. E. BREITMAIER and W. VOELTER. Carbon-13 nmr spectroscopy. 3rd ed. VCH Verlagsgesellschaft, Weinheim. 1987. p. 145.
22. K. R. HANSON and E. A. HAVIR. *In* The biochemistry of plants. Vol. 7. *Edited by* P. K. Stumpf and E. E. Conn. Academic Press, New York. 1981. p. 577.
23. A. NEUBERGER. *In* Comprehensive biochemistry. *Edited by* M. Florkin and E. H. Stotz. Vol. 19A. *Volume editors*: A. Neuberger and L. L. M. Van Deenen. Elsevier, Amsterdam. 1981. p. 257.
24. K. HASSE and G. SCHMID. Biochem. Z. **337**, 69 (1963).
25. C. NEUBERG and J. HIRSCH. Biochem. Z. **115**, 282 (1921).
26. C. NEUBERG and H. OHLE. Biochem. Z. **127**, 327 (1922).
27. C. NEUBERG and H. OHLE. Biochem. Z. **128**, 610 (1922).
28. J. KAMLET. Wallerstein Lab. Commun. **4**, 213 (1941).
29. Y. SHIMAZU. Nippon Kagaku Zasshi, **71**, 503 (1950).
30. Y. SHIMAZU. J. Inst. Polytech. Osaka City Univ. Ser. C: **2**, 125 (1952).
31. P. F. SMITH and D. HENDLIN. J. Bacteriol. **65**, 440 (1953).
32. O. HANC and B KAKÁC. Naturwissenschaften, **43**, 498 (1956).
33. D. GRÖGER, H. P. SCHMAUDER, and K. MOTHES. Z. Allg. Mikrobiol. **6**, 275 (1966).
34. J. P. VOETS, E. J. VANDAMME, and C. VLERICK. Z. Allg. Mikrobiol. **13**, 355 (1973).
35. P. M. SUBRAMANIAN, S. K. CHATTERJEE, and M. C. BHATIA. J. Chem. Technol. Biotechnol. **39**, 215 (1987).
36. H. HOLZER and K. BEAUCAMP. Angew. Chem. **71**, 776 (1959).
37. H. HOLZER and K. BEAUCAMP. Biochim. Biophys. Acta, **46**, 225 (1961).
38. G. L. CARLSON and G. M. BROWN. J. Biol. Chem. **236**, 2099 (1961).
39. G. J. KAPADIA, G. S. RAO, E. LEETE, M. B. E. FAYEZ, Y. N. VAISHNAV, and H. M. FALES. J. Am. Chem. Soc. **92**, 6943 (1970).
40. A. R. BATTERSBY, R. BINKS, and R. HUXTABLE. Tetrahedron Lett. 563 (1967).
41. E. LEETE. J. Nat. Prod. (Lloydia), **43**, 130 (1980).
42. X. SCHORNO and E. STEINEGGER. Experientia, **35**, 572 (1979).
43. B. D. BERRANG, A. H. LEWIN, and F. I. CARROLL. J. Org. Chem. **47**, 2643 (1982).
44. H. SUOMALAINEN and L. JÄNNES. Nature, **157**, 336 (1946).
45. F. C. HAPPOLD and C. P. SPENCER. Biochim. Biophys. Acta, **8**, 543 (1952).
46. G. G. GROSS. *In* The biochemistry of plants. Vol. 7. *Edited by* P. K. Stumpf and E. E. Conn. Academic Press, New York. 1981. p. 311.
47. Heilbronn's Dictionary of Organic Compounds. 5th ed. Chapman & Hall, New York. 1982; (*a*) Vol. 4, M-00798; (*b*) Vol. 5, P-01796; (*c*) Vol. 4, N-00273.
48. T. Q. CHOU. J. Biol. Chem. **70**, 109 (1926).
49. G. G. SMITH. J. Am. Chem. Soc. **75**, 1134 (1953).
50. G. WANAG and A. VEINBERGS. Ber. Dtsch. Chem. Ges. B: **75**, 1558 (1942).
51. J. RIGAUDY and S. P. KLESNEY. Nomenclature of organic chemistry. Pergamon Press, Oxford. 1979.
52. H. W. GRIMMEL, A. GUENTHER, and J. F. MORGAN. J. Am. Chem. Soc. **68**, 539 (1946).
53. E. LEETE, H. GREGORY, and E. G. GROS. J. Am. Chem. Soc. **87**, 3475 (1965).
54. C. D. LEWIS, R. G. KRUPP, H. TIECKELMANN, and H. W. POST. J. Org. Chem. **12**, 303 (1947).

Can. J. Chem. Downloaded from www.nrcresearchpress.com by 41.223.56.140 on 09/07/12
For personal use only.

Asymmetric induction in Diels–Alder reactions of α-alkoxyorthoquinodimethanes

JAMES L. CHARLTON, GUY L. PLOURDE, AND GLENN H. PENNER
Department of Chemistry, University of Manitoba, Winnipeg, Man., Canada R3T 2N2

Received September 23, 1988

JAMES L. CHARLTON, GUY L. PLOURDE, and GLENN H. PENNER. Can. J. Chem. **67**, 1010 (1989).

It has been shown that dienophiles cycloadd selectively to one face of *o*-quinodimethanes (*o*-QDMs) bearing chiral α-alkoxy groups. The face selectivity (diastereoselectivity) increases for the series of chiral groups -OCH(Ph)CH_3, -OCH(Ph)$CH(CH_3)_2$, and -OCH(Ph)$C(CH_3)_3$. A similar effect on the face selectivity of the Diels–Alder reactions of chiral alkoxy vinyl ethers for the same series of chiral groups has been noted previously by others. A mechanism has been proposed to explain the face selectivity in the cycloaddition reactions of the alkoxy *o*-QDMs. *Ab initio* molecular orbital calculations with geometry optimization on vinyl 1-phenylethyl ether to determine its lowest energy conformations support the proposed mechanism. The absolute stereochemistries of the *o*-QDM cycloadducts have been determined to verify the predictions of the model.

Key words: *o*-quinodimethanes, asymmetric, Diels–Alder, cycloaddition.

JAMES L. CHARLTON, GUY L. PLOURDE et GLENN H. PENNER. Can. J. Chem. **67**, 1010 (1989).

On a démontré que les diénophiles peuvent donner lieu à une cycloaddition qui est sélective pour une face des *o*-quinodiméthanes (*o*-QDM) portant des groupements α-alcoxy chiraux. La sélectivité faciale (diastéréosélectivité) augmente dans la série des groupements chiraux -OCH(Ph)CH_3, -OCH(Ph)$CH(CH_3)_2$ et -OCH(Ph)$C(CH_3)_3$. Un effet semblable a déjà été observé antérieurement, par d'autres, dans le cas de la sélectivité faciale de réactions de Diels–Alder d'éthers vinyliques comportant la même série de groupements alcoxy chiraux. On propose un mécanisme pour expliquer la sélectivité faciale observée lors des réactions de cycloadditions des alcoxy *o*-QDM. Des calculs d'orbitales moléculaires *ab initio*, comportant une optimisation de la géométrie, ont été effectués sur l'éther de vinyle et de phényl-1 éthyle dans le but de déterminer ses conformations d'énergies minimales; ces calculs supportent le mécanisme proposé. Dans le but de vérifier les prédictions du modèle, on a déterminé les stéréochimies absolues des cyclo-adduits des *o*-QDM.

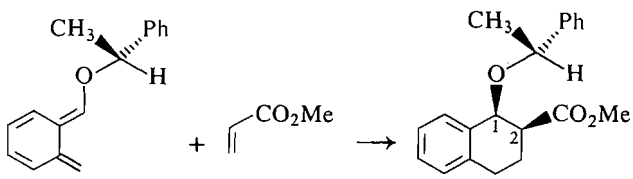
Mots clés : *o*-quinodiméthanes, asymétrique, Diels–Alder, cycloaddition.

[Traduit par la revue]

Introduction

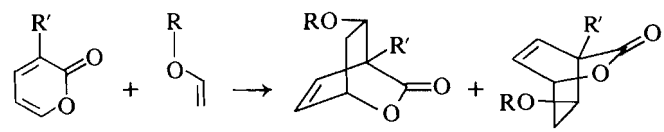
The Diels–Alder reaction, and more recently, the asymmetric Diels–Alder reaction, has proven to be a popular synthetic tool (1). While the Diels–Alder reactions of *ortho*-quinodimethanes (*o*-QDMs) have also received extensive study, less work has appeared on the asymmetric cycloaddition reactions of *o*-QDMs (2). Asymmetric control of these versatile reactions would open up the possibility for enantioselective synthesis of a large number of interesting and important compounds.

In preceding publications we have described initial studies of asymmetric induction in the Diels–Alder reaction of *o*-quinodimethanes (2–5) and, while the results of these studies have now been successively applied to an asymmetric synthesis of (+)-isolariciresinol (5), the exact mechanism of the induction is still unknown. The reactions in question involve the cycloaddition of achiral dienophiles to *o*-QDMs that bear an α chiral alkoxy group. As an example, in the conversion of **1** to **2**, it was



found that an (*R*)-1-phenylethoxy group directed addition of methyl acrylate to the upper face of **1** (*si* face at the α center) such that the major product had the (1′*R*,1*S*,2*S*) configuration.

A mechanism to explain the face selectivity, based on π-stacking of the chiral auxiliary to the *o*-QDM, has been shown to be inconsistent with product stereochemistry (3, 4, 6) and it was proposed that reaction from the conformation shown



3 R′ = -SO_2Tol **4** **5**

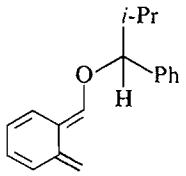
	R	%de
a	-CH(Ph)Me	66
b	-CH(Ph)*i*-Pr	84
c	-CH(Ph)*t*-Bu	90

in **1** might explain the face selectivity due to the difference in size of the phenyl and methyl groups (4). Results from a study by Posner and Wettlaufer seemed to be inconsistent with the above proposal (7). They studied the conversion of **3***a–c* to **4** and **5**.

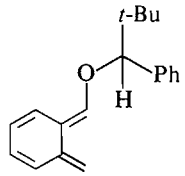
They found that the face selectivity of the reaction increased as the bulk of the alkyl group in the chiral auxiliary increased. The question then arises as to whether the same increase in face selectivity would be observed in the reactions of **1** as methyl is changed to isopropyl and *tert*-butyl. Such an increase would be inconsistent with the face selectivity being due to a conformation of the *o*-QDM as shown in **1**. It is also necessary to determine at which face the *o*-QDM reacts for each of the chiral auxiliaries by determining the configurations of the newly formed chiral centers in the cycloaddition products relative to that of the chiral auxiliary.

In this paper we describe the preparation of the *o*-QDMs **1**, **6**, and **7**, a study of their reactions with dimethyl fumarate, and a comparison of the diastereoselectivities in these reactions. We also describe *ab initio* molecular orbital calculations on **3***a*, which were carried out with geometry optimization to determine the conformational preferences of this molecule and, by inference, the conformational preferences of the *o*-QDM **1**.

Can. J. Chem. Downloaded from www.nrcresearchpress.com by 194.225.253.170 on 09/07/12
For personal use only.



6



7

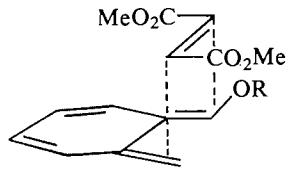
Results and discussion

The *o*-QDMs **6** and **7** were generated and reacted with dimethyl fumarate using the procedure (illustrated in Scheme 1) previously described for **1** (3, 4).

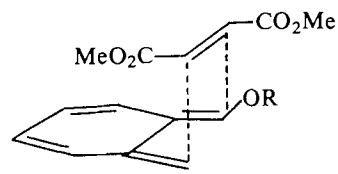
For comparison purposes the *o*-QDM **1** was generated and reacted with dimethyl fumarate. As well as the racemic form, **1** was also generated in the optically pure *S* form. **6** was generated in both the racemic and the *R* forms while only the racemic form of **7** was prepared. In all cases, reaction with dimethyl fumarate led to one major and three minor diastereomers (**9/10**, **11/12**, **13/14**, **15/16**), which were each characterized by nmr. These four products made up more than 95% of the crude reaction mixture and the major product was 60 ± 5% of the total for all three starting *o*-QDMs.

The major isomer could be crystallized from the product mixture from racemic **1**, racemic **7**, and optically pure (*R*)-**6** and totally freed from the minor isomers in each case. In the case of optically pure (*S*)-**1**, the major adduct **10***a* cocrystallized with the minor isomer **12***a* but could be enriched to 85% by column chromatography. The minor isomers could not be separated and were characterized using difference nmr techniques. However, treatment of the crude cycloadduct mixtures with toluenesulfonic acid in refluxing toluene converted all of the stereoisomeric adducts to the single elimination product **17** in high yield in each case (see Table 1), thereby confirming the stereoisomeric nature of the minor products.

Dimethyl fumarate is known to add to *o*-QDMs through the two transition states **A** and **B** with the major products (*r*-1,*c*-2,*t*-3) arising from **A** (8, 9).



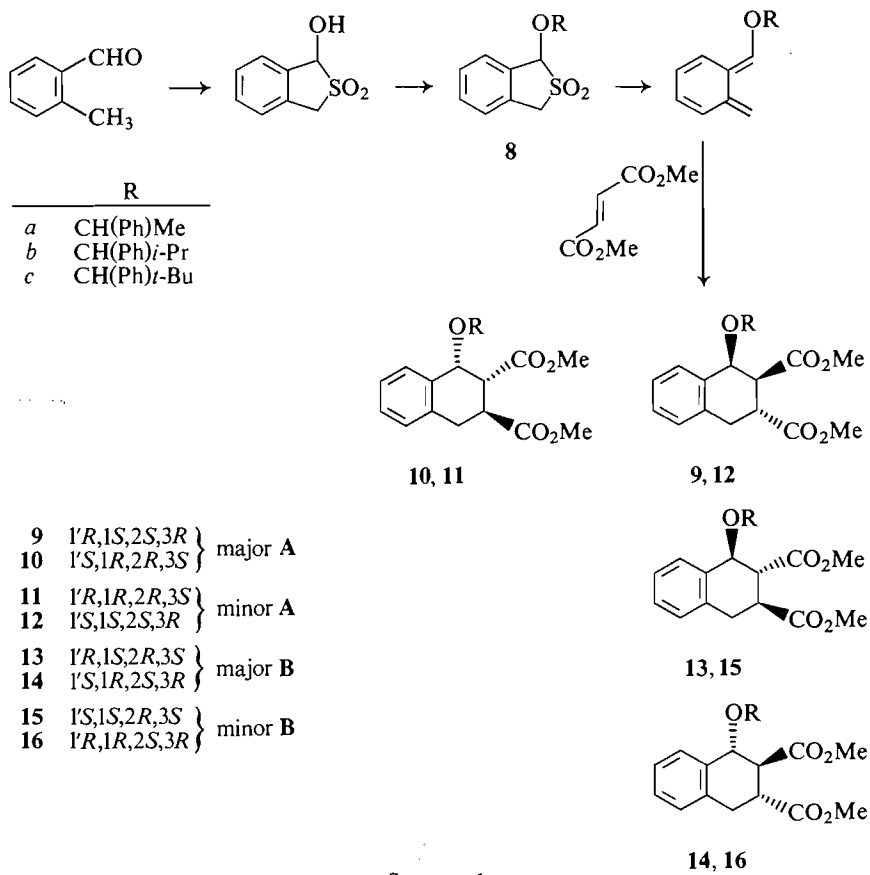
A



B

For *o*-QDMs bearing a chiral auxiliary, two diastereomers can arise from each transition state, one from addition to each face of the *o*-QDM. In this study the major **A** diastereomer was assigned the structure **9/10** by nmr. The minor **A** isomer, **11/12**, was identified by the similarity of its spectrum to that of the major isomer. The two **B** isomers (*r*-1,*t*-2,*c*-3, **13/14** and **15/16**) were easily distinguished from the **A** isomers by their nmr spectra. The product yields and isomer ratios for the **A** isomers are given in Table 1. As can be seen from the data in Table 1, the diastereoselectivity (face selectivity) of the addition did indeed increase as the alkyl group in the chiral auxiliary was changed from methyl to *tert*-butyl.

In two previous studies we have shown that the (*R*)-1-phenylethyl chiral auxiliary partially blocks the *re* face of the *o*-QDM towards cycloaddition reactions and therefore the *S* chiral auxiliary would block the *si* face (4, 5). Thus the



SCHEME 1

Can. J. Chem. Downloaded from www.nrcresearchpress.com by 194.225.253.170 on 09/07/12
For personal use only.

Can. J. Chem. Downloaded from www.nrcresearchpress.com by 194.225.253.170 on 09/07/12
For personal use only.

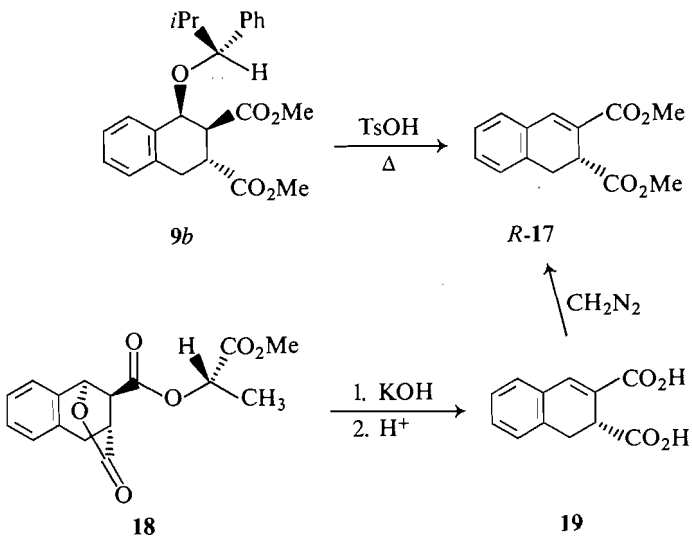
TABLE 1. Yields and diastereomer ratios

Sulfones	Sulfone yields[a]	Cycloadduct yields[b]	Elimination yields	Ratio of **A** type isomers
rac-**8***a*	98	80	97[a]	2.7:1
rac-**8***b*	100(82[d])	78	82[d]	3.0:1
rac-**8***c*	97(84[d])	77	90[a]	3.5:1
(1′*S*)-**8***a*	94(67[d])	84	92[d]	2.8:1[c]
(1′*R*)-**8***b*	92(71[d])	81	71[d]	3.1:1

[a]Crude yield.
[b]Mixture of diastereomers.
[c]Diastereomer ratio for (1′*R*)-**8***a* is 2.7:1 (4).
[d]After chromatography.

reaction of *o*-QDM (*S*)-**1** with dimethyl fumarate gives the (1′*S*,1*R*,2*R*,3*S*)-cycloadduct (**10***a*) as the major product. Treating this adduct (containing 15% **12***a*) with toluenesulfonic acid in refluxing toluene produced the (*S*)-2,3-dicarbomethoxy-3,4-dihydronaphthalene (*S*)-**17** ($[\alpha]_D = -92°$). Subjecting the adduct from the pure (*R*)-**6** to the elimination reaction produced (*R*)-**17** ($[\alpha]_D = +124°$). To confirm the absolute configuration of (*R*)-**17** it was also synthesized from the recently reported lactone **18** whose structure has been unambiguously established by X-ray crystallography (10). **18** was hydrolysed in methanolic KOH and the intermediate acid **19** esterified with CH_2N_2 to yield (*R*)-**17**, which had a specific rotation of +128°. Thus the cycloadduct from *R*-**6** has the configuration (1′*R*,1*S*,2*S*,3*R*) (**9***b*) and the *R* chiral auxiliary must partially block the *re* face in **6**, as was found for **1**.

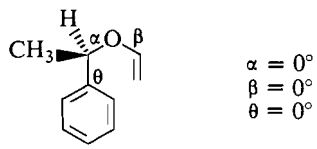
We were unable to obtain the chiral auxiliary for **7** in an optically pure form and therefore the relative configurations of the chiral centers in this cycloadduct were assigned on the basis of the nmr spectrum of the racemic material. In the cases of **1** and **6** there are distinct differences between the nmr spectra of the major and minor **A**-type cycloaddition products, with the H1 and H2 in the major isomer both appearing downfield of the protons in the minor isomer. This pattern was also true in the racemic cycloadduct **7**, leading us to the conclusion that the relative configurations of the chiral centers in **7** were the same as that in **1** and **6**. Therefore the major cycloadduct from the racemic **7** was assumed to be a racemic mixture of **9**/**10***c*. This being the case, an *R* chiral auxiliary in **7** also partially blocks the *re* face of the *o*-QDM.



It is expected that *o*-QDM cycloadditions are relatively exothermic with early transition states (Hammond postulate), and that the conformation of the *o*-QDM will not change substantially on entering the transition state. In such cases, face selectivity might be predicted by determining the preferred conformation of the *o*-QDM. Predictions of face selectivity based on conformational preferences of the diene or dienophile have been very successful for other asymmetric Diels–Alder reactions (1*b*).

Molecular orbital calculations were carried out on **3***a* as a model for **1**, to reduce computational requirements. The appropriateness of using **3***a* as a model is discussed below. *Ab initio* calculations were carried out at the STO-3G level with optimization of bond lengths and bond angles, with the constraint that the ring carbons in the phenyl group were held planar as were the carbons in the vinyl group. The ring carbons of the phenyl were also constrained to a hexagonal geometry. Calculations were performed on an Amdahl 470/V8 system using the program MONSTERGAUSS (11).

The conformation of the molecule can be described by the use of the three dihedral angles θ, α, and β, which are defined in structure **20**. Rotation about any of the three bonds from zero degrees (eclipsed) to a positive torsion angle is a rotation in which the atom in the foreground is rotated counterclockwise relative to the atom in the background.



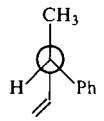
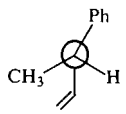
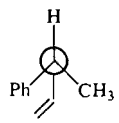
20

To probe the conformational preferences of **3***a*, calculations were carried out starting at several different combinations of angles for α, β, and θ. The first general observation resulting from these calculations is that β always optimizes to a value near 180° or 0°. This is presumably due to the conjugation of the double bond with the lone pair electrons on the ether oxygen. Such a conformational preference in unsaturated ethers has been noted previously (12). The two structures **21** and **22** represent the two extremes in β (180° and 0° respectively).

Since these calculations are a model for the *o*-QDM **1**, conformations with β near 0° are not of interest because this conformation is sterically impossible for **1**. Thus we concentrated further calculations on only those conformations that had β near 180°. Within this domain we found three low energy conformations with respect to rotation about the α axis, corresponding roughly to the three possible staggered conformations about α. The optimized angles of α, β, and θ and the relative energies of the three conformations are given in Table 2. It can be seen that the lowest energy conformer is that which roughly corresponds to structure **21** (illustrated more accurately in the ORTEP drawing, which is oriented to better display the orientation around α, β, and θ). We expect the conformational preferences of *o*-QDM **1** to be similar to that of **3***a* and that the most stable conformer of **1** is approximately that shown by structure **23**.

Face selectivity in cycloaddition reactions of **23** will arise due to the difference in steric bulk of the phenyl and hydrogen substituents. This differs slightly from the conformation previously proposed (see structure **1**) to account for the diastereo-

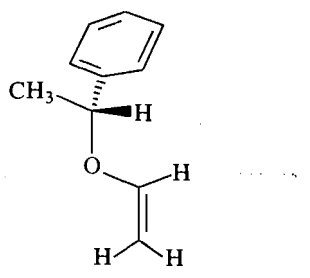
TABLE 2. Conformers of **3***a*

Conformation	Angles (°) α	β	θ	Energy (relative) (kJ/mol)
	70	184	37	0.0
	164	161	35	2.78
	300	187	119	2.30

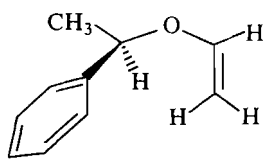
selectivity, where face selectivity depended on the relative bulk of the phenyl and methyl substituents. Proposing that reaction occurs from conformer **23** is more consistent with the experimental data since exchanging the methyl group for an isopropyl (**6**) or *tert*-butyl (**7**) group would improve the diastereoselectivity (as observed) by increasing the preference for conformation **23**, which conformation provides the most room for the alkyl substituent.

Posner and Wettlaufer (7) proposed no mechanism for the asymmetric induction observed in their work since the relative configurations of all chiral centers in **4** and **5**, and the face at which the chiral vinyl ether reacted, were unknown. While it is tempting to predict that the *R* chiral auxiliary blocks the *re* face, as in this work, the fact that conformations of the vinyl ether with $\beta \approx 0°$ may be populated makes such a prediction uncertain.

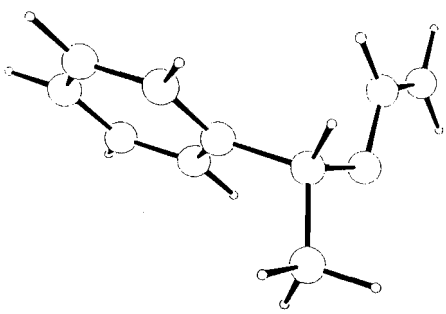
Based on the above observations and calculations it would appear that further improvement in face selectivity in Diels–Alder reactions of *o*-QDMs will require the conformation of the chiral auxiliary to be more rigidly locked. Strategies such as putting a substituent onto the alkyl group of the chiral auxiliary, which can hydrogen bond to the ether oxygen and thereby lock the conformation, are being pursued.

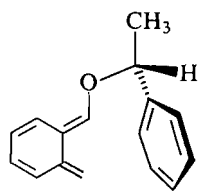


21



22





23

Experimental

The ^{1}H nmr spectra were recorded on a Bruker AM-300 instrument using tetramethylsilane as internal standard. The ir spectra were recorded on a Perkin Elmer 881 spectrometer. Merck Kieselgel 60 was used for all chromatography. Elemental analyses were performed by Guelph Chemical Laboratories Ltd., Guelph, Ontario, Canada. Melting points were measured on a hot stage instrument and are uncorrected. Optical rotations were recorded on a Rudolph Research Corporation Autopol III instrument.

1-Hydroxy-1,3-dihydrobenzo[c]thiophene-2,2-dioxide

This compound was prepared from *o*-methylbenzaldehyde (7.6 g) using the method previously described (8, 13) to yield 3.7 g (32%). Traces of *o*-toluic acid were removed by trituration with a small amount of carbon tetrachloride at room temperature.

1-Alkoxy-1,3-dihydrobenzo[c]thiophene-2,2-dioxide, 8

The alkoxysulfones **8** were prepared by refluxing, for 5–6 h, a methylene chloride solution of hydroxysulfone, the alcohols (1.5:1 molar ratio) *rac*-1-phenylethanol, *rac*-2-methyl-1-phenyl-1-propanol, *rac*-2,2-dimethyl-1-phenyl-1-propanol, (*S*)-(−)-1-phenylethanol, and (*R*)-(+)-2-methyl-1-phenyl-1-propanol, and a trace of toluenesulfonic acid, filtering the mixture through a short silica gel column (5 cm × 1.5 cm) with methylene chloride, and evaporating to give a mixture of diastereomers. Crude yields were typically 90–100%. The residual oil was further purified by chromatography on silica gel using 10% ethyl acetate/hexane as eluant to isolate the major stereoisomer whose properties are given below.

rac-***8***a: ^{1}H nmr ($CDCl_3$) δ: 1.61 (d, J = 6.5, CH_3), 4.20 (d, J = 15.7, H-3A), 4.46 (d, J = 15.7, H-3B), 5.20 (s, H-1), 5.23 (q overlapping with s at 5.20, J = 6.5, H-1′), 7.23–7.47 (m, aromatics).

rac-***8***b: mp 102–105°C (dec.); ^{1}H nmr ($CDCl_3$) δ: 0.75 (d, J = 6.7, CH_3), 1.15 (d, J = 6.7, CH_3), 2.0–2.2 (m, H-2′), 4.17 (d, J = 15.6, H-3A), 4.42 (d, J = 15.6, H-3B), 4.74 (d, J = 8.1, H-1′), 5.19 (s, H-1), 7.2–7.5 (m, aromatics). *Anal.* calcd. for $C_{18}H_{20}SO_3$: C 68.33, H 6.38, S 10.11; found: C 68.09, H 6.42, S 10.17.

rac-***8***c: mp 116–118°C (dec.); ^{1}H nmr ($CDCl_3$) δ: 0.98 (s, *tert*-butyl), 4.15 (d, J = 15.5, H-3A), 4.41 (d, J = 15.5, H-3B), 4.90 (s, H-1′), 5.18 (s, H-1), 7.3–7.5 (m, aromatics). *Anal.* calcd. for $C_{19}H_{22}SO_3$: C 69.06, H 6.72, S 9.68; found: C 68.96, H 6.73, S 9.70.

*(1′S)-**8***a: ^{1}H nmr ($CDCl_3$) identical to that of *rac*-**8***a*.

*(1′R)-**8***b: ^{1}H nmr ($CDCl_3$) identical to that of *rac*-**8***b*.

*Alkoxy-2,3-dicarbomethoxy-1,2,3,4-tetrahydronaphthalene, **9/10, 11/12, 13/14, 15/16***

The cycloadducts were prepared by refluxing a toluene solution (20 mL) of alkoxy sulfone **8** (200–400 mg), four equivalents of dimethyl fumarate, and 100–200 mg of zinc oxide powder for 3–5 h. The solution was filtered through a silica gel column (5 cm × 1.5 cm) with methylene chloride, evaporated to dryness, then heated to 100°C at high vacuum to remove the excess fumarate. Crude yields were typically 75–85%. The major diastereomer from the reaction of *rac*-**1**, *rac*-**7**, and (*R*)-**6** could be obtained by crystallization from hexane or pentane. The major **A** isomer from (*S*)-**1** was obtained as an 85:15 mixture with the minor **A** isomer by chromatography on silica gel using 5% ethyl acetate in benzene as eluant. The remaining minor isomers were also partially separated by a similar chromatography and their nmr spectra determined using difference nmr techniques.

9a/***10***a: mp 78–79°C; ir (CH_2Cl_2): 1737 cm^{-1} carbonyl; ^{1}H nmr ($CDCl_3$) δ: 1.40 (d, J = 6.4, CH_3), 2.81 (dd, J = 10.9, 16.9, H-4a),

Can. J. Chem. Downloaded from www.nrcresearchpress.com by 194.225.253.170 on 09/07/12
For personal use only.

3.14 (dd, J = 3.3, 11.4, H-2), 3.27 (dd, J = 6.6, 16.9, H-4e), 3.64 (ddd, J = 6.6, 11.3, H-3), 3.73 and 3.83 (s, OCH_3), 4.50 (q, J = 6.4, H-1′), 4.92 (d, J = 3.3, H-1), 6.68 (d, J = 7.1, H-5), 7.0–7.4 (m, aromatics). Identical to that previously reported (4).

9b/***10***b: mp 89–91°C; ir (CH_2Cl_2): 1750 cm^{-1} carbonyl; ^1H nmr ($CDCl_3$) δ: 0.64 (d, J = 6.8, CH_3), 0.95 (d, J = 6.8, CH_3), 1.90 (m, H-2′), 2.78 (dd, J = 10.1, 16.8, H-4a), 3.07 (dd, J = 2.9, 11.2, H-2), 3.26 (dd, J = 7.4, 16.8, H-4e), 3.61–3.71 (m, H-3), 3.75 and 3.82 (s, OCH_3), 3.99 (d, J = 7.3, H-1′), 4.87 (d, J = 2.9, H-1), 6.53 (d, J = 7.6, H-5), 6.8–7.2 (m, aromatics). *Anal.* calcd. for $C_{24}H_{28}O_5$: C 72.69, H 7.12; found: C 72.92, H 6.98.

11b/***12***b: ^1H nmr ($CDCl_3$) δ: 0.51 (d, J = 6.8, CH_3), 0.67 (d, J = 6.8, CH_3), 1.72 (m, H-2′), 2.89 (dd, J = 9.3, 17.0, H-4a), 3.02 (dd, J = 2.7, 11.2, H-2), 3.41 (dd, J = 8.0, 17.0, H-4e), 3.67–3.75 (m, H-3), 3.67 and 3.75 (s, OCH_3), 3.79 (d, J = 7.2, H-1′), 4.58 (d, J = 2.7, H-1), 6.8–7.4 (m, aromatics).

13b/***14***b: ^1H nmr ($CDCl_3$) δ: 0.69 (d, J = 6.7, CH_3), 1.00 (d, J = 6.7, CH_3), 2.00 (m, H-2′), 2.96 (m, H-4e), 3.13 (m, H-3, H-4a), 3.58 (dd, J = 4.5, 7.9, H-2), 3.68 and 3.74 (s, OCH_3), 4.16 (d, J = 7.8, H-1′), 4.67 (d, J = 4.5, H-1), 6.9–7.4 (m, aromatics).

15b/***16***b: ^1H nmr ($CDCl_3$) δ: 0.55 (d, J = 6.8, CH_3), 0.72 (d, J = 6.8, CH_3), 1.75 (m, H-2′), 3.00 (dd, J = 6.1, 14.5, H-4e), 3.22 (m, H-3), 3.35 (dd, J = 9.5, 14.5, H-4a), 3.47 and 3.77 (s, OCH_3), 3.72–3.80 (m, H-2, H-1′), 4.59 (d, J = 2.8, H-1), 6.9–7.4 (m, aromatics).

9c/***10***c: mp 136–137°C; ir (CH_2Cl_2): 1735 cm^{-1} carbonyl; ^1H nmr ($CDCl_3$) δ: 0.82 (s, *tert*-butyl), 2.78 (dd, J = 9.1, H-4a), 3.08 (dd, J = 2.8, 10.9, H-2), 3.27 (dd, J = 8.2, 16.9, H-4e), 3.74 and 3.79 (s, OCH_3), 4.07 (s, H-1′), 4.86 (d, J = 2.8, H-1), 6.7–7.0 (m, aromatics), H-3 hidden under other signals. *Anal.* calcd. for $C_{25}H_{30}O_5$: C 73.13, H 7.37; found: C 73.46, H 7.45.

11c/***12***c: ^1H nmr ($CDCl_3$) δ: 0.65 (s, *tert*-butyl), 2.88 (dd, J = 9.7, 17.1, H-4a), 3.05 (dd, J = 2.7, 11.4, H-2), 3.40 (dd, J = 8.0, 17.1, H-4e), 3.76 and 3.77 (s, OCH_3), 4.56 (d, J = 2.7, H-1), 6.7–7.05 (m, aromatics), H-3, and H-1′ hidden under other signals.

13c/***14***c: ^1H nmr ($CDCl_3$) δ: 0.87 (s, *tert*-butyl), 2.96 and 3.16 (m, H-3, H-4a, H-4e), 3.69 (dd, J = 3.2, 7.9, H-2), 3.62 and 3.75 (s, OCH_3), 4.28 (s, H-1′), 4.59 (d, J = 3.0, H-1), 6.9–7.4 (m, aromatics).

15c/***16***c: ^1H nmr ($CDCl_3$) δ: 0.65 (s, *tert*-butyl), 3.02 (dd, J = 9.6, 14.4, H-4e), 3.37 (dd, J = 6.1, 14.4, H-4a), 3.47 and 3.80 (s, OCH_3), 3.84 (dd, J = 2.4, 5.7, H-2), 4.52 (d, J = 2.4, H-1), 6.9–7.4 (m, aromatics), H-3 and H-1′ hidden under other signals.

10a: ^1H nmr ($CDCl_3$) identical to that of ***9a***/***10a***; $[\alpha]_D^{20}$ +46.9° (*c* 0.54, $CHCl_3$, 85% pure by nmr).

9b: mp 95–96.5°C. ^1H nmr ($CDCl_3$) identical to that of ***9b***/***10b***; $[\alpha]_D^{20}$ −59.4° (*c* 0.74, $CHCl_3$).

2,3-Dicarbomethoxy-3,4-dihydronaphthalene, ***17*** (Compound **20** in ref. 8)

Elimination of the alcohol from the cycloadducts was accomplished by refluxing a toluene solution (10 mL) of adduct (10–20 mg) and toluenesulfonic acid (3 mg) for 7 h, filtering through a short silica gel column with methylene chloride, and evaporating. The residue was chromatographed on silica gel (25 cm × 0.6 cm) using 10% ethyl acetate/hexane as eluant. Yields are summarized in Table 1.

rac-***17***: ^1H nmr ($CDCl_3$) δ: 3.13 (dd, J = 8.0, 16.2, H-4a), 3.35 (dd, J = 3.5, 16.2, H-4e), 3.60 and 3.84 (s, OCH_3), 3.88 (dd, J = 3.5, 8.0, H-3), 7.17–7.23 (m, aromatics), 7.65 (s, H-1).

*(R)-****17***: ^1H nmr ($CDCl_3$) identical to that of *rac*-**17**; $[\alpha]_D^{20}$ +124° (*c* 0.74, $CHCl_3$).

*(S)-****17***: Prepared from an 85:15 mixture of ***10a*** and ***12a***; ^1H nmr ($CDCl_3$) identical to that of *rac*-**17**; $[\alpha]_D^{20}$ −92° (*c* 0.33, $CHCl_3$).

*Preparation of (R)-****17*** *from lactone* ***18***

The lactone **18** (10) (67.5 mg, 0.22 mmol) was dissolved in methanolic KOH (0.2 M, 10 mL) and the solution refluxed for 2 h. The solution was concentrated to one half volume by evaporation, diluted with 5% aqueous $NaHCO_3$, and extracted with ethyl acetate. The aqueous portion was acidified (HCl), extracted with ethyl acetate, dried ($MgSO_4$), and evaporated to give an oil. The oil was dissolved in ethyl ether (5 mL) and an excess of CH_2N_2 in ether added. After 15 min at room temperature the solvent was removed by evaporation to leave an oil (47.4 mg, 87%). Chromatography on silica gel using 15% ethyl acetate/hexane as eluant gave a clear oil (37 mg, 65%) identical by nmr to the material produced above; $[\alpha]_D^{20}$ +128° (*c* 0.58, $CHCl_3$).

Acknowledgments

We would like to acknowledge the financial assistance of the Natural Sciences and Engineering Research Council of Canada and the technical assistance of R. Sebastian who aided with the *ab initio* calculations.

1. (*a*) D. A. Evans, K. T. Chapman, and J. Bisha. J. Am. Chem. Soc. **110**, 1238 (1988), and references cited; (*b*) G. Helmchen, R. Karge, and J. Weetman. *In* Modern synthetic methods. Vol. 4. *Edited by* R. Scheffold. Springer Verlag, New York. 1986. p. 261 and references cited.
2. J. L. Charlton and M. M. Alauddin. Tetrahedron, **43**, 2873 (1987).
3. J. L. Charlton. Tetrahedron Lett. **26**, 3413 (1985).
4. J. L. Charlton. Can. J. Chem. **64**, 720 (1986).
5. J. L. Charlton and M. M. Alauddin. J. Org. Chem. **51**, 3490 (1986).
6. Y. Ito, Y. Amino, M. Nakatsuka, and T. Saegusa. J. Am. Chem. Soc. **105**, 1586 (1983).
7. G. H. Posner and D. G. Wettlaufer. Tetrahedron Lett. **27**, 667 (1986).
8. T. Durst, E. C. Kozma, and J. L. Charlton. J. Org. Chem. **50**, 4829 (1985).
9. J. L. Charlton, M. M. Alauddin, and G. H. Penner. Can. J. Chem. **64**, 793 (1986).
10. J. L. Charlton, G. L. Plourde, K. Koh, and A. S. Secco. Can. J. Chem. **67**, 574 (1989).
11. M. R. Peterson and R. A. Poirier. MONSTERGAUSS, Department of Chemistry, University of Toronto, Canada, 1981.
12. T. Schaefer, R. Laatikainen, T. A. Wildman, J. Peeling, G. Penner, J. Baleja, and K. Marat. Can. J. Chem. **62**, 1592 (1984).
13. J. L. Charlton and T. Durst. Tetrahedron Lett. **25**, 2663 (1984).

Can. J. Chem. Downloaded from www.nrcresearchpress.com by 194.225.253.170 on 09/07/12
For personal use only.

Conformational properties of benzyl alcohol in dilute solution

TED SCHAEFER, RUDY SEBASTIAN, JAMES PEELING,[1] GLENN H. PENNER,[2] AND KEVIN KOH[3]
Department of Chemistry, University of Manitoba, Winnipeg, Man., Canada R3T 2N2

Received September 27, 1988

TED SCHAEFER, RUDY SEBASTIAN, JAMES PEELING, GLENN H. PENNER, and KEVIN KOH. Can. J. Chem. **67**, 1015 (1989).

STO-3G MO computations, with substantial geometry optimization, are reported for benzyl alcohol. They are performed at 15° intervals for the angle by which the C—O bond twists out of the plane of the phenyl group, as well as for 30° intervals for the HCOH dihedral angle. The ensuing conformational energies are used to estimate expectation values of these two angles as well as of functions of these angles. The latter are compared with those obtained from long-range proton–proton coupling constants for dilute solutions in CS_2 and acetone-d_6. At infinite dilution in CS_2 these coupling constants give a distribution for motion about the C(1)—C_{sp^3} bond that happens to agree with the theoretical results for the free molecule. The latter are used to derive the dihedral angle dependence of ^3J(HCOH), the coupling constant between the hydroxyl and methylene protons. This dependence is compared with the observed coupling constants in benzyl alcohol in the gas phase at 422 K and with those measured for the 2,6-difluoro and 2,6-dichloro derivatives of benzyl alcohol. Infinite dilution shifts are reported for the latter two compounds and for α,α-dimethylbenzyl alcohol. The first self-association complex of any significance for benzyl alcohol in CS_2 at 300 K is most likely a trimer. Between zero and 2.5 mol% in CS_2, all five proton chemical shifts of this molecule are linearly proportional to one another, four of them becoming less shielded at decreasing concentrations. Some nuclear magnetic resonance data are also reported for 3,5-dichlorobenzyl alcohol.

Key words: conformations of benzyl alcohol, ^{1}H NMR of benzyl alcohol, STO-3G MO calculations of benzyl alcohol.

TED SCHAEFER, RUDY SEBASTIAN, JAMES PEELING, GLENN H. PENNER et KEVIN KOH. Can. J. Chem. **67**, 1015 (1989).

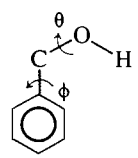
On a effectué des calculs d'OM STO-3G, avec optimisation importante de la géométrie de l'alcool benzylique. Ces calculs ont été réalisés à des intervalles des 15° pour l'angle de torsion C—O hors du plan du groupement phényle ainsi que pour des intervalles de 30° pour l'angle dièdre HCOH. On a utilisé les énergies conformationnelles ainsi obtenues pour évaluer l'ordre de grandeur de ces deux angles ainsi que les grandeurs qui varient en fonction de ces angles. On a comparé les valeurs ainsi déterminées avec celles qui ont été obtenues expérimentalement à partir de constantes de couplage proton–proton à longue distance, pour des solutions diluées dans le CS_2 ou l'acétone-d_6. À dilution infinie dans le CS_2, ces constantes de couplage donnent une distribution du mouvement autour de la liaison C(1)—C_{sp^3} qui est en accord avec les résultats théoriques pour la molécule libre. On utilise ces derniers pour obtenir la relation qui existe entre l'angle dièdre et ^3J(HCOH), la constante de couplage entre les protons hydroxyle et méthylènes. On compare cette dépendance avec les constantes de couplage observées pour l'alcool benzylique en phase gazeuse, à 422 K, ainsi que pour celles mesurées pour les dérivés difluoro-2,6 et dichloro-2,6 de l'alcool benzylique. On a déterminé les déplacements chimiques à dilution infinie pour ces deux composés ainsi que pour l'alcool α,α-diméthylbenzylique. Le premier complexe d'auto-association significatif de l'alcool benzylique, dans le CS_2, à 300 K, est probablement un trimère. À des concentrations allant de 0 à 2,5 mol%, dans le CS_2, les cinq déplacements chimiques des protons de cette molécule sont proportionnellement linéaires les uns aux autres; quatre d'entre eux deviennent moins blindés avec des diminutions de concentrations. On rapporte aussi quelques données de résonance magnétique nucléaire pour l'alcool dichloro-3,5 benzylique.

Mots clés: conformations de l'alcool benzylique, RMN du ^{1}H de l'alcool benzylique, calculs d'OM STO-3G de l'alcool benzylique.

[Traduit par la revue]

Introduction

The conformational behaviour of benzyl alcohol has been much discussed in recent years, particularly from the viewpoint of intramolecular hydrogen bonding of the hydroxyl group to the aromatic π system, (θ behaviour in **1**) but also in terms of the motion about the exocyclic C—C bond (ϕ motion).



1

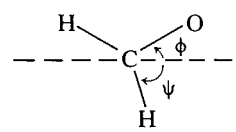
$\theta = 0°$ } as shown
$\phi = 0°$ } in **1**

endo: $\theta = 60°$ or 300°

exo: $\theta = 180°$

Electron diffraction patterns for gaseous benzyl alcohol (1) are most consistent with a conformation in which ϕ is 54° (see **2**). Presumably this angle represents an average over the potential surface. Because the hydrogen atom adds only small contributions to the scattering intensities, its position is uncertain, although it appears (1) that the *endo* forms (θ in **1** assumed to be 60° or 300°) are more stable than the *exo* form (θ is 180° in **1**).

On the basis of ^3J(HCOH) ≡ ^3J, the vicinal proton–proton coupling constants in the side chain of benzyl alcohol, measured at a concentration of 0.02 M in CCl_4 solution at 296 K, it is concluded that the *endo* conformer is about 10 times as abundant as the *exo* conformer (2). The relative concentrations deduced in this way depend on the values assumed for ^3J at $\theta = 60°$ and 180°. Again, the ^{1}H nmr chemical shift of the



2

---

[1]Present address: Department of Chemistry, University of Winnipeg, Winnipeg, Manitoba.

[2]Present address: Department of Chemistry and Biochemistry, University of Guelph, Guelph, Ontario.

[3]Undergraduate research participant, 1986–1987.

Can. J. Chem. Downloaded from www.nrcresearchpress.com by 41.223.56.140 on 09/07/12
For personal use only.

hydroxyl proton at infinite dilution in CCl_4 (2) is consistent with an *endo* conformer having $\phi = 60°$ but also with free rotation about the exocyclic C—C bond (ϕ motion). The geminal coupling constant, $^2J(H,H)$, deduced from $^2J(^1H,^2H)$ in α-deuterobenzyl alcohol (2), gives the same consistency. The probability of a rather low barrier to rotation about the C—C bond is indicated by early STO-3G MO computations (3), albeit with a standard (unrelaxed) geometry.

The stability of the *endo* conformers has been attributed, not to O—H$\cdots\pi$ hydrogen bonding (4) but, more recently (5–8), to repulsive forces between the lone-pair electrons on the oxygen atom and the π electrons. This interpretation is in line with a recent theoretical investigation of allyl alcohol (9), in which the most stable conformer about the allylic C—O bond is attributed to a minimization of the repulsion between the lone pairs on the oxygen atom and the π bond. The latest infrared and nmr data (10) are also interpreted in this way.

The many infrared studies of benzyl alcohol and related compounds have been reviewed (4). The latest of these (4) concludes that, in CCl_4 and CS_2 solutions, at least two conformers are present, defined by $\phi = 0°$ and 60°. The conformer with $\phi = 90°$ cannot be excluded, however (4). It is stated that a distinction between attractive O—H$\cdots\pi$ and repulsive lone-pair $\cdots\pi$ forces cannot be made on the basis of stretching frequencies.

Now, if the barrier to rotation about the C—C bond is rather small compared to thermal energies, as is also suggested by the long-range proton–proton coupling constants in 3,5-dichlorobenzyl alcohol (11), then a discussion in terms of only a few conformations appears inappropriate. A more detailed potential surface is required for comparison with experimental data. STO-3G MO computations, with extensive geometry optimization, are reported here for many combinations of θ and ϕ. Computations with larger basis sets are too time consuming at present. It may be noted that the minimal basis set appears to give reasonable conformational predictions for some benzyl derivatives, such as the fluoride and chloride (12, 13).

The computations yield expectation values of θ, ϕ, and of functions of these angles. These can be compared with those deduced from electron diffraction patterns and from long-range coupling constants reported here for benzyl alcohol in CS_2 and acetone-d_6 solutions. In addition, measurements of ^3J are reported for some diortho-substituted benzyl alcohols. These measurements represent an attempt at testing values of ^3J for the *exo* and *endo* conformers.

Experimental

Benzyl alcohol and its derivatives came from Aldrich. Samples for nmr analysis of benzyl alcohol were prepared as 0.5, 1.0, and 2.5 mol% solutions in CS_2 and as a 2.5 mol% solution in acetone-d_6 (see the tables for details of the solvent composition) and were transferred to 5 mm o.d. sample tubes. The tubes were degassed by several freeze–pump–thaw cycles and were then flame-sealed. The nmr sample tubes contained a few pellets of Linde 3A molecular sieve (Alfa products), meant to remove residual water. Solutions of varying and low concentrations were also prepared in CS_2/C_6D_{12}/TMS of benzyl alcohol and its α,α-dimethyl, 2,6-difluoro, and 2,6-dichloro derivatives.

The ^1H nmr spectra were accumulated on an AM 300 spectrometer in the manner previously described in detail (12). The ^1H nmr spectra of α,α-dimethylbenzyl alcohol and of 3,5-dichlorobenzyl alcohol (in a number of solvents) were recorded on a WH 90 FFT nmr spectrometer. STO-3G MO computations (14) were performed with the program GAUSSIAN 82 (15) on an Amdahl 5870 system.

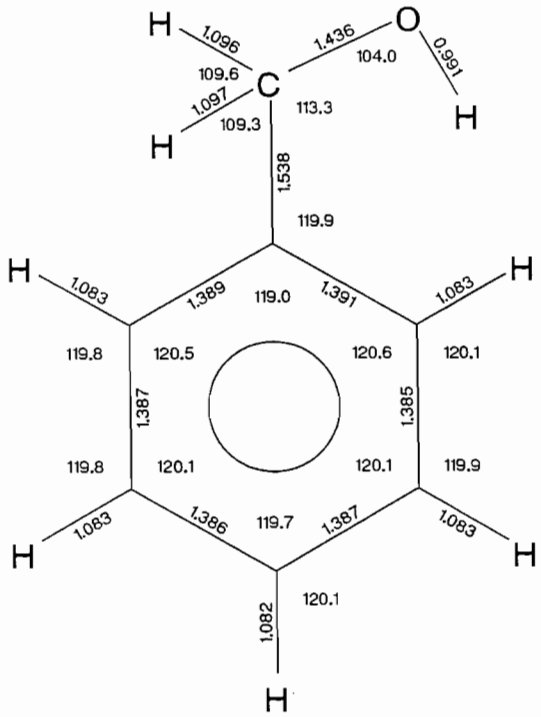


FIG. 1. The geometry-optimized STO-3G MO structure of lowest energy, −340.302247 au, is shown and can be used as a starting point for computations with larger basis sets. The angle ϕ is 42.9° and θ is 60.2° (see **1** in the text), the molecule being in the *endo* conformation. The C(1)—C(α) bond bends by 0.4°, C(α) lying below the plane of the phenyl group, which was actually constrained to have its nuclei in a plane. The deviations of the internal angles of the phenyl moiety from 120° are in qualitative agreement, but somewhat smaller in magnitude than those caused by a methyl group (46–48).

Results and discussion

The stable STO-3G MO structure

Figure 1 displays the computed structure with the minimum energy of −340.302247 au. It has the *endo* conformation. The angle ϕ is 42.9°, θ is 60.2° (see **1**), and the exocyclic C—C bond makes an angle of 0.4° with the extension of the C(1)–C(4) line. Optimization of the bond angles within the benzene ring has reduced the total energy by 0.4 kJ/mol but has not changed the geometry of the side chain significantly, e.g., ϕ changes from 42.8 to 42.9°. Because of the computing time involved (58.4 h for the cpu time in the computations given in Table 1), the ensuing calculations constrained the carbon skeleton of the benzene ring to a regular hexagon.

As expected (16), the exocyclic C—C and the C—O bond lengths are computed about 0.01–0.02 Å longer than anticipated on the basis of those known for related molecules. The COH angle of 104.0° in Fig. 1 is about 4° smaller than measured in methanol (17). However, it does not follow that the relative energies of the various conformers in Table 1 will therefore be computed incorrectly (18, 19). Naturally, geometry optimization procedures are requisite.

The STO-3G MO populations at 300 K

Table 1 contains the computed energies of the geometry-optimized conformations of benzyl alcohol for $0° \leq \theta \leq 180°$ and $0° \leq \phi \leq 180°$. The intervals are 15° in ϕ and 30° in θ (see **1**). The energies are given relative to the conformation defined by $\phi = 45°$ and $\theta = 60°$. This conformation has an energy

Can. J. Chem. Downloaded from www.nrcresearchpress.com by 41.223.56.140 on 09/07/12
For personal use only.

TABLE 1. Optimized STO-3G MO energies[a] for various conformations of benzyl alcohol

	θ/deg						
φ/deg	0	30	60	90	120	150[b]	180[b]
0	21.02[c]	13.64	3.61	5.19	10.05	7.14	3.46
15	19.40	9.94	1.17	4.37	10.15	7.41	3.43
30	15.41	6.45	0.03	4.35	10.51	7.68	3.47
45	11.46	4.84	0.00	4.82	11.07	8.09	3.79
60	9.50	4.60	0.39	5.54	11.65	8.55	4.30
75	8.97	4.70	0.76	5.96	12.03	8.83	4.71
90	8.89	4.91	1.26	6.50	12.28	8.89	4.84
105	8.97	5.42	2.13	7.15	12.43	8.73	4.71
120	9.50	7.15	4.05	8.04	12.41	8.27	4.30
135	11.46	10.57	6.36	8.49	11.91	7.62	3.79
150	15.41	14.11	7.35	7.94	11.12	7.11	3.47
165	19.40	15.37	6.22	6.56	10.44	7.01	3.43
180	21.02	13.64	3.61	5.19	10.05	7.14	3.46

[a]In kJ/mol relative to $\phi = 45°$, $\theta = 60°$.
[b]The *exo* conformers are taken as those with $\theta > 120°$, although, of course, those with $\theta = 180°$ are the stable ones.
[c]See structure **1** in the text for definitions of φ and θ.

insignificantly different from that with $\phi = 42.8°$ (0.04 kJ/mol). The energies of the conformers described by $180° < \phi < 360°$ can, of course, be obtained from those in Table 1. The presentation in Table 1 is, in our opinion, preferable to a contour diagram because it is the quantitative base for the calculation of populational distributions that a reader may want to perform. The eye also easily follows various energetic pathways in such a table.

For example, the *exo* conformer is that one with $\theta = 180°$; the barrier to rotation about the C—C bond (φ motion) is 1.4 kJ/mol, very similar to that computed for benzyl fluoride (12). It may be that, for values of θ near 180°, an attractive force exists between the C^+–O^- and the *ortho* C^-–H^+ dipole. The interatomic distances involved for conformations not far from $\phi = 0°$ are just those for which attractive intramolecular C—H···O interactions have been detected in the solid state (20, 21). If so, then the postulated lone-pair···π repulsive forces at a φ near 90° are not strikingly large, less than those necessary to cause a barrier of 1.4 kJ/mol. Note that the most stable *endo* conformer, at $\phi \sim 45°$, has the O—H bond pointing in such a manner that the 1*s* orbital lies rather near the $2p - \pi$ orbital on the *ipso* carbon atom.

The data in Table 1 can be converted into populational distributions over a grid of some 90 points. The populations are found from the data in Table 1 via the Boltzmann expression ($T = 300$ K) and simple statistical weights (entropy corrections) for equivalent conformations are applied. This procedure is not rigorous because the populations are determined by free energies whereas the energies in Table 1 are internal energies, which can be equated to enthalpies if the volume differences between conformers are small. A proper calculation of a classical partition function would account for entropy terms arising from the shape of the potential energy surface defined by θ and φ. Such calculations are beyond our resources and, in common with many other workers, we write $\langle x \rangle = \Sigma_i p_i x_i$, where p_i is the fractional population of conformer *i* as obtained in the simple way above; note that the conformational grid is reasonably fine. Furthermore, these averages are also compared below with experimental quantities obtained for the solution state, adding a further uncertainty to that contributed by the approximate averages, themselves based on an approximate theoretical model. The reasonable agreement between the model and the experimental data may therefore be fortuitous.

At 300 K, $\langle\phi\rangle$, the average value of φ, is computed as 48.2°. The electron diffraction patterns correspond to a nozzle temperature of about 383 K (1) and are best fit by a φ of 53.7°. The value of $\langle\phi\rangle$ at 383 K actually decreases by a degree for the energies in Table 1. Of course, a distribution of φ values with very similar energies is expected on the basis of Table 1.

From the viewpoint of the nmr data to follow, other averages from Table 1 are also of interest. If the *exo* forms are taken as those with $\theta > 120°$, then their fractional populations add to 0.27 at 300 K, leaving 0.73 as the populations of the *endo* conformers. Furthermore, $\langle\sin^2\phi\rangle$ is found to be 0.538 and $\langle\sin^2\psi\rangle$ is 0.481 (see **2**). The latter number will be compared with that found from long-range proton–proton couplings below.

^{1}H nuclear magnetic resonance spectra of benzyl alcohol

Table 2 presents the ^{1}H nmr spectral parameters of benzyl alcohol in CS_2 and acetone-d_6 solutions at 300 K. Although the spectral extent of the ring protons is small, giving rise to some significant parameter correlations, the crucial parameter, $^6J(H,CH_2)$, is available with some precision. $^6J(H,CH_2) \equiv {}^6J$ is proportional to $\langle\sin^2\psi\rangle$. The proportionality constant is $^6J_{90}$, the value of ^6J when ψ is 90°. $^6J_{90}$ is known reliably from very detailed investigations of the conformational behaviour of salicyl alcohol and its monoethylated derivatives (22). Its value is −1.02 Hz. Hence $\langle\sin^2\psi\rangle$ for benzyl alcohol in CS_2 solution is $0.503/1.02 = 0.493$. This number is indeed in satisfactory agreement with the 0.481 obtained from the computations for the free molecule.

The question of solvent and self-association effects on the conformational distribution is naturally of interest. At a concentration of 2.5 mol%, appreciable intermolecular hydrogen bonding is expected. How the conformational distribution is perturbed by the presence of hydrogen bonded trimers (see below) is problematical. Intuitively, one might expect higher proportions of the *exo* conformers in such a situation. Indeed, for the acetone-d_6 solution, in which considerable populations of benzyl alcohol – acetone complexes should occur, the magnitude of ^6J rises to −0.552 Hz, yielding a $\langle\sin^2\psi\rangle$ of 0.542. A higher value of $\langle\sin^2\psi\rangle$ is expected as the population of *exo* conformers increases because fewer unfavorable O—H, *ortho* C—H interactions occur. Hence φ values near 0° and 180°, and therefore ψ values near 60° or 120°, become more probable.

Dilution to 0.5 mol% in the CS_2 solvent mixture causes a hydroxyl proton chemical shift of 1.39 ppm. Because this chemical shift is 1.07 ppm at infinite dilution (see below) and because the association shift must be *at least* 3.38 ppm, the value at a concentration of 2.5 mol%, it follows that not less than about 90% of the benzyl alcohol is in monomeric form at a concentration of 0.5 mol% and 300 K. It is therefore interesting that the long-range coupling constants between the methylene and ring protons, particularly $^6J(H,CH_2)$, are invariant to concentration between 0.5 and 2.5 mol%. The most simple explanation of this fact has it that association into trimers and probably into higher polymers as well (23), which must be substantial at 2.5 mol%, does not alter the distribution of φ values. In other words, the internal potential controlling the motion about the

Can. J. Chem. Downloaded from www.nrcresearchpress.com by 41.223.56.140 on 09/07/12
For personal use only.

Can. J. Chem. Downloaded from www.nrcresearchpress.com by 41.223.56.140 on 09/07/12
For personal use only.

TABLE 2. ^{1}H nuclear magnetic resonance spectral parameters for benzyl alcohol at 300 K in CS_2 and acetone-d_6 solutions

Parameter	CS_2			Acetone-d_6
ν(OH)	418.4[a,g]	657.5[b]	1014.4[c,d]	1256.1[e]
$\nu(CH_2)$	1360.0	1340.7	1312.7	1388.1
ν_2	2163.593(3)	2151.403(1)	2136.048(1)[f]	2206.793(1)
ν_3	2164.772(3)	2158.052(1)	2148.522(1)	2193.660(1)
ν_4	2143.761(1)	2139.394(1)	2133.303(1)	2166.998(1)
$^3J_{23}$	7.683(2)	7.681(1)	7.687(1)	7.702(1)
$^3J_{34}$	7.459(7)	7.432(1)	7.440(1)	7.439(1)
$^4J(H,CH_2)$	−0.685(3)	0.688(1)	−0.686(1)	−0.734(1)
$^4J_{26}$	1.877(4)	1.878(2)	1.881(1)	1.857(1)
$^4J_{24}$	1.261(7)	1.283(1)	1.278(1)	1.286(1)
$^4J_{35}$	1.395(3)	1.393(2)	1.398(1)	1.400(1)
$^5J(H,CH_2)$	0.308(4)	0.317(1)	0.312(1)	0.325(1)
$^5J_{25}$	0.593(1)	0.601(1)	0.601(1)	0.613(1)
$^6J(H,CH_2)$	−0.508(2)	−0.504(1)	−0.503(1)	−0.552(1)
Calculated transitions	298	317	300	284
Assigned transitions	191	265	240	227
Observed peaks	110	160	157	142
Largest difference	0.025	0.017	0.017	0.017
Root-mean-square deviation	0.010	0.007	0.006	0.005

[a]0.5 mol% in CS_2, containing also 10 mol% cyclohexane-d_{12} and 0.5 mol% tetramethylsilane.
[b]1.0 mol% in the CS_2/C_6D_{12}/TMS mixture.
[c]2.5 mol% in the CS_2/C_6D_{12}/TMS mixture.
[d]Frequencies at 300.135_2 MHz to high frequency of internal TMS.
[e]2.5 mol% in acetone-d_6, containing 0.5 mol% TMS.
[f]Numbers in parentheses are standard deviations in the last significant figure.
[g]^3J(HCOH) is 6.07 ± 0.01 Hz at concentrations of 0.12_5, 0.06_3, 0.03, and 0.01_6 mol%.

C_{sp^2}—C_{sp^3} bond has not altered significantly. The lifetime of intermolecular hydrogen bonds in solution at ambient temperatures is certainly less than 10^{-7} s (24, 25). In fact, the depolarized light scattering spectrum of liquid benzyl alcohol and dielectric relaxation data for the liquid (26) are consistent with a lifetime of about 50 ps near room temperature. The present results suggest that the present extent of self-association, viewed as a solvent effect, is no more effective in perturbing the internal rotational potential in benzyl alcohol than are the molecules of CS_2 and C_6D_{12} surrounding the monomer in the dilute solution.

In a statistical mechanical treatment of gaseous and liquid alkyl alcohols (27) it is found that the molecules in the liquid make close to two hydrogen bonds per molecule. The conformational energy wells for rotation about the C—O bonds become narrower, that is, *gauche* and *trans* conformers become better defined at 298 K in the liquid. Furthermore, the change in conformational populations is rather small as the gas condenses. For example, the *trans* population of ethanol changes by only 2% and similar alterations are found for 1-propanol and 2-propanol (27). These results are taken to indicate that a comparison between computations on free benzyl alcohol molecules and measurements in CS_2 solutions have some validity.

Finally, in a study of the orientational ordering of benzyl alcohol in some phospholipid bilayers (28), it was concluded that the aromatic ring is preferentially coplanar with the hydroxyl group. In that event the computations in Table 1 imply a stabilization of this conformer ($\phi = 0°$) by at least 4 kJ/mol, presumably by an interaction (29) with the head group and glycerol moiety in the backbone region of the bilayer membrane.

exo *and* endo *populations from* ^{3}J*(HCOH)* $\equiv$ ^{3}J

The deduction of the *exo/endo* equilibrium constant in benzyl alcohols has been based on the assumption that each conformer is characterized by a definite ^3J, namely, a ^3J_g or *gauche* coupling constant for the *exo* form and a $(^3J_g + {}^3J_t)/2$, or the mean of *gauche* and *trans* coupling constants, for the *endo* form (2, 30–32). A range of ^3J_g and ^3J_t values has been employed in discussions of alcohols, covering 2.0–3.0 Hz for ^3J_g and 11.0–12.5 Hz for ^3J_t. Clearly, the equilibrium constant and the derived conformational energy difference depend significantly on the assumed values of ^3J_g and ^3J_t. At infinite dilution in CS_2 solution at 300 K, ^3J in 2,6-dichlorobenzyl alcohol is 7.27 ± 0.01 Hz (see below), while in 2,6-difluorobenzyl alcohol it is 6.89 ± 0.02 Hz. In a CCl_4/C_6D_{12} solution containing 0.1 w/v% of 2,6-dimethoxybenzyl alcohol, ^3J is 7.02 ± 0.01 Hz (22). At infinite dilution in CS_2 solution, ^3J in 2-chloro-6-fluorobenzyl alcohol is 7.09 ± 0.02 Hz at 305 K. On the assumption that ^3J depends only on the *exo/endo* equilibrium, these results suggest a lower limit of 14.5_4 Hz for $^3J_g + {}^3J_t$.

The approach outlined above assumes rigid conformations. The average values of the trigonometric functions of the Karplus equation (33) are needed for a more rigorous treatment. In other words, an equation of the type $^3J = A\langle\cos^2\gamma\rangle + B\langle\cos\gamma\rangle + C$ is required, angular brackets indicating expectation values and γ being the dihedral angle for the HCOH fragment. These expectation values are not available in general.

As an example, suppose that the STO-3G MO results for benzyl alcohol hold for the dilute solution in CS_2 at 300 K, in which ^3J is 6.07 ± 0.01 Hz. At 300 K, the data in Table 1 yield a $\langle\cos^2\gamma\rangle$ of 0.517_3 and $\langle\cos\gamma\rangle$ as -0.064_2. The equation, $^3J/\text{Hz} = 11.0\,\langle\cos^2\gamma\rangle - 1.9\,\langle\cos\gamma\rangle + 0.25$, then has ^3J as 6.06 Hz. ^3J_t and ^3J_g ($\gamma = 60°$) are now 13.1_5 and 2.0_5 Hz, respectively. The largest ^3J_t values in the literature appear to be 12.1 and 12.5 Hz (34, 35) and, of course, are expected to be smaller than the true ^3J_t because of torsional motions in the

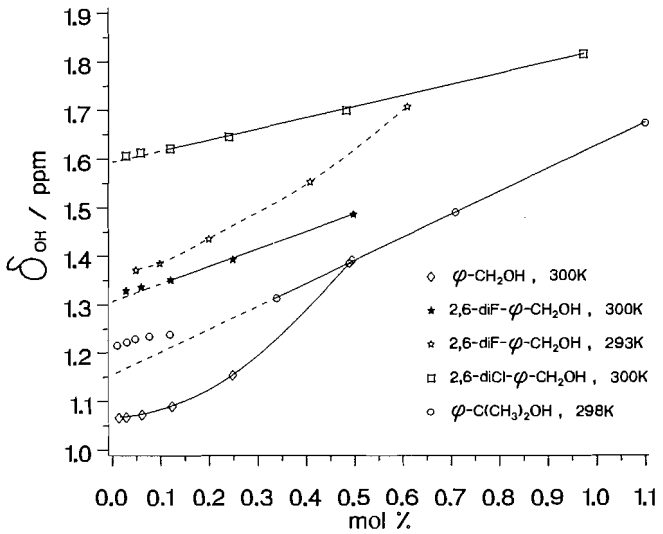


FIG. 2. The hydroxyl proton chemical shifts, relative to internal tetramethylsilane, are plotted as a function of concentration in units of mol% for dilute solutions in CS_2, which also contains 10 mol% of C_6D_{12} and 0.5 mol% TMS. For benzyl alcohol, ϕ-CH_2OH, δ(OH) is 1.394, 1.1569, 1.0923, 1.0744, 1.0693, and 1.0684 at concentrations of 0.50, 0.25, 0.12_5, 0.06_3, 0.03_1, and 0.01_6 mol%, respectively. ^3J(HCOH) is 6.06_9 and 6.06_7 Hz at 0.06_3 and 0.01_6 mol%, respectively. The shift at infinite dilution appears to be 1.067_5 ppm. See Table 2 for δ(OH) at 1.0 and 2.5 mol%. A plot of δ(OH) between 0.01_6 and 2.5 mol%, not shown here, displays the characteristic shape of a monomer–trimer equilibrium (40). Infinite dilution shifts and ^3J(HCOH), when applicable, are given in the text for the other compounds.

reference molecule. For the 2,6-disubstituted benzyl alcohol derivatives above, potential surfaces are required, to estimate ^3J from the present equation. Qualitatively it is clear that the 2,6-dichloro compound comes closest to a pure *endo* form in CS_2 solution at infinite dilution and 300 K. The rigid *endo* conformer would now have a ^3J of 7.6_0 Hz, only 0.1 Hz larger than in a recent discussion (22).

^3J is reported as 5.94 ± 0.05 Hz for benzyl alcohol in the gas phase at a pressure of 100 Torr (1 Torr = 133.3 Pa) and at 422 K (36). The data in Table 1 translate into a $\langle\cos^2\gamma\rangle$ of 0.499 and a $\langle\cos\gamma\rangle$ of −0.002 at 422 K. Hence the equation above yields ^3J as 5.75 Hz (the computed population of the *exo* form has increased to 31% at 422 K from 27% at 300 K). The dipole moment in the vapor phase at 463 K is 1.70 ± 0.01 D for benzyl alcohol (37), equal to that measured at 298 K in benzene, benzene–hexane, and in CCl_4 solutions (37–39). However, the computed dipole moment of the *exo* form is only 5% larger than that of the *endo* form, so that these data do not provide a sensitive measure of populational changes with temperature.

The population of the *endo* conformer in benzyl alcohol and its diortho-substituted derivatives increases in the order H < F < OCH_3 < F-2, Cl-6 < Cl, from 73% in the parent molecule to 94% in the dichloro derivative, assuming the new values of ^3J_g and ^3J_t. Of course, this treatment assumes the same dihedral angle in a given conformer for all the molecules (22).

Hydroxyl proton shifts in dilute solutions

(*i*) *Benzyl alcohol and its 3,5-dichloro derivative*

In Fig. 2 the plot of δ(OH) versus concentration in the CS_2/C_6D_{12}/TMS mixture (see figure caption) shows remarkable curvature between 0.01_6 and 0.49_6 mol% (roughly 0.003–0.08 molar) and, as already noted by Abraham and Bakke (2) for CCl_4 solutions at concentrations as low as 0.02 M, displays a rapidly decreasing slope at the lowest concentrations. At 300 K the shift at infinite dilution is 1.067_5 ppm. This number is very similar to the 1.09 ppm quoted for the CCl_4 solution at 298 K.[4] As is well known (23, 40), these results strongly indicate that a polymer higher than dimer is predominant at low concentrations. It is also true that the determination of the associative equilibria from δ(OH) alone is beset by uncertainties (40) and will not be attempted here.

^3J(HCOH) is 6.07(1) Hz at concentrations of 0.12_5, 0.06_3, 0.03, and 0.01_6 mol%, so that this number is also that at infinite dilution in the CS_2/C_6D_{12}/TMS mixture at 300 K. At 298 K, ^3J(HCOH) is 5.79 Hz for a 0.02 M solution in CCl_4 (2). In an experiment with 3,5-dichlorobenzyl alcohol, we find ^3J as 5.99(2) Hz for a 0.1 mol% solution in CS_2/C_6D_{12}/TMS and as 5.85(1) Hz at a concentration of 0.1 mol% in acetone-d_6, while it is 6.23(1) Hz at the same concentration in benzene-d_6. δ(OH) is 1.319, 4.470, and 0.623 at 298 K for the three solutions, in that order.[5]

(*ii*) *α,α-Dimethylbenzyl alcohol*

The investigations of associative equilibria for *tert*-butyl alcohol in CCl_4 solutions set an upper limit of 0.25 M^{-1} for the dimerization constant, but a much smaller, perhaps vanishingly small, value applies in hexadecane solution (23). δ(OH) is a linear function of concentration between 0.05 and 0.2 M in CCl_4 at 294 K (23, 40) and changes by 1.07 ppm between 0 and 0.2 M.

In Fig. 2, δ(OH) for α,α-dimethylbenzyl alcohol in CS_2 varies by only 0.46 ppm over roughly the same range of concentration but at 300 K, the lowest concentration being 0.01_2 mol% or roughly 0.002 M. Consequently, a small dimer concentration will be more easily detected for this compound because, clearly, the trimer concentration is smaller than for *tert*-butyl alcohol. This point is also emphasized by the difference of 0.06_5 ppm between the extrapolated shift and the true shift at infinite dilution in Fig. 2. This difference, whose magnitude is related to the trimer concentration for the dilute region, is as large as 0.17 ppm for *tert*-butyl alcohol (23, 40). The distribution of points in Fig. 2 suggests the presence of dimer at the lowest concentrations (limiting finite slope), followed by the rapid onset of polymer formation above about 0.05 mol% or roughly 0.008 M. An estimate of the dimerization constant, K_2, demands a value of δ(OH) for the dimer. A rough estimate of 5 ppm for this number, noting that δ(OH) for the monomer is 1.214 ppm, gives K_2 as ca. 0.2 M^{-1}.

(*iii*) *2,6-Difluorobenzyl alcohol*

The high sensitivity of δ(OH) to temperature is demonstrated by the plots in Fig. 2 at 293 and 300 K. Again, at 300 K the decreasing slope at low concentrations is evident. ^3J(HCOH) is 6.89(2) Hz for the four solutions ranging from 0.25 to 0.03 mol% in the alcohol, giving its value at infinite dilution. The increase of 0.8 Hz relative to the parent molecule is plausibly attributable to an increase in the *endo* population. The δ(OH) at infinite dilution at 300 K is less than 1.331 and greater than 1.321.

[4] At 422 K and 100 Torr, δ(OH) is 0.802.

[5] The assumption that ^3J_t is 13.1_5 Hz and that ^3J_g is 2.0_5 Hz (see the equation in the previous section) leads to 24% as the population of the *exo* conformer in the benzene solution at 298 K. This approximation may be compared with that of 30% for 4-chlorobenzyl alcohol in benzene at 308 K obtained from dipole moments (41). In the solid, 4-chlorobenzyl alcohol forms intermolecular hydrogen bonds, which cause it to exist in the *exo* form only (42).

Can. J. Chem. Downloaded from www.nrcresearchpress.com by 41.223.56.140 on 09/07/12
For personal use only.

Can. J. Chem. Downloaded from www.nrcresearchpress.com by 41.223.56.140 on 09/07/12
For personal use only.

(iv) 2,6-Dichlorobenzyl alcohol

At infinite dilution, δ(OH) is greater than 1.604 at 300 K and less than 1.608. Between 0.24 and 0.03 mol%, ^3J(HCOH) is 7.27(1) Hz. The decreased shielding of the hydroxyl proton in the 2,6-dihalobenzyl alcohols is perhaps partly caused by intramolecular hydrogen bonding (δ(OH) is 2.08 for 2-nitrobenzyl alcohol at infinite dilution in CCl_4 and is 1.63 for 2-methoxybenzyl alcohol (2)). Judging by the δ(OH) plots in Fig. 2, formation of polymers, probably mainly trimers at these low concentrations (23, 40), is most pronounced for benzyl alcohol and least pronounced for 2,6-dichlorobenzyl alcohol. For sufficiently hindered molecules, such as 2,4-dimethyl-3-ethyl-3-pentanol, only dimer formation occurs (43), so that at least part of the present observations is accounted for by the greater congestion near the site of the hydroxyl group in the benzyl alcohol derivatives.

(v) Caveats

The existence of sharp multiplets in the hydroxyl proton spectra of benzyl alcohol and its dihalo derivatives at low concentrations demonstrates the absence of rapid intermolecular proton exchange. However, it does not prove the absence of water in the nmr samples, even though the presence of molecular sieve will reduce the concentration of water significantly. Thus, it is conceivable that some of the alcohol monomers or polymers at the lowest concentrations actually exist as species in which a water molecule is hydrogen bonded to the alcohol. Peaks due to water were not observed in the spectra. In one experiment, the CS_2/C_6D_{12}/TMS mixture was shaken with water. The ^{1}H nmr spectrum of the nonaqueous layer displayed no obvious peak attributable to water. One very small peak near the residual peak due to the 0.5% residual protons in the 99.5% deuterated cyclohexane, if indeed it arose from water, represented a concentration of less than 0.015 mol%. For the α,α-dimethylbenzyl alcohol solutions there is no large ^3J(HCOH), so that some ambiguity arises; it is possible that the linear portion of the plot at low concentrations in Fig. 1 is caused by exchange with water protons whose chemical shift is less than 1.2 ppm. However, we have no evidence for this exchange.

The ring proton shifts in CS_2 solution

Compared to the quoted dilution shifts of aromatic protons in monosubstituted benzene derivatives (44), those of the ring protons in benzyl alcohol are larger by about an order of magnitude (Table 2). Plots of these shifts as a function of concentration in the CS_2 solvent mixture are curved and, unfortunately, below 0.5 mol% spectral analytical difficulties do not allow their extraction from the very tightly coupled spectra. However, the chemical shifts of all five types of protons are proportional to each other, correlation coefficients being 0.999 or better. Thus, for six concentrations between 0.016 and 0.50 mol%, one has $\delta(CH_2) = 4.6660 - 0.09685\delta(OH)$ with $r = 0.999_1$. Again, for the three concentrations at which ring proton chemical shifts are available one has, for example, δ(H-3) = 7.2503 − 0.02718δ(OH) with $r = 0.999_9$. Correlations of this kind allow the conclusion that, at infinite dilution and 300 K, $\delta(CH_2)$ = 4.563(3), δ(H-2) = 7.224(2), δ(H-3) = 7.223(1), and δ(H-4) = 7.149(1); these numbers are based on a δ(OH) of 1.067_5 at infinite dilution.

The methylene and ring protons are increasingly deshielded as the concentration decreases. The changes in chemical shifts between zero and 2.5 mol% are in the ratio of 1:2.1:3.5:6.1 for H-4, H-3, H-2, CH_2 respectively. This means that the hydrogen bonded complexes, probably mainly trimers in this concentration range, have a structure in which, on average, these protons lie in the shielding region arising from the diamagnetic anisotropies of the other phenyl groups involved in the complex. Furthermore, although the shielding depends on angular as well as distance parameters (45) and therefore a unique average structure is unlikely to be ascertainable from the chemical shifts, the ratio above is consistent with the idea that the structure has the methylene protons of one molecule placed nearest to the phenyl rings of the partners in the complex. A structure in which two phenyl groups are stacked is unlikely, for example, because of the ratio given above.

The ratio of the change in δ(OH) to that of δ(H-4) in this concentration range is −77:1, so that δ(OH) is dominated by the deshielding caused by the O—H···O interactions. However, δ(OH) also contains a term of unknown sign and magnitude originating in the diamagnetic anisotropies of the other phenyl groups in the self-complex.

Finally, it is of interest that the $\delta(CH_2)$ of 4.563(3), at 300 K and at infinite dilution in the CS_2 solvent mixture, is rather near that of 4.585 in the vapor at 422 K (36). At 296 K, $\delta(CH_2)$ is 4.598 at infinite dilution in CCl_4(2).

Acknowledgments

We thank the Natural Sciences and Engineering Research Council of Canada for a grant-in-aid of research, and the referee for cogent criticism.

1. M. Traetteberg, H. Ostensen, and R. Seip. Acta Chem. Scand. Ser. A: **A34**, 449 (1980).
2. R. J. Abraham and J. M. Bakke. Tetrahedron, **34**, 2947 (1978).
3. W. J. Hehre, L. Radom, and J. A. Pople. J. Am. Chem. Soc. **94**, 1496 (1972).
4. T. Visser and J. H. van der Maas. Spectrochim. Acta, Part A, **42A**, 599 (1986), and references therein.
5. R. J. Abraham, J. M. Bakke, and T. Skjetne. Acta Chem. Scand. Ser. B: **B38**, 547 (1984).
6. R. J. Abraham and J. M. Bakke. Acta Chem. Scand. Ser. B: **B37**, 865 (1983).
7. R. J. Abraham and J. M. Bakke. Acta Chem. Scand. Ser. B: **B35**, 367 (1981).
8. J. M. Bakke, H. Ronneberg, and D. J. Chadwick. Magn. Reson. Chem. **25**, 251 (1987).
9. S. D. Kahn and W. J. Hehre. J. Am. Chem. Soc. **109**, 666 (1987).
10. J. M. Bakke, A. M. Schie, and T. Skjetne. Acta Chem. Scand. Ser. B: **B40**, 703 (1986).
11. T. Schaefer, W. Danchura, W. Niemczura, and W. J. E. Parr. Can. J. Chem. **56**, 1721 (1978).
12. T. Schaefer, J. Peeling, and R. Sebastian. Can. J. Chem. **63**, 3219 (1985).
13. T. Schaefer, R. Sebastian, and G. H. Penner. Can. J. Chem. **64**, 1372 (1986).
14. W. J. Hehre, R. F. Stewart, and J. A. Pople. J. Chem. Phys. **51**, 2657 (1969); W. J. Hehre, R. Ditchfield, R. F. Stewart, and J. A. Pople. J. Chem. Phys. **52**, 2769 (1970).
15. J. S. Binkley, M. J. Frisch, D. J. DeFrees, K. Raghavachara, R. A. Whiteside, H. B. Schlegel, E. M. Fluder, and J. A. Pople. GAUSSIAN 82. Department of Chemistry, Carnegie–Mellon University, Pittsburgh, PA.
16. W. J. Hehre, L. Radom, P. v. R. Schleyer, and J. A. Pople. Ab initio molecular orbital theory. John Wiley & Sons, New York. 1986.
17. R. M. Lees and J. G. Baker. J. Chem. Phys. **48**, 5299 (1968).
18. G. H. Penner, P. George, and C. W. Bock. J. Mol. Struct. (Theochem), **152**, 201 (1987).
19. S. Marriott, A. Silvestro, and R. D. Topsom. J. Chem. Soc. Perkin Trans. 2, 457 (1988).

20. R. TAYLOR and O. KENNARD. J. Am. Chem. Soc. **104**, 5063 (1982).
21. M. SOUHASSOU, A. AUBRY, G. BOUSSARD, and M. MARRAUD. Angew. Chem. Int. Ed. Engl. **25**, 447 (1986).
22. R. LAATIKAINEN and K. TUPPURAINEN. J. Chem. Soc. Perkin Trans. 2, 121 (1987).
23. E. E. TUCKER and E. D. BECKER. J. Phys. Chem. **77**, 1783 (1973).
24. K. ENDO, B. KNUETTEL, I. MOROSHIMA, T. INUBUSHI, and T. YONEZAWA. Chem. Phys. Lett. **31**, 387 (1975).
25. K. ENDO, I. MORISHIMA, and T. YONEZAWA. J. Chem. Phys. **67**, 4760 (1977).
26. P. BEZOT, C. BROT, and G. M. SEARBY. Chem. Phys. **31**, 363 (1978).
27. W. L. JORGENSEN. J. Phys. Chem. **90**, 1276 (1986).
28. J. M. POPE, D. DUBRO, J. W. DOANE, and P. W. WESTERMAN. J. Am. Chem. Soc. **108**, 5246 (1986).
29. J. M. POPE, P. W. WESTERMAN, and J. W. DOANE. Chem. Phys. Lett. **139**, 589 (1987).
30. R. R. FRASER, M. KAUFMAN, P. MORAND, and G. GOVIL. Can. J. Chem. **47**, 403 (1969).
31. C. P. RADER. J. Am. Chem. Soc. **91**, 3248 (1969).
32. J. P. ZAHRA, B. WAEGELL, and H. BODOT. Bull. Soc. Chim. Fr. 1107 (1974).
33. M. KARPLUS. J. Am. Chem. Soc. **85**, 2870 (1963).
34. P. DAIS and A. S. PERLIN. Can. J. Chem. **60**, 1648 (1982).
35. J. M. BAKKE. Acta Chem. Scand. Ser. B: **B40**, 407 (1986).
36. J. P. CHAUVEL and N. S. TRUE. Chem. Phys. **95**, 435 (1985).
37. A. D. BUCKINGHAM, H. G. HOLLAND, and R. J. W. LEFÈVRE. J. Chem. Soc. London, 1646 (1954).
38. K. HIGASHI. Bull. Inst. Phys. Chem. Res. (Tokyo), **11**, 729 (1932).
39. J. BARASSIN and H. LUMBROSO. C. R. Hebd. Seances Acad. Sci. **254**, 863 (1962).
40. E. E. TUCKER and E. LIPPERT. *In* The hydrogen bond — recent developments in theory and experiment. *Edited by* P. Schuster, G. Zundel, and C. Sandorfy. North-Holland Publ. Co., Amsterdam. 1976. Chap. 17.
41. K. PANDIARAJAN and R. SEKAR. Indian J. Chem. Part B, **20**, 686 (1981).
42. M. HASHIMOTO, Y. NAKAMURA, and K. HAMADA. Acta Crystallogr. Sect. C: Cryst. Struct. Commun. **C44**, 482 (1988).
43. E. D. BECKER, E. E. TUCKER, and C. N. R. RAO. J. Chem. Soc. Faraday Trans. 2, **73**, 438 (1977).
44. K. HAYAMIZU and O. YAMAMOTO. J. Mol. Spectrosc. **28**, 89 (1968); **29**, 183 (1969).
45. C. W. HAIGH and R. B. MALLION. Prog. NMR Spectrosc. **13**, 303 (1979).
46. A. DOMENICANO and P. MURRAY-RUST. Tetrahedron Lett. 2283 (1979).
47. R. NORRESTAM and L. SCHEPPER. Acta Chem. Scand. Ser. A: **A35**, 91 (1981).
48. C. W. BOCK, M. TRACHTMAN, and P. GEORGE. J. Mol. Struct. (Theochem), **122**, 155 (1985).

Can. J. Chem. Downloaded from www.nrcresearchpress.com by 41.223.56.140 on 09/07/12
For personal use only.

Internal motion in benzylidene diacetate and its 2,6-dibromo derivative by DNMR and the *J* method

TED SCHAEFER AND CRAIG S. TAKEGUCHI
Department of Chemistry, University of Manitoba, Winnipeg, Man., Canada R3T 2N2

Received October 17, 1988

TED SCHAEFER and CRAIG S. TAKEGUCHI. Can. J. Chem. **67**, 1022 (1989).

The ^{1}H nuclear magnetic resonance spectral parameters are reported for benzylidene diacetate in CS_2 and acetone-d_6 solutions. The long-range spin–spin coupling constant over six formal bonds, ^6J, is used to derive apparent twofold barriers to rotation about the exocyclic C(1)—C bond in the two solutions. The conformation of lowest energy has the α C—H bond in the benzene plane. The barrier is higher in CS_2 than in acetone-d_6 solution, in contrast to a molecule like benzyl chloride. In the 2,6-dibromo derivative, the free energy of activation for reorientation about the bond in question is 36 kJ/mol at 165 K in dimethyl ether solution. Such a high barrier implies a very small six-bond proton–proton coupling constant for this derivative because ^6J is proportional to the expectation value of $\sin^2\theta$. The angle θ is zero when the α C—H bond lies in the benzene plane. ^6J is −0.051 Hz in acetone-d_6 solutions; its sign is determined by double resonance experiments. The question of an angle-independent component of ^6J, that is, whether ^6J is finite at $\theta = 0°$, is addressed. A maximum magnitude of 0.02 Hz may be present at $\theta = 0°$ for the 2,6-dibromo derivative, although a zero magnitude is also compatible with the experimental data. In a compound with a higher internal barrier, α,α,2,6-tetrachlorotoluene, the experimental results are best in accord with a negligibly small ^6J at $\theta = 0°$.

Key words: ^{1}H NMR of benzylidene diacetate, spin–spin coupling constants for benzylidene diacetate, DNMR, 2,6-dibromobenzylidene diacetate.

TED SCHAEFER et CRAIG S. TAKEGUCHI. Can. J. Chem. **67**, 1022 (1989).

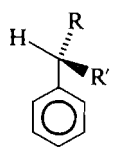
On a rapporte les paramètres des spectres rmn du ^{1}H du diacétate de benzylidène, mesurés en solutions dans le CS_2 et l'acétone-d_6. On a utilisé les constantes de couplage spin–spin à longue distance à travers six liaisons formelles, ^6J, pour déterminer les barrières binaires, apparentes, à la rotation autour de la liaison exocyclique C(1)—C, dans les deux types de solutions. Pour la conformation d'énergie plus basse, la liaison C—Hα se trouve dans le plan du benzène. Par opposition à ce qui a été observé avec le chlorure de benzyle, la barrière est plus élevée dans le CS_2 que dans l'acétone-d_6. Dans le dérivé dibromo-2,6, en solution dans l'éther diméthylique, à 165 K, l'énergie libre d'activation pour la réorientation autour de la liaison en question est de 36 kJ/mol. Puisque la valeur de ^6J est proportionnelle à la valeur attendue pour $\sin^2\theta$, une barrière aussi élevée implique que la constante de couplage proton–proton à longue distance est très faible. L'angle θ est égal à zéro lorsque la liaison C—H α se trouve dans le plan du benzène. En solution dans l'acétone-d_6, la valeur de ^6J est −0,051 Hz; on a déterminé son signe grâce à des expériences de double résonance. On discute de la question relative à la possibilité que la valeur de ^6J soit différente de zéro lorsque $\theta = 0°$. Même si une amplitude de zéro est compatible avec les données expérimentales obtenues avec le dérivé dibromo-2,6, on établit à 0,02 Hz l'amplitude maximale présente dans ce système, lorsque $\theta = 0°$. Dans l'α,α,2,6-tétrachlorotoluène, un composé possédant une barrière interne plus élevée, les résultats expérimentaux s'accordent mieux avec une valeur négligeable de ^6J pour $\theta = 0°$.

Mots clés : RMN du ^{1}H du diacétate de benzylidène, constantes de couplage spin–spin du diacétate de benzylidène, diacétate de benzylidène dibromo-2,6.

[Traduit par la revue]

Introduction

The deduction of the internal barrier to rotation about the bond between a benzene ring and a side chain from motionally averaged long-range spin–spin coupling constants (*J* method) depends on a knowledge of the coupling mechanisms and of the extrema in the magnitudes of the coupling constants (1–4). For example, in **1** the coupling constant over six bonds between the proton in the side chain and that at the *para* position has



1

been written as in eq. [1], where θ is the angle by which the

$$[1] \quad {}^6J(\mathrm{H,H}) = {}^6J_{90} \sin^2\theta$$

C—H bond rotates out of the benzene plane and $^6J_{90}$ is the value of ^6J at $\theta = 90°$ (1). If the latter is known, then a measurement of ^6J yields the expectation value of $\sin^2\theta$, which, in turn, can be related to the internal barrier by a hindered rotor model (1) or by a classical averaging procedure (5). In toluene, $^6J_{90}$ is −1.20 Hz (6) but electronegative substituents can alter this magnitude (1, 3, 4), thereby introducing some uncertainty into the use of the *J* method. A further possible source of error originates in the suspicion that there occurs an angle-independent term in eq. [1], ^6J_o, analogous to that in the Heller-McConnell relationship for β-hyperfine interactions in radicals (7).

Nevertheless, the *J* method is one of the few available for the estimation of small barriers in solution and is most reliable for barrier magnitudes much smaller than those accessible to dynamic nuclear magnetic resonance (DNMR) procedures. Consequently it is worthwhile to devise tests of its reliability. One such test involved the overlap of the *J* method and DNMR in 2,6-difluoroisopropyl benzene (2), but was not entirely successful, the barrier lying in a range for which both methods were somewhat insensitive. The present work describes another attempt at an overlap of the two methods. Again, the results are not without some ambiguity, although they are compatible with the non-existence of a second term on the right of eq. [1]. The nmr spectral data were obtained for benzylidene diacetate (R = R′ = $OCOCH_3$ in **1**) (α,α′-diacetoxytoluene) and for its 2,6-

Can. J. Chem. Downloaded from www.nrcresearchpress.com by 194.225.253.170 on 09/07/12
For personal use only.

TABLE 1. ^{1}H nuclear magnetic resonance spectral parameters for benzylidene diacetate in CS_2 and acetone-d_6 at 300 K

Parameter	Values			Parameter	Values		
$\nu(CH_3)$	627.12[a,b]	—[a,c]	586.83[i]	^4J(H-2,CH)	−0.529(3)[a,b]	−0.527(2)[b,c]	−0.491(3)[i]
ν(CH)	2295.5[d]	2295.481(2)	2246.0	$^5J_{25}$	0.605(2)	0.607(2)	0.606(2)
ν_2	2259.647(1)	2259.671(2)	2212.262(1)	^5J(H-3,CH)	0.275(4)	0.279(3)	0.271(4)
ν_3	2230.822(2)	2230.846(2)	2178.543	$^5J(CH_3CH)$	±0.067	—	±0.072
ν_4	2227.866(3)	2227.891(3)	2177.577(3)	^6J(H-4,CH)	−0.264(6)	−0.262(4)	−0.223(6)
$^3J_{23}$	7.818(2)[e]	7.822(2)	7.785(2)	Calculated trans.	183[f]	183[f]	155[f]
$^3J_{34}$	7.490(3)	7.486(4)	7.386(4)	Assigned trans.	111[g]	117[h]	97[g]
$^4J_{24}$	1.262(3)	1.261(3)	1.276(3)	Peaks obs.	95[g]	118[h]	96[g]
$^4J_{26}$	1.934(2)	1.934(3)	1.807(3)	Largest diff.	0.034	0.026	0.026
$^4J_{35}$	1.369(2)	1.467(2)	1.332(3)	Root-mean-square deviation	0.010	0.010	0.010

[a]For a 2.5 mol% solution in acetone-d_6 containing also 0.5 mol% TMS.
[b]In the absence of decoupling of the methyl protons.
[c]Decoupling of the methyl protons.
[d]In Hz at 300.135$_2$ MHz to high frequency of internal TMS.
[e]Numbers in parentheses are standard deviations in the last significant figure.
[f]For the ring and methine protons, ignoring the methyl protons.
[g]Ring protons only.
[h]Ring and methine protons. The two analyses were independent in that they were performed some months apart in a "blind" sense. The Bloch–Siegert shift is observed for the ring protons during decoupling of the methyl protons and amounts to 0.024 Hz in column 3.
[i]For a 4.8 mol% solution in CS_2, containing also 10.0 mol% of C_6D_{12} and 0.5 mol% of TMS.

dibromo derivative, **2**; α,α,2,6-tetrachlorotoluene was also examined.

Experimental

The synthesis (8) of **2** used 1.01 g of 2,6-dibromotoluene (Lancaster Synthesis), dissolved in a precooled mixture of 10 mL acetic anhydride, 10 mL of glacial acetic acid, and 3 mL of concentrated H_2SO_4. At a solution temperature of 5°C, 1.7 g of CrO_3 was added slowly so as to keep the temperature below 10°C, stirring the while. Stirring ceased 0.5 h after the addition was complete. The flask contents were poured into a 400-mL beaker that had been one-third filled with crushed ice. Cold water was added to give a volume of 200 mL. Filtration and washing with cold water until the washings were colorless was followed by a wash with cold 2% Na_2CO_3 solution and, finally, with 10 mL of ethanol.

1 came from 2.01 g of benzaldehyde and 0.044 g of *p*-toluenesulfonic acid, which were added to 10 mL of acetic anhydride in a 100-mL round-bottom flask. The mixture was stirred overnight. The isolated solid was dried on a vacuum line to remove acetic anhydride and was then air-dried, yielding a white crystalline product.

Approximately 2–3 mol% solutions of **1**, **2**, and of 2,6-dibromotoluene were prepared in CS_2/C_6D_{12}/TMS and acetone-d_6/TMS mixtures (see tables). These were transferred to 5 mm o.d. nmr sample tubes; the latter were degassed by numerous freeze–pump–thaw cycles and were then flame-sealed. A dilute (<5 mol%) solution of **2** in dimethyl ether was sealed off in a 5 mm o.d. sample tube and was stored in a freezer before use.

The ^{1}H nmr spectra were accumulated on an AM300 Bruker nmr spectrometer by methods previously described (6). Linewidths at half-height of less than 0.04 Hz could be attained for **2** and of about 0.05 Hz for **1**. The DNMR experiments on **2** in dimethyl ether were performed by the usual procedures (2) in this laboratory, also on the AM300 instrument.

Results and discussion

Spectral analyses

These were performed with the computer program NUMARIT (9), as revised in this laboratory by R. Sebastian. The ^{1}H nmr spectral parameters are given in Tables 1 and 2. For the benzylidene diacetate, **1**, in acetone-d_6 solution, two independent analyses were made, one in which the spectrum under analysis was single resonance, the other of a spectrum for which the methyl protons had been decoupled. Comparison of the spectral data in Table 1 suggests that the standard deviations are good measures of precision (note also the Bloch–Siegert shifts for the ring protons).

The sign of ^6J in **2** for the acetone-d_6 solution was determined by weak irradiation experiments (10). ^6J is −0.051(0) Hz. See Fig. 1 for an adumbration.

*^{6}J and the internal barrier in **1***

^6J is −0.263(10) Hz in acetone-d_6 solution, the standard deviation being taken as the sum of the standard deviations for the two analyses in Table 1. Were $^6J_{90}$ in eq. [1] that in toluene, −1.20 Hz, then $\langle\sin^2\theta\rangle$ would follow as 0.219(8). The assumption of a twofold barrier hindering rotation about the exocyclic C_{sp^2}—C_{sp^3} bond and a hindered rotor model (1) would then yield a V_2 of 7.0 ± 0.3 kJ/mol. A classical averaging procedure would and did give the same result at 300 K. The measured value of ^6J shows that the conformation of lowest energy has the methine C—H bond in the benzene plane.

However, the electronegativity of the acetoxy group is effectively that of the methoxy group (11). The latter reduces the magnitude of $^6J_{90}$ to 1.02 Hz (12). It is unlikely that a second acetoxy group is as effective as the first (saturation effect). The assumption of additivity will therefore yield a maximum in $\langle\sin^2\theta\rangle$ and a lower limit to a V_2. A $^6J_{90}$ of −0.84 Hz (additivity assumption) has $\langle\sin^2\theta\rangle$ as 0.313(12) and an apparent V_2 as 4.1 ± 0.4 kJ/mol. An alternative, that $^6J_{90}$ is −0.93 Hz, the second acetoxy group being now half as effective as the first in magnitude reduction, has the apparent V_2 as 4.9 ± 0.4 kJ/mol. It seems safe to conclude that, if the barrier is twofold, then it lies between 4 and 5 kJ/mol.

In CS_2 solution, ^6J is −0.223(6) Hz. The procedure above leads to an apparent V_2 lying between 5 and 6 kJ/mol, an increase of about 1 kJ/mol relative to that in acetone-d_6 solution. It may be that the perpendicular conformer of **1**, that with $\theta = 90°$, is stabilized by the polar solvent. This stabilization occurs in benzyl chloride, for which the acetone solvent stabilizes that conformer in which the C—Cl bond lies in a plane perpendicular to the benzene plane. In benzyl chloride, however, the perpendicular conformer lies at the bottom of the

Can. J. Chem. Downloaded from www.nrcresearchpress.com by 194.225.253.170 on 09/07/12
For personal use only.

TABLE 2. ^{1}H nuclear magnetic resonance spectral parameters for 2,6-dibromotoluene and 2,6-dibromobenzylidene diacetate at 300 K

Parameters	Values			
$\nu(CH_3)^e$	760.648(1)[a]	764.844(0)[b]	604.004(0)[c]	634.875(0)[d]
ν(CH)	—	—	2397.660(1)	2466.0
ν_3	2224.374(1)[f]	2280.602(0)	2248.855(0)	2317.351(0)
ν_4	2051.649(1)	2116.975(0)	2098.784(0)	2182.417(0)
$^3J_{34}$	7.983(1)	8.030(1)	8.009(0)	8.063(0)
^5J(H-3,CH)	0.415(1)	0.420(0)	0.231(0)	0.233(0)
^6J(H-4,CH)	−0.627(1)	−0.637(0)	−0.045(1)	−0.051(0)[g]
$^5J(CH_3,CH)$	—	—	±0.077(0)	±0.075(0)
Calc. trans.	80	80	576	576
Assigned trans.	79	80	269[h]	448[h]
Observed peaks	38	38	24	16
Largest diff.	0.017	0.010	0.009	0.010
Root-mean-square deviation	0.005	0.002	0.003	0.003

[a]For 2,6-dibromotoluene as a 2.5 mol% solution in CS_2, containing also 10 mol% C_6D_{12} and 0.5 mol% TMS.
[b]For 2,6-dibromotoluene as a 3.0 mol% solution in acetone-d_6 containing also 0.5 mol% TMS.
[c]For a 3.0 mol% solution of the diacetate in the CS_2/C_6D_{12}/TMS solvent mixture.
[d]For a 3.1 mol% solution of the diacetate in acetone-d_6 and 0.5 mol% TMS.
[e]To high frequency of internal TMS at 300.135$_2$ MHz.
[f]Numbers in parentheses are standard deviations in the last significant figure.
[g]Determined as negative, see text.
[h]Because of inexperience; only a few peaks were assigned in the methine region, as were the two peaks in the methyl proton region.

Can. J. Chem. Downloaded from www.nrcresearchpress.com by 194.225.253.170 on 09/07/12
For personal use only.

internal rotational potential well, so that the acetone solvent *increases* the internal barrier (13); that is, ^6J is smaller in magnitude in the acetone solution. On the other hand, for both benzyl chloride and **1**, the coupling constants within the ring are in general larger in acetone-d_6 than in CS_2 solution. Consequently, it is reasonable to conclude that the solvent dependence of ^6J in **1** implies a solvent dependence of the internal barrier and is not simply an indication of an intrinsic solvent perturbation.

The barrier magnitudes seem reasonable by comparison with those deducible from ^6J for 2-phenyl-1,3-dioxane and the analogous dioxolane (14), for which the present approach with a $^6J_{90}$ of −0.93 Hz yields apparent V_2 values of 1.5 ± 0.3 and 3.1 ± 0.4 kJ/mol, respectively. It should be noted that molecular mechanics (15) and calorimetric techniques (16) indicate an essentially free internal rotation in the phenyldioxane. Of course, in these two compounds the relative motion of the phenyl and saturated rings implies nearest approaches of the *ortho* C—H bonds of the phenyl group and of the oxygen atoms in the saturated moiety, the rest of the latter being held distant by virtue of its cyclic structure. Models of **1** clearly indicate that, the lowest energy corresponding to a conformation with the α C—H bond in the benzene plane (as shown by the magnitude of ^6J), the acetyl groups must point away from the phenyl group during internal rotational motion. However, whatever the value of $^6J_{90}$, the ^6J values in the three compounds under discussion show that the barrier is **1** is rather higher than in the other two. This seems reasonable because the excursions of the acetyl group must be significant in **1** and should therefore lead to a higher barrier to motion about the C_{sp^2}—C_{sp^3} bond.

Now, because of the reasonable agreement between the calorimetric and J measurements of the internal barrier in the phenyl dioxane and because the J measurement assumes a twofold barrier, it is reasonable that the twofold component is indeed dominant, at least for the two-ring molecules. For **1**, the presence of the librating groups in the side chain might introduce substantial magnitudes of higherfold terms into the internal rotational potential. Assume $\langle \sin^2 \theta \rangle$ to be 0.283 in acetone-d_6 solution, corresponding to a $^6J_{90}$ of −0.93 Hz. Such a value at 300 K also corresponds to a V_2, V_4 combination of 4.0 and 2.0 kJ/mol, instead of a V_2 of 4.9 kJ/mol; or, if V_2 and V_4 have opposite signs, then, among other combinations, V_2 and V_4 could typically be 11.5 and −7.3 kJ/mol, respectively, or 10.5 and −6.6 kJ/mol. These magnitudes of V_4 may be considered as rather high, yet they cannot be excluded on the basis of ^6J.

Finally, the presence of an angle-independent term in eq. [1] would introduce further complications. Such a term, apparently negative and about 0.1 Hz in magnitude, is thought to exist in styrene (17). Consequently, the following measurements on **2** become of interest.

2,6-Dibromobenzylidene diacetate, 2, and ^6J_o

The free energy barrier to internal rotation in **2** comes from the DNMR data for the dimethyl ether solution. At 150 K the chemical shift difference between H-3 and H-5 is 12 ± 2 Hz at 300 MHz. The coalescence temperature is 165 ± 3 K. Assuming a transmission coefficient of unity, $\Delta G^{\ddagger}_{165}$ follows as 36.2 ± 0.9 kJ/mol. It is bootless (18) to attempt a reliable decomposition of $\Delta G^{\ddagger}$ into $\Delta H^{\ddagger}$ and $\Delta S^{\ddagger}$ for such a small difference in chemical shift for H-3 and H-5 because the temperature range over which the line shape is sensitive to the pre-exchange lifetime is too small. The apparent V_2 should be compared roughly with $\Delta H^{\ddagger}$ and not with $\Delta G^{\ddagger}$ (2).

^6J is −0.045(0) and −0.051(0) Hz for **2** in CS_2 and acetone-d_6 solutions, respectively (Table 2). Perturbations of $^6J_{90}$ by the bromine substituents are indicated by the ^6J of −0.627(1) and −0.637(0) Hz for 2,6-dibromotoluene in these two solvents. ^6J is −0.602(2) Hz in toluene (6).

Because the internal barrier to rotation in **2** cannot be infinite, $|^6J_o| < 0.05$ Hz. If $\Delta S^{\ddagger}$ is zero, then $\Delta H^{\ddagger} = \Delta G^{\ddagger}$ and is 36 ± 1 kJ/mol in ether solution. With the assumptions that $\Delta G^{\ddagger}$ is

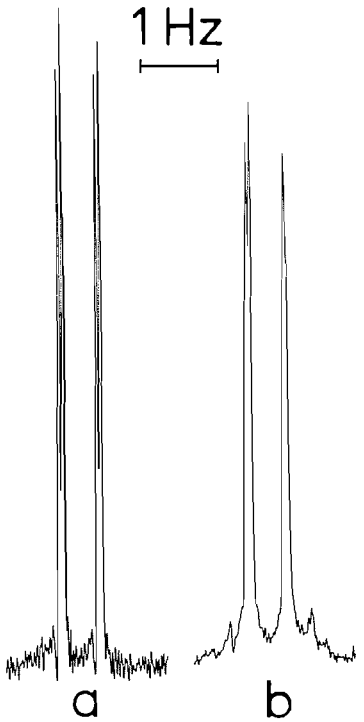


FIG. 1. In (a) four peaks of the nmr spectrum of H-4 in 2,6-dibromobenzylidene diacetate, **2**, are shown for a 3.1 mol% solution in acetone-d_6 at 300 K and 300 MHz. The small splitting of 0.051 Hz corresponds to $^6J_{AX}$ in the spectrum arising from an AB_2X spin system (see Table 2 for the spectral parameters). The doublet on the left represents the two transitions of H-4 for which the B_2 (H-3 and H-5) protons are in antisymmetric spin states (vanishing spin magnetic moment for the B_2 protons). The two pairs of doublets would coincide in frequency were the spin system describable as AM_2X. In (b) the doublets in (a) are again shown, but under conditions in which a very weak radiofrequency field is constantly applied while co-adding (24) 32 F1Ds with acquisition times of 42 s. The weak irradiation is applied to one transition in the B_2 region, corresponding to a given spin state of the X (methine) proton. The peak at low frequency in the right-hand doublet in (b) has been perturbed (the "antisymmetric" transitions on the left must be "unaware" of the second radiofrequency field under these conditions and therefore provide a good reference for resolution conditions as well as peak frequencies). Because the second field is applied at "high" frequency, the experiment indicates that J_{AX} and J_{BX}, i.e., ^6J and ^5J, have opposite signs. This indication was confirmed by three further experiments during which the second field was applied to three other transitions in the B_2 region. Because ^5J is positive (25), it follows that ^6J is $-0.051(0)$ Hz, the number in parentheses being the standard deviation given by the analysis of the single resonance spectrum.

the same in all three solvents, that the barrier is twofold, that $0.88 \leq |^6J_{90}| \leq 1.02$ Hz, that ^6J_o vanishes, and that $^6J = -0.048(3)$ Hz (being the mean of ^6J in CS_2 and acetone-d_6 solutions), $\langle \sin^2\theta \rangle$ is then 0.051(7) and V_2 is $26.5^{+4.0}_{-3.0}$ kJ/mol. If ^6J_o is -0.01 Hz, V_2 follows as $33.5^{+6.5}_{-5.0}$ kJ/mol. Of course, if the α substituents did not alter $^6J_{90}$, then (Table 2) it would be $-1.26(1)$ Hz and a ^6J of 0.048(3) Hz with a vanishing ^6J_o would correspond to a V_2 of 35.4 ± 2.1 kJ/mol. However, it is very unlikely that $^6J_{90}$ is not of the lower magnitude indicated above.

$\Delta S^{\ddagger}$ is not necessarily zero. In 2,6-difluoroisopropylbenzene, $\Delta S^{\ddagger}$ and $\Delta H^{\ddagger}$ are -21 ± 4 J/mol K and 25.5 ± 0.4 kJ/mol (2), whereas in α,α,2,4,6-pentabromotoluene they are -2 ± 2 J/mol K and 80 ± 1 kJ/mol (19).

If the former value of $\Delta S^{\ddagger}$ applies to **2**, then $\Delta H^{\ddagger}$ is 33 ± 2 kJ/mol, which again is compatible with a ^6J_o of -0.01 Hz.

The presence of a fourfold component, V_4, must also be considered. A negative V_4 allows freer oscillation about the C(1)—C_{sp^3} bond than if only V_2 is present. A negative V_4 therefore leads to a larger value of $\langle \sin^2\theta \rangle$ for a given V_2, the latter being the measure of the barrier height. Consequently, the existence of a negative V_4 implies a ^6J_o of less than 0.01 Hz in magnitude.

However, the available data imply a small positive V_4 for a related compound. Thus, for α,α-diiodo-2,6-dichlorotoluene, molecular mechanics computations (20) of the internal energy of the molecule agree with the measured free energy of activation of 89 kJ/mol for internal rotation and imply that $V_4 < 0.1\,V_2$. In such a situation V_2 yields the barrier height. If V_2 is 36 kJ/mol in **2** and V_4 is 4 kJ/mol, then $\langle \sin^2\theta \rangle$ is 0.026 at 300 K; a V_2 of 33 kJ/mol and a V_4 of 3 kJ/mol yield $\langle \sin^2\theta \rangle$ as 0.030. Because the measured value of the latter is 0.051(7), ^6J_o would follow as ca. -0.02 Hz.

These illustrative arguments show that a vanishing ^6J_o cannot be established with the available information.

Turning to molecules with a higher internal rotational barrier, in CS_2 solution $\Delta H^{\ddagger}$ for α,α,2,4,6-pentachlorotoluene is 57.3 ± 1.1 kJ/mol (21) and is expected (19, 21, 22) to be much the same in α,α,2,6-tetrachlorotoluene. For a dilute solution of the latter in CS_2, containing also a smaller amount of α,2,6-trichlorotoluene, the outer peaks of H-4 correspond to αα and ββ spin states of H-3 and H-5. Hence these peaks are not broadened by the internal rate process. The peak at lowest frequency has a linewidth at 300 K of 0.06 Hz, whereas the triplets of H-4 in α,2,6-trichlorotoluene possess one of 0.03_3 Hz. The larger linewidth is attributed to an unresolved ^6J(H,H) in the α,α-dichlorotoluene derivative. Simulations, which allow for the partially Gaussian character of the resolution-enhanced experimental peaks, show that a ^6J(H,H) of just over 0.025 Hz, but certainly less than 0.030 Hz, in magnitude will account for the shapes of the measured peaks.

$^6J_{90}$ in benzyl chloride is -1.06 Hz (13). The assumption of additivity implies $^6J_{90}$ as -0.92 Hz in benzal chloride. In 2,6-dichlorotoluene, $^6J(H,CH_3)$ is $-0.630(1)$ Hz, implying $^6J_{90}$ as -1.26 Hz, compared to -1.20 Hz in toluene. A reasonable $^6J_{90}$ for α,α,2,6-dichlorotoluene appears to be -0.98 Hz, assuming additivity, or perhaps -1.05 Hz if the second α chlorine substituent is only half as effective as the first in reducing the magnitude of $^6J_{90}$. An estimate of $\langle \sin^2\theta \rangle$ as 0.027(3) follows from all these considerations. A hindered rotor approach, using 51 basis functions and a V_2 of 57.3 kJ/mol, has $\langle \sin^2\theta \rangle$ as 0.030 at 300 K. A molecular mechanics calculation (23) yields 55.2 kJ/mol for the barrier height in α,α,2,6-tetrachlorotoluene and implies a small fourfold component of the internal potential. If it is as large as 10% of V_2, then $\langle \sin^2\theta \rangle$ follows as 0.024. For this molecule, at least, ^6J_o appears to be negligibly small. There is no *a priori* reason why the situation should be any different in **1** or **2**.

Acknowledgements

We are grateful to the Natural Sciences and Engineering Research Council of Canada for financial assistance, and thank Kirk Marat for the DNMR measurements. We thank the referees for useful criticism.

1. W. J. E. PARR and T. SCHAEFER. Acc. Chem. Res. **13**, 400 (1980).

Can. J. Chem. Downloaded from www.nrcresearchpress.com by 194.225.253.170 on 09/07/12
For personal use only.

2. T. SCHAEFER, R. P. VEREGIN, R. LAATIKAINEN, R. SEBASTIAN, K. MARAT, and J. L. CHARLTON. Can. J. Chem. **60**, 2611 (1982).
3. T. SCHAEFER, J. PEELING, and R. SEBASTIAN. Can. J. Chem. **63**, 3219 (1985).
4. T. SCHAEFER, G. H. PENNER, and R. SEBASTIAN. Can. J. Chem. **65**, 873 (1987).
5. G. H. PENNER. Can. J. Chem. **65**, 538 (1987).
6. T. SCHAEFER, R. SEBASTIAN, and G. H. PENNER. Can. J. Chem. **63**, 2597 (1985).
7. C. HELLER and H. M. MCCONNELL. J. Chem. Phys. **32**, 1535 (1960).
8. A. I. VOGEL. Practical organic chemistry. 3rd ed. Longmans, London. 1956. p. 769.
9. A. R. QUIRT and J. S. MARTIN. J. Magn. Reson. **5**, 318 (1971); J. S. MARTIN, A. R. QUIRT, and K. E. WORVILL. The nmr program library. Daresbury Laboratory, Daresbury, U.K.
10. W. A. ANDERSON and R. FREEMAN. J. Chem. Phys. **37**, 85 (1962).
11. S. MARRIOTT, W. F. REYNOLDS, R. W. TAFT, and R. D. TOPSOM. J. Org. Chem. **49**, 959 (1984).
12. R. LAATIKAINEN. Magn. Reson. Chem. **24**, 588 (1986); R. LAATIKAINEN and K. TUPPURAINEN. J. Chem. Soc. Perkin Trans. 2, 121 (1987).
13. T. SCHAEFER, R. SEBASTIAN, and G. H. PENNER. Can. J. Chem. **64**, 1372 (1986).
14. T. SCHAEFER, W. NIEMCZURA, and W. DANCHURA. Can. J. Chem. **57**, 355 (1979).
15. N. L. ALLINGER and D. Y. CHUNG. J. Am. Chem. Soc. **98**, 6798 (1976).
16. W. F. BAILEY, H. CONNON, E. L. ELIEL, and K. B. WIBERG. J. Am. Chem. Soc. **100**, 2202 (1978).
17. R. LAATIKAINEN and E. KOLEHMAINEN. J. Magn. Reson. **65**, 89 (1985).
18. G. BINSCH and H. KESSLER. Angew. Chem. Int. Ed. Engl. **19**, 411 (1980).
19. J. PEELING, L. ERNST, and T. SCHAEFER. Can. J. Chem. **52**, 849 (1974).
20. J. PEELING, J. B. ROWBOTHAM, L. ERNST, and T. SCHAEFER. Can. J. Chem. **52**, 2414 (1974).
21. H. G. GYULAI, B. J. FUHR, H. M. HUTTON, and T. SCHAEFER. Can. J. Chem. **48**, 3877 (1970).
22. T. SCHAEFER, R. SCHWENK, C. J. MACDONALD, and W. F. REYNOLDS. Can. J. Chem. **46**, 2187 (1968).
23. A. MANNSCHRECK and L. ERNST. Chem. Ber. **104**, 228 (1971).
24. R. R. ERNST, G. BODENHAUSEN, and A. WOKAUN. Principles of nuclear magnetic resonance in one and two dimensions. Oxford University Press, Oxford. 1987. Section 4.7.
25. T. SCHAEFER and R. WASYLISHEN. Can. J. Chem. **48**, 1343 (1970), and references therein.

Can. J. Chem. Downloaded from www.nrcresearchpress.com by 194.225.253.170 on 09/07/12
For personal use only.

^{1}H nuclear magnetic resonance and molecular orbital studies of the conformations of 3-fluoroanisole

TED SCHAEFER AND RUDY SEBASTIAN
Department of Chemistry, University of Manitoba, Winnipeg, Man., Canada R3T 2N2

Received November 29, 1988

TED SCHAEFER and RUDY SEBASTIAN. Can. J. Chem. **67**, 1027 (1989).

The proximate spin–spin coupling constant between the methyl protons and the ring protons, $^5J(H,OCH_3)$, is extracted from a full analysis of the ^{1}H and ^{19}F nuclear magnetic resonance spectra of 3-fluoroanisole in CS_2 and acetone-d_6 solutions. The values of $^5J(H,OCH_3)$ imply that the less polar *cis* conformer is slightly more stable at 300 K than the more polar *trans* conformer in both solvents, in agreement with geometry-optimized STO-3G MO computations for the free molecule. The latter also find a higher barrier to internal rotation of the methoxy group for 3-fluoroanisole than for the parent molecule. The present results are compared with other measurements of the conformer ratio for the vapor and for solutions. The STO-3G and 6-31G structures of the *cis* and *trans* conformers are compared. The C—F bond length is computed more reliably with the minimal basis set, as is the COC bond angle. The internal angles of the benzene moiety are, of course, found more accurately with the 6-31G basis. The computations indicate additivity of the substituent effects on the internal angle, as found experimentally for a variety of benzene derivatives.

Key words: ^{1}H NMR of fluoroanisole, conformations of fluoroanisole, molecular orbital calculations for fluoroanisole.

TED SCHAEFER et RUDY SEBASTIAN. Can. J. Chem. **67**, 1027 (1989).

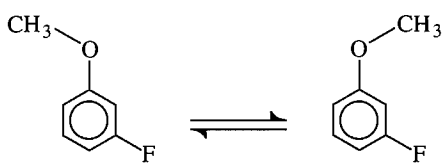
En se basant sur les spectres rmn du ^{1}H et du ^{19}F du fluoro-3 anisole, déterminés dans des solutions de CS_2 et d'acétone-d_6, on a déterminé les constantes de couplage spin–spin entre les protons du méthyle et les protons du cycles, $^5J(H,OCH_3)$. Ces valeurs impliquent que, à 300 K et dans chacun des solvants, le conformère *cis* qui est le moins polaire est légèrement plus stable que le conformère *trans* qui est plus polaire; ces résultats sont en accord avec des calculs d'OM STO-3G effectués sur la molécule libre à l'aide de géométries optimisées. Ces calculs ont aussi permis d'évaluer que la barrière à la rotation interne du groupement méthoxy est plus élevée dans de fluoro-3 anisole que dans la molécule parente. On compare les résultats obtenus au cours de cette étude avec ceux obtenus par d'autres méthodes pour le rapport des conformères en phase vapeur ainsi qu'en solution. On compare aussi les structures des conformères *cis* et *trans* auxquelles ont arrive par des calculs STO-3G et 6-31G. Les valeurs les plus fiables pour la longueur de la liaison C—F ainsi que pour l'angle de la liaison COC sont obtenues à l'aide de l'ensemble avec la base minimale. Par ailleurs, les angles internes de la portion benzénique les plus précis sont obtenus à l'aide de l'ensemble 6-31G. Comme on l'a noté sur la base des données expérimentales pour un grand nombre de dérivés du benzène, les calculs indiquent qu'il existe une additivité des effets des substituants.

Mots clés : RMN du ^{1}H du fluoroanisole, conformations du fluoroanisole, calculs d'OM sur le fluoroanisole.

[Traduit par la revue]

Introduction

The *cis–trans* equilibrium for 3-fluoroanisole has been investigated in solution and in the gas phase, with different results. Two bands in the infrared, at 940 and 915 cm^{-1}, displayed changes in their optical densities between 23 and 100°C for liquid 3-fluoroanisole (1). From these changes, the enthalpy difference between the two isomers was estimated as 2.4 ± 0.6 kJ/mol. The *trans* conformer was assigned as the more stable. In another investigation, a liquid sample gave vibrational bands from two conformers (2). On cooling to 93 K, the vibrational spectrum simplified significantly and was assigned to one conformer. From the intensities of the vibrational bands for 3-fluoroanisole in CCl_4 solution at ambient temperatures (3) the *cis* conformer was assigned a fractional population of 0.72.



trans *cis*

The microwave spectrum in the gas phase detected (4) the *trans* form only, possibly because it has by far the larger dipole moment (see below). The electronic spectrum of a supersonic free jet of 3-fluoroanisole showed that the *cis* conformer was the more stable (5), but the proportions of the conformers was not given; both conformers were present. Geometry-optimized STO-3G MO computations (see below) predict the *cis* form to be 0.45 kJ/mol lower in energy than the *trans*.

These data suggest that the more polar *trans* conformer is being stabilized in the liquid or in polar solvents. Because the long-range spin–spin coupling constant between the *ortho* and methyl protons in anisole and its derivatives is stereospecific (6–9) and should allow an estimate of the *cis–trans* equilibrium, its extraction is described here for CS_2 and acetone-d_6 solutions of 3-fluoroanisole. It seems that the proportions of *cis* and *trans* forms in these solutions are very nearly equal, the *cis* form being slightly more abundant.

Experimental

The 3-fluoroanisole (Aldrich) was prepared as 3.0 mol% solutions in $CS_2/C_6D_{12}/TMS/C_6F_6$ and acetone-d_6/TMS/C_6F_6 solvent mixtures; the tables below give the composition of these mixtures. The solutions were transferred to 5 mm o.d. nmr sample tubes and were degassed by several cycles of the freeze–pump–thaw procedure. The sample tubes were then flame-sealed so as to produce symmetrical tops.

The ^{1}H nmr and ^{19}F nmr spectra were accumulated on an AM 300 Bruker spectrometer, precisely in the manner described previously for benzyl fluoride (10).

STO-3G and 6-31G MO computations employed the computer program Gaussian 82 (11) on an Amdahl 5870 system. The constraint in the geometry optimization procedure was that the nuclei of the aromatic ring remain in a plane.

Can. J. Chem. Downloaded from www.nrcresearchpress.com by 41.223.56.140 on 09/07/12
For personal use only.

TABLE 1. ^1H and ^{19}F nuclear magnetic resonance spectral parameters for 3-fluoroanisole at 300 K

Parameter	Value		Parameter	Value	
$\nu(CH_3)^c$	1114.407(1)[a]	1138.958(0)[b]	$^5J_{25}$	0.300(1)[a]	0.305(1)[b]
ν_2	1939.859(1)	2006.677(1)	$^5J_{36}$	−0.488(1)	−0.426(1)
ν_4	1953.438(1)	2001.395(1)	$^5J(2,CH_3)$	−0.152(1)	−0.163(1)
ν_5	2130.391(1)	2182.870(0)	$^5J(6,CH_3)$	−0.145(1)	−0.141(0)
ν_6	1967.598(1)	2024.066(1)	$^6J(5,CH_3)$	0.061(1)	0.054(0)
ν(F-3)[d]	14476.464(1)	14436.205(1)	$^6J(F,CH_3)$	±0.074(1)	±0.074(0)
$^3J_{23}$	10.704(1)[e]	11.315(1)[f]	$^7J(4,CH_3)$	−0.019(8)	−0.024(1)
$^3J_{34}$	8.140(1)	8.627(1)[f]	Calculated transitions	608	665
$^3J_{45}$	8.245(1)	8.282(1)	Assigned transitions	525	581
$^3J_{56}$	8.342(1)	8.382(1)	Peaks observed	250	282
$^4J_{26}$	2.408(1)	2.417(1)	Largest difference	0.017	0.016
$^4J_{24}$	2.404(1)	2.446(1)	Root mean square		
$^4J_{45}$	0.880(1)	0.850(1)	deviation	0.006	0.005
$^4J_{35}$	6.740(1)	6.959(1)			

[a]3.0 mol% in CS_2, containing also 10 mol% of C_6D_{12}, 0.5 mol% of TMS, and a small drop of C_6F_6 in 0.5 mL of solution.
[b]3.0 mol% in acetone-d_6 containing also 0.5 mol% of TMS and a tiny amount of C_6F_6.
[c]In Hz at 300.135$_2$ MHz to high frequency of internal TMS.
[d]In Hz at 282.363 MHz to high frequency of internal C_6F_6.
[e]Numbers in parentheses are standard deviations of the last significant figure.
[f]The solvent dependence of ^nJ(H,F) has precedents (38); the generally larger ^nJ(H,H) values for the protons within the ring in the more polar solvent are a frequent result in this laboratory.

Results and discussion

Spectral analysis

The ^1H nmr and ^{19}F nmr spectra were analyzed with the computer program Numarit (12), as reworked in this laboratory by R. Sebastian. The spectral parameters are given in Table 1. Figure 1 shows a small part of the ring proton spectrum to illustrate the spectral quality.

$^3J(H,OCH_3) \equiv {}^5J$ and the conformational equilibrium

For anisole in CS_2 and acetone-d_6 solutions, ^5J is −0.152(0) and −0.155(0) Hz, respectively, at 300 K (9). ^5J is −0.288(1) Hz for a 5 mol% solution of 2-methoxyphenol in benzene-d_6 at 305 K (13). Again, ^5J is −0.28(1) Hz for a solution of 1,2-dimethoxybenzene in benzene-d_6 at 305 K (6). These data suggest that ^5J has a large magnitude only when the methyl group lies *cis* to the *ortho* C—H bond containing the coupled proton. Indeed, a detailed set of computations (6, 7) implies that ^5J is dominated by a through-space or proximate mechanism in which the sizeable coupling magnitudes occur when the bonds carrying the coupled nuclei are rather near each other. The computations yield ^5J as −0.292 Hz for a *cis* and 0.037 Hz for a *trans* orientation.

These considerations lead to the following application of the ^5J values in Table 1. Assume that ^5J_t, the coupling constant for the *trans* orientation, vanishes. Then ^5J_c, that for the *cis* arrangement, is −0.297(2) Hz for 3-fluoroanisole in the CS_2/C_6D_{12} solution and is −0.304(1) Hz in the acetone-d_6 solution. The fractional population of *cis* conformer follows as 0.54 in the latter and as 0.51 in the former solution.

Alternatively, a small nonzero ^5J_t can be accommodated as follows. In acetone-d_6 solution, ^5J is −0.155 Hz for anisole. Assume ^5J_t to be as large as 0.05 Hz. Then ^5J_c is −0.36 Hz. The two ^5J values for 3-fluoroanisole in acetone-d_6 solution therefore yield the fractional population of the *cis* conformer as 0.52 or 0.53. The same procedure, but with ^5J_t as −0.05 Hz, gives these populations as 0.54 or 0.57. In other words, the *cis* conformer is *slightly* preferred in both acetone-d_6 and CS_2 solutions at 305 K. For a 5 mol% solution in CCl_4, ^5J of 3,5-dichloroanisole is 0.158(7) Hz, implying a negligible intrinsic perturbation of ^5J by electronegative *meta* substituents (7).

The values of $^6J(H,OCH_3) \equiv {}^6J$ for 3-fluoroanisole are consistent with the very similar stabilities of the two conformers. For example, ^6J in the acetone-d_6 solution is 0.054(0) Hz whereas, in the same solvent, ^6J is 0.049(0) Hz for anisole (9). ^6J appears to be sizeable only when the *meta* C—H bond is arranged *cis* to the methoxy group (9), and is 0.095(14) Hz in 2,3,4-trichloroanisole.

The usual rule, that a polar solvent stabilizes that conformer with the higher dipole moment, does not appear to hold for 3-fluoroanisole. Indeed, ^5J indicates that, if anything, the *cis* conformer is more stable in acetone than in CS_2 solutions. Of course, the two dipolar centers are somewhat remote from one another in this molecule. By way of contrast, the long-range coupling constant, ^5J(OH,F), of 3-fluorophenol indicates that the more polar *trans* form is favored by more than 2 kJ/mol in free energy at 305 K for solutions in CCl_4, CS_2, C_6D_6, and $CDCl_3$ (14). The electronic spectra of 3-fluorophenol in a supersonic free jet also suggest (5) a somewhat greater stability of the *trans* conformer.

Molecular orbital results

Figure 2 displays the STO-3G MO potential energy curve for the rotation of the methoxy group in 3-fluoroanisole. The figure caption gives the computed energies at 15° intervals of the internal rotational angle, θ. The relative energies can be fit to a function consisting of six terms, also given in the caption; the solid line of the figure represents this function.

The rotational barrier is dominated by a twofold term, in $\sin^2\theta$, of 8.3 kJ/mol and by a fourfold term, in $\sin^2 2\theta$, of 2.5 kJ/mol. These terms are somewhat higher than for similar calculations on anisole (15), being 5.8 and 2.4 kJ/mol (see notes to Table 1 of ref. 15). It is noteworthy that the twofold term, no doubt a reflection of the decreased π electron conjugation at θ = 90°, has increased by 2.5 kJ/mol in 3-fluoroanisole, rather larger than the decrease of about 1 kJ/mol

Can. J. Chem. Downloaded from www.nrcresearchpress.com by 41.223.56.140 on 09/07/12
For personal use only.

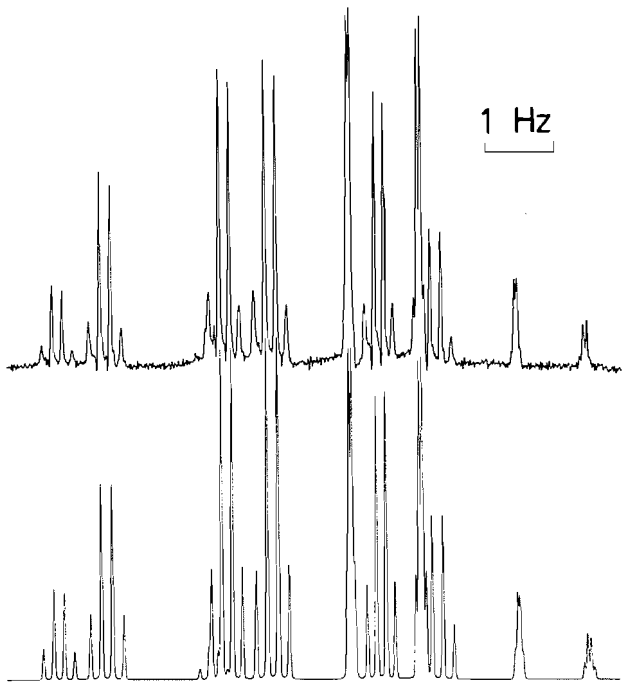


FIG. 1. The parts at high frequency of the ^{1}H nmr spectrum of H-2 and H-4 are shown for 3-fluoroanisole in acetone-d_6 solution at 300 MHz and 300 K (see Table 1 for spectral parameters). The quartets with the large splittings of 0.16 Hz arise from H-2 and those with the small splittings of 0.02 Hz originate with H-4 (in a first-order approximation). The computed spectrum has a linewidth at half height of 0.03 Hz.

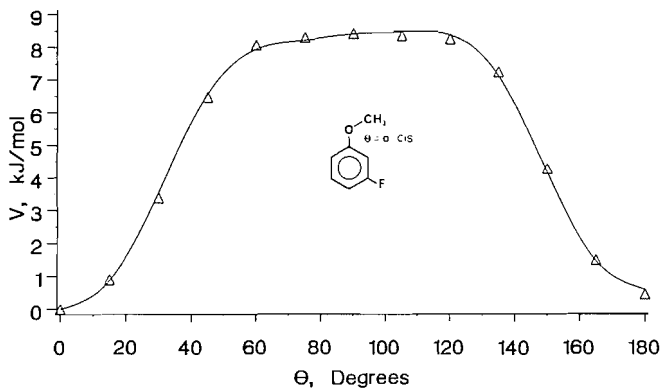


FIG. 2. The relative energies of 3-fluoroanisole at the STO-3G level of molecular orbital theory are plotted as a function of θ, the angle of the out-of-plane twist of the methoxy group. The total energy of the *cis* conformer, with θ = 0°, is −437.772194 au. Relative to this energy, the energies of the other conformers in kJ/mol (θ, degrees) are 0.92(15), 3.40(30), 6.49(45), 8.10(60), 8.35(75), 8.46(90), 8.40(105), 8.30(120), 7.27(135), 4.28(150), 1.52(165), and 0.46(180). These energies are given as triangles in the figure. The solid line is given by $V(\theta)/\text{kJ mol}^{-1} = 0.69 \sin^2(\theta/2) + 8.32 \sin^2\theta - 0.10 \sin^2(3\theta/2) + 2.50 \sin^2 2\theta - 0.17 \sin^2 3\theta - 0.28 \sin^2 4\theta$. Clearly, the internal rotational potential is dominated by the twofold term, 8.32 kJ/mol, and the fourfold term, 2.50 kJ/mol.

computed for 4-fluoroanisole (15). The torsional frequencies of the liquids have been interpreted to mean that the internal barrier in 3-fluoroanisole is 4 kJ/mol higher than in anisole (1). Rather dramatic increases in V_2 have been measured for *meta* derivatives of thiophenol and thioanisole (16, 17), in qualitative agreement with STO-3G MO computations. Qualitatively, therefore, the increased, computed rotational barrier in 3-fluoroanisole is very likely correct. Of course, the internal barrier in anisole is state dependent (18–20) and, although its value in the vapor, as well as in solution, is unknown, there is little doubt that it is substantially higher in solution than in the gas phase or than the value computed (20). By way of contrast, the onefold component computed for 3-fluoroanisole, that is, the energy difference of 0.46 kJ/mol between the two planar conformers, happens to agree with that obtainable from the $^5J(H,OCH_3)$ values in CS_2 and in acetone-d_6 solutions. At 300 K, the computed difference in energy indicates a fractional *cis* population of 0.55, very close to those deduced above from $^5J(H,OCH_3)$.

The dipole moments computed with the minimal basis set are 0.69 D for the *cis* conformer and 2.13 D for the *trans* conformer. The dipole moment of 3-fluoroanisole appears not to be available. Judging from the STO-3G MO dipole moments of anisole and fluorobenzene (21), the values above are somewhat too low. Split-valence basis sets yield dipole moments larger than measured (21). At the 6-31G level, the *cis* conformer was here computed to have a dipole moment of 1.54 D, and 4.13 D was calculated for the *trans* conformer. Comparison of the computations for the monosubstituted benzenes at the two levels of MO theory with experiment (21) suggests that a 1:1 mixture of the two conformers of 3-fluoroanisole will have a dipole moment of 2.3 ± 0.2 D. This number represents the mean of numbers at the STO-3G and 6-31G levels of computation. In this connection it might be noted that the dipole moment of 3-bromoanisole is 2.05 D in benzene solution at 298 K (22) and that the dipole moments of fluorobenzene and bromobenzene are nearly equal (23). $^5J(H,OCH_3)$ for 3-bromoanisole in acetone-d_6 solution at 300 K implies that the fractional population of the *cis* conformer is 0.49 ± 0.03 (8). The infrared intensity measurements in CCl_4 solution yield this number as 0.50(3).

In a recent study of 20 monosubstituted benzenes (24) it was concluded that minimal basis computations, in general, give a better account of π electron transfer and related experimental data than do split-valence calculations, such as 4-31G, for example. Indirect support for such a conclusion comes from a good correlation of σ and π electron densities, calculated from STO-3G wavefunctions, with the variations of the internal angles in such compounds (25–27). It does not follow, however (28–32), that the angles themselves will be reproduced satisfactorily by the minimal basis set. Thus, Figs. 3 and 4 display the STO-3G and 6-31G structures of the *cis* and *trans* conformers, respectively, of 3-fluoroanisole, and the following comparisons may well be of interest.

First, the computed geometry at the methoxy group may be compared with that found by averaging (33) over values for 212 crystal structures, that is, for planar anisole derivatives. The COC angle is 117.7(1.2)°, the number in parentheses being the standard deviation. Neither basis set reproduces this number, although the STO-3G value is somewhat more satisfactory, it being also computed as 115.2° in anisole itself (34). The large CCO angle has an average value of 124.5(9)°. The STO-3G values have an average of 125.9° whereas the 6-31G number is 123.8° in Figs. 3 and 4. The C_{sp^3}—O length in the crystal structures is 1.425(16) Å; both computations are satisfactory. The C_{sp^2}—O average is 1.371(15) Å, the 6-31G value falling very close to this.

The C—F bond length is computed more reliably by the minimal basis set, judging by the microwave substitution

Can. J. Chem. Downloaded from www.nrcresearchpress.com by 41.223.56.140 on 09/07/12
For personal use only.

Can. J. Chem. Downloaded from www.nrcresearchpress.com by 41.223.56.140 on 09/07/12
For personal use only.

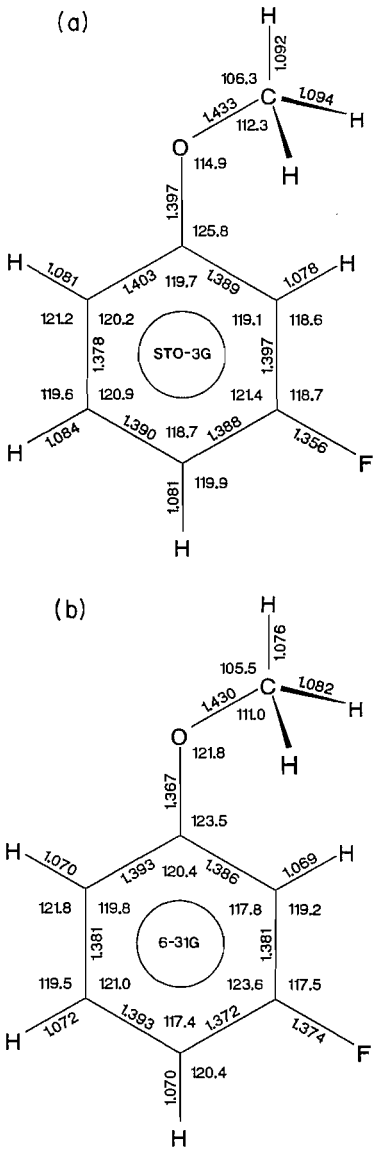


FIG. 3. The STO-3G and 6-31G MO structures of the *cis* conformer of 3-fluoroanisole are shown. During the optimization procedure the nuclei of the benzene moiety were constrained to lie in a plane. The total energies are −437.772194 and −443.275538 au, respectively, and the dipole moments are 0.69 and 1.54 D. The bond angles and lengths given in degrees and angstroms are discussed in the text.

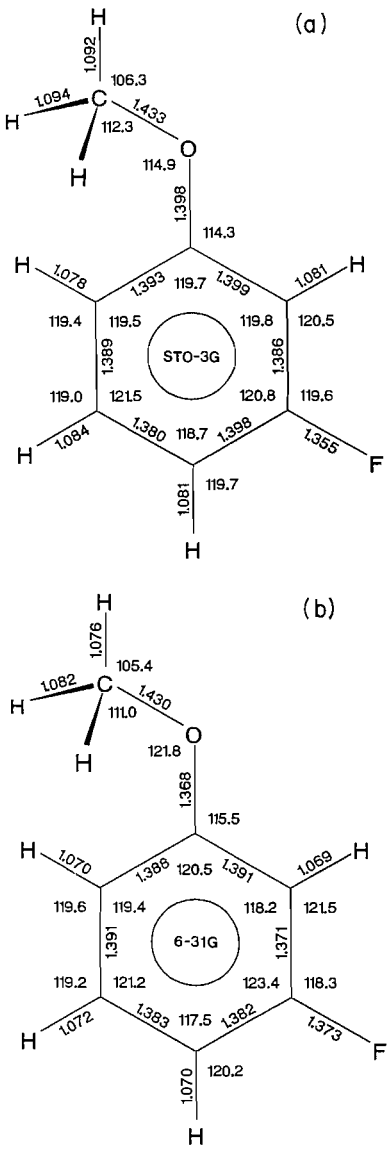


FIG. 4. The STO-3G and 6-31G MO structures of the *trans* conformer of 3-fluoroanisole are displayed. They are computed to be 0.46 and 0.85_5 kJ/mol less stable than the *cis* conformer structures, respectively, and the dipole moments are 2.13 and 4.13 D. These properties and the bond angles and lengths are discussed in the text and compared with the available experimental data.

structures of fluorobenzene and its 2- and 3-fluoro derivatives; these three have an average C—F length of 1.351 ± 0.005 Å (35). The so-called (28) "basis set offset" is therefore probably very near −0.02 Å at the 6-31G level for 3-fluoroanisole.

It is quite clear that internal bond angles in monosubstituted benzene derivatives are much better reproduced with the 6-31G than with the minimal basis (29–32). If those for fluorobenzene and phenol (anisole is not available) are superimposed, then the averages of the 6-31G angles for the two conformers of 3-fluoroanisole are reproduced with a mean deviation of 0.15°. The additivity of substituent effects on internal bond angles has been noted experimentally (26, 36), but there are some noticeable exceptions (37). In fact, the bond angle deformations assigned to fluorine and methoxy substituents (Tables 5 and 8 of ref. 26) reproduce the averaged internal angles of the two 6-31G structures to within a mean deviation of 0.3°, the largest deviation being 0.4°. The angular parameters come from polysubstituted benzenes as derived from an additivity scheme. The effect of thermal motion on these parameters is apparently less than 0.1°. A number of other comparisons of the structural parameters in Figs. 3 and 4 could be made. The present remarks are sufficient, however, to demonstrate that, even within the same molecule, a correct choice of basis set for the prediction of a particular parameter depends on experience (of course, given unlimited computing time, such experience would be unnecessary).

The 6-31G basis has the *cis* as 0.85_5 kJ/mol more stable than the *trans* conformer, corresponding to a 58% abundance of the former at 300 K.

Acknowledgments

This work was helped by a grant-in-aid from the Natural Sciences and Engineering Research Council of Canada.

1. N. L. OWEN and R. E. HESTER. Spectrochim. Acta, Part A: **25**, 343 (1969).
2. R. JOSEFI, E. DRAHORADOVA, and M. HORAK. Collect. Czech. Chem. Commun. **39**, 1541 (1974).
3. A. R. KATRITZKY, M. V. SINNOT, T. T. TIDWELL, and R. D. TOPSOM. J. Am. Chem. Soc. **91**, 628 (1969).
4. R. CERVELLATI, D. G. LISTER, D. CHRISTEN, and V. HOFFMANN. J. Mol. Struct. **82**, 307 (1982).
5. A. OIKAWA, H. ABE, N. MIKAMI, and M. ITO. Chem. Phys. Lett. **116**, 50 (1985).
6. T. SCHAEFER and R. LAATIKAINEN. Can. J. Chem. **61**, 224 (1983).
7. T. SCHAEFER, S. R. SALMAN, T. A. WILDMAN, and G. H. PENNER. Can. J. Chem. **63**, 782 (1985).
8. T. SCHAEFER, T. A. WILDMAN, and J. PEELING. J. Magn. Reson. **56**, 144 (1984).
9. T. SCHAEFER and R. SEBASTIAN. J. Magn. Reson. **73**, 541 (1987).
10. T. SCHAEFER, J. PEELING, and R. SEBASTIAN. Can. J. Chem. **63**, 3219 (1985).
11. J. S. BINKLEY, M. J. FRISCH, D. J. DEFREES, K. RAGHAVACHARI, R. A. WHITESIDE, H. B. SCHLEGEL, E. M. FLUDER, and J. A. POPLE. Gaussian 82. Department of Chemistry, Carnegie–Mellon University, Pittsburgh, PA.
12. J. S. MARTIN, A. R. QUIRT, and K. E. WORVILL. The NMR program library. Daresbury Laboratory, Daresbury, U.K.
13. T. SCHAEFER and T. A. WILDMAN. Can. J. Chem. **57**, 450 (1979).
14. T. SCHAEFER, S. R. SALMAN, and R. SEBASTIAN. J. Phys. Chem. **85**, 499 (1981).
15. T. SCHAEFER and G. H. PENNER. J. Mol. Struct. (Theochem), **152**, 179 (1987).
16. T. SCHAEFER, J. D. BALEJA, and G. H. PENNER. Can. J. Chem. **63**, 2471 (1985).
17. T. SCHAEFER and J. D. BALEJA. Can. J. Chem. **64**, 1376 (1986).
18. H. KONSCHIN, H. TYLLI, and C. GRUNDFELT-FORSIUS. J. Mol. Struct. **77**, 51 (1981).
19. H. KONSCHIN. Doctoral dissertation. University of Helsinki, Helsinki, Finland, 1985, and references therein.
20. T. SCHAEFER, R. LAATIKAINEN, T. A. WILDMAN, J. PEELING, G. H. PENNER, J. BALEJA, and K. MARAT. Can. J. Chem. **62**, 1592 (1984), and references therein.
21. S. MARRIOTT, T. SILVESTRO, R. D. TOPSOM, and C. W. BOCK. J. Mol. Struct. (Theochem), **151**, 15 (1987).
22. N. L. ALLINGER, J. J. MAUL, and M. J. HICKEY. J. Org. Chem. **36**, 2747 (1971).
23. A. L. MCCLELLAN. Tables of experimental dipole moments. W. H. Freeman and Company, San Francisco, CA. 1963.
24. S. MARRIOTT, A. SILVESTRO, and R. D. TOPSOM. J. Chem. Soc. Perkin Trans. 2, 457 (1988).
25. W. J. HEHRE, L. RADOM, and J. A. POPLE. J. Am. Chem. Soc. **94**, 1496 (1972).
26. R. NORRESTAM and L. SCHEPPER. Acta Chem. Scand. Ser. A: A**35**, 91 (1981).
27. T. M. KRYGOWSKI, G. HÄFELINGER, and J. SCHULE. Z. Naturforsch. B. Anorg. Chem. Org. Chem. **41B**, 895 (1986).
28. J. E. BOGGS and F. R. CORDELL. J. Mol. Struct. (Theochem), **76**, 329 (1981).
29. J. E. BOGGS, F. PANG, and P. PULAY. J. Comput. Chem. **3**, 344 (1982).
30. G. PORTALONE, G. SCHULTZ, A. DOMENICANO, and I. HARGITTAI. J. Mol. Struct. **118**, 53 (1984).
31. C. W. BOCK, M. TRACHTMAN, and P. GEORGE. J. Mol. Struct. (Theochem), **122**, 155 (1985).
32. C. W. BOCK, M. TRACHTMAN, and P. GEORGE. J. Comput. Chem. **6**, 592 (1985).
33. S. C. NYBURG and C. H. FAERMAN. J. Mol. Struct. **140**, 347 (1986).
34. H. KONSCHIN. J. Mol. Struct. **105**, 213 (1983).
35. O. L. STIEFVATER. Z. Naturforsch. A: Phys. Phys. Chem. Kosmophys. **43A**, 155 (1988).
36. A. DOMENICANO and P. MURRAY-RUST. Tetrahedron Lett. 2283 (1979).
37. R. ANULEWICZ, G. HÄFELINGER, T. M. KRYGOWSKI, C. REGELMANN, and G. RITTER. Z. Naturforsch. B: Anorg. Chem. Org. Chem. **42B**, 917 (1987).
38. H. M. HUTTON, B. RICHARDSON, and T. SCHAEFER. Can. J. Chem. **45**, 1795 (1967).

Can. J. Chem. Downloaded from www.nrcresearchpress.com by 41.223.56.140 on 09/07/12
For personal use only.

A selenosulfonation-based approach to (22*S*,23*E*)-6β-methoxy-3α,5-cyclo-5α-ergost-23-en-22-ol, a key intermediate for brassinolide synthesis

THOMAS G. BACK,[1] KURT BRUNNER, M. VIJAYA KRISHNA, AND ENOCH K. Y. LAI
Department of Chemistry, University of Calgary, Calgary, Alta., Canada T2N 1N4

Received August 30, 1988

THOMAS G. BACK, KURT BRUNNER, M. VIJAYA KRISHNA, and ENOCH K. Y. LAI. Can. J. Chem. **67**, 1032 (1989).

(22*S*,23*E*)-6β-Methoxy-3α,5-cyclo-5α-ergost-23-en-22-ol (**2**), an intermediate in the synthesis of brassinolide (**1**) and related compounds, was synthesized by a new approach. (20*S*)-6β-Methoxy-3α,5-cyclo-5α-pregnane-20-carboxaldehyde (**5**) was converted to the corresponding 22*S* and 22*R*-24-yn-22-ol derivatives **6***a* and **6***b* by treatment with 3-lithio-1-trimethylsilylpropyne, followed by tetra-*n*-butylammonium fluoride. The products were subjected to selenosulfonation, base-catalyzed isomerization, and selenoxide elimination to afford the respective 22*S* and 22*R* allenic sulfones **9***a* and **9***b*. The 22*S* isomer **9***a* underwent addition with lithium diisopropylcuprate – dimethyl sulfide complex, followed by reductive desulfonylation with magnesium in methanol, to afford **2**, as well as smaller amounts of its 24(28) isomer **11***a* and (22*E*)-6β-methoxy-3α,5-cyclo-5α-ergosta-22,24(28)-diene (**12**). Similar treatment of **9***b* afforded **13**, the 22*R* isomer of **2**, as the principal product, as well as its 24(28) isomer **11***b*, and diene **12**.

Key words: brassinolide, (22*S*,23*E*)-6β-methoxy-3α,5-cyclo-5α-ergost-23-en-22-ol, selenosulfonation, allenic sulfones.

THOMAS G. BACK, KURT BRUNNER, M. VIJAYA KRISHNA et ENOCH K. Y. LAI. Can. J. Chem. **67**, 1032 (1989).

Utilisant une nouvelle approche, on a réalisé la synthèse du méthoxy-6β cyclo-3α,5 5α-ergostène-23 ol-22 (22*S*,23*E*) (**2**), un intermédiaire dans la synthèse du brassinolide (**1**). En faisant réagir le méthoxy-6β cyclo-3α,5 5α-pregnanecarboxaldéhyde-20 (**5**) avec le lithio-3 triméthylsilyl-1 propyne, puis avec le fluorure de tétra-*n*-butylammonium, on obtient les dérivés correspondants yne-24 ol-22 (22*S* et 22*R*) (**6***a* et **6***b*). Ces produits, soumis successivement à une réaction de sélénosulfonation, à une isomérisation catalysée par les bases et à une élimination de sélénoxyde, fournissent respectivement les sulfones alléniques 22*S* et 22*R* (**9***a* et **9***b*). Lorsqu'on soumet l'isomère 22*S* (**9***a*) à une addition du complexe de diisopropylcuprate de lithium/sulfure de diméthyle puis à une désulfonylation réductrice par le magnésium et le méthanol, on obtient le composé **2** ainsi que de faibles quantités de l'isomère 24(28) (**11***a*) et du méthoxy-6β cyclo-3,5α 5α-ergostadiène-22,24(28) (**12**). Soumis aux mêmes réactions, le produit principal obtenu à partir du composé **9***b* est le composé **13**, l'isomère 22*R* du produit **2**, ainsi que son isomère 24(28) (**11***b*) et le diène **12**.

Mots clés : brassinolide, méthoxy-6β cyclo-3α,5 5α-ergostène-23 ol-22 (22*S*,23*E*), sélénosulfonation, sulfones alléniques.
[Traduit par la revue]

Can. J. Chem. Downloaded from www.nrcresearchpress.com by 41.223.56.140 on 09/07/12
For personal use only.

Introduction

Brassinolide (**1**) is a potent plant-growth promoter that was first isolated in minute quantities from the pollen of *Brassica napus* L. (1). Its biological activity and unusual structure have made it a challenging synthetic target (for reviews, see ref. 2; for previous syntheses, ref. 3). The allylic alcohol (22*S*,23*E*)-6β-methoxy-3α,5-cyclo-5α-ergost-23-en-22-ol (**2**) was employed as a key intermediate in the first synthesis of brassinolide by Fung and Siddall (3*a*), who prepared it from stigmasterol (**3**). Moreover, **2** is a potential precursor of other structurally related steroids such as dolicholide (3*f*, 4), typhasterol (3*c*, 5), and castasterone (3*c*, 3*f*), some of which also display plant growth-promoting activity (3*g*, 6). An alternative synthesis of **2** from ergosterol (**4**) was later described by Fiecchi and co-workers (7) (Scheme 1).

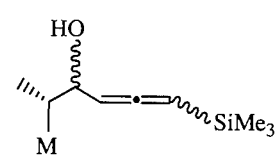
We recently demonstrated that acetylenes can be converted to allenic sulfones by a simple protocol involving selenosulfonation, base-catalyzed isomerization, and selenoxide elimination (8) (Scheme 2). A related selenosulfonation-based method was previously employed for the synthesis of the marine sterols 24,28-dehydroaplysterol, xestosterol, and ostreasterol (9). We now report a new synthesis of the allylic alcohol **2**, using the novel addition of an organocuprate to an allenic sulfone obtained via the method shown in Scheme 2 as the key step in the elaboration of the steroid side chain.

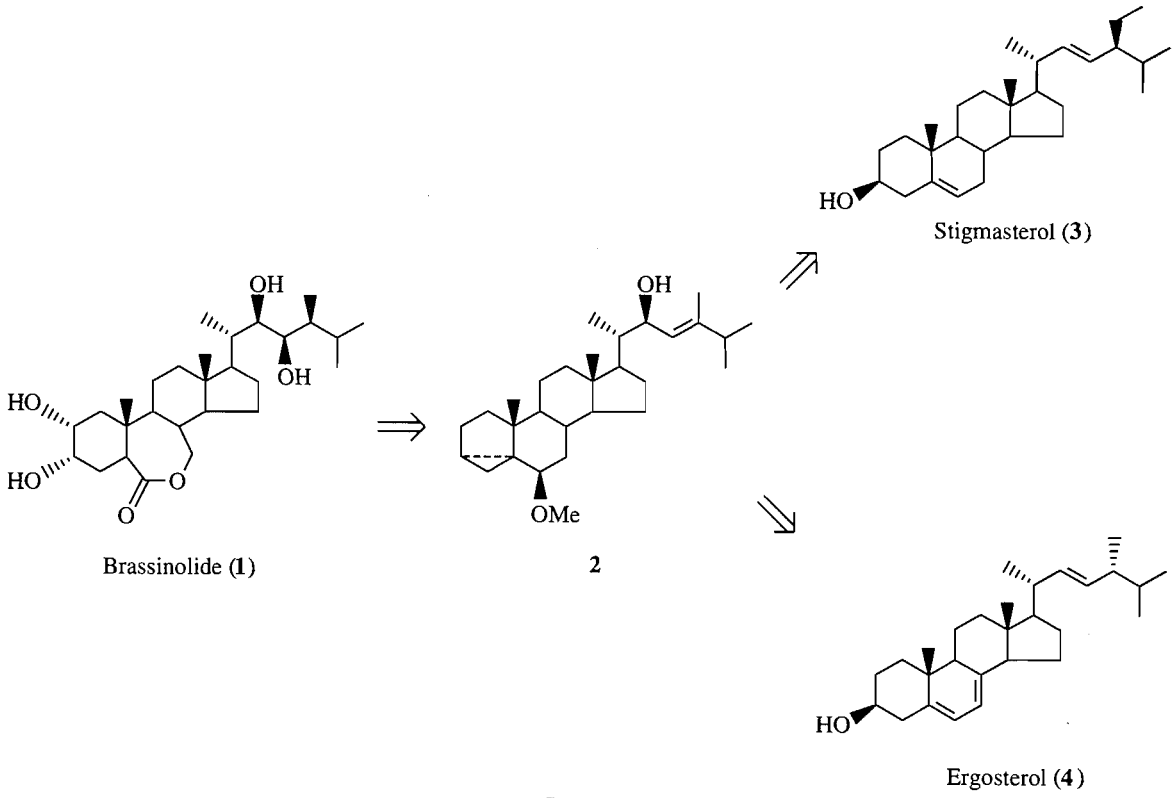
[1]Author to whom correspondence may be addressed.

Results and discussion

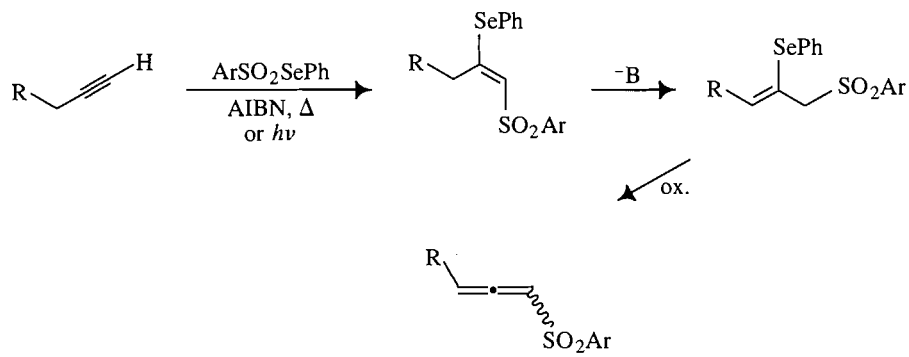
The synthesis of the required allenic sulfone precursor of the allylic alcohol **2** is summarized in Scheme 3. The aldehyde **5**, readily available from stigmasterol by a literature method (10), was treated with 3-lithio-1-trimethylsilylpropyne (11) to afford a 1.32:1 mixture of the epimeric C-22 alcohols **6***a* and **6***b*, obtained in 64% yield[2] after desilylation with tetra-*n*-butylammonium fluoride. The mixture of **6***a*,*b* was subjected to free-radical selenosulfonation with Se-phenyl *p*-tolueneselenosulfonate to afford, as expected (12), exclusively the products of *anti* addition **7***a*,*b*, respectively. The two C-22 epimers could be separated chromatographically at this stage, and elaborated further independently. However, it proved more convenient to postpone the separation until a later point in the synthesis (*vide infra*). Base-catalyzed isomerization of **7***a*,*b* produced the allylic sulfones **8***a*,*b*, tentatively depicted with the

[2]The ratio is based on the isolated yields of the corresponding C-22 epimers **7***a* and **7***b* obtained after selenosulfonation. The addition of 3-lithio-1-trimethylsilylpropyne to **5** also produced 22–24% of the corresponding allene stereoisomers:





SCHEME 1



SCHEME 2

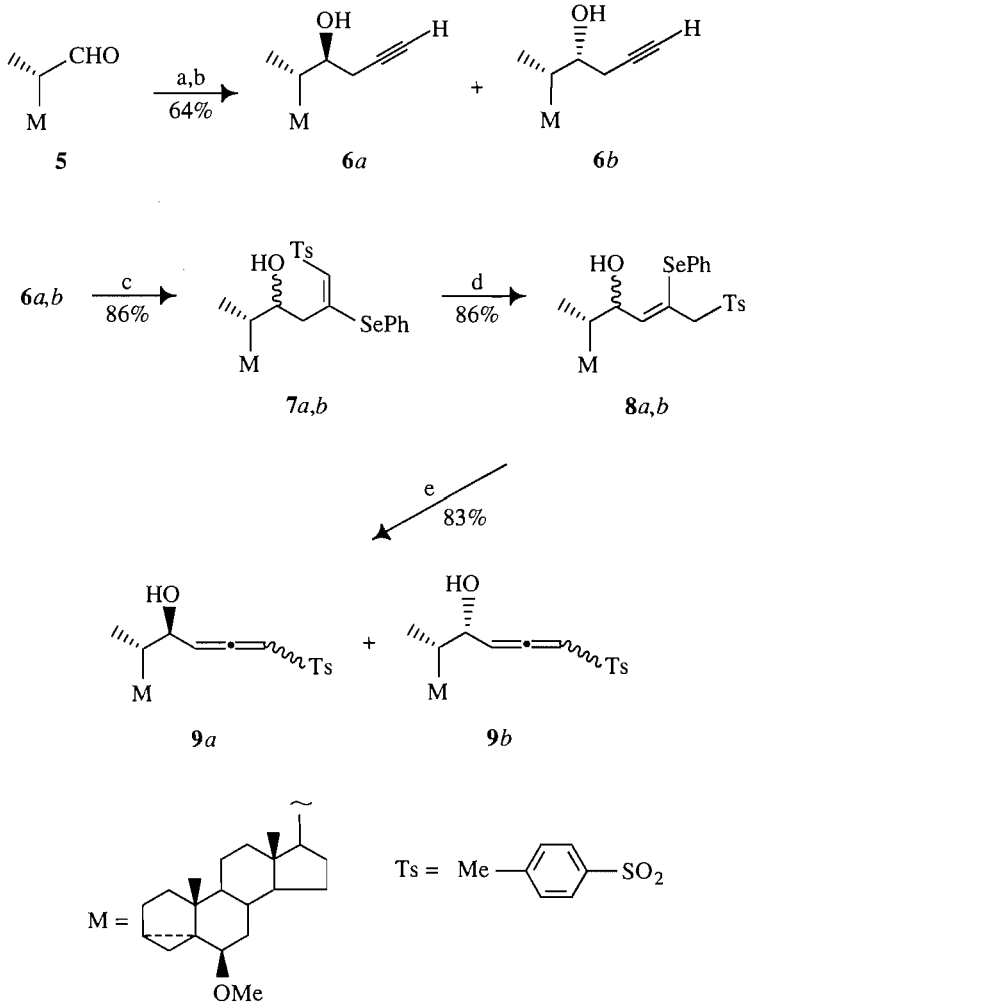
Z configuration. Oxidation of **8***a*,*b*, followed by selenoxide *syn*-elimination, was induced with *tert*-butyl hydroperoxide (13),[3] cleanly providing the allenic sulfones **9***a*,*b*, and no significant quantities of their corresponding acetylenic sulfone regioisomers. The regioselectivity of the selenoxide elimination can be attributed to either the activating effect of the sulfone group, or the *Z* configuration of **8***a*,*b*, which would preclude acetylene formation because of the unavailability of a *cis* vinylic hydrogen required for the *syn*-elimination. Furthermore, since the allene moiety is chiral, each C-22 epimer of **9***a*,*b* was formed as a mixture of two diastereomers. The epimers **9***a* and **9***b* could be easily separated by flash chromatography at this point, but attempted separation of the two allene diastereomers of each epimer was unsuccessful, and fortunately unnecessary.

[3]For the previous use of this oxidant in selenoxide eliminations, see ref. 13*a*; for the formation of other allenes via selenoxide elimination, see ref. 13*b*.

The further transformations of the latter products are shown in Scheme 4. The mixtures of allene stereoisomers of the C-22 epimers **9***a* and **9***b* were individually treated with lithium diisopropyl cuprate – dimethyl sulfide complex (i-$Pr_2CuLi \cdot SMe_2$) to afford the allylic sulfones **10***a* and **10***b*, in yields of 52% and 56%, respectively. Whereas organocuprate additions to vinyl sulfones are known (14), this represents, to our knowledge, the first example of such an addition to an allenic sulfone. The olefin geometry was established in each case by ^{1}H nmr nOe difference spectroscopy. Evidently, addition of the cuprate occurs with high selectivity to the sulfone-substituted π-bond from the less hindered side (Scheme 5), resulting in products with the 23*Z* configuration. The unmasked C-22 hydroxyl group does not appear to play a role in determining the direction of addition by complexing with the cuprate reagent, as evidenced by the formation of only the (*Z*) isomer from either of the C-22 alcohol epimers.

To complete the synthesis of the desired allylic alcohol **2**,

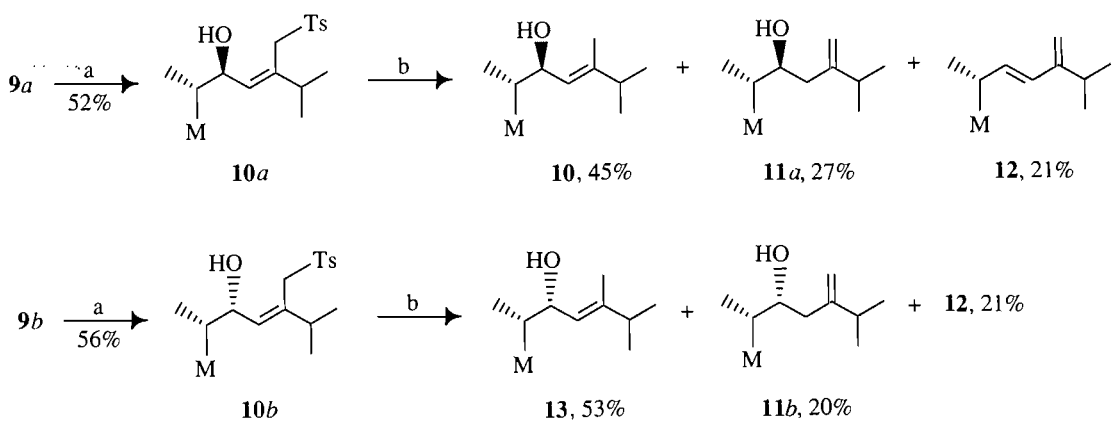
Can. J. Chem. Downloaded from www.nrcresearchpress.com by 41.223.56.140 on 09/07/12
For personal use only.



(a) $LiCH_2C{\equiv}CSiMe_3$ (b) n-$Bu_4N^+F^-$ (c) TsSePh, $h\nu$

(d) Et_3N, toluene, Δ (e) t-BuOOH

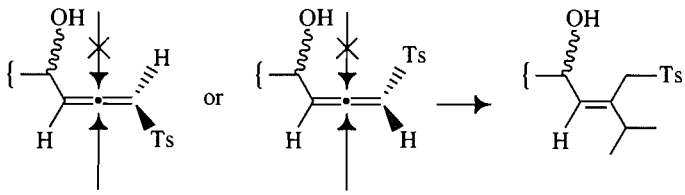
SCHEME 3



(a) i-$Pr_2CuLi{\cdot}SMe_2$ (b) Mg, MeOH

SCHEME 4

Can. J. Chem. Downloaded from www.nrcresearchpress.com by 41.223.56.140 on 09/07/12
For personal use only.



SCHEME 5

allylic sulfone **10***a* was subjected to reductive desulfonylation. Although a number of methods are reported to be effective for the desulfonylation of various types of unsaturated sulfones (15), the best results in the present case were obtained with magnesium in methanol (16). Sulfone **10***a* thus afforded **2** as the principal product, along with its isomer **11***a* and diene **12**, the product of reductive elimination. Similarly, the C-22 epimer **10***b* furnished allylic alcohol **13**, its isomer **11***b*, and diene **12**. Products **2**, **12**, and **13** had physical and spectral properties consistent with those reported in the literature (3*a*, 7). The structures of **2** and **13** were further confirmed by ^{1}H nmr nOe difference spectroscopy. Since **2** has been previously converted to brassinolide (**1**) (3*a*), these results constitute a formal synthesis of the latter sterol.

Experimental

Melting points were determined on an A. H. Thomas hot-stage apparatus and are uncorrected. The ir spectra were recorded on a Nicolet 5DX spectrometer as thin films. The ^{1}H and ^{13}C nmr spectra were recorded on a Bruker ACE 200 or a Bruker AM 400 spectrometer, operating at 200 and 400 MHz, respectively, in deuteriochloroform solvent with either chloroform or tetramethylsilane as the internal standard. Mass spectra were recorded on a Kratos MS80 or a VG 7070 spectrometer. Optical rotations were measured on a Rudolph Autopol III polarimeter in chloroform solution. Elemental analyses were obtained by Dr. W. S. Lin, using the analytical facilities of the Department of Chemical Engineering, courtesy of Mr. L. Dornan. Preparative tlc was carried out on Analtech 20 × 20 cm glass plates coated with 1 mm of silica gel GF. Flash chromatography was performed on Merck silica gel, 60–200 mesh. A Rayonet RMR-500 reactor equipped with four 254-nm lamps was employed for selenosulfonations.

THF was distilled from $LiAlH_4$ prior to use, and air- or moisture-sensitive materials were handled under argon. Aldehyde **5** was obtained by a literature method (10), as was Se-phenyl *p*-tolueneselenosulfonate (17). All other reagents were purchased from commercial sources and purified by standard methods as required.

*6β-Methoxy-3α,5-cyclo-5α-26,27-dinorcholest-24-yn-22-ol (**6**a,b)*

n-Butyllithium in hexane (9.00 mmol) was added to a solution of 1-trimethylsilylpropyne (1.33 mL, 9.00 mmol) in 20 mL of THF at 0°C. After 10 min, the solution was cooled to −78°C and aldehyde **5** (2.00 g, 5.81 mmol) in 30 mL of THF was added dropwise. The mixture was stirred at −78°C for 3 h, quenched with aqueous NH_4Cl solution, and warmed to room temperature. The product was diluted with ether, washed with aqueous NaCl solution, dried (anhydrous $MgSO_4$), and evaporated *in vacuo*. Flash chromatography (elution with 5% ethyl acetate – hexane) afforded 1.70 g (64%) of a mixture of C-22 epimers of the silylacetylene as a viscous oil; ir: 3434, 2175, 1249, 1099, 842, 759 cm^{-1}; ^{1}H nmr (400 MHz) δ: 3.85 (m, 1H), 3.32 (s, 3H), 2.76 (m, 1H), 1.02 (s, 3H), 0.91 (two overlapping d each with J = 6.7 Hz, total 3H), 0.74 and 0.73 (two s, total 3H), 0.15 (s, 9H); mass spectrum, *m/e* (relative intensity, %): 456 (M^+, 4), 441 (M^+ − Me, 4), 424 (16), 43 (100).

The preceding product (1.485 g, 3.25 mmol) and tetra-*n*-butylammonium fluoride (6.5 mL of a 1 M THF solution, 6.5 mmol) were stirred in 40 mL of THF at 0°C for 25 min. The solution was then diluted with ether, washed with aqueous NaCl solution, dried (anhydrous $MgSO_4$), and evaporated *in vacuo* to afford 1.25 g (100%) of the title compound **6***a,b* (mixture of C-22 epimers) as a viscous oil of sufficient purity for further use; ir: 3419, 3310, 2119, 1098, 733 cm^{-1}; ^{1}H nmr (200 MHz) δ: 3.90 (m, 1H), 3.33 and 3.32 (two s, total 3H), 2.77 (m, 1H), 1.02 (s, 3H), 0.93 and 0.92 (two overlapping d each with J = 6.8 Hz, total 3H), 0.74 and 0.73 (two s, total 3H); mass spectrum, *m/e* (relative intensity, %): 384 (M^+, 12), 369 (27), 352 (27), 329 (55), 41 (100).

*(24E)-6β-Methoxy-24-(phenylseleno)-25-(*p*-toluenesulfonyl)-3α,5-cyclo-5α-26,27-dinorcholest-24-en-22-ol (**7**a,b)*

The mixture of **6***a,b* (113 mg, 0.29 mmol) produced in the preceding experiment and Se-phenyl *p*-tolueneselenosulfonate (110 mg, 0.35 mmol) were dissolved in 2 mL of benzene and irradiated with uv light for 4.5 h. The products were purified by flash chromatography (elution with 15% ethyl acetate – hexane) to afford 175 mg (86%) of the unseparated epimers **7***a,b*. When the reaction was performed similarly with 6.09 mmol of **6***a,b*, the products **7***a,b* were obtained in 82% yield. A portion of this mixture was separated by preparative tlc (25% ethyl acetate – hexane) to provide **7***a* and **7***b* in the ratio of 1.32:1. Compound **7***a* (22*S*) was a pale yellow oil, R_f 0.52; ir: 3507, 1596, 1588, 1316, 1302, 1289, 1144, 1085, 733 cm^{-1}; ^{1}H nmr (200 MHz) δ: 7.68 (d, J = 8.3 Hz, 2H), 7.57–7.27 (complex, 7H), 6.00 (s, 1H), 3.99 (m, 1H), 3.46 (dd, J = 14.0, 10.0 Hz, 1H), 3.33 (s, 3H), 2.78 (m, 1H), 2.42 (s superimposed on dd at δ 2.48, J = 14.0, 2.7 Hz, total 4H), 1.03 (s, 3H), 0.99 (d, J = 6.3 Hz, 3H), 0.73 (s, 3H). *Anal.* calcd. for $C_{39}H_{52}O_4SSe$: C 67.30, H 7.55; found: C 67.31, H 7.39. Compound **7***b* (22*R*) was a pale yellow oil, R_f 0.44; ir: 3512, 1596, 1575, 1314, 1303, 1289, 1143, 1084, 733 cm^{-1}; ^{1}H nmr (200 MHz) δ: 7.68 (d, J = 8.4 Hz, 2H), 7.56–7.27 (complex, 7H), 6.01 (s, 1H), 4.02 (m, 1H), 3.44 (dd, J = 14.1, 10.9 Hz, 1H), 3.32 (s, 3H), 3.10 (d, J = 8.0 Hz, 1H, exchanged in D_2O), 2.77 (m, 1H), 2.42 (s superimposed on dd at δ 2.36, J = 14.2, 1.95 Hz, total 4H), 1.03 (s, 3H), 1.01 (d, J = 6.4 Hz, 3H), 0.76 (s, 3H). *Anal.* calcd. for $C_{39}H_{52}O_4SSe$: C 67.30, H 7.55; found: C 66.57, H 7.60.

*6β-Methoxy-24-(phenylseleno)-25-(*p*-toluenesulfonyl)-3α,5-cyclo-5α-26,27-dinorcholest-23-en-22-ol (**8**a,b)*

The mixture of **7***a,b* (2.39 g, 3.43 mmol) was refluxed for 35 h in a mixture of 30 mL of triethylamine and 50 mL of toluene. Evaporation of volatile material, followed by flash chromatography (elution with 50% ethyl acetate – hexane), produced 2.06 g (86%) of the mixture of epimers **8***a,b*. The reaction was repeated separately with pure **7***a* and **7***b* to afford pure **8***a* and **8***b*, respectively. Compound **8***a* (22*S*) was a solid foam; ir: 3476, 1598, 1579, 1318, 1303, 1137, 1086 cm^{-1}; ^{1}H nmr (200 MHz) δ: 7.68 (d, J = 8.3 Hz, 2H), 7.35–7.24 (complex, 7H), 6.25 (d, J = 7.3 Hz, 1H), 4.65 (crude d, J = 7.6 Hz, 1H), 3.86 (AB quartet, J = 14.5 Hz, 2H), 3.33 (s, 3H), 2.78 (m, 1H), 2.47 (s, 3H), 1.04 (s, 3H), 0.895 (d, J = 6.3 Hz, 3H), 0.73 (s, 3H). *Anal.* calcd. for $C_{39}H_{52}O_4SSe$: C 67.30, H 7.55; found: C 67.29, H 7.81. Compound **8***b* (22*R*) was a solid foam; ir: 3502, 1597, 1578, 1319, 1303, 1137, 1086 cm^{-1}; ^{1}H nmr (200 MHz) δ: 7.71 (d, J = 8.3 Hz, 2H), 7.36–7.26 (complex, 7H), 6.20 (d, J = 8.8 Hz, 1H), 4.59 (dd, J = 8.8, 3.5 Hz, 1H), 3.91 (AB quartet, J = 14.5 Hz, 2H), 3.34 (s, 3H), 2.80 (m, 1H), 2.48 (s, 3H), 1.035 (s, 3H), 1.02 (d, J = 6.4 Hz, 3H), 0.76 (s, 3H). *Anal.* calcd. for $C_{39}H_{52}O_4SSe$: C 67.30, H 7.55; found: C 67.17, H 7.69.

*6β-Methoxy-25-(*p*-toluenesulfonyl)-3α,5-cyclo-5α-26,27-dinorcholesta-23,24-dien-22-ol (**9**a,b)*

The mixture of **8***a,b* (2.06 g, 2.96 mmol) and *tert*-butyl hydroperoxide (25 mL of ca. 90% solution in *tert*-butanol) was stirred for 8 h in 50 mL of chloroform. The solution was then evaporated and the residue was separated by flash chromatography (elution with 10% ethyl acetate – hexane) to afford 0.76 g (47.4%) of the less polar 22*S* epimer **9***a* (mixture of allene diastereomers), followed by 0.57 g (35.4%) of the more polar 22*R* epimer **9***b* (mixture of allene diastereomers).

Can. J. Chem. Downloaded from www.nrcresearchpress.com by 41.223.56.140 on 09/07/12
For personal use only.

Can. J. Chem. Downloaded from www.nrcresearchpress.com by 41.223.56.140 on 09/07/12
For personal use only.

Compound **9***a* was a pale yellow oil;[4] ir: 3504, 1956, 1597, 1320, 1303, 1146, 1085, 733 cm^{-1}; ^1H nmr (200 MHz) δ: 7.80 (d, J = 8.3 Hz, 2H), 7.34 (d, J = 8.4 Hz, 2H), 6.34 (m, 1H), 5.89 (m, 1H), 4.47 (m, 1H), 3.33 (s, 3H), 2.78 (m, 1H), 2.44 (s, 3H), 1.03 (s, 3H), 0.72 (s, 3H). Compound **9***b* was a pale yellow oil;[4] ir: 3508, 1958, 1598, 1324, 1304, 1146, 1086, 755 cm^{-1}; ^1H nmr (200 MHz) δ: 7.80 (d, J = 8.3 Hz, 2H), 7.34 (d, J = 8.3 Hz, 2H), 6.28 (m, 1H), 5.88 (m, 1H), 4.41 (m, 1H), 3.33 and 3.32 (two s, total 3H), 2.44 (s, 3H), 1.02 (s, 3H), 0.75 and 0.74 (two s, total 3H).

*(22S,23Z)-6β-Methoxy-28-(p-toluenesulfonyl)-3α,5-cyclo-5α-ergost-23-en-22-ol (**10**a)*

Isopropyllithium (2.06 mmol) in petroleum ether (bp 30–60°C) was added to a stirred suspension of cuprous bromide – dimethyl sulfide complex (212 mg, 1.03 mmol) in 10 mL of THF at −78°C. After 45 min, the allenic sulfone **9***a* (111 mg, 0.206 mmol) in 1 mL of THF was added and stirring at −78°C was continued for 14 h. The reaction was then quenched with aqueous NH_4Cl solution, dried (anhydrous $MgSO_4$), filtered through Celite, and evaporated *in vacuo*. The residue was separated by preparative tlc in 28% ethyl acetate – hexane to afford 62 mg (52%) of **10***a* as a pale yellow oil,[4] R_f 0.52; ir: 3508, 1597, 1316, 1303, 1143, 1086, 733 cm^{-1}; ^1H nmr (200 MHz) δ: 7.78 (d, J = 8.3 Hz, 2H), 7.36 (d, J = 8.0 Hz, 2H), 5.72 (d, J = 7.0 Hz), 4.27 (crude d, J = 6.3 Hz, 1H), 4.02 (AB quartet, J = 13.5 Hz, 2H), 3.33 (s, 3H), 2.78 (m, 1H), 2.46 (s, 3H), 2.24 (m, 1H), 1.02 (s, 3H), 1.02 (d, J = 7 Hz, collapsed to s with double irradiation at δ 2.24, 3H), 0.98 (d, J = 7 Hz, collapsed to s with double irradiation at δ 2.24, 3H), 0.95 (d, J = 6.3 Hz, 3H), 0.71 (s, 3H). Irradiation of the vinylic proton at δ 5.72 produced nOe enhancement of the signals at δ 1.02 and 0.98 assigned to the *i*-propyl group, but not of the AB quartet at δ 4.02 assigned to the C-28 methylene protons.

*(22R,23Z)-6β-Methoxy-28-(p-toluenesulfonyl)-3α,5-cyclo-5α-ergost-23-en-22-ol (**10**b)*

The 22*R* epimer **10***b* was prepared in 56% yield from **9***b* according to the preceding procedure. The product was purified by preparative tlc in 28% ethyl acetate – hexane, to afford a pale yellow oil,[4] R_f 0.39; ir: 3511, 1597, 1316, 1303, 1145, 1086, 733 cm^{-1}; ^1H nmr (400 MHz) δ: 7.80 (d, J = 8.3 Hz, 2H), 7.37 (d, J = 8.0 Hz, 2H), 5.81 (d, J = 9.2 Hz, 1H), 4.28 (m, 1H), 3.99 (AB quartet, J = 13.5 Hz, 2H), 3.32 (s, 3H), 2.75 (m, 1H), 2.46 (s, 3H), 2.09 (m, 1H), 1.04 (d, J = 6.7 Hz, 3H), 1.01 (s superimposed on d, J = 6.7 Hz, total 6H), 0.95 (d, J = 6.8 Hz, 3H), 0.74 (s, 3H). Irradiation of the vinylic proton at δ 5.81 produced nOe enhancement of the signals at δ 1.04 and 1.01 assigned to the *i*-propyl group, but not of the AB quartet at δ 3.99 assigned to the C-28 methylene protons.

*(22S,23E)-6β-Methoxy-3α,5-cyclo-5α-ergost-23-en-22-ol (**2**)*

Magnesium turnings (265 mg, 11 mg-atom) were warmed to 45–50°C in 6 mL of methanol. When hydrogen evolution commenced, the allylic sulfone **10***a* (100 mg, 0.172 mmol) was added in 1 mL of THF. The mixture was stirred at room temperature for 2.5 h. The mixture was concentrated; 5 mL of 20% aqueous NH_4Cl was added, and the product was extracted three times with ether, dried (anhydrous $MgSO_4$), and evaporated *in vacuo*. Flash chromatography (elution with 5% ethyl acetate – hexane) afforded, in order of elution, 15 mg (21%) of diene **12**, 20 mg (27%) of the 24(28) isomer **11***a*, and 33 mg (45%) of the title compound. Diene **12** had mp 72–76°C (from methanol) (lit. (7) mp 79–81°C), and spectra in close agreement with the literature (7). Compound **11***a* was a pale yellow oil; ir: 3459, 1638, 1099, 892, 734 cm^{-1}; ^1H nmr (200 MHz) δ: 4.89 (crude s, 1H), 4.79 (crude s, 1H), 3.81 (m, 1H), 3.33 (s, 3H), 2.77 (m, 1H), 2.20 (m, 1H), 1.06 (d, J = 6.8 Hz, 3H), 1.03 (d, J = 6.8 Hz, 3H), 1.02 (s, 3H), 0.94 (d, J = 6.3 Hz, 3H), 0.73 (s, 3H); mass spectrum *m/e* (relative intensity, %): 428 (M^+, 1.4), 343 (35), 312 (85), 83 (100). Product **2** had R_f 0.65 (silica gel, 30% ethyl acetate – hexane),[5] mp 128–130°C (from moist methanol) (lit. (3*a*) mp 127–129°C); $[\alpha]_D$ +34° (lit. (7) $[\alpha]_D$ +37°); and an ^1H nmr spectrum in close agreement with the literature (3*a*, 7). In addition, the 23*E* configuration was confirmed by nOe experiments, where irradiation of the vinylic methyl signal resulted in enhancement of the signal assigned to the C-22 proton. ^{13}C nmr δ: 142.9 (s), 125.1 (d), 82.6 (d), 70.7 (d).

*(22R,23E)-6β-Methoxy-3α,5-cyclo-5α-ergost-23-en-22-ol (**13**)*

Allyl sulfone **10***b* (146 mg, 0.25 mmol) was reduced and the products were separated by flash chromatography (elution with 10% ethyl acetate – hexane) as described in the preceding procedure. The products obtained were, in order of elution, 22 mg (21%) of diene **12**, 21 mg (20%) of the 24(28) isomer **11***b*, and 57 mg (53%) of **13**. Diene **12** was identical to the sample obtained in the previous procedure in all respects. Compound **11***b* was a pale yellow oil; ir: 3464, 1639, 1099, 757 cm^{-1}; ^1H nmr (200 MHz) δ: 4.93 (s, 1H), 4.83 (s, 1H), 3.75 (m, 1H), 3.33 (s, 3H), 2.77 (m, 1H), 2.20 (m, 1H), 1.08 (d, J = 6.0 Hz, 3H), 1.05 (d, J = 7.2 Hz, 3H), 1.03 (s, 3H), 0.95 (d, J = 6.7 Hz, 3H), 0.76 (s, 3H); mass spectrum, *m/e* (relative intensity, %): 428 (M^+, 2.0), 343 (30), 312 (78), 83 (100). Product **13** had R_f 0.50 (silica gel, 30% ethyl acetate – hexane);[5] ir: 3460, 1665, 1099, 1016, 734 cm^{-1}; ^1H nmr (200 MHz) δ: 5.29 (crude d, J = ca. 9.5 Hz, 1H), 4.42 (dd, J = 9.7, 3.6 Hz, 1H), 3.32 (s, 3H), 2.76 (m, 1H), 2.27 (m, 1H), 1.69 (d, J = 1.3 Hz, 3H), 1.04–0.99 (complex, overlapping resonances from *i*-Pr, C-21 and C-19 methyl groups, total 12H), 0.73 (s, 3H). Irradiation of the vinylic methyl signal at δ 1.69 resulted in nOe enhancement of the signal assigned to the C-22 proton at δ 4.42; ^{13}C nmr δ: 146.5 (s), 120.5 (d), 82.4 (d), 69.6 (d).

Acknowledgements

We thank the Natural Sciences and Engineering Research Council of Canada for financial support and Drs. R. Yamdagni and W. S. Lin for assistance in recording certain spectra.

1. M. D. Grove, G. F. Spencer, W. K. Rohwedder, N. Mandava, J. F. Worley, J. D. Warthen, Jr., G. L. Steffens, J. L. Flippen-Anderson, and J. C. Cook, Jr. Nature (London), **281**, 216 (1979).
2. (*a*) S. C. Chen. Chem. Can. **35**, 13 (September, 1983); (*b*) H. Singh and T. R. Bhardwaj. Indian J. Chem. Sect. B, **25B**, 989 (1986).
3. (*a*) S. Fung and J. B. Siddall. J. Am. Chem. Soc. **102**, 6580 (1980); (*b*) M. Ishiguro, S. Takatsuto, M. Morisaki, and N. Ikekawa. J. Chem. Soc. Chem. Commun. 962 (1980); (*c*) S. Takatsuto, N. Yazawa, M. Ishiguro, M. Morisaki, and N. Ikekawa. J. Chem. Soc. Perkin Trans. 1, 139 (1984); (*d*) K. Mori, M. Sakakibara, Y. Ichikawa, H. Ueda, K. Okada, T. Umemura, G. Yabuta, S. Kuwahara, M. Kondo, M. Minobe, and A. Sogabe. Tetrahedron, **38**, 2099 (1982); (*e*) M. Sakakibara, K. Okada, Y. Ichikawa, and K. Mori. Heterocycles, **17**, 301 (1982); (*f*) K. Mori, M. Sakakibara, and K. Okada. Tetrahedron, **40**, 1767 (1984); (*g*) M. J. Thompson, N. B. Mandava, W. J. Meudt, W. R. Lusby, and D. W. Spaulding. Steroids, **38**, 567 (1981); (*h*) J. R. Donaubauer, A. M. Greaves, and T. C. McMorris. J. Org. Chem. **49**, 2833 (1984); (*i*) T. Kametani, T. Katoh, M. Tsubuki, and T. Honda. J. Am. Chem. Soc. **108**, 7055 (1986).
4. K. Okada and K. Mori. Agric. Biol. Chem. **47**, 925 (1983).
5. W.-S. Zhou and W.-S. Tian. Tetrahedron, **43**, 3705 (1987).
6. (*a*) M. J. Thompson, W. J. Meudt, N. B. Mandava, S. R. Dutky, W. R. Lusby, and D. W. Spaulding. Steroids, **39**, 89 (1982); (*b*) S. Takatsuto, N. Yazawa, N. Ikekawa, T.

[4]The viscous, oily nature of compounds **9** and **10** precluded satisfactory analyses, presumably due to the retention of traces of solvent. High resolution mass spectra for these compounds could not be obtained because of their failure to display molecular ions.

[5]Fung and Siddall (3*a*) reported that the 22*R* epimer **13** is less polar than the 22*S* epimer **2**, whereas Fiecchi and co-workers (7) noted the reverse. Our observations are in accord with the latter authors.

TAKEMATSU, Y. TAKEUCHI, and M. KOGUCHI. Phytochemistry, **22**, 2437 (1983).
7. M. ANASTASIA, P. ALLEVI, P. CIUFFREDA, A. FIECCHI, and A. SCALA. J. Org. Chem. **49**, 4297 (1984).
8. T. G. BACK, M. V. KRISHNA, and K. R. MURALIDHARAN. Tetrahedron Lett. **28**, 1737 (1987).
9. T. G. BACK, J. R. PROUDFOOT, and C. DJERASSI. Tetrahedron Lett. **27**, 2187 (1986).
10. (*a*) J. A. STEELE and E. MOSETTIG. J. Org. Chem. **28**, 571 (1963); (*b*) J. J. PAPPAS, W. P. KEAVENEY, E. GANCHER, and M. BERGER. Tetrahedron Lett. 4273 (1966); (*c*) R. F. N. HUTCHINS, J. J. THOMPSON, and J. A. SVOBODA. Steroids, **15**, 113 (1970); (*d*) W. G. SALMOND and M. C. SOBALA. Tetrahedron Lett. 1695 (1977).
11. E. J. COREY and H. A. KIRST. Tetrahedron Lett. 5041 (1968).
12. (*a*) T. G. BACK, S. COLLINS, and R. G. KERR. J. Org. Chem. **48**, 3077 (1983); (*b*) T. G. BACK, S. COLLINS, U. GOKHALE, and K.-W. LAW. J. Org. Chem. **48**, 4776 (1983); (*c*) T. MIURA and M. KOBAYASHI. J. Chem. Soc. Chem. Commun. 438 (1982).
13. (*a*) T. HORI and K. B. SHARPLESS. J. Org. Chem. **43**, 1689 (1978); (*b*) H. J. REICH and W. W. WILLIS, JR. J. Am. Chem. Soc. **102**, 5967 (1980).
14. (*a*) G. H. POSNER and D. J. BRUNELLE. J. Org. Chem. **38**, 2747 (1973); (*b*) D. K. HUTCHINSON, S. A. HARDINGER, and P. L. FUCHS. Tetrahedron Lett. **27**, 1425 (1986); (*c*) D. K. HUTCHINSON and P. L. FUCHS. Tetrahedron Lett. **27**, 1429 (1986); (*d*) J. J. EISCH and J. E. GALLE. J. Org. Chem. **44**, 3277 (1979); (*e*) M. JULIA, A. RIGHINI, and J.-N. VERPEAUX. Tetrahedron Lett. 2393 (1979); (*f*) V. FIANDANESE, G. MARCHESE, and F. NASO. Tetrahedron Lett. 5131 (1978).
15. (*a*) R. V. C. CARR, R. V. WILLIAMS, and L. A. PAQUETTE. J. Org. Chem. **48**, 4976 (1983); (*b*) V. PASCALI and A. UMANI-RONCHI. J. Chem. Soc. Chem. Commun. 351 (1973); (*c*) J. BREMNER, M. JULIA, M. LAUNAY, and J.-P. STACINO. Tetrahedron Lett. **23**, 3265 (1982); (*d*) J.-L. FABRE and M. JULIA. Tetrahedron Lett. **24**, 4311 (1983); (*e*) T. CUVIGNY, C. HERVE DU PENHOAT, and M. JULIA. Tetrahedron, **43**, 859 (1987); (*f*) M. MOHRI, H. KINOSHITA, K. INOMATA, and H. KOTAKE. Chem. Lett. 451 (1985); (*g*) K. INOMATA, S. IGARASHI, M. MOHRI, T. YAMAMOTO, H. KINOSHITA, and H. KOTAKE. Chem. Lett. 707 (1987).
16. A. C. BROWN and L. A. CARPINO. J. Org. Chem. **50**, 1749 (1985).
17. T. G. BACK, S. COLLINS, and M. V. KRISHNA. Can. J. Chem. **65**, 38 (1987).

Can. J. Chem. Downloaded from www.nrcresearchpress.com by 41.223.56.140 on 09/07/12
For personal use only.

Structural analysis of the specific capsular polysaccharide of *Streptococcus pneumoniae* type 22F[1]

JAMES C. RICHARDS AND MALCOLM B. PERRY[2]
Division of Biological Sciences, National Research Council of Canada, Ottawa, Ont., Canada K1A 0R6

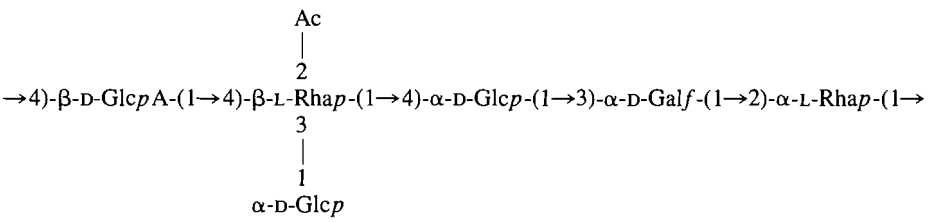
AND

PETER J. KNISKERN
Merck, Sharp and Dohme Research Laboratories, West Point, PA 19486, U.S.A.

Received December 5, 1988

JAMES C. RICHARDS, MALCOLM B. PERRY, and PETER J. KNISKERN. Can. J. Chem. **67**, 1038 (1989).

The structure of the specific capsular polysaccharide produced by *Streptococcus pneumoniae* type 22F (American type 22) was investigated by high-field ^1H and ^{13}C nuclear magnetic resonance spectroscopy, composition, methylation analysis, and periodate oxidation studies. The polysaccharide was found to be a high molecular weight acidic polymer composed of D-glucose, D-galactose, D-glucuronic acid, and L-rhamnose residues to form a regular repeating hexasaccharide unit having the structure

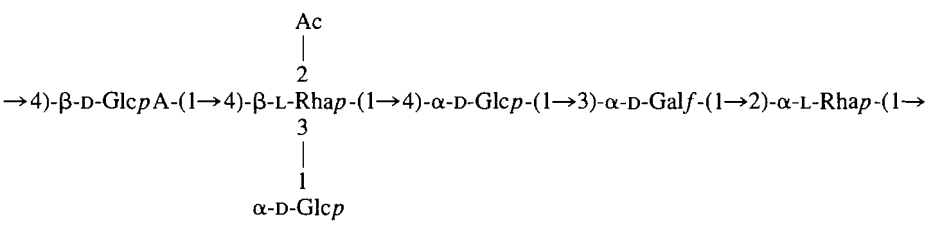


in which the β-L-rhamnopyranosyl residues were substituted by *O*-acetyl groups in 80% of the repeating units. The ^1H and ^{13}C nmr resonances of the *O*-deacetylated type 22F polysaccharide were completely assigned by application of two-dimensional homo- and heteronuclear chemical shift correlation techniques.

Key words: *Streptococcus pneumoniae* polysaccharide, NMR analysis.

JAMES C. RICHARDS, MALCOLM B. PERRY et PETER J. KNISKERN. Can. J. Chem. **67**, 1038 (1989).

Faisant appel à des études par résonance magnétique nucléaire du ^1H et du ^{13}C, d'analyses de composition et de méthylation ainsi que par des oxydations periodiques, on a étudié la structure du polysaccharide capsulaire spécifique produit par le *Streptococcus pneumoniae* de type 22 (américain de type 22). On a trouvé que le polysaccharide est un polymère acide de poids moléculaire élevé, composé de résidus de D-glucose, de D-galactose, d'acide D-glucuronique et de L-rhamnose formant une unité hexasaccharide régulière de structure



dans laquelle les résidus β-L-rhamnopyrannosyles ont été substitués par des groupements acétyles dans 80% des unités qui se répètent. En se basant sur des techniques de corrélations des déplacements chimiques homo- et hétéro-nucléaires bi-dimensionnels, on a pu attribuer toutes les raies observées dans les spectres rmn du ^1H et du ^{13}C du polysaccharide de type 22F *O*-désacétylé.

Mots clés : Polysaccharide de *Streptococcus pneumoniae*, analyse RMN.

[Traduit par la revue]

Introduction

The cell surface capsular polysaccharides of *Streptococcus pneumoniae* are the type specific immunological determinants of these microorganisms and have received considerable attention because of their successful use as vaccines for the prevention of pneumococcal pneumonia (1, 2). Eighty-four serologically defined types of *S. pneumoniae* are recognized, of which the pneumococcal vaccine currently in use in North America contains the capsular polysaccharides of 23 serotypes (3, 4). Within the group 22 *S. pneumoniae*, two serotypes, 22F and 22A, are recognized from the use of factor serum (3). Type 22F accounts for 99% of pneumococcal infections caused by the group 22 organisms and the capsular polysaccharide of *S. pneumoniae* type 22F is included as a component of the current 23-valent human pneumococcal vaccine (4).

The structural analysis of the 22F pneumococcal polysaccharide was undertaken to provide information on the relationship of its molecular structure to its immunobiological activities and cross-serological properties, and to establish physical and chemical criteria for the determination of its purity in commercial biologicals.

[1]Issued as NRCC No. 30117.

[2]Author to whom correspondence may be addressed.

Can. J. Chem. Downloaded from www.nrcresearchpress.com by 41.223.56.140 on 09/07/12
For personal use only.

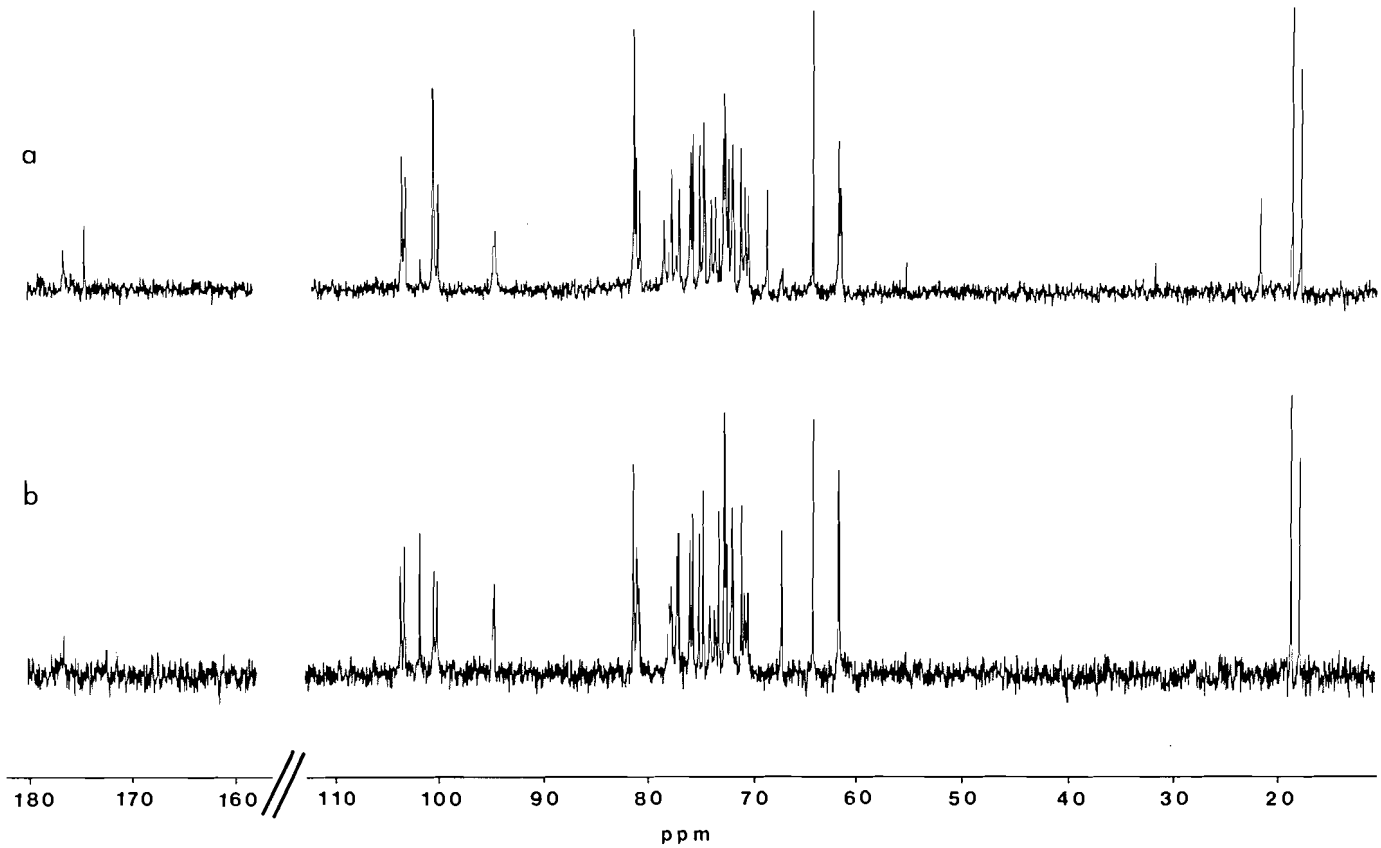


FIG. 1. Proton decoupled ^{13}C nmr spectra of the type 22F pneumococcal polysaccharide recorded at 310 K. (a) Native polysaccharide. (b) *O*-Deacetylated polysaccharide.

Previous structural analyses of the 22F polysaccharide made by Chatterjee *et al.* (5, 6) led to a proposed structure of a repeating unit composed of 21 glycose units containing D-galactopyranosyl, D-glucopyranosyl, L-arabinofuranosyl, L-rhamnopyranosyl, and D-glucopyranosyluronic acid residues as well as a phosphodiester unit. Our present studies have led to the unambiguous conclusion that the 22F polysaccharide is composed of a repeating hexasaccharide unit that is unrelated to the previously reported structure.

Results and discussion

The type 22F specific capsular polysaccharide was obtained from the spent growth medium of *S. pneumoniae* type 22F and was purified via its insoluble cetyltrimethylammonium salt (7). Ion exchange chromatography of the capsular material on DEAE-Sephacel afforded the specific polysaccharide as a sharp peak at the beginning of the salt gradient (0.02 M NaCl), which was homogeneous with respect to glycose composition and positive reaction with 22F type specific antiserum. The purified polysaccharide was indicated to be a high molecular weight polymer since it eluted as the void volume fraction on a Sephadex G-200 gel filtration system. All subsequent analyses were made on this material.

Complete acid hydrolysis of the capsular polysaccharide afforded the component glycoses, which were identified as D-galactose, D-glucose, D-glucuronic acid, and L-rhamnose by glc–ms of the derived acetylated or trimethylsilylated *R*-(−)-2-butyl glycosides (8–10). Quantitative analysis of the reduced and acetylated hydrolysis products on glc (program A) indicated that the neutral glycosyl components, identified as 1,2,3,4,5-penta-*O*-acetyl-L-rhamnitol (T_{GA} 0.51), 1,2,3,4,5,6-hexa-*O*-acetylgalactitol (T_{GA} 0.95), and 1,2,3,4,5,6-hexa-*O*-acetyl-D-glucitol (T_{GA} 1.00), were present in the molar ratio 1.9:1.0:2.2. When a sample of the capsular polysaccharide was treated with methanolic HCl (100°C, 15 h) and the product reduced with sodium borodeuteride prior to the quantitative analysis procedure, the aforementioned acetylated alditols were obtained in the molar ratio 2.0:1.0:2.9 in which the D-glucuronic acid component, detected as 1,2,3,4,5,6-hexa-*O*-acetyl-D-glucitol-6,6-d_2 (by ms), represented ≈30% of the derived D-glucitol hexaacetate.

The ^1H and ^{13}C nmr data for the native polysaccharide indicated the presence of an *O*-acetyl substituent. Comparison of the relative signal area of the *O*-acetyl methyl protons (2.18 ppm) to those of the methyl signals from the two L-rhamnosyl residues (1.38 and 1.26 ppm) indicated that the polymer was substituted by *O*-acetyl groups to the extent of 0.8 mol per repeating unit. In the ^{13}C nmr spectrum of the native polysaccharide (Fig. 1a), resonances at 174.10 ppm and 20.90 ppm were characteristic of the carbonyl and methyl carbons of the acetate ester. Removal of the *O*-acetyl groups by treatment of the polysaccharide with dilute alkali resulted in the loss of these signals (Fig. 1b).

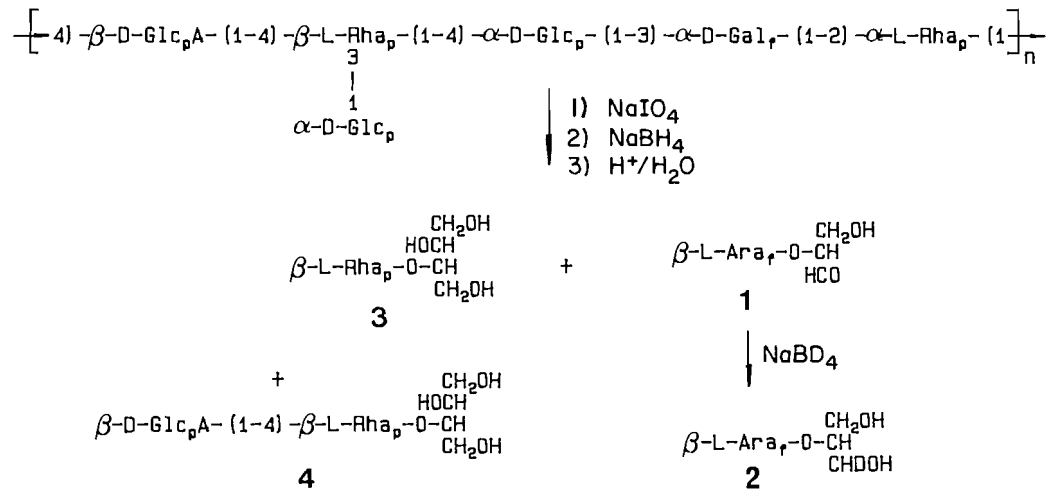
Diagnostic ^{13}C signals were observed in the spectrum of the native polysaccharide (Fig. 1a) at 103.20 (1C), 102.85 (1C), 100.14 (2C), 99.68 (1C), and 94.20 ppm (1C) from the anomeric carbon atoms, at 17.90 and 17.00 ppm from the methyl carbons of the two L-rhamnosyl residues, and at 176.20 ppm from the carboxyl carbon of the D-glucuronic acid residue. The methylene carbon resonances due to the hydroxymethyl groups (C-6) of the D-galactosyl and the two D-glucosyl residues were readily identified at 63.86, 61.47, and

Can. J. Chem. Downloaded from www.nrcresearchpress.com by 41.223.56.140 on 09/07/12
For personal use only.

TABLE 1. Methylation analysis data for the native type 22F specific polysaccharide

Derivative	T_{GM}	Mole ratio[a]	
		Methylated polysaccharide	Carboxyl reduced methylated polysaccharide
1,2,5-Tri-*O*-acetyl-3,4-di-*O*-methyl-L-rhamnitol-1-*d*	0.94[b]	0.9	0.8
1,5-Di-*O*-acetyl-2,3,4,6-tetra-*O*-methyl-D-glucitol-1-*d*	1.00	1.0	1.1
1,3,4,5-Tetra-*O*-acetyl-2-*O*-methyl-L-rhamnitol-1-*d*	1.36	0.9	0.9
1,3,4-Tri-*O*-acetyl-2,5,6-tri-*O*-methyl-D-galactitol-1-*d*	1.89	1.0	1.0
1,4,5-Tri-*O*-acetyl-2,3,6-tri-*O*-methyl-D-glucitol-1-*d*	2.13	1.1	1.1
1,4,5,6-Tetra-*O*-acetyl-2,3-di-*O*-methyl-D-glucitol-1,6,6-d_3	3.42	—	0.8

[a]Relative to that of 1,3,4-tri-*O*-acetyl-2,5,6-tri-*O*-methyl-D-galactitol.
[b]Using glc program B.



SCHEME 1

61.30 ppm from a ^{13}C DEPT experiment (11). In the spectrum of the *O*-deacetylated polymer (Fig. 1b), six resonances from the anomeric carbon atoms of the constituent monosaccharides were observed between 95 and 105 ppm, clearly indicating that the polysaccharide is composed of a regular hexasaccharide repeating unit.

Methylation analysis of the 22F polysaccharide gave the results recorded in Table 1. Since the hydrolysis products derived from the methylated native polysaccharide contained equal molar amounts of 3,4-di-*O*-methyl-L-rhamnose, 2,3,4,6-tetra-*O*-methyl-D-glucose, 2-*O*-methyl-L-rhamnose, 2,5,6-tri-*O*-methyl-D-galactose, and 2,3,6-tri-*O*-methyl-D-glucose, it can be concluded that the polysaccharide is composed of the following structural units: →2)-L-Rha*p*-(1→, D-Glc*p*-(1→, →3,4)-L-Rha*p*-(1→, →3)-D-Gal*f*-(1→, and →4)-D-Glc*p*-(1→. In addition, carboxyl reduction of the permethylated polysaccharide, by treatment with $NaBD_4$ prior to hydrolysis, gave a molar equivalent of 2,3-di-*O*-methyl-D-glucose-6,6-d_2, which establishes the presence of 1,4-linked D-glucuronic acid residues in the repeating unit.

The combined analytical evidence indicates that the 22F polysaccharide is a high molecular weight polymer composed of a branched hexasaccharide repeating unit in which one of the D-glucosyl residues forms the non-reducing end group and a L-rhamnopyranosyl unit is a di-*O*-substituted branch point. To determine the sequence of the glycosyl residues within the repeating unit, chemical fragmentation of the polymer was investigated by taking advantage of the anticipated resistance of the 1,3-linked L-rhamnopyranosyl and D-galactofuranosyl ring systems to periodate oxidation.

As expected, periodate oxidation of the *O*-deacetylated 22F polysaccharide followed by reduction and total acid hydrolysis afforded L-rhamnose and L-arabinose (1:1) as the only detectable neutral glycoses. Mild acid hydrolysis of the reduced periodate-oxidized type 22F polysaccharide (Smith degradation) with dilute aqueous acetic acid (1%, 100°C, 3 h) followed by fractionation of the products on a Bio-Gel P2 column afforded two neutral disaccharides, **1** and **3**, and an acidic trisaccharide **4**, which were fully characterized by nmr and ms analyses (Scheme 1).

The fraction containing oligosaccharide **1** was reduced with sodium borodeuteride and rechromatographed on Bio-Gel P2 to afford disaccharide **2**. The disaccharide **2** on hydrolysis gave L-arabinose and glycerol-1-*d* (1:1). The peracetylated derivative of **2** gave a protonated molecular ion in its ci ms at m/z 436. The ^1H nmr spectrum of **2** showed a single anomeric proton doublet at 5.186 ppm ($J_{1,2}$ = 3.7 Hz) and eight resonances were observed in the ^{13}C nmr spectrum in which those corresponding to the glycosyl residue could be readily assigned (Table 2) by comparison with data reported (12) for methyl β-L-arabinofuranoside. The chemical shifts of the remaining signals were consistent with O-2 substitution of the glycerol moiety (13). The assignment of the β-L-configuration for the arabinofuranosyl residue was consistent with the observed high specific optical

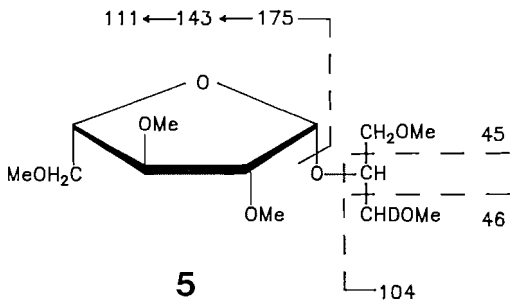
Can. J. Chem. Downloaded from www.nrcresearchpress.com by 41.223.56.140 on 09/07/12
For personal use only.

TABLE 2. Carbon-13 chemical shifts of the oligosaccharides derived from the pneumococcal type 22F polysaccharide by Smith degradation

Oligosaccharide	Chemical shift									
	Glycose						Aglycon			
	C-1	C-2	C-3	C-4	C-5	C-6	C-1	C-2	C-3	C-4
β-L-Ara*f*-(1→2)-glycerol-1-*d* (**2**)	101.56	77.20	74.42	82.42	62.66	—	62.01	80.53	62.33	—
β-L-Rha*p*-(1→2)-D-erythritol (**3**)	100.14	71.68[c]	73.52	73.01[d]	72.87[d]	17.49	61.26	80.29	71.83[c]	63.50
β-D-Glc*p*A-(1→4)-β-L-Rha*p*-(1→2)-D-erythritol (**4**)	103.97[a] 99.97[b]	73.51 71.72[e]	76.42 71.86[e]	72.36 81.84[f]	74.40 71.53[e]	175.5 17.72	61.24	80.29[f]	71.86[e]	63.50

[a]Chemical shifts for the β-D-Glc*p*A-(1→ residue.
[b]Chemical shifts for the →4)-β-L-Rha*p*-(1→ residue.
[c–f]Assignments may be reversed.

rotation ($[\alpha]_D$ +107.3°) of **2** (14). Methylated **2** gave an ei ms fragmentation pattern consistent with 2-*O*-(2,3,5-tri-*O*-methyl-β-L-arabinofuranosyl)-1,3-di-*O*-methylglycerol-1-*d* (**5**).



5

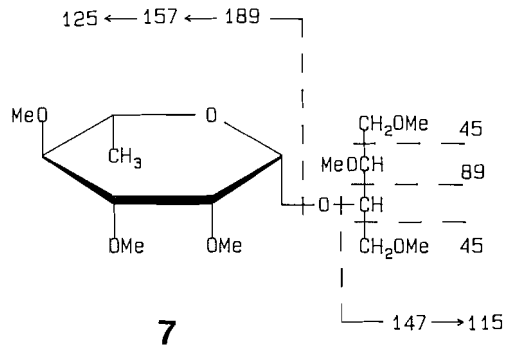
The combined evidence permits **2** to be identified as 2-*O*-β-L-arabinofuranosyl-D-glycerol-1-*d* and **1** to be assigned to the corresponding 2-*O*-substituted glyceraldehyde derivative. From the identification of a β-L-arabinofuranosyl end group in **1**, it can be inferred that it was derived from the 1,3-linked α-D-galactofuranosyl residue by periodate cleavage of the C-5—C-6 bond. Since the glyceraldehyde moiety can only arise from an O-2 substituted glycose residue in the intact polymer, it follows that the disaccharide fragment, **6**, forms part of the repeating unit.

→3)-α-D-Gal*f*-(1→2)-L-Rha*p*-(1→

6

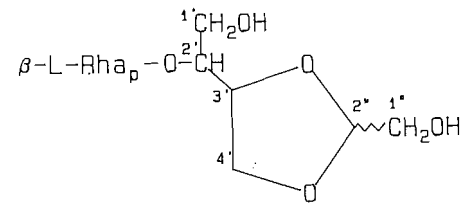
The oligosaccharides **3** and **4** were each obtained pure by preparative tlc. The disaccharide **3** was composed of L-rhamnose and erythritol (1:1). The ^{1}H nmr spectrum of **3** showed characteristic signals at 4.785 (d, $J_{1,2}$ = 1.2 Hz) and 1.321 ppm (d, $J_{5,6}$ = 6.0 Hz) due to the anomeric and 6-deoxy methyl protons of the L-rhamnopyranosyl component, respectively. The rhamnopyranosyl residue was assigned the β-L configuration from its specific optical rotation ($[\alpha]_D$ +58.5°, water) (15) and from analysis of its ^{13}C nmr spectrum (Table 2) (13). The methylated derivative (**7**) of **3** gave an ei ms fragmentation pattern that was consistent with **3** being 2-*O*-β-L-rhamnopyranosyl-D-erythritol, the erythritol moiety arising from the 4-*O*-substituted D-glucopyranosyl residue of the 22F polysaccharide.

In addition to oligosaccharide **3**, in which the aglycon was erythritol, the corresponding 2-*O*-substituted 3,4-*O*-(2-hydroxyethylidene)-D-erythritol analog (**8**) was obtained as a minor product (ca. 30% by ^{1}H nmr).



7

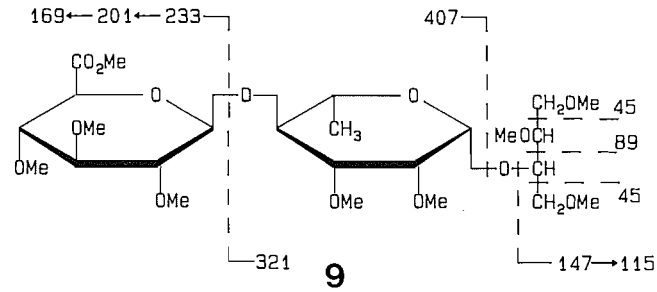
The cyclic derivative **8** was characterized from analysis of its ^{1}H and ^{13}C nmr spectra (see experimental section), the magnitude of the ^{1}H–^{1}H vicinal (^3J = 4.9, 6.6 Hz) and geminal (^2J = 8.5 Hz) coupling constants of the ring methylene protons (C-4′) being indicative of the 1,3-dioxolane ring system (16, 17). 3,4-*O*-(2-Hydroxyethylidene) derivatives have previously been reported as minor products (10–25%) obtained from the Smith degradation of polysaccharides containing O-4-linked α-D-hexopyranosyl residues having the *gluco* or *galacto* configuration (18, 19); they arise from acetal migration during the mild acid hydrolysis step (18).



8

The acidic trisaccharide **4** was composed of D-glucuronic acid, L-rhamnose, and erythritol (1:1:1). Two equal intensity anomeric proton signals were observed in the ^{1}H nmr spectrum of **4**: a singlet at 4.786 ppm corresponding to the L-rhamnosyl residue, and a doublet ($J_{1,2}$ = 7.8 Hz) at 4.769 ppm indicating that the D-glucopyranosyluronic acid residue has the β configuration. In the ^{13}C nmr spectrum of the trisaccharide (Table 2), characteristic signals at 175.50 and 17.72 ppm were diagnostic for the carboxyl carbon of the glucuronic acid and of the methyl carbon of the rhamnose residue, respectively. Comparison of the ^{13}C chemical shifts with those reported (13, 20) for the corresponding mono- and unsubstituted methyl glycosides

Can. J. Chem. Downloaded from www.nrcresearchpress.com by 41.223.56.140 on 09/07/12
For personal use only.



9

suggested that the β-D-glucopyranosyluronic acid was present as a non-reducing end group and that the β-L-rhamnopyranosyl group was substituted at the O-4 position. Methylation of **4** and subsequent glc–ms analysis confirmed the presence of a terminal glucuronic acid residue. The fragmentation pattern in the ei ms spectrum of the methylated derivative (**9**) showed primary fragment ions at m/z 233 [aA_1] (fragment ions labelled according to Kochetkov and Chizov (21)), 201 [aA_2], and 233 [aA_3], indicative of a permethylated hexopyranosyluronate end group (22). In addition, reduction of the methyl ester by treatment of the permethylated trisaccharide with sodium borodeuteride followed by hydrolysis gave 2,3,4-tri-*O*-methyl-D-glucose-6,6-d_2 and 2,3-di-*O*-methyl-L-rhamnose (1:1). Thus, the combined evidence leads to **4** being assigned the structure *O*-β-D-glucopyranosyl uronic acid-(1→4)-β-L-rhamnopyranosyl-(1→2)-D-erythritol.

The characterization of the oligosaccharides **3** and **4** indicates that part of the 22F polysaccharide structure contains the trisaccharide unit **10** in which the β-L-rhamnosyl residue forms the branch point, as indicated by methylation analysis of the native polysaccharide, and is therefore O-3 and O-4 disubstituted.

→4)-β-D-Glc*p*A-(1→4)-β-L-Rha*p*-(1→4)-D-Glc*p*-(1→

10

With the identification of the structural units **6** and **10**, several possibilities can still be envisaged for the arrangement of the glycosyl residues within the repeating unit of the 22F polysaccharide. The survival of the 1,4-linked D-glucuronic acid residue in the course of periodate oxidation of the *O*-deacetylated polysaccharide to give **4** probably results from its protection via hemiacetal formation with proximal aldehydo groups arising from more readily oxidizable residues (23). The terminal non-reducing D-glucopyranosyl residues identified as forming part of the repeating hexasaccharide unit (Table 1) would be expected to be most susceptible to periodate oxidation (24) and could afford protection to the D-glucuronic acid residues if they were positioned at either the O-4 position of the uronic acid or O-3 of the di-*O*-substituted L-rhamnopyranosyl residues. A detailed nmr analysis of the 22F capsular polysaccharide led to a unique structure.

Complete and unambiguous assignment of the ^1H and ^{13}C nmr spectra of the *O*-deacetylated 22F polysaccharide was made using two-dimensional (2D) homo- and heteronuclear chemical shift correlation techniques. Analysis of the connectivities observed between directly coupled protons in the 2D homonuclear chemical shift correlation (COSY) spectrum (Figs. 2 and 3) permitted the ^1H resonances to be grouped into subspectra corresponding to each of the component glycosyl ring systems (25). The ^1H chemical shift data and the ^1H–^1H coupling constants, determined from the appropriate cross-peaks in the COSY spectrum (cf. Fig. 3) or from a 2D homonuclear *J*-resolved spectrum (26), are recorded in Table 3. Comparison of the chemical shift data and the vicinal coupling constants with values reported in the literature (27, 28) led to the identification of the respective subspectra. Assignment of the ^{13}C resonances of the *O*-deacetylated polysaccharide was then achieved by correlation with the corresponding ^1H resonances from a 2D heteronuclear $^1H/^{13}C$ shift correlation map (Fig. 4) (29).

The anomeric proton (H-1) resonances, which were readily identified from their single vicinal proton couplings, in the low field region of the spectrum (5.3–4.7 ppm) provided a convenient starting point for this analysis and were labelled **A**1, **B**1, **C**1, **D**1, **E**1, and **F**1 in order of decreasing chemical shifts (Fig. 2). Delineation of the connectivity relationships defined by the cross-peaks led to the assignment of most of the ^1H resonances associated with the individual monosaccharide components (residues **A**, **B**, **C**, **D**, **E**, and **F**). This analysis was relatively straightforward and the connectivity pathway corresponding to residue **A** is shown in Fig. 3. Seven ^1H resonances could be associated with this subspectrum from the related cross-peaks and, from the magnitude of the vicinal ring proton coupling constants ($J_{1,2} \leq 4$ Hz, $J_{2,3} \approx J_{3,4} \approx J_{4,5} \approx$ 10 Hz), the residue **A** was identified as a D-glucopyranosyl unit having the α configuration. Analogously, the subspectra corresponding to residues **C** and **F** were attributed to pyranose residues having the *gluco* configuration. Residue **C** also had the α-anomeric configuration ($J_{1,2}$ = 3.8 Hz) and was assigned to the second D-glucopyranosyl unit, while residue **F**, which gave a spin system composed of only five ^1H resonances, could be assigned to the β-D-glucopyranosyluronic acid residue. The latter assignment was confirmed from the observed pH dependence of the H-4 and H-5 resonances of residue **F**, which showed downfield shifts of ≈0.1 and ≈0.4 ppm, respectively, when the spectrum of the *O*-deacetylated polysaccharide was recorded at pD ≈ 2 (Table 3).

Residues **D** and **E** were identified as the L-rhamnopyranosyl residues since the two high-field methyl doublets at 1.398 ($J_{5,6}$ = 5.7 Hz) and 1.294 ppm ($J_{5,6}$ = 6.1 Hz) could be readily associated with the respective connectivity pathways through cross-peaks to the H-5 resonances of **D** (3.550 ppm) and of **E** (4.051 ppm) in the full-scale COSY spectrum. The low intensity of the cross-peaks relating H-1 and H-2 of these residues (Fig. 2), which is particularly apparent in the case of residue **D** (**D**12), can be attributed to the small values (ca. 1 Hz) for the scalar couplings, $J_{1,2}$, which, together with small values for $J_{2,3}$ (≤3 Hz), are indicative of the *manno* configuration (28). Due to the axial disposition of the C-2 hydroxyl group of the L-rhamnopyranosyl residues, the anomeric configurations were not evident from the $J_{1,2}$ values (28). The configurations were determined from the magnitude of their corresponding one-bond ^{13}C–^1H coupling constants ($^1J_{C,H}$) (30). The $^1J_{C,H}$ values (Table 4) for the anomeric carbon (C-1) resonances of the L-rhamnopyranosyl units **D** (159 Hz) and **E** (172 Hz) were characteristic (30) of the two residues having the β and the α configurations, respectively.

The magnitudes of the ring proton vicinal coupling constants (Table 3) were consistent with the constituent monosaccharides, **A**, **C**, **D**, **E**, and **F** being present in the corresponding pyranosyl ring forms with the $^4C_1$ (D-enantiomer) or the $^1C_4$ (L-enantiomer) chair conformations (28). On the other hand, the $J_{1,2}$ (≈4 Hz), $J_{2,3}$ (≈8 Hz), $J_{3,4}$ (≈7 Hz) values measured for residue **B** were consistent (31) with that residue being the α-D-galactofuranosyl unit. Corroborative evidence for this assignment was obtained from a comparison of the respective ^{13}C chemical shifts (Table 4) with data for the corresponding

Can. J. Chem. Downloaded from www.nrcresearchpress.com by 41.223.56.140 on 09/07/12
For personal use only.

Can. J. Chem. Downloaded from www.nrcresearchpress.com by 41.223.56.140 on 09/07/12
For personal use only.

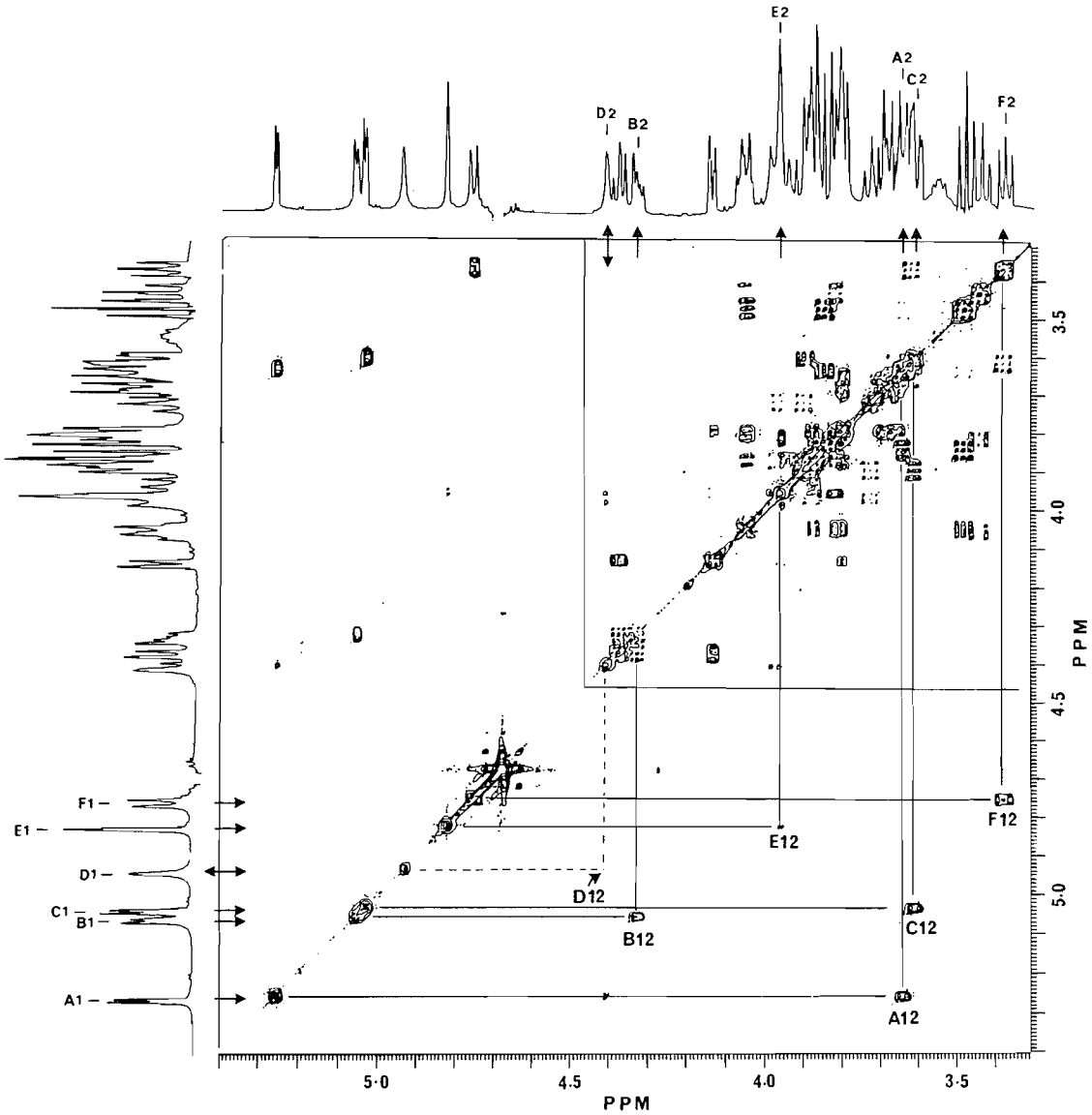


FIG. 2. Contour plot of the ring proton region (5.4–3.3 ppm) of the COSY spectrum of the *O*-deacetylated type 22F pneumococcal polysaccharide at 310 K. The spectrum was measured using a narrow sweep width and 512 × 2048 data points (see experimental section). Resonance assignments are shown for H-1 and H-2 of each of the component monosaccharides (**A**–**F**).

methyl furanosides of galactose, arabinose, and 3-*O*-methyl arabinose (12, 32), in which the chemical shift of C-1 (103.19 ppm) was diagnostic for the α-D configuration.

The arrangement of the six glycosyl residues within the repeating unit of the 22F polysaccharide was unequivocally determined from *inter*residue nOe measurements (33, 34). A 2D nOe experiment (NOESY) was carried out on the *O*-deacetylated 22F polysaccharide (Fig. 5). The 2D experiment provided the best method for nOe determination since the H-1 resonances corresponding to residues **B** and **C** were not completely resolved from one another in the 1D ^{1}H nmr spectrum.

*Inter*residue nOe's (Table 5) were observed between protons **B**1 and **E**2, and between protons **F**1 and **D**4, and **D**1 and **C**4, which provides verification of the sequences of the two structural units, **B**–**E** (**6**) and **F**–**D**–**C** (**10**), deduced from the periodate oxidation studies. The relationship between these units is indicated from the observed nOe's between H-1 of residue **C** and H-3, H-4, and H-5 of the α-D-galactofuranosyl residue (**B**), which, together with the *inter*residue effect between protons **E**1 and **F**4, establishes the linear sequence of glycoses as **F**–**D**–**C**–**B**–**E**–**F**. Thus, the main chain of the polymer is composed of the repeating pentasaccharide unit **11** in which the β-L-rhamnopyranosyl residue provides the branch point.

Nuclear Overhauser effects relating the anomeric protons with other protons within the same ring system provided additional confirmation for the anomeric configurations of the glycopyranosyl residues (Table 5). *Intra*residue effects between only H-1 and H-2 were indicative of the α configuration

Can. J. Chem. Downloaded from www.nrcresearchpress.com by 41.223.56.140 on 09/07/12
For personal use only.

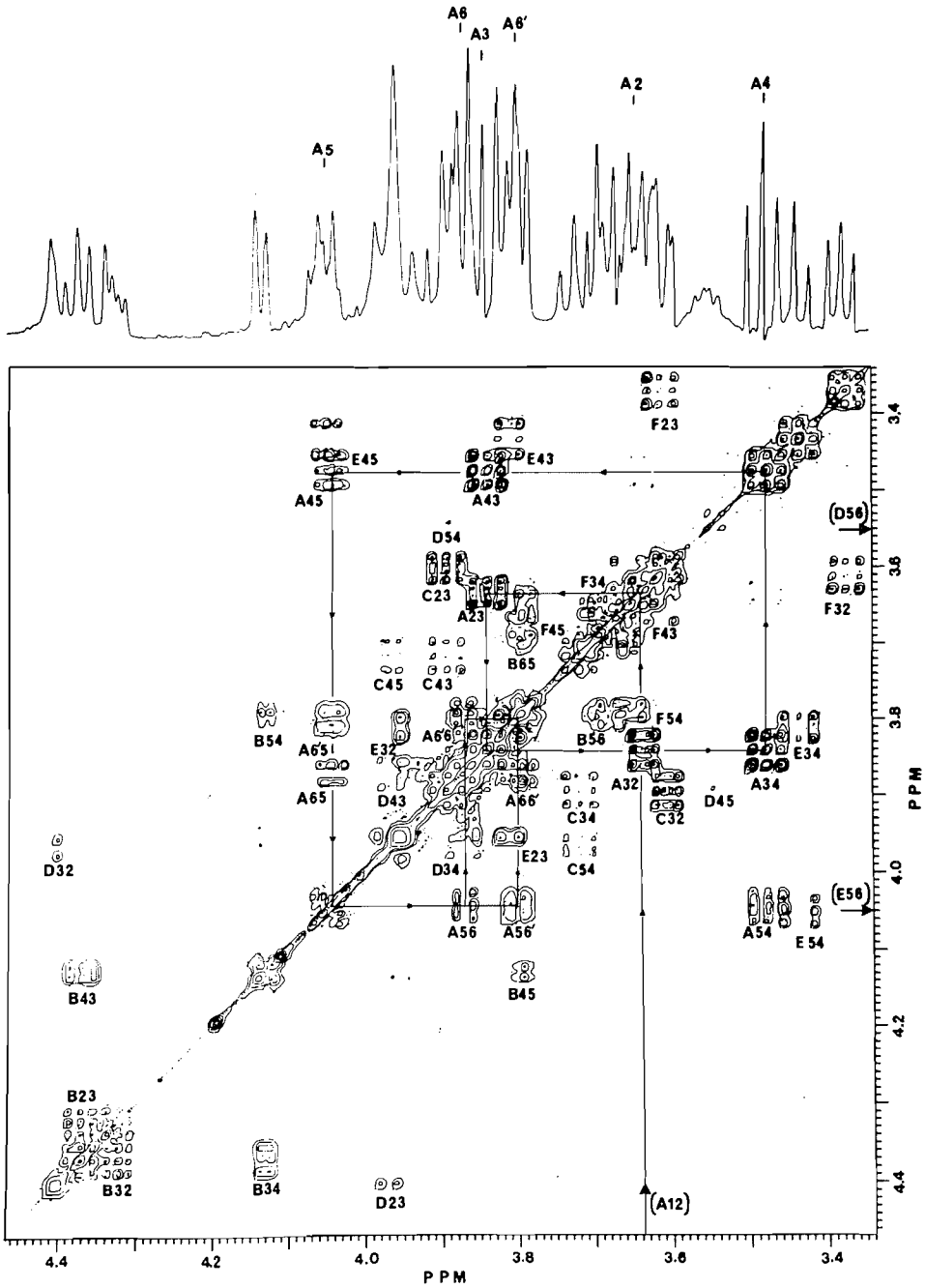
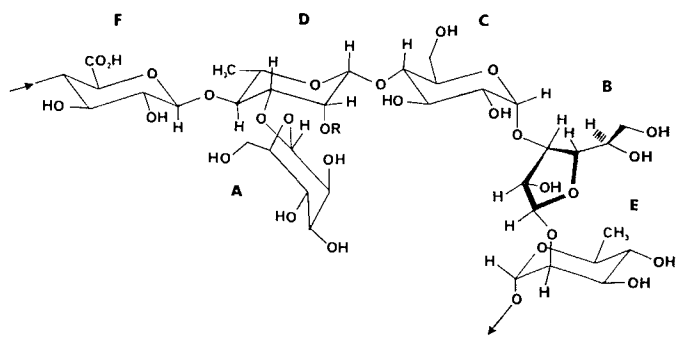


FIG. 3. Expansion (4.47–3.34 ppm) of the COSY contour plot shown in Fig. 2. Assignments of the cross-peaks are shown and the connectivity pathway corresponding to the residue **A** subspectrum is indicated by the solid line.

(residues **A**, **C**, and **E**), while *intra*residue nOe's between H-1 and H-3 and between H-1 and H-5 were diagnostic of the β-linked residues **D** and **F**.

In accord with the results of methylation analysis, the nOe data (Table 5) clearly indicate that residue **A** is the non-reducing α-D-glucopyranosyl end group. The occurrence of *inter*residue nOe's between H-1 of residue **A** and H-2 and H-3 of residue **D** establishes that the terminal non-reducing α-D-glucopyranosyl unit is 1,3-linked to the 3,4-di-*O*-substituted β-L-rhamnopyranosyl residue, and it follows that the hexasaccharide repeating unit of the *O*-deacetylated 22F polysaccharide has the structure **12**.

As indicated in Table 5, the occurrence of nOe's between the



12, R = H
13, R = Ac

TABLE 3. Proton chemical shifts[a] and coupling constants[b] for the *O*-deacetylated *S. pneumoniae* type 22F polysaccharide

Residue	Glycose unit	H-1 ($J_{1,2}$)	H-2 ($J_{2,3}$)	H-3 ($J_{3,4}$)	H-4 ($J_{4,5}$)	H-5	H-6 ($J_{5,6}$)	H-6′ ($J_{5,6'}$, $J_{6,6'}$)
A	α-D-Glc*p*-(1→	5.257 (3.9)	3.636 (9.9)	3.845 (10.0)	3.479 (9.6)	4.045	3.875 (2.2)	3.807 (4.7, 11.9)
B	→3)-α-D-Gal*f*-(1→	5.051 (4.3)	4.325 (8.4)	4.374 (7.2)	4.133 (1.8)	3.800	3.69 (ur)[c]	3.69 (ur)[c]
C	→4)-α-D-Glc*p*-(1→	5.028 (3.8)	3.608 (9.9)	3.897 (9.6)	3.721 (9.4)	3.975	3.94[d] (—)[e]	3.89[d] (—)[e]
D	→3)-β-L-Rha*p*-(1→ 4 ↑	4.930 (s)[f]	4.407 (2.8)	3.976 (10.0)	3.878 (9.4)	3.550	1.398 (5.7)	
E	→2)-α-L-Rha*p*-(1→	4.818 (s)[f]	3.958 (2.4)	3.816 (9.8)	3.437 (9.5)	4.051	1.294 (6.1)	
F	→4)-β-D-Glc*p*A-(1→	4.751 (7.8)	3.376 (9.2)	3.616 (9.4)	3.654 [3.73][g] (9.3)	3.794 [4.12][g]		

[a]Chemical shifts determined at 310 K relative to internal acetone (2.225 ppm) on a sample of the sodium salt in D_2O (pD ~ 7).
[b]Observed first-order coupling constants.
[c]Unresolved multiplet.
[d]Assignment confirmed from C–H correlation.
[e]Not determined.
[f]Singlet, $W_{1/2} < 3$ Hz.
[g]Chemical shifts measured from spectrum recorded at pD ~ 2.

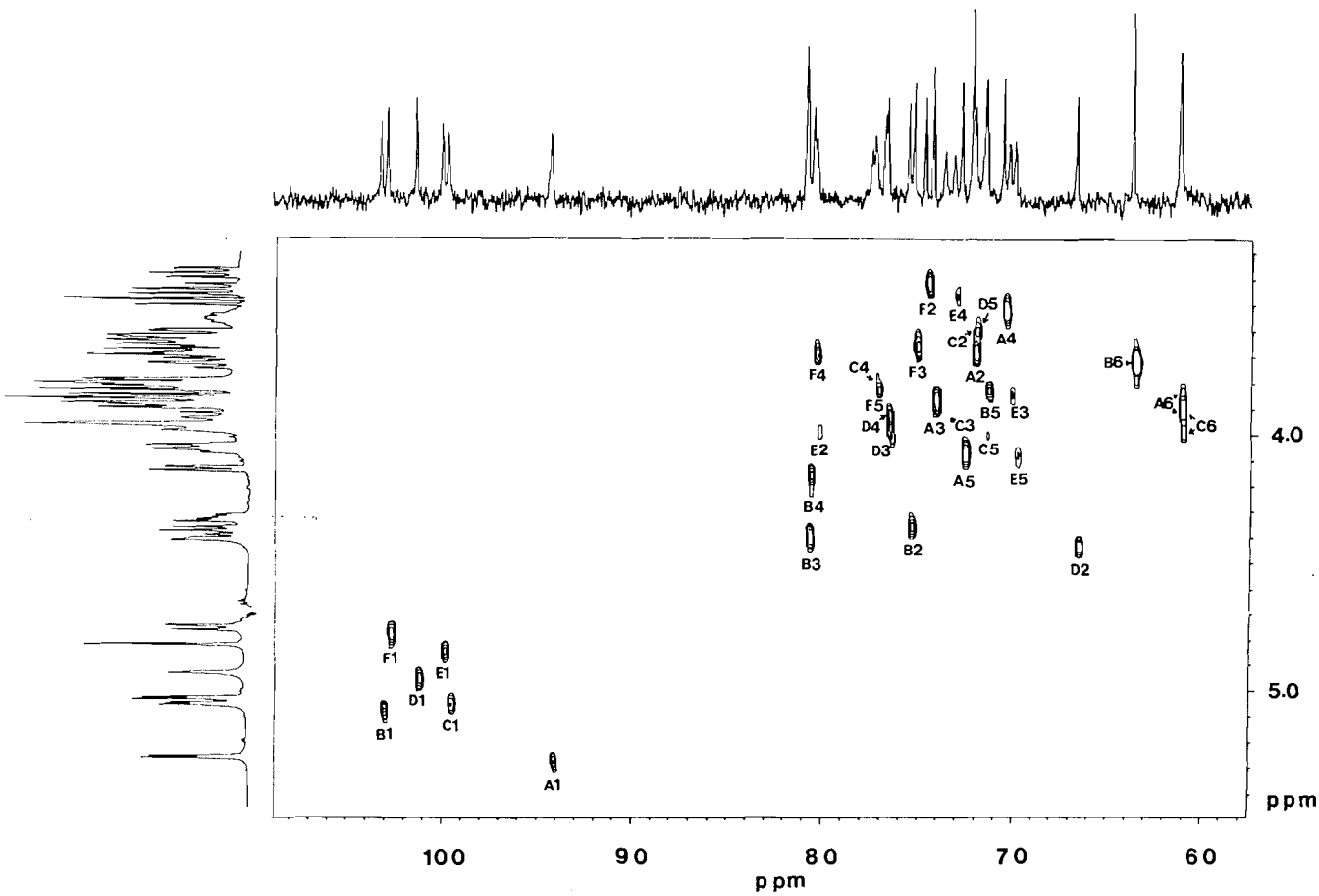


FIG. 4. Heteronuclear $^1H/^{13}C$ chemical shift correlation map of the *O*-deacetylated type 22F pneumococcal polysaccharide recorded at 310 K for the spectral regions F_2, 109–57 ppm, and F_1, 5.5–3.2 ppm. The respective 1D ^{13}C and ^1H spectra are displayed along the F_2 and F_1 axes and the correlated resonances are labelled.

Can. J. Chem. Downloaded from www.nrcresearchpress.com by 41.223.56.140 on 09/07/12
For personal use only.

TABLE 4. Carbon-13 chemical shifts and anomeric $^1J_{C,H}$ coupling constants (Hz) for the *O*-deacetylated *S. pneumoniae* type 22F polysaccharide[a]

Residue	Glycose unit	Carbon atom C-1	C-2	C-3	C-4	C-5	C-6
A	α-D-Glc*p*-(1→	94.23 (171)	72.24	74.28	70.63	72.61	61.37
B	→3)-α-D-Gal*f*-(1→	103.19 (174)	75.55	80.87	80.87	71.55[b]	63.78
C	→4)-α-D-Glc*p*-(1→	99.62 (173)	72.24	73.63	77.40	71.55	61.37
D	→3)-β-L-Rha*p*-(1→ 4 ↑	101.33 (159)	66.78	76.66	76.79	72.08	18.11
E	→2)-α-L-Rha*p*-(1→	99.98 (172)	80.40	70.34[b]	73.17	70.02	17.19
F	→4)-β-D-Glc*p*A-(1→	102.84 (163)	74.69	75.29	80.52	77.29	176.20

[a]Chemical shifts measured at 310 K relative to external dioxane.
[b]Assignment may be reversed.

TABLE 5. Proton nOe data for the *O*-deacetylated *S. pneumoniae* type 22F polysaccharide[a]

Anomeric proton	Observed proton: *Intra*residue nOe	*Inter*residue nOe	Partial sequence	Linkage site
A1	**A**2	**D**2, **D**3	**A** → **D**	0–3(**D**)
B1	**B**2	**E**1, **E**2	**B** → **E**	0–2(**E**)
C1	**C**2	**B**3, **B**4, **B**5	**C** → **B**	0–3(**B**)
D1	**D**2, **D**3, **D**5	C4, C6′	**D** → **C**	0–4(**C**)
E1	**E**2	**B**1, **F**4, **F**5	**E** → **F**	0–4(**F**)
F1	**F**3, **F**5, **F**2	**D**4	**F** → **D**	0–4(**D**)

[a]Determined from the 2D NOESY experiment (cf. Fig. 5).

anomeric and aglyconic protons of contiguous glycosyl residues can provide, in addition to the sequence, the positions of the glycosidic linkages (35). However, since the nOe is dependent on the conformation about the glycosidic bond, the largest *inter*residue nOe need not necessarily occur between the anomeric and aglyconic proton pair (36, 37). This is evident from the occurrence of significant *inter*residue nOe's between H-1 of the terminal α-D-glucopyranosyl unit (**A**) and both H-2 and H-3 of the β-L-rhamnopyranosyl unit (**D**), which, as predicted from potential energy calculations using the HSEA method (38), is a consequence of the conformation about the α-1,3 glycosidic linkage of the **A**–**D** disaccharide unit (cf. structure **12**). Similar effects have been observed for this disaccharide unit, which is also part of the pneumococcal type 7F polysaccharide repeating unit (39).

The location of the *O*-acetyl substituent, present in the native 22F polysaccharide, was determined from a comparison of its ^{13}C nmr spectrum with that of the *O*-deacetylated polysaccharide (Fig. 1). The anomeric carbon regions (95–105 ppm) of the two spectra were similar except that the signal intensity of the resonance at 101.33 ppm due to C-1 of the β-L-rhamnopyranosyl residue (**D**) was considerably reduced in the spectrum of the native polysaccharide, while the intensity of the signal at 99.98 ppm was almost twice that observed in the spectrum of the *O*-deacetylated polysaccharide, indicating that the introduction of the *O*-acetyl group leads to an upfield shift of the **D**1 resonance by almost 1.4 ppm. The C-2 resonance (**D**2) corresponding to the β-L-rhamnosyl residue was shifted downfield by ≈1.6 ppm in the spectrum of the native polysaccharide. Since replacement of an hydroxy group by an *O*-acetyl substituent in glycosides is known to lead to downfield shifts (0.7–3.5 ppm) of the substituted carbon and to upfield shifts (1.2–2.8 ppm) of the adjacent carbon resonances (40), it can be concluded that the O-2 position of the 3,4-di-*O*-glycosylated β-L-rhamnopyranosyl residues carry *O*-acetyl groups in the native polysaccharide. Moreover, the low-field position of the H-2 resonance of the β-L-rhamnopyranosyl residue in the ^1H nmr spectrum of the native polysaccharide (5.739 ppm) compared to the chemical shift of that resonance in the *O*-deacetylated polymer (4.407 ppm) is also in accord with the β-L-rhamnopyranosyl units being 2-*O*-acetylated (40).

The combined chemical and nmr evidence therefore permits the repeating hexasaccharide unit of the pneumococcal type 22F capsular polysaccharide to be assigned to the structure **13** in which the *O*-acetyl groups are present in ≈80% of the repeating units.

Experimental

Type 22F pneumococcal polysaccharide

Type 22F polysaccharide was obtained by ethanol precipitation from the growth medium of *S. pneumoniae* type 22F, after digestion with trypsin, ribonuclease, and deoxyribonuclease, and fractional precipitation with 2-propanol with serological probing (7). The capsular polysaccharide was further purified via its insoluble cetyltrimethylammonium complex (41).

Purified 22F polysaccharide (100 mg) was converted to its sodium salt by passing an aqueous solution (2.0 mL) through a column (0.5 × 2.0 cm) containing Rexyn 101 (Na^+ form) ion exchange resin followed by lyophilization of the eluate: $[\alpha]_D$ +90.8° (*c* 0.52, water). *Anal.* found: C 43.42, H 6.24, N nil, ash 2.10%.

O-Deacetylation

A solution of the purified type 22F polysaccharide (100 mg) in 5% (v/v) aqueous ammonia (5 mL) was stirred at 35°C for 3 h, the solution lyophilized, and the product converted to its sodium salt (as above).

Can. J. Chem. Downloaded from www.nrcresearchpress.com by 41.223.56.140 on 09/07/12
For personal use only.

Can. J. Chem. Downloaded from www.nrcresearchpress.com by 41.223.56.140 on 09/07/12
For personal use only.

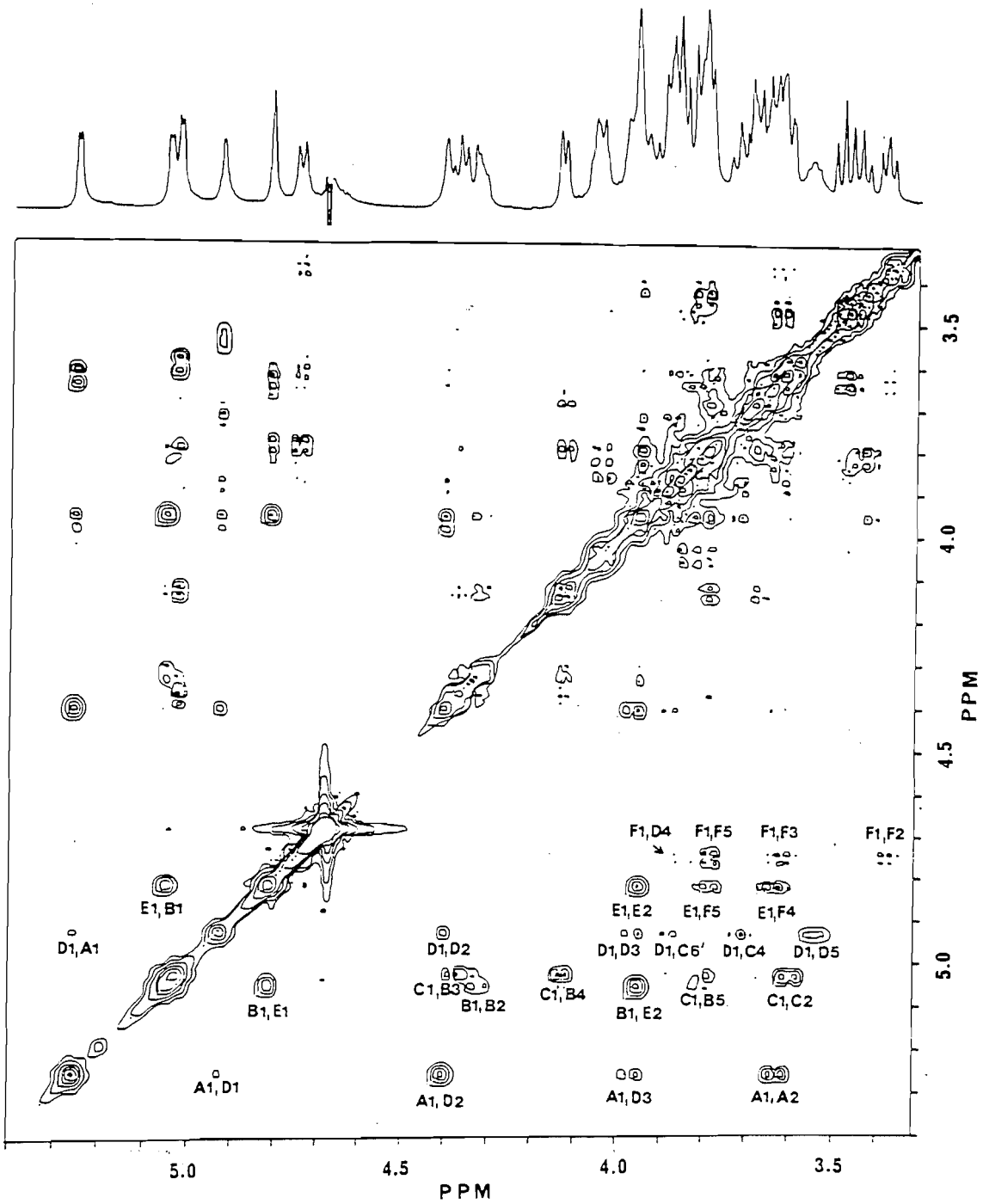


FIG. 5. Contour plot of the ring proton region (5.4–3.3 ppm) of the NOESY spectrum of the *O*-deacetylated type 22F pneumococcal polysaccharide at 310 K. Cross-peaks arising from nOe's involving the anomeric proton resonances are indicated.

Chromatography

Samples (6 mg) of polysaccharide were subjected to chromatography on columns (1.2 × 40 cm) of Sephadex G-200 eluted with 0.05 M pyridinium acetate (pH 4.5), and of DEAE-Sephacel (Pharmacia) eluted with 0.05 M Tris-HCl (pH 7.2) (25 mL) followed by a buffered 0–0.5 M sodium chloride gradient. Fractions (1 mL) were collected and assayed for neutral glycose (42) and hexuronic acid (43).

Analytical methods

Quantitative colorimetric methods used for the analysis of column chromatography eluates were (*i*) phenol – sulfuric acid for neutral glycoses (42), (*ii*) *m*-hydroxydiphenyl – sulfuric acid method for hexuronic acids (43), and (*iii*) the method of Nash (44) for the determination of formaldehyde liberated by periodate oxidation.

Gas–liquid chromatography (glc) was done with a Hewlett Packard model 5710A gas chromatograph fitted with a hydrogen flame detector and a model 3380A electronic integrator using the following conditions: A, glass column (2 mm × 180 cm) packed with 3% (w/w) SP2340 on Supelcoport (80–100 mesh) and the temperature program, 180°C (for 2 min) – 240°C at 4°C/min; B, the foregoing column and the temperature program, 190° (for 2 min) – 220°C at 1°C/min; C, glass column (2 mm × 60 cm) packed with 1% (w/w) Dexsil 300 on Supelcoport (100–120 mesh) and the temperature program, 130°C–340°C at 10°C/min; D, fused silica capillary column (0.3 mm × 25 m)

containing 3% (w/w) OV17 and the temperature program, 180°C (for 2 min) – 240°C at 2°C/min. The carrier gas was dry nitrogen and retention times are given relative to those of D-glucitol hexaacetate (T_{GA}), 1,5-di-*O*-acetyl-2,3,4,6-tetra-*O*-methyl-D-glucitol (T_{GM}), or permethylated cellobiitol (T_{CM}).

The glc–ms data were obtained using a Hewlett Packard 5958B system employing the glc program conditions A–D by electron impact (ei) with an ionization potential of 70 eV, or by chemical ionization (ci) with isobutane as the reagent gas.

Glycoses were determined by glc of their alditol acetates (45) using inositol as internal standard. Samples (0.2–0.5 mg) were hydrolyzed in sealed glass tubes with 1 M sulfuric acid (0.5 mL) for 15 h at 100°C followed by neutralization with barium carbonate, filtration, and concentration to obtain the free glycosides. For the estimation of hexuronic acid, samples (0.5 mg) suspended in methanolic hydrogen chloride (3%, w/v, 1 mL) were heated at 100°C in sealed glass tubes for 15 h. Excess methanolic HCl was removed *in vacuo* and the residues in water (1 mL) were treated with sodium borodeuteride (15 mg) for 6 h at 22°C. Following neutralization with aqueous acetic acid (10%, w/v), the reaction mixtures were decationized with Rexyn 101 (H^+ form) ion exchange resin (1.5 mL), concentrated *in vacuo*, and borate was removed by repeated distillation from methanol (5 × 5 mL). The products were then hydrolyzed in 3 M HCl (1 mL) for 3 h at 100°C followed by concentration *in vacuo*. The liberated glycoses were reduced ($NaBH_4$) and acetylated (Ac_2O) (46) prior to glc analysis using program A.

Absolute configurations of the glycoses were determined by glc–ms (program D) of the corresponding acetylated or trimethylsilylated *R*-(−)-2-butyl glycoside derivatives (8–10). The identity of the glycose derivatives was established by comparison of their glc retention times and mass spectra with those of authentic reference compounds.

Methylation analysis

Polysaccharide samples (2 mg) were methylated with methyl iodide in dimethyl sulfoxide containing an excess of sodium methylsulfinylmethanide according to the Hakomori procedure (47) and the products were purified by dialysis against distilled water followed by concentration of the aqueous dialyzate. Oligosaccharide samples (0.5–1.0 mg) were methylated by the above procedure, and the products were recovered by extraction into dichloromethane and analyzed by glc–ms using program C. The methylated products were hydrolyzed, reduced with sodium borodeuteride, and acetylated as previously described (46). Methylated products containing uronic acid residues were subjected to carboxyl reduction before hydrolysis by treatment with $NaBD_4$ in tetrahydrofuran (12 h, 50°C) and analysis by glc–ms (program B).

Nuclear magnetic resonance spectroscopy

Measurements were made at 310 K on solutions (0.4 mL) in deuterium oxide with a Bruker AM-500 spectrometer equipped with an Aspect 3000 computer, operating in the pulsed Fourier transform mode with quadrature detection using standard Bruker software.

Proton nmr spectra were recorded at 500 MHz using a spectral width of 2.5 kHz, a 16 K data block, and a 90° pulse. For quantitative measurement of signal area, a 45° pulse and a fixed delay of 3 s was employed. Prior to Fourier transformation, resolution enhancement was achieved by the Gaussian line shape transformation (48) with typical values of −2.0 to −4.0 Hz for the line broadening factor and a Gaussian broadening factor of +0.1 or +0.2. Chemical shifts are expressed relative to that of internal acetone (0.1%, 2.225 ppm).

Broad-band proton decoupled carbon-13 spectra were obtained at 125 MHz using a spectral width of 25 kHz, a 32 K data block, and a 90° pulse employing WALTZ decoupling (49). Heteronuclear $^1J_{C,H}$ coupling constants for the anomeric carbons were measured using gated decoupling (50). DEPT spectra (11) were obtained with broad-band proton decoupling by using a 135° proton pulse and a 3.3-ms delay between pulses. Chemical shifts are referenced to that of 1,4-dioxane (67.40 ppm).

Two-dimensional homonuclear COSY (41), NOESY (52, 53), and *J*-resolved (54) experiments were measured using the conventional pulse sequences on a D_2O solution (25 mg/mL) of the *O*-deacetylated polysaccharide (sodium salt, pD ≈ 7). COSY and NOESY data were measured using data sets ($t_1 \times t_2$) of 256 × 1024 points for a spectral width of 2203 Hz, a recycle delay of 1.5 s, and 32 or 96 transients for each value of the incrementable delay. A mixing time of 200 ms was employed for the NOESY experiment. The data matrices were zero filled to 512 × 2048 points and, following resolution enhancement in both dimensions by a non-shifted sine bell function, were processed to give magnitude spectra with symmetrization. The COSY was also carried out over a narrow spectral width (1200 Hz) using a data set of 512 × 2048 points that was zero filled to 1024 × 2048 points, and the data were processed as described above. The *J*-resolved spectrum was acquired using a 32 × 2048 point data set and spectral widths of 1200 Hz and ±18.7 Hz in the chemical shift (F_2) and the coupling constant (F_1) domains, respectively. A recycle delay of 1.5 s was used and 32 transients were collected for each of 32 experiments. The data matrix was zero filled to 128 × 2048 points, a non-shifted sine bell function was applied to both time domains, and the transformed data were tilted 45° and symmetrized.

A two-dimensional heteronuclear $^1H/^{13}C$ chemical shift correlation experiment (29, 55) was carried out on a concentrated solution (100 mg/mL) of the *O*-deacetylated polysaccharide (sodium salt). The experiment was performed using a data matrix of 128 × 1024 points and spectral widths of 12 500 and 2500 Hz for the respective carbon-13 (F_2) and proton (F_1) chemical shift domains. A recycle delay of 1.5 s was employed and the fixed delays, τ_1 and τ_2, were set at 3.2 and 1.6 ms, respectively, to select for all multiplicities. Composite broad-band proton decoupling was employed during the acquisition of 1000 transients for each of the 128 increments. The data matrix was zero filled to 256 × 2048 points and, following resolution enhancement in both dimensions by means of a Lorentz-to-Gauss transformation, the data were processed to give a power spectrum.

Smith degradation (ref. 56)

To a solution of the *O*-deacetylated type 22F polysaccharide (80 mg) in water (50 mL) was added an aqueous solution of 0.04 M sodium *meta*-periodate (50 mL). The solution was kept in the dark at 4°C for 96 h and, following the destruction of excess periodate by the addition of ethylene glycol (0.1 mL), the oxidized polymer was reduced by addition of sodium borohydride (500 mg). After stirring for 15 h at 22°C, excess borohydride was decomposed by the slow addition of aqueous acetic acid (10%, w/v) to the cooled solution, and the solution was dialyzed and lyophilized to yield the periodate-oxidized and reduced polymer (60 mg). The periodate-oxidized and reduced polysaccharide was hydrolyzed with dilute aqueous acetic acid (1%, v/v, 10 mL) at 100°C for 3 h, and the reaction mixture was concentrated to dryness. The hydrolysis products were chromatographed on a column (1.5 × 95 cm) of Bio-Gel P2, jacketed at 50°C, with water as the eluant to give three major oligosaccharide containing fractions, I (20 mg), II (13 mg), and III (10 mg).

Oligosaccharide 2

Fraction I, which eluted in the monosaccharide region of the Bio-Gel P2 column, was treated with sodium borodeuteride (25 mg) in water (2 mL) at 22°C for 3 h. Excess borodeuteride was decomposed by addition of acetic acid and the neutralized solution (pH 7) was passed through a bed of Rexyn 101 (H^+ form) ion exchange resin (2 mL). The eluate was repeatedly concentrated with methanol (5 × 10 mL) to yield a mixture of alditols (20 mg). A portion (ca. 0.5 mg) of the mixture was acetylated by heating an acetic anhydride solution (1 mL) containing anhydrous sodium acetate (0.5 mg) at 115°C for 3 h; glc–ms analysis showed unlabeled and glycerol-1-*d* triacetate (T_{GA} 0.13) (30%), L-arabinitol-1-*d* pentaacetate (T_{GA} 0.66) (18%), and 2-*O*-arabinofuranosyl-glycerol-1-*d* (**2**) pentaacetate (T_{GA} 1.50) (52%). Peracetylated **2** gave ms (ei), *m/z* (relative intensity): 259 (26.3), 170 (17.2), 160 (49.2), 157 (10.2), 139 (41.1), 128 (14.9), 115 (9.5), 97 (19.3), 69 (6.5), 68 (5.3), 43 (100); ms (ci), *m/z*: 436 (M + 1).

The remainder of the reduced fraction (19 mg) was rechromatographed on Bio-Gel P2 as described above and the fraction eluting in

Can. J. Chem. Downloaded from www.nrcresearchpress.com by 41.223.56.140 on 09/07/12
For personal use only.

the disaccharide region was collected and lyophilized to give pure **2** (7 mg): $[\alpha]_D$ +107.3 (*c* 0.22, water); ^{1}H nmr, δ (partial): 5.186 (d, 1H, $J_{1,2}$ = 3.7 Hz); ^{13}C nmr, Table 2. Hydrolysis, reduction, and acetylation of **2** gave (by glc–ms, program A) glycerol-1-*d* triacetate (T_{GA} 0.13) and L-arabinitol pentaacetate (T_{GA} 0.66) (1:1). Permethylated **2** gave a single peak on glc (program C) having T_{CM} 0.20; ms (ei), *m/z* (relative intensity): 175 (4.9) [aA_1], 164 (9.9) [J_1], 143 (10.7) [aA_2], 115 (9.3), 111 (4.9) [aA_3], 104 (5.6), 101 (100), 89 (4.7), 71 (6.4), 46 (22.3), 45 (46.1).

Oligosaccharides 3 and 8

Fraction II eluted in the disaccharide region of the Bio-Gel P2 column and showed ^{1}H nmr, δ (partial): 5.039 (t, 0.3H, $J_{1,2}$ = 3.2 Hz), 4.785 (d, ca. 0.7H, $J_{1,2}$ = 1.2 Hz), 4.780 (d, ca. 0.3H, $J_{1,2}$ = 1.2 Hz), 1.322 (d, 3H, $J_{5,6}$ = 6.0 Hz); ^{13}C nmr, δ: 104.4, 100.5, 100.0 (0.4:1.0:0.4). Thin-layer chromatography (silica gel) developed with ethyl acetate – acetic acid – methanol–water (12:3:3:5) showed two components that were subsequently separated by preparative tlc to give oligosaccharides **3** (7 mg, R_f 0.29) and **8** (3 mg, R_f 0.38).

Oligosaccharide **3** had $[\alpha]_D$ +58.5 (*c* 0.11, water); ^{1}H nmr, δ (partial, β-L-rhamnopyranosyl residue): 4.785 (d, 1H, $J_{1,2}$ = 1.2 Hz, H-1), 4.048 (d of d, 1H, $J_{1,2}$ = 1.2 Hz, $J_{2,3}$ = 3.3 Hz, H-2), 3.604 (d of d, 1H, $J_{2,3}$ = 3.3 Hz, $J_{3,4}$ = 9.3 Hz, H-3), 3.405 (d of q, ca. 1H, $J_{4,5}$ = 9.2 Hz, $J_{5,6}$ = 6.0 Hz, H-5), 3.383 (d of d, 1H, $J_{3,4}$ = 9.3 Hz, $J_{4,5}$ = 9.2 Hz, H-4), 1.321 (d, 3H, $J_{5,6}$ = 6.0 Hz, H-6); ^{13}C nmr, Table 2. The glc–ms (program A) of a hydrolyzed, reduced, and acetylated sample of **3** showed erythritol tetraacetate (T_{GA} 0.36) and L-rhamnitol pentaacetate (T_{GA} 0.51) (1:1). The methylated derivative (**7**) of the disaccharide gave a single peak on glc (program C) (T_{CM} 0.35); ms (ei), *m/z* (relative intensity): 207 (29.5) [J_1], 189 (5.9) [aA_1], 157 (3.0) [aA_2], 147 (13.0), 129 (7.2), 125 (3.4) [aA_3], 115 (27.8), 101 (31.1), 89 (22.7), 88 (100), 71 (24.7), 59 (27.1), 45 (99.5). Hydrolysis, reduction ($NaBD_4$), and acetylation of methylated **3** gave on glc–ms (program B) 1,5-di-*O*-acetyl-2,3,4-tri-*O*-methyl-L-rhamnitol-1-*d* (T_{GM} 0.89).

Oligosaccharide **8** gave ^{1}H nmr, δ: 5.032 (t, 1H, $J_{1'',2''}$ = 3.2 Hz, H-2″), 4.777 (d, 1H, $J_{1,2}$ = 1.2 Hz, H-1), 4.287 (d of t, 1H, $J_{3',4a'}$ = 4.9 Hz, $J_{3',4b'}$ = 6.6 Hz, H-3′), 4.157 (d of d, 1H, $J_{3',4a'}$ = 4.9 Hz, $J_{4a',4b'}$ = 8.5 Hz, H-4a′), 4.052 (d of d, 1H, $J_{3',4b'}$ = 6.6 Hz, $J_{4a',4b'}$ = 8.5 Hz, H-4b′), 4.021 (d of d, 1H, $J_{1,2}$ = 1.2 Hz, $J_{2,3}$ = 3.4 Hz, H-2), 3.882 (m (unresolved), ca. 1H, H-2′), 3.867 (d of d, ca. 1H, $J_{1a',2'}$ = 3.2 Hz, $J_{1a',1b'}$ = 13.2 Hz, H-1a′), 3.712 (d of d, 1H, $J_{1b',2'}$ = 5.6 Hz, $J_{1a',1b'}$ = 13.2 Hz, H-1b′), 3.680 (m, 2H, H-1a″, H-1b″), 3.590 (d of d, 1H, $J_{2,3}$ = 3.2 Hz, $J_{3,4}$ = 9.6 Hz, H-3), 3.375 (m (unresolved), ca. 1H, H-5), 3.362 (m (unresolved), ca. 1H, H-4), 1.320 (d, 3H, $J_{5,6}$ = 6.0 Hz, H-6); ^{13}C nmr, δ: 104.05 (C-2″), 99.70 (C-1), 79.75 (C-2′), 75.74 (C-3′), 73.52 (C-3), 72.95 (C-4, C-5), 71.69 (C-2), 68.20 (C-4′), 61.97 (C-1″), 61.14 (C-1′), 17.46 (C-6). The glc–ms of hydrolyzed, reduced, and acetylated **8** was similar to that of **3**, showing erythritol tetraacetate (T_{GA} 0.36) and L-rhamnitol pentaacetate (T_{GA} 0.51) (1:1).

Oligosaccharide 4

Fraction III, which contained hexuronic acid, eluted at the void volume of the Bio-Gel P2 column and was further purified by preparative tlc using the above-mentioned conditions to afford oligosaccharide **4** (6 mg, R_f 0.10). The oligosaccharide emerged in the trisaccharide region of a Sephadex G-15 column (1.7 × 95 cm). The trisaccharide had $[\alpha]_D$ 0° (*c* 0.12, water); ^{1}H nmr, δ (partial): 4.786 (s, 1H), 4.769 (d, 1H, $J_{1,2}$ = 7.8 Hz); ^{13}C nmr, Table 2. Glycose analysis of **4** gave erythritol tetraacetate (T_{GA} 0.36), L-rhamnitol pentaacetate (T_{GA} 0.51), and D-glucitol-6,6-d_2 hexaacetate (T_{GA} 1.00) (1:1:1). The permethylated trisaccharide (**9**) gave a single peak on glc (program C) (T_{CM} 1.92); ms (ei), *m/z* (relative intensity): 407 (0.2), 321 (0.6), 233 (7.1) [aA_1], 207 (44.5) [J_1], 201 (100.0) [aA_2], 169 (19.4) [aA_3], 157 (14.0), 147 (22.2), 141 (25.0), 129 (10.7), 115 (39.1), 101 (43.4), 89 (32.1), 88 (64.5), 85 (26.9), 71 (16.0), 59 (27.2), 45 (65.2). Following reduction of the methyl ester ($NaBD_4$), hydrolysis, reduction, and acetylation gave on glc–ms (program B) 1,4,5-tri-*O*-acetyl-2,3-di-*O*-methyl-L-rhamnitol-1-*d* (T_{GM} 0.98) and 1,5,6-tri-*O*-acetyl-2,3,4-tri-*O*-methyl-D-glucitol-1,6,6-d_3 (T_{GM} 1.98) (1:1).

Immunodiffusion

Double diffusion studies (57) were made at 4°C in 1% (w/w) agarose gels containing 0.8% (w/w) sodium chloride using 1 mg/mL concentrations of the polysaccharides. Precipitin lines were allowed to develop over 48 h. Type 22F factor serum was supplied by Dr. J. Henrichsen, Statens Serum Institut, Copenhagen.

General methods

Commercial reagents and solvents were analytical grade. Concentrations were made under reduced pressure at bath temperatures below 40°C. Optical rotations were determined at 22°C in 10-cm microtubes using a Perkin–Elmer 243 polarimeter.

Acknowledgments

We thank Mr. F. P. Cooper for glc–ms analyses and Dr. J. Henrichsen for providing us with type 22F pneumococcal factor sera.

1. R. AUSTRIAN, R. M. DOUGLAS, G. SCHIFFMAN, A. M. COETZEE, M. J. KOORNHOR, S. HAYDEN-SMITH, and R. D. W. REID. Trans. Assoc. Am. Physicians, **89**, 184 (1976).
2. M. R. MILLEMAN, A. J. CARLSON, JR., A. A. MCLEAN, P. O. VELLA, R. E. WEIBEL, and A. F. WOODHOUR. Rev. Infect. Dis. (Suppl.), **3**, 531 (1981).
3. E. LUND and J. HENRICHSEN. Methods Microbiol. **12**, 241 (1978).
4. J. B. ROBINS, C.-J. LEE, P. H. RASTOGI, G. SCHIFFMAN, R. AUSTRIAN, J. HENRICHSEN, P. H. MAGELA, and C. V. BROOME. J. Infect. Dis. **148**, 1136 (1983).
5. B. P. CHATTERJEE and C. V. N. RAO. J. Chem. Soc. (C), 985 (1975).
6. B. P. CHATTERJEE, S. PURKAYASTHA, and C. V. N. RAO. Indian J. Chem. **14B**, 914 (1976).
7. V. DAOUST, D. J. CARLO, J. Y. ZELTNER, and M. B. PERRY. Infect. Immun. **32**, 1028 (1981).
8. G. J. GERWIG, J. P. KAMERLING, and J. F. G. VLIEGENTHART. Carbohydr. Res. **62**, 349 (1978).
9. G. J. GERWIG, J. P. KAMERLING, and J. F. G. VLIEGENTHART. Carbohydr. Res. **77**, 1 (1979).
10. K. LEONTEIN, B. LINDBERG, and J. LONNGREN. Carbohydr. Res. **62**, 359 (1978).
11. D. M. DODDRELL, D. T. PEGG, and M. R. BENDALL. J. Magn. Reson. **48**, 323 (1982).
12. P. A. J. GORIN and M. MAZUREK. Can. J. Chem. **53**, 1212 (1975).
13. K. BOCK and C. PEDERSEN. Adv. Carbohydr. Chem. Biochem. **41**, 27 (1983).
14. C. T. BISHOP and F. P. COOPER. Can. J. Chem. **41**, 2743 (1963).
15. S. COFFEY (*Editor*). Rodd's chemistry of carbon compounds. 2nd ed. Vol. 1. pt. F. Elsevier, New York. 1967. p. 521.
16. F. ALDERWEIRELDT and M. ANTEUNIS. Bull. Soc. Chim. Belg. **74**, 488 (1965).
17. C. ALTONA and A. P. M. VAN DER VEEK. Tetrahedron, **24**, 4377 (1968).
18. P. A. J. GORIN and J. F. T. SPENCER. Can. J. Chem. **43**, 2978 (1965).
19. P. E. JANSSON, B. LINDBERG, and U. LINDQUIST. Carbohydr. Res. **95**, 73 (1981).
20. K. BOCK, C. PEDERSEN, and H. PEDERSEN. Adv. Carbohydr. Chem. Biochem. **42**, 193 (1984).
21. N. K. KOCHETKOV and O. S. CHIZOV. Adv. Carbohydr. Chem. Biochem. **21**, 39 (1966).
22. V. KOVACIK, S. BAUER, and P. KOVAC. Carbohydr. Res. **8**, 282 (1968).
23. M. F. ISHAK and T. PAINTER. Acta Chem. Scand. **27**, 1268 (1973).

Can. J. Chem. Downloaded from www.nrcresearchpress.com by 41.223.56.140 on 09/07/12
For personal use only.

24. J. C. RICHARDS and M. B. PERRY. Biochem. Cell Biol. **66**, 758 (1988).
25. M. A. BERNSTEIN, L. D. HALL, and S. SUKUMAR. Carbohydr. Res. **103**, C1 (1982).
26. L. D. HALL and S. SUKUMAR. J. Chem. Soc. Chem. Commun. 292 (1979).
27. K. BOCK and H. THOGERSEN. Annu. Rep. NMR Spectrosc. **13**, 1 (1982).
28. C. ALTONA and C. A. G. HAASNOOT. Org. Magn. Reson. **13**, 417 (1980).
29. A. BAX and G. A. MORRIS. J. Magn. Reson. **42**, 501 (1981).
30. K. BOCK and C. PEDERSEN. J. Chem. Soc. Perkin Trans. 2, 293 (1974).
31. S. ANGYAL. Carbohydr. Res. **77**, 37 (1979).
32. P. A. J. GORIN and M. MAZUREK. Carbohydr. Res. **48**, 171 (1976).
33. J. M. PRESTEGARD, T. A. W. KOERNER, P. C. DEMOU, and R. K. YU. J. Am. Chem. Soc. **104**, 4993 (1982).
34. M. A. BERNSTEIN and L. D. HALL. J. Am. Chem. Soc. **104**, 5553 (1982).
35. T. A. W. KOERNER, J. M. PRESTEGARD, P. C. DEMOU, and R. K. YU. Biochemistry, **22**, 2687 (1983).
36. V. K. DUA, B. N. N. RAO, S. S. WU, V. E. DUBE, and C. A. BUSH. J. Biol. Chem. **261**, 1599 (1986).
37. J. DABROWSKI, M. HAUCK, E. ROMANOWSKA, and A. GAMIAN. Carbohydr. Res. **180**, 163 (1988).
38. D. R. BUNDLE, J. W. CHERWONOGRODSKY, and M. B. PERRY. Biochemistry, **26**, 8717 (1987).
39. M. MOREAU, J. C. RICHARDS, M. B. PERRY, and P. J. KNISKERN. Carbohydr. Res. **182**, 79 (1988).
40. P.-E. JANSSON, L. KENNE, and E. SCHWEDA. J. Chem. Soc. Perkin Trans. 1, 377 (1987).
41. J. C. RICHARDS, M. B. PERRY, and D. J. CARLO. Can. J. Biochem. Cell Biol. **61**, 178 (1983).
42. M. DUBOIS, K. A. GILLES, J. K. HAMILTON, P. A. REBERS, and F. SMITH. Anal. Chem. **28**, 350 (1956).
43. N. BLUMENKRANTZ and G. ASBOE-HANSEN. Anal. Biochem. **54**, 484 (1973).
44. T. NASH. Biochem. J. **55**, 416 (1953).
45. S. W. GUNNER, J. K. N. JONES, and M. B. PERRY. Can. J. Chem. **29**, 1892 (1961).
46. J. C. RICHARDS, M. B. PERRY, and P. J. KNISKERN. Can. J. Biochem. Cell Biol. **62**, 1309 (1984).
47. S. HAKOMORI. J. Biochem. (Tokyo), **55**, 205 (1964).
48. A. G. FERRIGE and J. C. LINDON. J. Magn. Reson. **31**, 337 (1978).
49. A. SHAKA, J. KEEKER, T. FRENKIEL, and R. FREEMAN. J. Magn. Reson. **52**, 335 (1983).
50. O. A. GANSOW and W. SCHITTENHELM. J. Am. Chem. Soc. **93**, 4294 (1971).
51. A. BAX, R. FREEMAN, and G. MORRIS. J. Magn. Reson. **42**, 164 (1981).
52. A. KUMAR, R. R. ERNST, and K. WUTHRICH. Biochem. Biophys. Res. Commun. **95**, 1 (1980).
53. A. KUMAR, G. WAGNER, R. R. ERNST, and K. WUTHRICH. J. Am. Chem. Soc. **103**, 3654 (1981).
54. W. P. AUE, J. KARHAN, and R. R. ERNST. J. Chem. Phys. **64**, 4226 (1976).
55. A. BAX. J. Magn. Reson. **53**, 517 (1983).
56. I. J. GOLDSTEIN, G. W. HAY, B. A. LEWIS, and F. SMITH. Methods Carbohydr. Chem. **5**, 361 (1970).
57. O. OUCHTERLONY. Acta Pathol. Microbiol. Scand. **25**, 186 (1958).

Can. J. Chem. Downloaded from www.nrcresearchpress.com by 41.223.56.140 on 09/07/12
For personal use only.

Bis(imidazol-2-yl)phosphinic acid hemihydrate, $[(C_3H_3N_2)(C_3H_4N_2)PO_2].(1/2)H_2O$

HELEN E. HOWARD-LOCK, COLIN J. L. LOCK,[1] SARAH PENNY, AND MARY A. TURNER
Laboratories for Inorganic Medicine, Departments of Chemistry and Pathology, McMaster University, ABB 426, Hamilton, Ont., Canada L8S 4M1

Received September 17, 1988

HELEN E. HOWARD-LOCK, COLIN J. L. LOCK, SARAH PENNY, and MARY A. TURNER. Can. J. Chem. **67**, 1051 (1989).

The title compound was obtained as the major product of our handling of the literature preparation of tris(imidazol-2-yl)phosphine. The compound was characterized by ^{1}H NMR, mass and vibrational spectroscopy. The structure was determined by single crystal X-ray diffraction. Crystals were triclinic, $P\bar{1}$, a = 7.677(1), b = 12.658(2), c = 10.072(2) Å, α = 91.18(1), β = 114.44(1), γ = 99.49(1)°, Z = 4. Intensities were measured on a Syntex $P2_1$ diffractometer with MoKα radiation and 3088 reflections were used to determine the structure. R = 0.0698, R_w = 0.0534. The phosphinic acid exists in the solid as the zwitterionic form and bond lengths and angles are normal.

Key words: tris(imidazol-2-yl)phosphine, X-ray structure, bis(imidazol-2-yl)phosphinic acid hemihydrate.

HELEN E. HOWARD-LOCK, COLIN J. L. LOCK, SARAH PENNY et MARY A. TURNER. Can. J. Chem. **67**, 1051 (1989).

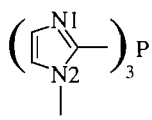
En répétant la préparation de la tris(imidazolyl-2)phosphine décrite dans la littérature, on a obtenu le composé mentionné dans le titre comme produit principal. On l'a caractérisé par RMN du ^{1}H ainsi que par spectrométrie de masse et par spectroscopie vibrationnelle. On a déterminé sa structure à l'aide de la diffraction des rayons-X sur un cristal unique. Les cristaux sont tricliniques, $P\bar{1}$, avec a = 7,677(1), b = 12,658(2) et c = 10,072(2) Å, α = 91,18(1), β = 114,44(1) et γ = 99,49(1)° et Z = 4. On a mesuré les intensités à l'aide d'un diffractomètre Syntex $P2_1$ et de la radiation MoKα; on a utilisé 3088 réflexions pour déterminer la structure. R = 0,0698 et R_w = 0,0534. L'acide phosphinique existe dans le solide sous la forme zwitterionique et les longueurs des liaisons ainsi que les angles sont normaux.

Mots clés : tris(imidazolyl-2)phosphine, structure par rayons-X, hémi-hydrure d'acide phosphinique bis(imidazolyl-2).
[Traduit par la revue]

Can. J. Chem. Downloaded from www.nrcresearchpress.com by 41.223.56.140 on 09/07/12
For personal use only.

Introduction

As part of our studies of metal complexes of ligands with two types of binding site, one soft and the other relatively hard (1), we became interested in tris(imidazol-2-yl)phosphine, **A**. In one of its substituted forms it has been used to bind zinc as a model for the protein carbonic anhydrase (2) and this zinc complex does act as a catalyst for the CO_2/HCO_3^- reaction (3). In this ligand there are three types of potential binding site, the



A

phosphorus atom, N1 and N2. The metal binding capabilities of N1 and N2 are very pH dependent since they will not bind metals when protonated. We attempted to prepare the ligand by a minor modification of the literature method (4), but the major product we obtained was not the desired compound and the fact that a copper(II) complex was neutral suggested the ligand was charged. We have investigated the product and identified it as bis(imidazol-2-yl)phosphinic acid. We describe this work here.

Experimental section

Imidazole orthoformate

The procedure was a modification of that of Curtis and Brown (4). The product was distilled under vacuum to give a clear colourless liquid (bp 90°C at 1 mm Hg).

Bis(imidazol-2-yl)phosphinic acid hemihydrate

The literature procedure for tris(imidazol-2-yl)phosphine was followed with minor modification (4). The procedure is described in full because of the different product obtained by us. *N*-butyllithium (1.6 *M* in hexane, 28.8 mL, 0.046 mol) was added with a syringe to dry ether (100 mL) in a round bottom flask, with a pressure equalized dropping funnel, at −78°C, under N_2. Imidazole orthoformate (7.86 g, 0.046 mol), dried over molecular sieves, was added by syringe to dry ether (10 mL) in the dropping funnel. The imidazole orthoformate was added slowly to the *n*-butyllithium and the solution was stirred for 15 min. This produced the lithium anion of the protected imidazole orthoformate. The dropping funnel was washed twice with ether (10 mL). PCl_3 (1.34 mL) was added by syringe to dry ether (10 mL) in the dropping funnel. The PCl_3 solution was added slowly to the lithium anion. When the addition of PCl_3 was complete the solution was stirred and allowed to warm up overnight. The round bottom flask was cooled in an ice bath and concentrated NH_4OH (100 mL) was added. The solution was stirred for 15 min. The ether layer was removed and dried over Na_2SO_4. The ether was then removed *in vacuo*. The residue was refluxed for 5 h in H_2O (10 mL) and acetone (100 mL). The white solid which separated was collected by filtration. Recrystallization was done from water (yield ~20%). Instead of the expected tris(imidazol-2-yl)phosphine, this white solid was found to be bis(imidazol-2-yl)phosphinic acid, mp 230°C, ^{1}H NMR (D_2O solvent) 7.25 ppm. In another attempt to prepare the desired tris(imidazol-2-yl)phosphine, we modified the literature procedure but this attempt was not successful. The following modifications in ratios and temperatures were made. The imidazole orthoformate was used in a 5:1 ratio with the PCl_3 rather than 3:1, and the reaction was carried out at 0°C, rather than at −78°C. When the residue was refluxed with water and acetone no solid appeared. The solvent was then removed *in vacuo* to produce an oil. Mass spectra and ^{1}H NMR revealed that the oil was a complex mixture.

Spectral measurements

Proton NMR spectra were recorded at 500.137 MHz on a Bruker AM-500 spectrometer with use of D_2O as an internal lock. Spectra were recorded over a 5 kHz sweep in 32K data points (3.277 s acquisition time). Suppression of the HDO resonance was achieved by pre-saturation during the 1.0 s delay before acquisition. Sample temperature was maintained at 30 ± 1°C by a Bruker B-VT1000 variable temperature unit. The free induction decays were processed using Gaussian multiplication for resolution enhancement. Chemical shift values are reported relative to TMS.

The FAB mass spectrum was recorded on a VG ZAB-E spectro-

[1]To whom all correspondence should be addressed.

Can. J. Chem. Downloaded from www.nrcresearchpress.com by 41.223.56.140 on 09/07/12
For personal use only.

TABLE 1. Crystal data

Formula	$[(C_3H_3N_2)(C_3H_4N_2)PO_2](1/2)H_2O$, $C_6H_8N_4O_{2.5}P$
Formula weight	207.13
Crystal shape, size (mm)	Plate, 0.30 × 0.20 × 0.40
Systematic absences	None
Space group	$P\bar{1}$
Unit cell parameters (Å and deg)	a = 7.677(1) α = 91.18(1)
	b = 12.658(2) β = 114.44(1)
	c = 10.072(2) γ = 99.49(1)
Volume (Å^3)	874.5(2)
Z	4
ρ_{calc}, ρ_{obs} (g cm^{-3})	1.57, 1.56(2)
Max 2θ, reflections measured	50°, $0 < h < 9$, $-15 < k < 15$, $-11 < l < 11$
Temperature, °C	22
Linear absorption coefficient cm^{-1}	3.01
Absorption coefficient Å*, range	1.054–1.081
Number of variables	292
Standard reflections (e.s.d.)	1 −5 −4 (0.018), 1 −1 −6 (0.017)
Number of reflections measured	3340
Number of independent reflections	3088
R_{int}[a]	0.0087
Final R[b], R_w[c]	0.0698, 0.0534
Final Δ/σ, max., ave.	0.023, 0.004
Final difference map, max, min, e Å^{-3}	0.42, −0.35
Weighting	$(\sigma_F^2 + 0.000314F_o^2)^{-1}$
Error in an observation of unit wt., S	1.2356
$F(000)$	432.6

[a] $R_{int} = \left[\frac{\Sigma\{Nx\Sigma[w(\langle F\rangle - F)^2]\}}{\Sigma(N-1)\Sigma wF^2}\right]^{1/2}$.

[b] $R = \Sigma||F_o| - |F_c||/\Sigma|F_o|$.

[c] $R_w = (\Sigma w(|F_o| - |F_c|)^2/\Sigma wF_o^2)^{1/2}$.

meter. The sample was dissolved in a thioglycerol/5% trifluoroacetic acid matrix and submitted to bombardment by Xe atoms (8 keV).

Infrared spectra were recorded on a Perkin-Elmer 283 grating spectrometer over the range 4000–200 cm^{-1}. The samples were prepared as KBr pellets. Spectra were calibrated against polystyrene. Raman spectra from powder samples were excited by the λ = 514.5 nm radiation of a Coherent Radiation Argon Laser Model 52 and measured over the range 3000–50 cm^{-1} on a Spex Spectrometer Model 14018. The wavenumber readout is accurate to ± 2 cm^{-1}. Spectral calibrations were made with the use of $HgCl_2$.

X-ray diffraction studies

The crystal used for diffraction studies was a colourless plate. Precession photographs showed the crystal to be triclinic and a Delaunay reduction showed no hidden symmetry. Cell parameters were obtained by least-squares refinement of the setting angles of 15 automatically centred reflections (21.7° < 2θ < 29.9°) measured on a Syntex $P2_1$ diffractometer with use of graphite-monochromated MoKα radiation (λ = 0.71069 Å). Crystal data and other information related to data collection are given in Table 1. Intensities were measured with a θ(crystal)–2θ(counter) scan. The density of the crystal was measured by suspension in a chloroform/bromoform mixture. Intensities were corrected for Lorentz-polarization effects, but not for absorption. This will cause a maximum error in F_o of <0.65%.

Although the correct space group is $P\bar{1}$, the structure was solved in $P1$. The strongest peak in the Patterson map was interpreted as a phosphorus atom and its centrosymmetrically related atom. Although difference syntheses revealed part of the structure, refinement ceased at R_w = 0.18. The structure was converted to $P1$ with one phosphorus atom placed at the origin. A series of refinements and difference syntheses revealed all the atoms. It became apparent that there were two molecules in the asymmetric unit and that the true space group was $P\bar{1}$. The initial problem was caused by the incorrect interpretation of the strongest peak in the Patterson map as that arising from a

TABLE 2. Positional parameters (×10^4) and U_{eq} (×10^3) for $[(C_3H_3N_2)(C_3H_4N_2)PO_2].(1/2)H_2O$

Atom	x	y	z	U_{eq}[a]
P(1)	5636(1)	5939(1)	2702(1)	22
O(11)	5890(3)	4979(2)	1981(2)	30
O(12)	7261(3)	6681(2)	3871(2)	30
N(11)	3538(4)	6147(2)	4355(3)	28
N(12)	2199(4)	4770(2)	2675(3)	29
N(13)	4154(4)	6603(2)	−184(3)	26
N(14)	4065(4)	7717(2)	1395(3)	28
C(11)	3739(4)	5565(2)	3307(3)	22
C(12)	1826(5)	5719(3)	4389(4)	34
C(13)	1014(5)	4872(3)	3356(4)	36
C(14)	4519(4)	6767(2)	1223(3)	22
C(15)	3416(5)	8162(3)	86(3)	32
C(16)	3479(5)	7465(3)	−906(3)	31
P(2)	2683(1)	1298(1)	2413(1)	21
O(21)	4296(3)	2053(2)	3608(2)	29
O(22)	2969(3)	258(2)	1914(2)	30
N(21)	547(4)	1626(2)	4013(3)	26
N(22)	−880(4)	268(2)	2284(3)	27
N(23)	1260(4)	1619(2)	−585(3)	25
N(24)	1679(4)	3067(2)	751(3)	24
C(21)	687(4)	1051(2)	2916(3)	22
C(22)	−1153(5)	1190(3)	4078(3)	33
C(23)	−2015(5)	364(3)	3008(4)	34
C(24)	1828(4)	2029(2)	798(3)	20
C(25)	1010(5)	3309(3)	−672(3)	31
C(26)	746(5)	2412(3)	−1500(3)	33
O(3)	3717(5)	8631(2)	3693(3)	48

[a] $U_{eq} = (1/3)(U_{11} + U_{22} + U_{33} + 2\cos\alpha U_{23} + 2\cos\beta U_{13} + 2\cos\gamma U_{12})$.

TABLE 3. Selected interatomic distances (Å) and angles (deg) for $[(C_3H_3N_2)(C_3H_4N_2).PO_2].(1/2)H_2O$

(*a*) Non hydrogen bonds

Atoms	Distance		Atoms	Distance	
	$i = 1$	$i = 2$		$i = 1$	$i = 2$
P(i)—O(i1)	1.483(2)	1.490(2)	P(i)—O(i2)	1.476(2)	1.482(2)
P(i)—C(i1)	1.798(3)	1.787(3)	P(i)—C(i4)	1.832(3)	1.819(3)
C(i1)—N(i1)	1.349(3)	1.360(3)	N(i1)—C(i2)	1.351(4)	1.359(4)
C(i2)—C(i3)	1.348(4)	1.352(4)	C(i3)—N(i2)	1.366(4)	1.365(4)
N(i2)—C(i1)	1.332(3)	1.334(3)	C(i4)—N(i3)	1.330(3)	1.339(3)
N(i3)—C(i6)	1.377(4)	1.372(4)	C(i6)—C(i5)	1.341(4)	1.330(4)
C(i5)—N(i4)	1.373(4)	1.368(4)	N(i4)—C(i4)	1.334(3)	1.338(3)

Atoms	Angle		Atoms	Angle	
	$i = 1$	$i = 2$		$i = 1$	$i = 2$
C(i1)—P(i)—O(i1)	109.9(1)	107.1(1)	C(i1)—P(i)—O(i2)	108.2(1)	108.7(1)
C(i4)—P(i)—O(i1)	105.4(1)	107.3(1)	C(i4)—P(i)—O(i2)	105.7(1)	106.0(1)
O(i1)—P(i)—O(i2)	123.5(1)	121.8(1)	C(i1)—P(i)—C(i4)	101.9(1)	104.6(1)
N(i1)—C(i1)—P(i)	124.1(2)	125.0(2)	N(i2)—C(i1)—P(i)	125.7(2)	125.2(2)
N(i3)—C(i4)—P(i)	128.0(2)	125.7(2)	N(i4)—C(i4)—P(i)	125.3(2)	127.5(2)
N(i2)—C(i1)—N(i1)	109.7(3)	109.8(3)	C(i1)—N(i1)—C(i2)	108.3(3)	107.9(2)
N(i1)—C(i2)—C(i3)	106.2(3)	106.1(3)	C(i2)—C(i3)—N(i2)	110.0(3)	110.4(3)
C(i3)—N(i2)—C(i1)	105.7(2)	105.8(3)	N(i4)—C(i4)—N(i3)	106.5(3)	106.8(2)
C(i4)—N(i3)—C(i6)	109.9(2)	109.0(2)	N(i3)—C(i6)—C(i5)	106.9(3)	107.5(3)
C(i6)—C(i5)—N(i4)	106.7(3)	107.3(3)	C(i5)—N(i4)—C(i4)	110.1(2)	109.4(2)

(*b*) Hydrogen bonds*

Atoms	Distance	Atoms	Distance	Atoms	Distance	Bonds	Angle
N(11)..O(21)[a]	2.812(3)	N(11)—H(13)	0.82(3)	H(13)..O(21)[a]	2.01(3)	N(11)—H(13)..O(21)[a]	166(4)
N(13)..O(11)[b]	2.658(3)	N(13)—H(16)	0.87(4)	H(16)..O(11)[b]	1.81(4)	N(13)—H(16)..O(11)[b]	165(3)
N(14)..O(3)	2.695(4)	N(14)—H(17)	0.90(4)	H(17)..O(3)	1.83(3)	N(14)—H(17)..O(3)	162(3)
N(21)..O(12)[a]	2.761(3)	N(21)—H(24)	0.85(3)	H(24)..O(12)[a]	1.93(3)	N(21)—H(24)..O(12)[a]	165(4)
N(23)..N(22)[c]	2.812(4)	N(23)—H(21)	0.94(4)	H(21)..H(22)[c]	1.93(4)	N(23)—H(21)..N(22)[c]	157(3)
N(24)..N(12)	2.732(4)	N(24)—H(27)	0.98(4)	H(27)..N(12)	1.77(4)	N(24)—H(27)..N(12)	167(3)
O(3)..O(22)[d]	2.732(4)	O(3)—H(3)	0.81(4)	H(3)..O(22)[d]	2.02(4)	O(3)—H(3)..O(22)[d]	148(4)

*Atoms are related to those given in Table 2 by the relationships *a*: $1 - x, 1 - y, 1 - z$; *b*: $1 - x, 1 - y, -z$; *c*: $-x, -y, -z$; *d*: $x, 1 + y, z$.

pair of centrosymmetrically related atoms. The water molecule was located, and subsequent full-matrix least-squares refinement of all parameters (except the hydrogen temperature factors), which minimized $\Sigma w(|F_o| - |F_c|)^2$, was terminated when Δ/σ fell below 0.1. Reflections with $3\sigma_I \geq I \geq -3\sigma_I$ were treated by the method of French and Wilson (5). Scattering curves were taken from the International tables (6) and a correction for anomalous dispersion was made to the curve for phosphorus (7). No correction was necessary for secondary extinction. The atomic positional parameters are given in Table 2.[2]

Results and discussion

Molecule **1** is shown in Fig. 1 and selected interatomic distances and angles are given in Table 3.[3] Both molecules of the compound exist in the zwitterionic form such that there are both protonated and unprotonated imidazole rings attached to the phosphorus atom in each molecule. The P—O bond lengths in a given molecule are insignificantly different, but the mean distances in molecule **1** appear to be shorter than those in molecule **2** and the shortest P—O distance in molecule **1** is

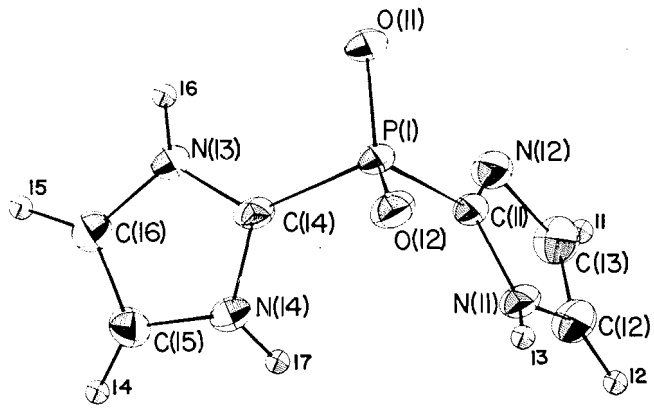


FIG. 1. Molecule **1** showing the atom numbering. The atoms in molecule **2** are numbered similarly, but the first affix is changed from **1** to **2**. Hydrogen atoms are given by affixes only in smaller print.

[2]The program DATRDN from the XTAL program (8) was used for preliminary data treatment. The structure was solved with use of SHELX (9). Planes calculations were made with LSQPL (10). Molecule and cell packing diagrams were obtained from SNOOPI (11).

[3]Tables of anisotropic temperature factors, hydrogen atom positional parameters, interatomic distances and angles involving hydrogen atoms, best planes and dihedral angles, and the moduli of F_o and F_c have been deposited. They may be purchased from the Depository of Unpublished Data, CISTI, National Research Council of Canada, Ottawa, Ont., Canada K1A 0S2.

Can. J. Chem. Downloaded from www.nrcresearchpress.com by 41.223.56.140 on 09/07/12
For personal use only.

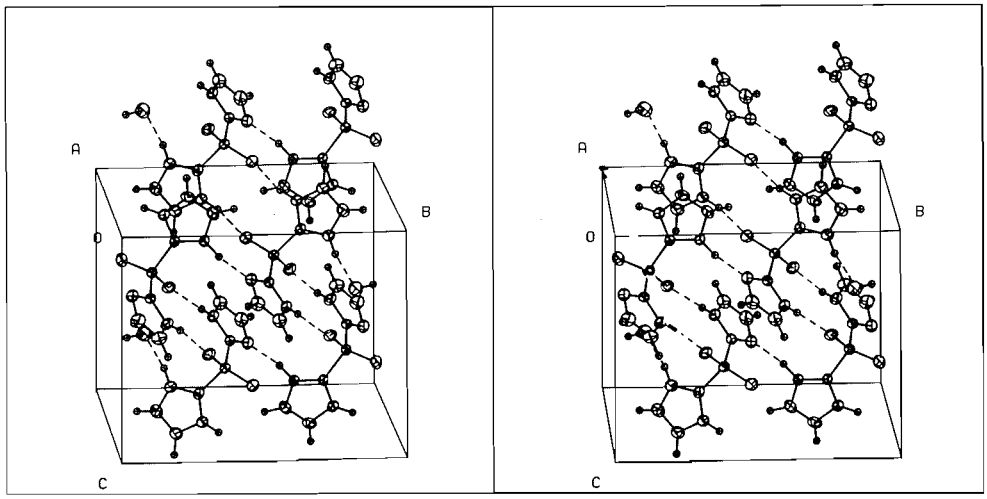


FIG. 2. The packing of the molecules in the unit cell. Hydrogen bonding is shown by broken lines. Molecule **1** is the left-hand one at the bottom of the figure and molecule **2** is the right-hand one.

significantly shorter than the longest P—O distance in molecule **2** ($\Delta = 4.94\sigma$). The difference is not caused by hydrogen bonding; the hydrogen bonds to the oxygen atoms in molecule **1** are stronger than those in molecule **2** (2.658(3), 2.761(3) Å vs. 2.812(3), 2.732(3) Å). The longer P—O distances in molecule **1** compared to molecule **2** are clearly related to the stronger P—C bonds in molecule **1**. The differences in P(1)—C(11) and P(2)—C(21) ($\Delta = 2.59\sigma$) and P(1)—C(12) and P(2)—C(22) ($\Delta = 3.06\sigma$) are significant at the 90% confidence level and may be related to changes in overlap of the *d* orbitals of the phosphorus atom and a π-system. Angles about the phosphorus atom are very roughly tetrahedral, the biggest variation being the O—P—O angles which are large (123.5(1), 121.8(1)°) because of the repulsion of the multiply bonded oxygen atoms; the O...O distances (2.57 Å, **1**; 2.60 Å, **2**) are shorter than the van der Waals distance (12). The C—P—C angles are correspondingly smaller than the tetrahedral angle (101.9(1), 104.6(1)°).

Protonation causes some significant changes in the bond lengths and angles in the imidazole group. While there are significant differences in the averages of C(*i*1)—N(*i*1) and C(*i*1)—N(*i*2), N(*i*1)—C(*i*2)—C(*i*3) and C(*i*2)—C(*i*3)—N(*i*2) (4.0°) and C(*i*2)—N(*i*1)—C(*i*1) and C(*i*3)—N(*i*2)—C(*i*1) (2.4°) ($i = 1, 2$) in the imidazole group these are removed on protonation. Protonation causes an increase in the internal ring angle at the protonated nitrogen atom (~4°) and consequent decreases in the adjacent angles at the carbon atoms (~3°) and a small increase in the angles at the opposite nitrogen atoms (~1°). Changes of this type on protonation of aromatic ring nitrogen atoms have been observed previously (13). Changes in bond lengths within the ring are hardly significant, although there is apparently a change in the lengths of bonds to the nitrogen atom opposite to the protonation site. N(*i*3)—C(*i*4) is longer (~0.02 Å) and N(*i*3)—C(*i*3) is shorter (~0.02 Å) than the corresponding bonds in the unprotonated imidazole. The surprising change is the significant lengthening of the P—C bonds to the protonated rings (average 0.033 Å). The dihedral angles between the two rings in each molecule are very similar (82.8(2)°, **1**; 77.1(2)°, **2**).

The packing is shown in Fig. 2 and is dominated by π–π interactions between imidazole rings and an extensive hydrogen bonding network. The two independent molecules form a pair such that each molecule lies roughly in the same orientation and pairs are hydrogen bonded together through the water molecule (N14—H...O3—H...O22). There are π–π interactions between pairs of centrosymmetrically related molecules (molecule **1**, ring 1, inversion centre at 1/2, 1/2, 1/2; molecule **2**, ring 1, inversion centre at 0 0 1/2) and between pairs of independent molecules (molecule **1**, ring 2 – molecule **2**, ring 2). There are hydrogen bonds between other centrosymmetrically related pairs (molecule **1**, N13...O11, inversion centre 0, 1/2, 1/2, molecule **2**, N23...N22, inversion centre 0, 0, 0) and between independent molecules (N24...N12, N21...O12, N11...O21). The remaining hydrogen bond is from O3...O21. This results in chains of molecules interacting through π–π interactions which lie roughly along [1 1 2]. Interactions between chains in the *a* direction are primarily van der Waals with the hydrogen bonds lying very roughly along [0 1 1].

TABLE 4. Mass spectrum of $(C_3H_3N_2)(C_3H_4N_2)PO_2$

M/Z	*I*	Assignment
595	6	$P_3 + H^+$
419	6	$P_2 + Na^+$
397	31	$P_2 + H^+$
237	5	$P + K^+$
221	16	$P + Na^+$
199	100	$P + H^+$
131	11	$P^+ - C_3H_3N_2$

Only a single proton nmr peak is observed at 7.25 ppm. No signal is seen for the protons attached to the nitrogen atoms because of exchange with the aqueous solvent and the exchange makes the protons attached to the carbon atoms equivalent.

The mass spectrum is given in Table 4. All peaks except one are derived from the parent ion plus a cation, as expected for a FAB spectrum. Higher peaks corresponding to two and three parent molecules plus a cation are of lower intensity. A peak at $m/z = 131$ corresponded to a parent ion which has lost an imidazole molecule.

The bis(imidazole)phosphinic acid spectra have been assigned by comparison with the imidazole spectra with the addition of bands associated with the P—C and P=O modes (14).

The vibrational spectra of imidazole have been assigned previously on the basis of a C_{2v} molecular model. The splitting

Can. J. Chem. Downloaded from www.nrcresearchpress.com by 41.223.56.140 on 09/07/12
For personal use only.

TABLE 5. Vibrational spectra of bis(2-imidazol-2-yl)phosphinic acid

Infrared[a] (cm^{-1})	Raman[a] (cm^{-1})	Assignment[b]	Infrared (cm^{-1})	Raman (cm^{-1})	Assignment
3145(w)	3153(m)		1350(m)	1355(s)	δCH
3130(w)	3135(m)	νC—H		1270(m,br)	νP=O
	3120(m)		1240(vs,br)	1261(m)	
	3100(w)			1155(w)	δNH
3015(w)			1115(s,br)	1115(w,doublet)	δCH
2920(w)		νN—H	1065(s,br)	1044(m)	δCH
2830(w,br)			965(m)		
2790				925(w)	δCH
2660(w)			870(vw)		Ring bend
2540(w)			790(sh)		
1970(vbr,s)			760(s)		δP—C
1595(m)		νC=C	699(m)		
1540(w)		δNH	575(s)	581(m)	
	1448(s)	νP—C	535(s)	542(m)	
1420, 1410 (m)	1438(vs)	νP—C	475(vw)	460(m)	

[a]Bands in cm^{-1}, s = strong, m = medium, w = weak, br = broad, sh = shoulder, v = very.
[b]ν = stretching frequency, δ = deformation.

of the νNH stretching band as well as the fact that there are two bands assignable to δNH deformations can be accounted for in C_{2v}, with protons equidistant from the two nitrogen atoms (15). The infrared spectrum of imidazole observed by us is similar. The broad absorption 2800–2600 cm^{-1} is typical of five-membered heteroaromatic rings with more than one nitrogen. There are strong interactions of force constants and a large amount of mixing among the mid-region frequencies.

The major product obtained by us was not that reported for the same reaction in the literature (4). By coincidence, the ^1H NMR parameters and melting points of the two compounds were identical, but there is no doubt about the nature of the compound described in the literature, since it was also characterized by analysis and mass spectrometry (16). The reason we obtained the phosphinic acid rather than the phosphine is probably because we used the general procedures for synthesizing the phosphines given in ref. 4 in which the hydrolysis step was carried out under reflux for 5 h in a water (10 mL)/acetone (100 mL) mixture, since we did not obtain any product when the mixture was stirred at room temperature. The room temperature reaction, given in a footnote, suggests the mixture did not *require* heating. In light of our experience the procedure should probably be modified to state the mixture should not be heated (4). The hydrolysis/oxidation does not occur on the recrystallization step even though we had to use water rather than methanol for recrystallization. The mass spectrum of the powder before recrystallization is identical to that of the crystals use for the X-ray study, with a parent ion m/z of 198, rather than the expected 232. The hydrolysis–oxidation reaction has been observed before in the preparation of a zinc complex (17). In this case, it was postulated that the zinc ions catalysed the hydrolysis–oxidation reaction, but no metal ions were present in our reaction so the reaction is obviously more facile than had previously been anticipated.[4]

Acknowledgements

We acknowledge, with thanks, financial support from the Natural Sciences and Engineering Research Council of Canada. We also acknowledge helpful discussions with Professor R. S. Brown, University of Alberta.

1. C. J. L. LOCK and M. A. TURNER. Acta Crystallogr. C**43**, 2096 (1987).
2. R. J. READ and M. N. G. JAMES. J. Am. Chem. Soc. **103**, 6947 (1981).
3. J. HUGUET and R. S. BROWN. J. Am. Chem. Soc. **102**, 7571 (1980).
4. N. J. CURTIS and R. S. BROWN. J. Org. Chem. **45**, 4038 (1980).
5. S. FRENCH and K. WILSON. Acta Crystallogr. A**34**, 517 (1978).
6. D. T. CROMER and J. T. WABER. International tables for X-ray crystallography. Vol. IV. *Edited by* J. A. Ibers and W. C. Hamilton, Kynoch Press, Birmingham, England. 1974. Table 2.2B. pp. 99–101.
7. D. T. CROMER and J. A. IBERS. International tables for X-ray crystallography. Vol. IV. *Edited by* J. A. Ibers and W. C. Hamilton. Table 2.3.1, pp. 149–150.
8. J. M. STEWART and S. R. HALL. The XTAL system of crystallographic programs, Tech. Report TR-1364, University of Maryland, College Park, MD. 1983.
9. G. M. SHELDRICK. SHELX. Program for crystal structure determination. University of Cambridge, England. 1976.
10. G. DAVENPORT. LSQPL. Calculation of Least-Squares Planes, Crystallography Centre, University of West Australia, Nedlands, WA., Australia, 6009: Part of the XTAL System of Crystallographic Programs. *Edited by* J. M. Stewart and S. R. Hall. Computer Science Technical Report Series, TR-1364. University of Maryland, College Park, MD 30742, 1983.
11. K. DAVIES. CHEMGRAF Suite: Program SNOOPI, Chemical Design Ltd., Oxford, England. 1986.
12. A. BONDI. J. Phys. Chem. **68**, 441 (1964).
13. D. VOET and A. RICH. Prog. Nucl. Acid Res. Mol. Biol. **10**, 183 (1970).
14. N. B. COLTHUP, L. H. DALY, and S. E. WIBERLEY. Introduction to infrared and Raman spectroscopy. Academic Press, New York. 1964. pp. 237, 300.
15. M. CORDES DE N. D. and J. L. WALTER. Spectrochim. Acta, **24A**, 237 (1967).
16. R. S. BROWN. Private communication.
17. R. G. BALL, R. S. BROWN, and J. L. COCHO. Inorg. Chem. **23**, 2315 (1984).

[4]We have eliminated another possible explanation, namely, that $POCl_3$ was used in error for PCl_3 in the reaction.

Can. J. Chem. Downloaded from www.nrcresearchpress.com by 41.223.56.140 on 09/07/12
For personal use only.

The nature of selenium dissolved in hydrobromic acid containing selenium dioxide

JOHN MILNE
Department of Chemistry, University of Ottawa, Ottawa, Ont., Canada K1N 6N5

Received September 29, 1988

JOHN MILNE. Can. J. Chem. **67**, 1056 (1989).

Elemental selenium dissolves in solutions of selenium dioxide in hydrobromic acid. In 8.72 *M* HBr, there is complete reaction to give Se_2Br_2 and $SeBr_4^{2-}$ as shown by solubility studies and Raman spectroscopy. When the Se_2Br_2 concentration exceeds 0.0116 *M*, insoluble Se_2Br_2 is formed. The equilibrium constant for the reaction,

$$Se_2Br_2 + 2Br^- \rightleftharpoons SeBr_4^{2-} + Se^0$$

has been determined, $K = 0.025\ (\pm 0.002)\ mol^{-2}\ L^2$.

Solutions of SeO_2 and Se^0 in 4.8 *M* HBr contain Se(IV), Se(II), and Se(I) in equilibrium,

$$3SeBr_4^{-2} + H_2O \rightleftharpoons Se_2Br_2 + SeOBr_3^- + 7Br^- + 2H^+$$

The equilibrium constant for this reaction is $10.0\ (\pm 0.7) \times 10^{12}\ mol^8\ L^{-8}$. The solubility of Se_2Br_2 at saturation in 4.8 *M* HBr is 0.0052 *M*.

Key words: selenium bromides, bromoselenates, hydrobromic acid, solution equilibria, solubility.

JOHN MILNE. Can. J. Chem. **67**, 1056 (1989).

Le sélénium se dissout en solution du dioxyde de sélénium dans l'acide bromohydrique. L'étude de la solubilité et de la spectroscopie Raman de ces solutions ont montré que dans l'acide bromohydrique, 8,72 *M*, la réaction est complète et donne Se_2Br_2 et $SeBr_4^{2-}$. Quand la concentration de Se_2Br_2 dépasse 0,0116 *M*, le Se_2Br_2 devient insoluble. La constante d'équilibre de la réaction,

$$Se_2Br_2 + 2Br^- \rightleftharpoons SeBr_4^{2-} + Se^0$$

a été determinée, $K = 0{,}025\ (\pm 0{,}002)\ mol^{-2}\ L^2$.

Les solutions de SeO_2 et Se^0 en HBr, 4,80 *M*, contiennent Se(IV), Se(II) et Se(I) en équilibre,

$$3SeBr_4^{2-} + H_2O \rightleftharpoons Se_2Br_2 + SeOBr_3^- + 7Br^- + 2H^+$$

la constante d'équilibre pour cette réaction est $10{,}0\ (\pm 0{,}7) \times 10^{12}\ mol^8\ L^{-8}$. La solubilité de Se_2Br_2 au point de saturation en HBr, 4,80 *M*, est 0,0052 *M*.

Mots clés: bromures de sélénium, bromosélénates, acide bromhydrique, équilibres en solution, solubilité.

Introduction

Amongst the selenium chlorides and bromides only the diselenium dihalides, Se_2X_2, and the tetrahalides, SeX_4, are found as isolable substances. The dihalides, SeX_2, have been detected in vapour state (1, 2) and in non-aqueous solution (3, 4) but have not been prepared as pure compounds. Elemental selenium dissolves in hydrochloric acid containing SeO_2 and this has been accounted for by the formation of Se_2Cl_2 (5). Recently, however, it has been shown that such solutions contain significant concentrations of $SeCl_2$ or chloroselenate(II) (6). It was of interest to extend these studies to hydrobromic acid, where higher concentrations of Se(II) may be possible in view of the greater stability of $SeBr_2$ compared to $SeCl_2$ in acetonitrile (4).

Experimental section

Hydrobromic acid (Fisher, 48%) was analyzed for acid strength by titration against sodium carbonate and, for free bromine content, by iodimetry, against sodium thiosulfate. Acid strength was 8.72 *M* and free bromine content was 0.00125 *M*. Selenium dioxide (Aldrich) was analyzed by potentiometric acid base titration. Elemental selenium (Baker analyzed, pellets) was freshly ground before use.

Solutions of SeO_2 and HBr were saturated with elemental selenium by shaking for several hours in closed containers. Complete saturation was achieved for the SeO_2 concentrations studied, in 4 h. All experiments and measurements were carried out at room temperature (20°C). Initial SeO_2 concentrations were corrected to allow for the Se(IV) produced by oxidation of Se by free bromine in the HBr. No evidence of photooxidation in the timeframe of the experiments was noted. The concentration of dissolved elemental selenium (c_0) was determined by dilution in distilled water (1 in 4 minimum) and weighing of the precipitated selenium. The degree of dilution necessary for complete precipitation was determined by stepwise dilution to the point where no further precipitation occurred. Analysis for total Se content confirmed the stoichiometry,

$$c(\text{total Se}) = c_{IV} + c_0$$

where c_{IV} represents the initial SeO_2 concentration in HBr. Below the point of Se_2Br_2 saturation, elemental selenium was nearly twice as soluble, for the same c_{IV}, in 8.48 *M* HBr as in 11.80 *M* HCl (6).

Spectrophotometric measurements were made with a Varian DMS 90 UV-visible spectrophotometer using 1 cm and 1 mm path length quartz cells. All measurements were blanked against water.

Raman spectra were taken using a Jobin-Yvon spectrometer with PAR photon counting. The spectra were excited by a Spectra Physics Krypton Ion laser operating at 647.1 nm.

The preparation of $SeBr_4^{2-}$ salts from the solutions studied, with the addition of potassium or tetraethylammonium bromides, was attempted. The solids obtained were mixtures with crystals varying from orange to black in colour. Raman spectra showed them to consist mainly of hexabromoselenate(IV) and diselenium dibromide.

Results and discussion

When elemental selenium is dissolved in HBr solutions containing SeO_2, they turn from pale orange to dark orange. At low SeO_2 concentrations Se^0 is the insoluble phase but at higher SeO_2 concentrations, the insoluble phase becomes liquid Se_2Br_2. This is the basis of a preparative method for Se_2Br_2 (7).

Can. J. Chem. Downloaded from www.nrcresearchpress.com by 41.223.56.140 on 09/07/12
For personal use only.

TABLE 1. Solutions of varying SeO_2 concentration (c_{IV}) in 8.72 *M* HBr, Se solubilities (c_0), and absorbances at 385 nm (A_{385})

10^3 c_{IV} (mol L^{-1})	10^3 c_0 (mol L^{-1})	Obsd A_{385}	MOS[a]	10^3 $[Se_2Br_2]$ (mol L^{-1})	10^3 $[SeBr_4^{2-}]$ (mol L^{-1})	$[Br^-]$ (mol L^{-1})	K[c] (L^2 mol^{-2})	Calcd A_{385}
2.53	4.18	3.40	1.51	1.65	3.42	8.703	0.027	3.47
4.45	7.47	6.05	1.49	3.03	5.85	8.690	0.026	6.13
5.00	8.36	—	1.50	3.35	6.67	8.687	0.026	—
6.36	10.9	8.85	1.47	4.54	8.18	8.678	0.024	8.85
8.28	13.4	11.55	1.53	5.11	11.48	8.664	0.030	11.25
10.0	16.8	—	1.49	6.82	13.15	8.654	0.026	—
10.2	18.3	15.55	1.43	8.11	12.27	8.655	0.020	14.48
12.1	20.8	17.15	1.47	8.71	15.47	8.641	0.024	16.85
20.0	28.9	—	1.64	11.6[b]	—	—	—	—
29.4	28.6	22.95	2.03	—	—	—	—	—
39.0	28.7	23.90	2.30	—	—	—	—	—
48.5	28.7	23.90	2.51	—	—	—	—	—

[a]Mean oxidation state.
[b]Saturated with Se_2Br_2 (calculated).
[c]Mean $K = 0.025 (\pm 0.002)$ L^2 mol^{-2}.

8.72 M *HBr solutions*

The solubilities of elemental selenium in solutions of 8.72 *M* HBr containing various concentrations of SeO_2 are given in Table 1. A plot of c_0 against c_{IV}, Fig. 1, shows a straight line dependence of c_0 on c_{IV} up to $c_{IV} = 0.0165\,M$, followed by a plateau limit for which $c_0 = 0.0287\,M$. The insoluble phase for these latter solutions consisted of liquid Se_2Br_2 and solid selenium. The UV–visible spectra of the supernatant solutions were measured. The spectrum consists of an absorbance, increasing towards the UV from 600 nm with a shoulder at 385 nm, corresponding to a peak in the spectrum of Se_2Br_2 in carbon tetrachloride (3) and acetonitrile (4). The absorbances at 385 nm are listed in Table 1 and plotted in Fig. 1. The nature of the dependence of A_{385} on c_{IV} parallels that of c_0.

Elemental selenium is insoluble in pure HBr and the observed solubility must be due to reaction with Se(IV) to form species of intermediate oxidation state. The mean oxidation states (MOS) calculated from c_0 and c_{IV} by

$$[1] \qquad \text{MOS} = \frac{4 \times c_{IV}}{c_{IV} + c_0}$$

for the solutions studied are given in Table 1. Up to $c_{IV} = 0.0121$, the MOS remains constant at 1.49 ± 0.02. The apparent mean oxidation state then increases as part of the Se(IV) is used to produce insoluble Se_2Br_2. The constant MOS and the linear dependence of A_{385} on c_{IV} indicate that there is complete reaction with Se(IV) to give lower selenium bromides. Since the MOS is greater than unity, both Se_2Br_2 and some Se(II) species must be formed.

The Raman spectrum of a 0.05 *M* SeO_2 solution in 8.72 *M* HBr, saturated with Se, Fig. 2, exhibits three clearly distinguishable peaks at 103, 165, and 250 cm^{-1}. The two strongest peaks in the Raman spectrum of Se_2Br_2 are at 105 and 254 cm^{-1} (8), which accounts for the highest and the lowest bands observed. The remaining peak at 165 cm^{-1} cannot be due to $SeBr_2$, which has no peak at this frequency (4). The $SeBr_3^-$ and $SeBr_4^{2-}$ anions have bands at 159 and 162 cm^{-1} (9), respectively, and may be present in the solution. An additional band for $SeBr_3^-$ at 258 cm^{-1} may be hidden by the strong Se_2Br_2 peak at 254

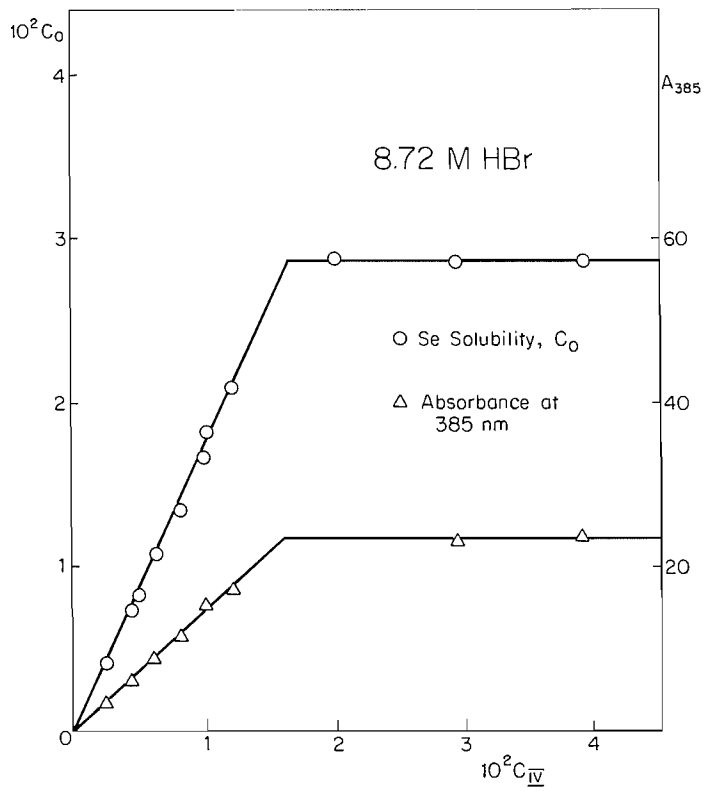


FIG. 1. Selenium solubilities and absorbances at 385 nm for 8.72 *M* HBr solutions of SeO_2.

cm^{-1}. However, in view of the high bromide ion concentration and the favourable formation constant for $SeBr_4^{2-}$ in acetonitrile (9), it is probable that $SeBr_4^{2-}$ is formed in these HBr solutions. Thus, the reactions which occur when Se is added to a solution of SeO_2 in 8.72 *M* HBr are

$$[2] \qquad SeBr_6^{2-} + 3Se \rightarrow 2Se_2Br_2 + 2Br^-$$

$$[3] \qquad 2Br^- + SeBr_6^{2-} + Se \rightarrow 2SeBr_4^{2-}$$

From the MOS in Table 1, the constant, K, for the equilibrium,

Can. J. Chem. Downloaded from www.nrcresearchpress.com by 41.223.56.140 on 09/07/12
For personal use only.

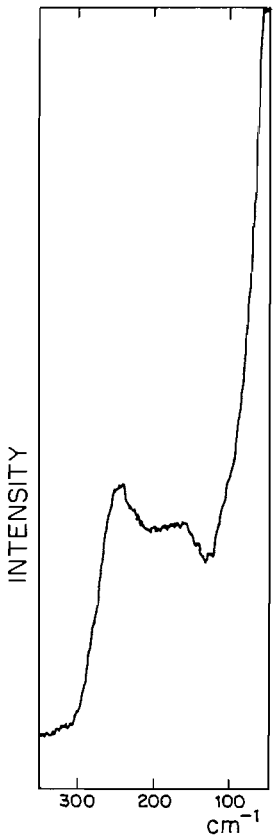


FIG. 2. The Raman spectrum of a 0.05 M solution of SeO_2 in 8.72 M HBr saturated with Se. Resolution, 10 cm^{-1}.

[4] $2Br^- + Se_2Br_2 \rightleftharpoons SeBr_4^{2-} + Se$

may be calculated, using the following equations,

[5] $$c_0 = \frac{[SeBr_4^{2-}]}{2} + \frac{3[Se_2Br_2]}{2}$$

[6] $$\frac{2[Se_2Br_2] + 2[SeBr_4^{2-}]}{c_{IV} + c_0} = MOS$$

[7] $$K = \frac{[SeBr_4^{2-}]}{[Se_2Br_2][Br^-]^2}$$

[8] $$[Br^-] = 8.72 - 4[SeBr_4^{2-}] - 2[Se_2Br_2]$$

The constant, K, is not a true thermodynamic equilibrium constant in as much as no allowance for activity coefficients has been made. The activity coefficient for Se_2Br_2 may be safely assumed to be unity but coefficients for the ionic species are unknown. However, the molar activity coefficient ratio, $y(SeBr_4^{2-})/y(Br^-)^2$, is expected to be nearly constant within the very small change in ionic strength over the range of c_{IV} and c_0 studied in the presence of such a large concentration of HBr. The equilibrium constant, K, is therefore a product of the true thermodynamic equilibrium constant, K_{th}, and the inverse of the activity coefficient factor. The value of this composite equilibrium constant and the concentration of Se_2Br_2, $SeBr_4^{2-}$, and Br^- for each solution are given in Table 1. The average value of K ($= K_{th} \times y(Br^-)^2/y(SeBr_4^{2-})$) is 0.025 ($\pm$0.002) $L^2\,mol^{-2}$. The measured absorbance of these solutions at 385 nm, A_{385}, is also shown in Table 1. Because the ratio $[Se_2Br_2]/[SeBr_4^{2-}]$ changes only slightly over the c_{IV} range studied and the absorbances are not sufficiently accurately determined, it was not possible to determine the extinction coefficients of the two species from the data.

From the plateau region of c_0 in Fig. 1, the solubility of Se_2Br_2 in 8.72 M HBr may be calculated. The average c_0 above $c_{IV} = 0.0165\,M$ is 0.0287 M. Using eqs. [5], [7], and [8] and $K = 0.025\,L^2\,mol^{-2}$, the saturation concentration of Se_2Br_2 in 8.62 M HBr is found to be 0.0116 M.

4.80 M *HBr solutions*

Table 2 gives c_0 and A_{385} values for solutions of SeO_2 in 4.8 M HBr, saturated with elemental selenium. Figure 3 shows the dependence of c_0 and A_{385} on c_{IV}. Below $c_{IV} = 0.100\,M$, the insoluble phase is Se^0 but above that concentration of SeO_2, the insoluble phase is Se_2Br_2 and Se^0. The MOS, given in Table 2, shows that the solutions contain Se(IV) species and the shoulder at 385 nm in the spectra of the solutions indicates the presence of Se_2Br_2. The curvature in the A_{385} and c_0 vs. c_{IV} plots shows that there is an equilibrium between Se(IV) and lower valent Se species. The principle Se(IV) species present at these concentrations in 4.80 M HBr is $SeOBr_3^-$ (10). Because of low concentrations, it is not possible to identify the lower valent Se species by Raman spectroscopy. If it is assumed that $SeBr_4^{2-}$ and Se_2Br_2 are formed as in the 8.72 M HBr solutions, the disproportionation equilibrium involved is

[9] $3SeBr_4^{2-} + H_2O \rightleftharpoons Se_2Br_2 + SeOBr_3^- + 7Br^- + 2H^+$

which is governed by the constant,

[10] $$K' = \frac{[Se_2Br_2][SeOBr_3^-][Br^-]^7[H^+]^2y^4}{[SeBr_4^{2-}]^3a}$$

where y is the mean molar ionic activity coefficient for HBr and a is the water activity. Since selenium solute concentration is small, y and a for pure HBr solutions may be used (11). The constant, K', is not a thermodynamic equilibrium constant, since no allowance for the activity coefficients of the selenium species and free Br^- ("non-HBr" Br^-) has been made. The activity coefficient for Se_2Br_2 may be assumed to be unity but the other ionic coefficients are unknown. The constant in eq. [10] may be expressed as,

[11] $$K' = K_{th} \times \frac{y(SeBr_4^{2-})^3}{y(SeOBr_3^-) \times y(Br^-)^5}$$

where K_{th} is the thermodynamic equilibrium constant and the y(ionic species)'s represent molar activity coefficients. The activity coefficient factor is expected to be nearly constant with the very small change in ionic strength over the range of c_{IV} and c_0 studied in the presence of the large HBr concentration. Therefore, K' is expected to be nearly constant.

The 4.8 M HBr solutions will contain four Se(IV) species, $HSeO_2Br$, $SeOBr_3^-$, $SeBr_5^-$, and $SeBr_6^{2-}$, the concentrations of which are governed by known equilibrium constants (10).

[12] $$K_2 = \frac{[SeOBr_3^-]a}{[HSeO_2Br][H^+][Br^-]^2y^2} = 9.5 \times 10^{-4}\,L^3\,mol^{-3}$$

[13] $$K_3 = \frac{[SeBr_5^-]a}{[SeOBr_3^-][H^+]^2[Br^-]^2y^4} \frac{y(SeBr_5^-)}{y(SeOBr_3^-)} = 8 \times 10^{-8}\,L^4\,mol^{-4}$$

[14] $$K_4 = \frac{[SeBr_6^{2-}]}{[SeBr_5^-][Br^-]} \frac{y(SeBr_6^{2-})}{y(SeBr_5^-) \times y(Br^-)} = 0.3\,L\,mol^{-1}$$

Can. J. Chem. Downloaded from www.nrcresearchpress.com by 41.223.56.140 on 09/07/12
For personal use only.

TABLE 2. Solutions of varying SeO_2 concentration (c_{IV}) in 4.80 M HBr, Se solubilities (c_0), and absorbances at 385 nm (A_{385})

10^3 c_{IV} (mol L^{-1})	10^3 c_0 (mol L^{-1})	Obsd A_{385}	MOS[a]	10^3 $[Se_2Br_2]$ (mol L^{-1})	10^3 $[SeBr_4^{2-}]$ (mol L^{-1})	10^3 $[HSeO_2Br]$ (mol L^{-1})	10^3 $[SeOBr_3^-]$ (mol L^{-1})	10^3 $[SeBr_5^-]$ (mol L^{-1})	10^3 $[SeBr_6^{2-}]$ (mol L^{-1})	10^3 $[Br^-]$ (mol L^{-1})	10^{-12} [c] K' (mol^8 L^{-8})	Calcd A_{385}
9.43	3.78	4.5	2.86	2.11	1.20	1.43	5.72	0.254	0.363	4.77	9.48	3.7
18.9	5.13	6.5	3.15	2.88	1.62	3.19	12.2	0.506	0.720	4.74	10.03	5.8
26.4	6.30	—	3.23	3.54	1.97	4.67	17.3	0.680	0.962	4.72	9.18	—
28.3	6.46	7.7	3.26	3.63	2.02	5.07	18.7	0.722	1.02	4.71	9.28	7.7
37.7	7.13	8.9	3.36	4.02	2.21	7.13	25.3	0.917	1.29	4.69	9.69	9.0
44.8	7.60	—	3.42	4.29	2.34	8.77	30.2	1.05	1.46	4.67	9.74	—
47.1	7.39	9.6	3.46	4.17	2.27	9.35	31.9	1.09	1.52	4.66	10.73	10.0
80.0	8.26	—	3.63	4.69	2.46	18.2	54.7	1.51	2.08	4.58	12.0	—
100.0	9.02	—	3.67	5.2[b]	—	—	—	—	—	—	—	—
135.9	9.22	—	3.75	—	—	—	—	—	—	—	—	—
150.0	9.47	—	3.76	—	—	—	—	—	—	—	—	—
179.3	9.12	—	3.81	—	—	—	—	—	—	—	—	—

[a]Mean oxidation state.
[b]Saturated with Se_2Br_2.
[c]Mean $K' = 10.0\ (\pm 0.7) \times 10^{12}$ mol^8 L^{-8}.

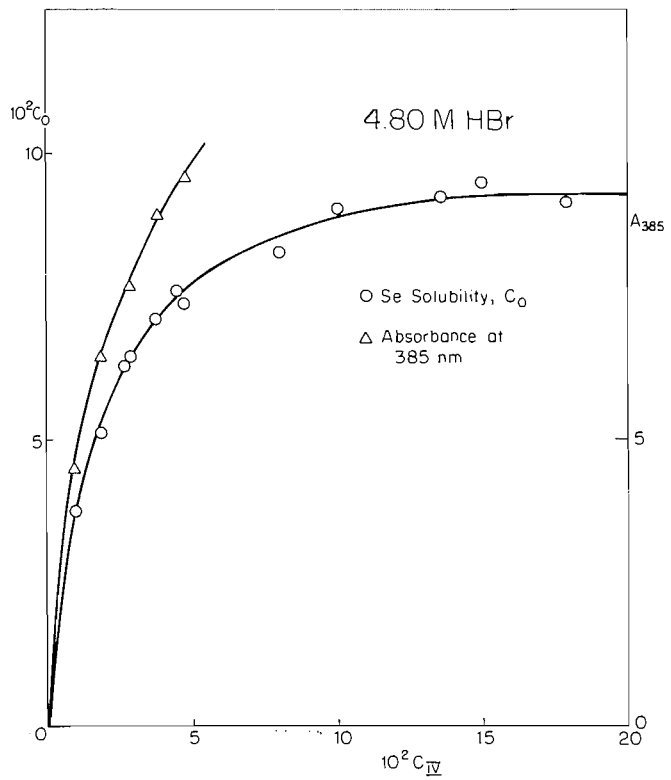


FIG. 3. Selenium solubilities and absorbances at 385 nm for 4.80 M HBr solutions of SeO_2.

where the activity coefficient factors for Se species and "non-HBr" Br^- in [13] and [14] were assumed to be unity (10) (or the equilibrium constants are a composite of the thermodynamic equilibrium constant and an activity coefficient factor as above). The equilibrium constant of the disproportionation, K', may be determined by an iterative procedure from equations [5], [7], [12], [13], [14], the mass balance for Br,

$$[15]\quad c_{HBr} = 4.80 = [Br^-] + 2[Se_2Br_2] + 4[SeBr_4^{2-}] + [HSeO_2Br] + 3[SeOBr_3^-] + 5[SeBr_5^-] + 6[SeBr_6^{2-}]$$

the valence balance for selenium,

$$[16]\quad 4c_{IV} = 2[Se_2Br_2] + 2[SeBr_4^{2-}] + 4[HSeO_2Br] + 4[SeOBr_3^-] + 4[SeBr_5^-] + 4[SeBr_6^{2-}]$$

and the charge balance

$$[17]\quad [H^+] = 2[SeBr_4^{2-}] + [SeOBr_3^-] + [SeBr_5^-] + 2[SeBr_6^{2-}] + [Br^-]$$

The K' values calculated in this way are listed in Table 2 along with the concentrations of all Se species and Br^-. The predominant Se species in these solutions are $SeOBr_3^-$, $HSeO_2Br$, and Se_2Br_2 but significant amounts of $SeBr_4^{2-}$, containing selenium in the unusual 2+ oxidation state, are also present.

The saturation solubility of Se_2Br_2 in these 4.80 M HBr solutions may be estimated from the plateau c_0 value (0.0092 M) at c_{IV} above ca. 0.1 M using eqs. [5] and [7] and assuming $[Br^-] = 4.58\ M$, the bromide concentration of the highest c_{IV} concentration solution, before saturation, studied. This gives an estimated saturation concentration of Se_2Br_2 in 4.58 M HBr of 0.0052 M, which is lower than the solubility in 8.61 M HBr, 0.0116 N. This direct dependence of Se_2Br_2 solubility on HBr concentration parallels the normal solubility behaviour of non-electrolytes in concentrated strong acids (12) and is opposite to the normal "salting-out" effect on solubility at low electrolyte concentrations.

The extinction coefficients of Se_2Br_2 and $SeBr_4^{2-}$ at 385 nm may be determined from the measured absorbance of a solution of known composition in 4.80 M and 8.72 M HBr and the known extinction coefficients of $HSeO_2Br$ (0.0 cm^{-1} mol^{-1} L), $SeOBr_3^-$ (40 cm^{-1} mol^{-1} L), $SeBr_5^-$ (1450 cm^{-1} mol^{-1} L), and $SeBr_6^{2-}$ (1300 cm^{-1} mol^{-1} L) (10). From the absorbances for the 4.80 M HBr solution with $c_{IV} = 0.0283\ M$ and the 8.72 M HBr solution with $c_{IV} = 0.00636\ M$, the molar extinction coefficient of Se_2Br_2 is found to be 934 cm^{-1} mol^{-1} L and that of $SeBr_4^{2-}$, 564 cm^{-1} mol^{-1} L. From these extinction coefficients and those for Se(IV) species, the absorbance at 385 nm for the 4.80 and 8.72 M solutions may be calculated from the known concentrations of all species. These calculated absorbances are listed in Tables 1 and 2 and they compare reasonably well with the observed absorbances, which supports the interpretation of

Can. J. Chem. Downloaded from www.nrcresearchpress.com by 41.223.56.140 on 09/07/12
For personal use only.

the 4.80 *M* HBr results in terms of Se_2Br_2 and $SeBr_4^{2-}$ as the lower valent Se species present.

Conclusion

The $SeBr_4^{2-}$ ion has been characterized in solid and in acetonitrile solution (9) and the crystal structure of $[P(C_6H_5)_4]_2SeBr_4$ has been determined (13). The present study shows that this unique anion is present in aqueous HBr solutions as well. The concentrations of Se(II) species in HBr are higher than in HCl solution (6), which parallels the behaviour in acetonitrile (4). While it is possible to prepare $SeBr_4^{2-}$ salts from aprotic solvents, if a sufficiently large cation is chosen, preparation from aqueous HBr is not possible because of the low solubility of Se_2Br_2 and of the corresponding $SeBr_6^{2-}$ salt, which arise from disproportionation of the Se(II) species.

Acknowledgement

Mani Mahadevan is thanked for his technical assistance in the early stages of this project.

1. D. M. Yost and J. B. Hatchem. J. Am. Chem. Soc. **53**, 2549 (1931).
2. M. Lundkvist and M. Lellep. Acta Chem. Scand. **22**, 291 (1968).
3. N. W. Tideswell and J. D. McCullough. J. Am. Chem. Soc. **78**, 3026 (1956).
4. J. Milne. Polyhedron, **4**, 65 (1985).
5. H. Ditz and F. Ullrich. Zeit. anorg. allg. Chem. **221**, 33 (1934).
6. M. Mahadevan and J. Milne. Inorg. Chem. **22**, 1648 (1983).
7. V. Lenher and C. J. Kao. J. Am. Chem. Soc. **47**, 772 (1925).
8. W. Kiefer. Spectrochim. Acta, **27A**, 1285 (1971).
9. J. Milne. Polyhedron, **6**, 849 (1987).
10. J. Milne and P. Lahaie. Inorg. Chem. **24**, 840 (1985).
11. R. Haase, N. Haas, and H. Thumm. Zeit. Phys. Chem. (Wiesbaden), **37**, 210 (1963).
12. A. Seidel. Solubilities of inorganic and metal organic compounds. 3rd ed. Van Nostrand, New York. 1953.
13. B. Krebs, A. Schaffer, and S. Pohl. Z. Naturforsch. **39b**, 1633 (1984).

Can. J. Chem. Downloaded from www.nrcresearchpress.com by 41.223.56.140 on 09/07/12
For personal use only.

Carbon tetrabromide as an electron acceptor in heterogeneous photocatalysis[1]

H. AL-EKABI,[2] A. M. DRAPER,[3] AND P. DE MAYO

Photochemistry Unit, Department of Chemistry, University of Western Ontario, London, Ont., Canada N6A 5B7

Received July 8, 1988

This paper is dedicated to Professor Sir Derek Barton on the occasion of his 70th birthday

H. AL-EKABI, A. M. DRAPER, and P. DE MAYO. Can. J. Chem. **67**, 1061 (1989).

Three reactions: the CdS-mediated valence isomerization of hexamethyldewarbenzene to hexamethylbenzene, the cycloreversion of dianthracene, and the TiO_2-mediated *cis–trans* isomerization of stilbene are known to be suppressed when the semiconductor excitation takes place in the absence of oxygen. The oxygen, when present, is presumed to trap the electron delaying electron–hole recombination. It has been found that CBr_4 may replace oxygen and functions in a similar way. In addition, the concomitant formation of oxidation products in the TiO_2-mediated aerobic reaction is avoided. The mechanism is discussed.

Key words: cadmium sulphide, carbon tetrabromide, dianthracene, heterogeneous photocatalysis, hexamethyldewarbenzene, titanium oxide.

H. AL-EKABI, A. M. DRAPER et P. DE MAYO. Can. J. Chem. **67**, 1061 (1989).

Il est connu que trois réactions (l'isomérisation de valence, sous l'influence du CdS, de l'hexaméthyldewarbenzène en hexaméthylbenzène; la cycloréversion du dianthrène ainsi que l'isomérisation *cis–trans* du stilbène sous l'influence du TiO_2) sont supprimées lorsque l'excitation semiconductrice a lieu en l'absence d'oxygène. Il est supposé que, lorsque l'oxygène est présent, il piège l'électron et retarde ainsi la recombinaison de l'électron dans le trou. On a trouvé que le CBr_4 peut remplacer l'oxygène et qu'il remplit les mêmes fonctions. De plus, on évite la formation concomitante de produits d'oxydation dans la réaction aérobique provoquée par le TiO_2. On discute du mécanisme.

Mots clés : sulfure de cadmium, tétrabromure de carbone, dianthracène, photocatalyse hétérogène, hexaméthyldewarbenzène, oxyde de titanium.

[Traduit par la revue]

Introduction

The recombination of photogenerated holes and electrons is an important process in the use of semiconductors. Rectification, transistor function, and photoconductivity all depend on the lifetime of the mobile carriers. This recombination rate is of paramount importance in heterogeneous photocatalysis with semiconductors if transformations of interest to the organic chemist are to be achieved. Recent studies on colloidal samples have indicated that these recombination processes occur on the ps–ns time scale (1–8). However, the trapping of either the conduction band electron by suitable electron acceptors, or the "hole" by suitable electron donors could, in principle, delay the energetically wasteful collapse.

Molecular oxygen has been found to enhance the rate of many semiconductor-mediated reactions (9–17). As an electron acceptor, adsorbed on the semiconductor surface, it traps the electron as superoxide ion. The latter has been detected as the spin adduct with 5,5-dimethyl-1-pyrroline 1-oxide (18, 19). The disadvantage of the use of oxygen is that accelerated reaction may be accompanied by oxidation. Whilst in certain cases oxidation may be a desired process (20–23), in many others it is not. For instance, the semiconductor photoinduced *cis–trans* isomerization of stilbenes in the presence of oxygen is usually associated with oxidation product formation (20, 24). Accordingly, we recognized the need for an electron trap which would not produce other complex by-products.

Carbon tetrabromide is known to be a good electron acceptor ($E^{red} = -0.3$ V vs. SCE (25)) and that the derived radical anion CBr_4^- dissociates rapidly at room temperature into $CBr_3^{\cdot}$ and bromide ion (26–32).[4] Provided the rate of reaction of D^+, obtained by oxidation of the donor (D) by the "hole", is slower than the rate of decomposition of CBr_4^- to radical and ion, then CBr_4 would act as an "irreversible" electron acceptor. We report below the results of our preliminary studies in this area.

Experimental

Chemicals

Methylene dichloride was of spectroscopic grade (BDH). HMDB (Aldrich) was purified by passage rapidly through a very short column (4 × 0.5 cm) of dry silica gel (Merck, 230–400 mesh). *cis*-Stilbene (Aldrich) was purified by fractional distillation and *trans*-stilbene (Kodak) was used without further purification. Dianthracene was prepared as previously described (33). Carbon tetrabromide (Aldrich) was crystallized from ethyl acetate.

General techniques

Irradiation sources used throughout this work: 150 W and 1000 W PRA xenon arcs. While the 150 W was used for CdS-mediated HMDB and dianthracene reactions the 1000 W was used for TiO_2-mediated stilbene reactions. For both lamps compressed air was used as collant and water filters were used to remove IR radiation. Prior to irradiation the mixture of the reactant and the semiconductor in methylene dichloride was sonicated for 10 min and was constantly stirred during the course of the irradiation. Except for the oxygen-free experiments, the reaction vessels were open to the atmosphere via a reflux condenser. For the oxygen-free experiments argon saturated with methylene dichloride was bubbled through the mixture for 15 min before starting the irradiation and was kept running during the irradiation. After irradiation, the semiconductor was removed by filtration. The filtrate, except in the case of the dianthracene reaction, was analyzed by a Varian 3700 gas chromatograph equipped with a flame ionization detector which was connected to a Hewlett Packard 3390 Å integrator. Analysis was performed on 2 m/2 mm column packed with OV-101 (10%) on chromosorb W(HP) 80–100 mesh. The yields of the oxida-

[1]Publication Number 413 from the Photochemistry Unit, University of Western Ontario.

[2]Present address: Nulite, a Division of Nutech Energy Systems, 317 Consortium Court, Inc., London, Ont., Canada N6E 2S8.

[3]Present address: Chipman, Stoney Creek, Ontario.

[4]We are grateful to Professor M. J. Stillman of this department for drawing our attention to the interesting properties of CBr_4.

Can. J. Chem. Downloaded from www.nrcresearchpress.com by 41.223.56.140 on 09/07/12
For personal use only.

TABLE 1. Some physical properties of different CdS samples

CdS supplier	Purity (%)	Surface area[a] (m^2/g)	Crystalline structure[a]
Strem (lot no. 16027-S_1)	≥99.99	44	Polytype
Aldrich (lot no. 1721 PJ)	99.999	1.2	α
Aldrich (lot no. 053087)	98.8	7	β

[a]See ref. 43.

tion products of stilbene were determined by NMR. For dianthracene cycloreversion, the reaction (anthracene formation) was followed spectroscopically.

Valence isomerization of HMDB

Typically, 0.057 *M* of HMDB in methylene dichloride (6 mL) in the presence of CdS (50 mg) was irradiated at $\lambda > 400$ nm for 15 min using 150 W PRA xenon lamp. The reaction was conducted with three different CdS samples (see Table 1 for their physical properties) in the presence and absence of oxygen and/or carbon tetrabromide. Adequate removal of oxygen is important for reproducibility in CBr_4 experiments.

Cycloreversion of dianthracene

Solutions of dianthracene (6 mL; 0.001 *M*) in methylene dichloride in the presence of CdS (50 mg) were irradiated at $\lambda > 400$ nm using 150 W PRA xenon arc. The reaction was conducted, with two different CdS samples, in the absence of oxygen and the presence of various concentrations of carbon tetrabromide.

Isomerisation of cis*-stilbene*

Typically, 0.057 *M* of *cis*-stilbene in methylene dichloride (6 mL) in the presence of TiO_2 (25 mg) was irradiated at $\lambda > 380$ nm using a 1000 W PRA xenon arc. The reaction was conducted in the absence of oxygen and presence of different concentrations of carbon tetrabromide.

Results and discussion

The CdS-mediated valence isomerization of hexamethyldewarbenzene (HMDB) to hexamethylbenzene (HMB)

The above-named reaction has been reported (13, 16) and a cation radical chain mechanism proposed: a quantum yield greater than unity was obtained (13). It has also been reported (16) that the presence of oxygen is essential for efficient reaction. That this is so may be seen from the results in Table 2 using three different commercial samples of CdS (described in Table 1). For instance, the chemical yield with Strem CdS increased from 3% under argon to 20% in the presence of oxygen under defined conditions. With the same CdS sample under argon but in the presence of 0.0026 *M* CBr_4 the yield increased to 70%, indicating that CBr_4 is acting as an electron acceptor. In the presence of both oxygen and CBr_4 an intermediate yield was obtained, suggesting that bound CBr_4 is more effective than bound molecular oxygen, but that, in competition, O_2 is preferentially bound to the surface sites.

The effect of varying the concentration of CBr_4 on the yield of HMB obtained under specific defined conditions, is shown in Fig. 1. There is an increase with increasing concentration of CBr_4 which levels off at about $[CBr_4] \simeq 0.0005$ *M*. This is less, by two orders of magnitude, than the initial concentration of HMDB, and suggests that the CdS surface is then saturated with CBr_4 at the concentration of HMDB used. The resemblance to the Langmuir isotherm suggests that only CBr_4 molecules preadsorbed on the surface will accept the conduction band electron. Such a pathway has been proposed (the Langmuir–Hishelwood pathway) as one of two contributors to the overall

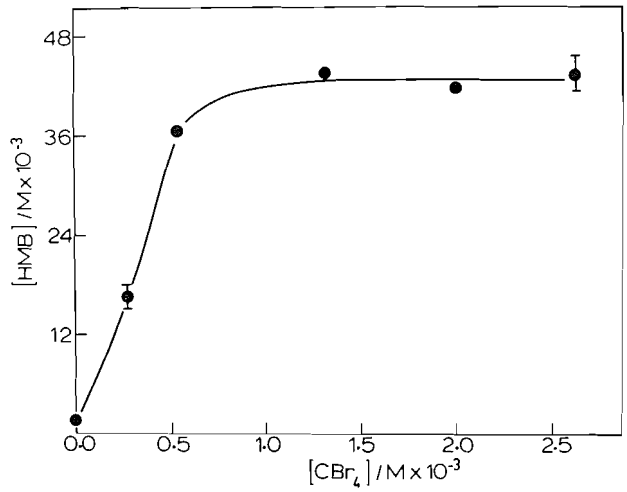


FIG. 1. Effect of CBr_4 concentration on yields of HMB formation. Each sample was irradiated at $\lambda > 400$ nm under argon for 15 min with a 150 W xenon lamp. [HMDB] = 0.057 *M*, CdS = 50 mg.

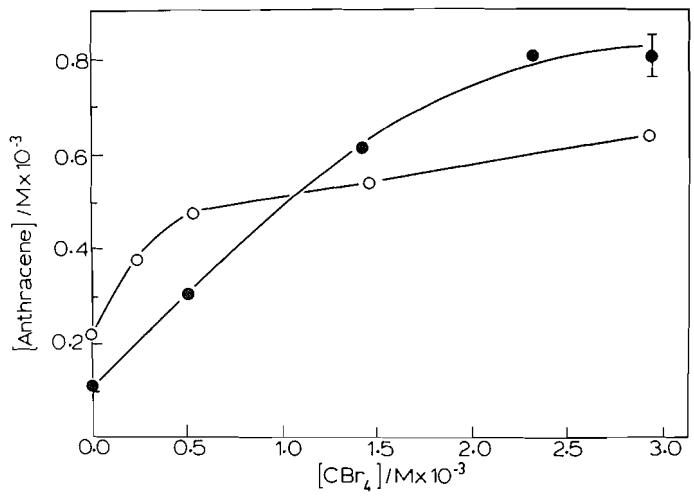


FIG. 2. Effect of CBr_4 concentration on yields of anthracene formation using two different CdS samples. Experiments conducted with Aldrich CdS sample (●) were irradiated for 30 min at $\lambda >$ 400 nm under argon with a 150 W xenon lamp while those with strem CdS sample (○) were irradiated for 2 h under similar conditions. [Dianthracene] = 0.001 *M*, CdS = 50 mg.

process, the second being the Eley–Rideal pathway. In principle, the lifetime of the reactive species (hole, electron, cation radical) bound to the surface determines the contribution of each pathway. In the present reaction, if our interpretation of Fig. 1 is correct, the lifetime of the conduction band electron appears to be too short to allow CBr_4 molecules in the bulk of the solution to diffuse to the surface and react (Eley–Rideal pathway). Recent studies (6, 7) have indicated that reduction of methyl viologen (MV^{2+}) by conduction band electron occurs on the surface within 100 ps of excitation of the colloidal CdS samples.

The CdS-mediated cycloreversion of dianthracene

This also has been shown (17) to proceed via a radical cation mechanism. The effect of CBr_4 concentration on the rate of anthracene formation was examined with two CdS samples: the Strem and Aldrich 99.999% (Table 1). The results are presented in Fig. 2. With the Strem the yield of anthracene obtained

Can. J. Chem. Downloaded from www.nrcresearchpress.com by 41.223.56.140 on 09/07/12
For personal use only.

TABLE 2. Valence isomerization of HMDB to MMB under different conditions[a]

CdS supplier	Chemical yield (%) of HMB (±10%)			
	Ar[b]	Atm[c]	Atm + CBr_4[d]	Ar + CBr_4[d]
Strem (lot no. 16027-S_1)	3	20	28	70
Aldrich (lot no. 1721 PJ)	4	10	18	38
Aldrich (lot no. 053087)	2	9	23	35

[a]HMDB in CH_2Cl_2 (0.057 *M*; 6 mL) were irradiated for 15 min in the presence of CdS (50 mg), $\lambda > 400$ nm, 150 W xenon lamp.
[b]Reaction mixtures were purged with argon (saturated with CH_2Cl_2) for 15 min prior to irradiation and during the irradiation.
[c]Reaction mixtures are open to atmosphere via a reflux condenser.
[d]$[CBr_4] = 0.0026$ *M*.

under specific defined conditions, low in the absence of CBr_4 increased with increasing $[CBr_4]$ reaching, as was found with HMDB, a plateau at $[CBr_4] \simeq 0.0005$ *M*. The initial concentration of dianthracene was 0.001 *M*.

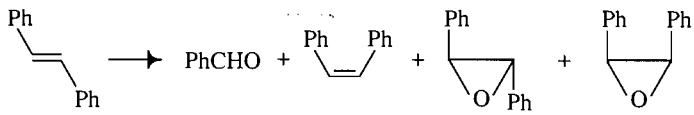
Since using the Strem CdS the initial concentration of HMDB is higher, by a factor of 57, than that of the dianthracene, but both achieve surface saturation with CBr_4 at the same concentration, one may tentatively suggest that the active sites at which CBr_4 is adsorbed are different from those utilized by HMDB and dianthracene.

Using the Aldrich CdS the same behaviour was observed except that the plateau was reached at ~0.0025 *M* CBr_4; higher, by a factor of five than found with the Strem. This is contrary to what would be expected on the basis of surface areas (Table 1) and is, presumably, to be attributed to their different crystalline form. Significantly, four times the irradication time was required for the Strem CdS to produce a comparable yield of anthracene as from the Aldrich CdS.

The TiO_2-mediated cis–trans *isomerisation of stilbene*

The results obtained with HMDB and dianthracene demonstrate the efficacity of CBr_4 as an electron acceptor with a semiconductor. However, these reactions are not associated with oxidation product formation even in the presence of oxygen. One reaction so associated is the *cis–trans* isomerization of stilbene in the presence of illuminated TiO_2.

Fox and Chen (20) have reported that when a suspension of TiO_2 in acetonitrile containing *trans*-stilbene **1** was irradiated ($\lambda = 350 \pm 30$ nm) in the presence of oxygen, four products **2–5** were obtained.



1 **2**:32% **3**:14% **4**:43% **5**:11%

More recently Tokumaru *et al.* (24) have reported that when a suspension of CdS or TiO_2 in acetonitrile containing **1** was irradiated (CdS, $\lambda > 430$ nm; TiO_2, $\lambda > 350$ nm) in the presence of oxygen **2** and **4** were obtained. Starting with **3** they obtained **1**, along with **2** and **4**. Further, under argon only **3** → **1** has been observed, the reverse process being barely discernible. We have also found that in the CdS-mediated *cis–trans* isomerization of stilbene, the photostationary state lies heavily on the side of the *trans*-isomer (34, 35). We have proposed, based on quenching data with methoxybenzenes, a cation radical mechanism (see refs. 36–38, however).

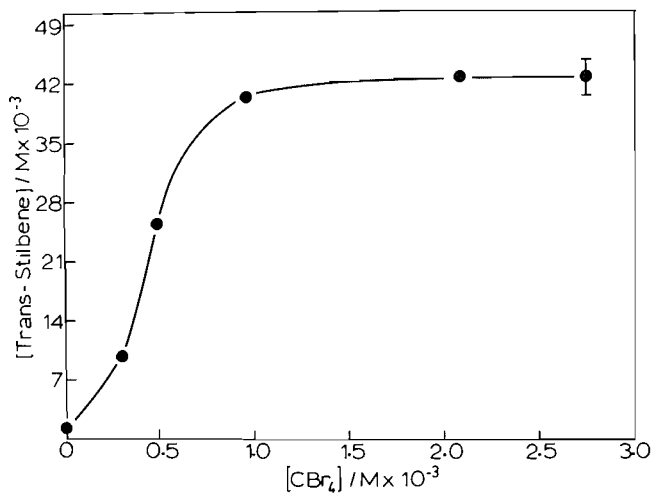


FIG. 3. Effect of CBr_4 concentration on yields of *trans*-stilbene formation. Each sample was irradiated at $\lambda > 380$ nm under argon for 30 min with a 1000 W xenon lamp. [*cis*-Stilbene] = 0.057 *M*, TiO_2 = 25 mg.

We have irradiated ($\lambda > 380$ nm) TiO_2 (Degussa P-25) in methylene chloride containing 0.057 *M* **1** for 1 h in an open system. Products **2** and **4** were formed in a total yield of 30% together with a trace of *cis*-stilbene. When the same experiment was performed in the presence of **3**, **1** was a major product (75%) with **2** and **4** in a total yield of 25%. In the absence of oxygen the isomerization of **3** was extremely slow. Addition of CBr_4 (0.0026 *M*) led to rapid isomerization and **1** was the only product.

Because of the reported **1** → **3** mentioned above (20) we took advantage of the facilitated process to determine the photostationary state. Approached from both sides we obtained **1**:**3** = 99.6:0.4. This is consistent with previous results (34, 35) obtained with CdS (>99:<1) and approximates the thermodynamic equilibrium (39). Accordingly, the formation of 14% **3** formed in TiO_2/MeCN may be attributed either to inadvertent direct irradiation or to sensitization by benzaldehyde a product of the experiment, or both.

The effect of CBr_4 concentration on the yield of **1**, obtained under specific defined conditions, was determined and is reported in Fig. 3. The plateau is reached ~0.001 *M* which is less by a factor of ~50 than the initial concentration of **3** (0.05 *M*); an observation which suggests that CBr_4 is strongly adsorbed on the TiO_2 surface. However, our attempt to determine the adsorption isotherm of CBr_4 on TiO_2 was not

Can. J. Chem. Downloaded from www.nrcresearchpress.com by 41.223.56.140 on 09/07/12
For personal use only.

successful as the sensitivity of the flame ionization detector to CBr_4 is very low.

Reversible or non-reversible trapping

It is generally known that substances such as CCl_4 (31, 40–42) or CBr_4 (26–31) accept an electron with dissociative attachment to give $CX_3^{\cdot}$ and X^-, but it appears not to known whether such a process can occur on the ps–ns time scale, i.e., whether CX_4 is a reversible or non-reversible trap. The problem can be tentatively discussed in terms of the unimolecular process $D \rightarrow P$, as outlined in Scheme 1. If step [*e*] be faster than any other process available to CBr_4^-, then the trapping is irreversible. If, on the other hand, step [*f*] can compete there is quenching without consumption of CBr_4. Step [*g*] permits product formation, if it can compete with [*e*] and there is no destruction of CBr_4. To our knowledge the occurrence of a step such as [*f*] and [*g*] in competition with [*e*] has not been unambiguously demonstrated, but evidence for its possible intrusion has been provided (see, for example, ref. 32).

[*a*] $SC \rightleftharpoons h^+ + e^-$

[*b*] $CBr_4 + e^- \rightarrow CBr_4^-$

[*c*] $D + h^+ \rightarrow D^{\ddagger}$

[*d*] $D^{\ddagger} \rightarrow P^{\ddagger}$

[*e*] $CBr_4^- \rightarrow CBr_3^{\cdot} + Br^- \left(\rightarrow \begin{matrix} C_2Br_6 \\ + \\ CHBr_3 \end{matrix} \text{ ref. 32}\right)$

[*f*] $CBr_4^- + D^{\ddagger} \rightarrow CBr_4 + D$

[*g*] $CBr_4^- + P^{\ddagger} \rightarrow CBr_4 + P$

[*h*] $D^{\ddagger} + e^- \rightarrow D$

[*i*] $P^{\ddagger} + e^- \rightarrow P$

SCHEME 1

If such a process be participating in the reactions under discussion, then the amount of CBr_4 decomposed during irradiation of the semiconductor in the presence of reactant D should be less than in its absence. Experimentally, it was found that irradiation of TiO_2 (argon) in methylene chloride containing CBr_4 (0.0026 *M*) for 1 h using a 1000 W lamp led to the decomposition of 15% CBr_4. However, when the mixture was 0.05 *M* in **3** the amount of CBr_4 decomposed decreased to 5%.

Acknowledgment

We thank the Natural Sciences and Engineering Research Council of Canada for support of this work.

1. D. DUONGHONG, J. RAMSDEN, and M. GRÄTZEL. J. Am. Chem. Soc. **104**, 2977 (1982).
2. N. SERPONE, D. K. SHARMA, M. JAMIESON, M. GRÄTZEL, and J. J. RAMSDEN. Chem. Phys. Lett. **115**, 473 (1985).
3. R. ROSSETTI and L. E. BRUS. J. Phys. Chem. **90**, 558 (1986).
4. N. SERPONE, D. K. SHARMA, J. MOSER, and M. GRÄTZEL. Chem. Phys. Lett. **136**, 47 (1987).
5. G. ROTHENBERGER, J. MOSER, M. GRÄTZEL, N. SERPONE, and D. K. SHARMA. J. Am. Chem. Soc. **107**, 8054 (1985).
6. Y. NOSAKA, H. MIYAMA, M. TERAUCHI, and T. KOBAYASHI. J. Phys. Chem. **92**, 255 (1988).
7. Y. NOSAKA and M. A. FOX. J. Phys. Chem. **92**, 1893 (1988).
8. J. MOSER, M. GRÄTZEL, and R. GALLAY. Helv. Chim. Acta, **70**, 1596 (1987).
9. A. M. DRAPER, M. ILYAS, P. DE MAYO, and V. RAMAMURTHY. J. Am. Chem. Soc. **106**, 6222 (1984).
10. H. AL-EKABI and P. DE MAYO. Tetrahedron, **42**, 6277 (1986).
11. H. AL-EKABI and P. DE MAYO. J. Org. Chem. **52**, 4756 (1987).
12. N. C. BAIRD, A. D. DRAPER, and P. DE MAYO. Can. J. Chem. In press.
13. H. AL-EKABI and P. DE MAYO. J. Phys. Chem. **90**, 4075 (1986).
14. K. OKADA, K. HISAMITSU, and T. MUKAI. J. Chem. Soc. Chem. Commun. 941 (1980).
15. A. M. DRAPER and P. DE MAYO. Tetrahedron Lett. **27**, 6157 (1986).
16. K. OKADA, K. HISAMITSU, T. HANAOKA, T. MIYASHI, and T. MUKAI. Tetrahedron Lett. **25**, 5311 (1984).
17. R. A. BARBER, P. DE MAYO, and K. OKADA. J. Chem. Soc. Chem. Commun. 1073 (1982).
18. J. R. HARBOUR and M. L. HAIR. J. Phys. Chem. **81**, 1791 (1977).
19. J. R. HARBOUR and M. L. HAIR. J. Phys. Chem. **82**, 1397 (1978).
20. M. A. FOX and C. C. CHEN. J. Am. Chem. Soc. **103**, 6757 (1981).
21. M. A. FOX. Acc. Chem. Res. **16**, 314 (1983).
22. J. A. PINCOCK, A. L. PINCOCK, and M. A. FOX. Tetrahedron, **41**, 4107 (1985).
23. M. A. FOX, D. D. SACKETT, and J. N. YOUNATHAN. Tetrahedron, **43**, 1643 (1987).
24. K. TOKUMARU *et al. In* Organic phototransformations in nonhomogeneous media. *Edited by* M. A. Fox. Am. Chem. Soc. Symp. 278, Washington. 1985. p. 43.
25. M. STACKELBERG and W. STRACKE. Z. Electrochem. **53**, 118 (1949).
26. T. NYOKONG, Z. GASYNA, and M. J. STILLMAN. Am. Chem. Soc. Symp. Ser. 321. Am. Chem. Soc. Washington, DC, 309 (1986).
27. T. NYOKONG, Z. GASYNA, and M. J. STILLMAN. Inorg. Chem. Acta, **112**, 11 (1986).
28. T. NYOKONG, Z. GASYNA, and M. J. STILLMAN. Inorg. Chem. **26**, 548 (1987).
29. Z. GASYNA, W. R. BROWETT, and M. J. STILLMAN. Am. Chem. Soc. Symp. Ser. 321, Am. Chem. Soc. Washington, DC, 298 (1986).
30. T. NYOKONG, Z. GASYNA, and M. J. STILLMAN. Inorg. Chem. **26**, 548 (1987).
31. Y. SHIROTA and H. MIKAWA. J. Macromol. Sci.-Rev. Macromol. Chem. C**16**, 129 (1977–1978).
32. L. EBERSON and M. EKSTRÖM. Acta Chem. Scand. B**42**, 101 (1988).
33. S. WEI and R. LIVINGSTON. Photochem. Photobiol. **6**, 229 (1967).
34. H. AL-EKABI and P. DE MAYO. J. Chem. Soc. Chem. Commun. 1231 (1984).
35. H. AL-EKABI and P. DE MAYO. J. Phys. Chem. **89**, 5815 (1985).
36. F. D. LEWIS, J. R. PETISCE, J. D. OXMAN, and M. J. NEPRAS. J. Am. Chem. Soc. **107**, 203 (1985).
37. F. D. LEWIS and M. KOJIMA. J. Am. Chem. Soc. **110**, 8664 (1988).
38. F. D. LEWIS, R. E. DYKSTRA, I. R. GOULD, and S. FARID. J. Phys. Chem. **92**, 7042 (1988).
39. G. FISHER, K. A. MUSZKAT, and E. FISHER. J. Chem. Soc. (B), 1156 (1968).
40. H.-U. GREMLLCH and R. E. BÜHLER. J. Phys. Chem. **87**, 3267 (1983).
41. N. V. KLASSEN and C. K. ROSS. J. Phys. Chem. **91**, 3668 (1987).
42. N. V. KLASSEN and C. K. ROSS. Chem. Phys. Lett. **132**, 478 (1986).
43. M. ILYAS and P. DE MAYO. J. Am. Chem. Soc. **107**, 5093 (1985).

Can. J. Chem. Downloaded from www.nrcresearchpress.com by 41.223.56.140 on 09/07/12
For personal use only.

An evaluation of the substrate specificity and asymmetric synthesis potential of the cloned L-lactate dehydrogenase from *Bacillus stearothermophilus*[1]

DANIEL BUR, MARCEL A. LUYTEN, HLA WYNN, LOUIS R. PROVENCHER, AND J. BRYAN JONES[2]
Department of Chemistry, University of Toronto, Toronto, Ont., Canada M5S 1A1

MARVIN GOLD AND JAMES D. FRIESEN
Department of Medical Genetics, University of Toronto, Toronto, Ont., Canada M5S 1A1

AND

ANTHONY R. CLARKE AND J. JOHN HOLBROOK
Department of Biochemistry, School of Medical Sciences, University of Bristol, Bristol BS8 1TD, U.K.

Received November 3, 1988

DANIEL BUR, MARCEL A. LUYTEN, HLA WYNN, LOUIS R. PROVENCHER, J. BRYAN JONES, MARVIN GOLD, JAMES D. FRIESEN, ANTHONY R. CLARKE, and J. JOHN HOLBROOK. Can. J. Chem. **67**, 1065 (1989).

The potential utility of the L-lactate dehydrogenase of *Bacillus stearothermophilus* (BSLDH) for stereospecific, preparative-scale reductions of α-keto acids to (*S*)-α-hydroxy acids of >99% ee has been demonstrated. BSLDH is a stable, thermophilic, enzyme whose gene has been cloned into a high-expression vector to assure its plentiful supply. Its specificity for keto acid substrates possessing straight- and branched-chain alkyl, cyclopropyl, or phenyl groups has been evaluated in preparative and kinetic terms, and compared with that of the mammalian pig heart enzyme (PHLDH). The specificities of BSLDH and PHLDH are similar, with branched alkyl-chain keto acids being poor substrates for both enzymes.

Key words: enzymes in organic syntheses, lactate dehydrogenase, asymmetric synthesis.

DANIEL BUR, MARCEL A. LUYTEN, HLA WYNN, LOUIS R. PROVENCHER, J. BRYAN JONES, MARVIN GOLD, JAMES D. FRIESEN, ANTHONY R. CLARKE et J. JOHN HOLBROOK. Can. J. Chem. **67**, 1065 (1989).

On a démontré que la déshydrogénase L-lactique du *Bacillus stearothermophilus* (DHLBS) peut être utile pour effectuer des réductions stéréospécifiques, à l'échelle préparative, d'acides α-cétoniques en (*S*)-α-hydroxyacides >99% ee. La DHLBS est un enzyme stable et thermophile dont on a reproduit les gènes en lignées afin de s'assurer de leur grande disponibilité. On a évalué sa spécificité, tant cinétique que préparative, par rapport à des substrats céto-acides possédant des chaînes alkyles linéaires et ramifiées ainsi que des groupements cyclopropyles et phényles et on l'a comparée à celle de l'enzyme cardiaque du cochon (DHLCC). Les spécificités des DHLBS et DHLCC sont semblables et, pour chacun de ces enzymes, les céto-acides portant des chaînes ramifiées sont de mauvais substrats.

Mots clés : enzymes en synthèses organiques, déshydrogénase lactique, synthèse asymétrique.

[Traduit par la revue]

Can. J. Chem. Downloaded from www.nrcresearchpress.com by 41.223.56.140 on 09/07/12
For personal use only.

Introduction

The application of enzymes for the generation of chiral synthons for asymmetric synthesis is well documented (2). Alcohol dehydrogenases, which catalyze C=O ⇄ CH(OH) interconversions and in whose preparative applications we have been involved (1), have been especially widely exploited. We have selected the L-lactate dehydrogenase of *Bacillus stearothermophilus* (BSLDH)[3] as a model system in connection with our interest in exploiting further the applicability of the oxidoreductase group of enzymes in organic synthesis. BSLDH is an excellent candidate for such exploratory studies since it is a very stable, thermophilic, enzyme of known protein sequence (4*a*, *b*) and its properties have already been the subject of several studies (4–7). Its gene has been cloned (4*c*, 5) and the protein very efficiently overexpressed (5), thereby enabling large quantities of BSLDH to be produced inexpensively from small fermentation volumes. Furthermore, the feasibility of altering the specificity of the native enzyme by site-directed mutagenesis of key active-site amino acid residues has just been established (8).

Lactate dehydrogenases (LDH's) are nicotinamide coenzyme-dependent enzymes whose in vivo function (9) is to catalyze pyruvate (**1***a*) – lactate (**2***a*) oxidoreductions as shown in eq. [1].

[1] $$\underset{\mathbf{1}}{\text{RCOCOOH}} + \text{NADH} + \text{H}^+ \rightleftharpoons \underset{\mathbf{2}}{\text{RCH(OH)COOH}} + \text{NAD}^+$$

a: R = CH_3
b: R = CH_2CH_3
c: R = $CH_2CH_2CH_3$
d: R = $CH(CH_3)_2$
e: R =
f: R = $CH_2C_6H_5$

While the natural LDH substrates **1**, **2***a* are small molecules possessing only a methyl side chain, LDH's from various mammalian and bacterial sources can tolerate a significant diversity in the structures of their 2-keto or 2-hydroxy acid substrates (10). In fact, sevral LDH's have already been applied in preparative-scale reactions (10*g*, 11) and in NADH recycling systems (12).

As the first step towards our evaluation of BSLDH, we examined its substrate specificity towards the 2-keto acids **1***a–f* in both preparative and kinetic terms. To provide a benchmark comparison of the BSLDH, the kinetic data of the mesophilic L-lactate dehydrogenase from pig heart (PHLDH) (13) were also determined for the same substrates.

Results

The keto acids **1***a–d*,*f* were commercially available and the

[1]Enzymes in Organic Synthesis 45. For part 44, see ref. 1.

[2]Author to whom correspondence may be addressed.

[3]Abbreviations used: LDH, lactate dehydrogenase; NAD/H, oxidized and reduced forms respectively of nicotinamide adenine dinucleotide; BSLDH, *Bacillus stearothermophilus* LDH; PHLDH, pig heart LDH; FDP, fructose-1,6-di(or bis)phosphate; FDH, formate dehydrogenase; MTPA, 2-methoxy-2-trifluoromethyl-2-phenylacetyl.

TABLE 1. Preparative scale BSLDH-catalyzed reductions of 2-oxo acids **1***b–f*[a]

Substrate	Product	Reaction time (days)	Scale (mmol)	Yield (%)	ee[b] (%)
1*b*	(*S*)-**2***b*	0.5	1.0	88	>99
1*c*	(*S*)-**2***c*	1.3	1.0	89	>99
1*d*	(*S*)-**2***d*	10.5[c]	3.0	86	>99
1*e*	(*S*)-**2***e*	3.5	2.0	89	>99
1*f*	(*S*)-**2***f*	3.3	1.8	90	>99

[a]In 5 mM Tris/HCl buffer pH 6.0 at 23°C, standardized to 500 units of LDH per reaction, and with HCOONa/FDH-catalyzed recycling of NADH.
[b]Determined from the ^{1}H nmr spectra of the Mosher esters of the corresponding methyl esters of **2***b–f* and by capillary glc analyses.
[c]FDP was used for this reaction.

TABLE 2. Enantiomeric shift differences for methyl protons of (±)-**3***b–f*[a]

Mosher ester	Δδ (ppm) CH_3OOC-	Δδ (ppm) CH_3O-
(±)-**3***b*	0.04	0.08
(±)-**3***c*	0.04	0.08
(±)-**3***d*	0.06	0.11
(±)-**3***e*	0.04	0.05
(±)-**3***f*	0.00	0.20

[a]At 400 MHz in $CDCl_3$.

cyclopropyl substrate **1***e* was prepared by the literature (14) method. BSLDH was readily obtained using the cloned gene of Barstow *et al.* (5), and employing a hydrophobic chromatographic purification procedure. PHLDH was commercially available material.

Preparative-scale reductions of **1***b–f* to the corresponding (2*S*)-hydroxy acids **2***b–f* were performed using BSLDH as catalyst, and employing formate/formate-dehydrogenase (FDH) recycling of NADH (10*g*, 12*e*, 15). The results are summarized in Table 1.

The (2*S*) absolute configurations of the product acids were assigned on the basis of their known rotations for **2***b* (16), **2***d* (17), and **2***f* (18), and by correlating the ^{1}H nmr chemical shifts of the methoxyl groups of the Mosher esters of **2***c* and **2***e* with the configuration of **2***b* (19).

For the enantiomeric excess (ee) determinations, the hydroxy acids (2*S*)-**2***b–f* were first converted to the corresponding methyl esters with diazomethane, and the C-2 hydroxyl groups then esterified with (*S*)-(+)-MTPA chloride (20) to give the Mosher ester derivatives (2*S*)-**3***b–f*. The ee values of these esters were obtained from ^{1}H nmr examinations of their methyl ester and methoxyl protons, using the Mosher esters "(±)"-**3***b–f*, prepared from the racemic acids (±)-**2***b–f*, as reference standards. The corresponding Δδ values for the latter are recorded in Table 2. In addition, capillary glc analyses of "(±)"-**3***b–f* showed base-line separations of the two diastereomers, with the (2*S*) diastereomers having the higher retention times. The glc analyses of (2*S*)-**3***b–f* confirmed the >99% ee values determined by nmr.

The kinetic parameters k_{cat} and K_M for **1***a–f* were evaluated under steady-state conditions for both BSLDH and PHLDH. The values are recorded in Table 3.

Discussion

The selection of BSLDH as a potentially useful enzyme for preparative-scale asymmetric syntheses was based on several criteria. It is an enzyme composed of two (at low concentrations) or four (at high concentrations or when allosterically activated by FDP) identical subunits (21*a*) and a great deal is known about its catalytic mechanism (7, 21). Of prime importance is the fact that it is a very stable enzyme of high activity and, being a thermophile (4*c*,*d*), can, if necessary, operate at the elevated temperatures often required in organic synthesis. Furthermore, a plentiful supply is assured as a result of the highly successful cloning of its gene into the pKK223-3 vector (5). When this is expressed in *Escherichia coli* TG1, BSLDH is produced in amounts of up to ~35% of the soluble proteins, from which it is easily purified, thereby enabling large quantities of the enzyme to be prepared from small fermentation volumes.

As the first step in our synthetic applications programme, we elected to evaluate the specificity and preparative-scale viability of BSLDH against that of a representative and well-documented mammalian enzyme (9, 10*g*, 13), PHLDH.

The reduction direction of eq. [1] was selected since, being an enantiotopically face-specific process, it is of more asymmetric synthetic interest than that of the reverse, oxidation, reaction. Also, on the preparative scale, reductions are easier to effect, being thermodynamically heavily favored (9), and with good methods for recycling of the nicotinamide coenzyme available (12, 15).

Despite the wide variation in activities of BSLDH towards the Table 1 substrates, the enzyme performed satisfactorily under preparative-scale conditions. The reactions were carried out on the 1–3 mmol scale and gave good yields of enantiomerically pure (2*S*) hydroxy acids (Table 1). Pyruvate itself was not subjected to preparative-scale reduction since its LDH-catalyzed conversion to L-lactic acid is so well documented (9). Product inhibition by the cyclopropyl acid **2***e* (11*e*) was not a problem with this enzyme. For 2-oxo-3-methylbutanoate (**1***d*), with a K_M of 17 mM, FDP was used to activate the BSLDH allosterically, thereby lowering the K_M (22). The purification of the hydroxy acid product **2***d* was not affected by the presence of FDP. We estimate that any substrate of BSLDH with a $k_{cat}/K_M \geq 10$ will be a satisfactory synthetic-scale candidate.

The kinetic measurements were carried out to provide a quantitative basis for comparison of the effects of the structural differences in **1***a–f* on the rates of reduction between the bacterial (BSLDH) and the well-known mammalian pig heart (PHLDH) enzyme. The kinetic parameters for the two enzymes (Table 3), which are in generally good agreement with the literature values available, show some interesting contrasts.

For the natural substrate pyruvate (**1***a*), the reduction is very fast and k_{cat} and K_M are about the same for both enzymes. For all the non-natural substrates **1***b–f*, the reduction processes are less facile to a greater or lesser extent, with k_{cat} lowered and K_M increased in each case.

For **1***b* and **1***c*, the next higher homologues of pyruvate, there is a marked decrease in activity of ~(2–8) × 10^2-fold within the series **1***a–c*, which is accounted for by the progressive increase in size of the alkyl substituents.

Branching at the 3-position of 2-keto acid substrates is seen to lower the enzyme activity dramatically. For **1***d*, the presence of the isopropyl group results in a reduction of the pyruvate k_{cat}/K_M value by ~10^5-fold for both enzymes. The highly deleterious effect of the 3-methyl substituent is also very clearly

Can. J. Chem. Downloaded from www.nrcresearchpress.com by 41.223.56.140 on 09/07/12
For personal use only.

TABLE 3. Kinetic parameters for BSLDH-catalyzed reductions of **1***a–f*[a] (values for PHLDH in parentheses)[a]

Substrate	k_{cat} (s^{-1})		K_M (mM)		k_{cat}/K_M (M^{-1} s^{-1})	
1*a*	188	(203)	0.04	(0.03)	4.76×10^6	(6.34×10^6)
1*b*	155	(101)	0.34	(0.43)	4.55×10^5	(2.33×10^5)
1*c*	44	(11)	2.38	(1.45)	1.85×10^4	(7.63×10^3)
1*d*	0.49	(0.65)	17	(3.9)	2.91×10^1	(1.66×10^2)
1*e*	5.0	(7.3)	1.74	(1.67)	2.87×10^3	(4.37×10^3)
1*f*	81	(5.4)	0.67	(1.47)	1.21×10^5	(3.67×10^3)

[a]At 25°C, pH 6.0 in triethanolamine-HCl buffer (20 mM) with [FDP] 5 mM, [S] $0.2K_M$–$6K_M$, [NADH] 0.2 mM, and [E] (0.2–5000) $\times 10^{-9}$ M.
[b]At same conditions as described under *a* but at pH 7.0 in phosphate buffer (100 mM) without FDP.

demonstrated by the 6×10^2-fold (BSLDH) and 50-fold (PHLDH) lowering of k_{cat}/K_M for **1***d* compared with its structurally isomeric parent 2-oxopentanoate (**1***c*).

The C-3 substituent effect is significantly ameliorated if the branching is part of a small ring. This is demonstrated by the results for the cyclopropyl substrate **1***e* for which the specificity constants are only slightly lower than for the isomeric 2-oxopentanoate (**1***c*) substrate.

When the branching is at the 4-position and is part of a planar phenyl ring, as in **1***f*, the two enzymes perform significantly differently, with **1***f* being much better tolerated by BSLDH (33-fold) than by PHLDH. In fact, the specificity constant for the BSLDH-catalyzed reduction of phenyl pyruvate (**1***f*) is even higher than that for the much less bulky 2-oxopentanoate (**1***c*).

2-Hydroxy acids have been widely recognized as useful chirons (23). This has stimulated many investigations of chemical (24) and fermentation (25, 26) methods for their preparation in enantiomerically pure forms. Enzyme-based approaches have also been demonstrated to be very powerful (10*g*, 11, 27). The initial results reported here with BSLDH show that this enzyme is an excellent choice as a catalyst for the preparation of a broad structural range of enantiomerically pure α-hydroxy acid chirons (23*a*). We are now exploring further the tolerance of the enzyme towards structural variations in its substrates, and the synthetic potential of predetermining the specificity of the enzyme in a controlled manner via the site-directed mutagenesis techniques of protein engineering (8, 28).

Experimental

Melting points were measured in an electrothermal capillary apparatus, and are uncorrected. The ir spectra were recorded on a Nicolet 5DX FT-IR system as liquid films, or in KBr if solid. Proton nmr spectra were obtained in $CDCl_3$, unless noted otherwise, using Varian T60, XL200, or XL400 spectrometers. Optical rotations were measured with a Perkin–Elmer 141 polarimeter. The glc analyses were performed on a Varian Aerograph 3400 fitted with a capillary DB wax column (25 m × 0.25 mm) and flame ionization detectors. The pH-stat used was a Metrohm 655 instrument.

NAD^+ was purchased from the Kyowa Hakko Kogyo Co. The pig heart L-lactate dehydrogenase (EC 1.1.1.27) used for kinetics was the H_4 enzyme from Boehringer Mannheim (batch no. 10525921-14). Formate dehydrogenase (from yeast, EC 1.2.1.2) was obtained in lyophilized form from Boehringer Mannheim (batch no. 10978222-78). (*R*)-(+)-Methoxytrifluoromethylphenylacetic acid ((*R*)-(+)-MTPA) was purchased from Aldrich.

Substrates

Except for **1***e*, all 2-oxo acids **1***a–f* were purchased from Sigma Chemical Co., and were used as received. 2-Cyclopropyl-2-oxoacetic acid (**1***e*) was prepared as its potassium salt, as described by Basnak and Farkas (14), in 65% yield; mp 260°C (dec.) (lit. (14) mp 258°C (dec.); ir: 2990, 1690, 1620, 1361 cm^{-1}; ^1H nmr (DMSO-d_6): 0.81 (4H, m) and 2.23 (1H, m) ppm.

Preparation of BSLDH

The gene, cloned into a pKK223-3 plasmid, was expressed in *E. coli* TG1 as described by Barstow *et al.* (5). Cells were grown overnight (16 h) in YT (2×) medium (16 g Bactotryptone, 10 g yeast extract, 5 g NaCl per litre) supplemented with ampicillin and harvested by centrifugation (10 min at 4000*g*). The cells were resuspended in 10 mM sodium phosphate buffer pH 6.3, lysed by sonication, and the cell debris removed by centrifugation (10 min at 9000*g*). The supernatant was heated for 90 min at 65°C with occasional swirling, and the denatured proteins removed by centrifugation (15 min at 14 000*g*). The supernatant was brought to 25% ammonium sulfate saturation and loaded onto a phenyl-Sepharose column (Pharmacia, 5.5 mL/g of wet cells) previously equilibrated with 25% saturated ammonium sulfate in 10 mM sodium phosphate buffer pH 6.3. A step gradient down to 0% ammonium sulfate saturation in the above phosphate buffer removed bulk proteins. The LDH protein was eluted with 2 column volumes of a linear gradient of ethylene glycol (0–50%) in 10 mM phosphate buffer pH 6.3 and yielded ~250 mg (120 000 units) of LDH per litre of overnight culture. Fractions were assayed by the method of Schaer and Zuber (4*d*). Those with LDH activity were dialyzed against 10 mM sodium phosphate buffer pH 6.3 and were >95% pure as judged by polyacrylamide gel electrophoresis in SDS (29). This level of purity was satisfactory for all the preparative scale reductions. The enzyme was stored in 2 M ammonium sulfate at 4°C.

Preparative scale BSLDH catalyzed reductions of ***1*** b–f

BSLDH and FDH were assayed prior to the experiments by the literature methods (refs. 4*d*, 30*a* for PHLDH, and 30*b* for FDH).

The same basic procedure was used for all preparative-scale LDH-catalyzed reactions, as follows: the keto acid substrate and 1.2 equivalents of sodium formate were dissolved in Tris-HCl buffer (5 mM, pH 6.0) and the solution deoxygenated with bubbling nitrogen for 30 min. The enzyme-catalyzed reaction, carried out under positive nitrogen atmosphere at 23°C, was initiated by adding NAD^+, dithiothreitol (0.5 μM), FDH, and BSLDH. The gently stirred solution was kept at a constant pH of 6.0 by adding hydrochloric acid (0.1 or 0.5 M) using a pH-stat. After 1 equivalent of acid had been added, the solution was acidified to pH 2 with 6 M hydrochloric acid, filtered through a Hyflo SuperCel-packed sintered funnel, and extracted with ethyl acetate (3×). The organic phases were dried ($MgSO_4$) and the solvent rotoevaporated. The hydroxy acid products were then recrystallized.

The individual reactions gave the following results.

BSLDH-catalyzed preparations of ***2*** b–f

*(S)-2-Hydroxybutanoic acid (**2** b)*

2-Oxobutanoic acid (**1***b*, 101.8 mg, 1 mmol), NAD^+ (5.1 mg), BSLDH (400 U), FDH (8.4 mg, 4.3 U), Tris-HCl buffer (10 mL), reaction time 15 h, recrystallization from $CHCl_3$, gave **2***b* (90.6 mg,

Can. J. Chem. Downloaded from www.nrcresearchpress.com by 41.223.56.140 on 09/07/12
For personal use only.

Can. J. Chem. Downloaded from www.nrcresearchpress.com by 41.223.56.140 on 09/07/12
For personal use only.

88%, >99% ee); mp 48–49°C (lit. (16) mp 52.7–53.5°C (dec.)); $[\alpha]_D^{25}$ +6.4° (*c* 2.63, $CHCl_3$) (lit. (16) $[\alpha]_D^{21}$ +6.4° (*c* 11.03, $CHCl_3$); ir (KBr): 1131, 1735, 2938, 2973, 3402, 2600–3676 cm^{-1}; ^1H nmr (400 MHz) δ: 0.99 (3H, t, J = 7 Hz), 1.74 (1H, m), 1.88 (1H, m), 4.24 (1H, dd, J = 7 Hz, J' = 5 Hz), and 5.95 (2H, br s, OH and COOH) ppm.

*(S)-2-Hydroxypentanoic acid (***2**c*)*

2-Oxopentanoic acid, sodium salt (**1***c*, 138.3 mg, 1 mmol), NAD^+ (5.1 mg), BSLDH (430 U), FDH (8.9 mg, 4.5 U), Tris-HCl buffer (10 mL), reaction time 35 h, recrystallization from CCl_4, yielded **2***c* (105.7 mg, 89%, >99% ee); mp 52–55°C (lit. (10*g*) mp 57.8–58.5°C); $[\alpha]_D^{25}$ +5.9° (*c* 1.25, $CHCl_3$), $[\alpha]_D^{25}$ −3.3° (*c* 1.0, H_2O) (lit. (31) $[\alpha]_D^{25}$ −2.7° (*c* 1–5%, H_2O); ir (KBr): 1131, 1215, 1728, 2959, 3367, 2400–3711 cm^{-1}; ^1H nmr (400 MHz) δ: 0.94 (3H, t, J = 7 Hz), 1.46 (2H, m), 1.66 (1H, m), 1.79 (1H, m), 4.25 (1H, dd, J = 7 Hz, J' = 4 Hz), and 5.40 (2H, br s, OH and COOH) ppm.

*(S)-2-Hydroxy-3-methylbutanoic acid (***2**d*)*

3-Methyl-2-oxobutanoic acid, sodium salt (**1***d*, 414 mg, 3 mmol), NAD^+ (15 mg), BSLDH (3000 U), FDH (23.6 mg, 12 U), Tris-HCl buffer (20 mL), FDP (60.5 mg, 0.11 mmol), reaction time 42 h, recrystallization from CCl_4, afforded **2***d* (305 mg, 86%, >99% ee); mp 66°C (lit. (17) mp 65°C); $[\alpha]_D^{25}$ +17.2° (*c* 1.85, $CHCl_3$) (lit. (17) $[\alpha]_D^{14}$ +16.9° ± 2° (*c* 1.85, $CHCl_3$); ir (KBr): 1032, 1707, 2973, 3423, 2400–3600 cm^{-1}; ^1H nmr (400 MHz) δ: 0.91 (3H, d, J = 7 Hz), 1.05 (3H, d, J = 7 Hz), 2.14 (1H, m), 4.13 (1H, d, J = 3 Hz), and 7.3 (2H, s, br) ppm.

*(S)-2-Hydroxy-2-cyclopropylethanoic acid (***2**e*)*

2-Cyclopropyl-2-oxoethanoic acid, potassium salt (**1***e*, 304 mg, 2 mmol), NAD^+ (10 mg), BSLDH (1000 U), FDH (15.7 mg, 8 U), Tris-HCl buffer (20 mL), reaction time 42 h, recrystallization from CCl_4, produced **2***e* (206 mg, 89%, >99% ee); mp 98°C (lit. (10*g*) mp 97–98.5°C); $[\alpha]_D^{25}$ +44° (*c* 0.87, $CHCl_3$); ir (KBr): 1075, 1264, 1721, 3430, 2400–3600 cm^{-1}; ^1H nmr (400 MHz) δ: 0.50 (4H, m), 1.15 (1H, m), 3.81 (1H, d, J = 7 Hz), and 6.20 (2H, br s, OH and COOH) ppm.

*(S)-2-Hydroxy-3-phenylpropanoic acid (***2**f*)*

2-Oxo-3-phenylpropanoic acid (**1***f*, 301 mg, 1.84 mmol), NAD^+ (10.3 mg), BSLDH (800 U), FDH (22.1 mg, 11.3 U), Tris-HCl buffer (20 mL), reaction time 2.1 days, recrystallization from $CHCl_3$, yielded **2***f* (276 mg, 90%, >99% ee); mp 125–126°C (lit. (18) mp 124–125°C); $[\alpha]_D^{25}$ −24.7° (*c* 3.2, H_2O) (lit. (18) $[\alpha]_D^{25}$ −19.9° (*c* 3.2, water)); ir (KBr): 1735, 2600, 3451, 2500–3600 cm^{-1}; ^1H nmr (200 MHz) δ: 2.98 (1H, dd, J = 14 Hz, J' = 8 Hz), 3.11 (1H, dd, J = 14 Hz, J' = 4 Hz), 4.50 (1H, dd, J = 7 Hz, J' = 4 Hz), 5.90 (2H, v br s, OH and COOH), and 7.25 (5H, m) ppm.

*Synthesis of racemic 2-hydroxy acids (±)-***2**b–f *as reference standards*

*(±)-2-Hydroxy-3-methylbutanoic acid ((±)-***2**d*)* was obtained from Aldrich as a calcium salt. For **2***b*, *c*, *e*, *f* the same basic preparative procedure was used. The following is representative.

*(±)-2-Hydroxybutanoic acid ((±)-***2**b*)*

To a stirred solution of potassium cyanide (6.5 g, 0.1 mol) in EtOH-free diethyl ether (40 mL) and distilled water (20 mL) at 0°C was added simultaneously propanal (3.48 g, 0.06 mol) and glacial acetic acid (5.72 mL, 0.1 mol). The mixture was stirred vigorously at 0°C, and stirring was continued while it was allowed to warm to room temperature during 2 h. The ether layer was then separated and the aqueous layer extracted with more ether (3 × 50 mL). The combined ether extracts were dried ($MgSO_4$), filtered, and concentrated by rotoevaporation to give (±)-2-hydroxybutanonitrile (3.91 g, 77%); ir (film): 3430, 2249 cm^{-1}; ^1H nmr δ: 1.18 (3H, dt, J = 6 Hz, J' = 1 Hz), 1.95 (2H, dq, J = 7 Hz, J' = 1 Hz), 2.98–4.25 (1H, br s), and 4.50 (1H, t, J = 6 Hz) ppm. The above cyanohydrin (3.8 g, 45 mmol) in distilled water (15 mL) was slowly poured into a precooled (0°C) solution of hydrochloric acid (12 M, 36 mL). Methanol (6 mL) was used to rinse the flask and was added to the reaction. The mixture was stirred for 12 h, during which period it was allowed to warm from 0 to 20°C. It was then heated at reflux for 1 h, cooled, and rotoevaporated at 60–70°C. The residue was dissolved in water (30 mL), extracted with ethyl acetate (3 × 50 mL), and the organic extracts dried ($MgSO_4$), filtered, and concentrated. Kugelrohr distillation gave 2-hydroxybutanoic acid ((±)-**2***b*, 2.3 g, 56%); bp 110°C (0.5 Torr; 1 Torr = 133.3 Pa) (lit. (16) bp 140°C (14 Torr)); ir and ^1H nmr for all the racemic hydroxy acids are the same as described for the (*S*) isomers.

The remaining (±)-2-hydroxy acids **2***c–f* were prepared by the same method, as follows:

*(±)-2-Hydroxypentanoic acid ((±)-***2**c*)*

Butanal (Aldrich) (4.32 g, 0.06 mol) yielded its cyanohydrin (5 g, 84%); ir (film): 3430 (strong), 2249 cm^{-1}; ^1H nmr δ ($CDCl_3$/DMSO-d_6): 0.95 (3H, br t, J = 6 Hz), 1.80 (4H, m), 4.45 (1H, m (dt)), and 5.98 (1H, d, J = 6 Hz, disappeared upon D_2O exchange) ppm. This cyanohydrin (3.5 g, 0.035 mol) yielded (±)-**2***c* (3.46 g, 75%), which solidified after distillation, mp 34–35°C (lit. (3) mp 34°C).

*(±)-2-Hydroxy-2-cyclopropylacetic acid ((±)-***2**e*)*

To a solution of hydroxymethylcyclopropane (5 g, 0.069 mol) in dry dichloromethane (50 mL) under a nitrogen atmosphere was added pyridinium chlorochromate (Aldrich, 16.5 g, 0.076 mol) at 0°C, and the mixture stirred for 2 h. Filtration through silica gel and evaporation of the solvent gave formylcyclopropane (2.7 g, 56%); ir (film): 2839, 1707 cm^{-1}; ^1H nmr δ: 1.05 (4H, distorted d), 1.75 (1H, m), 8.90 (1H, d, J = 6 Hz). This aldehyde (2.6 g, 0.037 mol) was converted to its cyanohydrin (3.6 g, 100%); ir (film): 3409 (strong), 2249 cm^{-1}; ^1H nmr (60 MHz) δ: 0.60–0.90 (4H, distorted d), 1.42 (1H, m), 3.78–4.48 (1H, br s), and 4.27 (1H, d, J = 6 Hz) ppm. The cyanohydrin (3.6 g, 0.037 mol), recrystallized from CCl_4:hexane (1:1), gave (±)-**2***e* (2 g, 47%), mp 76–78°C (lit. (32) mp 77–78°C).

*(±)-2-Hydroxy-3-phenylpropanoic acid ((±)-***2**f*)*

Phenylacetaldehyde (Aldrich, 3.0 mL, 0.026 mol) gave its cyanohydrin (3.7 g, 98%); ir (film): 3437, 2249 cm^{-1}; ^1H nmr δ: 2.79 (1H, d, J = 6 Hz), 3.15 (2H, d, J = 6 Hz), 4.60 (1H, td, J = 6 Hz, J' = 6 Hz), and 7.23 (5H, s) ppm. This cyanohydrin (3.48 g, 0.024 mol) yielded (±)-**2***f* (3.1 g, 80%); mp 97–98°C (lit. (16) mp 98°C).

Enantiomeric excess determinations

The ee's were determined by the Mosher ester method (20). The enzyme-derived acids **2***b–f* were first converted in quantitative yields to their methyl esters with diazomethane in THF at 0°C, and these then reacted with (*S*)-(+)-MTPA chloride (freshly prepared from (*R*)-(+)-MTPA with excess thionyl chloride) in the presence of a catalytic amount of 4-dimethylaminopyridine to give the corresponding Mosher esters (20). The % ee's were determined by integrations of the well-separated ^1H nmr -OCH_3 and -$COOCH_3$ signals, using the similarly prepared Mosher esters of racemic (±)-**2***b–f* as reference standards. In the capillary glc analyses, the *S*-**2***b–f*-derived MTPA-esters had longer (by 2.73–5.04 min) retention times than those of the *R* enantiomers. The results confirmed the >99% ee's of *S*-**2***b–f* determined by ^1H nmr.

The ^1H nmr (400 MHz) spectral data for the Mosher esters of the methyl esters of (*S*)-**2***b–f* are as follows:

(S)-2-O(MTPA)-butanoic acid methyl ester: δ: 0.99 (3H, t, J = 7.4 Hz), 1.94 (2H, m), 3.55 (3H, br s), 3.73 (3H, s), 5.13 (1H, dd, J = 7.0 Hz, J' = 5.2 Hz), and 7.40–7.60 (5H, m) ppm.

(S)-2-O(MTPA)-pentanoic acid methyl ester: δ: 0.92 (3H, t, J = 7.38 Hz), 1.41 (2H, m), 1.82 (2H, m), 3.55 (3H, br s), 3.73 (3H, s), 5.17 (1H, t, J = 6.42 Hz), and 7.40–7.63 (5H, m) ppm.

(S)-2-O(MTPA)-3-methylbutanoic acid methyl ester: δ: 0.95 (3H, d, J = 6.83 Hz), 1.02 (3H, d, J = 7.08 Hz), 2.33 (1H, m), 3.54 (3H, br s), 3.74 (3H, s), 5.00 (1H, d, J = 4.1 Hz), and 7.40–7.56 (5H, m) ppm.

(S)-2-O(MTPA)-2-cyclopropylacetic acid methyl ester: δ: 0.44–0.75 (4H, m), 1.31 (1H, m), 3.57 (3H, br s), 3.75 (3H, s), 4.58 (1H, d, J = 8.74 Hz), and 7.4–7.6 (5H, m) ppm.

(S)-2-O(MTPA)-3-phenylpropanoic acid methyl ester: δ: 3.10 (1H, dd, J = 14 Hz, J' = 10 Hz), 3.33 (1H, dd, J = 14 Hz, J' = 4 Hz),

Can. J. Chem. Downloaded from www.nrcresearchpress.com by 41.223.56.140 on 09/07/12
For personal use only.

3.33 (3H, br s), 3.77 (3H, s), 5.42 (1H, dd, J = 10 Hz, J' = 4 Hz), and 7.19–7.41 (10H, m) ppm.

Absolute configuration assignments

The absolute configurations of the LDH-produced hydroxy acids **2***b–f* were confirmed as *S* from comparison of their optical rotations with the known values of *S*-**2***b* (16), -**2***d* (17), and -**2***f* (18). For **2***c* and **2***e* the ^{1}H nmr chemical shifts for one to three characteristic protons of each (*R*)-(+)-MTPA derivative were correlated with the *S* configuration by the scheme described by Yamaguchi (19).

LDH kinetic studies

BSLDH was prepared as described above for the preparative studies, but with additional purification by affinity chromatography on *N*-(6-aminohexyl)oxamate-Sepharose 4B according to Schaer and Zuber (4*d*), and with the procedure being slightly modified to give a highly concentrated enzyme solution (33). The gel was prepared by coupling AH-Sepharose 4B (Pharmacia) with oxalic acid in the presence of (1-ethyl-3-(3-dimethylaminopropyl)-carbodiimide.[4] The column was equilibrated with triethanolamine-HCl buffer (20 mM, pH 6.0) containing NaCl (500 mM), 2-mercaptoethanol (5 mM), FDP (5 mM), and NADH (750 μM). Five millilitres (containing 15 mg) of the above purified enzyme solution was brought to 500 mM in NaCl, 5 mM in 2-mercaptoethanol, 5 mM in FDP, and 750 μM in NADH, incubated for 1 h, and applied to the column (0.5 mL gel). The inactive proteins were washed out with 5 mL of the equilibration buffer and the enzyme was eluted with triethanolamine-HCl (20 mM, pH 9.0) containing 2-mercaptoethanol (5 mM) (33). Fractions with LDH activity (6) were dialyzed against triethanolamine-HCl (20 mM, pH 6.0) buffer containing mercaptoethanol (1 mM) and EDTA (1 mM). Concentrations were determined spectrophotometrically at 280 nm assuming an absorption coefficient of 0.91 for 1 mg/mL enzyme (7*b*). The molecular weight of the monomeric enzyme was taken to be 34 862 daltons (5).

For kinetic measurements the pig heart H_4 (PHLDH) enzyme suspension in ammonium sulfate was centrifuged and redissolved in phosphate buffer (100 mM, pH 7.0). Concentrations were determined spectrophotometrically using E_{A280} = 1.37 cm^{-1} mg^{-1} (34).

Kinetic studies

All measurements were done under steady-state conditions at 25°C. Triethanolamine-HCl buffer (20 mM, pH 6.0) and saturating conditions of FDP (5 mM) and NADH (0.2 mM) were used for the assays with BSLDH. The kinetics measurements with PHLDH were carried out on the H_4 enzyme in phosphate buffer (100 mM, pH 7.0), without FDP. Typically, enzyme concentrations between 6×10^{-9} and 6×10^{-7} M (BSLDH) and 5×10^{-10} and 5×10^{-6} M (PHLDH) were used. The reactions were initiated by addition of a substrate solution (3–500 mM) to give a final concentration between $0.1K_M$ and $5.0K_M$ in a 1-mL, 1 cm pathlength, cuvette. Reactions were recorded on a Shimadzu UV-240/PR1 spectrophotometer equipped with a constant temperature cell holder. The reactions were followed by monitoring the decrease in the NADH absorbance at 340 nm. The extinction coefficient of NADH was taken to be 6220 L^{-1} M^{-1} cm^{-1} (35). All experiments were done in duplicate and individual data points were determined in triplicate. Michaelis constants (K_M) and turnover numbers (k_{cat}) were determined by Lineweaver–Burk plots (36) and least-squares analyses. Correlation coefficients were higher than 0.995 in each case. A minimum of six substrate concentrations between $0.1K_M$ and $5K_M$ were used except for **1***b* ($0.1K_M$–$1.5K_M$) and **1***g* ($0.1K_M$–$2.5K_M$) for BSLDH where substrate inhibition occurred. The results are recorded in Table 3.

Acknowledgements

This work was supported in Toronto by a Natural Sciences and Engineering Research Council of Canada (NSERC) strategic grant (to J.B.J., J.D.F., and M.G.), in Bristol by Molecular Recognition (to W. N. Chia and J.J.H.) and Protein Engineering Initiatives (to C. R. Dunn, H. Muirhead, and J.J.H.) grants from the Science and Engineering Research Council, and by a NATO Scientific Exchange award (to J.J.H. and J.B.J.). The awards of a Stiftung fuer Stipendien auf dem Gebiete der Chemie, Switzerland (to M.A.L.), and an NSERC Postgraduate Scholarship and an FCAR (Quebec) Postgraduate Scholarship (to L.R.P.) are gratefully acknowledged. We also thank Professor G. M. Whitesides for providing us with his PHLDH results (ref. 10*g*) prior to publication.

[4] J. J. Holbrook, unpublished work.

1. L. K-P. Lam and J. B. Jones. Can. J. Chem. **66**, 1422 (1988), and previous papers.
2. (*a*) J. B. Jones and J. F. Beck. Tech. Chem. (NY), **10**, 107 (1976); J. B. Jones. Tetrahedron, **42**, 3351 (1986); (*b*) C. H. Wong and G. M. Whitesides. Angew Chem. Int. Ed. Engl. **24**, 617 (1985); A. Akiyama, M. Bednarski, M. J. Kim, E. S. Simon, H. Waldmann, and G. M. Whitesides. Chem. Br. **23**, 645 (1987); (*c*) A. M. Klibanov. Science, **219**, 722 (1983); Chem. Technol. 354 (1986); (*d*) R. Porter and S. Clark (*Editors*). Enzymes in organic synthesis. Ciba Foundation Symposium 111. Pitman, London. 1985; (*e*) J. Tramper, H. C. von der Plas, and P. Linko (*Editors*). Biocatalysis in organic synthesis. Elsevier, Amsterdam. 1985; (*f*) M. Schneider (*Editor*). Enzymes as catalysts in organic synthesis. Reidel, Dordrecht, The Netherlands. 1986.
3. Dictionary of organic compounds. Vol. 3. Eyre and Spottiswoode, london. 1965
4. (*a*) J. D. Tratschin, B. Wirz, G. Frank, and H. Zuber. Hoppe-Seyler's Z. Physiol. Chem. **364**, 879 (1983); (*b*) B. Wirz, F. Suter, and H. Zuber. Hoppe-Seyler's Z. Physiol. Chem. **364**, 893 (1983); (*c*) D. Stangl, F. Wiederkehr, F. Suter, and H. Zuber. Biol. Chem. Hoppe-Seyler, **368**, 1157 (1987); (*d*) H.-P. Schaer and H. Zuber. Hoppe-Seyler's Z. Physiol. Chem. **360**, 795 (1979).
5. D. A. Barstow, A. R. Clarke, W. N. Chia, D. B. Wigley, A. S. Sharman, J. J. Holbrook, T. Atkinson, and N. T. Mington. Gene, **46**, 47 (1986).
6. A. R. Clarke, T. Atkinson, J. W. Campbell, and J. J. Holbrook. Biochim. Biophys. Acta, **829**, 387 (1985).
7. (*a*) A. R. Clarke, H. M. Wilks, D. A. Barstow, T. Atkinson, W. N. Chia, and J. J. Holbrook. Biochemistry, **27**, 1617 (1988), and previous papers; (*b*) A. R. Clarke, A. D. B. Waldman, I. Munro, and J. J. Holbrook. Biochim. Biophys. Acta, **828**, 375 (1985).
8. A. R. Clarke, C. J. Smith, K. W. Hart, H. M. Wilks, W. N. Chia, T. V. Lee, J. J. Birktoff, L. J. Banaszak, D. A. Barstow, T. Atkinson, and J. J. Holbrook. Biochim. Biophys. Res. Commun. **148**, 15 (1987).
9. (*a*) J. J. Holbrook, A. Liljas, S. J. Steindal, and M. G. Rossmann. *In* The enzymes. 3rd ed. *Edited by* P. D. Boyer. Academic, New York. 1975. Chap. 4; (*b*) J. Everse and N. O. Kaplan. Adv. Enzymol. **37**, 61 (1973); (*c*) G. W. Schwert and A. D. Winer. *In* The enzymes. 2nd ed. *Edited by* P. D. Boyer, H. Lardy, and K. Myrbak. Academic, New York. 1963. Chap. 6.
10. (*a*) R. J. S. Duncan and K. F. Tipton. Eur. J. Biochem. **11**, 58 (1969); (*b*) R. S. Lane and E. E. Dekker. Biochemistry, **8**, 2958 (1969); (*c*) B. Pensa, M. Costa, A. Colosimo, and D. Cavallini. Mol. Cell. Biochem. **44**, 107 (1982); (*d*) A. Meister. J. Biol. Chem. **184**, 117 (1950); (*e*) A. Meister. J. Biol. Chem. **197**, 309 (1952); (*f*) J. Martensson. Anal. Biochem. **154**, 43 (1986); (*g*) M.-J. Kim and G. M. Whitesides. J. Am. Chem. Soc. **110**, 2959 (1988).
11. (*a*) W. Hummel, H. Schuette, and M.-R. Kula. Eur. J. Appl. Microbiol. Biotechnol. **18**, 75 (1983); (*b*) Ch.-S. Chen, B.-N. Zhou, G. Girdaukas, W.-R. Shieh, F. VanMiddlesworth, A. S. Gopalan, and Ch. Sih. Bioorg. Chem. **12**, 98 (1984); (*c*) M. Nardini, H. Kodama, G. Ricci, G. Federici, and D. Cavallini. Biochem. Int. **11**, 789 (1985); (*d*) H. K. Chenault,

M.-J. KIM, A. AKIYAMA, T. MIYAZAWA, E. S. SIMON, and G. M. WHITESIDES. J. Org. Chem. **52**, 2608 (1987); (*e*) D. C. NONHEBEL, S. T. ORSZULIK, and C. J. SUCKLING. J. Chem. Soc. Chem. Commun. 1146 (1982); (*f*) I. MACINNES, D. C. NONHEBEL, S. T. ORSZULIK, and C. J. SUCKLING. J. Chem. Soc. Perkin Trans. 1, 2771 (1983).

12. (*a*) O. ABRIL and G. M. WHITESIDES. J. Am. Chem. Soc. **104**, 1552 (1982); (*b*) M.-O. MANSSON, N. SIEGBAHN, and K. MOSBACH. Proc. Natl. Acad. Sci. U.S.A. **80**, 1487 (1983); (*c*) N. SIEGBAHN, M.-O. MANSSON, and K. MOSBACH. Appl. Biochem. Biotechnol. **12**, 91 (1986); (*d*) H. K. CHENAULT and G. M. WHITESIDES. Appl. Biochem. Biotechnol. **141**, 147 (1987); (*e*) M. R. KULA and C. WANDREY. Methods Enzymol. **136**, 9 (1987).
13. A. M. GRAU, W. E. TROMMER, and M. G. ROSSMANN. J. Mol. Biol. **151**, 289 (1981).
14. I. BASNAK and J. FARKAS. Collect. Czech. Chem. Commun. **40**, 1038 (1975).
15. R. WICHMANN, CH. WANDREY, A. BUECKMANN, and M.-R. KULA. Biotechnol. Bioeng. **23**, 2789 (1981).
16. D. H. S. HORN and M. Y. Y. PRETORIUS. J. Chem. Soc. 1460 (1954).
17. A. H. COOK, S. F. COX, and T. H. FARMER. J. Chem. Soc. 1022 (1949).
18. R. C. WEAST (*Editor*). CRC handbook of chemistry and physics. 63rd ed. CRC Press, Boca Raton, FL. 1982. p. C-357.
19. S. YAMAGUCHI. *In* Asymmetric synthesis. *Edited by* J. D. Morrison. Academic, New York. 1983. Chap. 7; F. YASUHARA and S. YAMAGUCHI. Tetrahedron Lett. **21**, 2827 (1980).
20. J. A. DALE, D. L. DULL, and H. S. MOSHER. J. Org. Chem. **34**, 3543 (1969).
21. (*a*) A. R. CLARKE, J. R. N. EVINGTON, C. R. DUNN, T. ATKINSON, and J. J. HOLBROOK. Biochim. Biophys. Acta, **870**, 112 (1986); (*b*) A. R. CLARKE, D. B. WIGLEY, W. N. CHIA, D. A. BARSTOW, T. ATKINSON, and J. J. HOLBROOK. Nature, **324**, 699 (1986); (*c*) A. R. CLARKE, D. B. WIGLEY, D. A. BARSTOW, W. N. CHIA, T. ATKINSON, and J. J. HOLBROOK. Biochim. Biophys. Acta, **913**, 72 (1987).
22. K. W. HART, A. R. CLARKE, D. B. WIGLEY, A. D. B. WALDMAN, W. N. CHIA, D. A. BARSTOW, T. ATKINSON, J. B. JONES, and J. J. HOLBROOK. Biochim. Biophys. Acta, **914**, 294 (1987).
23. (*a*) S. HANESSIAN (*Editor*). Total synthesis of natural products: the chiron approach. Pergamon, New York. 1983. Chap. 2; (*b*) K. MORI. *In* The total synthesis of natural products. *Edited by* J. Simon. Wiley Interscience, New York. 1981. Chap. 1; (*c*) D. SEEBACH and E. HUNGERBUEHLER. *In* Modern synthetic methods. *Edited by* R. Scheffold. Otto Salle Verlag, Frankfurt am Main, Germany. 1980. p. 91.
24. (*a*) K. SOAI, T. ISODA, and H. HASEGAWA. Chem. Lett. 1987 (1986); (*b*) J. K. WHITESELL, R. M. LAWRENCE, and H. CHEN. J. Org. Chem. **51**, 4779 (1981); (*c*) R. GAMBONI and C. TAMM. Tetrahedron Lett. **27**, 3999 (1986); (*d*) T. MUNEGUMI, M. FUJTA, T. MARUJAMA, S. SHIONO, M. TAKASAKI, and K. HARADA. Bull. Chem. Soc. Jpn. **60**, 249 (1987); (*e*) H.-C. BROWN, B. T. CHO, and W. S. PARK. J. Org. Chem. **51**, 3396 (1986); (*f*) W. H. PEARSON and M.-C. CHENG. J. Org. Chem. **51**, 3746 (1986); (*g*) D. A. EVANS, M. M. MORRISSEY, and R. L. DOROW. J. Am. Chem. Soc. **107**, 4346 (1985).
25. H. GUNTHER, S. NEUMAN, and H. SIMON. J. Biotechnol. **5**, 53 (1987); H. SIMON, J. BADER, H. GUNTHER, S. NEUMAN, and J. THANOS. Angew. Chem. Int. Ed. Engl. **24**, 539 (1985).
26. S. TSUBOI, E. NISHIYAMA, M. UTAKA, and A. TAKEDA. Tetrahedron Lett. **27**, 1915 (1986).
27. M. D. BEDNARSKI, H. K. CHENAULT, E. S. SIMON, and G. M. WHITESIDES. J. Am. Chem. Soc. **109**, 1283 (1987); M. A. K. PATTERSON, R. P. SZAJEWSKI, and G. M. WHITESIDES. J. Org. Chem. **46**, 4683 (1981); Z. SHAKED and G. M. WHITESIDES. J. Am. Chem. Soc. **102**, 7104 (1980); J. R. MATOS, M. B. SMITH, and C.-H. WONG. Bioorg. Chem. **13**, 121 (1985); C.-H. WONG and J. R. MATOS. J. Org. Chem. **50**, 1992 (1985); K. MOTOSUGI, N. ESAKI, and K. SODA. Biotechnol. Bioeng. **26**, 805 (1984); W. HUMMEL, H. SCHUTTE, and M.-R. KULA. Ann. N.Y. Acad. Sci. **434**, 195 (1984); R. WICHMANN, C. WANDREY, W. HUMMEL, H. SCHUTTE, A. F. BUCKMANN, and M.-R. KULA. Ann. N.Y. Acad. Sci. **434**, 87 (1984).
28. (*a*) J. A. GERLT. Chem. Rev. **87**, 1079 (1987); (*b*) W. V. SHAW. Biochem. J. **246**, 1 (1987); (*c*) R. J. LEATHERBARROW and A. R. FERSHT. Protein Eng. **1**, 7 (1986).
29. U. K. LAEMMLI. Nature, **227**, 680 (1970).
30. H. U. BERGMEYER, J. BERGMEYER, and L. M. GRASS (*Editors*). Methods of enzymatic analysis. Vol. 2. 3rd ed. Verlag Chemie, Weinheim, Germany. 1983. (*a*) p. 232; (*b*) p. 183.
31. M. WINITZ, L. BLOCH-FRANKENTHAL, N. IZUMIYA, S. M. BIRNBAUM, C. G. BAKER, and J. P. GREENSTEIN. J. Am. Chem. Soc. **78**, 2423 (1956).
32. H. DAHN, L.-H. DAV, and R. HUNMA. Helv. Chim. Acta, **65**, 2458 (1982).
33. D. M. PARKER and J. J. HOLBROOK. Int. J. Biochem. **13**, 1101 (1981).
34. D. JECKEL and G. PFLEIDERER. Hoppe-Seyler's Z. Physiol. Chem. **350**, 903 (1969).
35. B. L. HORECKER and A. KORNBERG. J. Biol. Chem. **175**, 385 (1948).
36. H. LINEWEAVER and D. BURK. J. Am. Chem. Soc. **56**, 658 (1934).

Can. J. Chem. Downloaded from www.nrcresearchpress.com by 41.223.56.140 on 09/07/12
For personal use only.

Intramolecular rhodium carbenoid insertions into aromatic C—H bonds. Preparation of 1,3-dihydrothiophene 2,2-dioxides fused onto aromatic rings

SURESH D. BABU, MICHAEL D. HRYTSAK, AND TONY DURST[1]

Ottawa–Carleton Chemistry Institute, Department of Chemistry, University of Ottawa, Ottawa, Ont., Canada K1N 9B4

Received June 28, 1988[2]

SURESH D. BABU, MICHAEL D. HRYTSAK, and TONY DURST. Can. J. Chem. **67**, 1071 (1989).

The preparation of 1-carboalkoxy-1,3-dihydrobenzo[*b*]thiophene 2,2-dioxides via rhodium acetate or rhodium trifluoroacetate catalyzed decomposition of α-diazo-β-arylmethanesulfonyl esters is described. The reaction has been extended to yield 1,3-dihydrothiophene 2,2-dioxides fused to the 2,3 position of thiophene and indole, but not of furans. In the latter case products derived from the opening of the furan ring were obtained.

Key words: synthesis, 1-carboalkoxy-1,3-dihydrobenzo[*b*]thiophene 2,2-dioxides, intramolecular carbenoid insertions, rhodium acetate catalysis.

SURESH D. BABU, MICHAEL D. HRYTSAK et TONY DURST. Can. J. Chem. **67**, 1071 (1989).

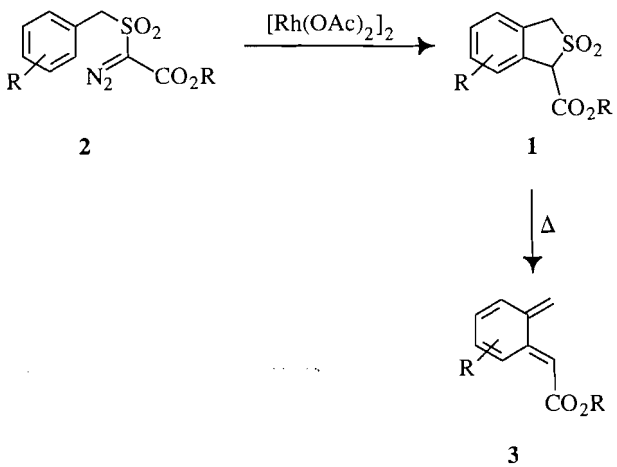
On décrit la préparation des dioxydes-2,2 des carboalcoxy-1 dihydro-1,3 benzo[*b*]thiophènes par le biais de décompositions, catalysées par l'acétate ou le trifluoroacétate de rhodium, d'esters α-diazo β-arylméthanesulfoniques. On a étendu le champ d'application de cette réaction de façon à pouvoir obtenir des dioxydes-2,2 de dihydro-1,3 thiophènes condensés aux positions 2,3 du thiophène ou de l'indole, mais pas des furannes. Dans ces derniers cas, on obtient plutôt des produits provenant de l'ouverture des noyaux furannes.

Mots clés : synthèse, dioxydes-2,2 des carboalcoxy-1 dihydro-1,3 benzo[*b*]thiophènes, insertions intramoléculaires de carbénoïdes, catalyse par l'acétate de rhodium.

[Traduit par la revue]

Introduction

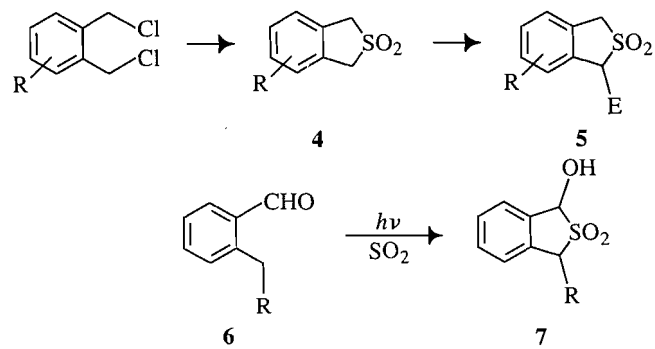
We have reported in a preliminary publication the preparation of 1-carboalkoxy-1,3-dihydrobenzo[*b*]thiophene 2,2-dioxides **1** (1) via the rhodium acetate catalyzed decomposition of α-diazo-β-arylmethanesulfonyl esters of the type **2**. Compounds such as **1** are of interest as synthetic intermediates since they undergo thermal extrusion of sulfur dioxide to yield *o*-quinodimethanes, **3**.



2 **1** **3**

The use of these reactive dienes as intermediates in the synthesis of natural products was first championed by Kametani and Nemoto (2*a*) and Oppolzer (2*b*). The field has recently been reviewed by Charlton and Alauddin (3).

1,3-Dihydrobenzo[*b*]thiophene 2,2-dioxides have been prepared by the reaction of *o*-dihalomethylbenzenes with sodium sulfide followed by oxidation (4), or by photolysis of *o*-substituted benzaldehydes **6** in the presence of SO_2 to yield α-hydroxy sulfones **7** (5). Compounds such as **5**, which are substituted in the heterocyclic ring, can be obtained via formation of an α-sulfonyl carbanion derived from **4** followed by addition of an electrophile (4*c*–*e*). Potential problems concerning regiochemistry can arise in the above reaction when substituents are also present in the aromatic ring.



4 **5** **6** **7**

The rhodium acetate catalyzed route from **2** to **1** represents a new route to these sulfones. Rhodium carboxylate decomposition of the diazo compounds bearing electron-withdrawing groups have been extensively investigated during the past decade. Typical reactions observed for the intermediate carbenoid include OH, NH, SH, and both aliphatic and aromatic CH insertions, and cyclopropanations. Recent reviews by Doyle and Mass are available (6). The required α-diazo-β-sulfonyl esters are readily prepared from commercially available benzylic alcohols or halides via mercaptoacetates and zinc iodide or mercaptoacetate and sodium hydroxide, respectively, followed by oxidation and diazo transfer using tosyl azide and base (7). Compounds such as **1** can be modified in the heterocyclic ring at either C-1 or C-3 via the C-1 anion or the C-1, C-3 dianion. Examples of this methodology and extensions of the carbenoid insertion to form 1,3-dihydrothiophene rings fused to thiophene and indole are also described in this paper. Furan analogs could not be prepared by this route. Their attempted preparation resulted in opening of the furan ring to give α,β-unsaturated aldehydes.

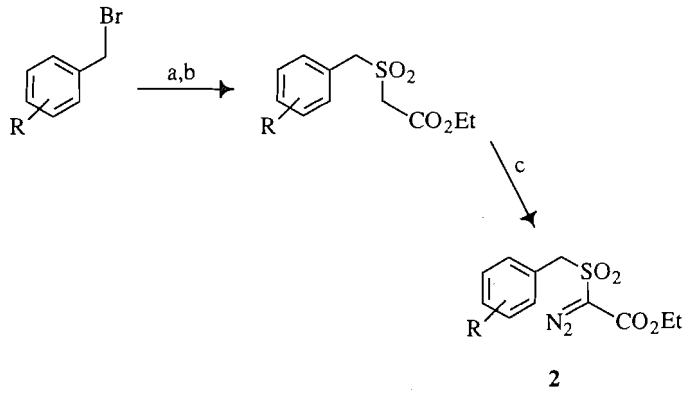
Results and discussion

The α-diazo-β-sulfonyl esters used in this study were prepared by standard procedures outlined below (Scheme 1).

[1]Author to whom correspondence may be addressed.

[2]Revision received January 27, 1989.

Can. J. Chem. Downloaded from www.nrcresearchpress.com by 41.223.56.140 on 09/07/12
For personal use only.

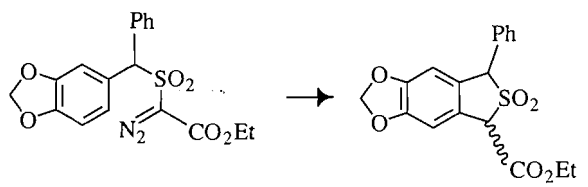


SCHEME 1. (a) $NaSCH_2CO_2Et$; (b) MCPBA; (c) TsN_3/base.

The yields in the various steps were generally excellent with the exception of the diazo transfer reaction, which rarely afforded the desired product in higher than 50% yield despite extensive variations in the diazotization conditions (tosyl azide, NaH/THF; tosyl azide, EtOH/KOH; tosyl azide, CH_2Cl_2/NEt_3) (7). The key α-diazo sulfones were characterized by the strong peak near 2120 cm^{-1} in the infrared and by their nmr spectra. These data are reported in the experimental section.

The decomposition of the various diazo sulfones was initially studied with $(Rh(OAc)_2)_2$ in methylene chloride at room temperature. Under these conditions the yields of the insertion product of the type **1** derived from the substituted benzenes or substituted thiophenes were generally in the 40–50% range. Near the end of this investigation it was found that the use of rhodium trifluoroacetate (8) improved the insertion yields to the more useful 70–80% range. The results are collected in Table 1.

The cyclic sulfones were readily characterized by their nmr spectra, which showed the C-1 hydrogen as a singlet at δ 4.95–5.25 ppm and the C-3 methylene group as an AB quartet centred near δ 4.4 ppm. When the diazosulfone bore an additional substituent at the benzylic carbon, for example a phenyl group, compound **8**, and entries 10 and 11 in Table 1, a 1:1.5 to 1:2 mixture of diastereomers of **9** was obtained as judged by the appearance of two sets of singlets near δ 5 and 4.4 ppm respectively, each set equal to 1H. The stereochemical assignment of the individual isomers was not made.

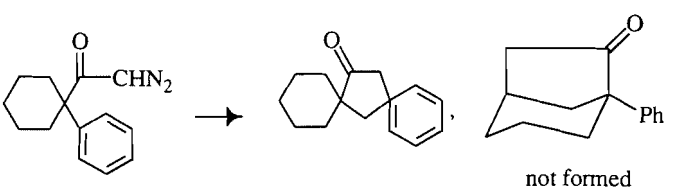


8 **9**

Inspection of Table 1 reveals that the aromatic C—H insertion is tolerant of an *ortho*-methyl or bromine, but not an *ortho*-methoxy substituent. In the former case, the rhodium carbenoid insertion would require a 7-membered ring transition state for aliphatic C—H insertion compared to a 6-membered ring for the aryl C—H insertion. Nakatani (9) has reported a preference for a formyl aryl C—H insertion when compared to insertion into an equidistant aliphatic C—H bond.

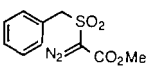
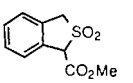
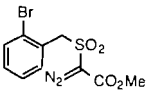
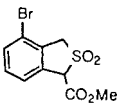
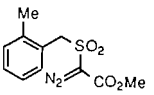
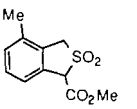
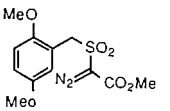
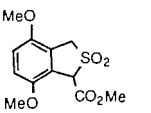
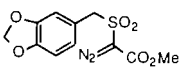
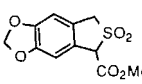
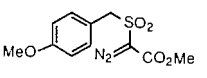
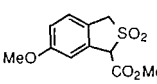
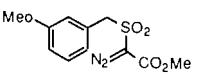
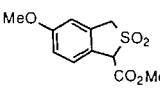
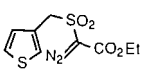
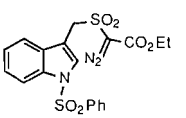
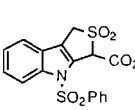
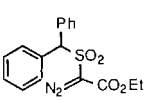
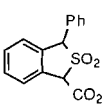
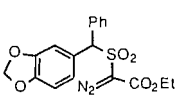
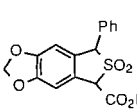
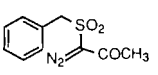
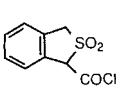
Reaction of the 2,5-dimethoxybenzyl substituted sulfone (entry 4, Table 1) led to a complex mixture (tlc) from which no pure product was isolated. A considerable amount of literature exists concerning the formation of oxygen ylids upon reaction of carbenes or carbenoids with ether oxygens (10). A variety of products are typically obtained from such intermediates.

The regiochemistry of the insertion reaction is predictable if one assumes an electrophilic characteristic for the rhodium carbenoid, coupled with a steric effect. The preference for



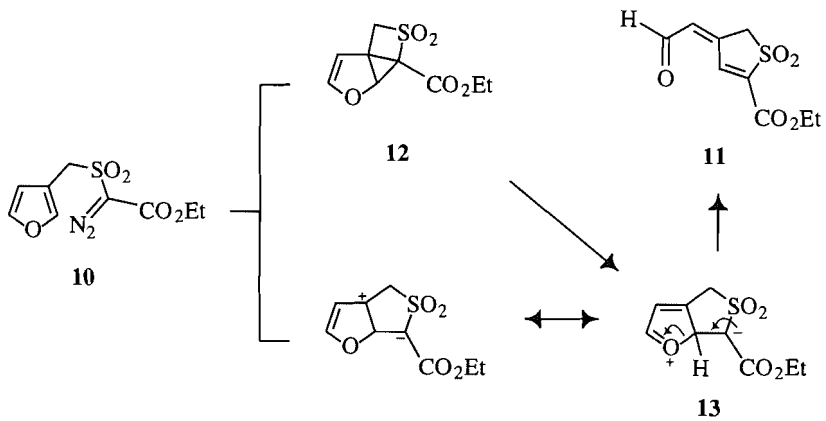
not formed

TABLE 1. Preparation of 1,3-dihydrobenzo[*b*]thiophene 2,2-dioxides

Entry	Diazo Compound	Product	Yield(%)
1			46
2			48
3			14
4			---
5			47
6			45
7			42
8			50
9			24
10			47
11			52,74[a]
12			56[a]

[a]Using rhodium trifluoroacetate.

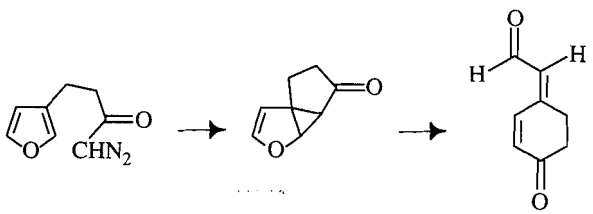
Can. J. Chem. Downloaded from www.nrcresearchpress.com by 41.223.56.140 on 09/07/12
For personal use only.



insertion into the more activated methylenedioxy substituted aryl ring as compared to a phenyl ring, i.e., conversion of **8** to **9**, is as expected. The aromatic insertion reaction is also applicable to the preparation of 2,5-dihydrothiophene sulfones fused onto the 2,3-position of thiophene and indole, see entries 8 and 9 in Table 1.

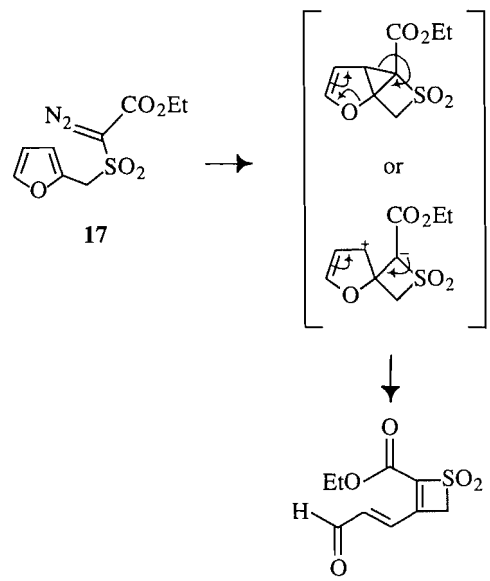
Attempts to extend the insertion reaction to furans failed. Thus the reaction of **10** with rhodium acetate in methylene chloride at room temperature for 2 h afforded the unsaturated aldehyde **11** in >95% crude yield. The nmr spectrum (200 MHz) (δ: 1.40, (t, J = 7 Hz, 3H), 4.24 (d, J = 1.3 Hz, 2H), 4.43 (q, J = 7 Hz, 2H), 6.30 (dd, J = 6, 1.3 Hz, 1H), 8.50 (s, 1H), 10.16 (d, J = 6 Hz, 1H)), was consistent with the assigned structure. The formation of this product is readily rationalized as resulting from either fragmentation of the strained cyclopropane intermediate **12** or, more directly, via the zwitterion **13**, which is due to an electrophilic attack of the carbenoid on the furan ring.

Padwa *et al.* (11) have obtained the unsaturated aldehyde **14** in 86% yield from the reaction of the diazoketone **15** with rhodium acetate. These authors have postulated the cyclopropane **16** as the intermediate in the conversion of **15** to **14**. Cyclopropanation products have been isolated from the intermolecular reaction of rhodium carbenoids with furans (12).



15 **16** **14**

Reaction of the diazo compound **17**, bearing a 2-furyl substituent, with $[Rh(OAc)_2]_2$ led to the formation of **18** as the only product after filtration of the reaction mixture and evaporation of the solvent. The 200-MHz nmr spectrum of this unusual product showed, in addition to the ethyl group, a 2H singlet at δ 4.81 assigned to the methylene group of the thiete sulfone ring, a doublet of doublets at δ 6.45 (J = 12, 6.3 Hz), a doublet δ 7.68 (J = 12 Hz), and a doublet at δ 10.16 (J = 6.3 Hz) due to the *trans*-α,β-unsaturated aldehyde unit. Attempts to purify either **11** or **18** via silica gel chromatography resulted in extensive decomposition. Two possible mechanisms for the formation of **18** are shown below. It is interesting to speculate whether cyclobutenones could be prepared from the keto analog of **17**.



Mechanistic aspects

A number of mechanistic possibilities can be proposed to explain the formal insertion products described in this paper. These include (*i*) the formation of an unstable norcaradiene intermediate, (*ii*) electrophilic attack on the carbenoid by the aromatic ring, and (*iii*) C—H insertion via a 6-membered metallocycle e.g., **19**.

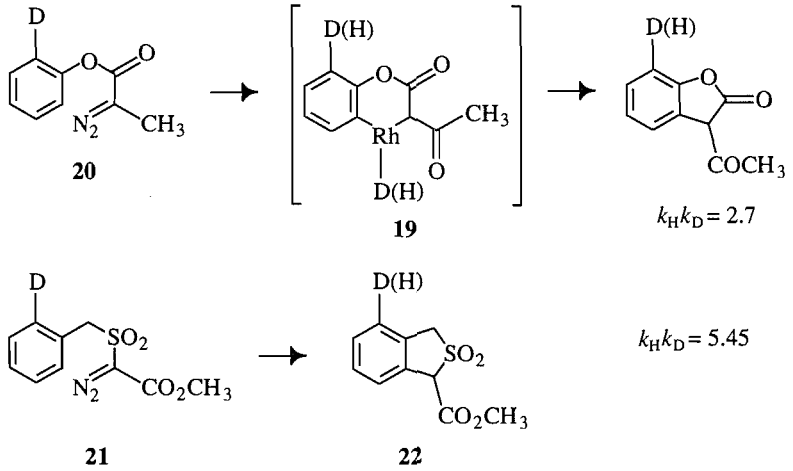
These aspects were considered in an earlier publication (13) dealing with the insertion reaction of the carbenoid derived from the diazo ester **20**. The observation of a significant isotope effect (k_H/k_D = 2.7) in that reaction indicated that the aromatic C—H bond was broken in the rate-determining step. This was interpreted as being most consistent with the aromatic C—H insertion process. A significant hydrogen–deuterium isotope effect (k_H/k_D = 5.45) has been observed for the diazo sulfone **21**.

1,3-Dianion chemistry in the thiopheen series (Compound **23**)

As mentioned in the introduction, the insertion products ought to be amenable to regio-controlled introduction of electrophilic reagents in the dihydrothiophene ring via mono- and 1,3-dianions such as **24** and **24***a*. These intermediates could indeed be generated by treatment of **23** in THF with one or two equivalents of *n*BuLi.

Thus, reaction of **24** with excess CH_3I afforded a 60% yield of **25**, while treatment of **24***a* with one equivalent of alkylating agent gave a mixture of diastereomers of **26** in 32% isolated

Can. J. Chem. Downloaded from www.nrcresearchpress.com by 41.223.56.140 on 09/07/12
For personal use only.



yield. The structures of these products were readily established by nmr spectroscopy. For example, **25** showed singlets for both the newly introduced methyl and the remaining methylene group α to the sulfone at δ 1.90 and 4.33 ppm, respectively, while **26** showed two methyl doublets near δ 1.66 ppm, and two methine singlets at δ 5.14 and 5.17 ppm (2:1 ratio) due to the hydrogen α to both the carboethoxy and the sulfone group; the remaining methine hydrogen in **26** overlapped with the methylene group of the ethyl ester.

Finally, reaction of **23** with 3 equivalents of *n*BuLi followed by 2 equivalents of CH_3I afforded the α,α-disubstituted products **27** (41%). The mass spectrum (CI) showed a small molecular ion at the expected $m/e = 274 + 1$ with the base peak at $M - 64$ due to facile extrusion of SO_2. The nmr spectrum of **27** (60 MHz) featured, in addition to the ethyl group, a 6H singlet (δ 1.67), a 1H singlet (δ 5.05), and two doublets at δ 6.88 and 7.43 ppm due to the remaining thiophene hydrogens. The formation of **27** presumably involves rapid initial monomethylation of **24***a* to **28**, dianion formation due to the third equivalent of *n*BuLi, and a further methylation at the more reactive α′ centre. The possibility that **27** is formed via an α,α,α′ trianion has been suggested by a referee but it is considered less likely by the authors.

Experimental

"Usual work-up" indicates that the reaction mixture was diluted with an appropriate volume of saturated NH_4Cl solution and extracted with ether or methylene chloride. The organic extracts were dried over anhydrous $MgSO_4$ and the solvent evaporated. The nmr spectra, unless stated otherwise, were recorded using a Varian EM 360 spectrometer in $CDCl_3$ solution. Chromatography was carried out using hexane – ethyl acetate solvent mixtures.

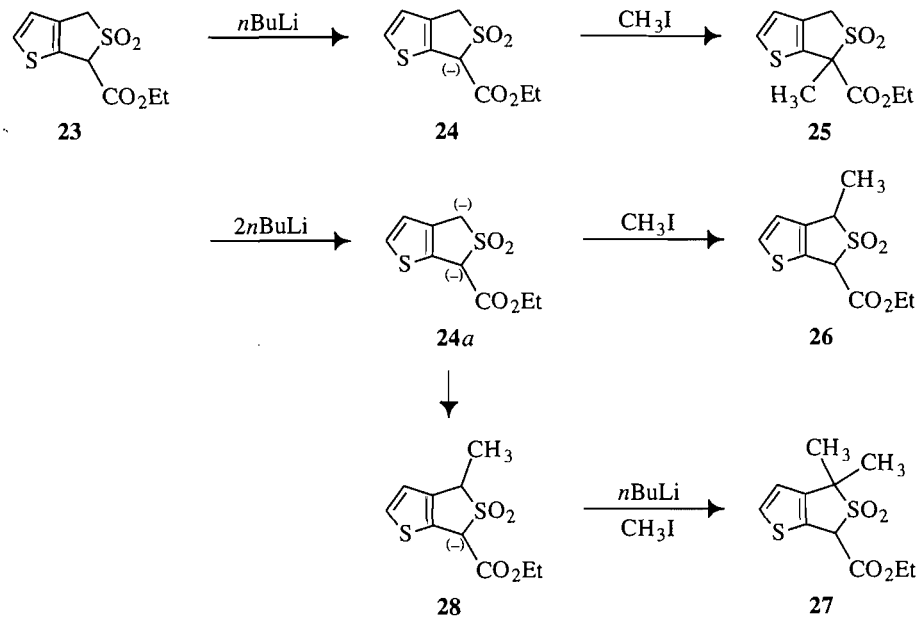
Preparation of benzylic sulfides. General procedures

Method A

To a solution of 1 equiv. of benzylic bromide in ethanol (4 mL/mmol) was added 1 equiv. of KOH dissolved in ethanol. The resulting solution was stirred under a nitrogen atmosphere for about 2 h. The reaction mixture was poured into an equal volume of saturated NaCl solution and extracted with ether. The ether layer was dried over $MgSO_4$ and the solvent evaporated to give crude sulfide (78–90%), of sufficient purity for subsequent manipulation.

Method B

To a solution of methyl or ethyl mercaptoacetate (1 equiv.) and benzylic alcohol (1 equiv.) in CH_2Cl_2 (2 mL/mmol of alcohol) under N_2 at room temperature was added 0.5 equiv. of powdered zinc iodide. The mixture was stirred for 45 min and then washed with water. The organic phase was dried over $MgSO_4$ and evaporated to give the crude benzylic sulfide. This material was filtered through a silica gel column



Can. J. Chem. Downloaded from www.nrcresearchpress.com by 41.223.56.140 on 09/07/12
For personal use only.

Can. J. Chem. Downloaded from www.nrcresearchpress.com by 41.223.56.140 on 09/07/12
For personal use only.

with 1:1 ethyl acetate – hexane to give 85–95% of sulfide of sufficient purity for further manipulation. The crude sulfides were characterized by their nmr spectrum. The key features were the CH_2 group α to the aromatic ring found in the δ 3.7–3.9 ppm range and the methylene group α to the ester at δ 2.9–3.1 ppm. Most of the ethyl esters of the following sulfides have been previously reported. The data for the non-ester nmr peaks agree closely with our data (14).

Mercaptobenzylacetone

Powdered KOH (23 mmol) was dissolved in 50 mL of ethanol under N_2. Benzyl mercaptan (21.3 mmol) was added, followed by chloroacetone (33 mmol). The reaction mixture was stirred for 30 min at room temperature and the solvent evaporated on a rotary evaporator. The residue was taken up in CH_2Cl_2 and the solution washed with 10% NaOH solution. Evaporation of the organic phase afforded 3.75 g (98%) of the title compound (15); nmr: 2.23 (s, 3H), 3.03 (s, 2H), 3.63 (s, 2H), 7.23 (s, 5H).

Oxidation of benzylic sulfides to the corresponding sulfones. General procedures

The crude or semipurified sulfides were oxidized to the corresponding sulfones using either 2 equiv. of MCPBA in CH_2Cl_2 at 0°C for 45 min (method A) or excess 30% H_2O_2 in acetic acid for 1–2 days (method B). Work-up consisted of washing the organic phase successively with 10% $Na_2S_2O_3$ and 5% $NaHCO_3$ solution, then drying and evaporating the resultant solutions. The sulfones were thus obtained in 60–90% yield. The sulfones were purified either by recrystallization and (or) by silica gel chromatography. Data concerning individual sulfones are given using the following format: entry number, relating to the table; preparation method, A or B; yield; mp (°C); chemical shift of the methylene groups α to the ester and aromatic rings.

1; A; 59%; 48–49; 3.73, 4.43 ppm
2; A; 68%; 90–91; 3.90, 4.70 ppm
3; A; 93%; 67–69; 3.83, 4.50 ppm
4; B; 77%; 91–92; 3.83, 4.38 ppm
5; B; 72%; 74–75; 3.86, 4.33 ppm
6; B; 72%; 68–69; 3.70, 4.36 ppm
7; A; 69%; oil; 3.72, 4.30 ppm
8; A; 60%; oil; 3.70, 4.50 ppm
9; A; 72%; oil; 4.00, 4.85 ppm
10; A; 73%; oil; 3.82, 5.53 ppm
11; A; 76%; oil; 3.87, 6.01 ppm
12; A; 92%; 63–64; 3.60, 3.00 ppm
13; 2-furyl-$CH_2SO_2CH_2COOEt$; A; oil; 3.80, 4.30 ppm
14; 3-furyl-$CH_2SO_2CH_2COOEt$; A; oil; 3.75, 4.38 ppm

Diazo transfer reactions

Method A

To a sulfone in dry ethanol (5 mL/mmol) cooled in an ice bath was added 1.2 equiv. of powdered KOH (A1), NaH using THF as the reaction solvent (A2), or triethylamine (A3), and then, dropwise, tosyl azide (1.1 equiv.) dissolved in a minimum quantity of ethanol or THF. The mixture was stirred at room temperature for 40 min and then evaporated to dryness. The residue was taken up in ether, washed with 10% KOH solution, and then worked up in the usual manner to afford the crude diazo compounds. These were further purified by chromatography on silica gel using 3:1 hexane – ethyl acetate as eluant.

Method B

To a solution of sodium methoxide in methanol (1 mmol/2 mL) was added an ice-cold solution of 1 equiv. of sulfone (1 mmol/2 mL) in methanol. The solution thus obtained was stirred for 5 min and treated with 1 equiv. of methyl formate, followed 5 min later by 1 equiv. of tosyl azide. The reaction mixture was stirred at room temperature for 2.5 h and the solvents were evaporated. Work-up of the product was carried out as in method A above. Data concerning the individual α-diazosulfones are given in the following format: entry number relating to the table; yield; mp (°C); chemical shift of the benzylic methylene singlet (ppm).

1; A1; 40%; oil; 4.53
2; A1; 15%; oil; 4.80
3; B; 52%; 63–68; 4.33
4; A1; 27%; 75–78; 4.40
5; A1; 18%; oil; 4.33
6; A1; 52%; oil; 4.43
7; B; 38%; oil; 4.46
8; A2; 33%; oil; 4.56
9; A2; 33%; oil; 4.78
10; A2; 27%; oil; 6.10
11; A2; 26%; oil; 6.00
12; A3; 51%; 85–86; 4.40
13; 2-furyl-$CH_2SO_2C(N_2)COOEt$; A2, 41.6%; oil; 4.66
14; 3-furyl-$CH_2SO_2C(N_2)COOEt$; A2; 43%; oil; 4.56

Rhodium carboxylate catalyzed cyclizations of the α-diazosulfones. General procedure

A solution of the diazo sulfone in dry CH_2Cl_2 (1 mmol/4 mL) was stirred at room temperature and treated with 5 mol% of rhodium acetate or rhodium trifluoroacetate in one portion. Gas evolution occurred slowly. The progress of the reaction was monitored by tlc. When the reaction was judged complete, the green solution was filtered through a cotton plug and the solvent was evaporated. The desired bicyclic sulfones were purified via silica gel chromatography. Yields refer to isolated, purified products. Data concerning these compounds are presented below according to the following format: entry number; mp (°C); hrms for the molecular ion peak unless otherwise indicated, calculated, found; chemical shift of methine singlet α to the ester at C-1, and the remaining hydrogens at C-3 (ppm). All compounds showed the expected ester peak near 1740 cm^{-1} and the symmetric sulfone stretching frequency near 1335 cm^{-1}.

1; oil; 240.0455, 240.0443; 5.0 (s, 1H) and 4.43 (s, 2H)
2; 127–128; 317.9559, 317.9559; 5.10 (s, 1H) and 4.42 (s, 2H)
3; 110–112; 240.0455, 240.0459; 5.16 (s, 1H) and 4.33 (d, J = 15.7 Hz, 1H)
5; 184–185; 270.0196, 270.0171; 4.90 (s, 1H), 4.22 (d, J = 15 Hz, 1H), and 4.43 (d, J = 15 Hz, 1H)
6; oil; 256.0403, 256.0410; 4.98 (s, 1H), 4.25 (d, J = 15 Hz, 1H), and 4.42 (d, J = 15 Hz, 1H)
7; 147–148; 256.0403, 256.0422; 4.90 (s, 1H), 4.27 (d, J = 15 Hz, 1H), and 4.47 (d, J = 15 Hz, 1H)
8; 92; (M − 64) 182.0402, 182.0406; 5.16 (s, 1H) and 4.36 (m, 2H)
9; 245; (M − $PhSO_2$) 278.04876, 278.0461; 6.59 (s, 1H) and 4.75 (d, J = 8 Hz, 2H)
10; 42; (M − 64) 252.1150, 252.1157; 5.19 (s, 1H) and 5.78 (s, 1H)
11; 74; (M − 64) 296.1048, 296.1047; 5.08 (s, 1H) and 5.64 (s, 1H)
12; oil; 210.0394, 210.0372; 5.25 (s, 1H), 4.51 (d, J = 15.7 Hz, 1H), and 4.39 (d, J = 15.7 Hz, 1H)

Reaction of the furan substituted diazo compounds with rhodium acetate

A solution of the diazosulfone **10** (260 mg, 10 mmol) in 10 mL of dry CH_2Cl_2 was stirred with $(Rh(OAc)_2)_2$ for 1 h. Thin-layer chromatographic analysis showed the absence of starting material and the formation of one major product. The reaction mixture was filtered through a cotton plug and the solvent was evaporated to afford 230 mg of crude unsaturated aldehyde **11**; nmr: (200 MHz) δ: 1.40 (t, J = 7 Hz, 3H), 4.24 (d, J = 1.3 Hz, 1H), 4.43 (q, J = 7 Hz, 2H), 6.37 (dd, J = 1.3 Hz, 1H), 8.50 (s, 1H), 10.16 (d, J = 6 Hz, 1H) ppm. Attempted chromatography on silica gel led to decomposition. The EI mass spectrum of **11** failed to show a molecular ion peak at m/e 230. The highest m/e peak occurred at M − OC_2H_5 = 185. A hrms of this peak gave 184.9943; calculated for $C_7H_5O_4S$: 185.0092.

The diazo sulfone **17** was treated as above for compound **10** with 20 mg of rhodium acetate. The crude product, 130 mg (81%) of **18** as a colorless oil, had nmr (200 MHz) peaks at δ 1.31 (t, J = 7 Hz, 3H),

4.30 (q, J = 7 Hz, 2H), 4.81 (s, 2H), 6.45 (dd, J = 12 Hz, 6.3 Hz, 1H), 7.68 (d, J = 12 Hz, 1H), and 10.16 (d, J = 6.3 Hz, 1H) ppm. Attempted further purification via silica gel column chromatography resulted in extensive decomposition.

Methylation of sulfone ***23***

(a) To a solution of 0.6 mmol of sulfone **23** in 12 mL of THF at −78°C was added 0.6 mmol of *n*BuLi, followed after 30 min by 0.6 mmol of CH_3I. The reaction mixture was stirred for 30 min at −78°C and then warmed to room temperature for 2 h prior to quenching with saturated NH_4Cl solution. The usual work-up followed by chromatography afforded 100 mg (64%) of the monomethyl derivative **25** as a colorless solid, mp 88°C.

(b) Sulfone **23** (0.28 mmol) was dissolved in THF at −78°C and reacted with 3.3 equiv. of *n*BuLi for 1 h at −78°C and 1 h at room temperature. The reaction mixture was recooled to −78°C and 0.62 mmol (2.2 equiv.) of CH_3I was added. The mixture continued to be stirred at −78°C for 30 min and then at room temperature for 1 h prior to quenching with saturated NH_4Cl solution. The usual work-up followed by chromatography afforded 35 mg (41%) of the 3,3-dimethyl derivative **27** as a colorless solid, mp 82°C; nmr δ: 1.4 (t, J = 7 Hz, 3H), 1.7 (s, 6H), 4.3 (q, J = 7 Hz, 2H), 5.1 (s, 1H), 6.68 (d, J = 6 Hz, 1H), 7.43 (d, J = 6 Hz, 1H); ms m/e (rel.%): 210 (M − 64) (49), 137 (100).

(c) To a THF solution of sulfone **23** (0.6 mmol) in THF at −78°C was added 2.2 equiv. of *n*BuLi. The anion-forming reaction was allowed to proceed for 30 min at −78°C and 1 h at room temperature; the resultant solution was reacted with 0.6 mmol of CH_3I for 20 min at −78°C and 1 h at room temperature. The usual work-up followed by chromatography afforded 56 mg (36%) of the methylated sulfone **26** as a mixture of isomers, mp 91°C.

1. M. D. Hrytsak, N. Etkin, and T. Durst. Tetrahedron Lett. **27**, 5679 (1986).
2. (*a*) T. Kametani and H. Nemoto. Tetrahedron, **37**, 3 (1981); (*b*) W. Oppolzer. J. Am. Chem. Soc. **93**, 3833 (1971).
3. J. L. Charlton and M. M. Alauddin. Tetrahedron, **43**, 2873 (1987).
4. (*a*) M. P. Cava and A. A. Deana. J. Am. Chem. Soc. **81**, 4266 (1959); (*b*) M. P. Cava, M. J. Mitchell, and A. A. Deana. J. Org. Chem. **25**, 1481 (1960); (*c*) K. C. Nicolaou, W. E. Barnette, and P. Ma. J. Org. Chem. **45**, 1463 (1980); (*d*) W. Oppolzer, D. A. Roberts, and T. G. C. Bird. Helv. Chim. Acta, **62**, 2017 (1979); (*e*) W. Oppolzer and D. A. Roberts. Helv. Chim. Acta, **63**, 1703 (1980).
5. T. Durst, E. Kozma, and J. L. Charlton. J. Org. Chem. **50**, 4829 (1985); J. L. Charlton and T. Durst. Tetrahedron Lett. **25**, 2663 (1984).
6. (*a*) M. P. Doyle. Chem. Rev. **86**, 919 (1986); (*b*) G. Mass. *In* Topics in current chemistry. Organic synthesis, reactions and mechanisms. Vol. 137. Springer Verlag, New York. 1987. p. 75.
7. M. Regitz. Synthesis, 351 (1972).
8. M. A. McKervey, D. N. Russell, and M. F. Twohig. J. Chem. Soc. Chem. Commun. 491 (1985).
9. K. Nakatani. Tetrahedron Lett. **28**, 165 (1987).
10. M. C. Pirrung and J. A. Werner. J. Am. Chem. Soc. **108**, 6060 (1986).
11. A. Padwa, T. J. Wisnieff, and E. J. Walsh. J. Org. Chem. **51**, 5036 (1986).
12. J. Adams and J. Rokach. Tetrahedron Lett. **25**, 35 (1984).
13. M. Hrytsak and T. Durst. J. Chem. Soc. Chem. Commun. 1150 (1987).
14. Y. Tamura. Synthesis, 326 (1984).
15. M. Brink. Tetrahedron Lett. **29**, 2753 (1971).

Can. J. Chem. Downloaded from www.nrcresearchpress.com by 41.223.56.140 on 09/07/12
For personal use only.

Some new Lycopodium alkaloids

WILLIAM A. AYER[1] AND GERTRUDE C. KASITU
Department of Chemistry, University of Alberta, Edmonton, Alta., Canada T6G 2G2

Received January 4, 1989

WILLIAM A. AYER and GERTRUDE C. KASITU. Can. J. Chem. **67**, 1077 (1989).

The alkaloids of the club moss *Lycopodium obscurum* L., collected in Northern Alberta, have been investigated. The known alkaloids lycopodine, lycodine, clavolonine, dihydrolycopodine, *O*-acetyldehydrolycopodine, flabelliformine, β-lofoline, lycofoline, and des-*N*-methyl-α-obscurine were isolated and identified, as were the known compounds des-*N*-methyl-β-obscurine and acrifolinol. α-Obscurine and β-obscurine were not detected. The structures of the previously unreported alkaloids hydroxypropyllycodine (**9***a*), lyconnotinol (**11***a*), lobscurinol (**19***a*), epilobscurinol (**19***b*), and acetyllobscurinol (**19***c*) are presented. Hydroxypropyllycodine (**9***a*) is the first 19-carbon Lycopodium alkaloid reported to date. Its possible biogenetic significance is discussed. The isolation of obscurinine (**14**) and isoobscurinine (**15**) are reported and the preparation of obscurinine (**15**) by treatment of lobscurine (**18**) with ammonia is described. It is suggested that obscurinine and isoobscurinine are artefacts produced during the isolation process.

Key words: alkaloids, Lycopodium alkaloids, obscurinine, *Lycopodium obscurum*, biogenesis.

WILLIAM A. AYER et GERTRUDE C. KASITU. Can. J. Chem. **67**, 1077 (1989).

On a étudié les alcaloïdes de lycopodes en massue, *Lycopodium obscurum* L., récoltés dans le nord de l'Alberta. On a isolé et identifié les alcaloïdes connus lycopodine, lycodine, clavolonine, dihydrolycopodine, *O*-acétyldéhydrolycopodine, flabelliformine, β-lofoline, lycofoline et des-*N*-méthyl-α-obscurine ainsi que la des-*N*-méthyl-β-obscurine et l'acrifolinol. Par ailleurs, on n'a pas détecté la présence des α- et β-obscurines. On a déterminé les structures des alcaloïdes suivants qui n'avaient pas été rapportés antérieurement : l'hydropropyllycodine (**9***a*), le lyconotinol (**11***a*), le lobscurinol (**19***a*), l'épilobscurinol (**19***b*) et l'acétyllobscurinol (**19***a*). L'hydroxypropyllycodine (**9***a*) est le premier alcaloïde du Lycopodium à 19 atomes de carbones à être rapporté. On discute de sa signification biologique éventuelle. On décrit aussi l'isolement des obscurinine (**14**) et isoobscurinine (**15**) ainsi que la préparation de l'obscurinine (**15**) par traitement de lobscurine (**18**) avec de l'ammoniac. On suggère que la présence de l'obscurinine et de l'isoobscurinine est due à un artefact résultant de la méthode d'isoler les produits.

Mots clés : alcaloïdes, alcaloïdes Lycopodium, obscurinine, *Lycopodium obscurum*, biogenèse.

[Traduit par la revue]

Introduction

The club moss *Lycopodium serratum* Thumb. has been used in Chinese traditional medicine in the treatment of myasthenia gravis and conditions of senile memory loss now recognized as symptoms of Alzheimer's dementia (AD) (1). The alkaloids huperzine A (**1**) and huperzine B (**2**), isolated from this plant (2), show pronounced anticholinesterase activity and are under clinical investigation in China for the treatment of myasthenia gravis and senile memory loss (1, 2). Another report of the use of a club moss in an AD-related disorder dates back to the late forties when powdered *L. selago* was investigated as a substitute for pilocarpine and eserine in treating glaucoma (3). *Lycopodium selago* is the source of the alkaloid selagine, which has been assigned structure **3** (4). In 1960 we reported the structures of α-obscurine (**4**) and β-obscurine (**5**), the first of the α-pyridone containing Lycopodium alkaloids (5). The obscurines (**4** and **5**) were first isolated in 1944 by Manske and Marion (6) from *L. obscurum* L. They also reported the presence of lycopodine (**6***a*) and three alkaloids designated L13, L16, and L17. In our earlier work on *L. obscurum* we isolated lycopodine (6), the obscurines (**4** and **5**), lycodine (**7**), and several other alkaloids (5). Because of the current interest in the α-pyridine alkaloids **1** and **2** we have recently reexamined the alkaloidal content of *L. obscurum*, which we collected in northern Alberta, to obtain more of the obscurines for pharmacological testing and to search for other pyridone-type alkaloids. During this study we have isolated several new alkaloids, which are the subject of this report.

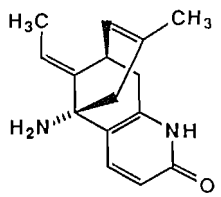
[1]Author to whom correspondence may be addressed.

Results and discussion

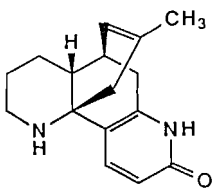
Finely ground *L. obscurum* was extracted with aqueous 2% tartaric acid (7). The extract was concentrated, washed with chloroform to remove neutral and acidic material, basified with aqueous ammonia, and extracted with ether and then chloroform. The combined extracts were examined by gas chromatography – mass spectrometry (gc–ms) (8), which revealed the presence of at least 20 components, the major ones being lycopodine (**6***a*), clavolonine (**6***b*), lycodine (**7**), and an unidentified compound $C_{17}H_{24}N_2O$ described below. Subsequent isolation of these compounds confirmed the gc–ms result. Surprisingly, no α- or β-obscurine was detected in the gc–ms scan and none was obtained during the isolation studies. Both des-*N*-methyl-α-obscurine (**4***b*) and des-*N*-methyl-β-obscurine (**5***b*) were, however, detected and isolated. Other known compounds detected and isolated include dihydrolycopodine, *O*-acetyldihydrolycopodine, flabelliformine (**6***c*), β-lofoline (**6***b* with carbonyl reduced to β-OH), lycofoline (**6***b* with carbonyl reduced to β-OH and containing $\Delta^{11,12}$ double bond), and flabellidine (**8**). The identity of the known compounds was established by direct comparison of spectral data with those obtained from authentic samples. Des-*N*-methyl-β-obscurine (**5***b*) has not previously been reported as a natural product, but has been prepared from β-obscurine (9).

The crude alkaloids from *L. obscurum* were first separated

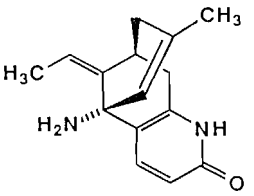
Can. J. Chem. Downloaded from www.nrcresearchpress.com by 41.223.56.140 on 09/07/12
For personal use only.



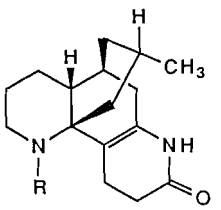
1



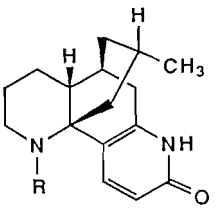
2



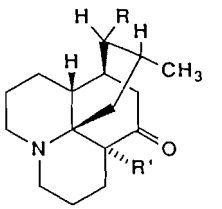
3



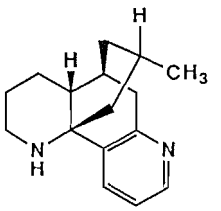
4*a* R = CH_3
4*b* R = H



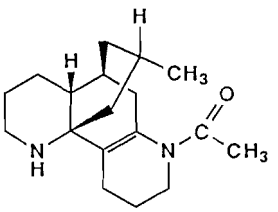
5*a* R = CH_3
5*b* R = H



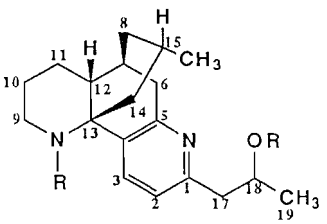
6*a* R = R' = H
6*b* R = OH, R' = H
6*c* R = H, R' = OH



7



8



6*a* R = H
6*b* R = Ac

into seven fractions by gradient (methanol in dichloromethane) elution chromatography over alumina. These fractions were further separated by elution chromatography over alumina, flash chromatography over silica gel, or preparative thin-layer chromatography (ptlc) over silica gel as described in the Experimental. Each of the new compounds is described below.

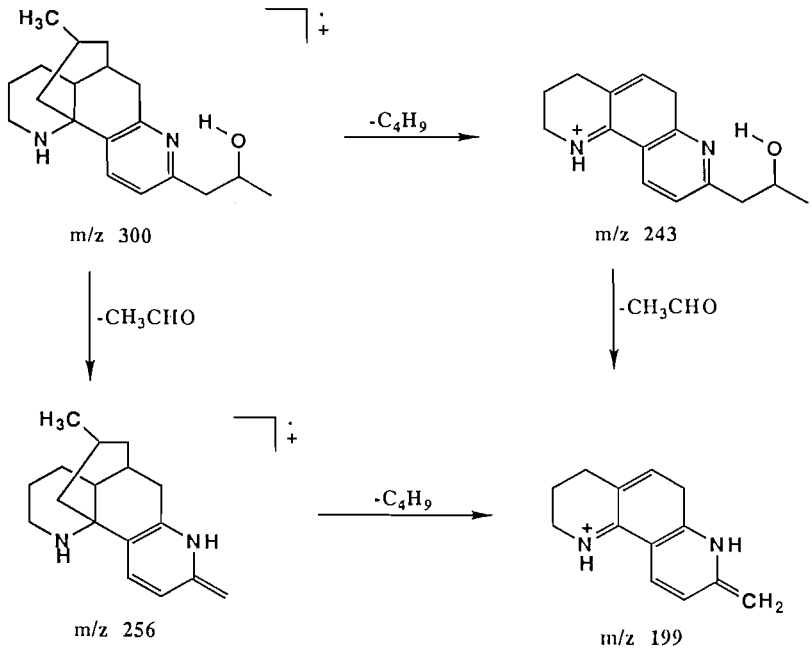
*Hydroxypropyllycodine (**9**a)*

This alkaloid was obtained as an opaque solid and was shown by high resolution electron impact mass spectrometry (hreims) and chemical ionization mass spectrometry (cims) to possess the molecular formula $C_{19}H_{28}N_2O$. The ultraviolet (uv) spectrum suggested the presence of a substituted pyridine ring (λ_{max} 272, 280 (sh) nm) and the ^{13}C nuclear magnetic resonance (nmr) spectrum showed that the ring was trisubstituted (δ 157.6 (s), 157.3 (s), 134.0 (d), 133.7 (s), 121.4 (d)). Comparison of the ^1H nmr and ^{13}C nmr spectra (see Table 1) of lycodine (**7**) and hydroxypropyllycodine (**9***a*) reveals many similarities. The presence of a 2-hydroxypropyl group in **9***a* is apparent from the ^1H nmr spectrum. On irradiation of the signal for the hydrogen (δ 4.21) *geminal* to the hydroxyl group, the non-equivalent *geminal* methylene hydrogens at δ 2.89 (dd, J = 15, 3 Hz) and 2.71 (dd, J = 15, 9 Hz) each collapse to a doublet (J = 15 Hz), while the methyl signal (δ 1.27, d, J = 6 Hz) collapses to a singlet. Comparison of the ^{13}C nmr spectrum of **9***a* with that of lycodine (**7**) reveals that the hydroxypropyl group is located at C-1. In lycodine, C-1 appears as a doublet at δ 147.0, while in **9***a* it appears as a singlet at δ 157.6. This is consistent with the observed coupling (J = 8 Hz) of the aromatic hydrogens, since in pyridines $J_{\alpha,\beta}$ is normally ca. 5 Hz, while $J_{\beta,\gamma}$ is 7–9 Hz (10). This also follows from a comparison of the uv spectra (lycodine (**7**) λ_{max} 268 nm, hydroxypropyllycodine 272 nm) since α substitution in pyridines causes a bathochromic shift, γ substitution a hypsochromic shift (11). Analysis of the COSY 90 spectrum of hydroxypropyllycodine provides further evidence for structure **9***a*. This reveals long range coupling between the hydrogens of the methylene group of the 2-hydroxypropyl group and H-2 and H-3. These are in turn coupled to the C-6 methylene hydrogens (δ 3.09 and 2.66), which are further coupled to H-7 (δ 2.06). H-7 is coupled to a pair of H's (C-8), which are both coupled to the hydrogen (H-15) that is coupled to the methyl group at δ 0.76. In a similar manner, H-7 may be traced through the C-12, C-11, and C-10 hydrogens to the downfield (δ 2.43, 2.27) hydrogens of the C-9 methylene group.

The hreims of hydroxypropyllycodine (**9***a*) (Scheme 1) shows the base peak at m/z 243 corresponding to the loss of the "bridging" carbons C-14, C-15, C-8, a common fragmentation pathway in related Lycopodium alkaloids (12). An ion at m/z 256 is due to the loss of acetaldehyde (McLafferty rearrangement) from the molecular ion, and a prominent peak at m/z 199 corresponds to the loss of both acetaldehyde and the bridging carbons, as illustrated in Scheme 1.

Acetylation (acetic anhydride – triethylamine) of hydroxypropyllycodine (**9***a*) gives the diacetyl derivative **9***b*, which shows both ester (1737 cm^{-1}) and amide (1656 cm^{-1}) absorption in the ir. Significant downfield shifts are observed in the ^1H nmr spectrum for the hydrogens at C-18 (δ 4.21 to δ 5.27) and C-9 (δ 2.77 and 2.43 to δ 3.03 and 2.91). A signal at δ 3.17 is assigned to the equatorial hydrogen at C-14. This signal appears as a broadened doublet (J = 12 Hz), which collapses to a sharp doublet when the hydrogen at C-15 (δ 1.18) is irradiated. We attribute the deshielding of this hydrogen to the anisotropic effect of the N-acetyl carbonyl group. In the ^{13}C nmr spectrum (Table 1), C-14 shows an upfield shift. The rela-

Can. J. Chem. Downloaded from www.nrcresearchpress.com by 41.223.56.140 on 09/07/12
For personal use only.



SCHEME 1

TABLE 1. The ^{13}C nmr spectra of lycodine (**7**), hydroxypropyllycodine (**9***a*), and diacetylhydroxylpropyllycodine (**9***b*) ($CDCl_3$, 100.6 MHz)

C	Multiplicity	Chemical shift (δ)		
		10	**36**	**37**
1	d	147.0	157.6(s)[a]	155.8(s)
2	d	121.6	121.4	121.8
3	d	133.4	134.0	134.8
4	s	136.2	133.7	132.6
5	s	158.9	157.3[a]	157.3
6	t	35.5	35.2	35.0
7	d	34.1	33.8	34.5
8	t	44.0	44.2	44.4
9	t	41.5	41.4	45.6[a]
10	t	26.4	26.2	25.8
11	t	28.2	28.0	27.4
12	d	45.0	44.7	43.9[b]
13	s	56.1	55.9	65.7
14	t	51.7	51.4	47.7[a]
15	d	26.0	25.9	26.5[c]
16	q	22.1	22.1	22.3
17	t		43.7	43.0[b]
18	d		67.1	70.8
19	q		23.1	26.4[c]
*C*O	s			172.6
*C*O	s			170.4
CH_3CO	q			21.2
CH_3CO	q			20.0

[a,b,c]Carbon assignments may be interchanged.

tive (and absolute) stereochemistry of hydroxypropyllycodine (**9***a*) is assumed to be the same as in lycodine (**7**). The stereochemistry at C-18 has not been assigned.

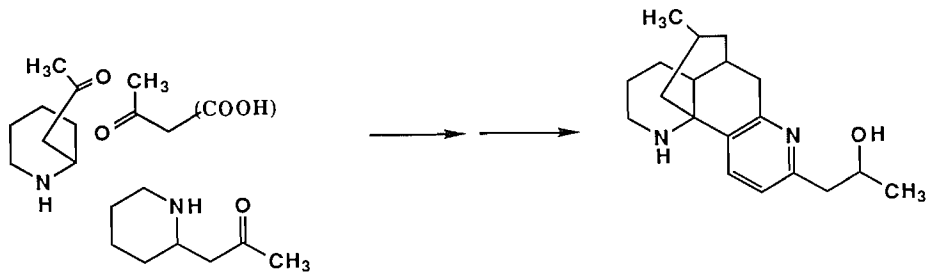
Hydroxypropyllycodine (**9***a*) is the first Lycopodium alkaloid encountered possessing a 19-carbon skeleton. The biogenetic origin of the Lycopodium alkaloids still is not completely clarified.[2] It has been shown that carbons 9–16 in lycopodine (**6***a*) and, by implication, lycodine (**7**) are derived from lysine and acetoacetate via pelletierine (**10**). Carbons 1–5 are derived from lysine and carbons 6, 7, and 8 from acetate, without the intermediacy of pelletierine (**10**) (13). As illustrated in Scheme 2, the 19-carbon skeleton of hydroxypropyllycodine can be constructed from two pelletierine units and one acetoacetate unit.

*Lyconnotinol (**11**a)*

This alkaloid was isolated by repeated chromatography of one of the more polar fractions from the initial separation. Lyconnotinol (**11***a*), $C_{16}H_{25}NO_2$, mp 173–175°C, is most easily separated from accompanying polar components in the form of the monoacetyl derivative **11***b*. Lyconnotinol (**11***a*) itself does not show a molecular ion in the hreims, although the protonated form of the molecular ion can be detected in the cims. Monoacetyllyconnotinol (**11***b*) does show a molecular ion in the hreims. The base peak in the mass spectra of both **11***a* and **11***b* occurs at *m/z* 190, corresponding to the ion **12** formed by loss (α-cleavage) of the four-carbon side chain. The ^1H nmr spectrum of monoacetyllyconnotinol (**11***b*) indicates the presence of an acetylated primary alcohol (δ 3.87 and 3.71, shifted from δ 3.43 and 3.28 in lyconnotinol itself), a secondary alcohol (δ 4.10), and three olefinic hydrogens (δ 6.20, 5.68, and 5.49). The uv spectrum (λ_{max} 235 nm) suggests a conjugated diene system. The ^1H nmr spectra and the ^{13}C nmr spectra (Table 2) of **11***a* and **11***b* are very similar to those of the known alkaloid lyconnotine (**13**) (14), except for the signals associated with C-8. Reduction of lyconnotine with lithium aluminum hydride gave the diol **11***a*, identical with the compound isolated from *L. obscurum*. The configuration at C-15 in lyconnotinol (**11***a*) has not been determined. Lyconnotinol (**11***a*) is only the second representative of this particular skeleton among the Lycopodium alkaloids, the other being lyconnotine (**13**).

[2]Reference 13 provides an informative and up to date summary of the biosynthetic studies and biogenetic theories in this field.

Can. J. Chem. Downloaded from www.nrcresearchpress.com by 41.223.56.140 on 09/07/12
For personal use only.



SCHEME 2

TABLE 2. The ^{13}C nmr spectra of lyconnotine (**13**),lyconnotinol (**11***a*), monoacetyllyconnotinol (**11***b*) ($CDCl_3$, 100.6 MHz)

C	Multiplicity	Chemical shift (δ)		
		13	**11***a*	**11***b*
1	t	48.2	47.7	48.0
2	t	25.8[a]	25.6[a]	26.0[a]
3	t	23.4[a]	22.8[a]	22.7[a]
4	d	47.5	48.0	48.3
5	d	69.4	69.2	69.3
6	t	35.4	34.6	34.8
7	d	123.0[b]	122.7[b]	122.9[b]
8		178.3(s)	69.0(t)	70.5(t)
9	t	49.3	49.7	49.8
10	d	124.7[b]	124.3[b]	124.6[b]
11	d	127.1[b]	128.4[b]	128.3[b]
12	s	136.8	138.0	137.6
13	s	56.1	56.2	55.9
14	t	27.6[a]	27.1[a]	26.8[a]
15	d	37.2	32.6	29.5
16	q	21.0	19.7	20.0
$COOCH_3$	q	51.2		
$COCH_3$	s			171.2
$COCH_3$	q			21.0

[a,b]Carbon assignments may be interchanged.

*Obscurinine (**14**)[3] and isoobscurinine (**15**)*

Obscurinine (**14**), $C_{17}H_{24}N_2O$, mp 128–130°C, and isoobscurinine, mp 106–107°C, have R_f values very similar to those of lycopodine (**6***a*) and lycodine (**7**), from which they were separated by flash chromatography over silica gel. Both compounds show cyclopentanone absorption in the ir (**14** at 1731 cm^{-1}, **15** at 1734 cm^{-1}) and in the ^{13}C nmr spectrum (**14**, δ 220.3; **15**, δ 220.6), but only **14** shows conjugated imine (233 nm) absorption (17) in the uv. The 2D COSY spectrum of isoobscurinine (**15**) shows the presence of two isolated spin systems, one for the C-9, C-10, and C-11 hydrogens similar to that in obscurinine (16), the other including C-1 to C-8 and C-14, C-16. The methylene hydrogens at C-14 (δ 3.00 and 2.92) are coupled to the olefinic hydrogen (δ 5.54) and the alkenic methyl hydrogens (δ 1.78). The olefinic hydrogen is in turn correlated with a methine hydrogen at δ 2.67 (H-7), which is coupled to the C-6 methylene hydrogens (δ 2.44 and 1.87). One of the C-6 H's shows a small (2 Hz) coupling to a hydrogen (C-4) at δ 3.81, and this in turn is coupled (3 Hz) to the C-3 methine hydrogen (δ 4.21), and so on to C-1. The ^{13}C nmr spectrum of **15** (Table 3) shows the expected similarities with (and differences from) that of obscurinine (**14**). Treatment of isoobscurinine (**15**) with warm 10% hydrochloric acid brings about isomerization to obscurinine (**14**).

The location of the imino nitrogen in obscurinine and isoobscurinine is not consistent with a biogenetic origin from lysine as is envisioned for the other dinitrogenous Lycopodium alkaloids (e.g., lycodine (**7**), cernuine (**16**), phlegmarine (**17**)) (13). It seemed possible that obscurinine (**14**) and isoobscurinine (**15**) are artefacts derived by addition of ammonia to an appropriate (e.g., **18**) fawcettimine-type precursor. To test this hypothesis, lobscurinol (**19***a*, structure *vide infra*) was oxidized to lobscurine (**18**). Treatment of a chloroform solution of **18** with aqueous ammonia led to the formation of obscurinine (**14**) in virtually quantitative yield. Since we had exhausted our supply of plant material, we have not yet been able to show that lobscurine (**18**) is present in *L. obscurum* and obscurinine (**14**) is not. However, the fact that lobscurinol (**19***a*) and epilobscurinol (**19***b*) are both isolated from the plant (*vide infra*), and since lobscurine (**18**) reacts readily with aqueous ammonia, we feel that obscurinine (**14**) may well be an artefact of the isolation process. Chandler and co-workers (15) also used aqueous ammonia in their study.

*Lobscurinol (**19**a), epilobscurinol (**19**b), and acetyllobscurinol (**19**c)*

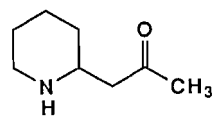
These three minor alkaloids are uv active and thus readily detected on tlc. Lobscurinol (**19***a*), the most abundant of the three, has an R_f very similar to that of the much more abundant β-lofoline and was obtained pure only after extensive chromatography. More lobscurinol (**19***a*) was obtained in the form of the much less polar naturally occurring acetyl derivative **19***c*. Epilobscurinol (**19***b*) is eluted from alumina after lobscurinol and is most readily purified as its acetyl derivative **19***d*.

The hreims spectrum of lobscurinol (**19***a*) indicated a molecular formula $C_{17}H_{25}NO_2$ and did not show the $M^+ - C_4H_9$ peak characteristic of the lycopodine and lycodine type alkaloids (12). The base peak appears at *m/z* 84, attributed to ion 20, similar to the case of paniculatine (**21**) (18). The oxygen atoms are present as a carbonyl (ir, 1658 cm^{-1}; ^{13}C nmr, δ 200.2 (s)) and a secondary hydroxyl (ir, 3400 cm^{-1}; ^{13}C nmr, δ 72.2 (d)) group. The ^{13}C nmr spectrum (Table 4) shows the presence of four other sp^2 carbons and the uv spectrum (λ_{max} 234 nm) is consistent with the α,β-unsaturated ketone. The ^1H nmr spectrum shows two olefinic hydrogens (δ 5.95 and 5.82), an allylic carbinyl hydrogen (δ 4.36), and two methyl groups (δ 2.33 ($N-CH_3$), δ 1.92 (alkenic methyl)). Analysis of the COSY 90 ^1H nmr spectrum again revealed an isolated spin

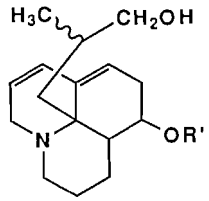
[3]During the course of our studies, Chandler and co-workers (15) reported the isolation and X-ray crystallographic structure determination of this compound, which they have named obscurinine. We independently arrived at the same structural assignment based on extensive nmr, ir, and uv studies. These studies are described in detail in ref. 16. We will present evidence herein that obscurinine is probably an artefact formed during the isolation process.

Can. J. Chem. Downloaded from www.nrcresearchpress.com by 41.223.56.140 on 09/07/12
For personal use only.

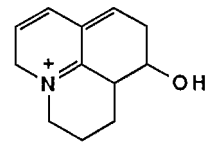
Can. J. Chem. Downloaded from www.nrcresearchpress.com by 41.223.56.140 on 09/07/12
For personal use only.



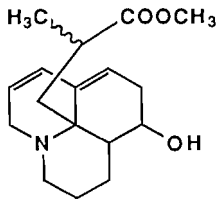
10



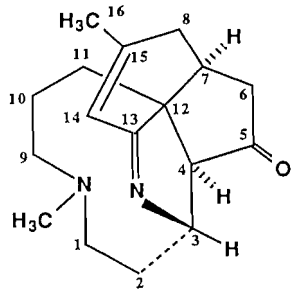
11*a* R = R' = H
11*b* R = Ac, R' = H
11*c* R = R' = Ac



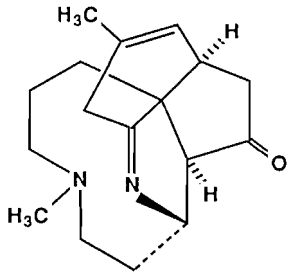
12



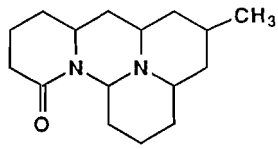
13



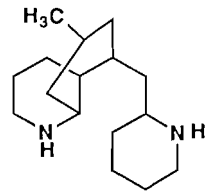
14



15



16



17

TABLE 3. The ^{13}C nmr spectra of obscurinine (**14**) and isoobscurinine (**15**) ($CDCl_3$, 100 MHz)

	Chemical shift (δ)	
C	**14**	**15**
5	220.3(s)	220.6(s)
13	175.6(s)	178.5(s)
15	146.7(s)	131.9(s)
14	119.1(d)	36.1(t)
3	76.8(d)	75.9(d)
4	61.1(d)	61.2(d)
12	60.9(s)	61.8(s)
9	58.8(t)	58.4(t)
1	48.2(t)	47.0(t)
17	44.3(q)	44.2(q)
6	43.4(t)	44.9(t)
7	39.8(d)	46.3(d)
11	34.5(t)	34.7(t)
8	31.1(t)	122.8(d)
2	30.3(t)	30.0(t)
10	24.0(t)	24.2(t)
16	23.8(q)	23.2(q)

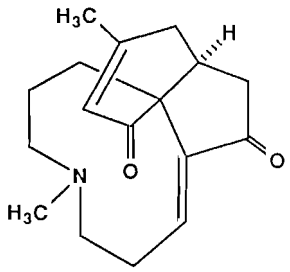
system corresponding to carbons 9, 10, and 11 and another correlating H-14 with the alkenic methyl and on through the C-8 hydrogens all the way to C-2 as summarized in Fig. 1.

The relative stereochemistry at C-5 in lobscurinol (**19***a*) is assigned on the basis of extensive decoupling of ^1H nmr spectra and by nOe difference spectroscopy. The hydrogen at C-5 appears as a doublet of doublets ($J_{3,5}$ = 1 Hz, $J_{5,6\beta}$ = 5 Hz, $J_{5,6\alpha}$ = 0 Hz). The chemical shifts of the C-6 hydrogens (Fig. 1) were established by the 2D COSY experiment mentioned above.

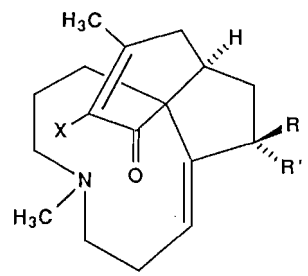
The α and β assignments[4] are based on the observed coupling constants, i.e., the hydrogen showing the large *vicinal* coupling (13 Hz) with H-7 is assigned as *antiperiplanar* to H-7. It is this hydrogen at C-6 which shows the 5-Hz coupling with H-5 (dihedral angle approaching 0°). In the nOe experiment, irradiation of H-5 causes a 9% enhancement of H-6β, no enhancement of H-6α. Acetylation of lobscurinol (**19***a*) afforded acetyllobscurinol (**19***c*), identical with the naturally occurring compound. The ^1H nmr spectral data obtained for **19***a* and **19***c* are very similar to those reported for lycoplegmarine (**19***e*) and acetyllycoplegmarine (19).

Epilobscurinol (**19***b*) was obtained in very small amounts (~1 mg), and was characterized as its acetyl derivative **19***d*. The hreims spectrum of acetylepilobscurinol is very similar to that of **19***c*. The ^1H nmr spectrum of **19***d* is remarkably similar to that of **19***c* except for the signals associated with H-5. This signal appears slightly downfield (δ 5.45 vs. 5.40) from that in acetyllobscurinol (**19***c*) and shows *vicinal* coupling with both C-6 hydrogens (7 Hz, 7 Hz), allylic coupling (2 Hz) with H-3, and W plan coupling (3 Hz) with H-7, consistent with its α-orientation. Due to the limited availability of **19***d*, the ^{13}C nmr spectrum was not obtained.

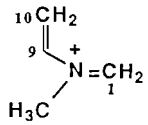
[4]Substituents on the same side as the C-13, C-14 bond are arbitrarily designated β, those on the opposite side are designated α.



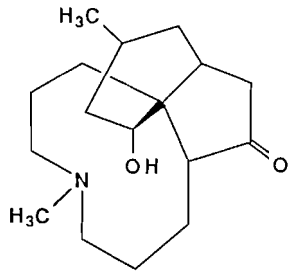
18



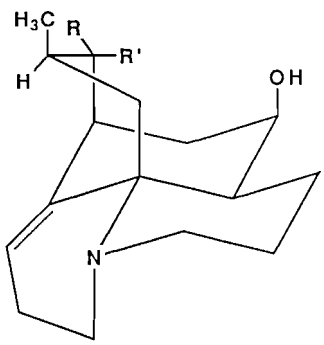
19*a* R = H, R' = OH, X = H
19*b* R = OH, R' = H, X = H
19*c* R = H, R' = OAc, X = H
19*d* R = OAc, R' = H, X = H
19*e* R = H, R' = OH, X = OCH_3



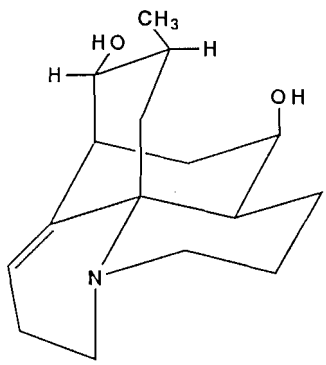
20



21



22 R = H, R' = OH
24 R = R' = carbonyl



23

Acrifolinol (22)

The fractions containing lyconnotinol (**11***a*) afforded two minor, isomeric alkaloids, acrifolinol (**22**) and the known alkaloid lycofoline (**23**). To the best of our knowledge, acrifolinol (**22**), a reduction product of acrifoline (**24**) (20) has not been reported previously as a natural product. To confirm the structural assignments, acrifoline (**24**) was reduced with sodium borohydride in the presence of sodium hydroxide (21) to give the C-15 epimers, acrifolinol (**22**) and lycofoline (**23**).

Experimental

High resolution electron impact mass spectra (hreims) were recorded on an AEI MS-50 mass spectrometer coupled to a DS-50 computer. Data are reported as *m/z* (formula, relative intensity). Unless diagnostically significant, peaks with intensities less than 20% of the base peak are omitted. Chemical ionization mass spectra (cims) were recorded on an AEI MS-12 mass spectrometer with ammonia as the reagent gas. Gas chromatography – mass spectra (gc–ms) were recorded on a Varian Vista 600 equipped with a mass spectrometry detector 7070E. Fourier transform infrared (ftir) spectra were recorded (thin film cast from $CHCl_3$ solution unless otherwise noted) on a Nicolet FT 7199 interferometer. Ultraviolet (uv) spectra were recorded on a Hewlett Packard 8450A or a Unicam SP 1700 spectrophotometer. Optical rotations were recorded on a Perkin Elmer 141 polarimeter. The ^1H and ^{13}C nuclear magnetic resonance (nmr) spectra were measured (in $CDCl_3$ unless otherwise noted) on Bruker WH-200, WH-300, WH-360, or WH-400 spectrometers. Chemical shifts are reported in parts per million (δ value) from tetramethylsilane (TMS). For ^1H nmr, residual $CHCl_3$ in $CDCl_3$ was employed as the internal standard (assigned as 7.26 ppm downfield from TMS). For ^{13}C nmr, $CDCl_3$ was employed as the internal standard (assigned as 77.0 ppm downfield from TMS). Melting points are uncorrected and were measured on a Zeitz–Wetzlar or a Thomas model 40 melting point apparatus.

Reagent grade solvents were distilled prior to use. Skellysolve B refers to Skelly Oil Company light petroleum, bp 62–70°C. Analytical grade diethyl ether was used without further purification. Pyridine was distilled from NaOH and stored over NaOH. Acetic anhydride was dried over P_2O_5 and distilled over sodium acetate.

Woelm (activity III/20 mm) and Brockman (activity I and II) neutral alumina were used for column chromatography. E. Merck silica gel 60 (230–400 mesh) was used for flash column chromatography. Pharmacia Sephadex LH20 and G10 were used for gel filtration chromatography. Analytical thin-layer chromatography (tlc) was carried out on silica gel precoated tlc plates (E. Merck DC-Alufolien, Kieselgel 60 F-254 0.2 mm thickness) and on alumina precoated tlc plates (E. Merck DC-Alufolien, Aluminumoxide 60 F-254 neutral type E 0.2 mm thickness). The chromatograms were examined under ultraviolet light (254 or 350 nm). Visualization was completed by spraying with Dragendorf's reagent (solution A: 1.7 g of basic $Bi(NO_3)_3 \cdot 5H_2O$ in 100 mL of water:acetic acid, 4:1; solution B: 40 g of KI in 100 mL of water; spray solution: 20 mL of solution A, 5 mL of solution B, and 70 mL of water) or by dipping in a 3% phosphomolybdic acid solution (3 g of $20MoO_3 \cdot 2H_3PO_4 \cdot 48H_2O$, 0.5 g of $H_4Ce(SO_4)_4$ in 100 mL of 3% (v/v) sulphuric acid).

Molecular formulae were established by hreims. Each new compound reported gave a single spot on tlc on both alumina and silica gel and showed no spurious peaks in the ^1H and ^{13}C nmr spectra.

Plant collection and extraction

Lycopodium obscurum was collected in September and October at

TABLE 4. The ^{13}C nmr spectra of lobscurinol (**19***a*), acetyllobscurinol (**19***c*), and lobscurinine (**18**) ($CDCl_3$, 100 MHz)

		Chemical shift (δ)		
C	Multiplicity	**19***a*	**19***c*	**18**[c]
13	s	200.2	199.8	198.7
15	s	157.1	156.4	156.9
4	s	146.9	141.7	139.7
3	d	132.0	135.5	142.0
14	d	124.8	124.8	125.0
5	d	74.2	77.1	202.9(s)
12	s	58.3	57.5	57.1
9	t	57.0[a]	56.1	54.4[a]
1	t	56.3[a]	53.9	54.7[a]
17	q	48.3	47.7	47.6
7	d	38.4	38.1	35.2
6	t	37.3	35.5	41.3
8	t	30.3[b]	30.5[a]	29.8[b]
11	t	30.0[b]	29.8[a]	28.9[b]
2	t	29.9[b]	28.5[a]	28.9[b]
10	t	25.6	25.5	25.5
16	q	24.3	24.2	24.5
			170.6(s, $COCH_3$)	
			21.5(q, $COCH_3$)	

[a,b]Carbon assignments may be interchanged.
[c]Spectrum obtained at 75 MHz.

Can. J. Chem. Downloaded from www.nrcresearchpress.com by 41.223.56.140 on 09/07/12
For personal use only.

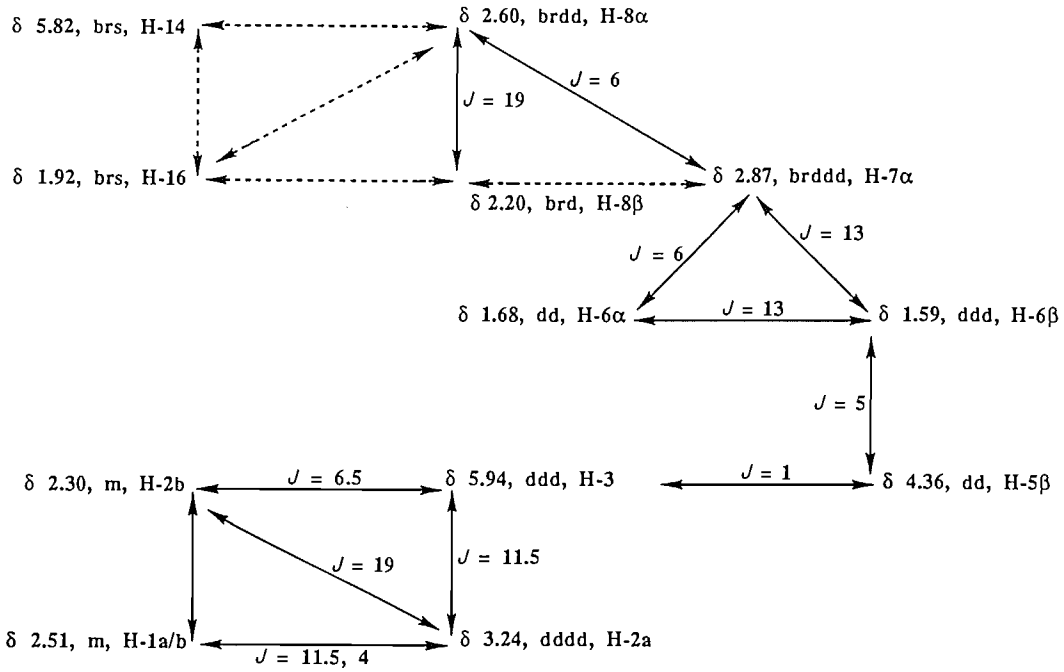


FIG. 1. ^1H–^1H chemical shift correlations obtained from the COSY 90 spectrum of lobscurinol (**19***a*). Chemical shifts in δ values, coupling constants (*J*) in Hz. Full arrows indicate measurable couplings, broken arrows indicate correlations where coupling constants were too small to be measured.

Pine Tree campgrounds, Fox Creek, Alberta, and 125 km south of Grande Prairie, Alberta, off forestry road 734. Specimens (nos. 91186, 92370, 92311) have been deposited in the herbarium, Department of Botany, University of Alberta. The whole plant was air-dried for three weeks, ground (Wiley mill), and suspended in 2% aqueous tartaric acid contained in 4-L Erlenmeyer flasks fitted with stopcocks at the bottom. Each flask contained 1 L aqueous tartaric acid and 0.5 kg ground plant. The mixture was stirred at room temperature for 24 h. The suspension was allowed to settle, the solution drained and then filtered. The extraction was repeated three times; then the clarified aqueous solution was concentrated to half volume *in vacuo* at 50°C. A white solid (negative to Dragendorf reagent) was removed by filtration and the filtrate was washed with chloroform (3×) and made basic to pH 11) with aqueous ammonia. The basic solution was extracted with ether and then chloroform. Each of the ether and chloroform layers were washed with water, dried ($MgSO_4$), and concentrated. The two extracts were combined to give the crude alkaloids (4.29 g from 4.7 kg plant material).

Isolation and characterization of the new alkaloids[5]

The crude alkaloid mixture (5.1 g) was partitioned into seven fractions by chromatography over neutral alumina (Woelm, 400 g) using methanol in dichloromethane as the eluant: fraction A, 0.3% methanol (0.5 L), 2.42 g; B, 0.5% methanol (0.5 L), 0.78 g; C, 1.0% methanol (1 L), 0.17 g; D, 1.0% methanol (1 L), 0.76 g; E, 2.0% methanol (1 L), 0.20 g; F, 3% methanol (0.5 L), 0.24 g; G, 5% methanol (1 L), 20% methanol (1 L), 0.43 g.

*Hydroxypropyllycodine (9*a)

Fraction D (0.60 g) was chromatographed over neutral alumina (100 g) eluting with 0.2, 0.5, 1.0, and 2.0% methanol in dichloromethane. The fraction that eluted with 1% methanol was subjected to ptlc over silica gel (eluent 3% methanol in ether saturated with ammonia). Hydroxypropyllycodine (**9***a*) was obtained as an opaque solid: $[\alpha]_D$ +11° (*c* 0.39, methanol); λ_{max} nm (log ε): 272 (3.7), ca. 280 (shoulder); ftir ν_{max} cm^{-1}: 3320 (br, NH and OH), 1650, 1590, 1570; ^1H nmr (see Table 5); ^{13}C nmr (see Table 1); hreims: *m/z* calcd. for $C_{19}H_{28}N_2O$: 300.2203; found: 300.2199 (19, M^+), 285 (2), 256 ($C_{17}H_{24}N_2$, 3), 243 ($C_{15}H_{19}N_2$, 100), 199 ($C_{13}H_{15}N_2$, 19), 171 (4).

*Acetylation of hydroxypropyllycodine (9*a)

Hydroxypropyllycodine (**9***a*, 2 mg), Ac_2O (1 mL), and Et_3N (5 drops) were stirred at room temperature overnight. Excess Ac_2O was decomposed by dropwise addition of water, the solvent was evaporated azeotropically with benzene *in vacuo*, and the residue was purified by preparative tlc (silica gel: 1% methanol in ethyl acetate – ammonia vapours; alumina: ethyl acetate:Skellysolve B, 1:4) to afford **9***b* (ca. 2 mg): ftir ν_{max} cm^{-1}: 1737, 1656, 1242; ^1H nmr (Table 5); ^{13}C nmr (Table 1); cims: *m/z* 385 (100 M^+ + 1); hreims: *m/z* calcd. for $C_{23}H_{32}N_2O_3$: 384.2415; found: 384.2405 (71, M^+), 341 (100), 327 (13), 325 (74), 324 (26), 298 (21), 285 (15), 267 (58), 225 (35).

*Acetyllyconnotinol (11*b)

A 1:1 mixture (by ^1H nmr, 3 mg) of lyconnotinol (**11***a*) and an unidentified alkaloid was obtained by chromatography of fraction F over alumina (eluent 2% methanol in CH_2Cl_2) followed by ptlc over silica gel (3% CH_3OH in CH_2Cl_2 saturated with ammonia). The mixture was acetylated (acetic anhydride, overnight at room temperature) and purified by filtration through alumina (pipette) in ethyl acetate to give monoacetyllyconnotinol (**11***b*) (1.5 mg). Additional material was obtained by similar treatment of other fractions from the chromatography of fraction F. A total of 5 mg of monoacetyllyconnotinol (**11***b*) was obtained as a viscous liquid from fraction F: ftir ν_{max} cm^{-1}: 3200 (OH), 2810, 2720, 2660 (Bohlmann bands), 1736, 1247, 1214, 1162, 1097, 1060, 1033; uv (ethanol) λ_{max} nm (log ε): 234 (3.72); ^1H nmr (400 MHz): 6.20 (1H, brd, *J* = 10 Hz, H-11), 5.68 (1H, brddd, *J* = 10, 5, 2 Hz, H-10), 5.49 (1H, t, *J* = 4 Hz, H-7), 4.10 (1H, ddd, 7.5, 3.4, 3.3 Hz, H-5 eq), 3.87 (1H, dd, *J* = 10.6, 5.2 Hz, H-8a), 3.71 (1H, dd, *J* = 10.5, 7 Hz, H-8b), 3.20 (1H, brd, *J* = 18 Hz, H-9 eq), 3.09 (1H, brdd, *J* = 18, 5 Hz, H-9 ax), 2.79 (1H, brddd, *J* = 20, 7.5, 4 Hz, H-6 ax), 2.68 (1H, ddd, *J* = 11.5, 11.5, 4.4 Hz, H-1 ax), 2.58 (1H, dt, *J* = 11.5, 2, 2 Hz, H-1 eq), 2.27 (1H, brd, *J* = 20.4 Hz, H-6 eq), 2.04 (3H, s, CH_3CO_2-), 1.98 (3H, m, H-15), 1.80–1.66 (6H, m), 1.52 (1H, brdm, *J* = 15 Hz, H-3a), 1.38 (1H, brd, 3.3, -O*H*), 0.89 (1H, d, *J* = 7 Hz); ^{13}C nmr: see Table 2; hreims: *m/z* calcd. for $C_{18}H_{27}NO_3$: 305.1992; found: 305.1988 (0.6, M^+), 190 (100), 172 (3), 144 (3).

[5]A complete description of the isolation of all of the alkaloids, including the identification of the known compounds, may be found in ref. 16.

Can. J. Chem. Downloaded from www.nrcresearchpress.com by 41.223.56.140 on 09/07/12
For personal use only.

Can. J. Chem. Downloaded from www.nrcresearchpress.com by 41.223.56.140 on 09/07/12
For personal use only.

TABLE 5. The ^{1}H nmr data[a] for **9***a*, **9***b*, **14**, **15**, **19***a*, **19***b*, and **19***c*

	Compound						
Hydrogen	**9***a*	**9***b*	**14**	**15**	**19***a*	**19***b*	**19***c*
1	—	—	2.54 (ddd, 13.5, 13.5, 3)	2.59 (brddd, 14, 14, 3.5)	[b]	[b]	[b]
			1.90 (ddd, 13.5, 3, 3)	2.04–1.82 (m)	[b]	[b]	[b]
2	6.96 (d, 8)	7.00 (d, 8)	1.99 (dddd, 13.5, 13.5, 3. 3)	2.04–1.82 (m)	3.24 (dddd, 19, 11.5, 11.5, 4)	3.37 (dddd, 17, 11.5, 11.5, 2)	3.25 (dddd, 17, 11.5, 11.5, 2)
			1.96 (m)	2.04–1.82 (m)	2.56–2.51 (m)	[b]	[b]
3	7.71 (d, 8)	7.49 (d, 8)	4.19 (brs, $W_{1/2}$ 8)	4.21 (br, $W_{1/2}$ 7)	5.94 (ddd, 11.5, 6, 5, 1)	6.02 (brddd, 11.5, 6.5, 1)	5.79 (ddd, 11.5, 7, 2)
4	—	—	3.32 (brs, $W_{1/2}$ 3)	3.81 (brt, 3)	—	—	
5	—	—			4.36 (dd, 5, 1)	5.40 (brd, 5)	5.45 (dddd, 7, 7, 3, 2)
6	3.09 (dd, 19, 7)	3.17 (brdd, 11.9, 7)	2.25 (ddd, 16.5, 7.5, 2)	2.44 (ddd, 18, 8, 2)	1.68 (dd, 13, 6)	[b]	[b]
	2.66 (d, 19)	2.65 (d, 19)	1.97 (dd, 16.5, 13.5)	1.87 (dd, 18, 12)	1.59 (ddd, 13, 13, 5)	[b]	[b]
7	2.06 (m)	2.13 (m)	2.43 (ddd, 13.5, 13.5, 3)	2.67 (brsext, 6)	2.87 (brddd, 13, 6, 6)	2.87 (brddd, 11.5, 7. 7)	[b]
8	1.77 (brd, 12)	1.71 (brd, 13)	2.66 (brddq, 20, 7.5, 1)	5.54 (brs, $W_{1/2}$ 10)	2.60 (brdd, 19, 6)	2.68–2.56 (m)	[b]
	1.33 (dddd, 12, 12, 4, 1)	1.38–1.25 (m)	2.12 (brd, 20)		2.20 (brd, 19)	2.18 (brd, 20)	[b]
9	2.77 (dm, 12)	3.60 (brdq, 14.5, 2)	2.29 (ddd, 12, 4, 2)	2.31 (brddd, 12, 3, 3)	2.96 (ddd, 14, 11.5, 3)	3.09 (brddd, 14, 11.5, 4)	2.98 (brdd, 13.5, 13.5)
	2.43 (dddd, 12, 12, 3, 1)	2.63 (ddd, 14.5, 11, 4)	2.13 (m)	2.27–2.11 (m)	2.31–2.25 (m)	[b]	[b]
10	1.60–1.46 (m)	1.65–1.55 (m)	1.55–1.40 (m)	1.66–1.49 (m)	1.73 (m)	[b]	[b]
	1.60–1.46 (m)	1.65–1.55 (m)	1.55–1.40 (m)	1.66–1.49 (m)	1.60 (m)	[b]	[b]
11	1.27–1.17 (m)	1.38–1.25 (m)	2.18 (m)	2.27–2.11 (m)	1.85 (ddd, 15, 8, 2)	[b]	[b]
	1.27–1.17 (m)	1.18 (m)	1.55–1.40 (m)	1.66–1.49 (m)	2.31–2.25 (m)	[b]	[b]
12	1.60–1.46 (m)	1.38–1.25 (m)	—	—	—	—	—
14	1.43 (ddd, 12, 3.5, 2)	3.17 (brd, 12)	6.26 (brs)	3.00 (brd, 19)	5.82 (brs, $W_{1/2}$ 5)	5.82 (brs, $W_{1/2}$ 5)	5.85 (brs, $W_{1/2}$ 5)
	1.13 (dd, 12, 11)	1.79 (dd, 13, 12)		2.92 (brd, 19)	—	—	—
15	1.28–1.17 (m)	1.18 (m)	—	—	—	—	—
16 (3H)	0.78 (d, 6)	0.82 (6.5)	1.85 (brs)	1.78 (brs)	1.92 (brs)	1.96 (brs)	1.92 (s)
Other	2.89 (dd, 15, 3)	3.03 (dd, 14, 8)	2.20 (s, N-CH_3)	2.21 (s, N-CH_3)	2.33 (s, N-CH_3)	2.35 (s, N-CH_3)	2.34 (s, N-CH_3)
	2.71 (dd, 15, 3)	2.91 (dd, 14, 6)				2.02 (s, $COCH_3$)	2.02 (s, $COCH_3$)
	4.21 (ddq, 9, 3, 6)	5.27 (ddq, 8, 6, 6)					
	1.27 (d, 6)	1.27 (d, 6)					
		2.23 (s, $COCH_3$)					
		1.95 (s, $COCH_3$)					

[a]Shift (δ), (multiplicity, *J*(Hz), in $CDCl_3$ at 400 MHz).
[b]Could not be assigned.

Can. J. Chem. Downloaded from www.nrcresearchpress.com by 41.223.56.140 on 09/07/12
For personal use only.

Acetyllyconnotinol (**11***b*) was further characterized as its crystalline methiodide, mp 192–193°C (from acetone).

Reduction of lyconnotine (13) to lyconnotinol (11a)

Lyconnotine (**13**) (119 mg) and $LiAlH_4$ (117 mg) in dry ether (10 mL) were heated under reflux for 4 h. Excess $LiAlH_4$ was decomposed by careful addition of acetic acid in ether, the mixture was diluted with ether, and filtered. The filtrate was diluted with water (5 mL), the ether and aqueous layers were separated, and the aqueous layer was extracted with chloroform (3 × 10 mL). The combined ether and chloroform extracts were concentrated *in vacuo*, then filtered through alumina (2% methanol in chloroform) to afford lyconnotinol (**13**) (100 mg). Lyconnotinol crystallizes from methanol–acetone as off-white prisms, mp 173–175°C; $[\alpha]_D$ +103° (*c* 0.43, methanol); uv (ethanol) λ_{max} nm (log ε): 235 (3.72); ftir ν_{max} cm^{-1}: 3340 (br, OH), 3027, 3013, 3006 (olefinic CH), 2880, 2824, 2789, 2773, 2763, 2747 (Bohlmann bands), 1642, 1099, 1081, 1062, 1033; ^1H nmr (400 MHz): 6.19 (1H, brd, *J* = 10 Hz, H-11), 5.71 (1H, brdd, *J* = 10, 5 Hz, H-10), 5.49 (1H, t, *J* = 4 Hz, H-7), 4.09 (1H, brs, $W_{1/2}$ = 16 Hz, H-5 eq), 3.43 (1H, dd, *J* = 10.4, 5 Hz, H-8a), 3.28 (1H, dd, *J* = 10.4, 6.3 Hz, H-8b), 3.23 (1H, brd, *J* = 18 Hz, H-9 eq), 3.12 (1H, brdd, *J* = 18, 5 Hz, H-9 ax), 2.80 (1H, brdd, *J* = 20, 7, 4 Hz, H-6 ax), 2.74 (1H, ddd, *J* = 12, 12, 4.5 Hz, H-1 ax), 2.58 (1H, brd, *J* = 12 Hz, H-1 eq), 2.27 (1H, brd, *J* = 12 Hz, H-6 eq), 1.93–1.66 (7H, m), 1.52 (1H, brdm, *J* = 15 Hz, H-3a), 1.45 (1H, brs, OH), 0.90 (3H, d, *J* = 6.4 Hz, H-16); ^{13}C nmr: see Table 2; cims: *m/z* 264 (100, M^+ + 1); hreims: *m/z* calcd. for $C_{16}H_{25}NO_2$: 263.1887 (not observed); 190 ($C_{12}H_{16}NO$, 100), 172 ($C_{12}H_{14}N$, 3), 144 ($C_{10}H_{10}N$, 3).

Acetylation of lyconnotinol (11a)

Lyconnotinol (84 mg), Ac_2O (10 mL), and Et_3N (5 drops) were stirred at room temperature for 15 h. Excess Ac_2O was decomposed with water and most of the solvent was removed by azeotropic distillation with benzene *in vacuo*. The mixture was diluted with water (10 mL), made basic (10% NaOH), and extracted with chloroform (5 × 10 mL). The organic solution was concentrated *in vacuo* and separated by chromatography over alumina (Skellysolve B:ethyl acetate, 1:1) into 3 fractions **a**–**c** containing diacetyllyconnotinol (**11***c*) (8 mg), a mixture of mono and diacetyllyconnotinol (58 mg), and monoacetyllyconnotinol (18 mg), respectively. Fraction **b** was separated by preparative tlc (3% methanol in ethyl acetate saturated with ammonia vapours) to afford **11***b* and **11***c* (50 mg and 3.8 mg, respectively). Monoacetyllyconnotinol (**11***b*) thus obtained is identical with the sample from natural sources. Diacetyllyconnotinol (**11***c*): ftir ν_{max} cm^{-1}: 2800, 2720, 2660 (Bohlmann bands), 1737, 1248, 1238, 1086, 1061, 1034; ^1H nmr (400 MHz): 6.17 (1H, brd, *J* = 10 Hz, H-11), 5.70 (1H, brdd, *J* = 10, 5 Hz), 5.48 (1H, t, *J* = 4 Hz, H-7), 5.17 (1H, dd, *J* = 7.9, 4.2 Hz, H-5 eq), 3.87 (1H, dd, *J* = 10.7, 5.2 Hz, H-8a), 3.72 (1H, dd, *J* = 10.7, 6.8 Hz, H-8b), 3.19 (1H, brd, *J* = 19 Hz, H-9 eq), 3.10 (1H, brdd, *J* = 19, 5 Hz, H-9 ax), 2.86 (1H, ddd, *J* = 21, 7.9, 5 Hz, H-6 ax), 2.64 (1H, ddd, *J* = 12, 12, 4 Hz, H-1 ax), 2.57 (1H, brd, *J* = 12 Hz, H-1 eq), 2.21 (1H, brd, *J* = 21 Hz, H-6 eq), 2.06 (3H, s, CH_3CO_2-), 2.05 (3H, s, CH_3CO_2-), 1.94–1.84 (2H, m), 1.79–1.63 (5H, m), 0.92 (3H, d, *J* = 6.7 Hz, H-16). The methiodide melts at 176–177°C (from acetone–ether).

Obscurinine (14) and isoobscurinine (15)

The portion of fraction D eluted with 0.5% methanol (see isolation of hydroxypropyllycodine above) was separated by flash chromatography (eluent acetone–CH_2Cl_2 (1:1)) to give lycopodine (**6***a*), isoobscurinine (**15**, 4 mg), and obscurinine (**14**, 85 mg). *Isoobscurinine* (**15**) crystallizes from Skellysolve B – acetone as off-white plates, mp 106–107°C; $[\alpha]_D$ +107° (*c* 1.1, methanol); ftir ν_{max} cm^{-1}: 2964, 2924, 2853, 2838, 2786 (Bohlmann bands) 1734, 1649, 1605; ^1H nmr: see Table 5; ^{13}C nmr: see Table 3; hreims: *m/z* calcd. for $C_{17}H_{24}N_2O$: 272.1890; found: 272.1888 (100, M^+), 271 (5), 257 (15), 189 (5), 173 (20), 172 (21), 98 (36), 84 (51), 72 (66), 71 (64), 70 (30), 58 (88), 57 (30).

Obscurinine (**14**) crystallizes from Skellysolve B – acetone as off-white plates, mp 128–130°C (lit. (15) mp 124–125.2°C); $[\alpha]_D$ +242° (*c* 0.5, methanol); uv (ethanol) λ_{max} nm (log ε): 233 (4.0); ftir ν_{max} cm^{-1}: 3029, 3006 (CH, olefinic), 2963, 2944, 2936, 2912, 2838, 2809, 2801, 2792, 2765, 2719, 2708 (Bohlmann bands), 1733, 1646, 1627, 1603; ^1H and ^{13}C nmr: see Tables 5 and 3; cims: *m/z* 273 (100, M^+ + 1); hreims: *m/z* calcd. for $C_{17}H_{24}N_2O$: 272.1890; found: 272.1886 (100, M^+), 271 (3), 257 (15), 189 (10), 172 (10), 98 (18), 84 (34), 72 (61), 71 (62), 70 (22), 58 (39), 57 (18).

Obscurinine (14) from lobscurinol (19a)

Lobscurinol (1.8 mg) dissolved in dichloromethane (0.2 mL) was added to a suspension of pyridinium chlorochromate (5 mg) in dichloromethane (0.4 mL) at 0°C. The mixture was stirred at 0°C for 30 min, then warmed to room temperature for 3 h. The reaction mixture was filtered through a pipette containing alumina and washed with chloroform. The organic solution was evaporated under reduced pressure to afford *lobscurinine* (**18**) (1 mg); ftir ν_{max} cm^{-1}: 1722, 1663, 1643; ^1H nmr (400 MHz): 6.95 (1H, dd, *J* = 11.7, 7.3 Hz, H-3), 5.92 (1H, brs, $W_{1/2}$ = 5.6 Hz, H-14), 3.33 (1H, dddd; *J* = 14, 11.7, 11.7, 2 Hz, H-2), 2.35 (3H, s, -NCH_3), 2.23 (1H, d, *J* = 17.3 Hz, H-8β), 1.98 (3H, s, H-16), 1.83 (1H, ddd, *J* = 15.2, 6.6, 2.5 Hz); ^{13}C nmr: see Table 4; cims: *m/z* 274 (100, M^+ + 1); hreims: *m/z* calcd. for $C_{17}H_{23}NO_2$: 273.1730; found: 273.1721 (13, M^+), 258 (34), 190 (5), 85 (20), 84 (100), 70 (14), 57 (50). A few drops of aqueous NH_3 were added to lobscurinine (**18**) dissolved in a minimum amount of chloroform. The mixture was stirred at room temperature overnight. Concentration under reduced pressure gave a single compound, identified (^1H nmr, ir, tlc) as obscurinine (**14**), in quantitative yield.

Lobscurinol (**19***a*) (2 mg) was obtained as a colourless oil from fraction E by chromatography (alumina, methanol in dichloromethane, 0.5% to 1%) and further purification by two successive preparative tlc's (methanol in dichloromethane 3% and 5%, atmosphere of ammonia); ftir ν_{max} cm^{-1}: 3600–3200 (br, OH), 1658; ^1H nmr: see Table 5; ^{13}C nmr: see Table 4; hreims: *m/z* calcd. for $C_{17}H_{25}NO_2$: 275.1887; found: 275.1881 (17, M^+), 192 (20), 85 (21), 84 ($C_5H_{10}N$, 100), 83 (22), 58 (28), 57 (44).

Epilobscurinol (19b)

Relatively pure epilobscurinol (**19***b*) (1 mg) was obtained from fraction E where it eluted after lobscurine (**19***a*, see above). It was further purified by preparative tlc (5% methanol in dichloromethane, atmosphere of ammonia), and then transformed to its acetyl derivative **19***d*. The acetylation (Ac_2O–pyridine) product was purified by preparative tlc (3% methanol in dichloromethane, atmosphere of ammonia); ^1H nmr: see Table 5; hreims: *m/z* calcd. for $C_{19}H_{27}NO_3$: 317.1992; found: 317.1991 (47, M^+), 302 (5), 258 (68), 215 (23), 85 (20), 84 ($C_5H_{10}N$, 100), 83 (21), 70 (25), 58 (57), 57 (37).

Acetyllobscurinol (19c)

Acetyllobscurinol (**19***c*) (3.5 mg) was obtained as a colourless opaque solid from fraction D by flash chromatography (acetone:dichloromethane, 1:4, 1:1, and 1% methanol in dichloromethane presaturated with ammonia) and by preparative tlc (3% methanol in ether in an atmosphere of ammonia); $[\alpha]_D$ +110° (*c* 0.16, methanol); uv (ethanol) λ_{max} nm (log ε): 234 (3.3); ftir ν_{max} cm^{-1}: 2956, 2925, 2854, 1735, 1659, 1240; ^1H and ^{13}C nmr: see Tables 5 and 4; cims: *m/z* 318 (100, M^+ + 1); hreims: *m/z* calcd. for $C_{19}H_{27}NO_3$: 317.1992; found: 317.1985 (18, M^+), 274 (5), 258 ($C_{17}H_{24}NO$, 100), 257 (8), 215 (39), 84 (38), 83 (10), 70 (12), 58 (39), 57 (21).

Des-N-methyl-β-obscurine (5b)

Trituration of fraction G left a residue (70 mg) that was purified by flash chromatography over silica gel (eluent 3% CH_3OH in CH_2Cl_2 saturated with ammonia) to give des-*N*-methyl-β-obscurine (**5***b*); mp 290–293°C; $[\alpha]_D$ −34° (*c* 0.21, methanol); ^1H nmr (400 MHz): 7.57 (1H, d, *J* = 9 Hz, H-3), 6.44 (1H, d, *J* = 9 Hz, H-2), 2.91 (1H, brdd, *J* = 19, 7 Hz, H-6 ax), 2.76 (1H, dm, *J* = 13 Hz, H-9 eq), 2.43 (1H, brddd, *J* = 13, 13, 2 Hz, H-9 ax), 2.40 (1H, brd, *J* = 19 Hz, H-6 eq), 2.10 (1H, brsext, *J* = 3 Hz, H-7 eq), 1.70 (1H, brdm, *J* = 12 Hz, H-8 eq), 1.60–1.35 (5H, m, H-12, H-14 eq, 2 H-10, H-15), 1.30–1.20 (3H, m, H-8 ax, 2 H-11), 1.03 (1H, dd, *J* = 11, 11 Hz, H-14 ax), 0.80 (3H, d, *J* = 6.5 Hz, H-16); hreims: *m/z* calcd. for $C_{16}H_{22}N_2O$: 258.1734; found: 258.1733 (14, M^+), 201 (100). The spectra (ir, ^1H and ^{13}C nmr) were identical with those of an authentic sample (9).

*Des-*N*-methyl-α-obscurine (4b)*

An uv-active material (1.3 mg), showing a single spot on tlc, was obtained from the chromatography described above and was identified (gc–ms) as a mixture of lobscurinol and des-*N*-methyl-α-obscurine. The mixture was acetylated (excess Ac_2O, 5 drops Et_3N, overnight). The reaction mixture was concentrated *in vacuo* and separated by preparative tlc (3% methanol in dichloromethane) to afford acetyllobscurinol (**19***b*) and acetyl des-*N*-methyl-α-obscurine (**4**, R = Ac); ^{1}H nmr (400 MHz): 6.49 (1H, brs, $W_{1/2}$ = 9 Hz, N*H*), 3.64 (1H, brd, J = 13.5 Hz), 3.14 (1H, brd, J = 10 Hz), 2.70 (1H, brddd, J = 13.5, 12, 3 Hz), 2.13 (3H, s, -NCOC*H*$_3$), 2.08 (1H, m, H-15), 1.92 (1H, brs, $W_{1/2}$ = 14 Hz), 0.91 (3H, d, J = 6.5 Hz); hreims: *m/z* calcd. for $C_{18}H_{26}N_2O_2$: 302.1996; found: 302.1997 (39, M^+), 245 (100). The spectra (ir, nmr) were identical with those of an authentic sample (9).

Acrifolinol (22) and lycofoline (23)

These alkaloids were obtained from fraction F after several chromatographic separations (16). They were compared with samples that were prepared from acrifoline (**24**) in the following manner: acrifoline hydrobromide (57 mg) and sodium borohydride (0.12 g) were added to a solution of sodium hydroxide (0.5 g) in 80% aqueous ethanol (10 mL). The reaction mixture was heated under reflux for 2 h, excess $NaBH_4$ was destroyed by the dropwise addition of acetic acid, and most of the alcohol was removed at the pump. The residue was diluted with water, basified (10% NaOH), and extracted with chloroform. The products were separated by ptlc (eluent 5% methanol in ether, atmosphere of ammonia) to give acrifolinol (**22**, 19 mg) and lycofoline (**23**, 6 mg), identical with the alkaloids isolated from *L. obscurum*.

Acknowledgements

We acknowledge with thanks the financial support provided by the Natural Sciences and Engineering Research Council of Canada. We also thank Drs. L. M. Browne and M. Kamada, Mrs. Anna Szenthe, and other members of our research group for help in collecting the plant material. We thank Dr. R. F. Chandler for a preprint of ref. 15, and Dr. D. B. MacLean for a sample of flabellidine.

1. Y. E. Wang, D. X. Yue, and X. C. Tang. Acta Pharmacol. Sin. **7**, 109 (1986).
2. J. S. Liu, Y. L. Zhu, C. M. Yu, Y. Z. Zhou, Y. Y. Han, F. W. Wu, and B. F. Qi. Can. J. Chem. **64**, 837 (1986).
3. Merck Index. 10th ed. Merck Co., Inc., Rahway, NJ. 1983. p. 1212.
4. Z. Valenta, H. Yoshimura, E. F. Rogers, M. Ternbah, and K. Wiesner. Tetrahedron Lett. No. 10, 26 (1960).
5. W. A. Ayer and G. G. Iverach. Can. J. Chem. **38**, 1823 (1960).
6. R. H. F. Manske and L. Marion. Can. J. Res. B, **22**, 53 (1944).
7. R. H. Burnell, B. S. Mootoo, and D. R. Taylor. Can. J. Chem. **38**, 1927 (1960).
8. R. V. Gerard and D. B. MacLean. Phytochemistry, **25**, 1143 (1986).
9. W. A. Ayer, J. A. Berezowsky, and G. G. Iverach. Tetrahedron, **18**, 567 (1962).
10. L. M. Jackman and S. Sternhell. Applications of nuclear magnetic resonance in organic chemistry. 2nd ed. Pergamon Press, Oxford. 1969. p. 307.
11. H. E. Podall. Anal. Chem. **29**, 1423 (1957).
12. D. B. MacLean. Can. J. Chem. **41**, 2654 (1963).
13. D. B. MacLean. *In* The alkaloids. Vol. 26. *Edited by* A. Brossi. Academic Press, New York. 1985. pp. 290–294.
14. F. A. L. Anet, M. Z. Hag, N. H. Khan, W. A. Ayer, R. Hayatsu, S. Valverde-Lopez, P. Deslongchamps, W. Riess, M. Ternbah, Z. Valenta, and K. Wiesner. Tetrahedron Lett. No. 14, 751 (1964).
15. T. Hu, R. F. Chandler, and A. W. Hansen. Tetrahedron Lett. **28**, 5993 (1987).
16. G. C. Kasitu. Ph.D. Thesis, University of Alberta, Edmonton, Alberta. 1988.
17. A. I. Scott. Interpretation of ultraviolet spectra of natural products. Pergamon Press, London. 1964. p. 27.
18. M. Castillo, G. Morales, L. Loyola, I. Singh, C. Calvo, H. Holland, and D. B. MacLean. Can. J. Chem. **54**, 2900 (1976).
19. Y. Inubushi and H. Harayama. Chem. Pharm. Bull. **29**, 3418 (1981).
20. G. S. Perry and D. B. MacLean. Can. J. Chem. **34**, 1189 (1956).
21. F. A. L. Anet, M. Ahmad, and N. H. Khan. Can. J. Chem. **40**, 236 (1962).

Can. J. Chem. Downloaded from www.nrcresearchpress.com by 41.223.56.140 on 09/07/12
For personal use only.

Binuclear phthalocyanines with aromatic bridges

HERMAN LAM, SEBASTIAN M. MARCUCCIO, POLINA I. SVIRSKAYA, SHAFRIRA GREENBERG, A. B. P. LEVER, AND CLIFFORD C. LEZNOFF[1]

Department of Chemistry, York University, 4700 Keele Street, North York, Ont., Canada M3J 1P3

AND

RONALD L. CERNY

Midwest Center for Mass Spectrometry, University of Nebraska–Lincoln, Lincoln, NE 68558, U.S.A.

Received September 14, 1988

HERMAN LAM, SEBASTIAN M. MARCUCCIO, POLINA I. SVIRSKAYA, SHAFRIRA GREENBERG, A. B. P. LEVER, CLIFFORD C. LEZNOFF, and RONALD L. CERNY. Can. J. Chem. **67**, 1087 (1989).

Three different binuclear phthalocyanines were prepared and characterized. Two of the binuclear phthalocyanines are cofacially linked by rigid naphthalene and anthracene spacers, while the third consists of a direct linkage between two phthalocyanine rings. The dicobalt, dicopper, and dizinc derivatives were prepared by inserting the metal into the metal-free species. The synthesis and the physical and spectroscopic properties of the precursor bisphthalonitriles are also included.

Key words: phthalocyanines, cofacial, binuclear, bisphthalonitriles.

HERMAN LAM, SEBASTIAN M. MARCUCCIO, POLINA I. SVIRSKAYA, SHAFRIRA GREENBERG, A. B. P. LEVER, CLIFFORD C. LEZNOFF et RONALD L. CERNY. Can. J. Chem. **67**, 1087 (1989).

On a préparé et caractérisé trois phtalocyanines binucléaires différentes. Deux d'entre elles sont liées d'une façon cofaciale par le biais de noyaux naphtalène et anthracène qui agissent comme rondelle d'espacement; dans le cas de la troisième, il s'agit d'un lien direct entre deux cycles phtalocyanines. On a préparé les dérivés comportant deux atomes de cobalt, de cuivre ou de zinc en insérant les métaux dans des espèces ne contenant pas de métal. On décrit aussi la synthèse ainsi que les propriétés physiques et spectroscopiques des bisphtalonitriles qui sont les précurseurs des phtalocyanines.

Mots clés: phtalocyanines, cofacial, binucléaire, bisphtalonitriles.

[Traduit par la revue]

Can. J. Chem. Downloaded from www.nrcresearchpress.com by 41.223.56.140 on 09/07/12
For personal use only.

The use of porphyrins and phthalocyanines in electrocatalysis has been the subject of intensive research (1).

Four-electron reductions of oxygen to water using cofacial dicobalt porphyrins have been reported by different groups of researchers (2, 3). The cofacial structures have been achieved either by using a cyclophane type of framework (2) or by covalently linking two porphyrins on rigid spacers, via the 1,8-positions of anthracene and biphenylene (3). Some of these binuclear porphyrins are sensitive to light, oxygen, or both (2). To overcome this problem, we have synthesized metal-free binuclear phthalocyanines covalently linked by one (4), two (5), four (5), five (6), and "−1" (7) atom bridges and some of their metallated derivatives. In general these phthalocyanines are very stable towards light and oxygen. The dicobalt derivatives of these binuclear phthalocyanines catalyze the two-electron reduction of oxygen to hydrogen peroxide but the four-electron process has not been observed (8). The lack of a permanent cofacial interaction between the two phthalocyanine rings may be one of the reasons for not achieving the goal of a four-electron reduction. We wished to prepare phthalocyanine derivatives analogous to the cofacial porphyrins that catalyze the four-electron reduction of oxygen to water. Methods were developed to link phthalonitrile units to rigid spacer molecules to form the bridging bisnitriles, which can be converted to binuclear phthalocyanines.

We report herein the synthesis of three examples of binuclear phthalocyanines and their dicobalt, dicopper, and dizinc derivatives. In the direct linked binuclear phthalocyanines, the two phthalocyanine rings are joined as two phenyl groups in biphenyl derivatives, while in the cofacial systems the two phthalocyanine rings are linked via the 1,8-positions of naphthalene (9) and anthracene. With these new binuclear phthalocyanines, we have now synthesized a series of binuclear phthalocyanines in which the covalent bridging linkages range from five to "−1" atoms.

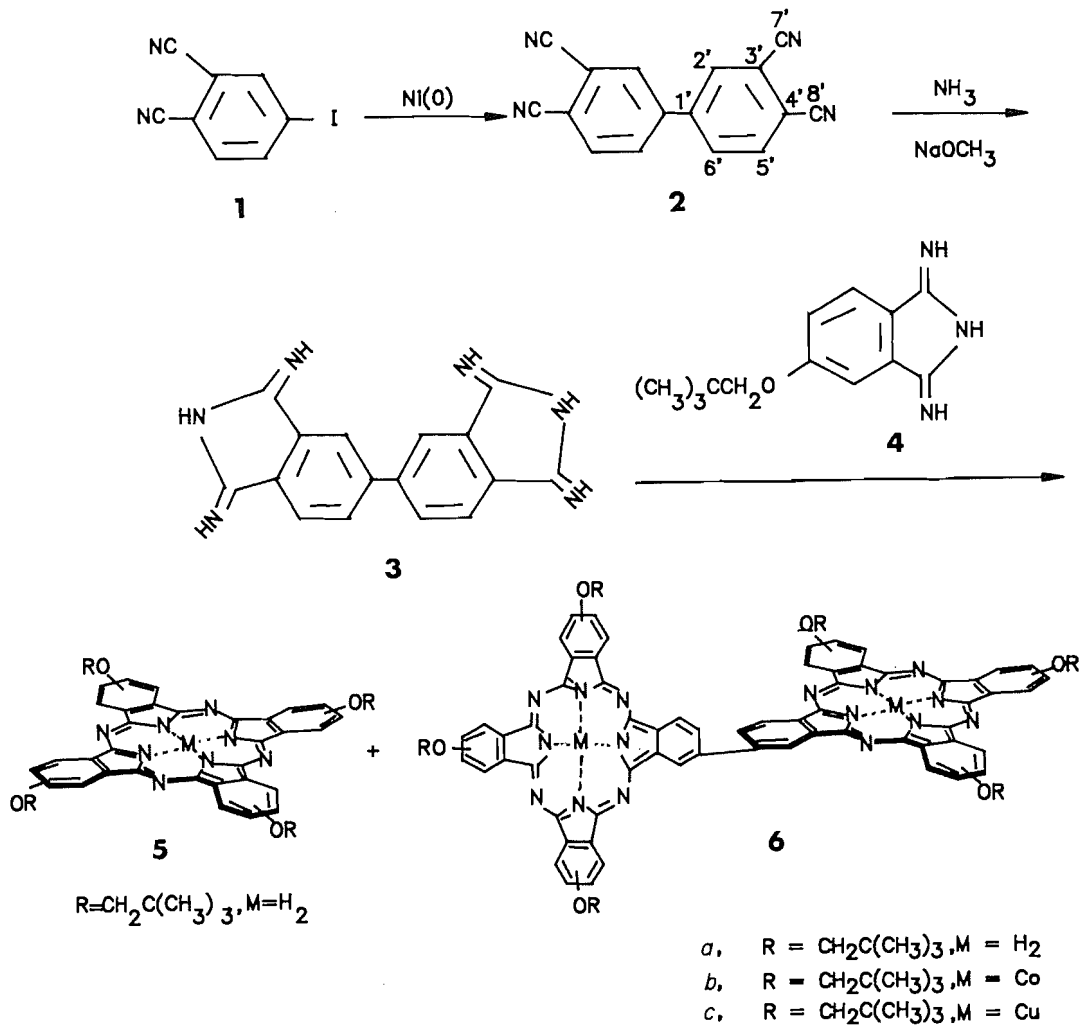
[1]Author to whom correspondence may be addressed.

Synthesis of directly linked binuclear phthalocyanines

By a previously described method (10), elemental nickel was generated by reduction of nickel iodide with lithium in dry glyme in the presence of naphthalene. The activated nickel powder catalyzed the self-coupling of 4-iodophthalonitrile (**1**) to give 3,3′,4,4′-tetracyanobiphenyl (**2**) in 78% yield. Compound **2** was converted into its 1,3-diiminoisoindoline (**3**) (5, 6). Condensation of **3** with 5-neopentoxy-1,3-diiminoisoindoline (**4**) (5, 6) was carried out in 2-*N*,*N*-dimethylaminoethanol for 36 h. The resulting dark blue solution was purified by flash chromatography (11) to give the mononuclear 2,9,16,23-tetraneopentoxyphthalocyanine (**5**) and the binuclear 2,2-bi-(9,16,23-trineopentoxyphthalocyanine) (**6***a*) in 55 and 33% yield respectively. We can refer to **6***a* as the zero atom bridged binuclear phthalocyanine. The binuclear phthalocyanine **6***a* was converted to its dicobalt **6***b* and dicopper **6***c* derivatives by refluxing **6***a* in toluene/2-methoxyethanol with $CoCl_2$ and $Cu(OAc)_2$ respectively (5, 6). Compounds **2** and **6***a*–*c* were fully characterized by spectroscopic data and elemental analysis (see Experimental). Some spectroscopic data of **6***a* but not its synthesis or characterization have been previously mentioned (12).

Synthesis of binuclear phthalocyanines covalently bridged by naphthalene

Treatment of **1** and 1,8-diiodonaphthalene (**7**) with elemental nickel (10) at room temperature for 3.5 h gave 1,8-bis(3,4-dicyanophenyl)naphthalene (**8**), 1-iodo-8-(3,4-dicyanophenyl)-naphthalene (**9**), and 3,3′,4,4′-tetracyanobiphenyl (**2**) in 15.5, 2.5, and 42.5% yield respectively. Compound **8** was converted to its 1,3-diiminoisoindoline (**10**) as previously described (5, 6).



SCHEME 1

Condensation of **10** and **4** in 2-*N*,*N*-dimethylaminoethanol for 44 h gave a dark green solution. Purification by flash chromatography (11) followed by vacuum liquid chromatography (13) gave the mononuclear **5** and the binuclear **11***a* in 45 and 8.7% yield respectively. The binuclear **11***a* was converted to its dicobalt **11***b*, dicopper **11***c*, and dizinc **11***d* derivatives by refluxing **11***a* in toluene/2-methoxyethanol with $CoCl_2$, $Cu(OAc)_2$, and $Zn(OAc)_2$ respectively. Although **11***a–d* and **8** have been reported in a communication (9), the full details are reported here (see Experimental). The binuclear phthalocyanines **11***a–d* exhibit parent ion clusters in their fast atom bombardment (FAB) mass spectra (14). More importantly, no evidence of partially or half-metallated species of **11***b–d* were observed. The ultraviolet–visible (uv) spectrum of **11***a* gave a single broad (symmetric shape) absorption at the Q band region that had not been observed before in other metal-free binuclear phthalocyanines (7, 12). A more detailed ^1H nmr analysis of **8** than previously reported (9) indicates that the compound exists as a mixture of two rotamers at room temperature in a 1:1 ratio. The existence of rotamers suggests that there is a rotation barrier sufficiently higher than that of the unsubstituted 1,8-diphenylnaphthalene (15). The ^{13}C nmr of **8** also indicates the presence of rotamers at room temperature.

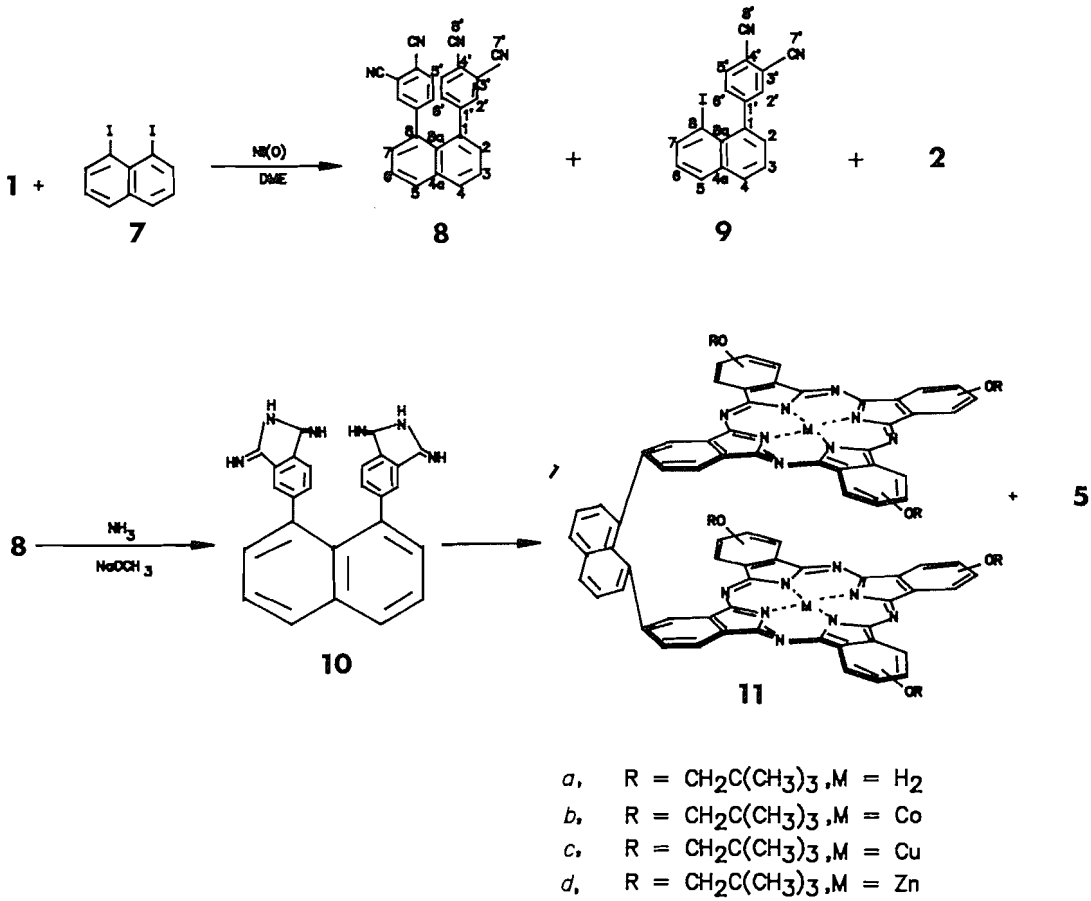
These rotamers did not separate by chromatographic methods. Although the two rotamers of **8** could be observed on the nmr time scale, their ultimate use in the formation of phthalocyanines at high temperatures, resulting in their subsequent equilibration again, removed any incentive to resort to heroic efforts to isolate the rotamers of **8**. After condensation, the binuclear phthalocyanine **11***a* should also exist as two isomers due to restriction in the rotation of the phthalocyanine rings. The two possible isomers of **11***a* were isolated as one fraction by chromatography. Construction of molecular models of **11***a* has shown substantial overlap of the two phthalocyanine rings in each isomer, and this may be the reason that these almost identical isomers are not separable by column chromatography. Separation of these isomers of **11***a* using high performance liquid chromatography (hplc) on a silica gel column was also not successful.

Synthesis of binuclear phthalocyanines covalently bridged by anthracene

The coupling reaction of aromatic halides using elemental nickel works well only with reactive halides such as iodides. The 1,8-diiodoanthracene is unknown. Even though 1,8-dichloroanthracene is readily available (16), it is not active enough to undergo the desired cross-coupling reaction.

Less electropositive arylzinc derivatives can tolerate various electrophilic functional groups such as nitriles and esters (17). These organometallic reagents readily undergo cross-coupling reactions with aryl halides (18), making arylzinc derivatives the reagents of choice in our synthesis. In general, direct attack

Can. J. Chem. Downloaded from www.nrcresearchpress.com by 41.223.56.140 on 09/07/12
For personal use only.



SCHEME 2

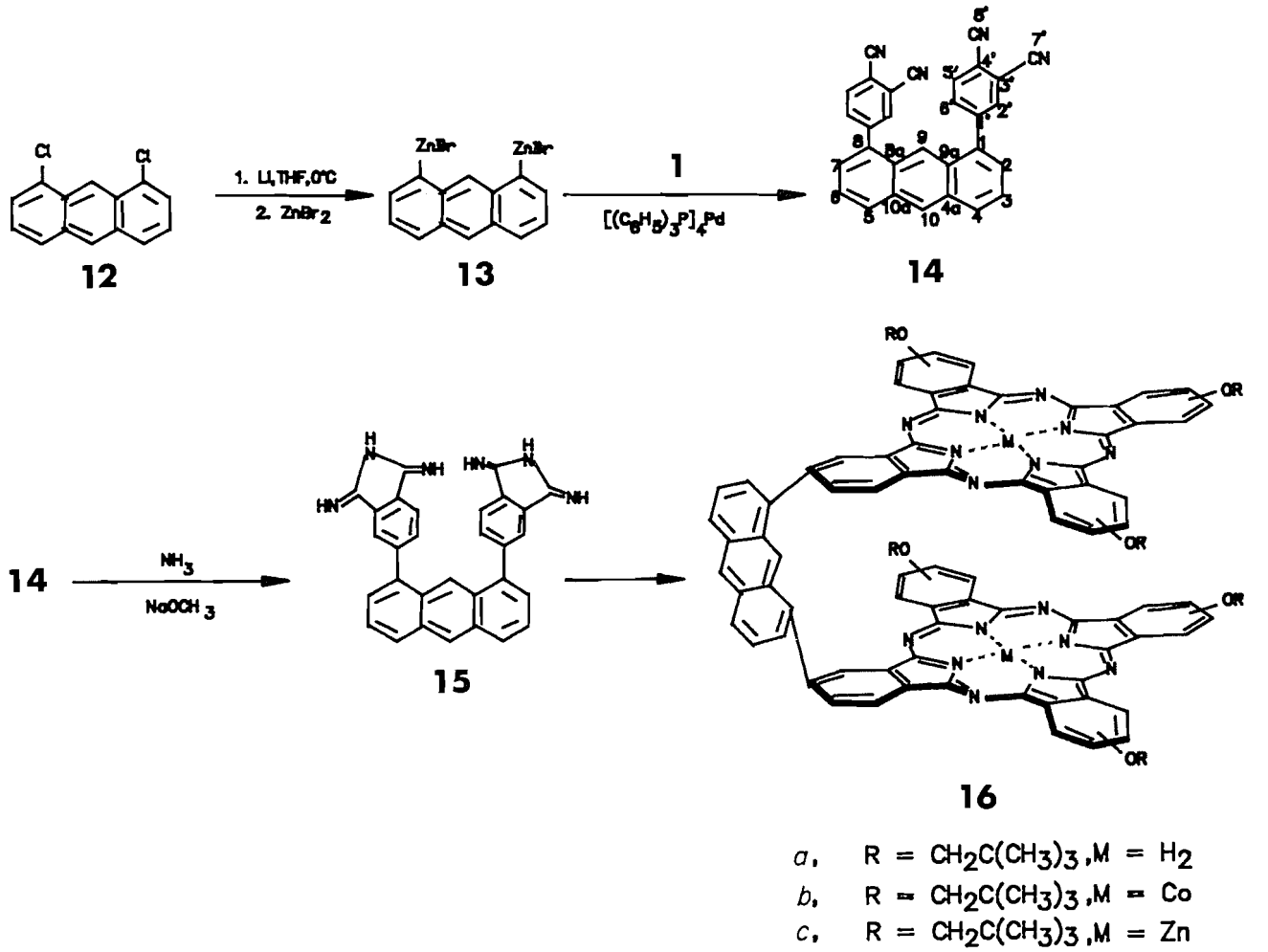
of aryl halide by zinc metal is difficult and the organozinc reagents are usually obtained by a two-step process from organolithium or Grignard reagents and the zinc halides (19). Instead of using an alkyllithium/aryl halide reaction to generate the organolithium intermediate, the organolithium can be generated conveniently by reacting the aryl halide directly with lithium metal in tetrahydrofuran (THF) using ultrasonic irradiation without any noticeable side reaction (20).

Treatment of 1,8-dichloroanthracene (**12**) with lithium and zinc bromide in dry THF at 0°C with ultrasonic activation for 2 h generated the 1,8-organozinc intermediate (**13**) (21). A cross-coupling reaction between **1** and **13** catalyzed by tetrakis-(triphenylphosphine)palladium (17, 18) gave 1,8-bis(3,4-dicyanophenyl)anthracene (**14**) in 9.9% yield. Compound **14** was converted to its 1,3-diiminoisoindoline (**15**) and condensed with **4** in 2-*N*,*N*-dimethylaminoethanol to give a dark green mixture. Upon dilution with water the mixture gave a blue colored residue. The mixture was purified by flash chromatography (11) to give a mixture of mononuclear phthalocyanine **5** and binuclear phthalocyanine **16***a*. A trace of the mononuclear phthalocyanine **5** was removed by gel permeation chromatography (22) to give the binuclear **16***a* in 12% yield. Metal-free binuclear phthalocyanine **16***a* was converted to its dicobalt (**16***b*) and dizinc (**16***c*) derivatives by standard procedures.

Unlike **8**, bisnitrile **14** does not exist as a mixture of rotamers, as shown by its simpler ^{1}H and ^{13}C nmr spectra, because of the low rotation barrier between the two phenyl rings in the 1,8-anthracene system (23). The uv spectrum of binuclear phthalocyanine **16***a* exhibits broad symmetric absorption similar to **11***a*. Parent ions were exhibited in the (FAB) mass spectra of **16***a–c* and no evidence for partially metallated species for **16***b* and *c* was observed.

Attempts to apply a similar organozinc procedure to 1,8-diiodonaphthalene did not give the desired product **8** (17–19). The products isolated were found to be 1-(3,4-dicyanophenyl)-naphthalene (**18**) and **2**. Due to the close proximity of the 1,8-positions on naphthalene, the formation of a monozinc-naphthalene intermediate **17** may be favoured over the naphthalene-1,8-dizinc species, although a dimer of **17** cannot be excluded. Reaction of **1** and **17** with zinc dissociated from naphthalene after reaction may explain the formation of **18**. The elemental nickel used in the cross-coupling reaction is not a true catalyst since it is not regenerated after the reaction (10). Large amounts of nickel iodide (more than 1:1 ratio) have been used for satisfactory results. Thin-layer chromatography of the reaction mixture has shown that the cross coupling between the organozinc derivatives and 4-iodophthalonitrile (**1**) is faster than the homo-coupling of **1** itself. In this regard, the cross-coupling reaction of organometallics and aryl halides catalyzed by transition metal complexes is superior to the mixed coupling between different aryl halides catalyzed by elemental nickel. The cross-coupling product is expected to be the major product in the case of the organometallic/aryl halide reaction, whereas the homo-coupling product is expected to be the major product in the elemental nickel catalyzed aryl halides coupling. The low yield of 1,8-bis(3,4-dicyanophenyl)naphthalene (**8**) is predictable because the 1,8-diiodonaphthalene has to react twice with 4-iodophthalonitrile to form the product, and has to compete against the homo-coupling reaction. The poor yield of 1,8-bis(3,4-dicyanophenyl)anthracene, which is obtained via a

Can. J. Chem. Downloaded from www.nrcresearchpress.com by 41.223.56.140 on 09/07/12
For personal use only.



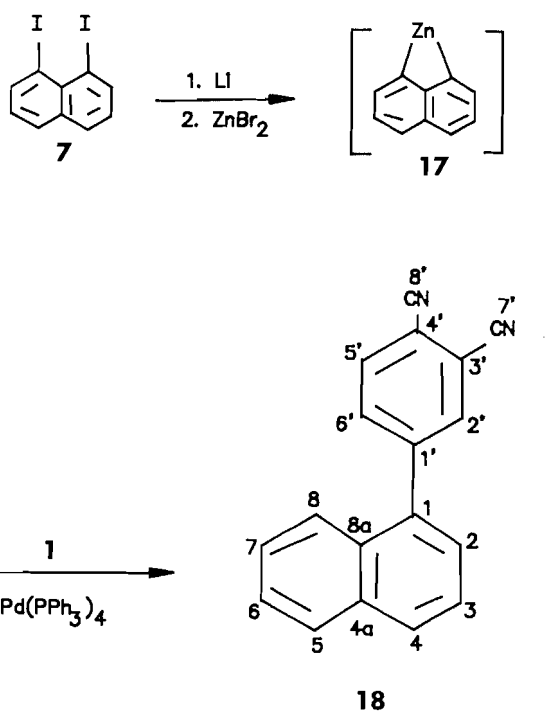
SCHEME 3

different coupling, may be due to incomplete formation of the 1,8-dilithiated intermediate. Half of the 1,8-dichloroanthracene was recovered. Also, the possible formation of polymeric organozinc in which the zinc atom acts as a bridge to link up adjacent anthracene molecules may decrease the yield.

Physical and spectroscopic properties of the phthalonitriles

Phthalonitriles **2**, **8**, **14**, and **18** all have melting points higher than their unsubstituted parent compounds (16, 24) and exhibit characteristic CN absorption in the infrared region at 2240 cm^{-1}. Phthalonitriles **8** and **9** have the same molecular weight of 380. High resolution mass spectra of **8** and **9** were obtained to check their elemental composition. Together with elemental analysis data, phthalonitrile **8** was clearly identified as the symmetrical 1,8-disubstituted product.

The proton nmr spectra of the bisphthalonitriles all showed complicated patterns in the aromatic region. Chemical shift assignments were achieved for **2**, **8**, **9**, **14**, and **18** with additional coupling information obtained from correlation nmr and homo-decoupling experiments (Table 1). Carbon/proton correlation experiments have been done on the more soluble phthalonitriles (Table 2). The ^1H nmr and ^{13}C nmr of **2** are relatively simple. Selective irradiation of H2′, H5′, and H6′ in **2**, which resulted in changes in signal intensity in the ^{13}C spectra due to the nOe effect, helps to identify the chemical shifts of the carbons (26, 27).



SCHEME 4

Can. J. Chem. Downloaded from www.nrcresearchpress.com by 41.223.56.140 on 09/07/12
For personal use only.

Can. J. Chem. Downloaded from www.nrcresearchpress.com by 41.223.56.140 on 09/07/12
For personal use only.

TABLE 1. The ^{1}H nmr chemical shifts in pm (δ) of some phthalonitriles

Compound	Proton[a]								
	2′	5′	6′	2	3	4	5	6	7
2 (acetone-d_6)	8.09 (d, J = 1.7)	8.09 (d, J = 7.9)	8.13 (dd, J = 7.9)						
8*a* (DMSO-d_6)	7.82 (d, J = 1.5)	7.77 (d, J = 8.1)	7.54 (d, J = 8.1)	7.48 (dd, J = 7.2)	7.73 (t, J = 7.7)	8.23 (d, J = 7.4)	8.23 (d, J = 7.4)	7.73 (t, J = 7.7)	7.48 (dd, J = 7.2)
8*b* (DMSO-d_6)	7.72 (d, J = 1.5)	7.91 (d, J = 8.1)	7.61 (d, J = 8.1)	7.48 (dd, J = 7.2)	7.73 (t, J = 7.7)	8.23 (dd, J = 7.4)	8.23 (dd, J = 7.4)	7.73 (t, J = 7.7)	7.48 (dd, J = 7.2)
9 (DMSO-d_6)	8.19 (d, J = 1.6)	8.23 (d, J = 8.1)	7.86 (d, J = 8.1)	7.52 (d, J = 7.0)	7.63 (t, J = 7.6)	8.10 (d, J = 8.2)	8.13 (d, J = 8.2)	7.27 (t, J = 7.6)	8.25 (d, J = 7.2)
14 (CD_3CN)[b]	8.06 (d, J = 1.8)	8.04 (d, J = 8.3)	7.06 (d, J = 8.1)	7.51 (d, J = 7.4)	7.63 (dd, J = 6.9)	8.22 (d, J = 8.7)	8.22 (d, J = 8.7)	7.63 (dd, J = 6.9)	7.51 (d, J = 7.4)
18 (DMSO-d_6)[c]	8.29 (d, J = 1.5)	8.26 (d, J = 8.1)	8.03 (d, J = 8.1)	7.52 (d, J = 7.1)	7.63 (t, J = 7.2)	8.06 (d, J = 7.2)	8.04 (d, J = 7.3)	7.54 (t, J = 7.5)	7.59 (t, J = 8.4)

[a]The numbering of the carbon atoms in the compounds listed follows that given for these structures in the schemes and does not follow from the name of the compounds.
[b]The chemical shift values for protons 9 and 10 are 8.74 (s) and 8.13 (s) respectively.
[c]The chemical shift values for proton 8 is 7.71 (d, J = 8.4).

TABLE 2. The ^{13}C nmr chemical shifts in ppm (δ) of some bisphthalonitriles and related compounds in DMSO-d_6

Compound	Carbon[a]																	
	1′	2′	3′	4′	5′	6′	7′	8′	1	2	3	4	4a	5	6	7	8	8a
2	141.18	132.79	114.88[b]	115.58[b]	134.64	132.44	115.61[c]	115.66[c]	—	—	—	—	—	—	—	—	—	—
7[d]	—	—	—	—	—	—	—	—	96.04	145.07	128.06	132.12	136.91	132.12	128.06	145.07	96.04	132.99
			113.81[b,e]	118.81[b,e]			115.13[c,e]											
8	147.59	134.98	113.56	117.60	133.17	134.75	115.26	115.54[c]	135.07	131.80	125.84	130.61	134.66	130.61	125.84	131.80	135.07	127.61
9	147.00	136.14	113.20[b]	113.94[b]	133.46	135.98	116.03[c]	116.16[c]	137.22	131.46	125.41	130.79	135.26	129.98	127.55	142.54	92.07	130.35
12[f]	—	—	—	—	—	—	—	—	130.71	127.83	126.24	126.68	132.21	126.68	126.24	127.83	130.71	128.62
14[g]	145.02	134.83	113.51[b]	115.11[b]	135.29	133.72	115.73[c]	115.88[c]	135.86	127.82	125.72	129.55	131.29	129.55	125.72	127.82	135.86	128.40
18	145.90	135.21	113.71[b]	115.40[b]	134.44	135.52	116.23[c]	116.39[c]	136.11	127.99	125.94	129.69	133.65	128.92	127.59	126.81	124.75	130.28

[a]The numbering of the carbon atoms in the compounds listed follows that given for these structures in the schemes and does not follow from the names of the compounds.
[b]These values may be interchanged.
[c]These values may be interchanged.
[d]Data taken from ref. 27.
[e]The two given values correspond to the two rotamers **8***a* and **8***b* and may be interchanged.
[f]The chemical shift values for carbons 9 and 10 are 128.45 and 119.00 respectively.
[g]The chemical shift values for carbons 9 and 10 are 128.08 and 120.82 respectively.

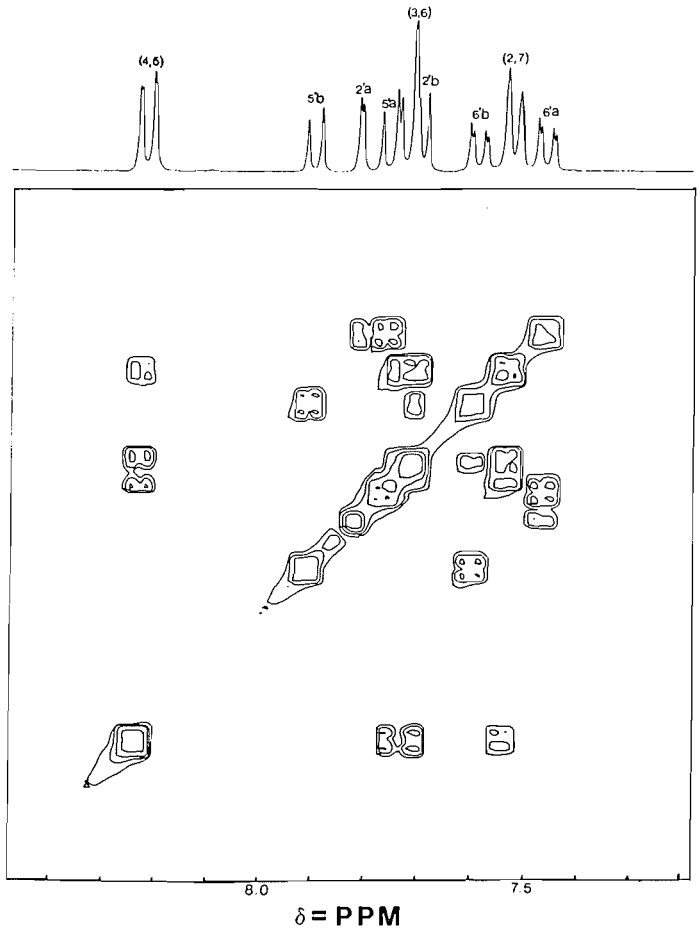


FIG. 1. ^{1}H homonuclear correlation (COSY) of a mixture of **8***a* and **8***b* in DMSO-d_6 at 25°C.

For the 1,8-disubstituted naphthalene systems, the two parallel phenyl rings are at an angle of about 70° to the plane of the naphthalene ring, to relieve some of the strain in the molecule (25). The distance between the 1,8-positions on the naphthalene ring is about 2.45 Å (24), which is too small for free rotation of the 3,4-dicyano-substituted phenyl rings at room temperature. The ^{1}H nmr of **8** at room temperature showed evidence that there is a sufficiently high rotation barrier between the two phenyl rings and **8** exists as two rotamers. The rotamer with two sets of cyano groups on the same side of the naphthalene plane is referred to as **8***a* and the other rotamer with cyano groups on the opposite side is referred to as **8***b*. Proton/proton correlation experiments clearly established the coupling relationship of the protons in the rotamers. The correlation spectrum indicated the protons on the phenyl rings of **8***a* and **8***b* as separate systems (Fig. 1). The chemical shifts for protons on the naphthalene ring do not seem to be affected by the different orientations of the phenyl rings. A model based on the different resultant dipoles pointed in different directions for **8***a* and **8***b* can help to assign the chemical shifts for the protons on the phenyl rings (Fig. 2). The orientation of the resultant dipoles may influence the localization of electron density over the ring and hence the deshielding effect of the π cloud. For **8***a*, the resultant influence is located between C3′ and C4′, which may have roughly equal effects on H2′ and H5′ and less effect on H6′. The expected chemical shifts are therefore H2′ = H5′ > H6′. For **8***b*, the resulting influence is concentrated around C4′, affecting H5′, H2′, and H6′ in decreasing order. The

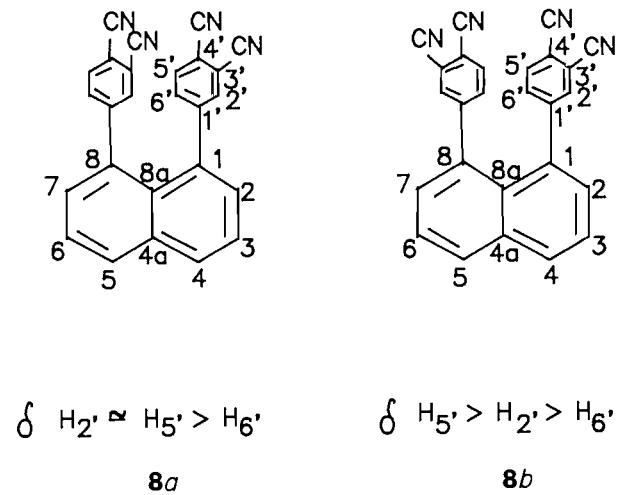


FIG. 2. 1,8-Bis(3,4-dicyanophenyl)naphthalene rotamers **8***a* and **8***b*.

expected chemical shifts are therefore H5′ > H2′ > H6′. The strongest influence will be experienced by H5′ in **8***b* due to the close distance between H5′ and the net dipole as shown in Fig. 2. With this model, the sequence of the predicted chemical shifts of the phenyl protons is found to be matched with the observed sequence. The nitrile groups cause the phenyl protons to shift downfield, which offsets the upfield shifting effect observed in the 1,8-diphenylnaphthalene, in which the ten phenyl protons resonate at 6.85 ppm in carbon tetrachloride (24). A carbon nmr spectrum of **8** at room temperature showed 18 peaks. If only one rotamer is present, 14 peaks are expected. At 100°C in DMSO-d_6 the spectrum consisted of 14 peaks as expected (see Experimental).

The proton spectrum of **9** is much simpler than that of **18** even though these compounds have similar structures. The chemical shifts of H2′ and H5′ of **9** are more downfield shifted than H6′. The characteristic C—I carbon appeared at 92.07 ppm. The distance between the 1,8-positions on anthracene is about 4.8 Å (16). The energy barrier of rotation of the phenyl rings at the 1,8-positions is quite small (23). In fact, ^{1}H nmr and ^{13}C nmr of **14** did not indicate the presence of rotamers at room temperature. Again, H2′ and H5′ are further downfield than H6′ and are consistent with the chemical shifts in the naphthalene systems.

Spectroscopic properties of the phthalocyanines

The infrared spectra of all metal-free phthalocyanines exhibited characteristic NH absorption at 3300 and 1020 cm^{-1}, which disappeared upon formation of their metallated derivatives. All phthalocyanines exhibited parent ions or ion clusters in their FAB mass spectra (14). All phthalocyanines gave satisfactory C, H, N analyses, while metal analyses were also good except for **6***b*, which was slightly low.

The double Q band seen in the mononuclear metal-free phthalocyanines as a consequence of D_{2h} symmetry is further split due to coupling in the binuclear phthalocyanines (12). Coupling in general can be expected to occur either through space in the close cofacial conformation, or via conjugation through the unsaturated bridge, or both. For binuclear phthalocyanines with low symmetry, transitions to higher and lower energy combinations are allowed, resulting in both blue and red shifts with respect to the mononuclear species (12). In fact, the zero linked binuclear phthalocyanine **6***a* and the previously reported

Can. J. Chem. Downloaded from www.nrcresearchpress.com by 41.223.56.140 on 09/07/12
For personal use only.

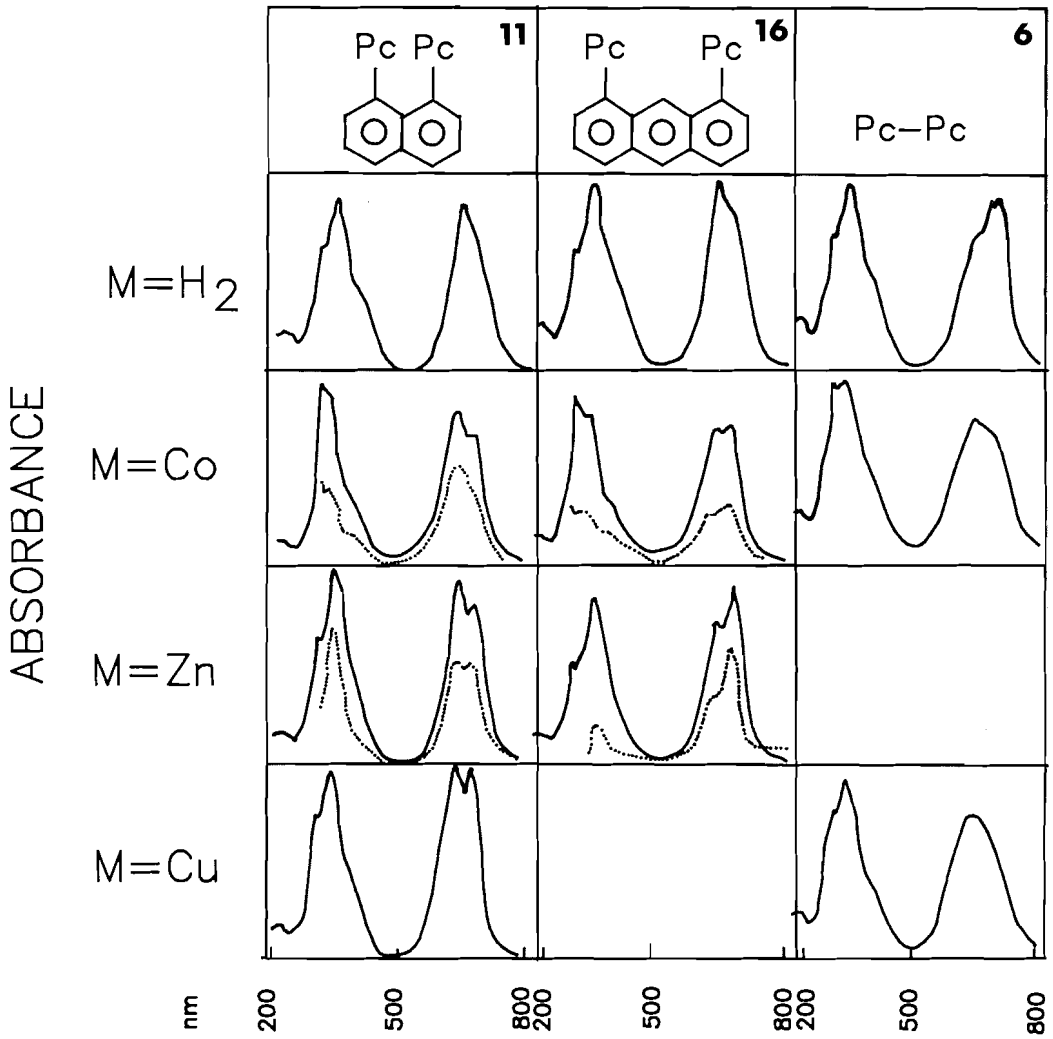


FIG. 3. Absorption spectra of metal-free and metallated binuclear phthalocyanines in *o*-dichlorobenzene at room temperature ([PcM], (---) $\sim 1 \times 10^{-5}$ M; (···) $\sim 5 \times 10^{-7}$ M).

binuclear phthalocyanines (4–6), except the negative linked binuclear phthalocyanine (7), show such splitting patterns. However, the electronic spectra of metal-free binuclear phthalocyanines **11***a* and **16***a*, which closely resembled one another, exhibited a single broad Q band absorption at 648 nm but with some evidence of splitting in the spectrum of **16***a* (Fig. 3).

Indeed, the spectra of **11***a* and **16***a* looked similar to the deprotonated spectrum of the five-atom bridged binuclear phthalocyanine (12), which is able to assume a close cofacial D_{4h} configuration. The similarity suggests that the two phthalocyanine rings in **11***a* and **16***a* are very close together and the four internal hydrogens are equivalent, which raises the symmetry of the molecules effectively to D_{4h}. For phthalocyanine with D_{4h} symmetry, the π–π^* transition is not split. There are large blue shifts in the Q band absorption in the metal-free cofacial D_{4h} binuclear phthalocyanines **11***a* and **16***a* (Table 3) relative to mononuclear metal-free phthalocyanines, indicative of the extensive electronic coupling between the cofacial rings (28, 29).

In general, all the metallated cofacial binuclear phthalocyanines showed two Q-band absorptions, the relative intensity varying with concentration. The absorption centered around 680 nm corresponds to the expected transition for uncoupled metallated phthalocyanines, whereas the 640-nm transition resulted from aggregated species (30). For cofacial systems, aggregation may be both intermolecular and intramolecular. Intermolecular aggregation is expected to be concentration dependent, while intramolecular aggregation should be concentration independent. When the concentration is sufficiently reduced, the spectrum becomes concentration independent and the remaining absorption near 640 nm arises from intramolecular coupling (aggregation) due to the cofacial arrangement (Fig. 3).

The proton nmr spectra of the binuclear phthalocyanines exhibited absorption peaks typical of the neopentoxy group and very weak aromatic signals. The NH absorption of **6***a* occurred around −3 ppm. The NH absorption of the binuclear phthalocyanines **11***a* and **16***a* occurred at higher field. Binuclear phthalocyanine **11***a* gives two sets of broad NH signals at −5 and −6 ppm. The two sets of signals may correspond to the two configurational isomers. The isomer which is exactly cofacial is related to the bisnitrile **8***a*. The other isomer is related to bisnitrile **8***b* in which the two rings are slightly away from each other but still have some degree of overlap in a cofacial manner. The broadening of all of the peaks is due to the positional isomers arising from the neopentyl substituents. The NH protons for the anthracene linked binuclear phthalocyanine **16***a* were observed at −6.5 ppm and are much sharper. The sharpening of the signal may be due to increased separation between the rings so that the neopentyl groups contribute less influence

Can. J. Chem. Downloaded from www.nrcresearchpress.com by 41.223.56.140 on 09/07/12
For personal use only.

TABLE 3. Absorption spectra of binuclear phthalocyanines in *o*-dichlorobenzene at room temperature[a]

Compound	λ_{max} (nm) (ε log)				
6*a*	298 (4.79)	342 (5.94)	648 (4.78)	682 (4.89)	704 (4.90)
6*b*	300 (4.90)	332 (4.90)	652 (4.79)		
6*c*	300 (4.76)	334 (4.84)	642 (4.74)		
11*a*		340 (4.90)	648 (4.89)		
11*b*	306 (5.15)		638 (5.09)	674 (5.01)	
11*c*	300 (4.88)	338 (5.01)	640 (5.02)	688 (5.02)	
11*d*	298 (4.88)	340 (5.05)	640 (5.03)	686 (4.96)	
16*a*		342 (5.01)	646 (5.00)		
16*b*	298 (5.03)	326 (4.97)	640 (4.94)	672 (4.95)	
16*c*	298 (4.71)	344 (5.01)	640 (4.93)	684 (5.04)	

[a]The concentration of the binuclear phthalocyanines was $\sim 1 \times 10^{-5}$ M.

on the overall configuration and hence less variation in the orientation of the two phthalocyanine rings. The upfield shift of the internal NH signal is very characteristic of a cofacial configuration. It is a result of the ring current effect of the two phthalocyanine rings being held closely in a cofacial arrangement. Similar upfield shifts for NH protons in cofacial porphyrins are well documented (2, 28). The NH signal disappeared in the ^{1}H nmr spectra of the zinc derivatives of **11***a* and **16***a*.

Experimental

Matheson high purity argon was used to maintain inert atmosphere conditions. Infrared (ir) spectra were recorded on a Pye Unicam SP1000 infrared spectrophotometer using KBr discs. Nuclear magnetic resonance (nmr) spectra for protons and carbons were recorded on a Bruker AM300 nmr spectrometer. The position of signals is reported in δ units. (The splitting of the signals is described as singlets (s), doublets (d), triplets (t), quartets (q), doublets of doublets (dd), or multiplets (m).) The ^{1}H nmr spectra of 10^{-4} M solutions of the phthalocyanines were obtained by averaging 500–3000 scans over the absorption range. The ultraviolet–visible spectra (uv) were recorded on a Hewlett Packard HP8451A diode array spectrophotometer. Mass spectra (ms) were recorded at 70 eV on a VG Micromass 16F mass spectrometer in the EI mode. The FAB spectra were obtained with a Kratos MS-50 triple analyzer mass spectrometer equipped with a FAB ion source of standard Kratos design and Ion Tech atom gun. The sample was dissolved in chloroform and a microlitre of the resulting solution added to a microlitre of *m*-nitrobenzyl alcohol on the probe tip. The spectra of the molecular ions of the binuclear phthalocyanines were obtained by signal averaging up to 256 scans over the appropriate mass range. The number in parentheses after the indicated ion shows the percentage of the base peak represented by that ion. Melting points (mp) were determined using a Kofler hot stage melting point apparatus and are uncorrected. Flash chromatography was performed using silica gel of particle size 20–45 μm. All reactions, except the one that required sonication, were stirred with a magnetic stirrer. Ultrasound activation was carried out using a Branson 1200 sonicator. All solvents were freshly distilled before use. Microanalyses were performed by Guelph Chemical Laboratories Ltd., Guelph, Ontario. Thin-layer chromatography (tlc) was performed using silica gel G as the absorbant.

3,3′-4,4′-Tetracyanobiphenyl (2)

By a previously described method (10), nickel iodide (dried for 4 h at 60–70°C/0.5 Torr; 1 Torr = 133.3 Pa) (4.53 g, 14.5 mmol), lithium (0.248 g, 35.7 mmol), and naphthalene (0.186 g, 1.45 mmol) in 30 mL of fresh distilled dry glyme were stirred at room temperature for 12 h. To the nickel powder, precipitated as a bulky black slurry, was added 1.0 g (3.9 mmol) of 4-iodophthalonitrile (**1**) dissolved in 5 mL of dry glyme. The reaction mixture became warm (30–35°C) and after 2 h the reaction was completed (tlc benzene/acetonitrile (9:1)). The reaction mixture was poured into 100 mL of ice-water; the solid was filtered and washed twice with ice-water. The resulting product was washed very slowly with benzene to remove most of the naphthalene. It was then extracted with ethyl acetate, dichloromethane, and acetonitrile (three times 30–40 mL portions for each solvent). The ethyl acetate, dichloromethane, and acetonitrile solutions were combined and dried over $MgSO_4$. The solvent was evaporated to give 0.5 g of crude product. The crude product was chromatographed by flash chromatography (11) using benzene, benzene/dichloromethane (1:1), and acetonitrile/dichloromethane (5:100) as eluants to give, in 78% yield, 0.39 g of **2** as white crystals, mp 291–293°C; ir (cm^{-1}): 2240 (CN), 1600, 1480, 1380, 1210, 910, 860, 840; uv (CH_2Cl_2) λ_{max} (log ε): 242 (4.16), 270 (4.18), 290 (4.14sh) nm; ^{1}H nmr and ^{13}C nmr: see Tables 1 and 2; ms *m/z*: 254 (M^+, 100), 227 (M^+ − HCN, 38), 220 (M^+ − 2HCN, 20). *Anal.* calcd. for $C_{16}H_6N_4$: C 75.60, H 2.36, N 22.04; found: C 75.54, H 2.07, N 21.98.

2,2-Bi-(9,16,23-trineopentoxyphthalocyaninyl) (6a)

By a previously described method (5, 6), the two crude diiminoisoindolines **3** and **4** were obtained from 0.273 g (1.10 mmol) of **2** and 6.0 g (28 mmol) of 4-neopentoxyphthalonitrile respectively. Compounds **3** and **4** were heated at 150°C (oil bath) in 20 mL of 2-*N*,*N*-dimethylaminoethanol and 10 mL of dimethylformamide (DMF) for 36 h under an argon atmosphere. After cooling to room temperature, the dark blue mixture was diluted with water, and the residue filtered and washed thoroughly with water until the filtrate was colorless. Preliminary purification of the product was achieved by flash chromatography using a 5 cm diameter column in which the crude product was preadsorbed on silica and eluted with hexane (200 mL), hexane/toluene (1:1) (1.5 L), and then hexane/toluene (1:2) until all the monomeric 2,9,16,23-tetraneopentoxyphthalocyanine (**5**) (3.3 g, 55% yield) was eluted. Further elution with toluene/2-methoxyethanol (200:5) (1.5 L) gave, after solvent evaporation, a portion of the dimer contaminated with traces of the monomer **5**. A second portion obtained by continued elution with toluene/2-methoxyethanol (200:5) (1 L) was contaminated with some green material. The latter portion was purified by evaporating the solution to dryness; the resultant solid was suspended in dry acetone, filtered, and washed with acetone until the filtrate was colorless. Finally, the product was purified by flash chromatography using silica gel and toluene/2-methoxyethanol (200:5) as eluant to give 565 mg (33% yield) of the product as a very dark blue shining solid; ir (cm^{-1}): 3300 (NH), 1615, 1240, 1100, 1015 (NH), 750; uv: see Table 3; ^{1}H nmr δ: 3.50 (br, CH_2O), 1.40–1.20 (m, $(CH_3)_3C$); ^{13}C nmr δ: 31.92, 27.13, 26.49; ms *m/z*: 1543.8 (M^+). *Anal.* calcd. for $C_{94}H_{94}N_{16}O_6$: C 73.13, H 6.14, N 14.15; found: C 73.50, H 6.39, N 14.60.

2,2-Bi-(9,16,23-trineopentoxyphthalocyaninyl) dicobalt(II) (6b)

A mixture of **6***a* (57.5 mg, 0.037 mmol), anhydrous cobalt(II) chloride (50 mg, 0.38 mmol), 2-methoxyethanol (3 mL), and toluene (7 mL) was heated at 110°C (oil bath) for 27 h under an argon atmosphere.

Can. J. Chem. Downloaded from www.nrcresearchpress.com by 41.223.56.140 on 09/07/12
For personal use only.

Can. J. Chem. Downloaded from www.nrcresearchpress.com by 41.223.56.140 on 09/07/12
For personal use only.

The product was purified by flash chromatography using a 1.5 × 8 cm column by direct application of the refluxing mixture to the column. Elution with hot toluene gave, after solvent evaporation, 24 mg of **6***b*. Continued elution with hot toluene/THF (1:1) yielded an additional 12 mg of **6***b*. The combined 36 mg of dimer **6***b* was washed with acetone to remove very minor fluorescent impurities (detected by tlc), leaving 32.4 mg (52% yield) of pure **6***b* as a very dark blue solid; ir (cm^{-1}): 1615, 1240, 1100, 750; uv: see Table 3; ms *m/z*: 1657.7, (M^+). *Anal.* calcd. for $C_{94}H_{90}N_{16}O_6Co_2$: C 68.11, H 5.47, N 13.52, Co 7.11; found: C 68.35, H 5.86, N 13.50, Co 6.40.

*2,2-Bi-(9,16,23-trineopentoxyphthalocyaninyl) dicopper(II) (**6**c)*

A mixture of **6***a* (100 mg, 0.065 mmol), anhydrous copper(II) acetate (100 mg, 0.550 mmol), 2-methoxyethanol (3 mL), and toluene (7 mL) was heated at 110°C for 24 h under an argon atmosphere. The solvent was removed and the mixture continuously extracted with toluene. Evaporation of toluene under reduced pressure gave **6***c* (57 mg) in 53% yield as a very dark blue shining solid; ir (cm^{-1}): 1620, 1245, 1070, 755; uv: see Table 3; ms *m/z*: 1667.6, (M^+). *Anal.* calcd. for $C_{94}H_{90}N_{16}O_6Cu_2$: C 67.73, H 5.44, N 13.44, Cu 7.62; found: C 67.72, H 5.26, N 13.15, Cu 7.55.

*1,8-Bis(3,4-dicyanophenyl)naphthalene (**8**) and 1-iodo-8-(3,4-dicyanophenyl)naphthalene (**9**)*

To 30 mL of freshly distilled dimethoxyethane (DME), 23.0 g (73 mmol) of anhydrous nickel iodide, 1.0 g (144 mmol) of lithium, and 0.8 g (6.25 mmol) of naphthalene were added. The mixture was stirred at room temperature for 12 h. To the resulting black slurry, 4-iodophthalonitrile (**1**) (4.0 g, 15 mmol) and 1,8-diiodonaphthalene (**7**) (25) (2.0 g, 5.26 mmol) were added. The mixture was allowed to react for 3.5 h. The resulting mixture was filtered through Celite using a sintered glass funnel and the residue was washed with ethyl acetate. The combined filtrate was washed with saturated sodium thiosulfate and water. The organic fraction was collected and dried over anhydrous magnesium sulphate. Evaporation of the solvent gave a yellowish brown solid. The crude material was purified by flash chromatography using benzene as the eluting solvent to remove naphthalene and unreacted 4-iodophthalonitrile (1.30 g). Elution with EtOAc/$CHCl_3$ (1:9) gave 50 mg of 1-iodo-8-(3,4-dicyanophenyl)naphthalene (**9**) in 2.5% yield. Recrystallization of **9** from EtOAc/hexane gave slightly brown crystals, mp 178–180°C; ir (cm^{-1}): 3060, 2240 (CN), 1595, 1490, 830, 780; uv (CH_2Cl_2) λ_{max} (log ε): 244 (4.13), 268 (4.15), 310 (4.19) nm; ^1H nmr and ^{13}C nmr: see Tables 1 and 2; hrms, *m/z* calcd. for $C_{18}H_9N_2I$ (M^+): 379.9809; found: 379.9802. *Anal.* calcd. for $C_{18}H_9N_2I$: C 56.86, H 2.38, N 7.37; found: C 57.21, H 2.89, N 7.89.

Further elution with the same solvent system gave 310 mg of 1,8-bis(3,4-dicyanophenyl)naphthalene (**8**) in 15.5% yield. Recrystallization of **8** from EtOAc/hexane gave white crystals, mp 284–285°C; ir (cm^{-1}): 3060, 2240 (CN), 1600, 1490, 835, 780; uv (CH_2Cl_2) λ_{max} (log ε): 238 (4.34), 265 (4.23sh), 340 (4.04) nm; ^1H nmr and ^{13}C nmr: see Tables 1 and 2; ^{13}C nmr (DMSO-d_6, 100°C) δ: 147.28, 134.67, 134.39, 134.35, 134.26, 132.52, 131.11, 130.01, 127.10, 125.22, 114.67, 114.46, 113.51, 111.62; hrms, *m/z* calcd. for $C_{26}H_{12}N_4$ (M^+): 380.10619; found: 380.10580. *Anal.* calcd. for $C_{26}H_{12}N_4$: C 82.09, H 3.18, N 14.73; found: C 82.00, H 3.34, N 14.80.

Further elution with 5% acetonitrile/dichloromethane gave 850 mg of **2** in 42.5% yield.

*Preparation of the bis-1,3-diiminoisoindoline (**10**)*

The bis-1,3-diiminoisoindoline (**10**) was prepared as previously described (5, 6). Bisphthalonitrile **8** (380 mg, 1.00 mmol) was added to 20 mL of a 1:1 mixture of methanol/dioxane containing 15 mg of sodium. Ammonia was bubbled into the solution at 80°C. The reaction was over in 3 h. The solution was evaporated to give crude **10**, which was used directly in the condensation reaction without further purification.

*1,8-Bis-2′-(9′,16′,23′-trineopentoxyphthalocyaninyl)naphthalene (**11**a)*

The two crude diiminoisoindolines **4** and **10** obtained from 6.0 g (28.00 mmol) of 4-neopentoxyphthalonitrile and 380 mg (1.00 mmol) of **8** respectively, in 25 mL of 2-*N*,*N*-dimethylaminoethanol, were heated to 150°C for 44 h. The reaction mixture was allowed to cool and then poured into 200 mL of water. The resulting mixture was filtered and washed with water until the filtrate became clear. The residue was washed again with methanol and then dried overnight in the oven at 60°C. Flash chromatography of the crude material using a 5 cm diameter column and eluting with toluene gave a mixture of mononuclear **5** and binuclear **11***a*. This mixture was chromatographed further using toluene/hexane (1:1) to give 2.70 g of **5** in 45% yield. Further elution using 2-methoxyethanol/toluene (2:100) gave a fraction consisting of mainly binuclear **11***a*. The final purification was achieved by vacuum liquid chromatography using toluene as the eluting solvent followed by gradual increase of 2-methoxyethanol/toluene (2:100) to give 139 mg of binuclear phthalocyanine **11***a* in 8.7% yield as a dark blue solid; ir (cm^{-1}): 3300 (NH), 1015, 1245, 1100, 1020 (NH), 750; uv: see Table 3; ^1H nmr (C_6D_6) δ: 7.0–8.5 (br, aromatic), 3.3–3.8 (br, CH_2O), 1.0–1.6 (br, $(CH_3)_3C$), −5 to −7 (br, NH); ms *m/z*: 1670 (M^+). *Anal.* calcd. for $C_{104}H_{100}N_{16}O_6$: C 74.72, H 6.03, N 13.42; found: C 74.71, H 5.76, N 13.15.

*1,8-Bis-2′-(9′,16′,23′-trineopentoxyphthalocyaninyl)naphthalene dicobalt(II) (**11**b)*

A mixture of 33 mg (0.02 mmol) of **11***a* and 60 mg (0.46 mmol) of anhydrous cobalt(II) chloride in 10 mL of a 1:4 mixture of 2-methoxyethanol/toluene was heated to 120°C for 20 h under an argon atmosphere. Flash chromatography of the crude reaction mixture using a 1 cm diameter column and eluting with 2-methoxyethanol/toluene (1:50) gave 30 mg of **11***b* in 85% yield as a dark blue shining solid; ir (cm^{-1}): 2940, 1610, 1240, 1090, 750; uv: see Table 3; ms *m/z*: 1782 (M^+). *Anal.* calcd. for $C_{104}H_{96}N_{16}O_6Co_2$: C 70.00, H 5.43, N 12.57, Co 6.61; found: C 70.50, H 5.50, N 12.32, Co 6.52.

*1,8-Bis-2′-(9′,16′,23′-trineopentoxyphthalocyaninyl)naphthalene dicopper(II) (**11**c)*

A mixture of 53 mg (0.032 mmol) of **11***a* and 57 mg (0.32 mmol) of anhydrous copper(II) acetate in 10 mL of a 1:4 mixture of 2-methoxyethanol/toluene was heated to 120°C for 20 h under argon. The crude reaction mixture was chromatographed as described above to give 37.2 mg of **11***c* in 70% yield as a dark blue solid; ir (cm^{-1}): 2940, 1610, 1235, 1090, 740; uv: see Table 3; ms *m/z*: 1793.6 (M^+ + 1, 100). *Anal.* calcd. for $C_{104}H_{96}N_{16}O_6Cu_2$: C 69.64, H 5.39, N 12.50, Cu 7.09; found: C 70.14, H 5.20, N 12.69, Cu 7.08.

*1,8-Bis-2′-(9′,16′,23′-trineopentoxyphthalocyaninyl)naphthalene dizinc(II) (**11**d)*

A mixture of 50 mg (0.030 mmol) of **11***a* and 100 mg (0.54 mmol) of anhydrous zinc acetate in 10 mL of a 1:4 mixture of 2-methoxyethanol/toluene was heated to 120°C for 20 h under argon. The crude reaction mixture was chromatographed as described for **11***b* to give 44 mg of **11***d* in 86% yield as a dark blue solid; ir (cm^{-1}): 2950, 1610, 1100, 740; uv: see Table 3; ^1H nmr ($CDCl_3$) δ: 7.5–8.5 (br, aromatic), 3.3–4.3 (br, CH_2O), 1.0–1.6 (br, $(CH_3)_3C$); ms *m/z*: 1797.6 (M^+ + 1.100). *Anal.* calcd. for $C_{104}H_{96}N_{16}O_6Zn_2$: C 69.50, H 5.38, N 12.48, Zn 7.28; found: C 69.25, H 5.73, N 12.60, Zn 7.46.

*1,8-Bis(3,4-dicyanophenyl)anthracene (**14**)*

To 60 mL of freshly distilled THF in a two-necked round-bottom flask, 2.0 g (8.1 mmol) of 1,8-dichloroanthracene (**12**) and 5.49 g (24 mmol) of anhydrous zinc bromide were added. The solution was cooled to 0°C. With a strong stream of argon flowing through the flask, 0.24 g (36 mmol) of lithium wire was cut into small pieces and dropped into the solution. The mixture was sonicated with ultrasound at 0°C for 1 h under argon and allowed to warm up to room temperature. The dark solution containing the zinc organometallic intermediate **13** was transferred with a syringe to another round-bottom flask containing 4.0 g (16 mmol) of **1** and 0.8 g (4 mol%) tetrakis(triphenylphosphine)palladium. The resulting solution was stirred under argon at room temperature for 3 h. Ethyl acetate and water were added to the reaction mixture, and the cloudy mixture was filtered through Celite. The filtrate separated into an aqueous and an organic layer. The organic

Can. J. Chem. Downloaded from www.nrcresearchpress.com by 41.223.56.140 on 09/07/12
For personal use only.

layer was collected and dried over anhydrous $MgSO_4$. Evaporation of the solvent gave a brownish crude material. The crude material was purified by flash chromatography using chloroform as the eluting solvent. The first fraction contained mostly unreacted starting material. Further elution gave 34.5 mg of 1,8-bis(3,4-dicyanophenyl)anthracene (**14**) in 10% yield. Recrystallization of **14** from acetonitrile/EtOAc gave yellow crystals, mp 345–346°C; ir (cm^{-1}): 3060, 2230 (CN), 1590; 1490, 880, 745; uv (CH_2Cl_2) λ_{max} (log ε): 284 (4.05), 268 (4.06), 386 (3.99), 405 (3.96); ^1H nmr and ^{13}C nmr: see Tables 1 and 2; ms *m/z*: 430 (M^+, 100) 330 (20). *Anal.* calcd. for $C_{30}H_{14}N_4$: C 83.69, H 3.28, N 13.02; found: C 83.42, H 3.46, N 13.15.

*Preparation of the bis-1,3-diiminoisoindoline (**15**)*

Bisphthalonitrile **14** (430 mg, 1.0 mmol) was added to 50 mL of a 1:1 mixture of methanol/dioxane containing 15 mg of sodium. Ammonia was bubbled into the solution under reflux at 80°C for 2 h. The solution was evaporated to give the crude bis-1,3-diiminoisoindoline (**15**), which was used directly in the condensation reaction without further purification.

*1,8-Bis-2′-(9′,16′,23′-trineopentoxyphthalocyaninyl)anthracene (**16**a)*

The two crude diiminoisoindolines **15** and **4** (5, 6), obtained from 430 mg (1.0 mmol) of **14** and 6.0 g (28.0 mmol) of 4-neopentoxyphthalonitrile respectively in 25 mL of 2-*N*,*N*-dimethylaminoethanol, were heated to 160°C for 44 h. The reaction mixture was allowed to cool and then poured into 200 mL of water. The resulting mixture was filtered and washed with water until the filtrate became clear. The residue was washed again with MeOH and then dried in the oven at 60°C overnight. Flash chromatography of the crude material using toluene as eluting solvent gave a mixture of mononuclear **5** and binuclear **16***a*. Rechromatography of the mixture using toluene/hexane (1:1) did not give a good separation. The binuclear fractions were still contaminated with large amounts of **5**. The mixed binuclear fraction was rechromatographed using a gel permeation column (Bio-Beads SX-1, 200–450 mesh) with THF as the eluting solvent. The front running binuclear fractions were combined and rechromatographed on a silica gel column using 2-methoxyethanol/toluene (2:100) as the eluting solvent to give 210 mg of 1,8-bis-2′-(9′,16′,23′-trineopentoxyphthalocyaninyl)anthracene (**16***a*) in 12% yield as a dark blue solid; ir (cm^{-1}): 3300 (NH), 1610, 1240, 1100, 1020 (NH), 750; uv: see Table 3; ^1H nmr (C_6D_6) δ: 7.0–8.5 (br, aromatic), 3.5–3.7 (br, CH_2O), 1.0–1.6 (br, $(CH_3)_3C$), −6 to −7 (NH); ms *m/z*: 1719 (M^+, 100%). *Anal.* calcd. for $C_{108}H_{102}N_{16}O_6$: C 75.39, H 5.98, N 13.03; found: C 75.18, H 6.33, N 12.65.

*1,8-Bis-2′-(9′,16′,23′-trineopentoxyphthalocyaninyl)anthracene dicobalt(II) (**16**b)*

A mixture of 52 mg (0.030 mmol) of **16***a* and 60 mg (8.46 mmol) of anhydrous cobalt(II) chloride in 10 mL of a 1:4 mixture of 2-methoxyethanol/toluene was heated to 120°C for 20 h. The crude reaction mixture was flash chromatographed using 2-methoxyethanol/toluene (1:80) and gave 56 mg of **16***b* in 95% yield; ir (cm^{-1}): 2940, 1610, 1240, 1090, 750; uv: see Table 3; ms *m/z*: 1832 (M^+). *Anal.* calcd. for $C_{108}H_{98}N_{16}O_6Co_2$: C 70.71, H 5.38, N 12.23, Cu 6.43; found: C 70.90, H 5.88, N 11.83, Co 6.40.

*1,8-Bis-2′-(9′,16′,23′-trineopentoxyphthalocyaninyl)anthracene dizinc(II) (**16**c)*

A mixture of 56 mg (0.0325 mmol) of **16***a* and 100 mg (0.54 mmol) of anhydrous zinc acetate in 10 mL of a 1:4 mixture of 2-methoxyethanol/toluene was heated to 120°C for 20 h. The crude reaction mixture was flash chromatographed using 2-methoxyethanol/toluene (1:50) to give 58 mg of **16***c* in 97% yield; ir (cm^{-1}): 2950, 1610, 1240, 1090, 750; uv: see Table 3; ^1H nmr (C_6D_6) δ: 7.5–8.5 (br, aromatic), 3.3–4.3 (br, CH_2O), 1.0–1.6 (br, $(CH_3)_3C$); ms *m/z*: 1847 (M^+). *Anal.* calcd. for $C_{108}H_{98}N_{10}O_6Zn_2$: C 70.22, H 5.35, N 12.14, Zn 7.08; found: C 70.72, H 5.65, N 11.60, Zn 7.45.

*1-(3,4-Dicyanophenyl)naphthalene (**18**)*

Following a previously described procedure (17, 18), 1.0 g (2.63 mmol) of 1.8-diiodonaphthalene and 1.78 g (7.9 mmol) of anhydrous zinc bromide were added to a two-necked flask containing 60 mL of freshly distilled THF. The solution was cooled to 0°C. Lithium (0.09 g, 0.013 mmol) was cut into small pieces and added into a flask flushed with a vigorous stream of argon. The mixture was sonicated with ultrasound at 0°C for 1 h under argon and allowed to warm to room temperature. The resulting solution was transferred with a syringe to another round-bottom flask containing 1.33 g (5.26 mmol) of **1** and 0.8 g (~4 mol%) tetrakis(triphenylphosphine)palladium. After stirring this mixture at room temperature for 3 h, water was added, followed by ethyl acetate. The cloudy mixture was filtered through Celite. The filtrate separated into aqueous and organic layers. The organic layer was collected and dried over anhydrous $MgSO_4$. Evaporation of the solvents gave a brownish colored crude material. The crude material was purified by flash chromatography using chloroform. The first fraction contained mostly starting material. Further elution gave 200 mg of **18** in 30% yield as white crystals, mp 148–149°C; ir (cm^{-1}): 3060, 2230 (CN), 1600, 1485, 1390, 910, 770; uv (CH_2Cl_2) λ_{max} (log ε): 242 (3.67), 282 (3.42), 324 (3.41) nm; ^1H nmr and ^{13}C nmr: see Tables 1 and 2; ms *m/z*: 254 (M^+) (100%), 233 (15%). *Anal.* calcd. for $C_{18}H_{10}N_2$: C 83.69, H 3.28, N 13.02; found: C 83.42, H 3.46, N 13.15.

Acknowledgements

Financial support by the Natural Sciences and Engineering Research Council of Canada and by The Office of Naval Research (Washington) is gratefully acknowledged. We would like to thank Mr. Byron Bachelor for his assistance in the preparation of compound **2**. The work was also funded by the Midwest Center for Mass Spectrometry, a National Science Foundation Regional Instrumentation Facility (Grant No. CHE-8620177).

1. D. Lexa, P. Millard, M. Momenteau, and J. M. Saveant. J. Am. Chem. Soc. **106**, 6321 (1984); P. Sayer, M. Gouterman, and C. R. Connell. Acc. Chem. Res. **15**, 73 (1982); P. Forswey, T. Kuwana, N. Kobayashi, and T. Osa. Adv. Chem. Ser. **201**, 601 (1982); J. Zagal, P. Binora, and E. Yeager. J. Electrochem. Soc. **127**, 1506 (1980); F. Van Den Brink, E. Barendrecht, and W. Visscher. Recl. Trav. Chim. Pays-Bas, **99**, 253 (1980); K. Kasuea, and M. Tsutsui. Coord. Chem. Rev. **32**, 67 (1980).
2. J. P. Collman, P. Denisevich, Y. Konai, M. Marrocco, C. Koval, and F. C. Anson. J. Am. Chem. Soc. **102**, 6027 (1980); J. P. Collman, F. C. Anson, S. Bencosme, A. Chong, T. Collins, P. Denisevich, E. Evitt, T. Geiger, J. A. Ibers, G. Jameson, Y. Konai, C. Koval, K. Meier, P. Oakley, R. B. Pettman, E. Schmittou, and J. Sessler. *In* Organic synthesis today and tomorrow. *Edited by* B. M. Trost and C. R. Hutchinson. Pergamon, Oxford. 1981; R. R. Durand, C. S. Bencosme, J. P. Collman, and F. C. Anson. J. Am. Chem. Soc. **105**, 2710 (1983); J. P. Collman, F. C. Anson, C. E. Barnes, C. S. Bencosme, T. Geiger, E. R. Evitt, R. P. Kreh, K. Meier, and R. B. Pettman. J. Am. Chem. Soc. **105**, 2694 (1983).
3. C. K. Chang and I. Abdalmuhdi. J. Org. Chem. **48**, 5388 (1983); C. K. Chang, H. Y. Liu, and I. Abdalmuhdi. J. Am. Chem. Soc. **106**, 2725 (1984); C. K. Chang and I. Abdalmuhdi. Angew. Chem. **23**, 164 (1984); H. Y. Liu, I. Abdalmuhdi, C. K. Chang, and F. C. Anson. J. Phys. Chem. **89**, 665 (1985); J. P. Fillers, K. G. Ravichandran, I. Abdalmuhdi, A. Tulinsky, and C. K. Chang. J. Am. Chem. Soc. **108**, 417 (1986).
4. S. Greenberg, S. M. Marcuccio, C. C. Leznoff, and K. B. Tomer. Synthesis, 406 (1986).
5. S. M. Marcuccio, P. I. Svirskaya, S. Greenberg, A. B. P. Lever, C. C. Leznoff, and K. B. Tomer. Can. J. Chem. **63**, 3057 (1985).
6. C. C. Leznoff, S. Greenberg, S. M. Marcuccio, P. C. Minor, P. Seymour, A. B. P. Lever, and K. B. Tomer. Inorg.

Chem. Acta, **89**, L35 (1984); C. C. LEZNOFF, S. M. MARCUCCIO, S. GREENBERG, A. B. P. LEVER, and K. B. TOMER. Can. J. Chem. **63**, 623 (1985).
7. C. C. LEZNOFF, H. LAM, S. M. MARCUCCIO, W. A. NEVIN, P. JANDA, N. KOBAYASHI, and A. B. P. LEVER. J. Chem. Soc. Chem. Commun. 699 (1987).
8. M. R. HEMPSTEAD, A. B. P. LEVER, and C. C. LEZNOFF. Can. J. Chem. **65**, 2677 (1987).
9. C. C. LEZNOFF, H. LAM, W. A. NEVIN, N. KOBAYASHI, P. JANDA, and A. B. P. LEVER. Angew. Chem. Int. Ed. Engl. **26**, 1021 (1987).
10. S. INABA, H. MATSUMOTO, and R. D. RIEKE. Tetrahedron Lett. **23**, 4215 (1982); H. MATSUMOTO, S. INABA, and R. D. RIEKE. J. Org. Chem. **48**, 840 (1983); S. INABA, H. MATSUMOTO, and R. D. RIEKE. J. Org. Chem. **49**, 2093 (1984).
11. W. C. STILL, M. KAHN, and A. MITRA. J. Org. Chem. **43**, 2923 (1978).
12. E. S. DODSWORTH, A. B. P. LEVER, P. SEYMOUR, and C. C. LEZNOFF. J. Phys. Chem. **89**, 5698 (1985).
13. N. M. TARGETT, J. P. KILCOYNE, and B. GREEN. J. Org. Chem. **44**, 4962 (1979).
14. M. BARBER, R. S. BORDOLI, R. D. SEDGWICK, and A. N. TYLER. J. Chem. Soc. Chem. Commun. 325 (1981).
15. H. O. HOUSE, W. J. CAMPBELL, and M. GALL. J. Org. Chem. **35**, 1815 (1970).
16. H. O. HOUSE, D. KOEPSELL, and W. JAEGER. J. Org. Chem. **38**, 1167 (1973).
17. E. NEGISHI. Acc. Chem. Res. **15**, 340 (1982); E. NEGISHI. *In* Current trends in organic synthesis. Pergamon Press, Oxford. 1982. p. 269.
18. E. NEGISHI, A. O. KING, and N. OKUKDO. J. Org. Chem. **42**, 1821 (1977); T. R. BAILEY. Tetrahedron Lett. **27**, 4407 (1986).
19. B. J. WAKEFIELD. *In* The chemistry of organolithium compounds. Pergamon Press, Oxford. 1974. p. 247.
20. J. L. LUCHE, C. PETRIER, J. P. LANSARD, and A. E. GREENE. J. Org. Chem. **48**, 3837 (1983).
21. C. PETRIER, J. C. DE SOUZA BARBOSA, C. DUPUY, and J. L. LUCHE. J. Org. Chem. **50**, 5761 (1985); P. BOUDJOUK, R. SOORIYAKUMARAN, and B. H. HAN. J. Org. Chem. **51**, 2818 (1986); D. BREMNER. Chem. Br. 633 (1986); T. J. MASON. Educ. Chem. 102 (1987).
22. J. A. ANTON, J. KWONG, and P. A. LOACH. J. Heterocycl. Chem. **13**, 717 (1976); W. A. NEVIN, W. LIU, S. GREENBERG, M. R. HEMPSTEAD, S. M. MARCUCCIO, M. MELNIK, C. C. LEZNOFF, and A. B. P. LEVER. Inorg. Chem. **26**, 891 (1987).
23. H. O. HOUSE, J. A. HRABIE, and D. VANDERVEER. J. Org. Chem. **51**, 921 (1986).
24. H. O. HOUSE, R. W. MAGIN, and H. W. THOMPSON. J. Org. Chem. **28**, 2403 (1963); V. BALASUBRAMANIYAN. Chem. Rev. **66**, 567 (1966).
25. H. O. HOUSE, D. G. KOEPSELL, and W. J. CAMPBELL. J. Org. Chem. **37**, 1003 (1972).
26. J. D. MEMORY and N. K. WILSON. *In* NMR of aromatic compounds. John Wiley & Sons, New York. 1982. p. 78; F. TODA, T. OSHIMA, Y. ISHIDA, Y. TAKEHIRA, K. SAITO, and K. TANAKA. *In* Handbook of ^{13}C NMR spectra. Sankyo, Japan. 1981.
27. P. E. HANSEN. Org. Magn. Reson. **12**, 109 (1979); B. P. CHO and R. G. HARVEY. J. Org. Chem. **52**, 5679 (1987).
28. D. DOLPHIN, J. HIOM, and J. B. PAINE II. Heterocycles, **16**, 417 (1981).
29. C. K. CHANG. J. Chem. Soc. Chem. Commun. 800 (1977).
30. W. A. NEVIN, W. LIU, and A. B. P. LEVER. Can. J. Chem. **65**, 855 (1987).

Can. J. Chem. Downloaded from www.nrcresearchpress.com by 41.223.56.140 on 09/07/12
For personal use only.

The initial stages of lead oxidation in pH 9 to 14 aqueous solutions

V. I. BIRSS[1] AND W. WAUDO
Chemistry Department, University of Calgary, Calgary, Alta., Canada, T2N 1N4

Received January 21, 1988[2]

V. I. BIRSS and W. WAUDO. Can. J. Chem. **67**, 1098 (1989).

The initial stages of lead oxidation in a range of alkaline solutions of varying pH and ion content have been investigated with the use of cyclic voltammetry and potential step techniques. In both carbonate and borate buffered solutions (pH > 9), and in more alkaline solutions, Pb oxidation commences at a potential of ca. 140 mV vs. RHE. The initial product is considered to be $Pb(OH)_2$, due to the proximity of this potential with the theoretically predicted one, and due to its invariance (vs. RHE) with pH. In pH 14 solutions, $Pb(OH)_2$ is soluble, producing $Pb(OH)_3^-$ and only a small amount of a stable surface film. At lower pH's, $Pb(OH)_2$ is not predicted to be soluble, and in borate-buffered solutions, a stable, reducible film appears to form. In carbonate-buffered solutions, the surface film is very difficult to remove electrochemically. Although XPS analyses show the film to be essentially free of carbonate, it is clear that carbonate must be involved in some way in inhibiting film reduction.

Key words: lead, lead hydroxide, lead oxide, surface films, carbonate solutions, borate solutions, alkaline solutions, cyclic voltammetry.

V. I. BIRSS et W. WAUDO. Can. J. Chem. **67**, 1098 (1989).

Utilisant des techniques de voltamétrie cyclique et opérant dans des solutions alcalines de pH et de contenus ioniques divers, on a étudié la nature des étapes initiales de l'oxydation du plomb. Dans des solutions tamponnées avec des ions carbonate ou borate (pH > 9) ainsi que dans des solutions plus alcalines, l'oxydation du plomb commence à un potentiel d'environ 140 mV vs. RHE. En se basant sur le fait que ce potential est très proche de celui prédit sur une base théorique ainsi que sur le fait qu'il ne varie pas (vs. RHE) avec le pH, on considère que le produit initial est du $Pb(OH)_2$. Dans des solutions de pH 14, le $Pb(OH)_2$ est soluble et il conduit à la formation de $Pb(OH)_3^-$ ainsi qu'à une très faible quantité d'une couche superficielle stable. A des pH plus bas, il n'est pas prévu que le $Pb(OH)_2$ soit soluble et, dans des solutions tamponnées au borate, il semble se former une couche stable qui peut être réduite. Dans des solutions tamponnées au carbonate, il est très difficile d'enlever la couche superficielle d'une façon électrochimique. Méme si des analyses par XPS démontrent que la couche superficielle ne contient essentiellement pas de carbonate, il est évident que le carbonate doit être impliqué d'une façon quelconque dans l'inhibition de la couche superficielle.

Mots clés : plomb, hydroxyde de plomb, oxyde de plomb, couches superficielles, solutions de carbonate, solutions de borate, solutions alcalines, voltamétrie cyclique.

[Traduit par la revue]

Introduction

Quite a number of studies concerning the electrochemical behaviour of lead have been carried out in the past (1–3), with emphasis on acidic environments. Lead has a variety of applications in industry, particularly as a lining and piping material because of its good corrosion resistance in acidic media (4). It has also played a major role in the development of electrical power sources, e.g. in lead–acid batteries (5).

Relatively little has been reported in the literature regarding the fundamental electrochemistry of lead in alkaline media. Early research (6) concerning the anodic behaviour of lead in alkaline solutions, carried out under galvanostatic conditions, has indicated that lead can be dissolved to form Pb^{2+} at low applied current densities. At higher current densities, a PbO_2 film is expected to form at the electrode surface, with the subsequent evolution of oxygen. A more recent study carried out by Ptitsyn *et al.* (7), using potentiostatic and potentiometric methods, has indicated that the oxidation of lead in alkaline solutions involves first the formation of $Pb(OH)_2$, which subsequently dissolves as $Pb(OH)_3^-$, with the latter dissolution step being rate determining.

More recently (8), it has been suggested on the basis of results obtained with cyclic voltammetry as well as steady state and transient potentiostatic techniques, that the first stage in the anodic oxidation of lead in 1 *M* NaOH solutions involves the formation of a surface intermediate, PbOH, followed by the deposition of a thin $Pb(OH)_2$ film on the Pb electrode surface, as shown in reactions [1] and [2]. The $Pb(OH)_2$ film then dissolves to form a soluble species, $Pb(OH)_3^-$ (reaction [3]), as was also suggested by Ptitsyn *et al.* (7).

[1] $Pb + OH^- \rightarrow (PbOH)_{ads} + e^-$

[2] $(PbOH)_{ads} + OH^- \rightarrow Pb(OH)_2 + e^-$

[3] $Pb(OH)_2 + OH^- \rightarrow Pb(OH)_3^-$

Following reaction [3], it has been suggested (9) that a PbO film forms at higher potentials, both by the dehydration of $Pb(OH)_2$ and also via a nucleation and growth process at the free Pb surface, according to reactions [4] and [5], respectively. PbO is also thought to be somewhat soluble (reaction [6]).

[4] $Pb(OH)_2 \rightarrow PbO + H_2O$

[5] $Pb + 2OH^- \rightarrow PbO + H_2O + 2e^-$

[6] $PbO + OH^- \rightarrow HPbO_2^-$

These suggested reactions pathways and products are supported by thermodynamic calculations (8–10) which indicate that $Pb(OH)_2$ is predicted to form at a potential more negative than that for PbO formation.

The electrochemistry of lead in somewhat less alkaline solutions has also been investigated recently (11, 12). In borate buffered solutions (pH 9.0), it has been suggested (11) that the initial stage of Pb oxidation involves the formation of a lead borate surface film, followed by PbO deposition. In carbonate solutions (pH 10 to 12), a small anodic peak preceding the main peak in cyclic voltammetric experiments has been attributed to the formation of a lead hydroxy–carbonate surface compound (12). It has been suggested that within the potential range of this small peak, some Pb dissolution may also occur, possibly via a

[1]To whom correspondence should be addressed.
[2]Revision received February 3, 1989.

Can. J. Chem. Downloaded from www.nrcresearchpress.com by 41.223.56.140 on 09/07/12
For personal use only.

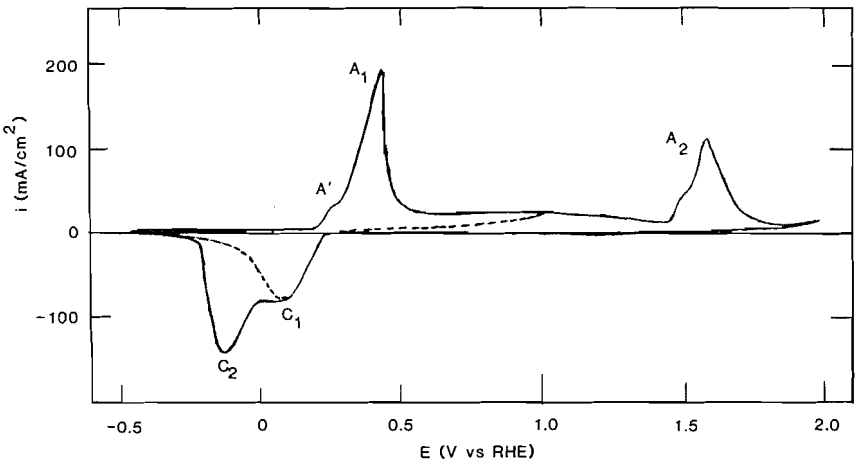


FIG. 1. Cyclic voltammogram of Pb chip electrode (0.015 cm^2) in 1 *M* NaOH at $s = 20$ mV/s.

surface intermediate, while at higher anodic potentials, further surface film formation occurs and the rate of dissolution diminishes.

Interest in the behaviour of lead in alkaline carbonate-containing solutions is growing due to the possible use of lead to precipitate ^{14}C-containing carbonate ions, a radioactive contaminant produced in CANDU D_2O-containing nuclear reactors (13). Lead may also be used as a storage material for nuclear waste in deep underground vaults in the future (14).

This paper focuses on the initial stage of lead oxidation in a number of alkaline solutions. These include NaOH (pH 14) solutions, as well as buffered (primarily pH 9 to 10) carbonate and borate solutions. It will be shown that the initial step in the oxidation process in all of these solutions is likely to involve the formation of the same species, i.e. $Pb(OH)_2$, as seen partly from the fact that the potential at which Pb oxidation commences (vs. the RHE) is independent of the nature of the electrolyte and the solution pH.

Experimental

Cyclic voltammetry (CV) and chronoamperometry (I/t) experiments were carried out using standard three electrode circuitry and an EG&G PARC 173 potentiostat coupled to an EG&G PARC 175 function generator. The current (I) vs. potential (E) profiles were plotted on a HP 7045B X/Y recorder at slow potential sweep rates (s), while all I/t data, and I/E curves at sweep rates greater than ca. 300 mV/s, were monitored on a Nicolet 3091 digital oscilloscope, and then transferred to the X/Y recorder.

A three compartment electrochemical cell was used in all of this work. The electrolytic contact between the working electrode (WE) and the reference electrode (RE) compartments was maintained via a luggin capillary. The counter electrode (CE), a large area platinum gauze, was placed in the third compartment. The RE was either a platinized Pt/hydrogen electrode placed in the same solution as that in the main compartment of the cell (RHE) or a saturated calomel electrode (SCE). All potentials are given with respect to the RHE in this work.

The WE consisted of either a Pb chip (from a Pb rod, 99.99% purity; Johnson and Matthey), having a geometrical area of ca. 1.5 to 3.0 mm^2, embedded in epoxy in a Pyrex tube, or a Pb disc (ca. 0.385 cm^2) press-fitted into a Teflon holder. In some of this work, the WE surface was mechanically polished in stages with various grades of emery paper (250 to 600 grit), then with 0.1 alumina paste on a polishing cloth, ultrasonically cleaned in acetone, and then finally rinsed with distilled water. The true surface area of the WE could be obtained from double layer capacitance measurements in 0.1 *N* Na_2SO_4 solutions (15), in order to compare the surface areas of different electrodes. However, because Pb is roughened by repeated oxidation/reduction cycles in high pH (>13) solutions, all current and charge densities are given with respect to the apparent electrode surface area in this work.

All solutions used were prepared from Analar grade chemicals and triply distilled water, and all experiments were carried out at room temperature. The solutions were deoxygenated by bubbling argon through the cell prior to, and over the cell solution, during the electrochemical experiments. Several runs were also carried out in carbonate-free NaOH, but no differences were seen in these results vs. those obtained in normal NaOH solutions.

X-ray photoelectron spectroscopy (XPS) analyses were carried out with a VG ESCA III instrument at the Alcan International Limited laboratories in Kingston, Ontario.

Results and discussion

(i) General behaviour of lead in 1 M *NaOH solutions*

Figure 1 shows a typical CV obtained with a mechanically polished Pb chip electrode in 1 *M* NaOH at a sweep rate of 20 mV/s. When the potential is extended positively towards the oxygen evolution reaction (OER) at ca. 2.0 V, and then negatively towards the range of hydrogen evolution (HER), two main anodic peaks (A_1 and A_2) and corresponding cathodic peaks (C_I and C_2) are observed. A shoulder (A′) is also seen on the cathodic side of peak A_1.

(a) Shoulder, A′

In earlier work (8), it was proposed that this shoulder, A′, is related to $Pb(OH)_2$ film formation and its subsequent dissolution, as shown by reactions [1]–[3]. A recent thermodynamic calculation has shown (8, 9) that $Pb(OH)_2$ can be expected to form at ca. 115 mV vs. RHE, while PbO is not predicted to form until ca. 255 mV (10, 16). At a higher current scale sensitivity than in Fig. 1, the potential at the foot of shoulder A′ is seen to be ca. 150 mV, which is at only a small overpotential relative to the theoretical value for $Pb(OH)_2$ formation. It should be noted that when a positive going potential sweep (at $s < 200$ mV/s) is reversed in the region of A′, very little cathodic current is seen (8). This evidence for the dissolution of the product formed in the anodic reaction (i.e. $Pb(OH)_3^-$, reaction [3]) under the conditions of these experiments was also supported by the results of ring-disc electrode experiments (9, 10).

To confirm $Pb(OH)_2$ dissolution in this potential range and in pH 14 solutions, new experiments were focussed on the use of high potential sweep rates and small area Pb electrodes. It should be noted that a small electrode area was chosen for the present work primarily to maintain low cell currents and thereby

Can. J. Chem. Downloaded from www.nrcresearchpress.com by 41.223.56.140 on 09/07/12
For personal use only.

TABLE 1. Potentials and charge densities in region of peaks A′/C′

Solution/pH	s (v/s)	E_+ (mV vs. RHE)	E_{foot}* (mV vs. RHE)	$q_{A'}$ (mC cm^{-2})	$q_{C'}$ (mC cm^{-2})	$q_{A'}/q_{C'}$
1 *M* NaOH	0.02	175	140	2.44	0.44	5.5
pH = 14	0.10	175	140	1.30	0.40	3.3
	2.0	300	150	2.20	1.70	1.3
	10.0	400	150	2.40	2.40	1.0
Na borate pH = 9.6	0.05	450	150	4.70	4.20	1.1
Na carbonate pH = 9.6	0.10	350	130	4.60	0.40	11.5

*At foot of A′.

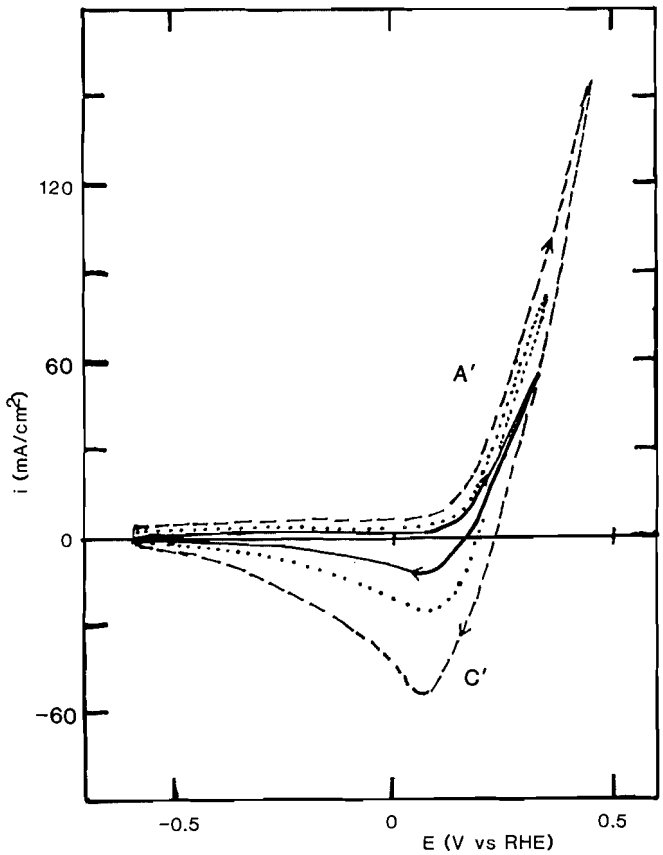


FIG. 2. Cyclic voltammetric response of Pb chip electrode (0.02 cm^2) at high sweep rates in 1 *M* NaOH. s = 2 V/s (—), 5 V/s (···) and 10 V/s (---).

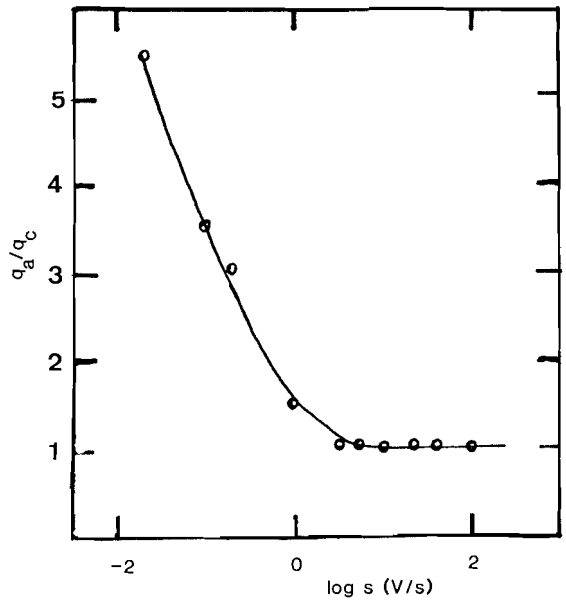


FIG. 3. Ratio of anodic to cathodic charge densities passed in the region of A′/C′ in 1 *M* NaOH as a function of potential sweep rate.

minimize *IR* drops and distributed potential effects (18), which were present in our prior work (8, 9).

The first series of experiments involved the use of high potential sweep rates as a test of the suggested reaction mechanism (reactions [1]–[3]) in pH 14 solutions. Figure 2 shows the CV response obtained in the region of A′ at high sweep rates (2 to 10 V/s) at a Pb chip electrode. With increasing sweep rates, the potential at the positive end of the scan had to be incremented somewhat in order to reach all of A′ in each scan.

In contrast to the large q_A/q_C ratios observed at low sweep rates (Table 1), it can be seen that as the sweep rate is increased, the anodic (A′) and cathodic (C′) charge densities become similar in value (Fig. 3). The charge density passed in A′ and C′ is ca. 2.3 ± 0.2 mC/cm^2 at high sweep rates, i.e. a charge density equivalent to ca. 5 to 10 monolayers of $Pb(OH)_2$ (19, 20), assuming a surface roughness factor (true surface area/apparent surface area) of unity. The similarity of the anodic and cathodic charge densities at high sweep rates indicates that insufficient time is available for any dissolution of $Pb(OH)_2$ (reaction [3]) to occur, so that only the formation and reduction of $Pb(OH)_2$ is monitored in A′/C′. Table 1 summarizes the principal features of A′/C′, including the charge densities and the potential at the foot of A′, as a function of potential sweep rate.

(b) Peaks A_1 and A_2

The potential obtained by extrapolating the current to the foot of peak A_1 in Fig. 1 is ca. 220 mV. Since this potential is reasonably close to the calculated potential for PbO formation (255 mV), it was suggested (8, 9) that peak A_1 depicts the formation of a PbO surface film, while peak C_1 reflects its reduction. When the potential is extended to peak A_2, considered to represent PbO_2 film formation, peak C_2 begins to develop (Fig. 1), while peak C_1 then decreases somewhat. This indicates that PbO_2 is reduced in peak C_2, and that more PbO is converted to PbO_2 in peak A_2 than is formed along with PbO_2 in

Can. J. Chem. Downloaded from www.nrcresearchpress.com by 41.223.56.140 on 09/07/12
For personal use only.

Can. J. Chem. Downloaded from www.nrcresearchpress.com by 41.223.56.140 on 09/07/12
For personal use only.

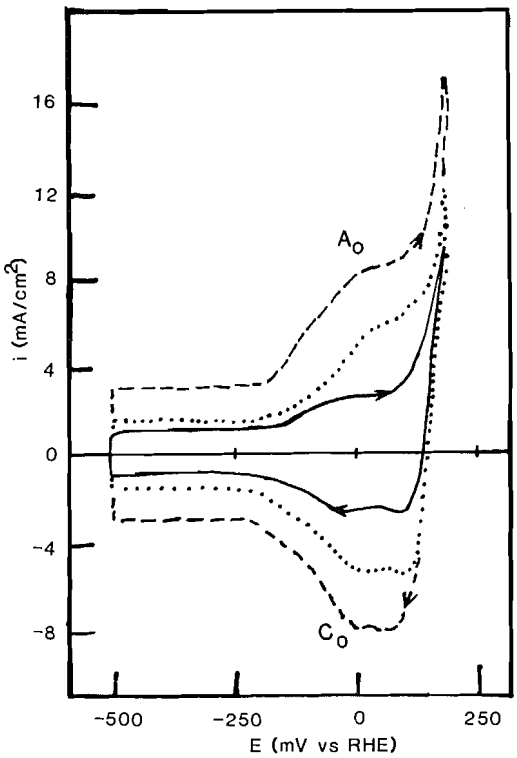


FIG. 4. Cyclic voltammograms of Pb chip electrode (0.02 cm^2) at high sweep rates after several hours of electrochemical experimentation in 1 *M* NaOH. s = 10 V/s (—), 20 V/s (···), and 30 V/s (---).

the potential range of peak A_2. The reduction of PbO (C_1) at a potential positive of that for the reduction of PbO_2 (C_2) is unusual, and may indicate that film reduction occurs first at the metal/inner film (PbO region) interface and then moves outward towards the outer film (PbO_2)/solution interface.

(c) *Peaks A_0/C_0*

After several hours of experimentation with a Pb electrode in the same 1 *M* NaOH solution, a new phenomenon was seen to develop in the potential range just negative of A′. Figure 4 shows that at high sweep rates, a matching pair of small peaks (A_0/C_0) appear, centred at a potential of ca. 0 V vs. RHE, i.e. at an underpotential of ca. 115 mV relative to the calculated potential for $Pb(OH)_2$ formation. An analysis of the relationship between the peak current densities of peaks A_0 and C_0 and the potential sweep rate reveals a linear dependence between these parameters (Fig. 5 depicts the case for peak A_0). The charge density contained in the peaks in Fig. 4 is ca. 40 $\mu C/cm^2$, if the apparent electrode area is again assumed. If the electrode area is higher by a factor of 2 or 3, which would be more realistic, the charge density would be still smaller than this.

It should be noted that the formation of a monolayer of $Pb(OH)_2$ would be expected to be seen at an underpotential. Also, a linear i_p/s relationship would be consistent with monolayer formation and removal. However, a single monolayer of $Pb(OH)_2$, having the same density as the bulk material, would be expected to involve a charge density of ca. 220 $\mu C/cm^2$ (19, 20). As the charges are sufficiently less than this, peaks A_0/C_0 may represent the formation of a two-dimensional layer of $Pb(OH)_2$ on only part of the electrode surface, or the deposition of two-dimensional $Pb(OH)_2$ having a very open structure (lower density than phase $Pb(OH)_2$ over the entire electrode surface).

Peaks A_0/C_0 may also reflect the adsorption of OH^- on the Pb surface, as suggested in reaction [1], followed by a partial

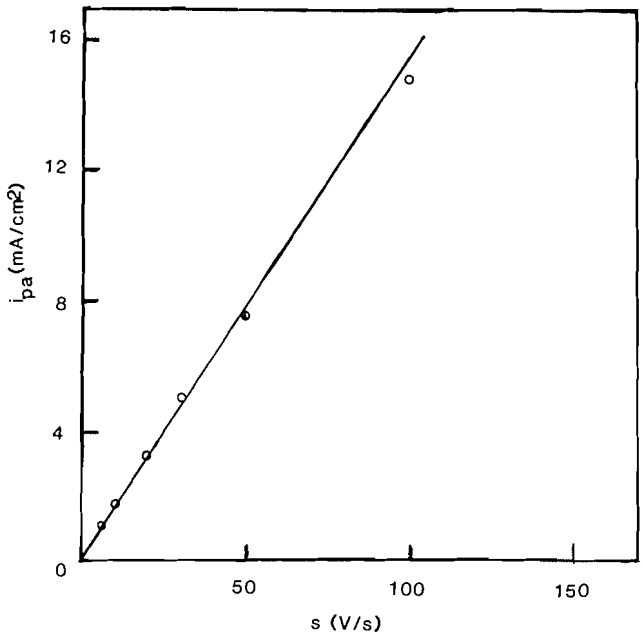


FIG. 5. Relationship between anodic peak current density of A_0 and potential sweep rate in 1 *M* NaOH.

charge transfer reaction (21). This type of process could also be observed at an underpotential, and would be expected to involve a lower charge density than that for the formation of a monolayer of $Pb(OH)_2$ film. These two possibilities cannot be distinguished from the data presented here. In a study of the electrochemistry of Ag electrodes in chloride-containing solutions (22), a similar difficulty was encountered in distinguishing adsorption with partial charge transfer from the formation of a low density monolayer.

The fact that peaks A_0/C_0 are only seen after some time of experimentation, during which many sweeps of potential are made to positive potentials, was originally thought to indicate that the Pb electrode had become activated, perhaps by an etching process, with time of potential cycling in these alkaline solutions. However, the appearance of peaks A_0/C_0 with time may also be related to the gradual deposition of high energy Pb nuclei on the Pb electrode surface by the reduction of $Pb(OH)_3^-$ at negative potentials. It is reasonable to suggest that Pb sites of this kind would be more active towards either two-dimensional film formation and/or anion (OH^-) absorption, as they would be likely to have a different surface energy from the original Pb electrode surface.

The suggestion that the newly deposited Pb nuclei, rather than a surface etching process, are responsible for the gradual appearance of peaks A_0/C_0 is supported by the following observation. A fresh Pb electrode, placed into a solution which had been studied previously, and therefore would be expected to contain dissolved Pb, probably in the form of $Pb(OH)_3^-$, rapidly developed peaks A_0/C_0. In contrast, a fresh Pb electrode placed in a fresh 1 *M* NaOH solution required several hours of continuous potential cycling before peaks A_0/C_0 appear. As the rate of Pb surface etching should depend only on time spent in the solution (and the potential), this result rules out an etching process as the cause of the development of peaks A_0/C_0.

(ii) Behaviour of Pb in less alkaline solutions

The cyclic voltammetric response obtained with lead in pH 9.6 bicarbonate and borate solutions is shown in Figs. 6*a* and *b*,

Can. J. Chem. Downloaded from www.nrcresearchpress.com by 41.223.56.140 on 09/07/12
For personal use only.

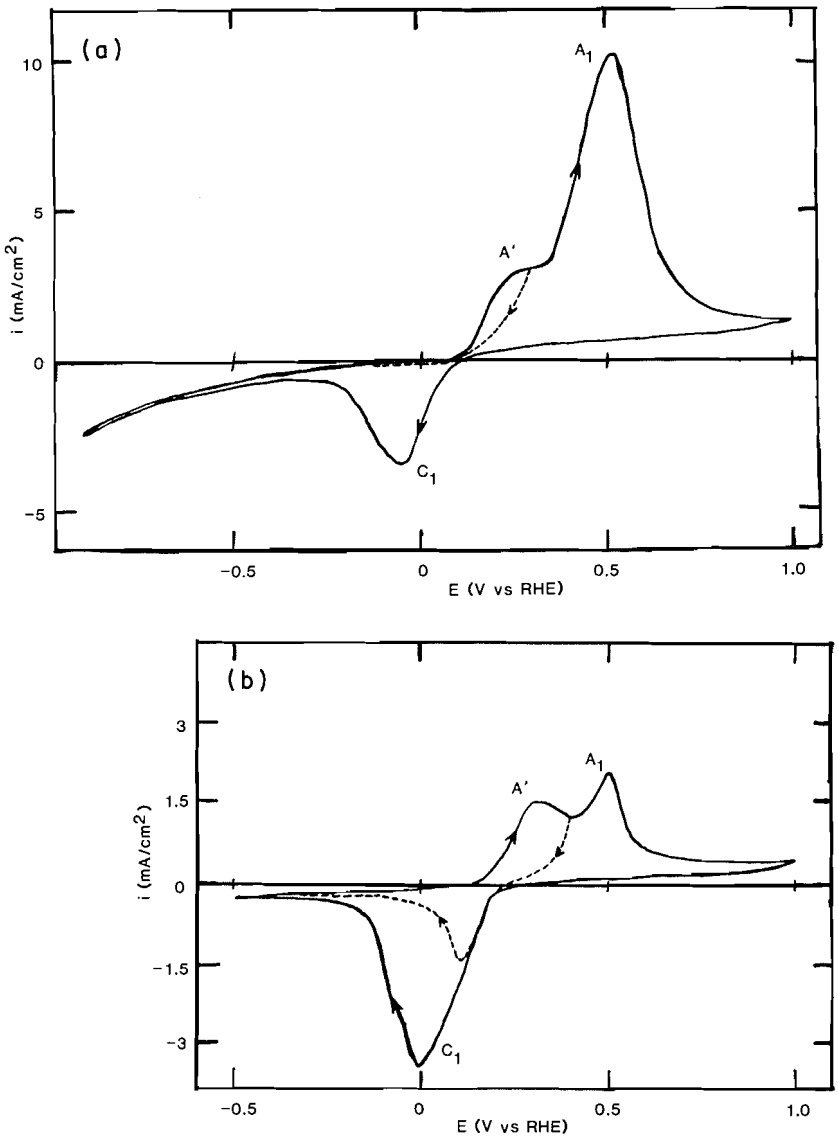


FIG. 6. Cyclic voltammograms obtained with Pb chip electrode in buffered pH 9.6 solutions: (*a*) 0.05 *M* sodium bicarbonate at s = 50 mV/s; (*b*) 0.025 *M* sodium borate at s = 20 mV/s.

respectively. In these experiments, the positive potential limit has been extended to only ca. 1.0 V. The general appearance of the CVs in these pH 9.6 solutions is similar to that at pH 14, although A′ now appears as a more distinct peak rather than a shoulder, and peak A_1 is significantly smaller at pH 9.6 than at pH 14. This indicates that the extent of PbO formation (A_1) is diminished at lower OH^- concentrations.

The similarity of the CVs in the carbonate and borate solutions is striking, lending support to a common reaction sequence and products. One noticeable difference in Figs. 6*a* vs. 6*b*, however, is that the anodic charge is substantially greater than the cathodic charge in carbonate solutions, while in the borate medium, the charges are similar. Figures 6*a* and *b* display this more clearly when the potential is reversed just positive of A′. In the carbonate solution, almost no cathodic charge is observed under the conditions of this experiment, while in borate solutions, the charges are very similar. It will be shown below that this difference in the anodic and cathodic charges in the carbonate solution is not the result of Pb dissolution, but rather the incomplete removal of the oxidation products from the electrode surface during each cathodic sweep. In fact, the electrochemistry of Pb in these dilute carbonate solutions is very complex, in that the magnitude of the anodic peaks, as well as their response to sweep rate, depends significantly on the electrochemical history of the electrode (23). Also, the ease of film reduction depends on both the upper potential limit utilized and the time of oxidation (23). A detailed mechanistic analysis of the oxidation of lead in pH 9 to 10 carbonate-buffered solutions will be presented in a future publication.

Despite these complexities, it is of interest to note that the onset of A′ occurs at ca. 140 mV vs. RHE under all conditions in the carbonate solutions and also in the borate-containing solutions investigated in this work (Table 1). This value is very similar to the potential at the foot of A′ in pH 14 solutions. The charge passed in peaks A′/C′ in borate solutions and also in carbonate solutions after numerous cycles of potential, are also given in Table 1, for comparison with the pH 14 case. It can be seen that the charge densities are of a similar order at pH 9.6 at low sweep rates to those in pH 14 solutions at high sweep rates. It should also be noted that $Pb(OH)_2$ is not expected to be very

Can. J. Chem. Downloaded from www.nrcresearchpress.com by 41.223.56.140 on 09/07/12
For personal use only.

soluble at pH 9.6 (8, 10), consistent with the matching anodic and cathodic charge densities in Fig. 6*b*.

A′ was also seen to commence at a similar potential (vs. RHE) over the range of pH from ca. 10 to 14, and with either (or neither) carbonate/bicarbonate or borate ions present. This is strong evidence for the formation of the same phase in A′ in all of these solutions, i.e. at least in the early stages of A′. As A′ has been correlated with $Pb(OH)_2$ formation in pH 14 solutions (from thermodynamic calculations), it is therefore assumed that the first step of Pb oxidation in these dilute borate and carbonate solutions also involves $Pb(OH)_2$ formation.

Our hypothesis that the same phase, i.e. $Pb(OH)_2$, is formed initially in a range of alkaline solutions is similar to that made in recent studies of the Zn electrode (24). During the oxidation of Zn in various alkaline solutions, using a range of buffer solutions, the potential at the onset of Zn oxidation was also found to be independent of the nature of the electrolytes used. It was therefore proposed that the initial stage of Zn oxidation must also involve the formation of the same oxide phase, i.e. $Zn(OH)_2$, in all solutions.

Our suggestion that peak A′ reflects $Pb(OH)_2$ formation, at least initially, is in partial disagreement with two prior studies in the literature. Shoesmith *et al.* (12) have recently studied the oxidation of lead in carbonate solutions (1 *M* carbonate, pH 12). At this comparitively high pH, the CV response appears quite similar to our results at pH 14, including the presence of an anodic shoulder (A′) preceding the main anodic peak (A_1). It was suggested in their work that the formation of a hydroxycarbonate complex of lead (e.g. plumbonacrite (PN) or hydrocerussite (HC), $Pb_{10}O(OH)_6(CO_3)_6$ or $Pb_3(OH)_2(CO_3)_2$, respectively) occurs in A′, as determined by XRD analyses after long times of oxidation. However, the potential obtained by extrapolating to the foot of peak A′ in their data also yields a potential of ca. 130 to 150 mV vs. RHE, as is observed in both carbonate and borate-buffered solutions in our work.

If a PN or HC phase is indeed the equilibrium phase formed in peak A′ in pH 12, 1 *M* carbonate solutions, it is possible that the initial step in the reaction is still the formation of $Pb(OH)_2$, hence defining the thermodynamic conditions, and that $Pb(OH)_2$ subsequently transforms to the carbonate/Pb oxide phase after reaction with carbonate. The high carbonate concentrations (ca. 1 *M*) used in their work would favor such a process. It is also feasible that the free energy of formation of the PN or HC phase is similar to that of $Pb(OH)_2$ in these carbonate-containing solutions, and that this is the case of the similar potentials observed in their work as in our solutions.

In a study of the electrochemical behavior of Pb in 0.1 *M* sodium borate solutions (11), the foot of the first anodic peak observed (very similar to peak A′ in Fig. 6*b*) was also observed at a potential of ca. 150 mV vs. RHE, while the second anodic peak was considered to reflect PbO film formation. In this paper (11), peak A′ was attributed to the formation of a lead borate surface film, although no supporting evidence (eg. surface analysis) was provided for this assignment. Under certain conditions during the reduction of this film, two cathodic peaks were seen, thought to depict two forms of Pb borate formation and reduction. We have carried out a series of experiments to determine the pH dependence of A′ in borate solutions, and have found that when the borate concentration was held constant, while the pH was varied from ca. 9.5 to 12, peaks A′ and A_1 both moved negatively with increasing pH in an identical manner. On the basis of all of our results, we believe it is more likely

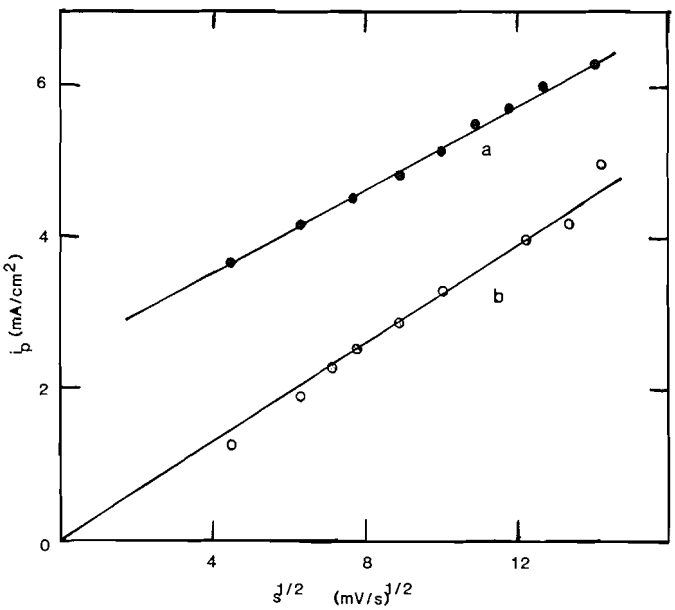


FIG. 7. Dependence of the peak current density of A′ on sweep rate in pH 9.6 bicarbonate (*a*) and borate (*b*) solutions.

that the first peak (A′) in borate solutions reflects $Pb(OH)_2$ deposition, followed by PbO formation in peak A_1.

Further support for the hypothesis that $Pb(OH)_2$ is formed in peak A′ in carbonate solutions comes from the results of XPS analyses. In a typical experiment, a Pb electrode, which had been oxidized in a single sweep from −1.0 V to 0.35 V in a pH 9.6 carbonate solution, was removed from the solution at the positive potential limit, and was examined by XPS. The nature of the surface film was assessed by comparing the binding energy shift for Pb(4*f*) and the O(1*s*)/Pb(4*f*) intensity ratios of the electrode surface with a number of standard materials, e.g. various lead oxides. As $Pb(OH)_2$ is not an equilibrium phase, it could not be produced as a standard material. Nevertheless, the results showed that the binding energy and intensity ratios of the surface film were essentially equivalent to that of PbO. This would be the likely dehydration product of $Pb(OH)_2$ after transferring the electrode into a vacuum chamber. Some carbon was observed at the electrode surface, but no more than at the PbO standard. Sputtering through the material at the electrode surface showed a sharp drop in carbon, and no evidence was obtained for carbonate at any points in the film. This result implies that an oxide film forms in A′ in pH 9 to 10 carbonate-buffered solutions, and by inference, this supports the same conclusion in borate-buffered solutions.

An analysis of the sweep rate dependence of peak A′ in carbonate (first sweep after holding the potential at the negative limit for controlled periods of time) and borate solutions was carried out to further probe similarities in the identity and nature of the surface products. This type of analysis could not be done in pH 14 solutions, as A′ did not form as a peak in this solution, even at high sweep rates (Fig. 2). Figure 7 demonstrates a generally similar behavior in the two solutions, although the non-zero intercept on the current density axis in Fig. 7 (curve *a*) is consistent with the more complex electrochemistry of Pb in the bicarbonate vs. borate solutions. These plots cannot be interpreted as being indicative of simple diffusion control by a species in solution. This is because the peak currents are essentially independent of solution stirring, and also as the diffusion

coefficients obtained from the slopes of these plots are anomalously large. It is perhaps more likely that the linear $i_p/s^{1/2}$ behavior is indicative of rate control by transport of species within pores of a surface film (25).

When the potential is reversed at ca. 0.35 V (see Fig. 6*a*), almost no cathodic charge passes, even at high sweep rates. An analysis of the solution after several hours of cycling of the potential between ca. −1.0 and 0.3 V revealed that virtually no Pb had dissolved during this time. The electrode surface, however, appeared to be covered with a grey, porous coating. Therefore, in pH 9.6 carbonate solutions, it appears that peak A′ initially involves the formation of $Pb(OH)_2$, which then interacts with carbonate species in some way so that the surface films are very difficult to reduce, as compared to the ease of reduction (in peak C′) of the material formed in A′ in borate solutions.

Overall, it is proposed that the initial step in the oxidation of lead in the range of pH from ca. 9 to 14, i.e. in solutions containing low concentrations of borate or carbonate ions as the buffering species, involves $Pb(OH)_2$ formation, as seen primarily by the common potential at the foot of peak A′ in all solutions. Also, the XPS result obtained for surface films formed in pH 9.6 carbonate solutions showed the presence of only oxide species, and essentially no carbonate was observed in the surface films. In pH 14 solutions, $Pb(OH)_2$ is soluble and repeated cycling of the potential in these solutions leads to the redeposition of lead on the electrode surface at negative potentials. A new pair of peaks is observed at an underpotential on such a lead electrode surface, perhaps reflecting OH^- adsorption with partial charge transfer, or the formation of a dilute monolayer of Pb hydroxide.

Summary

An investigation of the electrochemistry of Pb in three types of alkaline solutions of varying pH and ion content show a strong similarity in the initial stages of Pb oxidation. This is seen from cyclic voltammetry experiments, where a shoulder (A′) in pH 14 solutions occurs at the same potential (vs. the RHE) as the small peak (A′) in borate and carbonate solutions of lower pH. The potential at the onset of this shoulder (or peak) is ca. 140 ± 10 mV vs. RHE in all solutions. As the shoulder in pH 14 solutions has been suggested previously to be due to $Pb(OH)_2$ formation, it is proposed that the same reaction occurs in all of these solutions. The surface film formed in peak A′ in carbonate solutions was found by XPS to be an oxide film, containing essentially no carbonate. In pH 9.6 solutions, significantly less dissolution of $Pb(OH)_2$ is observed than at pH 14. In borate-buffered solutions, the $Pb(OH)_2$ surface film can be reversibly removed, while in carbonate solutions, the $Pb(OH)_2$ film must interact in some way with carbonate species in solution, making it difficult to remove electrochemically.

Acknowledgements

We extend our thanks to the Natural Sciences and Engineering Research Council and acknowledge a Canadian International Development Agency General Training Fund Scholarship from Kenya for the support of one of us (W.W.). We are also very grateful to Dr. D. Lloyd, Alcan International Limited, Kingston Laboratories, for the XPS analyses and for helpful advice and discussions.

1. P. Jones, R. Lind, and W. F. K. Wynne-Jones. Trans. Faraday Soc. **50**, 972 (1954).
2. L. M. Baugh and K. L. Bladen. J. Electroanal. Chem. **145**, 325 (1983); **145**, 339 (1983); **145**, 355 (1983).
3. S. R. Ellis, N. A. Hampson, M. C. Ball, and F. Wilkinson. J. Appl. Electrochem. **16**, 159 (1986).
4. W. Hoffman. Lead and lead alloys. 2nd ed. Springer-Verlag, New York. 1970.
5. Hans Bode. Lead–acid batteries. J. Wiley and Sons, New York. 1977.
6. K. Elbs and J. Forsell. Zeit. Elektrochem. **8**, 760 (1902).
7. M. V. Ptitsyn, G. S. Zenin, and K. I. Tikhonov. Sov. Electrochem. **13**, 1144 (1977).
8. V. I. Birss and M. T. Shevalier. J. Electrochem. Soc. **134**, 802 (1987).
9. V. I. Birss and M. T. Shevalier. J. Electrochem. Soc. **134**, 1594 (1987).
10. M. T. Shevalier. M.Sc. Dissertation, University of Calgary, Calgary, Canada. 1985.
11. J. S. Buchanan, N. P. Freestone, and L. M. Peter. J. Electroanal. Chem. **182**, 383 (1985).
12. D. W. Shoesmith. Personal communication.
13. R. R. Stasko and G. V. Vivian. Proc. of Int. Conf. on Radioactive Waste Management. Canadian Nuclear Society, Winnipeg, Sept. 1982.
14. J. Boulton. Atomic Energy of Canada Ltd, Report AECL-6314, 1978.
15. V. F. Ivanov and Z. N. Ushakova. Sov. Electrochem. **9**, 753 (1973).
16. M. Pourbaix. Atlas of electrochemical equilibria in aqueous solutions. 2nd ed., N.A.C.E., Houston, TX. 1974.
17. H. Angerstein-Kozlowska, B. E. Conway, and J. Klinger. J. Electroanal. Chem. **87**, 821 (1978).
18. D. Britz. J. Electroanal. Chem. **88**, 307 (1978).
19. V. I. Birss and L. E. Kee. J. Electrochem. Soc. **133**, 2097 (1986).
20. L. M. Peter. Electrochim. Acta, **23**, 165 (1980).
21. J. W. Schultze and F. D. Koppitz. Electrochim. Acta. **21**, 327 (1976).
22. V. I. Birss and C. K. Smith. Electrochim. Acta, **32**, 259 (1987).
23. W. Waudo. M.Sc. Thesis, University of Calgary, Calgary, Alberta. 1988.
24. D. C. W. Kannangara and B. E. Conway. J. Electrochem. Soc. **134**, 894 (1987).
25. A. J. Calandra, N. R. de Tacconi, R. Pereiro, and A. J. Arvia. Electrochim. Acta, **19**, 901 (1974).

Can. J. Chem. Downloaded from www.nrcresearchpress.com by 41.223.56.140 on 09/07/12
For personal use only.

Excess properties of the binary liquid systems dimethylsulfoxide + isopropanol and propylene carbonate + isopropanol

GEORGE RITZOULIS

Laboratory of Physical Chemistry, Aristotelian University of Thessaloniki, 54006 Thessaloniki, Greece

Received August 29, 1988[1]

GEORGE RITZOULIS. Can. J. Chem. **67**, 1105 (1989).

The dielectric constants, viscosities, densities, and refractive indices of the binary solvent mixtures dimethylsulfoxide–isopropanol and propylene carbonate–isopropanol were measured at 25, 30, and 35°C over the entire mole fraction range. Excess dielectric constant, excess molar polarization, and excess viscosity were calculated. For both binary systems the variation of the Kirkwood correlation factor has been examined.

Key words: propylene carbonate, acetonitrile, correlation factor, excess properties, dielectric constant.

GEORGE RITZOULIS. Can. J. Chem. **67**, 1105 (1989).

Opérant à 25, 30 et 35°C et sur l'ensemble des concentrations, on a mesuré les constantes diélectriques, les viscosités, les densités et les indices de réfraction de mélanges binaires des solvants diméthylsulfoxyde/isopropanol et carbonate de propylène/isopropanol. On a calculé les constantes diélectriques en excès, les polarisations molaires en excès et les viscosités en excès. Pour les deux systèmes binaires, on a examiné la variation du facteur de corrélation de Kirkwood.

Mots clés : carbonate de propylène, acétonitrile, facteur de corrélation, propriétés en excès, constante diélectrique.

[Traduit par la revue]

Can. J. Chem. Downloaded from www.nrcresearchpress.com by 194.225.253.170 on 09/07/12
For personal use only.

This work is a continuation of our previous studies (1) of thermodynamic and physicochemical properties of various binary liquid systems which are of special interest in chemical and electrochemical processes.

The binary systems chosen for investigation are the dimethylsulfoxide (DMSO)–isopropanol (*i*-prOH) and propylene carbonate (PC) – isopropanol (*i*-prOH). These binary liquid systems are good media for many chemical and electrochemical reactions and the fact that isopropanol is very often used as a substitute for ethanol extends the area of their applications.

The components dimethylsulfoxide and propylene carbonate belong to the so-called "high-energy reaction solvent" having a wide range of applications (2, 3). Moreover, there are many chemical reactions which are accelerated or retarded by dimethylsulfoxide and propylene carbonate. In many cases, the addition of alcohol changes the rate of these reactions and it is possible to control them by regulating the amount of added alcohol.

In the present paper densities, dielectric constants, viscosities, and refractive indices for the systems dimethylsulfoxide–isopropanol and propylene carbonate – isopropanol are measured over the entire mole fraction range at 25, 30, and 35°C. From the above experimental data the excess dielectric constant (ϵ^E), excess viscosity (η^E), and the excess molar polarization (P^E) are calculated. The variation of the Kirkwood correlation factor g_k as a function of mole fraction for the above-mentioned systems is also studied.

Experimental

Dimethylsulfoxide (Carlo Erba 99.5%) was dried for a week over 4A molecular sieves, followed by fractional distillation and collection of the middle fraction. The value of the specific conductance was 1×10^{-8} to 2×10^{-8} ohm^{-1} cm^{-1}.

Propylene carbonate (Merk zur synthese 99%) was dried over 4A molecular sieves and fractionally distilled under vacuum. The middle fraction was collected. The value of the specific conductance was less than 10^{-8} ohm^{-1} cm^{-1}.

Isopropanol (Fluka AG, puriss p.a.) was dried over 5A molecular sieves followed by two distillations. The value of the specific conductance was between $2 \times 10^{-8} - 3 \times 10^{-8}$ ohm^{-1} cm^{-1}.

Dielectric constants were measured with a dipolmeter employing the heterodyne beat method (Model WTW DM-01, Wissenshaftlich-Technische Werkstatten GmbH). The measurements were made at 2 MHz. The cell was thermostated (±0.02°C) by circulating the water of a constant temperature bath. The reproducibility of the measurement was approximately equal to 0.2 unit of dielectric constant.

Refractive indices were measured by means of a thermostated (±0.02°C) Abbe refractometer. The instrument was calibrated with benzene. The reproducibility was 0.0001 unit. Values were obtained for Na-D light.

Viscosity measurements were carried out with an Ubbelohde-type suspended-level viscometer with flow time 180 s for water at 25°C. Flow times were measured to 0.01 s with an electronic stopwatch. The standard deviations for more than five measurements did not exceed 0.05 s. Temperature control during the viscosity measurements was better than 0.01°C. The viscometer was standardized with conductivity water $\eta(H_2O, 25°C) = 0.008903$ P and $\eta(H_2O, 20) = 0.01002$ P. Kinetic energy corrections were made to the viscosity data.

Densities were measured with a Sprengel–Ostwald pycnometer having a volume of about 25 mL. Temperature control was 0.01°C.

Results

The experimental data for the binary systems dimethylsulfoxide–isopropanol and propylene carbonate – isopropanol are given in Table 1 at various mole fractions and at 25, 30, and 35°C.

The functions ϵ^E and η^E are calculated from the following equations

$$\epsilon^E = \epsilon - (\epsilon_1 x_1 - \epsilon_2 x_2)$$

$$\eta^E = \eta - (\eta_2 x_1 - \eta_2 x_2)$$

where x_1 and x_2 are the mole fractions; ϵ, ϵ_1, and ϵ_2 are the dielectric constant of the mixtures and of the pure (1) and (2) components; η, η_1, and η_2 are the viscosities of the mixtures and of the pure components.

The molar volume V is defined by the relationship

$$V = (x_1 M_1 + x_2 M_2)/d$$

where M_1 and M_2 are the molecular weights of the pure substances and d is the density of the mixture.

The linear correlation factor of the dielectric polarization g_k,

[1]Revision received February 16, 1989.

Can. J. Chem. Downloaded from www.nrcresearchpress.com by 194.225.253.170 on 09/07/12
For personal use only.

TABLE 1. Experimental values of η (poise), ϵ, n_D, d (g/cm^3)

(*i*) 25°C, system: DMSO – *i*-prOH

x(DMSO)	η	ϵ	n_D	d
1.000	0.0198	46.64	1.4768	1.0954
0.936	0.0188	45.00	1.4720	1.0802
0.8738	0.0180	43.12	1.4650	1.0596
0.8134	0.0172	41.20	1.4590	1.0392
0.7547	0.0166	39.19	1.4522	1.0196
0.6422	0.0155	35.33	1.4410	0.9824
0.5357	0.0148	31.68	1.4290	0.9479
0.4639	0.0145	29.62	1.4320	0.9252
0.3390	0.0142	25.35	1.4095	0.8860
0.2479	0.0145	22.80	1.4020	0.8586
0.2059	0.0151	21.50	1.3970	0.8460
0.0787	0.0177	18.99	1.3840	0.8093
0.0385	0.0191	18.53	1.3802	0.7969
0.000	0.0207	18.22	1.3758	0.7832

(*ii*) 25°C, system: PC – *i*-prOH

x(PC)	η	ϵ	n_D	d
1.000	0.0252	64.40	1.4201	1.1981
0.8412	0.0204	57.53	1.4126	1.1490
0.7019	0.0180	51.11	1.4070	1.0938
0.5787	0.0170	45.39	1.4011	1.0429
0.4690	0.0165	39.40	1.3980	0.9993
0.3706	0.0164	35.66	1.3962	0.9576
0.2818	0.0164	31.48	1.3881	0.9180
0.2015	0.0168	27.38	1.3850	0.8799
0.1283	0.0174	24.20	1.3812	0.8485
0.0614	0.0184	21.23	1.3783	0.8168
0.000	0.0207	18.22	1.3758	0.7832

(*iii*) 30°C, system: DMSO – *i*-prOH

x(DMSO)	η	ϵ	n_D	d
1.000	0.0179	46.43	1.4742	1.0910
0.9360	0.0172	44.50	1.4694	1.0759
0.8738	0.0164	42.59	1.4630	1.0544
0.8134	0.0157	40.73	1.4566	1.0339
0.7547	0.0151	38.80	1.4501	1.0143
0.6422	0.0142	34.97	1.4385	0.9773
0.5357	0.0135	31.27	1.4271	0.9429
0.4639	0.0132	28.87	1.4197	0.9201
0.3390	0.0129	25.25	1.4075	0.8824
0.2479	0.0132	21.98	1.3989	0.8534
0.2059	0.0134	20.66	1.3947	0.8409
0.0787	0.0149	18.00	1.3826	0.8038
0.0385	0.0159	17.73	1.3780	0.7922
0.000	0.0174	17.51	1.3738	0.7769

(*iv*) 30°C, system: PC – *i*-prOH

x(PC)	η	ϵ	n_D	d
1.000	0.0230	64.00	1.418	1.1920
0.8412	0.0185	56.79	1.4112	1.1413
0.7019	0.0165	50.31	1.4050	1.0889
0.5787	0.0154	44.53	1.4008	1.0382
0.4690	0.0148	39.00	1.3948	0.9952
0.3706	0.0145	34.62	1.3907	0.9533
0.2818	0.0144	30.50	1.3862	0.9151
0.2015	0.0146	26.47	1.3829	0.8753

TABLE 1 (*concluded*)

(*iv*) 30°C, system: PC – *i*-prOH

x(PC)	η	ϵ	n_D	d
0.1283	0.0153	23.30	1.3796	0.8430
0.0614	0.0160	20.46	1.3761	0.8120
0.000	0.0174	17.51	1.3738	0.7769

(*v*) 35°C, system: DMSO – *i*-prOH

x(DMSO)	η	ϵ	n_D	d
1.000	0.0159	46.10	1.4729	1.8070
0.9360	0.0155	43.72	1.4678	1.0704
0.8738	0.0150	41.71	1.4610	1.0496
0.8134	0.0145	40.19	1.4544	1.0299
0.7547	0.0139	38.20	1.4481	1.0099
0.6422	0.0132	34.60	1.4410	0.09780
0.5357	0.0124	30.75	1.4250	0.9385
0.4639	0.0121	28.34	1.4174	0.9159
0.3390	0.0118	24.19	1.4048	0.8776
0.2479	0.0120	21.39	1.3965	0.8492
0.2059	0.0122	20.18	1.3921	0.8368
0.0787	0.0136	17.56	1.3806	0.7996
0.0385	0.0146	17.06	1.3770	0.7888
0.000	0.0155	16.90	1.3721	0.7722

(*vi*) 35°C, system: PC – *i*-prOH

x(PC)	η	ϵ	n_D	d
1.000	0.0211	63.41	1.4163	1.1861
0.8412	0.0168	55.59	1.4097	1.1394
0.7019	0.0149	49.42	1.4036	1.0840
0.5787	0.0139	43.64	1.3970	1.0327
0.4690	0.0132	38.51	1.3930	0.9940
0.3706	0.0129	33.85	1.3887	0.9487
0.2818	0.0129	29.90	1.3845	0.9120
0.2015	0.0131	25.86	1.3810	0.8721
0.1283	0.0137	22.73	1.3778	0.8360
0.0614	0.0144	19.60	1.3743	0.8080
0.000	0.0155	16.90	1.3721	0.7722

is a parameter which provides useful information regarding intermolecular interactions, in particular the dipole association in the liquids.

Modifying the following equation proposed by Onsager and Kirkwood (4, 5)

$$\epsilon - \epsilon_\infty = \left(\frac{3\epsilon}{2\epsilon + \epsilon_\infty}\right)\left(\frac{\epsilon_\infty + 2}{3}\right)^2 \left(\frac{4\pi N \mu_i^2 g_k}{3kTV}\right)$$

where ϵ is the static dielectric constant, ϵ_∞ is the dielectric constant at high frequency, N is Avogadro's number, k is Boltzmann's constant, μ_i is the dipole moment of substance i, and g_k is the Kirkwood factor, given the following expression:

$$g_k = \frac{(\epsilon - \epsilon_\infty)(2\epsilon + \epsilon_\infty)}{\epsilon(\epsilon_\infty + 2)^2} \frac{9kT}{4\pi Nd} \frac{(M_1 x_1 + M_2 x_2)}{(\mu_1 x_1 + \mu_2 x_2)^2}$$

The quantity P defined by the following expression

$$P = \frac{(\epsilon - \epsilon_\infty)(2\epsilon + \epsilon_\infty)}{\epsilon(\epsilon_\infty + 2)^2} \frac{M_1 x_1 + M_2 x_2}{d}$$

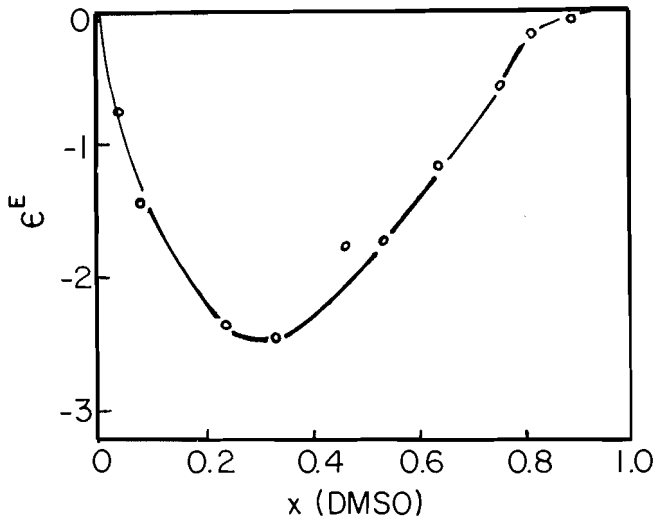


FIG. 1. Variation of ϵ^E vs. x for the system DMSO – i-prOH at 25°C.

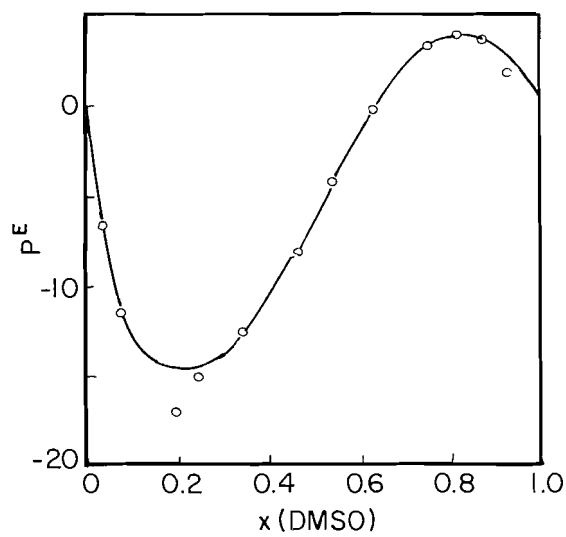


FIG. 2. Variation of P^E vs. x for the DMSO – i-prOH mixture at 25°C.

has been named the "molecular polarization" (6) of the mixture. The excess polarization is calculated by the expression

$$P^E = P - (P_1x_1 + P_2x_2)$$

During the calculations ϵ_∞ was set equal to n^2, where n is the refractive index of the mixture.

Discussion

The excess dielectric constant gives an estimate of the dipole–dipole interactions and the hydrogen bonded complexes (7). In the case of the system dimethyl sulfoxide – isopropanol, the excess dielectric constant shows negative deviations from ideal behaviour (Fig. 1), and is not sensitive to temperature. The curve ϵ^E vs. x shows a minimum at the dimethylsulfoxide mole fraction ~0.33.

In the case of propylene carbonate – isopropanol there are no significant deviations from the linear dependence of ϵ^E on mole fraction at the different temperatures. This does not mean that this binary liquid system can be considered an ideal mixture, because other properties show large deviations from ideality.

Excess molar polarizations are negative for both systems. Figure 2 shows the variation of excess molar polarization vs. x for the dimethylsulfoxide–isopropanol mixtures. The shape of the curve P^E vs. x for the system propylene carbonate – isopropanol is similar. One must notice the slightly different x values at which the minima ϵ^E and P^E appear. If we consider the variations of P^E in terms of temperature, a decrease of the extrema as the temperature increases is observed. This means that there is a reduction of the interactions between the different molecules as a consequence of the temperature increase.

The excess viscosity gives an estimation of the intermolecular interactions. According to Ford and Moor, positive values of η^E due to strong specific interaction causes complex formation and negative values of excess viscosity are observed for systems of different molecular size in which the dispersion forces are dominant (8, 9). In our case the excess viscosity is negative (Fig. 3) through the entire composition range at temperatures 25, 30, and 35°C for both binary mixtures under investigation. The values of mole fraction where the minimum is observed is at x(DMSO) ≃ 0.33 for the system dimethyl sulfoxide – isopropanol and x(PC) ≃ 0.50 for the system propylene carbonate – isopropanol (Fig. 4). In order to explain

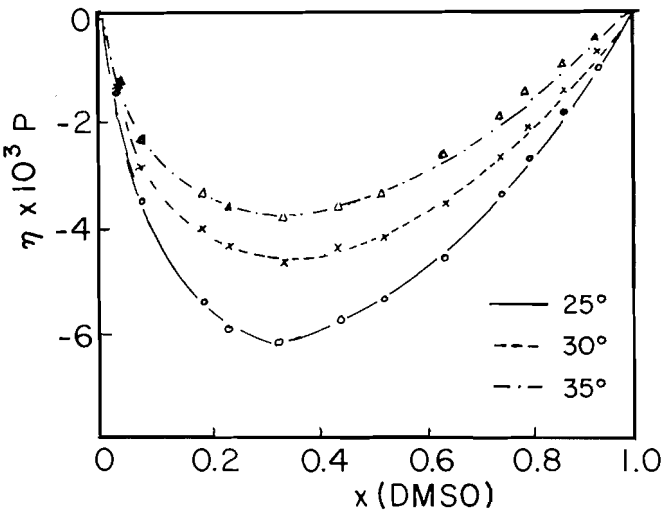


FIG. 3. Variation of η^E vs. x for the DMSO – i-prOH mixture.

this negative deviation we accept that the hydrogen bonds are broken and new species are formed. These new species consist of molecules having different geometrical configuration.

Increase of the temperature decreases the value of η^E extrema, implying that the intermolecular forces between different molecules becomes less strong.

The correlation factor g_k is an important parameter introduced by Kirkwood. It measures the correlation between the orientations of neighbouring molecules resulting from hindered rotation. The correlation factor is greater than unity for systems in which the dipole–dipole interactions give antiparallel orientation. It is less than unity when the dipole–dipole interactions give parallel orientation and g_k equals unity for a normal polar liquid. Hence the values of g_k provide a measure of the extent of the association in polar liquid (10).

The variation of g_k vs. mole fraction for both investigated binary liquid systems is shown in Fig. 5.

For the system dimethylsulfoxide–isopropanol, the correlation factor increases slowly as the concentration of dimethylsulfoxide decreases up to mole fraction x(DMSO) ≃ 0.33. From this point the correlation factor increases more rapidly. The value of g_k for pure dimethylsulfoxide is nearly unity,

Can. J. Chem. Downloaded from www.nrcresearchpress.com by 194.225.253.170 on 09/07/12
For personal use only.

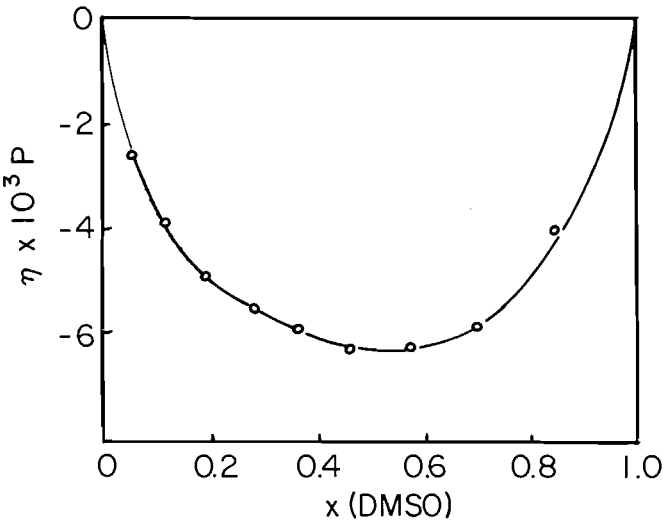


FIG. 4. Variation of η^E vs. x for the PC – *i*-prOH mixture at 25°C.

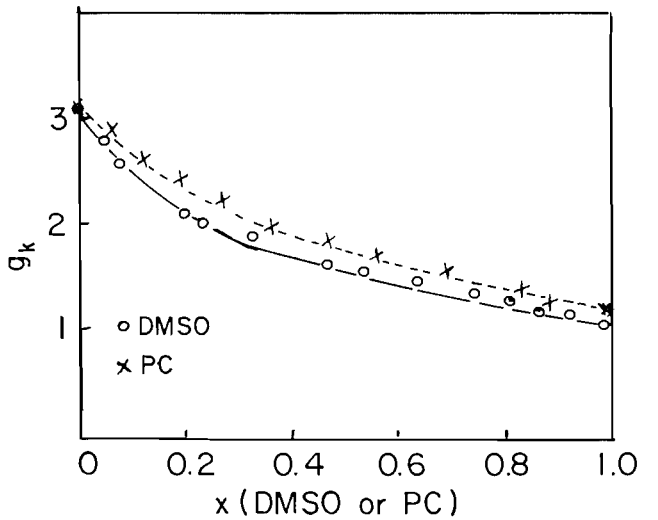


FIG. 5. Variation of η^E vs. x for the DMSO – *i*-prOH and PC – *i*-prOH mixtures.

which means that no specific dipole–dipole interactions exist. The value of g_k for pure isopropanol is much greater than unity. This observation indicates the existence of a chain of molecules with parallel dipole orientation. Addition of isopropanol to dimethylsulfoxide increases the value of g_k. This phenomenon in connection with the variation of ϵ^E and η^E can be explained by accepting the formation of a 2(*i*-prOH)·DMSO complex.

For the binary liquid system propylene carbonate – isopropanol, the molecular association through specific forces was also investigated by calculating the Kirkwood correlation factor g_k. The variation of g_k vs. x is shown in Fig. 5. The resultant g_k values for pure propylene carbonate at 25°C are close enough to unity and are in good agreement with the value reported by Simeral and Amey (11) at the same temperature (taken by extrapolation). This means that propylene carbonate is a relatively unstructured liquid. Thus its physical properties are due to the large molecular dipole moment and there are strong but not specific dipole–dipole forces.

The values of g_k increase gradually, up to mole fraction $x(\mathrm{PC}) \simeq 0.50$ and then the increase becomes more rapid. From the variation of η^E and the change of the increasing rate of g_k one can conclude that the formation of an 1:1 complex takes place. The ability of dimethylsulfoxide and propylene carbonate to associate with substances and to form aggregates, containing species of different kinds of molecules of liquid, has been reported by many authors. Thus the binary liquid system dimethylsulfoxide–water was examined in several laboratories. Experimental data on excess volume, excess viscosity, and excess heat of mixing indicate that these properties show large deviations from ideality (12–15). The deviations show extremum values at about $x \simeq 0.66$ of mole fraction of water. The latter implies that a complex containing a ratio of two molecules of water for each one of dimethylsulfoxide formed. Formation of similar complexes of dimethylsulfoxide with phenol, *p*-cresol, and picric acid is observed (16, 17). Association of dimethylsulfoxide with methanol, ethanol, and acetic acid is also reported (18, 19).

The propylene carbonate – water system shows a miscibility gap between 30 and 90 mol% of water at 25°C. In the area where the two components are miscible the excess dielectric constant shows negative deviation from ideality. Negative deviation in excess dielectric constant shows also the systems propylene carbonate – diethyl carbonate and ethylene carbonate – methanol (20).

It should be mentioned that the Trouton's constants of propylene carbonate and dimethylsulfoxide, which are higher than the value 21 corresponding to nonassociated liquid, are 23 and 29.5, respectively (21).

1. G. RITZOULIS, N. PAPADOPOULOS, and D. JANNACOUDAKIS. J. Chem. Eng. Data, **31**, 146 (1986).
2. A. J. PARKER. Chem. Rev. **16**, 163 (1969).
3. CROWN ZELLERBACH CORP. Dimethylsulfoxide as a reaction solvent. Camas, Washington. 1968.
4. J. B. HASTED. *In* Progress in dielectrics. Vol. 3. *Edited by* J. B. Birks. Heywood and Co., London. 1961.
5. R. H. COLE. J. Chem. Phys. **27**, 33 (1957).
6. J. BARRIOR and A. WEISBECKER. C.R. Acad. Sci. **259**, 2831 (1964).
7. G. DOUHERET and M. MORENAS. Can. J. Chem. **57**, 608 (1979).
8. R. J. FORT and W. R. MOOR. Trans. Faraday Soc. **62**, 1112 (1966).
9. H. N. SOLIMO, R. RIGGIO, F. DAVOLIO, and M. KATZ. Can. J. Chem. **53**, 1258 (1975).
10. A. D'APRANO, D. I. DONATO, and V. AGRIGENTO. J. Solution Chem. **4**, 259 (1982).
11. L. SIMERAL and R. L. AMEY. J. Phys. Chem. **74**, 1443 (1970).
12. J. M. COWIE and P. TOPOROWSKI. Can. J. Chem. **39**, 2240 (1961).
13. J. J. LINDBERG and R. LAUREN. Finska Kemiststamfunders Medd. **71**, 37 (1962).
14. J. KENTTAMAA and J. J. LINDBERG. Suomen Kemistilehti, **33B**, 32 (1960).
15. R. G. DEBEL and J. A. GORING. Chem. Eng. Data Ser. **7**, 100 (1962).
16. R. H. FIGUEROA, E. ROIG, and H. H. SZMANT. Spectrochim. Acta, **22**, 1107 (1966).
17. T. CAIRNS, G. EGLINTON, and D. T. GIBSON. Spectrochim. Acta, **20**, 31 (1964).
18. R. J. FORT and W. R. MOORE. Trans. Faraday Soc. **61**, 2102 (1965).
19. J. J. LINDBERG and J. PIETILA. Suomen Kemistilehti, **35B**, 30 (1962).
20. R. P. SEWARD AND E. C. VIEIRA. J. Phys. Chem. **62**, 127 (1958).
21. T. R. DOUGLAS. J. Am. Chem. Soc. **70**, 2001 (1948).

Can. J. Chem. Downloaded from www.nrcresearchpress.com by 194.225.253.170 on 09/07/12
For personal use only.

Dioxygen reduction at a graphite electrode modified by mononuclear tetraneopentoxyphthalocyaninatocobalt(II) and related polynuclear species

PAVEL JANDA, NAGAO KOBAYASHI, PAMELA R. AUBURN, HERMAN LAM, CLIFFORD C. LEZNOFF, AND A. B. P. LEVER[1]

Department of Chemistry, York University, North York, Ont., Canada M3J 1P3

Received October 6, 1988

PAVEL JANDA, NAGAO KOBAYASHI, PAMELA R. AUBURN, HERMAN LAM, CLIFFORD C. LEZNOFF, and A. B. P. LEVER. Can. J. Chem. **67**, 1109 (1989).

Potentiodynamic data were obtained under argon for the mononuclear species tetraneopentoxyphthalocyaninatocobalt(II) species adsorbed on glassy carbon (GC), ordinary pyrolytic graphite (OPG), and highly oriented pyrolytic graphite (HOPG). Comparative data show that the most convenient material to use is HOPG whereon a limiting monolayer is apparently achieved. Data were also presented for the mononuclear and polynuclear analogues on HOPG under both argon and dioxygen. Comparison is made of the potential data obtained in water and in organic solvent. A pH dependence study shows that the dioxygen reduction potential tracks the Co(II)TNPc/Co(I)TNPc redox couple with a slope of approximately −65 mV/pH for the mononuclear species, in the acid regime, but substantially less than −65 mV/pH for the polynuclear species. There is no pH dependence in the alkaline regime. Possible mechanisms are discussed.

Key words: phthalocyanine, electrochemistry, dioxygen reduction, pH dependence, graphite electrode, cobalt phthalocyanine.

PAVEL JANDA, NAGAO KOBAYASHI, PAMELA R. AUBURN, HERMAN LAM, CLIFFORD C. LEZNOFF et A. B. P. LEVER. Can. J. Chem. **67**, 1109 (1989).

Opérant sous de l'argon, on a déterminé des données potentiodynamiques pour des espèces mononucléaires du tétranéopentoxyphtalocyaninatocobalt(II) adsorbées sur du charbon vitreux (CV), sur du graphite pyrolytique ordinaire (GPO) et sur du graphite pyrolytique hautement orienté (GHPO). Des données comparatives ont permis de démontrer que le matériau le plus commode à utiliser est le GPHO sur lequel il semble possible se déposer une monocouche. On présente aussi des données relatives aux analogues mononucléaires et polynucléaires, sur le GPHO, tant sous un atmosphère d'argon que d'oxygène moléculaire. On a établi une comparaison des potentiels obtenus dans l'eau et dans un solvant organique. Une étude effectuée dans le but de déterminer l'influence du pH a permis de démontrer que, en milieu, le potentiel de réduction des espèces mononucléaires par l'oxygène moléculaire coupe le couple redox Co(II)TNPc/Co(I)TNPc avec une pente d'environ −65 mV/pH, valeur beaucoup plus faible que la valeur de −65 mV/pH qui est observée avec les espèces polynucléaires. En milieu alcalin, il n'y a aucune variation en fonction du pH. On discute des divers mécanismes qui pourraient être impliqués.

Mots clés : phtalocyanine, électrochimie, réduction de l'oxygène moléculaire, relation avec le pH, électrode de graphite, phtalocyanine de cobalt.

[Traduit par la revue]

Can. J. Chem. Downloaded from www.nrcresearchpress.com by 41.223.56.140 on 09/07/12
For personal use only.

Introduction

Macrocyclic complexes of iron and cobalt have proven useful in the development of a better dioxygen reduction catalyst for a fuel cell (1) cathode (2–45). In this regard phthalocyanine species are of particular interest (2–4, 7–9, 16, 17). Recently we have reported (30) data for a series of binuclear cobalt phthalocyanine complexes whose electrocatalytic activity exceeds that of the mononuclear control molecule [3,9,16,23-tetra(neopentoxy)phthalocyanato]cobalt(II),[2] **1** by an amount proportional to the degree of molecular electronic coupling within the binuclear system. During these studies, control data were collected for mononuclear complex **1** on various graphite substrates over a range of pH. The earlier work on the binuclear phthalocyanines was undertaken by depositing the phthalocyanine onto ordinary pyrolytic graphite (OPG) (30), but at that time no variable pH data were obtained. To obtain pH dependence data, this study was repeated on highly oriented pyrolytic graphite (HOPG) which is much more efficient to use since its surface can be prepared (renewed) much more readily than that of OPG. A tetranuclear species (46) was also studied. These data are now reported. Possible mechanisms for dioxygen reduction are discussed.

[1]To whom all correspondence should be addressed.

[2]For simplicity one isomer of species **1**, and of its analogues are labelled here; however, recognize that due to different neopentoxy group substitution patterns, there will be several isomers which are generally inseparable.

Experimental

Equipment

Potential scans (cyclic voltammetry) for dioxygen reduction were performed with a Pine Instruments RD3 potentiostat and the rotation studies with a Pine Instruments PIR rotator.

Materials

o-Dichlorobenzene (DCB) (Aldrich, Gold Label) was used as supplied. Tetrabutylammonium perchlorate (TBAP) (Kodak) was recrystallized from absolute ethanol and dried at 50°C under vacuum for 2 days. Water was purified by double distillation over $KMnO_4$, followed by passage through a Barnstead organic removal cartridge and two Barnstead mixed resin ultrapure cartridges. Fisher certified 1 *N* sodium hydroxide was used for pH 14 aqueous dioxygen reduction studies. Potassium hydrogen phosphate buffers were made up as required for other pH values and checked against a Beckman pH meter. Dilute H_2SO_4 was used for pH 0.7 and 1.0.

Argon gas (Linde) was purified by passage through preheated copper filings, anhydrous $CaSO_4$ (Drierite), molecular sieves (BDH type 3A), and glass wool. Oxygen gas (Linde) was purified by passage through anhydrous $CaSO_4$, NaOH pellets (AnalaR analytical grade), anhydrous $CaSO_4$, molecular sieves, and glass wool.

[3,9,16,23-tetra(neopentoxy)phthalocyanato]cobalt(II), **1** (47, 48), metal-free 3,9,16,23-tetra(neopentoxy)phthalocyanine, **2** (47, 48), and the polynuclear complexes were prepared by literature methods. The polynuclear complexes were 1,2-bis[2′-(9′,16′,23′-trineopentoxyphthalocyanino) cobalt(II)]ethane, C(2)[CoTrNPc]$_2$ (**3**) (49) two cobalt trineopentoxyphthalocyanine rings linked via —CH_2CH_2—; bis-[2′-(9′,16′,23′-trineopentoxyphthalocyanino) cobalt(II)] ether, O(1)[CoTrNPc]$_2$ (**4**) (50) two cobalt trineopentoxyphthalocyanine

Can. J. Chem. Downloaded from www.nrcresearchpress.com by 41.223.56.140 on 09/07/12
For personal use only.

rings linked via a single dioxygen (ether) bridge; Ethylmethylbis-[2′-(9′,16′,23′-trineopentoxy phthalocyaninoxymethyl) cobalt(II)]-methane, EtMeO(5)[CoTrNPc]$_2$ (**5**) (47, 48) two cobalt trineopentoxyphthalocyanine rings linked via —$OCH_2C(Me)(Et)CH_2O$—; 1,2-bis-[2′-(9′,16′,23′-trineopentoxyphthalocyaninoxy) cobalt(II)]benzene, Cat(4)[CoTrNPc]$_2$ (**6**) (49) two cobalt trineopentoxyphthalocyanine rings linked via —O—C_6H_4—O— (*o*-catechol). These complexes are henceforth abbreviated by the label appearing before the square bracket immediately above, namely C(2), O(1), EtMeO(5), and Cat(4), the numeral representing the number of atoms in the bridge. The study also included the tetranuclear spiro species, 1,1,1,1-tetrakis[2′-(9′,16′,23′-trineopentoxyphthalocyaninoxymethyl) cobalt(II)] methane, [Co(II)TrNPc(−2)]$_4$ (**7**) (46), abbreviated Tet.

Electrodes

Ordinary pyrolytic graphite (OPG), and highly oriented pyrolytic graphite (HOPG), sometimes called stress annealed pyrolytic graphite (SAPG) were obtained from Union Carbide. The OPG was mounted in Teflon to expose a circular area of 0.493 cm^2. The glassy carbon (GC) electrode, of area 0.07 cm^2, was purchased from Tokai Carbon Ltd., Japan.

Electrodes fabricated from OPG, GC, and Pt were cleaned by polishing with 1.0, 0.3, and 0.05 μM alumina suspended in water. The cell for the adsorption experiments employed an SCE electrode, a graphite working electrode, and a platinum wire counter electrode.

The HOPG was similarly mounted in a Teflon holder to expose a circular area of 0.44 cm^2. The basal plane of the graphite was perpendicular to the axis of the electrode. This enables a fresh surface of electrode material to be exposed when a piece of Scotch brand "Magic Transparent" tape is momentarily pressed onto the surface and then gently lifted off. Usually at least two layers are removed between each adsorption study. The new surface thus revealed is used within a few minutes of exposure.

Catalyst coated electrodes were prepared by immersing and rotating (ca. 400 rpm) (on open circuit) the freshly prepared graphite surface in DCB solutions of a phthalocyanine of concentration approximately 5 $\times 10^{-5} M$ (varied from $1 \times 10^{-7} M$ to $5 \times 10^{-5} M$ in the case of **1**). The coated electrode was washed with ethanol and distilled water and dried under reduced pressure.

The time required to achieve a steady state surface concentration of a designated phthalocyanine may be conveniently monitored by cyclic voltammetry (v = 100 mV/s). For these experiments, solutions containing the desired phthalocyanine were made 0.1 M in TBAP and the state of the adsorbed layer was monitored at 5 min intervals, until the peak current corresponding to a redox reaction of the adsorbed catalyst remained constant. Redox processes corresponding to the adsorbed and bulk species occur at different potentials and are thus easily distinguished. The adsorption equilibrium (as evidenced by constant first CV scan) was established in $10^{-7} M$ **1** in about 40 min and in about 10 min (or less) in the case of $5 \times 10^{-5} M$ solution. Unlike the situation with similarly active (11) tetrasulfonated phthalocyanines (TSPc) (12) well-defined voltammetric peaks were obtained without cycling of the electrode during the adsorption step. Indeed, continuous cycling during adsorption, in any potential range, significantly decreased the amount of **1** adsorbed at the surface.

Data in non-aqueous solution were referenced to SCE via incorporation of ferrocene as an internal calibrant (51).

Note that for good reproducibility of the dioxygen reduction data, the catalyst surface was renewed for every individual experiment, *i.e.*, for every scan. Successive scans, under dioxygen, using the same surface show variations (shift in potential, loss of current etc.) which may be due to loss of catalyst and/or some catalyst decomposition.

Results and discussion

*(i) Adsorption of **1** on GC, OPG, and HOPG*

Since it is feasible to study dioxygen reduction by laying down one or more layers of catalyst upon various types of graphitic surface, especially OPG, HOPG, and GC, the best conditions to prepare electrodes modified by **1** were first investigated.

Phthalocyanines applied to the electrode by simple evaporation of their solution in an organic solvent can form uneven multi-layer films which are often microcrystalline. In addition, only a fraction of the film may be electrochemically active, leading to problems of reproducibility. The slow diffusion of oxygen (and counter ions) from the solution into the film, and the potential drop caused by the resistance of the film and hence potential shift of the votammetric curve also provide complicating factors (52, 53). While vapour deposition provides a convenient method (54) for film preparation especially where insoluble, but volatile, phthalocyanines are concerned, adsorption is a simpler procedure for organic solvent soluble metallophthalocyanines. A monolayer of the catalyst formed at the electrode surface by adsorption yields much better electrochemical results under the conditions where adsorption is highly irreversible and the bare surface of the electrode shows minimal electrocatalytic activity toward dioxygen reduction. Such layers were laid down according to the procedures outlined in the experimental section.

No adsorption was found on a Pt electrode. In the case of OPG and especially HOPG strong adsorption was observed (Fig. 1). Essentially the same results were seen with **2**, thus adsorption does not seem to involve metal ion interaction with defects on the surface. Low coverage and weak adsorption were observed on amorphous GC (Fig. 1*D*) which does not have the oriented graphitic structure of other electrodes.

On the OPG surface, the phthalocyanine surface concentration calculated to be present varies with the cleaning procedure. An OPG electrode polished by alumina, and washed only by distilled water yields a lower coverage (Fig. 1*B*) than an electrode in which the surface after the alumina treatment is further cleaned using a clean wet polishing cloth or ultrasonic cleaner. In the former case a highly hydrophilic surface is formed, presumably covered by alumina particles which can block the adsorption of TNPc. The surface cleaned using the second method is hydrophobic, as judged qualitatively from the water contact angle, and the amount of adsorbed TNPc is higher (Fig. 1*A*). Thus the degree of coverage is variable and dependent upon the details of cleaning (55, 56). Moreover, there is a relatively large residual current from the OPG surface, hindering the observation of waves of low faradaic current. Thus this material provides an unsatisfactory surface for routine and reproducible study of the electroactivity of supported phthalocyanines. The HOPG surface was undoubtedly the preferred surface with a low residual current and high reproducibility. When the bare electrode is rotated in a *ca.* $10^{-5} M$ DCB solution of **1**, the cyclic voltammogram rapidly reaches an equilibrium current maximum. This maximum, adopting the macroscopic area of the electrode, and assuming a one-electron redox couple (see below), corresponded approximately to an average surface concentration of a 6×10^{-11} mol/cm^2. It is conceivable that the phthalocyanine molecules lie flat and form π–π bonds with the graphite lattice yielding an area of about 200 Å^2. Other aromatic molecules similarly show high affinity for graphite (54, 56). The coverage, Γ, then approaches a monolayer (Fig. 1*C*). Compounds **2**–**7** may be similarly adsorbed but no evidence was collected to determine their detailed surface behaviour.

The limit of one monolayer for **1** is instructive. If the molecules are lined up perpendicular to the surface with a smaller effective area (e.g. as suggested for tetrasulfonated cobalt phthalocyanine (13)), then the amount of charge, C_p, would correspond to an incompletely covered surface and further adsorption would have been anticipated.

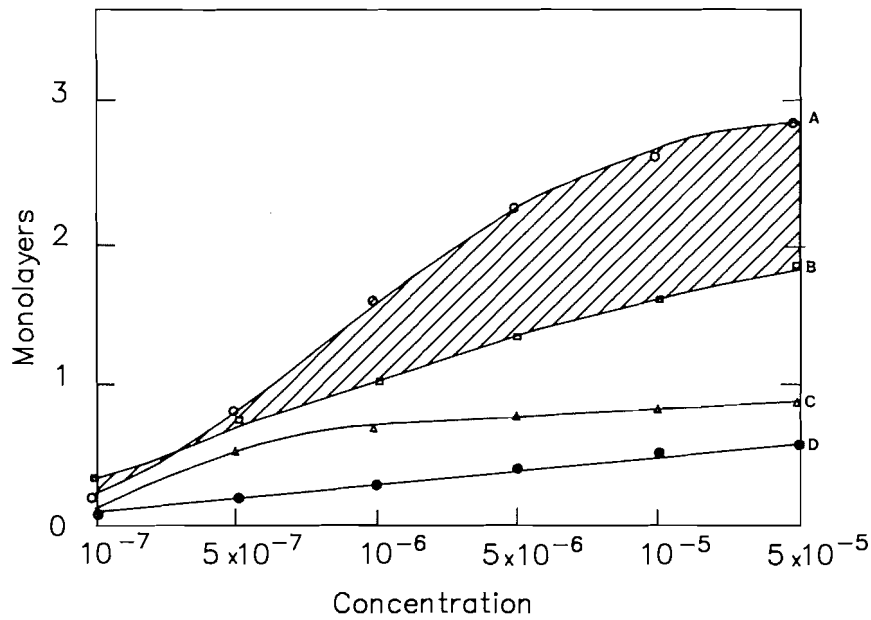


FIG. 1. Adsorption isotherms for Co(II)TNPc, **1**. Number of monolayers versus concentration of Co(II)TNPc in depositing solution (0.1 *M* TBAP/DCB) at 20°C. (*A*) OPG hydrophobic surface, (*B*) OPG hydrophilic surface, (*C*) HOPG, (*D*) GC. The shaded region shows a continual gradation between highly hydrophobic and highly hydrophilic surfaces.

TABLE 1. Charge under the Co(II)TNPc/Co(I)TNPc redox couple of complex **1** as a function of scan rate[a]

Scan rate (V/s)	Current (μA) i_p	Charge (μC) C	i_p/C
0.15	8.5	7.64	1.13
0.125	6.0	6.31	0.93
0.1	5.0	6.80	0.75
0.075	4.0	7.20	0.54
0.05	2.0	6.10	0.34

[a]Plot of i_p/C versus scan rate, including the origin point, yields a least-squares slope of 7.58 (for $nF/4RT$) corresponding to n = 0.78 and with a regression coefficient of 0.998.

The assumption that the redox couples observed under argon were one-electron in nature, was checked using eq. [1]. Thus:

$$i_p = n^2F^2\Gamma v/4RT$$

and since

$$C_p = nF\Gamma$$

then:

[1] $$i_p/C_p = nFv/4R$$

where i_p and C_p are the current and charge densities, respectively. Thus a plot of the ratio of these quantities against scan rate v, provides a measure of n, the number of electrons (14). Experimentally, using the Co(II)TNPc(−2)/[Co(I)TNPc(−2)]$^-$ redox couple of **1**, a value of n = 0.78 is obtained (Table 1).

Alternatively, if a Langmuir isotherm is assumed to be valid to describe the adsorption of the catalyst on the surface (see refs. 30, 57 for detailed discussion), then the number of electrons, n, is related to the half-bandwidth of the cyclic voltammetric peak, $W_{1/2}$, by

[2] $$n = 2RT[\ln (3 + 2\sqrt{2})/FW_{1/2}]$$

This yields a n value of 1.1–1.2 electrons for the several voltammetric peaks involved, using **1**. The deviation from unity probably reflects some deviation from true Langmuir isotherm behaviour, *i.e.* probably some interaction between adjacent molecules. Note, however, that the use of any isotherm requires a dynamic equilibrium between surface and solution, and the absence of any phthalocyanine catalyst in solution precludes such an equilibrium here.

In the HOPG case, the true surface area of the electrode and that measured macroscopically are not likely to be very disparate. A significantly higher coverage on OPG seems to be caused by a higher roughness factor of the OPG surface which is also confirmed by a higher residual current, *i.e.* the true microscopic surface area is larger than the macroscopically measured area.

Comparative CV data taken in DCB and in water show that the catalyst layer survives the transfer to the water medium.

(ii) Electrochemical behaviour of an HOPG electrode covered by a monolayer of ***1***

Under argon

The redox peaks of a monolayer of catalyst on the surface, under argon, can readily be observed in water solutions (Fig. 2*a*). A pair of voltammetric peaks in the region negative of 0 V vs. SCE, under argon, correspond to the [Co(II)TNPc(−2)]/[Co(I)TNPc(−2)]$^-$ couple, by analogy with a wealth of data collected in solvent media (58–67). They are adsorption peaks having a current proportional to the scan rate (not its square root) (68), and approach more reversible behaviour in acidic solution, the separation between the anodic and cathodic components decreasing with pH (Table 2). The half-wave potential for the [Co(II)TNPc(−2)]/[Co(I)TNPc(−2)]$^-$ couple in the alkaline range, near −700 mV vs. SCE, is essentially the same as that observed in the aprotic organic solvents such as DCB (67) (Table 3), but distinctly more negative than either CoPc or CoTsPc under the same adsorption conditions. A second reduction peak at more negative potentials arises from the [Co(I)TNPc(−2)]$^-$/[Co(I)TNPc(−3)]$^{2-}$ redox process.

The catalyst oxidation peaks are seen near (+475) − (+720) mV, vs. SCE (Fig. 2*a*) and are composite, at some pH showing two clear cathodic components. Solution studies (67) reveal

Can. J. Chem. Downloaded from www.nrcresearchpress.com by 41.223.56.140 on 09/07/12
For personal use only.

Can. J. Chem. Downloaded from www.nrcresearchpress.com by 41.223.56.140 on 09/07/12
For personal use only.

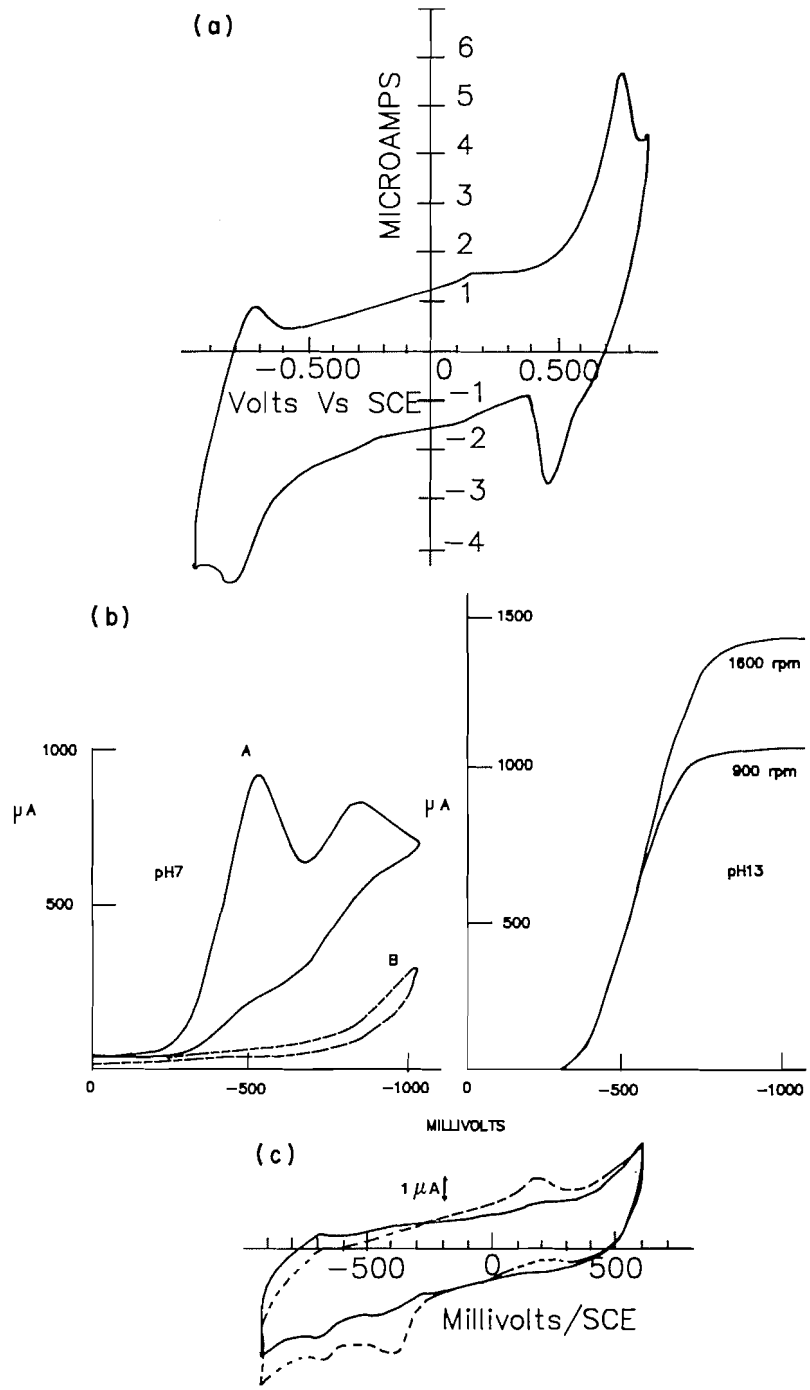


FIG. 2. (*a*) Cyclic voltammogram for Co(II)TNPc (**1**) layer deposited from a TBAP/DCB solution onto a HOPG electrode, and immersed in 0.1 *M* aq. phosphate buffer at pH 7, under argon. The left-hand couple is Co(II)TNPc(−2)/[Co(I)TNPc(−2)]$^-$, while the right-hand couple is probably an overlap of the Co(III)/Co(II) and Pc(−1)/Pc(−2) couples. (*b*) Left-hand plot: (A) Cyclic voltammogram for Co(II)TNPc (**1**) layer deposited from a TBAP/DCB solution onto a HOPG electrode, and immersed in 0.1 *M* aq. phosphate buffer at pH 7, saturated with dioxygen at 20°C. (B) as (A) but a bare unmodified HOPG surface. Right-hand plot: rotating disc electrode study of a Co(II)TNPc (**1**) layer deposited from a TBAP/DCB solution onto a HOPG electrode, and immersed in 0.1 *M* aq. NaOH at pH 13, saturated with dioxygen at 20°C. The lower scan is observed at 900 rpm and the upper at 1600 rpm. (*c*) Cyclic voltammogram for Co(II)TNPc (**1**) layer deposited from a TBAP/DCB solution onto a HOPG electrode, and immersed in 0.1 *M* NaOH at pH 13, under argon. Solid line — as described; hatched line with addition of 0.5 mL of 1×10^{-3} *M* O_2 dissolved in 0.1 *M* NaOH. The new peak at −420 mV in the second spectrum corresponds to dioxygen reduction while the new peak at +170 mV corresponds to hydrogen peroxide oxidation.

that the [Co(II)TNPc(−1)]$^+$/Co(II)TNPc(−2) and [Co(III)-TNPc(−2)]$^+$/Co(II)TNPc(−2) oxidation couples are likely to be close together and critically dependent upon potentially ligating groups in solution (or on the surface). In the absence of clearly defined behaviour for these couples their discussion will be postponed for later study.

Under dioxygen

It is very convenient that the bare HOPG surface also has a low catalytic activity towards dioxygen reduction in water solutions, allowing one to measure the electrocatalytic activity of the catalyst without interference of the bare surface (Fig. 2*b*).

An HOPG electrode surface modified with a layer of the

TABLE 2. Voltammetric data (mV) for CoTNPc under dioxygen and argon, as a function of pH

pH	Argon/CV[a]	Dioxygen/CV[b]		Dioxygen/RDE[c]
		Wave 1	Wave 2	
1	−420(60)	−300		−280
2	−460(40)	−340	−855	−330
3	−510(40)	−425	−1000	−390
4	−570(40)	−480	−865	−390
5	−630(60)	−520	−905	−400
6	−685(90)	−520	−830	−470
7	−720(70)	−500	−830	−440
8	−720(85)	−500	−840	−460
9	−700(100)	−485		−435
10		−475		−425
11	−700(80)	−480		−435
12	−695(80)	−470		−430
13	−720(40)	−465		−420

[a]Cyclic voltammogram under argon — average of anodic and cathodic waves; peak-to-peak separation in parentheses.

[b]Cyclic voltammogram under dioxygen, peak observed at a scan rate of 0.10 V/s; wave 1 is dioxygen to hydrogen peroxide and wave 2 is hydrogen peroxide to water.

[c]Half-wave potential of rotating disc electrode peak, under dioxygen.

metal free **2** does not show any electrocatalytic activity. However, the cobalt complex **1** is active. In Fig. 2*c* are shown the cyclic voltammograms for the **1** modified HOPG electrode in water solution at pH 13, under argon, to which has been added 0.5 mL of solution containing 10^{-3} *M* dioxygen. The appearance of a signal due to dioxygen reduction can clearly be observed at a potential positive of the catalyst reduction peak (Table 2). The hydrogen peroxide re-oxidation wave can also be observed at +170 mV (Fig. 2*c*).

As shown in Fig. 2*b*, with excess dioxygen, the anodic peak (observed under argon) corresponding to the re-oxidation of $[Co(I)TNPc(-2)]^-$ completely disappears since the $[Co(I)TNPc(-2)]^-$ has already been oxidized by dioxygen to Co(II)TNPc(−2).

(a) Cyclic voltammetry

The current exhibited by the dioxygen reduction wave is proportional to the square root of the scan rate and is therefore a diffusion wave (68). The dioxygen reduction wave occurs positive of the catalyst Co(II)/Co(I) redox couple, by about 250 mV in the alkaline regime decreasing to about 100 mV in the acid regime (Table 2, Fig. 2*b*).

The pH dependence of the dioxygen reduction potential for **1** parallels that of the $Co(II)TNPc(-2)/[Co(I)TNPc(-2)]^-$ couple with a slope, in the acid region, of −66 mV/pH. We return to this issue below.

At a more negative potential, a second reduction wave is observed (Table 2), which corresponds to the successive reduction of hydrogen peroxide to water. Scanning positively again after the first reduction peak yields a hydrogen peroxide re-oxidation wave at about 0.2 V (Fig. 2*c*). Further proof was obtained by adding microlitre quantities of dioxygen-free hydrogen peroxide to the electrochemical cell and observing an increase in the height of this second wave, relative to the first. The pH dependence of the second reduction wave is not very clearly defined since it is observed very close to the solvent limit and is therefore subject to some error. This behaviour is very similar to that observed with a crown phthalocyanine cobalt species (69–71) where a well-defined pH dependence was observed (71). Previous studies of the two-electron reduction of dioxygen to hydrogen peroxide, have noted the existence of a second reduction process ascribed to hydrogen peroxide reduction (4, 23, 31, 72). In acid solution, under argon, the second reduction process, namely $[Co(I)TNPc(-2)]^-/[Co(I)TNPc(-3)]^{2-}$ occurring very close to the $Co(II)TNPc(-2)/[Co(I)TNPc(-2)]^-$ couple (12), may catalyse the hydrogen peroxide reduction to water. In alkaline solution, this couple moves dramatically more negative (12), explaining why the hydrogen peroxide to water reduction process is not observable in alkaline solution.

(b) Rotating disc and ring disc electrode (RDE and RRDE) studies

The magnitude of the limiting current, i_L, in the RDE dioxygen reduction wave depends linearly on the square root of the rotation rate in the range of 400–2500 rpm and is in agreement with the two-electron reduction of dioxygen to peroxide throughout the pH range studied. The halfwave potential $E_{1/2}$ of the dioxygen reduction wave tracks the $Co(II)TNPc(-2)/[Co(I)TNPc(-2)]^-$ pH dependence (Fig. 3*a*).

The standard expression for the limiting current of a diffu-

TABLE 3. Variation of redox potentials (V) of cobalt phthalocyanine reduction processes as a function of environment[a]

Cobalt species[b]	Conditions[c]	$[Co(I)TNPc(-2)]^-/[Co(I)TNPc(-3)]^{2-}$	$[Co(II)TNPc(-2)]/[Co(I)TNPc(-2)]^-$	Reference
CoTsPc/ads	Aq. pH 13	−1.37	−0.51	12
CoTsPc/ads	Aq. pH 2	−0.60	−0.31	12
CoTNPc/ads	Aq. pH 8		−0.71	This work
CoTNPc/ads	Aq. pH 4		−0.57	This work
CoTNPc	DCB soln.	−1.76	−0.60	67
CoTNPc	DMF soln.	−1.76	−0.54	67
CoCRPc/ads	Aq. pH 11		−0.60	69, 71
CoCRPc/ads	Aq. pH 2	−0.48	−0.34	69, 71
CoPc	Py		−0.61	92
CoPc/ads[d]	pH 14		−0.57	93
CoPc/ads[d]	pH 2		−0.29	93

[a]Versus SCE.

[b]TsPc = tetrasulphonated phthalocyanine; TNPc = tetraneopentoxyphthalocyanine, CRPc = tetracrown-phthalocyanine, ads = adsorbed on HOPG.

[c]DCB = *o*-dichlorobenzene, DMF = dimethylformamide, Py = pyridine.

[d]Adsorbed on ordinary pyrolytic graphite.

Can. J. Chem. Downloaded from www.nrcresearchpress.com by 41.223.56.140 on 09/07/12
For personal use only.

Can. J. Chem. Downloaded from www.nrcresearchpress.com by 41.223.56.140 on 09/07/12
For personal use only.

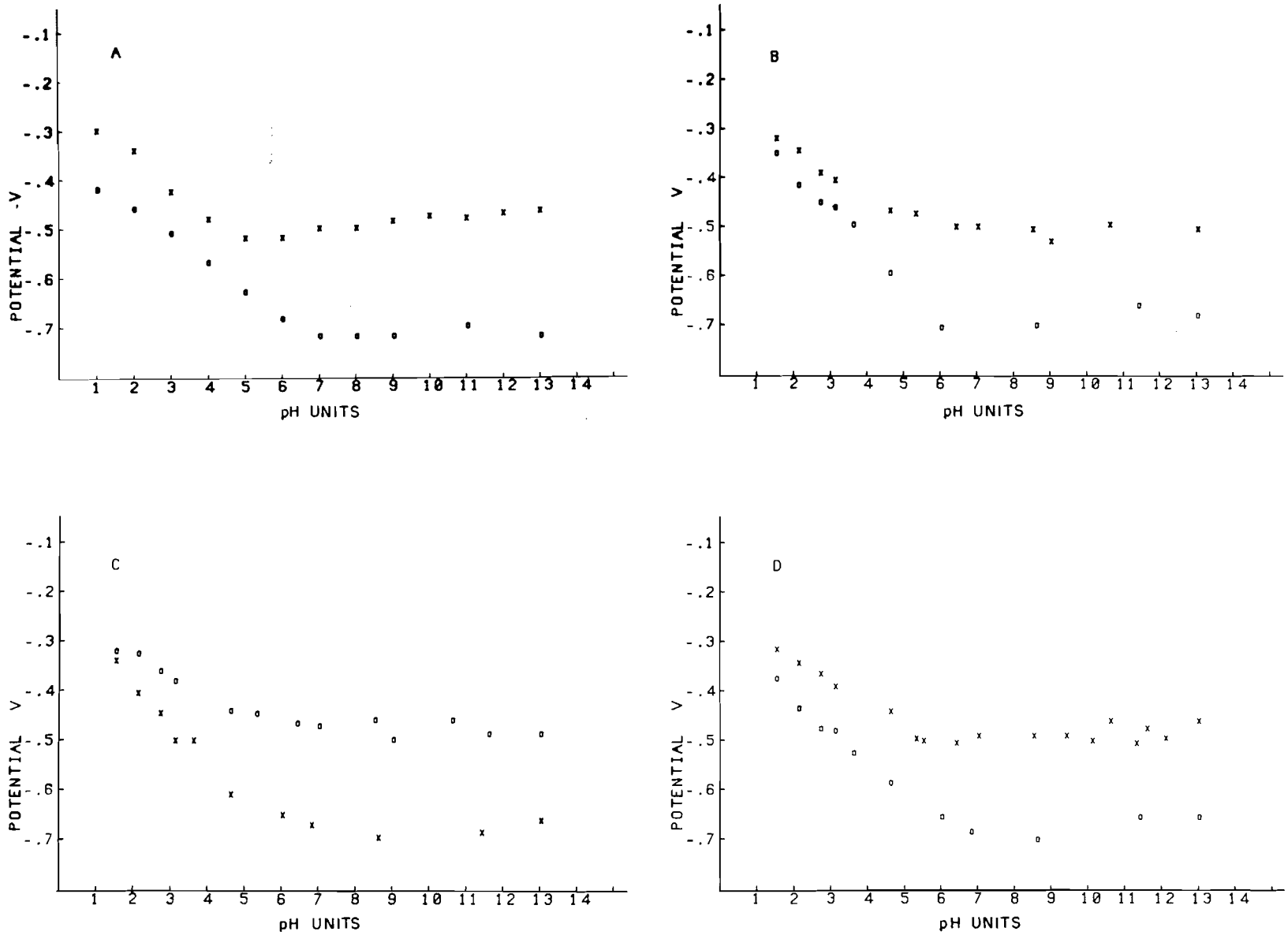


FIG. 3. pH versus potential plots for all the species under consideration. In each case the upper plot refers to dioxygen reduction half-wave potential, and the lower plot to the Co(II)/Co(I) half-wave potential. The species are (*a*) **1**, (*b*) **3**, (*c*) **4**, (*d*) **5**, (*e*) **6**, (*f*) **7**.

Can. J. Chem. Downloaded from www.nrcresearchpress.com by 41.223.56.140 on 09/07/12
For personal use only.

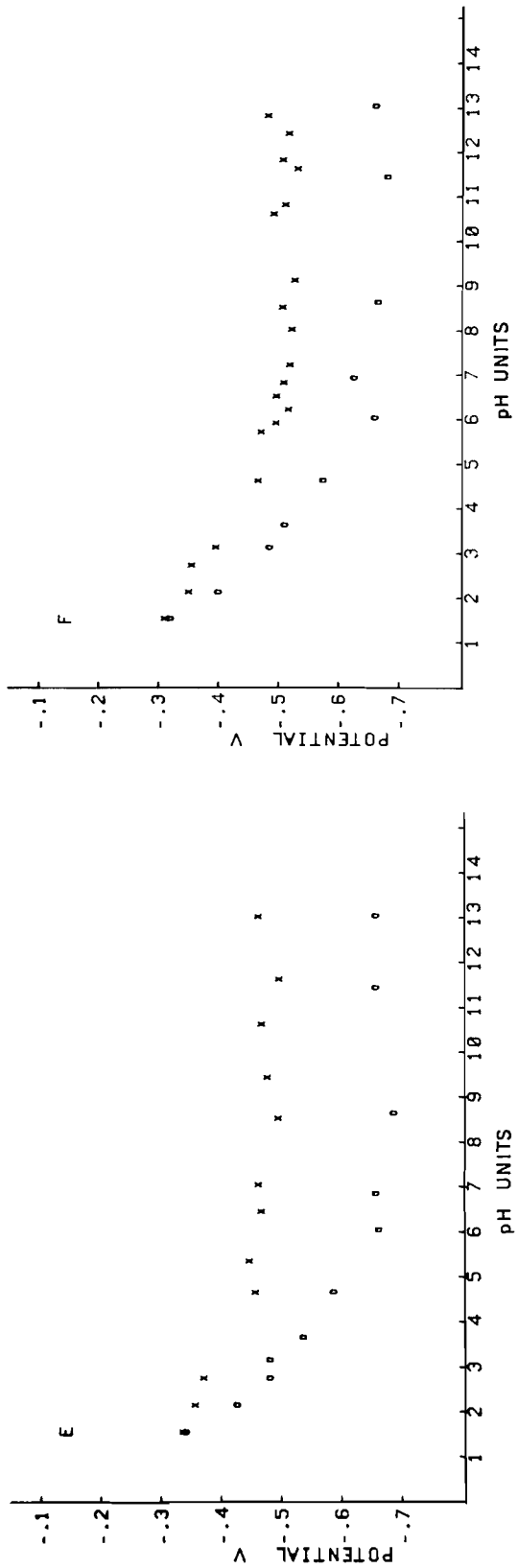


FIG. 3 (*concluded*)

Can. J. Chem. Downloaded from www.nrcresearchpress.com by 41.223.56.140 on 09/07/12
For personal use only.

sion limited RDE plateau is given by (68)

[3] $i_L = 0.620nFAD_0^{2/3}\Omega^{1/2}v^{-1/6}C_{ox}$

where $\Omega = 2\pi f/60$ (f in rpm). The terms $D_0^{2/3}v^{-1/6}C_{ox} = 1.77 \times 10^{-9}$ mol cm^{-2} s$^{-1/2}$ calibrated with a platinum electrode assumed to be well behaved (73) and to provide a four-electron limiting wave, and the kinematic viscosity, v, $= 9.97 \times 10^{-3}$ cm^2/s. The expression yields a limiting two-electron current of 1066 μA at 900 rpm compared with an experimental value of 1075 μA (complex **1**) (Fig. 2*b*).

Logarithmic analysis of the current, i, *i.e.*, a plot of potential versus log $[i/(i_L - i)]$ yields a value falling between −110 and −130 mV/pH unit (Tafel slope) through the pH range from ca. 1.0 to 13, with a regression coefficient generally of 0.999. This corresponds to a charge transfer coefficient, $\alpha = 0.5$ and a one-electron rate-determining step, a common observation with cobalt macrocycle catalysts which reduce dioxygen to hydrogen peroxide (14, 74). Similar results are obtained for the binuclear and polynuclear species described immediately below.

Finally, a rotating ring disc experiment (RRDE, OPG, gold ring), with the ring polarised to oxidise any hydrogen peroxide which may be formed, provides additional proof of the generation of hydrogen peroxide in this experiment (at pH 9.2, Fig. 4).

(iii) Binuclear and tetranuclear species, 3–7, adsorbed on to HOPG

Figure 3*b–f* illustrates the pH dependence of the Co(II)/Co(I) couple under argon, and the dioxygen reduction peak potentials, as a function of pH, for complexes **3–7**. In all cases, and similar to the monomeric species **1** the Co(II)/Co(I) couple has a ca. −(60–70) mV/pH unit dependence in the acid regime, between pH 1 and ca. 5.0, and then becomes pH independent.[3]

The dioxygen reduction wave appears at some 200–250 mV more positive a potential than the Co(II)/Co(I) wave, in the alkaline range, dropping to about 50 mV more positive in the acid range. However, there is characteristic difference between the polynuclear species and the control species **1**. In the latter, the slope of the dioxygen reduction wave is ca. −65 mV/pH in the acid range, but for the polynuclear species it is invariably significantly smaller (Table 4). Indeed, the dioxygen reduction wave and Co(II)/Co(I) wave in these polynuclear species will occur at essentially the same potential near pH 0 (see intercept in Table 4).

(iv) Mechanism and pH dependence

The −65 mV/pH unit dependence of the Co(II)TNPc(−2)/[Co(I)TNPc(−2)]$^-$ couple, seen with all the species investigated here, implies that the reduced and negatively charged [Co(I)TNPc(−2)]$^-$ species binds a proton, probably to a peripheral nitrogen atom (12). This pH dependence is very similar to that observed with the TsPcM(II)/[TsPcM(I)]$^-$ redox couples (M = Co, Fe) (12) and differs from that generated by the TsPcM(III)/TsPcM(II) redox couple (M = Co, Fe) where the pH dependent region lies above 7 rather than below 7.

There have been a number of studies of the role of pH on the dioxygen reduction potential of macrocyclic catalysts (3, 14, 18, 20, 23, 25, 27, 29, 37, 38, 76, 77) including a similar study of the pH dependence of the unsubstituted cobalt phthalocyanine in its Co(II)/Co(I) redox couple (3, 77).

Ni and Anson have (28) discussed the relative potentials for reduction of the adsorbed species, for various cobalt macrocyclic catalysts under argon and under dioxygen. They note that where the Co(III)/Co(II) couple of an adsorbed catalyst is involved, reduction of dioxygen often occurs at a potential *considerably more negative* than the Co(III)/Co(II) couple. The mechanism is perceived to be a "CE catalytic" mechanism where Co(II) is formed and subsequently reacts with dioxygen

[3]The data for the mononuclear species **1** were obtained at York, while the data for the polynuclear species were obtained by the same procedure in Prague, but using a different electrode and different equipment. These latter data are more scattered than the York data, with a probable error of at least ±20 mV. The reason for this scatter is not known, but it does not invalidate the general conclusions.

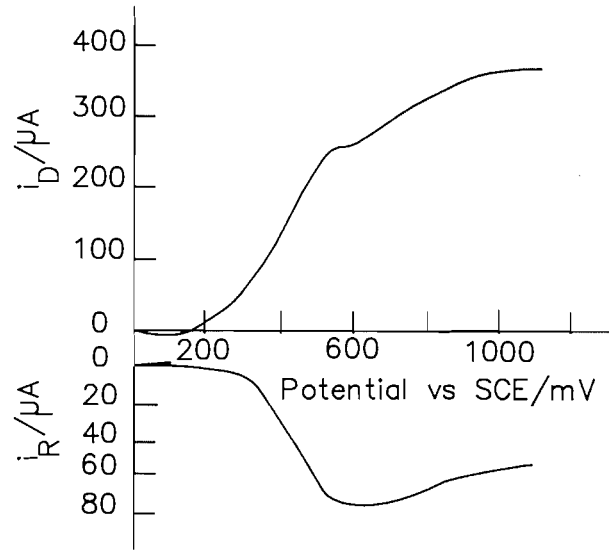
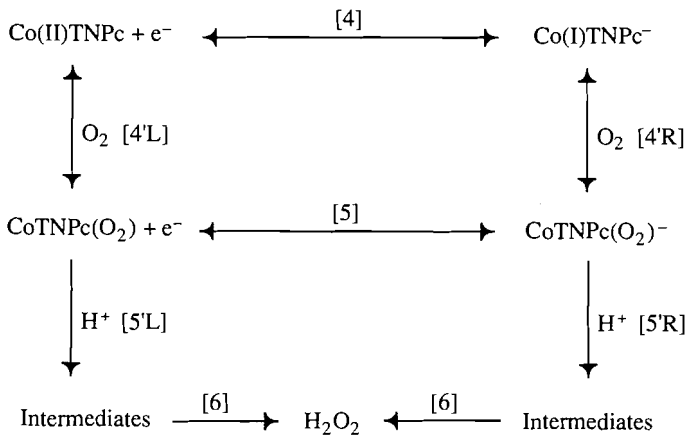


FIG. 4. A rotating ring disk experiment with Co(II)TNPc (**1**). Gold ring — OPG disk (0.18 cm^2 area) response for adsorbed **1** immersed in 0.1 *M* phosphate buffer at pH 9.2, saturated with dioxygen at 20°C. The upper curve shows reduction of dioxygen at the disk, and the lower response, re-oxidation of hydrogen peroxide at the ring (polarised at +1.0 V). Rotation rate is 400 rpm, and scan rate is 10 mV/s.

TABLE 4. Line equations in the acidic range[a]

Complex	Couple	Slope (mV/pH)	Intercept[b] (mV)	Correlation coefficient
Monomer	Co[c]	−53	−359	0.99
	O_2[d]	−58	−239	0.98
Binuclears				
O(1)	Co	−83.4	−224	0.98
	O_2	−41	−252	0.98
C(2)	Co	−73.6	−247	0.975
	O_2	−48.1	−253	0.985
Cat(4)	Co	−63.4	−299	0.97
	O_2	−32.5	−288	0.95
EtMeO(5)	Co	−65.1	−290	0.98
	O_2	−45.7	−247	0.99
Tet	Co	−69.2	−263	0.99
	O_2	−49.3	−239	0.97

[a]Data for least-square lines from approximately pH 2 to 5. Data are presented in millivolts.
[b]Intercept with respect to SCE.
[c]Refers to the Co(II)TnPc(−2)/[Co(I)TnPc(−2)]$^-$ couple.
[d]Refers to the dioxygen reduction couple.



SCHEME 1

(the C step) prior to eventual electron transfer with reduction of dioxygen (the E step) (28, 78). This is construed to differ from other systems where the reduction of the catalyst drives the dioxygen reduction immediately in an "EC catalytic" mechanism. This occurs both in homogenous solution (4, 25, 29, 39, 42, 43, 79) and for some adsorbed catalysts (25, 27, 29, 39, 41, 42, 76, 77), where the dioxygen reduction occurs at, or slightly negative of, the catalyst redox couple.

However, dioxygen reduction may occur at a potential positive of the catalyst redox process. This may be a consequence of an EC mechanism where the chemical and E step are so fast (80, 81) that dioxygen reduction can occur to a significant extent at a potential positive of the half-wave potential of the catalyst redox process, where a nernstian-determined small concentration of the active reduced form of the catalyst will occur.

However, if this process occurs some 250 mV or more positive of the catalyst redox wave, the quantity of reduced catalyst (e.g. Co(I)Pc here) is so small that the rate constant for dioxygen reduction needs to be excessively if not impossibly high (25, 29, 78, 80–86). Thus this likelihood is discounted, i.e., even though the dioxygen reduction tracks the Co(II)/Co(I) couple, it is not Co(I)Pc which is the primary active species. This conclusion is further supported by the observation of dioxygen reduction some 800 mV positive of the Co(II)Pc/Co(I)Pc wave at pH 14 using a newly investigated system (87).

A general set of relevant equations may be written as in Scheme 1. It is generally assumed that Co(III)TNPc species are not involved in dioxygen reduction.

Dioxygen reduction catalysis is not a consequence of activation by Co(I)TNPc, at least at the higher potentials (positive of the Co(II)/Co(I) wave). Thus the right-hand channel ([4], [4'R], [5'R]) is not important until very close to or beyond the Co(II)-TNPc/$[Co(I)TNPc]^-$ redox potential. Thus reaction must occur with Co(II)TNPc species.

Then the reaction mechanism may be written following [4'L], [5'L]. Equilibrium [4'L] lies well to the top since, at room temperature, there is little tendency to form a dioxygen adduct with Co(II)Pc. Such species are, however, observed at reduced temperatures (88). A significant overpotential is required to drive the reaction towards hydrogen peroxide. The Co(III)Pc/Co(II)Pc couple is pH independent in the acid regime (89) emphasizing that the pH dependence seen for dioxygen reduction in the acid regime must involve the irreversible binding of a proton to the coordinated di-oxygen as a first step towards hydrogen peroxide formation (85, 90); the fact that it appears to track the Co(II)/Co(I) wave is then fortuitous.

It is significant that the slope of the dioxygen reduction potential versus pH plot is less than −65 mV/pH for all the polynuclear species (Table 4), but is close to −65 mV/pH for dioxygen reduction at the mononuclear species, and for the Co(II)TNPc/Co(I)TNPc couple for the mononuclear and polynuclear species. That the dependence is about −65 mV/pH for this latter couple in the polynuclear species shows that the reduction of each Co(II) is unconcerted, *i.e.*, the reduction of one Co(II) moiety has no detectable electrochemical consequence for the other even though the electronic spectra of the polynuclear Co(II)TrNPc species shows evidence of some electronic coupling (46, 91).

A slope of less than −65 mV/pH can arise through the inclusion partially or wholly of a concerted two-electron dioxygen reduction process in the polynuclear species. That this is observed with the polynuclear species and not the mononuclear is quite credible. Consider, for example, the concerted process [7], [8]

[7] $\text{Bridge}[Co(II)TrNPc]_2 + O_2 \rightleftharpoons \text{Bridge}[TrNPcCo(III)(O_2^{2-})Co(III)TrNPc]$

[8] $\text{Bridge}[TrNPcCo(III)(O_2^{2-})Co(III)TrNPc] + H^+ + 2e^- \dashrightarrow O_2H^- + \text{Bridge}[Co(II)TrNPc]_2$

It is not at all unreasonable that the formation of a most likely bridged peroxo derivative in at least those polynuclear CoTrNPc species capable of cofacial configurations in one or more of their conformations could lead to some concerted character in the dioxygen reduction and re-formation of the starting polynuclear Co(II) species. We see no direct evidence in these complexes for such a binuclear peroxo species which need, however, only be present to a small equilibrium degree to give rise to the observed electrochemical behaviour. In the cofacial crown phthalocyanine cobalt species, however, there is much more direct evidence for the formation of such a dioxygen adduct (69, 75).

Acknowledgements

We are indebted to the Natural Sciences and Engineering Research Council (Ottawa) and the Office of Naval Research (Washington) for financial support, P.R.A. is indebted to Professor A. Vlcek of the Heyrovsky Electrochemical Institute for hospitality and the CSSR Academy of Science for financial support.

1. H. LIHACH. EPRI J. 8 (1984).
2. F. F. VAN DEN BRINK, W. VISSCHER, and E. BARENDRECHT. J. Electroanal. Chem. **157**, 283 (1983).
3. A. ELZING, A. VAN DER PUTTEN, W. VISSCHER, and E. BARENDRECHT. J. Electroanal. Chem. **200**, 313 (1986); **233**, 113 (1987).
4. A. VAN DER PUTTEN, A. ELZING, W. VISSCHER, and E. BARENDRECHT. J. Electroanal. Chem. **214**, 523 (1986); A. VAN DER PUTTEN. Ph.D. thesis. 1986.
5. N. KOBAYASHI and Y. NISHIYAMA. J. Phys. Chem. **89**, 1167 (1985).
6. T. OSAKA, T. K. NAOI, T. HIRABAYASHI, and S. NAKAMURA. Bull. Chem. Soc. Jpn. **59**, 2717 (1986).
7. F. VAN DEN BRINK, W. VISSCHER, and E. BARENDRECHT. J. Electroanal. Chem. **157**, 305 (1983).
8. F. VAN DEN BRINK, W. VISSCHER, and E. BARENDRECHT. J. Electroanal. Chem. **172**, 301 (1984).
9. F. VAN DEN BRINK, W. VISSCHER, and E. BARENDRECHT. J. Electroanal. Chem. **175**, 279 (1984).

Can. J. Chem. Downloaded from www.nrcresearchpress.com by 41.223.56.140 on 09/07/12
For personal use only.

Can. J. Chem. Downloaded from www.nrcresearchpress.com by 41.223.56.140 on 09/07/12
For personal use only.

10. J. A. R. VAN VEEN. Electrochimica Acta, **24**, 921 (1979).
11. J. ZAGAL, R. K. SEN, and E. YEAGER. J. Electroanal. Chem. **83**, 207 (1977).
12. S. ZECEVIC, B. SIMIC-GLAVASKI, E. YEAGER, A. B. P. LEVER, and P. C. MINOR. J. Electroanal. Chem. **196**, 339 (1985).
13. B. Z. NIKOLIC, R. R. ADZIC, and E. YEAGER. J. Electroanal. Chem. **103**, 281 (1979).
14. J. ZAGAL, P. BINDRA, and E. YEAGER. J. Electroanal. Chem. **127**, 1506 (1980).
15. A. J. APPLEBY, M. SAVY, and P. CARO. J. Electroanal. Chem. **111**, 91 (1980).
16. F. VAN DEN BRINK, E. BARENDRECHT, and W. VISSCHER. Rec. Trav. Chim. Pays Bas, **99**, 253 (1980).
17. A. ELZING, A. VAN DER PUTTEN, W. VISSCHER, and E. BARENDRECHT. J. Electroanal. Chem. **233**, 99 (1987).
18. H. BEHRET, H. W. CLAUBERG, and G. SANDSTEDE. Z. Phys. Chem. **113**, 97 (1979).
19. K. A. RADYUSHKINA and M. R. TARASEVICH. Sov. Electrochem. **22**, 1087 (1985).
20. E. NGAMENI, Y. LE MEST, M. L'HER, J. P. COLLMAN, N. H. HENDRICKS, and K. KIM. J. Electroanal. Chem. **220**, 247 (1987).
21. C. L. NI, I. ABDALMUDHI, C. K. CHANG, and F. C. ANSON. J. Phys. Chem. **91**, 158 (1987).
22. E. YEAGER. J. Mol. Catal. **38**, 5 (1986).
23. K. SHIGEHARA and F. C. ANSON. J. Phys. Chem. **86**, 2776 (1982).
24. A. J. APPLEBY and M. SAVY. Electrochim. Acta, **21**, 567 (1976).
25. P. FORSHEY and T. KUWANA. Inorg. Chem. **22**, 699 (1983).
26. N. KOBAYASHI, M. FUJIHIRA, K. SUNAKAWA, and T. OSA. J. Electroanal. Chem. **101**, 269 (1979).
27. R. J. H. CHAN, Y. O. SU, and T. KUWANA. Inorg. Chem. **24**, 3777 (1985).
28. C-L. NI, and F. C. ANSON. Inorg. Chem. **24**, 4754 (1985).
29. D. OZER, R. PARASH, F. BROTTMAN, U. MOR, and A. BETTELHEIM. J. Chem. Soc. Faraday Trans. I, **80**, 1139 (1984).
30. M. R. HEMPSTEAD, A. B. P. LEVER, and C. C. LEZNOFF. Can. J. Chem. **65**, 2677 (1987).
31. G. X. WAN, K. SHIGEHARA, E. TSUCHIDA, and F. C. ANSON. J. Electroanal. Chem. **179**, 239 (1984).
32. Y. LE MEST, M. L'HER, J. P. COLLMAN, N. H. HENDRICKS, and L. MCELWEE-WHITE. J. Am. Chem. Soc. **108**, 533 (1986).
33. F. C. ANSON, C-L. NI, and J. M. SAVEANT. J. Am. Chem. Soc. **107**, 3442 (1985).
34. E. YEAGER. Am. Chem. Soc. Symp. Ser. **288**, 472 (1985).
35. C. PALITEIRO, A. HAMNETT, and J. B. GOODENOUGH. J. Electroanal. Chem. **233**, 147 (1987).
36. O. HIRABARU, T. NAKASE, K. HANABUSA, H. SHIRAI, K. TAKEMOTO, and N. HOJO. J. Chem. Soc. Dalton, 1485 (1984).
37. H-Y. LIU, I. ABDALMUDHI, C. K. CHANG, and F. C. ANSON. J. Phys. Chem. **89**, 665 (1985).
38. M. R. TARASEVICH and K. A. RADYUSHKINA. Russ. Chem. Rev. **49**, 718 (1980); Engl. Transl. 1498 (1980).
39. N. KOBAYASHI, T. MATSUE, M. FUJIHIRA, and T. OSA. J. Electroanal. Chem. **103**, 427 (1979).
40. P. A. FORSHEY, T. KUWANA, N. KOBAYASHI, and T. OSA. Adv. Chem. Ser. Am. Chem. Soc. **201**, 601 (1982).
41. N. KOBAYASHI, M. FUJIHIRA, T. OSA, and S. DONG. Chem. Lett. 575 (1982).
42. N. KOBAYASHI and T. OSA. J. Electroanal. Chem. **157**, 269 (1983).
43. A. BETTELHEIM, D. OZER, and R. PARASH. J. Chem. Soc. Faraday Trans. I, **79**, 1555 (1983).
44. K. OKABAYASHI, O. IKEDA, and H. TAMURA. J. Chem. Soc. Chem. Commun. 684 (1983).
45. O. IKEDA, K. OKABAYASHI, N. YOSHIDA, and H. TAMURA. J. Electroanal. Chem. **191**, 157 (1985).
46. W. A. NEVIN, W. LIU, S. GREENBERG, M. R. HEMPSTEAD, S. M. MARCUCCIO, M. MELNIK, C. C. LEZNOFF, and A. B. P. LEVER. Inorg. Chem. **26**, 891 (1987).
47. C. C. LEZNOFF, S. M. MARCUCCIO, S. GREENBERG, A. B. P. LEVER, and K. B. TOMER. Can. J. Chem. **63**, 623 (1985).
48. C. C. LEZNOFF, S. GREENBERG, S. M. MARCUCCIO, P. C. MINOR, P. SEYMOUR, and A. B. P. LEVER. Inorg. Chim. Acta, **89**, L35 (1985).
49. S. M. MARCUCCIO, P. I. SVIRSKAYA, S. GREENBERG, A. B. P. LEVER, and C. C. LEZNOFF. Can. J. Chem. **63**, 3057 (1985).
50. S. GREENBERG, S. M. MARCUCCIO, and C. C. LEZNOFF. Synthesis, 406 (1986).
51. C. K. MANN and K. K. BARNES. Electrochemical reactions in non-aqueous systems. Marcel Dekker, New York. 1970; G. GRITZNER and J. KUTA. Electrochim. Acta, **29**, 869 (1984).
52. C. P. ANDRIEUX and J. M. SAVEANT. J. Electroanal. Chem. **93**, 163 (1978); **111**, 377 (1980).
53. S. HOLDCROFT and L. FUNT. J. Electroanal. Chem. **225**, 177 (1987).
54. A. P. BROWN, C. KOVAL, and F. C. ANSON. J. Electroanal. Chem. **72**, 379 (1976); A. P. BROWN and F. C. ANSON. J. Electroanal. Chem. **83**, 203 (1977).
55. Chemistry and physics of carbon. Vol. 11. Marcel Dekker, Inc., New York. 1973.
56. B. KAZEE, D. E. WEISSHAAR, and T. KUWANA. Anal. Chem. **57**, 2736 (1985).
57. P. NIKITAS. J. Chem. Soc. Faraday Trans. I, **81**, 1767 (1985).
58. A. B. P. LEVER, S. LICOCCIA, K. MAGNELL, P. C. MINOR, and B. S. RAMASWAMY. Am. Chem. Soc. Symp. Ser. **201**, 237 (1982).
59. A. B. P. LEVER and J. P. WILSHIRE. Inorg. Chem. **17**, 1145 (1978); Can. J. Chem. **54**, 2514 (1976).
60. J. LE MOIGNE and R. EVEN. J. Chem. Phys. **82**, 6472 (1985).
61. R. TAUBE. Z. Chem. **6**, 8 (1966).
62. M. J. STILLMAN and A. J. THOMPSON. J. Chem. Soc. Faraday Trans. II, **70**, 790 (1974).
63. P. DAY, H. A. O. HILL, and M. G. PRICE. J. Chem. Soc. A, 90 (1968).
64. D. W. CLACK and J. R. YANDLE. Inorg. Chem. **11**, 1738 (1972).
65. L. D. ROLLMANN and R. T. IWAMOTO. J. Am. Chem. Soc. **90**, 1455 (1968).
66. W. A. NEVIN, W. LIU, M. MELNIK, and A. B. P. LEVER. J. Electroanal. Chem. **213**, 217 (1986).
67. W. A. NEVIN, M. R. HEMPSTEAD, W. LIU, C. C. LEZNOFF, and A. B. P. LEVER. Inorg. Chem. **26**, 570 (1987).
68. A. J. BARD and L. R. FAULKNER. Electrochemical methods. John Wiley, New York. 1980.
69. N. KOBAYASHI and A. B. P. LEVER. J. Am. Chem. Soc. **109**, 7433 (1987).
70. N. KOBAYASHI and Y. NISHIYAMA. J. Chem. Soc. Chem. Commun. 1462 (1986).
71. N. KOBAYASHI, P. JANDA, and A. B. P. LEVER. To be published.
72. H. BEHRET, W. CLAUBERG, and G. SANDSTEDE. Ber. Bunsenges. Phys. Chem. **83**, 139 (1979).
73. J. KORYTA and J. DVORAK. Principles of electrochemistry. J. Wiley and Sons, New York. 1987. p. 343.
74. J. A. R. VAN VEEN, J. F. VAN BAAR, C. J. KROESE, J. G. F. COOLEGEM, N. DEWIT, and H. A. COLIJN. Ber. Bunsenges. Phys. Chem. **85**, 693 (1981).
75. A. B. P. LEVER, P. SEYMOUR, and N. KOBAYASHI. To be published.
76. A. BETTELHEIM, R. J. H. CHAN, and T. KUWANA. J. Electroanal. Chem. **99**, 391 (1979).
77. A. VAN DER PUTTEN, A. ELZING, W. VISSCHER, and E. BARENDRECHT. J. Electroanal. Chem. **221**, 95 (1987).
78. R. R. DURAND, JR., and F. C. ANSON. J. Electroanal. Chem. **134**, 273 (1982).
79. N. KOBAYASHI, M. FUJIHIRA, T. OSA, and T. KUWANA. Bull. Chem. Soc. Jpn. **53**, 2195 (1980).
80. C. P. ANDRIEUX, C. BLOCMAN, J. M. BOUCHIAT-DUMAS, F. M'HALLA, and J. M. SAVEANT. J. Electroanal. Chem. **119**, 19 (1980).
81. F. C. ANSON. J. Phys. Chem. **84**, 3336 (1980).

82. C. P. ANDRIEUX and J. M. SAVEANT. J. Electroanal. Chem. **134**, 163 (1982).
83. C. P. ANDRIEUX and J. M. SAVEANT. J. Electroanal. Chem. **142**, 1 (1982).
84. R. C. BIRKE, R. A. GU, J-M. YAU, and M-N. KIM. Anal. Chem. **56**, 1716 (1984).
85. C-L. NI, I. ABDALMUHDI, C. K. CHANG, and F. C. ANSON. J. Phys. Chem. **91**, 1158 (1987).
86. R. R. DURAND, JR., C. S. BENCOSME, J. P. COLLMAN, and F. C. ANSON. J. Am. Chem. Soc. **105**, 2710 (1983).
87. A. B. P. LEVER, N. GOLOVIN, K. JAYARAJ, and P. SEYMOUR. To be published.
88. F. CARIATI, F. MORAZZONI, and C. BUSETTO. J. Chem. Soc. Dalton, 556 (1975).
89. S. ZECEVIC, B. SIMIC-GLAVASKI, E. YEAGER, A. B. P. LEVER, and P. C. MINOR. J. Electroanal. Chem. **196**, 339 (1985).
90. L. NADJO and J. M. SAVEANT. J. Electroanal. Chem. **44**, 327 (1973).
91. W. LIU, M. R. HEMPSTEAD, W. A. NEVIN, M. MELNIK, A. B. P. LEVER, and C. C. LEZNOFF. J. Chem. Soc. Dalton, 2511 (1987).
92. A. B. P. LEVER and J. P. WILSHIRE. Can. J. Chem. **54**, 2514 (1976).
93. A. VAN DER PUTTEN. Ph.D. Thesis, Amsterdam. 1986.

Can. J. Chem. Downloaded from www.nrcresearchpress.com by 41.223.56.140 on 09/07/12
For personal use only.

Excess molar volumes of mixtures containing methyl alkanoates (acetate, propanoate, and butanoate) with normal alkanols (from ethanol to pentan-1-ol)

J. ORTEGA AND P. SUSIAL

Cátedra de Termodinámica y Fisicoquimica, Escuela Superior de Ingenieros Industriales, Polytechnic University of Canarias, 35071-Las Palmas, Spain

Received November 21, 1988

J. ORTEGA and P. SUSIAL. Can. J. Chem. **67**, 1120 (1989).

Measurements of v^E for binary mixtures of $C_mH_{2m+1}CO_2CH_3$ (m = 1, 2, 3) + $C_nH_{2n+1}(OH)$ (n = 2, 3, 4, 5) are reported. The results have been determined by using the densities obtained in a vibrating tube densimeter at 298.15 K, they are positive for all these systems. The data have also been compared with available literature values with a discussion on these mixtures.

Key words: excess molar mixtures, methyl alkanoates, normal alkanols.

J. ORTEGA et P. SUSIAL. Can. J. Chem. **67**, 1120 (1989).

On rapporte des mesures de v^E pour des mélanges binaires de $C_mH_{2m+1}CO_2CH_3$ (m = 1, 2, 3) + $C_nH_{2n+1}(OH)$ (n = 2, 3, 4, 5). On a déterminé les résultats, à 298,15 K, à l'aide d'un densimètre à tube vibrant et ils sont positifs pour tous les systèmes. On a aussi comparé les résultats ainsi obtenus avec ceux disponibles dans la littérature et on présente une discussion concernant ces mélanges.

Mots clés : mélanges molaires en excès, alcanoates de méthyle, alcanols normaux.

[Traduit par la revue]

Can. J. Chem. Downloaded from www.nrcresearchpress.com by 41.223.56.140 on 09/07/12
For personal use only.

Introduction

With a view to extending our previous study (1) of the binary systems methyl alkanoates with normal alkanols from hexan-1-ol to decan-1-ol, we report here the excess molar volumes of a further twelve systems formed by the same methyl esters and four other normal alkanols, from ethanol to pentan-1-ol. Although the v^E of the systems involving alkyl esters + methanol were presented in several reports (2–4), we later decided to undertake a separate study since these mixtures present a net effect of volume contraction, giving negative v^E values. The presence of methanol causes some type of specific interaction for several reasons, two of which are singled out for mention: on the one hand, the formation of hydrogen bridges and, on the other, the better interstitial accommodation of the small molecules of methanol among the molecules of the ester. The determination of other physico-chemical magnitudes will help to verify accurately this behaviour.

After the presentation of data, an analysis will be made of the effects caused by the increase in chain length of the ester and the *n*-alkanol on the v^E, verifying the indications made in other works.

Theoretical and experimental interest has increased in recent years in the thermodynamic properties of liquid mixtures containing associated compounds. The majority of the theoretical models, generally based on a rigid lattice concept, are not suitable for the prediction of volumetric properties such as v^E. Thus, the model of Nitta *et al.* (5) permits the prediction of several properties of pure compounds and mixtures, simultaneously, including v^E, and confirming that, an increase in the predictive capacity of a model causes a decrease in the capacity of representation or reproduction of experimental data. Therefore, the Nitta model does not offer a good prediction of v^E for mixtures. However, in recent years, Heintz (6) and Treszczanowicz and Benson (7) in particular have developed other models with specific applications to systems involving alkanols + alkanes that allow g^E, h^E, and v^E to be calculated simultaneously. Their extension to another type of systems requires previous knowledge of a large number of experimental data that confirm the models developed. This necessity arises when applying any of the models chosen.

Experimental

All the products employed were of the best quality commercially available (Fluka AG). The characteristics of the methyl esters have been reported previously (1). The normal alkanols, and likewise the esters, were used without further purification; however, prior to use, they were degassed with ultrasound and dried with a molecular sieve, type 4A by Fluka. After this treatment and to verify the purity of components used, the physical properties n_D and ρ were determined at 298.15 K, with comparable literature values shown in Table 1. Refractive indices of pure components were measured with a Bausch and Lomb refractometer with an accuracy of ±0.0001 unit. All measurements were made for a wavelength of 5893 Å for the sodium-D line, having been checked with pure water at 298.15 K. Measurements of densities for pure components and their mixtures were made with a DMA-55 densimeter (Anton Paar, Graz, Austria) with a reproductibility of ±0.01 kg m^{-3} and calibrated with doubly distilled and degassed wter, ρ(298.15 K) = 997.04 kg m^{-3}, and *n*-nonane (Fluka 74252 purum), ρ(298.15 K) = 713.85 kg m^{-3}. The densities of water and *n*-nonane offer a wide interval and are much closer to those of the majority of organic products, which recommends their joint use as substances for calibration purposes.

Both the digital densimeter and the refractometer were thermostated by a Heto Birdkerod ultrathermostat which controlled the temperature within ±0.01 K using a precision thermometer Anton Paar DT-100, whose performance was checked in accordance with the IPTS-68 norms.

All the mixtures were prepared by weighing in hermetically sealed 2.5 cm^3 glass vials, injecting the products with a hypodermic syringe to avoid evaporation. The mole fractions were calculated with an imprecision smaller than 5×10^{-5}.

From the densities, ρ_i, and molar masses, M_i, of the pure liquids (i = 1 for methyl alkanoates, 2 for *n*-alkanols) and the density ρ of the mixture, the molar excess volumes are given by

$$[1] \quad v^E/(\text{cm}^3\ \text{mol}^{-1}) = xM_1(\rho^{-1} - \rho_1^{-1}) + (1 - x)M_2(\rho^{-1} - \rho_2^{-1})$$

where x is the mole fraction of methyl alkanoate.

The results for v^E are estimated to be accurate to better than

TABLE 1. Physical properties ρ and n_D of pure normal alkanols obtained experimentally at 298.15 K and their comparison with literature data

Compound	ρ/(kg m^{-3})		n_D	
	This work	Literature	This work	Literature
Ethanol, $C_2H_5(OH)$	785.05	785.09 (8) 784.93 (9) 785.1 (10)	1.3595	1.35941 (8) 1.3593 (10)
Propan-1-ol, $C_3H_7(OH)$	799.65	799.75 (8) 799.60 (9) 799.5 (10)	1.3833	1.3837 (8) 1.3832 (10)
Butan-1-ol, $C_4H_9(OH)$	805.97	806.0 (8) 805.75 (9) 805.9 (10)	1.3974	1.3971 (8) 1.39741 (9) 1.3973 (10)
Pentan-1-ol, $C_5H_{11}(OH)$	810.84	811.2 (8) 810.8 (9) 810.9 (10)	1.4077	1.4080 (8) 1.4074 (10)

Can. J. Chem. Downloaded from www.nrcresearchpress.com by 41.223.56.140 on 09/07/12
For personal use only.

± 0.001 cm^3 mol^{-1}. The accuracy of the technique described was checked by measuring the v^E data for the test binary mixture benzene + cyclohexane at 298.15 K and the results agree satisfactorily with those of other authors.

Results and discussion

The excess molar volumes of the twelve systems studied are summarized in Table 2. The said results can be satisfactorily represented by a fitting equation, such as

$$[2] \quad v^E/(\text{cm}^3\ \text{mol}^{-1}) = x[1 - x]\Sigma A_i\{x/[x + k[1 - x]]\}^i \qquad i = 0, 1, 2, \ldots$$

where x is the mole fraction of the methyl ester. Table 3 shows the A_i coefficients determined by a least-squares method and the standard deviations, $s(v^E)$, of the fits. With these values and those of k, the curves in Fig. 1 could be plotted for all the systems studied. The best values of k were achieved upon optimizing the corresponding correlation of the set of values of each system, bearing in mind that k will always have positive values since, if $k < 0$, the term between brackets in eq. [2] will present a discontinuity in $x = k/(1 + k)$.

Of the twelve systems studied, data have only been found in the literature for methyl propanoate + ethanol (11). Although the representation of these data are qualitatively rather similar, quantitatively there exists a difference, at $x = 0.5$, between our data and those reported in ref. 11 of -0.02 cm^3 mol^{-1}. We attribute this to the major imprecision of their picnometric technique in measurements of small excess volumes.

The same effects on the volumetric behaviour of these systems, already described in earlier papers (1–4), can be observed in the curves plotted in Fig. 1. On the one hand, the negative effect on v^E due to the increase in the chain of the methyl ester and, on the other, the quasi-linear increase of v^E with the increase in length of the n-alkanol chain, when interacting with any one ester. This latter effect can be noted perfectly upon plotting v^E, at $x = 0.5$, for the binary systems methyl alkanoate + $C_nH_{2n+1}(OH)$ as a function of n. However, the proportionality indicated is clear for values of $n > 4$,

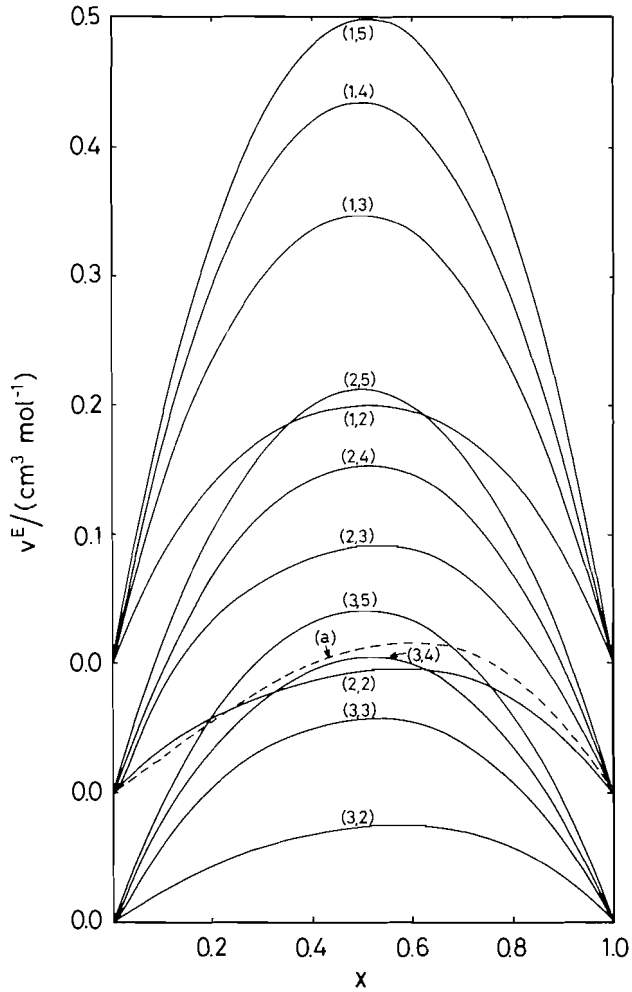


FIG. 1. Representation of the v^E curves using eq. [1] for the binary systems indicated by the pair (m, n): $\{xH_{2m+1}C_mCO_2CH_3$ $(m = 1, 2, 3) + (1 - x)C_nH_{2n+1}(OH)$ $(n = 2, 3, 4, 5)\}$. The dash line indicates the curve obtained by Polak and Lu (11) for the system (2,2).

Can. J. Chem. Downloaded from www.nrcresearchpress.com by 41.223.56.140 on 09/07/12
For personal use only.

TABLE 2. Excess molar volumes, v^E, for the binary systems: $x$methyl alkanoates + $(1 - x)$alkan-1-ol at 298.15 K

x	v^E / cm^3 mol^{-1}	x	v^E / cm^3 mol^{-1}	x	v^E / cm^3 mol^{-1}	x	v^E / cm^3 mol^{-1}
			$xH_3CCO_2CH_3 + (1 - x)C_2H_5(OH)$				
0.05910	0.0568	0.25390	0.1618	0.51393	0.2019	0.82051	0.1298
0.09779	0.0854	0.29418	0.1743	0.56863	0.1980	0.84710	0.1165
0.12681	0.1048	0.33074	0.1824	0.60976	0.1911	0.87005	0.1037
0.16019	0.1236	0.40947	0.1951	0.66005	0.1828	0.90816	0.0785
0.17797	0.1301	0.44104	0.2001	0.71082	0.1715	0.94566	0.0499
0.21078	0.1455	0.49162	0.2022	0.75320	0.1578	—	—
			$xH_3CCO_2CH_3 + (1 - x)C_3H_7(OH)$				
0.04092	0.0631	0.26449	0.2828	0.47201	0.3465	0.66482	0.3092
0.11204	0.1543	0.30963	0.3048	0.50734	0.3480	0.70180	0.2904
0.14606	0.1892	0.35623	0.3263	0.54305	0.3423	0.74745	0.2626
0.18338	0.2253	0.39985	0.3360	0.58756	0.3368	0.83031	0.1971
0.22956	0.2603	0.42285	0.3432	0.61741	0.3243	0.91192	0.1115
			$xH_3CCO_2CH_3 + (1 - x)C_4H_9(OH)$				
0.03808	0.0694	0.32148	0.3901	0.55460	0.4295	0.78332	0.2925
0.07491	0.1317	0.34754	0.3999	0.58623	0.4218	0.82519	0.2509
0.14353	0.2293	0.38242	0.4156	0.63650	0.4012	0.86395	0.2049
0.18579	0.2795	0.42789	0.4285	0.67124	0.3811	0.90073	0.1553
0.20942	0.3023	0.46221	0.4332	0.70331	0.3595	0.92280	0.1237
0.27530	0.3609	0.51209	0.4356	0.74711	0.3271	0.96039	0.0657
			$xH_3CCO_2CH_3 + (1 - x)C_5H_{11}(OH)$				
0.03483	0.0744	0.31613	0.4347	0.57382	0.4913	0.77481	0.3651
0.09872	0.1892	0.35085	0.4554	0.59280	0.4850	0.84494	0.2791
0.15597	0.2768	0.40081	0.4825	0.62078	0.4736	0.88019	0.2226
0.17460	0.2973	0.43519	0.4939	0.66828	0.4498	0.93010	0.1385
0.23475	0.3691	0.47995	0.4998	0.70106	0.4275	0.96215	0.0782
0.28423	0.4093	0.51466	0.4991	0.73294	0.4021	—	—
			$xH_5C_2CO_2CH_3 + (1 - x)C_2H_5(OH)$				
0.02568	0.0124	0.18855	0.0588	0.40080	0.0922	0.71949	0.0892
0.06133	0.0242	0.22182	0.0650	0.42283	0.0934	0.76928	0.0804
0.07947	0.0307	0.26311	0.0729	0.47584	0.0981	0.81541	0.0704
0.10240	0.0389	0.28933	0.0765	0.59351	0.1004	0.89990	0.0445
0.13561	0.0475	0.32773	0.0826	0.65443	0.0954	0.90104	0.0438
0.16587	0.0565	0.34354	0.0864	0.70565	0.0899	0.93789	0.0298
			$xH_5C_2CO_2CH_3 + (1 - x)C_3H_7(OH)$				
0.04718	0.0345	0.23959	0.1508	0.48758	0.1927	0.77516	0.1433
0.05761	0.0439	0.26193	0.1569	0.55018	0.1925	0.77595	0.1429
0.08631	0.0715	0.30164	0.1675	0.57835	0.1908	0.85827	0.1031
0.12040	0.0964	0.35845	0.1794	0.63489	0.1838	0.89275	0.0826
0.16752	0.1218	0.39165	0.1842	0.70563	0.1664	0.94302	0.0464
0.18456	0.1289	0.45012	0.1892	0.71676	0.1638	0.96452	0.0308
			$xH_5C_2CO_2CH_3 + (1 - x)C_4H_9(OH)$				
0.03883	0.0374	0.24645	0.1953	0.46140	0.2523	0.69442	0.2214
0.08145	0.0789	0.29630	0.2211	0.51005	0.2542	0.74415	0.1988
0.10480	0.1010	0.31590	0.2262	0.53866	0.2518	0.80906	0.1641
0.13042	0.1197	0.35167	0.2363	0.58164	0.2485	0.87393	0.1171
0.17867	0.1558	0.39950	0.2465	0.61083	0.2457	0.92861	0.0734
0.21238	0.1800	0.43044	0.2499	0.67214	0.2302	0.96275	0.0409
			$xH_5C_2CO_2CH_3 + (1 - x)C_5H_{11}(OH)$				
0.08975	0.1073	0.31352	0.2708	0.54370	0.3100	0.76846	0.2236
0.11820	0.1330	0.36001	0.2897	0.58495	0.3019	0.78010	0.2141
0.14738	0.1625	0.40529	0.3023	0.62573	0.2918	0.83442	0.1741
0.19022	0.1988	0.43207	0.3074	0.65285	0.2811	0.86091	0.1515
0.23379	0.2298	0.46037	0.3126	0.68430	0.2677	0.92602	0.0900
0.27474	0.2517	0.49599	0.3136	0.72323	0.2473	—	—

TABLE 2 (*concluded*)

x	v^E / cm^3 mol^{-1}	x	v^E / cm^3 mol^{-1}	x	v^E / cm^3 mol^{-1}	x	v^E / cm^3 mol^{-1}
			$xH_7C_3CO_2CH_3 + (1 - x)C_2H_5(OH)$				
0.04466	0.0123	0.18787	0.0433	0.39000	0.0704	0.67776	0.0701
0.06062	0.0165	0.22619	0.0499	0.43279	0.0726	0.72540	0.0655
0.09474	0.0242	0.25509	0.0542	0.48455	0.0750	0.79306	0.0558
0.10832	0.0277	0.28302	0.0585	0.52167	0.0761	0.85960	0.0438
0.13248	0.0325	0.32556	0.0635	0.56486	0.0758	0.93703	0.0221
0.16984	0.0398	0.35422	0.0667	0.62215	0.0739	—	—
			$xH_7C_3CO_2CH_3 + (1 - x)C_3H_7(OH)$				
0.03193	0.0187	0.17160	0.0952	0.38310	0.1511	0.77724	0.1138
0.04286	0.0238	0.19786	0.1071	0.41368	0.1545	0.83403	0.0918
0.05763	0.0348	0.22768	0.1168	0.51115	0.1579	0.88604	0.0669
0.08142	0.0492	0.27002	0.1285	0.52119	0.1578	0.93815	0.0379
0.11240	0.0668	0.30497	0.1368	0.63730	0.1485	0.95976	0.0258
0.13863	0.0809	0.34919	0.1455	0.72277	0.1301	—	—
			$xH_7C_3CO_2CH_3 + (1 - x)C_4H_9(OH)$				
0.03759	0.0309	0.23954	0.1521	0.46678	0.2016	0.70664	0.1703
0.06643	0.0589	0.27228	0.1661	0.50757	0.2048	0.76537	0.1498
0.11086	0.0870	0.30130	0.1750	0.54929	0.2039	0.80491	0.1296
0.12570	0.0974	0.34732	0.1869	0.57957	0.1996	0.85949	0.1004
0.16862	0.1199	0.38454	0.1951	0.63429	0.1898	0.89832	0.0798
0.20270	0.1352	0.41933	0.1991	0.67853	0.1808	0.94804	0.0417
			$xH_7C_3CO_2CH_3 + (1 - x)C_5H_{11}(OH)$				
0.05127	0.0514	0.26410	0.1955	0.50350	0.2403	0.74980	0.1841
0.07073	0.0690	0.31713	0.2150	0.54109	0.2399	0.78031	0.1648
0.12737	0.1157	0.35078	0.2230	0.59384	0.2295	0.83708	0.1353
0.15026	0.1308	0.37928	0.2316	0.62939	0.2261	0.86511	0.1158
0.19089	0.1531	0.43127	0.2394	0.67197	0.2140	0.91408	0.0766
0.23666	0.1798	0.46750	0.2392	0.70658	0.1985	0.96121	0.0378

TABLE 3. Coefficients A_i of eq. [1] and standard deviations, $s(v^E)$, in cm^3 mol^{-1} for binary systems methyl alkanoate + alkan-1-ol

Mixture	k	A_0	A_1	A_2	A_3	$s(v^E)$
$xH_3CCO_2CH_3 + (1 - x)C_2H_5(OH)$	0.894	1.0506	−0.9385	0.8827		0.0009
$+ (1 - x)C_3H_7(OH)$	0.379	1.6310	−0.2016	−0.6529	0.6483	0.0013
$+ (1 - x)C_4H_9(OH)$	0.262	1.8505	0.5307	−1.6254	0.9858	0.0011
$+ (1 - x)C_5H_{11}(OH)$	0.776	2.2274	−0.8903	0.8613		0.0018
$xH_5C_2CO_2CH_3 + (1 - x)C_2H_5(OH)$	0.524	0.4809	−0.4486	0.4834		0.0008
$+ (1 - x)C_3H_7(OH)$	0.177	0.1553	4.3267	−7.8239	4.2191	0.0007
$+ (1 - x)C_4H_9(OH)$	0.379	0.9058	1.1976	−2.6351	1.6550	0.0014
$+ (1 - x)C_5H_{11}(OH)$	2.826	1.3012	−0.2947	0.3638		0.0012
$xH_7C_3CO_2CH_3 + (1 - x)C_2H_5(OH)$	1.787	0.2807	2.3697	9.7425		0.0003
$+ (1 - x)C_3H_7(OH)$	0.238	0.4472	1.3665	−2.5516	1.4186	0.0006
$+ (1 - x)C_4H_9(OH)$	0.084	0.3542	2.9341	−4.7936	2.3419	0.0014
$+ (1 - x)C_5H_{11}(OH)$	1.123	1.0665	−0.3647	0.3186		0.0016

Can. J. Chem. Downloaded from www.nrcresearchpress.com by 41.223.56.140 on 09/07/12
For personal use only.

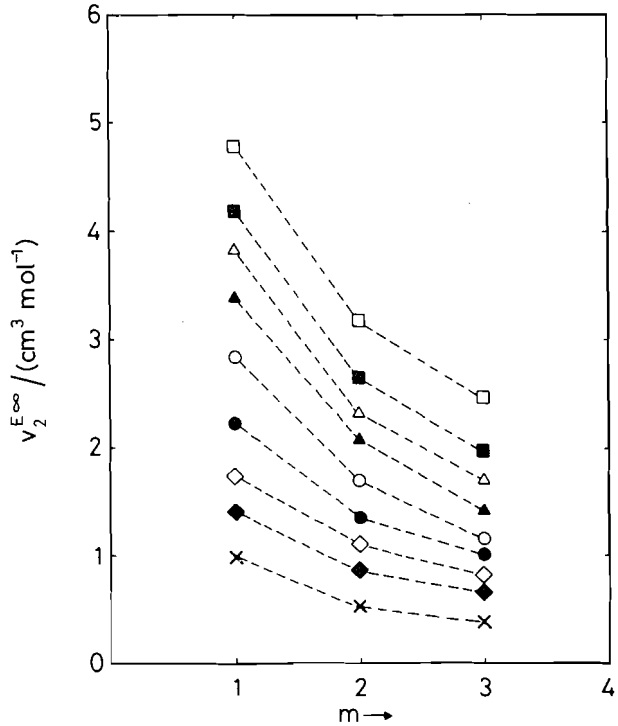


FIG. 2. Representation of $v_2^{E\infty}$ for normal alkanols $C_nH_{2n+1}(OH)$ diluted in methyl alkanoates, $H_{2m+1}C_mCO_2CH_3$ (m = 1, 2, 3), as a function of m; ×, n = 2; ◆, n = 8; ◇, n = 4; ●, n = 5. The other points correspond to the values derived from ref. 1 for n-alkanols, from hexan-1-ol to decan-1-ol.

falling abruptly for $n < 4$, to produce contractions of volume in the case of methanol.

To complete the earlier paper (1), the curves of the partial molar volumes were also determined by means of eq. [2]. In particular, the values at infinite dilution were determined by means of $v_2^{E\infty} = \Sigma A_i$ (i = 0, 1, 2, ...) for the four n-alkanols, being represented in Fig. 2 as a function of the number of carbon atoms, m, of the methyl ester $C_mH_{2m+1}COOCH_3$, and together with the data of the previous paper for the remaining normal alkanols (from hexan-1-ol to decan-1-ol).

A general qualitative interpretation of the results of the excess molar volumes of the mixtures of esters + n-alkanols is that they are the result of different factors which may be resumed as follows. First, a positive effect on the v^E due to the destruction of polymers and to the steric effect of the molecular groups of the pure compounds. However, added to these effects are others having opposite consequences on v^E, such as interstitial accommodation and especially the appearance of specific interactions with the formation of new polymers ester + n-alkanol. These act negatively in mixtures of ester with alkanols in addition to the effect of changes in the free volume. These negative effects may even predominate over the first ones, with the v^E taking on negative values as the number of carbon atoms of the n-alkanol decreases.

Acknowledgements

Financial support for this work was provided by the Canarias Government, under a research project 52/86.

1. J. ORTEGA and J. D. GARCIA. Can. J. Chem. **66**, 1520 (1988).
2. J. ORTEGA, R. BRAVO, E. JIMENEZ, and M. I. PAZ-ANDRADE. J. Chem. Thermodyn. **18**, 403 (1986).
3. J. ORTEGA, M. I. PAZ-ANDRADE, E. RODRIGUEZ, and L. ROMANI. Aust. J. Chem. **38**, 1435 (1985).
4. J. ORTEGA. J. Chem. Eng. Data, **30**, 465 (1985).
5. T. NITTA, E. A. TUREK, and R. A. GREENKORN. A. I. Ch. E. J. **23**, 144 (1977).
6. A. HEINTZ. Ber. Bunsenges. Phys. Chem. **89**, 172 (1985).
7. A. J. TRESZCZANOWICZ and G. C. BENSON. Fluid Phase Equilibria, **23**, 117 (1985).
8. R. C. WILHOIT and B. J. ZWOLINSKI. J. Phys. Chem. Ref. Data. Vol. II. 1973. Supplement no. 1.
9. J. A. RIDDICK, W. B. BUNGER, and T. K. SAKANO. Organic solvents. Techniques of chemistry. Vol. II. 4th ed. Wiley Interscience, New York. 1986.
10. J. ORTEGA. J. Chem. Eng. Data. **27**, 312 (1982).
11. J. POLAK and B. C-Y. LU. J. Chem. Eng. Data. **17**, 456 (1972).

Can. J. Chem. Downloaded from www.nrcresearchpress.com by 41.223.56.140 on 09/07/12
For personal use only.

Une application du cycle pyrazoline à la lactamisation et à la formylation de 6*H* thiazines-1,3

RÉMY TULOUP, RENÉE DANION-BOUGOT ET DANIEL DANION[1]

Groupe de recherches de physicochimie structurale, Unité associée au Centre national de la recherche scientifique, n° 704, Université de Rennes 1, 35042 Rennes CÉDEX, France

JEAN-PAUL PRADÈRE

Laboratoire de chimie organique, Unité associée au Centre national de la recherche scientifique, n° 475, 2, Rue de la Houssinière, 44072 Nantes CÉDEX 03, France

ET

LOÏC TOUPET

Département de physique cristalline, Unité associée au Centre national de la recherche scientifique, n° 804, Université de Rennes 1, 35042 Rennes CÉDEX, France

Reçu le 27 septembre 1988

RÉMY TULOUP, RENÉE DANION-BOUGOT, DANIEL DANION, JEAN-PAUL PRADÈRE et LOÏC TOUPET. Can. J. Chem. **67**, 1125 (1989).

Le cycle pyrazoline est utilisé à la fois comme groupe masquant, groupe stéréodirecteur et groupe formyle latent dans une synthèse d'amino-7 formyl-4 céphèmes à partir de 6*H*-thiazines-1,3.

Mots clés : thiazine, céphème, pyrazoline, anhydride benzèneséléninique.

RÉMY TULOUP, RENÉE DANION-BOUGOT, DANIEL DANION, JEAN-PAUL PRADÈRE, and LOÏC TOUPET. Can. J. Chem. **67**, 1125 (1989).

A pyrazoline ring is used as a masking, a stereodirecting, and a latent formyl group in the synthesis of 7-amino-4-formyl cephems from 6*H*-1,3-thiazines.

Key words: thiazine, cephem, pyrazoline, benzeneseleninic anhydride.

Introduction

Les 6*H*-thiazines-1,3 **1** sont des intermédiaires de synthèse facilement accessibles par réaction de Diels–Alder (1). Leur valorisation comme précurseurs de céphèmes implique une réaction de lactamisation avec un équivalent synthétique d'aminocétène et l'introduction d'une fonction acide carboxylique potentielle en position 4.

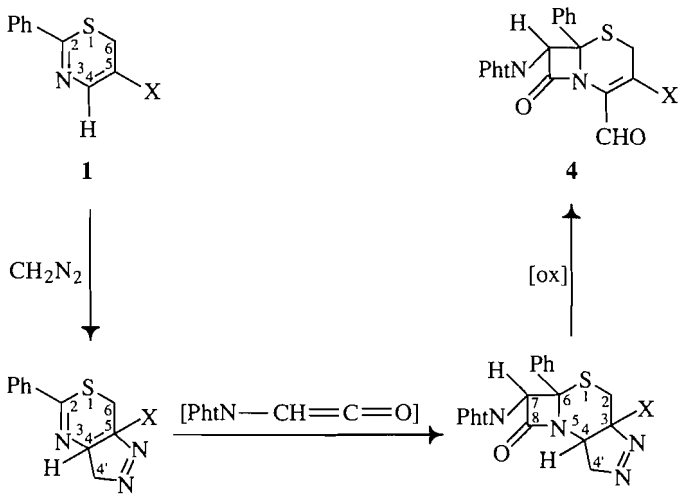
Ces réactions ne sont pas réalisables avec les thiazines **1**. D'une part, la fonction imine est trop peu réactive vis à vis des cétènes à cause de la conjugaison; d'autre part, il est très difficile d'introduire un groupement fonctionnel en position 4. Les réactifs nucléophiles attaquent en 2 ou 6 (2), les réactifs électrophiles attaquent en 3.[2]

Nous décrivons dans ce mémoire une méthodologie permettant d'atteindre ces objectifs. Elle fait appel à un cycle pyrazoline intermédiaire (schéma 1).

1. Addition du diazométhane

Les résultats d'un calcul MNDO, effectué sur une thiazine modèle[3] (géométrie optimisée selon la méthode inhérente au programme), montrent que les réactions de cycloaddition dipolaire avec le diazométhane sont susceptibles d'avoir lieu sélectivement sur la liaison C4—C5. On note, en particulier, une BV basse en énergie, avec des coefficients importants en C4 et C5 (schéma 2).

Comme nous l'avons montré dans un travail préliminaire (3), le diazométhane réagit lentement, mais de façon quantitative, avec les thiazines **1***a* et **1***b*. Les pyrazolines **2***a* et **2***b*, obtenues de façon régio et stéréosélective, sont stables jusqu'à 100°C.



X = CO_2CH_3 (composés *a*) ou $COCH_3$ (composés *b*)

SCHÉMA 1

2. Réactions de lactamisation

L'introduction du cycle pyrazoline permet un masquage temporaire de la double liaison C4—C5 et rend possible la réaction de lactamisation (4). Les réactions sont effectuées avec le système chlorure de l'acide phtalimidoacétique – triéthylamine dans le dichlorométhane, à la température ambiante (5).

Les pyrazolinothiazines **2** conduisent aux lactames **3***a* et **3***b* avec des rendements supérieurs à 80%, contrairement aux thia-

1. Auteur à qui adresser toute correspondance.
2. J. P. Pradère, communication personnelle.
3. Calculs effectués à l'Université d'Erlangen (R.F.A.) par A. J. Kos, que nous remercions vivement. HO et BV désignent respectivement l'orbitale moléculaire la plus haute occupée et la plus basse vacante.

Printed in Canada / Imprimé au Canada

Can. J. Chem. Downloaded from www.nrcresearchpress.com by 194.225.253.170 on 09/07/12
For personal use only.

Can. J. Chem. Downloaded from www.nrcresearchpress.com by 194.225.253.170 on 09/07/12
For personal use only.

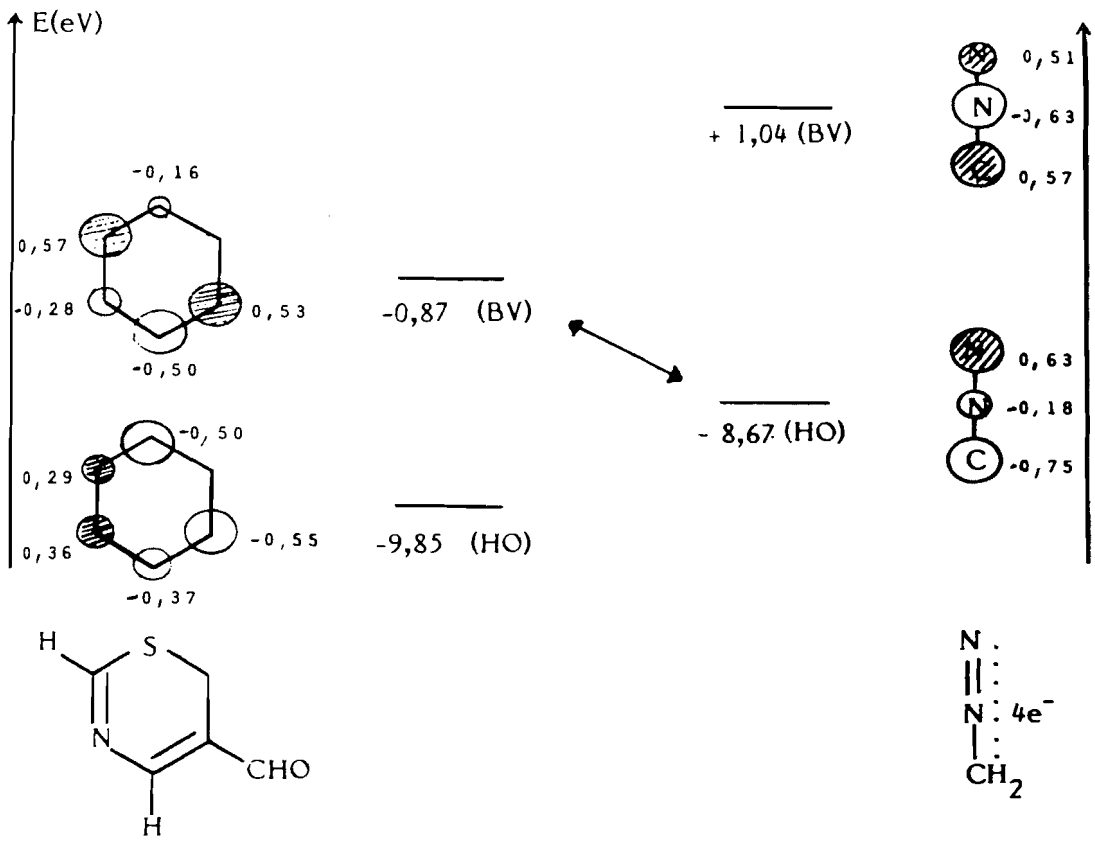
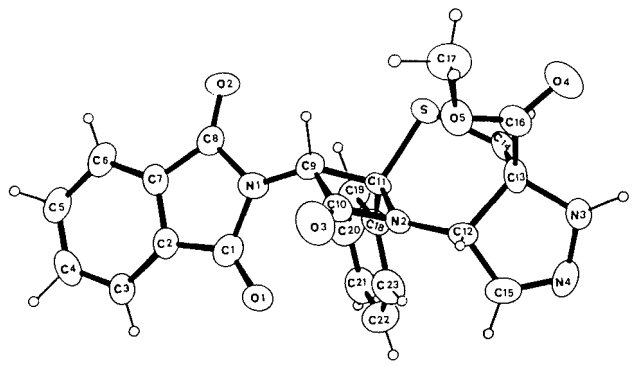
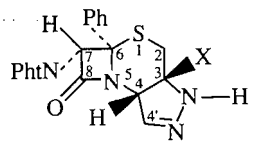


SCHÉMA 2



O.R.T.E.P. du compose *5a*[4]



5a

SCHÉMA 3

zines **1** qui ne réagissent pas. Comme attendu, le cycle pyrazoline a un effet stéréodirecteur très important. La réaction conduit à un seul stéréoisomère, dont la configuration a été établie sans difficulté par radiocristallographie X; l'étude a été réalisée sur la pyrazoline-2 *5a* (isomérisation de *3a* en présence de triéthylamine) (schéma 3).

Les cycles β-lactame et pyrazoline sont disposés en *trans*, de même que le groupe phtalimido et le noyau thiazine. Ce résultat est en bon accord avec un contrôle stérique de la réaction.

3. Préparation de méthyl-4 céphèmes et étude de leur oxydation allylique

La conversion des pyrazolinocéphames **3** en formyl-4 céphèmes **4** a été réalisée selon deux approches convergentes. La première méthode est basée sur la préparation du dérivé méthylé **6**, qui est ensuite oxydé selon des techniques déjà utilisées pour les méthyl-3 ou hydroxyméthyl-3 céphèmes (déacétoxy ou déacétyl céphalosporines) (6, 7) (schéma 4).

La thermolyse des pyrazolines **3** a fait l'objet d'un travail préliminaire (3). Elle conduit de façon exclusive aux céphèmes méthylés **6**. L'oxydation allylique a été réalisée sur le seul composé **6***a* (X = CO_2CH_3).

L'action de la *N*-bromosuccinimide, à la température ambiante dans le dichlorométhane, donne dans de bonnes conditions le bromométhyl-4 céphème **7**, qui peut être converti en composé **8** par action du nitrate d'argent dans l'acétonitrile.

L'hydrolyse du composé **7**, en présence de nitrate d'argent, conduit à la lactone **9**. Le composé **8** donne lieu à une élimination d'acide nitreux par traitement à la triéthylamine. Dans ces conditions, il se forme, à l'équilibre, un mélange du formyl-4 céphème **4** et d'un composé tautomère **10** auquel nous avons attribué une structure Δ-2 céphème sur la base des données de

4. Les coordonnées de tous les atomes avec les β_{eq}, les longueurs et angles de liaisons avec écart-type ainsi que la liste des facteurs de structure sont disponibles. On peut les acheter en s'adressant au Dépôt de données non publiées ICIST, Conseil National de Recherche du Canada, Ottawa (Ont.), Canada K1A 0S2.

On peut aussi obtenir les coordonnées des atomes, les longueurs et angles de liaisons, en s'adressant au Directeur, Cambridge Crystallographic Data Centre, University Chemical Laboratory, Lensfield Road, Cambridge CB2 1EW, U.K.

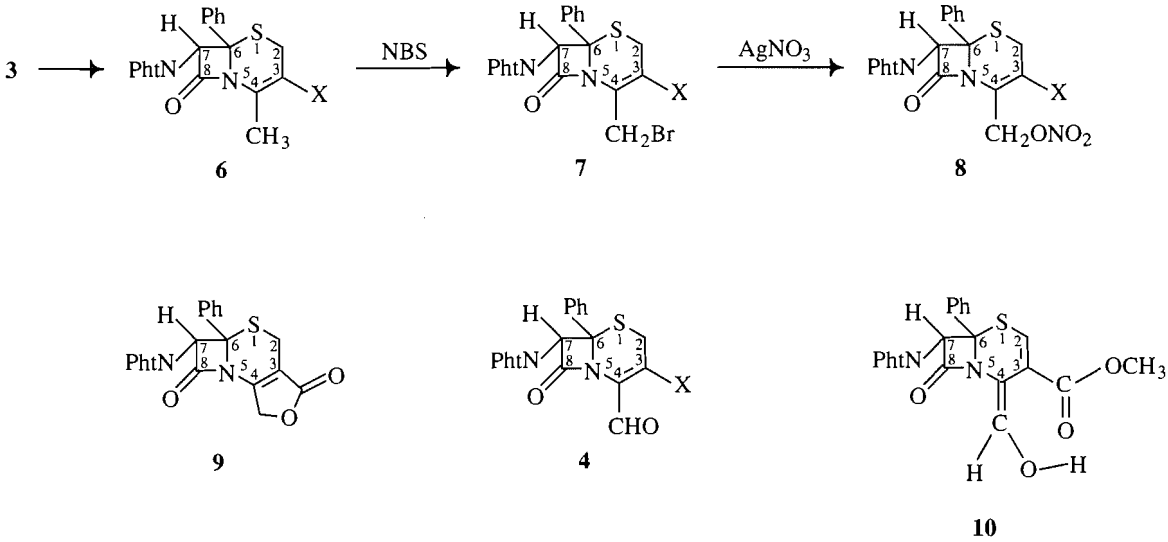


SCHÉMA 4

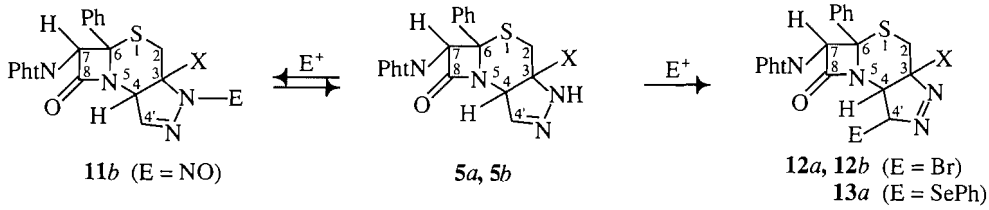


SCHÉMA 5

RMN. Ce type d'isomérisation en milieu basique est fréquemment rencontré en série céphème (6, 7).

Ces résultats nous ont conduits à privilégier une seconde approche, plus rapide, et qui permet de s'affranchir des milieux basiques.

4. Oxydation des pyrazolinocéphames par l'anhydride benzènesélénique

La mise au point d'une technique d'ouverture oxydante du cycle pyrazoline nous a conduits à étudier de façon systématique sur les pyrazolines-2 de formule **5** l'action des principaux oxydants utilisés pour le clivage des hydrazones (8). Une majorité de réactifs conduisent à des produits de N ou C substitution, stables dans le cas des pyrazolines étudiées (schéma 5).

La formation de ces deux types de composés s'interprète bien si l'on admet que la réaction peut être sous contrôle cinétique ou thermodynamique.

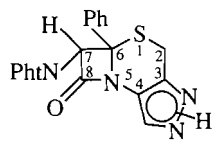
N-substitution

Il s'agit de la réaction la plus classique (alkylation ou acylation des pyrazolines-2) (9). Nous l'avons observée lors de la nitrosation de **5***b*, conduisant à **11***b*.

C-substitution

Cette réaction, sous contrôle thermodynamique, est observée lorsque les réactifs donnent des liaisons fragiles avec l'azote. La *N*-bromosuccinimide, en milieu eau/acétone, conduit à **12***a* et **12***b*. De même, le chlorure de benzènesélénényle donne lieu à la formation de **13***a*.

Les essais d'ouverture de ces pyrazolines substituées **11** ou **12** n'ont permis d'isoler que le pyrazole **14**, dans le cas où il n'y a pas dégradation du noyau céphame.



14

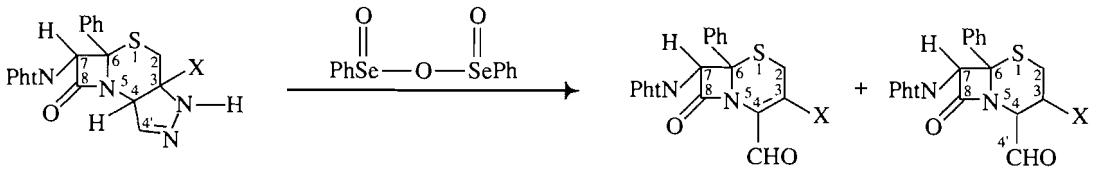
Action de l'anhydride benzènesélénique

Ce réactif, préconisé par Barton *et al.* pour réaliser le clivage des hydrazones encombrées (10), permet l'ouverture oxydante du cycle pyrazoline dans des conditions très douces. La réaction est générale et elle a fait l'objet d'une note préliminaire (11). Appliquée à la pyrazoline-2 **5***a*, elle conduit à un mélange de formyl-4 céphème **4** et de formyl-4 céphame **15** (schéma 6).

Un contrôle assez satisfaisant des proportions des deux produits est obtenu par le choix de la température. Lorsque l'oxydation est effectuée à l'ébullition du toluène, le céphème **4** est isolé à l'état pur avec un rendement de 50%. Sous l'action de la triéthylamine à la température ambiante, il s'isomérise en quelques minutes, en donnant un mélange identique à celui obtenu à partir du composé **8**.

Une autre réaction a été mise en évidence : lorsque la pyrazoline-2 bromée **16***a* (isomérisation de **12***a* par Et_3N) est soumise à l'action de l'anhydride benzènesélénique, le produit isolé est le 4-*H* céphème **17** (schéma 7).

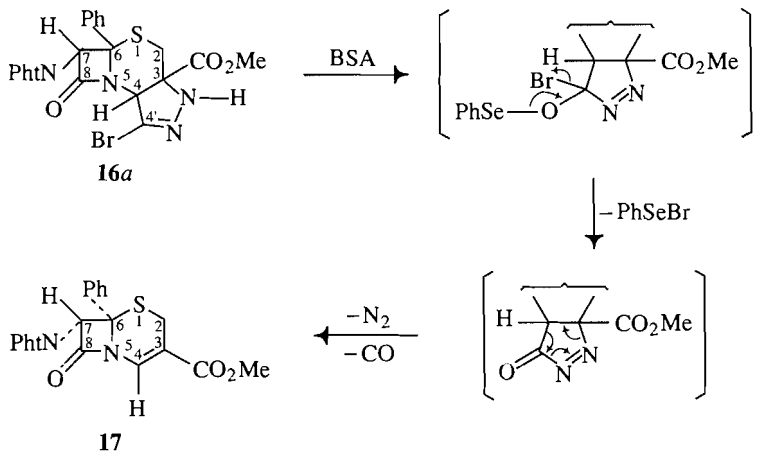
Can. J. Chem. Downloaded from www.nrcresearchpress.com by 194.225.253.170 on 09/07/12
For personal use only.



5a **4** **15**

	% relatifs (spectre de RMN ^1H)	
(CH_2Cl_2, 20 °C)	20%	80%
($PhCH_3$, 110 °C)	68%	32%

SCHÉMA 6



16a **17**

SCHÉMA 7

Compte tenu de l'instabilité des azocomposés cycliques α-carbonylés (12), le mécanisme le plus vraisemblable est la formation d'un ester séléninique intermédiaire, qui conduit à une oxo-3 pyrazoline-1. Une rétrocycloaddition [2σ + 2σ + 2σ] permet alors d'expliquer la formation de l'alcène **17**.

L'introduction de groupes carbonylés sur des modèles plus élaborés de thiazines ou de céphèmes (13) sera envisagée ultérieurement. D'autre part, ce travail montre que les pyrazolines peuvent être utilisées comme intermédiaires pour la formylation d'alcènes. L'application synthétique de ce résultat est actuellement en cours de développement (11).

Partie expérimentale

Les spectres de RMN sont enregistrés sur des solutions dans $CDCl_3$ (sauf indication contraire) à l'aide d'appareils Bruker WP 80 CW (80 MHz; ^1H), WP 80 DS à transformée de Fourier (20,115 MHz; ^{13}C) ou AM WB 300 (300,113 MHz pour ^1H; 75,472 MHz pour ^{13}C); les deux derniers appareils sont du Centre Régional de Mesures Physiques de l'Ouest (C.R.M.P.O.). Les déplacements chimiques δ sont exprimés en ppm/TMS et les constantes de couplage J en hertz (les signaux correspondant aux groupements phényles ne seront pas donnés). Un spectrophotomètre Perkin Elmer 1420 est utilisé pour les déterminations infrarouges; les échantillons sont examinés en suspension dans le Nujol; les fréquences de vibration caractéristiques sont exprimées en cm^{-1}. Les spectres de masse sont enregistrés soit à l'aide d'un appareil Varian MAT 311 du C.R.M.P.O. (énergie du faisceau électronique 70 eV, intensité du courant d'émission 300 μA et tension d'accélération des ions 3 kV), soit à l'aide d'un appareil Varian MAT 112 de l'Université de Nantes (énergie du faisceau électronique 70 eV, intensité dans le filament 1,5 mA). Les points de fusion sont déterminés à l'aide d'un banc chauffant Kofler ou sur une platine chauffante équipée d'un microscope. Les analyses élémentaires sont effectuées par le Service Central de Microanalyse du C.N.R.S.

Les 6-*H* thiazines-1,3 **1** (1*b*, 1*c*) et le diazométhane (14) sont préparés selon les méthodes décrites dans la littérature.

1. *Synthèse des pyrazolinothiazines* **2**

Une solution de 2×10^{-2} mol de thiazine **1** dans 20 cm^3 de dichlorométhane est additionnée d'une solution éthérée (6×10^{-2} mol dans 150 cm^3) de diazométhane (14). Le mélange réactionnel est abandonné 8 jours à la température ambiante, à l'abri de la lumière. Après élimination du solvant, la pyrazoline **2** cristalline.

2*a*: F = 65°C (acétate d'éthyle/éther de pétrole); Rdt = 95%; IR ν: 1732 (c=O), 1610 (C=N); RMN ^1H (80 MHz) δ: 3,52 et 3,91 (système AB, J = 13,5; H6); 3,78 (s; CO_2CH_3); système ABX (H4 et H4′) δ: 4,64 (A); 4,84 (B) et 4,98 (X); J_{AB} = 18,6; J_{AX} = 9,3 et J_{BX} = 1,6; RMN ^{13}C δ: 27,6 (t, ^1J = 146; C6); 53,4 (d, ^1J = 151; C4); 56,9 (q, ^1J = 149; CO_2CH_3); 85,8 (t, ^1J = 145; C4′); 91,5 (s large; C5); 160,5 (s; C2); 168,0 (s; CO_2CH_3). *Anal.* calc. pour $C_{13}H_{13}N_3O_2S$: C 56,73, H 4,72, N 15,27; tr.: C 56,73, H 4,73, N 15,22%.

2*b*: F = 78°C (éther); Rdt = 95%; IR ν: 1699 (C=O), 1593 (C=N); RMN ^1H (300 MHz; C_6D_6), δ: 1,87 (s; $COCH_3$); 2,90 et 2,97 (système AB, J = 13,4; H6); système ABX (H4 et H4′) δ: 4,31 (A); 4,42 (B) et 4,64 (X); J_{AB} = 18,3; J_{AX} = 8,2 et J_{BX} = 3,4; RMN ^{13}C δ: 26,8 (q, ^1J = 129; $COCH_3$); 28,2 (t, ^1J = 145; C6); 55,0 (d, ^1J = 151; C4); 84,3 (t, ^1J = 145; C4′); 96,5 (s large; C5); 159,2 (s; C2); 201,3 (s; $COCH_3$). *Anal.* calc. pour $C_{13}H_{13}N_3OS$: C 60,23, H 5,02, N 16,22; tr.: C 60,16, H 5,09, N 16,14%.

Can. J. Chem. Downloaded from www.nrcresearchpress.com by 194.225.253.170 on 09/07/12
For personal use only.

Can. J. Chem. Downloaded from www.nrcresearchpress.com by 194.225.253.170 on 09/07/12
For personal use only.

2. *Synthèse des pyrazolino-1 céphames* **3**

À 5×10^{-3} mol de pyrazolinothiazine **2** en solution, dans 25 cm^3 de dichlorométhane anhydre, est ajoutée $5,5 \times 10^{-3}$ mol de chlorure d'acide (5) en solution dans 10 cm^3 de dichlorométhane anhydre. Le mélange réactionnel est alors additionné de $5,5 \times 10^{-3}$ mol de triéthylamine et abandonné 12 h à la température ambiante. Après lavage avec une solution saturée d'hydrogénocarbonate de sodium, puis à l'eau, la phase organique est séchée sur $MgSO_4$. Après élimination du solvant, le résidu est cristallisé dans un mélange de 20 cm^3 d'éthanol et 2 cm^3 d'acétone.

3*a*: *F* = 210°C; Rdt = 82%; IR ν: 1793 (C=O lactame), 1730 (C=O ester); RMN ^{1}H (80 MHz) δ: 3,60 (s large; H2); 3,87 (s; CO_2CH_3); 4,87–5,37 (système ABC; H4 et H4′); 5,79 (s; H7); RMN ^{13}C δ: 27,4 (t, ^1J = 145; C2); 48,5 (d, ^1J = 147; C4); 53,7 (q, ^1J = 149; CO_2CH_3); 69,1 (d, ^1J = 153; C7); 71,2 (s, large; C6); 80,5 (t, ^1J = 144; C4′); 93,4 (s large; C3); 166,0 (s; C8); 167,3 (s large; CO_2CH_3). Spectrométrie de masse (Varian Mat 311): pour $[M]^+$, masse calculée: 462,099; trouvée: 462,100. *Anal.* calc. pour $C_{23}H_{18}N_4O_5S \cdot 1/4\ H_2O$: C 59,16, H 3,96, N 12,00; tr.: C 59,05, H 3,76, N 11,86%.

3*b*: *F* = 209°C; Rdt = 76%; IR ν: 1792 (C=O lactame), 1725 (C=O cétone); RMN ^{1}H (80 MHz) δ: 2,45 (s; $COCH_3$); 3,53 (s large; H2); 4,75–5,38 (système ABC; H4 et H4′); 5,75 (s; H7); RMN ^{13}C δ: 26,7 (q, ^1J = 129; $COCH_3$); 28,1 (t, ^1J = 142; C2); 46,5 (d, ^1J = 148; C4); 69,1 (d, ^1J = 152; C7); 71,1 (s large; C6); 79,5 (t, ^1J = 143; C4′); 100,1 (s large; C3); 166,0 (s; C8); 199,6 (s large; $COCH_3$). *Anal.* calc. pour $C_{23}H_{18}N_4O_4S$: C 61,88, H 4,04, N 12,55; tr.: C 61,66, H 4,05, N 12,55%.

3. *Synthèse des pyrazolino-2 céphames* **5**

De la triéthylamine ($1,5 \times 10^{-2}$ mol) est ajoutée à 5×10^{-3} mol de pyrazolino-1 céphame **3** en solution dans 25 cm^3 de dichlorométhane anhydre. Ce mélange est abandonné 24 h à la température ambiante. Après élimination du solvant, le résidu est cristallisé dans un mélange de 20 cm^3 d'éthanol et 2 cm^3 d'acétone.

5*a*: *F* = 259°C; Rdt = 92%; IR ν: 3310 (NH), 1792 (C=O lactame), 1728 (C=O ester); RMN ^{1}H (80 MHz; $CDCl_3/CF_3CO_2H$, 90:10) δ: 2,96 et 3,42 (système AB, J = 15,0; H2); 3,98 (s; CO_2CH_3); 5,84 (s; H7); 6,33 (s large; H4); 7,22 (s large; H4′); RMN ^{13}C ($CDCl_3/CF_3CO_2H$, 90:10) δ: 29,4 (t, ^1J = 144; C2); 54,0 (q, ^1J = 148; CO_2CH_3); 60,9 (d, ^1J = 144; C4); 65,3 (s large; C6); 67,9 (d, ^1J = 154; C7); 72,2 (s large; C3); 141,5 (d, ^1J = 198; C4′); 166,7 (s large; C8); 178,2 (s large; CO_2CH_3). *Anal.* calc. pour $C_{23}H_{18}N_4O_5S$: C 59,74, H 3,90 N 12,12; tr.: C 59,48, H 4,01, N 11,93%.

5*b*: *F* = 250°C; Rdt = 90%; IR ν: 3290 (NH), 1785 (C=O lactame), 1720 (C=O cétone); RMN ^{1}H (80 MHz; $CDCl_3/CF_3CO_2H$, 90:10) δ: 2,40 (s; $COCH_3$); 2,84 et 3,39 (système AB, J = 15,0; H2); 5,84 (s; H7); 6,13 (s large; H4); 7,15 (s large; H4′); RMN ^{13}C ($CDCl_3/CF_3CO_2H$, 90:10) δ: 25,6 (q, ^1J = 128; $COCH_3$); 28,7 (t, ^1J = 145; C2); 60,4 (d, ^1J = 144; C4); 67,9 (d, ^1J = 154; C7); 70,6 (s large; C6); 71,8 (s large; C3); 141,4 (d, ^1J = 195; C4′); 167,0 (s; C8); 205,4 (s large, $COCH_3$). *Anal.* calc. pour $C_{23}H_{18}N_4O_4S$: C 61,88, H 4,04, N 12,55; tr.: C 61,82, H 3,98, N 12,25%.

4. *Analyse cristallographique du composé* **5**a

$SO_5N_4C_{25}H_{18}$ M_r = 462.5

Orthorhombique, *Pbca*, a = 14,689(4), b = 16,243(4), c = 18,118(9) Å, V = 4322,6(6) Å^{-3}, Z = 8, D_x = 1,42 (Mg m^{-3}), λ (MoKα) = 0,71073 Å, μ = 1,8 cm^{-1}, F(000) = 1920, T = 296 K. L'étude a été réalisée à l'aide d'un diffractomètre automatique Enraf–Nonius: Les paramètres de la maille ont été déterminés et affinés à partir d'un ensemble de 25 réflections à angle élevé. L'échantillon, taillé à 0,15 × 0,23 × 0,26 mm, a fourni 4251 réflexions ($2\theta_{max}$ = 50°) dont 1044 indépendantes avec $I > \sigma(I)$: domaine analysé h (0 → 17) k (0 → 19) l (0 → 21), balayage $\omega/2\theta$ = 1, vitesse de balayage variable (t_{max} = 60 s), variation de 1,5% sur les contrôles d'intensité.

La structure a été résolue à l'aide des Méthodes Directes qui permettent de localiser tous les atomes non-hydrogène. L'ensemble du motif est affiné en mode isotrope (R = 0,084) puis en mode anisotrope (R = 0,072). À ce stade, les atomes d'hydrogène sont définis à l'aide d'une différence de Fourier (entre 0,57 et 0,19 e Å^{-3}).

Le meilleur affinement par matrice complète de l'ensemble de la molécule (x, y, z, β_{ij} atomes non-hydrogène et x, y, z atomes d'hydrogène) donne pour 1525 observations: R = 0,059; R_w = 0,058; S_w = 2,2; Δe = 0,15 e Å^{-3}.

5. *Synthèse des méthyl-4 céphèmes* **6**

Une solution de 10^{-3} mol de pyrazolino-1 céphame **3** dans 30 cm^3 de toluène est portée à reflux pendant 72 h. Après élimination du solvant, le résidu est cristallisé dans 10 cm^3 d'éthanol.

6*a*: *F* = 244°C; Rdt = 85%; IR ν: 1790 (C=O lactame), 1724 (C=O ester); RMN ^{1}H (80 MHz) δ: 2,87 et 3,77 (système AB, J = 15,0; H2); 2,95 (s; $=CCH_3$); 3,75 (s; CO_2CH_3); 5,60 (s; H7); RMN ^{13}C δ: 18,0 (q, ^1J = 131; $=CCH_3$); 25,7 (t, ^1J = 141; C2); 51,8 (q, ^1J = 147; CO_2CH_3); 65,1 (d, ^1J = 152; C7); 70,0 (s; C6); 108,1 (s large; C3); 144,7 (s large; C4); 161,0 (s; C8); 166,9 (s large; CO_2CH_3). *Anal.* calc. pour $C_{23}H_{18}N_2O_5S$: C 63,59, H 4,15, S 7,37; tr.: C 63,09, H 4,12, S 7,22%.

6*b*: *F* = 240°C; Rdt = 85%; IR ν: 1785 (C=O lactame), 1718 (C=O acétone); RMN ^{1}H (80 MHz) δ: 2,34 (s; $COCH_3$); 2,92 et 3,66 (système AB, J = 17,0; H2); 2,86 (s; $=CCH_3$); 5,58 (s; H7); RMN ^{13}C δ: 18,2 (q, ^1J = 130; $=CCH_3$); 26,4 (t, ^1J = 143; C2); 30,6 (q, ^1J = 127; $COCH_3$); 65,1 (d, ^1J = 152; C7); 69,9 (s; C6); 116,8 (s large; C3); 142,2 (s large; C4); 165,9 (s; C8); 198,2 (s large; $COCH_3$). Spectrométrie de masse (Varian Mat 112): $[M]^+$ = 418. *Anal.* calc. pour $C_{23}H_{18}N_2O_4S \cdot H_2O$: C 63,30, H 4,59, N 6,42; tr.: C 63,89, H 4,38, N 6,48%.

6. *Synthèse du bromométhyl-4 céphème* **7**

Du *N*-bromosuccinimide (3×10^{-3} mol) est ajouté à une solution de 2×10^{-3} mol de céphème **6***a* dans 15 cm^3 de dichlorométhane et le mélange est maintenu 6 h à reflux. Après lavage à l'eau et séchage sur $MgSO_4$, le solvant est éliminé. Le résidu est recristallisé à froid dans le mélange acétate d'éthyle/éther de pétrole; *F* = 198°C; Rdt = 91%; IR ν: 1795 (C=O lactame), 1727 (C=O ester); RMN ^{1}H (80 MHz) δ: 2,91 et 3,82 (système AB, J = 18,4; H2); 3,80 (s; CO_2CH_3); 5,14 et 5,41 (système AB, J = 10,4; CH_2Br); 5,62 (s; H7). *Anal.* calc. pour $C_{23}H_{17}N_2O_4SBr$: C 53,80, H 3,34, S 6,25; tr.: C 53,69, H 3,44, S 6,37%.

7. *Synthèse du composé* **8**

Du nitrate d'argent (7×10^{-4} mol) est ajouté, sous agitation magnétique, à une solution de 7×10^{-4} mol de bromométhylcéphème **7** dans 10 cm^3 d'acétonitrile anhydre. Le mélange est abandonné sous agitation pendant 24 h à la température ambiante et à l'abri de la lumière. Le solvant est alors éliminé et le résidu repris avec du dichlorométhane, puis lavé à l'eau. Après séchage sur $MgSO_4$, le dichlorométhane est éliminé et le produit obtenu recristallisé à froid dans le mélange acétate d'éthyle/éther de pétrole; *F* = 179°C; Rdt = 89%; IR ν: 1805 (C=O lactame), 1727 (C=O ester); RMN ^{1}H (80 MHz) δ: 2,82 et 3,70 (système AB, J = 19,2; H2); 3,69 (s; CO_2CH_3); 5,53 (s; H7); 5,91 et 6,24 (système AB, J = 12,4; CH_2ONO_2). Spectrométrie de masse (Varian Mat 112): $[M]^+$ = 495. *Anal.* calc. pour $C_{23}H_{17}N_3O_8S \cdot 1/2H_2O$: C 54,76, H 3,57, S 6,35; tr.: C 54,77, H 3,52, S 6,37%.

8. *Synthèse de la lactone* **9**

À une solution de 4×10^{-4} mol de bromométhylcéphème **7**, dans 20 cm^3 d'acétone, est ajoutée 8×10^{-4} mol de fluoroborate d'argent (celui-ci, soluble dans l'eau et dans l'acétone, est préparé par action de 2 mol de HBF_4 sur 1 mol de $AgCO_3$, lui-même obtenu par action de $NaHCO_3$ sur une solution de $AgNO_3$). Le mélange est maintenu à reflux sous agitation magnétique, pendant 24 h, à l'abri de la lumière, puis concentré au 1/4. Du dichlorométhane (100 cm^3) et 200 cm^3 d'eau sont alors ajoutés. La phase organique est épuisée au dichlorométhane, séchée et le solvant éliminé. Le produit ainsi obtenu est recristallisé dans l'éthanol; *F* = 260°C; Rdt = 92%; IR ν: 1815 (C=O lactame), 1770 (C=O lactone); RMN ^{1}H (80 MHz; $CDCl_3/CF_3CO_2H$, 90:10) δ: 3,15 et 3,40 (système AB, J = 16,0; H2); 5,50 (s large; CH_2 lactone); 5,84 (s; H7). Spectrométrie de masse (Varian Mat 311):

Can. J. Chem. Downloaded from www.nrcresearchpress.com by 194.225.253.170 on 09/07/12
For personal use only.

pour $[M]^{+}$, masse calculée : 418,062; trouvée : 418,063. *Anal.* calc. pour $C_{22}H_{14}N_2O_5S$: C 63,16, H 3,35, N 6,70; tr. : C 62,65, H 3,29, N 6,64%.

9. *Essai d'obtention du formyl-4 céphème* ***4*** *à partir du composé* ***8***

De la triéthylamine ($6,4 \times 10^{-4}$ mol) est ajoutée à une solution de $3,2 \times 10^{-4}$ mol de composé **8** dans 20 cm^3 de chloroforme. Le mélange est abandonné 15 min à la température ambiante, puis versé dans 10 cm^3 d'acide chlorhydrique molaire. Après épuisement au dichlorométhane et séchage sur $MgSO_4$, le solvant est éliminé et le résidu analysé par RMN ^{1}H. C'est un mélange de formyl-4 céphème **4** (20%) et d'un isomère (80%) auquel nous avons attribué la structure Δ-2 céphème énolisée **10**; les caractéristiques de ces deux produits seront données plus loin.

10. *Synthèse du nitrosopyrazolino-2 céphame* ***11***b

À une solution de 5×10^{-4} mol de pyrazolino-2 céphame **5***b* dans 2 cm^3 d'acide trifluoroacétique, portée à 0°C, est ajoutée $2,5 \times 10^{-3}$ mol de nitrite de sodium en solution dans 2 cm^3 d'eau, sous vive agitation magnétique. Cette agitation est maintenue pendant 5 min, puis le mélange est versé dans 20 cm^3 d'eau. Après essorage, le produit obtenu est recristallisé dans l'acétone; F = 235°C; Rdt quantitatif; IR ν : 1789 (C=O lactame), 1710 (C=O cétone); RMN ^{1}H (80 MHz) δ : 2,22 (s; $COCH_3$); 3,55 et 3,72 (système AB, J = 15,8; H2); 5,99 (d, ^3J = 2,0; H4); 6,08 (s; H7); 7,85 (d, ^3J = 2,0; H4′). Spectrométrie de masse (Varian Mat 112) : ion fragment $[M - COCH_3 - NO]^{+}$ = 402.

11. *Synthèse des bromopyrazolino-1 céphames* ***12***

Du *N*-bromosuccinimide ($3,3 \times 10^{-3}$ mol) est ajouté, sous agitation magnétique, à une solution de 3×10^{-3} mol de pyrazolino-2 céphame **5** dans 100 cm^3 d'acétone. Le mélange est abandonné 1 h à la température ambiante et le solvant éliminé. Le résidu est repris par 50 cm^3 de dichlorométhane, puis lavé successivement par une solution saturée d'hydrogénosulfite de sodium, une solution saturée d'hydrogénocarbonate de sodium et à l'eau. Après séchage sur $MgSO_4$ et élimination du solvant, le résidu est recristallisé dans l'éthanol.

12*a* : F = 188°C (déc.); Rdt = 87%; IR ν : 1790 (C=O lactame), 1730 (C=O ester); RMN ^{1}H (80 MHz) δ : 3,26 et 3,63 (système AB, J = 16,0; H2); 3,94 (s; CO_2CH_3); 5,35 (d, ^3J = 6,0; H4); 5,75 (s; H7); 6,25 (d, ^3J = 6,0; H4′); RMN ^{13}C δ : 28,1 (t, ^1J = 148; C2); 54,2 (q, ^1J = 148; CO_2CH_3); 58,8 (d, ^1J = 152; C4); 68,5 (d, ^1J = 153; C7); 71,6 (s large; C6); 79,9 (d, ^1J = 168; C4′); 93,0 (s large; C3); 166,0 (s; C8); 166,7 (s large; CO_2CH_3). *Anal.* calc. pour $C_{23}H_{17}N_4O_5SBr$: C 51,02, H 3,14, N 10,35; tr. : C 51,18, H 3,30, N 10,23%.

12*b* : F = 195–200°C (déc.); Rdt = 89%; IR ν : 1787 (C=O lactame), 1725 (C=O cétone); RMN ^{1}H (80 MHz) δ : 2,59 (s; $COCH_3$); 3,53 (s large; H2); 5,39 (d, ^3J = 5,0; H4); 5,87 (s; H7); 6,35 (d, ^3J = 5,0; H4′); RMN ^{13}C δ : 26,6 (q, ^1J = 129; $COCH_3$); 27,5 (t, ^1J = 146; C2); 55,4 (d, ^1J = 151; C4); 68,1 (d, ^1J = 155; C7); 70,7 (s large; C6); 79,5 (d, ^1J = 171; C4′); 98,8 (s large; C3); 165,7 (s; C8); 199,9 (s large; $COCH_3$). *Anal.* calc. pour $C_{23}H_{17}N_4O_4SBr$: C 52,57, H 3,24, N 10,66; tr. : C 52,47, H 3,45, N 10,79%.

12. *Synthèse du phénylsélénopyrazolino-1 céphame* ***13***a

Du chlorure de benzènesélénényle (10^{-3} mol) est ajouté à une solution de 10^{-3} mol de pyrazolino-2 céphame **5***a* dans 50 cm^3 de dichlorométhane. Le mélange est maintenu 18 h à reflux. Après élimination du solvant, le résidu est recristallisé dans l'acétone; F = 236°C; Rdt = 95%; IR ν : 1791 (C=O lactame), 1733 (C=O ester); RMN ^{1}H (80 MHz) δ : 3,13 et 3,56 (système AB, J = 15,4; H2); 3,72 (s; CO_2CH_3); 5,06 (d, ^3J = 6,8; H4); 5,69 (s; H7); 5,82 (d, ^3J = 6,8; H4′); RMN ^{13}C δ : 28,1 (t, ^1J = 145; C2); 53,8 (q, ^1J = 148; CO_2CH_3); 55,1 (d, ^1J = 150; C4); 66,3 (d, ^1J = 153; C7); 71,4 (s large; C6); 85,6 (d, ^1J = 156; C4′); 91;6 (s large; C3); 165,9 (s large; CO_2CH_3); 167,0 (s; C8). Spectre de masse (Varian Mat 311) : pour $[M]^{+}$, masse calculée : 590,041; trouvée : 590,041. *Anal.* calc. pour $C_{29}H_{22}N_4O_5SSe \cdot H_2O$: C 54,80, H 3,78, N 8,81; tr. : C 55,12, H 3,55, N 8,96%.

13. *Obtention du pyrazole* ***14***

À une solution de 3×10^{-4} mol de bromopyrazolino-1 céphame **12**, dans 40 cm^3 de méthanol, est ajoutée 3×10^{-4} mol de potasse en solution dans le minimum de méthanol. Le mélange est maintenu 20 min sous agitation magnétique, à la température ambiante, puis additionné de 25 cm^3 d'acide chlorhydrique 0,5 M. Après extraction au dichlorométhane, la phase organique est lavée à l'eau, puis séchée sur $MgSO_4$ et le solvant éliminé. Les cristaux obtenus après addition de 20 cm^3 d'éther sont recristallisés dans l'éthanol; F = 260°C; Rdt = 87%; IR ν : 3260, large (NH), 1795 (C=O lactame); RMN ^{1}H (80 MHz; $CDCl_3/CF_3CO_2H$, 90 : 10) δ : 3,50 et 4,21 (système AB, J = 18,4; H2); 5,78 (s; H7); 8,49 (s; H pyrazole). Spectrométrie de masse (Varian Mat 112) : $[M]^{+}$ = 402.

14. *Oxydation avec l'anhydride benzènesélénique*

(a) Synthèse des formyl-4 céphème 4 et formyl-4 céphame ***15***

Une solution de 2×10^{-3} mol de pyrazolino-2 céphame **5***a* dans 100 cm^3 de toluène est portée à reflux sous vive agitation. Sont alors ajoutées 10^{-2} mol d'hydrogénocarbonate de sodium en poudre, puis $2,2 \times 10^{-3}$ mol d'anhydride benzènesélénique. Le mélange est maintenu 5 min à reflux sous vive agitation magnétique, puis lavé avec 2 fois 50 cm^3 d'eau, séché sur $MgSO_4$ et le solvant éliminé. Le produit brut, analysé en RMN ^{1}H, montre la formation des composés **4** (68%) et **5** (32%). Il est repris par un mélange de tétrachlorure de carbone (20 cm^3) et d'acétone (10 cm^3). Le milieu, abandonné à l'air libre, laisse déposer les aldéhydes, qui sont séparés par recristallisation à chaud dans l'acétate d'éthyle.

4 : F = 241°C; Rdt = 50%; IR ν : 1808 (C=O lactame), 1735 (C=O ester), 1729 (C=O aldéhyde); RMN ^{1}H (80 MHz) δ : 2,98 et 3,82 (système AB, J = 19,2; H2); 3,79 (s; CO_2CH_3); 5,55 (s; H7); 10,25 (s; CHO); RMN ^{13}C δ : 26,0 (t, ^1J = 147; C2); 53,0 (q, ^1J = 148; CO_2CH_3); 65,6 (d, ^1J = 153; C7); 69,0 (s; C6); 117,8 (s large; C3); 141,3 (s large; C4); 159,5 (s; C8); 165,2 (s large; CO_2CH_3); 184,9 (d, ^1J = 199; CHO). *Anal.* calc. pour $C_{23}H_{16}N_2O_6S$: C 61,61, H 3,57, N 6,25; tr. : C 61,50, H 3,48, N 6,32%.

15 : F = 229°C; Rdt = 10%; IR ν : 1800 (C=O lactame), 1733 (C=O ester), 1726 (C=O aldéhyde); RMN ^{1}H (300 MHz) : système ABCX analysé par découplage successif des différents protons, δ : 2,82 (A) (H2); 3,06 (C) (H3); 3,17 (B) (H2); 5,56 (X) (H4); J_{AB} = 14,5; J_{AC} = 11,4; J_{BC} = 2,7; J_{BX} = 0,8; J_{CX} = 5,2; $J_{H3H4'}$ = 1,1; δ : 3,70 (s; CO_2CH_3); 5,54 (s; H7); 9,78 (d, $J_{H4'H3}$ = 1,1; H4′); RMN ^{13}C δ : 24,3 (t, ^1J = 143; C2); 40,2 (d, ^1J = 125; C3); 52,4 (q, ^1J = 148; CO_2CH_3); 57,5 (d, ^1J = 138; C4); 69,1 (d, ^1J = 156; C7); 71,0 (s; C6); 163,5 (s; C8); 169,3 (s large; CO_2CH_3); 193,7 (d, ^1J = 184; CHO). Spectrométrie de masse (Varian Mat 311) : pic moléculaire correspondant à $C_{23}H_{18}N_2O_6S$ (M = 450) trop faible pour mesurer la masse exacte; ion fragment $[M - OCH_3]^{+}$, masse calculée : 419,070; trouvée : 419,071.

(b) Obtention du Δ-2 céphème ***10***

De la triéthylamine (10^{-3} mol) est ajoutée à une solution de 2×10^{-4} mol de céphème **4** dans 15 cm^3 de dichlorométhane anhydre. La solution se colore immédiatement et, après 5 min à la température ambiante, elle est versée dans 25 cm^3 d'acide chlorhydrique 0,2 M. Après extraction au dichlorométhane, la phase organique est séchée sur $MgSO_4$, puis le solvant est éliminé. L'analyse en RMN ^{1}H montre que le produit obtenu est un mélange des composés **4** (20%) et **10** (80%). La recristallisation, à chaud dans l'acétate d'éthyle, permet d'isoler **10** pur; F = 230°C; Rdt = 75%; IR ν : 1795 (C=O lactame), 1720 (C=O ester); RMN ^{1}H (80 MHz) δ : 3,75 (s; CO_2CH_3); 5,61 (s; H7); 7,12 (s imbriqué dans les signaux du noyau phényle) et 7,73 (s) (H2 et =$CHOH$); le signal relatif au proton énolique n'est pas détecté; RMN ^{13}C δ : 52,3 (q, ^1J = 148; CO_2CH_3); 65,2 (d, ^1J = 156; C7); 68,2 (s; C6); 110,7 (s) et 118,3 (s large) (C3 et (ou) C4); 126,5 (d, ^1J = 180; C2); 141,4 (d, ^1J = 190; =$CHOH$); 161,0 (s; C8); 163,2 (s large; CO_2CH_3). Spectrométrie de masse (Varian Mat 311) : pour $[M]^{+}$ ($C_{23}H_{16}N_2O_6S$) masse calculée : 448,072; trouvée : 448,072.

*(c) Obtention du 4-*H *céphème* ***17*** *à partir du bromopyrazolino-1 céphame* ***12***a

(1) *Synthèse des bromopyrazolino-2 céphames* ***16*** : 10^{-2} mol de triéthylamine est ajoutée à une solution de 3×10^{-3} mol de bromopyrazolino-1 céphame **12** dans 30 cm^3 de dichlorométhane et le mé-

lange est maintenu au reflux pendant 2 h. Après élimination du solvant et de la triéthylamine, le produit obtenu est recristallisé dans l'éthanol.

16*a* : F = 248°C; Rdt = 90%; IR ν : 3335–3280 (NH), 1780 (C=O lactame), 1731 (C=O ester); RMN ^{1}H (80 MHz; $CDCl_3/CF_3CO_2H$, 90 : 10) δ : 2,81 et 3,36 (système AB, J = 14,4; H2); 3,92 (s; CO_2CH_3); 5,66 (s; H7); 6,18 (s; H4); RMN ^{13}C ($CDCl_3/CF_3CO_2H$, 90 : 10) δ : 29,4 (t, ^1J = 145; C2); 54,9 (q, ^1J = 149; CO_2CH_3); 64,2 (d, ^1J = 150; C4); 66,4 (s large; C6); 67,0 (d, ^1J = 154; C7); 74,0 (s large; C3); 133,4 (s large; C4′); 167,6 (s; C8); 169,9 (s large; CO_2CH_3). *Anal.* calc. pour $C_{23}H_{17}N_4O_5SBr$: C 51,02, H 3,14, N 10,35; tr. : C 50,97, H 3,32, N 10,22%.

16*b* : F = 257°C; Rdt = 90%; IR ν : 3330–3280 (NH), 1787 (C=O lactame), 1724 (C=O cétone); RMN ^{1}H (80 MHz; $CDCl_3/CF_3CO_2H$, 90 : 10) δ : 2,41 (s; $COCH_3$); 2,84 et 3,30 (système AB, J = 15,6; H2); 5,72 (s; H7); 6,03 (s; H4); RMN ^{13}C ($CDCl_3/CF_3CO_2H$, 90 : 10) δ : 25,4 (q, ^1J = 129; $COCH_3$); 28,7 (t, ^1J = 143; C2); 63,2 (d, ^1J = 149; C4); 67,2 (d, ^1J = 154; C7); 70,8 (s large; C6); 73,5 (s large; C3); 133,6 (s large; C4′); 167,4 (s; C8); 204,5 (s large; $COCH_3$). *Anal.* calc pour $C_{23}H_{17}N_4O_4SBr$: C 52,57, H 3,24, N 10,66; tr. : C 52,93, H 3,40, N 10,24%.

(2) *Synthèse du céphème* ***17*** : 1,98 × 10^{-4} mol d'anhydride benzèneséléninique est ajoutée à une solution de 3 × 10^{-4} mol de bromo-pyrazolino-2 céphame **16***a* dans 25 cm^3 de dichlorométhane. Le mélange est maintenu 2 h sous agitation magnétique, à la température ambiante. Après lavage par une solution saturée d'hydrogénocarbonate de sodium, puis à l'eau, la phase organique est séchée sur $MgSO_4$. Le produit obtenu après élimination du solvant est recristallisé dans l'éthanol; F = 253°C; Rdt = 77%; IR ν : 1805 (C=O lactame), 1723 (C=O ester); RMN ^{1}H (80 MHz) : Système ABX (H2 et H4) δ : 2,35 (A); 3,80 (B) et 8,27 (X); J_{AB} = 18,4; J_{AX} = 2,2 et J_{BX} = 0,0; δ : 3,90 (s CO_2CH_3); 5,78 (s; H7). Spectrométrie de masse (Varian Mat 112), $[M]^+$ = 420. *Anal.* calc. pour $C_{22}H_{16}N_2O_5S \cdot H_2O$: C 60,27, H 4,10, N 6,39; tr. : C 60,89, H 3,89, N 6,42%.

1. (*a*) J. C. Meslin et H. Quiniou. Bull. Soc. Chim. Fr. 347 (1979); (*b*) J. P. Pradère, J. C. Rozé, H. Quiniou, R. Danion-Bougot, D. Danion et L. Toupet. Can. J. Chem. **64**, 597 (1986); (*c*) M. Chehna, J. P. Pradère et A. Guingant. Synth. Comm. **17**, 1971 (1987); (*d*) D. L. Boger et S. M. Weinreb. Hetero Diels–Alder methodology in organic synthesis. Vol. 47. Academic Press, New York, London. 1987.
2. C. G. Tea, J. P. Pradère, J. Villieras et H. Quiniou. Tetrahedron Lett. **24**, 3713 (1983); C. G. Tea, J. P. Pradère, B. Bujoli, H. Quiniou et L. Toupet. Bull. Soc. Chim. Fr. 149 (1987).
3. R. Danion-Bougot, D. Danion, J. P. Pradère, J. C. Rozé, H. Quiniou et A. J. Kos. Sulfur Lett. **3**, 51 (1985).
4. B. Christiensen, K. Hoogsteen, F. Flavac et R. Ratcliffe. *Dans* Recent advances in the chemistry of β-lactam antibiotics. *Editeur* : J. Elks. The Chemical Society, Special publication n° 28. 1977. chap. 26.
5. A. K. Bose. Org. Synth. Coll. Vol. V, 973 (1973); J. C. Sheehan, D. W. Chapman et R. W. Roth. J. Am. Chem. Soc. **74**, 3822 (1952).
6. E. Flynn. Cephalosporins and penicillins. Academic Press, New York, London. 1972. Chap. 3, 4 et 5.
7. H. Peter et H. Bickel. Helv. Chim. Acta, **57**, 2044 (1974); H. Peter, B. Müller et H. Bickel. Helv. Chim. Acta, **58**, 2450 (1975).
8. L. Cagliotti, F. Gasparrini, D. Misiti et G. Palmieri. Synthesis, 207 (1979) et réf. citées; B. Dakova, M. Evers, L. Christiaens et M. Guillaume. Bull. Soc. Chim. Belg. **96**, 219 (1987) et réf. citées; T. Chiba, M. Okimoto, H. Nagai et Y. Takata. J. Org. Chem. **48**, 2968 (1983) et réf. citées.
9. L. Behr, R. Fusco et C. Jarboe. Pyrazoles, pyrazolines, indazoles and condensed rings. *Editeur* : R. Wiley. Interscience Publishers, J. Wiley and Sons, New York, London. 1967.
10. D. H. R. Barton, D. J. Lester et S. V. Ley. J. Chem. Soc. Chem. Commun. 277 (1978); J. Chem. Soc. Perkin Trans. 1, 1212 (1980).
11. R. Tuloup, R. Danion-Bougot, D. Danion et J. P. Pradère. Tetrahedron Lett. **29**, 6249 (1988).
12. E. Fahr et H. Lind. Angew. Chem. Int. Ed. Engl. **5**, 372 (1966); R. Kent et J. P. Anselme. Can. J. Chem. **46**, 2322 (1968).
13. J. C. Rozé. Thèse de Doctorat d'État, Nantes (1986); M. Chehna. Thèse de Doctorat d'État, Nantes (1987).
14. T. J. De Boer et H. J. Backer. Org. Synth. Coll. Vol. IV, 250 (1967).

Can. J. Chem. Downloaded from www.nrcresearchpress.com by 194.225.253.170 on 09/07/12
For personal use only.

Macrocycles polyoxygénés à structure benzodioxinique. Synthèse et étude de la complexation du sodium et du potassium dans le méthanol

MICHEL MPASSI ET GÉRALD GUILLAUMET
Laboratoire de chimie organique, Université d'Orléans, Rue de Chartres, BP 6759, 45067 Orléans CEDEX 2, France

GÉRARD COUDERT
Centre du médicament, Université de Nancy I, Unité associée au Centre national de la recherche scientifique, n° 597, 30, Rue Lionnois, 54000 Nancy, France

ET

MADELEINE TISSIER ET JEAN JUILLARD[1]
Laboratoire de chimie physique des solutions, Université Blaise Pascal (Clermont), Unité associée au Centre national de la recherche scientifique, n° 434, 63177 Aubière CEDEX, France

Reçu le 24 octobre 1988

MICHEL MPASSI, GÉRALD GUILLAUMET, GÉRARD COUDERT, MADELEINE TISSIER et JEAN JUILLARD. Can. J. Chem. **67**, 1132 (1989).

La synthèse de deux nouvelles séries de macrocycles polyoxygénés, **1** et **2**, a été réalisée. Ces dérivés présentent en commun une structure benzodioxinique 1,4 et sont apparentés aux éthers-couronnes, aux éthers-couronnes benzo et aux éthers-lassos. L'étude de la complexation des cations sodium et potassium par les différents composés préparés a été effectuée par potentiométrie dans le méthanol; ces résultats sont comparés aux données de la littérature concernant d'autres composés macrocycliques polyoxygénés.

Mots clés : macrocycles polyoxygénés, benzodioxine-1,4, éthers-lassos, complexes du sodium et du potassium, solvant méthanol.

MICHEL MPASSI, GÉRALD GUILLAUMET, GÉRARD COUDERT, MADELEINE TISSIER, and JEAN JUILLARD. Can. J. Chem. **67**, 1132 (1989).

The synthesis of two new series of polyoxygenated macrocyclic derivatives, **1** and **2**, was realised. All these compounds have a 1,4-benzodioxinic moiety and are related to crown ethers, benzocrown ethers, and lariat ethers. The complexing properties of sodium and potassium ions were studied using potentiometry in methanol; results thus obtained are compared to data, previously reported in the literature, for classical polyoxygenated macrocyclic compounds.

Key words: polyoxygenated macrocycles, 1,4-benzodioxin, lariat ethers, sodium and potassium complexes, solvent methanol.

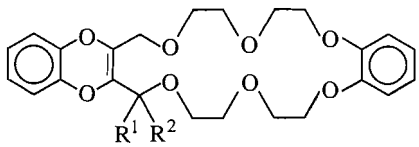
Introduction

Depuis la découverte quelque peu fortuite des éthers-couronnes effectuée par C. J. Pedersen il y a 20 ans (1) un nombre considérable de travaux ont été réalisés dans ce domaine. Après la synthèse des premiers composés cycliques polyoxygénés, des ligands organiques cycliques neutres incorporant des atomes de soufre (2), d'azote (3) ou de phosphore (4) ont aussi été préparés; l'ensemble de ces dérivés sont regroupés sous le terme de coronands. Parallèlement aux recherches réalisées en série monocyclique, Lehn a développé un nouveau groupe de composés, celui des cryptands (5), ligands bi- ou tri-cycliques oxygénés et azotés caractérisés par l'existence d'une cavité tridimensionnelle de taille modulable. Des travaux visant à l'obtention de dérivés à chaîne ouverte apparentés soit aux coronands soit aux cryptands (6) ont également été réalisés.

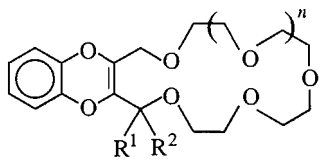
Tous ces composés, du fait de leur structure et de leur aptitude à complexer les cations, constituent des modèles potentiels des ionophores naturels. Cependant, le pouvoir complexant et la sélectivité observés dans le cas des coronands se révèlent souvent trop faibles, alors que les cryptands, ligands puissants et sélectifs des cations, présentent l'inconvénient de conduire à des complexes, les cryptates, souvent trop stables. On pouvait dès lors estimer qu'un compromis favorable du point de vue topologique devait être réalisé entre ces deux types de ligands avec les éthers-lassos (lariat-ethers) élaborés tout d'abord par Gokel *et al.* (7).

Il est souvent difficile de fixer des chaînes latérales sur des cycles polyoxygénés dans des conditions définies; trois d'entre-nous ont proposé, pour ce faire, une méthode originale utilisant comme structure de base le motif benzodioxine (8). Lors de cette synthèse il est aisé d'introduire en α du cycle benzodioxinique un ou deux bras susceptibles de participer ou non à la complexation des cations par le macrocycle. Ce travail a été développé et le pouvoir complexant des molécules obtenues systématiquement testé.

Nous avons préparé deux types de composés, **1** possèdant une chaîne latérale de nature et taille variable et un motif catéchol comme moyen de fermeture, et **2** comportant une cavité de taille variable et quelques bras représentatifs. Les groupements R^1 et R^2 peuvent être soit des chaînes alkyle ou aryle, soit des groupes porteurs de sites de complexation supplémentaires susceptibles, comme dans le cas des éthers-lassos simples, de participer à



1

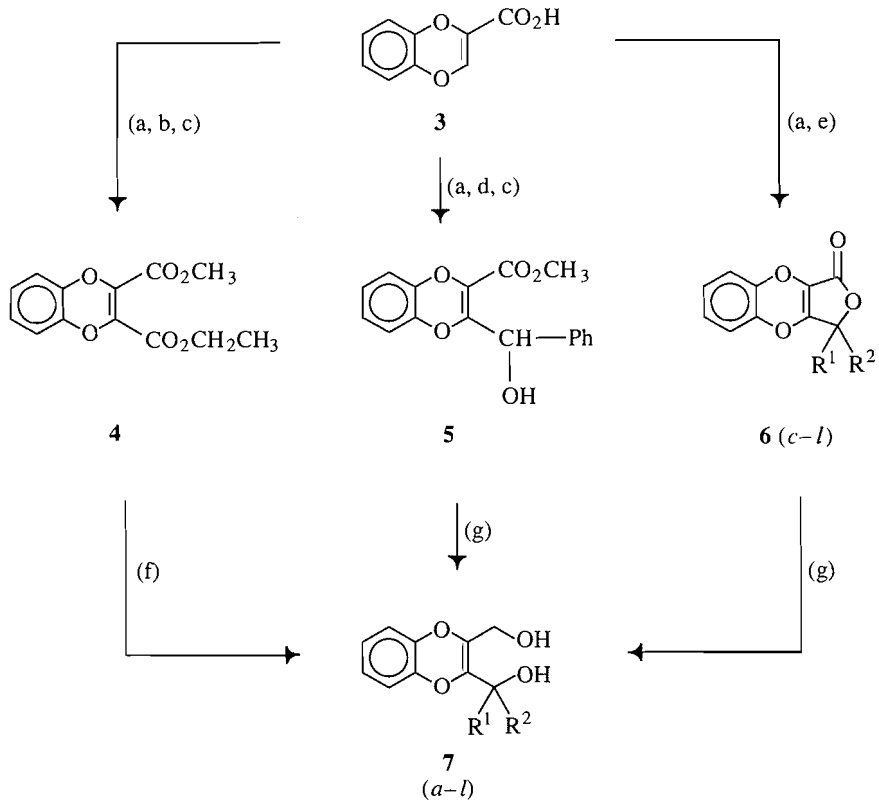


2

1. Auteur à qui adresser toute correspondance.

Printed in Canada / Imprimé au Canada

Can. J. Chem. Downloaded from www.nrcresearchpress.com by 194.225.253.170 on 09/07/12
For personal use only.



	R^1	R^2
a	H	H
b	H	Ph
c	CH_3	CH_3
d	—$(CH_2)_5$—	
e	CH_3	$PhCH_2OCH_2CH_2$
f	CH_3	2-$MeOC_6H_4OCH_2CH_2$
g	CH_3	3-$MeOC_6H_4OCH_2CH_2$
h	CH_3	4-$MeOC_6H_4OCH_2CH_2$
i	CH_3	2,3-di$MeOC_6H_3OCH_2CH_2$
j	CH_3	3,4-di$MeOC_6H_3OCH_2CH_2$
k	CH_3	$CH_3OCH_2CH_2$
l	CH_3	$PhCH_2$—$(OCH_2CH_2)_2$—OCH_2CH_2

SCHÉMA 1. (a) $i Pr_2NLi$, THF, −78°C; (b) $ClCO_2CH_2CH_3$ puis H_3O^+; (c) CH_2N_2; (d) PhCHO puis H_3O^+; (e) R^1—CO—R^2 puis H_3O^+; (f) $i Bu_2AlH$; (g) $LiAlH_4$.

la capture du cation. Quelques produits du type **1** préparés précédemment ont déjà été décrits (8).

Tous sont ici étudiés en ce qui concerne leur aptitude à complexer les cations sodium et potassium. Cette étude est effectuée dans le méthanol par une méthode potentiométrique utilisant des électrodes de verre sélectives à ces deux cations; beaucoup des données similaires concernant les macrocycles polyoxygénés ont été obtenues dans ce solvant, ce qui doit permettre de comparer les performances de nos produits à celles d'autres composés obtenus par d'autres auteurs.

Méthodes et résultats

Synthèse des macrocycles polyoxygénés 1 et 2

Les schémas 1 et 2 rendent compte de la stratégie adoptée pour préparer de tels composés à partir du carboxy-2 benzodioxine-1,4 **3**.

La première étape de cette séquence réactionnelle est constituée par la fonctionnalisation de la position 3 du cycle benzodioxinique par action du dianion de l'acide **3** sur des électrophiles appropriés (9). Cette réaction permet très aisément de faire varier la nature des substituants R^1 et R^2 et ainsi de moduler les caractéristiques topologiques et physico-chimiques des composés recherchés. De surcroît, le mode de fermeture du cycle polyoxygéné permet de faire varier la taille de la cavité et le nombre d'atomes d'oxygène impliqués dans le processus de complexation.

Nous avons déjà décrit le mode de préparation des composés **1***a–k* pour lesquels la fermeture du cycle est assurée par un noyau catéchol ainsi que les caractéristiques physiques et spectrales de **1***e–k* (8). Dans tous les cas le nombre d'atomes d'oxygène du macrocycle est égal à six.

Nous avons par ailleurs réalisé la préparation des macro-

Can. J. Chem. Downloaded from www.nrcresearchpress.com by 194.225.253.170 on 09/07/12
For personal use only.

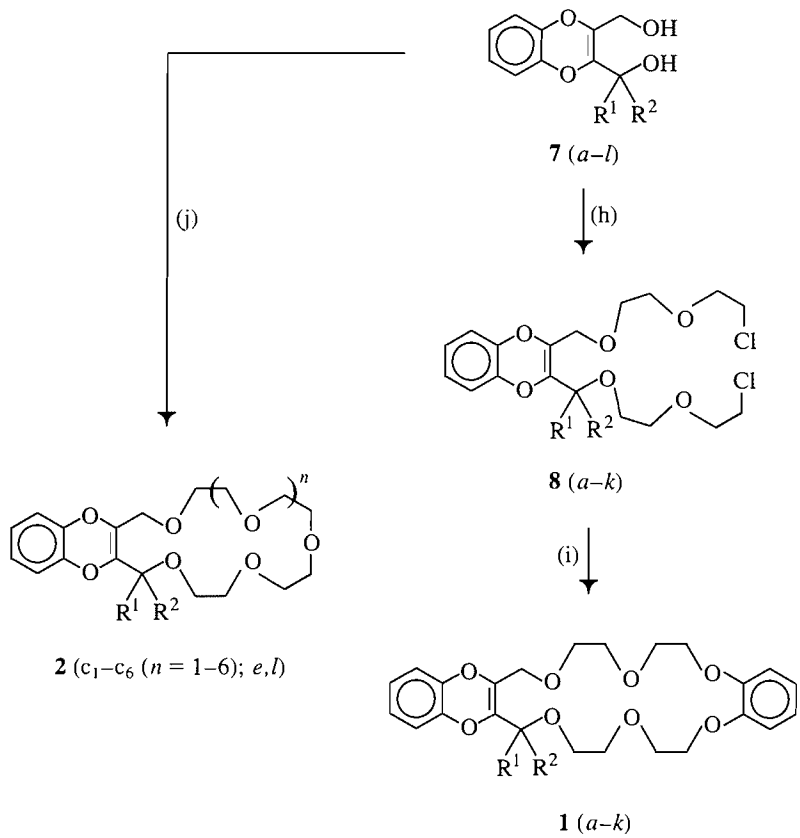


SCHÉMA 2. (h) $ClCH_2CH_2OCH_2CH_2Cl$, NaOH 50%, $nBu_4N^+HSO_4^-$; (i) catéchol, NaOH, butanol; (j) NaH, $TsO(CH_2CH_2O)_nTs$.

cycles **2** dans lesquels la fermeture du cycle est assurée par une chaîne polyéthylèneglycol de longueur variable. Les composés **2**c ont été préparés en fixant la nature des substituants R^1 et R^2 ($R^1 = R^2 = CH_3$) et en faisant varier la taille de la cavité. Les dérivés **2***e* ($R^1 = CH_3$; $R^2 = CH_2CH_2OCH_2Ph$) et **2***l* ($R^1 = CH_3$; $R^2 = CH_2CH_2(OCH_2CH_2)_2OCH_2Ph$) sont du type ethers-lassos et font apparaître au contraire une cavité de taille fixe, la longueur de la chaîne latérale étant variable et incorporant un ou trois atomes d'oxygène susceptibles d'intervenir dans le processus de complexation.

La cyclisation des diols **7***c*, **7***e*, et **7***l* est réalisée au sein du tétrahydrofuranne en utilisant l'hydrure de sodium comme base. Les macrocycles **2** sont isolés après purification sur colonne de silice avec des rendements compris entre 45 et 55%.

Complexes avec le sodium et le potassium

L'étude potentiométrique utilisant une électrode sélective, soit au sodium, soit au potassium, a permis de mettre en évidence une possible formation de deux complexes EM^+ et E_2M^+, entre l'éther couronne E et le cation métallique M^+, selon les réactions successives [1] et [2] :

[1] $E + M^+ \rightleftarrows EM^+$

[2] $EM^+ + E \rightleftarrows E_2M^+$

Le plus souvent, la formation de E_2M^+ est négligeable. Elle n'est appréciable que pour les interactions entre l'ion potassium et des composés de type **2** où $n \geq 4$. Dans ce cas les deux constantes K_1 et K_2 ont été déterminées conjointement. Les résultats sont reportés sur les tableaux 1 et 2.

Discussion

Couronnes cyclisées par les polyéthylèneglycols (composés **2**c_1–**2**c_6*)*

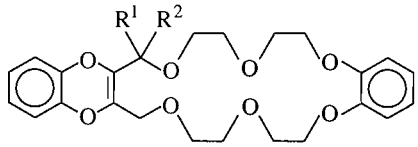
Si l'on compare les constantes de formation des complexes EM^+ à celles obtenues avec les couronnes (10, 11) et les benzocouronnes simples (12, 13) de même nombre d'atomes d'oxygène dans le macrocycle, il apparaît qu'elles sont beaucoup plus faibles pour les produits benzodioxiniques (10–100 fois). D'autre part, le fort maximum de complexation observé pour des cycles à 6 oxygènes (fig. 1) est perdu. Un petit maximum apparaît cependant ici pour les cycles à 7 oxygènes. Les constraintes stériques imposées par la liaison éthylénique conduisent à un rétrécissement *de facto* du macrocycle, les deux atomes d'oxygène de ce dernier les plus proches de la double liaison se révélant par ailleurs à l'examen des modèles CPK peu utilisables lors du processus de complexation. De ce fait, les performances de ces composés n'approchent celles des couronnes et benzocouronnes à même nombre d'oxygène dans le cycle que pour un nombre élevé d'atomes d'oxygène (fig. 1).

La sélectivité $S = K_1 (K^+) : K_1 (Na^+)$ est en faveur du potassium de façon à peu près similaire pour les cycles de 6 à 10 oxygènes, **2**c_2–**2**c_6 ($10 < S < 20$). Elle est plus faible, $S \simeq 3$, pour le cycle à 5 oxygènes **2**c_1. Une tendance analogue avait été observée avec les couronnes simples pour lesquelles la sélectivité potassium/sodium est forte pour 18-couronne-6 (10) et 21-couronne-7 (11), $S \simeq 60$. Celle de 24-couronne-8 (11), $S = 15$, est de l'ordre de celle mise ici en évidence pour les composés **2**c_2–**2**c_6. La sélectivité est faible pour 12-couronne-4, $S = 1{,}3$, et 15-couronne-5, $S = 3$; une inversion est même observée, $S = 0{,}65$, pour benzo-15-couronne-5 (12).

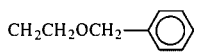
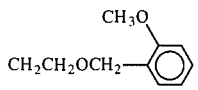
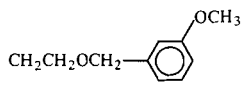
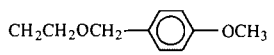
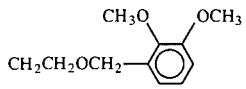
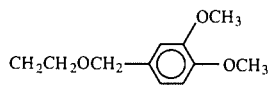
Can. J. Chem. Downloaded from www.nrcresearchpress.com by 194.225.253.170 on 09/07/12
For personal use only.

Can. J. Chem. Downloaded from www.nrcresearchpress.com by 194.225.253.170 on 09/07/12
For personal use only.

TABLEAU 1. Constantes de formation des complexes des composés **1** avec le sodium et le potassium dans le méthanol à 25,0°C (échelle molaire des concentrations, mol dm^{-3})



1

	R^1	R^2	Na^+ log K_1	K^+ log K_1
1*a*	H	H	1,53	2,15
1*b*	H	Ph	1,54	1,39
1*c*	CH_3	CH_3	1,87	2,28
1*d*		$-(CH_2)_5-$	1,71	1,38
1*e*	CH_3		1,74	2,14
1*f*	CH_3		1,79	2,19
1*g*	CH_3		1,32	2,04
1*h*	CH_3		1,25	2,00
1*i*	CH_3		1,75	2,26
1*j*	CH_3		1,73	2,25
1*k*	CH_3	$CH_2CH_2OCH_3$	1,70	2,20

Couronnes cyclisées par le catéchol (composés **1**a–**1**d*)*

Le composés $\mathbf{2c}_2$ ne diffère du dérivé **1***c* que par la présence d'un noyau aromatique. La constante de formation du complexe avec le sodium croît lors du passage de $\mathbf{2c}_2$ à **1***c*, celle du complexe avec le potassium décroît; de ce fait, la sélectivité potassium/sodium décroît fortement, de 15 à 2. Le même phénomène a été observé lors du passage des couronnes aux dibenzocouronnes; la sélectivité diminue, elle est même inversée, $S = 0,6$ pour le dibenzo-15-couronne-5 (12).

La présence d'un noyau aromatique **1***b* ou d'un cycle spiranique **1***d* aboutit à une forte restriction de la cavité; ceci induit un abaissement de la complexation notable dans le cas du sodium, important dans le cas du potassium. Ce phénomène entraîne pour ces deux composés une inversion de la sélectivité favorable ici au sodium.

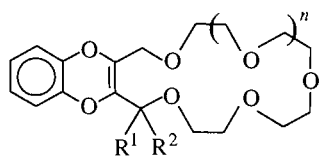
Ethers-lassos (composés **1**e–**1**k, **2**c *et* **2**l*)*

L'adjonction des divers bras et, en particulier, polyoxyéthylèniques sur l'un des carbones du cycle a conduit à des améliorations plus ou moins notables des propriétés complexantes de 15-couronne-5, pour le sodium et donc, dans certains cas, à un accroissement sensible de la sélectivité sodium/potassium (14, 15).

Dans le cas des composés **1** étudiés ici, aucune des chaînes latérales greffées n'améliore, par rapport au produit **1***c*, les propriétés complexantes vis à vis du potassium; elles les diminuent plus ou moins vis à vis du sodium. Ceci est sans doute dû à un mauvais positionnement de la chaîne latérale par rapport au macrocycle. Dans le cas des éthers-lassos simples la présence d'un groupement méthyle sur carbone pivot favoriserait une orientation correcte du bras (16, 17). Les conformations sont ici très différentes, la présence du carbone pivot au voisinage du cycle benzodioxinique introduit en effet une forte rigidification, la chaîne latérale entraînant plutôt une gêne stérique déterminant une restriction de la cavité complexante.

Par contre, dans le cas des composés **2***e* et **2***l* la cavité complexante se trouve agrandie du fait de la présence d'un maillon oxyéthylène supplémentaire, et les chaînes latérales

TABLEAU 2. Constantes de formation des complexes des composés **2** avec le sodium et le potassium dans le méthanol à 25,0°C (échelle molaire des concentrations, mol dm^{-3})



2

	R^1	R^2	n	Na^+ log K_1	K^+ log K_1	K^+ log K_2
$\mathbf{2c}_1$	CH_3	CH_3	1	0,95	1,40	
$\mathbf{2c}_2$	—	—	2	1,54	2,72	
$\mathbf{2c}_3$	—	—	3	1,64	2,85	
$\mathbf{2c}_4$	—	—	4	1,34	2,63	2,1
$\mathbf{2c}_5$	—	—	5	1,51	2,60	2,3
$\mathbf{2c}_6$	—	—	6	1,2	2,54	2,2
2*e*	CH_3	$CH_2CH_2OCH_2Ph$	3	1,18	2,9	
2*l*	CH_3	$CH_2CH_2O(CH_2CH_2O)_2CH_2Ph$	3	<0,6	3,03	

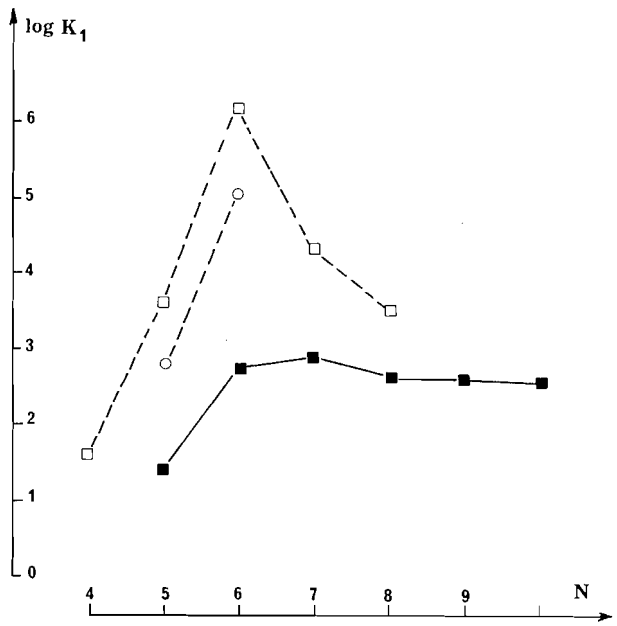


FIG. 1. Constantes de formation K_1 dans le méthanol à 25,0°C des complexes avec le potassium de quelques polyéthers cycliques en fonction du nombre N d'atome d'oxygène dans le cycle. □ éthers-couronnes (d'après les références 10 et 11); ○ éthers-couronnes benzo (d'après les références 12 et 13); ■ nos produits n° $\mathbf{2c_1}$–$\mathbf{2c_6}$.

favorisent légèrement la complexation du potassium et par contre défavorisent fortement celle du sodium.

La présence d'un carbone asymétrique dans un certain nombre de composés doit entraîner pour chaque stéréoisomère des variations notables des propriétés complexantes. Cependant, les études de complexation n'ont pas conduit à des résultats suffisamment convaincants pour qu'ait été entreprise la synthèse énantiosélective ou spécifique des dérivés **1** et **2**.

À la lumière des résultats obtenus il semble que les performances recherchées : augmentation de la complexation et de la sélectivité, pourraient être améliorées en adaptant la longueur et le nombre de sites de la chaîne latérale. Il est de surcroît indéniable que la nature du substituant R^1 détermine la position du bras R^2 et influe de ce fait de façon considérable sur le processus de complexation.

Partie expérimentale

Mesures physiques

Les spectres de résonance magnétique nucléaire (rmn) ont été enregistrés à l'aide de spectromètres Perkin Elmer R 12B (60 MHz) et Bruker AM 300 (300 MHz) en utilisant le tétraméthylsilane comme référence interne. Les spectres infra-rouge (ir) ont été tracés sur des appareils Perkin Elmer 297 et 580 B. Les spectres de masse (sm) ont été réalisés sur un appareil Nermag R.10.10C.

Les points de fusion ont été déterminés sur un banc de Kofler et ne sont pas corrigés.

Les chromatographies sur couche mince (ccm) ont été effectuées sur gel de silice 60 F_{254} (Merck). Toutes les analyses centésimales sont en accord avec les valeurs calculées à ±0,35% près.

*Préparation des composés carbonylés **4**, **5** et **6***

Le dianion de l'acide **3** (18) est obtenu par action de 17,5 mmol de diisopropylamidure de lithium sur 8 mmol de l'acide **3**. La réaction est réalisée sous atmosphère inerte, à −78°C, au sein de 30 mL de THF.

Au bout de 4 h à −78°C, on additionne 12 mmol du composé électrophile approprié (chloroformiate d'éthyle, aldéhyde benzoïque ou cétones) en solution dans 10 mL de THF. On laisse en contact 2 h supplémentaires à −78°C, puis on hydrolyse. Après extraction à l'éther en milieu basique, la phase aqueuse est acidifiée, puis extraite au chlorure de méthylène. La phase organique est séchée sur $MgSO_4$, puis évaporée sous vide.

Dans le cas du chloroformiate d'éthyle et du benzaldéhyde les produits bruts sont estérifiés par traitement au diazométhane, puis purifiés sur colonne de silice.

Dans le cas où les électrophiles sont des cétones, les produits bruts sont lactonisés après dissolution dans 30 mL de dioxanne par action de 30 mL d'une solution HCl à 10%. Les lactones sont purifiées sur colonne de silice.

1,4-Benzodioxin-2,3-dicarboxylic acid éthyl ester,'méthyl ester **4** (58%); huile; ir (film) : 1735, 1670 cm^{-1}; rmn ^1H (CCl_4) δ : 1,35 (t, 3H, CH_2—CH_3, J = 6,6 Hz), 3,82 (s, 3H, OCH_3), 4,29 (q, 2H, CH_2—CH_3, J = 6,6 Hz), 6,65–7,05 (m, 4H, aromatiques).

3-(Hydroxyphénylméthyl)-1,4-benzodioxin-2-carboxylic acid éthyl ester **5** (72%); F = 123–124°C; ir (KBr) : 3100–3700; 1710, 1660 cm^{-1}; rmn ^1H ($CDCl_3$) δ : 3,82 (s, 3H, OCH_3), 6,23 (s, 1H, CHOD), 6,60–6,95 (m, 4H, aromatiques), 7,20–7,70 (m, 5H, aromatiques).

3,3-Diméthyl-furo[3,4-*b*][1,4]benzodioxin-1 (3*H*)-one **6***c* (88%); F = 118–119°C; ir (KBr) : 1780, 1725 cm^{-1}; rmn ^1H (CCl_4) δ : 1,56 (s, 6H, CH_3), 6,80–7,00 (m, 4H, aromatiques).

Spiro[cyclohexane-1,1'(3'*H*)-furo[3,4-*b*][1,4]benzodioxin]-3'-one **6***d* (95%); F = 117–118°C; ir (KBr) : 1770, 1720 cm^{-1}; rmn ^1H (CCl_4) δ : 1,37–2,25 (m, 10H, -$(CH_2)_5$-), 6,65–7,05 (m, 4H, aromatiques).

3-Méthyl-3-[2-(phénylméthoxy)éthyl]-furo[3,4-*b*][1,4]benzodioxin-1 (3*H*)-one **6***e* (94%); F = 57–58°C; ir (KBr) : 1780, 1710 cm^{-1}; rmn ^1H ($CDCl_3$) δ : 1,48 (s, 3H, CH_3), 2,04 (t, 2H, CH_2CH_2O, J = 5,5 Hz), 3,43 (t, 2H, CH_2CH_2O, J = 5,5 Hz), 4,29 (s, 2H, OCH_2Ph), 6,60–6,90 (m, 4H, aromatiques), 7,02 (s, 5H, aromatiques).

3-Méthyl-3-[2-[(2-méthoxyphényl)méthoxy]éthyl]-furo[3,4-*b*]-[1,4]benzodioxin-1 (3*H*)-one **6***f* (70%); F = 80°C; ir (KBr) : 1780, 1720 cm^{-1}; rmn ^1H (CCl_4) δ : 1,53 (s, 3H, CH_3), 2,08 (t, 2H, CH_2CH_2O, J = 5,3 Hz), 3,52 (t, 2H, CH_2CH_2O, J = 5,3 Hz), 3,70 (s, 3H, OCH_3), 4,38 (s, 2H, OCH_2Ar), 6,45–7,25 (m, 8H, aromatiques).

3-Méthyl-3-[2-[(3-méthoxyphényl)méthoxy]éthyl]-furo[3,4-*b*]-[1,4]benzodioxin-1 (3*H*)-one **6***g* (85%); F = 88°C; ir (KBr) : 1780, 1720 cm^{-1}; rmn ^1H ($CDCl_3$) δ : 1,49 (s, 3H, CH_3), 2,03 (t, 2H, CH_2CH_2O, J = 5,3 Hz), 3,44 (t, 2H, CH_2CH_2O, J = 5,3 Hz), 3,61 (s, 3H, OCH_3), 4,25 (s, 2H, OCH_2Ar), 6,50–7,15 (m, 8H, aromatiques).

3-Méthyl-3-[2-[(4-méthoxyphényl)méthoxy]éthyl]-furo[3,4-*b*]-[1,4]benzodioxin-1 (3*H*)-one **6***h* (73%); F = 58–59°C; ir (KBr) : 1780, 1720 cm^{-1}; rmn ^1H (CCl_4) δ : 1,54 (s, 3H, CH_3), 2,11 (t, 2H, CH_2CH_2O, J = 5,2 Hz), 3,49 (t, 2H, CH_2CH_2O, J = 5,2 Hz), 3,68 (s, 3H, OCH_3), 4,19 (s, 2H, OCH_2Ar), 6,55–7,30 (m, 8H, aromatiques).

3-Méthyl-3-[2-[(2,3-diméthoxyphényl)méthoxy]éthyl]-furo[3,4-*b*][1,4]benzodioxin-1 (3*H*)-one **6***i* (60%); F = 74–75°C; ir (KBr) : 1780, 1710 cm^{-1}; rmn ^1H ($CDCl_3$) δ : 1,56 (s, 3H, CH_3), 2,13 (t, 2H, CH_2CH_2O, J = 5,2 Hz), 3,59 (t, 2H, CH_2CH_2O, J = 5,2 Hz), 3,75 et 3,79 (2s, 6H, OCH_3), 4,45 (s, 2H, OCH_2Ar), 6,60–7,05 (m, 7H, aromatiques).

3-Méthyl-3-[2-[(3,4-diméthoxyphényl)méthoxy]éthyl]-furo[3,4-*b*][1,4]benzodioxin-1 (3*H*)-one **6***j* (67%); huile; ir (film) : 1780, 1720 cm^{-1}; rmn ^1H (CCl_4) δ : 1,52 (s, 3H, CH_3), 2,03 (t, 2H, CH_2CH_2O, J = 5,2 Hz), 3,44 (t, 2H, CH_2CH_2O, J = 5,2 Hz), 3,69 (s, 6H, OCH_3), 4,23 (s, 2H, OCH_2Ar), 6,55–7,00 (m, 7H, aromatiques).

3-Méthyl-3-[(2-méthoxy)éthyl]-furo[3,4-*b*][1,4]benzodioxin-1 (3*H*)-one **6***k* (66%); F = 70°C; ir (KBr) : 1780, 1700 cm^{-1}; rmn ^1H ($CDCl_3$) δ : 1,59 (s, 3H, CH_3), 2,11 (t, 2H, CH_2CH_2O, J = 5,3 Hz), 3,22 (s, 3H, OCH_3), 3,45 (t, 2H, CH_2CH_2O, J = 5,3 Hz), 6,80–7,15 (m, 4H, aromatiques).

3-Méthyl-3-[2-[2-[2-(phénylméthoxy)éthoxy]éthoxy]éthyl]-furo-[3,4-*b*][1,4]benzodioxin-1 (3*H*)-one **6***l* (55%); huile; ir (film) : 1780, 1720 cm^{-1}; rmn ^1H ($CDCl_3$) δ : 1,53 (s, 3H, CH_3), 2,07 (t, 2H,

Can. J. Chem. Downloaded from www.nrcresearchpress.com by 194.225.253.170 on 09/07/12
For personal use only.

Can. J. Chem. Downloaded from www.nrcresearchpress.com by 194.225.253.170 on 09/07/12
For personal use only.

CH_2CH_2O, J = 5,2 Hz), 3,30–3,65 (m, 10H, OCH_2CH_2O), 4,38 (s, 2H, OCH_2Ar), 6,68 (s, 4H, aromatiques), 7,08 (s, 5H, aromatiques).

Réduction des composés carbonylés ***4***, ***5*** *et* ***6***

Réduction du diester ***4***

Après avoir dissous 4 mmol du diester **4** ou de l'ester alcool **5** dans 10 mL de THF, la solution est refroidie à 0°C; puis on additionne goutte à goutte 16 mL d'une solution 1,0 M de DIBAL dans le toluène. Après 3 h d'agitation à 0°C, le milieu réactionnel est hydrolysé par l'eau, filtré sur Célite, puis extrait à l'éther. La phase organique est séchée sur $MgSO_4$, puis évaporée sous vide pour conduire aux diols **7***a* ou **7***b* qui sont purifiés sur colonne de silice.

1,4-Benzodioxin-2,3-diméthanol **7***a* (83%); F = 152°C; ir (KBr) : 3750–3100, 1710 cm^{-1}; rmn ^1H (acétone d_6) δ : 3,99 (s, 4H, CH_2OD), 6,50–7,00 (m, 4H, aromatiques).

α-Phényl-1,4-benzodioxin-2,3-diméthanol **7***b* (95%); F = 141–142°C; ir (KBr) : 3650–3000, 1710 cm^{-1}; rmn ^1H (acétone d_6) δ : 4,29 (s, 2H, CH_2OD), 5,62 (s, 1H, CHOD), 6,55–6,95 (m, 4H, aromatiques), 7,20–7,70 (m, 5H, aromatiques).

Réduction des lactones ***6***

Après dissolution de 4 mmol de lactone dans 20 mL d'éther anhydre on additionne par petites fractions $LiAlH_4$ à température ambiante. L'évolution de la réaction est suivie en ccm. La réaction est hydrolysée après disparition de la lactone de départ, les sels sont filtrés sur Célite et la phase organique séchée sur $MgSO_4$. Après évaporation des solvants les diols sont purifiés sur colonne de silice en utilisant un mélange éther – éther de pétrole (6 : 4).

α,α-Diméthyl-1,4-benzodioxin-2,3-diméthanol **7***c* (90%); F = 147–148°C; ir (KBr) : 3700–3000, 1700 cm^{-1}; rmn ^1H (DMSO d_6) δ : 1,37 (s, 6H, CH_3), 4,29 (s, 2H, CH_2OD), 6,60–6,90 (m, 4H, aromatiques).

3-(1-Hydroxycyclohexyl)-1,4-benzodioxin-2-méthanol **7***d* (85%); F = 98–99°C; ir (KBr) : 3600–3100, 1680 cm^{-1}; rmn ^1H ($CDCl_3$) δ : 1,10–2,10 (m, 10H, $-(CH_2)_5-$), 4,39 (s, 2H, CH_2OD), 6,50–7,00 (m, 4H, aromatiques).

α-Méthyl-2-[2-(phénylméthoxy)éthyl]-1,4-benzodioxin-2,3-diméthanol **7***e* (90%); huile; ir (film) : 3600–3100, 1680 cm^{-1}; rmn ^1H (CCl_4) δ : 1,42 (s, 3H, CH_3), 1,80–2,15 (m, 2H, CH_2CH_2O), 3,50–3,90 (m, 2H, CH_2CH_2O), 4,22 et 4,29 (2s, 4H, OCH_2Ph et CH_2OD), 6,45–6,85 (m, 4H, aromatiques), 7,13 (s, 5H, aromatiques).

α-Méthyl-α-[2-[(2-méthoxyphényl)méthoxy]éthyl]-1,4-benzodioxin-2,3-diméthanol **7***f* (70%); huile; ir (film) : 3600–3200, 1680 cm^{-1}; rmn ^1H (CCl_4) δ : 1,37 (s, 3H, CH_3), 1,80–2,10 (m, 2H, CH_2CH_2O), 3,50–3,90 avec forte résonance à 3,71 (m, 5H, OCH_3 et CH_2CH_2O), 4,18 et 4,41 (2s, 4H, OCH_2Ar et CH_3OD), 6,40–7,35 (m, 8H, aromatiques).

α-Méthyl-α-[2-[(3-méthoxyphényl)méthoxy]éthyl]-1,4-benzodioxin-2,3-diméthanol **7***g* (85%); huile; ir (film) : 3600–3100, 1680 cm^{-1}; rmn ^1H (CCl_4) δ : 1,38 (s, 3H, CH_3), 1,80–2,10 (m, 2H, CH_2CH_2O), 3,30–3,85 avec forte résonance à 3,67 (m, 5H, OCH_3, CH_2CH_2O), 4,20–4,45 (m, 4H, OCH_2Ar et CH_2OD), 6,40–7,30 (m, 8H, aromatiques).

α-Méthyl-α-[2-[(4-méthoxyphényl)méthoxy]éthyl]-1,4-benzodioxin-2,3-diméthanol **7***h* (73%); huile; ir (film) : 3600–3200, 1680 cm^{-1}; rmn ^1H (CCl_4) δ : 1,36 (s, 3H, CH_3), 1,80–2,10 (m, 2H, CH_2CH_2O), 3,30–3,80 avec forte résonance à 3,71 (m, 5H, OCH_2CH_2O), 4,10–4,40 (m, 4H, OCH_2Ar et CH_2OD), 6,50–7,20 (m, 8H, aromatiques).

α-Méthyl-α-[2-[(2,3-diméthoxyphényl)méthoxy]éthyl]-1,4-benzodioxin-2,3-diméthanol **7***i* (62%); huile; ir (film) : 3600–3100, 1680 cm^{-1}; rmn ^1H ($CDCl_3$) δ : 1,41 (s, 3H, CH_3), 1,80–2,15 (m, 2H, CH_2CH_2O), 3,70–4,05 avec forte résonance à 3,78 (m, 8H, OCH_3 et CH_2CH_2O), 4,29 et 4,45 (2s, 4H, OCH_2Ar et CH_2OD), 6,60–7,20 (m, 7H, aromatiques).

α-Méthyl-α-[2-[(3,4-diméthoxyphényl)méthoxy]éthyl]-1,4-benzodioxin-2,3-diméthanol **7***j* (67%); huile; ir (film) : 3600–3100, 1680 cm^{-1}; rmn ^1H (CCl_4) δ : 1,36 (s, 3H, CH_3), 1,70–2,10 (m, 2H, CH_2CH_2O), 3,20–3,90 avec forte résonance à 3,69 (m, 8H, CH_3O et CH_2CH_2O), 4,23 et 4,32 (2s, 4H, OCH_2Ar et CH_2OD), 6,40–6,80 (m, 7H, aromatiques).

α-Méthyl-α-[(2-méthoxy)éthyl]-1,4-benzodioxin-2,3-diméthanol **7***k* (66%); huile; ir (film) : 3600–3200, 1680 cm^{-1}; rmn ^1H (CCl_4) δ : 1,38 (s, 3H, CH_3), 1,80–2,10 (m, 2H, CH_2CH_2O), 3,20–3,80 avec forte résonance à 3,24 (m, 5H, CH_3O et CH_2CH_2O), 4,28 (s, 2H, CH_2OD), 6,40–6,90 (m, 4H, aromatiques).

α-Méthyl-α-[2-[2-[2-(phénylméthoxy)éthoxy]éthoxy]éthyl]-1,4-benzodioxin-2,3-diméthanol **7***l* (60%); huile; ir (film) : 3600–3200, 1680 cm^{-1}; rmn ^1H ($CDCl_3$) δ : 1,31 (s, 3H, CH_3), 1,70–2,10 (m, 2H, CH_2CH_2O), 3,30–3,60 (m, 12H, OCH_2CH_2O), 4,31 (s, 2H, OCH_2Ar), 6,30–6,80 (m, 4H, aromatiques), 7,01 (s, 5H, aromatiques).

Préparation des dérivés dichlorés ***8***

Le mode de préparation de ces composés ainsi que les caractéristiques spectrales de **8***e*, **8***f*, **8***g*, **8***h*, **8***i*, **8***j* et **8***k* ont déjà fait l'objet d'une description détaillée (8).

2,3-Bis[[2-(2-chloroéthoxy)éthoxy]méthyl]-1,4-benzodioxin **8***a* (57%); huile; ir (film) : 1710, 1100 cm^{-1}; rmn ^1H (CCl_4) δ : 3,50–3,75 (m, 16H, OCH_2CH_2O), 4,01 (s, 4H, CH_2O), 6,60–6,90 (m, 4H, aromatiques).

2-[[2-(2-Chloroéthoxy)éthoxy]méthyl]-3-[[2-(2-chloroéthoxy)éthoxy]phénylméthyl]-1,4-benzodioxin **8***b* (55%); huile; ir (film) : 1700, 1090 cm^{-1}; rmn ^1H (CCl_4) δ : 3,30–3,90 (m, 16H, OCH_2CH_2O), 4,12 (s, 2H, CH_2O), 5,12 (s, 1H, PhC*H*O), 6,40–6,85 (m, 4H, aromatiques), 7,10–7,60 (m, 5H, aromatiques).

2-[[2-(2-Chloroéthoxy)éthoxy]méthyl]-3-[1-[2-(2-chloroéthoxy)-éthoxy]-1-méthyléthyl]-1,4-benzodioxin **8***c* (66%); huile; ir (film) : 1690–1100 cm^{-1}; rmn ^1H (CCl_4) δ : 1,41 (s, 6H, CH_3), 3,30–3,85 (m, 16H, OCH_2CH_2O), 4,19 (s, 2H, CH_2O), 6,40–6,85 (m, 4H, aromatiques).

2-[1-[2-(2-Chloroéthoxy)éthoxy]cyclohexyl]-3-[[2-(2-chloroéthoxy)éthoxy)]méthyl]-1,4-benzodioxin **8***d* (58%); huile; ir (film) : 1690–1100 cm^{-1}; rmn ^1H (CCl_4) δ : 1,10–2,00 (m, 10H, $-(CH_2)_5-$), 3,30–3,85 (m, 16H, OCH_2CH_2O), 4,18 (s, 2H, CH_2O), 6,40–6,90 (m, 4H, aromatiques).

Préparation des macrocycles ***1***

La synthèse de ces dérivés et les caractéristiques spectrales de **1***e*, **1***f*, **1***g*, **1***h*, **1***i*, **1***j* et **1***k* ont déjà fait l'objet d'une description détaillée (8).

6,8,9,11,12,19,20,22,23,25-Décahydro-[1,4]benzodioxino[2,3-*i*][1,4,7,12,15,18]-benzohexaoxacycloeicosin **1***a* (40%); F = 118°C; ir (KBr) : 1710, 1100 cm^{-1}; rmn ^1H acétone d_6 δ : 3,70–4,30 avec forte résonance à 3,75 et 4,15 (m, 20H, CH_2O), 6,60–7,00 (m, 8H, aromatiques); sm (m/z) : 444 (M^+). *Anal.* calc. pour $C_{24}H_{28}O_8$: C 64,85, H 6,35; trouvé : C 64,71, H 6,47.

6,8,9,11,12,19,20,22,23,25-Décahydro-6-phényl-[1,4]benzodioxino[2,3-*i*][1,4,7,12,15,18]-benzohexaoxacycloeicosin **1***b* (40%); huile; ir (film) : 1705, 1100 cm^{-1}; rmn ^1H (CCl_4) δ : 3,25–4,50 (m, 18H, CH_2O), 5,21 (s, 1H, PhC*H*—O), 6,35–7,05 (m, 8H, aromatiques), 7,05–7,60 (m, 5H, aromatiques); sm (m/z) : 520 (M^+). *Anal.* calc. pour $C_{30}H_{32}O_8$: C 69,22, H 6,20; trouvé : C 69,37, H 6,29.

6,8,9,11,12,19,20,22,23,25-Décahydro-6,6-diméthyl-[1,4]benzodioxino[2,3-*i*][1,4,7,12,15,18]-benzohexaoxacycloeicosin **1***c* (68%); huile; ir (film) : 1690, 1105 cm^{-1}; rmn ^1H (CCl_4) δ : 1,41 (s, 6H, CH_3), 3,35–4,20 (m, 16H, CH_2O), 4,31 (s, 2H, CH_2O), 6,60–7,00 (m, 8H, aromatiques); sm (m/z) : 472 (M^+). *Anal.* calc. pour $C_{26}H_{32}O_8$: C 67,99, H 6,87; trouvé : C 68,15, H 6,73.

8,9,11,12,19,20,22,23-Octahydro-spiro-[1,4]benzodioxino[2,3-*i*][1,4,7,12,15,18]-benzohexaoxacycloeicosin-6 (25*H*)-1′-cyclohexane **1***d* (52%); huile; ir (film) : 1685, 1100 cm^{-1}; rmn ^1H (CCl_4) δ : 1,20–2,10 (m, 10H, $-(CH_2)_5-$), 3,30–4,10 (m, 16H, CH_2O), 4,21 (s, 2H, CH_2O), 6,50–6,70 (m, 8H, aromatiques); sm (m/z) : 512 (M^+). *Anal.* calc. pour $C_{29}H_{36}O_8$: C 67,95, H 7,08; trouvé : C 67,72, H 7,21.

Préparation des macrocycles ***2***

Mode opératoire général

On soumet 4 mmol de diol en solution dans 30 mL de THF à l'action de 4,4 mmol de NaH. Après 2 h de contact à reflux on additionne 4 mmol du bistosylate du polyéthylèneglycol approprié en solution dans 70 mL de THF. On laisse à reflux pendant 24 h. Après retour à température ambiante, on hydrolyse, extrait à l'éther et sèche la

Can. J. Chem. Downloaded from www.nrcresearchpress.com by 194.225.253.170 on 09/07/12
For personal use only.

phase organique sur $MgSO_4$. Après évaporation des solvants, les macrocycles **2** sont purifiés sur colonne de silice en utilisant comme éluant un mélange CH_3OH–CH_2Cl_2.

6,8,9,11,12,14,15,17,18,20-Décahydro-6,6-diméthyl-[1,4]benzodioxino[2,3-*c*][1,6,9,12,15]-pentaoxacycloheptadecin **2c**$_1$ huile; ir (film) : 1685, 1100 cm^{-1}; rmn ^1H ($CDCl_3$) δ : 1,41 (s, 6H, CH_3), 3,40–3,90 (m, 16H, OCH_2CH_2O), 4,41 (s, 2H, CH_2O), 6,50–6,90 (m, 4H, aromatiques); sm (*m*/*z*) : 398 (M^+ + 18). *Anal.* calc. pour $C_{20}H_{28}O_7$: C 63,14, H 7,42; trouvé : C 62,91, H 7,59.

6,8,9,11,12,14,15,17,18,20,21,23-Dodécahydro-6,6-diméthyl-[1,4]benzodioxino[2,3-*c*][1,6,9,12,15,18]-hexaoxacycloeicosin **2c**$_2$ huile; ir (film) : 1685, 1100 cm^{-1}; rmn ^1H ($CDCl_3$) δ : 1,37 (s, 6H, CH_3), 3,40–3,90 (m, 20H, OCH_2CH_2O), 4,17 (s, 2H, CH_2O), 6,40–6,80 (m, 4H, aromatiques); sm (*m*/*z*) : 442 (M^+ + 18). *Anal.* calc. pour $C_{22}H_{32}O_8$: C 62,25, H 7,60; trouvé : C 62,47, H 7,43.

6,8,9,11,12,14,15,17,18,20,21,23,24,26-Tétradécahydro-6,6-diméthyl-[1,4]benzodioxino[2,3-*c*][1,6,9,12,15,18,21]-heptaoxacyclotricosin **2c**$_3$ huile; ir (film) : 1685, 1100 cm^{-1}; rmn ^1H ($CDCl_3$) δ : 1,37 (s, 6H, CH_3), 3,40–3,70 (m, 24H, OCH_2CH_2O), 4,11 (s, 2H, CH_2O), 6,40–6,70 (m, 4H, aromatiques); sm (*m*/*z*) : 486 (M^+ + 18). *Anal.* calc. pour $C_{24}H_{36}O_9$: C 61,52, H 7,74; trouvé : C 61,39, H 7,90.

6,8,9,11,12,14,15,17,18,20,21,23,24,26,27,29-Hexadécahydro-6,6-diméthyl-[1,4]benzodioxino[2,3-*c*][1,6,9,12,15,18,21,24]-octaoxacyclohexacosin **2c**$_4$ huile; ir (film) : 1685, 1100 cm^{-1}; rmn ^1H ($CDCl_3$) δ : 1,44 (s, 6H, CH_3), 3,40–3,85 (m, 28H, OCH_2CH_2O), 4,33 (s, 2H, CH_2O), 6,60–7,00 (m, 4H, aromatiques); sm (*m*/*z*) : 530 (M^+ + 18). *Anal.* calc. pour $C_{26}H_{40}O_{10}$: C 60,42, H 7,91; trouvé : C 60,18, H 7,75.

6,8,9,11,12,14,15,17,18,20,21,23,24,26,27,29,30,32-Octadécahydro-6,6-diméthyl-[1,4]benzodioxino[2,3-*c*][1,6,9,12,15,18,21,24,27]-nonaoxacyclononacosin **2c**$_5$ huile; ir (film) : 1685, 1090 cm^{-1}; rmn ^1H ($CDCl_3$) δ : 1,47 (s, 6H, CH_3), 3,55–3,90 (m, 32H, OCH_2CH_2O), 4,36 (s, 2H, CH_2O), 6,60–6,90 (m, 4H, aromatiques); sm (*m*/*z*) : 574 (M^+ + 18). *Anal.* calc. pour $C_{28}H_{44}O_{11}$: C 59,98, H 8,05; trouvé : C 60,21, H 7,88.

6,8,9,11,12,14,15,17,18,20,21,23,24,26,27,29,30,32,33,35-Eicosahydro-6,6-diméthyl-[1,4]benzodioxino[2,3-*c*][1,6,9,12,15,18,21,24,27,30]-décaoxacycloditiacosin **2c**$_6$ huile; ir (film) : 1685, 1090 cm^{-1}; rmn ^1H ($CDCl_3$) δ : 1,45 (s, 6H, CH_3), 3,50–4,00 (m, 36H, OCH_2CH_2O), 4,29 (s, 2H, CH_2O), 6,60–6,90 (m, 4H, aromatiques); sm (*m*/*z*) : 618 (M^+ + 18). *Anal.* calc. pour $C_{30}H_{48}O_{12}$: C 63,89, H 7,74; trouvé : C 63,67, H 7,56.

6,8,9,11,12,14,15,17,18,20,21,23,24,26-Tétradécahydro-6-méthyl-6-[2-(phénylméthoxy)éthyl]-[1,4]benzodioxino[2,3-*c*][1,6,9,12,15,18,21]-heptaoxacyclotricosin **2*e*** huile; ir (film) : 1680, 1100 cm^{-1}; rmn ^1H ($CDCl_3$) δ : 1,42 (s, 3H, CH_3), 2,05–2,30 (m, 2H, CH_2CH_2O), 3,45–4,00 (m, 26H, OCH_2CH_2O), 4,25–4,65 (m, 4H, CH_2O et OCH_2Ph), 6,60–6,90 (m, 4H, aromatiques), 7,26 (s, 5H, aromatiques); sm (*m*/*z*) : 606 (M^+ + 18). *Anal.* calc. pour $C_{32}H_{44}O_{10}$: C 65,29, H 7,53; trouvé : C 65,01, H 7,70.

6,8,9,11,12,14,15,17,18,20,21,23,24,26-Tétradécahydro-6-méthyl-3-[2-[2-[2-(phénylméthoxy)éthoxy]éthoxy]éthyl]-[1,4]benzodioxino[2,3-*c*][1,6,9,12,15,18,21]-heptaoxacyclotricosin **2*l*** huile; ir (film) : 1685–1100 cm^{-1}; rmn ^1H ($CDCl_3$) δ : 1,42 (s, 3H, CH_3), 2,00–2,20 (m, 2H, CH_2O), 3,45–3,90 (m, 32H, OCH_2CH_2O), 4,10–4,45 (m, 4H, CH_2O), 4,57 (s, 2H, OCH_2Ph), 6,60–7,00 (m, 4H, aromatiques), 7,32 (s, 5H, aromatiques); sm (*m*/*z*) : 694 (M^+ + 18). *Anal.* calc. pour $C_{36}H_{52}O_{12}$: C 63,89, H 7,74; trouvé : C 63,67, H 7,56.

Détermination potentiométrique des constantes de complexation des ions sodium et potassium par les produits préparés

Celle-ci est effectuée à l'aide d'un millivoltmètre Orion 701/A. La détermination des constantes est basée sur la mesure de la tension réversible d'une cellule galvanique formée d'une électrode spécifique au cation étudié et d'une électrode de référence. L'électrode de mesure est une électrode de verre sensible soit aux ions sodium (Jena^{er} glass), soit aux ions potassium (Tacussel type pKV3).

L'électrode de référence est une électrode au calomel saturé dans le méthanol munie d'une jonction constituée par une solution 0,08 mol dm^{-3} de perchlorate de tétraéthylammonium dans le méthanol. Lors des mesures, les solutions sont maintenues à 25,0°C et une agitation magnétique est assurée en permanence.

Les chlorures de potassium et de sodium sont des produits Merck Suprapur, le méthanol utilisé est aussi un produit Merck «Réactif pour analyse» de teneur en eau inférieure à 0,01%.

À un certain volume de méthanol pur, placé dans la cellule, sont ajoutées des quantités croissantes d'une solution concentrée du chlorure alcalin dans le méthanol, ce qui réalise l'étalonnage. Nous ajoutons alors des aliquotes successives d'une solution concentrée de l'éther couronne dans le méthanol.

Les réactions [1] et [2] sont isoélectriques. La correction d'activité peut donc être négligée. La constante de formation de EM^+, K_1, est calculée pour les divers rapports éther : cation. Les valeurs obtenues sont le plus souvent, compte-tenu de la précision, invariables. Dans le cas contraire, où une variation systématique de K_1 avec le rapport éther : cation est observée, nous prenons en compte la formation du second complexe E_2M^+ et utilisons alors, pour traiter les résultats, la méthode de calcul de Leden.

1. C. J. Pedersen. J. Am. Chem. Soc. **89**, 2495 (1967); **89**, 7017 (1967).
2. J. S. Bradshaw et J. Y. K. Hui. J. Heterocycl. Chem. **11**, 649 (1974).
3. G. W. Gokel, D. H. Dishong, R. A. Schultz et V. J. Gatto. Synthesis, 997 (1982).
4. G. W. Gokel et S. H. Korzeniowski. Macrocyclic polyether syntheses. Springer-Verlag, Berlin, Heidelberg, New York. 1982.
5. J. M. Lehn. Acc. Chem. Res. **11**, 49 (1978).
6. F. Vögtle et E. Weber. Angew. Chem. **91**, 813 (1979).
7. G. W. Gokel, D. M. Dishong et C. J. Diamond. J. Chem. Soc. Chem. Commun. 1053 (1980).
8. G. Coudert, G. Guillaumet et M. Mpassi. Synthesis, 112 (1985).
9. G. Guillaumet, G. Coudert et B. Loubinoux. Tetrahedron Lett. 4379 (1979).
10. G. Michaux et J. Reisse. J. Am. Chem. Soc. **104**, 6895 (1982).
11. G. W. Gokel, D. M. Goli, C. Minganti et L. Echegoyen. J. Am. Chem. Soc. **105**, 6786 (1983).
12. D. G. Parsons, M. R. Truter et J. N. Wingfield. Inorg. Chim. Acta, **47**, 81 (1980).
13. D. E. Fenton, D. Parkin et R. F. Newton. J. Chem. Soc. Perkin Trans. 1, 449 (1981).
14. Y. Nakatsuji, T. Nakamura et M. Okahara. Chemistry Lett. 1207 (1982).
15. Y. Nakatsuji, T. Nakamura, M. Okahara, D. M. Dishong et G. W. Gokel. Tetrahedron Lett. 1351 (1982).
16. Y. Nakatsuji, T. Nakamura, M. Okahara, D. M. Dishong et G. W. Gokel. J. Org. Chem. **48**, 1237 (1983).
17. M. Ouchi, Y. Inoue, K. Wada, S. Iketani, T. Hakushj et E. Weber. J. Org. Chem. **52**, 2420 (1987).
18. L. Lalloz, V. Loppinet, G. Coudert, G. Guillaumet, B. Loubinoux, C. Labrid, M. Beaughard, G. Dureng et J. C. Lamar. J. Med. Chem. **24**, 994 (1981).

Azide ion trapping and lifetime in aqueous solution of a primary carbenium ion stabilized by a 2-imidazoyl ring

JUDY L. BOLTON AND ROBERT A. MCCLELLAND
Department of Chemistry, University of Toronto, Toronto, Ont., Canada M5S 1A1

Received December 5, 1988

JUDY L. BOLTON and ROBERT A. MCCLELLAND. Can. J. Chem. **67**, 1139 (1989).

2-Chloromethyl-1-methylimidazole undergoes a pH-dependent aqueous hydrolysis with the neutral substrate being the reactive species, and the imidazole-protonated form ($pK_a = 5.7$) unreactive. Addition of sodium chloride retards the hydrolysis, evidence that there is a free carbenium ion intermediate (the common ion effect). The rate constant ratio k_{Cl}/k_w for the reactions of this cation with the added chloride and with the solvent is 7.4 M^{-1}. Further evidence for a free cation is the observation of the 2-azidomethyl product when the hydrolysis is carried out with sodium azide present, but with no change in the rate constant. The k_{az}/k_w ratio as determined by product analysis is 1.1×10^2 M^{-1}. With the assumption that k_{az} represents a diffusion-controlled reaction and has a value of 7×10^9 M^{-1} s^{-1}, the rate constant k_w for the reaction of the cation with solvent is 6×10^7 s^{-1}. A comparison with azide–water selectivity ratios reported for other cations shows that the imidazole-stabilized primary cation of this study is relatively long-lived. A possible explanation for this is given, in terms of the extensive resonance delocalization of the positive charge in this cation.

Key words: solvolysis, carbenium ion, heterocycle.

JUDY L. BOLTON et ROBERT A. MCCLELLAND. Can. J. Chem. **67**, 1139 (1989).

Le chlorométhyl-2 méthyl-1 imidazole subit une hydrolyse aqueuse qui dépend du pH et dans laquelle l'espèce réactive est le substrat neutre et l'espèce qui n'est pas réactive est la forme protonée de l'imidazole ($pK_a = 5,7$). L'addition de chlorure de sodium retarde l'hydrolyse; ce résultat indique l'existence d'une ion carbénium libre comme intermédiaire (effet d'ion commun). Le rapport des constantes de vitesse k_{Cl}/k_w pour les réactions de ce cation en présence de chlorure additionné et avec le solvant est de 7,4 M^{-1}. La formation d'un produit azidométhyl-2, sans changement de la constante de vitesse de la réaction, lorsqu'on opère l'hydrolyse en présence d'azoture de sodium est une preuve additionnelle de l'existence d'un cation libre. Le rapport k_{az}/k_w, tel que déterminé par analyse des produits, est égal à $1,1 \times 10^2$ M^{-1}. En faisant l'hypothèse que k_{az} correspond à la vitesse de la réaction contrôlée par la diffusion et que sa valeur est 7×10^9 M^{-1} s^{-1}, la constante de vitesse k_w de la réaction avec le solvant est égale à 6×10^7 s^{-1}. Une comparaison des rapports de sélectivité azoture–eau rapportés pour d'autres réactions indique que la durée de vie du cation primaire stabilisé par l'imidazole et examiné dans cette étude est relativement longue. Ces propriétés seraient le résultat d'une délocalisation importante par résonance de la charge positive de ce cation.

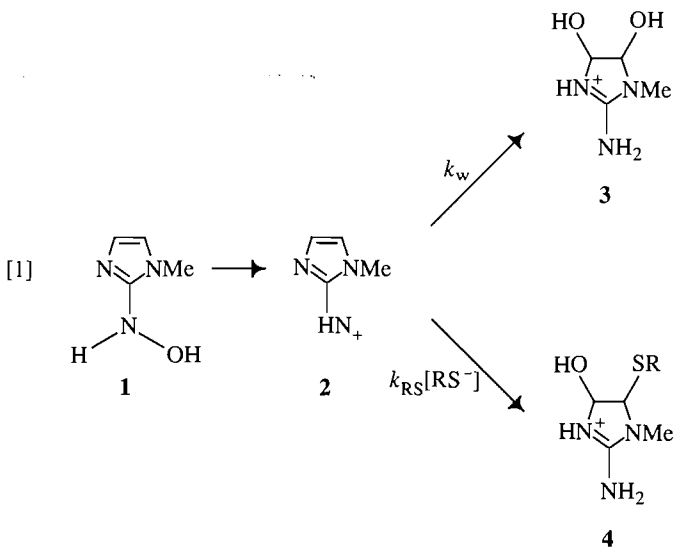
Mots clés : solvatation, l'ion carbénium, hétérocycle.

[Traduit par la revue]

Introduction

2-Hydroxylaminoimidazoles **1** undergo nitrogen–oxygen bond cleavage in water (1, 2) resulting in resonance-stabilized cationic intermediates that are nitrenium ions if written in the form of the resonance contributor **2**. The overall reaction, a heterocyclic analog of the Bamberger rearrangement (3–5), results in ring-substituted products such as **3** and **4** (1, 2).

More recent experiments have revealed high nucleophile:solvent selectivity ratios ($k_{RS}/k_w = 10^5$–10^6 M^{-1}) obtained by analyzing products when the reactions are carried out in the presence of added thiol anions (6). These results imply a first-order rate constant k_w of less than 10^4–10^5 s^{-1} for the reaction of the cation with water, since the thiol anion can react no faster than the diffusion limit ($\sim 10^{10}$ M^{-1} s^{-1}). In comparison with the 2,6-dimethylphenylnitrenium ion, a phenyl-stabilized analog, for which k_w has been estimated to be $\sim 10^9$ s^{-1} (7), imidazole-stabilized nitrenium ions are thus suggested to be relatively long-lived intermediates in water in the absence of other nucleophiles.



The effects of structure on relative nucleophilic selectivity and lifetime have seen more extensive investigations with carbenium ions, and we were therefore interested in seeing whether the stabilizing effect of the imidazole ring extends to this type of intermediate, or whether it is a particular feature of the Bamberger-type rearrangement of the hydroxylamino derivatives. Accordingly an investigation has been carried out, of a reaction that in principle at least would proceed through a carbenium ion analog of **2**, the aqueous hydrolysis of 2-chloromethyl-1-methylimidazole. The intermediate involved here is a primary carbenium ion, and indeed we find evidence that it forms in water as a free ion, with a significant lifetime for such a species.

Experimental

2-Hydroxymethyl-1-methylimidazole and 2-chloromethyl-1-methylimidazole were prepared as described by Jocelyn (8).

2-Azido-1-methylimidazole was prepared by the addition of solid 2-chloromethyl-1-methylimidazole to a solution of 0.5 M sodium azide

Can. J. Chem. Downloaded from www.nrcresearchpress.com by 194.225.253.170 on 09/07/12
For personal use only.

Can. J. Chem. Downloaded from www.nrcresearchpress.com by 194.225.253.170 on 09/07/12
For personal use only.

in 50 mL of water at pH 7. After 10 min stirring at ambient temperature the pH was adjusted to 8 with the addition of sodium hydroxide, and the solution was extracted with 200 mL of methylene chloride. After drying over anhydrous $MgSO_4$, the solvent was removed and the resulting liquid was purified by distillation at reduced pressure; bp 95–100°C, 15 Torr (1 Torr = 133.3 Pa); ^{1}H NMR ($CDCl_3$) δ: 3.70 (3H, s), 4.44 (2H, s), 6.91 (1H, br s), 7.00 (1H, br s); MS, *m/e*: 137 (M^+). *Anal.* calcd. for $C_5H_7N_5$: C 43.80, H 5.11, N 51.09; found: C 43.92, H 5.09, N 51.05.

Kinetic experiments with 2-chloromethyl-1-methylimidazole were carried out with a Varian 2390 spectrophotometer and, for faster reactions, with a Durrum–Gibson stopped-flow spectrophotometer. Data analyses were performed with Apple IIe (Varian) and Tektronix 4051 (Durrum–Gibson) microcomputers interfaced to the spectrophotometers. Experiments with the Varian apparatus were carried out by addition of 10 μL of a solution of the substrate (0.03 M) in dry acetonitrile to 3 mL of the appropriate aqueous solution, which had prior temperature equilibration in the UV cuvette. Stopped-flow experiments were carried out by preparing a substrate solution (2×10^{-4} M) in 0.1 M HCl, where the half-life is 10 h, and mixing this solution with the appropriate buffers of higher pH. Experiments were carried out by monitoring the spectral change, a decrease in absorbance, which occurs at 230 nm. First-order rate constants were calculated using a Varian Associates PLUS Kinetics Calculations Program, which fits the experimental absorbance–time data to the exponential equation via an iterative procedure, and with the stopped-flow apparatus, as the slopes of plots of ln $(A - A_\infty)$.

Product analyses for the hydrolysis in the presence of azide were carried out by addition of solid substrate (0.01 mmol) to 100 mL of an acetate buffer (pH 4.7, 0.005 M sodium acetate and 0.005 M acetic acid) containing varying amounts of sodium azide. After 10 min of vigorous stirring, the water was removed by lyophilization, and the resulting solids taken up in D_2O. The ^{1}H NMR spectra were immediately recorded with a Varian XL-400 NMR spectrophotometer. Ratios of alcohol product to azide product were obtained from the relative integrations of the N-methyl singlets at 3.81 and 3.85 ppm.

The dissociation constant of the conjugate acid of 2-hydroxymethyl-1-methylimidazole was determined by recording 400-Mz ^{1}H NMR spectra of 0.01 molar solutions of the compound in D_2O. A series of buffers in D_2O of Na_2DPO_4:NaD_2PO_4 were prepared at ionic strength 1.0 with the ratios of the components ranging from 1:10 to 10:1. The pD values of these solutions were obtained from the relationship (9): pD = pH(meter) + 0.40, where pH(meter) were the values recorded with a pH meter. Spectra in 0.01 M DCl and in 0.01 M NaOD were also recorded, to establish the chemical shifts of the conjugate acid (δ_{BH}) and conjugate base (δ_B) forms. The acidity constant was calculated as the average value obtained with the equation $K_a = [D^+](\delta_{BH} - \delta)/(\delta - \delta_B)$, where δ is the chemical shift in the solutions of intermediate pH. The signals of one of the aromatic protons and the N-methyl group undergo significant changes (0.2 ppm) with changing pH and both were analyzed. The acidity constant in H_2O was estimated by subtracting 0.5 from the value obtained in D_2O. This factor is the difference in the values obtained with imidazole itself in the two solvents (10).

Results and discussion

Rate–pH profile

2-Chloromethyl-1-methylimidazole undergoes hydrolysis in aqueous solutions, producing the expected alcohol, 2-hydroxymethyl-1-methylimidazole, as the only product. This species was isolated from the hydrolysis solution, and exhibited a 400-MHz ^{1}H NMR spectrum consistent with its structure being substituted on the exocyclic methylene. This hydrolysis is accompanied by changes in the UV spectra at 200–240 nm; first-order rate constants were obtained by monitoring a decrease at 230 nm. At a given pH these rate constants were found to be independent of the concentration of added buffers. There was, however, a dependency on pH, which is depicted in Fig. 1. In

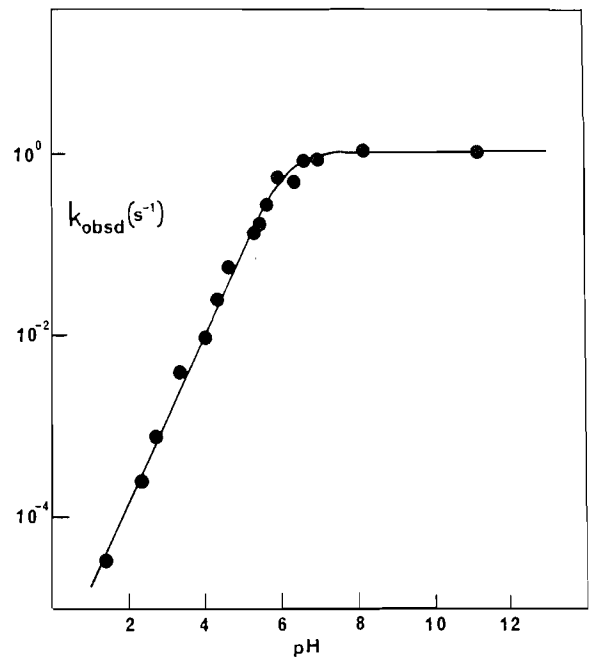
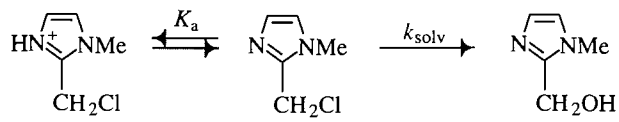


FIG. 1. The pH dependency of the first-order rate constants for the hydrolysis of 2-chloromethyl-1-methylimidazole, at 25°C and an ionic strength of 1.0 as maintained with $NaClO_4$. The points are experimental; the line is calculated according to eq. [3] with the constants given in the text.

acidic solutions the rate constants were found to be inversely proportional to H^+ concentration; there was a break at pH 5–6 and in neutral and basic solutions the rate constants became independent of pH. A mechanism that accounts for this behavior has the neutral imidazole as the solvolytically reactive species, with the imidazolium ion unreactive.

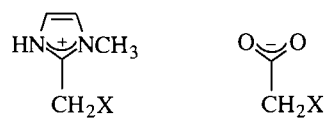
[2] 

With the assumption of a rapid equilibrium between the neutral and protonated forms, we may write

$$[3] \quad k_{obsd} = \frac{k_{solv}K_a}{(K_a + [H^+])}$$

The best fit of the experimental data to this equation, shown by the solid line in Fig. 1, has $k_{solv} = 1.0\ s^{-1}$ and $pK_a = 5.7$.

To place this acidity constant in perspective, the corresponding value for the alcohol product of the hydrolysis was also measured, in this case from the pH dependency of the ^{1}H NMR chemical shifts; a value for 1,2-dimethylimidazole is available from the literature (11). These are summarized in Table 1. The conclusion is that the effects of substitution in a 2-methyl group attached to an imidazole are very similar to the effects of the same substitutions in acetic acids. Although there are differences in the charges, this result is perhaps not surprising since in each case the substituent is located at a distance the same number of atoms removed from a delocalized system.



Can. J. Chem. Downloaded from www.nrcresearchpress.com by 194.225.253.170 on 09/07/12
For personal use only.

TABLE 1. Acid dissociation constants (pK_a) of 2-(substituted methyl)-1-methylimidazolium ions and substituted acetic acids

Substituent	2-XCH_2-1-CH_3Imid.	XCH_2COOH
H	7.85	4.76
OH	6.8	3.62
Cl	5.7	2.86

TABLE 2. Effect of added chloride ion on the rate constant for the hydrolysis of 2-chloromethyl-1-methylimidazole. Conditions: 25°C, pH = 5.3 (0.005 M CH_3COOH, 0.045 M CH_3COONa), ionic strength = 1.0, maintained with $NaClO_4$

[NaCl]	k_{obsd}, s^{-1}	k_{calc}[a]
0.000	0.30	0.25
0.024	0.25	0.21
0.048	0.159	0.185
0.096	0.155	0.146
0.191	0.083	0.104
0.382	0.076	0.065
0.573	0.042	0.048
0.764	0.040	0.038
0.955	0.030	0.031

[a] $0.25/(1 + 7.4[Cl^-])$.

Common ion rate depression

The question that we address here concerns the details of the mechanism of the hydrolysis of the neutral imidazole. The possibility that this is a stepwise S_N1 reaction can be investigated by studying the solvolysis in the presence of significant concentrations of the leaving group (12). As shown in Table 2 the addition of sodium chloride does have a significant rate-retarding effect. This behavior is good evidence for the formation of free ions in the solvolysis (13, 14) and the following reaction scheme can therefore be written,

$$[4] \quad ImCH_2Cl \underset{k_{Cl}}{\overset{k_{ion}}{\rightleftarrows}} \overset{+}{Im}CH_2 + Cl^-$$

$$[5] \quad \overset{+}{Im}CH_2 + H_2O \xrightarrow{k_w} ImCH_2OH + H^+$$

where Im = 1-methyl-2-imidazoyl. This then produces the equation

$$[6] \quad k_{obsd} = \frac{k_{ion}}{1 + (k_{Cl}/k_w)[Cl^-]}$$

defining k_w as a first-order rate constant. The data in Table 2 can be treated in the normal fashion, by plotting the reciprocal of k_{obsd} versus the concentration of chloride ion. This gives the two parameters $k_{ion} = 0.25\ s^{-1}$ and $k_{Cl}/k_w = 7.4\ M^{-1}$.

Azide ion trapping

A second way of demonstrating S_N1 solvolysis is through the observation of products derived from added nucleophiles, with no change in the rate constant for disappearance of the substrate. Azide ion has been extensively used in this regard (15–19) and, as shown in Fig. 2, this criterion is satisfied in experiments carried out with the substrate of this study in the presence of

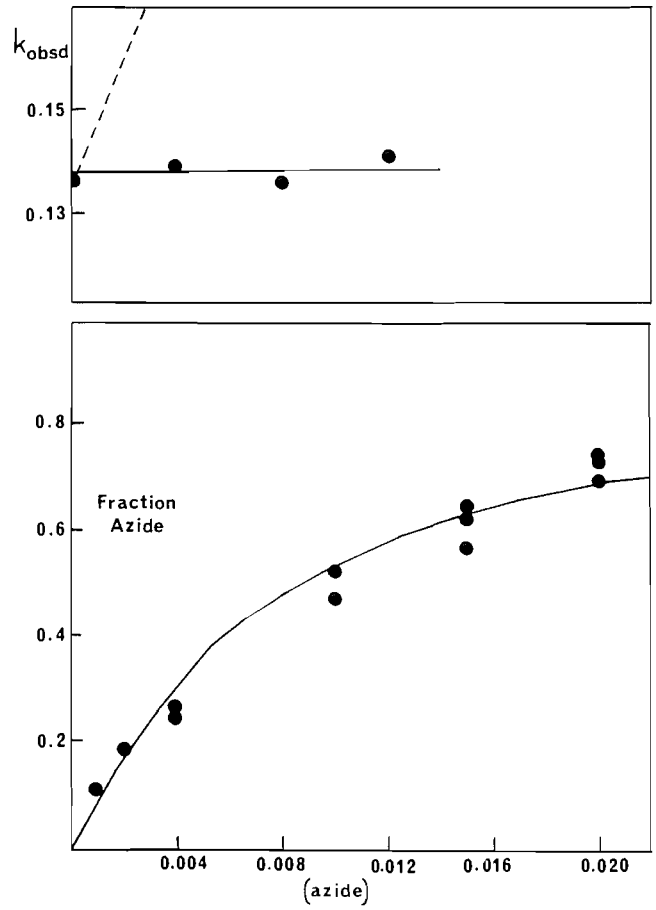


FIG. 2. First-order rate constants and the fraction of the total product that is the azidomethyl-substituted imidazole ($[RN_3]/([RN_3] + [ROH])$) for the hydrolysis of 2-chloromethyl-1-methylimidazole in the presence of sodium azide. The dashed line drawn in the top panel represents the behavior calculated from the product ratios if azide ion were to be reacting directly with the substrate in a bimolecular S_N2 fashion.

sodium azide. Thus, for example, the addition of 0.01 molar sodium azide resulted in approximately 50% of the azido-substituted product, but, within experimental error, there was no increase in the rate constant for the reaction. The azido-methyl product was also isolated, in this case from a reaction carried out in the presence of 0.5 M sodium azide. This material also had an ^1H NMR spectrum consistent with substitution at the exocyclic methylene.

[7]

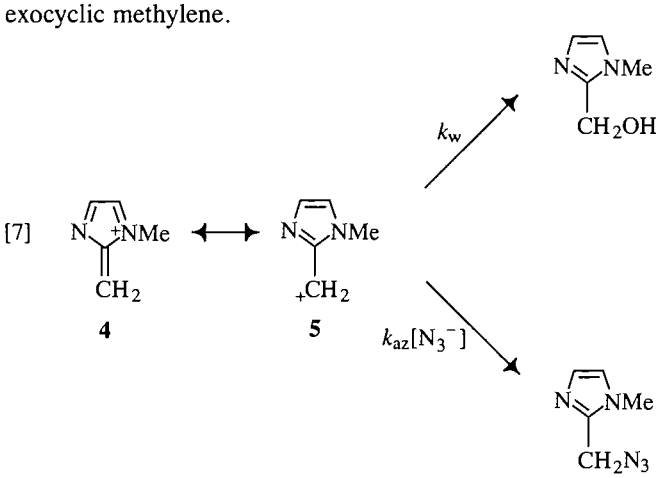


TABLE 3. Azide: water selectivities and rate constants for the reactions of cations with water

Substrate	k_{az}/k_w (M^{-1})	k_w (s^{-1})
2-(Chloromethyl)-1-methyl-imidazole	1.1×10^2	6×10^7
p-Methoxyphenethyl carboxylates[a]	4.9×10^1	1.4×10^8
Phenethyl chloride	1.8^b	$\sim 10^{11}$ [c]

[a]Reference 17.
[b]Reference 31. Reaction with azide is S_N2.
[c]Reference 17, estimated by extrapolation.

The product data can be treated in the normal way, through a plot of the inverse of the fraction azide product versus the inverse of the azide concentration. This produces a linear plot (not shown), with an intercept of unity as required by a simple competition model (eq. [7]). The inverse of the slope of this plot gives the azide selectivity factor $k_{az}/k_w = (1.1 \pm 0.1) \times 10^2$ M^{-1}.

Carbenium ion lifetime

The absolute value of the rate constant k_w for the reaction of the carbenium ion with water can be estimated from the k_{az}/k_w ratio with the assumption that the combination with azide ion is diffusion controlled (17–21). Direct proof of the validity of this approach has recently been provided through the measurement using laser flash photolysis of individual k_{az} and k_w for a series of diarylmethyl cations (22). Previously a value of 5×10^9 M^{-1} s^{-1} was taken for the diffusion-controlled k_{az} (18, 19); the direct measurements suggest that, in 20% acetonitrile in water, a value of 7×10^9 M^{-1} s^{-1} is more appropriate (22). Taking the latter value, k_w for the imidazole carbenium ion is then calculated as 6×10^7 s^{-1}. From the common ion experiments this in turn provides $k_{Cl} = 4 \times 10^8$ M^{-1} s^{-1}. The latter number obviously does not reflect diffusion control, a feature that is evident in a comparison of literature k_{Cl}/k_w ratios (23) with k_{az}/k_w ratios (17) obtained for the same cations.

A comparison of azide:water selectivities for three cations is presented in Table 3. The number for the *p*-methoxyphenethyl ion is that for 100% water, taken from Table V of ref. 17 and based on the "azide clock" method with k_{az} at 7×10^9. The entry for the parent phenethyl cation is also from ref. 17, this value estimated through an extrapolation of a correlation of log k_w for more stable cations with σ^+ and σ^0 substituent parameters. Estimates of lifetimes of simple primary cation analogs of the phenethyl cations appear not to be available. There have been studies of *p*-methoxybenzyl systems, but these have usually been carried out in less polar solvents where ionization is slow, and under these conditions it appears as if azide ion reacts principally via the S_N2 mechanism (24–26). Examination of the extensive compilation of Ta-Shma and Rappoport of azide:water selectivities (17) shows two examples suggestive of free primary carbenium ions, those derived from solvolyses of 6-(chloromethyl)benzo[*a*]pyrene and of 9-(chloromethyl)anthracene, where polycyclic aromatic hydrocarbons are the stabilizing groups (27).

Noyce and Stone previously analyzed the stabilizing influence of various heterocyclic rings through an examination of rate constants for solvolysis reactions of secondary derivatives (28). Their approach involved the generation of a log $k_{ion} - \sigma^+$ correlation line for a series of substituted 1-phenethyl *p*-nitrobenzoates. The k_{ion} value for the analogous heterocyclic system was then placed on this line, generating a group substituent constant for the heterocycle σ^+_{Ar}. The value obtained in this way for a 1-methyl-2-imidazoyl group was −0.82. This number implies that this group is slightly more stabilizing for an adjacent carbenium being formed than a *p*-methoxyphenyl group, for which σ^+_{Ar} is simply the σ^+ value of the substituent, −0.78. The results for the cation reacting with water are consistent with this, although with the present data the comparison is not perfect since the *p*-methoxyphenyl number is for a secondary cation.

Ab initio computations for an N-1 unsubstituted 2-imidazoyl carbenium ion suggest that the structure is better written as the resonance contributor **4** of eq. [7], rather than as **5** (29). This delocalization obviously accounts for the inherent stability of this type of cation, and may also explain the significant lifetime in water. As demonstrated now in two cases (19, 30), in a reaction of the type

[8] $R^+ + H_2O \rightleftarrows \neq \rightleftarrows ROH + H^+$

there is an imbalance in the transition state in the extent of development of the polar and resonance effects. In particular in the forward direction of eq. [8], where the cation is reacting with water, a large fraction of the resonance delocalization must be destroyed to reach the transition state. This has the consequence that a cation with a high degree of resonance stabilization, such as the carbenium ion adjacent to the imidazole ring, appears more kinetically stabilized in a reaction that starts at the fully formed cation than in a reaction that forms the cation.

Acknowledgement

The financial support of the Natural Sciences and Engineering Research Council of Canada is gratefully acknowledged.

1. R. A. McClelland, R. Panicucci, and A. M. Rauth. J. Am. Chem. Soc. **107**, 1762 (1985).
2. R. A. McClelland, R. Panicucci, and A. M. Rauth. J. Am. Chem. Soc. **109**, 4308 (1987).
3. D. V. Banthorpe, E. D. Hughes, C. K. Ingold, and J. Roy. J. Chem. Soc. 3294 (1962).
4. T. Sone, Y. Tokudo, T. Sakai, S. Shinkai, and O. Manabe. J. Chem. Soc. Perkin Trans. 2, 298 (1981).
5. T. Sone, K. Hamamato, Y. Seija, S. Shinkai, and O. Manabe. J. Chem. Soc. Perkin Trans. 2, 1596 (1981).
6. J. Bolton. Ph.D. Thesis, University of Toronto, 1988.
7. J. C. Fishbein and R. A. McClelland. J. Am. Chem. Soc. **109**, 2824 (1987).
8. P. C. Jocelyn. J. Chem. Soc. 3305 (1957).
9. R. G. Bates. Determination of pH—theory and practice. John Wiley and Sons, New York. 1973.
10. N. C. Le, P. Tang, and R. Mathur. J. Phys. Chem. **65**, 1074 (1961).
11. F. A. Walker. J. Am. Chem. Soc. **95**, 1150 (1973).
12. L. C. Bateman, E. D. Hughes, and C. K. Ingold. J. Chem. Soc. **123**, 1017 (1940).
13. S. Winstein, E. Clippinger, A. H. Fainberg, R. Heck, and G. C. Robinson. J. Am. Chem. Soc. **78**, 328 (1956).
14. T. H. Lowry and K. S. Richardson. Mechanism and theory in organic chemistry. 2nd ed. Harper and Row, New York. 1981. pp. 291–323.
15. R. A. Sneen, V. J. Carter, and P. S. Kay. J. Am. Chem. Soc. **88**, 2594 (1966).
16. D. J. Raber, J. M. Harris, R. E. Hall, and P. v. R. Schleyer. J. Am. Chem. Soc. **93**, 4821 (1971).
17. R. Ta-Shma and Z. Rappoport. J. Am. Chem. Soc. **105**, 6082 (1983).

Can. J. Chem. Downloaded from www.nrcresearchpress.com by 194.225.253.170 on 09/07/12
For personal use only.

18. J. P. RICHARD and W. P. JENCKS. J. Am. Chem. Soc. **104**, 4689 (1982); **104**, 4691 (1982).
19. J. P. RICHARD, M. E. ROTHENBERG, and W. P. JENCKS. J. Am. Chem. Soc. **106**, 1361 (1984).
20. D. S. KEMP and M. S. CASEY. J. Am. Chem. Soc. **95**, 6670 (1973).
21. Z. RAPPOPORT. Tetrahedron Lett. 2559 (1979).
22. R. A. MCCLELLAND, V. M. KANAGASABAPATHY, and S. STEENKEN. J. Am. Chem. Soc. **110**, 6913 (1988).
23. P. G. STANG, Z. RAPPOPORT, M. HANACK, and L. R. SUBRAMANIAN. Vinyl Cations. Academic Press, New York. 1979. Chap. 6.
24. G. KOHNSTAM, A. QUEEN, and T. RIBER. Chem. Ind. (London), 1287 (1962).
25. D. G. GRACZYK, J. W. TAYLOR, and C. R. TURNQUIST. J. Am. Chem. Soc. **100**, 7333 (1978).
26. E. R. THORNTON. Solvolysis mechanisms. Ronald Press, New York. 1964. pp. 86–88.
27. D. E. ROYER, G. H. DAUB, and D. L. VANDER JAGT. J. Org. Chem. **44**, 3196 (1979).
28. D. S. NOYCE and G. T. STONE. J. Org. Chem. **38**, 3762 (1973).
29. J. L. BOLTON and R. A. MCCLELLAND. J. Mol. Struct. Theochem. **165**, 379 (1988).
30. R. A. MCCLELLAND, V. M. KANAGASABAPATHY, N. BANAIT, and S. STEENKEN. J. Am. Chem. Soc. In press.
31. J. P. RICHARD and W. P. JENCKS. J. Am. Chem. Soc. **106**, 1383 (1984).

Can. J. Chem. Downloaded from www.nrcresearchpress.com by 194.225.253.170 on 09/07/12
For personal use only.

1-Chloromethyl-3,5-dimethylpyrazole hydrochloride. A useful synthetic intermediate

ALAN R. KATRITZKY[1] AND JAMSHED N. LAM
Department of Chemistry, University of Florida, Gainesville, FL 32611, U.S.A.

Received October 13, 1988

ALAN R. KATRITZKY and JAMSHED N. LAM. Can. J. Chem. **67**, 1144 (1989).

1-Chloromethyl-3,5-dimethylpyrazole hydrochloride readily undergoes nucleophilic displacement with O-, N-, or S-nucleophiles. 1-Phenylthiomethyl-3,5-dimethylpyrazole can be lithiated at the CH_2 group and reacted with alkyl halides and carbonyl compounds. Desulfurization of the products affords a novel method of preparing N-substituted pyrazoles.

Key words: pyrazole, lithiation, chloromethylazoles, desulfurization.

ALAN R. KATRITZKY et JAMSHED N. LAM. Can. J. Chem. **67**, 1144 (1989).

Sous l'influence de nucléophiles comportant des O, N ou S, le chlorhydrate du chlorométhyl-1 diméthyl-3,5 pyrazole subit une substitution nucléophile facile. Le phénylthiométhyl-1 diméthyl-3,5 pyrazole peut être lithié sans difficultés au niveau du groupement CH_2 et réagir alors avec les halogénures d'alkyles et les composés carbonylés. La désulfurisation des produits ainsi obtenus fournit une nouvelle méthode de préparation des pyrazoles N-substitués.

Mots clés : pyrazole, lithiation, azoles chlorométhyles, désulfurisation.

[Traduit par la revue]

Can. J. Chem. Downloaded from www.nrcresearchpress.com by 194.225.253.170 on 09/07/12
For personal use only.

Many heterocycles with a ring ·NH· group react with formaldehyde to yield addition products of type ·N(CH_2OH)·, which can be converted (1) into the corresponding derivatives ·N(CH_2Cl)·. The synthetic utility of some of these derivatives has been previously explored (1, 2).

Most previous N-substituted pyrazoles have been made either (*i*) by ring closure using N-substituted hydrazines (3) or (*ii*) by alkylation, etc. of an N-unsubstituted pyrazole (4). Relatively few procedures are known for the elaboration of N-substitution in the pyrazole series.

Hüttel and Jochum (5) showed that a variety of C-substituted, N-unsubstituted pyrazoles react with formaldehyde to give the corresponding *N*-hydroxymethyl derivatives, including 3,5-dimethylpyrazole (**2**), the preparation of which was repeated by Dvoretzky and Richter (6). The conversion of **2** into the chloromethyl hydrochloride **5**, first reported in the patent literature (7), was studied by Rüfenacht (8) as a precursor to various thiophosphates for use as insectides. Similar work has been reported for other pyrazoles (9–12), but apparently no attempts have been made to use 1-chloromethylpyrazoles as general intermediates for the preparation of more complex N-substituted pyrazoles. The present paper describes a variety of transformations of **5**, illustrating its potential as a synthetic intermediate.

Treatment with sodium ethoxide readily afforded the ethoxy compound **7***a*. The reaction of **5** with 2-pyridone in THF yielded solely the N-substituted 2-pyridone **8***a*; however, in two cases where the pyridone N-atom was hindered by a 6-phenyl group, the reaction with **5** gave mixtures of the corresponding N-substituted 2-pyridone (**8***b*,*c*) and the 2-(pyrazol-1-ylmethoxy)pyridine (**7***b*,*c*). The use of DMF as a solvent, treating with sodium salt of the corresponding pyridones with **5** or varying the temperature, still gave in all cases mixtures of the N-substituted derivatives (**8***b*,*c*) and the O-substituted analogs (**7***b*,*c*).

The chloromethyl hydrochloride **5** reacted readily with the appropriate S-nucleophiles to give **3**, **4**, and **6**. Attempts to cleave off the benzothiazole ring of **4** with butyllithium (cf. ref. 13) failed, but we found that the methylene group in **6** can be smoothly lithiated, and in this way prepared derivatives **9***a*,*b* by alkylation, and the hydroxythioether **12***a* by reaction of the lithium compound with 4-methylbenzaldehyde.

Further alkylation of **9***a* with benzyl bromide was effected via a second lithiation. Compounds **9***b*, **11**, and **12***a* were all desulfurized by treatment with Raney nickel, and the products **14***a*,*b*,*c* illustrate the potential of this novel way of synthesizing N-substituted pyrazoles.

The phenylthiomethyl derivative **6** was easily converted into its sulfoxide (**10**). Lithiation of **10** with LDA or *n*-BuLi followed by alkylation with benzyl bromide led directly to **15**. The intermediate **13** is formed at −78°C (as monitored by tlc) but decomposes readily to the styryl derivative **15** on warming to room temperature. With 4-methylbenzaldehyde as the electrophile, the alcohol **12***b* was isolated in 55% yield.

Experimental

Melting points were determined on a Kofler hot-stage microscope and are uncorrected. Spectra were recorded with the following instruments: ^{1}H nmr with a Varian model EM 360 L or a Varian XL-200 (FT mode) spectrometer with Me_4Si as internal standard; ^{13}C nmr with a JEOL model JNM-FX 100 (25 MHz) and on a Varian XL-200 (50 MHz) spectrometer, referring to the center signal of $CDCl_3$ (77.0). Mass spectra were obtained at 70 eV on a AEI MS 30 spectrometer operating with a DS-55 data system. Elemental analyses were performed under the supervision of Dr. R. W. King of this department.

Tetrahydrofuran (THF) was dried by distillation from sodium benzophenone ketyl.

All lithiations were carried out in a dry argon atmosphere.

Column chromatography was carried out with MCB silica gel (230–400 mesh).

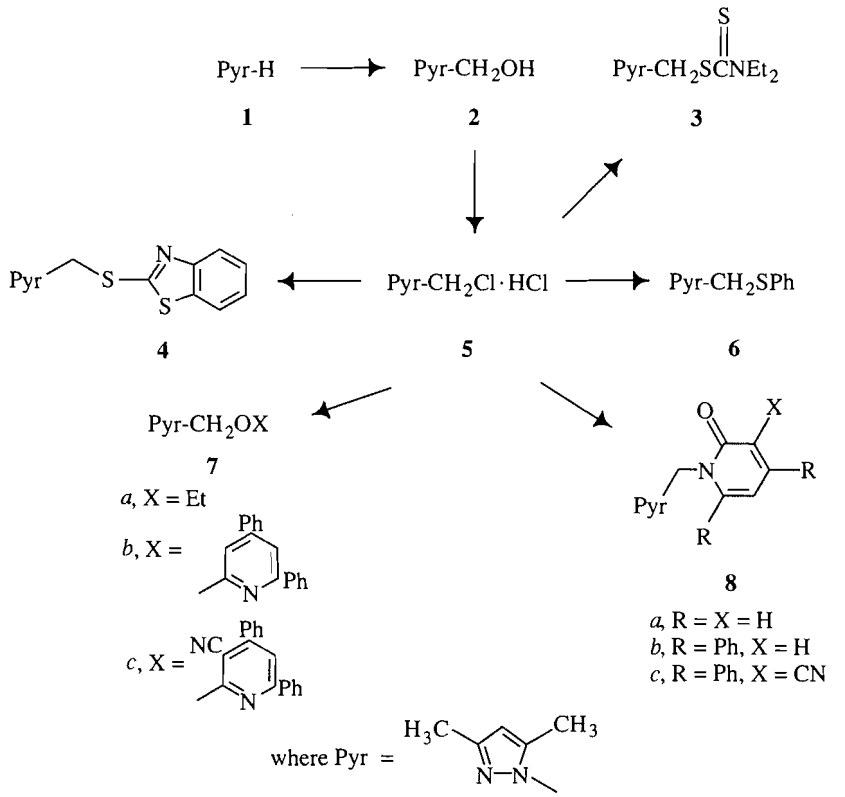
The following compounds were prepared by known literature methods: 3,5-dimethyl-1*H*-pyrazole (**1**), mp 106–108°C (lit. (14) mp 105–108°C); 1-hydroxymethyl-3,5-dimethyl-1*H*-pyrazole (**2**), mp 105–107°C (lit. (6) mp 108–109°C); 1-chloromethyl-3,5-dimethyl-1*H*-pyrazole hydrochloride (**5**) (8); δ_H: 16.13 (1H, s), 6.50 (3H, s), 2.66 (3H, s), and 2.59 (3H, s); 4,6-diphenyl-2-pyrone, mp 137–139°C (lit. (15) mp 139–140°C); 3-cyano-4,6-diphenyl-2-pyridone, mp 318–319°C (lit. (16) mp 318–320°C).

4,6-Diphenyl-2-pyridone

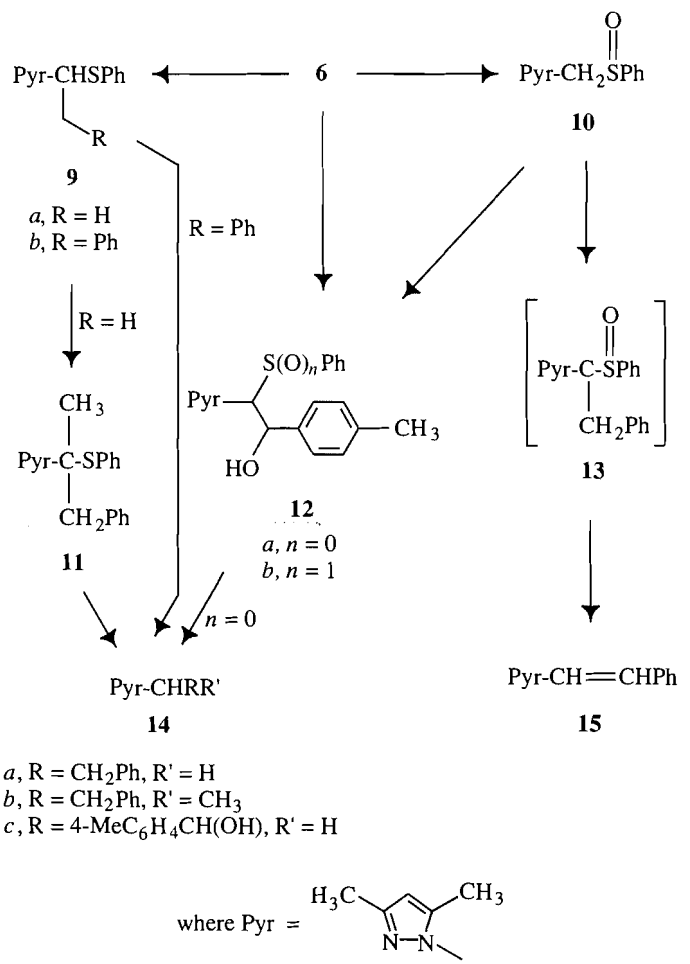
4,6-Diphenyl-2-pyrone (15) (10 g, 40 mmol) and ammonium acetate (31 g, 400 mmol) were heated at 150°C for 60 h. On cooling, chloroform (100 mL) was added and the organic layer washed with saturated sodium bicarbonate (2 × 25 mL), water (2 × 25 mL), dried ($MgSO_4$), and the solvent removed to afford tan microcrystals (8.11 g, 82%), mp 205–207°C (lit. (16) mp 207–208°C).

[1]Author to whom correspondence may be addressed.

Printed in Canada / Imprimé au Canada



SCHEME 1



SCHEME 2

*1-Ethoxymethyl-3,5-dimethyl-1*H*-pyrazole (7*a*)*

To a solution of 1 N sodium ethoxide (60 mL, 60 mmol) was added slowly 1-chloromethyl-3,5-dimethyl-1*H*-pyrazole hydrochloride (**5**) (5.0 g, 27.6 mmol). The reaction mixture was then heated under reflux for 12 h. The solvent was then removed *in vacuo* and to the residue was added chloroform (50 mL). The mixture was washed with water (3 × 20 mL), dried ($MgSO_4$), and the solvent removed to leave behind a pale yellow oil. Distillation under vacuum gave a colorless liquid (2.96 g, 70%), bp 98°C/31 Torr (1 Torr = 133.3 Pa); δ_H: 6.03 (1H, s), 5.50 (2H, s), 3.61 (2H, q, *J* 7 Hz), 2.36 (3H, s), 2.28 (3H, s), and 1.16 (3H, t, *J* 7 Hz); δ_C 147.4, 139.4, 106.0, 77.3, 63.5, 14.3, 13.0, and 10.1. $C_8H_{14}N_2O$ requires M^+, *m/z*: 154.1106; found: 154.1103.

*General procedure for the reaction of 1-chloromethyl-3,5-dimethyl-1*H*-pyrazole hydrochloride (**5**) with pyridones*

Method A

To a suspension of NaH (60% in mineral oil) (55 mmol) in tetrahydrofuran (150 mL) was added the corresponding pyridone (27.5 mmol). After stirring at ambient temperature for 30 min, 1-chloromethyl-3,5-dimethyl-1*H*-pyrazole hydrochloride (**5**) (25 mmol) was added slowly, and the mixture allowed to react further. The solvent was then removed *in vacuo* and the residue treated with water (75 mL). The organic material was extracted with chloroform (3 × 50 mL), dried ($MgSO_4$), and the solvent removed to give the crude product.

The following reactions were thus carried out:

Reaction with 2-pyridone

The reaction mixture was heated under reflux for 48 h, followed by the general work-up to give the crude product as a brown wax. Crystallization from ethyl acetate afforded *1-(pyrid-2-on-1-yl)methyl-3,5-dimethyl-1*H*-pyrazole* (**8***a*) as brown needles (32%), mp 131–132°C; δ_H: 7.9–7.3 (2H, m), 6.8–6.1 (4H, m), 6.00 (1H, s), 2.43 (3H, s), and 2.23 (3H, s); δ_C: 161.5, 149.2, 140.5, 139.9, 138.7, 136.3, 120.6, 106.3, 105.9, 102.7, 57.5, 13.2, and 10.5. *Anal.* calcd. for $C_{11}H_{13}N_3O$: C 65.01, H 6.45, N 20.68%; found: C 65.21, H 6.59, N 20.35%.

Reaction with 4,6-diphenyl-2-pyridone

The reaction mixture gave, after 18 h at ambient temperature and the

Can. J. Chem. Downloaded from www.nrcresearchpress.com by 194.225.253.170 on 09/07/12
For personal use only.

general work-up, a mixture of two compounds A and B purified by column chromatography (chloroform:hexanes 3:1). Compound A (R_f = 0.53), isolated as a colorless oil and characterized as *1-(4,6-diphenylpyrid-2-yl)oxymethyl-3,5-dimethyl-1*H*-pyrazole* (**7***b*), (44%), δ_H: 8.3–8.1 (2H, m), 7.8–7.2 (9H, m), 7.06 (1H, s), 6.50 (2H, s), 6.00 (1H, s), 2.36 (3H, s), and 2.30 (3H, s); δ_C: 162.5, 155.0, 152.4, 149.4, 140.6, 138.8, 138.3, 129.0, 128.6, 126.9, 126.8, 112.7, 107.4, 106.6, 72.4, 13.5, and 10.8. $C_{23}H_{21}N_3O$ requires M^+, *m/z*: 355.1676; found: 355.1685.

Compound B (R_f = 0.19) and characterized as *1-(4,6-diphenylpyrid-2-on-1-yl)methyl-3,5-dimethyl-1*H*-pyrazole* (**8***b*), colorless needles (21%), mp 160–161°C; δ_H: 7.6–7.5 (4H, m), 7.5–7.3 (6H, m), 6.76 (1H, d, *J* 2 Hz), 6.37 (1H, d, *J* 2 Hz), 5.95 (2H, s), 5.68 (1H, s), 2.22 (3H, s), and 2.10 (3H, s). *Anal.* calcd. for $C_{23}H_{21}N_3O$: C 77.72, H 5.96, N 11.82%; found: C 77.78, H 6.03, N 11.71%.

Reaction with 3-Cyano-4,6-diphenyl-2-pyridone

3-Cyano-4,6-diphenyl-2-pyridone (14) and **5** gave, after work-up, a mixture of two products, which were purified by column chromatography (chloroform:hexanes 3:1). The first product isolated (R_f = 0.41) was characterized as *1-(3-cyano-4,6-diphenylpyrid-2-yl)oxymethyl-3,5-dimethyl-1*H*-pyrazole* (**7***c*), colorless needles (35%), mp 153–154°C; δ_H: 8.4–8.1 (2H, m), 7.8–7.3 (9H, m), 6.57 (2H, s), 6.00 (1H, s), 2.43 (3H, s), and 2.27 (3H, s); δ_C: 162.9, 157.9, 157.0, 149.3, 140.9, 136.9, 136.0, 130.6, 130.0, 128.9, 128.8, 128.3, 127.4, 114.6, 114.4, 107.1, 93.6, 73.5, 13.4, and 10.8. *Anal.* calcd. for $C_{24}H_{20}N_4O$: C 75.76, H 5.30, N 14.73%; found: C 75.98, H 5.45, N 14.50%. Fraction 2 (R_f = 0.14), *1-(3-cyano-4,6-diphenylpyrid-2-on-1-yl)methyl-3,5-dimethyl-1*H*-pyrazole* (**8***c*), colorless microcrystals (20%), mp 198–200°C; δ_H: 7.9–7.4 (10H, m), 6.40 (1H, s), 6.00 (2H, s), 5.80 (1H, s), 2.33 (3H, s), and 2.13 (3H, s); δ_C: 161.0, 159.0, 154.1, 148.9, 141.3, 135.3, 133.6, 130.7, 130.1, 129.2, 128.8, 128.6, 128.1, 115.7, 110.0, 105.3, 101.0, 56.2, 13.7, and 10.7. *Anal.* calcd. for $C_{24}H_{20}N_4O$: C 75.76, H 5.30, N 14.73%; found: C 75.55, H 5.28, N 14.42%.

Method B

Sulfur nucleophiles: To a solution of 1 N sodium ethoxide (150 mL, 150 mmol) at 0°C was added the corresponding sulfur nucleophile (75 mmol). After 30 min, 1-chloromethyl-3,5-dimethyl-1*H*-pyrazole hydrochloride (**5**) (70 mmol) was added slowly and the mixture stirred at ambient temperature for 3 h. Work-up was carried out as described in Method A.

The following compounds were prepared in this manner:

*1-(Benzothiazol-2-ylthio)methyl-3,5-dimethyl-1*H*-pyrazole (**4**)*

From 2-mercaptobenzothiazole and **5**, a red solid that was crystallized from ethanol/water to give tan plates (71%), mp 96–98°C; δ_H: 8.1–7.6 (2H, m), 7.6–7.3 (2H, m), 6.10 (2H, s), 5.90 (1H, s), 2.36 (3H, s), and 2.26 (3H, s). *Anal.* calcd. for $C_{13}H_{13}N_3S_2$: C 56.7, H 4.8, N 15.3%; found: C 56.62, H 4.70, N 15.02%.

*1-(Phenylthio)methyl-3,5-dimethyl-1*H*-pyrazole (**6**)*

Thiophenol and **5** gave a pink oil, which was purified by distillation to give a pale yellow oil (72%), bp 138–140°C/0.85 Torr; δ_H: 7.7–7.3 (5H, m), 5.93 (1H, s), 5.43 (3H, s), 2.26 (3H, s), and 1.93 (3H, s); δ_C: 148.2, 139.4, 133.5, 132.8, 128.8, 128.0, 105.8, 53.4, 13.3, and 10.4. $C_{12}H_{14}N_2S$ requires M^+, *m/z*: 218.0877; found: 218.0861.

*1-(N,N-Diethyldithiocarbamyl)methyl-3,5-dimethyl-1*H*-pyrazole (**3**)*

To a solution of sodium diethyldithiocarbamate trihydrate (9.75 g, 43.5 mmol) in ethanol (150 mL) was added 1-chloromethyl-3,5-dimethyl-1*H*-pyrazole hydrochloride (**5**) (3.75 g, 20.7 mmol), and the mixture stirred overnight at ambient temperature. The solvent was then removed *in vacuo* and the residue treated with water (100 mL). The organic material was extracted with chloroform (3 × 25 mL), dried ($MgSO_4$), and the solvent removed to afford the crude mixture as an oil. Purification by chromatography (chloroform:hexanes 2:1) gave **3** as a yellow oil (4.62 g, 87%); δ_H: 5.95 (2H, s), 5.81 (1H, s), 4.01 (2H, q, *J* 7 Hz), 3.70 (2H, q, *J* 7 Hz), 2.34 (3H, s), 2.21 (3H, s), and 1.26 (6H, t, *J* 7 Hz); δ_C: 192.3, 149.1, 140.2, 106.1, 55.2, 49.2, 46.7, 13.4, 12.4, 11.3, and 11.2. *Anal.* calcd. for $C_{11}H_{19}N_3S_2$: C 51.33, H 7.44%; found: C 51.27, H 7.47%.

*3,5-Dimethyl-1-(phenylsulfinyl)methyl-1*H*-pyrazole (**10**)*

To a solution of 3,5-dimethyl-1-(phenylthio)methyl-1*H*-pyrazole (**6**) (5.45 g, 25 mmol) in methylene chloride (150 mL) at −20°C was added *m*-CPBA (80%; 5.93 g, 27.5 mmol) in small portions. The reaction mixture was stirred at that temperature for 4 h. Water (50 mL) was then added and the layers separated. The organic layer was washed with 10% aqueous Na_2CO_3 (2 × 25 mL), saturated NaCl (1 × 25 mL), dried ($MgSO_4$), and the solvent removed to give a pale yellow oil that solidified on trituration with hexanes. Crystallization from benzene/hexanes afforded the sulfoxide **10** as colorless needles (4.85 g, 83%), mp 75–76°C; δ_H: 7.51 (5H, s), 5.80 (1H, s), 5.09 (1H, AB, J_{AB} 12.7 Hz), 4.89 (1H, AB, J_{AB} 12.7 Hz), 2.20 (3H, s), and 2.01 (3H, s); δ_C: 149.6, 141.3, 141.0, 131.5, 129.1, 124.0, 106.4, 71.2, 13.2, and 10.4. *Anal.* calcd. for $C_{12}H_{14}N_2$: C 61.51, H 6.02, N 11.96%; found: C 61.36, H 5.99, N 11.88%.

General procedure for lithiation with n*-butyllithium and subsequent treatment with electrophiles*

To a solution of the corresponding precursor (**6** or **10**) (10 mmol) in dry THF (100 mL) at −78°C was added dropwise *n*-butyllithium (2.5 M in hexanes, 4.4 mL, 11 mmol), and the resulting solution stirred at that temperature for 2 h. To the solution of the corresponding lithio derivative was added a solution of the electrophile (10.5 mmol) in dry THF (10 mL). In the case of the sulfides (**6**, **9***a*), the resulting solution was stirred at −78°C for 6 h and at ambient temperature for 12 h. For the sulfoxide (**10**), the resulting solution was stirred at −78°C for 4 h. The reaction mixture was then poured into saturated aqueous ammonium chloride (75 mL) and the layers separated (it might be necessary to add a little water to dissolve any inorganic precipitate). The aqueous layer was washed with Et_2O (3 × 25 mL), the combined organic extracts washed with water, dried ($MgSO_4$), and the solvent evaporated to give the crude product, which was then purified.

The following compounds were prepared in this manner:

*2-(3,5-Dimethyl-1*H*-pyrazol-1-yl)-1-(4-methylphenyl)-2-(phenylthio)ethanol (**12**a)*

4-Methylbenzaldehyde and **6** afforded the alcohol as colorless microcrystals from *n*-pentane (55%), mp 123–124°C; δ_H: 7.57 (5H, s), 7.26 (4H, s), 6.3–6.0 (1H, m, OH), 5.73 (1H, s), 5.6–5.4 (2H, m), 2.33 (6H, s), and 1.30 (3H, s). *Anal.* calcd. for $C_{19}H_{20}N_2S$: C 70.97, H 6.55, N 8.28%; found: C 70.90, H 6.81, N 8.12%.

*1-(3,5-Dimethyl-1*H*-pyrazol-1-yl)-1-(phenylthio)ethane (**9**a)*

Obtained from **6** and methyl iodide as a colorless oil purified by column chromatography (chloroform:hexanes 2:1) (66%); δ_H: 7.20 (5H, m), 5.65 (1H, s), 5.40 (1H, q, *J* 7 Hz), 2.25 (3H, s), 1.91 (3H, d, *J* 7 Hz), and 1.70 (3H, s); δ_C: 148.2, 139.5, 135.1, 132.3, 128.6, 105.0, 61.4, 21.2, 13.6, and 10.3. *Anal.* calcd. for $C_{13}H_{16}N_2S$: C 67.20, H 6.94%; found: C 67.06, H 6.99%.

*1-(3,5-Dimethyl-1*H*-pyrazol-1-yl)-2-phenyl-1-(phenylthio)ethane (**9**b)*

Benzyl bromide and **6** gave **9***b* as colorless needles from *n*-pentane (74%), mp 69–70°C; δ_H: 7.3–7.1 (8H, m), 7.0–6.9 (2H, m), 5.52 (1H, s), 5.28 (1H, dd, *J* 4.5 Hz, 9.8 Hz), 3.71 (1H, dd, *J* 9.8 Hz, 13.6 Hz), 3.36 (1H, dd, *J* 4.5 Hz, 13.6 Hz), 2.30 (3H, s), and 1.36 (3H, s). *Anal.* calcd. for $C_{19}H_{20}N_2S$: C 73.98, H 6.54, N 9.08%; found: C 74.06, H 6.78, N 8.94%.

*2-(3,5-Dimethyl-1*H*-pyrazol-1-yl)-1-phenyl-2-(phenylthio)propane (**11**)*

9*a* and benzyl bromide gave the product as a colorless oil that slowly solidified. Crystallized from *n*-pentane as colorless plates (72%), mp 64–66°C; δ_H: 7.3–7.1 (6H, m), 7.05–6.95 (2H, m), 6.95–6.85 (2H, m), 5.83 (1H, s), 4.03 (1H, d, *J* 14 Hz), 3.21 (1H, d, *J* 14 Hz), 2.36 (3H, s), 2.15 (3H, s), and 1.73 (3H, s). *Anal.* calcd. for $C_{20}H_{22}N_2S$: C 74.49, H 6.88, N 8.69%; found: C 74.51, H 7.12, N 8.33%.

*3,5-Dimethyl-1-styryl-1*H*-pyrazole (**15**)*

10 and benzyl bromide gave the intermediate adduct **13**, which

Can. J. Chem. Downloaded from www.nrcresearchpress.com by 194.225.253.170 on 09/07/12
For personal use only.

readily decomposed at room temperature to give a pale yellow oil. Purification by column chromatography (chloroform:hexanes, 1:2) afforded a colorless oil (1.2 g, 60%); δ_H: 7.5–7.1 (7H, m), 5.89 (1H, s), 2.30 (3H, s), and 2.28 (3H, s); δ_C: 149.9, 139.2, 135.7, 128.6, 126.9, 125.9, 122.5, 116.3, 106.9, 13.5, and 10.8. $C_{13}H_{14}N_2$ requires M^+, m/z: 198.1157; found: 198.1150.

*2-(3,5-Dimethyl-1H-pyrazol-1-yl)-1-(4-methylphenyl)-2-phenylsulfinylethan-1-ol (**12**b)*

10 and 4-methylbenzaldehyde afforded a crude mixture that was purified by column chromatography (ethyl acetate:hexanes, 1:2) to afford the alcohol **12***b* as colorless needles (1.13 g, 55%), mp 155–157°C; δ_H: 7.4–7.2 (7H, m), 7.06 (2H, AB, J_{AB} 8 Hz), 6.05 (1H, bs, OH), 5.89 (1H, d, J 6 Hz), 5.60 (1H, s), 4.93 (1H, d, J 6 Hz), 2.29 (3H, s), 2.18 (3H, s), and 1.47 (3H, s); δ_C: 149.2, 142.5, 141.3, 137.5, 136.7, 130.8, 128.9, 128.6, 126.3, 124.8, 105.6, 83.1, 72.3, 21.1, 13.5, and 10.2. *Anal.* calcd. for $C_{20}H_{22}N_2O_2S$: C 67.77, H 6.26, N 7.90%; found: C 67.91, H 6.17, N 7.83%.

General procedure for the Raney nickel desulfurization

To a solution of the corresponding sulfide (2 mmol) in ethanol (20 mL) was added Raney nickel (ca. 3 g). The mixture was heated under reflux for 12 h. The Raney nickel was then filtered off and the solvent removed *in vacuo* to give the crude product. Purification by column chromatography (chloroform:hexanes, 1:1) afforded the pure products.

The following compounds were prepared in this manner:

*1-(3,5-Dimethylpyrazol-1-yl)-2-phenylethane (**14**a)*

A yellow liquid (17) (68%); δ_H: 7.4–7.0 (5H, m), 5.73 (1H, s), 4.16 (2H, t, J 7 Hz), 3.06 (2H, t, J 7 Hz), 2.30 (3H, s), and 1.86 (3H, s).

*2-(3,5-Dimethylpyrazol-1-yl)-1-phenylpropane (**14**b)*

A yellow oil (70%); δ_H: 7.2–7.1 (3H, m), 6.9–6.8 (2H, m), 5.61 (1H, s), 4.3–4.1 (1H, m), 3.18 (1H, dd, J 9, 13.2 Hz), 2.92 (1H, dd, J 5.3, 13.2 Hz), 2.26 (3H, s), 1.72 (3H, s), and 1.54 (3H, d, J 7 Hz); δ_C: 146.9, 138.7, 138.6, 128.8, 128.0, 126.1, 103.9, 55.2, 43.4, 20.7, 13.5, and 10.6. *Anal.* calcd. for $C_{14}H_{18}N_2$: C 78.46, H 8.47%; found: C 78.37, H 8.52%.

*1-(4-Methylphenyl)-2-(3,5-dimethylpyrazol-1-yl)ethan-1-ol (**14**c)*

Colorless microcrystals (68%), mp 125–126°C; δ_H: 7.18 (2H, AB, J_{AB} 8.4 Hz), 7.11 (2H, AB, J_{AB} 8.4 Hz), 5.74 (1H, s), 5.01 (1H, m), 2.32 (3H, s), 2.19 (3H, s), and 1.98 (3H, s). *Anal.* calcd. for $C_{14}H_{18}N_2O$: C 73.01, H 7.88%; found: C 73.10, H 7.89%.

1. A. R. KATRITZKY, S. RACHWAL, K. C. CASTER, F. MAHNI, K. W. LAW, and O. RUBIO. J. Chem. Soc. Perkin Trans. 1, 781 (1987).
2. A. R. KATRITZKY, W. H. RAMER, and J. N. LAM. J. Chem. Soc. Perkin Trans. 1, 775 (1987).
3. (*a*) G. COISPEAU and J. ELGUERO. Bull. Soc. Chim. Fr. 2717 (1970); (*b*) J. ELGUERO. *In* Comprehensive heterocyclic chemistry. Vol. 5. *Edited by* K. T. Potts. Pergamon Press, Oxford, 1984. p. 167.
4. K. SCHOFIELD, M. R. GRIMMETT, and B. T. R. KEENE. Heteroaromatic nitrogen compounds: The azoles. Cambridge University Press, Cambridge. 1976.
5. R. HÜTTEL, and P. JOCHUM. Chem. Ber. **85**, 820 (1952).
6. I. DVORETZKY, and G. H. RICHTER. J. Org. Chem. **15**, 1285 (1950).
7. A.-G. GEIGY. Fr. Pat. 1,331,721 (1963); Chem. Abstr. **60**, 1762 (1964).
8. K. RÜFENACHT. Helv. Chim. Acta, **56**, 2186 (1973).
9. I. L. FINAR, and K. UTTING. J. Chem. Soc. 5272 (1960).
10. W. BRANDES, and W. DAUM. Eur. Pat. Appl. EP 51,784 (1982); Chem. Abstr. **97**, 110 000 (1982).
11. H. FOERSTER, L. EUE, R. R. SCHMIDT, and K. LUERSSEN. Ger. Offen. DE 3,122,174 (1982); Chem. Abstr. **98**, 143 411 (1983).
12. F. MAURER, I. HAMMANN, and W. STENDEL. Ger. Offen. DE 3,126,390 (1983); Chem. Abstr. **98**, 179 635 (1983).
13. (*a*) A. R. KATRITZKY, J. M. AURRECOECHEA, and L. M. VAZQUEZ DE MIGUEL. J. Chem. Soc. Perkin Trans. 1, 769 (1987); (*b*) A. R. KATRITZKY, W. KUZMIERKIEWICZ, and J. M. AURRECOECHEA. J. Org. Chem. **52**, 844 (1987).
14. R. V. ROTHENBERG. Ber. Dtsch. Chem. Ges. **27**, 1097 (1894).
15. F. ARNDT and B. EISTERT. Chem. Ber. **58**, 2318 (1925).
16. U. BASU. J. Indian Chem. Soc. **7**, 481 (1930).
17. I. I. GRANDBERG. Khim. Geterotsikl. Soedin. Akad. Nauk Latv. SSR, 279 (1965); Chem. Abstr. **63**, 8339 (1965).

Can. J. Chem. Downloaded from www.nrcresearchpress.com by 194.225.253.170 on 09/07/12
For personal use only.

Remarks on the barrier to rotation about the C_{sp^2}—O bond in anisole

TED SCHAEFER AND RUDY SEBASTIAN
Department of Chemistry, University of Manitoba, Winnipeg, Man., Canada R3T 2N2

Received February 13, 1989

TED SCHAEFER and RUDY SEBASTIAN. Can. J. Chem. **67**, 1148 (1989).

Molecular orbital computations with the basis set 6-31G are reported for seven values of θ, the torsion angle about the C_{sp^2}—O bond in anisole. All bond angles and lengths are optimized but the atoms of the phenyl group are constrained to a plane. The relative energies are fit by $V(\theta)/\text{kJ mol}^{-1} = 7.78(5)\sin^2\theta + 2.41(5)\sin^2 2\theta - 0.54(5)\sin^2 3\theta$, where θ is zero when the heavy-atom skeleton is planar. Computations with the basis set 6-31G*(5D) for three values of θ can be reproduced by $V(\theta)/\text{kJ mol}^{-1} = 6.07\sin^2\theta + 2.68\sin^2 2\theta$. These results are compared with experimental gas phase data from the literature. The analysis of the ^{1}H nuclear magnetic resonance spectrum of anisole-α-^{13}C in a CS_2/C_6D_{12}/TMS solvent mixture yields a value of $^6J(^1\text{H}, ^{13}\text{C})$, the long-range spin–spin coupling constant between the ^{13}C nucleus in the methyl group and the *para* proton. Because this coupling constant is proportional to $\sin^2\theta$, it is shown, together with previous dynamic nmr measurements, that the barrier to rotation about the C_{sp^2}—O bond in solution cannot be purely twofold. The internal potential must also contain a fourfold term of the same sign as that of the twofold component. If the V_2/V_4 ratio given by the various molecular orbital computations holds in solution, then V_2 is 15.0 ± 2.0 kJ/mol and V_4 is 5.6 ± 2.2 kJ/mol. The apparent doubling of the internal barrier in solution is perhaps unprecedented for such a simple molecule.

Key words: anisole, internal barrier in solution, anisole-α-^{13}C, ^{1}H NMR, conformational behaviour, MO computations.

TED SCHAEFER et RUDY SEBASTIAN. Can. J. Chem. **67**, 1148 (1989).

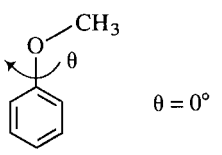
Utilisant un ensemble de base 6-31G, on a effectué des calculs d'orbitales moléculaires pour sept valeurs de θ, l'angle de torsion autour de la liaison C_{sp^2}—O de l'anisole. On a optimisé tous les angles ainsi que toutes les longueurs; on a toutefois contraint le groupement phényle dans un plan. Les énergies relatives peuvent être représentées par l'équation $V(\theta)/\text{kJ mol}^{-1} = 7{,}78(5)\sin^2\theta + 2{,}41(5)\sin^2 2\theta - 0{,}54(5)\sin^2 3\theta$, dans laquelle θ est égal à zéro lorsque le squelette de l'atome lourd est plan. Les calculs effectués à l'aide de l'ensemble 6-31G* (5D) pour trois valeurs de θ peuvent être reproduits par l'équation $V(\theta)/\text{kJ mol}^{-1} = 6{,}07\sin^2\theta + 2{,}68\sin^2 2\theta$. On compare ces résultats avec les données expérimentales en phase gazeuse qui sont rapportées dans la littérature. L'analyse des spectres rmn du ^{1}H de l'anisole-α-^{13}C, dans un mélange de solvant CS_2/C_6D_{12}/TMS, fournit une valeur de $^6J(^1\text{H}, ^{13}\text{C})$, la constante de couplage spin–spin à longue distance entre le ^{13}C du groupement méthyle et le proton en *para*. Cette constante de couplage étant proportionnelle à $\sin^2\theta$, on démontre, en se basant aussi sur des mesures rmn dynamiques antérieures, que la barrière à la rotation autour de la liaison C_{sp^2}—O, en solution, ne peut pas être purement binaire. Le potentiel interne doit aussi contenir un terme quaternaire du même signe que la composante binaire. Si le rapport de V_2/V_4 obtenu par les divers calculs d'orbitales moléculaires s'applique aussi en solution, V_2 est alors égal à 15,0 ± 2,0 kJ/mol et V_4 à 5,6 ± 2,2 kJ/mol. Il est probable que la multiplication par deux de la valeur de la barrière interne en solution n'a pas de précédent pour une molécule aussi simple.

Mot clés : anisole, barrière interne en solution, anisole-α-^{13}C, RMN du ^{1}H, comportement des conformations, calculs d'OM.
[Traduit par la revue]

Introduction

The barrier to rotation about the C_{sp^2}—O bond is uncertain. Its magnitude apparently ranges from 6 to 48 kJ/mol, depending on the experimental or theoretical methods used to assess its magnitude as well as on the state in which the molecule is examined. Compilations of references are available (1–3). Of immediate interest to the present investigations are the following summaries.

In the gas phase, the electron diffraction pattern (4) and the microwave spectrum (5) are consistent with a planar heavy-atom skeleton at 328 and 260 K, respectively, although slightly better agreement between experimental and computed intensities of the diffraction patterns is evident at a dihedral angle of 10° in **1**. At 523 K, the electron diffraction data are well represented on the basis of a θ of 40° (4); an unsuccessful fit to these data assumes a twofold barrier of 9.6 or 25.1 kJ/mol (4). Coupling of torsional modes complicates the interpretation of the infrared spectrum, but a twofold barrier of 15.1 kJ/mol is tentatively deduced (6). Molecular mechanics calculations (1) yield 7.9 kJ/mol for the barrier. Most quantum mechanical approaches also find a barrier of less than 8 kJ/mol *if* extensive geometry optimization procedures are employed (2, 7, 8).



θ = 0°

1

The barrier to rotation about the C_{sp^2}—O bond in anisole is apparently much larger in the liquid or in solution that in the vapour. On the assumption that it is twofold, its magnitude is estimated as 25.3 kJ/mol from the torsional frequencies measured on the liquid (6). However, dynamic ^{13}C nmr measurements on a dimethyl ether solution imply a barrier height of less than 19.7 kJ/mol and relaxation measurements in the rotating frame suggest a barrier of less than 18.4 kJ/mol for the same solution (9). Infrared intensities give 10.9 kJ/mol for the internal barrier in CCl_4 solution (10). Another approach to motion about the C_{sp^2}—O bond in solution uses the long-range spin–spin coupling constant over six bonds, $^6J(^1\text{H}, ^{13}\text{C})$, a σ–π coupling and therefore proportion to $\sin^2\theta$ (9). However, on a Bruker WH90 FT nmr spectrometer and for CS_2/C_6D_{12} or acetone-d_6 solutions, $^6J(^1\text{H}, ^{13}\text{C})$ is not apparent in the ^{13}C nmr spectrum of anisole-α-^{13}C (9) and must be <0.05 Hz in magnitude. Because $^6J(^1\text{H}, ^{13}\text{C})$ at θ = 90° is at least 0.6 Hz in magnitude (9), it follows that the expectation value of $\sin^2\theta$ is less than 0.08 at 300 K and therefore that a purely twofold

Can. J. Chem. Downloaded from www.nrcresearchpress.com by 194.225.253.170 on 09/07/12
For personal use only.

TABLE 1. The ^{1}H nmr spectral parameters for anisole and anisole-α-^{13}C in CS_2 solutions at 300 K

Parameter	Value		Parameter	Value	
	Anisole[a]	Anisole-α-^{13}C[b]		Anisole	Anisole-α-^{13}C
$\nu(CH_3)$[c]	1108.214(0)[d]	1106.187(0)	$^5J_{25}$	0.435(0)	0.435(0)
$\nu_2 = \nu_6$	2019.508(0)	2021.179(0)	$^5J(H,CH_3)$	−0.152(0)	−0.151(0)
$\nu_3 = \nu_5$	2137.652(0)	2138.551(0)	$^6J(H,CH_3)$	0.050(0)	0.054(0)
ν_4	2035.663(2)	2037.503(0)	$^7J(H,CH_3)$	−0.043(0)	−0.046(1)
$^3J_{23}$	8.304(0)	8.301(1)	Calculated transitions	512	1024[e,f]
$^3J_{34}$	7.351(1)	7.348(1)	Assigned	454	863
$^4J_{26}$	2.725(1)	2.725(1)	Peaks observed	195	240
$^4J_{24}$	1.068(1)	1.066(1)	Largest difference	0.017	0.019
$^4J_{35}$	1.761(1)	1.761(1)	Root-mean-square deviation	0.004	0.005

[a]As a 2.5 mol% solution in CS_2, containing 10 mol% of C_6D_{12} and 0.5 mol% TMS.
[b]As a 6.0 mol% solution in the CS_2/C_6D_{12}/TMS solvent mixture.
[c]In hertz at 300.135$_2$ MHz to high frequency of internal TMS.
[d]Numbers in parentheses are standard deviations in the NUMARIT analyses.
[e]Excluding 192 for ^{13}C.
[f]$^1J(H,^{13}C)$ = 142.899(1), $^4J(H,^{13}C)$ = 0.000(1), $^5J(H,^{13}C)$ = 0.113(1) Hz. Simulation of the H-4 spectral region with all these parameters, and a linewidth at half-height of 0.038 Hz, gives $^6J(H,^{13}C)$ as ±0.030 ± 0.005 Hz.

barrier must be greater than about 18 kJ/mol (as obtained from classical or quantum mechanical averages). The presence of a term in V_4 in the internal rotational potential, of the same sign as V_2, will reduce the magnitude of the barrier height compatible with such a value of $\langle\sin^2\theta\rangle$. Again, $^5J(^{13}C, ^{13}C)$ is not detectable for the acetone-d_6 solution (11), this coupling constant also being indicated as proportional in $\sin^2\theta$. While both long-range coupling constants are consistent with a predominantly planar conformation of anisole in solution, it is unsatisfying that their presence is not evident in the available spectra.

For solid anisole, the Raman spectra imply a barrier height of 48.2 kJ/mol (12). Dielectric loss studies of anisole dispersed in an *o*-terphenyl glass yield an enthalpy of activation of 11.0 ± 0.5 kJ/mol for the rotation about the C_{sp^2}—O bond (13). As stated by Konschin (3), the torsion is to be regarded as a motion of large amplitude that affects the spatial and structural preferences of the molecule in different aggregation states. Because the methoxyphenyl group is a constituent of a variety of useful and (or) interesting chemical moieties, such as lignin, and psychotomimetic entities as well as of mesogenic materials (14, 15), it is unfortunate that the quantitative data above are so disparate.

The results below present new molecular orbital calculations on anisole, of interest to structural work in the gas phase, as well as $^6J(^1H, ^{13}C)$ measurements, of interest in the assessment of the fourfold component of the barrier to rotation about the C_{sp^2}—O bond in solution.

Results and discussion

The ^{1}H nmr spectral parameters

The results of the NUMARIT (16) analyses of the ^{1}H nmr spectra of anisole and anisole-α-^{13}C at 300 MHz in CS_2/C_6D_{12}/TMS solutions at 300 K are given in Table 1. This solvent mixture is chosen because, unlike in acetone-d_6 solution (17), the spectral region of H-4 is relatively well separated from the H-2 and H-3 regions; this is an essential condition for the determination of a small $^6J(^1H, ^{13}C)$. It is also essential that the spectra of the two molecules be available for comparison because, apart from the ensuing comparison of the precision of the spectral parameters, the presence of a $^7J(H, CH_3)$, comparable in magnitude to $^6J(^1H, ^{13}C)$, entails spectral simulations with and without a contribution from $^6J(^1H, ^{13}C)$. By such procedures (footnotes in Table 1) it is established that $^6J(^1H, ^{13}C)$ is ±0.030 ± 0.005 Hz in the ^{13}C-enriched molecule. Comparison of the coupling constants for the two molecules suggests that the standard deviations are a reasonable estimate of the accuracy in the analyses. Another comparison is for $^5J(^1H, ^{13}C)$, 0.113(1) Hz in Table 1 and 0.116(2) Hz from the ^{13}C nmr spectrum obtained on a different spectrometer (9). Figure 1 displays parts of the ^{1}H nmr spectra of H-4 for anisole and anisole-α-^{13}C.

The long-range coupling constants involving the methyl protons have been discussed as to their magnitudes and coupling mechanisms (17).

6J(^1H, ^{13}C) and the internal barrier in solution

The ratio of $^6J(^1H, ^{13}C)$, as measured, to its value when θ = 90° in **1**, yields $\langle\sin^2\theta\rangle$, which in turn is determined by the potential governing motion about the C_{sp^2}—O bond. In 2,6-dichloroanisole, $^6J(^1H, ^{13}C)$ is 0.603(5) Hz in magnitude, and is 0.625(7) Hz for the corresponding bromine derivative (9). These numbers hold for benzene-d_6 solutions at 300 K. For 2,6-dimethylanisole, $^6J(^1H, ^{13}C)$ has a magnitude of 0.62$_2$ Hz (11). In the crystal of 2,3,5,6-tetrachloro-1,4-dimethoxybenzene, θ is 84.0° (18), implying that $\langle\sin^2\theta\rangle$ is perhaps within 1% of its maximal value of unity. We assess the value of $^6J(^1H, ^{13}C)$ as 0.625(5) Hz for a θ of 90°. Hence $\langle\sin^2\theta\rangle$ for anisole-α-^{13}C at 300 K in the CS_2 solvent mixture follows as 0.048(8). Were the barrier purely twofold, this number would mean that V_2 is $28.0^{+5.5}_{-3.9}$ kJ/mol. Therefore, because of the dynamic nmr measurements (9), it follows that a positive V_4 must be present. No negative V_4 values compatible with these measurements are, however, compatible with the above value of $\langle\sin^2\theta\rangle$; the latter is consistent with a range of V_2 and V_4 numbers of the same sign.

Figure 2 displays the V_4 and V_2 values consistent with a $\langle\sin^2\theta\rangle$ of 0.048(8) at 300 K. In principle, with the exception of combinations excluded by the dynamic nmr data, all combinations to left of the vertical line are possible. However, the 6-31G and 6-31G*(5D) computations, described below, imply that V_4 is not larger than 0.44 V_2. If the solvent does not alter the V_2/V_4 ratio drastically, then the V_2 and V_4 values in the hatched area of

Can. J. Chem. Downloaded from www.nrcresearchpress.com by 194.225.253.170 on 09/07/12
For personal use only.

Can. J. Chem. Downloaded from www.nrcresearchpress.com by 194.225.253.170 on 09/07/12
For personal use only.

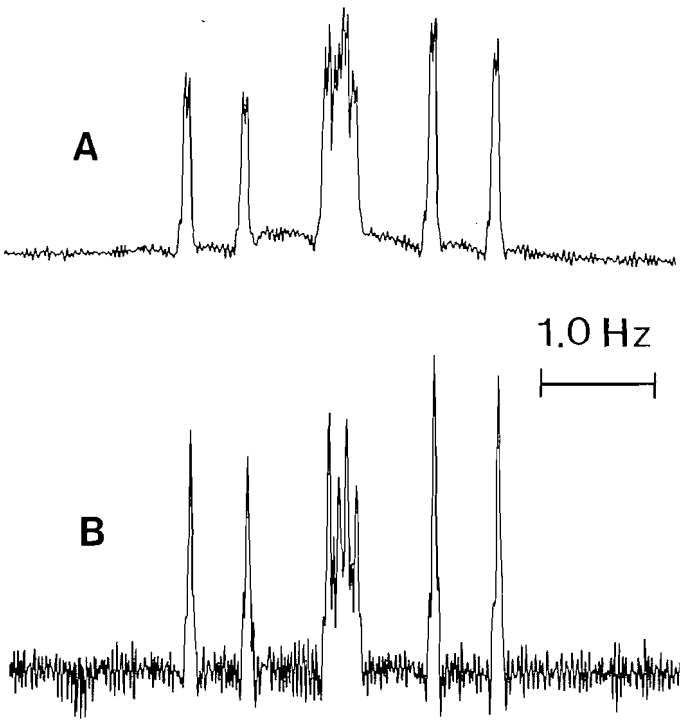


FIG. 1. In A, a part of the ^{1}H nmr spectrum of H-4 of anisole, that near the chemical shift position at 2037 Hz to high frequency of internal TMS, is shown for a 2.5 mol% solution in the CS_2/C_6D_{12}/TMS solvent mixture (see Table 1 and its footnotes). The smallest splittings arise from ^7J(H-4, CH_3). This coupling constant is rather better resolved in the methyl proton region (17) because the peaks in the latter region have a somewhat lower linewidth at half height, ca. 0.03 Hz, than do the peaks from H-4. ^7J(H-4, CH_3) is $-0.042(1)$ Hz (17). In B, the same spectral region is displayed as in A, but for anisole-α-^{13}C dissolved in the same solvent mixture. The presence of $^6J(^1H, ^{13}C)$ has altered the spectral appearance. A full analysis of the ^{1}H nmr spectrum for anisole gives the parameters in Table 1. There is a large coupling of 0.11 Hz between the α ^{13}C nucleus and the *meta* protons in anisole-α-^{13}C, but none discernible for the *ortho* protons. Analysis of the *ortho* and *meta* proton spectrum is followed by simulation of the *para* proton spectrum with various magnitudes of $^6J(^1H, ^{13}C)$, with the result that this coupling constant is $\pm 0.030 \pm 0.005$ Hz.

Fig. 2 are most likely, yielding V_2 as 15.0 ± 2.0 and V_4 as 5.6 ± 2.2 kJ/mol. These numbers are considerably larger than the theoretical values computed for the free molecule. The upper limit to the barrier *height* is 18.6 kJ/mol, just below the value tested by the dynamic nmr experiments (9). The lower limit is 13.0 kJ/mol.

*The internal potential according to 6-31G and 6-31G**

The relative energies computed (geometry optimization) for seven values of the torsion angle, θ, with the 6-31G basis set are reproduced by eq. [1], the standard error in the fit being shown in parentheses. The total energy at $\theta = 0°$ is $-344.450\,628$ au. The barrier height is very similar to that found (7) with the basis 4-31G. Inclusion of polarization functions (5 D per heavy atom) leads to relative energies at $\theta = 0, 45, 90°$, fit by eq. [2]. The barrier height is lowered to 6.5 kJ/mol and is very similar to that found with the minimal basis set, STO-3G (7, 8). The energies are plotted in Fig. 3 as a function of θ.

$$[1]\quad V/\text{kJ mol}^{-1} = 7.78(5)\sin^2\theta + 2.41(5)\sin^2 2\theta - 0.54(5)\sin^2 3\theta$$

$$[2]\quad V/\text{kJ mol}^{-1} = 6.07\sin^2\theta + 2.68\sin^2 2\theta$$

It may well be of interest that, at 523 K, the temperature of measurement for one set of electron diffraction data (4), the use of the potential in eq. [2] yields 31° as the expectation value of θ; alternatively, arc $\sin(\sin^2\theta)^{1/2}$ is 34°. The electron diffraction pattern was fit well with a *fixed* θ of 40°. A fit of that pattern with the potential of eq. [2] is indicated by this comparison.

The geometry of the stable, planar form of anisole is shown in Fig. 4, as computed with the polarized basis set. The geometry of the $COCH_3$ moiety agrees rather well with that quoted in connection with the diffraction data (4), but rather less well with that used and partially deduced in a microwave study (5). Of course, the external geometry changes significantly as θ increases from zero; the interested reader may ask for details.

Solvent perturbations of the barrier

Qualitatively, all the available experimental evidence indicates an increase in the internal barrier about the C_{sp^2}—O bond if anisole moves from the vapour phase into solution.

The present values, $V_2 = 15.0 \pm 2.0$ and $V_4 = 5.6 \pm 2.2$ kJ/mol, for the internal rotational potential in the CS_2/C_6D_{12}/TMS solvent mixture are reliable only if the solvent does not alter significantly the ratio of V_2 to V_4. In this connection, an excellent correlation exists between $^6J(^{13}C, ^{19}F)$ for 4-fluorophenyl OR (R = CH_3, CH_2CH_3, $CH(CH_3)_2$, $C(CH_3)_3$) in solution and ΔI^V_{31} for the parent molecules in the gas phase (19). $^6J(^{13}C, ^{19}F)$ is proportional (19) to $\langle\sin^2\theta\rangle$ and ΔI^V_{31} represents the conjugative interaction between the lone pairs on oxygen and the π electrons of the phenyl group (20). Among other things, this correlation ($r = 0.998$ and significant at the 98% confidence level) suggests that the qualitative nature of the internal rotational potential in the gas phase is not severely altered in solution, although the magnitudes of the *n*-fold components must increase in solution. Of course, it is still true that the numbers above depend on the assessment of V_2/V_4 provided by the various basis sets. Possible reasons for a finite V_4 have been discussed (8, 17).

The reason for the large increase in the barrier in solution is also problematic. A continuum model (21, 22), which takes electrostatic, dispersion, and cavitation energies into account, has reproduced the increase in internal barrier in benzaldehyde in solution (23). The same model appears to fail when applied to anisole (24). The recent intersecting-state model (25) evidently interprets the increased solution barrier for benzaldehyde as a consequence of an interaction of the lone-pair electrons on oxygen with solvent molecules; this interaction changes the "transition state bond order" found for the isolated molecule. The solvent effect on the barrier might therefore be said to be the consequence of specific molecular interactions, in contrast to the continuum model. The barrier in benzaldehyde is experimentally and theoretically almost purely twofold (26), unlike anisole, and it is not known how well the intersecting-state model applies to anisole.

It may be relevant that a comparison of experiment and molecular orbital computations suggests the independence of solvent of the barrier to rotation about the C_{sp^2}—C_{sp^3} bond in ethylbenzene and that the barrier may be slightly smaller in solution than in the gas phase (27). The magnitude of the barrier is computed as very similar in magnitude to that for anisole, although, of course, the conformation of lowest energy has θ as 90°. The sign of V_4 is the same (27) as that for anisole, however, and is computed as amounting to about 20% of the magnitude of V_2. The molecular volumes of anisole and ethylbenzene cannot differ greatly. The dipole moment of anisole in various environ-

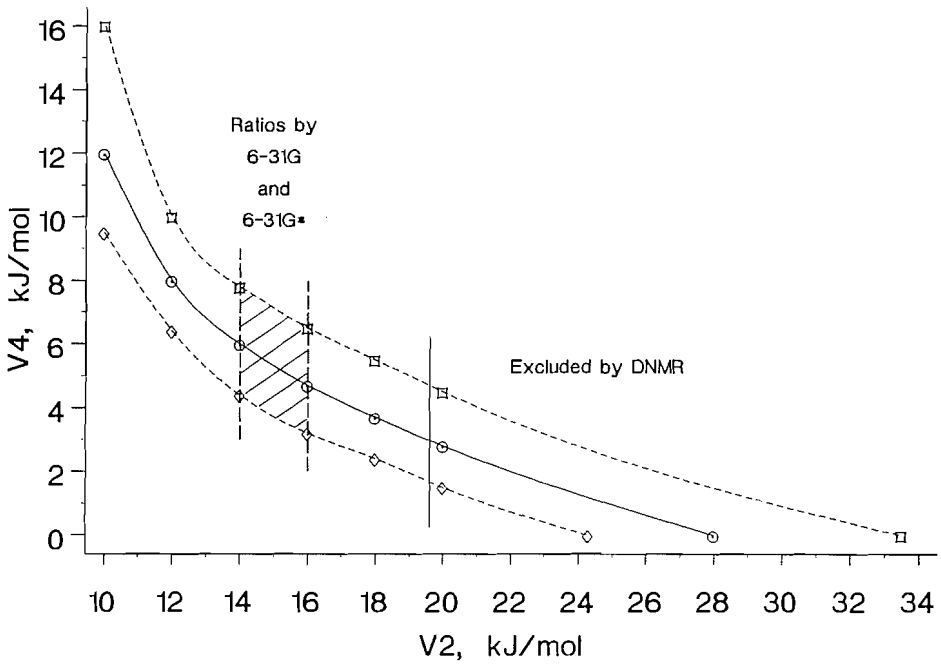


FIG. 2. The various combinations of the twofold component, V_2, and the fourfold component, V_4, of an internal potential, hindering rotation about the C_{sp^2}—O bond in anisole, are plotted. These combinations are compatible with a $\langle \sin^2 \theta \rangle$ of 0.048(8) as determined from $^6J(^1H, ^{13}C)$ in anisole-α-^{13}C and discussed in the text. The hatched area is that compatible with the V_2/V_4 ratios given by 6-31G and 6-31G*(5D) molecular orbital computations and also discussed in the text. The region to the right of the vertical solid line is excluded by dynamic ^{13}C nmr measurements (9).

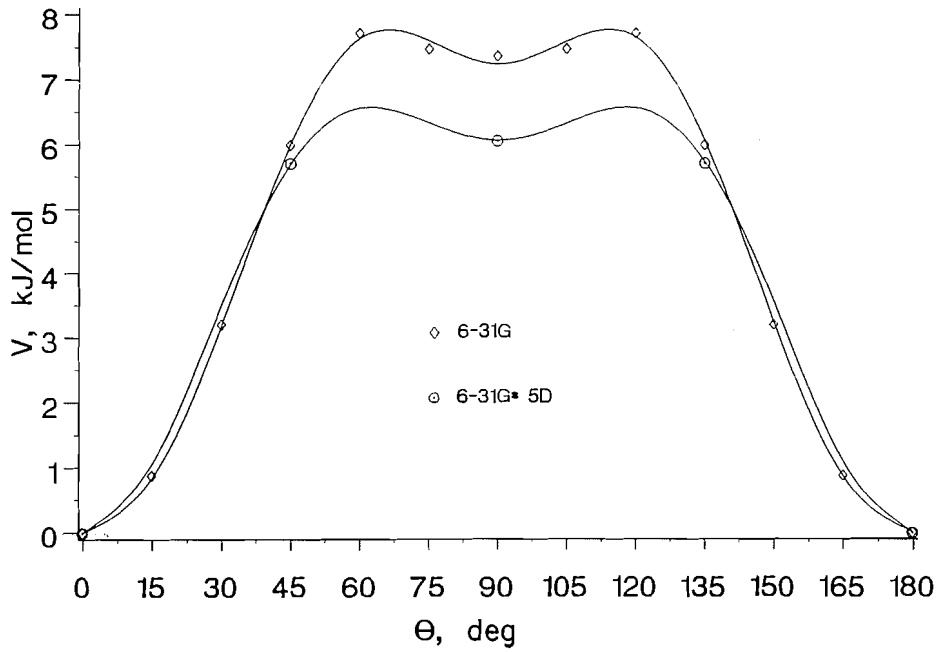


FIG. 3. The relative energies of various conformations of anisole, as computed with 6-31G and 6-31G*(5D) basis sets, are plotted as a function of θ, the angle of rotation about the C_{sp^2}—O bond. At θ = 0° the heavy-atom skeleton is planar. The solid lines represent the potential functions, $V(\theta)/\text{kJ mol}^{-1} = 7.78(5) \sin^2 \theta + 2.41(5) \sin^2 2\theta - 0.54(5) \sin^2 3\theta$ for the 6-31G results, and $V(\theta)/\text{kJ mol}^{-1} = 6.07 \sin^2 \theta + 2.68 \sin^2 2\theta$ for the three 6-31G*(5D) results.

ments is 1.25 ± 0.1 D (28). The 6-31G computations have the dipole moment as 1.18 D at θ = 0° in **1**, rising to only 1.35 D at θ = 90°. To a first approximation, therefore, the electrostatic term in the continuum model should act to decrease slightly the barrier in solution. The approximate doubling of the barrier in solution is therefore something of an anomaly; that of benzaldehye increases by only bout 50% in solution.

Experimental

The anisole-α-^{13}C was prepared as previously decribed (11). Solutions of anisole and anisole-α-^{13}C in the CS_2/C_6D_{12}/TMS solvent mixture, at concentrations given in Table 1, were transferred to 5 mm o.d. nmr sample tubes. Degassing of the tubes by a number of freeze–pump–thaw cycles was followed by flame-sealing of the evacuated tubes. The detailed procedures for accumulation of highly resolved

Can. J. Chem. Downloaded from www.nrcresearchpress.com by 194.225.253.170 on 09/07/12
For personal use only.

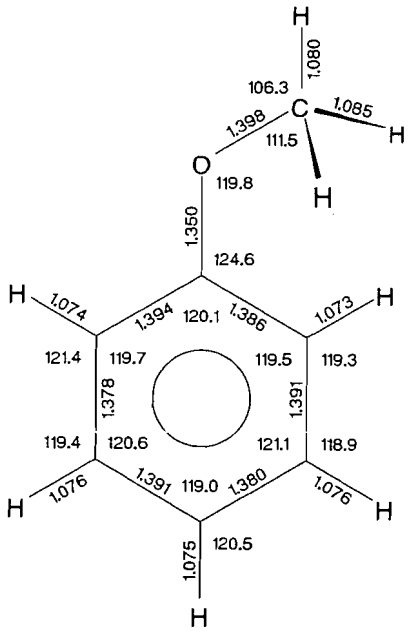


FIG. 4. The structure of the conformation of lowest energy, that with all heavy atoms in a plane, is shown and is that computed with the basis 6-31G*(5D). All bond angles, given in degrees, and bond lengths, given in angstroms, are optimized; the constraint is that the atoms of the phenyl group of anisole remain in a plane. The total energy is −344.582 089 au. The computed structure is quite similar to that assumed in the study of the electron diffraction patterns of anisole (4) but unlike that used in the work (5) on the microwave spectrum.

spectra on the Bruker AM 300 spectrometer have been described (29). These procedures were followed in the acquisition of ^{1}H nmr spectra of anisole-α-^{13}C at a probe temperature of 300 K.

The 6-31G and 6-31G* molecular orbital computations used the program GAUSSIAN 86 (30) and an Amdahl 5870 system. During these computations all bond angles and lengths were optimized, with the constraint, however, that the atoms of the phenyl group remain in a plane.

Acknowledgements

We are grateful to Craig Takeuchi for the synthesis of anisole-α-^{13}C, to the University of Manitoba for large amounts of computing time, and to the Natural Sciences and Engineering Research Council of Canada for a grant-in-aid of research.

1. H. DODZIUK, H. v. VOITHENBURG, and N. L. ALLINGER. Tetrahedron, **38**, 2811 (1982).
2. T. A. WILDMAN. Ph.D. Thesis, University of Manitoba, Winnipeg, Canada. 1982.
3. H. KONSCHIN. Ph.D. Thesis, University of Helsinki. Helsinki, Finland. 1985.
4. H. M. SEIP and R. SEIP. Acta Chem. Scand. **27**, 4024 (1973).
5. M. ONDA, A. TODA, S. MORI, and I. YAMAGUCHI. J. Mol. Struct. **144**, 47 (1986).
6. G. ALLEN and S. FEWSTER. *In* Internal rotation in molecules. *Edited by* W. J. Orville-Thomas. J. Wiley & Sons, London. 1974. pp. 274–276.
7. M. KLESSINGER and A. ZYUVIETZ. J. Mol. Struct. (Theochem), **90**, 341 (1982).
8. T. SCHAEFER and G. H. PENNER. J. Mol. Struct. (Theochem), **152**, 179 (1987).
9. T. SCHAEFER, R. LAATIKAINEN, T. A. WILDMAN, J. PEELING, G. H. PENNER, J. BALEJA, and K. MARAT. Can. J. Chem. **62**, 1592 (1984).
10. T. B. GRINDLEY, A. R. KATRITZKY, and K. D. TOPSOM. J. Chem. Soc. Perkin Trans. 2, 289 (1974).
11. T. SCHAEFER and G. H. PENNER. Can. J. Chem. **66**, 1635 (1988).
12. H. TYLLI and H. KONSCHIN. J. Mol. Struct. **42**, 7 (1977).
13. M. S. AHMED, M. A. KASHEM, and S. WALKER. J. Phys. Chem. **89**, 1670 (1985).
14. L. WALTZ, H. PAULUS, and W. HAASE. Z. Kristallogr. **180**, 97 (1987).
15. C. J. R. COUNSELL, J. W. EMSLEY, G. R. LUCKHURST, and H. S. SACHDEV. Mol. Phys. **63**, 33 (1988).
16. J. S. MARTIN, A. R. QUIRT, and K. E. WORVILL. The NMR program library, Daresbury Laboratory, Daresbury, U.K.
17. T. SCHAEFER and R. SEBASTIAN. J. Magn. Reson. **73**, 541 (1987).
18. M. W. WIECZOREK. Acta Crystallogr. Sect. B: Struct. Crystallogr. Cryst. Chem. **36**, 1515 (1980).
19. T. SCHAEFER and G. H. PENNER. Can. J. Chem. **66**, 1641 (1988).
20. H. FRIEGE and M. KLESSINGER. Chem. Ber. **112**, 1614 (1979).
21. O. SINANOĞLU. Chem. Phys. Lett. **1**, 340 (1967).
22. D. L. BEVERIDGE, M. M. KELLY, and R. J. RADNA. J. Am. Chem. Soc. **96**, 3769 (1974).
23. F. BIRNSTOCK, H-J. HOFMANN, and H-J. KÖHLER. Theor. Chim. Acta, **42**, 311 (1976).
24. L. T. NAGY and M. JANČÁROVÁ. Chem. Zvesti, **39**, 289 (1985).
25. J. SEITA and S. J. FORMOSINHO. Tetrahedron, **44**, 1707 (1988).
26. G. H. PENNER, P. GEORGE, and C. W. BOCK. J. Mol. Struct. (Theochem), **152**, 201 (1987).
27. T. SCHAEFER, G. H. PENNER, and R. SEBASTIAN. Can. J. Chem. **65**, 873 (1987).
28. A. L. MCCLELLAN. Tables of experimental dipole moments. W. H. Freeman and Company, San Francisco. 1963. p. 254.
29. T. SCHAEFER, R. SEBASTIAN, and G. H. PENNER. Can. J. Chem. **63**, 2597 (1985).
30. M. J. FRISCH, J. S. BINKLEY, H. B. SCHLEGEL, K. RAGHAVACHARI, C. F. MELIUS, R. L. MARTIN, J. J. P. STEWARD, F. W. BOBROWICZ, C. F. ROHLFING, L. R. KAHN, D. J. DEFREES, R. SEEGER, R. A. WHITESIDE, D. J. FOX, E. M. FLUDER, and J. A. POPLE. Carnegie–Mellon Quantum Publishing Unit, Pittsburgh, PA. 1984.

Can. J. Chem. Downloaded from www.nrcresearchpress.com by 194.225.253.170 on 09/07/12
For personal use only.

Examination of the inert solvent assumption in the ideal associated solution model. Enthalpy of chloroform–triethylamine complex dissociation

JOHN F. SMITH
Department of Chemistry, University of Alberta, Edmonton, Alta., Canada T6G 2G2

AND

LOREN G. HEPLER
Department of Chemistry and Department of Chemical Engineering, University of Alberta, Edmonton, Alta., Canada T6G 2G2

Received January 10, 1989

JOHN F. SMITH and LOREN G. HEPLER. Can. J. Chem. **67**, 1153 (1989).

We have made new measurements of the enthalpies of adding cyclohexane to mixtures of chloroform + triethylamine + cyclohexane at 25°C. The results of these measurements have been analysed in terms of the ideal associated solution model to obtain ΔH^θ for the dissociation of the chloroform–triethylamine complex. Our value of ΔH^θ is in excellent agreement with a published value that was obtained from results of measurements on binary mixtures of chloroform + triethylamine. This agreement indicates that it is usefully accurate to treat mixtures of chloroform + triethylamine + cyclohexane as ideal mixtures of chloroform, triethylamine, cyclohexane, and chloroform–triethylamine complex. This result has important implications for studies of associated systems dissolved in "inert" solvents and helps to provide a connection between complex formation in dilute solutions and in binary systems (A + B, no solvent).

Key words: ideal associated solution model, chloroform, triethylamine, inert solvent, hydrogen bonded complex.

JOHN F. SMITH et LOREN G. HEPLER. Can. J. Chem. **67**, 1153 (1989).

On a effectué de nouvelles mesures des enthalpies d'addition, à 25°C, du cyclohexane à des mélanges de chloroforme + triéthylamine + cyclohexane. Afin de déterminer les valeurs de ΔH^θ pour la dissociation du complexe chloroforme-triéthylamine, on a analysé ces résultats en fonction du modèle de la solution associée idéale. Notre valeur de ΔH^θ est en excellent accord avec une valeur publiée qui a été obtenue à partir de mesures sur des mélanges binaires de chloroforme + triéthylamine. Cet accord indique qu'il est correct et utile de traiter des mélanges de chloroforme + triéthylamine + cyclohexane comme des mélanges idéaux de chloroforme, de triéthylamine, de cyclohexane et du complexe chloroforme + triéthylamine. Les implications de ce résultat sont importantes pour les études de systèmes associés dissous dans des solvants «inertes» et il fournit un moyen de relier la formation de complexes en solutions diluées et dans des systèmes binaires (A + B, sans solvant).

Mots clés : modèle de la solution associée idéale; chloroforme; triéthylamine, solvant inerte, complexe avec liaison hydrogène.

[Traduit par la revue]

Can. J. Chem. Downloaded from www.nrcresearchpress.com by 194.225.253.170 on 09/07/12
For personal use only.

Introduction

It has recently been shown (1–9) that for some non-electrolyte solutions in which chemical reactions are expected (or known) to occur all of the observed deviations from ideality may appropriately be attributed to the formation of new chemical species. That is, contributions to non-ideality arising from differences in size, shape, and polarity of the components (often called "physical" contributions and usually accounted for by activity coefficients) are negligible compared with the chemical contributions. Since the physical contributions are assumed to be unimportant, the activity coefficients of all species are set equal to unity at all compositions and temperatures. The solution is, therefore, considered to be an ideal solution of all the species present at equilibrium. This is known as the ideal associated solution model (10–12).

The studies cited above show that the ideal associated solution model can be applied successfully to binary mixtures (no solvent) of two associating components. However, associated non-electrolyte systems (A + B = AB) are often studied as dilute solutions in some more or less inert solvent. For such investigations there are two ways of choosing standard states and evaluating activity coefficients. First, we may choose standard states for A, B, and AB based on Henry's law, which means that activity coefficients for all species that are sufficiently dilute are taken to be unity. An advantage of this choice is that it avoids the need to specify any particular model or theory of activity coefficients, but there are important difficulties. The first difficulty arises from the practical necessity of working with solutions that contain a reasonable concentration of complex. Many complexes are not formed in an appreciable amount in very dilute solution. Therefore, investigators are forced to work with reasonably concentrated solutions for which activity coefficients based on Henry's law may not be equal to unity, which then leads to the need for some further model or theory of activity coefficients. A second difficulty is that there is no straightforward way to compare K, ΔG^θ, and ΔS^θ values based on a Henry's law standard state with K, ΔG^θ, and ΔS^θ values based on Raoult's law, which is the usual standard state for binary mixtures of A + B (no solvent).

The second approach to solutions of A + B in an "inert" solvent is to choose standard states of all species based on Raoult's law. Compositions are expressed in terms of mole fractions and all activity coefficients are set equal to unity at all temperatures and compositions. This approach is equivalent to extending the ideal associated solution model from binary mixtures of A + B to solutions of A + B in an "inert" solvent and has the advantage that it permits direct comparison of results obtained for binary mixtures of A + B with results obtained for solutions of A + B in a solvent. If this approach is valid, then values of the equilibrium constant (K) and the standard enthalpy (ΔH^θ) for A + B = AB will be the same whether they are determined from the results of investigations of binary A + B (no solvent) or from the results of investigations of solutions of A + B in an inert solvent.

TABLE 1. Mass balance for A + B = AB mixed with an inert solvent S

Species	Stoichiometric amount/mol	Stoichiometric mole fraction	Equilibrium amount/mol[a]	Equilibrium mole fraction[b]
A	N_A	x_A	$(N_A - n_{AB}) = n_A$	$(x_A - r)/(1 - r) = z_A$
B	N_B	x_B	$(N_B - n_{AB}) = n_B$	$(x_B - r)/(1 - r) = z_B$
AB	—	—	n_{AB}	$r/(1 - r) = z_{AB}$
S	N_S	x_S	$N_S = n_S$	$x_S/(1 - r) = z_S$

[a]Total number of moles at equilibrium is $(N_A + N_B + N_S - n_{AB})$.
[b]$r = n_{AB}/(N_A + N_B + N_S)$.

To examine the validity of the extension of the ideal associated solution model to solutions of A + B in an inert solvent we have investigated the chloroform + triethylamine + cyclohexane system at 25°C. Chloroform + triethylamine was chosen as the complexing pair because the complex formed between chloroform and triethylamine is quite stable ($K = 2.6$ at 25°C) and because the ideal associated solution model has been shown (8) to work well for this binary system. Cyclohexane was chosen as the "inert" solvent because of its common use as a solvent in spectroscopic and thermodynamic studies of non-electrolyte solutions. In addition, cyclohexane has no obvious chemical reactivity towards either chloroform or triethylamine.

The enthalpies of adding known amounts of cyclohexane to both dilute and concentrated solutions of chloroform + triethylamine in cyclohexane were measured. To the extent that the model is applicable to the binary mixtures of chloroform + triethylamine and also to the solutions in cyclohexane, the results of these measurements will be consistent with the previously reported (8) values of K and ΔH^θ that were established on the basis of measurements of vapour pressures and excess enthalpies of binary A + B mixtures.

Treatment of speciation

The formation of a 1:1 complex, AB, between unlike molecules, A and B, can be represented by

[1] $A + B = AB$

When N_A moles of A are mixed with N_B moles of B and N_S moles of inert solvent, S, the equilibrium composition of the solution (expressed in terms of the equilibrium mole fractions, z_i) can be related to the stoichiometric composition (expressed in terms of the stoichiometric mole fractions, x_i). The relationship is derived from the mass balance considerations presented in Table 1, where r represents extent of reaction.

In the ideal associated solution model the activity coefficients of all species are taken to be unity at all compositions. Therefore, the equilibrium constant for reaction [1] can be expressed in terms of the equilibrium mole fractions, z_i:

[2] $$K = z_{AB}/z_A z_B$$

Substituting the expressions for the equilibrium mole fractions of each species, z_i, from the last column of Table 1 into eq. [2], we obtain an expression for the equilibrium constant in terms of the extent of reaction (r) and the stoichiometric mole fractions, x_A and x_B:

[3] $$K = r(1 - r)/(x_A - r)(x_B - r)$$

Rearrangement of eq. [3] yields

[4] $$r = \frac{[K(x_A + x_B) + 1] - \{[K(x_A + x_B) + 1] - 4(K + 1)Kx_Ax_B\}^{0.5}}{2(K + 1)}$$

Therefore, the value of r can be calculated for any given mixture of A, B, and S for which the equilibrium constant of association is known. The value of r can then be used in the expressions (obtained from Table 1)

[5] $$z_A = (x_A - r)/(1 - r)$$
$$z_B = (x_B - r)/(1 - r)$$
$$z_{AB} = r/(1 - r)$$
$$z_S = x_S/(1 - r)$$

to evaluate the equilibrium mole fraction of each species in the solution. The equilibrium amount of the complex, n_{AB}, can also be calculated from the extent of reaction using

[6] $$n_{AB} = r(N_A + N_B + N_S)$$

The equilibrium amounts of A and B, n_A and n_B, can then be calculated from the expressions

[7] $$n_A = N_A - n_{AB}$$
$$n_B = N_B - n_{AB}$$

that are derived in Table 1. The amount of solvent is unchanged by the formation of AB and hence the equilibrium amount of S, n_S, equals the stoichiometric amount of S:

[8] $$n_S = N_S$$

Thus, for any mixture of A, B, and S for which the stoichiometric amount of each species and the equilibrium constant of association are known, the equilibrium speciation can be calculated.

Experimental

Calorimetric measurements were made using an isoperibol calorimeter. The calorimeter consists of a Dewar flask (capacity 370 cm^3) reaction vessel clamped inside a sealed brass can. The brass can is fitted with an inlet port through which a liquid can be admitted to the reaction vessel by an automatic titrator. Changes in the temperature of the mixture in the reaction vessel are monitored with a thermistor and a resistance bridge. A calibration heater mounted on the inside of the lid of the can is positioned near the bottom of the reaction vessel when the vessel is sealed inside the can. The calorimeter is described in full in ref. 13.

Can. J. Chem. Downloaded from www.nrcresearchpress.com by 194.225.253.170 on 09/07/12
For personal use only.

Can. J. Chem. Downloaded from www.nrcresearchpress.com by 194.225.253.170 on 09/07/12
For personal use only.

To begin an experiment the reaction mixture is weighed into the reaction vessel. The reaction vessel is then clamped inside the can and the can is sealed and placed in a constant temperature water bath. The reaction mixture is stirred continuously and the change in resistance of the thermistor with time is recorded. When the resistance of the thermistor reaches a value that has been shown previously to correspond to the temperature of the water bath, a known volume of the liquid in the titrator is admitted to the reaction vessel. The titration leads to a change in temperature of the reaction mixture and a corresponding change in resistance of the thermistor. The change in resistance of the thermistor with time is recorded. When the rate of change in resistance of the thermistor with time has been constant for several minutes the calibration heater is switched on. The current through the heater, I_h, the voltage across the heater, V_h, and the time of the heating, t, are recorded. The heater is then switched off and the change in resistance of the thermistor with time is again recorded.

The resistance changes due to the titration and the electrical calibration are calculated by standard methods (14). The ratio of these resistance changes is equal to the ratio of the energy changes associated with the two processes. Since the electrical energy of the calibration, Q_c, is known (from $Q_c = I_h V_h t$), the energy associated with the titration can be calculated.

When the electrical calibration is finished, the mixture in the reaction vessel is heated (or cooled) until the resistance of the thermistor is $\sim 4\Omega$ above the resistance corresponding to the temperature of the water bath. The calorimetric experimental process (titration followed by calibration) is then repeated. The number of repetitions is limited only by the capacity of the reaction vessel. By this method several calorimetric experiments can be performed without changing the starting mixture in the reaction vessel.

In this work we have measured the heat associated with adding a known volume of cyclohexane to mixtures of chloroform, triethylamine, and cyclohexane at 25°C. Experiments were performed with two types of mixture in the reaction vessel. The first type of mixture contained concentrated chloroform + triethylamine with a maximum mole fraction of cyclohexane of 0.0971. The second type of mixture contained dilute chloroform + triethylamine with a minimum mole fraction of cyclohexane of 0.7345. For both types of mixture three ratios of chloroform to triethylamine were investigated: 3:1, 1:1, and 1:3. There were, therefore, six different starting mixtures, three concentrated and three dilute.

For each of the concentrated mixtures six additions of approximately 5 cm^3 of cyclohexane were made and the heat associated with each of these additions was measured. For the dilute mixtures the heat associated with each of four additions of 25 cm^3 of cyclohexane was measured.

Chloroform (Caledon) was washed five times with doubly distilled water, dried over anhydrous calcium chloride, and fractionally distilled twice. The middle fraction from each distillation was retained. At all stages of the process the chloroform was protected from light. The purified chloroform was stored under nitrogen in the dark and was used within 3 days of purification. Triethylamine (Fluka) was refluxed for 2 h over potassium hydroxide pellets and then distilled from the potassium hydroxide. The middle fraction of this distillation was collected and redistilled. The middle fraction was again collected and was stored under nitrogen. Cyclohexane (Caledon) was dried over molecular sieve (4A), distilled, and stored under nitrogen.

Results and analysis

The results of the calorimetric measurements described in the preceding section are given in Table 2 (concentrated mixtures) and Table 3 (dilute mixtures). Both tables list results of three sets of measurements, each set corresponding to a different ratio of chloroform to triethylamine. For each set of measurements the stoichiometric amounts of chloroform and triethylamine are invariant and are given above the results to which they relate. The first two columns of Tables 2 and 3 list the amount of cyclohexane in the reaction vessel before an experiment and the amount of cyclohexane added during the experiment. The third columns list the heat absorbed when this amount of cyclohexane is introduced to the reaction vessel. The uncertainty in these measured enthalpies is estimated to be less than 2%.

The fourth columns of Tables 2 and 3 list the heat arising

TABLE 2. Enthalpies measured on addition of a known amount of cyclohexane to concentrated mixtures of (chloroform + triethylamine) in cyclohexane

$n(C_6H_{12})^a$	$n(C_6H_{12})$ added^b	Q_{meas}/J	Q_{diss}/J
$n(CHCl_3)^c$ = 2.5048 mol, $n(TEA)^c$ = 0.8405 mol			
0.0000	0.0463	113.5	49.8
0.0463	0.0463	111.2	49.5
0.0926	0.0463	109.2	49.3
0.1389	0.0463	107.2	49.1
0.1852	0.0463	105.2	48.7
0.2314	0.0509	113.4	53.1
$n(CHCl_3)^c$ = 1.4192 mol, $n(TEA)^c$ = 1.3928 mol			
0.0000	0.0417	108.5	88.3
0.0417	0.0509	129.2	105.1
0.0926	0.0463	115.1	94.0
0.1389	0.0463	112.1	91.7
0.1852	0.0509	120.9	99.0
0.2361	0.0417	97.6	80.4
$n(CHCl_3)^c$ = 0.6468 mol, $n(TEA)^c$ = 1.9351 mol			
0.0000	0.0463	75.7	49.2
0.0463	0.0463	74.3	48.8
0.0926	0.0463	72.5	47.9
0.1389	0.0463	71.1	47.4
0.1852	0.0463	69.7	46.9
0.2314	0.0463	68.1	46.5

[a]Moles of cyclohexane in reaction vessel before experiment.
[b]Moles of cyclohexane added during experiment.
[c]Stoichiometric amount of chloroform ($CHCl_3$) and triethylamine (TEA) in reaction vessel for each set of experiments.

TABLE 3. Enthalpies measured on addition of a known amount of cyclohexane to dilute mixtures of (chloroform + triethylamine) in cyclohexane

$n(C_6H_{12})^a$	$n(C_6H_{12})^b$ added	Q_{meas}/J	Q_{diss}/J
$n(CHCl_3)^c$ = 0.4[illegible] mol, $n(TEA)^c$ = 0.1566 mol			
1.8953	0.231[illegible]	69.1	46.4
2.1268	0.231[illegible]	60.9	41.5
2.3582	0.2314	53.8	37.0
2.5896	0.2314	47.9	33.2
$n(CHCl_3)^c$ = 0.2598 mol, $n(TEA)^c$ = 0.2530 mol			
1.9103	0.2314	64.1	51.5
2.1417	0.2314	55.9	45.1
2.3732	0.2314	49.0	39.6
2.6046	0.2314	43.1	34.9
$n(CHCl_3)^c$ = 0.1566 mol, $n(TEA)^c$ = 0.4610 mol			
1.7089	0.2314	64.0	49.4
1.9403	0.2314	56.3	43.9
2.1718	0.2314	49.7	38.9
2.4032	0.2314	44.0	34.7

[a]Moles of cyclohexane in reaction vessel before experiment.
[b]Moles of cyclohexane added during experiment.
[c]Stoichiometric amount of chloroform ($CHCl_3$) and triethylamine (TEA) in reaction vessel for each set of experiments.

TABLE 4. Molar enthalpies of dissociation of the complex formed between chloroform and triethylamine

Condition	$n(CHCl_3)/n(TEA)$	ΔH^θ/kJ mol^{-1} [a]	$\pm\sigma$/kJ mol^{-1} [b]
Concentrated solutions	3/1	16.6	0.3
	1/1	17.3	0.2
	1/3	16.4	0.2
Dilute solutions	3/1	16.5	0.1
	1/1	17.0	0.2
	1/3	16.3	0.1

[a]Average molar enthalpy of complex dissociation, based on six experiments for concentrated solutions and four experiments for dilute solutions.
[b]One standard deviation of the set of enthalpies from the listed average enthalpy.

from complex dissociation. The heat of complex dissociation was calculated by subtracting the heat due to chloroform + cyclohexane interactions, $Q(CHCl_3/C_6H_{12})$, and the heat due to triethylamine + cyclohexane interactions, $Q(TEA/C_6H_{12})$, from the measured heat:

$$[9] \quad Q_{diss} = Q_{meas} - Q(CHCl_3/C_6H_{12}) - Q(TEA/C_6H_{12})$$

That the interactions of cyclohexane with chloroform and with triethylamine make significant contributions to the measured heat is consistent with treatment of the chloroform + triethylamine system by the ideal associated solution model. Although the model assumes that all physical contributions to the deviations from ideality are negligible, this assumption applies only to those species involved in association. The model contains no requirement that other species (e.g., "inert" solvent) be treated in any particular way. Therefore, we must evaluate the contributions to the measured heat arising from chloroform + cyclohexane and triethylamine + cyclohexane interactions from separate experiments. These contributions can then be subtracted from the measured heat to obtain the heat due to complex dissociation as described by eq. [9].

The last two terms in eq. [9] were evaluated for each experiment from equations of the form

$$[10] \quad Q(J/S) = [2z_J z_S \Delta H^*(J/S)](n_J + n_S)$$
$$J = CHCl_3 \text{ or TEA}, \; S = C_6H_{12}$$

where $2z_J z_S$ represents the probability of a J/S interaction in a random mixture of J and S and $\Delta H^*(J/S)$ represents the binary interaction enthalpy of J with cyclohexane. The equilibrium mole fraction (z_i) and equilibrium amount (n_i) of each species was found using the method described in the second section of this paper. A value of $K = 2.6$ for the equilibrium constant of association between chloroform and triethylamine as determined by Hepler *et al.* (8) from studies of the binary (no inert solvent) chloroform + triethylamine system was used in the speciation calculations. A value of $\Delta H^*(CHCl_3/C_6H_{12}) = 1.40$ kJ mol^{-1} was found by fitting an equation of the type represented by eq. [10] to the data of Findlay, Keniry, Kidman, and Pickles (15) for the excess enthalpies of the chloroform + cyclohexane system. A similar fit to the data of Murakami and Fujishiro (16) for excess enthalpies of mixing in the triethylamine + cyclohexane system led to a value of 0.55 kJ mol^{-1} for $\Delta H^*(TEA/C_6H_{12})$. The maximum residual in the fit to the chloroform + cyclohexane data was 26 J mol^{-1} while the maximum residual in the fit to the triethylamine + cyclohexane data was 33 J mol^{-1}.

The enthalpy of complex dissociation was calculated by dividing the enthalpy of dissociation from an experiment by the amount of complex dissociated, n_{diss}, during that experiment:

$$[11] \quad \Delta H_{diss} = Q_{diss}/n_{diss}$$

The amount of complex dissociated is the difference in amount of complex before and after a titration.

$$[12] \quad n_{diss} = n_{AB}(\text{before}) - n_{AB}(\text{after})$$

We estimate the uncertainty in each of our enthalpies of complex dissociation to be around 3%. For each set of experiments the values of ΔH_{diss} were averaged and these average enthalpies of complex dissociation together with the standard deviations of the averages are given in Table 4.

Earlier work (2) has shown that it is possible to apply the ideal associated solution model to the results of measurements of excess enthalpies to evaluate simultaneously the equilibrium constant and the standard enthalpy of association reactions. In principle, the calorimetric results presented in this paper could be treated in a similar way. We could then compare the values of *both* the association equilibrium constant and the standard enthalpy of association for chloroform + triethylamine with the values determined by other workers. In practice, analysis of our calorimetric results in this manner is complicated by the need for corrections due to chloroform/cyclohexane and triethylamine/cyclohexane interactions and leads to large uncertainties in the values of K and ΔH^θ. We have, therefore, chosen to assume that the value of $K = 2.6$ (8) is correct and to calculate the molar enthalpy of association as described above.

Discussion

Table 4 shows that the values of the molar enthalpy of chloroform–triethylamine complex dissociation determined in this work are independent of both the ratio of chloroform to triethylamine and the amount of cyclohexane in the mixture within the uncertainties of the calculations and the measurements. Our average value of the average enthalpy of complex dissociation is $\Delta H^\theta = 16.7 \pm 0.6$ kJ mol^{-1}. This average enthalpy is in excellent agreement with $\Delta H^\theta = -17.0 \pm 0.5$ kJ mol^{-1} that Hepler *et al.* (8) obtained for the enthalpy of complex association in the binary (no solvent) chloroform + triethylamine system from results of calorimetric experiments and the ideal associated solution model. This agreement shows that the same thermodynamic quantities ($\Delta H^\theta = 17$ kJ mol^{-1}, $K = 2.6$) can be used to describe the chloroform + triethylamine system both as a pure binary system and as a binary system dissolved in cyclohexane (and by inference, other "inert" solvents). We therefore conclude that the ideal associated

Can. J. Chem. Downloaded from www.nrcresearchpress.com by 194.225.253.170 on 09/07/12
For personal use only.

solution model can provide a useful approach to the analysis of data for A + B = AB systems when these systems are dissolved in some inert solvent.

That the model can provide a good approximation to associated systems in dilute solutions in an "inert" solvent is fortunate because there exists a large body of spectroscopic work in which dilute solutions of associated systems have been studied. The results of these studies are almost always analysed according to the ideal associated solution model. That is, it is assumed that physical interactions between the components are unimportant compared with the chemical interactions. A second assumption is then usually made: the thermodynamic properties of associated systems in dilute solution are the same as those that would be observed in binary mixtures (A + B = AB, no solvent). In this paper we have shown that, at least in the case of chloroform + triethylamine in cyclohexane, both assumptions are justified. Further experimentation is necessary to ascertain whether these assumptions are valid in general or are valid only for certain specific cases.

Acknowledgements

We thank Dr. Celina Dobrogowska for her assistance with the calorimetric measurements. We are also grateful to the Natural Sciences and Engineering Research Council of Canada for financial support of this and related research.

1. J. R. Baker, I. D. Watson, and A. G. Williamson. Aust. J. Chem. **24**, 2047 (1971).
2. L. G. Hepler and D. V. Fenby. J. Chem. Thermodyn. **5**, 471 (1973).
3. T. Matsui, L. G. Hepler, and D. V. Fenby. J. Phys. Chem. **77**, 2397 (1973).
4. D. V. Fenby and L. G. Hepler. Chem. Soc. Rev. **3**, 193 (1974).
5. D. V. Fenby and L. G. Hepler. J. Chem. Thermodyn. **6**, 185 (1974).
6. N. F. Pasco, D. V. Fenby, and L. G. Hepler. Can. J. Chem. **52**, 2139 (1974).
7. Y. P. Handa, D. V. Fenby, and D. E. Jones. J. Chem. Thermodyn. **7**, 337 (1975).
8. L. G. Hepler, Z. S. Kooner, G. Roux-Desgranges, and J.-P. E. Grolier. J. Solution Chem. **14**, 579 (1985).
9. J.-P. E. Grolier, G. Roux-Desgranges, Z. S. Kooner, J. F. Smith, and L. G. Hepler. J. Solution Chem. **16**, 745 (1987).
10. I. Prigogine and R. Defay. Chemical thermodynamics. John Wiley and Sons Inc., New York, NY. 1954. p. 417.
11. M. L. McGlashan. Chemical thermodynamics. Academic Press Inc., London, England. 1979. p. 266.
12. W. E. Acree Jr. Thermodynamic properties of nonelectrolyte solutions. Academic Press Inc., Orlando, FL. 1984. p. 134.
13. C. Dobrogowska and L. G. Hepler. To be published.
14. C. E. Vanderzee. J. Chem. Thermodyn. **13**, 1139 (1981).
15. T. J. V. Findlay, J. S. Keniry, A. D. Kidman, and V. A. Pickles. Trans. Faraday Soc. **63**, 846 (1967).
16. S. Murakami and R. Fujishiro. Kogyo Kagaku Zasshi, **69**, 1627 (1966).

Can. J. Chem. Downloaded from www.nrcresearchpress.com by 194.225.253.170 on 09/07/12
For personal use only.

Versatility of squaric acid as ligand. Crystal, molecular structures and magnetic studies of four poly- or dimetallic Cu(II) complexes

GERALD BERNARDINELLI

Laboratoire de cristallographie, Université de Genève, 24, quai E. Ansermet, 1211, Genève, Switzerland

AND

DIANE DEGUENON, REGIS SOULES, AND PAULE CASTAN[1]

Laboratoire de Chimie de Coordination du CNRS, Unité n° 8241 liée par convention à l'Université Paul Sabatier, 205 route de Narbonne, 31077 Toulouse Cedex, France

Received July 20, 1988[2]

GERALD BERNARDINELLI, DIANE DEGUENON, REGIS SOULES, and PAULE CASTAN. Can. J. Chem. **67**, 1158 (1989).

The synthesis and magnetic data of four copper(II) complexes obtained from squaric acid and bipyridyl or imidazole as ligand are described. $Cu(C_4O_4)(imidazole)_2 \cdot 2H_2O$ (compound **I**) is made of chains of squarato-1,3-bridged Cu(II) ions. The compound crystallizes in the monoclinic system, space group $P2_1/n$, and lattice parameters $a = 7.455(2)$ Å, $b = 8.196(2)$ Å, $c = 11.235(2)$ Å and $\beta = 100.55(2)°$. $R_F = 0.067$ for 1076 observed reflections. $[Cu_2(bipyridyl)_2(C_4O_4)(H_2O)_4](C_4O_4H)_2 \cdot 4H_2O$ (compound **II**) is a $C_4O_4H^-$ salt of a squarato-1,3 bridged centrosymmetric Cu(II) dimeric cation. The compound crystallizes in the triclinic system, space group P-1 and lattice parameters $a = 9.021(2)$ Å, $b = 9.017(2)$ Å, $c = 12.581(4)$ Å, $\alpha = 98.58(2)°$, $\beta = 106.81(2)°$, and $\gamma = 106.03(2)°$. $R_F = 0.038$ for 2376 reflections. Each copper atom is pentacoordinated in a distorted square-based pyramidal and is linked by two nitrogen atoms of the bipyridyl, one oxygen atom of the squarato bridge, and one oxygen atom of a water molecule in the plane and one water molecule out of plane. $[Cu_2(bipyridyl)_2(C_4O_4)(H_2O)_2Br_2]$ (compound **III**) is a squarato-1,3 bridged copper(II) dimer. The compound crystallizes in the monoclinic system, space group $P2_1/n$, and lattice parameters $a = 10.480(4)$ Å, $b = 8.503(1)$ Å, $c = 14.590(2)$ Å, and $\beta = 99.75(2)°$. $R_F = 0.048$ for 1423 reflections. Each copper atom is pentacoordinated in a distorted square-based pyramidal and is linked by two nitrogen atoms of the bipyridyl, one oxygen atom of the squarato bridge and one oxygen atom of a water molecule in the plane, and one bromine atom out of the plane.

In complexes **I**, **II**, and **III**, the magnetic susceptibility data could be best described by neglecting the exchange coupling. The magnetic data of $[Cu(bipyridyl)(C_4O_4) \cdot 4H_2O]_n$ (**IV**) are best explained in terms of an alternating Heisenberg ferromagnet. The epr spectra ratify results obtained from magnetic and crystallographic measurements.

Key words: squaric acid, 3,4-dihydroxy-3-cyclobutene-1,2-dion, copper(II) dimers, copper(II) chains, magnetic properties.

GERALD BERNARDINELLI, DIANE DEGUENON, REGIS SOULES et PAULE CASTAN. Can. J. Chem. **67**, 1158 (1989).

Nous décrivons la synthèse et les propriétés magnétiques de quatre complexes du cuivre(II), de l'acide squarique agissant comme ligand pontant entre deux atomes de cuivre et du bipyridyle ou de l'imidazole. La structure radiocristallographique de trois d'entre eux a été obtenue. Le complexe $Cu(C_4O_4)(imidazole)_2 \cdot 2H_2O$ (complexe I) est composé de chaînes dans lesquelles l'anion squarate ponte les atomes de cuivre par ses positions 1,3. Le composé cristallise dans le système monoclinique, groupe d'espace $P2_1/n$, les paramètres de la maille étant $a = 7{,}455(2)$ Å, $b = 8{,}196(2)$ Å, $c = 11{,}235(2)$ Å et $\beta = 100{,}55(2)°$. $R_F = 0{,}067$ pour 1076 réflexions observées. Le complexe $[Cu_2(bipyridyle)_2(C_4O_4)(H_2O)_4](C_4O_4H)_2 \cdot 4H_2O$ (complexe **II**) est un sel de $C_4O_4H^-$ et d'un cation centrosymétrique ou deux atomes de cuivre sont pontés par un ion $C_4O_4^{2-}$. Ce composé cristallise dans le système triclinique, avec un groupe d'espace P-1 et les paramètres de maille suivants : $a = 9{,}021(2)$ Å, $b = 9{,}017(2)$ Å, $c = 12{,}581(4)$ Å, $\alpha = 98{,}58(2)°$, $\beta = 106{,}81(2)°$ et $\gamma = 106{,}03(2)°$. $R_F = 0{,}038$ pour 2376 réflexions. Chaque atome de cuivre se trouve dans un environnement de pyramide à base carrée déformée. La coordination dans le plan est assurée par deux atomes d'azote du bipyridyle, un atome d'oxygène du pont squarate et un oxygène d'une molécule d'eau. La seconde molécule d'eau occupe la position axiale. Le complexe $[Cu_2(bipyridyle)_2(C_4O_4)(H_2O)_2Br_2]$ (complexe **III**) est aussi un dinucléaire du cuivre, où l'ion squarate agit comme pont. Le composé cristallise dans le système monoclinique, groupe d'espace $P2_1/n$, les paramètres de la maille étant $a = 10{,}480(4)$ Å, $b = 8{,}503(1)$ Å, $c = 14{,}590(2)$ Å et $\beta = 99{,}75(2)°$. $R_F = 0{,}048$ pour 1423 réflexions. Chaque atome de cuivre se trouve dans un environnement de pyramide à base carrée déformée. La coordination dans le plan est la même que celle du complexe **II** et un atome de brome occupe la position axiale. Dans les complexes **I**, **II** et **III**, aucun couplage magnétique n'est observé entre les atomes de cuivre. Le comportement magnétique du complexe **IV** $[Cu(bipyridyle)(C_4O_4) \cdot 4H_2O]_n$ ne peut être justifié qu'en utilisant le modèle d'une chaîne alternée d'Heisenberg. L'étude epr est en accord avec les données cristallographiques et les résultats de l'étude magnétique.

Mots clés : acide squarique, 3,4-dihydroxy-3-cyclobutene-1,2-dione, dimères du cuivre(II), chaînes de cuivre(II), propriétés magnétiques.

[Traduit par la revue]

Introduction

Squaric acid gives rise to a wide variety of complexes with transition metal compounds. The squarate anion $(C_4O_4)^{2-}$ does not behave like a chelating ligand but rather like a bridge between two or more metal atoms as uni- or multimonodentate ligand. In all the cases described so far, each site of coordination of squaric acid is coordinated to a different metal atom and either mono-dimensional chain or bi-dimensional or tri-dimensional polymers are obtained.

Moreover, interaction between paramagnetic metal ions in coupled systems has been extensively studied for many years. As early as 1977, Hendrickson and co-workers (1) have focussed on Cu(II) dimers bridged by small molecules and have described oxalate-bridged complexes exhibiting large antiferromagnetic exchange interaction. Keeping in mind analogies between squarate

[1]Author to whom correspondence should be addressed.

[2]Revision received December 22, 1988.

Can. J. Chem. Downloaded from www.nrcresearchpress.com by 194.225.253.170 on 09/07/12
For personal use only.

Can. J. Chem. Downloaded from www.nrcresearchpress.com by 194.225.253.170 on 09/07/12
For personal use only.

and oxalate ions, some copper squarate complexes have been investigated but not structurally identified (1, 2). We report here the study of some copper complexes obtained from copper(II) and squaric acid as ligand. From this work, it may be underlined that in such chemistry, it is very hazardous to postulate some "interesting magnetic properties" from a study of amorphous compounds since three hardly different complexes may be isolated from the same synthesis. In the present paper, the crystal structures of three copper complexes of squaric acid and bipyridyl or imidazole are reported.

Experimental

Synthesis

Compound ***I****, catena-poly-diaquabis(imidazole)copper(II)-μ-squarato(1,3)*

Transparent green–blue crystals of $Cu(C_4O_4)(imidazole)_2 \cdot 2H_2O$ were slowly grown from a mixture of $CuCl_2 \cdot 2H_2O$ in water (10 cm^3; 0.01 mol dm^{-3}), $H_2C_4O_4$ in water (10 cm^3, 0.01 mol dm^{-3}), and imidazole in water (10 cm^3, 0.02 mol dm^{-3}). The solution rapidly turned green. After 2 h, a green microcrystalline precipitate appeared and was filtered off. Green needles could be isolated from the resulting solution. The two fractions obtained have the same analysis. *Anal.* calcd. for $[Cu(C_3N_2H_4)_2(C_4O_4)(H_2O)_2]_n$: C 34.53, H 3.45, N 16.11, Cu 18.28; found: C 34.58, H 3.49, N 15.36, Cu 18.01.

Compound ***II****, $[Cu_2(C_{10}H_8N_2)_2(C_4O_4)(H_2O)_4](C_4O_4H)_2 \cdot 4H_2O$, [μ-squarato(1,3)-bis(diaqua(2,2'-bipyridyl)copper(II))] bis(hydrogenosquarate) tetrahydrate, and* ***III*** *$[Cu_2(C_{10}H_8N_2)_2(C_4O_4)(H_2O)_2Br_2]$, μ-squarato(1,3)-bis(aquabromo(2,2'-bipyridyl)copper(II))*

A solution of 0.001 mol of bipyridyl dissolved in 10 mL of ethanol was slowly added to a water solution of $CuBr_2$ (0.001 mol in 10 mL). The resultant solution was added to a solution of squaric acid (0.001 mol in 10 mL of $EtOH/H_2O$ 50/50). After about 1 week, emerald green crystals were separated (compound **II**). Shortly after, slightly darker crystals appeared (compound **III**). The two compounds could be unambiguously assigned by EDAX spectroscopy since compound **II** only contains copper as heavy atoms while compound **III** has a Cu/Br ratio close to 1. *Anal.* calcd. for $[Cu(C_{10}H_8N_2)(C_4O_4)_{0.5}(H_2O)_2]_2(C_4O_4H)_2 \cdot 4H_2O$ (compound **II**): C 41.69, H 3.72, N 6.08; found: C 41.75, H 3.67, N 6.02. *Anal.* calcd. for $[Cu(C_{10}H_8N_2)(C_4O_4)_{0.5}Br \cdot H_2O]_2$ (compound **III**): C 38.57, H 2.70, N 7.50; found: C 38.56, H 2.66, N 7.43.

Compound ***IV****, $[Cu(C_{10}H_8N_2)(C_4O_4) \cdot 4H_2O]_n$, catena-poly-tetraaqua(2,2'-bipyridyl)copper(II)-μ-squarato(1,3)*

Copper(II) squarate $\cdot 2H_2O$ was prepared following the procedure of West and Niu (3). This product (1×10^{-3} mol) was suspended in 20 mL of $EtOH/H_2O$ (50/50). A solution of 0.001 mol of bipyridyl dissolved in 10 mL of ethanol then was added slowly under stirring and gentle warming (60°C) until copper squarate dissolved. From this solution, compound **IV** crystallized with time as thin needles. *Anal.* calcd. for $Cu(C_4O_4)(C_{10}H_8N_2) \cdot 4H_2O$ (compound **IV**): C 41.64, H 3.99, N 6.94, Cu 15.74; found: C 41.61, H 3.41, N 6.88, Cu 15.62.

Measurements

Pertinent data about the crystals used and the measurement of diffraction intensities are summarized in Table 1. Intensity data for compounds **I** and **III** were collected on a Philips PW 100 diffractometer, those for compound **II** on an Enraf-Nonius CAD-4 diffractometer. The structures were solved by direct methods using the program MULTAN 80 (4) for complex **I** and MULTAN 84 (5) for complexes **II** and **III**. Anisotropic temperature factors were used for the non-hydrogen atoms. All hydrogen atoms were located on a Fourier difference map for compound **II**, but only those of water molecules for compounds **I** and **III** while the other ones were introduced into the calculations with common isotropic thermal parameters. The functions minimized were $\Sigma\omega[|F_o| - |F_c|]^2$.

Routine ir spectra were recorded on a Perkin Elmer 577 spectrophotometer using KBr pellets.

Magnetic susceptibility data were collected on powdered samples of the compounds using a Faraday-type magnetometer with mercury tetrakis(thiocyanato)cobaltate (susceptibility at 20°C, 16.44×10^{-6} cm^3 mol^{-1}) as susceptibility standard. Data were corrected for dimagnetism of the ligands estimated from Pascal constants (6).

Electron paramagnetic resonance spectra of powdered samples were recorded on a Bruker 200TT spectrometer at 77 K (sample immersed in liquid nitrogen) and room temperature using X-band frequencies.

Results and discussion

Description and discussion of the crystal structures

ORTEP drawings of the complexes showing the atom numbering scheme are given in Fig. 1. The final fractional atomic coordinates with estimated standard deviations are presented in Table 2 (compound **I**), Table 3 (compound **II**), and Table 4 (compound **III**). Selected interatomic bond distances and valence angles are given in Table 5. Hydrogen bonds are reported in Table 6.

Figure 1 shows that the crystal structure of complex **I** consists of chains, running parallel to the *b* axis, built up of *trans* squarato bridged copper(II) ions. Within each chain, each metal atom is octahedrally coordinated by two water molecules, two imidazole ligands, and two oxygen atoms of two different squarato ligands.

The chains of copper(II) are held together by strong hydrogen bridges between the water molecules and the noncoordinating squarato oxygen atoms on the one hand, and between the imidazole hydrogen atoms and the squarato coordinated oxygen atoms on the other hand (see Table 6).

This chain looks like the one observed in the homologous nickel(II) complex (NISIA) studied by Reedijk *et al.* (7). However, an important difference may be underlined in the squarae ring since in NISIA the carbon–carbon bond lengths (1.463 and 1.470 Å) are close to the value reported for $NiC_4O_4(H_2O)_2$ while in the copper complex (CUSIA), the carbon–carbon bond lengths of the squarato anion are 1.55 and 1.50 Å, respectively. To our knowledge, these are the longest bond lengths observed for such an anion, although the bond lengths in $[Pt_2(C_4O_4)_4]^{4+}$ are quite long (*i.e.* 1.533 and 1.463 Å, respectively) (8). Keeping in mind the 1.56 Å bond lengths in cyclobutane (9), it seems that this oxocarbon dianion is non-aromatic although the squarato anion is almost planar. The π-electron distributions are different in CUSIA and in the squarate ion, the greatest C—C bond lengths implying shorter C—O bond lengths (1.241 and 1.228 Å in CUSIA, 1.260 Å in potassium squarate monohydrate) (10). The C—C—C angles are very close to 90°. The geometry of the imidazole ligand is similar to that of reported data and therefore will not be discussed more in detail.

In contrast with compound **I** where Ni(II) and Cu(II) complexes are quite isostructural, the reaction of squaric acid with copper salts in the presence of bipyridyl does not give rise to linear chains with metal atoms cis-bridged squarate as for Ni(II) (11). This type of chain is only obtained by reaction of copper(II) squarate previously isolated (3) with bipyridyl (complex **IV**). Compounds **II** and **III** are two dinuclear complexes.

In compound **II**, two copper(II) ions are bridged by a squarato ion in a *trans* mode. Thus, each copper(II) is five-coordinated. The four equatorial donor atoms, *i.e.*, two nitrogen atoms from 2,2'-bipyridine, one oxygen atom of a water molecule, and one oxygen atom of the squarate ion are almost planar (maximum deviation = 0.044 Å for N(1)). The Cu atom is located at 0.169 Å above this mean plane.

Square-planar copper(II) has a decided tendency to extend its coordination sphere to five, the so-called (4 + 1) geometry

Can. J. Chem. Downloaded from www.nrcresearchpress.com by 194.225.253.170 on 09/07/12
For personal use only.

TABLE 1. Summary of crystal data, intensity measurement, and structure refinement

Parameter	Value		
	I	**II**	**III**
Formula	$Cu(C_3N_2H_4)_2(C_4O_4)(H_2O)_2$	$Cu(C_{10}H_8N_2)(C_4O_4)_{0.5}(C_4O_4H)(H_2O)_4$	$Cu(C_{10}H_8N_2)(C_4O_4)_{0.5}Br(H_2O)$
Molecular weight	349.8	460.9	373.7
Crystal size (mm)	0.07, 0.13, 0.15	0.12, 0.23, 0.25	0.14, 0.15, 0.30
Crystal system	Monoclinic	Triclinic	Monoclinic
Space group	$P2_1/n$	$P\text{-}1$	$P2_1/n$
a (Å)	7.455(2)	9.021(2)	10.480(4)
b (Å)	8.196(2)	9.017(2)	8.503(1)
c (Å)	11.235(2)	12.581(4)	14.590(2)
α (deg)	90.	98.58(2)	90.
β (deg)	100.55(2)	106.81(2)	99.75(2)
γ (deg)	90.	106.03(2)	90.
Z	2	2	4
D_c (g cm^{-3})	1.72	1.68	1.94
F_{000}	358	472	736
μ (mm^{-1})	1.65	1.26	4.80
Unit cell determination*			
No. of reflections	20	22	20
2θ range (deg)	31–41	31–36	22–36
$(\sin\theta/\lambda)_{max}$ (Å^{-1})	0.62	0.58	0.55
No. of measured reflections	1490	2868	1991
No. of observed reflections	1076	2376	1423
Criterion for observed reflections	$\|F_o\| > 4\sigma(F_o)$ and $\|F_o\| > 8$	$\|F_o\| > 4\sigma(F_o)$	$\|F_o\| > 4\sigma(F_o)$
Refinement (on F)	Full matrix	Full matrix	Full matrix
No. of parameters	97	313	172
Weighting scheme	$\omega = 1/\sigma^2(F_o)$	$\omega = 1/\sigma^2(F_o)$	$\omega = 1$
Max. and average Δ/σ	0.039, 0.005	0.032, 0.001	0.008, 0.001
Max. and min. $\Delta\rho$ (e Å^{-3})	0.97, −1.12	0.40, −0.52	0.81, −0.63
R, ωR (%)	6.7, 7.0	3.8, 4.2	4.8, 4.8

*Unit cell determined by least-squares fit.

TABLE 2. Fractional coordinates with esd's in parentheses for compound **I**

Atom	x	y	z
Cu	0.5	0.5	0.5
O(W1)	0.6481(9)	0.4311(7)	0.6616(6)
O(01)	0.5383(8)	0.2382(7)	0.3978(5)
O(02)	0.6455(11)	0.1136(8)	0.6803(6)
C(01)	0.5159(13)	0.1093(12)	0.4513(8)
C(02)	0.5690(14)	0.0525(11)	0.5845(9)
N(1)	0.2829(9)	0.3974(9)	0.5512(7)
N(2)	0.1001(11)	0.3027(11)	0.6679(7)
C(1)	0.2561(13)	0.3844(13)	0.6639(9)
C(2)	0.0282(14)	0.2619(14)	0.5537(10)
C(3)	0.1410(13)	0.3193(13)	0.4784(9)

(12), or to six (4 + 2) geometry. In complex **II**, the coordination sphere is extended to five by an axial water molecule, the Cu—O(w2) bond length of which is 0.222 Å smaller than the Cu—O(w1) bond of water in the plane.

The metal-bonded squaric dianion exhibits bond lengths and angles similar to those observed in squaric complexes. The O—C—C angles vary between 132.5 and 135.30° and the C—C—C angles are very close to 90° as in $CuC_4O_4(H_2O)_2$ where they are equal to 85.54 and 90.56°, respectively (13). In complex **II**, charge equilibrium is obtained by a non-bonded monoacidic squaric ion (HSq^-) and the bond lengths within the HSQ^- ion do not deviate greatly from those found in H_2Sq (14). The average C—O hydroxylic bond (1.305 Å) is similar to that observed in H_2Sq (1.291 Å) and little longer than that of $LiHSq\cdot H_2O$ (1.285 Å) (15). The average C—O bonds in the diketonic group (1.221 to 1.245 Å) are also in agreement with those found in $LiHSq\cdot H_2O$ (1.232 Å) or in H_2Sq (1.229 Å). Very small deviations are observed for the C—C bonds, the nearly "double" and "single" bonds being recognizable (1.428 Å and 1.492 Å, respectively). We have to note that even in HSq^-, carbon–carbon bond lengths are significantly shorter than in the bonded squarate of complex **I**. The molecular packing is fixed by a network of hydrogen bonds involving all potential donors (see Table 6).

The internal geometry of the bipyridine ligand is normal and will not be discussed further.

As already noticed, complexes **II** and **III** are obtained from the same preparative batch and their structures are very similar. Again the copper complex is dinuclear with the two metallic centers bonded by a squarate ligand. Bond lengths in the squarate entity are quite similar, as evidenced by Table 5. Here again, the square planar copper extends its coordination to five but in complex **III** a bromide ion changes places with the axial water molecule, allowing charge equilibrium. No hydrogen bonds or short interatomic contacts was observed for compound **III**. We have been informed[3] that a similar complex has

[3]M. Julve-Olcina. Personal communication.

Can. J. Chem. Downloaded from www.nrcresearchpress.com by 194.225.253.170 on 09/07/12
For personal use only.

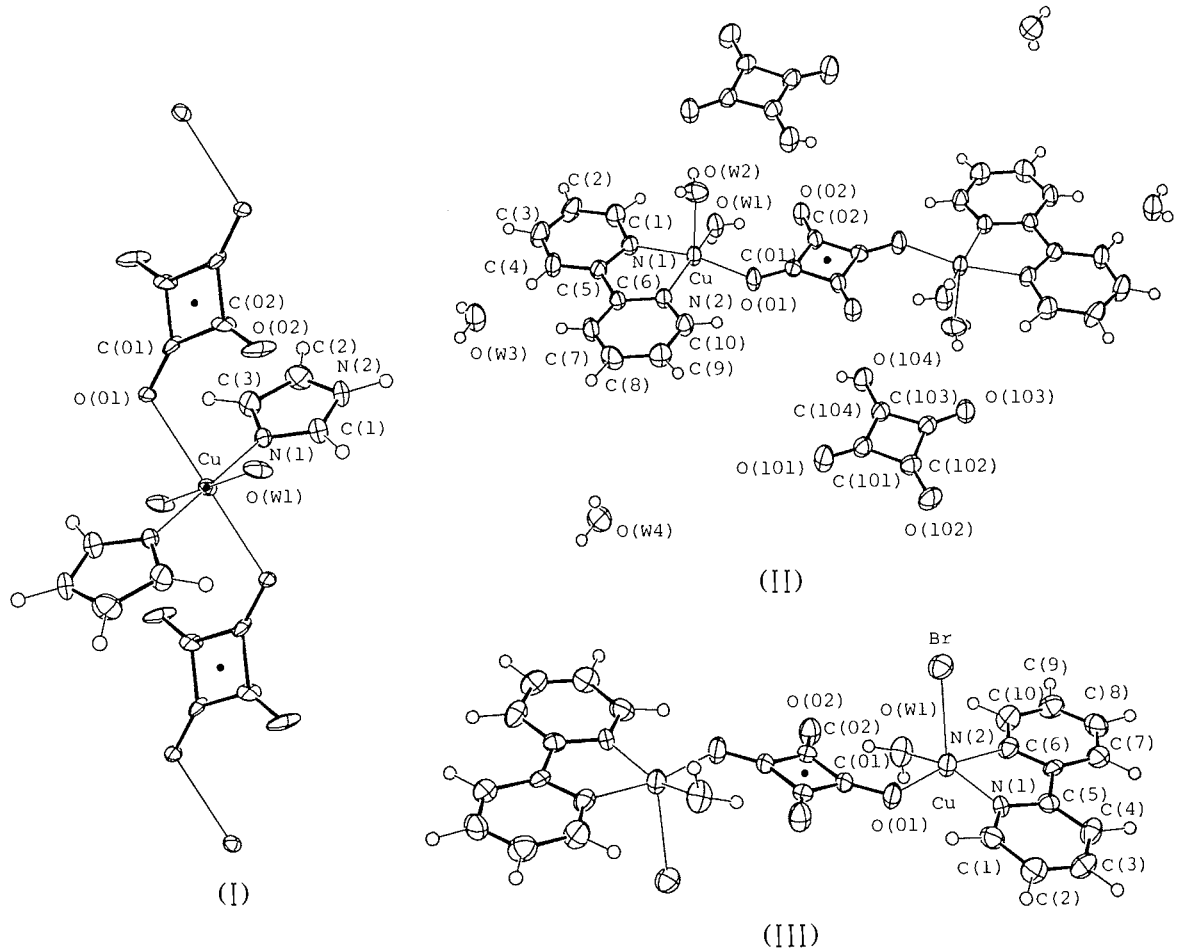


FIG. 1. Perspective view of compounds **I**, **II**, and **III** (■ indicates the position of the center of inversion).

recently been obtained with the bromide ion substituted by a NO_3^- ion. The structure of complex **IV** has not been determined, but from powder diffraction data show it is assumed to be the homologous Ni(II) complex already described as an infinite chain with squarato entities bonding metal atoms in a *cis* mode (11).

Spectroscopic data

As already discussed, the interpretation of the infrared spectra of squaric containing molecules is not straightforward. The infrared spectrum of complex **I** displays a broad and intense band located around 3100–2900 cm^{-1}. This observation agrees with structural data, pointing to the presence of strong hydrogen bonds. These bands may be attributed to the OH group of the water molecules. By contrast, complex **II** exhibits two bands in the same region (at 3150 and 3200 cm^{-1}, respectively), corresponding to O—H stretching vibrations of water molecules. In the same region, the C—H bands of the aromatic ring of bipyridyl may be identified. For complex **III**, the ir spectrum in the 3000 cm^{-1} region is almost identical to that of complex **II**.

All three complexes exhibit a very strong and extremely broad band near 1500 cm^{-1}. This type of absorption is characteristic of salts of $C_nO_n^{2-}$ ions (16) and was observed in $K_2C_4O_4$. This large band is slightly splitted, suggesting when compared to $K_2C_4O_4$ that symmetry is lower than D_{4h}, as evidenced by the X-ray investigation. In complex **II** a strong sharp band appears at 1780 cm^{-1} which is not present in the other two spectra. Our infrared studies show that this band appears at 1805 cm^{-1} for the $NaHC_4O_4$ molecule and at 1804 cm^{-1} in a complex of platinum, $[Pt(ethylenediamine)_2](C_4O_4H)_2$.[4] This band is attributed to a free non-coordinated carbonyl of the squaric entity.

In the far ir spectra, all the complexes exhibit two well-resolved absorption bands in the 400 cm^{-1} region (complex **I**: 400–380; complex **II**: 388–375; complex **III**: 410–375; complex **IV**: 419–370). Since metal–oxygen vibration bands are more intense compared to metal–nitrogen ones, these absorptions have been attributed to metal–oxygen. While Cu—Ow occurs generally near or higher than 400 cm^{-1}, the first band is attributed to the Cu–Ow stretching vibration while the other one is attributed to the Cu—Osq vibration. Since M—O stretching vibrations are metal-sensitive and are shifted to higher frequencies in the order Ni(II) < Cu(II) (17), the assignments may favorably compare with those proposed for NISIA (7), the homologue of complex **I**, viz. 400 ($\nu_{Ni—Ow}$) and 369 ($\nu_{Ni—Osq}$), respectively.

Magnetic susceptibility

The $1/\chi$ versus temperature curves for compounds **I**, **II**, and **III** are not reproduced here since the χ_M values obey the Curie–Weiss law, i.e. $\chi_M = (C/T) - \theta$. Table 7 reports the C, θ, and g values which correspond well to a Cu(II) ion without any interaction between metallic centers. The negative value of θ

[4]P. Castan *et al.* (unpublished results).

Can. J. Chem. Downloaded from www.nrcresearchpress.com by 194.225.253.170 on 09/07/12
For personal use only.

TABLE 3. Fractional coordinates with esd's in parentheses for compound **II**

Atom	*x*	*y*	*z*
Cu	0.89791(7)	0.20792(6)	0.24807(4)
O(W1)	0.9363(5)	0.0143(4)	0.1860(3)
O(W2)	1.1559(4)	0.3602(5)	0.3087(3)
O(W3)	0.6588(6)	0.8041(5)	0.0282(3)
O(W4)	0.2311(5)	0.6782(5)	0.3776(4)
O(01)	0.9036(4)	0.1637(4)	0.3972(2)
O(02)	0.9501(4)	0.1225(4)	0.6522(2)
C(01)	0.9585(5)	0.0734(5)	0.4522(3)
C(02)	0.9773(5)	0.0553(5)	0.5686(3)
O(101)	0.4556(5)	0.0879(4)	0.6234(3)
O(102)	0.4595(5)	−0.0194(4)	0.8596(3)
O(103)	0.6571(4)	−0.2526(4)	0.8060(3)
O(104)	0.6235(5)	−0.1751(5)	0.5628(3)
C(101)	0.5034(6)	−0.0093(5)	0.6713(4)
C(102)	0.5082(6)	−0.0532(5)	0.7813(4)
C(103)	0.5957(5)	−0.1642(5)	0.7548(4)
C(104)	0.5805(5)	−0.1228(5)	0.6476(4)
N(1)	0.8507(4)	0.2634(4)	0.0958(3)
N(2)	0.8052(4)	0.3800(4)	0.2811(3)
C(1)	0.8898(6)	0.2041(6)	0.0068(4)
C(2)	0.8587(7)	0.2556(6)	−0.0923(4)
C(3)	0.7871(7)	0.3710(6)	−0.1009(4)
C(4)	0.7488(6)	0.4337(6)	−0.0102(4)
C(5)	0.7837(5)	0.3789(5)	0.0881(3)
C(6)	0.7555(5)	0.4438(5)	0.1924(3)
C(7)	0.6871(6)	0.5620(5)	0.2026(4)
C(8)	0.6699(6)	0.6172(6)	0.3049(4)
C(9)	0.7226(6)	0.5532(6)	0.3953(4)
C(10)	0.7888(6)	0.4348(5)	0.3809(4)

TABLE 4. Fractional coordinates with esd's in parentheses for compound **III**

Atom	*x*	*y*	*z*
Br	0.48947(9)	0.2493(1)	0.73861(7)
Cu	0.3899(1)	−0.0353(1)	0.73453(7)
O(W1)	0.2312(6)	0.0235(9)	0.7864(4)
O(01)	0.4918(6)	−0.1012(8)	0.8538(4)
O(02)	0.3047(6)	0.1199(8)	0.9557(4)
C(01)	0.4961(8)	−0.043(1)	0.9339(6)
C(02)	0.4122(8)	0.055(1)	0.9806(6)
N(1)	0.4985(7)	−0.1770(8)	0.6696(4)
N(2)	0.2961(7)	−0.0118(9)	0.6047(5)
C(1)	0.6034(9)	−0.260(1)	0.7113(6)
C(2)	0.6701(9)	−0.365(1)	0.6611(7)
C(3)	0.6299(9)	−0.376(1)	0.5680(7)
C(4)	0.5246(9)	−0.287(1)	0.5242(6)
C(5)	0.4622(8)	−0.188(1)	0.5787(6)
C(6)	0.3501(8)	−0.090(1)	0.5399(6)
C(7)	0.299(1)	−0.077(1)	0.4457(6)
C(8)	0.195(1)	0.019(1)	0.4190(6)
C(9)	0.1398(9)	0.095(1)	0.4855(7)
C(10)	0.1922(9)	0.078(1)	0.5777(7)

TABLE 5. Selected bond distances (Å) and bond angles (deg) with esd's in parentheses for copper complexes **I**, **II**, and **II***

Bond	Distance (Å)		
	I	**II**	**III**
Coordinate squarate			
C(01)—C(02)	1.55(1)	1.463(6)	1.46(1)
C(01)—C(02)′	1.49(1)	1.456(7)	1.44(1)
C(01)—C(01)	1.24(1)	1.258(6)	1.26(1)
C(02)—O(02)	1.23(1)	1.255(1)	1.25(1)
Metal-ligand			
Cu—O(01)	2.475(6)	1.965(4)	1.963(6)
Cu—O(W1)	2.025(6)	2.186(4)	2.004(7)
Cu—O(W2)	—	1.964(4)	—
Cu—N(1)	2.000(8)	2.009(4)	2.002(7)
Cu—N(2)	—	2.001(4)	1.991(7)
Cu—Br	—	—	2.632(2)
Noncoordinated squarate			
C(101)—C(102)		1.486(7)	
C(102)—C(103)		1.492(8)	
C(103)—C(104)		1.431(7)	
C(104)—C(101)		1.428(8)	
C(101)—O(101)		1.240(7)	
C(102)—O(102)		1.221(7)	
C(103)—O(103)		1.245(6)	
C(104)—O(104)		1.305(7)	

Bonds	Angle (deg)		
	I	**II**	**III**
Metal surroundings			
O(01) —Cu—N(1)	86.4(3)	168.3(2)	88.9(3)
O(01) —Cu—N(2)	—	89.4(2)	168.3(3)
O(1) —Cu—O(W1)	94.8(2)	96.3(2)	95.6(3)
O(01) —Cu—O(W2)/Br	—	95.0(1)	95.1(2)
N(1) —Cu—N(2)	—	80.9(2)	80.7(3)
N(1) —Cu—O(W1)	87.8(3)	91.8(2)	154.6(3)
N(1) —Cu—O(W2)/Br	—	92.7(2)	108.0(2)
N(2) —Cu—O(W1)	—	166.0(1)	91.5(3)
N(2) —Cu—O(W2)/Br	—	97.0(2)	93.4(2)
O(W1)—Cu—O(W2)/Br	—	95.2(2)	96.5(2)
Coordinated squarate			
C(02)—C(01)—C(02)′	90.8(7)	90.0(4)	90.1(7)
C(01)—C(02)—C(01)′	89.2(7)	90.0(4)	89.9(7)
O(01)—C(01)—C(02)	133.7(8)	132.5(5)	136.4(8)
O(01)—C(01)—C(02)′	135.5(8)	137.5(4)	133.5(8)
O(02)—C(02)—C(01)	136.0(9)	135.3(5)	134.4(7)
O(02)—C(02)—C(01)′	134.8(9)	134.7(4)	135.7(8)

Mean values (deg) for the noncoordinated squarate of complex **II**:
O—C—C = 135.0 C—C—C = 90.0

*The primed atoms are generated through the center of inversion. The Cu atom of the complex **I** and the coordinated squarate of the complexes **I**, **II**, and **III** are located on a center of inversion.

for compound **I** suggests the occurrence of a weak antiferromagnetic interaction, as expected for a two-dimensional interchain interaction caused by the hydrogen bonds between the water molecule and the oxygen of the squarate ion.

Generally, in the least-squares fitting, it is best to use the *g* value obtained for epr measurements. However, in order to obtain a satisfactory fit to the magnetic data the average *g* value had to be adjusted. As for compound **II** it was necessary to fix *g* at 2.26 in order to get the best least-squares fit of the data.

Magnetic susceptibility data for compound **IV** are given in Fig. 2. The maxima in the susceptibility curves provide evidence for antiferromagnetic interactions. The data follow the Curie–Weiss law above 30 K, yielding $C = 0.45$ emu K/mol ($g = 2.19$) and $\theta = -29.47$ K. Below 30 K, there is a marked

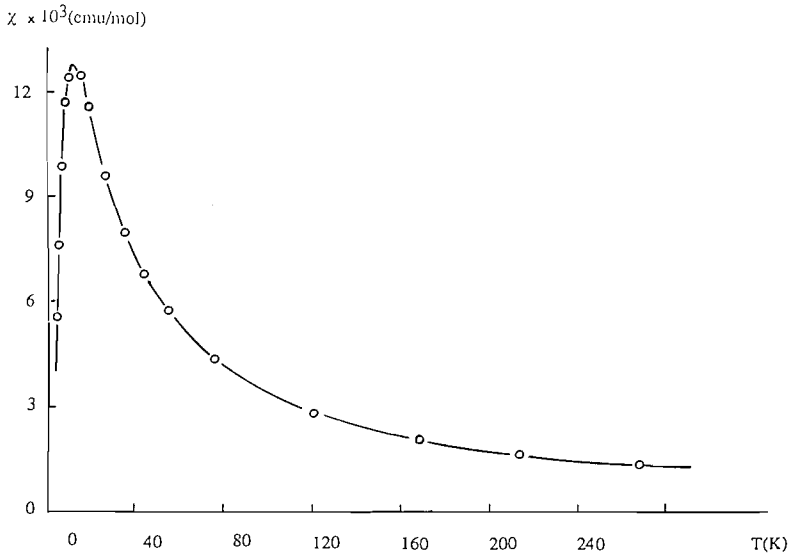


FIG. 2. Molar susceptibility versus T for complex **IV**. The drawn line represents the theoretical values, calculated with the susceptibility expression of an Heisenberg alternating chain, $J = 7.1\,cm^{-1}$, $g = 2.05$, $\alpha = 0.63$.

TABLE 6. Interatomic distances involving hydrogen bonds with esd's in parentheses

Atom 1	Atom 2	Distance (Å)	Equivalent position for atom 2
Compound **I**			
O(01)	... N(2)	2.726(11)	$1/2 + x, 1/2 - y, z - 1/2$
O(02)	... O(W1)	2.600(9)	$1\,1/2 - x, y - 1/2, 1\,1/2 - z$
Compound **II**			
Squarate ... squarate			
O(104)	... O(101)	2.551(5)	$1 - x, -y, 1 - z$
O(104)	... O(02)	3.156(5)	x, y, z
Squarate ... H_2O			
O(02)	... O(W1)	2.638(5)	$2 - x, -y, 1 - z$
O(02)	... O(W4)	2.741(6)	$1 - x, 1 - y, 1 - z$
O(101)	... O(W4)	3.028(6)	$1 - x, 1 - y, 1 - z$
O(102)	... O(W3)	2.846(7)	$1 - x, 1 - y, 1 - z$
O(103)	... O(W2)	2.786(6)	$2 - x, -y, 1 - z$
O(103)	... O(W3)	2.761(6)	$x, y - 1, z + 1$
H_2O	... H_2O		
O(W3)	... O(W1)	2.680(5)	$x, 1 + y, z$
O(W4)	... O(W2)	2.698(6)	$x - 1, y, z$
Compound **III**			
No hydrogen bond was observed below 3.2 Å.			

deviation from Curie–Weiss behavior and the susceptibility appears to tend to zero as the temperature approaches zero.

Since it has been proved that this compound is analogous to Ni(bipyridyl)(sq^{2-})·$2H_2O$ already described, attempts were made to fit magnetic data with the 1-D Heisenberg chain model. Bonner and Fischer (18) have performed exact calculations on small systems of $S = 1/2$ Heisenberg spins and have been able to extrapolate the infinite 1-D limit.

Furthermore, the fit of the Bonner–Fischer curve to the following rational function of $|J|/kT$ has been proposed (19):

$$\chi \approx [(N^2g^2\beta^2)/kT][(0.25 + 1.14995X + 0.30094X^2) \times (1.0 + 1.9862X + 0.68854X^2 + 6.0626X^3)]$$

where $X = |J|/kT$.

Agreement between susceptibilities calculated by the above equation and experimental data is excellent up to 30 K, with an exchange constant J near $-7\,cm^{-1}$. Below 30 K, the agreement is not as good and the susceptibility does not tend to zero at lower temperatures.

Actually, it is well known that the behavior expected for an infinite chain is that susceptibility tends to a non-zero value as the temperature reaches zero. In contrast, in small clusters containing even multiples of $S = 1/2$, the susceptibility tends to zero as the temperature tends to zero (18).

Consequently, we have used the model of an isolated Heisenberg dimer of $S = 1/2$ ions to analyze the data. The susceptibility of this model (20) has been shown to be:

$$\chi \approx [(Ng^2\beta^2)/kT][e^x/(1 + 3e^x)]$$

where $x = -2J/kT$.

This expression predicts the antiferromagnetic exchange constant to be related to the temperature of the maximum susceptibility (T_{max}) as $J/k = -0.801T_{max}$. Since T_{max} is 15 K for this compound, the exchange constant should be close to −12 K ($-8.3\,cm^{-1}$) if this is the appropriate model. A very good fit is obtained with this model with a J value of $-8\,cm^{-1}$ and $g = 1.94$.

A magnetic study of a copper complex described as $[Cu_2(phen)_4sq](ClO_4)_2$ has been published without X-ray structural investigation (2). Temperature-dependence studies of the magnetic susceptibility of this compound indicate antiferromagnetic exchange interaction. Susceptibility vs. temperature maxima occur at 17.2 K in this complex and a good fit has been obtained with $J = -10.1\,cm^{-1}$ with a dimer model.

To this point, it may be underlined that for compound **IV**, a similar model gives a good fit with experimental data while it seems that, in view of X-ray powder study, this compound is best described as an infinite chain.

In many exchange-coupled transition metal compounds with linear-chain structure, attempts to fit the magnetic data by the uniform Heisenberg-chain model have failed. This is the case for $Cu(NO_3)_2·2.5H_2O$ (21), a compound which has a ladder-like structure at room temperature (22). The magnetic properties of this compound, which is the most thoroughly studied example, may only be explained with an alternating Heisen-

Can. J. Chem. Downloaded from www.nrcresearchpress.com by 194.225.253.170 on 09/07/12
For personal use only.

TABLE 7. Summary of magnetic susceptibility and epr parameters

Compound	C (emu K/mol)	θ (K)	g^a	g_1	g_2	g_3
Compound **I**	0.455	−1.18	2.20±0.02 (2.17)	2.089	2.136	2.280
Compound **II**	0.479	−0.45	2.26±0.02 (2.17)	2.076	2.140	2.288
Compound **III**	0.441	+0.86	2.17±0.02 (2.16)	2.063	2.136	2.280
Compound **IV** until 30 K	0.451	−29.48	2.19±0.02 (~2.13)	~2.04	~2.08	~2.25

[a]Average g values from magnetic susceptibility fitting; numbers in parentheses are from average g values.

berg chain structure model. Other examples of copper compounds which have alternating-chain structures and attendant magnetic properties have been described as pyrazine-bridged binuclear copper acetate chains (23). X-ray structural studies at room temperature on a single crystal of Cu(N—Me-imidazole)$_2$Br$_2$ reveal a uniform chain (24). However, magnetic data have suggested that this material is an alternating Heisenberg antiferromagnet (25). For catena-di-μ chloro-bis(4-mefylpyridine)copper(II) (26), dielectric measurements provide evidence for structural transformations near 50 K, in agreement with the hypothesis of the alternating linear chain model. It may be underlined that, in such a model, the susceptibility tends to zero as the temperature tends to zero, like in dimers or even short clusters.

With this in view, the magnetic data for compound **IV** have been analyzed in terms of the alternating chain model. The Hamiltonian for the Heisenberg alternating chain may be written as:

$$H = 2J \sum_{i=1}^{n/2} [S_{2i}S_{2i-1} + \alpha S_{2i}S_{2i+1}]$$

where J is the exchange integral between a spin and its neighbor on the right, and αJ is the exchange integral between a spin and its neighbor on the left. The model is particularly interesting for antiferromagnetic exchange ($J < 0$) and for $0 \leq \alpha \leq 1$. This model has been largely studied by Duffy and Barr (27) and we have used the parameters proposed by Hatfield *et al.* (25) fitted for ten alternating chain cases.

With the values $J = -7.1\,\text{cm}^{-1}$, $g = 2.05$, and $\alpha = 0.63$, a good fit is obtained between calculated and experimental data, as viewed in Fig. 2.

While apparently structural studies for compound **IV** reveal a uniform chain structure, this remains a fascinating puzzle which certainly deserves room temperature and low temperature structural studies.

Electron paramagnetic resonance spectroscopy

Copper(II) complexes are particularly amenable to examination by epr since two types of information can be obtained. The pattern of g values for a given complex allows us to get insight into the coordination geometry around the copper(II) ion. Moreover, particularly in the case of dinuclear complexes, spectral features characteristic of magnetic exchange between the copper(II) ions may be observed. In a Cu(II) dimer, each Cu(II) ion has one unpaired electron in a d-type orbital, and to first order, the antiferromagnetic interaction reflects the level of spin–spin interactions.

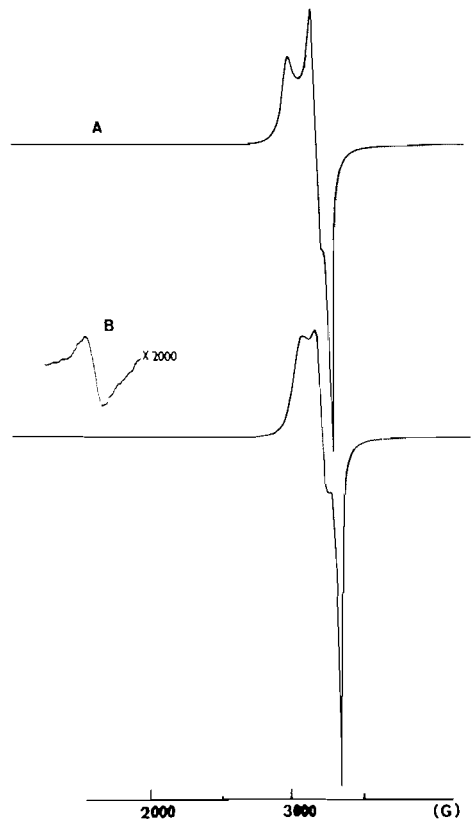


FIG. 3. Liquid-nitrogen X-band epr spectra: *A*, compound **I**; *B*, compound **III**.

The four complexes prepared in this study were investigated by epr spectroscopy at X-band frequencies both at room temperature and *ca.* 90 K. The spectra do not change when the temperature changes and only a slightly better resolution of signals is observed at the lower temperature.

For complexes **I**, **II**, and **III**, the epr data bear out the results of magnetic susceptibility studies. Each of the three compounds shows an asymmetric signal of *ca.* 3200 G in its X-band spectrum that is characteristic of a lone copper(II) ion. No hyperfine splitting was obtained. The asymmetric signal is characteristic either of a paramagnetic Cu(II) monomer or of a polymer without metal interactions (Fig. 3).

A formally forbidden transition, $\Delta m_s = 2$, is also observed for compounds **II** and **III** at "half-field" (1600 G) but at an intensity of 5×10^{-3} times the full-field transition.

Can. J. Chem. Downloaded from www.nrcresearchpress.com by 194.225.253.170 on 09/07/12
For personal use only.

In the epr spectra some points are of interest and may be underlined. The spectrum is strongly nonaxial, which reflects a noticeable distortion of the geometries. The values of g_1, g_2, and g_3 do not allow to precise geometry. First of all, the high field signal at $g = 2.09–2.07$, i.e. >2.04, will be consistent either with an elongated rhombic–octahedral geometry, which is the case for complex **I**, or for a distorted square-based pyramidal stereochemistry, which is the case for the two dimers (28, 29).

Actually, complexes structurally quite different such as an infinite chain with each copper atom in a quasi octahedral surrounding and a dinuclear with a penta-coordinated metal offer strongly similar epr spectra. In these two cases, the one-electron ground state is $d_{x^2-y^2}$.

The room temperature epr spectra of complex **IV** show only one broad uninterpretable signal with a pronounced hump at $g = \sim 2.04$ and apparent g values of 2.25 and 2.08. No additional information could be obtained upon decreasing the temperature of the sample to 77 K.

Acknowledgement

Dr. M. Fagot is gratefully acknowledged for carrying out EDAX measurements which have been performed at the Laboratoire de Microscopie et Structure des Matériaux (Université Paul Sabatier, Toulouse).

1. T. R. Felthouse, E. Laskowski, and D. N. Hendrickson. Inorg. Chem. **16**, 1077 (1979).
2. J. T. Reinprecht, J. G. Miller, G. C. Vogel, M. S. Haddad, and D. N. Hendrickson. Inorg. Chem. **19**, 927 (1980).
3. R. West and N. Y. Niu. J. Am. Chem. Soc. **85**, 2589 (1963).
4. P. Main, S. J. Fiske, S. E. Hull, L. Lessinger, G. Germain, J.-P. De Clercq, and M. M. Woolfson. A system of computer programs for the automatic solution of crystal structures from X-ray diffraction data. University of York, England, and University of Louvain-la-Neuve, Belgium. 1980.
5. P. Main, G. Germain, and M. M. Woolfson. A system of computer programs for the automatic solution of crystal structures from X-ray diffraction data. University of York, England, and University of Louvain-la-Neuve, Belgium. 1984.
6. P. W. Selwood. Magnetochemistry. Interscience, New York. 1956.
7. J. A. C. Van Ooijen, J. Reedijk, and A. L. Spek. Inorg. Chem. **18**, 1184 (1979).
8. O. Simonsen and H. Toftlund. Inorg. Chem. **20**, 4044 (1981).
9. J. D. Dunitz and V. Schomaker. J. Chem. Phys. **20**, 1703 (1952).
10. W. M. Macintyre and M. S. Werkema. J. Chem. Phys. **42**, 3563 (1964).
11. R. Soules, F. Dahan, J.-P. Laurent, and P. Castan. J. Chem. Soc. Dalton Trans. 587 (1988).
12. B. J. Hathaway. J. Struct. Bonding (Berlin), **14**, 49 (1973).
13. C. Robl and A. Weiss. Z. Naturforsch. **41b**, 1341 (1986).
14. (*a*) D. Semmingsen, F. J. Hollander, and T. F. Koetzle. J. Chem. Phys. **66**, 4405 (1977); (*b*) D. Semmingsen. Acta Chem. Scand. **10**, 3961 (1973); (*c*) D. Semmingsen. Tetrahedron Lett. **11**, 807 (1973); (*d*) Y. Wang, G. D. Stucky, and J. M. Williams. J. Chem. Soc. Perkin II, 35 (1974).
15. D. Semmingsen. Acta Chem. Scand. **30**, 808 (1976).
16. M. Ito and R. West. J. Am. Chem. Soc. **85**, 2580 (1963).
17. K. Nakamoto. Infrared and Raman spectra of inorganic and coordination compounds. 4th ed. Wiley Interscience, New York. 1986. p. 229.
18. J. C. Bonner and M. E. Fischer. Phys. Rev. Sect. A, **135**, 640 (1964) and references therein.
19. W. E. Estes, D. P. Gavel, W. E. Hatfield, and D. J. Hodgson. Inorg. Chem. **17**, 1415 (1978) and references cited therein.
20. B. Bleaney and K. D. Bowers. Proc. R. Soc. London, Ser. A, **214**, 451 (1952).
21. K. M. Diederix, H. W. Blöte, J. P. Groen, T. O. Klaasen, and N. J. Poulis. Phys. Rev. B., Condens. Matter, **19**, 420 (1979).
22. B. Morosin. Acta Crystallogr. Sect. B, **B26**, 1203 (1970).
23. J. S. Valentine, A. J. Silverstein, and Z. G. Soos. J. Am. Chem. Soc. **96**, 97 (1974).
24. J. C. Jansen, H. Van Koningsveld, and J. A. C. Van Ooijen. Cryst. Struct. Commun. **7**, 637 (1978).
25. J. J. Smit, L. J. Dejongh, J. A. C. Van Ooijen, J. Reedijk, and J. C. Bonner. Physica B + C (Amsterdam), **97**, 229 (1979).
26. J. W. Hall, W. E. Marsch, R. R. Weller, and W. E. Hatfield. Inorg. Chem. **20**, 1033 (1981).
27. W. Duffy and K. P. Barr. Phys. Rev. **165**, 647 (1968).
28. B. J. Hathaway and D. E. Billing. Coord. Chem. Rev. **5**, 143 (1978).
29. C. G. Pierpont, L. C. Francesconi, and D. N. Hendrickson. Inorg. Chem. **17**, 3470 (1978).

Can. J. Chem. Downloaded from www.nrcresearchpress.com by 194.225.253.170 on 09/07/12
For personal use only.

The photolysis of ethylene at 193 nm[1]

L. GIROUX AND M. H. BACK
Ottawa–Carleton Chemistry Institute, University of Ottawa, Ottawa, Ont., Canada K1N 6N5

AND

R. A. BACK
Division of Chemistry, National Research Council of Canada, 100 Sussex Drive, Ottawa, Ont., Canada K1A 0R6

Received February 2, 1989

L. GIROUX, M. H. BACK, and R. A. BACK. Can. J. Chem. **67**, 1166 (1989).

The photolysis of ethylene has been studied at pressures from 50 to 3000 Torr using a pulsed ArF excimer laser at 193.3 nm. Major products were acetylene, *n*-butane, 1-butene, ethane, and 1,3-butadiene, with smaller amounts of propane, propene, methane, and allene. Quantum yields varied with pressure and reaction time; the latter dependence is ascribed to secondary photolysis of butene and butadiene. The reaction products are accounted for by three primary processes:

[1] $C_2H_4 + h\nu \rightarrow C_2H_2 + H_2$

[2] $\rightarrow C_2H_2 + H + H$

[3] $\rightarrow C_2H_3^{\ddagger} + H$

followed by reactions of H, C_2H_3, and C_2H_5 radicals. The vibrationally excited $C_2H_3^{\ddagger}$ radical can decompose to H + C_2H_2 or can be stabilized by collision. The pressure dependence of the quantum yields of the primary processes [1]–[3] is complex, and a photodissociation mechanism involving several intermediates and excited states of ethylene is presented to account for the present results and previous measurements at 185 nm.

Key words: ethylene, uv photolysis.

L. GIROUX, M. H. BACK et R. A. BACK. Can. J. Chem. **67**, 1166 (1989).

On a étudié la photolyse de l'éthylène à l'aide d'un laser excimère ArF pulsé à 193,3 nm et en opérant à des pressions allant de 50 à 3000 Torr. Les produits principaux sont l'acétylène, le *n*-butane, le butène-1, l'éthane, le butadiène-1,3 ainsi que des quantités plus faibles de propane, de propène, de méthane et d'allène. Les rendements quantiques varient avec la pression et la durée de la réaction; cette dernière dépendance est attribuée à des photolyses secondaires du butène et du butadiène. On explique la formation des produits réactionnels à l'aide de trois processus primaires :

[1] $C_2H_4 + h\nu \rightarrow C_2H_2 + H_2$

[2] $\rightarrow C_2H_2 + H + H$

[3] $\rightarrow C_2H_3^{\ddagger} + H$

qui sont suivis de réactions avec des radicaux H, C_2H_3 et C_2H_5. Le radical $C_2H_3^{\ddagger}$ peut se décomposer en H + C_2H_2 ou être stabilisé par collision. La relation entre la pression et les rendements quantiques des processus primaires [1] à [3] est complexe; afin d'expliquer les résultats actuels ainsi que les mesures faites antérieurement à 185 nm, on propose un mécanisme de photodissociation impliquant plusieurs intermédiaires et des états excités de l'éthylène.

Mots clés : éthylène, photolyse uv.

[Traduit par la revue]

Introduction

The photolysis of ethylene in the far UV has been studied many times in a number of laboratories. The most thorough work and most relevant to the present paper has been done at 185 nm with a mercury resonance lamp (1–4), but results have also been reported at a number of shorter wavelengths. The photolysis was reviewed by McNesby and Okabe (5) and more recently by Collin (6). Three primary processes have been demonstrated to occur:

[1] $C_2H_4 + h\nu \rightarrow C_2H_2 + H_2$

[2] $\rightarrow C_2H_2 + 2H$

[3] $\rightarrow C_2H_3 + H$

with the relative yields showing some dependence on wavelength. Few measurements have been reported at wavelengths longer than 185 nm. Potzinger *et al.* did one or two experiments with a weak carbon-resonance lamp at 193 nm (2), and there is a brief unpublished report by Irion (7) of the photolysis with an ArF laser at 193 nm. The present paper describes a systematic study of the photolysis with an ArF laser at 193 nm.

Experimental methods

The photolysis vessel was a short cylinder, 0.5 cm long and 2.0 cm in diameter, made from a brass annulus 0.5 cm thick with plane Suprasil quartz windows cemented to each side with Apiezon W black wax. Two small-bore tubes through the annulus led with minimum dead space to valves which permitted attachment to a vacuum line for pumping or filling, or connection as the sample loop of a gas chromatograph, so that the entire contents of the vessel could be injected for analysis.

The light source was a pulsed ArF excimer laser (Lumonics 820 Series) with pulse energies typically between 15 and 30 mJ, operating at a pulse rate of 1 Hz. The beam was unfocussed and stopped down to a diameter of 1.04 cm to avoid striking the vessel walls. Care was taken to minimize heating of the front window and to avoid any build-up of solid material which could lead to local heating, and windows were cleaned or replaced whenever traces of a deposit became evident. Incident and transmitted power or pulse energy were measured with a Scientech Model 36-0001 disc calorimeter. Absorption by ethylene

[1]NRCC No. 30169.

Can. J. Chem. Downloaded from www.nrcresearchpress.com by 194.225.253.170 on 09/07/12
For personal use only.

TABLE 1. Quantum yields of products from the photolysis of ethylene, at 193 nm and 760 Torr, vs. number of laser pulses

Product	Initial extrapolated value	Yield when number of pulses = 10	25	50	100	250
C_2H_2	0.42	0.42	0.42	0.41	0.42	0.41
n-C_4H_{10}	0.069	0.071	0.075	0.076	0.081	0.084
1-C_4H_8	0.096	0.089	0.088	0.078	0.069	0.049
C_2H_6	0.047	0.048	0.051	0.052	0.055	0.061
1,3-C_4H_6	0.025	0.019	0.013	0.0092	0.0057	0.0028
C_3H_8	0.00	—	—	0.0065	0.010	0.020
C_3H_6	0.0050	0.0059	0.0089	0.0090	0.011	0.016
CH_4	0.0007	0.0012	0.0019	0.0027	0.0044	0.0069
C_3H_4	0.00	0.00037	0.00079	0.0011	0.0016	0.0021

followed Beer's Law, and a value of the molar decadic absorption coefficient of 5.63 (±0.14) M^{-1} cm^{-1} was obtained for the ArF laser radiation, which had a central wavelength of 193.3 nm and a band width (FWHM) of about 0.5 nm. For quantum yield measurements, the transmitted energy was monitored during the experiment, and the absorbed energy was calculated from the absorption coefficient, making allowance for window losses and back reflection.

Ethylene was Matheson Research-grade, used after rigorous degassing but no other purification. Trace impurities present were C_2H_2 and C_2H_6, each about 13 ppm; these were measured by GC in suitable blank experiments and corrections applied to the observed yields of these products. A variety of columns were employed for analysis; products were identified by comparison with standard mixtures and by mass spectrometry, and quantitative calibrations were made with synthetic mixtures similar in composition to the reagent–product mixture.

Results and discussion

Products and time dependence of their quantum yields

The major products observed, in approximate order of decreasing importance, were C_2H_2, n-C_4H_{10}, 1-butene, C_2H_6, and 1,3-butadiene. Minor products were C_3H_8, propene, CH_4, and allene. At higher conversions, traces of 2-butene and methylcyclopropane were observed, and some C_4 and C_5 hydrocarbons were tentatively identified, including 1,2-butadiene, diacetylene, 1,4-pentadiene, 1-pentene, and n-pentane. Hydrogen, known from previous work to accompany C_2H_2 in reaction [1], was also undoubtedly a major product but was not measured. Quantum yields of products from the photolysis at 760 Torr of C_2H_4 are shown in Table 1 as a function of the number of laser pulses, with incident pulse energies between 19 and 22 mJ; these data are also shown in Figs. 1 and 2. Of the major products, the quantum yield of C_2H_2 is constant, those of C_2H_6 and n-C_4H_{10} increase somewhat, while those of 1-butene and 1,3-butadiene decrease, the latter quite sharply, with increasing number of pulses (i.e., time of photolysis). The quantum yields of all the minor products increase markedly with time from initial values close to zero, and are all clearly secondary in origin. Because of these dependences on photolysis time, the data have been extrapolated to give initial values, primary quantum yields, as shown, and these will be used to assess the photolysis mechanism in its simplest initial stages.

The mechanism of the photolysis

The primary products of the photolysis can be accounted for by the three primary photodissociation reactions, [1], [2], and [3] followed by a sequence of reactions of hydrogen atoms and

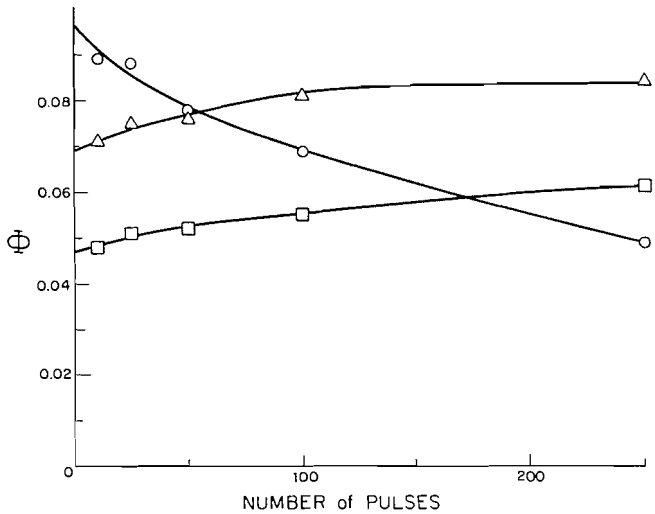


FIG. 1. Quantum yields of products from the photolysis of ethylene at 193 nm and 760 Torr, vs. number of laser pulses. Incident pulse energy was 20.4 (±1.2) mJ. ○ = 1-butene; △ = n-butane; □ = ethane.

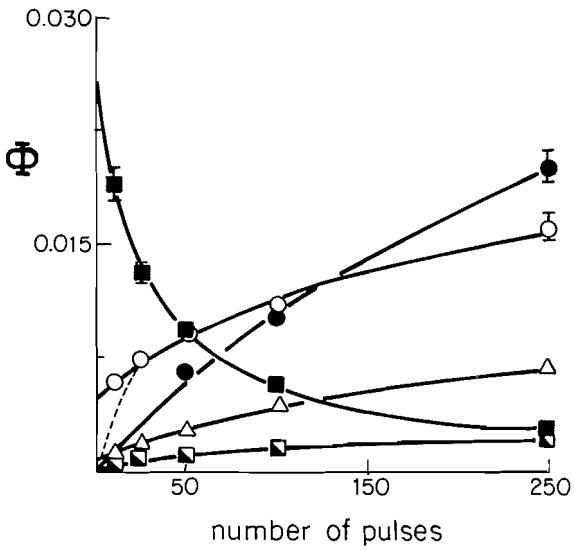


FIG. 2. Quantum yields of products from the photolysis of ethylene at 193 nm and 760 Torr, vs. number of laser pulses. Incident pulse energy was 20.4 (±1.2) mJ. ■ = 1,3-butadiene; ○ = propene; ● = propane; △ = methane; ◪ = allene.

Can. J. Chem. Downloaded from www.nrcresearchpress.com by 194.225.253.170 on 09/07/12
For personal use only.

TABLE 2. Product ratios and secondary quantum yields in the photolysis of ethylene at 193 nm and a pressure of 760 Torr vs. the number of laser pulses

Product ratio	Initial extrapolated value	Value when number of pulses = 10	25	50	100	250
$C_2H_6/(n\text{-}C_4H_{10} + 1\text{-}C_4H_8)$	0.28	0.30	0.31	0.34	0.37	0.46
$(1\text{-}C_4H_8)^2/(n\text{-}C_4H_{10})(1,3\text{-}C_4H_6)$	5.3	5.9	7.9	8.7	10.3	10.2
$n\text{-}C_4H_{10}$ (secondary)	0	2.0×10^{-3}	6.0×10^{-3}	7.0×10^{-3}	12×10^{-3}	15×10^{-3}
C_2H_6 (secondary)	0	1.0×10^{-3}	4.0×10^{-3}	5.0×10^{-3}	8.0×10^{-3}	14×10^{-3}
C_2H_6 (secondary, corrected for reaction 4)	0	0.9×10^{-3}	3.4×10^{-3}	4.3×10^{-3}	6.9×10^{-3}	12×10^{-3}
$(C_3H_8)^2/4(n\text{-}C_4H_{10})$	0	—	—	0.14×10^{-3}	0.31×10^{-3}	1.2×10^{-3}

ethyl and vinyl free radicals similar to that suggested previously (1–4):

[4] $H + C_2H_4 \xrightarrow{+M} C_2H_5$

[5] $2C_2H_5 \longrightarrow n\text{-}C_4H_{10}$

[6] $\longrightarrow C_2H_6 + C_2H_4$

[7] $C_2H_5 + C_2H_3 \longrightarrow 1\text{-}C_4H_8$

[8] $\longrightarrow C_2H_6 + C_2H_2$

[9] $\longrightarrow 2C_2H_4$

[10] $2C_2H_3 \longrightarrow 1,3\text{-}C_4H_6$

[11] $\longrightarrow C_2H_2 + C_2H_4$

[12] $H + C_2H_5 \longrightarrow [C_2H_6{}^*]$

[13] $[C_2H_6{}^*] \xrightarrow{+M} C_2H_6 + M$

[14] $\longrightarrow 2CH_3$

[15] $2CH_3 \longrightarrow C_2H_6$

[16] $CH_3 + C_2H_5 \longrightarrow C_3H_8$

[17] $\longrightarrow CH_4 + C_2H_4$

To test this mechanism and to evaluate the quantum yields of the primary photodissociation reaction, the following values were assumed for the several disproportionation/combination reactions involved: $k_6/k_5 = 0.14$ (8); $k_8/k_7 = 0.12$ (9); $k_9/k_7 = 0.03$ (9), and $k_{11}/k_{10} = 0.02$ (10). If C_2H_6 were formed only by reactions [6] and [8], and n-butane and 1-butene only by reactions [5] and [7], respectively, the ratio $C_2H_6/(n\text{-}C_4H_{10} + 1\text{-}C_4H_8)$ should have had a value between 0.14 and 0.12. In Table 2 it is seen that this ratio had an initial extrapolated value of 0.28, indicating an additional primary source of ethane. The combination of CH_3 radicals can be ruled out, since reaction [16] rather than [15] should be the predominant fate of CH_3 in the presence of excess C_2H_5 radicals, and the absence of C_3H_8 as a primary product shows that CH_3 was not a significant primary species. Reaction [13] in fact appears to be the most probable source of the extra primary C_2H_6; it can be shown that the required yield is compatible with estimates of the concentrations of H and C_2H_5 following the laser pulse, within the considerable uncertainties in the calculations.

The second ratio of interest included in Table 2 is (1-butene)^2/(n-butane)(1,3-butadiene), which should have a value of about 4 if these three products were formed by random combination of ethyl and vinyl radicals, reactions [5], [7], and [10]. The initial extrapolated value of this ratio is 5.3, and it rises to a value of 10.2 with increasing conversion. This rise is due to the sharp fall in 1,3-butadiene (Fig. 1), partly compensated by the decrease in 1-butene and the increase in n-butane. Given the uncertainties in the initial extrapolations, particularly for 1,3-butadiene, the initial extrapolated value of 5.3 is close enough to the expected value of 4 to support the conclusion that n-butane, 1-butene, and 1,3-butadiene were formed by radical combination.

Quantum yields of the primary photodissociation processes

If reactions [4] to [11] are assumed to account for all the primary products (i.e., neglecting C_2H_6 formation by reaction [13]), the quantum yields for reactions [1], [2], and [3] can be estimated from the following expressions:

$$\Phi(1) = \Phi(C_2H_2) - \Phi(2)$$

$$\Phi(2) = \tfrac{1}{2}\{2\Phi(n\text{-}C_4H_{10})(1 + k_6/k_5) + \Phi(1\text{-}C_4H_8)[1 + (k_8 + k_9)/k_7] - \Phi(3)\}$$

$$\Phi(3) = 2\Phi(1,3\text{-}C_4H_6)(1 + k_{11}/k_{10}) + \Phi(1\text{-}C_4H_8)[1 + (k_8 + k_9)/k_7]$$

It is seen that $\Phi(1)$ is given by the total yield of C_2H_2 minus that formed in reaction [2]; $\Phi(2)$ is equal to the total yield of C_2H_5 radicals (which in turn is a measure of the H atom yield), minus the H atoms formed in [3]; $\Phi(3)$ is given by the yield of C_2H_3 radicals found in the products. Values of these primary photodissociation quantum yields calculated in this way, using initial extrapolated product yields, are shown in Table 3.

If the formation of "extra" C_2H_6 noted earlier can be attributed to reaction [13], as seems probable, the quantum yield of this reaction should be added to $\Phi(2)$, and the value of $\Phi(1)$ should be reduced by a similar amount. These corrected values are also listed in Table 3.

Secondary processes

The variations in quantum yields with time evident in Table 1 and Figs. 1 and 2 occur at times when depletion of C_2H_4 is negligible, and must therefore arise from secondary reactions of products. The most striking variations are those of 1-butene and 1,3-butadiene, and their large absorption coefficients at 193 nm ($\sim$500 and $\sim10^4$ M^{-1} cm^{-1} respectively (11)) suggest that secondary photolysis was responsible for the observed decrease in yields. To test this hypothesis, the data were fitted to a simple expression, $\Phi = \Phi_0[1 - \exp(-KN)]/KN$, in which N = number of pulses and K is a constant, which corresponds to constant rate of formation of a product and its first-order loss by secondary photolysis. Best-fit calculated curves are compared with experiment in Fig. 3, and from the values of K and knowledge of the absorption coefficients and radiation fluence,

Can. J. Chem. Downloaded from www.nrcresearchpress.com by 194.225.253.170 on 09/07/12
For personal use only.

TABLE 3. Quantum yields of primary photodissociation processes in the photolysis of C_2H_4 at 193 nm and 760 Torr, based on initial extrapolated values

Quantum yield	Neglecting reaction [13]	Assuming extra C_2H_6 from reaction [13]
$\Phi(1)$	0.37	0.34
$\Phi(2)$	0.05	0.08
$\Phi(3)$	0.16	0.16
$\Phi(1 + 2 + 3)$	0.58	0.58

values for the required quantum yields of disappearance of 1-butene and 1,3-butadiene were found to be 0.31 and 0.15, respectively. These are reasonable values for an ethylene pressure of 760 Torr, as some collisional quenching has been observed with both molecules (12, 13). The deviation of the data for 1,3-butadiene above the curve at longer times is probably due to diffusion of product out of the laser beam, which did not fill the photolysis vessel.

The sharp increase with time of the minor products from initial yields close to zero, and the significant increases in the primary products, C_2H_6 and n-C_4H_{10}, are also probably largely the result of the secondary photolyses of 1-butene and 1,3-butadiene. The parallel increases in C_2H_6 and n-C_4H_{10} (Fig. 1) suggest a common cause, an increase in C_2H_5 radicals presumably caused in turn by an increased production of H atoms. The appearance of C_3H_8 indicates the presence of CH_3 radicals which combined with C_2H_5 (reaction [16]), and some of the CH_4 observed will have been formed in the accompanying disproportionation reaction, [17]. The yield of CH_4 is in fact higher than expected from this, and the balance may be a molecular product of a secondary photolysis or may be formed by abstraction of H from 1-butene by CH_3. Methyl radicals, H atoms, allyl radicals and allene are all known products of the photolysis of 1-butene (12), while CH_3 and perhaps H are also probably generated in the photolysis of 1,3-butadiene (13). Thus the secondary products C_3H_8, CH_4, and allene, and the secondary formation of C_2H_6 and C_4H_{10} can be accounted for. The secondary C_2H_6 is larger than expected from reaction [6]. In Table 2 are shown values of the secondary yields of n-C_4H_{10} and C_2H_6 obtained by subtracting the initial extrapolated values from the total yields. Also shown are yields of secondary C_2H_6 in excess of that expected from reaction [6] (i.e., (secondary C_2H_6) $-$ (k_6/k_5) (secondary C_4H_{10})), and finally are shown values of $(C_3H_8)^2/4C_4H_{10}$, which for statistical combination of C_2H_5 and CH_3 should be a measure of C_2H_6 expected from reaction [15]. It is clear that the secondary C_2H_6 cannot be accounted for by reactions [6] and [15]; some of the excess may come from reaction [12], and some may be formed by abstraction of H from 1-butene by ethyl radicals.

The minor product, propene, is not so easy to explain. Simple extrapolation of the data (Fig. 2) indicates a small primary yield of 0.005, but it is difficult to devise a plausible means for its formation as a primary product. It is possible that propene is entirely secondary (the dashed extrapolation in Fig. 2), with the curve bending over sharply with time due to secondary photolysis, which can be expected ($\epsilon_{193} = \sim 300\ M^{-1}\ cm^{-1}$ (11)); the resulting curve then reflects a balance between secondary formation and secondary destruction. The mechanism of formation is again not obvious. Propene is a known product of the photolysis of 1-butene, but it is formed there by

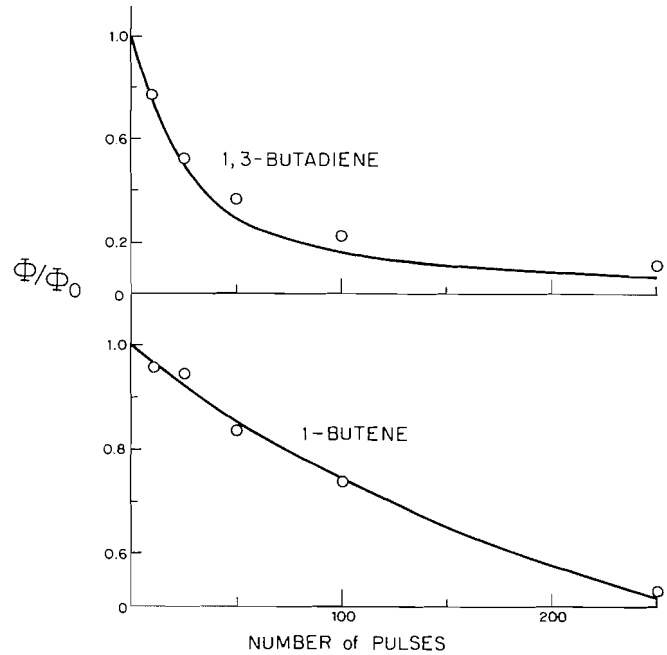


FIG. 3. The dependence of the quantum yields of 1,3-butadiene and 1-butene on number of pulses (i.e., photolysis time). Φ_0 is the initial extrapolated value at zero time. Curves are calculated, points measured; see text.

addition of H atoms to 1-butene followed by decomposition of a "hot" *sec*-butyl radical (12), a sequence of events doubly unlikely in the presence of 760 Torr of C_2H_4. A possible mechanism of formation is the reaction of electronically excited 1-butene and C_2H_4 to form a "hot" C_6H_{12} species which decomposes into 2 propenes via a sequence of two internal H-atom transfers, but further speculation is unwarranted.

The pressure dependence of the photolysis

Figures 4 and 5 show the quantum yields of the six most important products from a series of 10-pulse experiments with average incident energy per pulse of 29 ($\pm$2) mJ at C_2H_4 pressures from 50 to 3000 Torr. The quantum yield of C_2H_2 decreased from 0.47 at 50 Torr to 0.37 at 3000 Torr. That of 1-butene remained constant at 0.086, that of n-C_4H_{10} decreased from 0.082 to 0.067, while that of C_2H_6 increased from 0.037 to 0.059. The quantum yield of 1,3-butadiene increased while that of propene decreased markedly.

Values of the quantum yields of the three primary processes [1], [2], and [3] have been calculated as before, assuming that "extra" C_2H_6 was formed by reaction [13], and are shown in Fig. 6 as a function of C_2H_4 pressure. Reaction [1], the molecular elimination of H_2, is the main process at all pressures, although its yield declines slowly between 50 and 3000 Torr. Reaction [2] decreases while reaction [3] increases in the same pressure range. The observed decrease in the total quantum yield (Fig. 4) from a value of 0.58 at 50 Torr to 0.52 at 3000 Torr is almost entirely accounted for by the decrease in $\Phi(1)$ since the changes in $\Phi(2)$ and $\Phi(3)$ largely compensate one another. The observed decrease in $\Phi(C_2H_2)$ with pressure is thus attributable to the decreasing importance of both primary processes [1] and [2]. The decrease in process [2] and the compensating increase in [3] point to collisional stabilization of the vinyl radical as suggested previously (3, 14, 15) or possibly to vibrational de-excitation of a precursor. In the photolysis of ethylene at 185 nm, both Potzinger and co-workers (2) and

Can. J. Chem. Downloaded from www.nrcresearchpress.com by 194.225.253.170 on 09/07/12
For personal use only.

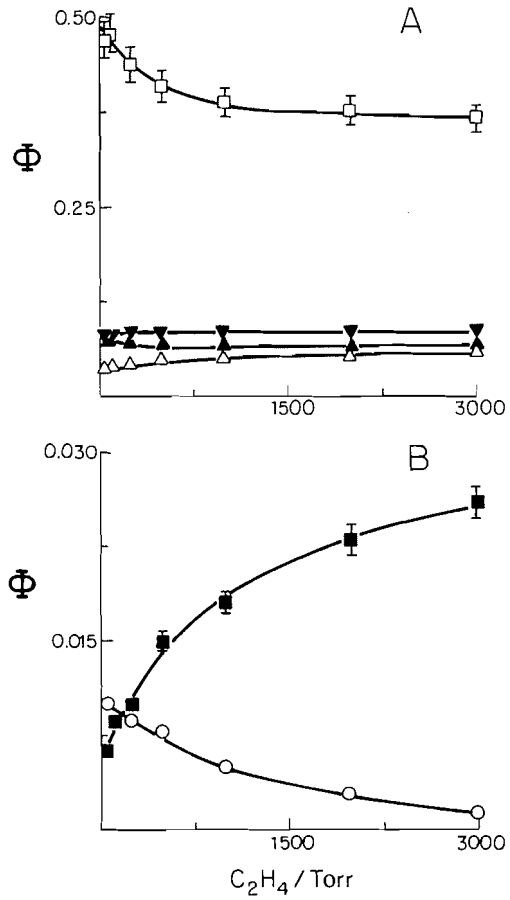


FIG. 4. Quantum yields of products from the photolysis of ethylene at 193 nm, vs. pressure of ethylene, measured at low conversions (10 pulses). Average incident pulse energy was 29 mJ. □ = acetylene; ▲ = *n*-butane; △ = ethane; ▼ = 1-butene; ■ = 1,3-butadiene; ○ = propene.

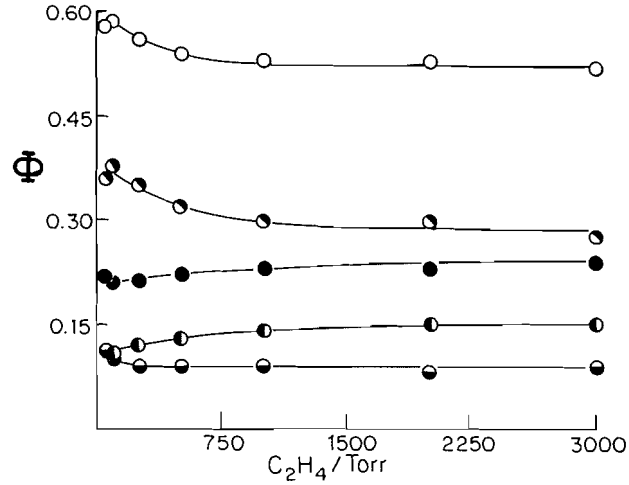


FIG. 5. Quantum yields of primary processes in the photolysis of ethylene at 193 nm, vs. pressure of ethylene. Based on data from Fig. 4. ○ = $\Phi_1 + \Phi_2 + \Phi_3$; ◔ = Φ_1; ● = $\Phi_1 + \Phi_2$; ◐ = Φ_3; ◒ = Φ_2.

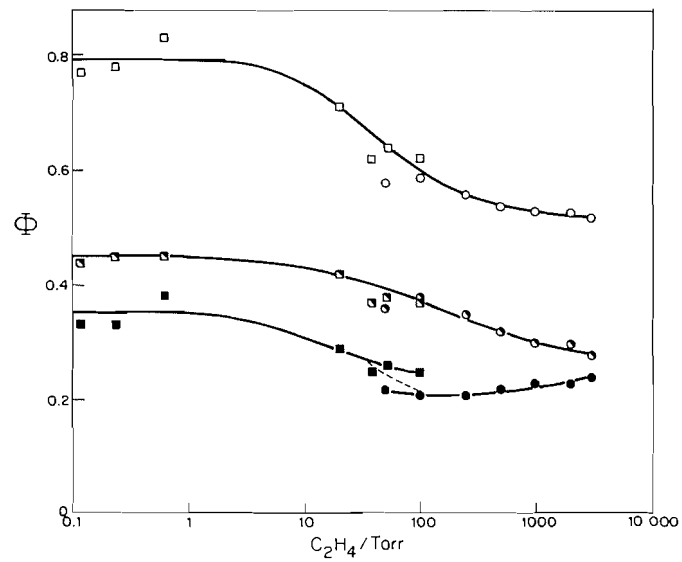


FIG. 6. Quantum yields of primary processes in the photolysis of ethylene. Squares are the data of Potzinger *et al.* at 185 nm (2); circles are the present work at 193 nm. Top curve = $\Phi_1 + \Phi_2 + \Phi_3$; middle curve = Φ_1; bottom curve = $\Phi_2 + \Phi_3$.

Borrell *et al.* (1) also observed a decrease in the acetylene quantum yield, and proposed collisional quenching of several different excited states of ethylene. A constant quantum yield of 1-butene was also reported by Potzinger *et al.* (2) at 185 nm between ethylene pressures of 0.1–100 Torr; they also found a decrease in $\Phi(n\text{-}C_4H_{10})$ from 0.24 to 0.18. The decrease in *n*-butane in the present work, and probably in the earlier studies, can be attributed to the decrease in process [2] and thence in the yield of H-atoms and C_2H_5 radicals. The increase in $\Phi(C_2H_6)$ is probably best explained by the enhancement of reaction [12] due to the higher concentrations of H· and C_2H_5· at higher pressures, and by increased stabilization of the C_2H_6* produced. The increasing trend in $\Phi(1,3\text{-}C_4H_6)$ can be attributed to increase in $\Phi(3)$ with increasing pressure.

Table 4 shows the ratios $C_2H_6/(n\text{-}C_4H_{10} + 1\text{-}C_4H_8)$ and $(1\text{-}C_4H_8)^2/(n\text{-}C_4H_{10})(1,3\text{-}C_4H_6)$, both as a function of pressure. As before, the first ratio exceeds 0.13, the value expected if ethane were all formed by disproportionation, and increases with increasing pressure, further evidence for an increase in reaction [12] with increasing pressure. The second ratio, which should be equal to about 4 for a random combination of ethyl and vinyl radicals, is appreciably larger. As before, this is probably due to loss by secondary photolysis of 1,3-butadiene, which was appreciable even at 10 pulses (Figs. 2 and 3). The decrease of this ratio with increasing pressure is probably due to collisional stabilization of the photo-excited butadiene and perhaps to some optical screening effects of the high pressure of C_2H_4.

Because the photon energies at 185 and 193 nm differ only by 27 kJ/mol, and because both wavelengths appear to excite cleanly into the V-state of C_2H_4, it is useful to compare the primary quantum yields obtained by Potzinger *et al.* at 185 nm (2) with the present results; this is done in Fig. 6. Within the experimental scatter, values of $\Phi(1)$ and $\Phi(2 + 3)$ at the two wavelengths can be reasonably well fitted by single smooth curves. The only major difference between the two sets of data appears in the ratio $\Phi(3)/\Phi(2)$ (Fig. 7); while this increased with increasing pressure at both wavelengths, its absolute value at 185 nm was smaller by a factor of about 5 at pressures from 50 to 100 Torr common to both studies. Some of this difference reflects a higher level of vibrational excitation of the vinyl radicals produced at 185 nm, and some can be attributed to loss of 1-butene and 1,3-butadiene (the latter was not observed at all)

Can. J. Chem. Downloaded from www.nrcresearchpress.com by 194.225.253.170 on 09/07/12
For personal use only.

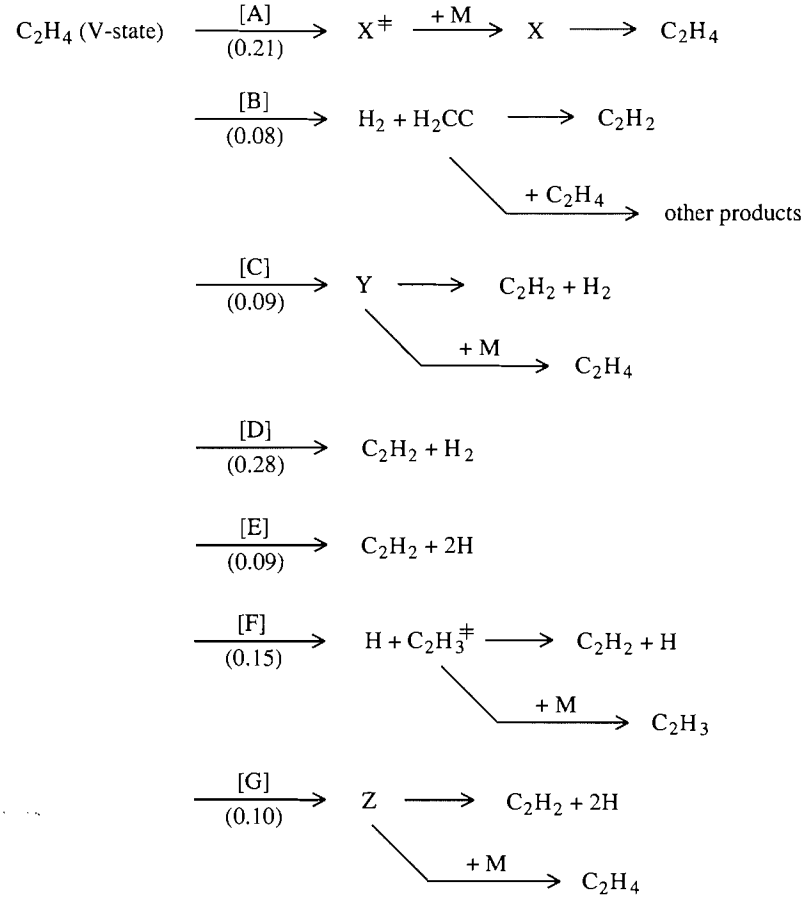
TABLE 4. Product ratios from the photolysis of ethylene at 193 nm with 10 laser pulses

Product ratio	Value when C_2H_4 pressure (Torr) =						
	50	100	250	500	1000	2000	3000
$C_2H_6/(n\text{-}C_4H_{10} + 1\text{-}C_4H_8)$	0.23	0.24	0.27	0.31	0.33	0.36	0.38
$(1\text{-}C_4H_8)^2/(n\text{-}C_4H_{10})(1,3\text{-}C_4H_6)$	13.0	11.0	10.8	7.2	6.3	4.9	4.4

at the higher conversions of the earlier work. The significant loss of these compounds by secondary photolysis (Figs. 1 and 2) sets in at times corresponding to less than 0.1% decomposition of C_2H_4.

The mechanism of the photodissociation

To account for the dependence of processes [1], [2], and [3] on wavelength and pressure, Potzinger *et al.* (2) proposed a scheme involving several excited states of C_2H_4. The present work extends the measurement of primary dissociation yields to higher pressures and to 193 nm, and a modified scheme to account for the combined results at 185 and 193 nm is suggested:



We assume that only the V-state is excited originally and that its lifetime is such that there is no collisional quenching at 3000 Torr, since the total quantum yield of dissociation remains constant from 1000 to 3000 Torr of C_2H_4. This implies a lifetime less than ~100 ps; in fact the diffuse character of the absorption spectrum indicates a lifetime at least 100 times shorter than this. Seven reaction channels [A] to [G] are postulated for the V-state, with quantum yields indicated in parentheses.

Reaction [A] is needed to account for the loss without product formation of about 20% of the molecules originally excited at 185 nm, even at a pressure as low as 0.12 Torr. This must involve a long-lived intermediate X^* that can be completely deactivated by collisions at this pressure and eventually reverts to ground state C_2H_4 with insufficient energy to decompose or react. There is no obvious candidate for X. The known behaviour of the triplet state and the vibrationally-excited ground-state in the mercury-photosensitized decomposition (16) rule these out. Ethylidene is an interesting possibility because of its heat of formation, estimated to be 324 and 279 kJ/mol above that of C_2H_4 for the singlet and triplet, respectively (17). If it were totally relaxed by collision before reverting to C_2H_4, its energy would be below an estimated threshold of ~350 kJ/mol for decomposition to $C_2H_2 + H_2$

Can. J. Chem. Downloaded from www.nrcresearchpress.com by 194.225.253.170 on 09/07/12
For personal use only.

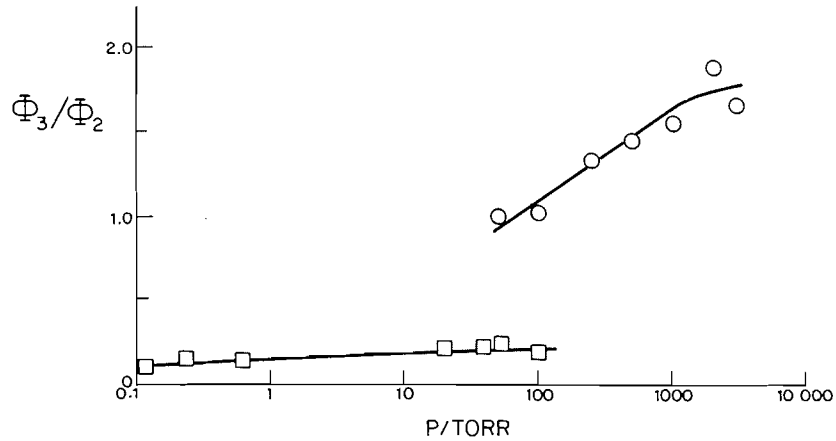


FIG. 7. The ratio of primary processes [3] and [2] in the photolysis of ethylene plotted against the log of ethylene pressure. □ = data of Potzinger *et al.* at 185 nm (2); ○ = present data at 193 nm.

(18). It is not clear, however, whether ethylidene is sufficiently unreactive towards C_2H_4 to permit such deactivation without reaction; the very small quantum yields of methylcyclopropane ($\leq 10^{-4}$) suggest that this may be so.

Reactions [B], [C], and [D] account for the formation of $C_2H_2 + H_2$ (process [1]), which has a complex pressure dependence. Potzinger *et al.* (2) found $\Phi(H_2)$ to be unaffected by pressure up to 100 Torr, but found $\Phi(1)$, based on hydrocarbon analysis, to decline from about 0.45 to 0.37 between 0.12 and 100 Torr (Fig. 6). It would be interesting to know whether this difference continued at higher pressure and at 193 nm, but the present experiments were not designed to measure H_2. Reaction [B] is suggested to account for this difference, since Laufer (19) showed that H_2CC, vinylidene, is an intermediate in the system and is relatively long-lived, and might be lost by reaction with C_2H_4; no products of such a reaction were observed in the present work, but yields would have been small and they may not have been detected in our analysis. The decline in $\Phi(1)$ with increasing pressure continues in our experiments, falling from about 0.37 at 50 Torr to 0.28 at our highest pressure (Figs. 5, 6). Stern–Volmer plots indicate two quenching processes, an efficient one (reaction [B]) at low pressure (<50 Torr) and a less efficient one between 50 and 100 Torr for which we suggest reaction [C] proceeding through an unspecified intermediate Y. The yield of process [1] of 0.28 unquenched at 3000 Torr we attribute to direct dissociation of the V-state, reaction [D].

Reactions [E], [F], and [G] are postulated to account for primary processes [2] and [3] and their pressure dependence. The formation of vibrationally "hot" vinyl radicals which decompose at low pressure but can be stabilized by collision was suggested in earlier photolysis studies (3, 14, 15). The present data indicate complete stabilization of $C_2H_3^{\ddagger}$ by about 2000 Torr, evident in the plot of $\Phi(3)$ in Fig. 5 which leads to $\Phi(F) = 0.15$, while $\Phi(E)$ is similarly given by the high-pressure limit of $\Phi(2)$, corresponding to direct formation of $C_2H_2 + 2H$. Reaction [G] is suggested to explain the decrease in $\Phi(2 + 3)$ from ~0.35 at low pressure to ~0.25 at 100 Torr; the decrease in fact occurred entirely in $\Phi(2)$ while $\Phi(3)$ remained constant. Values of $\Phi(2 + 3)$ in the present study lie slightly lower than the initial extrapolated values of Potzinger *et al.* (2). Reaction [G] requires the formation of an intermediate, Z, with a quantum yield of about 0.10 which is fully quenched at ~100 Torr and which can decompose to $C_2H_2 + 2H$ at low pressure. A lifetime of ~16 μs can be estimated for Z from a Stern–Volmer plot. The identity of Z is unknown, but the triplet state is a possible candidate; the vibrationally excited ground state is less likely, as some molecular dissociation to $C_2H_2 + H_2$ might be expected although perhaps Y and Z are in fact the same excited state, decomposing by two channels having different quenching probabilities.

Summary

The present work shows that the photochemistry of C_2H_4 excited to the V-state at 193 nm is well accounted for, as at shorter wavelengths, by three primary processes followed by simple reactions of H, C_2H_3, and C_2H_5. The pressure dependence confirms earlier conclusions that a surprisingly complex photodissociation mechanism underlies the photochemistry, involving several excited states and intermediates, a conclusion also reached in a recent review of the photolysis (6) and in a theoretical study (20) of the photodissociation.

Several points need experimental clarification. Careful measurements of quantum yields at low pressures, at both 185 and 193 nm, are needed to establish whether $\Phi(1 + 2 + 3)$ has indeed a low-pressure limit of about 0.8 as found at 185 nm, or whether it approaches unity, and thus whether reaction [A] is really required. Measurements of both H_2 and hydrocarbon products are also needed to determine whether the difference between $\Phi(1)$ and $\Phi(H_2)$ observed at 185 nm is real and if it persists at 193 nm and at higher pressures, and thus whether reaction [B] is needed. To be useful, these experiments demand accurate actinometry and must be done at very low conversions to avoid loss of 1-butene and 1,3-butadiene by secondary photolysis.

1. P. BORRELL, A. CERVENKA, and J. W. TURNER. J. Chem. Soc. B, 2293 (1971).
2. P. POTZINGER, L. C. GLASGOW, and G. VON BUNAU. Z. Naturforsch. **27a**, 628 (1972).
3. D. G. HOOPER, M. SIMON, and M. H. BACK. Can. J. Chem. **53**, 1237 (1975); M. SIMON and M. H. BACK. Can. J. Chem. **53**, 1245 (1975).
4. H. HARA and I. TANAKA. Bull. Chem. Soc. Jpn. **46**, 3012 (1973).
5. J. R. MCNESBY and H. OKABE. Adv. Photochem. **3**, 228 (1964).
6. G. J. COLLIN. Adv. Photochem. **14**, 136 (1988).
7. M. P. IRION. Beiträge zur Anwendung des ArF-Exiplex Lasers in der Photochemie. Max-Planck-Institut für Quantenoptik. 1981.
8. Handbook of bimolecular and termolecular gas reactions. CRC Press, Boca Raton. 1981. Vol. 2, Table 205.

Can. J. Chem. Downloaded from www.nrcresearchpress.com by 194.225.253.170 on 09/07/12
For personal use only.

9. D. G. L. JAMES and G. E. TROUGHTON. Trans. Faraday Soc. **62**, 145 (1966).
10. A. G. SHERWOOD and H. E. GUNNING. J. Phys. Chem. **69**, 2323 (1965).
11. L. C. JONES, JR. and L. W. TAYLOR. Anal. Chem. **27**, 228 (1955).
12. G. J. COLLIN and A. WIECKOWSKI. J. Photochem. **8**, 103 (1978).
13. R. D. DOEPKER. J. Phys. Chem. **72**, 4037 (1968).
14. R. A. BACK and D. W. L. GRIFFITHS. J. Chem. Phys. **46**, 4839 (1967).
15. H. HARA and I. TANAKA. Bull. Chem. Soc. Jpn. **47**, 1543 (1974).
16. R. J. CVETANOVIC. Prog. Reaction Kinet. **2**, 39 (1964).
17. B. T. LUKE, J. A. POPLE, M.-B. KROGH-JESPERSEN, Y. APELOIG, M. KARNI, J. CHANDRASEKHAR, and P. v. R. SCHLEYER. J. Am. Chem. Soc. **108**, 270 (1986).
18. S. W. BENSON and G. R. HAUGEN. J. Phys. Chem. **71**, 1735 (1971).
19. A. H. LAUFER. J. Photochem. **27**, 267 (1984); A. FAHR and A. H. LAUFER. J. Photochem. **34**, 261 (1986).
20. E. M. EVLETH and S. SEVIN. J. Am. Chem. Soc. **103**, 7414 (1981).

Can. J. Chem. Downloaded from www.nrcresearchpress.com by 194.225.253.170 on 09/07/12
For personal use only.

Thermal instability of germacrone: implications for gas chromatographic analysis of thermally unstable analytes

PAUL B. REICHARDT,[1] BARBARA J. ANDERSON, THOMAS P. CLAUSEN, AND L. CLARON HOSKINS
Department of Chemistry, University of Alaska, Fairbanks, AK 99775-0520, U.S.A.

Received October 3, 1988

PAUL B. REICHARDT, BARBARA J. ANDERSON, THOMAS P. CLAUSEN, and L. CLARON HOSKINS. Can. J. Chem. **67**, 1174 (1989).

The rearrangement of germacrone (**1**) to β-elemenone (**2**) is common during gas chromatographic (GC) analysis, with the conversion taking place in the injector port at temperatures above 250°C as well as on the column. While production of **2** in the injector is evident from the gas chromatographic trace, **2** produced from **1** during its migration down the column is difficult to detect because of the diffuse nature of the chromatographic peak produced by this process. A mathematical model and kinetic parameters ($A = (1.35 \pm 0.03) \times 10^{13}\,s^{-1}$; $E_a = 137 \pm 4\,kJ\,mol^{-1}$) determined from the reaction in solution can be used to estimate the degree of conversion of **1** to **2** for chromatographic runs (including temperature-programmed analyses). The results of these calculations verify that substantial amounts of **1** are converted to **2** under conditions that are commonly used for the analysis. The method for modeling thermally induced rearrangements in nonisothermal processes represents the first approach to quantitatively assessing their importance in GC analyses of thermally labile substances.

Key words: kinetics, gas chromatography, thermal rearrangement, germacrone, β-elemenone.

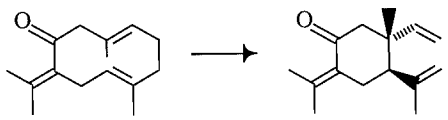
PAUL B. REICHARDT, BARBARA J. ANDERSON, THOMAS P. CLAUSEN et L. CLARON HOSKINS. Can. J. Chem. **67**, 1174 (1989).

La transposition de la germacrone (**1**) en β-élémènone (**2**) se produit régulièrement au cours d'analyses par chromatographie en phase gazeuse (CG); la conversion se produit tant dans l'injecteur, à des températures au-dessus de 250°C, que sur la colonne. Alors que la formation du composé **2** dans l'injecteur est évidente sur le chromatogramme, la formation du composé **2** à partir du composé **1** au cours de sa migration sur la colonne est plus difficile à détecter à cause de la nature diffuse du pic chromatographique qui résulte de ce processus. On peut utiliser une modèle mathématique et des paramètres cinétiques ($A = (1{,}35 \pm 0{,}03) \times 10^{13}\,s^{-1}$; $E_a = 137 \pm 4\,kJ/mol$) déterminés à partir de la réaction en solution pour évaluer le degré de conversion du composé **1** en **2** au cours de chromatographies (y compris des analyses avec une variation programmée de la température). Les résultats de ces calculs confirment que des quantités importantes du composé **1** sont transformées en **2** dans des conditions qui sont couramment utilisées pour l'analyse. La méthode développée pour faire un modèle des transpositions induites d'une façon thermique dans des processus qui ne sont pas isothermes représentes la première approche à une détermination quantitative de leur importance dans des analyses de CG de substances thermiquement labiles.

Mots clés : cinétique, chromatographie en phase gazeuse, transposition thermique, germacrone, β-élémènone.
[Traduit par la revue]

Can. J. Chem. Downloaded from www.nrcresearchpress.com by 194.225.253.170 on 09/07/12
For personal use only.

As part of a program designed to probe the chemical facets of plant defenses against herbivores, we require an analytical method for quantifying the volatile metabolites of Labrador tea (*Ledum groenlandicum*). Von Schantz and Hiltunen employed a gas chromatographic (GC) method for this purpose and found germacrone (**1**) to be a major component of the essential oil of this plant (1). Similar GC analyses of germacrone-containing essential oils of other plants have also been reported (e.g., refs. 2–7), but it is clear that the known propensity of **1** to thermally isomerize to β-elemenone (**2**; refs. 2, 8) poses problems for quantifying **1** by this method and casts doubt on the authenticity of reports (2, 4–7) of **2** as a metabolite of germacrone-containing plants.



1 **2**

Although **1** can be analyzed by high performance liquid chromatography (see below), normally it has been analyzed as only one of several volatile metabolites of a plant. Thus GC has been, and is likely to remain, the standard method for the analysis of **1**. Assessment of the validity of previous reports of the concentrations of **1** and **2** in plants as well as development of improved analytical methods require quantitative evaluation of the rearrangement of **1** to **2** during GC analysis.

The study reported here was initiated with two goals in mind. We desired to develop (1) a method that would provide the information needed to quantitatively interpret GC analyses of **1** and **2** in plant material and (2) a general kinetic technique for extracting quantitative information from GC analyses of thermally unstable substances.

Results and discussion

Our initial GC analyses of the steam distillable fraction of *Ledum groenlandicum* confirmed the previous finding that **1** is the major volatile metabolite of this species (1), but they also indicated the presence of **2** and exhibited a "hump" in the baseline between the retention times for **1** and **2** (Fig. 1).

HPLC analysis of the steam distillate revealed the presence of **1** but no detectable **2**, implying that **2** detected by GC is entirely an artifact. The sharpness of the β-elemenone GC peak suggested that it was generated in the injection port (high temperature and short residence time). This idea was supported by analyses of purified **1** in which column conditions were held constant but the injector temperature varied (Fig. 2).

Varying the column temperature, flow rate, or temperature program altered the relative size of the "hump" in GC traces of **1** (Fig. 1b; Table 1). From these results it is clear that increased

[1]Author to whom correspondence may be addressed.

Printed in Canada / Imprimé au Canada

Can. J. Chem. Downloaded from www.nrcresearchpress.com by 194.225.253.170 on 09/07/12
For personal use only.

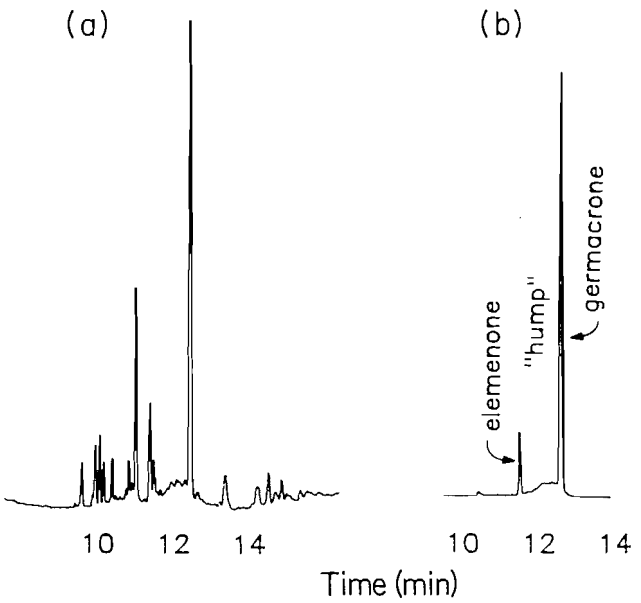


FIG. 1. Gas chromatographic traces of (a) *L. groenlandicum* steam distillate and (b) pure **1**.

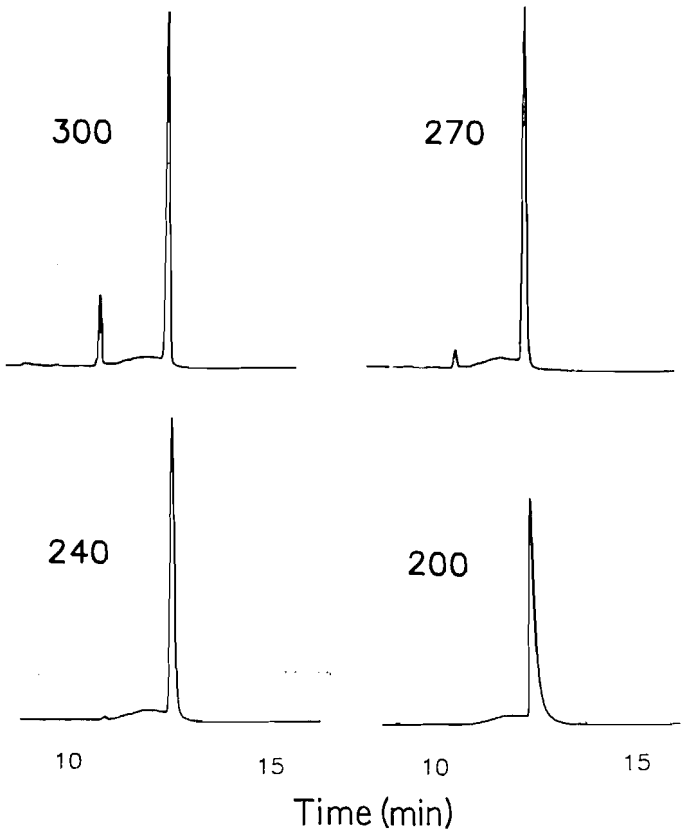


FIG. 2. Effect of injection port temperature on gas chromatographic trace of pure **1**. Injection port temperatures (°C) are given for each trace.

retention times and higher column temperatures lead to greater relative areas of the hump, as would be expected if **2** were produced from **1** *during migration through the column*.

To verify that both the β-elemenone peak and hump are artifacts of the analytical method and to calculate the amounts of **1** that were actually in the samples before injection into the GC,

TABLE 1. Observed and calculated effects of GC program on conversion of **1** to **2** on-column

GC conditions	Retention time of **1** (min)	Observed %**1***	Calculated %**1**
A	15.5	78	54
B	14.9	69	39
C	12.4	74	55
D	11.0	86	70

*Observed %**1** = $(A_G \times 100)/(A_G + A_H)$ where A_G and A_H are, respectively, the areas of the germacrone peak and the hump. A. Standard (see Experimental). B. Standard modified by upper temperature limit of first programmed step = 200°C. C. Standard modified by starting temperature held at 100°C for 2 min. D. Same as C except flow rate = 9.0 mL/min.

TABLE 2. Rate data for conversion of **1** to **2** (Mean ± 1 SD, $N = 3$)

Temperature (°C)	$k \times 10^3$ (min^{-1})
141.1	4.64±0.14
151.1	11.4 ±0.1
161.9	30.8 ±1.2

we conducted a kinetic analysis of the conversion of **1** to **2**. Over the temperature range 140–160°C, in bis(2-ethoxyethyl) ether, **1** converted to **2** with clean first-order kinetics. No products other than **2** were chromatographically detected (HPLC, GC), although minor decomposition was visually apparent (darkening) in some samples. Analyses at three half-lives indicated that **1** and **2** accounted for more than 90% of **1** originally in the sample. At ten half-lives the sample contained no detectable **1**, suggesting the conversion of **1** to **2** is irreversible (8).

Standard treatment of the kinetic data (Table 2) gave $E_a = 137 \pm 4\,kJ\,mol^{-1}$ and $A = (1.35 \pm 0.03) \times 10^{13}\,s^{-1}$, values that are similar to those determined for other Cope rearrangements (9).

These parameters and eq. [1] can be used to calculate the concentration (C) of **1** experiencing first-order decomposition

$$[1] \quad \frac{dC}{C} = -k\,dt = -A \exp(-E_a/RT)\,dt$$

to **2** at temperature T. However, eq. [1] must be modified for modeling the conversion during periods of temperature variation (temperature-programmed GC analysis, for example). As temperature rises at a constant rate, the temperature (T) at any time (t) can be expressed as $T = T_0 + rt$, where T_0 is the initial temperature and r is the temperature ramp rate (K/s). Substituting this relation into eq. [1] and integrating from a concentration C_0 to a final concentration C_f at time t_f yields

$$[2] \quad \ln \frac{C_f}{C_0} = -A \int_0^{t_f} \exp\{-E_a/[R(T_0 + rt)]\}\,dt$$

If we define $u = E_a/[R(T_0 + rt)]$, then eq. [2] can be transformed to

$$[3] \quad \ln \frac{C_f}{C_0} = \frac{AE_a}{Rr} \int_{u_0}^{u_f} e^{-u} u^2\,du$$

where $u_0 = E_a/RT_0$ and $u_f = E_a/RT_f$. The integral in eq. [3] can be evaluated using series or by numerical integration.

For computational purposes we chose to evaluate eq. [2] as

$$[4] \quad \ln \frac{C_f}{C_0} = -\tau A \sum_{i=0}^{n-1} e^{-E_a/RT_i}$$

where C_f = concentration of analyte at end of GC run; C_0 = concentration of analyte at beginning of GC run; τ = time increment per calculation; T_0 = initial temperature (K) of GC run; $T_i = T_0 + i\tau r$; r = temperature ramp rate (K/s); n = total time of GC run $\times \tau^{-1}$.

The activation parameters determined in solution can be used to model the conversion of **1** to **2** at any temperature, and eq. [4] can be used to model the conversion during a period of regular temperature change. The method can be applied to temperature-programmed GC analyses if one assumes the reactions in the gas phase and the GC stationary phase have the same activation parameters as the reaction in bis(2-ethoxyethyl) ether.

Attempts to use eq. [1] to calculate the degree of conversion of **1** to **2** in the injection port were thwarted by our inability to estimate a residence time. The problem is that the flow rate in the injector cannot be approximated due to the pressure rise associated with rapid solvent evaporation (T. Brown, personal communication). However, calculated $t_{1/2}$'s of 30 μs for the conversion at 300°C and 6 s at 200°C are consistent with the effect of injector temperature on the relative size of the β-elemenone peak (Fig. 2).

Using time increments (τ) of about 6 s and the temperature/time relationships defined by the GC temperature programs allowed calculation (eq. [4]) of the percent on-column conversion of **1** to **2** expected for several GC analyses (Table 1). The model makes only moderately good quantitative predictions about on-column conversions, presumably due to effects of the media on reaction rates (10) or small errors in the value of E_a. However, the calculations verify that the hump in the chromatographic traces can result from on-column conversion of **1** to **2** and that the fraction of **1** reaching the detector can be approximated by our model.

The value of this kinetic approach to modeling thermally induced reactions can be exemplified by its application to two long-standing problems in germacrone analysis. First, the kinetic parameters reported here indicate that at least trace quantities of **2** can be produced from **1** during steam distillation (about 2 h are calculated to be required for conversion of 1% of **1** to **2** at 100°C). Secondly, the method can be used to assess the validity of GC-based literature reports of **1** and **2** as natural products. Examination of several such reports indicates that generally the injection port temperatures used (e.g., refs. 1 and 4) are not high enough to cause substantial production of **2** from **1**, although in some cases this may be a problem (2). However, it does appear that typical GC conditions for analyzing germacrone-containing essential oils (e.g., refs. 1, 2, 4, 5, and 7) can result in significant underestimation of the concentration of **1** due to on-column conversion of **1** to **2** (Table 1). Conclusive statements about individual reports are not possible because authors have not given retention times and operating conditions in enough detail to mathematically model the analyses.

The method described here suggests a useful approach to modeling a reaction under nonisothermal conditions if appropriate kinetic parameters are known. Its application to GC analyses allows distinction between transformations that occur in the injector and on-column, and it provides an estimate of the extent of on-column transformation. It can be used to evaluate the reliability of analyses that have already been conducted and as a predictive tool for developing GC conditions for new analyses.

Experimental

Gas chromatographic analyses were conducted on a Perkin Elmer 8410 gas chromatograph equipped with a 30 m × 0.53 mm bonded FSOT RSL-200 column (Alltech). Unless otherwise specified the injector and detector were held at 300°C, the He flow rate was 6.0 mL/min, and the temperature program was 60°C for 1 min, 60–180°C at 10°/min, 180°C for 5 min, 180–260°C at 30°/min. HPLC analyses were conducted on a 4.6 mm × 25 cm silica gel column (5 μm) eluted with hexane–ether (95:5) at a rate of 2 mL/min and detection by UV at 255 nm. HPLC data collection and processing were accomplished using Chromatochart software.

The nmr spectra ($CDCl_3$ solvent) were recorded on a JEOL FX-90Q instrument.

*Isolation of germacrone (**1**)*

Ledum groenlandicum steam distillate (1.8 g) was separated by silica gel flash chromatography (11) using dichloromethane – petroleum ether (55:45) solvent. Fractions that appeared to be pure **1** by TLC (silica gel, dichloromethane) were combined (0.69 g) and the solid residue recrystallized from ethanol (−20°C) to give **1** (0.36 g); mp 54–56°C (lit. (12) mp 54–55°C); ^1H and ^{13}C nmr spectra were identical to those previously reported for **1** (12).

*Preparation of β-elemenone (**2**)*

1 (26 mg) was sealed in an ampoule under a nitrogen atmosphere and heated at 200°C for 3 h. The light brown reaction product was chromatographed using the system described above to give purified **2** (20 mg; oil) with an ^1H nmr spectrum identical to that reported for **2** (13).

Kinetics

Ampoules were charged with 100 μL of a bis(2-ethoxyethyl) ether solution of **1** (6.0 mg/mL) and fluoranthene (0.39 mg/mL; internal standard). Ampoules were sealed and immersed in a thermostated (±0.1°C) silicone oil bath. The temperature of each kinetics run was monitored with a calibrated thermometer (0.1°C). Ampoules were periodically removed, immersed in an ice water bath, and stored at −20°C until analysis. At least 12 ampoules removed over three half-lives were utilized for each kinetics run.

The contents of each ampoule were diluted with 1.0 mL of bis(2-ethoxyethyl) ether and analyzed by HPLC. The ratio of fluoranthene to germacrone peak areas was utilized to quantify the disappearance of **1**, and a first-order kinetics program (CONINFIN) was used to calculate rate constants.

Calculations of expected germacrone isomerization during GC analysis

Equation [1] was evaluated for several GC runs using a program written for an Apple II^+ computer. Each run was modeled by selecting successively smaller time increments (τ) until the calculated percentage rearrangement of **1** no longer responded to the magnitude of τ. Given the amount of **1** reaching the detector and the temperature/time profile in the GC run, the program calculates the amount of **1** that exited the injector.

Acknowledgements

We thank the National Science Foundation for support of this research (BSR-8500160) and for providing matching funds for purchase of the nmr spectrometer (BBS-8614587).

1. M. Von Schantz and R. Hiltunen. Sci. Pharm. **39**, 137 (1971).
2. R. P. Doss, W. H. Hatheway, and B. F. Hrutfiord. Phytochemistry, **25**, 1637 (1986).
3. I. Ognyanov and D. Ivanov. Recent Dev. Chem. Nat. Carbon Compd. **2**, 49 (1967).
4. D. H. E. Tattje and R. Bos. Pharm. Weekbl. **109**, 1189 (1974).

Can. J. Chem. Downloaded from www.nrcresearchpress.com by 194.225.253.170 on 09/07/12
For personal use only.

5. D. H. E. TATTJE and R. BOS. Planta Med. **41**, 303 (1981).
6. Y. NAYA, Y. NAGAHAMA, and M. KOTAKE. Heterocycles, **10**, 29 (1978).
7. S. SATAR. Pharmazie, **40**, 432 (1985).
8. E. TALMAN, P. E. J. VERWIEL, and A. C. LAKWIJK. *In* Advances in Mass Spectrometry in Biochemistry and Medicine. Vol. 2. *Edited by* A. Frigerio. Spectrum Publications, New York. 1976. Chap. 17.
9. G. G. SMITH and F. W. KELLEY. Prog. Phys. Org. Chem. **9**, 153 (1971).
10. K. J. LAIDLER. Chemical kinetics. 2nd ed. McGraw-Hill, New York. 1965. pp. 199–204.
11. W. C. STILL, M. KAHN, and A. MITRA. J. Org. Chem. **43**, 2923 (1978).
12. C. GANTER and B. KELLER-WOJTKIEWICZ. Helv. Chim. Acta, **54**, 183 (1971).
13. T. TAKAHASHI, K. KITAMURA, H. NEMOTO, and J. TSUJI. Tetrahedron Lett. **24**, 3489 (1983).

Can. J. Chem. Downloaded from www.nrcresearchpress.com by 194.225.253.170 on 09/07/12
For personal use only.

Characterization of thermal modulation of electrical conductivity: a small volume absorbance measurement technique

ROBERT MCLAREN AND NORMAN J. DOVICHI[1]
Department of Chemistry, University of Alberta, Edmonton, Alta., Canada T6G 2G2

Received December 21, 1988

ROBERT MCLAREN and NORMAN J. DOVICHI. Can. J. Chem. **67**, 1178 (1989).

Laser-induced thermal modulation of electrical conductivity is a new photothermal method for the measurement of minute absorbance in sub-nanoliter liquid samples. In this paper, a model is presented for the technique. This model is based upon the interaction of a Gaussian laser beam with a cylindrical, homogeneous electrolytic resistor. Particularly simple results are produced if the laser beam spot size is much smaller than the diameter of the electrodes. The theory is verified with respect to the electrode spacing and to the laser power, spot size, and chopping frequency; the highest sensitivity occurs with low chopping frequency, high laser power, and small electrode spacing. The signal is independent of laser spot size, as long as the beam does not illuminate the electrode surface. The precision of the measurement is dominated by shot noise in the current flow through the electrolytic resistor. One point absorbance detection limits of 5.5×10^{-6} measured across the 76-μm diameter electrode wires are obtained in aqueous solution with a 5-mW helium–neon laser. With this instrument, the difference in the absorbance of water and deuterated water is easily determined at 632.8 nm.

Key words: thermal modulation of electrical conductivity.

ROBERT MCLAREN et NORMAN J. DOVICHI. Can. J. Chem. **67**, 1178 (1989).

La modulation thermique induite au laser de la conductivité électrique est une nouvelle méthode photothermique permettant de mesurer de très faibles absorbances dans des échantillons liquides de volumes plus faibles que le nanolitre. Dans ce travail, on présente un modèle pour cette technique. Ce modèle est basé sur l'interaction d'un faisceau gaussien de laser avec une résistance électrolytique homogène et cylindrique. On obtient des résultats particulièrement simples si la grosseur du rayon laser est beaucoup plus petite que le diamètre des électrodes. La théorie se vérifie par rapport à l'espacement entre les électrodes, à la puissance et à la grosseur du rayon laser et à la fréquence de modulation; la meilleure sensibilité est obtenue avec une faible fréquence de modulation, une grande puissance du rayon laser et un faible espacement entre les électrodes. En autant que le rayon n'illumine pas la surface de l'électrode, le signal est indépendant de la grosseur du rayon laser. La précision des mesures est dominée par le bruit de fond dans le flot de courant à travers la résistance électrolytique. Opérant en solution aqueuse, avec un laser d'hélium-néon de 5-mW, on a obtenu des limites de détection de $5{,}5 \times 10^{-4}$ pour des mesures faites à travers des fils d'électrodes d'un diamètre de 76-μm. Avec cet instrument on peut facilement mesurer la différence d'absorbance de l'eau et de l'eau lourde, à 632,8 nm.

Mots clés : la modulation thermique de la conductivité électrique.

[Traduit par la revue]

Introduction

Photothermal techniques produce high sensitivity absorbance determination by measurement of the heat deposited within a sample following absorbance of light. This heat may be detected directly with a liquid helium cooled bolometer in molecular beam experiments (1) or the heat may be detected indirectly as a temperature rise with a thermocouple (2), as a pressure wave with a piezoelectric or microphonic transducer (3), as a variation in electron capture cross-section for gaseous samples (4), or as a refractive index disturbance with the variety of thermo-optical techniques (5). The latter class of thermo-optical techniques probably is the best developed analytical photothermal method for absorbance determination of liquid samples. In all cases, because the heat deposited within the sample following absorbance is directly proportional to the excitation energy, the absorbance of dilute and highly transparent materials may be measured by use of a high energy or high intensity light source.

Recently, we presented a preliminary report of a photothermal technique based upon the change in electrical conductivity with the temperature of an ionic solution (6). The principle of the measurement is rather simple. Small changes in the temperature of a volume of solution will result in relatively large changes in the viscosity of the solution because of the high thermal coefficient of viscosity for most liquids. The change in viscosity can be conveniently monitored by measuring the conductance of the solution because of the inverse relationship between conductance and viscosity. In this paper, the conductance is measured by employing miniature, 76-μm diameter platinum electrodes that define the geometry for a small volume electrolytic resistor. A modulated laser beam intersects the electrolytic resistor. When an absorbing analyte is present and the beam is on, the temperature increases, causing a decrease in the viscosity of the solution and an increase in the current through the electrolytic resistor. When the beam is off, the solution cools and the current decreases. The current (or conductivity) signal can be demodulated at the chopping frequency of the laser by a lock-in amplifier. The amplitude of the demodulated signal is proportional to the absorbance of the solution whereas the phase is related to thermal diffusion within the sample.

Small volume absorbance measurements are of importance in a number of technological fields, including detection for the chromatographic and electrophoretic analysis of biological materials. Although a number of thermo-optical techniques have been developed for small volume absorbance determinations (7), the thermally modulated electrical conductivity (TMEC) technique appears to offer the greatest promise for analysis of aqueous samples.

Theory

The coordinate system used in the model is shown in Fig. 1. A laser beam, aligned along the Z axis of a Cartesian system, intersects the cylindrical electrolytic resistor centered on the X axis and defined by the radius of the electrode, r, and the

[1]To whom correspondence should be addressed.

Can. J. Chem. Downloaded from www.nrcresearchpress.com by 194.225.253.170 on 09/07/12
For personal use only.

Can. J. Chem. Downloaded from www.nrcresearchpress.com by 194.225.253.170 on 09/07/12
For personal use only.

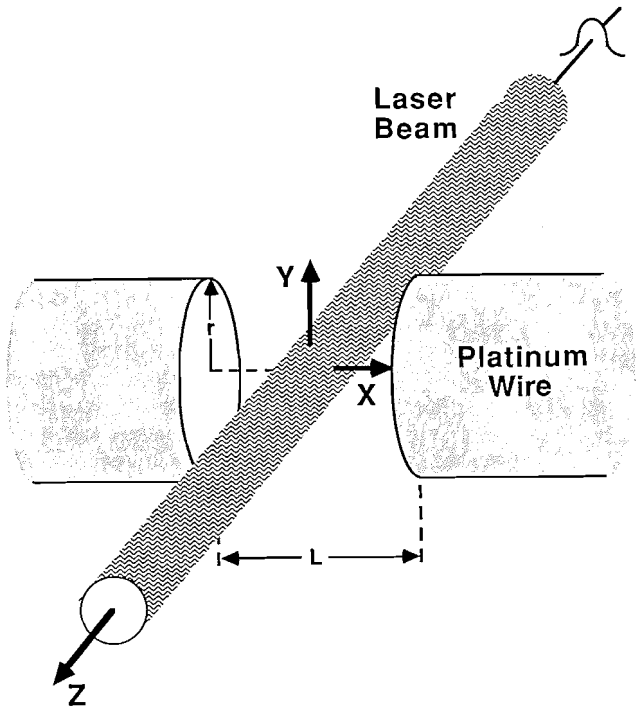


FIG. 1. Interaction of the beam with a cylindrical electrolytic resistor.

distance between the electrodes, L. Normally, the beam is aligned to intersect the center of the resistor. The change in current as a function of time following a pulse of light has been derived in Appendix 1. This impulse response function may be simplified greatly if the laser beam spot size is much smaller than the radius of the wire. In this case, the impulse function takes on a simple form

$$[1] \quad \Delta I_{\text{impulse}} \begin{bmatrix} \text{small spot} \\ \text{limit} \end{bmatrix} = \frac{2.303 E \epsilon C I}{\pi r L} \left[\frac{-1}{\rho C_p \eta} \frac{d\eta}{dT} \right]$$

where E is the energy of the laser pulse, ϵ is the molar absorptivity of the analyte, C is analyte concentration, and I is the average current passing through the resistor. The term in brackets is the solvent constant that is a function of the solvent density ρ, heat capacity C_p, viscosity η, and the derivative of the viscosity with respect to temperature $d\eta/dT$. The solvent constant, Table 1, changes by about a factor of three for the different solvents listed (5, 8–10). Interestingly, water has a solvent constant which is within a factor of two of the best solvent listed, ethanol. Of course, the low dielectric constant of most organic liquids presents difficulty in preparation of high ionic strength solutions required for high precision measurements.

The small spot size limit of the impulse response function is quite remarkable. The signal is predicted to be independent of time, undergoing no decay. Time independence results because the thermally modulated electrical conductivity signal is a function of the average temperature rise in the volume between the electrodes. A decay in the impulse signal will occur only when the thermal energy diffuses to the bulk solution or to some other heat sink. Assuming that the radius of the wire is less than the separation between the electrodes, the thermal decay is characterized by a diffusion time

$$[2] \quad t_{\text{diffusion}} \approx \frac{r^2}{D}$$

TABLE 1. Physical constants of solvents[a]

Solvent	Density (g/mL)	Heat capacity (J/g °C)	Viscosity η (cP)	$d\eta/dT$ (cP/°C)	$10^3 \times$ Solvent constant[b] (mL/J)
Water	0.998	4.18	1.002	−0.0245	5.86
Methanol	0.791	2.46	0.597	−0.0076	6.54
Ethanol	0.789	2.36	1.200	−0.0232	10.4
Acetonitrile	0.786	2.17	0.360	−0.0030	4.89
Acetone	0.790	2.18	0.326	−0.0021	3.74

[a]All constants are at 20°C. Obtained from refs. 5, 8–10.
[b]The solvent constant = $(-\eta\rho C_p)^{-1}\, d\eta/dT$.

where the thermal diffusivity of the solution, D, is given by

$$[3] \quad D = \frac{k}{C_p \rho}$$

where k is the thermal conductivity of the solution. For time shorter than the diffusion time, no decay in the impulse signal is predicted. Also, the signal is predicted to be independent of the laser beam spot size. This observation is understandable, given the dependence of the signal on the thermal energy contained between the electrodes. The signal is predicted to be inversely related to the radius of the electrode, r, and the electrode spacing, L. The former observation arises because the average temperature rise of the solution will depend inversely upon the volume of the electrolytic resistor; an inverse second power dependence is not observed because the laser beam crosses perpendicular to the electrolytic resistor. Integration over the beam path results in the observed inverse first power dependence on the wire radius. The inverse dependence of the signal upon both the wire radius and the electrode spacing is important for application of this technique to small volume absorbance determinations; the signal increases as the sample volume decreases, essentially because the thermal energy is contained within a smaller sample volume.

To obtain the change in current passing through the electrode for an arbitrary excitation waveform, it is necessary to convolute the impulse response function with the appropriate excitation function. For example, the current response obtained at time t after the start of a step excitation by a light source of power P is simply given by

$$[4] \quad \Delta I_{\text{step}} \begin{bmatrix} \text{small spot} \\ \text{limit} \end{bmatrix} = \frac{2.303 P \epsilon C I}{\pi r L} \left[\frac{-1}{\rho C_p \eta} \frac{d\eta}{dT} \right] t$$

The current change is expected to increase linearly with time following illumination with a continuous wave light source. Again, the approximation will be valid for time less than $t_{\text{diffusion}}$.

Experimental

Figure 2 presents a block diagram of the cell used to characterize the technique. The electrodes were constructed by drawing glass tubing over 76-μm diameter platinum wire. The finished electrodes had an outer diameter of 530 (±10) μm. The ends of the electrodes were polished progressively using coarse polishing cloth, 6 μm diamond polishing compound, 3 μm alumina, and finally 1 μm alumina. The cell was machined from a Teflon block with an inner chamber volume of ca. 0.3 mL. A "V" groove was cut across the front of the block in which the electrodes could sit to a depth such that they remained flush with the front face of the block. A quartz window presses firmly against the front of the block and is held in place by a thick Teflon ring. The laser beam enters the cell through the front window and

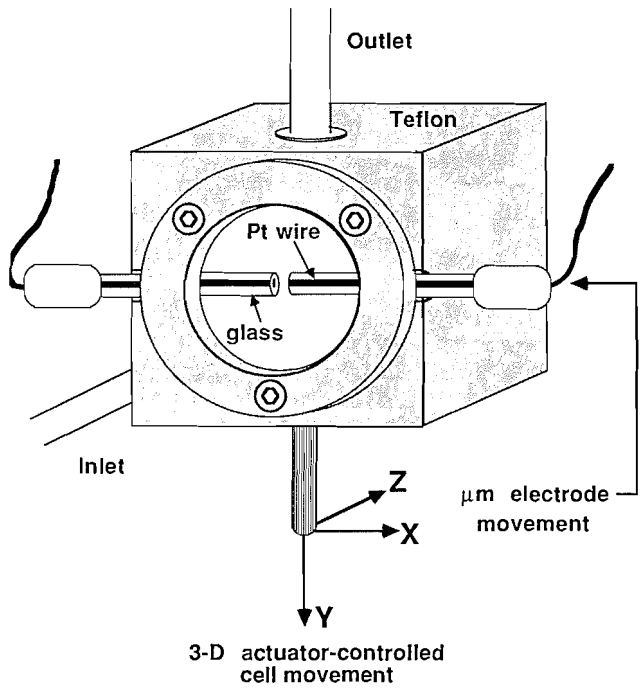


FIG. 2. Diagram of the cell used for characterization of TMEC.

exits through a second window at the back of the cell. The distance the beam travels in solution before it passes the electrode central axis is about 265 μm. One of the electrodes is held stationary while the other is driven along its axis using a translation stage-micrometer assembly. In this way the electrode spacing could be varied accurately while maintaining the platinum faces of the electrodes directly opposite each other in a parallel plate configuration. The entire cell–electrode assembly was mounted on translation stages for movement in three dimensions by computer controlled actuators.

The conductance of the solution between the electrodes is measured using an ac method. The electronics used are similar to those described previously (6). Briefly, a 40 kHz frequency carrier wave is applied to the electrodes. The ac current passing through the cell is amplified, half-wave rectified and smoothed using a four pole low-pass active filter with 300 Hz cutoff frequency. The resultant dc signal is linear with the conductivity of the solution for cell impedances of >10 kΩ; for typical solutions and electrode spacing, the cell impedance was greater than 100 kΩ. It was found that, with the present electrode configuration, a carrier wave frequency of 40 kHz was needed in order to minimize the impedance due to double layer capacitance; the system acts as a high pass filter with a cut-on frequency of about 10 kHz. In addition, there are three parallel capacitive impedances that should be made as large as possible in order to reduce any non-electrolytic current flow (11). They are (*i*) cell capacitance, (*ii*) contact and lead capacitance, and (*iii*) physical electrode capacitance (due to the parallel plate configuration). The cell capacitance was minimized by grounding the metal inlet and outlet ports of the cell. The contact and lead capacitance was reduced by careful construction. The physical electrode capacitance is dependent on the dielectric material and the electrode dimensions. In total, the current flow due to all three of these capacitances was typically <10% of the electrolytic current flow. This value would be unacceptable for an absolute conductance measurement but is quite acceptable for the differential measurement of conductance in this photothermal technique.

A block diagram of the experiment is presented in Fig. 3. A 5 mW, linearly polarized He–Ne laser beam (632.8 nm) passes through an optical chopper. Mirrors are used to manipulate the beam through a 2-mm diameter aperture that acts to reduce stray light. A 10×, 16 mm focal length lens focuses the beam to a small spot between the electrodes in the cell. The light exiting the cell strikes a photocell that generates a reference signal for the two-channel lock-in amplifier. The conductivity circuit described above provides the signal for the lock-in amplifier. The lock-in measures both the amplitude and phase of the thermally modulated conductivity signal simultaneously.

For the purpose of beam positioning and for generating X–Y scans, an 855C Newport programmable controller and actuators were used to control the movements of the cell with respect to the laser beam. The controller is capable of 0.1 μm movements although such resolution was not needed in this application. A computer was used to communicate with the controller and to store data from the lock-in as incremental movements were made.

Chemicals

Aqueous solutions were typically 0.01 *M* NaCl. Fast Green FCF dye (Aldrich, 96%), which has a strong absorbance at the He–Ne wavelength, was used for the experiments without further purification. The visible spectrum of the dye was recorded in water as a function of its concentration, NaCl concentration, and pH with a HP 8451A diode array spectrophotometer. A 0.01 *M* salt concentration was found not to have any effect on the spectrum. The dye behaves as an acid–base indicator, changing from violet in strongly alkaline solutions, to aqua in neutral solutions, to green in acidic solutions. The spectrum is relatively constant as the concentration of the dye is increased in neutral solutions up until about 10^{-5} *M*. Above this concentration, the intensity of the main α band centered at 624 nm starts to decrease in intensity. This decrease in intensity is not due to a change in pH that occurs as the dye concentration is increased but instead appears to be due to aggregation of the dye molecules (12).

Results and discussion

The cell–electrode arrangement was first characterized with respect to conductivity detection. For a 0.01 *M* NaCl solution, the current through the cell was measured for various electrode separations. As expected, the current was found to be inversely proportional to the electrode separation ($R = 0.998$, $n = 15$) in the range of 40 to 3000 μm at a constant applied voltage. A small positive intercept was observed in the data that is attributable to the parallel capacitances mentioned previously. The current through the cell was also found to be linear with the applied voltage ($R = 0.9991$, $n = 12$) in the range of 0 to 3 V rms. Above this voltage, resistive heating of the solution between the electrodes led to positive curvature. The upper limit to the voltage that may be applied to the electrodes is determined by the effects of resistive heating. Heating of the solution between the electrodes could result in convection currents, which would presumably lead to additional noise in the system; the current was found to be more stable over a long period of time with lower applied voltages. For this reason, voltages of less than 1 V rms were used for most subsequent experiments.

Two sources of modulated electrical conductivity are expected: that due to absorbance of the sample and that associated with stray light which illuminates the electrodes. To characterize the latter signal, the thermally modulated electrical conductivity signal was measured as the laser beam was moved with respect to the cell. Figure 4 shows the lock-in amplitude as a function of position near the electrodes in the X–Y plane of Fig. 1, using a blank solution and a chopping frequency of 200 Hz. Individual pixels in the plot are 10 μm on a side. An image of the wire is observed as two hills separated by a valley of weakly absorbing blank solution. The signal drops off quite quickly as the laser spot moves along the wire away from the resistor region. Because the resistance of the wire is negligible in comparison to that of the electrolytic resistor, it appears that the background signal associated with the illuminated wire arises as heat diffuses through the wire to the solution within the electrolytic resistor volume. As the laser beam illuminates

Can. J. Chem. Downloaded from www.nrcresearchpress.com by 194.225.253.170 on 09/07/12
For personal use only.

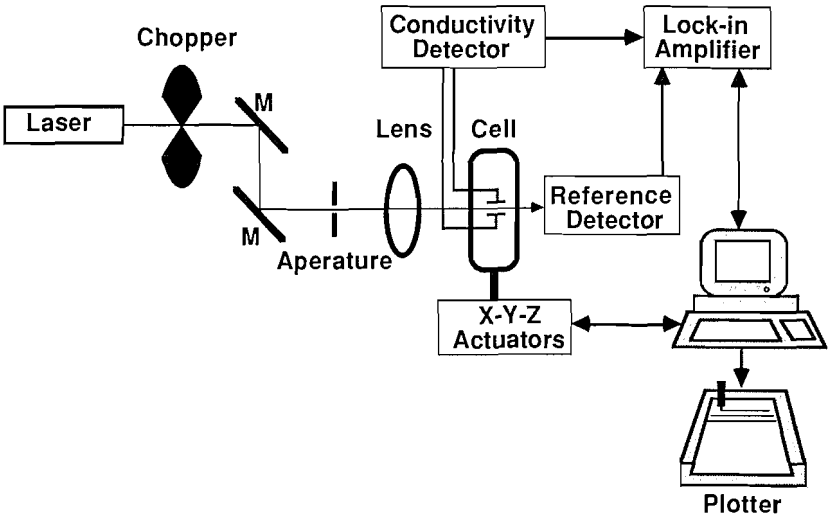


FIG. 3. Schematic diagram of the experiment.

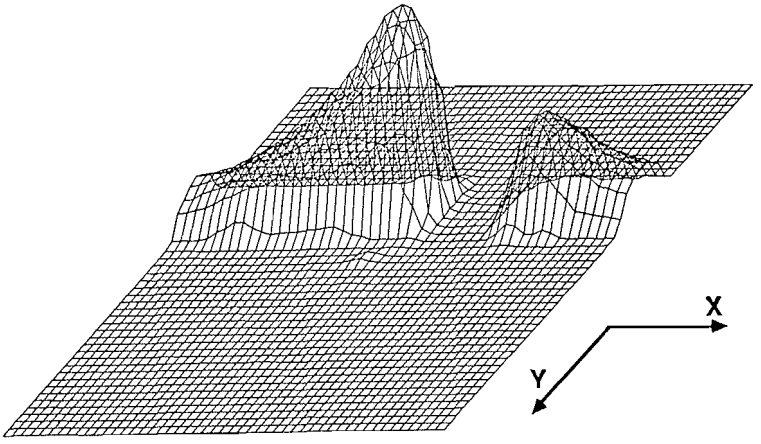


FIG. 4. A laser scan (X–Y) of the signal generated in the vicinity of the electrodes for a non-absorbing solution. The signal due to conductance of heat along the wire into the resistor region has generated a "picture" of the electrodes. TMEC absorbance measurements are made by aligning the beam to pass between the electrodes. Each pixel is 10 μm on a side.

the wire at larger distances from the electrolytic resistor, less heat is transported to the solution during each chopper cycle and an exponential decrease in signal is observed.

Absorbance measurements of a sample are generated when the laser illuminates the valley region between the electrodes. Figure 5 shows three close-up scans of the region between the electrodes using step sizes of 2.5 μm. Figure 5*a* shows the scan using a blank solution. The edges of the wire are observable as sharp rises in signal on the left and right sides of the scan. Any residual signal on the valley floor constitutes a background signal for the absorbance measurement. The magnitude of the background signal has been greatly reduced in this study as compared to our preliminary report (6). This decreased background signal results from careful minimization of beam reflections from the windows, use of polished electrode surfaces, and use of platinum as an electrode metal, which has a lower absorption than many other metals including copper (8). Figures 5*b* and 5*c* show scans of the same region with a dye concentration in solution of $4.0 \times 10^{-5} M$ for chopping frequencies of 10 Hz and 200 Hz, respectively. The signal maximizes between the electrodes and then falls off gradually in the radial direction. This signal, generated when the laser is shining in the region outside the resistor volume, is due to diffusion of heat into the resistor region. During the 50 ms illumination period during each chopping cycle, heat will diffuse approximately 100 μm — similar to the distance over which an appreciable hump is observed in Fig. 5*b*. At a chopping frequency of 200 Hz, Fig. 5*c*, heat will travel about 20 μm during the chopper cycle and little signal is generated in the solution outside of the electrolytic resistor.

With 20 μm spatial resolution provided by the 200 Hz chopping frequency, the signal strength generated between the electrodes reflects the local sensitivity of the measurement and not the effects of heat flow. A dip in the signal between the electrodes along the X axis in Fig. 5*c* is not due to increased background signal at the electrodes, see Fig. 5*a*, but rather may arise from increased sensitivity near the electrodes. The origin of this increased sensitivity would be associated with the higher current density near the electrode face compared with the region in the center of the electrolytic resistor. To test this idea, the magnitude of the electric field along the axis between two parallel, circular electrodes is derived in Appendix 2. The magnitude of the electric field vector pointing along the electrode axis is given by

Can. J. Chem. Downloaded from www.nrcresearchpress.com by 194.225.253.170 on 09/07/12
For personal use only.

Can. J. Chem. Downloaded from www.nrcresearchpress.com by 194.225.253.170 on 09/07/12
For personal use only.

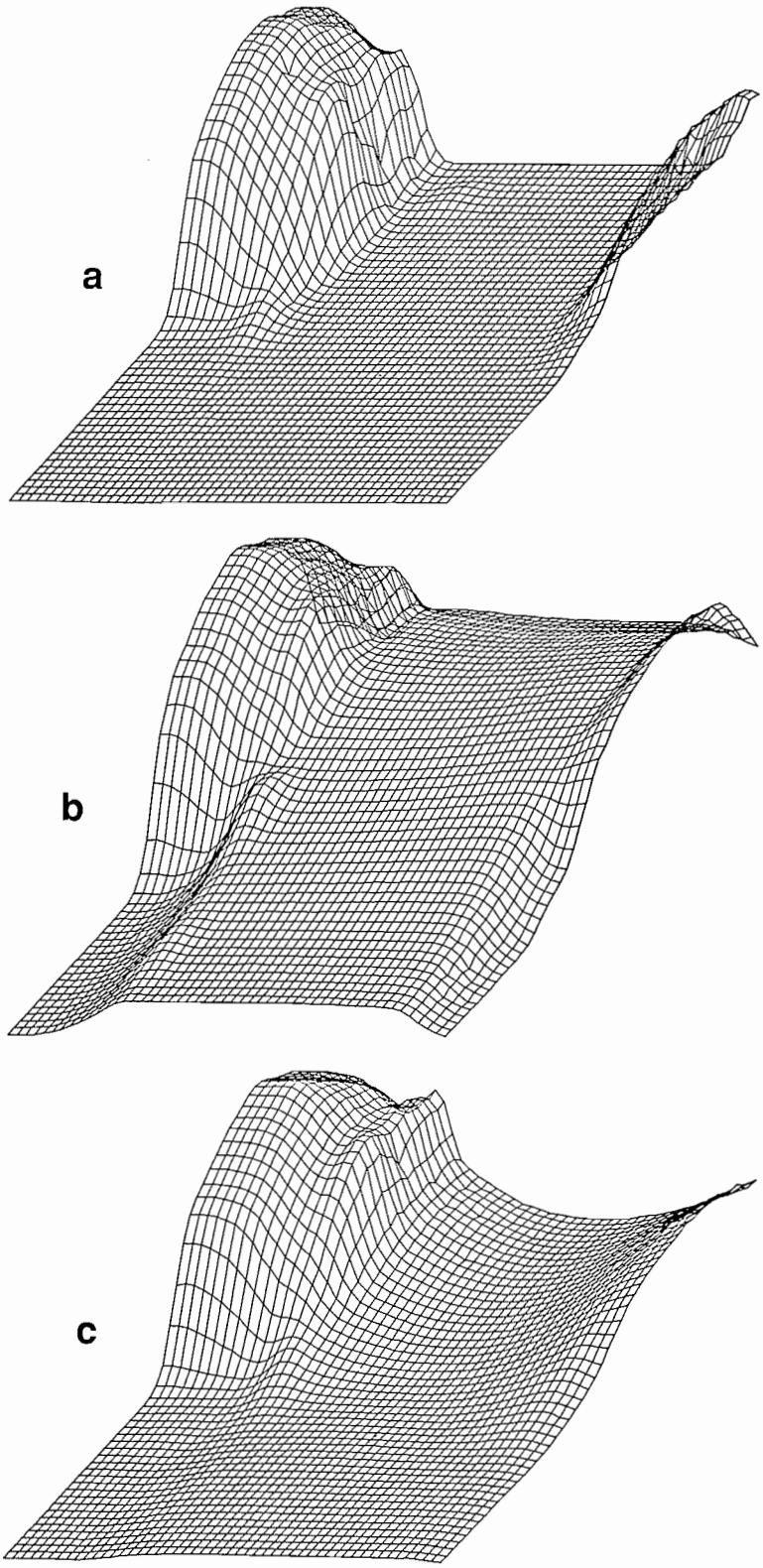


FIG. 5. Closeup scans (X–Y) of the signal in the resistor region using 2.5 μm pixels: (*a*) blank solution in the cell; (*b*) strongly absorbing solution with a chopping frequency of 10 Hz; (*c*) strongly absorbing solution with a chopping frequency of 200 Hz. The variation of the magnitude of the electric fields along the resistor axis become apparent at this higher chopping frequency. A "U" shape results for the TMEC absorbance signal in the X direction between the electrodes.

$$[5] \quad E = \frac{\sigma}{K\epsilon_0}\left[1 - (1/2)\left(\left[\frac{1}{1 + \{R/(0.5 + \beta)\}^2}\right]^{1/2} + \left[\frac{1}{1 + \{R/(0.5 - \beta)\}^2}\right]^{1/2}\right)\right]$$

where K is the dielectric constant of the medium, ϵ_0 is the permittivity of free space, R is the ratio of the wire radius r to the electrode separation L, and β is the distance from the electrode face divided by the electrode separation. Equation [5] is plotted as a function of β for various values of the dimensionless parameter R in Fig. 6. As R approaches ∞, corresponding to small electrode separations and large values of r, the electric field along the axis becomes uniform and approaches that given for a parallel plate configuration, $|E_{pp}| = \sigma/K\epsilon_0$ (13). The electric fields in the diagram are presented as a fraction of this value. As R decreases, the electric field along the axis of the resistor decreases: the magnitude of the field at the electrode surface asymptotically approaches a limit of $E_{pp}/2$ and the electric field at the center of the resistor approaches zero. The curve marked with squares has a R value of 0.381, corresponding to the particular r:L ratio used for the data in Fig. 5. The shape of the squared line in Fig. 6 qualitatively matches the shape of the dip between the electrodes in Fig. 5*c*. Higher sensitivity is achieved near the electrode face due to the greater magnitude of the electric fields there. To quantitatively compare Figs. 5*c* and 6, it is necessary to integrate the nonuniform electric field strength with the volume of the laser beam.

With the laser beam focused at the center of the electrolytic resistor, with a 100 μm electrode spacing, and utilizing a weakly absorbing solution, the dc current and the lock-in signal were measured as the voltage was increased from 0.0 to 3.0 V rms. The lock-in signal was found to be linear with the current (R = 0.9998, n = 12) as predicted from the theory. For all other data, the voltage applied to the electrodes was held at 1.0 V.

A linear polarizer was used to vary the laser power and a power meter was used to measure the power of the beam at the entrance to the cell. Using an electrode spacing of 50 μm, the lock-in signal increased linearly with the power (R = 0.9998, n = 7). However, the noise was constant to the maximum power of 5 mW. This constant noise and linear dependence of signal on laser power suggests that increasing the power further will result in increased sensitivity and improved detection limits.

The noise in the system appears to be associated with the conductivity of the electrolytic resistor. In fact, the noise appears to be due to shot noise in the current passing through the resistor. The current fluctuation associated with shot noise is given by (14)

$$[6] \quad I_{noise}(\text{rms}) = (2eIB)^{1/2}$$

where e is the electron charge, I is the average current through the cell, and B is the bandwidth of the measurement. Typical ac currents through the cell are 2.5 μA rms and the frequency bandwidth of the lock-in is given by $(1/8)T_c$ using the time constant T_c. Taking amplification into account, the expected shot noise appearing at the lock-in was 0.5 μV. Depending on the day, the noise that was measured was anywhere from one to six times this fundamental limit for chopping frequencies of 10 to 100 Hz. Using a resistor of 300 kΩ in place of the cell resulted in noise that was consistently within a factor of two of the shot noise limit.

Sensitivity was measured as a function of the electrode spacing, L, and chopping frequency, f, under constant current conditions for the ranges L = 50 to 200 μm and f = 10 to 100 Hz. The results are shown graphically in Fig. 7. The signal increases with a decrease in the chopping frequency at all electrode separations; lower chopping frequencies allow more heat to be deposited within the electrolytic resistor during each chopping cycle and, hence, a larger modulated signal. Of course, the temperature can not increase without bound between the electrodes. Eventually, heat will diffuse to the electrodes or other heat sinks, limiting the maximum signal produced at low chopping frequency. The signal also increases with a decrease in the electrode spacing; a small volume solution will heat faster than a larger volume. Equations [1] and [4] predict that the signal is inversely proportional to the electrode spacing. However, as the electrodes come close together, heat flow to the electrodes will decrease the sensitivity of the measurement and light scatter onto the electrodes will increase the background

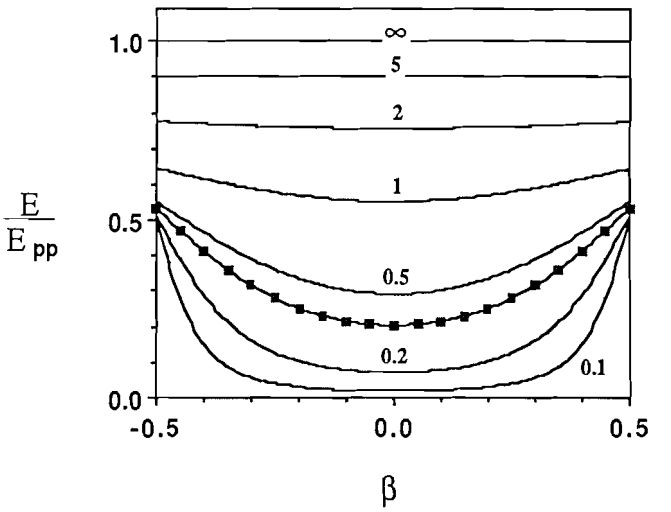


FIG. 6. Plotted are the calculated curves (eq. [11]) for the variation of the magnitude of the electric field on axis due inside a cylindrical parallel plate configuration. β is the fractional distance along the x axis between the electrodes and each curve represents a particular R value: the ratio of the wire radius to the electrode separation. E_{pp} is the field inside a parallel plate capacitor, achieved as R approaches infinity. The squared line represents the fields for an R ratio of 0.381, that used in the scans of Fig. 5.

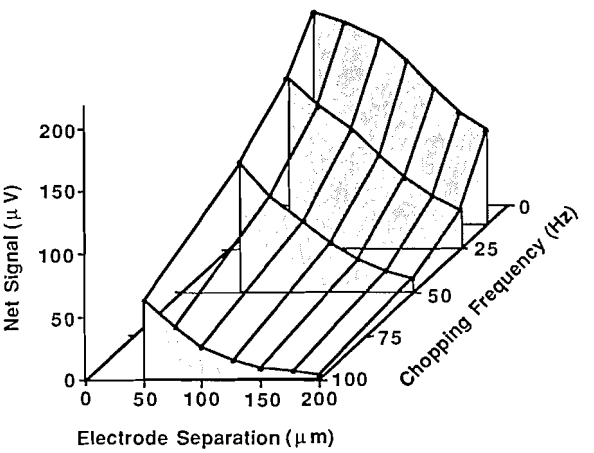


FIG. 7. Variation of the absorbance signal as a function of the electrode separation and chopping frequency. Greater sensitivity is achieved by using small electrode separations and low chopping frequencies.

Can. J. Chem. Downloaded from www.nrcresearchpress.com by 194.225.253.170 on 09/07/12
For personal use only.

Can. J. Chem. Downloaded from www.nrcresearchpress.com by 194.225.253.170 on 09/07/12
For personal use only.

signal. In this instrument, the background signal increases when the electrode spacing is less than 50 μm. Highest sensitivity is produced at low chopping frequency and small electrode spacing.

To study the variation in signal with laser beam spot size, a relatively large electrode separation, 125 μm, was used to allow a wide range of spot sizes to be studied. The spot size was varied by moving the lens, which focuses the beam, with respect to the cell using a micrometer. The spot size of the beam between the electrodes was estimated by recording the background signal as the laser beam was moved from the solution onto the resistor. The background signal gave a good approximation to an error function for the overlap of the Gaussian beam with the electrodes and the spot size was estimated from this data. The signal observed when the laser beam was centered in the electrolytic resistor varied by less than two standard deviations as the laser beam spot size changed from 9 μm to 40 μm and at a chopping frequency of both 10 Hz and 50 Hz. Despite the fact that the spot sizes are relatively large, this spot size independence is as predicted from eqs. [1] and [4]. This independence of signal upon spot size is important because it suggests that relatively large beams from incoherent light sources could be used to generate the thermally modulated signal.

A calibration curve was generated with an electrode separation of 50 μm and a chopping frequency of 10 Hz for aqueous Fast Green dye ranging from $1.0 \times 10^{-8} M$ to $4.0 \times 10^{-5} M$ and 0.01 *M* NaCl. Two blank solutions were prepared; one in H_2O and the other in D_2O. The noise measured during the calibration was 3.6 times the shot noise limit. The calibration curve was linear ($R = 0.9998$, $n = 14$) over three orders of magnitude from the one point detection limit (3σ) of $6.9 \times 10^{-9} M$ to $1.0 \times 10^{-5} M$ dye concentration. At higher concentrations, the calibration curve shows negative deviation because of a change in the spectrum of the dye due to self-association and a decrease in the laser power reaching the electrodes due to absorbance of the beam through the 260 μm distance from the window to the electrodes.

The blank signal was not zero, even though the laser beam passed through the center of the electrolytic resistor. This background signal has two origins, one from light scatter on the electrodes and the other from the finite absorbance of H_2O at 632.8 nm. The effect of each contribution may be determined by comparing the background signal observed with 0.01 *M* NaCl in water and that observed with 0.01 *M* NaCl prepared in D_2O. Although the light scatter background for the two solvents should be similar, because the refractive index of the two solvents is similar, the absorbance of D_2O is much less than that of H_2O at 632.8 nm. The absorbance of water in the red portion of the spectrum is associated with overtones of infrared transitions; the higher mass of deuterium results in lower frequency infrared transitions and, hence, lower absorbance in the visible portion of the spectrum. The Fast Green – H_2O calibration line intercepts the D_2O blank signal level at a negative dye concentration of $-1.31 \times 10^{-8} M$. The absorbance of a positive amount of dye of this concentration should thus be interpreted as the difference in absorbance between H_2O and D_2O at a wavelength of 632.8 nm. The experimental value for this difference is $\Delta\epsilon C(H_2O - D_2O) = 1.3 \times 10^{-3}\,cm^{-1}$. The datum is in excellent agreement with the literature value of $1.22 \times 10^{-3}\,cm^{-1}$ determined using pulsed photoacoustic spectroscopy in a long path length cell (15).

The absorptivity–concentration product (ϵC) detection limit for the calibration was $7.2 \times 10^{-4}\,cm^{-1}$, made over a path length given by the diameter of the wire, 76 μm. Using this path length, the absorbance detection limit is 5.5×10^{-6}, made in a volume of only 230 pL, estimated by the full resistor volume. The amount of analyte between the electrodes at the detection limit is only 1.6 attomoles or about a million molecules. Thermal modulation of electrical conductivity is a useful technique for the determination of absorbance within sub-nanoliter volumes of aqueous samples.

This excellent performance is achieved using a low power and low cost 5 mW laser. Of course, an increase in the laser power will result in a proportional increase in the sensitivity and decrease in the detection limit. For example, a 250-mW laser could produce detection limits on the order of 1×10^{-7} for aqueous samples, a significant advance in the state of the art. These detection limits are not likely to be exceeded with this particular cell geometry. Shot noise in the current flowing through the electrolytic resistor limits the precision of the conductivity technique. One approach to decrease the relative shot noise would be to increase the size of the electrodes which would increase the current through the increased electrolytic resistor. Unfortunately, the sensitivity of the measurements is predicted to scale inversely with the radius of the wire. Increasing the wire diameter will improve the precision of the measurement while decreasing the sensitivity of the measurement. It may prove necessary to investigate alternative cell geometries to improve further the performance of the technique.

Acknowledgements

This work was funded by the Natural Sciences and Engineering Research Council. The authors wish to thank Raymond Anthony Walford of the machine shop at the University of Alberta for his excellent work in construction of the Teflon cell. The software used for the collection of laser scans was developed by Messrs. Lee Tse Kheong and Dean S. Burgi.

1. T. E. Gough, R. E. Miller, and G. Scoles. Appl. Phys. Lett. **30**, 338 (1977).
2. G. H. Brilmyer and A. J. Bard. Anal. Chem. **52**, 685 (1980).
3. D. Betteridge and P. J. Meylor. CRC Crit. Rev. Anal. Chem. **14**, 267 (1984).
4. N. J. Dovichi and R. A. Keller. Anal. Chem. **55**, 543 (1983).
5. N. J. Dovichi. CRC Crit. Rev. Anal. Chem. **17**, 357 (1987).
6. R. McLaren and N. J. Dovichi. Anal. Chem. **60**, 730 (1988).
7. N. J. Dovichi. Prog. Anal. Spectrosc. **11**, 179 (1988).
8. R. C. Weast and M. J. Astle (*Editors*). CRC handbook of chemistry and physics. 63rd ed. Chemical Rubber Publishing Company, Boca Raton, Florida. 1982.
9. D. R. Lide (*Editor*). Journal of physical and chemical reference data. Vol. 11. 1982.
10. D. R. Lide (*Editor*). Journal of physical and chemical reference data. Vol. 13. 1984.
11. J. Braunstein and G. D. Robbins. J. Chem. Ed. **48**, 52 (1971).
12. B. C. Burdett. *In* Aggregation processes in solution. *Edited by* E. Wyn-Jones and J. Gormally. Elsevier Scientific Publishing Company, New York. 1983. p. 241.
13. A. F. Kip. Fundamentals of electricity and magnetism. 2nd ed. McGraw-Hill, New York. 1969.
14. P. Horowitz and W. Hill. The art of electronics. Cambridge University Press, Cambridge. 1980.
15. A. C. Tam and C. K. N. Patel. Appl. Opt. **18**, 3348 (1979).
16. A. W. Adamson. A textbook of physical chemistry. 2nd ed. Academic Press, New York. 1979.
17. A. J. Twarowski and D. S. Kliger. Chem. Phys. **20**, 253 (1977).

Can. J. Chem. Downloaded from www.nrcresearchpress.com by 194.225.253.170 on 09/07/12
For personal use only.

Appendix 1

In this appendix, a derivation is presented for the change in the current through a cylindrical electrolytic resistor induced by a pulsed Gaussian laser beam. The derivation of the impulse response involves a description of the current through a thermally non-homogeneous resistor, the temperature field produced by the laser and, finally, the change in the current.

The current through a cylindrical homogeneous resistor can be derived by calculating the current density in the resistor due to the movement of ions. The ions have a particular ion mobility and are subjected to a force from the electric field present in the resistor (16). Ignoring the complications from ion–ion forces, the current is given by

$$[7] \quad I = \sum_i \frac{M_i N z_i^2 e^2 \pi r^2 V}{6\pi\eta r_i L}$$

where M_i is the molarity of the ith ionic species, z_i is the ionic charge number, r_i is the radius of the ion, e is the electron charge, N is Avogadro's number, V is the voltage applied to the electrodes, η is the viscosity of the medium, r is the radius of the resistor, and L is its length. The summation is over the current carrying ionic species in the solution. The current through a thermally non-homogeneous resistor can be described by a weighted average of the current in small volume elements of the resistor

$$[8] \quad \bar{I} = \frac{\int_{vol} I(x,y,z)\,dx\,dy\,dz}{\int_{vol} dx\,dy\,dz}$$

where the integral is evaluated over the cylindrical resistor volume. With the assumption that only the viscosity changes with temperature and defining the resistor volume, vol $= \pi r^2 L$, the current is given by

$$[9] \quad \bar{I} = \sum_i \frac{M_i N z_i^2 e^2 V}{4\pi r_i L^2} \int_{vol} \frac{1}{\eta(x,y,z)}\,dx\,dy\,dz$$

where $\eta(x,y,z)$ is the local viscosity of the solution at a point. Equation [9] converges to eq. [7] for a homogeneous viscosity between the electrodes. The thermally induced current change, ΔI, is then given by differentiating with respect to temperature. Over the small temperature rise induced by absorbance of the laser beam, the viscosity will be inversely proportional to the temperature of the solvent. Collecting variables and simplifying

$$[10] \quad \Delta I = \frac{\partial I}{\partial T} \times \Delta T = \frac{\bar{I}}{vol}\left(\frac{-1}{\eta}\frac{d\eta}{dT}\right)\int_{vol} \Delta T\,dx\,dy\,dz$$

The current change is proportional to the temperature rise, ΔT, integrated over the resistor volume. The temperature rise excited by a pulsed Gaussian TEM_{00} laser within a homogeneous absorbing sample has been derived (17) and, in the coordinate system of Fig. 1, is given by

$$[11] \quad \Delta T_{impulse}(x,y,t) = \frac{2.303E\epsilon C}{2\pi k t_c(1 + 2t/t_c)} \times \exp\left[\frac{-2(x^2 + y^2)}{\omega^2(1 + 2t/t_c)}\right]$$

where k is the *thermal* conductivity of the solvent, ω is the spot size of the beam, t is the time after the pulse, and t_c is the time constant of the solvent.

$$[12] \quad t_c = \frac{\omega^2 \rho C_p}{4k}$$

Here, ρ is the solvent density and C_p is its thermal capacity. The impulse response of the current, $\Delta I_{impulse}$, is then given by substituting eq. [11] into eq. [10].

Taking the resistor center as the origin, the overlap integral of the temperature field with the resistor of eq. [10] may be evaluated using rectangular coordinates

$$[13] \quad \int_{vol} \Delta T_{impulse}\,d\tau = \frac{2.303E\epsilon C}{2\pi k t_c(1 + 2t/t_c)} \int_{-r}^{r} \int_{-\sqrt{r^2-Z^2}}^{\sqrt{r^2-Z^2}} \int_{-L/2}^{L/2} \times \exp\left[\frac{-2(X^2/\omega^2)}{(1 + 2t/t_c)}\right] \exp\left[\frac{-2(Y^2/\omega^2)}{(1 + 2t/t_c)}\right] dX\,dY\,dZ$$

The integration with respect to x is separable and yields an error function

$$[14] \quad \int_{-L/2}^{+L/2} \exp\left[\frac{-2x^2}{\omega^2(1 + 2t/t_c)}\right] dx = \left[\frac{\pi\omega^2(1 + 2t/t_c)}{2}\right]^{1/2} \mathrm{erf}\left(\left[\frac{L^2}{2\omega^2(1 + 2t/t_c)}\right]^{1/2}\right)$$

The remaining integrals can not be expressed in terms of simple functions. Instead, we make the approximation that the spot size of the laser beam is much less than the radius of the wire. Under this condition, the limits of integration in the Y direction become $\pm\infty$

$$[15] \quad \int_{vol} \Delta T_{impulse}\,d\tau = \frac{2.303E\epsilon C\omega}{2\sqrt{2\pi}kt_c\sqrt{(1 + 2t/t_c)}} \times \mathrm{erf}\left(\left[\frac{L^2}{2\omega^2(1 + 2t/t_c)}\right]^{1/2}\right) \times \int_{-r}^{r} \int_{-\infty}^{\infty} \exp\left[\frac{-2(Y^2/\omega^2)}{(1 + 2t/t_c)}\right] dY\,dZ = \frac{2.303E\epsilon Cr}{\rho C_p} \mathrm{erf}\left(\left[\frac{L^2}{2\omega^2(1 + 2t/t_c)}\right]^{1/2}\right)$$

Collecting all together, the modulated current is given by

$$[16] \quad \Delta I = \frac{2.303E\epsilon C\bar{I}}{\pi rL}\left(\frac{-1}{\rho C_p \eta}\frac{d\eta}{dT}\right) \times \mathrm{erf}\left(\left[\frac{L^2}{2\omega^2(1 + 2t/t_c)}\right]^{1/2}\right)$$

Last, if the laser beam spot size is much less than the electrode spacing, the current is found to be

$$[17] \quad \Delta I_{impulse}\begin{bmatrix}\text{small spot}\\ \text{limit}\end{bmatrix} = \frac{2.303E\epsilon C\bar{I}}{\pi rL}\left(\frac{-1}{\rho C_p \eta}\frac{d\eta}{dT}\right)$$

Assumptions

Various approximations have been made in the derivation of the impulse response of eq. [17]. These are listed below:

(*i*) The ions and absorbing analyte are homogeneously distributed between the electrodes.

(*ii*) In the derivation of the current of eq. [1], Stokes approximation has been invoked for the frictional coefficient of a spherical particle of radius r_i particle moving through a viscous medium: $f = 6\pi\eta r_i$ (16).

(*iii*) The electric field between the electrodes is of magnitude

$\boldsymbol{E} = V/L$ — inside the cylindrical resistor volume (V = applied voltage)

$\boldsymbol{E} = 0$ — elsewhere

This approximation will hold in the limit of small electrode spacing. An accurate model would account for the variation in electric field strength throughout the sample volume. Appendix 2 presents the variation in the axial electric field between the electrodes. A uniform axial electric field is achieved if the radius of the wire is more than five times the distance between the electrodes.

(*iv*) The voltage drop across the double layer capacitance is assumed to be zero. This is achieved by using a sufficiently high ac frequency to eliminate the double layer impedance.

(*v*) The spot size of the laser is assumed constant over the diameter of the electrolytic resistor.

(*vi*) The effects of heat sinks such as quartz windows and platinum wires have been ignored.

(*vii*) The background signal associated with scattered light striking the electrodes is ignored.

(*viii*) The modulation frequency of the conductivity measurement is sufficiently low so that eq. [7] holds.

Appendix 2

This appendix presents a derivation for the magnitude of the electric field at a point on the axis of a cylindrical parallel plate capacitor. The calculation involves summing all the contributions to the field at point P to all charge on the surface of the electrode faces as shown in Fig. 8.

A charge density $+\sigma$ exists on the left electrode surface and an equal and opposite charge density exists on the right electrode surface. An incremental electric field vector, $d\boldsymbol{E}$, at point P is calculated from Coulombs law (13)

$$[18] \quad d\boldsymbol{E} = \frac{1}{4\pi K\epsilon_0}\frac{dq}{l^2}\boldsymbol{l}$$

where dq is the element of surface charge a distance l away from point P and $\boldsymbol{l}$ is a vector pointing along the line from the surface charge to point P. When calculating the field on axis due to a thin circular ring of surface charge on an electrode face, the vector components perpendicular to the x axis can be ignored due to cancellation by symmetry. Thus, the field at P due to a charged ring of radius ζ and thickness $d\zeta$ on the left electrode face is given by

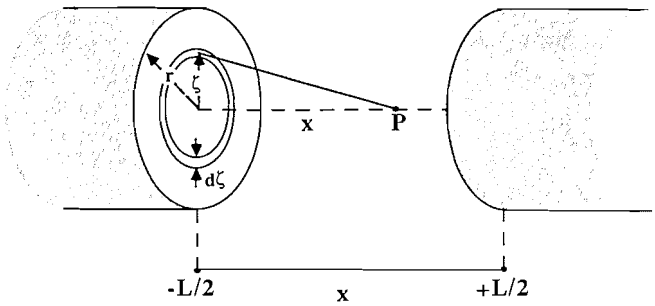


FIG. 8. Calculation of the magnitude of the electric fields on axis due to cylindrical parallel plate configuration. X is distance measured from the center of the electrode.

$$[19] \quad d\boldsymbol{E} = \frac{1}{4\pi K\epsilon_0}\frac{2\pi\zeta\, d\zeta\, \sigma}{[(L/2+x)^2+\zeta^2]}\frac{(L/2+x)}{\sqrt{(L/2+x)^2+\zeta^2}}\boldsymbol{x}$$

$$= \frac{(L/2+x)\sigma}{2K\epsilon_0}\frac{\zeta\, d\zeta}{[(L/2+x)^2+\zeta^2]^{3/2}}\boldsymbol{x}$$

The total field at point P due to the left electrode is obtained by integrating with respect to ζ

$$[20] \quad d\boldsymbol{E}_{\text{LEFT}} = \frac{(L/2+x)\sigma\boldsymbol{x}}{2K\epsilon_0}\int_0^r \frac{\zeta}{((L/2+x)^2+\zeta^2)^{3/2}}\, d\zeta$$

Substituting $y = \zeta^2$, the integral yields

$$[21] \quad \boldsymbol{E}_{\text{LEFT}} = \frac{\sigma\boldsymbol{x}}{2K\epsilon_0}\left(1 - \left[\frac{1}{1+\{r/(L/2+x)\}^2}\right]^{1/2}\right)$$

The field at P due to charge on the right electrode can be calculated in a similar fashion and will add to the field calculated above. It is convenient to use the fractional distance between the electrodes; $\beta = x/L$ and to calculate the field for a particular ratio of the wire radius r to the electrode separation L; $R = r/L$. The final expression for the magnitude of the field at P using these substitutions is

$$[22] \quad \boldsymbol{E}(\beta, R) = \frac{\sigma}{K\epsilon_0}\left[1 - (1/2)\left(\left[\frac{1}{1+\{R/(0.5+\beta)\}^2}\right]^{1/2} + \left[\frac{1}{1+\{R/(0.5-\beta)\}^2}\right]^{1/2}\right)\right]$$

Can. J. Chem. Downloaded from www.nrcresearchpress.com by 194.225.253.170 on 09/07/12
For personal use only.

Nitrosyl complexes of rhenium. 3. The synthesis and substitution reactions of $[ReH(CH_3OH)(NO)(PPh_3)_3]ClO_4$ derived from the reaction of $ReH_2(NO)(PPh_3)_3$ with $HClO_4$. Members of the series $ReHX(NO)(PPh_3)_3$

JULIE Y. CHEN, KEVIN R. GRUNDY,[1] AND KATHERINE N. ROBERTSON
The Department of Chemistry, Dalhousie University, Halifax, N.S., Canada B3H 4J3

Received August 18, 1988[2]

JULIE Y. CHEN, KEVIN R. GRUNDY, and KATHERINE N. ROBERTSON. Can. J. Chem. **67**, 1187 (1989).

$ReH_2(NO)(PPh_3)_3$ reacts with alcoholic $HClO_4$ to yield the solvated cation, $[ReH(ROH)(NO)(PPh_3)_3]ClO_4$ (R = CH_3, C_2H_5) which can be isolated as an explosive solid (R = CH_3 only). In the solid state, the perchlorate counter ion is hydrogen bound to the ligated alcohol, as observed for $[ReH(CH_3OH)(CO)(NO)(PPh_3)_2]ClO_4$. This latter complex also results from the reaction of $[ReH(CH_3OH)(NO)(PPh_3)_3]ClO_4$ with CO under ambient conditions. On reaction with *p*-tolylisocyanide (RNC), however, substitution is also accompanied by dihydrogen elimination to give $[Re(OR)(NO)(CNR)_2(PPh_3)_2]ClO_4$, irrespective of the mole ratio of the reactants. In contrast, $[ReH(CH_3OH)(NO)(PPh_3)_3]ClO_4$ reacts with coordinating anions with loss of methanol to give air-sensitive $ReHX(NO)(PPh_3)_3$ (X = OCH_3, F, Cl, Br, I, N_3, NCO, SCN), of which only those with X = Cl, Br, N_3 were characterized in solution. The compounds $ReHX(NO)(PPh_3)_3$ are similar to their osmium analogues in having a labile third phosphine. Thus, reaction with neutral ligands such as CO or RNC leads to the series of neutral rhenium hydrido nitrosyls $ReHX(L)(NO)(PPh_3)_2$. Prior to this work, the only known examples from this series were those with L = CO, X = H, F, OCH_3. Interestingly, the isomer of $ReHF(CO)(NO)(PPh_3)_2$ isolated in this work differs from that previously isolated (from the reaction of $[ReF(CO)(NO)(PPh_3)_3]^+$ with BH_4^-) in having F *trans* to NO. All structural assignments have been made on the basis of elemental analyses, infrared spectroscopy, ^1H and ^{31}P nmr spectroscopy and deuteration studies, where appropriate.

Key words: hydrido, nytrosyl, rhenium, complexes.

JULIE Y. CHEN, KEVIN R. GRUNDY et KATHERINE N. ROBERTSON. Can. J. Chem. **67**, 1187 (1989).

Le $ReH_2(NO)(PPh_3)_3$ réagit avec le $HClO_4$ en solution alcoolique pour fournir le cation solvaté, $[ReH(ROH)(NO)(PPh_3)_3]ClO_4$ (R = CH_3, C_2H_5), que l'on peut isoler sous la forme d'un solide explosif (R = CH_3 seulement). A l'état solide, une liaison hydrogène relie le contre-ion perchlorate à l'alcool agissant comme ligand; un résultat semblable a aussi été observé avec le $[ReH(CH_3OH)(CO)(NO)(PPh_3)_2]ClO_4$. Ce dernier composé est aussi formé par la réaction du $[ReH(CH_3OH)(NO)(PPh_3)_3]ClO_4$ avec du CO dans des conditions ambiantes. Lors de la réaction avec l'isocyanure de *p*-tolyle, la substitution est toutefois accompagnée d'une élimination d'hydrogène moléculaire conduisant à la formation de $[Re(OR)(NO)(CNR)_2(PPh_3)_2]ClO_4$, quel que soit le rapport molaire des réactifs. Par ailleurs, la réaction du $[ReH(CH_3OH)(NO)(PPh_3)_3]ClO_4$ avec des anions pouvant donner lieu à une coordination conduit à une perte de méthanol et à la formation de $ReHX(NO)(PPh_3)_3$ (X = OCH_3, F, Cl, Br, I, N_3, NCO, SCN) qui sont sensibles à l'air et dont seulement les dérivés contenant X = Cl, Br et N_3 ont été caractérisés en solution. Les composés $ReHX(L)(NO)(PPh_3)_2$, comme leurs analogues contenant de l'osmium, portent une troisième phosphine qui est labile. Par réaction avec des ligands neutres comme le CO et le RNC, ils conduisent donc à la formation d'une série de nitrosyl hydrido rhénium neutres $ReHX(L)(NO)(PPh_3)_2$. Avant ce travail, les seuls exemples connus dans cette série étaient ceux comportant un L = CO et X = H, F ou OCH_3. Il est intéressant de noter que l'isomère du $ReHF(CO)(NO)(PPh_3)_2$ qui a été isolé au cours de ce travail est différent de celui qui avait été isolé antérieurement (par réaction du $[ReF(CO)(NO)(PPh_3)_3]^+$ avec le BH_4^-); le F est trans par rapport au NO. Toutes les attributions de structures ont été faites en se basant, suivant le cas, sur des analyses élémentaires, les spectroscopies infrarouge et rmn du ^1H et ^{31}P ainsi que des éudes de deutération.

Mots clés : hydrido, nitrosyl, rhénium, composés.

[Traduit par la revue]

Introduction

In the second paper of this series (1), we described the reaction of $ReH_2(NO)(PPh_3)_3$ with alcoholic $HClO_4$ in the presence of CO to give $ReH(OR)(CO)(NO)(PPh_3)_2$ and numerous derived compounds, most of which took the form $ReXY(CO)(NO)(PPh_3)_2$. Like their isoelectronic osmium counterparts $OsXY(CO)_2(PPh_3)_2$, however, the reactivity of these mixed carbonyl nitrosyl derivatives of rhenium is limited by the lack of a labile ligand. $OsHCl(CO)(PPh_3)_3$ does not suffer from this limitation since the third phosphine *trans* to the hydride ligand is quite labile, making this material arguably the most versatile synthon available in osmium chemistry. It was obviously in our best interest, therefore, to synthesize $ReHCl(NO)(PPh_3)_3$, or some closely related species, and investigate its usefulness as a synthon for non-carbonyl containing Re(I) nitrosyl derivatives.

This paper describes the reaction of $ReH_2(NO)(PPh_3)_3$ with $HClO_4$ in the absence of CO to give the highly unstable, solvated species $[ReH(CH_3OH)(NO)(PPh_3)_3]ClO_4$, analogous to previously reported $[ReH(CH_3OH)(CO)(NO)(PPh_3)_2]ClO_4$ (1). The extreme instability of the title compound somewhat limits its utility but simple substitutions either of the coordinated solvent or the third phosphine do allow the synthesis of a variety of both new and previously reported Re(I) derivatives, including the original target compound, $ReHCl(NO)(PPh_3)_3$.

Experimental section

CAUTION! THESE COMPOUNDS SHOULD BE TREATED WITH THE EXTREME CAUTION NORMALLY AFFORDED ORGANOMETALLIC PERCHLORATE SALTS, WHICH ARE POTENTIALLY EXPLOSIVE (2). IN THIS RESPECT THE TITLE COMPOUND $[ReH(CH_3OH)(NO)(PPh_3)_3]ClO_4$ IS PARTICULARLY HAZARDOUS, BEING SUBJECT TO VIOLENT, EXPLOSIVE DECOMPOSITION. To minimize the hazards associated with these perchlorate complexes the following precautions should be observed: (*i*) Keep reaction scales to <0.5 g, or <0.25 g for the title compound, (*ii*) avoid the use of metal spatulas, and (*iii*) use the complexes when

[1]To whom all correspondence should be addressed.
[2]Revision received February 20, 1989.

Can. J. Chem. Downloaded from www.nrcresearchpress.com by 194.225.253.170 on 09/07/12
For personal use only.

Can. J. Chem. Downloaded from www.nrcresearchpress.com by 194.225.253.170 on 09/07/12
For personal use only.

prepared and refrain from storing samples, especially near sources of heat or in sealed containers.

General experimental details and instrumental methods were as outlined previously (1). Infrared and ^1H and ^{31}P nmr data are summarized in Tables 1 and 2.

Reaction of $ReH_2(NO)(PPh_3)_3$ with $HClO_4$ in methanol. Synthesis of $[ReH(CH_3OH)(NO)(PPh_3)_3]ClO_4$ (1)

$ReH_2(NO)(PPh_3)_3$ (0.20 g, 0.20 mmol) was combined with enough methanol to barely suspend the solid (0.5 mL) and 3 drops of perchloric acid (0.04 mL, 70% w/v) at 0°C. Dichloromethane (0.5 mL) was then added dropwise to the stirred suspension until a visible reaction had begun. A bright, yellow–orange solution formed as the original solid was consumed, accompanied by gas evolution. The product was precipitated immediately by the addition of diethyl ether (30 mL). After stirring for a further 5 min at 0°C, the pale yellow needles were collected by vacuum filtration under nitrogen and washed with diethyl ether. The product could neither be recrystallized nor sent for analysis because of its instability (0.22 g, 97%); mp 97–98°C expl.

Reaction of $[ReH(CH_3OH)(NO)(PPh_3)_3]ClO_4$ with CO. Synthesis of $[ReH(CH_3OH)(CO)(NO)(PPh_3)_2]ClO_4$

A mixture of dichloromethane and methanol (40 mL, 1:1 v/v) was saturated with CO by bubbling for 20 min. To the solution was added freshly prepared $[ReH(CH_3OH)(NO)(PPh_3)_3]ClO_4$ (0.1 g, 0.09 mmol) suspended in 10 mL of methanol. The resultant pale yellow solution was stirred under CO for a further 30 min and then reduced to 2–3 mL under reduced pressure. (*Note*: Do not evaporate to dryness or an explosion may result.) The viscous, dark gold oil was diluted with diethyl ether (100 mL) and stirred for 10 min to induce precipitation of a small amount of material. On further reducing the solvent volume to 10 mL the remainder of the product precipitated. The beige–yellow needles of $[ReH(CH_3OH)(CO)(NO)(PPh_3)_2]ClO_4$ were filtered and recrystallized from dichloromethane/methanol/diethyl ether (0.06 g, 80%). Characterization was by comparison with an authentic sample (1).

Reaction of $[ReH(CH_3OH)(NO)(PPh_3)_3]ClO_4$ with p-tolylisocyanide. Synthesis of $[Re(OC_2H_5)(NO)(C_7H_7NC)_2(PPh_3)_2]PF_6$ (2)

To 20 mL of ethanol was added 6.1 mL of *p*-tolylisocyanide solution (10 mg mL^{-1}, 2.4 equiv.) in ethanol followed by freshly prepared $[ReH(CH_3OH)(NO)(PPh_3)_3]ClO_4$ (0.25 g, 0.22 mmol) suspended in 10 mL methanol. After stirring for 5 min, solid $NaPF_6$ (0.1 g) was added to the bright yellow solution and stirring continued for a further 30 min. No gas evolution could be observed under these conditions. Evaporation under reduced pressure to 2–3 mL yielded a thick golden-orange oil which was dissolved in dichloromethane (15 mL) and filtered through Celite to remove excess $NaPF_6$. The resultant bright yellow solution was diluted with an equal volume of ethanol and the volume reduced to 2–3 mL. Crystallization was initiated by scratching the vessel and completed by the addition of diethyl ether (40 mL) in several small portions. After stirring for a further 5 min, the pale yellow product was removed by filtration and recrystallized in the above manner from dichloromethane/ethanol/diethyl ether in the form of small needles (0.21 g, 82%); mp 177–179°C dec. *Anal.* calcd. for $C_{54}H_{49}N_3F_6O_2P_3Re$: C 55.67, H 4.24, N 3.61; found: C 55.79, H 4.38, N 3.63.

Prepared in similar fashion using methanol and/or $NaClO_4$ where appropriate were $[Re(OC_2H_5)(NO)(C_7H_7NC)_2(PPh_3)_2]ClO_4$ (**2***a*) (81%, mp 182–183°C dec.), $[Re(OCH_3)(NO)(C_7H_7NC)_2(PPh_3)_2]PF_6$ (**3**) (59%, mp 195–198°C dec.), and $[Re(OCH_3)(NO)(C_7H_7NC)_2(PPh_3)_2]ClO_4$ (**3***a*) (70%, mp 183°C dec.).

Reaction of $[ReH(CH_3OH)(NO)(PPh_3)_3]ClO_4$ with anions. Synthesis of $ReHX(NO)(PPh_3)_3$ (4–9)

Method A: $ReH_2(NO)(PPh_3)_3$ (0.20 g, 0.20 mmol) was converted to $[ReH(CH_3OH)(NO)(PPh_3)_3]ClO_4$ as described above. The yellow solid was immediately suspended in methanol (5 mL) and 1.1 equiv. of the required solid salt were washed into it with a second 5 mL portion of methanol. The original solid dissolved rapidly with stirring as the product precipitated. After a further 5 to 10 min, the product was collected by filtration under nitrogen. All $ReHX(NO)(PPh_3)_3$ derivatives proved air-sensitive and were used immediately. Characterization was limited to infrared and nmr spectroscopy, and derivatization. Prepared in this manner were $[ReH(OCH_3)(NO)(PPh_3)_3]$ (**4**) (0.5 mL, 0.5 *M* $NaOCH_3$ in methanol, pale yellow, 49%, mp 104–107°C dec.), $ReHF(NO)(PPh_3)_3$ (**5**) ($KF.2H_2O$, yellow, 64%, mp 175–176°C dec.), and $ReH(NCO)(NO)(PPh_3)_3$ (**9**) (KNCO, golden orange, 72%, mp 171–174°C dec.).

Method B: $ReH_2(NO)(PPh_3)_3$ (0.20 mmol) was converted to $[ReH(CH_3OH)(NO)(PPh_3)_3]ClO_4$ as described above. While still on the filter stick, the yellow solid was washed with a minimum of degassed dichloromethane into a solution of 2 equiv. of the appropriate salt in 30 mL of methanol at 0°C. Precipitation of the bright yellow products began immediately. After stirring for 20 min, the crystals were collected under nitrogen and washed with methanol and hexane. Prepared in this manner were $ReHCl(NO)(PPh_3)_3$ (**6**) (LiCl, bright yellow, 68%, mp 165–170°C dec.), $ReHBr(NO)(PPh_3)_3$ (**7**) (NaBr, golden orange, 74%, mp 160–165°C dec.), and $ReH(N_3)(NO)(PPh_3)_3$ (**8**) (NaN_3, yellow, 67%, mp 133–134°C dec.).

Reaction of $ReHX(NO)(PPh_3)_3$ with CO. Synthesis of $ReHX(CO)(NO)(PPh_3)_2$. (10–15)

A mixture of dichloromethane and ethanol (40 mL, 1:1 v/v; methanol was used for X = OCH_3) was saturated with CO by bubbling for 20 min. While maintaining the flow of CO, a freshly prepared sample of $ReHX(NO)(PPh_3)_3$, suspended in 10 mL of the appropriate alcohol was added. Any solid remaining was dissolved by the addition of dichloromethane to give a bright yellow solution which quickly lightened to a pale yellow or gold as stirring under CO was continued for a further 30 min. Evaporation under reduced pressure precipitated the product which was recrystallized from dichloromethane and the appropriate alcohol. All derivatives are air- and solution-stable crystalline solids.

Prepared in this manner were $ReH(OCH_3)(CO)(NO)(PPh_3)_2$ (**10**) (pale yellow needles, 89%, characterized by comparison with an authentic sample (1). $ReHF(CO)(NO)(PPh_3)_2$ (**11**) (pale yellow, 93%, mp 186–188°C dec.) *Anal.* calcd. for $C_{37}H_{31}NO_2FP_2Re$: C 56.34, N 1.78, O. 4.06; found: C 56.38, N 1.75, O 4.16. $ReHCl(CO)(NO)(PPh_3)_2$ (**12**) (pale yellow, 85%, mp 205–208°C dec.). *Anal.* calcd. for $C_{37}H_{31}NClO_2P_2Re$: C 55.19, H 3.88, N 1.74; found: C 54.60, H 3.91; N 1.71. $ReHBr(CO)(NO)(PPh_3)_2$ (**13**) (pale yellow needles, 91%, mp 211°C dec.). $ReH(N_3)(CO)(NO)(PPh_3)_2$ (**14**) (pale yellow needles, 93%, mp 178–180°C dec.). $ReH(NCO)(CO)(NO)(PPh_3)_2$ (**15**) (pale yellow–gold needles, 92%, mp 209–212°C dec.).

Prepared in similar fashion using the appropriate precursors were $ReHI(CO)(NO)(PPh_3)_2$ (**16**) (pale yellow needles, 92%, mp 224–227°C dec.). $ReH(SCN)(CO)(NO)(PPh_3)_2$ (**17**) (golden orange, 90%, mp 173–177°C dec). *Anal.* calcd. for $C_{38}H_{31}N_2O_2P_2SRe$: C 55.13, H 3.77, N 3.38; found: C 55.02, H 3.78, N 3.37.

Reaction of $ReHX(NO)(PPh_3)_3$ with p-tolylisocyanide. Synthesis of $ReHX(C_7H_7NC)(NO)(PPh_3)_2$ (18–23)

To 20 mL of 1:1 dichloromethane/ethanol (methanol in the case X = OCH_3) was added 2.6 mL of *p*-tolylisocyanide solution (10 mg mL^{-1} in the appropriate alcohol, 1.1 equiv. based on original amount of $ReH_2(NO)(PPh_3)_3$ used at the start of the sequence, 0.25 g). To this solution was added the freshly prepared $ReHX(NO)(PPh_3)_3$ slurried in 10 mL of the appropriate alcohol. A further 10 mL of dichloromethane was added to generate a bright yellow solution which, after 30 min stirring, was evaporated under reduced pressure to give crystals of the product. Recrystallization was from dichloromethane/alcohol plus several drops of the isocyanide solution. All derivatives are air- and solution-stable, crystalline solids.

Prepared in this manner were $ReH(OCH_3)(C_7H_7NC)(NO)(PPh_3)_2$ (**18**) (pale yellow needles, 98% based on $ReH(OCH_3)(NO)(PPh_3)_3$ used, mp 179–180°C dec.). *Anal.* calcd. for $C_{45}H_{41}N_2O_2P_2Re$: C 60.73, H 4.64, N 3.15; found: C 60.76, H 4.77, N 3.17. $ReHF(C_7H_7NC)(NO)(PPh_3)_2$ (**19**) (pale yellow needles, 87%, mp 196–197°C dec.). $ReHCl(C_7H_7NC)(NO)(PPh_3)_2$ (**20**) (bright yellow needles, 85%, mp 221°C dec.). *Anal.* calcd. for $C_{44}H_{38}N_2ClOP_2Re$: C 59.09, H

Can. J. Chem. Downloaded from www.nrcresearchpress.com by 194.225.253.170 on 09/07/12
For personal use only.

4.28, N 3.13; found: C 58.57, H 4.35, N 3.09. $ReHBr(C_7H_7NC)(NO)(PPh_3)_2$ (**21**) (bright yellow needles, 77%, mp 223–225°C dec.). $ReH(N_3)(C_7H_7NC)(NO)(PPh_3)_2$ (**22**) (bright yellow needles, 87%, mp 208–209°C dec.). $ReH(NCO)(C_7H_7NC)(NO)(PPh_3)_2$ (**23**) (pale yellow needles, 94%, mp 196–197°C dec.).

Prepared in similar fashion using the appropriate precursors were $ReHI(C_7H_7NC)(NO)(PPh_3)_2$ (**24**) (yellow–green needles, 90%, mp 216–218°C dec.). $ReH(SCN)(C_7H_7NC)(NO)(PPh_3)_2$ (**25**) (bright yellow crystals, 83%, mp 188°C dec.). *Anal.* calcd. for $C_{45}H_{38}N_3OP_2SRe.(CH_2Cl_2)_{0.25}$: C 57.93, H 4.14, N 4.48; found: C 57.51, H 4.22, N 4.44.

Results and discussion

The reader's attention is drawn to the warning in the Experimental section concerning the instability of the percholorate complexes described in this paper. To date our efforts directed at eliminating the need for the use of perchloric acid have been unsuccessful so that, unfortunately, the only currently available synthetic route to compounds **4–25** is through the highly unstable title complex, $[ReH(CH_3OH)(NO)(PPh_3)_3]ClO_4$.

As mentioned in the Introduction, the previous paper in this series examined the reaction of $ReH_2(NO)(PPh_3)_3$ with alcoholic $HClO_4$ in the presence of CO. In order to rationalize the dependence of the observed products on the nature of the alcohol used in their preparation, we proposed the initial formation of $[ReH(ROH)(NO)(PPh_3)_3]ClO_4$ as a common intermediate. At that time we also reported that unstable materials could be isolated from this system by eliminating the addition of CO. It was apparent that, if these materials were as we thought, the presence of two labile ligands should make them useful precursors to a wide range of hydrido nitrosyl complexes of rhenium(I). Such proved to be the case, but on looking further into the nature of these intermediate complexes, it quickly became apparent that it was futile to attempt to either characterize or use the material obtained from ethanol, since its decomposition at room temperature is very rapid. From methanol, however, relatively stable samples can be obtained, provided solvent volumes are kept to a minimum. Thus, if $ReH_2(NO)(PPh_3)_3$ is suspended in a minimum of ice-cold methanolic $HClO_4$ (0.5 mL for 200 mg of solid) and 0.5 mL of dichloromethane is added to the suspension, the solid quickly goes into solution accompanied by gas evolution. Flooding the resultant yellow–orange solution immediately with diethyl ether affords a yellow crystalline precipitate of $[ReH(CH_3OH)(NO)(PPh_3)_3]ClO_4$ (**1**), in excellent yield.

As mentioned earlier, this compound is thermally unstable and prone to violent or explosive decomposition at any time, or on heating above about 90°C. In solution, decomposition can also be rapid and unpredictable, even at low temperatures. For example, even at −80°C under nitrogen, sufficient decomposition usually takes place to give poorly defined ^1H nmr spectra. Thus, a typical spectrum would show a poorly resolved multiplet in the aromatic region, a broad singlet at 3.40 ppm attributable to methanol and a featureless lump at 1.6 ppm, presumably arising from the hydride ligand. Although the presence of the hydride could not be unequivocally established through ^1H nmr spectroscopy, the proton coupled ^{31}P nmr spectrum exhibited evidence of coupling between the hydride ligand and the *trans*-phosphine of 53 Hz. Unfortunately, the lines were too broad to discern any *cis* H—P or P—P couplings. On proton decoupling, the lines were still too broad to resolve P—P coupling, which for members of the series $ReHX(NO)(PPh_3)_3$, were typically around 8 Hz.

The ir spectrum of **1** exhibits bands due to νReH and νNO at 1993 and 1700 cm^{-1}, respectively. Evidence for the methanol ligand is seen in absorptions at 2810 and 3138 cm^{-1}, the former of which is diagnostic of the OCH_3 group (3) and the latter due to ν(O—H—O). On reacting $ReH_2(NO)(PPh_3)_3$ with $DClO_4$ in CH_3OD, $[ReH(CH_3OD)(NO)(PPh_3)_3]ClO_4$ (**1***a*) was obtained which had essentially the same spectrum as **1** but for ν(O—D—O) which appeared at 2326 cm^{-1}. That the perchlorate counterion is hydrogen bound to the methanol ligand is further supported by the appearance of five absorptions at 1122, 1031 (ν_3), 921 (ν_1), 616 (ν_4), and 448 (ν_2) cm^{-1}. These and other nmr and ir data are summarized in Tables 1 and 2. Further support for the proposed formulation is provided by the fact that **1** reacts with CO in dichloromethane–methanol solution to give good yields of previously characterized $[ReH(CH_3OH)(CO)(NO)(PPh_3)_2]ClO_4$ (1).

Unlike CO, however, *p*-tolylisocyanide reacts with **1** via a quite different pathway, giving instead the cations $[Re(OR)(NO)(RNC)_2(PPh_3)_2]^+$ (R = CH_3 or C_2H_5, depending on the alcohol used), isolable as both PF_6^- and ClO_4^- salts (**2**, **2***a*: R = C_2H_5; **3**, **3***a*, R = CH_3). These compounds have been fully characterized by the usual techniques and both ir and nmr data establish a *trans* arrangement for the isocyanide ligands. This reaction involves the formal elimination of dihydrogen, although the presence of elemental dihydrogen was not demonstrated, and is strongly reminiscent of the reaction of $[ReH(CH_3OH)(CO)(NO)(PPh_3)_2]ClO_4$ with anions to generate $ReH(OCH_3)X(CO)(NO)(PPh_3)_2$ (1). Most probably, the first step in the reaction of **1** with RNC involves replacement of the labile third phosphine, which we believe to be *trans* to the hydride ligand (*vide infra*), to generate $[ReH(CH_3OH)(RNC)(NO)(PPh_3)_2]ClO_4$. Having an excellent donor ligand such as *p*-tolylisocyanide *trans* to hydrogen in this manner should promote dihydrogen loss by making this ligand even more hydridic in nature. Certainly dihydrogen loss must be more rapid than the initial substitution since reaction of **1** with one equivalent of RNC yields only a mixture of **1** and **2** or **3**. It is interesting to note that **2** and **3** can also be synthesized by reacting $[ReH(CH_3OH)(CO)(NO)(PPh_3)_2]^+$ with excess RNC in the appropriate alcohol. Here, the initial reaction presumably involves substitution of the carbonyl group which, although unusual, is perhaps not too surprising in view of the relative weakness of the Re—CO bonding, manifested by a rather high νCO value of 2040 cm^{-1} in the starting material.

Although **1** reacts with neutral ligands with phosphine substitution, sometimes followed by dihydrogen elimination, reacting **1** with anionic ligands normally results in the substitution of the methanol ligand. Thus, **1** reacts with a methanol solution of X^- to give the derivatives $ReHX(NO)(PPh_3)_3$ (**4–9**). These complexes are all air-sensitive in the solid state and decompose readily in solution. Attempts to recrystallize **4** and **6–8** from dichloromethane–methanol in air produced materials apparently containing hydroperoxy ligands, which are the subject of further research. Because of their solution sensitivity, the characterization of **4–9** in solution was restricted to the more stable chloride, bromide, and azide derivatives only. The ^1H nmr spectra of all three compounds exhibit a doublet of triplets for the hydride proton with $^2J_{HP}$ (*cis*) in the range of 26–28 Hz and $^2J_{HP}$ (*trans*) around 67–72 Hz, in keeping with a *mer*-arrangement of phosphine ligands with the hydride *trans* to the unique phosphorus atom. The ^{31}P nmr spectra are consistent with this stereochemistry, consisting of a doublet and triplet in a 2:1 ratio, with $^2J_{PP}$ around 8 Hz. Not surprisingly, this coupling was most clearly resolved at low temperatures, implying the existence of

TABLE 1. Infrared data[a]

No.	Compound	ν(ReH)[b]	ν(NO)[c]	ν(CO)[c]	ν(NC)[c]	Others
1	$[ReH(CH_3OH)(NO)(PPh_3)_3]ClO_4$	1993	1700			ν(CH), 2864w, 2810w; ν(OHO), 3138w, br; ClO_4^-, 1122 vs, 1031 vs, 921 mw, 616 m, 448 w
1*a*	$[ReH(CH_3OD)(NO)(PPh_3)_3]ClO_4$	1990	1699			ν(ODO) 2360 sh, 2326 w
2	$[Re(OC_2H_5)(C_7H_7NC)_2(NO)(PPh_3)_2]PF_6$		1693		2134	ν(C—O), 1057 s; ρ(CH_2), 909 m; PF_6^-, 840 vs, 555 m
2*a*	$[Re(OC_2H_5)(C_7H_7NC)_2(NO)(PPh_3)_2]ClO_4$		1702		2136	ν(C—O), obscured; ρ(CH_2), 909 m; ClO_4^-, 1090 vs br, 621 m
3	$[Re(OCH_3)(C_7H_7NC)_2(NO)(PPh_3)_2]PF_6$		1694		2136	ν(CH), 2795 w; ν(C—O), 1068 s; PF_6^-, 840 vs. 555 m
3*a*	$[Re(OCH_3)(C_7H_7NC)_2(NO)(PPh_3)_2]ClO_4$		1701		2154	ν(CH), 2786 w; ν(C—O) obscured; ClO_4^-, 1091 vs, 622 m
4	$ReH(OCH_3)(NO)(PPh_3)_3$	1980	1634			ν(CH), 2787 w; ν(C—O), 1087 s; δ(ReH), 800 vw
5	$ReHF(NO)(PPh_3)_3$	1957	1655			δ(ReH), 782 w
6	$ReHCl(NO)(PPh_3)_3$	2017	1664 1656 s 1651 s			δ(ReH), 800 w; ν(ReCl), 269 m
7	$ReHBr(NO)(PPh_3)_3$	2020	1665 1656 s 1651 s			δ(ReH), 799 w
8	$ReH(N_3)(NO)(PPh_3)_3$	1980	1660			$\nu_a(N_3)$, 2079 vs; $\nu_s(N_3)$, 1338 w, δ(ReH), 780, 775 w
9	$ReH(NCO)(NO)(PPh_3)_3$	1956	1661 1657			ν_a(NCO), 2237 vs δ(ReH), 771 w
	$ReHX(CO)(NO)(PPh_3)_2$					
10	X = OCH_3 (1)	1870	1669	2004		ν(CH), 2776 mw ν(C—O), 1080 s δReH, 772 w
11	X = F (*trans* to NO)		1698	2000		
11*a*	X = F (*trans* to CO) (3)		1662	1970		
12	X = Cl		1715 1710 1704	2001		ν(ReCl), 306 m
13	X = Br		1717 1709 1702	2000		
14	X = N_3		1704 1700	2008		δ(ReH), 768 w; $\nu_a(N_3)$, 2084 vs $\nu_s(N_3)$, 1344 m
15	X = NCO		1702	2006		ν_a(NCO), 2238 vs; ν_s(NCO), 1366 m; δ(NCO), 598 w
16	X = I		1719	2004		δ(ReH), 784 w
17	X = SCN		1726	2020		ν_a(SCN), 2126 s; δ(ReH), 771 w
	$ReHX(C_7H_7NC)(NO)(PPh_3)_2$		1722			
18	X = OCH_3	1864	1646		2106	ν(CH), 2778 w; ν(C—O); 1089
19	X = F	1846	1656		2120	
20	X = Cl	1864	1668		2121	ν(ReCl), 269 m
21	X = Br	1866	1667		2120	
22	X = N_3	1859	1675		2121	$\nu_a(N_3)$, 2090 vs, 2076 vs, 2061 vs $\nu_s(N_3)$, 1351 w, 1333 w
23	X = NCO	1870	1679		2117	ν_a(NCO), 2239 vs, ν_s(NCO), 1353 m
24	X = I	1868	1676		2119	
25	X = SCN	1921	1686		2122	ν_a(SCN), obscured

[a]Nujol mulls. Values in cm^{-1}.
[b]All absorptions medium to weak.
[c]All absorptions very strong unless otherwise indicated.

Can. J. Chem. Downloaded from www.nrcresearchpress.com by 194.225.253.170 on 09/07/12
For personal use only.

TABLE 2. ^{31}P and ^{1}H nmr data[a]

No.	Compound	δ^1H (ReH)[b]	Others[b]
1	$[ReH(CH_3OH)(NO)(PPh_3)_3]ClO_4$	See text	$\delta^{31}P$, 22.95 br s, 15.20 br d ($^2J_{PH}$ = 53.4)
2	$[Re(OC_2H_5)(C_7H_7NC)_2(NO)(PPh_3)_2]PF_6$	—	OC_2H_5, 0.55 t, 2.89 q ($^3J_{HH}$ = 6.9) C_7H_7NC, 2.40 s, 6.80 q ($^3J_{AB}$ = 8.4) Ph, 7.46 m
3	$[Re(OCH_3)(C_7H_7NC)_2(NO)(PPh_3)_2]PF_6$	—	OCH_3, 2.88 s C_7H_7NC, 2.39 s, 6.79 q ($^3J_{AB}$ = 8.1) Ph, 7.48 m
6	$ReHCl(NO)(PPh_3)_3$	0.79 dt ($^2J_{HP1,2}$ = 27.5) ($^2J_{HP3}$ = 71.4)	Ph, 7.02 m $\delta^{31}P$, 17.38 d, −7.66 t ($^2J_{PP}$ = 8.1)
7	$ReHBr(NO)(PPh_3)_3$	0.47 dt ($^2J_{HP1,2}$ = 27.8) ($^2J_{HP3}$ = 67.8)	Ph, 7.32 m $\delta^{31}P$, 14.20 d, −10.60 t ($^2J_{PP}$ = 8.3)
8	$ReH(N_3)(NO)(PPh_3)_3$	0.50 dt ($^2J_{HP1,2}$ = 26.5) ($^2J_{HP3}$ = 66.8)	Ph, 7.19 m $\delta^{31}P$, 17.16 s, −0.010 s ($^2J_{PP}$ = 8.5)
	$ReHX(CO)(NO)(PPh_3)_2$		
10	X = OCH_3 (1)	3.82 t ($^2J_{HP}$ = 22.9)	OCH_3, 2.61 s Ph, 7.46 m
11	X = F (*trans* to NO)	4.62 dt ($^2J_{HP}$ = 23.5) ($^2J_{HF}$ = 13.4)	Ph, 7.46 m
11*a*	X = F (*trans* to CO) (3)	4.73 dt ($^2J_{HP}$ = 22.6) ($^2J_{HF}$ = 5.7)	Ph, 7.44 m
12	X = Cl	3.38 t ($^2J_{HP}$ = 23.5)	Ph, 7.46 m
13	X = Br	2.74 t ($^2J_{HP}$ = 23.6)	Ph, 7.46 m
14	X = N_3	3.35 t ($^2J_{HP}$ = 22.6)	Ph, 7.49 m
15	X = NCO	2.90 t ($^2J_{HP}$ = 23.0)	Ph, 7.49 m
16	X = I	1.56 t ($^2J_{HP}$ = 23.4)	Ph, 7.42 m
17	X = SCN	2.34 t ($^2J_{HP}$ = 21.5)	Ph, 7.48 m
	$ReHX(C_7H_7NC)(NO)(PPh_3)_2$		
18	X = OCH_3	2.95 t ($^2J_{HP}$ = 21.4)	OCH_3, 2.55 s C_7H_7NC, 2.32 s, 6.68 q ($^3J_{AB}$ = 8.3) Ph, 7.39 m
19	X = F	3.78 dt ($^2J_{HP}$ = 22.2) ($^2J_{HF}$ = 13.3)	C_7H_7NC, 2.33 s, 6.72 q ($^3J_{AB}$ = 8.1) Ph, 7.43 m
20	X = Cl	2.63 t ($^2J_{HP}$ = 21.9)	C_7H_7NC, 2.35 s, 6.77 q ($^3J_{AB}$ = 8.3) Ph, 7.37 m
21	X = Br	2.06 t ($^2J_{HP}$ = 20.6)	C_7H_7NC, 2.35 s, 6.80 q ($^3J_{AB}$ = 8.4) Ph, 7.36 m
22	X = N_3	2.64 t ($^2J_{HP}$ = 21.5)	C_7H_7NC, 2.35 s, 6.80 q ($^3J_{AB}$ = 8.3) Ph, 7.44 m
23	X = NCO	2.13 t ($^2J_{HP}$ = 21.3)	C_7H_7NC, 2.35 s, 6.76 q ($^3J_{AB}$ = 8.4) Ph, 7.44 m
24	X = I	1.02 t ($^2J_{HP}$ = 21.5)	C_7H_7NC, 2.38 s, 6.85 q ($^3J_{AB}$ = 8.6) Ph, 7.34 m
25	X = SCN	1.49 t ($^2J_{HP}$ = 19.3)	C_7H_7NC, 2.36 s, 6.94 q ($^3J_{AB}$ = 8.4) Ph, 7.42 m

[a] CD_2Cl_2 as solvent, all calibrated with reference to the $CHDCl_2$ triplet at 5.32 ppm or H_3PO_4 at 0.00 ppm. All signals give satisfactory integrals.

[b] Coupling constants in Hz.

an exchange process between the phosphine *trans* to the hydride and adventitious triphenylphosphine, present either as a trace impurity or resulting from minor decomposition in the sample.

Infrared spectra of **4–9** are also in keeping with a *trans* arrangement of the X and nitrosyl ligands. The observed range for νNO is 1634 to 1665 cm^{-1} comparable to the νCO range of 1893 to 1927 cm^{-1} seen in the isoelectronic series $OsHX(CO)(PPh_3)_3$ of similar geometry (4). Furthermore, the trend seen in νNO as X varies is analogous to that seen in the osmium series, especially so with the lower extreme of the two series. In both cases, OR (R = H for the osmium case) and F ligands generate the lowest νNO and νCO values, further illustrating their strong π-donor characteristics (5). Infrared spectra also establish that for $ReH(NCO)(NO)(PPh_3)_3$ (**9**) the cyanate ligand is N-bonded (ν(NC) = 2237 cm^{-1}) (6).

Attempts to synthesize members of this series with X = I and

Can. J. Chem. Downloaded from www.nrcresearchpress.com by 194.225.253.170 on 09/07/12
For personal use only.

Can. J. Chem. Downloaded from www.nrcresearchpress.com by 194.225.253.170 on 09/07/12
For personal use only.

SCN met with mixed success. Following the usual procedure yielded yellow solids exhibiting clean ir spectra virtually identical to those observed for the other members, except for bands attributable to methanol. Both ^1H and ^{31}P nmr spectra, on the other hand, indicated the presence of complex mixtures in solution. Despite being mixtures, however, both products formed single derivatives when reacted with CO and *p*-tolylisocyanide (*vide infra*).

The *trans* hydride ligand in $ReHX(NO)(PPh_3)_3$ contributes to the lability of the unique phosphine making substitution with small neutral ligands very facile. Thus reacting complexes **4–9** with ligands L gives rise to the hydride series $ReHX(L)(NO)(PPh_3)_2$ (**10–15**, L = CO; **18–23**, L = RNC).[3] Reacting the yellow materials described above, obtained from the reaction of **1** with I^- or SCN^- yielded further members of the series, **16**, **17**, **24**, and **25**. There can be little question that the complexes **10–25** share the same stereochemistry, viz *trans* PPh_3 ligands and X *trans* to NO, which further supports the geometry assigned for $ReHX(NO)(PPh_3)_3$. The presence of *trans* PPh_3 groups in **10–25** is confirmed by the hydride signal in the ^1H nmr existing as a triplet in all cases, with fairly typical $^2J(HP)$ coupling constants of *ca.* 20–24 Hz. As we have observed with most other rhenium hydrido nitrosyls, chemical shifts for the hydride ligand are low by comparison to analogous complexes from groups 8–10 (1, 3).

That the X group is *trans* to NO is shown most clearly in $ReH(OCH_3)(CO)(NO)(PPh_3)_2$ (**10**) prepared in this way and $ReHF(CO)(NO)(PPh_3)_2$ (**11**). Complex **10** has identical spectroscopic parameters with samples isolated by different means and shown by deuteration studies to have the OCH_3 ligand *trans* to NO (1). We have also shown previously that reacting the cation $[ReF(CO)(NO)(PPh_3)_3]^+$ with BH_4^- gives $ReHF(CO)(NO)(PPh_3)_2$ (**11***a*), for which deuteration established that the fluoro ligand was *trans* to CO (3). We postulated at the time that this was probably a kinetic isomer, even though attempts to isomerize this isomer to the thermodynamically stable form with F *trans* to NO failed. Not surprisingly, therefore, complex **11** has quite different spectroscopic properties from its previously isolated isomer **11***a*. The data for both isomers are presented in the tables for ease of comparison.

Changing from H *trans* to NO in **11***a* to H *trans* to CO in **11** has some predictable consequences in the infrared spectra. Because νReH in both complexes **11** and **11***a* is intermediate in value between νCO and νNO, the presence of a Fermi resonance interaction will raise the former and decrease the latter. Thus, on going from **11***a* to **11**, νCO increases because a resonance interaction is introduced and νNO is likewise increased because a similar interaction is removed. The effect of the resonance interactions is overlaid with the electronic effects inherent in changing the ligand *trans* to CO and NO. The fluoro ligand is known for its excellent π-donor characteristics and hence its ability to lower νCO and νNO when *trans* to those ligands (5, *vide supra*). In the case of **11** and **11***a*, these two effects work in the same direction for νCO but oppose each other in determining the value of νNO. Since νNO shifts to a lower values in **11***a*, it would appear that the resonance interaction is the more important. Unfortunately, and for reasons which are not clear, νReH in the series **10–17** could not be observed, even though it is seen at 1870 cm^{-1} in $ReH(OCH_3)(CO)(NO)(PPh_3)_2$, at 1835 cm^{-1} in **11***a* and in the entire series **18–25**. The spectroscopic differences between **11** and its isomer **11***a* in the ^1H nmr are less pronounced, except for $^2J(HF)$ which for **11** is over twice that of **11***a*. The significance of this difference is not apparent since such coupling constants are sufficiently rare for it to be impossible to establish what represents a normal value.

It is interesting to note that the thiocyanate ligand in both **17** and **25** appears to be S-bound. The νNC values for these complexes of around 2125 cm^{-1} fall well within the S-bound range and there is no evidence of νCS in the 800–850 cm^{-1} region (6, 8). This situation is to be contrasted with that found for the complexes $ReX(NCS)(CO)(NO)(PPh_3)_2$ (X = OR, Cl)[4] in which νNC occurs around 2080 cm^{-1} and is accompanied by a sharp νCS absorption in the vicinity of 845 cm^{-1}. The observation of S-bound thiocyanate groups comes as a surprise since, in our experience, the site *trans* to NO in Re(I) nitrosyls seems to favor coordination by hard ligands (1, 3). It would appear therefore that **17** and **25** are kinetic isomers derived from a precursor in which the thiocyanate ligand is also S-bound. There is in fact some evidence to support this conjecture. Infrared spectra of the precursor show νNC absorptions at 2105 cm^{-1}, borderline between the ranges normally accepted for the two coordination modes, and no evidence of a νCS band. Without knowing the exact nature of the component(s) in the precursor that give rise to **17** and **25**, it is impossible to determine what factors might be responsible for determining the mode of thiocyanate coordination. There is, however, a growing body of evidence suggesting that steric pressures play a significant role (ref. 6, pp. 338–354, 382–385; ref. 9). So, for example, arguments based on steric grounds have been used to help explain the mode of thiocyanate bonding in *mer*-$Mn(NCS)(CO)_3L_2$ versus *fac*-$Mn(SCN)(CO)_3L_2$ (L = $AsPh_3$, $SbPh_3$) (10). This could be taken to indicate that the principal component of the mixture responsible for the generation of **17** and **25** is simply $ReH(SCN)(NO)(PPh_3)_3$.

[3]Complex **11**, $ReHCl(CO)(NO)(PPh_3)_2$, has been alluded to in a recent publication (7).

Acknowledgements

The authors acknowledge the financial support of the Natural Sciences and Engineering Research Council of Canada and the award of a Summer Research Studentship to J.Y.C. Thanks also to the Atlantic Region Magnetic Resonance Centre for obtaining the nmr spectra.

1. K. R. Grundy and K. N. Robertson. Inorg. Chem. **24**, 3898 (1985).
2. K. N. Raymond. Chem. Eng. News, **61**, 4 (1983); W. C. Wolsey. J. Chem. Educ. **55**, A355 (1978); Chem. Eng. News, **41**, 47 (1963).
3. T. S. Cameron, K. R. Grundy, and K. N. Robertson. Inorg. Chem. **21**, 4149 (1982).
4. K. R. Grundy. Ph.D. Thesis, University of Auckland. 1975.
5. C. A. Reed and W. R. Roper. J. Chem. Soc. Dalton, 1370 (1973).
6. A. H. Norbury. Adv. Inorg. Chem. Radiochem. **17**, 231 (1975).
7. G. L. Hillhouse and B. L. Haymore. Inorg. Chem. **26**, 1876 (1987).
8. R. A. Bailey, S. L. Kozak, T. W. Michelson, and W. N. Mills. Coord. Chem. Rev. **6**, 407 (1971).
9. C. T. Hunt and A. L. Balch. Inorg. Chem. **21**, 1242 (1982).
10. M. F. Farona and A. Wojcicki. Inorg. Chem. **4**, 1402 (1965).

[4]K. R. Grundy and K. N. Robertson. Unpublished results.

Drop calorimetry of the compounds $NbCl_5$, $TaCl_5$, $RbNbCl_6$, $CsNbCl_6$, $RbTaCl_6$, and $CsTaCl_6$

E. E. SHAWKI,[1] S. N. FLENGAS, AND D. R. SADOWAY[2]

Department of Metallurgy and Materials Science, University of Toronto, Toronto, Ont., Canada M5S 1A4

Received February 9, 1988[3]

E. E. SHAWKI, S. N. FLENGAS, and D. R. SADOWAY. Can. J. Chem. **67**, 1193 (1989).

Enthalpy contents for $NbCl_5$, $TaCl_5$, $RbNbCl_6$, $CsNbCl_6$, $RbTaCl_6$, and $CsTaCl_6$ were measured as functions of temperature using a high temperature aluminum block drop calorimeter. It was found that the solid compounds $RbNbCl_6$, $CsNbCl_6$, $RbTaCl_6$, and $CsTaCl_6$ undergo allotropic solid–solid transformations and the enthalpies and entropies associated with these phase changes, as well as from fusion, have been evaluated.

Molar heat capacities for the systems investigated are reported as linear functions of temperature.

The molar heat capacities for solid and molten $NbCl_5$ or $TaCl_5$ were used together with available vapour pressure data to express enthalpies and free energies of vaporization for these compounds as functions of temperature through the third law calculation method.

Key words: calorimetry, heat capacities, transition enthalpies, niobium compounds, tantalum compounds.

E. E. SHAWKI, S. N. FLENGAS et D. R. SADOWAY. Can. J. Chem. **67**, 1193 (1989).

Utilisant un calorimètre adiabatique en aluminium opérant à haute température, on a mesuré les enthalpies du $NbCl_5$, du $TaCl_5$, du $RbNbCl_6$, du $CsNbCl_6$, du $RbTaCl_6$ et du $CsTaCl_6$ en fonction de la température. On a trouvé que les composés solides $RbNbCl_6$, $CsNbCl_6$, $RbTaCl_6$ et $CsTaCl_6$ subissent des transformations allotropiques solide–solide et on a évalué les enthalpies et les entropies associées avec ces changements de phase ainsi qu'avec la fusion.

On rapporte les capacités calorifiques molaires des systèmes étudiés sous la forme de fonctions linéaires de la température.

Faisant appel à la méthode de calcul de la troisième loi de la thermodynamique et utilisant les capacités calorifiques molaires des $NbCl_5$ et $TaCl_5$ solides et fondus de concert avec les données disponibles relatives aux pressions de vapeur, on a pu obtenir une expression permettant de relier les enthalpies et les énergies libres de vaporisation de ces composés en fonction de la température.

Mots clés: calorimétrée, capacités calorifiques, enthalpies de transition, composés de niobium, composés de tantalum.

[Traduit par la revue]

Can. J. Chem. Downloaded from www.nrcresearchpress.com by 194.225.253.170 on 09/07/12
For personal use only.

Introduction

The complex compounds $NaNbCl_6$, $NaTaCl_6$, $KNbCl_6$, $KTaCl_6$, $RbNbCl_6$, $RbTaCl_6$, $CsNbCl_6$, and $CsTaCl_6$ have been synthesized in this laboratory by the reaction of $NbCl_5$ or $TaCl_5$ vapours with the respective alkali metal chlorides, in closed reactors, under specific temperature and vapour pressure conditions. The preparation method has been given elsewhere (1). X-ray diffraction patterns were also determined and temperatures for phase transformations were measured by the cooling curve technique.

These compounds represent thermodynamically stable forms of the volatile covalently bonded pentachlorides of Nb and Ta (2, 3) and, as such, they are of interest for the separation of Nb from Ta (4), and as potential electrolytes for the recovery of these metals by used salt electrolysis.

Crystal structures of the $AMCl_6$ type compounds, where A is an alkali metal like Na, K, Rb, and Cs, and M is either Nb or Ta, and parts of the phase diagrams of the ACl–MCl_5 type binary systems have also been reported by several investigators (1, 5–9).

In the present investigation the thermal properties of the compounds $NbCl_5$, $TaCl_5$, $RbNbCl_6$, $CsNbCl_6$, $RbTaCl_6$, and $CsTaCl_6$ were measured by drop calorimetry from various high temperatures. From these measurements molar heat capacities have been calculated as functions of temperature, and enthalpy changes representing solid–solid allotropic transformations and melting have been obtained.

Thermal data for these compounds, with the exception of $NbCl_5$ and $TaCl_5$, are not available in the literature.

Experimental

The preparation of anhydrous $NbCl_5$ and $TaCl_5$ having a purity better than 99.99% by weight and the synthesis of the stoichiometric $AMCl_6$-type compounds having a purity better than 99.8% by weight, have been described elsewhere (1, 2). The stoichiometry of each complex compound was determined from the weight gain of the alkali chloride when it is reacted with either $NbCl_5$ or $TaCl_5$ vapours. In all cases the mole ratio MCl_5/ACl was better than 0.995.

The twin Al-block drop calorimeter used for these measurements was the same instrument previously designed and built in this laboratory (10, 11).

The calorimeter proper was calibrated with synthetic sapphire certified by the U.S. Bureau of Standards. Its enthalpy content is known to be the following function of temperature (12),

$$[1] \quad H_T - H_0 = 82.1461 + 1.7106 \times 10^{-6} T^2 - 46.9949 \times \log_{10} T + 0.1485704\, T \ (\text{in kJ mol}^{-1})$$

where T is in Kelvin.

A typical calorimetric trace is given in Fig. 1.

The measured thermopile signals were all referred to a common reference temperature of 298 K, using the linear correction method of Goodkin *et al.* (13).

Since evacuated silica glass capsules lined with Pt-foil 0.5 mm thick were used as containers for the sapphire and for the salt samples, experiments were performed to determine the thermopile output per gram of silica and per gram of Pt, for temperatures up to 650°C. The least squares fit to 27 experimental points for SiO_2 corresponds to the linear equation,

[1]Present address: Ubichem Limited, Chandlers Ford Industrial Estate, Eastleigh, Hampshire 5O5 3AR, U.K.

[2]Present address: Department of Materials Science and Engineering, Massachusetts Institute of Technology, Cambridge, MA 02139, U.S.A.

[3]Revision received January 30, 1989.

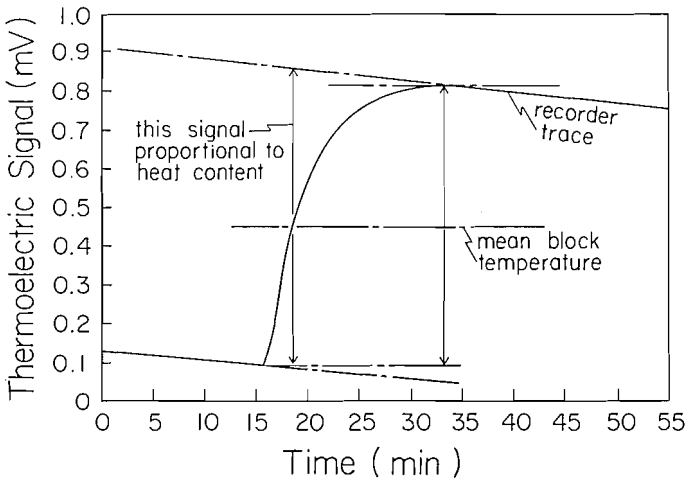


FIG. 1. Typical calorimetric trace of the thermopile signal.

[2] $V_{SiO_2} = -2.3943 \times 10^{-2} + 6.4691 \times 10^{-5} T + 1.83271 \times 10^{-8} T^2 + 849.5 \times 10^{-3} T^{-1}$ (in mV/g SiO_2)

where T is given in Kelvin. The correlation coefficient is 0.9997 and the standard error of estimate is 3.129×10^{-3} mV/g SiO_2.

The latter is a measure of the scatter about the linear regression curve and is calculated from the well known expression

$$S_{y,x} = \sqrt{\frac{\Sigma d^2}{n}}$$

where d's are the differences between the experimental and the estimated values of a dependent variable y, where $y = f(x)$.

The corresponding thermoelectric signal for platinum, based on eleven determinations, was

[3] $V_{Pt} = 4.692 \times 10^{-3} + 4.498 \times 10^{-6} T + 3.205 \times 10^{-9} T^2 + 177.194 \times 10^{-6} T^{1/2}$ (in mV/g Pt)

The correlation coefficient is 0.9996 and the standard error is 6.5×10^{-6} mV/g Pt, for temperatures up to 650°C.

Eleven drops were made with capsules containing the NBS sapphire to cover the temperature range from 150 to 650°C.

In a typical calibration experiment, the weight of the silica capsule was 7.0 g, the weight of Pt liner was 1.0 g, and that of the synthetic sapphire was 7 g.

The calorimetric constant of the instrument, or the number of joules corresponding to one millivolt of thermopile emf, was calculated from eqs. [1], [2], and [3]. The mean of eleven determinations, from 160 to 663°C, gave a value of 11 853 ± 259 J per mV.

There was no detectable temperature dependence.

With this value, and eqs. [1] and [2], the enthalpy contents of silica and platinum, at 600°C, were calculated and compared well with literature values (14). Thus, $H_{600} - H_{298}$ for platinum, which is given as 8 066 J mol^{-1}, compares well with the present value of 8 100 J mol^{-1} calculated from the present results. Similarly, for silica, the literature value of 16 556 J mol^{-1} compares well with the present 16 300 J mol^{-1}.

From such comparisons and from calculations of the standard errors, it is estimated that the calorimeter used for the present measurements was capable of measuring enthalpy contents with confidence to better than 2%.

Enthalpy contents for the various compounds were measured on at least two samples for each compound. Sample weights were between 10 and 15 g. The vapour space in the capsules was small enough that vaporization had a negligible effect on enthalpies.

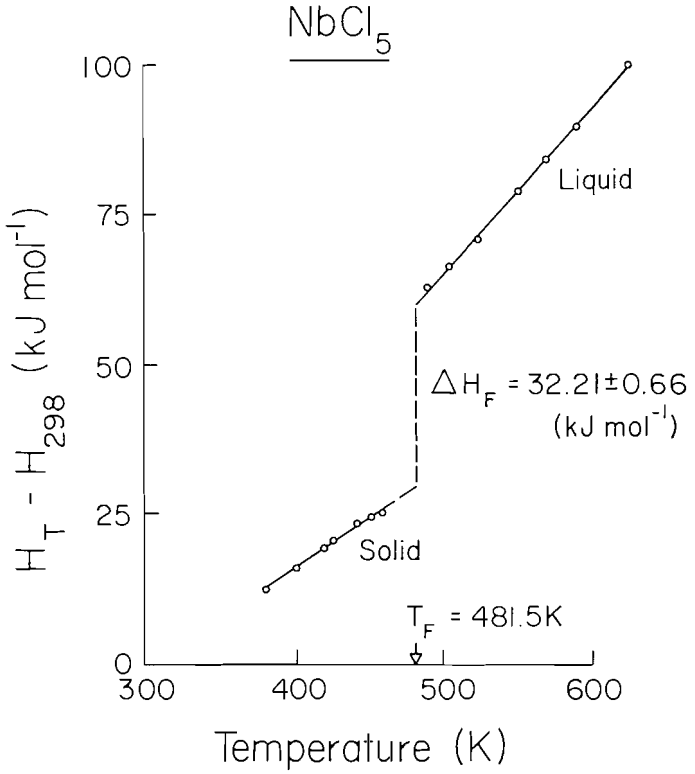


FIG. 2. Enthalpy content of $NbCl_5$ as a function of temperature. Points are experimental. Curves drawn through points represent the least squares fit from Table 1.

Results

Plots of $H_T - H_{298}$ for the various compounds investigated are presented in Figs. 2 to 7. The data have been fitted by least squares to second order polynomials of the form,

[4] $H_T - H_{298} = a + bT + cT^2$ (kJ mol^{-1})

Values of the coefficients a, b, and c are given in Table 1 together with the corresponding standard errors and the temperature ranges of measurements.

Molar heat capacities are readily calculated from eq. [4] from the expression $(\partial H/\partial T)_p = C_p$, as

[5] $C_p = A + BT$ (J K^{-1} mol^{-1})

The coefficients A and B for the molar heat capacities, transition enthalpies, and transition temperatures, are given in Table 2.

Enthalpy changes corresponding to solid–solid transformations, or to melting, have been obtained by extrapolating the enthalpy contents for any two different phases to the corresponding transition temperatures.

Prior to a drop, solid samples of a compound in either the α or the β configuration were kept at the desired constant high temperature for time periods differing by over 6 h with no detectable effect on their enthalpy contents. It appears, therefore, that complete conversion to the higher temperature configuration was achieved in all cases.

Discussion

A survey of the literature shows only one other calorimetric study of the enthalpy content of $NbCl_5$. Keneshea *et al.* (15) measured the enthalpy increments above 298 K for solid and

Can. J. Chem. Downloaded from www.nrcresearchpress.com by 194.225.253.170 on 09/07/12
For personal use only.

Can. J. Chem. Downloaded from www.nrcresearchpress.com by 194.225.253.170 on 09/07/12
For personal use only.

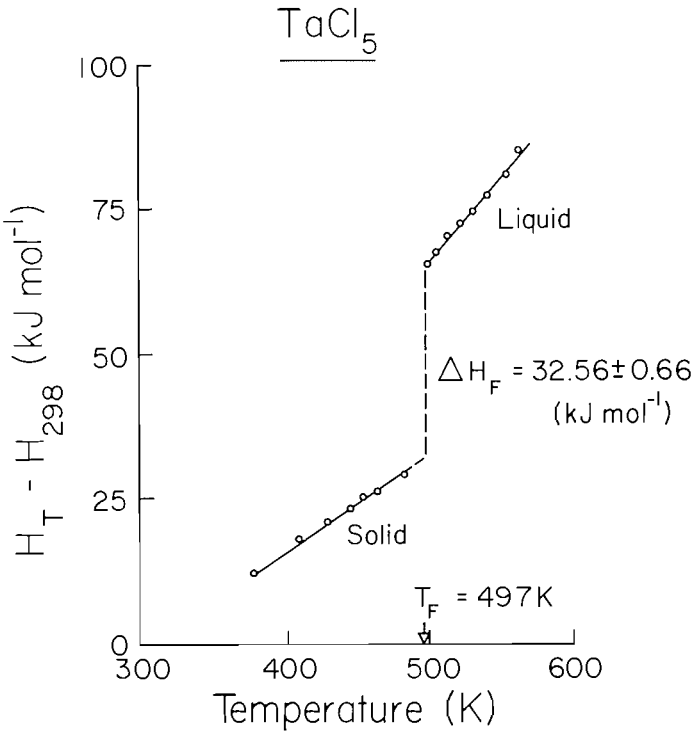


FIG. 3. Enthalpy content of $TaCl_5$ as a function of temperature. Points are experimental. Curves drawn through points represent the least squares fit from Table 1.

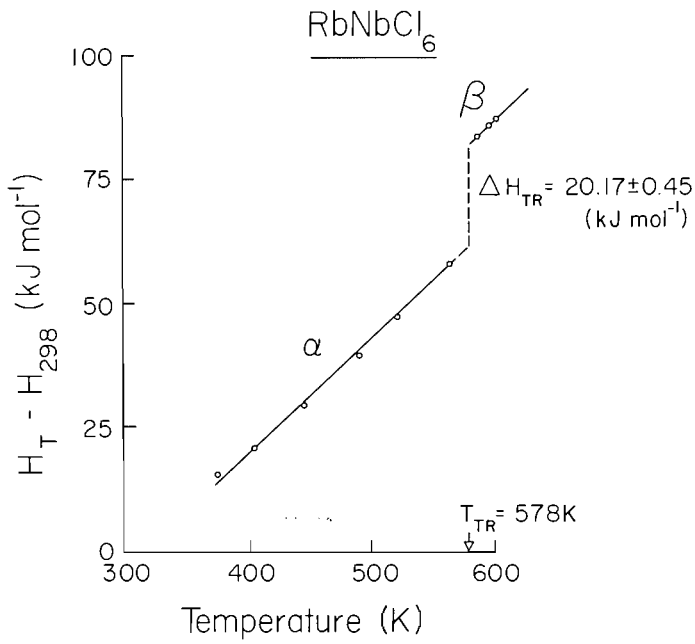


FIG. 4. Enthalpy content of $RbNbCl_6$ as a function of temperature. Curves drawn through the experimental points represent the least squares fit from Table 1.

liquid $NbCl_5$. Their results are given respectively as,

[6] $(H_T^0 - H_{298}^0)_s = -44.06 + 14.79 \times 10^{-2} T$, $\pm$ 0.29 kJ mol^{-1} for solid $NbCl_5$

and

[7] $(H_T^0 - H_{298}^0)_l = -50.71 + 23.96 \times 10^{-2} T - 30.71 \times 10^{-9} T^3$, $\pm$ 0.92 kJ mol^{-1} for liquid $NbCl_5$

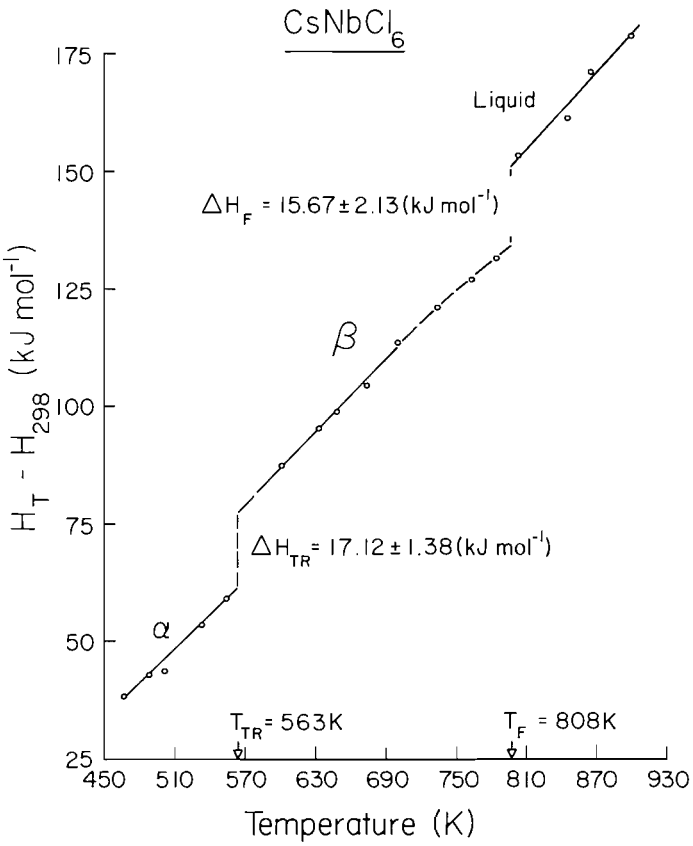


FIG. 5. Enthalpy content of $CsNbCl_6$ as a function of temperature. Curves drawn through the experimental points represent the least squares fit from Table 1.

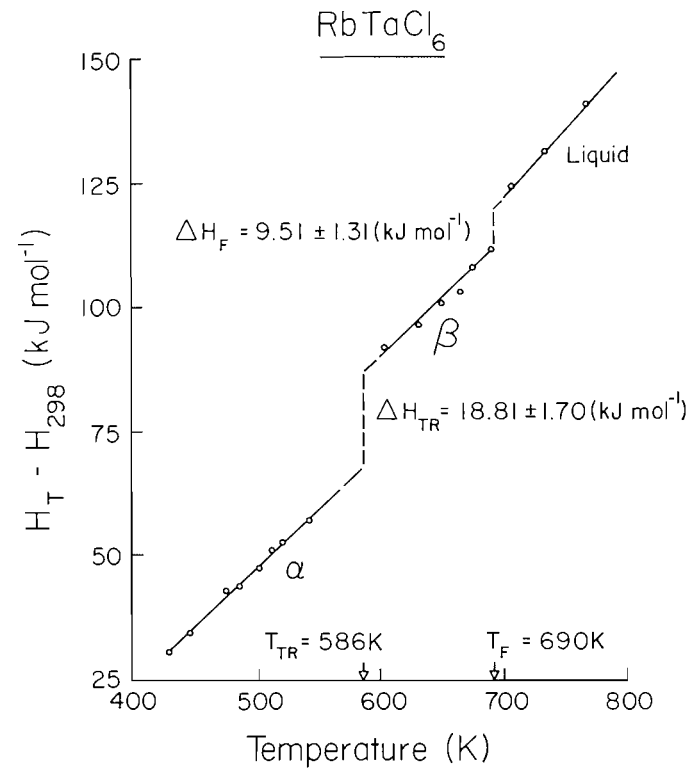


FIG. 6. Enthalpy content of $RbTaCl_6$ as a function of temperature. Curves drawn through the experimental points represent the least squares fit from Table 1.

TABLE 1. Calorimetric enthalpy data fitted by least squares to the equation $H_T - H_{298} = a + bT + cT^2$ (kJ mol^{-1})

Compound	a	$b \times 10^2$	$c \times 10^6$	Standard error of estimate (±)	Temperature range of measurements (K)	Sample characteristics
$NbCl_5$ (s)	−46.67	15.673	—	0.364	380–481	Yellow powder
$NbCl_5$ (ℓ)	−68.032	26.819	—	0.552	481–626	
$TaCl_5$ (s)	−45.062	14.820	21.757	0.318	379–497	White powder
$TaCl_5$ (ℓ)	−87.885	30.694	—	0.585	497–563	
α-$RbNbCl_6$ (s)	−37.664	7.795	162.76	0.443	376–578	Green powder (3)
β-$RbNbCl_6$ (s)	−51.149	23.012	—	0.088	578–602	
α-$CsNbCl_6$ (s)	−59.844	18.560	51.463	0.410	467–563	Green powder (3)
β-$CsNbCl_6$ (s)	−38.752	18.263	43.93	1.314	563–808	
$CsNbCl_6$ (ℓ)	−74.425	28.192	—	1.682	808–898	
α-$RbTaCl_6$ (s)	−69.350	23.259	—	1.301	429–586	White powder (3)
β-$RbTaCl_6$ (s)	−58.844	24.673	—	1.096	586–690	
$RbTaCl_6$ (ℓ)	−51.170	24.941	—	0.720	690–812	
α-$CsTaCl_6$ (s)	−77.722	25.983	—	0.749	480–569	White powder (3)
β-$CsTaCl_6$ (s)	−81.245	28.966	—	1.623	569–821	
$CsTaCl_6$ (ℓ)	−83.755	30.652	—	0.744	821–877	

Can. J. Chem. Downloaded from www.nrcresearchpress.com by 194.225.253.170 on 09/07/12
For personal use only.

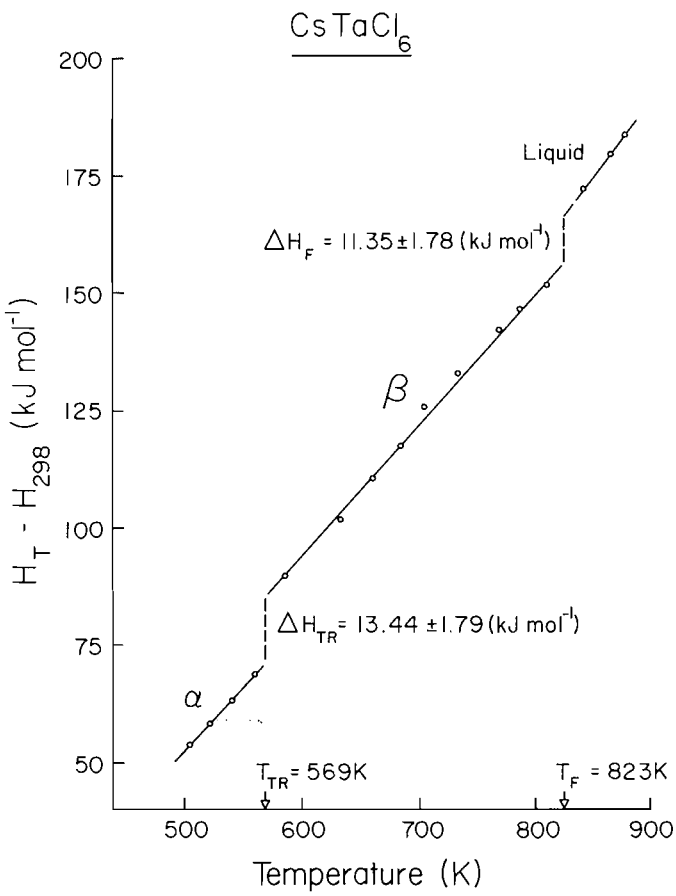


FIG. 7. Enthalpy contents of $CsTaCl_6$ as a function of temperature. Curves drawn through the experimental points represent the least squares fit from Table 1.

Experimental measurements of the heat capacities of solid and liquid $TaCl_5$ could not be found in the literature. However, Schaefer and Kahlenberg (16) estimated the heat capacity of $TaCl_5$ by comparison with the heat capacities of $ZrCl_4$ and $HfCl_4$. According to their estimates

[8] $C_{p(s)TaCl_5} = 159.0 - 12.55 \times 10^5 T^{-2}$ (J K^{-1} mol^{-1})

Heat capacities for solid $TaCl_5$ calculated from eq. [8] are about 8% lower than the present results.

A comparison between enthalpies of fusion for $NbCl_5$, reported by several investigators, is given in Table 3.

The standard enthalpy and entropy increments for $TaCl_5$ up to 550 K calculated from the present results are tabulated in Table 1.

Interpolation of the solid and liquid enthalpy lines to the melting points at 497 K gives the heat of fusion of $TaCl_5$ as

$$\Delta H_{f(TaCl_5)} = 32.56 \pm 0.66 \text{ (kJ mol}^{-1}\text{)}$$

This value is compared with the literature values in Table 3. It appears from the above comparison that the measured enthalpy of fusion is in excellent agreement with values by Shchukarev *et al.* (19) and by Saeki *et al.* (20) calculated from vapour pressure measurements. The present value is about 10% lower than that obtained by Dobrotin *et al.* (17) from calorimetric measurements for which no error limits were given.

Uncertainties in transition enthalpies are obtained by taking the square root of the sum of the squares of the standard errors of estimates for each of the enthalpy curves before and after a transition temperature, respectively.

As the equilibrium vapour pressures for the pure solid and pure liquid $NbCl_5$ (1, 21–26) and $TaCl_5$ (27), respectively, are available, the temperature dependence of the thermodynamic functions for each system may be calculated using the well known Σ-function method (28).

Molar heat capacities for gaseous $NbCl_5$ and $TaCl_5$ are also known and have been included in Table 2. If the heat capacities of either the gaseous or condensed state materials are represented by eq. [5]. The Σ-function for either the vaporization or sublimation reactions of $NbCl_5$ and $NbCl_5$ is given as

[9] $$\Sigma = \frac{\Delta H_0}{T} + \mathrm{I} = -R \ln P + \Delta A \ln T + \frac{\Delta B}{2} T$$

where ΔA and ΔB are the differences between the heat capacity constants of the gaseous and the corresponding condensed phases.

The enthalpy of vaporization, ΔH_v, or sublimation, ΔH_s, can then be expressed in the form

Can. J. Chem. Downloaded from www.nrcresearchpress.com by 194.225.253.170 on 09/07/12
For personal use only.

TABLE 2. Molar heat capacities and transition thermodynamic properties calculated from data in Table 1*

Compound	$C_p = A + BT$* (J K^{-1} mol^{-1}) A	$B \times 10^3$	Temperature range (K)	T_{Tr} Transition temperature $\alpha \rightarrow \beta$ (K)	ΔH_T* at T_{Tr} (kJ mol^{-1})	ΔS_T (J K^{-1} mol^{-1})	T_F fusion temperature (K)	ΔH_F* at mp (kJ mol^{-1})	ΔS_F (J K^{-1} mol^{-1})	C_p† at 298 K (J K^{-1} mol^{-1})	Crystal structure
$NbCl_5$ (s)	156.73	—	380–481	—	—	—	481 (3)	32.21±0.66	67.15±1.77	156.73	Monoclinic (31)
$NbCl_5$ (ℓ)	268.20	—	481–626	—	—	—	—	—	—	268.20	—
$TaCl_5$ (s)	144.43	43.51	379–497	—	—	—	497	32.56±0.66	65.52±1.33	157.40	Monoclinic (31)
$TaCl_5$ (ℓ)	306.94	—	497–563	—	—	—	—	—	—	306.94	—
α-$RbNbCl_6$ (s)	77.95	325.52	376–568	578 (3)	20.17±0.45	34.90±0.78	—	—	—	174.83	Incongruently melting compound, tetragonal (8)
β-$RbNbCl_6$ (s)	230.12	—	578–602	—	—	—	653 (3)	—	—	230.12	—
α-$CsNbCl_6$ (s)	185.60	102.93	467–563	563 (3)	17.12±1.38	30.41±2.45	—	—	—	218.36	Tetragonal (8)
β-$CsNbCl_6$ (s)	182.63	87.86	563–808	—	—	—	808 (3)	15.67±2.13	19.39±2.64	208.94	—
$CsNbCl_6$ (ℓ)	281.92	—	801–898	—	—	—	—	—	—	281.92	—
α-$RbTaCl_6$ (s)	232.60	—	429–586	586 (3)	18.81±1.70	32.10±2.90	—	—	—	232.60	—
β-$RbTaCl_6$ (s)	246.73	—	586–690	—	—	—	690 (3)	9.51±1.31	13.77±1.90	246.73	Hexagonal (3)
$RbTaCl_6$ (ℓ)	249.41	—	690–812	—	—	—	—	—	—	249.41	—
α-$CsTaCl_6$ (s)	259.83	—	480–569	569 (3)	13.44±1.79	23.64±3.14	—	—	—	259.83	Hexagonal (3)
β-$CsTaCl_6$	289.66	—	569–821	—	—	—	813 (3)	11.35±1.78	13.81±2.19	289.53	—
$CsTaCl_6$ (ℓ)	306.52	—	823–877	—	—	—	—	—	—	306.69	—

*Data rounded up to the second decimal. For $NbCl_{5\ (vap)}$ (29): $C_p = 132.76 - 11.205 \times 10^5\ T^{-2}$ in J K^{-1} mol^{-1}.

†Extrapolated values. For $TaCl_{5(vap)}$: $C_p = 132.2 - 15.48 \times 10^5\ T^{-2}$ in J K^{-1} mol^{-1} (estimated (16)).

TABLE 3. Comparison of enthalpy of fusion values for $NbCl_5$ and $TaCl_5$

Compound	ΔH_T* at mp (kJ mol^{-1})	Method	Reference
$NbCl_5$	32.21±0.66	Drop calorimetry	This work
$NbCl_5$	33.85±0.96	Drop calorimetry	15
$NbCl_5$	34.72±1.67	Phase equilibria	18
$NbCl_5$	28.66±2.30	Vapour pressures	2
$TaCl_5$	32.56±0.66	Drop calorimetry	This work
$TaCl_5$	35.98	Calorimetry	17
$TaCl_5$	26.15±3.56	Vapour pressure	2
$TaCl_5$	32.63	Vapour pressure	19
$TaCl_5$	33.05	Vapour pressure	20
$TaCl_5$	25.52	Vapour pressure	21

*The melting points are those reported in the respective investigations.

$$[10] \quad \Delta H_{v \text{ or } s} = \Delta H_0 + \Delta AT + \frac{\Delta B}{2} T^2$$

and similarly, the free energies of vapourization or sublimation are given as

$$[11] \quad \Delta G_{v \text{ or } s} = IT + \Delta H_0 - \Delta AT \ln T - \frac{\Delta B}{2} T^2$$

the unknowns in the above equations, i.e., ΔH_0 and I, are integration constants that can be determined from a plot of Σ versus $1/T$, as the slope and the intercept, respectively.

For the vaporization reaction,

$$[12] \quad NbCl_{5(liquid)} \rightarrow NbCl_{5(vapour)}$$

for temperatures up to 600 K, the corresponding Σ-plot was linear and least squares regression analysis yielded the enthalpy and free energy functions as

$$[13] \quad \Delta H_v = 126.54 - 0.1354\,T + 11.20 \times 10^5\,T^{-1} \quad (\pm 0.79 \text{ kJ mol}^{-1})$$

and as

$$[14] \quad \Delta G_v = 126.53 + 1.0924\,T + 0.1354\,T \ln T + 5.6 \times 10^{-3}\,T^{-1} \quad (\pm 0.79 \text{ kJ mol}^{-1})$$

The enthalpy of vaporization calculated from eq. [13] at the boiling temperature of 502.3 K is 60.67 ± 0.79 kJ mol^{-1}. Literature values vary from 46.86 to 62.76 ± 6.3 kJ mol^{-1}, while the vapour pressures calculated from the free energy function in eq. [14] compare very well with the vapour pressures measured in our laboratory (2).

For the sublimation reaction,

$$[15] \quad NbCl_{5(s)} \rightarrow NbCl_{5(vap)}$$

$$[16] \quad \Delta H_s = 95.621 + 1.548 \times 10^3\,T^{-2} \quad (\pm 3.0 \text{ kJ mol}^{-1})$$

For $TaCl_5$, the upper temperature limit for vapourization was 511 K, where the vapour pressure of $TaCl_5$ reaches 1 atm pressure. Σ-function plots for vapourization were linear, and the enthalpy and free energy functions by the least squares method are given, respectively, as:

$$[17] \quad \Delta H_{v(TaCl_5)} = 141.038 - 0.1747\,T + 1.548 \times 10^3\,T^{-1} \quad (\pm 0.21 \text{ kJ mol}^{-1})$$

and as

$$[18] \quad \Delta H_{v(TaCl_5)} = 141.038 - 1.3694\,T + 0.1747\,T \ln T + 7.74 \times 10^2\,T^{-1} \quad (\pm 0.21 \text{ kJ mol}^{-1})$$

ΔH_v at the boiling temperature of 502.7 K, is 56.27 ± 0.21 kJ mol^{-1}. Literature values vary between 62.34 and 48.95 (±4 kJ mol^{-1}).

Again, vapour pressures for $TaCl_5$ calculated from eq. [18] compare well with experimental measures (2).

For the sublimation reaction

$$[19] \quad TaCl_{5(s)} \rightarrow TaCl_{5(vap)}$$

the Σ-function method yielded the equation,

$$[20] \quad \Delta H_s = 93.960 + 1.548 \times 10^3\,T^{-2} \quad (\pm 3.94 \text{ kJ mol}^{-1})$$

The larger errors shown in eqs. [16] and [20] reflect differences between the available experimental vapour pressure data and possible uncertainty in the molar heat capacity data from which the Σ-function values were evaluated.

The linearity of the Σ-plots is usually taken as an indication of the accuracy and of compatibility between the calorimetric molar heat capacities and the corresponding vapour pressure data representing the equilibria between the condensed and the vapour phases. Thus, the Σ-function method is also a test of the accuracy of the experimental data used for the calculations, because, if either the calorimetric or the vapour pressure measurements are in error then the Σ versus $1/T$ plots cannot be linear (28).

Regarding the four complex compounds, $CsNbCl_6$, $RbNbCl_6$, $CsTaCl_6$, and $RbTaCl_6$, the large enthalpy and entropy effects associated with their allotropic changes suggest that their solid structures undergo dramatic changes before melting. Such large enthalpy and entropy effects may indicate fast-ion conduction in the high-temperature phases and to the possible use of these compounds in solid state chemical sensors (30).

1. D. R. SADOWAY and S. N. FLENGAS. Can. J. Chem. **56**, 2013 (1978).
2. D. R. SADOWAY and S N. FLENGAS. Can. J. Chem. **54**, 1692 (1976).
3. D. R. SADOWAY and S. N. FLENGAS. Can. J. Chem. **56**, 2538 (1978).
4. D. R. SADOWAY and S. N. FLENGAS. Metall. Trans. B, **11B**, 57 (1980).
5. K. HUBER, E. JOST, E. NEUENSCHWANDER, M. STUDER, and B. ROTH. Helv. Chim. Acta, **41**, 2411 (1958).
6. I. S. MOROZOV and A. T. SIMONICH. Russ. J. Inorg. Chem. **2**(8), 311 (1957).
7. E. K. SMIRNOVA, I. V. VASIL'KOVA, and N. F. KUDRYASHOVA. Russ. J. Inorg. Chem. **9**, 268 (1964).
8. E. K. SMIRNOVA and V. M. TSINTSIUS. Russ. J. Inorg. Chem. **16**, 303 (1971).
9. K. W. BAGNALL and D. BROWN. J. Chem. Soc. 581 (1964).
10. W. T. THOMPSON and S. N. FLENGAS. Can. J. Chem. **49**, 1550 (1971).
11. A. S. KUCHARSKI and S. N. FLENGAS. Can. J. Chem. **52**, 946 (1974).
12. G. T. FURUKAWA, T. B. DOUGLAS, R. E. MCCOSKEY, and D. C. GINNINGS. J. Res. Natl. Bur. Stand. **57**, 67 (1956).
13. J. GOODKIN, C. SOLOMONS, and G. T. JANZ. Rev. Sci. Instr. **29**, 105 (1958).
14. O. KUBASCHEWSKI and C. B. ALCOCK. Metallurgical thermochemistry. 5th ed. Pergamon Press, Oxford. 1979.

Can. J. Chem. Downloaded from www.nrcresearchpress.com by 194.225.253.170 on 09/07/12
For personal use only.

15. F. J. KENESHEA, D. CUBICCIOTTI, G. WHITHERS, and H. EDING. J. Phys. Chem. **72**, 1272 (1968).
16. H. SCHAEFER and F. KAHLENBERG. Z. Anorg. Allgem. Chem. **305**, 178 (1960).
17. R. B. DOBROTIN, A. V. SUVOROV, and YU. V. KONDRATIEV. Vestn. Leningr. Univ. Ser. Fiz. Khim. **4**, 95 (1964).
18. G. MEYER, J. F. OOSTEROM, and W. J. VAN OEVEREN. Rec. Trav. Chim. Pays-Bas, **80**, 502 (1961).
19. S. A. SHCHUKAREV and A. R. KURBANOV. Vestn. Leningr. Univ. Ser. Fiz. Khim. **10**, 144 (1962).
20. Y. SAEKI, R. MATSUZAKI, M. YANAI, and K. FUNAKI. Kogyo Kagaku Zasshi, **71**, 350 (1968).
21. L. I. STAFFANSSON and P. ENGHAG. Scand. J. Metall. **2**, 305 (1973).
22. M. A. OPYKHTINA and N. A. FLEISHER. Zh. Obshch. Khim. **7**, 2016 (1937).
23. D. N. TARASENKOV and A. V. KOMANDIN. Zh. Obshch. Khim. **10**, 1319 (1940).
24. K. M. ALEXANDER and F. FAIRBROTHER. J. Chem. Soc. **52**, S223 (1949).
25. J. W. JOHNSON, W. J. SILVA, and D. CUBICCIOTTI. High Temp. Sci. **2**, 20 (1970).
26. W. HART and G. MEYER. Rec. Trav. Chim. **83**, 1233 (1964).
27. J. M. BRINK and F. D. STEVENSON. J. Chem. Eng. Data, **17**, 143 (1972).
28. L. S. DARKEN and R. W. GURRY. *Physical chemistry of metals*. McGraw-Hill Co., New York. 1953. p. 225.
29. R. D. WERDER, R. A. FREY, and H. GUENTHARD. J. Chem. Phys. **47**, 4159 (1967).
30. F. W. POULSEN, N. H. ANDERSEN, K. CLAUSEN, D. R. SADOWAY, and L. H. OGENDAL. Super ionic conduction in alkali metal hexachloro niobates and tantalates. *In* Solid State Ionics. In press.
31. A. ZALKIN and D. E. SANDS. Acta Crystallogr. **11**, 615 (1958).

Can. J. Chem. Downloaded from www.nrcresearchpress.com by 194.225.253.170 on 09/07/12
For personal use only.

Electronic spectrum of bibenzimidazole homologue: effects of solvents and acid concentration

AWADESH KUMAR, HEMANT K. SINHA, AND SNEH K. DOGRA[1]
Department of Chemistry, Indian Institute of Technology, Kanpur – 208 016, India

Received June 14, 1988[2]

AWADESH KUMAR, HEMANT K. SINHA, and SNEH K. DOGRA. Can. J. Chem. **67**, 1200 (1989).

The absorption and fluorescence spectra of bibenzimidazole (BBI), *N,N'*-dimethylbibenzimidazole (MBBI), and methylene, 2,2'-bibenzimidazole (MtBBI) have been recorded in six solvents of different characteristics and at various acid concentrations. This study indicates the presence of intramolecular hydrogen bonding in BBI in both S_0 and S_1 states, leading to large conjugation of two benzimidazole (BI) rings. The geometry of BBI is the same in the S_0 and S_1 states. The spectral characteristics of BBI are insensitive to the solvents. The interaction of solvent molecule attached to the nitrogen lone pair and methyl group rotates the benzimidazolyl ring in MBBI around the single bond. This leads to a blue shift in the long wavelength absorption band maximum and a decrease in the intensity of this band. The two MBI rings are coplanar in the S_1 state. Presence of methylene group inhibits the direct interaction between the BI groups and these rings behave almost independently, i.e., the spectral characteristics of this molecule nearly resemble those of benzimidazole.

Key words: absorption spectrum, fluorescence spectrum, pK_a, bibenzimidazoles, excited state pK_a.

AWADESH KUMAR, HEMANT K. SINHA et SNEH K. DOGRA. Can. J. Chem. **67**, 1200 (1989).

Opérant à diverses concentrations d'acides et dans six solvants de caractéristiques diverses, on a déterminé les spectres d'absorption et de fluorescence du bibenzimidazole (BBI), du *N,N'*-diméthylbibenzimidazole (MBBI) et du méthylène-bibenzimidazole-2,2' (MtBBI). Cette étude indique qu'il existe des liaisons hydrogènes dans les états S_0 et S_1 du BBI. Les caractéristiques des spectres du BBI ne sont toutefois pas sensibles aux solvants. Dans le MBBI, l'interaction entre le groupement méthyle et la molécule de solvant attachée à la paire d'électrons libres de l'azote provoque une rotation du cycle benzimidazolyle autour de la simple liaison. Ceci provoque un déplacement vers le bleu du maximum de la bande d'absorption présente aux grandes longueurs d'onde ainsi qu'une diminution de l'intensité de cette bande. Dans l'état S_1, les deux cycles MBI sont coplanaires. La présence d'un groupement méthylène inhibe l'interaction directe des groupements BI et ces cycles se comportent comme s'ils étaient pratiquement indépendants, c'est-à-dire que les caractéristiques spectrales de cette molécule ressemblent beaucoup à celles du benzimidazole.

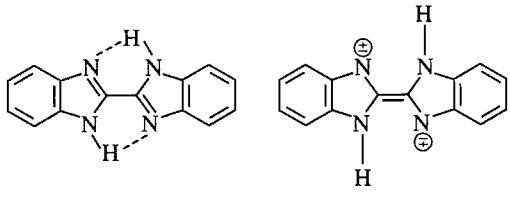
Mots clés : spectre d'absorption, spectre de fluorescence, pK_a, bibenzimidazoles, pK_a de l'état excité.

[Traduit par la revue]

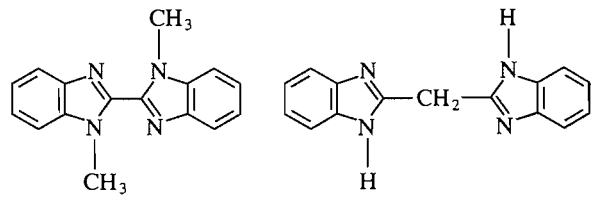
Introduction

Benzimidazole and its derivatives have been used extensively in medicine and industry (1–3). The chemistry of bibenzimidazoles has received attention recently because of its potential to act as a potent inhibitor of rhinoviruses (4) and as an effective chelating agent for metal ions (5, 6). However, until recently, there have been no reports in the literature on the photophysics and the photochemistry of these molecules.

In the present study we have selected 2,2'-bibenzimidazole (BBI), *N,N'*-dimethyl-2,2'-bibenzimidazole (MtBBI), and methylenebibenzimidazole (MBBI). Looking at the structure of BBI, one would expect the presence of intramolecular hydrogen bonding, resulting in a planar conformation (**I**) both in S_0 and S_1 states even though the imino N—H bond will be distorted and will lead to non-linear N—H—N bond. This interaction may bring about conjugation in the two rings. Apart from intramolecular hydrogen bonding, BBI may also possess a resonance dipolar structure (**II**) similar to quinoxaline (7–9). This will increase the bond order to the link that joins the two benzimidazole moieties. This interaction may bring about drastic changes in the spectral characteristics and dissociation constants of the various prototropic reactions, which this molecule may undergo, as compared to those of benzimidazole (BI) (10, 11). In MBBI (**III**), though the intramolecular hydrogen bonding will be absent, the molecule may possess a resonance dipolar structure. On the other hand, in MtBBI (**IV**)



I **II**



III **IV**

both intramolecular hydrogen bonding and dipolar resonance structure will be absent. Thus the spectral characteristics of MBBI and MtBBI and their prototropic species will be different from those of BBI and its prototropic species. To prove these points and to see the differences in the spectral characteristics of three molecules and their prototropic species, the absorption and fluorescence spectra have been recorded in six solvents of different polarities and hydrogen bond forming tendencies, as well as at various acid concentrations. The pK_a values for the different prototropic reactions have been determined in the S_0 and S_1 states and are discussed.

Materials and method

BBI was prepared by reacting *o*-phenylenediamine monohydrochloride with methyltrichloroacetimidate with acetic acid

[1]To whom all correspondence should be addressed.
[2]Revision received January 17, 1989.

Printed in Canada / Imprimé au Canada

Can. J. Chem. Downloaded from www.nrcresearchpress.com by 194.225.253.170 on 09/07/12
For personal use only.

Can. J. Chem. Downloaded from www.nrcresearchpress.com by 194.225.253.170 on 09/07/12
For personal use only.

as a solvent (12). MBBI was synthesized (13) by condensing *N*-methylbenzimidazole using powdered sodium, whereas the *N*-methylbenzimidazole required for this purpose was prepared by methylating (14) BI with methyliodide in alkaline medium. MtBBI (15) was prepared by condensing *o*-phenylenediamine with malonic acid in 2:1 molar ratio using polyphosphoric acid. These compounds were recrystallized from alcohol and their purity was checked by noting the melting point, thin layer chromatography, absorption spectra, and similar fluorescence spectra obtained when excited at different wavelengths. Analytical grade sulphuric acid, sodium hydroxide, *o*-phosphoric acid (all BDH), trifluoroacetic acid (TFA, Fluka), and spectroscopic grade methanol (BDH) were used as such. Cyclohexane, ether, dioxane, and acetonitrile (all AR) were further purified for spectral purposes as reported in literature (16). Triply distilled water was used for making aqueous solutions. The pH of the solutions in the range of 3 to 11 were adjusted by adding appropriate amounts of *o*-phosphoric acid and sodium hydroxide. The phosphate buffers in these concentrations do not quench the fluorescence of the desired compound and do not affect the prototropic equilibrium (17). Solutions below pH 1 were prepared by following Jorgenson and Hartter's H_0 scale (18) for H_2SO_4–H_2O mixtures and above pH 13 by Yagil's H_- scale (19) for NaOH–H_2O mixtures. The pH of the solutions between 1–13 were measured on a Toshniwal pH meter model CL44A. Absorption measurements were made on Shimadzu UV-190 spectrophotometer, equipped with a U-135 chart recorder. The fluorescence spectra were recorded on a laboratory-made scanning spectrofluorimeter, the details are available elsewhere (20). The fluorescence spectra were corrected according to the procedure suggested by Parker (21) and the fluorescence quantum yields were determined with the solutions of absorbances less than 0.1, using quinine sulphate in 0.1 *N* H_2SO_4 as a standard (22). For calculating the equilibrium constants for the various prototropic reactions, solutions were prepared just before making measurements. For fluorimetric titrations, the isosbestic wavelengths were used for the measurements of the relative fluorescence intensities at the analytical wavelengths as a function of H_0/pH/H_-.

Results and discussion

Effect of solvents

The absorption and fluorescence spectra of BBI, MBBI, and MtBBI were recorded in solvents of different polarity and hydrogen bond forming capacity. The relevant data are compiled in Tables 1 and 2, respectively. Due to the poor solubility of these compounds in all solvents except methanol, the molecular extinction coefficients are reported for methanol only. The long wavelength absorption band maxima of BBI are very large red shifted with respect to that of benzimidazole (BI) (23) and the absorption spectrum can be divided into four band systems, whereas there are only three band systems for BI. The band above 300 nm is highly structured with the vibrational frequency 1400 ± 50 cm^{-1}. The other three band systems are similar to that of BI, but slightly red shifted (i.e. at 280 nm, 250 nm, 210 nm). Similar to the absorption spectrum, the fluorescence spectrum of BBI is also red shifted as compared to BI (11) and is highly structured, with vibrational frequency of ~1420 ± 50 cm^{-1}. The short wavelength band at 339 nm can be assigned to the zero–zero transition. Both the absorption (long wavelength band) and fluorescence spectra are nearly insensitive to the polarity and hydrogen bond forming capacity of the solvents.

The absorption spectrum of MBBI resembles that of BBI in cyclohexane, but the band system above 300 nm, unlike BBI, is very sensitive to the solvent polarity and hydrogen bonding nature. For example, the vibrational structure of this band (above 300 nm) is completely lost and a large blue shift is observed in this band maximum. The intensity of this band also decreases and in water this band system is a weak shoulder. On the other hand, the fluorescence spectrum of MBBI exactly resembles that of BBI in all the solvents (zero–zero transition can be assigned to 344 nm band and ν_{vib} = 1440 ± 50 cm^{-1}). The fluorescence quantum yield of MBBI is less than that of BI (24). Lastly, the absorption and fluorescence spectra of MtBBI resembles that of BI (11, 24) in all respects. The zero–zero transition in fluorescence spectrum can be assigned to 288 nm and ν_{vib} = 1200 ± 50 cm^{-1}.

In biphenyl, the long wavelength absorption band is broad (~247 nm) and it has been shown to be a mixture of two or three transitions (25–27). Furthermore, it has also been proved that the two phenyl rings are not coplanar in the ground state whereas the distortion angle changes in the excited singlet and BP (28) is more planar (not completely) in S_1 than in S_0. However, from the data of Tables 1 and 2, it is possible to say that the fluorescence band of BBI is not separated much from and makes a mirror image with its long wavelength absorption band, indicating that the molecular conformation in the first excited singlet state differs little from that in the ground state. The fluorescence spectrum was found to be independent of the excitation wavelengths and of concentration. It is thus suggested that the two benzimidazolyl rings are coplanar in S_0 and S_1 states and the suggested conformation of BBI is structure **I**, i.e., a symmetrical structure. The following points can be made in its favour.

(*i*) The long wavelength absorption band and the fluorescence spectrum are highly structured and substantially red shifted as compared to BI, indicating extensive conjugation between the two rings.

(*ii*) A similar vibrational frequency (~1400 cm^{-1}) is also observed in the compounds, where the conjugated substituent is present at the position 2 of BI, thereby forming a three- or four-membered ring system, e.g., 2-phenylbenzimidazole (29), 2-(2′-aminophenyl) (30), 2-(2′-hydroxyphenyl) (31), 2-(3′-hydroxyphenyl) (32), 2-(3′-aminophenyl) (33), 2-(4′-aminophenyl) (34), and 2-(4′-hydroxyphenyl)benzimidazoles (32). This vibrational frequency is very different from that noticed in BI and MtBBI. The direct conjugation of two benzimidazolyl rings is absent in the latter molecule.

(*iii*) The presence of intramolecular hydrogen bonding in BBI, leading to the presence of rigidity in the BBI structure, is further reflected in the insensitivities of the absorption and fluorescence spectra in the presence of the different solvents. The structure **I** of BBI is totally symmetric and both the lone pairs on the tertiary nitrogen atoms are blocked by the intramolecular hydrogen bonding. Thus, no change in absorption and fluorescence spectral characteristics are observed in the above environments. It is further manifested in the fluorescence quantum yields, which nearly remain constant in different solvents. The high value of fluorescence quantum yield also reflects that the molecule is rigid.

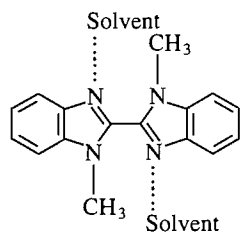
(*iv*) Near rigidity in BBI can also be achieved if we assume the resonance structure **II**. Similar resonance structure can also be achieved in MBBI. However, the effect of solvents on the absorption spectra of BBI and MBBI excludes a major contribution of structure **II** to the main structures of BBI and MBBI.

TABLE 1. Absorption maxima of BBI, MBBI, and MtBBI in different solvents at various proton concentrations at 298 K

Solvent/species (*1*)	BBI (*2*)				MBBI (*3*)				MtBBI (*4*)		
Cyclohexane	339	282	—	—	344	284	250	211	277		219
	326				326	278	235				209
	322				313						
	311				300						
Ether	338	281		218	344	285	249	—	281[a]	238	—
	327	273	233		325	278	239				
	321	263			298						
	312										
	308										
Dioxane	340	281	238	213	300[a]	284	253	216		240	219
	329	273	233			276			281		
	324								275		
	313										
Acetonitrile	338	279	237	205	300	284	253	213	283[b]	240	213
	322	271	231			276					
	311										
Methanol	339		238	209	294	283	250	209	279	240	210
	(3.97)		(3.67)	(4.02)	(3.92)	(4.09)	(4.23)	(4.80)			
	323		232			275			273		
	(4.09)		(3.72)			(4.09)					
	313										
	(3.99)										
Water pH = 6.7	340		239	197	294	280	248	203	276	239	196
(Neutral)	325					277			274		
	313					270			269		
Monocation	353		238	—	316	288	234	194	278	240	214
pH = 1	333					275			271		194
						269					
						263					
Dication	377		238	—	315	278	239	215	278	—	200
$H_0 = -6$	354					273	235	190	273		191
	338										
Monoanion	344	261	231		213		—		288[c]	—	195
pH = 12	328								283		
	323										
Dianion	348	273	—		227		—				
$H_- = 15$	330										

[a]Very broad band.
[b]Broad band.
[c]$H_- = 15$.

The absorption spectrum of MBBI in cyclohexane indicates that conjugation is possible in MBBI without involving intramolecular hydrogen bonding (which is not possible). In other solvents, it can be explained by a possible direct interaction between the lone pairs of MBBI and the solvents. This leads to steric interactions between the methyl groups and the solvent molecule as shown below and thus, rotation around the single bond takes place. A large blue shift in the absorption spectrum and a decrease in the absorbance in water and methanol substantiate their interactions. A weak shoulder at 294 nm in the protonic solvents indicates that a complete noncoplanarity is not achieved. On the other hand, the data in Table 2 show that the two rings of MBBI are coplanar and conjugation is achieved in the excited state in all solvents. The driving force behind this seems to be the transition moment vector which is long axis polarised, increasing the bond order of the single bond joining



the two rings. The small red shift observed in the fluorescence spectra of MBBI in water and methanol is due to the hydrogen bonding interaction with the lone pair of the tertiary nitrogen atoms. The decrease in the fluorescence quantum yield in any given solvent, as compared to BBI, may be due to the presence of methyl groups, which can increase the rates of radiationless processes. This is due to an increase in the number of vibrational

Can. J. Chem. Downloaded from www.nrcresearchpress.com by 194.225.253.170 on 09/07/12
For personal use only.

TABLE 2. Fluorescence band maxima and quantum yields of BBI, MBBI, and MtBBI in different solvents and at various proton concentrations at 298 K

Solvent/species	BBI (nm)				MBBI (nm)				MtBBI (nm)			
Cyclohexane	400	375	356	339	400	380	363	344		—		
						(0.201)						
Ether	390	370	354	338	400	380	358	339	288	277		268
		(0.70)				(0.047)				(0.01)		
Dioxane	396	375	358	340	400	380	360	344	291	283		—
		—				(0.034)				(0.03)		
Acetonitrile	390	373	255	338	400	380	360	344	288	280		—
		(0.78)				(0.032)				(0.02)		
Methanol	392	374	355	338		379	363	346	290	280		—
		(0.70)				(0.104)				(0.12)		
Water	400	376	358	342		377	367	350	290	273		—
		—				(0.299)				(0.015)		
Monocation pH 1		390				396				360[a]		
Dication H_0 −6	430	405	385			405				394		
Monoanion pH 1		370				—				306		
Dianion	400	385	366	348		—				—		

[a]Cyclohexane with 1% TFA (v/v).

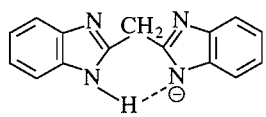
modes. The value of the fluorescence quantum yield of MBBI resembles that of 2-methylbenzimidazole (35).

The absorption and fluorescence characteristics of MtBBI are exactly the same as those of 2-methylbenzimidazole (35) in all solvents, indicating that the presence of a methylene group in between the two benzimidazolyl rings has drastically reduced their interaction. Similar behaviour has been observed in many cases where the presence of a methylene group inhibits the interaction of the two functional groups (36–38).

Effect of acid concentration

The absorption and fluorescence spectra of BBI, MBBI, and MtBBI have been studied in the H_0/pH/H_- range of −10 to 16. The relevant data have been compiled in Tables 1 and 2, respectively. The spectral changes observed in the absorption and fluorescence spectra, due to the formation of various prototropic species of the neutral molecules, are consistent with earlier studies on these chromophores (36–38), i.e. the red shift is observed in the absorption and fluorescence spectra when the protonation occurs at the tertiary nitrogen atom and deprotonation takes place at the imino group if $\pi \rightarrow \pi^*$ is the lowest energy transition. Thus the monocation at pH 1 and the dication at H_0 −6 are formed by protonating one and both the tertiary nitrogen atoms, respectively, in all cases. The monoanion at pH 12 and dianion of BBI at H_- 15 are formed by the deprotonation of one and both the imino groups, respectively. The monoanion and dianion of MBBI cannot be obtained as there are no dissociable imino protons whereas only the monoanion is formed in the case of MtBBI at H_- 15 and no dianion is formed even in the highly basic solutions used in our experiments. The spectral shifts occurring in this compound are similar to those noticed in case of BI (23) and an explanation similar to that given earlier can be offered.

The monocation of MBBI and dications of MBBI and MtBBI showed broad red shifted fluorescence bands. The nonfluorescent nature of monocation of MtBBI can be explained as follows. As said earlier, the spectral characteristics of MtBBI are similar to those of BI. The fluorescence quantum yield of neutral BI (0.7) is nearly ten times more than that of its monocation (0.07) (24). It is possible that the fluorescence quantum yield of the monocation of MtBBI is too low to be detected by our instrument. This indicates that the interaction of water with the monocation of MtBBI increases the rates of radiationless processes. This has been manifested in the fluorescence spectrum (368 nm) of MtBBI in cyclohexane + 1% (v/v) TFA. The absorption and fluorescence spectra in the latter solvent resemble that of monocation of BI, indicating that the rates of radiationless processes in the monocation of MtBBI are quite large in polar solvents. Furthermore, it is clear that the monoanion of MtBBI gives rise to the fluorescence band maximum (i.e. 306 nm), similar to that of BI. From our data, it is very difficult to pinpoint why the monocation and monoanion are nonplanar (or having a broad fluorescence band) and the dication and dianion of BBI are coplanar (or have structured fluorescence bands with similar vibrational frequencies as noticed for neutral BBI). The fluorescence spectra of the monocation and monoanion of BBI are broad band with band maxima at 390 and 396 nm, respectively, whereas those of dication and dianion are structured with ν_{vib} equal to 1400 ± 50 cm^{-1} and 1410 ± 50 cm^{-1}, respectively. This indicates that both the dication and dianion could be planar. No dianion of the latter molecule similar in ground state behaviour has been observed in the excited singlet state. This is because of the formation of strong intramolecular hydrogen bonding between $>N^-$ and >NH, as shown below.



Dissociation constants

The dissociation constants (pK_a) for the various prototropic reactions of all three molecules in their ground state have been determined spectrophotometrically. The relevant data have been compiled in Table 3. The pK_a (2) values (monocation–neutral equilibrium) of all three compounds are much less than that of similar reaction of BI (i.e. 5.48) (39). Similar results have also been observed in case of prototropic reactions of pyrazine (pK_a = −0.6) (8) and quinoxaline (pK_a = 0.7) (9). These values are low when compared with the similar proto-

Can. J. Chem. Downloaded from www.nrcresearchpress.com by 194.225.253.170 on 09/07/12
For personal use only.

TABLE 3. Dissociation constants of the various prototropic equilibria of BBI, MBBI, and in the ground and excited singlet states

Equilibrium	pK_a	pK_a[a] (a)	(b)	(c)
BBI				
Dication $\overset{1}{\rightleftharpoons}$ monocation	−2.7	1.1	−0.7	0.6
Monocation $\overset{2}{\rightleftharpoons}$ neutral	2.8	5.1	7.6	
Neutral $\overset{3}{\rightleftharpoons}$ monoanion	11.0	10.3	9.1	
Monoanion $\overset{4}{\rightleftharpoons}$ dianion	>16	$\Delta pK_a = 0.7$	2.2	14.0
MBBI				
Dication $\overset{1}{\rightleftharpoons}$ monocation	−4.9	—	−3.72	−1.1
Monocation $\overset{2}{\rightleftharpoons}$ neutral	3.0	5.0	7.2	
MtBBI				
Dication $\overset{1}{\rightleftharpoons}$ monocation	−6.2	—	—	−4.5
Monocation $\overset{2}{\rightleftharpoons}$ neutral	3.3	4.2	—	
Neutral $\overset{3}{\rightleftharpoons}$ monoanion	13.0	9.83	9.2	

[a](a),(b): by Forster cycle method, using absorption and fluorescence data; (c) by fluorimetric titration.

tropic reaction of pyridine (pK_a = 5.4) or quinoline (pK_a = 4.90) (40). In these cases it is due to the presence of a second nitrogen atom at the *para* position with respect to the first one, which will lead to the formation of an exactly equivalent dipolar structure in the non-ionised molecule and these may strengthen the resonance of these species at the expense of the ion. These molecules (quinoxaline, phenanzine, and pyrazine) are analogues of azabenzenes (41), which are very weak base for similar reason. The same argument can be given in case of BBI and MBBI. Even though the two tertiary nitrogen atoms are not on the same ring, the charge transfer can lead to an exactly similar dipolar structure **II**. This may be one reason that pK_a(2) for BBI and MBBI does not decrease as much in pyrazine as in pyridine and not as much in quinaoxaline as in quinoline. The pK_a (3) for BBI (11.0) is lower than that for BI (13.25) (38). This seems to be consistent with structure **I** as the imino proton will be partially polarized by intramolecular hydrogen bonding. pK_a(3) for MtBBI (13.0) agrees with the deprotonation reaction of BI (13.25), but pK_a (2) is quite low in comparison to BI. This indicates that one methylene group can inhibit a direct interaction of two BI rings but cannot stop the charge migration completely.

The excited state pK_a values for the three molecules have been calculated fluorimetrically as well as with the help of the Forster cycle method (42) (wherever applicable) using absorption and fluorescence data. Similar to the earlier studies, the fluorimetric titrations gave the ground state pK_a values for the first protonation (pK_a(2)) and first deprotonation reaction (pK_a(3)) (9). This indicates that the prototropic equilibria 2 and 3 in the S_1 state are not established during the lifetimes of these molecules, i.e., the rate of protonation or deprotonation are much slower than the rate of radiative deactivation of these species. Data in Table 3 indicate that pK_a*(1) is greater than pK_a(1), clearly showing that the tertiary nitrogen atom becomes more basic on excitation. Similarly the value of pK_a*(4) shows that the imino group becomes a stronger acid in the excited singlet state. The pK_a* calculated for the various prototropic reactions with the help of Forster cycle method also follows a similar trend that the tertiary nitrogen atom becomes more basic and the imino group becomes more acidic on excitation. The discrepancies observed between the pK_a* values calculated using absorption and fluorescence data are due to the fact that: (*i*) fluorescence spectra of the conjugate acid–base species involved are either structured or broad, thus difficult to locate 0–0 transitions or band maxima; (*ii*) solvent relaxation for the conjugate acid–base species may be different in the ground and excited singlet states.

Conclusions

The effect of solvents on the absorption and fluorescence spectra have clearly indicated that (*i*) intramolecular hydrogen bonding is present in BBI, both in S_0 and S_1 states and thus the geometry of BBI in both the states are same; (*ii*) extended conjugation is present in MBBI in cyclohexane but steric hindrance in the solvated molecule by the methyl groups removes this conjugation and the long wavelength absorption band is blue shifted. Conjugation between the two rings in the S_1 state in all solvents is stronger, and thus MBBI is more planar in S_1 state; (*iii*) the presence of methylene group inhibits direct interaction between BI groups, thus making these rings behave almost independently; (*iv*) the small pK_a values for protonation and deprotonation reactions of BBI, MBBI as compared to BI are due to the presence of the dipolar structure **II** stabilized by resonance; (*v*) the prototropic equilibria between the monocation–neutral and neutral–monoanion are not established in the S_1 state during the lifetimes of the conjugate acid–base pair.

Acknowledgement

The authors are thankful to the Department of Science and Technology, New Delhi, for financial support.

1. P. N. PRESTON. Chem. Rev. **74**, 310 (1974).
2. D. G. O'SULLIVAN, D. PENTIC, and A. K. WILLIS. J. Med. Chem. **15**, 103 (1972).
3. J. C. VORA. J. Electrochem. Soc. (India), **21**, 64 (1972).
4. W. R. RODERICK and C. W. NORDEEW. J. Med. Chem. **15**, 655 (1972).
5. B. F. FIESELMANN, D. N. HENDRICKSON, and G. D. STUCKY. Inorg. Chem. **17**, 2078 (1978).
6. M. S. HADDAD, D. N. HENDRICKSON, and G. D. STUCKY. Inorg. Chem. **17**, 2622 (1978).
7. G. W. H. CHEESEMAN and R. F. COOKSON. Condensed pyrazines. Wiley, London. 1972. p. 2.
8. A. ALBERT. Heterocyclic chemistry. Athlone, London. 1959. pp. 344, 345.
9. M. KRISHNAMURTHY, K. IYER, and S. K. DOGRA. J. Photochem. **38**, 277 (1987).
10. M. KONDO and H. KUWANO. Bull. Chem. Soc. Jpn. **42**, 1433 (1969).
11. P. C. TWAY and L. J. CLINELOVE. J. Phys. Chem. **86**, 5223 (1982); **86**, 5227 (1982).
12. G. HOLEN, E. L. SAMUEL, B. C. ENNIS, and R. W. HINDE. J. Chem. Soc. (C), 20 (1967).
13. B. A. TERTOV. Tetrahedron Lett. **42**, 4445 (1968).
14. B. PILLIAESKI. Leibig's Ann. Chem. 1078 (1983).
15. S. CHATTERJEE. J. Indian Chem. Soc. **43**, 660 (1966).
16. J. A. RIDDICK and W. B. BUNGER. Organic solvents. Vol. 2. Wiley Interscience, London. 1970. pp. 592, 706, 799.
17. A. K. MISHRA, M. SWAMINATHAN, and S. K. DOGRA. J. Photochem. **26**, 49 (1984).

Can. J. Chem. Downloaded from www.nrcresearchpress.com by 194.225.253.170 on 09/07/12
For personal use only.

18. M. J. JORGENSON and D. R. HARTTER. J. Am. Chem. Soc. **85**, 878 (1963).
19. G. YAGIL. J. Phys. Chem. **71**, 1034 (1967).
20. M. SWAMINATHAN and S. K. DOGRA. Indian J. Chem. **22**A, 853 (1983).
21. C. A. PARKER. Photoluminescence of solutions with application to photochemistry and analytical chemistry. Elsevier, Amsterdam. 1988. pp. 261–268.
22. S. R. MEECH and D. PHILLIPS. J. Photochem. **23**, 193 (1983).
23. P. N. PRESTON. Heterocycl. Comp. **44**, 65 (1981).
24. J. H. LONGWORTH, R. G. RAHN, and R. G. SCHULMAN. J. Chem. Phys. **45**, 2930 (1966).
25. I. B. BERLMAN. J. Chem. Phys. **52**, 5616 (1970).
26. P. PETELENZ. J. Chem. Phys. **57**, 5016 (1972).
27. F. MOMICCHIOLI, M. BUIM, and I. BARALDI. J. Phys. Chem. **76**, 3983 (1972).
28. E. C. LIM and Y. LI. J. Chem. Phys. **52**, 6416 (1970).
29. A. K. MISHRA and S. K. DOGRA. Spectrochim. Acta, **39**A, 609 (1983).
30. A. K. MISHRA and S. K. DOGRA. J. Photochem. **31**, 333 (1983).
31. H. K. SINHA and S. K. DOGRA. Chem. Phys. **102**, 337 (1986).
32. H. K. SINHA and S. K. DOGRA. J. Photochem. **36**, 149 (1986).
33. A. K. MISHRA and S. K. DOGRA. Indian J. Phys. **58**B, 480 (1984); Indian J. Chem. **24**A, 364 (1985).
34. A. K. MISHRA and S. K. DOGRA. Bull. Chem. Soc. Jpn. **58**, 3587 (1985).
35. M. KRISHNAMURTHY, P. PHANIRAJ, and S. K. DOGRA. J. Chem. Soc. Perkin Trans. 2, 1917 (1986).
36. H. K. SINHA and S. K. DOGRA. Spectrochim. Acta, **41**A, 961 (1985).
37. H. K. SINHA and S. K. DOGRA. Indian J. Chem. **25**A, 1092 (1986).
38. H. K. SINHA and S. K. DOGRA. J. Chem. Soc. Perkin Trans. 2, 1465 (1987).
39. P. N. PRESTON. Benzimidazoles and congeric tricyclic compounds. Wiley Interscience, London. 1981. p. 80.
40. J. F. IRELAND and P. A. H. WYATT. Adv. Phys. Org. Chem. **12**, 179 (1976); **12**, 180 (1976).
41. A. ALBERT, R. GOLDARE, and R. PHILLIPS. J. Chem. Soc. 2240 (1948).
42. TH. FORSTER. Z. Elektrochem. **54**, 531 (1950).

Can. J. Chem. Downloaded from www.nrcresearchpress.com by 194.225.253.170 on 09/07/12
For personal use only.

Chemoselective reductions with sodium borohydride

DALE E. WARD[1] AND CHUNG K. RHEE
Department of Chemistry, University of Saskatchewan, Saskatoon, Sask., Canada S7N 0W0

Received January 5, 1989

DALE E. WARD and CHUNG K. RHEE. Can. J. Chem. **67**, 1206 (1989).

Under the appropriate reaction conditions, sodium borohydride is a highly chemoselective reducing agent. The order of reactivity among carbonyl groups is conjugated enones < ketones < conjugated aldehydes < aldehydes. In general, a carbonyl group of one type can be selectively reduced in the presence of a carbonyl group of a less reactive type. Reactions are conducted with excess sodium borohydride at −78°C in solvent mixtures of methanol or ethanol in dichloromethane.

Key words: sodium borohydride, chemoselective reductions.

DALE E. WARD et CHUNG K. RHEE. Can. J. Chem. **67**, 1206 (1989).

Utilisé dans des conditions réactionnelles appropriées, le borohydrure de sodium est un agent de réduction très chémosélectif. Pour les groupements carbonyles, l'ordre de réactivité est le suivant : énones conjuguées < cétones < aldéhydes conjugués < aldéhydes. En général, un certain type de groupement carbonyle peut être réduit sélectivement lorsqu'il est en présence d'un autre groupement carbonyle d'un type moins réactif. On réalise ces réactions en opérant en présence d'un excès de borohydrure de sodium, à −78°C, dans des mélanges de solvants formés de méthanol ou d'éthanol avec du dichlorométhane.

Mots clés : borohydrure de sodium, réductions chémosélectives.

[Traduit par la revue]

Introduction

The use of sodium borohydride as a reducing agent in organic chemistry has been known for over 40 years (1). Its mild reducing properties allow for considerable selectivity in the reduction of organic compounds. Aldehydes and ketones are, in general, readily converted into their corresponding alcohols in the presence of a variety of functional groups including nitro, carboxylic acid, ester, amide, carbonate, carbamate, lactone, epoxide, nitrile, halide, alkene, and alkyne. The ready availability, high stability, mild reaction conditions, ease of "work-up", and high yields contribute to the widespread use of sodium borohydride for the reduction of aldehydes and ketones (1).

The development of methods for the chemoselective reduction of the carbonyl group (e.g., aldehydes vs. ketones) continues to be of interest in organic chemistry (2–7). In this paper we report the full results[2] of our studies on the chemoselective reduction of various types of aldehydes and ketones with sodium borohydride. The order of reactivity among carbonyl groups is conjugated enones < ketones < conjugated enals < aldehydes. In general, a carbonyl group of one type can be selectively reduced in the presence of a carbonyl group of a less reactive type.

Sodium borohydride (as well as other complex metal hydrides) is a "nucleophilic" reagent in that the rate of reduction is related to the electrophilicity of the carbonyl group (1). The difference in reactivity between aldehydes and ketones towards sodium borohydride can vary by more than three orders of magnitude (8). This suggests the possibility of selective reduction.

In recent years, a large number of reagents that can selectively reduce aldehydes in the presence of ketones have been reported (2). Generally, aldehydes are more susceptible to reduction than ketones, for both electronic and steric reasons. The reagents "normally" employed for carbonyl group reduction, such as sodium borohydride, lithium aluminum hydride, and diborane, are too reactive under the usual conditions to usefully take advantage of the inherent difference in reactivity between aldehydes and ketones. The majority of the reported methods achieve chemoselectivity through the modification of the ligands on the hydride donor in order to attenuate reactivity. This approach has resulted in the development of a large number of new reagents for reduction. A conceptually different strategy would involve the modification of the reaction conditions to attenuate reactivity. Using this strategy, we have found (2*ae*) that sodium borohydride alone[3] provides chemoselectivity comparable to the best of the reported methods.

The detailed mechanism of sodium borohydride reduction of ketones remains unknown (9). A hydroxylic solvent (or additive) is required for reduction. The rate of reduction is solvent dependent with the order of reactivity among alcohols being MeOH > EtOH > *i*-PrOH > *t*-BuOH. When reactions are performed in an aprotic solvent with 2-propanol added as a reagent, the kinetic order with respect to 2-propanol is 1.5 (10). Thus sodium borohydride reactivity may be attenuated by the nature of the hydroxylic solvent and its concentration, as well as by temperature. We have examined the effect of these parameters on the selectivity observed in competitive reductions of selected aldehydes and ketones.

Results and discussion

The reactivity of carbonyl groups of a particular type can vary over a wide range. The ranges of reactivity for different types of carbonyl groups are not distinct and some overlap occurs. To define reaction conditions to maximize selectivity, compounds of similar reactivity were chosen for study. Since a high degree of selectivity will be most difficult to achieve when reactivity is similar, the examples used should represent the lower limit of selectivity. Reactions were performed with equimolar amounts of each substrate. By limiting the amount of sodium borohydride and (or) the reaction time, the total amount of reduction was less than 35%. Thus, the ratio of the alcohol products obtained is a reasonable approximation of the relative reactivity of the substrates under the conditions employed. The results are summarized in Tables 1 and 2.

[1]Author to whom correspondence may be addressed.

[2]Preliminary results have been reported (2*ae*, 5*a*).

[3]The use of $NaBH_4$ for selective reduction of aldehydes in the presence of ketones has been reported (2*c*) for two examples. The method uses 1 equiv. of hydride in ethanol at room temperature. This method gives poor selectivity (40%) with 4-methylcyclohexanone vs. hexanal.

Can. J. Chem. Downloaded from www.nrcresearchpress.com by 194.225.253.170 on 09/07/12
For personal use only.

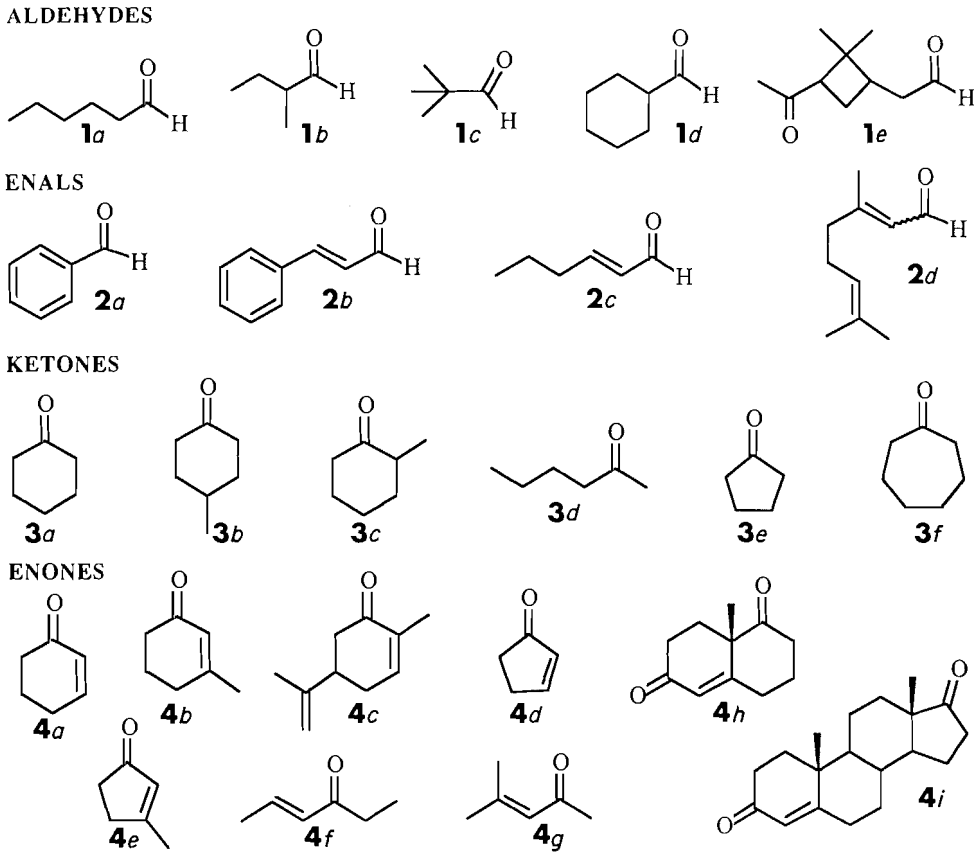


TABLE 1. The effect of alcohol on relative reactivity at room temperature

Alcohol	% in CH_2Cl_2 (v/v)	Relative reactivity 1*d*/1*a*	1*d*/2*a*	2*a*/3*a*	3*a*/3*c*
MeOH	100	1.6	0.7	3.4	2.0
	50	1.6	0.9	4.4	2.2
	25	1.4	1.4	4.4	2.1
	10	1.2	1.2	4.0	2.1
EtOH	100	1.2	0.9	4.1	2.8
	50	1.2	1.3	4.2	2.6
	25	1.2	1.8	4.0	2.5
	10	1.2	1.9	3.9	2.5
i-PrOH	100	1.1	1.5	4.9	3.4
	50	1.0	1.6	5.0	3.2
	25	0.9	1.6	5.8	3.3
	10	1.0	1.7	5.5	3.0
t-BuOH	100	1.0	2.2	4.8	3.1
	50	1.0	2.0	4.9	3.0
	25	1.0	2.0	5.2	3.1
	10	1.1	2.2	5.0	3.0

TABLE 2. The effect of temperature on relative reactivity

Alcohol	Temperature (°C)	Relative reactivity 1*d*/1*a*	1*d*/2*a*	2*a*/3*a*	3*a*/3*c*
50% MeOH	22	1.6	0.9	4.4	2.2
	0	2.0	1.2	3.9	2.5
	−78	2.6	4.8	2.3	3.8
50% EtOH	22	1.2	1.3	4.2	2.6
	0	1.6	1.9	5.1	3.2
	−78	1.9	4.5	5.8	3.8
50% *i*-PrOH	22	1.0	1.6	4.9	3.2
	0	1.2	2.4	5.1	3.3
	−78	1.1	3.9	7.0	—
50% *t*-BuOH	22	1.0	2.0	4.9	3.0
	0	1.2	3.7	3.4	3.9

As expected, the rate of reduction is strongly dependent on the reaction conditions. This is illustrated for the reduction of benzaldehyde (**2***a*). The approximate reaction time required for 50% reduction of **2***a* under various conditions is given in Table 3. In each case, **2***a* (0.2 mmol) was added to $NaBH_4$ (0.2 mmol) in the appropriate solvent mixture (2 mL). The solubility of $NaBH_4$ varies with solvent and temperature; in many cases a suspension is formed. The reaction rate was found to be dependent on the mixing time before the addition of

TABLE 3. Approximate reaction time (min) for 50% reduction of **2***a* (1 molar equiv. of $NaBH_4$)

	% Alcohol in CH_2Cl_2 (v/v) and temperature					
	100%	50%			25%	10%
Alcohol	22°C	22°C	0°C	−78°C	22°C	22°C
MeOH	<0.1	<0.1	<0.1	20	<0.1	<0.1
EtOH	<0.1	<0.1	0.1	120	<0.1	<0.1
i-PrOH	<0.1	0.2	0.4	900	1.3	2.0
t-BuOH	0.3	0.8	0.8		2.0	80

Can. J. Chem. Downloaded from www.nrcresearchpress.com by 194.225.253.170 on 09/07/12
For personal use only.

TABLE 4. Selective reduction of aldehydes

Starting materials	% Aldehyde reduction	% Other reduction	% Selectivity	Starting materials	% Aldehyde reduction	% Other reduction	% Selectivity
1*a*/**2***a*	96	34	48	**1***c*/**2***a*	94	38	42
1*a*/**2***b*	91	6	88	**1***c*/**2***c*	96	3	94
1*a*/**2***c*	93	4	92	**1***c*/**3***b*	96	6	88
1*a*/**2***d*	95	5	90	**1***c*/**3***d*	>97	<3	>94
1*a*/**3***b*	97	5	90	**1***c*/**3***e*	>97	<3	>94
1*a*/**3***d*	96	<3	>92	**1***c*/**3***f*	>97	<3	>94
1*a*/**3***e*	97	<3	>94	**1***c*/**4***a*	95	<3	>94
1*a*/**3***f*	97	<3	>94	**1***c*/**4***f*	96	<3	>94
1*a*/**4***a*	97	<3	>94	**1***d*/**2***a*	97	40	42
1*a*/**4***f*	96	<3	>92	**1***d*/**2***c*	96	4	92
1*b*/**2***a*	94	31	50	**1***d*/**3***b*	97	5	90
1*b*/**2***c*	95	4	92	**1***d*/**3***d*	95	<3	>94
1*b*/**3***b*	96	6	88	**1***d*/**3***e*	97	<3	>94
1*b*/**3***d*	95	<3	>94	**1***d*/**3***f*	>97	<3	>94
1*b*/**3***e*	97	<3	>94	**1***d*/**4***a*	96	<3	>94
1*b*/**3***f*	93	<3	>94	**1***d*/**4***f*	97	<3	>94
1*b*/**4***a*	93	<3	>92	**1***e*	>97	<3	>94
1*b*/**4***f*	95	<3	>94				

substrate. For example, if **2***a* was added immediately to $NaBH_4$ in 10% EtOH, 21 min were required for 50% reduction. Alternatively, if the $NaBH_4$ suspension was stirred for 10 min prior to the addition of **2***a*, reduction was essentially complete within 30 s. Similar results were observed in *i*-PrOH and *t*-BuOH. A possible explanation is that in the absence of dissolved $NaBH_4$ (or a derived species) a much slower heterogeneous reduction occurs in such a way as to inhibit the dissolution of $NaBH_4$ (or a derived species). To insure presaturation, mixing times of up to 30 min were employed.

While the reaction rate is attenuated with reduced concentration of alcohol, the relative reactivity remains fairly constant (typically with 25%, Table 1). Only in the case of **1***d*/**2***a* (in MeOH and EtOH) does the relative reactivity change more than a factor of 2. Similarly, at a fixed concentration (v/v), changing the nature of the alcohol has little effect on relative reactivity. Again the effect is largest with **1***d*/**2***a* (in 100% and 50% alcohol).

Interestingly, **1***d* is more reactive than **1***a* despite the apparent difference in steric hindrance. The additional α-C,C bond in **1***d* may be activating in a Felkin–Ahn sense. The difference in reactivity is related to the steric bulk of the alcohol used; however, the effect is small. The nature of the alcohol also has little effect on the relative reactivity of **3***a*/**3***c*. This is consistent with Wigfield's proposal of a "late" transition state in sodium borohydride reductions (*9a*).

Table 2 presents the effect of temperature on relative reactivity. Here a clear trend emerges. In all cases, maximum differentiation occurs at low temperature. The magnitude of the alcohol effect varies from case to case. With the exception of **1***d*/**1***a*, relative reactivity follows the order MeOH < EtOH < *i*-PrOH < *t*-BuOH. At −78°C, 50% *t*-BuOH (solid) cannot be used, while in 50% *i*-PrOH the rate of reduction of ketones and enones is very slow. In summary, the nature of the alcohol and its concentration, as well as temperature, have a significant effect on the reaction rate. The relative reactivity is influenced most strongly by temperature, to a lesser extent by the nature of the alcohol, and little by the alcohol concentration.

In developing reaction conditions for the chemoselective reduction of different types of carbonyl groups, we wished to employ sodium borohydride in excess. This would not only ensure a high degree of conversion but also provide for experimental simplicity. Similarly, we sought to control the rate of reaction such that the more reactive carbonyl group would require a few hours for complete reduction. Since maximum selectivity was observed at low temperature, we employed solvent mixtures in which the more reactive carbonyl group was completely reduced within a few hours in the presence of excess sodium borohydride at −78°C.

Selective reduction of aldehydes

Typical aldehydes are completely reduced in 1 h at −78°C with excess sodium borohydride in 30% EtOH in CH_2Cl_2 (*2ae*). Under these conditions, various aldehydes were reduced in the presence of enals, ketones, and enones. Reactions were quenched by the addition of acetaldehyde (*2ae*) and analyzed by gc and (or), after work-up, by ^1H nmr (300 MHz). The results of these competitive reductions are summarized in Table 4. Selectivity ([% reduction of aldehyde − % reduction other] ÷ [% reduction aldehyde + % reduction other])[4] is generally greater than 90%. While the conversion is typically high, some aldehydes are not reduced to completion even with prolonged reaction time (3 h), presumably due to hemiacetal formation. A typical ketoaldehyde (**1***e*)[5] is reduced with excellent selectivity. The observed selectivity compares favorably with the best of the previously reported methods (2).

The high selectivity with **3***b* is noteworthy. Relatively few of the reported methods (2) can selectively (>80%) reduce aldehydes in the presence of cyclohexanone (*2i,k,s,z,ab*). To the best of our knowledge, no methods for the selective reduction of aldehydes in the presence of conjugated aldehydes have been reported. Only in competition with benzaldehyde is the selectivity as low as 40%. The selectivity is high with other enals tested. Few methods report on the reduction of aldehydes in the presence of conjugated ketones (other than aceto-

[4]This is analogous to ee or de and thus is an indication of the potential yield obtainable in an intramolecular case. A different method of calculating selectivity was used in our previous work (*2ae*).

[5]Prepared from α-pinene (*i*. O_3, 10% MeOH in CH_2Cl_2, −78°C; *ii*. Me_2S); cf. ref. 12.

Can. J. Chem. Downloaded from www.nrcresearchpress.com by 194.225.253.170 on 09/07/12
For personal use only.

TABLE 5. Selective reduction of conjugated aldehydes

Starting materials	% Enal reduction	% Other reduction	% Selectivity	Starting materials	% Enal reduction	% Other reduction	% Selectivity
2*a*/**3***a*	97	38	44	**2***c*/**3***a*	71	94	−14
2*a*/**3***d*	97	<3	>94	**2***c*/**3***d*	95	13	76
2*a*/**3***e*	96	4	92	**2***c*/**3***e*	96	20	64
2*a*/**3***f*	96	<3	>94	**2***c*/**3***f*	94	15	72
2*a*/**4***a*	95	<3	>94	**2***c*/**4***a*	93	<3	>92
2*a*/**4***f*	96	<3	>94	**2***c*/**4***f*	96	<3	>94
2*b*/**3***a*	84	86	−1	**2***d*/**3***a*	40	91	−40
2*b*/**3***d*	94	8	84	**2***d*/**3***d*	94	15	72
2*b*/**3***e*	95	12	78	**2***d*/**3***e*	90	25	56
2*b*/**3***f*	92	9	82	**2***d*/**3***f*	92	18	68
2*b*/**4***a*	93	<3	>92	**2***d*/**4***a*	92	<3	>92
2*b*/**4***f*	96	<3	>94	**2***d*/**4***f*	93	<3	>92

TABLE 6. Selective reduction of ketones

Starting materials	% Ketone reduction	% Other reduction	% Selectivity	Starting materials	% Ketone reduction	% Other reduction	% Selectivity
3*b*/**4***a*	>97	8	84	**3***f*/**4***a*	>97	43	38
3*b*/**4***b*	>97	<3	>94	**3***f*/**4***b*	>97	5	90
3*b*/**4***c*	>97	4	92	**3***f*/**4***c*	>97	25	58
3*b*/**4***d*	>97	<3	>94	**3***f*/**4***d*	>97	10	80
3*b*/**4***e*	>97	<3	>94	**3***f*/**4***e*	>97	6	88
3*b*/**4***f*	>97	<3	>94	**3***f*/**4***f*	>97	9	82
3*b*/**4***g*	>97	<3	>94	**3***f*/**4***g*	>97	4	92
3*d*/**4***a*	>97	42	40	**4***h*	>97	<3	>94
3*d*/**4***b*	>97	5	90	**4***i*	>97	7	>87
3*d*/**4***c*	>97	21	64				
3*d*/**4***d*	>97	9	82	Starting materials	% **3***a* reduction	% Other reduction	% Selectivity
3*d*/**4***e*	>97	5	90				
3*d*/**4***f*	>97	9	82	**3***a*/**3***d*	>97	10	80
3*d*/**4***g*	>97	5	90	**3***a*/**3***e*	>97	15	72
3*e*/**4***a*	>97	40	42	**3***a*/**3***f*	>97	9	82
3*e*/**4***b*	>97	4	92				
3*e*/**4***c*	>97	18	68				
3*e*/**4***d*	>97	7	86	Starting materials	% **3***c* reduction	% Other reduction	% Selectivity
3*e*/**4***e*	>97	5	90				
3*e*/**4***f*	>97	9	82	**3***c*/**3***d*	>97	24	60
3*e*/**4***g*	>97	4	92	**3***c*/**3***e*	>97	26	56
				3*c*/**3***f*	>97	15	72

phenone). Excellent discrimination is observed with all enones tested.

Selective reduction of enals

Conjugated aldehydes are intermediate in reactivity between aldehydes and ketones. Benzaldehyde (**2***a*) is about five times more reactive than cyclohexanone (**3***a*) and about one-fifth as reactive as cyclohexane carboxaldehyde (**1***d*). Citral (**2***d*)[6] is only about one-fifth as reactive as cyclohexanone but more reactive than cyclopentanone (**3***e*). The enals studied were reduced in 1–3 h in 30% MeOH in CH_2Cl_2 at −78°C. Interestingly, we did not observe reduction, or addition of alkoxide, in a 1,4 sense under these conditions (11). Table 5 gives the results of the reduction of conjugated aldehydes in the presence of ketones and enones. While the selectivity is poor vs. cyclohexanone (**3***a*),[7] good selectivity is observed with other ketones. The selectivity is excellent with enones. With the exception of benzaldehydes (2), methods for the selective reduction of conjugated aldehydes have not been reported.[8]

Selective reduction of ketones

The reactivity of ketones varies over a wide range. In 50% MeOH in CH_2Cl_2, cyclohexanone (**3***a*) is reduced within 1 h whereas cycloheptanone (**3***e*) requires 14 h for complete reduction. Table 6 gives the results of the reduction of ketones in the presence of enones under these conditions. Despite the wide range in reaction time, selectivity remains high.

There are few reports on the selective reduction of ketones in

[6]Citral was a 65:35 mixture of geranial and neral. Geranial is more reactive than neral.

[7]Excellent selectivity has been achieved with benzaldehyde vs. cyclohexanone using highly hindered reagents (2*i*,*k*,*s*).

[8]For a micromethod for discriminating between conjugated aldehydes and conjugated ketones involving selective reduction see ref. 13.

Can. J. Chem. Downloaded from www.nrcresearchpress.com by 194.225.253.170 on 09/07/12
For personal use only.

Can. J. Chem. Downloaded from www.nrcresearchpress.com by 194.225.253.170 on 09/07/12
For personal use only.

the presence of enones (5).[9] We have expanded on our previous study (5*a*) in order to define the limitations of the method. While the less reactive ketones (**3***d–f*) show only modest selectivity against cyclohexenone (**4***a*), good selectivity is observed against α and β substituted cyclohexenones (**4***b,c*). Excellent discrimination was observed in all other cases studied. Two intramolecular examples (**4***h,i*)[10] were reduced with excellent selectivity.

The high reactivity of cyclohexanone compared to other ketones suggests the possibility of selective reduction. Under our conditions, modest to good selectivity is observed in the reduction of unhindered cyclohexanones (**3***a,c*) in the presence of other unhindered ketones (**3***d–f*) (Table 6). The reactivity of ketones towards sodium borohydride will be attenuated by steric factors. To predict selectivity in competitive reductions on the basis of steric effects is not straightforward (8*c*). The magnitude of steric effects in sodium borohydride reductions can be very different from those with other reagents (6–8).

Conclusion

Under the appropriate reaction conditions, sodium borohydride provides excellent chemoselectivity in the reduction of various types of carbonyl groups. The selectivity observed is comparable to the best of the previously reported methods. The ready availability and experimental simplicity associated with the use of sodium borohydride is noteworthy. Interestingly, reduction under Luche's conditions ($NaBH_4/CeCl_3$) often reverses the order of selectivity (3, 4).

Experimental

All solvents were distilled prior to use. Acetaldehyde, benzaldehyde (**2***a*), and cinnamaldehyde (**2***b*) were freshly distilled. Acetone was reagent grade. Ketoaldehyde **1***e* was prepared from α-pinene.[5] All other carbonyl compounds are commercially available and were used as received. The ^1H nmr spectra were obtained in $CDCl_3$ solution on a Bruker AM-300 instrument. A Hewlett–Packard 5890A gas chromatograph equipped with a FID detector, an HP-3393A integrator, and an HP-20M (Carbowax) column was used for gas chromatography. Helium was used as the carrier gas. In most cases, baseline separation of the components of interest could be achieved through temperature programming. The % selectivity is calculated as the ([% reduction of the group of interest − % reduction of the other group] ÷ [% reduction of the group of interest + % reduction of the other group]) × 100.[4]

Measurement of relative reactivities

Each carbonyl compound (0.2 mmol) and mesitylene (0.2 mmol, internal standard) were added to the appropriate solvent mixture (2 mL) and the resulting solution was analyzed by gc. The solution was cooled to the desired temperature and $NaBH_4$ (1–10 mg)[11] was added. Reactions at 22°C or 0°C were monitored directly by gc. For reactions at −78°C, small aliquots were quenched by addition to an acetaldehyde solution (CH_2Cl_2) prior to gc analysis. When analysis showed that the most reactive carbonyl compound was 30–40% reduced, the reaction was quenched by addition of acetaldehyde (0.2 mL)[12] and analyzed by gc. The amount of reduction was measured in two ways. The percentage loss of starting material was measured by comparison with the internal standard and the percentage of alcohol product formed was measured by comparison with the remaining starting material. These two measures of the amount of reduction were generally within 10%. The relative reactivity was calculated as the ratio of the percentage reduction of each component. The values in Tables 1 and 2 represent the average of at least two experiments.

*Reduction of benzaldehyde (***2***a)*

The appropriate solvent mixture (2 mL) was added to $NaBH_4$ (ca. 7 mg) and the resulting suspension (solution) was stirred for 3 min (50% MeOH), 20 min (50% EtOH), or 30 min (50% *i*-PrOH, 50% *t*-BuOH). The resulting mixtures were cooled to the appropriate temperature and benzaldehyde (**2***a*, 1 molar equivalent) was added. The reactions were monitored as above by gc. In cases where the reduction was greater than 90% complete within 30 s we estimate the time required for 50% reduction to be less than 0.1 min. In all other cases, reaction times for 45–55% reduction were obtained. Values are reported in Table 3.

Selective reduction of aldehydes

Most reactions (**1** vs. **3**, **1** vs. **4**, and **1***e*) were analyzed by ^1H nmr. $NaBH_4$ (20 mg) was dissolved in EtOH (1.5 mL) and CH_2Cl_2 (3.5 mL) was added. The resulting suspension was cooled to −78°C (Dry Ice – acetone) and each carbonyl compound (20 μL) was added. After stirring for 1 h, acetaldehyde (0.5 mL) was added and the mixture was allowed to warm to room temperature. The solution was diluted with CH_2Cl_2, washed with saturated $NaHCO_3$, dried with Na_2SO_4, and concentrated. The percentage reduction of each component was calculated by integration of appropriate signals in the ^1H nmr spectrum.

In the reaction of **1***e* (20 mg), work-up gave the corresponding hydroxyketone (21 mg, quantitative yield), which was essentially homogeneous by tlc and by ^1H nmr.

Reactions **1** vs. **2** were analyzed by gc. Reactions were carried out as above except that CH_2Cl_2 (3 mL) was added. After cooling to −78°C, a solution of each carbonyl compound and mesitylene (20 μL each) in CH_2Cl_2 (0.5 mL) was added. After stirring for 1 h, the reactions were quenched (acetaldehyde, 0.5 mL) and analyzed by gc as described above for the determination of relative reactivities.

Selective reduction of conjugated aldehydes

Reactions were conducted in 30% MeOH in CH_2Cl_2 at −78°C. To $NaBH_4$ (20 mg) was added a solution of MeOH (1.5 mL) in CH_2Cl_2 (3.0 mL). After stirring for 3 min, the mixture was cooled to −78°C (Dry Ice – acetone) and a solution of each carbonyl compound and mesitylene (20 μL each) in CH_2Cl_2 (0.5 mL) was added. After stirring for 1–3 h (reactions with **2***a*, 1 h; with **2***b,c*, 2 h; with **2***d*, 3 h), the reactions were quenched (acetaldehyde, 0.5 mL) and analyzed by gc as described above for the determination of relative reactivities.

The enals **2***b–d* were reduced individually as above. Products resulting from reduction or addition in a 1,4 sense were not detected by gc or, after work-up as above, by ^1H nmr.

Selective reduction of ketones

Reactions with **3***b* were conducted (5*a*) by adding $NaBH_4$ (20 mg) to a solution of carbonyl compounds (20 μL each) in 50% MeOH in CH_2Cl_2 (5 mL) at −78°C. After stirring for 1 h, the reactions were quenched (acetone, 0.5 mL) and allowed to warm to room temperature. The reaction mixture was diluted with CH_2Cl_2, washed with 1 M NaOH, dried with Na_2SO_4, concentrated, and analyzed by ^1H nmr.

Reaction of **4***h* (21 mg) as above gave, after work-up, the 1-β alcohol (21 mg), which was contaminated by less than 3% of the corresponding diol. Similar reduction of **4***i* (20 mg) for 6 h gave a 93:7 mixture (21 mg) of the 17-β alcohol and the 3β,17β diol. Recrystallization (acetone/hexane) gave the 17β alcohol (14 mg), mp 152–154°C (lit. (6*a*) mp 154–155°C).

When using the above method, we periodically encountered incomplete reduction (selectivity remains high) of the less reactive ketones (**3***d–f*) after 14 h. Thus the following conditions were employed. To $NaBH_4$ (20 mg) was added a solution of MeOH (2.5 mL) in CH_2Cl_2

[9]The reverse selectivity has been reported using $NaBH_4$ (3) or boranes (1*a,b*).

[10]Selective reductions of **4***h* (5*b*) and **4***i* (6*a,b,e,f*) have been reported.

[11]The amount of $NaBH_4$ added was a function of the reaction rate. For very fast reactions (MeOH or EtOH at 0°C or 22°C), 1–2 mg was added. For slower reactions, up to 10 mg was added.

[12]In a control experiment, **1***a* (0.2 mmol) and acetaldehyde (0.2 mL) in 50% MeOH in CH_2Cl_2 (2 mL) were reduced with $NaBH_4$ (0.1 mmol) at −78°C. After warming to room temperature, gc analysis indicated <5% reduction of **1***a*.

(2.0 mL). After stirring for 3 min, the mixture was cooled to −78°C (Dry Ice – acetone) and a solution of each carbonyl compound and mesitylene (20 μL each) in CH_2Cl_2 (0.5 mL) was added. After stirring for 1–14 h (reactions with **3***a*, 1 h; with **3***c*, 3 h; with **3***d–f*, 14 h), the reactions were quenched (acetone, 0.5 mL) and were analyzed by gc (as described above for the determination of relative reactivities) or, after work-up as above, by ^{1}H nmr.

Ketone **3***b* was reduced to an 85:15 mixture of *trans*:*cis* isomers; **3***c* to a 2:1 mixture of *trans*:*cis* isomers; **4***h* and **4***i* gave only the β alcohol. The ratio of 1,2:1,4 products from reduction of enones **4***b*,*e*,*f*,*g*,*h*,*i* was >10:1; for **4***a* and **4***c*, 3:1; for **4***d*, 0.5:1.

Acknowledgement

Financial support provided by the Natural Sciences and Engineering Research Council of Canada is gratefully acknowledged.

1. (*a*) H. C. Brown and S. Krishnamurthy. Tetrahedron, **35**, 567 (1979); (*b*) E. R. H. Walker. Chem. Soc. Rev. **5**, 23 (1976); (*c*) Sodium borohydride. Product brochure, Thiokol/Ventron Division, Danvers, MA. 1979.
2. Selective reduction of aldehydes in the presence of ketones: (*a*) ($NaBH_2S_3$) J. M. Lalancette, A. Freche, J. R. Brindle, and M. Laliberte. Synthesis, 526 (1972); (*b*) (Bu_4NBH_3CN) R. O. Hutchins and D. Kandasamy. J. Am. Chem. Soc. **95**, 6131 (1973); (*c*) ($NaBH_4$) C. S. Sell. Aust. J. Chem. **28**, 1383 (1975); (*d*) ($Na(OAc)_3BH$) G. W. Gribble and D. C. Ferguson. J. Chem. Soc. Chem. Commun. 535 (1975); (*e*) ($LiBu_2$-9-BBN) Y. Yamamoto, H. Toi, A. Sonoda, and S.-I. Murahasi. J. Am. Chem. Soc. **98**, 1965 (1976); (*f*) (SmI_2) P. Girard, H. B. Kagan, and J. L. Namy. Nouv. J. Chim. **1**, 5 (1977); (*g*) ($NaBH_4$/RSH) Y. Maki, K. Kikuchi, H. Sugiyama, and S. Seto. Tetrahedron Lett. 263 (1977); (*h*) (*i*PrOH/Al_2O_3) G. H. Posner, A. W. Runquist, and M. J. Chapdelaine. J. Org. Chem. **42**, 1202 (1977); (*i*) (9-BBN/pyr) H. C. Brown and S. U. Kulkarni. J. Org. Chem. **42**, 4169 (1977); (*j*) (BH_3/LiCl) N. M. Yoon and J. S. Cha. J. Korean Chem. Soc. **22**, 259 (1978); (*k*) (B-alkyl-9-BBN) M. M. Midland and A. Tramontano. J. Org. Chem. **43**, 1470 (1978); (*l*) (Bu_3SnH) N. Y. M. Fung, P. de Mayo, J. H. Shauble, and A. C. Weedon. J. Org. Chem. **43**, 3977 (1978); (*m*) ($LiBH_4$/sieves) P. A. Risbood and D. M. Ruthven. J. Org. Chem. **44**, 3969 (1979); (*n*) ($BH_3 \cdot NH_2R$) G. C. Andrews. Tetrahedron Lett. **21**, 697 (1980); (*o*) (Et_4NBH_4) T. N. Sorrell and P. S. Pearlman. Tetrahedron Lett. **21**, 3963 (1980); (*p*) ($EtCH(OMgBr)_2$) J. H. Babler and B. J. Invergo. Tetrahedron Lett. **22**, 621 (1981); (*q*) ($(Ph_3P)_2CuBH_4$) G. W. J. Fleet and P. J. C. Harding. Tetrahedron Lett. **22**, 675 (1981); (*r*) (NaOCHO) J. H. Babler and S. J. Sarussi. J. Org. Chem. **46**, 3367 (1981); (*s*) ($Li(Et_3CO)_3AlH$) S. Krishnamurthy. J. Org. Chem. **46**, 4628 (1981); (*t*) ($NaBH(OAr)_3$) S. Yamaguchi, K. Kabuto, and F. Yasuhara. Chem. Lett. 461 (1981); (*u*) ($Bu_4NB)OAc)_3H$) C. F. Nutaitus and G. W. Gribble. Tetrahedron Lett. **24**, 4287 (1983); (*v*) (BH_4^- resin) N. M. Yoon, K. B. Park, and Y. S. Gyoung. Tetrahedron Lett. **24**, 5367 (1983); (*w*) (BH_3/pyr/Al_2O_3) J. H. Babler and S. J. Sarussi. J. Org. Chem. **48**, 4416 (1983); (*x*) (8-oxyquinoline dihydroboronite/$BF_3 \cdot Et_2O$) S. Kim, H. J. Kang, and S. Yang. Tetrahedron Lett. **25**, 2985 (1984); Bull. Korean Chem. Soc. **5**, 240 (1984); (*y*) ($NaBH_4$/$CeCl_3$/DMSO) C. Adams. Synth. Commun. **14**, 1349 (1984); (*z*) ($Et_4N(\mu\text{-}HMo_2(CO)_{10}$) D. H. Gibson and Y. S. El-Omrani. Organometallics, **4**, 1473 (1985); (*aa*) (HCOOH/R_3N/$RuCl_2(Ph_3P)_3$) B. T. Khai and A. Arcelli. Tetrahedron Lett. **26**, 3365 (1985); (*ab*) (KPh_3BH) N. M. Yoon, K. E. Kim, and J. Kang. J. Org. Chem. **51**, 226 (1986); (*ac*) ($NaBH_4$/Bu_4NBr) C. S. Rao, A. A. Deshmukh, and B. J. Patel. Indian J. Chem. **25B**, 626 (1986); (*ad*) (TMSCl/Ni_2B) M. Borbaruah, N. C. Barua, and R. P. Sharma. Tetrahedron Lett. **28**, 5741 (1987); (*ae*) ($NaBH_4$) D. E. Ward and C. K. Rhee. Synth. Commun. **18**, 1927 (1988).
3. Selective reduction of enals in the presence of aldehydes: ($NaBH_4$/$ErCl_3$) A. L. Gemal and J. L. Luche. Tetrahedron Lett. **22**, 4077 (1981).
4. Selective reduction of ketones in the presence of aldehydes: ($NaBH_4$/$CeCl_3$) (*a*) A. L. Gemal and J. L. Luche. J. Org. Chem. **44**, 4187 (1979); (*b*) J. Am. Chem. Soc. **101**, 5848 (1979).
5. Selective reduction of ketones in the presence of enones: (*a*) ($NaBH_4$) D. E. Ward, C. K. Rhee, and W. M. Zoghaib. Tetrahedron Lett. **29**, 517 (1988). See also: (*b*) J. D. Cocher and T. G. Halsall. J. Chem. Soc. 3441 (1957); (*c*) H. Haubenstock. J. Org. Chem. **37**, 656 (1972); (*d*) H. Haubenstock and P. Quezada. J. Org. Chem. **37**, 4067 (1972).
6. Selective reduction of steroidal ketones: (*a*) J. K. Norymberski and G. F. Woods. J. Chem. Soc. 3426 (1955); (*b*) J. Fajkos. Collect. Czech. Chem. Commun. **24**, 2284 (1959); (*c*) J. L. Mateos. J. Org. Chem. **24**, 2034 (1959); (*d*) J. A. Zderic and J. Iriarte. J. Org. Chem. **27**, 1756 (1962); (*e*) U. Eder. Chem. Ber. **109**, 2954 (1976); (*f*) E. D'Incan, A. Loupy, A. Restelli, J. Seyden-Penne, and P. Vinout. Tetrahedron, **38**, 1755 (1982). See also ref. 2*h*.
7. Selective reduction of ketones: T. E. A. Nieminen and T. A. Hase. Tetrahedron Lett. **28**, 4725 (1987). See also refs. 2*e*, 2*n*, 2*v*, 2*x*, 2*ab*.
8. (*a*) H. C. Brown, O. H. Wheeler, and K. Ichikawa. Tetrahedron, **1**, 214 (1957); (*b*) H. C. Brown and K. Ichikawa. Tetrahedron, **1**, 221 (1957); (*c*) J. Am. Chem. Soc. **84**, 373 (1962); (*d*) O. H. Wheeler and J. L. Mateos. Can. J. Chem. **36**, 1049 (1956).
9. (*a*) D. C. Wigfield. Tetrahedron, **35**, 449 (1979); (*b*) J. R. Boone and E. C. Ashbey. Top. Stereochem. **11**, 53 (1979); (*c*) B. Caro, B. Boyer, G. Lamaty, and G. Jaouen. Bull. Soc. Chim. Fr. 281 (1983).
10. D. C. Wigfield and F. W. Gowland. J. Org. Chem. **42**, 1108 (1977).
11. M. R. Johnson and B. Rickborn. J. Org. Chem. **35**, 1041 (1970).
12. J. M. Conia and C. Faget. Bull. Soc. Chim. Fr. 1963 (1964).
13. J. P. Critchley, J. Friend, and T. Swain. Chem. Ind. 596 (1958).

Can. J. Chem. Downloaded from www.nrcresearchpress.com by 194.225.253.170 on 09/07/12
For personal use only.

A novel 1:1 benzenesulfonamide:18-crown-6 complex as uncovered via ^{13}C solid phase NMR spectroscopy and X-ray crystallography[1]

G. W. BUCHANAN[2] AND C. MORAT[3]

Ottawa–Carleton Chemistry Institute, Department of Chemistry, Carleton University, Ottawa, Ont., Canada K1S 5B6

AND

J. P. CHARLAND, C. I. RATCLIFFE, AND J. A. RIPMEESTER

Division of Chemistry, National Research Council of Canada, Ottawa, Ont., Canada K1A 0R6

Received November 22, 1988

G. W. BUCHANAN, C. MORAT, J. P. CHARLAND, C. I. RATCLIFFE, and J. A. RIPMEESTER. Can. J. Chem. **67**, 1212 (1989).

A 1:1 complex of 18-crown-6 ether and benzenesulfonamide has been prepared, whose melting point is within 4° of the previously reported 1:2 complex. The X-ray crystallographic structure shows pseudo D_{3d} symmetry in the crown ether portion of this complex, in contrast to the 1:2 complex, which exhibits C_i symmetry in the macrocycle. The temperature dependent ^{13}C CPMAS NMR spectra of these complexes have two regions of broadening for the crown ether carbons. At higher temperatures, a dipolar "washout" mechanism is operative, leading to broadening when molecular motion has a correlation time approximately equal to the inverse of the decoupling field. At lower temperatures broadening occurs when the motional correlation time is equal to the inverse of the chemical shift difference. From application of the Arrhenius equation, the activation energy for the molecular motion in solid 18-crown-6 is found to be approximately 10 kcal/mol. Evidence for independent anisotropic motion in the benzenesulfonamide moiety of the 1:1 complex is also presented.

Key words: crown ether, molecular motion, solid phase NMR.

G. W. BUCHANAN, C. MORAT, J. P. CHARLAND, C. I. RATCLIFFE et J. A. RIPMEESTER. Can. J. Chem. **67**, 1212 (1989).

On a préparé un complexe 1 : 1 de l'éther 18-couronne-6 et du benzènesulfonamide; son point de fusion ne diffère de celui rapporté antérieurement pour le complexe 1 : 2 que par 4°. Une étude de la structure par diffraction des rayons-X indique que la portion éther couronne possède une symétrie D_{3d}; par opposition, la portion macrocyclique du complexe 1 : 2 présentait une symétrie C_i. On a déterminé les spectres RMN CPMAS du ^{13}C en fonction de la température; ils présentent deux régions dans lesquelles les raies des carbones de l'éther couronne sont élargies. Aux températures élevées, un mécanisme dipolaire intervient pour provoquer un élargissement lorsque le temps de corrélation du mouvement moléculaire est approximativement égal à l'inverse du champ des découplage. Aux températures plus basses, l'élargissement se produit lorsque le temps de corrélation du mouvement est égal à l'inverse de la différence des déplacements chimiques. En appliquant l'équation d'Arrhénius, on a trouvé que l'énergie d'activation du mouvement moléculaire dans la 18-couronne-6 est approximativement 10 kcal/mol. On présente aussi des données suggérant l'existence d'un mouvement anisotrope indépendant dans la portion benzènesulfonamide du complexe 1 : 1.

Mots clés : éther couronne, mouvement moléculaire, RMN des phases solides.

[Traduit par la revue]

Can. J. Chem. Downloaded from www.nrcresearchpress.com by 194.225.253.170 on 09/07/12
For personal use only.

Introduction

Recent publications from these laboratories (1, 2) have dealt with the observation of dynamic ^{13}C NMR phenomena in crystalline 18-crown-6 ether (1), its KNCS complex (1), and its $NaNCS \cdot H_2O$ complex (2). In each case, the low temperature ^{13}C chemical shift differences could be interpreted in terms of torsional angle effects, with the geometrical data being available from X-ray crystallographic results.

In an effort to extend these studies to *molecular* inclusion complexes of 18-crown-6, we have prepared a number of complexes with neutral guest molecules, one such case being benzenesulfonamide.

Results and discussion

The literature (3) describes the X-ray crystallographic structure of a 1:2 18-crown-6:benzenesulfonamide complex (melting point 92°C) in which the macrocyclic ring adopts a centrosymmetric conformation that is nearly identical to that for 18-crown-6 itself (4, 5). Accordingly, based on our recent results (1, 2), we anticipated that the ^{13}C CPMAS spectra in the crown ether region of these two systems would be quite similar. To our surprise, the complex that we initially prepared (mp 88–89°C) possesses solid phase ^{13}C spectra for the crown ether region as a function of temperature (Fig. 1) that much more closely resemble those of the KNCS:18-crown-6 complex having approximate D_{3d} symmetry (1, 6).

In view of this apparent dichotomy of results, we proceeded to examine the structure of our 88–89°C complex via X-ray crystallography. The ORTEP diagram of the structure obtained is presented in Fig. 2 and clearly represents that of a *1:1* benzenesulfonamide:18-crown-6 complex. For this complex the refined coordinates of the non-H-atoms are listed in Table 1, while Table 2 gives the geometrical data (bond lengths, bond angles, and torsional angles).

In this 1:1 complex, the "guest" benzenesulfonamide molecule is hydrogen bonded to the "host" crown ether. The two N---O distances (Table 2) are identical within standard deviations and are similar to those observed in the 2:1 guest:host complex (3). Figure 2 shows that the crown ether in the 1:1 complex has a nearly circular conformation, similar to that found in the 1:1 complex with KSCN (6). By contrast, in the 2:1 complex with benzenesulfonamide (3) the crown ether adopts an elliptical shape. Hence one sees here cases of stoichiometrically induced conformation changes in the 18-crown-6 structure, with simultaneous optimization of hydrogen bonding and van der Waals or stacking interactions.

Detailed examination of the torsional angle data indicates that

[1]NRCC No. 30020.

[2]Author to whom correspondence may be addressed.

[3]Permanent address: LEDSS, Université Joseph Fourier (Grenoble I), BP 68, 38402, St-Martin-d'Hères, Cedex, France.

Can. J. Chem. Downloaded from www.nrcresearchpress.com by 194.225.253.170 on 09/07/12
For personal use only.

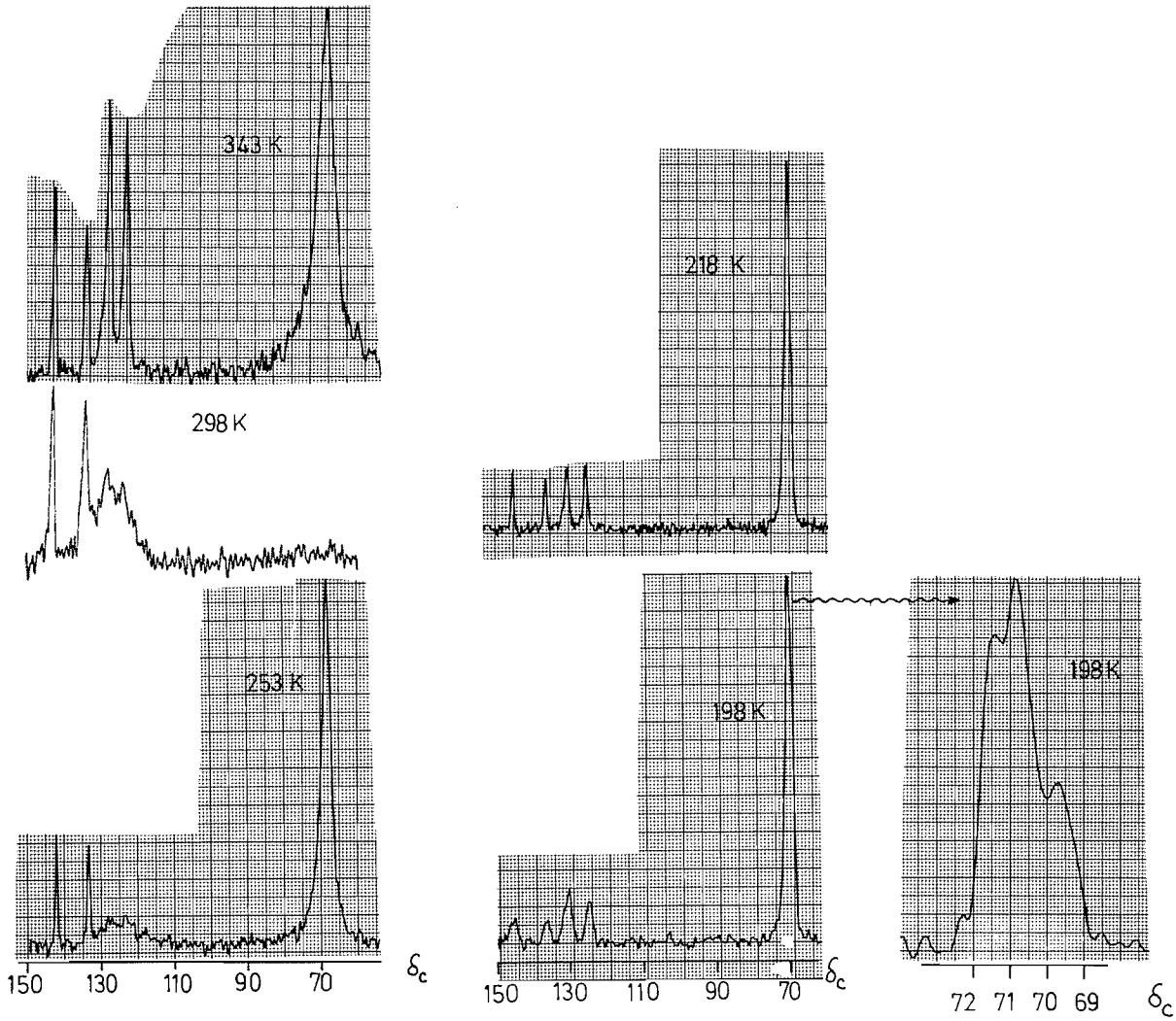


FIG. 1. The 45.3-MHz ^{13}C CPMAS spectrum of the 1:1 18-crown-6:benzenesulfonamide complex as a function of temperature.

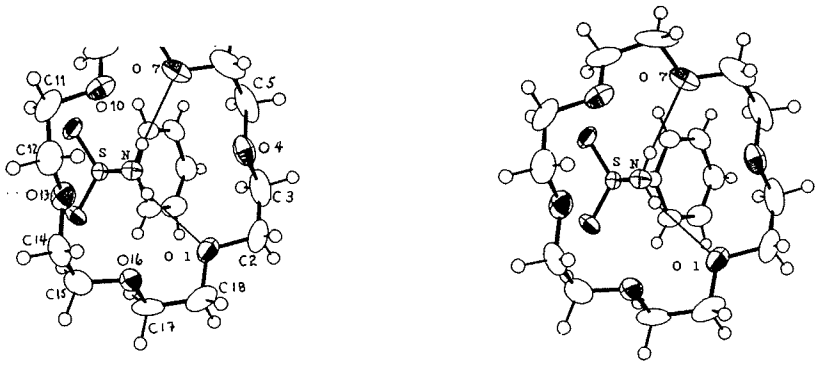


FIG. 2. Stereodiagram of the 1:1 complex.

the 18-membered ring in the 1:1 complex possesses pseudo D_{3d} symmetry. Each carbon has a skew *gauche* geometry for the O—C*—C—O network and pseudo *trans* geometries for the other torsional networks (Table 3).

The ^{13}C CPMAS spectra of the 1:1 complex as a function of temperature are presented in Fig. 1. Clearly, there are marked temperature dependencies in both the guest and host ^{13}C resonances. At the high temperature limit of 343 K, a relatively broad (linewidth ca. 230 Hz) crown ether resonance is observed with a chemical shift near 70 ppm. In the aromatic region there are four sharp lines at $\delta_C = 144.7$, 135.9, 129.7, and 125.2. From solution work (7), C-19 (below) will be the most deshielded position, followed by C-22 and then the C-21,23 pair. The *ortho* sites, C-20,24, will be the most shielded, appearing at 125.2 ppm.

At 298 K, there is severe broadening of the crown ether

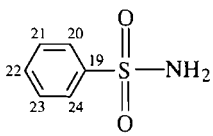
Can. J. Chem. Downloaded from www.nrcresearchpress.com by 194.225.253.170 on 09/07/12
For personal use only.

TABLE 1. Atomic Parameters and B_{iso}* of the non-H atoms

Atom	x	y	z	B_{iso}
S	0.44549(14)	0,21049(8)	0.75279(8)	3.50(6)
O 1	0.8282 (4)	0.30469(22)	0.8735 (3)	5.85(20)
O 2	0.3327 (3)	0.20652(20)	0.67918(20)	5.15(17)
O 3	0.3904 (4)	0.20627(20)	0.83662(19)	5.00(17)
O 4	0.8897 (5)	0.31765(23)	0.6948 (3)	6.53(23)
O 7	0.6278 (6)	0.33387(25)	0.56950(24)	6.56(24)
O10	0.3841 (5)	0.43977(22)	0.6181 (3)	5.94(22)
O13	0.3242 (4)	0.43653(22)	0.7991 (3)	5.96(21)
O16	0.5770 (5)	0.39803(23)	0.92934(22)	5.49(20)
N	0.5419 (6)	0.2899 (3)	0.7461 (4)	4.01(24)
C 2	0.9815 (9)	0.3098 (7)	0.8415 (7)	8.6 (6)
C 3	0.9774 (10)	0.2709 (7)	0.7571 (8)	9.1 (6)
C 5	0.8834 (12)	0.2856 (6)	0.6106 (7)	9.0 (6)
C 6	0.7860 (15)	0.3367 (7)	0.5505 (7)	9.0 (6)
C 8	0.5222 (16)	0.3809 (5)	0.5114 (5)	8.4 (6)
C 9	0.3701 (13)	0.3891 (5)	0.5493 (5)	7.8 (5)
C11	0.2352 (10)	0.4544 (7)	0.6557 (7)	8.7 (5)
C12	0.2634 (12)	0.4915 (6)	0.7396 (7)	8.2 (5)
C14	0.3394 (10)	0.4620 (6)	0.8864 (6)	7.3 (5)
C15	0.4167 (10)	0.4003 (5)	0.9406 (5)	6.9 (4)
C17	0.6584 (11)	0.3376 (4)	0.9786 (4)	6.5 (4)
C18	0.8241 (11)	0.3358 (5)	0.9567 (5)	7.4 (4)
C19	0.5792 (5)	0.1311 (3)	0.7443 (3)	2.85(21)
C20	0.6554 (8)	0.0977 (4)	0.8163 (4)	5.2 (3)
C21	0.7583 (8)	0.0354 (4)	0.8083 (5)	6.3 (4)
C22	0.7871 (8)	0.0062 (4)	0.7299 (5)	5.6 (4)
C23	0.7104 (8)	0.0391 (4)	0.6581 (4)	5.2 (3)
C24	0.6076 (7)	0.1015 (3)	0.6657 (4)	4.4 (3)

*B_{iso} is the mean of the principal axes of the thermal ellipsoid; esd's refer to the last digit printed.

resonance, followed by a resharpening to a minimum linewidth at 218 K. Subsequently, there is a more subtle broadening of the crown ether resonance until the low temperature limit is reached at 198 K. At this point there are three resolvable resonances for the crown ether carbons.



The higher temperature broadening can be described as "dipolar washout" (8) and will occur when the molecular motions have rates such that the correlation time for the C—H vector, τ_c, is the inverse of the decoupling field amplitude of 60 kHz; i.e., $\tau_c = 1/2\pi\gamma H_1 = 1/2\pi \times 60\,\text{kHz} = 2.7 \times 10^{-6}$ s.

An estimate of the barrier for this process can be obtained by application of the Waugh–Fedin Approximation (9). Employing a temperature of 298 K, the value obtained is ca. 11 kcal/mol.

The low temperature broadening will occur when motions have correlation times of the same order as the chemical shift differences. Since the chemical shift differences between conformationally different carbons are found to be ca. 2 ppm in this complex, these correlation times at a ^{13}C resonance frequency of 45.3 MHz will be ca. $1/(45.3 \times 2) = 10^{-2}$ s.

Converting these correlation times to rates and using the temperatures of 298 K and 198 K for the fast and slow broadening mechanisms, respectively, yields, by application of the Arrhenius equation, a value for the activation energy of ca. 10 kcal/mol. The reasonable agreement between this value and that obtained from the Waugh–Fedin Approximation lends support to the hypothesis that only one process is being detected here with two time scales being accessible via the variable temperature ^{13}C CPMAS experiment.

For the benzenesulfonamide resonances, a similar dipolar washout occurs, but only for the C20,24 and C21,23 pairs, and is apparent in the spectrum at 253 K. The fact that only these resonances experience this phenomenon indicates that the preferred direction of motion in the benzenesulfonamide moiety is about the C19—C22 axis. Similar behaviour was noted previously (10) in the solid state ^{13}C spectrum of benzaldehyde encapsulated in cyclodextrin.

From a conformational viewpoint, the chemical shift differences in the 18-crown-6 at 198 K are of interest. In light of the X-ray results and assuming a dominance of torsional angle effects on the ^{13}C chemical shifts (11), one would thus anticipate only minor chemical shift differences between the carbons of the macrocycle. Indeed this is observed, since at 198 K three lines of relative intensity ca. 4:5:3 are found at δ_C = 71.4, 70,9, and 69.7 ppm, respectively. At higher temperatures, the fact that only one crown ether resonance is resolved indicates that torsional angle averaging is occurring in the solid on the NMR time scale.

It is of interest to attempt to assign the three resolved resonances in the solid phase spectrum to particular groups of carbons in the X-ray structure. The basic tenets for analysis here are that any expansion of the O—C—C—O angle above 60° will induce deshielding while any contraction of the C—O—C—C angle below 180° will induce shielding at all carbon sites. Such tenets are in accord with experimental data (11).

Thus if one assumes an approximately equal angular dependence of the chemical shift for each type of torsional network, a relative order of shielding can be established. Such a procedure involves calculating Σ (contractions from 180°) and then subtracting the expansion above 60°. The carbon possessing the highest resulting value is predicted to be the most shielded. On this rather crude basis, we suggest that carbons 9, 11, and 12 constitute the most shielded intensity 3 resonance at 69.7 ppm. Similarly, C 2, C 6, C 8, C 17, and C 18 may give rise to the intensity 5 line at 70.9 ppm and the remaining four carbons appear at 71.4 ppm.

Of course one cannot rule out other contributions to the ^{13}C shifts of the macrocycle, such as steric and anisotropic effects arising from the guest, since the overall chemical shift difference is only 1.7 ppm.

For the 1:2 18-crown-6:benzenesulfonamide complex, the ^{13}C CPMAS spectra as a function of temperature are presented in Fig. 3. The dipolar washout of the crown ether resonance is again clear from the spectrum at 298 K, with the conformational broadening becoming apparent in the 220 K spectrum.

In the X-ray structure of the 1:2 complex (3), the two benzenesulfonamide moieties are equivalent due to the presence of the centre of symmetry. At 340 K in the ^{13}C CPMAS spectrum, there are only three aromatic carbon resonances observed, at 129.3, 132.5, and 148.1 ppm respectively. In this case it appears that C20, C21, C23, and C24 are accidently chemical shift degenerate. There are appreciable temperature dependent chemical shifts for the benzenesulfonamide carbons since at 298 K their chemical shifts, 126.3, 129.9, 133.8, and 144.4 ppm, are substantially different from those at 340 K. The fact that only four aromatic resonances appear indicates two possible situations: (*i*) rapid twofold flips of the aromatic ring about the C19–C22 axis, or (*ii*) accidental coincidence of the C20,24 and C21,23 pairs of resonances.

Can. J. Chem. Downloaded from www.nrcresearchpress.com by 194.225.253.170 on 09/07/12
For personal use only.

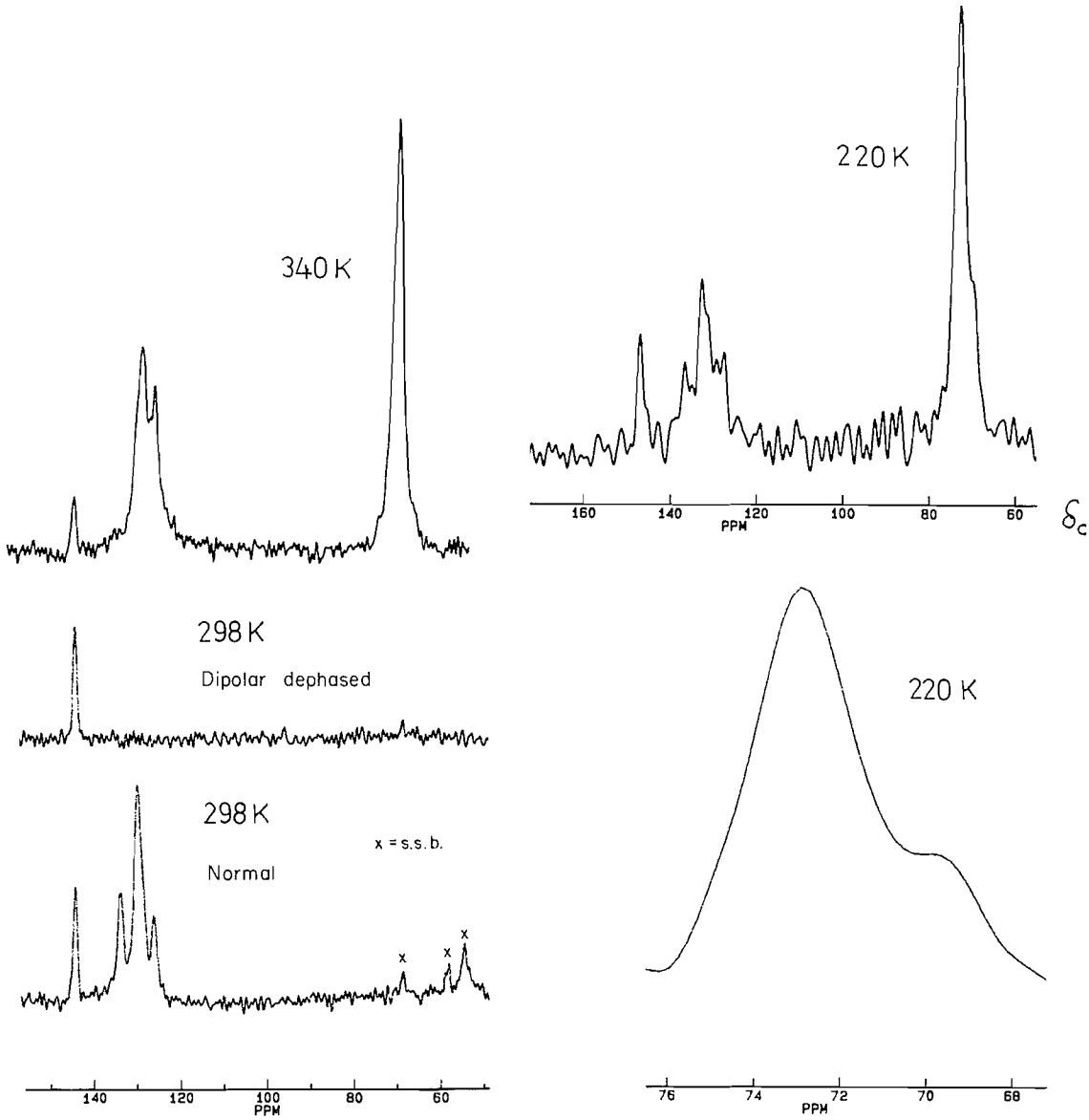


FIG. 3. The 45.3-MHz ^{13}C CPMAS spectrum of the 1:2 18-crown-6:benzenesulfonamide complex as a function of temperature.

To distinguish between these two possibilities, the spectrum was recorded under conditions of dipolar dephasing (12), with a delay time of 40 μs in the interrupted decoupling sequence. The resulting spectrum (Fig. 3) shows that the protonated carbon resonances have completely disappeared, indicating (13) that there must be relatively rigid benzenesulfonamide units in this complex. Had there been rapid molecular motion about the C19—C22 axis, the dipolar couplings would be averaged to near zero with the exception of C22. The C22–H dipolar interaction would not be averaged by flipping about such a twofold axis and would thus have had approximately the same intensity as the nonprotonated carbon in the dipolar dephased spectrum. Hence the resonance overlap observed in the normal ^{13}C CPMAS spectrum can be attributed to accidental chemical shift equivalence.

In the low temperature limit of 220 K, little change is evident in the aromatic carbon region of the spectrum. The crown ether resonance, however, has reappeared as a doublet with components having an intensity ratio of ca 1:3 with chemical shifts of 69.6 and 72.9 ppm, respectively.

It is of interest to attempt to analyze the crown ether spectral appearance in terms of the torsional angle and steric chemical shift tenets employed for the 1:1 complex (*vide supra*). The previously determined (3) torsional angles for the 18-crown-6 portion of the 1:2 complex are presented in Table 4. Consideration of the torsional angle contractions below 180° and the expansions above 60°, as was done in the 1:1 case, leads one to expect that C-2 will be the most shielded carbon followed by C-3, C-5, C-9, C-8, and, finally, the most deshielded position C-6. It appears that only the C-2 resonance is resolvable at 220 K.

The low temperature chemical shift difference of 3.3 ppm in the crown ether carbons of the 1:2 complex reflects the more diverse torsional environments present in the centrosymmetric crystal structure than was the case for the pseudosymmetric D_{3d} 1:1 complex where the limiting chemical shift difference was only 1.7 ppm.

To conclude, a limitation exists in the analysis as presented, since the torsion angles from the X-ray data were measured at ca. 300 K, and these data are employed in an attempt to interpret

Can. J. Chem. Downloaded from www.nrcresearchpress.com by 194.225.253.170 on 09/07/12
For personal use only.

TABLE 2. Bond lengths and angles, and torsional angles

Bond	Length (Å)	Bond	Length (Å)
S—O(2)	1.430(3)	O(10)—C(9)	1.373(10)
S—O(3)	1.426(3)	O(10)—C(11)	1.446(11)
S—N	1.578(5)	O(13)—C(12)	1.384(10)
S—C(19)	1.764(5)	O(13)—C(14)	1.425(9)
O(1)—N	3.003(6)	O(16)—C(15)	1.373(10)
O(1)—C(2)	1.422(10)	O(16)—C(17)	1.422(8)
O(1)—C(3)	2.362(12)	C(2)—C(3)	1.472(19)
O(1)—C(17)	2.329(10)	C(5)—C(6)	1.474(18)
O(1)—C(18)	1.406(10)	C(8)—C(9)	1.458(19)
O(2)—N	2.424(6)	C(11)—C(12)	1.455(16)
O(3)—N	2.433(6)	C(14)—C(15)	1.464(15)
O(4)—C(3)	1.413(11)	C(17)—C(18)	1.461(14)
O(4)—C(5)	1.419(11)	C(19)—C(20)	1.369(7)
O(7)—N	3.002(7)	C(19)—C(24)	1.366(7)
O(7)—C(5)	2.338(12)	C(20)—C(21)	1.376(9)
O(7)—C(6)	1.386(13)	C(21)—C(22)	1.360(11)
O(7)—C(8)	1.454(10)	C(22)—C(23)	1.365(10)
O(7)—C(9)	2.356(12)	C(23)—C(24)	1.376(9)

Bonds	Angle (°)	Bonds	Angle (°)
O(2)—S—O(3)	119.50(21)	S—N—O(7)	115.8(3)
O(2)—S—N	107.3(3)	O(1)—N—O(2)	147.90(23)
O(2)—S—C(19)	106.74(20)	O(1)—N—O(3)	95.31(21)
O(3)—S—N	108.1(3)	O(1)—N—O(7)	110.37(20)
O(3)—S—C(19)	106.69(21)	O(2)—N—O(3)	61.05(16)
N—S—C(19)	108.15(23)	O(2)—N—O(7)	88.19(21)
N—O(1)—C(2)	118.2(5)	O(3)—N—O(7)	148.74(24)
N—O(1)—C(3)	85.3(3)	O(1)—C(2)—C(3)	109.4(7)
N—O(1)—C(17)	89.05(24)	O(1)—C(3)—O(4)	96.5(5)
N—O(1)—C(18)	124.4(4)	O(1)—C(3)—C(2)	34.6(4)
C(2)—O(1)—C(3)	36.0(6)	O(4)—C(3)—C(2)	109.7(8)
C(2)—O(1)—C(17)	149.1(6)	O(4)—C(5)—O(7)	94.9(5)
C(2)—O(1)—C(18)	113.1(6)	O(4)—C(5)—C(6)	110.0(7)
C(3)—O(1)—C(17)	174.3(4)	O(7)—C(5)—C(6)	33.9(5)
C(3)—O(1)—C(18)	149.0(5)	O(7)—C(6)—C(5)	109.6(8)
C(17)—O(1)—C(18)	36.5(4)	O(7)—C(8)—C(9)	108.0(7)
S—O(2)—N	38.44(16)	O(7)—C(9)—O(10)	97.1(5)
S—O(3)—N	38.08(16)	O(7)—C(9)—C(8)	36.0(4)
C(3)—O(4)—C(5)	113.6(8)	O(10)—C(9)—C(8)	110.8(7)
N—O(7)—C(5)	86.9(3)	O(10)—C(11)—C(12)	110.9(7)
N—O(7)—C(6)	120.8(5)	O(13)—C(12)—C(11)	109.8(8)
N—O(7)—C(8)	122.0(6)	O(13)—C(14)—C(15)	109.8(6)
N—O(7)—C(9)	86.2(3)	O(16)—C(15)—C(14)	109.8(7)
C(5)—O(7)—(C6)	36.4(6)	O(1)—C(17)—O(16)	94.9(4)
C(5)—O(7)—C(8)	149.6(7)	O(1)—C(17)—C(18)	34.9(4)
C(5)—O(7)—C(9)	171.5(4)	O(16)—C(17)—C(18)	108.2(6)
C(6)—O(7)—C(8)	113.3(8)	O(1)—C(18)—C(17)	108.7(5)
C(6)—O(7)—C(9)	147.6(6)	S—C(19)—C(20)	120.8(4)
C(8)—O(7)—C(9)	36.1(6)	S—C(19)—C(24)	120.5(4)
C(9)—O(10)—C(11)	113.8(7)	C(20)—C(19)—C(24)	118.8(5)
C(12)—O(13)—C(14)	116.0(7)	C(19)—C(20)—C(21)	119.9(6)
C(15)—O(16)—C(17)	112.6(6)	C(20)—C(21)—C(22)	121.3(6)
S—N—O(1)	114.5(3)	C(21)—C(22)—C(23)	119.0(6)
S—N—O(2)	34.29(14)	C(22)—C(23)—C(24)	120.0(6)
S—N—O(3)	33.86(15)	C(19)—C(24)—C(23)	121.1(5)

^{13}C CPMAS spectra at temperatures that are nearly 100 K lower. Ideally, only X-ray data obtained at comparable temperatures should be utilized; however, the logistics of obtaining such data are often difficult.

These results present the first cases where overall motion of the crown ether host molecule that is independent of the motion of the molecular guest species has been detected. In an attempt to determine the detailed nature of the motions in the 18-crown-6 moieties, further studies of these phenomena in the solid state, utilizing deuterated crown ether complexes, are in progress.

Experimental

Materials

The published procedure (3) for preparation of the 1:2 complex was

TABLE 2 (*concluded*)

Bonds	Torsional angle (°)	Bonds	Torsional angle (°)
C18—O 1—C 2—C 3	176.0(10)	C 2—O 1—C18—C17	172.4(9)
C 5—O 4—C 3—C 2	178.3(11)	C 3—O 4—C 5—C 6	178.3(11)
C 8—O 7—C 6—C 5	−178.3(11)	C 6—O 7—C 8—C 9	−166.3(10)
C11—O10—C 9—C 8	176.4(10)	C 9—O10—C11—C12	165.6(10)
C14—O13—C12—C11	−172.6(10)	C12—O13—C14—C15	−175.5(9)
C17—O16—C15—C14	−178.3(9)	C15—O16—C17—C18	175.3(8)
O 1—C 2—C 3—O 4	72.1(7)	O 4—C 5—C 6—O 7	−67.7(7)
O 7—C 8—C 9—O10	72.7(7)	O10—C11—C12—O13	−73.6(7)
O13—C14—C15—O16	74.7(6)	O16—C17—C18—O 1	−71.6(6)

TABLE 3. Torsional angles (°) in the macrocyclic ring of the 1:1 18-crown-6: benzenesulfonamide complex

Carbon	O—C*—C—O	C*—O—C—C	C—O—C*—C	C—O—C—C*
C2	72.1	172.4	176.0	178.3
C3	72.1	178.3	178.3	176.0
C5	67.7	178.3	178.3	178.3
C6	67.7	166.3	178.3	178.3
C8	72.7	178.3	166.3	176.4
C9	72.7	165.6	176.4	166.3
C11	73.6	176.4	165.6	172.6
C12	73.6	175.5	172.6	165.6
C14	74.7	172.6	175.5	178.3
C15	74.7	175.3	178.3	175.5
C17	71.6	178.3	175.3	172.4
C18	71.6	176.0	172.4	175.3

TABLE 4. Torsional angles for 1:2 18-crown-6:benzenesulfonamide complex (3)

Carbon	O—C*—C—O	C*—O—C—C	C—O—C*—C	C—O—C—C*
C-2	65.8	172.9	176.7	157.6
C-3	65.8	180.0	157.6	176.7
C-5	66.6	157.6	180.0	180.0
C-6	66.6	72.5	180.0	180.0
C-8	68.4	180.0	72.5	172.9
C-9	68.4	176.7	172.9	72.5

followed. This report, however, does not specify the solvent employed for recrystallization. In our hands, even when the stoichiometry of reagents is 1:2 (3), recrystallization from THF gives initially a white solid, mp 88–89°C, in 34% yield, which turns out to be the 1:1 complex. The 1:2 complex, mp 92–93°C, can be subsequently isolated from the mother liquors. If the reagent stoichiometry is 1:1 then the 1:1 complex is obtained exclusively.

Spectra

The 45.3-MHz ^{13}C CPMAS spectra were obtained via techniques described previously (1, 2).

Crystallographic measurements and structure solution (1:1 complex)

$C_{18}H_{31}NO_8S$ fw = 420.44

Monoclinic, $P2_1/n$, $a = 8.401(2)$ Å, $b = 16.936(2)$ Å, $c = 15.6170(2)$ Å, $\beta = 94.70(1)°$, $V = 2214.77$ Å^3, $Z = 4$, $D_c = 1.264$ Mg·m^{-3}. A single crystal of the title compound, dimensions 0.25 × 0.30 × 0.35 mm, was mounted on a glass fiber and transferred on a Nonius CAD4 diffractometer driven by the NRCCAD control program (14). Cell parameters and intensity data were obtained at room temperature using graphite-monochromatized Mo Kα radiation. The accurate cell parameters were obtained from 30 well-centered reflections with 2θ in the range 30–35°. Intensity data were measured up to 45°, 2θ. A total of 4368 ± *hkl* and *hkl* reflections were measured. After averaging the symmetry-related reflections and correcting them for the Lorentz and polarization ratio effects, the data set consisted of 2871 unique reflections, of which 1760 were considered observed ($I_{net} \geq 2.5\,\sigma(I_{net})$).

The space group $P2_1/n$ was unambiguously defined from the systematic absences noted in the data set. The structure was solved by direct methods using MULTAN (15). The hydrogen atoms were located on the next D-map after preliminary full-matrix least-squares refinement. They were included and refined isotropically while non-H atoms were refined anisotropically by full-matrix least squares, using the following weighting scheme: $1/[\sigma(F_o)^2 + 0.0003(F_o^2)]$. Final residuals are $R_f = 0.051$ and $R_w = 0.052$, with a goodness-of-fit ratio of 1.4 and $(\Delta/\sigma)_{max}$ of 0.2 in the last refinement cycle. The final D-map was featureless with a background noise ≤0.18 e$^-$/Å^3. Scattering

Can. J. Chem. Downloaded from www.nrcresearchpress.com by 194.225.253.170 on 09/07/12
For personal use only.

curves were from standard sources (16). All computations were performed with the NRCVAX system of programs (17).[4]

1. G. W. BUCHANAN, R. A. KIRBY, J. A. RIPMEESTER, and C. I. RATCLIFFE. Tetrahedron Lett. **28**, 4783 (1987).
2. G. W. BUCHANAN, M. Z. KHAN, J. A. RIPMEESTER, J. W. BOVENKAMP, and A. RODRIGUE. Can. J. Chem. **65**, 2564 (1987).
3. A. KNOCHEL, J. KOPF, J. OEHLER, and G. RUDOLPH. J. Chem. Soc. Chem. Commun. 595 (1978).
4. J. D. DUNITZ and P. SEILER. Acta Crystallogr. Sect. B: Struct. Crystallogr. Cryst. Chem. **30**, 2739 (1974).
5. E. MAVERICK, P. SEILER, W. B. SCHWEITZER, and J. D. DUNITZ. Acta Crystallogr. Sect. B: Struct. Crystallogr. Cryst. Chem. **36**, 615 (1980).
6. P. SEILER, M. DOBLER, and J. D. DUNITZ. Acta Crystallogr. Sect. B: Struct. Crystallogr. Cryst. Chem. **30**, 2744 (1974).

[4]Tables of anisotropic temperature factors, hydrogen atom parameters, and bond lengths and angles may be purchased from the Depository of Unpublished Data, CISTI, National Research Council of Canada, Ottawa, Ont., Canada K1A 0S2.

Tables of atomic coordinates have also been deposited with the Cambridge Crystallographic Data Centre, and can be obtained on request from The Director, Cambridge Crystallographic Data Centre, University Chemical Laboratory, Lensfield Road, Cambridge, CB2 1EW, U.K.

7. G. C. LEVY, R. L. LICHTER, and G. L. NELSON. Carbon-13 nuclear magnetic resonance spectrocopy. 2nd ed. Wiley Interscience, New York. 1980. p. 111.
8. W. P. ROTHWELL and J. S. WAUGH. J. Chem. Phys. **74**, 2721 (1981).
9. J. S. WAUGH and E. I. FEDIN. Sov. Phys. Solid State (Engl. Transl.), **4**, 1633 (1963).
10. J. A. RIPMEESTER. J. Inclusion Phenom. **6**, 31 (1988).
11. N. K. WILSON and J. B. STOTHERS. Top. Stereochem. **8**, 1 (1973).
12. S. J. OPELLA and M. H. FREY. J. Am. Chem. Soc. **101**, 5854 (1979).
13. A. J. BEELER, A. M. ORENDT, D. M. GRANT, P. W. CUTTS, J. MICHL, K. W. ZILM, J. W. DOWNING, J. C. FACELLI, M. S. SCHINDLER, and W. KUTZELNIG. J. Am. Chem. Soc. **106**, 7672 (1984).
14. Y. LEPAGE, P. S. WHITE, and E. J. GABE. ACA Meeting Abstr. **14**, 24, (1986).
15. G. GERMAIN, P. MAIN and M. M. WOLFSON. Acta Crystallogr. Sect. A: Cryst. Phys. Diffr. Theor. Gen. Crystallogr. **27**, 368 (1971).
16. International tables for X-ray crystallography. Vol. 4. 2nd ed. Kynoch Press, Birmingham. 1974.
17. E. J. GABE, F. L. LEE, and Y. LEPAGE. *In* Crystallogr. Comput. 3: Data Collect. Struct. Determ. Proteins Databases, Pap. Int. Summer Sch. 9th. 1985. p. 167.

Can. J. Chem. Downloaded from www.nrcresearchpress.com by 194.225.253.170 on 09/07/12
For personal use only.

Nitrogen-15 shielding in *trans*-azobenzene

RODERICK E. WASYLISHEN,[1] WILLIAM P. POWER, GLENN H. PENNER, AND RONALD D. CURTIS
Department of Chemistry, Dalhousie University, Halifax, N.S., Canada B3H 4J3

Received September 23, 1988

RODERICK E. WASYLISHEN, WILLIAM P. POWER, GLENN H. PENNER, and RONALD D. CURTIS. Can. J. Chem. **67**, 1219 (1989).

The principal values of the nitrogen nuclear magnetic resonance shielding tensor for *trans*-azobenzene have been measured and compared with theoretical values recently reported for *trans*-diazene. The shielding anisotropy for the two crystallographically nonequivalent molecules in *trans*-azobenzene is 925 and 880 ppm respectively, about 40% smaller than the value calculated for *trans*-diazene. Interestingly, the isotropic shielding constants for the two nonequivalent molecules are the same within experimental error. The most shielded component of the ^{15}N shielding tensor, σ_{33}, is approximately perpendicular to the molecular plane, as it is in other planar π-systems; σ_{11}, the least shielded component, is directed in the same general direction as the N—C_{ipso} bond. The theoretical calculations overestimate the paramagnetic contribution to σ_{11}. The magnitude and relative orientation of the nitrogen shielding tensor in *trans*-azobenzene are also compared with the corresponding phosphorus values in a diphosphene.

Key words: ^{15}N chemical shielding anisotropy, solid state NMR, *trans*-azobenzene.

RODERICK E. WASYLISHEN, WILLIAM P. POWER, GLENN H. PENNER et RONALD D. CURTIS. Can. J. Chem. **67**, 1219 (1989).

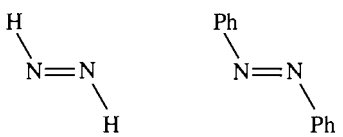
On a mesuré les principales valeurs du tenseur de blindage en résonance magnétique nucléaire de l'azote du *trans*-azobenzène et on les a comparées avec les valeurs théoriques rapportées récemment pour le *trans*-diazène. L'anisotropie de blindage est respectivement de 925 et 880 ppm pour les deux molécules de *trans*-azobenzène qui ne sont cristallographiquement pas équivalentes; ces valeurs sont environ 40% plus faibles que les valeurs calculées pour le *trans*-diazène. Il est intéressant de noter que les constantes de couplage isotrope des deux molécules qui ne sont pas équivalentes sont les mêmes, aux erreurs expérimentales près. La composante la plus blindée du tenseur de blindage du ^{15}N, σ_{33}, est approximativement perpendiculaire au plan de la molécule, comme c'est le cas dans d'autres systèmes π plans; la composante la moins blindée, σ_{11}, est orientée dans le même direction générale que la liaison N—C_{ipso}. Les calculs théoriques surévaluent la contribution magnétique à la composante σ_{11}. On a aussi comparé l'amplitude et l'orientation relative du tenseur de blindage de l'azote dans le *trans*-azobenzène avec les valeurs correspondantes du diphosphène.

Mots clés : anisotropie de blindage, RMN de l'état solide, *trans*-azobenzène.

[Traduit par la revue]

Introduction

Recently Schindler (1) used an individual gauge for localized molecular orbital method (IGLO) to calculate nitrogen nmr shielding tensors for various classes of nitrogen-containing molecules. The *ab initio* method has been very successful in calculating reliable carbon shielding tensors in a variety of molecules (2). Unfortunately, few experimental ^{15}N shielding tensors are available for direct comparison with the theoretical calculations (3–8). Of the molecules considered in ref. 1, *trans*-diazene (**I**) was predicted to have the largest ^{15}N shielding anisotropy, approximately 1500 ppm. This is more than twice the value observed in dinitrogen (9); hence, we felt that it would be of interest to measure the value in a related stable compound. By obtaining a ^{15}N homonuclear dipolar spectrum of a static powder sample of *trans*-azobenzene-$^{15}N_2$ (**II**) we are able to



I **II**

determine the principal components of the ^{15}N shielding tensor and obtain valuable information regarding its orientation. Although the phenyl rings of *trans*-azobenzene will perturb the diazene system and complicate a direct comparison between experiment and theory, our results are the first measurement of the principal components of the nitrogen shielding tensor in a diazene. Our results will be compared with the ^{31}P shielding tensor recently reported for the P=P double bond in an aryl-substituted diphosphene (10).

[1]Author to whom correspondence may be addressed.

Theory

For a pair of like spins, A_2, such as the directly bonded ^{15}N spins of *trans*-azobenzene-$^{15}N_2$ the chemical shielding (CS) and direct dipolar interactions are orientation dependent (11–13). That is, for any given crystallite the nmr resonance frequency will depend on the orientation of the principal components of the CS tensor in the applied magnetic field, B_0, and the orientation of the dipolar vector in the principal axis system (PAS) of the CS tensor (see eq. [1], below). The orientation of the CS tensor in B_0 is defined by the angles θ and ϕ, and the orientation of the dipolar vector, r_{NN}, in the PAS of the CS tensor is defined by the angles α and β (see Fig. 1).

$$[1] \quad \nu_m(\theta,\phi) = \nu_L - \nu_{CS} - \tfrac{3}{2}\nu_D m$$

where

$$\nu_L = \gamma_N B_0/2\pi$$

$$\nu_{CS} = (\gamma_N B_0/2\pi)[\sigma_{11}\sin^2\theta\cos^2\phi + \sigma_{22}\sin^2\theta\sin^2\phi + \sigma_{33}\cos^2\theta]$$

$$\nu_D = R[1 - 3(\sin\beta\sin\theta\cos(\phi-\alpha) + \cos\beta\cos\theta)^2]$$

and

$$R = \frac{\gamma_N^2\hbar}{2\pi}\left(\frac{\mu_0}{4\pi}\right)\langle r_{NN}^{-3}\rangle$$

The nmr spectrum of a powder sample is simulated by adding the two subspectra $\nu_{\pm 1/2}(\theta,\phi)$, and integrating over all angles θ and ϕ. We have used the standard convention $\sigma_{33} > \sigma_{22} > \sigma_{11}$

Can. J. Chem. Downloaded from www.nrcresearchpress.com by 194.225.253.170 on 09/07/12
For personal use only.

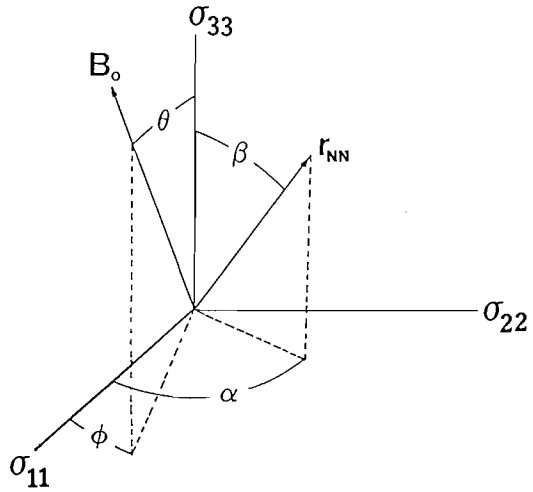


FIG. 1. Definition of the angles α, β, θ, and φ. α and β define the orientation of $r_{N,N}$ in the principal axis system of the CS tensor. θ and φ define the orientation of the molecule in the magnetic field, B_0.

(3, 4, 14). β is an angle between r_{NN} and the most shielded component of the CS tensor, σ_{33}, and α is the angle between the projection of r_{NN} onto the σ_{11}–σ_{22} plane and the least shielded component of the CS tensor σ_{11}. Note that the experimentalist has no control over the angles α and β; they will depend upon the particular molecule and spin-pair under consideration.

The principal components of the chemical shielding tensors are often expressed as chemical shifts, δ_{ii}, with respect to some reference (14). Since chemical shifts to high frequency of the reference are by convention positive, $\delta_{11} > \delta_{22} > \delta_{33}$. (Note that δ_{33} still corresponds to the most shielded component of the chemical shift tensor.)

Experimental

trans-Azobenzene-$^{15}N_2$ was obtained from MSD isotopes, Montreal.

The sample was ground to a fine powder and packed into an aluminum oxide rotor (7 mm o.d.). Nitrogen-15 nmr spectra were obtained at 21 ± 2°C on a Bruker MSL-200 spectrometer operating at 20.29 MHz. Spectra were acquired under the conditions of the Hartmann–Hahn match (3) using the FLIPBACK pulse sequence (15) and high power ^1H decoupling at 200.106 MHz. The $\pi/2$ pulse width was 5.5 μs and the recycle time was 120 s. The contact time was optimized and found to be 12 ms. The static spectrum (2750 transients) was acquired using an acquisition time of 106.5 ms; the corresponding time for the MAS spectrum (100 transients) was 426 ms. A sensitivity enhancement corresponding to 100 Hz and 10 Hz of line broadening respectively was applied to the static and MAS spectra prior to Fourier transformation. A polynomial baseline correction was used to compensate for baseline roll in the experimental static spectrum.

Nitrogen-15 chemical shifts were referenced with respect to the ammonium ^{15}N signal of external ammonium nitrate, which has a shift of 23.8 ppm with respect to liquid ammonia at 20°C.

Simulations were performed using the POWDER simulation routine (16) on a VAX 8800 computer.

Results and discussion

Before discussing the static ^{15}N nmr powder spectrum of *trans*-azobenzene-$^{15}N_2$ we will briefly discuss the structure of *trans*-azobenzene and the ^{15}N nmr spectrum obtained with magic angle spinning (MAS).

Crystal structure and MAS spectrum

X-ray diffraction experiments indicate that *trans*-azobenzene crystals are monoclinic, $P2_1/c$, with two crystallographically independent molecules (17, 18). The molecule at one of the two sites has much larger thermal parameters than that at the other, and N,N bond lengths of 1.172 Å and 1.243 Å were reported in an early refinement of the crystal structure (17). The shorter bond length was obtained for the molecule at the disordered site. A more recent reinvestigation of the disorder has led to the conclusion that the N,N bond lengths are essentially equal at the two sites, 1.247 Å at the ordered site and 1.240 Å and 1.249 Å for two possible orientations of the molecule at the disordered site (18). The occupancy ratio for the two disordered molecules was found to be 0.83:0.17, thus one of the two possible orientations at the disordered site is more favored than the other. The centrosymmetric molecules at each of the two crystallographic sites are essentially planar, with the torsional angles NNCC being approximately 17° at the ordered site and less than 10° at the disordered site. Nitrogen-15 spectra obtained with magic angle spinning appear to support the conclusion that the structures of the two crystallographically independent molecules are very similar. Only a single isotropic peak of linewidth $\nu_{1/2} \leq 20$ Hz is observed in the MAS spectrum (Fig. 2). Although no splitting due to crystallographic nonequivalence has been reported in previous CP/MAS ^{13}C nmr studies of *trans*-azobenzene (19, 20), we do observe a splitting of approximately 0.8 and 0.7 ppm respectively for C_{ipso} and C6; the other carbon resonances (C2, C3, C4, and C5) overlap extensively.

The slow spinning ^{15}N nmr spectrum in Fig. 2 has rotational sidebands that are modulated by both the ^{15}N chemical shielding and ^{15}N,^{15}N dipolar interaction (21). Since rotational sidebands of significant intensity are observed over a frequency range in excess of 18 kHz it is clear that the shielding anisotropy is much greater than the direct dipolar coupling constant, $R = 636.6$ Hz. Ignoring the dipolar interaction and applying the Herzfeld–Berger (21) analysis at rotor speeds of 1500 and 2000 Hz we obtain $\delta_{11} = 991$ ppm, $\delta_{22} = 487$ ppm, and $\delta_{33} = 55$ ppm. Thus the chemical shielding anisotropy, $\Delta\sigma = \delta_{11} - \delta_{33}$, is approximately 936 ppm. As indicated below, the error in the components of the CS tensor is substantial (±100 ppm) if one carries out the Herzfeld–Berger analysis ignoring the ^{15}N,^{15}N dipolar coupling.

The isotropic ^{15}N chemical shift of solid *trans*-azobenzene with respect to external liquid ammonia is 511.5 ppm. In chloroform solution the ^{15}N chemical shift of *trans*-azobenzene with respect to nitromethane is 129.0 ppm (22). Taking the chemical shift of nitromethane with respect to NH_3 (*l*, 20°) as 380.4 ppm (5) leads to a solution shift of 509.4 ppm, in excellent agreement with the value measured in the solid state.

Analysis of the static powder pattern

The static ^{15}N nmr powder spectrum of *trans*-azobenzene-$^{15}N_2$ obtained after approximately 4 days of signal averaging is shown in Fig. 3. Expansions of the high and low frequency shoulders are shown in Figs. 4a and 4b respectively. From the appearance of the low frequency shoulders (δ_{33} region) it is apparent that the principal components of the ^{15}N shielding tensor for the two nonequivalent molecules are different even though the average values (trace) of the two tensors are the same within ±0.5 ppm. Only two shoulders as opposed to four would be observed in the low frequency region if the spectrum could be interpreted in terms of a single dipolar split site (see Figs. 5 and 6 and the discussion to follow).

X-ray diffraction results indicate that molecules at the disordered site of *trans*-azobenzene exhibit much larger thermal

Can. J. Chem. Downloaded from www.nrcresearchpress.com by 194.225.253.170 on 09/07/12
For personal use only.

Can. J. Chem. Downloaded from www.nrcresearchpress.com by 194.225.253.170 on 09/07/12
For personal use only.

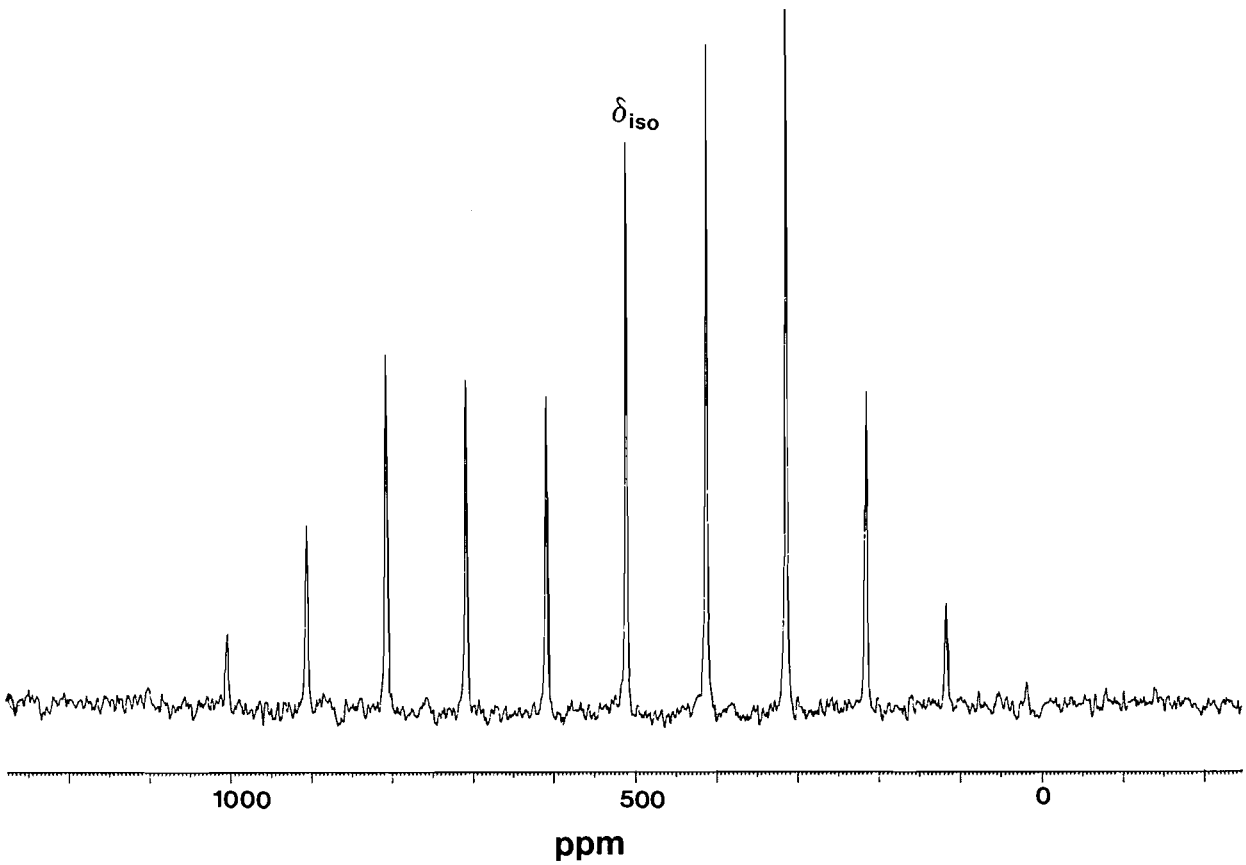


FIG. 2. Nitrogen-15 nmr spectrum of a powder sample of *trans*-azobenzene-$^{15}N_2$ obtained with high power ^1H decoupling, cross-polarization, and magic angle spinning (2 kHz).

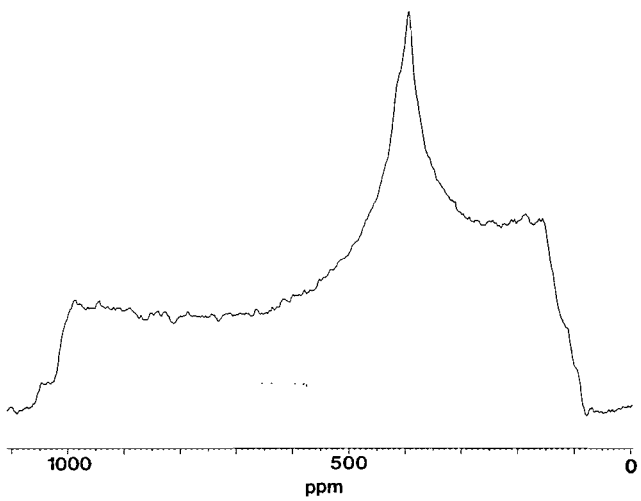


FIG. 3. Dipolar ^{15}N nmr spectrum of a static powder sample of *trans*-azobenzene-$^{15}N_2$ obtained with high power ^1H decoupling and cross-polarization.

ellipsoids than those at the ordered site; therefore it is reasonable to assume that the thermal motion at the disordered site will result in partial averaging of the chemical shielding tensor. On this basis we have assigned the outer features of the δ_{33} and δ_{11} shoulders (see Fig. 4) to molecules at the ordered site, site 1. The inner features of these regions are associated with the disordered site of *trans*-azobenzene, site 2.

To describe how the spectrum in Fig. 3 was analyzed it is useful to consider how a theoretical dipole-coupled CS powder spectrum depends on the angles α and β when $|\nu_{11} - \nu_{iso}|$ and $|\nu_{33} - \nu_{iso}|$ are much greater than R. Using eq. [1], it is easy to derive the following relationships for dipolar splitting at δ_{11}, δ_{22}, and δ_{33}:

$$[2] \quad \Delta\nu_{11} = \pm(3/2)R[1 - 3(\sin\beta\cos\alpha)^2]$$

$$[3] \quad \Delta\nu_{22} = \pm(3/2)R[1 - 3(\sin\beta\sin\alpha)^2]$$

$$[4] \quad \Delta\nu_{33} = \pm(3/2)R[1 - 3\cos^2\beta]$$

We have found these expressions extremely useful in obtaining initial estimates for the angles α and β in simulating dipolar coupled spectra. The value of R in eqs. [2]–[4] was fixed at 636.6 Hz; this value was calculated from the N,N bond length obtained from X-ray diffraction experiments, $r_{NN} = 1.247$ Å.

For *trans*-azobenzene-$^{15}N_2$ one expects $\beta = 90°$ (1, 6, 23, 25–28; see also footnotes 2 and 3); that is, the most shielded component of the ^{15}N shielding tensor should be approximately perpendicular to the molecular plane. This appears to be a general observation for systems where nitrogen is a part of a planar π-system (6, 25–28, footnote 3) and is supported by molecular orbital calculations (1, 23, footnote 2). One can obtain β at each of the two sites of *trans*-azobenzene from the splittings at the δ_{33} region, $\Delta\nu_{33}(1) = 910 \pm 30$ Hz and $\Delta\nu_{33}(2) = 825 \pm 30$ Hz using eq. [4]. Using these splittings

[2]M. Schindler, unpublished results.

[3]R. D. Curtis, W. P. Power, G. H. Penner, and R. E. Wasylishen. Submitted for publication.

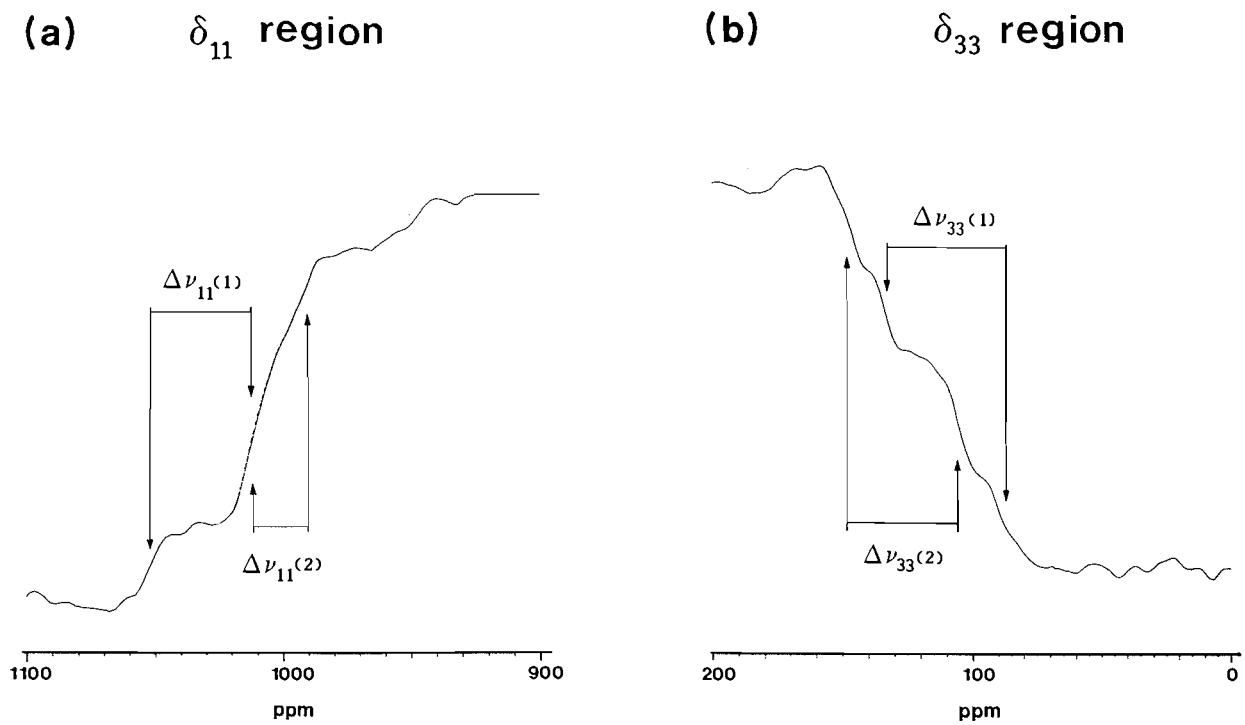
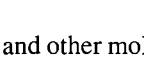


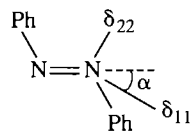
FIG. 4. (*a*) Expansion of the high frequency end (δ_{11} region) of the ^{15}N nmr spectrum of *trans*-azobenzene-$^{15}N_2$. (*b*) Expansion of the low frequency end (δ_{33} region) of the same spectrum.

one obtains $\beta = 83°$ and 78° repectively. As expected, the values of β at site 1 and site 2 are close to 90°. The values calculated here must be considered as lower limits since any molecular motion would reduce R and lead to values of β that are too small. The values of δ_{33} at sites 1 and 2 are 109.4 ± 1.5 and 125.4 ± 1.5 ppm respectively.

To demonstrate the sensitivity of the ^{15}N spectrum to the angle α we have generated a number of theoretical homonuclear dipolar coupled powder spectra varying α in steps of 15° (Fig. 5). Note that the splitting of the central feature, δ_{22}, is very sensitive to the value of α. Our experimental spectrum (Fig. 3) indicates that the splitting of this feature is definitely less than 600 Hz at both sites, implying that α must lie between 21° and 48°.

More accurate estimates of α can be obtained from the δ_{11} region of the spectrum. From the splittings, $\Delta\nu_{11} = 830 \pm 80$ Hz centered at $\delta_{11}(1) = 1034 \pm 4$ ppm and $\Delta\nu_{11} = 380 \pm 80$ Hz centered at $\delta_{11}(2) = 1005 \pm 4$ ppm, α values of 37° and 46° are obtained for sites 1 and 2, respectively. (Note that the errors in the $\Delta\nu_{11}$ and δ_{11} values are larger than the corresponding values at the low frequency end of the spectrum where the splittings are well defined.) These values for the angle α lead to splittings in the δ_{22} region of approximately 80 and 450 Hz. Final values for this angle were obtained by visually fitting the experimental and calculated spectra.

The results of our analysis for the angle α imply that the axis of the least shielded principal component (δ_{11}) of the nitrogen shielding tensor is directed in the same general direction as the N—C_{ipso} bond, and the axis of the intermediate component (δ_{22}) bisects the NNC angle (i.e., lies along the direction of the nitrogen lone pair). For site 1, $\alpha = 37°$, and the approximate orientation of δ_{11} and δ_{22} is illustrated in **III**. A value of $\alpha = 37°$ would also be compatible with δ_{11} being approximately perpendicular to the N—C_{ipso} bond axis; however, this is extremely unlikely on the basis of molecular orbital calculations on diazene (1) and other molecules containing the  fragment (ref. 23 and footnote 2). A value for α of 42° has been found for ^{15}N in a similar molecule, benzylideneaniline.[3] The different values of the angle α derived for sites 1 and 2 (37° and 46°) could result from the slightly different structure of the molecules at these two sites and subtle differences in their intermolecular interactions; there is more available space at the disordered site (18).



III

We have ignored the indirect spin–spin coupling interaction in our analysis of the ^{15}N dipolar spectrum. This is expected to be an excellent assumption since $J(^{15}N,^{15}N)_{iso}$ is only 15.5 Hz in a related *trans*-azobenzene where one of the benzene rings has a *para* substituent (30).

Comparison with theory and related molecules

The principal components of the ^{15}N chemical shift tensor may be converted to absolute shielding components since the absolute ^{15}N chemical shielding constant of liquid ammonia is known to be approximately 244.6 ppm at 20°C (31). The absolute ^{15}N shielding components are given in Table 2 together with those calculated for *trans*-diazene (1). The calculated least shielded component, σ_{11}, is obviously too paramagnetic. It is apparent that Schindler is correct in concluding that it will be necessary to include electron correlation and to use large basis sets to obtain an adequate description of nitrogen shielding in systems with NN multiple bonds. The large negative contribution to σ_{11} arises mainly from the molecular orbital

Can. J. Chem. Downloaded from www.nrcresearchpress.com by 194.225.253.170 on 09/07/12
For personal use only.

Can. J. Chem. Downloaded from www.nrcresearchpress.com by 194.225.253.170 on 09/07/12
For personal use only.

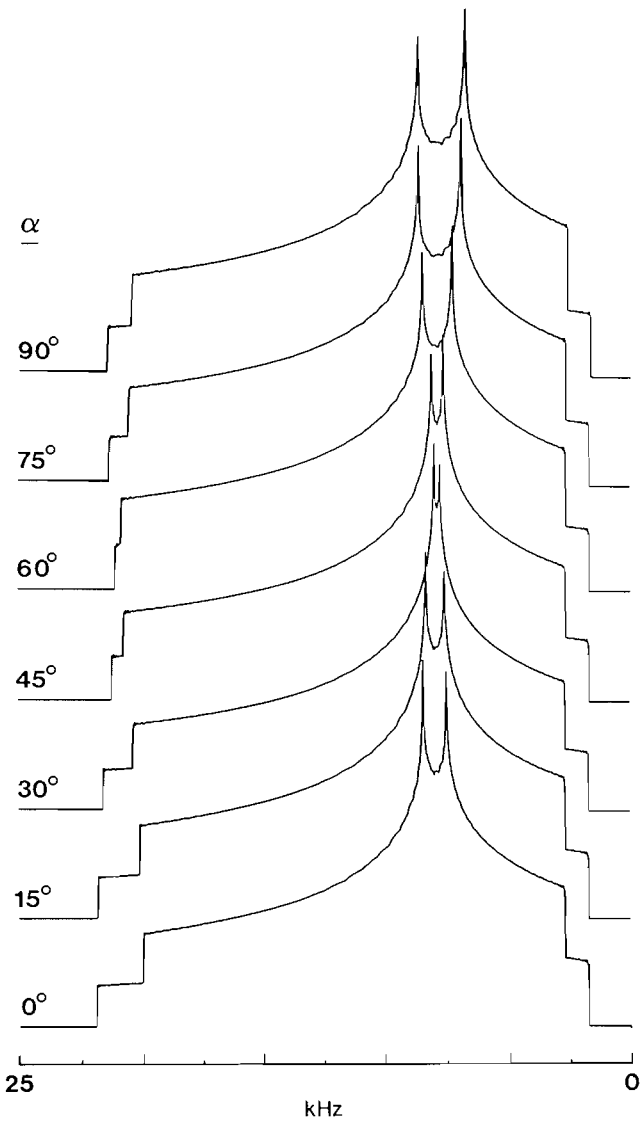
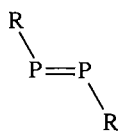


FIG. 5. Calculated homonuclear dipolar ^{15}N nmr spectra as a function of the angle α. β = 90° and r_{NN} = 1.247 Å; values of ν_{11}, ν_{22}, and ν_{33} are comparable to those given for azobenzene in Table 1 (B_0 = 4.70 T).

associated with the nitrogen lone pair that is involved in low-lying singlet $n \rightarrow \pi^*$ transitions (1, 32, 33).

It is of interest to compare the principal components of the nitrogen shielding tensor of *trans*-azobenzene with the corresponding ^{31}P components recently reported in the diphosphene (**IV**) (10). The principal components of the ^{31}P shielding tensor



R = 2,4,6-tri-*tert*-butylphenyl

IV

are σ_{11} = −880 ppm, σ_{22} = 107 ppm, and σ_{33} = 359 ppm; σ_{iso} = −138 ppm; the shielding anisotropy is 1239 ppm and the asymmetry parameter is 0.34. We have converted the components of the shift tensor given in ref. 10 to those of a shielding tensor, taking the absolute phosphorus shielding constant of H_3PO_4, 85%, as 356 ppm (14, 34). The most shielded component, σ_{33}, is perpendicular to the plane containing the CP=PC fragment; σ_{11} is directed at approximately 60° from the P=P bond vector towards the substituted phenyl ring, while the intermediate component, σ_{22}, is oriented in the same general direction as the phosphorus lone pair. As one would intuitively expect, the relative orientation of the principal components of the nitrogen and phosphorus shielding tensors is similar in the diazene (**II**) and the diphosphene (**IV**). Qualitatively, the larger shielding anisotropy observed for the diphosphene (**IV**) is probably related to the larger value of $\langle a_0^3/r^3 \rangle$ for phosphorus as compared to nitrogen (14, 29) and

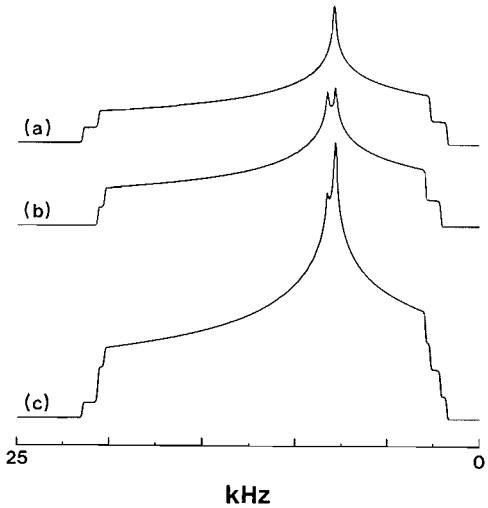


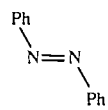
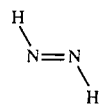
FIG. 6. Simulation of the dipolar coupled ^{15}N spectrum (powder) of *trans*-azobenzene-$^{15}N_2$. The spectrum of molecules in site 1 and site 2 is shown in (a) and (b) respectively; the spectrum obtained by summation of (a) and (b) is given in (c). Line broadening corresponding to 100 Hz was used to generate (a), (b), and (c), with all other parameters as given in Table 1 and the text.

TABLE 1. Principal components and orientation of the nitrogen-15 chemical shift tensor in *trans*-azobenzene[a]

	δ_{11}	δ_{22}	δ_{33}	δ_{iso}[b]	$\Delta\sigma$[c]	η[d]	α	β
Site 1	1034	391	109	511	925	0.54	37°	83°
Site 2	1005	400	125	510	880	0.56	46°	78°

[a]The δ_{ii}, δ_{iso}, and $\Delta\sigma$ values are in ppm; errors are estimated to be less than ±4 ppm. The errors in the angles α and β are estimated to be less than ±5°. As indicated in the text, the values reported for β are lower limits.
[b]$\delta_{iso} = \frac{1}{3}(\sigma_{11} + \sigma_{22} + \sigma_{33})$.
[c]$\Delta\sigma = \sigma_{33} - \sigma_{11}$.
[d]$\eta = (\sigma_{22} - \sigma_{33})/(\sigma_{11} - \sigma_{iso})$.

TABLE 2. Principal values of the nitrogen shielding tensor measured for *trans*-azobenzene (site 1) and calculated for *trans*-diazene (1)

Molecule	σ_{11} (ppm)	σ_{22} (ppm)	σ_{33} (ppm)	σ_{iso} (ppm)	$\Delta\sigma$ (ppm)	η
	−789	−146	136	−267	925	0.54
	−1370	−362	186	−515	1556	0.64

the lower energy of the $n \rightarrow \pi^*$ transition in the diphosphene (32).

Although a direct comparison between the observed ^{31}P shielding in **IV** and that calculated for the parent compound is difficult because of unknown substituent effects, it appears that *ab initio* molecular orbital calculations of $\sigma_{iso}(^{31}P)$ are too paramagnetic (24, 32). For *trans*-diphosphene the SOS CI (32) and IGLO (24) calculations predict $\sigma_{iso} = -359$ and -396 ppm respectively. These values are approximately 221 and 258 ppm respectively more negative than the isotropic value observed for **IV**; however, the bulky tri-*tert*-butylphenyl substituents could exert a substantial substituent effect. The same theoretical SOS CI calculations of Galasso (32) yield $\sigma_{iso} = -416$ ppm for the *trans*-diazene, approximately 149 ppm more negative than the value observed for **II**.

Acknowledgements

We wish to acknowledge the financial support of the Natural Sciences and Engineering Research Council of Canada (NSERC) in the form of equipment and operating grants (REW) and postgraduate scholarships (WPP, RDC). GHP, WPP, and RDC thank Dalhousie University for a Killam postdoctoral fellowship and postgraduate fellowships respectively. WPP and RDC are also holders of Sumner fellowships. We thank Professor O. Knop and Dr. E. J. Gabe for helpful discussions regarding the crystallographic data, Professor M. Schindler for a preprint (see footnote 2), Mr. Brian Millier for maintaining the nmr spectrometer, and Ms. Annette Salsman for her help preparing this manuscript.

1. M. SCHINDLER. J. Am. Chem. Soc. **109**, 5950 (1987).
2. (*a*) M. SCHINDLER and W. KUTZELNIGG. J. Am. Chem. Soc. **105**, 1360 (1983); (*b*) Mol. Phys. **48**, 781 (1983); (*c*) A. J. BEELER, A. M. ORENDT, D. M. GRANT, P. W. CUTTS, J. MICHL, K. W. ZILM, J. W. DOWNING, J. C. FACELLI, M. SCHINDLER, and W. KUTZELNIGG. J. Am. Chem. Soc. **106**, 7672 (1984); (*d*) J. C. FACELLI, D. M. GRANT, and J. MICHL. Acc. Chem. Res. **20**, 152 (1987).
3. M. MEHRING. High resolution NMR in solids. 2nd ed. Springer-Verlag, New York. 1983.
4. H. W. SPIESS. *In* NMR basic principles and progress. Vol. 15. *Edited by* P. Diehl, E. Fluck, and R. Kosfeld. Springer-Verlag, New York. 1978. p. 55.
5. M. WITANOWSKI, L. STEFANIAK, and G. A. WEBB. *In* Annual reports on NMR spectroscopy. Vol. 18. *Edited by* G. A. Webb. Academic Press, London. 1986. p. 1.
6. J. MASON. *In* Multinuclear NMR. *Edited by* J. Mason. Plenum Press, New York. 1987. Chap. 12. p. 335.
7. W. VON PHILIPSBORN and R. MULLER. Angew. Chem. **98**, 381 (1986).
8. C. J. JAMESON. *In* Specialist periodic report — NMR spectroscopy. Vol. 17. *Edited by* G. A. Webb. The Chemical Society, London. 1988. p. 1, and previous volumes in these annual reviews of the literature.
9. L. M. ISHOL and T. A. SCOTT. J. Magn. Reson. **27**, 23 (1977).
10. K. W. ZILM, G. G. WEBB, A. H. COWLEY, M. PAKULSKI, and A. ORENDT. J. Am. Chem. Soc. **110**, 2032 (1988).
11. D. L. VANDERHART and H. S. GUTOWSKY. J. Chem. Phys. **49**, 261 (1968).
12. K. W. ZILM and D. M. GRANT. J. Am. Chem. Soc. **103**, 2913 (1981).
13. K. G. VALENTINE, A. L. ROCKWELL, L. M. GIERASCH, and S. J. OPELLA. J. Magn. Reson. **73**, 519 (1987).
14. C. J. JAMESON and J. MASON. *In* Multinuclear NMR. *Edited by* J. Mason. Plenum Press, New York. 1987. Chap. 2 and Chap. 3, p. 3 and p. 51, respectively.
15. J. TEGENFELDT and U. HAEBERLEN. J. Magn. Reson. **36**, 453 (1979).
16. D. W. ALDERMAN, M. S. SOLUM, and D. M. GRANT. J. Chem. Phys. **87**, 3717 (1986).
17. C. J. BROWN. Acta Crystallogr. **21**, 146 (1966).
18. J. A. BOUWSTRA, A. SCHOUTEN, and J. KROON. Acta Crystallogr. Sect. C: Cryst. Struct. Commun. **C39**, 1121 (1983).
19. A. M. CHIPPENDALE, A. MATHIAS, R. K. HARRIS, K. J. PACKER, and B. J. SAY. J. Chem. Soc. Perkin Trans. 2, 1031 (1981).
20. C. L. FORBER, E. C. KELUSKY, N. J. BUNCE, and M. C. ZERNER. J. Am. Chem. Soc. **107**, 5884 (1985).
21. J. HERZFELD and A. E. BERGER. J. Chem. Phys. **73**, 6021 (1980).
22. A. LYČKA. Collect. Czech. Chem. Commun. **47**, 1112 (1982).
23. F. RIBAS PRADO and C. GIESSNER-PRETTRE. J. Magn. Reson. **47**, 103 (1982).
24. U. FLEISCHER, M. SCHINDLER, and W. KUTZELNIGG. J. Chem. Phys. **86**, 6337 (1987).
25. (*a*) M. G. GIBBY, R. G. GRIFFIN, A. PINES, and J. S. WAUGH. Chem. Phys. Lett. **17**, 80 (1972); (*b*) R. A. MARINO and S. J. BULUSU. J. Energ. Mater. **3**, 57 (1985).
26. D. SCHWEITZER and H. W. SPIESS. J. Magn. Reson. **15**, 529 (1974).
27. M. MUNOWITZ, W. W. BACHOVCHIN, J. HERZFELD, C. M. DOBSON, and R. G. GRIFFIN. J. Am. Chem. Soc. **104**, 1192 (1982).
28. R. E. WASYLISHEN, G. H. PENNER, W. P. POWER, and R. D. CURTIS. J. Am. Chem. Soc. In press.
29. W. GORDY and R. L. COOK. Microwave molecular spectra. 3rd ed. John Wiley and Sons, New York. 1984. p. 734.
30. Y. KURODA, H. LEE, and A. KUWAE. J. Phys. Chem. **84**, 3417 (1980).
31. C. J. JAMESON, A. K. JAMESON, D. OPPUSUNGGU, S. WILLE, P. M. BURRELL, and J. MASON. J. Chem. Phys. **74**, 81 (1981).
32. V. GALASSO. Chem. Phys. **83**, 407 (1984).
33. J. KRONER, W. SCHNEID, N. WIBERG, B. WRACKMEYER, and G. ZIEGLEDER. J. Chem. Soc. Faraday Trans. 2, **74**, 1909 (1978).
34. B. R. APPLEMAN and B. P. DAILEY. Adv. Magn. Reson. **7**, 2311 (1974).

Can. J. Chem. Downloaded from www.nrcresearchpress.com by 194.225.253.170 on 09/07/12
For personal use only.

Thermodynamics of complex formation in chloroform + 1,4-dioxane

L. BARTA, Z. S. KOONER, and L. G. HEPLER
Department of Chemistry, University of Alberta, Edmonton, Alta, Canada T6G 2G2

AND

G. ROUX-DESGRANGES and J.-P. E. GROLIER
Laboratoire de Thermodynamique et Cinetique Chimique, Universite de Clermont-Ferrand 2, F-63170 Aubiere, France

Received January 19, 1989

L. BARTA, Z. S. KOONER, L. G. HEPLER, G. ROUX-DESGRANGES and J.-P. E. GROLIER. Can. J. Chem. **67**, 1225 (1989).

We have made new measurements of excess heat capacities and excess volumes of mixtures of chloroform and dioxane. In combination with published vapor pressures and excess enthalpies the results have been analyzed using the ideal associated solution model to yield K, ΔH^θ, ΔC_p^θ, and ΔV^θ for the formation of AB and A_2B complexes. It is demonstrated that the ideal associated solution model is consistent with all of the available thermodynamic data for this system, indicating that chemical interactions of the two components can account for nearly all of the deviations from ideal solution behavior. The results of our thermodynamic analysis are discussed in relation to the results of similar analyses of other systems in which there are strong chemical interactions of chloroform with electron-donor molecules.

Key words: complex formation, hydrogen bonding, ideal associated solution model, chloroform, 1,4-dioxane.

L. BARTA, Z. S. KOONER, L. G. HEPLER, G. ROUX-DESGRANGES et J.-P. E. GROLIER. Can. J. Chem. **67**, 1225 (1989).

On a effectué de nouvelles mesures des capacités calorifiques en excès et des volumes en excès de mélanges du chloroforme et du dioxane. Afin de déterminer les valeurs de K, de ΔH^θ, de ΔC_p^θ et ΔV^θ pour la formation des complexes AB et A_2B, on a analysé les résultats à l'aide du modèle de la solution associée idéale et en combinaison avec des pressions de vapeur et des enthalpies en excès déjà publiées. Il a été démontré que le modèle de la solution associée idéale est en accord avec toutes les données thermodynamiques disponibles pour ce système; ceci indique que les interactions chimiques entre les deux composants peuvent expliquer pratiquement toutes les déviations par rapport au comportement d'une solution idéale. On discute des résultats de notre analyse thermodynamique en fonction d'analyses semblables effectuées sur d'autres systèmes dans lesquels il existe de fortes interactions chimiques entre le chloroforme et des molécules qui donnent des électrons.

Mots clés : formation de complexes, liaisons hydrogènes, modèle de la solution associée idéale, chloroforme, 1,4-dioxane.

[Traduit par la revue]

Introduction

Many studies (1–13) have shown that thermodynamic data for binary mixtures of chloroform with Lewis bases can be interpreted in terms of the formation of either 1:1 or both 1:1 and 2:1 complexes. That such an interpretation is physically realistic has in some cases been substantiated by other types of investigation, including measurements of NMR relaxation rates (14, 15), measurements of dielectric properties (16), and determination of stable phases in the solid state (17, 18). The simplest and most convenient thermodynamic model that has been applied for this purpose assumes that the species present at equilibrium mix ideally. In effect, all of the deviations of the mixture from ideal solution behavior are treated in terms of chemical equilibria, with neglect of activity coefficients (activity coefficients equal to unity at all compositions, temperatures, and pressures). Accordingly there has been considerable interest in investigating the accuracy with which this simple "ideal associated solution" model describes the equilibrium properties of associated solutions.

The ideal associated solution model has recently been extended and applied with encouraging results to the analysis of thermodynamic properties of binary mixtures in which 1:1 complexes are formed (1–4). For both practical and theoretical reasons we have had an interest in extending this model to systems in which 2:1 as well as 1:1 complexes are expected to form, as represented by the coupled chemical equilibria,

[1] $A + B = AB$

[2] $AB + A = A_2B$

Previous investigations have shown that the ideal associated solution model gives a consistent account of vapor pressures and excess enthalpies of binary solutions of chloroform with dioxane (13), acetone (11, 12), dimethylsulfoxide (8–10), and selected ketones and esters (5). We have recently shown that the model also is reasonably consistent with partial molar enthalpies of solution, excess heat capacities, and excess volumes of chloroform + dimethylsulfoxide (7).

In the present work we have made new measurements of thermal and volumetric properties of chloroform + dioxane mixtures at 25°C. Vapor pressures and excess enthalpies at 50°C have been available for some time (13). We have combined these data with our heat capacity data to obtain, by way of the ideal associated solution model, values of the equilibrium constants and enthalpies and heat capacities of reactions [1] and [2] at 25°C. The resulting values have been used to calculate excess enthalpies at 35°C which have then been compared with experimental values reported by others (6, 19). Using the ideal associated solution model the volume changes of reactions [1] and [2] have also been evaluated.

The values of the thermodynamic properties of reactions [1] and [2] for chloroform + 1,4-dioxane are compared with those for chloroform + dimethylsulfoxide (7). The thermodynamic properties of formation of the 1:1 complexes of chloroform with 1,4-dioxane and with dimethylsulfoxide are compared with those that have been reported for the formation of 1:1 complexes of chloroform with triethylamine (1, 4) and with benzene (3).

Experimental

Heat capacities and densities at 298.15 ± 0.05 K were measured with a Picker flow calorimeter (20) and vibrating tube densimeter (21).

Chloroform (Fluka, IR 0.5% ethanol) and dioxane (Fluka, puriss.,

Printed in Canada / Imprimé au Canada

Can. J. Chem. Downloaded from www.nrcresearchpress.com by 194.225.253.170 on 09/07/12
For personal use only.

TABLE 1. Densities and heat capacities of mixtures of chloroform and dioxane at 298.15 K

x_A	ρ, g cm^{-3}	V^E, cm^3 mol^{-1}	c_p, J K^{-1} g^{-1}	C_p^E, J K^{-1} mol^{-1}
0	1.022737	0	1.69668	0
0.0429	1.046017	−0.0026	1.65628	0.166
0.0844	1.063872	−0.0069	1.61864	0.368
0.1361	1.086239	−0.0179	1.57392	0.667
0.1693	1.100738	−0.0267	1.54646	0.909
0.1991	1.113753	−0.0349	1.52287	1.166
0.2707	1.145463	−0.0662	1.46845	1.838
0.3503	1.181119	−0.1053	1.41217	2.717
0.4216	1.213476	−0.1446	1.36504	3.606
0.5063	1.252292	−0.1939	1.31166	4.649
0.5807	1.286624	−0.2280	1.26498	5.356
0.6625	1.324629	−0.2561	1.21208	5.714
0.7256	1.353879	−0.2596	1.16742	5.371
0.7944	1.385619	−0.2368	1.11485	4.365
0.8447	1.408813	−0.2082	1.07715	3.575
0.8997	1.433830	−0.1536	1.03526	2.488
0.9499	1.456505	−0.0855	0.99641	1.304
1	1.478904	0	0.95766	0

>99.5 mol%) were purified and handled as described previously (3, 22).

Results of calorimetric and volumetric measurements

Table 1 lists the results of our measurements of heat capacities and densities. For convenience we have also expressed these results as molar excess properties, defined by the general relationship

$$Y^E = Y - x_A Y_A^0 - x_B Y_B^0$$

where Y represents the property of a mixture containing exactly one mole of stoichiometric A + B, x_A and x_B are stoichiometric mole fractions of A and B, and Y_A^0 and Y_B^0 are the molar properties of the pure liquids. Our heat capacity and density of pure chloroform are $C_{pA}^0 = 114.32$ J K^{-1} mol^{-1} and $\rho_A^0 = 1.47890$ g cm^{-3}, in excellent agreement with values that recently have been reported elsewhere (3, 7). Our heat capacity and density of pure dioxane are $C_{pB}^0 = 149.489$ J K^{-1} mol^{-1} and $\rho_B^0 = 1.027737$ g cm^{-3}.

Thermodynamic analysis

In applying the ideal associated solution model it is assumed that all deviations of the properties of the solution from ideality are due to complex formation, with all activity coefficients equal to unity at all temperatures, pressures, and compositions. For mixtures of chloroform (A) and dioxane (B) we consider the coupled chemical equilibria represented by reactions [1] and [2] and then take these mixtures to be ideal solutions of the four distinct chemical species A, B, AB, and A_2B. Since physical interactions are neglected and activity coefficients are set equal to unity, the equilibrium activity of species i is equal to the equilibrium mole fraction (z_i), and the equilibrium constants for reactions [1] and [2] may be written

$$[3] \quad K_1 = z_{AB}/(z_A z_B)$$

$$[4] \quad K_2 = z_{A_2B}/(z_{AB} z_A)$$

Combination of eqs. [3] and [4] with the mass balance constraint

$$[5] \quad 1 = z_A + z_B + z_{AB} + z_{A_2B}$$

leads to

$$[6] \quad (1 - z_A - z_B)/(z_A z_B) = K_1 + K_1 K_2 z_A$$

Since the solution is considered as an ideal mixture, the partial pressure of each of the four components is given by Raoult's law, $p_i = z_i p_i^0$. If the condensed phase is ideal, then it is reasonable that the vapor phase is also an ideal mixture and that the partial pressure of species i may be calculated as the product of the total vapor pressure and the equilibrium mole fraction of species i in the vapor phase, $p_i = y_i P$. At the low pressures of the vapor pressure measurements for this system (13) there will be little or no association in the vapor phase, and the equilibrium mole fraction of species A in solution can be calculated from the equilibrium mole fraction of A in the vapor phase (y_A), the total vapor pressure (P), and the vapor pressure of pure A (p_A^0): $z_A = y_A P/p_A^0$. Similarly, $z_B = (P - z_A p_A^0)/p_B^0$.

The molar excess enthalpy (enthalpy of mixing) and excess volume are given by equations of the form

$$[7] \quad Y^E = r\Delta Y_1^\theta + s\Delta Y_2^\theta$$

where r and s are the extents of reactions [1] and [2], respectively. The relationships between r, s, the stoichiometric mole fractions (x_A and x_B) of the two components, and the equilibrium mole fractions (z_i) are summarized in Table 2. The temperature derivative of eq. [7] and with Y = H, gives the excess heat capacity:

$$[8] \quad C_p^E = r\Delta C_{p1}^\theta + s\Delta C_{p2}^\theta + (\partial r/\partial T)_p \Delta H_1^\theta + (\partial s/\partial T)_p \Delta H_2^\theta$$

Once the values of the equilibrium constants are known, the quantities r and s in eq. [7] and [8] may be obtained by iterative solution of the simultaneous equations

$$[9] \quad K_1 = [(r - s)(1 - r - s)]/[(x_A - r - s)(x_B - r)]$$

$$[10] \quad K_2 = [s(1 - r - s)]/[(x_A - r - s)(r - s)]$$

that result from substituting for the z_i in eqs. [3] and [4] using the expressions listed in Table 2. If the enthalpies of reaction are known, then the temperature derivatives of r and s may be evaluated by solving the simultaneous equations

$$[11] \quad (\partial \ln K_1/\partial T)_p = (\partial r/\partial T)_p[1/(r - s) - 1/(1 - r - s) + 1/(x_A - r - s) + 1/(x_B - r)] + (\partial s/\partial T)_p[1/(x_A - r - s) - 1/(r - s) - 1/(1 - r - s)] = \Delta H_1^\theta/RT^2$$

$$[12] \quad (\partial \ln K_2/\partial T)_p = (\partial r/\partial T)_p[1/(x_A - r - s) - 1/(r - s) - 1/(1 - r - s)] + (\partial s/\partial T)_p[1/s - 1/(1 - r - s) + 1/(r - s) + 1/(x_A - r - s)] = \Delta H_2^\theta/RT^2$$

To use eqs. [3] – [12] to evaluate the desired properties of complex formation at 25°C, we begin with evaluation of the equilibrium constants at 50°C, the temperature of the available vapor pressure data (13). Fitting of eq. [6] to these data leads to $K_{1,323} = 1.10$ and $K_{2,323} = 0.83$. Iterative solution of eqs. [9] and [10] then yields r_{323} and s_{323} for any stoichiometric mixture. Using eq. [7] and excess enthalpy data at 50°C (also from ref.

Can. J. Chem. Downloaded from www.nrcresearchpress.com by 194.225.253.170 on 09/07/12
For personal use only.

TABLE 2. Reaction table for formation of AB and A_2B complexes in the system A + B

Species	Initial amount	Initial mole fraction	Amount at equilibrium	Equilibrium mole fraction[a]
A	N_A	x_A	$N_A - n - m$	$z_A = (x_A - r - s)/(1 - r - s)$
B	N_B	x_B	$N_B - n$	$z_B = (x_B - r)/(1 - r - s)$
AB	0	0	$n - m$	$z_{AB} = (r - s)/(1 - r - s)$
A_2B	0	0	m	$z_{A_2B} = s/(1 - r - s)$

[a] $r = n/(N_A + N_B)$; $s = m/(N_A + N_B)$; equilibrium mole fraction of species $i = z_i$.

TABLE 3. Thermodynamic properties for formation of AB and A_2B complexes in mixtures of chloroform + dioxane based on the ideal associated solution model

Property[a]	A + B = AB[b]	A + AB = A_2B[b]
K_{323}	1.10 (1.11)	0.83 (1.12)
ΔH^θ_{323}	−8.6 (−8.4)	−9.2 (−6.7)
K_{298}	1.41	1.09
ΔH^θ_{298}	−7.9	−8.3
ΔC_p^θ	−29±3	−37±10
ΔV^θ_{298}	0.07±0.05	−4.23±0.16

[a] Equilibrium constants have been expressed in terms of mole fractions; units are kJ mol^{-1} (enthalpies), J K^{-1} mol^{-1} (heat capacities), and cm^3 mol^{-1} (volumes).
[b] Values in parentheses are from ref. 13.

13) we have obtained $\Delta H_1{}^\theta_{323} = -8.6$ kJ mol^{-1} and $\Delta H_2{}^\theta_{323} = -9.2$ kJ mol^{-1}.

We now introduce the thermodynamic relationship

[13] $(\partial \Delta H^\theta/\partial T)_p = \Delta C_p{}^\theta$

and assume that the $\Delta C_p{}^\theta$ values are independent of temperature over the range 298 K to 323 K. The values of $\Delta C_p{}^\theta$ have been obtained by an iterative method, choosing initial values of $\Delta C_p{}^\theta = 0$. Integration of the van't Hoff relationship

[14] $(\partial \ln K/\partial T)_p = \Delta H^\theta/RT^2$

using eq. [13] yields estimates of the values of ΔH^θ_{298} and K_{298}. Substitution of these values of K into eqs. [9] and [10] then yields estimates of r_{298} and s_{298}, and these in combination with the ΔH^θ_{298} values and eqs. [11] and [12] lead to estimates of $(\partial r/\partial T)_p$ and $(\partial s/\partial T)_p$ at 298 K. New estimates of the values of $\Delta C_p{}^\theta$ may then obtained by fitting eq. [8] to our excess heat capacities. The iteration was terminated when the values of both of the $\Delta C_p{}^\theta$ from successive iterations differed by less than 1%.

Using the final values of r_{298} and s_{298}, $\Delta V_1{}^\theta_{298}$ and $\Delta V_2{}^\theta_{298}$ were evaluated by fitting eq. [7] to our excess volumes.

Discussion

The results of our analysis are summarized in Table 3, where the values of K_{323} and ΔH^θ_{323} reported by McGlashan and Rastogi (13) are included for comparison. The relative errors (based on eleven measurements) in our values of $K_{1,323}$ and $K_{2,323}$ are of the order of 5% and 10%, respectively. The relative errors (based on five measurements) in our values of $\Delta H_1{}^\theta_{323}$ and $\Delta H_2{}^\theta_{323}$ are both of the order of 10%; thus our enthalpies of stepwise formation of AB and A_2B complexes are the same within the uncertainties of the analysis. This result may be contrasted with that of McGlashan and Rastogi, who found that the formation of A_2B from AB and A was slightly less exothermic than the formation of AB from A and B. In view of the uncertainties in their calculations, the result of McGlashan and Rastogi may be fortuitous although physically reasonable, as these authors have discussed. Use of the values of K and ΔH^θ as reported by McGlashan and Rastogi leads to a fit to our heat capacity and volumetric data that is slightly worse than that obtained using our values of these quantities.

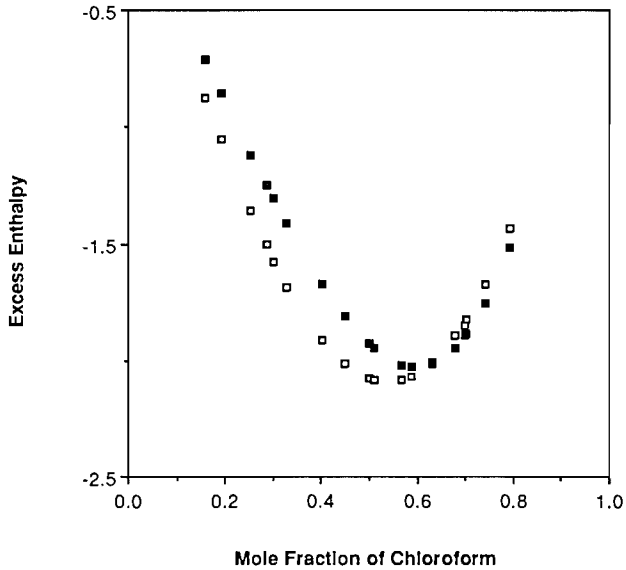


FIG. 1. Excess enthalpy (kJ mol^{-1}) of chloroform + 1,4-dioxane at 308.15 K versus stoichiometric mole fraction of chloroform. Open squares represent the data of ref. 6; solid squares represent the corresponding values predicted by the ideal associated solution model. Interpolated values based on the data of Van Ness and Abbott at 303.15 K and 318.15 K lie on the curve defined by the solid squares.

We have calculated excess enthalpies at 308.15 K using eq. [7]. Values of ΔH^θ_{308} were calculated using eq. [13] and values of ΔH^θ_{298} and $\Delta C_p{}^\theta_{298}$ from Table 3. Values of r and s at 308 K were calculated from eqs. [9] and [10] using values of K obtained from eqs. [11] and [12] and the information in Table 3. The results are displayed in Fig. 1 and are compared there with the experimental results of Singh (6). This author has reported a maximum value of $H^E_{max,308} = -2.10$ kJ mol^{-1} at a mole fraction of chloroform of 0.55 and has compared these values with $H^E_{max,308} = -2.08$ kJ mol^{-1} at $x_A = 0.6$ obtained by interpolation of the data of Van Ness and Abbott (19) at 303 K and 318 K. Singh has also noted that his excess enthalpies in comparison to those of Van Ness and Abbott are slightly more exothermic (by about 0.2 kJ mol^{-1}) at $x_A < 0.45$ and slightly less exothermic (by about 0.1 kJ mol^{-1}) at $x_A > 0.6$. On this basis our calculated values are in excellent agreement with the data of Van Ness and Abbott.

Can. J. Chem. Downloaded from www.nrcresearchpress.com by 194.225.253.170 on 09/07/12
For personal use only.

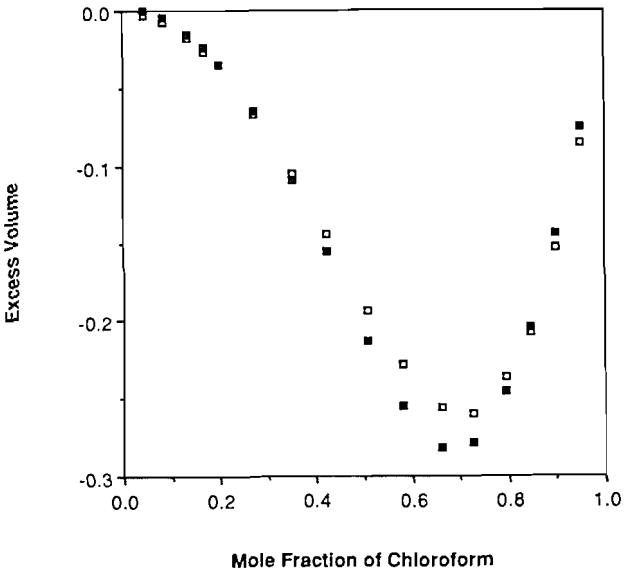


FIG. 2. Excess volumes ($cm^3\ mol^{-1}$) of chloroform + 1,4-dioxane at 298.15 K versus stoichiometric mole fraction of chloroform. Open squares represent our experimental data (Table 1); solid squares represent the corresponding values predicted by the ideal associated solution model (eq. [7]).

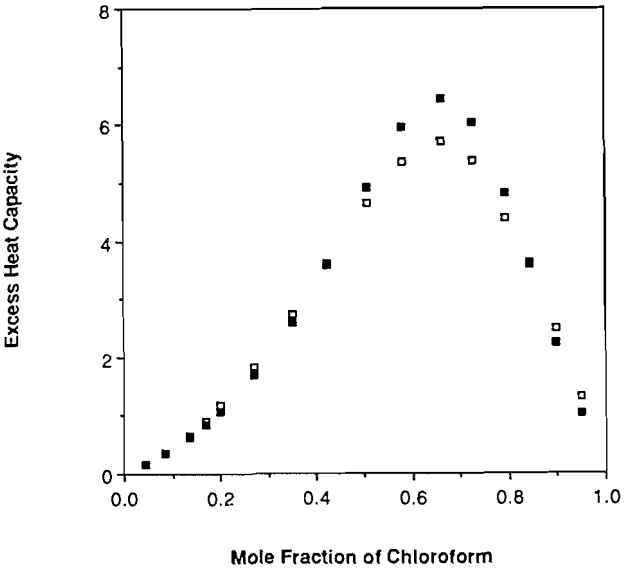


FIG. 3. Excess heat capacities ($J\ K^{-1}\ mol^{-1}$) of chloroform + 1,4-dioxane at 298.15 K versus stoichiometric mole fraction of chloroform. Open squares represent the data reported here (Table 1); solid squares represent the corresponding values predicted by the ideal associated solution model (eq. [8]).

We may also compare calculated values of excess enthalpies at 298.15 K with experimental values reported by Searles and Tamres (23). These authors obtained $H^E_{298} = -2.02 \pm 0.06$ kJ mol^{-1} at $x_A = 0.598$; our calculated value of -2.08 ± 0.06 kJ mol^{-1} is in excellent agreement. At $x_A = 0.400$ the experimental and calculated values are -1.90 kJ mol^{-1} and -1.70 kJ mol^{-1}, respectively.

The accuracy of the ideal associated solution model in representing our molar excess volumes and heat capacities is displayed in Figs. 2 and 3, respectively. We note that the overall representation of thermodynamic properties by the ideal associated solution model is more accurate for chloroform + 1,4-dioxane than for chloroform + dimethylsulfoxide (7).

TABLE 4. Thermodynamics of 1:1 complex formation of chloroform with electron donors at 25°C; units are J mol^{-1} (ΔG^θ), kJ mol^{-1} (ΔH^θ), J K^{-1} mol^{-1} (ΔS^θ, $\Delta C_p{}^\theta$), and cm^3 mol^{-1} (ΔV^θ)

Electron donor	ΔG^θ	ΔH^θ	ΔS^θ	$\Delta C_p{}^\theta$	ΔV^θ
Triethylamine	−2350	−17.0	−49.1	−42	−8.3
Benzene	1979	−4.9	−23.1	−17	2.1
DMSO[a]	−361	−10.5	−33.9	−89	1.8
	(−3267)	(−6.2)	(−9.8)	(56)	(−4.8)
1,4-Dioxane[a]	−860	−7.9	−23.6	−29	0.07
	(−220)	(−8.3)	(−27.1)	(−37)	(−4.2)

[a]Values in parentheses refer to the reaction A + AB = A_2B

In Table 4 the thermodynamic properties for complex formation in chloroform + 1,4-dioxane are compared with those for complex formation in chloroform + other electron donors. Certain features are common to the formation of the AB complex in each of the four systems listed. The reactions are exothermic and hence all of the AB complexes become less stable with increasing temperature. Formation of AB becomes more exothermic with increasing basicity of the electron donor molecule. The change in entropy is unfavorable to complex formation ($\Delta S^\theta < 0$) and, like ΔH^θ, becomes less negative with increasing temperature ($\Delta C_p{}^\theta < 0$). $\Delta C_p{}^\theta < 0$ also indicates that the reactions become more exothermic with increasing temperature.

For the system chloroform + 1,4-dioxane formation of the first bond and formation of the second bond of chloroform with the base are approximately equivalent in terms of standard enthalpy, entropy, and heat capacity changes. This result may be contrasted with that for chloroform + dimethylsulfoxide, where formation of the first bond is considerably more exothermic than that of the second, ΔS^θ is considerably more negative, and $\Delta C_p{}^\theta$ is of opposite sign. Thus formation of the second bond in the chloroform + dioxane system follows the general pattern observed for formation of AB complexes as discussed above. Formation of the second bond in the chloroform + dimethylsulfoxide system departs from this general pattern in that the reaction becomes *less* exothermic with increasing temperature.

While formation of a complex results in a reduction in intermolecular distance, the geometry of the complex relative to that of A and B molecules may lead to a net increase in void space due to reduction in packing efficiency of molecules in the solution. It therefore seems reasonable that values of ΔV^θ may range from negative (efficient packing) to positive (inefficient packing). It is noteworthy that in those cases where ΔV^θ is positive, the values are small.

Acknowledgements

We thank the Natural Sciences and Engineering Research Council of Canada and the France–Canada Exchange Program for support of this research. We thank J. F. Smith for helpful discussions.

1. J. F. SMITH and L. G. HEPLER. Can. J. Chem. In press.
2. J. F. SMITH and L. G. HEPLER. To be published.
3. J.-P. E. GROLIER, G. ROUX-DESGRANGES, Z. S. KOONER, J. F. SMITH, and L. G. HEPLER. J. Solution Chem. **16**, 745 (1987).
4. L. G. HEPLER, Z. S. KOONER, G. ROUX-DESGRANGES, and J.-P. E. GROLIER. J. Solution Chem. **14**, 579 (1985).

Can. J. Chem. Downloaded from www.nrcresearchpress.com by 194.225.253.170 on 09/07/12
For personal use only.

5. T. OHTA, H. ASANO, and I. NAGATA. Fluid Phase Equilibria, **4**, 105 (1980).
6. P. P. SINGH. Thermochim. Acta, **17**, 113 (1976).
7. L. BARTA, Z. S. KOONER, L. G. HEPLER, G. ROUX-DESGRANGES, and J.-P. E. GROLIER. J. Solution Chem. In press.
8. D. V. FENBY and L. G. HEPLER. J. Chem. Thermodyn. **6**, 185 (1974).
9. T. MATSUI, L. G. HEPLER, and D. V. FENBY. J. Phys. Chem. **77**, 2397 (1973).
10. L. G. HEPLER and D. V. FENBY. J. Chem. Thermodyn. **5**, 471 (1973).
11. K. W. MORCOM and D. N. TRAVERS. Trans. Faraday Soc. **61**, 230 (1965).
12. E. R. KEARNS. J. Phys. Chem. **65**, 314 (1961).
13. M. L. MCGLASHAN and R. P. RASTOGI. Trans. Faraday Soc. **54**, 496 (1958).
14. A. L. MCCLELLAN, S. W. NICKSIC, and J. C. GUFFY. J. Mol. Spectrosc. **11**, 340 (1963).
15. L. HELM and A. KRATOCHWILL. Z. Phys. Chem. N.F. **109**, 129 (1978).
16. P. BOULE. J. Chem. Phys. **57**, 5285 (1972).
17. G. W. STAPLETON, M. BELLAY, C. A. WULFF, and L. G. HEPLER. J. Chem. Eng. Data, **11**, 95 (1965).
18. J. R. GOATES, J. B. OTT, and N. F. MANGELSON. J. Phys. Chem. **67**, 2874 (1963).
19. H. C. VAN NESS and M. M. ABBOTT. International data series. No. 2, 1974. p. 93.
20. P. PICKER, P. A. LEDUC, P. R. PHILIP, and J. E. DESNOYERS. J. Chem. Thermodyn. **3**, 631 (1971).
21. P. PICKER, E. TREMBLAY, and C. JOLICOEUR. J. Solution Chem. **3**, 377 (1974).
22. J.-P. E. GROLIER, A. INGLESE, and E. WILHELM. J. Chem. Thermodyn. **16**, 67 (1984).
23. S. SEARLES and M. TAMRES. J. Am. Chem. Soc. **73**, 3740 (1951).

Can. J. Chem. Downloaded from www.nrcresearchpress.com by 194.225.253.170 on 09/07/12
For personal use only.

Synthesis and reaction chemistry of the heterobimetallic FeIr complexes $(CO)_3(PPh_3)Fe(\mu\text{-}PCy_2)Ir(PPh_3)(CO)_2$ and $(CO)_4Fe(\mu\text{-}PCy_2)Ir(1,5\text{-}COD)$

HILARY A. JENKINS AND STEPHEN J. LOEB[1]

Department of Chemistry, University of Winnipeg, Winnipeg, Man., Canada R3B 2E9

Received February 14, 1989

HILARY A. JENKINS and STEPHEN J. LOEB. Can. J. Chem. **67**, 1230 (1989).

Reactions of $Li[Fe(CO)_4(PCy_2)]$ with *trans*-$IrCl(CO)(PPh_3)_2$ and $[IrCl(1,5\text{-}COD)]_2$ (COD = cyclooctadiene) results in the formation of the μ-PCy_2 bridged complexes $(CO)_3(PPh_3)Fe(\mu\text{-}PCy_2)Ir(PPh_3)(CO)_2$, **1**, and $(CO)_4Fe(\mu\text{-}PCy_2)Ir(1,5\text{-}COD)$, **2**, respectively. **1** is coordinatively saturated with an FeIr dative bond and does not form an adduct with CO or undergo oxidative addition with H_2, HCl, or CH_3I. The protonation of **1** with HBF_4 gives the Ir hydride compound $[(CO)_3(PPh_3)Fe(\mu\text{-}PCy_2)Ir(H)(PPh_3)(CO)][BF_4]$. **1** undergoes phosphine substitution reactions in which PPh_3 is replaced by PR_3. Substitution is at Ir for PEt_3, $PnBu_3$, $PiPr_3$, PBz_3, and PCy_3, at Fe for PMe_2Ph, and at both metal centers for PPh_2Me. The substitution pattern is selective and appears to be sterically controlled. There is also evidence for cooperativity between metal centers in the formation of the PPh_2Me adduct since only the disubstituted product can be detected. Coordinative unsaturation was generated at the Ir centre by thermally induced CO loss from $(CO)_3(PPh_3)Fe(\mu\text{-}PCy_2)Ir(PCy_3)(CO)_2$ to give $(CO)_3(PPh_3)Fe(\mu\text{-}PCy_2)Ir(PCy_3)(CO)$. The reaction of **2** with excess CO(g) resulted in the formation of the carbonyl species $(CO)_4Fe(\mu\text{-}PCy_2)Ir(CO)_3$. **2** also reacts with 2 PEt_3 or DPPE (DPPE = 1,2-bis(diphenylphosphino)ethane) under CO(g) to give the disubstituted products $(CO)_3(PEt_3)Fe(\mu\text{-}PCy_2)Ir(PEt_3)(CO)_2$ and $(CO)_3Fe(\mu\text{-}PCy_2)(\mu\text{-DPPE})Ir(CO)_2$ with loss of 1,5-COD.

Key words: heterobimetallic FeIr complexes, cooperativity, phosphido-bridge.

HILARY A. JENKINS et STEPHEN J. LOEB. Can. J. Chem. **67**, 1230 (1989).

La réaction du $Li[Fe(CO)_4(PCy_2)]$ avec le *trans*-$IrCl(CO)(PPh_3)_2$ et le $[IrCl(1,5\text{-}COD)]_2$ (COD = cyclooctadiène) conduit à la formation des complexes pontés par un μ-PCy_2, respectivement le $(CO)_3(PPh_3)Fe(\mu\text{-}PCy_2)Ir(PPh_3)(CO)_2$, **1**, et $(CO)_4Fe(\mu\text{-}PCy_2)Ir(1,5\text{-COD})$, **2**. Le composé **1** est saturé par une coordination avec une liaison dative FeIr; il ne forme pas d'adduit avec le CO et il ne subit pas d'additions oxydantes avec le H_2, le HCl ou le CH_3I. La protonation du composé **1** avec du HBF, conduit à un hydrure de Ir, le composé $[(CO)_3(PPh_3)Fe(\mu\text{-}PCy_2)Ir(H)(PPh_3)(CO)_2][BF_4]$. Le composé **1** subit des réactions de substitution des phosphines au cours desquelles le PPh_3 est remplacé par des PR_3. Les substitutions se produisent au niveau du Ir avec PEt_3, $PnBu_3$, $PiPr_3$, PBz_3 et PCy_3 et au niveau du Fe avec le PMe_2Ph et aux deux centres métalliques avec le PPh_2Me. Le patron des substitutions est sélectif et il semble contrôlé par des facteurs stériques. Puisqu'on ne peut détecter que le produit disubstitué, il semble aussi y avoir de la coopération entre les centres métalliques dans la formation de l'adduit PPh_2Me. On a généré une insaturation de coordination au niveau du Ir par une perte de CO induite d'une façon thermique à partir du $(CO)_3(PPh_3)Fe(\mu\text{-}PCy_2)Ir(PCy_3)(CO)_2$ et conduisant à la formation de $(CO)_3(PPh_3)Fe(\mu\text{-}PCy_2)Ir(PCy_3)(CO)$. La réaction du composé **2** avec un excès de CO(g) conduit à la formation d'espèces carbonylées $(CO)_4Fe(\mu\text{-}PCy_2)Ir(CO)_3$. Sous une atmosphère de CO(g), le composé **2** réagit aussi avec 2 PEt_3 ou DPPE (DPPE = 1,2-bis(diphénylphosphino)éthane) pour donner les produits disubstitués, $(CO)_3(PEt_3)Fe(\mu\text{-}PCy_2)Ir(PEt_3)(CO)_2$ et $(CO)_3Fe(\mu\text{-}PCy_2)(\mu\text{-DPPE})Ir(CO)_2$, avec perte de 1,5-COD.

Mots clés : complexes hétéro-bimétalliques de FeIr, coopérativité, pont phosphido.

[Traduit par la revue]

Introduction

It is well known that sterically demanding trialkyl and triarylphosphine ligands can be used to induce coordinative unsaturation at a metal centre (1, 2). This is usually the result of creating a crowded environment at the metal which precludes coordination of the full compliment of ligands necessary for coordinative saturation. This technique has been used very successfully in the design of reactive metal systems such as the 16-electron complexes *trans*-$M(PR_3)_2(CO)_4$ (M = Mo, W: R = Cy, *i*Pr,) (3) and the 14-electron species $M(PR_3)_2$ (M = Pd, Pt; R = *i*Pr, Cy, *t*Bu) (4–6) and $RhH(PR_3)_2$ (R = *i*Pr, *t*Bu, Cy) (7). These coordinatively unsaturated complexes are known to react specifically with small molecules (3–7) such as N_2, H_2, C_2H_4, SO_2, and CO.

We are currently interested in extending this concept to multi-centred complexes. Our approach has been to use the bulky dicyclohexylphosphido group in combination with various large ancillary ligands, such as PR_3, in attempts to produce coordinatively unsaturated heterobimetallic complexes. Initially, we studied complexes containing two μ-PCy_2 ligands linking Mo or W to Ni, Pd, and Pt (8). However, these sterically crowded molecules exhibited little chemical reactivity. Recently, we employed a *single* μ-PCy_2 unit with the assumption that this would lessen the overall steric shielding and produce a more exposed metal–metal bond resulting in an increase in reactivity. In a preliminary study, we prepared some coordinatively unsaturated heterobimetallic complexes of FeRh containing a single μ-PCy_2 bridge (9). These complexes were observed to undergo adduct formation with small molecules and also showed substitution for a donor–acceptor metal–metal bond. In general, the reactivity patterns were not those observed for similar μ-PPh_2 bridged complexes. In this paper, we describe the preparation and reactivity of some analogous FeIr complexes.

Experimental section

General

trans-$IrCl(CO)(PPh_3)_2$, $[IrCl(1,5\text{-}COD)]_2$ (COD = cyclooctadiene), $Fe(CO)_4(PCy_2H)$, and DMA·HCl (DMA = dimethylacetamide) were prepared by the literature methods (9–12). $Fe_2(CO)_9$, $IrCl_3 \cdot xH_2O$, PCy_2H, PBz_3 (Bz = benzyl), $PiPr_3$, PCy_3 (Strem), PPh_3, DPPE (1,2-bis(diphenylphosphino)ethane), PEt_3, $PnBu_3$, PPh_2Me, PMe_2Ph, and *n*-BuLi (Aldrich) were purchased and used as received. THF (tetrahydrofuran), toluene, and *n*-hexane were dried by distillation from Na-benzophenone ketyl under N_2. All reactions were conducted under an atmosphere of dry N_2 using standard Schlenk techniques.

$^{31}P\{^1H\}$, $^{13}C\{^1H\}$, and ^1H NMR spectra were obtained at 121.5, 75.5, and 300.1 MHz, respectively, on a Bruker AM300 spectrometer

[1]To whom correspondence should be addressed.

Can. J. Chem. Downloaded from www.nrcresearchpress.com by 194.225.253.170 on 09/07/12
For personal use only.

Can. J. Chem. Downloaded from www.nrcresearchpress.com by 194.225.253.170 on 09/07/12
For personal use only.

using deuterated solvents as lock. Phosphorus chemical shifts were measured relative to external 85% H_3PO_4 with positive shifts downfield. Infrared spectra were recorded on a Perkin-Elmer 781 grating spectrometer.

*Preparation of $(CO)_3(PPh_3)Fe(\mu\text{-}PCy_2)Ir(PPh_3)(CO)_2$, **1***

Method A

n-Butyllithium (1.65 mL, 2.56 mmol of 1.55 *M* solution in hexanes) was added via syringe to a brown solution of $Fe(CO)_4(PCy_2H)$ (0.938 g, 2.56 mmol) in THF (15 mL). This solution was stirred for 10 min and then added dropwise to a yellow slurry of *trans*-$IrCl(CO)(PPh_3)_2$ (2.00 g, 2.56 mmol) in THF (30 mL) at 23°C. The resulting orange-brown solution was stirred for 24 h at room temperature and the solvent removed *in vacuo*. The remaining brown semi-solid was washed with *n*-hexane (3 × 10 mL), and extracted with CH_2Cl_2 (5 × 10 mL). The volume was reduced to 10 mL and the solution cooled to −20°C for 18 h. This yielded yellow-orange microcrystals of **1**. (2.21 g, 1.98 mmol, 75%).

Method B

$(CO)_4Fe(\mu\text{-}PCy_2)Ir(1,5\text{-COD})$ **2**, (0.265 g, 0.398 mmol) was dissolved in toluene (5 mL) and PPh_3 (0.209 g, 0.796 mmol) added. The resulting orange–brown solution was then placed under an atmosphere of CO(g) and stirred for 18 h. The orange solution was then taken to dryness *in vacuo* and the solid residue washed with diethyl ether (2 × 10 mL). The residue was recrystallized from CH_2Cl_2 to give yellow–orange microcrystals of **1**, 0.362 g (82%). *Anal.* calcd. for $C_{53}H_{52}FeIrO_5P_3$: C 57.31, H 4.73; found: C 57.24, H 4.63.

*Preparation of $(CO)_4Fe(\mu\text{-}PCy_2)Ir(1,5\text{-COD})$, **2***

n-Butyllithium (0.511 mL, 0.819 mmol of 1.6 *M* solution in hexanes) was added via syringe to a brown solution of $Fe(CO)_4(PCy_2H)$ (0.300 g, 0.819 mmol) in THF (10 mL). The resulting dark brown solution was stirred at room temperature for 10 min and then cooled to 0°C. This cooled solution was then added dropwise to an orange solution of $[IrCl(1,5\text{-COD})]_2$ (0.275 g, 0.409 mmol) in THF (10 mL). An immediate colour change was observed from orange to an intense dark red–brown. Stirring was continued for 4 h at 0°C, the solution taken to dryness *in vacuo* and the resulting reddish-brown oil extracted with toluene (3 × 5 mL). The solution was filtered and the volume reduced to 5 mL. After the solution was cooled at −20°C for 48 h, red microcrystalline material was isolated (0.365 g, 67%). $^{13}C\{^1H\}$ NMR ($CDCl_3$) δ 214.5 (br, CO), δ 77.2, 76.8 (CH, COD), δ 26.8 (CH_2, COD); ^1H NMR (toluene-d_8) δ 4.70, 4.36 (br s, 4H, COD), δ 2.21 (br s, 8H, COD), δ 0.95–1.80 (br m, 22H, Cy). *Anal.* calcd. for $C_{24}H_{34}FeIrO_4P$: C, 43.31, H 5.16; found: C 43.01, H 5.04.

*Reactions of $(CO)_3(PPh_3)Fe(\mu\text{-}PCy_2)Ir(PPh_3)(CO)_2$, **1**, with CO or H_2*

$(CO)_3(PPh_3)Fe(\mu\text{-}PCy_2)Ir(PPh_3)(CO)_2$, **1** (0.100 g, 0.090 mmol), was partially dissolved in toluene-d_8 (5 mL). The reagent gas was introduced as the atmosphere in place of N_2(g) and this mixture stirred for 4 h at 23°C with no visible change. A 3 mL sample of the solution was then removed, filtered and the $^{31}P\{^1H\}$ NMR recorded under an atmosphere (1 atm) of the reagent gas. $^{31}P\{^1H\}$ NMR showed only resonances due to **1**.

*Reactions of $(CO)_3(PPh_3)Fe(\mu\text{-}PCy_2)Ir(PPh_3)(CO)_2$, **1** with CH_3I or DMA·HCl*

$(CO)_3(PPh_3)Fe(\mu\text{-}PCy_2)Ir(PPh_3)(CO)_2$, **1**, (0.100 g, 0.090 mmol), was partially dissolved in toluene-d_8 (5 mL). Equimolar amounts of either CH_3I or DMA·HCl were then added and the resulting solution stirred for 18 h. A 3 mL sample of the solution was removed, filtered, and the $^{31}P\{^1H\}$ NMR recorded. $^{31}P\{^1H\}$ NMR showed only resonances due to **1**.

*Preparation of $[(CO)_3(PPh_3)Fe(\mu\text{-}PCy_2)Ir(H)(PPh_3)(CO)][BF_4]$, **3***

$(CO)_3(PPh_3)Fe(PCy_2)Ir(PPh_3)(CO)_2$ **1** (0.120 g, 0.108 mmol), was partially dissolved in THF (5 mL) and HBF_4–etherate (0.025 mL, 0.108 mmol) added. A clear pale yellow solution resulted immediately. The mixture was stirred for a further 18 h at 23°C. The volume was reduced to 3 mL and the solution cooled to −20°C for 48 h to yield pale yellow microcrystals of **3**, 0.044 g (35%). Although this compound appeared to be pure from all spectroscopic evidence, a satisfactory elemental analysis could not be obtained.

*Preparation of $(CO)_3(PPh_3)Fe(\mu\text{-}PCy_2)Ir(PR_3)(CO)_2$, (R = Et, **4**; n-Bu, **5**; i-Pr, **6**; Bz, **7**; and $(CO)_3(PPh_2Me)Fe(\mu\text{-}PCy_2)Ir(PPh_2Me)(CO)_2$, **8***

$(CO)_3(PPh_3)Fe(\mu\text{-}PCy_2)Ir(PPh_3)(CO)_2$, **1** (0.150 g, 0.135 mmol), was partially dissolved in toluene (10 mL) and two molar equivalents of the appropriate phosphine added via microsyringe. The solution was stirred for 15 min during which time **1** completely dissolved resulting in an orange solution. This solution was then stirred for a further 12 h at 23°C. The toluene was removed *in vacuo* and the resulting oily solid washed with diethyl ether (2 × 3 mL) to leave the product as a yellow or orange–yellow solid, **4**, 0.143 g (57%). *Anal.* calcd. for $C_{41}H_{52}FeIrO_5P_3$: C 50.96, H 5.43; found: C 51.27, H 5.53; **5** 0.150 g (63%). *Anal.* calcd. for $C_{47}H_{64}FeIrO_5P_3$: C 53.74, H 6.15; found: C 53.27, H 5.89; **6**, 0.081 g (61%). *Anal.* calcd. for $C_{44}H_{58}FeIrO_5P_3$: C 52.41, H 5.81; found: C 52.43, H 5.63; **7**, 0.132 g (58%). *Anal.* calcd. for $C_{56}H_{61}FeIrO_5P_3$: C 58.19, H 5.08; found: C 57.39, H 4.92; **8**, 0.116 g (63%). *Anal.* calcd. for $C_{43}H_{48}FeIrO_5P_3$: C 52.35, H 4.91; found: C 52.11, H 4.75.

*Preparation of $(CO)_3(PMe_2Ph)Fe(\mu\text{-}PCy_2)Ir(PPh_3)(CO)_2$, **9**, and $(CO)_3(PPh_3)Fe(\mu\text{-}PCy_2)Ir(PCy_3)(CO)_2$, **10***

$(CO)_3(PPh_3)Fe(\mu\text{-}PCy_2)Ir(PPh_3)(CO)_2$, **1** (0.150 g, 0.135 mmol), was partially dissolved in toluene (10 mL) and two molar equivalents of the appropriate phosphine added. The mixture was stirred for 30 min during which time the remaining **1** completely dissolved. The reaction solution was stirred for a further 12 h at 23°C. The toluene was removed *in vacuo* and the resulting orange–red oil dissolved in the minimum amount of diethyl ether. This solution was then cooled to −20°C for 24 h producing orange microcrystals of the product. **9**, 0.072 g (55%). *Anal.* calcd. for $C_{43}H_{48}FeIrO_5P_3$: C 52.36, H 4.92; found: C 52.99 H 4.86; **10**, 0.079 (68%). *Anal.* calcd. for $C_{53}H_{70}FeIrO_5P_3$: C 56.40, H 6.26; found: C 55.43, H 6.52.

*Preparation of $(CO)_3(PPh_3)Fe(\mu\text{-}PCy_2)Ir(PCy_3)(CO)$, **12***

$(CO)_3(PPh_3)Fe(\mu\text{-}PCy_2)Ir(PCy_3)(CO)_2$, **10** (0.150 g, 0.133 mmol), was dissolved in toluene (10 mL) and this solution refluxed for 12 h. The solution gradually darkened in colour from orange to orange–red over this time. The resulting solution was cooled, filtered, and the volume reduced to 3 mL. After cooling at −20°C for 18 h a small amount of orange–red solid (0.065 g, 44%) was isolated. Although this material can be identified spectroscopically as **12** and could seemingly be recrystallized from toluene, the final product was persistently contaminated with **10**. As a result no satisfactory elemental analysis could be obtained.

*Preparation of $(CO)_4Fe(\mu\text{-}PCy_2)Ir(CO)_3$, **13***

$(CO)_4Fe(\mu\text{-}PCy_2)Ir(1,5\text{-COD})$, **2** (0.200 g, 0.298 mmol), was dissolved in toluene (10 mL) and the N_2(g) atmosphere replaced by CO(g). The solution was stirred for 90 min and then taken to dryness and the residue dried *in vacuo* for 4 h to remove 1,5-COD. *n*-Hexane (2 mL) was added to dissolve the residue and after cooling at −20°C for 48 h red microcrystals of **13** were collected, 0.136 g (71%). $^{13}C\{^1H\}$ NMR ($CDCl_3$) δ 210.5 (br, Fe—CO), 179.6 (br, Ir—CO). Free 1,5-COD was detected in the original reaction mixture with no evidence for unreacted **2**. *Anal.* calcd. for $C_{19}H_{22}FeIrO_7$: C 35.58, H 3.46; found: C 34.89, H 3.37.

*Preparation of $(CO)_3(PEt_3)Fe(\mu\text{-}PCy_2)Ir(PEt_3)(CO)_2$, **14***

$(CO)_4Fe(\mu\text{-}PCy_2)Ir(1,5\text{-COD})$, **2**, (0.340 g, 0.511 mmol) was dissolved in toluene (5 mL) and PEt_3 (0.121 g, 1.02 mmol) added. The resulting orange–brown solution was then placed under an atmosphere of CO(g) and stirred for 18 h. The orange solution was then taken to dryness *in vacuo* and the semi-solid residue washed with *n*-hexane. The residue was recrystallized from toluene/*n*-hexane to give yellow–orange microcrystals of **14**, 0.344 g (82%). *Anal.* calcd. for $C_{29}H_{52}FeIrO_5P_3$: C 42.38, H 6.39; found: C 41.88, H 6.19.

TABLE 1. $^{31}P\{^1H\}$ NMR spectral data [a]

Complex	δ(μ-PCy_2)	δ(Fe)	δ(Ir)	$^2J_{PP}$(μ-Fe)	$^2J_{PP}$(μ-Ir)
$(CO)_3(PPh_3)Fe(\mu\text{-}PCy_2)Ir(PPh_3)(CO)_2$ **1**	148.9 (dd)[b]	74.3 (d)	10.7 (d)	20.6	178.2
$(CO)_4Fe(\mu\text{-}PCy_2)Ir(1,5\text{-COD})$ **2**	201.4 (s)	—	—	—	—
$[(CO)_3(PPh_3)Fe(\mu\text{-}PCy_2)Ir(PPh_3)(H)(CO)][BF_4]$ **3**	165.6 (dd)	51.5 (dd)	5.7 (dd)	42.5	11.0[c]
$(CO)_3(PPh_3)Fe(\mu\text{-}PCy_2)Ir(PEt_3)(CO)_2$ **4**	149.8 (dd)	78.6 (dd)	−5.7 (dd)	17.3	164.7
$(CO)_3(PPh_3)Fe(\mu\text{-}PCy_2)Ir(P\textit{n}Bu_3)(CO)_2$ **5**	150.1 (dd)	78.5 (dd)	−13.6 (dd)	17.1	165.5
$(CO)_3(PPh_3)Fe(\mu\text{-}PCy_2)Ir(P\textit{i}Pr_3)(CO)_2$ **6**	143.9 (dd)	78.0 (dd)	31.6 (dd)	16.8	163.3
$(CO)_3(PPh_3)Fe(\mu\text{-}PCy_2)Ir(PBz_3)(CO)_2$ **7**	152.2 (dd)	78.9 (dd)	−8.5 (dd)	16.5	174.2
$(CO)_3(PPh_2Me)Fe(\mu\text{-}PCy_2)Ir(PPh_2Me)(CO)_2$ **8**	148.9 (dd)	58.0 (dd)	−13.6 (dd)	18.6	173.4
$(CO)_3(PMe_2Ph)Fe(\mu\text{-}PCy_2)Ir(PPh_3)(CO)_2$ **9**	145.1 (dd)	37.5 (dd)	9.5 (dd)	19.1	177.9
$(CO)_3(PPh_3)Fe(\mu\text{-}PCy_2)Ir(PCy_3)(CO)_2$ **10**	143.7 (dd)	77.7 (dd)	23.3 (dd)	16.8	163.5
$(CO)_3(PPh_3)Fe(\mu\text{-}PCy_2)Ir(PPh_3)(CO)$ **11**	135.8 (dd)	75.5 (dd)	22.1 (dd)	25.1	18.1
$(CO)_3(PPh_3)Fe(\mu\text{-}PCy_2)Ir(PCy_3)(CO)$ **12**	120.5 (dd)	76.2 (dd)	39.4 (dd)	17.2	14.1
$(CO)_4Fe(\mu\text{-}PCy_2)Ir(CO)_3$ **13**	160.8 (s)	—	—	—	—
$(CO)_3(PEt_3)Fe(\mu\text{-}PCy_2)Ir(PEt_3)(CO)_2$ **14**	151.3 (dd)	59.9 (dd)	−4.8 (dd)	14.6	162.8
$(CO)_3Fe(\mu\text{-}PCy_2)(\mu\text{-DPPE})Ir(CO)_2$ **15**	145.3 (dd)	66.7 (dd)	−2.3 (dd)	23.4	172.8

[a]Recorded as toluene-d_8 solutions.
[b]s = singlet, d = doublet.
[c]$^3J_{PP}$ = 9.6 Hz.

Preparation of $(CO)_3Fe(\mu\text{-}PCy_2)(\mu\text{-DPPE})Ir(CO)_2$, 15

$(CO)_4Fe(\mu\text{-}PCy_2)Ir(1,5\text{-COD})$, **2** (0.285 g, 0.428 mmol), was dissolved in toluene (10 mL) and DPPE (0.341 g, 0.856 mmol) added with stirring. The orange solution was then placed under an atmosphere of CO(g). The resulting yellow–orange solution was stirred for 24 h and the solvent removed *in vacuo*. The residue was washed with diethyl ether (3 × 10 mL) and then recrystallized from toluene at −20°C to give yellow microcrystals of **15**, 0.185 g (44%). *Anal.* calcd. for $C_{43}H_{46}FeIrO_5P_3$: C 52.49, H 4.72; found: C 51.88, H 4.49.

Results

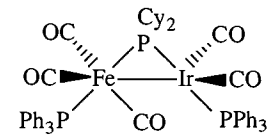
Synthesis and characterization of 1 and 2

The heterobimetallic FeIr complexes $(CO)_3(PPh_3)Fe(\mu\text{-}PCy_2)Ir(PPh_3)(CO)_2$, **1**, and $(CO)_4Fe(\mu\text{-}PCy_2)Ir(1,5\text{-COD})$, **2**, were prepared by the bridge-assisted synthetic method (13) according to eqs. [1] and [2].

[1] *trans*-$IrCl(CO)(PPh_3)_2 + Li[Fe(CO)_4(PCy_2)] \rightarrow (CO)_3(PPh_3)Fe(\mu\text{-}PCy_2)Ir(PPh_3)(CO)_2 + LiCl$

[2] $[IrCl(1,5\text{-COD})]_2 + 2Li[Fe(CO)_4(PCy_2)] \rightarrow 2(CO)_4Fe(\mu\text{-}PCy_2)Ir(1,5\text{-COD}) + 2LiCl$

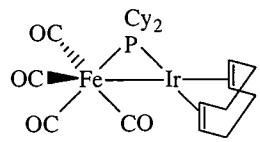
The $^{31}P\{^1H\}$ NMR spectral data for **1** and **2** are summarized in Table 1. Complex **1** shows a downfield resonance (δ 148.9 (dd)) due to the bridging PCy_2 ligand coupled to two different PPh_3 groups ($^2J_{pp}$(Fe) = 20.6 Hz and $^2J_{pp}$(Ir) = 178.2 Hz). The two different PPh_3 groups (δ(Fe) 74.3 (d), δ(Ir) 10.7 (d)) can be distinguished by comparison with the analogous FeRh complex (9) which showed PPh_3 bound to Fe at 77.4 ppm and PPh_3 bonded to Rh at 36.0 ppm with unambiguous characterization aided by the presence of $^1J_{PRh}$. The downfield chemical shift for the μ-PCy_2 ligand is indicative of a phosphido group bridging a metal–metal bond (14). This correlation has been observed for μ-PPh_2 (15) ligands and also for bulky groups such as μ-$PtBu_2$ (16–18) and μ-PCy_2 (8, 9, 19), and is well supported by X-ray studies. The $^2J_{PP}$ couplings between the bridging group and the terminal PPh_3 ligands supports a structure in which both the PPh_3 groups are *trans* to the μ-PCy_2 bridge (20). The infrared spectrum of **2** in CH_2Cl_2 solution (ν(CO); 1987 m, 1951 s, 1926 s, br, 1887 w, 1878 w, cm^{-1}) showed five bands assignable to five CO groups. We therefore formulate the structure of **1** as shown.



1

This is the same structural arrangement determined spectroscopically and verified crystallographically for the μ-PPh_2 bridged species (21) $(CO)_3(PPh_3)Fe(\mu\text{-}PPh_2)Ir(PPh_3)(CO)_2$.

The $^{31}P\{^1H\}$ NMR of **2** shows only a single downfield singlet due to the μ-PCy_2 ligand (δ 201.4 (s)) and this chemical shift is also attributed to the phosphido ligand bridging a metal–metal bond. The infrared spectrum (CH_2Cl_2 solution) shows four bands (ν(CO); 2034 m, sh, 2010 s, 1999 s, 1978 s, br cm^{-1}) due to the four CO groups which are bonded to Fe and both $^{13}C\{^1H\}$ and ^1H NMR show resonances due to coordinated 1,5-COD ($^{13}C\{^1H\}$; δ 77.2, 76.8 CH, δ 26.1 CH_2, ^1H; δ 4.70, 4.36 CH, 2.21 CH_2). Thus, the most probable structure for **2** is that of an $Fe(CO)_4$ fragment and an Ir(1,5-COD) fragment bridged by the μ-PCy_2 ligand with an Fe to Ir dative bond and a coordinatively unsaturated Ir center.



2

Reaction chemistry of 1

We find that no adduct formation occurs when **1** is reacted with CO and no oxidative addition reactions occur with H_2, HCl, or CH_3I. However, the reaction of **1** with one equivalent of HBF_4–etherate resulted in the protonation of **1** to give a single product **3**, as evidenced by $^{31}P\{^1H\}$ NMR. Complex **3** showed a single downfield resonance (δ 165.6 (dd)) due to the μ-PCy_2 ligand bridging the FeIr bond and two upfield resonances due to PPh_3 on Fe (δ 51.5(dd)) and PPh_3 on Ir (δ 5.7(dd)). The $^2J_{PP}$ couplings indicated a *trans* disposition for the PCy_2 and PPh_3(Fe) groups and a *cis* arrangement of the

Can. J. Chem. Downloaded from www.nrcresearchpress.com by 194.225.253.170 on 09/07/12
For personal use only.

Can. J. Chem. Downloaded from www.nrcresearchpress.com by 194.225.253.170 on 09/07/12
For personal use only.

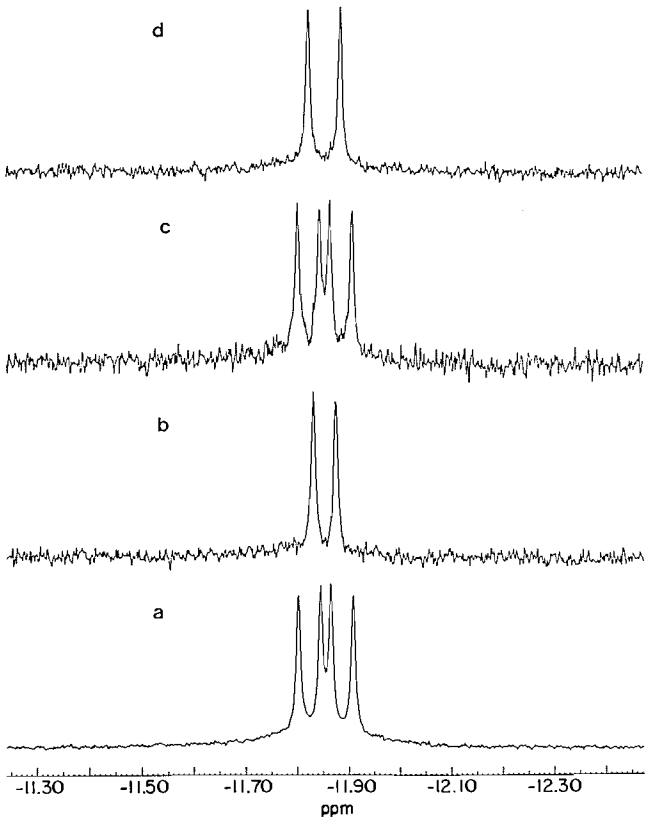
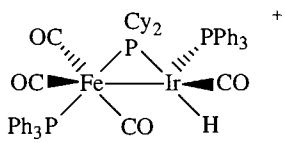


FIG. 1. $^1H\{^{31}P\}$ NMR decoupling experiment to identify the position of the hydride ligand for $[(CO)_3(PPh_3)Fe(\mu\text{-}PCy_2)Ir(H)(PPh_3)(CO)]^+$, **3**. (*a*) The fully coupled spectrum. (*b*) The ^{31}P resonance at δ 165.6 due to the μ-PCy_2 ligand is decoupled. (*c*) The ^{31}P resonance at δ 51.5 due to PPh_3(Fe) is decoupled. (*d*) The ^{31}P resonance at δ 5.7 due to PPh_3(Ir) is decoupled.

PCy_2 and PPh_3(Ir) ligands. Interestingly, there was also a small $^3J_{PP}$ coupling of 9.6 Hz between the Ph_3P(Fe) and PPh_3(Ir) ligands which appears to be unique in PR_2 bridged complexes. A ^1H NMR spectrum of the hydride region of **3** showed a single resonance (δ −11.2 (dd)) due to the hydride ligand coupled to two of the phosphorus ligands. A selective $^1H\{^{31}P\}$ decoupling experiment (Fig. 1) unambiguously showed that the hydride is coupled to the PCy_2 group (^2J = 19.0) and the PPh_3(Ir) ligand (^2J = 12.7). This infers that the H ligand is bound to Ir and not Fe, although the change in chemical shift of these resonances upon protonation might lead to the conclusion that the site of protonation was the Fe centre. The reason for a large shift in the PPh_3(Fe) resonance (δ 74.3 to 51.5) and very little change for PPh_3(Ir) (δ 10.7 to 5.7) is unclear. We formulate the structure of **3** as $(CO)_3(PPh_3)Fe(\mu\text{-}PCy_2)Ir(H)(PPh_3)(CO)$ based on these



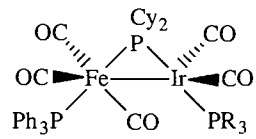
3

NMR results which show the site of protonation to be the Ir metal as shown below. A reasonable comparison can be made with the complex $(CO)(PPh_3)Fe(\mu\text{-}PPh_2)IrCl(H)(PPh_3)(CO)$ which is the result of HCl addition to the complex $(CO)(PPh_3)Fe(\mu\text{-}PPh_2)Ir(PPh_3)(CO)$ (21). The $^2J_{HP}$ and relative chemical shift changes upon protonation are similar to those observed for the conversion of **1** to **3**.

Phosphine substitution reactions of 1

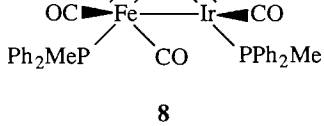
One of the objectives of this study was to use ancillary PR_3 ligands to create steric congestion at the metal sites and consequently produce coordinatively unsaturated complexes capable of small molecule activation. To this end, we studied the phosphine substitution patterns of **1** with PR_3 ligands (PEt_3, $PnBu_3$, $PiPr_3$, PBz_3, PPh_2Me, PMe_2Ph, PCy_3) of varying cone angle. In a typical experiment, two equivalents of the phosphine were added to a solution of **1**. Two equivalents were used since it was found that only one equivalent generally produced a mixture of **1** and product. The reactions were monitored by $^{31}P\{^1H\}$ NMR to determine the types and numbers of products formed. In each case only one major product was detected and eventually isolated.

The products formed depended on the nature of the PR_3 ligand but in all cases the result was simple PR_3 substitution for PPh_3. For PR_3 = PEt_3, $PnBu_3$, PBz_3, $PiPr_3$, and PCy_3 the compound formed was the result of PR_3 substitution for PPh_3 at Ir.

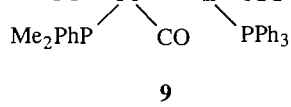


4 (R = Et), **5** (R = *n*Bu), **6** (R = *i*Pr), **7** (R = Bz), **10** (R = Cy)

For PR_3 = PMe_2Ph, substitution was for the PPh_3 group on Fe and when either one or two equivalents of PPh_2Me were used the only product detected was the result of PR_3 substitution for both PPh_3 ligands on Fe and Ir. $^{31}P\{^1H\}$ NMR spectral data for **4**–**8** are found in Table 1 and infrared data in Table 2.



8



9

Generation of coordinatively unsaturated complexes

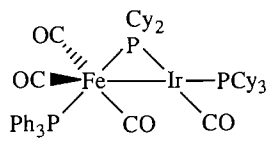
Geoffroy has shown that the μ-PPh_2 complex $(CO)_3(PPh_3)Fe(\mu\text{-}PPh_2)Ir(PPh_3)(CO)_2$ can be converted to the coordinatively unsaturated species $(CO)_3(PPh_3)Fe(\mu\text{-}PPh_2)Ir(PPh_3)(CO)$ by removing CO thermally or photochemically (21). However, **1** does not easily lose CO under these conditions. Only after prolonged reflux in toluene, was there $^{31}P\{^1H\}$ NMR spectral evidence for reaction, but full conversion to $(CO)(PPh_3)Fe(\mu\text{-}PCy_2)Ir(PPh_3)(CO)$, **11** did not occur before decomposition of the product. By introducing bulky ancillary ligands in place of PPh_3, it was anticipated that loss of a ligand such as CO may occur due to increased steric demands. However, even when PCy_3 was used in place of PPh_3, only the coordinatively saturated species $(CO)(PPh_3)Fe(\mu\text{-}PCy_2)Ir(PCy_3)(CO)_2$, **10** was formed. Complex **10** does display an increase tendency for loss of CO and this was achieved thermally by refluxing a toluene solution for 12 h, to give $(CO)(PPh_3)Fe(\mu\text{-}PCy_2)Ir(PCy_3)(CO)$, **12**. The $^{31}P\{^1H\}$ NMR of **12** shows the three resonances expected but the $^2J_{PP}$ coupling between μ-PCy_2 and PCy_3 indicates a *cis* orientation for these ligands. This is consistent with the loss of CO from Ir to give the coordinatively unsaturated species **12**. The change in geometry

TABLE 2. Infrared spectral data[a]

Complex	ν(CO)
$(CO)_3(PPh_3)Fe(\mu\text{-}PCy_2)Ir(PPh_3)(CO)_2$ **1**	1987 (m)[b], 1951 (s), 1926 (s, br), 1887 (m), 1878 (m)
$(CO)_4Fe(\mu\text{-}PCy_2)Ir(1,5\text{-COD})$ **2**[c]	2012 (s), 2000 (s), 1982 (s), 1962 (m), 1939 (w)
$[(CO)_3(PPh_3)Fe(\mu\text{-}PCy_2)Ir(PPh_3)(H)(CO)][BF_4]$ **3**	2072 (m)[d], 2039 (s), 2020 (s), 1992 (s, sh) 1979 (s, br)
$(CO)_3(PPh_3)Fe(\mu\text{-}PCy_2)Ir(PEt_3)(CO)_2$ **4**	1979 (m), 1943 (s), 1914 (s, br), 1888 (s), 1871 (m, sh)
$(CO)_3(PPh_3)Fe(\mu\text{-}PCy_2)Ir(P\textit{n}Bu_3)(CO)_2$ **5**	1978 (m), 1944 (s), 1917 (s, br), 1891 (m, sh), 1875 (m, sh)
$(CO)_3(PPh_3)Fe(\mu\text{-}PCy_2)Ir(P\textit{i}Pr_3)(CO)_2$ **6**	1985 (m), 1947 (s), 1922 (s, br), 1885 (m)
$(CO)_3(PPh_3)Fe(\mu\text{-}PCy_2)(PBz_3)(CO)_2$ **7**	1985 (m), 1950 (s), 1925 (s), 1888 (m, br)
$(CO)_3(PPh_2Me)Fe(\mu\text{-}PCy_2)Ir(PPh_2Me)(CO)_2$ **8**	1983 (m), 1948 (s), 1921 (s, br), 1894 (s, sh), 1875 (m, sh)
$(CO)_3(PMe_2Ph)Fe(\mu\text{-}PCy_2)Ir(PPh_3)(CO)_2$ **9**	1986 (m), 1948 (s, 1921 (s, br), 1879 (m)
$(CO)_3(PPh_3)Fe(\mu\text{-}PCy_2)Ir(PCy_3)(CO)_2$ **10**	1983 (m), 1945 (s), 1918 (s, br) 1884 (s, br)
$(CO)_3(PPh_3)Fe(\mu\text{-}PCy_2)Ir(PCy_3)(CO)$ **12**[e]	1961 (s), 1930 (s, br), 1886 (s), 1811 (m, br)
$(CO)_4Fe(\mu\text{-}PCy_2)Ir(CO)_3$ **13**	2082 (m), 2037 (s), 2012 (s), 1998 (s), 1967 (m, sh)
$(CO)_3(PEt_3)Fe(\mu\text{-}PCy_2)Ir(PEt_3)(CO)_2$ **14**	1995 (m, sh), 1958 (s), 1943 (s, br), 1912 (s), 1886 (m)
$(CO)_3Fe(\mu\text{-}PCy_2)(\mu\text{-DPPE})Ir(CO)_2$ **15**	2006 (m), 1959 (s), 1945 (s, br), 1925 (s, sh), 1889 (m)

[a]Recorded as solutions in CH_2Cl_2 unless otherwise noted.
[b]s = strong, m = medium, w = weak, sh = shoulder, br = broad.
[c]Recorded as *n*-heptane solution.
[d]Actually ν(IrH).
[e]Recorded in *n*-hexane solution.

at Ir is the same as that observed for μ-PPh_2 bridged FeIr complexes and μ-PCy_2 bridged FeRh complexes which have been characterized by X-ray diffraction (9, 21).

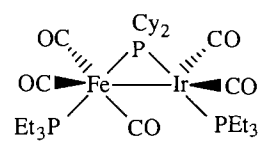


12

Reaction chemistry of 2

The problems associated with producing coordinative unsaturation via phosphine substitution on complex **1** prompted us to study **2** as an alternative to **1**. This complex has a number of advantages over **1**. It is not only coordinatively unsaturated but also contains the potentially labile 1,5-COD ligand and has no ancillary PR_3 ligands. The initial experiment performed was the reaction of **2** with CO to determine if the 1,5-COD ligand could be easily removed. The result of this reaction was the complete conversion of **2** to $(CO)_4Fe(\mu\text{-}PCy_2)Ir(CO)_3$, **13**. This formulation is based on the infrared and $^{31}P\{^1H\}$, $^{13}C\{^1H\}$, and ^1H NMR data. These spectra show that the 1,5-COD ligand has been displaced and are consistent with the idea that the complex is coordinatively saturated and still contains the FeIr bond. There is no evidence for substitution of the metal–metal interaction even under an atmosphere (1 atm) of CO. This is in contrast to the analogous FeRh complex $(CO)_4Fe(\mu\text{-}PCy_2)Rh(1,5\text{-COD})$ for which solution studies showed a mixture of complexes, $(CO)_4Fe(\mu\text{-}PCy_2)Rh(CO)_x$, $x = 1$–3, and thus evidence for both a coordinatively unsaturated species and substitution of the FeRh bond by CO (9).

Phosphine substitution reactions of **2** were not as straightforward. The simple addition of *one* equivalent of PEt_3 produced a mixture of compounds as observed by $^{31}P\{^1H\}$ NMR. The only discernable product was the coordinatively saturated species $(CO_3)(PEt_3)Fe(\mu\text{-}PCy_2)Ir(PEt_3)(CO)_2$, **14**. This was formulated as such due to the $^2J_{PP}$ coupling between the μ-PCy_2 and PEt_3(Ir) groups (162.8 Hz) which indicated a *trans* geometry for these ligands similar to **1**. The formation of this complex requires two equivalents of PEt_3 and the abstraction of CO from some source. In order to avoid the mixture of products and to optimize the formation of **14**, the reaction was carried out with two equivalents of PEt_3 under an atmosphere of CO(g). This produced almost quantitative conversion of **2** to **14** as shown by $^{31}P\{^1H\}$ NMR and an eventual isolated yield of 82%. The same reaction was repeated using PPh_3 and this gave **1** in good yield as well. Since the coordination of two PR_3 ligands seemed to be favored in these substitutions we also investigated the reaction of the bidentate phosphine ligand DPPE under these same conditions. The resulting complex, **15**, was formulated as resulting from coordination of the DPPE to both the Fe and Ir centers. The bridging mode for this ligand appears to allow for a geometry similar to that observed for all of the FeIr complexes with the PPh_2 groups of DPPE bound *trans* to the μ-PCy_2 ligand. In fact, the $^{31}P\{^1H\}$ NMR spectral data for **15** (δ(μ) 145.3 (dd), δ(Fe) 66.7 (dd), δ(Ir) −2.3 (dd); $^2J_{PP}$(μ-Fe) = 23.4 Hz, $^2J_{PP}$(μ-Ir) = 172.8 Hz) are similar to that for **8** (δ(μ) 148.9 (dd), δ(Fe) 58.0 (dd), δ(Ir) −13.6 (dd); $^2J_{PP}$(μ-Fe) = 18.6 Hz, $^2J_{PP}$(μ-Ir) = 173.4 Hz) which contains PPh_2Me coordinated to both Fe and Ir in the proposed geometry.



14

Discussion

Complex **1** is coordinatively saturated if the dative Fe to Ir interaction is assumed to be a formal, two electron donation. For this complex to undergo oxidative addition or adduct formation a reaction must occur to either remove an ancillary ligand or substitute for the FeIr dative bond. This latter type of reaction has been observed for a number of heterobimetallic phosphido-bridged complexes, most notably $(CO)_3(PPh_3)Fe(\mu\text{-}PPh_2)Ir(PPh_3)(CO)_2$ in which the FeIr bond is replaced upon adduct

Can. J. Chem. Downloaded from www.nrcresearchpress.com by 194.225.253.170 on 09/07/12
For personal use only.

formation with CO or oxidative addition of H_2 (21). The fact that **1** does not react in this manner can be rationalized as being the result of a stronger donor–acceptor interaction for the μ-PCy_2 species. The ready protonation of **1** is also evidence for the robustness of this μ-PCy_2 bridge and could be due to the increased basicity of the complex with the dialkyl-phosphido group PCy_2 versus the diaryl-phosphido group PPh_2.

An interesting problem in the study of heterobimetallic complexes is the question of whether both metal sites actively participate in the observed chemistry. One might expect to see evidence for site preference under different substitution conditions or perhaps cooperativity between the metals which effects the substitution pattern. Since there is a possible site of substitution on each metal in **1**, we can use these simple experiments as a probe for metal site preferences and cooperativity effects by observing product distribution. Since all the phosphines except PMe_2Ph, which has the smallest cone angle, substitute preferentially at Ir, and there is little difference in the basicities of the PR_3 ligands, it is likely that steric considerations are predominate in site selection. It could be rationalized that the preferred site of substitution is at the Fe atom when steric considerations are relatively unimportant, such as for PMe_2Ph, but that the less crowded Ir centre becomes the site of preference when steric demands are important as occurs for ligands such as PCy_3. The substitution at Fe occurs only when the PR_3 molecule is small enough to minimize steric demands at this site.

In the case of PPh_2Me, for which substitution occurs at both metals, we can assume that the first substitution significantly enhances substitution at the second metal, since no monosubstituted product is observed. Although there is no evidence to show at which site the first substitution occurs, it could be that the initial substitution at Fe effects the Ir site electronically via the FeIr dative interaction. Overall, we see that there is a definite pattern for substitution likely based on steric demands and a cooperative effect between the adjacent metals is evident from the disubstitution pattern observed for $(CO)(PPh_2Me)Fe(\mu\text{-}PCy_2)Ir(PPh_2Me)(CO)_2$.

Attempts to create coordinative unsaturation by simply substituting bulky ancillary phosphines for PPh_3 on **1** were not successful. Although complex **10** did lose CO upon heating to generate the coordinatively unsaturated species **12**, this type of transformation has already been readily achieved for the μ-PPh_2 complex (21) analogous to **1** and can not be considered unique to these μ-PCy_2 bridged compounds.

The reaction chemistry of **2** is dominated by the facile loss of the 1,5-COD ligand. This should allow for the introduction of a wide range of ancillary ligands however, we have only investigated the simple reactions with CO and a few phosphines to date. The trend appears to be the formation of coordinatively saturated species with a relatively unreactive FeIr bond. This is evidenced by the lack of substitution for the metal–metal bond under a CO atmosphere and the clean reactions to form compounds **1**, **13**, **14**, and **15** from **2**.

Acknowledgements

We thank the Natural Sciences and Engineering Research Council of Canada for financial support of this work. The Chemistry Department of the University of Manitoba is gratefully acknowledged for use of their NMR facilities and as the home department of graduate student H.A.J.

1. J. A. IBERS. Chem. Soc. Rev. **11**, 57 (1982).
2. C. A. TOLMAN. Chem. Rev. **77**, 313 (1977).
3. G. J. KUBAS, R. R. RYAN, B. I. SWANSON, P. J. VERGAMINI, and H. J. WASSERMAN. J. Am. Chem. Soc. **106**, 451 (1984).
4. J. M. RITCHEY, D. C. MOODY, and R. R. RYAN. Inorg. Chem. **22**, 2276 (1982).
5. G. J. KUBAS. J. Chem. Soc. Chem. Commun. 61 (1980).
6. G. J. KUBAS, G. D. JARVINEN, and R. R. RYAN. J. Am. Chem. Soc. **105**, 1883 (1983).
7. T. YOSHIDA, D. L. THORN, T. OKANO, S. OTSUKA, and J. A. IBERS. J. Am. Chem. Soc. **102**, 6451 (1980).
8. S. J. LOEB, H. A. TAYLOR, L. GELMINI, and D. W. STEPHAN. Inorg. Chem. **25**, 1977 (1986).
9. S. J. LOEB, H. A. JENKINS, and D. W. STEPHAN. Inorg. Chem. In press.
10. K. VRIEZE, J. P. COLLMAN, C. T. SEARS JR., and M. KUBOTA. Inorg. Synth. **11**, 101 (1968).
11. J. L. HERDE, J. C. LAMBERT, C. V. SENOFF, and M. A. CUSHING. Inorg. Synth. **15**, 18 (1974).
12. M. COWIE, S. J. LOEB, and I. R. MCKEER. Organometallics, **5**, 854 (1986).
13. D. A. ROBERTS and G. L. GEOFFROY. *In* Comprehensive organometallics chemistry. *Edited by* G. Wilkinson, F. G. A. Stone, and E. Abel. Pergamon Press, Oxford, England. 1982. Chap. 40.
14. (*a*) J. L. PETERSON and R. P. STEWART, JR. Inorg. Chem. **19**, 186 (1980); (*b*) A. J. CARTY, S. A. MACLAUGHLIN, and N. J. TAYLOR. J. Organomet. Chem. **204**, C27 (1981); (*c*) A. J. CARTY. *In* Catalytic aspects of metal phosphine complexes: Advances in Chemistry 196. Am. Chem. Soc., Washington, DC. 1982. p 163; (*d*) P. E. GARROU. Chem. Rev. **81**, 229 (1981).
15. A. J. CARTY, S. A. MACLAUGHLIN, and D. NUCCARIONE. *In* Phosphorus-31 NMR spectroscopy in stereochemical analysis. *Edited by* J. G. Verkade and L. D. Quin. 1987. Chap. 16, p. 559 and references therein.
16. A. M. ARIF, R. A. JONES, M. H. SEEBERGER, B. R. WHITTLESEY, and T. C. WRIGHT. Inorg. Chem. **25**, 3943 (1986), and refs. 6–11 therein.
17. A. M. ARIF, D. E. HEATON, R. A. JONES, and C. M. NUNN. Inorg. Chem. **26**, 4228 (1987).
18. A. M. ARIF, D. E. HEATON, R. A. JONES, K. B. KIDD, T. C. WRIGHT, B. R. WHITTLESEY, J. L. ATWOOD, W. E. HUNTER, and H. ZHANG. Inorg. Chem. **26**, 4065 (1987).
19. T. A. ALBRIGHT, S-K. KANG, A. M. ARIF, A. J. BARD, R. A. JONES, J. K. LELAND, and S. T. SCHWAB. Inorg. Chem. **27**, 1246 (1988).
20. J. F. NIXON, and J. F. PIDCOCK. Ann. Rev. NMR Spectrosc. **2**, 345 (1969).
21. D. A. ROBERTS, G. R. STEINMETZ, M. J. BREEN, P. M. SHULMAN, E. D. MORRISON, M. R. DUTTERA, C. W. DE BROSSE, R. R. WHITTLE, and G. L. GEOFFROY. Organometallics, **2**, 846 (1984).

Can. J. Chem. Downloaded from www.nrcresearchpress.com by 194.225.253.170 on 09/07/12
For personal use only.

Reassignment of the structure of $M_3(CO)_{12}(Cl)(SnCl_3)$ (M = Ru, Os)

ANNA BECALSKA AND ROLAND K. POMEROY[1]
Department of Chemistry, Simon Fraser University, Burnaby, B.C., Canada V5A 1S6

AND

WILLIAM A. G. GRAHAM
Department of Chemistry, University of Alberta, Edmonton, Alta., Canada T6G 2G2

Received January 30, 1989

ANNA BECALSKA, ROLAND K. POMEROY, and WILLIAM A. G. GRAHAM. Can. J. Chem. **67**, 1236 (1989).

Reaction of $M_3(CO)_{12}$ (M = Ru, Os) with $SnCl_4$ in benzene at room temperature affords $M_3(CO)_{12}(Cl)(SnCl_3)$ in essentially quantitative yield. The ^{13}C nmr spectra of these complexes indicate they have a $ClM_3(SnCl_3)$ arrangement of atoms with the Cl ligand *cis* and the $SnCl_3$ group *trans* to a linear Os_3 chain. This is contrary to previously proposed structures for these compounds. The ^{13}C nmr spectrum of $Os_3(CO)_{12}(I)_2$ which has the iodo ligands *cis* to the Os_3 chain is also reported for comparison.

Key words: ruthenium–tin, osmium–tin, osmium–iodine, ^{13}C nmr spectroscopy.

ANNA BECALSKA, ROLAND K. POMEROY et WILLIAM A. G. GRAHAM. Can. J. Chem. **67**, 1236 (1989).

La réaction des composés $M_3(CO)_{12}$ (M = Ru, Os) avec le $SnCl_4$, dans le benzène, à la température ambiante, conduit aux produits $M_3(CO)_{12}(Cl)(SnCl_3)$ avec un rendement qui est essentiellement quantitatif. Les spectres rmn du ^{13}C de ces complexes indiquent que l'arrangement des atomes dans la portion $ClM_3(SnCl_3)$ comporte un ligand Cl *cis* et un groupement $SnCl_3$ *trans* par rapport à une chaîne Os_3 linéaire. Ce résultat est contraire aux structures proposées antérieurement pour ces composés. Pour fins de comparaison, on rapporte aussi les spectres rmn du ^{13}C du composé $Os_3(CO)_{12}(I)_2$ dans lequel les ligands iodo sont *cis* par rapport à la chaîne OsO_3.

Mots clés : ruthénium–étain, osmium–étain, osmium–iode, spectroscopie en rmn du ^{13}C.

[Traduit par la revue]

Can. J. Chem. Downloaded from www.nrcresearchpress.com by 194.225.253.170 on 09/07/12
For personal use only.

Introduction

The syntheses of $M_3(CO)_{12}(Cl)(SnCl_3)$ (M = Ru, Os) from $M_3(CO)_{12}$ and $SnCl_4$ were originally communicated in 1969 (1, 2). At that time the compounds were formulated with a linear $(Cl)M(CO)_4M(CO)_4M(CO)_4(SnCl_3)$ arrangement of non-carbonyl atoms. This arrangement was apparently assumed in an investigation of some aspects of the chemistry of $Os_3(CO)_{12}(Cl)(SnCl_3)$ (3). It has, however, been suggested (4, 5) that these complexes may be Lewis acid – Lewis base adducts especially as they are formed under mild conditions and $Fe_3(CO)_{12}$ does not react with $SnCl_4$ under the same conditions. Another possibility that has been put forward (6) has both the Cl and $SnCl_3$ ligands *cis* to the linear Os_3 chain, analogous to the structure found for $Os_3(CO)_{12}(I)_2$ (7). Unfortunately, crystals of $M_3(CO)_{12}SnCl_4$ suitable for X-ray crystallographic study could not be obtained so as to distinguish these possibilities.

Here we report the ^{13}C nmr spectra of these complexes which are not consistent with any of the previously proposed structures but rather one with a linear Os_3 chain with the Cl ligand *cis* and the $SnCl_3$ group *trans* to this chain. (The ^{13}C nmr spectrum of $Os_3(CO)_{12}(I)_2$ is reported for comparison.) The preparation of $Ru_3(CO)_{12}(Cl)(SnCl_3)$ is also described in detail for the first time.

Experimental

The reaction and isolation of products were carried out under a nitrogen atmosphere with the use of Schlenk techniques; solvents were scrupulously dried before use. The starting materials $M_3(CO)_{12}$ (M = Ru, Os) were prepared by literature methods (8). The ^{13}CO-enriched compounds were obtained from ^{13}CO-enriched $M_3(CO)_{12}$ that were in turn prepared by heating $M_3(CO)_{12}$ in toluene under ~1.5 atm of ^{13}CO (99% ^{13}C) for 3 days; reaction temperatures were 100°C for M = Ru and 125°C for M = Os. It was estimated that this procedure produce a level of enrichment of 10–15% for $Ru_3(CO)_{12}$ and ~35% for $Os_3(CO)_{12}$. The iodo derivative, $Os_3(CO)_{12}(I)_2$, was prepared by a literature method (7) and recrystallized from CH_2Cl_2–hexane.

Infrared spectra were recorded on a Perkin-Elmer 983 spectrometer; the internal calibration of the instrument was periodically checked against the known absorptions frequencies of gaseous CO. Electron impact mass spectra were obtained on an Associated Electrical Industries MS-12 instrument. Nuclear magnetic resonance spectra were recorded at room temperature on a Bruker WM400 spectrometer; the solvent was CH_2Cl_2/CD_2Cl_2 (4/1). The microanalysis was performed by Pascher Mickroanalytisches Laboratorium, Bonn.

Preparation of $Ru_3(CO)_{12}(Cl)(SnCl_3)$

A suspension of $Ru_3(CO)_{12}$ (0.64 g, 1.0 mmol) in benzene (25 mL) was stirred with $SnCl_4$ (1 mL, 8.6 mmol) at room temperature. After 40 min (there was no appreciable evolution of gas during this time), a fine yellow solid had formed. The benzene was removed and the product washed twice with *n*-hexane (2 × 25 mL) and dried under vacuum. The yield was essentially quantitative. The analytical sample of $Ru_3(CO)_{12}(Cl)(SnCl_3)$ was obtained in the form of yellow platelets by recrystallization from CH_2Cl_2–hexane at −78°C: mp dec. > 80°C. *Anal.* calcd. for $C_{12}Cl_4O_{12}Ru_3Sn$: C 16.0, H 0.0, Cl 15.8, O 21.3, Ru 13.2; found: C 15.9, H 0.1, Cl 15.4, O 20.9, Ru 12.7. Infrared (CH_2Cl_2): ν_{CO} 2148 (m), 2119.5 (m), 2089 (sh), 2073.5 (s), 2057 (vs), 2039.5 (w), 2019 (m) cm^{-1}; ^{13}C nmr δ 201.4 (4C), 196.2 (4C), 195.0 (2C), 191.1 (1C), 178.0 (1C) ppm. The compound was insufficiently volatile below its decomposition temperature for an EI mass spectrum. The compound could be handled in air for short periods without apparent decomposition but decomposed on prolonged exposure. Solutions of $Ru_3(CO)_{12}(Cl)(SnCl_3)$ in CH_2Cl_2 were initially green but rapidly turned yellow on exposure to light. The green color was partially restored by storage in the dark.

The osmium analogue, $Os_3(CO)_{12}(Cl)(SnCl_3)$, was prepared in a similar manner: infrared (CH_2Cl_2): ν_{CO} 2152 (w), 2124.5 (m), 2087 (sh), 2069 (s), 2049.5 (vs), 2031.5 (m), 2005.5 (m) cm^{-1}; ^{13}C nmr δ 183.4 (4C) 176.9 (4C, J_{Sn-C} = 62.7 Hz), 176.6 (2C), 168.3 (1C), 160.8 (1C) ppm (see Fig. 1). MS (EI) m/z 1166 (M^+). A satisfactory elemental analysis was obtained in the original preparation (6). The compound was a white, air-stable solid.

[1]To whom correspondence should be addressed.

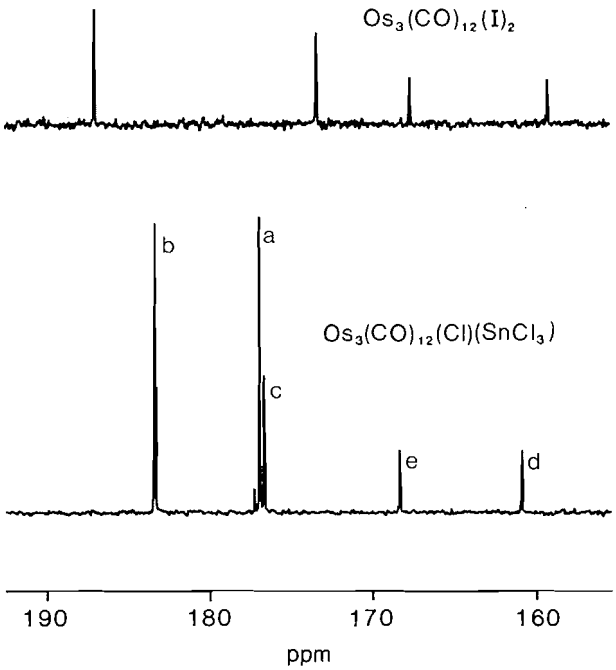


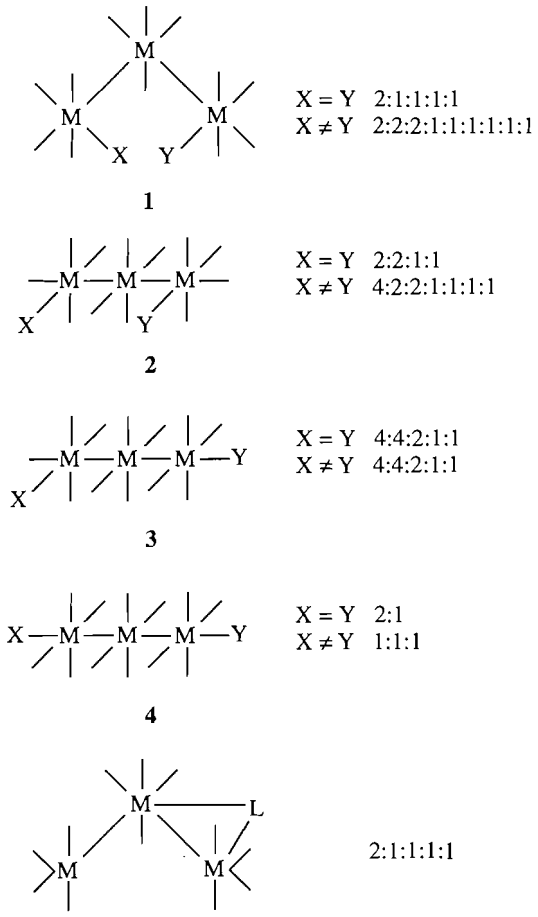
FIG. 1. ^{13}C nmr spectra of $Os_3(CO)_{12}(I)_2$ and $Os_3(CO)_{12}(Cl)(SnCl_3)$ (^{13}CO-enriched samples; CH_2Cl_2/CD_2Cl_2 solution).

Spectroscopic data for $Os_3(CO)_{12}(I)_2$: infrared (CH_2Cl_2): ν_{CO} 2144 (w), 2114 (s), 2085 (vw), 2058 (vs, br), 2029.5 (s), 2000 (w) cm^{-1}; ^{13}C nmr δ 186.9, 173.2, 167.4, 159.1 ppm (in an approximate ratio of 2:2:1:1; see Fig. 1).

Results and discussion

Addition of $SnCl_4$ to a suspension of $M_3(CO)_{12}$ (M = Ru, Os) in benzene at room temperature results in essentially quantitative formation of $M_3(CO)_{12}SnCl_4$ over 40 min. The ruthenium compound is a yellow solid that can be handled for short periods in air but prolonged exposure causes decomposition. The osmium analogue (which is white) is much more robust in air. Both complexes are insoluble in hexane but soluble in CH_2Cl_2. The infrared spectrum of each in CH_2Cl_2 shows seven terminal CO stretches. Evidence is presented below that these compounds should be formulated as (OC)—M(CO)$_3$(Cl)—M(CO)$_4$—M(CO)$_4$—($SnCl_3$) with C_s symmetry. Such an asymmetric structure should have 12 infrared-active CO stretches so that some of the modes must either be accidentally degenerate in CH_2Cl_2 solution or of zero intensity.

Several possible structures for a compound having the formula $M_3(CO)_{12}(X)(Y)$ are shown in Scheme 1 (eclipsed configurations are drawn for convenience). There are other isomers of this formulation but those shown in the scheme are thought to be the most reasonable from a survey of $M_3(CO)_{12}$ derivatives reported in the literature (5, 9). As can be seen from the scheme, the various structures can, for the most part, be distinguished by ^{13}C nmr spectroscopy provided the structures are rigid on the nmr time scale with the exception that there is free rotation about the M—M and M—Sn bonds. The intensities of ^{13}C nmr signals of metal carbonyl derivatives such as these are usually found to be proportional to the number of carbons of a particular type within the molecule. This is presumably due to the carbonyl carbons having similar T_1 values and there is, of course, no Overhauser effect on the signals.



SCHEME 1. Expected ^{13}C nmr spectra.

Structure **1** is found when X and Y are linked as for example in $Os_3(CO)_{12}$[MeOC(O)NNC(O)OMe] (10). This structure is thought unlikely for $M_3(CO)_{12}(Cl)(SnCl_3)$.

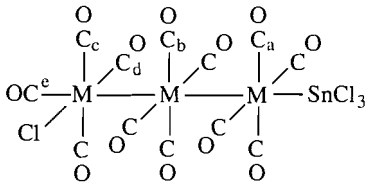
Structure **2** has been found by X-ray crystallography for $Os_3(CO)_{12}(I)_2$ (7). The previously unreported ^{13}C nmr spectrum of this compound is shown in Fig. 1; it shows the expected 2:2:1:1 pattern for structure **2** with X = Y = I. A similar spectrum has been found for $Os_3(CO)_{12}(H)_2$ (11). The dimethyl analogue of these complexes, $Os_3(CO)_{12}(Me)_2$, also has the same structure (12).

Compounds with structure **3** have not been previously observed but evidence is presented below that the $M_3(CO)_{12}$-(Cl)($SnCl_3$) derivatives have this structure. Structure **4**, although rare, has been shown by X-ray crystallography to be adopted by $Os_3(CO)_{12}(SiCl_3)_2$ (13). The ^{13}C nmr spectrum of this compound shows the expected two resonances in the ratio of 1:2 at δ 186.8 and 177.9 ppm (13). Note that the ^{13}C resonances of the Os(CO)$_4$($SiCl_3$) units can be assigned unambiguously and appear to higher field of those of the central Os(CO)$_4$ unit. The $^{13}C\{^1H\}$ nmr spectrum of $[Os_3(CO)_{12}(H)]^+$ shows five resonances of relative intensity 1:2:1:1:1 as expected for structure **5** (L = H) (14).

The room temperature ^{13}C nmr spectrum of $Os_3(CO)_{12}(Cl)$-($SnCl_3$) (^{13}CO-enriched sample, CH_2Cl_2/CD_2Cl_2 solution) is shown in Fig. 1. The spectrum of the ruthenium analogue was similar although the signal to noise ratio was not as good and the tin coupling was not observed. As can be seen, the spectrum

Can. J. Chem. Downloaded from www.nrcresearchpress.com by 194.225.253.170 on 09/07/12
For personal use only.

consists of five resonances in a 4:4:2:1:1 pattern (peak positions are δ 183.4, 176.9, 176.6, 168.3, and 160.8 ppm). Furthermore, the resonance of intensity 4 at δ 176.9 ppm exhibits coupling to $^{117,119}Sn$ of 62.7 Hz which indicates $Os_3(CO)_{12}(Cl)(SnCl_3)$ contains a *trans*-Os—$Os(CO)_4(SnCl_3)$ unit. The position of this resonance is also in the region found for the peak due to carbonyls of the analogous units of $Os_3(CO)_{12}(SiCl_3)_2$ (see above). The ^{13}C nmr data are therefore consistent with structure **3**, with X = Cl and Y = $SnCl_3$, for the $M_3(CO)_{12}(Cl)(SnCl_3)$ complexes, as shown. The assignment (as shown) of the signals in the ^{13}C nmr spectrum of $Os_3(CO)_{12}(Cl)(SnCl_3)$ is straightforward if it is assumed that the resonance furthest upfield is due to the carbonyl *trans* to the chlorine ligand. The positions of the resonances of the $Os_3(CO)_{12}(X)(Y)$ derivatives may be compared with those of the parent carbonyl $Os_3(CO)_{12}$ at 170.4 (equatorial carbonyls) and 182.3 ppm (axial carbonyls) (15).



M = Ru, Os

3

Of the five isomers shown in the scheme, structure **3** would appear to be the least likely to be formed from the reaction under mild conditions of a triangular $M_3(CO)_{12}$ cluster with an X—Y reagent. However, there always appears to be rapid isomerization about the central osmium atom in the formation of $Os_3(CO)_{12}(X)(Y)$ derivatives when the X and Y groups are not connected. This presumably relieves the steric interactions between the substituents on the terminal osmium atoms in the product. Furthermore, derivatives of the type $M(CO)_4(X)_2$ (M = Fe, Ru, Os) tend to be stable as the *cis* isomer for X = H, Cl, Br, I (9, 16) but when X = ER_3 (E = Si, Ge, Sn; R = Cl or organic group) the *trans* isomer can be the most stable (1, 4, 17).[2] This is especially the case for M = Ru, Os with ECl_3 ligands. We have rationalized this observation in terms of the steric and electronic properties of the ECl_3 ligands: the ECl_3 ligands have π-acceptor properties comparable to CO so that neither the *cis* nor the *trans* site is preferred on electronic grounds and hence the ECl_3 ligands adopt *trans* positions so as to minimize steric interactions (4, 13). (For the poor π-acceptor ligands, hydride or halogen, the *cis* site is electronically preferred since it avoids, as far as possible, carbonyl ligands competing for the same electron density on the metal atom.) It is, therefore, not unexpected that the $M_3(CO)_{12}(Cl)(SnCl_3)$ complexes are stable with the Cl *cis* but with $SnCl_3$ ligand *trans* to the Os_3 chain.

A further question arises as to whether the $M_3(CO)_{12}(Cl)(SnCl_3)$ complexes initially form as isomer **2** followed by rapid isomerization to give the observed isomer **3**. Although this might have been expected, evidence will be presented in a subsequent paper that the reaction, in CH_2Cl_2, of $Os_3(CO)_{12}$ and Cl_2, surprisingly, gives $Os_3(CO)_{12}(Cl)_2$ mainly as isomer **3** as the initial product and that this isomer subsequently rearranges to isomer **2**. This suggests the formation of $M_3(CO)_{12}(Cl)(SnCl_3)$ does not proceed via isomer **2**. We have no evidence for or against the initial formation of adduct **5** (L = $SnCl_4$) in the synthesis of the $M_3(CO)_{12}(Cl)(SnCl_3)$ compounds.

[2]The structure of $[Ru(CO)_4(SnMe_3)]_2$ also shows an all *trans* arrangement of metal atoms (18).

Acknowledgement

We thank the Natural Sciences and Engineering Research Council of Canada for financial support.

1. R. K. Pomeroy, M. Elder, D. Hall, and W. A. G. Graham. J. Chem. Soc. Chem. Commun. 381 (1969).
2. J. R. Moss and W. A. G. Graham. J. Organomet. Chem. **18**, P24 (1969).
3. S. P. Gubin, O. M. Chentsova, G. V. Burmakina, and A. A. Ioganson. Izv. Akad. Nauk. SSSR, Ser. Khim. **12**, 2790 (1981); Chem. Abstr. **97**, 119463w (1982).
4. R. K. Pomeroy. Ph.D. Thesis. University of Alberta, Edmonton, Alta., 1972.
5. E. A. Seddon and K. R. Seddon. The chemistry of ruthenium. Elsevier, Amsterdam. 1984. p. 986.
6. J. R. Moss and W. A. G. Graham. J. Chem. Soc. Dalton Trans. 89 (1977).
7. N. Cook, L. Smart, and P. Woodward. J. Chem. Soc. Dalton Trans. 1744 (1977).
8. M. I. Bruce, J. G. Matisons, R. C. Wallis, J. M. Patrick, B. W. Skelton, and A. H. White. J. Chem. Soc. Dalton Trans. 2365 (1983); B. F. G. Johnson, J. Lewis, and P. A. Kilty. J. Chem. Soc. (A) 2859 (1968).
9. S. C. Tripathi, S. C. Srivastava, R. P. Mani, and A. K. Schrimal. Inorg. Chim. Acta, **15**, 249 (1975); M. I. Bruce. *In* Comprehensive organometallic chemistry. Vol. 4. *Edited by* G. Wilkinson, F. G. A. Stone, and E. W. Abel. Pergamon, New York. 1982. p. 843; R. D. Adams and J. P. Selegue. *In* Comprehensive organometallic chemistry. Vol. 4. *Edited by* G. Wilkinson, F. G. A. Stone, and E. W. Abel. Pergamon, New York. 1982. p. 967; A. J. Deeming. Adv. Organomet. Chem. **26**, 1 (1986).
10. F. W. B. Einstein, S. Nussbaum, D. Sutton, and A. C. Willis. Organometallics, **3**, 568 (1984).
11. M. Gochin and J. R. Moss. J. Organomet. Chem. **192**, 409 (1980).
12. J. W. Kelland and J. R. Norton. J. Organomet. Chem. **149**, 185 (1978).
13. A. C. Willis, G. N. Van Buuren, R. K. Pomeroy, and F. W. B. Einstein. Inorg. Chem. **22**, 1162 (1983).
14. A. A. Koridze, O. A. Kizas, N. M. Astakhova, P. V. Petrovskii, and Y. K. Grishin. J. Chem. Soc. Chem. Commun. 853 (1981).
15. A. Forster, B. F. G. Johnson, J. Lewis, T. W. Matheson, B. H. Robinson, and W. G. Jackson. J. Chem. Soc. Chem. Commun. 1042 (1974).
16. D. F. Shriver and K. H. Whitmire. *In* Comprehensive organometallic chemistry. Vol. 4. *Edited by* G. Wilkinson, F. G. A. Stone, and E. W. Abel. Pergamon, New York. 1982. p. 243; M. I. Bruce. *In* Comprehensive organometallic chemistry. Vol. 4. *Edited by* G. Wilkinson, F. G. A. Stone, and E. W. Abel. Pergamon, New York. 1982. p. 661; L. Vancea and W. A. G. Graham. J. Organomet. Chem. **134**, 219 (1977); J. R. Moss, M. L. Niven, and E. E. Sutton. Inorg. Chim. Acta, **147**, 251 (1988).
17. G. N. Van Buuren, A. C. Willis, F. W. B. Einstein, L. K. Peterson, R. K. Pomeroy, and D. Sutton. Inorg. Chem. **20**, 4361 (1981); R. K. Pomeroy and K. S. Wijesekera. Inorg. Chem. **19**, 3729 (1980); A. Bonny. Coord. Chem. Rev. **25**, 229 (1978) and references therein.
18. J. A. K. Howard, S. C. Kellet, and P. Woodward. J. Chem. Soc. Dalton Trans. 2332 (1975).

Can. J. Chem. Downloaded from www.nrcresearchpress.com by 194.225.253.170 on 09/07/12
For personal use only.

Antiferromagnetic exchange in manganese(II) monophenylphosphinate and the effects of cadmium doping

JING-LONG DU AND ROBERT C. THOMPSON

Department of Chemistry, University of British Columbia, 2036 Main Mall, Vancouver, B.C., Canada V6T 1Y6

Received December 2, 1988

JING-LONG DU and ROBERT C. THOMPSON. Can. J. Chem. **67**, 1239 (1989).

$Mn[H(C_6H_5)PO_2]_2$, its cadmium analogue, and mixed metal materials of composition $Mn_{1-x}Cd_x[H(C_6H_5)PO_2]_2$ (x = 0.005, 0.01, 0.09, 0.27, and 0.47) have been synthesized and characterized by X-ray powder diffraction, infrared spectroscopy, differential scanning calorimetry and low-temperature (4.2 to 80 K) magnetic susceptibility studies. The materials are shown to be isomorphous and are considered to have polymeric structures in which chains of metal atoms are linked by bridging phosphinate groups. The pure manganese compound is antiferromagnetic (maximum in χ_M at ~35 K) and the magnetic data for the compound have been analyzed according to two theoretical models for linear chains of antiferromagnetically coupled manganese(II) (d^5, spin-free) ions. The Wagner and Friedberg model gives $J = -3.00\ cm^{-1}$ and the Weng model gives $J = -2.78\ cm^{-1}$. The effects of replacing Mn^{2+} by Cd^{2+} ions in the polymer is to increase the magnetic susceptibility (per mol of Mn) at all temperatures. Analysis of the data as a function of Cd doping indicates the incorporation of a paramagnetic component to the susceptibility which increases with increasing Cd content. In addition, the absolute value of the exchange coupling constant appears to decrease as the Cd content increases. These effects are considered in terms of a random defect model in which the replacement of Mn ions in the polymer by Cd ions results in the formation of Cd ion separated finite magnetic chain fragments.

Key words: manganese(II) monophenylphosphinate, magnetic properties, coordination polymer, cadmium doped antiferromagnet.

JING-LONG DU et ROBERT C. THOMPSON. Can. J. Chem. **67**, 1239 (1989).

On a synthétisé le $Mn[H(C_6H_5)PO_2]_2$, son analogue du cadmium, ainsi que des matériaux métalliques mixtes de composition $Mn_{1-x}Cd_x[H(C_6H_5)PO_2]_2$ (x = 0,005, 0,01, 0,09, 0,27 et 0,47) et on les a caractérisés par diffraction des rayons-X sur des poudres, par spectroscopie infrarouge, par calorimétrie à balayage différentiel et par des études de susceptibilités magnétiques à basses températures (4,2 à 80 K). On a démontré que les matériaux sont isomorphes et on considère qu'ils possèdent des structures polymériques dans lesquelles des chaînes d'atomes métalliques sont reliées par des groupements phosphinates agissant comme ponts. Le composé ne contenant que du manganèse est antiferromagnétique (la valeur maximale de χ_M apparaît à ~35 K) et on a analysé les données magnétiques suivant deux modèles théoriques pour des chaînes linéaires d'ions de manganèse(II) couplés d'une façon antiferromagnétique (d^5, sans spin). Le modèle de Wagner et Friedberg donne une valeur de $J = -3{,}00\ cm^{-1}$ alors que le modèle de Weng donne une valeur de $J = -2{,}78\ cm^{-1}$. A toutes les températures, le remplacement dans le polymère d'ions Mn^{2+} par des ions Cd^{2+} provoque une augmentation de la susceptibilité magnétique (par mole de Mn). L'analyse des données en fonction d'un dopage par le Cd indique que la susceptibilité est modifiée par l'incorporation d'une composante paramagnétique et qu'elle augmente avec une augmentation de la concentration du Cd. De plus, la valeur absolue de la constante de couplage de l'échange semble diminuer avec une augmentation de la concentration du Cd. On considère ces effets en fonction d'un modèle de défaut au hasard dans lequel le remplacement dans le polymère d'ions Mn par des ions Cd conduit à la formation de fragments de chaînes magnétiques définies séparées par des ions Cd.

Mots clés : monophénylphosphinate de manganèse(II), propriétés magnétiques, polymères de coordination, cadmium antiferromagnétique dopé.

[Traduit par la revue]

Introduction

The tendency of phosphinate anions, $R_2PO_2^-$, to coordinate to metal ions in a bridging rather than chelating mode is now well established by a number of X-ray crystallographic studies which have shown metal phosphinate compounds to be polymeric with infinite chains of metal ions linked by phosphinate bridges (1). In addition, it has been shown in several instances that bridging phosphinates are capable of transmitting magnetic exchange effects between paramagnetic centres via a super-exchange mechanism; examples of both ferromagnetic and antiferromagnetic coupling have been observed (2). It has been pointed out that in the formation of extended polymers of this type the incorporation of random defects in the polymer would effectively break it into finite segments and this may have a significant effect on the magnetic properties (3). To investigate this factor as it applies to poly-metalphosphinates we have examined the magnetic properties of manganese(II) monophenylphosphinate and samples of the compound doped with varying amounts of cadmium. The partial replacement of manganese by diamagnetic cadmium ions in the polymer would have the effect of chemically fragmenting the magnetic chain and should permit a quantitative examination of the effect of chain fragmentation on magnetic properties.

We chose to examine a manganese(II) system because the $^6A_1$ ground state renders the measurement and interpretation of the magnetic properties relatively straightforward. An examination of the magnetic properties of a number of different manganese(II) phosphinates revealed that the monophenylphosphinate derivative is appropriate for such studies for two reasons: (*i*) the pure compound is relatively strongly antiferromagnetic, exhibiting a broad maximum in χ_M at ~35 K and (*ii*) the cadmium(II) analogue is isomorphous; hence it is possible to readily prepare materials of composition $Mn_{1-x}Cd_x[H(C_6H_5)PO_2]_2$, where x varies from 0 to 1, for study.

Experimental

Synthesis: manganese(II) monophenylphosphinate, $Mn[H(C_6H_5)PO_2]_2$

Monophenylphosphinic acid (1.99 g, 14.0 mmol) was dissolved in 200 mL ethanol. A manganese(II) acetate tetrahydrate solution was prepared by dissolving 1.47 g (6.01 mmol) of salt in 150 mL ethanol. The salt solution was added dropwise to the stirring acid solution. The reaction mixture became cloudy after about one sixth of the salt solution had been added. The reaction mixture was totally opaque and

Can. J. Chem. Downloaded from www.nrcresearchpress.com by 194.225.253.170 on 09/07/12
For personal use only.

Can. J. Chem. Downloaded from www.nrcresearchpress.com by 194.225.253.170 on 09/07/12
For personal use only.

pink in color once the addition was completed. The solution was left stirring for a further 24 h, then allowed to stand for another 5 days. The precipitate was collected on a sintered glass filter, washed with ethanol, and set aside to air-dry between pieces of filter paper. The dry product is a pink, fine-grained powder. *Anal.* calcd. for $MnC_{12}H_{12}P_2O_4$: C 42.76, H 3.59; found: C 42.90, H 3.70.

Cadmium(II) monophenylphosphinate, $Cd[H(C_6H_5)PO_2]_2$

Monophenylphosphinic acid (1.42 g, 10.0 mmol) was dissolved in 55 mL ethanol. Cadmium(II) acetate dihydrate (1.33 g, 5.00 mmol) was dissolved in 150 mL ethanol, then added dropwise to the acid solution. A white product began to precipitate after about 10 mL of cadmium acetate solution had been added. The precipitate was collected, left to air-dry overnight, then dried in vacuum at 85°C for 12 h. *Anal.* calcd. for $CdC_{12}H_{12}P_2O_4$: C 36.53, H 3.07; found: C 36.64, H 3.10.

Manganese(II) (cadmium(II)) monophenylphosphinate, $Mn_{1-x}Cd_x[H(C_6H_5)PO_2]_2$

The mixed metal materials were made by adding separately, and simultaneously, solutions of the metal acetates in appropriate relative proportions to a stirring solution of monophenylphosphinic acid. The conditions of precipitation were kept as near as possible to those used for the preparation of the pure manganese compound.

Consider the preparation of $Mn_{0.53}Cd_{0.47}[H(C_6H_5)PO_2]_2$: monophenylphosphinic acid 1.99 g (14.0 mmol) was dissolved in 200 mL ethanol. A manganese(II) acetate tetrahydrate solution was prepared by dissolving 0.734 g (3.00 mmol) of the salt in 75 mL ethanol. Similarly, a cadmium(II) acetate dihydrate solution was prepared by dissolving 0.800 g (3.00 mmol) of the salt in 75 mL ethanol. The two salts were added to the stirring acid solution from separate funnels. The rest of the procedures for this and other mixed metal systems of the type $Mn_{1-x}Cd_x[H(C_6H_5)PO_2]_2$, where $x = 0.27, 0.09, 0.01, 0.005$, were identical to those used for the preparation of $Mn[H(C_6H_5)PO_2]_2$. *Anal.* calcd. for $Mn_{0.995}Cd_{0.005}C_{12}H_{12}P_2O_4$: C 42.72, H 3.58; found: C 42.62, H 3.71. *Anal.* calcd. for $Mn_{0.99}Cd_{0.01}C_{12}H_{12}P_2O_4$: C 42.68, H 3.58; found: C 42.78, H 3.77. *Anal.* calcd. for $Mn_{0.91}Cd_{0.09}C_{12}H_{12}P_2O_4$: Mn 14.6, Cd 2.96, C 42.11, H 3.53; found: Mn 13.7, Cd 2.89, C 41.96, H 3.55. *Anal.* calcd. for $Mn_{0.73}Cd_{0.27}C_{12}H_{12}P_2O_4$: Mn 11.4, Cd 8.61, C 40.87, H 3.43; found: Mn 10.9, Cd 8.62, C 40.96, H 3.53. *Anal.* calcd. for $Mn_{0.53}Cd_{0.47}C_{12}H_{12}P_2O_4$: Mn 8.00, Cd 14.5, C 39.58, H 3.32; found: Mn 7.57, Cd 14.1, C 39.63, H 3.36.

Elemental analyses

Manganese and cadmium were determined using, respectively, Varian AA5 and Perkin Elmer 305 Atomic Absorption Spectrophotometers. The sample solution was prepared by dissolving a known amount (20 to 70 mg) of the metal phosphinate in 15 mL of 37% HCl. This solution was then heated gently until all the solids were dissolved, and was diluted with distilled water to about 3 ppm in concentration. Mn and Cd standard solution (1–5 ppm) were made using spectrum grade manganese or cadmium nitrates. C and H microanalyses were performed by P. Borda of this Department.

The measured Mn to Cd ratio as determined by atomic absorption spectroscopy was used to determine x in the $Mn_{1-x}Cd_x[H(C_6H_5)PO_2]_2$ materials where $x = 0.47$, 0.27, and 0.09. From the relative proportions of Mn and Cd in the solutions from which the polymers were precipitated values of 0.50, 0.25, and 0.09 would have been predicted. For the samples of lower x where the Cd proportion was too low for meaningful determination by AA spectroscopy we used the value predicted from the relative proportions of the metal ions in solution.

Infrared spectroscopy

Infrared spectra were recorded on a Perkin Elmer 598 spectrophotometer. Samples were mulled in Nujol and pressed between KRS-5 plates (Harshaw Chemical Co.). Calibration was achieved using polystyrene and frequencies are reproducible to $\pm 3\ cm^{-1}$. Bands observed in the range 2500 to 250 cm^{-1} are given. $Mn[H(C_6H_5)PO_2]_2$: 2346 sh, 2336 m, 1598 w, 1442 m, 1147 s, 1127 sh, 1121 s, 1076 w, 1034 s, 1018 s, 995 s, 933 w, 923 w, 763 m, 758 w, 751 m, 710 m, 694 m, 668 w, 560 s, 504 wsh, 490 m, 421 w, 366 w. $Cd[H(C_6H_5)PO_2]_2$: 2342 sh, 2331 m, 1593 w, 1438 m, 1147 s, 1129 s, 1120 s, 1072 w, 1033 s, 1015 s, 990 s, 931 w, 921 w, 757 m, 751 m, 709 m, 692 m, 670 w, 556 s, 503 wsh, 486 m, 416 w, 360 w. $Mn_{1-x}Cd_x[H(C_6H_5)PO_2]_2$: as above for $Mn[H(C_6H_5)PO_2]_2$ to within $\pm 3\ cm^{-1}$ (w = weak, m = medium, s = strong, sh = shoulder).

Differential scanning calorimetry (DSC)

DSC studies were made using a Mettler DSC 20 cell interfaced with a Mettler TC 10 TA processor. In a typical experiment, a finely powdered sample of approximately 3 to 12 mg was accurately weighed into an aluminium crucible (with a small pinhole on the lid allowing atmospheric access) and the sample was heated from ca. 35 to 350°C at a rate of 4 degrees per minute. The temperature calibration of the platinum sensor was achieved using the known fusion temperature of indium. The heat flow was calibrated using an exactly known quantity of indium. The peak temperature and enthalpy of a particular thermal event were obtained respectively from the maximum in the DSC curve and the integrated area beneath the curve.

$Mn[H(C_6H_5)PO_2]_2$ is stable up to about 200°C at which temperature exothermic decomposition begins (peak temperature = 220°C, $\Delta H = 160\ kJ\ mol^{-1}$). $Cd[H(C_6H_5)PO_2]_2$ shows onset of exothermic decomposition at about 270°C (peak temperature = 290°C, $\Delta H = 240\ kJ\ mol^{-1}$).

$Mn_{1-x}Cd_x[H(C_6H_5)PO_2]_2$ materials, all except one, showed a single exothermic decomposition peak at 220 ± 4°C. The peak was shifted to ~237°C in the compound with $x = 0.47$.

X-ray powder diffractometry

Powder diffraction patterns were obtained on a Philips X-Ray Diffraction (XRD) unit using Cu Kα as the radiation source. The measurements were done with a diffractometer 2θ setting of 2° per minute and chart speed of 2 centimeters per minute. Samples were prepared by dispersing the specimen by grinding under alcohol in an agate mortar. The sample slurry was mounted on a glass side and allowed to dry. The diffraction patterns were calibrated by using Si as an internal standard. $Mn[H(C_6H_5)PO_2]_2$ d(Å) with relative intensities in parentheses: 10.63 (100), 7.97 (3), 6.24 (6), 6.05 (7), 5.34 (6), 5.18 (6), 4.62 (25), 4.46 (2), 3.98 (20), 3.45 (2), 3.27 (5). $Cd[H(C_6H_5)PO_2]_2$: 15.56 (7), 10.78 (100), 7.81 (2), 6.29 (10), 6.12 (8), 5.39 (10), 5.25 (6), 4.67 (15), 4.59 (4), 4.01 (5), 3.48 (4), 3.33 (6). $Mn_{1-x}Cd_x[H(C_6H_5)PO_2]_2$: patterns as for the pure manganese compound except additional weak peaks are observed at 14.73 (7) and 15.28 (2) for $x = 0.99$ and 0.91, respectively, the weak 7.97 peak is not observed for $x = 0.53$ and the weak 4.46 peak is not observed for $x = 0.995$, 0.99, 0.91.

Solubilities

Qualitative solubility tests show $Mn[H(C_6H_5)PO_2]_2$ to be soluble in water (>0.1 g in 100 mL) but only slightly soluble to insoluble in methanol, ethanol, acetone, benzene, petroleum ether, carbontetrachloride, dichloromethane, and chloroform. $Cd[H(C_6H_5)PO_2]_2$ is soluble in water and methanol but only slightly soluble to insoluble in the other solvents tested.

Magnetic susceptibility measurements

Magnetic susceptibilities over the range 4.2 to 82 K were made using a Princeton Applied Research Model 155 Vibrating Sample Magnetometer with an applied field of 7501 G. The equipment and calibration procedures were described previously (4). Molar magnetic susceptibilities were corrected for diamagnetism of the metal ions and ligands; the corrections were (in $10^{-6}\ cm^3\ mol^{-1}$): manganese, −14; cadmium, −22; $H(C_6H_5)PO_2^-$, −78. Magnetic susceptibility data from 4.2 to 82 K are given in Table 1.[1]

[1]Table 1 may be purchased from the Depository of Unpublished Data, CISTI, National Research Council of Canada, Ottawa, Ont., Canada K1A 0S2.

Can. J. Chem. Downloaded from www.nrcresearchpress.com by 194.225.253.170 on 09/07/12
For personal use only.

Results and discussion

$Mn[H(C_6H_5)PO_2]_2$ was prepared by the dropwise addition of a dilute ethanol solution of manganese(II) acetate tetrahydrate to a dilute ethanol solution of monophenylphosphinic acid. This material is antiferromagnetic, exhibiting a broad maximum in magnetic susceptibility at ~35 K. We have found that it is important to control the conditions under which the precipitation occurs. Using solutions approximately twice as concentrated as those described in the Experimental section resulted in more rapid precipitation and the isolation of products containing a significant amount of paramagnetic, structural, impurity. We will return to this point later.

Since crystals of $Mn[H(C_6H_5)PO_2]_2$ suitable for single crystal X-ray diffraction studies could not be obtained, we have had to rely on other studies for structural information. Evidence that the compound is polymeric comes from its lack of significant solubility in a range of solvents, the observation that it decomposes without melting and the fact that it is magnetically concentrated (discussed later). Information on the nature of phosphinate coordination may be obtained from infrared studies particularly in the PO_2 stretching region (5). For this purpose we compared the spectrum of $Mn[H(C_6H_5)PO_2]_2$ with that of $Mn(HCONH_2)_2[H(C_6H_5)PO_2]_2$, a compound shown by single crystal X-ray diffraction studies (6) to have the double phosphinate-bridged chain structure with terminal *trans*-bound formamide ligands completing a distorted octahedral coordination about manganese. In the latter compound a strong broad band at 1133 cm^{-1} and a medium intensity band at 1050 cm^{-1} may be assigned to the PO_2 antisymmetric and symmetric stretching vibrations, respectively. In comparison, $Mn[H(C_6H_5)PO_2]_2$ shows a broad split, band centered around 1130 cm^{-1} and a band at 1018 cm^{-1} assigned to these vibrations.

The absence of the terminal ligands in $Mn[H(C_6H_5)PO_2]_2$ would be expected to have some effect on the phosphinate frequencies but the rather large shift to lower frequencies in the symmetric mode and the splitting of the antisymmetric mode suggests that the phosphinate bridging is more unsymmetrical in this compound than it is in the bis(formamide) derivative. It seems likely that the double phosphinate bridged structure is maintained in $Mn[H(C_6H_5)PO_2]_2$ but that interchain interactions involving coordination of oxygens in one phosphinate chain to manganese atoms in another occur, thus completing a distorted octahedral environment around manganese. Such a structure was proposed earlier for $Mn[(CH_3)_2PO_2]_2$ (7). Further evidence in support of a chain structure comes from the analysis of the magnetic data to be discussed below.

$Cd[H(C_6H_5)PO_2]_2$ was prepared by a procedure analogous to that used to obtain the manganese compound. The X-ray powder diffraction patterns indicate that the manganese and cadmium compounds are isomorphous, a conclusion supported by the infrared spectra which are virtually identical. As would be expected, the materials also have similar thermal and solubility properties. The X-ray powder diffraction patterns and infrared spectra of all of the mixed metal samples were examined and found to be virtually indistinguishable from those of the pure manganese compound. No evidence for acetate, water, or other impurities were found. Proof that these are single phase materials and not physical mixtures of the manganese and cadmium compounds comes from magnetic susceptibility studies.

Plots of magnetic susceptibility (per mol of Mn) and the effective magnetic moment of manganese versus temperature

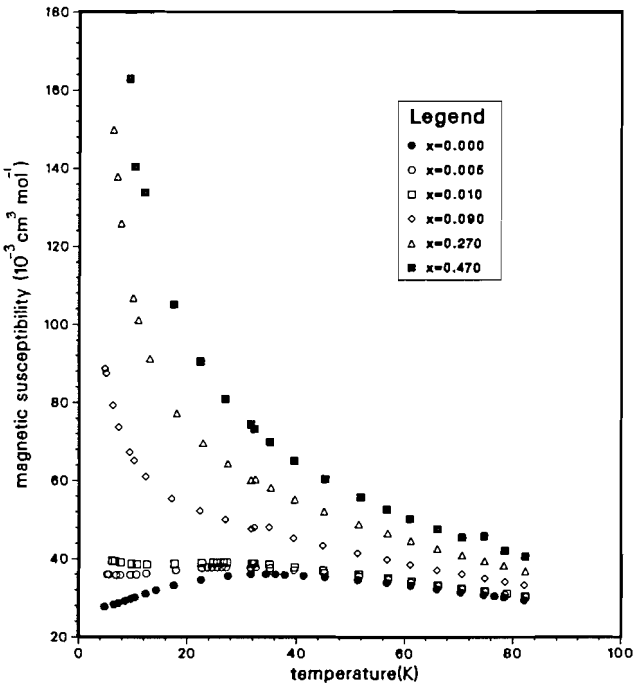


FIG. 1. Magnetic susceptibility versus temperature data for $Mn_{1-x}Cd_x[H(C_6H_5)PO_2]_2$.

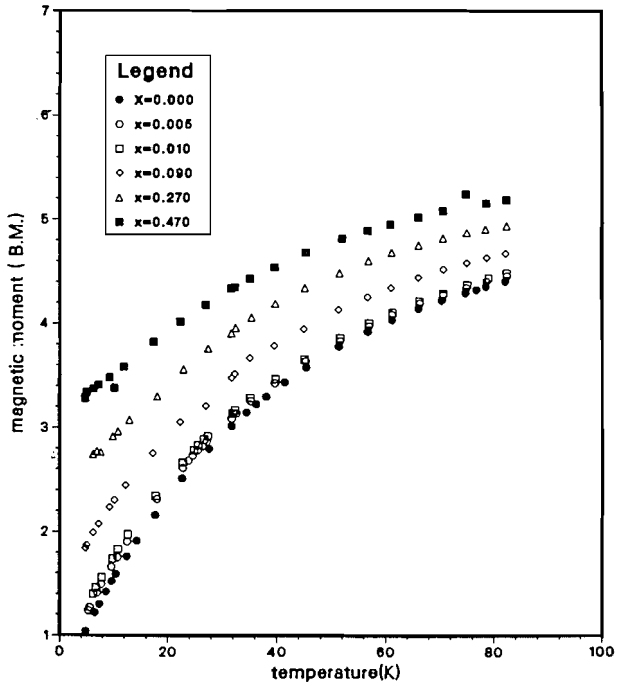


FIG. 2. Magnetic moment versus temperature data for $Mn_{1-x}Cd_x[H(C_6H_5)PO_2]_2$.

(4.2 to 82 K) are given in Figs. 1 and 2. At all temperatures both the susceptibility and the moment increase as the fraction of manganese decreases in the sample. In a physical mixture, of course, neither would be expected to change. As the proportion of manganese decreases the maximum in susceptibility appears to shift to lower temperatures and the susceptibility increase is greatest at the lowest temperatures.

The magnetic susceptibilities of pure $Mn[H(C_6H_5)PO_2]_2$

TABLE 2. Magnetic parameters for $Mn_{1-x}Cd_x[H(C_6H_5)PO_2]_2$

	Weng model[a]			Wagner–Friedberg model[a]		
x	$-J(cm^{-1})$	$100p^b$	F^c	$-J(cm^{-1})$	$100p^b$	F^c
0	2.78	0.00[d]	0.0233	3.00	0.00[d]	0.0349
0.005	2.65	0.84	0.0259	2.80	0.56	0.0099
0.01	2.64	1.50	0.0252	2.77	1.10	0.0107
0.09	2.37	6.73	0.0291	2.48	6.38	0.0190
0.27	2.19	16.9	0.0066	2.26	16.3	0.0072
0.47	1.94	27.5	0.0221	2.00	27.1	0.0231

[a]See text.
[b]$100p$ = % paramagnetic component.
[c]F = function minimized in obtaining the best fit; ref. 7.
[d]$100p$ set at zero. The measured susceptibilities at the lowest temperatures are lower than predicted by the model and including p as a variable parameter here generates an unrealistic negative value.

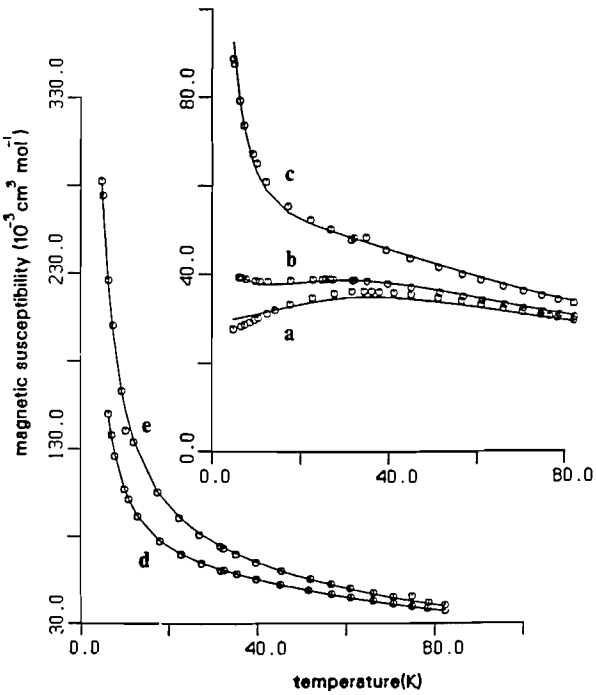


FIG. 3. Magnetic susceptibility versus temperature plots for $Mn_{1-x}Cd_x[H(C_6H_5)PO_2]_2$ (x = 0.00, 0.01, 0.09, 0.27, and 0.47 for a, b, c, d, e, and f, respectively). Solid lines are the best fit to the Wagner–Friedberg model.

were analyzed according to three models, all of which use the isotropic Heisenberg Hamiltonian. It was not possible to obtain a reasonable fit of the data to the Lines two-dimensional model (8); whereas satisfactory fits were possible employing either of the one-dimensional models tested. These were the scaling model of Wagner and Friedberg (9) and the interpolation scheme developed by Weng (10, 11). The fits using these two models were very similar (Table 2) although the Weng model does not reproduce the temperature of the susceptibility maximum as well as was found previously for $Mn[(CH_3)_2PO_2]_2$, a compound which exhibits very similar magnetic properties to the monophenylphosphinate (7). The magnetic analysis, then, is consistent with linear chains of antiferromagnetically coupled manganese ions.

Initial trials indicated the susceptibilities of the mixed metal systems could be fitted to the linear chain models provided allowance was made for a paramagnetic component p. Hence calculated susceptibilities were obtained from

$$\chi_{calc} = (1 - p)\chi_{chain} + p\chi_{para}$$

where χ_{chain} is the susceptibility calculated according to either chain model, χ_{para} is the susceptibility for magnetically dilute manganese(II) and p is the fraction of manganese making up the paramagnetic component. Fits were made to the susceptibility data with g fixed at 2.00 and J, the exchange coupling constant and p as fitting parameters. Best fit values of J and p are given in Table 2. The observed susceptibilities are compared with calculated for the Wagner–Friedberg model for some of the materials in Fig. 3.

It is clear from the data analysis that the change in magnetic properties with Cd doping is accounted for primarily by the incorporation of a paramagnetic component which increases with increasing Cd content. Such an effect can be rationalized if we consider the "random defect" model of de Jongh (3). According to this model any chain system will suffer from a certain concentration of defects which, in turn, will break the magnetic chain into finite segments. Half of these finite segments will contain an odd number of magnetic atoms and, coupled antiferromagnetically, these odd numbered segments will have a net spin at low temperatures. This net spin will be very weakly coupled along the chain, since the effective magnetic interaction will have to traverse the defects, and will therefore be much smaller than the nearest neighbour intrachain interaction. In our case, Cd plays the role of a defect, breaking up the long chains of contiguous Mn atoms into smaller isolated fragments. For example, consider the case where $x = 0.09$. For a random distribution of Cd atoms we would expect the average chain of contiguous Mn atoms to be about 9 atoms long but that there would be a distribution of chain lengths about this average. Half of the chains will be odd numbered producing a net spin at low temperatures as described by the random defect model. The magnetic analysis indicates that this leads to 6 to 7% paramagnetic component in this particular sample. According to this model, as the cadmium doping increases the average chain length would decrease and therefore the paramagnetic component should increase as is in fact, observed (Table 2).

The magnetic analysis also shows a decrease in the absolute value of the exchange coupling constant as doping is increased (Table 2). That this variation is, in fact, significant was verified by a careful examination of the sensitivity of the fits to changes in the parameter J. For example, employing the Wagner–

Can. J. Chem. Downloaded from www.nrcresearchpress.com by 194.225.253.170 on 09/07/12
For personal use only.

Friedberg model, setting $|J|$ at 5% above or below its best fit value and allowing p to vary produced significantly poorer fits both visually and in terms of the fitting function F (function minimized in obtaining the best fit; ref. 7). This function is increased to a valve in the range 1.5 to 3 times the best fit value for all samples except that with $x = 0.47$. In this case the large paramagnetic component renders the fit less sensitive to variations in J although even here F is increased by 10% of its best fit value. The changes in the best fit values of J from sample to sample as x increases are of the order of 6 to 11% (except for the small change going from $x = 0.005$ to 0.01) and the overall change from $x = 0$ to 0.47 is about 30% (Table 2). Even assuming an uncertainty of ±5% in J, the variation must be considered significant. The fact that $|J|$ decreases with increasing Cd doping and hence, presumably with decreasing average chain length suggests that the exchange is not limited to nearest neighbour interactions in the chain but that longer range intrachain as well as interchain effects may be important. Alternatively, the effect may result from weaker coupling between manganese neighbours when one of the metals is adjacent to a cadmium ion or may simply reflect the limitations of an analysis which involves fitting a system of random-length chains to infinite-chain models.

Samples of $Mn[H(C_6H_5)PO_2]_2$ and Cd-doped materials prepared under conditions of rapid precipitation (solution concentrations about twice as large as those described in the experimental section) invariably gave higher susceptibilities (per mole Mn) than those reported here. Analyses of the data showed higher values for p and lower values for $|J|$ than corresponding samples prepared under conditions of slow crystallization. It appears that rapid precipitation results in the incorporation of natural structural defects which have the same effect on the magnetic properties as does the incorporation of diamagnetic Cd atoms into the polymer. Mixed metal materials prepared from concentrated solutions then have both natural and chemical (Cd atom) structural defects contributing to the fragmentation of the magnetic chain.

Conclusions

$Mn[H(C_6H_5)PO_2]_2$ is antiferromagnetic and the susceptibility versus temperature behaviour may be reasonably modeled according to an infinite chain of coupled manganese ions. Incorporation of diamagnetic Cd ions into the polymer fragments the magnetic chains resulting in the formation of a significant paramagnetic component arising from the net spins associated with odd numbered fragments. Natural defects can also fragment the chains and lead to a paramagnetic component. Since no paramagnetic component is detected for samples of the pure manganese compound (prepared from dilute solutions) one can conclude that chain fragmentation in this sample is minimal and that one is dealing here with magnetic chains which on average contain 100 or more contiguous manganese ions. This estimate is based on the observation that we were able to detect levels of paramagnetic component as low as about 0.5% in the mixed metal systems and average chain lengths of less than 100 in the pure manganese compound should generate paramagnetic component levels greater than this.

As x varies from 0 to 0.47 in the $Mn_{1-x}Cd_x[H(C_6H_5)PO_2]_2$ samples the average number of contiguous Mn atoms is considered to go from greater than 100 to presumably two or three atoms at most in a chain. This is accompanied by an apparent decrease of about 30% in the absolute value of the exchange coupling constant J. This result suggests that factors other than nearest neighbour intrachain interactions such as longer range intrachain exchange and interchain exchange may also be affecting the magnetic properties of these materials.

Acknowledgement

We thank the Natural Sciences and Engineering Research Council of Canada for financial support.

1. P. Betz and A. Bino. Inorg. Chim. Acta, **147**, 109 (1988), and references therein.
2. J. S. Hayes, K. W. Oliver, and R. C. Thompson. Can. J. Chem. **63**, 1111 (1985).
3. L. J. de Jongh. *In* Magneto-structural correlations in exchange coupled systems. *Edited by* R. D. Willett, D. Gatteschi, and O. Kahn. D. Reidel Publishing Co., Dordrecht, Holland. 1985. p. 1.
4. J. S. Haynes, K. W. Oliver, S. J. Rettig, R. C. Thompson, and J. Trotter. Can. J. Chem. **62**, 891 (1984).
5. H. D. Gillman. Inorg. Chem. **13**, 1921 (1974).
6. P. Betz and A. Bino. Private communication.
7. W. V. Cicha, J. S. Haynes, K. W. Oliver, S. J. Rettig, R. C. Thompson, and J. Trotter. Can. J. Chem. **63**, 1055 (1985).
8. M. E. Lines. J. Phys. Chem. Solids, **31**, 101 (1970).
9. G. R. Wagner and S. A. Friedberg. Phys. Lett. **9**, 11 (1964).
10. C. Y. Weng. Ph.D. Dissertation, Carnegie-Mellon University. 1968.
11. W. Hiller, J. Strähle, A. Datz, M. Hanack, W. E. Hatfield, L. W. ter Haar, and P. Gütlich. J. Am. Chem. Soc. **106**, 329 (1984).

Can. J. Chem. Downloaded from www.nrcresearchpress.com by 194.225.253.170 on 09/07/12
For personal use only.

Preparation of and addition of carbanions to 6-methyl-6-nitrocyclohexa-2,4-dienones[1]

ALFRED FISCHER,[2] GEORGE N. HENDERSON, AND S. SANKARARAMAN
Department of Chemistry, University of Victoria, Victoria, B.C., Canada V8W 2Y2

Received January 9, 1989

ALFRED FISCHER, GEORGE N. HENDERSON, and S. SANKARARAMAN. Can. J. Chem. **67**, 1244 (1989).

Nitration of 2-methylphenols with nitric acid and trifluoroacetic anhydride in ether at −78°C gives 6-methyl-6-nitrocyclohexa-2,4-dienones that can be isolated. Carbanions add to 5,6-dimethyl-6-nitrocyclohexa-2,4-dienone to give the 5-substituted 2,3-dimethyl-2-nitrocyclohex-3-enone anion, which, with additional carbanion, gives the 5-substituted 2,3-dimethylphenoxide anion by elimination of nitrous acid.

Key words: nitration, dienone, addition, carbanion, nucleophilic.

ALFRED FISCHER, GEORGE N. HENDERSON et S. SANKARARAMAN. Can. J. Chem. **67**, 1244 (1989).

La nitration des méthyl-2 phénols par l'acide nitrique et l'anhydride trifluoroacétique, dans l'éther à −78°C, conduit à la formation de méthyl-6 nitro-6 cyclohexadiène-2,4 ones que l'on peut isoler. Les carbanions s'additionnent sur la diméthyl-5,6 nitro-6 cyclohexadiène-2,4 one pour conduire à l'anion diméthyl-2,3 nitro-2 cyclohexène-3 one substituée en position 5 qui, sous l'action d'un autre carbanion et par élimination d'acide nitreux, conduit à la formation de l'anion diméthyl-2,3 phénolate substitué en position 5.

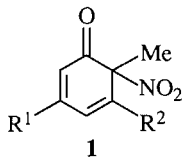
Mots clés : nitration, diénone, addition, carbanion, nucléophile.

[Traduit par la revue]

Can. J. Chem. Downloaded from www.nrcresearchpress.com by 194.225.253.170 on 09/07/12
For personal use only.

Introduction

Formation of 6-methyl-6-nitrocyclohexa-2,4-dienones in the low temperature nitration of 2-methylphenols in acetic anhydride has been reported (1, 2). However, these dienones were not isolated as they are thermally very labile. 6-Methyl-6-nitrocyclohexa-2,4-dienone (**1***a*) isomerizes above −40°C to 6-nitro-*o*-cresol, and in the nitration mixture at −20°C the dienone has a half-life of approximately 8 min. The normal procedure for work-up of nitration reactions carried out in acetic anhydride usually involves treatment with liquid ammonia or concentrated ammonium hydroxide. In this process the temperature of the reaction mixture rises to at least −10°C and 6-methyl-6-nitrocyclohexa-2,4-dienones do not survive. Nitrodienone **1***a* was formed in the nitration of *o*-cresol in dichloromethane, but again isomerized during work-up with liquid ammonia, nominally at −78°C. During a search for a convenient procedure to isolate the thermally unstable 4-halo-4-nitrocyclohexa-2,5-dienones, Clewley developed a nitration procedure for the nitration of 4-halophenols in ether using trifluoroacetyl nitrate (3, 4). Several unstable nitrodienones have been isolated for the first time using this procedure. This appears to be a general method for the low temperature nitration of phenols and we now report the isolation of 6-methyl- (**1***a*), 5,6-dimethyl- (**1***b*), and 3,6-dimethyl-6-nitrocyclohexa-2,4-dienone (**1***c*) in yields of 30–50%.



1

a, $R^1 = R^2 = H$
b, $R^1 = H$, $R^2 = Me$
c, $R^1 = Me$, $R^2 = H$

Results and discussion

Nitration of 2-methylphenols

Nitration was carried out at −78°C and the reaction mixture was worked up by the addition of *N*,*N*,*N*′,*N*′-tetramethylethylenediamine (TMEDA) at −78°C. The trifluoroacetate salt of TMEDA precipitated, and the ethereal solution containing the nitrodienone and the nitrophenols was filtered through a column of basic alumina at −78°C. Only the nitrodienone was eluted and the more acidic nitrophenols remained at the top of the column. Pure nitrodienone was obtained after removal of the solvent at −60°C in a vacuum rotary evaporator. The method has several advantages over the nitration in acetic anhydride. Nitration of 2-methylphenols occurs rapidly at −78°C and the reaction is complete within minutes using one equivalent of the nitrating agent; nitration is carried out in anhydrous conditions and thus the dienones are isolated pure and dry; the reaction mixture can be diluted with additional ether at −78°C and there is no large excess of acid or anhydride, thus the heat of neutralization during work-up and its effect in raising the temperature are minimized, allowing the isolation of thermally labile dienones. Since ether is a basic solvent it is necessary to use the powerful nitrating agent trifluoroacetyl nitrate. When acetyl nitrate was used reaction did not occur, even at 0°C. The basic alumina must be freshly activated. Deactivation of alumina due to prolonged storage usually led to the elution of nitrophenols along with the nitrodienone. The nmr spectral data of the isolated dienones are given in Tables 1 and 2.

The nitrodienones isomerized by specific 1,3 rearrangement of the nitro group, yielding the corresponding 6-nitro-*o*-cresols. No 4-nitro-*o*-cresols were obtained.

TABLE 1. The ^1H nmr spectra of 6-methyl-6-nitrocyclohexa-2,4-dienones[a]

	Chemical shifts/ppm					
Dienone	2-H	3-H	4-H	5-H	6-Me	Me
1*a*[b]	6.27	7.30	6.58	6.52	1.86	—
1*b*[c]	6.15	7.20	6.29	—	1.84	1.97
1*c*	6.07	—	6.43	6.43	1.82	2.21

[a]At 250 MHz in $CDCl_3$ at −40°C.
[b]$J_{2,3} = 9.9$, $J_{2,4} = 3.3$, $J_{3,4} = 6.3$, $J_{3,5} = 1.7$, $J_{4,5} = 9.5$ Hz.
[c]$J_{2,3} = 9.8$, $J_{3,4} = 6.2$ Hz.

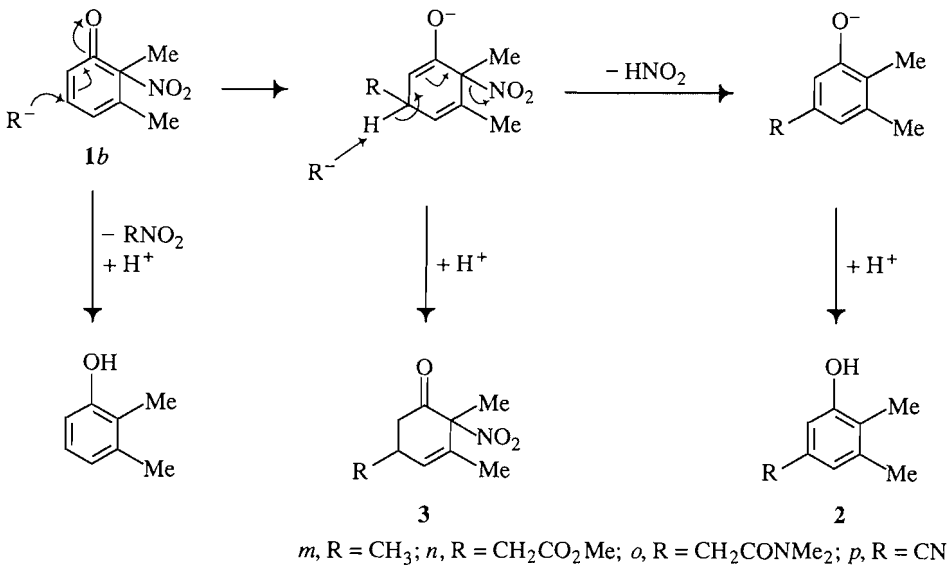
[1]From the Ph.D. dissertation of S. Sankararaman, University of Victoria, September 1985.

[2]Author to whom correspondence may be addressed.

TABLE 2. The ^{13}C nmr spectra of 6-methyl-6-nitrocyclohexa-2,5-dienones[a]

	Chemical shifts/ppm							
Dienone	C-1	C-2	C-3	C-4	C-5	C-6	6-Me	Me
1*a*	192.3	123.9	142.4	124.3	136.1	91.9	22.6	—
1*b*	193.9	121.1	143.3	121.9	146.1	95.5	22.8	17.9
1*c*	191.3	122.0	155.0	128.1	135.4	89.8	22.9	23.2

[a]At −40°C.



m, R = CH_3; *n*, R = CH_2CO_2Me; *o*, R = CH_2CONMe_2; *p*, R = CN

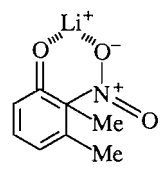
SCHEME 1

Addition of carbanions to 6-methyl-6-nitrocyclohexa-2,4-dienones

Organolithium reagents (RLi) add in a 1,2 fashion to the carbonyl group of 4-alkyl-4-nitrocyclohexa-2,5-dienones to form 1-*R*-4-alkyl-4-nitrocyclohexa-2,5-dienols (5, 6). We hoped that the 6-methyl-6-nitrocyclohexa-2,4-dienones would undergo the same reaction to form 1-*R*-6-methyl-6-nitrocyclohexa-2,4-dienols. The 1,2-addition of carbanions to 6,6-dialkylcyclohexa-2,4-dienones has been reported (7), although the resulting dienols are unstable and readily undergo allylic rearrangement (8) or dehydration (9) to form more stable products. The high reactivity of the conjugated cyclohexadienols is attributed to the steric repulsion of the substituents on the adjacent tetrahedral ring carbons, which is relieved during the further reactions of the dienols.

Dienone **1***b* was chosen as the substrate for study of the addition reactions because it was the most thermally stable. Addition of methyllithium and lithium dimethylcuprate yielded, in each case, 2,3-dimethylphenol as the only product. It is likely that the anionic species abstracts the nitro group to leave the phenoxide anion, which is protonated to the phenol on work-up. An alternative pathway is electron transfer from carbanion to dienone followed by cleavage of nitrogen dioxide (6). Addition of methylmagnesium bromide, methyl lithioacetate, *N*,*N*-dimethyllithioacetamide, and potassium cyanide/18-crown-6 yielded the corresponding *meta*-substituted phenol (**2**). Two mole proportions of the reagent were required for the completion of the reaction. When only one mole of the reagent was used, a mixture of 1,4-addition product (**3**), *meta*-substituted phenol, and 2,3-dimethyl-6-nitrophenol was obtained, the latter product arising from the isomerization of the unreacted nitrodienone. The 1,4-addition product resulting from the addition of methyl lithioacetate, 5-carbomethoxymethyl-2,3-dimethyl-2-nitrocyclohex-3-enone (**3***n*), was isolated as a mixture of two diastereomers. These results suggest that the *meta*-substituted phenol is formed by a stepwise process via an initial 1,4-addition of the reagent to the nitrodienone followed by the 1,4-elimination of nitrous acid in the presence of excess reagent (Scheme 1).

Two factors may be responsible for the different reactivity of the 6-methyl-6-nitrocyclohexa-2,4-dienones as compared with that of the 2,5-dienones. Steric hindrance at the carbonyl group due to the presence of the two bulky α substituents would prevent the carbanion from approaching the carbonyl carbon. Furthermore, the lithium ion is probably strongly chelated by the carbonyl oxygen and the oxygen of the nitro group as shown in **4**. This would add to the hindrance for 1,2-addition, yet



4

increase the reactivity of the carbanion towards 1,4-addition. Carbanions are known to add in 1,4 fashion to enones in cation complexing solvents such as hexamethylphosphoramide (10). The acetoxy analogue of **1** and other *o*-quinol acetates add Grignard reagents and alkyllithium reagents in a 1,4 fashion,

Can. J. Chem. Downloaded from www.nrcresearchpress.com by 194.225.253.170 on 09/07/12
For personal use only.

Can. J. Chem. Downloaded from www.nrcresearchpress.com by 194.225.253.170 on 09/07/12
For personal use only.

then eliminate acetic acid to give *meta*-substituted phenols in a mechanism analogous to that of Scheme 1 (7, 11).

Reaction of 3,6-dimethyl-6-nitrocyclohexa-2,4-dienone (**1***c*) with methyl lithioacetate yielded an unidentifiable insoluble polymer. Its analog, 3,6-dimethyl-*o*-quinol acetate, reacts with carbanions to yield 3-(substituted-methyl)phenols, presumably via a methylenecyclohexadiene intermediate. An analogous intermediate may be involved in the polymerization.

Experimental

Instrument and general experimental methods have been described previously (6, 12). *o*-Cresol, 2,3-, and 2,5-dimethylphenol were Aldrich reagent grade. *N,N,N′,N′*-Tetramethylethylenediamine (Aldrich) was purified by distillation from lithium aluminium hydride under argon.

Nitration of 2-methylphenols

Trifluoroacetic anhydride (7.8 cm^3, 55 mmol) was carefully added, with stirring, to fuming nitric acid (3.4 g, 55 mmol) at −40°C. A solution of the nitrating mixture in ether (10 cm^3) at −78°C was added dropwise with stirring to a solution of 2-methylphenol (50 mmol) in ether (50 cm^3) at −78°C. Stirring was continued for 30 min at −60°C and the mixture was cooled to −78°C. The ^1H nmr of the reaction mixture showed that **1***a* and 4-nitro- and 6-nitro-2-methylphenol had been formed, and that no unreacted 2-methylphenol remained. *N,N,N′,N′*-Tetramethylethylenediamine (57.5 mmol) in ether (10 cm^3) at −78°C was added dropwise, with stirring. The resulting slurry was filtered through a jacketed filter funnel that had been precooled to −78°C, and the solid residue was washed with ether (2 × 20 cm^3) at −60°C. The filtrate, collected at −78°C, was then filtered through a column of basic alumina (50 g, packed with ether) at −78°C, in a jacketed glass column. The column was further eluted with ether (250 cm^3) at −60°C. Upon evaporation of ether from the eluate at −40°C, **1***a* was obtained as a white crystalline solid in 30% yield. The dienone was dried at −40°C and 2 Pa for 10 h. Dienones **1***b* and **1***c* were prepared similarly.

*Addition of carbon nucleophiles to 5,6-dimethyl-6-nitrocyclohexa-2,4-dienone (**1**b)*

Methyllithium (10 mmol) in ether (27 cm^3) at −78°C was added dropwise to a stirred solution of **1***b* (5 mmol, 0.83 g) in tetrahydrofuran (THF) (70 cm^3) under an argon atmosphere. The reaction mixture was stirred at −78°C for 20 min. Aqueous ammonium chloride (10 cm^3, 30 mmol) was added and the mixture was warmed to 0°C and extracted with ice-cold ether. The organic layer was dried ($MgSO_4$) at −20°C and the solvent was removed at −30°C under reduced pressure to give a viscous oil shown to be 2,3-dimethylphenol by ^1H nmr, and confirmed by glc.

Cuprous iodide (5 mmol, 0.95 g) was added to a stirred solution of methyllithium (10 mmol) in ether (7 cm^3) and THF (75 cm^3) at 0°C and under an argon atmosphere. The mixture was stirred for 15 min and then added, as described for methyllithium, to the **1***b* (5 mmol, 0.83 g) in THF and stirred for 1.5 h. The product (0.53 g) was 2,3-dimethylphenol with a small amount of 2,3-dimethyl-6-nitrophenol.

Methylmagnesium bromide (11 mmol) in ether (24 cm^3) was added to the **1***b* (10 mmol, 1.67 g) in THF (50 cm^3) as described above and stirred for 1 h. The product oil was a mixture of 2,3-dimethyl-6-nitrophenol (50%) and 2,3,5-trimethylphenol (**2***m*) (50%).

Methyl lithioacetate (6) (10 mmol) in THF (50 cm^3), was added to the **1***b* (5 mmol, 0.83 g) in THF (70 cm^3) and stirred for 1.5 h. The crude product, a colorless viscous oil (0.30 g, 30%), on crystallization from ether – petroleum ether at −20°C gave colorless crystals of methyl (4,5-dimethyl-3-hydroxyphenyl)acetate (**2***n*): mp 89–90°C; ir (KBr): 3360 (br, OH), 2950, 1705 (C=O), 1590, 1450, 1320, 1265, 1140, 1085, 870, and 800 cm^{-1}; ^1H nmr ($CDCl_3$) δ: 6.62 (s, 1, 6-H), 6.57 (s, 1, 2-H), 5.50 (s, 1, OH), 3.64 (s, 3, $COOCH_3$), 3.46 (s, 2, CH_2COO), 2.20 (s, 3, 5-CH_3), 2.08 (s, 3, 4-CH_3); ^{13}C nmr ($CDCl_3$) δ_C: 172.4 (C=O), 153.7 (C-3), 138.4 (C-5), 131.6 (C-4), 123.1 (C-6), 121.5 (C-1), 113.4 (C-2), 52.0 ($COOCH_3$), 40.7 (CH_2), 19.9 (5-CH_3), 11.2 (4-CH_3); ms, *m/z* (relative intensity): 194.096 (25, M_r $C_{11}H_{14}O_3$: 194.094), 136 (11), 135 (100), 91 (17), 77 (7), 65 (4).

When the reaction was repeated by adding methyl lithioacetate (11 mmol) to the dienone (10 mmol) the crude product, an oil (1.3 g), was a mixture of 2,3-dimethyl-6-nitrophenol (35%) and 5-carbomethoxymethyl-2,3-dimethyl-2-nitrocyclohex-3-enone (65%). An ethereal solution of this product was washed with ice-cold 2% aqueous sodium hydroxide, followed by ice-cold water, and this afforded 5-carbomethoxymethyl-2,3-dimethyl-2-nitrocyclohexa-3-enone (**3***n*) (0.05 g) as a colorless oil: ir (film): 2950, 1735 (C=O), 1550 and 1375 (NO_2), 1440, 1260, 910, and 730 cm^{-1}; ^1H nmr ($CDCl_3$, 250 MHz) δ: 5.84 (m, 1, 4-H), 3.63 (s, 3, $COOCH_3$), 3.12 (m, 1, 5-H), 2.83 (dd, J = 14.4 Hz, 5.8 Hz, 1, 6-H), 2.44 (dd, J = 14.4 Hz, 8.2 Hz, 1, 6-H), 2.38 and 2.35 (d, J = 1.8 Hz, 2.3 Hz, 2, CH_2COO), 1.74 (s, 3, 2-CH_3), 1.70 and 1.69 (d, J = 1.4 Hz, 3, 3-CH_3); ^{13}C nmr ($CDCl_3$) δ_C: 199.0 (C-1), 170.2 (*C*OOMe), 132.0 (C-3), 131.6 (C-4), 92.9 (C-2), 50.8 ($COOCH_3$), 40.2 and 38.3 (C-6 and CH_2COO), 31.8 (C-5), 19.6 and 16.8 (2-CH_3 and 3-CH_3).

N,N-Dimethyllithioacetamide (12 mmol) in THF (50 cm^3) was added to the dienone (5 mmol) in THF (45 cm^3) and stirred for 1.5 h. The product, *N,N*-dimethyl(4,5-dimethyl-3-hydroxyphenyl)acetamide (**2***o*) (0.47 g, 45%), was obtained as colorless crystals on recrystallization from dichloromethane–hexane at −20°C: mp 138–140°C; ir (KBr): 3290 (br, OH), 2920, 1625 (C=O), 1585, 1510, 1450, 1400, 1285, 1135, 1090, 860, and 790 cm^{-1}; ^1H nmr ($CDCl_3$) δ: 8.45 (br, OH), 6.79 (s, 1, 6-H), 6.48 (s, 1, 2-H), 3.55 (s, 2, CH_2COO), 2.92 (s, 6, $N(CH_3)_2$), 2.18 (s, 3, 5-CH_3), 2.08 (s, 3, 4-CH_3); ^{13}C nmr ($CDCl_3$) δ_C: 172.2 (C=O), 155.3 (C-3), 137.9 (C-5), 131.8 (C-4), 121.8 (C-6), 121.6 (C-1), 112.3 (C-2), 40.8 (CH_2), 37.9 and 35.9 ($N(CH_3)_2$), 19.9 (5-CH_3), 11.2 (4-CH_3); ms, *m/z* (relative intensity): 208 (2), 207.129 (10, M_r $C_{12}H_{17}NO_2$: 207.125), 135 (34), 91 (14), 85 (30), 77 (9), 72 (100).

A mixture of potassium cyanide (20 mmol, 1.30 g), 18-crown-6 (2 mmol, 0.53 g), and the dienone (2 mmol, 0.34 g) in acetonitrile (10 cm^3) was stirred at −40°C for 3 h. The product, 5-cyano-2,3-dimethylphenol (**2***p*), was recrystallized from a mixture of ether and hexane at −20°C: mp 122°C (lit. (13) mp 122.5–123°C); ir (KBr): 3250 (br, OH), 2230 (CN) cm^{-1}; ^1H nmr ($CDCl_3$) δ: 7.03 (s, 1, 4-H), 6.96 (s, 1, 6-H), 5.92 (br s, 1, OH), 2.26 (s, 3, 3-CH_3), 2.19 (s, 3, 2-CH_3); ^{13}C nmr ($CDCl_3$) δ_C: 154.0 (C-1), 139.0 (C-3), 129.5 (C-2), 125.0 (C-4), 119.0 (CN), 115.7 (C-6), 108.9 (C-5), 19.8 (3-CH_3), 11.9 (2-CH_3); ms, *m/z* (relative intensity): 147.068 (92, M_r C_9H_9NO: 147.068), 146 (34), 132 (100), 77 (21).

1. G. G. Cross, G. N. Henderson, and T. A. Smyth. Can. J. Chem. **62**, 1446 (1984).
2. A. Fischer and G. N. Henderson. Tetrahedron Lett. 4661 (1980).
3. R. G. Clewley. Ph.D. Dissertation, University of Victoria, Victoria, B.C. 1985.
4. R. G. Clewley, G. G. Cross, A. Fischer, and G. N. Henderson. Tetrahedron, 1299 (1989).
5. C. E. Barnes, K. S. Feldman, M. W. Johnson, H. W. H. Lee, and P. C. Myhre. J. Org. Chem. **44**, 3925 (1979).
6. A. Fischer and S. Sankararaman. J. Org. Chem. **52**, 4464 (1987).
7. A. J. Waring. Adv. Alicycl. Chem. **1**, 201 (1966).
8. H. Budzikiewicz, F. Wessely, and H. Janda. Monatsh. **92**, 621 (1961).
9. H. Hart and A. J. Waring. J. Am. Chem. Soc. **86**, 1454 (1964).
10. W. Dumont, A. Krief, and J. Lucchetti. Tetrahedron Lett. 2695 (1979).
11. W. Specht and F. Wessely. Monatsh. **90**, 713 (1959).
12. A. Fischer, D. L. Fyles, G. N. Henderson, and S. Ray Mahasay. Can. J. Chem. **64**, 1764 (1986).
13. J. Leitich and F. Wessely. Monatsh. **95**, 129 (1964).

Kinetic study of the oxidation mechanism of glutathione by hydrogen peroxide in neutral aqueous medium

Z. ABEDINZADEH, M. GARDES-ALBERT, AND C. FERRADINI

Laboratoire de chimie-physique, 45, rue des Saints-Pères, F-75270, Paris CEDEX 06, France

Received July 21, 1988[1]

Z. ABEDINZADEH, M. GARDES-ALBERT, and C. FERRADINI. Can. J. Chem. **67**, 1247 (1989).

The oxidation kinetics of glutathione (GSH) by hydrogen peroxide has been studied at neutral pH for different concentration ratios $[GSH]_0/[H_2O_2]_0$ between 0.2 and 2 ($5 \times 10^{-4}\ M \leq [H_2O_2]_0 \leq 2.5 \times 10^{-3}\ M$; $4 \times 10^{-4}\ M \leq [GSH]_0 \leq 2.5 \times 10^{-3}\ M$). In all cases studied, glutathione disulfide GSSG is the main product formed via two different oxidation ways, each of them contributing respectively to 80–85% and 10–15%.

Our kinetic data indicate that an important fraction of hydrogen peroxide disappears without oxidizing the thiol function. This can be attributed to a combination between GSH and H_2O_2 protecting the sulfide group. Chemical evidences of the existence of a peroxide bond with GSSG are described. In our experimental conditions, the overall oxidation equation is 2 mol GSH reacting with 2 mol H_2O_2 giving 1 mol GSSG. It is very different from the usually accepted stoichiometric reaction:

$$H_2O_2 + 2GSH \rightarrow GSSG + 2H_2O$$

A kinetic scheme is proposed and the corresponding rate constants are determined.

Key words: glutathione, hydrogen peroxide, kinetic mechanism, glutathione disulfide.

Z. ABEDINZADEH, M. GARDES-ALBERT et C. FERRADINI. Can. J. Chem. **67**, 1247 (1989).

Opérant à un pH neutre et à des rapports de concentration de $[GSH]_0/[H_2O_2]_0$ allant de 0,2 à 2 ($5 \times 10^{-4}\ M \leq [H_2O_2]_0 \leq 2{,}5 \times 10^{-3}\ M$; $4 \times 10^{-4}\ M \leq [GSH]_0 \leq 2{,}5 \times 10^{-3}\ M$), on a étudié la cinétique de l'oxydation du glutathion (GSH) par le peroxyde d'hydrogène. Dans tous les cas étudiés, le disulfure de glutathion, GSSG, est le produit principal qui est formé par deux voies d'oxydation principales qui apportent des contributions respectives de 80 à 85% et 10 à 15%.

Nos données cinétiques indiquent qu'une fraction importante du peroxyde d'hydrogène disparaît sans oxyder la fonction thiol. On peut attribuer ce fait à une combinaison du GSH et du H_2O_2 qui protégerait le groupement sulfure. On décrit des données chimiques qui suggèrent l'existence d'une liaison du peroxyde avec le GSSG. Dans nos conditions expérimentales, l'équation globale d'oxydation implique donc deux moles de GSH qui réagissent avec deux moles de H_2O_2 pour donner une mole de GSSG. Cette équation diffère beaucoup de la réaction stoechimétrique généralement admise:

$$H_2O_2 + 2GSH \rightarrow GSSG + 2H_2O$$

On propose une schéma cinétique et on a déterminé les constantes de vitesse correspondantes.

Mots clés : glutathion, peroxyde d'hydrogène, mécanisme cinétique, disulfure de glutathion.

[Traduit par la revue]

Introduction

Glutathione (GSH) is present in almost all cells in rather high concentration. The conversion of glutathione (GSH) to glutathione disulfide GSSG, *in vivo*, is catalyzed by glutathione peroxidase, which acts on hydrogen peroxide and other peroxides. The overall oxidation reaction of GSH by H_2O_2 in presence of peroxidase is

$$[1]\quad 2GSH + H_2O_2 \xrightarrow{GPX} GSSG + 2H_2O$$

It is generally agreed that in the absence of the enzyme the overall oxidation process is not different from this reaction (1). But the real mechanism of oxidation of GSH by H_2O_2 is unknown.

However, the oxidation kinetics of a variety of sulfur compounds such as hydrogen sulfide (2), sulfur dioxide (3), thioureas (4), thioxane (5), thiocyanate (6, 7) and 2 mercaptoethanol (8) by hydrogen peroxide in aqueous solution have been studied. A common mechanism for the acid-catalyzed nucleophilic attack consists of a heterolytic cleavage of oxygen–oxygen bond of hydrogen peroxide with the release of either hydroxide ion or water as leaving group according to

$$RSH + H_2O_2 \rightarrow RSOH + H_2O$$

The hydroxy intermediate (RSOH) subsequently reacts with either a second molecule of reductant to form a dimer as a final product or with an additional molecule of H_2O_2 (2).

Concerning the reaction of H_2O_2 with GSH, McCormic *et al.* (9) have shown that a UV chromophore having a maximal absorption at 305 nm appears during the reaction. But the kinetics of the reaction were not studied. The same observation was obtained when aerated aqueous solutions of GSH were irradiated with a 254 nm radiation (9). From several comparative studies with other thiols in the same conditions, they attributed the absorbance at 305 nm to a product which is formed on the *N*-acetylcysteinamide (—CONH—CH(—CH_2—SH)—$CONH_2$) part of GSH.

In order to carefully investigate the mechanism of oxidation of GSH by H_2O_2, the kinetics of this reaction have been studied in neutral aerated aqueous medium, in absence of peroxidase for different concentrations: $4 \times 10^{-4}\ M \leq [GSH]_0 \leq 2.5 \times 10^{-3}\ M$, $5 \times 10^{-4}\ M \leq [H_2O_2]_0 \leq 2.5 \times 10^{-3}\ M$, and different ratios $[GSH]_0/[H_2O_2]_0$ (0.2 to 2).

Materials and methods

Chemicals were of the purest grade available and were used without further purification. The only exception was glutathione sulfonic acid which was used as a standard for HPLC and spectral analysis. It was prepared according to Calam and Waley (10). GSH and GSSG were obtained from FLUKA; 5,5′-dithiobis(2-nitrobenzoic acid), NADPH, glutathione reductase were supplied by Sigma Chemical Co.; hydrogen

[1]Revision received February 6, 1989.

Printed in Canada / Imprimé au Canada

Can. J. Chem. Downloaded from www.nrcresearchpress.com by 194.225.253.170 on 09/07/12
For personal use only.

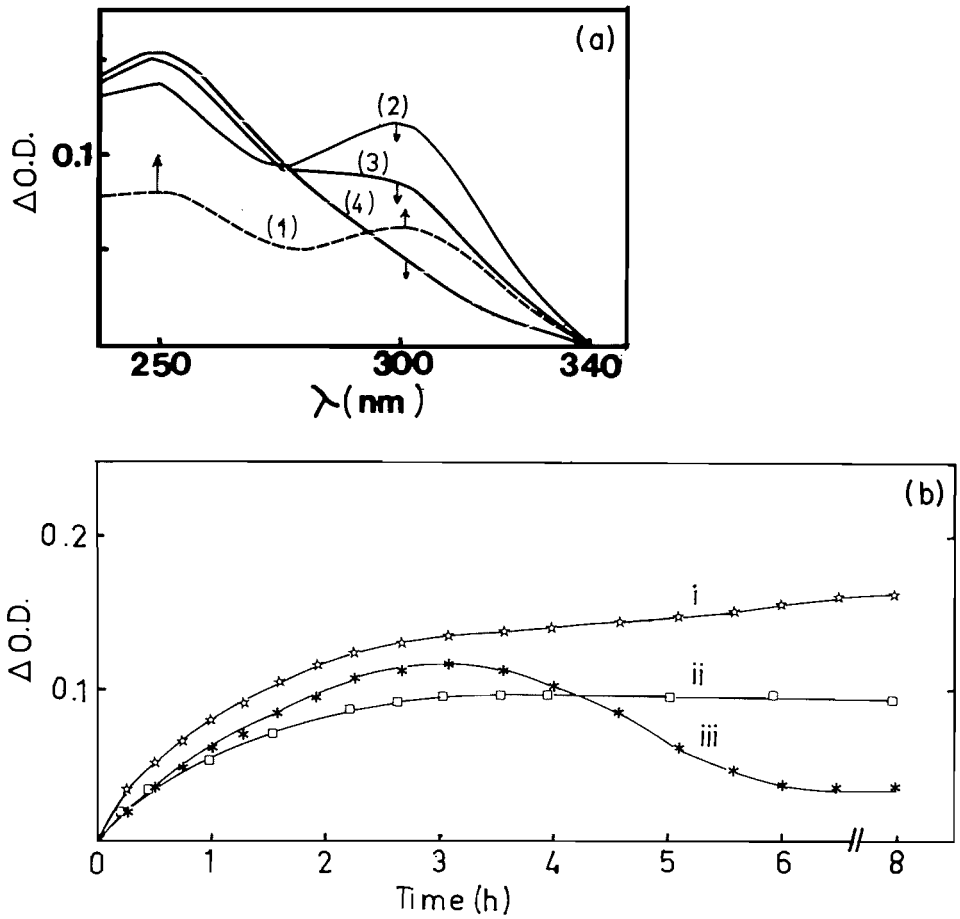


FIG. 1. (*a*) Differential absorption spectra at various times after mixing. $[GSH]_0 = [H_2O_2]_0 = 10^{-3}$ *M*, phosphate buffer 0.1 *M*, 22°C, pH 7, *l* = 0.875 cm. Reference: $[GSG]_0 = 2 \times 10^{-3}$ *M* (*l* = 0.4375 cm) (two chambers cell, see Experimental section). (*1*) 1 h, (*2*) 3 h 5 min, (*3*) 4 h 35 min, (*4*) 5 h 35 min after mixing of the reactants. (*b*) Evolutions of the differential absorption densities as a function of time at three different wavelengths: (☆) λ 250 nm, (□) λ 268 nm, (★) λ 305 nm.

peroxide, sodium acid phosphate were from Merck. All solutions were prepared with triply distilled water, the purity of which was controlled by conductivity measurements (10^{-6} Ω cm^{-1}).

Thiol concentration was determined with Ellman's reagent, 5,5'-dithiobis(2-nitrobenzoïc acid) which undergoes a thiolate disulphide exchange reaction to yield 2-nitromercaptobenzoïc acid (11). This product was measured spectrophotometrically (λ_{max} = 412 nm, ϵ = 13600 ± 600 M^{-1} cm^{-1}) against an appropriate blank. The oxidized form GSSG was titrated by its reduction by NADPH in the presence of glutathione reductase, the NADPH in excess being measured spectrophotometrically (λ_{max} = 340 nm, ϵ = 5400 ± 250 M^{-1} cm^{-1}). This titration was carried out with solutions containing an excess of GSSG to avoid any parasitical oxidation of NADPH due to an oxidase activity of glutathione reductase (12).

Hydrogen peroxide concentrations were measured spectrophotometrically by the titanium sulfate method (13, 14) using ϵ_{410} = 700 M^{-1} cm^{-1}.

For the differential spectrophotometric measurements of reaction mixtures, we used two chamber cells, each having an optical path of 0.4375 cm. The reference cell in one chamber contained H_2O_2, (with $[H_2O_2]_0$ = 2 $[H_2O_2]_0$ reaction mixture) and in the other GSH (with $[GSH]_0$ = 2 $[GSH]_0$ reaction mixture). The measure cell in each chamber contained the same reaction mixture.

Another method for determining GSSG was deduced from the differential optical densities at 250 nm. At this wavelength the extinction coefficient for GSH is equal to zero and for H_2O_2 ϵ_{250} = 25 M^{-1} cm^{-1} (15). According to Beer's law, the differential extinction coefficient of GSSG 330 ± 4 M^{-1} cm^{-1} has been determined.

Oxygen concentration was determined by Gilson oxygraph model IC TS-KI. All solutions were prepared just prior to use and buffered at pH 7 in a 10^{-1} *M* phosphate medium. Temperature was maintained constant at 22°C with a BIOBLOCK Polystat circulating water bath.

HPLC analysis has been done according to Reed (16) on a ZORBAX-NH_2 (25 cm × 4.6 mm) column.

Results

1. Differential absorption spectra of the reaction mixture in function of time

For various times after the mixing the differential absorption spectra of a solution containing initially H_2O_2 10^{-3} *M* and GSH 10^{-3} *M* (phosphate buffer 0.1 *M*, pH 7) can be seen in Fig. 1*a* (between 240 and 340 nm). The differential absorption spectrum (*1*) recorded 1 h after the mixing presents two maxima at 250 nm and 305 nm. The absorption band at 250 nm increases (spectra (*2*) and (*3*)), until the end of the reaction (spectrum (4), ΔOD^{250} (5 h 35 min) = 0.16). Simultaneously the absorption band at 305 nm increases and reaches a maximum value at 3 h 20 min (spectrum (*2*), ΔOD^{305} (3 h 20 min) = 0.12) and decays. We note the presence of an isobestic point at 268 ± 8 nm.

The kinetics at 250, 268, and 305 nm are reported on the Fig. 1*b*. The curve (*i*) at 250 nm appears to be composed of a fast increase until ≃ 3 h, followed by a much slower growth until the end of the reaction. This absorption band at 250 nm has been attributed to GSSG ($\Delta\epsilon^{250}$ = 330 M^{-1} cm^{-1}, see Experimental section). At the end of the reaction, the disulfide concentration is equal to 4.85 × 10^{-4} *M* which corresponds to the transfor-

Can. J. Chem. Downloaded from www.nrcresearchpress.com by 194.225.253.170 on 09/07/12
For personal use only.

TABLE 1. Determination of the equilibrium constant of formation of the complex [GSH—H_2O_2]

$[H_2O_2]_0$ M	$[GSH]_0$ M	$R = \frac{[GSH]_0}{[H_2O_2]_0}$	$[H_2O_2]_{eq}$ M	$[GSH]_{eq}$ M	$[GSH—H_2O_2]_{eq}$ M	K_2
5×10^{-4}	10^{-3}	2	2.2×10^{-4}	7.2×10^{-4}	2.8×10^{-4}	1770
5×10^{-4}	5×10^{-4}	1	3×10^{-4}	3×10^{-4}	2×10^{-4}	2220
10^{-3}	10^{-3}	1	5×10^{-4}	6×10^{-4}	5×10^{-4}	2000
10^{-3}	8×10^{-4}	0.8	6×10^{-4}	4×10^{-4}	4×10^{-4}	1670
5×10^{-4}	4×10^{-4}	0.8	3.4×10^{-4}	2.4×10^{-4}	1.6×10^{-4}	1960
1.33×10^{-3}	8×10^{-4}	0.6	8.5×10^{-4}	3.2×10^{-4}	4.8×10^{-4}	1760
10^{-3}	6×10^{-4}	0.6	6.5×10^{-4}	2.5×10^{-4}	3.5×10^{-4}	2150
2.5×10^{-3}	10^{-3}	0.4	1.78×10^{-3}	2.2×10^{-4}	7.8×10^{-4}	1990
2.5×10^{-3}	5×10^{-4}	0.2	2.1×10^{-3}	10^{-4}	3×10^{-4}	1900

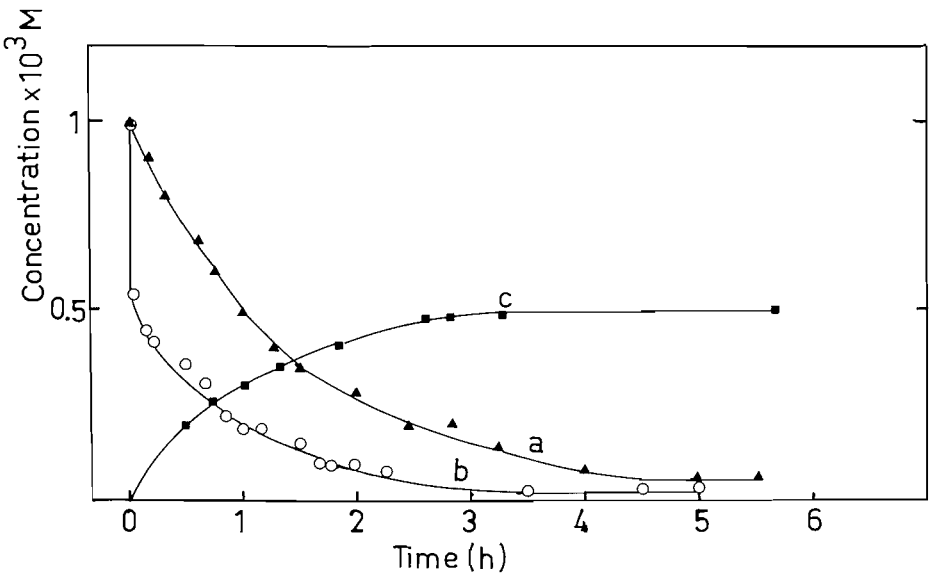


FIG. 2. Evolution of the concentration of GSH (▲), H_2O_2 (○), and GSSG (■). $[GSH]_0 = [H_2O_2]_0 = 10^{-3}$ M, phosphate buffer 0.1 M, pH 7, 22°C.

mation of 97% of GSH initially present in the solution. Consequently, we can consider that the thiol GSH is stoichiometrically oxidized to GSSG within experimental errors. Curve (*iii*) characterizes a transient which exhibits an absorption maximum (at 3 h 20 min), then decays until 7 h, and reaches a final value of ΔOD^{305} (7 h) = 0.035. We will call this intermediate X^{305}. Curve (*ii*) gives the ΔOD^{268} evolution at the isobestic point and it can be observed that a plateau value of $\Delta OD^{268} = 0.095$ is reached and is maintained constant between 3 h 20 min and the end of the reaction. This isobestic point shows that the decay of the intermediate X^{305} gives rise only to GSSG. It can be noticed that ϵ_{305} GSSG = 0 so the absorption at 305 nm is only due to X^{305}. The variations of GSSG concentration during the decay of X^{305} can be measured: it is equal to 6.5×10^{-5} M which represents 13% of the total amount of GSSG appeared. Hence the thiol oxidation via intermediate X^{305} is a minor oxidation phenomenon.

2. Evolution of GSH, H_2O_2, and GSSG

Figure 2 shows the kinetic changes in the concentration of GSH, H_2O_2, and GSSG (curves *a*, *b*, and *c*), when the solutions contain initially the same concentrations of GSH and H_2O_2, 10^{-3} M (phosphate buffer 10^{-1} M, pH 7). We remark that the decay of H_2O_2 measured by the titanium composed of two distinct phenomena: the first, a very fast decrease which ends in 2 min and corresponds to the disappearance of 50% of the H_2O_2 initial concentration. The second phenomenon lasts about 6 h, and corresponds to the disappearance of the last 50% of H_2O_2. Identical processes have been observed for numerous experiments; the corresponding initial concentrations are reported in Table 1 (see the three first columns).

The decay of GSH (Fig. 2*a*) and the formation of GSSG (Fig. 2*c*) are contemporary with the slow decrease of H_2O_2 (Fig. 2*b*). We note that, at the end of the reaction, the thiol GSH is quantitatively oxidized to GSSG. This fact confirms the previously stoichiometric oxidation demonstrated according to the results of Fig. 1*b*.

Furthermore, at the end of the reaction the whole H_2O_2 has disappeared (detection by the titanium method), leading us to conclude that 2 mol of H_2O_2 react with 2 mol of GSH to give 1 mol of GSSG. This overall reaction is very different from the usually accepted stoichiometry [1].

[1] $2GSH + H_2O_2 \rightarrow GSSG + 2H_2O$

Can. J. Chem. Downloaded from www.nrcresearchpress.com by 194.225.253.170 on 09/07/12
For personal use only.

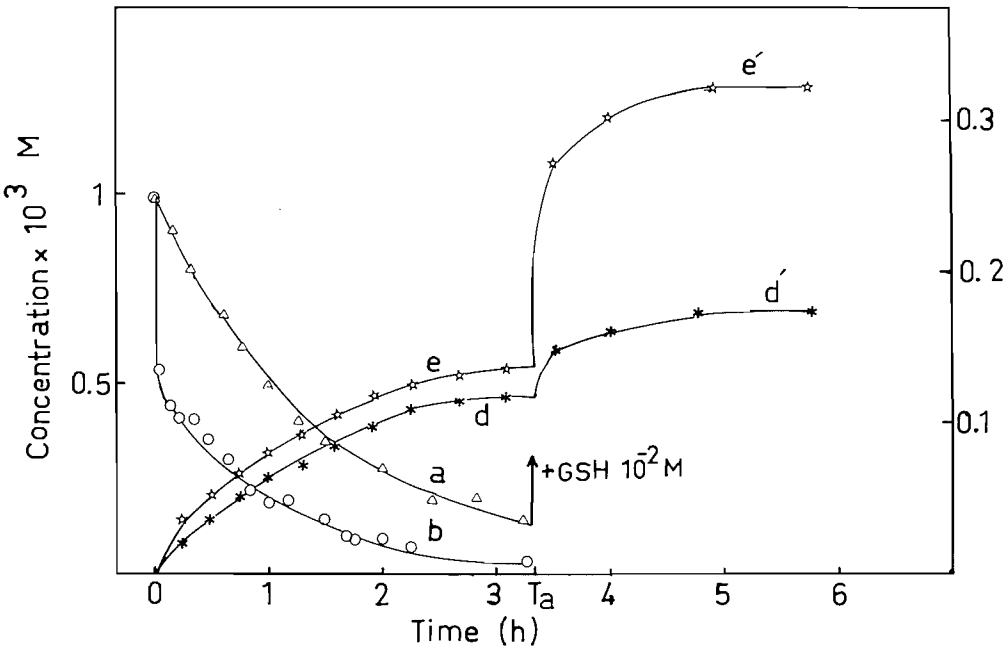


FIG. 3. Addition of GSH at the end of the reaction. Initial reaction: $[GSH]_0 = [H_2O_2]_0 = 10^{-3}$ *M*, phosphate buffer 0.1 *M*, pH 7, 22°C. $[GSH]_t$ (*a*), $[H_2O_2]_t$ (*b*), ΔOD^{250} (*e*), ΔOD^{305} (*d*). T_a = 3 h 20 min, addition of GSH 10^{-2} *M*, ΔOD^{250} (*e'*), ΔOD^{305} (*d'*).

It seems that 1 mol of H_2O_2 disappears without oxidizing the thiol function. To find out what has become with H_2O_2, three experiments have been done.

(a) Oxygen measurements

We have tested the possibility of formation of oxygen by Gilson Oxygraph (see Experimental section) in a solution initially containing GSH and H_2O_2 at the same concentration 10^{-3} *M* (phosphate buffer, pH 7). However, neither at the beginning nor during the reaction was any formation of oxygen observed. Hence H_2O_2 is not oxidized nor does it disproportionate.

(b) Addition of an excess of GSH

An excess of GSH was added (see Fig. 3, time T_a) ($[GSH] \simeq 10^{-2}$ *M*) when H_2O_2 had totally disappeared, i.e. 3 h 20 min after the beginning of the reaction ($[H_2O_2]_0 = [GSH]_0 = 10^{-3}$ *M*, phosphate buffer 10^{-1} *M*, pH 7). We observed a new formation of GSSG (curve *e'*) whose final concentration was equal to 9.85×10^{-4} *M*. Hence this total concentration of GSSG is about the initial H_2O_2 amount (85%), leading us to conclude that an excess of GSH is necessary to reduce quantitatively the whole amount of hydrogen peroxide.

(c) Addition of catalase

To determine the nature of the oxidant property in the final solution, we added catalase 10^{-7} *M*, six hours after mixing the reactants GSH and H_2O_2 ($[GSH]_0 = [H_2O_2]_0 = 10^{-3}$ *M*, phosphate buffer 10^{-1} *M*, pH 7). We observed the formation of oxygen in concentration 5×10^{-4} *M* corresponding to the bound H_2O_2 whereas there was no free H_2O_2 (measured by the titanium method) in the reaction medium.

3. Studies of the X^{305} intermediate

We have shown that the decrease of X^{305} intermediate gives rise to 15% of the total GSSG formed (see Fig. 1*b*). Thus the oxidation process occurring via X^{305} was a minor one. Hence X^{305} cannot be responsible of the oxidant property of the final solution. Nevertheless, to determine the nature of X^{305}, we attempted HPLC analysis of the reaction medium to detect a possible sulfonate product, GSO_3H. We found no GSO_3H because either it was not present or its concentration was too small to be detected by our experimental conditions ($<10^{-5}$ *M*). To determine the chemical behavior of X^{305} we checked the effect of GSH or H_2O_2 on the reaction. An excess of GSH ($\simeq 10^{-2}$ *M*) was added when the differential optical density at 305 nm was maximum (T_a), ($[H_2O_2]_0 = [GSH]_0 = 10^{-3}$ *M*, phosphate buffer 10^{-1} *M*, pH 7). As it can be seen in Fig. 3, we observed that ΔOD^{305} (curve *d'*) increases and remains constant until the end of the reaction. Consequently an excess of GSH protects the X^{305} intermediate and it seems that there is an equilibrium between GSH and X^{305}.

A similar phenomenon has been observed (Fig. 4) when the GSH initial concentration is greater than those of H_2O_2 ($[GSH]_0 = 10^{-3}$ *M*, $[H_2O_2]_0 = 5 \times 10^{-4}$ *M* phosphate buffer 10^{-1} *M*, pH 7). Thus at the end of this reaction ($\simeq$4 h 30 min), free H_2O_2 has totally disappeared (curve *b*), GSSG 5×10^{-4} *M* is formed (curve *e*, ΔOD^{250}), half of GSH is still present (curve *a*) and the X^{305} intermediate reached a plateau value ΔOD^{305} = 0.075 (curve *d*) and does not decrease. In inset of Fig. 4, the differential absorption spectra recorded for different times after mixing are reported. There is no isobestic point because the X^{305} intermediate does not disappear. Therefore we confirm that an initial excess of GSH protects the X^{305} intermediate.

Hydrogen peroxide 2×10^{-3} *M* was added when ΔOD^{305} was maximum (T_b), ($[GSH]_0 = [H_2O_2]_0 = 10^{-3}$ *M*, phosphate buffer 10^{-1} *M*, pH 7). As it can be seen in Fig. 5, the added H_2O_2 accelerates the decrease of X^{305} (curve *d*) giving GSSG (curve *e*). Figure 5 inset shows the differential absorption spectra recorded after the addition of H_2O_2 present an isobestic point at 268 nm, showing that the X^{305} intermediate is transformed into GSSG. We can therefore conclude that H_2O_2 reacts with the X^{305} intermediate to give GSSG.

A similar phenomenon occurs when the initial concentration of H_2O_2 is greater than those of GSH as it can be seen in Fig. 6 ($[GSH])_0 = 10^{-3}$ *M*, $[H_2O_2]_0 = 2.5 \times 10^{-3}$ *M*, phosphate buffer 10^{-1} *M*, pH 7). When ΔOD^{305} is maximum (curve *d*, $t \simeq$

Can. J. Chem. Downloaded from www.nrcresearchpress.com by 194.225.253.170 on 09/07/12
For personal use only.

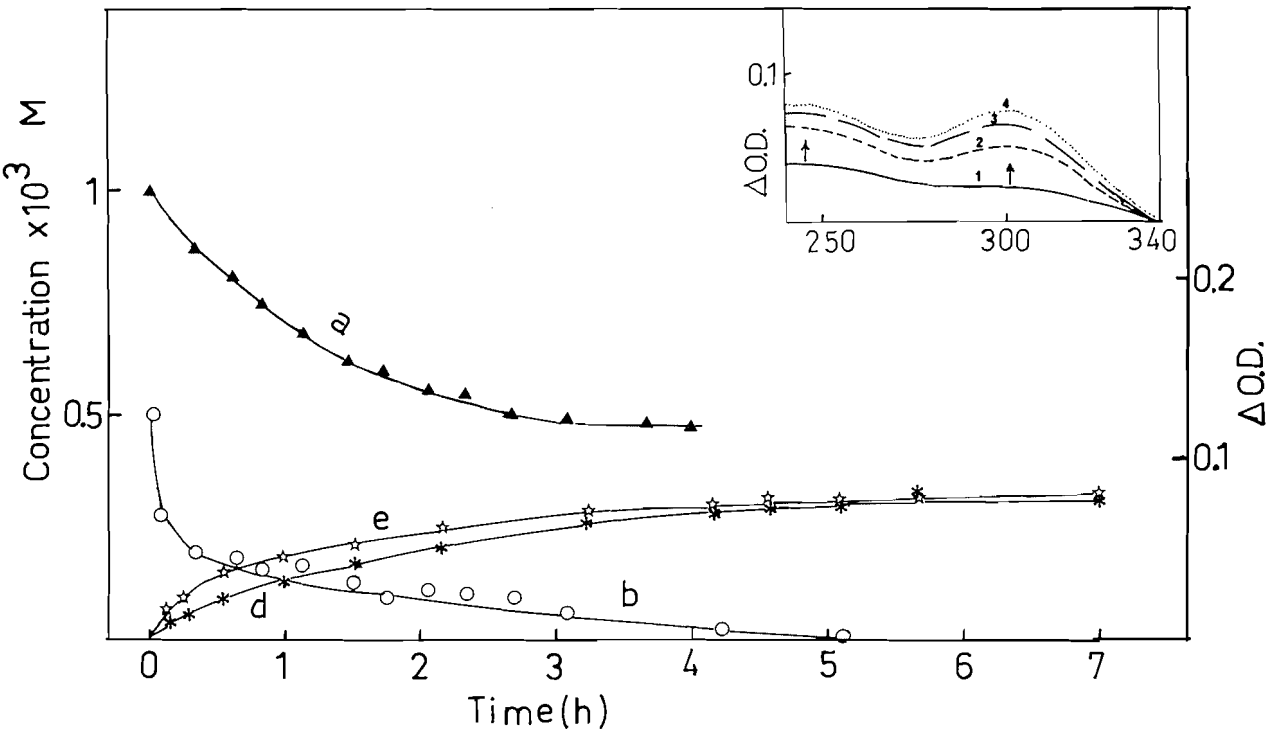


FIG. 4. Kinetic curves of [GSH] (*a*), $[H_2O_2]_0$ (*b*), ΔOD^{250} (*e*), and ΔOD^{305} (*d*). $[GSH]_0 = 10^{-3}$ *M*, $[H_2O_2]_0 = 5 \times 10^{-4}$ *M*, phosphate buffer 0.1 *M*, pH 7, 22°C. Inset: differential absorption spectra of the reaction mixture: (*1*) 32 min, (*2*) 2 h 10 min, (*3*) 3 h 15 min, (*4*) 5 h 7 min after the start of the reaction.

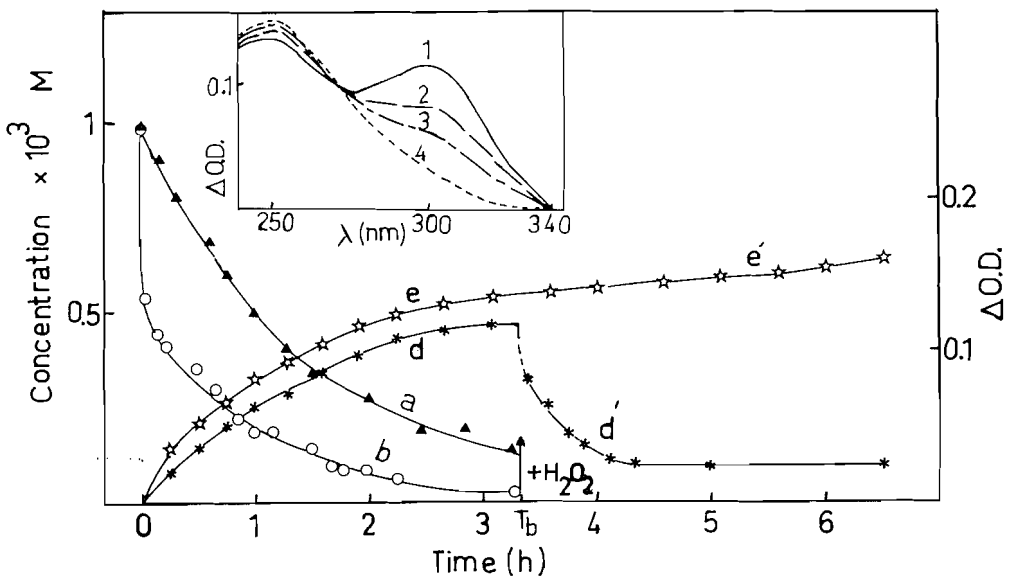


FIG. 5. Addition of $[H_2O_2]$ at the end of a reaction. Initial reaction: $[GSH]_0 = [H_2O_2]_0 = 10^{-3}$ *M*, phosphate buffer 0.1 *M*, pH 7, 22°C. $[GSH]_t$ (*a*), $[H_2O_2]_t$ (*b*), ΔOD^{250} (*e*), ΔOD^{305} (*d*). T_b = 3 h 20 min, addition of H_2O_2 2×10^{-3} *M*, ΔOD^{250} (*e'*), ΔOD^{305} (*d'*). Inset: the differential absorption spectra after the addition of H_2O_2 2×10^{-3} *M*: (*1*) 3 h 20 min (time 0 for the addition of H_2O_2), (*2*) 3 h 25 min, (*3*) 3 h 45 min, (*4*) 4 h after the beginning of the reaction.

50 mn), free H_2O_2 has a high concentration (1.5×10^{-3} *M*, curve *b*) resulting in the X^{305} intermediate decreasing faster than when there is no free H_2O_2 in the medium (Fig. 1*b*, curve *4*). During the decrease of X^{305}, however, hydrogen peroxide remains constant. The decay of X^{305} is thus catalyzed by H_2O_2. Figure 6 inset shows the differential absorption spectra, recorded at different times after the mixing, present an isobestic point at 268 nm when ΔOD^{305} decreases showing the transformation of X^{305} into GSSG.

Discussion

Fast initial decay of H_2O_2

The fast decay of H_2O_2 can be explained by the formation of a compound between GSH and H_2O_2 which could be, for

Can. J. Chem. Downloaded from www.nrcresearchpress.com by 194.225.253.170 on 09/07/12
For personal use only.

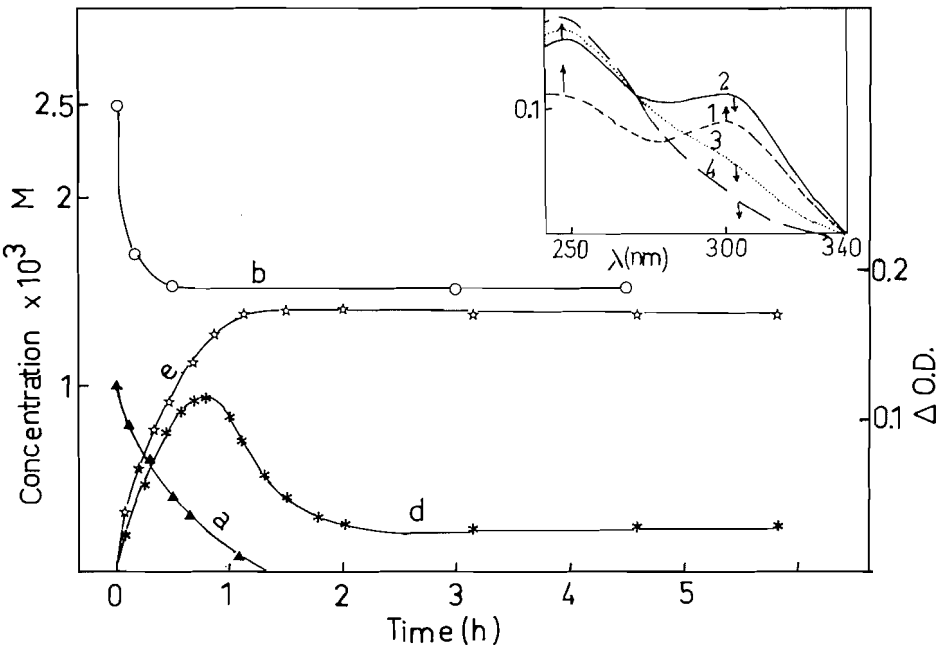


FIG. 6. Kinetic curves of $[GSH]_t$ (*a*), $[H_2O_2]_t$ (*b*), ΔOD^{250} (*e*), and ΔOD^{305} (*d*). $[GSH]_0 = 10^{-3}$ *M*, $[H_2O_2]_0 = 2.5 \times 10^{-3}$ *M*, phosphate buffer 0.1 *M*, pH 7, 22°C. Inset: differential absorption spectra of the reaction mixture: (*1*) 27 min, (*2*) 52 min, (*3*) 1 h 18 min, (*4*) 1 h 45 min after the start of the reaction.

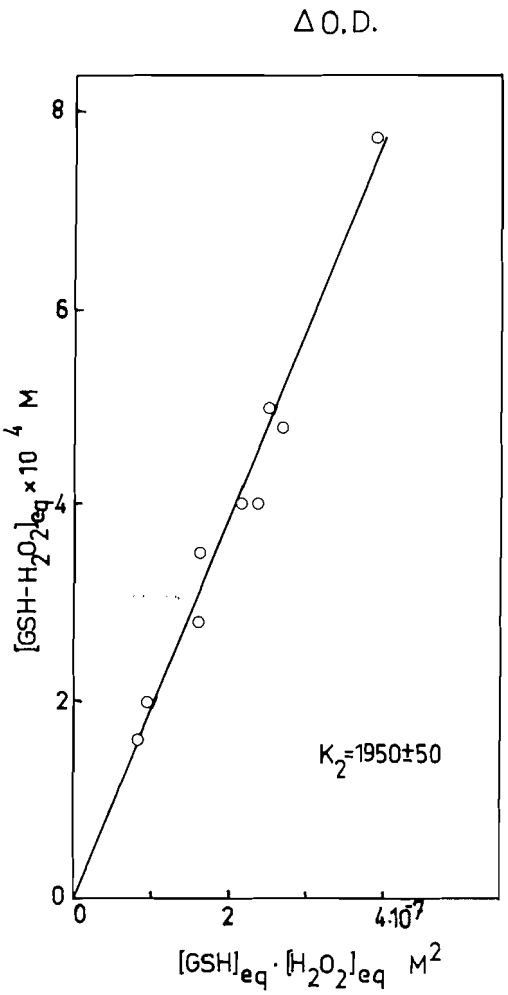


FIG. 7. Determination of the equilibrium constant of formation of the complex [GSH—H_2O_2]. $[GSH—H_2O_2]_{eq}$ vs. $[GSH]_{eq} \times [H_2O_2]_{eq}$, phosphate buffer 0.1 *M*, pH 7, 22°C, $4 \times 10^{-4} \leq [GSH]_0 \leq 2.5 \times 10^{-3}$ *M*, $5 \times 10^{-4} \leq [H_2O_2]_0 \leq 2.5 \times 10^{-3}$ *M*.

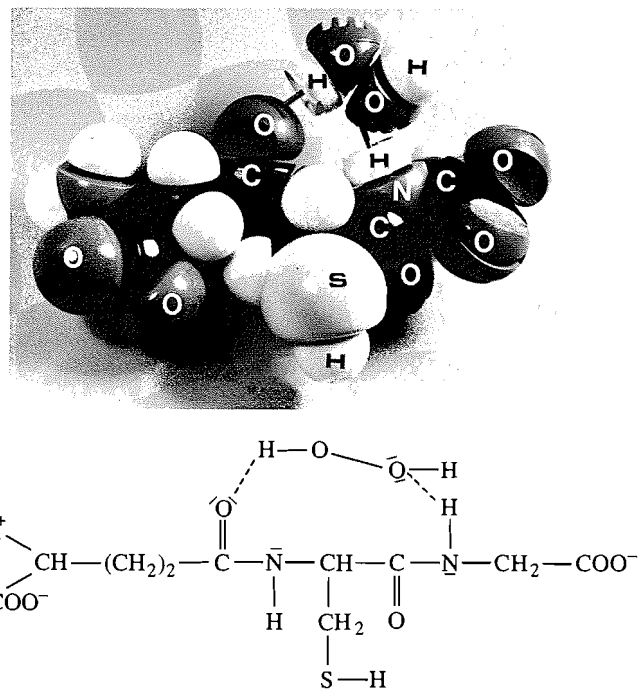


FIG. 8. A chelate model between GSH and H_2O_2.

example, either a peroxide (covalently bond) or a chelate (hydrogen bonds). If we suppose that this product is formed with 1 mol of GSH and 1 mol of H_2O_2, we will use the symbole [GSH—H_2O_2], according to the equilibrium [2]

[2] $GSH + H_2O_2 \rightleftharpoons [GSH—H_2O_2]$ K_2

Since the thiol function of this complex [GSH—H_2O_2] is measured by the Ellman's method (see Experimental section) the curves showing [GSH] versus time would represent the sum [GSH] + [GSH—H_2O_2] versus time. We have to notice that the peroxide or the chelate ([GSH—H_2O_2]) cannot be determined

Can. J. Chem. Downloaded from www.nrcresearchpress.com by 194.225.253.170 on 09/07/12
For personal use only.

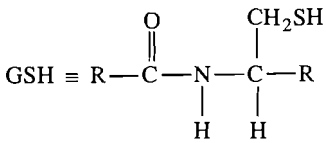
by the titanium method. Let us suppose the concentration of the complex is equal to the concentration of initial disappearance of free H_2O_2. The equilibrium constant is given by

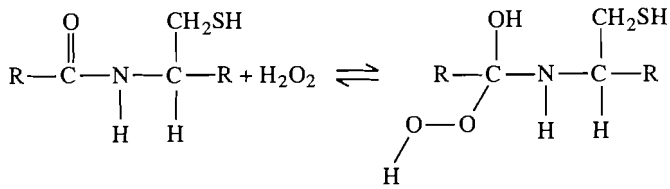
$$K_2 = \frac{[GSH—H_2O_2]_{eq}}{[GSH]_{eq}[H_2O_2]_{eq}}$$

$$= \frac{[H_2O_2]_0 - [H_2O_2]_{eq}}{([GSH]_0 - [H_2O_2]_0 + [H_2O_2]_{eq})[H_2O_2]_{eq}}$$

These values are reported in Table 1. A plot of $[GSH—H_2O_2]_{eq}$ against $[H_2O_2]_{eq} \times [GSH]_{eq}$ is given in Fig. 7, the straight line being consistent with the above mentioned hypothesis. The slope of this line gives $K_2 = 1950 \pm 50$.

Several hypotheses can be considered on the nature of the complex symbolized by $[GSH—H_2O_2]$. It would be a chelate formed from two hydrogen bonds between H_2O_2 and the peptide parts of the glutathione molecule (see Fig. 8 as a model). Another possibility could be a peroxide formed by the nucleophilic addition of H_2O_2 on one of the carbonyl groups of GSH according to





Such an organic peroxide could account for the residual oxidizing power noted experimentally. This type of addition is well known for aldehydes and ketones and, for example, the equilibrium constant between HCHO and H_2O_2 has been determined to be 7000 M^{-1} (17). Thus our value for $K_2 = 1950 \pm 50$ is consistent with this type of addition or adduct formation.

Kinetic scheme

Our experimental results can be explained by two separate kinetic pathways. Pathway I involves reaction [2] and [3]; and pathway II is composed of reactions [4] to [7]

Pathway I
[2] $GSH + H_2O_2 \rightleftharpoons [GSH—H_2O_2]$
[3] $2[GSH—H_2O_2] \rightarrow [GSSG—H_2O_2] + H_2O$

Pathway II
[4] $[GSH—H_2O_2] \rightarrow GSOH + H_2O$
[5] $2GSOH \rightleftharpoons GSH + GSO_2H$
[6] $GSO_2H + [GSH—H_2O_2] \rightarrow [GSSG—H_2O_2] + H_2O_2$
[7] $GSOH + H_2O_2 \rightarrow GSO_2H + H_2O$

In pathway I, equilibrium [2] indicates the disappearance of H_2O_2 without oxidizing the thiol, giving the complex $[GSH—H_2O_2]$ which cannot be distinguished from GSH by the Ellman's method. $[GSH—H_2O_2]$ could disproportionate according to reaction [3], giving the final product $[GSSG—H_2O_2]$ which accumulates. The formation of this peroxide or chelate between GSSG and H_2O_2 is consistent with the following experimental results: at the end of a reaction, when there is no free H_2O_2 (*i*) the addition of catalase stimulates the formation of oxygen (see Fig. 2, curve *c*) and (*ii*) the presence of an excess of GSH gives an amount of GSSG equal to those of the hound peroxide (see Fig. 3, curve *e'*).

In pathway II, reaction [4] occurs in competition with reaction [3] and could explain the formation of another oxidized from of GSH like, for example, GSOH, which is named X^{305} in the text. This reaction which can be described as a nucleophilic attack on H_2O_2 initiates the minor oxidation mechanism. It is consistent with previous works where H_2O_2 acts with thiocyanate (6), 2-mercaptoethanol (8), hydrogen sulfide (2), thiourea or *N,N'*-dialkylthioureas (4) giving an intermediate type of RSOH.

We have admitted that GSOH diproportionates according to reaction [5] giving GSH and GSO_2H, this reaction being similar to those of CySOH (18) and HSOH (2). The backward reaction [−5] could explain the stabilization of the intermediate GSOH when an excess of GSH is present at the end of a reaction (see Fig. 3). GSO_2H would react with $[GSH—H_2O_2]$ giving $[GSSG—H_2O_2]$ according to reaction [6]. Both reactions [5] plus [6] explain the transformation of GSOH (= X^{305}) into $(GSSG—H_2O_2]$ (λ_{max} = 250 nm) that is consistent with the presence of an isobestic point (268 nm) when the intermediate X^{305} decays (see Figs. 1, 5, and 6, curves *iii*, *d'*, *d*); reaction [7] takes place only when there is an excess of free H_2O_2 in the medium and could explain the fast decrease of X^{305} (see Figs. 5 and 6). The sum of the reactions [7] plus [6] involves the non-decomposition of H_2O_2 as it has been experimentally verified (see Fig. 6, curve *d*), the decay of X^{305} being catalyzed by H_2O_2.

Simulation of the kinetic curves have been done by four successive steps; one step for pathway I and three other steps for pathway II.

(i) Pathway I: We have calculated only with pathway I (reactions [2], [−2], and [3]), the three rate constants k_2, k_{-2}, and k_3 (knowing the experimental constant $K_2 = 1950 \pm 50$) with the following values:

$$k_2 \geq 15\ M^{-1}\ s^{-1}$$
$$k_{-2} \geq 7.5 \times 10^{-3}\ s^{-1}$$
$$K_2 = 2000 \pm 700$$
$$k_3 = 0.9 \pm 0.1\ M^{-1}\ s^{-1}$$

The kinetic scheme [2], [−2], and [3] is consistent with 85% of the overall oxidation of GSH and the calculated curves agree with experimental ones during 1.5 to 2 half times (calculated curves not shown).

Several comments can be made. The quantitative treatment of the kinetic scheme shows that reaction [3] is the rate-limiting step for GSH oxidation. Indeed rate constant k_3 (0.9 $M^{-1}\ s^{-1}$) is smaller than the rate constant of the initiation reaction k_2 (≥ 15 $M^{-1}\ s^{-1}$). We gave the lower limit values of the rate constants k_2 and k_{-2} which are consistent with the k_3 limiting step value (the ratio k_2/k_{-2} being constant). The slow decay of free H_2O_2 can be explained by the displacement of equilibrium [2] to the right by reaction [3]. Two reactions [2] and [3] correspond to the overall reaction:

[8] $2GSH + 2H_2O_2 \rightarrow [GSSH—H_2O_2] + 2H_2O$

We have calculated that 80–85% of the total of $[GSSG—H_2O_2]$ is formed according to both reactions [2] and [3] ($k_2 \geq 15$ $M^{-1}\ s^{-1}$, $k_{-2} \geq 7.5 \times 10^{-3}\ s^{-1}$, $K_2 = 2000 \pm 700$, $k_3 = 0.9 \pm 0.1\ M^{-1}\ s^{-1}$).

(ii) Pathway II: This pathway involves three other steps. We have determined the rate constant k_4 of reaction [4] which initiates the minor oxidation process by studying the kinetic formation of X^{305}. We have made the following hypothesis: since the disappearance of X^{305} gives the formation of GSSG,

Can. J. Chem. Downloaded from www.nrcresearchpress.com by 194.225.253.170 on 09/07/12
For personal use only.

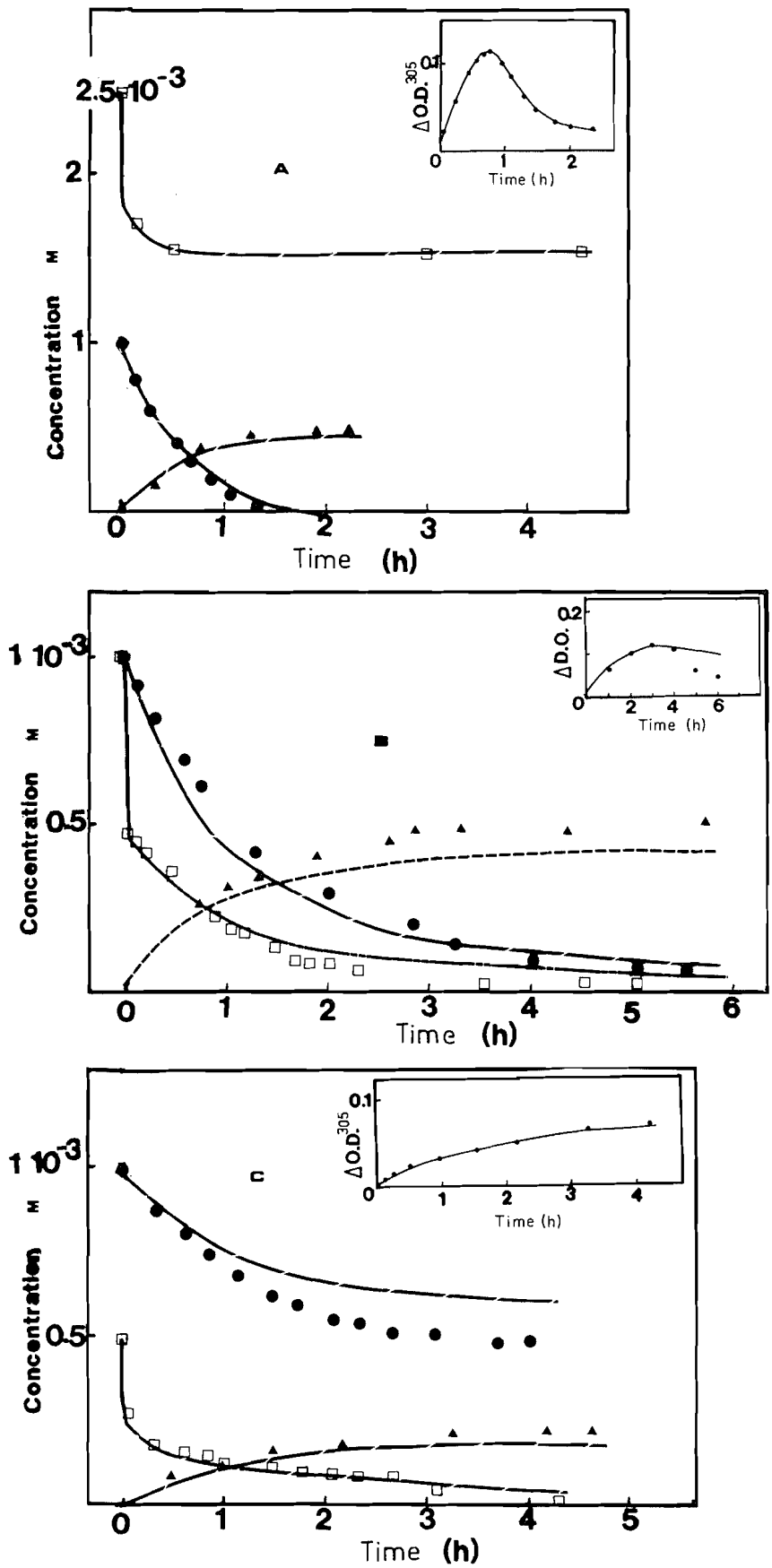


FIG. 9. Comparison between the computed kinetic curves and the experimental points [GSH] + [GSH − H_2O_2] (●), [H_2O_2] (□), [GSSG—H_2O_2] (▲) for three different experiments: (*A*) $[GSH]_0 = 10^{-3}$ *M*, $[H_2O_2]_0 = 2.5 \times 10^{-3}$ *M*; (*B*) $[GSH]_0 = [H_2O_2]_0 = 10^{-3}$ *M*; (*C*) $[GSH]_0 = 10^{-3}$ *M*, $[H_2O_2]_0 = 5 \times 10^{-4}$ *M*, phosphate buffer 0.1 *M*, pH 7, 22°C. Inset: computed curves of ΔOD^{305} (taking $\Delta\epsilon^{305} = 750 \pm 50$ M^{-1} cm^{-1}, see text) for three experiments (points are experimental).

Can. J. Chem. Downloaded from www.nrcresearchpress.com by 194.225.253.170 on 09/07/12
For personal use only.

we supposed that the variation $\Delta[X^{305}]$ was equal to [GSSG]/2. Therefore

$$\Delta\epsilon X^{305} = \frac{\Delta OD^{305}}{\Delta[GSSG]/2} = 750 \pm 50\ M^{-1}\,cm^{-1}$$

Using this method we could obtain the evolution of X^{305} concentration and consequently the initial rate of formation of X^{305}. Thus from different experimentations we have obtained the mean value of k_4 which is equal to $(1.5 \pm 0.5) \times 10^{-4}\ s^{-1}$.

The second step was the determination of k_7 and k_6. As we have seen before in the experimental results (paragraph 3), the decay of X^{305} is accelerated by added H_2O_2 (Fig. 5). This phenomenon has also been seen when $[H_2O_2]_0 > [GSH]_0$ (Fig. 6). Hence we have supposed that reactions [7] and [6] were predominant under these conditions and that reactions [5] and [−5] can be ignored.

k values of reactions [7] and [6] have been calculated using the kinetic scheme composed of reactions [2], [−2], [3], [4], [7], and [6]. The following k values gave the best agreement with the experimental curves in Fig. 6:

$$k_7 = 0.25 \pm 0.05\ M^{-1}\,s^{-1}$$

$$k_6 = 30 \pm 5\ M^{-1}\,s^{-1}$$

The third step consists of the calculation of the rate constants k_5 and k_{-5} in the case where $[GSH]_0 \geq [H_2O_2]_0$ (Fig. 9*C*). We then used the total kinetic scheme comprising reactions [2], [−2], [3], [4], [5], [−5], [6], and [7] to obtain

$$k_5 = 0.05 \pm 0.02\ M^{-1}\,s^{-1}$$

$$k_{-5} = 0.06 \pm 0.01\ M^{-1}\,s^{-1}$$

From these we obtain

$$K_5 = 0.83 \pm 0.17$$

Thus this reaction mechanism (reactions [2] to [7]) has been shown to adequately describe all kinetic results (Fig. 9 *A*, *B* and *C*).

Figure 9 *A*, *B*, and *C* insets show the calculated curves of ΔOD^{305}, points are experimental. We can see a good agreement with the experimental values.

When there is initially an excess of GSH it can be supposed that another reaction takes place, for example,

[9] $[GSSG—H_2O_2] + 2GSH \rightarrow 2GSSG + 2H_2O$

This reaction explains the results reported before showing that an excess of GSH gives an amount of GSSG equal to those of the peroxide $[GSSG—H_2O_2]$.

Reactions [8] and [9] add together to give reaction [1], in good agreement with the usually accepted overall reaction:

[1] $2GSH + H_2O_2 \rightarrow GSSG + 2H_2O$

Hence when there is a sufficient excess of GSH, the overall stoichiometry of the reaction could be accurately expressed by reaction [1].

Conclusion

The analytical methods used in this work allowed us to measure (*i*) free H_2O_2 and not other peroxide with the titanium method, (*ii*) the SH group with Ellman's method, (*iii*) the disulfide S—S with the enzymatic NADPH reduction or with the differential absorption at 250 nm, (*iv*) the intermediate X^{305} (which could be GSOH) with the differential absorption at 305 nm.

Our kinetic data indicate that in our experimental conditions $(0.2 \leq [GSH]_0/[H_2O_2]_0 \leq 2)$ the overall oxidation equation has been established to be 2 mol GSH with 2 mol of H_2O_2 giving 1 mol GSSG:

[8] $2GSH + 2H_2O_2 \rightarrow [GSSG—H_2O_2] + 2H_2O$

This implicates that an important part of H_2O_2 disappears without oxidizing the thiol function. We attributed this result to the formation of a peroxide or a chelate between GSH and H_2O_2, in which bound H_2O_2 cannot be measured by our titanium sulphate method.

Since GSH can rapidly scavenge H_2O_2 before reducing it, GSH appears as a carrier of H_2O_2 and therefore as a protector against the toxicity of H_2O_2.

Moreover, it has been shown that the oxidation of GSH by H_2O_2 has also a minor oxidation process (15% of the total GSSG formation). This phenomenon is mediated by an intermediate compound absorbing at 305 nm, which has been seen by McCormick *et al.* (9) in the same conditions.

Acknowledgments

We are grateful for valuable discussions with Dr. R. Azerad and the HPLC facilities.

1. M. Lal, D. A. Armstrong, and M. Wieser. Rad. Res. **37**, 246 (1969).
2. M. R. Hoffmann. Environ. Sci. Technol. **11**, 61 (1977).
3. J. V. McArdle and M. R. Hoffmann. J. Phys. Chem. **87**, 5425 (1983).
4. M. R. Hoffmann and J. O. Edwards. Inorg. Chem. **16**, 3333 (1977).
5. M. A. P. Dankleff, R. Curci, J. O. Edwards, and H. Y. Pyun. J. Am. Chem. Soc. **90**, 3209 (1968).
6. I. R. Wilson and G. M. Harris. J. Am. Chem. Soc. **82**, 4515 (1960).
7. I. R. Wilson and G. M. Harris. J. Am. Chem. Soc. **83**, 268 (1961).
8. P. S. K. Leung and M. R. Hoffmann. J. Phys. Chem. **89**, 5267 (1985).
9. J. P. McCormick, S. Klita, J. Terry, M. Schrod, and A. Eisenstark. Photochem. Photobiol. **36**, 367 (1982).
10. D. H. Calam and S. G. Waley. Biochem. J. **85**, 417 (1962).
11. G. L. Ellman. Arch. Biochem. Biophys. **82**, 70 (1959).
12. I. Carlberg and B. Mannervik. Febs Lett. **115**, 265 (1980).
13. G. Eisenberg. Ind. Eng. Chem. Anal. Ed. **15**, 327 (1948).
14. M. P. Bonét-Maury. C.R. de l'Academie des Sciences, 117 (1944).
15. R. Curci and J. O. Edwards. *In* Organic peroxides. vol. 1. *Edited by* D. Swern. Wiley Interscience, New York. 1970.
16. D. J. Reed, J. R. Babson, P. W. Beatty, A. E. Brodie, W. W. Ellis, and D. W. Potter. J. Anal. Biochem. **106**, 55 (1980).
17. S. Marklund. Acta Chem. Scand. **25**, 3517 (1971).
18. J. W. Purdie. J. Am. Chem. Soc. **89**, 2 (1967).

Can. J. Chem. Downloaded from www.nrcresearchpress.com by 194.225.253.170 on 09/07/12
For personal use only.

Morphinanes isomères originaux isolés de *Stephania zippeliana*

BRIGITTE CHARLES, HELENE GUINAUDEAU ET JEAN BRUNETON[1]

Centre d'études des plantes médicinales, Unité de formation et de recherche des sciences médicales et pharmaceutiques, 16, boulevard Daviers, 49000 Angers, France

et

PIERRE CABALION

Office de la recherche scientifique et technique d'outre-mer, B.P. 76, Port-Vila, Vanuatu

Reçu le 6 juin 1988[2]

BRIGITTE CHARLES, HELENE GUINAUDEAU, JEAN BRUNETON et PIERRE CABALION. Can. J. Chem. **67**, 1257 (1989).

À côté de huit aporphinoïdes, six alcaloïdes possédant une structure de morphinane ont été isolés des parties aériennes de *Stephania zippeliana* Miq. (Ménispermacées) : quatre d'entre eux sont nouveaux : la (+)-erromangine **2**, la (+)-tannagine **3**, la (+)-zippeline **5** et la (+)-zippelianine **6**. La (+)-stephodeline **1**, la (+)-isostephodeline **4** et les composés **2** et **3** sont isomères. La structure de la (+)-isostephodeline **4** a été corrigée.

Mots clés : *Stephania zippeliana*, morphinanes, alcaloïdes.

BRIGITTE CHARLES, HELENE GUINAUDEAU, JEAN BRUNETON, and PIERRE CABALION. Can. J. Chem. **67**, 1257 (1989).

Eight aporphinoids and six morphinans have been isolated from aerial parts of *Stephania zippeliana* Miq. (Menispermaceae): four of them are new: (+)-erromangine **2**, (+)-tannagine **3**, (+)-zippeline **5**, and (+)-zippelianine **6**. The previously isolated alkaloids (+)-stephodeline **1**, (+)-isostephodeline **4**, and compounds **2** and **3** are isomeric. The structure of (+)-isostephodeline **4** has been revised.

Key words: *Stephania zippeliana*, morphinans, alkaloids.

L'analyse de l'extrait alcaloïdique total obtenu à partir de 3 kg des parties aériennes sèches de *Stephania zippeliana* a fourni 14 alcaloïdes dont huit aporphinoïdes; ces derniers sont quatre aporphines, la (+)-corydine, la (+)-dicentrine, la (+)-crebanine et la (+)-stesakine, deux oxoaporphines, la dicentrinone et l'oxocrebanine et deux hydroxy-4 aporphines, la (+)-épiglaufidine et la (+)-hydroxy-4 dicentrine (1). Les six autres alcaloïdes sont des morphinanes, la (+)-stephodeline **1**, la (+)-erromangine **2**, la (+)-tannagine **3**, la (+)-isostephodeline **4**, la (+)-zippeline **5** et la (+)-zippelianine **6**. Les alcaloïdes **1** et **4** ont été isolés précédemment à partir de *Stephania delavayi*; les autres sont nouveaux.

Les alcaloïdes **1**, **2**, **3**, **4** sont isomères. Leurs spectres de masse (impact électronique) sont qualitativement semblables mais diffèrent par l'abondance des ions. Le pic moléculaire à m/z 373 correspond à la formule brute $C_{21}H_{27}O_5N$. Le spectre infrarouge de ces quatre composés présente deux bandes d'absorption vers 1615 et 1665 cm^{-1} mettant en évidence une fonction carbonyle conjuguée.

Le premier morphinane nouveau isolé est la (+)-erromangine **2**. Le spectre de rmn du proton (reporté autour de la formule **2**) présente quatre singulets de trois protons chacun dus à quatre méthoxyles (δ 3,78, 3,83, 3,84 et 4,08 ppm). Un système de quatre signaux conjugués est présent dans la région des protons aliphatiques; ce système est dû à un groupement méthylène (doublet de doublet à δ 2,68 ppm, et doublet à δ 3,18 ppm, J_{gem} = 17,7 Hz) conjugué à un groupement CH (doublet à δ 3,83 ppm, J_{ax} = 5,5 Hz), lui-même couplé à un second groupe CH (singulet élargi à δ 2,42 ppm). La présence de cet enchaînement -CH_2—CH—CH- est en faveur d'un squelette morphinane et exclut une structure hasubanane qui est caractérisée par la présence d'un système -CH_2—CH_2-. Les constantes de couplages des signaux de la séquence CH_2—CH—CH sont du même ordre que celles observées pour la stephodeline **1** (reportées autour de la formule **1**), et indiquent un enchaînement *trans* des cycles B et C de la (+)-erromangine comme pour la (+)-stephodeline (2). Dans la région des protons aromatiques, la présence de deux singulets de un proton à 6,59 et 6,60 ppm indique que le cycle A est substitué en 2,3. Deux doublets de un proton chacun à δ 2,83 et 2,88 ppm, présentant une constante de couplage de 16 Hz, sont dus à un groupement méthylène isolé. L'existence simultanée de la fonction carbonyle conjuguée et d'un groupement méthylène isolé dans la molécule impose que le groupement carbonyle soit en 6 ou 8. La différence des déplacements chimiques des protons en 14 et en 5, ainsi que celle d'un des méthoxyles du cycle C, indique une substitution différente de ce cycle C entre la stephodeline **1** et l'alcaloïde **2**. Dans le cas de la stephodeline, l'étude des effets Overhauser indique que le groupement carbonyle est en 6; en effet, l'irradiation du proton en 14 provoque l'augmentation du signal dû au méthoxyle à 4,18 ppm et inversement. Par suite, pour la (+)-erromangine **2**, la fonction carbonyle ne peut être qu'en 8.

L'étude du spectre de rmn du ^{13}C confirme cette attribution. Le déplacement chimique du carbone 5 est de 48,2 ppm dans le spectre de **1** et 39,1 ppm dans celui de **2**. La valeur observée dans le spectre de **2** est à rapprocher de celle présentée par la (+)-tridictyophylline (δ 34,6 ppm) (3) ou de celle observée dans le cas de la (+)-stephaphylline (δ 37,2 ppm) (4).

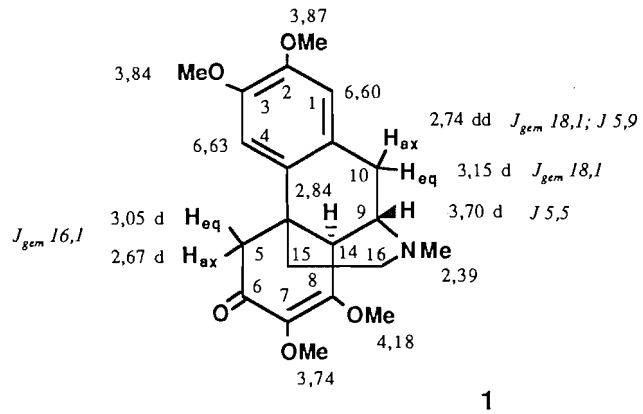
Le deuxième alcaloïde isolé, la (+)-tannagine **3**, présente, sur son spectre de masse, des fragmentations différentes de celles observées sur le spectre de masse de **1** et de **2**. En particulier, le fragment à m/z 59 a une abondance de 15% alors qu'il est pratiquement inexistant sur le spectre des alcaloïdes précédents; l'abondance de ce fragment est considérée comme indicative d'un enchaînement *cis* (5, 6).

Le spectre de rmn ^1H de **3** diffère de celui de l'alcaloïde précédent par la présence du signal dû au méthoxyle en 7 dans les champs plus élevés (δ 3,32 ppm), par le déplacement vers les champs plus faibles du multiplet dû à un des protons en C-15 (δ 1,47 ppm) ainsi que par la modification des constantes de couplage des protons en C-9 et C-14. Le découplage sélectif

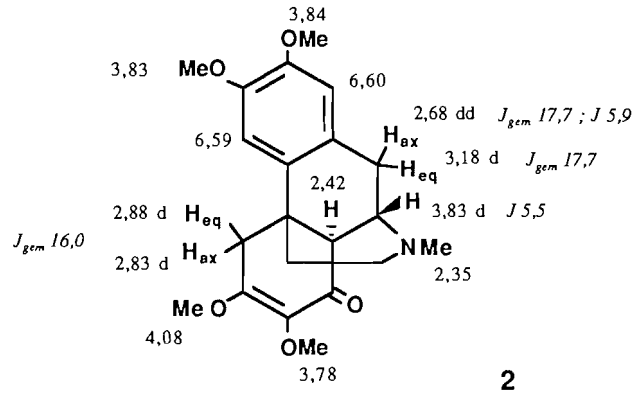
1. Auteur à qui adresser toute correspondance.
2. Revision reçue le 22 mars 1989.

Printed in Canada / Imprimé au Canada

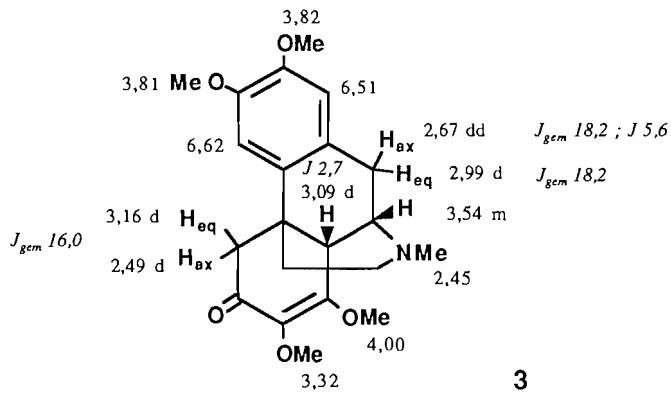
Can. J. Chem. Downloaded from www.nrcresearchpress.com by 194.225.253.170 on 09/07/12
For personal use only.



1



2



3

du spectre de rmn du proton ainsi qu'une étude des effets Overhauser confirment l'enchaînement *cis* des cycles B et C. En particulier, l'irradiation du doublet du proton en 14 (δ 3,09 ppm) entraîne une augmentation de l'intensité du multiplet à δ 1,92 ppm dû à H-15_{ax}, l'effet inverse étant également observé. L'analyse du spectre de ^{13}C permet de placer la fonction carbonyle en 6 étant donné le déplacement chimique du carbone 5 à 48,9 ppm; en effet, cette valeur est voisine de celle observée sur le spectre de la (+)-stephodeline **1**. La (+)-tannagine est donc un céto-6 morphinane tétraméthoxylé en 2, 3, 7 et 8 avec une jonction *cis* des cycles B et C. Cette structure est celle qui a été attribuée à la (+)-isostephodeline (7). Cependant, les données spectrales de la (+)-tannagine **3** sont différentes de celles décrites pour la (+)-isostephodeline.

Le morphinane **4**, isolé au cours de notre travail, présente en revanche des données spectrales identiques à celles indiquées pour la (+)-isostephodeline (7).

Le déplacement chimique à δ 39,2 ppm du carbone 5 sur le spectre de ^{13}C de l'alcaloïde **4** permet de placer la fonction carbonyle en 8 et non en 6 comme indiqué antérieurement pour l'isostephodeline. D'une part, les valeurs des constantes de couplage des signaux dus aux protons en 9 et 14 sont proches de celles observées dans le spectre de la (+)-tannagine; d'autre part, l'étude des effets Overhauser montre un effet réciproque entre les protons en 14 (δ 2,62 ppm) et celui en 15_{ax} (δ 1,92 ppm). De plus, le fragment à m/z 59 a une abondance de 12%. Ces données permettent de déterminer la stéréochimie *cis* de la jonction des cycles B et C. De même que pour les deux alcaloïdes précédents, le déplacement chimique du carbone 5 dans le spectre de ^{13}C est indicatif de la position du carbonyle; ce carbone résonnant à δ 39,2 ppm, la cétone doit être en 8.

La (+)-isotephodeline **4** est donc un céto-8 morphinane d'enchaînement B/C *cis* et la (+)-stephaphylline de *Stephania suberosa* lui est identique (4).

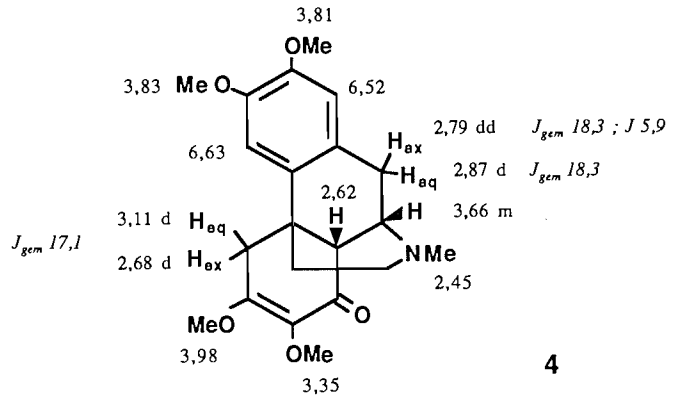
Les deux autres morphinanes isolés appartiennent au même type structural. La (+)-zippeline **5** a pour formule brute $C_{20}H_{25}O_4N$ et son spectre de masse présente un pic moléculaire décalé de 30 uma par rapport à celui de la (+)-stephodeline. Le spectre de rmn du proton de **5** est proche de celui de la (+)-stephodeline; cependant, il ne présente que trois singulets attribuables à des méthoxyles (δ 3,72, 3,84, 3,87 ppm) et comporte un doublet supplémentaire (δ 5,81 ppm, J = 2 Hz) dû à un proton qui couple avec celui en 14 (δ 2,97 ppm) comme l'a indiqué le découplage systématique. Une étude partielle des effets Overhauser montre une augmentation réciproque des intensités des signaux entre les protons en 8 et 14. Le méthoxyle porté par le carbone 8 dans la (+)-stephodeline est remplacé dans la (+)-zippeline **5** par un hydrogène.

Le dernier alcaloïde isolé, la (+)-zippelianine **6**, présente des données spectrales également proches de celles de la (+)-stephodeline **1**. Le spectre de masse de **6** présente un pic moléculaire à $M^{+\bullet}$ 359, c'est à dire inférieur de 14 uma à celui de la (+)-stephodeline; il correspond à la formule brute $C_{20}H_{25}O_5N$. Le spectre uv présente un effet bathochrome en milieu alcalin, ce qui indique la présence d'une fonction phénolique. Le spectre de rmn du proton montre l'absence du singulet dû au méthoxyle en 2 qui résonne sur le spectre de la (+)-stephodeline à δ 3,87 ppm. Une étude partielle des effets Overhauser montre la proximité du méthoxyle qui résonne à 3,85 ppm et du proton en 4 (δ 6,59 ppm). La (+)-zippelianine **6** est donc une (+)-déméthyl-2 stephodeline. La méthylation de l'alcaloïde **6** par le diazométhane conduit à la (+)-stephodeline **1**.

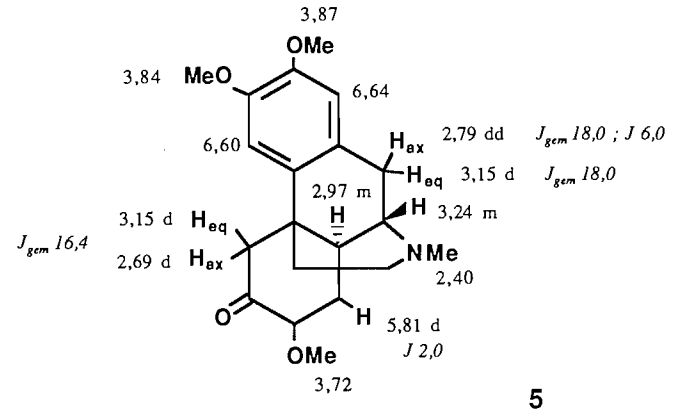
Jusqu'alors, l'étude approfondie des spectres de rmn du proton des céto-6 ou céto-8 morphinanes (enregistrement des spectres à hauts champs, découplage, étude des effets Overhauser) ne permettait pas de déterminer avec certitude la stéréochimie de la jonction des cycles B et C. Seul le déplacement chimique du carbone 5 sur le spectre de ^{13}C est indicatif de la position du carbonyle en position 6 ou 8. L'examen du spectre de masse en impact électronique n'est pas non plus concluant. En effet, l'abondance de l'ion fragment à m/z 59 ne semble pas être un élément de diagnostic très sûr en ce qui concerne l'enchaînement des cycles B et C; cette abondance n'est en effet pas reproductible d'un spectre à l'autre, les conditions dans lesquelles sont enregistrées les spectres semblant intervenir de façon non négligeable.

Par contre, l'étude des spectres en ms/ms en ionisation chimique positive nous a donné des résultats dépourvus d'ambiguïté (8); dans le cas d'un céto-6 morphinane, l'ion fragment correspondant aux carbones 7 et 8 éliminé aux cours des fragmentations (m/z 87 dans le cas d'une substitution diméthoxy-

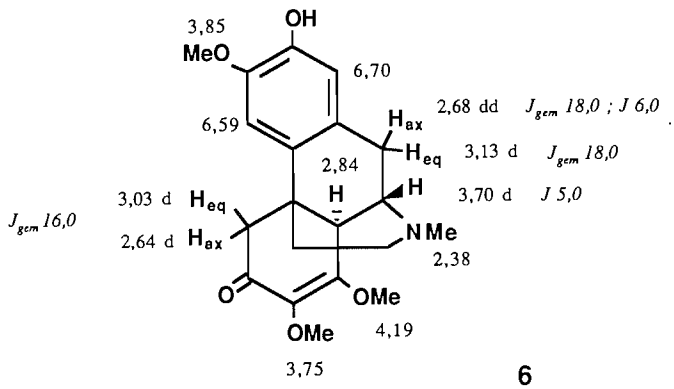
Can. J. Chem. Downloaded from www.nrcresearchpress.com by 194.225.253.170 on 09/07/12
For personal use only.



4



5



6

7,8) est abondant. Dans le cas d'un céto-8 morphinane, c'est le fragment correspondant à l'élimination des carbones 6 et 7 qui est important (*m/z* 101 dans le cas d'une substitution diméthoxy-7,8); ces résultats sont très reproductibles (8).

Dans la mesure où il nous a été possible d'analyser les données spectrales d'au moins un alcaloïde correspondant à chaque type d'enchaînement des cycles B et C ainsi que des deux positions du groupement carbonyle, des règles de détermination de structure par analyse des déplacements chimiques des spectres de rmn du proton sont proposées.

Le déplacement chimique du singulet dû au méthoxyle en 7 permet de différencier un enchaînement B/C *cis* ($\delta \approx 3{,}35$ ppm) d'un enchaînement *trans* ($\delta \approx 3{,}75$ ppm); de même le proton équatorial en 15 résonne à des champs plus élevés dans le cas d'un enchaînement *trans* ($\delta \approx 1{,}15$ ppm) que dans le cas d'un enchaînement *cis* ($\delta \approx 1{,}50$ ppm). Enfin, la valeur de la constante de couplage entre les protons en 9 et 14 est différente dans les deux types d'enchaînement, ce qui entraîne un aspect différent des signaux concernés (l'aspect attendu de doublet pour H-14 et de doublet dédoublé pour H-9 étant plus net dans le cas de l'enchaînement *cis* que dans celui d'un enchaînement *trans*). La position du groupement carbonyle en 6 ou 8 ne peut être déterminée que par l'examen du spectre de rmn du ^{13}C; le déplacement chimique du signal dû au carbone 5 permet de différencier les deux types de composés; ce déplacement est de l'ordre de 39 ppm dans le cas d'un céto-8 morphinane, alors qu'il est d'environ 49 ppm lorsque la fonction cétone est en 6; le déplacement vers les champs faibles est, dans ce dernier cas, dû à la proximité de la cétone.

Partie expérimentale

Appareillage

Les pouvoirs rotatoires sont mesurés à température ambiante dans le chloroforme à l'aide d'un polarimètre Schmidt et Haensch, les spectres uv enregistrés sur un appareil Beckman 530 et les spectres ir sur un spectromètre Perkin Elmer 580. Les spectres de rmn du proton ont été réalisés sur des solutions dans le $CDCl_3$ à l'aide des appareils Varian EM 360 (60 MHz) et Bruker WB 360 (360 MHz) et WM 500 (500 MHz). Les spectres de carbone 13 ont été enregistrés également sur des solutions dans le $CDCl_3$ à l'aide d'un appareil Bruker WM 500.

Matérial végétal

L'échantillon (3 kg de parties aériennes ligneuses) a été récolté en juillet 1984 à Erromango (Vanuatu) sur la pente nord de la péninsule du Rantop et est référencé sous le n° 187.

Extraction des alcaloïdes et purification

Après traitement de la poudre par l'hexane, l'extraction des alcaloïdes conduite suivant le processus classique (alcalinisation du marc suivi d'une extraction par le chlorure de méthylène et d'une purification par passage à l'état de sels) fournit 42 g d'alcaloïdes totaux (rendement 1,4%). Les alcaloïdes sont isolés et purifiés par chromatographie sur colonne de silice (silice pour ccm) puis par chromatographie préparative sur couche mince.

Description des produits isolés

(+)-Stephodeline **1** (rendement 4,5%) : $[\alpha]_D$ +20° ($CHCl_3$, *c* 0,60); ir (KBr) : 1665, 1615 cm^{-1}; uv (EtOH) : 273, 224, 212 nm; rmn ^1H : 2,30 (m, H-15_{ax}), 1,15 (m, H-15_{eq}), 2,09 (m, H-16_{ax}), 2,37 (m, H-16_{eq}); rmn ^{13}C : 110,3 (C-1), 147,5 (C-2), 147,5 (C-3), 106,5 (C-4), 48,2 (C-5), 193,9 (C-6), 137,1 (C-7), 162,9 (C-8), 52,2 (C-9), 26,8 (C-10), 133,4 (C-11), 133,4 (C-12), 34,6 (C-13), 48,2 (C-14), 32,7 (C-15), 45,9 (C-16); sm (IE) *m/z* : 373 (80) $M^{+\bullet}$, 358 (60), 342 (100), 330 (40), 222 (11), 192 (1,7), 59 (1,8). *Masse Exacte* calc. pour $C_{21}H_{27}O_5N$: 373,1894; trouvé (sm) : 373,1889.

Principaux effets nOe observés : H-4 vers OMe-3 (16%) et réciproquement (20%); H-4 vers H-$5_{éq}$ (10%) et réciproquement (13%); H-9 vers H-14 (6%) et réciproquement (8%); OMe-8 vers H-14 (3%) et réciproquement (3%).

(+)-Erromangine **2** (rendement 0,3%) : $[\alpha]_D$ +15° ($CHCl_3$, *c* 0,85); ir (KBr) : 1665, 1615 cm^{-1}; uv (EtOH) : 273, 224, 212 nm; rmn ^1H : 2,33 (m, H-15_{ax}), 1,18 (m, H-15_{eq}), 2,08 (m, H-16_{ax}), 2,38 (m, H-16_{eq}); rmn ^1H (C_6D_6) : 6,40 (H-1), 3,70 (OMe-2), 3,68 (OMe-3), 6,46 (H-4), 2,93 (H-5_{ax}), 2,58 (H-$5_{éq}$), 3,41 (OMe-6), 3,43 (OMe-7), 4,03 (d, H-9), 2,39 (H-10_{ax}), 2,95 (H-$10_{éq}$), 2,16 (s él, H-14); rmn ^{13}C : 110,5 (C-1), 147,5 (C-2), 147,6 (C-3), 106,8 (C-4), 39,1 (C-5), 160,5 (C-6), 136,2 (C-7), 193,2 (C-8), 51,6 (C-9), 26,7 (C-10), 133,8 (C-11), 129,2 (C-12), 34,4 (C-13), 50,1 (C-14), 33,7 (C-15), 46,3 (C-16); sm (IE) *m/z* : 373 (60) $M^{+\bullet}$, 358 (100), 344 (22), 330 (25), 299 (27), 230 (48), 222 (36,5), 178 (6,7), 59 (1,8). *Masse Exacte* calc. pour $C_{21}H_{27}O_5N$: 373,1894; trouvé (sm) : 373,1889.

(+)-Tannagine **3** (rendement 0,7%) : $[\alpha]_D$ +40° ($CHCl_3$, *c* 0,80); ir (KBr) : 1670, 1605 cm^{-1}; uv (EtOH) : 270, 225, 212 nm; rmn ^1H : 1,92 (m, H-15_{ax}), 1,47 (m, H-15_{eq}), 2,16 (m, H-16_{ax}), 2,49 (m, H-16_{eq}); rmn ^{13}C : 110,3 (C-1), 147,2 (C-2), 147,4 (C-3), 107,8 (C-4), 48,9 (C-5), 197,3 (C-6), 137,6 (C-7), 162,0 (C-8), 53,3 (C-9), 23,8 (C-10), 128,6 (C-11), 128,5 (C-12), 36,8 (C-13), 47,6 (C-14), 38,5 (C-15), 46,4 (C-16); sm (IE) *m/z* : 373 (60) $M^{+\bullet}$, 359 (63),

Can. J. Chem. Downloaded from www.nrcresearchpress.com by 194.225.253.170 on 09/07/12
For personal use only.

342 (100), 330 (40), 222 (13), 201 (8), 192 (2), 59 (3). *Masse Exacte* calc. pour $C_{21}H_{27}O_5N$: 373,1894; trouvé (sm) : 373,1889.

Principaux effets nOe observés : H-4 vers OMe-3 (11%) et réciproquement (10%); H-4 vers H-$5_{éq}$ (9%) et réciproquement (12%); H-14 vers H-15_{ax} (6%) et réciproquement (7%).

(+)-Isostephodeline **4** (rendement 14,5%) : $[\alpha]_D$ +93° ($CHCl_3$, *c* 1,0); ir (KBr) : 1645, 1605 cm^{-1}; uv (EtOH) : 273, 225, 211 nm; rmn ^1H : H-15_{ax} : 1,92 (m, H-15_{ax}), 1,53 (m, H-15_{eq}), 2,10 (m, H-16_{ax}), 2,48 (m, H-16_{eq}); rmn ^{13}C : 110,7 (C-1), 147,5 (C-2), 147,3 (C-3), 106,4 (C-4), 39,2 (C-5), 160,8 (C-6), 136,1 (C-7), 193,2 (C-8), 52,6 (C-9), 23,1 (C-10), 130,4 (C-11), 129,2 (C-12), 27,0 (C-13), 53,3 (C-14), 39,4 (C-15), 46,2 (C-16); sm (IE) *m/z* : 373 (72) $M^{+\bullet}$, 358 (100), 342 (17), 330 (8), 315 (42), 299 (23), 283 (48), 222 (14), 201 (8), 192 (2,2), 59 (12,5). *Masse Exacte* calc. pour $C_{21}H_{27}O_5N$: 373,1894; trouvé (sm) : 373,1889.

Principaux effets nOe observés : H-4 vers OMe-3 (15%) et réciproquement (15%); H-4 vers H-$5_{éq}$ (12%) et réciproquement (16%); H-14 vers H-15_{ax} (7%) et réciproquement (7%); H-14 vers H-9 (10%) et réciproquement (10%).

(+)-Zippeline **5** (rendement : 0,1%) : $[\alpha]_D$ +20° ($CHCl_3$, *c* 0,60); ir (KBr) : 1660, 1625 cm^{-1}; uv (EtOH) : 272, 225, 210 nm; rmn ^1H : 2,27 (m, H-15_{ax}), 1,14 (m, H-15_{eq}), 2,11 (m, H-16_{ax}), 2,49 (m, H-16_{eq}); rmn ^{13}C : 110,5 (C-1), 147,6 (C-2), 147,6 (C-3), 106,4 (C-4), 48,9 (C-5), 193,2 (C-6), 119,3 (C-7), 151,0 (C-8), 57,8 (C-9), 23,9 (C-10), 133,4 (C-11), 128,1 (C-12), 36,7 (C-13), 41,2 (C-14), 31,6 (C-15), 46,3 (C-16); sm (IE) *m/z* : 343 (100) $M^{+\bullet}$, 328 (7), 300 (20), 192 (23), 115 (6), 59 (0,9). *Masse Exacte* calc. pour $C_{20}H_{25}O_4N$: 343,1781; trouvé (sm) : 343,1783.

Principaux effets nOe observés : H-4 vers H-$5_{éq}$ (14%) et réciproquement (14%); H-9 vers H-14 (5%) et réciproquement (5%), H-9 vers H-10_{ax} (12%) et réciproquement (4%); H-8 vers H-14 (5%) et réciproquement (5%).

(+)-Zippelianine **6** (rendement : 0,2%) : $[\alpha]_D$ +25° ($CHCl_3$, *c* 0,70); ir (KBr) : 1660, 1605 cm^{-1}; uv (EtOH) : 268, 221, 212 nm (EtOH + KOH : 272, 248, 221 nm); rmn ^1H : 2,32 (m, H-15_{ax}), 1,13 (m, H-15_{eq}), 2,11 (m, H-16_{ax}), 2,37 (m, H-16_{eq}); sm (IE) *m/z* : 359 (40) $M^{+\bullet}$, 344 (42), 329 (45), 328 (100), 316 (39), 230 (40), 222 (20). *Masse Exacte* calc. pour $C_{20}H_{25}O_5N$: 359,1741; trouvé (sm) : 359,1732.

Principaux effets nOe observés : H-4 vers H-$5_{éq}$ (14%) et réciproquement (14%); H-9 vers H-14 (5%) et réciproquement (5%); H-9 vers H-10_{ax} (12%) et réciproquement (4%); H-4 vers OMe-3 (11%) et réciproquement (12%).

Méthylation de la zippelianine **6** : 10 mg de **6** en solution dans 2 mL de méthanol ont été mis en contact avec 3 mL de diazométhane en solution éthérée pendant 24 h; après évaporation du solvant, 6 mg de résidu présentent des caractéristiques spectrales identiques à celles de la stéphodéline **1** (ccm, ir, rmn ^1H).

1. H. Guinaudeau, M. Leboeuf et A. Cavé. J. Nat. Prod. **47**, 565 (1984).
2. T. L. Il'inskaya, M. E. Perelson, I. I. Fadeeva et O. N. Tolkachev. Khim. Prir. Soedin. 650 (1973).
3. A. I. Spiff, V. Zabel, H. Watson, M. A. Zemaiti, A. M. Ateya, D. J. Slatkin, J. E. Knapp et P. L. Schiff. J. Nat. Prod. **44**, 160 (1981).
4. A. Patra. Phytochemistry, **26**, 2391 (1987).
5. H-E. Audier, M. Fetizon, D. Ginsburg, A. Mandelbaum et T. Rull. Tetrahedron Lett. 13 (1965).
6. A. Mandelbaum et D. Ginsburg. Tetrahedron Lett. 2479 (1965).
7. M. E. Perels'on, I. I. Fadeeva et T. L. Il'inskaya. Khim. Prir. Soedin. 188 (1975).
8. B. Charles et J.-C. Tabet. Rapid Commun. Mass Spectrom. **2**, 86 (1988).

Can. J. Chem. Downloaded from www.nrcresearchpress.com by 194.225.253.170 on 09/07/12
For personal use only.

S_N2 reactions in the gas phase. Transition states for the reaction: $Cl^- + RBr = ClR + Br^-$, where $R = CH_3$, C_2H_5, and iso-C_3H_7, from *ab initio* calculations and comparison with experiment. Solvent effects

KIMIHIKO HIRAO
Department of Chemistry, College of General Education, Nagoya University, Nagoya, Japan

AND

PAUL KEBARLE
Chemistry Department, University of Alberta, Edmonton, Alta., Canada T6G 2G2

Received January 5, 1989

KIMIHIKO HIRAO and PAUL KEBARLE. Can. J. Chem. **67**, 1261 (1989).

The geometries and the energies of the reactants, transition state, and products for the gas phase reaction: $Cl^- + CH_3Br = ClCH_3 + Br^-$, were obtained from *ab initio* calculations using a closed shell SCF method with a MINI basis set developed by Huzinaga *et al.* The energy changes predicted by the calculations are found in good agreement with the experimental data. The energies and geometries of the reactants and the transition state for the gas phase reactions: $Cl^- + RBr = ClR + Br^-$, where $R = C_2H_5$ and iso-C_3H_7, were also obtained. The resulting activation energies follow the same trend as the experimental data: Me < Et < iso-Pr; however, the predicted increase of activation energy is considerably larger. The energies and geometries for the reactants, transition state, and products of the gas phase ion-dihydrate reaction: $Cl^-(H_2O)_2 + CH_3Br \rightarrow H_2O(ClCH_3Br)^-H_2O \rightarrow Br^-(H_2O)_2 + CH_3Cl$ were obtained as well. These data provide an interesting comparison with experimental results in aqueous solution. The reaction coordinate of the ion-dihydrate reaction is very much closer to that for aqueous solution than to that for the gas phase.

Key words: nucleophilic substitution reactions, ion–molecule reactions, activation energy.

KIMIHIKO HIRAO et PAUL KEBARLE. Can. J. Chem. **67**, 1261 (1989).

Faisant appel à des calculs *ab initio* et utilisant la méthode en champ auto-cohérent, en couches fermées et basée sur un ensemble MINI, qui a été développée par Huzinaga et ses collaborateurs, on a déterminé les géométries ainsi que les énergies des réactifs, des états de transition et des produits de la réaction en phase gazeuse : $Cl^- + CH_3Br = ClCH_3 + Br^-$. On a trouvé que les changements d'énergie prédits par les calculs sont en bon accord avec les données expérimentales. On a aussi déterminé les énergies et les géométries des réactifs et des états de transition pour les réactions en phase gazeuse : $Cl^- + RBr = ClR + Br^-$ dans lesquelles $R = C_2H_5$ et iso-C_3H_7. Les énergies d'activation qui en résultent sont dans le même ordre que les données expérimentales : Me < Et < iso-Pr; toutefois, l'augmentation prédite pour l'activation d'énergie est beaucoup plus grande. On a aussi déterminé les énergies et les géométries des réactifs, des états de transitions ainsi que des produits de la réaction en phase gazeuse du dihydrate ionique : $Cl^-(H_2O)_2 + CH_3Br \rightarrow H_2O(ClCH_3Br)^-H_2O \rightarrow Br^-(H_2O)_2 + CH_3Cl$. Ces données fournissent une base intéressante de comparaison avec les résultats expérimentaux déterminés en solution aqueuse. Les coordonnées de la réaction du dihydrate ionique sont beaucoup plus proches de celles de la réaction en solution aqueuse que de celles de la réaction en phase gazeuse.

Mots clés : réactions de substitution nucléophile, réactions ion–molécule, énergie d'activation.

[Traduit par la revue]

Introduction

Studies of the kinetics and mechanism of bimolecular nucleophilic S_N2 reactions in solution have played a fundamental role in the development of physical organic chemistry (1). More recently a number of kinetic studies of S_N2 reactions in the gas phase were also reported and these have been recently reviewed (2*a*). The gas phase kinetic studies also include hydrated ionic reactants (2*b*). A number of quantum mechanical calculations relating to the structures and energies of reactants and transition states are also available (3, 4).

Reaction [1] is probably the most extensively studied S_N2 process in solution and has also received much attention in gas phase work. Experimental measurements of the rates of [1] in

[1] $Cl^- + RBr = ClR + Br^-$

R = Me, Et, *n*-Pr, iso-Pr, *n*-Bu, iso-Bu

the gas phase provide information on key points of the reaction coordinate, i.e., potential energy profile of the reaction. Initial work by Brauman and co-workers (5) based on ICR measurements at a single temperature led to a framework for the interpretation of the low pressure data, leading to predictions for the height of the energy barrier associated with the transition state. This was followed by work from this laboratory (6–8) at higher pressures and at variable temperature, which extended the results and interpretation.

The present work presents results from *ab initio* calculations for R = Me, Et, and iso-Pr. These data allow a comparison to be made between the experimental and theoretical data. Since the motivation for much of the above work was to seek comparison with the analogous reactions in solution (7, 8), the present calculations also include results that illustrate the effect of the presence of solvent molecules (H_2O) on the reaction coordinate for the reaction involving MeBr.

Results and discussion

a. Method of calculation, general

The energy profiles of reaction [1] (R = Me, Et, iso-Pr) were constructed on the basis of closed shell SCF calculations with a MINI basis set developed by Huzinaga *et al.* (9). A variety of basis sets was tested to determine the theoretical level appropriate for the present problems, particularly for the relative energies involved. The larger basis sets lead to improved

Can. J. Chem. Downloaded from www.nrcresearchpress.com by 194.225.253.170 on 09/07/12
For personal use only.

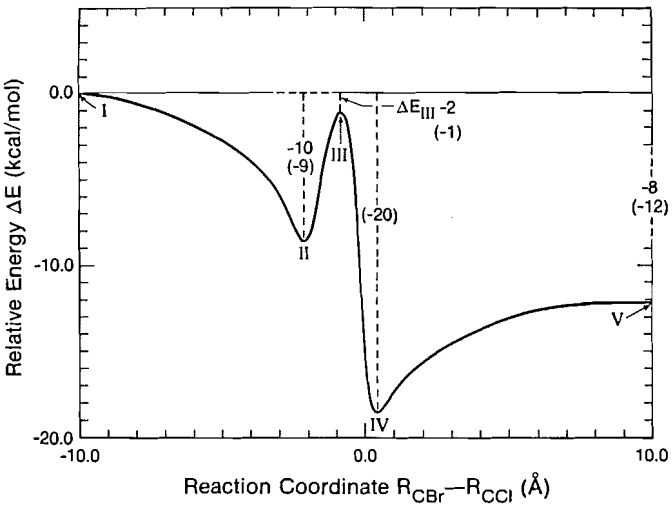


FIG. 1. Reaction coordinate for: $Cl^- + CH_3Br = ClCH_3 + Br^-$ in the gas phase. Energy changes in kcal/mol, without parentheses experimental results, with parentheses present calculations. For geometries of I–V see Fig. 2 and Table 1.

prediction for the energy of the individual molecules such as CH_3Cl and CH_3Br, but the agreement with experiment was not as good for the relative energies that are involved in Fig. 1. The SCF with MINI basis set provides a uniformly good description for the four key points on the reaction surface, viz., the separated reactants, the ion–dipole complex, the transition state, and the products. The good performance of this theoretical level may be due to fortuitous cancellation of errors arising from the incomplete basis set and neglect of electron correlation.

The energy profiles were obtained by using given fixed R_{CCl} values and optimizing the remaining geometry parameters with the energy gradient method.

b. Reaction coordinate of $Cl^- + CH_3Br \rightarrow ClCH_3 + Br^-$

The resulting energy profile is given in Fig. 1. It includes the energies of the reactants I, the precursor ion–dipole complex II, the transition state III, the post reaction ion–dipole complex IV, and the products V. The optimized geometries of I–V are given in Fig. 2.

The full reaction profile was constructed by calculating the energies at 17 points between reactants and products. For each fixed value of R_{ClC}, the remaining geometry parameters were optimized in C_{3v} symmetry. The calculated geometries and energies as well as the net atomic charges derived from a Mulliken population analysis are given in Table 1. The reaction coordinate, R_C is defined as

$$R_C = R_{CBr} - R_{ClC}$$

The R_C reflects the symmetry of the reaction. In the present calculations R_C takes on values of $-\infty$, -1.005 Å, -0.008 Å, 1.443 Å, and ∞ for the reactants, the ion–dipole complex, the transition states, the post reaction ion–dipole complex, and the products.

The increase of the H—C—Br angle (111.30°) in the dipole complex II relative to the angle in undisturbed CH_3Br (109.6°) must be due to the attractive interaction of the partially positive hydrogens of the CH_3 group with the negative Cl^-. The increase of the C—Br bond (2.073 Å) in II relative to that in undisturbed CH_3Br (2.026 Å) is quite small, see Fig. 2.

The transition state III has a geometry that is somewhat closer

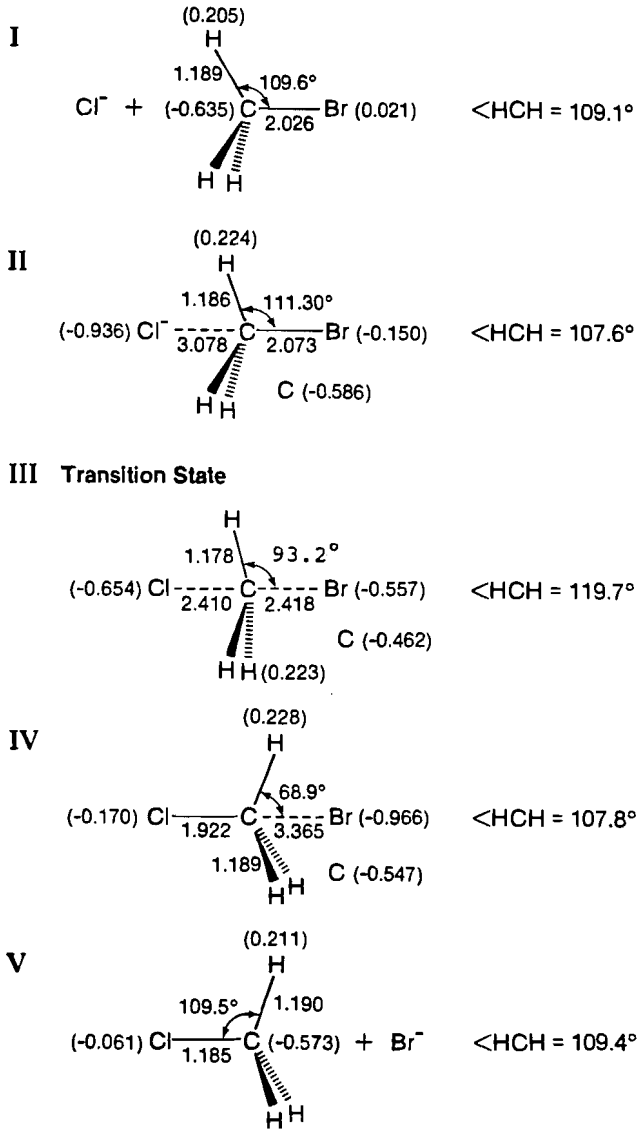


FIG. 2. Optimized geometries of reactants and transition state for gas phase reaction: $Cl^- + CH_3Br = ClCH_3 + Br^-$. Values in parentheses are net atomic charges. Distance is in angström, energies in atomic units.

to the reactants than the products. Thus the H—C—Br angle, although decreased relative to that in II and in CH_3Br, is still not 90° but 93.24°, see Fig. 2. Also, more of the negative charges appears on the Cl (−0.66) when compared to that on Br (−0.55).

In the dipole complex IV, $Br^-...CH_3Cl$, the H—C—Cl angle (111.1°) is similar to the analogous H—C—Br angle (111.3°) in the dipole complex II, i.e., now the attraction between the partially positive H atom and the Br^- pulls the CH_3 umbrella in, towards the negative Br^-.

Examining the data in Table 1 one finds that the distances R_{CCl} and R_{CBr} change smoothly as the system moves from the reactants to the products. The change in R_{CH} is also smooth but small. The change in the net atomic charges on Cl and Br is given in Fig. 3. The charge migration from Cl^- to Br also occurs smoothly and changes rapidly in the region of the transition state. The charge delocalization effect is maximum at the

Can. J. Chem. Downloaded from www.nrcresearchpress.com by 194.225.253.170 on 09/07/12
For personal use only.

TABLE 1. Geometries and energies of $ClCH_3Br^-$ calculated at the MINI basis[a]

R_{ClC}	R_{CBr}	R_{CH}	∠BrCH	$-E$ (au)	ΔE	Net atomic charges ΔQ_{Cl}	ΔQ_{Br}	ΔQ_C	ΔQ_H
∞ (I)	2.026	1.187	109.62	3058.751441	0.	−1.0	0.021	−0.635	0.205
7.0	2.029	1.187	109.99	3058.754401	−1.86	−1.0	−0.011	−0.630	0.214
4.0	2.038	1.188	110.86	3058.760628	−5.76	−0.994	−0.064	−0.618	0.225
3.5	2.048	1.187	111.35	3058.763646	−7.66	−0.975	−0.096	−0.608	0.226
3.2	2.063	1.186	111.44	3058.765302	−8.70	−0.950	−0.131	−0.594	0.225
3.078 (II)	2.073	1.186	111.30	3058.765504	−8.82	−0.936	−0.150	−0.586	0.224
2.8	2.115	1.182	109.64	3058.763075	−7.30	−0.887	−0.220	−0.557	0.221
2.6	2.186	1.179	105.39	3058.757654	−3.90	−0.825	−0.317	−0.519	0.221
2.5	2.265	1.177	100.77	3058.754299	−1.79	−0.763	−0.408	−0.492	0.221
2.439	2.348	1.178	96.40	3058.752891	−0.93	−0.700	−0.494	−0.472	0.222
2.410 (III)	2.418	1.178	93.24	3058.752690	−0.78	−0.660	−0.548	−0.462	0.223
2.40	2.444	1.178	91.94	3058.752739	−0.81	−0.636	−0.580	−0.457	0.224
2.38	2.548	1.180	88.17	3058.753118	−1.05	−0.653	−0.579	−0.446	0.226
2.35	2.711	1.183	82.64	3058.754546	−1.95	−0.497	−0.747	−0.439	0.228
2.3	2.830	1.186	78.50	3058.758112	−4.19	−0.429	−0.807	−0.444	0.227
2.2	2.994	1.189	74.41	3058.766404	−9.39	−0.353	−0.864	−0.461	0.226
2.1	3.135	1.190	71.98	3058.774535	−14.49	−0.270	−0.920	−0.490	0.226
1.922 (IV)	3.365	1.189	68.88	3058.782510	−19.50	−0.170	−0.966	−0.547	0.228
1.907	4.0	1.190	69.35	3058.780470	−18.21	−0.132	−0.993	−0.561	0.228
1.902	5.0	1.190	69.99	3058.777141	−16.13	−0.108	−1.0	−0.567	0.225
1.899	7.0	1.190	70.32	3058.774197	−14.28	−0.087	−1.0	−0.570	0.219
1.895 (V)	∞	1.190	70.53	3058.770733	−12.11	−0.061	−1.0	−0.573	0.211

[a]Distances in angstroms, angles in degrees, and relative energies in kcal/mol. Cl^-: −457.302114, Br^-: −2562.219615, CH_3Br: −2601.449297, CH_3Cl: −496.551118 (au).

transition state and this stabilizes the complex at the point where the chemical bond weakening is at its maximum.

The opening and shutting of the CH_3 umbrella as a function of the reaction coordinate is also shown in Fig. 3. In the initial stage of the reaction, the CH_3 umbrella shuts a little to help the approach of the Cl^-, which accelerates the reaction. This implies that the electrostatic attraction between the somewhat positive H atoms on the CH_3 group and the negative Cl^- plays a dominant role in the long-range interaction. Beyond this point, the umbrella begins to open and approaches a planar CH_3 at the transition state region. After the transition state, the umbrella begins to shut again in the opposite direction and overextends somewhat on formation of the dipole complex IV.

The theoretically predicted energy changes are very close to those determined experimentally and are also given in Fig. 1. Thus, the binding energy in the ion–dipole complex II is calculated as 9 kcal/mol while the experimental result is ~10 ± 1 kcal/mol, Larson and McMahon (10). The ΔE_{III}, i.e., the difference in energy between the transition state and the reactants, is −0.8 kcal/mol calculated, while the experimental results (5, 7) give −2 kcal/mol. Experimental data for the dipole complex IV, $Br^-...CH_3Cl$, are not available; however, the exothermicity of the reaction, ΔE_V, can be obtained from thermochemical data (7), so that the comparison of −12 kcal/mol, theoretical, versus −8 kcal/mol, experimental, can be made.

c. The $Cl^- + C_2H_5Br = C_2H_5Cl + Br^-$ and $Cl^- + iso\text{-}C_3H_7Br = iso\text{-}C_3H_7Cl + Br^-$ reactions

The energies of the reactants and the transition state were calculated. The transition state energies relative to the reactants and the geometries are given in Table 2 and in Figs. 4 and 5.

Methyl substitution increases the energy of the central barrier in Fig. 1 and increases ΔE_{III} from −0.9 for CH_3 to +5.3 for C_2H_5 and +15.7 kcal/mol for iso-C_3H_7. The changes are in the same direction as those observed by experiment (7); however, the calculation predicts progressively higher energies, see Table 3.

The increase of the energy barrier with methyl substitution is generally attributed to a steric effect. The net atomic charges of the reactant alkyl bromides, see Figs. 3, 4, and 5, provide an elaboration of this effect. As the negative Cl^- approaches the CH_3 group it experiences an attractive interaction with the three positive hydrogens, see preceding section. When one of the hydrogens is replaced by methyl, as in ethyl bromide, the carbon of the new methyl group has a negative charge (−0.54), see Figs. 4, 5, and the exchange repulsion with the negative Cl^- leads to an increase of energy. The effect repeats itself with the next new methyl for hydrogen replacement, i.e., isopropyl-bromide, see Fig. 5. The increasing repulsion with methyl substitution leads also to a very noticeable deviation from linearity in the $Cl^{-\delta}$—C—$Br^{-\delta}$ axis of the transition state, which is R = Me, 0.0°; R = Et, 13.2°; R = iso-Pr, 17.5°, see Figs. 4 and 5.

Concerning the discrepancy with the experimental ΔE_{III}, see Table 3, we give precedence of the experimental results over the calculated ones, particularly since the present calculations do not include diffuse augmentary basis functions. However, it should be mentioned that the interpretation of the experimental results (7) was not fully satisfactory. It was pointed out (7) that the preexponential factors of the rate constants k_1 increased by two orders of magnitude from MeBr to iso-PrBr. This is an unexpected result that could indicate a change of mechanism. One possibility is the occurrence of elimination, E2, rather than substitution for the larger alkyl groups. This alternative was considered, see discussion on p. 965 of ref. 7, and rejected

Can. J. Chem. Downloaded from www.nrcresearchpress.com by 194.225.253.170 on 09/07/12
For personal use only.

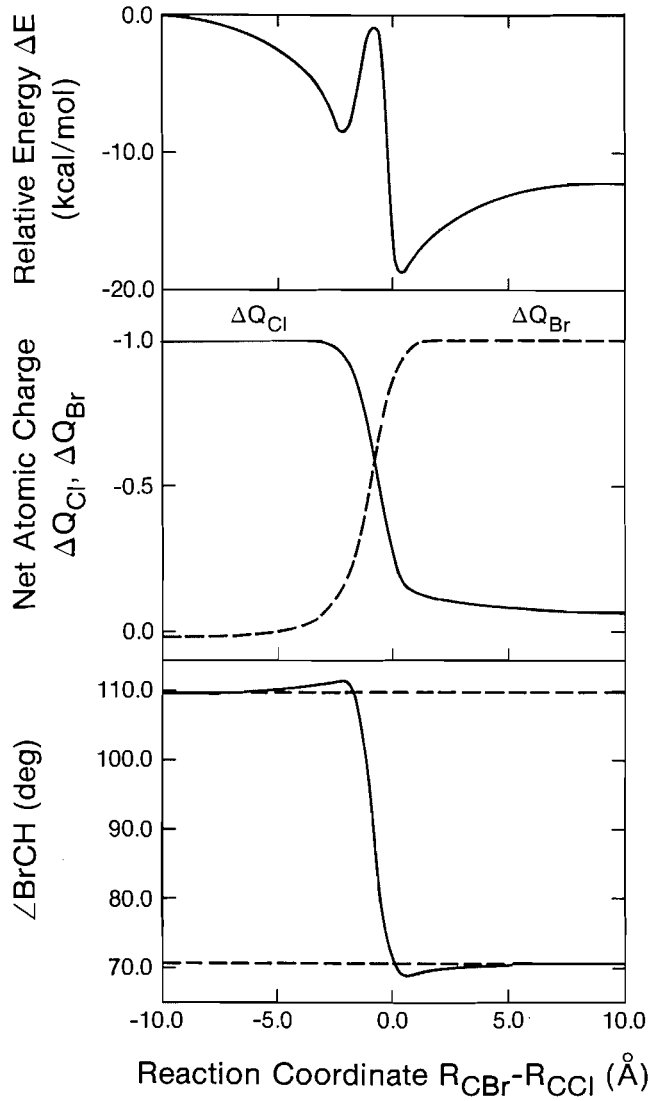


FIG. 3. Changes of relative energy ΔE (kcal/mol), net atomic charge on Cl resp. Br, Q_{Cl} resp. Q_{Br}, in atomic units, and angle BrCH for dilute gas phase reaction: $Cl^- + CH_3Br \rightarrow ClCH_3 + Br^-$ predicted by calculation.

on the basis of the known endothermicity of the reactions. However, the endothermicity is removed if the elimination proceeds initially not to HCl + Br^- but to $BrHCl^-$, which later dissociates (7). While the intermediate $BrHCl^-$ was not observed (7), this does not constitute a proof that it was not formed. Another alternative is a change of the transition state of the S_N2 reaction for the higher alkyl bromides. For example, one could speculate that in these reactions the Cl^- comes in on the same side as the Br atom and displaces it without Walden inversion. When the present calculations were made, such "extreme" transition state geometries were not considered.

d. Effect of dihydration on the reaction: $Cl^- + CH_3Br = ClCH_3 + Br^-$

Ab initio SCF calculations were performed also for the gas phase reaction:

$$Cl^-(H_2O)_2 + CH_3Br \rightarrow HOHCl\cdots C(H)(H)\cdots Br^-HOH \rightarrow ClCH_3 + Br^-(H_2O)_2$$

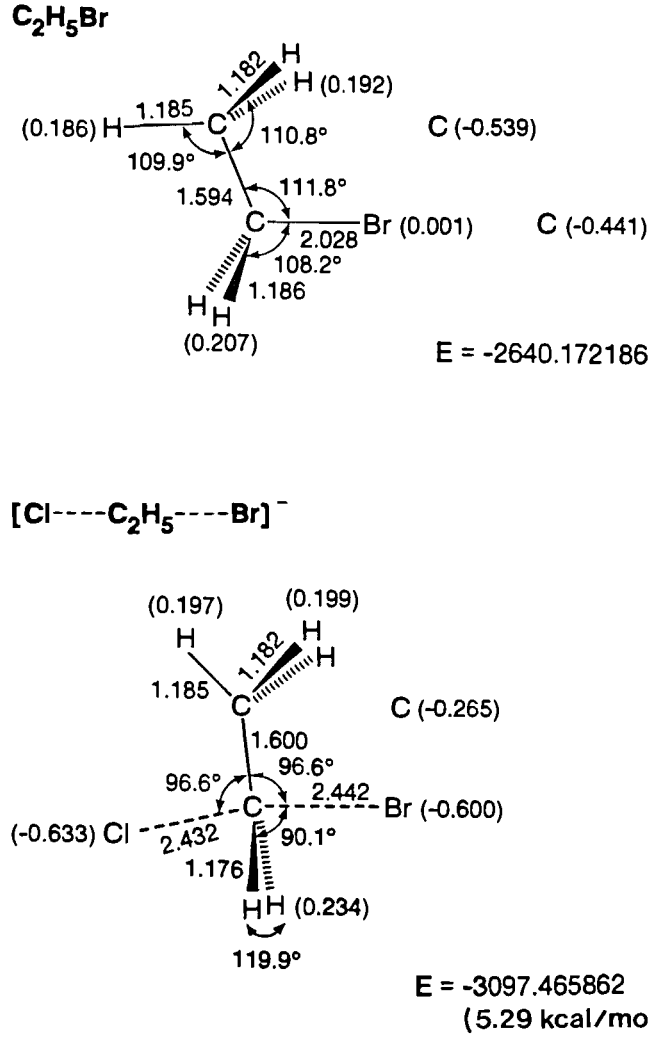


FIG. 4. Optimized geometries of ethyl bromide and transition state for gas phase reaction: $Cl^- + C_2H_5Br = ClC_2H_5 + Br^-$. Values in parentheses are net atomic charges. Distance is in angström, energies in atomic units.

Only partial geometry optimizations were performed for the dihydrate reaction. The geometries of the ion–dipole complex I, the transition state III, and the ion–dipole complex IV were taken as in the water-free reaction, see Fig. 2. However, the positions of the two water molecules were optimized in each case. The standard experimental geometries were used throughout for the H_2O molecules, i.e., O—H = 0.96 Å and HOH = 104.5°.

The optimized geometries of $Cl^-(H_2O)_2$, the dihydrate of the transition structure, and $Br^-(H_2O)_2$ are given in Fig. 6. It should be noted that the dihydrate of the transition structure $(ClCH_3Br)^-$ given in Fig. 6 should not be considered as the transition state of the gas phase reaction. As has been pointed out by Henchman and co-workers (11), states of higher energy occur as one of the two solvent molecules is transferred from the Cl side to the Br side of the transition structure ($ClCH_3Br$). Results from *ab initio* calculations, due to Morokuma (3*k*), giving points on the reaction coordinate of the symmetric Cl^- substitution reaction [2], *vide infra*, illustrate the energy increases associated with the transfer of a water molecule for the dihydrate reaction. The symmetrically hydrated transition structure in Fig. 6 represents, rather, one of the intermediate states of the reaction, and this state is of special interest from

Can. J. Chem. Downloaded from www.nrcresearchpress.com by 194.225.253.170 on 09/07/12
For personal use only.

TABLE 2. Energies and geometric parameters of the reactants, ion–dipole complexes, transition state, and products

	I	II	III	IV	V
E (au)	−3058.751441	−3058.765504	−3058.752891	−3058.782510	−3058.7707
ΔE (kcal/mol)	0.0	−8.84	−0.93	−19.51	−12.12
R_{ClC}	∞	3.078	2.439	1.922	1.18
R_{CBr} (Å)	2.026	2.073	2.348	3.365	∞
R_{CH} (Å)	1.187	1.186	1.178	1.189	1.19
∠BrCH	109.6	111.3	96.4	68.9	70.5
Net atomic charges					
ΔQ_{Cl}	−1.0	−0.936	−0.700	−0.170	−0.06
ΔQ_{Br}	0.021	−0.150	−0.494	−0.966	−1.0
ΔQ_{C}	−0.635	−0.586	−0.472	−0.547	−0.57
ΔQ_{H}	0.205	0.224	0.222	0.228	0.21

Cl^-: −457.302114, CH_3Br = 2601.449297, Br^-: −2601.449297, CH_3Cl = 496.551118 (au).

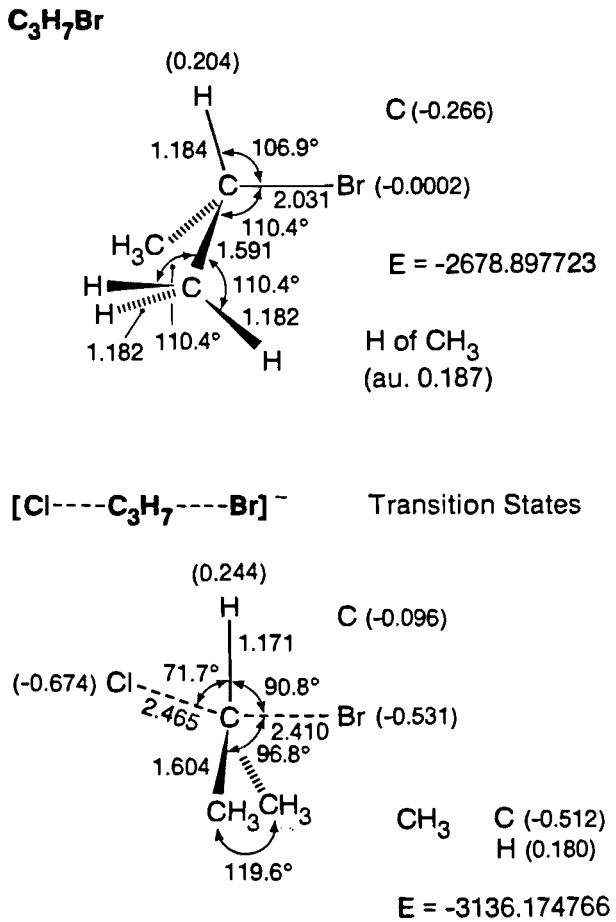


FIG. 5. Optimized geometries of isopropylbromide and transition state for gas phase reaction: Cl^- + iso-C_3H_7Br = C_3H_7Cl + Br^-. Values in parentheses are net atomic charges. Distances in angströms, energies in atomic units.

the standpoint of the reaction occurring in solution where the requirement that solvent molecules be transferred from one side to the other does not exist.

The reaction coordinates for reaction [1] in the gas phase (A), for the negative ion dihydrates (B), and in aqueous solution (C) are given in Fig. 7. The calculated energy changes together with the corresponding values from experiment, when available, are

TABLE 3. Cl^- + RBr = ClR + Br^-

(*a*) Transition state energy relative to that of the reactants (kcal/mol)

R	Theory	Experiment[a]
Me	−0.83	−2.5
Et	5.3	0.8
i-Pr	15.7	5.1

[a]Reference 3.

(*b*) Transition state geometries

R	R_{ClC}	R_{CBr}	∠BrCH	∠ClCBr
Me	2.410	2.418	93.24	180.0 (0.0)[a]
Et	2.432	2.442	96.6	166.8 (13.2)[a]
i-Pr	2.465	2.410	96.8	162.5 (17.5)[a]

[a]Deviation from linearity.

(*c*) Net atomic charges of the transition state

R	Q_{Cl}	Q_{Br}	Q_{C}	Q_{H}
Me	−0.660	−0.548	−0.462	0.223
Et	−0.633	−0.601	−0.268	0.234
i-Pr	−0.674	−0.531	−0.096	1.244

shown for four important positions in the reaction coordinate. The origins of the experimental data are given in the Appendix. The three cases A, B, C provide an interesting comparison. Although the ion dihydrate curve B is only ~27 kcal/mol below the gas phase, i.e., ΔE_I (B) = −27, while ΔE_I (C) = −86 kcal/mol, it is much closer in its general shape to the solution curve (C) than to the gas phase (A). Thus, the activation energies ΔE_{III} are (A) −2, (B) 18, (C) 26 kcal/mol. The depths of the well for the precursor complex are (A) −22, (B) −4, (C) 0, and the energy changes for the reaction ΔE_V are: (A) −8, (B) −5, (C) −4.6. Thus the presence of only two water molecules attached to the ion in the reactants, transition state, and products provides a good qualitative model for the major energy changes occurring in solution.

A reaction coordinate for the process [2] from *ab initio*

[2] $Cl^- + CH_3Cl \rightarrow [Cl\ldots CH_3\ldots Cl]^- \rightarrow ClCH_3 + Cl^-$

Can. J. Chem. Downloaded from www.nrcresearchpress.com by 194.225.253.170 on 09/07/12
For personal use only.

Can. J. Chem. Downloaded from www.nrcresearchpress.com by 194.225.253.170 on 09/07/12
For personal use only.

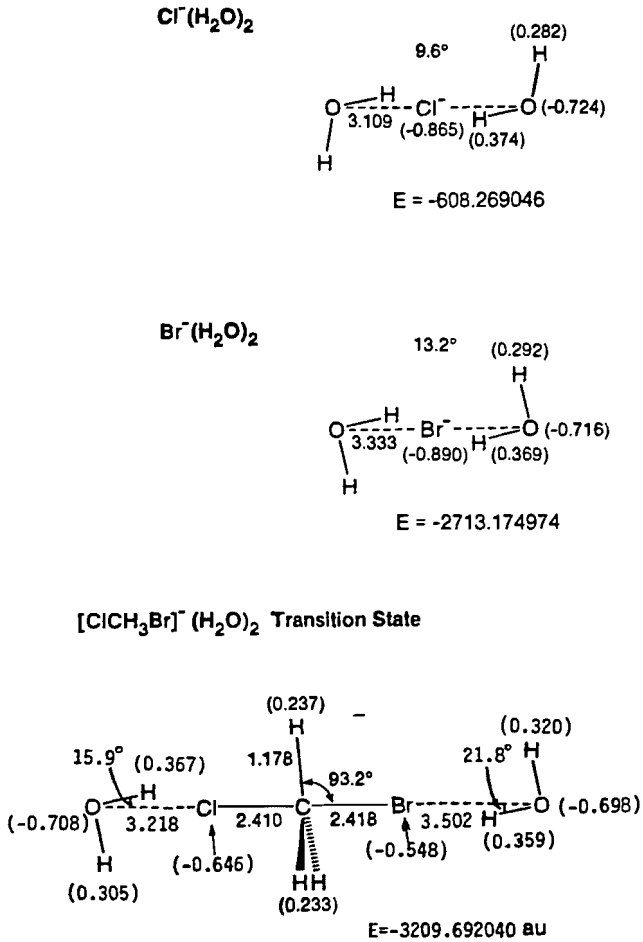


FIG. 6. Optimized geometries for ion dihydrate reaction: $Cl^-(H_2O)_2 + CH_3Br = CH_3Cl + Br^-(H_2O)_2$ giving geometries of hydrated ions, including the dihydrated transition state. Distances are in angströms, energies in atomic units. Values in parentheses are net atomic charges.

calculations was obtained by Jorgensen and co-workers (4) and was then used for Monte Carlo simulation of the effect of the liquid solvents. Jorgensen's work, which involves much more extensive calculations, provides very valuable insights on the solvation effects and the specific action of protic (H_2O) and dipolar aprotic solvents (DMF). It is interesting to note that reliable experimental rate constants for reaction [2] in the gas phase were published only very recently (12). Apparently, these results confirm Jorgensen's activation energy; however, details on how the rate data were used to obtain the activation energy were not given (12).

The present results, which deal with the computationally more difficult bromine-atom-containing reaction [1] and the effect of the alkyl groups, are expected to be less accurate. Also, the present results deal with hydration by only two molecules. Nevertheless they should be useful. Reaction [1] has been the subject of numerous experimental studies and can be considered as the historic prototype of aliphatic S_N2 processes. The very limited dihydration results, see Fig. 7, while not a quantitative model for aqueous solution, have didactic value since they illustrate, on the basis of only two solvent molecules, the major energy changes occurring with solvation, i.e., the large decrease of solvation of the charge dispersed ionic transition state II relative to the solvation of the ionic reactant Cl^-.

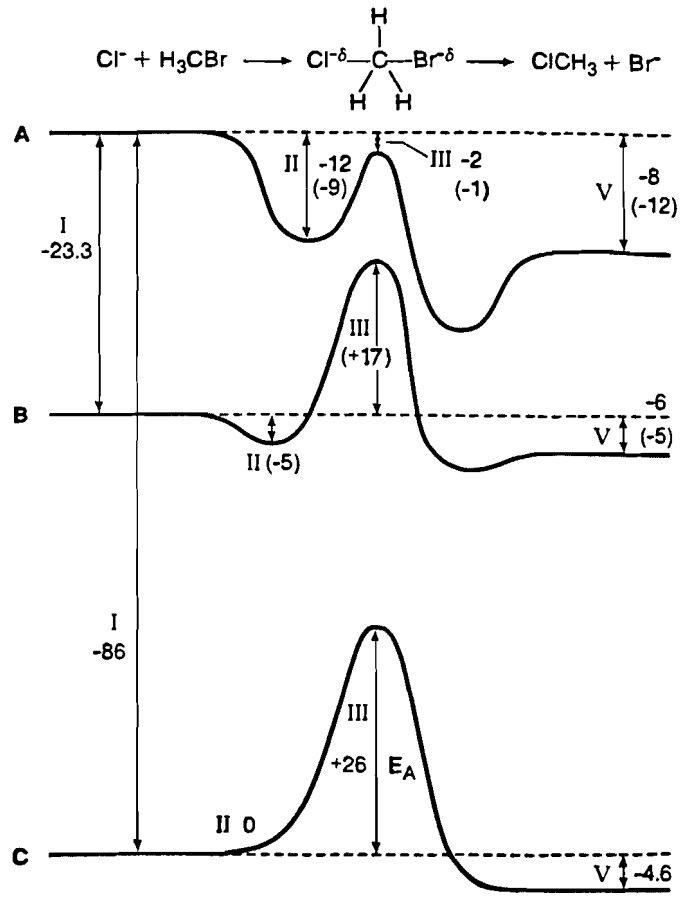


FIG. 7. Schematic reaction coordinates for reaction $Cl^- + CH_3Br = ClCH_3 + Br^-$; (A) in the gas phase, (B) ions including ionic transition state are dihydrated, see Fig. 6 (C) in aqueous solution. Energy changes in kcal/mol, values without parentheses from experiment, values in parentheses from present calculations. For origin of experimental values see Appendix. ΔE_I are energies of reactants B and C relative to gas phase reactants. Other energies are relative to reactants in the given phase. Energy changes drawn approximately to scale.

Acknowledgement

This research was supported by a grant from the Natural Sciences and Engineering Research Council of Canada (NSERC).

1. (*a*) C. K. INGOLD. Structure and mechanism in organic chemistry. 2nd ed. Cornell University Press, Ithaca, NY. 1969; (*b*) A. J. PARKER. Chem. Rev. **69**, 1 (1969); (*c*) O. DE TAR, D. F. MCMULLEN, and N. P. LUTHRA. J. Am. Chem. Soc. **100**, 2484 (1978).
2. (*a*) J. M. RIVEROS, S. M. JOSÉ, and K. TAKASHIMA. Adv. Phys. Org. Chem. **21**, 197 (1985); (*b*) D. K. BOHME and G. I. MACKAY. J. Am. Chem. Soc. **103**, 978 (1981).
3. (*a*) A. DEDIEU and A. J. VEILLARD. J. Am. Chem. Soc. **94**, 6730 (1972); (*b*) W. TH. VAN DER LUGT and P. ROS. Chem. Phys. Lett. **4**, 389 (1969); (*c*) J. J. C. MULDER and J. S. WRIGHT. Chem. Phys. Lett. **5**, 445 (1970); (*d*) D. D. RITCHIE and G. A. CHAPPELL. J. Am. Chem. Soc. **92**, 1819 (1970); (*e*) V. DYCZMONS and W. KUTZELNIGG. Theor. Chim. Acta, **33**, 239 (1974); (*f*) P. BAYBUTT. Mol. Phys. **29**, 389 (1975); (*g*) F. KEIL and R. AHLRICHS. J. Am. Chem. Soc. **98**, 4787 (1976); (*h*) R. BADER, F. W. J. DUKE, and R. R. MESSER. J. Am. Chem. Soc. **95**, 7715 (1973); (*i*) H. B. SCHLEGEL, K. MISLOW, F. BERNARDI, and A. BOTTONI. Theor. Chim. Acta, **44**, 245 (1977): (*j*) K. ISHIDA,

K. MOROKUMA, and A. KOMORNICK. J. Chem. Phys. **66**, 2153 (1977); (*k*) K. MOROKUMA. J. Am. Chem. Soc. **104**, 3732 (1982); (*l*) S. WOLFE, D. J. MITCHELL, and J. H. SCHLEGEL. J. Am. Chem. Soc. **103**, 7692 (1981); **103**, 7694 (1981).
4. J. CHANDRASEKHAR, S. F. SMITH, and W. L. JORGENSEN. J. Am. Chem. Soc. **106**, 3079 (1984); J. CHANDRASEKHAR and W. L. JORGENSEN. J. Am. Chem. Soc. **107**, 2974 (1985).
5. W. E. FARNETH and J. I. BRAUMAN. J. Am. Chem. Soc. **98**, 5546 (1976); W. N. OLMSTEAD and J. I. BRAUMAN. J. Am. Chem. Soc. **99**, 4219 (1977); **101**, 3715 (1979).
6. D. K. SEN SHARMA and P. KEBARLE. J. Am. Chem. Soc. **104**, 19 (1982); T. F. MAGNERA and P. KEBARLE. *In* Ionic processes in the gas phase. *Edited by* M. Almoster Ferreira. D. Reidel Publishing Co., Dordrecht, The Netherlands. 1984; NATO ASI Series Vol. 118, p. 135.
7. G. CALDWELL, T. F. MAGNERA, and P. KEBARLE. J. Am. Chem. Soc. **106**, 959 (1984).
8. T. F. MAGNERA, G. CALDWELL, J. SUNNER, S. IKUTA, and P. KEBARLE. J. Am. Chem. Soc. **106**, 6140 (1984); P. KEBARLE, G. CALDWELL, T. F. MAGNERA, and J. SUNNER. Pure Appl. Chem. **57**, 339 (1985).
9. S. HUZINAGA, J. ANZELM, M. KLOBUKOWSKI, E. RODZIO-ANZELM, Y. SAKAI, and H. TETEWAKE. Gaussian basis sets for molecular calculations. Elsevier, Amsterdam. 1984.
10. J. W. LARSON and T. B. MCMAHON. Can. J. Chem. **62**, 675 (1984).
11. M. HENCHMAN, P. M. HIERL, and J. F. PAULSON. Adv. Chem. Ser. **215**, 83 (1987); P. M. HIERL, A. F. AHRENS, M. J. HENCHMAN, A. A. VIGGIANO, J. F. PAULSON, and D. C. CLARY. J. Am. Chem. Soc. **108**, 3142 (1988); P. M. HIERL, A. H. AHRENS, M. J. HENCHMAN, A. A. VIGGIANO, and J. F. PAULSON. Faraday Discuss. Chem. Soc. In press.
12. S. E. BARLOW, J. M. VAN DOREN, and V. M. BIERBAUM. J. Am. Chem. Soc. **110**, 7240 (1988).
13. (*a*) M. ARSHADI, R. YAMDAGNI, and P. KEBARLE. J. Phys. Chem. **74**, 1475 (1970); (*b*) R. G. KEESE and A. W. CASTLEMAN. J. Chem. Phys. Lett. **74**, 139 (1980).
14. L. A. CURTIS, D. J. FRUID, and M. J. BLANDER. Chem. Phys. **71**, 2703 (1973).
15. J. E. DESNOYERS and C. JOLICOEUR. *In* Modern aspects of electrochemistry. Vol. 5. *Edited by* J. O'M. Bockris and B. E. Conway. Plenum Press, New York. 1969. p. 20.
16. Selected values of chemical thermodynamic properties. NBS Technical Note 270-3. Natl. Bureau of Standards. 1968. p. 115.
17. R. H. BATHGATE and E. A. MOELWYN-HUGHES. J. Chem. Soc. **1959**, 2642.

Appendix: Energy changes based on experimental measurements

The experimental energy changes for the gas phase coordinate (A) in Fig. 7 were discussed in Sect. (b), see Fig. 1.

The experimental energy change ΔE_I for B in Fig. 7 corresponds to $\Delta H^0_{0,2}$, i.e., the enthalpy change for the gas phase reaction: $Cl^- + 2H_2O = Cl^-(H_2O)_2$. This is obtained from $\Delta H^0_{0,1} + \Delta H^0_{1,2}$ for Cl^-. Experimental results by Arshadi *et al.* (13*a*) and Keese and Castleman (13*b*) provide $\Delta H^0_{0,2} = -27 \pm 3$ kcal/mol. Setting the zero energy level for the reaction at $Cl^- + CH_3Br + (H_2O)_2$ and using the dimerization energy of H_2O, $\Delta H = -3.7$ kcal/mol (14), one obtains $\Delta H_I \approx \Delta E_I = -23.3 \pm 3$ kcal/mol.

The ΔE_V for curve B in Fig. 7 corresponds to $\Delta E_V = \Delta H^0_{0,2}(Br^-) - \Delta H^0_{0,2}(Cl^-) + \Delta H^0_V(A) = -25 + 27 - 8 = -6 \pm 3$ kcal/mol, where $\Delta H^0_{0,2}(Br^-) = -27 \pm 3$ kcal/mol is from Arshadi *et al.* (13*a*).

The $\Delta E_{II} = -4$ kcal/mol for curve B in Fig. 7 is a rough estimate. $\Delta H^0_{2,3}(Cl^-) = 10.5$ kcal/mol (13*a*) for H_2O. The required value is not for H_2O but for CH_3Cl addition to $Cl^-(H_2O)_2$. We have taken 0.3 of $\Delta H^0_{2,3}$, i.e., $\Delta E_{II} = -0.3 \times 10.5 = -4$ kcal/mol. The factor 0.3 is justified by the larger effective distance expected between Cl^- and the locus of the dipole and the polarizability of CH_3Cl relative to that of H_2O.

The $\Delta E_I = -86$ kcal/mol for curve C, aqueous solution, was obtained from the hydration energies of Cl^-, $\Delta H_h = -81.3$ kcal/mol, Desnoyers and Jolicoeur (15), and the hydration energy of CH_3Br, $\Delta H_h(CH_3Cl) \approx -5$ kcal/mol (16), and $\Delta E_I = \Delta H_h(Cl^-) + \Delta H_h(CH_3Br) = -86.3$ kcal/mol.

The $\Delta E_{III} = +26$ kcal/mol is the activation energy in aqueous solution, Bathgate and Moelwyn-Hughes (17).

The ΔE_V is based on the hydration energies $\Delta H_h(Cl^-) = -81.3$ kcal/mol (15), $\Delta H_h(Br^-) = -77.9$ kcal/mol (15), $\Delta H_h(CH_3Cl) \approx \Delta H_h(CH_3Br)$, and $\Delta H_1 = -8$ kcal/mol in the gas phase (7). $\Delta E_{III} = \Delta H^0_1 + \Delta H_h(Br^-) - \Delta H_h(Cl^-) = -4.6$ kcal/mol.

Can. J. Chem. Downloaded from www.nrcresearchpress.com by 194.225.253.170 on 09/07/12
For personal use only.

Gibbs energies of transfer of individual ions from water to acetone + water solvents

MAHMOUD MOHAMAD ELSEMONGY[1] AND AHMED AHMED ABDEL-KHALEK[2]

Chemistry Department, Faculty of Education, Umm Al-Qura University, Al-Taif City, Shihar, Saudi Arabia

Received November 10, 1988

MAHMOUD MOHAMAD ELSEMONGY and AHMED AHMED ABDEL-KHALEK. Can. J. Chem. **67**, 1268 (1989).

The standard absolute potentials of hydrogen, Ag–AgX (X = Cl, Br, and I) and M/M^+ (M = Li, Na, K, Rb, and Cs) electrodes in nine different acetone + water solvents containing up to 80 wt.% acetone were determined from the emf data at 25°C of the cells: glass electrode/HCl (*m*), solvent/AgCl–Ag and glass electrode (M)/MX (*m*), solvent/AgX–Ag. The standard Gibbs free energies of a transfer of halogen acids and alkali metal halides as well as their constituent individual ions from water to the respective solvents were computed. The observed increases in ΔG_t^0 values of all ions with increasing acetone content of the solvent and their relative order in each solvent were interpreted and discussed. A comparison of the present results with those obtained earlier in the dimethyl sulphoxide (DMSO) + water solvents shows the different nature of the two dipolar aprotic solvents, acetone and DMSO, in their aqueous mixtures.

Key words: acetone + water solvents, electrode potentials, emf measurements, individual ions, transfer free energies.

MAHMOUD MOHAMAD ELSEMONGY et AHMED AHMED ABDEL-KHALEK. Can. J. Chem. **67**, 1268 (1989).

En se basant sur des données de fem, mesurées à 25°C, pour les cellules: électrode de verre/HCl (*m*), solvant/AgCl–Ag et électrode de verre (M)/MX (*m*), solvant/AgX–Ag, on a déterminé les potentiels absolus standard des électrodes hydrogène, Ag–AgX (X = Cl, Br et I) et M/M^+ (M = Li, Na, K, Rb et Cs) dans neuf solvants différents formés d'acétone + eau et contenant jusqu'à 80% en poids d'acétone. On a calculé les énergies libres standard de Gibbs pour le transfert des acides halogénés, des halogénures des métaux alcalins ainsi que de leurs ions constituants individuels de l'eau aux divers solvants. On interprète et on discute de l'augmentation qui est observée pour les valeurs des ΔG_t^0 de tous les ions avec une augmentation de la concentration d'acétone dans le solvant ainsi que de leur ordre relatif dans chacun des solvants. Une comparaison de résultats obtenus au cours de cette étude avec ceux obtenus antérieurement dans des solvants formés de diméthylsulfoxyde (DMSO) + eau met en évidence la nature différente des deux solvants dipolaires aprotriques, acétone et DMSO, dans leurs mélanges aqueux.

Mots clés : solvants acétone + eau, potentiels d'électrode, mesures de fem; ions individuels, énergies libres de transfert.

[Traduit par la revue]

Introduction

A new procedure for the determination of standard absolute electrode potentials in aqueous and non-aqueous, protic and aprotic solvents, as well as the thermodynamics of individual ions in these media, was described recently (1). The procedure was applied successfully to the emf data of cells connecting silver, silver halide electrodes with hydrogen or alkali metal amalgam electrodes (1–3). The interest, validity, and general applicability of the procedure in various solvent systems have been demonstrated (1–3).

As far as electrochemical methods are concerned, amalgam electrodes have been considered for a long time as the most reliable means for the determination of alkali metal ion activity in solution (4–7). However, the failure of alkali metal amalgam electrodes to function satisfactorily in acetone + water solvent mixtures has dictated the use of cation-sensitive glass electrodes to determine free energies of transfer for the alkali metal halides from water to these solvent mixtures (4). Therefore, instead of amalgam electrodes, we used glass electrodes reversible to the alkali metal ions in the cells:

[I] Glass electrode (M)/MX (*m*), solvent/AgX–Ag

(where M = Li, Na, K, Rb, and Cs for X = Cl and M = Na for X = Br and I) and also glass electrodes reversible to the H^+ ions in the cells:

[II] Glass electrode/HCl (*m*), solvent/AgCl–Ag

in order to perform emf measurements at 25°C in nine different acetone + water solvents, containing up to 80 wt.% acetone. Thus, in the present paper, the new procedure (1) is further applied to the emf data of cells [I] and [II] in the aqueous mixtures of acetone, on the one hand for verification of the used procedure for cells with glass electrodes, on the other to obtain standard absolute electrode potentials in such aqueous dipolar aprotic media as well as Gibbs free energies of transfer for individual ions from water to each solvent.

Glass electrodes were used for the determination of Gibbs free energy of transfer (ΔG_t^0) for the alkali metal chlorides from water to aqueous solvents containing *t*-butanol up to 40 wt.% (5, 6), dioxane (D) up to 40 wt.% (5), or dimethyl sulphoxide (DMSO) up to 85 wt.% (7*a*), and for HCl (7*b*) and RbCl (7*c*) to a large number of aqueous organic solvents containing up to 85 wt.% of organic solvent. Comparisons show that agreement between the two types of electrode, amalgam and glass, is generally good up to ca. 40 wt.% of organic solvent (5, 7*a*). The differences tend to increase with increasing concentration of the organic solvent, but this leaves the percentage error of the ΔG_t^0 values (4) approximately the same (ca. 2%). Therefore, Smits *et al.* (7*a*) believe that cationic glass electrode measurements not only represent a fast and easy method for determining Gibbs free energies of transfer of the alkali metal halides, but also quite an accurate one. Thus, cationic glass electrodes were used recently (4) to determine free energies of transfer of alkali metal halides from water to aqueous mixtures containing up to 60 wt.% acetone. The values of ΔE_m^0 obtained by Feakins *et al.* (4) for RbCl are uniformly higher than those obtained by Smits *et al.* (7*c*), who also used glass electrodes, by ca. 1 mV at the lowest and 2 mV at the highest acetone concentration (4). On the other hand, Bax *et al.* (8, 9), who used amalgam electrodes for KCl at 20, 40, 60, and 80 wt.% acetone, gave ΔE_m^0 values which are 4–5 mV higher than those of Feakins *et al.* (4) at the two lower concentrations. The present investigation was undertaken not

[1]Author to whom all correspondence should be addressed.

[2]Chemistry Department, Faculty of Science, Cairo University, Beni-Suef City, Egypt.

Printed in Canada / Imprimé au Canada

Can. J. Chem. Downloaded from www.nrcresearchpress.com by 194.225.253.170 on 09/07/12
For personal use only.

TABLE 1. Values of ΔE^0_m (mV) for cells [I] and [II] in acetone + water solvents at 25°C, and previously reported (4, 8, 15, 16) values, for comparison

Acetone (wt.%)	Reference	ΔE^0_m HCl	LiCl	NaCl	NaBr	NaI	KCl	RbCl	CsCl
5	This work	3.5	7.0	8.1	5.8	2.8	8.0	7.9	7.6
	(16)	3.3	—	—	—	—	—	—	—
10	This work	6.9	14.4	16.7	12.0	5.9	16.2	16.1	15.5
	(4)	—	14.05	16.8	12.2	5.3	16.0	16.0	15.25
	(16)	6.7	—	—	—	—	—	—	—
20	This work	14.9	29.9	34.6	25.6	11.9	33.9	33.7	32.5
	(4)	—	29.4	34.15	25.6	11.9	34.35	34.35	30.65
	(8)	—	—	—	—	—	38.6	—	—
	(15)	14.8	—	—	—	—	—	—	—
	(16)	14.4	—	—	—	—	—	—	—
30	This work	23.8	48.2	55.7	41.9	19.7	54.7	54.5	52.6
	(4)	—	48.4	55.6	42.1	19.65	54.95	54.95	52.55
	(15)	24.3	—	—	—	—	—	—	—
40	This work	35.2	68.5	79.3	60.0	29.0	77.9	77.5	75.0
	(4)	—	69.25	79.4	60.65	30.75	77.9	79.35	75.4
	(8)	—	—	—	—	—	83.4	—	—
	(15)	35.8	—	—	—	—	—	—	—
	(16)	36.4	—	—	—	—	—	—	—
50	This work	50.5	92.2	107.3	81.8	41.2	105.4	104.6	101.2
	(4)	—	91.9	—	—	—	106.55	—	—
	(15)	51.8	—	—	—	—	—	—	—
60	This work	72.7	123.0	144.0	111.6	60.3	140.2	138.4	133.8
	(4)	—	121.7	144.0	112.45	—	140.3	139.3	133.3
	(8)	—	—	—	—	—	140.1	—	—
	(15)	75.3	—	—	—	—	—	—	—
70	This work	107.5	162.2	191.0	150.6	87.0	185.0	181.0	175.5
	(15)	107.3	—	—	—	—	—	—	—
80	This work	162.1	207.5	244.6	194.4	115.9	236.1	229.5	223.3
	(8)	—	—	—	—	—	235.3	—	—
	(15)	162.3	—	—	—	—	—	—	—

only to check the previous data but also to extend the work to other solvent compositions. This enables us to study solvent influence on standard absolute electrode potentials and related transfer free energies.

Experimental

Acetone (BDH, AnalaR) was further purified as before (10). It was stored over anhydrous $CaSO_4$ in an atmosphere of nitrogen, redistilled freshly, and used within a few hours. AnalaR and Merck quality alkali metal salts were further purified (2, 3), dried at 120°C, and kept in a desiccator over P_2O_5 (7). Redistilled deionized water (2, 3, 10) was generally used in the preparation of the solutions. All solutions were freshly prepared before taking measurements. The compositions of the solvents were accurate to ±0.01 wt.%. The solutions were all stored in dark bottles under a nitrogen atmosphere.

Emf measurements on cells [I] and [II] were carried out using Corning glass electrodes. Electrodes no. 476022 were used for H^+ ion determinations, sodium-sensitive electrodes no. 476210 for all Na^+ ion determinations, and monovalent cation selective electrodes no. 476220 for all the remaining cations. Silver, silver halide electrodes were as before (2–4, 10). The cell design, general experimental procedure, and mathematical treatment of the results were described earlier (4, 7*b*, 11). The molality of cell solutions was in the range 0.002–0.10 mol kg^{-1}. The values of m are accurate to ca. 0.01%. As reported by Feakins *et al.* (4), a possible source of error in their work is that Ag^+ ion from the halide electrodes could interfere with glass electrodes, since both were in the same cell compartment. Therefore, in our study, the two electrodes were put in different compartments, as done later by Feakins *et al.* (11), and their simpler method of compensating for drift and asymmetry potentials (11) was used. The cell measurements were made in triplicate, and the mean values of these observations recorded. The triplicates generally agreed within ±0.1 mV. The temperature of the measuring cells was carefully maintained at 25 ± 0.01°C.

Succinate buffered solutions were used with Ag–AgBr and Ag–AgI electrodes in all acetone + water solvents, as in previous investigations (12–14). In this way, it is possible to obtain steady potentials for these electrodes in solvents containing up to 80 wt.% acetone. Attempts to perform measurements with cell [I] for X = I in 90 wt.% acetone were unsuccessful as we failed to obtain steady potentials. This could have been due to dissolution of silver iodide (4).

Results

For cells [I] or [II] in water (w) and in acetone + water solvent (s), if the same glass electrode is used in each and the emf values are corrected for drift (4, 11), we can define

[1] $\Delta E = {}^{w}E - {}^{s}E$

and

[2] $\Delta G_t = F\Delta E$

where ΔG_t is the free energy of transfer of 1 mole of electrolyte from water to the mixed solvent at the stated molalities (4). The

Can. J. Chem. Downloaded from www.nrcresearchpress.com by 194.225.253.170 on 09/07/12
For personal use only.

Can. J. Chem. Downloaded from www.nrcresearchpress.com by 194.225.253.170 on 09/07/12
For personal use only.

TABLE 2. Values of ΔG_t^0 (kJ mol^{-1}) on the molal scale at 25°C, and previously reported (7, 9) values for comparison

Acetone (wt.%)	Reference	ΔG_t^0 HCl	LiCl	NaCl	NaBr	NaI	KCl	RbCl	CsCl
5	This work	0.34	0.67	0.78	0.56	0.27	0.77	0.76	0.73
	(7)	0.32	—	—	—	—	—	0.77	—
10	This work	0.67	1.39	1.61	1.16	0.57	1.56	1.55	1.50
	(7)	0.61	—	—	—	—	—	1.47	—
20	This work	1.44	2.88	3.34	2.47	1.15	3.27	3.25	3.14
	(7)	1.34	—	—	—	—	—	3.17	—
	(9)	1.39	—	—	—	—	3.72	3.79	3.41
30	This work	2.30	4.65	5.37	4.04	1.90	5.28	5.26	5.08
	(7)	2.23	—	—	—	—	—	5.20	—
40	This work	3.40	6.61	7.65	5.79	2.80	7.52	7.48	7.24
	(7)	3.34	—	—	—	—	—	7.45	—
	(9)	3.51	—	—	—	—	8.05	7.65	7.23
50	This work	4.87	8.90	10.35	7.89	3.98	10.17	10.09	9.76
	(7)	4.83	—	—	—	—	—	10.1	—
60	This work	7.01	11.87	13.89	10.77	5.82	13.53	13.35	12.91
	(7)	7.00	—	—	—	—	—	13.3	—
	(9)	7.27	—	—	—	—	13.52	12.88	12.45
70	This work	10.37	15.65	18.43	14.53	8.39	17.85	17.46	16.93
	(7)	10.0	—	—	—	—	—	17.3	—
80	This work	15.64	20.02	23.60	18.76	11.18	22.78	22.14	21.55
	(7)	14.9	—	—	—	—	—	23.0	—
	(9)	15.66	—	—	—	—	22.70	22.12	21.71

TABLE 3. Values of E_m^0 (V) of cells [I] and [II] in acetone + water solvents at 25°C

Acetone (wt.%)	E_m^0(V) 5	10	20	30	40	50	60	70	80
HCl	0.2188	0.2154	0.2074	0.1985	0.1871	0.1718	0.1496	0.1148	0.0602
HBr	0.0711	0.0699	0.0667	0.0632	0.0575	0.0485	0.0334	0.0067	−0.0380
HI	−0.1503	−0.1482	−0.1443	−0.1398	−0.1369	−0.1364	−0.1409	−0.1554	−0.1853
LiCl	3.2597	3.2523	3.2368	3.2185	3.1982	3.1745	3.1437	3.1045	3.0592
LiBr	3.1120	3.1068	3.0961	3.0832	3.0686	3.0512	3.0275	2.9964	2.9610
LiI	2.8906	2.8886	2.8851	2.8802	2.8742	2.8663	2.8532	2.8343	2.8137
NaCl	2.9271	2.9186	2.9006	2.8792	2.8556	2.8275	2.7908	2.7437	2.6901
NaBr	2.7795	2.7732	2.7599	2.7439	2.7260	2.7042	2.6745	2.6356	2.5919
NaI	2.5580	2.5550	2.5489	2.5409	2.5316	2.5193	2.5002	2.4735	2.4446
KCl	3.1392	3.1310	3.1133	3.0925	3.0693	3.0418	3.0070	2.9622	2.9111
KBr	2.9915	2.9855	2.9726	2.9572	2.9397	2.9185	2.8908	2.8541	2.8129
KI	2.7701	2.7673	2.7616	2.7542	2.7453	2.7336	2.7165	2.6920	2.6656
RbCl	3.1396	3.1314	3.1138	3.0930	3.0700	3.0429	3.0091	2.9665	2.9180
RbBr	2.9919	2.9859	2.9731	2.9577	2.9404	2.9196	2.8929	2.8584	2.8198
RbI	2.7705	2.7677	2.7621	2.7547	2.7460	2.7347	2.7186	2.6963	2.6725
CsCl	3.1378	3.1299	3.1129	3.0928	3.0704	3.0442	3.0116	2.9699	2.9221
CsBr	2.9901	2.9844	2.9722	2.9575	2.9408	2.9209	2.8954	2.8618	2.8239
CsI	2.7687	2.7662	2.7612	2.7545	2.7464	2.7360	2.7211	2.6997	2.6766

values of ΔE were analysed in the way previously described for amalgam cells (4, 11) to give ΔE_m^0 values in the different acetone + water solvents. These are listed in Table 1. Note that the behaviour of the electrodes was so satisfactory when used as described (4, 11) that extrapolation of the individual ^wE or ^sE values obtained over a few weeks to give the individual E_m^0 values was possible; ΔE_m^0 values obtained as the difference of these data agreed well with those obtained by extrapolation of ΔE. Generally, the values of ΔE_m^0 are precise to better than ±0.1 and ±0.2 mV for solvents containing up to 50 and 80 wt.% acetone, respectively. The values of ΔG_t^0 on the molal scale calculated from ΔE_m^0 values are recorded in Table 2.

TABLE 4. The least-squares results of applying eq. [3] to the emf data of cells [I] and [II] in acetone + water solvents at 25°C, ΔG_t^0 values on the molal scale

Parameter	M or MX	ΔG_t^0 values with acetone concentration in wt.%								
		5	10	20	30	40	50	60	70	80
−Corr (10^{-2})		100.0000	99.9999	100.0000	99.9998	99.9995	99.9993	99.9990	99.9986	99.9981
Δ (mV)	NaCl	+0.06	+0.13	−0.05	−0.25	−0.34	−0.39	−0.44	−0.49	−0.52
	NaBr	−0.09	−0.22	+0.08	+0.42	+0.57	+0.64	+0.74	+0.82	+0.87
	NaI	+0.04	+0.09	−0.03	−0.17	−0.23	−0.26	−0.29	−0.33	−0.35
a_1^0 (10^{10} V m^{-1})		1.0546	1.0390	1.0048	0.9666	0.9257	0.8805	0.8302	0.7721	0.7015
r_+ (10^{-10} m)	H	2.017	2.017	2.016	2.015	2.012	2.005	1.990	1.959	1.896
	Li	4.901	4.940	5.031	5.140	5.265	5.415	5.597	5.831	6.171
	Na	4.586	4.619	4.697	4.789	4.895	5.021	5.172	5.364	5.645
	K	4.787	4.824	4.908	5.009	5.126	5.265	5.432	5.646	5.960
	Rb	4.787	4.824	4.909	5.010	5.126	5.266	5.435	5.652	5.970
	Cs	4.785	4.822	4.908	5.010	5.127	5.267	5.438	5.656	5.976
S_e (10^{-10} m)	Li	4.30	4.34	4.43	4.54	4.66	4.82	5.00	5.23	5.57
	Na	3.64	3.67	3.75	3.84	3.94	4.07	4.22	4.41	4.69
	K	3.46	3.49	3.58	3.68	3.80	3.93	4.10	4.32	4.63
	Rb	3.31	3.34	3.43	3.53	3.65	3.79	3.95	4.17	4.49
	Cs	3.10	3.13	3.22	3.32	3.44	3.58	3.75	3.97	4.29
${}^{ox}_{L}E^0_m$ (V)	H	2.1277	2.0960	2.0261	1.9481	1.8626	1.7655	1.6522	1.5123	1.3299
	Li	5.1686	5.1329	5.0555	4.9681	4.8737	4.7682	4.6463	4.5020	4.3289
	Na	4.8360	4.7992	4.7193	4.6288	4.5310	4.4212	4.2933	4.1412	3.9598
	K	5.0481	5.0116	4.9320	4.8421	4.7448	4.6355	4.5096	4.3597	4.1808
	Rb	5.0485	5.0120	4.9325	4.8426	4.7455	4.6366	4.5117	4.3640	4.1877
	Cs	5.0467	5.0105	4.9316	4.8424	4.7459	4.6379	4.5142	4.3674	4.1918
${}^{ox}_{R}E^0_m$ (V)	Cl	1.9089	1.8806	1.8187	1.7496	1.6755	1.5937	1.5026	1.3975	1.2697
	Br	2.0565	2.0260	1.9594	1.8849	1.8051	1.7170	1.6188	1.5056	1.3679
	I	2.2780	2.2442	2.1704	2.0879	1.9995	1.9019	1.7931	1.6677	1.5152
ΔG_t^0 (J mol^{-1})	H	2977	6036	12776	20304	28555	37922	48855	62349	79947
	Li	3307	6752	14215	22651	31760	41938	53700	67619	84320
	Na	3408	6960	14673	23399	32834	43432	55769	70445	87950
	K	3399	6922	14597	23274	32663	43208	55356	69815	87075
	Rb	3395	6918	14584	23260	32630	43136	55188	69435	86444
	Cs	3362	6856	14464	23073	32385	42804	54741	68901	85842
	Cl	2633	5365	11332	18002	25153	33044	41835	51971	64301
	Br	2836	5778	12208	19394	27097	35599	45070	55990	69274
	I	3142	6401	13523	21483	30015	39432	49924	62020	76734

These are therefore precise to ±10 and ±20 J mol^{-1} for solvents containing up to 50 and 80 wt.% acetone, respectively, based on the precision of the ΔE^0_m values.

Further, all the values of ${}^{w}E^0_m$ of cell [I] or [II], obtained using glass electrodes in the present investigation, agree very well with those reported recently (1, 2) for cells containing HCl or MX electrolytes with different electrodes. The values of ${}^{s}E^0_m$ of the cells, containing HCl, LiCl, NaCl, NaBr, NaI, KCl, RbCl, and CsCl in various acetone + water solvents, are given in Table 3.

Standard absolute electrode potential

The new procedure, developed recently (1, 2) for determination of absolute electrode potentials and the thermodynamics of individual ions in solution, has been applied to the emf data of cell [I] in acetone + water solvents. According to this procedure, the oxidation potential of any electrode varies directly with the radius (r) of the solvated ion on the activity of which the potential depends. Therefore, the cell emf is linearly related to the radius of the solvated ion which is being varied in a series of electrolytes having a common ion (1). Thus, in any solvent, the plot of the standard emf (E^0_m) values of cell [I], containing NaCl, NaBr, and NaI, against the radius of the solvated anion r_- should yield a straight line according to eq. [3], at any temperature (1).

$$[3] \quad E^0_m = a^0_1 r_+ - a^0_1 r_-$$

This holds in various acetone + water solvents, and the least-squares results at 25°C are collected in Table 4. In all solvents, perfect straight lines were obtained, and the extent of correlation is indicated by the correlation coefficients (corr) and the differences, Δ(mV), between the E^0_m values obtained experimentally and those calculated by eq. [4],

$$[4] \quad E^0_m = {}^{ox}_{L}E^0_m - {}^{ox}_{R}E^0_m$$

where ${}^{ox}_{L}E^0_m$ and ${}^{ox}_{R}E^0_m$ are the oxidation potentials of the left and right electrodes, respectively (1, 2). Thus, the standard absolute potential of the Na/Na^+ and Ag–AgX (X = Cl, Br, and I) electrodes, the radius (r_+) of the solvated Na^+ ion and thus its solvation extent (S_e), in the standard state, have been computed as before (1, 2).

From the computed values of the standard absolute potential of the Ag–AgCl electrode in each solvent (Table 4), those of H_2/H^+, Li/Li^+, K/K^+, Rb/Rb^+, and Cs/Cs^+ electrodes could

Can. J. Chem. Downloaded from www.nrcresearchpress.com by 194.225.253.170 on 09/07/12
For personal use only.

TABLE 5. Standard transfer free energies (J mol^{-1}) of halogen acids and alkali metal halides from water to acetone + water solvents at 25°C

	Standard transfer free energies								
MX	5	10	20	30	40	50	60	70	80
HCl	344	671	1444	2302	3402	4878	7020	10378	15646
HBr	141	258	568	910	1458	2323	3785	6359	10673
HI	−165	−365	−747	−1179	−1460	−1510	−1069	329	3213
LiCl	674	1387	2883	4649	6607	8894	11865	15648	20019
LiBr	471	974	2007	3257	4663	6339	8630	11629	15046
LiI	165	351	692	1168	1745	2506	3776	5599	7586
NaCl	775	1595	3341	5397	7681	10388	13934	18474	23649
NaBr	572	1182	2465	4005	5737	7833	10699	14455	18676
NaI	266	559	1150	1916	2819	4000	5845	8425	11216
KCl	766	1557	3265	5272	7510	10164	13521	17844	22774
KBr	563	1144	2389	3880	5566	7609	10286	13825	17801
KI	257	521	1074	1791	2648	3776	5432	7795	10341
RbCl	762	1553	3252	5258	7477	10092	13353	17464	22143
RbBr	559	1140	2376	3866	5533	7537	10118	13445	17170
RbI	253	517	1061	1777	2615	3704	5264	7415	9710
CsCl	729	1491	3132	5071	7232	9760	12906	16930	21541
CsBr	526	1078	2256	3679	5288	7205	9671	12911	16568
CsI	220	455	941	1590	2370	3372	4817	6881	9108

be obtained (by eq. [4]) from the E^{0}_{m} values of cells [II] and [I] containing HCl and LiCl, KCl, RbCl, and CsCl, respectively, Table 3. The radii of the solvated cations and their solvation extent as well as the individual ionic contributions to ΔG^{0}_{t} values of electrolytes, in each solvent, were calculated as before (1–3). All these results are also included in Table 4.

Furthermore, by coupling the standard absolute potentials ($^{ox}_{L}E^{0}_{m}$) of hydrogen or M/M^{+} (M = Li, K, Rb, or Cs) electrodes with those ($^{ox}_{R}E^{0}_{m}$) of Ag–AgX (X = Br or I) electrodes, using eq. [4], the values of E^{0}_{m} for cell [III] or [I], containing HBr, HI, LiBr, LiI, KBr, KI, RbBr, RbI, CsBr, or CsI, could be computed. Thus, all the values of E^{0}_{m} of these cells in various acetone + water solvents so computed at 25°C are listed in Table 3.

Standard Gibbs free energies

The standard free energy changes (ΔG^{0}_{E}) involved in the half-cell reactions are related to the standard absolute electrode potentials ($^{ox}_{E}E^{0}_{m}$) by the relation (1, 2):

[5] $\Delta G^{0}_{E} = -F\,^{ox}_{E}E^{0}_{m}$

Thus, the values of ΔG^{0}_{E} can be computed on the molal scale using the $^{ox}_{E}E^{0}_{m}$ values given in Table 4.

The values for the standard Gibbs free energy ΔG^{0}_{t} for the transfer of an individual ion from water to various acetone + water solvents were calculated (1–3) on the molal scale from the standard absolute electrode potentials in water ($^{w}_{E}E^{0}_{m}$) and in the respective mixed solvents ($^{s}_{E}E^{0}_{m}$), Table 4, using eq. [6].

[6] $\Delta G^{0}_{t} = F(^{w}_{E}E^{0}_{m} - {}^{s}_{E}E^{0}_{m})$

The values of ΔG^{0}_{t} calculated at 25°C on the basis of the oxidation potential scale (1–3) are also included in Table 4. These are accurate to better than 20 and 40 J mol^{-1} for solvents containing up to 50 and 80 wt.% acetone, respectively.

The values of ΔG^{0}_{t} for halogen acids as well as alkali metal halides can be obtained by coupling the transfer free energies of cations with those of anions, i.e., from the differences between those for the ion constituents, both based on the same oxidation potential scale (1–3), in any solvent.

[7] $\Delta G^{0}_{t}(HX \text{ or } MX) = \Delta G^{0}_{t}(H^{+} \text{ or } M^{+}) - \Delta G^{0}_{t}(X^{-})$

The values of ΔG^{0}_{t} so calculated at 25°C, by eq. [7], in various acetone + water solvents are listed in Table 5. To check the reliability of the calculations, the values of ΔG^{0}_{t} (Table 5) for HCl, LiCl, NaCl, NaBr, NaI, KCl, RbCl, or CsCl can be compared with those based on ΔE^{0}_{m} values and given in Table 2. Full agreement between the values is always seen.

Discussion

Now, the values of ΔE^{0}_{m} and ΔG^{0}_{t}, obtained in the present work (Tables 1 and 2), can be compared with other results. These were taken from the literature with all significant digits as they were originally given (on the molal scale) and are also included in Tables 1 and 2. For the alkali metal halides, the new values are in good agreement with most values obtained by Feakins *et al.* (4) and Smits *et al.* (7*c*), who also used glass electrodes; the differences are roughly within the combined error of the two determinations. Bax *et al.* (8) used amalgam electrodes for KCl at 20, 40, 60, and 80 wt.% acetone. Their results give ΔE^{0}_{m} values which are 4.7–5.5 mV higher than ours at the two lower concentrations. On the other hand, the agreement is good at 60 and 80 wt.% acetone. As noted before (4), the observed differences between the amalgam and glass electrodes in other systems point to an accuracy of ΔE^{0}_{m} and ΔG^{0}_{t} of 2%. This is important in comparing the present results with others.

Bax *et al.* (9) also determined differences in ΔG^{0}_{t} between the H^{+} ion and the K^{+}, Rb^{+}, and Cs^{+} ions at these solvent compositions from a combination of data obtained by emf and solubility methods. A combination of these values with those given for the sum of ΔG^{0}_{t} for the H^{+} and Cl^{-} ions leads to sets for KCl, RbCl, and CsCl which show good agreement with the new values for KCl at 60 and 80 wt.% acetone and CsCl at 40 wt.% acetone, and fair agreement for CsCl at 80 wt.% acetone.

Can. J. Chem. Downloaded from www.nrcresearchpress.com by 194.225.253.170 on 09/07/12
For personal use only.

Can. J. Chem. Downloaded from www.nrcresearchpress.com by 194.225.253.170 on 09/07/12
For personal use only.

For HCl, the new values are in good agreement (taking into account the combined precision limits of the measurements) with those of Smits *et al.* (7) at 5–60 wt.% acetone and Morel (15) at 20, 70, and 80 wt.% acetone, both obtained by glass electrode measurements, and Feakins and French (16) at 5 and 10 wt.% acetone, using hdyrogen electrodes. However, Feakins *et al.* (4) reported that hydrogen electrodes misbehave in acetone + water solvents, and therefore, the new values of ΔE^0_m in these solvents, obtained by glass electrodes should be preferred.

It is evident from Table 4 that the value of a^0_I decreases with increasing acetone content of the solvent system. As reported earlier (1, 2), the values of a^0_I appear to be universal constants for all electrodes, and dependent only on the medium, at any temperature. However, as the acetone content of the solvent increases, the radius (r_+) of the solvated H^+ ion decreases, i.e., the solvation extent of the protons decreases, and the oxidation potentials of both left and right electrodes decrease. These features have been noticed recently (1–3) in the D–, methanol (MeOH)–, ethylene glycol (EG) – , and propylene glycol (PG) – water solvent systems.

The protons, therefore, are less solvated in the mixed solvent than in water, Table 4. The solvation of protons in aqueous acetone solvents can be compared with that in aqueous DMSO solvents, where the protons become gradually more solvated (r_+ values increase) on the successive addition of DMSO to the aqueous medium (2). This reflects the different nature of the two dipolar aprotic solvents, acetone and DMSO, in their aqueous mixtures.

On the other hand, the radii of the solvated cations and thus their solvation extent increase with increasing acetone content in the solvent. This can be explained by successive substitution of water molecules by the larger sized acetone dipoles in the solvation sheath, on gradual addition of acetone to the solvent. This explanation is supported by the very interesting feature that, in any solvent, the extent of solvation increases in the expected well-known order: $Cs^+ < Rb^+ < K^+ < Na^+ < Li^+$, and the Li^+ ion is always highly solvated. Similar results were also obtained for the alkali metal ions in D–, MeOH–, EG–, PG–, and DMSO–water solvent systems (1–3). Thus, the values of r_+ indicate that, so far as any M^+ ion is concerned, any mixed solvent is a stronger solvating agent than water. This is probably due to the charge density distribution in the acetone molecule, combined with its spatial structure, which strongly favours solvation of positive M^+ ions. A relatively large negative charge is localised on the oxygen atom, while the positive charge is delocalised over the propyl group (9).

As the acetone content of the solvent increases, the oxidation potentials of H_2/H^+, M/M^+, and Ag–AgX electrodes decrease. In any solvent, the standard absolute potentials of Ag–AgX electrodes decrease in the regular expected (1–3) order: ${}^{ox}E^0_m(AG–AgI) > {}^{ox}E^0_m(Ag–AgBr) > {}^{ox}E^0_m(Ag–AgCl)$. On the other hand, the irregular order of variation of the standard absolute potentials of the alkali metal electrodes, from Li/Li^+ to Cs/Cs^+ in any solvent, is dictated by the extent of solvation of the alkali metal ions, and thus by the radii of solvated cations. These trends of variation of electrode potentials with solvent composition were observed in all the solvent systems studied recently (1–3).

It is noticed from Table 4 that the values of ΔG^0_t for all ions are positive and increase with increasing acetone concentration. The increasingly positive values of ΔG^0_t of individual ions signify that the transfer of the ions from water to acetone + water solvents is increasingly unfavourable. Thus, the values of ΔG^0_t show a qualitative resemblance to other solvent systems (1–3).

It is generally thought that changes of Gibbs free energies for the transfer from one medium to another are closely related to changes in ion solvation. Since the transfer process is not spontaneous, the ions are more strongly stabilised by solvation in water than in any aqueous acetone solvent. However, this is not reflected by the values of r_+, Table 4. Increased desolvation of the proton (r_+ values decrease), and on the other hand, increased solvation of the M^+ ions (r_+ values increase), with increasing amounts of acetone in the solvent, are observed. This is also noticed in D–, MeOH–, EG–, and PG–water solvent systems (1–3). This, and the increasingly positive values of ΔG^0_t for all (H^+ and M^+) ions indicate that there is no relationship between ΔG^0_t values and solvation of ions (2).

In any solvent, the relative order of non-spontaneity for the anions is $\Delta G^0_t(Cl^-) < \Delta G^0_t(Br^-) < \Delta G^0_t(I^-)$, while that for the cations is $\Delta G^0_t(H^+) < \Delta G^0_t(Li^+) < \Delta G^0_t(Na^+) > \Delta G^0_t(K^+) > \Delta G^0_t(Rb^+) > \Delta G^0_t(Cs^+)$. Similar behaviour has been observed in the DMSO–water solvent system (2), and the similarity in the profiles of ΔG^0_t points to a common cause for the behaviour of these simple ions in the two solvent systems.

Finally, the whole of the obtained results, in acetone + water solvents, lend another proof and extra confidence to the general applicability of the new procedure (1) applied to the emf data of cells with the glass electrodes, and hence, more reliability in the evaluated data.

Acknowledgement

The authors express their appreciation to Mrs. Laila Abu Elela for encouragement, fruitful suggestions, and many helpful discussions.

1. M. M. Elsemongy. Thermochim. Acta, **80**, 239 (1984); **103**, 387 (1986); **108**, 133 (1986).
2. M.M. Elsemongy and F. M. Reicha. Thermochim. Acta, **103**, 371 (1986); **106**, 309 (1986); **108**, 115 (1986).
3. M. M. Elsemongy and H. M. Abu Elnader. Thermochim. Acta, **120**, 261 (1987).
4. D. Feakins, M. Knox, and B. E. Hickey. J. Chem. Soc. Faraday Trans. I. **80**, 961 (1984).
5. T. A. Clune, D. Feakins, and P. J. McCarthy. J. Electroanal. Chem. **84**, 199 (1977).
6. Y. Pointud, J. Juillard, J. P. Morel, and L. Avédikian. Electrochim. Acta, **19**, 229 (1974).
7. R. Smits, D. L. Massart, J. Juillard, and J. P. Morel. Electrochim. Acta, (*a*) **21**, 437 (1976); (*b*) **21**, 431 (1976); (*c*) **21**, 425 (1976).
8. D. Bax, M. Alfenaar, and C. L. de Ligny. Recl. Trav. Chim. Pays-Bas, **90**, 1002 (1971).
9. D. Bax, C. L. de Ligny, and A. G. Remijnse. Recl. Trav. Chim. Pays-Bas, **91**, 1225 (1972).
10. M. M. Elsemongy, A. S. Fouda, and I. M. Kenawy. J. Chem. Soc. Faraday Trans. I, **78**, 567 (1982).
11. D. Feakins, R. D. O'Neill, W. E. Waghorne, and A. J. I. Ward. J. Chem. Soc. Faraday Trans. I, **78**, 1431 (1982).
12. D. Bax, C. L. de Ligny, M. Alfenaar, and N. J. Mohr. Recl. Trav. Chim. Pays-Bas, **91**, 601 (1972).
13. M. M. Elsemongy, A. A. Abdel-Khalek, and M. A. Hussein. Z. Phys. Chem. Neue Folge, **134**, 215 (1983); Thermochim. Acta, **68**, 187 (1983).
14. M. M. Elsemongy and A. A. Abdel-Khalek. Monatsh. Chem. **114**, 891 (1983).
15. J. P. Morel. Bull. Soc. Chim. Fr. **11**, 3231 (1965).
16. D. Feakins and C. M. French. J. Chem. Soc. 3168 (1956).

General acid catalysis in the enolization of acetone

KEVIN P. SHELLY, S. VENIMADHAVAN, K. NAGARAJAN, AND ROSS STEWART[1]
Department of Chemistry, University of British Columbia, Vancouver, B.C., Canada V6T 1Y6

Received January 27, 1989

KEVIN P. SHELLY, S. VENIMADHAVAN, K. NAGARAJAN, and ROSS STEWART. Can. J. Chem. **67**, 1274 (1989).

We have used iodometry to study the enolization of acetone in water catalyzed by a series of general acids, comprised of hydrochloric acid, methanesulfonic acid, 24 aliphatic monocarboxylic acids, nine aromatic monocarboxylic acids, eight aliphatic dicarboxylic acids, and 20 monoanions of dicarboxylic acids. The log $k-pK$ profile for unbuffered solutions of strong and moderately strong acids shows a maximum near $pK \approx 0$. The Brønsted α value for a set of eight aliphatic monocarboxylic acids in which effects of bulk, charge, and polarizability are at a minimum is 0.56. Steric effects, probably augmented by polarizability effects in some cases, cause positive deviations from the Brønsted line drawn with respect to these standard acids. Anionic carboxylic acids are also more reactive than would be predicted from their equilibrium acid strengths, whereas cationic acids tend to be less reactive. Using D_2O as solvent has only a small effect on the rate of carboxylic acid catalysis. Using acetone-d_6 gives values of k_H/k_D in the range of 7.0–8.0 at 25°C, values consistent with proton or deuteron being transferred between two bases of comparable strength, the carboxylate anion and the enol form of acetone.

Key words: general acid catalysis, enolization, Brønsted relation, steric effects, deuterium isotope effects.

KEVIN P. SHELLY, S. VENIMADHAVAN, K. NAGARAJAN et ROSS STEWART. Can. J. Chem. **67**, 1274 (1989).

On a utilisé l'iodométrie pour étudier l'énolisation de l'acétone, en milieux aqueux et sous l'influence d'une série d'acides généraux comme l'acide chlorhydrique, l'acide méthanesulfonique, 24 acides aliphatiques monocarboxyliques, neuf acides aromatiques monocarboxyliques, huit acides aliphatiques dicarboxyliques et 20 monoanions d'acides dicarboxyliques. La courbe log $k-pK$, pour des solutions non-tamponnées d'acides forts et modérément forts, présente un maximum près d'un pK de 0. La valeur α de Brønsted est de 0,56 pour un ensemble de huit acides monocarboxyliques pour lesquels les valeurs des effets d'encombrement, de charge et de polarisabilité sont minimales. Les effets stériques, probablement amplifiés dans certains cas par des effets de polarisabilité, provoquent des déviations positives par rapport à la ligne de Brønsted tracée en utilisant ces acides de référence. Les anions des acides dicarboxyliques sont aussi plus réactifs que prévu sur la base de la force de leurs acides; toutefois, les acides cationiques tendent à être moins réactifs. L'utilisation de D_2O comme solvant ne provoque qu'un léger effet sur la constante de la catalyse des acides carboxyliques. À 25°C, l'utilisation d'acétone-d_6 conduit à une valeur de k_H/k_D de l'ordre de 7,0–8,0; cette valeur est en accord avec un mécanisme dans lequel un proton ou un deutéron est transféré entre deux bases de force comparable, l'anion carboxylate et la forme énolique de l'acétone.

Mots clés : catalyse acide générale, énolisation, relation de Brønsted, effets stériques, effets isotopiques du deutérium.

[Traduit par la revue]

Introduction

The acid-catalyzed enolization of acetone occupies an important place in the evolution of our understanding of the phenomenon of general acid catalysis. In 1913, Dawson and Powis examined the effect of weak acids on this reaction and recognized that their catalytic effect was due both to the hydrogen ions that they produce and to the undissociated acid molecules themselves (1). A decade later Brønsted and Pedersen (2) showed that catalysis by the latter could be quantified, and we now refer to the governing relationship as the Brønsted equation, which appears in eq. [1] with the appropriate statistical corrections. The latter attempt to account for variations in the number of protonic sites (p) in the acid catalysts that are used and in the number of basic sites (q) in their corresponding conjugate bases (3–5).

$$[1] \quad \log (k_{HA}/p) = \alpha \log (K_{HA} q/p)$$

The mechanism of the general acid-catalyzed enolization process is generally agreed to be that shown in eq. [2] (ref. 5, p. 259, and ref. 6).

$$[2a] \quad CH_3-\overset{\overset{O}{\|}}{C}-CH_3 + H^+ \leftrightharpoons CH_3-\overset{\overset{+OH}{\|}}{C}-CH_3$$

$$[2b] \quad CH_3-\overset{\overset{+OH}{\|}}{C}-CH_3 + A^- \longrightarrow CH_3-\overset{\overset{OH}{|}}{C}=CH_2 + HA$$

[1]Author to whom correspondence may be addressed.

The present paper concerns itself with five aspects of the reaction: (a) catalysis in unbuffered systems, (b) steric and polarizability effects in HA, (c) the behaviour of cationic and anionic acids, (d) the catalytic role of monoanions of dicarboxylic acids, and (e) deuterium isotope effects.

Results and discussion

Catalysis in unbuffered systems

It has long been recognized that H^+ is generally a less effective catalyst in general acid-catalyzed proceses than would be expected from its formal pK (−1.74) (ref. 4, p. 200, and ref. 5, p. 278). The catalytic constant, k_{H^+}, for the enolization of acetone has been determined many times over the years; Hine *et al.* averaged 18 such reports in the literature and obtained a value of 2.84×10^{-5} M^{-1} s^{-1} at 25°C (9). We have made 24 measurements of this quantity using various concentrations of hydrochloric acid. The results are shown in Fig. 1. A number of additional measurements were made on solutions to which 1/3 to 4/5 equivalent of sodium hydroxide had been added. These points fall very close to the line in Fig. 1, indicating that salt effects on the reaction are negligible, at least in the more dilute solutions. The slope of the line in Fig. 1 gives a value of 2.56×10^{-5} M^{-1} s^{-1} (25°C) for k_{H^+}, slightly lower than the average value from the literature.

We find a small but consistent difference between the stoichiometric concentration of H^+ and the concentration determined directly from our glass electrode measurements. The latter, which is strictly speaking an activity, is always found to be slightly lower than the former, which has been determined

Can. J. Chem. Downloaded from www.nrcresearchpress.com by 194.225.253.170 on 09/07/12
For personal use only.

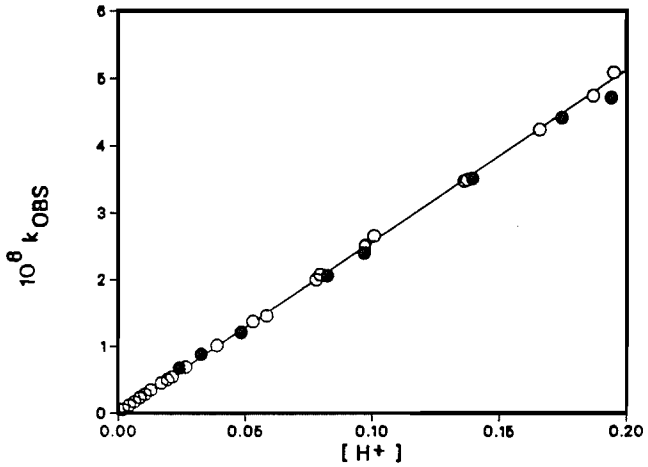


FIG. 1. Plot of observed rate of enolization of acetone against the stoichiometric concentration of hydrochloric acid; open circles, slope = $(2.56 \pm 0.01) \times 10^{-5}\,M^{-1}\,s^{-1}$, corr. coeff. = 0.9998; closed circles represent solutions containing sodium chloride as a result of adding sodium hydroxide.

by titration with standardized sodium hydroxide. Thus, k_{H^+} based directly on glass electrode measurements without any activity/concentration corrections would be slightly higher ($2.95 \times 10^{-5}\,M^{-1}\,s^{-1}$, based on all 32 points in Fig. 1).

We have measured the rate of enolization of acetone in 0.1 M unbuffered solutions of a number of strong and moderately strong acids. In these cases the hydrogen ion concentration is high enough to be unaffected by the iodometric process that is used to follow the reaction and which generates acid on a small scale. The results are shown in Fig. 2, with the dotted lines being those based on the H^+ and HA contributions, which have been calculated from the known dissociation constants of the acids themselves. The value of $2.56 \times 10^{-5}\,M^{-1}\,s^{-1}$ was used for the H^+ curve, and the Brønsted value of 0.56 for carboxylic acids (*vide infra*) was used for the HA curve. The solid line represents the expected sum of the H^+ and HA contributions in unbuffered solutions of acid concentration 0.1 M. As can be seen there is a maximum in the curve at a pK_{HA} of about −0.2. The eight acids for which experimental points are given range from chloroacetic acid, pK_{HA} 2.86, to methanesulfonic acid, pK_{HA} −1.92 (ref. 5, p. 12, and ref. 10). The latter, which falls precisely on the theoretical line, is the only acid that is not a carboxylic acid and it could be argued that there is no reason to assume that its catalytic ability will be governed by the Brønsted curve for carboxylic acids. However, the undissociated form of this particular acid will make only small contributions to the overall rate and so any deviations on this score will be minor.

The three trihaloacetic acids are more interesting since their acid strengths are such that their undissociated forms make significant contributions to the overall rate. There is a decrease in catalytic effectiveness going from tribromoacetic to trifluoroacetic acid, that is, as acid strength increases, and if the theoretical curve were displaced some 1.6 units to the right these acids would fall directly on the line. A much more reasonable explanation for this effect, however, is the following. Phenylphosphonic acids, containing an iodine or bromine atom at the *ortho* position, exhibit enhanced catalytic activity in acetone enolization and this effect has been tentatively attributed to the polarizability of these atoms (12). A similar effect may be at work here with the proton-transfer step shown in eq. [2*b*] being facilitated by polarization of the nearby halogen atoms.

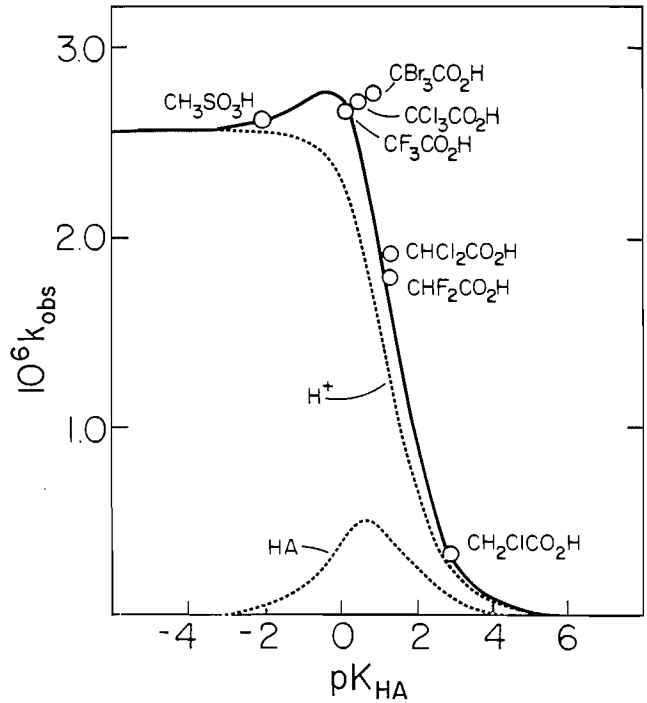


FIG. 2. Plot of observed rate for catalysis by 0.1 molar acid solutions as a function of the p*K* of the catalyzing acid. Dotted lines are calculated curves for the proton and undissociated acid; the solid line represents the sum of the values that produce the dotted lines. The curve for HA was calculated using the equation for the solid line in Fig. 4.

(Unfortunately, triiodo- and diiodoacetic acids cannot be used since they give curved rate plots, presumably because they undergo partial solvolysis in the reaction mixture.) Whatever the cause of the reactivity order here, there is no doubt that the three trihaloacetic acids, particularly the tribromo compound, are more effective catalysts in aqueous solution than are hydrochloric acid and other strong acids, whose catalytic power depends only on the hydrogen ion that they generate.

Buffer catalysis

Two methods have been used to measure k_{HA}, which is the catalytic constant of the undissociated acids used as catalysts. The first, the buffer-ratio method of Bell and Lidwell (13), has been used for the weaker acids, where contributions from the buffer anion A^- are significant. This method requires a large number of rate measurements to be made using several buffer ratios. At a constant buffer ratio (n) the observed rate constant (k_{obs}) is plotted against [HA] and the slope (s) measured. This procedure is repeated for several other buffer ratios and the slopes then plotted against $1/n$, according to eq. [3], to give both catalytic constants, k_{HA} as the intercept and k_{A^-} as the slope.

$$[3] \quad s = k_{HA} + (1/n)k_{A^-}$$

When $k_{HA} < k_{A^-}$, as it is for acetic acid and weaker acids, then it is often convenient to plot k_{obs} against $[A^-]$; the corresponding plot of s against $1/n$ is governed by eq. [4] in these cases,

$$[4] \quad s = k_{A^-} + nk_{HA}$$

For stronger acids, those whose pK_{HA} values are lower than, say, 3.2, the contribution of A^- to the rate becomes so small

Can. J. Chem. Downloaded from www.nrcresearchpress.com by 194.225.253.170 on 09/07/12
For personal use only.

TABLE 1. Catalytic constants for the enolization of acetone in water at 25°C, at 0.1 M ionic strength

No.	Compound	$10^7 k_{HA}$, $M^{-1} s^{-1}$	log k/p	Method[a]	pK_{HA}[b]	$pK_{HA} + \log p/q$
1	$(CH_3)_3CCO_2H$	0.718 ± 0.027	−7.14	2	5.03	4.73
2	$(CH_3)_3CCH_2CO_2H$	0.897 ± 0.020	−7.05	2	5.01[c]	4.71
3	c-$C_6H_{11}CO_2H$	0.771 ± 0.100	−7.11	2	4.91	4.61
4*	$CH_3CH_2CO_2H$	0.653 ± 0.084	−7.18	2	4.87	4.56
5	Me_2CHCO_2H	0.691 ± 0.045	−7.16	2	4.86	4.56
6	$CH_3CH_2CH_2CO_2H$	0.884 ± 0.010	−7.05	2	4.82	4.52
7*	CD_3CO_2H	0.812 ± 0.020	−7.09	2	4.77[d]	4.47
8*	CH_3CO_2H	0.822 ± 0.022	−7.08	2	4.76	4.46
9	$C_6H_5CH_2CO_2H$	1.90 ± 0.07	−6.72	1	4.31	4.01
10*	$HOCH_2CO_2H$	3.09 ± 0.01	−6.51	1	3.83	3.53
11*	$CH_3OCH_2CO_2H$	4.81 ± 0.01	−6.32	1	3.57	3.27
12	$C_6H_5CHOHCO_2H$	7.76 ± 0.16	−6.11	1	3.41	3.11
13	ICH_2CO_2H	9.76 ± 0.02		1		
	9.58	9.22 ± 0.20	−6.02	3	3.18	2.88
		9.36 ± 0.41		4		
14*	$ClCH_2CO_2H$	11.0 ± 1.0		1		
	10.8	10.4 ± 1.0	−5.97	3	2.86	2.56
		10.9 ± 1.1		4		
15	$Cl^-H_3N^+CH_2CO_2H$	13.0 ± 0.8	−5.89	4	2.36[e]	2.06
16	$Cl^-(Me)_2N^+HCH_2CO_2H$	21.4 ± 0.6	−5.70	4	1.94[e]	1.64
17	$Cl^-Me_3N^+CH_2CO_2H$	29.9 ± 1.4	−5.52	4	1.83[e]	1.53
18	$Cl^-Me_3N^+(CH_2)_3CO_2H$	1.59 ± 0.01	−6.80	1	4.13[c,f]	3.83
19	$Cl^-Me_3N^+(CH_2)_5CO_2H$	1.18 ± 0.03	−6.93	1	4.51[c,f]	4.21
20	Cl_2CHCO_2H	91.9 ± 1.5	−5.03	4	1.36[c,g]	1.06
21*	F_2CHCO_2H	63.7 ± 1.2	−5.20	4	1.30,[c] 1.34[g]	1.02
22	Br_3CCO_2H	273 ± 11	−4.56	4	0.73	0.43
23	Cl_3CCO_2H	281 ± 8	−4.55	4	0.69,[c] 0.52[d]	0.30
24*	F_3CCO_2H	205 ± 9	−4.69	4	0.54,[c] 0.50[d]	0.22
25	$C_6H_5CO_2H$	2.45 ± 0.41	−6.61	1	4.20	3.90
26	3-$CH_3C_6H_4CO_2H$	1.61 ± 0.08	−6.79	1	4.27	3.97
27	2-$C_2H_5OC_6H_4CO_2H$	3.05 ± 0.36	−6.52	1	4.16[c]	3.86
28	2-$CH_3C_6H_4CO_2H$	4.22 ± 0.13	−6.37	1	3.91	3.61
29	3-$FC_6H_4CO_2H$	3.42 ± 0.31	−6.47	2	3.86	3.56
30	3-$O_2NC_6H_4CO_2H$	5.27 ± 0.24	−6.28	2	3.49	3.19
31	2-$FC_6H_4CO_2H$	8.86 ± 0.69	−6.05	2	3.27	2.97
32	2-$O_2NC_6H_4CO_2H$	39.1 ± 1.2	−5.41	4	2.21	1.91
33	2,6-$(O_2N)_2C_6H_3CO_2H$	175 ± 19	−4.76	4	1.14	0.84
34	$(CO_2H)_2$	104 ± 2.3[h]	−5.28	1,2	1.25	1.25
35	$(C_2H_5)_2C(CO_2H)_2$	22.0 ± 0.5	−5.96	1,2	2.21	2.21
36	$CH_3CH(CH_2CO_2H)_2$	2.09 ± 0.01	−6.98	1,2	4.35	4.35
37	$(CH_3)_2C(CH_2CO_2H)_2$	2.44 ± 0.07	−6.91	1,2	3.85	3.85
38	$(CH_2CO_2H)_2$	2.44 ± 0.04	−6.91	1,2	4.20	4.20
39	$[(Me)_2CCO_2H]_2$	3.78 ± 0.10	−6.72	1,2	3.56	3.56
40	(±)-$(EtCHCO_2H)_2$	5.03 ± 0.18	−6.60	1,2	3.51	3.51
41	meso-$[EtCHCO_2H]_2$	3.62 ± 0.08	−6.74	1,2	3.63	3.63
42	$^-O_2CCO_2H$	6.34 ± 0.52	−6.20	3	4.29	3.69
43	$Et_2C(CO_2^-)CO_2H$	—[hh]	—	1,2	7.29	6.69
44	$CH_3CH(CH_2CO_2^-)CH_2CO_2H$	3.79 ± 0.02	−6.48	1,2	5.44	4.84
45	$Me_2C(CH_2CO_2^-)CH_2CO_2H$	0.795 ± 0.055	−7.10	1,2	6.45[i]	5.85
46	$^-O_2CCH_2CH_2CO_2H$	2.45 ± 0.11	−6.61	1,2	5.63[j]	5.03
47	$^-O_2CCMe_2CMe_2CO_2H$	0.315 ± 0.08	−7.50	1,2	7.41	6.81
48	(±)-$^-O_2CCHEtCH(Et)CO_2H$	0.576 ± 0.019	−7.24	1,2	6.60	6.00
49	(meso)-$^-O_2CCH(Et)CH(Et)CO_2H$	0.761 ± 0.11	−7.12	1,2	6.46	5.86
50	1,2-$C_6H_4(CO_2^-)CO_2H$	1.63 ± 0.32[k]	−6.79	2	5.41[c]	4.81
51	1,3-$C_6H_4(CO_2^-)CO_2H$	3.46 ± 0.07[l]	−6.46	2	4.75[m]	4.15
52	5-Me-1,3-$C_6H_3(CO_2^-)CO_2H$	2.86 ± 0.33[l]	−6.54	2	4.82[m]	4.22
53	5-Br-1,3-$C_6H_3(CO_2^-)CO_2H$	3.89 ± 0.22[l]	−6.41	2	4.36[m]	3.76
54	5-I-1,3-$C_6H_3(CO_2^-)CO_2H$	3.93 ± 0.28[l]	−6.40	2	4.41[m]	3.81
55	5-NO_2-1,3-$C_6H_3(CO_2^-)CO_2H$	5.59 ± 0.69[l]	−6.25	2	4.04[m]	3.44

Can. J. Chem. Downloaded from www.nrcresearchpress.com by 194.225.253.170 on 09/07/12
For personal use only.

TABLE 1 (*concluded*)

No.	Compound	$10^7 k_{HA}$, $M^{-1} s^{-1}$	log k/p	Method[a]	pK_{HA}[b]	$pK_{HA} + \log p/q$
56	2-MeO-1,3-$C_6H_3(CO_2^-)CO_2H$	6.57 ± 0.24^l	−6.18	2	4.32[m]	3.72
57	2-Me-1,3-$C_6H_3(CO_2^-)CO_2H$	7.95 ± 0.59^l	−6.10	2	4.25[c]	3.65
58	2-Cl-1,3-$C_6H_3(CO_2^-)CO_2H$	25.6 ± 1.3^l	−5.59	2	3.38[c]	2.78
59	2-Br-1,3-$C_6H_3(CO_2^-)CO_2H$	31.2 ± 0.9^l	−5.51	2	3.28[c]	2.68
60	2-I-1,3-$C_6H_3(CO_2^-)CO_2H$	34.7 ± 1.6^l	−5.46	2	3.32[c]	2.72
61	2-O_2N-1,3-$C_6H_3(CO_2^-)CO_2H$	38.6 ± 0.9^l	−5.41	2	3.01[c]	2.41

[a]1. Buffer ratio method, eq. [3]; 2. Buffer ratio method, eq. [4]; 3. Plot of k_{obs} against [HA], eq. [5]; 4. Plot of $k_{obs} - k_{H^+}[H^+]$ against [HA] (see text). Errors have been calculated using a Minitab programme.
[b]From refs. 5, 14, and 39, and are thermodynamic values unless otherwise indicated.
[c]This work.
[d]Reference 7.
[e]Reference 8.
[f]Ionic strength 0.1 M.
[g]Reference 11.
[h]Ionic strength 0.1–0.2 M.
[hh]Too small to measure.
[i]Reference 35.
[j]Reference 14, p. 60.
[k]Ionic strength 0.05 M.
[l]Overlapping dissociations ignored; values are slightly larger when overlap is considered, with the stronger acids displaying significantly larger error limits.
[m]Reference 27.

that it becomes possible to simply plot k_{obs} against [HA] and determine k_{HA} from the slope of the plot, that is, from eq. [5], where k_{sum} represents the contributions of H^+, H_2O, and A^-.

$$[5] \quad \log k_{obs} = k_{sum} + k_{HA}[HA]$$

In the case of stronger acids k_{sum} can be shown to be simply the contributions from $k_{H^+}[H^+]$. Figure 3 shows the effect of plotting $k_{obs} - k_{H^+}[H^+]$ against [HA], the calculated concentration of the acid component of a series of difluoroacetic and dichloroacetic acid buffer solutions. The intercepts are essentially at the origin, showing that contributions from water and buffer anion are negligible. Since we have used values of $[H^+]$ obtained directly from glass electrode measurements, we have used here the value of $2.95 \times 10^{-5} M^{-1} s^{-1}$ for k_{H^+}.

Table 1 lists the catalytic constants for a total of 41 neutral or cationic carboxylic acids of various types and 19 anions of dicarboxylic acids; the latter species are amphoteric but, as we shall see later, they function as acid, not base, catalysts in the enolization process.[2] The low solubility of the aromatic acids made determinations of their catalytic constants somewhat difficult and resulted in higher error limits than in the case of aliphatic acids. In the case of the phthalic and isophthalic acids and some of the aliphatic dicarboxylic acids it was not found possible to determine the catalytic constants of the undissociated acids at all, although catalysis by the monoanions could be measured. Many of these acids have a further problem; their first and second dissociation constants are sufficiently close that pains had to be taken to determine the concentration of the various catalytic species present (14–16).

Figure 4 is the Brønsted plot for acetone enolization using all the carboxylic acid catalysts for which we have been able to measure rate constants. Even though all the catalysts are

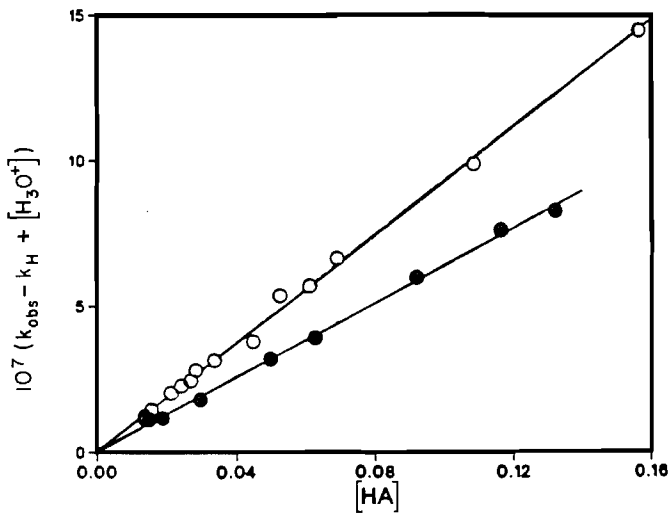


FIG. 3. Plot of $k_{obs} - k_{H^+}[H^+]$ against the concentration of undissociated buffer acid; open circles, dichloroacetic acid, corr. coeff. = 0.9985; closed circles, difluoroacetic acid, corr. coeff. = 0.9990.

carboxylic acids there is considerable diversity in structural and charge type and it is perhaps not surprising that the plot shows significant scatter. The least-squares line for all the points is shown as a dotted line in Fig. 4; its slope α is 0.482 ± 0.024 with a correlation coefficient of 0.9374. We prefer to attach more significance to the unbroken line, which refers to a subset of acids in which ancillary effects are at a minimum.

Of the 60 acids listed in Table 1 that are displayed in Fig. 4 there is a group of eight, identified by an asterisk in Table 1 and by solid symbols in Fig. 4, that possess no charge and in which steric and polarizability effects are small. The α value of 0.56 (0.560 ± 0.12, corr. coeff. 0.9986) is close to the value of 0.57 determined by Bell and Lidwell for a group of four aliphatic carboxylic acids, three of which are members of our standard

[2]Listings of the rate constants at various buffer ratios, from which the values in Table 1 were derived, may be purchased from the Depository of Unpublished Data, CISTI, National Research Council, Ottawa, Ont., Canada K1A 0S2.

Can. J. Chem. Downloaded from www.nrcresearchpress.com by 194.225.253.170 on 09/07/12
For personal use only.

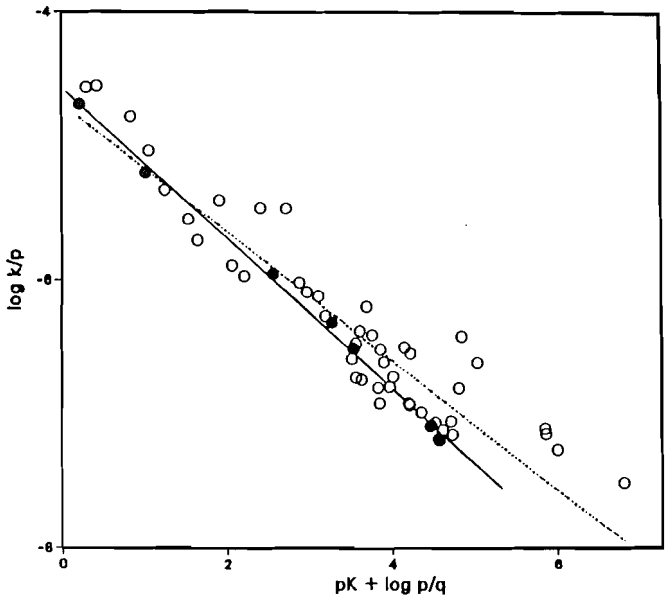


FIG. 4. Brønsted plot for acid catalysis of acetone enolization; solid symbols represent the acids listed in Table 1 that bear asterisks. The equation governing the solid line is $\log k_{HA} = 0.560 \log K_{HA} - 4.564$.

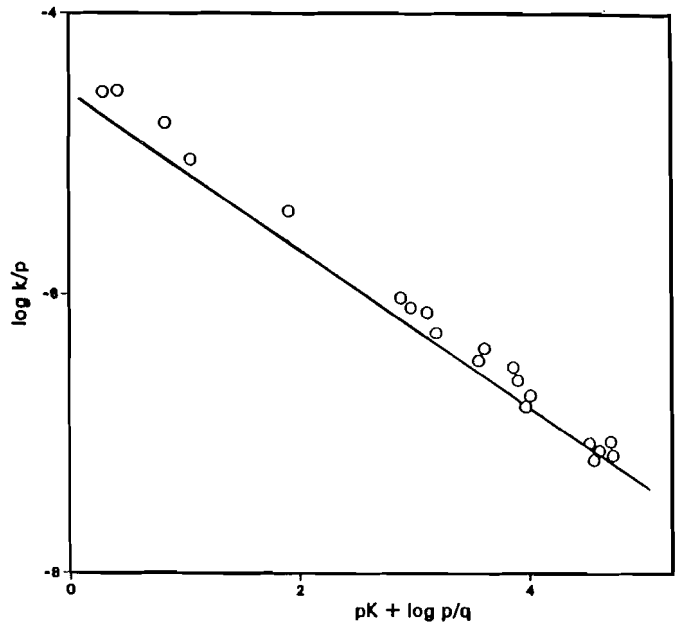


FIG. 5. Brønsted plot for all neutral monocarboxylic acids; line drawn with respect to the standard acids (see text) whose points are not shown.

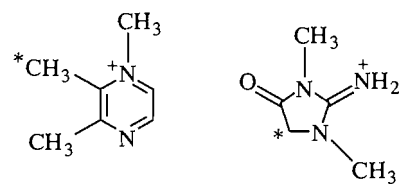
group and one of which, pivalic acid, possesses steric bulk. (The rate constants for the acids that are common to both sets are in reasonable agreement.)

As is usual for Brønsted plots the lines drawn in Fig. 4 are straight. The question of curvature in Brønsted plots is a question of current interest (17, 18) and examination of the solid points and unbroken line in Fig. 4 raises the question as to whether a quadratic, rather than a linear, relationship better represents the variation in catalyst strength with acid strength for the eight standard acids. Moreover, if a slight degree of curvature is present, it is in the expected direction; that is, the stronger acids are marginally less effective catalysts than would be predicted from a straight line based on the weaker acids. Too much should not be made of this point, however, since, if glycollic acid had not been included in the study, the question of curvature might not have arisen. Regardless of whether the Brønsted line is straight or slightly curved, our analysis of the causes of deviation of the remaining points will be essentially unaffected. This having been said, we will use the linear Brønsted relationship for the eight standard acids as the basis for subsequent discussion.

Steric and polarizability effects

In Fig. 5 the line for the eight standard acids is displayed, together with the points for the remaining neutral monocarboxylic acids, all of which possess steric bulk. It can be seen that virtually all such acids are *more* effective catalysts than would be suggested by a consideration of their equilibrium acid strengths. The effects are not large but they are consistently in this direction. Steric acceleration of proton transfer reactions has been observed in a number of other instances, both when the steric bulk is in the substrate (19) and in the catalyst. In particular, the base-catalyzed deprotonation of the 6-methyl group in the pyrazinium ion **I** and the methylene group of **II** (marked by asterisks), by a series of aliphatic and aromatic carboxylate bases showed the effects of marked steric activation (20, 21). However, previous studies of acetone enolization by arylphosphonate anions (base catalysis) and by arylphosphonic acids (acid catalysis) showed such effects to be absent in the former and small in the latter (12). It could well be that acetone, being a small molecule, does not exhibit as much sensitivity to steric bulk as does **I** or **II**.

It is significant that in virtually all cases in which steric activation in the catalyst has been observed the proton is being abstracted from a cation. In the cases of **I** and **II** the substrate is cationic; in the present case, and in the case of arylphosphonic acid catalysis, the rate-controlling step involves a cationic intermediate (see eq. [2*b*]).



I **II**

The effect of a group's polarizability is not always easy to separate from that of its size. Several of the deviating points in Fig. 5 represent acids that contain chlorine, bromine, or iodine atoms near the carboxyl group. All such catalysts exhibit exalted effects, except chloroacetic acid, which would be expected to be the one with the smallest polarizability/steric effect and is included as one of our standard catalysts. Is there any evidence in these results for the notion that polarizable groups in the catalyst stabilize the transition state of prototropic reactions (ref. 12; see also ref. 22)? Or are steric effects alone sufficient to explain the deviation of acids containing the large halogen units? If one examines the steric parameter E_s (23) of all the groups in Fig. 5 for which this quantity is available, one finds that the positive deviations from the Brønsted line are roughly in accordance with the magnitude of E_s; the major exception is the CH_2I group, **13**, which has a large deviation despite having a modest value of E_s. The high polarizability of iodine could explain this group's exalted catalytic effect. Unfortunately, the groups that would have further tested the polarizability hypothesis (the bromo- and iodoacetic acids

Can. J. Chem. Downloaded from www.nrcresearchpress.com by 194.225.253.170 on 09/07/12
For personal use only.

Can. J. Chem. Downloaded from www.nrcresearchpress.com by 194.225.253.170 on 09/07/12
For personal use only.

that are missing from Table 1, and various sulfur-containing carboxylic acids) were all found to react under the reaction conditions employed. One can conclude that steric activation occurs in the general acid catalysis of acetone enolization, probably augmented by polarizability effects in some cases. As to the cause of the steric activation, we simply draw attention to the following points: (1) The effect seems to be most clearly evident when cationic substrates and anionic bases are involved in the rate-controlling step. (2) As has been previously noted (21), it is unwise to try to explain deviations from Brønsted lines on the basis of exalted or depressed rate constants alone; the equilibrium acid or base strengths of the catalysts are of equal importance in determining a point on a Brønsted plot, and a substituent's effect on these parameters should receive an equal degree of scrutiny.

Charged catalysts

In Fig. 6 the effect of positive or negative charge in the acid catalyst is displayed; again the Brønsted line for our eight standard acids is shown for comparison. It can be seen that all anionic acid catalysts show exalted effects and most cationic acids show depressed effects, results similar to those reported by Kresge and Chiang for vinyl ether hydrolysis (24). (The anionic catalysts, which are amphoteric, are assumed to be acting as general acids, not as general bases or as bifunctional catalysts; see later.) It is clear that proximity of the positive charge to the catalytic site is important since the largest negative deviations occur for the three ammonioacetic acids, whereas an ammonio group at the 4- or 6-position produces virtually no effect. It should be noted that the depressed catalytic constant for the hydrated proton, which has often been remarked upon (8), fits well into this general picture (24).

The deviations of the anionic acid catalysts from the Brønsted line are generally greater than those of their cationic counterparts, as was also the case for vinyl ether hydrolysis (24, 25). (The opposite effect has been observed in a base-catalyzed reaction (26).) Many of the anionic catalysts are sterically hindered, e.g., the 2-substituted isophthalic acid anions, and some of the rate exaltation may be due to this factor. However, it should be noted that the catalyst that deviates most from the Brønsted line is the anion of succinic acid **46**, which does not have a large degree of encumbrance.

The present results, when taken in conjunction with previous work that showed that dianionic bases (eq. [5]) are less effective than monoanionic bases in removing protons from neutral acetone (27), confront us with a paradox. The rate-controlling step of the reaction of the monoanionic catalysts examined herein is, presumably, the reaction of protonated acetone with these very dianionic bases (eq. [6*b*]), and yet here these catalysts exhibit exalted, not depressed, effects.

[5] $Z + A^{2-} \rightarrow$ products

[6*a*] $Z + HA^{-} \leftrightarrows ZH^{+} + A^{2+}$

[6*b*] $ZH^{+} + A^{2-} \rightarrow$ products

Put another way, the proton activating factor, paf (28), appears to be markedly greater for dianionic bases than for monoanionic bases. Perhaps the presence of a positive charge in the substrate and a double negative charge in the base provides a special interaction in the transition state of eq. [6*b*] that is not taken into account when only protolytic equilibria, which are the basis of the Brønsted relation, are considered. (Such an interaction in the transition state has been invoked previously by

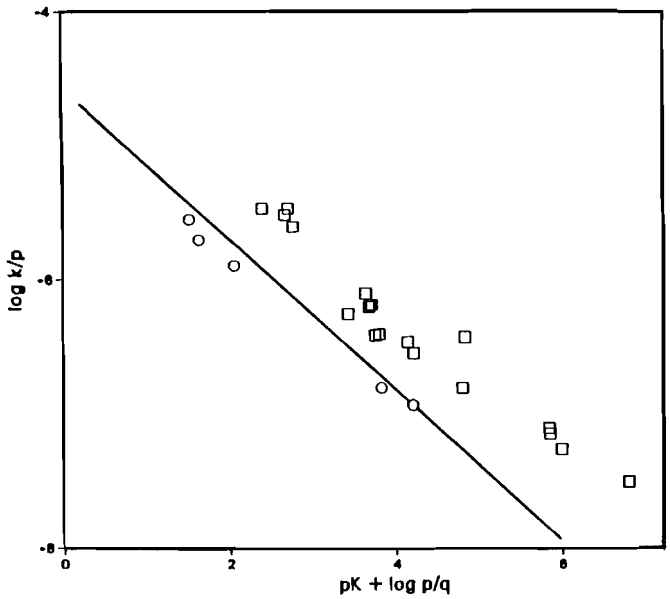


FIG. 6. Brønsted plot for charged acid catalysts; circles represent cationic acids, and squares, anionic acids; line drawn as in Fig. 5.

Kresge and co-workers to explain the greater catalytic effect of phosphonate monoanionic acids than carboxylic acids of the same acid strength in the hydrolysis of vinyl ethers (25).) One would have expected, then, that proton abstraction from the cation **II**, a reaction that is analogous to [6*b*], would be faster for dianionic carboxylate bases than for monocarboxylate bases of the same strength. The reverse, in fact, is found (20). It may be that the mesoionic character of the species formed from **II** makes it a less than satisfactory model for the enol formed in the present case. Unfortunately, the carboxylate bases used to construct the Brønsted line for the cation **I** (which would give a neutral intermediate analogous to an enol) did not include any dicarboxylate ions (21) and so we regard as still unsettled the question of the effect of charge in the catalyst on the enolization process.

Dicarboxylic acids

We have shown previously that dianions of dicarboxylic acids have, as a group, lower catalytic constants for acetone enolization than those of monoanions of comparable base strength (27). Moreover, among these dianions is a group whose catalytic effects are even further depressed and whose behaviour was traced to the ability of the corresponding monoanions to form internal hydrogen bonds. That is, the kinetic base strength of their dianions is lower than expected because the product stabilization caused by hydrogen bonding is absent in the transition state. Since the monoanion acts as the basic component in dicarboxylic acid catalysis (eq. [6*b*]), we have scrutinized the results for dicarboxylic acid catalysis to see if the same anomalies are present. In Fig. 7 it can be seen that the dicarboxylic acids, **34**–**41**, conform fairly well to the Brønsted line for the standard acids, although **35**, **37**, **39**, and **41** show small but probably significant negative deviations. These four acids (plus **40**) are the ones for which a high degree of internal hydrogen bonding is present in the monoanion and whose dianions exhibit large anomalies in the general base-catalyzed process. It appears as if internally hydrogen-bonded anions tend to be slightly less effective bases in reaction [6*b*] than their nonbonded counterparts. Unlike the case of base catalysis by

TABLE 2. Catalytic constants and isotope effects for enolization of acetone in D_2O[a] at 25°C

Acid catalyst	$10^7 k_{DA}$ (D_2O), $M^{-1} s^{-1}$	n[b]	$k_{HA}(H_2O)/k_{DA}$ (D_2O)[c]
D^+	462 ± 10	11	0.54 ± 0.01
F_3CCO_2D	218 ± 13	3	0.94 ± 0.07
F_2CHCO_2D	62.7 ± 1.4	5	1.02 ± 0.03
Cl_2CHCO_2D	101 ± 3	6	0.92 ± 0.03
$ClCH_2CO_2D$	11.4 ± 0.2	4	0.96 ± 0.10
$HOCH_2CO_2D$	2.47 ± 0.04	3	1.25 ± 0.05
CH_3CO_2D	0.541 ± 0.037	3	1.52 ± 0.11
$(CH_3)_3CCO_2D$	0.513 ± 0.044	3	1.40 ± 0.13

[a]99.9 at.% deuterium, Merck Frosst Canada.
[b]Number of kinetic runs (first five entries) or buffer ratios (final three entries).
[c]See Table 1 for values of k_{HA} (H_2O).

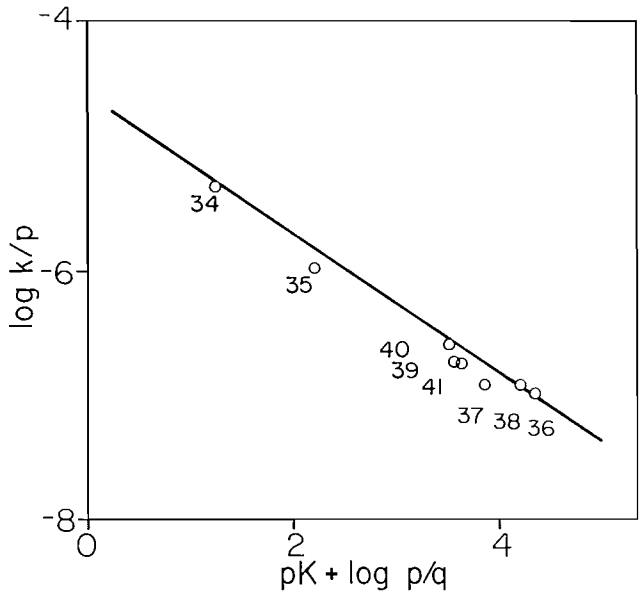


FIG. 7. Brønsted plot for dicarboxylic acids; line drawn as in Fig. 5.

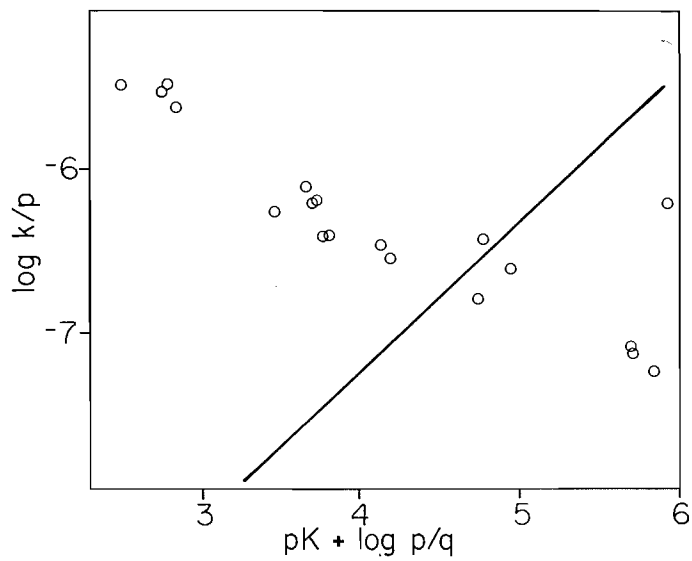


FIG. 8. Brønsted plot for dicarboxylic acid monoanions acting as bases (pK_1); line drawn with respect to the k_{A^-} values of the anions of the standard acids (see text).

dianions, where the anomalies are large and readily explainable, no obvious cause of the small deviations shown in Fig. 7 springs to mind.

Catalytic role of dicarboxylic acid monoanions

It can be seen in Fig. 6 that the behaviour of dicarboxylic monoanions is consistent with their acting as general acids; that is, the greater the acid strength (pK_2) the greater the catalytic effect. They do, of course, fall above the Brønsted line for simple acids and there is considerable scatter, presumably caused in part by steric effects in the catalyst. To be satisfied that the monoanions are acting as general acids, not general bases, we have compared their catalytic effects with those for simple general bases. Figure 8 shows the Brønsted line for the anions of the standard acids used herein, making use of data from refs. 12 and 16. It can be seen that the dicarboxylic acid monoanions lie very poorly on the plot and, indeed, the stronger the base the poorer the catalyst tends to be. Moreover, most of the points fall well above the Brønsted line for simple bases. Considering that (a) steric effects in the general base catalysis are small (27) and (b) an uncharged carboxyl group elsewhere in the molecule does not seem to have a large effect on catalytic activity (previous section), we can conclude that the monoanions are not acting as general bases. This conclusion is in line with that reached earlier

TABLE 3. Catalytic constants and isotope effects for enolization of acetone-d_6[a] in H_2O at 25°C

Acid catalyst	pK_{HA}	$10^8 k_{HA}(k_D)$, $M^{-1} s^{-1}$	n[b]	k_H/k_D[c]
F_3CCO_2H	0.52	258 ± 22	5	7.9 ± 0.8
Cl_2CHCO_2H	1.36	132 ± 7	8	7.0 ± 0.4
$2\text{-}O_2NC_6H_4CO_2H$	2.21	44.7 ± 3.3	3	8.8 ± 0.8
$ClCH_2CO_2H$	2.86	15.1 ± 1.9	4	7.3 ± 1.1
$HOCH_2CO_2H$	3.83	3.92 ± 0.38	3	7.9 ± 0.8
$C_6H_5CH_2CO_2H$	4.31	2.54 ± 0.06	3	7.6 ± 0.5

[a]99.9 at.% deuterium, Merck Frosst Canada.
[b]Number of kinetic runs (first four entries) or buffer ratios (final two entries).
[c]See Table 1 for values of k_H.

with respect to the monoanions of arylphosphonic acids, which are also amphoteric (12).

There remains the possibility that the dicarboxylate monoanions are acting as bifunctional catalysts, transferring and receiving a proton in one operation, which would be in line with their being more effective catalysts than simple acids and bases of the same strength. (This is not so with arylphosphonate monoanions (12).) A concerted reaction would be expected to have a flattish Brønsted plot (see ref. 29, where bifunctional

Can. J. Chem. Downloaded from www.nrcresearchpress.com by 194.225.253.170 on 09/07/12
For personal use only.

TABLE 4. Melting point and analytical data for 2-substituted isophthalic acids[a]

Substituent	Melting point, °C[b]	Analysis					
		Calculated			Found		
		C	H	N	C	H	N
2-Methoxy	220–222	55.11	4.11	—	55.19	4.20	—
2-Chloro	228–230	47.90	2.51	—	47.45	2.43	—
2-Bromo	219–221	39.22	2.06	—	39.06	1.98	—
2-Nitro	314–315	45.51	2.39	6.63	45.62	2.44	6.39
2-Methyl	239–242	60.00	4.48	—	59.88	4.42	—
2-Acetamido	210–214	53.82	4.07	6.28	53.55	3.95	6.32
2-Iodo	244–246	32.90	1.73	—	32.87	1.76	—

[a]Compounds that are not documented in the literature.
[b]Uncorrected.

catalysis, albeit of a different type, is described). Since catalytic activity is very roughly a function of acid strength for these species, we conclude that the group as a whole is acting as general acids, although it is possible that some of the rather large positive deviations in Fig. 6 are due in part to bifunctional catalysis.

Isotope effects

The effect of deuterium substitution in both substrate and solvent is shown in Tables 2 and 3. The results in D_2O (Table 2) are more extensive than those Reitz and Kopp reported in the early days of isotope study, but generally confirm their work (30). (See refs. 31 and 32 for a discussion of the factors responsible for deuterium solvent isotope effects.)

Reitz and Kopp also examined the general acid-catalyzed enolization of acetone-d_6, using acetone containing 92 at.% deuterium. Our kinetic isotope effects, listed in Table 3, have been obtained using 99.9% isotopically pure substrate and are markedly higher than theirs. It is clear that the primary kinetic isotope effects are substantial in all cases and that the magnitude of the effect is not significantly dependent on the catalytic power of the acid catalyst. There are grounds for believing that primary isotope effects should be at a maximum in proton transfer processes when the two bases sharing the proton in the transition state are of comparable strength (33, 34, and ref. 5, p. 169), and this may be the case here. The strength of protonated acetone as a carbon acid can be estimated from its strength as an oxygen acid and from the keto–enol equilibrium constant for acetone, since it can be readily shown (ref. 5, p. 181ff) that $K^c = K^0 K_E$, where K^c and K^0 are the carbon and oxygen acid dissociation constants of protonated acetone and K_E is the keto–enol equilibrium constant.

Values of -3 for pK^0 (ref. 5, p. 121) and -8 for $\log K_E$ (36, 37) give a pK of about 5 for the carbon acidity of the conjugate acid of acetone. If acetone is less basic than this, that is, if the pK of the protonated form is more negative than -3, as some believe (ref. 5, p. 121), its pK as a carbon acid will be lower than 5, possibly in the range of 2–3. Since the pK values of the buffer acids fall near these values, it is perhaps not surprising to find kinetic isotope effects that are large and that are generally insensitive to changes in catalyst pK.

Experimental

The enolization reaction was followed iodometrically and the results analyzed essentially by the methods previously described (12).

Many of the buffer acids are commercially available. The preparation of others, notably the dicarboxylic acids, is described elsewhere (27, 38), except for a number of 2-substituted isophthalic acids whose preparation and characterization are described below and in Table 4.

The 2-methoxy, 2-chloro, 2-bromo, and 2-nitro derivatives of isophthalic acid were prepared by the aqueous permanganate oxidation of the corresponding *meta*-xylenes. The 2-chloro- and 2-bromo-*meta*-xylenes were prepared by the diazotization of the corresponding amino compounds.

2-Aminoisophthalic acid was prepared by the aqueous permanganate oxidation of 2-acetamido-*meta*-xylene followed by acid hydrolysis of 2-acetamidoisophthalic acid. 2-Acetamido-*meta*-xylene was prepared by acetylation of 2-amino-*meta*-xylene using a mixture of acetic anhydride and acetic acid.

2-Iodoisophthalic acid was prepared from 2-aminoisophthalic acid by treating it with sodium nitrate/sulfuric acid and potassium iodide at 0–5°C.

2-Methylisophthalic acid was synthesized from 2,6-dichlorotoluene by refluxing it with cuprous cyanide in the presence of *N*-methylpyrrolidine for 2 days, followed by its hydrolysis by 20% ethanolic potassium hydroxide.

Acknowledgement

The financial support of the Natural Sciences and Engineering Research Council of Canada is gratefully acknowledged.

1. H. M. DAWSON and F. POWIS. J. Chem. Soc. 2135 (1913).
2. J. N. BRØNSTED and K. J. PEDERSEN. Z. Phys. Chem. **108**, 185 (1924).
3. D. M. BISHOP and K. J. LAIDLER. J. Chem. Phys. **42**, 1688 (1965).
4. R. P. BELL. The proton in chemistry. 2nd ed. Cornell Univ. Press, Ithaca, NY. 1973. p. 197.
5. R. STEWART. The proton: applications to organic chemistry. Academic Press, Orlando, FL. 1985. p. 270.
6. J. TOULLEC. *In* Advances in physical organic chemistry. Vol. 18. *Edited by* V. Gold and D. Bethell. Academic Press, London. 1982. p. 1.
7. A. STREITWIESER and H. S. KLEIN. J. Am. Chem. Soc. **85**, 2759 (1963).
8. J. T. EDWARD, P. G. FARRELL, J. HALLE, J. KIRCHNEROVA, R. SCHAAL, and F. TERRIER. J. Org. Chem. **44**, 615 (1979).
9. J. HINE, J. C. KAUFMANN, and M. S. CHOLOD. J. Am. Chem. Soc. **94**, 4590 (1972).
10. A. K. COVINGTON and R. THOMPSON. J. Solution Chem. **3**, 603 (1974).
11. J. L. KURZ and J. M. FARRAR. J. Am. Chem. Soc. **91**, 6057 (1969).
12. K. P. SHELLY, K. NAGARAJAN, and R. STEWART. Can. J. Chem. **65**, 1734 (1987).

Can. J. Chem. Downloaded from www.nrcresearchpress.com by 194.225.253.170 on 09/07/12
For personal use only.

13. R. P. BELL and D. M. LIDWELL. Proc. R. Soc. London A: **176**, 88 (1940).
14. A. ALBERT and E. P. SERJEANT. The determination of ionization constants. 3rd ed. Chapman and Hall, London. 1984. p. 56.
15. R. W. RAMETTE. Chemical equilibrium and analysis. Addison Wesley, New York. 1981. pp. 294–296.
16. K. P. SHELLY. Ph.D. Thesis, University of British Columbia. 1988.
17. A. J. KRESGE. *In* Proton-transfer reactions. *Edited by* E. F. Caldin and V. Gold. Chapman and Hall, London. 1975.
18. F. G. BORDWELL and D. L. HUGHES. J. Org. Chem. **47**, 3224 (1982).
19. T. W. S. LEE and R. STEWART. Can. J. Chem. **64**, 1085 (1986), and references therein.
20. R. SRINIVASAN and R. STEWART. J. Chem. Soc. Perkin Trans. 2, 674 (1976).
21. K. NAGARAJAN, T. W. S. LEE, R. R. PERKINS, and R. STEWART. Can. J. Chem. **64**, 1090 (1986).
22. M. ECKERT and G. ZUNDEL. J. Phys. Chem. **91**, 5170 (1987).
23. T. FUJITA and T. NISHIOKA. Prog. Phys. Org. Chem. **12**, 49 (1976).
24. A. J. KRESGE and Y. CHIANG. J. Am. Chem. Soc. **95**, 803 (1973).
25. W. K. CHWANG, R. ELIASON, and A. J. KRESGE. J. Am. Chem. Soc. **99**, 805 (1977).
26. D. B. DAHLBERG, M. A. KUZEMKO, V. CHIANG, A. J. KRESGE, and M. POWELL. J. Am. Chem. Soc. **105**, 5387 (1983).
27. S. VENIMADHAVAN, K. P. SHELLY, and R. STEWART. J. Org. Chem. **54**, 2483 (1989).
28. R. STEWART and R. SRINIVASAN. Acc. Chem. Res. **11**, 271 (1978).
29. A. F. HEGARTY and W. P. JENCKS. J. Am. Chem. Soc. **97**, 7188 (1975).
30. O. REITZ and J. KOPP. Z. Physik. Chem. Abt. A: **184**, 429 (1939).
31. F. J. ALVAREZ and R. L. SCHOWEN; and A. J. KRESGE, R. A. MORE O'FERRALL, and M. F. POWELL. *In* Isotopes in organic chemistry. Vol. 7. *Edited by* E. Buncel and C. C. Lee. Elsevier, Amsterdam. 1987.
32. J. TOULLEC and J. E. DUBOIS. J. Am. Chem. Soc. **96**, 3524 (1974).
33. F. H. WESTHEIMER. Chem. Rev. **61**, 265 (1961).
34. R. P. BELL. The tunnel effect in chemistry. Chapman and Hall, London. 1980.
35. T. C. BRUICE and W. C. BRADBURY. J. Am. Chem. Soc. **87**, 4851 (1965).
36. (*a*) J. P. GUTHRIE. Can. J. Chem. **57**, 797 (1979); (*b*) E. TAPUHI and W. P. JENCKS. J. Am. Chem. Soc. **104**, 5758 (1982).
37. (*a*) Y. CHIANG, A. J. KRESGE, Y. S. TANG, and J. WIRZ. J. Am. Chem. Soc. **106**, 460 (1984); (*b*) J. R. KEEFFE, A. J. KRESGE, and N. P. SCHEPP. J. Am. Chem. Soc. **110**, 1993 (1988).
38. S. J. GUMBLEY and R. STEWART. J. Chem. Soc. Perkin Trans. 2, 529 (1984).
39. G. KORTÜM, W. VOGEL, and K. ANDRUSSOW. Dissociation constants of organic acids in aqueous solution. Butterworths, London. 1961.

Can. J. Chem. Downloaded from www.nrcresearchpress.com by 194.225.253.170 on 09/07/12
For personal use only.

An NMR study of steric and hyperconjugative barriers in benzyl $X(CH_3)_3$, X = C, Si, Ge, Sn, Pb

TED SCHAEFER, GLENN H. PENNER,[1] CRAIG S. TAKEUCHI, AND CHRISTIAN BEAULIEU[2]
Department of Chemistry, University of Manitoba, Winnipeg, Man., Canada R3T 2N2

Received February 14, 1989

TED SCHAEFER, GLENN H. PENNER, CRAIG S. TAKEUCHI, and CHRISTIAN BEAULIEU. Can. J. Chem. **67**, 1283 (1989).

The ^1H nuclear magnetic resonance spectra and their analyses are reported for benzyltrimethyl X (X = C, Si, Ge, Sn, Pb) and for the 2,6-dichloro derivatives where X = Si, Ge, Sn, Pb. The steric barrier to rotation about the C_{sp^2}—C_{sp^3} bond for X = C, based on the long-range proton–proton coupling constant over six bonds, $^6J(H,CH_2)$, must be greater than 20 kJ/mol. Unexpectedly, $^6J(H,CH_2)$ implies that the barriers for X = Si, Ge, Sn, Pb have relatively minor steric components. If these barriers are dominated by hyperconjugative interactions of the C—X bond with the aromatic π system, then they are probably mainly twofold in nature. Furthermore, their magnitude is likely to be near 9.5 kJ/mol for X = Si, Ge, Sn and may be as high as 12 kJ/mol for X = Pb.

Key words: NMR, benzyl $X(CH_3)_3$, X = C, Si, Ge, Sn, Pb; NMR, conformations; NMR, hyperconjugation.

TED SCHAEFER, GLENN H. PENNER, CRAIG S. TAKEUCHI et CHRISTIAN BEAULIEU. Can. J. Chem. **67**, 1283 (1989).

On a déterminé et analyse les spectres de résonance magnétique nucléaire du ^1H des benzyl-X-triméthyl (X = C, Si, Ge, Sn ou Pb) et de leurs dérivés dichloro-2,6. Lorsque X = C, la barrière stérique à la rotation autour de la liaison C_{sp^2}—C_{sp^3}, telle qu'évaluée en se basant sur la constante de couplage proton–proton à longue distance à travers six liaisons, $^6J(H,CH_2)$, doit être plus grande que 20 kJ/mol. Lorsque X = Si, Ge, Sn ou Pb, il est toutefois surprenant que les valeurs de $^6J(H,CH_2)$ suggèrent que ces barrières ne comportent que des composantes stériques relativement mineures. Si ces barrières sont dominées par des interactions d'hyperconjugaison de la liaison C—X avec le système π aromatique, il est probable que leur nature est principalement binaire. De plus, il est probable que leur amplitude est de l'ordre de 9,5 kJ/mol pour X = Si, Ge et Sn et qu'elle aille jusqu'à 12 kJ/mol pour X = Pb.

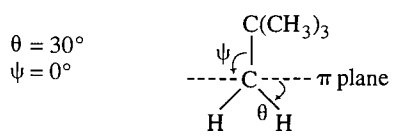
Mots clés : RMN, benzyl $X(CH_3)_3$, X = C, Si, Ge, Sn, Pb; RMN, conformations; RMN, hyperconjugaison.
[Traduit par la revue]

Introduction

The present nmr measurements are meant to probe further the idea (1–3) that hyperconjugation of the carbon–metal bond with the aromatic π electron system determines the conformational preference about the C_{sp^2}—C_{sp^3} bond in benzyltrimethyl X (X = Si, Ge, Sn, Pb). Such an origin for its conformational behaviour was not suggested for benzyltrimethylmethane (neopentylbenzene), where steric interactions presumably are dominant (4–7).

A variety of neopentylbenzene derivatives have been investigated by dynamic nmr methods with a view to establishing the free energies of activation, $\Delta G^{\ddagger}$, for rotation about the C_{sp^2}—C_{sp^3} bonds (4–7). For the parent compound the reorientation rate is too fast to measure by such methods. ^{13}C and ^2H relaxation times suggest a $\Delta G^{\ddagger}$ of 18–23 kJ/mol (5). For 2-bromo-3,5-di-*tert*-butylneopentylbenzene (7) only a line-broadening is observed in the ^1H nmr spectrum, attributed to a rate process characterized by an upper limit to $\Delta G^{\ddagger}$ of 23 kJ/mol for rotation past the *ortho* C—H bond.

Molecular mechanics calculations on neopentylbenzene itself yield 26.7 kJ/mol for the maximum in the rotational potential for the C_{sp^2}—C_{sp^3} bond (4); the most stable conformer corresponds to **1**. Because of the experimental data given above, it is stated (4) that the barrier is probably less than 23 kJ/mol.



1

If the barrier to internal rotation in neopentylbenzene is too small to measure by lineshape methods, then it is possible that the *J* method is applicable (8). In this method, the long-range proton–proton coupling constant, ^6J, between the methylene and *para* ring protons is related to the internal barrier via the expectation value of $\sin^2\theta$. The angle θ is defined in **1** and is 90° when the α C—H bond lies in a plane perpendicular to that of the benzene framework. ^6J is given by $^6J_{90}\langle\sin^2\theta\rangle$. We report here the analysis of the ^1H nmr spectrum of neopentylbenzene and discuss the spectral parameters in terms of the internal rotational potential.

The ^1H nmr spectral parameters are also obtained for the other title compounds and imply rather lower internal rotational potentials. In an attempt to discriminate between steric and hyperconjugative origins of the barrier, the spectral parameters are measured for the 2,6-dichloro derivatives of the metal compounds because a steric component for rotation of the side chain past the benzene plane should be enhanced by the chlorine substituents.

The ^{13}C nmr spectra for the tin compounds are presented in a number of solvents, to assess environmental influences on the conformational behaviour.

Experimental

Neopentylbenzene (Frinton) and benzyltrimethylsilane (Fluka) were purchased. The other compounds were prepared by standard procedures (1, 9). A typical procedure for the preparation of an nmr sample went as follows. A 5.0 mol% solution of neopentylbenzene (Frinton) in CCl_4, containing also 10 mol% of cyclohexane-d_{12} and ca. 0.5 mol% tetramethylsilane (TMS), was transferred to a 5 mm o.d. nmr tube. This solution was degassed by several cycles of the freeze–pump–thaw technique and the nmr tube was then flame-sealed.

The ^1H nmr spectra were accumulated on an AM300 FT spectrometer in exactly the way recently described in detail for toluene (10). The protons in the three equivalent methyl groups were spin coupled

[1]Present address: Department of Chemistry and Biochemistry, University of Guelph, Guelph, Ontario.

[2]Undergraduate research participant, 1988.

Can. J. Chem. Downloaded from www.nrcresearchpress.com by 194.225.253.170 on 09/07/12
For personal use only.

TABLE 1. ^{1}H nuclear magnetic resonance spectral parameters for benzyl $X(CH_3)_3$, X = C, Si, Ge, Sn, Pb, at 300 K

Parameter	C[a]	Si[b]	Ge[c]	Sn[d]	Pb[c]
$\nu(CH_3)$[e]	268.71	−7.13	−27.9	7.6	199.71[j]
$\nu(CH_2)$	750.12	606.5	639.3	701.6	859.80
$\nu_2 = \nu_6$	2109.112(2)[f]	2067.188(2)	2076.697(1)	2101.323(1)	2093.359(1)
$\nu_3 = \nu_5$	2147.789(2)	2130.434(2)	2127.513(1)	2145.849(1)	2146.135(1)
ν_4	2128.124(2)	2088.136(2)	2079.317(1)	2084.989(1)	2070.338(1)
$^3J_{23}$	7.665(3)	7.695(2)	7.706(1)	7.723(1)	7.733(1)
$^3J_{34}$	7.448(2)	7.440(2)	7.432(1)	7.417(1)	7.406(1)
$^4J_{26}$	1.918(4)	1.983(4)	1.978(1)	2.008(2)	2.010(1)
$^4J_{24}$	1.275(2)	1.241(2)	1.239(1)	1.229(1)	1.224(1)
$^4J_{35}$	1.454(4)	1.474(4)	1.490(1)	1.503(2)	1.498(1)
$^5J_{25}$	0.594(2)	0.587(2)	0.590(1)	0.585(1)	0.583(1)
$^4J(H,CH_2)$	−0.453(3)[i]	−0.594(3)	−0.507(1)	−0.491(2)	−0.456(1)
$^5J(H,CH_2)$	0.242(4)	0.281(3)	0.290(1)	0.294(1)	0.302(1)
$^6J(H,CH_2)$	−0.300(3)	−0.418(3)	−0.408(1)	−0.422(1)	−0.397(1)
Calculated transitions[g]	260	262	—	256	256
Assigned transitions[h]	149	153	196	149	236
Largest difference	0.029	0.030	0.018	0.015	0.016
Root-mean-square deviation	0.014	0.012	0.006	0.005	0.006

[a]5.0 mol% in CCl_4 containing also 10 mol% of cyclohexane-d_{12} and 0.5 mol% TMS.
[b]7.0 mol% in the CCl_4 mixture.
[c]4.1 mol% in acetone-d_6 with 0.5 mol% TMS.
[d]4.4 mol% in the acetone-d_6 mixture.
[e]In Hz at 300.135_2 MHz to high frequency of internal TMS.
[f]Numbers in parentheses are standard deviations in the last significant figure.
[g]For the ring protons only.
[h]Assigned transitions in the ring proton region, those for the CH_2 and CH_3 protons not being assigned.
[i]$^4J(H,CH_2)$ and $^4J_{35}$ have a correlation coefficient of −0.217.
[j]$^4J(CH_2,CH_3)$ is ±0.11 Hz.

to the methylene and, by a small amount, also to the ring protons. Decoupling procedures reduced the peak widths of the ring protons to ca. 0.10 Hz.

The ^{13}C nmr spectra of the stannane in three solvents and of its 2,6-dichloro derivative in acetone-d_6 were collected as previously described (11), and at 300 K and 75.469 MHz on the AM300 instrument.

Results and discussion

Spectral analysis

The ^{1}H nmr spectra of the ring protons were analyzed with the computer program NUMARIT (12), as extensively modified by R. Sebastian in this laboratory. The spectral parameters appear in Tables 1 and 3. There were no substantial correlations involving the crucial parameter, $^6J(H,CH_2)$.

The internal barriers about the C_{sp^2}—C_{sp^3} bonds

$^6J(H,CH_2)$ is known to obey eq. [1]

$$[1] \quad {}^6J = {}^6J_{90}\langle\sin^2\theta\rangle$$

in a substantial number of benzyl derivatives (8, 11, 13–16). The expectation value of $\sin^2\theta$ can be calculated classically, or quantum mechanically using a hindered rotor model. The value of $^6J_{90}$ depends on the electronegativity of the group attached to the methylene carbon atom (1, 16). For a methyl substituent, i.e., for ethylbenzene, $^6J_{90}$ has been taken as −1.16 Hz (14), as compared to the −1.20 Hz established for toluene (10). The electronegativities of the $C(CH_3)_3$ and $Si(CH_3)_3$ groups have been given as equal to that of the methyl group (17).

In neopentylbenzene, $^6J(H,CH_2)$ is −0.300(3) Hz, corresponding to a $\langle\sin^2\theta\rangle$ of −0.300/−1.16 or 0.259(5); the indicated error allows for an actual error of 0.006 Hz in ^6J. For a rigid conformation, **1**, $\langle\sin^2\theta\rangle$ is 0.25, corresponding to a ^6J of −0.29 Hz. Clearly, the barrier about the C_{sp^2}—C_{sp^3} bond is large. The *J* method is insensitive for a barrier as large as 20 kJ/mol or more. However, the given MMP1 potential (4) can be closely reproduced by $V(\psi)/\text{kJ mol}^{-1} = 27.7\sin^2\psi + 7.4\sin^2 2\psi$, where ψ is the angle by which the *tert*-butyl group twists out of conformation **1**. At 300 K this potential implies $\langle\sin^2\theta\rangle$ as 0.262 (classical average). In other words, the potential agrees with the observed ^6J in neopentylbenzene. The fourfold term (in $\sin^2 2\psi$) serves to decrease $\langle\sin^2\theta\rangle$ from the value expected in its absence in the above equation, producing a rapid rise in strain energy as the angle ψ increases from 15° to 60°.

While the theoretical fourfold term is not large enough to contribute to the height of the barrier, the suggested barrier in neopentylbenzene itself, although not measured, is 23 kJ/mol (4). It should be remembered that, for such a high barrier, the α C—H bonds sample only a small region of the internal potential at ambient temperatures. Consequently, it is best to conclude that the observed ^6J is compatible with a two-component barrier whose magnitude is rather larger than 20 kJ/mol. Of course, DNMR measurements are inapplicable to neopentylbenzene itself because of the symmetry of the conformation, **1**, of lowest energy.

Turning to the benzyltrimethylsilane, ^6J is −0.418(3) Hz, implying a $\langle\sin^2\theta\rangle$ of 0.360(6) if $^6J_{90}$ is again −1.16 Hz. *If* the barrier about the C_{sp^2}—C_{sp^3} bond is purely twofold, then its magnitude is 6.9(4) kJ/mol (hindered rotor model). However, if a substantial fourfold component exists as well, then various combinations of the two components yield a $\langle\sin^2\theta\rangle$ of 0.36, for example, V_2/V_4 values of 12.2/5.0, 10.0/3.2, 9.0/2.3, 8.0/1.5, 6.9/0.0 (in units of kJ/mol). For the MMP1 potential of neopentylbenzene, $V_2/V_4 \sim 3.7$. A similar ratio for the

Can. J. Chem. Downloaded from www.nrcresearchpress.com by 194.225.253.170 on 09/07/12
For personal use only.

Can. J. Chem. Downloaded from www.nrcresearchpress.com by 194.225.253.170 on 09/07/12
For personal use only.

silane derivative would have V_2 and V_4 as 9.0 and 2.3 kJ/mol, respectively. From the discussion in ref. 4 it may be inferred that the fourfold component has much to do with the close approach of two methyl groups to the phenyl moiety in neopentylbenzene. Because such an approach will be less marked in the silane (Si—C bonds are ca. 0.4 Å longer than C—C bonds), the V_2/V_4 ratio is likely to be larger in this compound. Hence it is perhaps more likely that the following V_2/V_4 values in kJ/mol apply to benzyltrimethylsilane: 9.0/2.3, 8.0/1.5, 7.5/0.9, 6.9/0.0. The ^6J value is compatible with all these combinations, of course.

It should be noted, however, that, if the barrier arises from $\sigma-\pi$ hyperconjugation of the C—Si bond with the aromatic π electrons and having a maximum value at $\psi = 0°$ (see **1**), then a twofold character is expected for the barrier, the hyperconjugation varying as $\cos^2\psi$.

The drastic reduction in internal barrier about the C_{sp^2}—C_{sp^3} relative to neopentylbenzene, caused by replacement of the quaternary carbon atom by silicon, is not entirely without precedent. Thus, in hexakis(dimethylsilyl) benzene an empirical force field yields 65.7 kJ/mol for the barrier to rotation about the C_{sp^2}—Si bond (18), compared to an approximate experimental value 60.0 kJ/mol. In the carbon analog, hexaisopropylbenzene, the computed internal barrier is 146.4 kJ/mol. These, presumably steric, barriers again illustrate the large changes caused by substitution of C—Si for C—C bonds. Similar phenomena have been observed for phenyldimethylsilane (19) as compared to isopropyl benzene.

The apparent twofold barriers in benzyltrimethylgermane and its tin and lead analogues are effectively the same as in the silane derivative, judging by the values of ^6J in Table 1. However, as can be seen from the discussion of the silane compound, combinations of V_2 and V_4 other than that appropriate to the latter are also compatible with the same ^6J for all three compounds. The group electronegativities of trimethyl X (X = C, Si, Ge, Sn, Pb) are here assumed equal.

An alternative assumption

The naive expectation, that the apparent V_2 will decrease monotonically from C to Pb, is not fulfilled. This order would be compatible with the measured ^6J only if $^6J_{90}$ were to *decrease* in magnitude in a monotonic way in going from carbon to lead; that could occur only if the electronegativity were increasing in that order. An alternative assumption uses the iota (inductive) substituent parameters, applicable to ^{13}C nmr chemical shifts (20). These parameters are 2.12, 1.72, 1.80, 1.66, and 1.50 for $C(CH_3)_3$, $Si(CH_3)_3$, $Ge(CH_3)_3$, $Sn(CH_3)_3$, and $Pb(CH_3)_3$, respectively. For hydrogen and the methoxy substituents, iota is 2.00 and 2.83, whereas $^6J_{90}$ is −1.20 and −1.02 Hz, respectively (10, 16). $^6J_{90}$ is then −1.17, −1.26, −1.24, −1.27, and −1.31 Hz, respectively, for X = C, Si, Ge, Sn, Pb in $X(CH_3)_3$. The $\langle\sin^2\theta\rangle$ becomes 0.256, 0.331, 0.328, 0.331, and 0.303, in that order. While these numbers imply somewhat higher apparent twofold barriers, near 9.5 kJ/mol for X = Si, Ge, Sn, than do the $\langle\sin^2\theta\rangle$ values when assuming equal electronegativities of the $X(CH_3)_3$ groups for all X, they *also* imply equal barrier *heights* for X = Si, Ge, Sn and a somewhat larger apparent V_2 of 14 kJ/mol for X = Pb.

Finally, the most recent determination of the relative electronegativities of CH_3 and $X(CH_3)_3$, when attached to CH_2, has the order C > H > Ge > Si > Pb > Sn (3). This order agrees with the iota scale above, *except* for $Pb(CH_3)_3$. The iota values for $Si(CH_3)_3$ and $Sn(CH_3)_3$ are 1.72 and 1.66, respectively. If the iota value for $Pb(CH_3)_3$ is taken as 1.69, then $\langle\sin^2\theta\rangle$ for this substituent becomes 0.313, corresponding to an apparent V_2 of 12 kJ/mol.

Given that the steric forces favor **1** ($\psi = 0°$, $\theta = 30°$) in all these compounds, ^6J showing that **1** is indeed of lowest energy (were the stable conformer described by $\psi = 30°$, for example, then a *rigid* form of this conformer would correspond to a $\langle\sin^2\theta\rangle$ of 0.375 and any motion would tend to increase $\langle\sin^2\theta\rangle$ towards a limiting value of 0.5 for free rotation), the barrier relationships for X = Si, Ge, Sn, Pb strongly imply an additional source of the stabilization of **1**. This second source may be the hyperconjugative interaction of the C—X bond with the π electron system of the benzene ring (1–3). A measure of such interactions is the σ_R^0 scale (3), giving the order of hyperconjugative electron release of CH_2XR_3 groups. At least one set of such substituent constants has Si < Ge < Sn < Pb,[3] an order consistent with the present results for the apparent barrier heights if the stabilization of **1** by increasing hyperconjugative interactions, going down the group, is compensating the decreasing steric forces. Alternatively, on the assumption that no steric barrier exists for X = Pb, for example, an upper limit to the hyperconjugative stabilization of **1** for this compound is near 12 kJ/mol. These matters are discussed further below, following a discussion of $^5J(^{13}C,^{117,119}Sn)$.

Comparison with $^5J(^{13}C,^{117,119}Sn)$

Kitching *et al.* (27) deduce an approximate value of 30° for ψ in benzyltrimethyl stannane, based (1) on a $\sigma-\pi$ mechanism for $^5J(^{13}C,^{117,119}Sn)$, and of 28° for its 4-fluoro derivative. The $\langle\sin^2\theta\rangle$ of 0.331 quoted above corresponds to an arc sin $\langle\sin^2\psi\rangle^{1/2}$ of 24°, while the assumption that $^6J_{90}$ is −1.16 Hz, as in the earlier discussion, implies 29°. ^6J is for a dilute solution in acetone-d_6 at 300 K, whereas $^5J(^{13}C,^{117,119}Sn)$ is for a solution in $CDCl_3$ (1). The absence of substantial differential solvent effects on the conformational stability of benzyltrimethylstannane is affirmed by the ^{13}C nmr data for three solvents in Table 2. $^5J(^{13}C,^{117,119}Sn)$ is independent of solvent to within experimental error.

For 4-methylbenzyltrimethylstannane, $^7J(^1H,^{117,119}Sn)$ is quoted as 9 Hz (28). A $\sigma-\pi$ coupling mechanism implies its proportionality to $\langle\sin^2\psi\rangle$. Furthermore, because the hyperfine interaction parameters, Q_{CH}^H and Q_{CCH}^H, are almost equal in magnitude, $^6J(^1H,^{117,119}Sn)$ should also be near 9 Hz in magnitude, although of opposite sign. From Table 2 it follows that $^5J(^{13}C,^{117,119}Sn)/^6J(^1H,^{117,119}Sn)$ has a magnitude of 1.75 ± 0.25. To within experimental error, this ratio is the same as $^5J(^{13}C,^{13}C)/^6J(^1H,^{13}C)$, precisely −1.50, found for eight anisole, thioanisole, and benzyl cyanide derivatives (29). The negative sign is expected on the basis of a positive Q_{CH}^C and a negative Q_{CH}^H (21); these quantities represent transmission of unpaired spin density from the aromatic π orbitals to the sites of *para* ^{13}C or ^1H nuclei. $^6J(^1H,^{117,119}Sn)$ is rather difficult to measure in the parent compound because of the complexity of the ^1H nmr spectrum of aromatic protons; we have not attempted to do so. Similar remarks would apply to $^6J(^1H,^{207}Pb)$ in the plumbanes, although from $^5J(^{13}C,^{207}Pb)$ in the parent compound (1) an estimate of near 20 Hz is obtained from a factor of 1.5.

2,6-Dichlorobenzyltrimethyl X (X = Si, Ge, Sn, Pb)

The striking result is that ^6J has not altered significantly

[3]W. F. Reynolds, quoted as a private communication in ref. 18 of Adcock and Sankar Tyer (3).

Can. J. Chem. Downloaded from www.nrcresearchpress.com by 194.225.253.170 on 09/07/12
For personal use only.

TABLE 2. ^{13}C nuclear magnetic resonance chemical shifts and $^{n}J(C,Sn)$ for benzyltrimethylstannane and its 2,6-dichloro derivative

Parameter	CS_2[a]	Benzene-d_6[b]	Acetone-d_6[c]	2,6-DiCl[d]
$\delta(CH_3)$[e]	−9.97	−10.25	−10.20	−8.55
$\delta(CH_2)$	20.33	20.16	20.41	18.05
δ_1	142.45	143.20	144.01	141.22
δ_2	126.63	127.09	127.52	133.05
δ_3	128.28	128.69	128.98	128.55
δ_4	123.23	123.61	123.78	125.44
$^1J(^{13}CH_3,^{117}Sn)$[f]	312	313	315	322
$^1J(^{13}CH_3,^{119}Sn)$[f]	326	326	330	337
$^1J(^{13}CH_2,^{117}Sn)$[f]	281	—	282	246
$^1J(^{13}C,^{119}Sn)$[f]	294	294	296	258
$^2J(C\text{-}1,Sn)$[g]	40.2	39.4	40.6	40.2
$^3J(C\text{-}2,Sn)$[g]	23.2	23.2	23.0	24.4
$^4J(C\text{-}3,Sn)$[g]	13.0	13.2	13.2	13.0
$^5J(C\text{-}4,Sn)$[g]	15.4	15.6	15.6	15.2

[a]4.4 mol%.
[b]4.7 mol%.
[c]4.8 mol%.
[d]3.5 mol% in acetone-d_6.
[e]To within ±0.05 ppm.
[f]To within ±1 Hz.
[g]To within 0.5 Hz, coupling to different Sn isotopes not resolved.

TABLE 3. ^1H nuclear magnetic resonance spectral parameters for 2,6-dichlorobenzyl $X(CH_3)_3$, X = Si, Ge, Sn, Pb, at 300 K

Parameter	Si		Ge		Sn	Pb
$\nu(CH_3)$	17.71[a,d]	22.43[b]	53.23	57.44[b]	31.74[c]	233.69[b]
$\nu(CH_2)$	740.581(1)[e]	759.365(2)	772.0	790.592(3)	793.7	922.103(1)
$V_3 = V_5$	2143.713(1)	2203.090(3)	2143.160(2)	2202.488(4)	2193.879(1)	2194.602(1)
V_4	2058.484(1)	2125.315(3)	2056.886(2)	2121.260(3)	2089.272(1)	2076.942(1)
$^3J_{34}$	8.001(1)	8.047(3)	8.002(2)	8.050(3)	8.040(2)	8.029(1)
$^5J(H,CH_2)$	0.422(1)	0.425(3)	0.433(3)	0.429(3)	0.456(2)	0.465(1)
$^6J(H,CH_2)$	−0.414(1)	−0.423(3)	−0.397(3)	−0.411(3)	−0.423(2)	−0.403(1)
Calculated transitions	48	48	48	48	48	48
Assigned transitions	44	41	26	41	30	41
Largest difference	0.014	0.045	0.012	0.023	0.010	0.013
Root-mean-square deviation	0.005	0.009	0.006	0.010	0.005	0.004

[a]Dilute in CS_2, containing also 10 mol% of C_6D_{12} and 0.5 mol% of TMS.
[b]Dilute in acetone-d_6, containing 0.5 mol% of TMS.
[c]3.5 mol% in the acetone-d_6, TMS solvent.
[d]In Hz at 300.135_2 MHz to high frequency of internal TMS.
[e]Numbers in parentheses are the standard deviations in the last significant figure.

(Table 3) on introduction of chlorine substituents at the *ortho* positions. This is also true for $^5J(^{13}C,^{117,119}Sn)$ in Table 2. This extraordinary result may be contrasted, for example, with ethylbenzene (14) and 2,6-dichloroethylbenzene (22). In the former, ^6J is −0.455(1) Hz in CS_2 solution, corresponding to a (probable) steric barrier of about 5.4 kJ/mol, the stable conformer being that analogous to **1**. In the 2,6-dichloro derivative, ^6J drops to 0.3 Hz in magnitude and indicates an internal barrier larger than 20 kJ/mol.

More precisely, the *ortho* chlorine substituents alter $^6J_{90}$ somewhat, $^6J(H,CH_3)$ being −0.641(1) Hz for 2,6-dichlorotoluene in acetone-d_6 solution. Hence $^6J_{90}$ is −1.28 Hz. Then the approach described above, and taking iota for $Pb(CH_3)_3$ as 1.69, leads to apparent V_2 values of 12.5 kJ/mol for X = Si, Ge, Sn and to 15.1 kJ/mol for X = Pb. Accordingly, the steric contribution to the barrier in the compounds of Table 3 is perhaps as large as 3 kJ/mol; that is, considering the relative steric effects of C—H and C—Cl bonds (4, 7, 23, 24), the present data imply that hyperconjugative interactions are mainly responsible for the conformational preferences about the C_{sp^2}—C_{sp^3} bonds in benzyltrimethyl X (X = Si, Ge, Sn, Pb).

Other spectral parameters

With due regard for solvent effects on chemical shifts, the shifts of H-4 in Table 3 are consistent with the conclusions from detailed studies of the chemical shifts of C-4 and of ^{19}F in the 4-fluoro derivatives (2), namely, that hyperconjugative electron release by $CH_2X(CH_3)_3$ follows the order Pb ~ Sn > Ge ~ Si. Actually, the shifts of H-3 can also be grouped in this fashion for the 2,6-dichloro compounds.

Comparisons for the parent compounds are more ambiguous because of the solvents involved. In a further comparison, it may be noted that the chemical shift of H-4 in ethylbenzene

in CCl_4 solution (14) is 0.033 ppm smaller than that in neopentylbenzene in the same solvent, implying that the CH_2CCH_3 releases electrons hyperconjugatively less readily than the CH_2CH_3 group, whereas the $CH_2Si(CH_3)_3$ group does so more readily (Table 1).

The chemical shifts of C-4 for the stannane and its 2,6-dichloro derivative in Table 2 are consistent with the indications from $^6J(H,CH_2)$ and $^5J(^{13}C,^{117,119}Sn)$ that the two chlorine substituents do not markedly alter the conformational behaviour of the $CH_2Sn(CH_3)_3$ moiety. This consistency follows from the fact that C-5 in 1,3-dichlorobenzene is deshielded by just over 2 ppm relative to benzene (25).

The values of $^5J(H,CH_2)$ in Tables 1 and 3 can also be rationalized. Thus, for toluene, $^5J(H,CH_3)$ is written in Hz as $0.336\langle\sin^2\theta\rangle + 0.322\langle\sin^2(\theta/2)\rangle$, the second term representing the σ electron contribution to ^5J (10). A $\langle\sin^2\theta\rangle$ of 0.33, and the fact that $\langle\sin^2\theta\rangle$ is 0.5 for any evenfold barriers, yields 0.27 Hz for ^5J. A $\langle\sin^2\theta\rangle$ of 0.26 entails a ^5J of 0.25 Hz, applicable to neopentylbenzene in Table 1. The measured value is 0.24 Hz and the other model value above is considered sufficiently close to measured values for the metalloid compounds.

In 2,6-dichlorotoluene, $^5J(H,CH_3)$ is 0.441(2) Hz. In terms of previous detailed discussions (10, 26) one may write $^5J/\text{Hz} = 0.359\langle\sin^2\theta\rangle + 0.583\langle\sin^2(\theta/2)\rangle$. Hence ^5J for the compounds in Table 3, where $\langle\sin^2\theta\rangle$ is near 0.31, should be close to 0.40 Hz. The measured values are somewhat higher, by as much as 0.06 Hz for Pb, but only 0.02 Hz for Si.

Conclusions

While the barrier to internal rotation about the C_{sp^2}—C_{sp^3} bond in neopentylbenzene is no doubt steric and greater than 20 kJ/mol in magnitude, the corresponding barriers in benzyltrimethyl X (X = Si, Ge, Sn, Pb) are very much smaller and, it appears, dominated by hyperconjugation between the C—X bond and the aromatic π electron system. If these barriers are purely twofold, then they may be as low as 7 kJ/mol, but more likely near 9.5 kJ/mol, for X = Si, Ge, Sn, and as high as 12 kJ/mol for X = Pb.

Acknowledgment

We are grateful to the Natural Sciences and Engineering Research Council of Canada for financial assistance.

1. W. Adcock, B. D. Gupta, W. Kitching, and D. Doddrell. J. Organometal. Chem. **102**, 297 (1975), and references therein.
2. W. Adcock, D. P. Cox, and W. Kitching. J. Organometal. Chem. **133**, 393 (1977), and references therein.
3. W. Adcock and V. Sankar Tyer. J. Org. Chem. **50**, 1538 (1985).
4. S. Andersson and T. Drakenberg. Org. Magn. Reson. **21**, 730 (1983), and references therein.
5. S. Andersson, R. E. Carter, and T. Drakenberg. Acta Chem. Scand. Ser. B, **34B**, 661 (1980).
6. J. E. Anderson, H. Pearson, and D. I. Rawson. J. Chem. Soc. Chem. Commun. 95 (1973).
7. B. Nilsson, P. Martinson, K. Olsson, and R. E. Carter. J. Am. Chem. Soc. **96**, 3190 (1974).
8. W. J. E. Parr and T. Schaefer. Acc. Chem. Res. **13**, 400 (1980).
9. C. R. Hauser and C. R. Hance. J. Am. Chem. Soc. **73**, 5846 (1951).
10. T. Schaefer, R. Sebastian, and G. H. Penner. Can. J. Chem. **63**, 2597 (1985).
11. T. Schaefer, J. Peeling, and R. Sebastian. Can. J. Chem. **63**, 3219 (1985).
12. J. S. Martin, A. R. Quirt, and K. E. Worvill. The NMR program library. Daresbury Laboratory, Daresbury, U.K.
13. T. Schaefer and G. H. Penner. Can. J. Chem. **64**, 2013 (1986).
14. T. Schaefer, G. H. Penner, and R. Sebastian. Can. J. Chem. **65**, 873 (1987).
15. G. H. Penner, T. Schaefer, R. Sebastian, and S. Wolfe. Can. J. Chem. **65**, 1845 (1987).
16. T. Schaefer, R. Sebastian, and G. H. Penner. Can. J. Chem. **64**, 1372 (1986).
17. J. E. Huheey. J. Phys. Chem. **69**, 3284 (1965).
18. I. I. Schuster, W. Weissensteiner, and K. Mislow. J. Am. Chem. Soc. **108**, 6661 (1986).
19. W. J. E. Parr and T. Schaefer. Can. J. Chem. **55**, 557 (1977).
20. N. Inamoto and S. Masuda. Tetrahedron Lett. 3287 (1977).
21. H. M. McConnell and D. B. Chesnut. J. Chem. Phys. **28**, 107 (1958).
22. T. Schaefer, L. Kruczynski, and W. Niemczura. Chem. Phys. Lett. **38**, 498 (1976).
23. H. Förster and F. Vögtle. Angew. Chem. Int. Ed. Engl. **16**, 429 (1977).
24. M. Charton and B. Charton. J. Am. Chem. Soc. **97**, 6472 (1975).
25. E. Breitmaier and W. Voelter. ^{13}C nmr spectroscopy. 2nd ed. Verlag Chemie, New York. 1978. p. 185.
26. T. Schaefer and R. Laatikainen. Can. J. Chem. **61**, 2785 (1983).
27. W. Kitching, G. Drew, W. Adcock, and A. N. Abeywickrema. J. Org. Chem. **46**, 2252 (1981).
28. J. M. Angelelli, M. A. Delmas, and J. C. Maire. J. Organometal. Chem. **131**, 225 (1977).
29. T. Schaefer and Glenn H. Penner. Can. J. Chem. **66**, 1229 (1988).

Can. J. Chem. Downloaded from www.nrcresearchpress.com by 194.225.253.170 on 09/07/12
For personal use only.

New aromadendranic sesquiterpenes from *Sideritis varoi* ssp. *cuatrecasasii*

ANDRÉS GARCÍA-GRANADOS[1] AND ANTONIO MOLINA

Departamento de Química Orgánica, Facultad de Ciencias, Universidad de Granada, 18071 Granada, Spain

Received August 5, 1988[2]

ANDRÉS GARCÍA-GRANADOS and ANTONIO MOLINA. Can. J. Chem. **67**, 1288 (1989).

Two new aromadendrane sesquiterpenes 4β,9β-dihydroxyaromadendrene and 4β-hydroxy-9β-acetoxyaromadendrene have been isolated from *Sideritis varoi* ssp. *cuatrecasasii*, and their stereochemistry has been established by a series of 2D nuclear magnetic resonance experiments.

Key words: *Sideritis*, *Labiatae*, new aromadendrenes, sesquiterpenes, 2D NMR.

ANDRÉS GARCÍA-GRANADOS et ANTONIO MOLINA. Can. J. Chem. **67**, 1288 (1989).

On a isolé deux nouveaux sesquiterpènes de l'aromadendrane, les dihydroxy-4β,9β et hydroxy-4β acétoxy-9β aromadendrène, à partir du *Sideritis varoi* ssp. *cuatrecasasii* et on a déterminé leur stéréochimie en se basant sur une série d'expériences de résonance magnétique nucléaire en 2D.

Mots clés : *Sideritis*, *Labiatae*, aromadendrènes nouveaux, sesquiterpènes, RMN 2D.

[Traduit par la revue]

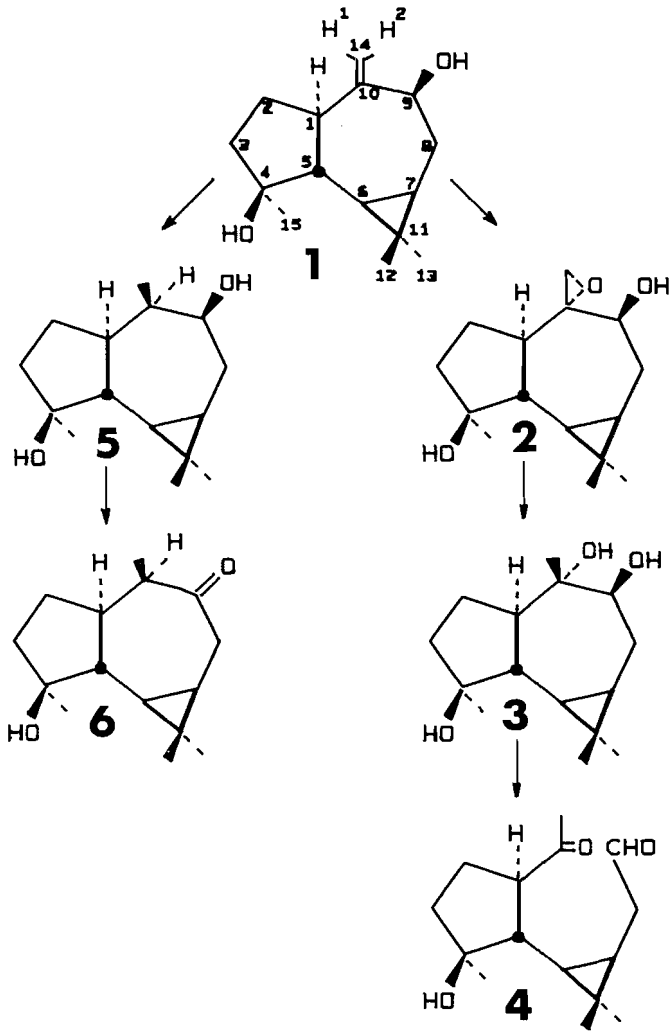
Can. J. Chem. Downloaded from www.nrcresearchpress.com by 194.225.253.170 on 09/07/12
For personal use only.

Introduction

Many diterpenic compounds with *ent*-kaurenic (1, 2), *ent*-beyerenic (3), *ent*-atis-13-enic (4), and *ent*-labdanic (5) skeletons have been isolated from the genus *Sideritis*. The number of sesquiterpenes found in this genus, however, are scarce, with only some eudesmanes (6, 7), germacranes (8), and guaianes (8) having been isolated from two subspecies of *S. varoi*. We report here on a study of the structure of two new natural products that have the uncommon aromadendrane skeleton. This is the first time that this class of compound has been isolated from *Labiatae* in Spain, and from the genus *Sideritis* anywhere. Their structures have been determined by a combination of chemical and spectroscopic techniques. 2D-NMR experiments have rarely been applied to this type of skeleton (9) as the considerable mobility within its cycloheptane moiety makes the stereochemical analysis of these molecules somewhat difficult.

Results and discussion

The first compound isolated (**1**) had a molecular weight of 236 and an elemental analysis compatible with the molecular formula $C_{15}H_{24}O_2$. Its ir spectrum showed bands at 3345 (OH), 1630 (C=C), and 895 (C=CH_2) cm^{-1}. These functions were confirmed by high resolution ^1H nmr experiments (300 MHz), which showed signals of exocyclic methylene at δ 5.10 and 4.85 (1H each, dd) and a signal of one proton geminal to a hydroxyl group (δ 4.05, J_1 = 10.9, J_2 = 1.8, J_3 = 1.4, J_4 = 1.1 Hz), as well as three methyl singlet signals at δ 1.27, 1.02, and 1.01 (3H each), the first of them possibly geminal to a hydroxyl group and hence relatively deshielded. There were also two complex signals of a cyclopropane ring (δ 0.76, 1H, ddd, J_1 = 11.25, J_2 = 9.38, and J_3 = 6.56 Hz; δ 0.48, 1H, dd, J_1 = 11.33, J_2 = 9.38 Hz) in this spectrum (see Table 1). Taking everything into account, product **1** should be a tricyclic sesquiterpene with one cyclopropane ring, a secondary hydroxyl group, and some other tertiary group. The ^{13}C nmr spectra of **1** revealed the presence of three methyl, four methylene (one of these unsaturated exomethylene), and five methine groups (one of these binding with a hydroxyl group), as well as three quaternary carbons (one oxygenated and another sp^2 one), all of which confirms the type of skeleton proposed.



SCHEME 1

The oxidation of **1** with pyridinium dichromate (10) under very mild conditions gave an unstable product that could not be isolated. A series of experiments were carried out to find out the position on the skeleton of the oxidable hydroxyl group (see Scheme 1). The epoxidation of **1** with metachloroperbenzoic acid (MCPBA) yielded as the major product (51%) the epoxy

[1]Author to whom correspondence may be addressed.

[2]Revision received March 6, 1989.

TABLE 1. Assignment of ^{13}C resonances and assignments of ^{1}H resonances directly bonded to specific carbon atoms for **1** (7 tesla, $CDCl_3$, TMS as internal standard), and monodimensional nOe difference spectroscopy

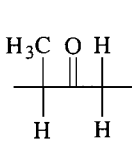
^{13}C	δ_C (ppm)	^{1}H	δ_H (ppm)	Monodimensional observed nOe difference
1	50.30	H-1	2.15 (m)	H-6, H-7, H-9, H-2α
2	26.34	H-2α	1.63 (m)	
		H-2β	2.01 (m)	
3	41.89	H-3α	1.60 (m)	
		H-3β	1.80 (m)	
4	80.82	—	—	
5	54.40	H-5	1.27 (dd)	
6	30.05	H-6	0.48 (dd)	H-7, 3H-15, 3H-13, H-1
7	23.72	H-7	0.76 (ddd)	H-6, H-9, H-1
8	34.26	H-8α	2.15 (ddd)	H-8β
		H-8β	1.27 (ddd)	H-8α
9	74.62	H-9	4.05 (complex doublet)	H-1, H-7
10	155.78	—	—	
11	20.13	—	—	
12	16.19	3H-12	1.01 (s)	H-8β
13	28.48	3H-13	1.02 (s)	H-6, H-7
14	101.86	14-H1	4.85 (dd)	14-H2, H-2β
		14-H2	5.10 (dd)	14-H1
15	25.83	3H-15	1.27 (s)	H-6

J(Hz): 5,6 = 11.33; 6,7 = 9.38; 7,8β = 11.30; 7,8α = 6.56; 8β,8α = 13.74; 9,8β = 10.9; 9,8α = 1.8; 14-H1, 14-H2 = 2.7; 14-H1, 9 = 1.4; 14-H2, 9 = 1.1.

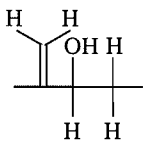
compound **2**, which, when treated with $LiAlH_4$, gave **3**. The oxidation of **3** with $NaIO_4$ resulted in the ketoaldehyde **4**, which proved that the secondary hydroxyl group in **1** is allylic.

To determine the size of the ring on which the secondary hydroxyl group is situated, compound **1** was hydrogenated to give a main product (**5**), which was then oxidized to a stable ketone (**6**). The ir spectrum of **6** showed a ketonic band at 1690 cm^{-1}, which eliminated the possibility of a cyclopentanone. The ^{1}H nmr spectrum of **6** (80 MHz) showed signals at δ 2.77 (1H, m, $W_{1/2}$ = 20 Hz) and 2.33 (2H, complex broad signal). After treating **6** with D_2O/DO^- the last signal was greatly simplified. The cyclopropane signal at δ 0.76 also showed significant variations. The ^{13}C nmr spectra of **6** and its deuterated derivative were significant: experiment DEPT (135°C) showed a positive triplet signal at δ 35.89, which can be attributed to a -CHD- group, very close to another, slightly deshielded, negative signal of a methylene group. The introduction of deuterium is greater on the methylene side than on the methine side.

From these experiments a partial structure (A) could be deduced for **6** and hence a partial structure (B) for **1**.



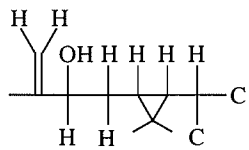
A



B

As mentioned above, the deuteration at the methylene group contiguous to the keto group modified the multiplicity of one of the protons (δ 0.76) of the cyclopropane ring. Several double-resonance experiments carried out with **6** showed that the methylene group that was deuterated in the previous experiment was also contiguous to this cyclopropane proton. Thus, the irradiation at δ 2.33 transformed the signal at δ 0.76 into a doublet signal (J = 9 Hz), which allowed us to extend the partial structure to C, bearing in mind the multiplicity of the signal of the other cyclopropane proton (δ 0.5, dd, $J_1 = J_2$ = 9.5 Hz).

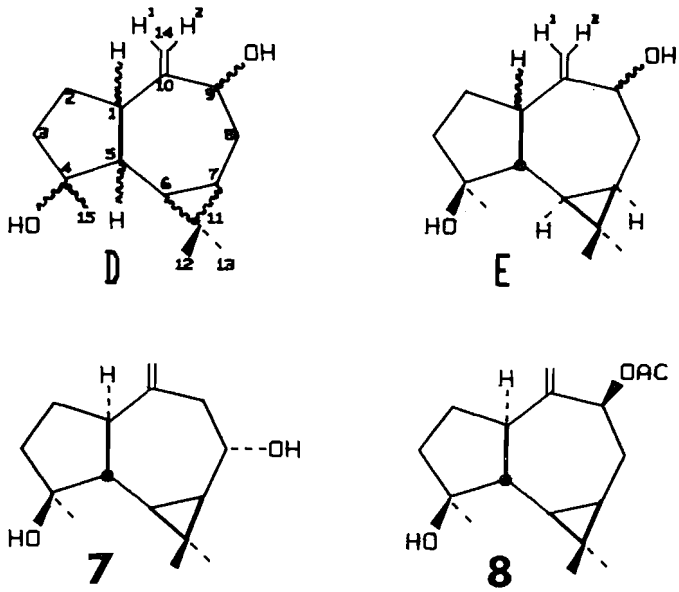
A reconsideration of the ^{13}C nmr spectrum of **1** leads to the conclusion that its structure might be D. This structure has six asymmetric centers and its relative stereochemistry was established by high resolution 1D and 2D-NMR procedures.



C

The ^{1}H nmr assignments for all the protons of **1** were achieved by combining the proton homonuclear correlation (COSY 90) results and those of the C/H heteronuclear correlation. Thus, the C/H correlation allowed us to assign the ^{13}C and ^{1}H chemical shifts of positions 4, 6, 7, 9, 10, 11, 12/13, 14, and 15, and the COSY experiments allowed us to assign the protons at C-8 (by correlation with H-9 and confirmed by correlation 2H-8/H-7) and also confirmed the assignments carried out by the C/H correlation. The correlation H-6/H-5 allowed us to assign the last one. Nevertheless, the fact that the signals of H-8α and H-8β overlapped with the signals of H-5/H-1 made this important correlation difficult. After these assignments only the C-1 methine and the C-2 and C-3 methylene groups remained to be assigned. On reconsidering, at this point, the C/H correlation for product **1** we assigned the signal at δ 50.30 to C-1 and δ 2.15 to H-1. A new analysis of the COSY experiment now allowed us to assign the protons at C-2 (δ 2.01 and 1.63). We then assigned the signal at δ 26.34 to

Can. J. Chem. Downloaded from www.nrcresearchpress.com by 194.225.253.170 on 09/07/12
For personal use only.



C-2 and finally the signal at δ 41.89 to C-3 with its proton signal at δ 1.80 and 1.60 by C/H correlation.

The homonuclear *J*-resolved experiment allowed us to confirm the chemical shifts for the protons of **1** by considering the F2 projection, which provided a "full decoupled proton spectrum". By plotting the columns of this experiment, clear figures of many proton signals could be obtained. A complete analysis of the *J* values was fairly difficult because of considerable overlapping of the protons (H-1/H-8 and H-5/H-8/3H-15) and a considerable coincidence between one of the protons at C-2 and another at C-3 even in the *J*-resolved experiment (only apparent *J* values, read directly on the spectral chart, could be used because the signals were so close that there were few first-order systems). All the assignments are shown in Table 1. Some coupling constants were useful in the determination of certain points of the relative stereochemistry. The value of the coupling constants between H-5/H-6 and H-6/H-7 (11.33 and 9.38 Hz respectively) are very similar to those indicated for the *cis*-cyclopropane **7** (11). Next, it is necessary to establish the relative configurations of C-1, C-4, and C-9, as well as the absolute configuration of the molecule.

The 2D nOe-correlated experiments for product **1** were of help in the determination of its stereochemistry. Dipolar couplings between H-6/3H-15, H-6/3H-13, and H-6/H-7, the latter very small in value, were found. This 2D-NMR experiment also confirmed the chemical shifts of the pairs of geminal protons at C-2, C-3, C-8, and C-14. The stereochemistry of **1** can now be proposed as indicated in structure E, although with the doubt remaining whether the cross signal in the NOESY experiment between H-6/3H-15 was due to its dipolar interaction or due to the dipolar coupling between H-6 and some of the signals (H-5 or H-8) beneath the intense signal of 3H-15. The possibility of dipolar coupling between H-6 and H-8 was eliminated after considering the scalar coupling constant of this proton at C-8 (J_1 = 13.74, J_2 = 11.3, J_3 = 10.97 Hz), which indicated that this had an 8β disposition. In addition, the clear signal of H-6 indicated a *trans* disposition with regard to H-5 ($J_{5,6}$ = 11.33 Hz). The 8β-H proton showed cross signals with 14-H2, the 14-H1 with one of the H-2 (δ 2.01) protons, and, although not so clearly, between H-5 and 14-H1. In this experiment H-9 (geminal to the hydroxyl group) did not show any cross signals and hence the relative configurations of C-1, C-9 remain undetermined.

The limitations shown by the NOESY experiments for the small molecules are known because in this type of experiment the zero-quantum (W_0) and not the double-quantum transitions are measured (12). Therefore careful monodimensional nOe difference experiments (12) were performed for **1**, as described in the Experimental, and the results appear in Table 1. These experiments confirm the dipolar coupling shown by the NOESY experiment but also reveal clear signals of nOe difference between H-6 and H-1 (or H-8α) and between H-9 with H-1 (or H-8α) and H-7. It can be deduced from the H-9 coupling constants (J_1 = 10.9, J_2 = 1.8, J_3 = 1.4, J_4 = 1.1 Hz) that there is a *trans* disposition between H-9 and H-8β and a dihedral angle of nearly 90° between H-9 and H-8α. Thus H-8α was not near H-6 (Dreiding stereomodels), and the nOe effect between H-6 and H-1 is clear. This conformation for C-8 is also confirmed by the nOe effect between H-9 and H-7. This proved that H-1, H-6, H-7, and H-9 were all within the cycloheptane ring, and the study of the relative stereochemistry of product **1** was thus complete.

The *S* configuration at C-9 was established by Horeau's procedure (13). Product **1** is 4β,9β-dihydroxyaromadendrene, a new natural product for which we propose the name *sesquivarodiol*.

Another new natural product was **8**, with a molecular weight of 278 and ir bands of hydroxyl (3454), exocyclic double bond (3102, 1639, and 900), and acetoxy group (1735 and 1244 cm^{-1}). The ^1H nmr spectrum (300 MHz) of product **8** was very similar to that of product **1**, with the exception of the acetate group at δ 2.09 (3H, s) and the presence of a proton at δ 5.08 (1H, dd, J_1 = 11.22, J_2 = 1.5 Hz). Saponification of product **8** led to product **1**. Hence **8** is a natural acetate at C-9 of product **1**.

Experimental

Melting points (Kofler apparatus) are uncorrected. The nmr spectra (80-MHz ^1H and 20.13-MHz ^{13}C) were obtained with a Bruker WP80SY spectrometer or at 7 tesla (300-MHz ^1H) and 300 K with a Bruker AM-300 equipped with process controller and "array processor". A 60-mg sample of product **1** was used for the 2D experiments. A 30-mg sample of product **1** was used for nOe difference spectroscopy. The programs from Bruker's library were utilized for COSY (45°) (14), NOESY (15), C/H correlation (16), homonuclear *J*-resolved (17), and CONOESY (90°) (18). The carrier frequency was centered in all cases at the centre of frequencies in both axes, with a precise number of scans in all cases to provide complete phase cycles. For the COSY, 128 experiments of 64 scans, relaxation delay of 1 s, spectral widths of 1420.45 Hz in *f*2 and 710.23 in *f*1 (2K and 1K data points respectively), and digital resolution of 1.387 Hz/point were used. The resulting matrix was symmetrized. The same conditions were utilized for NOESY experiments, with a mixing time of 0.7 s. For the ^1H–^{13}C measurement, shift correlated 2D-NMR, 128 experiments of 16 scans, a relaxation delay of 2 s, and spectral widths of 7462.687 and 764.994 Hz were used in the *f*1 and *f*2 dimensions (digital resolution of 3.64 and 0.74 Hz/point respectively). For the 2D *J*-resolved experiments, 64 experiments of 32 scans, a relaxation delay of 2.8 s, spectral widths of 500 and 31.25 Hz (digital resolution of 0.488 and 0.122 Hz/point) in the *f*1 and *f*2 dimensions, and TILT and *J*-symmetrized matrix were used. Monodimensional nOe difference experiments were achieved by irradiation for 4 s in series of 8 scans, on-resonance and off-resonance alternately. The ir spectra were recorded on a Perkin–Elmer 983G spectrometer. The rotatory powers were measured on a Perkin–Elmer 240 polarimeter. Mass spectra were

Can. J. Chem. Downloaded from www.nrcresearchpress.com by 194.225.253.170 on 09/07/12
For personal use only.

Can. J. Chem. Downloaded from www.nrcresearchpress.com by 194.225.253.170 on 09/07/12
For personal use only.

recorded on a Hewlett Packard 5988A instrument. Silica gel, Merck 7729 (less than 0.08 mm), was used for column chromatography. Voucher specimens have been deposited at the Herbarium of the Faculty of Pharmacy (University of Granada).

Isolation of sesquiterpenes

Dried plants (2.8 kg), collected from around Carboneras (Almería) in April, were processed to give 84 g of the terpenic fraction; 60 g of this fraction was processed as indicated in ref. 5, yielding, apart from the sesquiterpenes previously described (6, 8), the following products in order of elution: 4β-hydroxy-9β-acetoxyaromadendrene (**8**) (20 mg) and 4β,9β-dihydroxyaromadendrene (**1**) (1.05 g).

4β,9β-Dihydroxyaromadendrene (1): mp 129–131°C; $[\alpha]_D$ −5° ($CHCl_3$, *c* 1); ir ν_{max} (KBr): 3345, 3040, 1630, and 895 cm^{-1}; ^1H nmr (300 MHz) and ^{13}C nmr (75 MHz): see Table 1; ms *m/z* (rel. int.): 236 $[M]^+$ (12), 221 (31), 218 (17), 203 (26), 200 (12), 189 (40), 185 (23), 175 (51), 160 (73), and 145 (100). *Anal.* calcd. for $C_{15}H_{24}O_2$: C 76.23, H 10.23; found: C 76.25, H 10.21%.

Determination of absolute configuration at C-9 of **1**: 25 mg **1** and 100 mg (±)-α-phenylbutyric anhydride (13); $[\alpha]_D$ −6.4° (C_6H_6, *c* 6.6).

Epoxidation of 1: 60 mg **1** was dissolved in $CHCl_3$ (10 mL) and epoxidized with MCPBA (48 mg), KF (8 mg), and NaF (17.5 mg) for 75 min. The usual processing followed by column chromatography gave product **2** (32 mg); mp 126–128°C; $[\alpha]_D$ −9.3° ($CHCl_3$, *c* 1); ^1H nmr (80 MHz) δ: 3.76 (1H, dd, J_1 = 10.5, J_2 = 1.5 Hz, H-9), 2.93 and 2.68 (2H, ABq, J = 4 Hz, 2H-14), 1.28 (3H, s, 3H-15), 1.08 (6H, s, 3H-12 and 3H-13), 0.76 (1H, m, H-7), 0.47 (1H, dd, J_1 = 11, J_2 = 9 Hz, H-6).

$LiAlH_4$ reduction of epoxide 2: 20 mg **2** was reduced with $LiAlH_4$ (7 mg). Usual work-up followed by column chromatography gave 12 mg **3**. Colourless gum; ir ν_{max} (neat): 3450 cm^{-1}; ^1H nmr (80 MHz) δ: 3.43 (1H, dd, J_1 = 11, J_2 = 2 Hz, H-9), 1.25 (3H, s, 3H-15), 1.13 (3H, s, 3H-14), 1.05 (6H, s, 3H-12 and 3H-13), 0.75 (1H, m, H-7), and 0.38 (1H, dd, J_1 = 11, J_2 = 9 Hz, H-6).

Oxidation of 3: 11 mg **3** was treated with $NaIO_4$ (20 mg), affording, after chromatography, 8 mg of product **4**. Colourless gum; $[\alpha]_D$ +16.7° ($CHCl_3$, *c* 1); ir ν_{max} (neat): 3426 and 1708 cm^{-1}; ^1H nmr (80 MHz) δ: 9.7 (1H, s, H-9), 2.88 (1H, m, $W_{1/2}$ = 16 Hz, H-1), 2.12 (3H, s, 3H-14), 1.26 (3H, s, 3H-15), 1.06 and 1.02 (3H each, s, 3H-12 and 3H-13), 0.76 (1H, m, $W_{1/2}$ = 16 Hz, H-7), and 0.4 (1H, dd, J_1 = 11, J_2 = 9 Hz, H-6).

Hydrogenation of 1: 20 mg **1** was hydrogenated for 2.5 h with H_2 (5 atm; 1 atm = 101.3 kPa). After chromatography **5** (13 mg) was isolated; mp 111–113°C; $[\alpha]_D$ −14° ($CHCl_3$, *c* 1); ir ν_{max} (KBr): 3350 cm^{-1}; ^1H nmr (80 MHz) δ: 3.83 (1H, dt, J_d = 10, J_t = 4 Hz, H-9), 1.25 (3H, s, 3H-15), 1.08 and 1.03 (3H each, s, 3H-12 and 3H-13), 0.9 (3H, d, J = 6.5 Hz, 3H-14), 0.63 (1H, m, H-7), and 0.38 (1H, t, J = 10 Hz, H-6).

Oxidation of 5: 12 mg **5** was oxidized with 30 mg pyridinium dichromate (10) and, after chromatography, gave ketone **6** (10 mg); mp 85–87°C; ir ν_{max} ($CHCl_3$, *c* 3.5): 3450 and 1690 cm^{-1}; ^1H nmr (80 MHz) δ: 2.77 (1H, m, $W_{1/2}$ = 20 Hz, H-10), 2.33 (2H, complex wide signal, 2H-8), 1.3 (3H, s, 3H-15), 1.13 and 1.08 (3H each, s, 3H-12 and 3H-13), 1.07 (3H, d, J = 6.5 Hz, 3H-14), 0.82 (1H, m, $W_{1/2}$ = 18 Hz, H-7), and 0.5 (1H, t, J = 9.5 Hz, H-6); ^{13}C nmr: see Table 2.

$$[\alpha]_D = \frac{\begin{matrix}589 & 578 & 546 & 436\end{matrix}}{\begin{matrix}-176.1 & -186 & -219.3 & -463.5\end{matrix}} (CHCl_3, c\ 1)$$

4β-Hydroxy-9β-acetoxyaromadendrene (8): mp 76–78°C; $[\alpha]_D$ +3.2° ($CHCl_3$, *c* 1); ir ν_{max} (KBr): 3454, 3102, 1735, 1639, 1244, and 900 cm^{-1}; ^1H nmr (300 MHz) δ: 5.09 (1H, dd, J_1 = 11.24, J_2 = 0.5 Hz, H-9), 4.88 and 4.81 (1H each, s, H1-14 and H2-14), 2.19 (1H, m, $W_{1/2}$ = 19.8 Hz, H-1), 2.09 (3H, s, AcO group), 2.06 (1H, ddd, J_1 = 13.74, J_2 = 6.33, J_3 = 1.85 Hz, H-8α), 1.97 (1H, m, $W_{1/2}$ = 22 Hz, H-2β), 1.78 (1H, m, $W_{1/2}$ = 16.37 Hz, H-3β), 1.26 (3H, s, 3H-15), 1.05 (3H, s, 3H-13), 1.01 (3H, s, 3H-12), 0.81 (1H, ddd, J_1 = 11.37, J_2 = 9.4, J_3 = 6.39 Hz, H-7), and 0.49 (1H, dd, J_1 = 11.33, J_2 = 9.41 Hz, H-6); ^{13}C nmr (75 MHz): see Table 2; ms *m/z* (rel. int.): 278 $[M]^+$ (4), 236 (7), 221 (13), 218 (40), 203 (34), 201 (10), 200 (38), 185 (46), 175 (47), 160 (100), 157 (40), 149 (30), 145 (84).

TABLE 2. ^{13}C nuclear magnetic resonance spectral data for compounds **6** and **8**

Carbon No.	**6**	**8**
1	47.09	50.43
2	25.14	26.38
3	42.33	41.95
4	79.89	80.87
5	48.08	54.44
6	28.41	29.93
7	23.10	23.50
8	35.87	31.99
9	214.22	75.75
10	48.73	150.81
11	21.94	20.39
12	16.17	16.25
13	28.41	28.50
14	10.75	103.01
15	25.26	26.03
CH_3—CO	—	21.31
CH_3—*CO*	—	169.85

Saponification of 8: 20 mg **9** was refluxed for 1.5 h with aqueous MeOH–NaOH. After column chromatography, 15 mg **1** was obtained.

Acknowledgements

This work was supported by a grant from the Comisión Asesora de Investigación Científica y Técnica. We thank Isabel J. Macdonald for her assistance in the translation of the text as well as Bruker for some of the 2D-NMR experiments. The CONOESY experiments were carried out by the Servicio de Resonancia Magnética Nuclear and the final revision of the text by the Servicio de Traducción Técnica (Servicios Técnicos, Universidad de Granada, Spain).

1. T. García de Quesada, B. Rodríguez, S. Valverde, and S. Huneck. Tetrahedron Lett. 2187 (1972).
2. A. García-Granados, A. Parra, A. Peña, A. Sáenz de Buruaga, and J. M. Sáenz de Buruaga. Tetrahedron Lett. **21**, 3611 (1980).
3. T. García de Quesada, B. Rodríguez, and S. Valverde. An. Quím. **70**, 239 (1974).
4. W. A. Ayer, J. A. Ball, B. Rodríguez, and S. Valverde. Can. J. Chem. **52**, 2792 (1974).
5. J. L. Algarra, A. García-Granados, A. Sáenz de Buruaga, and J. M. Sáenz de Buruaga. Phytochemistry, **22**, 1779 (1983).
6. A. García-Granados, A. Molina, A. Sáenz de Buruaga, and J. M. Sáenz de Buruaga. Phytochemistry, **24**, 97 (1985).
7. A. García-Granados, A. Martínez, A. Molina, and M. E. Onorato. Phytochemistry, **25**, 2171 (1986).
8. A. García-Granados, A. Molina, and E. Cabrera. Tetrahedron, **42**, 81 (1986).
9. I. Fuyihiko and A. Akira. J. Chem. Soc. Perkin Trans. 2, 1773 (1985).
10. G. Cainelli, G. Gardillo, M. Orena, and S. Sandri. J. Am. Chem. Soc. **98**, 6737 (1976).

11. F. BOHLMAN, P. SINGH, and J. JAKUPOVIC. Phytochemistry, **21**, 2531 (1982).
12. J. K. M. SANDERS and J. O. MERSH. Prog. Nucl. Magn. Reson. Spectrosc. **15**, 353 (1982).
13. A. HOREAU. Tetrahedron Lett. 506 (1961).
14. W. P. AUE, E. BARTHOLDI, and R. R. ERNST. J. Chem. Phys. **64**, 2229 (1976); K. NAGAYAMA, A. KUMAR, K. WÜTHRICH, and R. R. ERNST. J. Magn. Reson. **40**, 321 (1980).
15. S. MACURA, Y. HUANG, D. SUTER, and R. R. ERNST. J. Magn. Reson. **43**, 259 (1981).
16. A. BAX. J. Magn. Reson. **53**, 517 (1983); V. RUTAR. J. Magn. Reson. **58**, 306 (1984); J. A. WILDE and P. H. BOLTON. J. Magn. Reson. **59**, 343 (1984).
17. W. P. AUE, J. KARHAN, and R. R. ERNST. J. Chem. Phys. **64**, 4226 (1976).
18. C. A. G. HAASNOOT, F. J. M. VAN DE VEN, and C. W. HILBERS. J. Magn. Reson. **56**, 343 (1984); A. Z. GUREVICH, I. L. BARSUKOV, A. S. ARSENIEV, and V. F. BYSTROV. J. Magn. Reson. **56**, 471 (1984).

Can. J. Chem. Downloaded from www.nrcresearchpress.com by 194.225.253.170 on 09/07/12
For personal use only.

Structure of the stoichiometric complex 18-crown-6·H_2O·succinic acid

LUCIE PARENTEAU AND FRANÇOIS BRISSE
Département de chimie, Université de Montréal, C.P. 6128, Succ. A, Montréal (Qué.), Canada H3C 3J7

Received December 20, 1988

LUCIE PARENTEAU and FRANÇOIS BRISSE. Can. J. Chem. **67**, 1293 (1989).

Attempts to prepare stoichiometric complexes of the type dicarboxylic acid·18C6·H_2O succeeded only with oxalic, succinic, and glutaric acids. The crystal structure of the succinic acid complex was established by X-ray diffraction at 173 K, and was refined to R_w = 0.038 for 3204 observed reflections. The stoichiometry of the complex is 1:1:1 (succinic acid·H_2O·18C6). In the solid state there is a dimeric H-bonded association, through a center of symmetry, of two succinic acid molecules. Each diacid is also hydrogen bonded to a water molecule. The water molecules, in turn, form two hydrogen bonds each with the crown ether. The diacid–diacid, diacid–water, and the two water–18C6 hydrogen bonds are 2.657(2), 2.636(2), 2.819(2), and 2.910(2) Å long respectively. They are all nearly linear. The structural units are associated and form the centrosymmetric dimer (18C6–H_2O – succinic acid)$_2$. The conformation of the macrocyclic polyether differs significantly from that normally found. Instead of the usual $(ttg)_6$ conformation, that adopted in this complex is $(ttgttgstg)_2$. The two s torsion angles have values of 90.1(3) and 86.9(3)°. In this complex the succinic acid itself is in the *gauche* conformation.

Key words: macrocycle – succinic acid complex.

LUCIE PARENTEAU et FRANÇOIS BRISSE. Can. J. Chem. **67**, 1293 (1989).

On n'a réussi à préparer des complexes du type acide carboxylique·18C6·H_2O qu'avec les acides oxalique, succinique et glutarique. Faisant appel à la diffraction des rayons-X, à 173 K, on a déterminé la structure cristalline du complexe avec l'acide succinique et on l'a affinée jusqu'à une valeur de R_w de 0,038 pour 3204 réflexions observées. La stoechiométrie du complexe est 1:1:1 (acide succinique·H_2O·18C6). À l'état solide, on observe l'existence d'un dimère centrosymétrique formé par ponts-hydrogène entre deux molécules d'acide succinique. Chaque diacide est aussi relié par un pont hydrogène avec une molécule d'eau. Par ailleurs, les molécules d'eau forment chacune deux liaisons hydrogènes avec l'éther couronne. Les longueurs des liaisons hydrogènes diacide–diacide, diacide–eau et des deux molécules d'eau–18C6 sont respectivement de 2,657(2), 2,636(2), 2,819(2) et 2,910(2) Å. Elles sont pratiquement toutes linéaires. Les unités structurales ainsi liées forment un dimère centrosymétrique (18C6–H_2O – acide succinique)$_2$. La conformation du polyéther macrocyclique diffère beaucoup de celle normalement trouvée. Plutôt que le conformation $(ttg)_6$ habituelle, celle qui est adoptée dans ce complexe est $(ttgttgstg)_2$. Les valeurs des deux angles de torsion, s, sont de 90,1(3) et 86,9(3)°. Dans ce complexe, l'acide succinique adopte une conformation *gauche*.

Mots clés : complexe macrocycle – acide succinique.

[Traduit par la revue]

Introduction

In a previous investigation (1) we reported on the crystal and molecular structure of a complex formed between a dicarboxylic acid, oxalic acid, and the macrocyclic polyether, 18-crown-6 (abbreviated 18C6). The oxalic acid complex formed by incorporating H_2O has the stoichiometry $(COOH)_2 \cdot 2H_2O \cdot 18C6$, i.e., 1:2:1 (acid/water/18C6). Such complexes have also been observed with monocarboxylic acids. These included one or two water molecules with such resulting stoichiometries as 2:2:1 and 1:1:1 (2). Most unsubstituted 18C6 crown ethers adopt the highly symmetrical $(ttg)_6$ conformation (1, 9, 15, 18). However, other conformations such as $(tgttttg^-g^+t)_2$ for the uncomplexed macrocycle (16) or (ttg ttg$^-$ttg stgttt sg$^-$g$^-$) in complexes of 18C6 and small cations (17) have also been reported. We decided to study complexes incorporating other dicarboxylic acids such as HOOC—$(CH_2)_n$—COOH to establish if a trend in the stoichiometry and the packing mode could be detected as the number of methylenic groups increased. The points of interest are therefore to find: (a) the stoichiometry of the complex and, in particular, whether the water molecules are always required and in the same proportion; (b) whether the conformation of the diacid is the same as in the uncomplexed state, i.e., in the fully extended conformation; (c) whether the diacid molecule is disordered, as was reported in the case of the oxalic acid complex; (d) whether the conformation of the macrocyclic polyether is always the same.

Experimental

The complexes were prepared by addition of the acid (2.69 mmol), in the solid state, to a solution of 18C6 crown ether (3.78 mmol) in tetrahydrofuran (10 mL) with a small amount of water (0.3 mL). In these preparations, the following diacids were used: succinic, glutaric, adipic, suberic, malonique, decanedioic, and dodecanedioic.

For the X-ray study of the succinic acid complex, a well-formed single crystal was mounted on a Nonius-CAD4 diffractometer. The unit-cell dimensions (see Table 1) and the orientation matrix were computed by a least-squares refinement of the angular settings of 25 well-centered reflections in the range $40 \leq 2\theta \leq 50°$. The integrated intensities of 4011 reflections were measured within the sphere of reflection limited by $2\theta \leq 140°$ and $0 \leq h \leq 13$, $0 \leq k \leq 18$, $-18 \leq l \leq 14$ using graphite monochromatized copper radiation. The $\omega/2\theta$ scan mode was used with a scan range defined by $\Delta\omega = (1.00 + 0.14 \tan\theta)°$. The orientation of the crystal and the intensities of seven reference reflections were monitored every 100 measurements and every hour respectively. The intensity fluctuations were no higher than 1.9% over the duration of the measurements. The 3204 reflections satisfying the criterion $I/\sigma(I) \geq 2.50$ were considered observed and retained for the structure determination and refinement; $\sigma(I)$ was derived from the counting statistics. The diffracted intensities were corrected[1] for Lorentz and polarization effects but not for absorption since the absorption coefficient for the Cu radiation was small.

[1]The programs used are NRC-2, data reduction; NRC-10, bond distances and angles; FORDAP Fourier and Patterson syntheses (A. Zalkin); MULTAN80, multisolution program; NUCLS, least-squares refinement; ORTEP, stereodrawings (refs. 3–6).

Can. J. Chem. Downloaded from www.nrcresearchpress.com by 194.225.253.170 on 09/07/12
For personal use only.

TABLE 1. Crystal data

$C_{12}H_{24}O_6 \cdot H_2O \cdot C_4H_6O_4$ ($C_{16}H_{32}O_{11}$)		FW = 400.423	MP = 393 K
Monoclinic	Space group $P2_1/c$	$F(000)$ = 864 e	λ = 1.54178 Å
a = 11.347(3)	b = 15.278(4)	c = 15.023(4) Å	β = 128.78(2)°
V = 2030.26 Å^3	d_0 = 1.29	d_c = 1.310 g cm^{-3}	Z = 4
Crystal size	0.21 × 0.34 × 0.50 mm	μ(CuKα) = 9.04 cm^{-1}	T = 173 K

The structure was solved by direct methods using the MULTAN80 program. All the atoms were located from the E-map computed with the set of phases having the highest combined figures of merit. Once the block-diagonal least-squares refinement of the non-hydrogen atoms, with isotropic then anisotropic temperature factors, had converged, a difference Fourier synthesis revealed all the H-atoms of the 18C6 molecule. These were included in all subsequent cycles of refinement with isotropic thermal parameters. The H-atoms of the water molecule and those of the succinic acid were located in another difference Fourier synthesis. These were also included in the refinement. It was then discovered that one of the acid hydrogens occupied two distinct positions in a 60/40 proportion. Convergence was reached at R = 0.044 and R_w = 0.038 for 3204 reflections.[2] On the final refinement cycle the average parameter shift was 0.03σ (maximum 0.46σ); the mean error of an observation of unit weight S was 2.67. The extreme fluctuations of the residual electron density as shown on the final difference Fourier synthesis were −0.23 and 0.36 e Å^{-3}. The quantity minimized was $\Sigma w\Delta F^2$. The scattering factors used were taken from ref. 7 for non-hydrogen atoms and from ref. 8 for H-atoms.

Results and discussion

Of all attempts undertaken at obtaining complexes with diacids, only those with the oxalic, succinic, and glutaric acids were successful. In all other cases only the starting compounds were recovered. Usually it was the 18C6 molecules that crystallized out first. A complex of 1:1:1 stoichiometry, succinic acid·H_2O·18C6, was obtained after a slow evaporation of the solvent. The crystal structure of the succinic acid complex is discussed below and compared to that of its oxalic acid analog. The final atomic coordinates and the equivalent U values of the anisotropic temperature factors are given in Table 2.[3] A stereoview showing the molecular conformation and the atomic numbering is shown in Fig. 1.

TABLE 2. Fractional atomic coordinates (×10^5) and their esd's, U_{eq} (×10^4)

$U_{eq} = \frac{1}{3}\sum_i\sum_j U_{ij}a_i^*a_j^*a_i \cdot a_j$

Atom	X	Y	Z	U_{eq}
C(1)	104779(16)	85839(10)	43007(14)	404
O(2)	89724(11)	88898(6)	34675(8)	359
C(3)	84395(18)	87376(10)	23352(13)	415
C(4)	68507(18)	90644(10)	15097(13)	413
O(5)	58903(11)	84948(7)	15359(9)	417
C(6)	43670(17)	88065(11)	8123(13)	437
C(7)	33974(17)	81505(11)	8181(13)	459
O(8)	37214(11)	80678(7)	18951(9)	423
C(9)	28856(15)	86316(9)	20690(13)	394
C(10)	33976(16)	84785(9)	32456(13)	383
O(11)	48533(10)	88546(6)	40570(8)	353
C(12)	54315(17)	87285(10)	52055(13)	396
C(13)	69855(17)	91177(10)	59869(12)	408
O(14)	80163(11)	85507(6)	60375(9)	389
C(15)	94867(17)	89190(10)	66740(13)	439
C(16)	105265(17)	82637(11)	67414(13)	447
O(17)	102185(11)	81234(6)	56774(9)	383
C(18)	109754(15)	87281(9)	54724(13)	397
O(19)	55871(11)	111498(7)	15594(9)	399
O(20)	47745(11)	108251(6)	25411(9)	363
C(20)	47098(14)	112658(8)	17485(11)	300
C(21)	34634(16)	119313(9)	11338(12)	372
C(22)	22337(16)	118223(9)	12423(13)	384
C(23)	13057(15)	110148(9)	7081(11)	329
O(23)	4548(12)	108157(8)	9666(9)	460
O(24)	13283(12)	105774(7)	140(9)	451
O(W)	68435(10)	96034(6)	37469(8)	344

Conformation of the 18C6 crown ether

The bond distances, bond angles, and torsion angles and their esd's are presented in Table 3. The C—C bond distances vary little (range 1.490(3)–1.502(3) Å) and average 1.495 Å. The C—O bond distances also remain in a narrow interval (1.415(3)–1.429(3) Å) and average 1.422 Å. The average of the C—O—C bond angles, 112.7°, is slightly higher than that of the C—C—O bond angles, 109.7°. These features, and in particular the relatively short C—C bond distances, are consistent with the corresponding quantities found in structures containing the 18C6 molecule (9, 11–18).

The salient feature of the 18C6 molecule in this complex is its conformation, which can be described by the (ttgttgstg)$_2$ sequence of torsion angles (t = trans ≃ 180°, g = gauche ≃ 60°, s = skew ≃ 90°). The average value of the torsion angle around the C—C bond is 71.7° and the spread is only ±5°. The conformation about these bonds is *gauche*. On the other hand, 10 out of the 12 torsion angles around the C—O bonds have values within ±3° of their average of 177.2°. These are in the *trans* conformation. The other two torsion angles, C(6)—C(7)—O(8)—C(9) and C(15)—C(16)—O(17)—C(18) have values of 90.1(3) and 86.9(3)° rather than the 180° value usually observed for this crown ether in the D_{3d} symmetry. In a search of the Cambridge Data File[4] for crystal structures containing the 18C6 macrocycle it was found that only one out of 57 reported structures came close to our situation. This conformation was observed by Weber and Sheldrick (9) in a 2:1 complex of 2,4-dinitroaniline and 18-crown-6. However, it should be pointed out that in this centrosymmetric complex, besides the two skew torsion angles, there are also two other torsion angles, which depart quite significantly from a *trans* value that the authors consider to be strongly distorted *trans*. Histograms representing the distribution of the C—C—O—C and O—C—C—O torsion angles, based on the crystal struc-

[2] $R = \Sigma||F_o| - |F_c||/\Sigma|F_o|$, $R_w = [\Sigma w(|F_o| - |F_c|)^2/\Sigma wF_o^2]^{1/2}$, $S = [\Sigma w\Delta F^2/(m - n)]^{1/2}$.

[3] Tables of atomic positions of H-atoms, anisotropic temperature factors, and structure factors have been deposited and may be purchased from the Depository of Unpublished Data, CISTI, National Research Council of Canada, Ottawa, Ont., Canada K1A 0S2.

[4] The search of the NRC version of the Cambridge Data File, conducted in November 1986, was restricted to crystal structures where the 18C6 macrocycle was not substituted.

Can. J. Chem. Downloaded from www.nrcresearchpress.com by 194.225.253.170 on 09/07/12
For personal use only.

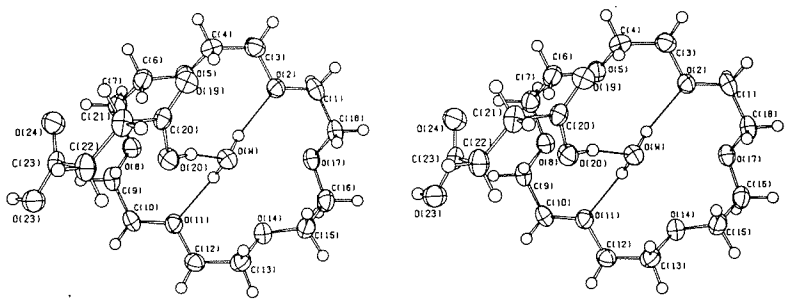


FIG. 1. Stereopair showing the various structural units and their atomic numbering.

TABLE 3. Bond distances (Å), bond angles, torsion angles (°), and their esd's of the 18-crown-6 molecule

Distances		Angles		Torsion angles	
C(1)—O(2)	1.423(2)	C(1)—O(2)—C(3)	112.0(1)	C(1)—O(2)—C(3)—C(4)	179.3(2)
O(2)—C(3)	1.423(2)	O(2)—C(3)—C(4)	109.0(2)	O(2)—C(3)—C(4)—O(5)	−71.8(2)
C(3)—C(4)	1.496(3)	C(3)—C(4)—O(5)	108.7(2)	C(3)—C(4)—O(5)—C(6)	176.5(2)
C(4)—O(5)	1.414(2)	C(4)—O(5)—C(6)	111.1(1)	C(4)—O(5)—C(6)—C(7)	176.4(2)
O(5)—C(6)	1.429(2)	O(5)—C(6)—C(7)	108.5(2)	O(5)—C(6)—C(7)—O(8)	66.3(2)
C(6)—C(7)	1.497(3)	C(6)—C(7)—O(8)	113.6(2)	C(6)—C(7)—O(8)—C(9)	90.1(2)
C(7)—O(8)	1.422(2)	C(7)—O(8)—C(9)	115.4(1)	C(7)—O(8)—C(9)—C(10)	−178.3(2)
O(8)—C(9)	1.421(2)	O(8)—C(9)—C(10)	108.2(1)	O(8)—C(9)—C(10)—O(11)	73.6(2)
C(9)—C(10)	1.493(3)	C(9)—C(10)—O(11)	109.5(1)	C(9)—C(10)—O(11)—C(12)	−179.4(2)
C(10)—O(11)	1.422(2)	C(10)—O(11)—C(12)	112.9(1)	C(10)—O(11)—C(12)—C(13)	177.9(2)
O(11)—C(12)	1.423(2)	O(11)—C(12)—C(13)	108.6(1)	O(11)—C(12)—C(13)—O(14)	−75.9(2)
C(12)—C(13)	1.499(3)	C(12)—C(13)—O(14)	109.0(1)	C(12)—C(13)—O(14)—C(15)	174.2(2)
C(13)—O(14)	1.419(2)	C(13)—O(14)—C(15)	112.1(1)	C(13)—O(14)—C(15)—C(16)	177.0(2)
O(14)—C(15)	1.419(2)	O(14)—C(15)—C(16)	108.9(2)	O(14)—C(15)—C(16)—O(17)	69.7(2)
C(15)—C(16)	1.502(3)	C(15)—C(16)—O(17)	113.3(2)	C(15)—C(16)—O(17)—C(18)	86.9(2)
C(16)—O(17)	1.422(2)	C(16)—O(17)—C(18)	112.9(1)	C(16)—O(17)—C(18)—C(1)	−174.9(2)
O(17)—C(18)	1.420(2)	O(17)—C(18)—C(1)	109.1(1)	O(17)—C(18)—C(1)—O(2)	72.6(2)
C(18)—C(1)	1.490(3)	C(18)—C(1)—O(2)	110.4(2)	C(18)—C(1)—O(2)—C(3)	−178.1(2)

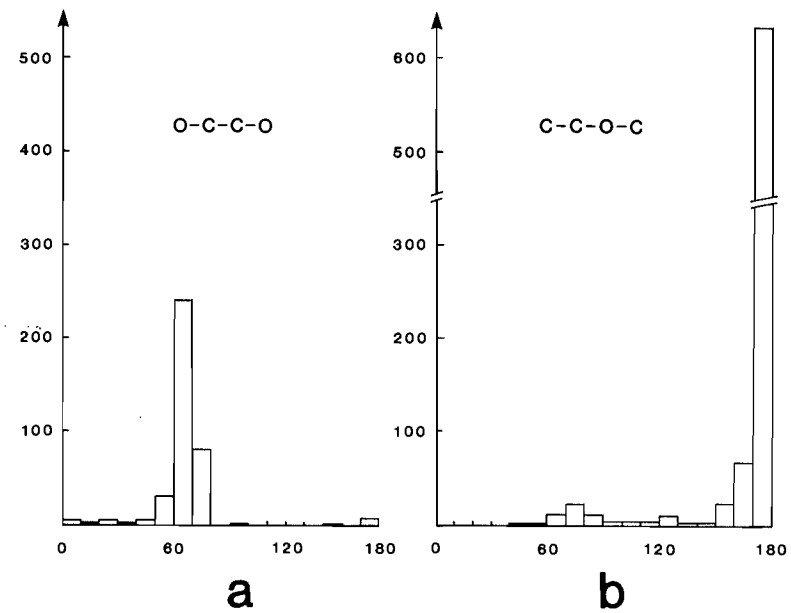


FIG. 2. Histograms: (a) distribution of the O—C—C—O torsion angles; (b) distribution of the C—C—O—C torsion angles.

tures listed in the Cambridge Data File, are shown in Fig. 2. It is clear that in most structures containing the 18C6 crown ether, the macrocycle adopts the $(ttg)_6$ conformation. There are very few examples where the torsion angles deviate significantly from ±60° or 180°. Perrin, Décoret, Bertholon, and Lamartine (10) have proposed six energetically acceptable conformations for the 18C6 macrocycle. These are based on theoretical calculations and dipolar moment measurements. Although

Can. J. Chem. Downloaded from www.nrcresearchpress.com by 194.225.253.170 on 09/07/12
For personal use only.

TABLE 4. Bond distances (Å), bond angles, torsion angles (°), and their esd's of the succinic acid

Distances		Angles		Torsion angles	
C(20)—O(19)	1.207(2)	O(19)—C(20)—O(20)	123.1(1)	O(19)—C(20)—C(21)—C(22)	163.9(2)
C(20)—O(20)	1.329(2)	O(19)—C(20)—C(21)	123.6(1)	O(20)—C(20)—C(21)—C(22)	−17.3(2)
C(20)—C(21)	1.500(3)	O(20)—C(20)—C(21)	113.4(1)	C(20)—C(21)—C(22)—C(23)	−65.5(2)
C(21)—C(22)	1.512(3)	C(20)—C(21)—C(22)	115.9(1)	C(21)—C(22)—C(23)—O(23)	167.1(2)
C(22)—C(23)	1.489(3)	C(21)—C(22)—C(23)	114.9(1)	C(21)—C(22)—C(23)—O(24)	−15.3(2)
C(23)—O(23)	1.283(3)	C(22)—C(23)—O(23)	116.5(1)		
C(23)—O(24)	1.252(3)	C(22)—C(23)—O(24)	122.9(2)		
		O(23)—C(23)—O(24)	123.0(2)		

TABLE 5. Geometrical characteristics of the hydrogen bonds in succinic acid·H_2O·18C6

Atoms	Distances (Å) O—H	H···O	O···O*	Angles (°) O—H···O*
O(W)—H(W1)···O(2)	0.89(3)	2.03(3)	2.910(2)	165(2)
O(W)—H(W2)···O(11)	0.82(2)	2.01(3)	2.819(2)	159(2)
O(20)—H(O20)···O(W)	0.86(2)	1.78(2)	2.636(2)	167(2)
O(23)—H(O23)[a]···O(24*)	0.85(3)	1.81(3)	2.657(2)	178(3)
O(24)—H(O24)[a]···O(23*)	0.70(5)	1.98(5)	2.657(2)	163(6)

[a]The occupancy factor of H(O23) is 0.60 and that of H(O24) is 0.40.

there are actual examples for only three of the six proposed conformations, our case cannot be associated with any of the six situations examined by Décoret and co-workers (10).

The succinic acid

The bond distances, bond angles, and torsion angles for the succinic part of the complex are given in Table 4. In the succinic acid·H_2O·18C6 complex, the succinic group of atoms is not planar since the main torsion angle, C(20)—C(21)—C(22)—C(23) = 65.5(2)°, is *gauche*. This is unusual since in most compounds containing the succinic group, including the β-form of succinic acid, the conformation around the central bond is *trans* (19). In monomethyl succinate, however, the succinic group is also in the *gauche* conformation (14). Also deviating from planarity are the two carboxylic groups, which are tilted by about 15° as indicated by the torsion angles O(20)—C(20)—C(21)—C(22) and C(21)—C(22)—C(23)—C(24) in Table 4. Another interesting result, caused by the formation of a dimer through O(23)···O(24*) and O(24)···O(23*), is that the two "ends" of the acid molecule are chemically distinct. There is a "carboxylic end" at C(20) since the two C—O bonds are clearly unequal: C(20)—O(19) = 1.207(2) Å and C(20)—O(20) = 1.329(2) Å, while at C(23), the "carboxylate end", the corresponding distances are nearly equal: C(23)—O(23) = 1.283(3) and C(23)—O(24) = 1.252(3) Å. This difference is also reflected in the values taken by the following bond angles: C(21)—C(20)—O(19) = 123.6(1)° and C(21)—C(20)—O(20) = 113.4(1)° at the carboxylic end compared to C(22)—C(23)—O(23) = 116.5(1) and C(22)—C(23)—O(24) = 120.9(2)° at the carboxylate end. A situation in all respects comparable to ours was observed by Kanters *et al.* (14) in monomethyl succinate. There, the two C—O bonds and C—C—O bond angles at the ester end were clearly very different from one another. At the other end of the molecule these quantities, although significantly different, tended to be more equal.

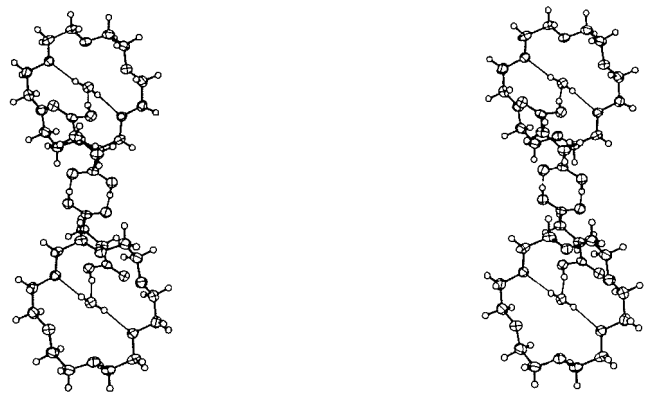


FIG. 3. Stereopair showing the "dimeric" unit formed of (18C6–H_2O – succinic acid)$_2$.

Association of the structural units

The crown ether, the water, and the succinic acid molecules form the crystalline complex through a number of hydrogen bonds. A stereoview of the association of the structural units is shown in Fig. 3. Two centrosymmetrically related acid molecules form strong hydrogen bonds where both O···O distances are 2.657(2) Å. In this dimer, it is found that the H-atoms are delocalized over two sites with respective occupancy factors of 0.60 and 0.40. The H-bonds are nearly linear since the two angles O(23)—H(O23)···O(24*) and O(24)—H(O24)···O(23*) have values of 178(3) and 163(3)° respectively. Except for the disorder of the H-atoms, the H-bonding scheme described here matches that reported for monomethyl succinate (14). There, the O—H···O angle is 172.5° while the O···O distance is 2.66 Å.

The "acid end" of the molecule forms another strong, almost linear, H-bond with the water molecule, d(O···O) = 2.636(2) Å.

Can. J. Chem. Downloaded from www.nrcresearchpress.com by 194.225.253.170 on 09/07/12
For personal use only.

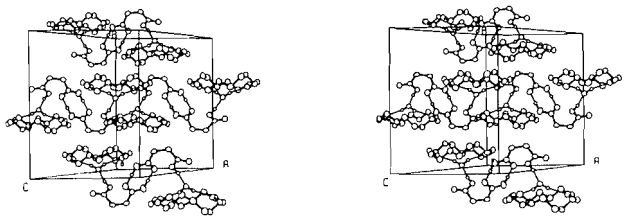


FIG. 4. Stereopair showing the molecular packing.

It is this water molecule which links, through two other hydrogen bonds, the succinic acid and the crown ether. These two H-bonds are relatively long; the O(W)···O(2) and O(W)···O(11) distances are 2.910(2) and 2.819(2) Å respectively. The other geometrical parameters characterizing these hydrogen bonds are given in Table 5. It is to be noted that this mode of association of the structural units bears no relation to that found in the parent oxalic acid complex. In the latter case, the units form a pseudo-polymer through a series of H-bonds that could be described as $(18C6\cdots H_2O\cdots HOOCCOOH\cdots H_2O)_n$. The relative disposition of the dimeric units of the succinic complex in the unit cell is shown in Fig. 4.

It could be that the large size difference between the structural units (diacid vs. 18C6) or the fact that there is a *gauche* torsion angle around the central CH_2—CH_2 bond of succinic acid is responsible for the disorder of the oxalic acid molecule (1). We are still attempting to synthesize higher members in the series to verify this point.

Conclusions

A complex of 1:1:1 stoichiometry is formed between succinic acid, H_2O, and the 18C6 macrocycle. The water molecule that forms two H-bonds with the 18C6 crown ether is also H-bonded to a succinic acid molecule. It, in turn, is centrosymmetrically H-bonded to another succinic acid, thus forming the dimer $(18C6{-}H_2O$ – succinic acid$)_2$. The diacid is not in a fully extended conformation but has a torsion angle of 65° around the central CH_2—CH_2 bond. The crown ether adopts the unusual $(ttgttgstg)_2$ conformation.

Acknowledgements

We thank the Natural Sciences and Engineering Research Council of Canada for its financial support. We also thank Mr. M. J. Olivier for collecting the X-ray data.

1. S. DEGUIRE, F. BRISSE, J. OUELLET, and R. SAVOIE. Can. J. Chem. **64**, 142 (1986).
2. R. SAVOIE, A. RODRIGUE, M. PIGEON-GOSSELIN, and R. CHÊNEVERT. Can. J. Chem. **63**, 1457 (1985).
3. F. R. AHMED, S. R. HALL, M. E. PIPPY, and C. P. HUBER. J. Appl. Crystallogr. **6**, 309 (1973). Accession Nos. 133–147.
4. P. MAIN, S. J. FISKE, S. E. HULL, L. LESSINGER, G. GERMAIN, J. DECLERCQ, and M. M. WOOLFSON. MULTAN80. A system of computer programs for the automatic solution of crystal structures from X-ray diffraction data. Universities of York, England, and Louvain, Belgium.
5. R. J. DOEDENS and J. A. IBERS. Inorg. Chem. **6**, 204 (1967).
6. C. K. JOHNSON. ORTEP. Report ORNL-3794. Oak Ridge National Laboratory, Tennessee. 1965.
7. D. T. CROMER and J. B. MANN. Acta Crystallogr. Sect. A: Cryst. Phys. Diffr. Theor. Gen. Crystallogr. **24**, 321 (1968).
8. R. F. STEWART, E. R. DAVIDSON, and W. T. SIMPSON. J. Chem. Phys. **53**, 1891 (1970).
9. G. WEBER and G. M. SHELDRICK. Acta Crystallogr. Sect. B: Struct. Crystallogr. Cryst. Chem. **37**, 2108 (1981).
10. P. PERRIN, C. DÉCORET, G. BERTHOLON, and R. LAMARTINE. Nouv. J. Chim. **7**, 263 (1983).
11. I. GOLDBERG. Acta Crystallogr. Sect. B: Cryst. Phys. Diffr. Theor. Gen. Crystallogr. **33**, 472 (1977).
12. E. MAVERICK, P. SEILER, W. B. SCHWEIZER, and J. D. DUNITZ. Acta Crystallogr. Sect. B: Cryst. Phys. Diffr. Theor. Gen. Crystallogr. **36**, 615 (1980).
13. O. NAGANO. Acta Crystallogr. Sect. B: Cryst. Phys. Diffr. Theor. Gen. Crystallogr. **35**, 465 (1979).
14. J. A. KANTERS, H. M. DOESBURG, and T. KOOPS. Acta Crystallogr. Sect. B: Cryst. Phys. Diffr. Theor. Gen. Crystallogr. **33**, 1286 (1977).
15. L. PARENTEAU and F. BRISSE. Can. J. Chem. Submitted.
16. J. D. DUNITZ and P. SEILER. Acta Crystallogr. Sect. B: Cryst. Phys. Diffr. Theor. Gen. Crystallogr. **29**, 154 (1973).
17. M. DOBLER, J. D. DUNITZ, and P. SEILER. Acta Crystallogr. Sect. B: Cryst. Phys. Diffr. Theor. Gen. Crystallogr. **30**, 2741 (1974).
18. R. CHÊNEVERT, D. CHAMBERLAND, M. SIMARD, and F. BRISSE. Can. J. Chem. **67**, 32 (1989).
19. F. BRISSE, N. MOLHANT, and S. PÉREZ. Acta Crystallogr. Sect. B: Cryst. Phys. Diffr. Theor. Gen. Crystallogr. **35**, 1825 (1979).

Can. J. Chem. Downloaded from www.nrcresearchpress.com by 194.225.253.170 on 09/07/12
For personal use only.

An analysis of the pathways for magnesium ion in the field of a macrocyclic ligand

SUPOT V. HANNONGBUA[1] AND SIRIRAT U. KOKPOL
Computational Chemistry Unit Cell, Department of Chemistry, Faculty of Science, Chulalongkorn University, Bangkok 10330, Thailand

AND

JUMRAS P. LIMTRAKUL
Department of Chemistry, Faculty of Science, Kasetsart University, Bangkok 10903, Thailand

Received September 26, 1988[2]

SUPOT V. HANNONGBUA, SIRIRAT U. KOKPOL, and JUMRAS P. LIMTRAKUL. Can. J. Chem. **67**, 1298 (1989).

An *ab initio* MO-SCF calculations have been performed with a minimal Gaussian lobe basis set for numerous Mg(II) 1,4,7,10-tetraazacyclododecane (cyclen) configurations. Mg(II) shows a strong interaction with all functional groups of cyclen. The strongest interaction occurs when magnesium points to the cavity and perpendicular to the ligand plane. However, in the complex formation processes, the ion does not prefer to move along this direction because of the repulsive interaction with the NH functional groups. The favourable path for entering the cavity of the ligand encloses an angle of 30° with the *z* axis and lies in the plane between the opposite NH groups.

Key words: cyclen, macrocyclic effect, complex formation, favourable path, *ab initio* calculations.

SUPOT V. HANNONGBUA, SIRIRAT U. KOKPOL et JUMRAS P. LIMTRAKUL. Can. J. Chem. **67**, 1298 (1989).

Utilisant un ensemble de base gaussien minimal de Lobe, on a réalisé des calculs *ab initio* d'orbitales moléculaires en champ auto-cohérent pour diverses configurations du Mg(II) tétraaza-1,4,7,10 cyclododécane (cyclen). Le Mg(II) interagit fortement avec tous les groupements fonctionnels du cyclen. On observe l'interaction la plus importante lorsque le magnésium est orienté vers la cavité et qu'il est perpendiculaire au plan du ligand. Toutefois, dans le processus de formation du complexe, les interactions répulsives générées par les groupements fonctionnels NH font que l'ion ne se déplace préférentiellement pas le long de cette direction. La voie d'accès la plus favorable pour l'entrée du ligand dans la cavité implique un angle de 30° par rapport à l'axe des *z* et elle se trouve dans le plan qui se trouve entre les groupements NH opposés.

Mots clés : cyclen, effet macrocyclique, formation du complexe, voie d'accès favorable, calculs *ab initio*.

[Traduit par la revue]

Introduction

The term "macrocyclic effect" was introduced by Margerum and co-worker (1) in 1969 to indicate the unusually high stability constants of metal complexes with cyclic ligands compared to equivalent open chain compounds. Several suggestions were made to explain details of this effect. The most frequent suggestions postulate that this effect arises from (*i*) the lower degree of solvation of cyclic ligands due to the steric hindrance of the ring, hence termed "solvation effect" (2, 3), (*ii*) the "prestrained" conformation of the cyclic ligands which is already the conformation suitable for complexation (4, 5), (*iii*) the presence of more secondary donor atoms, resulting in a higher "ligand field strength" of cyclic ligands (6), and (*iv*) the easier dissociation process due to less fixed atoms in the open chain ligand, leading to the term "multiple juxtapositional fixeness" of cyclic ligands (7).

In our previous works (8, 9, 10*a*), the factors contributing to the macrocyclic effect were investigated by means of quantum chemical calculations, neglecting solvation effects and selecting cyclic and open chain ligands with the same number of donor atoms. The results showed that open chain ligands spend considerable energy adapting their structure for optimal ion binding, a conclusion that agrees with the suggested advantages of the "prestrained" cyclic ligands. However, it was also found that electronic effects arising from charge density rearrangements, in their contribution to the stability, are similar in both cases (10*a*).

Solvent effects have been considered by Monte Carlo simulations for 1,4,7,10-tetraazacyclododecane (10*b*–*d*) and its magnesium complex (11, 12) in water. Those investigations have shown that both ligand and complex form discrete solvated structure containing 12 and 18 water molecules, respectively, among which one is located directly above and one below the center of the macrocyclic cavity. According to these results, it has to be expected that enthalpic rather than entropic effects of hydration will influence the stability of macrocyclic complexes, and that substitutions at the macrocycle's nitrogen atoms should

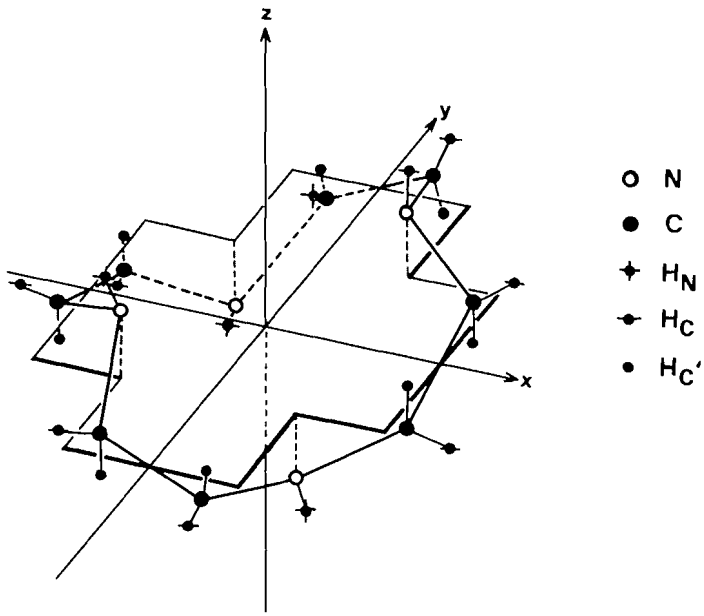


FIG. 1. The optimum conformation (alternate form) of 1,4,7,10-tetraazacyclododecane taken from ref. 9.

[1]To whom correspondence should be addressed.
[2]Revision received April 10, 1989.

Can. J. Chem. Downloaded from www.nrcresearchpress.com by 194.225.253.170 on 09/07/12
For personal use only.

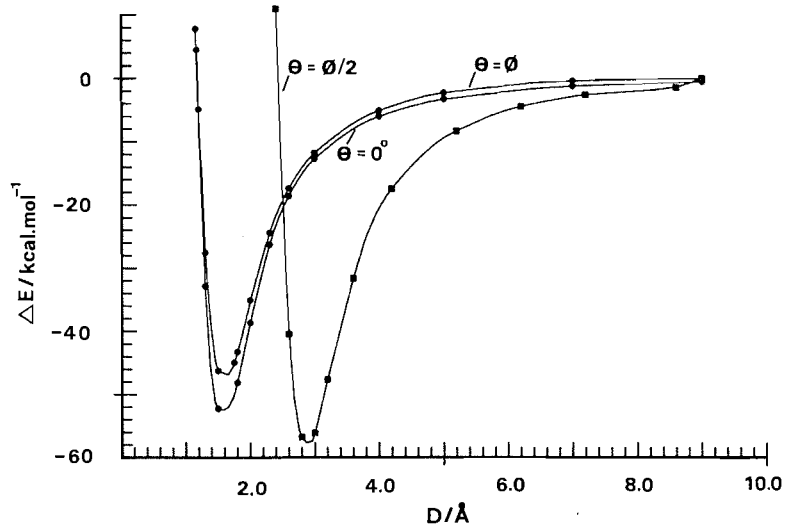


FIG. 2. Mg(II)–cyclen interaction potentials near the hydrophobic CH_2 functional groups in H—C—H plane. θ is the angle between C—H bonds and a vector ***r*** pointing to the C atoms. $\phi = \angle HCH$.

have a considerable influence on such solvation contributions (12).

In the present study, the interaction potential between Mg(II) and cyclen is analyzed in detail. The optimal path of Mg(II) approach through the potential field of cyclen to its cavity is evaluated and discussed.

Methods of calculation

Considering the solvation structure around cyclen from our Monte Carlo results (10*c*, *d*) the ligand field can be divided into three different regions, the strongest hydrophilic funnel-shaped regions above and below the molecular plane around the molecular center (see Fig. 1), the hydrophilic regions around the NH functional groups and the hydrophobic regions near the CH_2 groups. Interaction energies between Mg(II) and 1,4,7,10-tetraazacyclododecane for numerous configurations in these three regions have been evaluated by *ab initio* LCAO-MO-SCF calculations with a minimal Gaussian lobe basis set (13) successfully used in previous investigations (8–11). The optimized geometry of cyclen was taken from our previous work (9) (Fig. 1) and kept constant throughout the calculations, since optimization of the Mg(II)/cyclen complex has led to only minor changes of conformation (10*a*, 14). An estimation of the basis set superposition error (15) was performed for the configuration where Mg(II) is located in the center of the cavity.

All calculations were performed on the IBM-3031 computer of Chulalongkorn University, using an adapted version of the MO-SCF program given in ref. 16.

Results and discussion

The Mg(II)–cyclen interaction potentials for the three important regions around CH_2 and NH functional groups and near the molecular center are shown in Figs. 2, 3, and 4, respectively.

(i) Mg(II)–cyclen interactions near the hydrophobic CH_2 functional groups

In Fig. 2, curves are characterized by the angles θ and φ, where θ being the angle between C—H bonds and a vector ***r*** pointing to the C atoms, and φ being the H—C—H angle. The interactions between Mg(II) and cyclen in the H—C—H plane are plotted for three different orientations, i.e. along the two different types of C—H bonds, where $\theta = 0°$ and $\theta = \phi$ (cf. ref. 10*b*), and bisecting the H—C—H angle, where $\theta = \phi/2$. The results show that Mg(II) interacts strongly with cyclen even when approaching this hydrophobic area. The energy minimum differ by about 6 kcal, as the axial H atom ($\theta = 0°$) has a smaller partial charge, +0.14 atomic charge units according to Mulliken population analysis (17) compared to +0.02 of the equatorial one ($\theta = \phi$). Besides this lower repulsion, the approach near the axial hydrogen brings the metal ion into a position very close to the hydrophilic region and hence favours this pathway.

(ii) Mg(II)–cyclen interactions near the hydrophilic NH functional groups

The interaction of Mg(II) with NH functional groups of cyclen are shown in Fig. 3. The angle between the *z* axis and a vector ***r*** pointing to N atoms is denoted by θ and φ; where θ is the angle between the *z* axis and the N—H bonds. Angles $\theta = 0°$, 90° and φ represent interactions parallel and perpendicular to *z* axis and along the N—H bond, respectively. The depth of the minima is directly proportional to the angle between that path and the N—H bond. This relation can be described by the repulsive interaction between Mg(II) ion and the partial positive charge of hydrogen atoms (of the NH functional groups) of cyclen.

(iii) Mg(II)–cyclen interactions in the hydrophilic funnel regions above and below the molecular plane

In Fig. 4, where θ is the angle formed by the *z* axis and a vector ***r*** in the *xz* plane (Fig. 1), interactions of Mg(II) with the molecular center of cyclen in five different orientations are given. In all cases, Mg(II) ion is attracted into the molecular center of the ligand except for $\theta = 90°$ because of the hindrance by the dimethylene bridges. In cases where $\theta = 45°$ and 60°, Mg(II) shows a very strong repulsion with the molecular backbone of cyclen within a distance of 1.2–3.4 Å. At shorter distances, the curves are lowering steadily until Mg(II) ion reaches the cavity. When $\theta = 0°$, repulsion with the NH functional groups can also be recognized from a fluctuation of the curve between 2.2–2.4 Å.

The trajectory where $\theta = 30°$ is the only one displaying no shoulder and leads to optimal stabilization (about 50 kcal lower than for $\theta = 0°$ at 2.3 Å). Therefore, it will be the most

Can. J. Chem. Downloaded from www.nrcresearchpress.com by 194.225.253.170 on 09/07/12
For personal use only.

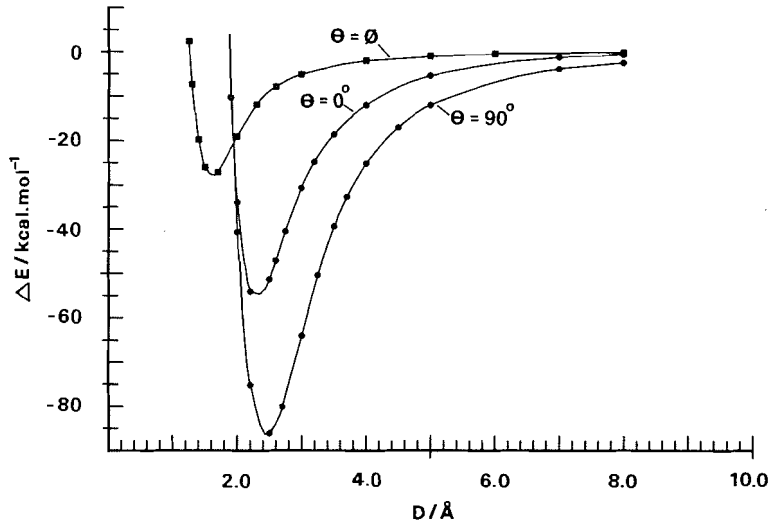


FIG. 3. Mg(II)–cyclen interaction potentials near the hydrophilic NH functional groups in the plane passing through the N—H bond and the z axis. θ is the angle between z axis and a vector $\boldsymbol{r}$ pointing to N atoms. ϕ is the angle between z axis and N—H bond.

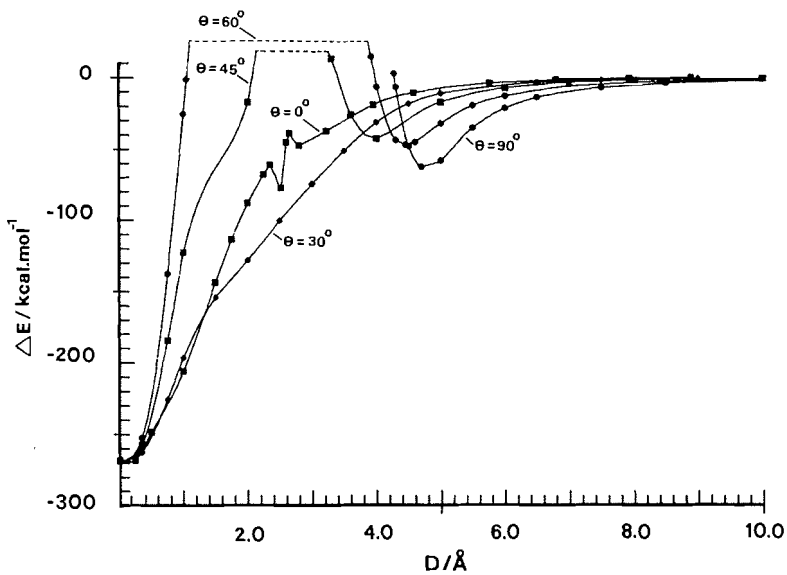


FIG. 4. Mg(II)–cyclen interaction potentials near the hydrophilic "funnel regions" above and below the molecular center in "xz" plane. θ is the angle between the z axis and a vector $\boldsymbol{r}$ pointing to the molecular center.

favourable path for moving the ion into the cavity of the ligand in the complexation process, avoiding repulsion with NH functional groups and dimethylene bridges of the molecular backbone of the ligand.

Further, such an approach will strongly facilitate the elimination of the one central water molecule located above the cavity according to the Monte Carlo results (10*d*), expelling it simultaneously as the ion moves in. The binding energy of the water molecule is only 12 kcal mol^{-1} (10*b*) compared to 270 kcal mol^{-1} for Mg(II) ion (Fig. 4). The water molecule on the other side of the plane needs not to be moved, and can immediately become a part of the complex's solvation shell. The other solvation water molecules located farther in the shape of a funnel (10*d*) can cooperate in the displacement of the metal ion's hydration water by offering alternative coordination site.

The above conclusion also confirms the kinetic inertness of macrocyclic complexes (18) in exchanging the metal ion. Any collision between macrocyclic ligand and ion will result in exchange only if this specific trajectory is followed. Thus, the reaction will be able to occur only within a reaction area which is less than 20% of the whole space around the macrocyclic ligand.

The results reported here provide some first information for the complexation process. Although stabilization energies computed with the small basis set are usually overemphasized due to basis set superposition error (13.5 kcal mol^{-1} or 5% at the lowest-energy configuration), relative stabilities are satisfactorily reproduced in almost every case (8–10, 19). On the other hand, the size of the system under consideration did not allow the use of extended basis sets because of the enormous computation time that would have been required.

Acknowledgements

Financial support by the Natural Research Council of Thailand and generous supply of computer time by the computer center of Chulalongkorn University are gratefully acknowledged.

Can. J. Chem. Downloaded from www.nrcresearchpress.com by 194.225.253.170 on 09/07/12
For personal use only.

1. D. K. CARBINESS and D. W. MARGERUM. J. Am. Chem. Soc. **91**, 6540 (1969).
2. D. J. CRAM and J. M. CRAM. Acc. Chem. Res. **11**, 8 (1978); Pure Appl. Chem. **817**, 50 (1978).
3. J. J. CHRISTENSEN, D. J. EATOUGH, and R. M. IZATT. Chem. Rev. **74**, 351 (1974); R. M. IZATT, J. J. CHRISTENSEN, and J. O. HILL. Science, **174**, 459 (1971).
4. L. FABBRIZZI, P. PAOLETTI, and R. M. CLAY. Inorg. Chem. **17**, 1042 (1978).
5. G. J. MCDOUGALL, R. D. HANCOCK, and J. C. A. BOEYENS. J. Chem. Soc. Dalton, 1438 (1978).
6. R. D. HANCOCK and G. J. MCDOUGALL. Adv. Mol. Relax. Int. Proc. **18**, 99 (1980).
7. D. H. BUSCH, K. FARMERY, V. GOEDKEN, V. KATOVIC, A. C. MELNYK, C. R. SPERATI, and N. TOKEL. Adv. Chem. Ser. **100**, 44 (1971).
8. G. J. REIBNEGGER and B. M. RODE. Inorg. Chim. Acta, **72**, 47 (1983).
9. B. M. RODE and S. V. HANNONGBUA. Inorg. Chim. Acta, **96**, 91 (1985).
10. S. V. HANNONGBUA and B. M. RODE. (*a*) Inorg. Chem. **24**, 2577 (1985); (*b*) Z. Naturforsch. **40***a*, 644 (1985); (*c*) J. Sci. Soc. Thailand, **11**, 135 (1985); (*d*) J. Chem. Soc. Faraday Trans. II, **82**, 1021 (1986).
11. V. W. RUANGPORNVISUTI, M. M. PROBST, and B. M. RODE. Inorg. Chim. Acta, **134**, 297 (1987).
12. B. M. RODE, V. W. RUANGPORNVISUTI, and S. V. HANNONGBUA. J. Sci. Soc. Thailand, **13**, 47 (1987).
13. B. M. RODE. Monatsch. Chem. **106**, 339 (1975).
14. M. F. RICHARDSON and R. E. SIEVER. J. Am. Chem. Soc. **94**, 4134 (1972).
15. S. F. BOYS and F. BERNARDI. Mol. Phys. **19**, 553 (1970).
16. B. M. RODE and G. J. REIBNEGGER. Monatsch. Chem. **110**, 813 (1979).
17. R. S. MULLIKEN. J. Chem. Phys. **23**, 1833 (1955); **23**, 1841 (1955); **23**, 2338 (1955); **23**, 2343 (1955).
18. D. K. CARBINESS and D. K. MARGERUM. J. Am. Chem. Soc. **92**, 2151 (1970).
19. K. P. SAGARIK and B. M. RODE. Inorg. Chim. Acta, **76**, L209 (1983); **78**, 81 (1983); **78**, 177 (1983).

Can. J. Chem. Downloaded from www.nrcresearchpress.com by 194.225.253.170 on 09/07/12
For personal use only.

The isolation, structure, and stereochemistry of traversiadiene. The precursor hydrocarbon of traversianal biosynthesis[1]

ALBERT STOESSL AND G. L. ROCK
Agriculture Canada, London Research Centre, London, Ont., Canada N6G 2V4

AND

J. B. STOTHERS
Department of Chemistry, The University of Western Ontario, London, Ont., Canada N6A 5B7

Received February 27, 1989

ALBERT STOESSL, G. L. ROCK, and J. B. STOTHERS. Can. J. Chem. **67**, 1302 (1989).

A tricyclic diene, traversiadiene, isolated from cultures of *Cercospora traversiana* has been shown to have the structure and stereochemistry of the previously postulated hydrocarbon intermediate on the biosynthetic pathway to traversianal (**1**). Detailed ^1H and ^{13}C magnetic resonance studies, including homo- and heteronuclear correlation spectra, led to the gross structure, and the stereochemistry was established through a series of nuclear Overhauser effect difference spectra.

Key words: diterpene, traversiadiene, ^1H and ^{13}C magnetic resonance spectra.

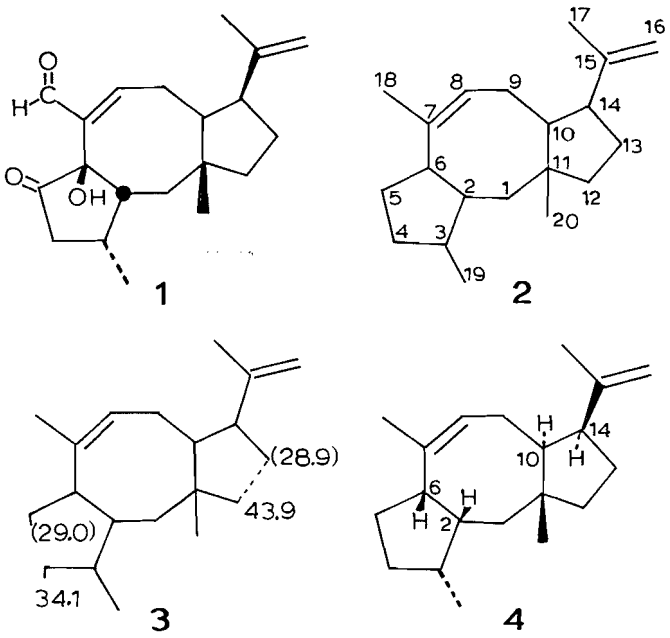
ALBERT STOESSL, G. L. ROCK et J. B. STOTHERS. Can. J. Chem. **67**, 1302 (1989).

On a démontré qu'un diène tricyclique, le traversiadiène, isolé de cultures de *Cercospora traversiana* possède la structure et la stéréochimie de l'hydrocarbure intermédiaire dont la présence sur le chemin biogénétique allant au traversianal (**1**) avait été postulée antérieurement. Des études détaillées de résonance magnétique nucléaire du ^1H et du ^{13}C, comportant des spectres de corrélation homonucléaire et hétéronucléaire, ont été utilisées pour déterminer la structure; pour établir la stéréochimie, on a fait appel à une série de spectres permettant d'évaluer la différence d'effet Overhauser nucléaire.

Mots clés : diterpène, traversiadiène, spectres de résonance magnétique du ^1H et du ^{13}C.

[Traduit par la revue]

Traversianal (**1**), a novel tricyclic diterpenoid aldehyde, recently isolated as a fungal metabolite of *Cercospora traversiana*, has been fully characterized (1). In the course of the study, the probable biosynthetic origin of the aldehyde was found to be similar to that demonstrated by other workers for several ophiobolins but, nevertheless, to differ therefrom in an important stereochemical feature and its consequences. A tricyclic diene was proposed as the likely hydrocarbon precursor of **1** (Scheme 1). A careful chromatographic search of the extracts of the fungal cultures for related metabolites has now led to the isolation of a diene, which in fact has the proposed structure **2** and has been named traversiadiene. Its structure and stereochemistry have been established through a series of nmr experiments which we wish to report in this paper.



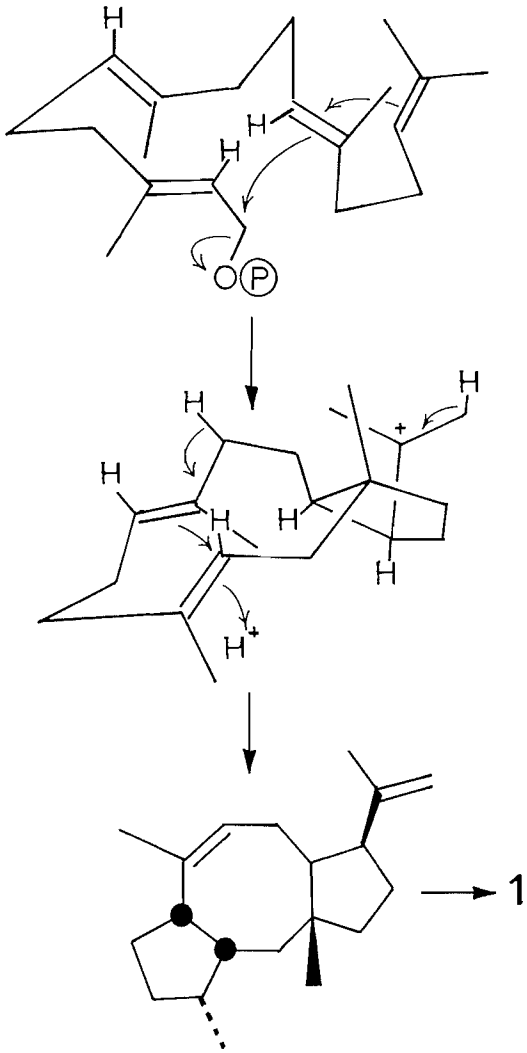
Mother liquors from which traversianal had separated were carefully chromatographed over silica to yield **2**, which was readily purified by recrystallization. The compound showed end absorption in the uv spectrum, and the ^1Hmr spectrum indicated the presence of one trisubstituted double bond (δ 5.51, 1H) and a terminal olefinic methylene group (δ 4.65, 4.73). Its constitution as a diterpenoid tricyclic diene was confirmed from a precise mass measurement giving its molecular formula as $C_{20}H_{32}$. Other readily discernible features in the proton spectrum included signals for four methyl groups: a doublet, δ 0.80 (J = 7.1 Hz), a broadened singlet, δ 0.97, and two olefinic methyls, δ 1.67 (dd, J = 0.7 and 1.4 Hz) and δ 1.71 (bd, $J \sim 1.4$ Hz), and five separately resolved one-proton multiplets, three having identical patterns to three multiplets in the ^1H spectrum of **1**. The ^{13}Cmr spectrum contained 20 signals including those for four methyl, six methylene, five methine, and a quaternary carbon in addition to those for a terminal and a trisubstituted double bond. All of these data are quite compatible with structure **2** for this diene and confirmation was sought through a series of correlation experiments.

Initially, the individual ^{13}C signals were correlated with specific ^1H patterns through a heteronuclear ^{13}C–^1H COSY experiment which (a) readily matched the methyl signals, (b) revealed that three of the five resolved multiplets noted above arise from methine protons while the other two arise from an individual methylene group, and (c) gave the approximate positions of the remaining methylene and methine patterns. The spectrum obtained from a homonuclear ^1H COSY experiment showed that the terminal olefinic protons, H-16, δ 4.65 and 4.73, are coupled to the olefinic 15-methyl protons, δ 1.67 (δ_C 23.0), and that at δ 4.65 is also coupled to the 14-methine

[1]Part 141 of ^{13}Cmr studies; for Part 140 see ref. 6; for Part 139 see ref. 7.

Can. J. Chem. Downloaded from www.nrcresearchpress.com by 194.225.253.170 on 09/07/12
For personal use only.

Can. J. Chem. Downloaded from www.nrcresearchpress.com by 194.225.253.170 on 09/07/12
For personal use only.



SCHEME 1

proton at δ 2.92 (δ_C 51.0). The latter is coupled to a pair of methylene protons, H-13, near 1.65 and 1.80 ($\delta_C \sim 29$) and to a methine proton, H-10, near 1.60 ppm (δ_C 56.2). Thus, the diene contains an isopropenyl group bonded to a methine centre, which in turn is bonded to another methine and a methylene group. The individual shieldings of these nine protons and six carbons are very similar to the data previously determined for this fragment in **1**. The lone olefinic proton, H-8, at δ 5.51 was clearly coupled to the 18-methyl group at δ 1.71 (δ_C 22.0), the 9-methylene protons at δ 1.8, 2.1 (δ_C 24.3), and the 6-methine proton at δ 3.02 (δ_C 42.4). The lower field methylene proton (2.1) appeared to be coupled to the 10-methine proton at δ 1.6. The H-6, δ 3.02, multiplet, a broadened "triplet", was found to be also coupled with the 2-methine absorption at δ 2.26 (δ_C 46.5) and the 5-methylene group near 1.65 and 1.85 ppm ($\delta_C \sim 29$). The δ 2.26 methine proton, H-2, is coupled to the remaining 3-methine pattern near δ 2.15 and the only clearly resolved methylene proton multiplets in the spectrum, δ 1.17 and 1.49, H-1, appearing as the AB part of an ABX pattern, $J_{AB} = 13.6$, $J_{AX} = 12.8$, $J_{BX} = 3.6$ Hz. The lack of additional resolvable coupling indicates that this methylene group is bonded to the quaternary centre, δ_C 44.3. The fifth methine proton, δ_C 2.15, H-3, is that coupled to the 19-methyl group at 0.80 (δ_C 18.7). These methyl protons were shown to be vicinally coupled to the 2-methine carbon at δ_C 46.5 (δ_H 2.26)

TABLE 1. ^{1}H and ^{13}C magnetic resonance data for **2**[a]

1α	1.17 (13.6, 12.8)		39.9	
β	1.49 (13.6, 3.6)			
2	2.26 (12.8, 7.8, 7.8, 3.6)		46.5	
3	2.1_5		36.5	
4	1.3_5, 2.0_5		34.1	
5	1.6_5, 1.8_5		29.0[b]	
6	3.02 (b "t")		42.4	
7	—		136.3	
8	5.51 (8.0, 8.0, 1.4, 1.4)		129.9	
9	1.8_3, 2.1_3		24.3	[25.2]
10	1.6	[1.84]	56.2	[54.9]
11	—	—	44.3	[44.4]
12	1.3, 1.4	[1.45]	43.9	[44.0]
13	1.6_5, 1.8_0	[~1.7]	28.9[b]	[28.5]
14	2.92 (b "dt")	[3.03]	51.0	[51.2]
15	—	—	149.3	[148.3]
16	4.65 (2.6, 0.7, 0.7)	[4.72]	112.6	[113.8]
	4.73 (2.6, 1.4)	[4.80]		
17	1.674 (1.4, 0.7)	[1.71]	23.0	[22.6]
18	1.707 (1.4)		22.0	
19	0.804 (7.1)	[0.78]	18.7	[17.0]
20	0.970	[1.16]	19.1	[18.5]

[a]Shieldings in ppm from internal TMS in CD_2Cl_2 solution; ^{1}H–^{1}H couplings in Hz listed in parentheses. The corresponding shielding data for several positions in **1** are included, in square brackets, for comparative purposes.

[b]These two values may be interchanged.

and the 4-methylene carbon at δ_C 34.1 through a long range heteronuclear ^{13}C–^{1}H correlation experiment utilizing the XCORFE sequence (2). This spectrum also revealed vicinal coupling of the angular methyl protons, H-20, at δ 0.97 (δ_C 19.1) with the 10-methine carbon at δ_C 56.2 and the methylene carbons at δ_C 39.9 and 43.9 (C-1 and -12), as well as geminal coupling with the quaternary carbon, δ_C 44.3. A complete tabulation of the ^{1}H and ^{13}C results is given in Table 1, in which are included some of the shielding data for **1**, for comparison. The results for **2** lead directly to fragment **3**, for which the ^{13}C shieldings for the "end" groups are indicated. While the completion of the structure requires two linkages between these four "end" groups, only structure **2** could arise from geranylgeranyl pyrophosphate with no carbon–carbon rearrangement during the biosynthesis, as has been established for **1** (1). The dashed linkage in **3** follows from comparison of the shieldings for C-9 through C-17 in the two compounds (see Table 1), providing support for the proposed structure **2** for the diene.

To obtain further evidence bearing on the relative disposition of some of the nuclei in the diene a series of nuclear Overhauser effect (nOe) experiments was carried out. Saturation of the angular methyl protons at δ 0.97 enhanced the methine absorptions at δ 2.26 and 3.02 (H-2 and -6, respectively) as well as the methylene pattern at δ 2.13 (H-9). Irradiation of the olefinic proton, δ 5.51, enhanced the second 9-methylene proton at δ 1.83. Enhancement of the δ 2.13 proton was also observed upon saturation of H-6 (δ 3.02), which also increased the intensity of H-2 absorption (δ 2.26). Saturation of the latter pattern enhanced the absorptions for H-6, the angular methyl, the 9-proton at δ 2.13, and H-1 at δ 1.49. Consequently, we could conclude that these nuclei are on the same side of the molecule. Irradiation of the other 1-methylene proton (δ 1.17) enhanced the pattern for its partner, δ 1.49, and the methine absorption, a broadened triplet, δ 1.60, due to H-10. This

pattern was also enhanced by irradiation of the methine proton at δ 2.92, H-14, which, in addition, increased the intensity of the olefinic methylene proton at δ 4.65. The latter observation indicates this to be the proton *trans* with respect to the olefinic methyl group, δ 1.67, δ_C 23.0. Saturation of the methyl doublet, δ 0.80, led to enhancement of the patterns for H-3, δ 2.15, and those for the 1-methylene protons, H-1. These results are exactly analogous to our findings for **1** with the added feature of the stereochemistry at C-5 (see **4**). Since **1** bears a hydroxyl group at this position, its orientation was not established, but models indicated that a *cis* junction of the cyclopentanoid ring at C-2 and -6 is the more favorable. For diene **2**, the nOe results clearly show that H-2 and -6 are *cis* with respect to each other *and* the angular methyl group, while the secondary methyl group, H-10 and -14, is on the opposite side of the molecule as depicted in **4**.

Another compound obtained from one of the chromatographic fractions was identified as brassicasterol by direct comparison with specimens, both from *C. arachidicola* (3) and *Taphrina deformans* (4). We have also isolated the same sterol from *C. kikuchii*. The isolation from three *Cercospora* spp. suggests that it may be a frequent metabolite of this genus. The common occurrence of the compound in several families of the *Ascomycotina* has been discussed by Weete *et al.* (5).

Experimental

General procedures and routine instrumentation were employed as previously described (1). Cultures of *Cercospora traversiana* were grown on potato-dextrose agar in 92 Petri dishes and extracted as before after 16 days' growth. The mother liquors from which crude traversianal (**1**, 43 mg) had separated were chromatographed over SiO_2 (Camag DFO, 100 g), impregnated by slurrying with tartaric acid (7.5% in MeOH), filtering, and drying, first at room temperature, finally at 110°C for 1.5 h) with $EtOAc/C_6H_5Me$ (5:95 v/v; 10-mL fractions). Pure traversiadiene (18 mg) was obtained from fractions 13–15 by evaporation, trituration with MeOH, and two recrystallizations from $MeOH/CH_2Cl_2/$, mp 70–72°C; $[\alpha]_D^{24}$ +6° (*c* 1.0, CCl_4); ir (CCl_4): 3107 (w), 3069, 2948, 2874, 1635 (m), 1453, 1380, 892; ^1H and ^{13}Cmr: see Table 1; ms *m/e*: 272 (M^+), 257, 229, 215, 189, 175, 161, 149, 148, 147, 135, 121, 109, 107 (100). *Exact Mass* calcd. for $C_{20}H_{32}$: 272.2504; found: 272.2501.

Another 10 mg of good quality traversiadiene was obtained by sublimation (35°C, ca. 0.7 Torr (1 Torr = 133.3 Pa)) of the trituration and recrystallization mother liquors.

The nmr spectra were recorded with a Varian XL-300 system using a 9-mg sample of **2** in CD_2Cl_2 solution. The $^1H-^1H$ coupling interactions were identified by a homonuclear correlation (COSY) spectrum using the HOMCOR pulse sequence of the XL software. The spectrum was obtained with a 1024 × 512 data point matrix transforming 1024 points in both F_1 and F_2 with pseudo echo processing and a 1650-Hz spectral width in both domains. A series of nOe difference spectra were recorded with a spectral width of 1650 Hz, 90° pulses, a 2-s acquisition time, and a 17% duty cycle. A total of seven 16-transient blocks, each with 8 steady-state pulse cycles, was collected at 10 frequencies, one of which was 5000 Hz off-resonance. Subtraction of the latter free-induction decay (fid) from each of the nine fids containing a saturated absorption before 32 K transformation gave the required difference spectra. The ^{13}Cmr spectra were obtained at 75.4 MHz and the protonation level for each carbon signal was determined by recording the APT spectrum. Specific assignments of the protonated carbon signals were obtained by heteronuclear correlation with the proton spectrum using the HETCOR sequence of the XL software. The $^{13}C-^1H$ correlation spectrum utilized a 2048 × 128 data matrix with a 10-kHz spectral width for ^{13}C and a 1.6-kHz width for ^1H, transforming 2048 and 512 points, respectively, with modest (1 Hz) line broadening. Two- and three-bond carbon–hydrogen correlations for the methyl protons were revealed through an experiment utilizing the XCORFE sequence (2). This spectrum was obtained with a 1024 × 220 data matrix, 3000-Hz spectral width for ^{13}C, 1000 Hz for ^1H, and transforming 2048 and 512 points, respectively, after pseudo-echo processing.

Acknowledgements

We are grateful to Prof. J. D. Weete for a generous gift of brassicasterol and to S. Wilson, V. Richardson, and D. Hairsine for technical assistance. We thank the Natural Sciences and Engineering Research Council of Canada for financial support.

1. A. Stoessl, G. L. Rock, J. B. Stothers, and R. C. Zimmer. Can. J. Chem. **66**, 1084 (1988).
2. W. F. Reynolds, D. W. Hughes, M. Perpick-Dumont, and R. G. Enriquez. J. Magn. Reson. **63**, 413 (1985).
3. A. Stoessl. Can. J. Microbiol. **31**, 129 (1985).
4. J. D. Weete, M. Sancholle, and C. Montant. Biochim. Biophys. Acta, **752**, 19 (1983).
5. J. D. Weete, M. Kulifaj, C. Montant, W. R. Nes, and M. Sancholle. Can. J. Microbiol. **31**, 1127 (1985).
6. A. Stoessl, Z. Abramowski, H. H. Lester, G. L. Rock, J. B. Stothers, G. H. N. Towers, and R. C. Zimmer. *In* Biotechnology for crop protection. *Edited by* P. A. Hedin, J. J. Menn, and R. M. Hollingsworth. ACS Symp. Ser. 379, Washington, DC. 1988. pp. 94–109.
7. A. N. Starratt, E. W. B. Ward, and J. B. Stothers. Can. J. Chem. **67**, 417 (1989).

Can. J. Chem. Downloaded from www.nrcresearchpress.com by 194.225.253.170 on 09/07/12
For personal use only.

Kinetics and mechanisms of the reaction of chromium(III) and 2,4-hexanedione in aqueous solution

CARLOS BLANCO, JOSÉ M. HERNANDO, AND MANUEL MATEO
Departamento de Química Física, Facultad de Ciencias, Universidad de Valladolid, Valladolid, Spain

Received July 12, 1988[1]

CARLOS BLANCO, JOSÉ M. HERNANDO, and MANUEL MATEO. Can. J. Chem. **67**, 1305 (1989).

The kinetics and mechanism of the reaction between Cr(III) and 2,4-hexanedione in aqueous solution have been studied. Complexation occurs by coordination of both oxygen atoms of the ligand to the chromium(III) center, with concomitant loss of a proton yielding 1:1 complex of the type $[Cr(CH_3COCHCOC_2H_5)(H_2O)_4]^{2+}$. When the metal ion is in pseudo first-order excess the concentration dependence of the observed rate constants agrees with a mechanism involving reversible reaction between the enol tautomer of 2,4-hexanedione and the metallic species $Cr(H_2O)_6^{3+}$ and $Cr(H_2O)_5OH^{2+}$, with rate constants of 8.0×10^{-4} and 3.5×10^{-2} dm^3 mol^{-1} s^{-1}, respectively.

Key words: chromium(III), β-diketones, β-diketonates, kinetics, complexation.

CARLOS BLANCO, JOSÉ M. HERNANDO et MANUEL MATEO. Can. J. Chem. **67**, 1305 (1989).

La cinétique et le mécanisme de la réaction de la 2,4-hexanedione avec le Cr(III) en solution aqueuse ont été étudiés. La complexation se produit par la coordination de tous deux atomes d'oxygène du ligand avec le chrome(III), avec une perte simultanée d'un proton pour produire le complexe 1:1 du type $[Cr(CH_3COCHCOC_2H_5)(H_2O)_4]^{2+}$. Quand l'ion métallique se trouve en pseudo premier-ordre excès, l'influence de la concentration sur la constante de vitesse observée s'accorde avec une mécanisme réversible selon lequel le tautomére énol réactionne avec les espèces $Cr(H_2O)_6^{3+}$ and $Cr(H_2O)_5OH^{2+}$. Les constantes de vitesse qui correspondent à ces réactions ont pour valeur $8{,}0 \times 10^{-4}$ et $3{,}5 \times 10^{-2}$ dm^3 mol^{-1} s^{-1}, respectivement.

Mots clés : chromo(III), β-dicétones, β-dicétonates, cinétique, complexation.

Introduction

In recent years a number of papers dealing with the kinetics and mechanisms of the reactions of metal and oxometal ions with β-diketones have appeared in the literature (1–6).

Chromium(III) complexes have been less well studied than the Cu(II), Co(II), Ni(II), or Fe(III) systems which are classified as "labile" metal ions. The particularly interesting feature of chromium(III) chemistry is that the complex-formation reactions from hexaaquachromium(III) or its monohydroxy species are very slow. Substitution at chromium(III) centres has received attention (7) because of the possibility of A (or I_a) (8) associative mechanisms for the d^3 electronic configuration.

We have studied the reaction of chromium(III) with 2,4-hexanedione in the pH region 2.0–3.0 at temperatures typically used for chromium kinetics work (50°C) and ionic strength I = 0.5 mol dm^{-3}.

The aim of the present work is the elucidation of the mechanism and the rate of 1:1 complex formation in aqueous solution by measuring the chemical reaction rate using a spectrophotometric method.

Experimental

The solutions of Cr(III) were prepared from Aldrich reagent grade $Cr(NO_3)_3.9H_2O$, and they were standardized by oxidizing the chromium(III) to chromium(VI). 2,4-Hexanedione (propionylacetone, PAH) obtained as Kodak reagent grade, was freshly distilled prior to use. Unless otherwise indicated, all materials were of reagent grade (Merck) and were used without further purification. The ionic strength of all solutions was adjusted to 0.5 mol dm^{-3} using $HClO_4$–$NaClO_4$ solutions. Spectra were recorded on a Spectronic 1201 UV-visible spectrophotometer and the kinetic data were obtained by following the absorbance increase in the vicinity of 327 nm using a kinetic programme. pH measurements were made with a Crison 501 pH-meter equipped with an Ingold combined glass-and-reference electrode.

[1]Revision received April 3, 1989.

Results

Tautomerization equilibrium

The keto–enol tautomerization equilibrium of 2,4-hexanedione may be represented by reaction [1] where PAH_k and PAH_e represent the keto and enol tautomers, respectively.

$$[1] \quad PAH_k \underset{k_f}{\overset{k_e}{\rightleftharpoons}} PAH_e$$

The enolization rates of β-diketones (k_e) are measured by a bromination procedure (2). Usually, the enol tautomer and any enolate ion present react rapidly with bromine added. To maintain equilibrium some of the keto tautomer converts to the enol tautomer which then reacts with bromine; hence the rate of enolization parallels the rate of bromination. Therefore

$$[2] \quad -d[Br_2]/dt = -d[PAH_k]/dt = k_e[PAH_k]$$

$$[3] \quad [Br_2] = A/\epsilon \quad \text{and} \quad [PAH_k] = (A/\epsilon + a - b)$$

where A is the optical density at time t due to the absorbance of bromine, ϵ is the molar absorptivity of bromine in a cell of 1 cm path length, a is the total concentration of β-diketone, and b is the total concentration of bromine. Making the appropriate substitution in eqs. [2] and [3], we obtain [4]

$$[4] \quad -\ln (A/\epsilon + a - b) = k_e t + C$$

where C is a constant.

A plot of the left-hand side of eq. [4] against time gives a straight line of slope k_e, the rate of enolization of the β-diketone.

Since $[PAH] = [PAH_k] + [PAH_e]$, from intercepts obtained in eq. [4] the 2,4-hexanedione enol fraction $y = [PAH_e]/[PAH]$ has been determined equal to 0.16 at 20°C. This result is in agreement with literature values (9, 10).

Stability constant of complex

The composition of the complex that chromium(III) forms

Can. J. Chem. Downloaded from www.nrcresearchpress.com by 194.225.253.170 on 09/07/12
For personal use only.

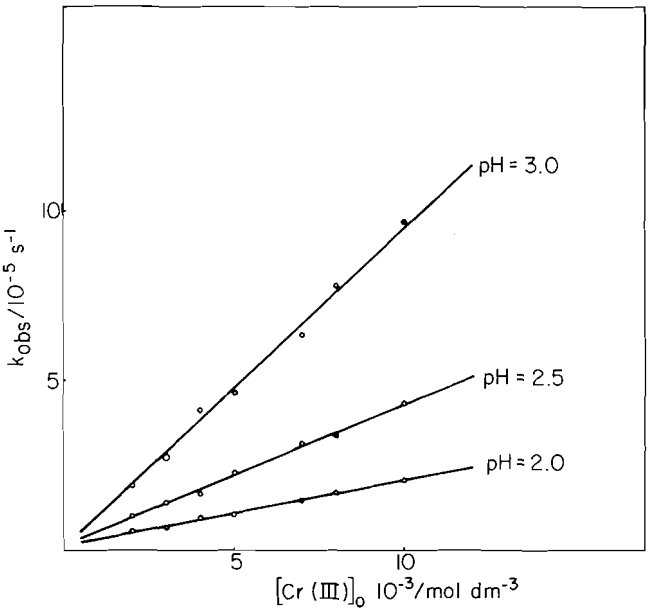


FIG. 1. k_{obs} as a function of the total concentration of chromium(III) at 50°C and ionic strength 0.5 M ($NaClO_4$). [PAH] = 1.0×10^{-4} M.

with 2,4-hexanedione in aqueous solution has been investigated spectrophotometrically using the Job (11) and Yoe–Jones (12) methods. The pH range was low enough to prevent hydrolysis products other than $Cr(H_2O)_5OH^{2+}$ and the ionic strength was kept at a constant value with $HClO_4/NaClO_4$ buffer solutions. The results from both methods agree on a 1:1 stoichiometry (13).

Although the complex ion which will be studied in this work is $Cr(H_2O)_4PA^{2+}$, for the sake of simplicity, the solvent molecules will not be written, so the stability constant of $CrPA^{2+}$ complex can be written as,

$$K = \frac{[CrPA^{2+}]}{[Cr(III)][PA^-]}$$

The direct determination of this equilibrium constant is rather complicated because several competing reactions can take place which can affect the extent the complex formation. This is quantitatively expressed by the conditional constants:

$$[5] \quad K' = \frac{[CrPA^{2+}]}{[Cr'][PA^{-\prime}]}$$

where [Cr'] and [$PA^{-\prime}$] are the total concentration of chromium and the total concentration of ligand that does not form the complex, respectively (14). The stability constant can be connected with the conditional constant by

$$[6] \quad K = K'\left\{1 + \frac{K_1}{[H^+]} + \frac{K_2}{[H^+]^2} + 2\frac{K_3[Cr^{3+}]}{[H^+]^2}\right\}\left\{1 + \frac{[H^+]}{K_I}\right\}$$

where K_1, K_2, and K_3 are the hydrolysis constants of Cr^{3+} to form $Cr(OH)^{2+}$, $Cr(OH)_2^+$, and $Cr_2(OH)_2^{4+}$, which are known from the literature (14, 15) amount to $10^{-4.0}$, $10^{-9.7}$, and $10^{-2.4}$, respectively, at 20°C.

The ionization constant of the ligand, $K_I = 10^{-9.40}$ has been determined in our previous paper (16).

K' can be determined from absorption values at the stoichiometric point according to Job's method in the same way as in a previous paper (17). When data range from 1.00×10^{-1} to 1.00×10^{-3} M acid, $K = 9.6\ (\pm 0.8) \times 10^{10}$ mol^{-1} dm^3.

Kinetic measurements

The reaction of Cr(III) with PAH was carried out with the metal ion concentration in excess over the ligand, at the hydrogen ion concentration 0.01–0.001 M. If the complex stability constant value is taken into account, only the propionylacetonatechromium(III) ($CrPA^{2+}$) ion is formed quantitatively under our experimental conditions. The pseudo first-order rate constants were obtained from plots of ln ($A_\infty - A$) against time, where A_∞ is the complex absorption when the reaction is over.

To study the influence of the Cr(III) concentration on k_{obs}, several series of experiments with constant [PAH], pH, ionic strength, and temperature were performed. It was evaluated by plotting k_{obs} against [Cr(III)], yielding a linear correlation (Fig. 1).

Discussion

Taking into consideration the 2,4-hexanedione tautomeric equilibrium, the mechanism that we have considered is presented in Scheme 1 (coordinated H_2O is omitted for clarity), it is consistent with the assumption that the formation of $CrPA^{2+}$ proceeds via two paths, one involving the reaction of Cr^{3+} with the enol tautomer of PAH, (PAH_e), and the other involving the reaction of $CrOH^{2+}$ with (PAH_e).

[I] $Cr^{3+} \overset{K_h}{\rightleftharpoons} CrOH^{2+} + H^+$

[II] $Cr^{3+} + PAH_e \underset{k_{-1}}{\overset{k_1}{\rightleftharpoons}} CrPA^{2+} + H^+$

[III] $CrOH^{2+} + PAH_e \underset{k_{-2}}{\overset{k_2}{\rightleftharpoons}} CrPA^{2+}$

[IV] $PAH_k \underset{k_f}{\overset{k_e}{\rightleftharpoons}} PAH_e$

SCHEME 1

The rate of formation of $CrPA^{2+}$ is then given by

$$\frac{d[CrPA^{2+}]}{dt} = k_1[Cr^{3+}][PAH_e] - k_{-1}[CrPA^{2+}][H^+] + k_2[CrOH^{2+}][PAH_e] - k_{-2}[CrPA^{2+}]$$

Substituting the enol fraction $y = [PAH_e]/[PAH]$, then

$$[8] \quad \frac{d[CrPA^{2+}]}{dt} = -(k_{-1}[H^+] + k_{-2})[CrPA^{2+}] + \left(k_1 y + \frac{k_2 K_h y}{[H^+]}\right)[Cr^{3+}][PAH]$$

Moreover

$$[CrPA^{2+}] = [PAH]_0 - [PAH]$$

and

$$\frac{d[CrPA^{2+}]}{dt} = -\frac{d[PAH]}{dt}$$

Therefore

Can. J. Chem. Downloaded from www.nrcresearchpress.com by 194.225.253.170 on 09/07/12
For personal use only.

$$[9] \quad -\frac{d[PAH]}{dt} = -(k_{-1}[H^+] + k_{-2})[PAH]_0 + (k_{-1}[H^+] + k_{-2})[PAH] + \left(k_1 y + \frac{k_2 K_h y}{[H^+]}\right)[Cr^{3+}][PAH]$$

Integrating this equation and considering the conditions used in this investigation, we get

$$[10] \quad \ln \frac{[PAH]_0 - [CrPA^{2+}]}{[PAH]_0} = -\left\{(k_{-1}[H^+] + k_{-2}) + \left(k_1 y + \frac{k_2 K_h y}{[H^+]}\right)[Cr^{3+}]\right\} t$$

if we consider $[PAH]_0 = [CrPA^{2+}]_\infty$

$$[11] \quad \ln (A_\infty - A) = \ln A_\infty - \left\{(k_{-1}[H^+] + k_{-2}) + \left(k_1 y + \frac{k_2 K_h y}{[H^+]}\right)[Cr^{3+}]\right\} t$$

where A and A_∞ are the absorbances of the reaction system at t seconds after the start of the reaction and at equilibrium, respectively. Thus the conditional first-order rate constant obtained by experiment is

$$[12] \quad k_{obs} = (k_{-1}[H^+] + k_{-2}) + \left(k_1 y + \frac{k_2 K_h y}{[H^+]}\right)[Cr^{3+}]$$

Since $[Cr(III)]_0 \gg [PAH]$, it follows that

$$[13] \quad [Cr^{3+}] = \frac{[Cr(III)]_0[H^+]}{[H^+] + K_h}$$

where $[Cr(III)]_0$ is the total concentration of chromium(III), thus

$$[14] \quad k_{obs} = \frac{k_1[H^+]}{K_E} + \frac{k_2 K_h}{K_E} + \left(\frac{k_1[H^+]y + k_2 K_h y}{[H^+] + K_h}\right)[Cr(III)]_0$$

where $K_E = k_1/k_{-1}$.

The value of K_h at 50°C was found to be 3.98×10^{-4} (18) while the value of y was found by extrapolation of the data at 50°C, taking into account ref. 10, to be 0.10.

Equation [14] suggests that a plot of k_{obs} against $[Cr(III)]_0$ at a constant acid concentration should be linear.

Consequently, the values of rate constants k_1 and k_2 were determined from the slopes of Fig. 1 plots by the method of least squares: $k_1 = 8.0(\pm 0.1) \times 10^{-4}$ and $k_2 = 3.5(\pm 0.1) \times 10^{-2}$ dm^3 mol^{-1} s^{-1}, respectively. Due to the relatively small value of the intercept and the resulting uncertainty, the kinetic data can not be reliably used to obtain a value of K_E.

The mechanisms of the complex formation reactions of β-diketones have been widely investigated [1]–[6] and the reactivity toward metal ions has been found to be enolate ion > enol tautomer > keto tautomer. In the present investigation the results show that the reaction of PAH with Cr(III) occurs by a mechanism in which the metal ions $[Cr(H_2O)_6]^{3+}$ and $[Cr(H_2O)_5OH]^{2+}$ react with the enol form of the β-diketone.

Although the reactions of chromium(III) with 2,4-pentanedione have been thoroughly studied (19–21), and the rate constants can be predicted on the basis of the Eigen–Wilkins mechanism (22, 23), it is not easy to get clear predictions on Cr(III)–2,4-hexanedione complexation.

The relative inertness of chromium(III) with similar ligands (20, 24), may be the reason for the retarded rates of complex formation, when compared with other β-diketonate systems (1–6). For solvent exchange on chromium(III) in aqueous solution $\Delta H^{\neq} = 109.7$ kJ mol^{-1} while $\Delta S^{\neq} = 1.2$ J K^{-1} mol^{-1} (25). Thus the solvent exchange rate in water is 1.4×10^{-5} s^{-1} at 50°C. It is clear that the rate of formation of the $CrPA^{2+}$ complex is considerably larger than the rate of solvent exchange on the metal ion. It follows that the mechanism must be interchange associative (I_a) which involves association of the enol tautomer with the hexacoordinated chromium(III) in a rate-determining step to give an intermediate of increased coordination number. High pressure solvent exchange studies in Cr(III) and other non-labile metal ions Co(III), Rh(III), and Ir(III) (26–28) are in accord with an associative interchange for Cr(III), Rh(III), and Ir(III), while a dissociative interchange is indicated for Co(III). It has been suggested that I_a mechanisms are the rule for the 3+ ions, Co(III) being the exception due to its small size.

1. D. P. Fay, A. R. Nichols, and N. Sutin. Inorg. Chem. **10**, 2096 (1971).
2. M. R. Jaffe, D. P. Fay, M. Cefola, and N. Sutin. J. Am. Chem. Soc. **93**, 2878 (1971).
3. R. G. Pearson and O. P. Anderson. Inorg. Chem. **9**, 39 (1970).
4. M. J. Hynes and B. D. O'Regan. J. Chem. Soc. Dalton Trans. 7 (1980).
5. I. Ando, K. Yoshizumi, K. Ito, K. Ujimoto, and H. Kurihara. Bull. Chem. Soc. Jpn. **56**, 1368 (1983).
6. M. J. Hynes and M. T. O'Sea. J. Chem. Soc. Dalton Trans. 331 (1983).
7. C. H. Langford. Inorg. Chem. **18**, 3289 (1979).
8. C. H. Langford and H. Gray. Ligand substitution processes. W. A. Benjamin, New York. 1965.
9. M. J. Rumpf and E. D'Incan. Compt. Rend. **244**, 902 (1957).
10. J. P. Calmon, Y. Cazaux-Maraval, and P. Maroni. Bull. Soc. Chim. Fr. 3779 (1968).
11. P. Job. Ann. Chim. **9**, 13 (1928).
12. J. H. Yoe and A. L. Jones. Ind. Eng. Chem. Anal. Ed. **16**, 11 (1944).
13. Y. Pascua. Tesis de Licenciatura, Universidad de Valladolid. 1985.
14. A. Ringbom. Formación de complejos en Química Analítica. *Edited by* S. A. Alhambra. Madrid. 1979.
15. H. Stunzi and W. Marty. Inorg. Chem. **22**, 2145 (1983).
16. J. M. Hernando, C. Blanco, and T. Prieto. Bull. Soc. Chim. Fr. **5**, 775 (1987).
17. J. M. Romero, C. Blanco, and J. Verdú. An. Quím. **77** *b*, 182 (1981).
18. M. A. Abdullah, J. Barret, and P. O'Brian. J. Chem. Soc. Dalton Trans. 1647 (1984).
19. H. Kido and K. Saito. Inorg. Chem. **16**, 397 (1977).
20. H. Kido and K. Saito. J. Am. Chem. Soc. **110**, 3187 (1988).
21. T. Sekine, K. Inaba, and O. Takahashi. Polyhedron, **7**, 781 (1984).
22. R. G. Wilkins. Acc. Chem. Res. **3**, 408 (1970).
23. M. Eigen and R. G. Wilkins. Adv. Chem. Ser. **49**, 55 (1965).
24. C. Blanco and J. M. Hernando. An. Quím. In press.
25. D. R. Stranks and T. W. Swaddle. J. Am. Chem. Soc. **93**, 2783 (1971).
26. T. W. Swaddle. Coord. Chem. Rev. **14**, 217 (1974).
27. D. R. Stranks. Pure Appl. Chem. **38**, 303 (1974).
28. T. Asano and W. J. Lenobel. Chem. Rev. 407 (1978).

Can. J. Chem. Downloaded from www.nrcresearchpress.com by 194.225.253.170 on 09/07/12
For personal use only.

Direct synthesis of indenones from alkenyliron complexes

IAN R. BUTLER,[1] JOANNE E. ELLIOTT, AND JEAN HOUDE JR.
The Chemistry Department, The University of Ottawa, Ottawa, Ont., Canada K1N 9B5

Received January 2, 1989

IAN R. BUTLER, JOANNE E. ELLIOTT, and JEAN HOUDE JR. Can. J. Chem. **67**, 1308 (1989).

Alkenyliron complexes have been prepared by the metathesis of dicarbonyl(η^5-cyclopentadienyl)iodoiron with aryl-substituted alkenyllithiums. Thermolysis of the product alkenyliron complexes leads to the formation of indenones in good yields.

Key words: alkenyliron, carbonyl, indenone, insertion, metallation, synthesis.

IAN R. BUTLER, JOANNE E. ELLIOTT et JEAN HOUDE JR. Can. J. Chem. **67**, 1308 (1989).

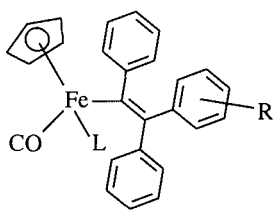
On a préparé des complexes d'alcénylfer par la réaction de métathèse du dicarbonyl(η^5-cyclopentadiényl)iodofer avec des alcénylllithiens substitués par des groupements aryles. La thermolyse des complexes alcénylfer conduit à la formation d'indénones, avec de bons rendements.

Mots clés : alcénylfer, carbonyl, indénone, insertion, métallation, synthèse.

[Traduit par la revue]

Introduction

A recent communication described the thermal reactions of Fp—Ar (Fp = dicarbonyl-(η^5-cyclopentadienyl)iron), Ar = Aryl or Aroyl with diarylacetylenes to give 2,3-disubstituted indenones (1). However, the indenone yields are fairly low, typically 10–40%, since a number of byproducts such as aryl and 1,1′-diarylferrocenes, Fp_2, and hexa-arylbenzenes (from acetylene trimerization) are also obtained.[2] A tentative mechanism for indenone formation was proposed which included alkenyliron derivatives, **1**, as possible key intermediates in the



1 L = acetylene or CO, R = 4-methyl, 2-fluoro, 2-chloro, 3-fluoro

synthesis. This intermediate is the product of diarylacetylene insertion into the metal–aryl bond. In an effort to improve the efficiency of the indenone synthesis it was decided to prepare some related alkenyliron complexes independently to use as alternate synthons to the iron–aryl precursors.

The reaction of 2 molar equivalents of aryllithium with diphenylacetylene (2) in the presence of tetramethylethylenediamine (TMED), followed by metathesis with organometallic titanium halides has been used by Rausch and co-workers (3) to prepare a series of metallocycles. We decided to approach the synthesis of iron–alkenyl compounds using a similar method, since the starting reagents are all commercially available or relatively easy to synthesize. We were, however, interested in the utilization of monolithioalkene derivatives instead of the 1,4-dilithioarylalkenes which had previously been used.

[1]Author to whom correspondence should be addressed.

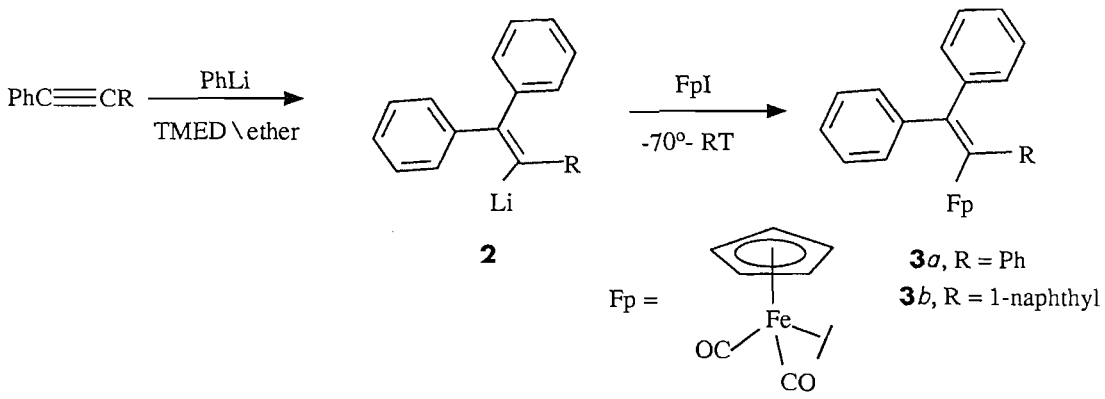
[2]We have carried out a detailed investigation into the reaction mechanism using deuterium labelling studies, and have examined the reactions of acetylenes with a variety of substrates such as Fp—2-thienyl, Fp—naphthyls, and Fp—*p*-tolyl.

Results and discussion

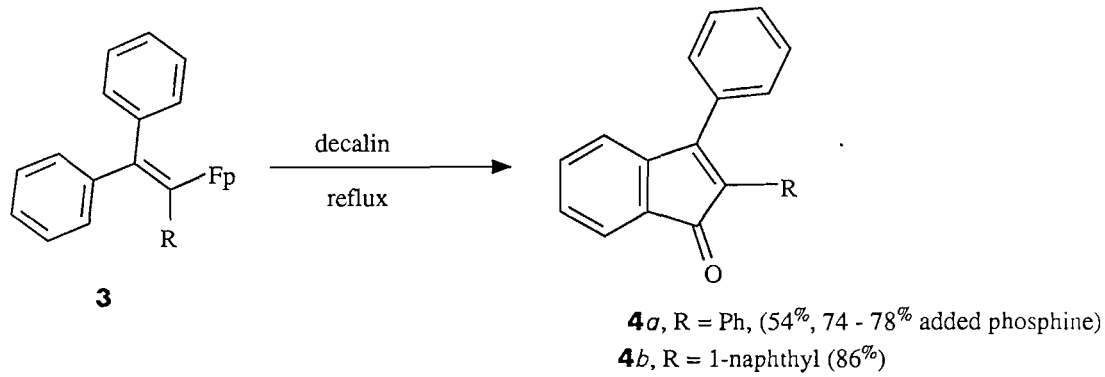
The ambient temperature reaction of phenyllithium with either diphenylacetylene or 1-naphthyl(phenyl)acetylene in the presence of TMED (24 h) in diethyl ether followed by metathesis with FpI at low temperature gave the alkenyliron compounds **3** (Scheme 1), isolated under an inert atmosphere following column chromatography on neutral alumina. In the case of **3*b*** where there are two possible isomers, preliminary tlc and mass spectroscopic studies of the reaction mixture indicated that both were present. However only one was obtained on crystallization of the mixed product solution following chromatography. Compound **3*b***, thus obtained, is the product from lithiation of 1-naphthyl(phenyl)acetylene to give the least sterically hindered alkenyllithium intermediate. The ^{1}H nmr spectra of **3*a*** and **3*b*** exhibit cyclopentadienyl resonances at 4.53 δ and 4.48 δ, respectively. The ^{13}C nmr spectra ($CDCl_3$) are as anticipated with the cyclopentadienyl ring carbon chemical shifts at 84.2 and 85.9 ppm, respectively. Interestingly **3*b*** exhibits two closely situated (215.1 and 214.8 ppm) resonances for the terminal carbonyl groups. There is no evidence for doubling of any of the other resonances. This is presumably due to restricted rotation, due to the presence of the bulky 1-naphthyl group on the α-carbon of the coordinated alkene. In the electron impact mass spectra these compounds either do not show parent ions or exhibit only weak parent ions: as expected intense peaks are observed corresponding to the loss of two carbonyl groups in each case. In the case of **3*b*** the most intense peak is observed at *m/e* 306 corresponding to the 1,1-diphenyl-2-(1′-naphthyl)ethylene fragment formed by cleavage of the organo-iron fragment and its replacement by a proton.

Heating **3** in decalin at reflux for 10 min under N_2 gave the desired indenones, **4**, in clean, relatively high yielding reactions (Scheme 2). The separation and isolation of the coloured indenones is readily achieved by column chromatography on a short alumina column. Indenone **4*a*** was identified by spectral comparison with an authentic sample and **4*b*** was characterized by a melting point comparison using the literature data, mass spectroscopy, and 2D-^{1}H nmr spectroscopy. A similar reaction of **3*a*** in refluxing xylenes (3 h) or refluxing toluene (5 h) in the presence of a molar equivalent of triphenylphosphine also gave **4*a*** in 74% and 78% yields, respectively.

Can. J. Chem. Downloaded from www.nrcresearchpress.com by 194.225.253.170 on 09/07/12
For personal use only.



SCHEME 1



SCHEME 2

It should be noted that related σ-alkenyl derivatives can be prepared from the reaction of nucleophiles with cationic iron acetylene complexes and thus offer an alternate synthesis of the required precursors **3** (4–6). In addition the desired alkenyllithium reagents can be made perhaps more conveniently by metathesis of the appropriate haloalkenyl compound (7), again allowing an alternate route to the required synthons. Such an approach has been successfully used by Cardin and co-workers in the synthesis of alkenyltitanium, chromium, palladium, platinum, and tin derivatives (8, 9).

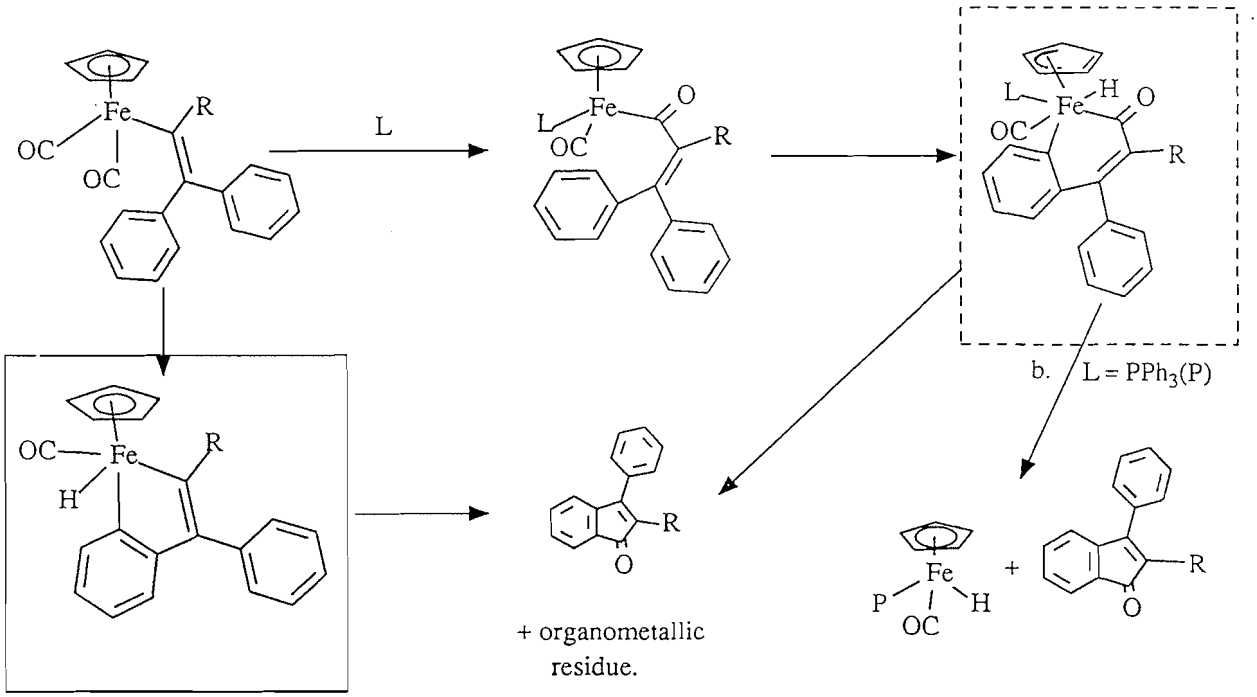
The reaction mechanism for the conversion of **3** to **4** requires the insertion of carbon monoxide into the metal–alkenyl bond. Reger *et al.* (10) have shown that related insertion (alkenyl migration) reactions proceed catalytically in the presence of trace oxidants such as ferricinium or Ce(IV) salts. In the present case trace decomposition may be responsible for the generation of an active catalyst. The reaction mechanism is not clear, however: the intermediate may be a five- or six-membered metallocycle depending on whether or not the carbonyl insertion precedes the aryl metallation. Slippage of the η^5-cyclopentadienyl ring to an η^3- or an η^1-coordination mode in the intermediate may occur to maintain a stable electron configuration around iron. In the presence of triphenylphosphine it might be expected that the monocarbonyl(η^5-cyclopentadienyl)triphenylphosphine(hydrido)iron (11–13) is generated but under the experimental conditions used here the hydride would be unstable and decompose to give a mixture of by-products (Scheme 3*b*). In addition to the indenone small quantities of an unidentified deep green complex containing terminal carbonyl, η^5-cyclopentadienyl, and triphenylphosphine in the ratio 1:1:1 are obtained.

An attempted reaction of phenyllithium with 2-thienylphenylacetylene followed by metathesis with FpI gave **5** as a consequence of preferential lithiation of the thienyl ring (Scheme 4). **5** was obtained following column chromatography (in the dark). It is light-sensitive in solution. Compound **5**, unlike the alkenyliron derivatives, exhibits a clear parent ion in its thermal ionization mass spectrum. The ^{1}H nmr spectrum clearly indicates that only two thienyl proton resonances, J_{H-H} = 2.5 Hz, are present. Heating **5** in refluxing decalin results in the formation of a dark polymeric material, presumably the result of intermolecular reaction of the iron centre with the acetylene.

Experimental section

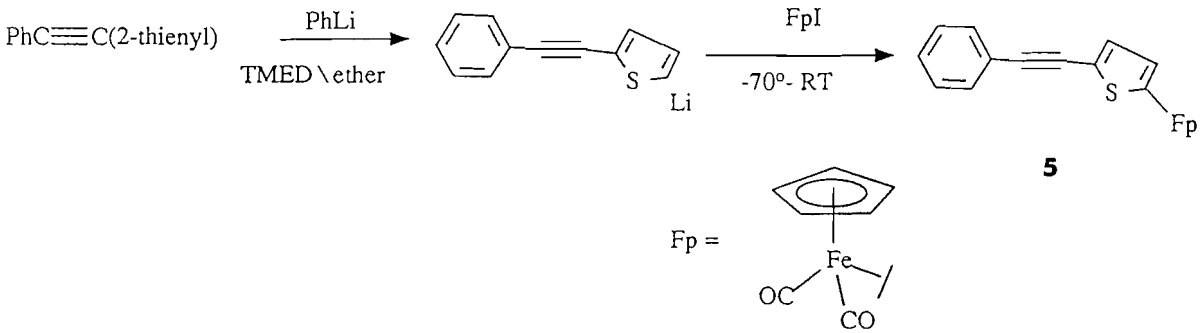
All reactions were performed using conventional Schlenk glassware under an inert atmosphere. Solvents were dried according to standard methods and were distilled prior to use. 1-Naphthyl(phenyl)acetylene was prepared in 96% yield by the palladium catalyzed coupling of phenylacetylene and 1-iodonaphthalene by the adaption of the general procedures of Cassar (14) and Ames and co-workers (15). Nuclear magnetic resonance spectra were recorded using a Varian XL-300 instrument using $CDCl_3$ as sample solvent. Mass spectra were obtained by the electron impact (70 MeV) method on a VG. Analytical 7070E instrument at the University of Ottawa Mass Spectroscopy Centre. Column chromatography was carried out on an activated neutral alumina support starting initially with hexanes as the eluent then using progressively more polar mixtures of hexanes, diethyl ether, and dichloromethane throughout the separations.

Can. J. Chem. Downloaded from www.nrcresearchpress.com by 194.225.253.170 on 09/07/12
For personal use only.



(L = CO or triphenylphosphine)

SCHEME 3



SCHEME 4

Preparation of **3**a

A solution of phenyllithium (10 mL of a 2.5 *M* solution), diphenylacetylene (3.00 g, 16.8 mmol), and TMED (1.95 g, 16.8 mmol) was stirred for 24 h in diethylether (100 mL). The reaction mixture was cooled to ca. −70°C and dicarbonyl(η^5-cyclopentadienyl)iodoiron (7.6 g, 25 mmol) was added. After stirring for 1 h at this temperature the mixture was warmed slowly to room temperature. The volume was reduced under vacuum to a few mL and the resulting oil was chromatographed on a neutral alumina support. The deep yellow product band was collected under nitrogen and was crystallized from a 50/50 mixture of hexane/diethyl ether at −20°C to give **3***a* as yellow–orange nodules (47%).

3*a*: ir (hexane) ν_{CO} = 2023, 1968 cm^{-1}. ^{1}H nmr data ($CDCl_3$), δ, 4.53 (s, 5), 6.77–6.91 (m's, 7), 6.92–7.03 (broad t, 1), 7.18–7.24 (m, 1), 7.29–7.40 (m's, 5). ^{13}C, δ (relative intensity): 84.24 (251); 122.99 (61); 124.36 (51); 125.61 (57); 126.88 (125); 126.93 (151); 127.24 (110); 127.87 (139); 130.36 (137); 131.45 (80); 145.58 (29); 148.73 (25); 151.52 (30); 157.84 (32); 214.66 (60).

Mass spectrum: *m/e* (relative intensity) 432 (0.7); 404 (3.5); 377 (27.3); 376 (81.9); 375 (100); 310 (7.4); 256 (15.0); 255 (12.4); 254 (17.2); 253 (17.4); 252 (19.6); 239 (10.4). *Anal.* calcd. for $C_{27}H_{20}FeO_2$: C 75.02, H 4.66; found: C 75.59, H 4.66.

Preparation of **3**b

The synthesis of **3***b* is identical to that of the above except that diphenylacetylene is replaced by 1-naphthyl(phenyl)acetylene (14). Examination of the reaction mixture by tlc indicated the presence of three yellow bands preceding Fp_2. The first of these was identified as dicarbonyl(η^5-cyclopentadienyl)phenyliron by spectral comparison with an authentic sample. Collection of the latter two bands (mixed isomers 53%, identified individually as such by mass spectroscopy following preparative plate chromatographic separation) followed by crystallization as described above gave **3***b* as yellow/orange needles in 35–40% yield.

3*b*: ir (hexane) ν_{CO} = 2022, 1968 cm^{-1}. ^{1}H nmr data ($CDCl_3$) δ, 4.48 (s, 5); 6.69 (m, 1); 6.74 (t + m, 2); 6.89–6.96 (2m, 3); 7.20 (t, 1); 7.26 (m, 1); 7.31–7.46 (m's, 5); 7.57 (d, 2); 7.65 (d, 1); 8.10 (d, 1). ^{13}C, δ (relative intensity, $CDCl_3$) 85.89 (202); 123.05 (46); 124.84 (57); 124.63 (98); 125.21 (56); 125.27 (20); 126.52 (58); 126.82 (102); 128.14 (123); 128.51 (106); 129.87 (35); 133.57 (37); 142.44 (29); 145.32 (33); 148.58 (31); 152.03 (28); 155.66 (34); 214.76 (24); 215.06 (28).

Mass spectrum: *m/e* (relative intensity) 454 (1.9); $M^{+\cdot}$ − CO; 427 (4.6) $M^{+\cdot}$ − 2CO; 425 (10.3); 360 (11.9); 334 (6.8); 307 (25.7); 306 (100.0); 305 (32.0); 304 (49.4); 303 (20.7); 302 (23.3); 290 (7.4);

Can. J. Chem. Downloaded from www.nrcresearchpress.com by 194.225.253.170 on 09/07/12
For personal use only.

289 (13.2); 229 (33.1); 228 (52.4); 226 (14.3). *Anal.* calcd. for $C_{31}H_{22}FeO_2$: C 77.19, H 4.60; found: C 76.95, H 4.56.

Preparation of indenones

3*a* or **3***b* in decalin were heated to reflux for 10 min. The cooled mixture was chromatographed on a neutral alumina support (length 15 cm, diameter 6 cm). Initial elution with hexanes developed the decalin. Addition of diethyl ether to the eluent results in the collection of the orange indenone band, which is pure as shown by nmr after solvent removal under vacuum. The indenone may be crystallized at −20°C from a mixture of the eluting solvents. **3***a* was characterized by spectral comparison with an authentic sample and **3***b* was characterized as follows: melting point 159°C, lit., 156°C (16) (lit. mp for the other isomer, 2-phenyl-3-(1′-naphthyl)inden-1-one = 180°C). Ultraviolet: λ_{max}(visible) = 428 nm, lit. = 432 nm. The nmr spectrum was identical to that of a product obtained from the reaction of Fp—benzoyl with 1-naphthyl(phenyl)acetylene.[2]

Preparation of **5**

A mixture of 2-thienyl(phenyl)acetylene (1.84 g, 10 mmol), phenyllithium (10 mL of a 2 *M* solution), and TMED (1.16 g, 10 mmol) in diethylether was stirred for 2 days. FpI (6.08 g, 20 mmol) was added to the chilled (−70°C) solution. After warming to room temperature and stirring at this temperature for 2 h the solvent volume was reduced under vacuum to a few mL and the mixture was chromatographed (the column should be wrapped with aluminum foil to exclude light). Collection of the second yellow band (eluting just prior to Fp_2) and solvent removal gave 2.5 g (69%) of **5** initially as a yellow oil, which was then crystallized from a hexanes/diethyl ether mixture to give yellow/brown needles.

5: ir (hexane) ν_{CO} = 2037, 1987 cm^{-1}. ^1H nmr, δ, 4.98 (s, 5) Cp; 6.72 (d, 1); 7.21 (d, 1), thienyls; 7.43–7.46 (2d's, 2), 7.26–7.30 (m's, 3) phenyls. ^{13}C, δ (relative intensity, $CDCl_3$) 83.67 (9); 85.76 (97); 93.69 (7); 123.84 (11); 127.51 (23); 128.11 (46); 128.20 (15); 131.00 (47); 133.58 (21); 138.44 (21); 142.16 (9); 123.72 (17).

Mass spectrum: 361 (5.6); 360 (26.8) $M^{+\cdot}$; 332 (19.1) $M^{+\cdot} - CO$; 305 (18.0); 304 (85.2); 302 (10.7); 249 (21.8); 248 (100.0); 247 (35.5); 246 (13.5); 216 (18.4); 215 (55.3); 202 (11.5); 186 (48.5); 185 (11.3); 184 (72.9). *Anal.* calcd. for $C_{19}H_{12}FeO_2S$: C 63.00, H 3.33; found: C 62.96, H 3.32.

Reaction of **3**a *in the presence of triphenylphosphine*

The reactions were carried out on a 10 mmol scale as described above using toluene (5 h) or xylenes (3 h) replacing decalin and in the presence of a two-fold molar excess of triphenylphosphine. The product indenone was collected by column chromatography as described above (yields 74% and 78%, respectively). The excess triphenylphosphine is eluted with hexanes/diethyl ether prior to product elution. In addition to the product indenone a green band following Fp_2 (trace, faint red/brown band) was eluted with diethyl ether. On solvent removal this product was crystallized from diethyl ether to give green nodules which gave the following spectroscopic data. Mass spectrum: electron impact, *m/e* (relative intensity) 665 (0.8); 345 (0.8); 284 (5.0); 283 (2.1); 263 (20.6); 262 (100.0); chemical ionization: 335 (5.8); 321 (15.3); 285 (14.5); 263 (100.0). mp 180–181°C. ^1H nmr 4.46 (s, 5); 7.36–7.59 (m, 9).

Acknowledgement

The work was funded by an operating grant to I.R.B. from the Natural Sciences and Engineering Research Council of Canada.

1. I. R. Butler, W. R. Cullen, W. E. Lindsell, P. N. Preston, and S. J. Rettig. J. Chem. Soc. Chem. Commun. 439 (1987).
2. S. E. Mulvaney, Z. G. Gardland, S. L. Gardland, and D. J. Newton. J. Am. Chem. Soc. **88**, 476 (1966).
3. M. D. Rausch, L. P. Kleiman, and W. H. Boon. Synth. React. Inorg. Met.-Org. Chem. **15**, 923 (1985).
4. D. L. Reger, S. A. Klaeren, J. E. Babin, and R. D. Adams. Organometallics, **7**, 181 (1988) and references therein.
5. D. L. Reger and E. Mintz. Organometallics, **3**, 1759 (1984).
6. P. Lennon, A. M. Rosen, and M. Rosenblum. J. Am. Chem. Soc. **99**, 8426 (1977).
7. L. Miller and D. A. Kaufman. J. Am. Chem. Soc. **90**, 7282 (1968).
8. C. J. Cardin, D. J. Cardin, R. J. Norton, H. E. Parge, and K. W. Muir. J. Chem. Soc. Dalton Trans. 665 (1983).
9. C. J. Cardin, D. J. Cardin, H. E. Parge, and A. C. Sullivan. J. Chem. Soc. Dalton Trans. 2315 (1986) and references therein.
10. D. L. Reger, S. A. Klaeron, and L. Lebioda. Organometallics, **5**, 1072 (1986).
11. S. R. Su and A. J. Wojcicki. J. Organometal. Chem. **27**, 31 (1977).
12. T. W. Bodnar and A. R. Cutler. Organometallics, **4**, 1558 (1985).
13. T. W. Bodnar, S. J. LaCroce, and A. R. Cutler. J. Am. Chem. Soc. **102**, 3292 (1980).
14. L. Cassar. J. Organometal. Chem. **93**, 253 (1975).
15. D. E. Ames, D. Bull, and C. Takundwa. Synthesis, 364 (1981).
16. E. D. Bergman. J. Org. Chem. **21**, 461 (1956).

Can. J. Chem. Downloaded from www.nrcresearchpress.com by 194.225.253.170 on 09/07/12
For personal use only.

Étude structurale de la liaison thioamide : Synthèse et conformation de dérivés de la thioalanine et de la thioglycine

ANDRE G. MICHEL,[1] CHAKIB AMEZIANE-HASSANI ET GASTON BOULAY
Laboratoire de chimie structurale, Université de Sherbrooke, Sherbrooke (Québec), Canada J1K 2R1

ET

GILLES LAJOIE
Department of Chemistry, University of Waterloo, Waterloo, Ont., Canada N2L 3G1

Reçu le 15 juin 1988[2]

ANDRE G. MICHEL, CHAKIB AMEZIANE-HASSANI, GASTON BOULAY et GILLES LAJOIE. Can. J. Chem. **67**, 1312 (1989).

Cette étude rapporte la synthèse, la détermination de structures cristallines et l'analyse conformationnelle par calculs empiriques de la *N*-tertiobutyloxycarbonyl *N'*-méthylthioalanine (Boc-AlaS-NHCH$_3$, $C_9H_{18}N_2O_2S$) et de la *N*-tertiobutyloxycarbonyl *N'*-méthylthioglycine (Boc-GlyS-NHCH$_3$, $C_8H_{16}N_2O_2S$), composés à l'intérieur desquels la liaison amide conventionnelle a été remplacée par un lien thioamide. Boc-AlaS-NHCH$_3$ cristallise dans le système quadratique, le groupe d'espace étant $P4_32_12$. Boc-GlyS-NHCH$_3$ a cristallisé dans le système monoclinique, correspondant au groupe d'espace $P2_1/c$. Les deux structures ont été résolues par méthodes directes et affinées par la méthode des moindres carrés (matrices entières), jusqu'à des valeurs de *Rw* de 0,045 et 0,035 pour 827 et 1335 réflexions respectivement pour lesquelles l'intensité *I* était supérieure à $2{,}5\sigma(I)$. Les conformations observées pour Boc-AlaS-NHCH$_3$ et Boc-GlyS-NHCH$_3$ correspondent toutes à des minima d'énergie conformationnelle calculés pour les résidus classiques. La longueur du lien C=S de 1,665(9) Å et de 1,650(3) Å constitue la modification majeure en comparaison avec les molécules oxygénées; la présence de l'atome de soufre ne semble pas modifier les propriétés du lien peptidique. À partir des structures cristallines ainsi déterminées, les cartes d'énergie conformationnelle pour des dérivés de la dithioalanine et la dithioglycine ont été calculées par une méthode classique dans le cadre de l'étude structurale des peptides (ECEPP/2) et comparées à celles que l'on obtient pour les résidus classiques. On peut conclure que la synthèse d'une part et l'analyse conformationnelle d'autre part permettent d'inclure le lien thiopeptidique dans des structures plus complexes et d'en prévoir les conformères préférentiels.

Mots clés : conformation moléculaire, structures peptidiques, cristallographie.

ANDRE G. MICHEL, CHAKIB AMEZIANE-HASSANI, GASTON BOULAY, and GILLES LAJOIE. Can. J. Chem. **67**, 1312 (1989).

The present study reports the synthesis, crystal structure determinations, and the conformational analysis of *N*-tertiobutyloxycarbonyl *N'*-methylthioalanine (Boc-AlaS-NHCH$_3$, $C_9H_{18}N_2O_2S$) and of *N*-tertiobutyloxycarbonyl *N'*-methylthioglycine (Boc-GlyS-NHCH$_3$, $C_8H_{16}N_2O_2S$). The particular feature of these compounds is the replacement of the classical oxopeptide linkage by a thioamide bond. Crystals of Boc-AlaS-NHCH$_3$ are tetragonal, space group $P4_32_12$. Those of Boc-GlyS-NHCH$_3$ are monoclinic, space group $P2_1/c$. Both structures were solved by direct methods and refined by full-matrix least-squares methods to *Rw* = 0.045 and 0.035 for 827 and 1335 reflections respectively, with intensities greater than $2.5\sigma(I)$. The conformations of both compounds correspond to conformational energy minima, calculated for classical amino acids. The C=S bond lengths of 1.665(9) and 1.650(3) Å constitute the major difference compared to oxopeptides; the crystal structures reveal that the presence of the sulfur atom does not change the electronic properties of the peptide bond. Using a classical method for the study of peptides (ECEPP/2), conformational energy maps were computed for derivatives of dithioalanine and dithioglycine and are compared to the oxo residues. We conclude that the synthesis and conformational analysis of thionated amino acids allow us to introduce the thioamide linkage into more complex peptide structures and to predict the conformational behaviour.

Key words: molecular conformations, peptidic structure, crystallography.

Introduction

Les processus physiologiques à l'intérieur desquels les peptides sont impliqués, sont très nombreux. La compréhension des mécanismes d'action est d'autant plus grande que chacun de ces processus constitue un endroit propice en vue d'une intervention pharmacologique. Les difficultés sont cependant nombreuses, tenant compte de la courte durée de vie des peptides endogènes et de la diversité de leurs modes d'action. Au cours des dernières années, diverses méthodes ont été développées en vue de synthétiser des molécules de nature peptidique, dont la conformation était contrainte, par l'introduction de groupements spécifiques. De telles recherches visent à conférer aux dérivés peptidiques une conformation telle que la reconnaissance par un récepteur biologique donné soit accrue (1). De plus il s'agit d'augmenter la durée d'action de ces molécules, en les protégeant des agents hydrolytiques. Diverses approches sont apparues en vue de conférer une plus grande intégrité conformationnelle aux molécules. Certains chercheurs ont préconisé d'introduire un caractère plus rigide en intervenant au niveau des chaînes latérales (2). D'autres ont préféré effectuer des modifications sur la chaîne principale des peptides. Parmi ces méthodes, il fut considéré de remplacer un ou plusieurs liens peptidiques par des analogues thiocarbonylés. Il a été démontré que l'introduction de tels résidus dans la séquence de peptides possédant une activité chimiotactique faisait disparaître l'activité comme la libération de lysosymes (3, 4). D'autre part, il était de première importance d'examiner de quelle manière de telles modifications pourraient influencer la susceptibilité des substrats, vis à vis de l'hydrolyse enzymatique (5).

Par ailleurs, les dérivés thiocarbonylés d'acides aminés représentent un intérêt particulier car ils ont été montrés complètement résistants à l'hydrolyse enzymatique par l'α-chymotrypsine (3) et la leucine aminopeptidase ainsi que plus stables que leurs homologues oxygénés à l'hydrolyse par la

1. Auteur à qui adresser toute correspondance.
2. Revision reçue le 18 avril 1989.

Can. J. Chem. Downloaded from www.nrcresearchpress.com by 194.225.253.170 on 09/07/12
For personal use only.

TABLEAU 1. Caractéristiques physico-chimiques des amides des Boc *N'*-méthyl aminoacides, et de leurs analogues après thionation

Composé	R^a (%)	R_f^c	T_{fusion} (°C)	RMN du $^1H^b$ C=SNH	C=ONH	NHBoc	$C^\alpha H$	$C^\beta H$	Me	*t*-Bu
Boc-Gly-$NHCH_3$	73	0,19	75–76		6,73	5,63	3,78	—	2,83	1,46
Boc-Ala-$NHCH_3$	74	0,24	115–116		6,30	5,13	4,20	1,40	2,78	1,43
Boc-GlyS-$NHCH_3$	73	0,54	109–110	8,33		5,60	4,16	—	3,70	1,48
Boc-AlaS-$NHCH_3$	59	0,59	125–126	8,66		5,56	4,59	1,46	3,13	1,46

[a]Rendement de la réaction.
[b]60 MHz, $CDCl_3$.
[c]EtOAc/hexane 2:1.

carboxypeptidase (6*a*,*b*). D'autre part, il a été récemment observé que la résistance enzymatique des thiopeptides était dépendante de la nature du résidu dans le cas de l'enzyme de conversion de l'angiotensine (7). D'autres composés thiocarbonylés dérivés de la glycine et de l'alanine ont par ailleurs servi dans des études de mécanismes avec la papaïne par spectroscopie Raman (8). En vue de poursuivre de telles études, il a été envisagé de synthétiser des analogues thiocarbonylés de substrats de l'α-chymotrypsine et de vérifier si le mécanisme d'action proposé pour l'hydrolyse des substrats habituels, serait également effectif pour des analogues thiocarbonylés. Dans le but de comprendre les propriétés conformationnelles caractéristiques de molécules peptidiques, nous avons entrepris la détermination de structures cristallines de deux composés : *N*-tertiobutyloxycarbonyl *N'*-méthylthioalanine Boc-AlaS-$NHCH_3$ et *N*-tertiobutyloxycarbonyl *N'*-méthylthioglycine Boc-GlyS-$NHCH_3$. Les structures moléculaires résultantes ont alors été utilisées en vue de paramétriser les calculs d'énergies conformationnelles dans le cadre de l'application des méthodes empiriques. Disposant ainsi des fonctions énergétiques adéquates, nous espérons qu'il sera possible de prédire les conformations des composés à l'intérieur desquels de telles unités thiopeptidique seraient ultérieurement introduites.

Partie expérimentale

Synthèse

Synthèse des amides des N-*tertiobutyloxycarbonyl* N'-*méthylamino-acides*

L'acide *N*-tertiobutyloxycarbonyl-amino et l'hydroxybenzotriazole (1,1 équiv.) ont été dissouts dans CH_2Cl_2, la température de la solution étant maintenue à 0°C. La *N*,*N'*-dicyclohexylcarbodiimide (1,05 équiv.) a été ajoutée et la solution agitée à 0°C pendant 30 min. Une solution à 1% dans le tétrahydrofurane de méthyl amine (1,1 équiv.) fut ensuite ajoutée sous agitation à 0°C. L'agitation fut maintenue pendant 1 h à cette température et ensuite 20–24 h à la température normale. La dicyclohexylurée fut alors éliminée par filtration, et la solution diluée avec CH_2Cl_2 et lavée à l'acide citrique (5%), $NaHCO_3$ (5%), séchée ($MgSO_4$) et évaporée sous vide. Les rendements et les propriétés physico-chimiques sont données au tableau 1.

Thionation des amides des N-*tertiobutyloxycarbonyl* N'-*méthyl-amino-acides*

Le réactif de thionation **1** (0,6 équiv.) (9) a été ajouté en une seule fois à la solution de l'amide appropriée (1–10 mmol) dans le tétrahydrofurane sec (10% en solution). Le mélange fut ensuite agité à 23 ± 2°C sous atmosphère d'azote. L'avancement de la réaction fut alors contrôlé par chromatographie en couche mince et la durée de réaction déterminée par la disparition de l'amide de départ (ninhydrine). Les composés furent alors purifiés par chromatographie sur gel de silice. Les propriétés physico-chimiques, les temps de réactions et les rendements sont donnés au tableau 1.

Détermination des structures cristallines

Des cristaux de Boc-AlaS-$NHCH_3$ et de Boc-GlyS-$NHCH_3$ ont été obtenus par évaporation lente d'une solution d'acétate d'éthyl/hexane. Les données ont été mesurées à l'aide d'un diffractomètre Nonius CAD4 en utilisant le rayonnement Kα du cuivre, rendu monochromatique grâce à un monochromateur au graphite. Les dimensions de la maille ont été obtenues par une technique de moindres-carrés à partir de 18 réflexions dans un domaine de $15° \leq \theta \leq 23°$. Deux réflexions de contrôle d'intensité ont été mesurées chaque 50 réflexions. Aucun changement significatif n'a été observé quant à l'intensité de ces deux réflexions. Le système de programmes cristallographiques NRCVAX (10) a été employé pour tous les calculs. Le groupe spatial $P4_32_12$ dans le cas de Boc-AlaS-$NHCH_3$ a été fixé de telle sorte que l'isomère L du résidu Ala utilisé pour la synthèse du composé soit respectée. Cependant, afin de juger de l'applicabilité de la diffusion anomale de l'atome de soufre, nous avons confirmé cette polarité en calculant les valeurs des résidus globaux obtenus pour chacun des isomères, soient 0,067 pour le groupe $P4_12_12$ et 0,064 pour le groupe $P4_32_12$. La liste des réflexions calculées et les plus affectées par le changement d'isomère fait partie du matériel supplémentaire.[3] Les structures ont été résolues par application des méthodes directes et affinées par la technique des moindres-carrés en matrice entière, basés sur les valeurs de *F*. Des facteurs thermiques anisotropes ont été affinés pour tous les atomes autres que l'hydrogène. Les atomes d'hydrogène ont été localisés par différence de Fourier, mais leurs positions n'ont pas été affinées. Un schéma de pondération basé sur les comptages statistiques a été appliqué. Les courbes de diffusion utilisées ont été celles que fournit le système NRCVAX (10). Les données cristallographiques relatives aux déterminations de structures sont données au tableau 2.

Calculs d'énergie conformationnelle

Les conventions standard (IUPAC) quant aux définitions des angles dièdres ω, ϕ, φ dans les peptides ont été observées tout au long de ce travail (19).

Les propriétés conformationnelles du résidu alanine ont été étudiées antérieurement par méthodes classiques (11) et quantiques (12). Se référant au calcul quantique *ab initio* (12), il s'est avéré que des calculs d'énergie conformationnelle effectués à l'aide du programme

3. On peut acheter des tableaux des coordonnées finales et des facteurs de température des atomes d'hydrogène pour les composés **2** et **3**, des facteurs de température anisotropes pour les atomes différents de l'hydrogène pour **2** et **3** ainsi que des listes des facteurs de structures calculés et observés en s'adressant au Dépôt des données non publiées, ICIST, Conseil national de recherches du Canada, Ottawa (Ontario), Canada K1A 0S2.

Un tableau des coordonnées des atomes d'hydrogène peut être obtenu en s'adressant au Director, Cambridge Crystallographic Data Centre, University Chemical Laboratory, Lensfield Road, Cambridge CB2 1EW, U.K.

Can. J. Chem. Downloaded from www.nrcresearchpress.com by 194.225.253.170 on 09/07/12
For personal use only.

Can. J. Chem. Downloaded from www.nrcresearchpress.com by 194.225.253.170 on 09/07/12
For personal use only.

TABLEAU 2. Données cristallographiques[a]

Paramètres	2	3
Composé	Boc-AlaS-$NHCH_3$	Boc-GlyS-$NHCH_3$
Formule	$C_9H_{18}O_2N_2S$	$C_8H_{16}O_2N_2S$
Poids moléculaire	218,325	204,298
Système cristallin	Tétragonal	Monoclinique
Groupe d'espace	$P4_32_12$	$P2_1/c$
a (Å)	11,9345(8)	5,9823(1)
b (Å)	—	17,096(1)
c (Å)	17,8623(7)	10,8923(5)
β (°)	—	92,609(3)
V (Å^3)	2544,34	1112,84
Z	8	4
ρ_c (g/cm^3)	1,14	1,22
$F(000)$	943,84	439,92
μ (CuKα) (cm^{-1})	20,57	19,01
Dimensions du cristal (mm)	0,20 × 0,20 × 0,30	0,22 × 0,15 × 0,25
Type de balayage	ω–2θ (rapport 1/2)	ω–2θ (rapport 1/2)
Domaine de balayage	0,8 + 0,15 tg θ	0,8 + 0,15 tg θ
Vitesse de balayage	2° min^{-1}	2° min^{-1}
Données enregistrées	$+h, +k, +l$ et paires de Friedel sélectionnées	$\pm h, +k, +l$
2θ max (deg)	120	119,7
Réflexions indépendantes	1130	1641
Réflexions avec $I \geq 2{,}5\sigma(I)$	827	1335
Nombre de variables	128	167
R	0,064	0,043
R_w	0,045	0,035
S (fin d'affinement)	3,213	2,855
Δ/σ moyen (cycle finie)	0,001	0,001
Δ/σ maximum (cycle finie)	0,002	0,001
Densité résiduelle (e/Å^3)	−0,20–0,22	−0,23–0,43

[a]Température 293 K, diffractomètre Enraf–Nonius CAD4, radiation CuKα (λKα = 1,54178 Å) monochromateur au graphite, angle de départ 3°, ouverture de la fente du détecteur 4,0 × 4,0 mm à une distance de 173 mm du cristal; largeur de balayage étendue de 25% de chaque côté de la réflexion pour tenir compte du bruit de fond $\sigma^2(I) = C + 2B$ (C = nombre de coups; B = nombre de coups normalisé du bruit de fond).

Fonction minimisée : $\Sigma w(|F_o| - |F_c|)^2$ où $w = 1/\sigma^2(F)$; $R = \Sigma||F_o| - |F_c||/\Sigma|F_o|$; $R_w = (\Sigma w(|F_o| - |F_c|)^2/\Sigma w|F_o|^2)^{1/2}$; $S = (\Sigma w(|F_o| - |F_c|)^2/(m - n))^{1/2}$.
Les valeurs données pour R, R_w et S sont basées sur les réflexions avec $I \geq 2{,}5\sigma(I)$.

ECEPP/2 (11) (13*a*, *b*, *c*) donnaient des résultats tout à fait comparables. Ce programme a donc été utilisé pour évaluer l'énergie de conformation des molécules peptidiques dans le cadre de la mécanique moléculaire. L'énergie est calculée comme la somme de quatre contributions : celle des interactions électrostatiques, les liaisons hydrogènes, les énergies de torsion et enfin des interactions entre atomes non liés. Ce champ de force a été présenté en détail par F. A. Momany *et al.* (13*c*). Nous développons ici la composante que nous avons modifiée, celle des interactions entre atomes non liés. Cette composante est donnée par la relation suivante :

$$E_{NB} = \Sigma_i\Sigma_j FA^{kl}/R_{ij}^{12} - C^{kl}/R_{ij}^{6}$$

où R_{ij} est la distance entre atomes i et j.
Coéfficient du terme attractif,

$$C^{kl} = 3/2[eh/2\pi m_e^{1/2}]\alpha_k\alpha_l/[(\alpha_k/N_k)^{1/2} + (\alpha_l/N_l)^{1/2}]$$

e : charge de l'électron; α_k : polarisabilité de l'atome de type k; h : constante de Planck; N_k : nombre effectif des électrons de l'atome de type k; m_e : masse de l'électron.
Coéfficient du terme répulsif déduit à partir de C^{kl},

$$A^{kl} = (1/2)C^{kl}(r_g^{kl})^6$$

r_g^{kl} : rayon correspondant à l'énergie minimale entre des atomes de type k et l. $F = 0{,}5$ pour les interactions de type 1–4 et $F = 1{,}0$ pour les autres types d'interactions.

L'utilisation du programme ECEPP/2 pour des molécules thiopeptidiques demandait cependant que des paramètres adéquats soient introduits dans le champ de force utilisé. Les paramètres que nous avons utilisés sont donnés dans le tableau 3. La longueur de liaison C—S a été déterminée par cristallographie. Les charges atomiques partielles ont été calculées par la méthode CNDO/2 en utilisant le programme PCILO3 (14). Les valeurs du rayon de van der Waals pour l'atome de soufre ainsi que la polarisabilité pour cet atome ont été choisies telles que proposé antérieurement (11). Ce dernier paramètre permet de calculer les coefficients du terme attractif intervenant dans la contribution des interactions entre atomes non liés dans l'énergie conformationnelle totale en utilisant les relations précédemment mentionnées.

Résultats et discussion

Structures moléculaires et cristallines

Les paramètres atomiques obtenus par diffraction de rayons-X pour les atomes autres que les hydrogènes sont donnés au tableau 4. La figure 1 présente les structures moléculaires obtenues pour Boc-AlaS-$NHCH_3$ (fig. 1a) et Boc-GlyS-$NHCH_3$ (fig. 1b).

Les longueurs de liaisons ainsi que les angles de valence sont donnés au tableau 5. La géométrie du lien peptidique déterminée pour les deux composés correspond aux valeurs moyennes obtenues après une recherche dans la base de données «Cambridge Crystal Structure Data Base» et ulté-

Can. J. Chem. Downloaded from www.nrcresearchpress.com by 194.225.253.170 on 09/07/12
For personal use only.

TABLEAU 3. Paramètres utilisés pour le lien thiopeptidique dans les calculs d'énergie avec ECEPP/2

Distances[a] (Å)	C′═S	1,66
	$C^{\alpha}_{(n-1)}$—C′	1,53
	C′—N	1,32
	N—H	1,00
	N—$C^{\alpha}_{(n)}$	1,45
Angles[a] (deg)	$C^{\alpha}_{(n-1)}$—C′—N	115,0
	$C^{\alpha}_{(n-1)}$—C′—S	120,5
	S—C′—N	124,5
	C′—N—$C^{\alpha}_{(n)}$	121,0
	C′—N—H	124,0
Charges atomiques partielles (unité électrostatique de charge)	$C^{\alpha}_{(n-1)}$	0,076
	C′	0,523
	S	−0,441
	N	−0,426
	H	0,211
	$C^{\alpha}_{(n)}$	0,076
Rayon de van der Waals du soufre		1,89
Polarisabilité du soufre		0,34 Å^3

[a]La désignation des atomes se réfère au modèle classique du lien peptidique (19) : -$C^{\alpha}_{(n-1)}$—[(C′═S)—NH—$C^{\alpha}_{(n)}$]-.

TABLEAU 4. Coordonnées finales et facteurs de température B_{eq},[a] pour les composés Boc-AlaS-$NHCH_3$ et Boc-GlyS-$NHCH_3$

Boc-AlaS-$NHCH_3$

Atome	*x/a*	*y/b*	*z/c*	B_{eq}
S	0,7317(2)	0,9970(3)	0,8947(1)	9,5
O1	0,3687(5)	0,9735(5)	0,9549(3)	7,5
O2	0,3302(5)	1,0104(5)	0,8335(3)	6,1
N1	0,6529(6)	0,9102(6)	1,0187(4)	6,8
N2	0,4802(6)	0,9110(6)	0,8627(3)	5,2
C1	0,7376(9)	0,9626(8)	1,0661(5)	9,9
C2	0,6456(8)	0,9209(8)	0,9475(5)	5,7
C3	0,5523(7)	0,8482(7)	0,9129(4)	5,1
C4	0,3925(8)	0,9678(8)	0,8907(5)	5,2
C5	0,2234(9)	1,0666(9)	0,8477(5)	7,0
C6	0,2432(9)	1,1680(8)	0,8951(6)	9,9
C7	0,1433(7)	0,9857(8)	0,8875(5)	9,1
C8	0,1833(9)	1,0978(9)	0,7742(5)	10,1
C9	0,6071(8)	0,7516(8)	0,8715(5)	8,5

Boc-GlyS-$NHCH_3$

Atome	*x/a*	*y/b*	*z/c*	B_{eq}
S	0,4225(1)	0,8799(1)	0,1919(1)	7,2
N1	0,5828(4)	0,8762(1)	−0,0294(2)	5,7
N2	0,7767(4)	1,0022(1)	0,2189(2)	5,6
O1	1,0789(4)	1,0758(1)	0,1855(2)	6,8
O2	0,9077(3)	1,0793(1)	0,3673(2)	5,4
C1	0,4222(6)	0,8178(2)	−0,0723(3)	7,5
C2	0,5935(5)	0,9046(1)	0,0837(2)	4,8
C3	0,7859(5)	0,9615(2)	0,1032(2)	5,6
C4	0,9343(5)	1,0541(2)	0,2518(3)	5,1
C5	1,0714(5)	1,1333(2)	0,4272(3)	5,4
C6	1,0716(6)	1,2104(2)	0,3614(3)	7,9
C7	1,2994(5)	1,0936(2)	0,4365(3)	7,9
C8	0,9798(5)	1,1412(2)	0,5552(3)	7,3

[a]$B_{eq} = \frac{8\pi^2}{3}\Sigma_i\Sigma_j u_{ij} a_i^* a_j^* a_i a_j$.

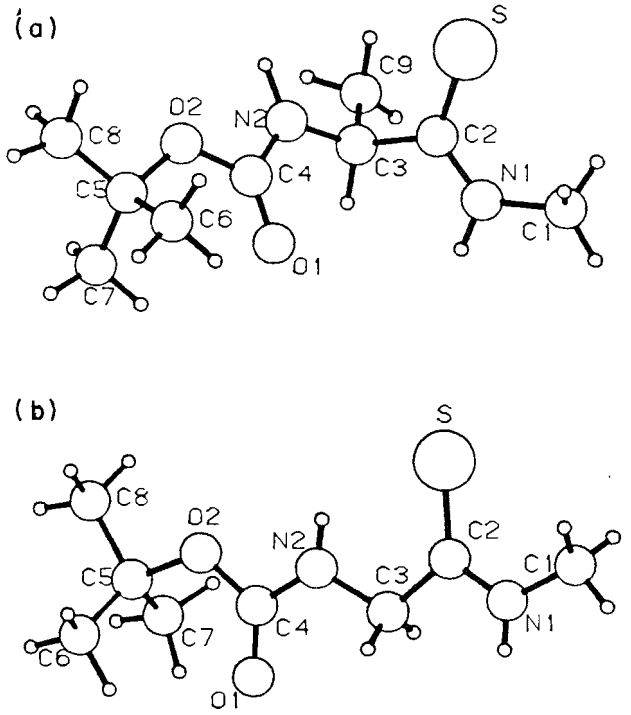


FIG. 1. Structures moléculaires et numérotation : (a) Boc-AlaS-$NHCH_3$; (b) Boc-GlyS-$NHCH_3$.

rieurement optimisée par calculs quantiques (Gaussian 80/82) (15). L'allongement de la liaison thiocarbonyle (1,66 Å) est la différence essentielle entre la liaison thiopeptidique et le lien classique (16). Une valeur particulièrement courte (1,64 Å) avait été précédemment proposée (17) à partir de résultats cristallographiques préliminaires. Cependant, on a pu montrer que la valeur de cette longueur de liaison constitue un paramètre important dans les calculs des propriétés électroniques. Aucune modification notoire n'a été observée quant à la longueur du lien C—N, laissant croire que peu de changements sont apportés aux propriétés électroniques du lien peptidique par l'introduction de l'atome de soufre. Cette proposition est appuyée par les valeurs des angles ω proches de 180° (tableau 5).

Les deux structures cristallines déterminées correspondent à des conformères proches de minimas énergétiques calculés pour les oxopeptides correspondants. Pour Boc-AlaS-$NHCH_3$, les valeurs des angles $\phi = -85,7(8)$ et $\psi = 130,8(8)$ correspondent à une conformation située à la limite des zones C et F (18), comme on peut le voir à la figure 3c. Il s'agit d'un conformère propice à la formation d'axes d'ordre 3 et 4 dans une chaîne polypeptidique. Grâce à cette conformation, la molécule peut former dans le cristal des chaînes en hélices 4_3, comme le montre la figure 2a. Une liaison hydrogène N2—H---O1 (tableau 6) assure la cohésion le long de cette hélice.

En ce qui concerne le composé Boc-GlyS-$NHCH_3$, les angles ϕ, ψ de la chaîne principale ont des valeurs proches de 180°. Ceci correspond à une structure très planaire pour l'unité peptidique. Cette conformation appartient à la zone E dans la classification de Scheraga (fig. 3c). La préférence pour cette conformation est aussi favorisée par le fait que les molécules peuvent s'associer en dimères par liaisons hydrogène (tableau 6), formant dans le cristal des associations et un empilement montré à la figure 2b.

Analyse conformationnelle

La figure 3 montre les cartes d'isoénergie [ϕ, ψ] calculées pour les composés **7** (fig. 3a) et **11** (fig. 3b) à l'aide du

TABLEAU 5. (a) Distances (Å), (b) angles (deg) intramoléculaires et (c) angles de torsion principaux (deg) pour Boc-AlaS-$NHCH_3$ et Boc-GlyS-$NHCH_3$. Les écart-types estimés sont indiqués entre parenthèses

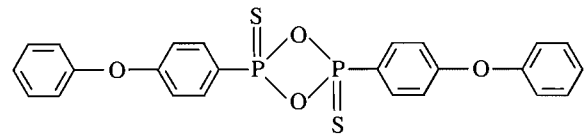
(a)	Boc-AlaS-$NHCH_3$	Boc-GlyS-$NHCH_3$
S—C2	1,665(9)	1,650(3)
O1—C4	1,184(9)	1,210(4)
O2—C4	1,362(11)	1,346(3)
O2—C5	1,462(11)	1,477(3)
N1—C1	1,460(12)	1,449(4)
N1—C2	1,281(11)	1,323(3)
N2—C3	1,453(11)	1,444(3)
N2—C4	1,343(12)	1,331(4)
C2—C3	1,540(13)	1,514(3)
C3—C9	1,518(13)	
C5—C6	1,456(14)	1,500(4)
C5—C7	1,533(15)	1,523(4)
C5—C8	1,445(13)	1,527(4)

(b)	Boc-AlaS-$NHCH_3$	Boc-GlyS-$NHCH_3$
C4—O2—C5	121,2(6)	120,6(2)
C1—N1—C2	125,5(8)	123,9(2)
C3—N2—C4	119,5(6)	120,1(2)
S—C2—N1	125,0(7)	124,5(2)
S—C2—C3	121,8(6)	123,8(2)
N1—C2—C3	113,0(8)	111,8(2)
N2—C3—C2	112,6(7)	111,9(2)
N2—C3—C9	110,2(7)	
C2—C3—C9	108,2(7)	
N2—C4—O1	125,3(9)	124,1(3)
N2—C4—O2	109,5(7)	110,6(3)
O1—C4—O2	125,0(8)	125,3(3)
O2—C5—C6	109,3(8)	110,7(2)
O2—C5—C7	109,5(7)	108,9(2)
O2—C5—C8	104,5(7)	101,6(2)
C6—C5—C7	110,2(8)	113,8(3)
C6—C5—C8	111,0(9)	111,5(2)
C7—C5—C8	112,1(9)	109,7(2)

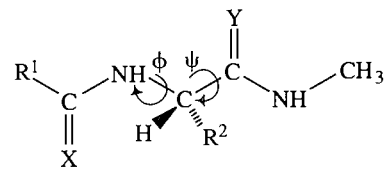
(c)	Boc-AlaS-$NHCH_3$	Boc-GlyS-$NHCH_3$
C5—O2—C4—N2	173,8(10)	176,0(3)
O2—C4—N2—C	−173,7(10)	−173,7(3)
ϕ C4—N2—C3—C2	−85,7(8)	179,4(3)
ψ N2—C3—C2—N1	130,8(10)	170,5(3)
ω C3—C2—N1—C1	175,8(10)	176,9(3)

programme ECEPP/2, paramétrisé pour les résidus AlaS et GlyS. Des rotations de −180° à 180° par pas de 15° ont été effectuées autour des angles ϕ et ψ indiqués sur le schéma moléculaire. Les conventions classiques (19) ont été utilisées dans la définition et la rotation des angles dièdres. Les courbes d'isoénergie ont été tracées par interpolations quadratiques par niveaux équidistants de 2 kcal/mol.[4] Pour chacune des cartes, le minimum global a été considéré comme zéro. Comparant l'allure générale des cartes obtenues à celles des dérivés oxopeptidiques (12, 20), on constate qu'il y a peu de modifications dans le cas de Ala et Gly. Les modifications les plus importantes apparaissent dans la zone C [$\phi = -75°$, $\psi = 75°$]. On sait d'autre part que cette zone comporte également les conformères correspondant au minimum global pour les oxopeptides (12, 15, 20). Ces conformères forment un cycle à sept membres incluant une liaison hydrogène intramoléculaire, la chaîne latérale étant

4. 1 kcal/mol = 4,18 kJ/mol.



1



1 Réactif de thionation

2	R^1 = O-C(CH_3)	X = O	$R^2 = CH_3$	Y = S	Boc-AlaS-$NHCH_3$
3	R^1 = O-C(CH_3)	X = O	R^2 = H	Y = S	Boc-GlyS-$NHCH_3$
4	$R^1 = CH_3$	X = O	$R^2 = CH_3$	Y = O	Ac-Ala-$NHCH_3$
5	$R^1 = CH_3$	X = S	$R^2 = CH_3$	Y = O	AcS-Ala-$NHCH_3$
6	$R^1 = CH_3$	X = O	$R^2 = CH_3$	Y = S	Ac-AlaS-$NHCH_3$
7	$R^1 = CH_3$	X = S	$R^2 = CH_3$	Y = S	AcS-AlaS-$NHCH_3$
8	$R^1 = CH_3$	X = O	R^2 = H	Y = O	Ac-Gly-$NHCH_3$
9	$R^1 = CH_3$	X = S	R^2 = H	Y = O	AcS-Gly-$NHCH_3$
10	$R^1 = CH_3$	X = O	R^2 = H	Y = O	Ac-GlyS-$NHCH_3$
11	$R^1 = CH_3$	X = S	R^2 = H	Y = O	AcS-GlyS-$NHCH_3$

placée en position équatoriale (C_7^{equ}). Cependant l'allongement de la liaison C=S et les orientations moins propices à une interaction stabilisante ont pour effet de déplacer légèrement ce minimum, tout en conservant une conformation C_7^{equ}.

Il ressort que les minima d'énergie, tout en étant situés pratiquement aux mêmes endroits de la carte, ont des valeurs relatives différentes de celles qui ont été observées pour les composés oxopeptidiques. Afin de mettre en évidence les effets de thio-substitution spécifiquement en X et Y, nous avons calculé à l'aide du programme ECEPP/2, les énergies conformationnelles des conformères correspondant aux divers minima globaux pour les différentes combinaisons : X = O, Y = O; X = S, Y = O; X = O, Y = S et X = S, Y = S, respectivement pour les résidus Ala (**4**–**7**) et Gly (**8**–**11**). Les résultats sont présentés au tableau 7.

Dans le cas des dérivés mono-substitués X = S on trouve que la conformation la plus stable est située dans la zone E [$\phi = -150°$, $\psi = 150°$] dans le cas du composé **5** et [$\phi = -180°$, $\psi = 180°$] pour le composé **9**.

On remarque également que la mono-substitution Y = S dans les composés **6** et **10** n'affecte pas la position du minimum global situé dans la zone C [$\phi = -75°$, $\psi = 75°$] tel qu'on le retrouve dans les oxopeptides.

Finalement, la disubstitution X = S, Y = S dans les composés **7** et **11** affecte légèrement la position du minimum global en le déplaçant de [$\phi = -75°$, $\psi = 75°$] à [$\phi = -90°$, $\psi = 90°$] tout en le conservant dans la même zone.

Revenant à l'examen des cartes conformationnelles, il ressort que si les conformations préférentielles sont modifiées lors de la substitution d'un atome d'oxygène par un atome de soufre, on ne constate cependant pas de restriction majeure apportée à l'espace conformationnel. Cependant on devrait s'attendre à ce que des changements plus accentués soient observés dans les cas où le lien thioamide est introduit dans un résidu pour lequel la chaîne latérale serait plus encombrée.

Conclusion

Nous avons montré que l'insertion du lien thioamide dans la chaîne peptidique peut tout d'abord se réaliser par synthèse

Can. J. Chem. Downloaded from www.nrcresearchpress.com by 194.225.253.170 on 09/07/12
For personal use only.

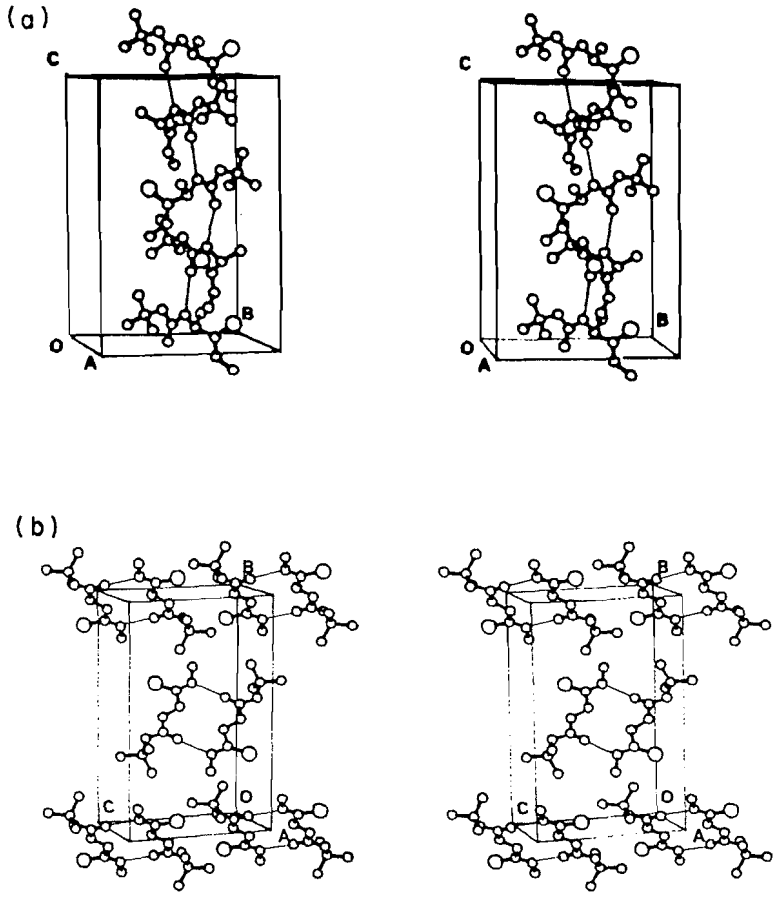


FIG. 2. Vues stéréoscopiques des empilements cristallins : les liaisons hydrogène sont représentées par les traits minces. (a) Boc-AlaS-$NHCH_3$; (b) Boc-GlyS-$NHCH_3$.

TABLEAU 6. Distances (Å) et angles (deg) entre donneurs et accepteurs observés pour les liaisons H pour Boc-AlaS-$NHCH_3$ et Boc-GlyS-$NHCH_3$

Composé	Liaison hydrogène	N—H----O	N----O	N—H	H----O
Boc-AlaS-$NHCH_3$	N2—H---O	166,9	2,916(8)	1,0	1,933
Boc-GlyS-$NHCH_3$	N1—H---O	169,4	2,824(3)	0,83	2,0

TABLEAU 7. Influence de la substitution thioamide sur la valeur de l'énergie (kcal/mol) et le déplacement du minimum global pour AcX-AlaY-$NHCH_3$ (**4–7**) et AcX-GlyY-$NHCH_3$ (**8–11**)

	Zone C		Zone E	
Angles [ϕ,ψ] : (deg)	[−75, +75]	[−90, +90]	[−150, +150]	[−180, +180]
AcX-AlaY-$NHCH_3$				
X = O, Y = O (**4**)	0,0	0,5	0,6	
X = S, Y = O (**5**)	21,1	0,4	0,0	
X = O, Y = S (**6**)	0,0	0,5	1,8	
X = S, Y = S (**7**)	20,6	0,0	0,8	
AcX-GlyY-$NHCH_3$				
X = O, Y = O (**8**)	0,0	0,8		1,2
X = S, Y = O (**9**)	15,7	0,1		0,0
X = O, Y = S (**10**)	0,0	0,8		3,1
X = S, Y = S (**11**)	15,7	0,0		1,8

Can. J. Chem. Downloaded from www.nrcresearchpress.com by 194.225.253.170 on 09/07/12
For personal use only.

Can. J. Chem. Downloaded from www.nrcresearchpress.com by 194.225.253.170 on 09/07/12
For personal use only.

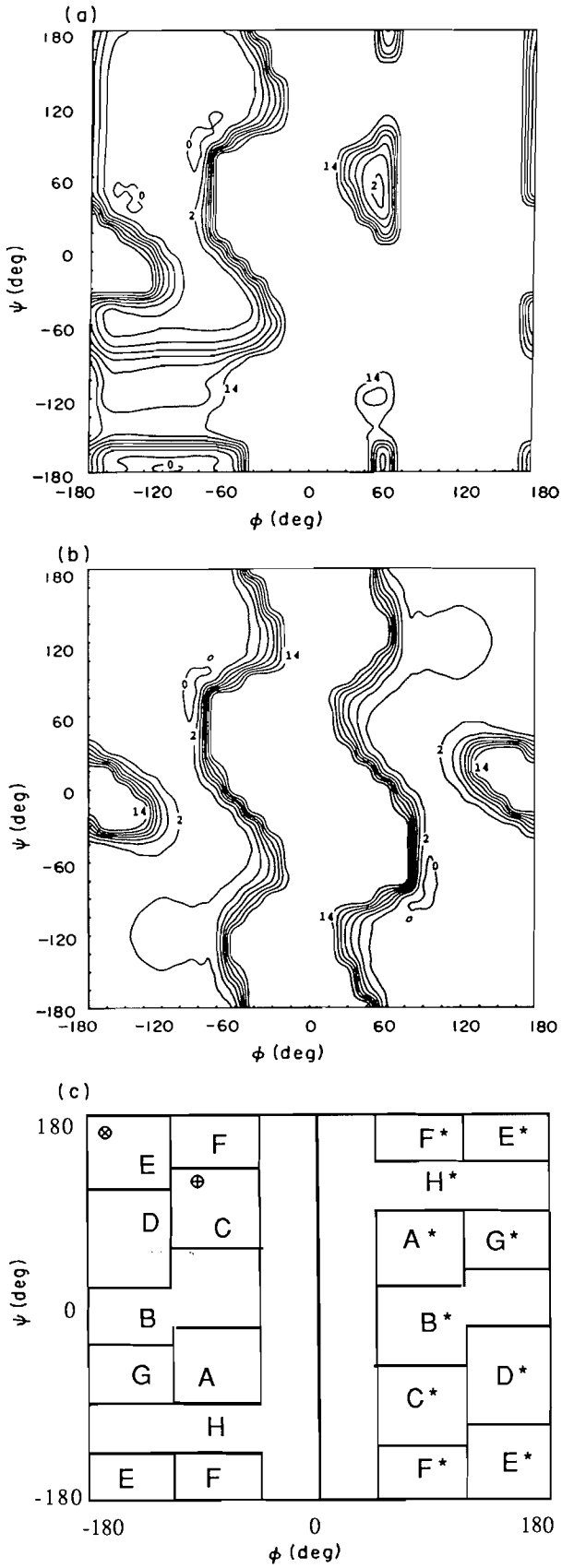


FIG. 3. Cartes d'énergie conformationnelle (ECEPP/2). Les angles de rotation [ψ, φ] sont indiqués sur le schéma des structures moléculaires. Les courbes ont été tracées à intervalles de 2 kcal/mol. 3(a) Boc-AlaS-$NHCH_3$; 3(b) Boc-GlyS-$NHCH_3$; 3(c) Régions définissant les zones de l'espace de conformation (18) : ⊕ Conformation cristalline de Boc-AlaS-$NHCH_3$; ⊗ Conformation cristalline de Boc-GlyS-$NHCH_3$.

classique et ensuite être étudiée d'un point de vue conformationnel. De ce point de vue, en poursuivant une approche combinant la diffraction des rayons-X des mono-cristaux et l'étude conformationnelle par méthodes classiques, il est possible de mettre en évidence les propriétés conformationnelles caractéristiques que le lien thioamide induit. Cette méthode doit permettre d'envisager l'étude de composés de plus grandes complexités et ainsi considérer les polypeptides à l'intérieur desquels le lien thioamide serait spécifiquement introduit en vue de générer des propriétés conformationnelles caractéristiques.

Remerciements

A.M. et G.L. remercient le Conseil de la recherche en sciences naturelles et en génie du Canada pour le support financier qui leur a été octroyé. Nous remercions particulièrement M. Y. Le Page (N.R.C. Chemistry Division, Ottawa) pour son aide dans l'analyse cristallographique. Nous remercions également M. D. P. Vercauteren (Chimie-physique, F.U.N.D.P., Namur, Belgique) pour son assistance dans la préparations des diagrammes d'isoénergie.

1. R. S. STRUTHERS, A. T. MAGLER et J. RUER. Conformationally directed drug design. II. Design of peptide analogs. American Chemical Society. 1984.
2. M. IQBAL, P. BALARAM, H. J. SHOWELL, R. J. FREER et E. L. BECKER. FEBS Lett. **165**, 171 (1984).
3. G. LAJOIE. Thèse de doctorat, département de chimie, Université McGill, Montréal. 1984.
4. G. SAUVE, V. S. RAO, G. LAJOIE et B. BELLEAU. Can. J. Chem. **63**, 3089 (1985).
5. A. C. STORER, R. H. ANGUS et P. R. CAREY. Biochemistry, **27**, 264 (1988).
6. (*a*) W. L. MOCK, J.-T. CHEN et J. W. TSANG. Biochem. Biophys. Res. Commun. **102**, 389 (1981); (*b*) P. A. BARTLETT, K. L. SPEAR et N. E. JACOBSEN. Biochemistry, **21**, 1609 (1982).
7. L. MAZIAK, G. LAJOIE et B. BELLEAU. J. Am. Chem. Soc. **108**, 182 (1986).
8. H. LEE, R. H. ANGUS, A. C. STORER, K. I. VARUGHESE et P. R. CAREY. Biochemistry, **27**, 250 (1988).
9. G. LAJOIE, F. LEPINE, L. MAZIAK et B. BELLEAU. Tetrahedron Lett. **24**, 3815 (1983).
10. E. J. GABE, F. L. LEE et Y. LE PAGE. The NRCVAX crystal structure system, in crystallographic computing 3: data collection, structure determination, proteins, and databases. *Éditeurs* : G. M. Sheldrick, C. Kruger et R. Goddard. Clarendon Press, Oxford. 1985. pp. 167–174.
11. G. NÉMETHY, M. S. POTTLE et H. A. SCHERAGA. J. Phys. Chem. **87**, 1883 (1983).
12. D. PETERS et J. PETERS. J. Mol. Struct. **85**, 107 (1981).
13. (*a*) F. A. MOMANY, R. F. MCGUIRE, A. W. BURGESS et H. A. SCHERAGA. J. Phys. Chem. **79**, 2361 (1975); (*b*) M. J. BROWMAN, L. M. CARRUTHERS, K. L. KASHUBA, F. A. MOMANY, M. S. POTTLE, S. P. ROSEN et S. M. RUMSEY. QCPE, **11**, 286 (1975); (*c*) F. A. MOMANY, L. M. CARRUTHERS, R. F. MCGUIRE et H. A. SCHERAGA. J. Phys. Chem. **78**, 1595 (1974).
14. R. BOCA. PCILO3: Perturbative configuration interaction (version 3). QCPE Program n° 462, Indiana University. 1983.
15. V. N. BALAJI, S. PROFETA, JR. et S. W. DIETRICH. Biochem. Biophys. Res. Commun. **145**, 834 (1987).
16. R. B. COREY et L. PAULING. Proc. R. Soc. B: **141**, 10 (1953).
17. T. F. M. LA COUR, H. A. S. HANSEN, K. CLAUSEN et S. O. LAWESSON. Int. J. Peptide Protein Res. **22**, 509 (1983).
18. S. S. ZIMMERMAN, M. S. POTTLE, G. NEMETHY et H. A. SCHERAGA. Macromolecules, **10**, 1 (1977).
19. IUPAC-IUB Commission on Biochemical Nomenclature. Biochemistry, **9**, 3471 (1970).
20. S. S. ZIMMERMAN et H. A. SCHERAGA. Proc. Natl. Acad. Sci. U.S.A. **74**, 4126 (1977).

Synthesis, solid state ^{31}P CP-MAS NMR infrared and Raman studies of mercury(II) complexes of 1,3,5-triaza-7-phosphaadamantane (PTA)[1]

ELMER C. ALYEA,[2] KEITH J. FISHER, AND STEVE JOHNSON

Guelph–Waterloo Centre for Graduate Work in Chemistry, Guelph Campus, Department of Chemistry and Biochemistry, Guelph, Ont., Canada N1G 2W1

Received September 20, 1988

ELMER C. ALYEA, KEITH J. FISHER, and STEVE JOHNSON. Can. J. Chem. **67**, 1319 (1989).

Insoluble mercury(II) complexes of a water-soluble phosphine, 1,3,5-triaza-7-phosphaadamantane (PTA), have been studied by solid state ^{31}P CP-MAS NMR, infrared and Raman spectroscopies. Complexes of the type $(PTA)HgX_2$ show larger coordination chemical shifts but similar $J(^{31}P—^{199}Hg)$ coupling constants to those previously observed for similar trialkylphosphine complexes. These complexes all appear to be dimeric or polymeric. The nitrate complex of the form $(PTA)_2Hg(NO_3)_2$ has also been isolated and complexes of the type $(PTA)_4Hg^{2+}$ are shown to exist.

Key words: mercury(II) phosphine complexes, solid state ^{31}P NMR studies.

ELMER C. ALYEA, KEITH J. FISHER et STEVE JOHNSON. Can. J. Chem. **67**, 1319 (1989).

Faisant appel aux méthodes spectroscopiques Raman, infrarouge et RMN CP-MAS du ^{31}P, on a étudié les complexes insolubles du mercure(II) obtenus à partir d'une phosphine soluble dans l'eau, le triaza-1,3,5 phospha-7 adamantane (PTA). Les complexes du type $(PTA)HgX_2$ présentent des déplacements chimiques de coordination qui sont plus grands que ceux observés antérieurement avec des complexes semblables de trialkylphosphines; toutefois, les constantes de couplage $J(^{31}P—^{199}Hg)$ sont semblables. Il semble que tous ces complexes sont des dimères ou des trimères. On a aussi isolé le complexe contenant un nitrate, $(PTA)_2Hg(NO_3)_2$ et on a démontré que les complexes du type $(PTA)_4Hg^{2+}$ existent.

Mots clés : complexes de mercure(II) phosphine, études en RMN du ^{31}P de l'état solide.

[Traduit par la revue]

Introduction

1,3,5-Triaza-7-phosphaadamantane (PTA), first reported in 1974 (1), is potentially a very important ligand. The solubility of this compound in water and the difficulty of oxidation make this an unusual aliphatic phosphine. The small cone angle of 102° (2) suggests that this phosphine should be a good substitute for trimethylphosphine. Darensbourg and Daigle (3) were able to prepare the complexes $PTAM(CO)_5$ where M = Cr, Mo, W, and $PTAFe(CO)_4$. The ^{31}P NMR spectra indicated that these complexes were P-bound to the metal. The ability of this phosphine to form stable organic derivatives (4), which leave the donor ability of the phosphorus intact, suggests that a fine tuning of useful properties of metal complexes may be possible.

We have undertaken an investigation of the synthesis of metal complexes of PTA and our initial results indicated that many metals form complexes (20); those with mercury(II) salts are reported here. The insolubility of the mercury(II) PTA complexes in water and non-aqueous solvents required us to study the properties of the complexes prepared by cross polarization magic angle spinning ^{31}P NMR spectroscopy (5). The importance of observing phosphorus–mercury coupling also required us to use a side band suppression technique (6).

Monodentate phosphine complexes of mercury(II) are generally of the form L_xHgX_2 (x = 1, 2, 3, or 4) (7) but complexes having the unusual formula $L_3(HgX_2)_2$ have also been observed (8). Small phosphines can form complexes where x = 1, 1.5, 2, 3, or 4 whereas bulky phosphines generally tend to form complexes where x = 1 or 2 only. Most of the $LHgX_2$ complexes have mercury(II) in a tetrahedral or distorted tetrahedral environment leading to a dimeric (centrosymmetric) or polymeric structure. There are exceptions such as the non-centrosymmetric structure observed for α-Pr_3PHgI_2 (9) and the five coordinate structures observed for Me_3PHgCl_2 and Et_3PHgCl_2 (10). L_2HgX_2 complexes have tetrahedral or distorted tetrahedral coordination about mercury(II). L_3HgX_2 and L_4HgX_2 complexes are generally tetrahedral ionic species (7).

^{31}P and ^{199}Hg NMR have proved useful tools in the investigation of mercury phosphine complexes. The correlation of chemical shifts (^{31}P and ^{199}Hg) and $J(^{31}P—^{199}Hg)$ are not always in agreement but in general there is a decrease in $J(^{31}P—^{199}Hg)$ with increasing value of x in the complexes L_xHgX_2. The coordination chemical shift of the ^{31}P resonance also tends to indicate the σ donor property of the phosphine (7, 11).

Our study of some new insoluble PTA–mercury complexes highlights the utility of solid state ^{31}P CP-MAS NMR spectroscopy in their characterization.

Experimental

Preparation of the complexes

$HgCl_2$, $HgBr_2$, HgI_2, $Hg(NO_3)_2$, and $Hg(SCN)_2$ were reagent grade and used as received. PTA was prepared (1), recrystallized from aqueous methanol, and its purity confirmed by its ^{31}P [^1H] NMR spectrum (singlet at −97.4 in methanol).

The complexes were prepared by adding hot methanolic solutions of mercury salt to hot methanolic solutions of PTA. Molar ratios of Hg:PTA of 1:2 and 1:1 were used. The mercury complexes precipitated almost immediately and the filtered precipitates were washed with hot methanol. The complexes were insoluble in water and organic solvents.

In all cases except the nitrate the order of addition of mercury salt solution to PTA solution or vice versa resulted in the major product $PTAHgX_2$. The attempted preparations of $PTAHg(NO_3)_2$ resulted in the isolation of $(PTA)_2Hg(NO_3)_2$ and when mercuric nitrate solution was added to a large excess of PTA in methanol solution, analytical results indicated that species approximating $(PTA)_4Hg(NO_3)_2$ were obtained.

The attempted preparations of the acetate and perchlorate complexes

[1]Dedicated to our Ph.D. mentor (E.C.A. and K.J.F.) Professor D. C. Bradley, D.Sc. FRS, Queen Mary College, University of London, on the occasion of his retirement.

[2]To whom all correspondence should be addressed. No reprints are available.

Can. J. Chem. Downloaded from www.nrcresearchpress.com by 194.225.253.170 on 09/07/12
For personal use only.

TABLE 1. Analytical data for the $(PTA)_nHgX_2$ complexes

Compound	Yield	Melting point (°C)	Calculated %C	Calculated %H	Found %C	Found %H
$PTAHgCl_2$	86%	213	16.80	2.80	16.91	2.75
$PTAHgBr_2$	93%	205d	13.92	2.32	14.08	2.36
$PTAHgI_2$	43%	(150d)196m	11.78	1.96	12.07	1.77
$PTAHg(SCN)_2$	90%	175d†	20.30	2.53	20.09	2.50
$PTAHg(CN)_2$	63%	175d, 193m	23.47	2.93	22.76	3.49
$(PTA)_2Hg(NO_3)_2$	88%	190–200†d,m	22.55	3.76	22.04	3.91

*Most samples darkened before melting; d = darken, m = melting.
†One sample exploded, no sample melted over a small temperature range.

TABLE 2. ^{31}P NMR data for $(PTA)_nHgX_2$

Complex	δ (ppm)*	Δ^b (ppm)†	$J(^{199}Hg—^{31}P)$ (Hz)
$(PTA)_2Hg(NO_3)_2$	−29.9	74.5	5111
$(PTA)HgCl_2$	−38.3	66.1	6559
$(PTA)HgBr_2$	−44.1	60.7	6184
$(PTA)HgI_2$	−61.4	43.0	4037
$(PTA)Hg(SCN)_2$	−32.6	71.8	5599
	−38.2	66.2	6510
$(PTA)Hg(CN)_2$	−50.4(maj)	54.0	4589
	−59.4(min)	45.0	4581
Other species observed			
$(PTA)_4HgCl_2$	−63.4	41.0	1937
$(PTA)_4HgBr_2$	−62.8	41.6	1953
$(PTA)_4Hg(NO_3)_2$	−58.0	46.4	1876

*δPTA = −104.4 (solid state).
†Δ is the complex coordination chemical shift = $(\delta_{complex} - \delta_{(free\ ligand)})$.

resulted in the precipitation of metallic mercury. This reduction to metallic mercury may be evidence for the strong basicity of PTA which we have observed in our study of molybdenum carbonyl complexes of PTA (20).

Elemental analyses were performed by M-H-W Laboratories, Phoenix, Arizona.

^{31}P-CP MAS NMR measurements

The mercury complexes were packed in Delrin spinners along with a small amount of KBr. The ^{79}Br resonance was used to set the spinning angle for each sample and side bands used to determine the spinning rate. Spinning rates of approximately 3.7 kHz were used.

The spectra were acquired at 81 MHz on a Bruker CXP-200 NMR spectrometer using a standard CP-MAS probe. 85% H_3PO_4 was used as an external reference. The spectra were obtained with proton decoupling and the spectrometer in a Fourier transform mode using 4K memory blocks. A total suppression of sidebands (TOSS) sequence was used as outlined by Dixon (6). Line broadenings of 0 or 20 Hz were found to give good spectra. Normally the number of scans needed to give good spectra were less than 1000 but up to 5000 scans were used in some cases to resolve the ^{199}Hg satellites.

Infrared and Raman spectra

Infrared spectra were recorded as Nujol mulls on a Nicolet 20 DXS FT-IR spectrometer.

Raman spectra were recorded on a Dilor, Omars 99 Multichannel Spectrometer using the multichannel mode and excitation line of 514.53 nm and laser power from 10 to 30 mW.

Results

The analytical results and melting points of the mercury compounds are given in Table 1. Some samples of the chloride, bromide, and nitrate were shown to be impure and these impurities were indicated in the ^{31}P NMR spectra. Samples of the cyanide gave low carbon analyses and appeared to be unstable to light.

The ^{31}P NMR results are shown in Table 2. Data for the major compounds are shown in the top part of the table and those for the $(PTA)_4HgX_2$ impurities observed in some samples are shown lower in the Table.

The infrared and Raman absorptions are shown in Table 3, together with possible assignments.

Discussion

The major mercury–PTA species produced seem to be largely independent of the mode of addition of the reagents or the ratio of reactants. The major species were $(PTA)_2Hg(NO_3)_2$ and $PTAHgX_2$ where X = Cl^-, Br^-, I^-, CN^-, and SCN^-. Minor impurities were observed in some spectra of the chloride, bromide, and nitrate. Analytical results of several samples of the chloride indicated the presence of species containing more than one PTA per mercury. Attempts to prepare the nitrate complex $PTAHg(NO_3)_2$ were unsuccessful and reactions involving aqueous solutions resulted in the precipitation of metallic mercury. The 1:2 nitrate complex in contrast with all the other complexes was slightly soluble in water but the solution darkened rapidly at room temperature and gave a broad resonance having no ^{199}Hg satellites in the ^{31}P NMR spectrum at −63 ppm. It is probable that $(PTA)_4Hg(NO_3)_2$ is being formed by decomposition in water, with the signal being

Can. J. Chem. Downloaded from www.nrcresearchpress.com by 194.225.253.170 on 09/07/12
For personal use only.

TABLE 3. Infrared and Raman spectral data with tentative assignments

Complex	Raman	Infrared	Assignment
$PTAHgCl_2$		447 s 388 s	PTA
		319 s	
	307 s		νHg—Cl terminal
	300 s(sh)		
	160 s		νHg—P
	152 s		νHg—Cl bridging
$PTAHgBr_2$	447 m	448 m	PTA
	385 w	388 m	
	308 w	303 w	
		253 m	
	213 m	227 m	νHg—Br
	146 s		νHg—P
$PTAHgI_2$	450 w	448 m	PTA
	389 w	390 m	
	132 s		νHg—I or νHg—P
$PTAHg(SCN)_2$	2121 s	2123 m	
	2096 s		SCN
	2090 s	2091 s	bridging and
	2075 m	2069 s(sh)	terminal
	454 w	449 m	PTA
	392 w	387 m	
	310 m	281 m	
	248 s	241 m	νHg—S terminal
	146 s		νHg—P
$PTAHg(CN)_2$*	2178 m		
	2147 m	2148 w	CN terminal
	2133 m	2135 w	and bridging
		449 m	PTA
		390 m	
		302 w	
$(PTA)_2Hg(NO_3)_2$*		1358 m(br)	Ionic
		1345 m(br)	NO_3^-
		450 m	PTA
		394 m	
PTA	450 m	452 m	
	435 s	405 m	
	404 s		
	257 m		

*These compounds decomposed during the observation of Raman spectra.

broadened by exchange with free PTA, since a resonance at −58 ppm is observed for this species in the solid state (see below). The reduction to metallic mercury in the attempted preparation of the acetate and perchlorate may be evidence of the high basicity of PTA as the deposition of metallic mercury from mercuric solutions is common with reducing ligands such as phosphines (7).

^{31}P CP-MAS NMR spectra

The spectrum of the nitrate indicated a major species and a minor impurity. The mercury satellites were well resolved using the total suppression of side band technique. The resonance at −29.9 ppm with $J(^{31}P—^{199}Hg)$ = 5111 Hz is attributed to the species $(PTA)_2Hg(NO_3)_2$. The coordination chemical shift is much larger than observed for the similar tricyclohexylphosphine (11*a*) or the tri-*n*-butylphosphine (11*b*) complex. The coupling constants of 4805 Hz for $(Cy_3P)_2Hg(NO_3)_2$ and 5200 Hz for $(Bu_3P)_2Hg(NO_3)_2$ are of similar magnitude and much smaller than for the monophosphine complexes, $Cy_3PHg(NO_3)_2$ (8540 Hz) and $Bu_3PHg(NO_3)_2$ (9230 Hz). The large coordination chemical shift for the PTA complex suggests a strong σ interaction, if we can assume that the C—P—C angles of this "tied back" phosphine cannot change appreciably. The only other comparable nitrate complex studied in the solid state was the triphenylphosphine complex $(Ph_3P)_2Hg(NO_3)_2$ studied by Allman and Lenkinski (5). This complex gave a lower coordination chemical shift (~46 ppm) and a higher coupling constant, 5560 Hz. The nitrate gave the highest coordination chemical shift and coupling constant of all the $(Ph_3P)_2HgX_2$ complexes studied and it is therefore tempting to suggest that the PTA and Ph_3P complexes are two coordinate ionic species $L_2Hg^{2+}2NO_3^-$.

The other PTA species observed at δ −58.0 ppm has a much smaller coordination chemical shift (46.4 ppm) and a much smaller coupling constant (1876 Hz). This coupling constant may be compared with the value for $(Me_3P)_4Hg(NO_3)_2$ (2255 Hz) observed by Schmidbaur and Räthlein (12) and the values for some chelate phosphine complexes observed by Dean

Can. J. Chem. Downloaded from www.nrcresearchpress.com by 194.225.253.170 on 09/07/12
For personal use only.

Can. J. Chem. Downloaded from www.nrcresearchpress.com by 194.225.253.170 on 09/07/12
For personal use only.

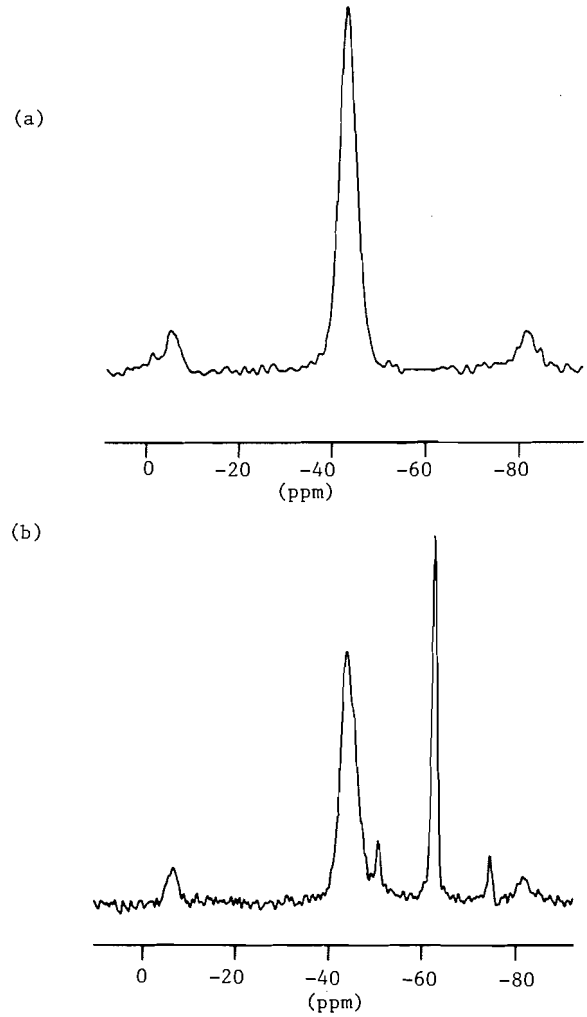


FIG. 1. The ^{31}P CP-MAS spectrum of $PTAHgBr_2$, (*a*) a pure sample; (*b*) an impure sample, showing the presence of $(PTA)_4Hg^{2+}$ (−62.8 ppm) in addition to $PTAHgBr_2$ (−44.1 ppm).

and Srivastava (13), e.g. $[Hg(dppp)_2]^{2+}$ (1979 Hz); dppp is bis(diphenylphosphino)propane. We therefore assign this species as $(PTA)_4Hg^{2+}2NO_3^-$.

Minor impurities were also observed by the appearance of peaks in some spectra of the chloride and bromide; spectra for the bromide are shown in Fig. 1. These resonances with coordination chemical shifts of 41.0 ppm (chloride) and 41.6 ppm (bromide) and $J(^{31}P—^{199}Hg)$ of 1937 and 1953 Hz, respectively, we also tentatively assign to the presence of the $(PTA)_4Hg^{2+}$ cation.

The remaining complexes of the form $PTAHgX_2$ show the previously observed correlation of increasing magnitude of the $J(^{31}P—Hg)$ with increasing electronegativity of the X ligand and the coordination chemical shift for the complex (11*a*, 14). This relationship is shown in Fig. 2; note that there are two points for both the cyanide and thiocyanate but that the line has been drawn using only one data point for these compounds (see later). The coordination chemical shifts are again larger than those observed in solution for other similar trialkyl–phosphine complexes (11) but the coupling constants are of a similar magnitude. Solid state spectra, with no potentially important solvent interactions, may differ from solution spectra but it has been shown that the chemical shift changes are small and coupling constant changes of a few hundred Hertz may be observed (5).

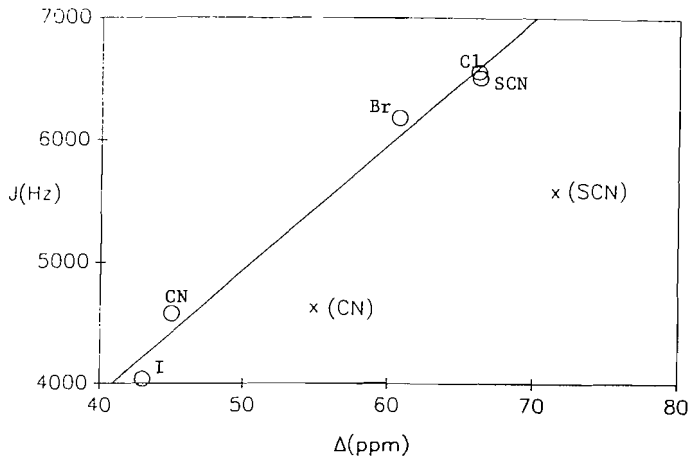


FIG. 2. The correlation of the coordination chemical shift Δ with $J(^{31}P—^{199}Hg)$ for the compounds $PTAHgX_2$.

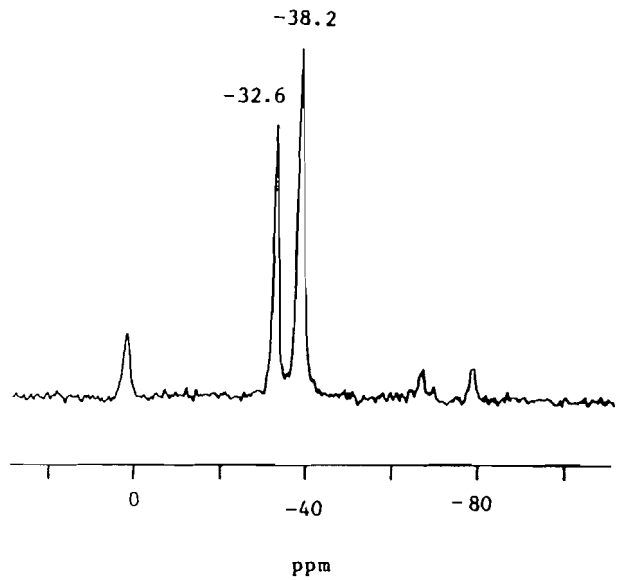


FIG. 3. The ^{31}P CP-MAS spectrum of $PTAHg(SCN)_2$.

The cyanide and thiocyanate deserve more discussion. Both complexes gave two ^{31}P resonances. The major peak for the cyanide at δ −50.4 ppm does not correlate with those for the other complexes but the minor resonance at δ −59.4 ppm correlates well with the peaks observed for the other 1:1 complexes. There may be two different infinite chains in this complex (5) but, in any case, the similar coupling constants observed for each species suggests a similar coordination environment for the mercury.

The thiocyanate also gave two well separated resonances, as illustrated in Fig. 3. The more intense resonance at δ −38.2 ppm with $\nu_{1/2}$ = 130 Hz was slightly broader than the resonance at δ −32.6 ppm and had a larger coupling constant (Table 2). $(Ph_3P)Hg(SCN)_2$ was observed to occur in two crystalline forms (15). Two species in solution (having similar chemical shifts but widely differing coupling constants) have also been observed for $(Bu_3P)Hg(SCN)_2$ (11*b*). Allman and Lenkinski (5) observed three species in the solid state spectrum of $(Ph_3P)_2Hg(SCN)_2$ although only one species was observed in solution. It appears that $(PTA)Hg(SCN)_2$ may exist in two crystalline forms consisting of two types of infinite chain.

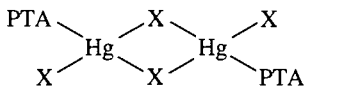
TABLE 4. Symmetric Hg—X (terminal) and Hg—P stretching frequencies for $(R_3P)HgX_2$ complexes

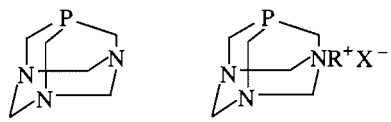
Complex	ν(Hg—X)	ν(Hg—P)	Reference
$PTAHgCl_2$	307	160	—
Ph_3PHgCl_2	286	156	17*a*
Cy_3PHgCl_2	270	145	17*a*
$t\text{-}Bu_3PHgCl_2$	266	123	18
$PTAHgBr_2$	213	146	—
Ph_3PHgBr_2	192	150	17*a*
Cy_3PHgBr_2	178	140	17*b*
$t\text{-}Bu_3PHgBr_2$	174	116	18
$PTAHgI_2$	132*	132*	—
Ph_3PHgI_2	143*	143*	17*a*
Cy_3PHgI_2	152	132	17*b*
$t\text{-}Bu_3PHgI_2$	138	110	18

*Only one band observed in this region.

Infrared and Raman spectra

The assignments in Table 3 are tentative but if correct indicate some interesting trends. For the chloride, bromide, and iodide we have tried to assign the mercury–halogen and mercury–phosphine stretching frequencies assuming the centrosymmetric structure found in the complex Ph_3PHgCl_2 (16)





PTA $PTAR^+X^-$

PTA has infrared absorptions at 452 and 405 cm^{-1} which are shifted on coordination to 448 and 388 cm^{-1}, respectively. The weak Raman absorption at 256 cm^{-1} was not observed in the complexes and so we have assigned all absorptions below 350 cm^{-1} to metal–halogen or metal–phosphorus vibrations.

The chloride should give rise to only one IR- and one Raman-active frequency, assuming C_{2h} skeletal symmetry. The IR spectrum gave an absorption at 319 cm^{-1} which we assign to the antisymmetric stretching frequency. The Raman spectrum gave a major band at 307 cm^{-1} with a shoulder at 300 cm^{-1}. Assigning these bands to the symmetric Hg—Cl vibrations also suggests a distortion from ideal C_{2h} symmetry. This is not surprising as PTA having a small cone angle may form polymeric structures observed for $HgCl_2(PMe_3)$ or $HgCl_2(PEt_3)$ (10). Bell *et al.* (17) have pointed out that small structural changes can have a marked influence on the IR spectral pattern but sometimes major structural variations can have very little influence on the spectrum. The observed frequencies are similar to other phosphine – mercury halide complexes (17, 18) as shown in Table 4, and so we feel confident that our assignments are correct. The changes observed for $\nu_s(HgX)$ for Cl, Br, and I are similar to the other complexes and show the same general trends. The ν(HgP) values are also similar. Thus it appears that the PTA complexes have a centrosymmetric structure or a chain polymer structure that approximates the centrosymmetric structure.

The thiocyanate gave more than two IR bands near 2100 cm^{-1} in accordance with the ^{31}P data indicating more than one environment for the SCN group. The absorptions are compatible with the expected Hg—S bonding and bridging of the SCN groups (18).

The IR absorptions of $PTAHg(CN)_2$ in the CN region were very weak and the observed Raman absorptions are comparable with the spectrum observed for $Cy_3PHg(CN)_2$ (19). This again suggests two types of CN groups and with the insight imparted by the ^{31}P NMR data is in agreement with a crystalline form containing two different polymeric structures.

The IR spectrum of the nitrate indicated the presence of ionic nitrate due to the broad absorptions at 1358 and 1345 cm^{-1}. Unfortunately this compound decomposed while the Raman spectrum was being observed and thus the presence of the two coordinate cation $(PTA)_2Hg^{2+}$ as indicated by the ^{31}P data was only partially confirmed by the vibrational spectral data.

Acknowledgements

E.C.A. thanks NSERC of Canada for continuing financial support. K.F. thanks the University of Khartoum for research leave.

We gratefully acknowledge Professor C. A. Fyfe for the use of his MAS probe and useful discussions concerning solid state NMR methodology. We also thank Professor D. E. Irish for recording the Raman spectral measurements at Waterloo.

1. D. J. DAIGLE, A. B. PEPPERMAN JR., and S. L. VAIL. J. Heterocycl. Chem. **11**, 407 (1974).
2. J. R. DELERNO, L. M. TREFONAS, M. Y. DARENSBOURG, and R. J. MAJESTE. Inorg. Chem. **15**, 816 (1976).
3. M. Y. DARENSBOURG and D. J. DAIGLE. Inorg. Chem. **14**, 1217 (1975).
4. D. J. DAIGLE and A. B. PEPPERMAN JR. J. Heterocycl. Chem. **12**, 579 (1975).
5. T. ALLMAN and R. E. LENKINSKI. Inorg. Chem. **25**, 3202 (1986).
6. W. T. DIXON. J. Chem. Phys. **77**, 1800 (1982).
7. (*a*) T. S. LOBANA. Coord. Chem. Rev. **63**, 161 (1985); (*b*) P. W. A. DEAN. Prog. Inorg. Chem. **24**, 109 (1978).
8. N. A. BELL, M. GOLDSTEIN, T. JONES, and I. W. NOWELL. Acta Crystallogr. B**36**, 708 (1980).
9. N. A. BELL, N. A. CHUDLEY, L. A. MARCH, and I. W. NOWELL. Inorg. Chim. Acta, **141**, 155 (1988).
10. N. A. BELL, M. GOLDSTEIN, T. JONES, and I. W. NOWELL. Inorg. Chim. Acta, **48**, 185 (1981).
11. (*a*) E. C. ALYEA, S. A. DIAS, R. G. GOEL, W. O. OGINI, P. PILON, and D. W. MEEK. Inorg. Chem. **17**, 1697 (1978); (*b*) R. COLTON and D. DAKTERNIEKS. Aust. J. Chem. **34**, 323 (1981).
12. H. SCHMIDBAUR and K. H. RÄTHLEIN. Chem. Ber. **106**, 2491 (1973).
13. P. A. W. DEAN and R. S. SRIVASTAVA. Can. J. Chem. **63**, 2829 (1985).
14. (*a*) S. O. GRIM, P. J. LUI, and R. L. KEITER. Inorg. Chem. **13**, 342 (1974); (*b*) R. L. KEITER and S. O. GRIM. J. Chem. Soc. Chem. Commun. 521 (1968).
15. R. C. MAKHIJA, R. RIVEST, and A. L. BEAUCHAMP. Can. J. Chem. **57**, 2555 (1979).
16. N. A. BELL, M. GOLDSTEIN, T. JONES, and I. W. NOWELL. Inorg. Chim. Acta, **43**, 87 (1980).
17. (*a*) N. A. BELL, M. GOLDSTEIN, T. JONES, and I. W. NOWELL. Inorg. Chim. Acta, **69**, 155 (1983); (*b*) T. ALLMAN, R. G. GOEL, and P. PILON. Spectrochim. Acta, **35**A, 922 (1979).
18. E. C. ALYEA, S. A. DIAS, R. G. GOEL, and W. O. OGINI. Can. J. Chem. **55**, 4227 (1977).
19. R. G. GOEL, W. P. HENRY, and W. O. OGINI. Can. J. Chem. **57**, 762 (1979).
20. E. C. ALYEA and K. J. FISHER. Inorg. Abstr. 172 and 420. Third Chemical Congress of North America, June 5–10, 1988. Toronto, Ont.

Can. J. Chem. Downloaded from www.nrcresearchpress.com by 194.225.253.170 on 09/07/12
For personal use only.

On the partitioning of the viscosity *B* coefficient and the correlation of ionic *B* coefficients with partial molar volumes of ions for aqueous and non-aqueous solutions

MONI MOHAN BHATTACHARYYA

Physical Chemistry Section, Department of Pure Chemistry, University College of Science, Calcutta-700009, India

Received September 26, 1988[1]

MONI MOHAN BHATTACHARYYA. Can. J. Chem. **67**, 1324 (1989).

A new method of partitioning the viscosity *B* coefficients has been proposed on the basis of the assumption that ionic *B* values should be a monotonic function of crystal radii cubed, independent of the sign of the charge, for aqueous and various non-aqueous systems. Ionic *B* values thus obtained in different solvents by a single method of division provide a basis for uniform comparison among themselves as well as with the existing values. The usual assumption of equal contributions of K^+ and Cl^- ions has been discarded. The internal consistency of the derived set of B_i values is demonstrated by correlation with the ionic radii, hydrated ionic radii, partial molal volumes, temperature coefficient of equivalent conductance, and partial molal ionic entropy. The salient feature of the set of B_i values is noted by its linear relationship not only with the partial molal volumes but the same is also observed with the ionic radii of ions of different valence and charge types. Eyring's equation for viscosity using Frank–Wen's model of ion–solvent interaction has been utilised for the calculation of void viscosity and electrostriction viscosity. The latter is compared with the corresponding component of partial molal volumes using the Drude–Nernst equation based on the continuum model for solvent.

Key words: ion–solvent model, ionic *B* values, *B* coefficients, division of *B* coefficient, void viscosity, micro viscosity.

MONI MOHAN BHATTACHARYYA. Can. J. Chem. **67**, 1324 (1989).

En faisant l'hypothèse que, pour des systèmes aqueux ainsi que divers systèmes non-aqueux, les valeurs ioniques B devraient être une fonction monotone du cube du rayon cristallin qui serait indépendante du signe de la charge, on propose une nouvelle méthode pour séparer les coefficients de viscosité *B*. Les valeurs ioniques *B* que l'on obtient ainsi, dans divers solvants et utilisant une seule méthode de division, peuvent servir de base pour faire une comparaison uniforme entre elles ainsi qu'avec des valeurs existantes. On n'a pas retenu l'hypothèse habituelle selon laquelle les contributions des ions K^+ et Cl^- sont égales. Pour démontrer la cohérence interne de l'ensemble des valeurs B_i qui en dérivent, on a utilisé une corrélation avec les rayons ioniques, les rayons ioniques d'hydratation, les volumes molals partiels, le coefficient de température de la conductivité équivalente et l'entropie ionique molale partielle. La caractéristique principale de l'ensemble des valeurs B_i est mise en évidence par leur relation linéaire non seulement avec les volumes molals partiels mais aussi avec les rayons ioniques des ions de valence et de types de charges différents. Pour le calcul des viscosités libre et d'électrostriction, on a utilisé l'équation de Eyring pour la viscosité et le modèle de Frank–Wen pour l'interaction ion–solvant. Faisant appel à l'équation de Drude–Nernst, basée sur le modèle continue pour le solvant, on a comparé la viscosité d'électrostriction avec la composante correspondante des volumes molals partiels.

Mots clés : modèle ion–solvant, valeurs ioniques *B*, coefficients *B*, division du coefficient *B*, viscosité libre, microviscosité.

[Traduit par la revue]

Introduction

The viscosities of aqueous and non-aqueous electrolyte solutions can be well represented by the following semi-empirical equation, introduced by Jones and Dole (1)

$$[1] \quad \eta/\eta_0 = 1 + A\sqrt{c} + Bc$$

where the first term, $A\sqrt{c}$, represents the contribution from the long range ionic interaction, theoretically calculated by Falkenhagen and Dole (2). The second term, known as the viscosity *B* coefficient, has been established as being additive (3–6) in the contributions from the cationic and anionic interactions with the solvent molecules. However, unlike some other similar additive properties, e.g., mobilities, diffusivities, for which sound experimental methods exist for the determination of the extremely important and revealing ionic values, there is as yet no definitive assignment (6–8) for the single ion *B* values.

A survey of the literature shows that the methods so far adopted to divide the *B* coefficient in different solvent systems are mostly based upon the viscosity–mobility relationship. Cox and Wolfenden (9) first carried out the partitioning of the *B* values in aqueous solutions by assuming that ionic components B_{Li^+} and $B_{IO_3^-}$ are proportional to the volumes of the solvated ions and hence inversely to the cubes of the ionic mobilities. Gurney (3) and later Kaminsky (10), partitioned the *B* coefficient by assuming the ionic *B* coefficient of K^+ ion is equal to that of Cl^- ion, based upon the equality of conductance values for the ions over a wide range of temperature. However, the division of *B* coefficient on the basis of KCl has been criticised by later workers (11–14) and as such, a number of alternatives to KCl has been suggested for the purpose.

In the case of non-aqueous systems, Tuan and Fuoss (15) utilised $B_{Bu_4N^+} = B_{Ph_4B^-}$ in acetonitrile solutions, Gopal and Rastogi (16) assumed $B_{Et_4N^+} = B_{I^-}$ at all temperatures in *N*-methyl propionamide solutions (NMP), Criss and Mastroianni (17) adopted the equality of B_{K^+} and B_{Cl^-} in methanol, and in dimethyl sulfoxide (DMSO), Yao and Bennion (18) assumed $B_{i\text{-}Am_3BuN^+} = B_{Ph_4B^-}$ to resolve the respective *B* values.

Martinus and Vincent (19) partitioned the *B* coefficient in formamide solution by constructing a correspondence plot of partial molar entropy and the ionic *B* coefficient, following the manner of Gurney (3). Besides, other methods similar to the extrapolation method (20) or Millero's tetraphenyl arsonium tetraphenyl boron method (21) as used for the separation of partial molal volumes have also been extended in a slightly modified form to the case of partitioning the *B* coefficients by Krumgalz (8) and Gill *et al.* (22), respectively. However, the results obtained by these methods (8, 22) are in poor agreement with each other for the same ions in the same solvent. It is also to be noted that the methods described are mostly specific for

[1]Revision received March 22, 1989.

Can. J. Chem. Downloaded from www.nrcresearchpress.com by 194.225.253.170 on 09/07/12
For personal use only.

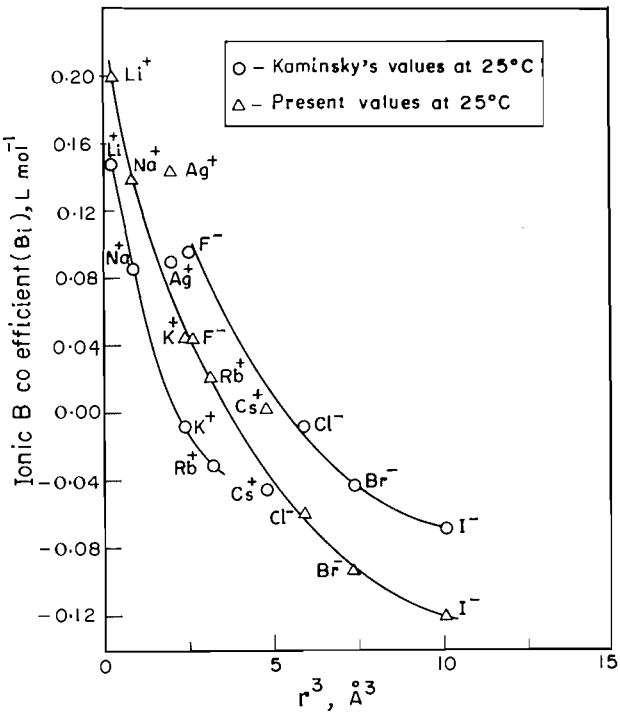


FIG. 1. The viscosity B coefficient of alkali metal ions and halide ions plotted against r_i^3 for two different values of B_i based on (*i*) $B_{K^+} = B_{Cl^-}$ scale and (*ii*) the proposed scale for aqueous system.

solvent, indicating the complexity of behavior of electrolyte solutions.

The purpose of the present article is therefore to propose a more general method for obtaining individual ionic values of B coefficient valid for both aqueous and non-aqueous systems from an entirely different approach.

Derivation of the model

It has been shown by various workers (4, 12, 23, 24) that there exist some correlations between the viscosity B coefficient and the partial molal volume (V) of a salt in solution, and these can be summarised either by the equation $B = 2.5\bar{V}$ or by the equation $B = a\bar{V}^0 - b$. Apart from these, the similarity of the two parameters with respect to additivity and measure of ion–solvent interaction has been well established. Moreover, since well known methods of separation of partial molal volumes are also applicable to B coefficient, it is assumed that the ionic B values should be monotonic functions of crystal radii cubed, independent of the sign of the charge. This follows from the treatment of Couture and Laidler (25) that for large monoatomic monovalent ions, B_i, like $\bar{V}_i^0$, does not depend on the sign of the charge (26).

The B values for alkali metal halides in aqueous system at 25°C are first of all partitioned on the basis of $B_{K^+} = B_{Cl^-}$ and then plotted against crystal radii cubed as shown in Fig. 1. As regards the choice of crystal ionic radii which are very critical for the present purpose, both the Pauling radii (27) and those of Gourary and Adrian (28) have been tried. However, the former is preferred since the derived set of B_i values are reasonable, give better fits with the radii, and show superior internal consistency with various other parameters as discussed in a later section. Figure 1 shows two smooth curves, one for the alkali metal ions, and the other for the halide ions. According to our assumption, since the B_i values for both monovalent cations and anions should be a smooth function of crystal radii cubed, irrespective of the charge of the ions, the curves for these two types of ions should merge on a single curve. It is interesting to note that if an estimated value of 0.052 is added to the B_i values of cations, and the same also is subtracted from those of the anions, the two curves smoothly fuse together into a single one, thus adding support to our assumption. The only alkali metal ion found to be off the line is Cs^+.

The method of partitioning the B values for aqueous system has been extended to other tempratures also, viz. 15°C, 35°C, and it has been found that the same estimated value (i.e., 0.052) is obtained in each of these cases. Thus, in order to get B_i values of any ion at any temperature, one requires to add 0.052(Z) to the cationic B values (10), and subtract the same from the anionic B values, as obtained on the assumption that $B_{K^+} = B_{Cl^-}$, where Z is the charge on the ion.

To test the applicability of the present method of division to other more complex monoatomic monovalent ions than the ions considered, the silver ion in aqueous solution has been chosen for this purpose and is shown in Fig. 1. The position of the ion is seen markedly off from the smooth curve given by the alkali metal and halide ions, and thus largely disagrees with the basic premise of the proposed model. Moreover, in such non-aqueous solvents as *N*-methyl formamide (NMF) (29, 30) and *N*-methyl propionamide (NMP) (16), the present method seems inapplicable.

However, the present method has been successfully applied to the partitioning of B coefficients for alkali metal halides in methanol (31, 32), formamide (19), dimethyl sulphoxide (33), ethylene carbonate (34), hexamethyl phosphotriamide (35), and sulfolane (36) solvents at 25°C. The initial B_i values required for B_i vs. r^3 plots were obtained on the basis of $B_{K^+} = B_{Cl^-}$ for methanol and formamide, whereas for the rest of the solvents $B_{Cs^+} = B_{I^-}$ was followed for the same purpose. The new set of B_i values thus obtained for monovalent ions together with the existing values for different systems are shown in Table 1. Also included in Table 1 are the different estimated values for addition or subtraction to the existing B_i values for all the solvents.

Results and discussion

The significance of the proposed model is best illustrated by the fact that the set of B_i values obtained in various solvents for different class of ions lead to internally consistent correlations with the ionic partial molal volumes, ionic radii, temperature coefficient of equivalent conductance and ionic partial molal entropy respectively.

Partial molal volume of ions

In Fig. 2, plots of B_i vs. $\bar{V}_i^0$ are shown for alkali metal and halide ions, using ionic B values of the new scale (Table 1, column 2) along with those of the existing ones. The $\bar{V}_i^0$ values were taken from the experimental values using ultrasonic vibration potential method (37). The figure illustrates that, while the nature of the B_i–$\bar{V}_i^0$ curve is U-shaped for the existing B_i values (10, 14), the new set of B_i values, excepting Li^+ ion, gives almost a linear plot with $\bar{V}_i^0$. Exactly similar plots are also obtained for the same ions in methanol and formamide systems using $\bar{V}_i^0$ values from the UVP method (37) and Mukerjee's method (38), respectively.

The B_i vs. $\bar{V}_i^0$ plots have also been extended to di- and trivalent cations and polyatomic anions in aqueous system. The $\bar{V}_i^0$ values ($H^+ = -4.5$ mL scale) for polyatomic anions,

Can. J. Chem. Downloaded from www.nrcresearchpress.com by 194.225.253.170 on 09/07/12
For personal use only.

TABLE 1. Ionic B coefficients and partial molal volumes of monovalent ions

	Water		Methanol		Formamide			
Ion	Present B_i (L mol^{-1}) (0.052)*	V_i^0 UVP method (mL mol^{-1})	Present B_i (L mol^{-1}) (0.040)*	V_i^0 UVP method (mL mol^{-1})	Present B_i (L mol^{-1}) (0.040)*	Krumgalz (8) B_i (L mol^{-1})	Martinus and Vincent (19) B_i (L mol^{-1})	V_i^0 Mukerjee method (38) (mL mol^{-1})
Li^+	0.2015	−11.2	0.486	—	0.345	0.31	0.309	−4.0
Na^+	0.1383	−7.4	0.454	−18.6	0.448	0.43	0.421	−2.5
K^+	0.045	3.4	0.422	−4.9	0.222	0.21	0.195	8.4
Rb^+	0.022	9.0	—	−2.8	0.199	0.18	0.173	12.4
Cs^+	0.007	15.5	0.221	3.3	0.173	0.15	0.146	18.7
Ag^+	0.143							
F^-	0.0445	3.3	—	−1.2				
Cl^-	−0.059	23.7	0.342	13.0	0.142	0.16	0.169	23.6
Br^-	−0.094	30.2	0.318	17.1	0.115	0.11	0.127	30.0
I^-	−0.1205	41.4	0.253	30.0	0.07	0.08	0.097	42.4
NMe_4^+	0.183	—	0.03†					
NEt_4^+	0.379	—	0.16†					
NPr_4^+	0.934	—	0.34†					
NBu_4^+	1.039	—	0.53†					

*Different estimated values.
†Reference 55.
‡Reference 56.

bivalent and trivalent cations taken from the compilations of Mukerjee (26), Millero (39), and Spedding's reported values (40), respectively, and the corresponding B_i values are all included in Table 2.

It is interesting to note that the B_i vs. $\bar{V}_i^0$ plots for various ions as mentioned, follow linear relationships in anticipation with the earlier assertions, and are summarised in the form of the following equation [2]

$$[2] \quad B_i = \pm a\bar{V}_i^0 \pm b$$

where a and b are adjustable parameters and the values, calculated by computerised least square technique, are shown in Table 3. The values of a in Table 3 indicate that contrary to what is stated in the Einstein relation (4), the B_i values of different class of ions do not increase monotonically with r_i either in aqueous or non-aqueous systems.

Crystal ionic radii and effective hydrated radii

The new set of B_i values for a number of uni-, di-, and trivalent cations and anions are plotted as a function of crystal ionic radius in Fig. 3. The most striking feature of the plot in the case of univalent ions for aqueous system is that a distinct minimum is obtained at the crystal radius 2.4 Å. The minimum demonstrates that the ion–dipole interaction persists up to this size and beyond this, formal ion–solvent interaction ceases to function, rendering the larger ions (polyatomic cations and anions) unhydrated. Nightingale (11) also observed a similar minimum at 2.3 Å in the plot of hydrated crystal radius versus crystal ionic radius for a number of uni-, di-, and trivalent ions, thus strengthening the above view point. The minimum is shifted considerably towards right (3.4 Å) for MeOH, formamide, and DMSO, indicating more ions within this size are also solvated in these solvents compared to water.

The B_i–r_i plots also show that not only the monovalent cations and anions fall on a single straight line but also the divalent ions and the trivalent ions follow similar paths, thereby supporting the very basis of the present model. The behavior of transition metal ions, e.g., the silver ion in aqueous solution as mentioned is quite anomalous, and has been explained in terms of an effective charge higher than the formal charge and due to the presence of the exposed d-electrons (41).

Temperature coefficient of limiting equivalent conductance

The ratio of the Walden product, $(\lambda^0\eta^0)^{25°C}/(\lambda^0\eta^0)^{0°C}$ at the two temperatures decreases with increasing ion size because of gradual decrease in peripheral charge; this function also seems to be related to the ionic B coefficient (4). The temperature coefficient of mobility for aqueous system has been calculated for temperatures 0 and 25°C, procuring data from the compilation of Robinson and Stokes (42), and are shown plotted versus ionic B coefficient in Fig. 4. Two different linear plots are obtained, one for alkali metal ions, and the other for anions. It also points out that the temperature coefficient values for K^+ and Cl^- ions are not the same, contrary to what was observed by Gurney from a similar plot, considering 0 and 18°C as the two intervening temperatures.

Partial molal entropy of ion

Gurney demonstrated a linear relation between the viscosity B coefficient and the partial molal entropy for monoatomic ions, based on the value −5.5 eu, as the absolute partial molal entropy of hydrogen ion at 25°C. However, the literature now abounds with compilations of such data by various workers (43), but due to variations in the values of partial molal entropies of ions, the recommended CODATA values (43) for monoatomic ions have been used for the present purpose. The scale is, however, based on $\bar{S}_{H^+} = 0.0$. Linear relations between ionic B coefficient and entropy for both the monoatomic cations and anions for aqueous system represented by two different lines are obtained (slopes and intercepts for cations, −0.007 and 0.225; anions, −0.006 and 0.025). Since the B coefficient is also a measure of order or disorder introduced by the ions in a solvent, the trend of the curves is in line with the concept of entropy.

Can. J. Chem. Downloaded from www.nrcresearchpress.com by 194.225.253.170 on 09/07/12
For personal use only.

in various solvents by different methods at 25°C

DMSO	HMPT		EC (40°C)		Sulpholane (30°C)	
Present B_i (L mol^{-1}) (0.100)*	Present B_i (L mol^{-1}) (0.06)*	Petrella (35) (L mol^{-1})	Present B_i (L mol^{-1}) (0.20)*	Petrella (34) B_i (L mol^{-1})	Present B_i (L mol^{-1}) (0.36)*	Petrella (36) B_i (L mol^{-1})
0.508	1.10	1.16	0.43	0.63	0.71	1.07
0.434	1.15	1.21	0.51	0.71	0.94	1.30
0.444	0.87	0.93	0.38	0.58	0.75	1.11
0.423	0.87	0.93	0.36	0.56	0.68	1.04
0.392	0.85	0.91	0.36	0.56	0.55	0.91
0.358	0.78	0.72	0.30	0.10	0.35	−0.01
0.399	0.73	0.67	0.31	0.11	0.42	0.06
0.372	0.60	0.54	0.28	0.08	0.40	0.04
0.10‡						
0.39‡						
0.85‡						

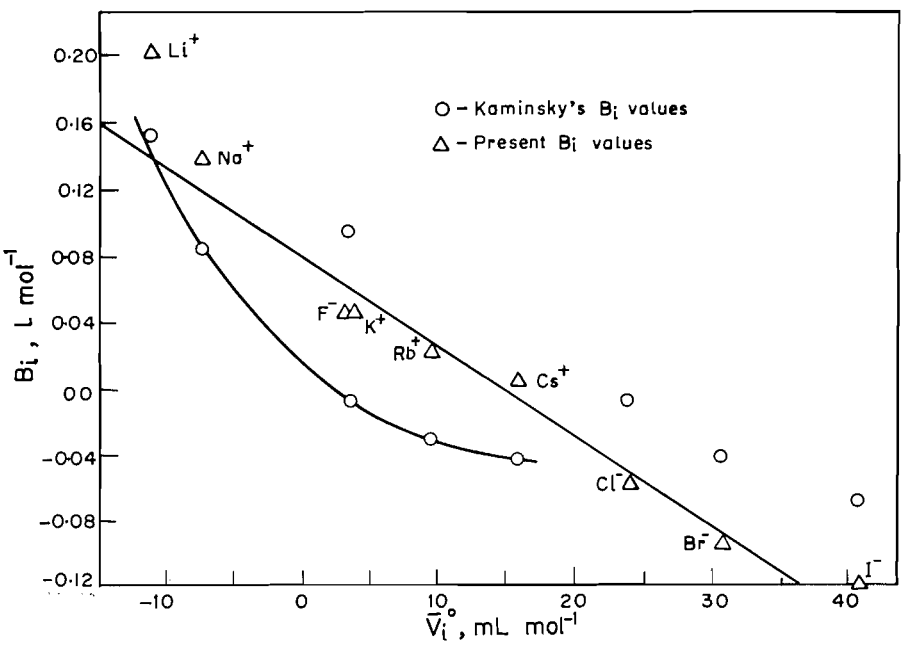


FIG. 2. Comparison of B_i vs. $\bar{V}_i^0$ plots for monovalent monoatomic ions between the B_i values of the existing scale and those of the proposed scale.

Comparison of B_i *values from other workers*

Based on the transition state theory, Feakins *et al.* (44) deduced the following equation [3] for viscosity B coefficient

$$[3] \quad B = \frac{\bar{V}_1^0 - \bar{V}_2^0}{1000} + \frac{\bar{V}_1^0}{1000}\left(\frac{\Delta\mu_2^{0\neq} - \Delta\mu_1^{0\neq}}{RT}\right)$$

where $\bar{V}_1^0$, $\bar{V}_2^0$ are partial molal volume of pure solvent and solute at infinite dilution. According to this equation, the viscosity B coefficient is a function of molar volume of solvent and therefore the order of increasing B_i values is

$$B_{water} < B_{Formamide} < B_{MeOH} < B_{EC} < B_{DMSO} < B_{TMS} < B_{HMPT}$$

The ionic values obtained here strictly follow this order, thereby justifying the present method (Table 1). However, the B_i values obtained by Sacco *et al.* (35) in EC and those by Bicknell *et al.* (33) in DMSO following identical method do not follow this order. Krumgalz's values (8) in methanol also deviate considerably from this trend.

The agreement between the different ionic values in form-

Can. J. Chem. Downloaded from www.nrcresearchpress.com by 194.225.253.170 on 09/07/12
For personal use only.

TABLE 2. Ionic B coefficient and partial molal volumes of higher valent cations and polyatomic anions in aqueous solution at 25°C

Ion	Pauling radius (Å)	B_i (L mol^{-1})	V_i^0 ($V_{H^+}^0 = -4.5$ mL) (26)	Ion	Pauling radius (Å)	B_i (L mol^{-1})	V_i^0 ($V_{H^+}^0 = -4.5$ mL) (26)
Ba^{2+}	1.35	0.324	−21.47	Dy^{3+}	0.99	0.816	−54.08
Sr^{2+}	1.13	0.369	−27.16	Ho^{3+}	0.97	0.827	−55.07
Ca^{2+}	0.99	0.389	−26.85	Er^{3+}	0.96	0.823	−56.21
Cu^{2+}	0.72	0.434	−36.76	ClO_3^-	2.88	−0.076	41.16
Mg^{2+}	0.65	0.489	−30.17	BrO_3^-	3.08	−0.046	39.8
Fe^{2+}	0.75	0.520	−33.7	IO_3^-	3.30	0.088	29.8
Ni^{2+}	0.70	0.510	−33.0	NO_3^-	2.64	−0.098	—
Zn^{2+}	0.74	0.429	−30.6	MnO_4^-	3.09	−0.111	47.0
La^{3+}	1.15	0.731	−52.52	ClO_4^-	2.92	−0.108	48.62
Pr^{3+}	1.09	0.739	−55.94	SO_4^{2-}	2.90	0.1045	22.98
Nd^{3+}	1.08	0.734	−56.42	CrO_4^{2-}	3.0	0.0621	28.7
Sm^{3+}	1.04	0.761	−55.48	PO_4^{3-}	2.96	−0.065*	
Tb^{3+}	1.0	0.810	−53.39	AsO_4^{3-}	3.14	−0.092*	

*Calculated from ref. 57.

Can. J. Chem. Downloaded from www.nrcresearchpress.com by 194.225.253.170 on 09/07/12
For personal use only.

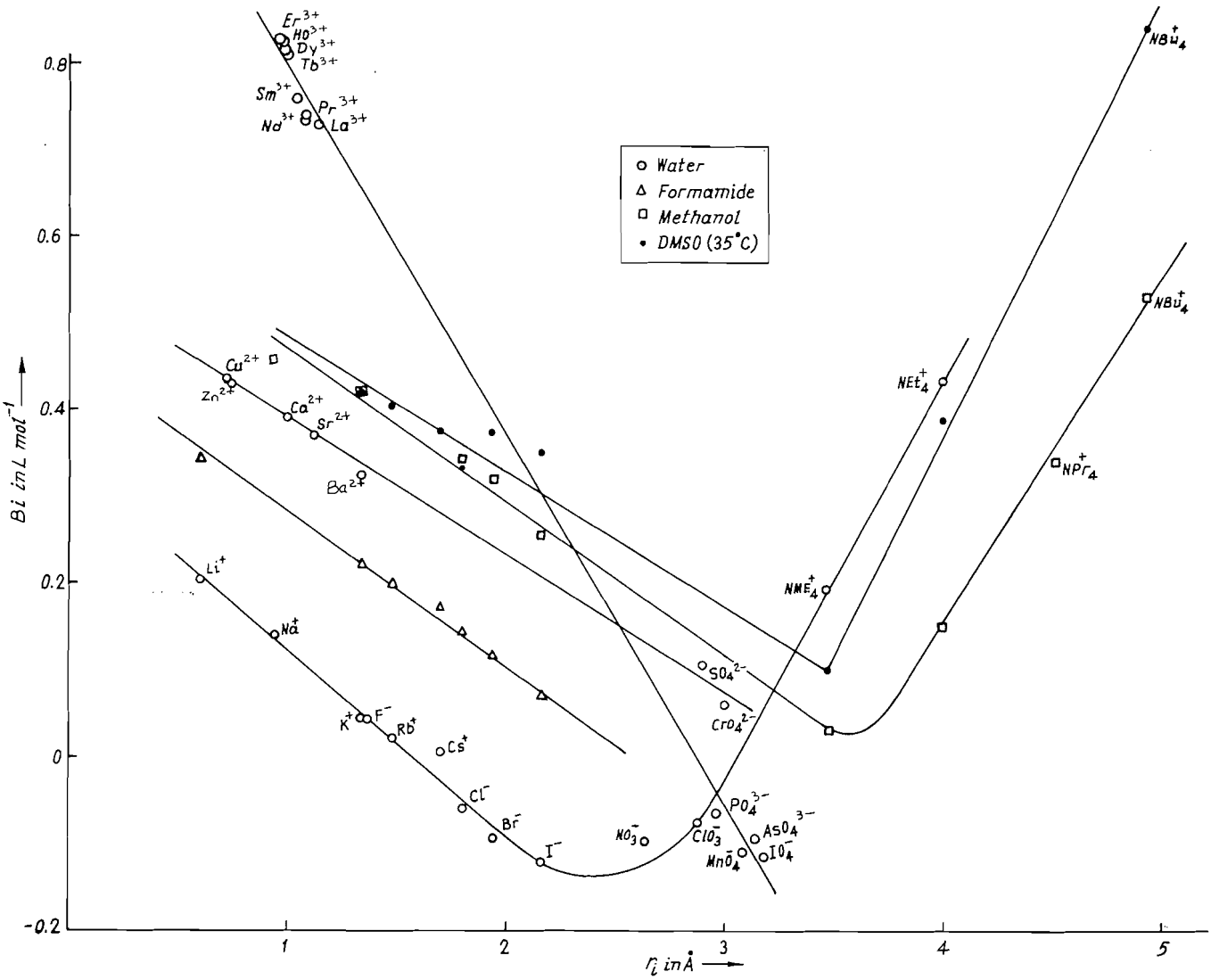


FIG. 3. Variation of ionic B values with crystal ionic radius at 25°C.

TABLE 3. Values of the parameters a and b in equation $B_i = \pm a\bar{V}_i^0 \pm b$ calculated by computerized least square method

Na^+, K^+, Rb^+, Cs^+, F^-, Cl^-, Br^-, I^-	−0.0052* ± 0.002	0.075* ± 0.015
	−0.0042† ± 0.001	0.3884† ± 0.009
	−0.0045‡ ± 0.0003	0.2551‡ ± 0.005
Ba^{2+}, Sr^{2+}, Ca^{2+}, Co^{2+}, Mg^{2+}, Fe^{2+}, Ni^{2+}, Zn^{2+}	−0.016 ± 0.0008	−0.032 ± 0.024
Pr^{3+}, Nd^{3+}, Sm^{3+}, Tb^{3+}, Dy^{3+}, Ho^{3+}	0.029 ± 0.0004	2.39 ± 0.022
ClO_3^-, BrO_3^-, IO_3^-, MnO_4^-, ClO_4^-	−0.010 ± 0.0004	0.391 ± 0.017

*Water.
†Methanol.
‡Formamide.

amide obtained by the present method with those of Krumgalz (8) and Vincent *et al.* (19) from entirely different assumptions is striking (Table 1). Very recently, Lawrence *et al.* (45) have obtained B_i value for bromide ion in HMPT (= 0.732) by using the extrapolation method, almost identical to our value of 0.73. However, very low anionic values in EC and especially negative value for chloride ion in sulfolane obtained by Sacco *et al.* (36) are not justified in these non-associated solvents. If steric hindrance is regarded as the origin for such low values, then one would also expect similar results in HMPT and DMSO.

Splitting of B_i *values*

Based on Frank and Wen's model (46) of ion–solvent interaction, Mandal *et al.* (47) has split the ionic viscosity B coefficient by the following relation [4] using Eyring's equation of viscosity proposed for non-associated liquids

$$[4] \quad B_i = A_1 r^3 - A_2 r^2 + A_3 \frac{Z^2}{r}$$

where the first, second, and the third term represent the intrinsic, void, and electrostriction viscosities of ions, respectively. If the intrinsic viscosity and void space viscosity are combined, the following relation [5] analogous to Hepler's semi-empirical relation (48) for ionic partial molal volume is obtained.

$$[5] \quad B_i = A_\eta r^3 + B_\eta \frac{Z^2}{r}$$

The first term originates from the geometry of the solvated ion and the second term from electrostriction.

Equation [5] has been tested graphically using the various B_i values of inorganic ions at 25°C in water, methanol, formamide, DMSO, EC, sulfolane, and HMPT (Fig. 5). Single straight line plots of $B_i r$ versus r^4 are obtained for cations and anions in most of the solvents, indicating the validity of eq. [5] as well as the similarity of cation–solvent and anion–solvent interactions in those solvents. Moreover, the inapplicability of the present method to the *N*-substituted amide solvents supports the earlier experimental observation by Kawaizumi and Zana (49) that the anionic solvation in these solvents is sterically hindered. The slopes (A_η) and intercepts (B_η) of eq. [5] obtained for different solvents are shown in Table 4.

Significance of A_η *values*

The A_η values shown in Table 4 are a reflection of void volumes of solvated ions transformed into the corresponding contribution to viscosity. Now since these two quantities are inversely related (47), one can expect the lowest value in water and steadily increasing values in the other solvents with increasing molar volumes (Table 4, column 2). Experimental

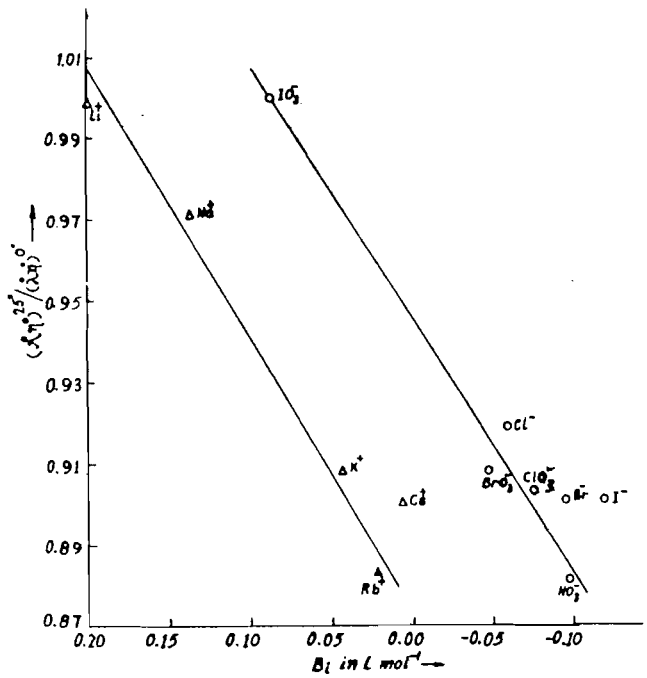


FIG. 4. Variation of $(\lambda^0\eta^0)^{25°C}/(\lambda^0\eta^0)^{0°C}$ with ionic B coefficient at 25°C for aqueous system.

values for the partial molal volumes (49, 50) show that the void volumes around ions are significantly smaller in methanol and propylene carbonate compared to that in water. The negative values obtained for the hydrogen bonded solvents are unwarranted by eq. [5]. However, if one recalls that the above equation was deduced for non-associated solvents, the negative values may be accounted for from the effect of destructuring of the hydrogen bonded solvents by these ions.

Electrostriction viscosity (B_η)

Electrostriction causes a decrement in volume but an increment in viscosity. The magnitudes of B_η shown in Table 4 indicate that electrostriction is lowest in water, moderate in formamide, EC, DMSO, and highest in methanol and HMPT. Zana *et al.* (49, 50) observed from experimental values of $\bar{V}_i^0$ a moderate electrostriction for water, ethanol, DMSO, and PC but higher for methanol and DMF.

The Drude–Nernst equation (51), which is based on a continuum model for a solvent, leads for monovalent ions to the equation

$$[6] \quad V_e = -\frac{Ne^2}{2Dr_i}\left(\frac{\partial \ln D}{\partial P}\right)_T = -\frac{\beta e^2}{2Dr_i}\left(\frac{\partial \ln D}{\partial \ln \rho}\right)_T$$

Can. J. Chem. Downloaded from www.nrcresearchpress.com by 194.225.253.170 on 09/07/12
For personal use only.

Can. J. Chem. Downloaded from www.nrcresearchpress.com by 194.225.253.170 on 09/07/12
For personal use only.

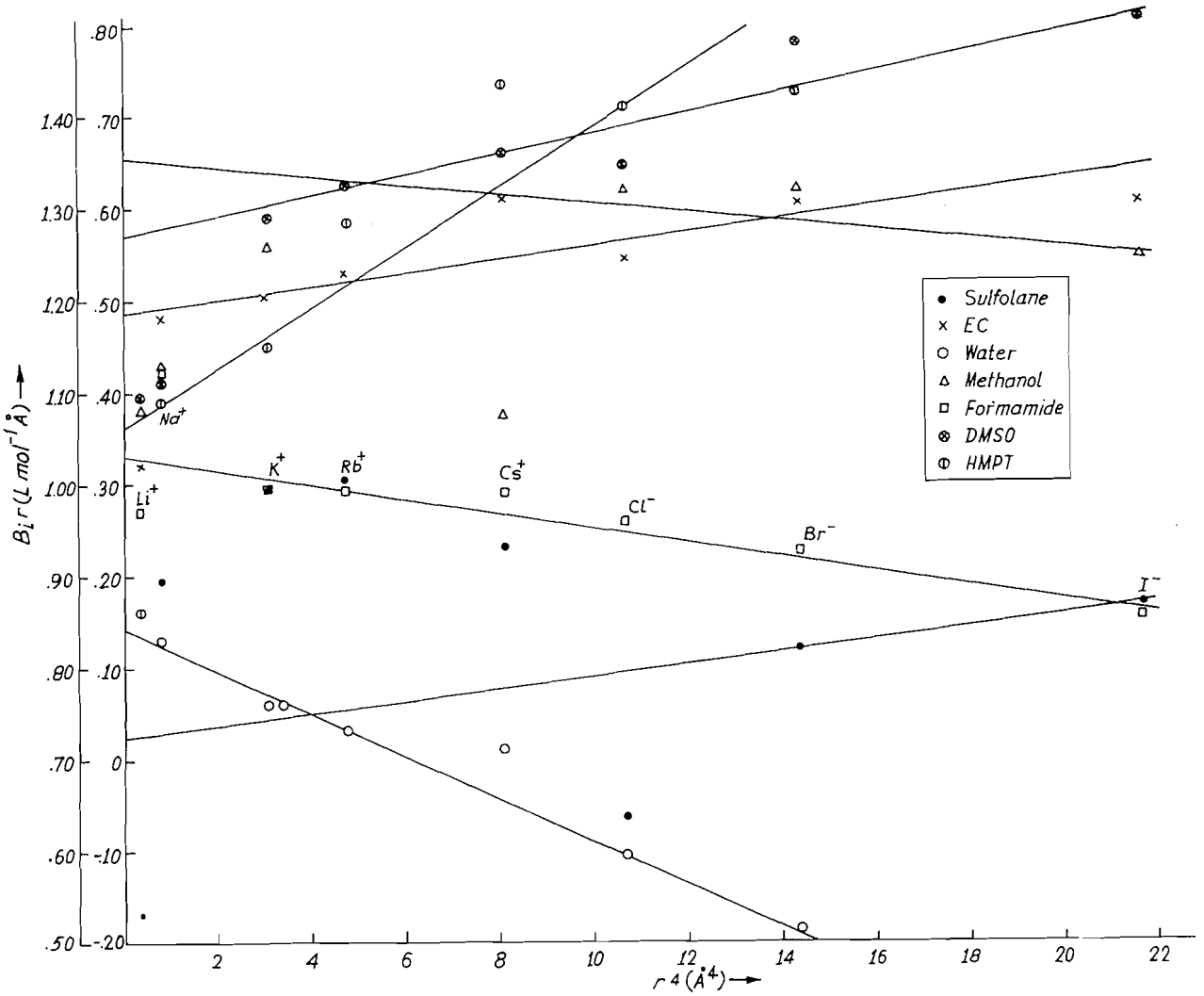


FIG. 5. Comparison of $B_i r$ vs. r^4 plots for alkali metal and halide ions in different solvents at 25°C.

TABLE 4. Comparison of the constants for the semi-empirical equation of the viscosity B coefficient of monovalent ions in various solvents at 25°C

System	A_η (L mol^{-1})	B_η (L mol^{-1})	Molal volume V (mL mol^{-1})	Dielectric constant	Isothermal compressibility 10^4 (cm^2 dyn^{-1})	V_e^0 (calcd) (mL mol^{-1})	B_η (calcd) (L mol^{-1})
Water	−0.023	0.142	18.05	78.3	4.53	3.99 (4.2)*	0.095
Formamide	−0.008	0.330	39.85	109.5	4.04	2.54	0.266
Methanol	−0.005	0.655	40.67	32.63	12.42	26.2 (24)*	0.498
EC	0.008	0.485	66.6	90.3			
DMSO	0.011	0.570	71.3	46.7	5.22	7.71	
Sulfolane	0.007	0.725	95.2	43.3			
HMPT	0.033	1.060	175.7	29.64	7.88	18.34	

*Reference 54.

where $\beta = (\partial \ln \rho/\partial P)_T$ is isothermal compressibility, D the dielectric constant, ρ, the density of the solvent. The equation predicts a direct proportionality between electrostriction volume (V_e) and compressibility but inverse with the dielectric constant of the medium. This is reasonably followed in the present case, as seen from Table 4. Since the electrostriction volume and electrostriction viscosity are proportional (47), one is tempted to convert the various calculated values of V_e using eq. [6] into the corresponding contribution of viscosity through eq. [2].

To calculate V_e values in various solvents, the $(\partial \ln D/\partial P)_T$ values required for the purpose are not available for most of the solvents. We have used instead the isothermal compressibilities

from the compilation of Dack *et al.* (52) following the suggestion of Kawaizumi and Zana (49). The dielectric constants (42, 53), compressibilities, and calculated values of V_e are all included in Table 4. The agreement between the B_η values and the converted V_e values in the three protic solvents is satisfactory, considering the approximate nature of D–N equations as well as other approximations. The results also point out that the continuum model works better in the case of viscosity than in partial molal volume (54) (Table 4).

Acknowledgements

The author is grateful to Professor M. Sengupta, Calcutta University, for encouragement and laboratory facilities offered during the course of this work. Financial assistance under minor research project by the U.G.C., India, is also gratefully acknowledged. The author also thanks the referees for their comments and helpful suggestions.

1. G. Jones and M. Dole. J. Am. Chem. Soc. **51**, 2950 (1929).
2. H. Falkenhagen and M. Dole. Phys. Z. **30**, 611 (1929).
3. R. W. Gurney. Ionic processes in solution. McGraw Hill, London. 1953.
4. R. H. Stokes and R. Mills. Viscosity of electrolytes and related properties. Pergamon Press, Oxford. 1965.
5. H. S. Harned and B. B. Owen. The physical chemistry of electrolytic solutions. 3rd ed. Reinhold, New York. 1957.
6. R. S. Dordick and W. Drost-Hansen. J. Phys. Chem. **85**, 1086 (1981).
7. B. E. Conway, R. E. Verrall, and J. E. Desnoyers. Z. Phys. Chem. **230**, 157 (1965).
8. B. S. Krumgalz. J. Chem. Soc. Faraday 1, **76**, 1275 (1980).
9. W. M. Cox and J. H. Wolfenden. Proc. R. Soc. (London), A**145**, 486 (1934).
10. M. Kaminsky. Discuss. Faraday Soc. **24**, 171 (1957).
11. E. R. Nightingale. J. Phys. Chem. **63**, 1381 (1959).
12. T. Isono and R. Tamamushi. Electrochim. Acta (London), **12**, 1479 (1967).
13. B. S. Krumgalz. Russ. J. Phys. Chem. **47**, 956 (1973).
14. H. D. B. Jenkins and M. S. F. Pritchett. J. Chem. Soc. Chem. Commun. **18**, 1041 (1983); J. Chem. Soc. **80**, 721 (1984).
15. D. F. T. Tuan and R. M. Fuoss. J. Phys. Chem. **67**, 1343 (1963).
16. R. Gopal and P. P. Rastogi. Z. Phys. Chem. (N.F.), **69**, 1 (1970).
17. C. M. Criss and M. J. Mastroianni. J. Phys. Chem. **75**, 2532 (1971).
18. N. P. Yao and D. N. Bennion. J. Phys. Chem. **75**, 1727 (1971).
19. N. Martinus and C. A. Vincent. J. Chem. Soc. Faraday I, **77**, 141 (1981).
20. B. E. Conway, R. E. Verrall, and J. E. Desnoyers. Trans. Faraday Soc. **62**, 2738 (1966).
21. F. J. Millero. J. Phys. Chem. **75**, 280 (1971).
22. D. S. Gill and A. K. Sharma. J. Chem. Soc. Faraday I, **78**, 476 (1982).
23. B. R. Breslau and I. F. Miller. J. Phys. Chem. **74**, 1056 (1970).
24. M. M. Bhattacharyya and M. Sengupta. Electrochim. Acta, **30**, 857 (1985).
25. A. M. Couture and K. J. Laidler. Can. J. Chem. **34**, 1209 (1956).
26. P. Mukerjee. J. Phys. Chem. **65**, 740 (1961).
27. L. Pauling. The nature of the chemical bond. 2nd ed. Cornell University Press, Ithaca, NY. 1945.
28. B. S. Gourary and F. J. Adrian. Solid State Phys. **10**, 127 (1960).
29. D. Feakins and K. G. Lawrence. J. Chem. Soc. A, 212 (1966).
30. P. P. Rastogi. Bull. Chem. Soc. Jpn. **43**, 2442 (1970).
31. G. Jones and H. J. Fornwalt. J. Am. Chem. Soc. **57**, 2041 (1935).
32. J. Einfeldt and E. Gerdes. Z. Phys. Chem. Leipzig, **246**, 221 (1971).
33. R. T. M. Bicknell, K. G. Lawrence, M. A. Seeley, D. Feakins, and L. Werblan. J. Chem. Soc. Faraday I, **72**, 307 (1976); **76**, 637 (1980).
34. G. Petrella and A. Sacco. J. Chem. Soc. Faraday I, **74**, 2070 (1978).
35. A. Sacco, G. Petrella, M. D. Monica, and M. Castagnolo. J. Chem. Soc. Faraday I, **73**, 1936 (1977).
36. A. Sacco, G. Petrella, and M. Castagnolo. J. Phys. Chem. **80**, 749 (1976).
37. R. Zana and E. Yeager. J. Phys. Chem. **71**, 521 (1967).
38. Utpal Sen. J. Phys. Chem. **35**, 81 (1977).
39. F. J. Millero. Chem. Rev. **71**, 147 (1971).
40. F. H. Spedding and M. J. Pikal. J. Phys. Chem. **70**, 2430 (1966); **70**, 2440 (1966).
41. F. Basolo and R. G. Pearson. Mechanism of inorganic reactions. Wiley Eastern Private Limited. 1973. p. 88.
42. R. A. Robinson and R. H. Stokes. Electrolyte solutions. Butterworths Scientific Publication, London. 1959. p. 373.
43. A. L. Horvath. Handbook of aqueous electrolyte solutions. Ellis Horwood Ltd. 1985. p. 262.
44. D. Feakins, D. J. Freemantle, and K. G. Lawrence. Trans. Faraday Soc. **70**, 795 (1974).
45. K. G. Lawrence, R. T. M. Bicknell, A. Sacco, and A. Dell'Atti. J. Chem. Soc. Trans. Faraday I, **81**, 1133 (1985).
46. H. S. Frank and W. Y. Wen. Discuss. Faraday Soc. **24**, 133 (1957).
47. P. K. Mandal, B. K. Seal, and A. S. Basu. Z. Phys. Chem. **87**, 295 (1973).
48. L. G. Hepler. J. Phys. Chem. **61**, 1426 (1957).
49. F. Kawaizumi and R. Zana. J. Phys. Chem. **78**, 627 (1974); **78**, 1099 (1974).
50. R. Zana, J. E. Desnoyers, G. Perron, R. L. Kay, and K. Lee. J. Phys. Chem. **86**, 3996 (1982).
51. P. Drude and W. Nernst. Z. Phys. Chem. **15**, 79 (1894).
52. M. R. J. Dack, K. J. Bird, and A. J. Parkin. Aust. J. Chem. **28**, 955 (1975).
53. K. Sing, D. K. Agarwala, and K. Kumar. J. Indian Chem. Soc. **52**, 304 (1975).
54. F. J. Millero. J. Phys. Chem. **73**, 2417 (1969).
55. R. L. Kay, T. Vituccio, C. Zawoski, and D. F. Evans. J. Phys. Chem. **70**, 2336 (1966).
56. R. Gopal and P. Singh. Indian J. Chem. **14A**, 388 (1976).
57. International Critical Tables. Vol. 5. McGraw Hill Book Co., New York, NY. 1928. p. 13.

Can. J. Chem. Downloaded from www.nrcresearchpress.com by 194.225.253.170 on 09/07/12
For personal use only.

Carbanions phosphonate préparés par voie électrochimique : formation et réactivité vis-à-vis d'un aldéhyde

JEAN-CHRISTOPHE LE MENN, JEAN SARRAZIN[1] ET ANDRÉ TALLEC

Laboratoire d'électrochimie, Unité associée au Centre national de la recherche scientifique, n° 439, Université de Rennes, Campus Beaulieu, 35042 Rennes, France

Reçu le 14 décembre 1988

JEAN-CHRISTOPHE LE MENN, JEAN SARRAZIN et ANDRÉ TALLEC. Can. J. Chem. **67**, 1332 (1989).

On a étudié la réactivité, vis-à-vis du *p*-méthoxybenzaldéhyde (noté ArCHO), de carbanions phosphonate formés par voie électrochimique. Les électrolyses sont effectuées sur cathode de mercure, en milieu DMF, et deux voies d'accès aux carbanions ont été comparées : (*i*) Déprotonation de phosphonates de formule générale $(EtO)_2P(O)CHYW$ (Y = W = Cl; Y = H, W = Cl; Y = Cl, W = CO_2Et; Y = H, W = CO_2Et; Y = CH_3, W = CO_2Et; Y = Cl, W = CH_3) par les bases résultant de l'électroréduction de l'azobenzène; dans tous les cas, le carbanion formé s'additionne au carbonyle pour conduire à l'adduit $(EtO)_2P(O)CYW(Ar)O^-$. (*ii*) La réduction biélectronique de phosphonates halogénés $(EtO)_2P(O)CXYW$ (X = Cl, Y et W comme ci-dessus; X = Br, W = CO_2Et, Y = Cl, Br, ou CH_3); si le carbone auquel est lié le groupement phosphonate ne porte aucun atome d'hydrogène (Y et W ≠ H) la même évolution conduisant à l'adduit ci-dessus est observée; par contre, si Y = H, le carbanion électrogénéré déprotone le substrat et c'est le carbanion résultant $(EtO)_2P(O)\bar{C}XW$ qui réagit avec l'aldéhyde pour conduire à $(EtO)_2P(O)CXW(Ar)O^-$.

L'évolution de l'intermédiaire anionique dépend de la nature des substituants W et Y (ou X) mais pas du mode de génération du carbanion : pour W = CO_2Et, quelle que soit la nature de Y, une élimination de phosphate de diéthyle avec formation d'un éthylénique est observée (réaction de Wittig–Horner); la même évolution se produit pour Y = W = Cl. Lorsque W = Cl et Y = H ou CH_3, le produit final est un époxyde phosphonate provenant d'une élimination d'ion chlorure (réaction de Darzens).

La stéréochimie des produits ne dépend que de Y et W; elle est indépendante du mode de formation du carbanion. Les rendements ne sont limités que par l'intervention de protonations parasites, liées à la basicité des carbanions phosphonate. L'analyse de l'ensemble des résultats permet de définir les conditions optimales d'électrolyse, utilisée comme technique de synthèse.

Mots clés : électrosynthèse, bases électrogénérées, phosphonates, Wittig–Horner.

JEAN-CHRISTOPHE LE MENN, JEAN SARRAZIN, and ANDRÉ TALLEC. Can. J. Chem. **67**, 1332 (1989).

Reactivity towards *p*-methoxybenzaldehyde (ArCHO) of electrochemically generated phosphonate carbanions has been investigated. Electrolyses were carried out at a mercury cathode in DMF and two routes to the desired carbanion have been compared: (*i*) Deprotonation of phosphonates of general formula $(EtO)_2P(O)CHYW$ (Y = W = Cl; Y = H, W = Cl; Y = Cl, W = CO_2Et; Y = H, W = CO_2Et; Y = CH_3, W = CO_2Et; Y = Cl, W = CH_3), by the bases resulting from the electroreduction of azobenzene; addition of the carbanion formed onto the carbonyl group takes place and leads to the adduct $(EtO)_2P(O)CYW(Ar)O^-$. (*ii*) Two-electron reduction of halophosphonates $(EtO)_2P(O)CXYW$ (X = Cl, Y and W as above; X = Br, W = CO_2Et, Y = Cl, Br, or CH_3); when no H atom is present on the carbon bearing the phosphonate group (Y and W ≠ H), the same evolution leading to the above adduct is observed; on the contrary, when Y = H, the electrogenerated carbanion deprotonates the substrate and the resulting carbanion $(EtO)_2P(O)\bar{C}XW$ reacts with the aldehyde, giving the adduct $(EtO)_2P(O)CXW(Ar)O^-$.

Evolution of the intermediate adduct depends on the substituants Y (or X) and W: when W = CO_2Et, whatever the nature of Y (or X), diethyl phosphate is eliminated with formation of the ethylenic ArCH=CWY (or X) (Wittig–Horner reaction); the same evolution is observed when Y = W = Cl. When W = Cl and Y = H or CH_3, the final product is the phosphonate epoxyde resulting from chloride elimination (Darzens reaction).

Chemo- and stereoselectivity depend only on the nature of Y and W but are independent of the mode of generation of the carbanion. Yields are limited by side-protonation reactions, which are related to the basicity of the phosphonate carbanions. Analysis of the results permits selection of the optimal electrolysis conditions for purposes of synthesis.

Key words: electrosynthesis, electrogenerated bases, phosphonates, Wittig–Horner.

Introduction

L'utilisation de carbanions phosphonate, comme intermédiaires de synthèse en chimie organique, a fait l'objet de nombreuses études (1, 2). La réaction de ces carbanions avec des composés carbonylés, qui a été réalisée pour la première fois par Horner *et al.* (3), est généralement considérée comme une modification de la réaction de Wittig et elle est dénommée réaction de Wittig–Horner ou réaction de Horner–Emmons.

$$RR'CO + (EtO)_2P(O)\bar{C}YW \rightarrow RR'C{=}CYW + (EtO)_2PO_2^-$$

Les carbanions phosphonate $(EtO)_2P(O)CYW^-$ peuvent résulter du traitement basique des phosphonates porteurs d'un atome d'hydrogène sur le carbone en α $(EtO)_2P(O)CHYW$. Différentes techniques ont ainsi été mises en oeuvre pour la conduite de réactions de Wittig–Horner. L'utilisation, en milieu homogène, dans de nombreux solvants, de bases telles que des alcoolates, des amidures ou des hydrures, correspond simplement à de légères modifications des conditions employées initialement par Horner *et al.* (3) ou par Wadsworth et Emmons (4). La catalyse par transfert de phase liquide–liquide a également retenu l'attention : elle implique un système biphasique constitué de soude aqueuse et d'un solvant organique, en présence de cations ammonium ou d'éthers-couronne ou même en l'absence de catalyseur (5). Enfin, plus récemment, l'utilisation d'une base minérale solide en suspension dans un solvant tel que le tétrahydrofuranne s'est avérée une technique de synthèse particulièrement efficace (6).

D'autre part, il a été montré que des bases électrogénérées,

1. Adresse actuelle : École nationale supérieure de chimie, 8, rue de l'École normale, 34000 Montpellier, France.

Printed in Canada / Imprimé au Canada

Can. J. Chem. Downloaded from www.nrcresearchpress.com by 194.225.253.170 on 09/07/12
For personal use only.

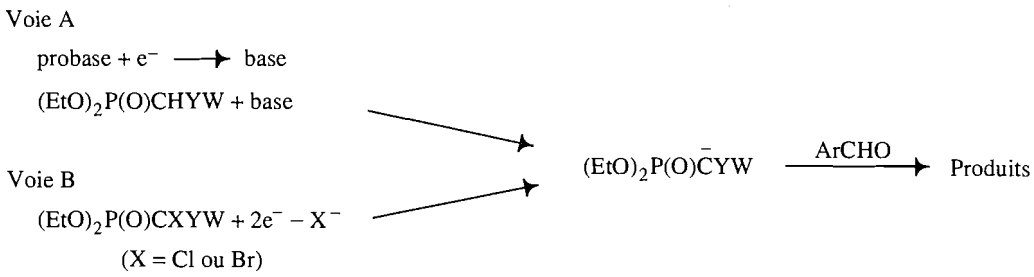


SCHÉMA 1

TABLEAU 1. Phosphonates étudiés

Phosphonate halogéné $(EtO)_2P(O)CXYW$ (X = Cl ou Br)		Phosphonate hydrogéné $(EtO)_2P(O)CHYW$		Carbanion attendu $(EtO)_2P(O)\bar{C}YW$	
—CXYW	n°	—CHYW	n°	—$\bar{C}$YW	n°
$-CCl_3$	**1**	$-CHCl_2$	**2**	$-\bar{C}Cl_2$	**1***A*
$-CCl_2H$	**2**	$-CH_2Cl$	**3**	$-\bar{C}ClH$	**2***A*
$-CCl_2CO_2Et$	**4**	$-CHClCO_2Et$	**5**	$-\bar{C}ClCO_2Et$	**4***A*
$-CHClCO_2Et$	**5**	$-CH_2CO_2Et$	**6**	$-\bar{C}HCO_2Et$	**5***A*
$-CCl(CH_3)CO_2Et$	**7**	$-CH(CH_3)CO_2Et$	**9**	$-\bar{C}(CH_3)CO_2Et$	**7***A*
$-CBr(CH_3)CO_2Et$	**8**				
$-CBr_2CO_2Et$	**10**			$-\bar{C}BrCO_2Et$	**10***A*
$-CClBrCO_2Et$	**11**				**4***A* ou **10***A*
$-CCl_2CH_3$	**12**	$-CHClCH_3$	**13**	$-\bar{C}ClCH_3$	**12***A*

résultant de la réduction cathodique de probases telles que l'azobenzène, sont capables de déprotoner des phosphonates que la présence de substituants attracteurs rend suffisamment acides; des réactions de Wittig–Horner peuvent ainsi être initiées par voie électrochimique (7, 8).

Par ailleurs, les phosphonates halogénés constituent une autre source de carbanions phosphonate. En effet, la réduction chimique, par le butyl lithium, à basse température, du trichlorométhylphosphonate de diéthyle **1** $(EtO)_2P(O)CCl_3$ a été étudiée par Seyferth et Marmor (9) puis par Normant et ses collaborateurs (10) : le dichloro carbanion lithié ainsi obtenu $(EtO)_2P(O)CCl_2Li$ peut être alkylé au moyen d'iodures ou de bromures d'alkyle; par réaction avec des aldéhydes ou des cétones, il conduit aux dichloro-1,1 alcènes correspondants.

La réduction électrochimique des phosphonates halogénés n'a donné lieu qu'à peu d'études; elles concernent presque exclusivement le trichlorométhylphosphonate **1**. En solution hydroalcoolique acide (11), l'électroréduction de celui-ci conduit, par coupures successives de liaisons carbone–chlore, aux dichlorométhylphosphonate **2** $(EtO)_2P(O)CCl_2H$ et chlorométhylphosphonate de diéthyle **3** $(EtO)_2P(O)CClH_2$. L'électroréduction de **1** a également été réalisée en milieu aprotique en présence d'électrophiles; nous avons ainsi montré qu'en présence d'halogénures d'alkyle RX, des dichloro-1,1 alkylphosphonates de diéthyle $(EtO)_2P(O)CCl_2R$ peuvent être synthétisés électrochimiquement (12). De même, une étude de l'électroréduction du phosphonate **1** en présence de composés carbonylés a été menée (13, 14); enfin, l'examen du comportement du phosphonodichloroacétate de triéthyle **4** $(EtO)_2P(O)CCl_2CO_2Et$ a fait l'objet d'une note préliminaire (14) : les alcènes chlorés attendus sont effectivement obtenus, mais les rendements ne dépassent pas 50–55%.

Le présent article est consacré à la génération par voie électrochimique de carbanions phosphonate et à l'étude de leur réactivité vis-à-vis d'aldéhydes.

Les phosphonates ont été choisis de telle sorte que soient disponibles à la fois le substrat hydrogéné $(EtO)_2P(O)CHYW$ et l'homologue halogéné $(EtO)_2P(O)CXYW$, afin qu'une comparaison puisse être établie entre les deux voies d'accès à un même carbanion (schéma 1) : déprotonation (voie A) ou réduction (voie B). Leurs formules sont regroupées dans le tableau 1. Compte-tenu de leur comportement, les substrats étudiés peuvent être classés en deux groupes selon qu'ils portent ou non un substituant carboxylate.

L'aldéhyde choisi est le paraméthoxybenzaldéhyde, noté ArCHO. Un tel composé présente en effet l'avantage de ne pas porter d'atome d'hydrogène sur l'atome de carbone en α du carbonyle; par ailleurs, la présence sur le noyau aromatique d'un substituant donnant un signal RMN est particulièrement intéressante pour l'analyse des produits de réaction.

Enfin, pour qu'une comparaison puisse être établie entre les comportements des différents phosphonates étudiés, les conditions de réaction ont été préalablement définies et un mode opératoire standard a été adopté.

Résultats et discussion

1. Détermination des conditions expérimentales

Le choix des conditions expérimentales résulte de l'étude de l'influence de deux paramètres (nature de l'électrolyte-support et concentration des réactifs) sur le rendement de la réaction de

Can. J. Chem. Downloaded from www.nrcresearchpress.com by 194.225.253.170 on 09/07/12
For personal use only.

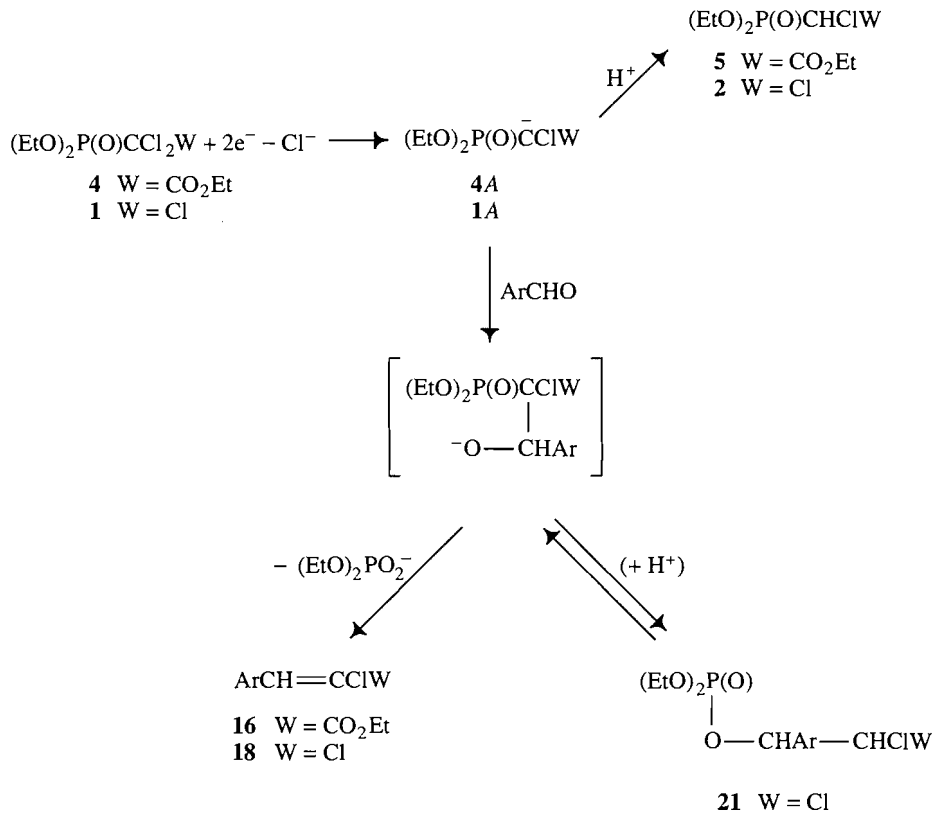


SCHÉMA 2

Wittig–Horner dans le cas de l'électroréduction du dichlorophosphonoacétate de triéthyle **4** et du trichlorométhylphosphonate de diéthyle **1** antérieurement examinée par d'autres auteurs.

L'électroréduction de **4**, à potentiel contrôlé en solution dans le DMF et en présence d'une quantité stoechiométrique de *p*-méthoxybenzaldéhyde, nécessite 2 faradays par mole. Elle conduit à un mélange de l'éthylénique attendu **16**, d'aldéhyde n'ayant pas réagi et de phosphonate réduit **5** qui résulte de la protonation du carbanion électrogénéré **4***A* (schéma 2). Les proportions dépendent de la concentration initiale des réactifs et de la nature du cation de l'électrolyte-support, comme on peut le constater à la lecture du tableau 2. Ce tableau montre que le carbanion intermédiaire **4***A* est plus facilement protoné par le cation tétrabutylammonium que par le cation tétraméthylammonium. D'autre part, on constate qu'une augmentation de la concentration des réactifs phosphonate et aldéhyde favorise l'attaque nucléophile du carbanion sur le carbonyle au détriment de sa protonation; le rendement en produit de Wittig–Horner est plus élevé.

Ces conclusions, relatives à l'intérêt de l'emploi du cation tétraméthylammonium et d'une concentration en réactifs élevée, sont confirmées par l'étude du comportement du phosphonate **1** : le tableau 3 montre en effet que les quantités de phosphonate réduit **2** et d'aldéhyde n'ayant pas réagi sont moins importantes lorsque ces conditions sont réunies. Le rendement de la réaction de Wittig–Horner est alors augmenté. Mais il semble surtout que ces conditions soient favorables à la formation du phosphate **21**, espèce qui résulte d'une évolution, sans élimination d'anion diéthylphosphate, de l'adduit formé entre le carbanion et l'aldéhyde (schéma 2). La présence de ce phosphate parmi les produits de réaction ne présente pas d'inconvénient majeur pour notre étude; en effet, sa formation n'a été observée qu'à partir du carbanion phosphonate dichloré **1***A*. De plus, ce phosphate peut être converti en éthylénique **18** par un traitement basique;

TABLEAU 2. Influence de la concentration des réactifs et de la nature du cation de l'électrolyte-support. Electroréduction du dichlorophosphonoacétate de triéthyle **4** dans le DMF (E_T = −0,7 V vs. AgI/Ag) en présence d'une quantité stoechiométrique de *p*-méthoxybenzaldéhyde ArCHO. Les rendements indiqués sont les rapports des quantités de matière obtenues après extraction à la quantité de phosphonate introduite dans la cellule d'électrolyse

C (mol L^{-1})	4×10^{-2}		10^{-1}	
Cation	Bu_4N^+	Me_4N^+	Bu_4N^+	Me_4N^+
ArCHO (%)	45	20	15	10
Phosphonate réduit **5** (%)	20	10	15	7
ArCH=CClCO$_2$Et **16** (%)	45	60	65	75

TABLEAU 3. Influence de la concentration des réactifs et de la nature du cation de l'électrolyte-support. Electroréduction du trichlorométhylphosphonate **1** dans le DMF (E_T = −1 V) en présence d'une quantité stoechiométrique de *p*-méthoxybenzaldéhyde ArCHO. Rendements calculés comme dans le tableau 2

C (mol L^{-1})	4×10^{-2}	10^{-1}	
Cation	Bu_4N^+	Bu_4N^+	Me_4N^+
ArCHO (%)	33	5	5
Phosphonate réduit **2** (%)	30	10	0
(EtO)$_2$P(O)—O—CHArCCl$_2$H **21** (%)	0	10	18
ArCH=CCl$_2$ **18** (%)	53	57	62

en particulier, on n'obtient pas **21** lorsque l'électrolyse est réalisée avec un léger excès de phosphonate **1** comparativement à l'aldéhyde : le milieu est alors rendu suffisamment basique par l'excès de carbanion **1***A* électrogénéré.

Can. J. Chem. Downloaded from www.nrcresearchpress.com by 194.225.253.170 on 09/07/12
For personal use only.

TABLEAU 4. Formation de carbanions phosphonate stabilisés par un groupement carboxylate. Electroréduction dans le DMF 0,1 mol L^{-1} en Me_4NBF_4. Phosphonate 3 mmol, *p*-méthoxybenzaldéhyde ArCHO 3 mmol; le cas échéant (+) azobenzène 1,5 mmol. Le résultat coulométrique est calculé par rapport à la quantité de phosphonate. Le rendement est calculé comme dans le tableau 2

Electrolyse	E1	E2	E3	E4	E5	E6	E7	E8	E9*
Phosphonate	**9**	**7**	**8**	**6**	**5**	**5**	**4**	**11**	**10**
$(EtO)_2P(O)CXYCO_2Et$									
X	H	Cl	Br	H	Cl	Cl	Cl	Br	Br
Y	CH_3	CH_3	CH_3	H	H	H	Cl	Cl	Br
Azobenzène	+			+					
E_T (V)	−1,1	−1,4	−1,0	−1,1	−1,3	−0,9	−0,7	−0,8	−0,9
Q (F/mol)	1,07	1,8	1,6	1,03	1,95	1,0	1,85	1,5	1,7
Aldéhyde recouvré (%)	0	10	30	0	22	43	10	30	27
Phosphonate réduit (%)	—	**9** 10	**9** 30	—	**6** 14	**6** 22	**5** 7	**5** 11	19
Éthylénique	$ArCH{=}C(CH_3)CO_2Et$ (**14**)			$ArCH{=}CHCO_2Et$ (**15**)		$ArCH{=}CClCO_2Et$ (**16**)			$ArCH{=}CBrCO_2Et$ (**17**)
Stéréochimie		*E*		*E*	*E*/*Z* 80 : 20		*E*/*Z* 30 : 70		*E*/*Z* 35 : 65
Rendement (%)	80	73	50	82	68	43	75	52	45

*Cathode de cuivre.

Aussi, pour conduire l'étude comparative des différents phosphonates, une concentration de 0,1 mol L^{-1} a été adoptée pour le phosphonate et l'aldéhyde, et le tétrafluoroborate de tétraméthylammonium a été choisi comme électrolyte-support. Les rendements observés dans ces conditions sont nettement supérieurs à ceux de la littérature (13, 14).

Notons de plus que la réduction électrochimique s'avère une méthode de synthèse intéressante : la conversion de l'aldéhyde en éthylénique chloré est en effet réalisée quantitativement si l'on met en oeuvre un excès de l'ordre de 10–20% du phosphonate initial. On forme alors du phosphonate réduit en quantité correspondante à cet excès; son élimination est très aisée puisqu'il est retenu sur la colonne par simple filtration sur silice (voir partie expérimentale).

II. Carbanions phosphonate substitués par un groupement carboxylate

Les résultats des électrolyses préparatives (repérées E1–E9) impliquant la formation intermédiaire de tels carbanions sont regroupés dans le tableau 4. Les expériences ont été conduites dans les conditions standard choisies comme cela a été indiqué précédemment.

1. Déprotonation (voie A) par les bases issues de l'électroréduction de l'azobenzène

On électrolyse, à un potentiel tel que seul l'azobenzène soit réduit, une solution contenant un mélange, dans les proportions molaires 0,5 : 1 : 1, d'azobenzène, d'aldéhyde et de phosphonate porteur d'un atome d'hydrogène. Parmi les phosphonates étudiés, seuls les composés **6** (Y = H) et **9** (Y = CH_3) peuvent se prêter à ce type d'étude; le dérivé **5** (Y = Cl) doit être exclu car il est aussi facilement réductible que l'azobenzène.

La réaction consomme environ 2 faradays par mole d'azobenzène, et l'on extrait un mélange d'hydrazobenzène et d'éthylénique. Ainsi, **6** et **9** (électrolyses E4 et E1) conduisent à une consommation complète de l'aldéhyde : la réaction de Wittig–Horner se produit quantitativement et les pertes que l'on remarque, si l'on effectue les bilans de matière dans le tableau 4, sont dues à l'extraction.

Le groupement carboxylate rend le phosphonate suffisamment acide pour qu'il n'intervienne pas de protonation parasite des bases électrogénérées par un autre donneur de proton; dans le même ordre d'idée, aucune protonation du carbanion intermédiaire n'est observée. Le mécanisme de la déprotonation du phosphonate a déjà été discuté (7) et est résumé sur le schéma 3.

Cette réaction est suivie d'une attaque nucléophile rapide du carbanion sur le carbonyle, puis de l'élimination de phosphate de diéthyle :

$$(EtO)_2P(O)\bar{C}YCO_2Et + ArCHO \rightarrow ArCH{=}CYCO_2Et + (EtO)_2PO_2^-$$

5*a* Y = H — **15**(*E*) Y = H

7*a* Y = CH_3 — **14**(*E*) Y = CH_3

On remarquera la stéréospécificité de la réaction qui conduit exclusivement à l'éthylénique de configuration *E*.

*2. Réduction (voie B) des phosphonates halogénés **4**, **5**, **7**, **8**, **10**, **11***

On électrolyse, au potentiel de réduction du phosphonate, une solution équimolaire de phosphonate $(EtO)_2P(O)CXYCO_2Et$ (X = Cl ou Br) et d'aldéhyde. Les produits extraits en fin d'électrolyse contiennent toujours une certaine quantité d'aldéhyde n'ayant pas réagi, du phosphonate réduit $(EtO)_2P(O)CHYCO_2Et$ (remplacement de l'halogène du substrat initial par un atome d'hydrogène) et un éthylénique (tableau 4). Aucun autre produit n'est mis en évidence.

2.1. Réduction avec élimination de l'ion chlorure (composés **4**, **5** et **7**). (*a*) Les réductions des phosphonates chloré **7** (X = Cl, Y = CH_3) et dichloré **4** (X = Y = Cl) conduisent avec des rendements satisfaisants aux éthyléniques attendus (électrolyses E2 et E7). L'étape électrochimique conduit au carbanion (**7***A* ou **4***A*) qui réagit principalement avec l'aldéhyde (schéma 4); une protonation parasite peu importante, par action de l'eau résiduelle ou du cation de l'électrolyte-support, entraîne la formation de phosphonate réduit (**9** ou **5**); la quantité d'aldéhyde recouvré reflète également l'importance de cette protonation.

Au plan stéréochimique, la réaction de Wittig–Horner est encore spécifique dans le cas du dérivé monochloré (formation exclusive de l'isomère *E*) alors que le phosphonate dichloré conduit à un mélange des deux isomères *E* et *Z* (proportion *E*/*Z* = 30 : 70).

On notera aussi dans ce dernier cas que le rendement en éthylénique est nettement supérieur à celui obtenu au terme d'électrolyses comparables, réalisées avec $LiClO_4$ comme électrolyte-support (14). Comme nous l'avons déjà montré

Can. J. Chem. Downloaded from www.nrcresearchpress.com by 194.225.253.170 on 09/07/12
For personal use only.

Can. J. Chem. Downloaded from www.nrcresearchpress.com by 194.225.253.170 on 09/07/12
For personal use only.

$$C_6H_5N{=}NC_6H_5 + e^- \rightleftarrows (C_6H_5NNC_6H_5)^{\cdot-}$$

$$(C_6H_5NNC_6H_5)^{\cdot-} + (EtO)_2P(O)CHYW \rightleftarrows (C_6H_5NHNC_6H_5)^{\cdot} + (EtO)_2P(O)\bar{C}YW$$

$$\begin{cases} (C_6H_5NHNC_6H_5)^{\cdot} + (C_6H_5NNC_6H_5)^{\cdot-} \rightleftarrows C_6H_5N{=}NC_6H_5 + (C_6H_5NHNC_6H_5)^- \\ (C_6H_5NHNC_6H_5)^{\cdot} + e^- \rightleftarrows (C_6H_5NHNC_6H_5)^- \end{cases}$$

$$(C_6H_5NHNC_6H_5)^- + (EtO)_2P(O)CHYW \rightleftarrows (C_6H_5NHNHC_6H_5) + (EtO)_2P(O)\bar{C}YW$$

Bilan

$$C_6H_5N{=}NC_6H_5 + 2e^- + 2\,(EtO)_2P(O)CHYCO_2Et \longrightarrow (C_6H_5NHNHC_6H_5) + 2\,(EtO)_2P(O)\bar{C}YCO_2Et$$

6 Y = H; **9** Y = CH_3 — **5***A* Y = H; **7***A* Y = CH_3

W = CO_2Et; Y = H ou CH_3

SCHÉMA 3

$$(EtO)_2P(O)CXYCO_2Et + 2e^- - X^- \longrightarrow (EtO)_2P(O)\bar{C}YCO_2Et$$

$$(EtO)_2P(O)\bar{C}YCO_2Et \xrightarrow{+\,ArCHO} \xrightarrow{-\,(EtO)_2PO_2^-} ArCH{=}CYCO_2Et$$

$$(EtO)_2P(O)\bar{C}YCO_2Et \xrightarrow{+\,H^+} (EtO)_2P(O)CHYCO_2Et$$

7	X = Cl; Y = CH_3	**7***A*	**14** (*E*)	**9**
8	X = Br; Y = CH_3			
4	X = Cl; Y = Cl	**4***A*	**16** (*E*/*Z* 30 : 70)	**5**
11	X = Br; Y = Cl			
10	X = Br; Y = Br	**10***A*	**17** (*E*/*Z* 35 : 65)	

SCHÉMA 4

(12), la présence d'ions Li^+ dans le milieu inhibe partiellement la nucléophilie des carbanions électrogénérés.

(*b*) Le phosphonate chloré **5** (X = Cl, Y = H) présente un comportement particulier.

La réduction à −0,9 V (électrolyse E6) ne consomme qu'un électron par molécule de substrat; elle ne conduit pas au composé attendu **15** mais à l'éthylénique chloré **16**. Ce résultat s'explique par une protonation du carbanion électrogénéré **5***A* par le phosphonate initial (schéma 5). L'équilibre acido-basique (réaction [2]) est très déplacé vers la droite, conformément à l'effet attendu du substituant chloro (**5** est plus acide que **6**). De plus, le transfert de proton étant plus rapide que l'attaque d'un carbanion sur l'aldéhyde, seul le carbanion chloré **4***A* réagit pour conduire au produit **16** de la réaction Wittig–Horner (réaction [3] du schéma 5); à l'appui de cette interprétation, notons que la proportion des isomères **16**(*E*) et **16**(*Z*) est la même que celle obtenue lors de la réduction du phosphonate dichloré **4**.

Dans ces conditions, le rendement en **16** ne saurait excéder 50% puisque la moitié du phosphonate initial est consommé comme probase. Les pourcentages indiqués dans le tableau 4, si l'on tient compte des difficultés d'extraction des phosphonates, sont en parfait accord avec cette interprétation, et le bilan de la réduction de **5** à −0,9 V peut s'écrire :

$$\underset{\mathbf{5}\,(100\%)}{2(EtO)_2P(O)CHClCO_2Et} + 2e^- + \underset{(50\%)}{ArCHO} \rightarrow$$

$$\underset{\mathbf{6}\,(50\%)}{(EtO)_2P(O)CH_2CO_2Et} + \underset{\mathbf{16}\,(50\%)}{ArCH{=}CClCO_2Et} + Cl^- + (EtO)_2PO_2^-$$

Des résultats très différents sont obtenus lors de la réduction du même substrat (X = Cl, Y = H) au potentiel −1,3 V (électrolyse E5). Le résultat coulométrique est proche de 2 F/mol, et l'éthylénique extrait est le produit non chloré **15**. En outre, les deux isomères **15**(*E*) et **15**(*Z*) sont présents, contrairement à ce qui a été observé par déprotonation de l'homologue hydrogéné **6** au cours de l'électrolyse E4. Pour rendre compte de la présence de **15**(*Z*), il est donc nécessaire de proposer une voie d'accès à **15** autre que la réaction du carbanion **5***A* avec l'aldéhyde.

Nous avons vérifié que le chlorocinnamate d'éthyle **16**, non électroactif à −0,9 V, est réduit lentement à −1,3 V. Cependant, cette réaction électrochimique (étape [4] du schéma 5) ne peut à elle seule expliquer les résultats obtenus : d'une part, comme pour l'électrolyse E6, le rendement en éthylénique **15** ne devrait pas excéder 50%; d'autre part, le pourcentage en isomère **15**(*E*) est supérieur à celui attendu par électroréduction de **16**.[2]

L'ensemble des réactions qui permettent de rendre compte de l'électrolyse de **5** à −1,3 V (E5) est regroupé sur le schéma 5. L'obtention d'un rendement en **15** supérieur à 50% est attribuable au rôle de probase joué par **16**. En effet, le carbanion vinylique issu de **16** est suffisamment basique pour déprotoner les phosphonates **5** et **6** (réactions [5] et [6]). La déprotonation de **5**, qui est le plus acide, doit conduire, par l'intermédiaire de

2. Nous avons vérifié qu'en présence d'un donneur de protons la réduction électrochimique de **16** s'effectue avec rétention de configuration; ainsi un mélange des deux isomères **16**(*E* et *Z*), en proportion 30 : 70 conduit à un mélange des deux isomères **15**(*E* et *Z*), en proportion 70 : 30.

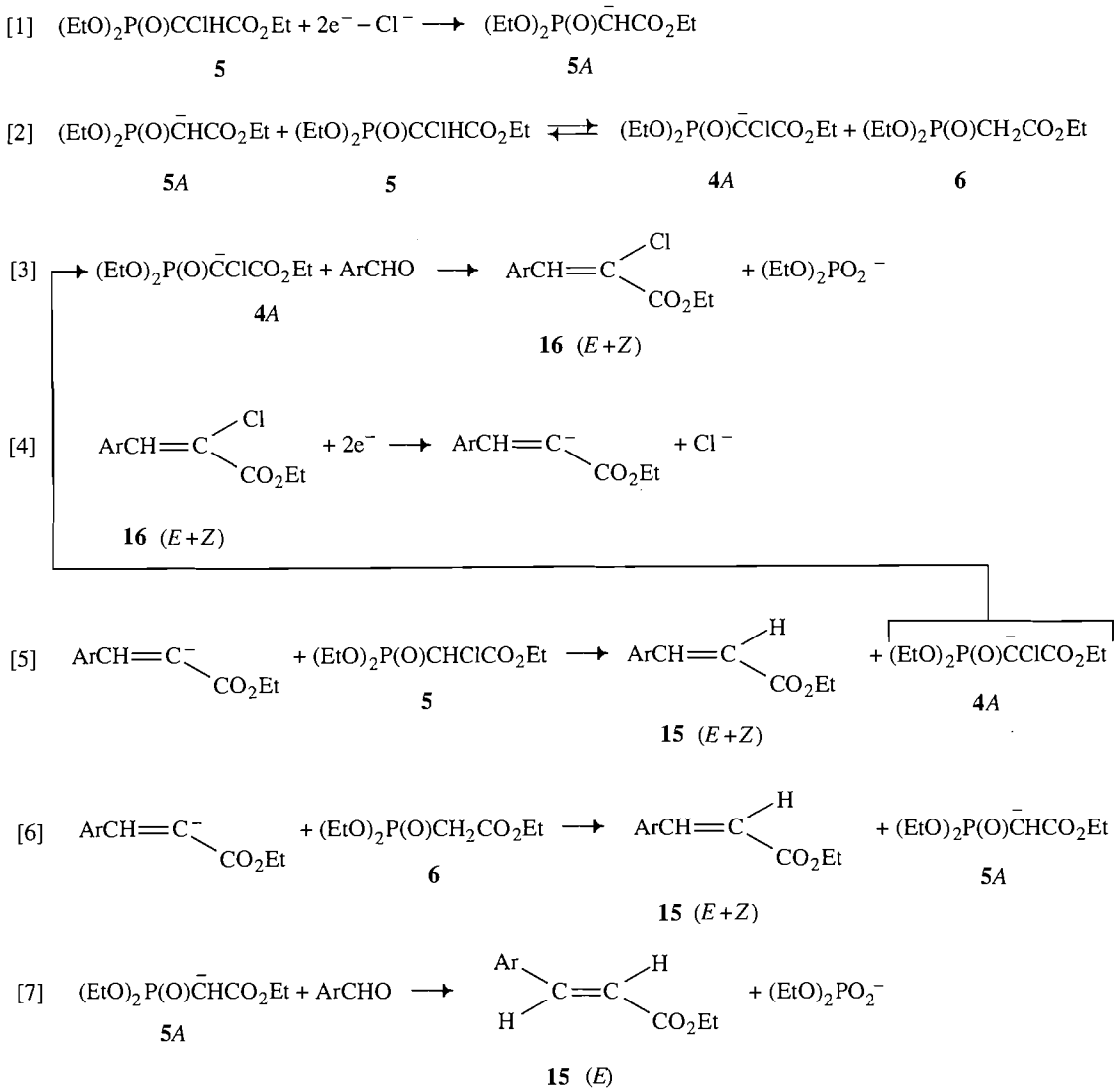


SCHÉMA 5

4A, au mélange d'isomères *Z* et *E*. Celle de **6**, qui interviendra surtout vers la fin de l'électrolyse, lorsque **5** aura été consommé, conduit, par l'intermédiaire de **5A**, au seul isomère *E* (réaction [7]). L'écart entre le résultat stéréochimique des électrolyses E6–E8 et celui de l'électrolyse E5 est attribuable à l'intervention de cette dernière réaction. Enfin, la quantité d'aldéhyde n'ayant pas réagi est liée à l'importance des protonations parasites de tous ces carbanions.

2.2. Réduction avec élimination de l'ion bromure (composés **8**, **10** et **11**). (*a*) Elle est observée dans le cas du dérivé monobromé **8**, du dérivé dibromé **10** et du dérivé chlorobromé **11**; comme attendu, dans ce dernier cas, il y a coupure sélective de la liaison C—Br.

Les électrolyses correspondantes s'accompagnent d'un déficit coulométrique marqué par rapport aux 2 faradays par mole attendus; de plus, le rendement en produit de Wittig–Horner est plus faible. Les réactions du schéma 4 (X = Br) n'interviennent donc que pour une part. A priori, deux types de comportement supplémentaires peuvent expliquer la différence observée entre substrats bromés et analogues chlorés : (*i*) L'existence d'une réaction de substitution nucléophile entre le carbanion électrogénéré et le composé bromé initial justifierait le déficit coulométrique; cette hypothèse ne nous paraît pas devoir être retenue car nous n'avons jamais pu mettre en évidence la formation du diphosphonate auquel conduirait cette réaction. (*ii*) Il est plus vraisemblable que l'étape électrochimique corresponde, en partie, à un transfert monoélectronique avec élimination d'ion bromure et formation d'un radical; le même phénomène a déjà été observé lors de la réduction de bromures d'alkyle sur cathode de mercure (15). Dans cette hypothèse, le phosphonate réduit, présent en quantité notable, se formerait également par transfert d'atome d'hydrogène du solvant sur le radical intermédiaire.

(*b*) À l'appui de l'interprétation précédente, il convient d'indiquer les difficultés particulières rencontrées lors de l'électrosynthèse du bromocinnamate **17** à partir du phosphonate dibromé **10**. Dans les conditions standard (cathode de mercure, sel de tétraméthylammonium), le rendement en éthylénique **17** est inférieur à 5%, l'aldéhyde est presque entièrement récupéré en fin d'expérience. En cours d'électrolyse, la précipitation du bromure de tétraméthylammonium (qui indique la formation d'ions bromure en solution) ne se produit que tardivement; de plus, le mercure a tendance à se rassembler en petites billes ternes comme celà se produit lors de formation d'espèces radicalaires ou de composés organomercuriques (16).

Ces inconvénients peuvent être évités soit en utilisant un sel de tétrabutylammonium si la cathode est en mercure, soit

Can. J. Chem. Downloaded from www.nrcresearchpress.com by 194.225.253.170 on 09/07/12
For personal use only.

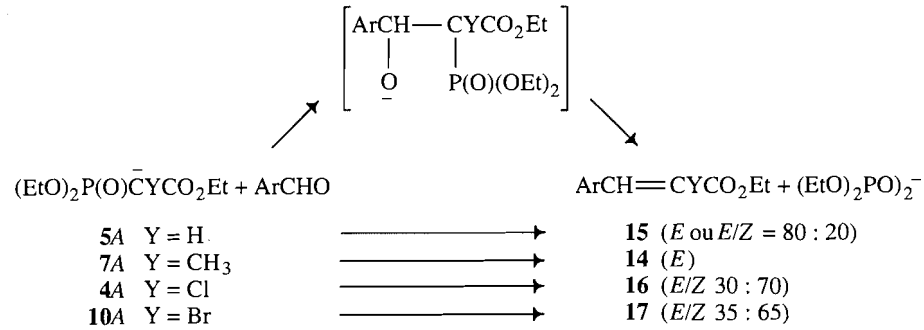


SCHÉMA 6

TABLEAU 5. Déprotonation des phosphonates **2**, **3** et **13** au moyen des bases électrogénérées par réduction de l'azobenzène dans le DMF 0,1 mol L^{-1} en Me_4NBF_4 en présence de *p*-méthoxybenzaldéhyde ArCHO; phosphonate 3 mmol, ArCHO 3 mmol, azobenzène, 1,5 mmol. Le résultat coulométrique est calculé par rapport à la quantité de phosphonate. Le rendement est calculé comme dans le tableau 2

Electrolyse	E10	E11	E12
Phosphonate	**2**	**13**	**3**
$(EtO)_2P(O)CHYW$			
Y	Cl	CH_3	H
W	Cl	Cl	Cl
E_T (V)	−0,9	−0,8	−0,6
Q (F/mol)	1,05	1,2	1,0
Aldéhyde recouvré (%)	0	13	8
Phosphonate recouvré (%)	0	28	13
Produits (%)	$ArCH{=}CCl_2$ (**18**) (56) $(EtO)_2P(O){-}O{-}CH(Ar)CCl_2H$ (**21**) (14)	$(EtO)_2P(O){-}C(CH_3){-}CHAr$ (O) (**19**) (*E*/*Z* 60 : 40) (34)	$(EtO)_2P(O){-}CH{-}CHAr$ (O) (**20**) (*E*/*Z* 70 : 30) (72)

en conservant le cation tétraméthylammonium mais en utilisant une cathode de cuivre. Les rendements obtenus dans ces dernières conditions sont indiqués dans le tableau 4 (électrolyse E9).

3. Conclusion

On retiendra de cette étude que les quatre carbanions phosphonate, porteurs d'un groupement carboxylate, mis en jeu dans les électrolyses E1–E9 donnent une réaction d'addition sur le *p*-méthoxybenzaldéhyde, même si le carbanion est par ailleurs substitué par un atome de chlore ou un atome de brome. L'adduit ainsi formé se décompose avec élimination de phosphate de diéthyle pour conduire à un dérivé éthylénique.

L'ensemble des résultats est résumé sur le schéma 6.

La stéréosélectivité de la réaction est imposée par les étapes chimiques. Elle apparaît indépendante du mode de formation du carbanion mais varie selon la nature du substituant Y. Si celui-ci est un atome d'hydrogène ou un groupement méthyle, la réaction conduit exclusivement à l'éthylénique de configuration *E*. Par contre, si celui-ci est un atome d'halogène, on obtient un mélange où prédomine l'isomère *Z*, la stéréosélectivité étant légèrement supérieure pour Y = Cl.

On se rappelera enfin que du fait de la présence d'un atome d'hydrogène sur le phosphonate **5**, le carbanion qui réagit sur l'aldéhyde n'est pas le carbanion formé par réduction, mais celui-ci issu de la déprotonation du substrat.

III. Carbanions phosphonate halogénés sans substituant carboxylate

1. Déprotonation par les bases issues de l'électroréduction de l'azobenzène (voie A)

On électrolyse, à un potentiel tel que seul l'azobenzène soit réduit, une solution contenant un mélange d'azobenzène (1,5 mmol), de *p*-méthoxybenzaldéhyde ArCHO (3 mmol) et de phosphonate (3 mmol). Les phosphonates concernés $(EtO)_2P(O)CHYW$ sont **2** (Y = W = Cl), **3** (Y = H, W = Cl) et **13** (Y = CH_3, W = Cl) (tableau 5).

(a) L'étape de déprotonation. La réduction de l'azobenzène dans ces conditions consomme 2 faradays par mole et conduit à l'hydrazobenzène que l'on extrait parmi les produits d'électrolyse. On constate que le cours de la réaction dépend du phosphonate étudié. En effet, lorsque l'électrolyse est réalisée en présence de **2** (électrolyse E10), la solution reste incolore, alors que en présence de **13** ou de **3** (respectivement E11 et E12), une coloration noire apparaît intermédiairement; celle-ci est due à une accumulation en solution du radical-anion de l'azobenzène qui ne s'avère donc pas assez basique pour déprotoner les phosphonates **3** ou **13**. Ainsi, le mécanisme proposé précédemment (schéma 3) pour la déprotonation des phosphonocarboxylates **6** et **9** est également valable pour celle de **2**. En revanche, les déprotonations de **3** et de **13** ne peuvent être assurées que par les espèces plus basiques, le monoanion

Can. J. Chem. Downloaded from www.nrcresearchpress.com by 194.225.253.170 on 09/07/12
For personal use only.

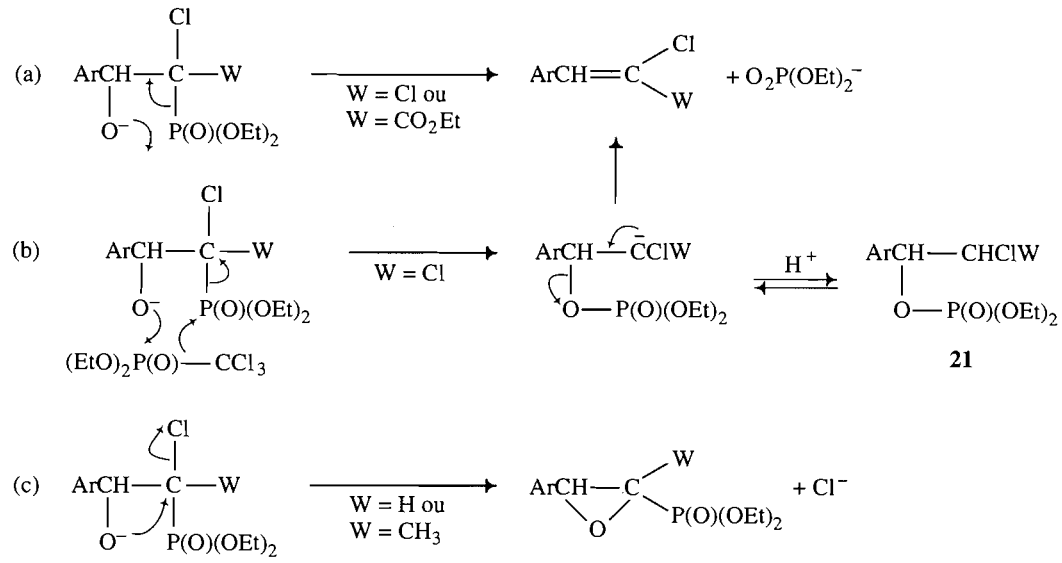


SCHÉMA 7. Evolutions de l'adduit aldéhyde-carbanion phosphonate chloré.

$(C_6H_5NHNC_6H_5)^-$ ou le dianion $(C_6H_5NNC_6H_5)^{2-}$, qui résultent de la dismutation du radical-anion formé à l'électrode; un tel comportement a déjà été observé lors de l'étude du benzylphosphonate de diéthyle (7).

En outre, on peut s'attendre à ce que les protonations parasites des bases électrogénérées prennent d'autant plus d'importance que le phosphonate présent est moins acide. De fait, comme on peut le constater à la lecture du tableau 5, les quantités d'aldéhyde et de phosphonate qui n'ont pas réagi augmentent lorsque l'on remplace le substituant Y = Cl de **2** par un atome d'hydrogène, dans **3**, et plus encore par un groupe Y = CH_3, dans **13**. Ces résultats sont en accord avec la variation d'acidité des substrats attendue d'après les effets inducteurs des substituants Y (17).

(b) Les produits de réaction. Il apparait, à la lecture du tableau 5, que la nature des produits de la réaction du carbanion phosphonate et de l'aldéhyde dépend de la nature du phosphonate. Alors que la réaction de Wittig–Horner est observée dans le cas du carbanion dichloré issu de la déprotonation de **2**, les phosphonates **3** et **13** fournissent des époxydes selon la réaction de Darzens. Cette sélectivité est identique à celle qui est observée lorsque les déprotonations sont conduites dans l'hexane à basse température au moyen de la base butyllithium (18, 19).

Ainsi trois évolutions sont possibles pour l'anion résultant de l'addition du carbanion phosphonate sur l'aldéhyde (schéma 7). (*i*) L'élimination de phosphate de diéthyle (schéma 7a) se produit lorsque W est suffisamment attracteur, comme nous l'avons déjà observé dans la première partie (W = Cl) et dans la deuxième partie (W = CO_2Et) de ce mémoire. (*ii*) La formation du phosphate **21** est en compétition avec l'évolution précédente lorsque W = Cl (schéma 7b); le mécanisme bimoléculaire proposé, également envisagé par d'autres auteurs (20), rend compte de l'influence de la concentration du substrat rapportée dans la première partie. (*iii*) Une substitution nucléophile interne se produit (schéma 7c) lorsque W n'est pas attracteur (W = H ou CH_3). L'élimination d'un ion chlorure entraîne alors la formation d'un époxyde.

(c) Application synthétique. Étant donné la sélectivité des réactions mises en jeu, l'électrolyse peut être utilisée comme technique de synthèse. En effet, l'utilisation d'un excès convenable de probase azobenzène doit permettre une conversion quantitative de l'aldéhyde et du phosphonate. Nous avons effectivement vérifié que l'électrolyse conduite en présence de **2** avec un excès d'azobenzène et arrêtée au moment où la couleur de la solution commence à foncer parce que le radical anion formé à la cathode ne trouve plus de donneur de proton disponible, fournit quantitativement l'éthylénique **18**. De même, l'emploi d'un excès d'azobenzène (0,75 mole consommée par mole de phosphonate) permet d'augmenter le taux de conversion du réactif **13** en époxyde **19** de 34% à 65%.

2. Réduction des phosphonates polyhalogénés (voie B)

On électrolyse, au potentiel de réduction du phosphonate, une solution équimolaire de phosphonate $(EtO)_2P(O)CClYW$ et d'aldéhyde. Les phosphonates étudiés sont **1** (Y = W = Cl), **2** (Y = H, W = Cl) et **12** (Y = CH_3, W = Cl). En fin d'électrolyse, après consommation de 2 F/mol, on récupère un peu d'aldéhyde qui n'a pas réagi, du phosphonate réduit $(EtO)_2P(O)CHYW$, ainsi que des produits de condensation issus du phosphonate et de l'aldéhyde. Les résultats, qui sont regroupés dans le tableau 6, permettent d'établir une comparaison avec ceux obtenus à partir des phosphonates homologues par la voie A.

2.1. Comparaison des deux voies d'accès aux carbanions phosphonate. (a) Electroréduction de 1 et de 12. Il n'apparaît pas de différence fondamentale entre les deux premières colonnes des tableaux 5 et 6: l'électroréduction de **1** (E13) fournit l'éthylénique dichloré **18** et le phosphate **21** avec des rendements semblables à ceux de l'électrolyse E10; celle de **12** (E14) conduit à l'époxyde **19** avec un rendement légèrement supérieur à celui de l'électrolyse E11, et la stéréochimie est la même.

Remarque : la présence de l'éthylénique **18** (ArCH = CCl_2) et l'absence de l'acétylénique chloré **27** (ArC≡CCl) parmi les produits des électrolyses E10 et E13 indiquent que **18** n'est pas déshydrohalogéné par les bases électrogénérées issues de l'azobenzène ni par le dichlorocarbanion **1***A*, du moins tant que de l'aldéhyde est présent; l'anion **1***A* subit une attaque électrophile par l'aldéhyde plus rapide que sa protonation par **18**. Cependant, si on réalise une électrolyse sur 3 mmol de

Can. J. Chem. Downloaded from www.nrcresearchpress.com by 194.225.253.170 on 09/07/12
For personal use only.

TABLEAU 6. Electroréduction des phosphonates **1**, **2** et **12**, dans le DMF 0,1 mol L^{-1} en Me_4NBF_4, en présence de *p*-méthoxybenzaldéhyde ArCHO; phosphonate 3 mmol, ArCHO 3 mmol. Le rendement est calculé comme dans le tableau 2

Electrolyse	E13	E14	E15
Phosphonate	**1**	**12**	**2**
$(EtO)_2P(O)CClYW$			
Y	Cl	CH_3	H
W	Cl	Cl	Cl
E_T (V)	−1,0	−1,3	−1,35
Q (F/mol)	1,9	2,0	1,9
Aldéhyde recouvré (%)	5	15	23
Phosphonate réduit (%)	**2** 0	**13** 6	**3** 24
Produits (%)	$ArCH{=}CCl_2$ (**18**) (62) $(EtO)_2P(O){-}O{-}CH(Ar)CCl_2H$ (**21**) (18)	$(EtO)_2P(O){-}C(H_3C)(O){-}CHAr$ (**19**) (*E*/*Z* 60 : 40) (41)	$ArCH{=}CHCl$ (**22**) (*E*/*Z* 70 : 30) (30) $ArC{\equiv}CH$ (**23**) (13) $(EtO)_2P(O)CH{-}CHAr$ (**20**) O (3)

phosphonate **1** et seulement 1,5 mmol d'aldéhyde, on obtient 20% d'oléfine **18** et 20% d'acétylénique **27**. Cette remarque sera utile à la discussion du paragraphe 2.2.

(b) Electroréduction de 2. Au contraire, par comparaison à l'électrolyse E12 du tableau 5, l'examen des résultats de E15 (tableau 6) fait apparaitre des différences notables : Le produit majoritaire est l'éthylénique **22** attendu d'après la réaction de Wittig–Horner, alors que l'époxyde provenant de la réaction de Darzens est maintenant nettement minoritaire. Des quantités relativement grandes d'aldéhyde n'ayant pas réagi et de phosphonate réduit **3** sont obtenues. Parmi les produits de E15, il apparait l'acétylénique **23** (ArC≡CH); signalons en outre que les rapports entre les pourcentages de **22** et **23** d'une part, et entre les pourcentages des isomères *E* et *Z* de **22** d'autre part, ne sont pas reproductibles.

Il est donc peu probable que l'éthylénique **22** et l'époxyde **20** puissent provenir de deux évolutions concurrentes d'un même adduit comme cela peut être suggéré par le schéma 7.

Afin d'élucider la nature des réactions intervenant dans E15, nous avons été conduits à examiner plus en détail le comportement du phosphonate dichloré **2**.

2.2. Réduction du dichlorométhylphosphonate 2 dans des conditions expérimentales variées. Le tableau 7 regroupe les résultats des électrolyses relatives à l'électroréduction du phosphonate **2** dans des conditions différentes des conditions standard déterminées dans la première partie.

Nous avons envisagé la réduction indirecte de **2** par catalyse rédox (21). Le couple formé par la benzophénone et son radical-anion permet une telle réduction (électrolyse E16) et l'on obtient alors, outre **22** et **23**, une quantité plus importante de l'époxyde **20**; il apparait donc que la formation de **22** et celle de **20** sont compétitives.

Si l'on remplace le cation tétraalkylammonium de l'électrolyte-support par un cation alcalin (électrolyses E17), tous les autres paramètres expérimentaux étant identiques à ceux de E15, le bilan coulométrique de l'électrolyse n'est que de 1 F/mol; on obtient essentiellement l'éthylénique dichloré **18** à côté d'une faible quantité de phosphate **21**.

L'ensemble des réactions rassemblées sur le schéma 8 permet de rendre compte des résultats des électrolyses E16 et E17 : Le carbanion **2***A* formé à la cathode par transfert de deux électrons et élimination d'un chlorure peut subir une réaction nucléophile et une protonation concurrentes. L'attaque nucléophile de l'aldéhyde conduit à un alcoolate intermédiaire dont nous avons vu qu'il évoluait vers la formation d'époxyde avec élimination de chlorure. La réaction acido-basique est un échange de proton entre le carbanion **2***A* électrogénéré et le phosphonate **2** pour former le carbanion dichloré **1***A* qui réagit avec l'aldéhyde. Nous avons vu que cette dernière réaction conduit à l'éthylénique **18** et au phosphate **21**. Lorsque le cation de l'électrolyte-support est un alcalin, la nucléophilie des carbanions est diminuée, et **2***A* subit exclusivement la protonation. Le second chemin réactionnel, semblable à celui décrit précédemment pour la réduction du phosphonocarboxylate **5**, est le seul observé; le rendement maximum en produits **18** et **21** est alors 50% puisque la moitié du phosphonate initial joue le rôle de probase.

Une autre façon de privilégier la protonation de **2***A* au détriment de sa réaction nucléophile consiste à lui opposer un aldéhyde peu électrophile. Nous avons ainsi pu vérifier lorsque l'électrolyse est conduite en présence de triméthoxy-2,4,6 benzaldéhyde (E18), de *p*-diméthylaminobenzaldéhyde (E19) ou d'heptanal (E20), le bilan coulométrique est de 1 F/mol et seul l'éthylénique dichloré est obtenu (tableau 7) avec un rendement qui n'est pas très inférieur à la valeur maximum théorique 50%.

Enfin, la présence de l'éthylénique monochloré **22** et de l'acétylénique **23** parmi les produits de l'électrolyse E16 est imputable à la réduction de l'éthylénique dichloré **18**. Une telle réduction ne se produit pas dans le cas de E17 (*vide infra*).

De même, lorsque l'aldéhyde est plus désactivé que le *p*-méthoxybenzaldéhyde (E18–E20), le potentiel de réduction de l'éthylénique dichloré correspondant est suffisamment cathodique pour que sa réduction ne soit pas observée au potentiel de travail choisi.

2.3. Retour sur l'électrolyse du dichlorométhylphosphonate 2 dans les conditions standard. Il est maintenant possible de rendre compte des résultats de l'électrolyse E15 (tableau 6), pour laquelle on peut grossièrement distinguer deux périodes successives.

Dans un premier temps, il se produit surtout l'électroréduction de **2** en **2***A*; ce dernier déprotone rapidement **2** en **1***A*. L'arrêt de l'électrolyse lorsque le résultat coulométrique atteint environ 1 F/mol montre alors la présence de l'éthylénique dichloré **18**, de l'aldéhyde et du phosphonate réduit **3**, en quantités peu différentes de celles de E17.

Mais la réaction ne s'arrête pas là, et dans un second temps, l'électroréduction de **18** se produit. Nous avons vérifié que **18**

Can. J. Chem. Downloaded from www.nrcresearchpress.com by 194.225.253.170 on 09/07/12
For personal use only.

Can. J. Chem. Downloaded from www.nrcresearchpress.com by 194.225.253.170 on 09/07/12
For personal use only.

est électroactif à −1,3 V lorsque le cation de l'électrolyte-support est le cation tétraméthylammonium, mais qu'il n'est pas réduit à ce potentiel si l'on utilise un cation alcalin comme dans E17; il est en effet bien connu que le potentiel de réduction de certains substrats dépend de la nature de l'électrolyte-support (22, 23). La réduction biélectronique de **18** conduit à un carbanion vinylique dont la protonation donne le produit **22** (schéma 9).

Il est probable que l'espèce qui protone le carbanion vinylique est essentiellement l'éthylénique dichloré **18**; pour ce dernier, le bilan est une déshydrohalogénation qui fournit l'acétylénique chloré Ar—C≡C—Cl. L'acétylénique chloré est réductible à deux électrons au potentiel de l'électrolyse; la protonation du carbanion résultant par l'éthylénique monochloré **22** conduit exclusivement à l'acétylénique vrai **23**. Comme le montre la dernière équation du schéma 9, le bilan de la réduction de **18** seul, en l'absence de donneur de proton, devrait être la formation quantitative de **23**; nous avons effectivement pu vérifier que l'électroréduction de **18** seul, à −1,5 V, conduit bien à **23** (rendement après extraction 75%). De plus, si d'autres donneurs de protons sont présents, les produits devraient contenir **22**; c'est bien le cas puisque l'électroréduction de **18** en présence de deux équivalents d'acide acétique fournit un mélange de **22** et **23** (rendements après extraction respectivement 71% et 13%). Ainsi, la présence de **22** dans les produits de E15 (et également de E16) est attribuable à l'intervention de protonations parasites pendant la lente réduction de **18** qui suit celle de **2**.

3. Conclusion

Les trois carbanions phosphonate mis en jeu dans les réactions étudiées donnent une réaction d'addition sur le paraméthoxybenzaldéhyde.

La décomposition de l'adduit est fonction des substituants portés par le carbanion phosphonate. Lorsque ce dernier est porteur de deux atomes de chlore, l'adduit se décompose avec élimination de phosphate de diéthyle pour conduire à un dérivé éthylénique dichloré (réaction de Wittig–Horner). Lorsque le carbanion phosphonate est porteur d'un seul atome de chlore, que le second substituant soit un atome d'hydrogène ou un groupement méthyle, il y a élimination d'un ion chlorure et formation de l'époxyde correspondant (réaction de Darzens).

La stéréosélectivité de la formation des époxydes semble indépendante du mode de formation du carbanion; elle varie avec la nature du substituant Y = H ou CH_3.

Enfin, dans le cas du phosphonate **2**, porteur d'un atome d'hydrogène, le carbanion qui réagit sur l'aldéhyde n'est pas le carbanion électrogénéré par réduction de **2**, mais celui qui résulte de la déprotonation du substrat.

Partie expérimentale

Réactifs

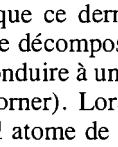
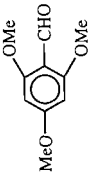
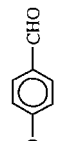
Les aldéhydes sont des échantillons commerciaux utilisés sans autre purification.

Le chlorométhylphosphonate de diéthyle **3**, le phosphono-acétate de triéthyle **6** et le phosphono-2 propionate de triéthyle **9** sont des échantillons commerciaux utilisés sans autre purification.

Le trichlorométhylphosphonate de diéthyle **1** est synthétisé par réaction de la triéthylphosphite et du tétrachlorométhane selon la réaction d'Arbusov (24).

Le dichlorométhylphosphonate de diéthyle **2** et le chloro-1 éthylphosphonate de diéthyle **13** sont préparés par réduction électrochimique, respectivement de **1** et de **12**, sur cathode de mercure, en milieu hydro-alcoolique, selon une méthode semblable à celle décrite récemment pour la synthèse de **2** (11).

TABLEAU 7. Réduction du dichlorométhylphosphonate de diéthyle **2** dans le DMF 0,1 mol L^{-1} en électrolyte-support (tétrafluoroborate), en présence d'un équivalent d'aldéhyde. Les rendements sont calculés comme dans le tableau 2

Electrolyse	E16*	E17	E18	E19	E20
Aldéhyde					$nC_6H_{13}CHO$
Cation de l'électrolyte-support	Bu_4N^+	Li^+, Na^+ ou K^+	Me_4N^+	Me_4N^+	Me_4N^+
E_T (V)	−1,25	−1,3	−1,35	−1,35	−1,35
Q (F/mol)	2,0	1,0	1,05	1,0	1,0
Aldéhyde recouvré (%)	23	37	27	36	20
Phosphonate réduit **3** (%)	23	31	27	27	42
Produits (%)	ArCH=CHCl (**22**) (30) ArC≡CH (**23**) (23) $(EtO)_2P(O)CH(O)CHAr$ (**20**) (20)	ArCH=CCl_2 (**18**) (40) $(EtO)_2P(O)$—O—$CHArCCl_2H$ (**21**) (6)	ArCH=CCl_2 (**24**) (36)	ArCH=CCl_2 (**25**) (42)	$nC_6H_{13}CH$=CCl_2 (**26**) (42)

*En présence de benzophénone (0,6 mmol) comme catalyseur rédox.

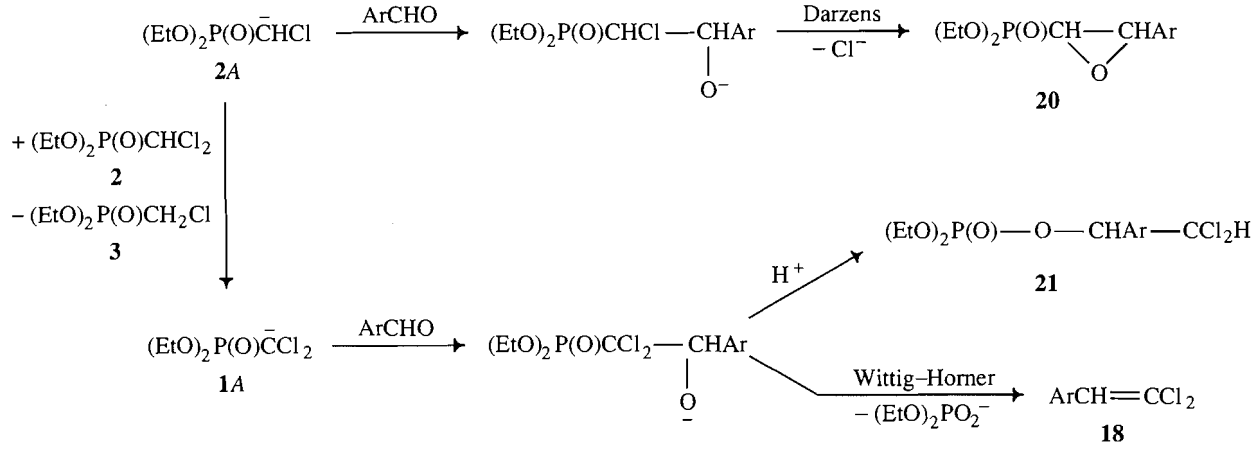


SCHÉMA 8

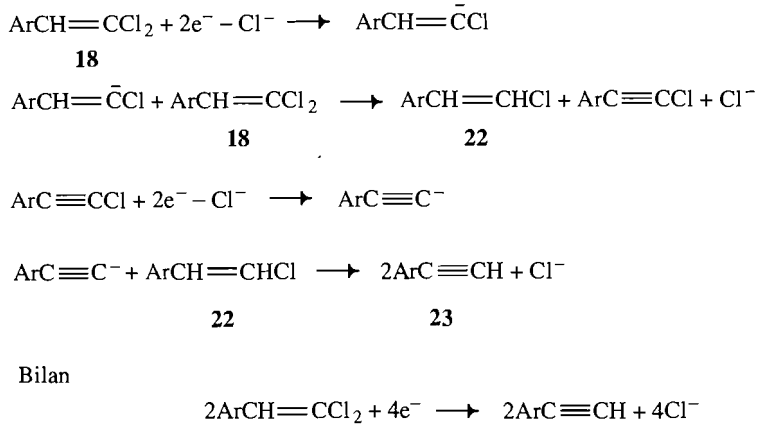


SCHÉMA 9

Le dichloro-1,1 éthylphosphonate de diéthyle **12** est un échantillon qui nous a gracieusement été fourni par Pr. Villieras de l'Université de Nantes; il peut également être obtenu par méthylation lors de l'électroréduction de **1** en présence d'iodure de méthyle (12).

Les phosphonates halogénés **4**, **5** et **10** sont synthétisés selon la méthode décrite dans la littérature (25).

Le bromo-2 phosphono-2 propionate de triéthyle **8** et le bromo chloro phosphonoacétate de diéthyle **11** sont obtenus par bromation, respectivement de **9** et de **5**, selon la technique décrite dans la référence 25.

Le chloro-2, phosphono-2 propionate de triéthyle **7** est synthétisé par méthylation de **5** par l'iodure de méthyle dans le THF en présence de carbonate de potassium.

Techniques électrochimiques

Les électrolyses préparatives sont réalisées à potentiel contrôlé (E_T), sous argon, à température ambiante, sur cathode de mercure, dans une cellule à compartiments séparés. Le volume de la solution de travail est 30 mL. Le générateur est un potentiostat Tacussel PRT 20-2X et un intégrateur Tacussel IG5-LN permet les mesures coulométriques. L'électrode de référence est un fil d'argent plongé dans une solution 0,1 mol L^{-1} d'iodure de tétrabutylammonium dans le DMF. Les électrolytes-supports sont employés à la concentration 0,1 mol L^{-1}.

Le tétrafluoroborate de tétrabutylammonium est recristallisé deux fois dans un mélange eau–méthanol (50 : 50) puis séché sous vide à 100°C. Le tétrafluoroborate de tétraméthylammonium est un produit commercial et il est utilisé sans autre purification. Le solvant DMF, de qualité Puran (diméthylamine < 50 ppm), est utilisé sans distillation. Il est séché sur tamis moléculaire 4Å et la teneur en eau résiduelle, déterminée par la méthode de Karl–Fischer juste avant emploi, peut être estimée à 60–100 ppm.

Le compartiment anodique, séparé du compartiment cathodique par un verre fritté, contient 20 mL d'une solution de chlorure de tétraalkylammonium. Le chlorure a été préféré au tétrafluoroborate à cause de la réaction anodique : avec NR_4BF_4, il se forme à l'anode des espèces acides susceptibles de migrer vers le compartiment cathodique. Avec NR_4Cl, le contenu du compartiment anodique doit néanmoins être changé une fois en cours d'électrolyse pour éviter la diffusion vers le compartiment cathodique du chlore formé à l'anode.

Lors de l'électroréduction des phosphonates halogénés en présence de tétrafluoroborate de tétraméthylammonium comme électrolyte-support, on observe, quelques minutes après le début de l'électrolyse, la précipitation de l'halogénure de tétraméthylammonium.

Produits

En fin d'électrolyse, le contenu du compartiment cathodique est versé dans 120 mL d'eau saturée en chlorure de sodium. La solution résultante est extraite à l'éther, la phase éthérée est ensuite lavée à l'eau puis séchée sur sulfate de magnésium, et l'éther est évaporé sous vide. Le résidu ainsi obtenu est pesé.

Un tel mode opératoire permet l'extraction de l'essentiel (supérieur à 80%) des produits non phosphorés; les phosphonates ne sont que partiellement extraits. Cependant, l'application systématique de ce mode opératoire permet d'effectuer des comparaisons entre les résultats des différentes expériences.

Les spectres de RMN du proton sont enregistrés à 60 MHz sur une solution, dans $CDCl_3$, du résidu obtenu après évaporation comme décrit précédemment. La quantité de chaque produit dans ce résidu est

Can. J. Chem. Downloaded from www.nrcresearchpress.com by 194.225.253.170 on 09/07/12
For personal use only.

déterminée d'après la masse du résidu et l'intégration des signaux RMN après identification de tous les signaux du spectre.

Pour effectuer cette identification, la préparation d'échantillons purs a été nécessaire. La séparation entre composés phosphorés et composés non phosphorés s'effectue très facilement par filtration du mélange à travers une colonne de silice avec un mélange d'hexane et d'acétate d'éthyle (90 : 10) comme éluant : les phosphonates sont retenus sur la colonne, et ils peuvent être récupérés par lavage à l'acétate d'éthyle pur. La séparation des phosphonates contenus dans les mélanges ainsi recueillis peut être effectuée, pour des raisons d'analyse, par distillation sous pression réduite dans un four à boules rotatives. L'élution de la colonne à l'aide du mélange hexane/acétate d'éthyle permet d'isoler les aldéhydes et les éthyléniques isomères. En cas de nécessité pour une identification certaine, il a été fait appel à d'autres études spectroscopiques : RMN ^{13}C, RMN ^{31}P, RMN ^{1}H 80 MHz ou spectroscopie de masse. Les données sont rassemblées ci-dessous :

Chloro-2 phosphono-2 propionate de triéthyle (**7**) $(EtO)_2P(O)CCl(CH_3)CO_2C_2H_5$; RMN ^1H : 1,2–1,5 (m, 9); 1,95 (d, 3, J_{PH} = 14 Hz); 4–4,5 (m, 6).

Bromo-2 phosphono-2 propionate de triéthyle (**8**) $(EtO)_2P(O)CBr(CH_3)CO_2C_2H_5$; RMN ^1H : 1,2–1,5 (m, 9); 2,06 (d, 3, J_{PH} = 14 Hz); 4–4,5 (m, 6).

p-Méthoxyphényl-3 méthyl-2 propénoate d'éthyle (**14**) *p*-$CH_3O—C_6H_4—CH=C(CH_3)CO_2C_2H_5$. **14**(*E*) : RMN ^1H : 1,33 (t, 3, J = 7 Hz); 2,13 (d, 3, J = 2 Hz); 3,80 (s, 3); 4,20 (q, 2, J = 7 Hz); 6,87–7,33 (AB, 4, J = 9 Hz); 7,60 (m, 1).

p-Méthoxyphényl-3 propénoate d'éthyle (**15**) *p*-$CH_3O—C_6H_4—CH=CHCO_2C_2H_5$. **15**(*Z*) : RMN ^1H : 1,26 (t, 3, J = 7 Hz); 3,78 (s, 3); 4,17 (q, 2, J = 7 Hz); 5,78 (d, 1, J = 13 Hz); 6,82 (d, 1, J = 13 Hz); 6,87–7,68 (AB, 4, J = 9 Hz). **15**(*E*) : RMN ^1H : 1,33 (t, 3, J = 7 Hz); 3,80 (s, 3); 4,23 (q, 2, J = 7 Hz); 6,27 (d, 1, J = 16 Hz); 6,85–7,43 (AB, 4, J = 9 Hz); 7,60 (d, 1, J = 16 Hz).

p-Méthoxyphényl-3 chloro-2 propénoate d'éthyle (**16**) *p*-$CH_3—C_6H_4—CH=CClCO_2C_2H_5$. **16**(*Z*) : RMN ^1H : 1,35 (t, 3, J = 7 Hz); 3,80 (s, 3); 4,30 (q, 2, J = 7 Hz); 6,90–7,80 (AB, 4, J = 9 Hz); 7,80 (s, 1). RMN ^{13}C : 14,22; 55,30; 62,34; 114,14; 119,77; 125,74; 132,78; 136,57; 161,33; 163,71. **16**(*E*) : RMN ^1H : 1,23 (t, 3, J = 7 Hz); 3,77 (s, 3); 4,18 (q, 2, J = 7 Hz); 6,80–7,27 (AB, 4, J = 9 Hz); 7,07 (s, 1). RMN ^{13}C : 13,84; 55,30; 62,05; 113,80; 120,94; 126,32; 130,65; 137,15; 160,41; 163,85.

p-Méthoxyphényl-3 bromo-2 propénoate d'éthyle (**17**) *p*-$CH_3O—C_6H_4—CH=CBrCO_2C_2H_5$. **17**(*Z*) : RMN ^1H : 1,37 (t, 3, J = 7 Hz); 3,82 (s, 3); 4,32 (q, 2, J = 7 Hz); 6,90–7,85 (AB, 4, J = 9 Hz); 8,13 (s, 1). **17**(*E*) : RMN ^1H : 1,23 (t, 3, J = 7 Hz); 3,79 (s, 3); 4,22 (q, 2, J = 7 Hz); 6,80–7,25 (AB, 4, J = 9 Hz); 7,25 (s, 1).

p-Méthoxyphényl-2 dichloro-1,1 éthylène (**18**) *p*-$CH_3O—C_6H_4—CH=CCl_2$; RMN ^1H : 3,77 (s, 3); 6,80 (s, 1); 6,88–7,50 (AB, 4, J = 8 Hz). Masse exacte, calculée : 201,9952; trouvée : 201,9939.

p-Méthoxyphényl-2 méthyl-1 époxy-1,2 éthanephosphonate (**19**) $(EtO)_2P(O)—C(CH_3)—CH(O)—C_6H_4$-*p*-$OCH_3$. Masse exacte calculée : 300,1127; trouvée : 300,1116. **19**(*Z*) : RMN ^1H 80 MHz : 1,13 (t, 3, J = 6,0 Hz); 1,19 (t, 3, J = 6,8 Hz); 1,64 (d, 3, J_{PH} = 10,3 Hz); 3,80 (s, 3); 3,9–4,4 (m, 5); 6,87–7,36 (AB, 4, J = 8,5 Hz). **19**(*E*) : RMN ^1H : 1,24 (d, 3, J_{PH} = 11,7 Hz); 1,37 (t, 3, J = 7,2 Hz); 1,38 (t, 3, J = 7 Hz); 3,81 (s, 3); 3,9–4,4 (m, 5); 6,9–7,23 (AB, 4, J = 8,9 Hz).

p-Méthoxyphényl-2 époxy-1,2 éthanephosphonate (**20**) $(EtO)_2P(O)CH—CH(O)—C_6H_4$-*p*-$OCH_3$. Masse exacte, calculée : 286,0970; trouvée : 286,0963. **20**(*Z*) : RMN ^1H : 1,34 (t, 3, J = 7 Hz); 1,37 (t, 3, J = 7 Hz); 3,05 (dd, 1, J_{HH} = 2,5 Hz; J_{PH} = 31 Hz); 3,75 (s, 3); 3,7–4,4 (m, 5); 6,83–7,18 (AB, 4, J = 8 Hz). **20**(*E*) : RMN ^1H : 1,13 (t, 3, J = 7 Hz); 1,18 (t, 3, J = 7 Hz); 3,17 (dd, 1, J_{HH} = 4,5 Hz; J_{PH} = 28 Hz); 3,75 (s, 3); 3,7–4,4 (m, 5); 6,83–7,33 (AB, 4, J = 8 Hz).

Phosphate de diéthyle et de paraméthoxyphényl-1 dichloro-2,2 éthyle (**21**) $(EtO)_2P(O)—O—CH(p\text{-}CH_3O—C_6H_4)—CCl_2H$. RMN ^1H : avec structure fine 1,13 (t, 3, J = 8 Hz); 1,30 (t, 3, J = 8 Hz); 3,80 (s, 3); 4,03 (dq, 4, J_{HH} = 8 Hz, J_{PH} = 8 Hz); 5,50 (dd, 1, J_{HH} = 4 Hz, J_{PH} = 9 Hz); 5,92 (d, 1, J = 4 Hz); 6,90–7,37 (AB, 4, J = 9 Hz).

p-Méthoxyphényl-2 chloro-1 éthylène (**22**) *p*-$CH_3O—C_6H_4—CH=CHCl$. Masse exacte, calculée : 168,0342; trouvée : 168,0350. **22**(*E*) : RMN ^1H : 3,77 (s, 3); 6,40 (d, 1, J = 14 Hz); 6,7–8 (m, 5). **22**(*Z*) : RMN ^1H : 3,77 (s, 3); 6,00 (d, 1, J = 8 Hz); 6,7–8 (m, 5).

p-Méthoxyphényl acétylène (**23**) *p*-$CH_3O—C_6H_4—C\equiv CH$. RMN ^1H : 2,95 (s, 1); 3,77 (s, 3); 6,82–7,38 (AB, 4, J = 9 Hz).

(Triméthoxy-2,4,6 phényl)-2 dichloro-1,1 éthylène (**24**) $(CH_3O)_3C_6H_2—CH=CCl_2$. RMN ^1H : 3,80 (s, 9); 6,10 (s, 2); 6,60 (s, 1).

p-Diméthylamino phényl-2 dichloro-1,1 éthylène (**25**) *p*-$(CH_3)_2N—C_6H_4—CH=CCl_2$. RMN ^1H : 3,03 (s, 6); 6,83 (s, 1); 6,77–7,60 (AB, 4, J = 9 Hz). Masse exacte, calculée : 215,0269; trouvée : 215,0270.

Dichloro-1,1 octène-1 (**26**) *n*-$C_6H_{13}—CH=CCl_2$. RMN ^1H : 0,9 (t, 3, J = 5 Hz); 1,2–2,5 (m, 10); 5,80 (t, 1, J = 7 Hz).

p-Méthoxyphényl-2 chloro-1 acétylène (**27**) *p*-$CH_3O—C_6H_4—C\equiv CCl$. RMN ^1H : 3,77 (s, 3); 6,82–7,40 (AB, 4, J = 9 Hz). Masse exacte, calculée : 166,0185; trouvée : 166,0187.

1. W. S. Wadsworth, Jr. Org. React. (NY), **25**, 73 (1977).
2. J. Boutagy et R. Thomas. Chem. Rev. **74**, 87 (1974).
3. L. Horner, H. Hoffmann, H. G. Wippel et G. Klarhe. Chem. Ber. **92**, 2499 (1959).
4. W. S. Wadsworth et W. D. Emmons. J. Am. Chem. Soc. **83**, 1733 (1961).
5. E. V. Dehmlov et S. S. Dehmlov. Phase transfer catalysis. Monographs in Modern Chemistry. **11**. Verlag Chemie, Weinheim. 1983.
6. F. Texier-Boullet et A. Foucaud. Synthesis, 884 (1979).
7. J. C. Le Menn et J. Sarrazin. Bull. Soc. Chim. Fr. 781 (1988).
8. B. Costisella, H. Gross, P. Jeroschenski, I. Keitel et K. H. Schwarz. Phosphorus Sulfur, **29**, 159 (1987).
9. D. Seyferth et R. S. Marmor. J. Organomet. Chem. **59**, 237 (1973).
10. P. Coutrot, C. Laurenco, J. F. Normant, P. Perriot, P. Savignac et J. Villieras. Synthesis, **9**, 615 (1977).
11. B. Tue Bi et M. Devaud. Tetrahedron Lett. **28**, 3799 (1987).
12. J. C. Le Menn et J. Sarrazin. J. Chem. Res. (S), 26 (1989).
13. W. J. M. Van Tilborg et C. J. Smith. Recl. J. R. Neth. Chem. Soc. **99**, 202 (1980).
14. K. Karrenbrock, H. J. Schäfer et I. Langer. Tetrahedron Lett. 2915 (1979).
15. K. L. Vieira et D. G. Peters. J. Org. Chem. **51**, 1231 (1986) et références incluses.
16. J. P. Gisselbrecht et H. Lund. Acta Chem. Scand. Ser. B: **B39**, 773 (1985).
17. M. P. Teulade, P. Savignac, E. E. Aboujaoude et N. Collignon. J. Organomet. Chem. **312**, 283 (1986).
18. P. Savignac, J. Petrova, M. Dreux et P. Coutrot. Synthesis, 535 (1975).
19. (*a*) P. Coutrot et P. Savignac. Synthesis, 34 (1978); (*b*) P. Perriot, J. Villieras et J. F. Normant. Synthesis, 33 (1978).
20. B. Tue Bi. Thèse, Rouen. 1988.
21. C. P. Andrieux, J. M. Dumas-Bouchiat et J. M. Saveant. J. Electroanal. Chem. **87**, 39 (1978); **87**, 55 (1978); **88**, 43 (1978); **113**, 1 (1980); **113**, 19 (1980).
22. A. J. Fry et R. L. Krieger. J. Org. Chem. **41**, 54 (1976).
23. D. A. Corigan et D. H. Evans. J. Electroanal. Chem. **106**, 287 (1980).
24. G. M. Kosolapoff. J. Am. Chem. Soc. **69**, 1002 (1947).
25. D. A. Nicholson et H. Vaughn. J. Org. Chem. **36**, 1835 (1971).

Can. J. Chem. Downloaded from www.nrcresearchpress.com by 194.225.253.170 on 09/07/12
For personal use only.

Structural studies of oligonucleotides with an O4-isopropylated thymine. d(i^{4}TpT), d(Tpi^{4}T), and d(Tpi^{4}TpT)[1]

GARRY W. BUCHKO, FRANK E. HRUSKA,[2] AND KRISHAN L. SADANA
Department of Chemistry, The University of Manitoba, Winnipeg, Man., Canada R3T 2N2

Received January 6, 1989

GARRY W. BUCHKO, FRANK E. HRUSKA, and KRISHAN L. SADANA. Can. J. Chem. **67**, 1344 (1989).

Syntheses are described for d(i^{4}TpT) (**1**), d(Tpi^{4}T) (**2**), and d(Tpi^{4}TpT) (**3**), the O4-isopropylated analogues of d(TpT) (**4**) and d(TpTpT) (**5**). The detection of the molecular $[M - H]^-$ ions and some $[2M - H]^-$ aggregates shows that Fast Atom Bombardment mass spectrometry operating in the negative ion mode is useful for structural analysis of these DNA oligomers. In contrast with the monomer, i^{4}dT, the two O4-isopropyl methyl groups of **1** and **2** are magnetically nonequivalent and give rise to separate ^{1}H and ^{13}C NMR signals. Their chemical shift difference (Δ) decreases gradually with increasing temperature, and can be interpreted as reflecting intramolecular base stacking, in line with circular dichroic data. This chemical shift difference is not seen in the ^{1}H NMR spectra of **3**, and is attenuated in the ^{13}C spectra of this trimer. Coupling constant data indicate a shift towards the 3′-*endo* conformation of the sugar of the i^{4}Tp moiety of **1**, a trend observed for the corresponding O4-ethylated moiety of d(e^{4}TpT). ^{13}C–^{31}P and ^{1}H–^{31}P coupling constants indicate that the structural features monitored by these couplings are not significantly altered by O4-isopropylation of the thymine base.

Key words: oligonucleotides, O-alkylation, stereochemistry, NMR, mass spectrometry.

GARRY W. BUCHKO, FRANK E. HRUSKA et KRISHAN L. SADANA. Can. J. Chem. **67**, 1344 (1989).

On décrit la synthèse des d(i^{4}TpT) (**1**), d(Tpi^{4}T) (**2**) et d(Tpi^{4}TpT) (**3**), les analogues O4-isopropylés des d(TpT) (**4**) et d(TpTpT) (**5**). La détection des ions moléculaires $[M - H]^-$ et de quelques agrégats $[2M - H]^-$ démontre que la spectrométrie de masse, par bombardement avec des atomes rapides (FAB) et opérée en mode d'ions négatifs, est utile pour l'analyse des structures de ces oligomères de l'ADN. Par opposition avec le monomère, i^{4}dT, les deux groupements méthyles de l'isopropyle en O-4 ne sont pas équivalents d'un point de vue magnétique et ils donnent lieu à des signaux séparés en RMN tant du ^{1}H que du ^{13}C. La différence (Δ) dans leurs déplacements chimiques diminue avec une augmentation de la température; en conformité avec ce qui a pu être déduit sur la base de données de dichroïsme circulaire, on peut interpréter ce résultat en fonction d'un empilement moléculaire des bases. On n'observe pas cette différence dans les déplacements chimiques des spectres RMN du ^{1}H du composé **3** et elle est atténuée dans le spectre du ^{13}C de ce trimère. Les données relatives aux constantes de couplage indiquent qu'il se produit un déplacement vers la conformation 3′-*endo* du sucre de la portion i^{4}Tp du composé **1**; cette tendance a été observée pour la portion O4-éthylée correspondante du d(e^{4}TpT). Les constantes de couplage ^{13}C–^{31}P et ^{1}H–^{31}P indiquent que les caractéristiques structurales déterminées par ces couplages ne sont pas altérées d'une façon significative par une O4-isopropylation de la base thymine.

Mots clés : oligonucléotides, O-alkylation, stéréochimie, RMN, spectrométrie de masse.

[Traduit par la revue]

Introduction

There is considerable interest in the biological effects of O-alkylation of thymine (1, 2). Information about the electronic and geometric changes effected by this modification is being provided by X-ray crystallographic and spectroscopic studies of nucleosides and nucleotides (3–7) and, more recently, oligonucleotides with an O4-methylated thymine (m^{4}T) have been examined by NMR (8, 9). We have initiated a program for the synthesis of oligomers containing an O4-alkylated thymine (r^{4}T) for study by physical methods. These syntheses require considerable care since the r^{4}T base is labile in acid and basic solution (1, 6). Thus, our initial focus has been on oligonucleotides containing only r^{4}T and T bases; such molecules were deemed to be the most easily prepared because protection of the T base is generally not required. In our previous work (10), we described the synthesis of d(e^{4}TpT) and d(Tpe^{4}T), the O4-ethylated analogues of d(TpT), and their characterization by ^{1}H NMR, Fast Atom Bombardment (FAB) mass spectrometry, and circular dichroism (CD). Singer *et al.* (11) have shown that O4-isopropyl, as well as methyl and ethyl, substituents on thymidine lead to transitions during replication. For the present work, we extended our synthesis to the isopropylated dimers, d(i^{4}TpT) (**1**) and d(Tpi^{4}T) (**2**), and the trimer d(Tpi^{4}TpT) (**3**) (Fig. 1). ^{1}H and ^{13}C NMR data as well as FAB and CD data are compared with those of d(TpT) (**4**) and d(TpTpT) (**5**) (provided here and in the literature (12–15)), and with those of d(e^{4}TpT) (**6**) and d(Tpe^{4}T) (**7**). In an earlier study (5) we reported NMR data for the mononucleoside i^{4}dT and some analogs, and discussed the effects of O-alkylation at the monomer level.

Experimental

Materials and methods

Materials

Thymidine and the reagents used for protection, coupling, and deblocking were purchased (Aldrich or Sigma Chemical Co.), or synthesized as described by Buchko *et al.* (10). Chromatographic solvents were purchased from Fisher Scientific. Kieselgel 60 (Merck) was used for dry-column flash chromatography (DCFC). Thin-layer chromatography (TLC) was carried out on Kieselgel 60 F_{254} plates from Merck. For paper chromatography, Whatman paper (No. 3001 917) was used.

Synthetic methods

The O4-isopropylated derivative **1** was prepared according to the procedure (10) for the corresponding O4-ethylated dimer (**6**), except that sodium isopropoxide replaced sodium ethoxide to introduce the O4-isopropyl group and to remove the 3′-terminal acetyl group in the final deprotection step. Isomer **2** with the O4-isopropyl group on the 5′-linked nucleotidyl unit was conveniently obtained by treating 133 A_{260} units of the trimer d(Tpi^{4}TpT) (**3**; see below) with 249 units of snake venom phosphodiesterase (Russell's viper; Calbiochem) at 32°C for 24 h in a 0.1 M Tris buffer (pH 8.0). This exonuclease

[1]Presented in part at the 70th Canadian Chemical Conference, Quebec, P.Q., June 7–11, 1987.

[2]Author to whom correspondence may be addressed.

Can. J. Chem. Downloaded from www.nrcresearchpress.com by 194.225.253.170 on 09/07/12
For personal use only.

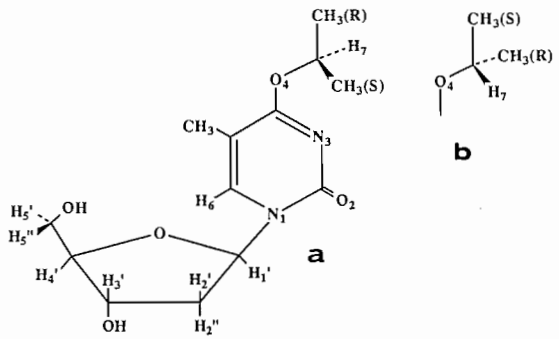


FIG. 1. (a) Structure and numbering scheme of i^{4}dT (O4-isopropylthymidine), the modified component of d(i^{4}TpT) (**1**), d(Tpi^{4}T) (**2**), and d(Tpi^{4}TpT) (**3**). C7 and C8 refer respectively to the tertiary and the methyl carbons of the isopropyl group. *R* and *S* give the *pro-R* and *pro-S* assignments of the diastereotopic 8-methyl groups. C7 is *syn-periplanar* to N3, the *pro-S* methyl flanks the base on its 3′ face, and the *pro-R* group is directed away from the ring. (b) An alternate conformation of the isopropyl group, obtained by rotation about the C7—O4 bond, in which the *pro-R* methyl flanks the base on its 5′ face and the *pro-S* methyl is directed away from the ring.

degrades single strands with a free 3′-hydroxyl group, but the presence of the O4-isopropyl lesion apparently retards the enzyme's progress, and **2** is obtained as the only product following the cleavage of the pT fragment from the 3′ end of the trimer. (Our recent experiments on the methylated and ethylated analogs of **3** show that an O4-ethyl also retards this phosphodiesterase, whereas an O4-methyl does not.[3])

Compound **3** was synthesized starting with fully-blocked **1** (3′ end: acetyl; 5′ end; 4,4′-dimethoxytrityl (DMT); phosphate: *para*-chlorophenyl), which was prepared following Buchko *et al.* (10), except that the DMT replaced the *tert*-butyldimethylsilyl group at the 5′ end. This blocked dimer was extended in the 5′ direction, after removal of the DMT group with $ZnBr_2$ (16), by coupling with 5′-DMT thymidine; the coupling was carried out as described (10) for the synthesis of **7**. Compound **3** was obtained from this blocked trimer by sequential treatment with (*i*) $ZnBr_2$, (*ii*) oximate reagent for phosphate deprotection, and (*iii*) sodium isopropoxide. The unmodified trimer **5** was obtained from the blocked trimer by treatment with sodium hydroxide rather than sodium isopropoxide. All of the molecules were purified initially by descending paper chromatography followed by HPLC (Perkin Elmer Series 4 liquid chromatograph) using a semipreparative ODS-Hypersil column and a gradient of methanol and 0.1 M aqueous ammonium acetate (pH 6.0).

The following UV absorption data for H_2O solutions were obtained on a Cary 219 spectrophotometer: **1**: λ_{max} = 272 nm, λ_{min} = 239 nm; **2**: λ_{max} = 270 nm, λ_{min} = 238 nm; **3**: λ_{max} = 269 nm, λ_{min} = 237 nm; **4**: λ_{max} = 267 nm, λ_{min} = 235 nm; **5**: λ_{max} = 266 nm, λ_{min} = 234 nm. The data for **1** and **2** are in good agreement with those reported for the corresponding O4-ethylated dimers (10).

Mass spectrometric experiments

Positive- and negative-ion FAB mass spectra (glycerol matrix, 8-keV xenon atoms) were obtained on a VG 7070E-HF spectrometer. As was the case for **6** and **7** (10), the negative-ion spectra proved to be more diagnostic; some of the more prominent negative-ion peaks are reported here as follows: *m/z* (relative intensity, [ionic species]), with the relative intensity normalized to the molecular ion $[M - H]^-$. *d(i^{4}TpT)*: 587 (100, $[M - H]^-$); 1175 (1.6, $[2M - H]^-$); 125 (65, [thymine $- H]^-$); 167 (41, [O4-isopropylthymine $- H]^-$); 321 (23, [5′-dTMP $- H]^-$); 363 (23, [3′-i^{4}dTMP $- H]^-$); 545 (6, $[M - CH(CH_3)_2]^-$). *d(Tpi^{4}T)*: 587 (100, $[M - H]^-$); 1175 (4, $[2M - H]^-$); 125 (62, [thymine $- H]^-$); 167 (7, [O4-isopropylthymine $- H]^-$); 321 (19, [3′-dTMP $- H]^-$); 363 (21, [5′-i^{4}dTMP $- H]^-$); 545 (18, $[M - CH(CH_3)_2]^-$). *d(Tpi^{4}TpT)*: 891 (100, $[M - H]^-$); 125 (93, [thymine $- H]^-$); 167 (14, [O4-isopropylthymine $- H]^-$); 321 (58, [3′-dTMP $- H]^-$ + [5′-dTMP $- H]^-$); 587 (5, [d(i^{4}TpT) $- H]^-$ + [d(Tpi^{4}T) $- H]^-$); 667 (36, [d(pi^{4}TpT) $- H]^-$ + [d(Tpi^{4}Tp) $- H]^-$); 849 (11, $[M - CH(CH_3)_2]^-$). *d(TpTpT)*: 850 (100, $[M - H]^-$); 872 (54, $[M + Na - H]^-$); 125 (187, [thymine $- H]^-$); 321 (106, [3′-dTMP $- H]^-$ + [5′-dTMP $- H]^-$); 625 (42, [d(pTpT) $- H]^-$ + [d(TpTp) $- H]^-$).

^{1}H NMR experiments

Most of the ^{1}H NMR spectra were obtained at 300.134 MHz (Bruker AM300). The samples were contained in 5 mm (o.d.) tubes at concentrations in D_2O that preclude significant intermolecular interaction: **1**, 0.0048 M; **2**, 0.0083 M; **3**, 0.0025 M; **5**, 0.0030 M. The concentrations were calculated from UV absorbance measurements, assuming additivity of the molar extinction coefficients (ε_{max}) of the component nucleosides; literature values for ε_{max} of a thymidine (dT) unit (9600) and an O4-alkylated thymidine (6700) were used (17, 18). The solutions contained 0.01 M sodium phosphate buffer (pH = 6.9), EDTA (0.001 M) to chelate paramagnetic ions, 0.1 M NaCl to maintain a constant ionic strength, and, for an NMR reference, a trace of *tert*-butanol (assigned a chemical shift of 1.231 ppm on the DSS scale). The samples were lyophilized twice from 99.8% D_2O and taken up in 99.9% D_2O. One-dimensional (1D) FIDs were obtained at 10° intervals from 10 to 70°C in 16K of computer memory and processed with a Lorentz-to-Gaussian lineshape transform (GB = 0.2, LB = −2.0) prior to zero-filling (to 32K). The HDO resonance was suppressed by presaturation (Bruker PRESAT. AU microprogram). Conventional homonuclear decoupling, nOe, and two-dimensional (COSY-45°) (19) experiments were carried out for spectral assignments. Spectra for the trimers at 10 and 70°C were also obtained at 500.137 MHz (Bruker AM500; McMaster University). Spectra were analyzed (NUMARIT) (20) at two temperatures (10 or 20°C, and 70°C), and computer-generated spectra confirmed the data.

Proton-decoupled ^{13}C data were obtained (27 and 70°C) at 75.5 MHz (Bruker AM300) for molecules **1–5** in the buffer solution used for the ^{1}H NMR experiments; a trace of dioxane was used as the internal reference. The concentrations were the same as for the ^{1}H NMR studies except for **3** (0.05 M).

Circular dichroism experiments

CD spectra were obtained on a Jasco J-500A spectropolarimeter in cells equipped for temperature control by a water bath. Each molecule was studied at (8.3–9.5) × 10^{-5} M (calculated from UV absorbance measurements (10)) in the phosphate buffer solution used for the NMR experiments.

Results and discussion

NMR spectra, data, and assignments

Tables 1–5 provide ^{1}H and ^{13}C chemical shift (δ) and coupling constant (J) data. Complete ^{1}H NMR spectra for **1** and **2** are not given since they are similar (except for the bands of the O4-alkyl groups) to those of **6** and **7** (10). As discussed further in the next section, the isopropyl methyl groups of **1** and **2** are diastereotopic (5) (see Fig. 1 for the *pro-R* and *pro-S* designations), and give rise to separate doublets (inset of Fig. 2) with $J(78)$ = 6.2 Hz. On the other hand, the methylene protons of the O4-ethyl groups of **6** and **7** are diastereotopic, giving rise to ABX_3 patterns for these groups (10).

A partial one-dimensional ^{1}H NMR spectrum of the trimer **3** is given in Fig. 2. Note that, in contrast with the dimers, the prochiral H8 protons of the trimer (δ = 1.33 ppm) are isochronous and a single doublet ($J(78)$ = 6.2 Hz; Table 3) is observed. The isochronicity of these protons is retained over the 10–70°C range.

Figure 3 shows a ^{13}C (^{1}H-decoupled) spectrum of **3** at 27°C. Expanded spectra reveal that the peak (22.2 ppm) assigned to

[3]G. W. Buchko, F. E. Hruska, and K. L. Sadana, unpublished results.

Can. J. Chem. Downloaded from www.nrcresearchpress.com by 194.225.253.170 on 09/07/12
For personal use only.

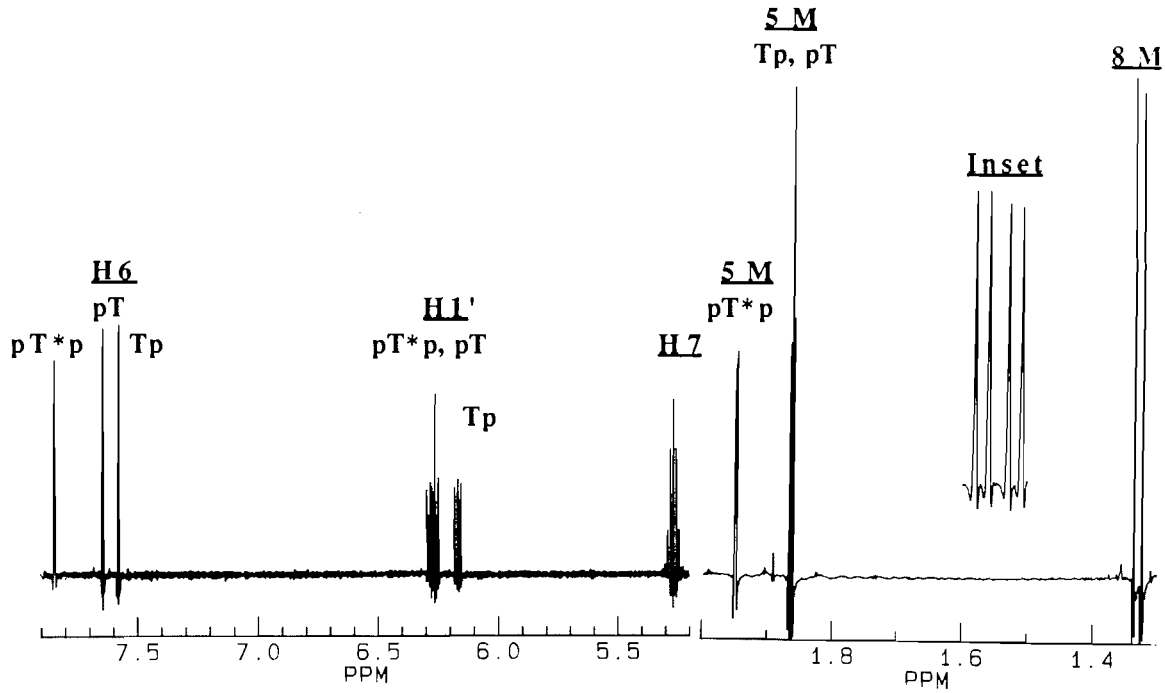


FIG. 2. Partial 500-MHz ^{1}H NMR spectrum (70°C) of d(Tpi^{4}TpT) (**3**) showing the peaks for the H6, 5M (5-methyl), H1′, H7, and 8M (8-methyl) protons. The chemical shifts were measured relative to internal *tert*-butanol and converted to a DSS scale by addition of 1.231 ppm. For the two diastereotopic 8-methyl groups, only a single doublet (1.33 ppm, $J(78) = 6.2$ Hz) is observed. Inset: The two doublets observed (300 MHz, 12°C) for the 8M protons of d(i^{4}TpT) (**1**) at 1.37 ppm and 1.32 ppm ($J(78) = 6.2$ Hz). A pair of doublets ($J(78) = 6.2$ Hz) is also seen for the 8M protons of d(Tpi^{4}T) (**2**) in the 12–70°C range (Tables 1, 2).

TABLE 1. Proton chemical shifts (δ, ppm from DSS) of d(i^{4}TpT) (**1**) and d(Tpi^{4}T) (**2**)[a]

	δ, ppm							
	d(i^{4}TpT)				d(Tpi^{4}T)			
	i^{4}Tp		pT		Tp		pi^{4}T	
Proton	20°C	70°C	20°C	70°C	20°C	70°C	20°C	70°C
1′	6.135	6.201	6.278	6.261	6.157	6.168	6.286	6.281
2′	2.371	2.317	2.341[b]	2.342	2.332	2.315	2.318	2.301
2″	2.628	2.624	2.344[b]	2.364	2.504	2.505	2.450	2.468
3′	4.716	4.754	4.555	4.534	4.742	4.757	4.561	4.534
4′	4.200	4.201	4.109	4.123	4.152	4.141	4.159	4.162
5′	3.871	3.851	4.145	4.119	3.792	3.795	4.170	4.144
5″	3.798	3.780	4.065	4.065	3.748	3.740	4.078	4.076
6	7.889	7.799	7.670	7.624	7.639	7.573	7.886	7.848
5M	1.925	1.934	1.814	1.858	1.857	1.866	1.944	1.952
7	5.243	5.292	—	—	—	—	5.232	5.269
8R	1.365	1.350	—	—	—	—	1.331	1.328
8S	1.324	1.339	—	—	—	—	1.309	1.320
Δ[c]	12.4	3.5	—	—	—	—	6.6	2.3

[a]Proton labelling (Fig. 1): 5M: 5-methyl; 7: tertiary hydrogen of the O-alkyl group; 8R and 8S: diastereotopic methyl protons of the O-alkyl group at low field and high field, respectively.
[b]Estimated, since δ2′ ~ δ2″.
[c]Δ: chemical shift in Hz at 300.134 MHz between the 8R and 8S protons.

the isopropyl methyl carbons (C8) is a doublet with a 1.9-Hz splitting, reflecting the slight differential shielding of the *pro-R* and *pro-S* groups. The doublet shown in the inset reveals a much larger differential shielding (8.1 Hz) of the prochiral carbons in **1**. A doublet is also observed for the C8 carbons of **2** (6.9 Hz separation at 27°C; Table 4).

The ^{1}H NMR spectra were assigned following the study of **6** and **7** (10), and the extensive literature data for thymine oligonucleotides (12–15). Particularly useful are the characteristic effects of O4-alkylation on the base proton shifts, and the observation that ^4J splitting in the H6 and 5-CH_3 bands is consistently smaller by 0.1–0.2 Hz in an O4-alkylated base relative to the parent base (10). ^{1}H-Decoupling and COSY (45°C) spectra were used to connect the sugar protons, and nOe

Can. J. Chem. Downloaded from www.nrcresearchpress.com by 194.225.253.170 on 09/07/12
For personal use only.

TABLE 2. Coupling constants (J, Hz) of d(i^{4}TpT) (**1**), d(Tpi^{4}T) (**2**), and d(TpT) (**4**)[a]

	J, Hz											
	d(i^{4}TpT)				d(Tpi^{4}T)				d(TpT)			
	i^{4}Tp		pT		Tp		pi^{4}T		Tp		pT	
Protons	20°C	70°C	20°C	70°C	20°C	70°C	20°C	70°C	20°C	70°C	20°C	70°C
1′2′	6.2	6.5	6.6]	6.7	7.4	7.4	6.5	6.6	7.4	7.0	6.8	6.8]
1′2″	6.3	6.4	6.6]	6.9	6.1	6.3	6.5	6.6	6.2	6.4	6.8	6.8]
2′2″	−14.0	−14.2	−14.1[b]	−14.1	−14.0	−14.1	−14.0	−14.1	−14.1	−14.1	−14.3	−14.2[b]
2′3′	6.4	6.7	5.7]	6.2	6.4	6.7	6.6	6.7	6.4	6.8	6.7	5.5]
2″3′	5.0	4.1	5.7]	4.6	3.4	3.4	4.5	4.3	3.5	3.4	4.2	5.5]
3′4′	4.6	4.2	4.1	3.7	3.3	3.4	4.4	4.3	3.5	3.5	3.9	4.1
4′5′	3.1	3.5	2.5	2.8	3.4	3.6	2.6	2.7	3.4	3.5	2.3	2.6
4′5″	4.3	4.9	3.0	4.3	4.5	4.8	3.6	4.5	4.6	4.9	3.3	4.5
5′5″	−12.8	−12.5	−11.4	−11.8	−12.5	−12.4	−11.9	−11.9	−12.6	−12.4	−11.5	−11.8
56	1.2	1.1	1.3	1.3	1.3	1.3	1.2	1.2	1.3	1.3	1.3	1.3
78[c]	6.2	6.2	—	—	—	—	6.2	6.2	—	—	—	—
3′P	6.5	6.8	—	—	6.5	6.7	—	—	6.5	6.7	—	—
5′P	—	—	4.1	4.8	—	—	4.5	4.8	—	—	4.4	4.5
5″P[d]	—	—	3.8	5.0	—	—	4.2	4.9	—	—	4.2	5.1

[a]Proton labelling in Fig. 1. 5: 5-methyl; 7: tertiary proton of the O-alkyl; 8: methyl protons of the O4-isopropyl group. Data for **4** from ref. 10.
[b]When δ2′ ~ δ2″, only the sum of connected couplings (]) is significant and J(2′2″) is arbitrary.
[c]H7 is identically coupled to the protons on the two 8-methyl groups.
[d]A ^4J(P–H4′) coupling of 2.0–2.5 Hz was observed in some of the spectra.

TABLE 3. Proton chemical shifts (δ, ppm) and coupling constants (J, Hz) for d(Tpi^{4}TpT) (**3**)[a]

	δ, ppm							J, Hz					
	Tp		pi^{4}Tp		pT			Tp		pi^{4}Tp		pT	
Proton	10°C	70°C	10°C	70°C	10°C	70°C	Protons	10°C	70°C	10°C	70°C	10°C	70°C
1′	6.153	6.163	6.244	6.277	6.273	6.257	1′2′	7.7	7.5	6.6	7.3	6.8]	7.0
2′	2.313	2.301	2.328	2.307	2.337[b]	2.333	1′2″	6.0	6.2	6.3	6.2	6.8]	6.6
2″	2.492	2.490	2.611	2.630	2.333[b]	2.356	2′2″	−14.1	−14.2	−14.2	−14.1	−14.1[b]	−14.1
3′	4.753	4.761	4.845	4.848	4.559	4.540	2′3′	6.4	6.6	6.4	6.5	5.4	6.7
4′	4.159	4.140	4.352	4.345	4.117	4.126	2″3′	3.2	3.4	3.7	3.4	5.4]	3.6
5′	3.786	3.789	4.168	4.147	4.144	4.122	3′4′	3.2	3.4	3.3	3.3	3.9	4.2
5″	3.753	3.739	4.088	4.081	4.066	4.072	4′5′	3.4	3.5	2.8	2.8	2.7	2.9
6	7.646	7.574	7.877	7.841	7.679	7.639	4′5″	4.4	4.9	3.2	4.0	3.1	4.0
5M	1.849	1.861	1.936	1.946	1.837	1.863	5′5″	−12.6	−12.5	−11.7	−11.8	−11.2	−11.6
7	—	—	5.219	5.264	—	—	3′P	6.4	6.7	6.5	6.6	—	—
8M	—	—	1.330	1.328	—	—	4′P	—	—	3.1	2.2	2.7	2.5
							5′P	—	—	4.7	4.9	3.9	4.7
							5″P	—	—	3.4	4.3	4.3	5.4
							M6	1.3	1.3	1.2	1.2	1.3	1.3
							78[c]	—	—	6.2	6.2	—	—

[a]Data at 500.137 MHz. Proton labelling (Fig. 1): 5M: 5-methyl; H7 and H8: tertiary and methyl hydrogens of the O4-isopropyl group, respectively. In contrast with the dimers **1** and **2** (Table 1), no difference can be detected in the shielding of the protons of the two 8-methyl groups.
[b]When δ2′ ~ δ2″, only the sum of connected couplings (]) is significant, and J(2′2″) is arbitrary.
[c]H7 is identically coupled to the protons on the two isopropyl methyl carbon atoms.

experiments were used to connect the H6 and H1′ protons. The ^{13}C spectra were assigned using as guides (a) the extensive chemical shift data for O4-alkylated and unmodified monomers (6, 7) and for thymine oligonucleotides (14, 15), and (b) the trends in ^{13}C–^{31}P coupling constants for nucleotides and DNA oligonucleotides (14, 15, 21, 22). Selective ^{1}H-decoupling experiments were useful for assigning the 5-methyl, C1′, and C3′ resonances of the **3**. Unfortunately, we are not able to provide an unambiguous assignment of the *pro-R* and *pro-S* groups in either the ^{1}H or ^{13}C spectra; the *R*, *S* labelling in the tables is arbitrary.

The O4-isopropyl group

Two important points about this group must be made. First, due to the presence of chiral centers in the sugar, the C8 methyl groups are diastereotopic. In general, such prochiral groups give rise to separate NMR signals (23, 24). However, at the *monomer* level (i^{4}dT), separate peaks are not observed in either

Can. J. Chem. Downloaded from www.nrcresearchpress.com by 194.225.253.170 on 09/07/12
For personal use only.

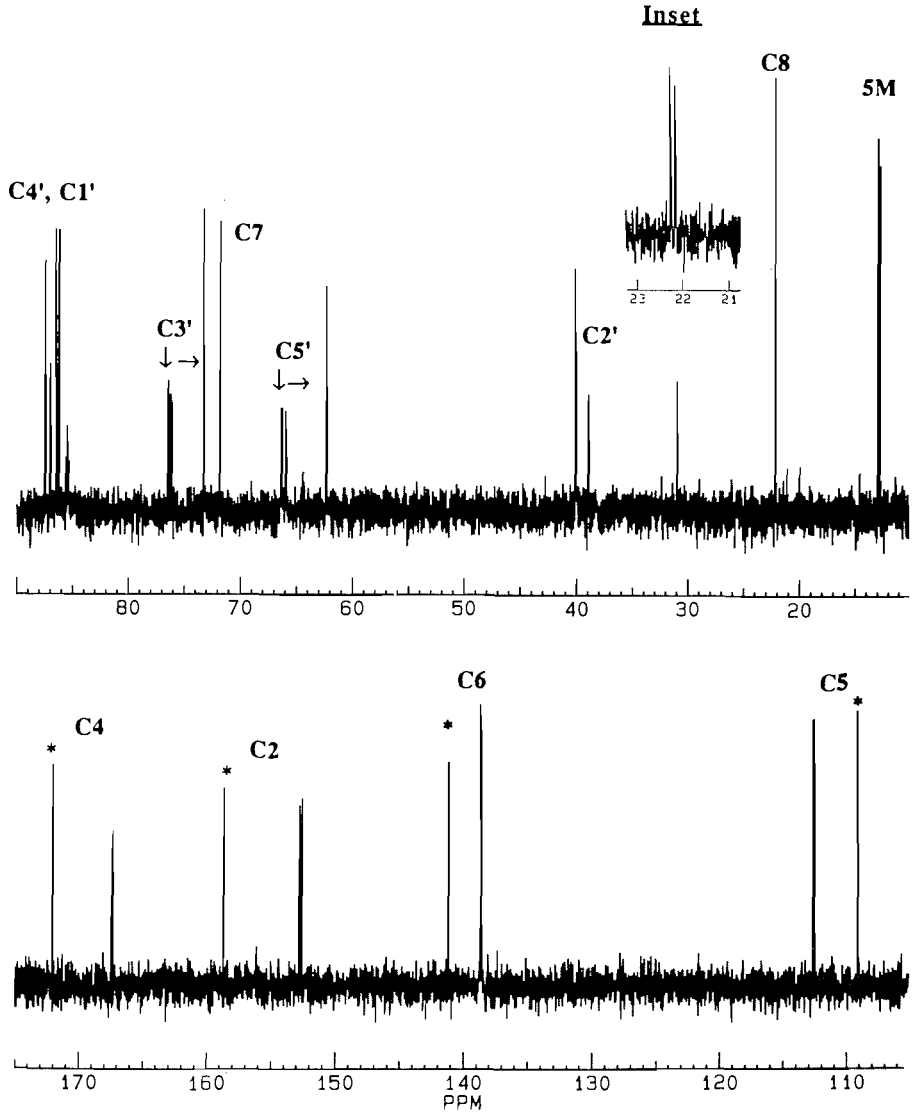


FIG. 3. The 75.5-MHz ^{13}C NMR spectra of d(Tpi^{4}TpT) (**3**) at 27°C in the range 10–90 ppm (top panel) and 105–175 ppm (bottom panel). The chemical shifts were measured relative to internal dioxane and converted to a TMS scale by addition of 67.86 ppm. The "starred" peaks in the bottom panel refer to carbons of the pi^{4}Tp unit. The peak at 22.2 ppm is a doublet (1.9 Hz separation) assigned to the two diastereotopic C8 atoms of the O4-isopropyl group. *tert*-Butanol peak at 31 ppm. Inset: An expanded view of the distinct resonances (8.1 Hz separation) observed for the two C8 atoms of d(i^{4}TpT) (**1**) at 27°C; distinct resonances are also observed for these carbons in d(Tpi^{4}T) (**2**) (Table 4).

the ^1H or the ^{13}C spectra (5), and thus we can conclude that the sugar is too distant from the O4-isopropyl group to cause differential shielding, in line with the observations (23) that such shielding falls off rapidly with the distance between the chiral and prochiral centers.

The second point concerns the conformation of the isopropyl group relative to the base ring. Figure 1 shows the two conformers expected to occur in solution, on the basis of the crystallographic structure of O2-isopropylthymidine (5). In both, C8 is *syn-periplanar* to N3, with the *pro-S* methyl flanking the base on its "3′ face" in one conformer (Fig. 1a) and the *pro-R* methyl flanking the base on its "5′ face" in the other (Fig. 1b). A third conformer in which both methyls flank the base is unlikely for steric reasons (5). (We define as 3′ or 5′ the face that would point to the 3′ or 5′ end of a strand of a normal B-DNA.) There is no apparent reason for a bias, at the *mononucleoside* level, for one or other of the two *syn-periplanar* (*sp*) conformations, and thus equal proportions of the two forms (and rapid interconversion between them) should obtain in solution. In line with this expectation is the isochronicity of prochiral groups of i^{4}dT, in both the ^1H and the ^{13}C NMR spectra (ref. 5 and Table 4).

In contrast with the monomer, the C8 methyl groups of the dimers **1** and **2** give rise to separate NMR signals in the proton spectra (doublets; $J(78) = 6.2$ Hz; Table 2) and in the carbon spectra. These bands for **1** are given in the insets of Figs. 2 and 3; similar patterns are observed in the spectra of **2**, but the chemical shifts are somewhat less than those seen for **1** (Tables 1, 4). As noted above, we cannot provide an absolute assignment of the *R* and *S* resonances of the dimers in either their ^1H and ^{13}C NMR spectra. Figure 4 provides a temperature profile for the H8 proton shifts, and shows that Δ, the separation between the two doublets, decreases monotonically with increasing temperature. The decrease is more pronounced for **1**, but in both dimers some separation remains even at 70°C. Furthermore, in the case of **1**, the two peaks approach the H8

Can. J. Chem. Downloaded from www.nrcresearchpress.com by 194.225.253.170 on 09/07/12
For personal use only.

TABLE 4. ^{13}C chemical shifts (δ, ppm) and coupling constants (J, Hz) for d(i^{4}TpT) (**1**), d(Tpi^{4}T) (**2**), d(TpT) (**4**), and i^{4}dT at 27°C[a]

		d(i^{4}TpT)		d(Tpi^{4}T)		d(TpT)[b]	
Carbon	i^{4}dT	i^{4}Tp	pT	Tp	pi^{4}T	Tp	pT
Chemical shifts							
C2	5.94	5.75	0.10	−0.23	6.16	152.84	152.67
C4	4.43	4.56	−0.11	−0.05	4.69	167.55	167.38
C5	−3.57	−3.78	−0.16	−0.16	−3.64	112.69	112.72
C6	2.63	2.54	−0.09	−0.02	2.83	138.64	138.51
5M	−0.18	−0.18	−0.01	−0.01	−0.13	12.89	12.86
C1′	1.35	1.26	0.05	0.09	1.38	86.39	86.01
C2′	1.02	0.93	0.16	0.04	0.96	38.81	39.89
C3′	−0.14	−0.92	−0.19	0.06	−0.28	76.18	71.54
C4′	0.30	0.02	−0.01	0.05	0.27	86.86	86.19
C5′	−0.10	−0.43	−0.11	0.00	−0.22	62.17	66.01
C7	73.10	73.17	—	—	73.18	—	—
C8R[c]	22.15	22.244	—	—	22.199	—	—
	—	22.208	—	—	22.203	—	—
C8S[c]	22.15	22.137	—	—	22.107	—	—
	—	22.179	—	—	22.160	—	—
Coupling constants							
^3J(C2′P)	—	2.7	—	3.1	—	2.7	—
^2J(C3′P)	—	5.7	—	5.3	—	5.4	—
^3J(C4′P)	—	7.3	9.0	7.1	8.7	7.4	9.1
^2J(C5′P)	—	—	5.5	—	5.7	—	5.2

[a]δ in ppm were measured relative to internal dioxane and converted to a TMS scale by δ(TMS) = δ(dioxane) + 67.86 ppm. δC2 through δC5′ for d(i^{4}TpT) (**1**) and d(Tpi^{4}T) (**2**) are given relative to the corresponding δ in d(TpT), with positive numbers indicating a deshielding relative to this reference. The δ for the O4-isopropyl groups are relative to TMS. The data for i^{4}dT are from ref. 5 (δC2 through δC5′ are relative to dT; δC7 and δC8 are relative to TMS). See Fig. 1 for atom labelling.

[b]The base carbon assignments for Tp and pT may be interchanged.

[c]The *R* and *S* assignment is arbitrary. The first entry is for 27°C, and the second for 70°C.

chemical shift of i^{4}dT. The ^{13}C NMR data were collected at only two temperatures (27 and 70°C). However, the trends here are in line with the proton data in that the separation of the resonances decreases at the higher temperature, with the larger change occurring for dimer **1** (Table 4).

Since no differential shielding of the prochiral methyl groups is observed in the monomer i^{4}dT (5), the temperature dependence of Δ at the dimer level can be accounted for by intramolecular base stacking, the rationale presented for the chemical shifts of the prochiral methylene protons of **6** and **7** (10). Space-filling molecular models of the dimers in a right-handed base-stacked conformation (with both bases oriented *anti* about the N-glycosyl bond and with the O4-isopropyl group oriented as in Fig. 1a) suggest that the ^1H and ^{13}C shielding of the *pro-S* methyl of **1** would be more influenced by the second base, whereas the *pro-R* group would be more affected in **2**. However, models also suggest that we cannot, for the time being, discount contributions from base stacks involving the alternate *sp* conformation of the isopropyl group (Fig. 1b). Because of our uncertainty as to the favored orientation of the isopropyl group, we do not feel confident to use the shift trends in Fig. 4 as a basis for assigning the *pro-R* and *pro-S* resonances, or to derive more precise details of the base stacks. Nevertheless, because the 8-methyl peaks are intense and occur in isolated regions of the ^1H and the ^{13}C spectra, it would seem that their chemical shifts might provide a convenient means to monitor, in longer oligonucleotides, helix–coil transitions in the vicinity of the modified base.

In striking contrast with the dimers, only a single doublet is observed in the ^1H NMR spectrum of the trimer **3** over the 10–70°C range (Fig. 4, Table 3), and the ^{13}C spectra reveal only a small differential shielding (Fig. 3, Table 5). Furthermore, the ^1H chemical shift of the 8M protons shows no dependence on temperature in the 10–70°C range (Fig. 4). This is unexpected in view of the behaviour of the prochiral groups of **1** and **2**, and because the CD spectra of **3** show changes that suggest some degree of base stacking at low temperature (see below). Perhaps there is a cancellation of the shielding effects of the Tp and pT bases; magnetic shielding of the O4-alkyl and CD changes have different origins, and therefore must report different features of the same ordered structure. Interestingly, we have recently noted that, for the ethyl analogue of **3**, d(Tpe^{4}TpT), *both* the CD and the Δ for the diastereotopic methylene protons of the O4-ethyl group are temperature dependent.[4]

Sugar pucker

This feature of a 2′-deoxyribose ring can be evaluated from the vicinal proton coupling constants $J(1'2')$ through $J(3'4')$ (Tables 2 and 3), or from certain sums of these couplings such as $\Sigma 1' = J(1'2') + J(1'2'')$ (25). Comparing the 20°C data for the dimers (Table 2), one sees that O4-isopropylation of the Tp unit of **4** leads to an increase of 1.1 Hz in $J(3'4')$ and 1.5 Hz in $J(2''3')$, and a decrease of 1.2 Hz in $J(1'2')$, consistent with a destabilization of the *S* (2′-*endo*) pucker (26). The same trend

[4]Communicated at the 13th International Conference on Magnetic Resonance in Biological Systems, Madison, WI, August 14–19, 1988.

Can. J. Chem. Downloaded from www.nrcresearchpress.com by 194.225.253.170 on 09/07/12
For personal use only.

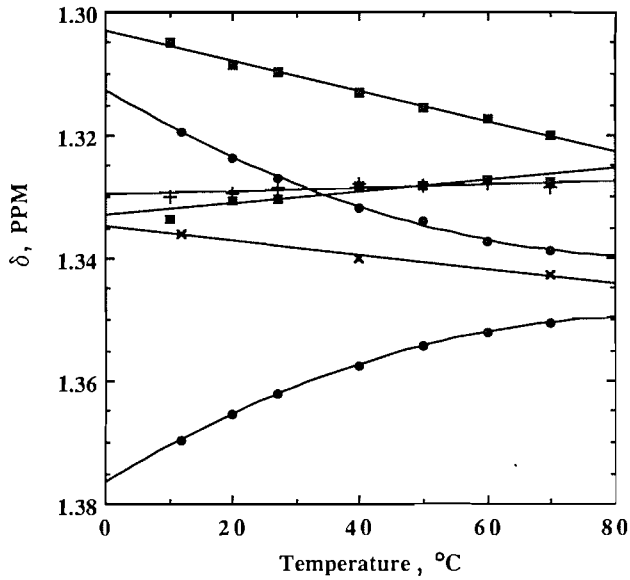


FIG. 4. Temperature (°C) profile of the chemical shifts (δ, ppm from DSS) of the diastereotopic methyl (8M) protons of the O4-isopropyl groups of d(i^{4}TpT) (**1**) (solid circle), d(Tpi^{4}T) (**2**) (solid square), d(Tpi^{4}TpT) (**3**) (+), and i^{4}dT (×). Distinct doublets (J(78) = 6.2 Hz) are observed for the *pro-R* and *pro-S* groups in the spectra of **1** and **2**, but the protons on the two groups are isochronous in **3** and i^{4}dT so that only a single doublet (J(78) = 6.2 Hz) is observed.

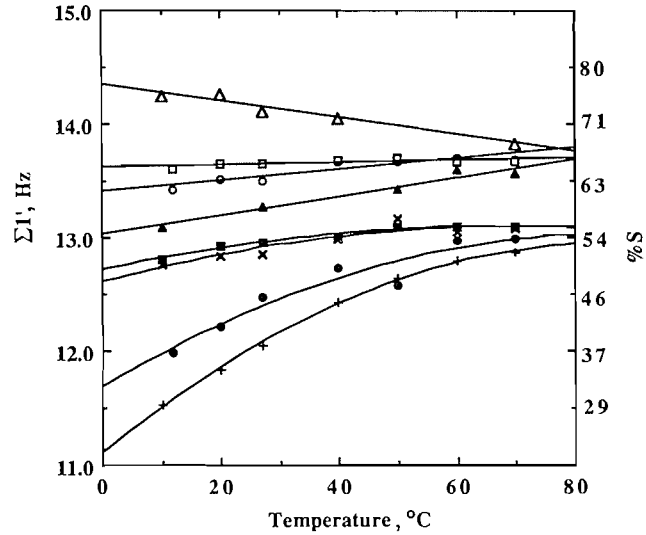


FIG. 5. Temperature profiles of $\Sigma 1' = J(1'2') + J(1'2'')$ in Hz for the modified units i^{4}Tp (**1**) (solid circle), e^{4}Tp (**6**) (+), pi^{4}T (**2**) (solid square), pe^{4}T (**7**) (×), and pi^{4}Tp (**3**) (solid triangle), and the corresponding unmodified units Tp (**4**) (open circle), pT (**4**) (open square), and pTp (**5**) (open triangle). The data are taken from Tables 2 and 3, ref. 10, or from the width of the H1′ band. The vertical axis at the right provides the *%S* (2′-*endo*) conformation of the sugar ring calculated according to ref. 25. For comparison, Σ1′ is 13.1 Hz (55% *S*) for i^{4}dT and 13.6 Hz (65% *S*) for dT in the 10–70°C range.

was noted for O4-ethylation (10), but the changes were larger. However, the effect of O4-isopropylation on the pT unit is small. For the modified segment of **1**, increasing the temperature to 70°C leads to decreases in $J(2''3')$ and $J(3'4')$, and to an increase in $J(1'2')$, reflecting a shift back to the *S* pucker at high temperature. These general trends are evident in the temperature profiles of Σ1′ in Fig. 5, which show the shift towards the *N* type pucker for the i^{4}Tp unit of **1**. In the figure, Σ1′ data are also provided for e^{4}Tp of **6** (10), and reveal a slightly larger shift towards *N* for this unit. On the other hand, Σ1′ for the modified (pi^{4}T, pe^{4}T) and unmodified (pT) 5′-nucleotidyl units show relatively little variation with temperature.

Data (500 MHz) are provided for the trimer **3** at 10 and 70°C (Table 3) for comparison with the 30°C data (500 MHz) on the unmodified trimer **5** published by Rycyna *et al.* (14). The coupling constants of the unmodified Tp and pT ends of **3** show little variation from 10 to 70°C (≅0.2 Hz), and are identical to within 0.2 Hz to the corresponding couplings of **5**. Comparing the low temperature data for the pNp units of the trimers, we note that O4-alkylation causes a decrease in $J(1'2')$ from 8.1 to 6.6 Hz with a concomitant increase in $J(2''3')$ from 3.1 Hz to 3.7 Hz, in line with a destabilization of the *S* pucker. Unfortunately, at 10°C the HDO resonance is uncomfortably close to the H3′ (pi^{4}Tp) band, and so we are less confident about the magnitude of $J(3'4')$ of this unit, though a small increase of 0.4 Hz relative to the pTp unit is indicated. Figure 5 shows that at 10°C Σ1′(pNp) is smaller by 1.2 Hz in **3**, indicating a reduction of about 20% in the *S* pucker relative to **5**. At 70°C, their Σ1′ are identical to within experimental error.

We have also measured the Σ1′ for a series of monomeric r^{4}dT (r = methyl, ethyl, isopropyl, *n*-propyl) and for the 3′-nucleotide (3′-e^{4}dTMP), and found that they are independent of temperature in the 10–70°C range (13.1 Hz; 55% *S*). Since no temperature dependence is seen for the monomers, the effect of temperature on the pucker of certain modified units of the oligomers, as discussed above, would seem to be related to intramolecular base stacking. As noted in a previous section and in our study of the O4-ethylated dimers (10), the variation of Δ points to some base association at low temperature. Since stacked, single-stranded 2′-deoxyoligonucleotides containing the major bases favor the *S* pucker (25), our results reveal that certain nucleotidyl units containing the O4-alkylthymine must adjust their conformation to be accommodated in the ordered structure.[5]

The C4′—C5′ (γ) bond

Table 6 gives the populations for the *gauche*$^+$ (g$^+$), *trans* (t), and *gauche*$^-$ (g$^-$) conformers about the γ bond of **1**–**5**, calculated from the $J(4'5')$ and $J(4'5'')$ data according to Haasnoot *et al.* (27). At the low temperature, the Np fragments of the dimers and the trimers show preferences for g$^+$ in the narrow ranges 59 ± 3% whereas the pN and pNp units lie in the range 77 ± 4%, with the two units of **1** lying at the high ends of their respective ranges. Elevating the temperature to 70°C reduces g$^+$ to 54 ± 2% (Np) and 65 ± 3% (pN, pNp). The g$^-$ conformer is always the least populated, particularly for the pN and pNp units. Similar results were observed for the O4-ethylated molecules (10), and so it seems that O4-alkylation does not have much effect on the γ bonds at the dimer and trimer level.

[5]A referee has stated that our calculations based on Σ1′ data lead to *%S*, which can be quite different from those obtained by the more complete calculation using the PSEUROT program (25). For example, at 20°C the calculated *S* populations differ by 13% for the i^{4}Tp (**1**): 41% via Σ1′ (Fig. 5) and 54% via PSEUROT (calculated by the referee). There are uncertainties in all of these methods but they reveal the same trends. Our tabled data are available for the PSEUROT calculations.

Can. J. Chem. Downloaded from www.nrcresearchpress.com by 194.225.253.170 on 09/07/12
For personal use only.

Can. J. Chem. Downloaded from www.nrcresearchpress.com by 194.225.253.170 on 09/07/12
For personal use only.

TABLE 5. ^{13}C Chemical shifts (δ, ppm)[a] and ^{13}C–^{31}P coupling constants (J, Hz) of d(Tpi^{4}TpT) (**3**) and d(TpTpT) (**5**) at 27°C[a]

	d(Tpi^{4}TpT)			d(TpTpT)		
Carbon	Tp	pi^{4}Tp	pT	Tp	pTp	pT
Chemical shifts						
C2	−0.06	5.95	−0.10	152.80	152.69	152.62
C4	−0.14	4.74	−0.12	167.53	167.30	167.43
C5	−0.21	−3.67	−0.25	112.71	112.74	112.87
C6	−0.06	2.67	−0.01	138.64	138.42	136.52
5M	−0.07	−0.13	0.06	12.94	12.87	12.87
C1′	0.07	1.37	0.06	86.38	86.05	86.12
C2′	−0.03	1.12	0.06	38.92	38.81	40.00
C3′	−0.21	−0.27	0.01	76.64	76.39	71.72
C4′	0.05	0.08	−0.07	86.93	85.36	86.41
C5′	−0.01	−0.39	0.13	62.26	66.24	66.10
C7	—	73.22	—	—	—	—
C8R	—	22.17	—	—	—	—
C8S	—	22.15	—	—	—	—
Δ[b]	—	1.9	—	—	—	—
Coupling constants						
^3J(C2′P)	2.5	3.0	—	3.1	3.0	—
^2J(C3′P)	5.5	5.6	—	5.0	5.3	—
^3J(C4′P3′)	7.0	7.0	—	7.4	8.2	—
^3J(C4′P5′)	—	8.6	8.8	—	8.2	9.0
^2J(C5′P)	—	5.6	5.4	—	5.8	5.6

[a]The chemical shift data are measured at 75.5 MHz relative to internal dioxane and converted to a TMS scale by addition of 67.86 ppm. δC2 through δC5′ for **3** are relative to the carbon shift of the corresponding fragment of **5**; a negative sign indicates a resonance at high field of the reference. The δC7 and δC8 are relative to TMS. The assignments of the base carbons of Tp and pT may be interchanged. See Fig. 1 for atom labelling. The J data for **5** at 30°C are from ref. 15.

[b]Δ is the chemical shift in Hz at 75.5 MHz between the two diastereotopic isopropyl methyl carbons at 27°C; at 70°C, distinct resonances for these carbons are not detected, and thus Δ must be less than about 1 Hz.

The C5′—O5′ (β) bond

The population of the favored *trans* (t) conformation of the β bond of the pN and pNp fragments can be estimated from $\Sigma' = J(5'P) + J(5''P)$ (28). This sum falls into the narrow range from 7.9 to 9.1 Hz for these fragments of **1** and **2** (20°C, Table 2), **3** (10°C, Table 3), **4** (20°C) (10), **5** (30°C) (15), and **6** and **7** (20°C) (10). With the parameterization of Cheng *et al.* (13), these data yield %t populations in the range 76–84%. The unmodified pT units of **1** and **6** are found at the high end of the range (82–84%) but, overall, the data do not reveal any large effect of alkylation for the molecules studied. Increasing the temperature to 70°C invariably leads to an increase in Σ' (range 9.3–10.1 Hz), corresponding to a decrease in %t (72–76% range). Similar trends are generally observed for dimers and trimers containing only the normal bases.

The preference for the t(β) conformer for the 5′-nucleotidyl fragments is confirmed by the ^3J(C4′P5′) data (27°C) for **1**–**5**, which fall into the narrow range 9.0 ± 0.3 Hz, except for the pTp unit of **5** (8.2 Hz) (Tables 4, 5), and correspond to 80 ± 3% for the t(β) conformer (calculated according to Lankhorst *et al.* (29)). The value for pTp (**5**), 8.2 Hz, taken from Rycyna *et al.* (15), corresponds to 73% t(β).

The C3′—O3′ (ε) bond

The behaviour of this bond of a 3′-nucleotidyl fragment can be followed with the ^3J(H3′P3′), ^3J(C4′P3′), and ^3J(C2′P3′) coupling constants (15, 21, 29–31). The ^3J(H3′P3′) data, collected over the 20–70°C range for the 3′-nucleotidyl fragments of **1**, **2**, and **4** (Table 2), **3** (Table 3), **5** (15), **6** and **7** (10), lie in the narrow range 6.3–6.8 Hz. A thorough evaluation of the orientation of the ε bond would require ^3J(C4′P3′) and ^3J(C2′P3′) data over a range of temperature (29), but we are limited so far to data near ambient temperature. However,

TABLE 6. Calculated % population[a] of the *gauche*$^+$ (g$^+$), *trans* (t), and *gauche*$^-$ (g$^-$) rotamers about the C4′—C5′ bond for d(i^{4}TpT) (**1**), d(Tpi^{4}T) (**2**), d(TpT) (**4**), d(Tpi^{4}TpT) (**3**), and d(TpTpT) (**5**)

Unit	T, °C	g$^+$	t	g$^-$	Unit	T, °C	g$^+$	t	g$^-$
1 i^{4}Tp	20	62	30	8	**3** Tp	10	58	31	11
	70	52	36	13		70	52	36	13
pT	20	81	18	1	pi^{4}Tp	10	76	19	4
	70	64	31	4		70	68	28	4
2 Tp	20	57	32	11	pT	10	78	19	3
	70	52	34	14		70	67	28	5
pi^{4}T	20	73	26	2	**5** Tp	30	56	33	11
	70	63	34	3	pTp	30	79	19	2
4 Tp	20	56	33	11	pT	30	73	24	3
	70	52	36	13					
pT	20	80	22	−2					
	70	64	34	2					

[a]According to ref. 25. Populations for **5** calculated from J data in Rycyna *et al.* (15).

Can. J. Chem. Downloaded from www.nrcresearchpress.com by 194.225.253.170 on 09/07/12
For personal use only.

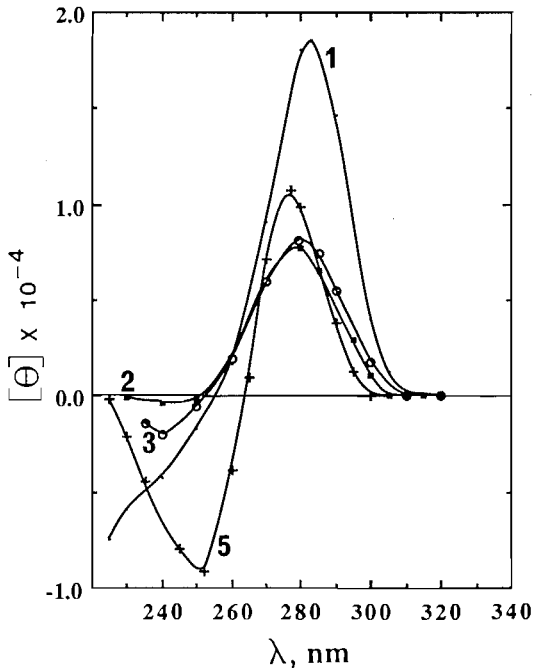


FIG. 6. Circular dichroism (CD) spectra at 9–12°C for d(i^{4}TpT) (**1**) (●), d(Tpi^{4}T) (**2**) (■), d(Tpi^{4}TpT) (**3**) (○), and d(TpTpT) (**5**) (+) at (8.3–9.5) × 10^{-5} M in phosphate buffer (pH = 6.9). The vertical axis gives [θ] in deg M^{-1} cm^{-1}, the molar ellipticity per residue calculated following Cantor and Schimmel (32). For comparison, spectra for d(e^{4}TpT) (**6**), d(Tpe^{4}T) (**7**), and d(TpT) (**4**) are found in ref. 10.

one clear feature in the available data is that ^3J(C4′P3′) is invariably larger than ^3J(C2′P3′) (typically about 7 and 3 Hz, respectively). This collection of data points to a preference for the *trans* conformer of the C4′—C3′—O3′—P3′ fragment over the *gauche*$^-$.

^{1}H and ^{13}C chemical shifts

^{1}H NMR spectra were obtained for our O4-isopropylated molecules (and their unmodified parents) at 10° intervals in the 10–70°C range, and computer-analyzed at two temperatures (Tables 1–3); estimates of the shifts at other temperatures can be easily obtained with the information provided by the computer-derived data. Temperature profiles for the O4-isopropylated dimers (other than those in Fig. 4) are not given here since they closely resemble the profiles of their O4-ethylated counterparts provided by Buchko *et al.* (10). The most noteworthy effect of O4-alkylation, observed at the dimer and trimer levels, is the deshielding of H6 (0.22–0.29 ppm) and the 5-CH_3 protons (0.06–0.08 ppm) of the modified base (Fig. 2).

To facilitate comparison of the effects of O4-alkylation on the carbon shifts, the δ(^{13}C) values for the dimers **1** and **2** are given (Table 4) relative to the corresponding value in the parent dimer **4** (except for the O4-isopropyl carbons, which are relative to TMS), whereas data for **4** are given relative to TMS. Also provided are the published (5) δ values of the monomer i^{4}dT relative to dT. In Table 5 are found the data for the unmodified trimer **5** relative to TMS and the data for the modified trimer **3** relative to **5**. Clearly, the major effects of O4-alkylation are restricted to the base of the altered nucleoside unit, with close agreement at monomer, dimer, and trimer levels: deshielding of C2, C4, and C6 (2.5–6.2 ppm) and shielding of C5 (−3.5 to −3.8 ppm). Only a small deshielding is found at the 5-methyl carbon (5M (< −0.2 ppm). It is interesting to note that in all instances the effect at the C2 carbonyl carbon is about 30% larger than at the directly affected C4 position; this points to an extensive polarization of the entire O4—C4—N3—C2—O2 fragment. The effect of O4-alkylation on the carbons of the unmodified segments of the oligomers is in all cases less than 0.3 ppm. These trends, as well as those of ^{1}H NMR data, would facilitate the assignment of pyrimidine bases in the spectra of longer oligonucleotides.

Circular dichroism

Figure 6 provides [θ], the molar ellipticity per residue, for **1**, **2**, **3**, and **5** at 9–11°C; the spectrum for **4** (in ref. 10) is not provided here since it is identical to that of **5**. Our CD spectrum of **5** (λ_{max}: 277 nm, $[\theta]_{max}$ = 10 700; λ_{min}: 252 nm, $[\theta]_{min}$ = −9100) is in good agreement with that of d(pTpTpT) (33). O4-Isopropylation causes a dramatic reduction in the negative CD peak at 252 nm and a shift of λ_{max} of the positive peak to longer wavelengths (284 nm (**1**), 280 nm (**2**), 279 nm (**3**)). In addition, the magnitude of the positive peak is considerably enhanced in **1** ($[\theta]_{max}$: 18 600), but decreased slightly in **2** and **3**. These trends are identical to those noted for the corresponding ethylated derivatives **6** and **7** (10). It is interesting to note that the CD spectra of **1** and **2** are qualitatively similar to those of d(CpT) and d(TpC) (33). This correspondence was noted earlier for **6** and **7** and suggests that in some respects an O4-alkylated base is "cytosine-like," in line with crystallographic data (3, 4).

CD spectra were obtained at 15–20°C intervals up to about 65°C, and invariably show a gradual diminution of the extrema with increasing temperature. For the prominent positive peak, the decrease in $[\theta]_{max}$ is larger (40–44%) for the Np-modified dimers (**1**, **6**) and the unmodified molecules (**4**, **5**), and less for the pN-modified dimers (**2**, **7**) (10–15%) and the modified trimer (**3**) (24%). This temperature dependence points to the formation of some base stacking at low temperature. At the dimer level, the trends are in qualitative agreement with the effects of temperature on Δ (Fig. 4), which were interpreted in terms of base stacking. On the other hand, no differential shielding of the diastereotopic 8-methyl groups of **3** was observed (see above), an inconsistency that we cannot now explain.

Mass spectrometric experiments

Our FAB-MS data for the O4-isopropylated molecules, as well as those for their O4-ethylated analogs in Buchko *et al.* (10), demonstrate the utility of this technique for the characterization of DNA oligomers containing the r^{4}T base. Particularly useful is the presence of an intense $[M - H]^-$ molecular ion of **1**, **2** and **3**, and of the fragment [O4-alkylthymine − H]$^-$, which results from the scission of the N-glycosyl bond of the modified unit. The spectra of **1** and **2** show peaks at *m/z* 363, which correspond to the nucleotidyl fragments [3′-i^{4}dTMP − H]$^-$) and [5′-i^{4}dTMP − H]$^-$), respectively. Also of diagnostic value is the presence of peaks at *m/z* 1175 in the spectra of **1** and **2** (2–4% of the $[M - H]^-$ ion) that can be assigned to the molecular aggregates $[2M - H]^-$. An aggregate of *three* molecules was also apparent (at very low intensity) in the negative ion FAB spectra of **6** (10), but no such aggregate was seen here. No aggregates were apparent in the spectrum of either **3** or **5**. In a subsequent report, discussion of molecular scissions and rearrangements of our modified oligomers will be provided, as has been done for the parent nucleosides (34). Our studies could be useful for determining the site of modification of longer DNA fragments.

Acknowledgements

We acknowledge the support of the following: NSERC (for operating grants to F.E.H. (A1549) and K.L.S. (A6434); The University of Manitoba (research funds for F.E.H. and K.L.S., and a Manitoba Fellowship for G.W.B.); Mr. W. Buchannon (for acquiring and interpreting the FAB-MS spectra); Mr. K. Marat (for help with acquiring the NMR spectra); Drs. D. Hughes and B. Sayer (McMaster University, for acquiring the 500-MHz spectra); Drs. F. Ahmad, A. S. Secco, B. Singer, and J. B. Westmore, and Mr. F. LaFortune (for discussions); Donna Hruska (for help with manuscript preparation).

1. B. SINGER. Cancer Res. **46**, 4879 (1986).
2. T. P. BRENT, M. E. DOLAN, H. FRAENKEL-CONRAT, J. HALL, P. KARRAN, F. LAVAL, G. P. MARGISON, R. MONTESANO, A. E. PEGG, P. M. POTTER, B. SINGER, J. A. SWENBERG, and D. B. YAROSH. Proc. Natl. Acad. Sci. U.S.A. **85**, 1759 (1988).
3. R. G. BRENNAN, D. PYZALSKA, W. J. P. BLONSKI, F. E. HRUSKA, and M. SUNDARALINGAM. Biochemistry, **25**, 1181 (1986).
4. G. I. BIRNBAUM, K. L. SADANA, W. J. P. BLONSKI, and F. E. HRUSKA. J. Am. Chem. Soc. **108**, 167 (1986).
5. G. I. BIRNBAUM, K. L. SADANA, M. T. RAZI, T. LEE, R. SEBASTIAN, G. W. BUCHKO, and F. E. HRUSKA. Can. J. Chem. **66**, 1628 (1988).
6. B. D. ALLORE, A. QUEEN, W. J. P. BLONSKI, and F. E. HRUSKA. Can. J. Chem. **61**, 2397 (1983).
7. C.-J. CHANG, D. J. ASHWORTH, L.-J. CHERN, J. D. GOMES, C.-G. LEE, P. W. MOU, and R. NARAYAN. Org. Magn. Reson. **22**, 671 (1984).
8. B. F. L. LI, C. B. REESE, and P. F. SWANN. Biochemistry, **27**, 1086 (1987).
9. M. W. KALNIK, M. KOUCHAKDJIAN, B. F. L. LI, P. F. SWANN, and D. J. PATEL. Biochemistry, **27**, 108 (1988).
10. G. W. BUCHKO, F. E. HRUSKA, and K. L. SADANA. Can. J. Chem. **67**, 109 (1989).
11. B. SINGER, S. J. SPENGLER, H. FRAENKEL-CONRAT, and J. T. KUSMIEREK. Proc. Natl. Acad. Sci. U.S.A. **83**, 28 (1986).
12. D. J. WOOD, F. E. HRUSKA, and K. K. OGILVIE. Can. J. Chem. **52**, 335 (1974).
13. D. M. CHENG, M. M. DHINGRA, and R. H. SARMA. Nucleic Acids Res. **5**, 4399 (1978).
14. R. E. RYCYNA and J. L. ALDERFER. Nucleic Acids Res. **13**, 5949 (1985).
15. R. E. RYCYNA, J. C. WALLACE, M. SHARMA, and J. L. ALDERFER. Biochemistry, **27**, 3152 (1988).
16. M. D. MATTEUCHI and M. H. CARUTHERS. Tetrahedron Lett. **21**, 3243 (1980).
17. P. S. MILLER, K. N. FANG, N. S. KONDO, and P. O. P. Ts'O. J. Am. Chem. Soc. **93**, 6657 (1971).
18. B. SINGER, J. SAGI, and J. T. KUSMIEREK. Proc. Natl. Acad. Sci. U.S.A. **80**, 4884 (1983).
19. W. P. AUE, E. BARTHOLDI, and R. R. ERNST. J. Chem. Phys. **64**, 2229 (1976).
20. A. R. QUIRT and J. S. MARTIN. J. Magn. Reson. **5**, 318 (1971).
21. W. J. BLONSKI, F. E. HRUSKA, K. L. SADANA, and P. C. LOEWEN. Biopolymers, **22**, 605 (1983).
22. P. P. LANKHORST, C. A. G. HAASNOOT, C. ERKELENS, H. P. WESTERINK, J. H. VAN BOOM, and C. ALTONA. Nucleic Acids Res. **13**, 927 (1985).
23. W. B. JENNINGS. Chem. Rev. **75**, 307 (1975).
24. A. E. TONELLI, F. C. SCHILLING, and F. A. BOVEY. J. Am. Chem. Soc. **106**, 1157 (1984).
25. L. J. RINKEL and C. ALTONA. J. Biomol. Struct. Dyn. **4**, 621 (1987).
26. C. ALTONA and M. SUNDARALINGAM. J. Am. Chem. Soc. **94**, 8205 (1982).
27. C. A. G. HAASNOOT, F. A. A. M. DE LEEUW, H. P. M. DE LEEUW, and C. ALTONA. Recl. Trav. Chim. Pays-Bas, **98**, 576 (1979).
28. D. J. WOOD, F. E. HRUSKA, R. J. MYNOTT, and R. H. SARMA. Can. J. Chem. **51**, 2571 (1973).
29. P. P. LANKHORST, C. A. G. HAASNOOT, C. ERKELNS, and C. ALTONA. J. Biomol. Struct. Dyn. **1**, 1387 (1984).
30. J. L. ALDERFER and P. O. P. Ts'O. Biochemistry, **16**, 2410 (1977).
31. D. B. DAVIES and H. SADIKOT. Biopolymers, **22**, 1843 (1983).
32. C. R. CANTOR and P. R. SCHIMMEL. Biophysical chemistry. Part II. Freeman, San Francisco, CA. 1980. p. 413.
33. C. R. CANTOR, M. W. WARSHAW, and H. SHAPIRO. Biopolymers, **1**, 1059 (1970).
34. F. LAFORTUNE, W. ENNS, F. E. HRUSKA, K. L. SADANA, K. G. STANDING, and J. B. WESTMORE. Int. J. Mass Spectrom. Ion Processes, **78**, 179 (1987).

Can. J. Chem. Downloaded from www.nrcresearchpress.com by 194.225.253.170 on 09/07/12
For personal use only.

Reactions of polar dienes with *o*-quinones

JACQUES PAQUET AND PAUL BRASSARD[1]
Département de chimie, Université Laval, Québec (Québec), Canada G1K 7P4

Received November 22, 1988

JACQUES PAQUET and PAUL BRASSARD. Can. J. Chem. **67**, 1354 (1989).

The behaviour of various types of polar dienes towards halogenated *ortho* quinones has been investigated in a number of representative cases. As compared to the commonly used *para* analogues, *o*-quinones provide a wide range of products that indicate a keener response to the nature, number, and position of substituents on both reactants. 3-Halogenated-*o*-naphthoquinones **1** and **2** react smoothly with a representative vinologous ketene acetal **3**, vinylketene acetals **4** and **5**, and a monooxygenated diene **6** to provide variously substituted phenanthrenequinones **7–11**. Only monooxygenated dienes on the other hand add to *o*-benzoquinones **14–16** and give convenient syntheses of the corresponding *o*-naphthoquinones **18–20**.

Key words: cycloaddition, *o*-naphthoquinones, phenanthrenequinones, regiospecificity.

JACQUES PAQUET et PAUL BRASSARD. Can. J. Chem. **67**, 1354 (1989).

Le comportement de divers types de dienes polaires vis-à-vis les *o*-quinones halogénées a été étudié dans un certain nombre de cas significatifs. Par comparaison avec les isomères-1,4 d'usage plus répandu, les *o*-quinones fournissent une gamme plus étendue de produits qui traduisent une sensibilité accrue à la nature, au nombre et à la position des substituants dans les deux réactants. Les *o*-naphtoquinones halogénées **1**, **2**, par réaction avec le vinylogue d'acétal de cétène **3**, des acétals de vinylcétènes **4**, **5** et un diène monoxygéné **6**, fournissent les phénanthrènequinones **7–11** attendues. Seuls les diènes monoxygénés, par contre, réagissent bien avec les benzoquinones **14–16** et conduisent aux *o*-naphtoquinones correspondantes **18–20**.

Mots clés : cycloaddition, *o*-naphtoquinones, phénanthrènequinones, régiospécificité.

Can. J. Chem. Downloaded from www.nrcresearchpress.com by 194.225.253.170 on 09/07/12
For personal use only.

The Diels–Alder reaction of simple dienes with *o*-quinones has been intensively examined by a number of investigators over the years (1). Various regiochemical problems such as the involvement of 3,4 or 5,6 double bonds in the case of substituted *o*-benzoquinones (2–5), the ease of addition to carbonyl groups (6), the formation of dioxanes (6*b*, 7), and the dienic character of *o*-quinones (8) have all received considerable attention. The orientation of weakly polar dienes in the process has not been addressed systematically although regioselective behaviour has been established in a few instances (3–5, 9). Enhanced reactivity in the case of halogenated quinones has been repeatedly pointed out (2, 9) and this type of substituent has been used to direct addition from the 3,4 to the 5,6 double bond (4) but does not seem to have been otherwise used to assist in the orientation of the diene.

The concomitant application of electron-rich dienes and halogenated *p*-benzo- and *p*-naphthoquinones to effect regiospecific annulations (10) was extended to *ortho* isomers in the expectation that naturally occurring *o*-naphthoquinones, phenanthrenequinones, and eventually phenanthrenoid phytoalexins could be synthesized expeditiously by this simple approach. It has previously been shown that cycloadditions with *o*-benzoquinones generally affect the carbon–carbon double bond of lowest electron density (2). However, *o*-naphthoquinones substituted in the 4-position with electron-attracting groups give mainly adducts involving the 2-carbonyl function (6*a*). Nevertheless, with sufficiently electrophilic *o*-quinones, 1,6 rather than 1,4 additions of nucleophiles are known to occur (11), and it was hoped that polar dienes like vinylogous ketene acetals and vinylketene acetals should not only produce the expected products with 3-halogenated substrates but might also considerably facilitate the inverse addition with the 4-substituted isomers.

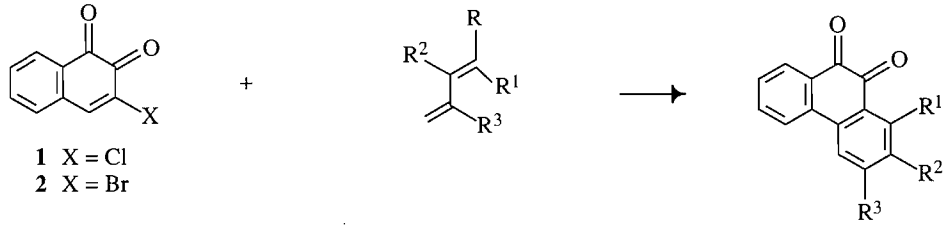
Both 3- and 4-halogenated *o*-naphthoquinones are more readily available and better able to demonstrate the usefulness of the method than the variously substituted monocyclic analogues. Initial tests involving the electron-rich 2-methyl-1,3-bistrimethylsiloxy-1,3-butadiene (**3**) and quinone **2** easily gave an adduct, which was aromatized with HCl at room temperature and provided a 74% yield of the expected phenanthrenequinone **7**. A similar reaction with chloroquinone **1** proved more difficult to complete and yielded the same product in 40% yield only upon refluxing the intermediate in toluene for 18 h.

Subsequent experiments with a vinylketene acetal, 1,3-dimethoxy-1-trimethylsiloxy-1,3-butadiene (**4**) proceeded as smoothly as before but produced somewhat startling results. A reaction between this diene and quinone **2**, when conducted in THF at 0°C, gave only 1-hydroxy-3-methyl phenanthrenequinone (**8**) in 70% yield after the reaction was allowed to come to room temperature. On the other hand, when the cycloaddition was carried out in benzene at 6°C, only the 1,3-dimethoxy derivative **9** was obtained. Although reactions with dienic mixed acetals that do not involve hydrolysis of the intermediate adduct generally afford mixtures of such products as the foregoing, this is the only case, to our knowledge, of such a selective outcome (12).

The eventual application of this approach to the synthesis of natural products requires the use of such compounds as 1-methoxy-3-methyl-1-trimethylsiloxy-1,3-butadiene (**5***a*). This reactant is often less satisfactory than the preceding one, giving on occasion small amounts of an open-chain by-product (10*b*). An initial experiment with 3-chloro-*o*-naphthoquinone (**1**) gave only 40% of the desired phenanthrenequinone **10** along with 10% of the open-chain compound **12**. Frequently, in this area, improvement of a yield can be obtained by decreasing the rate either by lowering the temperature of the reaction or by using a more hindered diene. A second reaction with such a reactant **5***b* and naphthoquinone **2** provided a similar overall yield but to the advantage of the open-chain by-product **13**. This behaviour remains obscure but could reflect the diminished polarity of these dienes, with aromatization of adducts (facilitated by a bromine substituent) being rapid with respect to the formation of a dipolar intermediate.

A recently developed approach to the annulation of quinones involves a cycloaddition of monooxygenated dienes followed by oxidation of the resultant adduct (13). This type of reactant

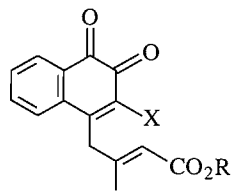
[1]Author to whom correspondence may be addressed.



1 X = Cl
2 X = Br

	R	R^1	R^2	R^3		R^1	R^2	R^3
3	OTMS	H	CH_3	OTMS	**7**	H	CH_3	OH
4	OCH_3	OTMS	H	OCH_3	**8**	OH	H	OCH_3
5*a*	OCH_3	OTMS	H	CH_3	**9**	OCH_3	H	OCH_3
5*b*	OTMS	OTMS	H	CH_3	**10**	OH	H	CH_3
6	OTMS	H	H	H	**11**	OH	H	H

SCHEME 1

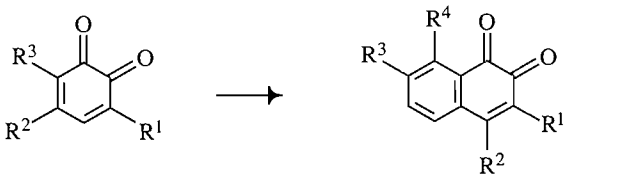


12 X = Cl, R = CH_3
13 X = Br, R = H

had been found to be particularly useful since it combined readily with all sorts of quinonoid dienophiles. In this case the adduct obtained from *o*-naphthoquinone **1** and 1-trimethylsiloxy-1,3-butadiene (**6**) was oxidized with CrO_3 and provided an easy access to 1-hydroxyphenanthrenequinone (**11**) (Scheme 1).

At this point attention was turned to the potentially even more useful 3,5- and 3,6-dihalogenated-*o*-benzoquinones (**14**–**16**). The 3,5-disubstituted catechols are easily prepared by Dakin oxidation of the corresponding salicylaldehydes (14) while the 3,6 isomers are conveniently available by halogenation of cyclohexanones using copper(II) halides, followed by aromatization of the intermediates (15). Reactions of the quinones, prepared *in situ*, with the usual electron-rich dienes, however, produced only unstable colourless compounds, which probably resulted from addition to a carbonyl group.

The cycloaddition–oxidation sequence with monooxygenated dienes fortunately gave more promising results. When adducts formed from diene **6** and quinones **14**–**16** were oxidized with MnO_2, the corresponding novel *o*-naphthoquinones **17**–**19** were obtained, albeit only in fair yield. Although the chloro derivatives **17** and **19** are quite stable, the bromo compound **18** decomposed completely within a few days. Analogous results were also available with the use of 3-trimethylsiloxy-1,3-pentadiene, and the structure of the resulting *o*-naphthoquinone **20** is inferred from results obtained with *p*-quinones (13) and is consistent with the nmr data (a relatively shielded H-5) (Scheme 2).



	R^1	R^2	R^3		R^1	R^2	R^3	R^4
14	Cl	H	Cl	**17**	Cl	H	H	OH
15	Br	H	Br	**18**	Br	H	H	OH
16	Cl	Cl	H	**19**	H	Cl	H	OH
				20	Cl	H	OH	CH_3

SCHEME 2

In the case of 3-halogenated *o*-quinones, the electronic effects of this substituent and the 2-oxo group are complementary and produce a rather electrophilic 4-position. In the 4-substituted isomers **21** and **22**, on the other hand, the opposition of the foregoing effects results in the enhanced reactivity of the 2-carbonyl group. Expectations of inducing the nucleophilic end of electron-rich dienes to attack the 4-substituted substrates in the 3-position, however, proved illusory. Vinylogous ketene acetals (e.g., **3**) and vinylketene acetals such as **4** and **5***a* give only spiro-γ- (**23** and **24**) and -α-pyrones (**25** and **26**) respectively. (Attempts to modify this result with the use of mild Lewis acids, i.e., boron trifluoride etherate and "boron acetate", were unsuccessful.) A significantly different result was obtained with the use of 1-trimethylsiloxy-1,3-butadiene (**6**), when substitution in the 4-position was observed to result in the unusual open-chain quinonemethide **27** (Scheme 3).

Although annulations of *o*-quinones with electron-rich dienes have been found to be somewhat restricted with respect to those of the *para* analogues, nevertheless the method does provide greatly improved syntheses of a variety of phenanhrenequinones as well as entry to some heretofore unavailable *o*-naphthoquinones. This approach therefore allows easy access in principle to numerous naturally occurring phenanthrene derivatives.

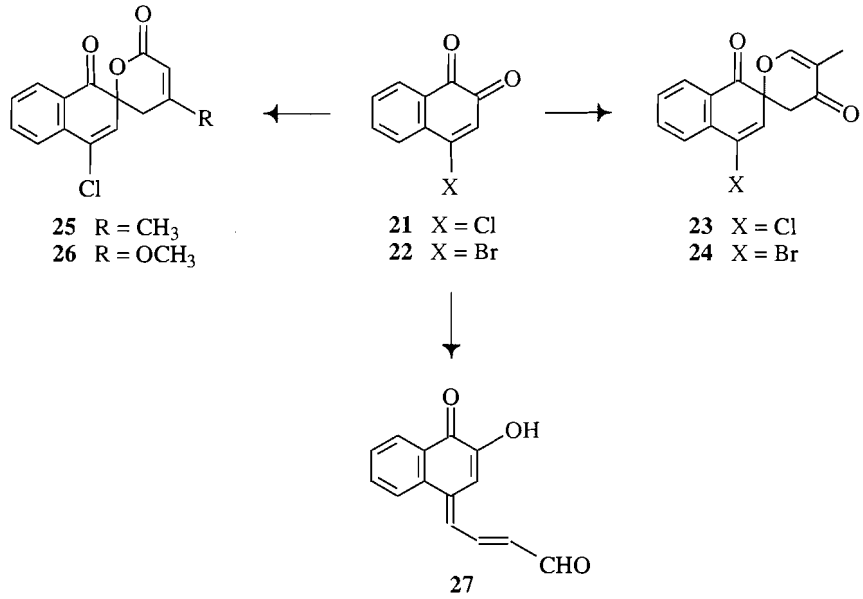
Experimental

All mp's were taken for samples in capillary tubes with a Thomas–Hoover apparatus and are not corrected. The uv spectra were determined on a Hewlett–Packard 8450A spectrophotometer, the ir spectra on a Beckman model IR-4250 instrument, and were calibrated with a film of polystyrene. The nmr spectra were recorded with Varian XL-200 and Bruker HX-90 spectrometers using tetramethylsilane as internal standard. Mass spectra were obtained with a Hewlett–Packard 5995A spectrometer. Merck silica gel $60F_{254}$, for dry column chromatography, was used throughout in a product-to-adsorbent ratio of 1:50–100. Elemental analyses were carried out by Galbraith Laboratories, Inc., Knoxville, Tenn. Ether refers to diethyl ether.

A. Preparation of halogenated o*-quinones*

o-Naphthoquinone was halogenated as proposed for juglone methyl ether (16). Chlorination gave 3-chloro-*o*-naphthoquinone (**1**) (40%),

Can. J. Chem. Downloaded from www.nrcresearchpress.com by 194.225.253.170 on 09/07/12
For personal use only.



SCHEME 3

mp 170–172°C ($CHCl_3$–CCl_4) (lit. (17) mp 172°C) while treatment with bromine provided 3-bromo-*o*-naphthoquinone (**2**) (43%), mp 175–176°C ($CHCl_3$–CCl_4) (lit. (17) mp 177–178°C).

2,4-Dichloro- and 2,4-dibromo-1-naphthol, obtained essentially according to de la Mare and Suzuki (18), were oxidized with $Pb(OAc)_4$ as recommended by Perumal and Bhatt (19) to give 4-chloro- (**21**) and 4-bromo-*o*-naphthoquinone (**22**) respectively.

3,5-Dichloro- (**16**), 3,6-dichloro- (**14**), and 3,6-dibromo-*o*-benzoquinones (**15**) were obtained by oxidation of the corresponding catechols with Ag_2O in THF and used immediately without isolation. 3,5-Dihalogenated catechols are available from the suitable salicylaldehyde as described by Dakin (14). The 3,6 isomers can readily be obtained from cyclohexanone and copper(II) halides by aromatizing the intermediates with $LiCO_3$ in DMF (15).

3,6-Dibromocatechol, mp 83–84°C (pet. ether, bp 60–80°C); ir ν_{max}(KBr): 3400, 1450, 1230, 1120 cm^{-1}; ^1H nmr δ ($CDCl_3$; 60 MHz): 5.7 (2H, s, OH-1,2), 7.1 (2H, s, H-4,5); ms, *m/z*: 270/268/266 $(M)^+$. *Anal.* calcd. for $H_6H_4Br_2O_2$: C 26.90, H 1.51, Br 59.65; found: C 26.96, H 1.53, Br 59.43%.

B. General methods

(*a*) *Cycloaddition*

Method A: The diene (2.50 mmol) dissolved in benzene (5 mL) was added slowly (15–30 min) to a solution of the quinone (2.00 mmol) in the same solvent (5 mL) at 6°C. Stirring was continued at room temperature until disappearance of the substrate was revealed by tlc.

Method B: The reaction was carried out as in A but replacing the solvent by THF and initiating the process at 0°C.

(*b*) *Aromatization*

Method C: The adduct was adsorbed on a column of silica gel. Elution was started with benzene and the polarity of the solvent was gradually increased by addition of ethyl acetate.

Method D: Upon evaporation of the solvent, a mixture of concentrated HCl (4 mL) and THF (10 mL) was added at 0°C to the residue dissolved in the same solvent (10 mL), and stirring was continued at room temperature for 1 h. The crude product was then extracted with CH_2Cl_2 and purified by chromatography.

Method E: The adduct was pyrolyzed in refluxing toluene for 18 h.

C. Reactions with 3-halo-o-naphthoquinones

3-Hydroxy-2-methylphenanthrenequinone (7)

(*a*) 2-Methyl-1,3-bistrimethylsiloxy-1,3-butadiene (**3**) and 3-chloro-*o*-naphthoquinone (**1**) were brought together according to method A (1 h). Aromatization of the adduct as per method E gave phenanthrenequinone **7** (192 mg; 40%), mp 298–300°C (methanol); ir ν_{max}(KBr): 3310, 1685, 1650, 1580, 1560 cm^{-1}; uv λ_{max} (MeOH) (log ε): 239(4.06), 264(4.19), 322(3.54), 378(3.57) nm; ^1H nmr δ (200 MHz; DMSO-d_6): 2.20 (3H, s, CH_3-2), 7.50 (1H, s, H-4), 7.52 (1H, qd, *J* = 7.6, 7.5, 0.7 Hz, H-7), 7.80 (1H, td, *J* = 7.6, 1.5 Hz, H-6), 7.82 (1H, s, H-1), 7.94 (1H, dd, *J* = 7.6, 0.7 Hz, H-5), 7.99 (1H, dd, *J* = 7.5, 1.5 Hz, H-8); ms, *m/z*: 238$(M)^+$. *Anal.* calcd. for $C_{15}H_{10}O_3$: C 75.62, H 4.23; found: C 75.48, H 4.16%.

(*b*) In a similar reaction with 3-bromo-*o*-naphthoquinone (**2**) (method A; 3 h), the adduct was aromatized according to method D and provided the same quinone (**7**) (350 mg; 74%).

1-Hydroxy-3-methoxyphenanthrenequinone (8) and 1,3-dimethoxyphenanthrenequinone (9)

(*a*) Method B applied to 1,3-dimethoxy-1-trimethylsiloxy-1,3-butadiene (10*b*) (**4**) and quinone **2** resulted in spontaneous aromatization at room temperature and afforded upon filtration only phenanthrenequinone **8** (352 mg; 70%), mp 304–306°C (methanol); ir ν_{max}(KBr): 3210, 1685, 1642, 1590, 1580 cm^{-1}; uv λ_{max} (MeOH) (log ε): 256(4.36), 400(3.86) nm; ^1H nmr δ (200 MHz; DMSO-d_6): 3.83 (3H, s, OCH_3-3), 6.53 (1H, br s, H-2), 7.20 (1H, br s, H-4), 7.52 (1H, t, *J* = 7.6 Hz, H-6), 7.76 (1H, td, *J* = 7.6, 1.5 Hz, H-7), 7.94 (1H, dd, *J* = 7.6, 1.5 Hz, H-5), 8.10 (1H, d, *J* = 7.6 Hz, H-8); ms *m/z*: 254$(M)^+$. *Anal.* calcd. for $C_{15}H_{10}O_4$: C 70.86, H 3.97; found; C 70.84, H 3.92%.

(*b*) The same reaction conducted as in method A (20 min), at room temperature, yielded by filtration only the dimethyl ether **9** (153 mg; 57%), mp 209–210°C (methanol) (lit. (20) mp 215–216°C); ir ν_{max}(KBr): 1680, 1655, 1595, 1570 cm^{-1}; uv λ_{max} (MeOH) (log ε): 258(4.76), 400(4.24) nm; ^1H nmr δ (200 MHz; DMSO-d_6): 3.90 and 3.98 (2 × 3H, 2s, OCH_3-1,3), 6.69 (1H, br s, H-2), 7.35 (1H, br s, H-4), 7.53 (1H, t, *J* = 7.6 Hz, H-6), 7.76 (1H, td, *J* = 7.6, 1.0 Hz, H-7), 7.94 (1H, dd, *J* = 7.6, 1.0 Hz, H-5), 8.30 (1H, d, *J* = 7.6 Hz, H-8); ms *m/z*: 268$(M)^+$. *Anal.* calcd. for $C_{16}H_{12}O_4$: C 71.64, H 4.51; found: C 71.33, H 4.57%.

1-Hydroxy-3-methylphenanthrenequinone (10)

(*a*) Addition of 1-methoxy-3-methyl-1-trimethylsiloxy-1,3-butadiene (10*b*) (**5***a*) to quinone **1** following method A (1 h) gave a mixture, which was treated according to method C. Separation by chromatography (benzene – ethyl acetate 10:1) provided phenanthrenequinone **10** (192 mg; 40%), which decomposes at 240–245°C (acetone – pet. ether, bp 60–80°C); ir ν_{max}(KBr): 1680, 1635, 1590 cm^{-1}; uv λ_{max} (MeOH) (log ε): 214(4.60), 260(4.52), 280sh(4.74), 335(3.54), 442(3.69) nm; ^1H nmr δ (200 MHz; $CDCl_3$): 2.44 (3H, br s, CH_3-3), 7.28 (1H, br s,

Can. J. Chem. Downloaded from www.nrcresearchpress.com by 194.225.253.170 on 09/07/12
For personal use only.

Can. J. Chem. Downloaded from www.nrcresearchpress.com by 194.225.253.170 on 09/07/12
For personal use only.

H-2), 7.34 (1H, brs, H-4), 7.47 (1H, td, J = 7.6, 0.8 Hz, H-7), 7.70 (1H, ddd, J = 8.1, 7.6, 0.8 Hz, H-6), 7.99 (1H, dd, J = 8.1, 0.8 Hz, H-5), 8.17 (1H, dd, J = 7.6, 0.8 Hz, H-8); ms m/z: 238$(M)^+$. *Anal.* calcd. for $C_{15}H_{10}O_3$: C 75.62, H 4.23; found: C 75.57, H 4.28%.

A second band consisted of methyl 4-(3-chloro-*o*-naphthoquinonyl-4)-3-methyl-2-butenoate (**12**) (61 mg; 10%), mp 153–155°C (acetone–pet. ether, bp 60–80°C); ir ν_{max}(KBr): 1730, 1705, 1695, 1675 cm^{-1}; ^1H nmr δ (200 MHz; $CDCl_3$): 2.39 (3H, d, J = 1.1 Hz, CH_3-3), 3.66 (3H, s, OCH_3-1), 3.84 (2H, br s, H-4), 5.59 (1H, q, J = 1.1 Hz, H-2), 7.40 (1H, dd, J = 7.7, 1.5 Hz, H-5), 7.54 and 7.68 (2H, 2td, J = 7.7, 1.5 Hz, H-6,7), 8.17 (1H, dd, J = 7.7, 1.5 Hz, H-8); ms m/z: 306/304 $(H)^+$.

(*b*) When a reaction was carried out with 3-methyl-1,1-bistrimethylsiloxy-1,3-butadiene (**5***b*) prepared from 3-methylcrotonic acid essentially as in ref. 10*b* (bp 74–78°C/5 Torr (1 Torr = 133.3 Pa) (94%); ir ν_{max} (film): 2960, 1650, 1255, 1200, 1060, 840 cm^{-1}; ^1H nmr δ (200 MHz; $CDCl_3$): 0.16 and 0.20 (18 H, 2s, OTMS-1,1), 1.84 (3H, s, CH_3-3), 4.20 (1H, s, H-2), 4.44 and 4.66 (2H, 2d, J = 2.8 Hz, H-4). *Anal.* calcd. for $C_{11}H_{24}O_2Si_2$: C 54.04, H 9.89%; found: C 53.79, H 10.07%) and 3-bromo-*o*-naphthoquinone (**2**) according to methods A (1 h) and D, a similar mixture of products was obtained. Separation by chromatography (dichloromethane) gave phenanthrenequinone (**10**) (143 mg; 30%) and, eluting with ethyl acetate, 4-(3-bromo-*o*-naphthoquinonyl-4)-3-methyl-2-butenoic acid (**13**) (128 mg; 19%), mp 210–211°C (dec.) (ethanol); ir ν_{max}(KBr): 3080, 2580, 1680, 1665, 1635, 1585, 1550 cm^{-1}; uv λ_{max} (MeOH) (log ε): 214(4.57), 260(4.50), 333(3.58), 442(3.63) nm; ^1H nmr δ (200 MHz; DMSO-d_6): 2.26 (3H, s, CH_3-3), 3.84 (2H, br s, H-4), 5.60 (1H, br s, H-2), 7.52–7.74 (3H, m, H-5′,6′,7′), 7.98 (1H, dd, J = 7.7, 1.5 Hz, H-8′), 12.04 (1H, s, OH-1); ms m/z: 336/334 $(M)^+$. *Anal.* calcd. for $C_{15}H_{11}BrO_4$: C 53.75, H 3.31, Br 23.84; found: C 53.73, H 3.42, Br 23.73%.

*1-Hydroxyphenanthrenequinone (**11**)*

1-Trimethylsiloxy-1,3-butadiene (13) (**6**) (315 mg; 2.22 mmol) in CH_2Cl_2 (5 mL) was added at 0°C to 3-chloro-*o*-naphthoquinone (**1**) (387 mg; 2.01 mmol) in the same solvent (5 mL). The mixture was stirred for 16 h at room temperature and evaporated. The residue was oxidized with CrO_3 (330 mg; 3.30 mmol) in acetic acid (10 mL) at reflux temperature (1.5 h) and the crude product, taken up in ether and washed with water, was purified by chromatography (benzene – ethyl acetate (9:1), giving phenanthrenequinone **11** (224 mg; 50%), mp 221–222°C (acetone – pet. ether, bp 60–80°C) (lit. (21) mp 220°C); ir ν_{max}(KBr): 1680, 1630, 1595 cm^{-1}; uv λ_{max} (MeOH) (log ε): 256(4.40), 279sh(4.06), 336(3.47), 448(3.61) nm; ^1H nmr δ (200 MHz; $CDCl_3$): 7.03 (1H, br d, J = 8.2 Hz, H-2), 7.45–7.64 (3H, m, H-3,4,7), 7.72 (1H, td, J = 7.9, 1.6 Hz, H-6), 8.01 (1H, br d, J = 7.9 Hz, H-5), 8.20 (1H, dd, J = 7.9, 1.6 Hz, H-8), 12.50 (1H, s, OH-1); ms m/z: 224$(M)^+$. *Anal.* calcd. for $C_{14}H_8O_3$: C 75.10, H 3.60; found: C 75.00, H 3.60%.

D. Reactions with dihalo-o-benzoquinones

*3-Chloro-8-hydroxy-o-naphthoquinone (**17**)*

A mixture of 3,6-dichlorocatechol (15) (360 mg; 2.01 mmol) and silver(I) oxide (1.2 g; 5.2 mmol) in THF (10 mL) was stirred at room temperature for 2 h, then cooled to 0°C. To this suspension was then added dropwise, over 30 min, a solution of 1-trimethylsiloxy-1,3-butadiene (**6**) (351 mg; 2.51 mmol) in the same solvent (5 mL) and stirring was continued at room temperature for 5 h. The adduct was then hydrolyzed by addition of 5% aqueous HCl (30 mL) over 30 min to the reaction mixture at 0°C, and stirring was again continued for 1 h. The solid was next filtered off and washed well with ether (3 × 30 mL). Evaporation of the solvent gave a residue, which was dissolved in THF (20 mL) containing MnO_2 (361 mg; 4.15 mmol). This mixture was stirred for 16 h, filtered, and evaporated. Purification of the crude product by chromatography (CH_2Cl_2) gave naphthoquinone **24** (145 mg; 35%), mp 119–122°C (dec.) (dichloromethane – pet. ether, bp 60–80°C); ir ν_{max}(KBr): 1685, 1630, 1585, 1560 cm^{-1}; uv λ_{max} (MeOH) (log ε): 256(4.05), 366(3.62), 371(3.62) nm; ^1H nmr δ (200 MHz; $CDCl_3$): 6.89 (1H, dd, J = 7.7, 1.0 Hz, H-7), 7.08 (1H, dd, J = 9.0, 1.0 Hz, H-5), 7.55 (1H, s, H-4), 7.57 (1H, dd, J = 7.7, 9.0 Hz, H-6), 11.88 (1H, s, OH-8). *Anal.* calcd. for $C_{10}H_5ClO_3$: C 57.58, H 2.42, Cl, 17.00; found: C 57.38, H 2.39, Cl 17.22%.

*3-Bromo-8-hydroxy-o-naphthoquinone (**18**)*

Under conditions similar to the foregoing, 3,6-dibromocatechol (270 mg; 1.02 mmol) was converted to quinone **15** and the latter combined with diene **6** (117 mg; 1.25 mmol). Oxidation of the hydrolyzed adduct with MnO_2 (180 mg; 2.00 mmol) gave quinone **18** (96 mg; 38%), which decomposed completely within a few days; ^1H nmr δ (90 MHz; $CDCl_3$): 6.9 (1H, br d, J = 7.5 Hz, H-7), 7.1 (1H, br d, J = 9.0 Hz, H-5), 7.6 (1H, dd, J = 7.5, 9.0 Hz, H-6), 7.8 (1H, s, H-4), 12.9 (1H, s, OH-8); ms m/z: 252/254$(M)^+$.

*4-Chloro-8-hydroxy-o-naphthoquinone (**19**)*

In a reaction similar to the preceding ones, diene **6** (156 mg; 1.10 mmol) and quinone **16** obtained from 3,5-dichlorocatechol (179 mg; 1.00 mmol) gave an adduct that was converted by MnO_2 (860 mg; 10.0 mmol) to the corresponding quinone **19** (66 mg; 32%), which decomposes at 135–140°C; ir ν_{max}(KBr): 1670, 1640, 1580, 1555 cm^{-1}; ^1H nmr δ (200 MHz; $CDCl_3$): 6.75 (1H, s, H-3), 7.20 (1H, dd, J = 8.7, 1.3 Hz, H-5), 7.47 (1H, dd, J = 7.4, 1.3 Hz, H-7), 7.67 (1H, dd, J = 8.7, 7.4 Hz, H-6), 12.29 (1H, s, OH-8). *Anal.* calcd. for $C_{10}H_5ClO_3$: C 57.58, H 2.42, Cl 17.00; found: C 57.26, H 2.51, Cl 16.60%.

*3-Chloro-7-hydroxy-8-methyl-o-naphthoquinone (**20**)*

3-Trimethylsiloxy-1,3-pentadiene (13) (630 mg; 4.04 mmol) in THF (1 mL) was added to the residue obtained from the oxidation of 3,6-dichlorocatechol (361 mg; 2.02 mmol), and evaporation of the solvent. The mixture was stirred at room temperature for 24 h, MnO_2 (170 mg; 1.95 mmol) was added to the adduct, and stirring again continued for 16 h. Upon purification of the crude product by chromatography (CH_2Cl_2), a first zone (106 mg) consisted of what seemed to be an unidentified dimer of the quinone.

A second band provided the desired quinone **20** (74 mg; 17%), mp 243–244°C (dec.) (dichloromethane – pet. ether, bp 60–80°C); ir ν_{max}(KBr): 3280, 1680, 1650, 1560 cm^{-1}; uv λ_{max} (MeOH) (log ε): 276(3.62), 406(3.08) nm; ^1H nmr δ (200 MHz; $(CD_3)_2CO$): 2.39 (3H, s, CH_3-8), 7.00 (1H, d, J = 8.3 Hz, H-5), 7.80 (1H, d, J = 8.3 Hz, H-6), 8.11 (1H, s, H-4); ms m/z: 222/224$(M)^-$. *Anal.* calcd. for $C_{11}H_7ClO_3$: C 59.34, H 3.17, Cl 15.93; found: C 59.05, H 3.22, Cl 15.46%.

E. Reactions with 4-halo-o-naphthoquinones

*4-Chloro-3′,4′-dihydro-5′-methylspiro[naphthalene-2(1H),2′-(2H)pyran]-1,4′-dione (**23**)*

Diene **3**, when added to 4-chloro-*o*-naphthoquinone **21** following method A (1.5 h), gave spirodione **23** (480 mg; 88%), mp 114–116°C (benzene – pet. ether, bp 60–80°C); ir ν_{max}(KBr): 1690, 1665, 1615, 1595, 1585, 1550 cm^{-1}; uv λ_{max} (MeOH) (log ε): 232(4.80), 294(4.44); ^1H nmr δ (200 MHz; $CDCl_3$): 1.72 (3H, s, CH_3-5′), 2.92 and 3.04 (2H, 2d, J = 17.1 Hz, H-3′), 6.37 (1H, s, H-3), 7.44–7.60 (2H, m, H-6,7), 7.48 (1H, br s, H-6′), 7.67–7.72 (1H, m, H-5), 7.87–7.92 (1H, m, H-8); ms m/z: 274/276$(M)^+$. *Anal.* calcd. for $C_{15}H_{11}ClO_3$: C 65.59, H 4.04, Cl 12.91; found: C 65.64, H 4.18, Cl 12.61%.

*4-Bromo-3′,4′-dihydro-5′-methylspiro[naphthalene-2(1H),2′-(2H)pyran]-1,4′-dione (**24**)*

In a reaction similar to the preceding one, diene **3** and bromo-*o*-naphthoquinone **22**, after 2 h, gave spirodione **24**, (473 mg; 74%), mp 124–126°C (benzene – pet. ether, bp 60–80°C); ir ν_{max}(KBr): 1695, 1675, 1625, 1600, 1590, 1560 cm^{-1}; ^1H nmr δ (200 MHz; $CDCl_3$): 1.72 (3H, d, J = 1.3 Hz, CH_3-5′), 2.93 and 3.06 (2H, 2d, J = 17.1 Hz, H-3′), 6.64 (1H, s, H-3), 7.44–7.57 (2H, m, H-6,7), 7.48 (1H, m, H-6′), 7.65–7.72 (1H, m, H-5), 7.85–7.90 (1H, m, H-8).

*4-Chloro-3′,6′-dihydro-4′-methylspiro[naphthalene-2(1H),2′-(2H)pyran]-1,6′-dione (**25**)*

(*a*) Application of method A to diene **5***a* and quinone **21**, after 1 h, afforded spirodione **25** (470 mg; 86%), mp 148.5–150.0°C (benzene – pet. ether, bp 60–80°C); ir ν_{max}(KBr): 1725, 1695, 1655 cm^{-1}; uv

λ_{max} (MeOH) (log ϵ): 231(4.17), 237(4.17), 310(3.84) nm; ^{1}H nmr δ (200 MHz; $CDCl_3$): 1.85 (3H, br s, CH_3-4′), 2.77 (2H, s, H-3′), 5.97 (1H, br s, H-5′), 6.38 (1H, s, H-3), 7.45–7.62 (2H, m, H-6,7), 7.72–7.80 (1H, m, H-5), 7.87–8.01 (1H, m, H-8); ms *m/z*: 274/276(M)$^+$. *Anal.* calcd. for $C_{15}H_{11}ClO_3$: C 65.60, H 4.00, Cl 12.90; found: C 65.72, H 4.15, Cl 12.81%.

(*b*) A reaction analogous to the foregoing one, in which diene **5***a* was replaced by diene **5***b*, gave the same spirodione **25** (484 mg; 88%).

*4-Chloro-3′,6′-dihydro-4′-methoxyspiro[naphthalene-2(1*H*),2′-(2*H*)pyran]-1,6′-dione (**26**)*

Cycloaddition of diene **4** to chloronaphthoquinone **21** according to method A (1 h) gave the corresponding spirodione **26** (369 mg; 63%), mp 169–171°C (benzene – pet. ether, bp, 60–80°C); ir ν_{max}(KBr): 1730, 1695, 1630, 1600, 1555 cm^{-1}; uv λ_{max} (MeOH) (log ϵ): 232(4.42), 237(4.44), 311(3.99) nm; ^{1}H nmr δ (200 MHz; $CDCl_3$): 2.91 (2H, s, H-3′), 3.71 (3H, s, OCH_3-4′), 5.32 (1H, s, H-5′), 6.39 (1H, s, H-3), 7.45–7.62 (2H, m, H-6,7), 7.76–7.81 (1H, m, H-5), 7.87–7.91 (1H, m, H-8); ms *m/z*: 290/292(M)$^+$. *Anal.* calcd. for $C_{15}H_{11}ClO_4$: C 61.98, H 3.81, Cl 12.20; found: C 62.34, H 3.92, Cl 11.82%.

*4-(4-Oxo-2-buten-1-ylidene)-2-hydroxynaphthalen-1(4*H*)-one (**27**)*

A mixture of 1-trimethylsiloxy-1,3-butadiene (**6**) (568 mg; 4.00 mmol) and 4-chloro-*o*-naphthoquinone (**21**) (387 mg; 2.01 mmol) in benzene (10 mL) was heated at reflux for 2 h. Purification of the crude product by chromatography (benzene) gave naphthalenone **27** (144 mg; 32%), mp 204–206°C (benzene); ir ν_{max}(KBr): 3020, 2840, 1660, 1640, 1595, 1580 cm^{-1}; uv λ_{max} (MeOH) (log ϵ): 237(3.50), 336(3.23), 404(3.51) nm; ^{1}H nmr δ (200 MHz; $CDCl_3$): 6.54 (1H, ddd, J = 14.8, 7.8, 1.2 Hz, H-3′), 7.08 (1H, s, OH-2), 7.34 (1H, d, J = 1.0 Hz, H-3), 7.54 (1H, br d, J = 12.9 Hz, H-1′), 7.57–7.76 (2H, ~ 2dt, H-6,7), 7.85 (1H, dd, J = 12.9, 14.8 Hz, H-2′), 8.11 (1H, ~dd, H-5), 8.31 (1H, ~dd, H-8), 9.81 (1H, d, J = 7.8 Hz, H-4′); ms *m/z*: 226(H)$^+$. *Anal.* calcd. for $C_{14}H_{10}O_3$: C 74.33, H 4.46; found: C 74.19, H 4.52%.

Acknowledgment

We gratefully acknowledge financial support from the Natural Sciences and Engineering Research Council of Canada and the Fonds F.C.A.R. (Gouvernement du Québec).

1. K. T. Finley. *In* The chemistry of the quinonoid compounds. *Edited by* S. Patai. John Wiley and Sons, New York. 1974. Chap. 17. p. 877.
2. M. F. Ansell, A. J. Bignold, A. F. Gosden, V. J. Leslie, and R. A. Murray. J. Chem. Soc. (C), 1414 (1971).
3. S. Danishefsky, P. F. Scuda, S. Mazza, and K. Kato. J. Org. Chem. **41**, 3468 (1976); S. Danishefsky, P. F. Scuda, and W. Caruthers. J. Org. Chem. **42**, 2179 (1977).
4. D. D. Weller and E. P. Stirchak. J. Org. Chem. **48**, 4873 (1983).
5. D. Pitea, M. Gastaldi, F. Orsini, F. Pelizzoni, A. Mugnoli, and E. Abbondanti. J. Org. Chem. **50**, 1853 (1985).
6. (*a*) M. F. Ansell and R. A. Murray. J. Chem. Soc. (C), 1429 (1971); (*b*) M. F. Ansell and V. J. Leslie. J. Chem. Soc. (C), 1423 (1971).
7. W. M. Horspool, J. M. Tedder, and Z. U. Din. J. Chem. Soc. (C), 1692 (1969); 1694 (1969); W. M. Horspool, D. T. Anderson, and C. Martin. J. Chem. Soc. (C), 398 (1971); D. T. Anderson and W. M. Horspool. J. Chem. Soc. Perkin Trans. 1, 532 (1972).
8. M. F. Ansell, A. F. Gosden, V. J. Leslie, and R. A. Murray. J. Chem. Soc. (C), 1401 (1971); W. M. Horspool, P. Smith, and J. M. Tedder. J. Chem. Soc. (C), 1638 (1971).
9. M. D. Gates. J. Am. Chem. Soc. **72**, 228 (1950); W. Davies and B. C. Ennis. J. Chem. Soc. 915 (1959).
10. (*a*) J. Banville and P. Brassard. J. Chem. Soc. Perkin Trans. 1, 1852 (1976); (*b*) J. Savard and P. Brassard. Tetrahedron, **40**, 3455 (1984), and other papers in this series.
11. W. M. Horspool. Q. Rev. **23**, 204 (1969).
12. D. W. Cameron, G. I. Feutrill, G. B. Gamble, and J. Stavrakis. Tetrahedron Lett. **27**, 4999 (1986).
13. L. Boisvert and P. Brassard. J. Org. Chem. **53**, 4052 (1988).
14. H. D. Dakin. Am. Chem. J. **42**, 477 (1909).
15. K. Nishizawa and J. Y. Satoh. Bull. Chem. Soc. Jpn. **48**, 1276 (1975); **48**, 1875 (1975); **48**, 2215 (1975).
16. R. L. Hannan, R. B. Barber, and H. Rapoport. J. Org. Chem. **44**, 2153 (1979).
17. Th. Zincke. Chem. Ber. **19**, 2493 (1886).
18. P. B. D. De La Mare and H. Suzuki. J. Chem. Soc. (C), 648 (1968).
19. P. T. Perumal and M. V. Bhatt. Synthesis, 943 (1980).
20. D. W. Cameron, K. R. Deutscher, and G. I. Feutrill. Aust. J. Chem. **31**, 2259 (1978).
21. L. F. Fieser. J. Am. Chem. Soc. **51**, 2460 (1929).

Can. J. Chem. Downloaded from www.nrcresearchpress.com by 194.225.253.170 on 09/07/12
For personal use only.

Xestolide and secoxestenone, degraded triterpenoids from the sponge *Xestospongia vanilla*

PETER T. NORTHCOTE AND RAYMOND J. ANDERSEN[1]

Departments of Chemistry and Oceanography, University of British Columbia, Vancouver, B.C., Canada V6T 1Y6

Received March 22, 1989

PETER T. NORTHCOTE and RAYMOND J. ANDERSEN. Can. J. Chem. **67**, 1359 (1989).

Xestolide (**5**) and secoxestenone (**6**), two metabolites with new terpenoid carbon skeletons, have been isolated from the northeastern Pacific sponge *Xestospongia vanilla*. Proposed structures for **5** and **6** are based on spectroscopic analysis and chemical interconversions. The similarity in structure between xestolide (**5**), secoxestenone (**6**), xestenone (**2**), and the aglycone of secoxestovanin A (**4**) has prompted the biogenetic proposal that metabolites **2**, **5**, and **6** are degraded triterpenoids.

Key words: sponge, terpenoids, *Xestospongia*.

PETER T. NORTHCOTE et RAYMOND J. ANDERSEN. Can. J. Chem. **67**, 1359 (1989).

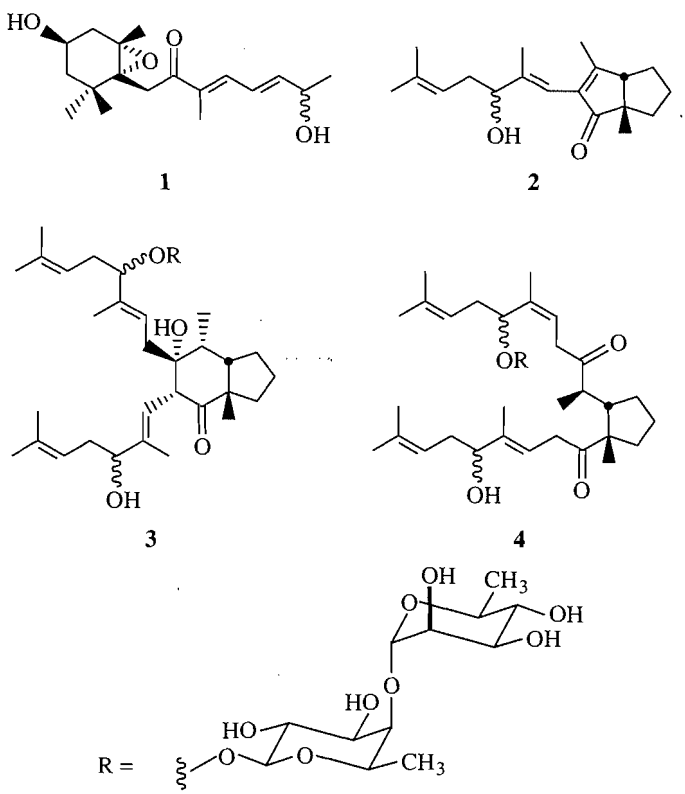
On a isolé la xestolide (**5**) et la sécoxesténone (**6**), deux métabolites possédant un nouveau squelette carbonné terpénique, à partir de l'éponge *Xestospongia vanilla* du Pacifique Nord-est. Les structures proposées pour ces deux composés s'appuient sur l'analyse spectroscopique et sur des transformations chimiques. La similarité de structure entre la xestolide (**5**), la sécoxesténone (**6**), la xesténone (**2**) et l'aglycone de la sécoxestovanine A (**4**) suggère une dégradation biogénétique des métabolites **2**, **5** et **6** en triterpènes.

Mots clés : éponge, terpènoïdes, *Xestospongia*.

[Traduit par la revue]

Can. J. Chem. Downloaded from www.nrcresearchpress.com by 194.225.253.170 on 09/07/12
For personal use only.

The northeastern Pacific sponge *Xestospongia vanilla* is a rich source of normal carbon number and degraded terpenoids having new carbon skeletons. We previously reported the isolation of xestodiol (**1**) (1), xestenone (**2**) (2), xestovanin A (**3**) (3), and secoxestovanin A (**4**) (3) from extracts of *X. vanilla*. This varied group of metabolites includes a C_{18} apocarotenoid, a C_{19} degraded terpenoid, and two triterpenoid glycosides. We now wish to report the structures of two new *X. vanilla* metabolites, xestolide (**5**) and secoxestenone (**6**). The discovery of xestolide and secoxestenone provides further support for the hypothesis that compounds **2**, **5**, and **6** are degraded triterpenoids (3).



[1]Author to whom correspondence may be addressed.

Xestospongia vanilla was collected along the shoreline of the Deer Group of islands in Barkley Sound, British Columbia. The sponge was extracted and the metabolites purified as previously described (2, 3).

Xestolide (**5**) was isolated as a colorless oil that gave a parent ion in the electron impact high resolution mass spectrum (EIHRMS) at 334.2158 daltons, corresponding to a molecular formula of $C_{20}H_{30}O_4$ (ΔM +1.4 mmu). The infrared (IR) spectrum of xestolide showed bands at 3360 and 1688 cm^{-1} that could be assigned to hydroxyl and conjugated carbonyl stretching vibrations, respectively. All 20 carbons were observed in the ^{13}C nmr spectrum of **5** and an APT experiment revealed 28 protons attached to carbon atoms (Table 1). The two remaining protons had to be attached to the oxygen atoms of hydroxyl functionalities. Seven deshielded carbon resonances (δ 165.5, 164.7, 144.1, 135.3, 119.6, 117.2, and 117.0) were assigned to one ester carbonyl and six olefinic carbons. The two additional sites of unsaturation not accounted for by the ester and olefinic functionalities but required by the molecular formula had to be rings.

A ten-carbon acyclic portion (Fragment A) of xestolide (**5**) was routinely identified from information obtained in a series of ^1H nmr experiments. The nature of the two independent scalar-coupled spin systems in Fragment A was established by analysis of COSY and double resonance data (Table 1). The indicated connectivity between the scalar-coupled spin systems (i.e., C11 → C12) was required by the observation of a nOe in H12 (δ 4.12) upon irradiation of H10 (δ 5.68). This nOe result also established the *E* configuration for the C10–C11 olefin. Intense peaks at *m/z* 265.1431 ($C_{15}H_{21}O_4$, ΔM +0.1 mmu: $M^+ - C_5H_9$) and 181.0871 daltons ($C_{10}H_{13}O_3$, ΔM +0.6 mmu: M^+ − Fragment A) in the EIHRMS of **5** were consistent with the presence of Fragment A in xestolide. Fragment A is also a substructure of the co-occurring metabolite secoxestovanin A (**4**) (3).

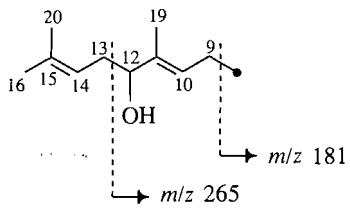
The remaining bicyclic portion of xestolide (**5**) had to have an elemental composition of $C_{10}H_{13}O_3$. In addition, it had to contain a trisubstituted α,β-unsaturated ester (IR: 1688 cm^{-1}; ^{13}C nmr δ: 165.5(C), 117.2(C), 164.7(C)), an olefinic methyl (^1H nmr δ: 1.80, s), an aliphatic methyl attached to a quaternary carbon (^1H nmr δ: 1.14, s), a ketal (^{13}C nmr δ: 105.3(C)), a

TABLE 1. The ^1H and ^{13}C nmr assignments for xestolide (**5**) and secoxestenone (**6**)

Carbon number	**5**			**6**	
	$^1H^a$	$^{13}C^b$	COSY[a]	$^1H^a$	COSY[a,c]
1	—	165.5 (C)		2.16, s	
2	—	117.2 (C)		—	
3	—	164.7 (C)		2.86, dd (8.9, 5.0)	H4
4	2.5, m (2H)	29.3 (CH_2)	H5, H17	2.10, m	H3, H4′, H5
4′	—			1.88, m	H3, H4, H5
5	1.85–1.95, m (2H)	22.5 (CH_2)	H4, H6, H6′	1.79, m	H4, H4′, H5′, H6
5′	—			1.64, m*	H5, H6
6	1.6, m	34.0 (CH_2)[&]	H5	2.24, m*	H5, H5′, H6′
6′	2.1, m		H5	1.96, m	H6
7	—	49.5 (C)		—	
8	—	105.3 (C)		—	
9	2.66, dd (5.3, 14)	34.8 (CH_2)	H9′, H10, H19	3.34, dd (18.4, 6.7)	H9′, H10, H18
9′	2.51, dd (10.6, 14)		H9, H10, H19	3.26, dd (18.4, 6.7)	H9, H10, H18
10	5.68, dd (5.3, 10.6)	119.6 (CH)[#]	H9, H9′, H19	5.61, t (6.7)	H9, H9′, H18
11	—	144.1 (C)		—	
12	4.12, t (6.0)	76.8 (CH)	H13	4.05, t (6.7)	H13
13	2.2–2.4, m (2H)	34.1 (CH_2)[&]	H12, H14, H16, H20	3.3, m (2H)	H12, H14
14	5.08, t (6.9)	117.0 (CH)[#]	H13, H16, H20	5.09, t (7.3)	H13, H16, H19
15	—	135.3 (C)		—	
16	1.71, s	26.0 (CH_3)	H13, H14	1.59, s[#]	H14
17	1.80, s	13.0 (CH_3)	H4	1.29, s	
18	1.14, s	21.3 (CH_3)		1.63, s	H9, H9′, H10
19	1.67, s	12.1 (CH_3)	H9, H9′, H10	1.71, s[#]	H14
20	1.64, s	18.0 (CH_3)	H13, H14		

[a]Recorded in $CDCl_3$ at 400 MHz.
[b]Recorded in $CDCl_3$ at 75 MHz.
[c]The downfield couplings ($\delta > 3.0$) were also observed in double resonance experiments.
#,&,* May be interchanged within a column.

hydroxyl, and three aliphatic methylenes (^{13}C nmr δ: 29.3, 22.5, 34.0). Correlations in the ^1H COSY spectrum of xestolide (**5**) revealed that the three methylene carbons were contiguous (Table 1) and the oxygen count required that the hydroxyl and ester groups be attached to the ketal carbon. The apparent biogenetic similarity between xestolide and secoxestovanin A (**4**) guided the assembly of the identified components into the proposed structure shown in **5**.



Fragment A

A pair of SINEPT experiments (4), optimized for polarization transfer through C/H scalar couplings of 7 Hz, provided support for the proposed structure. Irradiation of the aliphatic methyl singlet protons at δ 1.14 (Me18) gave polarization transfer through three-bond couplings to the ketal (δ 105.3: C8) and β olefinic carbons (δ 164.7: C3), and through two-bond coupling to the quaternary carbon (δ 49.5: C7). Irradiation of the olefinic methyl protons at δ 1.80 (Me17) gave polarization transfer through three-bond coupling to the ester carbonyl carbon (δ 165.5: C1). These results are only compatible with the constitution shown in **5**. Further support for the proposed structure came from the EIHRMS. A prominent ion at *m/z*

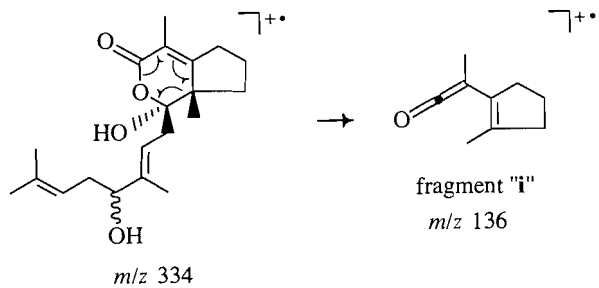


FIGURE 1

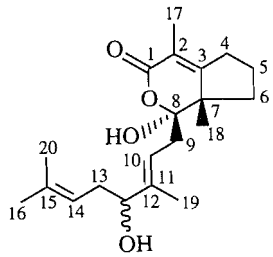
136.0885 daltons ($C_9H_{12}O$, ΔM −0.3 mmu) could be attributed to fragment **i** formed via a retro-Diels–Alder reaction as shown in Fig. 1.

A difference nOe experiment was used to establish the relative stereochemistry at carbons 7 and 8. Irradiation of the Me18 protons at δ 1.14 induced nOe's in both of the C9 methylene protons at δ 2.51 and 2.66, demonstrating that the acyclic side chain and the quaternary methyl group were *cis* as shown. Rather surprisingly, we were not able to detect any of the corresponding *trans* isomer that should be in equilibrium with the *cis* isomer through the open-chain form of the C8 hemiketal. Chemical proof that the lactone–hemiketal/carboxylic acid – keto equilibration does exist came from the treatment of xestolide (**5**) with diazomethane, resulting in a quantitative conversion to the ketoester **7**. Clearly the *cis* isomer is significantly more stable than the *trans* isomer.

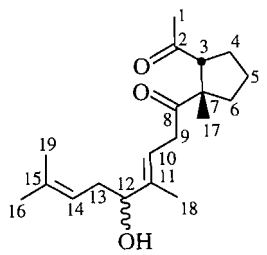
Secoxestenone (**6**) was isolated in very low yield as a colorless oil. The highest mass ion in the EIHRMS of **6**

Can. J. Chem. Downloaded from www.nrcresearchpress.com by 194.225.253.170 on 09/07/12
For personal use only.

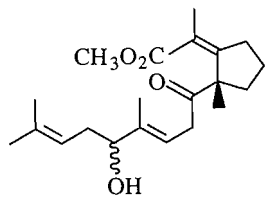
Can. J. Chem. Downloaded from www.nrcresearchpress.com by 194.225.253.170 on 09/07/12
For personal use only.



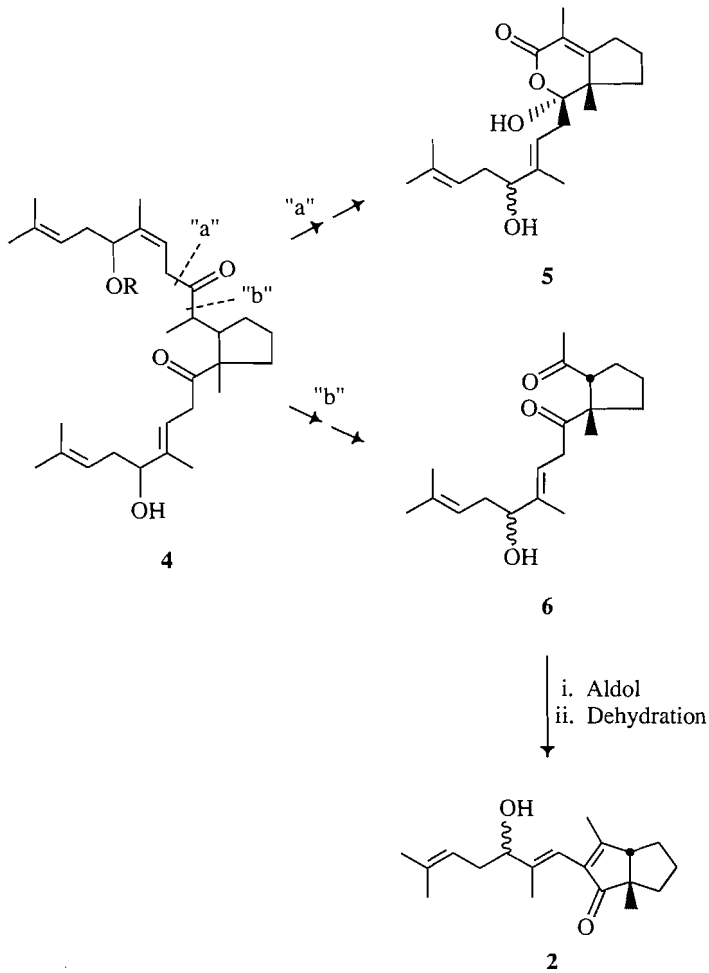
5



6



7



4 5 6 2

SCHEME 1

appeared at m/z 288.2081 daltons ($C_{19}H_{28}O_2$, ΔM −0.8 mmu) and the ^{13}C nmr spectrum of **6** showed 19 resonances, in agreement with the elemental composition of the ion. However, additional information in the ^{13}C nmr spectrum demonstrated that the mass spectral peak at m/z 288 daltons was not a molecular ion. Two ^{13}C nmr resonances at δ 212.6 and 210.6 could be assigned to ketone carbonyl carbons and a resonance at δ 77.2 could be assigned to a carbinol methine carbon, indicating that the molecule actually contained a total of three oxygen atoms. Therefore, we assumed that secoxestenone was readily losing water in the mass spectrometer and that the true molecular formula was $C_{19}H_{30}O_3$.

The ^1H nmr spectrum of secoxestenone (**6**) showed a strong resemblance to that of xestolide (**5**) and a series of double resonance and difference nOe experiments conducted on **6** demonstrated that it contained a ten-carbon acyclic residue identical to fragment A previously identified in **5** (C9 → C16: Table 1). The downfield shift of the C9 methylene protons in secoxestenone (**6**) (δ 3.26 and 3.34), relative to their position in xestolide (**5**) (δ 2.51 and 2.66), was attributed to the replacement of the C8 hemiketal functionality in **5** with a C8 ketone functionality in **6**. A methyl singlet at δ 2.16 in the ^1H nmr spectrum and one of the ketone carbonyl resonances in the ^{13}C nmr spectrum of **6** were assigned to an acetyl appendage. The absence of ^{13}C nmr evidence for additional unsaturated functionality demanded that the remainder of secoxestenone (C_6H_{10}) be monocyclic, to satisfy the unsaturation number required by the molecular formula. An aliphatic methyl singlet at δ 1.29 in the ^1H nmr spectrum of **6** had a nearly identical chemical shift to the protons on the ring junction methyl in secoxestovanin A (**4**) (DMSO-d_6 δ 1.33). This observation implied that both molecules contained similarly substituted cyclopentane rings and, along with the assumption of a common biogenetic origin for both of these *X. vanilla* metabolites, it led to the proposed structure **6** for secoxestenone. A strong nOe between the methyl protons at δ 1.29 (Me17) and the methine proton at δ 2.86 (H3) defined the relative stereochemistry around the cyclopentane ring as shown. Treatment of secoxestenone (**6**) with hot aqueous sodium hydroxide converted it cleanly into xestenone (**2**), providing chemical verification of the proposed structure.

Xestolide (**5**), secoxestenone (**6**), and xestenone (**2**) all have new terpenoid carbon skeletons. We previously suggested that xestenone (**2**) was a norditerpenoid (2). Implicit in our proposal was the assumption that the xestenone carbon skeleton had been formed from geranylgeranylpyrophosphate and that one methyl carbon had been lost at a late stage in the biogenesis. The subsequent discovery of xestovanin A (**3**), secoxestovanin A (**4**), xestolide (**5**), and secoxestenone (**6**) has made our original suggestion untenable. The similarity in structure between the aglycone of secoxestovanin A (**4**) and compounds **2**, **5**, and **6** suggests that the latter metabolites are degraded triterpenoids. Cleavage of the secoxestovanane skeleton at points "a" and "b" as shown in Scheme 1 would give the carbon skeletons of xestolide (**5**) and secoxestenone (**6**) directly. A biological aldol condensation on secoxestenone (**6**) followed by dehydration would give xestenone (**2**).

Experimental

Isolation of xestolide (5) and secoxestenone (6)

Xestospongia vanilla was collected in Barkley Sound, British Columbia, in January 1988. Fresh sponge material was homogenized with methanol in a Waring blender (2 kg dry weight). Concentration of the methanol extract *in vacuo* gave an aqueous suspension that was diluted with water (1 L) and extracted with dichloromethane (3 × 600 mL). The dried (Na_2SO_4) dichloromethane extract was concentrated *in vacuo* and fractionated via gel filtration chromatography on Sephadex LH20 (9:1 MeOH/CH_2Cl_2). Late eluting fractions were combined and further fractionated by gradient silica gel flash (CH_2Cl_2 to MeOH/EtOAc 1:4), silica gel preparative thin-layer (EtOAc), and reversed phase preparative thin-layer (MeOH/H_2O 8:2) chromatographies to give pure samples of xestolide (**5**) (7 mg, 3.5×10^{-4}%) and secoxestenone (**6**) (1.6 mg, 8×10^{-5}%).

Xestolide (5): colorless oil; FTIR (film): 3360, 1688 cm^{-1}; UV (MeOH): 233 nm (ε 7260); ^1H and ^{13}C nmr, see Table 1; EIHRMS, M^+: 334.2158 ($C_{20}H_{30}O_4$ ΔM 1.4 mmu); EILRMS: 334, 316, 265, 247, 181, 165, 153, 136.

Methylation of xestolide: A solution of xestolide (**5**) (3 mg) in diethyl ether (1 mL) was treated with excess diazomethane in ether at room temperature for 15 min. Removal of the ether and excess diazomethane *in vacuo* gave a quantitative yield of the keto methyl ester **7** as a colorless oil; ^1H nmr (300 MHz, $CDCl_3$) δ: 5.61 (t, 6.9, H10), 5.09 (t, 6.6, H14), 4.03 (t, 6.7, H12), 3.62 (s, OMe), 3.20 (dd, 16.6, 7.0, H9), 3.12 (dd, 16.6, 6.2, H9′), 2.72 (dd, 16.8, 7.5, H13), 2.55 (dd, 16.8, 8.8, H13′), 1.92 (s), 1.71 (s), 1.63 (s), 1.58 (s), 1.32 (s).

Secoxestenone (6): colorless oil; FTIR (film): 3444, 1705 cm^{-1}; ^1H nmr, see Table 1; ^{13}C nmr (75 MHz, $CDCl_3$) δ: 212.6, 210.6, 139.9, 134.7, 119.9, 118.2, 77.2, 61.3, 59.5, 37.9, 35.5, 34.1, 29.9, 27.8, 26.0, 25.4, 22.5, 18.1, 12.2; EIHRMS, M − H_2O: 288.2081 ($C_{19}H_{28}O_2$, ΔM −0.8 mmu); EILRMS: 288, 270, 255, 219, 153, 125.

Conversion of secoxestenone (6) to xestenone (2)

Secoxestenone (**6**) (1 mg) was dissolved in a mixture of methanol (0.25 mL) and 0.1 N aqueous NaOH (0.75 mL) and the reaction mixture was stirred at room temperature for 7 days. The reaction mixture was diluted to 3 mL with water, neutralized with 0.1 N HCl, and extracted with dichloromethane (3 × 10 mL). Removal of the dichloromethane *in vacuo* gave a residue that was purified by thin-layer chromatography to give pure xestenone (**2**), identical to the authentic material by tlc and ^1H nmr comparison.

Acknowledgements

The authors wish to thank Mike LeBlanc and the staff of the Bamfield Marine Station for assistance with the collection of *X. vanilla*. Financial support was provided by NSERC and by Rohm and Haas Co. P.T.N. was supported by NSERC and Polysar graduate fellowships.

1. P. T. Northcote and R. J. Andersen. J. Nat. Prod. **50**, 754 (1987).
2. P. T. Northcote and R. J. Andersen. Tetrahedron Lett. **29**, 4357 (1988).
3. P. T. Northcote and R. J. Andersen. J. Am. Chem. Soc. In press.
4. A. Bax. J. Magn. Reson. **57**, 314 (1984).

Can. J. Chem. Downloaded from www.nrcresearchpress.com by 194.225.253.170 on 09/07/12
For personal use only.

Tris-imidazole tripodands: synthesis and complexation

PIERRE G. POTVIN,[1] ROBERTO GAU, CATHLEEN M. UNRAU, AND NIKOLAUS K. GEHL
Department of Chemistry, York University, 4700 Keele Street, North York, Ont., Canada M3J 1P3

Received November 1, 1988[2]

PIERRE G. POTVIN, ROBERTO GAU, CATHLEEN M. UNRAU, and NIKOLAUS K. GEHL. Can. J. Chem. **67**, 1363 (1989).

Simple syntheses of seven imidazole-terminated tripodands are described. Some are *N*-methylated and water-soluble and others are *N*-benzylated and only lipo-soluble. Pronounced and unusual selectivity for hydrazinium ion was found in complexation experiments using Cram's extraction methods.

Key words: imidazole, tripodands, extraction, selectivity, hydrazinium.

PIERRE G. POTVIN, ROBERTO GAU, CATHLEEN M. UNRAU et NIKOLAUS K. GEHL. Can. J. Chem. **67**, 1363 (1989).

On décrit la synthèse simple de sept tripodands portant chacun trois groupements imidazoles. Certains sont *N*-méthylés et solubles dans l'eau et d'autres sont *N*-benzylés, seulement solubles en phases organiques. On rapporte des expériences suivant les méthodes d'extraction de Cram qui ont démontré une sélectivité inhabituelle et prononcée pour l'ion hydrazinium par ceux-ci.

Mots clés : imidazole, tripodands, extraction, sélectivité, hydrazinium.

Can. J. Chem. Downloaded from www.nrcresearchpress.com by 194.225.253.170 on 09/07/12
For personal use only.

In complexation chemistry, podands (1), multi-"armed" acyclic ligands, can offer many of the benefits of cryptands without much of the associated synthetic cost. The "lariat ethers" and BIBLEs are good examples of podando-coronands isomorphic with [2]- and [3]-cryptands that display cryptand-like binding (2). In related work (3), we prepared a large tripodand bearing six imidazole imino N^{π} (N-3) binding sites. In the molecule's binding conformation(s), these are arranged in two loci that are contained within the concave portion. Thus, the acyclic ligand becomes cryptating or encapsulating as it binds, and isomorphic with [2]-cryptands. Herein we describe the one-step preparation, using the same chemistry, of both lipophilic and hydrophilic varieties of simpler tripodands bearing imidazole binding groups at the arms' termini. The flexible tripod of N-3 donor atoms can define a tetrahedral or octahedral binding locus most suitable for hydrogen bond donors and transition metal ions. We also report preliminary results of complexation studies with these substrates.

5-Oxo-5,6,7,8-tetrahydro-imidazo[1,5-*c*]pyrimidine (3, 4), **1**, can be specifically alkylated at N-3 with CH_3I (3, 5) or $PhCH_2Br$ (6) to produce salts **2***a* or **2***b*, respectively, as latent N^{τ} (N-1)-alkylated histamine units. These salts (and **1**) can be ring-opened by a variety of primary and secondary amines. In dry DMF at 80–90°C, salt **2***a* reacted with triamines **3**, **4**, and **5** to produce the N—CH_3 podands **6***a*,[3] **7***a*,[4] and **8***a*,[5] in 82%, 80%, and 70% unoptimized yields, respectively.[6,7] These podands are readily soluble in both organic solvents and H_2O. Salt **2***b* similarly furnished the N—CH_2Ph podands **6***b*,[8] **7***b*,[9] and **8***b*[10] from the same triamines in 37%, 27%, and 44%

[1]Author to whom correspondence may be addressed.

[2]Revision received April 17, 1989.

[3]Results for **6***a* ^{1}H-nmr ($CDCl_3$): δ 7.28 (s, 3H, H-2′), 6.65 (s, 3H, H-5′), 6.19, 5.38 (2bt, 3H + 3H, NH), 3.58 (s, 9H, NCH_3), 3.39 (dt, 6H, J = 5.9, 6.3 Hz, CH_2NH), 2.83 (d, 6H, J = 6.2 Hz, CH_3CCH_2), 2.67 (t, 6H, J = 6.4 Hz, CH_2CH_2NH), 0.72 (s, 3H, CCH_3) ppm. ^{13}C-nmr ($CDCl_3$): δ 159.1 (CO), 140.1 (C-4′), 137.1 (C-2′), 117.1 (C-5′), 43.2 (CH_2CH_2NH), 41.0 (CCH_3), 40.1 (CH_3CCH_2), 33.1 (NCH_3), 28.6 (CH_2CH_2NH), 18.9 (CCH_3) ppm.

[4]Results for **7***a*: ^{1}H-nmr (CD_3OD): δ 7.49 (s, 3H, H-2′), 6.86, 6.83 (2s, 3H, H-5′), 3.65 (s, 9H, NCH_3), 3.35, 3.31 (2t, 12H), 3.18 (t, 2H, CCH_2CH_2NH), 2.72, 2.66 (2t, 6H, CCH_2CH_2NH) ppm. ^{13}C-nmr ($CDCl_3$): δ 159.1, 158.6 (CO), 139.5, 139.2 (C-4′), 136.6 (C-2′), 117.0 (C-5′), 47.4 (NCH_2CH_2NH), 40.5, 39.6, 38.7 (NCH_2CH_2NH, CCH_2CH_2NH), 32.8 (NCH_3), 28.2, 28.0 (CCH_2CH_2NH) ppm.

[5]Results for **8***a*: ^{1}H-nmr ($CDCl_3$): δ 7.32 (s, 3H, H-2′), 6.68 (s, 3H, H-5′), 6.05, 5.85 (2bt, 3H + 3H, NH), 3.61 (s, 9H, NCH_3), 3.37 (bdt, 6H, NCH_2CH_2NH), 3.15 (bdt, 6H, CCH_2CH_2NH), 2.67 (bt, 6H, NCH_2CH_2NH), 2.46 (bt, 6H, CCH_2CH_2NH) ppm. ^{13}C-nmr ($CDCl_3$): δ 159.2 (CO), 140.3 (C-4′), 136.8 (C-2′), 117.2 (C-5′), 54.6 (NCH_2CH_2NH), 40.1 (CCH_2CH_2NH), 38.1 (NCH_2CH_2NH), 33.3 (NCH_3), 28.7 (CCH_2CH_2NH) ppm.

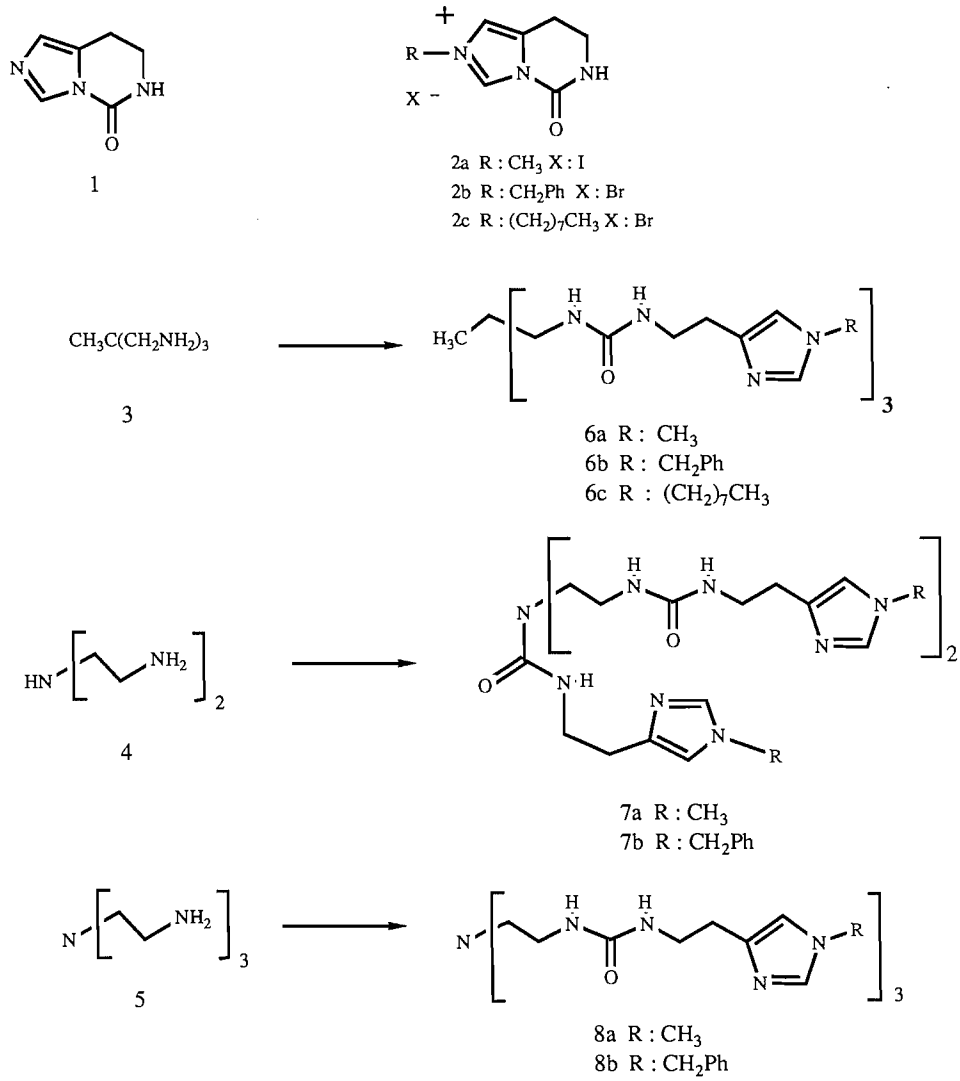
[6]General synthetic procedure for **6**, **7**, **8**: A mixture of 1 mmol of salt **2***a*, **2***b*, or **2***c* and 0.33 mmol of triamine **3**, **4**, or **5** in 1–5 mL dry DMF was heated in a capped, Ar-flushed flask at 80–90°C overnight. The cooled mixture was diluted with H_2O and neutralized by Dowex IRA-400 resin (OH^- form). After evaporation to dryness, the crude products were purified by centrifugal chromatography on a Harrison Research Model 7924T Chromatotron, using rotors coated with 4 mm Merck GF_{254} Al_2O_3 containing 10 wt.% $CaSO_4$, and eluting with 5–20 vol.% MeOH in CH_2Cl_2.

[7]All of the podands described were thick, hygroscopic oils that were chromatographically homogeneous on tlc plates and were characterized by ^{1}H-nmr, ^{13}C-nmr, ir and mass spectroscopy. Attempts at preparing crystalline hydrochloride or picrate salts failed and resulted in darkened material. As well, $CHCl_3$ solutions of these ligands became discoloured over a period of a few days, probably owing to reactions with the photo- or base-induced decomposition products of the solvent.

[8]Results for **6***b*: ^{1}H-nmr ($CDCl_3$): δ 7.42 (s, 3H, H-2′), 7.33 (m, 9H, Ph), 7.14 (m, 6H, Ph), 6.68 (s, 3H, H-5′), 5.91, 5.12 (2bt, 3H + 3H, NH), 5.03 (s, 6H, CH_2Ph), 3.43 (dt, 6H, J = 5.8, ≅6 Hz, CH_2CH_2NH), 2.87 (d, 6H, J = 6.4 Hz, CH_3CCH_2NH), 2.71 (t, 6H, J = 6.4 Hz, CH_2CH_2NH), 0.72 (s, 3H, CH_3) ppm. ^{13}C-nmr ($CDCl_3$): δ 159.0 (CO), 140.3 (C-4′), 136.6 (C-2′), 136.0, 128.9, 128.1, 127.3 (Ph), 50.7 (CH_2Ph), 43.4 (CH_2CH_2NH), 41.0 (CH_3C), 40.2 (CH_3CCH_2NH), 28.6 (CH_2CH_2NH), 19.1 (CH_3) ppm.

[9]Results for **7***b*: ^{1}H-nmr ($CDCl_3$): δ 7.39, 7.35 (2s, 1H + 2H, H-2′), 7.28 (m, 9H, Ph), 7.10 (m, 6H, Ph), 6.69, 6.65 (s, 1H + 2H, H-5′), 6.56, 6.29, 6.04 (3bt, 1H + 2H + 2H, NH), 4.95, 4.93 (2s, 6H, CH_2Ph), 3.37 (bm, 8H, NCH_2CH_2NH), 3.20 (bm, 6H, CCH_2CH_2NH), 2.67, 2.65 (2t, 6H, CCH_2CH_2NH) ppm. ^{13}C-nmr ($CDCl_3$): δ 159.2, 158.7 (CO), 140.3, 140.1 (C-4′), 136.6 (C-2′), 136.0, 128.6, 127.9, 127.1 (Ph), 50.4 (CH_2Ph), 47.8 (NCH_2CH_2NH), 40.7, 39.8, 39.0 (CH_2NH), 28.7, 28.3 (CCH_2CH_2NH) ppm.

[10]Results for **8***b*: ^{1}H-nmr ($CDCl_3$): δ 7.57 (s, 3H, H-2′), 7.30 (m, 9H, Ph), 7.16 (m, 6H, Ph), 6.75 (s, 3H, H-5′), 6.37, 6.28 (2bt,



unoptimized yields, respectively.[6,7] Although the reactions had proceeded to completion, contamination by impurities with very similar chromatographic mobilities was responsible for the lower isolated yields. When $CDCl_3$ solutions of the N—CH_2Ph ligands were shaken with D_2O, no ligand could be detected in the D_2O layer. *N*-octyl podand **6***c* was similarly prepared, albeit in only poor yield, from salt **2***c*, itself obtained by heating **1** and 1-bromooctane at 80–90°C overnight in dry DMF, followed by trituration with ether.

$CHCl_3$ or $CDCl_3$ solutions of the N—CH_2Ph podands **6***b* and **7***b* were able to extract picrate (Pic^-) salts of Na^+, K^+, and NH_4^+, and $H_2NNH_3^+$ (7) from aqueous solutions. With the latter substrate, the yellow colour of Pic^- was very strong in the organic phase. The extractions could be monitored by ^{1}H-nmr spectroscopy. The ratio R^{nmr}, reported in Table 1, of complexed substrate to total ligand (8) was calculated, assuming 1:1 stoichiometry, as three times the ratio of the integration of the Pic^- signal (near 9 ppm) divided by that of the ligand CH_2Ph signals (near 5 ppm). By this method, it was also found that Na^+ tosylate, Na^+ salicylate, and K^+ hydrogen phthallate were not measurably extracted. Unfortunately, extractions of Zn^{2+} or Co^{2+} (as the nitrates) in the presence of NaPic resulted in the deposition of thick oils. This also occurred with the more lipophilic *N*-octyl analogue **6***c*.

Integration of the Pic^- peak is subject to much error, especially with very poor or very good substrates. The more accurate uv method of Cram *et al.* (9) was therefore also used: aliquots of both the aqueous and organic phases were diluted in CH_3CN and the absorbances at 380 nm of each were measured against appropriate blanks. Table 1 summarizes the results obtained with **6***b*. Ligand **7***b* behaved very similarly. The quantities R^{uv}, representing the ratios of substrate to total ligand, calculated (9) from the absorbances of the diluted aliquots from the organic layers, were closer to those calculated from nmr integration ratios. The aliquots from the aqueous phases furnished ratios that deviated significantly from these values. We have traced this to a significant drop in the extinction coefficients with increasing concentration of both H_2O and Pic^-, depending on the cation. Accordingly, extraction constants and association constants were calculated using the *R* values from the organic phases. The errors in Table 1 were calculated according to the analysis of ref. 9*c*. Using pessimistic error estimates in weights and volumes, errors of 1.1% and 0.7%

3H + 3H, NH), 5.01 (s, 6H, CH_2Ph), 3.36 (bt, 6H, NCH_2CH_2NH), 3.11 (bt, 6H, CCH_2CH_2NH), 2.68 (bt, 6H, NCH_2CH_2NH), 2.40 (bt, 6H, CCH_2CH_2NH) ppm. ^{13}C-nmr ($CDCl_3$): δ 159.1 (CO), 139.2 (C-4′), 136.0 (C-2′), 135.7, 128.7, 128.0, 127.3 (Ph), 54.3 (NCH_2CH_2NH), 50.7 (CH_2Ph), 39.7 (CCH_2CH_2NH), 37.5 (NCH_2CH_2NH), 28.6 (CCH_2CH_2NH) ppm.

Can. J. Chem. Downloaded from www.nrcresearchpress.com by 194.225.253.170 on 09/07/12
For personal use only.

TABLE 1. Extractions of 0.400 ± 0.005 mL picrate salt solutions by 0.400 ± 0.005 mL $2.25 \pm 0.025 \times 10^{-2}$ *M* **6***b* in $CDCl_3$

Cation	Concentration ($\times 10^{-2}$ *M*)	R^{nmr}	R^{uv}	log K_e	log K_a
Na^+	1.04[a]	0.06	0.111 ± .006	3.30 ± .08	6.06 ± .13[b]
K^+	1.00	0.09	0.096 ± .005	3.24 ± .07	5.83 ± .12
NH_4^+	1.00	0.16	0.175 ± .010	3.76 ± .15	6.16 ± .20
$NH_2NH_3^+$	1.09	0.31	0.331 ± .019	4.62 ± .47	—[c]

[a] ± 0.7%.
[b] Calculated using a ± 4.2% error (9*c*) in the $CHCl_3$–H_2O distribution constants taken from ref. 9*b*.
[c] A value for the distribution constant of NH_2NH_3Pic is lacking.

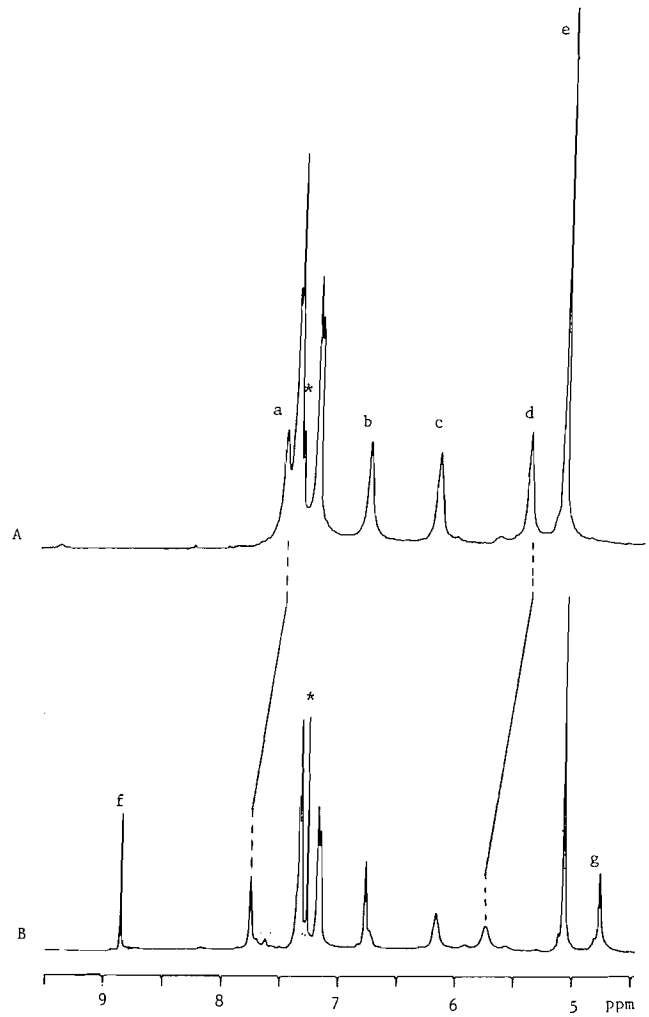


FIG. 1. Downfield regions of ^1H-nmr spectra of free **6***b* (trace A) and the complex of **6***b* with NH_2NH_3Pic (trace B) showing downfield displacements of ligand signals (see text). Assignments are (*a*) imidazole H-2, (*b*) imidazole H-5, (*c*) and (*d*) NH, (*e*) CH_2Ph, (*f*) Pic^-, (*g*) entrained H_2O, and (*) $CHCl_3$.

were calculated for ligand and metal concentrations, respectively. This led to an error estimate of 5.6% in R^{uv} (*cf.* 4.9% in ref. 9*c*). The corresponding uncertainties in K_e, which depend on the value of R^{uv}, are large but lead to much smaller uncertainties in log K_e and log K_a.

1:1 Complex stoichiometries were assumed, but were difficult to prove. Job plots of the chemical shifts of ligand signals during titration of a $CDCl_3$ solution of **6***b* with concentrated DMSO-d_6 solutions of $NaClO_4$ and $Zn(ClO_4)_2$ showed no asymptotic behaviour. We found that DMSO-d_6 alone induced strong upfield shifts (*cf.* ref. 8), but subtraction of these effects also failed to yield asymptotic behaviour. Evidence for binding at the N^π sites was provided by the sizeable shifts for the imidazole H-2 and H-4 signals from their positions in the free ligands. For instance, shaking equal volumes of 1.000×10^{-2} *M* NH_2NH_3Pic in D_2O and 4.355×10^{-3} *M* **6***b* in $CDCl_3$ resulted in downfield shifts of 0.33 ppm and 0.08 ppm for the imidazole H-2 and H-5 signals, respectively, and 0.50 ppm for one NH signal, while all other signals were shifted less than 0.05 ppm (Fig. 1). The order of extraction selectivity and the NH shift, virtually absent with Na^+ or K^+, suggested that the urea groups may be involved in secondary binding of the ammonium ions. Indeed, when a 3.964×10^{-3} *M* $CDCl_3$ solution of **7***b* was mixed with an equal volume of a 1.000×10^{-2} *M* aqueous solution of H_2NNH_3Pic, the two *C*=O resonances were shifted downfield by an average 0.42 ppm, compared to a 0.91 ppm upfield shift for the imidazole C-2 signal. All of the complexes were in rapid exchange with free ligand, on the nmr time scale.

Ligand **6***b* is less selective overall than macrocyclic carriers, but clearly preferring $NH_2NH_3^+$. To our knowledge, this is the first instance of such preference. Although NH_4^+ is extracted to a greater extent than Na^+, it is also more soluble in $CDCl_3$, and their association constants are about the same and comparable to those of K^+-selective 2,3-naphtho-18-crown-6 (with log K_a values of 5.93 for Na^+ and 6.88 for NH_4^+; see ref. 9*c*). The extraction constants calculated for NH_4Pic and NH_2NH_3Pic suggest that the N—CH_2Ph podands may be good passive ion carriers for ammonium ions (10). Further studies with alkylammonium ion substrates are underway. The insolubility of the transition metal complexes somewhat restricts the usefulness of these ligands as carriers. Complexation studies in H_2O with the N—CH_3 ligands and transition metal ions will be reported elsewhere.

Acknowledgements

We thank Professor D. N. Butler for triamine **5**, the Natural Sciences and Engineering Research Council of Canada for a University Research Fellowship awarded to P.G.P., and Research Corporation for a Cottrell Research Grant in support of this work.

1. E. WEBER and F. VÖGTLE. Top. Curr. Chem. **98**, 1 (1981).
2. P. G. POTVIN and J. M. LEHN. *In* Synthesis of macrocycles. The design of selective complexing agents. *Edited by* R. M. Izatt and J. J. Christensen. Wiley, New York. 1987. p. 167.

Can. J. Chem. Downloaded from www.nrcresearchpress.com by 194.225.253.170 on 09/07/12
For personal use only.

3. P. G. POTVIN and M. H. WONG. J. Chem. Soc. Chem. Commun. 672 (1987).
4. R. MECHOULAM and A. HIRSCHFELD. Tetrahedron, **23**, 239 (1967).
5. G. J. DURANT, J. C. EMMETT, R. GANELLIN, A. M. ROE, and R. A. SLATER. J. Med. Chem. **19**, 923 (1976).
6. J. C. EMMETT, G. J. DURANT, R. GANELLIN, A. M. ROE, and J. L. TURNER. J. Med. Chem. **25**, 1168 (1982).
7. M. A. COPLAN and R. M. FUOSS. J. Phys. Chem. **68**, 1177 (1964).
8. E. P. KYBA, R. C. HEGELSON, K. MADAN, G. W. GOKEL, T. L. TARNOWSKI, S. S. MOORE, and D. J. CRAM. J. Am. Chem. Soc. **99**, 2564 (1977); J. M. TIMKO, S. S. MOORE, D. M. WALBA, P. HIBERTY, and D. J. CRAM. J. Am. Chem. Soc. **99**, 4207 (1977).
9. (*a*) S. S. MOORE, T. L. TARNOWSKI, M. NEWCOMB, and D. J. CRAM. J. Am. Chem. Soc. **99**, 6398 (1977); (*b*) K. E. KOENIG, G. M. LEIN, P. STUCKLER, T. KANEDA, and D. J. CRAM. J. Am. Chem. Soc. **101**, 3553 (1979); (*c*) R. G. HEGELSON, G. R. WEISMAN, J. L. TONER, T. L. TARNOWSKI, Y. CHAO, J. M. MAYER, and D. J. CRAM. J. Am. Chem. Soc. **101**, 4928 (1979).
10. J. P. BEHR, M. KIRCH, and J. M. LEHN. J. Am. Chem. Soc. **107**, 241 (1985).

Can. J. Chem. Downloaded from www.nrcresearchpress.com by 194.225.253.170 on 09/07/12
For personal use only.

Absolute rate constants for lipid peroxidation and inhibition in model biomembranes

LAWRENCE ROSS COATES BARCLAY,[1] KIMBERLY ANN BASKIN, STEVEN JEFFREY LOCKE, AND MELINDA RUTH VINQVIST
Department of Chemistry, Mount Allison University, Sackville, N.B., Canada E0A 3C0

Received October 7, 1988

LAWRENCE ROSS COATES BARCLAY, KIMBERLY ANN BASKIN, STEVEN JEFFREY LOCKE, and MELINDA RUTH VINQVIST. Can. J. Chem. **67**, 1366 (1989).

The benzophenone-photosensitized free radical autoxidation of linoleic acid in 0.50 M SDS and of dilinoleoylphosphatidylcholine (DLPC) bilayers follows the classical equation, $-d[O_2]/dt = k_p/2k_t^{1/2} \times [RH]R_i^{1/2}$. Rate constants for chain propagation, k_p, and termination, $2k_t$, at 37°C in 0.50 M SDS ($k_p = 39.1\ M^{-1}\ s^{-1}$, $2k_t = 4.17 \times 10^5\ M^{-1}\ s^{-1}$), and in DLPC bilayers ($k_p = 36.1\ M^{-1}\ s^{-1}$, $2k_t = 1.32 \times 10^5\ M^{-1}\ s^{-1}$) are reduced markedly compared to those in homogeneous solution. Results are interpreted in terms of hydrogen bonding of polar peroxyl radicals that diffuse towards the aqueous phase. The activities, measured by the inhibited autoxidation method, of typical phenolic antioxidants 2,2,5,7,8-pentamethyl-6-hydroxychroman (PMHC), α-tocopherol (α-T), 2,5,7,8-tetramethyl-6-hydroxychroman-2-carboxylate (Trolox), and butylated hydroxytoluene (BHT) range from 4.3×10^3 to $1.9 \times 10^3\ M^{-1}\ s^{-1}$ for photoinitiated runs and from 8.9×10^3 to $2.7 \times 10^3\ M^{-1}\ s^{-1}$ for runs thermally initiated with azobis-2,4-dimethylvaleronitrile (DMVN). The large reductions in k_{inh} for α-T, PMHC, and Trolox in DLPC bilayers compared to known values in chlorobenzene are explained in terms of hydrogen bonding of the *para* ether oxygen and phenolic hydroxyl group.

Key words: autoxidation, membranes, antioxidants, rate constants.

LAWRENCE ROSS COATES BARCLAY, KIMBERLY ANN BASKIN, STEVEN JEFFREY LOCKE et MELINDA RUTH VINQVIST. Can. J. Chem. **67**, 1366 (1989).

L'auto-oxydation radicalaire de l'acide linoléique, photosensibilisée par la benzophénone et effectuée dans du SDS à 0,50 M ou dans des bicouches de dilinoléoylphosphatidylcholine (DLPC), suit l'équation classique : $-d[O_2]/dt = k_p/2k_t^{1/2} \times [RH]R_i^{1/2}$. Les constantes de vitesse pour la propagation de la chaîne, k_p, et pour la terminaison, $2k_t$, mesurées à 37°C, sont : $k_p = 39{,}1\ M^{-1}\ s^{-1}$, $2k_t = 4{,}17 \times 10^5\ M^{-1}\ s^{-1}$ dans du SDS à 0,50 M et $k_p = 36{,}1\ M^{-1}\ s^{-1}$, $2k_t = 1{,}32 \times 10^5\ M^{-1}\ s^{-1}$ dans des bicouches de DLPC. On interprèts les résultats en fonction de liaisons hydrogènes des radicaux peroxyles polaires qui diffusent vers la phase aqueuse. Les activités des anti-oxydants phénoliques typiques, pentaméthyl-2,2,5,7,8 hydroxy-6 chromane (PMHC), α-tocophérol (α-T), tétraméthyl-2,5,7,8 hydroxy-6 chromanecarboxylate-2 (Trolox) et hydroxytoluène butylé (BHT), telles que mesurées par la méthode de l'inhibition de l'auto-oxydation, varient de $4{,}3 \times 10^3$ à $1{,}9 \times 10^3\ M^{-1}\ s^{-1}$ pour les essais photosensibilisés et de $8{,}9 \times 10^3$ à $2{,}7 \times 10^3\ M^{-1}\ s^{-1}$ pour des essais initiés d'une façon thermique à l'aide d'azobis-2,4-diméthylvaléronitrile (DMVN). On explique les réductions importantes qui sont observées pour les valeurs de k_{inh} du α-T, du PMHC et du Trolox dans des bicouches de DLPC, comparées aux valeurs connues dans le chlorobenzène, en faisant appel à une liaison hydrogène du groupement hydroxyle phénolique avec l'oxygène de l'éther en position *para*.

Mots clés : auto-oxydation, membranes, anti-oxydants, constantes de vitesse.

[Traduit par la revue]

Peroxidation of polyunsaturated fatty acid (PUFA) chains in phospholipid membranes is related to important pathological events (1–5). We now report some recent results on the quantitative kinetic behavior of peroxyl radicals photochemically or thermally generated in phosphatidylcholine (PPC) membranes by measurements of (*i*) the absolute rate constants of peroxyl radical propagation and termination steps in autoxidation, and (*ii*) the activity of phenolic antioxidants as inhibitors of free radical peroxidation.

[1]Author to whom correspondence may be addressed.

Autoxidation of PUFA chains in PPC membranes (6–10) and micelles (11–13) follows the classical rate law [1]:

$$[1] \quad -d[O_2]/dt = k_p/(2k_t)^{1/2} \times [RH]R_i^{1/2}$$

where RH is the substrate, R_i the rate of free radical chain initiation, k_p the propagation rate constant, and $2k_t$ the chain termination rate constant. The kinetic studies to date give useful information on the *oxidizability* of PUFA in aggregates in terms of the rate ratios, $k_p/(2k_t)^{1/2}$. The separate absolute rate constants provide much more significant information on the

Can. J. Chem. Downloaded from www.nrcresearchpress.com by 194.225.253.170 on 09/07/12
For personal use only.

dynamics of peroxyls in membranes and we now report values of k_p and $2k_t$ for bilayers. The activities of peroxyl radical trapping phenolic antioxidants are also of continuing interest (14–22) and we report herein for the first time on the absolute reactivity of several phenolic antioxidants in PPC membranes by determinations of the rate constants for eq. [2].

$$[2] \quad ROO^{\bullet} + ArOH \xrightarrow{k_{inh}} ROOH + ArO^{\bullet}$$

Dilinoleoylphosphatidylcholine (DLPC), purified and in multilamellar vesicles (MLV) in phosphate buffer (pH 7.0) containing benzophenone (BP) or the water-soluble derivative 4-sulphomethylbenzophenone (BP^-) as photoinitiators, was used as oxidizable substrate. 2,5-Dimethylazobisvaleronitrile (DMVN) was used as a lipid-soluble thermal initiator. The antioxidants used were α-tocopherol (α-T), 2,2,5,7,8-pentamethyl-6-hydroxychroman (PMHC), 2,5,7,8-tetramethyl-6-hydroxychroman-2-carboxylate (Trolox), and 2,6-di-*tert*-butyl-4-methylphenol (BHT). The procedures for preparing the MLV bilayers and the rotating sector method for measuring absolute rate constants have been described in detail (13). The inhibition rate constants (k_{inh}) were determined from oxygen uptake during antioxidant inhibition periods by using the integrated expression for the kinetics during inhibition (14, 16), eq. [3],

$$[3] \quad \Delta[O_2]_t = -k_p/k_{inh} \times [RH] \ln (1 - t/T)$$

where k_p is the propagation rate constant determined separately for the same system. Plots of $\Delta[O_2]$ versus $-\ln (1 - t/T)$, where T is the induction period and t the time during the inhibition period after injection of the antioxidant, were used to calculate k_{inh}, and the values were comparable to those calculated from the oxygen consumed at points during the induction period. The kinetic order in R_i for photoinitiated runs was determined by varying the light intensity with six neutral density filters.

Absolute rate constants determined for linoleate in bilayers and 0.50 M SDS at 37°C for comparison purposes are given in Table 1. The kinetic order in light intensity, 0.532, for these MLV liposomes indicates half-order dependence on the R_i, which is required for the classical rate law in eq. [1] to be obeyed. Absolute rate constants for linoleate (Table 1) are depressed significantly in membranes, $k_p = 36.1 \pm 1.2$ and $2k_t = (1.32 \pm 0.16) \times 10^5$ (Runs 2(a)–(c)), and micelles, $k_p = 39.1 \pm 1.1$ and $2k_t = (4.17 \pm 0.17) \times 10^5$ (Runs 1(a)–(c)), compared with those in solution (units of $M^{-1}\ s^{-1}$). For example, the k_p for DLPC bilayers is reduced by 1/4 and the $2k_t$ reduced by 1/50 of those values reported for DLPC in *tert*-butyl alcohol (8), and the $2k_t$ for the linoleate chain in bilayers is more than two orders of magnitude less than for linoleic acid in this solvent (13). The marked reduction in the $2k_t$ term observed in SDS micelles (13) and in bilayers is attributed to the intrinsic polarity of peroxyl radicals (23). Such polar species would diffuse rapidly from the hydrophobic region of micelles or bilayers, where they initially form, towards the polar aqueous region, where strong hydrogen bonding interactions would lower the $2k_t$ substantially.

The k_{inh} values, determined by photoinitiation, are summarized in Table 2. The k_{inh} values of the three lipid-soluble antioxidants α-T, PMHC, and BHT show remarkable differences from those found in homogenous solution (14), in two respects: (*i*) in bilayers the values are all similar, within experimental error, whereas in chlorobenzene BHT is much less active, and (*ii*) the activities of α-T and PMHC in bilayers *are reduced by at least three orders of magnitude compared to*

TABLE 1. Absolute rate constants for autoxidation of linoleate in SDS micelles and DLPC bilayers photoinitiated with benzophenone at 37°C

Run no.[a]	Substrate[b]	Medium	R_i[c] ($M\ s^{-1} \times 10^7$)	Oxidizability ($M^{-1/2} s^{-1/2} \times 10^2$)	ν[d]	γ	m	k_x (s^{-1})	$2k_t$[e] ($M^{-1} s^{-1} \times 10^{-5}$)	k_p[e] ($M^{-1} s^{-1}$)
1(a)	L.A.	0.50 M SDS	7.26	5.05	14.0	0.110	3.41	0.1070	4.05 ± 1.36	38.3 ± 7.9
(b)	L.A.	0.50 M SDS	7.37	5.20	15.0	0.090	3.64	0.0990	4.29 ± 1.33	39.8 ± 5.2
(c)	L.A.	0.50 M SDS	1.50	4.50	29.0	0.104	3.00	0.0581	5.27 ± 2.06	40.1 ± 11.0
2(a)	DLPC	Bilayers	19.00	8.45	63.0	0.165	3.82	0.1790	1.50 ± 0.30	37.4 ± 4.0
(b)	DLPC	Bilayers	18.30	8.57	6.5	0.173	3.44	0.1670	1.26 ± 0.28	35.0 ± 5.0
(c)	DLPC	Bilayers	19.10	10.00	74.0	0.123	3.83	0.1150	1.19 ± 0.57	35.8 ± 9.5
(d)	DLPC	Bilayers	16.40	10.10	80.0	0.170	3.38	0.1610	1.27 ± 0.28	41.6 ± 4.8

[a]BP amounts used: 1(a), (b), 2.22×10^{-5} mol; 1(c), 4.44×10^{-7} mol; 2(a)–(c) 8.23×10^{-7} mol. Run 2(d) used BP^- (see text) 1.00×10^{-6} mol.
[b]L.A., linoleic acid, 4.76×10^{-4} mol; DLPC, dilinoleoylphosphatidylcholine, 4.48×10^{-5} mol.
[c]R_i, rate of chain initiation measured by the induction period method (13) with Trolox.
[d]The kinetic chain length; $\nu = (-d[O_2]/dt)/R_i$.
[e]Methods of calculation and the parameters γ, m, k_x are given in ref. 13. The errors in $2k_t$ and k_p in each run were determined by three measurements.

TABLE 2. Inhibition rate constants for phenolic antioxidants during photoinitiated peroxidation of DLPC bilayers at 37°C

No.[a]	Antioxidant (mol × 10^7)	R_i[b] ($M\ s^{-1} \times 10^6$)	k_{inh}[c] ($M^{-1}\ s^{-1} \times 10^{-3}$)	ν range[d]
1	α-T (1.87)	0.561–2.15	2.9 ± 0.3	2.9–6.3
2	PMHC (1.88)	2.32 –3.14	4.3 ± 1.1	2.5–5.8
3	BHT (1.89)	2.24 –2.46	1.9 ± 0.1	2.7–8.4
4	Trolox (1.78–1.88)	1.90 –2.78	2.5 ± 0.3	2.6–8.4

[a]Each run was repeated at least three times, using 8.17×10^{-7} mol benzophenone and DLPC $(4.58–4.76) \times 10^{-5}$ mol, giving calculated reaction volumes of $(4.48–4.70) \times 10^{-5}$ L.

[b]The R_i was varied by using different light intensities.

[c]k_{inh} values calculated from plots of $\Delta[O_2]$ versus $-\ln(1 - t/T)$, and using an averaged $k_p = 36.1\ M^{-1}\ s^{-1}$.

[d]The chain length calculated at points along the induction period from the equation (ref. 14, using $n = 2$) $\nu_t = ([O_2]_t - [O_2]_{t=0})/n[AH]_0(1 - t/T) \ln(1 - t/T)$.

TABLE 3. Antioxidant activities of phenolic antioxidants during thermally initiated peroxidation of DLPC bilayers by DMVN[a] at 37°C

No.[b]	Antioxidant (mol × 10^8)	R_i ($M\ s^{-1} \times 10^8$)	k_{inh}[c] ($M^{-1}\ s^{-1} \times 10^{-3}$)	ν range[d]
1	α-T (0.630)	1.65	3.9 ± 0.1	47–116
2	PMHC (1.50)	5.10–5.28	8.9 ± 0.7	7–31
3	BHT (1.51)	5.19–5.37	2.7	26–86
4[e]	Trolox (0.211–0.633)	1.46–4.80	6.5 ± 0.7	29–317

[a]Amounts of DMVN used; Run No. 1, 9.6×10^{-7} mol; Nos. 2 and 3, 32×10^{-7} mol; No. 4, $(9.6–32) \times 10^{-7}$ mol.

[b]Each run was repeated at least twice. The amount of DLPC used was $(5.74–5.93) \times 10^{-5}$ mol, giving calculated reaction volumes of $(5.61–5.80) \times 10^{-5}$ L.

[c,d]See footnotes *c* and *d*, Table 2.

[e]Results averaged from 13 separate runs.

those in chlorobenzene. The superior antioxidant activity of α-T and PMHC in solution was attributed to stereoelectronic effects, involving overlap of electron lone pairs on the *para* ether oxygen with the aromatic π system (14). In bilayers, the chroman ring of α-T (and presumably PMHC) is now known to be situated near the aqueous surface (24). We suggest that, in this aqueous bilayer, the stereoelectronic effect is inhibited by hydrogen bonding interactions of the ether oxygen lone pair with water. The antioxidant activity of BHT, which has no ether oxygen, is not so dramatically affected by the bilayer system. Such aqueous solvation effects are also used to explain the depressed antioxidant activities in micelles (13, 16).

k_{inh} values can vary somewhat with the initiation method (16, 21). To further illustrate this point, we report some recent results for k_{inh} determined in DLPC bilayers where peroxidation was thermally initiated with DMVN, when the sample sizes and rates of chain initiation (R_i) were selected to give chain lengths ranging approximately an order of magnitude higher (see Table 3) than in the photoinitiated runs. The k_{inh} values for lipid-soluble inhibitors α-T, BHT, and PMHC are 1.3 to 2 times those measured by photoinitiation.[2] These results do not alter our main conclusion, namely, that these phenolic antioxidant activities are dramatically lowered, by as much as 2 to 3 orders of magnitude, in phospholipid membranes compared to those in homogeneous solution. The antioxidant activities in SDS micelles (13, 16, 21) are intermediate between those in solution and the present values in membranes, while the order of activity of the lipid-soluble ones appears to be PMHC > α-T > BHT in the three systems. We postulate that the more dramatic reduction in model membranes is due to a combination of solvation forces and differential diffusion dynamics of bilayer-bound lipid peroxyl radicals and inhibitors in membranes compared to either homogeneous solution or micelles.

[2]Our k_{inh} values in Table 2 are *not* corrected for oxygen uptake during inhibition periods, it being assumed that the ketyl radicals do *not* compete significantly for O_2, $(C_6H_5)_2$—$\dot{C}OH + O_2 \rightarrow (C_6H_5)_2$—$C(OH)O\dot{O}$, with substrate radicals. As a referee points out, this could lead to "incorrect values" at short chain lengths. Oxygen absorbed by initiating radicals would tend to reduce measured k_{inh} values.

Acknowledgements

This research was supported by grants from the Natural Sciences and Engineering Research Council of Canada and the Terry Fox Fund (New Brunswick) for Cancer Research.

1. P. J. O'BRIEN. *In* Autoxidation of unsaturated lipids. Academic Press, London. 1987. Chap. 7, pp. 233–280.
2. B. HALLIWELL and J. M. C. GUTTERIDGE. Free radicals in biology and medicine. Clarendon Press, Oxford. 1985.
3. W. BORS, M. SARAN, and D. TAIT (*Editors*). Oxygen radicals in chemistry and biology. Proceedings 3rd International Conference. W. de Gruyter, Berlin. 1984.
4. D. C. H. MCBRIEN and T. F. SLATER (*Editors*). Protective agents in cancer. Academic Press, New York. 1983.
5. W. A. PRYOR (*Editor*). Free radicals in biology. Vols. I–V. Academic Press, New York. 1976–1982.
6. L. R. C. BARCLAY and K. U. INGOLD. J. Am. Chem. Soc. **103**, 6478 (1981).

Can. J. Chem. Downloaded from www.nrcresearchpress.com by 194.225.253.170 on 09/07/12
For personal use only.

7. L. R. C. BARCLAY, K. A. BASKIN, D. KONG, and S. J. LOCKE. Can. J. Chem. **65**, 2541 (1987).
8. L. R. C. BARCLAY, S. J. LOCKE, J. M. MACNEIL, and J. VANKESSEL. Can. J. Chem. **63**, 2633 (1985).
9. L. R. C. BARCLAY, S. J. LOCKE, J. M. MACNEIL, J. VANKESSEL, G. W. BURTON, and K. U. INGOLD. J. Am. Chem. Soc. **106**, 2479 (1984).
10. Y. YAMAMOTO, E. NIKI, Y. KAMIYA, and H. SHIMASAKI. Biochim. Biophys. Acta, **795**, 332 (1984).
11. Y. YAMAMOTO, S. HAGA, E. NIKI, and Y. KAMIYA. Bull. Chem. Soc. Jpn. **57**, 1260 (1984).
12. L. R. C. BARCLAY, S. J. LOCKE, and J. M. MACNEIL. Can. J. Chem. **63**, 366 (1985).
13. L. R. C. BARCLAY, K. A. BASKIN, S. J. LOCKE, and T. D. SCHAEFER. Can. J. Chem. **65**, 2529 (1987).
14. G. W. BURTON and K. U. INGOLD. J. Am. Chem. Soc. **103**, 6472 (1981).
15. G. W. BURTON, T. DOBA, E. J. GABE, L. HUGHES, F. L. LEE, L. PRASAD, and K. U. INGOLD. J. Am. Chem. Soc. **107**, 7053 (1985).
16. W. A. PRYOR, T. STRICKLAND, and D. F. CHURCH. J. Am. Chem. Soc. **110**, 2224 (1988).
17. E. NIKI, A. KAWAKAMI, M. SAITO, Y. YAMAMOTO, J. TSUCHIYA, and Y. KAMIYA. J. Biol. Chem. **260**, 2191 (1985).
18. E. NIKI, J. TSUCHIYA, Y. YOSHIKAWA, Y. YAMAMOTO, and Y. KAMIYA. Bull. Chem. Soc. Jpn. **59**, 497 (1986).
19. E. NIKI, M. TAKAHASHI, and E. KOMURO. Chem. Lett. 1573 (1986).
20. E. NIKI. Clinical and nutritional aspects of vitamin E. *Edited by* O. Hayaishi and M. Mino. Elsevier Science, New York. pp. 3–13. 1987.
21. L. CASTLE and M. J. PERKINS. J. Am. Chem. Soc. **108**, 6382 (1986).
22. E. NIKI, A. KAWAKAMI, M. SAITO, Y. YAMAMOTO, J. TSUCHIYA, and Y. NAMIYA. J. Biol. Chem. **260**, 2191 (1985).
23. R. W. FESSENDEN, A. HITACHI, and V. NAGARAJAN. J. Phys. Chem. **88**, 107 (1984).
24. I. H. EKIEL, L. HUGHES, G. W. BURTON, P. A. JOVALL, K. U. INGOLD, and I. C. P. SMITH. Biochemistry, **27**, 1432 (1988).

Can. J. Chem. Downloaded from www.nrcresearchpress.com by 194.225.253.170 on 09/07/12
For personal use only.

Metabolites of the fairy ring fungus, *Marasmius oreades*. Part 2. Norsesquiterpenes, further sesquiterpenes, and agrocybin

WILLIAM A. AYER AND PETER A. CRAW
Department of Chemistry, University of Alberta, Edmonton, Alta., Canada T6G 2G2

Received February 10, 1989

WILLIAM A. AYER and PETER A. CRAW. Can. J. Chem. **67**, 1371 (1989).

The fungus *Marasmius oreades* has previously been reported to produce the sesquiterpenes marasmone (**1**), anhydromarasmone (**2**), isomarasmone (**3**), and dihydromarasmone (**4**) when grown in liquid culture. We report herein several other sesquiterpene metabolites of the same skeleton but with differing oxidation patterns. The norsesquiterpenes *O*-formyloreadone (**15***a*), 3α-hydroxyoreadone (**15***c*), and dehydrooreadone (**17***b*) are also reported. It is suggested that the formyl group in **15***a* is derived biogenetically from C-15 of a precursor sesquiterpene. Oxidation of 1α,15-dihydroxymarasmene (**13***a*), one of the new sesquiterpenes reported, with one equivalent of pyridinium dichromate gives *O*-formyloreadone (**15***a*) as one of the products. Agrocybin (**5**), a polyacetylene amide previously isolated from the fungus *Agrocybe dura*, has also been isolated from the cultures of *M. oreades*. It is suggested that agrocybin (**5**) is the phytotoxic compound responsible for the killing of grass caused by the fairy ring mushroom fungus.

Key words: sesquiterpenes, fungal metabolites, drimanes, fairy ring mushroom, agrocybin.

WILLIAM A. AYER et PETER A. CRAW. Can. J. Chem. **67**, 1371 (1989).

On a déjà rapporté que le champignon *Marasmius oreades*, en croissance dans une culture liquide, produit les sesquiterpènes marasmone (**1**), l'anhydromarasmone (**2**), l'isomarasmone (**3**) et la dihydromarasmone (**4**). On rapporte dans cet article plusieurs autres métabolites sesquiterpéniques ayant le même squelette mais avec des modèles d'oxydation différents. Nous décrivons également les norsesquiterpènes : la *O*-formyloréadone (**15***a*), l'hydroxy-3α-oréadone (**15***c*) et la déhydrooréadone (**17***b*). On suggère que le groupe formyle du terpène (**15***a*) dérive biogénétiquement du carbone C15 d'un sesquiterpène précurseur. L'oxydation du dihydro-1α,15-marasmène (**13***a*), un des nouveaux sesquiterpènes rapportés, avec un équivalent de dichromate de pyridinium donne entre produits la *O*-formyloréadone (**15***a*). On a également isolé l'agocybine (**5**), un amide polyacétylénique isolé antérieurement du champignon *Agrocybe dura* à partir des cultures de *M. oreades*. On suggère que l'agrocybine (**5**) est le composé phytotoxique responsable de la destruction du gazon provoquée par le mousseron du champignon.

Mots clés : sesquiterpènes, métabolites du champignon, drimanes, mousseron, agrocybine.

[Traduit par la revue]

Introduction

The mycelium of many mushrooms has a tendency to grow in all directions from a control point in the ground, forming a large circular colony. When the time for sporulation arrives, the fruiting bodies are produced at the periphery of the colony and thus produce a ring. This ring is called a fairy ring because of an old superstition that mushrooms growing in a circle represent the path of dancing fairies (1). *Marasmius oreades* (Bolt.: Fr) Fr., known as the fairy ring mushroom, is the best known of a number of mushrooms that form rings. In the case of *M. oreades*, these rings have an inner and outer zone of stimulated grass growth and a zone of dead grass in the middle (2). The perennial mycelium is known to live for as many as 400 years, forming rings on the prairies over a kilometer in diameter and producing a crop of edible mushrooms each year (1, 2). In the previous paper on the metabolites of *M. oreades* we reported the structures of four related drimane-type sesquiterpenes, marasmone (**1**), anhydromarasmone (**2**), isomarasmone (**3**), and dihydromarasmone (**4**), produced when the fungus is grown in liquid culture on a potato dextrose – yeast (PDY) medium (3). In this article we describe several more metabolites produced by liquid cultures of *M. oreades*, including some biogenetically interesting norsesquiterpenes. We also describe the isolation of agrocybin (**5**), which we believe may be the compound responsible for the phytotoxicity of culture filtrates of *M. oreades* (4) and for the dead zone in the middle of the band of the fairy ring.

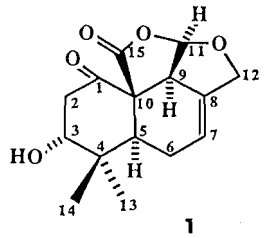
Results and discussion

In the previous paper (3) we reported the structures of four new sesquiterpene metabolites (**1–4**) produced when *M. oreades* is grown in liquid culture on a PDY medium. We find that these compounds are not produced in isolable amounts when the fungus is grown on a malt extract – glucose (MEG) medium, but that several related metabolites, some of which are also produced on the PDY medium, are obtained.[1] One of the major metabolites produced on the MEG medium is the hemiacetal **6***a*, 3α,15-dihydroxymarasmene,[2] obtained as an inseparable mixture of the C-15 epimeric hemiacetals. 3α,15-Dihydroxymarasmene (**6***a*), mp 146–147°C, $C_{15}H_{22}O_4$ (determined by high resolution electron impact mass spectrometry (hreims)), shows complex ^{1}H nmr and ^{13}C nmr spectra (see Experimental) reflecting the presence of the two epimeric hemiacetals and a trace of the aldehyde. Oxidation of **6***a* with an excess of pyridinium dichromate gave the ketolactone **8**, which shows carbonyl absorption at 1761 (γ-lactone) and 1707 (cyclohexanone) cm^{-1} in its infrared (ir) spectrum. Acetylation of **6***a* gave a separable mixture of the diacetate **6***b* (only one epimer at C-15 (^{1}H nmr: δ 6.08 (s, H-15), δ 5.74 (d, *J* 4 Hz, H-11)) and the diacetoxyaldehyde **9** (^{1}H nmr: δ 9.80 (d, *J* 2 Hz, H-15), δ 5.91 (d, *J* 4 Hz, H-11)). The signal for H-3 in both **6***a* and **9** shows two small couplings (<3 Hz) indicating the equatorial nature of H-3. Reduction of ketone **8** with sodium borohydride gave the 3β alcohol **10***a* in which the C-3 hydrogen is axial (*J*'s 11.5, 4 Hz). The strong nuclear Overhauser effect (nOe) enhancement

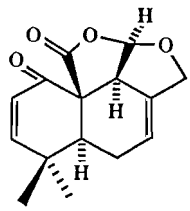
[1]Since the PDY and MEG cultures were grown at different times, and since the inoculum was not necessarily identical, it is unclear as to whether the difference in metabolite spectrum is due entirely to the difference in media (5).

[2]We suggest the trivial name marasmene for the acetal **7**, and have named several of the metabolites as derivatives of **7**. Marasmene (**7**) itself is a metabolite of *M. oreades* (*vide infra*).

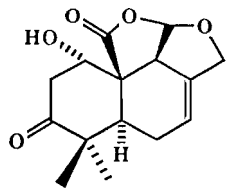
Can. J. Chem. Downloaded from www.nrcresearchpress.com by 194.225.253.170 on 09/07/12
For personal use only.



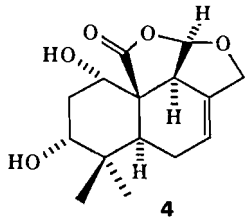
1



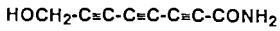
2



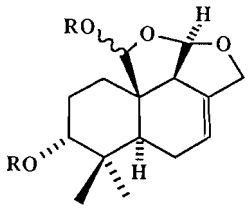
3



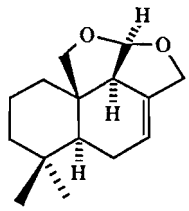
4



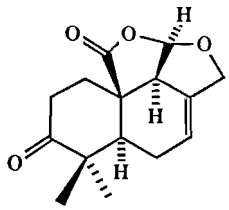
5



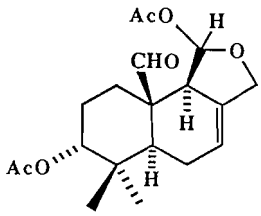
6*a* R = H
6*b* R = Ac



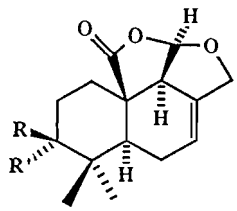
7



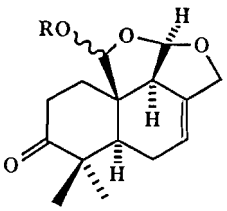
8



9



10*a* R = OH, R' = H
10*b* R = H, R' = OH
10*c* R = H, R' = OAc

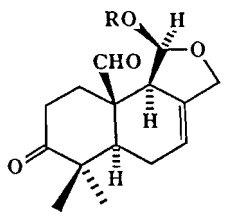


11*a* R = H
11*b* R = Ac

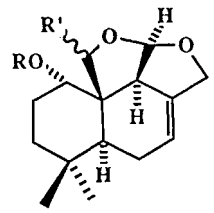
of the C-3 hydrogen observed when *either* of the C-4 methyl groups of **9** is irradiated confirms the location of the secondary alcoholic hydroxyl group in 3α,15-dihydroxymarasmene (**6***a*). Oxidation of **6***a* with one equivalent of pyridinium dichromate in dichloromethane gave a mixture of the ketolactone **8**, starting material, the hydroxy lactone **10***b*, and the ketolactol **11***a*. The latter two were separated in the form of their acetyl derivatives **10***c* (ir 1774, 1717 cm^{-1}) and **11***b* (ir 1752, 1706 cm^{-1}). The C-3 hydrogen in **10***c* appears as a double doublet at δ 4.83 (*J* 4 and 2 Hz) and H-15 in **11***b* appears as a singlet at δ 6.25. The ketolactol **11***a* (15-hydroxymarasmen-3-one) has been isolated as the equilibrium mixture (**11***a* ⇄ **12***a*), as one of the metabolites of *M. oreades* grown on PDB. Acetylation of the natural product **11***a* afforded the acetate **11***b* and a lesser amount of the aldehyde form, **12***b* (^{1}H nmr: δ 9.93 (d, *J* 2 Hz, H-15), δ 5.97 (d, *J* 4 Hz, H-11)).

A hydroxylactol, mp 152–155°C, isomeric with **6***a* has been isolated from both the MEG and the PDB media and has been shown to be 1α,15-dihydroxymarasmene (**13***a*). The molecular formula was established by hreims. The nmr spectra are again complicated by the presence of an equilibrium mixture of the two epimeric hemiacetals (in this case no aldehyde signal was detected in the ^{1}H nmr spectrum). Oxidation of **13***a* with an excess of pyridinium dichromate gave the ketolactone **14** (marasmene-1,15-dione) showing carbonyl absorption at 1767 (γ-lactone) and 1713 (cyclohexanone) cm^{-1} in the ir. The carbonyl signals in the ^{13}C nmr spectrum of **14** (δ 169.3 (lactone) and 205.5 (ketone)) are considerably upfield from those in **8** (δ 174.3 and 213.6), indicative of a 1,3 dipole–dipole interaction between the two carbonyls in **14**, similar to that observed in marasmone (**1**) (3). Reduction of anhydromarasmone (**2**) with triethylsilane – trifluoroacetic acid (6) gave ketolactone **14**. Since the structure and stereochemistry of anhydromarasmone (**2**) is well established (3), the correlation serves to confirm the structure, except for the stereochemistry, at C-1, of 1α,15-hydroxymarasmene (**13***a*). Oxidation of **13***a* with one equivalent of pyridinium dichromate gave, in addition to some of the diketone **14** and starting material, the hydroxy-

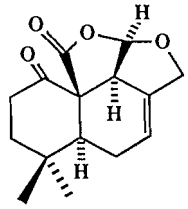
Can. J. Chem. Downloaded from www.nrcresearchpress.com by 194.225.253.170 on 09/07/12
For personal use only.



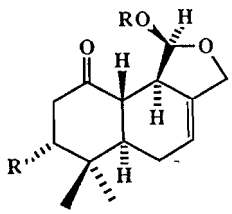
12*a* R = H
12*b* R = Ac



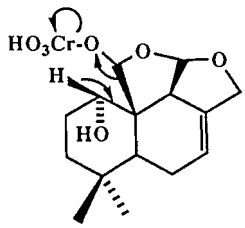
13*a* R = H, R' = OH
13*b* R = H, R' = carbonyl



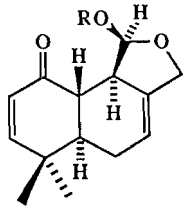
14



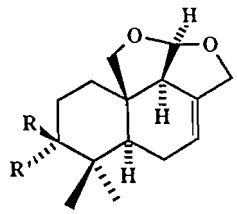
15*a* R = CHO, R' = H
15*b* R = R' = H
15*c* R = H, R' = OH
15*d* R = Ac, R'= OAc
15*e* R = Ac, R' = OH



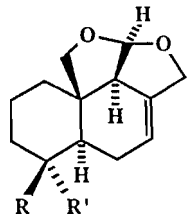
16



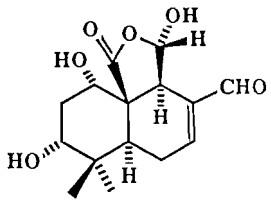
17*a* R = Ac
17*b* R = H



18*a* R = OH, R' = H
18*b* R = R' = carbonyl



19*a* R = CH_3, R' = CH_2OH
19*b* R = CH_2OH, R' = CH_3



20

lactone **13***b*, as well as another product discussed below. The hydroxylactone **13***b* shows lactone carbonyl absorption at 1769 cm^{-1} in the ir. In the ^1H nmr spectrum of **13***b*, the signal for H-1 appears as a broad singlet, indicating that the hydrogen is equatorial and thus that the hydroxyl is α-axial.

Another of the minor metabolites isolated from the PDY culture proves to be the interesting *O*-formyl compound **15***a* (we suggest the name oreadone for the corresponding hemiacetal **15***b*). *O*-Formyloreadone (**15***a*) does not show a molecular ion in the hreims, the highest mass peak (and base peak) at *m/z* 218 ($C_{14}H_{18}O_2$) corresponding to the loss of formic acid from the molecular ion. The ^{13}C nmr spectrum shows the presence of 15 carbons, and the chemical ionization mass spectrum (cims) indicates a molecular weight of 264 ($C_{15}H_{20}O_4$). The *O*-formyl group is apparent from the ^{13}C (160.8, d) and ^1H (8.10, s) nmr spectra. The ir spectrum shows formate (1732 cm^{-1}) and saturated ketone (1702 cm^{-1}) absorption. With the exception of the formyl signal and the signal for the hydrogen at C-10, the ^1H nmr spectrum of **15***a* is very similar to that of ketone **14**. The C-11 hydrogen appears downfield (δ 6.62) to that in **14** (δ 6.12) but has a similar coupling to H-9 (4.8 Hz vs. 4.5 Hz). *O*-Formyloreadone (**15***a*) *is identical with* the minor oxidation product obtained (see above) when 1α,15-dihydroxymarasmene (**13***a*) is oxidized with one equivalent of pyridinium dichromate. Oxidative cleavage of the C-10 to C-15 bond may occur as illustrated in **16**, or **15***a* may arise by a retroaldol cleavage of a first formed C-1 ketone. The *trans* AB stereochemistry in **15***a* is assigned on the basis of the fact that the C-10 hydrogen (δ 2.35) shows diaxial couplings (13 Hz and 10 Hz) with both H-5 and H-9.

The related norsesquiterpene 3α-hydroxyoreadone (**15***c*) has been isolated from both PDY and MEG cultures of *M. oreades*. The compound shows a molecular ion ($C_{14}H_{20}O_4$) in the hreims as confirmed by cims, 14 signals in the ^{13}C nmr, and hydroxyl and carbonyl (1710 cm^{-1}) absorption in the ir. The ^{13}C and ^1H nmr spectra indicate that only one form of the C-11 hemiacetal is present in solution and this is tentatively assigned the β configuration on the basis of the coupling constant (5 Hz) observed between H-11 and H-9. The coupling is similar to that observed in **1**–**4** and other compounds of similar stereochemistry discussed herein (*J*'s 4–5 Hz). Irradiation of H-11 brings about significant (10%) nOe enhancement of the signal for H-9, and vice versa. The signal for H-3 (δ 3.91) appears as an apparent triplet (*J*'s 3 Hz) and is coupled to signals at δ 2.47 and δ 2.89 (H-2's), which show no further coupling other than to each other (J_{gem} = 15 Hz). The signal for H-3 shows significant nOe enhancement when either of the C-4 methyls is irradiated, confirming both the position and the orientation of the hydroxyl function. The signal for H-10 (δ 2.45) shows two large couplings (each 10 Hz), in agreement with the *trans* AB stereochemistry. The remainder of the ^1H nmr spectrum is consistent with structure **15***c*. Treatment of 3α-hydroxyoreadone (**15***c*) with acetic anhydride – pyridine gave a mixture of the diacetyl derivative **15***d*, the monoacetyl derivative **15***e*,

Can. J. Chem. Downloaded from www.nrcresearchpress.com by 194.225.253.170 on 09/07/12
For personal use only.

Can. J. Chem. Downloaded from www.nrcresearchpress.com by 194.225.253.170 on 09/07/12
For personal use only.

and the dehydration product **17***a*. The ^{1}H nmr spectrum of the dehydration product **17***a* was consistent with this compound being the acetate of dehydrooreadone (**17***b*), a metabolite isolated from the PDY culture. The ^{1}H nmr spectrum of dehydrooreadone (**17***b*) shows the vinyl signals of an α,β-unsaturated ketone at δ 5.89 (d, *J* 10 Hz) and 6.74 (d, *J* 10 Hz) for the hydrogens at H-2 and H-3, respectively.

The isolation of the norsesquiterpenes **15***c* and **17***b* is biogenetically interesting, especially in view of the co-occurrence of the formyl compound **15***a*. It appears that the course of biological demethylation may involve oxidation at C-15 to the aldehyde stage, hemiacetal formation (as seen in **13***a*), and then oxidative cleavage of the C-10, C-15 bond to give the *O*-formyl compound. Subsequent hydrolysis then furnishes the norsesquiterpene (**15***c*, **17***b*) at the C-1 ketone oxidation level.

A series of compounds in which C-15 is oxidized to the alcohol level has also been isolated. Marasmene (**7**) was obtained from the MEG culture. It is a crystalline solid, mp 70–74°C, which elutes early on flash chromatography of the crude metabolites. The hreims shows the molecular ion ($C_{15}H_{22}O_2$, *m/z* 234) and also shows a pronounced peak at $M^+ - 30$, corresponding to the loss of formaldehyde (C-15 plus attached hydrogens and oxygen) from the molecular ion, which is characteristic of the compounds at this oxidation level (compounds with a carbonyl at C-15, e.g., **1–4**, **8**, **10**, **14**, lose this carbon as CO_2). The C-15 hydrogens appear at δ 3.68 and 3.73. Besides the *geminal* coupling (8 Hz), the signal at δ 3.73 shows additional long-range W-plan coupling (2.1 Hz), believed to be with H-1α. Both 3β-hydroxymarasmene (**18***a*) and the corresponding ketone, marasmen-3-one (**18***b*) were also present as metabolites of *M. oreades*. The C-3 hydroxyl group was assigned the β (equatorial) configuration since H-3 showed both axial–axial (11.5 Hz) and axial–equatorial (4 Hz) couplings. Irradiation of the methyl signal at δ 1.04 caused significant (10.6%) enhancement of the H-3 signal, whereas irradiation of the methyl signal at δ 0.74 did not. Irradiation of the δ 0.74 methyl did, however, bring about enhancement of the signals for the hydrogens on C-15. Oxidation of **18***a* with pyridinium dichromate gave marasmen-3-one (**18***b*), identical with the natural material (ν_{max} 1708 cm^{-1}).

Two other marasmene derivatives, 13-hydroxymarasmene (**19***a*), and 14-hydroxymarasmene (**19***b*) have also been isolated. These showed nmr spectra very similar to those of marasmene except each shows only one methyl singlet (δ 0.60 in **19***a*, δ 1.03 in **19***b*) and an AB quartet for a primary alcohol (δ 3.14, 3.37 (*J* 11 Hz) in **19***a*, δ 3.37, 3.48 (*J* 11 Hz) in **19***b*). The stereochemical assignments at C-4 were made on the basis of nOe experiments that demonstrated the proximity of the C-4 methyl group to the C-15 hydrogens in **19***a*, and the proximity of the C-4 methyl in **19***b* to H-5 and one of the H-6's.

A metabolite in which C-12 is oxidized to the aldehyde level was isolated from PDY culture. This compound, for which we suggest the name marasmal, has the molecular formula $C_{15}H_{20}O_6$ and appears to possess structure **20**. The presence of the α,β-unsaturated aldehyde was indicated by strong conjugated aldehyde absorption at 1687 cm^{-1} in the ir spectrum, signals at δ 9.36 (s, CHO) and δ 7.15 (br d, H-7) in the ^{1}H nmr spectrum, and signals at δ 195.2 (d, C-12), 156.2 (d, C-7), and 140.4 (s, C-8) in the ^{13}C nmr spectrum. Lactone and lactol groups are indicated by signals at δ 178.9 (s, C-15) and δ 101.5 (d, C-11) in the ^{13}C nmr spectrum and absorptions at 1754 and 3465 cm^{-1} in the ir spectrum. The presence of the axial hydroxyl groups at C-1 and C-3 is indicated by the doublets of doublets at δ 3.51 (*J*'s 3 Hz) and δ 4.34 (*J*'s 3 Hz), which are each coupled to *geminally* coupled (J_{gem} 15 Hz) signals at δ 1.95 and 2.18. Similar small *vicinal* coupling constants for the signals of H-1 and H-3 are observed in the spectrum of dihydromarasmone (**4**) (3). The signal for H-11 appears as a broad singlet, not as a doublet, *J* 4–5 Hz, as oberved in the previously described compounds in which H-11 has an α orientation. The alternative lactol structure **21** for marasmal may be ruled out on the basis of nOe experiments that demonstrate the proximity of H-11 to H-9 and H-12.

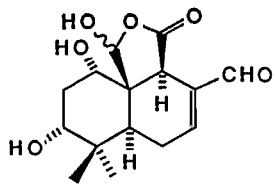
A series of compounds in which C-15 is not oxygenated was also isolated from the PDB and MEG cultures. Two of these compounds are the isomeric triols 3,11,12-trihydroxydrimene (**22**) and 11,12,14-trihydroxydrimene (**23**), which both give molecular ions at *m/z* 254 in the hreims corresponding to a molecular formula of $C_{15}H_{26}O_3$. The triol **22**, like all of the other sesquiterpenes from *M. oreades*, has not been previously isolated from natural sources. However, **22** was prepared by reduction of the naturally occurring sesquiterpene 3β-acetoxydrimenin (**24**) (7), as well as by total synthesis (8), and by microbiological hydroxylation of the (±) drimenediol (**25**) (9). The mp and optical rotation of the naturally occurring material from *M. oreades* agree with those reported for the reduction product of 3β-acetoxydrimenin (**24**) (7).

The drimenetriol **23** isolated from *M. oreades* possesses ^{1}H and ^{13}C nmr spectra similar to those of **22** except that the ^{1}H spectrum of **23** displays only two methyl singlets (δ 0.76, 0.99) and an additional AB quartet (δ 3.49, 3.83, *J* 10.5 Hz), which has replaced the signal due to H-3 (δ 3.26) in the ^{1}H nmr spectrum of **22**. Furthermore, the ^{13}C nmr spectrum of **23** shows signals for three hydroxymethyl carbons (δ 61.4, 64.7, 66.9) whereas the spectrum of **22** shows signals for two primary alcohol carbons (δ 61.2, 66.8) and a secondary alcohol carbon (δ 79.6). Thus either C-13, C-14, or C-15 must be a primary alcohol group in **23**. The location of the additional primary hydroxyl group in **23** was established by nOe eperiments that demonstrate the proximity of the C-15 hydrogens to the primary hydroxyl groups at C-11 and C-14, and the proximity of the C-13 methyl group to the C-14 hydroxymethyl group.

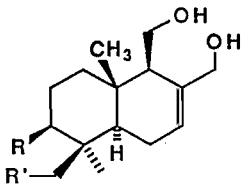
Another compound lacking a C-8—C-12, C-15 dioxabicyclooctane moiety is the lactol **26**, which has a molecular formula of $C_{15}H_{24}O_3$ as determined by hreims. The related C-14 deoxy compound, isodrimeninol (**27**), is a natural product (10), and (±)-**27** along with 3β-hydroxyisodrimeninol (**28**) have been prepared by synthesis (9). The ^{1}H nmr spectrum of **26** and those reported (9) for **27** and **28** are very similar, except that in the spectrum of **26** an AB quartet (δ 3.56, 3.85, *J* 10.7 Hz) indicates that either C-13, C-14, or C-15 is a primary hydroxyl group in this compound. The position of the primary hydroxyl group in **26** was established by nOe experiments that demonstrate the proximity of H-15 to both the lactol hydrogen (thereby confirming the assigned stereochemistry at C-11) and to one of the H-14 signals of the AB quartet. The hydrogens of the second methyl group (C-13) show significant nOe's to the other H-14 signal as well as to H-5 and both H-6's.

Small amounts of a uv-active sesquiterpene, 3β-hydroxycinnamolide (**29**), were isolated from the PDB culture. An abundant ion at *m/z* 232 in the low resolution mass spectrum (lrms) is consistent with loss of H_2O from the molecular ion. The ^{1}H nmr spectrum of **29** is very similar to that reported (9) for (±)-3β-hydroxycinnamolide obtained by microbiological hydroxylation of cinnamolide (**30**).

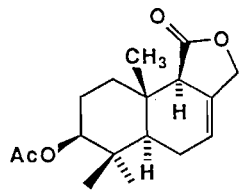
Very small amounts of a drimenediol to which we have



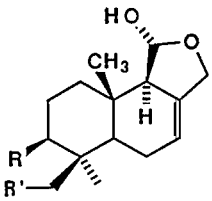
21



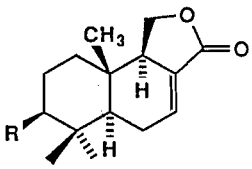
22 R = OH, R' = H
23 R = H, R' = OH
25 R = R' = H



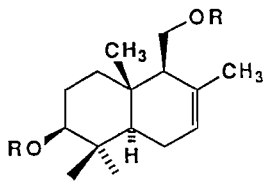
24



26 R = H, R' = OH
27 R = R' = H
28 R = OH, R' = H



29 R = OH
20 R = H



31*a* R = H
31*b* R = Ac

tentatively assigned the structure **31***a* were isolated from the MEG culture. The ^{1}H nmr spectrum of this compound shows three saturated methyl singlets (δ 0.86, 0.87, 0.98), alkenic hydrogen (δ 5.54) and alkenic methyl (δ 1.78) signals, and signals due to primary (δ 3.75, dd, *J* 11.5, 5.0 Hz, and δ 3.86, dd, *J* 11.1, 3.4 Hz) as well as secondary (δ 3.26, dd, *J* 10.5, 5.4 Hz) hydroxyl groups, which are all consistent with the assigned structure. For the corresponding diacetate (**31***b*), nOe experiments demonstrated the proximity of one of the methyl groups (δ 0.86, H-13) to the secondary carbinyl hydrogen (δ 4.51, dd, *J* 11.5, 4.8 Hz, H-3), and of another methyl group (δ 0.84, H-15) to the primary carbinyl hydrogens (δ 4.11, 4.21, H-11).

During the preliminary separation of the crude metabolites from the MEG culture, which involved flash chromatography over silica gel, some of the intermediate fractions eluted with ethyl acetate – Skellysolve B (1:1 and 2:1) deposited relatively large amounts of a heat- and light-sensitive crystalline compound. This compound shows only one signal (δ 4.26, s) in its ^{1}H nmr spectrum (in methanol-d_4). The ^{13}C nmr spectrum shows eight signals and the hreims suggested the molecular formula $C_8H_5NO_2$. The mp and spectral properties led to the identification of this compound as agrocybin (**5**), previously obtained as a metabolite of *Agrocybe dura* (11).[3] This compound has been shown to possess antibiotic activity (12). Preliminary tests in our laboratories have shown that agrocybin (**5**), but none of the sesquiterpenes isolated and tested, causes browning and death of grass (creeping red fescu) seedlings. It has also been shown that agrocybin (12.5 ppm) inhibits the growth of *Lemna minor* (duckweed) and that it displays phytotoxic activity when sprayed on whole plants (soybean, wheat) at 1.75 kg/ha.[4] We feel that agrocybin may be responsible, at least in part, for the destruction of grass caused by the fairy ring fungus *M. oreades* (2, 4).

Experimental

For general experimental details see the first paper in this series (3).

Growth of Marasmius oreades *on potato dextrose yeast broth and isolation of metabolites*

The details of the growth of the fungus on PDY broth, and column chromatography of the ethyl acetate extract of the broth, are described in the previous paper (3). The metabolites of fractions 33–45 (compound **2**), and fractions 46–49 (compounds **1**, **2**, **3**, and **4**) were discussed in the previous report.

Fractions 50–59 (0.42 g) were combined and, after extensive chromatography on several columns of silica gel, eluting with mixtures of ethyl acetate – Skellysolve B, the following compounds were obtained (in order of decreasing R_f value): **2** (3.4 mg), **18***b* (3.0 mg), **15***a* (1.4 mg), **1** (20.1 mg), **3** (3.5 mg), **4** (16.4 mg), **19***a* (3.8 mg), **29** (0.6 mg), **11***a* (6.7 mg), **18***a* (125.7 mg), and **19***b* (17.0 mg).

Fractions 60–67 (0.39 g) were combined and chromatographed on a column of silica gel (ethyl acetate – Skellysolve B, 2:1) to give **13***a* (30.6 mg) and **6***a* (159.0 mg).

Fractions 68–77 (0.55 g) were combined and chromatographed on a column of silica gel (ethyl acetate – Skellysolve B, 3:1) to give **17***b* (2.6 mg), **20** (3.8 mg), **6***a* (28.5 mg), and **15***c* (172 mg).

Fractions 78–84 (0.51 g) were combined and chromatographed on a column of silica gel (ethyl acetate – Skellysolve B, 2:1) to give several fractions enriched in **22** and **23**. Further chromatography (ethyl acetate – Skellysolve B, 3:1) of these fractions successively gave **23**, which crystallized from dichloromethane – Skellysolve B as needles (17.3 mg), and a mixture (ca. 1:1 by ^{1}H nmr) of **22** and an unidentified compound (28 mg).

3α,15-Dihydroxymarasmene (**6***a*) crystallized from ethyl acetate – Skellysolve B as prisms, mp 146–147°C; Ftir (KBr disc): 3529

[3]This compound was not isolated from the PDY culture reported previously (3). We attribute this to the fact that the metabolites were isolated by continuous extraction with ethyl acetate, and agrocybin is thermally unstable. It has been isolated from later PDY cultures that were extracted with ethyl acetate at room temperature.

[4]We thank J. Kopp, D. Krupa, K. Crosby, R. J. Stonard, and S. W. Ayer, Monsanto Agricultural Co., St. Louis, MO, for this information.

Can. J. Chem. Downloaded from www.nrcresearchpress.com by 194.225.253.170 on 09/07/12
For personal use only.

Can. J. Chem. Downloaded from www.nrcresearchpress.com by 194.225.253.170 on 09/07/12
For personal use only.

(br, OH), 1705 (w), 1385, 1370 (m, *gem* dimethyl), 1125, 1003 (C—O) cm^{-1}; Ftir ($CHCl_3$ cast): 3374 (br, OH), 1725 (w), 1705 (w), 1380, 1360 (m, *gem* dimethyl) cm^{-1}; ^1H nmr ($CDCl_3$) δ: 0.99 (3H, s, CH_3), 1.02 (3H, s, CH_3), 1.03 (6H, s, $2CH_3$), 1.48–2.48 (ca. 14H, m), 2.68 (2H, br s), 2.87 (1H, br s, H-9), 3.54–3.57 (1H, br s, H-3), 3.57–3.60 (1H, br s, H-3), 4.37 (2H, br s, H-12), 4.47 (br d, *J* 11.1 Hz, H-12), 4.55 (ddd, *J* 11.0, 1.2, 1.2 Hz, H-12), 5.22 (1H, d, *J* 10.2 Hz, H-15), 5.40 (1H, d, *J* 5.7 Hz, H-15), 5.71 (1H, d, *J* 4.7 Hz, H-11), 5.73 (1H, d, *J* 5.1 Hz, H-11), 5.79 (1H, br s, H-7), 5.91 (1H, br s, H-7), 9.79 (≪1H, CHO), 9.90 (≪1H, CHO); ^{13}C nmr ($CDCl_3$) δ: 19.9, 22.2, 26.3, 27.2, 38.0, 38.1, 54.7, 57.8, 76.0, 76.4, 99.1, 103.1, 104.3, 106.6, 116.4 (weak), 117.4 (weak), 122.2, 122.9, 206.4 (weak), 206.7 (weak) (CH, CH_3); 22.8, 24.9, 25.8, 26.1, 26.7, 30.3, 36.9, 37.7, 44.6, 46.0, 71.6, 72.6, 134.0, 136.9 (C, CH_2); hreims (probe 160°C), *m/z* calcd. for $C_{15}H_{22}O_4$ (M^+): 266.1518; found: 266.1514 (6), 248 ($M^+ - H_2O$, 36), 220 (57), 202 (29), 201 (25), 174 (20), 173 (100), 172 (63), 159 (35), 132 (26), 131 (43), 124 (27), 119 (44), 117 (27), 107 (28), 105 (80), 104 (28), 93 (28), 91 (71), 81 (24), 79 (46), 69 (58), 67 (29), 57 (30), 55 (49), 53 (27).

15-Hydroxymarasmen-3-one (**11***a*) was obtained as a clear oil; Ftir ($CHCl_3$ cast): 3410 (br, OH), 1705 (s, C=O) cm^{-1}; (major epimer) ^1H nmr ($CDCl_3$) δ: 1.12 (3H, s, H-14), 1.23 (3H, s, H-13), 1.50–1.66 (1H, m, H-1), 2.15 (1H, dd, *J* 10.0, 7.5 Hz, H-5), 2.27 (1H, ddd, *J* 14.7, 5.2, 2.6 Hz, H-6), 2.30–2.38 (1H, m, H-6), 2.54 (1H, ddd, *J* 13.5, 6.2, 2.2 Hz, H-2α), 2.68 (1H, m, H-9), 2.89 (1H, d, *J* 4.2 Hz, OH), 3.29 (1H, ddd, *J* 14.2, 14.0, 6.5 Hz, H-2β), 4.42 (2H, br s, H-12), 5.60 (1H, d, *J* 4.4 Hz, H-15), 5.80 (1H, d, *J* 4.0 Hz, H-11), 5.83 (1H, m, H-7); ^{13}C nmr ($CDCl_3$) δ: 19.4, 23.3, 23.4, 32.9, 36.1, 45.7, 47.5, 57.4, 71.5, 98.6, 103.3, 121.3, 133.8, 215.5, one signal obscured; (minor epimer) ^1H nmr ($CDCl_3$) δ: 1.13 (3H, s, H-14), 1.20 (3H, s, H-13), 1.50–1.66 (1H, m, H-1), 2.11 (1H, ddd, *J* 14.0, 6.2, 2.6 Hz, H-2α), 2.20 (1H, dd, *J* 10.5, 3.6 Hz, H-5), 2.30–2.38 (1H, m, H-6), 2.68 (1H, m, H-9), 2.82 (1H, ddd, *J* 15.0, 15.0, 6.2 Hz, H-2β), 2.86 (1H, d, *J* 9.3 Hz, OH), 4.49 (1H, br d, *J* 11.0 Hz, H-12), 4.60 (1H, dddd, *J* 11.0, 1.4, 1.4, 1.4 Hz, H-12), 5.48 (1H, d, *J* 9.3 Hz, H-11), 5.79 (1H, d, *J* 4.9 Hz, H-11), 5.83 (1H, m, H-7); ^{13}C nmr ($CDCl_3$) δ: 21.6, 22.8, 25.3, 34.6, 36.5, 44.3, 45.8, 48.5, 54.5, 106.5, 122.5, 135.8, 213.9, two signals obscured; hreims (probe 190°C), *m/z* calcd. for $C_{15}H_{20}O_4$ (M^+): 264.1362; found: 264.1359 (5), 246 ($M^+ - H_2O$, 25), 218 (19), 132 (100), 119 (27), 105 (41), 91 (40), 77 (20).

1α,15-Dihydroxymarasmene (**13***a*) crystallized from ethyl acetate – Skellysolve B as prisms, mp 152–155°C; Ftir (KBr disc): 3419 (br, OH), 1730 (w), 1710 (w), 1625 (m) cm^{-1}; ^1H nmr ($CDCl_3$) δ: 0.965 (s, CH_3), 0.96 (s, CH_3), 0.975 (s, CH_3), 0.995 (s, CH_3), 2.27 (d, *J* 8.5 Hz), 2.31–2.37 (m), 2.60 (dd, *J* 4.5, 1.5 Hz), 2.93 (d, *J* 10.8 Hz), 3.36–3.41 (m), 3.60–3.64 (m), 4.36–4.43 (m), 4.49 (br d, *J* 11.0 Hz), 4.56 (ddd, *J* 11.0, 1.3, 1.3 Hz), 5.05 (d, *J* 10.9 Hz), 5.73 (d, *J* 5.5 Hz), 5.73 (m), 5.75 (d, *J* 4.5 Hz), 5.86 (m); hreims (probe 180°C), *m/z* calcd. for $C_{15}H_{22}O_4$ (M^+): 266.1518; found: 266.1516 (3), 248 ($M^+ - H_2O$, 57), 220 (29), 219 (31), 202 (21), 201 (33), 191 (22), 190 (20), 174 (38), 173 (100), 164 (20), 159 (32), 146 (26), 145 (21), 133 (21), 131 (48), 129 (20), 121 (33), 119 (45), 118 (71), 117 (47), 107 (27), 96 (20), 95 (23), 93 (47), 92 (25), 91 (99), 83 (21), 81 (65), 78 (49), 77 (54), 71 (33), 70 (28), 69 (64), 67 (35), 65 (28), 57 (57), 56 (25), 55 (81), 53 (35).

O-*Formyloreadone* (**15***a*) was obtained as a glass; $[\alpha]_D^{24}$ +278° (*c* 0.07, CH_3OH); Ftir ($CHCl_3$ cast): 1732 (s, formate C=O), 1702 (s, ketone C=O), 1387, 1364 (m, *gem* dimethyl), 1157, 1052 (s, C—O) cm^{-1}; ^1H nmr ($CDCl_3$) δ: 1.03 (3H, s, H-14), 1.13 (3H, s, H-13), 1.66 (1H, ddd, *J* 13.5, 13.0, 4.3 Hz, H-3α), 1.72 (1H, ddd, *J* 12.5, 6.0, 2.0 Hz, H-5), 1.78 (1H, ddd, *J* 13.5, 6.0, 2.5 Hz, H-3β), 2.08–2.34 (2H, m, H-6), 2.35 (1H, dd, *J* 12.8, 9.8 Hz, H-10), 2.53 (1H, dddd, *J* 15.0, 15.0, 6.0, 0.8 Hz, H-2β), 2.92 (1H, m, H-9), 4.41 (1H, ddd, *J* 12.5, 2.2, 2.2 Hz, H-12), 4.49 (1H, ddd, *J* 12.5, 2.2, 2.2 Hz, H-12), 5.63 (1H, m, H-7), 6.62 (1H, d, *J* 4.8 Hz, H-11), 8.10 (1H, s, H-15); ^{13}C nmr ($CDCl_3$) δ: 19.3 (C-14), 27.1 (C-6), 29.1 (C-13), 32.8 (C-4), 38.0 (C-2), 41.4 (C-3), 44.4 (C-5), 46.2 (C-9), 47.0 (C-10), 69.6 (C-12), 99.4 (C-11), 117.6 (C-7), 134.3 (C-8), 160.8 (C-15), 210.9 (C-1); hreims (probe 100°C), *m/z* calcd. for $C_{14}H_{18}O_2$ ($M^+ - HCO_2H$): 218.1307; found: 218.1301 (100); cims, *m/z*: 282 ($M^+ + 18$, 11).

3α-Hydroxyoreadone (**15***c*) crystallized from dichloromethane – Skellysolve B as prisms, mp 103–108°C; $[\alpha]_D^{24}$ +130.2° (*c* 1.00, CH_3OH); Ftir (KBr disc): 3465 (br, OH), 1710 (s, C=O), 1226 (s, C—O) cm^{-1}; ^1H nmr ($CDCl_3$) δ: 1.13 (3H, s, CH_3), 1.14 (3H, s, CH_3), 2.14–2.35 (3H, m, H-5, H-6), 2.45 (1H, dd, *J* 10.0, 10.0 Hz, H-10), 2.47 (1H, dd, *J* 14.9, 3.4 Hz, H-2α), 2.81 (1H, m, H-9), 2.89 (1H, ddd, *J* 15.0, 3.2, 0.8 Hz, H-2β), 3.91 (1H, dd, *J* 3.0, 3.0 Hz, H-3), 4.36–4.37 (2H, m, H-12), 5.66 (1H, m, H-7), 5.85 (1H, d, *J* 5.0 Hz, H-11); ^1H nmr (C_6D_6) δ: 0.57 (3H, s, H-14), 0.76 (3H, s, H-13), 1.00 (1H, br s, OH), 1.68–1.88 (2H, m, H-6), 2.02 (1H, br d, *J* 2.8 Hz, OH), 2.10 (1H, ddd, *J* 12.2, 10.5, 6.5 Hz, H-5), 2.11 (1H, dd, *J* 14.5, 3.2 Hz, H-2α), 2.25 (1H, ddd, *J* 14.5, 3.2, 0.8 Hz, H-2β), 2.43 (1H, dd, *J* 12.0, 9.8 Hz, H-10), 2.85 (1H, m, H-9), 3.11 (1H, br s, H-3), 4.31 (1H, dddd, *J* 10.5, 3.0, 2.0, 2.0 Hz, H-12), 4.36 (1H, dddd, *J* 10.6, 3.0, 2.2, 2.2 Hz, H-12), 5.25 (1H, m, H-7), 6.04 (1H, dd, *J* 4.8, 2.6 Hz, H-11); ^{13}C nmr ($CDCl_3$) δ: 20.3 (C-14), 24.9 (C-13), 26.5 (C-6), 37.4 (C-4), 40.4 (C-5), 44.8 (C-9), 45.7 (C-2), 46.5 (C-10), 68.3 (C-12), 79.5 (C-3), 98.1 (C-11), 117.3 (C-7), 136.1 (C-8), 210.2 (C-1); hreims (probe 150°C), *m/z* calcd. for $C_{14}H_{20}O_4$ (M^+): 252.1362; found: 252.1364 (2); calcd. for $C_{14}H_{18}O_3$ ($M^+ - H_2O$): 234.1225; found: 234.1257 (100), 206 (35), 188 (20), 173 (21), 120 (47), 119 (22), 93 (35), 92 (59), 91 (64), 79 (21), 71 (34); cims, *m/z*: 270 ($M^+ + 18$, 18).

Dehydrooreadone (**17***b*) was obtained as a solid; ^1H nmr ($CDCl_3$) δ: 1.09 (3H, s, H-14), 1.18 (3H, s, H-13), 2.09 (1H, ddd, *J* 12.5, 9.5, 7.0 Hz, H-5), 2.21–2.29 (2H, m, H-6), 2.51 (1H, d, *J* 3.6 Hz, OH), 2.56 (1H, dd, *J* 12.8, 10.0 Hz, H-10), 2.64 (1H, m, H-9), 4.42–4.46 (2H, m, H-12), 5.70 (1H, m, H-7), 5.89 (1H, d, *J* 10.1 Hz, H-2), 5.99 (1H, br dd, *J* 4.0, 4.0 Hz, H-11), 6.74 (1H, d, *J* 10.1 Hz, H-3).

3β-Hydroxymarasmene (**18***a*) crystallized, on standing, as a microcrystalline solid, mp 129–133°C; $[\alpha]_D^{24}$ +34.0° (*c* 1.05, CH_3OH); Ftir ($CHCl_3$ cast): 3450 (br, OH), 1370, 1360 (m, *gem* dimethyl), 1016 (s, C—O) cm^{-1}; ^1H nmr ($CDCl_3$) δ: 0.67 (3H, s, H-14), 1.01 (3H, s, H-13), 1.29 (1H, dddd, *J* 14.0, 14.0, 4.5, 2.0 Hz, H-1α), 1.45 (1H, d, *J* 5.0 Hz, OH), 1.58 (1H, dddd, *J* 13.5, 13.5, 13.5, 4.0 Hz, H-2β), 1.73 (1H, dd, *J* 10.8, 6.9 Hz, H-5), 1.75–1.80 (1H, m), 1.94 (1H, ddd, *J* 13.5, 3.5, 3.5 Hz, H-1β), 2.02–2.18 (1H, m), 2.23–2.38 (1H, br d, *J* 18 Hz, H-6), 2.58 (1H, m, H-9), 3.35 (1H, ddd, *J* 11.5, 4.2, 4.2 Hz, H-3), 3.64 (1H, d, *J* 8.2 Hz, H-15α), 3.73 (1H, dd, *J* 8.2, 2.0 Hz, H-15β), 4.30–4.41 (2H, m, H-12), 5.65 (1H, d, *J* 4.8 Hz, H-11), 5.79 (1H, m, H-7); ^{13}C nmr ($CDCl_3$) δ: 14.0 (C-14), 23.4 (C-6), 25.8 (C-13), 27.7 (C-2), 34.2 (C-1), 39.1 (C-4), 43.6 (C-10), 44.0 (C-5), 55.7 (C-9), 69.3 (C-15), 72.2 (C-12), 78.3 (C-3), 105.6 (C-11), 121.1 (C-7), 133.3 (C-8); hreims (probe 120°C), *m/z* calcd. for $C_{15}H_{22}O_3$ (M^+): 250.1569; found: 250.1572 (42), 232 ($M^+ - H_2O$, 12), 220 (29), 204 (72), 186 (36), 175 (24), 173 (73), 172 (22), 171 (35), 161 (24), 145 (34), 143 (30), 133 (24), 132 (88), 131 (39), 119 (78), 118 (46), 117 (43), 107 (34), 106 (22), 105 (92), 104 (54), 96 (100), 95 (77), 93 (28), 91 (88), 82 (30), 81 (25), 79 (43), 77 (41), 69 (57), 67 (42), 65 (23), 57 (20), 55 (46), 53 (31).

Marasmen-3-one (**18***b*) was obtained as a clear oil, which crystallized from dichloromethane – Skellysolve B as microcrystals, mp 135–138°C; $[\alpha]_D^{24}$ −1.6° (*c* 1.00, CH_3OH); cd (*c* 3.63 mM, CH_3OH), 24°C: $[\theta]_{293}$ −3000; Ftir ($CHCl_3$ cast): 1708 (s, C=O), 1388, 1369 (m, *gem* dimethyl), 1006 (s, C—O) cm^{-1}; ^1H nmr ($CDCl_3$) δ: 0.95 (3H, s, H-14), 1.09 (3H, s, H-13), 1.60 (1H, ddd, *J* 14.5, 4.5, 1.2 Hz, H-1β), 2.14 (1H, dd, *J* 10.2, 6.5 Hz, H-5), 2.15–2.30 (2H, m, H-6), 2.25 (1H, ddd, *J* 13.5, 6.0, 2.5 Hz, H-1α), 2.33 (1H, ddd, *J* 14.5, 4.2, 2.5 Hz, H-2α), 2.67 (1H, m, H-9), 2.75 (1H, ddd, *J* 14.7, 14.7, 6.0 Hz, H-2β), 3.93 (1H, d, *J* 1.7 Hz, H-15β), 3.94 (1H, br s, H-15α), 4.37 (1H, br d, *J* 10.5 Hz, H-12), 4.43 (1H, ddd, *J* 10.6, 1.2, 1.2 Hz, H-12), 5.71 (1H, d, *J* 4.9 Hz, H-11), 5.83 (1H, m, H-7); ^{13}C nmr ($CDCl_3$) δ: 20.7 (C-14), 22.6 (C-13), 23.6 (C-6), 34.8, 35.6 (C-1, C-2), 43.6 (C-10), 45.6 (C-5), 48.1 (C-4), 55.4 (C-9), 68.5 (C-15), 72.2 (C-12), 105.6 (C-11), 120.7 (C-7), 133.4 (C-8), 214.1 (C-3); hreims (probe 100°C), *m/z* calcd. for $C_{15}H_{20}O_3$ (M^+): 248.1412;

found: 248.1418 (41), 205 (27), 133 (22), 132 (100), 123 (23), 119 (36), 118 (46), 117 (20), 107 (68), 105 (45), 96 (23), 95 (33), 91 (47), 79 (23), 77 (31), 69 (20), 55 (25), 53 (20).

13-Hydroxymarasmene (**19***a*) crystallized, on standing, as microcrystals, mp 147–150°C; $[\alpha]_D^{24}$ +37° (*c* 0.20, CH_3OH); Ftir ($CHCl_3$ cast): 3350 (br, OH) cm^{-1}; ^1H nmr ($CDCl_3$) δ: 0.60 (3H, s, H-14), 1.15–1.65 (4H, m), 1.83 (1H, br d, *J* 13.5 Hz), 1.87–1.98 (1H, m), 2.03–2.11 (2H, m), 2.16 (1H, br d, *J* 18 Hz, H-6), 2.55 (1H, m, H-9), 3.14 (1H, br d, *J* 11.0 Hz, H-13), 3.37 (1H, br d, *J* 11.0 Hz, H-13), 3.63 (1H, d, *J* 8.0 Hz, H-15α), 3.68 (1H, dd, *J* 8.0, 2.0 Hz, H-15β), 4.25–4.33 (2H, m, H-12), 5.60 (1H, d, *J* 4.5 Hz, H-11), 5.70 (1H, m, H-7); ^{13}C nmr ($CDCl_3$) δ: 16.6 (C-14), 18.4 (C-2), 23.2 (C-6), 29.7 (C-3), 35.8 (C-1), 37.8 (C-4), 38.6 (C-5), 43.5 (C-10), 55.2 (C-9), 69.5 (C-15), 70.8 (C-13), 72.4 (C-12), 105.8 (C-11), 121.0 (C-7), 133.5 (C-8); hreims (probe 150°C), *m/z* calcd. for $C_{15}H_{22}O_3$ (M^+): 250.1569; found: 250.1572 (15), 232 ($M^+ - H_2O$, 7), 220 (42), 191 (21), 189 (25), 174 (36), 173 (91), 159 (72), 145 (34), 143 (21), 132 (27), 131 (51), 129 (24), 119 (37), 118 (39), 117 (42), 107 (24), 106 (23), 105 (100), 104 (43), 96 (33), 95 (34), 93 (34), 91 (90), 82 (29), 81 (40), 79 (48), 77 (46), 69 (35), 67 (41), 65 (24), 57 (24), 55 (59), 53 (34).

14-Hydroxymarasmene (**19***b*) crystallized on standing. Recrystallization from dichloromethane – Skellysolve B gave prisms, mp 162.5–163°C; $[\alpha]_D^{24}$ +23.8° (*c* 0.32, CH_3OH); Ftir ($CHCl_3$ cast): 3351 (br, OH) cm^{-1}; ^1H nmr ($CDCl_3$) δ: 1.03 (3H, s, H-13), 1.00–1.15 (1H, m), 1.18–1.32 (2H, m), 1.57–1.62 (2H, m), 1.97 (1H, dd, *J* 11.8, 6.5 Hz, H-5), 1.90–2.03 (2H, m), 2.07–2.20 (1H, m), 2.37 (1H, br d, *J* 18.5 Hz, H-6), 2.63 (1H, m, H-9), 3.37 (1H, br d, *J* 11.0 Hz, H-14), 3.48 (1H, br d, *J* 11.0 Hz, H-14), 3.67 (1H, d, *J* 8.5 Hz, H-15α), 3.72 (1H, dd, *J* 7.5, 2.0 Hz, H-15β), 4.33–4.42 (2H, m, H-12), 5.68 (1H, d, *J* 4.5 Hz, H-11), 5.78 (1H, m, H-7); ^{13}C nmr ($CDCl_3$) δ: 18.7 (C-2), 23.0 (C-6), 25.2 (C-13), 35.8, 36.2 (C-1, C-3), 37.7 (C-4), 43.8 (C-10), 44.7 (C-5), 55.9 (C-9), 64.5 (C-14), 72.3 (C-12), 105.9 (C-11), 121.3 (C-7), 133.5 (C-8); hreims (probe 140°C), *m/z* calcd. for $C_{15}H_{22}O_3$ (M^+): 250.1569; found: 250.1570 (9), 232 ($M^+ - H_2O$, 7), 220 (42), 204 (74), 174 (38), 173 (72), 161 (39), 159 (52), 145 (34), 133 (20), 132 (30), 131 (48), 129 (20), 119 (47), 118 (43), 117 (40), 109 (24), 107 (32), 106 (28), 105 (100), 104 (51), 96 (39), 95 (37), 93 (41), 92 (21), 91 (97), 83 (25), 82 (33), 81 (46), 79 (66), 77 (58), 71 (36), 70 (29), 69 (65), 67 (54), 65 (29), 59 (66), 57 (73), 55 (98), 53 (42).

Marasmal (**20**) crystallized from chloroform as prisms, mp 195–200°C; $[\alpha]_D^{24}$ −73.1° (*c* 0.32, CH_3OH); Ftir (KBr disc): 3465 (s, OH), 3264 (s, OH), 1754 (s, lactone C=O), 1687 (s, conj. aldehyde C=O), 1655, 1632 (m, C=C), 1370, 1365 (m, *gem* dimethyl) cm^{-1}; ^1H nmr (CD_3OD) δ: 0.99 (3H, s, H-14), 1.13 (3H, s, H-13), 1.87 (1H, dd, *J* 12.8, 3.5 Hz, H-5), 1.95 (1H, ddd, *J* 14.8, 2.8, 2.8 Hz, H-2α), 2.12 (1H, br ddd, *J* 12.8, 3.0, 2.0 Hz, H-6β), 2.18 (1H, ddd, *J* 14.8, 2.8, 2.8 Hz, H-2β), 2.43 (1H, br dddd, *J* 19.4, 7.0, 3.5, 1.5 Hz, H-6α), 3.51 (1H, br dd, *J* 2.8, 2.8 Hz, H-3), 3.69 (1H, m, H-9), 4.34 (1H, br dd, *J* 2.8, 2.8 Hz, H-1), 5.31 (1H, br s, H-11), 7.15 (1H, br d, *J* 6.5 Hz, H-7), 9.36 (1H, s, H-12); ^{13}C nmr (CD_3OD) δ: 23.0 (C-6), 25.8 (C-14), 28.9 (C-2), 30.4 (C-13), 37.3 (C-5), 38.2 (C-4), 47.7 (C-9), 54.6 (C-10), 70.8 (C-1), 77.9 (C-3), 101.5 (C-11), 140.4 (C-8), 156.2 (C-7), 178.9 (C-15), 195.2 (C-12); hreims (probe 180°C), *m/z* calcd. for $C_{15}H_{18}O_5$ ($M^+ - H_2O$): 278.1154; found: 278.1152 (100), 260 ($M^+ - 2H_2O$, 15), 250 (20), 249 ($M^+ - CHO$, 18), 234 ($M^+ - H_2O - CO_2$, 9), 232 ($M^+ - 2H_2O - CO$, 35), 206 (23), 188 (25), 187 (33), 186 (50), 181 (50), 171 (26), 164 (20), 162 (41), 159 (22), 157 (38), 151 (25), 143 (36), 135 (46), 133 (37), 119 (27), 117 (33), 107 (27), 105 (49), 98 (100), 91 (78), 79 (64), 77 (57), 72 (65), 71 (27), 69 (44), 67 (20), 65 (22), 55 (29), 53 (27); cims, *m/z*: 314 ($M^+ + 28$, 26).

11,12,14-Trihydroxydrimene (**23**) crystallized from ethyl acetate as needles, mp 178–180°C; $[\alpha]_D^{24}$ −10.7° (*c* 0.15, CH_3OH); Ftir (KBr disc): 3306 (br, OH) cm^{-1}; ^1H nmr ($CDCl_3$) δ: 0.76 (3H, s, H-15), 0.99 (3H, s, H-13), 1.12–1.28 (2H, m), 1.44 (1H, dd, *J* 12.8, 4.5 Hz, H-5), 1.47–1.56 (2H, m), 1.65 (1H, ddd, *J* 13.5, 4.9, 3.2 Hz), 1.95 (1H, ddd, *J* 12.8, 4.1, 2.1 Hz), 2.05 (1H, ddd, *J* 11.0, 4.9, 3.2 Hz), 2.12–2.21 (2H, m), 2.80 (2H, br s, OH), 3.49 (1H, br d, *J* 10.5 Hz, H-14), 3.68 (1H, dd, *J* 10.5, 8.0 Hz, H-11), 3.83 (1H, br d, *J* 10.5 Hz, H-14), 3.92 (1H, dd, *J* 10.5, 2.0 Hz, H-11), 4.00 (1H, d, *J* 12.0 Hz, H-12), 4.34 (1H, br d, *J* 12.0 Hz, H-12), 5.79 (1H, m, H-7); ^1H nmr (CD_3OD) δ: 0.79 (3H, s, H-15), 0.93 (1H, ddd, *J* 13.5, 13.5, 3.5 Hz), 0.95 (3H, s, H-13), 1.18 (1H, ddd, *J* 13.2, 13.2, 4.0 Hz), 1.37 (1H, dd, *J* 12.6, 4.5 Hz, H-5), 1.46 (1H, ddd, *J* 14.0, 4.5, 4.5 Hz), 1.56 (1H, ddddd, *J* 13.5, 13.5, 13.5, 3.0, 3.0 Hz, H-2β), 1.90 (1H, br d, *J* 14.0 Hz), 1.95–2.09 (3H, m), 2.14 (1H, br ddd, *J* 17, 4.5, 4.5 Hz, H-6), 3.38 (1H, d, *J* 11.0 Hz, H-14), 3.60 (1H, dd, *J* 11.0, 7.5 Hz, H-11), 3.78 (1H, d, *J* 11.0 Hz, H-14), 3.83 (1H, dd, *J* 11.1, 2.7 Hz, H-11), 3.95 (1H, d, *J* 12.6 Hz, H-12), 4.24 (1H, d, *J* 12.6 Hz, H-12), 5.76 (1H, m, H-7); ^{13}C nmr ($CDCl_3$) δ: 16.0 (C-15), 19.5 (C-2), 24.0 (C-6), 27.5 (C-13), 36.4 (C-1), 36.8 (C-3), 39.1 (C-10), 40.6 (C-4), 52.1 (C-5), 56.0 (C-9), 61.4 (C-11), 64.7 (C-14), 66.9 (C-12), 126.4 (C-7), 138.6 (C-8); hreims (probe 150°C), *m/z* calcd. for $C_{15}H_{26}O_3$ (M^+): 254.1883; found: 254.1884 (1), 236 ($M^+ - H_2O$, 5), 218 ($M^+ - 2H_2O$, 2), 188 (21), 173 (24), 163 (21), 119 (22), 109 (100), 93 (21), 91 (20), 81 (23), 55 (26); cims, *m/z*: 272 ($M^+ + 18$, 8).

3β-Hydroxycinnamolide (**29**) was obtained as an oil; ^1H nmr ($CDCl_3$) δ: 0.81 (3H, s), 0.92 (3H, s), 1.05 (3H, s), 3.32 (1H, dd, *J* 10.5, 5.5 Hz, H-3), 4.05 (1H, dd, *J* 9.0, 9.0 Hz, H-11), 4.39 (1H, dd, *J* 9.0, 9.0 Hz, H-11), 6.91 (1H, ddd, *J* 3.8, 3.8, 3.8 Hz, H-7); lrms (probe 170°C), 232 ($M^+ - H_2O$, 20), 217 (17), 172 (30), 125 (20), 122 (100), 96 (84).

Growth of Marasmius oreades *on malt extract broth and isolation of metabolites*

Twenty 2.8-L Fernbach flasks each containing 1 L of malt extract liquid medium (20 g glucose, 20 g malt extract broth (Difco Laboratories, Detroit, Michigan, USA), 1 g peptone, 1 L water) were inoculated with ca. 10 mL of a mycelial suspension of *Marasmius oreades* (UAMH 5750) (3) and the still cultures were kept at room temperature (20–25°C) for 7 weeks.

The mycelium was separated by filtration through cheesecloth and air-dried for 72 h before being ground to a coarse powder (39.8 g). The filtered broth was concentrated to 1.8 L at reduced pressure (waterbath 40–45°C) and the concentrate was stirred for 12-h periods with three successive 1.5-L volumes of ethyl acetate. The combined ethyl acetate extracts were dried with magnesium sulfate and then evaporated at reduced pressure to give a brown foam (1.495 g). The foam was adsorbed onto silica gel (10 g) and then loaded onto a column of silica gel (150 g) that had been packed with ethyl acetate – Skellysolve B (1:2). Fractions of 25 mL were collected, eluting successively with 1:2 (fractions 1–24), 1:1 (fractions 25–53), 2:1 (fractions 54–81) ethyl acetate – Skellysolve B, and ethyl acetate (fractions 82–100). Each fraction was examined by tlc (ethyl acetate – Skellysolve B, 2:1) and those fractions with similar components were combined.

Fractions 8–10 (6.0 mg) were combined and chromatographed on a column of silica gel (ethyl acetate – Skellysolve B, 1:10) to give *marasmene* (**7**).

Fractions 36–43 (26.4 mg) were combined and chromatographed on a column of silica gel (ethyl acetate – dichloromethane, 1:2) and then the fractions rich in **19***a* were combined and subjected to preparative tlc (methanol–dichloromethane, 1:40, several developments) to give *13-hydroxymarasmene* (**19***a*, 3.1 mg). Fractions enriched in lactol **26** were combined and chromatographed over silica gel (methanol–dichloromethane, 1:20) to give pure lactol **26** (1.2 mg). Fractions enriched in diol **31***a* were combined and chromatographed on silica gel (methanol–dichloromethane, 1:20) to give diol **31***a* (1.5 mg).

The ethyl acetate soluble material from fractions 44–63 (0.15 g) was chromatographed on a column of silica gel (methanol–dichloromethane 1:20) to give successively **18***a* (6.0 mg), **19***b* (5.4 mg), and an oil, which was separated by chromatography on a column of silica gel (ethyl acetate – Skellysolve B, 1:1) into *1α,15-dihydroxymarasmene* (**13***a*, 7 mg) and *3α,15-dihydroxymarasmene* (**6***a*, 15 mg).

The ethyl acetate soluble material from fractions 64–75 (0.06 g) was chromatographed on a column of silica gel (methanol–dichloromethane, 1:20) to give successively **6***a* (7 mg) and fractions containing

Can. J. Chem. Downloaded from www.nrcresearchpress.com by 194.225.253.170 on 09/07/12
For personal use only.

Can. J. Chem. Downloaded from www.nrcresearchpress.com by 194.225.253.170 on 09/07/12
For personal use only.

3α-hydroxyoreadone (**15***c*) and *11,12,14-trihydroxydrimene* (**23**), which were combined and crystallized from dichloromethane to give pure **23** (4 mg). The mother liquors were chromatographed on silica gel to give pure **15***c* (4.3 mg).

The material that deposited from ethyl acetate solutions of fractions 44–63 and 64–75 was recrystallized from ethyl acetate to give *agrocybin* (**5**) as a heat- and light-sensitive off-white solid (0.294 g), mp 133–140°C (dec.) (lit. (11) mp 133°C (dec.)); Ftir (KBr disc): 3275 (br), 3105 (br), 2206 (s, C≡C), 1679 (s, C=O), 1625 (s, NH bend) cm^{-1}; ^1H nmr (CD_3OD) δ: 4.26 (s, CH_2OH); ^{13}C nmr (CD_3OD) δ: 51.0 (t, CH_2OH), 61.2 (s), 67.6 (s), 68.9 (s), 69.9 (s), 70.5 (s), 81.9 (s), 155.3 (s, C=O); hreims (probe 150°C), *m/z* calcd. for $C_8H_5NO_2$ (M^+): 147.0319; found: 147.0319 (100), 131 ($M^+ - NH_2$, 11), 118 (93), 91 (36), 86 (21), 85 (20), 75 (44), 74 (43), 73 (22), 65 (47).

Fractions 76–91 (84 mg) were combined and chromatographed on a column of silica gel (ethyl acetate – Skellysolve B, 2:1) to give several fractions rich in *3,11,12-trihydroxydrimene* (**22**), which were combined and further chromatographed (5% methanol–dichloromethane) to give pure **22** (14.5 mg).

Marasmene (**7**) crystallized, on standing, as needles, mp 70–74°C; $[\alpha]_D^{24}$ +57° (*c* 0.07, CH_3OH); Ftir ($CHCl_3$ cast): 1380, 1360 (m, *gem* dimethyl), 1280, 1225 (s, C—O) cm^{-1}; ^1H nmr ($CDCl_3$) δ: 0.71 (3H, s, H-14), 0.91 (3H, s, H-13), 1.16 (1H, dddd, *J* 13.0, 13.0, 4.8, 2.0 Hz, H-1α), 1.29 (1H, br, ddd, *J* 13.5, 13.5, 5.2 Hz), 1.43–1.62 (1H, m), 1.77 (1H, dd, *J* 11.4, 6.8 Hz, H-5), 1.89 (1H, br d, *J* 13.5 Hz), 1.94–2.07 (1H, m, H-6), 2.29 (1H, br d, *J* 19 Hz, H-6), 2.58 (1H, m, H-9), 3.68 (1H, d, *J* 8.0 Hz, H-15α), 3.73 (1H, dd, *J* 8.0, 2.1 Hz, H-15β), 4.30–4.40 (2H, m, H-12), 5.65 (1H, d, *J* 4.5 Hz, H-11), 5.78 (1H, m, H-7); ^{13}C nmr ($CDCl_3$) δ: 19.1 (C-2), 20.7 (C-14), 23.6 (C-6), 31.1 (C-13), 33.2 (C-4), 36.2 (C-1), 42.3 (C-3), 43.7 (C-10), 45.0 (C-5), 55.7 (C-9), 69.4 (C-15), 72.3 (C-12), 105.8 (C-11), 121.4 (C-7), 133.4 (C-8); hreims (probe 100°C), *m/z* calcd. for $C_{15}H_{22}O_2$ (M^+): 234.1620; found: 234.1624 (34), 204 (41), 188 (22), 177 (25), 175 (27), 173 (23), 151 (21), 145 (42), 133 (24), 132 (38), 131 (24), 119 (69), 118 (32), 117 (29), 109 (66), 107 (30), 106 (28), 105 (100), 104 (43), 96 (51), 95 (41), 93 (30), 92 (25), 91 (73), 82 (32), 81 (25), 79 (37), 77 (36), 69 (48), 67 (41), 65 (23), 55 (44), 53 (26); cims, *m/z*: 252 (M^+ + 18, 26).

Lactol **26** was obtained as a clear oil; Ftir ($CHCl_3$ cast): 3395 (br, OH), 1717 (w), 1385, 1366 (m, *gem* dimethyl) cm^{-1}; ^1H nmr ($CDCl_3$) δ: 0.80 (3H, m, H-13), 0.99 (3H, s, H-15), 1.18 (1H, br s, OH), 1.30 (1H, ddd, *J* 13.0, 13.0, 4.4 Hz), 1.45–1.54 (2H, m), 1.50 (1H, dd, *J* 11.5, 5.1 Hz, H-5), 1.83 (1H, ddd, *J* 13.0, 5.2, 2.0 Hz), 1.91 (1H, ddd, *J* 13.7, 5.2, 2.0 Hz), 1.98 (1H, br d, *J* 13.5 Hz), 2.17–2.25 (2H, m, H-6, H-9), 2.60–2.90 (1H, br m, OH), 3.56 (1H, d, *J* 10.7 Hz, H-14), 3.85 (1H, d, *J* 10.8 Hz, H-14), 4.17 (1H, ddd, *J* 11.4, 1.4, 1.4 Hz, H-12), 4.47 (1H, br d, *J* 11.4 Hz, H-12), 5.26 (1H, d, *J* 4.3 Hz, H-11), 5.49 (1H, m, H-7); ^{13}C nmr ($CDCl_3$) δ: 15.0 (C-15), 18.1 (C-2), 23.2 (C-6), 26.6 (C-13), 33.4, 35.8 (C-1, C-3), 38.0, 39.0 (C-4, C-10), 50.8 (C-5), 61.8 (C-9), 64.8 (C-14), 69.0 (C-12), 99.4 (C-11), 117.0 (C-7), 136.6 (C-8); hreims (probe 150°C), *m/z* calcd. for $C_{15}H_{24}O_3$ (M^+): 252.1726; found: 252.1729 (9), 234 ($M^+ - H_2O$, 4), 188 (54), 175 (100), 173 (33), 163 (76), 159 (61), 145 (28), 133 (29), 132 (37), 123 (25), 122 (21), 120 (23), 119 (73), 118 (49), 117 (22), 109 (76), 107 (58), 106 (27), 105 (76), 95 (34), 93 (54), 91 (65), 81 (56), 79 (44), 77 (33), 69 (35), 67 (42), 57 (22), 55 (68), 53 (25).

3β,11-Dihydroxydrimene (**31***a*) was obtained as an oil containing small amounts of inseparable impurities; ^1H nmr ($CDCl_3$) δ: 0.86 (3H, s), 0.87 (3H, s), 0.98 (3H, s), 1.1–1.4 (m), 1.6–1.7 (m), 1.78 (3H, br s, H-12), 1.90–2.08 (4H, m), 3.26 (1H, dd, *J* 10.5, 5.4 Hz, H-3), 3.75 (1H, dd, *J* 11.5, 5.0 Hz, H-11), 3.86 (1H, dd, *J* 11.1, 3.4 Hz, H-11), 5.54 (1H, m, H-7); hreims (probe 150°C), *m/z* calcd. for $C_{15}H_{26}O_2$ (M^+): 238.1932; found: 238.1934 (22), 220 ($M^+ - H_2O$, 14), 189 (21), 139 (21), 123 (29), 122 (58), 121 (25), 119 (51), 107 (36), 105 (21), 98 (33), 96 (100), 93 (21), 91 (22), 81 (27), 69 (34), 55 (32). Acetylation of the impure **31***a* with acetic anhydride in pyridine and column chromatography (9% ethyl acetate – Skellysolve B) of the product gave the diacetate **31***b* (0.8 mg) as a clear oil; ^1H nmr ($CDCl_3$) δ: 0.84 (3H, s, H-15), 0.86 (3H, s, H-13), 0.98 (3H, s, H-14), 1.30 (1H, dd, *J* 10.5, 6.2 Hz, H-5), 1.34 (1H, br ddd, *J* 13.2, 13.2, 4.8 Hz, H-1α), 1.60–1.72 (2H, m), 1.67 (3H, br s, H-12), 1.95–2.09 (4H, m), 2.04 (3H, s, OAc), 2.05 (3H, s, OAc), 4.11 (1H, dd, *J* 11.7, 6.5 Hz, H-11), 4.21 (1H, dd, *J* 11.5, 3.8 Hz, H-11), 4.51 (1H, dd, *J* 11.5, 4.8 Hz, H-3), 5.50 (1H, m, H-7); hreims (probe 150°C), *m/z* calcd. for $C_{17}H_{26}O_2$ (M^+ − HOAc): 262.1933; found: 262.1931 (70), 202 (82), 187 (100), 160 (22), 159 (63), 146 (20), 135 (24), 133 (42), 131 (20), 119 (41), 108 (28), 107 (38), 105 (25), 91 (23), 55 (20).

3,11,12-Trihydroxydrimene (**22**) crystallized from ethyl acetate – Skellysolve B as prisms, mp 164–165°C; $[\alpha]_D^{24}$ −10.7° (*c* 0.15, CH_3OH) (lit. (7) mp 165–166°C; $[\alpha]_D^{20}$ −10.9°); Ftir (KBr disc): 3327 (br, OH) cm^{-1}; ^1H nmr ($CDCl_3$) δ: 0.78 (3H, s, H-14), 0.87 (3H, s, H-15), 1.00 (3H, s, H-13), 1.29 (1H, dd, *J* 12.0, 4.5 Hz, H-5), 1.32–1.42 (2H, m), 1.65 (1H, ddd, *J* 13.0, 3.6, 1.8 Hz), 1.70 (1H, ddd, *J* 12.8, 4.5, 4.5 Hz), 2.04 (1H, ddd, *J* 13.5, 3.5, 3.5 Hz), 1.94–2.05 (1H, m), 2.08 (1H, ddd, *J* 5.3, 5.3, 2.0 Hz), 2.13–2.18 (1H, m), 2.80 (2H, br s, OH), 3.26 (1H, br dd, *J* 11.0, 3.5 Hz, H-3), 3.69 (1H, dd, *J* 10.6, 8.2 Hz, H-11), 3.91 (1H, dd, *J* 10.7, 2.0 Hz, H-11), 4.01 (1H, br d, *J* 12.0 Hz, H-12), 4.35 (1H, br d, *J* 12.0 Hz, H-12), 5.82 (1H, m, H-7); ^1H nmr (CD_3OD) δ: 0.81 (3H, s, H-14), 0.86 (3H, s, H-15), 0.98 (3H, s, H-13), 1.20–1.40 (2H, m), 1.60–1.75 (2H, m), 2.00–2.20 (4H, m), 3.20 (1H, dd, *J* 10.5, 5.5 Hz, H-3), 3.63 (1H, dd, *J* 11.0, 7.4 Hz, H-11), 3.84 (1H, dd, *J* 11.0, 2.5 Hz, H-11), 3.96 (1H, d, *J* 12.4 Hz, H-12), 4.25 (1H, dd, *J* 12.4 Hz, H-12), 5.80 (1H, m, H-7); ^{13}C nmr ($CDCl_3$) δ: 15.0 (C-14), 15.9 (C-15), 24.3 (C-6), 28.1 (C-2), 28.6 (C-13), 36.6 (C-1), 38.9 (C-10), 39.8 (C-4), 50.7 (C-5), 55.8 (C-9), 61.2 (C-11), 66.8 (C-12), 79.6 (C-3), 126.4 (C-7), 138.5 (C-8); hreims (probe 150°C), *m/z* calcd. for $C_{15}H_{26}O_3$ (M^+): 254.1883; found: 254.1883 (10), 236 ($M^+ - H_2O$, 4), 218 ($M^+ - 2H_2O$, 4), 188 (100), 173 (48), 122 (24), 119 (25), 107 (25), 105 (28), 96 (63), 55 (24); cims, *m/z*: 272 (M^+ + 18, 100).

Acetylation of 3α,15-dihydroxymarasmene (**6**a)

Treatment of 3α,15-dihydroxymarasmene (**6***a*, 20 mg) with acetic anhydride (0.10 mL) in pyridine (0.10 mL) for 10 h, followed by addition of benzene (4 mL) and removal of the solvents, gave an oil, which was chromatographed on a column of silica gel. Elution with ethyl acetate – Skellysolve B (1:4) gave first aldehyde **9** (6.7 mg), then **6***b* (7 mg). Aldehyde **9** crystallized from Skellysolve B as prisms, mp 136–137°C; $[\alpha]_D^{24}$ −41.5° (*c* 0.33, CH_3OH); Ftir ($CHCl_3$ cast): 1742 (OAc), 1731 (OAc), 1714 (CHO) cm^{-1}; ^1H nmr ($CDCl_3$) δ: 0.85 (3H, s, H-14), 0.94 (3H, s, H-13), 1.27 (1H, dddd, *J* 14.5, 14.0, 4.1, 1.6 Hz, H-1α), 1.65 (1H, ddd, *J* 15.5, 4.5, 3.0 Hz, H-1β), 1.82 (1H, dddd, *J* 15.5, 14.3, 4.1, 2.5 Hz, H-2β), 2.07 (3H, s, OAc), 2.08 (3H, s, OAc), 2.17 (1H, ddd, *J* 13.5, 4.1, 3.0 Hz, H-2α), 2.30 (1H, dd, *J* 9.0, 9.0 Hz, H-5), 2.41–2.48 (2H, m, H-6), 2.83 (1H, m, H-9), 4.31 (1H, ddd, *J* 11.3, 1.4, 1.4 Hz, H-12), 4.46 (1H, dddd, *J* 11.2, 2.0, 2.0, 2.0 Hz, H-12), 4.73 (1H, dd, *J* 2.8, 2.8 Hz, H-3), 5.78 (1H, m, H-7), 5.91 (1H, d, *J* 4.2 Hz, H-11), 9.80 (1H, d, *J* 1.8 Hz, H-15); ^{13}C nmr ($CDCl_3$) δ: 20.4 (C-14), 21.18 (OAc), 21.24 (OAc), 22.8 (C-6), 22.9 (C-13), 25.7 (C-2), 26.1 (C-1), 36.8 (C-4), 43.4 (C-5), 47.0 (C-10), 55.6 (C-9), 70.0 (C-12), 77.6 (C-3), 97.7 (C-11), 118.2 (C-7), 134.5 (C-8), 169.8 (OAc), 170.3 (OAc), 205.2 (C-15); hreims (probe 130°C), M^+ not detected, *m/z* calcd. for $C_{17}H_{22}O_4$ (M^+ − HOAc): 290.1518; found: 290.1516 (26), 261 (M^+ − HOAc − CHO, 8), 202 (23), 201 (100), 173 (20); cims, *m/z*: 368 (M^+ + 18, 2). *3α,15-Diacetoxymarasmene* (**6***b*) was obtained as an oil; Ftir ($CHCl_3$ cast): 1734 (OAc) cm^{-1}; ^1H nmr ($CDCl_3$) δ: 0.81 (3H, s, H-14), 0.93 (3H, s, H-13), 1.16–1.22 (1H, m), 1.70 (1H, ddd, *J* 14.0, 7.0, 2.5 Hz), 2.03–2.12 (2H, m), 2.09 (6H, s, OAc), 2.16 (1H, ddd, *J* 14.0, 4.5, 2.5 Hz), 2.20–2.28 (1H, m), 2.30 (1H, dd, *J* 13.1, 5.5 Hz, H-5), 2.71 (1H, m, H-9), 4.36–4.43 (2H, m, H-12), 4.75 (1H, dd, *J* 2.5, 2.5 Hz, H-3), 5.75 (1H, d, *J* 4.0 Hz, H-11), 5.94 (1H, m, H-7), 6.08 (1H, s, H-15); ^{13}C nmr ($CDCl_3$) δ: 14.2 (C-14), 19.3 (OAc), 21.3 (OAc), 22.6 (C-2), 24.2 (C-6), 26.6 (C-13), 27.8 (C-1), 36.0 (C-4), 39.2 (C-5), 44.0 (C-10), 57.4 (C-9), 71.6 (C-12), 77.6 (C-3), 96.7 (C-15), 104.0 (C-11), 122.6 (C-7), 133.6 (C-8),

Can. J. Chem. Downloaded from www.nrcresearchpress.com by 194.225.253.170 on 09/07/12
For personal use only.

169.6 (OAc), 170.5 (OAc); hreims (probe 130°C), M^+ not detected, m/z calcd. for $C_{17}H_{23}O_5$ ($M^+ - CH_3CO$): 307.1545; found: 307.1548 (11), 290 (M^+ − HOAc, 4), 262 (16), 201 (41), 173 (23), 172 (31), 105 (21), 91 (26), 71 (100); cims, m/z: 368 ($M^+ + 18$, 12).

*Acetylation of 15-hydroxymarasmen-3-one (**11**a)*

Compound **11***a* (6.0 mg) was treated with acetic anhydride (0.05 mL) in pyridine (0.02 mL) at room temperature for 1 h and then benzene (4 mL) was added and the mixture was evaporated to dryness. Column chromatography, eluting with ethyl acetate – Skellysolve B (1:2), gave successively aldehyde **12***b* (0.6 mg) and acetate **11***b* (2.8 mg). Aldehyde **12***b* was obtained as an oil; Ftir ($CHCl_3$ cast): 1745 (sh, acetate C=O), 1708 (s, aldehyde C=O) cm^{-1}; ^1H nmr ($CDCl_3$) δ: 1.01 (3H, s, H-14), 1.13 (3H, s, H-13), 1.36 (1H, dddd, *J* 13.8, 13.8, 4.6, 1.9 Hz, H-1α), 2.07 (3H, s, OAc), 2.16 (1H, dd, *J* 11.5, 6.6 Hz, H-5), 2.28 (1H, ddd, *J* 14.2, 4.7, 2.8 Hz, H-2α), 2.44–2.61 (2H, m, H-6), 2.66 (1H, ddd, *J* 13.8, 5.9, 2.9 Hz, H-1β), 2.77 (1H, ddd, *J* 14.2, 14.2, 5.9 Hz, H-2β), 2.78 (1H, m, H-9), 4.36 (1H, dddd, *J* 11.6, 1.5, 1.5, 1.5 Hz, H-12), 4.48 (1H, dddd, *J* 11.6, 1.9, 1.9, 1.9 Hz, H-12), 5.84 (1H, m, H-7), 5.97 (1H, d, *J* 4.0 Hz, H-11), 9.93 (1H, d, *J* 2.0 Hz, H-15); hreims (probe 120°C), m/z calcd. for $C_{15}H_{18}O_3$ (M^+ − HOAc): 246.1257; found: 246.1257 (43), 218 (28), 217 (M^+ − HOAc − CHO, 100), 175 (28), 132 (65), 119 (24), 117 (20), 105 (36), 91 (45), 77 (23), 55 (24). *15-Acetoxymarasmen-3-one* (**11***b*) crystallized from dichloromethane – ethyl acetate – Skellysolve B as long thin flakes, mp 168–171°C; $[\alpha]_D^{24}$ +15.1° (*c* 0.35, CH_3OH); Ftir ($CHCl_3$ cast): 1752 (s, acetate C=O), 1706 (s, ketone C=O), 1384, 1370 (m, *gem* dimethyl) cm^{-1}; ^1H nmr ($CDCl_3$) δ: 0.98 (3H, s, H-14), 1.13 (3H, s, H-13), 1.72 (1H, ddd, *J* 14.0, 14.0, 5.5 Hz, H-1α), 2.13 (3H, s, OAc), 2.19 (1H, dd, *J* 9.9, 7.5 Hz, H-5), 2.32–2.41 (3H, m, H-1β, H-6), 2.60 (1H, ddd, *J* 13.9, 6.6, 2.5 Hz, H-2α), 2.72 (1H, m, H-9), 3.06 (1H, ddd, *J* 14.8, 14.0, 6.6 Hz, H-2β), 4.43 (1H, dddd, *J* 11.0, 1.4, 1.4, 1.4 Hz, H-12), 4.49 (1H, dddd, *J* 11.0, 1.4, 1.4, 1.4 Hz, H-12), 5.82 (1H, d, *J* 4.0 Hz, H-11), 5.88 (1H, m, H-7), 6.25 (1H, s, H-15); ^{13}C nmr ($CDCl_3$) δ: 19.3 (C-14), 21.2 (OAc), 23.3 (C-6), 23.4 (C-13), 33.5 (C-2), 35.7 (C-1), 43.8 (C-10), 45.6 (C-5), 47.3 (C-4), 57.1 (C-9), 71.5 (C-12), 96.4 (C-15), 104.1 (C-11), 121.9 (C-7), 133.3 (C-8), 169.4 (OAc), 214.3 (C-3); hreims (probe 200°C), m/z calcd. for $C_{15}H_{18}O_3$ (M^+ − HOAc): 246.1256; found: 246.1261 (14), 218 (M^+ − HOAc − CO, 16), 132 (100), 119 (23); cims, m/z: 324 ($M^+ + 18$, 14).

*Oxidation of 3α,15-dihydroxymarasmene (**6**a)*

(i) With excess pyridinium dichromate. A suspension of 3α,15-dihydroxymarasmene (**6***a*, 7.4 mg) and pyridinium dichromate (50 mg) in dichloromethane (2 mL) was stirred at room temperature for 12 h and then diluted with ether and filtered to remove precipitated chromium complexes. The filtrate was evaporated to give an oil, which was chromatographed on a column of silica gel, eluting with ethyl acetate – Skellysolve B (1:2), to give marasmene-3,15-dione (**8**, 2.5 mg), which crystallized from ethyl acetate – Skellysolve B as prisms, mp 166–167°C; $[\alpha]_D^{24}$ −18.9° (*c* 0.18, CH_3OH); cd (*c* 6.68 mM, CH_3OH), 24°C: $[\theta]_{294}$ −1800, $[\theta]_{226}$ −800; Ftir ($CHCl_3$ cast): 1761 (s, lactone C=O), 1707 (s, ketone C=O) cm^{-1}; ^1H nmr ($CDCl_3$) δ: 1.20 (3H, s, H-13), 1.46 (3H, s, H-14), 2.01 (1H, ddd, *J* 13.5, 13.5, 4.2 Hz, H-1α), 2.14 (1H, dd, *J* 11.8, 5.8 Hz, H-5), 2.30–2.56 (4H, m, H-1β, H-2α, H-6), 2.98 (1H, m, H-9), 3.04 (1H, ddd, *J* 14.5, 14.5, 5.0 Hz, H-2β), 4.52–4.62 (2H, m, H-12), 6.02 (1H, d, *J* 4.5 Hz, H-11), 6.05 (1H, m, H-7); ^{13}C nmr ($CDCl_3$) δ: 21.9, 24.7 (C-13, C-14), 24.4 (C-6), 33.5, 34.4 (C-1, C-2), 45.8 (C-5), 47.5, 48.8 (C-4, C-10), 53.3 (C-9), 72.7 (C-12), 103.9 (C-11), 126.2 (C-7), 131.4 (C-8), 174.3 (C-15), 213.6 (C-3); hreims (probe 140°C), m/z calcd. for $C_{15}H_{18}O_4$ (M^+): 262.1205; found: 262.1208 (44), 262 (67), 234 (M^+ − CO, 13), 132 (100), 120 (21), 119 (34), 105 (22), 91 (31), 77 (20), 67 (21).

(ii) With 1 equivalent of pyridinium dichromate. A suspension of **6***a* (20 mg, 0.075 mmol) and pyridinium dichromate (30 mg, 0.08 mmol) in dichloromethane (5 mL) was stirred at room temperature for 18 h and then diluted with ether and filtered through a short column of silica gel to remove precipitated chromium complexes. The column was washed with ether and the combined filtrates were evaporated to give an oil, which was chromatographed over silica gel. Elution with ethyl acetate – Skellysolve B (1:2) gave successively marasmene-3,15-dione (**8**, 2.7 mg), an oil (7.8 mg) that was a mixture of **10***b* and **11***a*, and unreacted **6***a* (4.0 mg).

The mixture of **10***b* and **11***a* was acetylated with acetic anhydride (0.10 mL) and pyridine (0.10 mL) at room temperature for 2 h, and the resulting oil was chromatographed on silica gel, eluting with ethyl acetate – Skellysolve B (1:3), to give first **10***c* (3.1 mg), then **11***b* (3.8 mg). Compound **10***c* crystallized from dichloromethane – ethyl acetate – Skellysolve B as blades, sublimes from 167–205°C to give prisms, mp 220.5–221°C; Ftir ($CHCl_3$ cast): 1774 (s, lactone C=O), 1717 (s, acetate C=O) cm^{-1}; ^1H nmr ($CDCl_3$) δ: 0.97 (3H, s, H-13), 1.31 (3H, s, H-14), 1.75 (1H, ddd, *J* 13.8, 3.5, 2.9 Hz, H-2α), 1.85 (1H, br ddd, *J* 13.7, 3.8, 3.8 Hz, H-1β), 1.94 (1H, ddd, *J* 13.5, 13.5, 2.8 Hz, H-1α), 2.04 (1H, dddd, *J* 13.6, 13.6, 3.9, 1.8 Hz, H-2β), 2.09 (3H, s, OAc), 2.14 (1H, dd, *J* 9.8, 8.5 Hz, H-5), 2.23–2.30 (2H, m, H-6), 2.90 (1H, m, H-9), 4.48 (1H, dddd, *J* 10.4, 1.4, 1.4, 1.4 Hz, H-12), 4.53 (1H, dddd, *J* 10.5, 1.4, 1.4, 1.4 Hz, H-12), 4.83 (1H, dd, *J* 3.9, 1.8 Hz, H-3), 5.94 (1H, d, *J* 4.5 Hz, H-11), 5.98 (1H, m, H-7); ^{13}C nmr ($CDCl_3$) δ: 21.2 (C-14), 21.9 (OAc), 22.5 (C-2), 23.7 (C-6), 27.2 (C-13), 28.1 (C-1), 36.0 (C-4), 39.6 (C-5), 48.6 (C-10), 53.9 (C-9), 72.6 (C-12), 77.6 (C-3), 103.5 (C-11), 126.3 (C-7), 131.6 (C-8), 170.3 (OAc), 171.4 (C-15); hreims (probe 100°C), m/z calcd. for $C_{17}H_{22}O_5$ (M^+): 306.1467; found: 306.1439 (0.3); m/z calcd. for $C_{16}H_{22}O_3$ ($M^+ - CO_2$): 262.1569; found: 262.1571 (76), 202 (41), 173 (35), 172 (100), 157 (36), 145 (26), 143 (23), 132 (48), 131 (23), 129 (25), 119 (39), 105 (39), 104 (22), 91 (28), 69 (24); cims, m/z: 324 ($M^+ + 18$, 100).

*Oxidation of 1α,15-dihydroxymarasmene (**13**a)*

(i) With excess pyridinium dichromate. A suspension of **13***a* (5.6 mg) and pyridinium dichromate (50 mg) in dichloromethane (2 mL) was stirred at room temperature for 18 h and then diluted with ether and filtered. The filtrate was evaporated to give an oil, which was chromatographed on silica gel, eluting with ethyl acetate – Skellysolve B (1:4), to give marasmene-1,15-dione (**14**, 2.7 mg), which crystallized from dichloromethane – Skellysolve B as prisms, mp 110.5–111.5°C; $[\alpha]_D^{24}$ +70.8° (*c* 0.26, CH_3OH); cd (*c* 9.92 mM, CH_3OH), 24°C: $[\theta]_{308}$ +7300, $[\theta]_{299}$ −7800, $[\theta]_{219}$ −2800; Ftir ($CHCl_3$ cast): 1767 (s, lactone C=O), 1713 (s, ketone C=O) cm^{-1}; ^1H nmr ($CDCl_3$) δ: 1.04 (3H, s, H-13), 1.43 (3H, s, H-14), 1.71 (1H, ddd, *J* 14.2, 14.2, 3.5 Hz, H-3α), 1.92 (1H, ddd, *J* 14.0, 5.1, 3.8 Hz, H-3β), 2.02 (1H, dd, *J* 11.3, 6.0 Hz, H-5), 2.28–2.48 (2H, m, H-6), 2.36 (1H, ddd, *J* 14.0, 3.8, 3.8 Hz, H-2α), 2.89 (1H, ddd, *J* 14.5, 14.5, 5.1 Hz, H-2β), 3.35 (1H, m, H-9), 4.43 (1H, ddd, *J* 10.5, 1.2, 1.2 Hz, H-12), 4.52 (1H, br d, *J* 10.5 Hz, H-12), 5.93 (1H, m, H-7), 6.12 (1H, d, *J* 4.5 Hz, H-11); ^{13}C nmr ($CDCl_3$) δ: 21.5, 31.4 (C-13, C-14), 25.4 (C-6), 32.7, 36.5 (C-2, C-3), 41.4 (C-4), 47.9 (C-5), 48.8 (C-9), 64.7 (C-10), 72.3 (C-12), 105.4 (C-11), 126.0 (C-7), 131.3 (C-8), 169.3 (C-15), 205.5 (C-1); hreims (probe 150°C), m/z calcd. for $C_{15}H_{18}O_4$ (M^+): 262.1205; found: 262.1211 (44), 234 (M^+ − CO, 4), 218 ($M^+ - CO_2$, 100), 176 (55), 161 (29), 134 (26), 120 (39), 119 (27), 91 (39), 77 (21).

(ii) With 1 equivalent of pyridinium dichromate. A suspension of **13***a* (20 mg, 0.075 mmol) and pyridinium dichromate (30 mg, 0.08 mmol) in dichloromethane (5 mL) was stirred at room temperature for 18 h and then diluted with ether and filtered through a short column of silica gel to remove precipitated chromium complexes. The column was washed with ether and the combined filtrates were evaporated to give an oil, which was chromatographed on a column of silica gel. Elution with ethyl acetate – Skellysolve B (1:2) gave successively a mixture of **14** and **15***a* (4.4 mg, approx. 6:4 by ^1H nmr spectrum), **13***b* (1.7 mg), impure 15-hydroxymarasmen-1-one (1.6 mg), and unreacted **13***a* (2.1 mg). The mixture of **14** and **15***a* was separated by column chromatography, eluting with ethyl acetate – Skellysolve B (1:10), to give marasmene-1,15-dione (**14**) (2.6 mg) and *O*-formyloreadone (**15***a*) (0.8 mg). Compound **13***b* was obtained as an oil; Ftir ($CHCl_3$ cast): 3430 (br, OH), 1769 (s, lactone C=O) cm^{-1}; ^1H nmr ($CDCl_3$) δ: 1.01 (3H, s, H-13), 1.25 (3H, s, H-14), 1.35 (1H, ddd, *J* 13.9, 3.6,

Can. J. Chem. Downloaded from www.nrcresearchpress.com by 194.225.253.170 on 09/07/12
For personal use only.

3.6 Hz, H-3β), 1.63–1.70 (1H, m), 1.75 (1H, ddd, *J* 13.9, 13.9, 3.5 Hz, H-3α), 2.02 (1H, dd, *J* 11.4, 6.3 Hz, H-5), 2.07 (1H, dddd, *J* 13.9, 13.9, 3.6, 2.2 Hz, H-2β), 2.16–2.40 (2H, m, H-6), 3.54 (1H, m, H-9), 3.96 (1H, br s, H-1), 4.47 (1H, ddd, *J* 10.6, 1.4, 1.4 Hz, H-12), 4.55 (1H, br d, *J* 10.6 Hz, H-12), 5.91 (1H, m, H-7), 5.96 (1H, d, *J* 4.5 Hz, H-11); ^{13}C nmr ($CDCl_3$) δ: 21.9, 24.3, 26.3, 32.4, 32.7, 33.7, 38.9, 48.2, 67.3 (C-1), 72.7 (C-12), 103.7 (C-11), 125.6 (C-7), 131.7 (C-8), 173.9 (C-15) (one signal obscured); hreims (probe 150°C), *m/z* calcd. for $C_{15}H_{20}O_4$ (M^+): 264.1362; found: 264.1363 (72), 220 (100), 202 (23), 201 (22), 190 (91), 187 (20), 174 (51), 173 (31), 164 (75), 159 (34), 157 (34), 151 (28), 149 (29), 146 (45), 145 (36), 133 (24), 132 (27), 131 (37), 129 (33), 121 (41), 120 (32), 119 (74), 118 (74), 117 (60), 115 (24), 105 (63), 104 (23), 95 (21), 93 (53), 92 (29), 91 (99), 81 (46), 79 (39), 77 (52).

Reduction of anhydromarasmone (2)

Triethylsilane (10 μL of a 0.6 mol L^{-1} solution in carbon tetrachloride) was added to a stirred solution of anhydromarasmone (**2**, 1.1 mg) in trifluoroacetic acid (0.2 mL). The yellow solution was stirred at room temperature for 5 h, then a further 10 μL of the triethylsilane solution was added and stirring continued for a further 12 h. The mixture was diluted with dichloromethane (1 mL), and saturated aqueous sodium hydrogen carbonate (0.5 mL) was added. The dichloromethane layer was separated, dried with magnesium sulfate, and evaporated to give an oil, which was chromatographed on silica gel. Elution with ethyl acetate – Skellysolve B (1:10) gave marasmene-1,15-dione (**14**) as an oil, identical (^{1}H nmr, tlc) with that prepared by oxidation of **13***a*.

Reduction of marasmene-3,15-dione (8)

Sodium borohydride (1.0 mg) was added to a solution of **8** (4.5 mg) in methanol (0.5 mL) and the mixture was stirred at room temperature for 15 min, then 1 M hydrochloric acid (0.1 mL) was added. The solution was diluted with ethyl acetate, dried with magnesium sulfate, and evaporated to give an oil, which was chromatographed on silica gel. Elution with ethyl acetate – Skellysolve B (1:1) gave **10***a* (3.8 mg), which crystallized from dichloromethane – ethyl acetate – Skellysolve B as prisms, mp 202.5–203.5°C; Ftir ($CHCl_3$ cast): 3483 (br, OH), 1753 (s, lactone C=O) cm^{-1}; ^{1}H nmr ($CDCl_3$) δ: 1.10 (3H, s, H-13), 1.18 (3H, s, H-14), 1.48 (1H, br d, *J* 5.4 Hz, OH, D_2O exchangeable), 1.64 (1H, dd, *J* 13.5, 3.5 Hz, H-5), 1.68–1.76 (2H, m), 1.79 (1H, dddd, *J* 13.4, 13.4, 2.5, 2.5 Hz, H-2β), 2.13 (1H, ddd, *J* 13.6, 3.2, 3.2 Hz, H-1β), 2.30–2.36 (2H, m, H-6), 2.80 (1H, m, H-9), 3.35 (1H, br d, *J* 10.5 Hz, H-3, collapsed to a dd, *J* 11.4, 3.9 Hz upon addition of D_2O), 4.47 (1H, ddd, *J* 10.6, 1.2, 1.2 Hz, H-12), 4.52 (1H, br d, *J* 10.7 Hz, H-12), 5.93 (1H, d, *J* 4.3 Hz, H-11), 5.97 (1H, m, H-7); ^{13}C nmr ($CDCl_3$) δ: 14.5 (C-14), 24.0 (C-6), 27.0 (C-2), 27.7 (C-13), 33.4 (C-1), 38.8 (C-4), 44.6 (C-5), 48.8 (C-10), 54.2 (C-9), 72.6 (C-12), 78.6 (C-3), 103.4 (C-11), 126.3 (C-7), 131.3 (C-8), 174.4 (C-15); hreims (probe 100°C), *m/z* calcd. for $C_{15}H_{20}O_4$ (M^+): 264.1362; found: 264.1357 (40), 220 (21), 208 (100), 173 (22), 172 (28), 145 (24), 132 (61), 119 (57), 118 (21), 117 (21), 105 (59), 104 (43), 91 (53), 79 (23), 77 (25), 69 (44), 55 (24).

Oxidation of 3β-hydroxymarasmene (18a)

Pyridinium dichromate (75 mg) was added to a solution of **18***a* (50 mg) in dichloromethane (10 mL) and the mixture was stirred at room temperature for 24 h. The mixture was diluted with ether and washed successively with 1 M hydrochloric acid, water, saturated aqueous sodium hydrogen carbonate, and brine. Evaporation of the dried solution gave a pale yellow oil, which was chromatographed on silica gel, eluting with ethyl acetate – Skellysolve B (1:2) to give marasmen-3-one (**18***b*, 25 mg), which crystallized from dichloromethane – Skellysolve B as microcrystals, mp 135–138°C.

Acetylation of 3α-hydroxyoreadone 15c)

3α-Hydroxyoreadone (**15***c*) (5.0 mg) was acetylated with acetic anhydride (0.02 mL) and pyridine (0.05 mL) at room temperature for 3 h, then benzene (2 mL) was added and the mixture was evaporated to give a pale yellow oil (6.1 mg). Column chromatography, eluting with ethyl acetate – Skellysolve B (1:2), gave successively impure dehydrooreadone acetate (**17***a*) (0.3 mg), diacetate **15***d* (4 mg), and monoacetate **15***e* (0.7 mg). Diacetate **15***d* was obtained as an oil; ^{1}H nmr ($CDCl_3$) δ: 1.04 (3H, s), 1.21 (3H, s), 1.99 (3H, s, OAc), 2.04 (3H, s, OAc), 2.18–2.27 (3H, m), 2.36 (1H, dd, *J* 12.0, 9.5 Hz, H-10), 2.52 (1H, dd, *J* 15.5, 3.0 Hz, H-2α), 2.79 (1H, ddd, *J* 15.5, 3.4, 0.8 Hz, H-2β), 2.95 (1H, m, H-9), 4.39 (1H, dddd, *J* 12.3, 2.0, 2.0, 2.0 Hz, H-12), 4.47 (1H, dddd, *J* 12.5, 2.0, 2.0, 2.0 Hz, H-12), 5.06 (1H, dd, *J* 3.2, 3.2 Hz, H-3), 5.65 (1H, m, H-7), 6.63 (1H, d, *J* 5.0 Hz, H-11); ^{13}C nmr ($CDCl_3$) δ: 19.9, 21.0, 21.3, 24.6, 26.4, 36.5, 41.3, 42.5, 43.8, 46.2, 69.2, 80.1, 97.8, 117.0, 135.3, 170.0, 170.1, 207.6. Monoacetate **15***e* was obtained as an oil; ^{1}H nmr ($CDCl_3$) δ: 1.13 (3H, s), 1.14 (3H, s), 1.98 (3H, s, OAc), 2.16–2.35 (4H, m), 2.45 (1H, dd, *J* 14.8, 3.5 Hz), 2.84 (1H, dd, *J* 14.8, 3.0 Hz), 2.95 (1H, m), 3.90 (1H, ddd, *J* 3.2, 3.2, 3.2 Hz), 4.37 (1H, dddd, *J* 12.2, 2.0, 2.0, 2.0 Hz), 4.46 (1H, dddd, *J* 12.5, 2.0, 2.0, 2.0 Hz), 5.64 (1H, m), 6.63 (1H, s).

Acknowledgements

The financial support of the Natural Sciences and Engineering Research Council of Canada is gratefully acknowledged. We thank Dr. K. I. Mallett, Northern Forest Research Centre, Edmonton, and Mrs. Lynne Sigler, University of Alberta Microfungus Herbarium, for cultures of *M. oreades* and for valuable discussion.

1. C. J. Alexopoulos and C. W. Mims. Introductory mycology. 3rd ed. John Wiley and Sons, New York. 1979. pp. 449–450.
2. J. D. Smith. Plant. Dis. **64**, 348 (1980).
3. W. A. Ayer, P. A. Craw, T. J. Stout, and J. Clardy. Can. J. Chem. **67**, 773 (1989).
4. J. A. Traquair and W. E. McKeen. Can. J. Plant Pathol. **8**, 59 (1986).
5. R. Greasham and E. Inamine. *In* Manual of industrial microbiology and biotechnology. *Edited by* A. L. Demain and N. A. Solomon. American Society of Microbiology, Washington, DC. 1986. pp. 41–48.
6. D. N. Kursanov, N. M. Loim, V. A. Baranova, L. V. Moiseeva, L. P. Zalukaev, and Z. N. Parnes. Synthesis, 420 (1973).
7. J. R. Sierra, J. T. Lopez, and M. J. Cortes. Phytochemistry, **25**, 253 (1986).
8. K. Mori and H. Watanabe. Tetrahedron, **42**, 273 (1986).
9. D. M. Hollinshead, S. C. Howell, S. V. Ley, M. Mahon, N. M. Ratcliffe, and P. A. Worthington. J. Chem. Soc. Perkin Trans. 1, 1579 (1983).
10. Y. Asakawa and T. Takemoto. Experientia, **35**, 1420 (1979).
11. J. D. Bu'Lock, E. R. H. Jones, G. H. Mansfield, J. W. Thompson, and M. C. Whiting. Chem. Ind. (London), 990 (1954).
12. F. Kavanagh, A. Hervey, and W. J. Robbins. Proc. Natl. Acad. Sci. U.S.A. **36**, 102 (1950).

Surfactant assisted permanganate oxidation of aromatic compounds

BRANKO JURŠIĆ
Laboratory of Organic Chemistry, Faculty of Science, University of Zagreb, Strossmayerov trg 14, 41000 Zagreb, Yugoslavia

Received April 12, 1988[1]

BRANKO JURŠIĆ. Can. J. Chem. **67**, 1381 (1989).

Potassium permanganate in aqueous solutions of surfactant can be used to oxidize aromatic compounds to the corresponding acids. It has been found that oxidation of aromatic alcohols and aldehydes proceeds under mild reaction conditions, while the oxidation of alkylbenzenes requires higher temperatures. The yields are very high and the work-up is simple, which makes oxidation with potassium permanganate a convenient synthetic method.

Key words: surfactant, oxidation, aromatic compounds, catalysis.

BRANKO JURŠIĆ. Can. J. Chem. **67**, 1381 (1989).

On peut utiliser le permanganate de potassium, dans des solutions aqueuses d'agent de surface, pour oxyder les composés aromatiques en acides correspondants. On a trouvé que l'oxydation des alcools et des aldéhydes aromatiques s'effectue dans des conditions douces, tandis que celle des alkylbenzènes requiert des températures plus élevées. Les rendements très élevés et la simplicité des manipulations rendent cette oxydation par le permanganate attrayante du point de vue synthétique.

Mots clés : agent de surface, oxydation, composés aromatiques, catalyse.

[Traduit par la revue]

Introduction

The oxidation of alcohols by permanganate ion has been the subject of extensive study (1–4). It is generally accepted that in acidic or basic media the permanganate ion oxidizes primary alcohols to acids; alcohols are relatively inert to neutral permanganate solutions. However, as reported by Lee (4*a*, citing Fatiati (4*b*)), potassium permanganate may be used in acidic, neutral, and basic aqueous solutions, but not in completely nonaqueous solvents. This is particularly useful for the oxidation of such hydroxy compounds as lactic and mandelic acids, which are completely soluble in aqueous base. Aqueous acetic acid or aqueous acetone has been used as the solvent; the use of two-phase systems, such as ether/water, dichloromethane/water, or petroleum ether/water has been described for permanganate oxidation of hydroxy compounds such as ethyl lactate or ethyl pyruvate. In a series of new methods, the effective use of phase-transfer catalysis with permanganate ion for the oxidation of hydroxy compounds has been demonstrated (5, 6).

The permanganate ion oxidizes the side chain of aromatic compounds; the products obtained are usually the corresponding acids (7). A series of alkyl-aromatic compounds has recently been oxidized by potassium permanganate in the presence of a phase-transfer catalyst (8–12). In this way toluene, stilbene, *p*-xylene, mesitylene, and durene were oxidized with potassium permanganate in a two-phase system (hydrocarbon/water) containing cetyltrimethylammonium bromide (CTAB) in 1:1:3.3 × 10^{-3}:138 molar ratio (ArH:$KMnO_4$:CTAB:H_2O) at 70–80°C, yielding the corresponding benzenecarboxylic acids, i.e., benzoic (93%), terephthalic (95%), trimesic (90%), pyromellitic (80%), and benzoic (84%) acids, respectively (8).

The conditions under which surfactant can be used in preparative organic chemistry are quite varied. Although the mechanism for many surfactant assisted reactions is well understood, there are still limitations to the application of micelles in preparative chemistry. The advantage of large rate enhancement is offset by the limited amount of substrate solubilization, the restricted temperature range, and the difficulty of separating the products from the surfactants (13). In spite of these limitations, Menger *et al.* succeeded in increasing the yield of $KMnO_4$ mediated oxidation of piperonal to piperonylic acid from 37 to 65% by the addition of catalytic amounts of cationic CTAB (14).

In this paper I would like to demonstrate the beneficial use of surfactants in several oxidation reactions. In water solution, surfactant probably forms some kind of aggregate, for instance micelles, and disperses organic compounds in water, which could conceivably result in higher yields and shorter reaction times. Surfactant also is capable of catalyzing many organic reactions (13), yet neither "emulsion catalysis" nor the micellar catalysis by surfactants have been exploited to any degree in synthetic organic chemistry.

TABLE 1. Percent yields of benzoic acid produced from the oxidation of benzyl alcohol (0.01 mol) by $KMnO_4$ (0.01 mol/0.5 L water)

Concentration of surfactant	Molar ratio surfactant/benzyl alcohol	Yield (%)
0	—	32
0.0001 M CTAB[a]	0.01	38
0.001 M CTAB	0.1	47
0.01 M CTAB	1	87
0.1 M CTAB	10	81
0.5 M CTAB	50	80
0.0001 M SS[b]	0.01	45
0.001 M SS	0.1	87
0.01 M SS	1	92
0.1 M SS	10	92

[a]CTAB = cetyltrimethylammonium bromide.
[b]SS = sodium stearate.

Results and discussion

I first investigated the heterogeneous oxidation of benzyl alcohol to benzoic acid. The reaction was carried out by stirring benzyl alcohol (1.0 g; 0.01 mol) with 500 mL of aqueous $KMnO_4$ (1.06 g; 0.01 mol) at room temperature in the presence or absence of surfactant (Table 1). After 8 h the reaction mixture was worked up. The yields of benzoic acid are listed in Table 1. As can be seen from the table, under the conditions employed

[1]Revision received January 20, 1989.

Printed in Canada / Imprimé au Canada

Can. J. Chem. Downloaded from www.nrcresearchpress.com by 194.225.253.170 on 09/07/12
For personal use only.

TABLE 2. Oxidation of aromatic compounds by $KMnO_4$ in the presence of surfactant (SS or CTAB)

Substrate (0.05 mol)	Surfactant (0.002 mol/0.1 L)	Temp. (°C)	Reaction time (h)	Permanganate: substrate ratio	Yield (%)
Benzaldehyde	SS	50	5	0.75	75
	CTAB	40	5	0.75	82
p-Chlorobenzaldehyde	SS	50	5	0.75	93
	CTAB	40	5	0.75	82
p-Nitrobenzaldehyde	SS	50	5	0.75	95
	CTAB	40	5	0.75	83
p-Anisaldehyde	SS	50	5	0.75	90
	CTAB	40	5	0.75	85
Benzyl alcohol	SS	50	8	1.5	93
	CTAB	40	8	1.5	85
p-Chlorobenzyl alcohol	SS	50	8	1.5	92
	CTAB	40	8	1.5	81
p-Methoxybenzyl alcohol	SS	50	8	1.5	91
	CTAB	40	8	1.5	83
Toluene	SS	100	6	3	93
	CTAB	100	6	3	82
Styrene	SS	80	4	4	91
	CTAB	80	4	4	90
Ethylbenzene	SS	100	6	3	82
	CTAB	100	6	3	81
Stilbene	SS	80	2	3	82
	CTAB	80	2	3	80

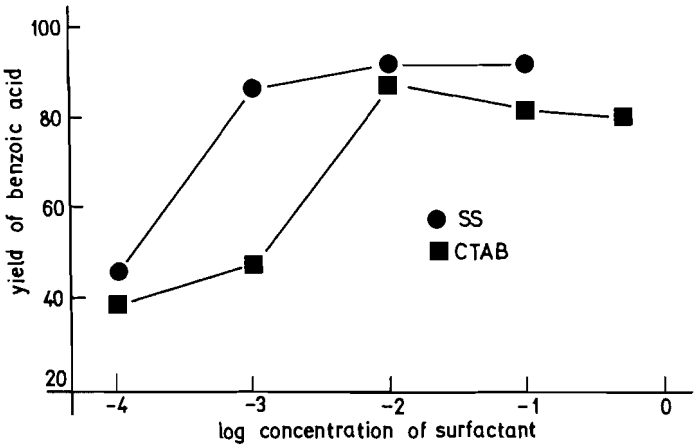


FIG. 1. Yield of benzoic acid from benzyl alcohol by $KMnO_4$ oxidation as a function of surfactant concentration.

the presence of surfactant, cetyltrimethylammonium bromide (CTAB) or sodium stearate (SS), plays an important role in accelerating the reaction, and an overall 40–60% increase in yield of benzoic acid was observed (Fig. 1). The same results were obtained when benzaldehyde and toluene were oxidized in the presence of surfactant. On the basis of these results the most suitable concentration of surfactant (0.01 mol surfactant/0.5 L water) was determined. The yields obtained for oxidation of a number of aromatic substrates by potassium permanganate in CTAB or SS are given in Table 2. The permanganate ion, as evidenced by vis spectroscopy, resides in the aqueous medium and the oxidation can proceed at the surface of the aggregates

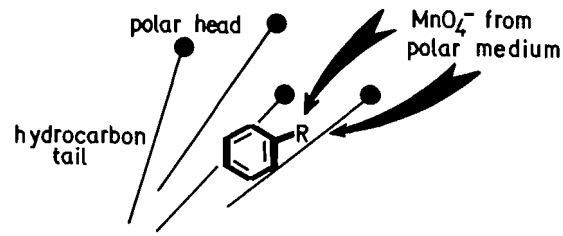


FIG. 2. Schematic representation of $KMnO_4$ oxidation at surface of the surfactant aggregate.

(Fig. 2) giving rise to the formation of benzoic salt, which, being soluble in water, resides in the bulk water. The work-up was simple and involved saturation of the reaction mixture with NaCl, filtration, acidification of the water layer, separation of precipitate, and purification by recrystallization.

It can be concluded that in some cases cationic and anionic surfactants can increase the yield and shorten the reaction time. Surfactant catalysis might be advantageous in large-scale reactions and in reactions of sensitive water-soluble liquids that require minimum exposure to aqueous solution. Therefore oxidation with potassium permanganate in the presence of surfactant is a valuable addition to the methods already available to synthetic organic chemists.

Experimental

Melting points are uncorrected. The starting alcohols, aldehydes, and alkylbenzenes are commercially available. Cetyltrimethylammonium bromide (CTAB) was commercial quality (Fluka) and used without further purification. Sodium stearate (SS) was prepared immediately before use from stearic acid and sodium hydroxide. The

Can. J. Chem. Downloaded from www.nrcresearchpress.com by 194.225.253.170 on 09/07/12
For personal use only.

^{1}H nmr spectra were recorded on a JEOL FX-90Q spectrometer. Infrared spectra of samples in KBr were recorded on a Perkin–Elmer 257 spectrometer. All acids isolated gave ir and ^{1}H nmr spectra identical with those of authentic specimens.

Oxidation of benzaldehyde by $KMnO_4$ in the presence of SS

To water (100 mL) were added stearic acid (0.56 g; 0.002 mol) and sodium hydroxide (0.08 g; 0.002 mol). After heating to 80°C and vigorously stirring for 1 h, the reaction suspension was cooled down and benzaldehyde (5.3 g; 0.05 mol) and potassium permanganate (5.9 g; 0.0375 mol) were added; the reaction suspension was then heated and stirred vigorously at 50°C. After 6 h the suspension was cooled down and the aqueous layer separated by filtration through a short column of sodium chloride. The water layer was acidified to pH 3 by the addition of hydrochloric acid. The precipitate of benzoic acid was separated by filtration and washed with cold water (3 × 10 mL). Recrystallization from water yielded pur benzoic acid (4.6 g; 75%), mp 120–122°C.

Oxidation of benzaldehyde by $KMnO_4$ in the presence of CTAB

To an aqueous solution (100 mL) of cetyltrimethylammonium bromide (0.728 g; 0.002 mol), benzaldehyde (5.3 g; 0.05 mol) was added with stirring at 40°C. After 6 h the reaction suspension was cooled down and the aqueous layer separated by filtration through a short column of sodium chloride. The water layer was extracted with ether (2 × 20 mL) and acidified to pH 3 by addition of hydrochloric acid. The precipitate of benzoic acid was separated by filtration and washed three times with 10-mL portions of cold water. Recrystallization from water yielded pure benzoic acid (5.1 g; 82%), mp 121–122°C.

The oxidation of other aromatic compounds with $KMnO_4$ in the presence of SS or CTAB was achieved in the same manner and under same conditions as presented in Table 2.

1. F. FREEMAN. Rev. React. Species Chem. React. **1**, 179 (1976), and references therein.
2. R. STEWART. *In* Oxidation in organic chemistry. Part A. *Edited by* K. Wiberg. Academic Press, New York. 1965. Chap. 1.
3. D. G. LEE. *In* Oxidation. Vol. 1. *Edited by* R. L. Augustine. Marcel Dekker, New York. 1969. Chap. 1.
4. (*a*) D. G. LEE. The oxidation of organic compounds by permanganate ion and hexavalent chromium. Open Court, La Salle, Illinois. 1980; (*b*) A. J. FATIATI. Synthesis, 85 (1987).
5. D. J. SAM and H. E. SIMMONS. J. Am. Chem. Soc. **94**, 4024 (1972).
6. A. W. HERRIOTT and D. PICKER. Tetrahedron Lett. 1511 (1974).
7. (*a*) C. F. CULLIS and J. W. LADBURY. J. Chem. Soc. 555 (1955); (*b*) J. Chem. Soc. 1407 (1955); (*c*) J. Chem. Soc. 2850 (1955).
8. G. A. ARTAMKINA, A. A. GRINFELD, and I. P. BELETSKAYA. Zh. Org. Khim. **16**, 698 (1980); Chem. Abstr. **93**, 71 220 (1980).
9. H. J. SCHMIDT and H. J. SCHAFER. Angew. Chem. Int. Ed. Engl. **18**, 68 (1979).
10. H. J. SCHMIDT and H. J. SCHAFER. Angew. Chem. Int. Ed. Engl. **18**, 69 (1979).
11. T. SALA and M. V. SARGENT. J. Chem. Soc. Chem. Commun. 253 (1978).
12. (*a*) C. L. LIOTTA and H. P. HARRIS. J. Am. Chem. Soc. **96**, 2250 (1974); (*b*) D. J. SAM and H. E. SIMMONS. J. Am. Chem. Soc. **96**, 2252 (1974).
13. J. H. FENDLER. Membrane mimetic chemistry. Wiley–Interscience, New York. 1982.
14. F. M. MENGER, J. U. RHEE, and H. K. RHEE. J. Org. Chem. **40**, 3803 (1975).

Can. J. Chem. Downloaded from www.nrcresearchpress.com by 194.225.253.170 on 09/07/12
For personal use only.

ortho-Specific alkylation of phenols via 1,3,2-benzodioxaborins

CHEUK K. LAU,[1] HAYDN W. R. WILLIAMS, SYLVIE TARDIFF, CLAUDE DUFRESNE, JOHN SCHEIGETZ, AND PATRICE C. BÉLANGER

Medicinal Chemistry Department, Merck Frosst Canada Inc., P.O. Box 1005, Pointe Claire – Dorval, P.Q., Canada H9R 4P8

Received January 12, 1989

CHEUK K. LAU, HAYDN W. R. WILLIAMS, SYLVIE TARDIFF, CLAUDE DUFRESNE, JOHN SCHEIGETZ, and PATRICE C. BÉLANGER. Can. J. Chem. **67**, 1384 (1989).

Reaction of a phenol with an aldehyde in the presence of phenylboronic acid gives a 1,3,2-benzodioxaborin. The latter could be reduced to the corresponding *ortho*-alkylphenol with *tert*-butylamine borane in the presence of aluminum chloride. Alternatively, the dioxaborin, when reacted with an alkylthiol or an alcohol in the presence of an acid, gave the corresponding *ortho*-alkylthiomethyl- or *ortho*-alkoxymethylphenol.

Key words: phenol, alkylation, *ortho*-specific, 1,3,2-benzodioxaborin.

CHEUK K. LAU, HAYDN W. R. WILLIAMS, SYLVIE TARDIFF, CLAUDE DUFRESNE, JOHN SCHEIGETZ et PATRICE C. BÉLANGER. Can. J. Chem. **67**, 1384 (1989).

La réaction d'un phénol avec un aldéhyde, en présence d'acide phénylboronique, conduit à une 1,3,2-benzodioxaborine qui, sous l'influence d'une *tert*-butylamine borane en présence de chlorure d'aluminium, peut être réduite en *ortho*-alkylphénol correspondant. Par ailleurs, lorsqu'on fait réagir la dioxaborine avec un alkylthiol ou un alcool en présence d'un acide, on obtient les dérivés *ortho*-alkylthiométhyl- ou *ortho*-alkoxyméthyl-phénols correspondants.

Mots clés : phénol, alkylation, *ortho*-spécifique, 1,3,2-benzodioxaborine.

[Traduit par la revue]

Introduction

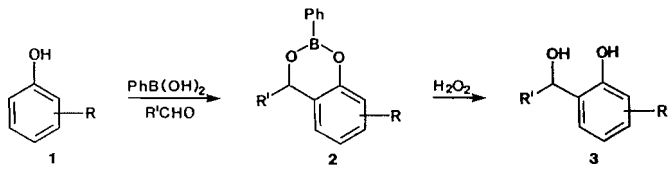
ortho-Alkyl- and *ortho*-thioalkylphenols are useful intermediates in organic synthesis. However, most direct alkylations of phenols are not selective, usually resulting in a mixture of *ortho*-, *para*-, and poly-substitution (for a recent review on *ortho*-thioalkylation, see ref. 1). *ortho*-Thioalkylation of phenols based on the [2,3]-sigmatropic rearrangement of the ylide formed from the corresponding oxasulfonium salt of the phenol is *ortho*-specific (2). The method generally gives good yield of the corresponding alkylthiomethylphenol, which could be elaborated further to other products. Recently, an improved procedure based on the same principle was reported (2*c*). *o*-Metallation of protected phenol derivatives followed by trapping with electrophiles provides a useful alternative for substrates that are stable to the metallation condition (3). Metal coordinated *o*-alkylation of phenol, though not as well studied, could also be quite useful (4). In a similar approach, Peer (5) and Nagata *et al.* (6) demonstrated the utility of phenylboronic acid in the condensation of an aldehyde with a phenol to give a 1,3,2-benzodioxaborin **2**, which, after oxidative work-up, gave the corresponding α-hydroxyalkyl derivative **3** (Scheme 1).

Herein we would like to report the further elaboration of such dioxaborins to give the corresponding *o*-alkyl phenol directly, as well as various *o*-thioalkylphenols and *o*-alkoxymethylphenols.

Results and discussion

ortho-*Alkylation of phenols*

Using the procedure of Nagata *et al.* (6), phenols were allowed to react with phenylboronic acid and an aldehyde in refluxing toluene in the presence of propanoic acid or trichloroacetic acid to give the corresponding 2-phenyl-4-alkyl-1,3,2-benzodioxaborins **2**. The latter were reduced with *tert*-butylamine borane in the presence of aluminum chloride in dichloromethane to give the corresponding *o*-alkylphenols **4**. The reagent was originally developed for the reductive deoxygenation of aryl ketones and aldehydes (7). The results are summarized in Table 1. Various aldehydes, including paraformaldehyde, benzaldehyde, and aliphatic aldehydes, were used. If desired, the intermediate dioxaborin can be isolated and characterized. In the preparation of **2***b*, we were able to obtain a higher yield (71%) than reported (49%) by using excess benzaldehyde. The conditions for the reduction of **2** to the corresponding *o*-alkylphenol depend on the reactivity of the substrate. The double benzylic benzaldehyde derivative **2***b* was reduced to 2-benzylphenol in 45 min at 0°C. Most substrates require reaction at room temperature overnight for completion. Reduction of the 5-methyl derivative **2***a* at room temperature overnight gave only 50% of the desired 2,5-dimethyl phenol with 25% starting material recovered. Interestingly, the dioxaborin derivative obtained from ethyl 4-hydroxybenzofuran-2-carboxylate **5** was reduced to 4-hydroxy-2,3,5-trimethylbenzofuran **6** after 3 days at room temperature, the ester being completely reduced to a methyl group. If the reaction was interrupted after 1 day, a mixture of intermediate alcohols at positions 2 and 5 resulted. Other reducing agents, such as triethylsilane in the presence of boron trifluoride, may also be used in the reduction of the dioxaborin in most cases. An exception is the 4-hydroxybenzofuran derivative **5**, in which case a complex mixture resulted.



SCHEME 1

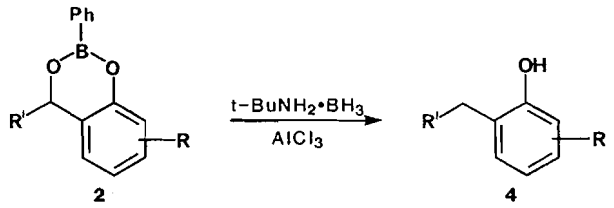
ortho-*Thioalkylation and* ortho-*alkoxymethylation*

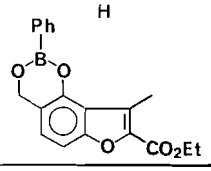
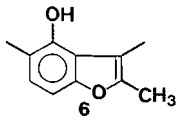
Reaction of a 2-phenyl-4-alkyl-1,3,2-benzodioxaborin **2** with various thiols in the presence of aluminum chloride in dichloromethane at 0°C gave the corresponding *o*-alkylthiomethylphenol **7**. Reaction of **2** in refluxing alcohol with a catalytic amount of concentrated sulphuric acid gave the

[1]Author to whom correspondence may be addressed.

Can. J. Chem. Downloaded from www.nrcresearchpress.com by 194.225.253.170 on 09/07/12
For personal use only.

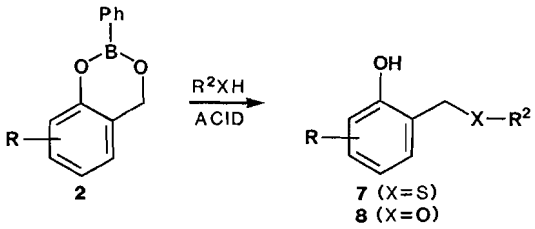
TABLE 1. Preparation of *ortho*-alkylphenols

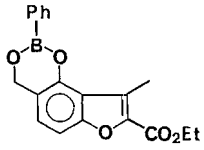


	R	R'	TEMP. (°C)	TIME (HOURS)	PRODUCT 4	YIELD[a] (%) OF 4
2a	3-CH_3	H	20	20	2-CH_3,5-CH_3	50 25 (S.M.)
2b	H	C_6H_5	0	0.75	2-$CH_2C_6H_5$	97
2c	H	$CH_2C_6H_5$	20	20	2-$(CH_2)_2C_6H_5$	71
2d	H	$(CH_2)_4C_6H_5$	20	20	2-$(CH_2)_5C_6H_5$	98
5		H	20	72	 6	40

[a] Yields from the experiments described herein refer to isolated, purified material.

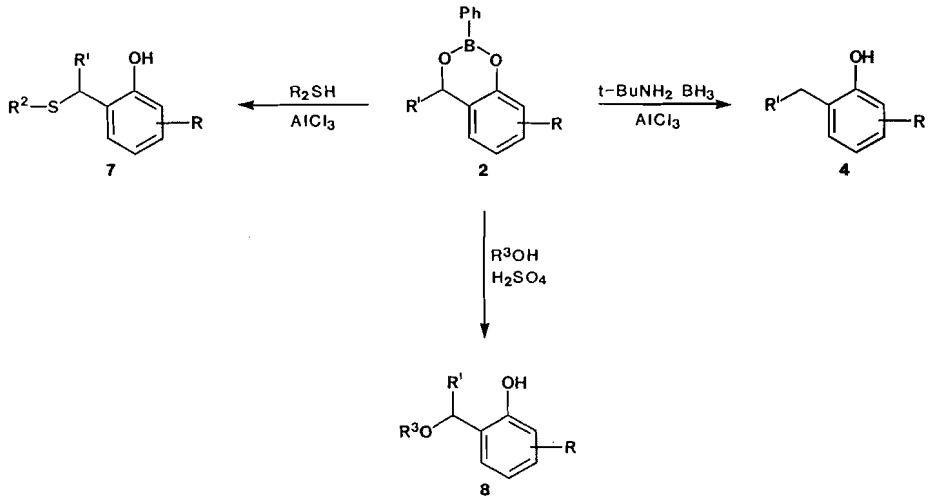
TABLE 2. Preparation of *ortho*-alkylthiomethylphenols and *ortho*-alkoxymethylphenols



	R	R^2XH (mol equiv.)	ACID (mol equiv.)	PRODUCT YIELD[a] (%)
2f	H	C_2H_5SH (4)	$AlCl_3$ (4)	**7a** (83)
	H	C_2H_5OH (excess)	H_2SO_4 (cat.)	**8a** (48)
2a	5-CH_3	C_2H_5SH (4)	$AlCl_3$ (4)	**7b** (94.2)
5		CH_3SH (excess)	$AlCl_3$ (4)	**7c** (56)
5		C_4H_9SH (4)	$AlCl_3$ (4)	**7d** (49)
5		$HSCH_2C_6H_5$ (4)	$AlCl_3$ (4)	**7e** (75)
5		$HSCH_2COOH$ (4)	$AlCl_3$ (5)	**7f** (28)
5		C_2H_5OH (excess)	H_2SO_4 (cat.)	**8b** (48)

[a] Yields refer to isolated, purified products.

Can. J. Chem. Downloaded from www.nrcresearchpress.com by 194.225.253.170 on 09/07/12
For personal use only.



SCHEME 2

corresponding *o*-alkoxymethylphenol derivative **8**. The results are summarized in Table 2. In general, the overall yield of the *o*-alkylthiomethylphenol obtained in this reaction is higher than in the sulfonium ylide rearrangement method (2), especially in the case of the 4-hydroxybenzofuran derivative **5**. Furthermore, various *o*-alkylthiomethyl and *o*-alkyloxymethyl derivatives can be prepared from the same intermediate, making this a very versatile approach in preparing analogs.

The 2-phenyl-4-alkyl-1,3,2-benzodioxaborin **2** has been shown to be a very useful and versatile synthetic intermediate, since its formation is *ortho*-specific and regioselective. It can be readily oxidized to the corresponding α-hydroxyalkylphenol (5, 6), reduced to *o*-alkylphenol, or transformed to alkylthiomethylphenol or alkoxymethylphenol derivatives, and thus provides an efficient route to any of these classes of compounds (Scheme 2).

Experimental

General information

Proton nuclear magnetic resonance spectra were obtained on a Bruker AM250 spectrometer. Reported boiling points are those observed during distillation with a Kugelrohr apparatus and are uncorrected. Melting points were measured on a Buchi 510 melting point apparatus and are uncorrected. Low-resolution mass spectral analyses were performed by the Morgan–Schaffer Corporation, Montreal. Elemental analyses were performed by Guelph Chemical Laboratories Ltd., Guelph, Ontario. All reactions, as well as column chromatography, were monitored routinely with the aid of thin-layer chromatography using precoated silica gel GF plates (Analtech).

tert-Butylamine borane was purchased from Callery Chemical Co. Ltd. and was used without purification. Dichloromethane and aluminum chloride were used without purification. Most of the compounds used in this study were commercial products, others were prepared using known procedures. The products obtained were readily available materials in most cases. If not, identification was based on ^{1}H nmr, ir, mass spectra, and elemental analyses.

Since all the reactions performed are similar in many aspects, a typical reaction is described as a specific example. In general, most reactions were performed with 10 mmol of starting material for ease of handling and isolation of products.

General procedure A

*Preparation of 2-phenyl-4-(4-phenylbutyl)-1,3,2-benzodioxaborin (**2**d)*

A mixture of phenol (0.941 g, 10 mmol), phenylboronic acid (1.46 g, 12 mmol), 4-phenylbutyraldehyde (2.22 g, 15 mmol), and trichloroacetic acid (0.5 g) in toluene was heated under reflux for 20 h, with azeotropic removal of water using a Dean–Stark trap. The reaction mixture was concentrated and the resulting oil was chromatographed (eluting with 5% ethyl acetate in hexane) to give 1.6 g (50%) of the title compound; mp 78–79°C; ^{1}H nmr (250 MHz, $CDCl_3$), δ: 8.0 (d, 2H), 7.4 (m, 3H), 7.0–7.3 (m, 9H), 5.3 (m, 1H, C*H*O), 2.7 (m, 2H), 1.95 (m, 4H).

*2,4-Diphenyl-1,3,2-benzodioxaborin (**2**b)*

According to the general procedure, using excess benzaldehyde, the title compound was obtained from **5***d* in 71% yield; ^{1}H nmr (250 MHz, $CDCl_3$) was identical to that reported (6).

*Preparation of 2-phenyl-4-phenylmethyl-1,3,2-benzodioxaborin (**2**c)*

According to general procedure, from **5***d*, 33% yield; mp 55–57°C; ^{1}H nmr (250 MHz, $CDCl_3$), δ: 7.8–7.98 (d, 2H, J = 6 Hz), 6.9–7.6 (m, 12H), 5.47 (t, 1H, J = 3.7 Hz, C*H*O), 3.06–3.3 (m, 2H). *Anal.* calcd. for $C_{20}H_{17}BO_2$: C 80.03, H 5.70; found: C 79.90, H 5.54.

*Preparation of ethyl 9-methyl-2-phenyl-4*H*-1,3,2-dioxaborin [6,5-e]-benzofuran-8-carboxylate (**5**)*

According to the general procedure, from **2***d*, 77% yield after recrystallization from acetonitrile; mp 171–172°C; ^{1}H nmr (250 MHz, $CDCl_3$), δ: 7.97 (d, 2H, J = 7.9 Hz), 7.50 (m, 3H), 7.22 (d, 1H, J = 7.5 Hz), 7.00 (d, 1H, J = 7.5 Hz), 5.31 (s, 2H, CH_2O), 4.46 (q, 2H, J = 7.5 Hz), 2.95 (s, 3H), 1.46 (t, 3H). *Anal.* calcd. for $C_{19}H_{17}BO_5$: C 67.89, H 5.10, B 3.22; found: C 67.24, H 5.09, B 3.11.

General procedure B

*Preparation of 2-(4-phenylbutyl)phenyl (**4**d)*

To a suspension of anhydrous aluminum chloride (0.4 g, 3 mmol) in dichloromethane (15 mL) at 0°C was added *tert*-butylamine borane (0.52 g, 6 mmol). The resulting mixture was allowed to react at 0°C for 20 min. A colorless solution resulted. A solution of 2-phenyl-4-(4-phenylbutyl)-1,3,2-benzodioxaborin (**5***d*) (0.328 g, 1 mmol) in 2 mL of dichloromethane was added. The mixture was warmed to room temperature and allowed to react for 20 h. Cold dilute (1 N) HCl was added. The product was extracted with dichloromethane. The organic extracts were dried over anhydrous magnesium sulfate, and concentrated to an oil. Chromatography of the latter on silica gel (eluted with 10% ethyl acetate in hexane) gave 0.214 g (95% yield) of the title compound; mp 78–79°C; ^{1}H nmr (250 MHz, $CDCl_3$), δ: 7.0–7.3 (m, 7H), 6.85 (t, 1H, J = 11.4 Hz), 6.72 (d, 1H, J = 7.6 Hz), 4.78 (s, 1H, O*H*), 2.7 (m, 4H), 2.65 (m, 4H). *Anal.* calcd. for $C_{16}H_{18}O$: C 84.95, H 7.96; found: C 84.62, H 7.92.

*2,5-Dimethylphenol (**4**a)*

According to the general procedure, from **4***d*, 50% yield after chromatography; mp 68–69°C; spectral data identical to commercial material. Another 25% of starting material (**5***a*) was recovered.

Can. J. Chem. Downloaded from www.nrcresearchpress.com by 194.225.253.170 on 09/07/12
For personal use only.

Can. J. Chem. Downloaded from www.nrcresearchpress.com by 194.225.253.170 on 09/07/12
For personal use only.

*2-Phenylmethylphenol (**4**b)*

According to the general procedure, from **4***d*, 97% yield after only 45 min at 0°C; ^{1}H nmr (250 MHz, $CDCl_3$), δ: 7.09–7.35 (m, 7H), 6.75–6.95 (s, 2H), 4.68 (s, 1H, O*H*), 4.00 (s, 2H, CH_2Ph). *Anal.* calcd. for $C_{13}H_{12}O$: C 84.80, H 6.50; found: C 84.49, H 6.86.

*2-Phenylethylphenol (**4**c)*

According to the general procedure, from **4***d*, 71% yield; mp 80–81°C; ^{1}H nmr (250 MHz, $CDCl_3$), δ: 7.03–7.30 (m, 8H), 6.83–6.93 (m, 1H), 6.75 (d, 1H), 4.57 (s, 1H, O*H*), 2.93 (s, 4H). *Anal.* calcd. for $C_{14}H_{14}O$: C 84.81, H 7.11; found: C 84.32, H 7.27.

*4-Hydroxy-2,3,5-trimethylbenzofuran (**6**)*

According to the general procedure, from **4***d*, 40% yield after 3 days at 20°C; mp 122–123°C; ^{1}H nmr (250 MHz, $CDCl_3$), δ: 6.90 (ABq, 2H, J = 3 Hz), 4.78 (s, 1H, O*H*), 2.35 (s, 6H), 2.30 (s, 3H). *Anal.* calcd. for $C_{11}H_{12}O_2$: C 75.00, H 6.81; found: C 75.12, H 7.06.

General procedure C

*Preparation of ethyl 4-hydroxyl-3-methyl-5-methylthiomethylbenzofuran-2-carboxylate (7*c)*

A mixture of **5** (5.04 g, 15 mmol), methanethiol (3.85 g, 89.5 mmol), and dichloromethane (100 mL) was cooled in an ice-bath, and anhydrous aluminum chloride (7.98 g, 60 mmol) was added in portions with stirring. The reaction mixture was stirred in the ice-bath for 0.5 h and then at room temperature for 0.5 h, after which it was quenched with ice and 6 N hydrochloric acid. The crude product isolated from the organic phase was purified by column chromatography (eluted with 1:4 ethyl acetate/hexane) to afford **7***c*, 2.37 g (56%); ^{1}H nmr (90 MHz, $CDCl_3$), δ: 7.49 (s, 1H, OH), 7.13 (d, 1H), 7.12 (d, 1H), 4.52 (q, 2H, J = 7 Hz), 3.92 (s, 2H, SCH_2), 2.86 (s, 3H), 2.07 (s, 3H), 1.51 (t, 3H, J = 7 Hz). *Anal.* calcd. for $C_{14}H_{16}O_4S$: C 60.00, H 5.75, S 11.40; found: C 60.08, H 5.70, S 11.31.

*2-Ethylthiomethylphenol (7*a)*

The title compound was prepared by the general procedure C, yield 83%; ^{1}H nmr (250 MHz, $CDCl_3$), δ: 7.1–7.3 (m, 1H), 7.09 (d, 1H, J = 6.3 Hz), 6.82–6.95 (m, 2H), 6.75 (s, 1H, O*H*), 3.84 (s, 2H, SCH_2Ph), 2.43 (q, 3H, J = 5.6 Hz), 1.22 (t, 3H, J = 5.6 Hz). *Anal.* calcd. for $C_9H_{12}OS$: C 64.24, H 7.18, S 19.05; found: C 64.00, H 7.16, S 18.96.

*2-Ethylthiomethyl-5-methylphenol (7*b)*

According to the general procedure C, yield 94%; ^{1}H nmr (250 MHz, $CDCl_3$), δ: 6.95 (d, 1H, J = 7.5 Hz), 6.63–6.78 (m, 3H), 3.80 (s, 2H, SCH_2Ph), 2.42 (q, 2H, J = 5.6 Hz), 2.31 (s, 3H), 1.23 (t, 3H, J = 5.6 Hz). *Anal.* calcd. for $C_{10}H_{14}OS$: C 65.89, H 7.74, S 17.58; found: C 65.76, H 7.34, S 17.30.

*Ethyl 5-butylthiomethyl-4-hydroxy-3-methyl-benzofuran-2-carboxylate (7*d)*

Using butanethiol in the above procedure C, the title compound was obtained in 49% yield; mp 59–60°C; ^{1}H nmr (90 MHz, $CDCl_3$), δ: 7.55 (s, 1H, O*H*), 7.1 (d, 1H), 7.0 (d, 1H), 4.45 (q, 2H, J = 7 Hz), 3.88 (s, 2H, SCH_2Ph), 2.79 (s, 3H), 2.42 (m, 2H), 1.4 (m, 7H), 0.89 (t, 3H, J = 7 Hz). *Anal.* calcd. for $C_{17}H_{22}O_4S$: C 63.33, H 6.88, S 9.94; found: C 63.40, H 6.97, S 9.93.

*Ethyl 5-benzylthiomethyl-4-hydroxy-3-methyl-benzofuran-2-carboxylate (7*e)*

The use of toluenethiol in the general procedure C provided **7***e* in 75% yield; mp 103–104°C; ^{1}H nmr (250 MHz, $CDCl_3$), δ: 7.23 (m, 5H), 6.95 (s, 2H), 4.40 (q, 2H, J = 7 Hz), 3.64 (s, 2H, SCH_2), 3.50 (s, 2H, SCH_2), 2.80 (s, 3H), 1.45 (t, 3H, J = 7 Hz). *Anal.* calcd. for $C_{20}H_{20}O_4S$: C 67.39, H 5.60, S 9.00; found: C 67.42, H 5.82, S 9.21.

*Ethyl 5-carboxymethylthiomethyl-4-hydroxy-3-methyl-benzofuran-2-carboxylate (7*f)*

In this case, a slightly increased proportion of aluminum chloride was used. Using 13 mmol of aluminum chloride, 2.5 mmol of **5**, and 10 mmol of mercaptoacetic acid, the title compound was obtained in 28% yield; mp 165–166°C; ^{1}H nmr (90 MHz, $CDCl_3$), δ: 7.32 (d, 1H, J = 8 Hz), 7.06 (d, 1H, J = 8 Hz), 4.42 (q, 2H, J = 7 Hz), 3.99 (s, 2H, SCH_2), 3.34 (s, 2H, SCH_2), 2.80 (s, 3H), 1.43 (t, 3H, J = 7 Hz). *Anal.* calcd. for $C_{15}H_{16}O_6S$: C 55.55, H 4.97, S 9.89; found: C 55.76, H 5.09, S 10.15.

General procedure D

*Preparation of ethyl 5-ethoxymethyl-4-hydroxy-3-methyl-benzofuran-2-carboxylate (8*b)*

A mixture of **5** (840 mg, 2.5 mmol), ethanol (17 mL), and concentrated sulphuric acid (0.1 mL) was heated under reflux for 1 h, and then evaporated to ca. 5 mL before the addition of ether and water. The crude product from the ether extract was purified by column chromatography to give 331 mg (48%) of **8***b*; mp 97–98°C, ir (KBr) ν: 1729, 3310 cm^{-1}; ^{1}H nmr (250 MHz, $CDCl_3$), δ: 8.40 (s, 1H, OH), 6.99 (s, 2H), 4.81 (s, 2H, OCH_2), 4.45 (q, 2H), 3.68 (q, 2H), 2.78 (s, 3H), 1.45 and 1.32 (2t, 6H). *Anal.* calcd. for $C_{15}H_{18}O_5$: C 64.74, H 6.52; found: C 64.74, H 6.39.

*2-Ethoxymethylphenol (8*a)*

Following the general procedure D, yield 48%; ^{1}H nmr (250 MHz, $CDCl_3$), δ: 7.74 (s, 1H, O*H*), 7.14–7.27 (m, 1H), 7.0 (d, 1H, J = 6.5 Hz), 6.78–6.93 (m, 2H), 4.71 (s, 2H, OCH_2), 3.62 (q, 2H, J = 6.5 Hz), 1.27 (t, 3H, J = 6.5 Hz); ms (70 eV) (m/e): 152 (M^+).

1. D. J. R. Massey. Synthesis, 589 (1987).
2. (*a*) P. G. Gassman and D. R. Amick. J. Am. Chem. Soc. **100**, 7611 (1978); (*b*) K. Sato, S. Inoue, and K. Ozawa. J. Chem. Soc. Perkin Trans. 1, 2715 (1984), and references cited therein; (*c*) S. Inoue, H. Ikeda, S. Sato, K. Horie, T. Ota, O. Miyamoto, and K. Sato. J. Org. Chem. **52**, 5495 (1987); (*d*) M. G. Burdon and J. G. Moffat. J. Am. Chem. Soc. **87**, 4645 (1965).
3. (*a*) H. Gilman and R. L. Bedd. J. Am. Chem. Soc. **61**, 109 (1939); (*b*) G. Wittig and G. Fuhrman. Chem. Ber. **73**, 1197 (1940); (*c*) H. Gilman and J. W. Mortin, Jr. Org. React. **8**, 258 (1954); (*d*) G. P. Ng and C. R. Dawson. J. Org. Chem. **43**, 3205 (1978); (*e*) H. Christensen. Synth. Commun. **5**, 65 (1975); (*f*) H. Achenback, W. Kohl, and B. Kunze. Chem. Ber. **112**, 1841 (1979); (*g*) R. C. Roland. Tetrahedron Lett. 3973 (1975); (*h*) N. S. Narasimhan, R. S. Mali, and M. V. Barve. Synthesis, 906 (1979); (*i*) G. A. Kraus and J. O. Penzzanite. J. Org. Chem. **44**, 2480 (1979); (*j*) D. L. Barton, P. C. Conrad, and P. L. Fuchs. Tetrahedron Lett. 1811 (1980); (*k*) T. Kamikawa. Synthesis, 431 (1986); (*l*) C. A. Townsend and L. M. Bloom. Tetrahedron Lett. 3923 (1981); (*m*) R. J. Mills, R. F. Horvath, M. P. Sibi, and V. Snieckus. Tetrahedron Lett. 1145 (1985).
4. (*a*) A. J. Kolka, J. P. Napolitano, and G. G. Ecke. J. Org. Chem. **21**, 712 (1956); (*b*) G. Casiraghi, M. Cornia, G. Casnati, G. G. Fava, M. F. Beliechi, and L. Zetta. J. Chem. Soc. Chem. Commun. 794 (1987); (*c*) G. Casiraghi, M. Cornia, and G. Rassu. J. Org. Chem. **53**, 4919 (1988).
5. H. G. Peer. Recl. Trav. Chim. Pays-Bas, **79**, 825 (1960).
6. W. Nagata, K. Okada, and T. Aoki. Synthesis, 365 (1979).
7. C. K. Lau, H. W. R. Williams, S. Tardif, C. Dufresne, and J. Scheigetz. J. Org. Chem. **54**, 491 (1989).

Synthesis of 4-methylumbelliferyl glycosides for the detection of α- and β-D-galactopyranosaminidases

R. SZWEDA,[1] U. SPOHR,[2] AND R. U. LEMIEUX[3]
Department of Chemistry, University of Alberta, Edmonton, Alta., Canada T6G 2G2

D. SCHINDLER[4]
Department of Human Genetics, University of Würzburg, Würzburg, F.R.G.

AND

D. F. BISHOP[5] AND R. J. DESNICK
Division of Medical and Molecular Genetics, The Mount Sinai School of Medicine, Fifth Avenue at 100th Street, New York, NY 10029-6574, U.S.A.

Received February 27, 1989

R. SZWEDA, U. SPOHR, R. U. LEMIEUX, D. SCHINDLER, D. F. BISHOP, and R. J. DESNICK. Can. J. Chem. **67**, 1388 (1989).

Reaction at room temperature of either 3,4,6-tri-*O*-acetyl-2-azido-2-deoxy-α- or -β-D-galactopyranosyl chloride with a twofold excess of 4-methylumbelliferone and silver trifluoromethanesulfonate in dichloromethane containing an equimolar amount of *sym*-collidine yielded 4-methylumbelliferyl tri-*O*-acetyl-2-azido-2-deoxy-α-D-galactopyranoside in 33% yield. The β anomer was formed in 20 and 10% yields, respectively. Reduction of the azido group, acetylation followed by de-*O*-acetylation, provided the desired 4-methylumbelliferyl 2-acetamido-2-deoxy-α- and -β-D-galactopyranosides (*N*-acetyl-α- and -β-D-galactopyranosaminides). The α-glycoside proved to be an effective substrate for the highly sensitive fluorimetric detection of *N*-acetyl-α-D-galactopyranosaminidase activity in human tissues and was used to examine the deficiency of this activity, which is the enzymatic defect in Schindler disease.

Key words: synthesis of 4-methylumbelliferyl *N*-acetyl-α- and -β-D-galactopyranosaminides, *N*-acetyl-α-D-galactosaminidase deficiency (Schindler disease).

R. SZWEDA, U. SPOHR, R. U. LEMIEUX, D. SCHINDLER, D. F. BISHOP et R. J. DESNICK. Can. J. Chem. **67**, 1388 (1989).

La réaction, à la température ambiante, des chlorures des 3,4,6-tri-*O*-acétyl-2-azido-2-déoxy-α- ou -β-D-galactopyranosyles avec deux moles de 4-méthylumbelliférone et de trifluorométhanesulfonate d'argent, dans du dichlorométhane contenant une quantité équimolaire de *sym*-collidine, conduit au tri-*O*-acétyl-2-azido-2-déoxy-α-D-galactopyranoside de 4-méthylumbelliféryle, avec un rendement de 33%. L'anomère β se forme avec des rendements respectifs de 10 et 20%. La réduction du groupement azido, suivie d'une acétylation et d'une de-*O*-acétylation, conduit aux 2-acétamido-2-déoxy-α- et -β-D-galactopyranosides de 4-méthylumbelliféryles désirés (*N*-acétyl-α- et -β-D-galactopyranosaminides). L'α-glycoside s'avère être un substrat efficace pour la détection fluorimétrique hautement sensible de l'activité de la *N*-acétyl-α-D-galactopyranosaminidase dans les tissus humains et on l'a utilisé pour examiner le manque de cette activité qui est le défaut enzymatique de la maladie de Schindler.

Mots clés : synthèse de 4-méthylumbelliféryle *N*-acétyl-α- et -β-D-galactopyranosaminides, manque de la *N*-acétyl-α-D-galactopyranosaminidase (maladie de Schindler).

[Traduit par la revue]

Introduction

In 1955, Mead, Smith, and Williams (1) observed that although umbelliferone fluoresced strongly in ultraviolet light at pH 9–10, its glucuronide was practically nonfluorescent. The possibility therefore existed that glucuronide could be used for the determination of enzymes in very small amounts of material. Indeed, 4-methylumbelliferyl β-D-glucuronide proved to be an excellent substrate for a fluorimetric assay for β-D-glucuronidase. In the following year, Robinson (2) synthesized 4-methylumbelliferyl β-D-glucopyranoside and used it to study β-D-glucopyranosidases from a variety of sources. In 1961, Leaback and Walker (3) published the use of 4-methylumbelliferyl *N*-acetyl-β-D-glucosaminide as a substrate and Winchester (4) then demonstrated the use of the corresponding *N*-acetyl-β-D-galactopyranosaminide to detect *N*-acetyl-β-D-galactosaminidase activity in tissues. Since these early studies, 4-methylumbelliferyl glycosides have found widespread applications for the detection and assay of a number of glycosidases (5, 6) and their use was extended to fluorimetric studies of their binding by lectins (7, 8).

Although 4-methylumbelliferyl *N*-acetyl-β-D-galactopyranosaminide (**9**) has long been commercially available, its preparation does not appear to have been published. *p*-Nitrophenyl *N*-acetyl-α-D-galactopyranosaminide has been used for the characterization of human *N*-acetyl-α-D-galactosaminidase. Use of the corresponding 4-methylumbelliferyl glycoside (**7**) could be expected to provide a much higher sensitivity, and its availability became a high priority with the discovery that Schindler disease is a neurodegenerative disorder that results from a deficiency of a lysosomal *N*-acetyl-α-D-galactopyranosaminidase (9, 10). The purpose of this communication is to report both the preparation of **7** and its β anomer (**9**) and to demonstrate the utility of **7** for the detection of hydrolases specific for terminal *N*-acetyl-α-D-galactopyranosaminidyl units as occur in human blood group A active glycolipids and O-linked glycoproteins.

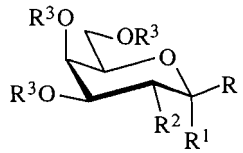
Results and discussion

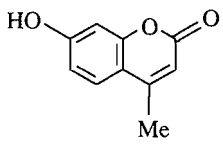
Possibly, 4-methylumbelliferyl *N*-acetyl-α-D-galactopyrano-

[1]University of Alberta Postdoctoral Fellow, 1987–present.
[2]Research Associate, University of Alberta, 1984–1988.
[3]Author to whom correspondence may be addressed.
[4]Visiting Assistant Professor, Mount Sinai School of Medicine, 1988–present.
[5]Associate Professor, Mount Sinai School of Medicine.

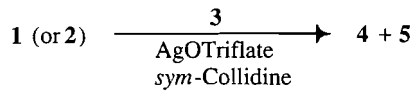
Printed in Canada / Imprimé au Canada

Can. J. Chem. Downloaded from www.nrcresearchpress.com by 194.225.253.170 on 09/07/12
For personal use only.





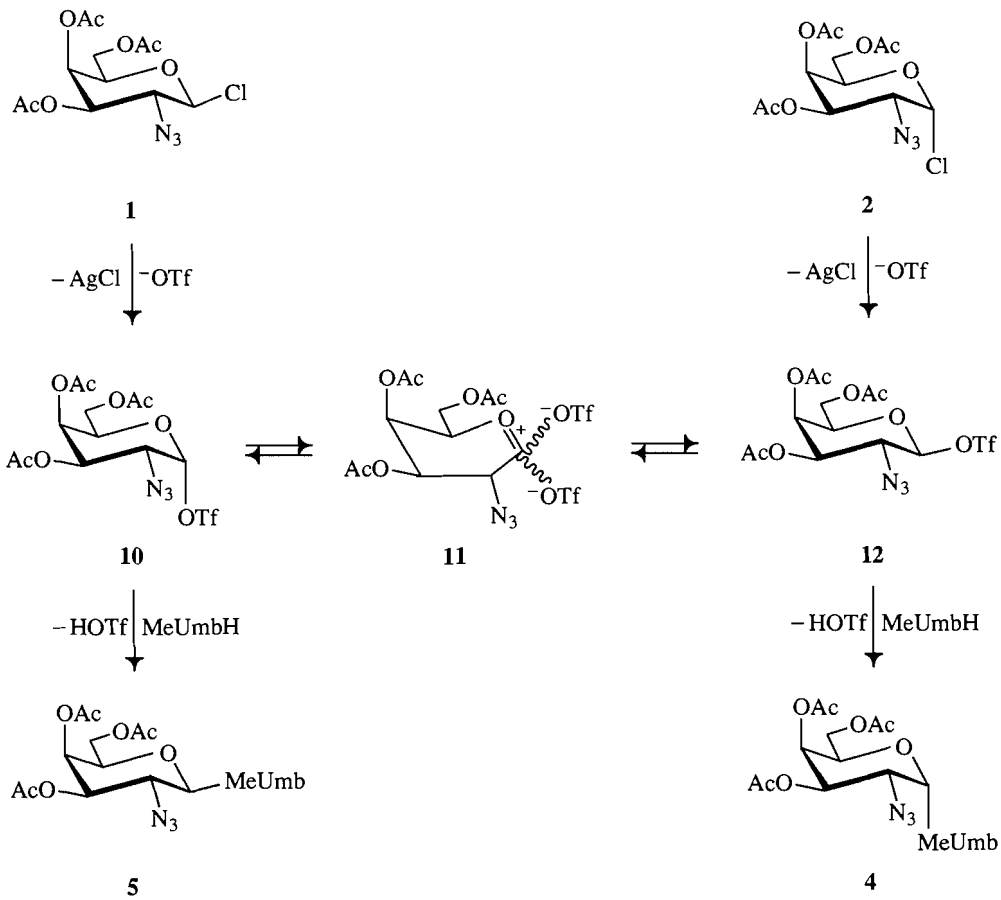
3 (MeUmb-H)



	R	R^1	R^2	R^3
1	Cl	H	N_3	Ac
2	H	Cl	N_3	Ac
4	H	MeUmb	N_3	Ac
5	MeUmb	H	N_3	Ac
6	H	MeUmb	NHAc	Ac
7	H	MeUmb	NHAc	H
8	MeUmb	H	NHAc	Ac
9	MeUmb	H	NHAc	H

saminide (**7**) would be obtained by way of a Koenigs–Knorr type reaction of 3,4,6-tri-*O*-acetyl-2-azido-2-deoxy-β-D-galactopyranosyl chloride (**11**) with 4-methylumbelliferone. Indeed, Lemieux and Ratcliffe (12) prepared the A-blood group related blocked trisaccharide, 8-methoxycarbonyloctyl 3-*O*-(3,4,6-tri-*O*-acetyl-2-azido-2-deoxy-α-D-galactopyranosyl)-2-*O*-(2,3,4-tri-*O*-benzyl-α-L-fucopyranosyl)-4,6-*O*-benzylidene-β-D-galactopyranoside in 74% yield using silver carbonate/silver trifluoromethanesulfonate (silver triflate) (45:1) as promoter for the reaction of **1**. Thus, reaction with simple inversion of the anomeric center was obtained and the formation of an intermediate glycosyl triflate did not occur. In contrast, Lemieux, Takeda, and Chung (13) introduced the use of a mixture of silver triflate (AgOTf) and *sym*-collidine to promote the reaction of 2-deoxy-2-phthalimido-glycosyl halides with alcohols to form β-glycosides, and demonstrated that glycosyl triflate was formed in the first stage of the reaction sequence. It was considered, therefore, of interest to examine the reaction of 3,4,6-tri-*O*-acetyl-2-azido-2-deoxy-α-D-galactopyranosyl chloride (**2**) with 4-methylumbelliferone (**3**) in the presence of the silver triflate – *sym*-collidine complex since the β-triflate (**12**) could be the first product of the overall reaction. Furthermore, the α-chloride (**2**) is much more readily available than is the β anomer (**1**) (11). In this regard, it is important to note that the use of the Vilsmeier reagent, as recommended by Sabesan and Lemieux (14), to convert the by-product *N*-(3,4,6-tri-*O*-acetyl-2-azido-2-deoxy-α-D-galactopyranosyl) acetamide to **2** has now provided a one-stage process from the crude product of azidonitration of D-galactal triacetate (11). Chromatographically pure **2** was obtained in 75% yield.

As mentioned above, it seemed likely that reaction of **2** with silver triflate would proceed with inversion to provide the β-glycosyl triflate (**12**). Reaction of **12** with umbelliferone would then provide the desired α-glycoside (**4**). In fact, **4** was the main product (33% yield) but the β anomer (**5**) was also formed (10% yield). The two products were readily isolated in a high state of purity by column chromatography on silica gel. Thus, although the yields are low, the procedure provides both the α- and β-glycosides. When the β-chloride (**1**) was starting material, much the same result was obtained (33% yield of **4** and 20% yield of **5**). These results suggest that the reactions proceeded by way of a common intermediate and could be



Can. J. Chem. Downloaded from www.nrcresearchpress.com by 194.225.253.170 on 09/07/12
For personal use only.

TABLE 1. *N*-Acetyl-α-D-galactosaminidase and *N*-acetyl-β-D-galactosaminidase activities in cultured fibroblasts from affected homozygotes with Schindler disease

Source	Activity (nmol·h^{-1}·(mg protein)$^{-1}$)	
	α-NAcGalase	β-NAcGalase
Affected homozygote 1	3.2	1500
Affected homozygote 2	1.8	1830
Normal male	146.0	1340

rationalized on the basis of the formation of a free oxocarbonium ion. On the other hand, a rapid interconversion of the initially formed glycosyl triflates (**10** and **12**) by way of the ion triplet (**11**), as was found for the anomerization of glycosyl halides in the presence of halide ion (15), is considered the more plausible route.

The conversions of the acetylated azido compounds (**4** and **5**) to the desired glycosides (**7** and **9**) involved standard transformations that proceeded in high yields. The main difficulty encountered was with the high insolubility of α-glycoside (**7**), which resisted crystallization. Crystals of the β-glycoside (**9**) were obtained without difficulty.

To establish the utility of **7** for the detection of enzymes specific for a terminal αDGalNAc residue, the deficient activity of *N*-acetyl-α-D-galactosaminidase was demonstrated in cultured fibroblasts from sibs affected with Schindler disease. Residual activities of 1–2% were observed in the affected sibs as compared to the high activity in a normal male control (Table 1). Mixing experiments with fibroblast extracts from an affected sib (1.4 nmol·h^{-1}·mg^{-1}) and an unrelated normal control (181 nmol·h^{-1}·mg^{-1}) revealed the expected intermediate activity (95.1 nmol·h^{-1}·mg^{-1}), thereby excluding the presence of an inhibitor or the absence of an activator as the cause of the enzymatic defect. In contrast, the *N*-acetyl-β-D-galactosaminidase activities were normal in cultured fibroblasts from the affected sibs and the normal male control (Table 1).

Experimental

General methods

All solvents and reagents were purified according to standard procedures (16).

Thin-layer chromatograms (tlc) were performed on precoated silica gel 60 F_{254} plates (E. Merck, Darmstadt) and visualized by charring after spraying with 5% sulphuric acid in ethanol. For column chromatography, silica gel G (type 60) (E. Merck, Darmstadt) and distilled solvents were used.

The ^{1}H nmr spectra were recorded at 300 MHz and 296 K. In $CDCl_3$ the ^{1}H chemical shifts (δ, in ppm) are relative to internal tetramethylsilane (δ = 0). When DMSO-d_6 was the solvent, the reference was the $(CH_3)_2SO$ signal set at 2.49 ppm.

The melting points are uncorrected.

*4-Methylumbelliferyl 3,4,6-tri-*O*-acetyl-2-azido-2-deoxy-α- (**4**) and -β-D-galactopyranoside (**5**)*

*(a) From 3,4,6-tri-*O*-acetyl-2-azido-2-deoxy-β-D-galactopyranosyl chloride (**1**)*

4-Methylumbelliferone (**3**) (0.895 g, 5.09 mmol), dry silver trifluoromethanesulfonate (1.308 g, 5.09 mmol), *sym*-collidine (0.34 g, 2.55 mmol), and 4 Å molecular sieves (4 g, powdered) in dichloromethane (10 mL) were stirred for 1 h under dry nitrogen in the dark. A solution of 3,4,6-tri-*O*-acetyl-2-azido-2-deoxy-β-D-galactopyranosyl chloride (11) (**1**) (0.89 g, 2.55 mmol) in dichloromethane (9 mL) was then added to the stirred mixture at room temperature. The disappearance of the chloride (**1**) was monitored by tlc using chloroform – ethyl acetate, 4:1 (v/v). After 6 h the mixture was filtered. The filtrate was evaporated to give a red syrup (~2.4 g), which was chromatographed on a silica gel column (250 g, solvent chloroform – ethyl acetate, 8:1 (v/v)) to give 4-methylumbelliferyl 3,4,6-tri-*O*-acetyl-2-azido-2-deoxy-α-D-galactopyranoside (**4**) (0.41 g, 33%) as a white foam. The analytical sample was recrystallized from ethanol, mp 131–132°C; $[\alpha]_D^{20}$ +195° (*c* 0.5, $CHCl_3$); ^{1}H nmr ($CDCl_3$) δ: 7.56 (d, 1H, H-5, $J_{5,6}$ = 8.75 Hz), 7.13 (d, 1H, H-8, $J_{6,8}$ = 2.5 Hz), 7.04 (dd, 1H, H-6), 6.21 (d, 1H, H-3, J_{3,CH_3} = 1.4 Hz), 5.70 (d, 1H, H-1′, $J_{1',2'}$ = 4 Hz), 5.58 (dd, 1H, H-3′, $J_{2',3'}$ = 11 Hz, $J_{3',4'}$ = 3 Hz), 5.53 (dd, 1H, H-4′, $J_{4',5'}$ = 1 Hz), 4.30 (m, 1H, H-5′), 4.10 (m, 2H, H-6′a and H-6′b), 3.90 (dd, 1H, H-2′), 2.43 (d, 3H, CH_3 (MeUmb)), 2.19, 2.11, 1.97 (3s, each 3H, $3CH_3CO$). Continued elution of the column provided 4-methylumbelliferyl 3,4,6-tri-*O*-acetyl-2-azido-2-deoxy-β-D-galactopyranoside (**5**) (0.25 g, 20%) as a yellowish foam; $[\alpha]_D^{20}$ +2° (*c* 0.5, $CHCl_3$); ^{1}H nmr ($CDCl_3$) δ: 7.56 (dd, 1H, H-5, $J_{5,6}$ = 9 Hz, $J_{5,8}$ = 1 Hz), 7.03 (d, 1H, H-8), 7.02 (dd, 1H, H-6, $J_{6,8}$ = 2 Hz), 6.22 (d, 1H, H-3, J_{3,CH_3} = 1.4 Hz), 5.43 (dd, 1H, H-4′, $J_{3',4'}$ = 3.5 Hz, $J_{4',5'}$ = 1 Hz), 5.00 (d, 1H, H-1′, $J_{1',2'}$ = 8 Hz), 4.92 (dd, 1H, H-3′, $J_{2',3'}$ = 11 Hz), 4.19 (m, 2H, H-6′a, H-6′b), 4.07 (m, 1H, H-5′), 4.03 (dd, 1H, H-2′), 2.43 (d, 3H, CH_3 (MeUmb)), 2.19, 2.12, 2.09 (3s, 9H, $3CH_3CO$). *Anal.* calcd. for $C_{22}H_{23}N_3O_{10}$: C 53.99, H 4.74, N 8.58; found for **4**: C 53.64, H 4.76, N 8.70; for **5**: C 53.25, H 4.90, N 8.82.

*(b) From 3,4,6-tri-*O*-acetyl-2-azido-2-deoxy-α-D-galactopyranosyl chloride (**2**)*

The crude product of azidonitration of 3,4,6-tri-*O*-acetyl-D-galactal (11) (0.31 g) was dissolved in dichloromethane (2 mL) and DMF (0.2 mL) and a solution of oxalyl chloride (140 μL, 1.61 mmol) in dichloromethane (0.5 mL) was added at 0°C with stirring. After 1 h, a solution of anhydrous tetraethylammonium chloride (0.64 g, 3.86 mmol) in dry acetonitrile (2 mL) was added and the stirring was continued for 6 h. The solution was then diluted with dichloromethane (100 mL) before washing with water (2 × 20 mL). Solvent removal left a syrup (0.287 g). Chromatography on a silica gel column (50 g, solvent *n*-hexane – ethyl acetate (3:1)) gave 0.215 g (75%) of very pure (^{1}H nmr) syrupy α-chloride (**2**) (11); $[\alpha]_D^{20}$ +146° (*c* 0.67, $CHCl_3$); ^{1}H nmr ($CDCl_3$) δ: 6.18 (d, 1H, H-1, $J_{1,2}$ = 4 Hz), 5.51 (dd, 1H, H-4, $J_{3,4}$ = 3 Hz, $J_{4,5}$ = 1.5 Hz), 5.38 (dd, 1H, H-3, $J_{2,3}$ = 11 Hz), 4.52 (m, 1H, H-5), 4.15 (m, 2H, H-6a, H-6b), 4.11 (dd, 1H, H-2), 2.17, 2.08, 2.06 (3s, each 3H, $3CH_3CO$).

4-Methylumbelliferone (**3**) (3.35 g, 19 mmol), silver trifluoromethanesulfonate (8.81 g, 34.2 mmol), *sym*-collidine (2.3 g, 17.17 mmol), and 4 Å molecular sieves (10 g, powdered) in dichloromethane (30 mL) were stirred for 1 h under nitrogen in the dark. A solution of the above α-chloride (**2**) (6 g, 17.17 mmol) in dichloromethane (20 mL) was then added dropwise over a period of 0.5 h to the stirred mixture at room temperature. The disappearance of the chloride was monitored by tlc using chloroform – ethyl acetate 4:1 (v/v). After 16 h the mixture was filtered. Evaporation of the dichloromethane left a red syrup (~10 g), which was chromatographed on a column of silica gel (500 g, solvent chloroform – ethyl acetate 8:1 (v/v)) to give 4-methylumbelliferyl 3,4,6-tri-*O*-acetyl-2-azido-2-deoxy-α-D-galactopyranoside (**4**) (2.79 g, 33%) and its β-anomer (**5**) (0.84 g, 10%).

*4-Methylumbelliferyl 2-acetamido-3,4,6-tri-*O*-acetyl-2-deoxy-α-D-galactopyranoside (**6**)*

4-Methylumbelliferyl 3,4,6-tri-*O*-acetyl-2-azido-2-deoxy-α-D-galactopyranoside (**4**) (2.75 g, 5.62 mmol) was dissolved in 95% ethanol (150 mL) and hydrogenated at room temperature in the presence of 5% palladium-on-charcoal (2.75 g). After 2 h the catalyst was removed. Evaporation of the ethanol left a white foam (~2.25 g), which was acetylated in pyridine (5 mL) and acetic anhydride (5 mL). The mixture was kept 1 h at room temperature. Evaporation provided a white foam (~2.4 g). Chromatography on a column of silica gel (200 g, solvent chloroform – ethyl acetate 1:1 (v/v)) gave the title compound (**6**) (2.02 g, 71%) as a white foam; $[\alpha]_D^{20}$ +202° (*c* 0.5, chloroform);

Can. J. Chem. Downloaded from www.nrcresearchpress.com by 194.225.253.170 on 09/07/12
For personal use only.

^{1}H nmr ($CDCl_3$) δ: 7.57 (d, 1H, H-5, $J_{5,6}$ = 8.75 Hz), 7.09 (d, 1H, H-8, $J_{6,8}$ = 2.5 Hz), 7.02 (dd, 1H, H-6), 6.20 (d, 1H, H-3, J_{3,CH_3} = 1.4 Hz), 5.78 (d, 1H, NH, $J_{NH,2'}$ = 9 Hz), 5.69 (d, 1H, H-1′, $J_{1',2'}$ = 3.5 Hz), 5.46 (dd, 1H, H-4′, $J_{3',4'}$ = 3 Hz, $J_{4',5'}$ = 1 Hz), 5.40 (dd, 1H, H-3′, $J_{2',3'}$ = 11.5 Hz), 4.79 (ddd, 1H, H-2′), 4.24 (dt, 1H, H-5′), 4.09 (m, 2H, H-6′a, H-6′b), 2.42 (d, 3H, CH_3 (MeUmb)), 2.20, 2.06, 2.00, 1.95 (4s, each 3H, $4CH_3CO$).

4-Methylumbelliferyl 2-acetamido-2-deoxy-α-D-galactopyranoside (7)

A solution of 4-methylumbelliferyl 2-acetamido-3,4,6-tri-*O*-acetyl-2-deoxy-α-D-galactopyranoside (**6**) (1.96 g, 3.88 mmol) in dry methanol (100 mL) containing 0.5 N methanolic sodium methoxide (6 mL) was stirred at room temperature. After 15 min a precipitate appeared. The tlc analysis (chloroform–methanol, 9:1) of the liquid phase showed the reaction to be complete. The precipitate was filtered and washed 3 times with cold methanol to provide the title compound in 90% yield (1.32 g) as a white solid, mp 264–265°C (dec.), $[\alpha]_D^{20}$ +251° (*c* 0.4, DMSO); uv (H_2O) λ_{max} (log ε): 318 nm (4.01); ^{1}H nmr (DMSO-d_6) δ: 7.91 (d, 1H, NH, $J_{NH,2'}$ = 9 Hz), 7.70 (d, 1H, H-5, $J_{5,6}$ = 8.5 Hz), 7.07 (dd, 1H, H-6, $J_{6,8}$ = 2 Hz), 7.05 (br s, 1H, H-8), 6.24 (d, 1H, H-3, J_{3,CH_3} = 1 Hz), 5.53 (d, 1H, H-1′, $J_{1',2'}$ = 3 Hz), 4.78 (d, 1H, OH-4′, $J_{4',OH}$ = 4 Hz), 4.69 (d, 1H, OH-3′, $J_{3',OH}$ = 6 Hz), 4.58 (t, 1H, OH-6′, $J_{OH,6'a}$ = $J_{OH,6'b}$ = 5.5 Hz), 4.24 (m, 1H, H-2′), 3.87–3.77 (m, 2H, H-3′, H-4′), 3.67 (m, 1H, H-5′), 3.52 (m, 1H, H-6′a), 3.41 (m, 1H, H-6′b), 2.39 (d, 3H, CH_3 (MeUmb)), 1.83 (s, 3H, CH_3CONH). *Anal.* calcd. for $C_{18}H_{21}NO_8$: C 56.99, H 5.58, N 3.69; found: C 56.45, H 5.70, N 3.62.

*4-Methylumbelliferyl 2-acetamido-3,4,6-tri-*O*-acetyl-2-deoxy-β-D-galactopyranoside (8)*

4-Methylumbelliferyl 3,4,6-tri-*O*-acetyl-2-azido-2-deoxy-β-D-galactopyranoside (**5**) (0.235 g, 0.48 mmol) was dissolved in 95% ethanol (10 mL) and hydrogenated at room temperature for 3 h in the presence of 5% palladium-on-charcoal (0.24 g). Catalyst removal and evaporation provided a white foam (0.205 g). It was dissolved in methanol (5 mL) and acetic anhydride (1.5 mL) was added. After 6 h the solvent was evaporated to give a white foam (0.21 g). Chromatography on a column of silica gel (25 g, chloroform – ethyl acetate 1:1 (v/v)) gave the title compound (**8**) (0.17 g, 70%) as a white foam; $[\alpha]_D^{20}$ −3° (*c* 0.4, $CHCl_3$); ^{1}H nmr ($CDCl_3$) δ: 7.50 (dd, 1H, H-5, $J_{5,6}$ = 8 Hz, $J_{5,8}$ = 1.5 Hz), 6.97 (br s, 1H, H-8), 6.95 (dd, 1H, H-6, $J_{6,8}$ = 2.5 Hz), 6.17 (d, 1H, H-3, J_{3,CH_3} = 1.4 Hz), 5.79 (d, 1H, NH, $J_{NH,2'}$ = 9 Hz), 5.46 (d, 1H, H-4′, $J_{3',4'}$ = 3.5 Hz), 5.44 (d, 1H, H-1′, $J_{1',2'}$ = 8 Hz), 5.43 (dd, 1H, H-3′, $J_{2',3'}$ = 11 Hz), 4.31 (m, 1H, H-2′), 4.21–4.09 (m, 3H, H-5′, H-6′a, H-6′b), 2.40 (d, 3H, CH_3 (MeUmb)), 2.18, 2.11, 2.05, 1.98 (4s, each 3H, $4CH_3CO$).

4-Methylumbelliferyl 2-acetamido-2-deoxy-β-D-galactopyranoside (9)

A solution of 4-methylumbelliferyl 2-acetamido-3,4,6-tri-*O*-acetyl-2-deoxy-β-D-galactopyranoside (**8**) (0.145 g, 0.29 mmol) in dry methanol (20 mL) containing 0.5 N methanolic sodium methoxide (2.5 mL) was stirred at room temperature. After 20 min precipitate appeared. The tlc analysis (chloroform–methanol, 9:1) of the liquid phase indicated that the reaction was finished. The mixture was neutralized with Amberlite IRC-50 (H^+) resin. The solvent was isolated by decantation and the resin was washed several times with methanol. The combined methanolic solution was evaporated to give a white solid (0.106 g, 97%). It was crystallized from 50% ethanol (0.07 g, 64%); mp 226–226.5°C (dec.), $[\alpha]_D^{20}$ +20° (*c* 0.4, DMSO); uv (H_2O) λ_{max} (log ε): 317 nm (4.156); ^{1}H nmr (DMSO-d_6) δ: 7.77 (d, 1H, NH, $J_{NH,2'}$ = 9 Hz), 7.68 (d, 1H, H-5, $J_{5,6}$ = 8.5 Hz), 6.99 (d, 1H, H-8, $J_{6,8}$ = 2 Hz), 6.94 (dd, 1H, H-6), 6.24 (d, 1H, H-3, J_{3,CH_3} = 1 Hz), 5.08 (d, 1H, H-1′, $J_{1',2'}$ = 8.5 Hz), 4.80 (d, OH-3′, $J_{3',OH}$ = 6 Hz), 4.71 (t, 1H, OH-6′, $J_{6'a,OH}$ = $J_{6'b,OH}$ = 4 Hz), 4.69 (d, 1H, OH-4′, $J_{4',OH}$ = 4 Hz), 4.01 (ddd, 1H, H-2′, $J_{2',3'}$ = 10 Hz), 3.73 (m, 1H, H-4′), 3.66–3.46 (m, 4H, H-3′, H-5′, H-6′a, H-6′b), 2.39 (d, 3H, CH_3 (MeUmb)), 1.79 (s, 3H, CH_3CONH).

Enzyme assays

N-acetyl-α-D-galactosaminidase and *N*-acetyl-β-D-galactosaminidase activities were determined in cultured skin fibroblasts from two sibs with Schindler disease (*N*-acetyl-α-D-galactosaminidase deficiency) and an unrelated normal individual. Cultured fibroblasts were established, grown, and harvested by standard techniques. The cell pellets were frozen at −70°C until use. Fibroblasts were sonicated (70 W; five 20-s bursts) in the presence of 0.1 M citrate/0.1 M sodium phosphate buffer, pH 4.5, in a cup-horn sonicator. The sonicates were centrifuged (10,000 × *g*; 10 min) and the supernatants were assayed immediately. The standard reaction mixture, containing 90 μL of 1.10 mM of either 4-methylumbelliferyl 2-acetamido-2-deoxy-α- (or β) D-galactopyranoside, and 10 μL of fibroblast supernatant was incubated at 37°C for 30 min. The reactions were terminated by addition of 1.16 mL of 0.1 M ethylenediamine, pH 11.4. Fluorescence was measured in a Turner model 111 fluorometer equipped with a Corning 7.60 excitation filter (365 nm), Wratten 48 and 2A emission filters (450 nm), and a 1% Wratten neutral density filter. Protein concentrations were determined by the fluorescamine procedure (17).

1. J. A. R. Mead, J. N. Smith, and R. T. Williams. Biochem. J. **61**, 569 (1955).
2. D. Robinson. Biochem. J. **63**, 39 (1956).
3. D. H. Leaback and P. G. Walker. Biochem. J. **78**, 151 (1961).
4. B. G. Winchester. Biochem. J. **124**, 929 (1971).
5. M. L. Shulman, V. A. Kulshin, and A. Ya. Khorlin. Anal. Biochem. **101**, 342 (1980).
6. T. Izumi and K. Suzuki. J. Biol. Chem. **258**, 6991 (1983).
7. H. De Boeck, H. Lis, H. van Tilbeurgh, N. Sharon, and F. G. Loentiens. J. Biol. Chem. **259**, 7067 (1984).
8. M. Decastel, M. Vincent, K. L. Matta, and J. P. Frénoy. Arch. Biochem. Biophys. **232**, 640 (1984).
9. O. P. van Diggelen, D. Schindler, W. J. Kleijer, J. M. G. Huijmans, H. Galyaard, H. U. Linden, J. Peter Katalinic, H. Egge, U. Dabrowski, and M. Cantz. Lancet, **2**, 804 (1987).
10. D. Schindler, D. F. Bishop, S. Wallace, D. E. Wolfe, and R. J. Desnick. Pediatr. Res. **23**, 333A (1988).
11. R. U. Lemieux and R. M. Ratcliffe. Can. J. Chem. **57**, 1244 (1979).
12. R. U. Lemieux and R. M. Ratcliffe. U.S. Patent 4,195,174; March 25, 1980.
13. R. U. Lemieux, T. Takeda, and B. Y. Chung. ACS Symp. Ser. No. 39. 1976. pp. 90–115.
14. S. Sabesan and R. U. Lemieux. Can. J. Chem. **62**, 644 (1984).
15. R. U. Lemieux and J. Hayami. Can. J. Chem. **43**, 2162 (1965).
16. D. D. Perrin, W. L. Armarego, and D. R. Perrin. *In* Purification of laboratory chemicals. Pergamon Press, London. 1966.
17. P. Bohlen, S. Stein, W. Dairman, and S. Udenfriend. Arch. Biochem. Biophys. **155**, 213 (1973).

Can. J. Chem. Downloaded from www.nrcresearchpress.com by 194.225.253.170 on 09/07/12
For personal use only.

Synthesis and reaction of *ortho*-fluoronitroaryl nitroxides. Novel versatile synthons and reagents for spin-labelling studies

H. OLGA HANKOVSZKY, KÁLMÁN HIDEG,[1] AND M. JUDIT LOVAS
Central Laboratory, Chemistry, University of Pécs, H-7643 Pécs, P.O. Box 99, Hungary
GYULA JERKOVICH
Institute for Drug Research, H-1325 Budapest, P.O. Box 82, Hungary
ANTAL ROCKENBAUER AND MIKLÓS GYÖR
Central Research Institute for Chemistry of the Hungarian Academy of Sciences, H-1525 Budapest, P.O. Box 17, Hungary
AND
PÁL SOHÁR
EGIS Pharmaceuticals, Spectroscopic Department, H-1475 Budapest, P.O. Box 100, Hungary

Received January 13, 1989

H. OLGA HANKOVSZKY, KÁLMÁN HIDEG, M. JUDIT LOVAS, GYULA JERKOVICH, ANTAL ROCKENBAUER, MIKLÓS GYÖR, and PÁL SOHÁR. Can. J. Chem. **67**, 1392 (1989).

2-Flurophenyl- and 2,5-bis(fluorophenyl)pyrrolidin-1-oxyls (**2** and **6**) were synthesized from the corresponding nitrones **1**, **4**, and **5** with the Grignard reagent prepared from 1-bromo-4-fluorobenzene. The reaction of 2,2,5,5-tetramethyl-3-formyl-3-pyrrolin-1-oxyl (**8**) with $(4\text{-}FC_6H_4)_2Cd$ gave 2,2,5,5-tetramethyl-3-(α-hydroxy-4-fluorobenzyl)-3-pyrrolin-1-oxyl (**9**), which was oxidized with MnO_2 to 2,2,5,5-tetramethyl-3-(4-fluorobenzoyl)-3-pyrrolin-1-oxyl (**10**). The aryl nitroxides **2**, **6**, and **10** were nitrated with concentrated H_2SO_4/HNO_3 to *ortho*-fluoronitrophenyl compounds **3**, **7**, and **11**. The fluoro nitro derivatives served as versatile synthons in the nucleophilic replacement of fluorine with OH, NH_2, α-amino acid ester, or thiol. The hydroxy nitroaryl compounds **16**, **26**, and **30** were nitrated further to give dinitrophenol derivatives **17**, **27**, and **31**.

Key words: fluorophenyl nitroxides, nitroaryl nitroxides, NMR spectra of nitroxides.

H. OLGA HANKOVSZKY, KÁLMÁN HIDEG, M. JUDIT LOVAS, GYULA JERKOVICH, ANTAL ROCKENBAUER, MIKLÓS GYÖR et PÁL SOHÁR. Can. J. Chem. **67**, 1392 (1989).

On a préparé des fluoro-2-phényl- et des bis(fluoro-2,5-phényl)-pyrrolidinoxyles-1 (**2** et **6**) à partir des nitrones correspondants **1**, **4** et **5** en utilisant des réactifs de Grignard préparés à partir du bromo-1-fluoro-4-benzène. Le composé téetraméthyl-2,2,5,5-formyl-3-pyrrolin-3-oxyle-1 (**8**) réagit avec le $(F\text{-}4\text{-}C_6H_4)_2Cd$ pour donner le tétraméthyl-2,2,5,5-(α-hydroxyfluoro-4-benzyle)-3-pyrrolin-3-oxyle-1 (**9**) qui par oxydation avec le MnO_2 donne le tétraméthyl-2,2,5,5-(fluoro-4-benzoyle)-3-pyrrolin-3-oxyle-1 (**10**). Une nitration des nitroxydes aryliques **2**, **6** et **10** par le mélange H_2SO_4/MNO_3 conduit aux composés *ortho*-fluoronitrophényles **3**, **7** et **11**. Les dérivés fluoronitrés peuvent servir d'intermédiaires de synthèses dans le remplacement nucléophile du fluor par du OH, du NH_2, un ester d'acide α-aminé ou par un thiol. Une nitration plus poussée des composés nitroaryles hydroxylés **16**, **26** et **30** conduit aux dérivés du dinitrophénol **17**, **27** et **31**.

Mots clés : oxydes d'azote fluorophényles, oxydes d'azote nitroaryles, spectres en RMN des oxydes d'azote.

[Traduit par la revue]

Introduction

Various chemically reactive functional groups can be incorporated into appropriate paramagnetic molecules, whereby they can be attached to biomolecules (proteins, drugs, etc.) under mild reaction conditions without the involvement of the *N*-oxyl paramagnetic centre (1, 2). The analysis of spin-labelled compounds by esr spectroscopy is an important method in the study of biomolecules (3, 4). It has been found that such nitroxides are resistant against all but a minor group of reagents. The well-known reasons for the stability of these *N*-oxyl paramagnetic centres are the three π-electrons delocalized over two atoms (5) and the lack of *H* substituents on the carbons in the α position to the nitrogen, which prevents any disproportionation to the nitrone and the hydroxylamine.

Such reactions can therefore be utilized when the paramagnetic *N*-oxyl centre is reduced to the labile *N*-hydroxy group, because this function is oxidized back to the *N*-oxyl almost spontaneously by air.

We previously described various syntheses of nitroxides with organometallic reagents (6–8) and the nitration of phenyl-substituted nitroxides (8). In the present work, we described the synthesis of various fluorophenyl pyrrolidine and pyrroline nitroxides as starting compounds in nitration reactions. In fluoronitrophenol-substituted nitroxides, the fluorine has enhanced reactivity toward nucleophiles, similar to known reagents such as fluoro-2,4-dinitrobenzene (Sanger reagent) (9, 10) or spin-labelled fluorodinitrobenzene derivatives (11, 12). This may lead not only to new spin-label reagents, but also to compounds useful for the preparation of polysubstituted aryl nitroxides.

We earlier prepared cationic nitroxide probes such as the triaryl (1-oxyl-2,2,5,5-tetramethyl-3-pyrrolin-3-yl) phosphonium salt (13) for the investigation of reduction and stability in mitochondria. Several 1-oxyl-2,2,6,6-tetramethylpiperidinyl-amino nitrophenols with low pK_a have been prepared and utilized as anionic probes (30).[2] It has been confirmed by a number of research groups that both pyrrolidine and pyrroline nitroxides exhibit a higher resistance towards reduction than that of piperidines and oxazolines (14–16). This prompted us to prepare a new series of pyrrolidinyl polynitrophenol derivatives.

[1]Author to whom correspondence may be addressed.

[2]Also, R. F. Lewelling and W. L. Hubbell, private communication.

Printed in Canada / Imprimé au Canada

Can. J. Chem. Downloaded from www.nrcresearchpress.com by 194.225.253.170 on 09/07/12
For personal use only.

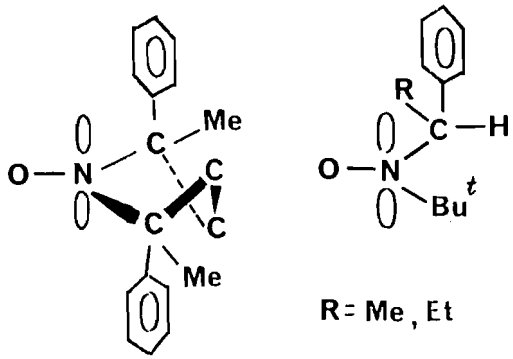


FIGURE 1

Results and discussion

2,5,5-Trimethyl-1-pyrroline-1-oxide (**1**) (17) was reacted with the Grignard reagent made from 1-bromo-4-fluorobenzene to give 2-(4-fluorophenyl)pyrrolidin-1-oxyl (**2**), which was then nitrated with H_2SO_4/HNO_3 to 2-(3-nitro-4-fluorophenyl)pyrrolidin-1-oxyl (**3**). 2,5-Dimethyl-1-pyrroline-1-oxide (**4**) was functionalized to **6** with the above Grignard reagent in two steps, *via* nitrone **5**. In the reaction of **5** to **6**, the formation of both *cis* and *trans* isomers appeared possible, but only one isomer could be detected and isolated by chromatography. The nitration of **6** led to the formation of single dinitro compound **7**, in accordance with the expected orientation of the substituents of **6** (the protonated nitroxide directs into the *meta* position and the fluorine into the *ortho* position). We could not detect the formation of *m,m'*-dinitrofluorophenyl derivatives. This is evidenced for compound **7** by the three aromatic proton signals (at 7.25, 7.78, and 8.24 ppm) in the ^1H nmr spectrum, and by the three protonated and three quaternary carbon lines in the ^{13}C nmr spectrum. The ^1H nmr chemical shifts are more consistent with the 3-position of the nitro group: for the 2-nitro analogue, the expected shifts (18) are 7.27, 7.37, and 7.82 ppm, while for 3-nitro substitution they are 7.12, 7.52, and 8.07 ppm, in better accordance with the measured data. Analogous observations were found to hold for all examples investigated in this work. The ^1H and ^{13}C nmr spectra of compound **7** clearly showed the existence of a single product, but the symmetry of the molecule did not allow a direct determination by nmr of the *cis* or *trans* orientation of the substituents in positions 2 and 5. The investigation would be of value if the **6** or **7** could be converted into an asymmetric compound, e.g., by acylation of the reduced nitroxide (N÷O → N—OH) with a chiral acyl chloride, such as the Mosher reagent (19), utilized to determine the configuration of nitroxide fatty acids (20). For the symmetrical diaryl-substituted nitroxides **6**, **7**, and **26**, the most salient feature of the esr spectra is the large ^{13}C hyperfine splitting of 1.12 mT caused by two magnetically equivalent ^{13}C nuclei. According to esr studies on open chain nitroxide radicals (21), the large carbon couplings are evidence that the aryl groups are positioned parallel to the lobe of the unpaired electron orbital (Fig. 1.) This in turn presumes *trans* isomers for **6**, **7**, and **26**, since the *cis* isomers would require an energetically less favoured envelope conformation with a large puckering angle and consequently a large C(C)NO pyramidal distortion (22), in clear contradiction to the observed small nitrogen hyperfine couplings (1.33–1.34 mT). On the basis of the above observations we believe the only stereoisomers of **6** and its derivatives have *trans* geometry. The fluorophenyl unsaturated ketone **10** was obtained *via* an allylic alcohol **9** from the reaction of unsaturated aldehyde **8** (23) with di(fluorophenyl) Cd formed *in situ*. Being both a benzylic and an allylic alcohol, **9** is partially oxidized to **10** during the isolation of the reaction product, and therefore completion of the oxidation could easily be achieved with MnO_2. The nitration of **10** in a clear reaction again led to the formation of the single product **11**, due to the fluoro and carbonyl substituents in **10**. 1-Oxyl-2,2,6,6-tetramethyl-4-hydroxy-4-phenylpiperidine (**12**) (24) can be obtained in moderate yield from phenylmagnesium bromide and 1-oxyl-2,2,6,6-tetra-methylpiperidin-4-one. The nitration of **12** gave a dehydrated dinitro derivative **13** (Scheme 1).

1,2,4-Trisubstitution is confirmed by the AMX spin system (two doublets and a double doublet) in the ^1H nmr spectrum, and by the six aromatic carbon lines in the ^{13}C nmr corresponding to an asymmetric substitution of the benzene ring. The 2,5- and the 3,4-dinitro isomers can be ruled out on the basis of the proton chemical shifts. For these compounds, the double doublet of the AMX spin system would be the upfield signal, as shown in Table 1.

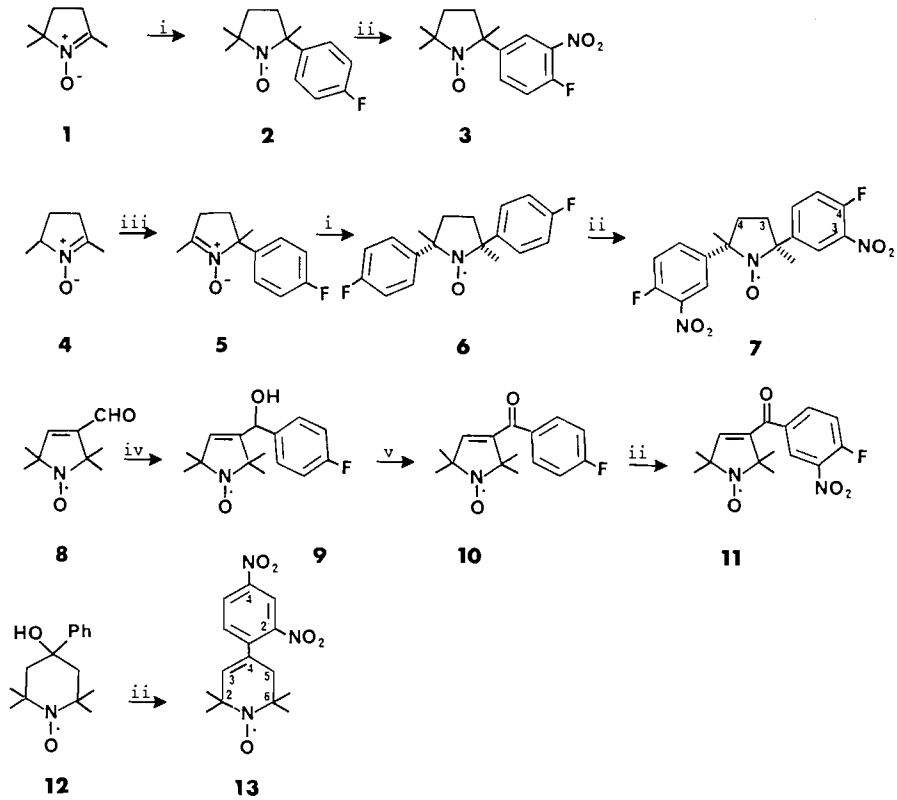
The enhanced reactivity of *ortho*-nitrofluorobenzene derivatives **3**, **7**, and **11** toward nucleophiles allows their utilization for the preparation of several useful synthons of spin-labelled analogues of heterocycles, or for use directly as spin-label reagents for the labelling of nucleophilic groups (e.g., in proteins SH, NH_2, and imidazole-NH).

The reaction of **3** with sodium hydroxide in aqueous ethanol led to the formation of an ether **14**, which could be nitrated to a dinitro ether **15**. When the reaction was carried out in aqueous sodium hydroxide, the phenol **16** was formed. The nitration of **16** led to the dinitrophenol **17**, while the reduction of **16** in a transfer hydrogenation (Pd/C, ammonium formate) (8, 25–27) gave the *ortho*-aminophenol derivative **18**. Analogously, reduction of the nitroaniline **19**, formed from **3** with aqueous ammonia in dioxane, allowed the preparation of an *ortho*-phenylenediamine derivative **20**. The conversion of **20** to the benzimidazolethione **21** was achieved with thiocarbonyldiimidazole. The replacement of fluorine by cyanide allowed the preparation of **22**, and reaction with imidazole gave a nitroimidazole **23**. This compound, analogous to reactive nucleophilic dinitrophenylimidazoles (28), is a potentially useful reagent for biomolecules. The reaction of a free thiol nitroxide (2,2,5,5-tetramethyl-3-thiolmethyl-3-pyrrolin-1-oxyl) (29) led to the formation of a biradical **24** in a clean reaction (Scheme 2). Therefore, **3** may serve as a reagent for the spin labelling of a thiol group. This confirms earlier observations that the reaction of a reactive group of a nitroxide reagent does not only permit the labelling of the thiol groups of protein; a highly reactive thiol group in a nitroxide molecule also allows interactions with another nitroxide molecule without any detectable loss of *N*-oxyl radical.

The reaction of **7** with alkali in aqueous ethanol led to the formation of the ethyl ether **25**. In aqueous dioxane the reaction led to **26**, which was nitrated to *trans*-2,5-di(4-hydroxy-3,5-dinitro)phenyl nitroxide **27**. The reaction of **7** with aqueous ammonia in dioxane led to the bis(nitroaniline) nitroxide **28**, and with imidazole to the bisimidazole **29** (Scheme 3).

A similar reaction to the above with alkali converted **11** to **30**, and further nitration of **30** resulted in the formation of a water-soluble unsaturated ketone nitroxide **31**. Besides its expected, more highly acidic phenolic hydroxy group (similar to **17** and **27**), the β-electrophilic centre of the unsaturated ketone

Can. J. Chem. Downloaded from www.nrcresearchpress.com by 194.225.253.170 on 09/07/12
For personal use only.



SCHEME 1. *Reagents:* i, Mg, 4-F—C_6H_4—Br, Et_2O; 0°C, NH_4Cl; $CHCl_3$, PbO_2; ii, H_2SO_4, HNO_3, 0°C; iii, Mg, 4-F—C_6H_4—Br, Et_2O; 0°C, NH_4Cl; MeOH, 25% NH_4OH, $Cu(Ac)_2$, O_2; iv, Mg, 4-F—C_6H_4—Br, EtO_2; −10°C, $CdCl_2$; 0°C, NH_4Cl; v, CCl_4, MnO_2, reflux.

TABLE 1. Comparative data concerning chemical shifts of dinitro compounds

	^{1}H nmr chemical shifts			
	Expected (18)		Observed	
Substitution	2,4-di-NO_2	3,4-di-NO_2	2,5-di-NO_2	(split by Hz)
Double doublet	8.62	8.07	8.37	8.29 (8.4, 2.3)
Doublet split by *ca.* 8 Hz	7.92	8.47	8.47	7.43 (8.04)
Doublet split by *ca.* 2Hz	9.17	8.62	8.62	8.59 (2.3)

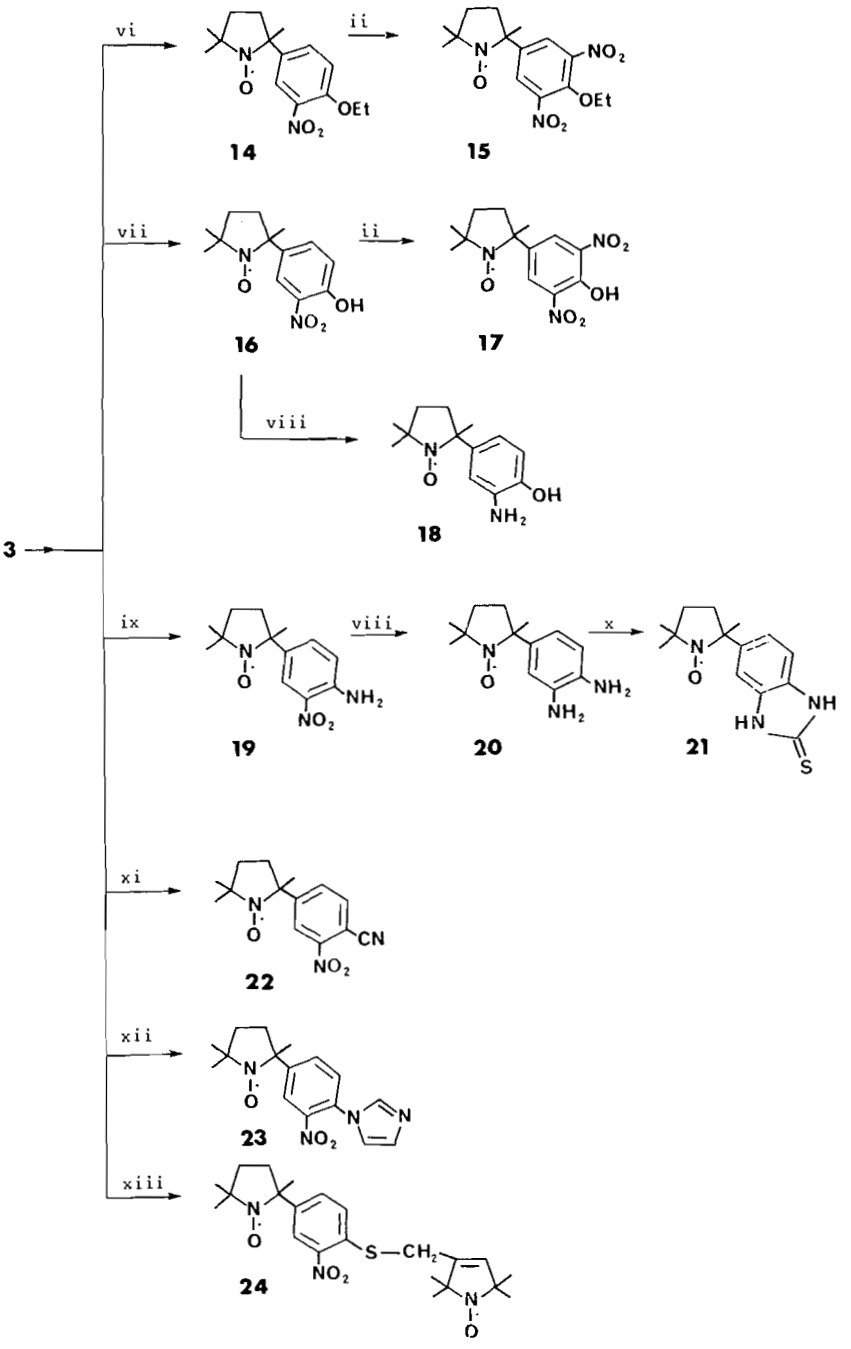
may offer potential applications for utilization as a synthon or for the covalent labelling of biomolecules. The reaction of **11** with aqueous ammonia led to a ketone-functionalized nitroaniline **32**, that with an amino acid ester (methyl glycianate) to a labelled amino acid **33**, and that with imidazole to a labelled imidazole **34**, which, as a salt (tosylate), may serve as a reactive synthon for further reactions. Compound **34** is a promising model compound for labelling of the imidazole-NH of a histidine in a protein chain (Scheme 4).

In conclusion, we hope that the above experiments offer not only new reactions and potentially useful spin-label reagents, but also several starting synthons for the preparation of nitroxide heterocycles in reactions analogous to those used earlier for the preparation of heterocycles from nitrophenols and nitroanilines.

Experimental

Melting points were determined with a Buchi micro melting point apparatus and are uncorrected. The ir spectra of radicals were measured with a Zeiss Specord 75 spectrometer, in neat oil or in Nujol suspension. The nmr spectra were recorded in 5- or 10-mm tubes at room temperature on a Bruker WM-250 instrument (^{1}H) at 250 MHz, or on a WP-80SY FT-spectrometer controlled by an Aspect 2000 computer at 20.14 MHz (^{13}C), in $CDCl_3$ solution, using the deuterium signal of the solvent as the lock and TMS as internal reference. To get high resolution spectra of radicals the samples were reduced with cosolved PhNHNHPh additive in the nmr tube as described (8). Mass spectra were taken on a Finnigan MAT 8430 mass spectrometer *via* the direct insertion probe. Operation conditions: R = 1250, $T_{\text{ion source}}$ = 250°C, U_{acc} = 3 kV, F_{el} = 70 eV, I_{el} = 500 μA. The evaporation temperatures of the samples varied between 150 and 350°C, and were controlled in each case within ±1°C accuracy. Spectral data were acquired and processed with a Finnigan MAT SS300 data system. The esr spectra were recorded with a JEOL JES-ME spectrometer working in the X band with 100-kHz field modulation. Oxygen-free benzene solutions of concentration 10^{-4} M were studied for radicals **6**, **7**, and **26**. The spectra were identical within experimental error, with the following parameters: g = 2.0058, nitrogen splitting 1.33–1.34 mT, ^{13}C splittings 1.12 and 1.52 mT. The intensity of ^{13}C satellites reveals

Can. J. Chem. Downloaded from www.nrcresearchpress.com by 194.225.253.170 on 09/07/12
For personal use only.



SCHEME 2. *Reagents:* ii, H_2SO_4, HNO_3, 0°C; vi, EtOH, 50% NaOH, reflux; 0°C, H^+; vii, dioxane, 50% NaOH, reflux; 0°C, H^+; viii, MeOH, Pd–C, NH_4CO_2H, 40°C; $CHCl_3$, PbO_2, O_2; ix, dioxane, 25% NH_4OH, reflux; x, THF, 1,1′-thiocarbonyldiimidazole, reflux; xi, DMSO, KCN, 50°C; xii, dioxane, imidazole, K_2CO_3, Aliquat 336; xiii, 2,2,5,5-tetramethyl-3-thiomethyl-3-pyrrolin-1-oxyl, EtOH, NaOH, 25°C.

the coupling of two magnetically equivalent nuclei. Flash column chromatography was performed with Silica Gel 60 (0.040–0.063 mm). Qualitative tlc was carried out on commercially prepared plates coated with Merck Kieselgel 60 F_{254}. Preparative layer chromatography was performed on plates (20 × 20 × 0.2 cm) coated with the same material.

2-(4-Fluorophenyl)-2,5,5-trimethylpyrrolidin-1-oxyl (2)

4-Fluorophenylmagnesium bromide, freshly prepared from 1-bromo-4-fluorobenzene (12.25 g, 70 mmol) and magnesium (1.70 g, 70 mmol) in dry ether (100 mL) was reacted under an argon atmosphere with 2,5,5-trimethyl-1-pyrroline-1-oxide (**1**) (7.57 g, 60 mmol). The mixture was stirred at room temperature for 6 h, and the reaction was then quenched by the addition of saturated aqueous ammonium chloride (50 mL) to the stirred, cooled reaction mixture. The ether phase was separated, washed with aqueous sodium chloride solution, and evaporated to dryness. The residue was taken up in chloroform (50 mL) and the well-stirred solution was treated with drying agent ($MgSO_4$) and aerated in the presence of PbO_2 catalyst (ca. 1 g) for 1 h, when all the *N*-hydroxy compound was oxidized to the *N*-oxyl radical. The filtrate was evaporated to dryness and the residue was chromatographed (silica gel, hexane – ethyl acetate, 9:1) to give pure **2** (10.64 g, 80%) as a deep orange-yellow oil.

2-(3-Nitro-4-fluorophenyl)-2,5,5-trimethylpyrrolidin)-1-oxyl (3)

To a stirred, ice-cooled solution of **2** (6.67 g, 30 mmol) in concentrated H_2SO_4 (20 mL) a mixture of 67% HNO_3 and concentrated H_2SO_4 (12 mL, 1:2, v/v) was added dropwise. When the addition was complete (ca. 30 min), the mixture was stirred for a further 30 min. It

Can. J. Chem. Downloaded from www.nrcresearchpress.com by 194.225.253.170 on 09/07/12
For personal use only.

TABLE 2. Analytical and spectroscopic data for compounds

Compound	Molecular formula	Analysis (%) calcd. (found) C	H	N	Infrared absorption ν_{max} (cm^{-1})	Mass spectrum, m/z (origin, %)
2	$C_{13}H_{17}FNO$	70.25 (70.37	7.71 7.87	6.30 6.47)		222 (M^+, 12.8%), 136 ($ArCCH_3{=}CH_2^{+\cdot}$, 100)
3	$C_{13}H_{16}FN_2O_3$	58.42 (58.32	6.03 6.17	10.48 10.37)	1530, 1330 (NO_2)	267 (M^+, 18.3%), 181 ($ArCCH_3{=}CH_2^{+\cdot}$, 100)
6	$C_{18}H_{18}F_2NO$	71.51 (71.45	6.00 5.98	4.63 4.82)		302 (M^+, 7%), 288 ($M^+ + \cdot H - \dot{C}H_3$, 9.4), 136 ($ArCCH_3{=}CH_2^{+\cdot}$, 100)
7	$C_{18}H_{16}F_2N_3O_5$	55.10 (55.12	4.11 4.21	10.71 10.64)	1533, 1345 (NO_2)	392 (M^+, 6.4%), 378 ($M^+ + \dot{H} - \dot{C}H_3$, 5.6), 362 ($M^+ - \dot{N}O$, 7), 181 ($ArCCH_3{=}CH_2^{+\cdot}$, 100)
9	$C_{15}H_{19}FNO_2$	68.16 (68.11	7.24 7.35	5.30 5.25)	3400–3200 (OH)	264 (M^+, 100%), 249 ($M^+ - \dot{C}H_3$, 18), 234 ($M^+ - \dot{N}O$, 14), 219 ($M^+ - \dot{N}O - \dot{C}H_3$, 25), 201 ($m/z$ 219 $- H_2O$, 30), 126 ($ArCHOH^+$, 26), 109 ($C_8H_{13}^+$, 29)
10	$C_{15}H_{17}FNO_2$	68.69 (68.55	6.53 6.39	5.34 5.39)	1640, 1600 (C=C—C=O)	262 (M^+, 31%), 232 ($M^+ - \dot{N}O$, 100), 217 ($M^+ - \dot{N}O - \dot{C}H_3$, 45.5), 123 ($ArCO^+$, 73)
11	$C_{15}H_{16}FN_2O_4$	58.63 (58.60	5.25 5.40	9.12 9.20)	1660, 1610 (C=C—C=O) 1530, 1330 (NO_2)	307 (M^+, 24.4%), 277 ($M^+ - \dot{N}O$, 77.6), 262 ($M^+ - \dot{N}O - \dot{C}H_3$, 57), 168 ($ArCO^+$, 100), 122 ($ArCO^+ - \dot{N}O_2$, 76.5), 109 ($M^+ - \dot{N}O - Ar\dot{C}O$, 66), 94 ($Ar^+ - \dot{N}O_2$, 18)
13	$C_{15}H_{18}N_3O_5$	56.25 (56.40	5.66 5.48	13.12 13.22)	1538, 1347 (NO_2)	320 (M^+, 100%), 217 ($M^+ - (CH_3)_2C{=}NOH - \dot{N}O$, 69), 189 ($C_8H_3N_2O_4$, 48)
14	$C_{15}H_{21}N_2O_4$	61.42 (61.22	7.22 7.35	9.55 9.73)	1535, 1315 (NO_2)	293 (M^+, 28.5%), 207 ($ArCCH_3{=}CH_2^{+\cdot}$, 65.6) 179 ($ArCCH_3{=}CH_2^{+\cdot} - C_2H_4$, 100)
15	$C_{15}H_{20}N_3O_6$	53.25 (53.15	5.96 5.81	12.42 12.34)	1530, 1310 (NO_2)	338 (M^+, 20.3%), 252 ($ArCCH_3{=}CH_2^{+\cdot}$, 21), 244 (m/z 252 $- C_2H_4$, 100)
16	$C_{13}H_{17}N_2O_4$	58.86 (58.72	6.46 6.42	10.56 10.37)	3500–3300 (OH), 1520, 1360 (NO_2)	265 (M^+, 45.3%), 179 ($ArCCH_3{=}CH_2^{+\cdot}$, 100),
17	$C_{13}H_{16}N_3O_6$	50.32 (50.30	5.20 5.09	13.54 13.46)	3500–3200 (OH), 1530, 1350 (NO_2)	310 (M^+, 35%), 280 ($M^+ - \dot{N}O$, 100), 263 ($M^+ - \dot{N}O - \dot{O}H$, 32), 224 ($ArCCH_3{=}CH_2^{+\cdot}$, 57)
18	$C_{13}H_{19}N_2O_2$	66.36 (66.42	8.14 8.23	11.90 12.04)	3475, 3380 (NH_2), 3200–3100 (OH)	235 (M^+, 15%), 149 ($ArCCH_3{=}CH_2^{+\cdot}$, 100), 109 ($ArH^{+\cdot}$, 10)
19	$C_{13}H_{18}N_3O_3$	59.08 (58.90	6.86 6.96	15.90 15.86)	3470, 3360 (NH_2), 1520, 1340 (NO_2)	264 (M^+, 18.5%), 178 ($ArCCH_3{=}CH_2^{+\cdot}$, 100),
20	$C_{13}H_{20}N_3O$	66.64 (66.72	8.60 8.71	17.93 18.04)	3420, 3315 (NH_2)	234 (M^+, 16.2%), 148 ($ArCCH_3{=}CH_2^{+\cdot}$, 100)
21	$C_{14}H_{18}N_3OS$	60.84 (60.77	6.56 6.43	15.20 15.34)	3500–3000 (NH)	276 (M^+, 26.5%), 190 ($ArCCH_3{=}CH_2^{+\cdot}$, 100)
22	$C_{14}H_{16}N_3O_3$	61.30 (61.19	5.88 5.78	15.32 15.44)	2230 (CN), 1530, 1340 (NO_2)	274 (M^+, 30%), 189 ($ArCHCH_3 - CH_2^+$, 66.7), 188 ($ArCCH_3{=}CH_2^{+\cdot}$, 100), 115 (m/z 188 $- \dot{N}O_2$ $-$ HCN, 25.6)
23	$C_{16}H_{19}N_4O_3$	60.94 (61.06	6.07 5.94	17.77 17.90)	1530, 1360 (NO_2)	315 (M^+, 100%), 242 ($M^+ - C_4H_8 - \dot{O}H$, 28), 174 (m/z 242 $- C_3H_4N_2$, 66)
24	$C_{22}H_{31}N_3O_4S$	60.95 (60.87	7.21 7.28	9.69 9.52)	1510, 1330 (NO_2)	433 (M^+, 25.6%), 403 ($M^+ - \dot{N}O$, 22), 178 ($M - Ar\dot{S} - \dot{C}H_3$, 40.4), 123 ($M^+ - Ar\dot{S} - \dot{N}O$, 100)
25	$C_{22}H_{26}N_3O_7$	59.45 (59.31	5.90 5.92	9.45 9.48)	1535, 1310 (NO_2)	444 (M^+, 3.8%), 414 ($M^+ - \dot{N}O$, 4), 207 ($ArCCH_3{=}CH_2^{+\cdot}$, 100), 179 ($ArCCH_3{=}CH_2^{+\cdot} - C_2H_4$, 65)
26	$C_{18}H_{18}N_3O_7$	55.67 (55.53	4.67 4.77	10.82 10.67)	3400–3100 (OH), 1530, 1375 (NO_2)	388 (M^+, 4%), 179 ($ArCCH_3{=}CH_2^{+\cdot}$, 100)
27	$C_{18}H_{16}N_5O_{11}$	45.20 (45.32	3.37 3.53	14.64 14.60)	3500–3300 (OH), 1535, 1350 (NO_2)	478 (M^+, 1.3%), 450 ($M^+ - C_2H_4$, 38), 449 ($M + H - \dot{N}O$, 67.5), 448 ($M^+ - \dot{N}O$, 39.3), 224 ($ArCCH_3{=}CH_2^{+\cdot}$, 100), 211 ($ArCHCH_3^+$, 50.2), 194 (m/z 224 $- \dot{N}O$, 23.2), 165 (m/z 211 $- \dot{N}O_2$, 24.2)

Can. J. Chem. Downloaded from www.nrcresearchpress.com by 194.225.253.170 on 09/07/12
For personal use only.

TABLE 2. (*concluded*)

Compound	Molecular formula	Analysis (%) calcd. (found) C	H	N	Infrared absorption ν_{max} (cm^{-1})	Mass spectrum, *m/z* (origin, %)
28	$C_{18}H_{20}N_5O_5$	55.95 (55.83	5.22 5.39	18.12 18.38)	3560, 3350 (NH_2), 1550, 1340 (NO_2)	386 (M^+, 4.5%), 385 ($M^+ - \cdot H$, 14.2), 359 ($M^+ - HCN$, 8), 178 ($ArCCH_3{=}CH_2^{+\cdot}$, 100)
29	$C_{24}H_{22}N_7O_5$	59.01 (59.18	4.54 4.52	20.07 20.13)	1530, 1380 (NO_2)	488 (M^+, 8.6%), 458 ($M^+ - \dot{N}O$, 100), 401 ($M^+ - 2 \times \dot{N}O - HCN$, 69), 230 ($ArCHCH_3 - CH_2^+$, 32), 229 ($ArCCH_3{=}CH_2^{+\cdot}$, 26)
30	$C_{15}H_{17}N_2O_5$	59.01 (59.07	5.61 5.70	9.17 9.20)	3070 (OH), 1642 (C=O), 1530, 1340 (NO_2)	305 (M^+, 18.8%), 275 ($M^+ - \dot{N}O$, 62.6), 260 ($M^+ - \dot{N}O - \dot{C}H_3$, 37), 166 ($ArCO^+$, 100), 120 ($ArCO^+ - \dot{N}O_2$, 54)
31	$C_{15}H_{16}N_3O_7$	51.43 (51.34	4.60 4.52	11.99 11.93)	3500–3000 (OH), 1660, 1620 (C=C—C=O), 1540, 1370 (NO_2)	350 (M^+, 56%), 320 ($M^+ - \dot{N}O$, 75.3), 305 ($M^+ - \dot{N}O - \dot{C}H_3$, 49), 211 ($ArCO^+$, 100), 109 ($M^+ - \dot{N}O - ArCO$, 62)
32	$C_{15}H_{18}N_3O_4$	59.20 (59.21	5.96 5.77	13.81 13.68)	3450, 3285 (NH_2), 1640, 1580 (C=C—C=O), 1530, 1340 (NO_2)	304 (M^+, 14.7%), 274 ($M^+ - \dot{N}O$, 29), 259 ($M^+ - \dot{N}O - \dot{C}H_3$, 17.4), 257 ($M^+ - \dot{N}O - \dot{O}H$, 25.5), 165 ($ArCO^+$, 100), 119 ($ArCO^+ - \dot{N}O_2$, 45), 91 ($Ar^+ - \dot{N}O_2$, 33)
33	$C_{18}H_{22}N_3O_6$	57.44 (57.45	5.89 5.74	11.16 10.97)	3330 (NH), 1740 (C=O), 1640, 1620 (C=C—C=O),	376 (M^+, 14.7%), 346 ($M^+ - \dot{N}O$, 21.7), 331 ($M^+ - \dot{N}O - \dot{C}H_3$, 10.4), 329 ($M^+ - \dot{N}O - \dot{O}H$, 13), 237 ($ArCO^+$, 100)
34	$C_{18}H_{19}N_4O_4$	60.84 (60.92	5.39 5.18	15.77 15.67)	1655, 1610 (C=C—C=O), 1530, 1370 (NO_2)	355 (M^+, 73.3%), 325 ($M^+ - \dot{N}O$, 53), 310 ($M^+ - \dot{N}O - \dot{C}H_3$, 42), 216 ($ArCO^+$, 100), 109 ($C_{18}H_{13}^+$, 65.5), 67 ($C_3H_3N_2^+$, 77.7)
34	Tosylate $C_{25}H_{27}N_4O_7S$	56.92 (57.03	5.16 5.24	10.62 10.58)	1660, 1610 (C=C—C=O), 1540, 1375 (NO_2), 1240, 1020 (SO_2)	

was then poured into ice-water (ca. 300 g), extracted with ether (3 × 30 mL), dried ($MgSO_4$), and evaporated to dryness. The deep-orange solid residue was purified by column chromatography (silica gel, hexane – ethyl acetate, 9:1) to give orange, crystalline **3** (5.90 g, 72%); mp 64–65°C (from chloroform–hexane).

trans-*2,5-Di(4-fluorophenyl)-2,5-dimethylpyrrolidin-1-oxyl (6)*

4-Fluorophenylmagnesium bromide was freshly prepared from 1-bromo-4-fluorobenzene (19.25 g, 0.11 mol) and magnesium (2.67 g, 0.11 mol) in dry ether (200 mL) and was reacted with 2,5-dimethyl-1-pyrroline-1-oxide (**4**) (11.32 g, 0.1 mol). The reaction mixture was worked up as described for compound **2**, but the oxidation was carried out in 25% aqueous ammonia (20 mL) and MeOH (100 mL) containing copper(II) acetate (ca. 0.5 g), by aeration of the stirred solution when the solution turned deep-blue; the aeration was continued for a further 30 min, after which the MeOH was evaporated *in vacuo*. The oily residue was taken up in ether, washed with saturated NaCl, dried ($MgSO_4$), and evaporated to dryness. The residue was bulb-to-bulb distilled at 120°C (bath temp.) at 0.1 Torr (1 Torr = 133.3 Pa), to give the viscous oily nitrone **5** (17.60 g, 85%).

A solution of the nitrone **5** (14.51 g, 70 mmol) in dry ether (50 mL) was added to a well-stirred ethereal solution (100 mL) of freshly prepared 4-fluorophenylmagnesium bromide (80 mmol) at room temperature, and after 6 h the reaction mixture was quenched and worked up as for **2** to give pure *trans* isomer **6** as pale yellow crystals (13.15 g, 62%); mp 105–106°C (from ether–hexane).

trans-*2,5-Di(3-nitro-4-fluorophenyl)-2,5-dimethylpyrrolidin-1-oxyl (7)*

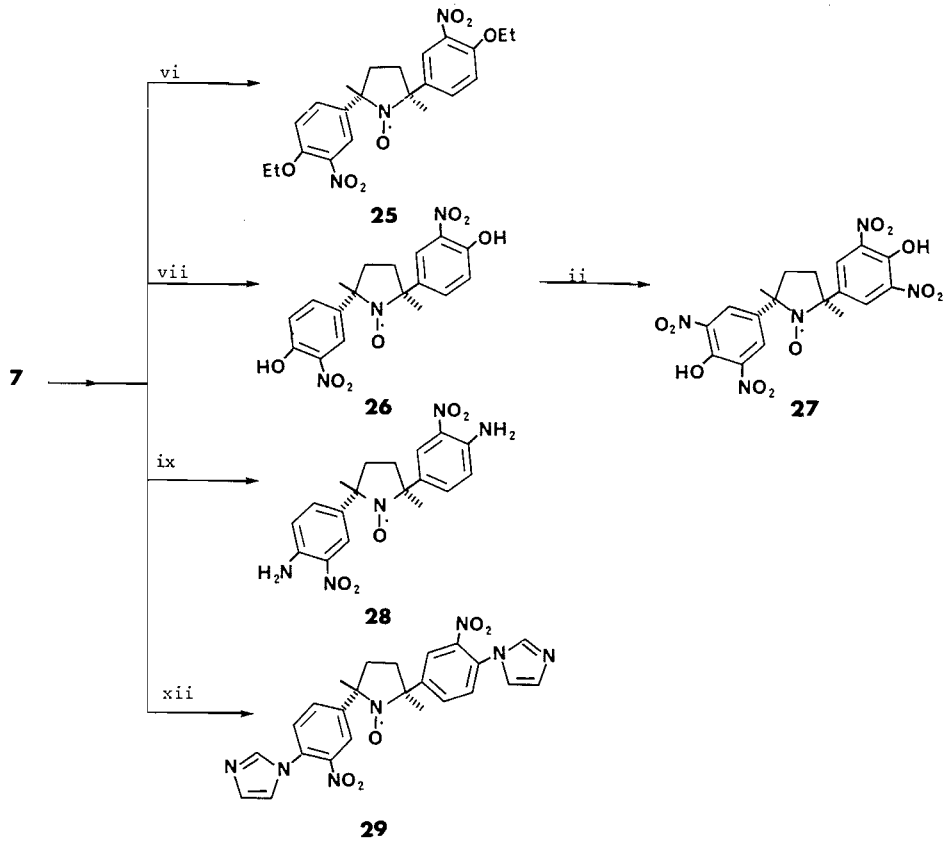
Compound **6** (20 mmol) was nitrated and isolated as described in the preparation of **3**, to give the orange-yellow, crystalline dinitro compound **7** (6.15 g, 63%); mp 176–177°C (from chloroform–hexane); ^1H nmr (δ, $CDCl_3$, 250 MHz): 1.31 (s, 6H, $2CH_3$), 2.08 and 2.32 (2m, 2 × 2H, CH_2CH_2), 7.25 (1H, ArH-5 overlapped by a multiplet of the $(PhNH)_2$ additive), 7.78 (ddd, 1H, ArH-6), 8.24 (dd, 1H, ArH-2, J = 7.2 and 2.4 Hz); ^{13}C nmr (δ, $CDCl_3$): 27.1 (CH_3), 35.3 (CH_2-3,4), 68.1 (C-2,5 Cq sp^3), 117.8 (20.5 Hz, ArC-5), 124.1 (2.4 Hz, ArC-2), 134.8 (8.2 Hz, ArC-6), 136.8 (7.0 Hz, ArC-3), 144.3 (4.3 Hz, ArC-1), 154.2 (264.1 Hz, ArC-4).

2,2,5,5-Tetramethyl-3-(α-hydroxy-4-fluorobenzyl)-3-pyrrolin-1-oxyl (9) and 2,2,5,5-tetramethyl-3-(4-fluorobenzoyl)-3-pyrrolin-1-oxyl (10)

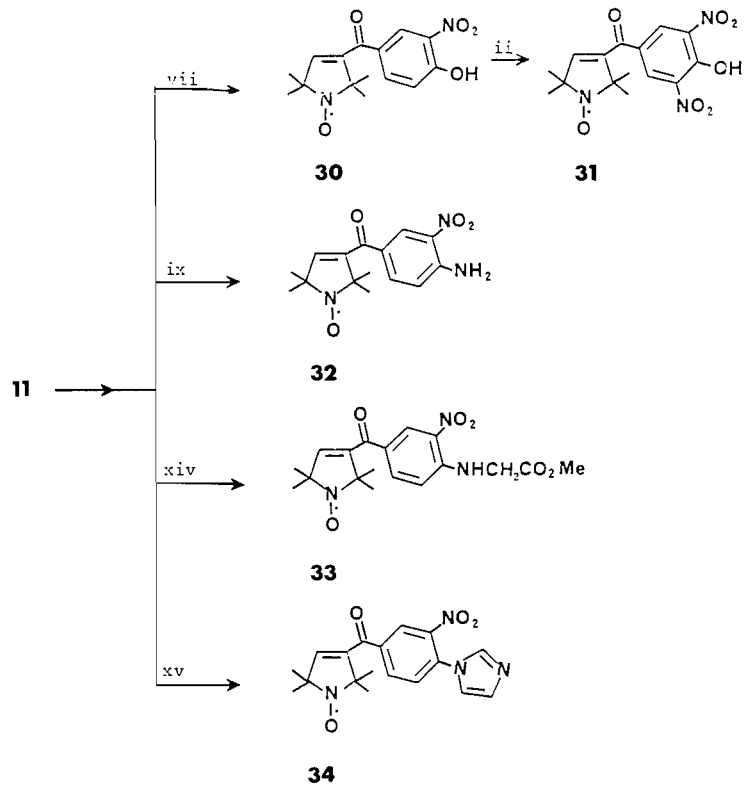
Dry $CdCl_2$ (4.58 g, 25 mmol) was added rapidly to a well-stirred and cooled (−10°C) solution of freshly prepared 4-fluorophenylmagnesium bromide (50 mmol) (as described above for compound **2**). To the stirred suspension of the di(4-fluorophenyl) cadmium (25 mmol) formed in dry ether (100 mL), a solution of 2,2,5,5-tetramethyl-3-formyl-3-pyrrolin-1-oxyl (**8**) (23) (4.21 g, 25 mmol) in dry ether (100 mL) was added slowly under argon at room temperature, and the reaction mixture was stirred for a further 6 h, then cooled with an ice-water bath, and decomposed with saturated aqueous NH_4Cl (50 mL). The organic phase was separated, dried ($MgSO_4$), and evaporated to dryness. The solid yellow residue was a mixture of the allylic alcohol **9** and ketone **10**, formed because the alcohol **9** was partially oxidized during the work-up. Therefore, only an analytical sample of **9** was isolated, by flash chromatography (silica gel, hexane – ethyl acetate, 9:1); mp 106–107°C (from ether–hexane).

The stirred mixture of **9** and **10** was dissolved in CCl_4 (100 mL), refluxed with active MnO_2 (Merck, 30 g) for 6 h, and then filtered. The filtrate was evaporated and chromatographed (silica gel, hexane – ethyl acetate, 9:1) to give pure, yellow crystalline ketone **10** (5.20 g, 79%); mp 123–124°C (from chloroform–hexane).

Can. J. Chem. Downloaded from www.nrcresearchpress.com by 194.225.253.170 on 09/07/12
For personal use only.



SCHEME 3. *Reagents:* ii, H_2SO_4, HNO_3, 0°C; vi, EtOH, 50% NaOH, reflux; 0°C, H^+; vii, dioxane, 50% NaOH, reflux; 0°C, H^+; ix, dioxane, 25% NH_4OH, 50°C; xii, dioxane, imidazole, K_2CO_3, Aliquat 336.



SCHEME 4. *Reagents:* ii, H_2SO_4, HNO_3, 0°C; vii, dioxane, 50% NaOH, reflux; 0°C, H^+; ix, dioxane, 25% NH_4OH, reflux; xiv, 80% aq. EtOH, $^+H_3NCH_2CO_2Me$ Cl^-, K_2CO_3, reflux, xv, dioxane, H_2O, imidazole, K_2CO_3, reflux.

Can. J. Chem. Downloaded from www.nrcresearchpress.com by 194.225.253.170 on 09/07/12
For personal use only.

Can. J. Chem. Downloaded from www.nrcresearchpress.com by 194.225.253.170 on 09/07/12
For personal use only.

2,2,5,5-Tetramethyl-3-(3-nitro-4-fluorobenzoyl)-3-pyrrolin-1-oxyl (11)

Compound **10** (2.62 g, 10 mmol) was nitrated and isolated as in the preparation of **3**, and gave the yellow, crystalline nitro ketone **11** (2.60 g, 84%); mp 146–147°C (from chloroform–hexane).

2,2,6,6-Tetramethyl-1,2,5,6-tetrahydro-4-(2,4-dinitrophenyl)pyridin-1-oxyl (13)

A solution of 2,2,6,6-tetramethyl-4-hydroxy-4-phenylpiperidin-1-oxyl (**12**) (24) (0.248 g, 1 mmol) was nitrated to give **13** (0.240 g, 75%); mp 156–157°C (from chloroform–hexane); ^{1}H nmr (δ, $CDCl_3$, 250 MHz): 1.27 and 1.29 (2s, 2 × 6H, $4CH_3$), 2.33 (s, 2H, CH_2), 5.50 (s, 1H, CH), 7.43 (d, 1H, ArH-6, J = 8.4 Hz), 8.29 (dd, 1H, Arh-5, J = 8.4 and 2.3 Hz), 8.59 (d, 1H, Arh-3, J = 2.3 Hz); ^{13}C nmr (δ, $CDCl_3$): 24.8, 25.8 (CH_3), 43.2 (CH_2-5), 57.6, 59.8 (C-2,6 Cq sp^3), 119.4 (ArC-3), 126.3 (ArC-6), 127.9 (ArC-5), 129.3 (C-4, hidden by a line of the $(PhNH)_2$ additive), 131.8 (C-3), 136.4 (ArC-1), 143.1 (ArC-4), 146.0 (ArC-2).

2,5,5-Trimethyl-2-(3-nitro-4-ethoxyphenyl)pyrrolidin-1-oxyl (14)

A solution of **3** (0.802 g, 3 mmol) in EtOH (10 mL) and 50% aqueous NaOH (3 mL) was refluxed for 3 h, then cooled and acidified with 5% H_2SO_4. The reaction mixture was extracted with ether (3 × 10 mL), dried ($MgSO_4$), and evaporated to dryness. The yellow solid residue was recrystallized from ether–hexane to give pure **14** (0.610 g, 69%); mp 90–91°C.

2,5,5-Trimethyl-2-(3,5-dinitro-4-ethoxyphenyl)pyrrolidin-1-oxyl (15)

The nitration of **14** (0.293 g, 1 mmol) gave the dinitro compound **15** (0.169 g, 50%); mp 76–77°C (from ether–hexane).

2,5,5-Trimethyl-2-(3-nitro-4-hydroxyphenyl)pyrrolidin-1-oxyl (16)

The above reaction of **3** (0.802 g, 3 mmol) was carried out in dioxane (10 mL) instead of EtOH, to give **16** (0.655 g, 82%); mp 76–78°C (from chloroform–hexane).

2,5,5-Trimethyl-2-(3,5-dinitro-4-hydroxyphenyl)pyrrolidin-1-oxyl (17)

The nitration of **16** (0.265 g, 1 mmol) gave the dinitrophenol **17** (0.242 g, 78%); mp > 260°C (from chloroform–hexane).

2,5,5-Trimethyl-2-(3-amino-4-hydroxyphenyl)pyrrolidin-1-oxyl (18)

To a stirred solution of nitrophenol **16** (2.65 g, 10 mmol) and 10% Pd/carbon (200 mg) in dry MeOH (20 mL) under argon, ammonium formate (3.78 g, 60 mmol) was added rapidly. The reaction mixture was stirred at 40°C for 3 h, then diluted with water and filtered from the catalyst. The filtrate was extracted with $CHCl_3$ (3 × 30 mL), and the organic phase was washed with saturated NaCl, dried ($MgSO_4$), and aerated in the presence of PbO_2 catalyst to oxidize the hydroxylamine to nitroxide. Finally, the filtrate was evaporated to dryness to give the aminophenol **18** (1.41 g, 60%); mp 148–149°C (from ether–hexane).

2,5,5-Trimethyl-2-(3-nitro-4-aminophenyl)pyrrolidin-1-oxyl (19)

A solution of fluoronitrophenol derivative **3** (2.67 g, 10 mmol) in dioxane (20 mL) was refluxed and stirred with 25% aqueous ammonia (10 mL) for 16 h. The reaction mixture was then extracted with ether (50 mL) and washed with saturated NaCl (2 × 10 mL). The ether phase was dried ($MgSO_4$) and evaporated to dryness. The residue was chromatographed (silica gel, hexane – ethyl acetate, 9:1) to give nonreacted **3** (0.670 g, 25%) and the nitroaniline **19** (1.35 g, 51%); mp 130–131°C (from ether–hexane).

2,5,5-Trimethyl-2-(3,4-diaminophenyl)pyrrolidin-1-oxyl (20)

The nitroaniline **19** (0.529 g, 2 mmol) was transfer-hydrogenated as described in the preparation of aminophenyl **18**, to give the pale-yellow diaminophenyl derivative **20** (0.250 g, 53%); mp 126–127°C (from ether–hexane).

5(6)-(2,5,5-Trimethylpyrrolidin-2-yl)benzimidazole-2-thione (21)

To a solution of diamine **20** (0.234 g, 1 mmol) in dry tetrahydrofuran (5 mL), 1,1′-thiocarbonyldiimidazole (0.214 g, 1.2 mmol) was added. The mixture was heated for 30 min, then diluted with water (10 mL) and extracted with ether (3 × 20 mL). The ether phase was dried ($MgSO_4$) and evaporated to dryness. The residue was purified with chloroform–methanol (8:1) on a preparative silica gel plate, to give **21** (0.125 g, 45%); mp 173–175°C (from chloroform–hexane).

2,5,5-Trimethyl-2-(3-nitro-4-cyanophenyl)pyrrolidin-1-oxyl (22)

A stirred solution of **3** (0.267 g, 1 mmol) and NaCN (0.072 g, 1.1 mmol) in dry dimethyl sulphoxide (5 mL) was heated at 50°C for 1 h, then diluted with water (50 mL) and extracted with ether (3 × 20 mL). The ether phase was dried ($MgSO_4$) and evaporated to dryness. The yellow solid was purified with hexane – ethyl acetate (2:1) on a preparative silica gel plate, to give **22** (0.132 g, 48%); mp 94–95°C (from ether–hexane).

2,5,5-Trimethyl-2-[3-nitro-4-(imidazol-1-yl)phenyl]pyrrolidin-1-oxyl 23

A stirred solution of **3** (0.535 g, 2 mmol) and imidazole (0.204 g, 3 mmol) in dioxane (10 mL) was heated and stirred with K_2CO_3 (400 mg) in the presence of Aliquat 336 (Fluka, 30 mg) for 6 h, then diluted with water (30 mL) and extracted with ether (3 × 10 mL). The dried ($MgSO_4$) ethereal phase was evaporated, and the residual solid was purified on a short silica gel column with chloroform–methanol (30:1) to give the yellow, crystalline, pure imidazole **23** (0.530 g, 84%); mp 107–108°C (from chloroform–hexane).

2,5,5-Trimethyl-2-[3-nitro-4-(1-oxyl-2,2,5,5-tetramethyl-3-pyrroline-3-methyl)thiophenyl]pyrrolidin-1-oxyl (24)

To a freshly prepared solution of 2,2,5,5-tetramethyl-3-thiolmethyl-3-pyrrolin-1-oxyl (29) (0.186 g, 1 mmol) and **3** (0.267 g, 1 mmol) in ethanol (10 mL), 2% aqueous NaOH (2 mL) was added. The reaction mixture was stirred at room temperature for 3 h, then diluted with water (40 mL) and extracted with ethyl acetate (3 × 10 mL). The organic phase was dried ($MgSO_4$) and evaporated to dryness, and the residue was chromatographed on a silica gel plate (hexane – ethyl acetate, 2:1), to give the biradical **24** (0.204 g, 47%); mp 110–111°C (from chloroform–hexane).

*2,5-Dimethyl-*trans*-2,5-di(3-nitro-4-ethoxyphenyl)pyrrolidin-1-oxyl (25)*

To a solution of difluorodinitro derivative **7** (0.785 g, 2 mmol) in ethanol (20 mL), 50% aqueous NaOH (5 mL) was added and the reaction mixture was heated for 3 h. The bulk of the ethanol was then evaporated, and the residue was acidified with 5% H_2SO_4 and extracted with chloroform (3 × 10 mL). The organic phase was dried ($MgSO_4$) and evaporated to dryness. The solid residue was purified on a short silica gel column (hexane–chloroform, 4:1), to give the yellow crystalline **25** (0.563 g, 63%); mp 156–157°C (from chloroform–hexane).

*2,5-Dimethyl-*trans*-2,5-di(3-nitro-4-hydroxyphenyl)pyrrolidin-1-oxyl (26)*

The difluorodinitro derivative **7** (0.785 mg, 2 mmol) was reacted as in the preparation of **25**, but dioxane (20 mL) was used instead of ethanol, to give **26** (0.560 g, 72%); mp 190–191°C (from ether–hexane).

*2,5-Dimethyl-*trans*-2,5-di(3,5-dinitro-4-hydroxyphenyl)pyrrolidin-1-oxyl (27)*

The dihydroxy derivative **26** (0.388 g, 1 mmol) was nitrated as described in the preparation of **3**. Preparative layer chromatography (chloroform–ethanol, 6:1) gave the red-yellow, crystalline tetranitro derivative **27** (0.384 g, 80%); mp 160–161°C (from chloroform–hexane).

*2,5-Dimethyl-*trans*-2,5-di(3-nitro-4-aminophenyl)pyrrolidin-1-oxyl (28)*

A stirred solution of **7** (0.785 g, 2 mmol) in dioxane (20 mL) and 25% aqueous ammonia (5 mL) was heated for 6 h, then extracted with ethyl acetate (3 × 10 mL). The organic phase was dried ($MgSO_4$) and evaporated to dryness. The yellow residual solid was purified by column chromatography (silica gel, chloroform–ether, 10:1), to give the bis(nitroaniline) **28** (0.572 g, 74%); mp 84–85°C (from chloroform–hexane).

2,5-Dimethyl-trans-*2,5-di[3-nitro-4-(imidazol-1-yl)phenyl]pyrrolidin-1-oxyl (29)*

The diimidazole compound **29** was prepared in good yield from **7** (0.392 g, 1 mmol) with imidazole (0.150 g, 2.2 mmol) as described in the preparation of **23**. Yield: 0.332 g, (68%); mp 193–194°C (from chloroform–hexane).

2,2,5,5-Tetramethyl-3-(3-nitro-4-hydroxybenzoyl)-3-pyrrolin-1-oxyl (30)

To a stirred solution of the fluoronitroketone **11** (3.07 g, 10 mmol) in dioxane (20 mL), 50% aqueous NaOH (5 mL) was added. The reaction mixture was refluxed for 6 h, cooled, acidified with 5% H_2SO_4, and extracted with ether (3 × 20 mL). The organic phase was washed with saturated NaCl, dried ($MgSO_4$), and evaporated. The crude product was purified by column chromatography (silica gel, hexane – ethyl acetate, 10:1), to give the orange, crystalline hydroxy derivative **30** (2.35 g, 77%); mp 130–131°C (from chloroform–hexane).

2,2,5,5-Tetramethyl-3-(3,5-dinitro-4-hydroxybenzoyl)-3-pyrrolin-1-oxyl (31)

The nitrophenol **30** (1.53 g, 5 mmol) was nitrated as described in the preparation of **3**, to give the dinitrophenol derivative **31** (1.40 g, 80%); mp 59–61°C (from chloroform–hexane).

2,2,5,5-Tetramethyl-3-(3-nitro-4-aminobenzoyl)-3-pyrrolin-1-oxyl (32)

A solution of **11** (0.307 g, 1 mmol) in dioxane (10 mL) and 25% aqueous ammonia (5 mL) was refluxed for 3 h, then worked up as described in the preparation of **19** to give **32** (0.278 g, 90%); mp 175–176°C (from ether–hexane).

2,2,5,5-Tetramethyl-3-{3-nitro-4-[N-(methoxy-carbonylmethyl)]aminobenzoyl}-3-pyrrolin-1-oxyl (33)

A solution of **11** (0.307 g, 1 mmol), glycine methyl ester hydrochloride (0.138 g, 1.1 mmol), and K_2CO_3 (140 mg) in 80% aqueous EtOH (10 mL) was refluxed for 3 h, then evaporated to dryness. The residue was taken up in chloroform (20 mL), washed with water, dried ($MgSO_4$), and evaporated to dryness. The solid residue was recrystallized from ether–hexane, to give **33** (0.272 g, 72%); mp 157–158°C.

2,2,5,5-Tetramethyl-3-[3-nitro-4-(imidazol-1-yl)benzoyl]-3-pyrrolin-1-oxyl (34)

A stirred solution of **11** (0.625 g, 2 mmol), imidazole (0.150 g, 2.2 mmol), and K_2CO_3 (300 mg) in water (5 mL) was refluxed for 3 h, then worked up as in the preparation of **23**, to give **34** (0.612 g, 86%); mp 41–42°C (from chloroform–hexane).

The tosylate of **34** was precipitated from a solution of the base in dry acetone, treated with an equivalent amount of toluenesulphonic acid, and then diluted with ether, mp 173–174°C.

Acknowledgements

This work was supported by grants from the Hungarian Academy of Sciences (301/A/82 and 3/104/86). The authors express their thanks to Mrs. M. Ott for microanalyses.

1. E. G. Rozantsev. Free nitroxyl radicals. Plenum Press, New York. 1970.
2. J. F. W. Keana. Synthesis and chemistry of nitroxide spin labels. *In* Spin labeling in pharmacology. *Edited by* J. L. Holtzman. Academic Press, Orlando, FL. 1984. Chap. 1.
3. L. J. Berliner (*Editor*). Spin labeling, theory and applications. Academic Press, New York, NY. Vol. 1. 1976; Vol. 2. 1979.
4. G. I. Likhtenshtein. Method spinovykh metok v molecularnoi biologii. Nauka, Moscow, 1973 (in Russian); translation: G. I. Likhtenshtein. Spin labeling methods in molecular biology. Wiley–Interscience, New York, NY. 1976.
5. H. G. Aurich. Nitroxides. *In* The chemistry of functional groups Suppl. F. The chemistry of amino, nitroso and nitro compounds. *Edited by* S. Patai. Wiley–Interscience, London. 1982. Chap. 14. pp. 565–622.
6. H. O. Hankovszky, K. Hideg, L. Lex, Gy. Kulcsár, and H. A. Halász. Can. J. Chem. **60**, 1432 (1982).
7. J. F. W. Keana, K. Hideg, B. G. Birrell, H. O. Hankovszky, G. Ferguson, and M. Parvez. Can. J. Chem. **60**, 1439 (1982).
8. K. Hideg, H. O. Hankovszky, H. A. Halász, and P. Sohár. J. Chem. Soc. Perkin Trans. 1, 2905 (1988).
9. F. Sanger. Biochem. J. **42**, 287 (1948).
10. M. Humphries and J. S. Thompson. Anal. Biochem. **105**, 319 (1980).
11. J. T. Gerig, J. D. Reiheimer, and R. H. Robinson. Biochim. Biophys. Acta, **579**, 409 (1979).
12. J. C. Hsia and N. H. Kwan. J. Biol. Chem. **256**, 2242 (1981).
13. S. Belkin, R. J. Mehlhorn, K. Hideg, H. O. Hankovszky, and L. Packer. Arch. Biochim. Biophys. **256**, 232 (1987).
14. W. R. Couet, R. C. Brash, G. Sosnovsky, J. Lukszo, I. Prakash, C. T. Gnewuch, and T. N. Tozer. Tetrahedron, **41**, 1165 (1985).
15. W. R. Couet, R. C. Brash, and T. N. Tozer. Magn. Reson. Imaging, **3**, 83 (1985).
16. J. F. W. Keana and F. L. Van Nice. Physiol. Chem. Phys. Med. NMR. **16**, 447 (1984).
17. J. F. W. Keana. New aspects of nitroxide chemistry. *In* Spin labeling, theory and applications. Vol. 2. *Edited by* L. J. Berliner. Academic Press, New York, NY. 1979. Chap. 3.
18. P. Sohár. Nuclear magnetic resonance spectroscopy. Vol. 2. CRC Press, Inc., Boca Raton, FL. 1983. p. 69.
19. J. A. Dale, D. L. Dull, and H. S. Mosher. J. Org. Chem. **34**, 2543 (1969).
20. J. F. W. Keana and V. S. Prabhu. J. Org. Chem. **51**, 4300 (1986).
21. E. G. Janzen, U. M. Oehler, D. L. Haire, and Kotake. J. Am. Chem. Soc. **108**, 6858 (1986).
22. A. Rockenbauer, M. Györ, H. O. Hankovszky, and K. Hideg. *In* Electron spin resonance. Vol. 11A. Royal Society of Chemistry. Alden Press, London. 1988. Chap. 5. p. 145.
23. K. Hideg, H. O. Hankovszky, L. Lex, and Gy. Kulcsár. Synthesis, 911 (1980).
24. R. Briere, H. Lemaire, A. Rassat, and J. J. Dunand. Bull. Soc. Chim. Fr. 4220 (1970).
25. M. K. Anwer and A. F. Spatola. Tetrahedron Lett. 6369 (1981).
26. S. Ram and R. E. Ehrenkaufer. Synthesis, 133 (1986).
27. S. Ram and R. E. Ehrenkaufer. Synthesis, 91 (1988).
28. S. Shaltiel. Biochem. Biophys. Res. Commun. **29**, 178 (1967).
29. H. O. Hankovszky, K. Hideg, and L. Lex. Synthesis, 914 (1980).
30. R. F. Lewelling. Ph.D. Thesis, University of California, Los Angeles, CA. 1984.

Can. J. Chem. Downloaded from www.nrcresearchpress.com by 194.225.253.170 on 09/07/12
For personal use only.

On the regioselectivity of Wittig reactions with unsymmetrically substituted succinic anhydrides

MARGARET M. KAYSER[1] AND LIVAIN BREAU

Department of Chemistry, University of New Brunswick, P.O. Box 5050, Saint John, N.B., Canada E2L 4L5

Received December 20, 1988

MARGARET M. KAYSER and LIVAIN BREAU. Can. J. Chem. **67**, 1401 (1989).

Phosphorane ylids react readily with succinic anhydrides to give enol-lactones. With highly substituted succinic anhydrides, condensations occur at the less substituted carbonyl group, suggesting that the reaction is sterically controlled. This, however, is not the case in monosubstituted anhydrides where effects other than steric become dominant. Condensation of phosphorane **1***a* with methoxysuccinic anhydride occurs selectively at the carbonyl group adjacent to the substituent. Stabilization of the transition state through complexation between the oxygen atom of the substituent and an electron-deficient phosphorus of the ylid is proposed.

Key words: cyclic anhydrides, Wittig reaction, regioselectivity, stabilized ylid.

MARGARET M. KAYSER et LIVAIN BREAU. Can. J. Chem. **67**, 1401 (1989).

Les ylides de phosphoranes réagissent facilement avec des anhydrides succiniques pour donner des énol-lactones. Dans le cas des anhydrides succiniques fortement substitués, la condensation se produit au niveau du carbonyle le moins substitué, suggérant ainsi un contrôle stérique de la réaction. La situation est cependant différente dans le cas des anhydrides monosubstitués où des effets autre que stériques deviennent prédominants. La condensation du phosphorane **1***a* sur l'anhydride méthoxysuccinique se fait de façon sélective au niveau du groupe carbonyle adjacent au substituant. On suggère une stabilisation de l'état de transition via une complexation entre l'atome d'oxygène du substituant et un atome de phosphore pauvre en électrons de l'ylide.

Mots clés : anhydrides cycliques, réaction de Wittig, régioséléctivité, ylide stabilisé.

[Traduit par la revue]

Can. J. Chem. Downloaded from www.nrcresearchpress.com by 194.225.253.170 on 09/07/12
For personal use only.

Introduction

Five-member enol-lactones, which occur widely in nature, frequently display an unusual range of biological activities (1). Since many of these compounds hold promise as insecticides, antiviral and antibacterial agents, and as synthetic intermediates for the construction of more complex molecules, a number of methods have been developed for their preparation (2). The condensation of stabilized phosphoranes, such as **1**, with five-member cyclic anhydrides was found to often be a procedure of choice for the synthesis of various enol-lactones (3–5).

In previous publications we outlined the problems of regioselectivity control in the reactions of unsymmetrically substituted maleic (6) and phthalic (7) anhydrides with stabilized phosphorane **1***a*.

$$Ph_3P{=}CHCOOR$$
1

1*a* R = CH_3, **1***b* R = CH_3CH_2

In this paper we describe the results of a complementary study of the condensations of **1***a* with a number of unsymmetrically substituted succinic anhydrides.

The first reaction between a saturated cyclic anhydride (glutaric anhydride) and ethoxycarbonylmethylenetriphenylphosphorane **1***b* was described in 1965 (8). The yield of the product, an enol-lactone, was low, even after prolonged reflux in dimethoxyethane. In a more recent study, Massy-Westropp and co-workers (9) investigated condensations of phosphoranes with various methyl-substituted glutaric and succinic anhydrides. The reactions of methyl-substituted succinic anhydrides with **1***b* were found to occur exclusively at the sterically more accessible carbonyl function and to give predominantly the (*E*)-enol-lactones (Table 1).

The reported regioselectivities of ylid additions to methylsuccinic and 2,2-dimethylsuccinic anhydrides stood in contrast to the theoretically predicted (10) and experimentally confirmed (11) regioselectivities for metal hydride reductions, which occur preferentially at the "more hindered" carbonyl group.

In addition, Massy-Westropp and co-workers reported that the phosphorane **1***b* reacted with methylsuccinic anhydride to give a mixture of *two* intermediate acyclic phosphonium salts **6**α and **6**β, formed by the addition of the ylid to the α- and β-carbonyl groups in the ratio 1:5 respectively, Scheme 1 (9). Since the reaction was postulated to be irreversible, the α addition should have led to the formation of the α-enol-lactone upon reflux.

The above inconsistency and the apparent lack of agreement with theoretical calculations prompted us to reinvestigate these reactions in the course of our studies on the regioselectivity of ylid condensations with cyclic anhydrides.

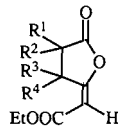
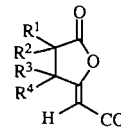
Results

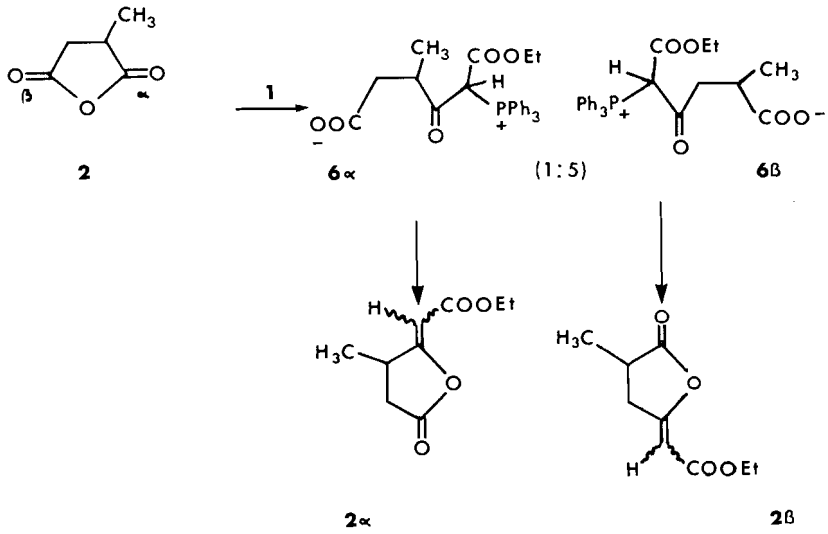
The reactions of stabilized phosphorane **1** with methylsuccinic anhydride **2**, 2,2-dimethylsuccinic anhydride **3**, and several other substituted anhydrides were carried out; the product ratios were analyzed by ^{1}H nmr and gas chromatography. The enol-lactones were subsequently isolated and, in cases of ambiguity, their structures were confirmed experimentally. The results are listed in Table 2.

The 2,2-dimethylsuccinic anhydride **3** reacted smoothly with phosphorane **1***a* to give an almost quantitative yield of the 3β*E* isomer after 35 h at room temperature, in agreement with the previous findings (9). On the other hand, the condensation of methylsuccinic anhydride **2** with **1***a* gave results significantly different from those reported earlier (compare Tables 1 and 2). Gas chromatographic analysis of the reaction product showed the presence of three enol-lactones in ratio 43:14:43. The minor component, later identified as 2α*Z*, was removed by chromatography; even after repeated attempts the 2α*E* and 2β*Z* could not be separated. Eventually the two geometrical isomers were separated and their structures confirmed by the series of experiments outlined in Scheme 2.

[1]Author to whom correspondence may be addressed.

TABLE 1. Condensations between methyl substituted succinic anhydrides and phosphorane **1***b* (ref. 9)

Anhydride					Products		
							
R^1	R^2	R^3	R^4		βE	βZ	Isolated enol-lactone (% yield)
CH_3	H	H	H	**2**	94	6	60
CH_3	CH_3	H	H	**3**	98	2	66
CH_3	CH_3	CH_3	H	**4**	70	30	99
CH_3	CH_3	CH_3	CH_3	**5**	85	15	56



SCHEME 1

The reaction of *p*-methoxyphenylsuccinic anhydride **7** with phosphorane **1***a* gave a 50:50 mixture **7**α and **7**β. The products were separated by chromatography; their structures were established by ^{1}H nmr and confirmed by hydrogenation experiments, as shown in Scheme 3.

The condensation of phenylsuccinic anhydride **8** with **1***a* gave a 68:32 mixture of the two isomers **8**α and **8**β. The product ratio was established by gas chromatography and by comparison of the ^{1}H nmr spectra of the crude reaction mixtures from the condensations of **1***a* with phenylsuccinic and **1***a* with *p*-methoxyphenylsuccinic anhydrides. We were unable to separate **8**α and **8**β by chromatography.

The hydrogenation of the mixture of **7**α and **7**β produced two new products **7**α*H* and **7**β*H*, of which one was identified by comparison with an authentic sample, as shown in Scheme 3.

The reaction of methoxysuccinic anhydride **11** with phosphorane **1** gave a single product, **11**α*E*, identified on the basis of its high resolution proton nmr spectrum. Its structure was confirmed by isomerization and hydrogenation experiments, as shown in Scheme 4.

The last compound studied in the succinic anhydride series was **12**, prepared by a Diels–Alder addition of furan to bromomaleic anhydride. The condensation of the adduct **12** with **1***a* gave two products, **12**β*E* and **13**, the latter resulting from a facile retro Diels–Alder decomposition of **12**β*E* (Scheme 5). Upon gentle heating the remaining **12**β*E* could be converted to **13**. In fact, the above reaction is the best route to the bromomaleic enol-lactone **13**, since the direct condensation between bromomaleic anhydride and phosphorane **1***a* yields predominantly a polymeric material.

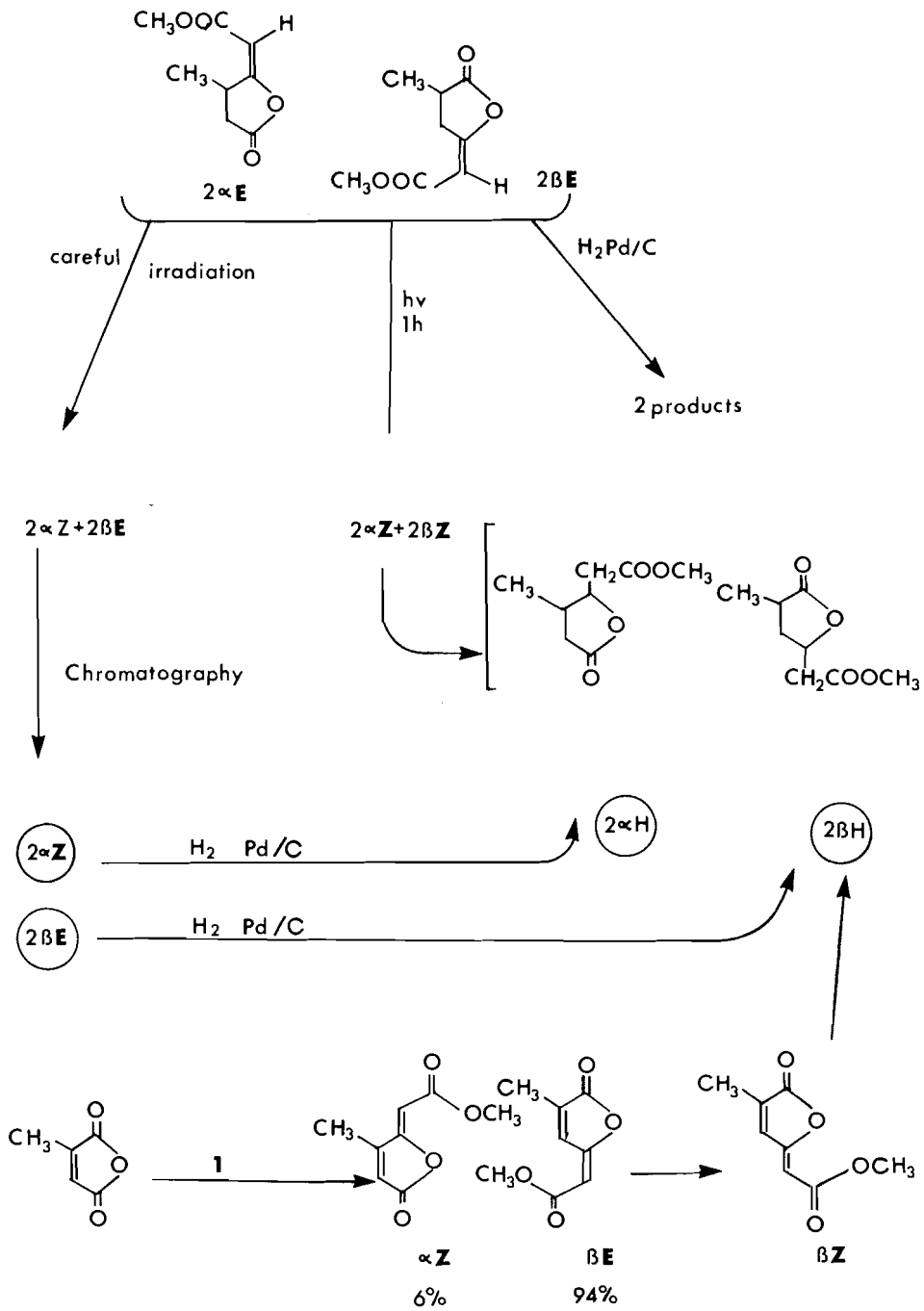
Discussion

The experimental results indicate that, depending on the nature of the substituents and the substitution patterns, we may distinguish two principal types of behaviour in the condensation of succinic anhydrides with stabilized phosphoranes.

Firstly, the 2,2-disubstituted (**3**, **10**) or 2,2,3-trisubstituted anhydrides (**4**, **12**) give enol-lactones resulting from condensation at *the less sterically hindered* carbonyl function. These reactions, completed within a few hours at room temperature, give preferentially the *E* isomers.

The simplest interpretation would suggest that the Wittig condensations with highly substituted succinic anhydrides are sterically controlled. An additional experiment, involving reaction of phosphorane **1***a* with 2,2-dimethyl-3,3-diphenylsuccinic anhydride **14** (12), which gives only one product, **14**β*Z*, supports this view. This reaction has not been included in Table 2, since the yield of the enol-lactone **14**β*Z* is very low (5–8%), and the product identification is based solely on its proton nmr spectrum.

Can. J. Chem. Downloaded from www.nrcresearchpress.com by 194.225.253.170 on 09/07/12
For personal use only.



SCHEME 2

The second type of behaviour is exhibited by monosubstituted succinic anhydrides **2**, **7**, **8**, and **11**. These compounds give condensation products ranging from a nonselective 50:50 mixture of regioisomers **7**, to 100:0 selectivity in favour of the carbonyl group adjacent to the substituent in methoxysuccinic anhydride **11**.

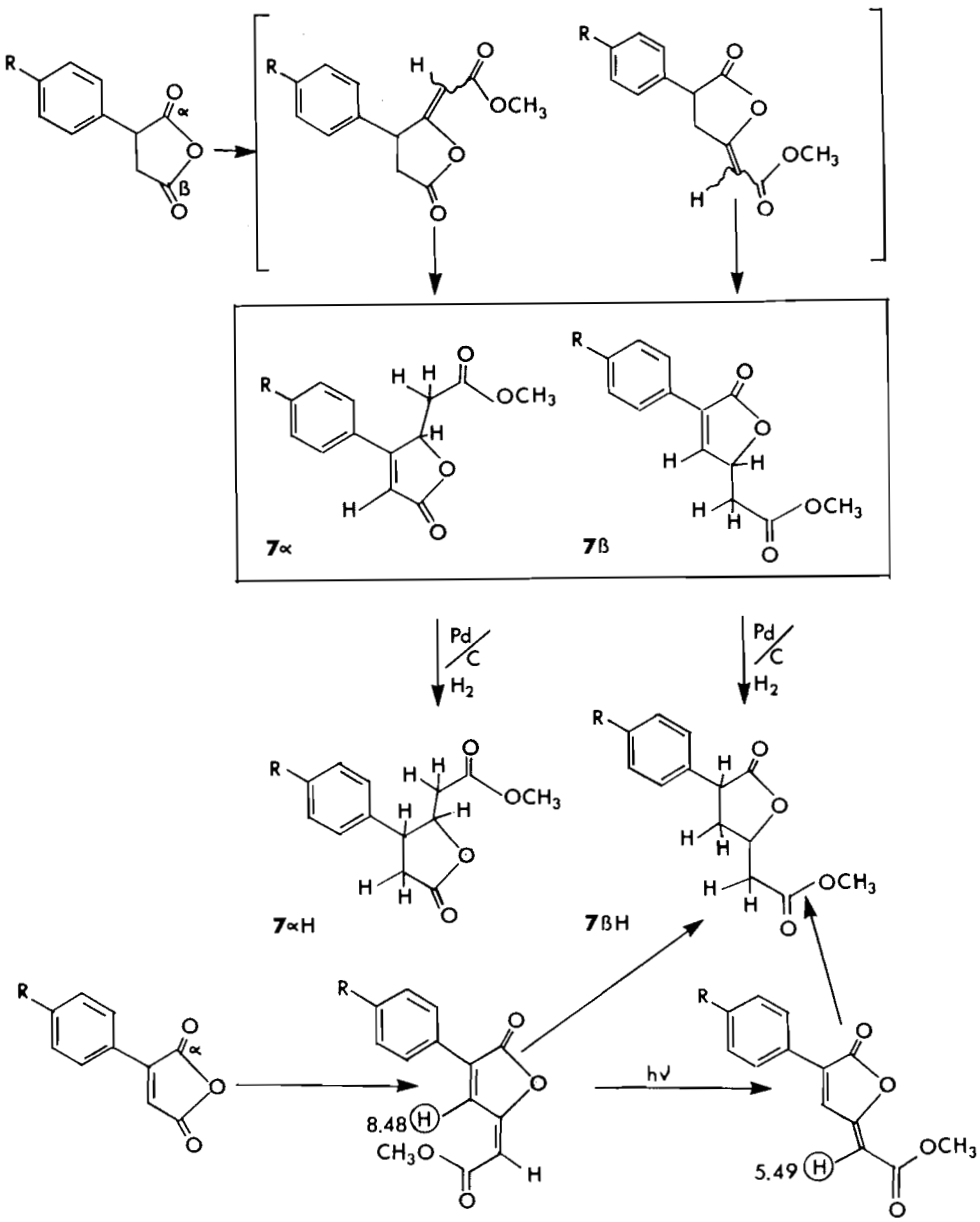
To assess the importance of the various effects that influence the regioselectivity of these reactions, the three cases are examined in detail.

Methylsuccinic anhydride

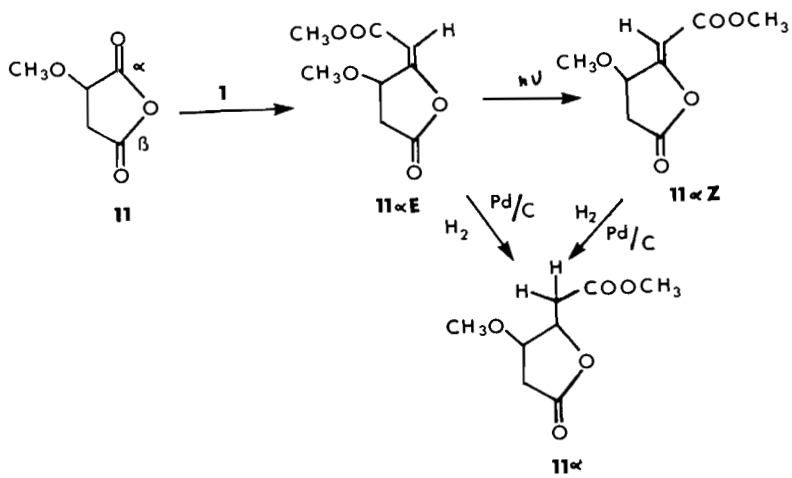
Experimental evidence (13) and various calculations (10, 14) indicate that the succinic anhydride ring is slightly twisted; even an unsubstituted ring exhibits a small deviation from planarity observable by electron diffraction in the gas phase (13). The distortion, resulting most probably from the large out-of-plane vibrations, demonstrates the flexibility of the ring, which can assume a skewed conformation to minimize strain in the transition state, or in the ground state when substituted with large groups. The *ab initio* calculations (10), carried out on methylsuccinic and 2,2-dimethylsuccinic anhydrides, have shown that a distortion from planarity is energetically favourable and that the methyl substituent prefers to assume a quasi-equatorial position (10). More recent MM2 calculations confirm both results, namely that the substitution causes a significant distortion of the anhydride ring and that the conformation having a 2-substituent in the quasi-equatorial position is preferred for phenyl as well as for all alkyl groups studied (14).

Can. J. Chem. Downloaded from www.nrcresearchpress.com by 194.225.253.170 on 09/07/12
For personal use only.

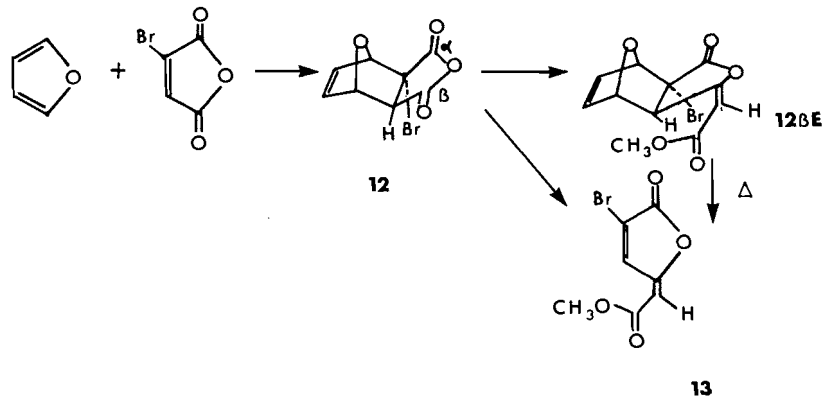
Can. J. Chem. Downloaded from www.nrcresearchpress.com by 194.225.253.170 on 09/07/12
For personal use only.



SCHEME 3

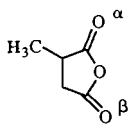
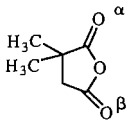
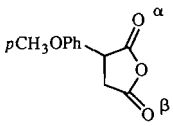
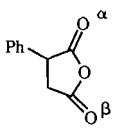
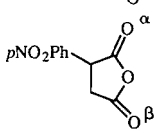
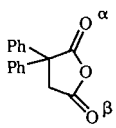
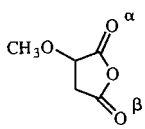
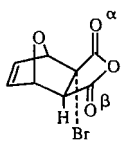


SCHEME 4



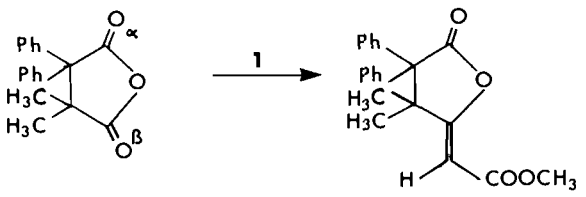
SCHEME 5

TABLE 2. Condensation of **1***a* with unsymmetrically substituted succinic anhydrides

Starting anhydride	No.	Products				Ratio α:β	Isolated enol-lactone (% yield)
		E	*Z*	β*E*	β*Z*		
	2	43	14	43	—	57:43	67
	3	—	—	100	—	0:100	90
	7	50			50	50:50	86
	8	68			32	68:32	77
	9	Polymerization					
	10	—	—	100	—	0:100	90
	11	100	—	—	—	100:0	71
	12	—	—	100	—	100:0	96

Can. J. Chem. Downloaded from www.nrcresearchpress.com by 194.225.253.170 on 09/07/12
For personal use only.

Can. J. Chem. Downloaded from www.nrcresearchpress.com by 194.225.253.170 on 09/07/12
For personal use only.



14 **14ßZ**

Examination of a model of a twisted methylsuccinic anhydride shows that the quasi-equatorial methyl group is almost eclipsed with the neighbouring carbonyl function.[2]

Ab initio calculations (10) for the hydride addition to methylsuccinic anhydride suggest that the energetically most favourable nucleophilic attack occurs in the antiperiplanar fashion at the α-carbonyl group of the anhydride twisted in a chair-like conformation, with the methyl substituent in a quasi-equatorial position, **16***c*.

Since the above calculations do not take into account the steric requirements of the large ylid nucleophile, one may assume that the preferred conformation during ylid addition probably most closely resembles the "quasi axial" supermolecule **16***b*. A better HOMO–LUMO overlap (21), and a stabilizing antiperiplanar relationship of the nucleophile to the C—CH_3 bond (22), are likely to be responsible for a weak preference for the α-carbonyl group.

Phenylsuccinic anhydride **8**

In the reaction of phenylsuccinic anhydride with the stabilized phosphorane **1**, the usual condensation products, butanolides, are not observed. Rather, a rapid migration of the *exo* double bond occurs, giving a 68:32 mixture of **8**α and **8**β. Since the rearrangement is irreversible, this ratio represents the distribution of α and β attack at condensation.

The higher proportion of the α attack may be due to a stabilizing complexation between the electron-rich carbonyl group of the ylid and the electron-poor phenyl ring, as shown in structure **17**. The complexation is facilitated by the flexibility of the succinic anhydride ring and preferred quasi-equatorial conformation of the phenyl substituent (*vide supra*).

The above interpretation is supported by the results obtained in the reaction of *p*-methoxyphenylsuccinic anhydride **7** with the ylid, in which the proportion of the condensation at the α-carbonyl group next to the substituent decreased significantly.

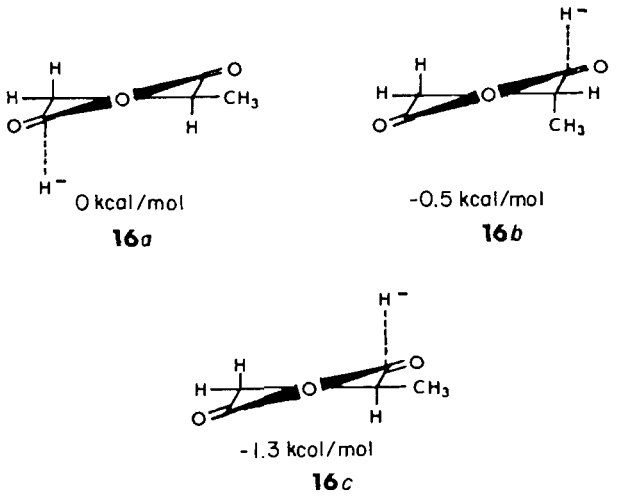
Somewhat related complexing effects were evoked by Chopard *et al.* (4) to explain stereoselectivity patterns observed in the condensation of stabilized phosphoranes with phthalic anhydride (4).

Methoxysuccinic anhydride

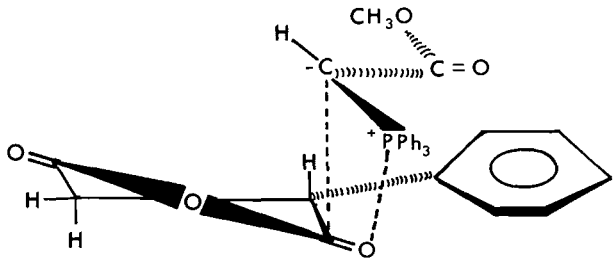
The reaction of methoxysuccinic anhydride **11** with phosphorane **1** is completed within minutes at room temperature to give a single *E* isomer. The reaction can be readily followed by nmr and thereby disappearance of the anhydride and formation of the enol-lactone can be monitored. A similarly regiospecific condensation at the carbonyl group adjacent to the substituent occurs in alkoxy maleic anhydrides (6), while an enhanced selectivity for the 2-carbonyl group has been observed in 3-methoxyphthalic anhydrides (7).

The regioselectivity of these reactions has been interpreted in terms of a particularly effective stabilization of the transition state due to electron donation from the electron-rich oxygen of the alkoxy substituent to the electron-poor phosphorus of the ylid (6, 7).

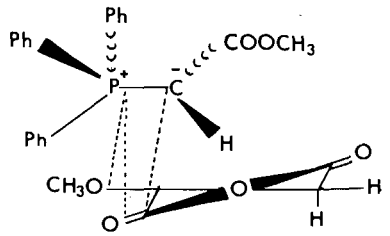
In the reaction between methoxysuccinic anhydride and the ylid the geometry is suitable for an effective O—P overlap (23), providing the anhydride ring is twisted into a chair-like conformation with the methoxy group in the quasi-equatorial position as shown in **18**.



16*a* **16***b* **16***c*



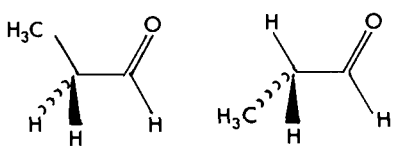
17



18

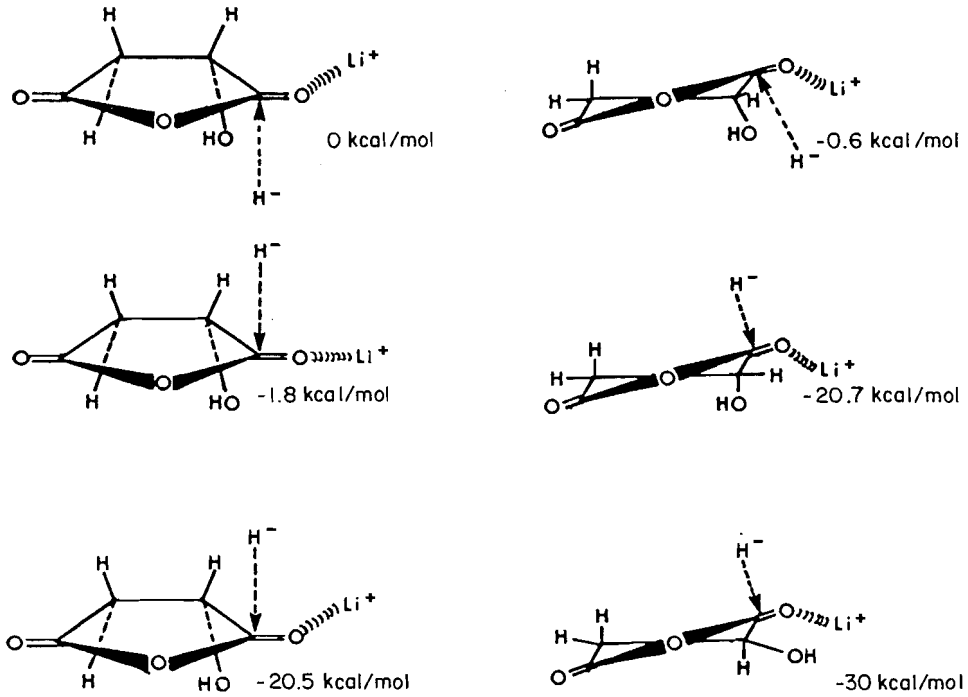
Since it has been demonstrated in the past that the antiperiplanar effect may be particularly important when the substituent α to the carbonyl group is an electronegative atom such as Cl or O (22), we carried out *ab initio* calculations on a simplified model to estimate the relative importance of an antiperiplanar versus a complexation effect for the hydroxysuccinic anhydride supermolecule (24). The results are shown in Table 3. Although

[2]Interestingly, the most stable conformation of propanal is the eclipsed rotamer **15***a*, which is favoured ovr the next low energy conformation **15***b* by approximately 900 cal/mol (15–20).



15*a* **15***b*

TABLE 3. Relative energies of planar and twisted supermolecules



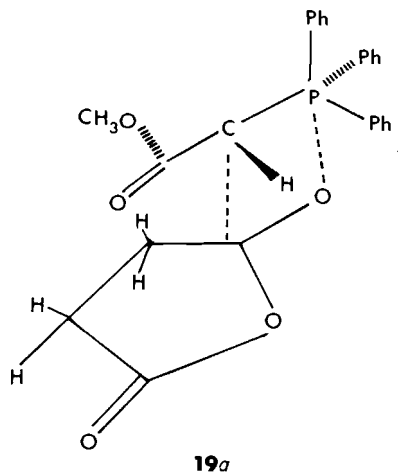
the model used (Table 3) clearly does not reflect adequately the geometrical requirements for ylid–anhydride addition, as illustrated in **18**, it does suggest that a twisted conformation, in which the oxygen atom of the substituent can act as a base vis-à-vis a Lewis acid, is particularly favourable. The internal complexation also enhances the positive character of the C atom of the carbonyl group, thereby facilitating nucleophilic attack. Since similar geometry is encountered in the addition of the ylid to the alkoxymaleic anhydrides (6) and the experimental results for these compounds show that the condensations occur entirely at the carbonyl group adjacent to the substituents, the model is probably adequate and complexation in the methoxysuccinic anhydride is the determining factor in regioselectivity control.

The stereochemistry of ylid addition

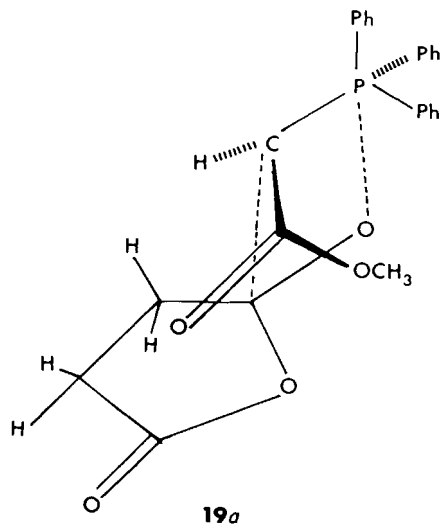
From the observations recorded in Tables 1 and 2 it is apparent that the additions of stabilized ylids **1***a* and **1***b* to the succinic anhydrides preferentially give the *E* isomers. This stereochemistry may be explained as follows. In the transition state the carboxy group of the ylid assumes preferentially a configuration *trans* to the ring-oxygen atom, **19***a*. Stacking of the carboxy group above the oxygen as shown in **19***b* is clearly unfavourable, probably due to the oxygen – carboxy group repulsion. Even when the substituents on the ring are large and cannot be twisted away from interfering with the nucleophile, the *E* isomer predominates. It is possible that in some cases, when the *Z* isomer was isolated, it had been formed only during the work-up procedures from the sterically more hindered *E* isomer. We have observed such an easy isomerization in a number of reactions, which were followed by proton nmr.

Conclusion

It is quite evident that, although ylid additions to succinic anhydrides are sensitive to steric restrictions and are more likely



19*a*



19*a*

Can. J. Chem. Downloaded from www.nrcresearchpress.com by 194.225.253.170 on 09/07/12
For personal use only.

Can. J. Chem. Downloaded from www.nrcresearchpress.com by 194.225.253.170 on 09/07/12
For personal use only.

to occur at a "less hindered" carbonyl function, various electronic effects cannot be neglected. In particular, complexation between electron-rich substituents and the electron-poor phosphorus of the ylid appears to be important in regioselectivity control. We are presently investigating other substituents as possible electron donors and the geometrical requirements for effective base–phosphorus stabilizing interactions.

Experimental

Melting points were determined on a Fisher Scientific Co. hot-stage melting point apparatus and are uncorrected. Infrared spectra were obtained on a Perkin–Elmer 1420 ratio recording infrared spectrophotometer, neat, or with chloroform as solvent. Ultraviolet spectra were measured in methanol using a Varian Cary 219 spectrophotometer. Proton nmr and ^{13}C nmr spectra were recorded on a Varian EM 300L nmr spectrometer or on a Nicolet 360 spectrometer with $CDCl_3$ as solvent and $(CH_3)_4Si$ as internal standard. Mass spectra were recorded on a VG mass spectrometer with a DANI 7070 gas chromatograph. Gas chromatography analyses were carried out with a Varian 3700 gas chromatograph, using a 50 cm × 1/8 in. 5% OV-101 on Chromosorb G-HP 100/120 mesh column. Chromatographic separations were performed on a preparative, centrifugally accelerated, radial, thin-layer chromatograph (a Chromatotron model 7924T). Tetrahydrofuran (THF) was dried over sodium metal and was distilled under nitrogen.

*General procedure for the reactions of $Ph_3P{=}CHCO_2CH_3$ **1**a with succinic anhydrides*

Molar equivalent amounts of an anhydride (0.01 mol) and methyl)(triphenylphosphoranylidene) acetate **1***a* (0.01 mol) were dissolved in dry THF (100 mL) and the solution was refluxed under N_2 atmosphere. Progress of the reaction was followed by gas chromatography and proton nmr. Crude products were separated on the Chromatotron. The isomeric lactones were identified by proton nmr, hydrogenation, and isomerization experiments.

Photochemical isomerization of enol-lactones

A pure sample of an enol-lactone was dissolved in cyclohexane and placed in a petri dish surrounded by aluminum foil. The solution was irradiated with a uv lamp (UVSL-25 watt) for a period of 15 min – 2 h. After evaporation of the solvent the residue was analyzed by proton nmr and gas chromatography.

Reaction of methylsuccinic anhydride 2

The reaction between methylsuccinic anhydride **2** (1.12 g, 8.77 mmol) and phosphorane **1***a* (2.93 g, 8.77 mmol) in THF was completed in 48 h at 40°C. Proton nmr analysis of the crude reaction mixture showed that the isomers **2**α*E*, **2**α*Z*, and **2**β*E* were present in the ratio 43:14:43. Chromatography with petroleum ether/ether failed to separate the isomeric enol-lactones **2**α*E* and **2**β*E*, but succeeded in removing the triphenylphosphine oxide ($Ph_3P{=}O$) and **2**α*Z* isomer from the mixture. The remaining two enol-lactones were isolated in 67% yield (1.0 g). The assignment of structures was based on the 360-MHz proton nmr spectroscopic data. The following resonances were identified as due to methyl (*E*)-(tetrahydro-3-methyl-5-oxo-2-furanylidene)acetate **2**α*E*: proton nmr ($CDCl_3$) δ: 1.39 (d, J = 7 Hz, 3H, CH_3), 2.26–3.11 (m, 3H, at C-3 and C-4), 3.71 (s, 3H, $COOCH_3$), 5.61 (d, J = 1.3 Hz, 1H, :C*H*COOMe); gc–ms m/z: M^+ 170 (9%), 142 (44%), 139 (23%), 110 (23%), 101 (35%), 69 (100%), and 42 (26%). The methyl (*E*)-tetrahydro-4-methyl-5-oxo-2-furanylidene) acetate **2**β*E* showed characteristic peaks at δ 1.36 (d, J = 7 Hz, 3H, CH_3), 2.26–3.11 (m, 3H, at C-3 and C-4), 3.70 (s, 3H, $COOCH_3$), 5.66 (t, J = 2 Hz, 1H, :C*H*COOMe); gc–ms m/z: M^+ 170 (M^+, 20), 142 (46), 139 (29), 110 (26), 101 (49), 69 (100), and 42 (31).

A solution of **2**α*E* (65%) and **2**β*E* (35%) in cyclohexane was irradiated for 30 min. Proton nmr and glc of the product showed that three enol-lactones were now present: **2**α*E* (24%), **2**α*Z* (41%), and **2**β*E* (35%). The major isomer, methyl (*Z*)-(tetrahydro-3-methyl-5-oxo-2-furanylidene)acetate **2**α*Z*, was characterized by a proton nmr signal at δ 5.13 (d, J = 1 Hz, :C*H*COOMe).

A solution of **2**α*Z* (50 mg) in ethyl acetate (50 mL) was hydrogenated according to the general procedure to give the single product, **2**α*H*, with a characteristic signal in the proton nmr spectrum at δ 4.43 (m, 1H).

Hydrogenation carried out on the mixture of **2**α*Z* and **2**β*Z* (from an exhaustive irradiation of the original mixture of **2**α*E* and **2**β*E*) gave an inseparable mixture of **2**α*H* and **2**β*H*. The proton nmr spectrum of the mixture showed signals at δ 4.43 (m, 1H, C-3) for **2**α*H* and at δ 4.93 (m, 1H, C-4) for **2**β*H*. The identity of **2**β*H* was confirmed by the hydrogenation carried out on the **18**β*E* enol-lactone (6). A solution of pure **18**β*E* (100 mg) in ethyl acetate (100 mL) containing 5% palladium-on-carbon catalyst (25 mg) was shaken under hydrogen at 40 psi (1 psi = 6.9 kPa) overnight. The mixture was filtered and the filtrate evaporated under reduced pressure to give 98 mg (98%) of methyl (tetrahydro-4-methyl-5-oxo-2-furan)acetate, **2**β*H*, as a colourless oil; ir (thin layer) ν_{max}: 2945, 1770, 1740, 1440, 1170, 1030, and 935 cm^{-1}; proton nmr ($CDCl_3$) δ: 1.3 (d, J = 7 Hz, 3H) 1.4–1.95 (m, 1H), 2.25–3.20 (m, 4H), 3.75 (s, 3H, $COOCH_3$), and 4.93 (m, 1H, C-4).

Reaction of 2,2-dimethylsuccinic anhydride 3

2,2-Dimethylsuccinic anhydride **3** (142 mg, 1.0 mmol) and phosphorane **1***a* (334 mg, 1.0 mmol) were dissolved in $CDCl_3$ at room temperature. The reaction was monitored by proton nmr. After 12 h the reaction was essentially completed. The infrared and proton nmr spectra of the product enol-lactone, **3**β*E*, were identical with those described in the literature (9).

Reaction with (p-methoxyphenyl)succinic anhydride 7

Using the general procedure, the reaction between (*p*-methoxyphenyl)succinic anhydride **7** (25) (1.00 g, 4.85 mmol) and phosphorane **1***a* (1.62 g, 4.85 mmol) was completed after 20 h of reflux in THF. Proton nmr analysis of the crude reaction mixture showed that the two isomers **7**α and **7**β were present in the ratio 50:50. Chromatography with petroleum ether/ether gave methyl (3-[2,5-dihydro *p*-methoxyphenyl]-5-oxo-2-furan)acetate **7**α (eluted first), as white flaky leaflets, mp 94–95°C; ir ($CHCl_3$) ν_{max}: 2960, 2930, 2830, 1755, 1740, 1610, 1410, 1260, 1180, 1125, and 840 cm^{-1}; proton nmr ($CDCl_3$) δ: 2.68 (dd, J = 16.4 and 7.2 Hz, 1H), 2.91 (dd, J = 16.4 and 7.0 Hz, 1H), 3.75 (s, 3H, $COOCH_3$), 3.83 (s, 3H, *p*-Ar -OCH_3), 5.39 (td, J = 7.0, 7.2, and 1.6 Hz, 1H, >C*H*—Ph), 6.93 (asym. d, J = 8.8 Hz, 2H, *m*-Ar H), 7.54 (d, J = 1.6 Hz, 1H, :C*H*COOMe), 7.82 (asym. d, J = 8.8 Hz, 2H, *o*-Ar H); ms m/z: 262 (M^+, 38), 202 (100), 189 (19), 161 (45), 133 (88), and 57 (21). *Exact Mass* calcd. for $C_{14}H_{14}O_5$: 262.0841; found: 262.0802. Further elution gave methyl (4-[2,5-dihydro *p*-methoxyphenyl]-5-oxo-2-furan)acetate **7**β as pale yellow cubic crystals, mp 64–66°C; ir ($CHCl_3$) ν_{max}: 3020, 2960, 2940, 2930, 1840, 1605, 1510, 1290, 1260, 1170, 1050, and 830 cm^{-1}; proton nmr ($CDCl_3$) δ: 2.50 (dd, J = 17.5 and 9.4 Hz, 1H), 2.92 (dd, J = 16.5 and 2.6 Hz, 1H), 3.74 (s, 3H, $COOCH_3$), 3.86 (s, 3H, *p*-Ar OCH_3), 5.88 (ddd, J = 9.4, 2.6, and 1.3 Hz, 1H), 6.20 (d, J = 1.3 Hz, 1H, :C*H*COOMe), 6.98 (asym. d, J = 8.8 Hz, 2H, *o*-Ar H), 7.42 (asym. d, J = 8.8 Hz, 2H, *m*-Ar H); ms m/z: 262 (M^+, 63), 171 (32), 202 (19), 189 (23), 161 (48), 133 (100), 131 (52), 71 (19), 57 (36), 43 (20), and 28 (29). *Exact Mass* calcd. for $C_{14}H_{14}O_5$: 262.0841; found: 262.0832. Overall yield of the two isomers was 1.09 g (86%).

A cyclohexane solution of pure **7**α was irradiated. Proton nmr and glc showed on change even after 4 h of irradiation. Some polymeric material was formed upon prolonged irradiation. Identical results were obtained on the irradiation of the **7**β isomer.

A solution of the pure **7**α (100 mg) in ethyl acetate (100 mL) containing 5% palladium-on-carbon catalyst (25 mg) was shaken under hydrogen at 30 psi for 6 h; the mixture was filtered and the filtrate evaporated under reduced pressure to give 105 mg of a pale yellow oil. Chromatography on the Chromatotron with petroleum ether/ether gave the pure methyl (tetrahydro-3-[*p*-methoxyphenyl]-5-oxo-2-furan)acetate, **7**α*H* (90 mg, 89%), as a very pale yellow oil; ir (thin film) ν_{max}: 3005, 2960, 1780, 1735, 1610, 1520, 1255, 1180, 1030, and 835 cm^{-1}; proton nmr ($CDCl_3$) δ: 2.18 (dd, J = 17.0 and 6.5 Hz, 1H), 2.46

Can. J. Chem. Downloaded from www.nrcresearchpress.com by 194.225.253.170 on 09/07/12
For personal use only.

(dd, J = 17.0 and 7.6 Hz, 1H), 2.74 (dd, J = 17.0 and 4.1 Hz, 1H), 3.02 (dd, J = 17.0 and 8.8 Hz, 1H), 3.61 (s, 3H, $COOCH_3$), 3.80 (s, 3H, *p*-Ar -OCH_3), 3.84 (m, 1H, H-A), 5.16 (m, 1H, H-B), 6.86 (asym. d, J = 8.7 Hz, 2H, *m*-Ar H), and 7.02 (asym. d, J = 8.7 Hz, 2H, *o*-Ar H).

A solution of the mixture of **7**α and **7**β in ethyl acetate (100 mL) containing 5% palladium-on-carbon catalyst (50 mg) was shaken under hydrogen at 30 psi for 6 h; the mixture was filtered and the filtrate evaporated under reduced pressure to give 205 mg of a pale yellow oil. Chromatography on the Chromatotron with petroleum ether/ether gave methyl (tetrahydro-3-[*p*-methoxyphenyl]-5-oxo-2-furan)acetate, **7**α*H* (110 mg), eluted first. The sample had identical spectral properties with the product obtained from the hydrogenation of pure **7**α. Methyl (tetrahydro-4-[*p*-methoxyphenyl-5-oxo-2-furan)acetate **7**β*H* (90 mg), a colourless oil, was eluted second. This fraction corresponded to the hydrogenation product of the pure **7**β: ir (thin film) ν_{max}: 2940, 1770, 1735, 1615, 1515, 1250, 1155, and 1030 cm^{-1}; proton nmr ($CDCl_3$) δ: 2.12 (m, 1H, H-D), 2.71 (dd, J = 16.3 and 6.1 Hz, 1H), 2.86 (m, 1H, H-C), 2.90 (dd, J = 16.3 and 6.7 Hz, 1H), 3.73 (s, 3H $COOCH_3$), 3.79 (s, 3H, *p*-Ar -OCH_3), 3.86 (dd, J = 8.9 and J = 8.6 Hz, 1H, H-A), 4.87 (m, 1H, H-B), 6.89 (asym. d, J = H.7 Hz, 2H, *m*-Ar H), and 7.20 (asym. d, J = 8.6 Hz, 2H, *o*-Ar H).

Synthesis of phenylsuccinic anhydride **8**

A solution of phenylsuccinic acid (23 g, 0.13 mol) in acetic anhydride (25 g, 0.23 mol) was heated under reflux for 2 h. Fractional distillation under reduced pressure yielded phenylsuccinic anhydride **8** (20.6 g, 91%) as a pale yellow oil, bp 153–155°C/0.4 Torr (1 Torr = 133.3 Pa), which crystallized on cooling; mp 53–54°C (lit. (27) mp 54°C); ir ($CHCl_3$) ν_{max}: 3010, 2960, 1865, 1790, 1062, 920, and 908 cm^{-1}; proton nmr ($CDCl_3$) δ: 3.23 (m, 2H, —CH_2), 4.33 (m, 1H, >CH—Ph), 7.33 (m, 5H, Ar H).

Reaction with phenylsuccinic anhydride **8**

Using the general procedure, the reaction between phenylsuccinic anhydride **8** (1.00 g, 5.68 mmol) and phosphorane **1***a* (1.90 g, 5.68 mmol) was completed after 20 h of reflux in THF. Proton nmr analysis of the crude reaction mixture showed that the two isomers **8**α and **8**β were present in the ratio of 68:32. Repeated chromatography failed to separate the isomeric enol-lactones **8**α and **8**β but succeeded in removing triphenylphosphine oxide (Ph_3P=O) from the mixture. The two enol-lactones were isolated in 77% yield (1.01 g). The assignment of the structures was based on the proton nmr spectra by comparison with almost identical chemical shifts observed for a separable mixture of **7**α and **7**β.

Hydrogenation of a mixture of isomers **8**α *and* **8**β

A solution of **8**α and **8**β was hydrogenated, as described previously, to yield an inseparable mixture of methyl (tetrahydro-3-phenyl-5-oxo-2-furan)acetate **8**α*H* and methyl (tetrahydro-4-phenyl-5-oxo-2-furan)acetate **8**β*H* as a colourless oil. The 60-MHz proton nmr ($CDCl_3$) of the reaction mixture showed characteristic peaks at δ 5.10 (m, 1H, H at C-3) for the **8**α*H* isomer and 4.85 (m, 1H, H at C-4) for the **8**β*H* isomer. The **8**β*H* was identical (gc and proton nmr) with a sample of pure methyl (tetrahydro-4-phenyl-5-oxo-2-furan)acetate from the hydrogenation of the enol-lactone obtained by condensation of phenylmaleic anhydride with phosphorane **1***a* (6). *Exact Mass* calculated for $C_{13}H_{14}O_4$: 234.0892; found: 234.0892.

Reaction with p*-nitrophenylsuccinic anhydride* **9**

Upon mixing *p*-nitrophenylsuccinic anhydride **9** (26) (0.35 g, 1.58 mmol) and phosphorane **1***a* (0.53 g, 1.59 mmol) in THF, a deep red colouring developed instantaneously. Neither starting material nor any monomeric enol-lactone could be detected by glc and proton nmr.

Reaction with methoxysuccinic anhydride **11**

The reaction between methoxysuccinic anhydride **11** (27) (0.50 g, 3.84 mmol) and phosphorane **1***a* (1.29 g, 3.84 mmol) was completed in 20 h at 40°C in THF. Proton nmr and glc analyses of the crude reaction mixture showed a single enol-lactone **11**α*E*. Chromatography on the Chromatotron with petroleum ether/ether gave the pure methyl (*E*)-(tetrahydro-3-methoxy-5-oxo-2-furanylidene)acetate **11**α*E* (0.51 g, 71%) as a colourless liquid: ir (thin film) ν_{max}: 3000, 2955, 1830, 1720, 1675, 1270, 1100, and 950 cm^{-1}; 100-MHz proton nmr ($CHCl_3$) δ: 2.66 (dd, J = 18 and 2 Hz, 1H), 2.88 (dd, J = 18 and 5 Hz, 1H), 3.43 (s, 3H, OCH_3), 3.76 (s, 3H, $COOCH_3$), 5.29 (ddd, J = 5, 2, and 0.9 Hz, 1H), and 5.84 (d, J = 0.9 Hz, 1H, :CHCOOMe); ms m/z: 186 (M^+, 5), 171 (1), 156 (34), 123 (49), 101 (24), 85 (26), 84 (22), 69 (92), and 58 (100). *Exact Mass* calculated for $C_8H_{10}O_5$: 186.0528; found: 186.0536.

Isomerization of **11**α*E to* **11**α*Z*

A solution of pure **11**α*E* (100 mg) in cyclohexane was irradiated for 2 h. Proton nmr and glc analyses of the reaction mixture showed that **11**α*E* and **11**α*Z* were in a 50:50 ratio. Upon chromatography with petroleum ether/ether, **11**α*E* (50 mg) was eluted first and the methyl (*Z*)-(tetrahydro-3-methoxy-5-oxo-2-furanylidene)acetate **11**α*Z* (50 mg) eluted second as a colourless oil; ir (thin film) ν_{max}: 3000, 2950, 1830, 1720, 1685, 1235, 1150, 1100, and 960 cm^{-1}; 60-MHz proton nmr ($CDCl_3$) δ: 2.60 (dd, J = 18 and 4 Hz, 1H), 3.02 (dd, J = 18 and 7 Hz, 1H) 3.44 (s, 3H, OCH_3), 3.76 (s, 3H, $COOCH_3$), 4.47 (ddd, J = 7, 4, and 2 Hz, 1H), 5.35 (d, J = 2 Hz, 1H, :CHCOOMe); ms m/z: 171 (M^+ −15 (CH_3, 1), 156 (28), 123 (64), 101 (23), 85 (32), 84 (22), 69 (97), and 58 (100).

Synthesis of exo*-3a-bromo-3a,4,7,7a-tetrahydro epoxyisobenzofuran-1,3-dione* **12**

This anhydride was prepared by a Diels–Alder cycloaddition reaction of bromomaleic anhydride with furan. A mixture of bromomaleic anhydride (3.00 g, 17.0 mmol) and furan (10.0 g, 147 mmol) was stirred, for 24 h at room temperature, in a tightly stoppered flask covered with aluminum foil. The excess furan was evaporated with a gentle stream of dry nitrogen until crystallization had started. The flask was stoppered and cooled for 2 days in a refrigerator. The brown product that precipitated upon cooling was filtered, and washed with ice-cold $CHCl_3/CCl_4$ (50:50) (3 × 10 mL), to yield 3.77 g (91%) of the *exo* adduct: *exo*-3a-bromo-3a,4,7,7a-tetrahydro-4,7 epoxyisobenzofuran-1,3-dione (12). Crystallization from $CHCl_3$/petroleum ether (50:50) gave a sample melting at 95–101°C (dec.) (lit. (28) mp 93–95°C); ir ($CDCl_3$) ν_{max}: 2960, 2878, 1868, 1790, 1248, 1108, 1020, 980, 950, 900, 860, 710, 690, and 650 cm^{-1}; proton nmr ($CDCl_3$) δ: 3.10 (s, 1H, H-7a), 5.43 (d, J = 1 Hz, 1H, H-7), 5.47 (d, J = 1 Hz, 1H, H-4), 6.72 (d, J = 1 Hz, 2H, H-5, 6).

Wittig reaction with exo*-3a-bromo-3a,4,7,7a-tetrahydro-4,7 epoxyisobenzofuran-1,3-dione* **12**

Using the general procedure, the reaction between **12** (1.00 g, 4.08 mmol) and phosphorane **1***a* (1.36 g, 4.07 mmol) was completed after 48 h at room temperature. Proton nmr analysis of the crude mixture revealed that the furan adduct **12**β*E* and the enol-lactone **13** were present in the ratio 45:55. Chromatography with petroleum ether/ether failed to separate the two enol-lactones, but succeeded in removing Ph_3P=O from the mixture. The two enol-lactones: methyl (*E*)-(2,5-dihydro-4-bromo-5-oxo-2-furanylidene)acetate, **13**, and methyl-(*E*)-3a-bromo-3-oxo-1,3,3aα,4α,7α,7aα-hexahydro-4,7 epoxyisobenzofuran-1-ylideneacetate), **12**β*E*, were isolated as white crystals in 96% yield (1.0 g). The **12**β*E* isomer was not purified further; however, 60-MHz proton nmr ($CDCl_3$) showed the following characteristic peaks: δ 3.72 (br s, 1H, H-7a), 3.81 (s, 3H, $COOCH_3$), 5.27 (d, J = 1 Hz, 1H, H-7), 5.32 (d, J = 1 Hz, 1H, H-4).

Acknowledgements

We thank the Natural Sciences and Engineering Research Council of Canada for support and Dr. K. C. Tompkins for helpful discussion.

1. G. Pattenden. Fortschr. Chem. Org. Naturst. **35**, 133 (1978).
2. Y. S. Rao. Chem. Rev. **76**, 625 (1976); K. Tomioka and

T. TASHIGURO. Tetrahedron Lett. 2973 (1980), J. Chem. Soc. Chem. Commun. 652 (1979); M. FIGUEREDO, J. FONT, and A. VIRGILI. Tetrahedron, **43**, 1881 (1987).
3. D. W. KNIGHT and G. PATTENDEN. J. Chem. Soc. Perkin Trans., 1, 635 (1975); 641 (1975).
4. P. A. CHOPARD, R. F. HUDSON, and R. J. SEARLE. Tetrahedron Lett. 2357 (1965).
5. C. F. INGHAM, R. A. MASSY-WESTROPP, G. D. REYNOLDS, and W. D. THORPE. Aust. J. Chem. **28**, 2499 (1975).
6. M. M. KAYSER and L. BREAU. Tetrahedron Lett. **29**, 6203 (1988).
7. L. BREAU and M. M. KAYSER. Can. J. Chem. **67**, 569 (1989).
8. P. A. CHOPARD, R. J. SEARLE, and F. H. DEVITT. J. Org. Chem. **30**, 1015 (1965).
9. A. D. ABELL, I. R. DOYLE, and R. A. MASSY-WESTROPP. Aust. J. Chem. **35**, 2277 (1982).
10. M. M. KAYSER and G. WIPFF. Can. J. Chem. **60**, 1192 (1982).
11. M. M. KAYSER and P. MORAND. Can. J. Chem. **56**, 1524 (1978).
12. M. M. KAYSER and P. MORAND. Tetrahedron Lett. 695 (1979).
13. K. BRENDHAUGEN, M. K. FIKKE, and H. M. SEIP. Acta Chem. Scand. **27**, 1101 (1973).
14. T. POLONSKI. J. Chem. Soc. Perkin Trans. 1, 629 (1988).
15. S. S. BUTCHER and E. B. WILSON, JR. J. Chem. Phys. **40**, 1671 (1964).
16. G. J. KARABATSOS and D. J. FENOGLIO. Top. Stereochem. **5**, 167 (1970).
17. R. J. ABRAHAM and J. A. POPLE. Mol. Phys. **3**, 609 (1960).
18. H. M. PICKETT and D. G. SCROGGIN. J. Chem. Phys. **61**, 3954 (1974).
19. N. L. ALLINGER, M. T. TRIBBLE, and M. A. MILLER. Tetrahedron, **28**, 1173 (1972).
20. N. L. ALLINGER and M. J. HICKEY. J.Mol. Struct. **17**, 233 (1973).
21. M.M. KAYSER and O. EISENSTEIN. Can. J. Chem. **59**, 2457 (1981).
22. N. T. ANH and O. EISENSTEIN. Nouv. J. Chim. **1**, 61 (1977).
23. K. P. JOHN, R. SCHMUTZLER, and W. S. SHELDRICK. J. Chem. Soc. Dalton Trans. 1841 (1974); 2466 (1974); D. ROBERT, H. A. GAWARD, and J. G. RIESS. Bull. Soc. Chim. Fr. 511 (1987).
24. J. S. BINKLEY, M. J. FRISCH, D. J. DEFREES, K. RAGHAUACHARI, R. A. WHITESIDE, H. B. SCHLEGAL, E. M. FLUDER, and J. A. POPLE. Gauss 82. Carnegie–Mellon University, Pittsburgh, PA. 1986.
25. V. ASKAM and W. H. LINNELL. J. Chem. Soc. 2435 (1954).
26. J. LANGE and J. KORYKOWSKA. Chem. Abstr. **70**, 19808m (1969); L. HORNER and K. KLUPFEL. Liebigs Ann. Chem. 69 (1955).
27. O. L. MNDZHOYAN and L. M. TOSKUNINA. Chem. Abstr. **70**, 11066X (1969).
28. C. RIVAS, C. PEREZ, and T. NAKANO. Rev. Latinoam. Quim. **6**, 166 (1975).

Can. J. Chem. Downloaded from www.nrcresearchpress.com by 194.225.253.170 on 09/07/12
For personal use only.

Adsorption of dicarboxylic ions on polycrystalline gold electrode from solutions at constant cationic strength

EDWARD DUTKIEWICZ AND PIOTR SKOŁUDA

Uniwersytet im. A. Mickiewicza, Wydział Chemii, Zakład Chemii Fizycznej, ul. Grunwaldzka 6,60-780 Poznan, Poland

Received August, 27, 1988[1]

EDWARD DUTKIEWICZ and PIOTR SKOŁUDA. Can. J. Chem. **67**, 1411 (1989).

Studies on the specific adsorption of succinate and maleate anions at polycrystalline gold electrode from solutions at constant cationic strength are reported. The adsorption has been studied by differential capacity – potential measurements. The adsorption can be described by one-constant virial isotherm. The basic parameters of this isotherm are determined. Our experimental results are partly interpreted with the help of the results of the adsorption of dicarboxylic anions on the (210) and (311) faces of gold.

Key words: electrochemistry, adsorption, double layer, gold electrode, dicarboxylic ions.

EDWARD DUTKIEWICZ et PIOTR SKOŁUDA. Can. J. Chem. **67**, 1411 (1989).

Opérant à partir de solutions à force cationique constante, on a déterminé l'adsorption spécifique des anions succinate et maléate sur une électrode d'or polycristallin. On a étudié cette adsorption à l'aide de mesures de différentielles de capacité – potentiel. On peut décrire l'adsorption à l'aide d'une isotherme viriale à une constante. On a déterminé les paramètres fondamentaux de cette isotherme. On peut interpréter une partie des résultats à l'aide des résultats obtenus pour l'adsorption des anions dicarboxylates sur les faces (210) et (311) de l'or.

Mots clés : électrochimie, adsorption, couche double, électrode d'or, ions dicarboxylates.

[Traduit par la revue]

Introduction

The adsorption of dicarboxylic anions on single crystals of gold so far has been the object of two quantitative studies (1, 2). In ref. 1 the adsorption of succinate (Su) and maleate (Ma) anions was investigated on a (210) face of gold using the approximate method for determining the charge adsorbed specifically from solutions of mixed electrolytes of different symmetry at constant cationic strength (3). The adsorption was found to increase from Su to Ma anions and was interpreted in terms of the geometric structure and the electric properties of both anions. In ref. 2, thermodynamic analysis of the adsorption of dicarboxylic anions on a (311) face of gold, carried out using the same method of calculation, shows that the Su anions are more strongly adsorbed than Ma anions. These results were interpreted not only in terms of the geometric structure and electric properties of a given ion but also of the arrangement of metal atoms on the electrode surface. In this work, we decided to study the adsorption of succinate and maleate anions on the polycrystalline gold electrode.

Experimental

The solutions were prepared with triple distilled water; analar grade NaF, three times recrystallized and calcined; and organic salts, prepared from the corresponding acid by reacting with sodium carbonate of analar grade.

A classical three-electrode cell was used. The working electrode was a gold sphere made according to the method described by Clavilier and Nguyen Van Huong (4). Before each experiment the electrode was cleaned in deoxygenated supporting electrolyte NaF by a few cycles involving anodic oxidation of the surface and its subsequent reduction. This procedure was performed until the current–potential curves exhibited the known features already reported (5). Next the desired electrolyte was added to the supporting electrolyte solution at potentials corresponding to the so-called double layer region and the capacity–potential measurements were carried out.

The differential capacity – potential dependences $C(E)$ were obtained using the method described in ref. 6 from the alternating current – potential measurements. Measurements were carried out during linear potential sweep at 6 mV s^{-1} with superimposed alternating potential of 6 mV and frequency 24 Hz.

As a very small variation of the differential capacity with the frequency was observed, we assumed that the measured capacities correspond to the equilibrium ones.

All results are reported with respect to the apparent surface area. Measurements were made at 25 ± 2°C.

Results and discussion

The differential capacity of the electrical double layer at polycrystalline gold electrode was measured in mixed [xM Na_2Su + $(0.15 - 2x)M$ NaF] and [xM Na_2Ma + $(0.15 - 2x)M$ NaF] solutions where x denotes the concentration between 0 and 0.014 mol dm^{-3}. The capacity of the double layer is shown as a function of the potential for seven values of x in Figs. 1 and 2.

The form of the capacity curves as a function of potential and disodium succinate or disodium maleate concentration is very similar to that frequently observed in the case of halides adsorbed at the gold electrode/electrolyte solution interface (4, 7). Each curve has two maxima which increase with concentration of both anions. It is worth mentioning that although in the case of halides the peak of $C(E)$ curves in the negative potential range is smaller in comparison with the second peak, in the case of dicarboxylic anion the inverse order is observed. Besides, the values of double layer capacities for Ma anions are lower in comparison with the capacities obtained for Su anions for the same concentration.

On comparing present results with those obtained on single crystals of gold (1, 2), it should be mentioned that the $C(E)$ curves are different. The main difference is the lack of a peak in the positive potential range for single crystals.

It is interesting to note that for the same concentration the potential of capacity peaks for polycrystalline gold and for the (210) face are always less negative for Ma anions than for Su anions, while for the (311) face the inverse order is observed.

In both cases all curves merge together at negative potentials. This allows us to carry out reverse integration and further analysis. For polycrystalline gold electrode the capacity mini-

[1]Revision received March 23, 1989.

Printed in Canada / Imprimé au Canada

Can. J. Chem. Downloaded from www.nrcresearchpress.com by 194.225.253.170 on 09/07/12
For personal use only.

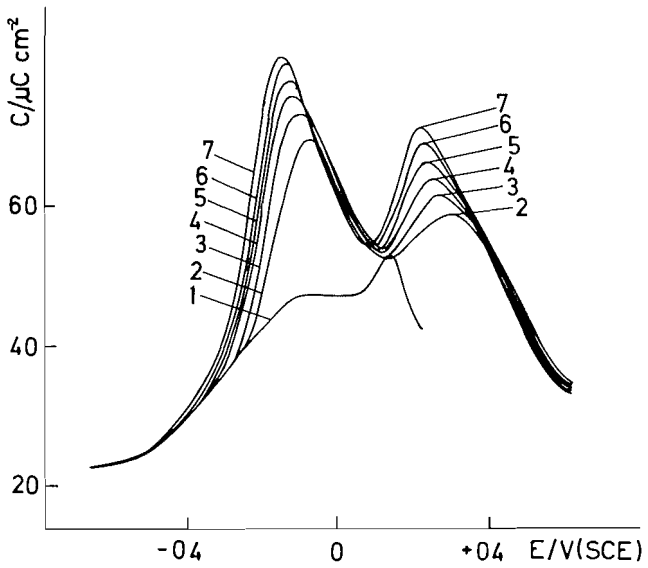


FIG. 1. Differential capacity of the electrical double layer of polycrystalline gold electrode in contact with solutions of xM Na_2Su + $(0.15 - 2x)M$ NaF; x = 0 (*1*); 0.002 (*2*); 0.0035 (*3*); 0.005 (*4*); 0.0075 (*5*); 0.01 (*6*); 0.014 (*7*).

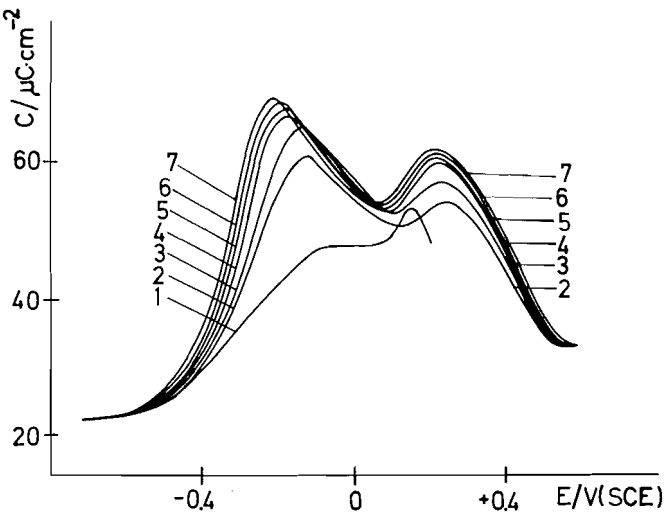


FIG. 2. Same as Fig. 1, but in xM Na_2Ma + $(0.15 - 2x)M$ NaF.

mum is not visible in 0.15 M NaF, the potential of zero charge (pzc) was calculated using the route proposed in ref. 8. For each system the charge–potential curves $\sigma(E)$ were determined by back-integration method from a more negative potentials at which coincidence of all curves take place. At these potentials the electrode charge is identical for all solutions and can be determined by integrating the NaF $C(E)$ curves from pzc. We integrated from charge $\sigma = -21$ μC cm^{-2} which corresponds to −0.689 V vs. SCE for Su anions and from the charge $\sigma = -20$ μC cm^{-2} which corresponds to −0.648 V vs. SCE for Ma anions respectively.

For solids at equilibrium and in reversible conditions, the reversible work required to form unit area of new surface by cleavage γ is equivalent to the surface tension. For our polycrystalline gold electrode relative values of $\Delta\gamma$ versus potential $\Delta\gamma(E)$ curves were obtained by back integration of the

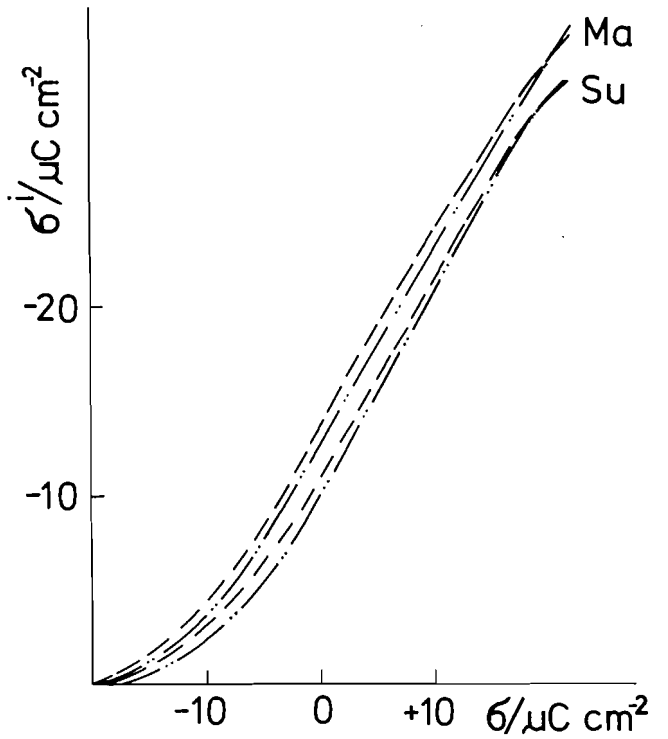


FIG. 3. Comparison of the charge due to specifically adsorbed succinate (Su) and maleate (Ma) anions as a function of electrode charge for x = 0.0075 (—··); 0.01 (---).

$\sigma(E)$ curves, the integration constants were $\gamma = 0$ at $E = -0.690$ V vs. SCE for Su anions and $\gamma = 0$ at $E = -0.648$ V vs. SCE for Ma anions, respectively.

The charge due to specific adsorption of ions (σ^i) has been determined using the method described in detail previously (3). Briefly, it concerns mixed electrolyte solutions of constant cationic strength but with variable concentrations of anions and of a total composition:

$$(m_T - 2m_{K_2B})[KA] + m_{K_2B}[K_2B]$$

where $m_T = m_{KA} + 2m_{K_2B}$ is a constant and represents the total formal molar concentration of salts 1:1 and 1:2, being simultaneously equal to the constant real cationic concentration. In the case of a very low concentration of salt K_2B and an excess of the other one, KA, the Gibbs equation simplifies and takes the approximate form:

$$[1] \quad -\frac{1}{RT}\left(\frac{\partial\gamma}{\partial \ln m_{K_2B}}\right)_{T,p,E^+} = \Gamma_B^i + \Gamma_B^d$$

where Γ_B^i and Γ_B^d are the surface excess of ion B in the inner and diffuse layer and E^+ is the potential of the electrode measured with respect to a reference electrode reversible to the cation in the working solution.

Equation [1] has the form of an equation describing the adsorption of ions from solutions of different ionic strength. Hence, by differentiating γ vs. ln x and using Graham's diffuse-layer theory (9) the surface excess of specifically adsorbed ions from solutions of constant cationic strength can be calculated. This method of calculation of σ^i is the same as that used recently (1, 2). The variation of σ^i as a function of σ for both anions at the two chosen concentration are plotted in Fig. 3.

Can. J. Chem. Downloaded from www.nrcresearchpress.com by 194.225.253.170 on 09/07/12
For personal use only.

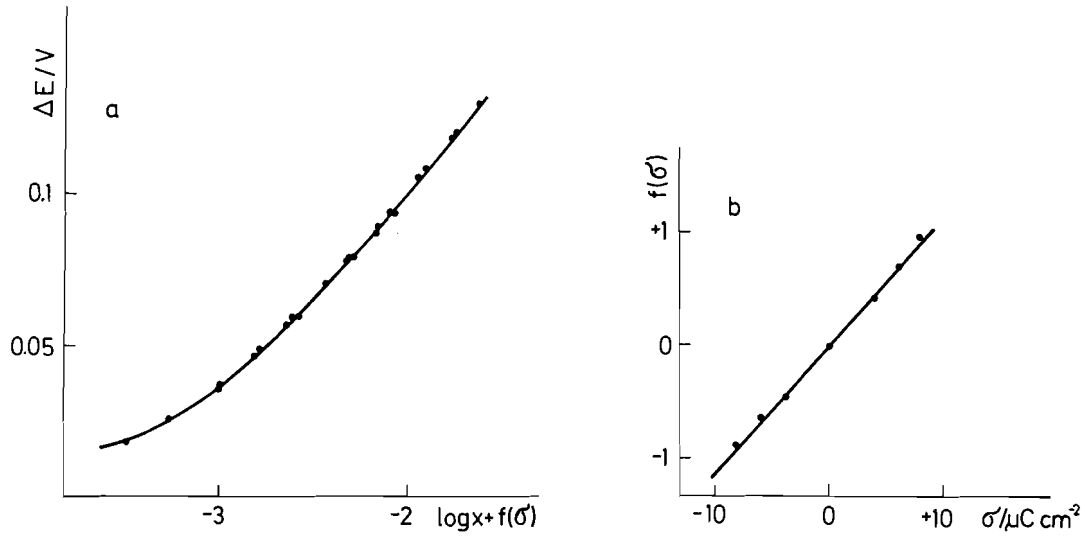


FIG. 4. (*a*) Shift of the electrode potential at constant charge plotted against log concentration of maleate anions. The curves at different values of charge are superimposed by shifting to the log x axis by an amount $f(\sigma)$. (*b*) Plots of $f(\sigma)$ as a function of σ obtained from the results in Fig. 4(*a*).

From Fig. 3 it can be concluded that the Ma anions are more strongly adsorbed when compared to the Su anions. A similar situation was found for the (210) gold electrode but here the difference in σ^i was larger (1). For the (311) gold electrode, however, Su anions are more strongly adsorbed than Ma anions (2).

Moreover, the $\sigma^i(\sigma)$ curves are similar to those observed for various systems of mixed electrolyte solutions, both at constant ionic (10–13) and constant cationic strength (1, 2). In other words, the inversion of variation of σ^i as a function of concentration of anions under investigation is observed and shown in Fig. 3. The appearance of the crossing point on the $\sigma^i(\sigma)$ curves was considered in more general terms in our recent paper (2). Our present results show that the crossing point also occurs for polycrystalline surface. In the studies where NaF was used as a supporting electrolyte, this phenomenon can be attributed to the adsorption of fluoride anions as suggested in refs. 1, 2, 10. The present studies also confirm the fact that the stronger the adsorbability of ions under consideration, the higher the value of charge at which the crossing point occurs (1, 2, 12). Thus for Ma anions which adsorb more strongly in comparison with Su anions, the inversion occurs at a charge (σ = 19 μC cm^{-2}) more positive than for Su anions (σ = 18 μC cm^{-2}).

Because of the anomalous variation of σ^i with ionic concentration, the thermodynamic analysis was only carried out for $\sigma < 10$ μC cm^{-1}, i.e. the electrode charge range concerned the first peak on $C(E)$ curves.

Our next step was to show the congruency in the charge of the adsorption isotherm. To solve this problem we have applied the test based on the relations given in ref. 14. This implies that if the adsorption isotherm is congruent with respect to the charge, then (14) the curves ($E_b - E$) versus logarithm of concentration at constant σ are segments of common adsorption isotherm with the amount adsorbed multiplied by the factor $f(\Delta G^0)$, where E_b and E are potential of the electrode measured in the base electrolyte and in the presence of ions under consideration versus the same reference electrode and ΔG^0 is the standard Gibbs energy of adsorption. For both succinate and maleate

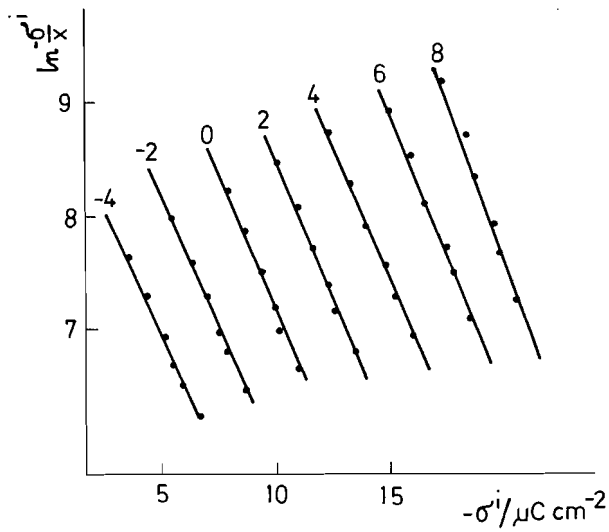


FIG. 5. Virial isotherm plots for succinate anions. The number near each line indicates the charge density of the polycrystalline gold electrode in μC cm^{-2}.

anions all segments fit a common curve. Each segment was superimposed by shifting along the abscissa by the quantity $f(\sigma) = \Delta \ln x = \Delta \ln \beta$, where β is the adsorption equilibrium constant. An example of this displacement of the individual segment parallel to the abscissa is given in Fig. 4(*a*) for Na_2Ma + NaF/gold system.

The linear dependence of $f(\sigma)$ vs. σ was found for both system under investigation. In Fig. 4(*b*) we report the quantity $f(\sigma)$ as a function of charge for the same system.

The linear relation found may confirm the constancy of $(\partial \ln \beta/\partial\sigma)$ within this range for these systems.

The adsorption process of Su and Ma anions agrees with the simple virial isotherm. This isotherm is plotted at constant charge in Figs. 5 and 6 for Su and Ma anions, respectively.

For Ma anions (Fig. 6) satisfactorily straight and parallel lines were obtained for the charge density range examined.

Can. J. Chem. Downloaded from www.nrcresearchpress.com by 194.225.253.170 on 09/07/12
For personal use only.

TABLE 1. Comparison of adsorption parameters[a] for succinate and maleate anions on polycrystalline Au, Au (210), and Au (311)

Interface	$-\Delta G^0/(\text{kJ mol}^{-1})^b$	$B/(\text{nm}^2\,\text{ion}^{-1})$	$(-\sigma^i)_{\sigma=0}/(\mu\text{C cm}^{-2})$ $x = 0.0075\ M$
Na_2Su/Au	106.0	7.4	10
Na_2Ma/Au	108.0	4.7	13
Na_2Su/Au (210)	100.0	8.5	5
Na_2Ma/Au (210)	102.0	5.4	10
Na_2Su/Au (311)	110.0	7.8	14
Na_2Ma/Au (311)	103.0	5.6	11

[a]The accuracy in the determination of ΔG^0, B, and σ^i is of the order 10%, 10%, and 5%, respectively.

[b]The standard states are 1 mol dm^{-3} in solution and 1 ion cm^{-2} on the surface.

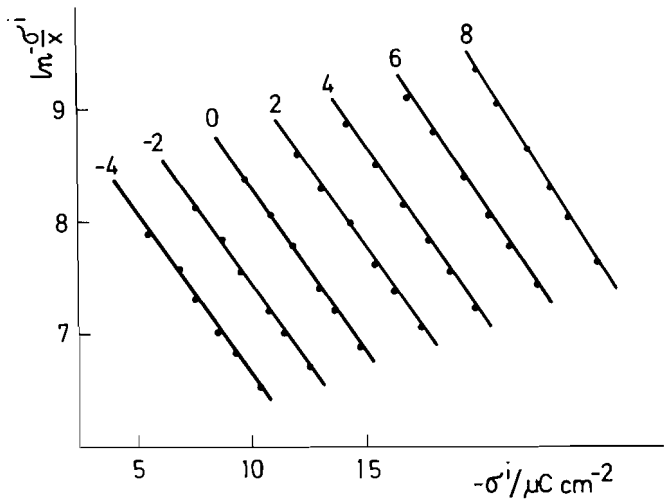


FIG. 6. Same as Fig. 5, but for maleate anions.

From Fig. 5 (Su anions) a linear dependence was also obtained but for the most positive value of $\sigma = 8\ \mu C\ cm^{-2}$ this line was not quite parallel. This line has a little higher slope and consequently higher value of the virial coefficient B at the most positive value of the electrode charge. However, the deviation from linearity is small and within the domain of uncertainty. The ΔG^0 values are found by extrapolating these plots. For uncharged ($\sigma = 0$) polycrystalline gold, the standard free energies of adsorption are reported in Table 1. The slope of these lines allows the B coefficient to be determined (Table 1).

The data on the adsorption of dicarboxylic anions on the polycrystalline gold electrode have been presented. To summarise, it is convenient to compare the adsorption of these anions on the polycrystalline gold with the adsorption on the single crystals of gold (1, 2). All adsorption parameters are tabulated in Table 1.

Generally, the adsorption process is a very complex problem both from the thermodynamic and the molecular point of view. The ionic adsorption from solution on the electrode depends upon the types of ions, the properties of the solvent and the electrode. The properties of the electrode refer both to the type of metal and the crystallographic orientation of its surface. However, only in the case of single crystals is it possible to study the adsorption dependence on the atomic geometry of the metal surface. For polycrystalline electrode, it is well known that some complications are encountered in the quantitative analysis of the $C(E)$ curves, which are connected with the crystallographic inhomogeneity of the surface. In other words, a different proportion of the crystal planes and the number of defects can vary from electrode to electrode, making comparisons between such $C(E)$ curves less rigorous. However, in spite of these difficulties, an attempt was made to describe the $C(E)$ curves of a polycrystalline electrode as an additive sum of the $C(E)$ curves of individual faces of a single crystals of silver in a diluted solution of NaF (15). The calculated curve approximately corresponds to the experimental one. This approach to polycrystalline surface is of course a simplification because the difference in the surface energy of the crystal faces may produce a preferential orientation, which is not accounted for in this model. In addition, the presence of some defects or grains at the surface should also be taken into account. In this paper we interpret the experimental results, to a limited extent, on the basis of our earlier papers concerning the adsorption of dicarboxylic ions on the (210) and (311) faces of gold (1, 2). Analysing the adsorption data of dicarboxylic anions on the single crystals of gold and on the polycrystalline gold, one can note that there is a greater similarity between the polycrystalline gold with the (210) face than with the (311) face. For polycrystalline and gold (210) electrodes σ^i due to specific adsorption of Ma anions is greater than that obtained for Su anions, whereas for the (311) face the reverse was observed. Besides, virial coefficients on polycrystalline and gold (210) electrodes are inversely proportional to σ^i, which was not the case on gold (311) electrode. These observations might lead to a conclusion that the behaviour of dicarboxylic anions on polycrystalline gold electrode is similar to that on gold (210) electrode. Therefore, the different case of adsorption of anions on polycrystalline gold is probably due to their different geometric and electric structure and, as has been suggested in ref. 1, different interaction in the electric field in the double layer. However, the existing differences, i.e. the higher value of σ^i for both anions under investigation in the case of polycrystalline gold in comparison with (210) face of gold, are probably due to the presence on the surface of polycrystalline gold of some faces which have a higher superficial atomic density than the (210) face e.g. (111), (100).

On the other hand, however, increase in strength of specific adsorption is larger for Su anions than for Ma anions. The fact that on the polycrystalline surface there is also a certain number of stepped faces e.g. (311), (211), may provide a partial explanation. According to our suggestion in ref. 2, the adsorption of Su anions can be located on the "step" atoms, which is not the case for Ma anions. Such "step" atoms exist on the stepped faces. This seems to result from a small deviation

Can. J. Chem. Downloaded from www.nrcresearchpress.com by 194.225.253.170 on 09/07/12
For personal use only.

from parallelism of the lines at the most positive value of observed in Fig. 5. However, we cannot exclude the possibility that other adsorption sites may exist on the surface of the polycrystal, e.g. grain boundaries, defects on which Su anions may exclusively adsorbed.

Acknowledgement

This work was carried out under Research Project CPBP 01.15.

1. E. DUTKIEWICZ, P. SKOŁUDA, and A. HAMELIN. J. Electroanal. Chem. **240**, 291 (1988).
2. E. DUTKIEWICZ, P. SKOŁUDA, and A. HAMELIN. J. Electroanal. Chem. **248**, 209 (1988).
3. (*a*) E. DUTKIEWICZ and P. SKOŁUDA. Extended abstracts. 36th I.S.E. Meeting, Salamanca. 1985; (*b*) E. DUTKIEWICZ and P. SKOŁUDA. J. Electroanal. Chem. **213**, 327 (1986).
4. J. CLAVILIER and C. NGUYEN VAN HUONG. J. Electroanal. Chem. **41**, 193 (1973).
5. C. NGUYEN VAN HUONG, C. HINNEN, J. P. DALBERA, and R. PARSONS. J. Electroanal. Chem. **125**, 177 (1981).
6. J. CLAVILIER. C.R. Acad. Sci. Paris, **263**C, 191 (1966).
7. C. HINNEN, C. NGUYEN VAN HUONG, A. ROUSSEAU, and J. P. DALBERA. J. Electroanal. Chem. **95**, 131 (1979).
8. A. HAMELIN. J. Electroanal. Chem. **138**, 395 (1982).
9. D. C. GRAHAME. J. Chem. Phys. **21**, 1054 (1953).
10. G. VALETTE. J. Electroanal. Chem. **132**, 311 (1982).
11. G. VALETTE and R. PARSONS. J. Electroanal. Chem. **191**, 377 (1985).
12. G. VALETTE and R. PARSONS. J. Electroanal. Chem. **204**, 291 (1986).
13. J. P. BELLIER. Thesis, Paris. 1980.
14. E. DUTKIEWICZ and R. PARSONS. J. Electroanal. Chem. **11**, 100 (1966).
15. G. VALETTE and A. HAMELIN. J. Electroanal. Chem. **45**, 301 (1973).

Can. J. Chem. Downloaded from www.nrcresearchpress.com by 194.225.253.170 on 09/07/12
For personal use only.

Interaction of diiodine with Et_4todit = 4,5,6,7-tetrathiocino [1,2-*b*:3,4-*b'*]diimidazolyl-1,3,8,10-tetraethyl-2,9-dithione. Crystal and molecular structure of Et_4todit·$2I_2$

DAVIDE ATZEI, PAOLA DEPLANO, AND EMANUELE F. TROGU
Dipartimento di Chimica e Tecnologie Inorganiche e Metallorganiche dell'Università, Via Ospedale 72, I-09124 Cagliari, Italy

FRANCESCO BIGOLI AND MARIA ANGELA PELLINGHELLI
Centro di Studio per la Strutturistica Diffrattometrica del CNR. Viale delle Scienze 78, I-43100 Parma, Italy

AND

ANTONIO SABATINI AND ALBERTO VACCA
Dipartimento di Chimica dell'Università, Via Maragliano 77, I-50144 Firenze, Italy

Received October 26, 1988[1]

DAVIDE ATZEI, PAOLA DEPLANO, EMANUELE F. TROGU, FRANCESCO BIGOLI, MARIA ANGELA PELLINGHELLI, ANTONIO SABATINI, and ALBERTO VACCA. Can. J. Chem. **67**, 1416 (1989).

Spectrophotometric studies on the reaction between diiodine and the title ligand in ratios ranging from 1:1 to 1:20 in $CHCl_3$ have shown the formation of a 1:1 charge-transfer complex. A general computer program has been used to refine the equilibrium constant and the extinction coefficients simultaneously. In the solid state a 1:2 (donor to acceptor) complex has been isolated and an X-ray structure analysis of the compound indicated that the crystals are monoclinic, space group $C2/c$ with a = 16.317(4), b = 13.912(3), c = 12.879(3) Å, β = 111.24(2)°, Z = 4.

The molecular structure shows that two sulphur-thioamide atoms of the ligand act as donor with respect to two diiodine molecules. The structural data of the organic molecule of the complex and those of the free molecule are very similar.

Key words: diiodine, thioamides, charge-transfer, structure, equilibrium-constants.

DAVIDE ATZEI, PAOLA DEPLANO, EMANUELE F. TROGU, FRANCESCO BIGOLI, MARIA ANGELA PELLINGHELLI, ANTONIO SABATINI et ALBERTO VACCA. Can. J. Chem. **67**, 1416 (1989).

Des études spectrophotométriques sur la réaction entre le diiode et le ligand mentionné dans le titre effectuée dans le $CHCl_3$, à des rapports allant de 1:1 à 1:20, ont permis de démontrer qu'il y a formation d'un complexe de charge 1:1. On a utilisé un programme général d'ordinateur pour déterminer d'une façon simultanée la constante d'équilibre ainsi que les coefficients d'extinction. A l'état solide, on a isolé un complexe 1:2 (donneur à accepteur) et on a réalisé une étude par diffraction des rayons-X qui a permis de préciser que les cristaux du composé sont tricliniques, groupe d'espace $C2/c$ avec a = 16,317(4), b = 13,912(3) et c = 12,879(3) Å, β = 111,24(2)° et Z = 4.

La structure moléculaire démontre que deux atomes de soufre du thioamide du ligand agissent comme donneurs par rapport à deux molécules de diiode. Les données structurales de la molécule organique du complexe et celles de la molécule libre sont très semblables.

Mots clés : diiode, thioamides, transfert de charge, structure, constantes d'équilibre.

[Traduit par la revue]

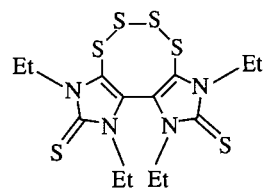
Introduction

Formation of charge-transfer (c.t.) complexes between I_2 and thiones has long been recognized (1). Moreover, these c.t. complexes may be inert compounds or intermediates in redox reactions. The present studies are therefore of current interest in understanding various types of mechanisms including the reactions of heterocyclic antithyroid drugs with I_2 (2) and the formation of sulphur–iodine complexes showing superconducting ability (3).

We are investigating c.t. complex formations between I_2 and molecules containing thioamide groups, both free (4, 5) and coordinated to transition metals (6–9). In particular, in the case of the following ligands with two N—C=S groups: $R_2NC(S)SSC(S)NR_2$ (**I**) (4), $R_2NC(S)CH_2C(S)NR_2$ (**II**) (10), $R_2NC(S)C(S)NR_2$ (**III**) (5), we have observed different reaction paths depending on the ligand structure. In fact, in **I** and **II** the c.t. adduct formation is the initial step in the oxidation of the ligands to the known trithiolane and dithiolylium (11) cations, while in the dithiooxamide (**III**) case, the 1:1 and 1:2 (donor to acceptor) c.t. complexes are inert.

X-Ray data on a dithiooxamide·$2I_2$ crystal show that the ligand conformation (torsion angle S—C—C—S near 90°) is the most favourable for a minimum hindrance, and that there is no delocalization along the C—C skeleton between the two NC=S moieties.

Et_4todit =



We here report the behaviour of a new ligand: 4,5,6,7-tetrathiocino[1,2-*b*:3,4-*b'*]diimidazolyl-1,3,8,10-tetraethyl-2,9-dithione, recently synthesized by us (12), in which the two donor sites are forced in very distant positions (see below).

Experimental

Materials

The compound Et_4todit was prepared as previously described (12). Twice sublimed diiodine was purchased from Carlo Erba. $CHCl_3$ was Merck Reagent Grade and dried over 4 Å molecular sieves before use. The adduct Et_4todit·$2I_2$ was obtained as brown crystals, suitable for X-ray analysis, by slow concentration of a $CHCl_3$ solution of Et_4todit

[1]Revision received April 28, 1989.

Printed in Canada / Imprimé au Canada

Can. J. Chem. Downloaded from www.nrcresearchpress.com by 194.225.253.170 on 09/07/12
For personal use only.

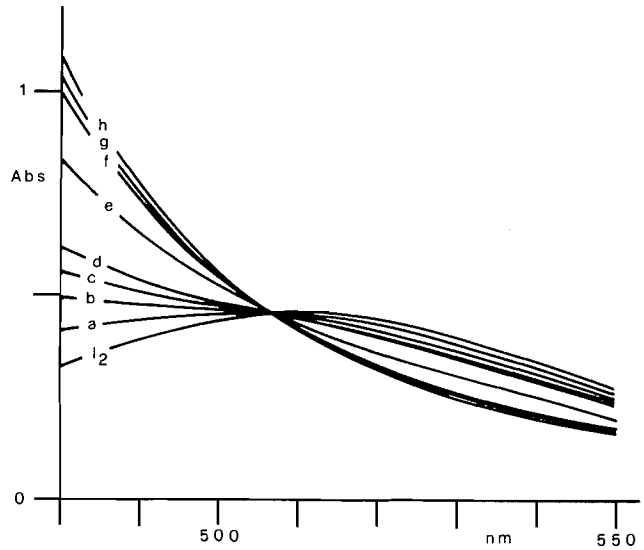


FIG. 1. Visible spectra at 298 K in 1 cm cell of $CHCl_3$ solutions containing constant amounts of I_2 (5.0×10^{-4} mol dm^{-3}) and variable Et_4todit concentrations in the ratios (Et_4todit/I_2): *a* = 0.5; *b* = 1.0; *c* = 1.5; *d* = 2.0; *e* = 5.0; *f* = 10.0; *g* = 12.0; *h* = 15.0.

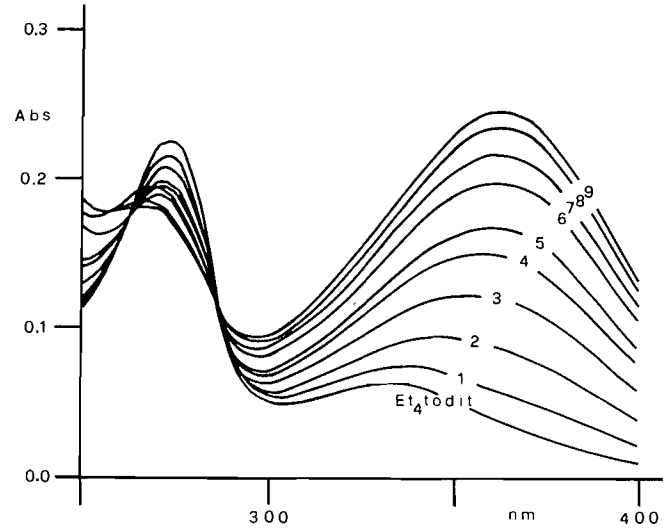


FIG. 2. Ultraviolet spectra at 298 K in 0.1 cm cell of $CHCl_3$ solutions containing constant amounts of Et_4todit (6.3×10^{-5} mol dm^{-3}) and variable diiodine concentrations in the ratios (I_2/Et_4todit): *1* = 2.0; *2* = 5.0; *3* = 10.0; *4* = 15.0; *5* = 19.0; *6* = 29.0; *7* = 38.5; *8* = 48.0; *9* = 58.0.

and I_2 in excess. *Anal.* calcd. for $C_{14}H_{20}N_4S_6I_4$: C 17.81, H 2.13, N 5.93; found: C 17.86, H 2.18, N 5.50.

The elemental analysis was performed by Istituto di Chimica Farmaceutica, Università di Cagliari.

Infrared data (KBr pellets; cm^{-1}) for [Et_4todit]·$2I_2$ are as follows: 2970w, 2922w, 2852w, 1513m, 1438s, 1395vs, 1330m, 1303mw, 1255vs, 1146vs, 1100w, 1080m, 1050w, 980sh, 960m, 797m, 770w, 748vw, 693w, 637vw, 608vw, 534vw, 435sh, 412m, 395sh, 361w.

The infrared spectrum was recorded by using a Perkin Elmer model 983 spectrophotometer.

Spectrophotometric measurements

The electronic spectra were measured at different temperatures in the range 15 to 35°C in $CHCl_3$ solutions with a Varian model Cary 2300 spectrophotometer, equipped with an automatic system of data acquisition.

A set of eight solutions containing a constant diiodine concentration (5×10^{-4} mol dm^{-3}) and variable Et_4todit concentrations (ranging from 1.2×10^{-4} to 3.7×10^{-3}) (see Fig. 1) was prepared and the spectra recorded between 400 and 550 nm using 1 cm silica cells. Two other sets of solutions were prepared with a constant concentration of Et_4todit and variable diiodine concentrations: (*a*) Et_4todit concentration is 6.3×10^{-5} mol dm^{-3} and diiodine in the range 1.3×10^{-4} to 3.6×10^{-3} mol dm^{-3} (nine solutions) and (*b*) Et_4todit is 2.5×10^{-4} and diiodine in the range 5×10^{-4} to 7.5×10^{-3} (seven solutions). Their spectra were measured in the range 240 to 400 nm in 1 mm silica cells. In Fig. 2 the spectra of the (*a*) solutions are reported. Spectrophotometer performance has been tested by measuring absorption spectra of solutions of potassium dichromate according to ref. 13.

Calculations

The experimental points used in the calculations have been taken from the recorded spectra at 10 nm intervals, the total number being always 90 readings for each system at each temperature. A general computer program, derived from "SUPERQUAD" (14), has been used to refine simultaneously equilibrium constants and molar extinction coefficients from the spectrophotometric measurements as described in ref. 5.

X-ray crystallography

Crystal data are as follows:

$C_{14}H_{20}N_4S_6I_4$ MW = 944.316

Monoclinic, space group $C2/c$, a = 16.317(4), b = 13.912(3), c = 12.879(3) Å, β = 111.24(2)° (by least-squares refinement from the θ values, in the range 10–16°, of 30 reflections accurately measured), U = 2725.0(1.2) Å^3, D_c = 2.302 Mg/m^{-3}, Z = 4, F(000) = 1760, Mo-Kα radiation (λ = 0.71073 Å), μ = 49.80 cm^{-1}. Crystal dimensions: 0.08 × 0.16 × 0.29 mm^3.

Data collection and processing

Data collection was made on an SIEMENS AED diffractometer with Nb-filtered Mo-Kα radiation using the θ–2θ scan mode. Of a total of 3097 measured reflections ($\pm h$, $+k$, $+l$), 1090 having $I \geq 3\sigma(I)$ were considered observed and employed in the analysis. The recorded intensities were corrected for Lorentz polarization factor, for absorption (maximum and minimum values 1.05590, 0.91928) and extinction (maximum and minimum values 1.07473, 0.91775) following Walker and Stuart (15).

Structure analysis and refinement

The solution of the structure was achieved by the heavy-atom method through Patterson and Fourier maps. The refinements were carried out by full-matrix least-squares cycles using initially isotropic and then anisotropic thermal parameters for all non-hydrogen atoms. The co-ordinates of the hydrogen atoms, except H(8) and H(10) of the C(7) methyl carbon, were clearly located from a ΔF map; at this stage a full-matrix least-squares cycle was computed including all the hydrogen atoms with individual isotropic thermal parameters and with H(8) and H(10) riding on their bonded carbon atom. In the final blocked full-matrix least squares only the non-hydrogen atoms were refined. The weighting scheme used in the final cycles was: $w = 0.6164[\sigma^2(F_o) + 0.001066F_o^2]^{-1}$. Final convergence was reached at an R value of 0.0371 (R' = 0.0425). The final electron density difference synthesis showed no peaks >0.89 and <−0.66 e Å^{-3}. Scattering factors and corrections for anomalous dispersion effects were those from ref. 16. Calculations were carried out on the CRAY X-MP/48 computer of Consorzio Interuniversitario Nord Est Calcolo Automatico (Casalecchio, Bologna) with financial support from the University of Parma, and on the GOULD-SEL 32/77 computer of the Centro di Studio per la Strutturistica Diffrattometrica del

Can. J. Chem. Downloaded from www.nrcresearchpress.com by 194.225.253.170 on 09/07/12
For personal use only.

TABLE 1. Fractional atomic co-ordinates ($\times 10^4$) with estimated standard deviations in parentheses

Atom	X/a	Y/b	Z/c	Atom	X/a	Y/b	Z/c
I1	1396(1)	2478(1)	2103(1)	C6	3651(9)	1878(11)	4693(10)
I2	213(1)	1043(1)	891(1)	C7	3169(9)	964(9)	4382(13)
S1	2681(2)	3780(3)	3293(3)	H1	3507(91)	4529(102)	1995(114)
S2	5323(2)	1093(3)	4164(3)	H2	4335(63)	4141(67)	1526(73)
S3	4733(2)	−34(2)	3098(3)	H3	2967(86)	4312(108)	230(113)
N1	4027(6)	3325(7)	2580(8)	H4	2526(94)	3596(100)	602(114)
N2	3922(7)	2310(7)	3848(8)	H5	3278(117)	3182(134)	343(149)
C1	3542(8)	3106(9)	3259(11)	H6	4115(117)	1703(149)	5150(155)
C2	4625(8)	2038(8)	3553(10)	H7	3363(98)	2319(104)	5037(134)
C3	4691(7)	2680(7)	2793(9)	H8	2618	1036	3606
C4	3780(8)	4075(9)	1716(10)	H9	3500(99)	614(119)	4339(129)
C5	3112(9)	3701(10)	671(11)	H10	2939	721	5025

TABLE 2. Selected bond distances (Å) and angles (deg) with esd's in parentheses*

Bond	Length	Bond	Length
I1—I2	2.822(2)	N1—C4	1.47(2)
I1—S1	2.775(4)	N2—C1	1.36(2)
S2—S3	2.077(5)	N2—C2	1.39(2)
S3—S3′	2.026(6)	N2—C6	1.45(2)
S1—C1	1.70(1)	C2—C3	1.36(2)
S2—C2	1.73(1)	C3—C3′	1.46(2)
N1—C1	1.41(2)	C4—C5	1.49(2)
N1—C3	1.36(1)	C6—C7	1.47(2)

Bonds	Angle	Bonds	Angle
I2—I1—S1	174.8(1)	C3—C2—N2	107.9(11)
I1—S1—C1	95.3(5)	S2—C2—N2	123.8(9)
S1—C1—N1	123.4(9)	S2—C2—C3	128.1(10)
S1—C1—N2	130.4(11)	C1—N2—C2	109.0(10)
N1—C1—N2	106.1(11)	C1—N2—C6	123.9(11)
C1—N1—C3	108.6(10)	C2—N2—C6	127.0(11)
C1—N1—C4	124.1(10)	N1—C4—C5	110.3(11)
C3—N1—C4	127.0(10)	N2—C6—C7	115.7(11)
N1—C3—C2	108.4(11)	C2—S2—S3	101.6(5)
N1—C3—C3′	123.1(9)	S2—S3—S3′	106.2(2)
C2—C3—C3′	128.4(10)		

*Key to symmetry operations (′): $1 - x, y, \frac{1}{2} - z$.

C.N.R. (Parma). The SHELX 76 system of computer programs (17), ASSORB (18), PARST (19), PLUTO (20), and ORTEP (21) were used. Final atomic co-ordinates are in Table 1, selected distances and angles in Table 2.

Results and discussion

We have investigated the interaction between Et_4todit and I_2 in $CHCl_3$ via conventional ultraviolet–visible spectrophotometric techniques between 250 and 550 nm. The spectra obtained in the visible region for the solutions with the constant diiodine concentration and the variable donor concentration are reported in Fig. 1, where a single isosbestic point between complexed (blue-shifted band) and free I_2 is observed at 505 nm. These spectrophotometric data are interpreted quite satisfactorily by assuming that the 1:1 species is the only adduct formed.

The spectra recorded in the 250–400 nm range on solutions

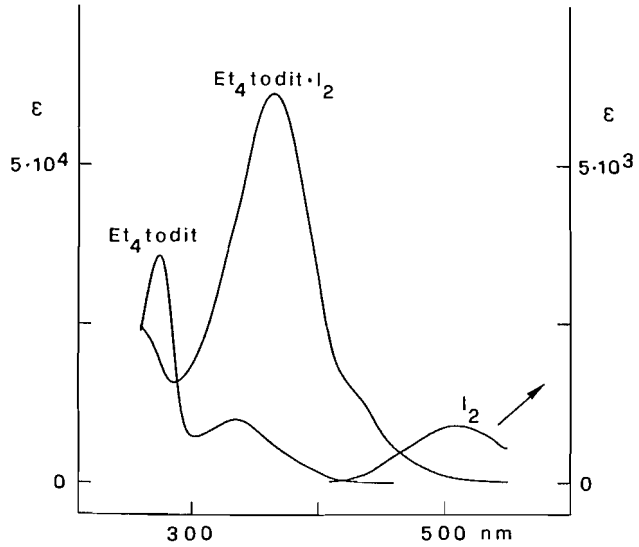


FIG. 3. Calculated uv–vis spectra of the 1:1 adduct between Et_4todit and diiodine at 298 K in $CHCl_3$ solution.

containing constant Et_4todit and variable I_2 concentrations are reported in Fig. 2, where the decrease of the donor band and the increase of the charge-transfer band of the adduct are evident.

By processing the experimental data (spectra *1–5*) up to a ligand to diiodine ratio of 1:20, reliable 1:1 equilibrium constants have been calculated, and the obtained values are reported in Table 3. The refined molar extinction coefficients of the adduct are plotted in Fig. 3 together with those determined for the free reactants. The agreement between calculated and experimental spectra was within the instrumental precision. The thermodynamic functions of the adduct formation ΔH^0 and ΔS^0, have been determined by least-square analysis of the Vant' Hoff plot of log K_1 vs. $1/T$. Such values (Table 3) are comparable with similar thione–diiodine complexes (5).

By processing spectra of solutions having donor to diiodine ratios larger than 1:20, it appears that further equilibria in addition to the 1:1 case occur. However, no satisfactory agreement in the explored wavenumber and temperature range has been obtained for any stoichiometry higher than 1:1. A check of the experimental conditions and instrumental accuracy confirmed the reliability of our data. However, we did not obtain a satisfactory simulation of the experimental spectra, not even by including a 1:2 species with formation constant K_2 differing from K_1 by the statistic factor ($K_2 = K_1/4$ in the case

Can. J. Chem. Downloaded from www.nrcresearchpress.com by 194.225.253.170 on 09/07/12
For personal use only.

TABLE 3. Logarithms of the equilibrium constants, enthalpy (kcal mol^{-1}) and entropy changes (cal K^{-1} mol^{-1}) for the formation of 1:1 adduct between Et_4todit and diiodine in $CHCl_3$ solution

log K_1						
10°C	15°C	20°C	25°C	35°C	ΔH^0	ΔS^0
2.937(7)	2.858(6)	2.786(7)	2.777(8)	2.648(9)	−4.4(5)	−2(2)

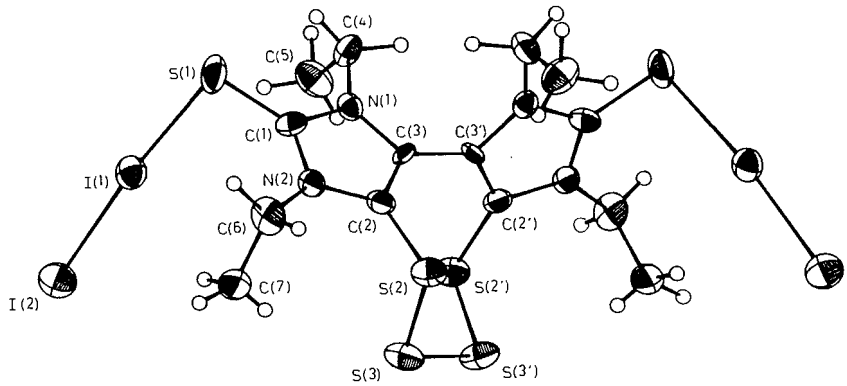


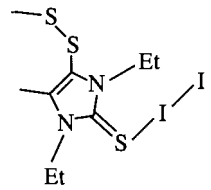
FIG. 4. Perspective view of the molecule. Thermal ellipsoids are drawn at the 50% probability level.

of two equivalent binding sites and non-cooperativity). This hypothesis seemed to us reliable on the basis of the structural results on the isolated solid Et_4todit·$2I_2$.

These intriguing results may be tentatively explained by assuming that complexes of stoichiometries higher than 1:1 exist in solution at oversaturation or incipient precipitation conditions. Such hypothesis is supported by the fact that, once formed, the Et_4todit·$2I_2$ solid is very sparingly soluble in $CHCl_3$.

Crystal and molecular structure

The molecular structure of this neutral molecular compound belonging, as our previous bis(morpholinothiocarbonyl)—bis-(diiodine) (5), to the series with two S as heteroatoms in the donor and with two diiodine molecules as acceptors, is shown in Fig. 4, together with the atomic numbering scheme. In the molecule the two



moieties are related by a crystallographic two-fold axis. The structural data of the organic molecule in the present adduct and those of the uncomplexed molecule (12) are very similar. In fact, apart from the presence of a crystallographic two-fold axis, it is observed that the imidazoline ring is planar and that the arrangement of the two ethyl substituents lying perpendicular to the ring [C(1)—N(1)—C(4)—C(5) −83°, C(1)—N(2)—C(6)—C(7) 107°] is responsible for the mutual orientation of the two imidazoline rings in the molecule [N(1)—C(3)—C(3′)—N(1′) 76°]. Here a chair-conformation for the eight-membered ring is also observed [S(2)—S(3)—S(3′)—S(2′) −76°, C(2)—C(3)—C(3′)—C(2′) 66°, C(2)—S(2)—S(3)—S(3′) 89°, S(3)—S(2)—C(2)—C(3) −93°] and the value of 1.46(2) Å for C(3)—C(3′) bond distance is consistent with a single bond between two sp^2-hibridized carbon atoms. The S(2)—S(3) bond distance (2.077(5) Å) is related to the value of the S(3)—S(2)—C(2)—C(3) torsion angle (−93°), as observed in uncomplexed disulphides. The only significant differences are obviously the small lengthening of the S(1)—C(1) bond owing to the interaction with the diiodine molecule and the orientation of an ethyl group (C(1)—N(2)—C(6)—C(7) 107° and −87° in the adduct and in the uncomplexed molecule, respectively) due to the interactions involving C(6) and C(7). The C(1)—S(1)—I(1)—I(2) moiety is roughly planar (maximum deviation 0.020(15) Å for C(1) and roughly perpendicular to the imidazoline ring (I(1)—S(1)—C(1)—N(1) 106°, I(1)—S(1)—C(1)—N(2) −76°). In this fragment the values of d(S—I) and d(I—I) are correlated and in good agreement with those reported by Herbstein and Schwotzer in their work on the interactions of thiones with molecular diiodine (ref. 22 and references therein) and with those observed in bis(morpholinothiocarbonyl)—bis(diiodine) (5), while no appreciable variation is observed for d(C—S). The almost linear arrangement for S(1)—I(1)—I(2) (174.8(1)°) and a very small contribution of the sp^3 hybridization for S(1) [C(1)—S(1)—I(1) 95.3(5)°] were also observed in the above cited adducts. The I(2)...I(2) contact of 3.608(2) Å across the symmetry centre (Fig. 5) is important in forming chains running parallel to ***a***. This last value, significantly less than the van der Waals radii sum, is intermediate among those observed in compounds showing the I_2...I_2 arrangement [3.50 Å in crystalline I_2 (23), 3.472 Å in 2(ethylenethiourea)—3(I_2) (22), in the range 3.705(3)–3.931(3) Å in bis(morpholinothiocarbonyl)—bis(diiodine) (5), and 3.720(1) Å in dithia[3.3.1]-propellane·$2I_2$ (24)]. The interaction deviates from linearity more than in the mentioned compounds (I—I...I 148.9(1)°). The packing is determined by

Can. J. Chem. Downloaded from www.nrcresearchpress.com by 194.225.253.170 on 09/07/12
For personal use only.

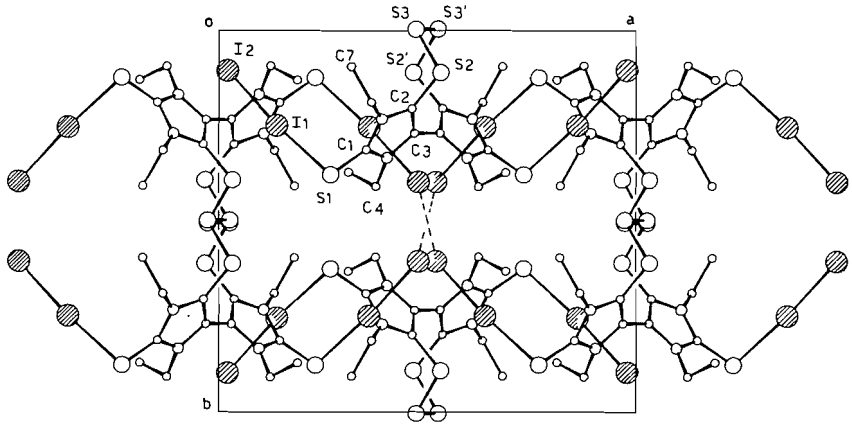


FIG. 5. Projection of the structure along [001].

contacts of type I...S and I...C; the shortest contact [I(2)...C(6) ($x - \frac{1}{2}$, $\frac{1}{2} - y$, $z - \frac{1}{2}$) 3.79(1) Å is quite perpendicular to I—I...I plane.[2]

Acknowledgments

We thank the Consiglio Nazionale delle Ricerche and the Ministero della Pubblica Istruzione for support in this work.

1. M. E. PEACH. Int. J. Sulfur Chem. **8**, 151 (1973).
2. C. RABY, J. CLAUDE, C. MOESCH, and J. C. R. BUXERAUD. Acad. Sci. Ser. C, **288**, 319 (1979).
3. J. R. FERRARO and J. M. WILLIAMS. Introduction to synthetic electrical conductors. Academic Press. 1987. Chapt. 2.
4. F. BIGOLI, M. A. PELLINGHELLI, G. CRISPONI, P. DEPLANO, and E. F. TROGU. J. Chem. Soc. Dalton Trans. 1349 (1985).
5. D. ATZEI, P. DEPLANO, E. F. TROGU, F. BIGOLI, M. A. PELLINGHELLI, and A. VACCA. Can. J. Chem. **66**, 1483 (1988).
6. G. CRISPONI, P. DEPLANO, V. NURCHI, and E. F. TROGU. Polyhedron, **3**, 1241 (1984).
7. G. CRISPONI, P. DEPLANO, and E. F. TROGU. Inorg. Chim. Acta, **75**, 135 (1984).
8. G. CRISPONI, P. DEPLANO, and E. F. TROGU. J. Chem. Soc. Dalton Trans. 365 (1986).
9. F. BIGOLI, P. DEPLANO, M. A. PELLINGHELLI, and E. F. TROGU. J. Chem. Soc. Dalton Trans. 2407 (1987).
10. D. ATZEI, F. BIGOLI, P. DEPLANO, M. A. PELLINGHELLI, E. F. TROGU, and A. VACCA. Atti del "XIX Congresso Nazionale di Chimica Inorganica" S. Margherita, Cagliari, Italy, ottobre 1986. p. 537.
11. A. HORDVIK. Acta Chem. Scand. **19**, 1039 (1965).
12. F. BIGOLI, M. A. PELLINGHELLI, D. ATZEI, P. DEPLANO, and E. F. TROGU. Phosphorus Sulfur, **37**, 189 (1988).
13. G. WERNIMONT. Anal. Chem. **39**, 554 (1967).
14. P. GANS, A. SABATINI, and A. VACCA. J. Chem. Soc. Dalton Trans. 1195 (1985).
15. N. WALKER and D. STUART. Acta Crystallogr. Sect. A, **39**, 158 (1983).
16. International tables for X-ray crystallography. Vol. 4. Kynoch Press, Birmingham. 1974. pp. 99, 149.
17. G. SHELDRICK. SHELX 76. A program for crystal structure determination. University of Cambridge. 1976.
18. F. UGOZZOLI. Comput. Chem. **11**, 109 (1987).
19. M. NARDELLI. Comput. Chem. **7**, 95 (1983).
20. W. D. S. MOTHERWELL. PLUTO, University of Cambridge. 1976.
21. C. K. JOHNSON. ORTEP. Report ORNL-3794, revised, Oak Ridge National Laboratory, Tennessee. 1965.
22. F. H. HERBSTEIN and W. SCHWOTZER. J. Am. Chem. Soc. **106**, 2367 (1984).
23. F. VAN BOLHUIS, P. B. KOSTER, and T. MIGCHELSEN. Acta Crystallogr. **23**, 90 (1967).
24. F. H. HERBSTEIN, P. ASHKENAZI, M. KAFTORY, M. KAPON, G. M. REISNER, and D. GINSBURG. Acta Crystallogr. B**42**, 575 (1986).

[2]The measured and calculated structure factors, fractional atomic co-ordinates for the H atoms, anisotropic thermal parameters, and other material mentioned in the text, may be purchased from the Depository of Unpublished Data, CISTI, National Research Council of Canada, Ottawa, Ont., Canada K1A 0S2.

Can. J. Chem. Downloaded from www.nrcresearchpress.com by 194.225.253.170 on 09/07/12
For personal use only.

Ultraviolet spectrum of domoic acid[1]

MICHAEL FALK, JOHN A. WALTER, AND PAUL W. WISEMAN

Atlantic Research Laboratory, National Research Council of Canada, 1411 Oxford Street, Halifax, N.S., Canada B3H 3Z1

Received March 17, 1989

MICHAEL FALK, JOHN A. WALTER, and PAUL W. WISEMAN. Can. J. Chem. **67**, 1421 (1989).

The ultraviolet spectrum of aqueous domoic acid solutions has an intense absorption band, whose λ_{max} shifts from 240.0 ± 0.3 nm at pH 1.3 to 244.7 ± 0.3 nm at pH 12.3. At the same time, its ε_{max} increases from 24 250 to 26 700 L mol^{-1} cm^{-1}. At pH 7 λ_{max} is 242.8 ± 0.3 nm and ε_{max} is 26 035 ± 200 L mol^{-1} cm^{-1}. Analysis of the variation of λ_{max} and ε_{max} with pH allowed us to estimate the values of these quantities for each of the five stages of protonation of domoic acid and to verify the p*K* values reported by Takemoto and Daigo.

Key words: ultraviolet spectrum, p*K* values, protonation, domoic acid.

MICHAEL FALK, JOHN A. WALTER et PAUL W. WISEMAN. Can. J. Chem. **67**, 1421 (1989).

Le spectre ultraviolet de solutions aqueuses d'acide domoïque possède une bande d'absorption intense, dont le λ_{max} se deplace de 240,0 ± 0,3 nm à un pH de 1,3 jusqu'à 244,7 ± 0,3 nm à un pH de 12,3. En même temps, son ε_{max} augmente de 24 250 jusqu'à 26 700 L mol^{-1} cm^{-1}. À un pH de 7, λ_{max} et ε_{max} sont respectivement de 242,8 ± 0,3 nm et 26 035 ± 200 L mol^{-1} cm^{-1}. L'analyse de la variation de λ_{max} et ε_{max} avec le pH nous a permis de les calculer pour les cinq étapes de la protonation de l'acide domoïque et aussi de verifier les valeurs de p*K* rapportées par Takemoto et Daigo.

Mots clés: spectre ultraviolet, valeurs de p*K*, protonation, acide domoïque.

[Traduit par la revue]

Introduction

Domoid acid is an important naturally occurring substance, with insecticidal, neuro-excitatory, and neurotoxic properties (1–4). It was first isolated from the benthic red seaweed *Chondria armata* ("domoi" in Japanese) and was named after it by Takemoto and Daigo (5, 6). Its molecular structure has been determined and confirmed by a total synthesis (7, 8). It is a tribasic imino acid, related structurally to glutamic acid and containing a proline ring; the stereochemistry of the doubly unsaturated side chain is indicated in Fig. 1.

Domoic acid has unexpectedly taken on a much increased importance since it was identified as the cause of a brief but serious outbreak of poisoning in November/December 1987 (9–12). The poisoning resulted from the consumption of cultured blue mussels (*Mytilus edulis*) originating from eastern Prince Edward Island (9–12). This recent event has prompted a renewed interest in the chemistry, biochemistry, and toxicology of domoic acid, with ongoing research in this laboratory and elsewhere (13–17).

Ultraviolet spectroscopy plays a prominent role in further studies of domoic acid, as it affords a fast and practical method of quantitation. By virtue of the occurrence of two conjugated double bonds in its side chain, domoic acid is a strong absorber of ultraviolet light. The maximum absorption has been reported to occur at wavelength λ_{max} = 242 nm with a molar absorptivity ε_{max} = 26 300 L mol^{-1} cm^{-1} or log ε_{max} = 4.42 (5, 6). Unfortunately, the pH value at which the ultraviolet spectra were measured in refs. 5 and 6 was not specified. At least some spectral changes may be expected to occur as a function of pH, as the degree of protonation of domoic acid varies.

In view of the importance of ultraviolet spectra in future analytical procedures involving domoic acid and its analogues, we have initiated the present study (1) to obtain an accurate value of ε_{max} at a known pH that can be recommended for analytical purposes and (2) to measure the dependence of λ_{max} and ε_{max} on pH and interpret any spectral changes in structural terms. In a following study, we intend to use the ultraviolet spectrum to determine the solubility of domoic acid in water and in organic solvents.

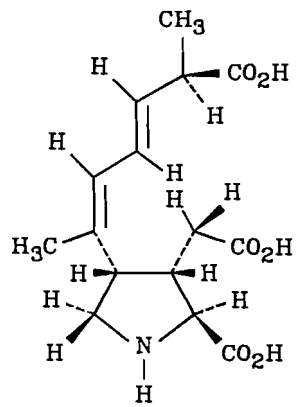


FIG. 1. Molecular structure of domoic acid in its neutral form.

Experimental

Material

High-purity domoic acid was isolated from an aqueous extract of toxic mussels by ion-exchange chromatography (13), followed by crystallization from deionized water as a dihydrate (shiny colorless needles), which dehydrated in vacuum at 50°C within 1 h to anhydrous domoic acid (dull white powder). Upon dehydration, three 10-mg batches of the crystals underwent weight loss of 10.47, 10.01, and 10.54%; calculated for dihydrate: 10.37. Anal. calcd. for $C_{15}H_{21}NO_6$: C 57.87, H 6.80, N 4.50; found: C 57.54, H 6.98, N 4.16%. The material was found to be chromatographically pure (HPLC with UV absorption detection at 200 nm) (13) and its infrared spectrum was identical with that of authentic domoic acid (15). The mass spectrum (14) as well as proton and carbon-13 NMR spectra (13) contained no major signals ascribable to impurities.

Ultraviolet spectroscopy

Spectra in the range of 375–190 nm were recorded on a GCA/-McPherson EU-700 series digital double-beam ratio-recording spectrophotometer. All measurements were made using the transmittance scale, which we found to be more accurate than the absorbance scale. To avoid tracking errors, the wavelength was scanned in small

[1]NRCC No. 30412.

Can. J. Chem. Downloaded from www.nrcresearchpress.com by 194.225.253.170 on 09/07/12
For personal use only.

Can. J. Chem. Downloaded from www.nrcresearchpress.com by 194.225.253.170 on 09/07/12
For personal use only.

increments and transmittance values were recorded manually with the wavelength stationary. The photometric accuracy of the spectrometer was checked by means of a set of calibrated rotating sectors, designed by R.N. Jones for the calibration of infrared spectrometers (18, 19), but found by us to be also perfectly suitable in the ultraviolet region. The digital transmittance reading of the spectrometer was found to be accurate within 0.001 in the transmittance range of 0.06–0.84. At transmittance values of about 0.4, typical of those measured in the present work, the relative error in transmittance is therefore 0.001/0.4 = 0.0025. Since transmittance of 0.4 corresponds to absorbance of $-\log(0.4) = 0.4$, relative errors in absorbance and in transmittance are equal, so that the relative error in molar absorptivity, resulting from photometric inaccuracy, is also 0.25%. The wavelength scale was calibrated with holmium oxide glass, using the holmium absorption line at 241.5 nm. The precision of the measurement of the peak wavelength of this line on our instrument was ±0.06 nm, so that our wavelength calibration error in this spectral region is mainly due to the uncertainty of the wavelength standard, ±0.2 nm (20). All the spectra were recorded at 21°C.

Optical path

The optical path of the sample cell (nominal length 1 cm) was measured by means of a travelling microscope and found to be 0.997 ± 0.005 cm. The relative error in molar absorptivity, resulting from the uncertainty of 0.005 cm in the optical path, is 0.5%.

Measurement of pH

The pH measurements were performed with a Fisher Accumet pH Meter model 610A, using Ingold catalogue no. 6030 pH electrodes. The pH scale was calibrated with Anachemia standard buffers. The pH was measured before and after each spectral measurement.

Measurement of ε_{max} (series A)

Two stock solutions of domoic acid in water were independently made up by gravimetry. Each stock solution was diluted to produce eight solutions of accurately known concentration in the vicinity of 1.6×10^{-5} M, which yielded minimum transmittance in the vicinity of 0.37; this value minimizes the relative error of the determination of maximum absorbance (21). The pH of these solutions was found to be 5.5. The wavelength was set at the absorbance maximum. Firstly, transmittance T_1 was measured with the domoic acid solution in the sample cell and pure water in the reference cell. Then transmittance T_2 was measured with both sample and reference cells filled with pure water. The peak absorbance, A, was calculated from $A = -\log(T) = -\log(T_1/T_2)$. The molar absorptivity, ε_{max}, was calculated from the Beer–Lambert law, $\varepsilon_{max} = A/b \cdot c$, where b is the optical path in cm, and c is the concentration of domoic acid in mol L^{-1}.

Variation of ε_{max} with pH (series B)

One stock solution of domoic acid was used; it was diluted 20-fold with water whose pH had been appropriately adjusted with HCl or NaOH. A series of 34 solutions were prepared by this procedure, spanning the pH scale from 1.28 to 12.35 and containing a known concentration of domoic acid near 1.6×10^{-5} M. The reference cell was filled with pure water. Transmittance T_1 was determined at the wavelength of peak maximum as in series A, but T_2 was taken to be the transmittance of the same domoic acid solution, with the same reference solution, at 275 nm, beyond the edge of domoic acid absorption.

Variation of λ_{max} with pH

The wavelength of maximum absorbance, λ_{max}, was determined manually by fitting a third-degree polynomial to 10 pairs of values of wavelength and transmittance spanning the peak. λ_{max} was taken as the wavelength at which the derivative of this polynomial was zero. The measurements were carried out on a series of 49 domoic acid solutions whose pH spanned the range from 1.34 to 12.29.

Results

Qualitative description of the spectrum

Figure 2 shows the ultraviolet absorptivity of domoic acid at pH 7. In the spectral region investigated, 375–190 nm, the absorption consists essentially of a single band, with high-wavelength onset at about 275 nm, maximum at 243 nm, and width at half-height of 33 nm. At low wavelengths, the absorption passes through a minimum at about 200 nm and begins to increase again as we reach the lower wavelength limit, 190 nm.

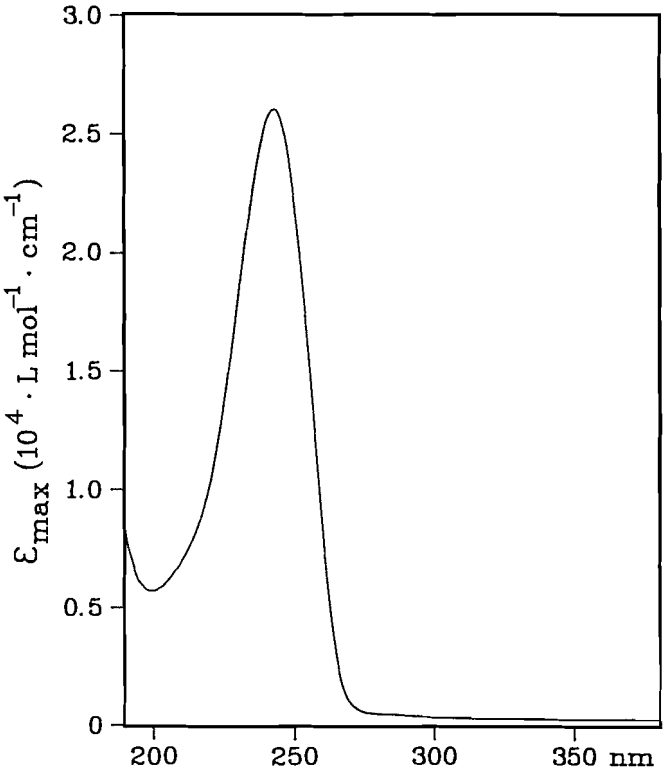


FIG. 2. Ultraviolet spectrum of aqueous domoic acid at pH 7.

ε_{max} at pH 5.5

Averaging the eight measurements on the two independently prepared solutions in series A yielded the values 25 359 and 25 990 L mol^{-1} cm^{-1} for ε_{max} at pH 5.5. Smoothing and interpolation of results from series B yielded the value 26 067 L mol^{-1} cm^{-1} at pH 5.5. Averaging these three values gave 25 805 L mol^{-1} cm^{-1}, which we adopted as the "best" value. This value of ε_{max} agrees with the value of 26 300 L mol^{-1} cm^{-1}, reported by Takemoto and Daigo for an unspecified pH (5, 6). Since the random error of our spectroscopic measurements was well below 1%, our standard deviation of 387 L mol^{-1} cm^{-1}, or 1.5%, probably arises from random errors in the concentration of domoic acid, resulting from errors in the weighings of the rather small (10 mg) domoic acid samples.

Variation of λ_{max} with pH

The λ_{max} results (Table 1,[2] Fig. 3) were obtained in one series of measurements. λ_{max} increases from about 240.0 nm at pH 1.3 to about 244.7 nm at pH 12.3. The λ_{max}/pH plot has a characteristic shape, with three plateau regions (first below pH 2, second between pH 6 and 9, third above pH 11) and relatively steep slope near pH 4 and 10. This behaviour of λ_{max} signifies that the UV absorption is appreciably shifted toward longer

[2]Tables 1, 2, 5, and 6 have been deposited. Copies may be purchased from the Depository of Unpublished Data, CISTI, National Research Council of Canada, Ottawa, Ont., Canada K1A 0S2.

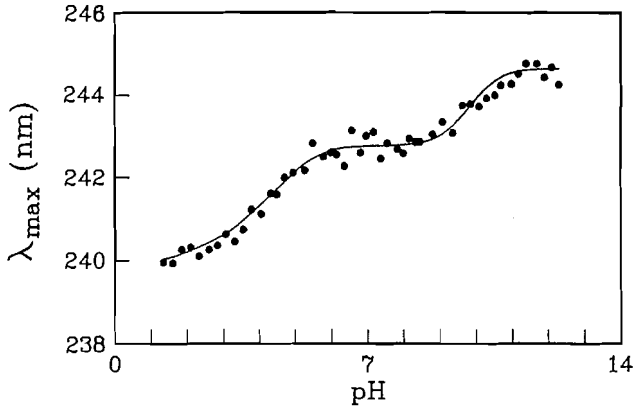


FIG. 3. Variation of λ_{max} with pH. The line was calculated from eqs. [2] and [3] using parameters A'–E' from Table 4 and pK values from ref. 5.

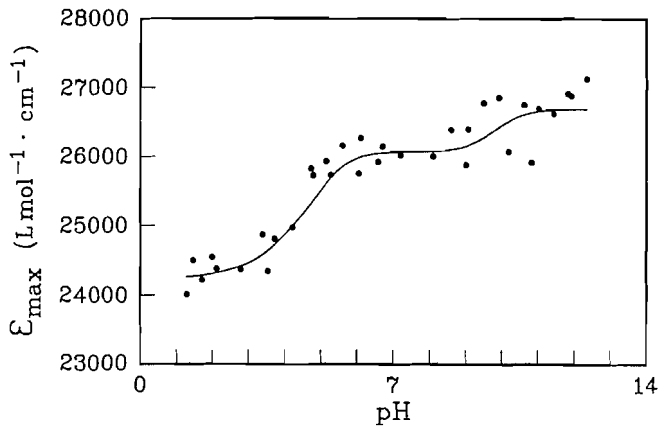


FIG. 4. Variation of ε_{max} with pH. The line as in Fig. 3.

wavelengths at each of the four stages of deprotonation of domoic acid.

A measure of the dispersion of our λ_{max} measurement can be obtained by averaging the 15 values of λ_{max} in the plateau region between pH 5.98 and 8.80. This yields the standard deviation $\sigma = 0.25$ nm. The absolute accuracy of our λ_{max} values ($\pm$ 0.2 nm) does not affect the treatment and discussion of our results. The total shift of λ_{max} with pH is 4.70 nm, which is about 19 times the dispersion of the data. This is good enough to verify the previously reported pK values for domoic acid, as will be done in a following section.

Variation of ε_{max} with pH

The results of series B are recorded in Table 2.[2] Smoothing and interpolation of these data yielded the value of 26 067 L mol^{-1} cm^{-1} for ε_{max} at pH 5.5. Since the best value of this quantity is 25 808 L mol^{-1} cm^{-1}, obtained by averaging the results of series A and B as described above, we have scaled the results from series B by the factor 25 808/26 067 = 0.98995 to obtain the final data recorded in Table 2[2] and plotted in Fig. 4.

ε_{max} varies from 24 250 at pH 1.3 to 26 700 at pH 12.3, for a total shift of 2450 L mol^{-1} cm^{-1}. Allowing for the experimental scatter of about 200 L mol^{-1} cm^{-1}, ε_{max} varies with pH similarly to λ_{max}, continuously increasing and exhibiting three plateau regions. The latter are somewhat less distinct than for λ_{max}, due to the greater experimental scatter. Apparently intensity increase accompanies the blue shift of the absorption band through the four stages of deprotonation. Table 3 lists the

TABLE 3. Values of ε_{max} recommended for analytical purposes

pH	ε_{max} (L mol^{-1} cm^{-1})
2.00	(2.43 ± 0.04) × 10^4
7.00	(2.61 ± 0.04) × 10^4
11.00	(2.70 ± 0.04) × 10^4

smoothed and interpolated values of ε_{max} at pH 2, 7, and 11, recommended for analytical purposes, with estimated standard errors.

Analysis of pH-dependence

Protonation states of domoic acid

Domoic acid contains one imino group, >NH, and three carboxylate groups, —COO$^-$. All of these groups are capable of protonation, so that domoic acid in an aqueous medium must occur as a mixture of five distinct protonation states, A–E, with proportions varying with the pH.

A is the fully protonated cation. It occurs in only one form:

$>NH_2^+$ —COOH —COOH —COOH

B is the neutral molecule. It can undergo site isomerism, alternating between one uncharged form and three zwitterion forms:

$B1$:	>NH	—COOH	—COOH	—COOH
$B2$:	$>NH_2^+$	—COOH	—COOH	—COO$^-$
$B3$:	$>NH_2^+$	—COOH	—COO$^-$	—COOH
$B4$:	$>NH_2^+$	—COO$^-$	—COOH	—COOH

C is the singly charged anion. It can occur in six isomeric forms, corresponding to the six possible locations of the two protons on four distinct sites:

$C1$:	>NH	—COOH	—COOH	—COO$^-$
$C2$:	>NH	—COOH	—COO$^-$	—COOH
$C3$:	>NH	—COO$^-$	—COOH	—COOH
$C4$:	$>NH_2^+$	—COOH	—COO$^-$	—COO$^-$
$C5$:	$>NH_2^+$	—COO$^-$	—COOH	—COO$^-$
$C6$:	$>NH_2^+$	—COO$^-$	—COO$^-$	—COOH

D is the doubly charged anion, occurring in four isomeric forms:

$D1$:	>NH	—COOH	—COO$^-$	—COO$^-$
$D2$:	$>NH_2^+$	—COO$^-$	—COO$^-$	—COOH
$D3$:	$>NH_2^+$	—COO$^-$	—COOH	—COO$^-$
$D4$:	$>NH_2^+$	—COOH	—COO$^-$	—COO$^-$

E is the triply charged anion, occurring in a unique form:

>NH —COO$^-$ —COO$^-$ —COO$^-$

Relation between mole fractions and dissociation constants

We shall, in the following, neglect the complications due to site isomerism and assume that activity coefficients for species A–E are equal. The relative proportions of species A–E are the result of four consecutive equilibria, governed by the four macroscopic dissociation constants, K_1 to K_4:

[1a] $A \rightleftharpoons H^+ + B$ $K_1 = h \cdot b/a$
[1b] $B \rightleftharpoons H^+ + C$ $K_2 = h \cdot c/b$
[1c] $C \rightleftharpoons H^+ + D$ $K_3 = h \cdot d/c$
[1d] $D \rightleftharpoons H^+ + E$ $K_4 = h \cdot e/d$

In the above equations, a, b, c, d, e are the fractions of domoic acid molecules in protonation states A, B, C, D, E, respectively,

Can. J. Chem. Downloaded from www.nrcresearchpress.com by 194.225.253.170 on 09/07/12
For personal use only.

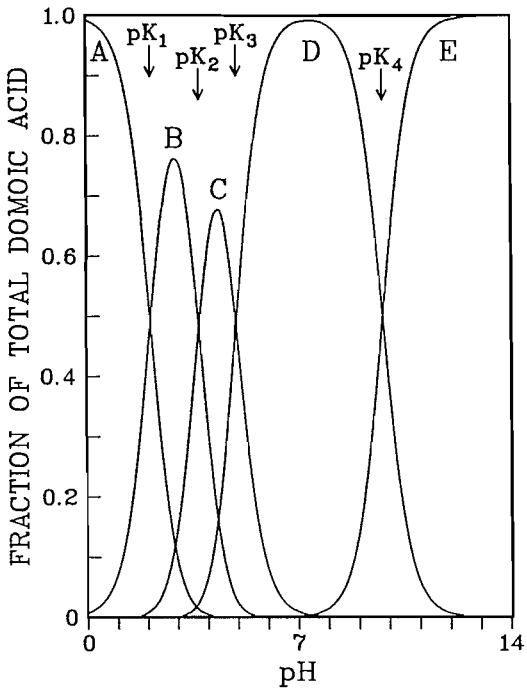


Fig. 5. Protonation stages of domoic acid.

and h stands for the activity of hydrogen ions. The dissociation constants are usually expressed in the logarithmic form, $-\log K_1 = pK_1$, etc.

Equations [1*a*]–[1*d*] can be transformed to yield

$$[2a] \quad a = 1/[F]$$
$$[2b] \quad b = K_1/([F]\cdot h)$$
$$[2c] \quad c = K_1\cdot K_2/([F]\cdot h^2)$$
$$[2d] \quad d = K_1\cdot K_2\cdot K_3/([F]\cdot h^3)$$
$$[2e] \quad e = K_1\cdot K_2\cdot K_3\cdot K_4/([F]\cdot h^4)$$

where $F = 1 + (K_1/h) + (K_1\cdot K_2/h^2) + (K_1\cdot K_2\cdot K_3/h^3) + (K_1\cdot K_2\cdot K_3\cdot K_4/h^4)$.

Equations [2*a*]–[2*e*] relate the fractions a–e of domoic acid molecules in protonation states A–E to the values of dissociation constants K_1–K_4 at any pH. Using the values of the four pK's reported by Takemoto and Daigo (5), $pK_1 = 2.10$, $pK_2 = 3.72$, $pK_3 = 4.97$, $pK_4 = 9.82$, we obtain the fractions a–e shown in Fig. 5.

Model for the variation of spectrum with pH

We will assume that each of the five protonation species has a characteristic value of λ_{max} or ε_{max} (or any other spectral quantity in general), namely A', B', C', D', and E', independent of pH, and that the observed value of that spectral quantity at any pH, S', is the sum of the contributions from the five species:

$$[3] \quad S' = a\cdot A' + b\cdot B' + c\cdot C' + d\cdot D' + e\cdot E'$$

where the five fractions, a–e, can be expressed in terms of the four dissociation constants, K_1–K_4, via eqs. [2*a*]–[2*e*]. Thus, eq. [3] relates the observed λ_{max} or ε_{max} at any pH to the values of nine variable parameters K_1, K_2, K_3, K_4, A', B', C', D', E'.

It is possible to determine the values of these parameters by optimizing the fit of eq. [3] to a set of spectroscopic data as a function of pH. The limit of refinement that can be achieved in the optimization is imposed by the precision of the data.

TABLE 4. Values of initial parameters A'–E' used in the optimization

	A'	B'	C'	D'	E'
λ_{max} data	239.94	240.50	241.60	242.77	244.66
ε_{max} data	24239	24374	24974	26072	26699

Initial values of the variable parameters in the optimization

The initial values of the four pK's were those reported by Takemoto and Daigo (5). The initial values of A'–E' were estimated by assuming that the above pK values are correct, so that the mole fractions of the five protonation species of domoic acid are those plotted in Fig. 5. This plot implies that state A dominates at low pH, state B near pH 2.9, state C near pH 4.4, state D near 7.3, and state E at high pH. The values of constants A'–E' were accordingly estimated from the smoothed values of λ_{max} or ε_{max} at the appropriate pH and are recorded in Table 4.

The optimization procedure

The optimization was carried out on a PC-AT minicomputer using a program for the optimization of up to eight variables adapted from the program described in ref. 22. The program was written in Pascal and uses a modified Simplex method. In each optimization run, some variable parameters were constrained to their initial values and one to eight parameters were optimized. The results of typical optimization runs are shown in Table 5[2] for the λ_{max} data and in Table 6[2] for the ε_{max} data.

Optimization results

The optimization of λ_{max}/pH data leads to sets of values of pK parameters recorded in the different rows of Table 5[2]. It is immediately apparent that the initial values of the nine parameters (first row) are already consistent with the experimental data. The initial value of SSR, the sum of squares of the residuals (i.e., of the differences between λ_{max} observed and λ_{max} calculated from eq. [4]) was 2.119. This corresponds to root-mean-square residual of $(2.119/49)^{1/2} = 0.208$ nm, which is of the order of the experimental scatter of λ_{max} data. Optimization of the values of pK's and of A' through E', carried out in various combinations, produced only a very slight improvement of SSR, from 2.119 to 1.798. The optimization brought about changes in the pK values no greater than 0.32 for K_1, 0.30 for K_2, 0.12 for pK_3, and 0.12 for pK_4. We conclude that the four pK values from ref. 5, $pK_1 = 2.10$, $pK_2 = 3.72$, $pK_3 = 4.97$, and $pK_4 = 9.82$, are roughly correct, the experimental uncertainty being of the order of 0.3. It is not possible to pinpoint the pK values any closer on the basis of the λ_{max}/pH data. Nevertheless, our results do represent an independent rough check of the pK values of Takemoto and Daigo. As a consequence of the pK values from ref. 5 being nearly correct, the plot of Fig. 5 must represent fairly closely the distribution of protonation species of domoic acid in aqueous solution as a function of pH.

Attempts to optimize the pK values on the basis of the ε_{max}/pH data are summarized in Table 6.[2] As before, the initial values of the nine parameters are already consistent with the experimental data. The initial value of SSR is 2.82×10^6, which corresponds to root-mean-square residual of $(2.82 \times 10^6/34)^{1/2} = 288$ L mol^{-1} cm^{-1}, which is of the order of the experimental scatter of the ε_{max} data. Optimization brought about only a minor improvement of SSR, from 2.82×10^6 to 2.28×10^6. The optimization brought about changes in the pK values no greater than 0.35 for pK_1, 0.56 for pK_2, 0.72 for pK_3,

Can. J. Chem. Downloaded from www.nrcresearchpress.com by 194.225.253.170 on 09/07/12
For personal use only.

and 0.57 for pK_4. Therefore, we conclude, as we did from the λ_{max} data, that the pK values from ref. 5 are correct, but because of the greater experimental scatter of the ε_{max} values, the margin of uncertainty is greater.

The initial values of constants $A'-E'$ for λ_{max} and ε_{max} changed only slightly upon optimization. We conclude that the initial values are already close to the true values of these spectral parameters.

Acknowledgements

We wish to thank Mr. Ping F. Seto for technical help, Drs. J. L. C. Wright and A. G. McInnes for supplying samples of pure domoic acid, Donald M. Leek for providing a Pascal language program for Simplex optimization, and Dr. R. N. Jones for the gift of a calibrated set of rotating sectors.

1. T. TAKEMOTO. *In* Kainic acid as a tool in neurobiology. *Edited by* E.G. McGeer, J.W. Olney, and P.L. McGeer. Raven Press, New York. 1978. Chap. 1.
2. H. SHINOZAKI. *In* Kainic acid as a tool in neurobiology. *Edited by* E.G. McGeer, J.W. Olney, and P.L. McGeer. Raven Press, New York. 1978. Chap. 2.
3. J. C. WATKINS. *In* Kainic acid as a tool in neurobiology. *Edited by* E.G. McGeer, J.W. Olney, and P.L. McGeer. Raven Press, New York. 1978. Chap. 3.
4. M. MAEDA, T. KODAMA, T. TANAKA, Y. OHFUNE, K. NOMOTO, K. NISHIMURA, and T. FUJITA. J. Pestic. Sci. **9**, 27 (1984).
5. T. TAKEMOTO and K. DAIGO. Chem. Pharm. Bull. **6**, 578 (1958).
6. T. TAKEMOTO and K. DAIGO. Archiv. Pharm. (Weinheim) **293**, 627 (1960).
7. T. TAKEMOTO, K. DAIGO, Y. KONDO, and K. KONDO. Yakugaku Zasshi, **86**, 874 (1966).
8. Y. OHFUNE and M. TOMITA. J. Am. Chem. Soc. **104**, 3511 (1982).
9. T. M. PERL, L. BEDARD, T. KOSATSKY, J. HOCKIN, and R. S. REMIS. Gastrointestinal and neurological illness related to mussels from Prince Edward Island: A new clinical syndrome associated with domoic acid. Laboratory Centre for Disease Control, Ottawa. Presented at the Epidemic Intelligence Service Conference, Center for Disease Control, Atlanta, GA. April 19, 1988.
10. Identification of domoic acid as the toxic agent responsible for the P.E.I. contaminated mussel incident. Atlantic Research Laboratory Technical Report No. 56. NRCC 29083, July 1988.
11. J. L. C. WRIGHT, R. K. BOYD, A. S. W. DEFREITAS, M. FALK, R. A. FOXALL, W. D. JAMIESON, M. V. LAYCOCK, A. W. MCCULLOCH, A. G. MCINNES, P. ODENSE, V. P. PATHAK, M. A. QUILLIAM, M. A. RAGAN, P. G. SIM, J. A. WALTER, M. GILGAN, D. J. A. RICHARD, and D. DEWAR. Can. J. Chem. **67**, 481 (1989).
12. Investigations on the source of domoic acid responsible for the outbreak of amnesic shellfish poisoning (ASP) in Eastern Prince Edward Island. Atlantic Research Laboratory Technical Report No. 57. NRCC 29086, September 1988.
13. M. A. QUILLAM, P. G. SIM, A. W. MCCULLOCH, and A. G. MCINNES. Int. J. Environ. Anal. Chem. In press.
14. P. THIBAULT, M. A. QUILLAM, W. D. JAMIESON, and R. K. BOYD. Biomed. Environ. Mass Spectrom. **18**, 373 (1989).
15. M. FALK. Can. J. Spectrosc. **33**, 117 (1988).
16. J. F. LAWRENCE, C. F. CHARBONNEAU, C. MENARD, M. A. QUILLIAM, and P. G. SIM. J. Chromatogr. **462**, 349 (1989).
17. D. V. SUBBA RAO, M. A. QUILLIAM, and R. POCKLINGTON. Can. J. Fish. Aquat. Sci. **45**: 2076 (1988).
18. R. N. JONES. Kagaku no Ryoiki, **21**, 617 (1967).
19. R. N. JONES. Pure Appl. Chem. **18**, 303 (1969).
20. J. R. EDISBURY. Practical hints on absorption spectrometry. Hilger and Watts, London. 1966. p. 176.
21. R. P. BAUMAN. Absorption spectroscopy. Wiley, New York. 1962. p. 378.
22. J. W. COOPER. Introduction to Pascal for scientists. Wiley–Interscience, New York. 1981. pp. 186–194.

Can. J. Chem. Downloaded from www.nrcresearchpress.com by 194.225.253.170 on 09/07/12
For personal use only.

Metal ion – biomolecule interactions. Part 14.[1] Methylmercury and hydrogen ion catalysis of C(2)-H isotopic exchange in 1-methylhistidine

ERWIN BUNCEL, HELEN A. JOLY, AND DIANE C. YEE
Department of Chemistry, Queen's University, Kingston, Ont., Canada K7L 3N6

Received December 1, 1988

ERWIN BUNCEL, HELEN A. JOLY, and DIANE C. YEE. Can. J. Chem. **67**, 1426 (1989).

The rate constants for detritiation from the C(2) position of 1-methyl[2-^{3}H]histidine have been determined in a series of aqueous buffers at 85°C. The resulting sigmoidal rate–pH profile was indicative of a mechanism involving hydroxide ion attack on the N(3)-protonated (**4**) and the amino-protonated (**5**) forms of 1-methylhistidine, and dissection of the kinetic data allowed the extraction of the second-order rate constants for the two pathways, k and k'. The unusually large value of k' for a species not protonated at N(3) of the imidazole ring suggested the involvement of a kinetically equivalent zwitterionic form of the substrate (**7**). Comparison of the rate constant k with values determined previously for closely related substrates, such as histidine, 1-methylimidazole, and imidazole, led to the use of FMO theory to explain the effect of the various structural changes, e.g., the effect of methylation and a positively charged side chain on k and k'. The addition of $MeHgNO_3$ resulted in a decrease in the pseudo-first-order rate constant for detritiation. The rate retardation was discussed in terms of two mechanisms (Schemes 2 and 3). Analysis of the data in terms of the various metal-ion-coordinated species present under the experimental conditions showed that the reactivity of the protonated substrate greatly exceeds that of the metal-coordinated species. The difference in the catalytic ability of H^+ vs. $MeHg^+$ is discussed in terms of the extent of positive charge developed on the ligating heteroatom in the ylide (carbenoid) reaction intermediate.

Key words: methylmercury, 1-methylhistidine, isotopic exchange, proton transfer, metal ion catalysis.

ERWIN BUNCEL, HELEN A. JOLY et DIANE C. YEE. Can. J. Chem. **67**, 1426 (1989).

On a déterminé les constantes de vitesse de la détritiation à partir de la position C(2) de la méthyl-1[^{3}H-2]-histidine dans une série de solutions tampons à 85°C. Le profil sigmoidal de la courbe de vitesse en fonction du pH obtenue, témoigne l'existence d'un mécanisme faisant intervenir l'attaque de l'ion hydroxyle sur les formes protonées en N(3) (**4**) et amino-protonée (**5**) de la méthyl-1-histidine. Le dépouillement des données cinétiques permet d'extraire les constantes de vitesse d'ordre deux des deux sites d'attaque, k et k'. La grande valeur inhabituelle de k' pour les espèces non protonées au niveau N(3) du cycle imidazole suggèrent l'intervention d'une forme zwitterionique cinétiquement équivalente du substrat (**7**). La comparaison de la constante de vitesse k avec les valeurs déterminées antérieurement pour des substrats très apparentés comme l'histidine, le méthyl-1-imidazole et l'imidazole, conduit à utiliser la théorie des OML pour expliquer l'effet des divers changements structuraux, par exemple, l'effet d'une méthylation et d'une chaîne latérale chargée positivement sur les valeurs de k et de k'. L'addition du $MeHgNO_3$ conduit à une diminution de la constante de vitesse de pseudo ordre un de la détritiation. On discute de la diminution de la vitesse en fonction de deux mécanismes (schémas 2 et 3). L'analyse des données en fonction des diverses espèces ion métallique-coordonné présentes dans les conditions expérimentales décrites, montre que la réactivité du substrat protoné excède de beaucoup celle des espèces métalliques coordonnées. On discute de la différence de pouvoir catalytique de H^+ versus $MeHg^+$ en fonction du taux de charge positive développée au niveau de l'hétéroatome jouant le rôle de ligand dans l'intermédiaire (carbénoide) de réaction de l'ylide.

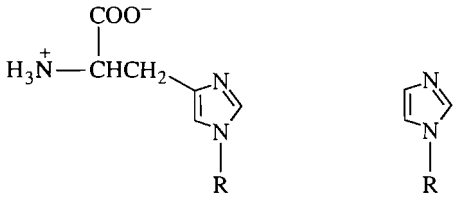
Mots clés : mercure-méthyle, méthyl-1-histidine, échange isotopique, transfert de proton, catalyse d'ion métallique.
[Traduit par la revue]

Can. J. Chem. Downloaded from www.nrcresearchpress.com by 194.225.253.170 on 09/07/12
For personal use only.

Histidine (**1**) is one of the most important amino acids found in biological systems and is present at the active site of enzyme systems such as ribonuclease and a series of serine proteases including α-chymotrypsin, trypsin, and subtilisin (1). In addition, histidine is an essential constituent of several metalloproteins including haemoglobin, myoglobin, and histidine deaminase, presumably because of the availability of the electron pair on N(3) of the heteroaromatic ring to bind transition-metal cations (2).

In imidazole (**2**), the heteroaromatic component of histidine, the C(2)-H flanked by the two heteroatoms, is relatively labile and upon prolonged heating in D_2O or tritiated water will undergo isotopic exchange (3). This property has proven useful in probing biological systems and was used to identify the metal-coordinated histidine residues of the enzymes β-lactamase II and superoxide dismutase (4, 5).

The optimal use of labelled biochemical reactants for elucidating accurate mechanistic information about an enzymatic process requires that one clearly understands the factors that affect tritium and deuterium loss, such as variation in pH,



1 R = H **2** R = H
1*a* R = Me **2***a* R = Me

temperature, and the presence of various metal ions. In one of the earliest reported studies concerning the effect of metal ions on isotopic hydrogen exchange in heterocyclic compounds, with 1-methyltetrazole as the substrate, Olofson *et al.* (6) found that complexation with the transition metal ions Cu^{2+} and Zn^{2+} enhanced the rate of C(5)-H exchange considerably. Based on a mechanism involving hydroxide ion attack on a 1:1 M^{n+}–1-methyltetrazole complex, it was found that metal complexation was 6 to 403 times less effective for exchange than the path involving the conjugate acid, but 5 to 294 times faster than the path involving the neutral substrate.

Jones and co-workers (7) studied the effect of metal ions on the rate of detritiation of [2-^{3}H]imidazole at 85°C and pH 5.70

[1]Part 13: ref. 26.

Can. J. Chem. Downloaded from www.nrcresearchpress.com by 194.225.253.170 on 09/07/12
For personal use only.

and found without exception that addition of metal ions caused rate retardation. The effectiveness of the metal ion increases in the order $Cu^{2+} > Zn^{2+} \approx Ni^{2+} \gg MeHg^{+}$. The results suggested that formation of metal complexes reduced the concentration of the active kinetic species, namely the conjugate acid of imidazole.

Martin and co-workers (8) extended the study of the effect of metal ions on reactivity of the isotopic hydrogen exchange reaction to 1-methylhistidine (**1***a*). The rate constant for deuteration of the 2:1 complex of 1-methylhistidine and Pd^{2+} was measured in D_2O at 61°C at various pH values ranging from 11.3 to 12.0 using NMR spectroscopy. The results showed that hydroxide ion attack occurs $10^{4.8}$ and $10^{5.4}$ times faster for the amino-protonated form (**1***a*) and the 1-methylhistidine species protonated both on N(3) of the imidazole group and the amino group of the side chain, than for the Pd^{2+} complex. Comparison of the rate constants in this fashion gives a quantitative measure of the effect of metal ions on reactivity.

A significant decrease in the detritiation rate constants observed on addition of copper ions to an aqueous solution of 1-methyl[8-^{3}H]guanosine (9) implicates N(7) of 1-methyl-[8-^{3}H]guanosine as the site of metal complex formation, since N(1) and N(9) positions are blocked by a methyl group and a ribose group, respectively. Metal ions added to the reaction mixture compete with H^+ for N(7) of the methylated purine derivatives and, as a result, the rate of isotopic exchange in the presence of metal ion depends upon the rate of hydroxide ion attack on both the protonated substrate (BH^+) and the metal-complexed (BM^{n+}) species. The ratio of the second-order rate constant for hydroxide ion attack for BH^+ to that for BM^{n+}, k and k_{Cu} respectively, was found to be $10^{2.5}$, indicating that Cu^{2+} was not as effective as the proton in accelerating the rate of detritiation. However, a comparison of k_{Cu} to k_n, the second-order rate constant for OH^- attack on neutral 1-methyl[8-^{3}H]guanosine (9), shows that Cu^{2+} coordinated to N(7) does in fact catalyze the reaction ($k_{Cu}/k_n = 10^{6.7}$). The ratio k_m/k_n has been called the metal-activating factor (10).

In a study of the rates of detritiation of 1-methyl[8-^{3}H]inosine in the presence of Cu^{2+}, Zn^{2+}, and Ag^+ ions, the metal ions were found to influence the rate of isotopic exchange in very different ways (10). For example, Zn^{2+} had virtually no effect on the rate of detritiation while Ag^+ was found to suppress the rate of exchange to an even greater degree than Cu^{2+}. This observation is consistent with the ability of the metal ion to coordinate with the N(7) centre. Ag^+, as a soft metal ion, binds more strongly to nitrogen centres than do the two borderline metal ions, Zn^{2+} and Cu^{2+}. Since Ag^+ binds most strongly, the complex will be in higher concentration than the complexes of Zn^{2+} and Cu^{2+}, and thus Ag^+ causes greatest rate retardation.

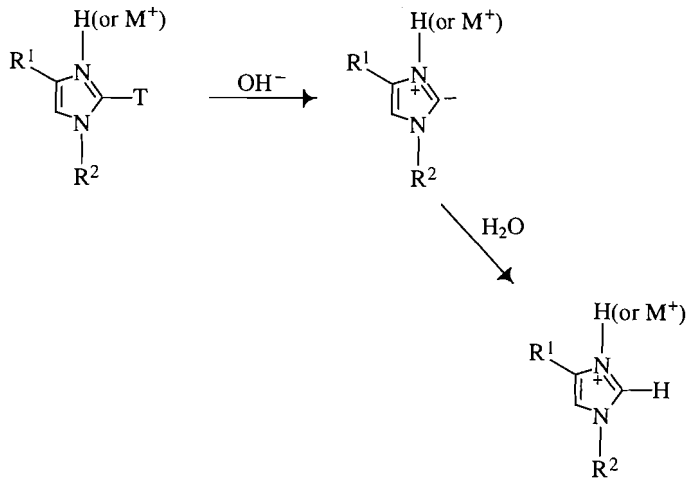
A similar treatment (9) to that used for 1-methylguanosine results in a metal-activating factor (k_m/k_n) of 10^7 for Cu^{2+} and 10^5 for Ag^+, and a proton activation factor (k/k_m) of 10^3 and $10^{4.7}$ for Cu^{2+} and Ag^+, respectively. From all the metal ion studies carried out so far, it can be concluded that metal ions significantly retard the rate of C(2)-H exchange with respect to the N(3)-protonated species (7, 8). Thus, metal ions are not as effective catalysts as is the proton in promoting C(2)-H exchange.

In the present study, the 1-methylhistidine – methylmercury nitrate system has been chosen on the basis of several considerations. First, methylmercury(II) is known to form relatively strong complexes with N-containing ligands, compared with transition-metal salts of Zn^{2+}, Cu^{2+}, etc. (2, 11). Secondly, the preferred coordination number of $MeHg^+$ is one, unlike transition-metal ions such as Cu^{2+}, which coordinate 1–6 ligands depending upon the experimental conditions. Thirdly, the $MeHg^+$ hydroxides that form are soluble at relatively high pH, allowing rate constants to be measured at higher pH values (11). It is worth noting, however, that hydroxide ion is a very effective competitor for $MeHg^+$ and a delicate balance exists between the pH value that is most appropriate to monitor a change in the magnitude of the rate constant and the pH value that minimizes the competition of hydroxide ion and 1-methylhistidine for $MeHg^+$.

The similarity in structure between 1-methylhistidine (**1***a*) and histidine (**1**) makes it an attractive substrate to study. Blocking N(1) with a methyl group reduces the potential $MeHg^+$ binding sites from 4 to 3, thereby significantly reducing the complexity of the kinetic analysis.

The first section of the paper describes the kinetic analysis of the data collected for 1-methyl[2-^{3}H]histidine (**1***a*) in aqueous buffers at 85°C, so as to obtain a rate–pH profile. With that necessary information, results were obtained for the detritiation of 1-methyl[2-^{3}H]histidine in a series of $MeHgNO_3$ solutions varying in concentration from 0 to 0.007 M.

The observed decrease in pseudo-first-order rate constant with increase in metal-ion concentration can be accounted for by mechanisms involving rate-determining triton abstraction from C(2) of N(3)-protonated or metal-coordinated species to give an ylide (carbenoid) intermediate, which is then rapidly protonated (12). The detailed discussion involves consideration of ionized states in the side chain (R^1) and the relative effectiveness of H^+ vs. M^+ in exchange (see Schemes 2 and 3).



Experimental

Preparation of 1-methyl-L-histidine

1-Methyl-L-histidine dihydrochloride was prepared by the three-step sequence outlined by Noordam *et al.* (13*a*). The ^{1}H NMR spectrum in D_2O compared well to that previously reported (δ ppm: 3.38 (2H, 8-peak multiplet, CH_2), 3.89 (3H, singlet, NMe), 4.24 (1H, triplet, NH_2CH), 7.41 (1H, singlet, CCHN), 8.66 (1H, singlet, NCHN). The IR spectrum showed an absorption at 1709 cm^{-1} characteristic of a carboxylic acid. The presence of the ammonium salt is evidenced by several absorption bands: a medium broad band at 3400 cm^{-1}, a group of strong bands between 1575 cm^{-1} and 1600 cm^{-1}, and one strong absorption found at 1495 cm^{-1}. Finally, ascending paper chromatography was performed on the dihydrochloride product against L-histidine as a standard. The two compounds were spotted (5 μg) on cellulose paper and developed in a chromatography tank saturated with 0.1 M α-picoline for 110 min. The dried paper was sprayed with

Can. J. Chem. Downloaded from www.nrcresearchpress.com by 194.225.253.170 on 09/07/12
For personal use only.

ninhydrin and heated in an oven for 15 min at which time purple spots pertaining to each of the two compounds appeared. The 1-methyl-L-histidine dihydrochloride (R_f = 0.868) was found to migrate further than the L-histidine (R_f = 0.814) consistent with that previously reported (13*b*).

1-Methyl-L-histidine dihydrochloride was desalted using cation exchange chromatography. The 1-methyl-L-histidine dihydrochloride (0.425 g) dissolved in 1.5 mL of 2 N HCl was loaded onto a Dowex 50 × 2–400 (200–400 mesh) column (1 cm diameter × 13 cm high). Deionized distilled water was eluted through the column to remove all chloride ions. This was continued until addition of $AgNO_3$ showed no evidence of AgCl precipitation. To remove the 1-methyl-L-histidine as the free base from the column, 4 N NH_4OH was used as an eluant. Water and ammonia were removed by rotoevaporation. The residue was dried under vacuum overnight (0.208 g, 69.8% yield, mp 239.5–240°C (lit. (12) mp 246–248°C)).

Synthesis of 1-methyl[2-^{3}H]-L-histidine

Tritiated water (30 μL, 150 mCi) was added via a syringe to freshly purified 1-methyl-L-histidine (97.75 mg) in a heavy-walled glass ampoule. The glass ampoule was capped with a rubber septum, its contents frozen in liquid nitrogen, and the ampoule evacuated. After sealing, the ampoule was immersed in an oil bath at 85°C for 17 days, at the end of which period the ampoule was opened, 1 mL of distilled water was added to exchange labile tritium, and the solvent was removed by lyophilization. Addition of 1-mL portions of water was continued until the activity of the lyophilized water was found to be insignificant. The total activity of the substrate was approximately 14 mCi. The material was yellowish brown in colour and tlc analysis indicated two or three other impurities, which were removed as follows.

Using a preparative tlc silica gel plate, approximately 50 mg (7 mCi) of crude material in distilled water was spotted along the baseline of the plate. The plate was developed in a closed tank containing solvent (6:6:4:1 CH_3OH:pyridine:H_2O:glacial acetic acid) and equilibrated overnight at room temperature. Development of the plate required 3 h 35 min.

Under UV light, the band pertaining to the 1-methyl[2-^{3}H]-L-histidine was marked. This band of silica gel was scraped off the plate and placed in a small Erlenmeyer flask. Distilled water (3 × 3 mL) was added to extract the substrate. After filtration, water was removed by lyophilization. The total activity was found to be ≈1.2 mCi.

A kinetic stock solution was prepared by transferring the tritiated material to a test tube containing 1 mL of distilled water. The tube was stoppered, sealed with Parafilm, and stored in the refrigerator until needed.

Preparation of buffer solutions

Potassium hydrogen phthalate and sodium borate buffers were used for kinetic measurements carried out at low and intermediate pH ranges, respectively, while sodium hydroxide solutions were used for measurements at higher pH values.

Preparation of methylmercury nitrate solutions (14)

Methylmercury chloride (3.75 g) was suspended in 25 mL of distilled, deionized water in an Erlenmeyer flask. To this was added a solution containing 2.54 g of $AgNO_3$ in 25 mL of water. The flask was stoppered, covered in aluminum foil, and allowed to stir in the dark for 6 days. At this point the solution was filtered through a sintered glass funnel and the AgCl resulting from the ligand exchange was collected on the filter. To ensure the absence of free Ag^+ ions, 0.4 g of methylmercury chloride was added to the filtrate, which was refiltered after stirring for ca. 2 h. The filtrate was transferred to a beaker and allowed to evaporate in the fume cupboard until a solid residue remained. The residue was recrystallized from hot CCl_4. Upon cooling, white crystals formed and were collected and dried *in vacuo* overnight, yield ca. 2.0 g.

A series of solutions ranging from 0 to 0.007 M were prepared by dissolving the appropriate amount of $MeHgNO_3$ in boiled and cooled, deionized, distilled water in a 100-mL volumetric flask. Potassium nitrate (dried at 100°C) was added to maintain constant ionic strength.

Adjustment of the pH of the metal-ion solutions

The metal-ion solution was placed in a reaction vessel designed to carry out potentiometric titrations, which was fitted with a cover with several openings. A combination pH electrode was inserted into one of the openings while the Teflon tubing attached to a microburette was inserted through a small hole punched through a rubber stopper; all other openings were sealed. A stirring bar was used throughout the pH-adjustment procedure to ensure efficient mixing.

Very small quantities of 5% HNO_3 or 0.01 M NaOH were delivered to the metal salt solution to a desired pH with the aid of the microburette of a Metrohm–Herisau automatic titrator. After addition of the final aliquot of acid or base, the solution was allowed to stir for ca. 3–5 min before the pH reading was recorded.

Kinetic measurements

The rate of detritiation of 1-methyl[2-^{3}H]histidine was measured by monitoring the increase in radioactivity of the reaction mixture with time (t_n). The kinetic stock solution (25 μL) was dispensed by means of an automatic pipette to 20 mL of buffer or metal-ion solution contained in a 50-mL round-bottom flask and equilibrated for no less than 30 min at 85°C. The mixture was shaken for 30–60 s. Aliquots of 1 mL were removed at various times ($t_0 \ldots t_n$) with either a Mohr pipette or an Ependorf automatic pipette and delivered to a 50-mL round-bottom flask containing 0.1 g of sodium chloride. (To prevent sublimation of 1-methylhistidine, the B14 joint of the freeze drying bends was lightly plugged with glass wool.) At this point the time on the stopclock was read and recorded. The round-bottom flask was immediately dipped into a Dewar flask containing liquid nitrogen for quenching the reaction and rotated so as to cause the solution to freeze as a thin film on the inner wall of the flask. Lyophilization of the quenched samples enabled separation of the water from the substrate.

A sample of the water separated from the substrate was withdrawn with a 0.1-mL Mohr pipette and transferred to a 7-mL plastic liquid scintillation vial containing 6 mL of Unisolve E or Beckman HP liquid scintillator. The kinetic sample was assayed for tritium (C_t) on a Beckman LS5801 liquid scintillation counter. Subsequent kinetic samples were treated in the same fashion.

The infinity reading (C_∞), i.e., the radioactivity transferred to the aqueous solution when the exchange reaction had reached completion, was determined by measuring the disintegrations per minute of 0.1 mL of the reaction mixture in 6 mL of Unisolve E or Beckman HP liquid scintillator.

Analysis of kinetic data

First-order kinetics

The first-order rate constants, k_{obs}, for the detritiation of 1-methyl[2-^{3}H]histidine in aqueous buffers and metal-salt solutions were extracted from the slopes ($-2.303\ k_{obs}$) of the plots of log ($C_\infty - C_t$) vs. time.

Initial rates method

For slow reactions, i.e., when $t_{1/2}$ was greater than 6 h, an initial rates method was used to determine the first-order rate constant for the detritiation of 1-methyl[2-^{3}H]histidine. This method required that C_t and the corresponding time be collected for no more than 5% of reaction. A plot of C_t vs. time results in a straight line with a slope equal to k_{obs}/C_∞.

Results and discussion

C(2)-H exchange in the absence of metal ion

The rate constants for the detritiation of 1-methyl[2-^{3}H]-histidine (**1***a*) in aqueous buffer solutions at 85°C are listed in Table 1 and shown graphically in Figure 1 in the form of a rate–pH profile for the pH range 2.9–13.2. Also included for comparison are the rate–pH profiles for 1-methyl[2-^{3}H]-imidazole and [2-^{3}H]histidine.

TABLE 1. Detritiation rate constants (k_{obs}) for 1-methyl[2-^{3}H]histidine (**1***a*) in aqueous buffers at 85°C

pH (at 85°C)	$10^4 k_{obs}$ (s^{-1})	pH (at 85°C)	$10^4 k_{obs}$ (s^{-1})
2.94	0.0307	7.47	10.2
3.69	0.152	7.94	15.1
4.22	0.401	8.27	18.6
4.91	1.78	8.69	22.3
5.36	2.59	9.54	24.5
6.01	4.84	10.63	21.8
6.45	5.49	12.58	25.3
7.00	6.43	13.21	21.4

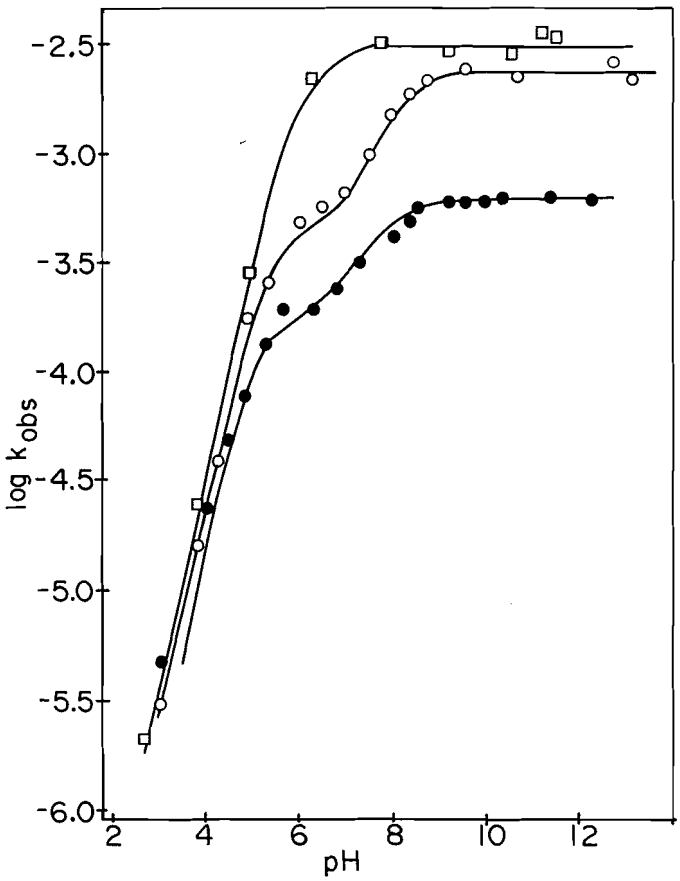


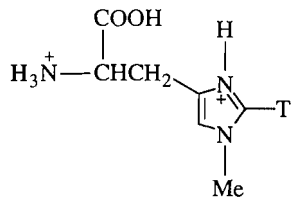
FIG. 1. Rate–pH profiles for the detritiation of 1-methyl[2-^{3}H]-imidazole, (□), [2-^{3}H]-1-methylhistidine (○), and [2-^{3}H]-histidine (●) in aqueous buffers at 85°C. The solid lines represent the theoretical profiles calculated from eq. [7] using the values summarized in Table 2.

In a previous study (3) involving 1-methyl[2-^{3}H]imidazole (**2***a*) the rate constants were found to increase with increasing pH in the lower pH region, while at intermediate pH (7–10) the rate constants plateaued. If the rate–pH profiles for 1-methyl[2-^{3}H]imidazole (**2***a*) and 1-methyl[2-^{3}H]histidine (**1***a*) are compared, similar behaviour is observed in the lower and upper pH regions. The slight deviation observed in the intermediate pH region for 1-methyl[2-^{3}H]histidine, resulting in sigmoidal behaviour, is thought to arise because of the involvement of one or other of the ionizable groups in the side chain. In fact, the rate–pH profile for 1-methyl[2-^{3}H]histidine resembles that obtained for guanosine (15, 16), inosine (15, 17, 18), 9-methylhypoxanthine (15), and histidine (19), compounds that possess an additional ionizable group on the adjacent pyrimidine ring or side chain.

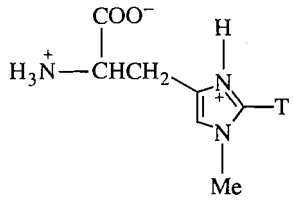
More specifically, the deviation in the intermediate pH region is thought to result from involvement of the amino group in the 1-methylhistidine side chain. Support for this conclusion follows from a comparison of the rate–pH profiles for histidine and histamine (19). The fact that the histamine and histidine profiles are similar suggests that the amino group is responsible for the sigmoidal shape of the curve (19).

1. Kinetic analysis

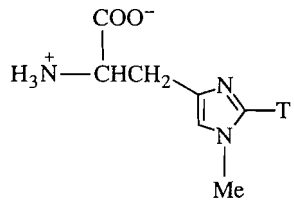
1-Methyl[2-^{3}H]histidine can exist in various ionic forms (**3–6**) depending upon the solution pH. The pK_a for the ionization of the carboxyl group in 1-methylhistidine has a value of 2.0 at 25°C.[2] Hence, in the pH range under study 1-methylhistidine can exist in 3 forms: the N(3)-protonated form **4** (2-THisH$_2^+$), the amino protonated form **5** (2-THisH), and the anionic form **6** (2-THis$^-$). The rate expression for the



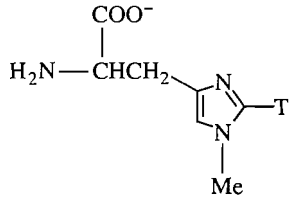
2-THisH$_3^{2+}$ (**3**)



2-THisH$_2^+$ (**4**)



2-THisH (**5**)



2-THis$^-$ (**6**)

isotopic exchange reaction over the entire pH region is given by eq. [1].

$$[1]\quad \text{Rate} = \frac{-\text{d}[\text{2-THis}_t]}{\text{d}t} = k[\text{2-THisH}_2^+][\text{OH}^-] + k'[\text{2-THisH}][\text{OH}^-] + k''[\text{2-THis}^-][\text{OH}^-]$$

[2-THis$_t$] represents the total concentration of 1-methylhistidine-containing species tritiated at C(2), while k, k', and k'' are the rate constants corresponding to 2-THisH$_2^+$, 2-THisH, and 2-THis$^-$ respectively. From past work (10), the second-order rate constant for hydroxide ion attack on a species where N(3) is not protonated, such as 2-THis$^-$, is 10^7 times smaller than that for a species where N(3) of the imidazole ring is protonated. Contribution from the third term in eq. [1] can hence be regarded as insignificant and eq. [1] reduces to

$$[2]\quad \text{Rate} = \frac{-\text{d}[\text{2-THis}_t]}{\text{d}t} = k[\text{2-THisH}_2^+][\text{OH}^-] + k'[\text{2-THisH}][\text{OH}^-]$$

[2]Measured using NMR spectroscopy in our laboratory.

Can. J. Chem. Downloaded from www.nrcresearchpress.com by 194.225.253.170 on 09/07/12
For personal use only.

TABLE 2. Comparison of pK_a and rate constants derived from rate–pH profiles for histidine (His), imidazole (Im), benzimidazole (ϕIm), and their 1-methyl derivatives at 85°C

Compound	pK_a	pK'_a	k ($M^{-1}s^{-1}$)	k' ($M^{-1}s^{-1}$)	k_{Me}/k_H	k'_{Me}/k'_H	$k_{A'\text{-}X}/k_{A\text{-}X}$ (A,A′ = His, Im, or ϕIm; X = H or Me)	Ref.
Histidine (**1**)	5.0	7.6	6.1×10^3	49			A′ = ϕIm 10 (A = His; X = H)	8
1-Methylhistidine (**1***a*)	5.2	7.9	1.0×10^4	1.0×10^2	1.6	2.0	A′ = ϕIm 20 (A = His; X = Me)	This work
Imidazole (**2**)	5.9	—	6.0×10^3	—			A′ = ϕIm 10 (A = Im; X = H)	3,13
1-Methylimidazole (**2***a*)	6.0	—	1.0×10^4	—	1.7	—	A′ = ϕIm 20 (A = Im; X = Me)	3
Benzimidazole	4.6	—	6.2×10^4	—			A′ = His 1 (A = Im, X = H)	6,13
1-Methylbenzimidazole	4.6	—	2.0×10^5	—	3.2	—	A′ = His 1 (A = Im; X = Me)	13

The concentrations of 2-THisH$_2^+$, 2-THisH, and 2-THis$^-$ are related by means of the acid dissociation constants K_a and K'_a where K_a = [2-THisH][H$^+$]/[2-THisH$_2^+$] and K'_a = [2-THis$^-$][H$^+$]/[2-THisH], from which eqs. [3]–[5] follow.

$$[3]\quad [\text{2-THis}_t] = [\text{2-THisH}_2^+] + [\text{2-THisH}] + [\text{2-THis}^-]$$

$$[4]\quad [\text{2-THisH}_2^+] = [\text{2-THis}_t] \Big/ \left(1 + \frac{K_a}{[H^+]} + \frac{K'_aK_a}{[H^+]^2}\right)$$

$$[5]\quad [\text{2-THisH}] = [\text{2-THis}_t] \Big/ \left(1 + \frac{[H^+]}{K_a} + \frac{K'_a}{[H^+]}\right)$$

The rate expression for detritiation of 1-methylhistidine becomes

$$[6]\quad \text{Rate} = \frac{-d[\text{2-THis}_t]}{dt} = \frac{kK_w[H^+][\text{2-THis}_t] + k'K_aK_w[\text{2-THis}_t]}{[H^+]^2 + K_a[H^+] + K_aK'_a}$$

upon substitution of eqs. [4] and [5] into [2] and recognizing that [OH$^-$][H$^+$] = K_w, the ionization constant of water. Integration of eq. [6] gives the pseudo-first-order rate constant (k_{obs}) as

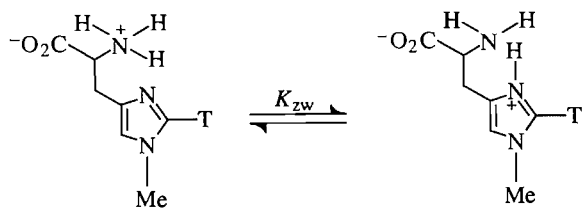
$$[7]\quad k_{obs} = \frac{kK_w[H^+] + k'K_wK_a}{[H^+]^2 + K_a[H^+] + K_aK'_a}$$

For the case where $K_a >> [H^+] >> K'_a$ and $k >> k'$, eq. [7] reduces to $k_{obs} = kK_w/K_a$, corresponding to the plateau extending between pH 6 and 7. Similarly, when $K'_a >> [H^+] >> K_a$, eq. [7] reduces to $k_{obs} = k'K_w/K'_a$, corresponding to the second plateau at pH 8.5–13. The solid curve in Fig. 1 represents the best fit of the experimental data to eq. [7] using a nonlinear least-squares program (NOTLIN). The acid dissociation constants that give the best fit are given by pK_a = 5.20 ± 0.05 and pK'_a = 7.86 ± 0.09 respectively. These values are in good agreement with pK_a and pK'_a determined by NMR when corrected to 85°C using the Perrin equation, i.e., 4.99 and 7.78, respectively.[3] The second-order rate constants k and k', corresponding to the best possible fit, were (1.00 ± 0.05) × 10^4 $M^{-1}s^{-1}$ and (1.05 ± 0.20) × 10^2 $M^{-1}s^{-1}$, respectively.

[3]E. Buncel and D. C. Yee. To be published.

2. Reactivity relationships

The second-order rate constants k and k' derived from the kinetic analysis can be compared with the corresponding rate constants previously reported for histidine (19, 20), imidazole (3, 21), and benzimidazole (21) and their 1-methyl derivatives (3, 17), Table 2. There are several interesting points that arise from the data presented in Table 2. As pointed out by Jones and co-workers (19) in a study of the detritiation of histidine, the magnitude of k' for the reaction between hydroxide ion and the amino-protonated histidine species is unusually large compared to similar compounds reacting in the neutral form (k' values normally range between 10^{-1} and 10^{-3} $M^{-1}s^{-1}$ (10)). The 10^3 to 10^5-fold increase in rate constant observed for the amino-protonated form of amino acids, relative to substrates not possessing a protonated side chain, suggests the involvement of a kinetically equivalent species. One such possibility for the 1-methylhistidine case is shown in eq. [8].

[8] 

5 7

The proton can be readily transferred from the ammonium group to N(3) of the imidazole ring, as the side chain can reorient itself to form a six-membered ring as shown above. It has long been known that histidine and its derivatives can chelate metal ions with the nitrogen atoms of the amino and imidazole groups. For instance, the reaction of 2 moles of 1-methylhistidine with 1 mole of K_2PdCl_4 results in a 2:1 complex of 1-methylhistidine:Pd^{2+}, where each ligand chelates via the amino nitrogen and N(3) of imidazole (8).

Hence k' is a composite of two rate constants: k_0, the rate constant for hydroxide ion attack on the amino-protonated species **5**, and k_{zw} the rate constant for attack on the zwitterionic form **7** ($k' = k_0 + k_{zw}K_{zw} = 1.0 \times 10^2\ M^{-1}s^{-1}$). A value for

Can. J. Chem. Downloaded from www.nrcresearchpress.com by 194.225.253.170 on 09/07/12
For personal use only.

the equilibrium constant K_{zw} was obtained by substituting the parameters derived from the above kinetic analysis into the rate expression for the exchange mechanism that includes the zwitterionic form, **7**, of 1-methylhistidine, eq. [9]. More

$$[9] \quad k_{obs} = \frac{kK_w[H^+] + K_aK_w(k_0 + k_{zw}K_{zw})}{[H^+]^2 + K_aK' + K_{zw}K_a[H^+] + K_a[H^+]}$$

specifically, a nonlinear least-squares fit of the experimental rate constants to eq. [9] where $k = 1.0 \times 10^4\ M^{-1}\ s^{-1}$, $K_a = 6.31 \times 10^{-6}$ M, $K'_a = 1.26 \times 10^{-8}$ M, $K_w = 3.16 \times 10^{-13}\ M^2$, and $k_0 + K_{zw}k_{zw} = 1.0 \times 10^2\ M^{-1}\ s^{-1}$, resulted in $K_{zw} = 9.95 \times 10^{-3}$. It is interesting to note that K_{zw} for histidine (8) has been estimated as 2.0×10^{-2} (8, 22).

By assuming a value for k_0 in the range of 10^{-1}–$10^{-3}\ M^{-1}\ s^{-1}$ and a value of 9.95×10^{-3} for K_{zw}, k_{zw} can be estimated from the relationship $k' = k_0 + k_{zw}K_{zw} = 1.0 \times 10^2\ M^{-1}\ s^{-1}$. The resulting second-order rate constant ($k_{zw} = 1 \times 10^4$ to $1 \times 10^5\ M^{-1}\ s^{-1}$) is comparable to those previously obtained for hydroxide ion attack on the conjugate acid of 1-methylimidazole, 1-methylbenzimidazole, etc. (cf. Table 2). Hence, the proton's ability to migrate to N(3) of the imidazole moiety in species **5** results in an ionic form of 1-methylhistidine that is as reactive as **4**. This is consistent with previous studies showing that the reactivity of an N(3)-protonated species is greater than that of the unprotonated species (10).

It should be noted that in attempting to obtain solutions for eq. [9], which involves four unknown parameters, k, k_0, k_{zw}, and K_{zw}, the uncertainty associated with their determination will necessarily be rather high. Nevertheless, the apparent agreement between K_{zw} obtained here and the previously reported value (8, 22), as noted above, gives some confidence in the overall procedure adopted here for the solution of eq. [9]. The overall mechanism that we have proposed is also in agreement with previous studies on related systems (9, 10, 19), i.e., the important reactive species and the corresponding rate constants are the following: **4** (k), **5** (k_0), and **7** (k_{zw}). Species that are found not to be important, or that contribute negligibly, are **3** and **6**.

The effect of N-methylation is demonstrated by a comparison of the second-order rate constants for 1-methylhistidine (**1***a*), 1-methylimidazole (**2***a*), and 1-methylbenzimidazole with those for the corresponding unmethylated parent compounds. Substitution of the hydrogen atom at N(1) of histidine (**1**), imidazole (**2**), and benzimidazole with a methyl group causes the rate constant (k) for proton transfer to increase by factors of 1.6, 1.7, and 3.2 respectively. Similarly, N-methylation results in a 2-fold increase in k' for histidine. It is also interesting to note that this structural change has little effect on the magnitude of the pK_a for N(3)-protonation; a pK_a of 5.1 was found for the pair histidine and 1-methylhistidine, 6.0 for imidazole and 1-methylimidazole, and 4.6 for benzimidazole and 1-methylbenzimidazole.

Finally, a comparison of rate constants (k) for histidine (**1**) and imidazole (**2**), 1-methylhistidine (**1***a*) and 1-methylimidazole (**2***a*), histidine and benzimidazole, and 1-methylhistidine and 1-methylbenzimidazole allows one to assess the effect on k of a charged side chain, relative to benzo annelation of the imidazole nucleus, for instance. This is shown in the eighth column of Table 2. Unlike annelation of a benzo group to the imidazole and 1-methylimidazole nucleus, which results in a 10- or 20-fold increase in k, respectively, substitution of a positively charged side chain has virtually no effect on k relative to the parent compound. Having uncovered the interesting reactivity differences mentioned above, one is left to try to explain their origin.

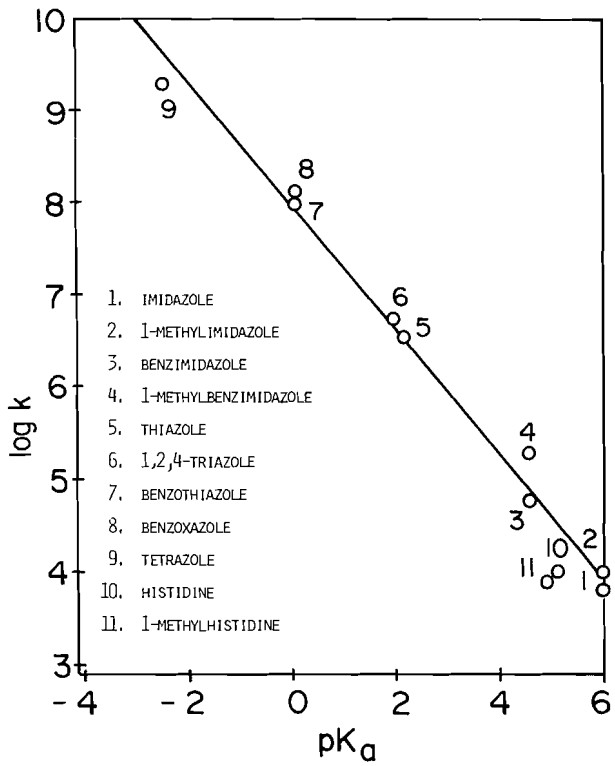


FIG. 2. Plot of log k for detritiation from C(2) of a series of azoles at 85°C versus the pK_a corresponding to N(3) protonation.

Jones and co-workers (10, 21) have shown that there is a linear correlation between log k, the second-order rate constant for C(2)-proton exchange in azoles, and the pK_a for N(3)-protonation; this relationship is followed by histidine (**1**), imidazole (**2**), benzimidazole, and their methyl derivatives. In fact, when the data for 1-methylimidazole and 1-methylbenzimidazole are included with that originally presented (21), the slope and correlation coefficient only vary from −0.72 and 0.993 to −0.66 and 0.995, respectively, Fig. 2. When histidine and 1-methylhistidine are included, the correlation is poorer (correlation coefficient = 0.986) but the slope is similar in magnitude (ca. 0.69). The poorer correlation is not surprising in that Jones and Taylor (10) found that various classes of substrates tended to show separate correlations. More specifically, compounds containing the purine nucleus seemed to show a separate correlation from that of substrates possessing the imidazole nucleus.

The relationship (log k vs. pK_a) is based on the premise that the pK_a is a reflection of the fractional charge at C(2) and hence an indicator of the acidity of C(2)-H. The smaller the negative charge localized at C(2), the more stable is the ylide intermediate, and hence the greater the rate of C(2)-H exchange. The magnitude of the slope of the linear free energy relationship (LFER) is thought to indicate the unequal substituent field effects on the protonation and detritiation process (21).

However, the LFER proposed by Jones cannot provide an explanation for the reactivity difference arising from substrates with identical pK_a values, for example, the reactivity differences observed for histidine and 1-methylhistidine, imidazole

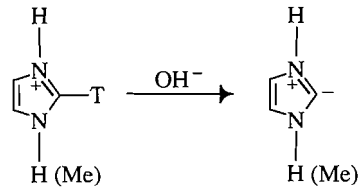
Can. J. Chem. Downloaded from www.nrcresearchpress.com by 194.225.253.170 on 09/07/12
For personal use only.

and 1-methylimidazole, and benzimidazole and 1-methylbenzimidazole.

3. FMO–PMO interpretation

In a previous study (3) the increased reactivity observed for the N-methylated and benzo-annelated analogues of imidazole was discussed in terms of frontier and perturbational molecular orbital theory (FMO and PMO theory, respectively). We summarize the salient features of the argument used and then extend it to the present system to account for the reactivity differences observed between 1-methylhistidine and related compounds.

The application of FMO–PMO theory to the components of the rate-determining step for proton transfer from 1-methylimidazole and imidazole (i.e., C(2)-H abstraction from the protonated substrate (R) to form the ylide intermediate (I)), results in the relative energies of the frontier orbitals of the reactants and ylide intermediates and the relative intramolecular stabilization energy effected by structural change. From the ordering of the frontier orbitals, the relative stabilization energy in going from the reactant to the ylide intermediate can be estimated.

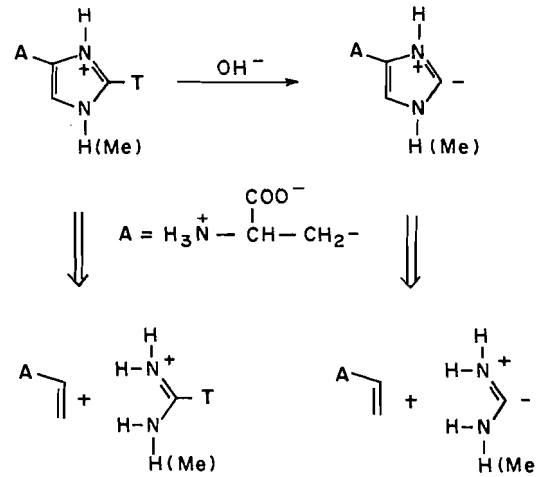


R I

The relative energies of the frontier orbitals of the species present in the rate-determining step for proton transfer were determined by dissecting into fragments of known molecular orbitals. The LUMO of one fragment and the HOMO of the remaining fragment are combined arbitrarily, resulting in the frontier orbital for the reacting species. Next, the stabilization energies in the reactant (SE^R) and intermediate (SE^I) states effected by structural change are compared. The closer the energies of the HOMO and LUMO, the better the orbital overlap and hence the greater the stabilization energy. The relative energies of the HOMOs and LUMOs are estimated from ionization potentials (IP) and electron affinities (EA), respectively; $E_{HOMO} = -IP$ and $E_{LUMO} = -EA$ (23). If the difference in the magnitude of the stabilization energy (δSE) effected by structural change is smaller in the reactant state than in the intermediate state ($\delta SE^I > \delta SE^R$), one would expect proton transfer from the substituted substrate to be faster than from the unsubstituted form. Conversely, if δSE is larger in the reactant state than in the intermediate state ($\delta SE^I < \delta SE^R$), then proton transfer from the substituted substrate would be slower than from the unsubstituted substrate.

(i) Effect of methyl substitution

For the case of imidazole and 1-methylimidazole, the difference in the stabilization energies between the N-methylated and unmethylated intermediates, $SE^I_{Me} - SE^I_H$, was found to be greater than that between the reactants $SE^R_{Me} - SE^R_H$ (3). The increased stabilization of the intermediate relative to the reactant effected by substitution of a methyl group at N(1) accounts for the increase in the second-order rate constant, as the transition state should also be stabilized by the structural change.



SCHEME 1

One can account for the reactivity difference observed for C(2)-proton transfer from N(3)-protonated histidine and 1-methylhistidine in a similar fashion. The relative energies of the FMOs of the reactant species and their corresponding intermediate structures, and hence the intramolecular stabilization energy, are estimated from the relative energies of the frontier orbitals of the fragments (Scheme 1). For histidine the fragments are a substituted ethylene and a pseudoallyl fragment, while 1-methylhistidine is fragmented into the same substituted ethylene fragment and a 1-methyl-pseudoallyl fragment. The same procedure is followed for the intermediate structures.

As shown in the previous study (3), methylation is associated with a decrease in ionization potential. This suggests that the HOMO of the 1-methyl-pseudoallyl fragment is higher in energy than that of the unsubstituted pseudo-allyl fragment in both the reactant and the intermediate. Hence in the reactant state the interaction of the LUMO of substituted ethylene and the HOMO of the 1-methyl-pseudoallyl fragment for the methylated substrate is greater, due to the smaller energy gap, than the corresponding orbital interaction for the unsubstituted parent compound. This results in a differential stabilization energy $\delta SE^R = SE^R_{Me} - SE^R_H$, where $SE^R_{Me} > SE^R_H$ (Fig. 3).

In going to the intermediate structures, the HOMO energy of the deprotonated pseudoallyl and 1-methyl-pseudoallyl fragments is expected to increase substantially relative to the corresponding protonated fragments; the energy required to remove an electron from a neutral molecule is greater than from its deprotonated analog. Consequently, the energy gap between the HOMO of the deprotonated pseudoallyl and 1-methyl-pseudoallyl fragment, and the LUMO of the substituted ethylene, is significantly smaller than that in the reactant state (Fig. 3). This results in greater orbital interaction and thus enhanced stabilization in the intermediate structures relative to the reactants. More specifically, $\delta SE^I (= SE^I_{Me} - SE^I_H)$ is greater than $\delta SE^R (= SE^R_{Me} - SE^R_H)$. An intermediate of lower energy results upon N-1 methylation of histidine. Assuming that the energy of the intermediate is in direct correspondence to the transition state energy, it follows that a change in structure from R = H to R = Me leads to stabilization of the transition state for proton transfer, thus accounting for the increase in rate on methyl substitution.

For proton transfer from the amino-protonated species (**5**) where the zwitterionic species **7** has been implicated as the

Can. J. Chem. Downloaded from www.nrcresearchpress.com by 194.225.253.170 on 09/07/12
For personal use only.

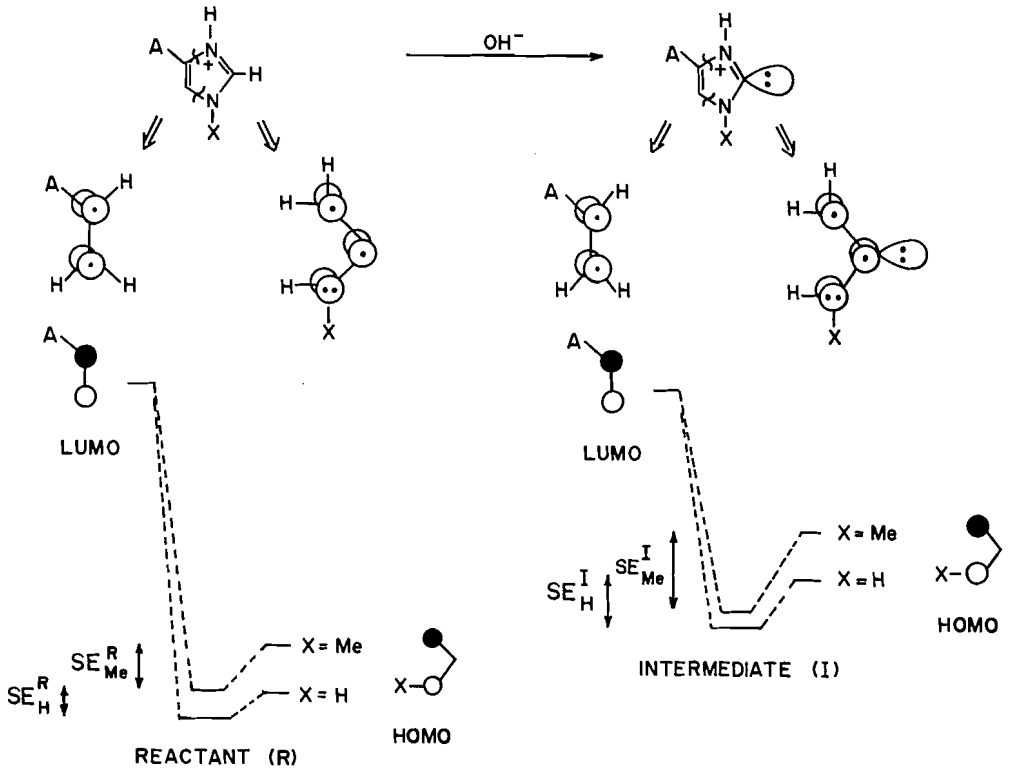


FIG. 3. FMO analysis of the effect of N(1)-methylation on proton transfer from C(2) of histidine (A = $H_3\overset{+}{N}$—CH(COO^-)CH_2-) and imidazole (A = H).

major contributor to k', a similar analysis can be made to explain the rate increase on N-methylation. The reactant substrates and the corresponding ylide intermediates are dissected into a substituted ethylene fragment and a pseudoallyl fragment for the histidine case (A = H_2N—CH(COO^-)—CH_2-, cf. Scheme 1), and a substituted ethylene fragment and a 1-methyl-pseudoallyl fragment for the 1-methylhistidine case (A = H_2N—CH(COO^-)—CH_2-, cf. Scheme 1). The relative ordering of the HOMOs for the pseudoallyl and 1-methyl-pseudoallyl fragments, and the LUMO of the substituted ethylene fragment, both in the reactant and intermediate state, are, however, as described for the diprotonated species (both N(3) and amino group are protonated) of histidine and 1-methylhistidine and hence the same analysis can be used to account for the difference in k' observed for histidine and 1-methylhistidine.

(ii) Effect of structural change on the ethylene moiety

Next one can consider the change of C(2)-H reactivity effected by structural change of the ethylene moiety. It was found previously that annelation of a benzo group to imidazole and 1-methylimidazole results in a 10- or 20-fold increase in k, which could be explained in terms of FMO–PMO theory (3). The present work shows, however, that substitution of the C(4)-H of imidazole and 1-methylimidazole with a charged side chain does not alter k significantly. This observation is interesting in view of the FMO–PMO analysis.

The FMO–PMO treatment of proton transfer from C(2) of imidazole and histidine requires that imidazole be dissected into ethylene and a pseudoallyl fragment ($H_2\overset{+}{N}$=CH—NH_2) while histidine is dissected into a substituted ethylene (CH_2=CHA, where A = ^+H_3N—CH(COO^-)—CH_2-) and a pseudoallyl fragment ($H_2\overset{+}{N}$=CH—NH_2). It is important to note that the pseudoallyl fragments are identical in both cases. Hence the analysis focuses on the change in energy of the LUMO of ethylene effected by substitution of the charged side chain, Fig. 4.

As previously stated, the energy of the LUMO is related to the electron affinity (EA) by the relationship, $E_{LUMO} = -EA$. One would expect that substitution of C(4)-H with a side chain such as ^+H_3N—CH(COO^-)—CH_2-, would result in an increase in the electron affinity, since the positive charge on the ammonio group would aid in binding electrons more tightly than the unsubstituted ethylene system. The negative charge on the carboxylate group, however, will diminish the effect of the positive charge and, while it is difficult to estimate the degree of the reduction in positive charge, one is tempted to argue that the proximity of the charges to the ethylene moiety would play a role. More specifically, as the positive charge is closer to the ethylene moiety it should dominate the overall effect.

As a result of the increase in electron affinity due to the electrostatic effect of the side chain, one would expect the energy of the substituted moiety to be lower. The energy of the HOMO of the pseudoallyl fragment is lower than that of the LUMO of ethylene, as discussed in the previous section. In the intermediate state, the relative energies of the LUMOs of ethylene and substituted ethylene are as stated. For the reactant, however, the HOMO energy for the deprotonated pseudoallyl fragment is significantly larger than that of the parent pseudoallyl fragment, for the same arguments presented in the previous section. Having established the relative energies of the LUMO and HOMO of the respective fragments, one proceeds by assessing the degree of interaction between the LUMOs of ethylene and substituted ethylene with the HOMO of the pseudoallyl fragment in the reactant state, and of the deproto-

Can. J. Chem. Downloaded from www.nrcresearchpress.com by 194.225.253.170 on 09/07/12
For personal use only.

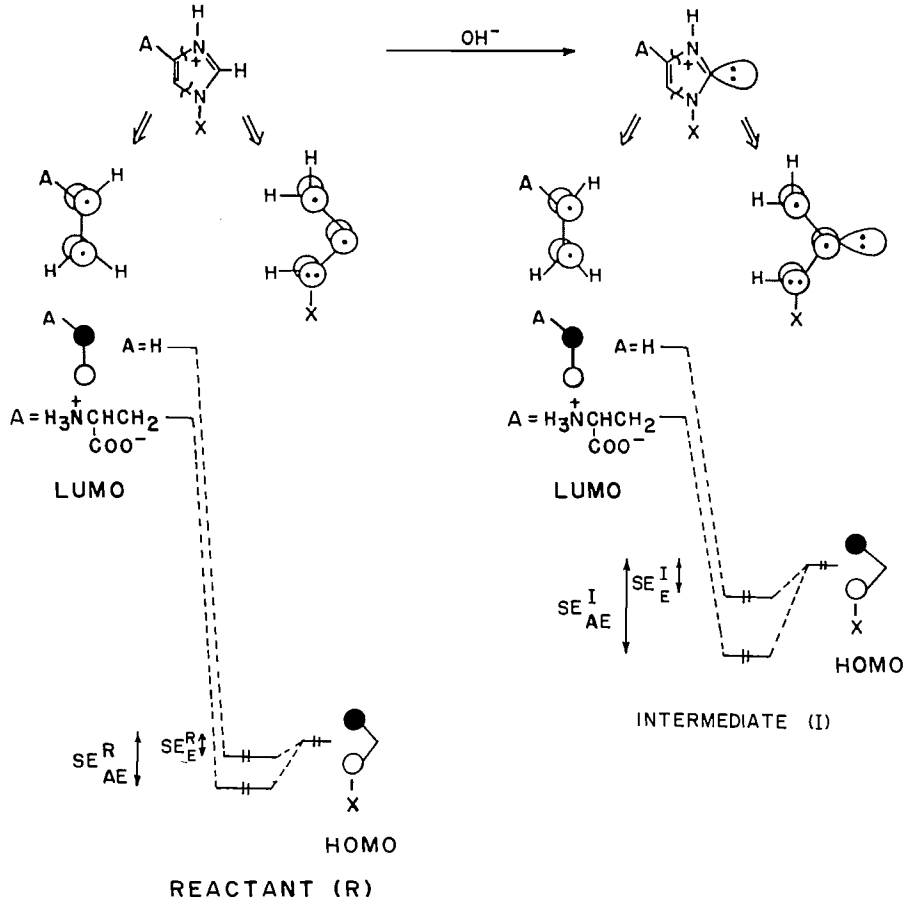


FIG. 4. FMO analysis of the effect of C(4) substitution (A = H vs. A = $H_3\overset{+}{N}$—CH(COO^-)CH_2-) on C(2)-H exchange from imidazole (X = H) and 1-methylimidazole (X = Me).

nated pseudoallyl fragment in the intermediate state. The smaller energy gap between the HOMO of the deprotonated pseudoallyl fragment and the LUMO of ethylene, or the LUMO of substituted ethylene, leads to greater orbital interaction, and thus enhanced stabilization in the intermediate structures relative to the reactants. The difference in the stabilization energies (δSE) of the two intermediate structures, $SE^I_{A\text{-}E} - SE^I_E$ (subscripts A-E and E represent substituted ethylene and ethylene, respectively) is greater than that for the reactants, i.e., $\delta SE^I > \delta SE^R$. The increased stabilization of the intermediate relative to the reactant effected by the side chain at C(4) would predict an increase in k for 1-methylhistidine and histidine relative to 1-methylimidazole and imidazole, respectively. However, as stated before, no significant change in k was observed for 1-methylhistidine and 1-methylimidazole, and for histidine and imidazole.

Jones and co-workers (19) determined k for histamine under the same experimental conditions as for imidazole (21). These workers found that the ratio of the k values for histamine and imidazole was 10/6.0 or 1.6. This result is consistent with the above FMO–PMO analysis. The positive charge of the side chain of histamine, $H_3\overset{+}{N}CH_2CH_2$-, would be expected to increase the electron affinity of ethylene. This would suggest that the effect of the carboxylate group of the histidine side chain has a greater effect in diminishing the positive charge than first anticipated.

Bradbury *et al.* (20) found that the second-order rate constant for C(2)-H deuterium exchange of imidazole acetic acid was 6.4/2.9, i.e., 2.2 times smaller than that for imidazole. The results of the above two studies suggest that the increase in rate due to the ammonium group is equal to the rate-retarding effect of the carboxylate, which is consistent with the k for histidine and imidazole, and for 1-methylhistidine and 1-methylimidazole, to be of the same order of magnitude.

Proton transfer from C(2) of 1-methylhistidine in the presence of $MeHgNO_3$

The pseudo-first-order rate constants for the detritiation of 1-methyl[2-^{3}H]histidine were determined at pH 5.90 and a temperature of 85°C for a series of reaction mixtures varying in $MeHgNO_3$ concentration (0–0.007 M). The results, given in Table 3, show a decrease in the value of the rate constant with increasing metal-ion concentration. The ratio of the pseudo-first-order rate constants at $[M^{n+}] = 0$ and $[M^{n+}] = 0.007$ M is $4.355 \times 10^{-4}/1.695 \times 10^{-5}$, i.e., 26. This decrease is shown graphically in Fig. 5 in the form of a rate constant vs. $[MeHg^+]$ profile.

The observed decrease in rate constant with increasing $MeHg^+$ concentration is not unlike that previously reported for the detritiation of [2-^{3}H]imidazole in the presence of Cu^{2+}, Ni^{2+}, and Zn^{2+} (7). It is interesting to note at this point that there is a discrepancy in the results obtained for [2-^{3}H]imidazole and 1-methyl[2-^{3}H]histidine in the presence of $MeHgNO_3$. Whereas a very small ratio ($k^{M=0}_{obs}/k^{M=0.003}_{obs} = 1.13$, pH =

Can. J. Chem. Downloaded from www.nrcresearchpress.com by 194.225.253.170 on 09/07/12
For personal use only.

TABLE 3. Pseudo-first-order rate constants for the detritiation of 1-methyl[2-^{3}H]histidine (**1***a*) in the presence of $MeHgNO_3$ at 85°C, pH = 5.90

$[MeHg^+]$ (M)	$10^5 k_{obs}$ (s^{-1})	$10^5 k^M_{obs}$ (avg.) (s^{-1})
0.00207	10.4	10.6
	10.7	
0.00316	4.17	4.18
	4.19	
0.00410	3.55	3.49
	3.43	
0.00590	2.34	2.36
	2.38	
0.00675	1.68	1.69
	1.69	

5.70) was detected for imidazole in the presence of 0.003 M $MeHgNO_3$, a rate ratio of 10 was obtained for 1-methylhistidine under similar experimental conditions.

Two explanations can be put forward to account for the observed decrease in the pseudo-first-order rate constant. These are discussed in terms of two mechanisms, Mechanism I and Mechanism II, and are shown in Schemes 2 and 3 respectively. In the first mechanism, $MeHg^+$ complexes with 1-methyl-[2-^{3}H]histidine at N(3) and the amino nitrogen, respectively. The result is to reduce the concentration of both the amino-protonated (**5**) and the N(3)-protonated form (**4**) of 1-methyl-[2-^{3}H]histidine. Hence the product of the concentration of hydroxide ion and the active species will be smaller, thus accounting for the decrease in observed rate constant.

Support for such a mechanism is afforded by a study of the effect of metal ions on C(2)-H isotopic exchange of imidazole (7). The rate-retarding effect of the metal ions ($Cu^{2+} > Zn^{2+} \sim Ni^{2+} \gg MeHg^+$) was rationalized in terms of complex formation and hence reduction in the concentration of the conjugate acid of imidazole.

The second mechanism also involves complexation of 1-methyl[2-^{3}H]histidine to form an N(3)- and an amino-coordinated complex. The reduction in the magnitude of the pseudo-first-order rate constant in this case results from competition of rate-determining hydroxide ion attack on the metal-coordinated species with the pathways involving hydroxide ion attack on the amino-protonated (**5**) and the N(3)-protonated species (**4**) respectively. The assumption must be made, however, that the magnitude of the second-order rate constants for hydroxide ion attack on the metal-coordinated species is smaller than k and k' determined for the pathways involving the amino-protonated (**5**) and N(3)-protonated species (**4**).

Detritiation of 1-methyl[8-^{3}H]inosine and 1-methyl[8-^{3}H]-guanosine, under conditions where the operative mechanism is reaction between the protonated substrate and hydroxide ion, was retarded by the presence of Ag^+ and Cu^{2+} for 1-methyl[8-^{3}H]inosine and by Cu^{2+} for 1-methyl[8-^{3}H]guanosine (9). This was explained by the formation of a metal-complex species that detritiated at a slower rate than the protonated form of the substrate, but about 10^4 to 10^6 times faster than the neutral form.

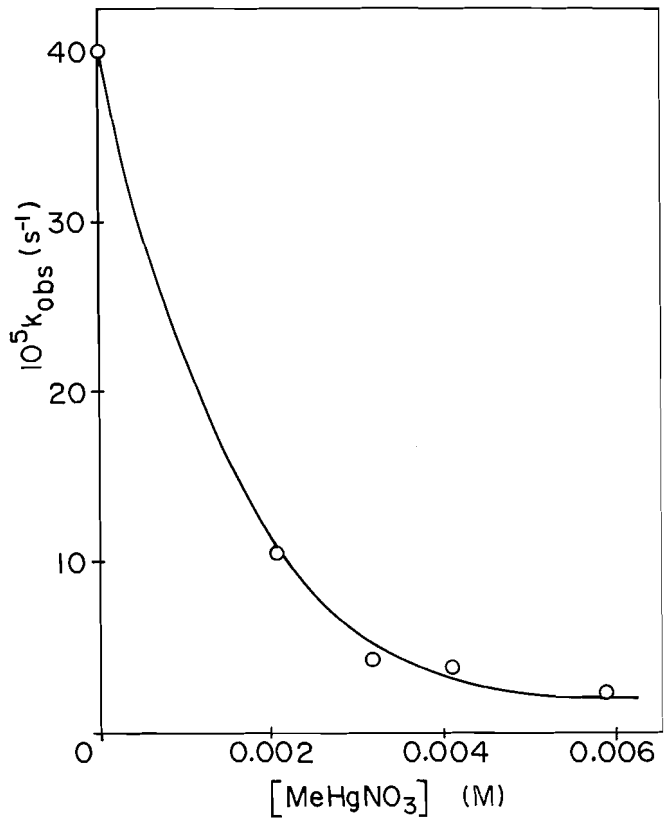


FIG. 5. Effect of metal ions on C(2)-H exchange of 1-methylhistidine. Plot of k_{obs} vs. [$MeHgNO_3$].

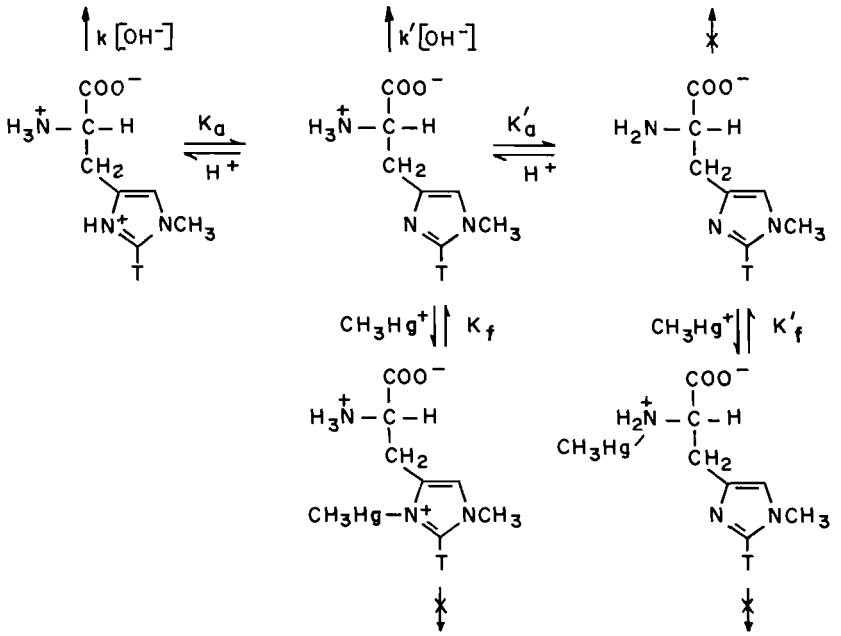
Martin and co-workers (8), on the other hand, investigated deuterium exchange at C(2) and C(8) of the series of Pt^{2+} and Pd^{2+} complexes, namely diethylenetriamineinosineplatinum(II) chloride, ethylenediaminebis(inosine)platinum(II) chloride, diethylenetriamineguanosineplatinum(II) chloride, ethylenediaminebis(guanosine)platinum(II) chloride, and bis(1-methylhistidine)palladium(II) chloride. The proton magnetic resonance method used by these workers to follow the rate of exchange allowed for the direct measurement of the loss of H(2) or H(8) intensity of the complex upon its replacement by deuterium, because the exchange between coordination sites in these compounds is slow on the NMR time scale. Hence specific second-order rate constants could be determined for the individual complexes of histidine and inosine, supporting the existence of a second, less reactive pathway, when metal ions come into play.

Expressions for the pseudo-first-order rate constant (k_{obs}) for Mechanism I and Mechanism II, eqs. [10] and [11] respectively, are derived in a similar fashion to that presented in the first section of the paper. (Detailed derivation of eqs. [10] and [11] is found in Appendices I and II.)

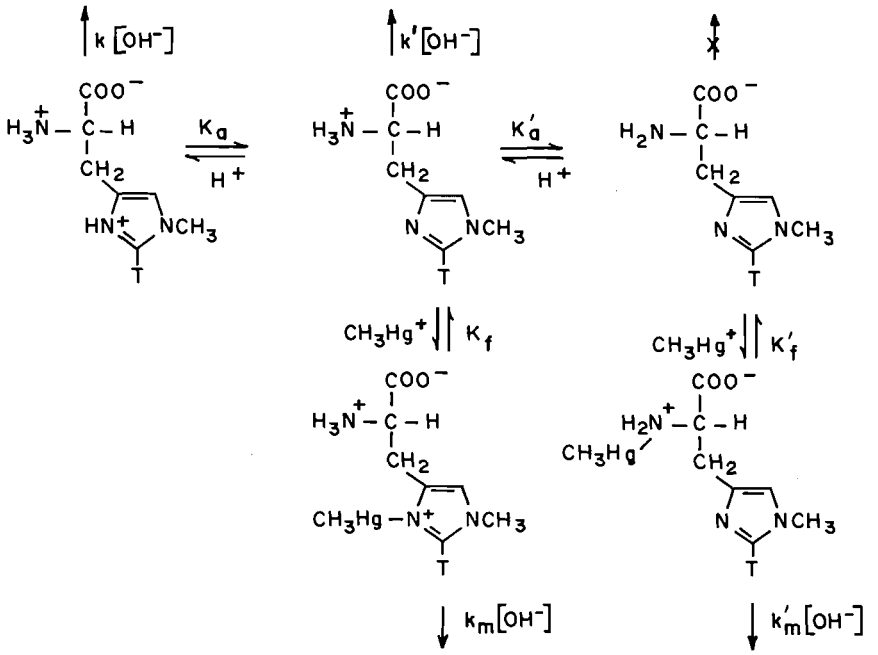
$$[10] \quad k_{obs} = \frac{kK_w[H^+] + K_aK_wk'}{[H^+]^2 + K_a[H^+] + K_aK'_a + K_aK_f[M^{n+}][H^+] + K'_fK'_aK_a[M^{n+}]}$$

$$[11] \quad k_{obs} = \frac{kK_w[H^+] + k'K_aK_w + k_mK_aK_fK_w[M^{n+}] + k'_mK_aK'_aK'_f[M^{n+}][OH^-]}{[H^+]^2 + K_a[H^+] + K_aK'_a + K_aK_f[M^{n+}][H^+] + K'_fK'_aK_a[M^{n+}]}$$

Can. J. Chem. Downloaded from www.nrcresearchpress.com by 194.225.253.170 on 09/07/12
For personal use only.



SCHEME 2. Mechanism 1: metal complexes are inactive.



SCHEME 3. Mechanism 2: metal complexes undergo detritiation.

The second-order rate constants for hydroxide ion attack on the N(3)- and amino-$MeHg^+$-coordinated 1-methyl[2-^{3}H]histidine complexes are represented by k_m and k'_m respectively, while K_f and K'_f are the formation constants for the N(3)- and amino-coordinated metal-coordinated 1-methylhistidine complexes. All other symbols are as defined in the first section of the paper.

It is noted that the expression for Mechanism I (eq. [10]) is in fact an extreme case of that for Mechanism II. More specifically, when k_m and k'_m in eq. [11] are zero, the resulting expression is eq. [10].

The experimental data in Table 3 were fitted to the expressions for k_{obs} corresponding to Mechanisms I and II respectively by means of NOTLIN, a nonlinear curvefitting program.

Results of least-squares fitting of rate data to rate expressions for Mechanisms I and II

(*a*) Varying the parameters k_m and k'_m did not give convergence. Allowing k, k', k_m, and k'_m to be zero in different combinations showed that the only important terms are those containing k and k' (i.e., setting k_m and (or) k'_m to zero gave proper convergence as judged by comparing the experimental and theoretical plots.)

(*b*) Cancellation of terms including k and (or) k' showed very poor fit or gave no convergence at all, implying that detritiation of species **4** and **5** is important in the mechanism. The term containing k, the largest second-order rate constant, is the most important. Cancellation of k_m and k'_m did not affect the fit.

Can. J. Chem. Downloaded from www.nrcresearchpress.com by 194.225.253.170 on 09/07/12
For personal use only.

TABLE 4. Comparison of second-order rate constants derived from rate data of several heterocycles

Substrate	Metal ion	k ($M^{-1}s^{-1}$)	k_m ($M^{-1}s^{-1}$)	k/k_m	$-pK_m$
1-Methylguanosine	Cu(II)	5.3×10^6	1.4×10^4	379	1.78
1-Methylinosine	Cu(II)	1.8×10^7	2.1×10^4	818	1.36
	Ag(I)	1.8×10^7	4.0×10^2	4.5×10^4	1.61
	Zn(II)	1.8×10^7	—	—	—
5′-Adenosine monophosphate	Cu(II)	8.6×10^6	8.2×10^3	1.1×10^3	1.58
3′-Adenosine monophosphate	Ag(I)	1.7×10^5	1.3×10^3	1.3×10^2	1.72
1-Methylhistidine	Pd(II)	3.2×10^3	1.3×10^{-2}	2.5×10^5	—
	MeHg(II)	1×10^4	$\leq 1\times10^{-1}$	$\geq 1\times10^3$	4.5

(*c*) Fixing k_m and k'_m to arbitrarily small values such as 10 M^{-1} s^{-1} and 0.0001 M^{-1} s^{-1}, respectively, gave convergence of k and k' to reasonable values. This seems to reemphasize that the variation in k_m and k'_m appears not to affect the observed rate. In other words, the behaviour of the lowering of the observed rate of detritiation in the presence of methylmercury nitrate, evidenced by the exponential decrease of the k_{obs} versus [$MeHg^+$] plot, is not significantly dependent on the terms containing k_m and k'_m.

(*d*) Because K_f and K'_f (determined at 25°C) were not corrected for temperature, these values were adjusted using NOTLIN assuming (*i*) k_m and $k'_m = 0$ and (*ii*) $k_m = 10\,M^{-1}\,s^{-1}$ and $k'_m = 0.0001\,M^{-1}\,s^{-1}$. The resulting values were $-pK_f \approx 4.5$ and $-pK'_f \approx 8.2$. Each value should be lower than the corresponding values at 25°C ($-pK_f = 5.91$ and $-pK'_f = 7.52$). Although the visual fit was satisfactory, the standard deviations pertaining to each value were unusually large.

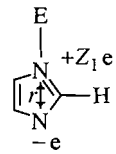
(*e*) Assuming K_f to be $10^{4.5}$ and K'_f to be $10^{8.2}$, attempts to vary the parameters k_m and k'_m gave negative values or no convergence at all.

One can conclude from the above that although the NOTLIN fitting of the rate data to rate expressions for Mechanisms I and II strongly indicates the operation of Mechanism I, the observation that small values of k_m and k'_m produce convergence with reasonable values for k and k' suggests that Mechanism II cannot be ruled out.

In a study by Martin and co-workers (8) the isotopic exchange of the 2:1 complex of 1-methylhistidine and Pd^{2+} was found to undergo hydroxide ion attack $10^{4.8}$ and $10^{5.4}$ times more slowly than the amino-protonated (**5**) and N(3)-protonated (**4**) species, respectively. In our case, also, there is every indication that C(2)-H exchange of the $MeHg^+$:1-methylhistidine complexes is slower than that of the unmetallated species. These findings are consistent and can be compared with the rate constants for attack on protonated and metal-coordinated species, i.e., k and k_m for a series of systems reported in the literature, Table 4. The relationship $k > k_m$ holds without exception; the ratio of k/k_m varies between 1.3×10^2 and 2.5×10^5.

It is interesting to note that in all cases thus far reported, rate acceleration due to metal coordination has not been observed. On electrostatic considerations one would have expected that the metal ion would mimic the effect of the proton. Both protonation and metal-ion coordination would cause the development of positive charge at the pyridine nitrogen adjacent to the site of hydroxide ion attack. This hypothesis is put in doubt, however, by the observation that addition of metal ion causes a decrease in the pseudo-first-order rate constant.

It is proposed that the disparity in behaviour between the protonated and the metal-coordinated species is a result of the difference in the magnitude of the positive charge on the heteroatom adjacent to the exchange site. Norris, Buncel, and Taylor (24) have treated the model imidazole system **8** in simple



8

electrostatic terms and found that the fractional positive charge residing on N(3) of the imidazole ring could be related to ΔpK_a (difference in pK_a for N(1)-H ionization in the absence of M^{n+} and in the presence of M^{n+}), the effective microscopic permittivity, D_{eff}, and the distance between the charged centres in Å (r^0) in the following way:

$$[12] \quad Z_1 = \frac{\Delta pK_a D_{eff} r^0}{241.7}$$

Using 1-methylimidazolium ion as a standard, and assuming that unit positive charge resides on N(3) of the 1-methylimidazolium ion, eq. [12] reduces to

$$[13] \quad Z_1 = \Delta pK_a/7.1$$

A plot of the C(2) chemical shift as a function of Z_1 for the series where E is Me^+, $Co(NH_3)_5^{3+}$, and no substituent, respectively, shows that the chemical shift at C(2) increases as the charge Z_1 increases, which indicates that the greater the positive charge at N(3), the more labile the C(2) hydrogen. The fractional charge of N(3) in the metal complexes is much lower than with H^+ and Me^+ and hence, according to the above argument, the rate of exchange should also be lower.

Lavallee *et al.* (25) have used ^1H chemical shift differences in heterocycles to indicate the change in charge density effected by metal complexation. These studies showed a decrease in electron density in the complexed heterocycle in the order $H^+ >$ Co(III) > Rh(II). These results are consistent with the model presented above and support our hypothesis of a causal relationship between the magnitude of charge developed on the heteroatom adjacent to the exchange site (C2) by M^{n+} vs. H^+, and the effectiveness of M^{n+} and H^+ in catalysis of proton exchange at C(2).

Can. J. Chem. Downloaded from www.nrcresearchpress.com by 194.225.253.170 on 09/07/12
For personal use only.

Can. J. Chem. Downloaded from www.nrcresearchpress.com by 194.225.253.170 on 09/07/12
For personal use only.

Conclusions

The plot of k_{obs} vs. pH for the detritiation of 1-methyl[2-^{3}H]-histidine resulted in a sigmoidal profile characteristic of substrates possessing two ionizable functionalities. Kinetic analysis of the data yielded second-order rate constants $k = (1.00 \pm 0.05) \times 10^{-4}$ M^{-1} s^{-1} for hydroxide attack on the N(3)-protonated species **4**, and $k' = (1.05 \pm 0.20) \times 10^2$ M^{-1} s^{-1} as a composite rate constant for attack on the zwitterionic species **5** and **7**. Comparison of k and k' with the corresponding rate constants for histidine, imidazole, and benzimidazole and their 1-methyl derivatives demonstrated some interesting relationships; (1) N(1)-methylation results in a 2- to 3-fold increase in k and a 2-fold increase in k'; (2) benzo annelation results in a 10- or 20-fold increase in k; (3) substitution of a positively charged side chain has virtually no effect on k. The observed reactivity differences could be explained by application of FMO–PMO theory to the proton transfer reaction scheme. Furthermore, it was found that detritiation of 1-methyl[2-^{3}H]histidine is inhibited by the addition of $MeHgNO_3$. The value of the rate constant decreased with increasing metal-ion concentration; the ratio of k_{obs} at $[M^{n+}] = 0$ and $[M^{n+}] = 0.007$ M was 26. A nonlinear least-squares fitting pointed to very small values for k_m and k'_m, consistent with reports on the effects of metal ions in related heterocyclic systems. The large difference in the effectiveness of the proton and the metal ion in promoting C(2)-H exchange has been attributed to the greater ability of the proton to transfer positive charge to the heteroatom adjacent to the exchange site as compared to the metal ion ($MeHg^+$).

Acknowledgements

Financial support of this research by the Natural Sciences and Engineering Research Council of Canada and the Ontario Ministry of Education (Ontario–Quebec Exchange Program) is gratefully acknowledged. Thanks are also due to Professor R. Y. Moir for assistance with computational aspects of the work, S. Hoz and S. S. Shaik for discussion of FMO aspects, and R. L. Benoit for hospitality at the University of Montreal and discussion.

1. C. A. Matuszak and A. J. Matuszak. J. Chem. Educ. **53**, 281 (1976).
2. A. E. Martell and R. M. Smith (*Editors*). Critical stability constants. Plenum, New York. 1982.
3. E. Buncel, H. A. Joly, and J. R. Jones. Can. J. Chem. **64**, 1240 (1986).
4. A. E. G. Cass, H. A. O. Hill, J. V. Bannister, W. H. Bannister, V. Hasemann, and J. T. Johansen. Biochem. J. **183**, 127 (1979).
5. G. S. Baldwin, S. G. Waley, and E. P. Abraham. Biochem. J. **179**, 459 (1979).
6. R. A. Olofson, W. R. Thompson, and J. S. Michelman. J. Am. Chem. Soc. **86**, 1865 (1964).
7. D. H. Buisson, J. R. Jones, and S. E. Taylor. J. Chem. Soc. Chem. Commun. 856 (1975).
8. B. Noszal, V. Scheller-Krattiger, and R. B. Martin. J. Am. Chem. Soc. **104**, 1078 (1982).
9. J. R. Jones and S. E. Taylor. J. Chem. Soc. Perkin Trans. 2, 1773 (1979).
10. J. R. Jones and S. E. Taylor. Chem. Soc. Rev. 329 (1981).
11. C. A. Evans, D. L. Rabenstein, G. Geier, and I. W. Erni. J. Am. Chem. Soc. **99**, 8106 (1977).
12. (*a*) E. Buncel, A. R. Norris, W. J. Racz, and S. E. Taylor. Inorg. Chem. **20**, 98 (1981); (*b*) E. Buncel, B. K. Hunter, R. Kumar, and A. R. Norris. J. Inorg. Biochem. **20**, 171 (1984).
13. (*a*) A. Noordam, L. Maat, and H. C. Beyerman. Recl. Trav. Chim. Pays-Bas, **97**, 293 (1978); (*b*) N. Nishizawa, T. Noguchi, S. Hareyama, and R. Funabiki. J. Chromatogr. **151**, 424 (1978).
14. L. W. Reeves, M. Suzuki, and J. A. Vanin. Inorg. Chem. **15**, 1035 (1976).
15. J. A. Elvidge, J. R. Jones, C. O'Brien, E. A. Evans, and H. C. Sheppard. J. Chem. Soc. Perkin Trans. 2, 174 (1974).
16. M. Tomasz, J. Olson, and C. M. Mercado. Biochemistry, **11**, 1235 (1972).
17. J. A. Elvidge, J. R. Jones, C. O'Brien, E. A. Evans, and J. C. Turner. J. Chem. Soc. Perkin Trans. 2, 432 (1973).
18. M. Maeda, M. Saneyoshi, and Y. Kawazoe. Chem. Pharm. Bull. **19**, 1641 (1971).
19. J. A. Elvidge, J. R. Jones, R. Salih, M. Shandala, and S. E. Taylor. J. Chem. Soc. Perkin Trans. 2, 447 (1980).
20. J. H. Bradbury, B. E. Chapman, and F. A. Pellegrino. J. Am. Chem. Soc. **95**, 6139 (1973).
21. J. A. Elvidge, J. R. Jones, R. Salih, M. Shandala, and S. E. Taylor. J. Chem. Res. (M), 2373 (1980).
22. R. J. Sundberg and R. B. Martin. Chem. Rev. **74**, 471 (1974).
23. A. Streitwieser. Molecular orbital theory for organic chemists. Wiley, New York. 1961.
24. A. R. Norris, E. Buncel, and S. E. Taylor. J. Inorg. Biochem. **16**, 279 (1982).
25. (*a*) D. K. Lavallee, M. D. Baughman, and M. P. Phillips. J. Am. Chem. Soc. **99**, 718 (1977); (*b*) D. K. Lavalee and E. B. Fleisher. J. Am. Chem. Soc. **94**, 2583 (1972).
26. E. Buncel, C. Boone, and H. Joly. Inorg. Chim. Acta, **125**, 167 (1986).

Appendix I

Derivation of the rate expression for Mechanism I

The rate expression for the competitive process shown in Scheme 2 is

$$[14] \quad \text{Rate} = \frac{-\mathrm{d}[2\text{-THis}_t]}{\mathrm{d}t} = k[2\text{-THisH}_2^+][OH^-] + k'[2\text{-THisH}][OH^-]$$

where [2-THis$_t$], [2-THisH$_2^+$], and [2-THisH] represent the total concentration of 1-methyl[2-^{3}H]histidine-containing species and the concentration of the N(3)-protonated and the amino-protonated form of the substrate, respectively; k and k' are the second-order rate constants for hydroxide ion attack on 2-THisH$_2^+$ and 2-THisH.

Expressions can be derived for [2-THisH$_2^+$] and [2-THisH] in terms of experimentally measurable quantities by using the mass law equation (eq. [15])

$$[15] \quad [2\text{-THis}_t] = [2\text{-THisH}_2^+] + [2\text{-THisH}] + [2\text{-THis}^-] + [2\text{-THisM}^+] + [2\text{-TMHis}]$$

in conjunction with expressions for the dissociation constants K_a and K'_a and the formation constants K_f and K'_f (eqs. [16]–[19]). 2-THis$^-$, 2-THisM$^+$, and 2-TMHis represent the neutral substrate, the N(3) $MeHg^+$-coordinated, and the amino-$MeHg^+$-coordinated forms of 1-methyl[2-^{3}H]histidine.

$$[16] \quad K_a = \frac{[2\text{-THisH}][H^+]}{[2\text{-THisH}_2^+]}$$

$$[17] \quad K'_a = \frac{[2\text{-THis}^-][H^+]}{[2\text{-THisH}]}$$

$$[18]\quad K_f = \frac{[\text{2-THisM}^+]}{[\text{2-THisH}][M^{n+}]}$$

$$[19]\quad K'_f = \frac{[\text{2-TMHis}]}{[\text{2-THis}^-][M^{n+}]}$$

More specifically, one uses the equations for the acidity constants and the formation constants to obtain expressions for [2-THis$^-$], [2-THisM$^+$], and [2-TMHis], first in terms of [2-THisH$_2^+$] and then in terms of [2-THisH]. Substitution into eq. [15] leads to eqs. [20] and [21] respectively.

$$[20]\quad [\text{2-THisH}_2^+] = \frac{[\text{2-THis}_t][H^+]^2}{[H^+]^2 + K_a[H^+] + K_aK'_a + K_aK_f[M^{n+}][H^+] + K'_fK_aK'_a[M^{n+}]}$$

$$[21]\quad [\text{2-THisH}] = \frac{K_a[\text{2-THis}_t][H^+]}{[H^+]^2 + K_a[H^+] + K_aK'_a + K_aK_f[M^{n+}][H^+] + K'_fK_aK'_a[M^{n+}]}$$

The rate expression for Mechanism I becomes

$$[22]\quad \text{Rate} = \frac{-d[\text{2-THis}_t]}{dt} = \frac{kK_w[H^+][\text{2-THis}_t] + k'K_aK_w[\text{2-THis}_t]}{[H^+]^2 + K_a[H^+] + K_aK'_a + K_aK_f[M^{n+}][H^+] + K'_fK_aK'_a[M^{n+}]}$$

where $K_w = [H^+][OH^-]$. Integration of eq. [22] results in the following expression for the pseudo-first-order rate constant (k_{obs}):

$$[10]\quad k_{obs} = \frac{kK_w[H^+] + K_aK_wk'}{[H^+]^2 + K_a[H^+] + K_aK'_a + K_aK_f[M^{n+}][H^+] + K'_fK_aK'_a[M^{n+}]}$$

Appendix II

Derivation of the rate expression for Mechanism II

In Mechanism II, terms must be included in the rate expression for the pathways involving hydroxide ion attack on the N(3) and amino-MeHg$^+$-coordinated 1-methyl[2-^{3}H]histidine complexes, respectively (2-THisM$^+$ and 2-TMHis). Hence the rate expression for Mechanism II is

$$[23]\quad \text{Rate} = \frac{-d[\text{2-THis}_t]}{dt} = k[\text{2-THisH}_2^+][OH^-] + k'[\text{2-THisH}][OH^-] + k_m[\text{2-THisM}^+][OH^-] + k'_m[\text{2-TMHis}][OH^-]$$

k_m and k'_m are the second-order rate constants for hydroxide ion attack on 2-THisM$^+$ and 2-TMHis respectively.

In a fashion similar to that outlined in Appendix I, expressions can be obtained for [2-THisH$_2^+$], [2-THisH], [2-THisM$^+$], and [2-TMHis] by using the mass law equation and expressions for the dissociation constants K_a and K'_a and the formation constants K_f and K'_f. Hence:

$$[20]\quad [\text{2-THisH}_2^+] = \frac{[\text{2-THis}_t][H^+]^2}{[H^+]^2 + K_a[H^+] + K_aK'_a + K_aK_f[M^{n+}][H^+] + K_aK'_aK'_f[M^{n+}]}$$

$$[21]\quad [\text{2-THisH}] = \frac{K_a[\text{2-THis}_t][H^+]}{[H^+]^2 + K_a[H^+] + K_aK'_a + K_aK_f[M^{n+}][H^+] + K_aK'_aK'_f[M^{n+}]}$$

$$[24]\quad [\text{2-THisM}^+] = \frac{K_aK_f[M^{n+}][H^+][\text{2-THis}_t]}{[H^+]^2 + K_a[H^+] + K_aK'_a + K_aK_f[M^{n+}][H^+] + K_aK'_aK'_f[M^{n+}]}$$

$$[25]\quad [\text{2-TMHis}] = \frac{K_aK'_aK'_f[M^{n+}][\text{2-THis}_t]}{[H^+]^2 + K_a[H^+] + K_aK'_a + K_aK_f[M^{n+}][H^+] + K_aK'_aK'_f[M^{n+}]}$$

Substitution of eqs. [20], [21], [24], and [25] into eq. [23] yields the following rate expression:

$$[26]\quad \text{Rate} = \frac{-d[\text{2-THis}_t]}{dt} = \frac{[\text{2-THis}_t](kK_w[H^+] + k'K_aK_w + k_mK_aK_fK_w[M^{n+}] + k'_mK_aK'_aK'_f[M^{n+}][OH^-])}{[H^+]^2 + K_a[H^+] + K_aK'_a + K_aK_f[M^{n+}][H^+] + K'_fK_aK'_a[M^{n+}]}$$

The expression for the pseudo-first-order rate constant obtained from integration of eq. [26] is

$$[11]\quad k_{obs} = \frac{kK_w[H^+] + k'K_aK_w + k_mK_aK_fK_w[M^{n+}] + k'_mK_aK'_aK'_f[M^{n+}][OH^-]}{[H^+]^2 + K_a[H^+] + K_aK'_a + K_aK_f[M^{n+}][H^+] + K_aK'_aK'_f[M^{n+}]}$$

Can. J. Chem. Downloaded from www.nrcresearchpress.com by 194.225.253.170 on 09/07/12
For personal use only.

Metal ion catalysis in nucleophilic displacement reactions at carbon, phosphorus, and sulfur centers.[1] I. Catalysis by metal ions in the reaction of *p*-nitrophenyl diphenylphosphinate with ethoxide

EDWARD J. DUNN AND ERWIN BUNCEL[2]

Department of Chemistry, Queen's University, Kingston, Ont., Canada K7L 3N6

Received December 1, 1988

EDWARD J. DUNN and ERWIN BUNCEL. Can. J. Chem. **67**, 1440 (1989).

The effect of macrocyclic crown ether and cryptand complexing agents on the rate of the nucleophilic displacement reaction of *p*-nitrophenyl diphenylphosphinate by alkali metal ethoxides in ethanol at 25°C has been studied by spectrophotometric techniques. For the reactions of potassium ethoxide, sodium ethoxide, and lithium ethoxide, the observed rate constant increased in the order KOEt < NaOEt < LiOEt. Crown ether and cryptand cation-complexing agents have a retarding effect on the rate. Increasing the ratio of complexing agent to base results in a decrease in k_{obs} to a minimum value corresponding to the rate of reaction of free ethoxide ion. In complementary experiments, alkali metal ions were added to these reaction systems in the form of unreactive salts, causing an increase in reaction rate. The kinetic data were analysed in terms of ion-pairing treatments, which allowed evaluation of rate coefficients due to free ethoxide ions and metal ion – ethoxide ion pairs. Possible roles of the metal cations are discussed in terms of ground state and transition state stabilization. Evaluation of the equilibrium constants for association of the metal ion with ground state (K_a) and the transition state (K'_a) shows that catalysis occurs as a result of enhanced association between the metal ion and the transition state, with K'_a values increasing in the order $K^+ < Na^+ < Li^+$. A model is proposed in which transition state stabilization arises largely from chelation of the solvated metal ion to two charged oxygen centers. This appears to be the first reported instance of catalysis by alkali metal cations in nucleophilic displacement at phosphoryl centers.

Key words: nucleophilic displacement at phosphorus, alkali-metal-ion catalysis.

EDWARD J. DUNN et ERWIN BUNCEL. Can. J. Chem. **67**, 1440 (1989).

Faisant appel à des techniques spectroscopiques, on a étudié l'effet d'un éther couronne macrocyclique et des agents complexants de type cryptand sur la vitesse de la réaction de déplacement nucléophyle du diphénylphosphinate de *p*-nitrophényle par des éthanolates de métal alcalin dans l'éthanol à 25°C. Pour les réactions impliquant les éthanolates de potassium, de sodium et de litium, les constantes de vitesse observées augmentent dans l'ordre suivant : KOEt < NaOEt < LiOEt. L'éther couronne et les agents complexants de type cation cryptand on un effet retardateur sur la vitesse. Une augmentation de l'agent complexant dans la base conduit à une diminution de la valeur de k_{obs} jusqu'à une valeur minimium correspondant à la vitesse de réaction de l'ion éthanolate libre. Dans des expériences complémentaires, on a ajouté des ions de métal alcalin, sous forme de sels non réactifs, au milieu réactionnel provoquant ainsi une augmentation de la vitesse. On a analysé les données cinétiques en fonction du traitement des paires d'ions qui permet d'évaluer les coefficients de vitesse dus aux ions éthanolates libres et aux paires d'ions métal–éthanolate. On discute du rôle possible des cations métalliques en fonction de la stabilisation de l'état fondamental et de l'état de transition de l'ion métallique avec l'état fondamental (K_a) et avec l'état de transition (K'_a) montre qu'il se produit une catalyse en raison d'une association accrue entre l'ion métallique et l'état de transition, avec des valeurs de (K'_a) qui augmentatent dans l'ordre suivant : $K^+ < Na^+ < Li^+$. On propose un modèle dans lequel la stabilisation de l'état de transition provient surtout de la chélation de l'ion métallique solvaté jusqu'à deux centres d'oxygène chargés. Il semble que ce soit la première publication concernant la catalyse par des cations métalliques dans des réactions de déplacement nucléophyle au niveau des centres phosphoryles.

Mots clés : déplacement nucléophyle à phosphore, catalyse des ions de métal alcalin.

[Traduit par la revue]

Introduction

A great deal of research has been conducted into the role that metal ions play in the mechanism of phosphoryl transfer reactions (2), due to their importance in biological processes (3). Most of the attention has been directed towards studying the catalytic effects of divalent metal ions such as Mg^{2+}, Ca^{2+}, Mn^{2+}, Fe^{2+}, Co^{2+}, Cu^{2+}, and Zn^{2+} in the hydrolysis of phosphate esters (4), though phosphonate esters have also received attention (5). However, phosphinate esters have not been examined in this respect.

Despite the ubiquitous presence of alkali metals in biological systems, intensive investigations of catalysis by these monovalent ions have only rarely been undertaken. We have initiated systematic studies of the influence of alkali metal ions in nucleophilic displacement reactions at carbon, phosphorus, and sulfur centres. In the present paper we report our detailed results on the influence of alkali metal ions on nucleophilic displacement in phosphinate esters, which, unexpectedly, have revealed a marked catalytic effect; moreover, catalysis is strongly dependent on the nature of the alkali metal cation (6).

Results

Reactions of LiOEt, NaOEt, and KOEt

The rate of the reaction of *p*-nitrophenyl diphenylphosphinate (**1**) with lithium ethoxide, sodium ethoxide, and potassium ethoxide in ethanol at 25°C was studied spectrophotometrically by following the appearance of the absorption due to *p*-nitrophenoxide ion. Plots of log ($A_\infty - A_t$) vs. t were linear for over 90% reaction.

The dependence of the observed pseudo-first-order rate constants (k_{obs}) on the concentration of alkali metal ethoxide ([MOEt]) (Table 1) indicates that LiOEt is more reactive towards **1** than is NaOEt, over a large range of base concentrations. Similarly, it can be seen from Fig. 1 (Table 1) that NaOEt

[1]This paper is an extension of our series on Bond Scission in Sulfur Compounds. For previous papers in this series see ref. 1.

[2] Author to whom correspondence may be addressed.

Can. J. Chem. Downloaded from www.nrcresearchpress.com by 194.225.253.170 on 09/07/12
For personal use only.

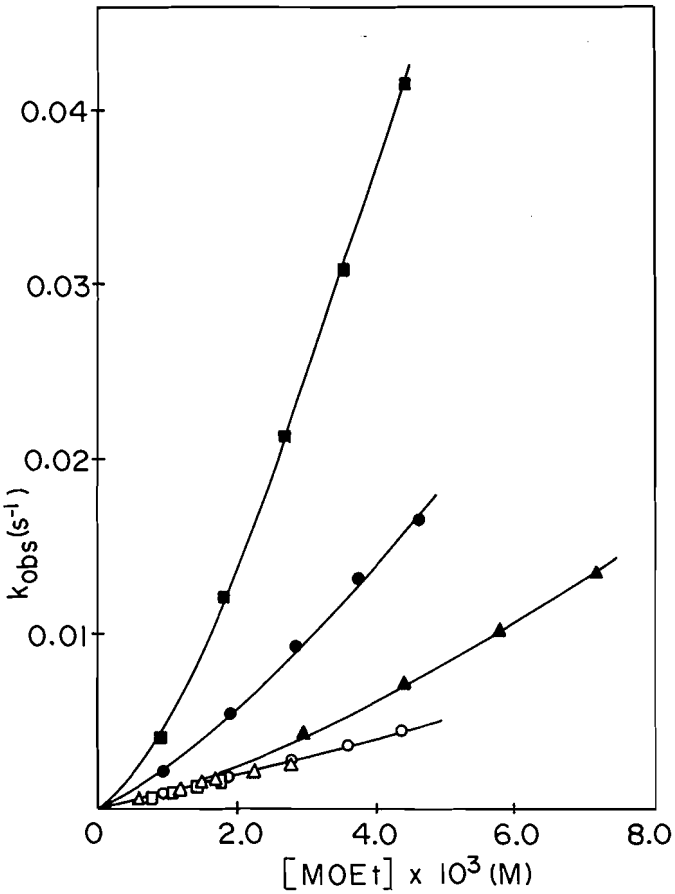


FIG. 1. Reaction of *p*-nitrophenyl diphenylphosphinate (**1**) with LiOEt (■), NaOEt (●), KOEt (▲); LiOEt plus excess [2.1.1]cryptand (□); NaOEt plus excess [2.2.2]cryptand (○); and with KOEt plus excess [2.2.2]cryptand (△), in EtOH at 25°C.

TABLE 1. Pseudo-first-order rate constants (k_{obs}) for the reaction of **1** with LiOEt, NaOEt, and KOEt in EtOH at 25°C

LiOEt + **1**		NaOEt + **1**		KOEt + **1**	
$LiOEt]_0$ (M)	k_{obs} (s^{-1})	$[NaOEt]_0$ (M)	k_{obs} (s^{-1})	$[KOEt]_0$ (M)	k_{obs} (s^{-1})
0.000916	0.004107	0.000964	0.002163	0.001492	0.001440
0.001815	0.01213	0.001909	0.005385	0.002954	0.004193
0.002697	0.02132	0.002836	0.009282	0.004388	0.007012
0.003560	0.03085	0.003746	0.01324	0.005795	0.01006
0.004408	0.04149	0.004638	0.01647	0.007175	0.01341
0.01945	0.2716	0.01431	0.07080	0.01189	0.02750
0.02917	0.4336	0.02862	0.1514	0.02387	0.05919
0.03889	0.6090	0.04293	0.2107	0.03567	0.1036
0.04862	0.7796	0.05724	0.2592	0.04756	0.1684
0.05834	0.9974	0.07155	0.3616	0.05945	0.2143
0.07778	1.338	0.08586	0.4226		
0.09723	1.733	0.1145	0.5922		
0.1458	2.753	0.1431	0.8030		
0.1945	4.000	0.2146	1.235		
0.2431	5.034	0.2862	1.825		
0.2907	6.320	0.3578	2.761		
0.3392	7.613				
0.3876	9.614				
0.4361	10.81				
0.4846	12.63				

TABLE 2. Pseudo-first-order rate constants for the reaction of **1** with LiOEt, NaOEt, and KOEt in the presence of excess complexing agent

Reaction system	10^3 $[Base]_0$ (M)	[Complexing agent] / $[Base]_0$	10^3 k_{obs} (s^{-1})
KOEt + DC18C6	0.588	10.7	0.454
	1.161	10.7	1.038
	1.717	10.7	1.501
	2.263	10.7	2.035
	2.795	10.7	2.543
KOEt + [2.2.2]	0.586	10.5	0.455
	1.156	10.5	0.981
	1.709	10.5	1.496
	2.247	10.5	1.980
	2.770	10.5	2.468
NaOEt + DC18C6	0.959	5.36	0.832
	1.891	5.36	1.798
	2.796	5.36	2.669
	3.675	5.36	3.613
	4.531	5.36	4.494
NaOEt + [2.2.2]	0.955	5.42	0.868
	1.873	5.42	1.808
	2.767	5.42	2.742
	3.608	5.42	3.642
	4.428	5.42	4.490
LiOEt + [2.1.1]	0.746	9.80	0.623
	1.104	9.80	0.974
	1.451	9.80	1.312
	1.788	9.80	1.638

is, in turn, more reactive towards **1** than is KOEt. A particularly striking feature of the plots of k_{obs} vs. [MOEt] (Fig. 1) is the upward curvature displayed in the LiOEt, NaOEt, and KOEt systems, indicating a disproportional increase in rate as the concentration of base is increased.

Effect of complexing agents

Reactions of **1** with LiOEt, NaOEt, and KOEt in the presence of excess complexing agent were carried out and the results are given in Table 2 and plotted in Fig. 1 for the lower MOEt concentration range. It can be seen from Fig. 1 that these data fall on the same plot, within experimental error, and that the plot is essentially linear.

Further experiments were performed under varying concentrations of added macrocyclic crown ether and cryptand to base. The effect of adding complexing agent to the reaction of LiOEt and NaOEt with **1** is shown in Fig. 2 (Table 3). Increasing the concentration of complexing agent at a constant base concentration causes a marked decrease in rate until a minimum value is reached, following which addition of more complexing agent no longer has any effect. The minimum value attained is similar for each system and is therefore assumed to correspond to the rate constant for the reaction of free ethoxide ion (k_{EtO^-}), since at the concentrations of crown ethers and cryptands employed the metal ions should be completely complexed. It is apparent from Fig. 2 that the [2.2.2]cryptand is more effective at complexing sodium ion than the macrocyclic ether dicyclohexyl-18-crown-6 (DC18C6), since the minimum rate is reached at a smaller relative concentration of complexing agent.

Effect of metal salts

Since the alkali metal ion apparently plays a significant

Can. J. Chem. Downloaded from www.nrcresearchpress.com by 194.225.253.170 on 09/07/12
For personal use only.

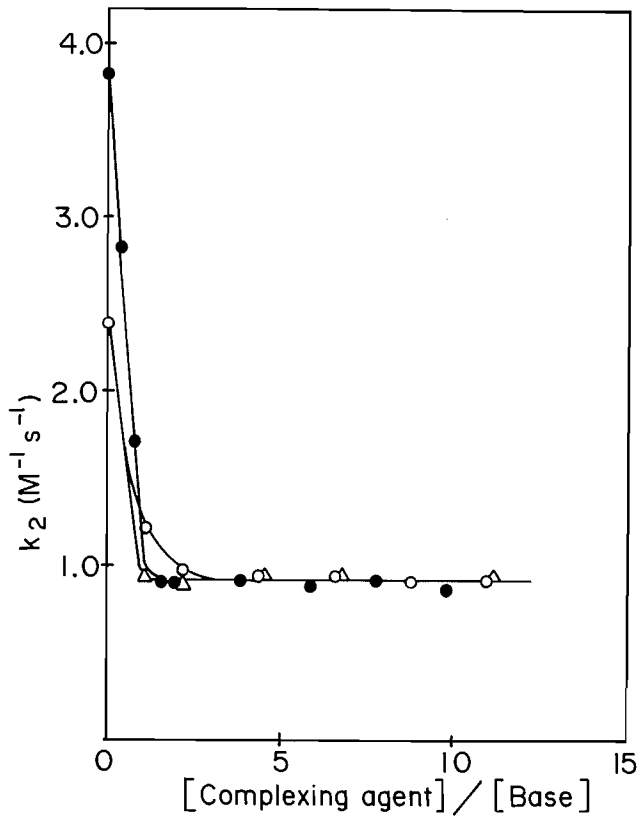


FIG. 2. Effect of added [2.1.1]cryptand on the reaction of **1** with LiOEt (●); effect of added DC18-crown-6 (○) and [2.2.2]cryptand (△) on the reaction of **1** with NaOEt, in EtOH.

catalytic role in this reaction, it was anticipated that addition of metal ion, in the form of an unreactive salt, should produce an increase in reaction rate. Such an increase was in fact observed (Fig. 3) when KSCN and KOAc were added to the KOEt reaction system (Table 4), and when LiSCN, LiOAc, $LiNO_3$, and $LiClO_4$ were added to the LiOEt reaction system (Table 5). As the concentration of metal ion was increased, the rate increased until a plateau was reached; after the initial increase, the rate either leveled off or began to decrease. Since the reactions with added metal ions do not reach a common level, and because of the complexity of possible anionic effects, it is difficult to account quantitatively for these specific salt effects. However, the maximum second-order rate constant attained for the reaction of **1** with LiOEt in the presence of added Li^+ ions was 17.5 M^{-1} s^{-1}. When K^+ ions were added to the reaction with KOEt the maximum rate constant observed was 3.76 M^{-1} s^{-1}. These results clearly demonstrate that the addition of metal ions has a catalytic effect on the reactions.

Discussion

The observed rate behaviour for the reaction of **1** with LiOEt, NaOEt, and KOEt alone (Fig. 1), coupled with the decrease in rate with added complexing agent (Fig. 2), and the increase in rate with added metal ion (Fig. 3), indicate a mechanism in which nucleophilic displacement of **1** by ethoxide is catalysed by the alkali metal cations.

The role that the metal ions play in bringing about the rate enhancement is of interest in this specific system and in general, and the ensuing discussion considers different pathways for metal ion involvement. Association of the metal ion with both ground state and transition state must be considered. As well,

TABLE 3. Kinetic data on the effect of adding complexing agents to the reaction of **1** with LiOEt and NaOEt in EtOH at 25°C

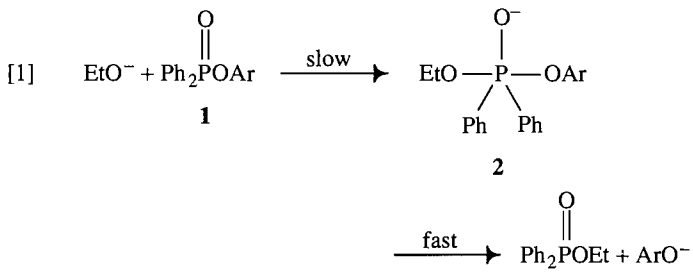
Reaction system	$[Base]_0$ 10^3 (M)	[Complexing agent] / $[Base]_0$	k_{obs} 10^3 (s^{-1})	k_2[a] (M^{-1} s^{-1})
NaOEt + DC18C6	1.237	0.00	3.003	2.428
	1.231	1.10	1.493	1.213
	1.225	2.21	1.186	0.968
	1.213	4.42	1.141	0.940
	1.202	6.62	1.132	0.942
	1.190	8.83	1.080	0.908
	1.179	11.0	1.075	0.911
NaOEt + [2.2.2]	1.231	1.11	1.148	0.932
	1.225	2.23	1.078	0.880
	1.213	4.47	1.146	0.945
	1.202	6.69	1.130	0.940
	1.179	11.2	1.095	0.929
LiOEt + [2.1.1]	0.938	0.00	3.642	3.880
	0.933	0.39	2.632	2.821
	0.929	0.78	1.580	1.701
	0.920	1.57	0.8297	0.9018
	0.915	1.96	0.8244	0.9010
	0.894	3.91	0.8169	0.9138
	0.874	5.87	0.7688	0.8796
	0.855	7.83	0.7661	0.8960
	0.836	9.79	0.7187	0.8597

[a]The second-order rate coefficient, $k_2 = k_{obs}/[Base]_0$.

one must consider whether only the free (dissociated) metal and alkoxide ions are involved in the reaction, or whether alkali metal – ethoxide ion pairs are the effective catalytic species, or if an intermediate situation exists.

1. Pathways for metal-ion involvement

First, we define the uncatalysed process, i.e., without the involvement of metal ions; this will occur when excess crown ether or cryptand complexing agent is present to complex the cation. Thus, one can depict the basic reaction of the substrate with ethoxide as proceeding by rate-determining attack of the free nucleophile at the phosphorus centre of **1** to form a pentacoordinate intermediate, **2**, followed by expulsion of the leaving group in a subsequent fast step (eq. [1]):



The rate equation for the reaction can be described by eq. [2], where S denotes the substrate:

[2] Rate = $k_{EtO^-}[EtO^-][S]$

The involvement of metal ions in the reaction can occur in various ways and these have to be examined in order to account for the observed catalysis. We consider below two possibilities: (1) the free (dissociated) M^+ is complexed with the substrate in a rapid preequilibrium, and (2) reaction occurs via the metal–alkoxide ion pairs.

Can. J. Chem. Downloaded from www.nrcresearchpress.com by 194.225.253.170 on 09/07/12
For personal use only.

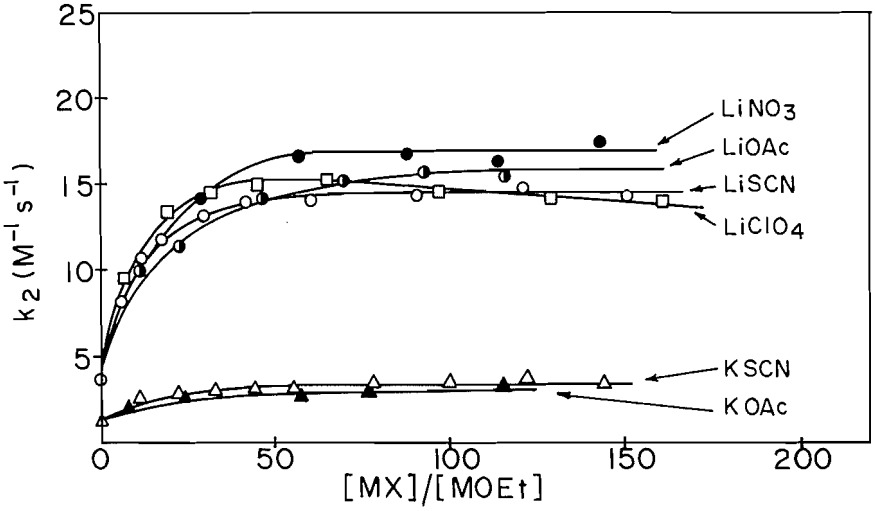


FIG. 3. Effect of added $LiNO_3$ (●), LiOAc (◑), LiSCN (○), and $LiClO_4$ (□) on the reaction of **1** with LiOEt; effect of added KSCN (△) and KOAc (▲) on the reaction of **1** with KOEt, in EtOH.

TABLE 4. Kinetic data on the effect of adding potassium metal salts (KX) to the reaction of **1** with KOEt in EtOH

Reaction system	$[KOEt]_0$ 10^3 (M)	$\frac{[KX]}{[KOEt]_0}$	k_{obs} 10^3 (s^{-1})	k_2[a] (M^{-1} s^{-1})
KOEt + KSCN	1.327	0.00	1.708	1.287
	1.265	11.1	3.238	2.560
	1.208	22.2	3.413	2.825
	1.156	33.3	3.562	3.081
	1.109	44.4	3.511	3.166
	1.065	55.5	3.493	3.280
	1.327	77.7	4.713	3.552
	1.327	99.9	4.737	3.570
	1.265	122.1	4.752	3.757
	1.327	144.3	4.582	3.453
KOEt + KOAc	1.314	7.66	2.619	1.993
	1.289	23.0	3.334	2.587
	1.236	57.4	3.378	2.733
	1.208	76.6	3.583	2.966
	1.156	115.0	3.886	3.362

[a]The second-order rate coefficient, $k_2 = k_{obs}/[KOEt]_0$.

TABLE 5. Kinetic data on the effect of adding lithium metal salts (LiX) to the reaction of **1** with LiOEt in EtOH

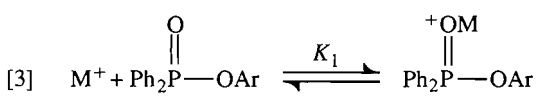
Reaction system	$[LiOEt]_0$ 10^3 (M)	$\frac{[LiX]}{[LiOEt]_0}$	k_{obs} 10^3 (s^{-1})	k_2[a] (M^{-1} s^{-1})
LiOEt + LiSCN	0.914	0.00	3.370	3.69
	0.910	6.05	7.459	8.20
	0.905	12.1	9.712	10.7
	0.901	18.2	10.60	11.8
	0.892	30.3	11.82	13.2
	0.884	42.4	12.28	13.9
	0.872	60.5	12.29	14.1
	0.852	90.8	12.25	14.4
	0.833	121.1	12.34	14.8
	0.815	151.4	11.72	14.4
LiOEt + LiOAc	0.872	11.6	8.647	9.92
	0.833	23.2	9.522	11.4
	0.914	46.5	12.98	14.2
	0.914	69.7	13.93	15.2
	0.914	92.9	14.37	15.7
	0.914	116.2	14.15	15.5
LiOEt + $LiClO_4$	0.910	6.46	8.634	9.49
	0.901	19.4	12.10	13.4
	0.892	32.3	12.96	14.5
	0.884	45.2	13.23	15.0
	0.872	64.6	13.30	15.3
	0.852	96.9	12.47	14.6
	0.833	129.1	11.94	14.3
	0.815	161.4	11.48	14.1
LiOEt + $LiNO_3$	0.892	28.6	12.71	14.2
	0.872	57.2	14.53	16.7
	0.833	114.4	13.68	16.4
	0.815	143.0	14.23	17.5

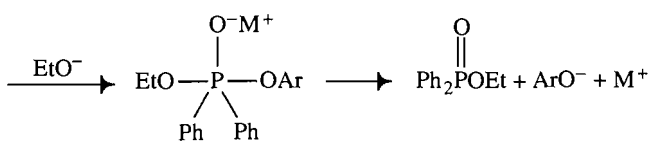
[a]The second-order rate coefficient, $k_2 = k_{obs}/[LiOEt]_0$.

(a) Pre-association of M^+ with substrate

Two possible sites for coordination of the metal cation can be considered:

(*i*) Coordination of the metal ion could occur at the phosphoryl oxygen, i.e.,



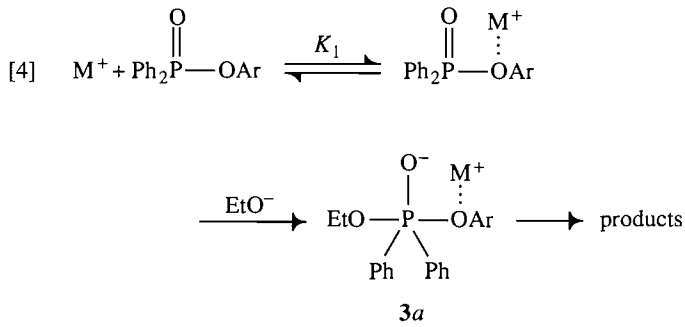


3

Coordination of M^+ at P = O will have the effect of increasing the electrophilicity of the phosphorus atom, thereby facilitating attack by the nucleophile at P.

(*ii*) Complexation of the metal ion could also occur with the oxygen of the leaving group, i.e.,

Can. J. Chem. Downloaded from www.nrcresearchpress.com by 194.225.253.170 on 09/07/12
For personal use only.



3*a*

The metal ion would thus act as an electrophilic catalyst in facilitating expulsion of the leaving group. This could be important if cleavage of the P—OAr bond is involved in the rate-determining step.

The rate equation *for both of these cases* will assume the form of [5], and eqs. [6] and [7] then follow:

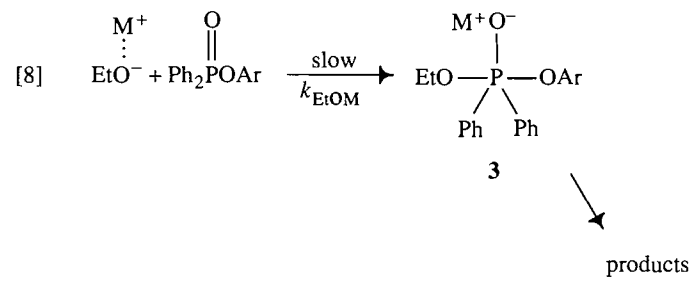
$$[5] \quad \text{Rate} = k_2[EtO^-][SM^+]$$

$$[6] \quad K_1 = \frac{[SM^+]}{[S][M^+]}$$

$$[7] \quad \text{Rate} = k_2K_1[EtO^-][M^+][S]$$

(b) Reaction via metal–alkoxide ion pairs

In this pathway, attack by the metal–alkoxide ion pair occurs in a concerted fashion to give rise to the pentacoordinate intermediate associated with the metal ion.



3

products

The metal ion would facilitate the reaction by aligning the nucleophile in the best orientation for attack as well as, through coordination at P = O, stabilizing the developing negative charge of the transition state leading to the intermediate.

The rate equation for this mechanism can be described by [9] where k_{EtOM} refers to the second-order rate coefficient of the ethoxide ion pair.

$$[9] \quad \text{Rate} = k_{EtOM}[EtOM][S]$$

The above pathways have been depicted as proceeding through a pentacoordinate intermediate with attack of the nucleophile being rate determining. The formation of a pentacoordinate intermediate in the rate-determining step of the alkaline hydrolysis of aryl diphenylphosphinothioates has been proposed, based on the correlation of rate constants with Hammett σ values rather than σ^- values, and on the magnitude of the Hammett ρ value (7). We have studied the ethanolysis reaction of substituted aryl diphenylphosphinates and, based on Hammett ρ values and correlation of rates with σ^0 constants, similarly propose the formation of an intermediate. The results of these experiments will be presented subsequently in this series.

2. Reactivities of metal–alkoxide ion pairs (k_{EtOM}) and of dissociated anions (k_{EtO^-})

Conventional wisdom would suggest that, in nucleophilic displacement reactions, the free (dissociated) nucleophile should be more reactive than the ion-paired species. However, the plots displayed in Fig. 1 show an *upward curvature* for the rate constants with increasing EtOM concentration, and this contrasts with expected behaviour if free ethoxide were more reactive than the ion-paired species. In fact, a number of S_N2 processes at saturated carbon centres have been found to be characterized by *downward curvature* of the *k* vs. [Nu] plots (8–12), which was interpreted as arising from decreased reactivity of the ion-paired species as compared to the dissociated anions. It was also found that the rate constant varied with the nature of the metal counterion, in parallel with the dissociation constant, i.e., the more tightly associated M^+Nu^- ion pairs were considered to be the least reactive (12).

In the present system, the upward curvature observed in the plot of *k* vs. [EtOM] (Fig. 1), as well as the decrease in rate with added complexing agent (Fig. 2), and the increase in rate with added metal ion (Fig. 3), are indicative of a mechanism in which the ion-paired nucleophile is more reactive than the free ion. Common metal ions should increase the concentration of associated ethoxide relative to free ethoxide by shifting to the left the equilibrium in eq. [10].

$$[10] \quad EtOM \overset{K_d}{\rightleftharpoons} M^+ + EtO^-$$

Considering that in the present system both free and associated ethoxide could be reactive species, the relevant rate equation will be

$$[11] \quad k_{obs} = k_{EtO^-}[EtO^-]_{eq} + k_{EtOM}[EtOM]_{eq}$$

The relative reactivities of the two species can now be derived.

The rate constant for the reaction of **1** with free ethoxide ion (k_{EtO^-}) was determined by linear regression analysis of the kinetic data for the reaction of **1** with LiOEt, NaOEt, and KOEt in the presence of excess complexing agent (Table 3), which yielded $k_{EtO^-} = 0.980\ M^{-1}\ s^{-1}$. To evaluate k_{EtOM} (eq. [11]), it is necessary to calculate the concentrations of the two species, making use of known metal–ethoxide dissociation constants.

K_d values, determined from conductance data, have been reported as follows (13, 14): LiOEt, 0.00472 M; NaOEt, 0.009804 M; KOEt, 0.0111 M. Using these values, the equilibrium concentrations of free ethoxide can be calculated from the initial stoichiometric concentration of ethoxide ($[EtOM]_0 = [EtO^-]_{eq} + [EtOM]_{eq}$) by means of eq. [12], which follows from manipulation of eq. [10] and solution of the resulting quadratic.

$$[12] \quad [EtO^-]_{eq} = 0.5[-K_d + (K_d^2 + 4K_d[EtOM]_0)^{1/2}]$$

The $[EtO^-]_{eq}$ values calculated in this manner are given in Table 6.

Now, eq. [11] can be rewritten as eq. [13], since $[EtOM]_{eq}$ is equal to $[EtO^-]_{eq}^2/K_d$, which predicts a linear plot for $k_{obs}/[EtO^-]_{eq}$ vs. $[EtO^-]_{eq}$, with k_{EtOM}/K_d as slope and k_{EtO^-} as intercept.

$$[13] \quad \frac{k_{obs}}{[EtO^-]_{eq}} = k_{EtO^-} + \frac{k_{EtOM}}{K_d}[EtO^-]_{eq}$$

The resulting plots (Fig. 4) are reasonably linear at the lower base concentrations and the initial slopes yield the ion-paired rate constants: $k_{LiOEt} = 22.8\ M^{-1}\ s^{-1}$, $k_{NaOEt} = 9.30\ M^{-1}\ s^{-1}$, $k_{KOEt} = 4.84\ M^{-1}\ s^{-1}$ (Table 7). The curvature observed in the plots of Fig. 4 in the higher range of ethoxide concentrations suggests the involvement of more than one metal cation,

Can. J. Chem. Downloaded from www.nrcresearchpress.com by 194.225.253.170 on 09/07/12
For personal use only.

TABLE 6. Ion-pairing treatment of the kinetic data for the reaction of **1** with LiOEt, NaOEt, and KOEt in EtOH at 25°C

LiOEt 1+ **1**			NaOEt + **1**			KOEt + **1**		
$[LiOEt]_0$ (M)	$[EtO^-]_{eq}$ (M)	$k_{obs}/[EtO^-]_{eq}$ ($M^{-1}s^{-1}$)	$[NaOEt]_0$ (M)	$[EtO^-]_{eq}$ (M)	$k_{obs}/[EtO^-]_{eq}$ ($M^{-1}s^{-1}$)	$[KOEt]_0$ (M)	$[EtO^-]_{eq}$ (M)	$k_{obs}/[EtO^-]_{eq}$ ($M^{-1}s^{-1}$)
0.000916	0.000785	5.23	0.000964	0.000884	2.45	0.001492	0.00133	1.08
0.001815	0.00140	8.66	0.001909	0.00164	3.29	0.002954	0.00242	1.73
0.002697	0.00192	11.1	0.002836	0.00230	4.04	0.004388	0.00337	2.08
0.003560	0.00237	13.0	0.003746	0.00290	4.57	0.005795	0.00421	2.39
0.004408	0.00278	15.0	0.004638	0.00344	4.79	0.007175	0.00496	2.70
0.01945	0.00751	36.2	0.01431	0.00791	8.95	0.01189	0.00721	3.82
0.02917	0.00961	45.1	0.02862	0.0126	12.1	0.02387	0.0116	5.08
0.03889	0.0114	53.5	0.04293	0.0162	13.0	0.03567	0.0151	6.85
0.04862	0.0130	60.1	0.05724	0.0193	13.4	0.04756	0.0181	9.31
0.05834	0.0144	69.3	0.07155	0.0220	16.4	0.05945	0.0207	10.3
0.07778	0.0169	79.0	0.08586	0.0245	17.2			
0.09723	0.0192	90.3	0.1145	0.0289	20.5			
0.1458	0.0240	115	0.1431	0.0329	24.4			
0.1945	0.0280	143	0.2146	0.0413	29.9			
0.2431	0.0316	159	0.2862	0.0483	37.8			
0.2907	0.0348	182	0.3578	0.0545	50.6			
0.3392	0.0377	202						
0.3876	0.0405	238						
0.4361	0.0431	251						
0.4846	0.0455	277						

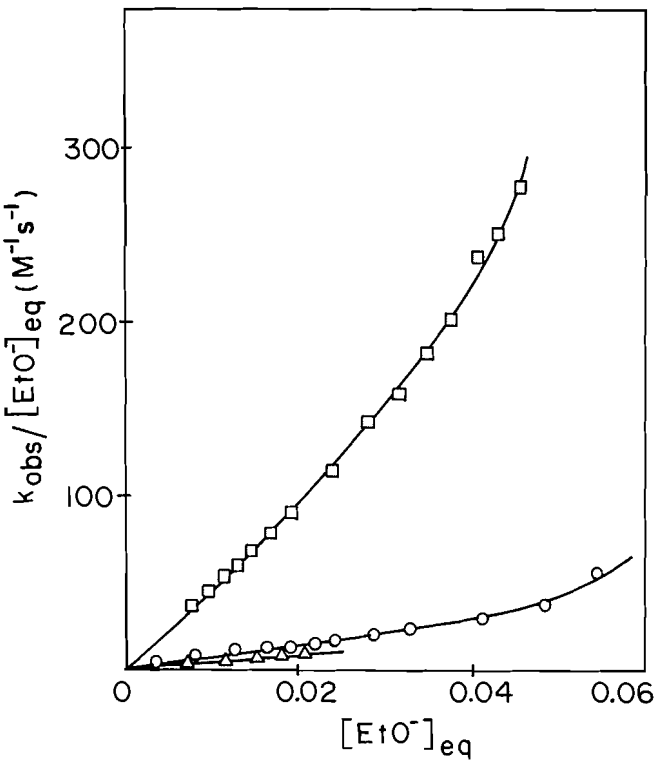


FIG. 4. Plot illustrating dissection of observed rates via eq. [13] into rate constants due to dissociated and ion-paired ethoxide for the reaction of **1** with LiOEt (□), NaOEt (○), and KOEt (△).

ethoxide anion, or ion pair. No definite information regarding this aspect is available at this time.

One can also use a nonlinear curve-fitting analysis of the k_{obs} and $[EtOM]_0$ data to derive values of k_{EtOM}, by means of the known K_d and k_{EtO^-} values. This method yielded the following rate constants; $k_{LiOEt} = 24.0\,M^{-1}s^{-1}$, $k_{NaOEt} = 11.6\,M^{-1}s^{-1}$, and $k_{KOEt} = 3.78\,M^{-1}s^{-1}$ (Table 7).

TABLE 7. Second-order rate constants for the reaction of **1** with LiOEt, NaOEt, KOEt, and EtO^- in EtOH at 25°C

Reaction system	k_{EtO^-} ($M^{-1}s^{-1}$)	k_{EtOM} ($M^{-1}s^{-1}$)
KOEt + DC18C6	0.938	—
KOEt + [2.2.2]	0.920	—
NaOEt + DC18C6	1.023	—
NaOEt + [2.2.2]	1.045	—
LiOEt +t[2.1.1]	0.976	—
KOEt[a]	0.579	4.84
KOEt[b]	—	3.78
NaOEt[a]	1.66	9.30
NaOEt[b]	—	11.6
LiOEt[a]	1.71	22.8
LiOEt[b]	—	24.0

[a]Ion-pairing treatment.
[b]Nonlinear least-squares analysis.

The dissection of k_{obs} into the contributions by free and ion-paired ethoxide by the above treatment yields k_{EtOM} values considerably larger than k_{EtO^-} values, the k_{EtOM}/k_{EtO^-} ratio ranging from ca. 5 for KOEt to ca. 25 for LiOEt. These derived values are concordant with the main experimental observations in the present system. However, on their own, these results do not give insight into the mechanism by which the metal ions catalyse the reaction, and this is considered in the following section.

3. *Catalysis by M^+: ground state versus transition state interactions*

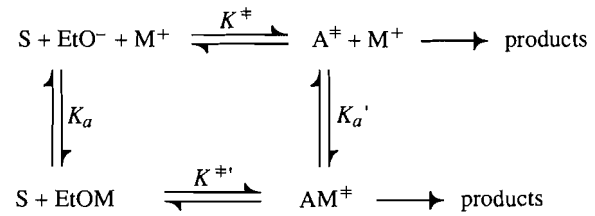
For catalysis to occur in this system, there has to be a decrease in the free energy of activation in the presence of metal ions. This can result from interaction of M^+ with the ground state, transition state, or a combination of the two. In the preceding

Can. J. Chem. Downloaded from www.nrcresearchpress.com by 194.225.253.170 on 09/07/12
For personal use only.

Can. J. Chem. Downloaded from www.nrcresearchpress.com by 194.225.253.170 on 09/07/12
For personal use only.

section we considered the interaction between M^+ and EtO^-, for which K_a (K_d^{-1}) values are known. Since there is no evidence for an appreciable interaction between M^+ and the substrate, the aforementioned M^+–EtO^- interaction is taken as the main ground state interaction.

Considering now interaction of M^+ with the transition state, Kurz (15) has shown that it is possible to calculate a virtual association constant of a catalyst with the transition state from basic transition theory by means of a thermodynamic cycle as illustrated in Scheme 1.



SCHEME 1

Here, $K^‡$ and $K^{‡\prime}$, are the equilibrium constants for the formation of the uncatalysed and catalysed transition states ($A^‡$ and $AM^‡$), while K_a and K_a' are the equilibrium association constants of M^+ with EtO^- and the transition state, respectively. This scheme requires the assumption that the concentration of transition states is at its equilibrium value with respect to the concentration of reactants. Since EtO^- and EtOM are in equilibrium, then $AM^‡$ will be at its equilibrium concentration with respect to $A^‡$, even though there is no direct dynamic equilibrium between the two transition states. It follows that

$$[14] \quad K_a' = \frac{k_{EtOM}K_a}{k_{EtO^-}} = \frac{k_{EtOM}}{k_{EtO^-}K_d}$$

K_a' values can therefore be determined using the known dissociation constants (K_d) of the metal–ethoxide ion pairs and the rate constants of free ethoxide and the metal–ethoxide ion pair.

For the reaction of **1** with ethoxide ion, the equilibrium constants for the association of the transition state with the cation (K_a') are calculated to be Li^+, 5188 M^{-1}; Na^+, 1207 M^{-1}; K^+, 347 M^{-1}. The association constants (K_a) for the alkali metal ethoxides are LiOEt, 212 M^{-1}; NaOEt, 102 M^{-1}, KOEt, 90 M^{-1} (see Table 8). Comparison of the magnitudes of K_a' and K_a clearly shows that the transition state is more tightly associated with the metal ion than is the ethoxide ion, and hence the transition state is the more stabilized.

The above considerations can nicely be illustrated by means of free energy – reaction coordinate profiles. In Fig. 5A, path *a* describes the uncatalysed reaction of the substrate with EtO^-, while the reaction with EtOM is illustrated in path *b*. Metal ion catalysis of the reaction will be observed when the difference in free energy between $AM^‡$ and $A^‡$ ($\delta G^‡$) is greater than the difference in free energy between EtOM and $M^+ + EtO^-$ ($\delta G°$). That is, when the transition state is stabilized to a greater extent than the ground state of the nucleophile (16, 17). This situation will occur when association of the metal ion with the transition state (K_a') is greater than its association with ethoxide ion (K_a). The present system clearly conforms to this requirement.

It is now necessary to account for catalysis in the reaction of free ethoxide ions as well. In this situation the involvement of both EtO^- and M^+ can be discussed in terms of the preassociation pathway, introduced in the previous section. The free

TABLE 8. Equilibrium constants for the association of alkali metal ion with ethoxide ion (K_a) and transition states (K_a')

Metal ion	K_a (M^{-1})[a]	K_a' (M^{-1})
Li^+	212	5188
Na^+	102	1207
K^+	90	347

[a]References 14 and 15.

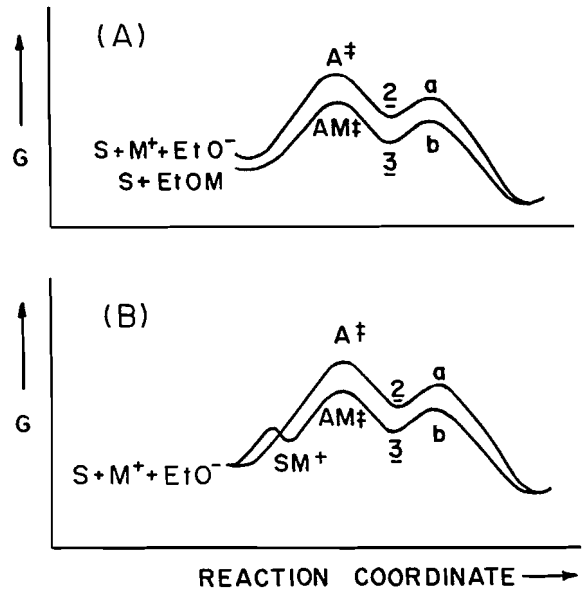


FIG. 5. (A) Path *a* illustrates the uncatalysed reaction of substrate (S) with EtO^-, while path *b* shows the lowering of both ground state and transition state free energies for the reaction of metal-alkoxide ion pairs due to association with M^+. (B) Catalysis by preassociation of M^+ with S is shown in path *b* while path *a* represents again the uncatalysed reaction.

energy – reaction coordinate diagram for this mechanism is shown in Fig. 5B, path *b*, which assumes a small equilibrium constant value ($K_1 \ll 1$), while path *a* depicts again the uncatalysed process. For path *b*, association of the substrate with the metal ion results in formation of a metal ion – substrate complex (SM^+), which can then react with ethoxide ion to give a metal-ion stabilized transition state ($AM^‡$). Lowering of the free energy of activation results from the enhanced electrophilicity of the phosphinyl group following coordination of M^+ with P=O.

In the above analysis we considered catalytic pathways involving (1) preassociation of M^+ with substrate and (2) reaction via metal—alkoxide ion pairs. A combination of these, and still other pathways, may be possible. However, it is difficult to differentiate between (1) and (2) since they are kinetically indistinguishable. Regardless of how S, M^+, and EtO^- come together, the key concern is to find satisfactory explanation for stabilization of the transition state in this system. This is considered in the next section in terms of the ion-pair model. The role of solvent molecules is also discussed.

4. Interaction of M^+ with the transition state: a mechanistic model

In considering transition state interactions involving the

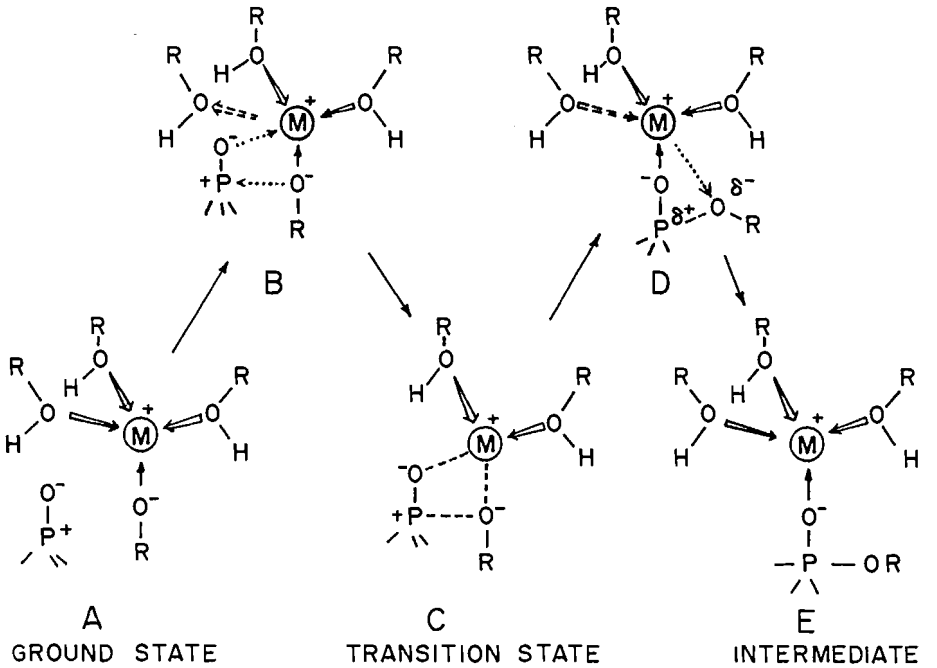


FIG. 6. Proposed model for nucleophilic attack of a metal-ion-paired alkoxide with the phosphinate centre illustrating the role of metal ion and solvent molecules.

metal cation, the size of M^+ and the spatial arrangement of the donor oxygen atoms of the nucleophile, substrate, and solvent in the coordination sphere of M^+ will contribute to the overall effectiveness of complexation. These factors are considered below.

The results in Table 8 clearly show a dependence of the association constant for binding of the metal ion with the transition state and with ethoxide ion (K'_a and K_a), on the size of the metal cation. Ignoring for the moment the role of the solvent, the fact that Li^+ is a better catalyst than Na^+ or K^+ may be a consequence of its smaller size, since the attraction between the metal ion and the intermediate will depend on the distance by which the centres of charge are separated. The crystallographic ionic radii of the metal ions have been given as Li^+, 0.60 Å; Na^+, 0.96 Å; and K^+, 1.33 Å (18). It follows that for the reaction of **1** with EtOM, the smaller the metal ion, the greater its association with the phosphinyl oxygen atom and, consequently, the larger the catalytic effect of the metal ion.

Studies of alkali metal ions in methanol have shown that the inner solvation sphere of Li^+ contains four solvent molecules (19), while Na^+ contains six solvent molecules in its first solvation sphere (20). Assuming for the present purpose that the metal ion has four coordination sites, one can depict the reaction of the ion-paired ethoxide with the phosphinyl group to form a negatively charged pentacoordinate intermediate as in Fig. 6. For simplicity, the solvation of P^+–O^- and RO^- is not shown in this figure.

In this illustration (Fig. 6), bond formation between the alkoxide oxygen and the phosphorus atom of the reactants (A) occurs concomitantly with association of the phosphinyl oxygen with M^+ and displacement of a solvent molecule from the inner coordination sphere of M^+ (Structure B). This leads to a transition state that has the metal ion coordinated to both the phosphinyl and alkoxide oxygen centres as well as to solvent molecules (Structure C). As P—OR bond formation progresses further, the negative charge on the alkoxide moiety decreases, weakening its electrostatic interaction with M^+ while association of M^+ with the phosphinyl oxygen increases (Structure D). It is also shown in Structure D that as the interaction between M^+ and alkoxide weakens, a solvent molecule may then reoccupy a coordination site around the metal ion. This results in the formation of intermediate E, which can be considered as being an essentially contact-ion-paired species.

The overall process A→E is essentially the transfer of M^+ (externally solvated) (21) from one ion-paired species to another, i.e., from the alkoxide oxygen to the phosphinyl oxygen, with bond formation occurring between the alkoxide oxygen and the phosphorus centre. Importantly, one sees that in the transition state C, M^+ is chelated to *two* oxygens, both of which carry substantial negative charge (see below), which leads to increased stabilization relative to alkoxide ion association with M^+.

It has recently been suggested (22, 23), based on MO calculations, that the P = O group (**4**) exists primarily in the dipolar form (**5**), i.e., with a highly developed negative charge on the phosphinyl oxygen atom.



4 **5**

In the transition state for the reaction of EtO^- at the phosphorus center, there would be effectively full negative charge developed on the phosphinyl oxygen, with very little delocalization of negative charge in the transition state of the type usually associated with, for example, addition to carbonyl compounds. This would tend to strengthen the interaction of the metal ion with the phosphinyl group. Therefore, the increase in reactivity due to stabilization of the transition state ($Li^+ > Na^+ > K^+$), as well as the correlation of the rate increase with decreasing crystallographic ionic radius, is consistent with this model of a contact-ion-paired intermediate.

Can. J. Chem. Downloaded from www.nrcresearchpress.com by 194.225.253.170 on 09/07/12
For personal use only.

To further investigate the effect of delocalized charge on the association of the metal ion with the transition state in displacement reactions of this type, a number of other substrates in which the charge is expected to be more delocalized (e.g., PhC(O)OAr, $PhS(O)_2OAr$) or less delocalized (e.g., $Me_2P(O)OAr$) have been studied with respect to their reactivities towards ethoxide and other nucleophiles, and the effect of metal ions on these reactions. The results of these investigations will be presented in subsequent papers in this series.

Experimental

Materials

Dry ethanol was obtained by refluxing absolute ethanol with magnesium turnings in the presence of iodine followed by distillation. Solutions of potassium or sodium ethoxide were prepared by dissolving clean potassium or sodium metal (Aldrich) in dry ethanol at 0°C. Lithium ethoxide solutions were prepared in a similar manner by dissolving lithium hydride (Alfa–Ventron) in dry ethanol. The ethoxide solutions were filtered at the end of the reaction in the glove box to remove any insoluble materials. The concentration of base was determined by titration with standard HCl. Solutions were prepared under a stream of nitrogen or in a dry N_2 atmosphere in a glove box.

The inorganic salts KOAc, KSCN (BDH), LiOAc, $LiClO_4$ (Fisher), $LiNO_3$ (Merck), and LiSCN (Alfa), reagent grade, were dried in a desiccator under vacuum (ca. 1 Torr; 1 Torr = 133.3 Pa) over P_2O_5.

The *p*-nitrophenyl diphenylphosphinate (**1**) used in this study was prepared as previously described (24).

Kinetic measuremnts

Kinetic reactions were generally conducted using an alkoxide concentration in the range $(1–5) \times 10^{-3}$ M. Due to the high extinction coefficient of *p*-nitrophenoxide (24 000 M^{-1} cm^{-1}), it was necessary to use a relatively low concentration of substrate (ca. 5×10^{-5} M). This range of concentrations gave pseudo-first-order conditions in which the base was in 20 to 100-fold excess of the substrate.

Kinetic runs that were relatively slow were followed spectrophotometrically using either a Beckman DU-8, Perkin–Elmer Lambda-5, or Perkin–Elmer 552 spectrophotometer. The instruments were equipped with thermostatted cell holders and the temperature inside the 10-mm quartz cuvette was maintained at 25.0°C. For relatively fast kinetic runs the reaction was followed using a Hi-Tech stopped-flow module equipped with a thermostatted water bath coupled to a McPherson monochrometer and Can-Tech transient recorder. The spectral traces were displayed on a Hewlett–Packard oscilloscope and the data were treated directly by a Commodore CBM 8032 computer.

Acknowledgements

This research was supported by the Department of National Defence, Chemical Detection and Decontamination Section, Defence Research Establishment, Ottawa, and by the Natural Sciences and Engineering Research Council of Canada. The award by Queen's University of a Graduate Student Fellowship to E.J.D. is acknowledged. The authors are grateful to Drs. R.A.B. Bannard, R.Y. Moir, and J.G. Purdon for helpful discussions.

1. (*a*) E. Buncel, H. Wilson and C. Chuaqui. J. Am. Chem. Soc. **104**, 4896 (1982); (*b*) E. Buncel, C. Chuaqui, and H. Wilson. J. Org. Chem. **45**, 3621 (1980; (*c*) E. Buncel and C. Chuaqui. J. Org. Chem. **45**, 2825 (1980).
2. F. H. Westheimer. Chem. Rev. **81**, 313 (1981).
3. T. Palmer. Understanding enzymes. 2nd ed. Ellis Horwood Ltd., Chichester, England. 1985. pp. 219–224.
4. (*a*) R. Breslow. Adv. Enzymol. **58**, 1 (1986); (*b*) D. Herschlag and W. P. Jencks. J. Am. Chem. Soc. **109**, 4665 (1987).
5. R. A. Kenley, R. H. Fleming, R. M. Laine, D. S. Tse, and J. S. Winterle. Inorg. Chem. **23**, 1870 (1984).
6. E. Buncel, E. J. Dunn, R. A. B. Bannard, and J. G. Purdon. J. Chem. Soc. Chem. Commun. 162 (1984).
7. R. D. Cook and L. Rahhal-Arabi. Tetrahedron Lett. 3147 (1985).
8. C. C. Evans and S. Sugden. J. Chem. Soc. 270 (1949).
9. J. R. Bevan and C. B. Monk. J. Chem. Soc. 1396 (1956).
10. P. Jones, P. Harrison, and L. Wynne-Jones. J. Chem. Soc. Perkin Trans. 2, 1679 (1979).
11. P. Beronius and L. Pataki. Acta. Chem. Scand. Ser. A: **A33**, 675 (1979).
12. N. N. Lichtin and K. N. Rao. J. Am. Chem. Soc. **83**, 2417 (1961).
13. J. Barthel, G. Bader, and M. Raach-Lenz. Z. Phys. Chem. (Munich), **84**, 100 (1973).
14. J. Barthel, J-C. Justice, and R. Wachter. Z. Phys. Chem. (Munich), **84**, 10 (1973).
15. J. L. Kurz. J. Am. Chem. Soc. **85**, 987 (1963).
16. E. Buncel and H. Wilson. Acc. Chem. Res. **12**, 42 (1979).
17. E. Buncel and E. A. Symons. J. Am. Chem. Soc. **98**, 656 (1976).
18. F. A. Cotton and G. Wilkinson. Basic inorganic chemistry. John Wiley and Sons, New York. 1976.
19. R. W. Impey, M. Sprik, and M. L. Klein. J. Am. Chem. Soc. **109**, 5900 (1987).
20. W. L. Jorgensen, B. Bigot, and J. Chandrasekhar. J. Am. Chem. Soc. **104**, 4584 (1982).
21. (*a*) B. C. Menon, H. F. Shurvell, J. P. Colpa, and E. Buncel. J. Mol. Struct. **78**, 29 (1982); (*b*) E. Buncel, B. C. Menon, and J. P. Colpa. Can. J. Chem. **57**, 999 (1979).
22. A. Streitwieser, A. Rajca, R. S. McDowell, and R. Glaser. J. Am. Chem. Soc. **109**, 4184 (1987); A. Rajca, J. E. Rice, A. Streitwieser, and H. F. Schaefer. J. Am. Chem. Soc. **109**, 4189 (1987).
23. M. W. Schmidt and M. S. Gordon. J. Am. Chem. Soc. **107**, 1922 (1985).
24. S. Hoz, E. J. Dunn, E. Buncel, R. A. B. Bannard, and J. G. Purdon. Phosphorus Sulfur, **24**, 321 (1985).

Can. J. Chem. Downloaded from www.nrcresearchpress.com by 194.225.253.170 on 09/07/12
For personal use only.

Novel regio- and stereoselective modifications of heparin in alkaline solution. Nuclear magnetic resonance spectroscopic evidence

MAHESH JASEJA, RABINDRA N. REJ,[1] FRANÇOIS SAURIOL, AND ARTHUR S. PERLIN
Department of Chemistry, McGill University, Montreal, P.Q., Canada H3A 2A7

Received January 3, 1989

MAHESH JASEJA, RABINDRA N. REJ, FRANÇOIS SAURIOL, and ARTHUR S. PERLIN. Can. J. Chem. **67**, 1449 (1989).

Nuclear magnetic resonance spectroscopic evidence is presented in characterizing three new structurally modified forms of heparin. One of these, polymer M-I, represents a conversion of about two-thirds of the α-L-iduronic acid 2-sulfate residues (**1**) into residues of a 2,3-anhydro derivative (**3**), through the action of sodium hydroxide. The formation of **3** is attributed to a base-catalysed displacement of the sulfate group of **1** by an intramolecular attack of O-3 on C-2. In more concentrated sodium hydroxide solution, heparin is transformed almost quantitatively into polymer M-II, which differs from it in having residues of (non-sulfated) α-L-iduronic acid (**4**) in place of **1**. It is likely that **3** is an intermediate, and that a selective nucleophilic attack of hydroxide ion at C-2 accounts for the *ido* configuration in **4**. The third modification, giving polymer M-III, is induced when a neutral or weakly alkaline solution of M-I is heated at 70°C or above, which promotes a different stereochemistry in the hydrolysis of the 2,3-oxirane ring of **3**. Hence, in contrast to residues of **4** in M-II, most of the uronic acid residues of M-III appear to have the alternate, α-L-*galacto*, configuration. As shown by a comparison of beef lung and hog mucosal heparin, the rate at which M-I is converted into M-III is facilitated by the higher level of structural heterogeneity in the mucosal heparin. Whereas the formation of M-I, -II, and -III is accompanied by only moderate depolymerization, these novel polymers retain little of the anti-coagulant and anti-XA activities of the unmodified heparin.

Key words: NMR spectroscopy, heparin, desulfation, anhydroaldoside, base-catalysed displacement.

MAHESH JASEJA, RABINDRA N. REJ, FRANÇOIS SAURIOL et ARTHUR S. PERLIN. Can. J. Chem. **67**, 1449 (1989).

On présente les spectres de résonance magnétique nucléaire de trois nouvelles formes d'héparine modifiées structuralement. Dans l'une d'elles, le polymère M-I, environ les deux tiers des résidus sulfates de l'acide α-L-iduronique (**1**) ont été transformés en résidu du dérivé déhydro-2,3 (**3**) sous l'action de l'hydroxyde de sodium. On attribue la formation du dérivé **3** au déplacement, catalysé par une base, du groupe sulfate du composé **1** par suite d'une attaque intramoléculaire de l'oxygène en position 3 (O-3) sur le carbone en position 2 (C-2). Dans une solution plus concentrée d'hydroxyde de sodium, l'héparine se transforme presque quantitativement en polymère M-II qui diffère de l'héparine par la présence de résidus (non sulfatés) de l'acide α-L-iduronique (**4**) au lieu du composé **1**. Il est communément admis que le composé **3** est un intermédiaire, et qu'une attaque nucléophile sélective de l'ion hydroxyde en C-2 est responsable de la configuration *ido* dans le composé **4**. La troisième modification, conduisant au polymère M-III, est obtenue par chauffage à 70°C ou au-dessus d'une solution neutre ou faiblement alcaline du polymère M-I, ce qui favorise une stéréochimie différente dans l'hydrolyse du cycle oxyrane-2,3 du composé **3**. Cependant, contrairement au résidu du composé **4**, dans le polymère M-II, la plupart des résidus de l'acide iduronique du polymère M-III semble avoir possiblement une configuration α-L-*galacto*. La comparaison de l'héparine du poumon de boeuf et de la muqueuse du porc montre que la vitesse avec laquelle le polymère M-I se transforme en polymère M-III est favorisée par un haut degré d'hétérogénéité structurale dans l'héparine de la muqueuse. Cependant, la formation de des polymères M-I, M-II et M-III s'accompagne seulement d'une dépolymérisation modérée. Ces nouveaux polymères retiennent qu'une faible partie des activités anticoagulante et anti-XA de l'héparine non modifiée.

Mots clés : spectroscopie RMN, héparine, désulfation, aldoside déhydro, déplacement catalysé par une base.

[Traduit par la revue]

Introduction

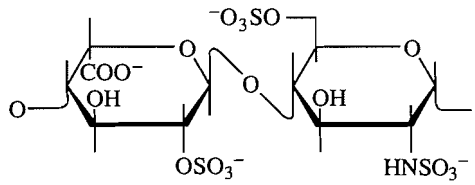
Heparin, the clinically important blood anticoagulant, is an anionic polysaccharide that is generally administered in the form of its sodium salt and, less commonly, as a calcium salt. Barium, benzidene, and quaternary ammonium compounds of heparin find use (1–4) in its purification and fractionation, following its extraction from animal tissue sources.

In carrying out the preparation of the sodium salt of a purified heparin from its barium precursor, we converted the latter into the acid form of heparin with a cation-exchange resin and then, inadvertently, raised the pH of the polymer solution to ~11, rather than to neutrality. The strongly basic preparation of the sodium salt recovered from this solution was found to be characterized by nmr spectra strikingly different from those of neutral sodium salts of heparin. Moreover, during the acquisition of the spectra, which sometimes involved lengthy exposure of solutions of the modified heparin to temperatures of 65–70°C, it became apparent that additional changes in the polymer were induced. Yet another type of alteration was found when the heparin was subjected to more strongly alkaline conditions. To our knowledge, effects of this nature had not been observed previously, and are described here together with proposals as to their origin.

[1]Author to whom correspondence may be addressed.

Results and discussion

The kinds of effects observed are illustrated in Fig. 1 with a beef lung heparin. Constituted mainly (5) of α-L-iduronic acid 2-sulfate (**1**) and 2-deoxy-2-sulfamino-α-D-glucose 6-sulfate (**2**), linked (1→4) in disaccharide repeating units (as shown),



1 **2**

this heparin gives (6–8) relatively uncomplicated spectra. Thus, the 300-MHz ^1H nmr spectrum of the *neutral* sodium salt in deuterium oxide (Fig. 1A) clearly reflects the high degree

Can. J. Chem. Downloaded from www.nrcresearchpress.com by 194.225.253.170 on 09/07/12
For personal use only.

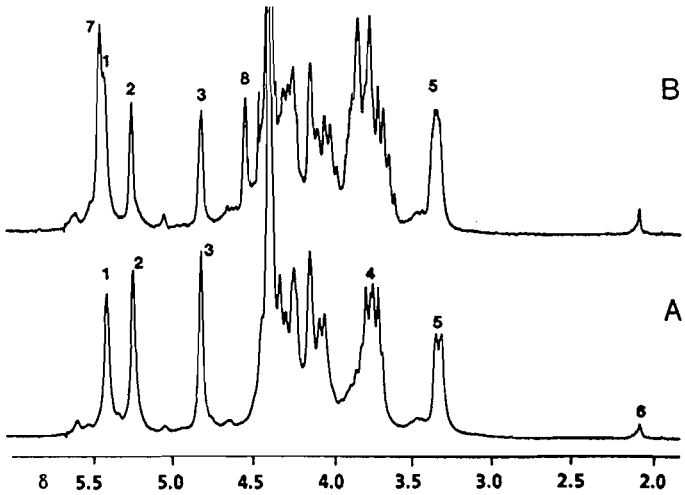


FIG. 1. The ^1H nmr spectra (300 MHz) of (A) beef lung heparin (sodium salt), in D_2O at 65°C; and (B) modified heparin M-I in NaOD (pD ~ 12) at 65°C. Signal designations: 1, A-1; 2, I-1; 3, I-5; 4, A-3, -4; 5, A-2; 6, acetamido CH_3; 7, I′-1; 8, I′-4 (I = **1**, A = **2**, I′ = **3**).

of structural homogeneity in the polymer. When an aqueous solution of the heparin was acidified with Amberlite IR-120 (H^+ form), followed by adjustment to pH 11 with sodium hydroxide, lyophilization, and deuterium exchange of the product, the spectrum shown in Fig. 1B was obtained.

The most striking difference between the spectrum (Fig. 1B) of the modified heparin, which will be referred to as "M-I", and that of the original material (Fig. 1A), is the decrease in the relative intensities of I-1 (δ 5.23) and I-5 (δ 4.80), i.e., the anomeric proton and 5-proton signals (7), respectively, of the iduronic acid 2-sulfate residue (**1**). This change is accompanied by the appearance of new signals such as those at δ 5.48 and 4.53, which, in terms of relative intensities, indicates that the shift displacements involved almost one-half of the uronic acid residues. Signals of the hexosamine residues (**2**) are affected far less: that of proton-2 (A-2), at δ 3.30, is slightly broadened whereas those due (8) to A-3, -4, and -5, in the vicinity of δ 3.6–3.9, are only dispersed somewhat differently. Hence, residues of **1** appeared to be the principal site of the polymer modification.

Formation and identity of polymer M-I

In pursuing these observations, it was found that the formation of M-I is highly sensitive to the experimental conditions used. This aspect of the reaction may be summarized by the following series of comments:

(a) A critical element was the fact that, as a requirement for the deuterium-exchange step with D_2O prior to the nmr examination, the alkaline solution of heparin was evaporated to dryness (either by lyophilization or by vacuum distillation of the solvent). Consequently the initial pH value of ~11 was not definitive, inasmuch as the polymer was subsequently exposed several times to a widely fluctuating concentration of base.

(b) The initial acidification step was only incidental. Providing that a sufficiently high concentration of alkali was used, the formation of M-I was observed. For example, it occurred when a solution of sodium heparin (40 mg) in water (10 mL) was adjusted to pH 11.2–11.5, followed by lyophilization, although not at all when the solution was initially at pH 10.5.

(c) Without the lyophilization step, the transformation of

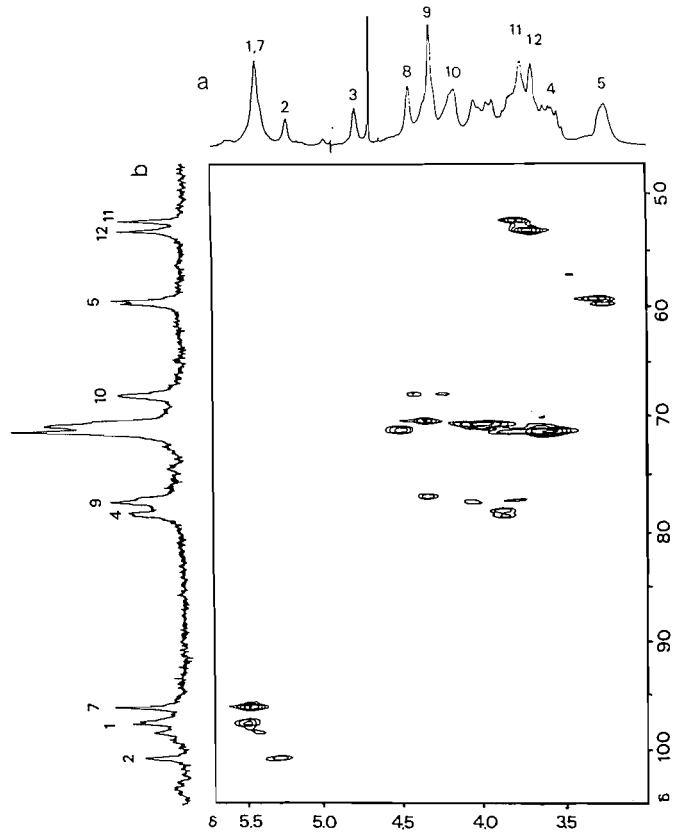


FIG. 2. The ^1H and ^{13}C heterocorrelation spectrum (300/75 MHz) of modified heparin M-I in NaOD (pD ~ 12) at 25°C; (a) ^1H spectrum; (b) ^{13}C spectrum. Signal designations: 1, A-1; 2, I-1; 3, I-5; 4, A-3, -4 (^{13}C-4 is A-4); 5, A-2; 7, I′-1; 8, I′-4; 9, I′-5, A-6; 10, A-6; 11, I′-3; 12, I′-2 (I = **1**, A = **2**, I′ = **3**).

heparin into M-I required a much higher pH, and even then the rate of the reaction was far slower, e.g., a period of 4–5 days for a solution of sodium heparin (30 mg) in D_2O (0.5 mL) at pH ~ 13.5 (as monitored by nmr spectroscopy).

(d) The degree of conversion of heparin into M-I varied substantially among the group of experiments conducted along these lines, undoubtedly in response to differences in the heparin concentration, pH, and rate of lyophilization. Hence, in contrast to its presence at a level of ~40% in the mixed product represented by Fig. 1B, conversion yields of 65–70% were obtained in other instances, as shown in Fig. 2.

The corresponding ^1H–^1H correlation (COSY) spectrum afforded the assignments designated, and the ^1H chemical shifts listed in Table 1. Acquisition of a ^{13}C nmr spectrum and a ^{13}C–^1H heterocorrelation (HETCOR) spectrum (Fig. 2) then provided the ^{13}C chemical shifts given in the table (a DEPT experiment confirmed that only the ^{13}C signal at δ 69 was due to a methylene group, i.e., C-6 of **2**).

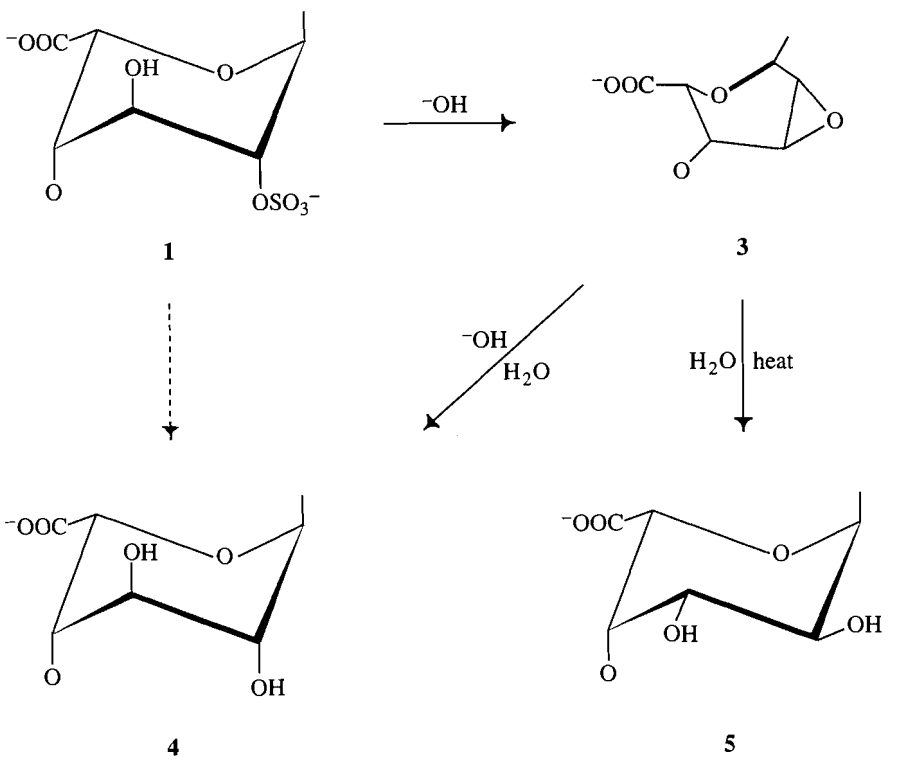
These data show that the formation of M-I entailed a number of large displacements of chemical shift of the uronic acid residues relative to those (**1**) of unmodified heparin, whereas those of the amino sugar (**2**) were little affected. Structural changes accompanying these displacements appeared to include such possibilities as (a) a conformational interconversion from the preponderant (7–10) $^1C_4$ (L) chair into the alternate chair, or skew, conformation; (b) the formation of a 2,3-cyclic sulfate, inasmuch as *trans* 2,3-cyclic sulfates are stable entities (11); or (c) the formation of a 2,3-anhydride. However, only the last was

Can. J. Chem. Downloaded from www.nrcresearchpress.com by 194.225.253.170 on 09/07/12
For personal use only.

TABLE 1. Chemical shifts for residues[a] of chemically modified heparins M-I, M-II, and M-III

	Heparin		M-I		M-II		M-III	
Resonance[b]	δ (^{1}H)	δ (^{13}C)	δ (^{1}H)	δ (^{13}C)	δ (^{1}H)	δ (^{13}C)	δ (^{1}H)	δ (^{13}C)
U-1	5.2	101.4	5.4	97.0	5.0	104.5	5.2	102.0
U-2	4.4	78.3	3.7	54.0	3.8	72	4.0	70.5
U-3	4.2	71.4	3.8	53.5	~4.1	~72	4.0	72.5
U-4	4.1	78.2	4.4	~72	~4.1	77.5	4.4	79.2
U-5	4.8	71.7	4.3	78.3	4.8	72.5	4.6	73.5
U-6	—	176.2	—	176.5	—	177.0	—	178.0
A-1	5.4	99.0	5.4	98.5	5.3	98.5	5.2–5.5	100.5
A-2	3.3	60.0	3.3	60.0	3.3	60.0	3.3	~60.0
A-3	3.7	71.9	3.6–3.9	~72	3.7	71.9	3.6–3.7	73.0
A-4	3.8	78.6	3.6–3.9	79.5	3.8	79.6	3.6–3.7	78.8
A-5	4.1	71.3	4.0	~72	4.0	71.3	4.1	71.0[c]
A-6	4.2–4.4	68.6	4.2–4.4	68.5	4.2–4.4	68.6	4.2–4.4	68.5

[a]Major residues.
[b]U, uronic acid; A, aminodeoxyhexose.
[c]May be interchanged.



1 3 4 5

SCHEME 1

consistent with the striking upfield location of ^{13}C resonances I′-2 and I′-3, at δ 53–54 (Table 1), which is in the range reported (12, 13) for several 2,3-anhydro-aldopyranoside derivatives. (Corresponding ^{13}C values for 2,3-cyclic sulfates are (14) δ ~79–80.) Although less definitive, the ^{1}H values of δ ~3.7 for I′-2 and I′-3 are closer to the range of δ 2.7–3.6 found (13) for the same group of 2,3-anhydrides than that (14) of δ 4–5 for related 2,3-cyclic sulfates.

Consequently, the transformation of heparin into M-I in alkaline solution must involve an intramolecular base-catalysed displacement of the 2-sulfate group of **1** by vicinal O-3 to form a 2,3-oxirane derivative. A facile displacement may readily be envisaged (15) for the $^1C_4$ (L) conformation (see Scheme 1), involving the *antiperiplanar* 2- and 3-substituents, which would give rise to residues of 2,3-anhydro-α-L-gulohexopyranose uronic acid (**3**). According to the relative intensities of the ^{1}H resonances in Fig. 2 (e.g., comparing signal I′-4 with I-5), about two-thirds of the uronic acid residues in polymer M-I are represented by **3**. Consistent with this proposal was the fact that 0.7 moles of sulfate ion (SO_4^{2-} by ion-exchange chromatography) per mole of **1** was liberated during the formation of M-I.

Can. J. Chem. Downloaded from www.nrcresearchpress.com by 194.225.253.170 on 09/07/12
For personal use only.

TABLE 2. Chemical shifts for the uronic acid residues of M-II and M-III relative to those of reference data

Resonance		1	2	3	4	5	6
^{13}C	M-II	104.5	~72	~72	77.5	72.6	177.0
	4[a]	105.6	72.0	73.6	82.5	72.1	176.6
	M-III	102.0	70.5	72.5	79.2	73.5	178.0
	6[b]	102	70	72	79	72	176
^{1}H	M-II	5.0	3.8	~4.1	~4.1	4.8	—
	4[a]	5.0	3.6	4.0	4.1	4.7	—
	M-III	5.2	4.0	4.0	4.4	4.6	—
	6[b]	5.3	3.8	3.9	4.3	4.4	—

[a]The 4-substituted residue of α-L-idopyranuronic acid in dermatan sulfate (17).
[b]Estimated for a 4-substituted residue of α-L-galactopyranuronic acid (**5**), by reference to data (23–25) for α-galacturonic acid and derivatives.

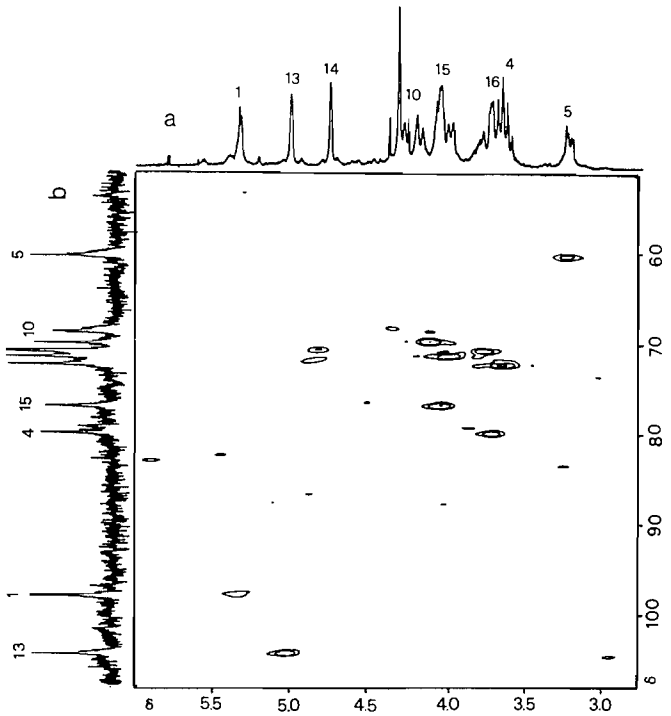


FIG. 3. The ^{1}H and ^{13}C heterocorrelation spectrum (300/75 MHz) of modified heparin M-II in NaOD (pD ~ 13) at 25°C; (a) ^{1}H spectrum (that shown was recorded at 65°C for improved resolution); (b) ^{13}C spectrum. Signal designations: 1, A-1; 4, A-3, -4 (^{13}C-4 is A-4); 5, A-2; 10, A-6; 13, I″-1; 14, I″-5; 15, I″-3, -4; 16, I″-2 (A = **2**, I″ = **4**).

A second, base-catalysed, modification of heparin

As already indicated, the formation of M-I in sodium hydroxide solution occurred only when the heparin was subjected to an appropriate concentration of base. For example, the initial pH of the solution lyophilized was in the region of 11–11.5. However, in analogous experiments with solutions adjusted initially to a range of pH 11.8–12.8, the nmr spectra of the products showed that another product was formed at these more elevated levels. At pH 12.5 and above, this second modification, M-II, was virtually the only species detected, and hence represented an essentially quantitative interconversion from heparin, as is evident from the ^{1}H and ^{13}C nmr spectra in Fig. 3.

The ^{1}H chemical shift data for M-II (Table 1) obtained with the aid of a COSY spectrum, together with the ^{13}C chemical shifts derived from the HETCOR spectrum (Fig. 3), indicate that, as in the formation of M-I, only the L-iduronic acid moiety of the heparin was altered. In this instance, moreover, all such residues were affected and, as shown by the presence of 0.9 moles of SO_4^{2-} per mole of **1** in the reaction medium, the 2-sulfate substituent must have been involved.

That the sulfamino group remained intact is shown by the location of the A-2 signal in all of the ^{1}H spectra (Figs. 1 and 2). Hence, its chemical shift remained essentially constant at δ ~3.3 (as in Fig. 1A for residues of **2**). Had hydrolysis to the amino function occurred, then the proton α to a free amino group would have given rise (6) to a signal at δ ~2.8, at the high pH at which these spectra were recorded. Similarly, hydrolysis of the 6-sulfate group of hexosamine residues (**2**) would have been readily detectable (16) in the ^{13}C spectra as a decrease in the relative intensity of its C-6 signal (δ 69), and the emergence of a corresponding signal at δ 62 for the liberated 6-hydroxymethyl group.

As there is a close similarity between the ^{1}H and ^{13}C chemical shifts for the uronic acid residues of M-II and those of the (non-sulfated) α-L-iduronic acid residue (**4**) in dermatan sulfate (Table 2), it is proposed that M-II is comprised mainly of residues of **4** and hexosamine **2**.

By adjusting the pH of a solution of M-I to 12.5 with sodium hydroxide, then subjecting it to lyophilization and deuterium exchange in the usual manner, it was determined that M-I is almost quantitatively converted into M-II at the concentration of base appropriately higher than that required for the formation of M-I itself. Hence, the ^{1}H nmr spectrum of the product was closely similar to that shown for M-II in Fig. 3. Therefore, the formation of the latter polymer involves M-I as an intermediate, and alkaline hydrolysis of the 2,3-anhydro ring of **3** (in M-I) occurs with high regio- and stereoselectivity, i.e., almost exclusively by nucleophilic attack of OH^- on C-2, to regenerate the α-L-*ido* configuration (**4**) (Scheme 1).

Chemical methods for desulfation of heparin

The removal of the various sulfate groups of heparin has received much attention, in attempts to determine possible functional roles that these substituents may play. Due to its marked acid lability, the sulfamino group undergoes (18) facile selective hydrolysis under conditions that leave other sulfate groups unaffected. However, prolonged treatment of heparin with, e.g., methanol – hydrogen chloride, also leads (19) to

Can. J. Chem. Downloaded from www.nrcresearchpress.com by 194.225.253.170 on 09/07/12
For personal use only.

Can. J. Chem. Downloaded from www.nrcresearchpress.com by 194.225.253.170 on 09/07/12
For personal use only.

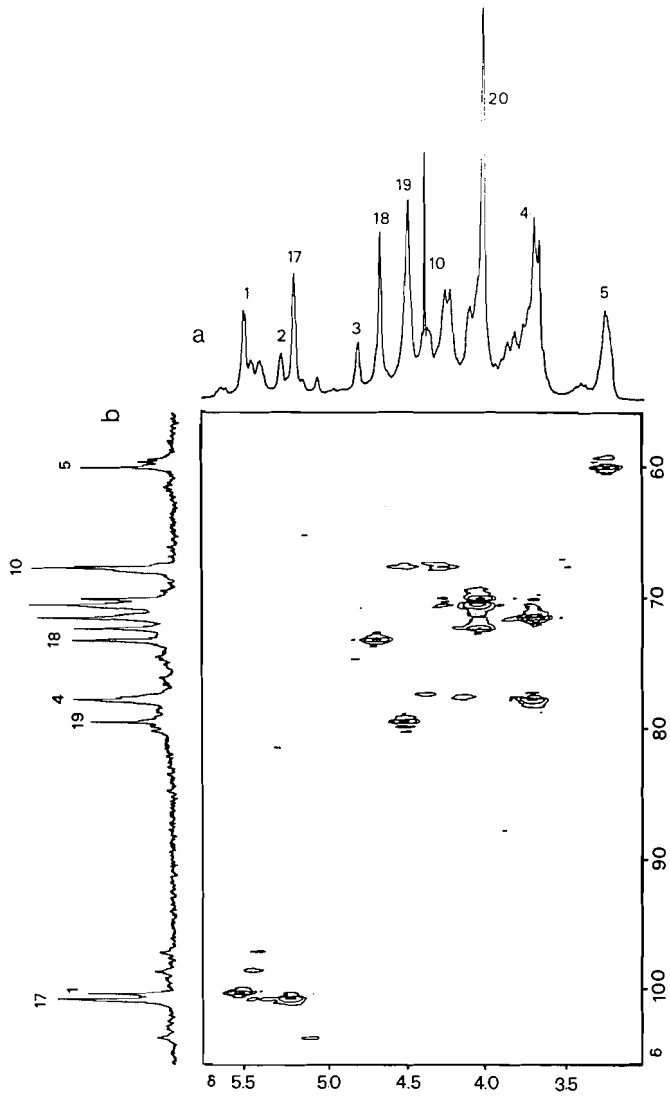


FIG. 4. The ^1H and ^{13}C heterocorrelation spectrum (300/75 MHz) of modified heparin M-III in NaOD (pD ~ 12) at 65°C; (a) ^1H spectrum; (b) ^{13}C spectrum. Signal designations: 1, A-1; 2, I-1; 3, I-5; 4, A-3, -4 (^{13}C-4 is A-4); 5, A-2; 10, A-6; 17, G-1; 18, G-5; 19, G-4; 20, G-2, -3 (I = **1**, A = **2**, G = **5**).

removal of the other sulfate groups. At close to neutrality, the pyridinium salt of heparin is effectively N- and O-desulfated (20) in hot, aqueous, dimethyl sulfoxide, whereby the rates of hydrolysis are (21) sulfamino ≥ ≥ 6-sulfate of **2** ≥ 2-sulfate of **1**. Although desulfation by alkali has long been recognized (22), the products obtained have not been well characterized. Presumably, some of the products would have included M-I and M-II.

A third modification of heparin (M-III)

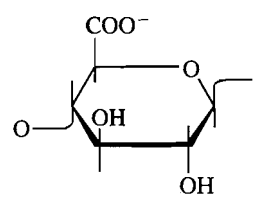
During the acquisition of 2D spectra of modified heparin M-I, which involved lengthy heating of the solution at ~70°C to minimize line widths, new signals slowly emerged in the spectra. (This also occurred with the neutralized solution, although at a slightly slower rate.) By prolonging the heating period to 72 h, the ^1H spectrum shown in Fig. 4 was obtained. It represents modified polymer M-III. As was seen in the ^1H spectrum of M-I (Fig. 2), minor I-1 and I-5 signals due to intact residues of **1** are also present in Fig. 4, whereas the I′-1 and I′-5 signals of M-I are no longer detected. Rather, they appear to be replaced in this region by two new signals, at δ 5.18 and δ 4.60, designated G-1 and G-5. Other prominent new signals are found at δ 4.45 (no. 19) and δ 4.10 (no. 20), and there now is greater complexity in the signals associated with the anomeric proton (A-1, δ 5.4) and proton-2 (A-2, δ 3.3) of the hexosamine residues, reflecting the structural heterogeneity present.

From the corresponding COSY spectrum of M-III, and the ^{13}C–^1H correlation data illustrated in Fig. 4, the chemical shift parameters in Table 1 were derived. Clearly, during the transformation of M-I into M-III, the hexosamine residues (**2**) remained unaltered, and the 2,3-oxirane ring disappeared, accompanied by the appearance of a uronic acid entity that was distinct from α-L-iduronic acid (**4**). As already noted (Scheme 1), the latter is the product expected by nucleophilic attack of HO^- on C-2 of the oxirane ring of **3**. The alternative diastereomeric uronic acid, resulting from an attack at C-3, would be α-L-galacturonic acid (**5**). In fact, the overall ^1H and ^{13}C parameters for the new uronic acid moiety in M-III are in general agreement with those expected for such a residue as **5** (Table 2), a possibility that has been confirmed by chemical evidence (R. Rej and A. S. Perlin, unpublished data).

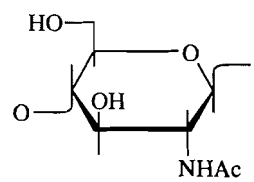
It is noteworthy that two different diastereoisomers (**4** and **5**) are produced, each almost exclusively, in the hydrolysis of anhydride **3**, one in concentrated alkali and the other under neutral, or weakly basic, conditions. Based on the known (15, 26) chemistry of ring-opening reactions of 2,3-anhydro-aldopyranosides, this high degree of regio- and stereoselectivity would not have been anticipated, nor are we able to account for it.

Influence of molecular constitution on the transformation of M-I into M-III

Although the preceding observations concern the influence of strong alkali on beef lung heparin, similar experiments were conducted with hog mucosal heparin, and fractions of it obtained by graded sedimentation of the barium salt. The hog mucosal material contains (6, 7) more residues of β-D-glucuronic acid (**6**) and 2-acetamido-2-deoxy-α-D-glucose (**7**)



6



7

than does beef lung heparin and, as its fractionation progresses, the precipitated materials are characterized (27) by an increase in the proportions of **6** and **7** and a decrease in molecular weight. Three of these fractions, nos. 4, 6, and 7 out of a total of seven, were subjected to the treatment with alkali, and heating at 70°C, described for the preparation of M-I and M-III from beef lung heparin. Representative of the ^1H nmr spectra of these fractions is Fig. 5, which shows that of fraction no. 6 (Fig. 5A), and its modified (M-I) product (Fig. 5B).

Whereas in the second stage transformation, to give M-III, the bovine heparin had required a heating period of 48–72 h to reach equilibrium, the hog mucosal fractions were fully modified in 24 h (no. 4), 12 h (no. 6), and 1 h (no. 7), respectively. The ^1H nmr spectra of these final products are shown in Fig. 6. Consequently, there is a direct correspondence

Can. J. Chem. Downloaded from www.nrcresearchpress.com by 194.225.253.170 on 09/07/12
For personal use only.

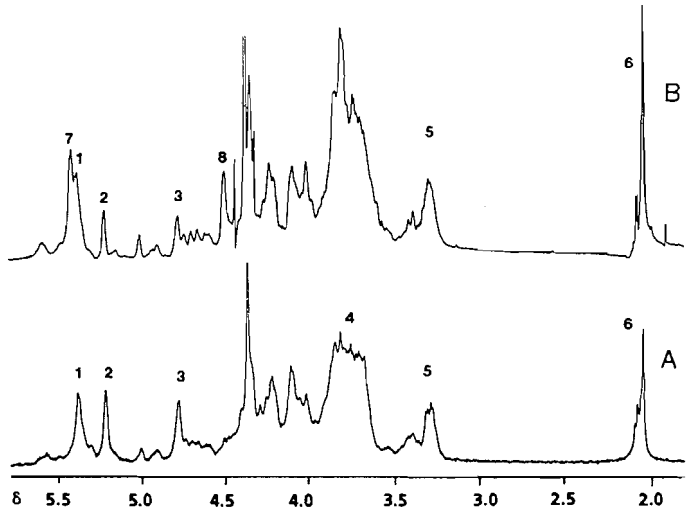


FIG. 5. The ^{1}H nmr spectra (300 MHz) of (A) hog mucosal heparin (fraction no. 6, sodium salt) in D_2O at 65°C; and (B) corresponding to modified heparin M-I in NaOD (pD ~ 12) at 65°C. Signal designations: 1, A-1; 2, I-1; 3, I-5; 4, A-3, -4; 5, A-2, A-2; 6, acetamido CH_3; 7, I′-1; 8, I′-4 (I = **1**, A = **2**, I′ = **3**).

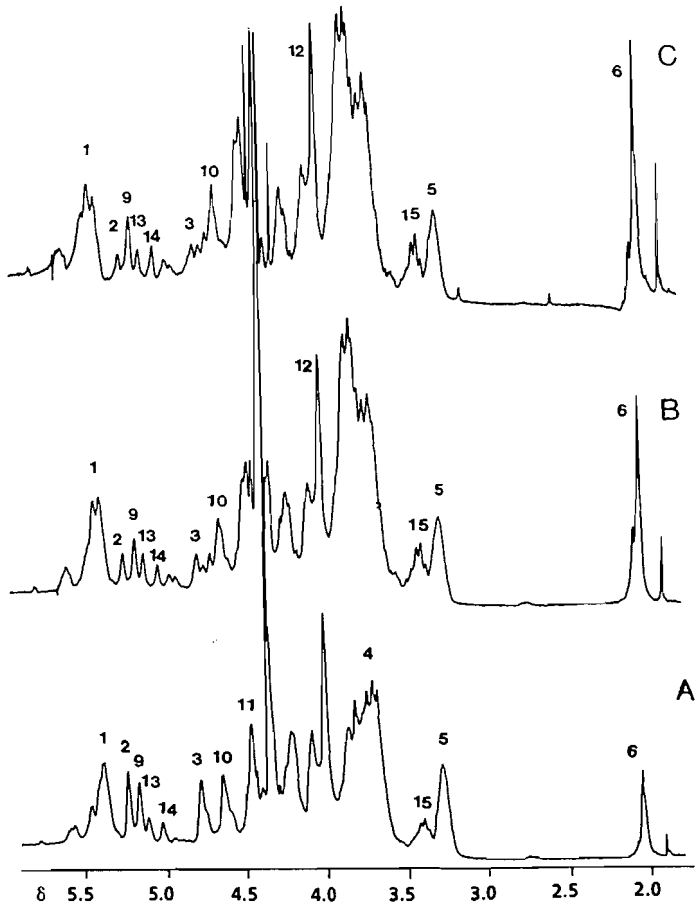
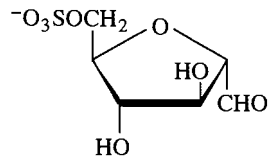


FIG. 6. The ^{1}H nmr spectra (300 MHz) of modified heparin corresponding to M-III, in NaOD (pD ~ 12) at 65°C, prepared from hog mucosal fractions (A) no. 4; (B) no. 6; (C) no. 7. Signal designations: 1, A-1; 2, I-1; 3, I-5; 4, A-3, -4; 5, A-2; 6, acetamido CH_3; 9, G-1; 10, G-5; 11, G-4; 12, G-2, -3; 13, G-1; 14, I′-1; 15, H-2 of D-glucuronic acid (**6**) and 2-acetamido-2-deoxy-D-glucose (**7**) (I = **1**, A = **2**, I′ = **4**, G = **5**).

between the ease with which M-III is produced from M-I and the molecular constitution of the polymers. Although the process is accelerated by both heat and base, it is also enhanced by structural inhomogeneity within the heparin molecule and (or) by a diminution in molecular size. The latter two possibilities are difficult to assess individually, because (27) the increase in heterogeneity is accompanied by a decrease in mass. However, evidence that chemical constitution plays a role has been obtained from the nmr spectra of modified heparin samples that were subjected to selective fragmentation.

Nuclear magnetic resonance spectra of products formed on deaminative degradation

When heparin is treated with nitrous acid, such residues as **2** that contain a 2-sulfamino group are converted by deaminative elimination (28) into *aldehydo*-2,5-anhydro-D-mannose residues (**8**), whereas those containing an N-acetyl group (such as **7**) are unaffected. For example, the depolymerization products of the hog mucosal heparin contain reducing-end residues of **8**



8

together with intact residues of **7**, as shown by the ^{1}H nmr spectrum (Fig. 7A) representing degraded fraction no. 4. Signals attributable to H-1 of **8** and neighboring **1** are observed at δ 5.15 and 5.20. In addition, H-1 peaks due to the unmodified residues of 2-acetamido-2-deoxy-α-D-glucose (**7**) and of residues of the uronic acid appended to it, are found at δ 5.42 and 5.30. The corresponding spectrum (Fig. 7B) for HNO_2-degraded fraction no. 6, a material that is richer in unreactive residues of **4**, clearly reflects the lower level of fragmentation effected.

Also evident from Fig. 7B is the fact that there is only a trace H-1 signal attributable to residues of **1** that are attached to residues of **7**. Consequently, prior to degradation, more of the residues of **1** were linked to **7** than to the 2-sulfamino isomer (**2**). This suggests that the modification of heparin occurs more readily with a disaccharide sequence of **1** and **7** than of **1** and **2**. Consistent with this suggestion, of course, is the greater resistance to change on the part of M-I from beef lung heparin. Perhaps a molecule of this latter type, due to its higher degree of structural homogeneity, is less easily perturbed than is a more heterogeneously constituted molecule derived from the mucosal heparin.

It is worth noting, in retrospect, that the present study originated in the detection, by nmr spectroscopy, of structural changes occurring during preparation of these lower molecular weight mucosal fractions, owing to their extreme sensitivity to alteration. Beef lung heparin was *then* examined as a "model" polymer, because of its greater constitutional homogeneity.

Influence of the chemical modifications of heparin on molecular size and biological activity

Not surprisingly, the structural changes induced in heparin by alkali and (or) heat were accompanied by a decrease in the molecular size of the polymer, as well as a reduction in its anticoagulant activity. Estimates of molecular weight by gel-filtration chromatography (Table 3) show that each modification step caused some depolymerization, which was most pro-

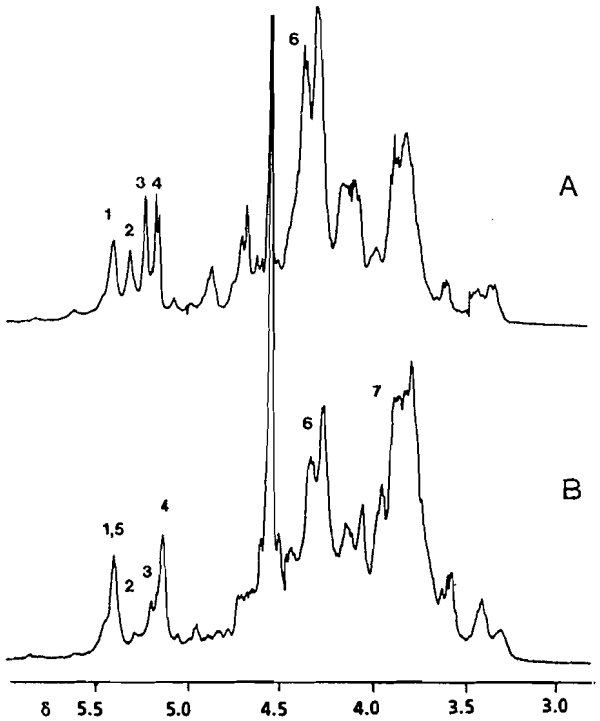


FIG. 7. The ^1H nmr spectra (300 MHz) of the products of deaminative degradation of (A) hog mucosal heparin (fraction no. 4); and (b) modified heparin M-III (from fraction no. 6), in D_2O at 65°C. Signal designations: 1, H-1 of **7**; 2, I-1 of residues appended to **7**; 3, I-1 of residues appended to residues of 2,5-anhydro-D-mannose (**8**); 4, H-1 of **8**; 5, G-1 of residues attached to **7**; 6, G-4; 7, G-2, -3 (I = **1**, G = **5**).

TABLE 3. Molecular weight and anticoagulant potency of modified heparins M-I, -II, and -III

Polymer	Molecular weight[a] (dalton)	USP potency (units/mg)	Anti XA activity (units/mg)
Heparin (beef lung)	9000	126	132
M-I	8000	73	26
M-II	6500	≤5	≤0.5
M-III	7500	70	24

[a]Estimated average value obtained by gel-filtration chromatography.

nounced under the strongly alkaline conditions required for the formation of M-II. As compared with a value averaging about 9000 daltons for the beef lung heparin, the value for M-II averaged about 6500, which also represented a more disperse range than observed with the unmodified polymer. M-I and M-III gave values of intermediate size. Consequently, all three stages of structural modification represent new polymers, of moderately high molecular weight, closely related to the heparin molecule.

Much more striking was the impact on the anticoagulant properties of heparin, as shown by the assays of USP and anti-XA potency (Table 3). Polymer M-II was virtually devoid of activity in both categories. In accord with other observations (9, 29) on modified heparins and synthetic oligosaccharides, this is suggestive (30) of a crucial contribution by the 2-sulfate group of the residues of **1** in heparin toward anticoagulant potency. Although M-I and M-III retain about one-half of the original USP activity, presumably most of this is attributable to the presence of about one-third of the unmodified heparin structure.[2] By contrast, the anti-XA activity was more drastically reduced and, on the basis of composition just discussed, implies a total loss of potency in M-I and M-III, as well as M-II. The two most extensively modified hog mucosal products, represented by Figs. 6B and 6C, gave U.S.P. values of 20 and 10 IU, respectively, as compared with values (27) of 90 and 60 IU for the corresponding, unmodified, heparin fractions. The reduced size of all of these polymers may be an additional factor, in view of the relatively low anticoagulant assays given by enzymatically or chemically produced low-molecular-weight heparins.

On the basis of these findings, it is not unreasonable to suggest that the lack of uniform anticoagulant activity commonly found among heparins (see, e.g., refs. 6, 31, and 32) may be related in certain instances to the observations reported here because, as already noted, some heparins will have been exposed to a wide variety of pH conditions during their isolation and purification.

Experimental

Beef lung heparin was furnished by the Upjohn Co., and hog mucosal heparin by Choay-Chimie. The latter heparin, after conversion into the barium salt, was fractionated from aqueous ethanol mixtures, as described earlier (4, 27).

To induce the formation of modified heparin M-I, a solution of heparin or heparin fraction (40 mg; either the sodium salt, or the acid form obtained from the barium salt by ion exchange) in 10 mL of water was adjusted to pH 11.5 with 0.1 N NaOH, and the solution was lyophilized. In various related experiments, either the initial pH was varied from 10.0 to 11.8, or the solution was concentrated to dryness *in vacuo* at 35°C or, following the formation of M-I, the excess of sodium hydroxide was removed by ion exchange or dialysis. A solution of the product in 99.8% D_2O was then subjected to deuterium exchange by repeated evaporation, or lyophilization, and the deuterated product was examined by nmr spectroscopy at a concentration of 25–30 mg/mL of 99.9% D_2O, with internal sodium 4,4-dimethyl-4-silapentane-1-sulfonate as reference (δ 0.0).

By storage of the nmr specimen of M-I at 65–70°C, or higher, the formation of modified heparin M-III, under basic or neutral conditions, was monitored spectroscopically.

Modified heparin M-II was prepared as described for M-I, except that the initial pH was adjusted to 12.5–12.8, followed by lyophilization, and deuterium exchange. In other experiments, M-II was obtained by lyophilization of a solution of sodium heparin (40 mg) in either 0.05 N, 0.1 N, or 1 N sodium hydroxide (10 mL), followed by the removal of excess base with ion-exchange resin, or by dialysis. The product was pale yellow, suggesting that some elimination had also occurred, a possibility reinforced (33) by the presence of the olefinic doublet at δ 5.8.

The nmr spectra were recorded at 300 MHz with a Varian XL-300 spectrometer. The shift correlation (HETCOR) experiments were acquired at 25 or 65°C, using a spectral width of 4290 Hz with 1 K data points for 64 increments. The data were zero-filled in the evolution domain, providing a matrix of 1 K × 256. A shifted sine-bell function was used prior to the Fourier transformation. The relaxation delay between experiments was 0.4–1.0 s.

For acquisition of the COSY spectra (at either 25 or 65°C), a spectral window of 970 Hz was used, with 512 data points for 128–256 increments. The data were zero-filled and transformed with a sine-bell function, and the relaxation delay was 1 s.

[2]This raises the, as yet unresolved, question as to whether M-I and M-III consist of a mixture of unaltered and altered polymer chains, or mixed structures.

Can. J. Chem. Downloaded from www.nrcresearchpress.com by 194.225.253.170 on 09/07/12
For personal use only.

Acknowledgements

The authors acknowledge generous support from the Natural Sciences and Engineering Research Council of Canada. They are grateful to R. J. Wood, Health and Welfare Canada, for the USP and anti-XA assays, to K. R. Holme for the molecular weight estimations, and to J. Ing for the sulfate ion analyses. Some of the NMR spectra were kindly recorded by P. V. M. Tan at the High Field NMR Centre, Université de Montréal.

1. L. B. JAQUES and H. J. BELL. Methods Biochem. Anal. **7**, 253 (1959).
2. R. W. JEANLOZ. Methods Carbohydr. Chem. **5**, 150 (1965).
3. T. LAURENT. Arch. Biochem. Biophys. **92**, 224 (1961).
4. L. AYOTTE, E. MUSHAYAKARARA, and A. S. PERLIN. Carbohydr. Res. **87**, 297 (1980).
5. A. S. PERLIN and G. R. SANDERSON. Carbohydr. Res. **12**, 183 (1970); A. S. PERLIN, D. M. MACKIE, and C. P. DIETRICH. Carbohydr. Res. **18**, 185 (1971).
6. A. S. PERLIN, M. MAZUREK, L. B. JAQUES, and L. W. KAVANAGH. Carbohydr. Res. **7**, 369 (1968).
7. A. S. PERLIN, B. CASU, G. R. SANDERSON, and L. F. JOHNSON. Can. J. Chem. **48**, 2260 (1970).
8. G. GATTI, B. CASU, G. K. HAMER, and A. S. PERLIN. Macromolecules, **12**, 1001 (1979).
9. B. CASU, J. CHOAY, D. R. FERRO, G. GATTI, J. C. JACQUINET, M. PETITOU, A. PROVASOLI, M. RAGAZZI, P. SINAY, and G. TORRI. Nature, **322**, 215 (1986); J. Am. Chem. Soc. **108**, 6773 (1986).
10. A. S. PERLIN, B. CASU, G. R. SANDERSON, and J. TSE. Carbohydr. Res. **21**, 123 (1972).
11. J. K. N. JONES, M. B. PERRY, and J. C. TURNER. Can. J. Chem. **38**, 1122 (1960); H. J. JENNINGS and J. K. N. JONES. Can. J. Chem. **41**, 1151 (1963).
12. K. S. KIM, D. M. VYAS, and W. A. SZAREK. Carbohydr. Res. **72**, 25 (1979).
13. M. M. ABDEL-MALIK, Q. J. PENG, and A. S. PERLIN. Carbohydr. Res. **159**, 11 (1987).
14. M. M. ABDEL-MALIK and A. S. PERLIN. Carbohydr. Res. **189**, 123 (1989).
15. R. S. TIPSON. Adv. Carbohydr. Chem. **8**, 171 (1953).
16. A. S. PERLIN, N. M. Y. NG KIN, S. S. BHATTACHARJEE, and L. F. JOHNSON. Can. J. Chem. **50**, 2437 (1972).
17. K. R. HOLME and A. S. PERLIN. Carbohydr. Res. **189**, 301 (1989).
18. M. L. WOLFROM, R. A. GIBBONS, and A. J. HUGGARD. J. Am. Chem. Soc. **79**, 5043 (1957).
19. M. L. WOLFROM, J. R. VERCELLOTTI, and G. H. S. THOMAS. J. Org. Chem. **29**, 536 (1964).
20. Y. INOUE and K. NAGASAWA. Carbohydr. Res. **46**, 87 (1976).
21. L. AYOTTE and A. S. PERLIN. Carbohydr. Res. **145**, 267 (1986).
22. A. B. FOSTER and A. J. HUGGARD. Adv. Carbohydr. Chem. **10**, 335 (1955).
23. L. W. JAQUES, J. B. MACASKILL, and W. WELTNER, JR. J. Phys. Chem. **83**, 1412 (1979).
24. K. BOCK and C. PEDERSEN. Adv. Carbohydr. Chem. Biochem. **41**, 27 (1983).
25. A. MORT, J.-P. UTILLE, G. TORRI, and A. S. PERLIN. Carbohydr. Res. **121**, 221 (1983).
26. R. D. GUTHRIE. *In* The carbohydrates. Vol. 1A. *Edited by* W. Pigman and D. Horton. Academic, New York. 1972. p. 434.
27. L. AYOTTE, J. C. LORMEAU, and A. S. PERLIN. Thromb. Res. **22**, 97 (1981).
28. A. B. FOSTER, R. HARRISON, T. D. INCH, M. STACEY, and J. M. WEBBER. J. Chem. Soc. 2229 (1963); J. A. CIFONELLI. Methods Carbohydr. Chem. **7**, 139 (1976).
29. M. PETITOU, J. C. LORMEAU, and J. CHOAY. Thromb. Haemostasis, **58**, 7 (1987); C. A. A. VAN BOECKEL, J. E. M. BASTEN, H. LUCAS, and S. F. VAN AELST. Angew. Chem. Int. Ed. Engl. **27**, 1177 (1988).
30. R. REJ, M. JASEJA, and A. S. PERLIN. Thromb. Haemostasis, **61**, 3 (1989).
31. A. B. FOSTER and A. J. HUGGARD. Adv. Carbohydr. Chem. **10**, 335 (1955).
32. B. CASU. Adv. Carbohydr. Chem. Biochem. **43**, 51 (1985).
33. A. S. PERLIN, D. M. MACKIE, and C. P. DIETRICH. Carbohydr. Res. **18**, 185 (1971).

Can. J. Chem. Downloaded from www.nrcresearchpress.com by 194.225.253.170 on 09/07/12
For personal use only.

The effect of the nature of the amine leaving group on the nature of the E2 transition state for the reaction of 1-phenylethylammonium ions with sodium ethoxide in ethanol

PETER JAMES SMITH[1] AND MD. AMIN

Department of Chemistry, University of Saskatchewan, Saskatoon, Sask., Canada S7N 0W0

Received March 28, 1989

PETER JAMES SMITH and MD. AMIN. Can. J. Chem. **67**, 1457 (1989).

To investigate the effect of the leaving group on the elimination reaction of 1-phenylethylammonium ions with sodium ethoxide in ethanol at 60°C, the reaction of seven different quaternary ammonium salts and their β-deuterated analogues with trimethylamine, *N*-methylpiperidine, *N*-methyldiethylamine, triethylamine, *N,N*-dimethylbenzylamine, tripropylamine, and *N,N*-diethylbenzylamine as leaving groups has been studied. In all cases the elimination, which was shown to proceed via the concerted E2 process, was accompanied by competing substitution reactions. Although a significant dependence of the rate of the elimination process on the nature of the leaving group was noted, there was not any linear correlation with the basicity of the amine leaving group. The primary hydrogen–deuterium kinetic isotope effect for the elimination process, $(k^H/k^D)_E$, was found to increase initially with an increase of reaction rate, k_E^H, for substrates containing the leaving groups trimethylamine, *N*-methylpiperidine, *N*-methyldiethylamine, triethylamine, and *N,N*-dimethylbenzylamine; i.e., $(k^H/k^D)_E$ = 5.03, 5.26, 5.40, 5.83, and 5.85, respectively. A further increase in rate, using substrates with tripropylamine and *N,N*-diethylbenzylamine as leaving groups resulted in a decrease of the magnitude of the hydrogen–deuterium isotope effect; i.e., $(k^H/k^D)_E$ = 5.42 and 4.67, respectively. It is concluded that steric effects mainly determine leaving group ability. As well, it is concluded that the leaving group ability of the amine determines the structure of the E2 transition state. For the reaction of the poorer leaving groups, trimethylamine, *N*-methylpiperidine, and *N*-methyldiethylamine, the proton is *more than* one-half transferred at the transition state while for reaction involving the two best leaving groups, tripropylamine and *N,N*-diethylbenzylamine, the C_β—H bond is *less than* one-half broken at the transition state. The conclusions are considered in the light of the More O'Ferrall – Jencks potential energy surface diagram.

Key words: elimination mechanism, transition state, isotope effects, leaving group, quaternary salts.

PETER JAMES SMITH et MD. AMIN. Can. J. Chem. **67**, 1457 (1989).

Dans le but d'étudier l'effet du groupement nucléofuge sur la réaction d'élimination des ions 1-phényléthylammonium sous l'influence de l'éthylate de sodium dans l'éthanol à 60°C, on a étudié la réaction de sept sels d'ammonium quaternaire différents, ainsi que leurs analogues deutérés en position β, portant la triméthylamine, la *N*-méthylpipéridine, la *N*-méthyldiéthylamine, la triéthylamine, la *N,N*-diméthylbenzylamine, la tripropylamine et *N,N*-diéthylbenzylamine comme groupements nucléofuges. Dans tous les cas, l'élimination qui procède par un processus concerte E2 est accompagnée par les réactions de substitution qui sont en compétition. Même si on a noté une corrélation importante entre la vitesse du processus d'élimination et la nature du groupement nucléofuge, il n'existe aucune corrélation linéaire avec la basicité de l'amine qui quitte. On a trouvé que, au début de la réaction, l'effet isotopique cinétique primaire hydrogène–deutérium du processus d'élimination, $(k^H/k^D)_E$, augmente avec une augmentation de la vitesse de la réaction, k_E^H, pour les substrates contenant les groupements nucléofuges triméthylamine, *N*-méthylpipéridine, *N*-méthyldiéthylamine, triéthylamine et *N,N*-diméthylbenzylamine pour lesquels $(K^H/k^D)_E$ = 5,03, 5,26, 5,40, 5,83 et 5,85 respectivement. L'utilisation des groupements nucléofuges tripropylamine et *N,N*-diéthylbenzylamine provoque une autre augmentation de la vitesse de la réaction qui est accompagnée d'une diminution de l'amplitude de l'effet isotopique hydrogène–deutérium alors que $(k^H/k^D)_E$ = 5,42 et 4,67 respectivement. On en conclut que les effets stériques sont prédominants dans la facilité des groupements à agir comme nucléofuges. De plus, on conclut que la facilité d'une amine à partir détermine la structure de l'état de transition E2. Pour les réactions impliquant les groupements les moins aptes à agir comme agents nucléofuges, comme la triméthylamine, la *N*-méthylpipéridine et la *N*-méthyldiéthylamine, le proton est *plus qu'à moitié* transféré au moment de l'état de transition; par ailleurs, dans les réactions impliquant les deux meilleurs groupements nucléofuges, soit la tripropylamine et la *N,N*-diéthylbenzylamine, *moins que la moitié* de la liaison C_β—H est brisée au moment de l'état de transition. On considère les conclusions à la lumière du diagramme d'énergie potentielle de surface de More O'Ferrall – Jencks.

Mots clés : mécanisme d'élimination, état de transition, effets isotopiques, groupement nucléofuge, sels quaternaires.

[Traduit par la revue]

Introduction

The effect of the nature of the leaving group on the structure of the E2 transition state has been extensively studied (1–12) for the base-promoted 1,2 elimination reactions of several 2-phenylethyl compounds. However, no systematic investigation on the effect of the nature of the leaving group has been carried out for the elimination reaction of 1-phenylethyl substrates.

The study of the elimination reaction of most 1-phenylethyl compounds is complicated by competing substitution reactions. Hughes *et al.* (13) studied the reaction of 1-phenylethyl bromide with sodium ethoxide in ethanol and interpreted their results in terms of competing E1, E2, S_N1, and S_N2 processes. Subsequently, Sneen and Robbins (14) proposed an "ion-pair" mechanism for this reaction on the basis that the second-order rate constant k_2, calculated from eq. [1], decreased sharply as

$$[1] \quad k_{obs} = k_1 + k_2[OEt^-]$$

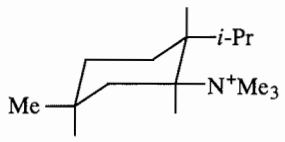
the ethoxide concentration increased. However, in an extensive study, McLennan (15) showed that the effect of base concentration on k_2 can be accounted for by a salt effect arising from ion pairing of the base to its counterion and concluded that the competing E1, E2, S_N1, and S_N2 processes satisfactorily account for the experimental results.

Tertiary amines are poor leaving groups and, hence, quaternary ammonium salts generally do not undergo elimination via a carbocation intermediate under solvolytic conditions. However,

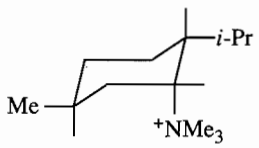
[1]Author to whom correspondence may be addressed.

Can. J. Chem. Downloaded from www.nrcresearchpress.com by 194.225.253.170 on 09/07/12
For personal use only.

it was reported (16) that the degradation of ax-7-cholestanyltrimethylammonium iodide in boiling ethanol proceeds via the E1 process. Similarly, Hughes and Wilby (17) proposed that menthyltrimethyl- and neomenthyltrimethylammonium hydroxides, **1** and **2**, underwent elimination in water by



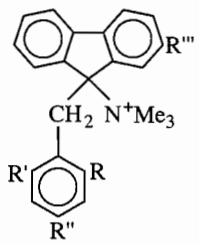
1



2

the E1 pathway, with the neomenthyl substrate showing a much greater affinity for reaction via the E1 mechanism than the menthyl substrate. The authors proposed that, since in the neomenthyl compound the trimethylammonium group is *cis* to the isopropyl group, the carbocation formation is made favourable due to a relief in steric strain in the molecule.

Recently, Smith and Pradhan (18) reported on the solvolysis of 2-substituted-9-(*ortho*-substituted phenylmethyl)fluoren-9-yltrimethylammonium ions, **3**, in various solvents. It was found



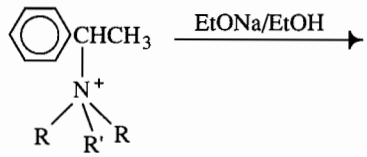
3

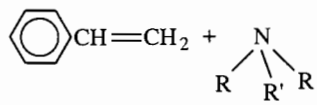
that when the phenyl ring contains no substituents in the *ortho* positions (R = R′ = H), the substrates were stable in ethanol. However, when one *ortho* position carried a substituent (R = CH_3, R′ = H), the salts were found to decompose in a first-order process to give both alkene and ether products. The addition of a second *ortho* substituent (R = R′ = CH_3) increased the rate significantly. The authors proposed that the loss of trimethylamine, a poor leaving group, is favoured by a relief of steric interaction between the *ortho* substituents and the onium group.

The effect of the nature of the amine leaving groups on the nature of the E2 transition state has been examined (3, 7, and footnote 2) for the reaction of several 2-phenylethylammonium salts. It was found that when the amine leaving group was made less basic the reaction rate increased. In fact, a reasonably good linear correlation was found[2] for a plot of log k_2 and the pK_a of the leaving group that had a slope, $\beta_{\text{leaving group}}$, of −0.25. An approximate linear correlation was found also to exist between the magnitude of the primary hydrogen–deuterium isotope effect observed for the reaction and the basicity of the leaving group. It was concluded[2] that a decrease in the basicity of the leaving group (increase in reaction rate) leads to a transition state with a decreased carbon–hydrogen bond rupture.

A preliminary study of the elimination reaction of 1-phenylethylammonium bromide with ethoxide in ethanol to give styrene has been carried out (20, 21). The observation of a positive Hammett ρ value of +0.98 together with a significant leaving group isotope effect, $[(k^{14}/k^{15})\text{-}1]100 = 1.34$, led the authors to conclude that the reaction proceeds via the concerted E2 mechanism with a transition state where the extent of C_β—H bond rupture is greater than the degree of C_α—N bond weakening (an E1cB-like E2 transition state).

To assess the possible effect of the nature of the leaving group in determining the mechanism of elimination (or changes in E2 transition state structure), it was decided in the present study to investigate the reaction of several 1-phenylethylammonium salts with ethoxide in ethanol at 60°C, eq. [2]. The possibility

[2] 



exists that by improving the leaving ability of the amine leaving group, reaction could proceed by way of the benzylic carbocation (E1 mechanism). Consequently, it might be possible to investigate the borderline between the E2 and E1 mechanisms (or a change from an E1cB-like E2 to an E1-like E2 transition state), by changing the leaving group in terms of both its basicity[2] and the extent of possible steric interactions of the leaving group with other atoms in the molecule (17, 18).

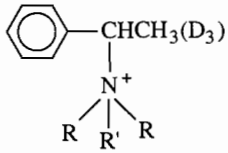
Results and discussion

Determination of the mechanism of the reaction of several 1-phenylethylammonium ions with ethoxide ion in ethanol at 60°C

As indicated in the Introduction, the possibility exists that the elimination reaction of the 1-phenylethylammonium salts with ethoxide in ethanol could proceed by a mechanism other than the usual one-step concerted E2 process.

To test for the possibility of reaction proceeding by rate-determining carbocation formation (E1 mechanism), the stability of all compounds investigated in the present study (**4–10**), as shown in Scheme 1, was determined by heating them in ethanol at 60°C for 2 days. Analysis of all the solutions showed no detectable absorption at 248 nm (λ_{max} for styrene). This observation excludes the possibility of reaction proceeding via the E1 mechanism.

The formation of the benzyl carbocation is not favoured for the reaction of substrates **4–10** in ethanol at 60°C where the amine leaving groups have pK_a values in H_2O ranging from 9 to 11. To further investigate the possible formation of the benzyl



4, R = CH_3; R′ = $C_6H_5CH_2$
5, R = CH_3CH_2; R′ = $C_6H_5CH_2$
6, R = R′ = CH_3
7, NR_2 =  ; R′ = CH_3
8, R = R′ = $CH_3CH_2CH_2$
9, R = CH_3CH_2; R′ = CH_3
10, R = R′ = CH_3CH_2

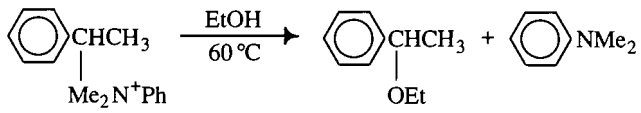
SCHEME 1

[2]T. S. Grover and P. J. Smith. Unpublished results.

Can. J. Chem. Downloaded from www.nrcresearchpress.com by 194.225.253.170 on 09/07/12
For personal use only.

carbocation it was decided to prepare *N,N*-dimethyl-*N*-(1-phenylethyl)anilinium bromide, **11**, since *N,N*-dimethylaniline (pK_a = 5.15 in H_2O) would be expected to be a much better leaving group than those listed above.

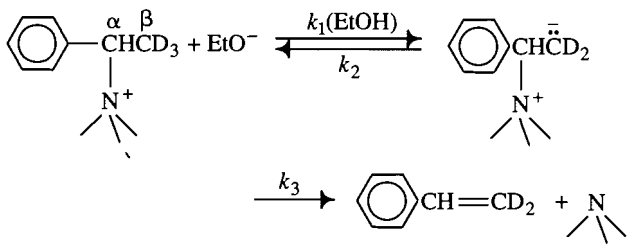
Upon heating **11** in ethanol at 60°C it was found that the absorbance measured at 248 nm (λ_{max} for styrene) increased gradually. Gas chromatographic analyses indicated, however, only the presence of ether **12** and *N,N*-dimethylaniline **13** (which has λ_{max} = 251 (22)), eq. [3]. Reaction of the quaternary

[3] 

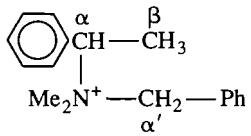
11 **12** **13**

ammonium salt **11** in ethanol, due to the good leaving group **13**, therefore proceeds via carbocation, which preferentially undergoes substitution rather than elimination. Due to the possibility of competition from this first-order process, no studies were carried out on the base-promoted reaction of salt **11**.

Reaction of salts **4–10** with sodium ethoxide in ethanol could proceed by way of the E1cB mechanism, eq. [4]. For reaction via the $(E1cB)_R$ mechanism, $k_2 \gg k_3$, the primary β-hydrogen–deuterium kinetic isotope effect is expected to be small or even inverse. On the other hand, reaction proceeding by way of the $(E1cB)_I$ process, $k_3 \gg k_2$, should exhibit a significant isotope effect (23).

[4] 

The base-promoted elimination reaction of all the quaternary ammonium salts studied, **4–10**, exhibited large primary hydrogen–deuterium isotope effects, $(k^H/k^D)_E > 4$, Table 1. This indicates that elimination is not proceeeding by way of the $(E1cB)_R$ mechanism. This conclusion receives support from the observation that the styrene isolated from the reaction of the β-trideuterated salts was exclusively β-dideuterated (gc–ms analysis), eq. [4]. Exchange of β-deuteriums with hydrogen from solvent ($k_2 \gg k_3$) would lead to the observation of less than two deuterium atoms at the β-position in styrene.

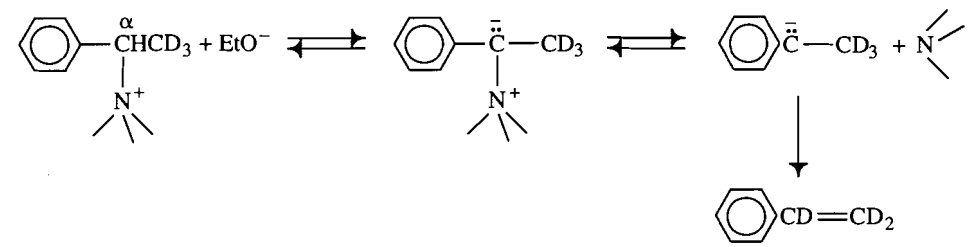


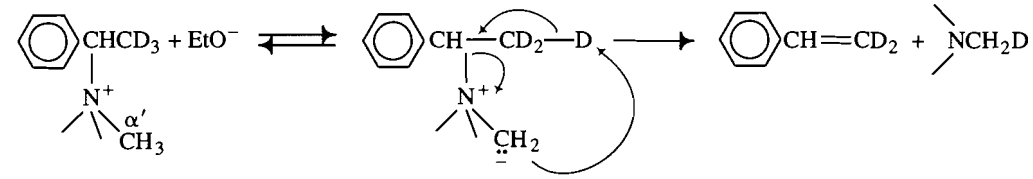
4

Reaction by way of the $(E1cB)_I$ mechanism is also excluded even though significant primary hydrogen–deuterium isotope effects were observed for the elimination reaction of all of the substrates. The rate of the elimination process should not be significantly affected by a change in the leaving group for the reaction proceeding by this mechanism since the carbon–nitrogen bond will be essentially intact at the transition state of the rate-determining k_1 step. However, in the present study, the rate of elimination has been found to change significantly when the leaving group is varied; i.e., $k_E = 3.60 \times 10^{-5}$ and 90.2×10^{-5} L mol^{-1} s^{-1} for reaction involving the leaving groups trimethylamine and *N,N*-diethylbenzylamine, respectively, Table 1. These results indicate that rupture of the C—N bond is involved in the rate-limiting step, a conclusion that is inconsistent with the $(E1cB)_I$ mechanism.

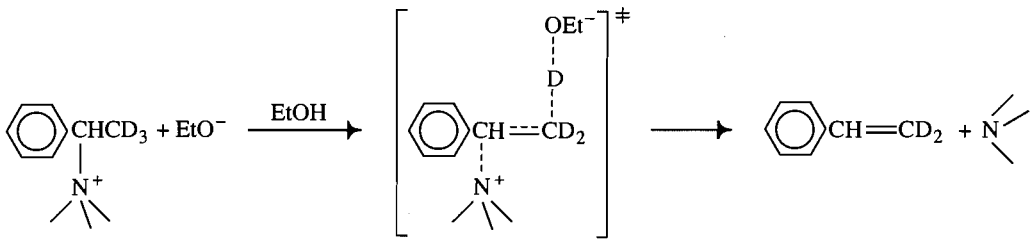
Two further mechanisms must be considered for the base-promoted elimination reaction of the 1-phenylethylammonium salts, since the acidity of both the α- and α′-hydrogens is expected to be greater than the β-hydrogens, **4**. Consequently, the possibility of reaction proceeding via either the carbene, eq. [5], or ylide, eq. [6], mechanisms was investigated by analyzing the products obtained from reaction involving all β-d_3 substrates. If a reaction involves a carbene intermediate, eq. [5], the resulting styrene will be completely deuterated at both the α and β carbons, while the amine product obtained from the reaction of the same substrate will contain deuterium, eq. [6], if a reaction involves the ylide intermediate. The gc–ms analyses showed that only the β-dideuterated styrenes were formed and the amine products did not contain deuterium. Thus reaction involving either the carbene or ylide intermediates is excluded.

All the experimental information reported herein supports the conclusion that the reaction of all the 1-phenylethylammonium salts with ethoxide ion in ethanol follows the concerted one-step pathway, eq. [7]. The significant primary hydrogen–deuterium isotope effects and leaving group effect indicate appreciable rupture at the transition state **14** of both the carbon (β)–hydrogen and carbon (α)–nitrogen bonds. The observation of the β-dideuterated styrene, when the reactants were trideuterated at C_β, is also consistent with the E2 mechanism.

[5] 

[6] 

Can. J. Chem. Downloaded from www.nrcresearchpress.com by 194.225.253.170 on 09/07/12
For personal use only.

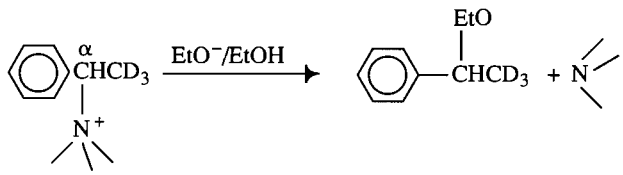
[7] 

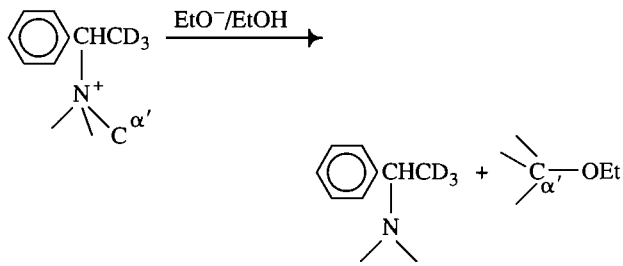
14

Effect of the nature of the amine leaving group on the nature of the E2 transition state for the reaction of 1-phenylethylammonium ions with ethoxide ion in ethanol at 60°C

Preliminary studies on the reaction of substrates **4–10**, and their β-d_3 analogues, with ethoxide ion in ethanol showed that the elimination process to give styrene was not the sole reaction. Whereas the undeuterated salts gave mainly styrene as product; i.e., % styrene = 97.3, 94.0, 97.3, 99.2, 98.2, 90.0, and 81.4 for reaction of salts **4–10**, respectively, the β-d_3 analogues of **4–10** gave significant amounts of substitution products; i.e., 84.7, 80.1, 87.3, 91.6, 83.1, 65.0, and 75.8% styrene, respectively, Table 1.

Optical density measurements at infinity for the reactions, as well as gas chromatographic – mass spectrometric analyses, indicated that the elimination process was accompanied by two competing substitution reactions. It was shown that nucelophilic attack of ethoxide ion occurs at both the benzylic carbon (C_α) and at $C_{\alpha'}$ of the leaving group, eqs. [8] and [9], respectively.

[8] 

[9] 

The extent of substitution at C_α for the reaction of the β-d_3 analogues of **4–10** was found to be 2.0, 6.0, 2.2, 4.8, 16.9, 2.0, and 3.2%, respectively, while substitution occurred at $C_{\alpha'}$ for the same compounds to the extent of 13.3, 13.9, 10.5, 3.6, 0, 33, and 21%, respectively. In cases where there were two different α′ carbons, substitution occurred exclusively at the benzylic carbon of the leaving group in **4**, only at the methyl group of **7**, and only at the ethyl group of **9**. For reaction of **5** both $C_6H_5CH(NEt_2)CD_3$ (3.5%) and $C_6H_5CH(BzNEt)CD_3$ (10.4%) were produced.

Since in all cases substitution reactions are competing with the elimination process under investigation, the decreased amount of alkene formation observed for the reaction of the β-d_3 compounds as compared with that found for the reaction of the undeuterated **4–10** salts can be readily ascribed to the operation of the primary hydrogen–deuterium isotope effect observed for the concerted E2 process, Table 1. The relative amounts of substitution products, formed from the competing S_N2 processes involving attack at both C_α and $C_{\alpha'}$, can also be qualitatively accounted for by considering both the steric and electronic factors associated with the bimolecular substitution reactions.

As mentioned in the Introduction, an objective of the present study was to investigate the effect of the amine leaving group on the nature of the E2 transition state for the reaction of the 1-phenylethylammonium ions with ethoxide in ethanol at 60°C. Accordingly, the overall rate of the reaction of the salts **4–10**, and their β-d_3 analogues, with ethoxide in ethanol was determined by measuring the formation of the alkene product at 248 nm (where the uv spectra of the substitution products did not show any absorption). The observed overall rate constant k_2, the percent of alkene, the rate constant of the E2 process k_E (calculated from the overall rate constant and the percentage of the elimination reaction), and the primary hydrogen–deuterium isotope effect for the elimination process $(k^H/k^D)_E$, are given in Table 1 along with the pK_a values in water of the various amine leaving groups.

The effect of changes in substrate and base concentrations on the magnitude of the second-order rate constants, k_2 and k_E, was investigated for the reaction of compounds **4**, **5**, and **6**, Table 2. It is seen that when the concentration of both reactants is decreased, a corresponding increase in the magnitude of k_2 and k_E is observed; i.e., $k_2 = 15.0 \times 10^{-5}$ and 25.2×10^{-5} and $k_E = 14.6 \times 10^{-5}$ and 24.5×10^{-5} L mol^{-1} s^{-1} for **4** when the substrate and the ethoxide concentration are changed from 0.1016 and 0.2238 to 0.0511 and 0.1119 M, respectively. Such a dependence of rate constants on substrate and base concentrations can be considered to be due to a salt effect. Such an effect is predicted by the Hughes–Ingold theory of solvent effect (24) and reported (25, 26) for several reactions of onium salts with base. Consequently, in the present study, all rate constant measurements were carried out using the same base and ammonium salt concentrations, ca. 0.150 M and ca. 0.052 M, respectively.

A consideration of the data in Table 1 indicates that the rate constant for elimination k_E changes significantly when the leaving group is varied; i.e., $k_E = 90.2 \times 10^{-5}$ and 3.6×10^{-5} L mol^{-1} s^{-1} for reaction involving the leaving groups *N,N*-diethylbenzylamine and trimethylamine, respectively. However, since the leaving groups are arranged in the table in terms of their pK_a values, it is clear that there is not a linear relationship between the basicity of the amine leaving group and the magnitude of k_E. For example, for reaction of compounds **4**, **5**, and **6**, where the pK_a values of the respective leaving groups are 9.02, 9.48, and 9.81, the rate constant for the elimination k_E varies in the order of 29.0×10^{-5}, 90.2×10^{-5}, and 3.60×10^{-5} L mol^{-1} s^{-1}, respectively.

The relationship between the rate of elimination and the basicity of the amine leaving group can be seen from the Brønsted plot of log k_E^H versus the pK_a of the leaving group, Fig. 1.

Can. J. Chem. Downloaded from www.nrcresearchpress.com by 194.225.253.170 on 09/07/12
For personal use only.

TABLE 1. Rate constants, pK_a values, and primary k^H/k^D for the different amine leaving groups for the reaction of 1-phenylethylammonium ions, $C_6H_5CH(Y)CX_3$, with EtONa/EtOH at 60°C

Substrate	Leaving group (Y)	pK_a[a,b]	X	k_2[c] × 10^5, L mol^{-1} s^{-1}	% alkene	k_E[d] × 10^5, L mol^{-1} s^{-1}	$(k^H/k^D)_E$
4	*N,N*-Dimethylbenzylamine	9.02	H	29.8±0.3	97.3±0.3[e]	29.0±0.3[e]	5.85±0.06[f]
			D	5.86±0.02	84.7±0.5	4.96±0.02	
5	*N,N*-Diethylbenzylamine	9.48	H	96.0±1.1	94.0±0.5	90.2±1.1	4.67±0.06
			D	24.1±0.1	80.1±0.6	19.3±0.1	
6	Trimethylamine	9.81	H	3.70±0.02	97.3±0.2	3.60±0.2	5.03±0.04
			D	0.82±0.01	87.3±0.4	0.716±0.001	
7	*N*-Methylpiperidine	10.08	H	6.00±0.03	99.2±0.7	5.95±0.03	5.26±0.10
			D	1.23±0.03	91.6±1.0	1.13±0.02	
8	Tripropylamine	10.26	H	53.4±1.3	98.2±0.5	52.4±1.3	5.42±0.18
			D	11.6±0.2	83.1±1.0	9.66±0.21	
9	*N*-Methyldiethylamine	10.35	H	10.0±0.1	90.0±1.0	9.02±0.06	5.40±0.20
			D	2.57±0.08	65.0±2.0	1.67±0.06	
10	Triethylamine	11.01	H	29.6±0.2	81.4±0.5	24.1±0.1	5.83±0.05
			D	5.45±0.04	75.8±2.5	4.13±0.03	

[a]The pK_a values were determined in water at 25°C (45).
[b]While the absolute value of pK_a will change when solvent is changed, the trend in pK_a should *not* (46).
[c]k_2 is the overall rate constant.
[d]k_E is the rate constant for elimination.
[e]Standard deviation.
[f]Deviation = $\pm(k^H/k^D)_E[(r^H/k^H)^2 + (r^D/k^D)^2]^{1/2}$ where r is the standard deviation in k_E.

TABLE 2. Rate constants for the reaction of several 1-phenylethylammonium ions, $C_6H_5CH(Y)CH_3$, with EtONa/EtOH at 60°C

Compound no.	Leaving group (Y)	Initial concentrations, mol L^{-1}		k_2[a] × 10^5, L mol^{-1} s^{-1}	% alkene	k_E[b] × 10^5, L mol^{-1} s^{-1}
		Substrate	Ethoxide			
4	*N,N*-Dimethylbenzylamine	0.1016	0.2238	15.0	97.3	14.6
		0.0511	0.1119	25.2		24.5
5	*N,N*-Diethylbenzylamine	0.1128	0.2235	39.4	94.0	37.0
		0.0479	0.1117	73.8		69.4
6	Trimethylamine	0.1010	0.2234	2.60	97.3	2.53
		0.0341	0.1124	4.80		4.67

[a]k_2 is the overall rate constant.
[b]k_E is the rate constant for elimination.

The obvious absence of a linear correlation, as compared with the reasonably good linear plot found for the reaction of the corresponding 2-phenylethylammonium ions,[2] indicates that in the present system the rate of elimination is not simply related to the basicity of the leaving group. In other words, there must be more than one factor, including the basicity of the leaving group, that determines the reaction rate for the elimination reaction of the 1-phenylethylammonium ions.

Leaving group ability (nucleofugality) has been investigated in detail for several elimination processes (27–35). It has been pointed out (32) that it is difficult to quantitatively evaluate the nucleofugality of a particular leaving group for reaction proceeding by the concerted E2 mechanism where the rupture of both the β-carbon–hydrogen and α-carbon – leaving group bonds occurs at the transition state. However, properties such as inductive effect and polarizability, which allow the leaving group to accept electron density at the transition state (34), as well as steric factors (18), are considered to be important.

To investigate the possible inductive effect of the onium groups of substrates **4–10** on the acidity of both the α and β hydrogens, the chemical shifts of these hydrogens were determined using a 300-MHz nmr spectrometer, Table 3. Although there does not appear to be any relationship between the chemical shift of the α hydrogens and the pK_a value of the amine leaving group, it is noted that for the two best leaving groups, **4** and **5**, the chemical shifts of the β hydrogens of 1.90 and 1.85 ppm, respectively, are significantly greater than the average value of 1.71 ppm found for the other leaving groups. The enhanced reactivity of compounds **4** and **5**, therefore, could be partly due to an increased facility for deprotonation arising from the inductive effect of the positive nitrogens.

Examination of the Brønsted plot, Fig. 1, reveals the absence of a linear correlation between log k_E and pK_a for all of the amine leaving groups studied. However, a reasonably good straight line with a positive slope can be drawn through the points representing the leaving groups trimethylamine, *N*-

Can. J. Chem. Downloaded from www.nrcresearchpress.com by 194.225.253.170 on 09/07/12
For personal use only.

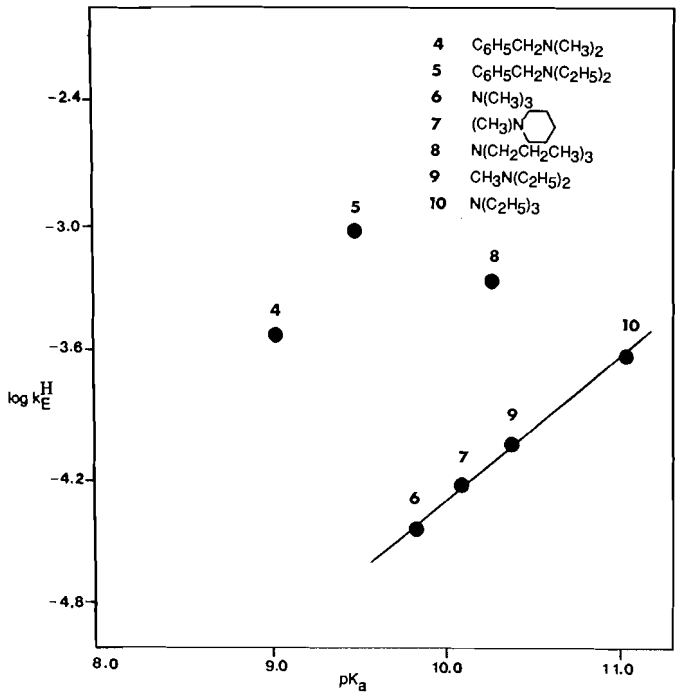
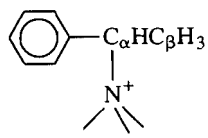


FIG. 1. Plot of log k_E^H versus pK_a of the leaving group for the reaction of 1-phenylethylammonium ions with EtONa / EtOH at 60°C.

TABLE 3. The pK_a values of the amine leaving groups and the proton nmr chemical shifts of the α and β hydrogens of 1-phenylethylammonium salts



Substrate	Leaving groups	pK_a	Chemical shifts, δ (DMSO-d_6), ppm α-H	β-H
4	*N,N*-Dimethylbenzylamine	9.02	5.18	1.90
5	*N,N*-Diethylbenzylamine	9.48	4.91	1.85
6	Trimethylamine	9.81	4.96	1.73
7	*N*-Methylpiperidine	10.08	5.09	1.72
8	Tripropylamine	10.26	4.80	1.71
9	*N*-Methyldiethylamine	10.35	4.82	1.69
10	Triethylamine	11.01	4.85	1.71

methylpiperidine, *N*-methyldiethylamine, and triethylamine, compounds **6**, **7**, **9**, and **10**, respectively. A possible explanation for this correlation is that both pK_a and log k_E increase progressively due to an increase in size of the leaving groups; i.e., from trimethylamine through to triethylamine. In other words, as the ability of the amine to attract a proton decreases, the leaving group ability increases. Consequently, it is suggested that for the reaction of the 1-phenylethylammonium ions with ethoxide in ethanol, the size of the leaving group mainly determines the reaction rate.

Molecular models indicate that there are significant steric interactions between the 1-phenylethyl and onium groups. An increase in the size of the alkyl groups on nitrogen, therefore, will enhance this steric effect and, consequently, reaction will be favoured due to a decrease in these interactions at a transition state that has been shown to have appreciable carbon–nitrogen bond rupture (21).

An alternative explanation of this increased reactivity, when the bulkiness of the leaving group is increased, is a solvation effect. The relative effective sizes of the ammonium groups will determine the relative extents of solvation in the polar ethanol solvent. Since it has been suggested (36) that due to steric factors the positive nitrogen cannot be directly solvated, solvation at the nearby α′ hydrogens must be important. Consequently, the α′ carbons of the larger alkyl groups attached to nitrogen will be solvated to a lesser extent.

Since there is significant carbon – leaving group bond rupture at the activated complex for the reaction of 1-phenylethyltrimethylammonium ion with ethoxide, $[(k^{14}/k^{15})\text{-}1]100 = 1.34$ (18), it is reasonable to conclude that differential solvation between the various ammonium ions might account to some degree for the observed rate differences. The less solvated higher energy substrate molecule will have a greater tendency to proceed to the transition state and, hence, will be more reactive towards ethoxide ion.

The points representing the compounds with the three largest leaving groups, **4**, **5**, and **8**, where it is expected that solvation of the onium group will be less effective, lie significantly above the line through the points **6**, **7**, **9**, and **10** on the log k_E^H versus pK_a plot, Fig. 1. The deviations increases in the order expected for increasing size; i.e., tripropylamine (**8**), *N,N*-dimethylbenzylamine (**4**), and *N,N*-diethylbenzylamine (**5**), respectively. This enhanced reactivity compared with compounds **6**, **7**, **9**, and **10** (where the size of the onium group was systematically increased) can be considered as being due to an appreciable decrease in solvation when, for example, an *N*-methyl group is replaced by a benzyl group. This solvation effect perhaps accounts for the increased chemical shifts of the β-hydrogens of compounds **4**, and **5**, which were noted earlier.

As mentioned in the Introduction, a reasonably good linear correlation between the reaction rate and the magnitude of the primary hydrogen–deuterium isotope effect was found for the E2 reaction of 2-phenylethylammonium ions with ethoxide ion when the amine leaving group was varied.[2] The increase in the magnitude of both the rate constant and the isotope effect was interpreted in terms of an E2 transition state where the extent of carbon–hydrogen bond rupture decreases for reaction involving the better leaving groups. It was considered that in all cases the proton was more than one-half transferred to base at the transition state (2, 23, 37, 38).

To measure the relative extent of C—H bond rupture at the E2 transition state for reaction involving the various 1-phenylethylammonium ions with ethoxide, the primary hydrogen–deuterium kinetic isotope effects for the elimination process, $(k^H/k^D)_E$, were examined, Table 1, A plot of $(k^H/k^D)_E$ against log k_E^H is shown in Fig. 2.

It is seen that $(k^H/k^D)_E$ *increases* approximately in a linear fashion with increasing reactivity of the substrates **6**, **7**, **9**, and **10** with leaving groups trimethylamine, *N*-methylpiperidine, *N*-methyldiethylamine, and triethylamine, respectively; i.e., $(k^H/k^D)_E = 5.03$, 5.26, 5.40, and 5.83 when $k_E^H = 3.60 \times 10^{-5}$, 5.95×10^{-5}, 9.02×10^{-5}, and 24.1×10^{-5} L mol^{-1} s^{-1}, respectively, Table 1 and Fig. 2. This relationship between the magnitude of $(k^H/k^D)_E$ and the reaction rate is in the same direction as that found for the corresponding reaction of the 2-phenylethylammonium ions (23) and suggests that the transition state for the E2 reaction of the 1-phenylethylammonium

Can. J. Chem. Downloaded from www.nrcresearchpress.com by 194.225.253.170 on 09/07/12
For personal use only.

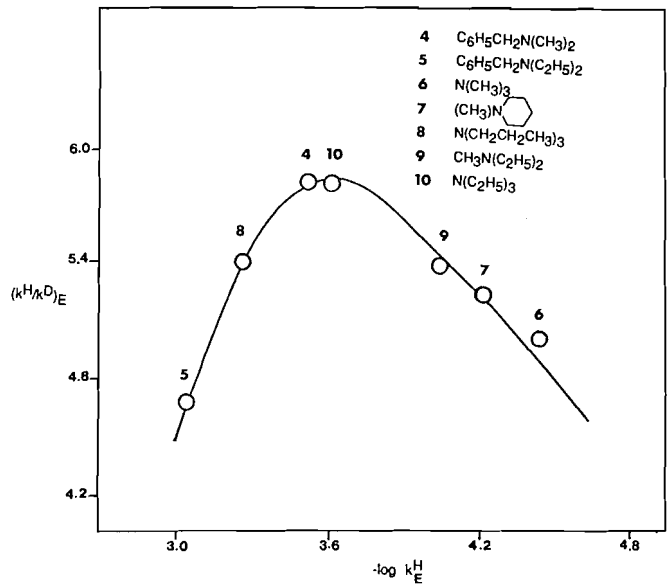


FIG. 2. Plot of $-\log k_E^H$ versus $(k^H/k^D)_E$ for the reaction of 1-phenylethylammonium ions with EtONa / EtOH at 60°C.

ions **6**, **7**, **9**, and **10** has the proton *more than* one-half transferred to base. The increase in the magnitude of $(k^H/k^D)_E$ on going to a better leaving group indicates, therefore, a *decrease* in the extent of carbon–hydrogen bond rupture at the activated complex.

Further increases in reaction rate for the substrates with the three best leaving groups *N,N*-dimethylbenzylamine (**4**), tripropylamine (**8**), and *N,N*-diethylbenzylamine (**5**), however, led to a *decrease* in the magnitude of $(k^H/k^D)_E$; i.e., $(k^H/k^D)_E = 5.85, 5.42, 4.67$ when $k_E^H = 29.0 \times 10^{-5}$, 52.4×10^{-5}, and 90.3×10^{-5} L mol^{-1} s^{-1}, respectively, Table 1 and Fig. 2. Such a decrease in $(k^H/k^D)_E$ with increasing reactivity of the onium salts is consistent with a reactant-like transition state for proton transfer where the hydrogen is *less than* one-half transferred to the base ethoxide. This conclusion is noteworthy since the base-promoted 1,2 elimination reactions of quaternary ammonium salts (involving the poor leaving groups, tertiary amines) have been found to proceed via the concerted E2 pathway with an E1cB-like E2 transition state where the C_β—H bond is more than one-half broken (23, 39, 40).

The plot of $(k^H/k^D)_E$ versus log k_E^H, Fig. 2, resembles a Westheimer (37) – Melander (38) type of curve where the substrates **6**, **7**, and **9**, with the poorest leaving groups trimethylamine, *N*-methylpiperidine, and *N*-methyldiethylamine, respectively, lie on the right hand side, indicating that their respective E2 transition states have the hydrogen more than one-half transferred to the base. The onium salts **8** and **5**, with the best leaving groups tripropylamine and *N,N*-diethylbenzylamine, respectively, lie on the left side of the curve, suggesting a transition state where the hydrogen is closer to the β carbon than the abstracting base. Substrates **10** and **4**, with leaving groups triethylamine and *N,N*-dimethylbenzylamine, respectively, lie at or near the maximum of the curve and, hence, have an E2 transition state where the hydrogen that is being transferred is approximately equidistant between the β carbon and ethoxide ion. To our knowledge this is the second example (41) where a Westheimer–Melander type of curve has been realized for the elimination reaction of a single substrate where the leaving group has been varied.

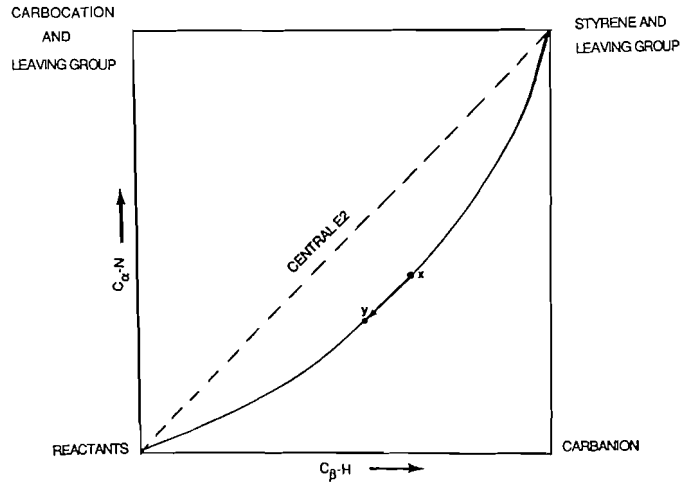


FIG. 3. More O'Ferrall – Jencks diagram showing the effect of changing the leaving group on the transition state structure for the elimination reaction of 1-phenylethylammonium ions with ethoxide ion.

The conclusion reached in the present study that an increase in leaving group ability (increase in k_E^H) leads to a progressive decrease in the extent of β-carbon–hydrogen bond rupture at the transition state can be examined in the light of a More O'Ferrall (42) – Jencks (43) energy surface diagram[3] as represented in Fig. 3. The *x*- and *y*-axes in the plane represent the extent of C_β—H and C_α—N bond rupture, respectively, while the axis perpendicular to the plane represents the potential energy. Reactants are located at the bottom left and the products at the top right corners. The possible carbocation and carbanion intermediates are located at the other two corners.

A consideration of the magnitude of both the primary hydrogen–deuterium and nitrogen isotope effects has been considered (20, 21) to provide strong evidence that the transition state for the E2 reaction of 1-phenylethyltrimethylammonium ion (this substrate has the poorest leaving group in the present study) with ethoxide ion lies to the right of the diagonal in Fig. 3, point x, where C_β—H bond weakening is more advanced than C_α—N bond rupture (an E1cB-like E2 transition state). An increase in the energy of the reactants, raising the bottom left corner, will lead to a shift in transition state structure towards the reactant corner, $x \rightarrow y$, for motion along the reaction coordinate,[4] as represented by the curved solid line in the figure. Consequently, an increase in the reactivity of the reactants (increase in steric interactions within the molecule and (or) decrease in solvation due to the size of the onium group) will result in a decrease in C—H bond rupture at the transition state. This conclusion is in accord with the conclusions reached from a consideration of the primary hydrogen–deuterium isotope results.

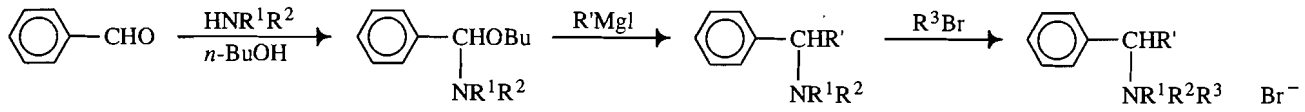
Experimental

All melting points and boiling points are uncorrected. Elemental analyses were carried out at the Guelph Chemical Laboratories Ltd, Guelph, Ontario. The nmr spectra were taken using Varian T60 and Bruker AM-300 multinuclear Fourier-transform spectrometers. The

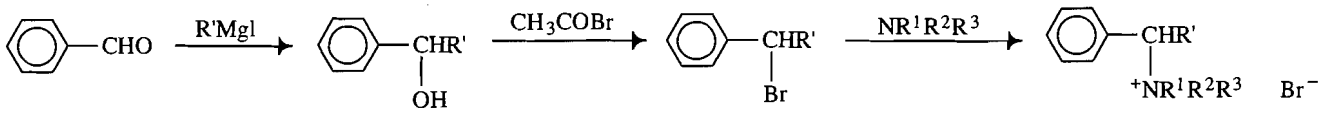
[3]A more recent model, which considers the geometrical nature of transition state variation, has been proposed (44).

[4]The relative difference in stability of various amine leaving groups is considered to be small and, hence, the perpendicular effect, as determined by raising or lowering the top left corner, is neglected.

Can. J. Chem. Downloaded from www.nrcresearchpress.com by 194.225.253.170 on 09/07/12
For personal use only.



SCHEME 2



SCHEME 3

ultraviolet absorbances were recorded using a Hewlett Packard 8451A diode array spectrophotometer. Mass spectra were recorded on an AEI MS-12 equipped with a vacuum retrofit. Analytical gas chromatography was carried out using a Hewlett Packard 5890 gas chromatograph equipped with a flame ionization detector. All reagents and solvents were reagent grade and were dried and purified by the usual procedures.

The synthetic procedures for most of the compounds in this study were similar and are outlined in Scheme 2, except for 1-phenylethyltripropylammonium (**8**) and *N,N*-dimethyl-*N*-(1-phenylethyl)anilinium (**11**) ions, which were prepared by the procedure outlined in Scheme 3. The deuterated substrates were better than 99% deuterated since nmr and mass spectrometric analyses indicate complete deuteration.

α-Dialkylaminobenzyl n-butyl ethers

To a 500-mL two-neck round bottom flask fitted with a reflux condenser capped with a calcium chloride drying tube and a magnetic stirrer were added 0.2 mol of aldehyde, 0.22–0.24 mol of amine, 0.2 mol of anhydrous potassium carbonate, and 1.0 mol of butanol-1. With the exception of the dimethylamine and diethylamine experiments, which were done at room temperature, the reactants were stirred for 24 h at an outside temperature of 70–80°C. After cooling to room temperature, excess chloroform was added to facilitate the filtration. The filtrate was evaporated by using a rotary evaporator with bath temperature at about 100°C. The residue, which consisted mainly of the desired amino ether, was purified by distillation under reduced pressure. The amino ethers were characterized by nmr spectroscopy. Most of the amino ethers were found to decompose if they were left for several days and, therefore, were immediately used for the next experiments. The boiling points, yields, and characteristics of the proton nmr spectra of the amino ethers are listed in Table 4.

1-Phenylethanol

In a 500-mL two-neck flask equipped with a magnetic stirrer, an addition funnel, and a double surface condenser with a drying tube at the top, were placed 3.64 g (0.15 mol) of dry magnesium turnings and 50 mL of sodium-dry ether. A stream of dry nitrogen gas was passed through the flask to remove any moisture. Methyl iodide (21.3 g, 0.15 mol) was placed in the addition funnel and a small amount of it was added to initiate the reaction. Ether (150 mL) was then poured through the condenser to slow down the reaction and the rest of the methyl iodide was added at such a rate as to maintain a gentle reflux of the solvent. After the addition was completed, the reactants were stirred for 2 h. Benzaldehyde (0.1 mol) in an equal volume of ether was then added slowly to the Grignard solution over a period of 2 h. The reaction mixture was further stirred overnight. The mixture was poured into 300 g of crushed ice contained in a large beaker and 10% HCl (300 mL) was then added slowly with rapid stirring. The two layers were separated and the aqueous layer was extracted with ether (3 × 100 mL). The ether extracts were combined with the original solution and dried over anhydrous sodium sulfate. Removal of the ether by using a rotary evaporator gave a pale yellow liquid. Distillation under reduced pressure gave a colorless liquid; 86% yield, bp 82–84°C / 0.5 Torr. (lit. (21) bp 79–81°C / 0.4 Torr (1 Torr = 133.3 Pa) lit. (22) bp 100°C / 18 Torr).

1-Phenylethanol-2.2.2.d_3 was prepared from benzaldehyde and methyl-d_3 iodide in the same way; bp 81–83°C / 0.5 Torr.

1-Phenylethyl bromide

Acetyl bromide (24.4 g, 0.2 mol) was added all at once to the 1-phenylethanol (0.1 mol) in a 100-mL round bottom flask. The reaction was vigorous and the reaction mixture was stirred for a further 5–10 min. Acetic acid and excess reagents were removed by using a rotary evaporator and the resulting pale yellow oil was distilled under reduced pressure to give colorless 1-phenylethyl bromide; 80% yield, bp 38–40°C / 0.05 Torr (lit. (21) bp 45–55°C / 0.1 Torr, lit. (22) bp 85°C / 13 Torr).

1-Phenylethyl-2,2,2-d_3 *bromide* was prepared from 1-phenylethanol-2,2,2-d_3 in the same way; bp 38–40°C / 0.05 Torr.

N,N-*Dialkyl-1-phenylethylamines*

Dry magnesium turnings (2.4 g, 0.1 mol) and 50 mL of sodium-dry ether were placed in a 250-mL two-neck round bottom flask fitted with a double surface condenser capped with a drying tube, an addition funnel, and a magnetic stirrer. The system was flushed with nitrogen to remove moisture. Methyl iodide (14.2 g, 0.1 mol) was placed in the addition funnel and a small amount of it was added to initiate the reaction. Ether (100 mL) was then poured through the condenser to slow down the reaction and the rest of the methyl iodide was added dropwise at such a rate as to maintain a gentle reflux of the solvent. After the addition was complete, the reactants were stirred for an additional 2 h. The corresponding α-dialkylaminobenzyl *n*-butyl ether (0.05 mol) was dissolved in an equal volume of diethyl ether and then added slowly to the Grignard solution over a period of 1 h. The reaction mixture was further stirred overnight. The mixture was then poured into a 1:1 mixture (w / w) of ammonium chloride (0.1 mol) and ice chips. After cooling, 10% sodium hydroxide solution (ca. 100 mL) was added and the mixture was shaken well. The ether layer was decanted and the aqueous layer was shaken for a few times with fresh ether and decanted. The ether extracts were combined and dried over magnesium sulfate. The solvent was evaporated and the residue was distilled under reduced pressure. The synthetic results are listed in Table 5.

N,N-*Dialkyl-1-phenylethylamines-2,2,2-*d_3 were prepared in the same way from the respective α-dialkylaminobenzyl *n*-butyl ether and methyl-d_3 iodide.

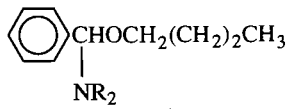
Benzyldimethyl-1-phenylethylammonium bromide (4)

Into a 200-mL round bottom flask fitted with a condenser with a magnetic stirrer were placed *N,N*-dimethyl-1-phenylethylamine (0.05 mol), dry ether (75 ml), and the benzyl bromide (17.1 g, 0.1 mol). The reactants were stirred overnight while the salt precipitated. The precipitate was filtered off and washed several times with ether to remove the unreacted benzyl bromide. The crude product was recrystallized at least three times from acetone / ether; 88% yield; mp 154–155°C; ^{1}H nmr δ (DMSO-d_6): 7.46–7.80 (m, 10H, aromatic), 5.18 (q, 1H, CH), 4.65 and 4.53 (AB system, 2H, NCH_2,[5] J = 12.4 Hz), 2.87 (s, 3H,

[5]These benzylic protons are diastereotopic and form an AB system. For the measurement of chemical shifts and coupling constant in an AB system, see ref. 48.

Can. J. Chem. Downloaded from www.nrcresearchpress.com by 194.225.253.170 on 09/07/12
For personal use only.

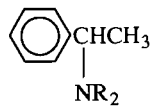
TABLE 4. The boiling points, yields, and characteristics of the proton nmr spectra for the α-dialkylaminobenzyl *n*-butyl ethers



NR_2	Boiling point °C/ Torr (lit.)	Yield, %	^{1}H nmr δ($CDCl_3$), ppm from TMS			
			Aromatic	CH	CH_2	CH_3
NMe_2	64/0.25 (108–109/1)[a]	83.3	7.15–7.45(m, 5H)	4.8(s, 1H)	3.2–3.7(m, 2H, OCH_2) 1.55–1.7(m, 2H, CH_2) 1.35–1.5(m, 2H, CH_2)	2.3(s, 6H, NCH_3) 0.92(t, 3H, CH_3)
	108–109/0.55 (153–154/1)[a]	65	7.2–7.6(m, 5H)	4.8(s, 1H)	3.35–3.8(m, 2H, OCH_2) 2.3–2.8(m, 4H, NCH_2) 1.2–1.9(m, 10H, CH_2)	0.92(t, 3H, CH_3)
NEt_2	98–100/0.4	35	7.2–7.7(m, 5H)	5.0(s, 1H)	3.38–3.7(m, 2H, OCH_2) 2.67(q, 4H, NCH_2) 1.5–1.7(m, 2H, CH_2) 1.35–1.5(m, 2H, CH_2)	1.01(t, 6H, CH_3) 0.93(t, 3H, CH_3)

[a]Reference 47.

TABLE 5. The boiling points, yields, and characteristics of the proton nmr spectra of *N,N*-dialkyl-1-phenylethyl amines



NR_2	Boiling point °C/Torr (lit.)	Yield, %	^{1}H nmr δ($CDCl_3$), ppm from TMS			
			Aromatic	CH	CH_2	CH_3
NMe_2	28–29/0.5 (80–81/10)[a]	69	7.2–7.6(m, 5H)	3.3(q, 1H)	—	2.19(s, 6H, NCH_3) 1.36(d, 3H)
	70–71/0.4	74	7.0–7.5(m, 5H)	3.4(q, 1H)	2.15–2.6(m, 4H, NCH_2) 1.25–1.80(m, 6H, CH_2)	1.38(d, 3H)
NEt_2	41–43/0.2	75	7.2–7.6(m, 5H)	3.8(q, 1H)	2.55(q, 4H, NCH_2)	1.34(d, 3H) 1.00(t, 3H)

[a]Reference 47.

NCH_3), 2.77 (s, 3H, NCH_3), 1.90 (d, 3H, CH_3). *Anal.* calcd. for $C_{17}H_{22}NBr$: C 63.75, H 6.93, N 4.37; found : C 63.75, H 6.90, N 4.33.

Benzyldimethyl-1-phenylethylammonium-2,2,2-d_3 *bromide* was prepared in the same way from *N,N*-dimethyl-1-phenylethylamine-2,2,2-d_3; mp 154–155°C.

Benzyldiethyl-1-phenylethylammonium bromide (*5*)

To a 100-mL round bottom flask equipped with a magnetic stirrer were added 0.025 mol of *N,N*-diethyl-1-phenylethylamine, 10 mL of nitromethane, and 0.05 mol of benzyl bromide. The flask was well stoppered and the reactants were stirred for 2–4 days, after which the mixture was transferred to a 250-mL flask. Addition of excess ether gave a viscous liquid. The viscous liquid, on standing overnight, formed a solid. The solid was recrystallized three times from acetone / ether; mp 141–142°C; 93% yield; ^{1}H nmr δ (DMSO-d_6): 7.4–7.9 (m, 10H, aromatic), 4.91 (q, 1H, CH), 4.60 and 4.38 (AB system, 2H, NCH_2[5], J = 13.1 Hz), 3.23–3.75 (m, NCH_2—CH_3), 1.85 (d, 3H, CH_3), 1.14 (t, 3H, NCH_2CH_3[6]), 1.02 (t, 3H, NCH_2CH_3[6]).

[6]The primary methyl hydrogens on the two *N*-ethyl groups appear as two separate triplets.

Anal. calcd. for $C_{19}H_{26}NBr$: C 65.52, H 7.52, N 4.02; found: C 65.51, H 7.55, N 3.66.

Benzyldiethyl-1-phenylethylammonium-2,2,2-d_3 *bromide* was prepared in the same way from *N,N*-diethyl-1-phenylethylamine-2,2,2-d_3; mp 142–143°C.

1-Phenylethyltrimethylammonium bromide (*6*)

N,N-Dimethyl-1-phenylethylamine (0.05 mol) was dissolved in 50 mL of diethyl ether and placed in a 200-mL round bottom flask fitted with a condenser and a magnetic stirrer. Ether (15 mL) was placed in a 50-mL erlenmeyer flask, the flask was cooled in an ice bath, and bromomethane (14.2 g, 0.15 mol) was weighed into it. The resulting cold solution was added all at once to the amine and the reactants were stirred overnight while the salt precipitated. The precipitate was then filtered and washed several times with dry ether. The crude product was recrystallized three times from ethanol / ether; 85% yield, mp 198–199°C (lit. (21) mp 202–203°C).

*1-Phenylethyltrimethylammonium-2,2,2*d_3 *bromide* was prepared in the same way from *N,N*-dimethyl-1-phenylethylamine-2,2,2-d_3; mp 198–199°C.

N-*Methyl*-N-*(1-phenylethyl)piperidinium bromide* (*7*)

N-(1-Phenylethyl)piperidine (5.68 g, 0.03 mol) was dissolved in 25

Can. J. Chem. Downloaded from www.nrcresearchpress.com by 194.225.253.170 on 09/07/12
For personal use only.

Can. J. Chem. Downloaded from www.nrcresearchpress.com by 194.225.253.170 on 09/07/12
For personal use only.

mL of nitromethane and was placed in a 100-mL flask fitted with a magnetic stirrer. Nitromethane (10 mL) was placed in another 50-mL erlenmeyer flask, cooled in an ice bath, and bromomethane (11.4 g, 0.12 mol) was weighed into it. The resulting cold solution was added all at once to the amine solution, the flask was well stoppered, and the reactants were stirred for 24 h. The reaction mixture was then transferred to a 250-mL round bottom flask and concentrated using a rotary evaporator. Addition of excess ether gave a viscous liquid, which formed a solid on standing overnight. The solid was recrystallized three times from acetone:ethanol (5:1) / ether; mp 155–157°C; 96% yield; ^{1}H nmr δ (DMSO-d_6): 7.40–7.75 (m, 5H, aromatic), 5.09 (q, 1H, CH), 3.25–3.65 (m, 4H, NCH_2), 2.94 (s, 3H, NCH_3), 1.72 (d, 3H, CH_3), 1.35–2.00 (m, 6H, CH_2). *Anal.* calcd. for $C_{14}H_{22}NBr$: C 59.16, H 7.80, N 4.93; found: C 59.17, H 7.99, N 5.08.

N-*Methyl*-N-*(1-phenylethyl)piperidinium-2,2,2-*d_3 *bromide* was prepared in the same way from *N*-(1-phenylethyl)piperidine-2,2,2-d_3; mp 155–157°C.

1-Phenylethyltripropylammonium bromide (*8*)

1-Phenylethyl bromide (5.55 g, 0.03 mol) was dissolved in 25 mL of nitromethane and was placed in a 100-mL round bottom flask to which tripropylamine (14.3 g, 0.1 mol) was added. The flask was well stoppered and the reactants were stirred for 48 h. Addition of excess ether gave a solid (6.33 g), which was recrystallized three times from ethanol / ether; mp 161–162°C; 64% yield; ^{1}H nmr δ (DMSO-d_6): 7.42–7.78 (m, 5H, aromatic), 4.80 (q, 1H, CH), 3.10–3.35 (m, 6H, CH_2), 1.71 (d, 3H, CH_3), 0.85 (t, 9H, CH_3). *Anal.* calcd. for $C_{17}H_{30}NBr$: C 62.19, H 9.21, N 4.26; found: C 62.22, H 9.28, N 4.34.

1-Phenylethyltripropylammonium-2,2,2-d_3 *bromide* was prepared in the same way from 1-phenylethyl-2,2,2-d_3 bromide; mp 161–162°C.

Diethylmethyl-1-phenylethylammonium bromide (*9*)

N,N-Diethyl-1-phenylethylamine (5.4 g, 0.03 mol) was treated with bromomethane (11.4 g, 0.12 mol) in the same way as described for the preparation of *N*-methyl-*N*-(1-phenylethyl)piperidinium bromide, **7**, to give a viscous liquid that, on standing overnight, gave 8.2 g of a solid. This was recrystallized three times from acetone:ethanol (5:1) / ether; mp 152–154°C; 98% yield; ^{1}H nmr δ (DMSO-d_6): 7.42–7.75 (m, 5H, aromatic), 4.82 (q, 1H, CH), 2.95–3.55 (m, 4H, NCH_2), 2.82 (s, 3H, NCH_3), 1.69 (d, 3H, $CHCH_3$), 1.28 (t, 3H, NCH_2—CH_3[5]), 1.22 (t, 3H, NCH_2CH_3[6]). *Anal.* calcd. for $C_{13}H_{22}NBr$: C 57.36, H 8.15, N 5.14; found: C 57.42, H 8.20, N 5.11.

Diethylmethyl-1-phenylethylammonium-2,2,2-d_3 *bromide* was prepared in the same way from *N,N*-diethyl-1-phenylethylamine-2,2,2-d_3; mp 152–154°C.

1-Phenylethyltriethylammonium bromide (*10*)

Into a 100-mL round bottom flask fitted with a reflux condenser, capped with a drying tube, were added 5.31 g (0.03 mol) of *N,N*-diethyl-1-phenylethylamine and 25 mL of bromoethane. The mixture was gently refluxed with a constant stirring for 48 h. It was then transferred to a 250-mL round bottom flask and concentrated using a rotary evaporator. Addition of excess ether gave 5.15 g of a solid, which was recrystallized from acetone:ethanol (4:1) / ether; 60% yield; mp 148–150°C; ^{1}H nmr δ (DMSO-d_6): 7.40–7.85 (m, 5H, aromatic), 4.85 (q, 1H, CH), 3.36 (q, 6H, NCH_2), 1.71 (d, 3H, CH_3), 1.17 (t, 9H, CH_3). *Anal.* calcd. for $C_{14}H_{24}NBr$: C 58.74, H 8.45, N 4.90; found: C 58.61, H 8.73, N 4.87.

1-Phenylethyltriethylammonium-2,2,2-d_3 *bromide* was prepared in same way from *N,N*-diethyl-1-phenylethylamine,2,2,2-d_3; mp 148–150°C.

N,N-*Dimethyl*-N-*(1-phenylethyl)anilinium bromide* (*11*)

To a 100-mL round bottom flask fitted with a magnetic stirrer were added 1-phenylethyl bromide (5.55 g, 0.03 mol) and *N,N*-dimethylaniline (12.1 g, 0.1 mol). The flask was well stoppered and the reactants were stirred while a solid started to form. The stirring was continued for 48 h and then excess ether was added. The solid was filtered, washed several times with ether, and recrystallized from cold ethanol / ether; 91.6% yield; mp 126–128°C; ^{1}H nmr δ (DMSO-d_6): 7.40–7.95 (m, 10H, aromatic), 5.38 (q, 1H, CH), 3.53 (s, 3H, NCH_3), 3.45 (s, 3H, NCH_3), 1.55 (d, 3H, CH_3). *Anal.* calcd. for $C_{16}H_{20}NBr$: C 62.75, H 6.58, N 4.57; found: C 62.81, H 6.81, N 4.41.

Absolute ethanol

This solvent was dried by the method of Lund and Bjerrum (19) and stored under anhydrous conditions.

Sodium ethoxide solution

Dry ethanol (300 mL) was placed in the flask and cooled in an ice bath. Nitrogen gas, purified by passing through successive wash bottles containing Fieser's solution, saturated lead acetate solution, and concentrated sulfuric acid to remove oxygen, carbon dioxide, and water, respectively, was bubbled through the ethanol. Sodium metal (~8 g, ~0.3 mol), washed in ether, was cut into small pieces and added to the ethanol through the top of the vessel. After the sodium had been completely dissolved, the flask, containing approximately 1 M sodium ethoxide solution, was stored in the refrigerator.

Product analyses

The solution remaining from the kinetic measurement was placed into a 250-mL separatory funnel. The solution was diluted with 25 mL of water and extracted three times with 50-mL portions of petroleum ether (30–60°C). After the removal of the solvent using a rotary evaporator at room temperature, the residue was diluted with 0.5–1 mL of diethyl ether and passed through a 30-m (J & W Scientific, Inc.) DB-5, 5% phenylmethyl capillary gc column. The products were identified from a comparison with authentic samples as well as from mass spectral data. The mass spectrometer was directly coupled with the gas chromatograph. At least three analyses were carried out on each sample.

Kinetic measurements

The rate of the elimination reaction of the quaternary ammonium salts and their deuterated analogues with sodium ethoxide in ethanol was determined by spectrophotometrically monitoring the increase in the amount of styrene at 248 nm as a function of time. All rate constant measurements were carried out using the same base and ammonium salt concentrations, ca. 0.150 M and ca. 0.052 M, respectively. The quaternary ammonium salts also showed significant absorptions at 248 nm at relatively higher concentrations. During the measurement of absorbance, the reaction solutions were diluted to the extent where the substrate salt did not show any absorption (which was determined independently using the salt). The absorption of other components of the mixture was negligible at 248 nm.

The thermostated oil bath was adjusted to the temperature 60.00 ± 0.02°C. A known weight of the substrate was placed in a 25-mL volumetric flask, containing a side bulb to balance the inside pressure, and dry ethanol (13 mL) was added to dissolve it. Sodium ethoxide solution of approximate six to seven times the substrate concentration was prepared in another flask by the dilution of the previously prepared 1 M base solution. Both flasks were then placed into the bath for about 30–45 min to allow the solutions to reach thermal equilibrium. The base concentration was determined by withdrawing 1 mL of the base, diluting to 50 mL with carbon-dioxide-free distilled water, and titrating with standardized 0.01 N sulfuric acid solution to bromthymol blue end point. A 10-mL aliquot of the base was introduced into the substrate flask and filled up to the mark with thermally equilibrated dry ethanol. The flask was well stoppered using a rubber septum and shaken vigorously to ensure complete mixing. Timing was started approximately halfway through the addition of the base to the substrate solution. At suitable intervals of time, aliquots were withdrawn using a calibrated gastight syringe and diluted to 50 mL in a volumetric flask with 95% ethanol. The absorbance of the solution was then recorded after proper dilution.

Kinetics were studied under second-order reaction conditions and the rate constants were calculated by using the following modified (to account for the competing substitution) form of the integrated second-order rate equation,

$$k_2 = \frac{1}{t(a_0 - b_0)} \ln \left[\frac{b_0}{a_0} \frac{(a_0 - p_1 - p_2)}{(b_0 - p_1 - p_2)} \right]$$

[7]This salt undergoes S_N1 reaction in hot ethanol.

where a_0 and b_0 are initial concentrations of the base and the substrate, respectively, p_1 and p_2 are the concentrations of elimination and substitution products, respectively, at time t, and k_2 is the overall second-order rate constant. The rate constant (k_2) was calculated from the slope of the least-squares plot of $\ln [(a_0 - p_1 - p_2)/(b_0 - p_1 - p_2)]$ vs. t. Excellent second-order plots were obtained in all cases. The rate constant for the elimination reaction (k_E) was then calculated using the following relationship,

$$k_E = k_2 \times \frac{\% \text{ of elimination product}}{100}$$

Test for solvolysis

A known weight of the substrate was placed in a 25-mL volumetric flask and approximately 20 mL of dry ethanol was added to dissolve the salt. The flask was then placed into the thermostated oil bath, which was adjusted to the temperature 60.00 ± 0.02°C. After half an hour, the flask was filled up to the mark with thermally equilibrated dry ethanol. The flask was well stoppered with a rubber septum and shaken vigorously to ensure complete mixing. Aliquots were withdrawn using a calibrated 1.00-mL syringe and diluted to 50 mL in a volumetric flask with 95% ethanol. The absorbance of the solution was recorded at 248 nm (λ_{max} for styrene) after proper dilution. No significant absorbance was observed for compounds **4–10** over a period of 3–4 days. The gc analysis also did not show the presence of any solvolysis product.

However, the absorbance at 248 nm increased progressively for the salt *N,N*-dimethyl-*N*-(1-phenylethyl)anilinium bromide (**11**). The gc–ms analysis indicated the presence of ether substitution product and amine leaving group (which has $\lambda_{max} = 251$ (22)).

Tests for E1cB, carbene, and ylide mechanisms

A known weight of the appropriate deuterated quaternary ammonium salt was dissolved in 25 mL of the base, so that the initial concentrations of the substrate and the base were ca. 0.0525 mol L^{-1} and ca. 0.150 mol L^{-1}, respectively. This solution was allowed to stand at 60°C in a thermostated oil bath for a period of 2–3 days. The products were then isolated and analyzed. In all cases, **4–10**, the resulting styrene was β-dideuterated and the amine product did not contain deuterium.

Acknowledgement

The authors gratefully acknowledge the financial support of this work by the Natural Sciences and Engineering Research Council of Canada.

1. W. H. Saunders, Jr. and D. H. Edison. J. Am. Chem. Soc. **82**, 138 (1960).
2. L. J. Steffa and E. R. Thornton. J. Am. Chem. Soc. **89**, 6149 (1967).
3. S. Alunni and W. P. Jencks. J. Am. Chem. Soc. **102**, 2052 (1980).
4. J. R. Keeffe and W. P. Jencks. J. Am. Chem. Soc. **103**, 2457 (1981).
5. J. R. Gandler and W. P. Jencks. J. Am. Chem. Soc. **104**, 1937 (1982).
6. J. R. Keeffe and W. P. Jencks. J. Am. Chem. Soc. **105**, 265 (1983).
7. P. Schmid and A. N. Bourns. Can. J. Chem. **53**, 3513 (1975).
8. J. R. Gandler and T. Yokoyama. J. Am. Chem. Soc. **106**, 130 (1984).
9. D. A. Winey and E. R. Thornton. J. Am. Chem. Soc. **97**, 3102 (1975).
10. R. V. Hoffman and J. M. Shankweiler. J. Am. Chem. Soc. **108**, 5536 (1986).
11. C. H. Depuy and C. A. Bishop. J. Am. Chem. Soc. **82**, 2532 (1960); **82**, 2535 (1960).
12. A. F. Cockerill. Tetrahedron Lett. 4913 (1969).
13. E. D. Hughes, C. K. Ingold, S. Masterman, and B. J. McNulty. J. Chem. Soc. 899 (1940).
14. R. A. Sneen and H. M. Robbins. J. Am. Chem. Soc. **91**, 3100 (1969).
15. D. J. McLennan. J. Chem. Soc. Perkin Trans. 2, 1577 (1972); Tetrahedron Lett. 2317 (1971).
16. R. Ledger, A. J. Smith, and J. McKenna. Tetrahedron Lett. **20**, 2413 (1964).
17. E. D. Hughes and J. Wilby. J. Chem. Soc. 4094 (1960).
18. P. J. Smith and J. Pradhan. Can. J. Chem. **64**, 1060 (1986).
19. H. Lund and J. Bjerrum. Chem. Ber. **64B**, 210 (1931).
20. P. J. Smith and S. K. Tsui. Tetrahedron Lett. **10**, 917 (1972).
21. G. S. Dyson. Ph.D. Thesis, University of Saskatchewan (1975).
22. R. C. Weast (*Editor*). Handbook of chemistry and physics. 55th ed. Chemical Rubber Company, Boca Raton, Fl. 1974.
23. P. J. Smith and A. N. Bourns. Can. J. Chem. **52**, 749 (1974).
24. E. D. Hughes and C. K. Ingold. J. Chem. Soc. 244 (1935).
25. D. V. Banthorpe, E. D. Hughes, and C. K. Ingold. J. Chem. Soc. 4054 (1960).
26. F. L. Roe, Jr. and W. H. Saunders, Jr. Tetrahedron, **33**, 1581 (1977).
27. D. R. Marshall, P. J. Thomas, and C. J. M. Stirling. J. Chem. Soc. Perkin Trans. 2, 1898 (1977).
28. P. J. Thomas and C. J. M. Stirling. J. Chem. Soc. Perkin Trans. 2, 1909 (1977).
29. D. R. Marshall, P. J. Thomas, and C. J. M. Stirling. J. Chem. Soc. Perkin Tans. 2, 1914 (1977).
30. P. J. Thomas and C. J. M. Stirling. J. Chem. Soc. Perkin Trans. 2, 1130 (1978).
31. R. P. Redman, P. J. Thomas, and C. J. M. Stirling. J. Chem. Soc. Perkin Trans. 2, 1135 (1978).
32. C. J. M. Stirling. Acc. Chem. Res. **12**, 198 (1979).
33. B. Issari and C. J. M. Stirling. J. Chem. Soc. Chem. Commun. 684 (1982).
34. D. B. Boyd, D. K. Herron, W. H. W. Lunn, and W. A. Spitzer. J. Am. Chem. Soc. **102**, 1812 (1980).
35. D. B. Boyd. J. Org. Chem. **50**, 885 (1985).
36. D. E. Lewis, L. B. Sims, H. Yamataca, and J. McKenna. J. Am. Chem. Soc. **102**, 7411 (1980).
37. F. H. Westheimer. Chem. Rev. **61**, 265 (1961).
38. L. Melander. Isotope effects on reaction rate. Ronald Press, New York. 1960.
39. P. J. Smith and A. N. Bourns. Can. J. Chem. **48**, 125 (1970).
40. W. H. Saunders, Jr. and A. F. Cockerill. Mechanism of elimination reactions. Wiley–Interscience, New York. 1973.
41. S.-L. Wu and P. J. Smith. Can. J. Chem. **59**, 3016 (1981).
42. R. A. More O'Ferrall. J. Chem. Soc. B, 274 (1970).
43. (*a*) D. A. Jencks and W. P. Jencks. J. Am. Chem. Soc. **99**, 7948 (1977); (*b*) W. P. Jencks. Chem. Rev. **72**, 705 (1972).
44. J. M. Harris and J. L Paul. Isr. J. Chem. **26**, 325 (1985).
45. (*a*) D. D. Perrin. pK_a prediction for organic acids and bases. Chapman and Hall, London, New York. 1981; (*b*) R. Stewart. The proton: application to organic chemistry. Academic Press, New York. 1985. pp. 90–100.
46. V. Frenna, N. Vivona, G. Consiglio, and D. Spinelli. J. Chem. Soc. Perkin Trans. 2, 1865 (1985).
47. A. T. Stewart, Jr. and C. R. Hauser. J. Am. Chem. Soc. **77**, 1098 (1955).
48. D. H. Williams and I. Fleming. Spectroscopic methods in organic chemistry. 3rd ed. McGraw–Hill, London. 1980. pp. 93–96.

Can. J. Chem. Downloaded from www.nrcresearchpress.com by 194.225.253.170 on 09/07/12
For personal use only.

Thermodynamic analysis of phase diagrams of binary solid solutions of ascending and minimum types: Na_2SO_4–Ag_2SO_4, Ag_2SO_4–K_2SO_4, Na_2SO_4–K_2SO_4

PATRICK C. DAWSON[1] AND E. A. SECCO[2]

Chemistry Department, St. Francis Xavier University, Antigonish, N.S., Canada B2G 1C0

AND

WILLIAM M. OXNER[1]

Department of Mathematics and Computer Science, St. Francis Xavier University, Antigonish, N.S., Canada B2G 1C0

Received April 18, 1989

PATRICK C. DAWSON, E. A. SECCO, and WILLIAM M. OXNER. Can. J. Chem. **67**, 1468 (1989).

The thermodynamic analysis of the condensed phase diagrams of binary system solid solutions of the ascending type, viz. Na_2SO_4–Ag_2SO_4 and of the minimum type, ameltrope, viz. Ag_2SO_4–K_2SO_4, Na_2SO_4–K_2SO_4 is presented. The analysis identifies the basis for ameltrope behavior and provides for the evaluation of α, the fraction of dissociation, and ΔH_{Diss}, the enthalpy of dissociation, of the dissociating component.

Key words: alkali sulfates solid solutions, thermodynamic analysis ameltropes, molten alkali sulfates dissociation, solid–solid phase diagrams, ionic melts.

PATRICK C. DAWSON, E. A. SECCO et WILLIAM M. OXNER. Can. J. Chem. **67**, 1468 (1989).

On présente une analyse thermodynamique des diagrammes de phase condensée de solutions solides de systèmes binaires de type ascendant, comme Na_2SO_4–Ag_2SO_4, ainsi que du type minimal, ameltrope, comme Ag_2SO_4–K_2SO_4, Na_2SO_4–K_2SO_4. L'analyse identifie la base à partir duquel on observe une comportement d'ameltrope et fournit une évaluation de α, la fraction de dissociation, ainsi que du ΔH_{Diss}, l'enthalpie de dissociation, de la composante qui se dissocie.

Mots clés : solutions solides, sulfates alcalins; analyse thermodynamique des ameltropes; dissociation des sulfates alcalins fondus; diagrammes de phase, solide–solide; produits ioniques en fusion.

[Traduit par la revue]

Introduction

Recent advances in materials science and their potential applications in recent years have increased interest in the subject of condensed phase equilibria. The pressure–temperature–composition behavior of multi-component systems has become an active area for experimental and theoretical analysis.

Recently, we reported the isobaric condensed phase diagrams of three binary systems, viz. Na_2SO_4–Ag_2SO_4, Ag_2SO_4–K_2SO_4, Na_2SO_4–K_2SO_4, incorporating both solid–solid and solid–liquid equilibria (1–3). The three sulfate components are orthorhombic solids in the low temperature form: Ag_2SO_4 and Na_2SO_4 are isomorphic, space group *Fddd*, while K_2SO_4 fits the space group *Pnam*. Each component undergoes a solid–solid phase transition to the isomorphic high temperature form space group $P6_3/mmc$ (4–6). The phase diagram of the Na_2SO_4–Ag_2SO_4 system is the simplest with a monotonic ascending solid solution behavior in both the solid–solid and solid–liquid regions. The Ag_2SO_4–K_2SO_4 system diagram shows a eutectoid in the solid–solid region and a constant melting composition[3] of the minimum type in the solid–liquid region paralleling the familiar azeotropic behavior found in boiling of liquid solution. The Na_2SO_4–K_2SO_4 diagram reveals complex solid–solid behavior with an eutectoid, the compound $KNaSO_4$ and another compound $K_3Na(SO_4)_3$ which exhibits eutectoid features along with a minimum constant melting composition in the solid–liquid region. The compounds $KNaSO_4$ and $K_3Na(SO_4)_3$ have been characterized by X-ray structural studies (7) and each undergoes a solid–solid phase transition speculated to be of the order–disorder type $\approx$400°C below their respective melting temperatures.

Solid solutions displaying an ameltrope are rare relative to the liquid solution analog. In this type of solid solution the original components are, as a rule, isostructural and even isomorphic in the solid state; that is, the same solid phase structure coexists with liquid in the solid–liquid region. An intuitive interpretation of a minimum ameltrope suggests a miscibility gap lying submerged beneath the solidus. However, the above described diagrams reveal no such miscibility gap, therefore, our knowledge of the nature and basis for ameltropic behavior is incomplete.

Reisman (8) outlines the overall thermodynamic approach to the analysis of ascending solid solutions including the minimum ameltrope. The latter analysis is based on the dissociation of at least one of the components on melting. The treatment is restricted to the complete dissociation case of the components of which two possibilities are considered: (*i*) a dimer solid dissociates to a monomer liquid and (*ii*) a monomer solid yields twice as many species in the liquid, e.g. ionization. However, a detailed analysis of the minimum ameltropic behavior incorporating various degrees of dissociation of the components is lacking. This paper, therefore, presents an analytical description which correlates the experimental isobaric temperature–composition condensed phase diagrams of three binary systems, viz. Na_2SO_4–Ag_2SO_4, Ag_2SO_4–K_2SO_4, Na_2SO_4–K_2SO_4 with the graphical representations generated by a refinement of the Reisman model.

[1]Natural Sciences and Engineering Research Council of Canada Undergraduate Summer Research Award Holder.

[2]To whom correspondence should be addressed.

[3]We identify the constant melting composition of a solid solution as "ameltrope", paralleling azeotrope derived from two Greek terms ατροπος, "unchanging" and μελδομαι, "to melt". Although "atropomeldic" may be appropriate and euphonic we sacrifice euphony for simplicity.

Can. J. Chem. Downloaded from www.nrcresearchpress.com by 194.225.253.170 on 09/07/12
For personal use only.

Results and discussion

A. Na_2SO_4–Ag_2SO_4 — ascending solid solution type

The solid–liquid equilibria are described by

[1] $Na_2SO_{4(s)} \rightleftarrows Na_2SO_{4(l)}$

[2] $Ag_2SO_{4(s)} \rightleftarrows Ag_2SO_{4(l)}$

where the symbols s and l represent the species in the solid solution and liquid solution, respectively. The solid–solid equilibria are given by

[1*a*] $Na_2SO_{4(s)} \rightleftarrows Na_2SO_{4(s')}$

[2*a*] $Ag_2SO_{4(s)} \rightleftarrows Ag_2SO_{4(s')}$

where s and s′ refer to the species in solid solution phase I and solid solution phase II, respectively. Applying the appropriate constraining and conservation conditions with respect to compositions to the equilibria [1] and [2] one obtains for the variation of Na_2SO_4 composition with T in the liquid and solid phases, respectively

$$[3]\quad x^{l}_{Na_2SO_4} = \frac{\exp\left[-\frac{\Delta H^0_{f,Na_2SO_4}}{R}\left(\frac{1}{T}-\frac{1}{T^0_{Na_2SO_4}}\right)\right]\left\{\exp\left[-\frac{\Delta H^0_{f,Ag_2SO_4}}{R}\left(\frac{1}{T}-\frac{1}{T^0_{Ag_2SO_4}}\right)\right]-1\right\}}{\exp\left[-\frac{\Delta H^0_{f,Ag_2SO_4}}{R}\left(\frac{1}{T}-\frac{1}{T^0_{Ag_2SO_4}}\right)\right]-\exp\left[-\frac{\Delta H^0_{f,Na_2SO_4}}{R}\left(\frac{1}{T}-\frac{1}{T^0_{Na_2SO_4}}\right)\right]}$$

$$[4]\quad x^{s}_{Na_2SO_4} = \frac{\exp\left[-\frac{\Delta H^0_{f,Ag_2SO_4}}{R}\left(\frac{1}{T}-\frac{1}{T^0_{Ag_2SO_4}}\right)\right]-1}{\exp\left[-\frac{\Delta H^0_{f,Ag_2SO_4}}{R}\left(\frac{1}{T}-\frac{1}{T^0_{Ag_2SO_4}}\right)\right]-\exp\left[-\frac{\Delta H^0_{f,Na_2SO_4}}{R}\left(\frac{1}{T}-\frac{1}{T^0_{Na_2SO_4}}\right)\right]}$$

Parallel equations in $x^{l}_{Ag_2SO_4}$ and $x^{s}_{Ag_2SO_4}$ are self-evident and unnecessary since the conservation conditions $x^{l}_{Ag_2SO_4} + x^{l}_{Na_2SO_4} = 1$ and $x^{s}_{Ag_2SO_4} + x^{s}_{Na_2SO_4} = 1$ prevail. In these equations x refers to the mole fraction, ΔH^0_f and T^0 refer to the respective enthalpy of fusion and melting temperature of the pure component and R the universal gas constant. Similar equations in $x^{s}_{Na_2SO_4}$ and $x^{s'}_{Na_2SO_4}$ are obtained for the equilibria [1*a*] and [2*a*] for the appropriate solid phases where ΔH^0_t, the respective enthalpy of transition replaces ΔH^0_f and T^0 represents the respective transition temperature instead of the melting temperature of the pure component.

Inserting the ΔH^0_f values of 5830 and 4280 cal/mol with 1155 and 940 K for T^0 of Na_2SO_4 and Ag_2SO_4, respectively (1, 2) in eqs. [3] and [4] we obtain the liquidus and solidus dotted line composition in the upper part of Fig. 1. The open squares represent the experimental melting temperatures in the heat mode of DSC, differential scanning calorimetry. The separate liquidus and solidus temperatures could not be distinguished experimentally because of their proximity. The agreement between the experimental and calculated data is considered to be excellent.

Using the ΔH^0_t values of 1670 and 4060 cal/mol and 530 and 693 K for T^0 of Na_2SO_4 and Ag_2SO_4, respectively, in equations similar to [3] and [4] we obtain the two solidi dotted line compositions in the lower part of Fig. 1. The unfilled circles represent the experimental transition temperatures in the heat mode of DSC. The separate solidi temperatures could not be resolved experimentally because of their proximity. Excellent agreement between the experimental and calculated data is evident above 40 mol% Ag_2SO_4 with deviation increasing towards pure Na_2SO_4. Four solid phases have been confirmed for Na_2SO_4 with the known transitions V ⇄ III ⇄ II ⇄ I occurring. However, short-circuit transitions also occur, viz. III ⇄ I and the metastable III phase can remain untransformed at room temperature, i.e. 250 K below its normal transition temperature, for months. The ΔH^0_t of 1670 cal/mol is for the III → I transition. The temperature 493 K in Fig. 1 obtained in the cool mode is given for comparison only. As noted in an earlier report (2), the behavior of the 10 mol% composition showing two transitions is attributed to existence of two kinds of Na_2SO_4–Ag_2SO_4 solid solutions where Ag_2SO_4 is distributed between two structural forms of Na_2SO_4 — a novel effect where a solute is distributed between two immiscible solid phases of the same compound.

B. Ag_2SO_4–K_2SO_4 and Na_2SO_4–K_2SO_4 — ameltrope solid solution type

This solid solution type involves the dissociation of one of the components on melting. The dissociation type considered here is case (*ii*), that is, the dissociation of the solid into liquid ions as described by Reisman (8). The dissociating solid is taken to be K_2SO_4 on the basis that it is the common component in both systems and by the compositional location of the ameltrope (8). The analytical treatment given here is for case (*ii*) but takes into consideration the fact that K_2SO_4 only partially dissociates into its ion species. We simplify the notation in the treatment by identifying the common component K_2SO_4 as AC and Ag_2SO_4 or Na_2SO_4 as BC, with the same usual symbols s and l for solid and liquid phases.

The heterogeneous equilibria for the case under consideration are described by

[5] $AC_{(s)} \rightleftarrows AC_{(l)} \rightleftarrows A_{(l)} + C_{(l)}$

[6] $BC_{(s)} \rightleftarrows BC_{(l)}$

The temperature dependencies of the equilibrium constants involving dissociation for eq. [5] and eq. [6] are

$$[7]\quad \frac{K_{AC}}{K^0_{AC}} = \exp\left[-\frac{\Delta H^0_{f,AC}}{R}\left(\frac{1}{T}-\frac{1}{T^0_{AC}}\right)\right] = e^{-AC}$$

$$[8]\quad \frac{K_{Diss}}{K^0_{Diss}} = \exp\left[-\frac{\Delta H_{Diss}}{R}\left(\frac{1}{T}-\frac{1}{T^0_{AC}}\right)\right] = e^{-Y}$$

$$[9]\quad \frac{K_{BC}}{K^0_{BC}} = \exp\left[-\frac{\Delta H^0_{f,BC}}{R}\left(\frac{1}{T}-\frac{1}{T^0_{BC}}\right)\right] = e^{-BC}$$

Can. J. Chem. Downloaded from www.nrcresearchpress.com by 194.225.253.170 on 09/07/12
For personal use only.

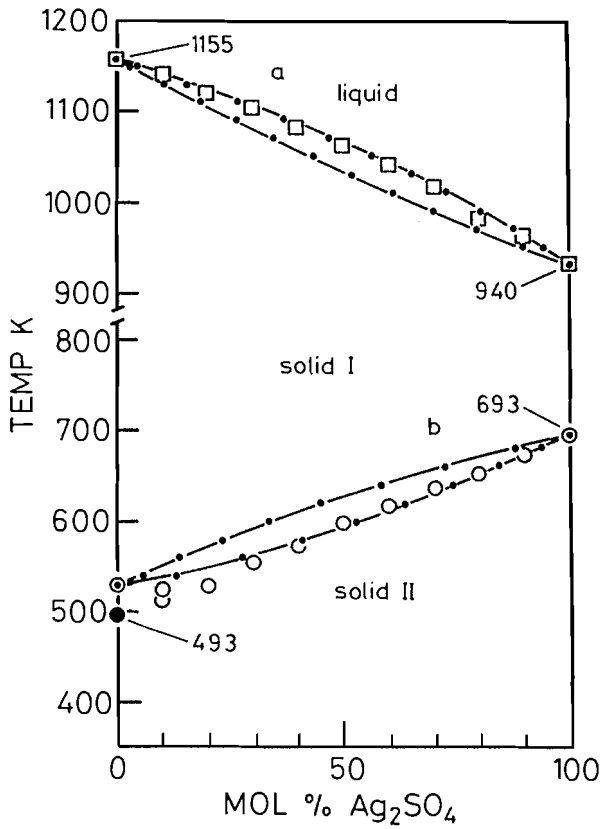


FIG. 1. Isobaric plots of temperature versus composition Ag_2SO_4 for Na_2SO_4–Ag_2SO_4 system: (*a*) solid–liquid equilibrium, ----- calculated and -□-□- experimental from ref. 2; (*b*) solid–solid equilibrium, ----- calculated and -○-○- experimental from ref. 2.

Since AC only partially dissociates we let α represent the fraction of dissociation to obtain the set of concentrations N of the pure dissociating substance:

$$N_{AC}^{0s} = N_{BC}^{0s} = N_{BC}^{0l} = 1.0$$

$$N_{A}^{0l} = N_{C}^{0l} = \alpha/(1 + \alpha)$$

$$N_{AC}^{0l} = (1 - \alpha)/(1 + \alpha)$$

We also have a new set of composition constraints in solution:

$$[10] \quad N_A^l + N_C^l + N_{AC}^l + N_{BC}^l = 1.0$$

$$[11] \quad [(\alpha + 1)/\alpha]N_A^l + N_{BC}^l = 1.0$$

$$[12] \quad N_{AC}^s + N_{BC}^s = 1.0$$

Expanding the form of eqs. [7]–[9] we get

$$[13] \quad N_{AC}^l = \left[\frac{(1 - \alpha)}{(1 + \alpha)} N_{AC}^s\right] e^{-AC}$$

$$[14] \quad (N_A^l)^2 = \left[\frac{\alpha^2}{(1 - \alpha^2)} N_{AC}^l\right] e^{-Y}$$

where

$$e^{-Y} = \frac{(N_A^l)^2/N_{AC}^l}{\alpha^2/(1 - \alpha^2)}$$

$$[15] \quad N_{BC}^l = N_{BC}^s e^{-BC}$$

Substituting N_{AC}^l from eq. [13] into eq. [14] we get

$$[16] \quad (N_A^l)^2 = \left[\left(\frac{\alpha^2}{1 - \alpha^2}\right)\frac{(1 - \alpha)}{(1 + \alpha)} N_{AC}^s e^{-AC}\right] e^{-Y}$$

Replacing N_{AC}^s in [16] and substituting N_{BC}^s from [15] we get

$$[17] \quad (N_A^l)^2 = \left[\frac{\alpha^2}{(1 + \alpha)^2}\frac{(1 - N_{BC}^l)}{e^{-BC}} e^{-AC}\right] e^{-Y}$$

Finally we replace N_{BC}^l in [17] from [11] to obtain

$$[18] \quad (N_A^l)^2 = \frac{\alpha^2}{(1 + \alpha)^2}\left[1 - \frac{[1 - (\alpha + 1)/\alpha]N_A^l}{e^{-BC}}\right] e^{-AC} e^{-Y}$$

which rearranges to the quadratic form in N_A^l

$$[19] \quad (N_A^l)^2 e^{-BC} - \left[\frac{\alpha}{(\alpha + 1)} N_A^l\right] e^{-AC} e^{-Y} - \frac{\alpha^2}{(\alpha + 1)^2}(e^{-BC} - 1) e^{-AC} e^{-Y} = 0$$

whose solution leads to the evaluation of α.

By using the component conservation equations the mole fractions of the components AC and BC in the solid and liquid phases are deduced:

$$[20] \quad x_{AC}^l = (1/\alpha)N_A^l/(\alpha - N_A^l)$$

$$[21] \quad x_{AC}^s = \left(\frac{1 - \alpha}{\alpha}\right) \cdot \frac{N_A^l}{e^{-AC}}$$

$$[22] \quad x_{BC}^s = \left[1 - \left(\frac{\alpha + 1}{\alpha}\right) \cdot N_A^l\right] \Big/ e^{-BC}$$

$$[23] \quad x_{BC}^l = \left[1 - \left(\frac{\alpha + 1}{\alpha}\right) \cdot N_A^l\right] \Big/ (1 - N_A^l)$$

These results allow a graphical description of the solid–liquid T versus x phase diagram as generated by this model of partial dissociation of component AC.

Inserting for the $Ag_2SO_4 - K_2SO_4$ system the values of 4280 and 8100 cal/mol for ΔH_f^0 with 1240 and 940 K for T_f^0 of Ag_2SO_4 and K_2SO_4, respectively, in eqs. [19]–[23] we obtain the T–x plot represented by the solid lines in Fig. 2 for the best fit values of $\alpha = 0.40$ and $\Delta H_{Diss} = 800$ cal/mol. The empty circles and the filled circles are the experimental liquidus and solidus melting temperatures, respectively, reported earlier (3). The half-filled circles in Figs. 2 and 3 indicate the separate liquidus and solidus temperatures to be experimentally indistinguishable in our studies.

Similarly, for the Na_2SO_4–K_2SO_4 system using the values of 5830 and 8100 cal/mol for ΔH_f^0 with 1155 and 1340 K for T_f^0 of Na_2SO_4 and K_2SO_4, respectively, we obtain the T–x plot represented by the solid lines in Fig. 3 for the best fit values of $\alpha = 0.35$ and $\Delta H_{Diss} = 2200$ cal/mol. The empty circles and the filled circles are the experimental liquidus and solidus melting temperatures, respectively, we reported earlier (1). The experimental liquidus and solidus temperature data of Perrier and Bellanca (9) are included in Fig. 3 for comparison purposes. The liquidus temperature data of Bergman and Rubleva (10), not shown in Fig. 3, are in good agreement with the plot. The liquidus and solidus lines of the computer plot cross over near $x_{K_2SO_4} \sim 0.30$ for the best fit and reported α and ΔH_{Diss} values. This cross-over is an artifact which can be eliminated and the two lines merged by adjusting α and ΔH_{Diss}. However, this adjustment of α and ΔH_{Diss} will effect a greater disparity between the theoretical plot and the experimental data for $x_{K_2SO_4} > 0.30$.

Hatem *et al.* (11) reported a thermodynamic analysis of the binary phase diagram K_2SO_4–Na_2SO_4 based on the deduced positive excess entropy of the solid and the enthalpy of mixing

Can. J. Chem. Downloaded from www.nrcresearchpress.com by 194.225.253.170 on 09/07/12
For personal use only.

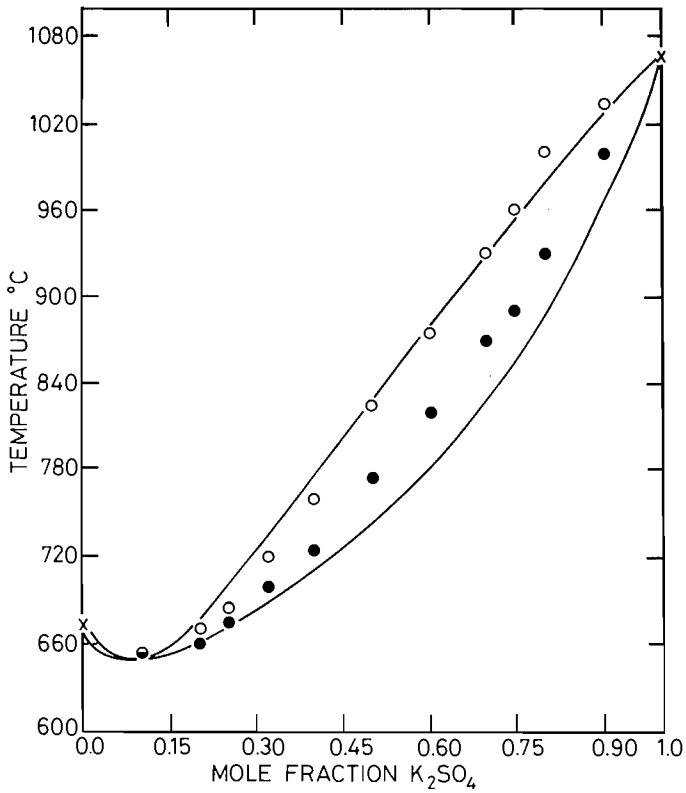


FIG. 2. Isobaric plot of temperature versus composition K_2SO_4 for solid–liquid equilibrium of Ag_2SO_4–K_2SO_4 system, — calculated and ○, ◒, ● experimental from ref. 3.

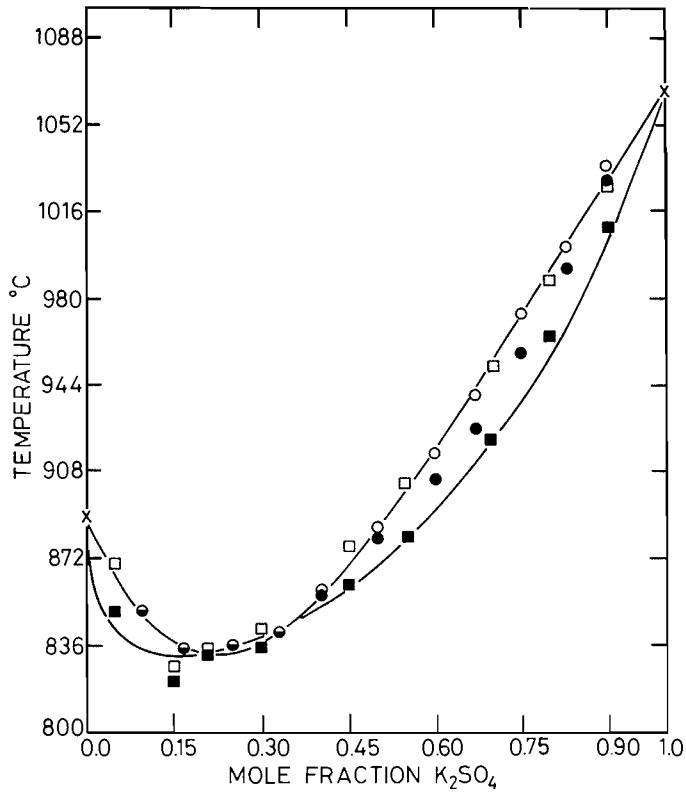


FIG. 3. Isobaric plot of temperature versus composition K_2SO_4 for solid–liquid equilibrium of Na_2SO_4–K_2SO_4 system, — calculated, ○, ◒, ● experimental from ref. 1, □, ■ experimental from ref. 9.

of Na_2SO_4–K_2SO_4 measured by Øsvold and Kleppa (12). The least-squares optimization technique was used with a one-term excess entropy expression and four terms for the enthalpy to obtain the "best" fit to the experimental liquidus and solidus data. Their "best" fit is in good agreement with the plot generated by the model for partially dissociated K_2SO_4 developed here. The more general theoretical analysis presented here incorporates the analytical approach reported by Hatem *et al.* and in addition provides for the evaluation of α, the fraction of dissociation, and the enthalpy of dissociation, ΔH_{Diss}.

It is interesting to note that the fraction of dissociation, α, values, viz. 0.40 and 0.35 obtained for K_2SO_4 in the Ag_2SO_4–K_2SO_4 and Na_2SO_4–K_2SO_4 systems, respectively, are internally consistent as might be expected. However, the spread in the ΔH_{Diss} values of 800 cal/mol for Ag_2SO_4–K_2SO_4 and 2200 cal/mol for Na_2SO_4–K_2SO_4 suggest secondary interactions such as complex association in the liquid phase. Assuming no association occurs in Na_2SO_4–K_2SO_4 then the difference of 1400 cal/mol might be attributed to enthalpy of formation of some complex resembling $K(Ag_2SO_4)^+$. It may be fortuitous that this enthalpy of complex formation is within limits of the difference between $\Delta H^0_{f,Na_2SO_4}$ and $\Delta H^0_{f,Ag_2SO_4}$ or that ΔH_{Diss} of 2200 cal/mol for Na_2SO_4–K_2SO_4 is the difference between $\Delta H^0_{f,Na_2SO_4}$ and $\Delta H^0_{f,K_2SO_4}$.

The concept of dissociation of K_2SO_4 as presented in this analysis may not coincide with that of a formal dissociation process where the usual bond cleavage is involved. In a structural study of molten alkali sulphates including K_2SO_4, Zarzycki (13) considers three principal symmetrical positions of a cation in contact with 3, 2, 1 oxygens of the anion. He focuses on "free volume" as a measure of the degree of packing of the particles in the melt and relates this parameter to free rotation states of SO_4^{2-} whereas Furukawa (14) focuses on restricted orientations of the anion. In the absence of more specific and detailed structural knowledge of molten solid solutions we use dissociation in the broadest sense to include dis-association, detachment, displacement, re-orientation, etc. of ionic groupings.

Acknowledgements

The authors are indebted to the Natural Sciences and Engineering Research Council of Canada for the Summer Research Awards (P.C.D. and W.M.O.), to Professor S. Aalto for mathematical/computer assistance, and to Professor G. Power for an enlightening exposition of Greek etymology.

1. M. S. KUMARI and E. A. SECCO. Can. J. Chem. **61**, 594 (1983).
2. M. S. KUMARI and E. A. SECCO. Can. J. Chem. **61**, 2804 (1983).
3. M. S. KUMARI and E. A. SECCO. Can. J. Chem. **63**, 324 (1985).
4. J. M. NEWSAM, A. K. CHEETHAM, and B. C. TOFIELD. Fast ion transport in solids. *Edited by* P. Vashishta, J. N. Mundy, and G. K. Shenoy. Elsevier North-Holland Inc., New York. 1979. p. 435.
5. A. J. VAN DEN BERG and F. TUINSTRA. Acta Crystallogr. B**34**, 3177 (1978).
6. W. EYSEL, H. H. HOFER, K. L. KEESTER, and TH. THAN. Acta Crystallogr. B**41**, 5 (1985).
7. K. OKADA and J. OSSAKA. Acta Crystallogr. B**36**, 919 (1980).
8. A. REISMAN. Phase equilibria. Academic Press, New York. 1970. Chapts. 29, 30.
9. C. PERRIER and A. BELLANCA. Period. Mineral. Rome, **11**, 169 (1940).
10. A. G. BERGMAN and V. V. RUBLEVA. Russ. J. Inorg. Chem. (Engl. Transl.), **4**, 56 (1959).
11. G. HATEM, M. GAUNE-ESCARD, and A. D. PELTON. J. Phys. Chem. **86**, 3039 (1982).
12. T. ØSVOLD and O. J. KLEPPA. Acta Chem. Scand. **25**, 919 (1971).
13. J. ZARZYCKI. Discuss. Faraday Soc. **32**, 38 (1961).
14. K. FURUKAWA. Discuss. Faraday Soc. **32**, 69 (1961).

Can. J. Chem. Downloaded from www.nrcresearchpress.com by 194.225.253.170 on 09/07/12
For personal use only.

ipso Nitration in *p*-halophenyl ethers

ROBIN G. CLEWLEY, ALFRED FISCHER, and GEORGE N. HENDERSON
Department of Chemistry, University of Victoria, Victoria, B.C., Canada V8W 2Y2

Received March 16, 1989

ROBIN G. CLEWLEY, ALFRED FISCHER, and GEORGE N. HENDERSON. Can. J. Chem. **67**, 1472 (1989).

Addition of nitronium ion *ipso* to halogen occurs on nitration of the *p*-haloanisoles in acetic anhydride at −60°C. In the cases of *p*-fluoro- and *p*-chloro-anisole, addition of the nitronium ion is reversible and only small amounts of *ipso* products are obtained. With *p*-bromoanisole nitrodebromination occurs. When *p*-halophenyl ethers containing a trapping substituent, e.g., 2-(4-chlorophenoxy)-2-methylpropanoic acid, are used as substrates, substantial amounts of the spiro diene with nitro *ipso* to halogen, e.g., 3,3-dimethyl-8-chloro-8-nitro-1,4-dioxaspiro[4.5]deca-6,9-dien-2-one, can be isolated. The results demonstrate that extensive *ipso* attack at the halogen-substituted position is general in the nitration of *p*-halophenyl ethers.

Key words: *ipso* nitration, ether, diene, *p*-haloanisole.

ROBIN G. CLEWLEY, ALFRED FISCHER et GEORGE N. HENDERSON. Can. J. Chem. **67**, 1472 (1989).

Lorsqu'on effectue la nitration des *p*-haloanisoles, dans l'anhydride acétique, à −60°C, l'addition de l'ion nitronium se fait en *ipso* de l'halogène. Dans les cas des *p*-fluoro- et *p*-chloro-anisoles, l'addition de l'ion nitronium est réversible et on n'obtient que des faibles quantités de produits *ipso*. Avec le *p*-bromoanisole, il se produit une nitrodébromation. Lorsqu'on utilise comme substrats des *p*-halophényl éthers portant un substituant pouvant agir comme piège, par exemple l'acide 2-(4-chlorophénoxy)-2-méthylpropanoïque, on isole des quantités importantes du spiro diène portant un groupement nitro en *ipso* de l'halogène, par exemple la 3,3-diméthyl-8-chloro-8-nitro-1,4-dioxaspiro[4.5]déca-6,9-dièn-2-one. Les résultats obtenus démontrent que l'attaque en position *ipso* de l'halogène est généralement importante lors de la nitration des éthers *p*-halophénylés.

Mots clés : *ipso* nitration, éther, diène, *p*-haloanisole.

[Traduit par la revue]

Can. J. Chem. Downloaded from www.nrcresearchpress.com by 194.225.253.170 on 09/07/12
For personal use only.

Nitration *ipso* to halogen is well established (1–14). Most examples of the formation of adducts and, from phenols, nitrohalodienones, relate to substrates that are fully substituted at the *ortho* and *para* positions and can therefore only undergo *ipso* attack. However, we have recently shown that it is possible to obtain the *ipso* nitrodienones from the *p*-halophenols although the adducts are labile and rearomatize well below ambient temperature (15). The *p*-haloanisoles provide another simple system from which we anticipated it might be possible to derive *ipso* adducts since it had been established that nitration of *p*-fluoro- and *p*-chloro-anisole in aqueous acetic acid (10) or aqueous sulphuric acid (12) gives the 4-halo-2-nitrophenol, as well as the expected 4-halo-2-nitroanisole, the former being derived via *ipso* attack. Nitration of the *p*-haloanisoles in acetic anhydride at 25°C had been investigated previously (10). It seemed likely to us that the adduct, if formed, might not be stable at this temperature. We hoped that nitration of the 4-haloanisoles in acetic anhydride at low temperatures would give the nitronium acetate adducts.

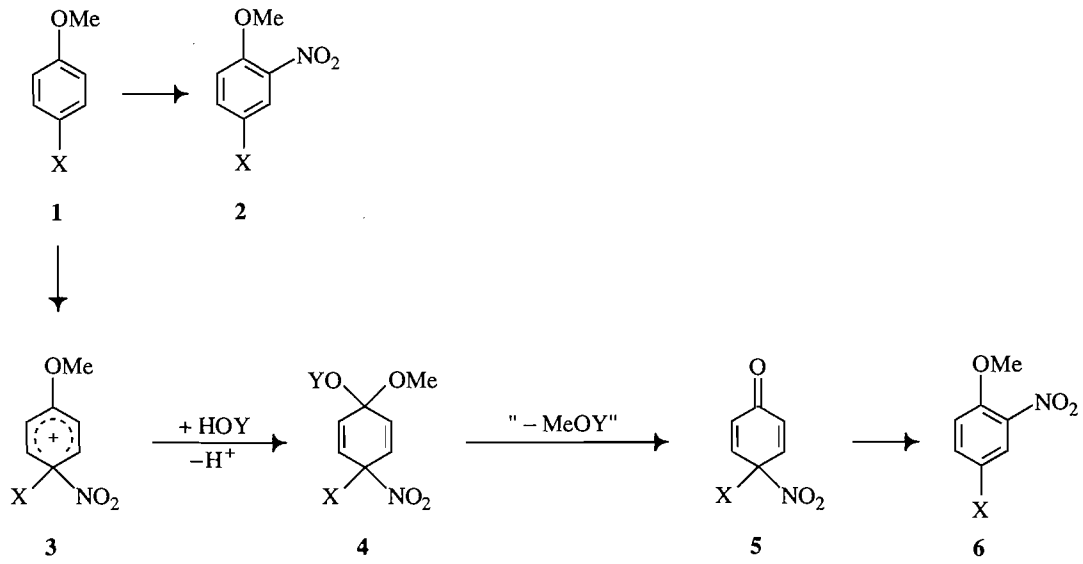
Results and discussion

Nitration of p-*fluoro-,* p-*chloro-, and* p-*bromo-anisole*

Nitration of the *p*-haloanisoles was carried out in acetic anhydride at −60°C. *p*-Fluoroanisole (**1***a*) gave a mixture of 4-fluoro-2-nitroanisole (**2***a*) (94%) and 4-fluoro-4-nitrocyclohexa-2,5-dienone (**5***a*) (6%). *p*-Chloroanisole (**1***b*) gave a similar mixture of **2***b* and **5***b* but *p*-bromoanisole (**1***c*) gave only a mixture of aromatic compounds which, after work-up, was shown to consist of **2***c* (68%), *p*-nitro- (15%), 2,4-dibromo- (11%), and 2-bromo-4-nitro-anisole (5%). Formation of **5***a* and **5***b* occurs through addition of the nitronium ion *ipso* to the halogen atom, and capture of the resulting carbocation by acetic acid, followed by loss of the elements of methyl acetate (Scheme 1 (Y = Ac), cf. Scheme 1 ref. 12). Thus, although a small amount of the *ipso* adduct **4** is apparently formed in the nitration of **1***a* and **1***b* in acetic anhydride at −60°C, the adduct is too labile with respect to elimination to the dienone to be detected, even at this temperature.

In the earlier studies the yield of the halonitrophenol **6** increased with the water content of the reaction medium, the maximum yield of **6***b* being 40% in aqueous sulphuric acid (12) and 37% in aqueous acetic acid (10). Similarly, nitration of **1***a* in aqueous sulphuric acid gave **2***a* (77%) and **6***a* (23%), the maximum yield of **6***a* being obtained in 64–74% acid (12). The halonitrophenol **6** is formed by the trapping of the *ipso* Wheland intermediate by water and thus its amount reflects the extent of *ipso* attack under these conditions. Nitration of **1***c* in aqueous acetic acid (10) gave a mixture of **2***c*, 2,4-dibromoanisole, *p*-nitroanisole, *p*-nitrophenol, and 2-bromo-4-nitrophenol; the amount of the products arising via *ipso* nitration (the nitrodebromination products) was 39%. The formation of the nitrodebromination products reflects the fact that Br^+ is a better leaving group than NO_2^+ (9). The fact that phenols are obtained as well as 4-nitroanisole shows that, in aqueous acid, capture of the *ipso* cation by water is competitive with loss of the Br^+.

For **1***a* and **1***b* the apparent extent of *ipso* attack in acetic anhydride, even at −60°C, is substantially lower than that observed in aqueous media. There is no reason to believe that there are gross disparities in the degrees of *ipso* attack in acetic anhydride and aqueous sulphuric acid or aqueous acetic acid. The extent of nucleophilic capture on nitration of 2-methyl- (16, 17), 4-methyl- (17, 18), and 2-chloro-4-methyl-anisole (12, 19) in acetic anhydride is comparable to that observed in nitrations in aqueous sulphuric acid. However, as the stability of the *ipso* nitrocyclohexadienyl cation is reduced, other reactions, such as rearrangement or the loss of nitronium ion, should start to compete with the trapping of the *ipso* cation. It would seem that this is the situation for **3***a* and **3***b* in acetic anhydride. In more nucleophilic solvents (aqueous sulphuric acid, aqueous acetic acid) the trapping reaction competes favourably with the rearrangement or cleavage of nitronium ion. In acetic anhydride **3***a* (**3***b*) rearranges or reverts to **1***a* (**1***b*) and nitronium ion 2–5 times



a X = F; *b* X = Cl; *c* X = Br

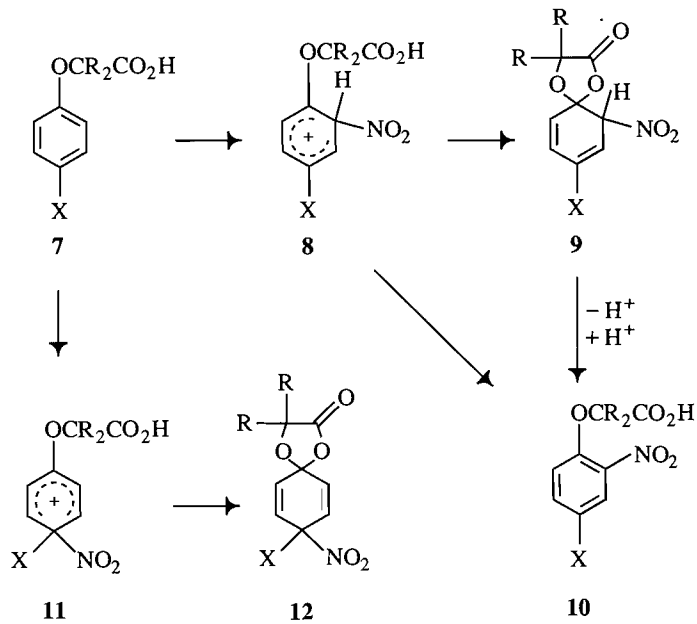
SCHEME 1

faster than it is trapped by the weaker (than water) nucleophile, acetic acid. The halonitroanisole **2** is the end product whether **3** undergoes rearrangement or cleavage. For **1***c* the amount of products derived from *ipso* attack in acetic anhydride (23%) is more nearly comparable with the amount formed in aqueous acetic acid (39%) (10). Since the ratio of *para:ortho* attack in anisoles increases in aqueous media (10), these percentages may be even more closely comparable. Loss of the bromine from the *ipso* cation, in acetic anhydride, is faster than loss of nitronium ion and also faster than capture by acetic acid.

Nitration of p-*halophenoxy acids in acetic anhydride*

Nitration of 2-(4-fluorophenoxy)-2-methylpropanoic acid (**7***a*) in acetic anhydride at −40°C gave 2-(4-fluoro-2-nitrophenoxy)-2-methylpropanoic acid (**10***a*) (and (or) its anhydride with acetic acid) (72%), 3,3-dimethyl-8-fluoro-8-nitro-1,4-dioxaspiro[4.5]deca-6,9-dien-2-one (**12***a*) (28%), and a trace amount of 3,3-dimethyl-8-fluoro-10-nitro-1,4-dioxaspiro[4.5]deca-6,8-dien-2-one (**9***a*) (Scheme 2). On low temperature work-up with aqueous ammonia, **10***a* (~46%), **12***a* (~19%), and 2-(4-fluoro-2-nitrophenoxy)-2-methylpropanamide (**13***a*) (~26%) were obtained, although the yields varied somewhat from one run to another. Acid **10***a* was separated from the nonaromatic compounds by extraction into base during work-up. The diastereomers of **12***a* (designated as **12***ai* and **12***aj*) and amide **13***a* were separated by low temperature column chromatography.

A mixture of **10***b* (and (or) its anhydride with acetic acid) (53%) and **12***b* (47%) was formed on the nitration of **7***b* in a mixture of acetic anhydride and trifluoroacetic anhydride at −60°C. On work-up, **10***b* (30%), **12***b* (44%), and **13***b* (27%) were obtained and were separated. Nitration of **7***c* at −60°C resulted in the formation of **10***c* (53%) (and (or) its anhydride with acetic acid), **12***c* (36%), and 2-(4-nitrophenoxy)-2-methylpropanoic acid (**14**) (11%). Ammonia work-up gave **10***c* (22%), **12***c* (30%), **13***c* (25%), **14** (18%), and 2-(2-bromo-4-nitrophenoxy)-2-methylpropanoic acid (3%). One diastereomer of **12***c* was obtained by recrystallization and the other diastereomer and amide **13***c* were separated by low temperature



a X = F, R = Me; *b* X = Cl, R = Me; *c* X = Br, R = Me
d X = I, R = Me; *e* X = Cl, R = H

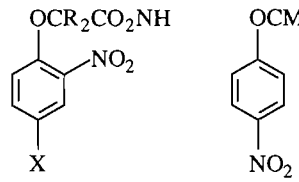
SCHEME 2

chromatography. Acid **7***d* was nitrated in acetic anhydride to give **14** (68%) and **10***d* (32%).

Nitration of 4-chlorophenoxyacetic acid (**7***e*) gave acid **10***e*, acetic 4-chloro-2-nitrophenoxyacetic anhydride, and diene **12***e*. On aqueous ammonia work-up, **10***e* (20%), **12***e* (21%), and amide **13***e* (52%) were obtained. One diastereomer of diene **12***e* was isolated by crystallization.

The structures of the spirodienes were assigned on the basis of spectral information. The ^{1}H nmr (Table 1) showed the *gem* dimethyls (methylene in **12***e*), and four protons in the vinylic region that exhibited an AA′BB′ pattern (AA′BB′X in **12***a*). The ^{13}C nmr (Table 2) showed that there are two pairs of sp^2 carbons bearing hydrogens, and two quaternary sp^3 carbons in

Can. J. Chem. Downloaded from www.nrcresearchpress.com by 194.225.253.170 on 09/07/12
For personal use only.



13 14

a X = F, R = Me
b X = Cl, R = Me
c X = Br, R = Me
e X = Cl, R = H

addition to the carbon bearing the *gem* dimethyl groups. The presence of the nitro group was confirmed by the infrared spectra. The spectral data are consistent with the addition of nitronium ion, ring closure with the carboxylic acid, and loss of the acid proton to give a spiro 1,4 adduct. There is insufficient information to allow the assignment of the stereochemistry. The lower-melting isomer, which was eluted first on chromatography, is designated as *i*, and the higher-melting isomer as *j*.

*Nitration of acids 7*a *and 7*b *in chloroform*

Acids **7***a* and **7***b* were also nitrated with trifluoroacetyl nitrate in [^{2}H]chloroform. In each case, in addition to the expected products **10** and **12**, a 3,3-dimethyl-8-halo-10-nitro-1,4-dioxaspiro[4.5]deca-6,8-dien-2-one (**9**) was obtained as a single diastereomer (Table 3). The extent of *ipso* attack in chloroform was similar to that in acetic anhydride. Formation of diene **9** reduced the amount of the nitro substitution product **10**, reflecting the partitioning of the Wheland cation **8** between capture by ring closure to **9** and deprotonation to substitution product **10**. Diene adducts with nitro *ipso* to hydrogen have been obtained by the rearrangement of nitrodiene adducts (16) and by the nitration of substrates subject to internal nucleophilic capture and possessing bulky substituents that hinder the deprotonation step (20). Normally, diene adducts with a secondary nitro group are not obtained from nitrations, as deprotonation of a secondary nitrocyclohexadienyl cation is usually too rapid for nucleophilic capture to compete. The formation of dienes **9***a* and **9***b* can be ascribed to the low nucleophilicity of the medium resulting in slow deprotonation, and to a low degree of solvation of the carboxylic acid side chain allowing ready capture of the carbocation; entropy considerations favour nucleophilic capture. The lower symmetry of the new dienes was apparent in the ^{1}H nmr spectra. Diene **9***b* had four signals in the region 5.5–6.5 ppm. Two of the protons exhibited a 10-Hz coupling and one other showed a 4-Hz coupling (the fourth proton was obscured). The ^{13}C nmr spectrum of the reaction mixture showed a prominent signal at 86.8 ppm; similar values have been observed for carbons with a nitro group *ipso* to a hydrogen in other secondary nitrodienes (16, 20). The spectral data are consistent with structure **9***b*. The nmr spectra of **9***a* were similar and, even more definitive, there was a signal at 87.0 ppm that showed a typical $^3J_{CF}$ coupling (10 Hz). Dienes **9***a* and **9***b* isomerized on work-up to give acids **10***a* and **10***b*.

*Nitration of derivatives of acids 7*b *and 7*c

Nitration of methyl 2-(4-chlorophenoxy)-2-methylpropanoate (**15***m*) in a mixture of acetic anhydride and trifluoroacetic anhydride failed to give nitronium acetate adducts; only methyl 2-(4-chloro-2-nitrophenoxy)-2-methylpropanoate (**16***m*) was obtained. It is likely that the *ipso* Wheland intermediate (**17***m*) cyclizes through addition of the carbonyl oxygen to the cationic centre. However, demethylation of the resulting cation **18***m* is presumably slower than reversion to **17***m*, and to the rearrangement, or further reversion, to **15***m* and nitronium ion and ultimate formation of **16***m* (Scheme 3). A mixture of **12***b* and **16***n* was obtained on nitration of **15***n*, the former through dealkylation of **18***n*, a reflection of the greater electrofugacity of *tert*-butyl compared to methyl. It is clear that the explanation for the failure of dienes to form from the methyl ester can only lie in the ineffective trapping step. The extent of addition of nitronium ion at the *ipso* position must be closely similar for acid **7***b* and esters **15***m* and **15***n*, and these observations also support the earlier conclusion that the failure to obtain adducts from the nitration of **1***a* and **1***b* in acetic anhydride is due to a slow trapping step and is not to be attributed to a lack of *ipso* attack.

TABLE 1. The ^{1}H nmr spectra of 8-X-8-nitro-1,4-dioxaspiro[4.5]deca-6,9-dien-2-ones

		Chemical shifts (ppm)		
Compound[a]	X	3-R_2[b]	6-H[c]	7-H[c]
12*ai*	F	1.58	6.39[d]	6.29
12*aj*	F	1.58	6.38	6.29
12*bi*	Cl	1.55	6.51	6.14
12*bj*	Cl	1.55	6.51	6.14
12*ci*	Br	1.54	6.75	6.05
12*cj*	Br	1.54	6.76	6.06
12*e*	Cl	4.47[e]	6.61	6.26

[a]The isomer of lower map is designated *i*.
[b]R = H for **12***e*, otherwise R = Me.
[c]d, $J_{6,7}$ = 10 Hz.
[d]dd, J_{HF} = 6 Hz.
[e]3-H of CH_2.

Nitration of 2-(4-chlorophenoxy)-2-methylpropanamide in acetic anhydride/trifluoroacetic anhydride/[^{2}H]chloroform and in trifluoroacetic anhydride/[^{2}H]chloroform gave 8-chloro-2,2-dimethyl-8-nitro-1-oxa-4-azaspiro[4.5]-deca-6,9-dien-3-one (**21***b*) and **13***b* (Scheme 4). The proportion of **21***b* in the nitration mixture varied between 48 and 60%. Although the amide group was as efficient as the carboxyl group in capturing the *ipso* Wheland intermediate, the resultant diene was not as stable and could not be isolated. On warming to ambient temperature in the presence of acid, **21***b* underwent opening of the lactam ring to give **13***b*. This is a striking contrast to the behaviour of Meisenheimer complexes possessing the same lactam ring, which open to give N-aryl amides (*vide infra* (21)). Under basic conditions 4-chloro-2-nitrophenol was also obtained, presumably via dienone **5***b*. Nitration of **19***c* in acetic anhydride/trifluoroacetic anhydride/[^{2}H]chloroform gave **13***c* (50%), **21***c* (40%), and 2-(4-nitrophenoxy)-2-methylpropanamide (10%). On aqueous ammonia work-up amide **13***c* (67%), 2-(4-nitrophenoxy)-2-methylpropanamide (24%), and 2,6-dibromo-4-nitrophenol (9%) were obtained.

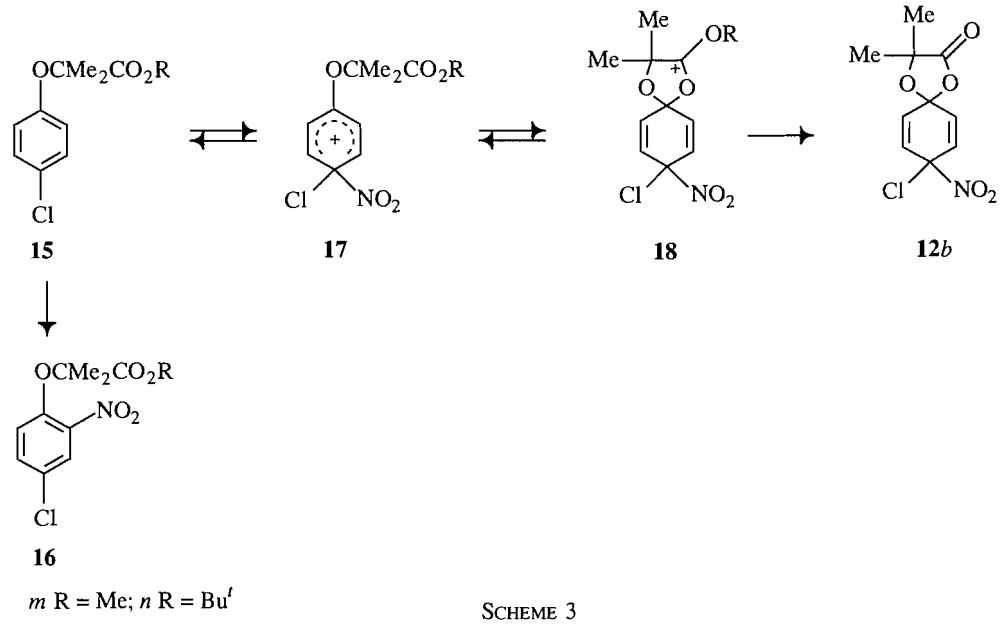
Data for the extent of apparent *ipso* attack in *p*-halophenyl ethers are summarized in Table 4. Whether or not an adduct is formed from the *ipso* cation depends upon the rate of the trapping reaction relative to the rates of other reactions of the cation. We can deduce the following rate relationships in acetic anhydride. For cations **3***a* and **3***b* the trapping reaction (with acetic acid) is 2–5 times slower than the reversion or rearrangement of the cation. For cation **3***c* the cleavage of the carbon–halogen bond is >10 times faster than the trapping reaction (and faster than the rearrangement or reversion) since no diene product was

Can. J. Chem. Downloaded from www.nrcresearchpress.com by 194.225.253.170 on 09/07/12
For personal use only.

TABLE 2. The ^{13}C nmr spectra of 8-X-8-nitro-1,4-dioxaspiro[4.5]deca-6,9-dien-2-ones

		Chemical shifts (ppm)						
Compound	X	3-R_2[a]	C-2	C-3	C-5	C-6	C-7	C-8
12*ai*	F	26.3	174.6	77.8	96.5	137.2[b]	125.4[c]	107.7[d]
12*aj*	F	26.2	174.5	77.8	96.5	137.2[b]	125.7[c]	107.5[d]
12*bi*	Cl	26.3	174.6	77.8	96.2	132.2	129.1	90.2
12*bj*	Cl	26.5	174.7	77.9	96.4	132.3	129.3	90.3
12*ci*	Br	26.3	174.6	77.7	96.2	130.6	129.9	77.8
12*cj*	Br	26.3	174.6	77.7	96.1	130.6	129.9	77.8
12*e*	Cl	—	170.4	62.9	98.7	131.0	129.0	90.9

[a]R = H for **12***e*, otherwise R = Me.
[b]d, J_{CF} = 9 Hz.
[c]d, J_{CF} = 25 Hz.
[d]d, J_{CF} = 228 Hz.



SCHEME 3

TABLE 3. Product distributions in the nitration of *p*-X-$C_6H_4OCMe_2CO_2H$

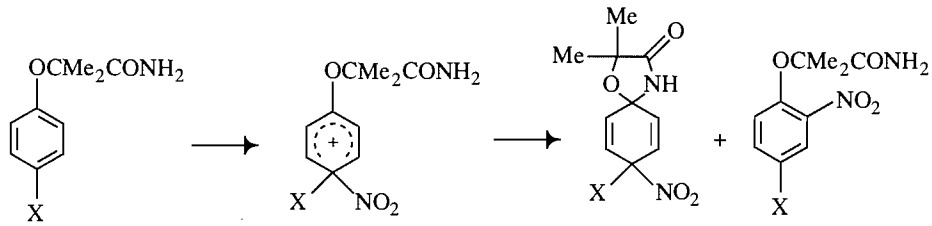
		In acetic anhydride			In [^{2}H]chloroform		
Compound	X	**9**	**10**	**12**	**9**	**10**	**12**
7*a*	F	—	72	28	26	53	21
7*b*	Cl	—	53	47	17	37	45

observed. For cations **11***a*, **11***b*, **11***e*, **17***n*, and **20***b* the trapping reaction (with internal carboxylic acid) is faster (>5 times) than the cleavage or rearrangement of nitronium ion. For cations **11***c* and **20***c* the trapping reaction is 3–4 times faster than the cleavage of Br^+. However, for cation **11***d*, cleavage of I^+ is >10 times faster than the trapping reaction since no trapped product was detected.

Formation and reactions of 4-halo-2-nitrophenoxy amides ***13***

The formation of amides was unexpected, as the only aromatic products resulting from the nitration of 2-methyl-2-(2-methylphenoxy)propanoic acid, 2-methyl-2-(4-methylphenoxy)propanoic acid, and 2-methylphenoxyacetic acid were nitrophenoxy acids (16). The ^1H nmr spectrum obtained when the nitration of *p*-chlorophenoxyacetic acid in acetic anhydride was complete showed, in addition to the signals due to diene **12***e*, two methylene signals, the combined intensity of what was in a 2:3 ratio with the signals in the aromatic region. The intensity of the downfield methylene signal increased with time, consistent with the slow formation of acetic 4-chloro-2-nitrophenoxyacetic anhydride. The formation of a mixed anhydride has also been demonstrated in the nitrations of both 2-methyl-2-(2-methylphenoxy)propanoic acid and 2-methylphenoxyacetic acid in acetic anhydride (16). Nucleophilic attack of ammonia on the mixed anhydride could result in the formation of either acetamide and an aryloxy acid, or acetic acid and an aryloxy amide. How the attack is partitioned will depend on the degree of electron deficiency at the two anhydride carbonyl carbons and the steric requirements at these two sites. With a 2-methyl-4-nitro- or a 4-methyl-2-nitro-aryloxy group, attack is solely at the acetyl carbonyl. However, two electron-withdrawing groups on the aromatic ring suffice to shift nuc-

Can. J. Chem. Downloaded from www.nrcresearchpress.com by 194.225.253.170 on 09/07/12
For personal use only.



b X = Cl; *c* X = Br

SCHEME 4

TABLE 4. Extent of apparent *ipso* attack in the nitration of *p*-X-C_6H_4OR

R	X			
	F	Cl	Br	I
Me[a]	6	6	23	32
Me[b]	23	40	—	—
Me[c]	—	37	39	—
Me[d]	—	<0.3	31	40
CMe_2CO_2H[a]	28	47	47	68
CMe_2CO_2Me[a]	—	0	—	—
$CMe_2CO_2Bu^tMe$[a]	—	34	—	—
CMe_2CONH_2[a]	—	<48	—	—

[a]This work, acetic anhydride, −60°C.
[b]From ref. 12, aqueous sulphuric acid, 25°C.
[c]From ref. 10, aqueous acetic acid, 0°C.
[d]From ref. 10, acetic anhydride, 25°C.

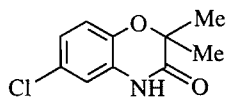
TABLE 5. The ^1H nmr spectra of *p*-X-$C_6H_4OCMe_2CO_2H$ and derivatives

Compound	X	Chemical shifts (ppm)		
		CH_3	3-H[a]	2-H[a]
7*a*	F	1.66	6.93[b]	6.93
7*b*	Cl	1.58	7.24	6.89
7*c*	Br	1.59	7.37	6.92
7*d*	I	1.59	7.51	6.71
14	NO_2	1.71	8.15	6.92
15*m*[c]	Cl	1.54	7.17	6.96
15*n*[d]	Cl	1.53	7.20	6.79
19*b*	Cl	1.49	7.22	6.88
19*c*	Br	1.46	7.36	6.81

[a]$J_{2,3}$ = 9 Hz.
[b]J_{HF} = 6.5 Hz.
[c]CH_3O at 3.71 ppm.
[d]$(CH_3)_3CO$ at 1.42 ppm.

leophilic attack substantially to the other carbonyl, as was demonstrated by forming acetic 2-(4-chloro-2-nitrophenoxy)-2-methylpropanoic anhydride and subjecting it to the standard work-up conditions whereupon amide **13***b* was formed.

Treatment of amide **13***b* with isoamyl nitrite in dioxane gave acid **7***b* on aqueous work-up, confirming the assigned structure. However, suspension of **13***b* in 20% sodium hydroxide for 1 h at 90°C gave 4-chloro-2-nitroaniline and 2-hydroxy-2-methylpropanoic acid. The Smiles rearrangement of 2-aryloxy-2-methylpropanamides is facile (even 2-(4-methoxyphenoxy)-2-methylpropanamide undergoes rearrangement under sufficiently vigorous conditions) (21). Treatment of **13***b* with sodium hydride in dry dimethylformamide for 10 min gave *N*-(4-chloro-2-nitrophenyl)-2-hydroxy-2-methylpropanamide. Alkaline hydrolysis of this amide gave 4-chloro-2-nitroaniline and 2-hydroxy-2-methylpropanoic acid. Treatment of amide **13***b* with 57% hydriodic acid failed to cleave the ether linkage and gave a product of formula $C_{10}H_{10}ClNO_2$. The ^1H nmr showed the presence of a pair of *gem* dimethyl groups and three aromatic protons. The infrared spectrum contained a lactam band at 1685 cm^{-1}. The spectral information is consistent with the structure 4-aza-6-chloro-2,2-dimethyl-1-oxa-3-oxo-1,2,3,4-tetrahydronaphthalene (**22**). Treatment of acid **10***b* with



22

57% hydriodic acid under the same conditions also gave this lactam. Thus from both **10***b* and **13***b* the lactam must have been formed by reduction of the nitro group followed by closure to form the lactam ring. Reduction of aromatic nitro groups by hydriodic acid was observed previously in 3-(arylmethylene)nitrophthalides (22).

Experimental

Instrumentation and general experimental methods were described previously (15, 18). 4-Fluoro-, 4-chloro-, 4-bromo-, 4-iodo-, and 4-nitro-phenol, 4-chlorophenoxyacetic acid, 4-chloro- and 4-bromoanisole, and 1,1,1-trichloro-2-methyl-2-propanol were Aldrich reagent grade. 4-Fluoroanisole, bp 150°C (lit. (23*a*) bp 157°C) was obtained by alkylation of 4-fluorophenol with dimethyl sulphate. The nmr spectra of substrates and products not given in the text are included in Tables 1,2,5–8.

2-(4-Halophenoxy)-2-methylpropanoic acid (7) and related acids

Pulverized sodium hydroxide (64.0 g, 1.60 mol) was added in five portions, at hourly intervals, to a solution of 4-fluorophenol (22.4 g, 0.20 mol) and 1,1,1-trichloro-2-methyl-2-propanol hydrate (85.2 g) in acetone (400 cm^3). The reaction mixture was cooled to 0°C before each portion of sodium hydroxide was added and the mixture was then allowed to warm to ambient temperature. Additional acetone (400 cm^3) was added after the last portion of sodium hydroxide. The reaction mixture was stirred for 16 h and the solvent was then evaporated under reduced pressure. The residue was taken up in water (500 cm^3) and the aqueous solution was washed with ether (2 × 100 cm^3), acidified with hydrochloric acid, and extracted with ether (3 × 100 cm^3). This ether solution was extracted with saturated sodium bicarbonate (3 × 100 cm^3) and the bicarbonate extract was acidified and extracted with ether

Can. J. Chem. Downloaded from www.nrcresearchpress.com by 194.225.253.170 on 09/07/12
For personal use only.

TABLE 6. The ^{13}C nmr spectra of p-X-$C_6H_4OCMe_2CO_2H$ and derivatives

Compound	X	Chemical shifts (ppm)						
		CH_3	C-1	C-2	C-1′	C-2′	C-3′	C-4′
7*a*	F	25.1	180.2	79.9	150.9	122.4[a]	115.8[b]	155.8[c]
7*b*	Cl	25.1	179.9	79.5	153.4	121.6	129.2	128.1
7*c*	Br	25.1	179.4	79.5	153.9	122.0	132.2	115.6
7*d*	I	25.2	179.5	79.5	154.8	122.4	138.2	85.9
14	NO_2	25.2	178.9	79.7	160.5	118.2	125.4	142.2
15*n*[d]	Cl	25.4	173.0	81.8	154.5	120.3	129.0	126.9
19*b*	Cl	24.8	177.6	81.6	152.9	122.5	129.2	128.5
19*c*	Br	24.8	177.5	81.5	153.4	122.9	132.2	116.0

[a]d, J_{CF} = 8 Hz.
[b]d, J_{CF} = 23 Hz.
[c]d, J_{CF} = 244 Hz.
[d]$(CH_3)_3CO$ at 27.8 and 79.9 (or 81.8 and C-2 at 79.9) ppm.

($4 \times 100\ cm^3$). The ether solution was dried ($MgSO_4$) and the ether was evaporated to afford a mixture of **7***a* and methacrylic acid. The latter was removed by heating the oil under reduced pressure and the residue was taken up in ether. On filtration through a thin layer of silica and evaporation of the solvent, **7***a* was obtained (34.7 g, 88%). Recrystallization from ether gave colourless crystals, mp 86–87°C (lit. (24) mp 83°C). The following acids were obtained similarly: **7***b* (90%), mp 123°C (lit. (24) mp 117°C), **7***c* (80%) mp 136°C (lit. (24) mp 135°C), **7***d* (64%), mp 144–145°C (lit. (24) mp 135°C), **14** (53%, after preforming the sodium phenoxide), mp 128°C (lit. (25) mp 123°C), and **10***c* (54%), mp 108°C; ir (KBr): 3000–2500 (OH), 1705 (C=O), 1540 and 1360 (NO_2) cm^{-1}. *Anal.* calcd. for $C_{10}H_{10}BrNO_5$: C 39.50, H 3.31, N 4.61; found: C 39.67, H 3.41, N 4.55.

2-(4-Chlorophenoxy)-2-methylpropanoic acid derivatives

A solution of **7***b* (1.72 g, 8.0 mmol) and pyridine (1.31 cm^3, 16.3 mmol) in ether (25 cm^3) was added dropwise with stirring to a solution of thionyl chloride (0.59 cm^3, 8.2 mmol) in ether (25 cm^3) heated under reflux. After 90 min methanol (0.35 cm^3, 8.6 mmol) was added and after a further 60 min the reaction mixture was washed with aqueous sodium bicarbonate, dried, and the ether was evaporated to afford ester **15***m* (1.70 g, 93%). Ester **15***n* (61%) was prepared by addition of a solution of potassium *tert*-butoxide in tetrahydrofuran to the acid chloride from **7***b* and had mp 38–39°C; ir (KBr): 1725 (C=O), 1235 (C—O) cm^{-1}. *Anal.* calcd. for $C_{14}H_{19}ClO_3$: C 62.11, H 7.07; found: C 61.89, H 6.98. Amide **19***b* was prepared (83%) by adding the acid chloride to a solution of ammonia in ether at −40°C, and had mp 120°C (lit. (24) mp 121°C). Amide **19***c* had mp 127°C (lit (24) mp 128°C).

Nitration of 4-haloanisoles (1)

A solution of **1***a* (0.63 g, 5 mmol) in acetic anhydride (2.55 g, 25 mmol) at −60°C was added with stirring to a solution of nitric acid (0.95 g, 15 mmol) in acetic anhydride (2.55 g, 25 mmol), also at −60°C. Within 45 s a yellow precipitate had formed, which dissolved on the addition of cold [^{2}H]chloroform (5 cm^3). The ^{1}H nmr showed that the reaction had gone to completion and that **2***a* (94%) and **5***a* (6%) (15) had been formed. The reaction mixture was added to ether (250 cm^3) at −60°C and concentrated aqueous ammonia (22 cm^3) was added dropwise. The ethereal fraction was washed with cold brine (2×75 cm^3) and water (75 cm^3). After drying, the ether was evaporated to give **2***a* (0.79 g), mp 61°C (lit. (23*b*) mp 61.5–62°C). The aqueous extracts were combined, acidified, and extracted with ether (3×75 cm^3). Evaporation of the ether afforded an acetic acid solution of **6***a* and a small amount of 2,6-dinitro-4-fluorophenol.

Anisoles **1***b* and **1***c* were nitrated similarly.

Nitration of halophenoxy acids and derivatives

A solution of **7***a* (19.8 g, 0.10 mol) in acetic anhydride (51.1 g, 0.50 mol) was added over 30 min to a solution of nitric acid (18.9 g, 0.30 mol) in acetic anhydride (51.1 g, 0.50 mol) at −60°C. The temperature was raised and held at −40°C for 40 min; ^{1}H nmr showed that **10***a* (71%) and diene (29%) were formed. The solution was added to ether (1.5 dm^3) at −60°C, and concentrated aqueous ammonia (215 cm^3) was added dropwise. The ether phase was separated and washed with brine (2×500 cm^3) and with water (500 cm^3), dried, and the ether evaporated to yield a mixture (9.7 g) of **12***a* (41%) and **13***a* (59%). The aqueous washings were combined, acidified, and extracted with ether (3×500 cm^3). The ether extract was washed with brine (500 cm^3), dried, and evaporated, finally under reduced pressure. The residue was taken up in 1:1 ether–pentane, washed with brine, dried, and the solvent evaporated to afford **10***a* (11.8 g), obtained as colourless crystals on recrystallization from ether, mp 79–81°C; ir (KBr): 3000–2500 (OH), 1715 (C=O), 1540 and 1360 (NO_2), 1205 (C—F) cm^{-1}. *Anal.* calcd. for $C_{10}H_{10}FNO_5$: C 49.39, H 4.14, N 5.76; found: C 49.36, H 3.94, N 5.67. Chromatography of the mixture of **12***a* and **13***a* on silica (800 g) at −40°C and elution with ether–pentane gave **12***a* (4.8 g). The lower melting diastereomer (**12***ai*) separated in the 15% and 20% ether fractions and was obtained as colourless crystals on recrystallization from ether, mp 101–103°C; ir (KBr): 1800 (C=O), 1570 and 1340 (NO_2), 1125 (C—F) cm^{-1}. *Anal.* calcd. for $C_{10}H_{10}FNO_5$: C 49.39, H 4.14, N 5.76; found: C 48.97, H 4.21, N

TABLE 7. The ^1H nmr spectra of 4-X-2-NO_2-$C_6H_4OCR_2CO_2H$ and derivatives

Compound	X	Chemical shifts (ppm)			
		R[a]	3-H[b]	5-H[c]	6-H[b]
10*a*	F	1.66	7.55[d]	7.28[d]	7.21[e]
10*b*	Cl	1.66	7.77	7.45	7.11
10*c*	Br	1.66	7.89	7.57	7.01
10*e*	Cl	4.81[f]	7.77	7.51	7.21
13*a*[g]	F	1.57	7.59[d]	7.30[d]	7.24[e]
13*b*	Cl	1.61	7.82	7.47	7.17
13*c*	Br	1.61	7.98	7.63	7.10
13*e*	Cl	4.81[f]	7.97	7.70	7.38
16*m*[h]	Cl	1.61	7.73	7.40	6.93
16*n*[i]	Cl	1.59	7.72	7.39	6.98

[a]R = H for **10***e* and **13***e*, otherwise R = Me.
[b]d.
[c]dd, $J_{3,6}$ = 9 Hz, $J_{3,5}$ = 3 Hz.
[d]J_{HF} = 7 Hz.
[e]J_{HF} = 4 Hz.
[f]3-H of CH_2.
[g]NH_2 of the amides **13** appeared as broad singlets at ~6.3 and ~6.9 ppm.
[h]CH_3O at 3.76 ppm.
[i]$(CH_3)_3O$ at 1.43 ppm.

Can. J. Chem. Downloaded from www.nrcresearchpress.com by 194.225.253.170 on 09/07/12
For personal use only.

TABLE 8. The ^{13}C nmr spectra of 4-X-2-NO_2-$C_6H_4OCR_2CO_2H$ and derivatives

Compound	X	Chemical shifts (ppm)								
		R[a]	C-1	C-2	C-1′	C-2′	C-3′	C-4′	C-5′	C-6′
10*a*	F	24.7	179.1	82.2	144.5	143.6[b]	112.4[c]	156.9[d]	120.3[e]	123.5[b]
10*b*	Cl	24.8	178.6	82.1	147.0	143.6	125.2	128.0	133.1	122.6
10*c*	Br	24.8	178.2	82.0	147.5	143.8	128.1	114.7	136.0	122.7
10*e*	Cl	—	168.7	66.2	150.3	141.2	125.1	125.9	133.9	117.4
13*a*	F	24.5	176.4	84.7	144.3	143.5[b]	112.7[f]	156.8[d]	120.5[e]	123.5[b]
13*b*	Cl	24.6	176.0	84.8	146.8	143.5	125.4	128.1	133.3	122.6
13*c*	Br	24.6	176.3	84.7	147.3	143.6	128.4	114.8	136.4	122.9
13*e*	Cl	—	169.3	69.2	151.0	140.9	126.1	126.4	135.2	118.2
16*m*[g]	Cl	25.1	173.7	82.2	147.5	143.6	125.2	127.4	132.9	121.7
16*n*[h]	Cl	25.1	172.2	82.2	147.8	142.6	125.1	126.5	132.7	120.6

[a]R = H for **10***e* and **13***e*, otherwise R = Me.
[b]d, J_{CF} = 8 Hz.
[c]d, J_{CF} = 27 Hz.
[d]d, J_{CF} = 248 Hz.
[e]d, J_{CF} = 23 Hz.
[f]d, J_{CF} = 28 Hz.
[g]CH_3O at 52.8 ppm.
[h]$(CH_3)_3CO$ at 27.7 and 82.6 (or 82.2 and C-2 at 82.6) ppm.

5.65. Recrystalliztion of the residue from the 30% through 100% ether fractions gave the second diastereomer **12***aj*, mp 122–124°C; ir (KBr): 1800, 1570 and 1340, 1125 cm^{-1}. *Anal.* calcd. for $C_{10}H_{10}FNO_5$: C 49.39, H 4.14, N 5.76; found: C 49.09, H 4.28, N 5.66. Elution with dichloromethane followed by methanol gave **13***a* (4.8 g), obtained as yellow crystals on recrystallization from ether, mp 118–119°C; ir (KBr): 3470 (NH_2), 1680 (C=O), 1520 and 1360 (NO_2), 1205 (C—F) cm^{-1}. *Anal.* calcd. for $C_{10}H_{11}FN_2O_4$: C 49.59, H 4.58, N 11.57; found: C 49.50, H 4.53, N 11.47.

A solution of acid **7***a* (198 mg, 1.0 mmol) in [^{2}H]chloroform (2.0 cm^3) was added to a solution of nitric acid (126 mg, 2.0 mmol) and trifluoroacetic anhydride (280 mm^3, 2.0 mmol) in [^{2}H]chloroform (2.0 cm^3) at −50°C. The mixture was warmed to −30°C and after 10 min the ^{1}H nmr spectrum showed that **10***a* (53%), **12***a* (21%), and **9***a* (26%) had been formed. Diene **9***a* had ^{1}H nmr ($CDCl_3$, 250 MHz) δ: 1.59 (s, 6, CH_3), 5.49 (dd, J = 5 and 5 Hz, 1, 10-H), 5.64 (m, 1, 9-H), 5.98 (dd, J = 4 Hz and 10 Hz, 1, 6-H) ppm. The 7-H signal occurred in the range 6.2–6.5 ppm but was obscured. The C-10 signal (87.0 ppm (d, $^3J_{CF}$ = 10 Hz)) was clearly evident in the ^{13}C nmr spectrum of the reaction mixture. The reaction mixture was worked up by adding it to aqueous sodium bicarbonate (20 cm^3) at 0°C, followed by extraction with dichloromethane (3 × 10 cm^3). Diene **12***a* was obtained from the organic phase and acid **10***a* from the aqueous phase. Diene **9***a* had isomerized to **10***a*.

Nitration of other acids and derivatives was carried out by methods similar to those described above. In a number of cases trifluoroacetic anhydride was included in the nitrating solution to boost the reactivity and (or) [^{2}H]chloroform was added to the substrate solution to increase the solubility. The amount of substrate, the ratio of nitric acid:acetic anhydride:trifluoroacetic anhydride:volume of [^{2}H]chloroform per mole of substrate, and the final reaction temperature are shown in parentheses in the following.

Acid **7***b* (0.10 mol; 6:14:3:—; −60°C) gave **10***b* (7.7 g), the diastereoisomers of **12***b* (10.7 g), and **13***b* (5.5 g). Acid **10***b* had mp 96–97°C; ir (KBr): 3000–2500, 1715, 1530 and 1340, 710 (C—Cl) cm^{-1}. *Anal.* calcd. for $C_{10}H_{11}ClNO_5$: C 46.26, H 3.88, N 5.39; found: C 46.21, H 3.67, N 5.33. The first diastereomer **12***bi* had mp 94–96°C (dec.); ir (KBr): 1800, 1560 and 1330, 690 (C—Cl) cm^{-1}. *Anal.* calcd. for $C_{10}H_{10}ClNO_5$: C 46.26, H 3.88, N 5.39; found: C 46.07, H 3.81, N 5.36. The second diastereomer **12***bj* had mp 105–106°C (dec.); ir: 1800, 1560 and 1330, 690 cm^{-1}. *Anal.* calcd. for $C_{10}H_{10}ClNO_5$: C 46.26, H 3.88, N 5.39; found: C 45.92, H 3.79, N 5.30. Amide **13***b* had mp 127°C; ir (KBr): 3470, 1700, 1515 and 1355, 705 (C—Cl) cm^{-1}. *Anal.* calcd. for $C_{10}H_{11}ClN_2O_4$: C 46.44, H 4.29, N 10.83; found: C 46.50, H 4.10, N 10.69. In the absence of acetic anhydride, **7***b* (2 mmol; 2:—:2:4 dm^3; −60°C) gave **10***b* (37%), **12***b* (45%), and **9***b* (17%). Diene **9***b* had ^{1}H nmr ($CDCl_3$, 90 MHz) δ: 1.67 (s, 6, CH_3), 5.55 (d, J = 4 Hz, 1, 10-H), 5.97 (d, J = 10 Hz, 1, 6-H), 6.31 (d, J = 10 Hz, 1, 7-H) ppm. The 9-H signal occurred in the range 6.2–6.3 ppm but was obscured. In the ^{13}C nmr spectrum of the mixture the C-10 signal at 86.8 ppm was unambiguous. On work-up, **10***b* and **12***b* were obtained but **9***b* did not survive. A small amount of 2-(2,6-dinitro-4-chlorophenoxy)-2-methylpropanoic acid was also obtained in the **10***b* fraction. It had ^{1}H nmr ($CDCl_3$, 90 MHz) δ: 1.58 (s, 6, CH_3), 7.97 (s, 2, 3-H and 5-H) ppm; ^{13}C nmr $CDCl_3$, 62.9 MHz) δ_C: 24.5 (CH_3), 87.7 ($C(CH_3)_2$), 128.4 (C-3 and C-5), 130.5 (C-4), 140.6 (C-2 and C-6), 147.4 (C-1), 176.1 (COOH) ppm.

Diastereomer **12***cj* crystallized from the ether solution of the product mixture from nitration of **7***c* (30 mmol; 4:16:3:—; −60°C). It had mp 99°C (dec.); ir (KBr): 1800 (C=O), 1530 and 1340 (NO_2) cm^{-1}. *Anal.* calcd. for $C_{10}H_{10}BrNO_5$: C 39.50, H 3.31, N 4.61; found: C 39.58, H 3.35, N 4.58. The other diastereomer **12***ci* had mp 90–92°C (dec.); ir (KBr): 1800, 1580 and 1340 cm^{-1}. *Anal.* calcd. for $C_{10}H_{10}BrNO_5$: C 39.50, H 3.31, N 4.61; found: C 39.47, H 3.34, N 4.57. amide **13***c* had mp 111°C; ir (KBr): 3470, 1700, 1520 and 1360 cm^{-1}.

Acid **7***d* (0.5 mmol; 3:10:—:—; −60°C) did not give any diene. Acid **7***e* (50 mmol; 6:14:3:—; −30°C) was added as a finely powdered solid to the nitrating mixture, as it was insoluble. On work-up the ether phase afforded **12***e* (2.43 g), obtained as a single diastereomer on recrystallization from ether, mp 98°C (dec.); ir (KBr): 1820, 1580 and 1330 cm^{-1}. *Anal.* calcd. for $C_8H_6ClNO_5$: C 41.49, H 2.61, N 6.05; found: C 41.52, H 2.68, N 6.03. Amide **13***e* (5.98 g) was filtered from the aqueous layer and obtained as colourless crystals on recrystallization from acetone, mp 188–189°C; ir (KBr): 3460 and 3160, 1700, 1520, and 1345 cm^{-1}. *Anal.* calcd. for $C_8H_6ClN_2O_5$: C 41.67, H 3.06, N 12.05; found: C 41.56, H 3.13, N 12.09. Acid **10***e* was obtained from the acidified aqueous layer and had mp 173–174°C (lit. (26) mp 169–170°C).

Ester **15***m* (2.5 mmol; 6:14:3:—; −60°C) did not give diene. The product, **16***m*, had mp 42–45°C; ir (KBr): 1740 (C=O), 1530 and 1355 (NO_2) cm^{-1}; ms m/e (relative intensity): 275 (14), 273.0439 (43, M_r($^{12}C_{11}{}^1H_{12}{}^{35}Cl{}^{14}N{}^{16}O_5$) = 273.0404), 216 (11), 214 (31), 175 (71), 174 (19), 173 (100), 128 (20), 101 (70), 73 (23), 69 (21), 63 (13), 59 (18).

Ester **15***n* (2.5 mmol; 6:14:3:—; −60°C) gave **12***b* and **16***n*. Amide **19***b* (3 mmol; 10:15:5:0.8 dm^3; −40°C; also 1.5 mmol; 10:15:5:1.7

Can. J. Chem. Downloaded from www.nrcresearchpress.com by 194.225.253.170 on 09/07/12
For personal use only.

Can. J. Chem. Downloaded from www.nrcresearchpress.com by 194.225.253.170 on 09/07/12
For personal use only.

dm^3; −40°C; and 2.5 mmol; 1.5:—:1.5:2.0 dm^3; −50°C) gave **13***b* and diene **21***b*. Work-up using aqueous ammonia, liquid ammonia, and aqueous sodium bicarbonate was variously attempted. In a number of cases a portion of the **21***b* survived through the work-up until the temperature was raised to ambient, whereupon it decomposed to **13***b*. The diene was precipitated from the last reaction mixture, and subsequently filtered off, on the addition of ether and pentane, but even then it decomposed on warming to ambient. One diastereomer of **21***b* had ^{1}H nmr ($CDCl_3$, 90 MHz) δ: 1.55 (s, 6, CH_3), 6.16 (d, J = 10 Hz, 2, 7-H and 9-H), 6.55 (d, J = 10 Hz, 2, 6-H and 10-H) ppm; the other diastereomer had ^{1}H nmr ($CDCl_3$, 90 MHz) δ: 1.57 (s, 6, CH_3), 6.14 (d, J = 10 Hz, 2, 7-H and 9-H), 6.50 (d, J = 10 Hz, 2, 6-H and 10-H) ppm. Diene **21***c*, obtained on the nitration of **19***c* (7.5 mmol; 10:15:5:1.7 dm^3; −40°C) did not survive work-up.

Reactions of 2-(4-chloro-2-nitrophenoxy)-2-methylpropanamide (13b)

A solution of isoamyl nitrite (0.54 cm^3, 4.0 mmol) in dioxane (5 cm^3) was added to a solution of amide **13***b* (519 mg, 2.0 mmol) in dioxane (5 cm^3) over 1 h. After stirring for 2 h at ambient temperature the reaction mixture was heated under reflux for 2.5 h. The solvent was evaporated and the residue taken up in ether (50 cm^3). The ether solution was extracted with aqueous sodium bicarbonate, which was then acidified and extracted with ether. Evaporation of the ether afforded **10***b* (425 mg).

Acid **10***b* (130 mg, 0.5 mmol) was dissolved in acetic anhydride (715 mg, 7.0 mmol) that contained a drop of trifluoroacetic acid and the solution was added to a mixture of nitric acid (347 mg, 5.5 mmol) and trifluoroacetic anhydride (42 cm^3, 3.0 mmol) in acetic anhydride (715 mg, 6.0 mmol) at −60°C. After 15 min the reaction mixture was added to ether (20 cm^3) at −60°C, and aqueous ammonia (3.7 cm^3) was added. The ethereal phase was washed with cold brine, dried, and evaporated to afford **13***b*. When diene **12***b* was subjected to the same treatment it was recovered without loss.

A suspension of **13***b* (200 mg) in 20% sodium hydroxide (3.0 cm^3) at 90°C was stirred for 1 h. The mixture was diluted to 25 cm^3 and extracted with ether (3 × 10 cm^3). The ether solution was dried and the ether was evaporated to afford 4-chloro-2-nitroaniline (123 mg), mp 116°C (lit. (23*c*) mp 116–117°C). The alkaline solution was acidified and extracted with ether (3 × 10 cm^3). Removal of the ether afforded 2-hydroxy-2-methylpropanoic acid (42 mg), mp 78°C (lit. (23*d*) mp 79°C).

A solution of **13***b* (778 mg, 3.0 mmol) in dry dimethylformamide (10 cm^3) was added to 60% sodium hydride dispersion (132 mg, 3.3 mmol) (cf. ref. 21). The solution became dark red immediately. The solvent was removed under reduced pressure and excess aqueous ammonium chloride was added. The mixture was extracted with ether (3 × 30 cm^3), the ethereal solution dried and evaporated to yield *N*-(4-chloro-2-nitrophenyl)-2-hydroxy-2-methylpropanamide (765 mg, 98%). Recrystallization from ether gave yellow crystals, mp 110°C; ir (KBr): 3440 (OH), 3390 and 3290 (NH), 1650 (C=O), 1570 and 1335 (NO_2) cm^{-1}. *Anal.* calcd. for $C_{10}H_{11}ClN_2O_4$: C 46.44, H 4.29, N 10.83; found: C 46.79, H 4.40, N 10.74.

A suspension of **13***b* (200 mg) in 57% hydriodic acid (2.0 cm^3) was heated under reflux for 2.5 h. The reaction mixture was diluted (25 cm^3) and extracted with ether. Evaporation of the ether after drying afforded 4-aza-6-chloro-2,2-dimethyl-1-oxa-3-oxo-1,2,3,4-tetrahydronaphthalene (**22**) (191 mg). Similar treatment of **10***b* gave the same product (156 mg). The heterocycle had mp 165–166°C; ir (KBr): 1685 (C=O) cm^{-1}; ^{1}H nmr ($CDCl_3$, 90 MHz) δ: 1.50 (s, 6, CH_3), 6.86 (bs, 4, 5-H, 6-H, 7-H, and 8-H) ppm; ^{13}C nmr ($CDCl_3$, 62.9 MHz) δ_C: 23.6 (CH_3), 78.2 (C-2), 115.3 (C-8), 118.4 (C-5), 123.8 (C-7), 127.2 (C-4a or C-6), 127.8 (C-6 or C-4a), 141.2 (C-8a), 170.8 (C-3) ppm. *Anal.* calcd. for $C_{10}H_{10}ClNO_3$: C 56.75, H 4.76, N 6.62; found: C 57.21, H 4.87, N 6.65.

Acknowledgements

We thank the Natural Sciences and Engineering Research Council of Canada for financial support and Gordon G. Cross for some preliminary studies.

1. K. Fries. Justus Liebigs Ann. Chem. **389**, 315 (1912).
2. G. A. Zlobina and V. V. Ershov. Izv. Akad. Nauk SSSR, Ser. Khim. 371 (1964).
3. V. D. Shteingarts, G. G. Yakobson, and N. N. Vorozhtsov-ml. Dokl. Akad. Nauk SSSR, **170**, 1347 (1966).
4. V. D. Shteingarts, A. G. Budnik, G. G. Yakobson, and N. N. Vorozhtsov-ml. Zh. Obshch. Khim. **37**, 1537 (1967).
5. O. I. Osina and V. D. Shteingarts. Zh. Org. Khim. **10**, 335 (1974).
6. A. A. Shtark, V. D. Shteingarts, and A. G. Maidanyuk. Izv. Sib. Otd. Akad. Nauk SSSR, Ser. Khim. Nauk, 123 (1976).
7. A. A. Shtark and V. D. Shteingarts. Izv. Sib. Otd. Akad. Nauk SSSR, Ser. Khim. Nauk, 123 (1976).
8. A. A. Shtark and V. D. Shteingarts. Zh. Org. Khim. **12**, 1499 (1976).
9. C. L. Perrin. J. Org. Chem. **36**, 420 (1971).
10. C. L. Perrin and G. A. Skinner. J. Am. Chem. Soc. **93**, 3389 (1971).
11. A. Fischer and S. S. Seyan. Can. J. Chem. **56**, 1348 (1978).
12. R. B. Moodie, K. Schofield, and G. D. Tobin. J. Chem. Soc. Chem. Commun. 180 (1978); C. Blomfield, A. K. Manglik, R. B. Moodie, K. Schofield, and G. D. Tobin. J. Chem. Soc. Perkin Trans. 2, 75 (1983).
13. M. P. Hartshorn, H. T. Ing, K. E. Richards, H. Sutton, and J. Vaughan. Aust. J. Chem. **35**, 1635 (1982).
14. M. P. Hartshorn, R. J. Martyn, J. Vaughan, and G. J. Wright. Aust. J. Chem. **36**, 839 (1983).
15. R. G. Clewley, G. G. Cross, A. Fischer, and G. N. Henderson. Tetrahedron, 1299 (1989).
16. G. S. Bapat, A. Fischer, G. N. Henderson, and S. RayMahasay. J. Chem. Soc. Chem. Commun. 119 (1983); G. S. Bapat. Ph.D. Dissertation, University of Victoria, 1983.
17. J. W. Barnett, R. B. Moodie, K. Schofield, J. B. Weston, R. G. Coombes, J. G. Golding, and G. D. Tobin. J. Chem. Soc. Perkin Trans. 2, 248 (1977).
18. A. Fischer, D. L. Fyles, G. N. Henderson, and S. RayMahasay. Can. J. Chem. **64**: 1764 (1986).
19. A. Fischer, G. N. Henderson, and S. RayMahasay. Can. J. Chem. **65**, 1233 (1987).
20. G. G. Cross, A. Fischer, and G. N. Henderson. Can. J. Chem. **62**, 2803 (1984).
21. R. Bayles, M. C. Johnson, R. F. Maisey, and R. W. Turner. Synthesis, **31**, 33 (1977).
22. L. Krasnec, Jr. and P. Hrnciar. Chem. Zvesti, **25**, 359 (1971).
23. J. Buckingham (*Editor*). Dictionary of organic compounds. 5th ed. Chapman and Hall, London. 1982; (*a*) Vol. 3, p. 2663; (*b*) Vol. 3, p. 2662; (*c*) Vol. 1, p. 1169; (*d*) Vol. 3, p. 3148.
24. H. Gilman and G. R. Wilder. J. Am. Chem. Soc. **77**, 6644 (1955).
25. P. Galimberti and A. Defranchesi. Gazz. Chim. Ital. **77**, 431 (1947).
26. A. Fredga, E. Gamstedt, and L. Ekermo. Ark. Kemi, **29**, 515 (1968).

Classical frequency modulation and the Franck–Condon principle

MURRAY N. NEUMAN
Department of Physics, University of Manitoba, Winnipeg, Man., Canada R3T 2N2

Received March 29, 1989

MURRAY N. NEUMAN. Can. J. Chem. **67**, 1480 (1989).

A classical frequency-modulation principle is used to calculate the dipole spectrum of a two-freedom oscillator. Its two motions are assumed adiabatically separable; the frequency of motion along the fast coordinate is assumed to have a weak linear dependence on the slow coordinate. At high temperatures, the dipole spectrum of the fast motion, as found by this method, agrees quantitatively with a result based on evaluation of the Franck–Condon factors for the corresponding quantum-mechanical transition. It is suggested that the frequency-modulation approach might be especially useful in studying hydrogen-bond networks whose classical oscillations may be chaotic.

Key words: Franck–Condon factors, frequency modulation, hydrogen bonding.

MURRAY N. NEUMAN. Can. J. Chem. **67**, 1480 (1989).

On utilise un principle classique de modulation de fréquence pour calculer le spectre dipolaire d'un oscillateur à deux degrés de liberté. On fait l'hypothèse que ses deux mouvements peuvent être séparés d'une façon adiabatique; on fait aussi l'hypothèse que la fréquence du mouvement le long de la coordonnée la plus rapide est faiblement lié d'une façon linéaire avec la coordonnée la plus lente. À des températures élevées, tel que trouvé par cette méthode, le specte dipolaire du mouvement rapide est en accord quantitatif avec un résultat basé sur l'évalution des facteurs de Franck–Condon pour la transition de mécanique quantique correspondante. On suggère que l'approche de la modulation de fréquence pourrait s'avérer particulièrement utile pour l'étude de réseaux de liaisons hydrogènes dont les oscillations classiques peuvent être chaotiques.

Mots clés : facteurs de Franck–Condon, modulation de fréquence, liaisons hydrogènes.

[Traduit par la revue]

1. Introduction

The Franck–Condon principle has long been used to interpret the vibrational structure in spectra of electronic transitions. The underlying assumption is that the slow (vibrational) and fast (electronic) coordinates of the active molecule are adiabatically separable. The same principle can be applied to other interacting molecular motions, provided they are sufficiently distinct in time scale. For instance, the Stepanov ladder scheme (1) for interpreting the vibrational spectra of hydrogen-bonded complexes is formally similar to the Franck–Condon principle; it is based on the wide separation between the covalent bond frequencies and the much lower hydrogen bond frequencies responsible for the substructure in the (covalent) vibrational spectra.

The aim of this paper is to show that, at high temperatures, the spectral features derived from the Stepanov scheme can be quantitatively reproduced by a purely classical calculation based on the "frequency-modulation" principle enunciated many years ago by Bateuv (2). In this analysis, one regards the fast coordinate as oscillating at an *instantaneously* well-defined frequency, but attributes to this frequency a secular variation owing to its dependence on the slow coordinate. This adiabatic separation of variables is the classical equivalent of the Born–Oppenheimer approximation, in which one ascribes to the wave function of the fast variable, and hence also to its energy eigenvalue, a parametric dependence on the slow variable. Assuming the existence of a separate eigenvalue for fast motion in the quantum case corresponds to assigning it an instantaneously pure frequency in the classical case.

There is a difficulty with the frequency-modulation concept that ought to be disposed of at the outset. There is a tendency to think that this approach flatly contradicts orthodox quantum mechanics, since, from the latter point of view, a proper account of the coupling between the slow and fast variables, though it will admit *perturbation* of the stationary states, can never cast doubt on their *existence*; and stationary states, of course, have *constant* eigenfrequencies, rather than periodically modulated frequencies as posited by the classical model. Such objections in fact formed the subject of some highly incivil polemics in the early literature (2, 3) on spectroscopic studies of hydrogen bonding, and probably are partially responsible for the eclipse of the classical approach in more recent studies. To deal with this point, we note that, provided the frequency modulation is *periodic* (as it will be if it arises from coupling with a slower normal coordinate), the time dependence of the classical variable may be represented by a *discrete* superposition of pure sinusoidal waves. This merely reflects the fact that the fast variable, which would presumably be a normal coordinate in the absence of coupling with the slow variable, is no longer an exact normal coordinate once the coupling is introduced, but rather contains admixtures of other actual normal coordinates — hence other frequencies. If the classical time dependence were calculated from an application of orthodox correspondence principles, by taking the quantum expectation value as a function of time, the same mixture of frequencies would appear in the result, since the operator corresponding to the classical variable would mix states differing in respect of more than one quantum number.

While this argument may dispel doubts about the correctness of the classical method, one may well wonder why we should ever want to resurrect it. The reasons become apparent when one considers cases in which the slow variable is subject to a stochastic time-dependent perturbation. This could occur because the slow variable is in close energetic contact with a heat bath — the vibrations of a hydrogen bond in a liquid would be an example (4). It could conceivably also occur in certain autonomous systems, such as networks of highly anharmonic hydrogen bonds, the vibrations of which might be chaotic and not resolvable into normal modes. In cases where the classical dynamics are chaotic, quantum-mechanical interpretations are difficult and controversial; classical methods have therefore regained favour with some investigators, at least pending the theoretical clarification of quantum chaos. We therefore feel that there is a useful role for classical approaches to spectros-

Can. J. Chem. Downloaded from www.nrcresearchpress.com by 194.225.253.170 on 09/07/12
For personal use only.

Can. J. Chem. Downloaded from www.nrcresearchpress.com by 194.225.253.170 on 09/07/12
For personal use only.

copy problems with the features mentioned above, and for the frequency modulation concept in particular.

In this paper we shall analyse the classical vibration of a special two-freedom oscillator — a simple autonomous system *without* external perturbation — and compare the results to those of the analogous quantum analysis using the Franck–Condon principle. In the classical analysis, we shall use the Anderson–Kubo lineshape formalism (5), one that is readily applied to systems *with* random external perturbation. The way to generalize the classical calculations to such cases will thus be clear, whereas the corresponding generalization of the quantum analysis would be relatively difficult. It is hoped that the close correspondence obtained between the results of the two analyses in the unperturbed limit, where both may be readily worked out, will encourage acceptance of the classical results in perturbed or chaotic cases where the quantum analysis is difficult or controversial.

2. Classical analysis

We consider a system having a "fast" coordinate q and a "slow" coordinate Q. The slow motion is regarded as a predescribed harmonic oscillation at frequency Ω. The fast motion is a harmonic oscillation at frequency ω, which, though well defined at any given time, depends on the instantaneous value of Q according to

$$[1] \qquad \omega(Q) = \omega_0 + \beta Q$$

where β is a coupling constant. The linear Q-dependence assumed here is general in the limit of weak coupling. Any back reaction of the fast motion on the slow motion is neglected, or at least is absorbed in the value of Ω; the slow motion responds only to the time-averaged behaviour of q, so no term involving the instantaneous value of q appears in the equation of motion for Q. The frequency Ω might well depend on the *amplitude* of the q-motion, without seriously complicating the analysis. A quantum analogue to this would be the different internuclear potential surfaces governing molecular vibrations in different electronic states.

According to the Anderson–Kubo formalism, the power spectrum of the classical oscillation is

$$[2] \qquad P(\omega) \propto \int_{-\infty}^{\infty} dt\, e^{-i(\omega-\omega_0)t}\phi(t)$$

where the *relaxation function* $\phi(t)$ is defined by

$$[3] \qquad \phi(t) = \left\langle \exp i \int_0^t dt'[\omega(t') - \omega_0] \right\rangle$$

where $\langle\cdot\rangle$ denotes an ensemble average. If the Q-motion is supposed to be harmonic with amplitude Q_0, then eq. [1] becomes

$$[4] \qquad \omega(t') = \omega_0 + \beta Q_0 \cos(\Omega t' + \theta)$$

where θ is the initial phase for a particular oscillator. Using eq. [4] in eq. [3] gives

$$[5] \qquad \phi(t) = \langle \exp i(\beta Q_0/\Omega)[\sin(\Omega t + \theta) - \sin\theta]\rangle$$

Expanding the exponential in a Taylor series and distributing the average over the terms of the resultant series gives

$$[6] \qquad \phi(t) = \sum_{n=0}^{\infty} \frac{1}{n!} (i\beta Q_0/\Omega)^n \langle[\sin(\Omega t + \theta) - \sin\theta]^n\rangle$$

The ensemble average may be interpreted as an average over random phases θ. This vanishes for odd n, and results in

$$[7] \qquad \langle[\sin(\Omega t + \theta) - \sin\theta]^n\rangle = \frac{n!(1 - \cos\Omega t)^{n/2}}{2^{n/2}[(n/2)!]^2}$$

for even n. With eq. [7], and the replacement of running index n by $k = n/2$, eq. [6] becomes

$$[8] \qquad \phi(t) = \sum_{k=0}^{\infty} \frac{(-)^k}{2^k(k!)^2} (\beta Q_0/\Omega)^{2k}(1 - \cos\Omega t)^k$$

The convergence of this series is assured for all t because $|(1 - \cos\Omega t)^k| \leq 2^k$ for all k and t, so that the absolute value of the ratio between successive terms is less than $(\beta Q_0/\Omega k)^2$, which in turn is less than unity for large enough k. The convergence is clearly fastest when $\beta Q_0 \ll \Omega$, that is, in the limit of weak modulation. This limit is assumed in the remaining analysis. We therefore truncate the series in eq. [8] at $k = 1$, leaving

$$[9] \qquad \phi(t) = 1 - \tfrac{1}{4}(\beta Q_0/\Omega)^2(2 - e^{i\Omega t} - e^{-i\Omega t})$$

where $\cos\Omega t$ has been rewritten in exponential form. If eq. [9] is substituted in eq. [2], and the form $\int_{-\infty}^{\infty} e^{i\omega t}\, dt$ is recognised as (2π times) a representation of the delta function $\delta(\omega)$, then

$$[10] \qquad P(\omega) \propto [1 - \tfrac{1}{2}(\beta Q_0/\Omega)^2]\delta(\omega - \omega_0) + \tfrac{1}{4}(\beta Q_0/\Omega)^2[\delta(\omega - \omega_0 + \Omega) + \delta(\omega - \omega_0 - \Omega)]$$

The spectrum thus exhibits side bands at $\omega = \omega_0 \pm \Omega$, each having an intensity approximately $\frac{1}{4}(\beta Q_0/\Omega)^2$ times that of the unmodulated component at $\omega = \omega_0$. the terms discarded by truncating eq. [8] are smaller by at least two orders of $\beta Q_0/\Omega$.

3. Quantum-mechanical analysis

We now reformulate the same problem quantum-mechanically. Following the standard procedure for adiabatic separation of the wave function (6), we write each eigenstate of the coupled oscillator as a product of slow and fast wave functions

$$[11] \qquad \Psi_{sf}(q,Q) = \Phi_s^{(f)}(Q) \cdot \Theta_f(q;Q)$$

where s and f are the quantum numbers associated with the slow and fast variables Q and q respectively. The notation indicates the parametric dependence of the slow function on f, and of the fast function on the instantaneous value of Q.

We shall calculate the intensity of a dipole transition $s,f \rightarrow s',f'$. This depends on the matrix element of the dipole moment operator $\hat{p}$ as follows:

$$[12] \qquad I_{s,f\rightarrow s',f'} \propto |\langle s, f|\hat{p}|s', f'\rangle|^2 = |\int dQ \Phi_s^{(f')*} J_{f\rightarrow f'}(Q)\Phi_s^{(f)}|^2$$

where

$$[13] \qquad J_{f\rightarrow f'}(Q) = \int dq \Theta_{f'}^* \hat{p}(q, Q)\Theta_f$$

If the system consists of oscillating point charges, and if q and Q are obtained by some linear transformation of the Cartesian coordinates of these charges, then $\hat{p}$ is a linear function of q and Q:

$$[14] \qquad \hat{p} = aq + bQ + c$$

where a, b, and c are constants. The terms bQ and c factor out of the integral in eq. [13]; in view of the orthogonality of the Θ_f, these terms contribute nothing to the integral except in the uninteresting case where $f' = f$. Thus $J_{f\rightarrow f'}$ reduces to

$a\int dq\Omega\Theta_{f'}q\Theta_f$. Since the Θ_f are simple harmonic oscillator (SHO) eigenfunctions, this works out at

$$[15] \quad J_{f\to f'} = \begin{cases} a(\hat{f}\hbar/2m\omega)^{1/2}, & |f'-f| = 1 \\ 0, & |f'-f| > 1 \end{cases}$$

where $\hat{f}$ is the larger of f and f', and where m is the reduced mass associated with q-motion. Now $J_{f\to f'}$ takes on a Q-dependence through ω, as is implied by eq. [1]. From eqs. [1] and [15], the fractional change in $J_{f\to f'}(Q)$ over the course of the integral in eq. [12] is roughly $\beta Q_0/\omega_0$, if the classical amplitude Q_0 is construed as the approximate width of the domain over which the $\Phi_f^{(s)}(Q)$ are nonvanishing. For the weak-coupling case assumed in Sect. 2 we had $\beta Q_0/\Omega \ll 1$; since for adiabatic separability we had also supposed $\Omega \ll \omega_0$, it follows that $\beta Q_0/\omega_0 \ll 1$ a fortiori if we make the same assumptions in the quantum as in the classical case. We conclude that $J_{f\to f'}$ is essentially constant over the integration domain in eq. [12] and may be factored out of the integral:

$$[16] \quad I_{s,f\to s',f'} \propto |J_{f\to f'}|^2 |\int dQ \Phi_{s'}^{(f')*}\Phi_s^{(f)}|^2$$

The square of the overlap integral appearing in eq. [16] may be identified as the Franck–Condon factor for the transition (7).

We now focus attention on a particular transition $f\to f'$, and examine the distribution of intensity within its s, s' substructure. For this purpose $J_{f\to f}$ may be regarded as fixed, so that, by eq. [16], the intensities for the various $s \to s'$ components are governed by the overlap between the initial and final slow wave functions. These are *not* necessarily orthogonal when $s' \neq s$, since $\Phi_{s'}^{(f')}$ and $\Phi_s^{(f)}$ are eigenfunctions of different operators when $f' \neq f$.

To evaluate the Franck–Condon factors, we must examine the Q-dependence of the Hamiltonian for the coupled oscillator described in Sect. 2. Following the standard procedure for the solution of adiabatically separable problems, we incorporate the energy eigenvalue of the fast oscillation in the effective Hamiltonian $H^{(f)}$ governing the slow motion. The fast eigenvalue is $(f+\frac{1}{2})\hbar\omega$; if ω is given by eq. [1], then we have

$$[17] \quad H^{(f)} = H_Q + (f+\tfrac{1}{2})\hbar\beta Q + (f+\tfrac{1}{2})\hbar\omega_0$$

where H_Q is the slow-motion SHO Hamiltonian in the absence of coupling. The overlap integral in eq. [16] may be evaluated by expanding $\Phi_s^{(f)}$ and $\Phi_{s'}^{(f')}$ in terms of the eigenfunctions $|j\rangle$ of H_Q. The expansion coefficients may be obtained by treating the second term on the right-hand side of eq. [17] as a small perturbation. (This will be justified presently.) According to first-order perturbation theory,

$$[18] \quad \Phi_s^{(f)} = |s\rangle + \left(f+\frac{1}{2}\right)\hbar\beta \sum_{j\neq s} |j\rangle\langle j|Q|s\rangle/(E_s - E_j)$$

Here the E_j are the energies of the unperturbed SHO states $|j\rangle$:

$$[19] \quad E_j = (j+\tfrac{1}{2})\hbar\Omega$$

Invoking the well-known results for the SHO matrix elements $\langle j|Q|s\rangle$, we obtain from eq. [18]

$$[20] \quad \Phi_s^{(f)} = |s\rangle + (f+\tfrac{1}{2})\epsilon[s^{1/2}|s-1\rangle - (s+1)^{1/2}|s+1\rangle]$$

where

$$[21] \quad \epsilon = (\beta/\Omega)(\hbar/2\Omega M)^{1/2}$$

and M is the reduced mass associated with Q-motion. Now ε is a dimensionless quantity whose value is much less than unity in the weak-coupling limit. This is apparent because the factor $(\hbar/2\Omega M)^{1/2}$ may be recognised as the root mean square value of Q in the ground SHO state $|0\rangle$, and may thus be taken as a lower bound for the classical amplitude Q_0. So ϵ is characteristically less than $\beta Q_0/\Omega$, a quantity that in turn is much less than unity in the weak-coupling limit as defined in Sect. 2. It then follows from eq. [20] that $\Phi_s^{(f)}$ differs little from $|s\rangle$, so that the first-order perturbation treatment is justified a posteriori. Using eq. [20] and the orthonormality of the $|j\rangle$, we calculate the overlaps to lowest order in ϵ:

$$[22] \quad \langle\Phi_{s'}^{(f')}|\Phi_s^{(f)}\rangle \simeq \begin{cases} 1, & s' = s \\ (f-f')s^{1/2}\epsilon, & s' = s-1 \\ (f'-f)(s')^{1/2}\epsilon, & s' = s+1 \end{cases}$$

For $|s'-s| \geq 2$, the inner product is of at least second order in ϵ, and is therefore negligible in the weak-coupling limit.

We have already ascertained (cf. eq. [15]) that the ordinary SHO selection rule applies to the fast coordinate; that is, $f' = f \pm 1$. With this restriction, eqs. [16] and [22] yield

$$[23] \quad I_{s,f\to s',f'} \propto |J_{f\to f'}|^2 |\langle\Phi_{s'}^{(f\pm1)}|\Phi_s^{(f)}\rangle|^2 = |J_{f\to f'}|^2 \times \begin{cases} 1, & s' = s \\ \hat{s}\epsilon^2, & s' = s\pm1 \end{cases}$$

where $\hat{s}$ is the larger of s and s'. Thus, to lowest order in ϵ, the spectrum of the transition $f \to f'$ comprises two side-band components $s' = s \pm 1$, each having a fraction $\hat{s}\epsilon^2$ of the intensity of the main ($s' = s$) component. To demonstrate the equivalence between this and the classical result, it remains to show that the frequency spacing and the relative intensities are the same in both cases.

According to the standard adiabatic treatment, the energy eigenvalue $E_s^{(f)}$ of the coupled-oscillator state Ψ_{sf} is just the expectation value of $H^{(f)}$ in state $\Phi_s^{(f)}$:

$$[24] \quad E_s^{(f)} = \langle\Phi_s^{(f)}|H^{(f)}|\Phi_s^{(f)}\rangle = (f+\tfrac{1}{2})\hbar\omega_0 + \langle\Phi_s^{(f)}|H_Q + (f+\tfrac{1}{2})\hbar\beta Q|\Phi_s^{(f)}\rangle$$

The remaining inner product on the right-hand side is the energy eigenvalue for the slow motion. Since the eigenfunction $\Phi_s^{(f)}$ has evolved from $|s\rangle$ under the action of the perturbation $(f+\frac{1}{2})\hbar\beta Q$, its eigenvalue is

$$[25] \quad \langle\Phi_s^{(f)}|H_Q + (f+\tfrac{1}{2})\hbar\beta Q|\Phi_s^{(f)}\rangle \simeq E_s + (f+\tfrac{1}{2})\hbar\beta\langle s|Q|s\rangle$$

to first order in the perturbation. The matrix element $\langle s|Q|s\rangle$ vanishes for SHO basis functions; so eqs. [24], [25], and [19] give

$$[26] \quad E_s^{(f)} = (f+\tfrac{1}{2})\hbar\omega_0 + (s+\tfrac{1}{2})\hbar\Omega$$

That is, the slow and fast energies are simply additive to first order in the perturbation; no interaction term appears at this level of approximation. From eq. [26], the Bohr transition frequencies composing the transition $f \to f \pm 1$ are ω_0 (for $s' = s$) and $\omega_0 \pm \Omega$ (for $s' = s \pm 1$). These frequencies are the same as those derived classically in Sect. 2.

The results given by eq. [23] have regard to the intrinsic oscillator strengths of the various s, s' subtransitions. The actual spectrum is realised by taking a thermal average, denoted by $\langle\cdot\rangle$, over initial states s. This is easily worked out from eqs. [23] and [26]. To effect a classical correspondence, we take the high-temperature limit ($kT \gg \hbar\Omega$):

Can. J. Chem. Downloaded from www.nrcresearchpress.com by 194.225.253.170 on 09/07/12
For personal use only.

[27a] $$\frac{\langle I_{s\to s-1}\rangle}{\langle I_{s\to s}\rangle} = \epsilon^2 \sum_{s=1}^{\infty} s \exp(-E_s^{(f)}/kT) \Big/ \sum_{s=0}^{\infty} \exp(-E_s^{(f)}/kT) \to \epsilon^2 kT/\hbar\Omega$$

[27b] $$\frac{\langle I_{s\to s+1}\rangle}{\langle I_{s\to s}\rangle} = \epsilon^2 \sum_{s'=1}^{\infty} s' \exp(-E_s^{(f)}{}_{-1}/kT) \Big/ \sum_{s=0}^{\infty} \exp(-E_s^{(f)}/kT) = \exp(\hbar\Omega/kT)\langle I_{s\to s-1}\rangle/\langle I_{s\to s}\rangle \to \epsilon^2 kT/\hbar\Omega$$

To relate the intensities to the amplitude of the Q-oscillation, we note that the thermal root-mean-square displacement from equilibrium in the high-temperature limit is

[28] $$Q_{\text{rms}} \to (kT/M\Omega^2)^{1/2}$$

as is readily found from the matrix elements of Q in the basis set $\{|j\rangle\}$. With eqs. [21] and [28], eq. [27] becomes

[29] $$\frac{\langle I_{s\to s\pm 1}\rangle}{\langle I_{s\to s}\rangle} \to \frac{1}{2}(\beta Q_{\text{rms}}/\Omega)^2$$

We recall that the corresponding classical result for the intensity ratio between each side band and the main component was $\frac{1}{4}(\beta Q_0/\Omega)^2$, where Q_0 was the amplitude of the slow oscillation. For classical SHO motion, $Q_0 = 2^{1/2}Q_{\text{rms}}$. Hence the classical and quantal results for the side-band intensities agree exactly in the high-temperature limit.

At lower temperatures, the classical spectrum, being symmetric, violates detailed balance. This problem is common to all classical lineshape calculations. They are routinely corrected by applying any of several simple desymmetrizing procedures that restore consistency with detailed balance (8, 9). One such formula for approximate recovery of the quantum-mechanical spectrum I_{qm} from the classical spectrum I_{cl} is as follows:

[30] $$I_{\text{qm}}(\omega_0 + \omega) \simeq 2[1 + \exp(-\hbar\omega/kT)]^{-1} I_{\text{cl}}(\omega_0 + \omega)$$

where ω_0 is the frequency of the line centre (as it is in the foregoing discussion). In the present case, it is clear that eq. [30] yields the same intensity ratio between the side bands at $\omega_0 \pm \Omega$ as does the proper quantum-mechanical formula, eq. [27], at any value of T.

4. Summary and conclusions

It has been demonstrated that the frequency-modulation principle, applied to a weakly coupled two-freedom oscillator, predicts essentially the same dipole radiation spectrum as does a correct quantum-mechanical treatment. The classical calculation reproduces the discrete substructure of the spectrum (often thought to be of distinctively quantal nature). At high temperatures, it also yields quantitatively correct values for the intensities of the several subtransitions. Even at lower temperatures, the correct intensities are obtained if one applies a simple desymmetrizing correction to the classical calculation. While, at first blush, this may seem insufficient reason to prefer a classical calculation, it should be pointed out that the classical formalism, eqs. [2]–[3], used here has been well developed and extended to systems in which $\omega(t)$ fluctuates stochastically according to various modulation schemes (e.g., Gaussian, Markovian) (5). The corresponding generalization of orthodox quantum mechanics is difficult and, in some cases, controversial (as in autonomous systems whose classical dynamics are chaotic). Given the recent spate of interest in the classical dynamics of simple coupled-oscillator systems (10) like the one examined here, it seems encouraging that classical calculations produce realistic results in a regime where it is readily possible to test them against quantum mechanics. This suggests the legitimacy of using the classical formalism as a point of departure for the study of coupled oscillators with more formidable dynamics.

The system examined here, with weak linear coupling and adiabatic separability, is an especially apt model for a covalent bond interacting with a hydrogen bond, and has been so applied (11, 12). We envisage the use of the classical lineshape formalism described here in elucidating the infrared and Raman spectroscopy of such systems. Its application would be especially interesting for networks of highly anharmonic hydrogen bonds whose lattice vibrations are conceivably chaotic.

Acknowledgements

This research was funded by a grant from the Natural Sciences and Engineering Research Council of Canada.

1. N. Sheppard. *In* Hydrogen bonding. *Edited by* D. Hadzi. Pergamon, London. 1959. pp. 90–96.
2. M. I. Batuev. Izv. Akad. Nauk S.S.S.R., Ser. Fiz. **14**, 429 (1950).
3. M. V. Wolkenstein, M. A. Eliashevich, and B. I. Stepanov. Zh. Fiz. Khim. **24**, 1158 (1950).
4. G. N. Robertson and J. Yarwood. Chem. Phys. **32**, 267 (1978).
5. R. Kubo. *In* Fluctuations, relaxation and resonance in magnetic systems. *Edited by* D. ter Haar. Oliver and Boyd, Edinburgh. 1962.
6. E. Merzbacher. Quantum mechanics. 2nd ed. Wiley, New York. 1970. pp. 77–78.
7. I. N. Levine. Quantum chemistry. Vol. 2. Allyn and Bacon, Boston. 1970. pp. 187–193.
8. F. Barocchi, M. Moraldi, and M. Zoppi. Mol. Phys. **45**, 1285 (1982).
9. J. Borysow, M. Moraldi, and L. Frommhold. Mol. Phys. **56**, 913 (1985).
10. A. J. Lichtenberg and M. A. Lieberman. Regular and stochastic motion. Springer-Verlag, New York. 1983.
11. M. J. Wójcik and M. Falk. Chem. Phys. Lett. **56**, 450 (1978).
12. Y. Bouteiller and E. Marechal. Mol. Phys. **32**, 277 (1976).

Can. J. Chem. Downloaded from www.nrcresearchpress.com by 194.225.253.170 on 09/07/12
For personal use only.

Synthesis, separation, and absolute configuration of the two 5-(2,2-dibromocyclopropyl) and four 5-(2-bromocyclopropyl) diastereomers of 2′-deoxyuridine

MANJU TANDON, LEONARD I. WIEBE, AND EDWARD E. KNAUS[1]

Faculty of Pharmacy and Pharmaceutical Sciences, University of Alberta, Edmonton, Alta., Canada T6G 2N8

Received March 9, 1989

MANJU TANDON, LEONARD I. WIEBE, and EDWARD E. KNAUS. Can. J. Chem. **67**, 1484 (1989).

The reaction of 3-*N*-3′,5′-di-*O*-tribenzoyl-2′-deoxy-5-vinyluridine (**2**) with dibromocarbene, generated from $PhHgCBr_3$ under thermal neutral conditions, yielded a mixture of the 5-[(1*S*)-2,2-dibromocyclopropyl]- (**3***a*) and 5-[(1*R*)-2,2-dibromocyclopropyl]-3-*N*-3′,5′-di-*O*-tribenzoyl-2′-deoxy-5-vinyluridine (**4***a*) diastereomers, which were separated (1:1 ratio). Treatment of **3***a* and **4***a* with methanolic ammonia afforded the respective 5-[(1*S*)-2,2-dibromocyclopropyl]- (**3***b*) and 5-[(1*R*)-2,2-dibromocyclopropyl]-2′-deoxyuridines (**4***b*). The absolute configuration of **3***b* has been established by X-ray crystal structure determination. Monodebromination of **3***b*, using zinc dust in HOAc at 50°C, gave a mixture of the 5-[(1*S*,2*S*)-2-bromocyclopropyl]- (**5**) and 5-[(1*S*,2*R*)-2-bromocyclopropyl]- (**6**) diastereomers, which were separated and their respective configuration assigned by ^1H nuclear magnetic resonance. A similar monodebromination of **4***b* yielded the 5-[(1*R*,2*R*)-2-bromocyclopropyl]- (**7**) and 5-[(1*R*,2*S*)-2-bromocyclopropyl]-2′-deoxyuridine (**8**) diastereomers. Relationships between physicochemical properties, such as melting point and tlc R_f value, and the configuration of the chiral cyclopropyl carbon(s) were observed. The chemical shifts for the ^{13}C nuclear magnetic resonances are also of diagnostic value for determination of the respective configuration of the cyclopropyl carbons of the 5-(2-bromocyclopropyl) isomers **5–8**.

Key words: bromocyclopropanes, 2′-deoxyuridines, absolute configuration, antiviral activity.

MANJU TANDON, LEONARD I. WIEBE et EDWARD E. KNAUS. Can. J. Chem. **67**, 1484 (1989).

La réaction de la 3-*N*-3′,5′-di-*O*-tribenzoyl-2′-déoxy-5-vinyluridine (**2**) avec le dibromocarbène, préparé à partir du $PhHgCBr_3$ dans des conditions neutres et thermiques, conduit à un mélange des 5-[(1*S*)-2,2-dibromocyclopropyl]- (**3***a*) et 5-[(1*R*)-2,2-dibromocyclopropyl]-3-N-3′,5′-di-*O*-tribenzoyl-2′-déoxy-5-vinyluridines (**4***a*) diastéréomères qui ont été séparées (rapport 1:1). Les réactions des composés **3***a* et **4***a* avec de l'ammoniac en milieu méthanolique conduisent aux 5-[(1*S*)-2,2-dibromocyclopropyl]- (**3***b*) et 5-[(1*R*)-2,2-dibromocyclopropyl]-2′-déoxyuridines (**4***b*) respectives. On a déterminé la configuration absolue du composé **3***b* en procédant à une détermination de structure par diffraction des rayons-X. La monodébromation du produit **3***b*, réalisée à l'aide de poudre de zinc dans HOAc à 50°C, fournit un mélange des diastéréomères 5-[(1*S*,2*S*)-2-bromocyclopropyl]- (**5**) et 5-[(1*S*,2*R*)-2-bromocyclopropyl]- (**6**) que l'on a séparé et dont les configurations respectives ont été déterminées par résonance magnétique nucléaire du ^1H. Une monodébromation semblable réalisée sur le composé **4***b* fournit les 5-[(1*R*,2*R*)-2-bromocyclopropyl]- (**7**) et 5-[(1*R*,2*S*)-2-bromocyclopropyl]- 2′-déoxyuridines (**8**) diastéréomères. On a observé une corrélation entre les propriétés physicochimiques, comme les points de fusion et les valeurs des R_f des ccm, et les configurations des carbones chiraux des cyclopropyles. Les déplacements chimiques en résonance magnétique nucléaire du ^{13}C peuvent aussi être utilisés pour déterminer les configurations respectives des carbones du cyclopropyle des 5-(2-bromocyclopropyles) isomères **5–8**.

Mots clés : bromocyclopropanes, 2′-deoxyuridines, configuration absolue, activité antivirale.

[Traduit par la revue]

Introduction

(*E*)-5-(2-Bromovinyl)-2′-deoxyuridine (BVDU) is a potent and selective antiviral agent against herpes simplex virus type 1 (HSV-1) and varicella-zoster virus (1). BVDU is selectively phosphorylated by HSV-1 encoded thymidine kinase and metabolically trapped within infected cells, but not in uninfected host cells (2, 3). Structure–activity correlations for olefinic 5-substituted-2′-deoxyuridines indicated optimum inhibition of HSV-1 occurred when the C-5 substituent was unsaturated and conjugated with the pyrimidine ring, was not longer than four carbon atoms in length, had the *E* stereochemistry, and included a hydrophobic electronegative atom (4). It was anticipated that 2′-deoxyuridine possessing a 5-(2,2-dibromocyclopropyl) or 5-(2-bromocyclopropyl) substituent could serve as a biological isostere of the (*E*)-5-(2-bromovinyl) substituent present in BVDU. The hybridization of the cyclopropane bonds is considered to result in a higher electron density for the C—C bonds. Furthermore, the cyclopropyl moiety interacts with neighboring π-electron systems and *p*-electron centers similar to a vinyl group (5, 6).

Acquisition of all dibromocyclopropyl and bromocyclopropyl diastereomers is required to determine the effect of cyclopropyl substituent stereochemistry upon antiviral activity. We now describe the synthesis, separation, and assignment of the absolute configuration for the 5-(2,2-dibromocyclopropyl) **3***b*–**4***b* and 5-(2-bromocyclopropyl) **5–8** derivatives of 2′-deoxyuridine.

Results and discussion

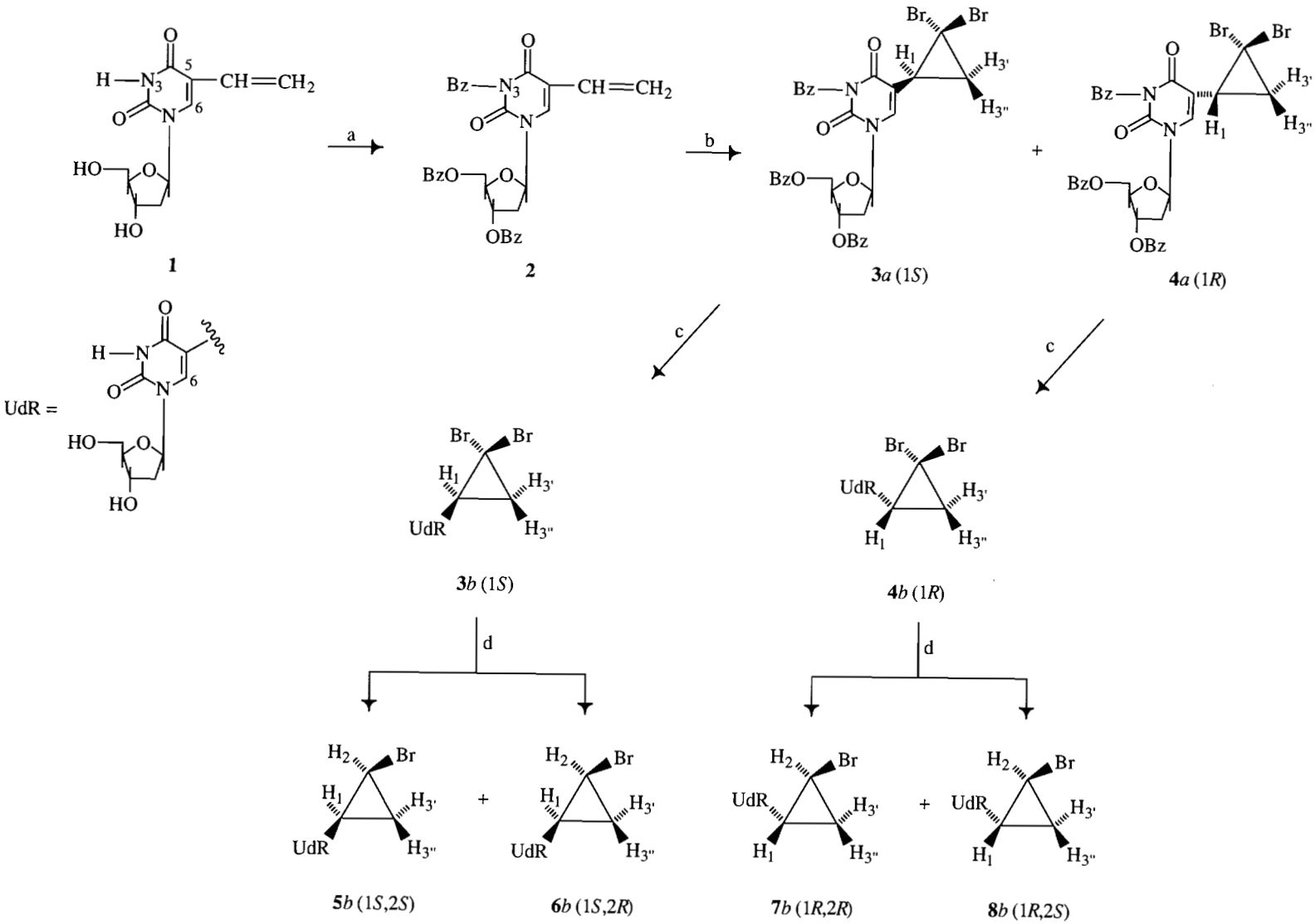
The 5-vinyl substituent of 5-vinyl-2′-deoxyuridine (**1**) is expected to be a poor substrate for dibromocarbene addition since it is conjugated with the 5,6-olefinic bond of the uracil ring. In an earlier study we reported that the reaction of (*E*)-5-(2-ethoxycarbonylvinyl)-3-methyl-2′-deoxyuridine with diazomethane yielded (*E*)-5-(2-ethoxycarbonylvinyl)-3-methyl-2′-deoxyuridine (7). Therefore, **1** was elaborated to 3-*N*-3′,5′-di-*O*-tribenzoyl-2′-deoxy-5-vinyluridine (**2**) as illustrated in Scheme 1 (78% yield). Reaction of **2** with dichlorocarbene, generated from chloroform and sodium hydroxide in the presence of the phase transfer catalyst benzyltriethylammonium bromide, afforded 3-*N*-dichloromethyl-3′,5′-di-*O*-benzoyl-2′-deoxy-5-vinyluridine.[2] The latter result indicates that dibromocarbene must be generated under neutral conditions to preserve the integrity of the 3-*N*-benzoyl substituent. Thus, reaction of

[1]Author to whom correspondence may be addressed.

[2]E. E. Knaus, L. I. Wiebe, and M. Tandon. Unpublished results.

Can. J. Chem. Downloaded from www.nrcresearchpress.com by 194.225.253.170 on 09/07/12
For personal use only.

Can. J. Chem. Downloaded from www.nrcresearchpress.com by 194.225.253.170 on 09/07/12
For personal use only.



(a) PhCOCl, pyridine, $(i\text{-Pr})_2CHCH_2NH_2$; (b) $PhHgCBr_3$, dry benzene, 80 °C; (c) NH_3, MeOH, 25 °C; (d) Zn dust, HOAc, 50 °C

SCHEME 1

Can. J. Chem. Downloaded from www.nrcresearchpress.com by 194.225.253.170 on 09/07/12
For personal use only.

the Seyferth reagent (8) phenyl(tribromomethyl)mercury ($PhHgCBr_3$) with **2** in dry benzene at 80°C yielded a mixture of two diastereomers (**3***a* and **4***a*), which were separated by silica gel column chromatography (1:1 ratio, 63% total isolated yield). Removal of the protective benzoyl substituents from **3***a* and **4***a*, by treatment with methanolic ammonia, yielded 5-[(1*S*)-2,2-dibromocyclopropyl]-2′-deoxyuridine (**3***b*) and 5-[(1*R*)-2,2-dibromocyclopropyl]-2′-deoxyuridine (**4***b*) in 71 and 74% isolated yields, respectively.

The X-ray crystal structure of **3***b* indicated that the absolute configuration of the C-5 substituent was [(1*S*)-2,2-dibromocyclopropyl] (9). The bond lengths and angles for **3***b* are similar to those of 2′-deoxyuridine (10) and the 1,1-dibromocyclopropyl moiety (11, 12) in other compounds. The pyrimidine ring of **3***b* is *anti* with respect to the deoxyribose ring, and the latter ring system is in the 2′-*endo* conformation. Compound **4***b*, which is a diastereomer of **3***b*, must therefore have a 5-[(1*R*)-2,2-dibromocyclopropyl] substituent.

Monodebromination of the 5-[(1*S*)-2,2-dibromocyclopropyl] diastereomer (**3***b*), using zinc dust in glacial acetic acid, yielded a mixture of two diastereomers, which were separated by silica gel column chromatography. In this reaction a new chiral center is introduced at the C-2 position of the 5-(2-bromocyclopropyl) substituent. An ^1H nmr difference nOe spectrum was acquired for the more polar diastereomer (R_f 0.15, solvent system C). Irradiation of the cyclopropyl H-1 proton at δ 1.98 produced a 10.8% enhancement for the cyclopropyl H-2 proton at δ 3.34 and a 7.7% enhancement for the cyclopropyl H-3′ proton at δ 1.42. Therefore, the cyclopropyl H-1 and H-2, as well as H-1 and H-3′ protons, must be *cis* to each other. Since the configuration of this product at the cyclopropyl C-1 position must be *S*, it is therefore the 5-[(1*S*,2*S*)-2-bromocyclopropyl] diastereomer (**5**). A large number of spectra of substituted cyclopropane derivatives have been recorded. The magnitude of the vicinal coupling constant for J_{cis} is always larger than J_{trans} for any given pair of cyclopropyl stereoisomers (13). The vicinal coupling constants for the diastereomer **5** are in agreement with the assigned 1*S*,2*S* configuration where $J_{1,2}$ = 8.5 (*cis*), $J_{1,3''}$ = 6.8 (*trans*), $J_{1,3'}$ = 9.2 (*cis*), $J_{2,3''}$ = 4.4 (*trans*), and $J_{2,3'}$ = 8.5 Hz (*cis*). A long-range allylic coupling $J_{1,6}$ = 1.2 Hz was also observed. The configuration of the other diastereomer **6** (R_f 0.29, solvent system C) obtained in this reaction, which also must have the 1*S* configuration, was assigned on the magnitude of the vicinal coupling constants in the ^1H nmr spectrum that can be correlated with the geometrical arrangement of the cyclopropyl substituents. Diastereomer **6** has a 5-[(1*S*,2*R*)-2-bromocyclopropyl] substituent since it exhibited vicinal coupling constants $J_{1,2}$ = 4.3 (*trans*), $J_{1,3'}$ = 10.1 (*cis*), $J_{1,3''}$ = 6.8 (*trans*), $J_{2,3'}$ = 4.3 (*trans*), and $J_{2,3''}$ = 7.5 Hz (*cis*).

A similar monodebromination of the 5-[(1*R*)-2,2-dibromocyclopropyl] diastereomer **4***b* afforded a mixture of two diastereomers, which were separated by multiple development preparative tlc and then silica gel column chromatography of the enriched tlc fractions. The more polar diastereomer (R_f 0.27, solvent system C) possesses a 5-[(1*R*,2*R*)-2-bromocyclopropyl] substituent (**7**) since the ^1H nmr spectrum exhibited vicinal coupling constants $J_{1,2}$ = 7.1 (*cis*), $J_{1,3'}$ = 7.1 (*trans*), $J_{1,3''}$ = 9.1 (*cis*), $J_{2,3'}$ = 4.3 (*trans*), and $J_{2,3''}$ = 7.1 Hz (*cis*). The less polar diastereomer (R_f 0.32, solvent system C) has a 5-[(1*R*,2*S*)-2-bromocyclopropyl] substituent (**8**) since the ^1H nmr spectrum displayed vicinal coupling constants $J_{1,2}$ = 4.3 (*trans*), $J_{1,3'}$ = 6.8 (*trans*), $J_{1,3''}$ = 9.8 (*cis*), $J_{2,3'}$ = 7.5 (*cis*), and $J_{2,3''}$ = 4.3 (*trans*).

A number of relationships or correlations between physicochemical properties and nmr spectral data for the cyclopropyl hydrogens and carbons were observed, which, in conjunction with the magnitude of the vicinal coupling constants described previously, will be of value in assigning the configuration of the cyclopropyl chiral carbons(s) of **3***b*–**4***b* and **5**–**8** (see Table 1). Compounds having the 1*S* configuration exhibit higher melting points since 1*S* (**3***b*) > 1*R* (**4***b*); 1*S*,2*S* (**5**) > 1*R*,2*R* (**7**); and 1*S*,2*R* (**6**) > 1*R*,2*S* (**8**). Diastereomers having the same configuration at the C-1 and C-2 positions possess higher melting points since 1*S*,2*S* (**5**) > 1*S*,2*R* (**6**) and 1*R*,2*R* (**7**) > 1*R*,2*S* (**8**). Compounds having the 1*S* configuration are more polar as indicated by their relative R_f values since 1*S* (**3***b*) < 1*R* (**4***b*); 1*S*,2*S* (**5**) < 1*R*,2*R* (**7**); and 1*S*, 2*R* (**6**) < 1*R*,2*S* (**8**). Diastereomers having the same configuration at C-1 and C-2 are more polar as the R_f values of 1*S*,2*S* (**5**) < 1*S*,2*R* (**6**) and 1*R*,2*R* (**7**) < 1*R*,2*S* (**8**). Although the rotations are equal, but of opposite sign, **3***b* and **4***b*, **5** and **6**, and **7** and **8**, respectively, are not enantiomers. Since each set of these diastereomers differs in configuration at only one chiral center, each set of diastereomers can also be called epimers. Examination of the ^1H nmr spectral data for the cyclopropyl chemical shifts (Table 1) indicates that the bromine substituent shields the adjacent *cis* H-3 proton relative to the *trans* H-3 proton (**5**–**8**) and the H-2 proton is shielded by a *cis*-2′-deoxyuridine substituent (**6**, **8**) relative to the *trans* H-2 proton (**5**, **7**). These correlations are consistent with the fact that all substituents, including bromine, generally shield *cis* vicinal protons in a cyclopropyl ring system (13). The chemical shifts of the cyclopropyl carbons for the *cis* 1*S*,2*S* (**5**) and 1*R*,2*R* (**7**), as well as these for the *trans* 1*S*,2*R* (**6**) and 1*R*,2*S* (**8**), are very similar. In compounds **5** and **7**, where the 2′-deoxyuridine and bromo substituents are *cis*, C-1 is deshielded δ 3.4–4.3, C-2 is shielded δ 4.4–5.0, and C-3 is shielded δ 3.3–3.6 relative to the corresponding carbon atoms in the *trans* compounds **6** and **8**. These differences in ^{13}C chemical shifts provide a rapid method to distinguish the *cis* (1*S*,2*S*, 1*R*,2*R*) from the *trans* (1*S*,2*R*, 1*R*,2*S*) stereoisomers.

Biological and biochemical studies for **3***b*–**4***b* and **5**–**8** are now in progress and will be reported elsewhere.

Experimental

Melting points were determined on a Büchi capillary apparatus and are uncorrected. The ^1H and ^{13}C nmr spectra were recorded on a Bruker AM-300 spectrometer. Chemical shifts are given in ppm downfield from tetramethylsilane as internal standard. The ^1H nmr assignments were confirmed by double irradiation experiments. The ^{13}C nmr resonances were assigned by use of the *J* modulation technique to determine the number of attached hydrogens. Specific rotations were measured on an Optical Activity Ltd. digital polarimeter. Thin-layer chromatography (tlc) was performed using Whatman MK6F silica gel microslides (250 μm thickness). Preparative tlc was carried out using Whatman PLK5F plates (1 mm thickness). The tlc solvent systems employed were A: toluene:ethyl acetate (4:1 v/v), B: chloroform:methanol (9:1 v/v), C: ethyl acetate:*n*-propanol:water (41:10:20 v/v/v). This last solvent mixture was mixed thoroughly, allowed to separate, and the upper layer was used in all instances where solvent C is indicated. Column chromatography was carried out using Merck 7734 silica gel (100–200 μm particle size). Pyridine and benzene were distilled from CaH_2, and methanol was distilled from Mg/I_2, prior to use. $PhHgCBr_3$ (8) and 5-vinyl-2′-deoxyuridine (14) (Lit. (15) mp 230°C; found mp 228°C) were prepared according to the literature procedures. Abbreviation: cp = cyclopropyl.

3-N-3′,5′-Di-O′-tribenzoyl-2′-deoxy-5-vinyluridine (**2**)

Benzoyl chloride (0.65 g, 4.64 mmol) was added to a solution of **1**

TABLE 1. Some physical and nmr spectral data[a] for the cyclopropyl hydrogens and carbons

Compound	Configuration	Melting point (°C)	R_f	$[\alpha]_D^{23}$	δ (ppm) H-1	H-2	H-3′	H-3″	C-1	C-2	C-3
3*b*	1*S*	180–185	0.40[b]	−80.8°	2.58	—	1.90	1.93	29.92	29.29	26.66
4*b*	1*R*	145–150	0.50[b]	+80.8°	2.67	—	2.02	1.98	29.83	29.95	26.48
5	1*S*, 2*S*	171–172	0.15[c]	+65.0°	1.98	3.34	1.42	1.14	23.89	15.90	13.36
6	1*S*, 2*R*	116–118	0.29[c]	−62.5°	2.14	3.10	1.24	1.44	20.33[d]	20.48[d]	16.68
7	1*R*, 2*R*	126–128	0.27[c]	−65.0°	2.00	3.40	1.10	1.44	24.65	15.82	13.18
8	1*R*, 2*S*	113–115	0.32[c]	+62.5°	2.14	3.10	1.46	1.24	20.36[d]	20.81[d]	16.77

[a]Chemical shifts are in parts per million with respect to $S_{TMS} = 0$.
[b]Solvent system B.
[c]Solvent system C.
[d]The chemical shifts of C-1 and C-2 may be interchanged.

(0.56 g, 2.2 mmol) in dry pyridine (25 mL) at 0–5°C with stirring. The reaction mixture was allowed to warm to 25°C and then maintained at this temperature for 2 h. The reaction mixture was cooled to 0–5°C and then diisopropylethylamine (0.43 g, 3.3 mmol) and benzoyl chloride (0.33 g, 2.32 mmol) were added. The reaction mixture was warmed to 25°C and the mixture was stirred for 12 h. Ice-water (25 mL) was added and the solvent was removed *in vacuo*. Two consecutive extractions of the residue with a chloroform:water mixtue (3:1 v / v, 40 mL), washing the chloroform extract in succession with cold 5% aqueous HCl (10 mL), 5% aqueous $NaHCO_3$ (10 mL), cold water (2 × 15 mL), drying the chloroform extract (Na_2SO_4), filtration, and removal of the solvent *in vacuo* yielded impure **2**. Purification on a silica gel column using toluene:ethyl acetate (19:1 v / v) as eluant gave **2**: 0.973 g, 77.6%; mp 245°C; R_f 0.58 (solvent system A); ^{1}H nmr ($CDCl_3$) δ: 2.44 (ddd, J_{gem} = 13.7, $J_{1',2'}$ = 8.7, $J_{2',3'}$ = 6.6 Hz, 1H, H-2′), 2.88 (ddd, J_{gem} = 13.7, $J_{1',2'}$ = 5.0, $J_{2',3'}$ = 1.5 Hz, 1H, H-2′), 4.68 (m, 1H, H-4′), 4.76–4.98 (m, 2H, H-5′), 5.18 (dd, J = 11.1, 1.7 Hz, 1H, —CH=C*H*H), 5.74 (m, 1H, H-3′), 5.92 (dd, J = 17.2, 1.7 Hz, 1H, —CH=CH*H*), 6.16 (dd, J = 17.2, J = 11.1 Hz, 1H, —*CH*=CHH), 6.54 (dd, $J_{1',2'}$ = 8.7, J = 5.0 Hz, 1H, H-1′), 7.52–8.20 (m, 16H, phenyl hydrogens, H-6).

*5-[(1S)-2,2-Dibromocyclopropyl]-3-*N*-3′,5′-di-*O*-tribenzoyl-2′-deoxyuridine* (**3***a*) *and 5-[(1R)-2,2-dibromocyclopropyl]-3-*N*-3′,5′-di-*O*-tribenzoyl-2′-deoxyuridine* (**4***a*)

Phenyl(tribromomethyl)mercury (1.96 g, 3.7 mmol) was added to a solution of **2** (2.1 g, 3.7 mmol) in dry benzene (50 mL) under a nitrogen atmosphere with stirring and the reaction mixture was heated at reflux for 2 h. Additional aliquots of $PhHgCBr_3$ (1.96 g, 3.7 mmol) were added to the reaction mixture at 2, 4, and 6 h respectively, after initiation of the reaction, which was allowed to proceed for 9 h in total reaction time. The reaction mixture was cooled to 25°C and the PhHgBr, which precipitated during the reaction, was removed by filtration. Removal of the solvent *in vacuo* gave a mixture of **3***a* and **4***a*, which were separated by silica gel column chromatography using a solvent gradient starting with toluene and ending with toluene:ethyl acetate (19:1 v / v). The two diastereomers **3***a* and **4***a* were obtained in a ratio of 1:1 (0.86 g each, 62.8% combined chemical yield) as foams: **3***a*, R_f 0.54 (solvent system A); mp 220°C; ^{1}H nmr ($CDCl_3$) δ: 1.56 (dd, $J_{3',3''}$ = 11.0, $J_{1,3'}$ = 9.1 Hz, 1H, cp H-3′), 1.61 (dd, $J_{3',3''}$ = 11.0, $J_{1,3''}$ = 8.1 Hz, 1H, cp H-3″), 2.28 (ddd, J_{gem} = 13.5, $J_{1',2'}$ = 8.6, $J_{2',3'}$ = 6.6 Hz, 1H, H-2′), 2.44 (ddd, $J_{1,3'}$ = 9.1, $J_{1,3''}$ = 8.1, $J_{1,6}$ = 1.34 Hz, 1H, cp H-1), 2.78 (dd, J_{gem} = 13.5, $J_{1',2'}$ = 5.0 Hz, 1H, H-2′), 4.52 (m, 1H, H-4′), 4.64–4.8 (m, 2H, H-5′), 5.56 (d, $J_{2',3'}$ = 6.6 Hz, 1H, H-3′), 6.34 (dd, $J_{1',2'}$ = 8.6 and 5.0 Hz, 1H, H-1′), 7.32–8.04 (m, 16H, phenyl hydrogens, H-6).

4*a*: R_f 0.63 (solvent system A); mp 228°C; ^{1}H nmr ($CDCl_3$) δ: 1.46 (t, $J_{3',3''}$ = 8.1, $J_{1,3'}$ = 8.1 Hz, 1H, cp H-3′), 1.73 (dd, $J_{1,3''}$ = 10.1, $J_{3',3''}$ = 8.1 Hz, 1H, cp H-3″), 2.22 (ddd, J_{gem} = 13.5, $J_{1',2'}$ = 8.6, $J_{2',3'}$ = 6.6 Hz, 1H, H-2′), 2.52 (dd, $J_{1,3''}$ = 10.1, $J_{1,3'}$ = 8.1 Hz, 1H, cp H-1), 2.74 (dd, J_{gem} = 13.5, $J_{1',2'}$ = 4.8 Hz, 1H, H-2′), 4.48 (m, 1H, H-4′), 4.58–4.78 (m, 2H, H-5′), 5.56 (d, $J_{2',3'}$ = 6.6 Hz, 1H, H-3′), 6.34 (dd, $J_{1',2'}$ = 8.6, $J_{1',2'}$ = 4.8 Hz, 1H, H-1′), 7.3–8.06 (m, 16H, phenyl hydrogens, H-6).

5[(1S)-2,2-Dibromocyclopropyl]-2′-deoxyuridine (**3***b*)

A solution of **3***a* (0.50 g, 0.68 mmol) in a saturated solution of ammonia in methanol (15 mL) was stirred at 25°C for 15 h. Removal of the solvent *in vacuo* yielded a residue, which was purified by silica gel column chromatography using $CHCl_3$:MeOH (19:1 v / v) as eluant to afford **3***b*: 0.205 g, 71%; R_f 0.40 (solvent system B); mp 180–185°C (dec.) after recrystallization from chloroform:methanol; $[\alpha]_D^{23}$ −80.8° (*c* 0.74, MeOH); ^{1}H nmr (CD_3OD) δ: 1.90 (dd, $J_{3',3''}$ = 15.5, $J_{1,3'}$ = 10.0 Hz, 1H, cp H-3′), 1.93 (dd, $J_{3',3''}$ = 15.5, $J_{1,3''}$ = 8.5 Hz, 1H, cp H-3″), 2.18 (m, 2H, H-2′), 2.58 (ddd, $J_{1,3'}$ = 10.0, $J_{1,3''}$ = 8.5, $J_{1,6}$ = 1.33 Hz, 1H, cp H-1), 3.70 (m, 2H, H-5′), 3.86 (m, 1H, H-4′), 4.34 (m, 1H, H-3′), 6.22 (t, $J_{1',2'}$ = 6.1 Hz, 1H, H-1′), 7.96 (d, $J_{1,6}$ = 1.33 Hz, 1H, H-6); ^{13}C nmr (CD_3OD) δ: 26.7 (cp C-3), 29.3 (cp C-2), 29.9 (cp C-1), 41.7 (C-2′), 62.6 (C-5′), 72.2 (C-3′), 86.8 (C-1′), 89.1 (C-4′), 112.9 (C-5), 140.8 (C-6), 152.8 (C-2), 165.5 (C-4). *Anal.* calcd. for $C_{12}H_{14}Br_2N_2O_5$: C 33.82, H 3.31, N 6.57; found: C 33.61, H 3.37, N 6.41.

5-[(1R)-2,2-Dibromocyclopropyl]-2′-deoxyuridine (**4***b*)

Treatment of **3***b* with a saturated solution of ammonia in methanol, as described for **3***a* above, gave **4***b*: 0.215 g, 74.5%; R_f 0.50 (solvent system B); mp 145–150°C (dec.) after recrystallization from chloroform:methanol; $[\alpha]_D^{23}$ +80.8° (*c* 0.74, MeOH); ^{1}H nmr (CD_3OD) δ: 1.98 (dd, $J_{1,3''}$ = 10.5, $J_{3',3''}$ = 10.0 Hz, 1H, cp H-3″), 2.02 (dd, $J_{3',3''}$ = 10.0, $J_{1,3'}$ = 8.6 Hz, 1H, cp H-3′), 2.13 (ddd, J_{gem} = 12.7, $J_{1',2'}$ = 6.35, $J_{2',3'}$ = 5.5 Hz, 1H, H-2′), 2.28 (ddd, J_{gem} = 12.7, $J_{1',2'}$ = 6.35, $J_{2',3'}$ = 3.9 Hz, 1H, H-2′), 2.67 (ddd, $J_{1,3''}$ = 10.5, $J_{1,3'}$ = 8.6, $J_{1,6}$ = 1.34, 1H, cp H-1), 3.75 (dd, J_{gem} = 12.4, $J_{4',5'}$ = 3.3 Hz, 1H, H-5′), 3.84 (dd, J_{gem} = 12.4, $J_{4',5'}$ = 3.3 Hz, 1H, H-5′), 3.93 (m, 1H, H-4′), 4.37 (m, 1H, H-3′), 6.28 (t, $J_{1',2'}$ = 6.35 Hz, 1H, H-1′), 8.05 (d, $J_{1,6}$ = 1.34 Hz, 1H, H-6); ^{13}C nmr (CD_3OD) δ: 26.48 (cp C-3), 29.83 (cp C-1), 29.95 (cp C-2), 42.22 (C-2′), 62.38 (C-5′), 71.73 (C-3′), 86.77 (C-1′), 89.13 (C-4′), 112.82 (C-5), 140.35 (C-6), 151.79 (C-2), 163.20 (C-4). *Anal.* calcd. for $C_{12}H_{14}Br_2N_2O_5$: C 33.82, H 3.31, N 6.57; found: C 34.17, H 3.19, N 6.67.

5-[(1S,2S)-2-Bromocyclopropyl]-2′-deoxyuridine (**5**) *and 5-[(1S,2R)-2-bromocyclopropyl]-2′-deoxyuridine* (**6**)

Zinc dust (0.46 g, 7.0 mmol) was added in aliquots over a 5 h period to a stirred solution of **3***b* (0.2 g, 0.47 mmol) in glacial acetic acid (5 mL) at 50°C. The reaction, which was monitored by tlc, was complete in 5 h. The reaction mixture was cooled to 25°C, filtered, and the filtercake was washed with glacial acetic acid (3 mL). Removal of the solvent from the combined filtrates *in vacuo* gave a residue that was purified on a silica gel column using ethyl acetate:*n*-propanol:water (700:1:2 v / v / v, upper layer) as eluant. This separation provided enriched fractions containing predominantly **5** and **6**, respectively. Each enriched fraction **5** and **6** was individually separated on a silica gel

Can. J. Chem. Downloaded from www.nrcresearchpress.com by 194.225.253.170 on 09/07/12
For personal use only.

column using chloroform:methanol (95:5 v/v) as eluant to yield the two separate diastereomers **5** and **6**: yield **5**, 53 mg, 32.5%; R_f 0.15 (solvent system C, upper layer); mp 171–172°C; $[\alpha]_D^{23}$ +65.0° (*c* 0.61, MeOH); ^{1}H nmr (CD_3OD) δ: 1.14 (dt, $J_{1,3''} = 6.8$, $J_{3',3''} = 6.8$, $J_{2,3''} = 4.4$ Hz, $W_{\frac{1}{2}} = 21.7$ Hz, 1H, cp H-3″), 1.42 (dt, $J_{1,3'} = 9.2$, $J_{2,3'} = 8.5$, $J_{3',3''} = 6.8$ Hz, $W_{\frac{1}{2}} = 24.5$ Hz, 1H, cp H-3′), 1.98 (dq, $J_{1,3'} = 9.2$, $J_{1,2} = 8.5$, $J_{1,3''} = 6.8$, $J_{1,6} = 1.2$ Hz, $W_{\frac{1}{2}} = 24.4$ Hz, 1H, cp H-1), 2.24 (m, 1H, H-2′), 3.34 (dt, $J_{1,2} = 8.5$, $J_{2,3'} = 8.5$, $J_{2,3''} = 4.4$ Hz, 1H, cp H-2, partially overlapped with CD_3OD), 3.74 (dd, J = 12.4, 3.5 Hz, 1H, H-5′), 3.80 (dd, J = 12.4, 3.1 Hz, 1H, H-5′), 3.96 (m, 1H, H-4′), 4.4 (m, 1H, H-3′), 6.3 (t, $J_{1',2'} = 6.7$ Hz, 1H, H-1′), 8.0 (d, $J_{1,6} = 1.2$ Hz, 1H, H-6); ^{13}C nmr (CD_3OD) δ: 13.36 (cp C-3), 15.90 (cp C-2), 23.89 (cp C-1), 41.57 (C-2′), 62.76 (C-5′), 72.30 (C-3′), 86.68 (C-1′), 89.04 (C-4′), 113.16 (C-5), 140.41 (C-6), 152.03 (C-2), 166.17 (C-4). *Anal.* calcd. for $C_{12}H_{15}BrN_2O_5$: C 41.51, H 4.35, N 8.07; found: C 41.72, H 4.62, N 8.09.

Diastereomer **6**: yield 47 mg, 28.8%; R_f 0.29 (solvent system C, upper layer); mp 116–118°C; $[\alpha]_D^{23}$ −62.5° (*c* 0.4, MeOH); ^{1}H nmr (CD_3OD) δ: 1.24 (octet, $J_{1,3'} = 10.1$, $J_{3',3''} = 6.8$, $J_{2,3'} = 4.3$ Hz, $W_{\frac{1}{2}} = 18.5$ Hz, 1H, cp H-3′), 1.44 (q, $J_{2,3''} = 7.5$, $J_{3',3''} = 6.8$, $J_{1,3''} = 6.8$ Hz, $W_{\frac{1}{2}} = 21.8$ Hz, 1H, cp H-3″), 2.14 (septet, $J_{1,3'} = 10.1$, $J_{1,3''} = 6.8$, $J_{1,2} = 4.3$ Hz, $W_{\frac{1}{2}} = 22.5$ Hz, 1H, cp H-1), 2.24 (m, 2H, H-2′), 3.1 (quintet, $J_{2,3''} = 7.5$, $J_{2,3'} = 4.3$, $J_{1,2} = 4.3$ Hz, $W_{\frac{1}{2}} = 17.7$ Hz, 1H, cp H-2), 3.78 (m, 2H, H-5′), 3.92 (m, 1H, H-4′), 4.4 (m, 1H, H-3′), 6.26 (t, $J_{1',2'} = 6.5$ Hz, 1H, H-1′), 7.84 (d, $J_{1,6} = 1.14$ Hz, 1H, H-6); ^{13}C nmr (CD_3OD) δ: 16.68 (cp C-3), 20.33 and 20.84 (cp C-1 and cp C-2), 41.54 (C-2′), 62.45 (C-5′), 71.85 (C-3′), 86.59 (C-1′), 88.93 (C-4′), 114.30 (C-5), 137.57 (C-6), 151.83 (C-2), 165.39 (C-4). *Anal.* calcd. for $C_{12}H_{15}BrN_2O_5$: C 41.51, H 4.35, N 8.07; found: C 41.72, H 4.62, N 8.09.

5-[(1R,2R)-2-Bromocyclopropyl]-2′-deoxyuridine (7) and 5-(1R,2S)-2-bromocyclopropyl]-2′-deoxyuridine (8)

Reaction of **4***b* (0.2 g, 0.47 mmol) with zinc dust, using the same procedure described for the monodebromination of **3***b* above, gave a mixture of diastereomers **7** and **8**. This mixture was subjected to multiple development preparative tlc on Whatman PLK5F plates, 1.0 mm in thickness, using solvent system C (upper layer) as the development solvent. This separation provided enriched fractions containing predominantly **7** and **8**, respectively. Each one of these enriched fractions was enriched further by silica gel column chromatography using ethyl acetate:*n*-propanol:water (700:1:2 v/v/v, upper layer) as eluant. Further separation on a silica gel column using chloroform: methanol (19:1 v/v) as eluant yielded the two diastereomers **7** and **8**, respectively: yield **7**, 54 mg, 33.1%; R_f 0.27 (solvent system C, upper layer); mp 126–128°C (dec.); $[\alpha]_D^{23}$ −65.0° (*c* 0.61, MeOH); ^{1}H nmr (D_2O, solvent suppression) δ: 1.1 (dt, $J_{1,3'} = 7.1$, $J_{3',3''} = 6.8$, $J_{2,3'} = 4.3$ Hz, $W_{\frac{1}{2}} = 21.0$ Hz, 1H, cp H-3′), 1.44 (dt, $J_{1,3''} = 9.1$, $J_{2,3''} = 7.1$, $J_{3',3''} = 6.8$ Hz, $W_{\frac{1}{2}} = 23.2$ Hz, 1H, cp H-3″), 2.0 (dq, $J_{1,3''} = 9.1$, $J_{1,2} = 7.1$, $J_{1,3'} = 7.1$, $J_{1,6} = 1.3$ Hz, $W_{\frac{1}{2}} = 26.4$ Hz, 1H, cp H-1), 2.38 (m, 2H, H-2′), 3.40 (dt, $J_{1,2} = 7.1$, $J_{2,3''} = 7.1$, $J_{2,3'} = 4.3$ Hz, $W_{\frac{1}{2}} = 19.6$ Hz, 1H, cp H-2), 3.74 (m, 2H, H-5′), 4.06 (m, 1H, H-4′), 4.45 (m, 1H, H-3′), 6.31 (t, $J_{1',2'} = 6.3$ Hz, 1H, H-1′), 7.85 (d, $J_{1,6} = 1.3$ Hz, 1H, H-6); ^{13}C nmr (CD_3OD) δ: 13.18 (cp C-3), 15.82 (cp C-2), 24.65 (cp C-1), 41.99 (C-2′), 62.45 (C-5′), 71.94 (C-3′), 86.61 (C-1′), 89.11 (C-4′), 113.16 (C-5), 139.72 (C-6), 151.98 (C-2), 166.14 (C-4). *Anal.* calcd. for $C_{12}H_{15}BrN_2O_5$: C 41.51, H 4.35, N 8.07; found: C 41.68, H 4.64, N 7.95.

Diastereomer **8**: yield 60 mg, 36.8%; R_f 0.32 (solvent system C, upper layer); mp 113–115°C (dec.); $[\alpha]_D^{23}$ +62.5° (*c* 0.4, MeOH); ^{1}H nmr (CD_3OD) δ: 1.24 (octet, $J_{1,3''} = 9.8$, $J_{3',3'} = 6.8$, $J_{2,3''} = 4.3$ Hz, $W_{\frac{1}{2}} = 22.6$ Hz, 1H, cp H-3″), 1.46 (q, $J_{2,3'} = 7.5$, $J_{1,3'} = 6.8$, $J_{3',3''} = 6.8$ Hz, $W_{\frac{1}{2}} = 21.7$ Hz, 1H, cp H-3′), 2.14 (septet, $J_{1,3''} = 9.8$, $J_{1,3'} = 6.8$, $J_{1,2} = 4.3$ Hz, $W_{\frac{1}{2}} = 22.8$ Hz, 1H, cp H-1), 2.24 (m, 2H, H-2′), 3.1 (quintet, $J_{2,3'} = 7.5$, $J_{2,3''} = 4.3$, $J_{1,2} = 4.3$ Hz, $W_{\frac{1}{2}} = 17.5$ Hz, 1H, cp H-2), 3.75 (m, 2H, H-5′), 3.92 (m, 1H, H-4′), 4.4 (m, 1H, H-3′), 6.26 (t, J = 6.4 Hz, 1H, H-1′), 7.88 (d, $J_{1,6} = 1.1$ Hz, 1H, H-6); ^{13}C nmr (CD_3OD) δ: 16.77 (cp C-3), 20.36 and 20.81 (cp C-1 and cp C-2), 41.64 (C-2′), 62.51 (C-5′), 71.88 (C-3′), 86.68 (C-1′), 89.01 (C-4′), 114.11 (C-5), 137.56 (C-6), 151.85 (C-2), 165.42 (C-4). *Anal.* calcd. for $C_{12}H_{15}BrN_2O_5$: C 41.51, H 4.35, N 8.07; found: C 41.50, H 4.18, N 7.68.

Acknowledgements

We are grateful to the Medical Research Council of Canada (Grant No. MT-5965) for financial support of this research and to the Alberta Heritage Foundation for Medical Research for a Fellowship to one of us (M.T.).

1. A. S. Jones, J. R. Sayers, R. T. Walker, and E. De Clercq. J. Med. Chem. **31**, 268 (1988).
2. Y. C. Cheng, G. Dutschman, J. J. Fox, K. A. Watanabe, and H. Machida. Antimicrob. Agents Chemother. **20**, 420 (1981).
3. E. De Clercq, J. Descamps, P. De Somer, P. J. Barr, A. S. Jones, and R. T. Walker. Proc. Natl. Acad. Sci (USA), **76**, 2947 (1979).
4. J. Goodchild, R. A. Porter, R. H. Raper, I. S. Sim, R. M. Upton, J. Viney, and H. J. Wadsworth. J. Med. Chem. **26**, 1252 (1983).
5. A. De Meijere. Angew. Chem. Int. Ed. Engl. **18**, 809 (1979).
6. P. G. Gassman. Chem. Commun. 793 (1967).
7. M. Tandon, T. Iwashina, L. Xu, E. Knaus, L. Wiebe, D. Tovell, and D. Tyrrell. Biochem. Arch. **4**, 131 (1988).
8. D. Seyferth and R. L. Lambert. J. Organometal. Chem. **16**, 21 (1969).
9. S. A. Moore, B. D. Santarsiero, T. Lin, M. N. G. James, M. Tandon, L. I. Wiebe, and E. E. Knaus. Acta Crystallogr. Sect. C: Cryst. Struct. Commun. **45**, 647 (1989).
10. E. A. Green, R. D. Rosenstein, R. Shiono, D. J. Abraham, B. L. Trus, and R. E. Marsh. Acta Crystallogr. Sect. B: Struct. Crystallogr. Cryst. Chem. **B31**, 102 (1975).
11. J. W. Lauher and J. A. Ibers. J. Am. Chem. Soc. **97**, 561 (1975).
12. M. E. Jason and J. A. Ibers. J. Am. Chem. Soc. **99**, 6012 (1977).
13. L. M. Jackman and S. Sternhell. Applications of nuclear magnetic resonance spectrometry in organic chemistry. 2nd ed. Pergamon Press, Toronto. 1969. pp. 228–229 and 286.
14. S. G. Rahim, M. J. H. Duggan, R. T. Walker, A. S. Jones, R. L. Dyer, J. Balzarini, and E. De Clercq. Nucleic Acids Res. **10**, 5285 (1982).
15. R. A. Sharma and M. Bobek. J. Org. Chem. **40**, 2377 (1975).

Can. J. Chem. Downloaded from www.nrcresearchpress.com by 194.225.253.170 on 09/07/12
For personal use only.

Apparent and partial molar heat capacities and volumes of aqueous $HClO_4$ and HNO_3 from 10 to 55°C

JAMEY K. HOVEY[1] AND LOREN G. HEPLER
Department of Chemistry, University of Alberta, Edmonton, Alta., Canada T6G 2G2

Received January 16, 1989

JAMEY K. HOVEY and LOREN G. HEPLER. Can. J. Chem. **67**, 1489 (1989).

Apparent molar heat capacities and volumes of aqueous solutions containing $HClO_4$ and HNO_3 have been determined from 10 to 55°C. The temperature dependences of the standard state heat capacities and volumes of ClO_4^- (aq) and NO_3^- (aq) from 10 to 55°C were found to be well represented by the following equations:

$$\tilde{V}^0(HClO_4, aq) = -107.79 + 0.87322T - 0.0012203T^2$$

$$\tilde{C}_p^0(HClO_4, aq) = 1408.2 - \frac{55801}{T - 190} - 3.0767T$$

$$\tilde{V}^0(HNO_3, aq) = 76.67 - \frac{2210.1}{T - 190} - 0.090063T$$

$$\tilde{C}_p^0(HNO_3, aq) = 1154.9 - \frac{49213}{T - 190} - 2.5850T$$

Combination of the experimental results with semiempirical equations for ion–solvent interaction has led to predictions of the standard state volumes and heat capacities for these ionic species at higher temperatures.

Key words: heat capacities, volumes, nitric acid, perchloric acid.

JAMEY K. HOVEY et LOREN G. HEPLER. Can. J. Chem. **67**, 1489 (1989).

Opérant à des températures allant de 10 à 55°C, on a déterminé les capacités calorifiques et les volumes molaires apparents de solutions aqueuses contenant du $HClO_4$ et du HNO_3. On a trouvé que, à des températures allant de 10 à 55°C, les relations qui existent entre la température et les capacités calorifiques et les volumes de l'état standard des ions ClO_4^- (aq) et NO_3^- sont bien représentées par les équations suivantes :

$$\tilde{V}^0(HClO_4, aq) = -107{,}79 + 0{,}87322T - 0{,}0012203T^2$$

$$\tilde{C}_p^0(HClO_4, aq) = 1408{,}2 - \frac{55801}{T - 190} - 3{,}0767T$$

$$\tilde{V}^0(HNO_3, aq) = 76{,}67 - \frac{2210{,}1}{T - 190} - 0{,}090063T$$

$$\tilde{C}_p^0(HNO_3, aq) = 1154{,}9 - \frac{49213}{T - 190} - 2{,}5850T$$

En faisant appel à une combinaison des résultats expérimentaux et d'équations semi-empiriques pour l'interaction ion–solvant, on a pu faire des prédictions concernant les capacités calorifiques et les volumes de l'état standard de ces espèces ioniques à des températures plus élevées.

Mots clés : capacités calorifiques, volumes, acide nitrique, acide perchlorique.

[Traduit par la revue]

Introduction

Heat capacities and volumes of aqueous solutions containing perchloric and nitric acids have been obtained from 10 to 55°C. The derived partial molar volumes and heat capacities of these aqueous species can be used in many calculations through the use of simple thermodynamic relationships. The temperature and pressure dependences of the equilibrium constant (or Gibbs free energy) are related to standard state heat capacities and volumes by the expressions:

$$[1] \quad \left(\frac{\partial \ln K}{\partial T}\right)_p = \frac{\Delta H^0}{RT^2}$$

$$[2] \quad \left(\frac{\partial \Delta H^0}{\partial T}\right)_p = \Delta C_p^0$$

$$[3] \quad \left(\frac{\partial \ln K}{\partial p}\right)_T = \frac{-\Delta V^0}{RT}$$

Knowledge of the standard state volume and heat capacity functions thus permits calculation of the equilibrium constants (or Gibbs free energies) as a function of both temperature and pressure over the experimental temperature range. Combination of these data with semitheoretical models of ionic hydration permits extrapolation of these data to higher temperatures that are more closely associated with many applications.

Experimental

Water used for all experiments was first passed through an activated charcoal filter and then through a Milli-RO4 / Milli-Q reagent grade mixed bed ion exchange and activated carbon system to yield purified water with a resistivity of 18 MΩ cm or greater. Solutions of NaCl (Fisher certified, ACS) were prepared by mass after drying the salt at 110°C until constant weight.

[1]Present address: Department of Chemistry and Lawrence Berkeley Laboratory, University of California, Berkeley, CA 94720, U.S.A.

Can. J. Chem. Downloaded from www.nrcresearchpress.com by 194.225.253.170 on 09/07/12
For personal use only.

TABLE 1. Compositions of solutions, densities, heat capacity ratios, and apparent molar volumes and heat capacities for HNO_3 and $HClO_4$ at 10, 40, and 55°C

m_2 (mol kg^{-1})	$10^2(d - d^0{}_1)$ (g cm^{-3})	$^{\Phi}V_2$ (cm^3 mol^{-1})	$10^2\left(\frac{c_p d}{c^0_{p,1} d^0_1} - 1\right)$	$^{\Phi}C_{p,2}$ (J K^{-1} mol^{-1})
		$HClO_4$		
		10°C		
1.0829	5.9961	42.53	−4.717	−14.17
0.8954	4.9956	42.54	−4.031	−19.08
0.7302	4.1049	42.49	−3.384	−23.67
0.6205	3.5059	42.47	−2.935	−26.99
0.5247	2.9827	42.35	−2.532	−30.23
0.4091	2.3349	42.39	−2.023	−34.69
0.2668	1.5381	42.15	−1.365	−41.74
0.1841	1.0647	42.17	−0.960	−45.12
		40°C		
1.0829	5.5268	46.80		
1.0829	5.5217	46.85	−4.276	19.59
0.8954	4.6003	46.89	−3.623	16.93
0.7302	3.7780	46.91	−3.017	14.57
0.6205	3.2231	46.96	−2.592	13.74
0.5247	2.7406	46.90	−2.235	10.75
0.4091	2.1492	46.87	−1.772	8.52
0.2668	1.4117	46.83	−1.182	5.34
0.1841	0.9751	46.98	−0.829	3.65
		55°C		
1.0829	5.3949	48.01	−4.257	23.74
0.8954	4.4915	48.10	−3.630	20.16
0.7302	3.6829	48.20	−2.993	19.98
0.6205	3.1478	48.17	−2.570	18.86
0.5247	2.6764	48.11	−2.197	17.50
0.4091	2.0992	48.08	−1.765	12.84
0.2668	1.3791	48.04	−1.161	12.23
0.1841	0.9529	48.18	−0.797	14.44
		HNO_3		
		10°C		
1.1115	3.7154	28.52	−4.517	−57.39
0.8581	2.8941	28.46	−3.652	−64.67
0.8112	2.7467	28.37	−3.473	−65.90
0.6142	2.0900	28.39	−2.745	−72.89
0.4714	1.6187	28.21	−2.164	−78.07
0.3427	1.1792	28.27	−1.615	−82.24
0.2279	0.7947	27.92	−1.102	−88.19
0.1116	0.3960	27.42	−0.553	−94.76
		40°C		
1.1115	3.3939	31.42	−3.766	−17.35
0.8581	2.6380	31.44	−3.040	−22.80
0.6142	1.9090	31.33	−2.280	−29.39
0.8112	2.4983	31.43	−2.896	−23.82
0.4714	1.4712	31.34	−1.800	−33.18
0.3427	1.0796	31.17	−1.341	−37.32
0.2279	0.7193	31.23	−0.912	−40.28
0.1116	0.3601	31.62	−0.458	−46.59
		55°C		
1.1115	3.3137	32.16	−3.615	−9.33
0.8581	2.5748	32.20	−2.928	−14.97
0.8112	2.4433	32.13	−2.788	−16.12
0.6142	1.8570	32.20	−2.206	−21.57
0.4714	1.4404	32.01	−1.748	−26.62
0.3427	1.0507	32.03	−1.289	−28.12
0.2279	0.7052	31.86	−0.883	−33.14
0.1116	0.3467	31.84	−0.441	−35.82

Can. J. Chem. Downloaded from www.nrcresearchpress.com by 194.225.253.170 on 09/07/12
For personal use only.

TABLE 2. Density, specific heat capacity, and Debye–Hückel slopes for water at 10, 25, 40, and 55°C from Kell (5, 6) and Ananthaswamy and Atkinson (8), repsectively

t (°C)	d_1^0 (g cm^{-3})	$c_{p,1}^0$ (J K^{-1} g^{-1})	A_V (cm^3 kg$^{1/2}$ mol$^{-3/2}$)	A_C (J kg$^{1/2}$ mol$^{-3/2}$ K^{-1})
10	0.999700	4.1919	1.6420	28.446
25	0.997047	4.1793	1.8743	32.783
40	0.992219	4.1783	2.1540	37.446
55	0.985695	4.1821	2.4946	42.699

All stock solutions were prepared from concentrated solutions of the acids. Concentrated (60%) perchloric acid and nitric acid were obtained from Fisher (certified, ACS). The molality of each stock solution was determined by titration with THAM (tris(hydroxymethyl)aminomethane). All subsequent solutions were prepared by diluting (by mass) the stock solutions with pure water.

The densities of all solutions were measured relative to water at each of the experimental temperatures ±0.01°C with a Sodev 03D vibrating tube densimeter (1), which was calibrated with pure water and a standard solution of NaCl (densities taken from Millero (2)). Heat capacities were measured at the mean reported temperatures ±0.01°C relative to water with a Sodev CP-C Picker type flow microcalorimeter (3). Temperatures were maintained (constant to ±0.001°C) in both instruments with separate Sodev CT-L circulating baths and monitored with calibrated thermistors. Daily evaluation of the calorimetric heat loss correction factor (4) by way of measurements on standard solutions of NaCl led to $f = 1.006 \pm 0.002$ at 25°C. This correction factor was assumed to be independent of temperature. Densities and heat capacities for pure water were taken from Kell (5, 6) and are listed later.

Results

Apparent molar properties

Table 1 lists the experimentally determined relative densities $(d - d_1^0)$ and heat capacity ratios $[c_p d/(c_{p,1}^0 d_1^0) - 1]$ for all of the aqueous solutions at each temperature. The apparent molar property $^{\Phi}Y$ of a solution is defined generally by

$$[4] \quad {}^{\Phi}Y_2 = \frac{Y_{soln} - 55.509 Y_1^0}{m_2}$$

where Y_{soln} is the extensive property (volume or heat capacity) of a solution that contains 1 kg of solvent (water), Y_1^0 is the molar volume or heat capacity of pure solvent (water), and m_2 is the molality of the solute. Apparent molar volumes and heat capacities were calculated from the results listed in Table 1 using the equations

$$[5] \quad {}^{\Phi}V_2 = \frac{\frac{1 + m_2 M_2}{d} - \frac{1}{d_1^0}}{m_2}$$

and

$$[6] \quad {}^{\Phi}C_{p,2} = \frac{c_p(1 + m_2 M_2) - c_{p,1}^0}{m_2}$$

where M represents the solute molar mass, c_p and d are the specific heat capacity and density of the solution, and $c_{p,1}^0$ and d_1^0 are the specific heat capacity and density of pure water. Table 1 lists values of these apparent molar volumes and heat capacities at the temperatures pertaining to the present measurements.

The functional dependences of the apparent molar volumes and heat capacities of $HClO_4$ and HNO_3 are well represented by extended Debye–Hückel equations of the type (7)

$$[7] \quad {}^{\Phi}Y = \bar{Y}^0 + 1.5 \frac{\omega A_Y}{I}[I - 2I^{1/2} + 2\ln(1 + I^{1/2})] + B_Y I + C_Y I^{3/2}$$

where

$$[8] \quad I = \omega m = \frac{1}{2}\sum m_i z_i^2$$

Values for the Debye–Hückel limiting slopes (A_Y) were taken from Ananthaswamy and Atkinson (8) and are listed in Table 2.

Equation [7] was fitted to the experimental apparent molar properties listed in Table 1 at 10, 40, and 55°C and at 25°C to the data from Hovey *et al.* (9) to generate the values of $\bar{Y}_2^0$, B_Y, and C_Y for nitric and perchloric acid that are listed in Table 3. It was found that the temperature dependence of the B_Y and C_Y parameters for perchloric acid could be represented satisfactorily by equations of the form

$$[9] \quad B_Y(\text{and } C_Y) = p_1 + \frac{p_2}{T} + p_3 T + p_4 T^2$$

using only three of the four parameters without significant loss in the precision of the fits. The p_i parameters are fitting coefficients and T is the temperature in kelvins. We have subsequently refit the data listed in Table 1 using values for the B and C parameters that resulted from the constrained fits.

Application of eq. [9] to the B and C parameters obtained from fits to data for nitric acid was found to increase the overall standard deviation of the fits and thus was not used for refining the limiting standard state values.

Plots of $^{\Phi}Y_2$ minus the Debye–Hückel limiting law (eq. [7]) are shown in Figs. 1 and 2 for perchloric acid and Fig. 3 and 4 for nitric acid. The ability of the above described procedure to represent the high concentration properties and the standard state values (infinite dilution) is illustrated in these plots.

Standard state properties

Direct comparisons

Many of the room temperature standard state partial molar volumes and heat capacities for nitric and perchloric acids were discussed by Hovey *et al.* (9) and the preferred values at 25°C are recommended over the present results. For temperatures above and below 25°C there are results from only a few studies that can be compared with the present work. Millero (10) cites standard state volumes from Zen (11) at 0, 10, and 25°C, of which the 10 and 25°C values are in good agreement with the present results. Smith-Magowan and Goldberg (12) cite several investigations of the heat capacities of aqueous nitric acid solutions. None of the results that were derived from temperature dependent studies are of sufficient precision or to low enough

Can. J. Chem. Downloaded from www.nrcresearchpress.com by 194.225.253.170 on 09/07/12
For personal use only.

TABLE 3. Standard state partial molar volumes, heat capacities, and ionic strength parameters for solutions of HNO_3 and $HClO_4$ from 10 to 55°C*

t (°C)	${}^{\Phi}V_2^0$ (cm^3 mol^{-1})	B_V (cm^3 kg mol^{-2})
	$HClO_4$†	
10	41.63±0.04	−0.0353±0.06
25	44.04±0.02	−0.4601±0.04
40	46.24±0.03	−0.5855±0.04
55	47.31±0.05	−0.6627±0.07
	HNO_3	
10	27.43±0.08	0.1175±0.11
25	29.41±0.01	−0.2592±0.01
40	30.47±0.05	−0.2912±0.07
55	31.14±0.05	−0.4196±0.07

t (°C)	${}^{\Phi}C_{p,2}^0$ (J K^{-1} mol^{-1})	B_C (J kg K^{-1} mol^{-2})	C_C (J kg$^{3/2}$ K^{-1} mol$^{-5/2}$)
		$HClO_4$†	
10	62.2±0.7	47.01±3.7	−17.18±3.2
25	−25.0±0.1	17.35±2.8	−3.868±2.6
40	−9.0±1.0	3.75±5.7	1.42±4.9
55	−5.2±2.0	4.65±20	−0.54±16
		HNO_3	
10	−106.4±0.6	41.29±3.4	−11.91±3.0
25	−69.0±0.5	13.57±2.9	2.321±2.6
40	−58.3±0.7	18.18±4.0	−1.27±3.5
55	−48.0±1.3	−4.245±7.9	15.74±6.9

*Expressions at 25°C were derived from fits to data from ref. 9.

†Reported uncertainties are those derived from the fits with unconstrained values of the B_Y and C_Y parameters. For $HClO_4$ calculations from 10 to 55°C use:

$$B_V = -38.635 + 8170.9/T + 0.00012152T^2$$
$$B_C = -3150.1 + 671750/T + 0.010287T^2$$
$$C_C = 1578.4 - 332590/T - 0.0052506T^2$$
$$T/K = t/°C + 273.15$$

ionic strengths for useful comparisons. It is expected that the present results are the most useful over this reported temperature range.

There are more recent data that lead to standard state volumes and heat capacities for perchloric acid. The recent precise volumetric results of Herrington *et al.* (13) from 25 to 75°C are in excellent agreement with the present results. Smith-Magowan and Goldberg (12) have compiled a listing of all heat capacity measurements on perchloric acid prior to 1979, from which it can be seen that no study covers the present temperature range. Very recent direct densimetric and calorimetric investigations of perchloric acid have been reported by Pogue and Atkinson (14) from 15 to 55°C. The volumetric results are in good agreement with the present results, but their standard state heat capacities are more positive than the present results by 3 J K^{-1} mol^{-1} at 25°C and 29 J K^{-1} mol^{-1} at 55°C. This difference is partly due to their apparent neglect of unsymmetrical heat losses in Picker type flow microcalorimeters. The results from Pogue and Atkinson (14) are also just outside of estimated uncertainties

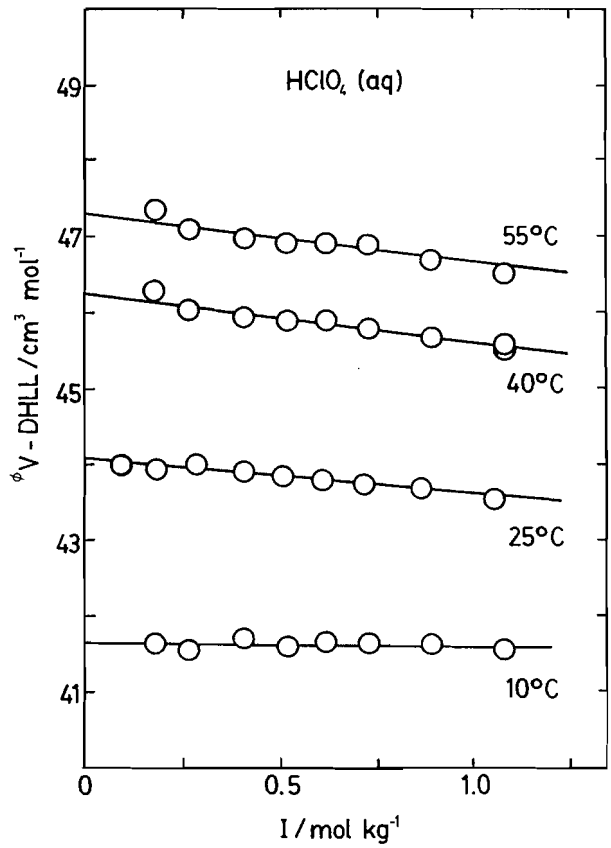


FIG. 1. ${}^{\Phi}V$ minus the extended Debye–Hückel limiting law (DHLL) for aqueous $HClO_4$ from 10 to 55°C versus ionic strength. Lines are least-squares fits of eq. [7].

of other results at room temperature, such as those by Singh *et al.* (15) and Hovey *et al.* (9) and the value based on a critical evaluation of data for perchloric acid and other perchlorate salts (7) that yielded $C_p^0 = 25 \pm 1$ J K^{-1} mol^{-1} for aqueous $HClO_4$. For these reasons, we believe that the present results are most reliable, and that the maximum uncertainty in the results occurs at 55°C and is approximately equal to ±10 J K^{-1} mol^{-1}.

Temperature dependence of standard state properties

It is useful to have analytical representations of the temperature dependence of the standard state partial molar volumes and heat capacities for all of the solutes under present investigation for use in various thermodynamic calculations. One of the most useful representations of the temperature dependence of standard state properties is the equation suggested by Holmes and Mesmer (16):

$$[10] \quad \bar{Y}^0 = a + \frac{b}{T - \theta} + cT + dT^2$$

For ease of calculations involving many species, and from fits of the standard state heat capacities for other electrolytes (17), the temperature represented by θ has been assigned the value 190 K. Most of the fits presented below have been made with data resulting solely from the present work. The fit to standard state volumes of perchloric acid included the accurate results of Wirth and Collier (18), and all of the results from Herrington *et al.* (13) except their 75°C point. Fitting of equations of type [10] (using only 3 of the 4 parameters available) to the selected standard state properties has led to:

Can. J. Chem. Downloaded from www.nrcresearchpress.com by 194.225.253.170 on 09/07/12
For personal use only.

Can. J. Chem. Downloaded from www.nrcresearchpress.com by 194.225.253.170 on 09/07/12
For personal use only.

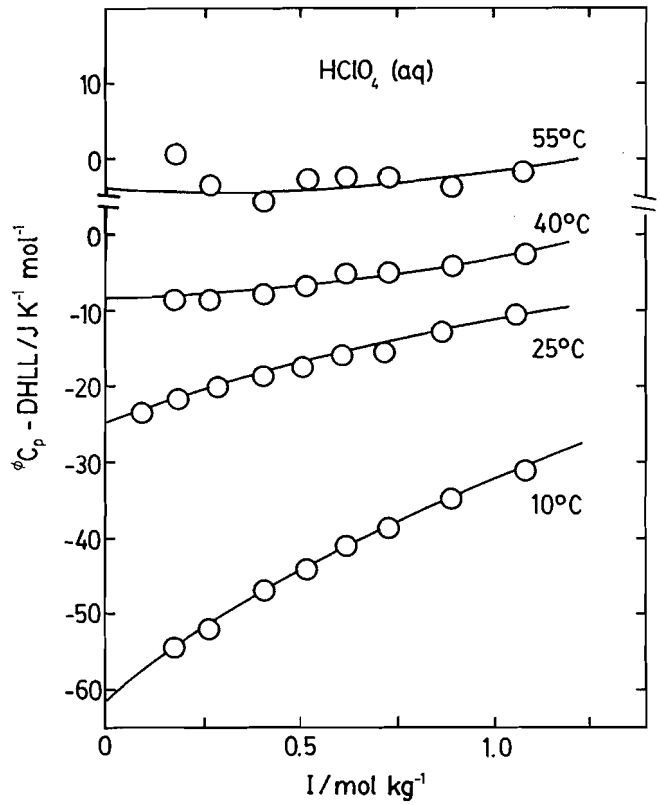


FIG. 2. $^{\Phi}C_p$ minus the extended Debye–Hückel limiting law (DHLL) for aqueous $HClO_4$ from 10 to 55°C versus ionic strength. Lines are least-squares fits of eq. [7].

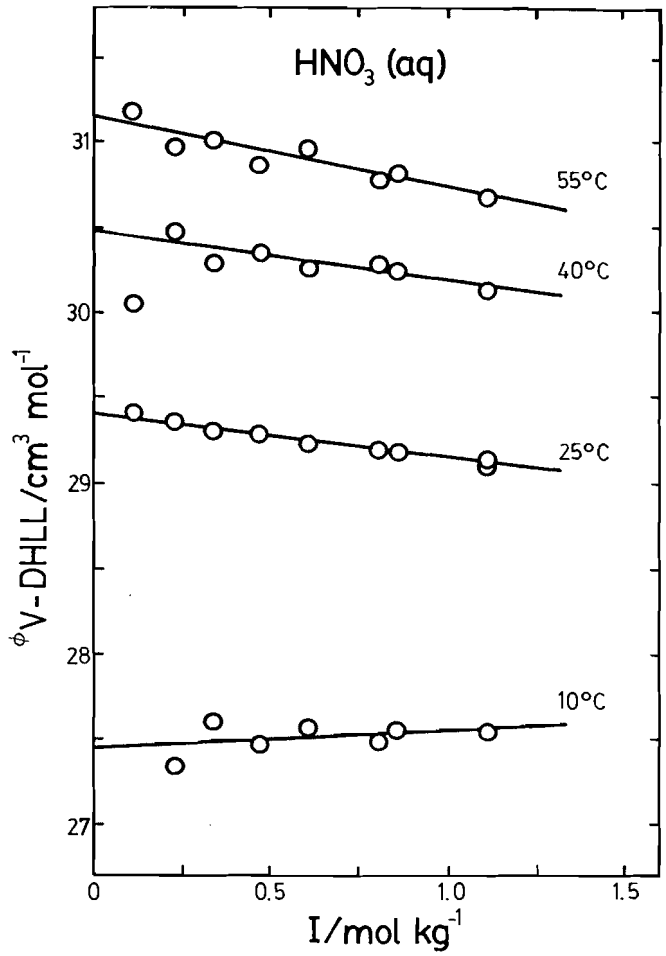


FIG. 3. $^{\Phi}V$ minus the extended Debye–Hückel limiting law (DHLL) for aqueous HNO_3 from 10 to 55°C versus ionic strength. Lines are least-squares fits of eq. [7].

$$[11]\quad \bar{V}^0(HClO_4, aq) = -107.79 + 0.87322T - 0.0012203T^2$$

$$[12]\quad \bar{C}_p^0(HClO_4, aq) = 1408.1 - \frac{55801}{T - 190} - 3.0767T$$

$$[13]\quad \bar{V}^\circ(HNO_3, aq) = 76.67 - \frac{2210.1}{T - 190} - 0.090063T$$

$$[14]\quad \bar{C}_p^0(HNO_3, aq) = 1154.9 - \frac{49213}{T - 190} - 2.5850T$$

All of these equations are accurate over the temperature range from 10 to 55°C, except the expression for $\bar{V}^0(HClO_4, aq)$, which is accurate from 10 to 65°C. Plots of the standard state partial molar volumes and heat capacities are shown in Figs. 5–8. The "goodness of fit" of the above expressions, and the marked temperature dependence of these properties can be seen. These expressions should be used for all calculations requiring the standard state volumes and heat capacities over these specified temperature ranges, rather than the expressions that are derived in the next section for use over wider ranges of temperature.

Conventional ionic volumes and heat capacities of the ions $NO_3^-(aq)$ and $ClO_4^-(aq)$ can be derived from the convention $\bar{Y}^0(H^+, aq) \equiv 0$ at all temperatures. Since all of the solutes that are under present investigation are strong acids, these conventional ionic properties are equal to the standard state properties.

Discussion

Helgeson–Kirkham–Flowers (HKF) model

The change in standard state heat capacity of a chemical reaction is related to the second derivative of the equilibrium constant with respect to temperature. Equilibrium constants or Gibbs free energies can be calculated at elevated temperatures by using heat capacity data, provided that room temperature equilibrium and enthalpy data are available. Because the relationship between equilibrium constants (or Gibbs free energies) and heat capacities is through the second derivative with respect to temperature (see eqs. [1]–[3]), shortcomings in heat capacity functions usually have only a small effect on calculations of Gibbs free energies.

The Helgeson–Kirkham–Flowers equations of state for standard state volumes and heat capacities have the form (at constant pressure) (19)

$$[15]\quad \bar{V}^0 = \sigma + \frac{\xi T}{T - \theta} + \Delta V_{Born}$$

$$[16]\quad \bar{C}_p^0 = c_1 + \frac{c_2 T}{T - \theta} + \Delta C_{p,Born}$$

where σ, ξ, c, and θ are fitting coefficients. The ΔY_{Born} terms come directly from the relationship of the partial molar free energy to partial molar volumes and heat capacities

$$[17]\quad \Delta V_{Born} = \left(\frac{\partial \Delta G_{Born}}{\partial p}\right)_T = -\omega \frac{1}{\epsilon}\left(\frac{\partial \ln \epsilon}{\partial p}\right)_T = -\omega Q$$

Can. J. Chem. Downloaded from www.nrcresearchpress.com by 194.225.253.170 on 09/07/12
For personal use only.

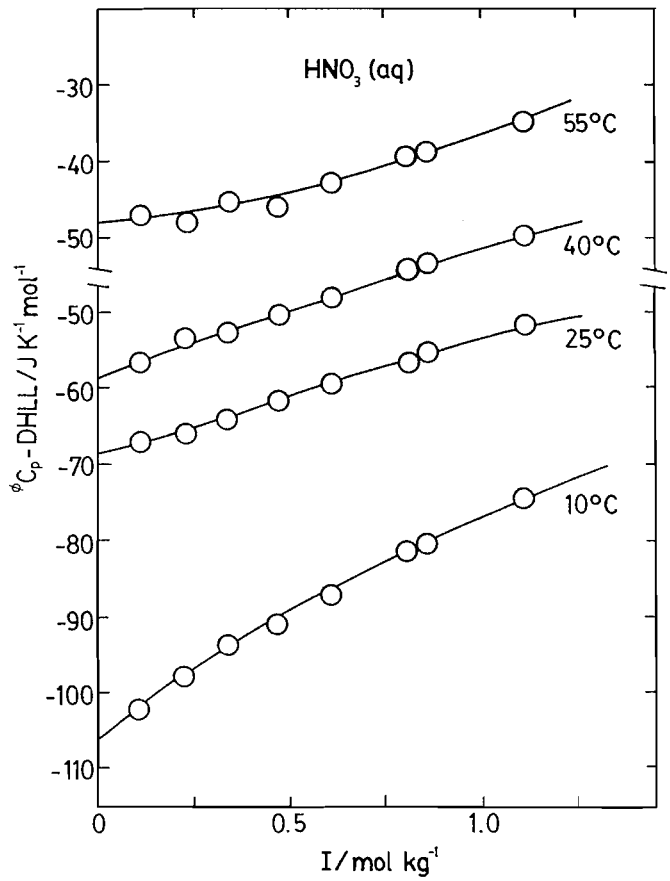


FIG. 4. ${}^{\Phi}C_p$ minus the extended Debye–Hückel limiting law (DHLL) for aqueous HNO_3 from 10 to 55°C versus ionic strength. Lines are least-squares fits of eq. [7].

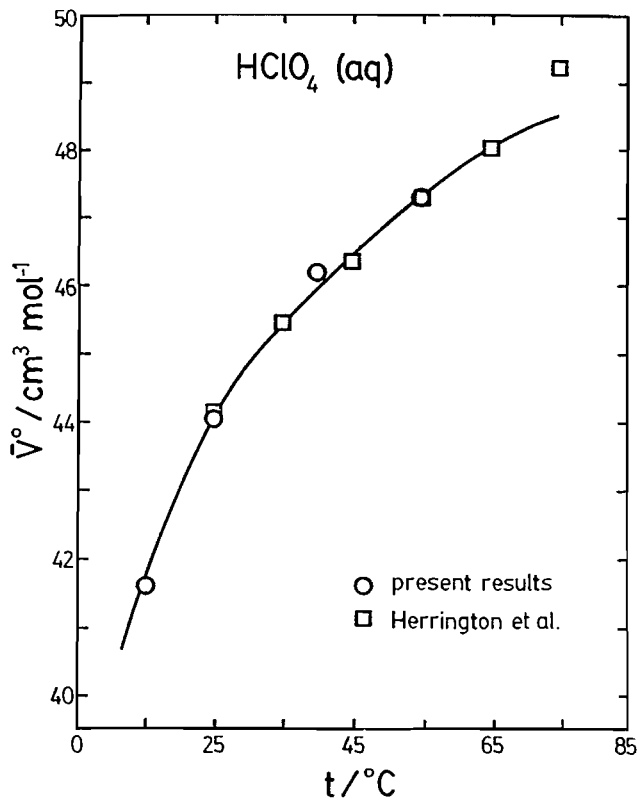


FIG. 5. Standard state volumes for $HClO_4$ from 10 to 65°C.

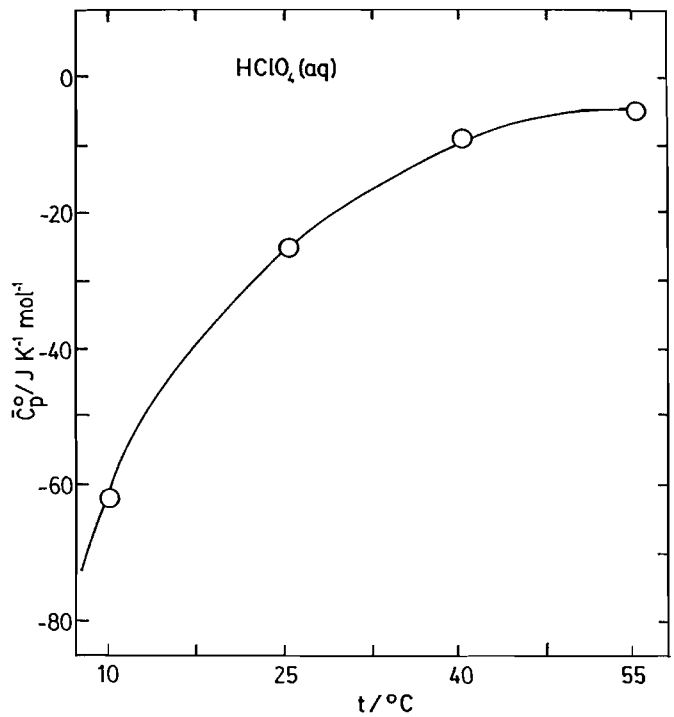


FIG. 6. Standard state heat capacities for $HClO_4$ from 10 to 55°C.

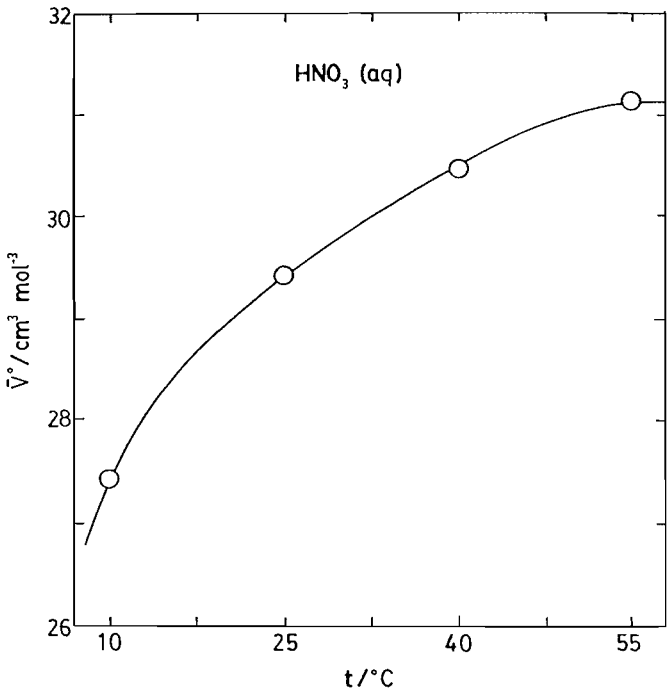


FIG. 7. Standard state volumes for HNO_3 from 10 to 55°C.

$$[18]\quad \Delta C_{p,\mathrm{Born}} = -T\left(\frac{\partial^2 \Delta G_{\mathrm{Born}}}{\partial T^2}\right)_p = \omega T \frac{1}{\epsilon}\left[\left(\frac{\partial^2 \ln \epsilon}{\partial T^2}\right)_p - \left(\frac{\partial \ln \epsilon}{\partial T}\right)_p^2\right] = \omega T X$$

and

$$[19]\quad \omega = 6.94657 \times 10^5 \left(\frac{z^2}{r_{\mathrm{eff}}}\right) \text{ Å J mol}^{-1}$$

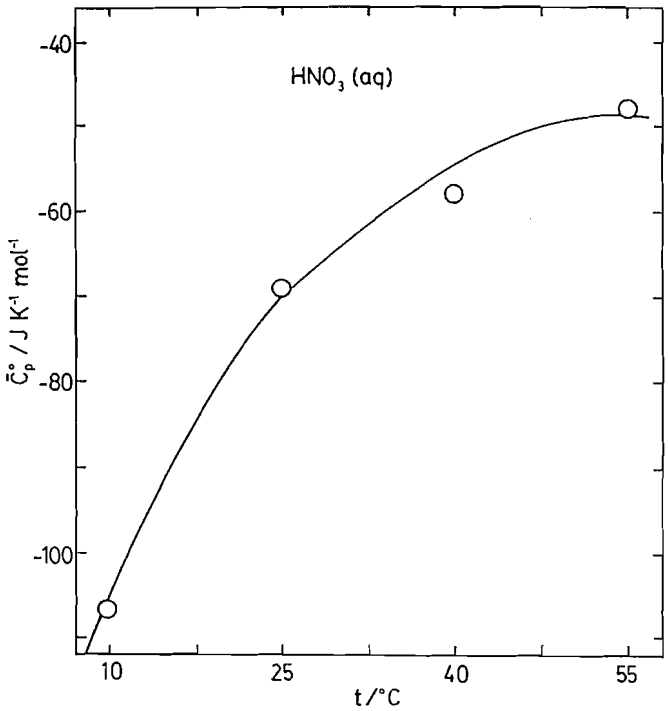


FIG. 8. Standard state heat capacities for HNO_3 from 10 to 55°C.

where Q and X are shorthand notations for the various pressure and temperature dependences of derivatives of the dielectric constant with respect to pressure and temperature, and r_{eff} is the "effective" radius of an ion in water. Numerical values for these terms were taken from Helgeson and Kirkham (20, 21).

The first two terms in eqs. [15] and [16] are purely empirical and are most important at low temperatures where the Born electrostatic model is least satisfactory. The third term in each equation results entirely from the Born equation, which dominates at high temperatures where the model is most satisfactory. Because of the balance of empirical and theoretical components, the HKF treatment is particularly well suited for extrapolation of low temperature data for standard state partial molar properties to higher temperatures.

In all of these equations the effective radii for anionic species are equivalent to crystallographic radii, and for cationic species the effective radii are the crystallographic radii plus 0.94 Å. Effective aqueous radii for all of these solutes were calculated from the crystal "ionic radii" listed by Shannon (22). The results of fitting equations of the type given by eqs. [15] and [16] are listed below

$$(22)\quad \frac{\bar{V}^0(HClO_4, aq)}{cm^3\ mol^{-1}} = 84.508 - \frac{16.465T}{T - 167.4} - 4.75415 \times 10^6 Q$$

$$(23)\quad \frac{\bar{C}_p^0(HClO_4, aq)}{J\ K^{-1}\ mol^{-1}} = 89.43 - \frac{8.6367T}{T - 261.0} - 4.75415 \times 10^5 TX$$

$$(24)\quad \frac{\bar{V}^0(HNO_3, aq)}{cm^3\ mol^{-1}} = 42.830 - \frac{2.5557T}{T - 226.5} - 4.7100 \times 10^6 Q$$

$$(25)\quad \frac{\bar{C}_p^0(HNO_3, aq)}{J\ K^{-1}\ mol^{-1}} = 45.36 - \frac{9.0799T}{T - 259.9} - 4.7100 \times 10^5 TX$$

These latter equations should be employed for calculations involving these solutes at temperatures higher than 55°C until direct results become available.

The magnitude of the standard state volumes and heat capacities for nitric and perchloric acid suggests that ion–solvent interactions in aqueous solutions containing these ions are qualitatively similar. Both the standard state volumes and heat capacities suggest that the total effects due to regions of ordered ion–water dipoles (first hydration sphere) and less ordered, less well-defined, secondary solvation spheres are larger for nitric acid. These observations are expected, due to the possibility of increased molecular motions in perchloric acid and due to the larger size of the anion.

Acknowledgements

We are extremely grateful to the Natural Sciences and Engineering Research Council of Canada for operating support (L.G.H.) and postgraduate and postdoctoral fellowships (J.K.H.). We also thank Dr. Peter Tremaine and the Alberta Research Council for allowing us to use all of the equipment mentioned above. J.K.H. is further grateful to Professor Kenneth S. Pitzer and the Lawrence Berkeley Laboratory for facilities to produce the final copy of this paper.

1. P. PICKER, E. TREMBLAY, and C. JOLICOEUR. J. Solution Chem. **3**, 377 (1974).
2. F. J. MILLERO. J. Phys. Chem. **74**, 356 (1970).
3. P. PICKER, P. A. LEDUC, P. R. PHILIP, and J. E. DESNOYERS. J. Chem. Thermodyn. **3**, 631 (1971).
4. J. E. DESNOYERS, C. DEVISSER, G. PERRON, and P. PICKER. J. Solution Chem. **5**, 605 (1976).
5. G. S. KELL. J. Chem. Eng. Data, **12**, 66 (1967).
6. G. S. KELL. *In* Water — A comprehensive treatise. Vol. I. *Edited by* F. Franks. Plenum Press, New York. 1972. pp. 363–412.
7. J. K. HOVEY. Thermodynamics of aqueous solutions. Ph.D. thesis, University of Alberta. 1988.
8. J. ANANTHASWAMY and G. ATKINSON. J. Chem. Eng. Data, **29**, 81 (1984).
9. J. K. HOVEY, L. G. HEPLER, and P. R. TREMAINE. Thermochim. Acta, **126**, 246 (1988).
10. F. J. MILLERO. *In* Water and aqueous solutions : Structure, thermodynamics and transport processes. *Edited by* R. A. Horne. John Wiley and Sons, New York. 1972.
11. E.-AN. ZEN. Geochim. Cosmochim. Acta, **12**, 103 (1957).
12. D. SMITH-MAGOWAN and R. N. GOLDBERG. A bibliography of sources of experimental data leading to thermal properties of binary aqueous electrolyte solutions. NBS SP 537, National Bureau of Standards, Washington, DC. 1979.
13. T. M. HERRINGTON, A. D. PETHYBRIDGE, and M. G. ROFFEY. J. Chem. Eng. Data, **30**, 264 (1985).
14. R. POGUE and G. ATKINSON. J. Chem. Eng. Data, **33**, 495 (1988).
15. P. P. SINGH, K. G. MCCURDY, E. M. WOOLLEY, and L. G. HEPLER. J. Solution Chem. **6**, 327 (1977).
16. H. F. HOLMES and R. E. MESMER. J. Phys. Chem. **87**, 1242 (1983).
17. P. R. TREMAINE, K. SWAY, and J. A. BARBERO. J. Solution Chem. **15**, 1 (1986).
18. H. E. WIRTH and F. N. COLLIER, JR. J. Am. Chem. soc. **72**, 5292 (1950).
19. H. C. HELGESON, D. H. KIRKHAM, and G. C. FLOWERS. Am. J. Sci. **281**, 1249 (1981).
20. H. C. HELGESON and D. H. KIRKHAM. Am. J. Sci. **274**, 1089 (1974).
21. H. C. HELGESON and D. H. KIRKHAM. Am. J. Sci. **276**, 97 (1976).
22. R. D. SHANNON. Acta Crystallogr. Sect. A: Cryst. Phys. Diffr. Theor. Gen. Crystallogr. **A32**, 751 (1976).

Can. J. Chem. Downloaded from www.nrcresearchpress.com by 194.225.253.170 on 09/07/12
For personal use only.

Characterization of metal complexes of 1,10-phenanthroline, 2,2′-bipyridine, and their derivatives by fast atom bombardment mass spectrometry

JACK M. MILLER[1] AND KESAGAPILLAI BALASANMUGAM
Department of Chemistry, Brock University, St. Catharines, Ont., Canada L2S 3A1

Received February 9, 1989

JACK M. MILLER and KESAGAPILLAI BALASANMUGAM. Can. J. Chem. **67**, 1496 (1989).

A series of 1,10-phenanthroline (phen), 5-nitro-1,10-phenanthroline (5-NO_2-phen), 2,9-dimethyl-1,10-phenanthroline (dmp), 2,2′-bipyridine (bpy), and 4,4′-dimethy-2,2′-bipyridine (dmb) metal complexes has been characterized using fast atom bombardment mass spectrometry (FAB MS). Intact cations are observed in the positive ion FAB mass spectra of all tetracoordinated complexes, $[Ag(L)_2]NO_3$, $[Cu(L)_2]_2\ SO_4{\cdot}5H_2O$, $[Cu(L)_2]SO_4$, and $[Tl(L)_2](ClO_4)$, where L = bpy, phen, or dmp. Structurally significant fragment ions (ML_2^+, ML^+, M^+, and $(L + H)^+$, where M^+ = metal ion) are also observed. Species such as $Ag[Ag(L)_2]NO_3^+$, where L = bpy or phen, and $Tl[Tl(phen)_2](ClO_4)^+$ are also seen. The hexacoordinate complexes, $[Co(phen)_3]Cl_2$, $[Ru(bpy)Cl_2]$, $[Fe(phen)_2(CN)_2]$, $[Fe(L)_3](ClO_4)$, where L = 5-NO_2-phen, dmb, or bpy, and $[Fe(L)_3]SO_4$, where L = bpy or phen, show intact cations in the positive ion spectra; $[Ni(bpy)_3]X_2$, where X = Cl^-, Br^-, NO_3^-, ClO_4^-, SCN^-, and tartrate^{2-}, and $[Co(bpy)_3](ClO_4)$ do not. Generally, fragment ions such as ML_3^+, ML_2X^+, ML_2^+, MLX^+, and $(L + H)^+$ are observed, where X = singly charged intact anion or HSO_4^-. Comparison of FAB results with those of laser mass spectrometry (LMS) show that they are comparable, through reduction processes are more important for FAB. LMS always gave the intact cation while FAB was not consistent.

Key words: FAB mass spectrometry, phenanthroline complexes, bipyridine complexes, laser desorption mass spectrometry.

JACK M. MILLER et KESAGAPILLAI BALASANMUGAM. Can. J. Chem. **67**, 1496 (1989).

Faisant appel à la spectrométrie de masse par bombardement avec des atomes rapides (SM FAB), on a caractérisé une série de complexes métalliques de la 1,10-phénanthroline (phen), de la 5-nitro-1,10-phénanthroline (5-NO_2-phen), de la 2,9-diméthyl-1,10-phénanthroline (dmp), de la 2,2′-bipyridine (bpy) et de la 4,4′-diméthyl-2,2′-bipyridine (dmb). On observe des cations intacts dans les spectres de masse FAB de tous les complexes tétracoordonnés, $[Ag(L)_2]NO_3$, $[Cu(L)_2]_2SO_4{\cdot}5H_2O$, $[Cu(L)_2]SO_4$ et $[Tl(L)_2]$ (ClO_4) dans lesquels L = bpy, phen ou dmp. On observe aussi la formation d'ions de fragmentation qui sont significatifs d'un point de vue structural (ML_2^+, ML^+, M^+ et $(L + H)^+$ dans lesquels M^+ = ion métallique). On a aussi observé des espèces comme $Ag[Ag(L)_2]NO_3^+$ dans lesquelles L = bpy ou phen et $Tl[Tl(phen)_2]$ $(ClO4)^+$. Dans les spectres positifs des complexes hexacoordonnés $[Co(phen)_3]Cl_2$, $[Ru(bpy)Cl_2]$, $[Fe(phen)_2(CN)_2]$, $[Fe(L)_3](ClO_4)$, dans lesquels L = 5-NO_2-phen, dmb ou bpy, ainsi que $[Fe(L)_3]SO_4$, dans lesquels L = bpy ou phen, on observe des cations intacts; toutefois, dans les spectres des complexes $[Ni(bpy)_3]X_2$, dans lesquels X = Cl^-, Br^-, NO_3^-, ClO_4^-, SCN^- et tartrate^{2-}, et $[Co(bpy)_3](ClO_4)$, on n'observe pas ces cations. D'une façon générale, on observe les ions de fragmentation ML_3^+, ML_2X^+, ML_2^+, MLX^+ et $(L + H)^+$ dans lesquels X = un anion intact portant une seule charge ou HSO_4^-. Une comparaison des résultats obtenus en FAB avec ceux obtenus en spectrométrie du masse au laser (LMS) démontre qu'ils sont comparables, même si les processus de réduction sont plus importants en FAB. En LMS, on observe toujours un cation intact alors qu'en FAB les résultats ne sont pas consistants.

Most clés : spectroscopie de masse en FAB, complexes de la phénanthroline, complexes de la bipyridine, spectrométrie de masse par désorption au laser.

[Traduit par la revue]

Introduction

Mass spectrometry has been widely applied to the characterization of coordination compounds (1–6). The interest in coordination and related compounds stems from their use in the fields of catalysis (7–9), chemical analysis (7–9), medicine (10), and biological systems (11–14).

Characterization of coordination compounds by conventional mass spectrometry has been limited, (2, 15) because many of them are involatile and thermally labile, although even conventional positive ion electron impact (EI) mass spectrometry has yielded a significant body of useful information (1). However, the newer ionization techniques such as field desorption (FD) (3), fast atom bombardment (FAB) (4, 16, 17), secondary ion mass spectrometry (SIMS) (5, 18), and laser mass spectrometry (LMS) (6, 19), have been used successfully for the characterization of coordination compounds.

In the present work, FAB has been used to investigate a series of 2,2′-bipyridine (bpy), 1,10-phenanthroline (phen), 5-nitro-1,10-phenthroline (5-NO_2-phen), 2,9-dimethyl-1,10-phenanthroline (dmp), and 4,4′-dimethyl-2-2′-bipyridine (dmb) complexes; these complexes are listed in Table 1. Comparison of FAB mass spectral data with those of LMS, which have been previously reported, (6) is also discussed in the appropriate places.

Experimental

The coordination compounds: $[Fe(phen)_3](ClO_4)_2$, $[Fe(bpy)_3]SO_4$, $[Fe(dmb)](ClO_4)_2$, $[Fe(phen)_3]SO_4$, $[Fe(5\text{-}NO_2\text{-}phen)_3]SO_4$, $[Fe(phen)_2(CN)_2]$, $[Co(bpy)_3](ClO_4)_2$, and $[Ru(bpy)_3]Cl_2$ were purchased from G. Frederic Smith Chemical Co., and used without further purification. Other complexes given in Table 1 were synthesized using standard methods (6).

FAB mass spectra were obtained on a Kratos MS 30 mass spectrometer, retrofitted (20) with a Kratos FAB source in beam I and interfaced to a Kratos DS 55 data system. Argon was used as the bombarding gas with atom gun (Ion Tech) energies of 6–8 kV and a gun current of 1 mA. The operating pressure of the ion source was typically $\sim 10^{-5}$ Torr (1 Torr = 133.3 Pa), and the positive secondary ions formed were accelerated to 4 ke V. The source was operated at room temperature (although localized heating on the probe tip and source components in the direct atom beam occurs). The mass analyzer was operated at a nominal resolving power of 1000.

3-Nitrobenzyl alcohol (NBA) was used as the liquid matrix in this study. Samples (2–3 μL) dissolved in NBA (~15 mg / 1 mL) were placed on the stainless steel FAB probe tips for spectral acquisition. The results for each sample are from an average of 6–10 scans, and are reported after matrix background subtraction.

[1]Author to whom correspondence may be addressed.

Can. J. Chem. Downloaded from www.nrcresearchpress.com by 194.225.253.170 on 09/07/12
For personal use only.

Can. J. Chem. Downloaded from www.nrcresearchpress.com by 194.225.253.170 on 09/07/12
For personal use only.

TABLE 1. Positive ion FAB mass spectra of 2,2′-bipyridine and 1,10-phenanthroline complexes[a]

No.	Compound	ML_3^+	ML_2X^+	ML_2^+	MLX^+	ML^+	$(L + H)^+$	Other ions (mass, rel. intensity)
1	$[Ag(bpy)_2]NO_3$			(419,33)		(263,100)	(157,9)	Ag^+(107,12), $Ag[Ag(bpy)_2NO_3]^+$(590,3)
2	$[Ag(phen)_2]NO_3$			(467,46)		(287,100)	(181,9)	Ag^+(107,15), $Ag[Ag(phen)_2NO_3]^+$(638, <1) $[Ag(phen)][Ag(phen)_2NO_3]^+$(818, <1)
3	$[Cu(bpy)_2]SO_4$		(472,7)[b]	(375,39)	(316,14)	(219,100)	(157,17)	Cu^+(63,6)
4	$[Cu(phen)_2]_2SO_4 \cdot 5H_2O$			(423,26)		(243,100)	(181,4)	Cu^+(63,4)
5	$[Cu(dmp)_2]_2SO_4 \cdot 5H_2O$			(479,51)		(271,100)	(209,3)	Cu^+(63,46)
6	$[Tl(phen)_2](ClO_4)$			(565,8)		(385,100)	(181,85)	Tl^+(205,25) $Tl\{[Tl(phen)_2](ClO_4)\}^+$(869, <1)
7	$[Fe(phen)_2(CN)_2]$	(442,81)[c]	(416,42)	(262,100)	(236,17)	(181,29)		$[Fe(phen)_2(CN_2)]^{+\cdot}$(468,12), Fe^+(56,7) $[Fe(phen)_2(CN_2 + H)]$469,14)
8	$[Ru(bpy)_3]Cl_2$	(570,56)	(449,20)	(413,100)	(292,5)	(257,43)	(157,41)	ML_3X^+(605,12)
9	$[Fe(5\text{-}NO_2\text{-}Phen)_3](ClO_4)_2$	(731,4)	(605,79)	(506,24)		(281,10)	(226,11)	$FeL(OH)^+$(298,57) FeL_2O^+(522,9), Fe^+(56,8)
10	$[Fe(dmb)_3](ClO_4)_2$	(608,1)	(523,60)	(424,29)		(240,29)	(185,15)	$[FeL_2 - H]^+$(439,16), $[FeL_2(NBA) - H]^+$(576,2) $FeLO_2$ + (272,100), $Fe(H)L^+$(241,29) $FeLO^+$(256,38), $FeL(OH)^+$(257,46), Fe^+(56,9)
11	$[Fe(phen)_3]SO_4$	(596,4)	(513,32)[b]	(416,70)		(236,82)	(181,100)	$FeL(OH)^+$(253,83), $Fe(H)L^+$(237,61) $FeL_2(OH)^+$(433,10), Fe(56,10)$^+$
12	$[Fe(bpy)_3](ClO_4)_2$	(524,1)	(467,60)	(368,27)		(212,32)	(157,14)	$FeL(H)^+$(213,25), $FeLO^+$(228,44) $FeLO_2^+$(244,100), FeLOH$^+$(229,50) $[FeL_2O - H]^+$(383,17), FeL_2O^+(384,10), Fe^+(56,12)
13	$[Fe(bpy)_3]SO_4$	(524,6)	(465,45)[b]	(368)66	(109,9)	(212,38)	(157,21)	$[FeL_2(NBA) - H]^+$(520,8), Fe^+(56,11) $FeL(OH)^+$(229,100), $FeL(H)^+$(213,38) $FeLO^+$(228,62), $[FeL_2O - H]^+$(383,21)
14	$[Co(bpy)_3](ClO_4)_2$		(470,71)	(371,42)	(314,8)	(215,100)	(157,14)	$[CoL_2O - H]^+$(386,11), $CoL_2O^{\cdot}$(387,10) $CoLO^+$(231,30), $CoL(OH)^+$(232,27) $CoLO_2^+$(247,35), Co^+(59,13)
15	$[Co(phen)_3]Cl_2$	(599,2)	(454,23)	(419,56)	(274,33)	(239,100)	(181,17)	Co^+(59,7)
16	$[Ni(bpy)_3](ClO_4)_2$		(469,42)	(370,31)	(313,13)	(214,100)	(157,10)	$[NiL_2O - H]^+$(385,6), $[NiL_2(NBA) - H]^+$(522, <1) $[NiL_3X]^+$(625, <1) $NiLO^+$(230,18)Ni^+(58.3)
17	$[Ni(bpy)_3]Br_2$		(451,13)	(370,29)	(295,19)	(214,100)	(157,6)	$[NiL_2(NBA) - H]^+$(522, <1)
18	$[Ni(bpy)_3]I_2$		(497,16)	(370,39)	(341,12)	(214,100)	(157,5)	$[NiL_2(NBA) - H]^+$(522, <1)
19	$[Ni(bpy)_3](SCN)_2$		(428,25)	(370,44)	(272,13)	(214,100)	(157,8)	$[NiL_2(NBA) - H]^+$(522, <1) Ni^+(58,5)
20	$[Ni(bpy)_3](NO_3)_2$		(432,27)	(370,36)	(276,35)	(214,100)	(157,6)	$[NiL_2(NBA) - H]^+$(522, <1) $[NiL_2O - H]^+$(385,6) $NiLO^+$(230,13) Ni^+(58,9)
21	$[Ni(bpy)_3](TAT)$		(519,4)	(370,59)	(363,3)	(214,100)	(157,8)	$[NiL_2(NBA) - H]^+$(522,2), Ni^+(58,11)
22	$[Ni(bpy)_3]Cl_2$		(405,23)	(370,37)	(249,24)	(214,100)	(157,6)	$[NiL_2(NBA) - H]^+$(522, <1, Ni^+(58,6)

[a]Intensities are reported based on the most abundant isotope of each metal ion cluster.
[b]X = HSO_4.
[c]X = CN.

Can. J. Chem. Downloaded from www.nrcresearchpress.com by 194.225.253.170 on 09/07/12
For personal use only.

Results and discussion

Tetracoordinate complexes

A positive ion FAB mass spectrum of $[Ag(bpy)_2]NO_3$ is shown in Fig. 1 ($m/z > 100$); the results for this and other tetracoordinate complexes are summarized in Table 1. The formula weight of the intact cation can be deduced from ions corresponding to AgL_2^+ (Fig. 1). Fragment ions such as AgL^+, $(L + H)^+$, and Ag^+, along with the intact cation AgL_2^+, provide structural information, i.e., the number of ligands present and the formula weight of the ligand and of the metal ion. Thus, ions observed for these complexes are characteristic of the composition. The striking feature in the spectrum shown in Fig. 1 is the observation of an ion corresponding to $Ag{\cdot}Comp^+$, where Comp = $[Ag(bpy)_2]NO_3$. This ion was not reported in the studies using SIMS (5) and LMS (6) for the same compound. The above species, $Ag{\cdot}Comp^+$, can be used to infer the molecular weight of the neutral molecule $[Ag(bpy)_2]NO_3$. Thus, a formula including both the anion and the cation can be obtained for $[Ag(bpy)_2]NO_3$ using the positive ion FAB mass spectrum.

The positive ion FAB mass spectra of $[Ag(phen)_2]NO_3$ and $[Tl(phen)_2](ClO_4)$ are very similar to the spectrum of $[Ag(bpy)_2]NO_3$, i.e., ions corresponding to M^+, $(L + H)^+$, ML^+, ML_2^+, and $M{\cdot}Comp^+$ (where M = metal cation, L = phen, and Comp = molecular weight of the complex) are observed (Table 1). In the case of $[Ag(phen)_2]NO_3$ an additional ion corresponding to $Ag(phen)Comp^+$ (m/z = 818) is also observed. The observation of these species suggests that some of the ions may arise as a result of decomposition of cluster ions. The fragmentation observed for $[Cu(L)_2]_2SO_4{\cdot}5H_2O$ (where L = phen or dmp) is the same as reported above, ions corresponding to CuL_2^+, CuL^+, $(L + H)^+$, and Cu^+ being observed in both cases. Thus, the formula weight of the intact cation, CuL_2^+, the ligand, $(L + H)^+$, and the metal ion, Cu^+, can be deduced. Ions of the same kind, as described above, are detected for $[Cu(bpy)_2]SO_4$. In addition, species such as $CuL_n(HSO_4)^+$, where n = 1,2, are also observed. The latter ions are probably produced by proton addition during the FAB ionization processes. These ions along with CuL_2^+ and CuL^+ may be used to infer the anionic species present, i.e., SO_4^{-2}, in the molecule.

Laser mass spectra reported (6) for the same tetracoordinate complexes showed similar fragmentation patterns, i.e., ions corresponding to ML_2^+, ML^+, $(L + H)^+$, and M^+ are observed for all tetracoordinated complexes. In both LMS and FAB, the intensities of ML^+ ions are higher than those of ML_2^+, an observation consistent with the stability constants in solution for tetracoordinate complexes. For example, the stability contant, $\log k_1$, for $Cu(bpy)^{2+}$ formation is higher, 9.3 (20), than $\log k_2$, 6.84, for $Cu(bpy)_2^{2+}$ formation.

There are also some differences observed between the results obtained by LMS and FAB for tetracoordinate complexes. Generally, the extent of dissociation of the complexes seems to be higher in LMS than in FAB. For example, the relative intensities of AgL_2^+ and $(L + H)^+$ in the positive ion mass spectrum of $[Ag(bpy)_2]NO_3$ are 17 and 43% (6) respectively in LMS compared to 33 and 9% respectively in FAB (with respect to the same ion, AgL^+). The higher level of fragmentation in LMS may be attributed to the high laser power (10^8–10^9 W/cm^2) used with the laser beam focused on the sample. Results comparable to those observed in FAB with respect to the level of fragmentation may be obtained in LMS, if the laser beam used is defocused on the sample, as reported recently (22).

The other big difference is the absence of LMS of species such as $M{\cdot}Comp^+$ (where $M = Ag^+, Tl^+$) and other cluster ions

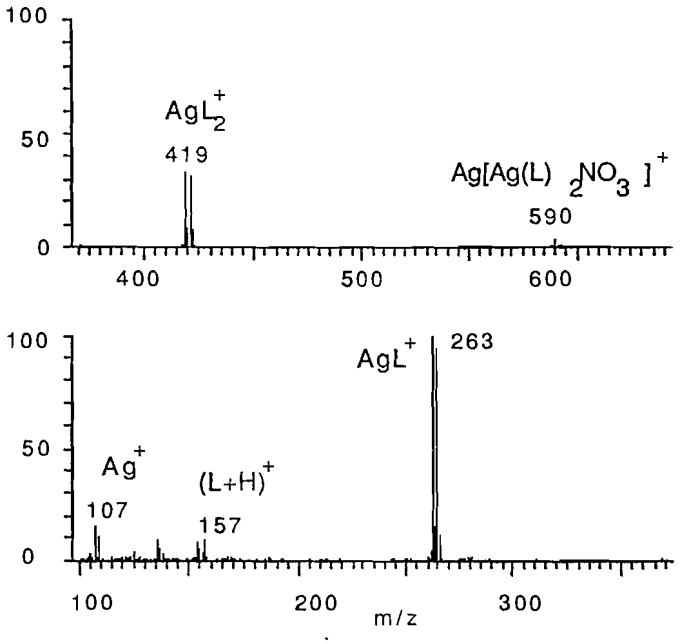


FIG. 1. Positive ion FAB mass spectrum of $[Ag(bpy)_2]NO_3$.

such as $Ag(phen)Comp^+$. Absence of cluster ions in LMS suggests that cluster ion formation may be favoured in a liquid matrix environment, or may occur in the high pressure "selvedge" region above the surface. A comparison study (23) using internal salts showed the same trend, i.e., a higher level of cluster ions in FAB than in LMS for internal salts.

The presence of ions corresponding to $CuL_n(HSO_4)^+$, where n = 1–2 for $[Cu(bpy)_2]SO_4$ only in FAB, not in LMS, may be attributed to the probable presence of protons in the protic liquid matrix, perhaps enhanced by radiation damage to the matrix.

Hexacoordinate complexes

The positive ion FAB mass spectra of $[Co(phen)_3]Cl_2$ and $[Fe(phen)_2(CN)_2]$ are shown in Fig. 2; the results of these two and other hexacoordinate complexes are summarized in Table 1. The highest mass ion detected for $[Co(phen)_3]Cl_2$ corresponds to the intact cation CoL_3^+. Ions corresponding to CoL_2^+, CoL^+, $(L + H)^+$, and Co^+ are also observed; these will provide information such as the number of ligands present and the formula weight of the ligand and the metal ion. Presence of the anion, Cl^-, may be deduced using ions corresponding to CoL_nCl^+, where n = 1–2.

Ions corresponding to $(Comp + H)^+$ and $Comp^{+\bullet}$ are observed in the positive ion FAB mass spectrum of $[Fe(phen)_2(CN)_2]$, where Comp = $[Fe(phen)_2(CN)_2]$. Detection of ions corresponding to FeL_2CN^+ and FeL_2^+ along with $FeL_2CN_2^{+\bullet}$ indicates that there are two cyanide groups present in the molecules, i.e., two successive losses of 26 mass units. The presence of two "phen" ligands can be deduced from the ions corresponding to Fe^+, $FeLCN^+$, and FeL_2CN^+ (Fig. 2a, Table 1). The results indicate that a fair amount of structural information can be obtained for hexacoordinate complexes from the positive ion FAB spectra.

Other hexacoordinate complexes give spectra very similar to those discussed above, and most of them show ions corresponding to ML_n^+, n = 1–3, ML_nX^+, n = 1–2, $(L + H)^+$, and M^+ in the positive ion FAB mass spectra. The absence of ions corresponding to ML_3^+ for nickel complexes and $[Co(bpy)_3](ClO_4)_2$ may be attributed to these complexes being weaker, decompos-

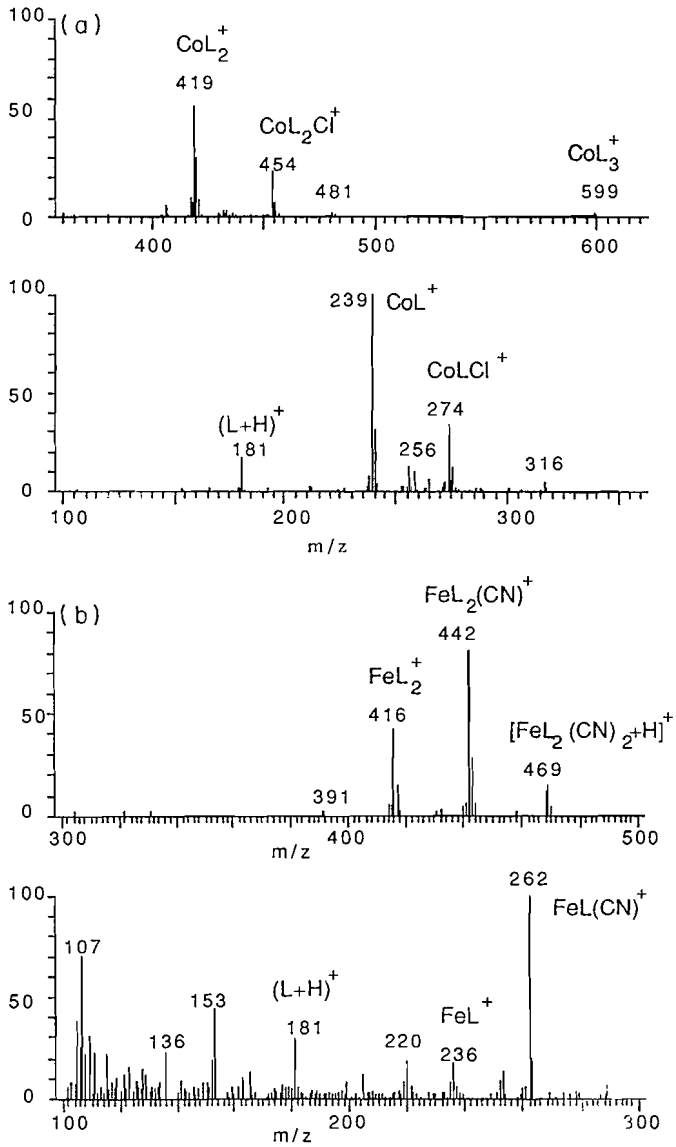


FIG. 2. (a) Positive ion FAB mass spectrum of $[Co(phen)_3]Cl$; (b) Positive ion FAB mass spectrum of $[Fe(phen)_2(CN)_2]$.

ing rapidly in the liquid matrix, NBA, during the ionization processes, leading to fragment ions only. Other liquid matrices such as glycerol, 1,1′-thiodiethanol, thioglycerol, and tetramethylene sulfolane were also tried for these complexes with little success in detecting intact cations.

Other ions of interest

Hydride anion addition leading to $FeL(H)^+$ ions is generally observed for iron complexes (Table 1). In some cases, ions corresponding to $ML(OH)^+$, where M = Fe, Co, are observed. As discussed earlier, radiation damaged liquid matrix may be responsible for production of these of ions.

Ions corresponding to $ML_mO_n^+$, m = 1–2, n = 1–2, are observed for some complexes (Table 1, Compounds **9–14**, **16**, **20**). These ions are very common when the intact anion is an oxidizing agent such as ClO_4^- or NO_3^- (Table 1). These types of ions were not observed for compounds such as $[Fe(phen)_2(CN)_2]$, $[Ru(bpy)_3]Cl_2$, $[Co(phen)_3]Cl_2$, and $[Ni(bpy)_3]X_2$, where X = Cl^-, Br^-, I^-, and SCN^-. These observations indicate that these oxygen-containing species are probably produced either by oxidation of the complexes by the oxidizing anions such as ClO_4^- or NO_3^-, or by internal decomposition of the complexes as suggested in LMS studies of the same complexes (6).

Laser mass spectra reported (6) for the same hexacoordinate complexes showed similar fragmentation patterns, i.e., ions corresponding to ML_3^+, ML_2X^+, ML_2^+, MLX^+, $(L + H)^+$, and M^+ are detected. As observed for tetracoordinate complexes, in both LMS and FAB the intensities of ions corresponding to ML^+, ML_2^+, and ML_3^+ decrease in the following order:

$$ML^+ > ML_2^+ > ML_3^+$$

This again agrees with individual stability constants from solution chemistry where stability constants generally decrease (21) as follows: $k_1 > k_2 > k_3$. For example, the stability constants log k_1, log k_2, and log k_3 for the formation of $Co(phen)^{2+}$, $Co(phen)_2^{2+}$, and $Co(phen)_3^{2+}$ are 7.25, 6.70, and 5.95 respectively (22). In both FAB and LMS, oxidized ionic species are observed for complexes having oxidizing anions such as ClO_4^-. The positive ion laser mass spectrum of $[Ni(bpy)_3](ClO_4)_2$ showed ions corresponding to NiL_3O^+ and $NiL_2O^{+\bullet}$; similar ions are observed for the same compound in FAB (Table 1). Molecular cluster ions were not observed either in LMS or FAB for hexacoordinate complexes.

Some of the differences observed between the results for hexacoordinate complexes using LMS and FAB are the same as discussed for tetracoordinate analogues. No reduced species such as $FeL(H)^+$ were observed in LMS and the degree of dissociation is relatively higher in the latter. This can be seen by the comparison of the intensities of $(L + H)^+$ ions, which vary from 30–90% in LMS and 5–41% in FAB (except for two cases). The other noticeable difference is the observation of NiL_3^+ ions for $[Ni(bpy)_3]X_2$, where X = Cl^-, Br^-, I^-, and SCN^-, only in LMS. The laser seems to heat the sample so fast that the intact ions are probably desorbed from the solid state to the gas phase before decomposition can occur. Interesting ions corresponding to $[ML_2(NBA - H)]^+$, where M = Fe or Ni, indicate the interaction of the liquid matrix with the sample in FAB.

Conclusions

Results discussed indicate that FAB has the potential for the characterization of coordination compounds. Comparison of the results obtained using FAB and LMS shows that the fragmentation patterns observed are similar for the same compounds. However, the reduction processes observed are limited in LMS compared to those in FAB. For this particular system, LMS seems to be slightly better than FAB, since we observed the intact cation for all compounds studied, using this technique. Except for the nickel complexes and $[Co(bpy)_3](ClO_4)_2$, all complexes show intact cations in the positive ion FAB. We observed structurally significant fragment ions for all complexes. Self-cationized species such as $Ag[Ag(bpy)_2]NO_3^+$ are also observed.

Acknowledgments

We thank the Natural Sciences and Engineering Research Council of Canada for operating and equipment grant support.

1. J. M. MILLER and G. L. WILSON. Adv. Inorg. Radiochem. **18**, 229 (1976).
2. K. M. INDRICHAN and N. V. GERBELEU. Zh. Neorg. Khim. **26**, 291 (1981); RUSS J. Inorg. Chem. **26**, 157 (1981).
3. D. E. GAMES, J. L. GOWER, and L. A. P. KANE-MAGUIRE. J. Chem. Soc. Chem. Commun. 757 (1978).

Can. J. Chem. Downloaded from www.nrcresearchpress.com by 194.225.253.170 on 09/07/12
For personal use only.

4. M. I. BRUCE and M. J. LIDDELL. Appl. Organomet. Chem. **1**, 191 (1987); J. M. MILLER. Adv. Inorg. Radiochem. **28**, 2 (1984).
5. J. L. PIERCE, K. J. BUSCH, R. G. COOKS, and R. A. WALTON. Inorg. Chem. **22**, 2492 (1983).
6. K. BALASANMUGAM, D. M. HERCULES, and R. J. DAY. Inorg. Chem. **24**, 4477 (1985).
7. A. A. SCHILT. Analytical applications of 1, 10-phenanthroline and related compounds. Pergamon Press, New York. 1969.
8. M. C. HUGHES and D. J. MACERO. Inorg. Chem. **15**, 2040 (1976).
9. D. L. KERPERT. Inorganic stereochemistry. Inorganic Chemistry Concepts. Vol. 6. Springer-Verlag, Berlin, Heidelberg. 1982.
10. A. I. COHEN, K. A. GLAVEN, and J. F. KRONAUGE. Biomed. Mass Spectrom. **10**, 287 (1983).
11. J. E. FALK. Porphyrins and metalloporphyrins. Elsevier, Amsterdam. 1975.
12. D. DOLPHIN. (*Editor*). The porphyrins. Vols. I–VII. Academic Press, New York. 1978.
13. D. DOLPHIN. (*Editor*). B_{12}. Wiley, New York. 1982.
14. B. D. BEREZIN. Coordination compounds of porphyrins and phthalocyanides. Wiley, Chichester. 1981.
15. K. W. GIVEN, B. M. MATTSON, G. L. MIESSLER, and L. H. PIGNOLET. J. Inorg. Nucl. Chem. **39**, 1309 (1977).
16. J. M. MILLER, K. BALASANMUGAM, J. NYE, G. B. DEACON, and N. C. THOMAS. Inorg. Chem. **26**, 560 (1989).
17. M. H. KOWALSKI, H. R. SHARP, and P. J. STANG. Org. Mass Spectrom. **22**, 642 (1987).
18. J. L. PIERCE, D. E. WIGLEY, and R. A. WALTON. Organometallics, **1**, 1328 (1982).
19. K. E. ROHLY, J. S. HEFFREN, and B. C. DOUGLAS. Org. Mass Spectrom. **19**, 398 (1984).
20. J. M. MILLER and A. FULCHER. Can. J. Chem. **63**, 2308 (1985).
21. L. G. SILLEN and A. E. MARTELL. Stability constant of metal–ion complexes. The Chemical Society. London. 1964.
22. Z. A. WILK, S. K. VISWANADHAM, A. G. SHARKEY, and D. M. HERCULES. Anal. Chem. **60**, 2338 (1988).
23. K. BALASANMUGAM, S. K. VISWANADHAM, D. M. HERCULES, R. J. COTTER, D. HELLER, A. BENNINGHOVEN, W. SICHTERMAN, V. ANDERS, T. KEOUGH, R. D. MACFARLANE, and C. J. MCNEAL. Appl. Spectrosc. **41**, 821 (1987).

Can. J. Chem. Downloaded from www.nrcresearchpress.com by 194.225.253.170 on 09/07/12
For personal use only.

^{125}Te and ^{19}F NMR spectroscopic study of the hydrolysis of pentafluorotellurium chloride: evidence for *trans*- and *cis*-$HOTeF_4Cl$ and *cis,mer*-$(HO)_2TeF_3Cl$

LAWRENCE J. LAWLOR, ALBAN MARTIN, MICHAEL P. MURCHIE, JACK PASSMORE,[1] AND JEREMY C. P. SANDERS
Department of Chemistry, University of New Brunswick, Bag Service No. 45222, Fredericton, N.B., Canada E3B 6E2

Received October 5, 1988[2]

LAWRENCE J. LAWLOR, ALBAN MARTIN, MICHAEL P. MURCHIE, JACK PASSMORE, and JEREMY C. P. SANDERS. Can. J. Chem. **67**, 1501 (1989).

The hydrolysis of TeF_5Cl has been followed by ^{125}Te and ^{19}F NMR spectroscopy. The spectra show that the known series $(HO)_nTeF_{6-n}$ (n = 2–6) are present. In addition the spectra are consistent with the presence of the previously unreported series $(HO)_nTeF_{5-n}Cl$ (n = 1–3) as well as unidentified fluorotellurium(IV) species. Evidence is presented for the new species *trans*- and *cis*-$HOTeF_4Cl$ and *cis, mer*-$(HO)_2TeF_3Cl$. The course of the hydrolysis of TeF_5Cl is compared with that of SF_5Cl.

Key words: *trans*-tetrafluorotellurium hydroxychloride, *cis*-tetrafluorotellurium hydroxychloride, *cis,mer*-tetrafluorotellurium dihydroxychloride, pentafluorotellurium chloride, hydrolysis.

LAWRENCE J. LAWLOR, ALBAN MARTIN, MICHAEL P. MURCHIE, JACK PASSMORE et JEREMY C. P. SANDERS. Can. J. Chem. **67**, 1501 (1989).

Faisant appel à la RMN du ^{125}Te et du ^{19}F, on a suivi l'évolution de la réaction d'hydrolyse du TeF_5Cl. Les spectres démontrent que les produits connus de la série $(OH)_nTeF_{6-n}$ (n = 2–6) sont présents. De plus, les spectres sont en accord avec la présence des produits de la série $(OH)_nTeF_{5-n}Cl$ (n = 1–3) qui n'avaient pas été rapportés antérieurement ainsi que d'espèces non-identifiées de fluorotellure(IV). On présente des données relatives aux nouvelles espèces *trans*- et *cis*-$HOTeF_4Cl$ ainsi que *cis,mer*-$(HO)_2TeF_4Cl$. On compare l'hydrolyse du TeF_5Cl avec celle du SF_5Cl.

Mots clés : *trans*- et *cis*-$HOTeF_4Cl$, *cis,mer*-$(HO)_2TeF_4Cl$, TeF_5Cl, hydrolyse.

[Traduit par la revue]

Introduction

It is well established that sulphur hexafluoride is chemically extremely inert (1), especially towards attack by nucleophiles, and that this low reactivity is mainly attributable to kinetic rather than thermodynamic factors. In contrast to this, the related pentafluorosulphur chloride is much more reactive and has an extensive chemistry (1–8). The Group 16 hexafluorides become more reactive as the group is descended and tellurium hexafluoride can form a number of derivatives by direct nucleophilic substitution (9, 10). For example, hydrolysis of TeF_6 yields the hydroxo-substituted series $TeF_n(OH)_{6-n}$, where n = 0–6 (11–14). This reaction has been studied in detail and all the species in the above series characterized by ^{125}Te and ^{19}F NMR spectroscopy (14–19).

The development of a convenient high-yield synthesis of pure pentafluorotellurium chloride in this laboratory has begun to allow an extensive exploration of its chemistry (20). The reactions of TeF_5Cl with a variety of reagents have been reported; the reaction of TeF_5Cl with CH_3OH or $CH_3OSi(CH_3)_3$ yields a mixture of *cis*- and *trans*-$(CH_3O)TeF_4Cl$ in a ratio of 1:6 (21). Thrasher and Seppelt have reported that TeF_5Cl can be added photolytically to nitriles, yielding the first compounds containing the $TeF_5N{=}C\diagdown$ moiety (22). Very recently, Thrasher *et al.* described the reactions of TeF_5Cl with a number of nitrogen nucleophiles; in all the case investigated, reduction to Te(IV) occurred (23). In view of the apparent reactivity of TeF_5Cl it was of interest to study its reaction with water and the results of this study are reported below.

Experimental

TeF_5Cl was prepared by the literature method (20) and its purity checked by infrared and ^{19}F NMR spectroscopy. H_2O was purified by triple distillation prior to use. TeF_5Cl was manipulated in a Monel vacuum line.

NMR samples were made up in either 1/4-in. FEP (polymerized CF_2CF_2 and CF_2CFCF_3, du Pont) tubes fitted with IKS4 Whitey valves or 10 mm o.d. thick-walled glass NMR tubes (Wilmad) containing a concentric 9 mm o.d. FEP insert tube. The 10 mm o.d. glass NMR tube was fitted with a J. Young (o-ringette PTFE stopcock) valve.

NMR spectra were recorded unlocked on a Varian XL-200 pulse FT spectrometer using a 10-mm broadband probe (frequency range 20–125 MHz) for ^{125}Te. The same probe was employed to record the ^{19}F NMR spectra by using the ^{1}H decoupler coils retuned to 188.220 MHz as the observe coils. ^{19}F NMR spectra were obtained at 188.220 MHz and accumulated in 30K of memory over a spectral width of 100 kHz, yielding a data point resolution of 6.7 Hz and an acquisition time of 0.15 s. The number of free induction decays collected varied but was typically 1000–3000 scans using a pulse width of 6 μs. The ^{125}Te spectra were obtained at 63.1940 MHz and accumulated in 32K of memory over spectral widths of 100 and 30 kHz (yielding data point resolutions of 6.3 and 1.9 Hz and acquisition times of 0.16 and 0.53 s, respectively) with a pulse width of 23 μs, in 600–2500 scans.

The respective nuclei were referenced externally to neat samples of $CFCl_3$ (^{19}F) and $(CH_3)_2Te$(^{125}Te) at 23°C. The chemical shift convention used is that a positive sign signifies a chemical shift to high frequency of the reference compound.

Hydrolysis of TeF_5Cl

Samples for direct study by NMR spectroscopy were made up with $TeClF_5$:H_2O ratios varying between 1:1 and 1:15. A known quantity of triply distilled water (0.07–3.45 g, 3.6–192 mmol, depending on the stoichiometry required) was weighed into the NMR tube. The tube was attached to the vacuum line and cooled to −78°C. The tube was then evacuated and the appropriate quantity of TeF_5Cl (0.94–3.48 g, 3.6–13.5 mmol, depending on stoichiometry required) distilled in. The mixture was then allowed to warm to room temperature. Samples contained in 1/4-in. FEP tubes were flame sealed whilst under vacuum with the sample frozen to −196°C. The FEP tube was inserted into a precision 10 mm (o.d.) glass NMR tube to obtain the NMR spectrum of the sample. NMR spectra of the samples were acquired after various time intervals at either 0°C or 25°C.

[1]Author to whom correspondence may be addressed.
[2]Revision received April 14, 1989.

Can. J. Chem. Downloaded from www.nrcresearchpress.com by 194.225.253.170 on 09/07/12
For personal use only.

Can. J. Chem. Downloaded from www.nrcresearchpress.com by 194.225.253.170 on 09/07/12
For personal use only.

TABLE 1. ^{19}F and ^{125}Te NMR data for species observed in the hydrolysis of TeF_5Cl

Species[a]	Spin system[b]	$\delta(^{19}F)$, ppm[c]	$^2J(F-F)$, Hz	$\delta(^{125}Te)$, ppm[d]	$^1J(^{125}Te-F)$, Hz
TeF_5Cl	$A_4B(X)$	−45.1(−45.1)[B]	170(AB)	592.0	3601(A)
		−6.1(−6.1)[A]			3444(B)
t-$HOTeF_4Cl$ **1***b*	$A_4(X)$	3.2(−0.6)		*e*	
c-$HOTeF_4Cl$ **1***a*	$A_2BC(X)$	−8.0(−0.6)[A]	138(AC)	*e*	
		−40.9(−39.6)[B]	143(BC)		
		11.4(4.8)[C]	168(AB)		
t-$(HO)_2TeF_4$	$A_4(X)$	−40.3(−43.5)		648.6	3464
c-$(HO)_2TeF_4$	$A_2C_2(X)$	−42.9(−43.5)[A]	152	650.6	3316(A)
		−33.9(−38.1)[C]			3247(C)
c,m-$(HO)_2TeF_3Cl$ **2***a*	$A_2C(X)$	19.2(10.3)[A]	146	688.0	3237(A)
		1.3(4.9)[C]			3157(C)
m-$(HO)_3TeF_3$	$A_2C(X)$	−38.3(−37.6)[A]	134	685.6	3224(A)
		−27.0(−31.6)[C]			3158(C)
m,c-$(HO)_3TeF_2Cl$ **3***a*	$BC(X)$	(−28.6)[B]?	169	*e*	
		19.0(15.8)[C][f]?			
f,c-$(HO)_3TeF_2Cl$ **3***b*	$C_2(X)$	21.5(15.8)[f]?		*e*	
t-$(HO)_4TeF_2$	$A_2(X)$	−35.5(−32.5)		710.0	2896
c-$(HO)_4TeF_2$	$C_2(X)$	−29.(−27.1)		705.3	2924
$(HO)_6Te$	(X)			707.0	
Te(IV)		−66.2 to −121.7		1130–1400	

[a] *t* = *trans*, *c* = *cis*, *m* = meridional, *f* = facial. Where a species formula is preceded by two letters, e.g., *c,m*-$(HO)_2TeF_3Cl$, the first letter refers to the stereochemical arrangement of the OH groups and the second to the stereochemical arrangement of the F ligands.

[b] A = F *trans* F, B = F *trans* Cl, C = F *trans* OH.

[c] $\delta(^{19}F)$ relative to neat $CFCl_3$. Dean and Evans calculated shifts in parentheses. Dean and Evans constants: $C = 48.4$ and $T = 9.4$ for Cl; $C = 5.5$ and $T = 10.9$ for OH.

[d] $\delta(^{125}Te)$ relative to neat $(CH_3)_2Te$.

[e] Species not observed in the ^{125}Te NMR spectrum.

[f] Tentative assignments only. The exact nature of the species giving rise to these resonances could not be ascertained.

Results and discussion

General procedures

The hydrolysis of TeF_5Cl was studied using a number of mixtures of TeF_5Cl and H_2O with different molar ratios, viz., $TeF_5Cl:H_2O$ = 1:1–1:15. Initially each sample comprised two liquid phases, the upper layer being the aqueous phase and the lower one being TeF_5Cl. However, samples with $TeF_5Cl:H_2O$ ratios greater than 1:8 formed a single liquid phase after approximately 12 h at room temperature, whereas samples having $TeF_5Cl:H_2O$ ratios of 1:4 or lower remained as two-phase systems for at least 2 days. Consequently, the NMR spectra of the latter samples were obtained on two-phase systems in the early stages of the hydrolysis reaction. Similar behaviour was observed in the hydrolysis of TeF_6 where a two-phase system was also formed when the TeF_6 and H_2O were first mixed (15). The products of the hydrolysis of TeF_5Cl were monitored and characterized by ^{19}F and ^{125}Te NMR spectroscopy. The NMR data obtained are summarized in Table 1. The data reveal the presence of the series $(HO)_nTeF_{6-n}$, where n = 2–6, and are also consistent with the presence of the series $(HO)_nTeF_{5-n}Cl$, where n = 1–3. In addition, both the ^{19}F and ^{125}Te NMR spectra display a broad singlet characteristic of fluorotellurium(IV) species undergoing exchange. The various species detected in two representative TeF_5Cl/H_2O samples, after various time periods, are presented in Table 2.

Identification of the hydrolysis products of TeF_5Cl by ^{19}F and ^{125}Te NMR spectroscopy: evidence for the previously unknown species trans- *and* cis-*$HOTeF_4Cl$, cis,mer-$(HO)_2TeF_3Cl$, and possibly* mer,cis- *and* fac,cis-*$(HO)_3TeF_2Cl$*

It has been demonstrated for a number of octahedral fluoro-species MX_nF_{6-n} (n = 1–6) that the ^{19}F chemical shifts of such species can be correlated in terms of a linear function. This function is given by eq. [1] where C and T are adjustable parameters

$$[1] \quad \delta(^{19}F) = pC + qT$$

characteristic of the substituent ligand (X), while p and q are the number of substituents (X) in a position *cis* and *trans*, respectively, to the fluorine ligand in question (p = 0–4; q = 0 or 1). This empirical method was first employed by Dean and Evans (24) to assign the ^{19}F NMR spectra of a range of fluorostannate(IV) species $(SnX_nF_{6-n})^{2-}$ where, for example, X = Cl, Br, I, OR, NCO, NCS, and N_3. Since then the same procedure has been successfully applied to a number of analogous systems, e.g., $(PtX_nF_{6-n})^{2-}$ (X = OH or Cl) (25), $(CH_3O)_nWF_{6-n}$ (26), WCl_nF_{6-n} (27), $[SbCl_nF_{6-n}]^-$, and $[AsCl_nF_{6-n}]^-$ (28).

The method may be extended to species having more than one type of substituent ligand (X) according to eq. [2].

$$[2] \quad \delta(^{19}F) = \sum_X p_X C_X + \sum_X q_X t_X$$

In the present work, the assignment of resonances arising from the $(HO)_nTeF_{6-n}$ species was carried out by comparison with the literature ^{19}F and ^{125}Te NMR data (chemical shifts, resonance multiplicities, and coupling constants) obtained for the species formed in the hydrolysis of TeF_6 (14, 15) and the solvolysis of $Te(OH)_6$ in HF (16). Elgad and Selig (14) found that the ^{19}F chemical shifts of the $(HO)_nTeF_{6-n}$ species could be satisfactorily reproduced using eq. [1], and our results (Table 1) are in accord with this finding.

The assignment of the ^{19}F resonances arising from the

TABLE 2. Species observed[a] in two representative TeF_5Cl/H_2O samples after various time periods[b]

Species	$TeF_5Cl:H_2O$ = 1:2						$TeF_5Cl:H_2O$ = 1:10		
	3 h	9 h	3 d	15 d	36 d	55 d	>1 m	6 h	5 d
TeF_5Cl	b	b	b	b			b		
t-$HOTeF_4Cl$ **1***b*				c	c				
c-$HOTeF_4Cl$ **1***a*				c	c	d			
t-$(HO)_2TeF_4$		c	c	c	c	c			
c-$(HO)_2TeF_4$		c	c	b	b	b	d	b	c
c,m-$(HO)_2TeF_3Cl$ **2***a*		c	c	b	b	b			
m-$(HO)_3TeF_3$	c	c	c	b	b	b		b	b
m,c-$(HO)_3TeF_2Cl$ **3***a*?				d	d	d			
f,c-$(HO)_3TeF_2Cl$ **3***b*?			d	d	d	d			
t-$(HO)_4TeF_2$								b	b
c-$(HO)_4TeF_2$									c
$(HO)_6Te$									c
Te(IV)	c	b	b	b	b	b		b	b

[a] b: Major product; c: Minor product; d: Trace amount.
[b] m = minute, h = hour, d = day.

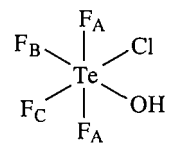
Can. J. Chem. Downloaded from www.nrcresearchpress.com by 194.225.253.170 on 09/07/12
For personal use only.

previously unobserved $(HO)_nTeF_{5-n}Cl$ species is based on the observed spin coupling patterns and ^{19}F chemical shift trends. In view of the proven usefulness of the Dean and Evans approach (eq. [2]), it was reasonable to use this method to calculate the expected ^{19}F chemical shifts for the $(HO)_nTeF_{6-n}Cl$ series. The values for the adjustable parameters (*C* and *T*) employed and the calculated $\delta(^{19}F)$ values are given in Table 1. The calculated $\delta(^{19}F)$ values predict that where more than one ^{19}F environment exists in the molecule the following trend will be observed: δ(F *trans* to OH) > δ(F *trans* to F) > δ(F *trans* to Cl). Although only fair agreement was found between the observed and calculated ^{19}F shifts, the predicted trends did hold good and were a useful aid in making assignments.

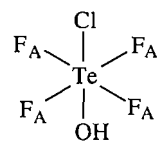
The ^{19}F NMR spectra provide evidence that the first products of the hydrolysis of TeF_5Cl are the new species *cis*-$HOTeF_4Cl$ **1***a* and *trans*-$HOTeF_4Cl$ **1***b*, as well as fluorotellurium(IV) reduction products. Evidence for the *trans* isomer comes from the observation of a singlet (A_4 spin system) at δ = 3.2 (calcd. value = −0.6). In the same spectrum three resonances with multiplet fine structure were also observed. These are in accord with the expected A_2BC system for *cis*-$HOTeF_4Cl$. The spin system was confirmed by computer simulation using the experimentally measured chemical shifts and coupling constants. In addition, the chemical shifts of the three fluorine environments are in quite good agreement with the trends predicted for *cis*-$HOTeF_4Cl$ by the Dean and Evans method (see Table 1).

Evidence for a new species with the formula $(HO)_2TeF_3Cl$ was provided by the observation of a doublet (δ = 19.2) and a triplet (δ = 1.3) in the ^{19}F NMR spectrum. Both resonances were flanked by ^{125}Te satellites. A corresponding doublet of triplets was observed in the ^{125}Te NMR spectrum. Three isomeric configurations are possible for $(HO)_2TeF_3Cl$: *cis,mer*-$(HO)_2TeF_3Cl$ **2***a*; *trans,mer*-$(HO)_2TeF_3Cl$ **2***b* and *cis,fac*-$(HO)_2TeF_3Cl$ **2***c*. However, only one of these appeared to be present in the samples investigated. All three isomers are expected to give rise to the same splitting patterns in the ^{19}F and ^{125}Te NMR spectra and consequently the splitting pattern does not afford a means of determining which isomer is present. In spite of this, the ^{19}F chemical shifts calculated by the Dean and Evans method provide some aid in this matter. The above method predicts different ^{19}F shifts for the fluorine environments depicted in the three isomeric structures **2***a*, **2***b*, and **2***c*: *cis, mer*- (δ_a = 4.9; δ_c = 10.3); *trans,mer*- (δ_a = 4.9; δ_b = −34.1); and *cis,fac*- (δ_b = −34.1; δ_c = 10.3). From these calculated values it can be seen that the closest agreement with the experimental shifts is for the *cis,mer* isomer. Furthermore, this is the only isomer for which the triplet resonance is predicted to occur to high frequency of the doublet resonance, in accord with the experimentally observed spectrum. In view of this, the isomer is tentatively assigned as *cis,mer*-$(HO)_2TeF_3Cl$.

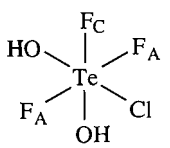
The ^{19}F NMR spectra of samples with a $TeF_5Cl:H_2O$ ratio of 1:2 reveal two other new resonances not previously reported. The species giving rise to these resonances are of very low concentration and their presence was only detected in the ^{19}F NMR spectrum. In view of the lack of other supportive evidence, only tentative assignments may be ventured for the identity of these species. The doublet at δ = 19 occurs close to the predicted ^{19}F chemical shift value (δ = 15.8) for the C part of the BC spin system belonging to *mer,cis*-$(HO)_3TeF_2Cl$ **3***a*.



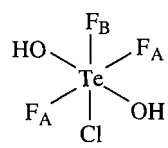
1*a*



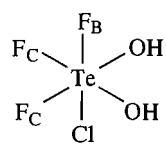
1*b*



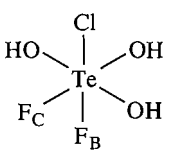
2*a*



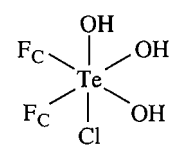
2*b*



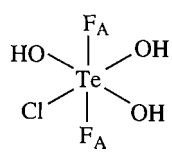
2*c*



3*a*



3*b*



3*c*

Can. J. Chem. Downloaded from www.nrcresearchpress.com by 194.225.253.170 on 09/07/12
For personal use only.

The corresponding doublet attributable to the B part of the BC spin system was not observed. The calculated shift for this resonance ($\delta = -28.6$) occurs in a congested region in the ^{19}F NMR spectrum of the TeF_5Cl hydrolysis system so that the resonance could be obscured. Two other isomers are possible for $(HO)_3TeF_2Cl$ (**3***b* and **3***c*); however, both isomers would only give rise to a singlet in the ^{19}F NMR spectrum. The singlet resonance observed at $\delta = 21.5$ could arise from *fac,cis*-$(HO)_3TeF_2Cl$ **3***b* (calcd. $\delta(^{19}F) = 15.8$) or *cis*$(HO)_4TeClF$ **4***a* (calcd. $\delta(^{19}F) = 21.3$). However, without other corroborative evidence, it is impossible to give an unequivocal assignment for this singlet.

The first hydrolysis products of TeF_5Cl: cis- *and* trans-*$HOTeF_4Cl$*

The species observed as the first hydrolysis products are *cis*- and *trans*-$HOTeF_4Cl$ **1***a*, **1***b*. The *cis:trans* ratio was approximately 4:1, which is in agreement with the predicted statistical ratio. In contrast, a very recent publication (29*a*) reports that the related phenyltellurium(VI) pentafluoride $PhTeF_5$ hydrolyses to *cis*- and *trans*-$PhTeF_4OH$, with an isomer ratio of 1:3. None of the spectra in this work revealed any evidence for $HOTeF_5$. Formation of $HOTeF_5$ from TeF_5Cl would involve hydrolysis with loss of HCl rather than HF. However, the formation of HF rather than HCl is thermodynamically favored since the bond energy difference between HF (565 kJ mol^{-1}) (28) and HCl (428 kJ mol^{-1}) (29*b*) can be anticipated to be greater than the bond energy difference between a Te—F bond and a Te—Cl bond in TeF_5Cl. *cis*- and *trans*-$HOTeF_4Cl$ were only observed in samples with TeF_5Cl:H_2O ratios less than 1:3.5 and even at these ratios their concentrations were very low compared with other hydrolysis products, e.g. *cis*- and *trans*-$(HO)_2TeF_4$ and *mer*-$(HO)_3TeF_3$. This indicates that the hydrolysis of *cis*- and *trans*-$HOTeF_4Cl$ **1***a* and **1***b* is rapid in the presence of excess water. In contrast, the related TeF_5OCH_3 hydrolyses exclusively to *cis*-$HOTeF_4OCH_3$ and this, in turn, only hydrolyses further after several hours at 60°C (30).

The hydrolysis of cis- *and* trans-*$HOTeF_4Cl$ leading to* cis- *and* trans-*$(HO)_2TeF_4$ and* cis,mer-*$(HO)_2TeF_3Cl$*

The products observed in the second stage of the hydrolysis of TeF_5Cl are *cis*- and *trans*-$(HO)_2TeF_4$ and the previously unknown species *cis,mer*-$(HO)_2TeF_3Cl$ **2***a*. *cis*-$(HO)_2TeF_4$ was observed in all the stoichiometries investigated and showed little change in intensity with time. This is in agreement with Tötsch and Sladky's (15, 18) finding that *cis*-$(HO)_2TeF_4$ hydrolyses very slowly over a period of several days at room temperature. *trans*-$(HO)_2TeF_4$ was observed in the spectra of all samples except those with TeF_5Cl:H_2O ratios greater than 1:10. The concentration of this species rapidly diminished in samples where excess H_2O was present, e.g., TeF_5Cl:$H_2O \geqq$ 1:8.5, in accordance with the rapid hydrolysis behaviour noted for this isomer by Tötsch and Sladky (15, 18). There are three possible isomers for $(HO)_2TeF_3Cl$: *cis,mer*-$(HO)_2TeF_3Cl$ **2***a*; *trans,mer*-$(HO)_2TeF_3Cl$ **2***b*; and *cis,fac*-$(HO)_2TeF_3Cl$ **2***c*. All three isomers can, in theory, arise from the hydrolysis of *cis*-$HOTeF_4Cl$ **1***a*, whereas only *cis,mer*-$(HO)_2TeF_3Cl$ **2***a* can arise from the hydrolysis of *trans*-$HOTeF_4Cl$ **1***b*. In all the samples investigated, evidence was only found for the *cis,mer* isomer. This was observed at all ratios of TeF_5Cl:H_2O except those $\geqq$1:8.5. Interestingly, where it was present, its intensity diminished little with time, indicating that, like the related *cis*-$(HO)_2TeF_4$, hydrolysis of this species is rather slow. Although only the *cis,mer* isomer of $(HO)_2TeF_3Cl$ **2***a* is observed, it is possible that the other two isomers (**2***b* and **2***c*) of this species are also formed, but that they are not observable because their rates of hydrolysis are faster than their rates of formation.

It is interesting that at the second stage of the hydrolysis of TeF_5Cl, products both containing, and not containing, chlorine are produced. The loss of HCl to form the hydroxofluoro species may arise for two reasons: (*i*) the replacement of fluorine ligands by OH ligands may result in an increased weakening of the Te—Cl bond; (*ii*) the Gibbs free energy of hydration is greater for HCl (35.9 kJ mol^{-1}) (31) than for HF (5.6 kJ mol^{-1}) (31). The combination of both factors could favour HCl elimination.

The third stage hydrolysis products of TeF_5Cl: mer-*$(HO)_3TeF_3$,* mer,cis-*$(HO)_3TeF_2Cl$, and* fac,cis-*$(HO)_3TeF_2Cl$*

The third hydrolysis step gives *mer*-$(HO)_3TeF_3$ as the major product. This species was observed in the NMR spectra of all TeF_5Cl:H_2O ratios and its intensity varied little with time. Tötsch and Sladky have shown that *trans*-$(HO)_2TeF_4$ hydrolyses stereospecifically to *mer*-$(HO)_3TeF_3$, whereas *cis*-$(HO)_2TeF_4$ hydrolyses to both *mer*- and *fac*-$(HO)_3TeF_3$ in the ratio 3:1 (18). The *fac*- isomer was not clearly identified in any of the spectra obtained in the present study, although a weak singlet observed at $\delta = -30$ in the ^{19}F NMR spectrum may be attributable to this isomer (lit. (15) δ value = -28).

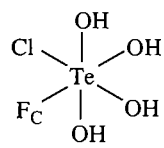
Two new resonances were observed in the ^{19}F NMR spectra of samples with a TeF_5Cl:H_2O ratio of 1:2. As discussed previously in the identification section, these resonances have been tentatively assigned to *mer,cis*-$(HO)_3TeF_2Cl$ and *fac,cis*-$(HO)_3TeF_2Cl$. Unfortunately, the lack of corroborative data to support these assignments makes further discussion of these species inappropriate.

The fourth, fifth, and sixth hydrolysis products of TeF_5Cl

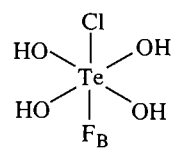
In samples containing a large stoichiometric excess of water, i.e., TeF_5Cl:$H_2O \geqq$ 1:15, the more highly substituted species *cis*- and *trans*-$(HO)_4TeF_2$ were the dominant products (excluding Te(IV) fluoro species) after 4 days of reaction. The ^{19}F and ^{125}Te NMR data obtained for these species are in good agreement with the literature values (15). The ^{125}Te NMR spectrum showed, in addition to the resonances arising from *cis*- and *trans*-$(Ho)_4TeF_2$, a weak singlet at $\delta = 707.2$, which is attributed to $(HO)_6Te$. $(HO)_5TeF$ was not observed; this is not unexpected since it is reported that this species hydrolyses rapidly and readily dismutates into *cis*-$(HO)_4TeF_2$ and $(HO)_6Te$ (15, 16).

cis- and *trans*-$(HO)_4TeFCl$ **4***a* and **4***b* and $(HO)_5TeCl$ are also possible products. However, none of these species was observed in the NMR spectra obtained for samples with TeF_5Cl:H_2O $\geqq$ 1:15. A very weak singlet was observed at $\delta = 21.5$ in the ^{19}F NMR spectrum of the TeF_5Cl:H_2O = 1:1 sample. As previously indicated in the identification section, this resonance might be attributable to *cis*-$(HO)_4TeFCl$ or *fac,cis*-$(HO)_3TeF_2Cl$. However, the precise nature of the species giving rise to this singlet resonance remains undetermined.

In view of the hydrolytic instability of $(HO)_5TeF$, it seems likely that $(HO)_4TeFCl$ and $(HO)_5TeCl$ would also rapidly hydrolyse. It is also possible that these species are never formed



4*a*



4*b*

and that the hydrolysis pathway only proceeds through *cis*- and *trans*-$(HO)_4TeF_2$.

Formation of fluorotellurium(IV) species

In all the samples investigated, both the ^{19}F and ^{125}Te NMR spectra displayed a broad unresolved resonance that could be attributed to fluorotellurium(IV) species (Table 1). No ^{125}Te-^{19}F spin–spin coupling was resolved, which is indicative of intermolecular fluorine exchange. Such exchange has previously been observed in other fluorotellurium(IV) species, e.g., TeF_4 (32) and TeF_5^- (33). The ratio of Te(IV) to Te(VI) species varied somewhat from reaction to reaction, although the ratio was approximately 1:1 in most cases. The formation of Te(IV) species has been reported previously in the reactions of TeF_5Cl with other nucleophiles (21, 23). The reaction of TeF_5Cl with CsF yields ClF and $CsTeF_5$ but not Te(VI) species (21). The suggested pathway for this reaction is attack by F^- on the partially positively charged chlorine ligand of TeF_5Cl (eq. [3]):

$$[3]\quad F^- + \overset{\delta^+}{Cl}\text{—}\overset{\delta^-}{TeF_5} \longrightarrow FCl + TeF_5^-$$

This pathway was first invoked to explain the attack of the hydroxyl ion on SF_5Cl, which also only yields reduced species (3).

Alternatively, TeF_5Cl may expand its coordination sphere to give a 7-coordinate intermediate (34). This intermediate can then undergo two elimination processes: in one case HF could eliminate with the formation of a Te(VI) species; in the other case ClF or HOCl could be eliminated, in addition to HF, giving rise to a Te(VI) species (eq. [4]).

$$[4]\quad H_2O + TeF_5Cl \text{——} \text{“}H_2OTeF_5Cl\text{”} \text{——} \text{Te(VI)} + \text{Te(IV) products}$$

This mechanism would therefore account for the observation of both Te(VI) and Te(IV) species as the hydrolysis products of TeF_5Cl. It could also account for both the Te(VI) and Te(IV) products in the reactions of CH_3OH and $(CH_3)_3SiOCH_3$ with TeF_5Cl. Further hydrolysis of $HOTeF_4Cl$ could proceed in the same manner, with the likelihood of HCl elimination becoming more thermodynamically favourable with the increased weakening of the Te—Cl bond as the number of F ligands substituted by OH ligands increases.

Comparison of the hydrolysis behaviour of TeF_5Cl and SF_5Cl

The hydrolysis behaviour of TeF_5Cl differs considerably from that of SF_5Cl. In the latter case, hydrolysis only occurs in the presence of alkali and leads only to S(IV) products (3). In contrast, hydrolysis of TeF_5Cl yields both Te(VI) and Te(IV) species, which can be attributed to the ability of tellurium to expand its coordination sphere to accommodate more than 6 ligands. The hydrolysis behaviour of SeF_5Cl appears to be as yet uninvestigated, although it may be anticipated that it will resemble that of SF_5Cl rather than TeF_5Cl.

Acknowledgements

We thank L. Calhoun for assistance with the ^{125}Te and ^{19}F NMR spectroscopy and the National Sciences and Engineering Research Council of Canada for financial support and a postgraduate scholarship (L.J.L.).

1. F. A. COTTON, and G. WILKINSON. Advanced inorganic chemistry. 4th ed. Wiley, New York, 1980. p. 521.
2. M. SCHMIDT, W. SIEBERT, and K. W. BAGNALL. *In* Comprehensive inorganic chemistry. Vol. 2. Pergamon Press, New York. 1973. pp. 795, 935.
3. H. L. ROBERTS. Q. Rev. **15**, 30 (1961).
4. B. COHEN and A. G. MACDIARMID. J. Chem. Soc. A. 1780 (1966).
5. R. D. DRESDNER and T. R. HOOPER. *In* Fluorine chemistry reviews. Vol. 4. Marcel Dekker, New York. 1969. p. 1.
6. F. SEEL. *In* Sulphur in organic and inorganic chemistry. Vol. 2. Marcel Dekker, New York. 1972. p. 201.
7. T. KITAZUME and J. M. SHREEVE. J. Am. Chem. Soc. **99**, 3690 (1977).
8. G. KLEEMAN and K. SEPPELT. Angew. Chem. Int. Ed. Engl. **17**, 516 (1978).
9. K. SEPPELT. Inorg. Chem. **12**, 2837 (1973); G. W. FRASER, R. D. PEACOCK, and P. M. WATKINS. J. Chem. Soc. A. 1125 (1971).
10. G. W. FRASER and J. B. MILLAR. J. Chem. Soc. Dalton Trans. 2029 (1974).
11. E. B. R. PRIDEAUX. J. Chem. Soc. **89**, 322 (1906).
12. A. ENGELBRECHT and F. SLADKY. Monatsh. Chem. **96**, 159 (1965).
13. G. W. FRASER and G. D. MEIKLE. J. Chem. Soc. Chem. Commun. 624 (1974).
14. U. ELGAD and H. SELIG. Inorg. Chem. **14**, 140 (1975).
15. W. TOTSCH and F. SLADKY. Z. Naturforsch. **386**, 1025 (1983).
16. W. TOTSCH, P. PERINGER, and F. SLADKY. J. Chem. Soc. Chem. Commun. 841 (1981).
17. W. TOTSCH and F. SLADKY. J. Chem. Soc. Chem. Commun. 927 (1980).
18. W. TOTSCH and F. SLADKY. Chem. Ber. **115**, 1019 (1982).
19. B. POTTER, D. LENTZ, H. PRITZKOW, and K. SEPPELT. Angew. Chem. Int. Ed. Engl. **20**, 1036 (1981).
20. M. MURCHIE and J. PASSMORE. Inorg. Synth. **24**, 31 (1986); C. LAU and J. PASSMORE. Inorg. Chem. **13**, 2278 (1974).
21. L. J. LAWLOR and J. PASSMORE. Can. J. Chem. **62**, 1477 (1984).
22. J. S. THRASHER and K. SEPPELT. Angew. Chem. Int. Ed. Engl. **22**, 789 (1983); Angew. Chem. Suppl. 1106 (1983); Inorg. Chem. **24**, 4171 (1985).
23. J. S. THRASHER, M. CLARK, and P. A. MORKEN. J. Fluorine Chem. **39**, 235 (1988).
24. P. A. W. DEAN and D. F. EVANS. J. Chem. Soc. A, 1154 (1968).
25. D. F. EVANS and G. K. TURNER. J. Chem. Soc. Dalton Trans. 1238 (1975).
26. W. MCFARLANE, A. M. NOBLE, and J. M. WINFIELD. J. Chem. Soc. A, 948 (1971).
27. G. W. FRASER, C. J. W. GIBBS, and R. D. PEACOCK. J. Chem. Soc. A, 1708 (1970).
28. M. F. A. DOVE, J. C. P. SANDERS, E. LLOYD JONES, and M. J. PARKIN. J. Chem. Soc. Chem. Commun. 1578 (1984).
29. (*a*) A. F. JANZEN, K. ALAM, M. JANG, B. J. BLACKBURN, and A. S. SECCO. Can. J. Chem. **66**, 1308 (1988); (*b*) J. E. HUHEEY. Inorganic chemistry. 2nd ed. Harper and Row, New York. 1978. pp. 839–851.
30. W. TOTSCH, B. MAICHEL, H. AICHINGER, and F. SLADKY. Rev. Chim. Miner. **23**, 391 (1986).
31. M. C. BELL. Physical data for inorganic chemists. Longman, London. 1974.
32. E. L. MUETTERTIES and W. D. PHILLIPS. J. Am. Chem. Soc. **81**, 1084 (1959); T. BIRCHALL, R. D. MYERS, H. DE WAARD, and G. J. SCHROBILGEN. Inorg. Chem. **21**, 1068 (1982).
33. L. B. ASPREY and N. A. MATWIYOTT, J. Inorg. Nucl. Chem. H. H. Hyman Memorial Volume, 123 (1976); R. J. MORRIS and K. C. MOSS. J. Fluorine Chem. **13**, 551 (1979).
34. L. LAWLOR. Ph.D. Thesis, University of New Brunswick, Fredericton. 1980.

Can. J. Chem. Downloaded from www.nrcresearchpress.com by 194.225.253.170 on 09/07/12
For personal use only.

Liquid junction potentials in molten salt cells

PETER J. TUMIDAJSKI

Department of Materials Engineering, The University of Western Ontario, London, Ont., Canada N6A 5B9

Received April 5, 1989

PETER J. TUMIDAJSKI. Can. J. Chem. **67**, 1506 (1989).

Liquid junction potentials were determined for fused salt concentration and galvanic cells. The results indicated that such potentials can be significant when concentration differences are large. For dilute solutions, the liquid junction potentials are within experimental uncertainty.

Key words: liquid junctions, thermodynamics, galvanic cells.

PETER J. TUMIDAJSKI. Can. J. Chem. **67**, 1506 (1989).

On a déterminé les potentiels de la jonction liquide pour diverses concentrations de sels fondus et diverses cellules galvaniques. Les résultats indiquent que de tels potentiels peuvent être importants lorsque les différences des concentrations sont grandes. Pour des solutions diluées, les potentiels de la jonction liquide sont inférieurs aux limites expérimentales.

Mots clés : jonctions liquides, thermodynamique, cellules galvaniques.

[Traduit par la revue]

Can. J. Chem. Downloaded from www.nrcresearchpress.com by 194.225.253.170 on 09/07/12
For personal use only.

Introduction

In a recent paper (1), the thermodynamic behaviour of reactive metal chlorides in alkali chlorides was determined using cells of this type,

$$(-)\text{M}|\text{MCl}_m\text{–ACl}\|\text{asbestos diaphragm}\|\text{AgCl–ACl}|\text{Ag}(+)$$

Because of compositional differences at the steady state condition, a potential across the asbestos diaphragm develops. This potential is called the liquid junction potential. It has been generally assumed that an excess of alkali chloride on both sides of the asbestos diaphragm minimizes the liquid junction potential. However, very little fundamental work has been done to definitely determine when these potentials become significant, especially for galvanic cells. Laity (2), Blander (3), and Klemm (4) assessed the magnitudes of the liquid junction potentials for a number of molten salt solutions. However, the precise calculations of the liquid junctions is handicapped by the paucity of reliable data on transport numbers and activity coefficients of ions through the contact zone. In addition, the physical construction of the junction is important. In a paper by Wagner (5), an experimental technique was described wherein liquid junction potentials could be measured directly without neglect or hypothesis using chloride formation cells in series. To the author's knowledge, this paper represents the first attempt to determine how concentration and temperature influence the magnitude of the liquid junction potential using chloride formation cells in series.

Experimental

Liquid junction potentials were determined for fused salt concentration and galvanic cells. The variables investigated were concentration and temperature.

To determine the liquid junction potential of a concentration cell, the AgCl–KCl system was used. The liquid junction potential is given by,

[1] $$E_j = E_A - E_B$$

where E_A corresponds to the potential of the concentration cell,

$$(-)\text{Ag}|\text{AgCl}(X_1)\text{–KCl}\|\text{asbestos diaphragm}\|\text{AgCl}(X_2)\text{– KCl}|\text{Ag}(+) \quad \text{(Cell A)}$$

and E_B corresponds to the potential of two formation cells connected in series,

$$(-)\text{Ag}|\text{AgCl}(X_1)\text{–KCl}|\text{Cl}_2,\text{C}\ldots\text{C},\text{Cl}_2|\text{AgCl}(X_2)\text{–KCl}|\text{Ag}(+) \quad \text{(Cell B)}$$

For both cases, X_2 is greater than X_1.

To study the liquid junction potential in galvanic cells, the ($PbCl_2$–KCl)–(AgCl–KCl) system was employed. The liquid junction potential is calculated from

[2] $$E_j = E_C - E_D$$

E_C corresponds to the potential of the galvanic cells.

$$(-)\text{Pb}|\text{PbCl}_2\text{–KCl}\|\text{asbestos diaphragm}\|\text{AgCl– KCl}|\text{Ag}(+) \quad \text{(Cell C)}$$

E_D corresponds to the potential of two chloride formation cells connected in series,

$$(-)\text{Pb}|\text{PbCl}_2\text{–KCl}|\text{Cl}_2,\text{C}\ldots\text{C},\text{Cl}_2|\text{AgCl–KCl}|\text{Ag}(+) \quad \text{(Cell D)}$$

Results and discussion

Results of the AgCl–KCl concentration cell are given in Table 1 for 973 and 1023 K. It can be seen that the junction potentials become an appreciable contribution to the total cell potential as the concentration difference across the asbestos diaphragm becomes larger. For the larger concentration differences, the magnitude of the liquid junction potential can attain values corresponding to greater than 20% of the total cell potential. In the early work of two decades ago, liquid junction potentials were of the order of several millivolts, which did not exceed the experimental errors. Murgulescu and Popescu (6) carefully measured the free liquid junction potentials with a capillary between the electrode compartments. In agreement with the present results, they found that the free junction potentials were significant and could not be assumed to be within the experimental error over the whole concentration range. An expression for the liquid junction potential for the AgCl–KCl system, with the chloride anion as the reference component, can be derived (7),

[3] $$E_j = \frac{RT}{F}\int\left(\frac{X_{KCl}t_{Ag^+} - X_{AgCl}t_{K^+}}{X_{KCl}}\right) d\ln a_{AgCl}$$

where t represents transport numbers. It is clear from eq. [3] that the liquid junction potential approaches negligible values when

TABLE 1. Junction potentials for the AgCl concentration cell

		700°C (973 K) (V)			750°C (1023 K) (V)		
X_{AgCl}	X'_{AgCl}	E_A	E_B	E_j	E_A	E_B	E_j
1.0	0.8	0.019	0.022	−0.003	0.020	0.023	−0.003
	0.6	0.049	0.055	−0.006	0.054	0.057	−0.003
	0.4	0.098	0.103	−0.005	0.102	0.107	−0.005
	0.2	0.161	0.178	−0.017	0.175	0.185	−0.010
0.8	0.6	0.033	0.033	0	0.035	0.034	+0.001
	0.4	0.077	0.081	−0.004	0.080	0.084	−0.004
	0.2	0.122	0.156	−0.034	0.138	0.162	−0.024
0.6	0.4	0.052	0.048	+0.004	0.055	0.050	+0.005
	0.2	0.117	0.123	−0.006	0.123	0.128	−0.005
0.4	0.2	0.089	0.075	+0.014	0.090	0.078	+0.012

TABLE 2. Junction potentials for the AgCl–$PbCl_2$ galvanic cell

		700°C (973 K) (V)			750°C (1023 K) (V)		
X_{AgCl}	X_{PbCl_2}	E_C	E_D	E_j	E_C	E_D	E_j
1.0	1.0	0.831	0.287	0.544	0.750	0.272	0.478
	0.8	0.427	0.301	0.126	0.377	0.281	0.096
	0.6	0.423	0.342	0.081	0.376	0.319	0.057
	0.4	0.379	0.393	−0.014	0.367	0.376	−0.009
	0.2	0.459	0.450	0.009	0.471	0.408	0.063
0.8	1.0	0.814	0.265	0.549	0.730	0.249	0.481
	0.8	0.406	0.279	0.127	0.352	0.258	0.094
	0.6	0.401	0.320	0.081	0.354	0.296	0.058
	0.4	0.357	0.371	−0.014	0.344	0.353	−0.009
	0.2	0.436	0.428	0.008	0.449	0.385	0.064
0.6	1.0	0.774	0.232	0.542	0.686	0.215	0.471
	0.8	0.362	0.246	0.116	0.302	0.224	0.078
	0.6	0.359	0.287	0.072	0.309	0.262	0.047
	0.4	0.313	0.338	−0.025	0.299	0.319	−0.020
	0.2	0.392	0.395	−0.003	0.403	0.351	0.052
0.4	1.0	0.740	0.184	0.556	0.639	0.165	0.474
	0.8	0.313	0.198	0.115	0.247	0.174	0.073
	0.6	0.309	0.239	0.070	0.257	0.212	0.045
	0.4	0.267	0.290	−0.023	0.253	0.269	−0.016
	0.2	0.349	0.347	0.002	0.356	0.301	0.055
0.2	1.0	0.671	0.109	0.562	0.574	0.087	0.487
	0.8	0.241	0.123	0.118	0.175	0.096	0.079
	0.6	0.244	0.164	0.080	0.189	0.134	0.055
	0.4	0.193	0.215	−0.022	0.174	0.191	−0.017
	0.2	0.281	0.272	0.009	0.285	0.223	0.062

the cation transport numbers are proportional to their mole fractions. Conradt and co-workers (8) found that none of the AgCl – alkali chloride mixtures satisfy this criteria over the entire composition range. Hence there could be a significant liquid junction potential. Furthermore, Smirnov *et al.* (9) measured the liquid junction potentials at the porous asbestos diaphragms separating alkali chloride melts of different cation compositions. It was found that cation transport numbers undergo a considerable variance with compositional changes.

In addition, Murgulescu and Popescu (6) reported that the magnitude of the diffusion potentials increases with temperature. The results of this study contradict their conclusion. Albeit liquid junction potentials were determined at two temperatures over a narrow interval, we observed a slight but discernable decrease in the magnitude of the liquid junction potential at the higher temperatures. Intuitively, this would be expected because fused salt solutions tend to become ideal as temperature is increased.

Results for the (AgCl–KCl)–($PbCl_2$–KCl) galvanic cell are given in Table 2 for 973 and 1023 K. It can be seen that there can be an appreciable junction potential especially for the more concentrated $PbCl_2$ solutions. When pure liquid $PbCl_2$ is pres-

Can. J. Chem. Downloaded from www.nrcresearchpress.com by 194.225.253.170 on 09/07/12
For personal use only.

ent, there is an approximately constant value of 550 mV for the liquid junction potential regardless of the AgCl concentration in the other electrode compartment. In fact, this is a general trend. That is, it is the concentration of $PbCl_2$, and consequently, the concentration of Pb^{2+} cation, which largely determines the magnitude of the liquid junction potential. The Ag^+ cation concentration appears to have little influence on the junction potential. It is the mobility (or transport number) of the cations through the contact zone (asbestos diaphragm) which is a major contribution to the magnitude of the liquid junction potential. There are several factors which determine ionic mobilities. For the present case, it is likely that the mass and valence differences for the silver and lead cations account for the major portion of the mobility differences between the silver and lead cations. It is these effects which are observed in the present investigation and predominate in the measurement of the liquid junction. It is also worth noting that the forces developed in an electronuetrality field in the contact zone between different solutions are greater when the valence of the competing species is higher, and when the charge density is larger. A full interpretation of the liquid junction potential is not possible because the concentration and transport numbers of all species throughout the liquid junction zone are not known.

It should be emphasized that, for both cells investigated, the liquid junction potentials for dilute solutions are small and within the limits of experimental uncertainty. The result is significant because the thermodynamic results presented previously (1), can be regarded to be free of a liquid junction contribution.

1. P. J. TUMIDAJSKI and S. N. FLENGAS. Proceedings of the Fifth International Symposium on Molten Salts. *Edited by* M. L. Saboungi, K. Johnson, D. S. Newman, and D. Inman. The electrochemical Society, New Jersey, 1986. pp. 551–575.
2. R. W. LAITY. Reference electrodes, theory and practice. *Edited by* D. J. G. Ives and G. J. Janz. Academic Press, New York. 1961. pp. 548–558.
3. M. BLANDER. Molten salt chemistry. *Edited by* M. Blander. Interscience, New York. 1964. pp. 142–146.
4. A. KLEMM. Molten salt chemistry. *Edited by* M. Blander. Interscience, New York. 1964. pp. 554–558.
5. C. WAGNER. Advances in electrochemistry and electrochemical engineering. Vol. 4. *Edited by* P. Delahay and C. Tobias. Interscience, New York. 1966. pp. 31–35.
6. I. G. MURGULESCU and L. POPESCU. Rev. Rom. Chim. **18**, 737 (1973).
7. H. ROSSOTTI. Chemical applications of potentiometry. Van Nostrand, Princeton. 1969. pp. 37, 38.
8. R. CONRADT, J. RICHTER, and H. WETTICH. Z. Naturforsch. **38***a*, 128 (1983).
9. M. V. SMIRNOV, K. A. ALEKSANDROV, and V. A. KHOKHLOV. Electrochim. Acta, **22**, 543 (1977).

Can. J. Chem. Downloaded from www.nrcresearchpress.com by 194.225.253.170 on 09/07/12
For personal use only.

Isolation and structure of the unusual Indian Ocean *Cephalodiscus gilchristi* components, cephalostatins 5 and 6[1]

GEORGE R. PETTIT,[2] YOSHIAKI KAMANO, CLAUDE DUFRESNE, MASUO INOUE, NIGEL CHRISTIE, JEAN M. SCHMIDT, AND DENNIS L. DOUBEK

Cancer Research Institute and Department of Chemistry, Arizona State University, Tempe, AZ 85287-1604, U.S.A.

Received March 28, 1989

GEORGE R. PETTIT, YOSHIAKI KAMANO, CLAUDE DUFRESNE, MASUO INOUE, NIGEL CHRISTIE, JEAN M. SCHMIDT, and DENNIS L. DOUBEK. Can. J. Chem. **67**, 1509 (1989).

The Indian Ocean (South African) marine worm *Cephalodiscus gilchristi* (Hemichordata phylum) has been found to contain a series of unusual disteroidal alkaloids, designated the cephalostatins, that possess exceptionally potent lymphocytic leukemia (murine P388) cell line inhibitory activity (to ED_{50} 10^{-9} μg/mL). Two of the less prominent members with P388 ED_{50} 10^{-3} – 10^{-2} μg/mL, cephalostatins 5 (**2**) and 6 (**3**), were isolated and assigned structures based on rigorous interpretation of two-dimensional 400-MHz ^1H and ^{13}C nuclear magnetic resonance.

Key words: cephalostatins 5 and 6, disteroidal alkaloids, lymphocytic leukemia, cytostatic, *Cephalodiscus gilchristi*.

GEORGE R. PETTIT, YOSHIAKI KAMANO, CLAUDE DUFRESNE, MASUO INOUE, NIGEL CHRISTIE, JEAN M. SCHMIDT et DENNIS L. DOUBEK. Can. J. Chem. **67**, 1509 (1989).

On a trouvé que le ver marin de l'océan Indien (Afrique du sud) *Cephalodiscus gilchristi* (Hemichordata phylum) contient une série d'alcaloïdes distéroïdaux inhabituels, nommés céphalostatines, qui possèdent une activité exceptionnelle contre la leucémie lymphocitique (activité inhibitrice des cellules de murine P388 jusqu'à une ED_{50} de 10^{-9} μg/mL). On a isolé les céphalostatines 5 (**2**) et 6 (**3**), deux des membres les moins importants de la série, avec une ED_{50} de 10^{-3}–10^{-2} μg/mL, et on a déterminé leurs structures en se basant sur une interprétation rigoureuse des spectres bidimensionnels en résonance magnétique nucléaire du ^1H et ^{13}C, déterminés à 400 MHz.

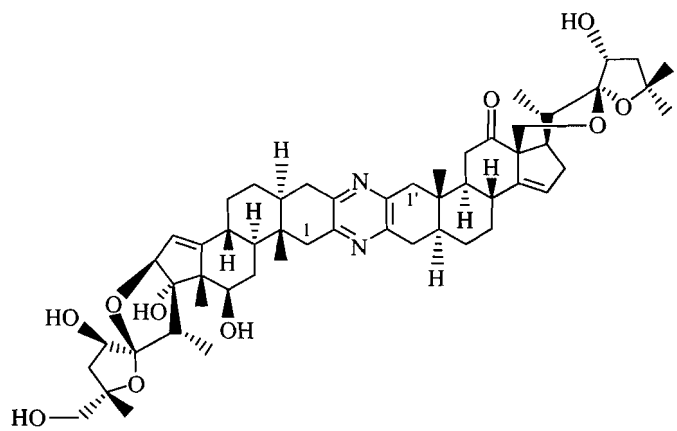
Mots clés: céphalostatines 5 et 6, alcaloïdes disteroïdaux, leucémie lymphocitique, cytostatique, *Cephalodiscus gilchristi*.

[Traduit par la revue]

Introduction

The marine worm order Cephalodiscida (Hemichordata phylum) contains two tube-living genera occurring primarily at considerable depths in the Southern hemisphere. Tubes containing colonies of these tiny marine animals are commonly found attached to, for example, bryozoans and sponges. Initial investigation of bioactive constituents in this worm class (Pterobranchia)[3] led to our discovery of the powerful murine P388 lymphocytic leukemia (PS system) cell growth inhibitor cephalostatin 1 (**1**) (1*b*) in the South African (Indian Ocean) *Cephalodiscus gilchristi*. Subsequently, we isolated and assigned structures to the related disteroidal alkaloids, cephalostatins 2, 3, and 4 (3). We now report that further bioassay (PS) guided study of *C. gilchristi* has led to the isolation of two unusual disteroidal alkaloids bearing aromatic C-rings, designated cephalostatins 5 (**2**) and 6 (**3**), that retain significant cell growth inhibition (PS ED_{50} 10^{-2} μg/mL).

Minor bioactive (PS leukemia) fractions prepared (1*b*) from a methylene chloride – methanol extract (from 166 kg of wet *C. gilchristi*) were separated by repeated gradient column chromatographic (partition on Sephadex LH-20, adsorption on silica gel, and hplc) techniques. Final purification by hplc using 30:70:0.1 hexane – ethyl acetate – methanol afforded cephalostatin 5 (**2**) as a colorless solid (5.5 mg, 3.1×10^{-5}% yield). With the X-ray crystal structure assigned cephalostatin 1 (**1**) as a reference point, and the completely interpreted nmr spectra for cephalostatins 1 (1*b*), 2, 3, and 4(3), it became possible, using detailed analysis of high field two-dimensional nmr data and the mass spectra, to unequivocally assign structures **2** and **3** respectively to cephalostatins 5 and 6.



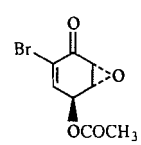
1

The ^1H and ^{13}C nmr spectra of cephalostatins 5 and 6 proved to be almost identical except for an additional methyl doublet at 1.07 ppm in the ^1H nmr spectrum of cephalostatin 5. By mass spectral analyses, each was found to possess one more degree of unsaturation than cephalostatin 1, with cephalostatin 5 bearing an additional methyl group. Their nmr spectra were found to be similar to those of cephalostatins 1 through 4, with the exception that aromatic signals were uncovered in ^{13}C spectra.

[1]Contribution 165, Antineoplastic agents. For part 164 of series consult ref. 1*a*.

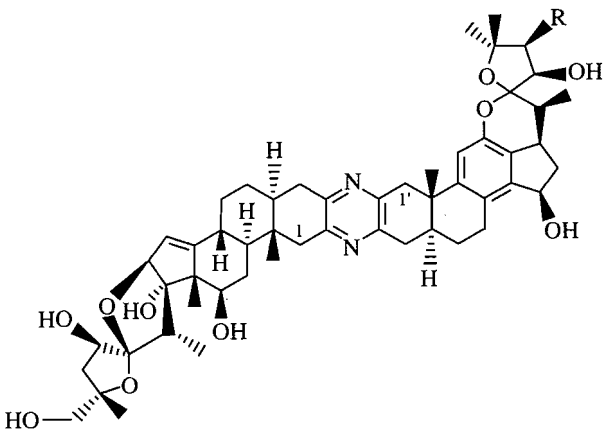
[2]Author to whom correspondence may be addressed.

[3]Recently, Scheuer and co-workers (2) summarized a productive study concerned with constituents of a new species of acorn worm (Enteropneusta order of the Hemichordata) found in a deep Hawaiian marine cave. A series of brominated indoles and phenols along with alicyclic derivatives were isolated. Three of the alicyclic compounds, especially **i** (ED_{50} 0.001 μg/mL), were found active against the PS cell line.

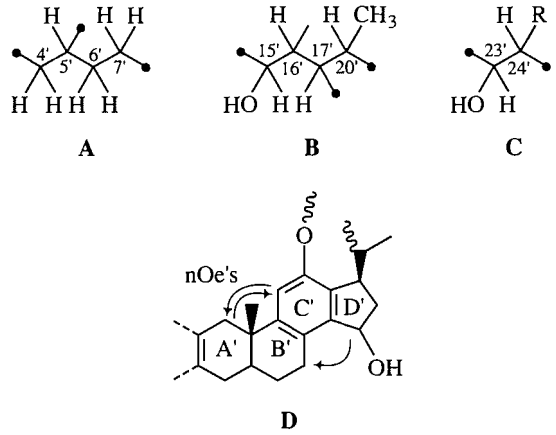


i

Can. J. Chem. Downloaded from www.nrcresearchpress.com by 194.225.253.170 on 09/07/12
For personal use only.



2: R = CH_3; cephalostatin 5
3: R = H; cephalostatin 6



A **B** **C** **D**

The nmr signals attributed to the "left-side" steroid unit in cephalostatins 1–4 all appeared in the spectra of cephalostatins 5 and 6, indicating that portion of the molecular skeleton remained unchanged. Subtraction of this unit from the spectra implied that the "right-side" steroid units each contained ten unsaturations, present as four double bonds and six rings. Only three spin systems, A, B, and C, were found in the right-side steroid unit, as determined by COSY and homonuclear relayed COSY (4) experiments. Spin system A was unambiguously assigned to C-4′ – C-7′. The presence of an nOe between the protons at 5.55 (H-15′ in B) and 3.09 ppm (H-7a′ in A) allowed assignment of spin system B to ring D′ and carbons 20′ and 21′ (cf. D). Location of the aromatic carbons in ring C′ was demonstrated by nOe effects between the aromatic proton at 6.93 ppm (C-11′; δ_C 111.46) and one of the C-1′ protons (3.56 ppm). The relatively high field chemical shift for the C-11′ carbon indicated the presence of an oxygen atom at C-12′, a structural feature consistent with all of the cephalostatins so far isolated. System C was attributed to side-chain carbons 23′ and 24′.

Next it remained to assign an acetal carbon (δ_C 107.35), one oxygen atom, a *gem* dimethyl group, and fragment C, while forming two rings. Using results of a sensitivity enhanced heteronuclear multiple bond correlation experiment (HMBC (5); see Table 1), and in keeping with the overall carbon skeleton deduced for cephalostatins 1–4, we were able to unambiguously assign structures **2** and **3** for cephalostatins 5 and 6 respectively. The stereochemistry at C-15′ was postulated to be *R*, assuming a biosynthetic relationship with cephalostatin 4, which bears a β epoxy group at C-14′–15′. However, it could not be assigned with certainty. The other chiral centers were assumed to correspond to their counterparts in cephalostatin 1, except for the stereochemistry at C-22′, which remains undetermined.

While naturally occurring and synthetic steroids with ring A aromatized are well known, steroids bearing an aromatic ring C are quite rare and examples of biosynthetic origin are heretofore essentially unknown. The dramatic reduction in PS cell growth inhibition displayed by cephalostatins 5 and 6 compared to 1–4 suggests that preservation of structural integrity in the right-side unit, including the C–D ring stereochemistry typical of, e.g., the steroid bufadienolides (6) and cardenolides (7), is very important to realizing powerful inhibition of the PS leukemia. The atypical C-22′ spiroketals involving C-18′ in cephalostatin 1 and C-12′ in cephalostatins 5 and 6 are also noteworthy. Doubtlessly, further pursuit of the opportunities for total syntheses and structural modifications offered by these important new leads to potent cell growth inhibition will yield important results.

Experimental

Chromatographic solvents were redistilled. Sephadex LH-20 and LH-60 (25–100 μm) employed for gel permeation and partition chromatography were obtained from Pharmacia Fine Chemicals AB, Uppsala, Sweden. Column chromatographic techniques utilizing silica gel (70–230 mesh) or silica gel 60 prepacked columns were accomplished with material supplied by E. Merck (Darmstadt, West Germany). Both the Partisil M9 10/50 and Partisil M9 10/50 ODS-2 (C-18 reverse phase) columns (9.4 mm i.d. × 500 mm) were used for hplc and obtained from Whatman, Inc., Clifton, New Jersey. Gilson FC-220 racetrack and F-80 microfractionators connected to Gilson HM uv-visible Holochrome detectors were used for chromatographic fractionation experiments. Preparative layer plates were also obtained from Whatman, Inc., and the silica gel GF Uniplates for tlc were supplied by Analtech, Inc., Newark, Delaware. The tlc plates were viewed with uv light or developed with concentrated sulfuric acid, ceric sulfate – sulfuric acid, or anisaldehyde acetic acid – sulfuric acid spray (heating at approximately 150°C for 5–10 min).

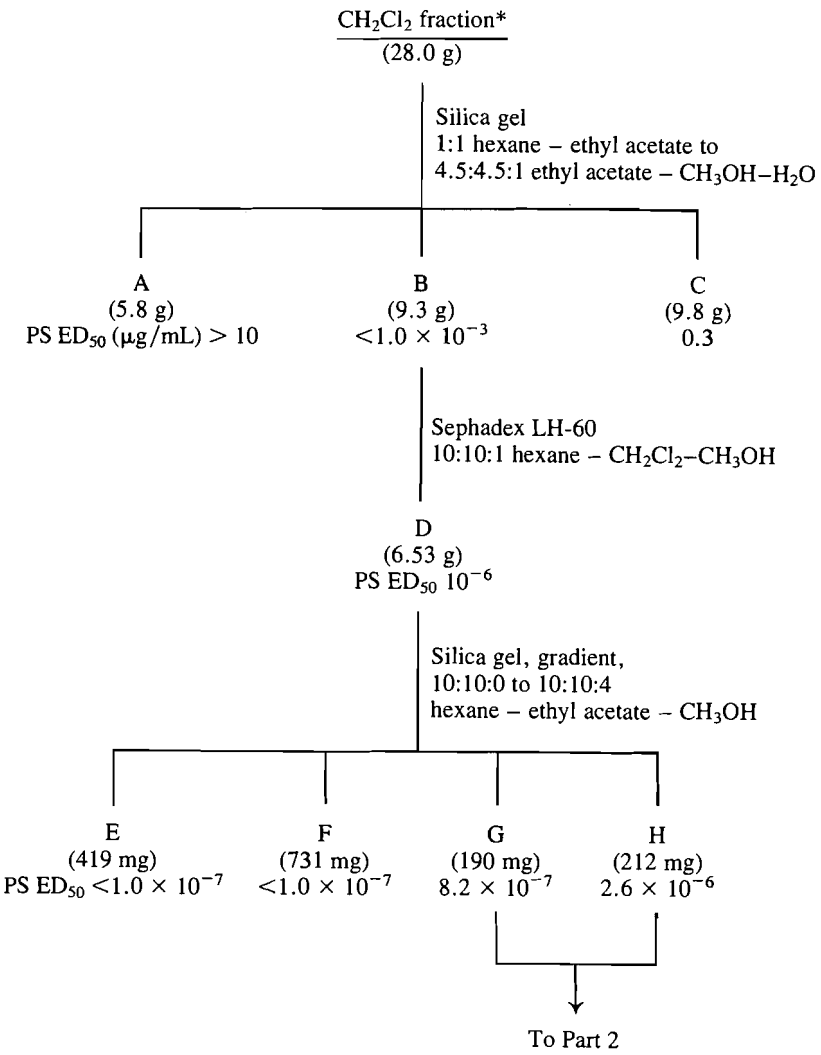
The melting points are uncorrected and were observed with a Kofler-type melting point apparatus. The uv spectra were recorded using a Hewlett–Packard 8450A uv/vis spectrophotometer equipped with a HP 7225A plotter. Optical rotation values were obtained using a Perkin–Elmer 241 polarimeter. Infrared spectral data were recorded with a Perkin–Elmer 299 IR spectrophotometer or a Nicolet MX-1 FT instrument. Mass spectra were recorded with a Kratos MS-50 spectrometer. The nmr experiments were conducted with Bruker WH-90 and Bruker WH-400 instruments employing chloroform-*d* or pyridine-d_5 as solvents and tetramethylsilane as internal standard.

Animal collection and initial experiments

The marine worm (~ 5 mm long in tube colonies) *Cephalodiscus gilchristi* (order Cephalodiscida) was collected in late 1972 by scuba (ca. −20 m) in the Indian Ocean off Southeast Africa. By 1974 methanol and water extracts of *C. gilchristi* reached the confirmed active level against the U.S. National Cancer Institute's murine P388 lymphocytic leukemia (PS system) with 32–41% life extension at 25–37.5 mg/kg.

A number of approaches to isolation of the cephalostatins were made, with re-collections of *C. gilchristi*, until the problem was eventually solved starting from a 1981 acquisition (166 kg wet weight, including Coenecium) from the same Indian Ocean location.

Can. J. Chem. Downloaded from www.nrcresearchpress.com by 194.225.253.170 on 09/07/12
For personal use only.



SEPARATION SCHEME 1, Part 1

*Same Scheme for the 42 g CCl_4 fraction

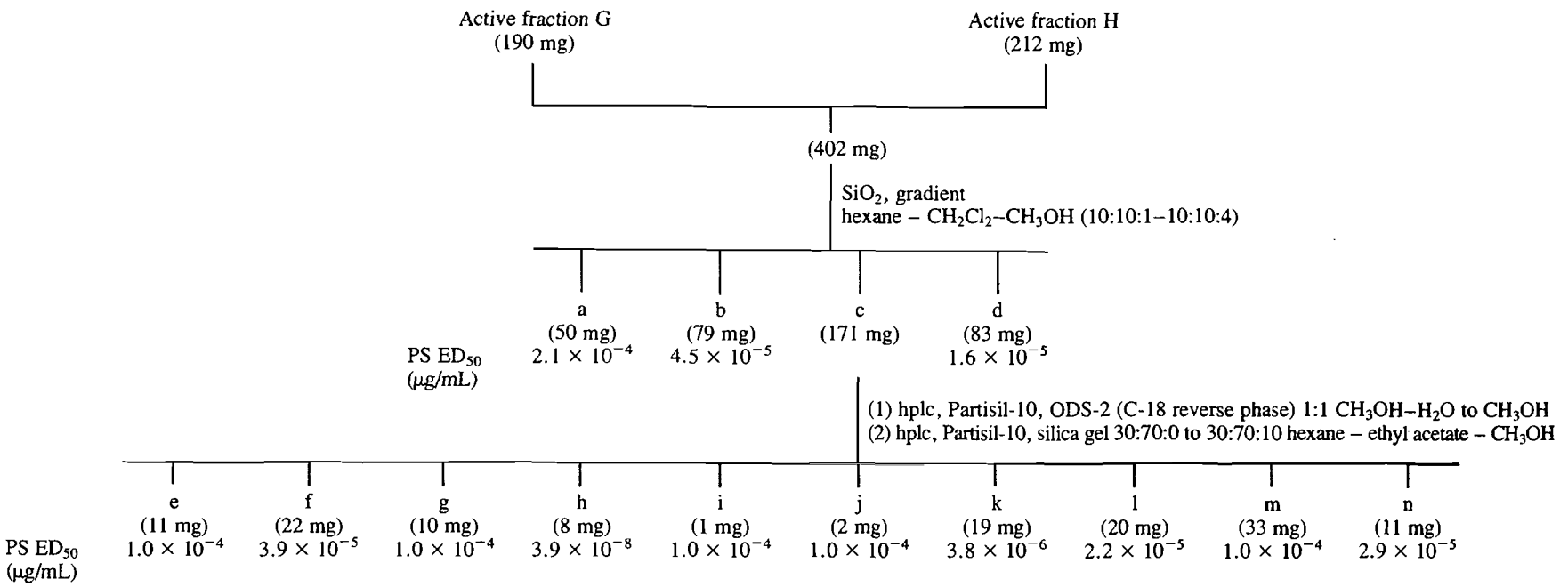
Animal extraction and solvent partition sequence

The marine worm (166 kg, wet weight) was extracted with methylene chloride – methanol at ambient temperature. The solvent was concentrated and the residue was partitioned between methylene chloride and water. The methylene chloride fraction was successively partitioned using the system (8) 9:1 → 4:1 → 3:2 methanol–water against hexane→carbon tetrachloride→methylene chloride, respectively. Both active methylene chloride and carbon tetrachloride fractions (28 g and 42 g respectively) were separated using a detailed (refer to Separation Scheme 1, parts 1–3) bioassay (PS) guided series of chromatographic procedures (8).

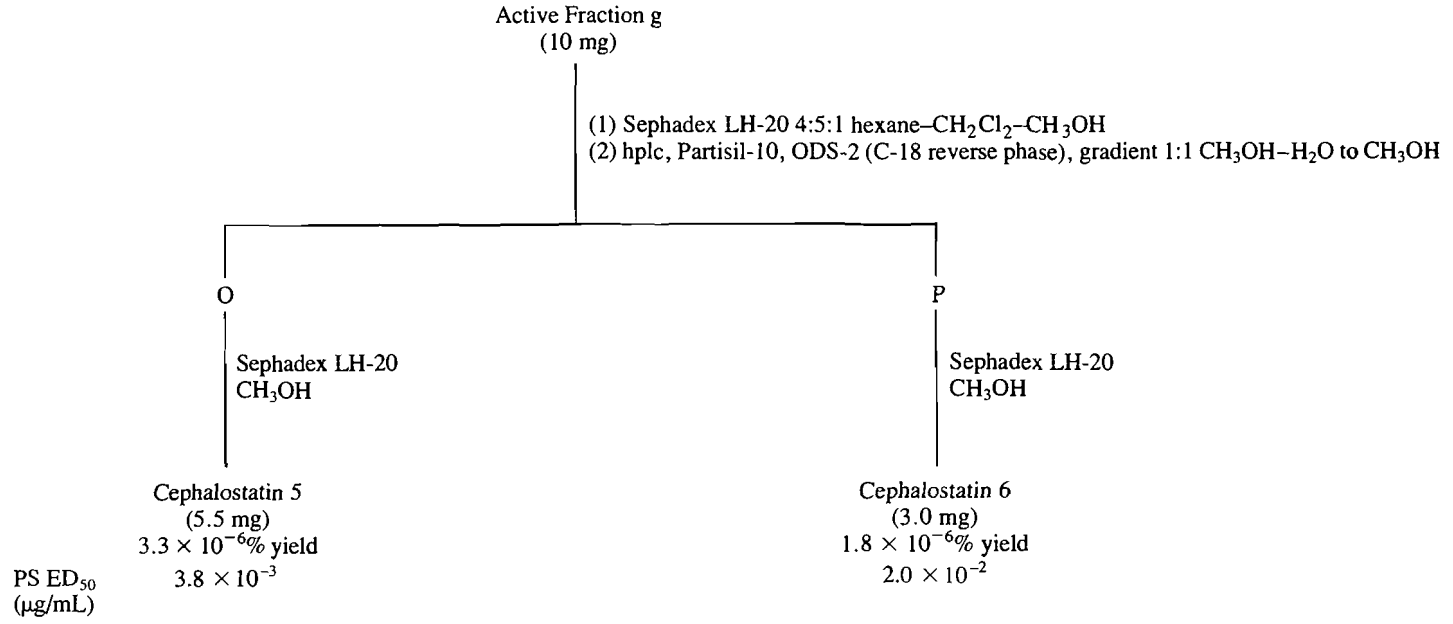
Separation of the 28 g active methylene chloride fraction was performed as outlined in Separation Scheme 1, Part 1. The active fractions, G (0.19 g; ED_{50} 8.2×10^{-7}) and H (0.21 g; ED_{50} 2.6×10^{-6}), were combined. The total amount (0.40 g) was chromatographed on a column of silica gel using gradient elution with hexane–CH_2Cl_2–CH_3OH (10:10:1→10:10:4) to give four active fractions (a,b,c, and d). Fraction c (0.17 g) was carefully separated by C-18 reversed phase hplc (Partisil-10, ODS-2) with CH_3OH–H_2O (1:1 to CH_3OH) as mobile phase, followed by normal phase hplc (Partisil-10, silica gel). Separation employing gradient elution with hexane – ethyl acetate – CH_3OH (30:70:0 to 30:70:10) provided ten active fractions (e – n). Fraction g (10 mg; ED_{50} 1.0×10^{-4}) was chromatographed on a column of Sephadex LH-20 (hexane–CH_2Cl_2-CH_3OH 4:5:1) and the resulting PS cell line active material was further separated using C-18 reverse phase hplc (Partisil-10, ODS-2: 1:1 CH_3OH-H_2O to CH_3OH). Final separation was achieved by incorporating a gel permeation step in methanol using Sephadex LH-20. By this means two pure and PS cytostatic substances were isolated: cephalostatin 5 (**2**) (5.5 mg, 3.3×10^{-6}% yield, ED_{50} 3.8×10^{-3}); mp 350°C; $[\alpha]_D$ +100° (*c* 0.02, CH_3OH); uv (CH_3OH): 290 (ε 9 500), 310 (sh) nm; SP-HRSIMS (glycerol–CF_3SO_3H), calcd. for $C_{54}H_{72}N_2O_{10}$: 908.5187; found: 908.5164 (M^+). Cephalostatin 6 (**3**) was also isolated as a colorless solid (2.5 mg, 1.8×10^{-5}% yield, ED_{50} 2.0×10^{-2}): mp > 350°C; $[\alpha]_D$ +100° (*c* 0.01, CH_3OH); uv (CH_3OH): 289 (ε 10 000), 310 (sh) nm; SP-HRSIMS (glycerol–CF_3SO_3H), calcd. for $C_{53}H_{70}N_2O_{10}$: 894.5031; found: 894.4985 (M^+). The ^1H and ^{13}C nmr assignments have been recorded in Table. 1.

Can. J. Chem. Downloaded from www.nrcresearchpress.com by 194.225.253.170 on 09/07/12
For personal use only.

Can. J. Chem. Downloaded from www.nrcresearchpress.com by 194.225.253.170 on 09/07/12
For personal use only.



SEPARATION SCHEME 1, Part 2



SEPARATION SCHEME 1, Part 3

TABLE 1. Nuclear magnetic resonance assignments and HMBC correlations for cephalostatin 6 (pyridine-d_5 solvent)

	Left-side unit				Right-side unit (′)			
Carbon no.	^{13}C	^{1}H	mult, J (Hz)	HMBC (H to C no.)	^{13}C	^{1}H	mult, J (Hz)	HMBC (H to C no.)
1	45.95	3.08	d, 17.0	3, 5, 10, 19	47.24	3.56	d, 16.9	3′, 5′, 10′, 19′
		2.63	d, 16.8			2.96		
2	149.63				149.54			
3	149.32				148.94			
4	35.77	2.90			35.77	2.96		
		2.65	d,16.8			2.80		
5	41.73	1.57			39.07	1.95	m	
6	28.19	1.49			25.29	1.71	2H	
		1.31						
7	28.66	1.69			26.35	3.09	br t, 2H	
		1.24						
8	33.77	2.05			124.58			
9	53.20	0.87	m		146.21			
10	36.27				37.12			
11	30.00	2.05			111.46	6.93	s	8′, 10′, 12′, 13′
12	75.56	4.05	ddd, 12.4, 4.9, 1.1		149.55			
13	55.36				127.88			
14	152.70				144.30			
15	122.25	5.63	s	8, 13, 14, 16	74.54	5.55	t, 5.5	
16	93.15	5.24	s		39.83	2.38	dd, 12.5, 6.0	13′, 14′, 15′
						2.18	ddd, 12.5, 10.5, 5.5	
17	91.64				36.90	4.44	dt, 10.0, 6.0	13′, 20′, 21′
18	12.57	1.34	s, 3H	12, 13,14,17				
19	11.67	0.71	s, 3H	1, 5, 9, 10	22.59	1.09	s, 3H	1′, 5′, 9′
20	44.50	2.86		13, 17, 21, 22, 23	37.00	2.27	quint, 7.0	13′, 21′
21	8.99	1.35	d, 7.1, 3H	17, 20, 22	8.72	1.07	d, 7.1, 3H	17′, 22′
22	117.12				107.35			
23	71.50	4.80			77.18	4.56	q, 8.7	
24	39.51	2.73	dd, 11.2, 8.0	22,23, 26	46.22	2.58	t, 11.2	23′, 25′, 26′, 27′
		2.35	t, 11.1	23, 25,26,27		2.46	dd, 11.7, 8.0	22′, 23′
25	82.80				78.48			
26	69.27	3.81	dd, 10.9, 5.3	25	30.12	1.27	s, 3H	24′, 25′, 27′
		3.71	dd, 10.9, 4.6					
27	26.41	1.64	s, 3H	24, 25, 26	31.29	1.43	s, 3H	24′, 25′, 26′
OH's								
-12		4.70	d, 1.1					
-15						6.54		
-17		6.23	s	13, 17				
-23		8.08	d, 7.4			6.51		
-26		6.55						

*Where no multiplicity is noted, it could not be determined because of overlapping signals.

Can. J. Chem. Downloaded from www.nrcresearchpress.com by 194.225.253.170 on 09/07/12
For personal use only.

Acknowledgments

For support of this research thanks and appreciation are extended to the Fannie E. Rippel Foundation, Mrs. Eleanor W. Libby, the Donald Ware Waddell Foundation, the Robert B. Dalton Endowment, the Arizona Disease Control Research Commission, Grants CA-16049-05-12 awarded by the NCI, DHHS, and Contract N01-CM-97262 with the Division of Cancer Treatment, NCI, DHHS. Also, we are pleased to thank Dr. M. Suffness, Mr. P. Daschner, the National Science Foundation for equipment Grant CHE-8409644, and the NSF Regional Instrumentation Facility in Nebraska (Grant CHE-8620177).

1. (*a*) G. R. PETTIT and D. E. SCHAUFELBERGER. J. Nat. Prod. **51**, 1104 (1988); (*b*) G. R. PETTIT, M. INOUE, Y. KAMANO, D. L. HERALD, C. ARM, C. DUFRESNE, N. CHRISTIE, J. M. SCHMIDT, D. L. DOUBEK, and T. S. KRUPA. J. Am. Chem. Soc. **110**, 2006 (1988).
2. T. HIGA, R. K. OKUDA, R. M. SEVERNS, P. J. SCHEUER, C.-H. HE, X. CHANFU, and J. CLARDY. Tetrahedron, **43**, 1063 (1987).
3. G. R. PETTIT, M. INOUE, Y. KAMANO, C. DUFRESNE, N. CHRISTIE, M. L. NIVEN, and D. L. HERALD. J. Chem. Soc. Chem. Commun. 865 (1988).
4. A. BAX and G. DROBNY. J. Magn. Reson. **61**, 306 (1985).
5. A. BAX and M. A. SUMMERS. J. Am. Chem. Soc. **108**, 2094 (1986).
6. G. R. PETTIT, Y. KAMANO, P. DRASAR, M. INOUE, and J. C. KNIGHT. J. Org. Chem. **52**, 3573 (1987).
7. D. M. PIATAK, J. PATEL, C. E. TOTTEN, R. P. SWENSON, P. BROWN and G. R. PETTIT. J. Nat. Prod. **48**, 470 (1985).
8. G. R. PETTIT, Y. KAMANO, R. AOYAGI, C. J. HERALD, D. L. DOUBEK, J. M. SCHMIDT, and J. J. RUDLOE. Tetrahedron, **41**, 985 (1985).

New investigations of the reaction of epichlorohydrin with hindered amines: X-ray and NMR analyses

MICHEL LAGUERRE,[1] CHANTAL BOYER, JEAN-MICHEL LEGER, AND ALAIN CARPY

Laboratoire de chimie analytique, Unité associée n° 605 du Centre national de la recherche scientifique, Faculté de pharmacie, 3 Place de la victoire, 33076 Bordeaux CEDEX, France

Received December 1, 1988

MICHEL LAGUERRE, CHANTAL BOYER, JEAN-MICHEL LEGER, and ALAIN CARPY. Can. J. Chem. **67**, 1514 (1989).

During the synthesis of a series of new antiarhythmic drugs, the reaction between epichlorohydrin and hindered amines was reinvestigated. With primary amines, 3-azetidinols were formed in fair yields. The X-ray structure elucidation of one of these compounds (**1**: $P2_1/n$, $a = 17.210$, $b = 6.665$, $c = 23.585$, $\beta = 102.29$, and $R = 0.064$ for 2005 observed reflections) and NMR studies led to the conclusion that both the hydroxy group and the bulky nitrogen substituent are on the same side of the azetidine ring. With secondary amines, the reaction was very complex, leading to diamino dioxane, diamino alcohols, amino alcohol ethers, and one glycol. X-ray analysis and ^1H and ^{13}C NMR studies allowed complete assignments for all compounds. All but one exhibited a slow interconversion of the nitrogen visible in the ^{13}C NMR spectra.

Key words: epichlorohydrin, hindered amines, azetidinol, adamantane, alkanol amines.

MICHEL LAGUERRE, CHANTAL BOYER, JEAN-MICHEL LEGER et ALAIN CARPY. Can. J. Chem. **67**, 1514 (1989).

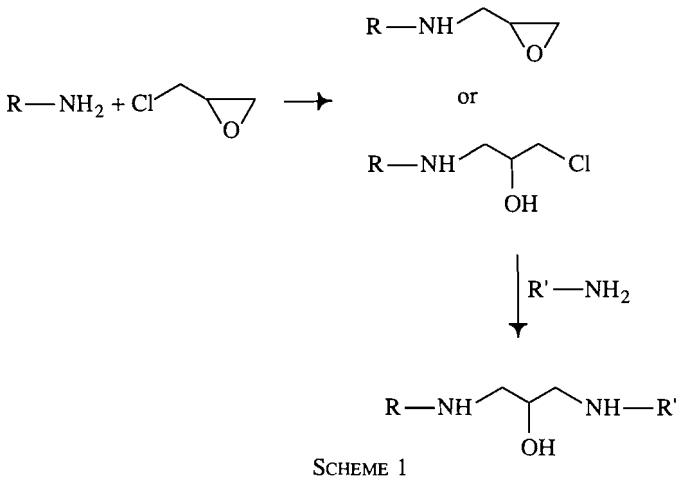
Au cours de la synthèse d'une nouvelle série d'antiarythmiques les auteurs ont été amenés à réexaminer la réaction de l'épichlorhydrine avec les amines encombrées. Avec les amines primaires, on observe la formation d'azétidinols-3 avec des rendements corrects. L'étude structurale par rayons X d'un de ces dérivés (**1** : $P2_1/n$, $a = 17{,}210$, $b = 6{,}665$, $c = 23{,}585$, $\beta = 102{,}29$ avec $R = 0{,}064$ pour 2005 réflexions observées) suivie d'une étude RMN a montré que le groupe OH et le substituant encombrant sur l'azote sont du même côté du cycle azétidine. Avec les amines secondaires, la réaction très complexe donne un diamino-dioxane, des diamino-alcools, des amino-alcools éthers et un glycol. Une analyse par rayons X et une étude complète par RMN ^1H et ^{13}C a permis, outre l'attribution de tous les dérivés, de montrer qu'ils présentaient tous (sauf un) une interconversion de l'azote visible en RMN ^{13}C.

Mots clés : épichlorohydrine, amines encombrées, azétidinol, adamantane, alkanolamines.

[Traduit par la revue]

I. Introduction

During the synthesis of a new class of antiarythmic drugs (1) the reaction of epichlorohydrin with several primary and secondary amines was reinvestigated. Our purpose was to synthesize chlorohydrins or epoxypropanes in order to react them according to Scheme 1:



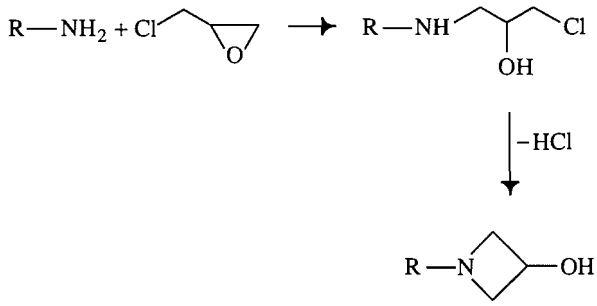
SCHEME 1

With sterically hindered amines, the reaction with epichlorohydrin follows different pathways depending on the nature of the amine.

[1]Author to whom correspondence may be addressed.

II. Primary hindered amines

Since Gaertner's work (2), it has been known that epichlorohydrin reacts with primary hindered amines and produces the corresponding 3-azetidinol by intramolecular cyclization (R must be bulky enough, i.e., R = *i*Pr, *t*Bu, cyclohexyl...) (Scheme 2).



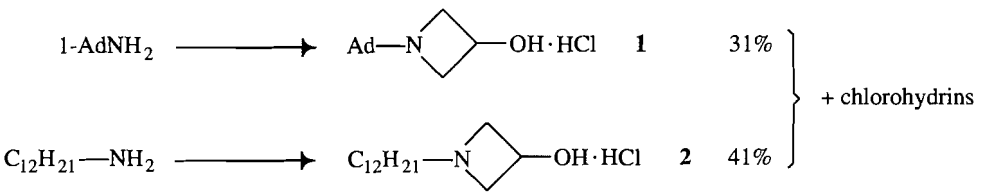
SCHEME 2

3-Azetidinols frequently present different biological effects, such as antidepressant (3), antihypertensive (4, 5), sedative (6), and antipsoriasis (7).

In our work (1) this intramolecular cyclization occurred with R = 1-adamantyl or 1-cyclododecyl. As the purpose was the synthesis of chlorohydrins, we did not try to improve the yields of azetidinol, which were the following (absolute ethanol, 1-night reflux) (Scheme 3):

Printed in Canada / Imprimé au Canada

Can. J. Chem. Downloaded from www.nrcresearchpress.com by 194.225.253.170 on 09/07/12
For personal use only.



SCHEME 3

TABLE 1. Crystal data of **1**

Parameter	Crystal data
Molecular formula	$C_{13}H_{21}NO \cdot HCl \cdot 1/2H_2O$
Molecular weight	252.78
Space group; Z	$P2_1/n$ (alt. $P2_1/c$, no. 14); 8 (2 independent molecules)
Unit-cell parameters	a = 17.210(5) Å b = 6.665(1) Å c = 23.585(6) Å β = 102.29(2)°
Volume (Å^3)	2643.1
Number of reflections used for the determination of unit-cell parameters; 2θ range (deg)	25; 12–48
Density (calcd) (g cm^{-3})	1.27
Number of measured reflections	4654
Number of observed reflections, $I \geq 2\sigma(I)$	2005
Number of refined parameters	474
2θ range scanned (deg)	1–130
μ (CuKα) (cm^{-1})	24.3
Crystal dimensions (mm)	0.25 × 0.20 × 0.20
Final R, R_w, S	0.064, 0.077, 1.763
Largest shift/error in final least-squares cycle, Δ/σ	0.29
Maximum and minimum residual electron density in final difference Fourier map (e Å^{-3})	0.3–0.2

TABLE 2. Fractional coordinates for $C_{13}H_{21}NO \cdot HCl \cdot 1/2H_2O$ ($\times 10^4$) with esd's in parentheses

Atom	x	y	z	B_{eq}
Molecule I				
C(1)	6701(4)	−722(10)	3751(3)	3.9
C(2)	6796(4)	−284(10)	4398(2)	4.4
C(3)	5970(4)	257(11)	4515(3)	4.8
C(4)	5397(4)	−1478(11)	4340(3)	5.2
C(5)	5312(4)	−1918(11)	3691(3)	4.9
C(6)	6130(4)	−2467(10)	3564(3)	4.6
C(7)	6397(4)	1175(11)	3395(3)	4.8
C(8)	5577(4)	1700(11)	3522(3)	5.4
C(9)	4997(4)	−45(12)	3342(3)	5.5
C(10)	5657(4)	2126(12)	4170(3)	5.6
N(11)	7503(3)	−1391(8)	3666(2)	4.2
C(12)	8214(4)	19(12)	3767(3)	5.2
C(13)	8478(4)	−943(12)	3242(3)	5.4
C(14)	7642(4)	−1864(13)	3063(3)	6.1
O(15)	8657(3)	429(10)	2838(2)	8.3
Cl(16)	10422(1)	21(3)	2844(1)	5.9
Molecule II				
C(501)	6760(3)	655(10)	8664(2)	3.8
C(502)	6856(4)	330(10)	8038(2)	4.2
C(503)	7727(4)	−239(11)	8051(3)	4.6
C(504)	7931(4)	−2180(11)	8399(3)	5.0
C(505)	7812(4)	−1866(10)	9021(3)	4.7
C(506)	6938(4)	−1296(10)	9007(3)	4.5
C(507)	7303(4)	2360(11)	8955(3)	4.7
C(508)	8176(4)	1763(11)	8965(3)	5.1
C(509)	8367(4)	−212(11)	9317(3)	5.5
C(510)	8283(4)	1427(11)	8345(3)	5.0
N(511)	5923(3)	1370(8)	8630(2)	4.2
C(512)	5222(4)	−47(12)	8422(3)	5.3
C(513)	4843(4)	733(11)	8919(3)	5.2
C(514)	5637(4)	1773(12)	9195(3)	5.4
O(515)	4638(3)	−831(9)	9264(2)	6.9
Cl(516)	7025(1)	−158(3)	600(1)	5.6
Water inclusion				
O(17)	4329(5)	3690(12)	80(3)	11.8

Where Gaertner (2) obtained the bases in MeOH (room temperature or reflux) or DMSO, we obtained the azetidinium salts in refluxing absolute ethanol. All formulae were confirmed by NMR, mass spectrometry, and microanalysis (see experimental section).

Compound **1** (base) has already been mentioned in the literature (5), but without any structural data. (In fact, few 3-azetidinol structures are known (8) and some questions concerning the conformation of the azetidine ring in the solid state (9) or in solution (10) were left unsolved.) Suitable crystals of **1** were obtained and the structure was determined by X-ray crystallography (Table 1).

In the crystals there are two independent molecules with slightly different geometries. The final fractional coordinates for non-hydrogen atoms are presented in Table 2. A view of molecule 1 showing the numbering of atoms and a stereo pair is shown in Fig. 1. The chemically equivalent bond lengths and angles in the independent molecules summarized in Table 3 are not very different.

Both azetidinium rings are present in a puckered form close to the puckered form of cyclobutane (11) (Table 4). Internal C—N bond lengths lie between 1.521(8) Å (molecule I) and 1.540(8) Å (molecule II), and internal C(sp^3)—C(sp^3) between 1.538(9) Å (molecule I) and 1.547(9) Å (molecule II). The corresponding C*—C(sp^3) distances in cyclobutane are in the range 1.519–1.538 Å. All θ valence angles are close to 90° with transannular distances that are shorter in molecule I than in molecule II. Consequently, the angle of pucker φ is larger in molecule I (21.6(5)°) than in molecule II (17.0(6)°). As already found in cyclobutane (12), a minimal change in θ ($\bar{\theta}$ = 89.4(5)° in II and 89.0(5)° in I) corresponds to a significant increase of the φ value (4.6°). Finally, the ring torsion angles ω are 3.3°

Can. J. Chem. Downloaded from www.nrcresearchpress.com by 194.225.253.170 on 09/07/12
For personal use only.

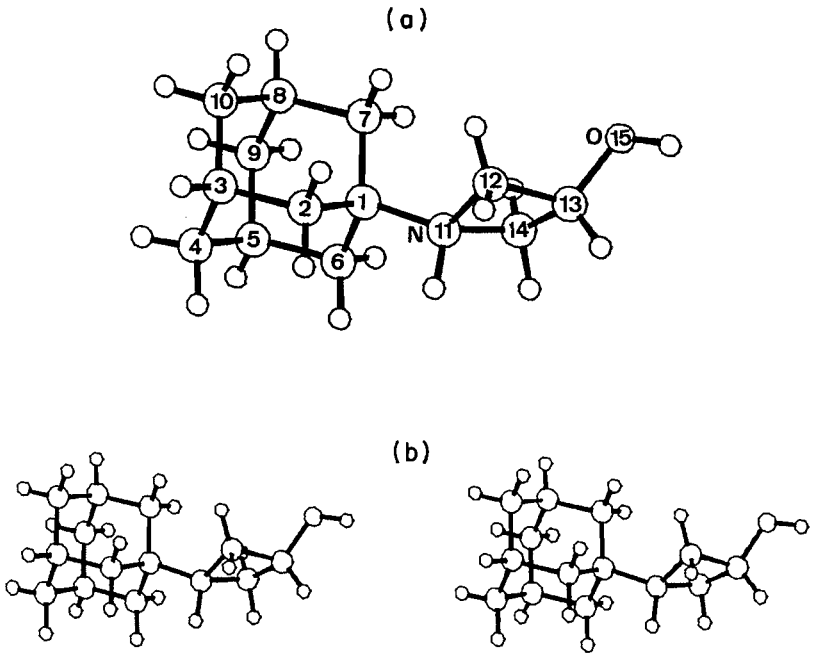


FIG. 1.(a) Projection and (b) stereoview of compound **1** (molecule I) showing the numbering of atoms.

larger in molecule I than in molecule II. C(1) and C(15) are *cis* with respect to each other and are substituted on the convex side of the azetidine ring. Both the O—H groups and the N are involved in hydrogen bonding with the Cl^- anions and the water molecules.

The geometry of the adamantane ring, known for a long time (13), is as expected: all internal torsion angles are $\simeq 60(1)°$. The relative position of the two rings is defined by the torsion angle C(6)—C(1)—N(11)—C(12) = 175.6(6)° (molecule I) or C(507)—C(501)—N(511)—C(512) = −173.3(5)° (molecule II).

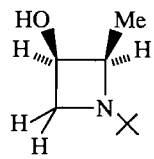
Both independent molecules exhibit an approximate mirror plane of symmetry passing through the atoms O(15), C(13), C(7), C(1), C(5), and C(4).

To examine the conformations of the prepared compounds in solution, the ^1H NMR spectra for both bases and hydrochlorides at 350 MHz were recorded. The chemical shifts and the coupling constants are listed in Table 5.

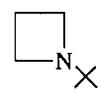
These data agree well with the literature. The chemical shift for H13 is fairly constant: 4.42 ± 0.06 ppm for the bases and 4.77 ± 0.03 ppm for the hydrochlorides. Depending on R, the chemical shifts vary for H12 and H14 (R = cyclododecyl close to R = cyclohexyl and R = 1-adamantyl close to R = *t*Bu). As expected, there is a downfield shift for all protons in the two hydrochlorides.

According to ref. 10*a*, lower field shifts for H12 and H14 may be assigned to protons *syn* to N-alkyl substituents, and higher field shifts to protons *anti* to this substituent. So the steric hindrance introduced by an N-alkyl substituent may account for the chemical shift dispersion in this series. It may also be deduced from these data that even in solution the OH group and R are on the same side of the molecule.

For **1** and **2** the geminal couplings ($J_{12,12'} = J_{14,14'}$) are larger than those already published: 9.8 and 9.1 Hz compared to 6–7 Hz (10). These coupling constants were assigned by irradiation of H13 after D_2O exchange of the OH group. But for compound **3** *cis*, $J_{gem14,14'}$ was found equal to −9.1 Hz, and only −7.2 Hz for the *trans* derivative (10*b*). For compound **4**, $J_{gem12,12'} = 7.45$ Hz and $J_{gem13,13'} = 10.0$ Hz (10*c*). Thus it appears that J_{gem} is very variable in this series, depending on R and presumably on the conformation.



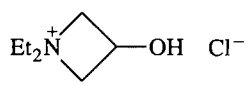
3 *cis*



4

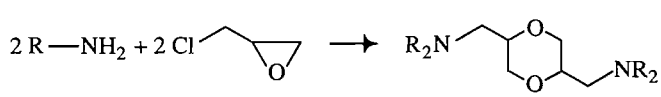
III. Secondary hindered amines

Until now, little work has been done in this area. In the case of diethylamine, A. T. Coscia and co-workers (14) demonstrated the formation of azetidinium **5**:



5

while D. L. Heywood and B. Philipps (15) described the formation of dioxanes (mainly with morpholine and piperidine) according to Scheme 4:



SCHEME 4

Can. J. Chem. Downloaded from www.nrcresearchpress.com by 194.225.253.170 on 09/07/12
For personal use only.

TABLE 3. (*a*) Bond distances (Å) for $C_{13}H_{21}NO \cdot HCl \cdot 1/2H_2O$ with esd's in parentheses for molecules I and II

Molecule I		Molecule II	
C(1)—C(2)	1.529(8)	C(501)—C(502)	1.536(8)
C(1)—C(6)	1.526(8)	C(501)—C(506)	1.528(8)
C(1)—C(7)	1.546(8)	C(501)—C(507)	1.536(8)
C(1)—N(11)	1.503(7)	C(501)—N(511)	1.503(7)
C(2)—C(3)	1.546(9)	C(502)—C(503)	1.539(8)
C(3)—C(4)	1.519(9)	C(503)—C(504)	1.532(9)
C(3)—C(10)	1.522(9)	C(503)—C(510)	1.532(9)
C(4)—C(5)	1.535(9)	C(504)—C(505)	1.537(9)
C(5)—C(6)	1.543(9)	C(505)—C(506)	1.546(9)
C(5)—C(9)	1.530(9)	C(505)—C(509)	1.527(9)
C(7)—C(8)	1.543(9)	C(507)—C(508)	1.550(9)
C(8)—C(9)	1.532(9)	C(508)—C(509)	1.553(9)
C(8)—C(10)	1.532(10)	C(508)—C(510)	1.530(9)
N(11)—C(12)	1.521(8)	N(511)—C(512)	1.528(8)
N(11)—C(14)	1.525(9)	N(511)—C(514)	1.540(8)
C(12)—C(13)	1.545(9)	C(512)—C(513)	1.546(9)
C(13)—C(14)	1.538(10)	C(513)—C(514)	1.547(9)
C(13)—O(15)	1.403(9)	C(513)—O(515)	1.412(8)

(*b*) Bond angles (deg) for $C_{13}H_{21}NO \cdot HCl \cdot 1/2H_2O$ with esd's in parentheses for molecules I and II

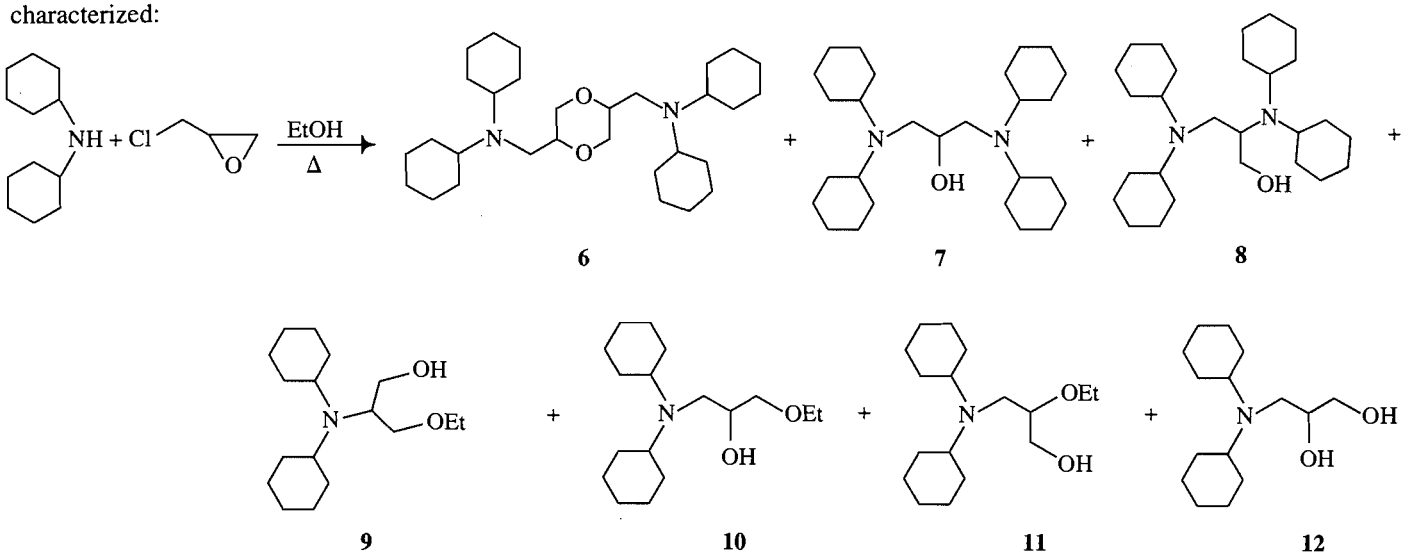
Molecule I		Molecule II	
C(2)—C(1)—C(6)	110.0(5)	C(502)—C(501)—C(506)	109.8(5)
C(2)—C(1)—C(7)	109.7(5)	C(502)—C(501)—C(507)	110.7(5)
C(2)—C(1)—N(11)	106.5(4)	C(502)—C(501)—N(511)	107.0(4)
C(6)—C(1)—C(7)	110.1(5)	C(506)—C(501)—C(507)	111.0(5)
C(6)—C(1)—N(11)	106.8(4)	C(506)—C(501)—N(511)	112.3(5)
C(7)—C(1)—N(11)	112.7(5)	C(507)—C(501)—N(511)	105.9(4)
C(1)—C(2)—C(3)	108.5(5)	C(501)—C(502)—C(503)	108.6(5)
C(2)—C(3)—C(4)	110.0(5)	C(502)—C(503)—C(504)	109.3(5)
C(2)—C(3)—C(10)	109.2(5)	C(502)—C(503)—C(510)	110.0(5)
C(4)—C(3)—C(10)	110.0(5)	C(504)—C(503)—C(510)	108.7(5)
C(3)—C(4)—C(5)	109.6(5)	C(503)—C(504)—C(505)	109.5(5)
C(4)—C(5)—C(6)	109.9(5)	C(504)—C(505)—C(506)	109.9(5)
C(4)—C(5)—C(9)	109.2(5)	C(504)—C(505)—C(509)	109.7(5)
C(6)—C(5)—C(9)	108.8(5)	C(506)—C(505)—C(509)	110.0(5)
C(1)—C(6)—C(5)	108.8(5)	C(501)—C(506)—C(505)	107.7(5)
C(1)—C(7)—C(8)	107.4(5)	C(501)—C(507)—C(508)	108.2(5)
C(7)—C(8)—C(9)	110.0(5)	C(507)—C(508)—C(509)	108.7(5)
C(7)—C(8)—C(10)	110.1(5)	C(507)—C(508)—C(510)	109.6(5)
C(9)—C(8)—C(10)	109.4(5)	C(509)—C(508)—C(510)	109.4(5)
C(5)—C(9)—C(8)	109.5(5)	C(505)—C(509)—C(508)	109.1(5)
C(3)—C(10)—C(8)	109.2(5)	C(503)—C(510)—C(508)	110.3(5)
C(1)—N(11)—C(12)	121.8(4)	C(501)—N(511)—C(512)	120.3(4)
C(1)—N(11)—C(14)	121.1(5)	C(501)—N(511)—C(514)	119.3(4)
C(12)—N(11)—C(14)	89.6(4)	C(512)—N(511)—C(514)	90.5(4)
N(11)—C(12)—C(13)	89.0(5)	N(511)—C(512)—C(513)	89.0(5)
C(12)—C(13)—C(14)	88.2(5)	C(512)—C(513)—C(514)	89.5(5)
C(12)—C(13)—O(15)	114.8(5)	C(512)—C(513)—O(515)	112.7(5)
C(14)—C(13)—O(15)	113.6(6)	C(514)—C(513)—O(515)	113.3(5)
N(11)—C(14)—C(13)	89.1(5)	N(511)—C(514)—C(513)	88.6(5)

In the present work, this side reaction was found with dicyclohexylamine. Under our experimental conditions (refluxing absolute ethanol) a very complex mixture, including one dioxane, dimers resulting from the condensation of two amines with epichlorohydrin, and ethers arising from the reaction of ethanol with the intermediate epoxide or chlorohydrin, was found. The reaction mixture, containing at least 10–12 compounds, was separated by repeated chromatography on an alumina column (see experimental section).

The following derivatives have been isolated and fully

Can. J. Chem. Downloaded from www.nrcresearchpress.com by 194.225.253.170 on 09/07/12
For personal use only.

characterized:



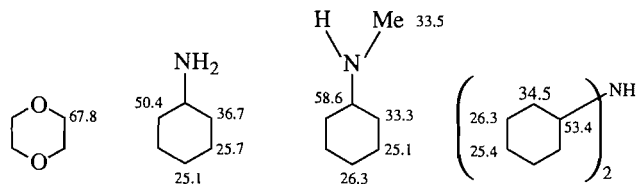
SCHEME 5

Two or three other products could not be purified enough to be unambiguously identified.

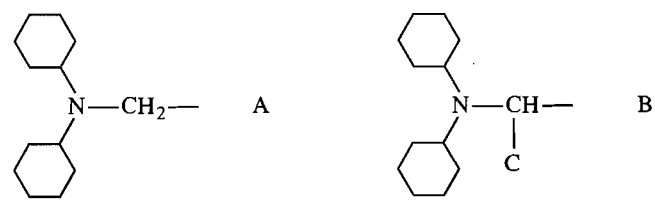
The identification of compounds **6–12** was facilitated by a single crystal X-ray analysis of compound **7**. This compound presented crystallographic problems. The Fourier maps showed a disordered hydroxypropyl unit and alternative chair conformations for the cyclohexane rings. Unfortunately it was not possible to refine properly the whole molecule. However, these observations are in agreement with a simultaneous inversion of the two nitrogen coordination tetrahedra.

After this analysis, owing to the fact that compound **7** is symmetrical, we could fully determine the ^{13}C sequence of the dicyclohexylamino fragment.

The ^{13}C chemical shifts tabled in the literature give the following data:

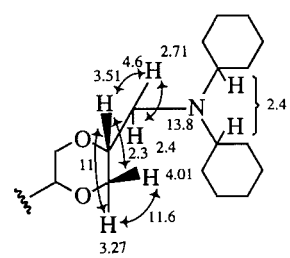


Differences between βCH_2 and γCH_2 in the cyclohexane rings (which have very close chemical shifts) were unambiguously established according to the relative intensity of the signals ($8CH_2\beta$ versus $4CH_2\gamma$) and by using quite long recycle delays (10–20 s depending on the compounds). In each case *two* close signals having the same intensity were recorded for $CH_2\alpha$ and in some cases for $CH_2\beta$. The results are shown in Table 6. From this table it may be deduced that for CH_{ipso} the chemical shift is 57.9 ± 0.7 ppm in fragment A and 54.0 ± 0.1 ppm in fragment B.



The ^{13}C chemical shift was fairly constant for $CH_2\gamma$: 25.5 ± 0.3 ppm, and for $CH_2\beta$: 26.2 ± 0.3 ppm (even if it appears as two close signals). For $CH_2\alpha$ there were always *two* different signals and for compound **8** (unsymmetrical) there were *four* signals. As compound **7** is absolutely symmetrical, a chiral center is not the fundamental reason. This fact was not mentioned for the ^{13}C spectrum of the parent dicyclohexylamine (16). According to the preliminary X-ray results for **7**, the best hypothesis may be a slow interconversion of the nitrogen atom so that the $CH_2\beta$ appears as enantiotopic. Other hypotheses, of a slow interconversion of the cyclohexane rings or the nitrogen atom being axial for one ring and equatorial for the other, can be ruled out. There was only *one* signal for ^{13}CH-N, when it is well known that in many substituted cyclohexane derivatives the α effect is different according to the axial/equatorial position of the substituent (17). For instance, in cyclohexanol derivatives, differences in δ for CH-OH axial or equatorial are about 5–6 ppm. Moreover, in 2-aminonorbornane there is a 2-ppm difference between the *endo* and the *exo* derivatives. It seems unexplained that there was not the slightest difference in δ $CH_2\alpha$ for at least one of our compounds.

To confirm the hypothetical inversion of the nitrogen, the ^1H spectra in the CH-N area were examined. But even at 500 MHz this area was so overcrowded that it was impossible to determine the coupling constants. Only the spectrum of **6** allowed some assignments to be made (but *not* in the CH-N area):

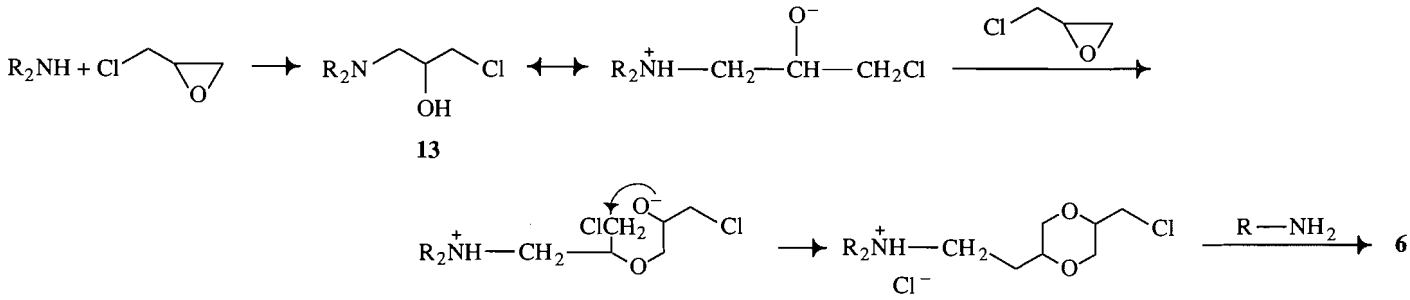


6

The assignment was performed by irradiation of the proton at 3.51 ppm, thus confirming the proposed structure.

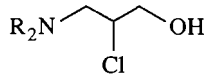
The product formation could be easily rationalized. The first product that appeared was chlorohydrin **13**. According to Heywood and Philipps (15), **6** was a product of the reaction between **13** and epichlorohydrin according to Scheme 6:

Can. J. Chem. Downloaded from www.nrcresearchpress.com by 194.225.253.170 on 09/07/12
For personal use only.



SCHEME 6

Compounds **7**, **8**, **10**, and **11** may be formed by reaction with the corresponding epoxide **14**. Compounds **10** and **7** can also arise directly from **3** but not compounds **11** and **8**, which would arise from the isomeric chlorohydrin **15**.

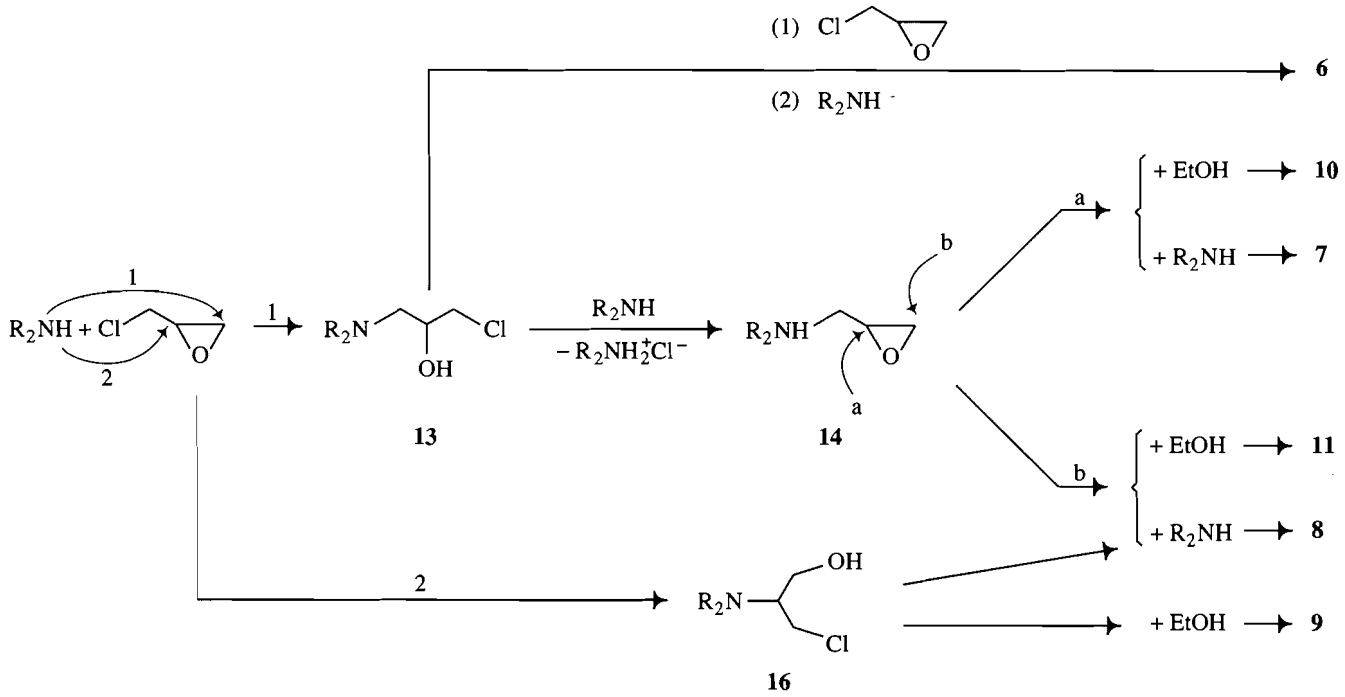


15

For compound **9** it is necessary to require another isomeric chlorohydrin **16** according to Scheme 7.

So compound **8** may arise from epoxide **14** via path b or from **16**. This is only a hypothesis as **16** has not been isolated from the reaction mixture. Compound **12** obviously came from **13** or **14** by hydrolysis during basic work-up.

In conclusion, the reaction of epichlorohydrin with secondary hindered amines is rather complex, as can be seen in Scheme 7:



SCHEME 7

TABLE 4. Geometrical parameters for the puckered forms of the azetidinium rings

Parameter	Molecule I	Molecule II
Transannular distances (D, Å)		
N(11)...C(13)	2.149(8)	2.155(8)
C(12)...C(14)	2.146(9)	2.178(9)
Angle of pucker (φ, deg)	21.6(6)	17.0(6)
Ring torsion angles (ω, deg)		
N(11)—C(14)—C(13)—C(12)	−15.2(5)	11.8(5)
C(14)—C(13)—C(12)—N(11)	15.2(5)	−11.9(5)
C(13)—C(12)—N(11)—C(14)	−15.3(5)	12.0(5)
C(12)—N(11)—C(14)—C(13)	15.4(5)	−12.0(5)

(Note: Buriks and Lovett (18) have recently encountered some very complex reactions between epichlorohydrin and secondary alkanolamines.)

Experimental

Melting points were taken on a Kofler apparatus and are uncorrected. The elemental analyses were carried out by the Service central d'analyses du CNRS (F-69390 Vernaison). The IR spectra were recorded on a Perkin–Elmer 157G spectrophotometer in CCl_4 solutions for solids or neat for liquids. Routine ^1H NMR spectra were recorded at 60 MHz on a Perkin–Elmer Hitachi R 24B instrument in $CDCl_3$ solution using TMS as internal standard. High-field ^1H NMR spectra were recorded at 350 MHz on a Cameca instrument and at 500 MHz on a Bruker WM-500 apparatus. ^{13}C NMR spectra were recorded at 22.63 MHz on a Bruker WM-90. All spectra were recorded in $CDCl_3$ solutions with TMS as reference.

Can. J. Chem. Downloaded from www.nrcresearchpress.com by 194.225.253.170 on 09/07/12
For personal use only.

Can. J. Chem. Downloaded from www.nrcresearchpress.com by 194.225.253.170 on 09/07/12
For personal use only.

TABLE 5. ^{1}H chemical shifts and coupling constants for compounds **1** and **2**

Compound	δ H2, H4	δ H3	Coupling constants (Hz)
1 base	3.21 and 3.55	4.48	$J_{2,2'} = J_{4,4'} = 9.8$ $J_{2,3} = J_{4,3} = 7$ $J_{2',3} = J_{4',3} = 6.2$
1, HCl	3.95 and 4.13	4.80	$J_{2,2'} = J_{4,4'} = 9.8$ $J_{2,3} = J_{4,3} = 7.0$ $J_{2',3} = J_{4',3} = 6.2$
2 base	2.87 and 3.63	4.40	$J_{2,2'} = J_{4,4'} = 9.1$ $J_{2,3} = J_{4,3} = 6.2$ $J_{2',3} = J_{4',3} = 5.8$
2, HCl	4.03 and 4.49	4.74	$J_{2',2} = J_{4,4'} = 9.8$ $J_{2,3} = J_{4,3} = 6.0$ $J_{2',3} = J_{4',3} = 6.0$
R = *t*Bu* base	3.0 and 3.38	4.37	$J_{2,2'} = J_{4,4'} = 6.5$ $J_{2,3} = J_{4,3} = 6.2$ $J_{2',3} = J_{4',3} = 7$
R = cyclohexyl* base	2.83 and 3.58	4.42	$J_{2,2'} = J_{4,4'} = 7$ $J_{2,3} = J_{4,3} = 7$ $J_{2',3} = J_{4',3} = 7$
R =  * base	2.83 and 3.45	4.42	$J_{2,2'} = J_{4,4'} = 6.0$ $J_{2,3} = J_{4,3} = 6.0$ $J_{2',3} = J_{4',3} = 6.0$

*Data from reference 10*a*.

TABLE 6. ^{13}C NMR chemical shifts of compounds **6–12**

	Cyclohexane rings								Ethyl groups	
Compounds	CH ipso	$CH_2\alpha$	$CH_2\beta$	$CH_2\gamma$	CH_2N	CHN	CH_2O or CH_2Cl	CHO	CH_2O	CH_3
6	58.3	30.8 32.6	26.3 26.2	25.9	47.4		71.2	74.8		
7	58.3	31.8 32.4	26.5	26.2	50.6			67.2		
8*	57.2 54.0	34.0 33.8 32.1 29.1	26.0	25.5 25.2	49.7	52.3	65.8			
9	54.1	34.7 33.6	26.5 26.3	25.5		55.8	72.4 66.6†		60.2†	15.0
10	57.6	32.4 30.5	25.9 25.8	25.5	47.9		73.1	65.8	66.3	14.7
11	57.9	31.6 29.7	25.9 25.8	25.5	49.8		65.2†	74.9	64.6†	15.1
12	58.6	32.4 30.6	26.3 26.2	25.8	47.8		64.6	66.9		

*With **8** there are two different dicyclohexylamine groups.
†Values may be reversed.

Can. J. Chem. Downloaded from www.nrcresearchpress.com by 194.225.253.170 on 09/07/12
For personal use only.

Synthesis of ***1***

A mixture of 0.066 mol of 1-adamantylamine (10 g) and 7.6 mL of epichlorohydrin was heated at reflux in 80 mL of absolute ethanol for 24 h. After ethanol elimination, there remained 20 g of a light-brown crystalline mass, which was recrystallized in 130 mL of $C_6H_6/CHCl_3$ = 1:2 leaving 5 g of white crystals of **1** in 2 crops: mp 225–228°C, yield 31%; pure base has mp 173–174°C. Mass spectrum of base: 207 (5.6%), 150 (27.3%) adamantyl-NH^+, 135 (100%) adamantyl, 93 (12.5%), 79 (14.5%), 67 (6.5%), and 55 (5.8%). *Anal.* calcd. for hydrochloride of $C_{13}H_{22}ClNO$: C 64.05, H 9.09, N 6.56, O 5.75; found: C 64.11, H 9.13, N 6.43, O 5.61.

Synthesis of ***2***

Cyclododecylamine (0.027 mol; 5.1 g) and 3 mL of epichlorohydrin were heated at reflux in 50 mL of absolute ethanol during 24 h. After ethanol elimination there remained 8.2 g of a whitish semicrystalline mass, which was recrystallized from benzene (200 mL) giving 3 g of white crystals of **2**: mp 175°C, yield 40.5%; pure base has mp 109°C. *Anal.* calcd. for hydrochloride of $C_{15}H_{30}ClNO$: C 65.31, H 10.96, N 5.08, O 5.80; found: C 65.31, H 11.02, N 4.96, O 5.75.

Reaction of dicyclohexylamine with epichlorohydrin

A mixture of 0.05 mol of dicyclohexylamine (9.1 g or 10 mL) and 5 mL of epichlorohydrin was heated under reflux in 80 mL of absolute ethanol during 24 h. After ethanol elimination, 15.5 g of a yellowish-white pasty mass or yellowish viscous oil was obtained. This crude product was extracted with CH_2Cl_2, and washed with dilute ammonia and then with water to neutrality, leaving 12.3 g of yellow viscous oil. Part (7.5 g) of this oil was applied to a column of 300 g of alumina (Merck 90, activity II–III, 70–230 mesh) prepared in cyclohexane. The introduction was also carried out in cyclohexane and products were separated according to the following sequence of elution:

C_6H_{12}/Et_2O = 95:5	**6**, then **8**
C_6H_{12}/Et_2O = 90:10	**7**
C_6H_{12}/Et_2O = 87.5:12.5	**9**
C_6H_{12}/Et_2O = 80:20	**10**
C_6H_{12}/Et_2O = 75:25	**11**
C_6H_{12}/Et_2O = 50:50	**12**

Physico-chemical characteristics of compounds ***6–12***

6: mp 170°C, white crystals (C_6H_{12}); IR (CCl_4): 2930, 2855, 1450, 1105, 890 cm^{-1}; ^1H NMR (500 MHz): see discussion above with 2.43 (m, 6H, 6CH-N), 1.73 (m, 12H), 1.57 (m, 8H), 1.20 (m, 16H), and 1.02 (m, 4H) for the four cyclohexyl groups. *Anal.* calcd. for $C_{30}H_{54}N_2O_2$: C 75.90, H 11.46, N 5.90, O 6.74; found: C 75.10, H 11.54, N 5.73, O 6.54.

7: mp 121–123°C, yellowish-white crystals (C_6H_{12}); IR (CCl_4): 3360, 2935, 2855, 1450, 1170, 1087, 891; ^1H NMR (500 MHz): 3.62 (m, 1H, CH-O), 2.60 (m, 8H, $2CH_2$-N + 4CH-N) and 1.83 (m, 16H), 1.65 (m, 4H), 1.27 (m, 16H), and 1.09 (m, 4H) for the four cyclohexyl groups. *Anal.* calcd. for $C_{27}H_{50}N_2O$: C 77.45, H 12.04, N 6.69, O 3.82; found: C 77.10, H 12.10, N 6.35, O 4.03.

8: mp 226–227°C, white powder (C_6H_{12}); IR (KBr disc): 3160, 2940, 2860, 1456, 1446, 1117, 1083, 1038, 887; ^1H NMR (60 MHz): 3.9–3.0 (m, 2H, CH_2-O), 2.60 (m, 7H, 5CH-N + CH_2-N), 1.50 (m, 40H) four cyclohexyl groups. *Anal.* calcd. for $C_{27}H_{50}N_2O$: C 77.45, H 12.04, N 6.69; found: C 77.17, H 12.19, N 6.56.

9: yellow oil; IR (neat): 3430, 2930, 2855, 1450, 1110, 1040, 890; ^1H NMR (60 MHz): 3.40 (m, 6H, $3CH_2$-O), 2.60 (br m, 3H, 3CH-N), 1.50 (br m, 20 H) two cyclohexyl groups, 1.15 (t, 3H, $1CH_3$). *Anal.* calcd. for $C_{17}H_{33}NO_2$: C 72.03, H 11.74, N 4.94; found: C 72.32, H 11.57, N 4.61.

10: yellow oil; IR (neat): 3430, 2930, 2860, 1450, 1120, 895; ^1H NMR (60 MHz): 3.45 (m, 5H, $2CH_2$-O + 1CH-O containing 1q at 3.5 O—CH_2—CH_3), 2.55 (m, 4H, containing an ABX system with $\delta_A \simeq 2.7$ and $\delta_B \simeq 2.25$ and J_{AB} = 12.5, J_{AX} = 4, and J_{BX} = 8.5 Hz), 1.90–1.0 (vbr m, 20 H) 2 cyclohexyl groups, 1.20 (t, 3H, CH_3). *Anal.* calcd. for $C_{17}H_{33}NO_2$: C 72.03, H 11.74, N 4.94; found: C 71.89, H 11.61, N 5.13.

11: yellow oil; IR (neat): 3420, 2920, 2840, 1450, 1110, 890; ^1H NMR (60 MHz): 3.60 (m, 5H, $2CH_2$-O + 1CH-O), 2.70 (m, 4H, CH_2-N + 2CH-N), 1.60 (vbr m, 20 H) 2 cyclohexyl groups, 1.15 (t, 3H, CH_3). *Anal.* calcd. for $C_{17}H_{33}NO_2$: C 72.03, H 11.74, N 4.94; found: C 72.16, H 11.74, N 4.69.

12: mp 80–81°C (Et_2O), white powder. IR (CCl_4): 3580, 3360, 2920, 2842, 1450, 1390, 1105, 1053, 892; ^1H NMR (60 MHz): 3.60 (m, 3H, O—CH—CH_2OH), 2.60 (m, 4H, CH_2-N + 2CH-N), 1.50 (vbr m, 20 H) 2 cyclohexyl groups. *Anal.* calcd. for $C_{15}H_{29}NO_2$: C 70.54, H 11.45, N 5.48, O 12.53; found: C 70.36, H 11.46, N 5.43, O 12.74.

Besides these products, we isolated in very small quantities, between compounds **8** and **7**, two very similar compounds having very close IR and NMR spectra. NMR spectra showed no OEt group. Data were as follows: compound A: white crystals, mp 142°C; IR (CCl_4): 2938, 2858, 1450, 1107, 890. Compound B: yellowish oil, IR (CCl_4): 2938, 2860, 1450, 1109, 890.

X-ray crystallography

Compound ***1*** was isolated from ethanol as colorless monoclinic crystals. A single crystal was selected for the collection of intensity data on an Enraf–Nonius CAD-4 diffractometer. The crystal data are summarized in Table 1. The data were collected by the ω–2θ scan technique, with variable scanning rate, using graphite monochromated CuKα radiation. Two standard reflections were measured every 5400 s of radiation time and showed no significant variation during the course of data collection. The intensities were corrected for Lorentz and polarization effects but not for absorption.

The structure was solved by direct methods using the program MULTAN 80 (19) and electron density synthesis. Difference Fourier map calculations revealed the water of inclusion and the hydrogen atoms. Block-diagonal matrix least-squares refinement was performed for the scale factor, positional, and anisotropic thermal parameters of the non-hydrogen atoms. The hydrogen atoms were included in the calculations and refined with isotropic thermal parameters. The function minimized was $\Sigma w||F_o| - |F_c||^2$ where $w = 1$ if $|F_o| < P$, $P = [F^2_{o(max)}/10]^{1/2}$; $w = (P/F_o)^2$ if $|F_o| > P$. The scattering factors used for non-hydrogen atoms were taken from the International Tables for X-ray Crystallography (20), and for hydrogens from Stewart *et al.* (21). The final atomic coordinates are given in Table 2. All calculations were performed on a Mini 6-92 CII-Honeywell Bull computer using unpublished programs from the Crystallography Laboratory, University of Bordeaux I.[2]

Compound ***7*** ($C_{27}H_{50}N_2O$; M = 418.70) was isolated from cyclohexane/ether as colorless triclinic crystals of space group $P\bar{1}$ and Z = 2. The same procedure as the one used for compound **1** was applied. The cell parameters are a = 6.340(1), b = 12.262(2), c = 17.684(3) Å, α = 102.38(2), β = 90.02(2), γ = 75.30(2)°. This compound presents crystallographic problems. During the resolution of the structure, the Fourier maps clearly indicated two conformations for the hydroxypropyl chain, with equal occupancies and single positions for both nitrogen atoms. We tried to refine the structure in the non-centrosymmetric space group $P1$ and two independent molecules but the same phenomenon occurred. We then allowed for disorder in the crystal (the low value of the calculated density D_{calcd} = 1.07, D_{obs} = 1.0 was in favour of this assumption; no solvent inclusion was identified in Fourier maps). Parallel to this, the Fourier maps revealed the four cyclohexane rings almost planar, with abnormal bond lengths and angles. Then we had to admit the existence of two conformers for

[2]A complete set of tables of hydrogen positional parameters, temperature factors, and observed and calculated structure factors may be purchased from the Depository of Unpublished Data, CISTI, National Research Council of Canada, Ottawa, Ont., Canada K1A 0S2.

The hydrogen atom coordinates have been deposited with the Cambridge Crystallographic Data Centre, and can be obtained on request from The Director, Cambridge Crystallographic Data Centre, University Chemical Laboratory, Lensfield Road, Cambridge CBE 1EW, U.K.

each ring due to a simultaneous inversion of the coordination tetrahedra of the two nitrogens. What was observed was an average conformation of each cyclohexane ring, which appeared almost planar. It was possible to model the disordered hydroxypropyl unit, but unfortunately the alternative cyclohexane conformations were not clearly observed and the whole molecule could not be properly refined.

1. C. BOYER, J. C. COLLETER, M. H. CREUZET, C. FENIOU, M. LAGUERRE, H. PONTAGNIER, and G. PRAT. French Patents 2 557 102, 2 557 103, and 2 564 465.
2. V. R. GAERTNER. Tetrahedron Lett. 141 (1964); 4691 (1966); J. Org. Chem. **32**, 2972 (1967); Tetrahedron, **23**, 2123 (1967).
3. D. MILLER and T. MELTON. Brit. Patent 1 236 078; Chem. Abstr. **75**, 76595s (1971).
4. S. A. CASTAIGNE. French Patent 2 280 370; Chem. Abstr. **85**, 159855j (1976).
5. T. OKUTANI, T. KANEKO, and K. MASUDA. Chem. Pharm. Bull. **22**, 1490 (1974).
6. D. FREHEL, A. HEYNES, J. P. MAFFRAND, F. ELOY, D. AUBERT, and F. ROLLAND. Eur. J. Med. Chem. **12**, 447 (1977).
7. E. H. GOLD and D. M. SOLOMON. Ger. Offen. 2 750 300; Chem. Abstr. **89**, 109039h (1978); U.S. Patent 4 183 923; Chem. Abstr. **93**, 47012r (1980).
8. (*a*) E. L. MCGANDY, H. M. BERMAN, J. W. BURGNER II, and R. L. VAN ETTEN. J. Am. Chem. Soc. **91**, 6173 (1969); (*b*) J. B. WETHERINGTON and J. W. MONCRIEF. Acta Crystallogr. Sect. B: Struct. Crystallogr. Cryst. Chem. **30**, 534 (1974); (*c*) S. RAMAKUMAR, K. VENKATESAN, and S. T. RAO. Acta Crystallogr. Sect. B: Struct. Crystallogr. Cryst. Chem. **33**, 824 (1977).
9. (*a*) H. M. BERMAN, E. L. MCGANDY, J. W. BURGNER II, and R. L. VAN ETTEN. J. Am. Chem. Soc. **91**, 6177 (1969); (*b*) R. L. TOWNS and L. M. TREFONAS. J. Am. Chem. Soc. **93**, 1761 (1971).
10. (*a*) R. H. HIGGINS, N. H. CROMWELL, and W. W. PANDLER. J. Heterocycl. Chem. **8**, 961 (1971); (*b*) R. H. HIGGINS and N. H. CROMWELL. J. Heterocycl. Chem. **8**, 1059 (1971); (*c*) R. H. HIGGINS, E. DOOMES, and N. H. CROMWELL. J. Heterocycl. Chem. **8**, 1063 (1971).
11. F. H. ALLEN. Acta Crystallogr. Sect. B: Struct. Crystallogr. Cryst. Chem. **40**, 64 (1984); **40**, 72 (1984).
12. J. D. DUNITZ. X-ray analysis and the structure of organic molecules. Cornell Univ. Press, Ithaca and London. 1979. pp. 423–424.
13. C. E. NORDMAN and D. J. SCHMITKONS. Acta Crystallogr. **18**, 764 (1965).
14. J. H. ROSS, D. BAKER, and A. T. COSCIA. J. Org. Chem. **29**, 824 (1964).
15. D. L. HEYWOOD and B. PHILIPPS. J. Am. Chem. Soc. **80**, 1257 (1958).
16. (*a*) A. K. BOSE and P. R. SRINIVASAN. Tetrahedron, **31**, 3025 (1975); (*b*) G. KNUPP and A. W. FRAHM. Magn. Reson. Chem. **26**, 37 (1988).
17. G. C. LEVY, R. L. LICHTER, and G. L. NELSON. Carbon-13 nuclear magnetic resonance spectroscopy. 2nd ed. Wiley–Interscience, New York. 1980. p. 61.
18. R. S. BURIKS and E. G. LOVETT. J. Org. Chem. **52**, 5247 (1987).
19. P. MAIN, S. J. FISKE, S. E. HULL, L. LESSINGER, G. GERMAIN, J. P. DECLERCQ, and M. M. WOOLFSON. MULTAN 80. A system of computer programs for the automatic solution of crystal structures from X-ray diffraction data. Universities of York, England, and Louvain, Belgium. 1980.
20. International tables for X-ray crystallography. Vol. IV. Kynoch Press, Birmingham (Present distributor: D. Reidel, Dordrecht). 1974.
21. R. F. STEWART, E. R. DAVIDSON, and W. T. SIMPSON. J. Chem. Phys. **42**, 3175 (1965).

Can. J. Chem. Downloaded from www.nrcresearchpress.com by 194.225.253.170 on 09/07/12
For personal use only.

The solution structures of chiral Ti^{4+} alkoxides

PIERRE G. POTVIN,[1] ROBERT GAU, PATRICK C. C. KWONG, AND STEPHEN BIANCHET
Department of Chemistry, York University, North York, Ont., Canada M3J 1P3

Received November 14, 1988[2]

PIERRE G. POTVIN, ROBERT GAU, PATRICK C. C. KWONG, and STEPHEN BIANCHET. Can. J. Chem. **67**, 1523 (1989).

1,4-Di-*O*-methyl-L-threitol and 1,2,5,6-tetra-*O*-methyl-L-mannitol were prepared by new, more convenient, and higher yielding routes. These and 1,2;5,6-di-*O*-isopropylidene-D-mannitol formed 2:2 complexes with $Ti(O^iPr)_4$, but did not readily form 1:2 complexes in the presence of excess Ti^{4+}. ^1H and ^{13}C nuclear magnetic resonance spectra showed that the structures in solution of the 2:2 complexes were analogous to solid-state structures of tartaric acid derivatives, i.e., possessing bridging diolate oxygens. In contrast, *R,R*- and *meso*-diisopropyl tartrates, *N,N'*-dibenzyl tartramide, and *N,N'*-di(2-phenyl)ethyl tartramide behaved very differently. The tartramides formed mixtures of complexes that became dominated by 2:3 complexes in the presence of excess $Ti(O^iPr)_4$. Two tertiary tartramides failed to provide well-defined complexes. The *R,R*-tartrate formed a monocyclic (nonbridged) 2:2 complex, but an equilibrating mixture of 1:2 and 2:2 complexes with excess Ti^{4+}. The equilibrium shifted upon cooling toward a 1:2 complex possessing a bridging diolate oxygen, as did the *meso* 1:2 complex. Other temperature-dependent phenomena were also studied.

Key words: titanium(IV), chiral alkoxides, solution structures, NMR, Sharpless catalysts.

PIERRE G. POTVIN, ROBERT GAU, PATRICK C. C. KWONG et STEPHEN BIANCHET. Can. J. Chem. **67**, 1523 (1989).

Le 1,4-di-*O*-méthyl-L-thréitol et le 1,2,5,6-tétra-*O*-méthyl-D-mannitol ont été préparés avec de meilleurs rendements par des voies nouvelles et plus commodes. Ces diols et le 1,2;5,6-di-*O*-isopropylidène-D-mannitol forment des complexes 2:2 avec le $Ti(O^iPr)_4$, mais ne forment pas aisément des complexes 1:2 en présence d'excès de Ti^{4+}. D'après la spectroscopie en résonance magnétique nucléaire, les complexes 2:2 ont des structures en solution analogues à celles adoptées à l'état solide par les complexes de dérivés d'acide tartrique, possédant des ponts diolates. Cependant, les tartrates d'isopropyle *R,R* et *meso* et les *N,N'*-dibenzyl et *N,N'*-di(2-phényl)éthyl tartramides mènent à des structures très différentes. Les tartramides forment des mélanges de complexes en équilibre où les complexes 2:3 predominent en présence d'excès de $Ti(O^iPr)_4$. Deux tartramides tertiaires n'ont fourni aucun complexe charactérisable. Le tartrate *R,R* forme un complexe 2:2 monocyclique non-ponté et, en présence d'excès de Ti^{4+}, un mélange en équilibre de complexes 2:2 et 1:2 non-ponté. Ce mélange, ainsi que celui obtenu avec le tartrate *meso*, fournissent à −50°C un complexe 1:2 possédant un pont diolate. Les variations des structures avec la température ont aussi été étudiées.

Mots clés : titanium(IV), alcoxides chiraux, structures en solution, RMN, catalyseurs de Sharpless.

Introduction

The Sharpless reaction (1–3), the enantioselective epoxidation of allylic alcohols catalyzed by 1:1 complexes of Ti^{4+} with tartaric esters, clearly demonstrates the value of chiral Lewis acidic complexes as catalysts for enantioselective bond formation. The utility of Ti^{4+} complexes has been further demonstrated in other enantioslective oxidations by 2:1 (4), 4:1 (5), and 1:2 (6, 7) ligand–Ti^{4+} complexes as well as by 1:1:1 and 2:1:1 ligand–Ti^{4+}–H_2O complexes (4). Further, chiral dichlorotitanium(IV) complexes have recently been used in enantioslective Diels–Alder (8) and ene (9) reactions.

We wished to design new, general, chiral Ti^{4+} Lewis acids suited for other bond-forming reactions involving, for instance, strong nucleophiles and bases, with which the tartaric acid derivatives are incompatible. We sought sources of chirality-bearing unreactive side chains able to reproduce, as much as possible, the chiral environment that the oxidation catalysts impose with such success. The crystal structures of two Sharpless catalysts had in fact been determined (10). Both were found to be dimeric, as in solution. Both possessed tricyclic cores formed by combinations of one terminal and one bridging diolate per ligand moiety, resulting in loss of ligand-centred C_2 symmetry.

We chose to investigate C_2-symmetric vicinal diols bearing additional base- and nucleophile-stable ether-type oxygen binding sites, of which new convenient syntheses are presented. These sugar-derived ligands did not lead to highly enantioslective epoxidation,[3] yet nmr spectroscopy revealed that their 1:1 complexes with $Ti(O^iPr)_4$ had lost the ligand-centred C_2 symmetry, as expected from the crystal structures (10). On the other hand, the 2:2 complex formed from *R,R*-diisopropyl tartrate (DIPT), a typical Sharpless ligand, gave symmetrical nmr spectra. We therefore launched a study of the structures in solution of the Sharpless catalysts. In a preliminary account (12), we presented evidence that the 2:2 *R,R*-DIPT–Ti^{4+} complex adopted a ten-membered monocyclic structure in solution, while tricyclic structures, found in solid-state complexes of tartaric acid derivatives (10), were formed in solution by our ether-bearing ligands. In this report, we present further details of those findings, a reexamination of the 1:2 *R,R*-DIPT–Ti^{4+} complex and new results with *meso*-DIPT and two secondary tartramide ligands, in an effort to shed light on the structures of the precatalytic complexes involved in oxidation reactions.

Experimental

General

THF, $CHCl_3$, $CDCl_3$, and $Ti(O^iPr)_4$ were freshly distilled. Fresh ampoules of CD_2Cl_2 (Merck) were used. Optical rotations were measured on a Perkin–Elmer 110 polarimeter in a 1-dm cell. The nmr spectra were obtained on a AM-3000 Bruker instrument, at 300 MHz for ^1H spectra or at 75 MHz for ^{13}C spectra. The $CHCl_3$ peak in ^1H nmr spectra or the $CDCl_3$ peak in ^{13}C nmr spectra were at times used as internal standards. The *t*-BuOH peaks were used for spectra in D_2O. Structural assignments were made with the help of coupled ^{13}C spectra,

[1]Author to whom correspondence may be addressed.
[2]Revision received May 16, 1989.

[3]P. G. Potvin and P. C. C. Kwong, unpublished results.

Can. J. Chem. Downloaded from www.nrcresearchpress.com by 194.225.253.170 on 09/07/12
For personal use only.

Can. J. Chem. Downloaded from www.nrcresearchpress.com by 194.225.253.170 on 09/07/12
For personal use only.

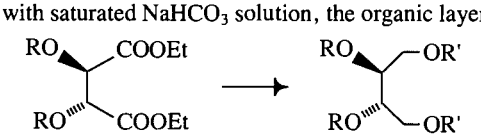
J-modulated spin echo, $^{13}C-^{1}H$ and $^{1}H-^{1}H$ correlation spectra, and with single-frequency hetero-decoupling (SFD) experiments using pulse sequences from the Bruker library. The ABX spin systems were analysed by computer simulation using the program NMRCALC (M. D. Johnson, Jr., University of South Florida).

Materials

1,2;3,4;5,6-Tri-*O*-isopropylidene-D-mannitol was prepared by a slight modification of the procedure of Wiggins (13), wherein three equivalents of 2,2-dimethoxypropane were added to the reaction mixture and the product was recrystallized from hexanes, with mp 70°C (lit. (13) mp 69–70°C). 3,4-*O*-Isopropylidene-D-mannitol was obtained by hydrolysis of the triacetonide according to Wiggins (13), but a shorter reaction time (1 h) provided a higher yield (77% vs. lit. 70%), mp 83°C (lit. (14) mp 85°C, (13) mp 86–87°C). 1,2;5,6-Di-*O*-isopropylidene-D-mannitol (mannitol diacetonide, MDA) was obtained by the method of Kohan and Just (15).

Diethyl 2R,3R-di-(tetrahydropyran-2-yloxy)succinate ***1***

R,R-Diethyl tartrate (2.07 g, 10 mmol) was dissolved in dry THF containing (optionally) a trace of *p*-TsOH. The solution was cooled (ice bath) and neat dihydropyran (1.23 mL, 20 mmol) was added dropwise (the reaction was exothermic). After stirring for 1 h in the cooling bath, the mixture was warmed to room temperature and allowed to stir a further 48 h. After diluting with ether and, if *p*-TsOH had been used, washing with saturated $NaHCO_3$ solution, the organic layer was dried



DET R: H
1 R: THP
2 R: THP R': H
3 R: THP R': Me
DMT R: H R': Me

($MgSO_4$) and rid of solvents. The yield of crude **1**, a mobile colourless oil, was 3.75 g (100%). It was used as such in the next step; ^{1}H nmr ($CDCl_3$) δ: 4.94, 4.83, 4.74 (3dd, 2H, OCHO), 4.80, 4.58, 4.56 (3s, 2H, OCHCOOEt), 4.29–4.14 (m, 4H, CH_2CH_3), 3.53–3.42 (m, 4H, OCH_2CH_2), 1.91–1.41 (m, 12H, $OCH_2CH_2CH_2$, $OCH_2CH_2CH_2$, $OCHCH_2CH_2$), 1.30, 1.28 (2q, 6H, CH_2CH_3) ppm; ^{13}C nmr ($CDCl_3$) δ: 169.30, 169.06 (COOR), 100.81, 100.59, 96.57, 96.36 (C-2′), 78.00, 77.57, 74.41, 74.03 (C-2), 62.81, 62.25, 62.07, 61.91 (OCH_2CH_3), 61.51, 61.29, 61.09 (C-6′), 30.61, 30.06, 29.73 (C-3′), 25.38, 25.23, 25.16 (C-5′), 18.79, 18.71, 18.40, 18.25 (C-4′), 14.10, 14.03, 14.01 (CH_2CH_3) ppm.

*2,3-Di-*O*-(tetrahydropyran-2-yl)-*L*-threitol* ***2***

A suspension of $LiAlH_4$ (0.38 g, 10 mmol) in dry THF (10 mL) was treated by dropwise addition with a solution of **1** (2.68 g, 7.12 mmol) in THF (10 mL), and the mixture was heated at reflux temperature overnight. The reaction was quenched by sequential addition of H_2O (0.38 mL), 15% NaOH solution (0.38 mL), and H_2O again (1.14 mL). After the precipitate was filtered off, the filtrate was diluted with H_2O and extracted with ether. The extracts were combined, dried ($MgSO_4$), and evaporated to dryness to afford a yellow oil. Filtration through a short column of SiO_2, using 1:4 EtOAc–hexane and then 2:3 EtOAc–hexane as eluents, afforded 1.51 g of a viscous, colourless oil (73% yield), which was used as such in the next step. The ir showed no absorptions due to starting material at 1741 or 3400 cm^{-1}; ^{1}H nmr ($CDCl_3$) δ: 4.75, 4.57, 4.52, 4.46 (4dd, 2H, OCHO), 4.00–3.44 (m, 10H, $OCHCH_2O$, $OCHCH_2O$, OCH_2CH_2), 2.50 (bs, 2H, OH), 1.84–1.74, 1.57–1.47 (2m, 12H) ppm; ^{13}C nmr ($CDCl_3$) δ: 101.76, 101.55, 101.07, 98.88 (C-2′), 82.33, 81.60, 76.49, 75.55 (C-2), 65.72, 64.80, 64.61, 63.49 (C-1), 62.46, 61.89, 60.84, 59.63 (C-6′), 31.32, 31.22, 31.36, 30.80 (C-3′), 25.17, 25.00, 24.96 (C-5′), 21.51, 20.88, 20.76, 20.00 (C-4′) ppm.

*1,4-Di-*O*-methyl-2,3-di-*O*-(tetrahydropyran-2-yl)-*L*-threitol* ***3***

A suspension of ca. 100 mg of NaH (ca. 5 mmol, previously freed of oil by hexane washes) in dry THF (15 mL) was treated, by dropwise addition under an Ar atmosphere, with a solution of diol **2** (500 mg, 1.72 mmol) in THF (10 mL) containing traces of imidazole and *n*-$Bu_4N^+Br^-$ (16). After cooling to 0°C (ice bath), 2 mL of CH_3I (32.1 mmol) was added and the mixture stirred for 2 h. After dilution with H_2O and extraction with ether, the ether solution was dried ($MgSO_4$) and evaporated to dryness *in vacuo*, providing 546 mg of viscous oily **3** (100% yield), which was used as such in the next step; ^{1}H nmr ($CDCl_3$) δ: 4.86, 4.81, 4.78, 4.71 (4dd, 2H, OCHO), 4.08–3.87 (m, 2H, $OCHCH_2O$), 3.70–3.41 (m, 8H, $OCHCH_2O$, OCH_2CH_2), 3.37, 3.36, 3.35, 3.34 (4s, 6H, OCH_3), 1.87–1.45 (m, 12H) ppm; ^{13}C nmr ($CDCl_3$) δ: 100.91, 99.83, 98.93, 97.29 (C-2′), 76.65, 76.34, 76.00, 74.26 (C-2), 72.86, 72.59, 71.63 (C-1), 62.86, 62.78, 62.13 (C-6′), 59.12, 59.02 (OCH_3), 30.95, 30.92, 30.79 (C-3′), 25.61, 25.46, 25.42 (C-5′), 19.98, 19.81, 19.34, 18.79 (C-4′) ppm.

*1,4-Di-*O*-methyl-*L*-threitol (DMT)*

Compound **3** (546 mg, 1.72 mmol) in 4:1 MeOH–H_2O (5 mL) containing 5 drops of CF_3COOH was allowed to stir overnight. An excess of Dowex IRA 400 resin (OH^- form) was then added, and after stirring 1 h, was filtered off. The neutralized reaction mixture was evaporated *in vacuo* at 30°C, using codistillation with MeOH to remove the last traces of H_2O. The mobile oily residue weighed 230 mg (90% yield); $[\alpha]_D^{22}$ −4.6° (*c* 0.05 M, MeOH) (Nanasi and Liptak (17) report $[\alpha]_D^{22}$ −9.8° (*c* 0.2, EtOH). Seebach *et al.* (18) report mp 28°C, and $[\alpha]_D$ −2.5° (*c* 2.5, MeOH)). These authors also report ir and 60-MHz ^{1}H nmr data taken in CCl_4 in agreement with ours. For ^{1}H nmr (D_2O), δ: 3.83 (m, 2H, H2), 3.62–3.51 (m, 4H, H1), 3.41 (OCH_3) ppm; ^{1}H nmr ($CDCl_3$) δ: 3.81 (X part of ABX, 2H, $J_{1a,2} = 6.0$, $J_{1b,2} = 4.0$ Hz), 3.54 (A part of ABX, 2H, $J_{1a,2} = 6.0$, $J_{1a,1b} = 9.8$ Hz), 3.52 (B part of ABX, 2H, $J_{1b,2} = 4.0$, $J_{1a,1b} = 9.8$ Hz), 3.39 (s, 6H, OCH_3) ppm; ^{13}C nmr ($CDCl_3$) δ: 74.40 (C-1), 70.35 (C-2), 59.14 (OCH_3) ppm; ^{13}C nmr (D_2O) δ: 73.17 (C-1), 69.86 (C-2), 58.28 (OCH_3) ppm.

*3,4-*O*-Isopropylidene-1,2,5,6-tetra-*O*-methyl-D-mannitol* ***5***

A solution of 3,4-*O*-isopropylidene-D-mannitol **4** (109 mg, 0.5 mmol) in dry DMSO (2 mL) was treated, under an Ar atmosphere, with 2 mL of a ca. 2 M solution of sodium dimsylate in DMSO. After stirring for 5 min, the solution was cooled to 0°C (ice bath), and CH_3I (2 mL, 32.1 mmol) was slowly added to the solidified mixture, which was then allowed to warm to room temperature and stirred for 10 min. After this period, the mixture was concentrated *in vacuo* and extracted into hexane. Washing with water, drying ($MgSO_4$), and removal of solvent afforded 83 mg (60% yield) of pure **5** as a slightly yellowish oil; $[\alpha]_D^{22}$ +31.8° (*c* 0.04 M, EtOH) (Irvine and Paterson (14) report $[\alpha]_D^{20}$ +39.1° (*c* 3.098, H_2O), +32.2° (*c* 2.865, EtOH)); ^{1}H nmr ($CDCl_3$) δ: 4.09 (X part of ABX, 2H, H3), J = 1.3, 3.2 Hz), 3.63 (A part of ABX, 2H, H1a, $J_{app} = 3.0$, 10.1 Hz), 3.53–3.41 (B part of ABX + m + s, 10H, H1b, H2, OCH_3), 3.37 (s, 6H, OCH_3), 1.39 (s, 6H, CCH_3) ppm; ^{13}C nmr ($CDCl_3$) δ: 109.73 (CCH_3), 81.34 (C-2), 77.96 (C-3), 71.89 (C-1), 59.15, 58.44 (OCH_3), 27.20 (CCH_3) ppm.

*1,2,5-6-Tetra-*O*-methyl-D-mannitol (TTM)*

Compound **5** (80 mg) was dissolved in 4:1 MeOH – 1 N HCl (5 mL) and allowed to stir at room temperature for 48 h. Work-up as with diol DMT afforded 56 mg of viscous, oily TTM (82% yield); $[\alpha]_D^{22}$ −12.6° (*c* 0.04 M, EtOH) (Irvine and Paterson (14) report $[\alpha]_D^{20}$ −13.02° (*c* 1.921, H_2O), −12.54° (*c* 1.813, EtOH)); ^{1}H nmr ($CDCl_3$) δ: 3.83 (d, 2H, H3, $J_{2,3} = 6.2$ Hz), 3.66 (A part of ABX, 2H, H1a, $J_{1a,2} = 4.4$, $J_{1a,1b} = 10.1$ Hz), 3.59 (B part of ABX, 2H, H1b, $J_{1b,2} = 4.4$, $J_{1a,1b} = 10.1$ Hz), 3.45 (X part of ABX, 2H, H2, $J_{2,3} = 6.2$, $J_{1a,2} = 4.4$, $J_{1b,2} = 4.4$ Hz), 3.47, 3.40 (2s, 12H, OCH_3) ppm; ^{13}C nmr ($CDCl_3$) δ: 80.85 (C-2), 71.66 (C-1), 69.73 (C-3), 59.23, 58.37 (OCH_3) ppm.

Nuclear magnetic resonance studies

Two methods of sample preparation were used. One involved titration at room temperature (27°C) of $CDCl_3$ solutions of $Ti(O^iPr)_4$ with $CDCl_3$ solutions of DMT, TTM, or MDA. Reverse titrations were also employed. This allowed monitoring over a wide range of stoichiometries. To preclude possible interference of adventitious H_2O, the second method involved formation of complexes at defined stoichiometries

Can. J. Chem. Downloaded from www.nrcresearchpress.com by 194.225.253.170 on 09/07/12
For personal use only.

under Ar. No differences were found in the signal patterns from samples prepared by either method. Preparations at different concentrations showed no observable differences.

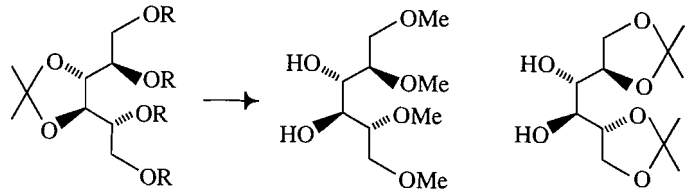
Results

Syntheses of DMT and TMM

1,4-Di-*O*-methyl-L-threitol (DMT) had been prepared by electrophilic (Purdie) methylation (CH_3I, Ag_2O/DMF/48 h/88.5% yield) of 2,3-*O*-isopropylidene-L-threitol, followed by hydrolysis (17). A similar methylation of the D enantiomer proceeded in 77% yield (19). Phase-transfer-catalyzed nucleophilic methylation with dimethyl sulfate (a variation on the Haworth method) proceeded in 67% yield (18). In other work in which 1,4-anhydro-L-threitol had been prepared, we had found that protection of diethyl tartrate with THP groups, needed for the cyclization of a 2,3-protected threitol, was convenient for small-scale work, proceeding quantitatively even without catalysis[4]. Thus, *R*,*R*-diethyl tartrate was protected as its di-THP derivative **1**, then reduced to the protected L-threitol **2** in 73% overall yield. In the methylation of **2**, we adapted the alcohol benzylation procedure of Czernecki *et al.* (16), in which exchange of the Na^+ counterions by the larger $^nBu_4N^+$ facilitates nucleophilic attack of CH_3I by an alkoxide. Thus, compound **3** was obtained in quantitative yield, a significant improvement over the Purdie or Haworth methods. After hydrolysis (90% yield), our overall yield of DMT was 36.5% from diethyl L-tartrate. The final product displayed the expected three-line ^{13}C nmr spectrum, the expected ABX pattern in the ^1H spectrum, and an optical rotation in agreement with literature values.

THP protecting groups find wide use in general organic work (21) but not in the carbohydrate or ribonucleoside fields (22) due to a lack of selectivity (23) or of crystallinity, to possible migration problems, and to diastereomerism. Diastereomeric THP-protected sugars have been separated in a few cases of mono-protection (24–26), but not with two THP groups (22). In our work, no attempts to separate diastereomers were made, yet there was no difficulty in verifying the structures of intermediates by ^{13}C nmr nor in monitoring the reactions by ir and tlc. The ^{13}C nmr resonances usually occurred in easily identifiable groups of four, simplified because the starting material and the product each have a C_2 axis of symmetry. However, the intermediates (particularly **3**) were not very stable in the presence of water and (or) acid, probably owing to steric congestion at the secondary positions. Trailing was also observed on tlc plates of SiO_2. The intermediates were therefore not stored and were used immediately.

We had hoped to use the same methylation procedure with mannitol 3,4-monoacetonide **4** (13) as was used in the preparation of DMT. However, the method of Czernecki *et al.* (16) failed because of the insolubility of the intermediate alkoxides. Purdie methylation of **4** had been reported, but was incomplete and required resubmission to fresh reagents for a cumulated yield of 60% (14). The yield of the subsequent hydrolysis step was not given. We found that the Hakomori polysaccharide permethylation procedure (27) (sodium dimsylate/DMSO/0°C to room temperature, then CH_3I/15 min) was fast and clean, and, after simple extraction into hexanes, afforded **5** in 60% isolated yield (Scheme 1). Thus, the Hakomori procedure presented a distinct advantage over the Purdie and Czernecki methods. After hydrolysis (82% yield), the overall yield of



4 R: H
5 R: Me

TMM MDA

SCHEME 1

TMM was 49%. These products displayed the expected seven- and five-line ^{13}C spectra, respectively, ^1H nmr spectra consistent with their structures, and optical rotations in agreement with literature values.

Nuclear magnetic resonance studies

Because epoxidation reactions are usually conducted at low temperatures (1), we examined several samples over a broad temperature range, down to as low as −50°C. As well, because CH_2Cl_2 is the usual solvent for epoxidation reactions (1), all of the complexes were examined in $CDCl_3$ and several were also examined in fresh, anhydrous CD_2Cl_2, with only slight differences in the nmr patterns resulting.

Complexes of DMT, TMM, and MDA

Treatment of each of the three sugar ligands DMT, TMM, and MDA with one equivalent of $Ti(O^iPr)_4$ at room temperature led to the liberation of two equivalents of HO^iPr and the disappearance of the $Ti(O^iPr)_4$ signal, according to the equation

[1] $H_2L + Ti(O^iPr)_4 \rightarrow LTi(O^iPr)_2 + 2HO^iPr$

Single species were formed in each case, as ascertained by decoupling experiments, with loss of the ligands' C_2 symmetry in the nmr spectra. In contrast with the rapid ligand equilibration reported for tartrate complexes (2, 3), these products evidently underwent no such side-chain exchange. In fact, the OCH_3 signals of the DMT complex coalesced only near 57°C, while coalescence of the central OC*H* signals was still incomplete at 62°C. Upon cooling to −23°C, only small changes in the ^1H shifts were seen. The nmr shift data and assignments appear in Tables 1 and 2. In Table 3 (entries 1–3) are reported the displacements of selected ligand signals from their positions in free ligands. Computer simulation was used to analyse the ABX pattern in the DMT complex, but similar analysis of the TMM and MDA complexes was impossible. However, the side-chain nuclei in all three complexes could be located by ^1H–^{13}C correlation experiments (see Fig. 1). Electron-impact (E.I.) mass spectra showed that, as with DBT or the tartrates (2, 3), the products were 2:2 complexes. Although a weak molecular ion was detected only with TMM, two common high-weight fragments could be assigned in each case, one owing to loss of $^iPrO^\bullet$, a fragmentation common in the E.I. spectra of tartrate ester complexes (3), and the other owing to loss of a side chain. Additionally, loss of $CH_3^\bullet$ or $CH_3O^\bullet$ occurred. For instance, the MDA complex showed Ti_2 clusters at m/z 837 ($M^{\bullet+} - CH_3^\bullet$), 793 ($M^{\bullet+} - {}^iPrO^\bullet$), and 751, coresponding to β-cleavage of one side chain, 2,2-dimethyl-1,3-dioxolane radical, which gave rise to the base peak (m/z 101). Moreover, the observed ion abundances in the cluster at 751 matched very well those calculated using formula $C_{31}H_{59}O_{14}Ti_2$ and natural isotope abundances.

At 1:2 ligand–Ti stoichiometry and even with very large excesses of $Ti(O^iPr)_4$, the mixtures clearly consisted of the 2:2

[4]P. G. Potvin and R. Gau, unpublished results.

Can. J. Chem. Downloaded from www.nrcresearchpress.com by 194.225.253.170 on 09/07/12
For personal use only.

TABLE 1. The ^{1}H nmr chemical shifts (in ppm) and coupling data for free ligands and complexes (w designates weak signals)

Compound	Central OC*H*	Side chain	O^{i}Pr OC*H*	Others
HO^{i}Pr			4.01	1.20[a]
Ti(O^{i}Pr)$_4$			4.49	1.25[a]
DMT[b]	3.81	3.52, 3.54		3.39[c]
Ti$_2$(O^{i}Pr)$_4$(DMT)$_2$[d]	4.67 (H2)	3.62 (H1), 3.61(H1′)	4.73	3.44, 3.38[c]
	4.36 (H3)	3.61 (H4), 3.55 (H4′)		
TMM[e]	3.83	3.45 (H2),		3.47, 3.40[c]
		3.66, 3.59 (H1)		
Ti$_2$(O^{i}Pr)$_4$(TMM)$_2$[f]	4.56 (H3)	3.30–3.70	4.87	3.54, 3.51,
	4.28 (H4)		4.76	3.40, 3.35[c]
MDA[g]	3.73	4.17 (H2)		1.41, 1.35[a]
		4.00, 4.10 (H1)		
Ti$_2$(O^{i}Pr)$_4$(MDA)$_2$[h]	4.64 (H3)	4.35 (H2), 4.20 (H1),	4.69	1.24–1.44[a]
	4.23 (H4)	3.95 (H5), 3.88–4.13		
R,R-DIPT	4.47	5.15[i]		1.29[a]
Ti$_2$(O^{i}Pr)$_4$(*R,R*-DIPT)$_2$	5.11	5.05[i]	5.05	1.26, 1.24[a]
(27°C)			4.7w	
(−30°C)	5.08[j]	5.07, 4.97[i]	≅4.7	1.29–1.14[a]
Ti$_2$(O^{i}Pr)$_6$(*R,R*-DIPT)	5.11	5.06[i]	5.00	1.27–1.19[a]
(27°C)[k]			4.75	
			4.45[s]	
(−50°C)	5.18	5.06, 4.98[i]	4.71	1.35–1.08[a]
	4.74			
meso-DIPT	4.51	5.13[i]		1.29[a]
Ti$_2$(O^{i}Pr)$_6$(*meso*-DIPT)	5.25	5.01[i]	4.75	1.29–1.16[a]
(27°C)[k]			4.46[s]	
(−50°C)	5.36	5.01, 4.92[i]	4.73	1.24–1.09[a]
	5.18			
Ti$_3$(O^{i}Pr)$_8$(DBT)$_3$	5.00[l]	9.26, 7.73[n]	4.73	7.27–7.36[p]
	(5.02)[m]	≅4.7–4.4, 4.27[o]	4.49[s]	
DPET	4.20	7.13,[n] 3.52,[o] 2.80[q]		7.18–7.34[p]
Ti$_3$(O^{i}Pr)$_8$(DPET)$_2$	4.87[r]	8.94, 7.41[n]	4.71	7.18–7.30[p]
	(4.91)[m]	3.52,[o] 2.83[q]	4.49[s]	

[a]C*C*H$_3$.
[b]$J_{1,1'} = 9.75, J_{1,2} = 5.97, J_{1',2} = 3.95$ Hz.
[c]O*C*H$_3$.
[d]$J_{1,2} = 7.99, J_{1',2} = 4.64, J_{2,3} = 2.25, J_{3,4} = 2.96, J_{3,4'} = 5.29, J_{1,1'} \cong J_{4,4'} \cong 9.1$ Hz.
[e]$J_{1,1'} = 10.11, J_{1,2} = 4.36, J_{1',2} = 4.43, J_{2,3} = 6.24$ Hz.
[f]$J_{2,3} = 6.11, J_{3,4} \cong 1.1, J_{4,5} = 6.23$ Hz.
[g]$J_{1,1'} = 8.28, J_{1,2} = 6.33, J_{1',2} = 5.37, J_{2,3} = 6.18$ Hz.
[h]$J_{2,3} = 9.15, J_{3,4} \cong 0, J_{4,5} = 8.66$ Hz.
[i]COO*C*H.
[j]Centre of AB quartet (see text).
[k]Consists of a mixture of 1:2 and 2:2 Ti–*R,R*-DIPT complexes (see text).
[l]Centre of AB quartet at 27°C: $\Delta\delta = 0.024$ ppm, $J_{ab} = 6.8$ Hz.
[m]Singlet from −10°C to −30°C.
[n]N*H*.
[o]NHC*H*$_2$.
[p]Ph.
[q]NHCH$_2$C*H*$_2$.
[r]Centre of AB quartet at 27°C: $\Delta\delta = 0.059$ ppm, $J_{ab} = 7.2$ Hz.
[s]Residual Ti(O^{i}Pr)$_4$.

complexes and unreacted Ti(O^{i}Pr)$_4$. New species did form in minor amounts but could be seen only above room temperature with DMT, or at lower temperatures with TMM. Adding excess ligand also failed to form any new well-defined complexes. Rather, the resonances gradually became weaker and broader, and were eventually replaced with signals from the free ligands. Clearly, the sugars were reluctant to form well-defined complexes of other molecularities.

This reluctance and the lack of ligand C_2 symmetry over a broad temperature range pointed to a rigidity and a mode of stabilization particular to the asymmetric 2:2 complex. Yet side-chain binding was expected to be relatively weak, to exert little influence on the central OC*H* and OC*H* signals, and thus not expected to be the source of asymmetry. By analogy to the solid-state structure of the 2:2 DBT complex (10), the differences observed in these signals can be explained by the presence of a bridging diolate O in each ligand moiety, as in structures A*a*, *b*, *c*, with the planar tricyclic core providing the particular

TABLE 2. The ^{13}C nmr chemical shift data (in ppm) for free ligands and complexes (w designates weak signals)

Compound	Central OCH	Side chain	$TiOCHMe_2$	Others
HO^iPr				63.90, 25.04[a]
$Ti(O^iPr)_4$			76.23	26.56[a]
DMT	70.35	74.40		59.14[b]
$Ti_2(O^iPr)_4(DMT)_2$	87.65 (C2) 81.65 (C3)	77.19 (C1), 74.12 (C4)	78.73 77.61	59.72, 58.98[b] 25.83, 25.64, 25.51[a]
TMM	69.73	80.85 (C2), 71.66 (C1)		59.23, 58.37[b]
$Ti_2(O^iPr)_4(TMM)_2$	88.21 (C3) 81.92 (C4)	84.46 (C5), 81.74 (C2), 73.03, 72.80 (C1, C6)	79.06 77.49	59.23, 58.97, 58.94, 58.85,[b] 26.00, 25.77, 25.65, 25.52[a]
MDA	70.73	75.54 (C2), 66.52 (C1)		109.10[c] 24.98, 26.50[a]
$Ti_2(O^iPr)_4(MDA)_2$	90.10 (C3) 86.60 (C4)	77.14 (C5), 75.75 (C2), 67.73, 67.45 (C1, C6)	79.37 78.98	109.25[c] 26.85, 26.64, 25.62, 25.49[a]
R,R-DIPT	71.88	170.70,[d] 69.56[e]		21.16, 21.08[a]
$Ti_2(O^iPr)_4(R,R\text{-DIPT})_2$	85.64	≅174.9, 172.2[d] ≅69[e]		25.19, 21.65, 21.63[a]
(27°C) (−10°C)	85.43 85.23	177w, 171.92[d] 70.90, 68.61[e]	≅77.3w	25.09, 25.07, 21.57[a]
$Ti_2(O^iPr)_6(R,R\text{-DIPT})$	84.91	≅175.3, 169.8[d]	≅77.3	26.41, 25.31, 21.66[a]
(27°C)[f]		69.49[e]	≅76.1	85.78[k]
(−30°C)[g]	86.00	179.22, 172.45[d]	79.18	25.68, 25.27, 25.01,
	82.57	71.65, 68.41[e]	78.26	23.86, 23.20, 21.65,
			73.81	21.60, 21.41[a]
meso-DIPT	73.01	170.72,[d] 70.40[e]		21.79, 21.67[a]
$Ti_2(O^iPr)_6$(*meso*-DIPT)	83.64	69.46[e]	77.18	26.24, 25.17, 25.06,
(27°C)			76.13[l]	21.71, 21.62, 21.55,
				21.47, 21.39, 21.31[a]
(−50°C)	84.53	179.43, 169.83[d]	79.07	26.39, 25.66, 25.47,
	81.64	72.53, 67.84[e]	78.41	25.09, 24.92, 24.10,
			77.20	23.20, 21.69, 21.53,
			73.85	21.33, 21.20[a]
$Ti_3(O^iPr)_8(DBT)_2$	85.90	183.45, 177.14[d]	77.30	26.55, 25.57, 25.34[a]
	84.46	44.41, 42.76[h]	76.23[l]	85.40[k]
		137.69, 137.03, 128.55		
		127.72, 127.57, 127.17[i]		
DPET	70.06	173.92,[d] 40.32,[h] 35.70[j]		
		138.26, 128.76, 128.73,		
		126.75[i]		
$Ti_3(O^iPr)_8(DPET)_2$	85.66	183.86, 177.04[d]	77.30	26.55, 25.59, 25.36[a]
	84.46	42.18, 40.10[h]	76.23[l]	85.37[k]
		35.83, 35.64[j]	72.22	
		138.65, 138.30, 128.67		
		128.59, 126.65, 126.55[i]		

[a] CCH_3.
[b] OCH_3.
[c] CCH_3.
[d] COOCH.
[e] COOCH.
[f] Consists of a mixture of $Ti(O^iPr)_4$, $Ti_2(O^iPr)_6(R,R\text{-DIPT})$, and $Ti_2(O^iPr)_4(R,R\text{-DIPT})_2$ (see text).
[g] Shows signals from residual room temperature species.
[h] $NHCH_2$.
[i] Ph.
[j] $NHCH_2CH_2$.
[k] Residual 2:2 complex.
[l] Residual $Ti(O^iPr)_4$.

Can. J. Chem. Downloaded from www.nrcresearchpress.com by 194.225.253.170 on 09/07/12
For personal use only.

TABLE 3. Displacements (in ppm) and assignments of selected ligand ^{13}C and ^{1}H nmr signals upon formation of complexes

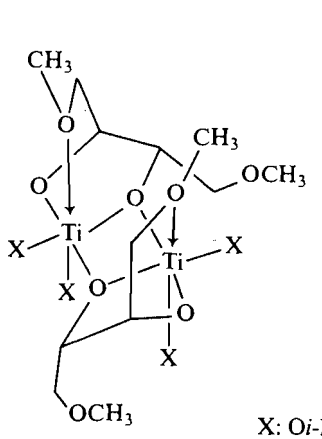
Compound	Central OCH	Central OC*H*	Side chain
$Ti_2(O^iPr)_4(DMT)_2$	17.30 (C2) 11.30 (C3)	0.86 (H2) 0.55 (H3)	2.29 (C1), −0.28 (C4) 0.58, −0.16 (OCH_3) 0.05, −0.01 (OCH_3)
$Ti_2(O^iPr)_4(TMM)_2$	18.48 (C3) 12.19 (C4)	0.73 (H3) 0.45 (H4)	3.61 (C5), 0.89 (C2) 1.37, 1.14 (C1, C6) 0.00, −0.25, −0.29, −0.38 (OCH_3) 0.07, 0.04, 0.00, −0.05 (OCH_3)
$Ti_2(O^iPr)_4(MDA)_2$	19.37 (C3) 15.87 (C4)	0.91 (H3) 0.50 (H4)	1.60 (C5), 0.21 (C2) 1.21, 0.93 (C1, C6)
$Ti_2(O^iPr)_4$(*R,R*-DIPT)$_2$	13.62	0.64	≅4.2, 1.5 (*C*=O) −0.10 (OC*H*)
$Ti_2(O^iPr)_6$(*R,R*-DIPT) (27°C)	13.50	0.64	≅4.6, −0.9 (*C*=O) −0.10 (OC*H*)
$Ti_2(O^i(Pr)_6$(*R,R*-DIPT) (−30°C)	13.62 12.35	0.71 0.27	8.52, 1.75 (*C*=O) 2.09, −1.15 (OCH) −0.09, −0.18 (OC*H*)
$Ti_2(O^iPr)_6$(*meso*-DIPT) (27°C)	10.63	0.74	−0.94 (OCH) −0.12 (OC*H*)
$Ti_2(O^iPr)_6$(*meso*-DIPT) (−50°C)	11.52 8.63	0.85 0.66	8.71, −0.89 (*C*=O) 2.13, −2.56 (OCH) −0.12, −0.21 (OC*H*)
$Ti_3(O^iPr)_8(DPET)_2$	15.60 14.40	0.73 0.61	9.94, 3.12 (*C*=O) 1.86, −0.22 ($NHCH_2$) 1.81, 0.28 (*NH*)

stability and rigidity observed. The other spectral data, in particular the pairs of distinct $TiOCHMe_2$ signals (and $TiOCHMe_2$ signals, with TMM), the weak coupling between central OC*H* (0–2.3 Hz), and the separate signals for each side chain, were entirely in accord with these structures.

Detailed examination of the spectra revealed two additional points. First, the most downfield side-chain carbon signal (C-4 in DMT or C-5 in the mannitols), assigned to the bound side chain, correlated to the most upfield side-chain OC*H*, and these were most closely connected to the upfield central OC*H*, assigned to the terminal diolate. Opposite assignments could also be made, but it seems most reasonable that the bridging central OCH signals should be downfield of the terminal ones. Second, the secondary ethers of the mannitols appeared to bind in preference to the primary ones. Although only small effects on adjoining nuclei were observed to result from side-chain binding, the shift differences between secondary positions were indeed larger than between the primary ones, indicating the probable binding of O5 as depicted in A*b*, *c*, even though less ring strain might be expected with O6.

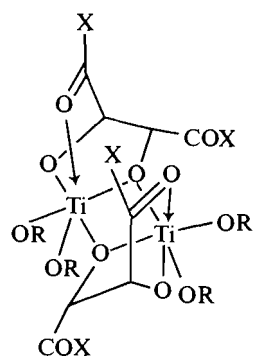
Complexes of R,R-*DIPT*

In contrast to the sugars, the nmr spectra of the 1:1 DIPT–$Ti(O^iPr)_4$ mixture showed complete symmetry at room temperature. Previous solution molecular weight measurements and mass spectral data (2) had established that tartrates form 2:2 complexes with $Ti(O^iPr)_4$ at 1:1 stoichiometry. Infrared evidence (2, 3) had indicated both Ti-bound and free ester groups in 2:2 tartrate complexes at room temperature. Although no nmr data have been published, $\Delta G^{\ddagger}$ values at coalescence of between 12.8 and 15.2 kcal mol^{-1} had been calculated for various tar-

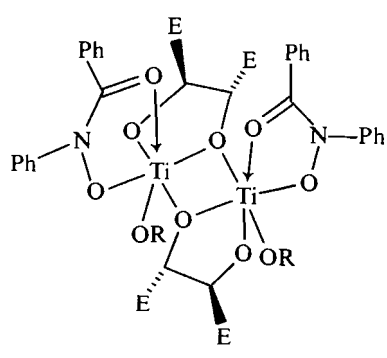


A*a*

A*b* R: Me
A*c* R,R: CMe_2



B R: *i*-Pr X: NHPh



C R: *i*-Pr E: COOEt

Can. J. Chem. Downloaded from www.nrcresearchpress.com by 194.225.253.170 on 09/07/12
For personal use only.

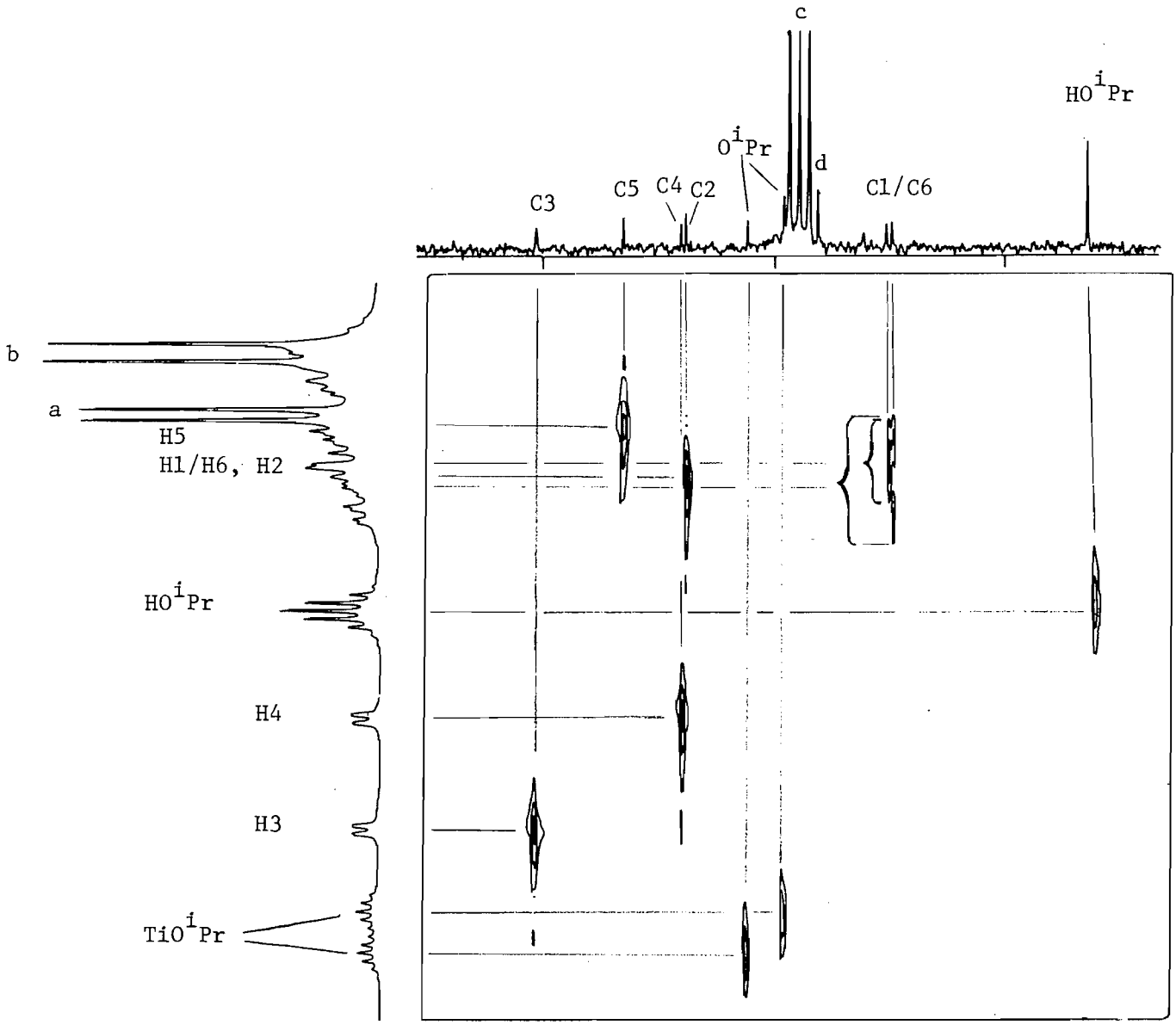


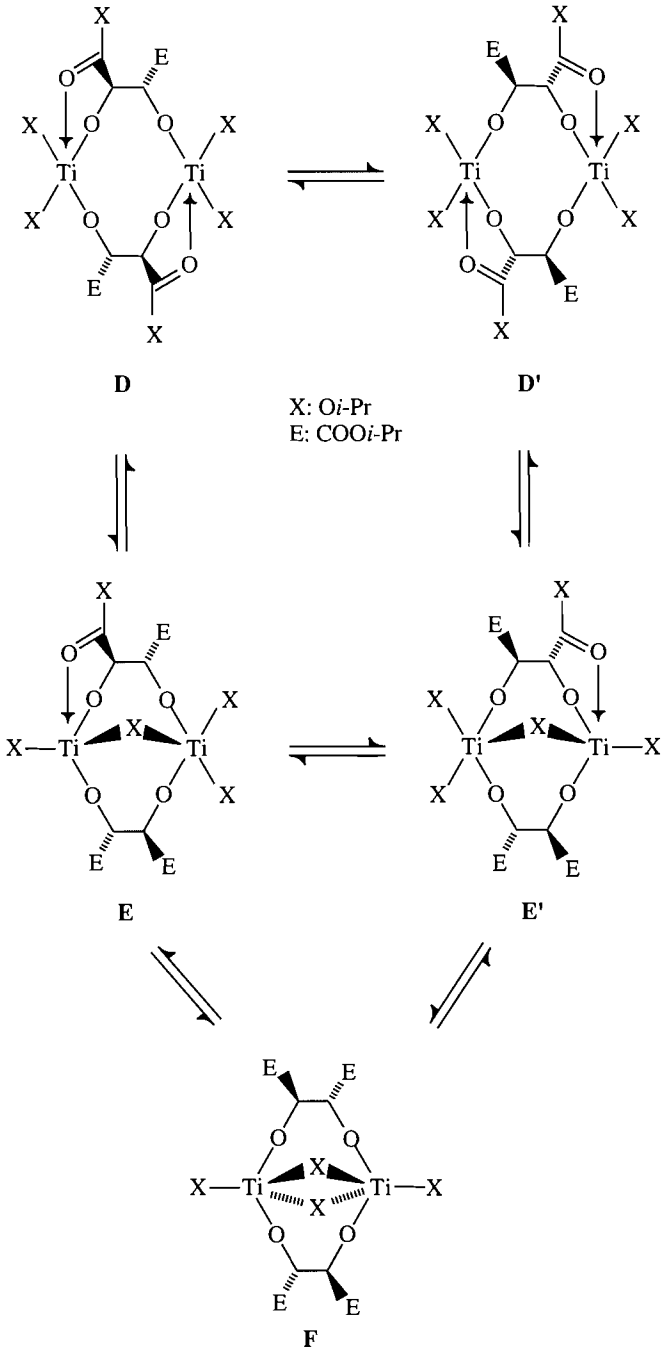
FIG. 1. OCH and OCH_2 regions of ^1H, ^{13}C and ^{13}C–^1H *J*-correlated nmr spectra of $(TMM)_2Ti_2(O^iPr)_4$ in $CDCl_3$, showing assignments. Other peaks are (a) O2-CH_3 and O5-CH_3; (b) O1-CH_3 and O6-CH_3; (c) CDCl_3; and (d) OCH from excess $Ti(O^iPr)_4$ present in ^{13}C sample.

trate–alkoxide combinations, and presumed to relate to fluxional ester interchange (2). The crystal structure of the 2:2:2 Ti – *N*-phenyl benzohydroxamate – diethyl tartrate (DET) complex (10), **B**, similar to that of the 2:2 Ti – *N*,*N*′-dibenzyltartramide (DBT) complex, **C**, in possessing a tricyclic core, would suggest that such interchange be rapid even on a rigid tricyclic framework. In view of the lack of side-chain equilibration in the sugar complexes, in which binding of the side-chain ethers was expected to be weak, the apparent symmetry in the 2:2 *R*,*R*-DIPT complex, in which binding of the side-chain ester group was expected to be much stronger, was not consistent with such a tricyclic core. The downfield shifts upon complex formation at room temperature of the single OCH and OC*H* resonances were in fact close in value to the upfield partners of the pairs seen in the sugar complexes. This suggested that both diolates were terminal and that the effect of side-chain binding on the central OCH nuclei was small compared to the effect of binding a second Ti. These suggestions were supported by data from the tartramide complexes (*vide infra*).

Detailed analysis of the nmr spectra led us back to the originally proposed (2) ten-membered monocyclic structure **D**. As shown in Fig. 2A, the room temperature ^1H nmr spectrum consisted of a broad singlet due to ligand OC*H*, overlapping broad signals for ester OC*H*, and new TiOC*H*Me_2. A weak and very broad feature near 4.7 ppm appeared to signal a second, minor kind of TiOC*H*Me_2. Single but broad ^{13}C resonances were found at room temperature for the central, ester, and HO^{i}Pr OCH, and they correlated weakly with signals due to the attached protons. Two very broad signals were at times found in the *C*=O region at room temperature, but at other times these were too broad and too weak to be detected. This might be due to rapid exchange between bound and free ester groups, but because the HO^{i}Pr signals were also broad, trans-esterification exchange was perhaps also occurring, as Ti^{4+} alkoxides are well-known trans-esterification catalysts, especially with α-hydroxy esters (1).

Cooling sharpened the spectra and arrested the side-chain exchange as well as any trans-esterification. The central OC*H*

Can. J. Chem. Downloaded from www.nrcresearchpress.com by 194.225.253.170 on 09/07/12
For personal use only.



D D' E E' F

signal split near −12°C into an apparent fine doublet (Fig. 2B), while the TiOC*H*Me_2 signal became more distinct from the ester OC*H*. The central OC*H* doublet widened into a clear AB quartet pattern (Fig. 2C) near −31°C and this persisted at least down to −43°C (at 5.08 ppm, with $\delta(H_a) - \delta(H_b) \cong 0.05$ ppm, $J_{ab} \cong 7$ Hz). Much below this temperature, the OC*H* region became more complex and detailed analysis was impossible. At the same time, the feature at 4.7 ppm gradually increased in proportion to the other signals in the OC*H* region to ca. 1:5, but remained broad. At −10°C and below, all ^{13}C signals were sharp except that for HOCMe_2. Two central OCH peaks were found, but these were very closely spaced (with $\Delta\delta = 0.2$ ppm at −50°C). This, along with the closely spaced central OC*H* signals, suggested that the diolates remained terminal at low temperatures. Two ester OCH signals could be clearly seen as well, though the downfield partner was weaker, and the C=O region contained one strong and one weak (downfield) signal. These downfield signals gradually disappeared upon cooling but had not completely disappeared even at −50°C. At this point, the TiOC*H*Me_2 signals were too weak and (or) too broad to be visible. Thus, the progressive loss of the downfield ester signals, and presumably of side-chain binding, appeared to be linked to the progressive gain in the upfield TiOC*H*Me_2 signal, while the complex remained asymmetric below −10°C. These data best fit a monocyclic structure where rapid side-chain exchange occurs at room temperature (**D** ↔ **D′**), but with loss of side-chain binding, replaced by reversible bridge formation, occurring in two steps at lower temperatures (**D** / **D′** ↔ **E** / **E′** ↔ **F**). Importantly, the bridging seemed to afford greater stability than side-chain binding.

The 1:2 DIPT–Ti(O^iPr)$_4$ mixture gave spectra at room temperature that were similar those of the 1:1 mixture. However, the presence of unreacted Ti(O^iPr)$_4$ (about one-eighth the total Ti, by integration, at 0.6 M Ti) was made evident by a broad OC*H* signal at 4.5 ppm and a OCH signal at 76.1 ppm. As well, a broad shoulder (near 5.0 ppm) on the ester OC*H* multiplet signalled a second kind of TiOC*H*Me_2 (Fig. 2D). Yet only one species was visible at −50°C (*vide infra*). Moreover, tenfold dilution sharpened the Ti(O^iPr)$_4$ and HO^{i}Pr signals and reduced the amount of unreacted Ti(O^iPr)$_4$ to about one-tenth. Clearly, *the 1:2 mixture was a mixture of complexes in rapid equilibrium*. The E.I. mass spectrum revealed the presence of both 2:2 and 1:2 complexes: a Ti_2 cluster at m/z 737 corresponded to (DIPT)$_2$Ti$_2$(O^iPr)$_4$ with loss of ^{i}PrO·, and weak clusters at m/z 681 ($M^{\bullet+}$ − H·) and 623 ($M^{\bullet+}$ − ^{i}PrO·) indicated the 1:2 complex. Further, clusters at m/z 283 ($M^{\bullet+}$ − H·), 269 ($M^{\bullet+}$ − CH_3·, base peak), and 225 ($M^{\bullet+}$ − ^{i}PrO·) confirmed the presence of Ti(O^iPr)$_4$. No significant higher mass fragments were found. Equilibrium [2] can then be postulated, with $K_2 \approx 240$. The broad feature at 5.0 ppm was therefore assigned to the 2:2 complex.

[2] $Ti_2(R,R\text{-DIPT})_2(O^iPr)_4 + 2Ti(O^iPr)_4 \overset{K_2}{\longleftrightarrow} 2Ti_2(R,R\text{-DIPT})(O^iPr)_6$

Earlier, we reported (12) that the low temperature spectra of the 1:2 mixture were also similar to those of the 1:1 mixture. That sample had been prepared by titration until disappearance of the Ti(OC*H*Me_2)$_4$ signal according to the equation

[3] $H_2L + 2Ti(O^iPr)_4 \rightarrow LTi_2(O^iPr)_6 + 2HO^iPr$

and was therefore, in light of the above, nearer 1:1 stoichiometry.

The sample used in the present work was prepared at exact 1:2 stoichiometry and showed very different spectra upon cooling. Some of the broad room temperature signals sharpened considerably. The Ti(OC*H*Me_2)$_4$ heptet progressively disappeared and new peaks due to an asymmetric complex progressively appeared and became dominant (Fig. 2E and F). The central OC*H* room temperature singlet at 5.11 ppm split, as with the 2:2 complex, into a fine doublet by −19°C, then disappeared near −30°C while being replaced, starting at least as soon as −10°C, by two new, widely separated singlets. One of these was strongly shifted upfield (to 4.74 ppm), overlapping one of the two broad LTiOC*H*Me_2 heptets that had arisen from the single room temperature heptet. The HO^{i}Pr signal remained broad throughout. These changes were paralleled in the ^{13}C spectra. At room temperature, two close broad central OCH signals were seen. The downfield partner was close to that seen in the 1:1 mixture and disappeared upon cooling, and was therefore likely due to the 2:2 species. The (upfield) room temperature partner at 84.9

Can. J. Chem. Downloaded from www.nrcresearchpress.com by 194.225.253.170 on 09/07/12
For personal use only.

Can. J. Chem. Downloaded from www.nrcresearchpress.com by 194.225.253.170 on 09/07/12
For personal use only.

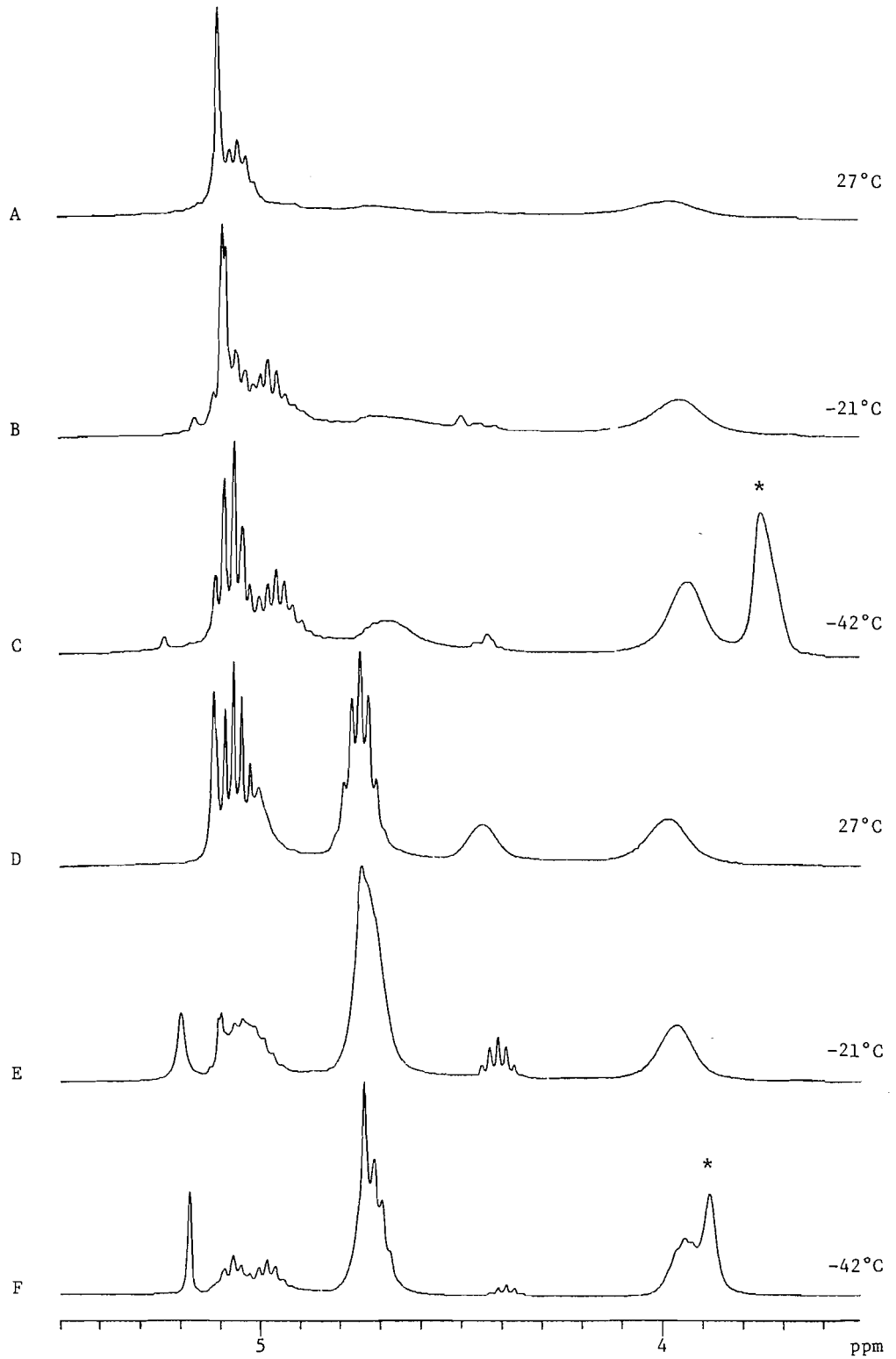
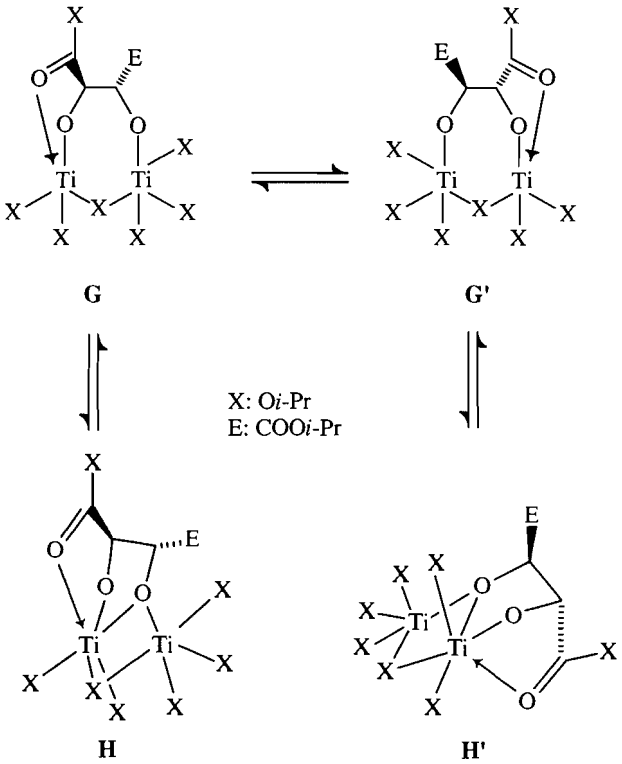


FIG. 2. OCH regions of ^{1}H nmr spectra taken at the indicated temperatures of *R*,*R*-DIPT complexes with 1 (A–C) and 2 (D–F) equivalents of $Ti(O^iPr)_4$ (refer to text). Starred peaks are due to OH, which migrate downfield upon cooling.

ppm was replaced at −30°C by two peaks at 86.0 and 82.6 ppm. SFD experiments at −50°C established that the former correlated to the downfield OC*H* and the latter to the upfield one. Three signals due to $LTiOCMe_2$ were found. Of these, the most upfield (at 71.1 ppm) was the smallest. Additionally, two distinct widely spaced singlets appeared in the *C*═O region, one strongly downfield (by 8.5 ppm) of the *C*═O peak in free DIPT. These data clearly indicate a radical change in structure upon cooling, from a symmetric form that resembled the 2:2 complex to a slightly asymmetric form of the same complex, and finally to a highly asymmetric complex.

Here again, combinations of bridging and terminal diolates



G G' H H'

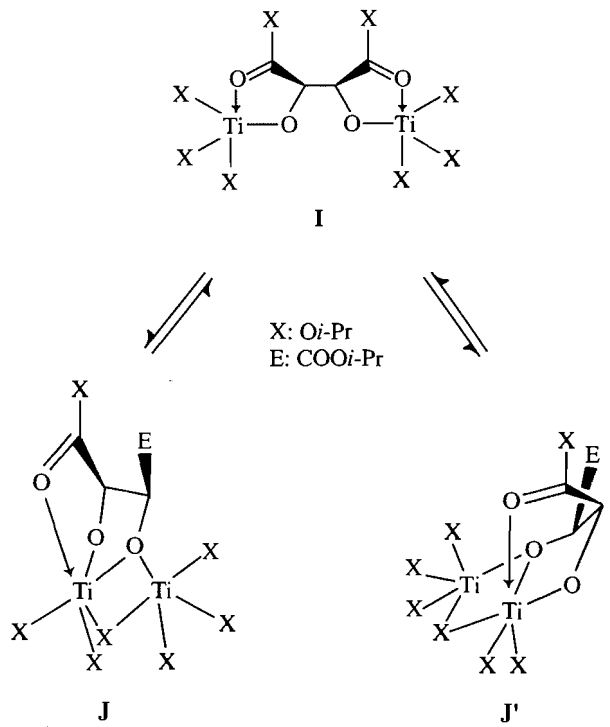
can be postulated for the low temperature species (structures **H**/**H**′), with both bound and free side chains. Clearly, the matched pairs of ^1H and ^{13}C signals indicate that single species were formed. The asymmetry and the lack of equilibration argue for a stiffened cyclic structure. The H–H coupling constant (0 Hz) was consistent with a five-membered envelope ring in which side-chain binding brings the attached ring C out of plane, affording a ca. 90° H—H dihedral angle. On the other hand, the difference between central OC*H* signals was smaller (1.3 ppm) than in the sugar complexes (3.5–6.3 ppm). This can be interpreted to have arisen from an overall increase in electron density at the metal centres owing to the more strongly electron-donating side chains. In contrast, the relatively far upfield position of one OC*H* signal, seen only in this cold complex, can be explained by H_2 in **H** finding itself in the shielding cone of the "inward"-oriented Ti-bound C=O. No satisfactory explanation can be put forth using other structural arrangements. The presence of O^{i}Pr bridges was suggested by analogy with the sugars and with the solid-state structures (10), wherein a planar bicyclic core confers a rigidity that disallows side-chain exchange or binding of both side chains, yet allows pentacoordination at one metal centre and hexacoordination at the other. This suggestion was supported by the presence of an upfield OC*H*Me$_2$ signal. The other TiOC*H*Me$_2$ signals were downfield and reminiscent of the *axial*/*equatorial* pair seen with the sugars.

Reasonable intermediates in the **H**–**H**′ interconversion and plausible structures for the warm 1:2 complex are **G** and **G**′, formed from **H**/**H**′ by the breaking of two dative bonds. According to models, the cyclic structure of **G** precludes the simultaneous binding of both side chains. Evidence for the side-chain binding or for the O^{i}Pr bridge in **G**/**G**′ was blurred by rapid exchanges above −19°C, the presence of 2:2 complex at room temperature, and by the presence of the low temperature species below −10°C. An acyclic complex is also possible, as had been originally proposed (6, 7), with both side chains feasibly binding to one metal each (12). However, the transformation of such a structure to the low temperature species (**H**/**H**′) would involve the concerted breaking and forming of three bonds. Moreover, it cannot help explain the apparent slight instability with respect to the 2:2 complex and free Ti(O^{i}Pr)$_4$ (eq. [2]). Instead we postulate a slight instability in the seven-membered ring of **G**/**G**′. Reversible extrusion of Ti(O^{i}Pr)$_4$, or reversible ring opening and exchange with HO^{i}Pr, would lead to the 2:2 complex.

Complexes of meso-*DIPT*

The upfield shift of one OC*H* signal seen in the cold 1:2 *R*,*R* complex (**H**) was explained by a shielding by the neighbouring Ti-bound ester group. As this would only be expected with the chiral tartrate, the *meso* analogue was prepared and examined to verify this hypothesis. Indeed, an analogous complex formed and no strong upfield shift occurred. The ^1H nmr spectrum of the 1:2 *meso* complex at room temperature included a singlet OC*H* at 5.25 ppm, which was replaced upon cooling by two well-separated OC*H* doublets at 5.35 and 5.17 ppm (cf. Δδ 0.44 ppm in the *R*,*R* case) that persisted down to −50°C. Similarly, the lone ester heptet at room temperature (at 5.01 ppm) broadened, and was replaced by two heptets (at 5.02 and 4.94 ppm) over the range −10°C to −20°C. In fact, coalescence seemed to occur near 0°C, with the room temperature ^1H and ^{13}C nmr signals at rough averages of the low temperature positions.

These and other data supported the assignment of structure **J**/**J**′ to the low temperature *meso* complex, in complete analogy to structures **H**/**H**′. Well-separated *C*O peaks, one strongly



I J J'

shifted downfield of the free ligand position (none were seen at room temperature due to extensive broadening above −10°C), and the distinct ester OC*H* and OC*H* signals argued for one Ti-bound side chain per ligand moiety. Well-separated OC*H* signals (Δδ = 2.9 ppm, approaching the spread seen in the sugar complexes) were consistent with a bridging diolate. The H–H coupling (J = 4.6 Hz at −20°C) was also consistent with the ca. 30° dihedral angle expected for a five-membered envelope in which side-chain binding brings the attached diolate carbon out of plane. Additionally, four TiOC*H*Me$_2$ signals were seen at

Can. J. Chem. Downloaded from www.nrcresearchpress.com by 194.225.253.170 on 09/07/12
For personal use only.

Can. J. Chem. Downloaded from www.nrcresearchpress.com by 194.225.253.170 on 09/07/12
For personal use only.

−50°C, replacing the one at room temperature, and one was significantly upfield of the others, as expected for a bridging O^{i}Pr.

The coalescence phenomenon suggested that the interconversion between **J** and **J′** may be faster than between **H** and **H′** as both side chains can bind in an analogous transitory (but undetected) intermediate **I**. A minor species was also present at room temperature but this was not due to an intermediate in the interconversion of **J** and **J′**, as its signals remained sharp at all temperatures.

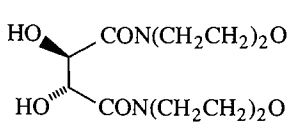
As might be expected, the 1:1 *meso*-DIPT–Ti(O^{i}Pr)$_4$ mixture gave complex spectra, featuring several doublet and AB quartet patterns in the OC*H* region. From low temperature ^{1}H and ^{13}C spectra, at least five different ligand types could be discerned and side-chain exchange was slow or absent in these, but no useful assignments could be made.

Complexes of tartramides

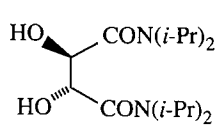
The behaviour of the tartramides was completely different from the foregoing. Little information was gained with the tertiary varieties. The $CDCl_3$-soluble *N,N,N′,N′*-tetraisopropyl tartramide (TIPT) gave an insoluble, likely polymeric, material upon treatment with Ti(O^{i}Pr)$_4$, while the $CDCl_3$-insoluble tartaryl bis-morpholide (TBM) very slowly dissolved only in the presence of two equivalents of Ti(O^{i}Pr)$_4$. Even after aging several days — tartramides form complexes more slowly than tartrates (7) — its spectra were broad, ill resolved, and uninformative.

N,N′-Dibenzyl tartramide (DBT), also $CDCl_3$-insoluble, dissolved in ca. 1 h after treatment with equimolar Ti(O^{i}Pr)$_4$, but gave similarly ill-resolved spectra (Fig. 3A), as did the 1:1 *N,N′*-di(2-phenylethyl) tartramide (DPET) mixture. The shapes of the OC*H* signals were time-, temperature-, and concentration-dependent, but prolonged aging, heating, or cooling failed to simplify the spectra (Fig. 3B) while tenfold dilution did so only temporarily (Fig. 3C). No useful assignments could be made, however. Incomplete reaction was not to blame as only a trace of unreacted Ti(O^{i}Pr)$_4$ could be detected (Fig. 3A). The ^{13}C signals were also broad, weak, and numerous. The 2:2 DBT complex had been crystallized for X-ray studies (10) by evaporation of liberated HO^{i}Pr and trituration with ether. In our hands, the solid product so obtained displayed similarly broad spectra after redissolution in $CDCl_3$. These observations suggested slowly equilibrating mixtures of species. The measured solution molecular weight (7) and the X-ray crystal structure (10) support a 2:2 molecularity for the 1:1 DBT mixture. However, this does not exclude the possibility of a concentration-dependent range of molecularities whose average molecular weight approaches that of the crystalline dimer.

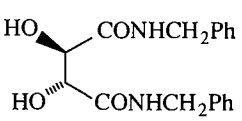
When excess Ti(O^{i}Pr)$_4$ was added to the secondary amide mixtures (up to and beyond 1:2 stoichiometry), the spectra



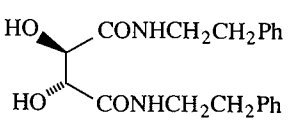
TBM



TIPT



DBT



DPET

became progressively sharper until a dominant set of ligand resonances appeared, evidently due to a single asymmetric complex (Fig. 3D). Other smaller broad resonances persisted at room temperature but slowly disappeared upon progressive cooling. Unreacted Ti(O^{i}Pr)$_4$ was present in significant amounts, indicating that the single dominant species was not of 1:2 stoichiometry. Signal integration was difficult in the DBT case due to overlapping signals but was clearer with DPET, and revealed that the dominant species could not be a 2:2 species as it had been with the 1:2 sugar mixtures. Rather, the integration ratios more aptly fit an equimolar mixture of 2:3 complex and unreacted Ti(O^{i}Pr)$_4$, according to

[4] $2H_2L + 4\,Ti(O^iPr)_4 \rightarrow L_2Ti_3(O^iPr)_8 + Ti(O^iPr)_4 + 4HO^iPr.$

[5] $L_2Ti_2(O^iPr)_4 + Ti(O^iPr)_4 \leftrightarrow L_2Ti_3(O^iPr)_8$

Equilibrium [5] was evidently operative; the value of the equilibrium constant was large but could not be estimated by integration due to signal overlaps. Mass spectrometry was unfortunately not very instructive, only confirming the presence of Ti(O^{i}Pr)$_4$ and showing extensive fragmentation (with no ions above *m / z* 501 in the DBT case). This result does not contradict the measured solution molecular weight of the 1:2 DBT mixture (7) since the number-average molecular weight (discounting volatile HO^{i}Pr) according to eq. [4] is exactly the same as that expected for a 1:2 complex. Small amounts of 2:2 complex, as suggested by minor OC*H* resonances, would increase the average molecular weight somewhat. Indeed, the measured molecular weight (819) of the 1:2 DBT mixture exceeded that expected (7) by 42 mass units.

These apparent 2:3 complexes showed the same kind of slight asymmetry that the DIPT complexes showed at moderately low temperatures. Again, small differences in OC*H* or O*C*H shifts, with values close to the downfield OCH signals in the cold 1:2 *R,R*-DIPT complex and to the upfield OCH signals in the 2:2 sugar complexes, and the evidently strong (nonequilibrating) side-chain binding pointed to terminal diolates. Again, side-chain binding exerted only a small effect on the central nuclei.

Most of the signals changed little upon cooling to −50°C; the postulated 2:3 species remained dominant throughout. However, the central OC*H* and *C*=O signals underwent interesting changes. In the case of DPET, the central OC*H* appeared as an AB system at room temperature (Fig. 3D), but as a singlet at −30°C (Fig. 3F). Strong coupling was still evident at intermediate temperatures (Fig. 3E). A new, broad TiOC*H*Me$_2$ signal appeared just upfield of the Ti(OC*H*Me$_2$)$_4$ signal and accounted for one proton per ligand. As well, a TiOCHMe$_2$ signal upfield of Ti(OCHMe$_2$)$_4$ appeared weak and broad at room temperature, but strong and sharp at −10°C. Meanwhile, there were two *C*=O signals at room temperature, one strongly downfield of the free ligand position, but the downfield partner decreased upon cooling and disappeared entirely at −30°C. At −50°C, almost all of the signals suddenly shifted upfield while the proportion of HO^{i}Pr increased, perhaps indicating some aggregation and (or) precipitation. However, a weak downfield *C*=O signal had reappeared. The case of DBT was more dramatic: the room temperature OC*H* AB quartet similarly collapsed to a singlet over the range −10°C to −30°C, but became a new AB quartet below −42°C. Meanwhile, a broad TiOC*H*Me$_2$ had appeared upfield of Ti(OC*H*Me$_2$)$_4$ in this case as well. Similarly, the downfield *C*=O signal gradually disappeared below −10°C, was completely absent at −30°C, then started to reappear at −50°C. Yet the complexes remained asymmetric

Can. J. Chem. Downloaded from www.nrcresearchpress.com by 194.225.253.170 on 09/07/12
For personal use only.

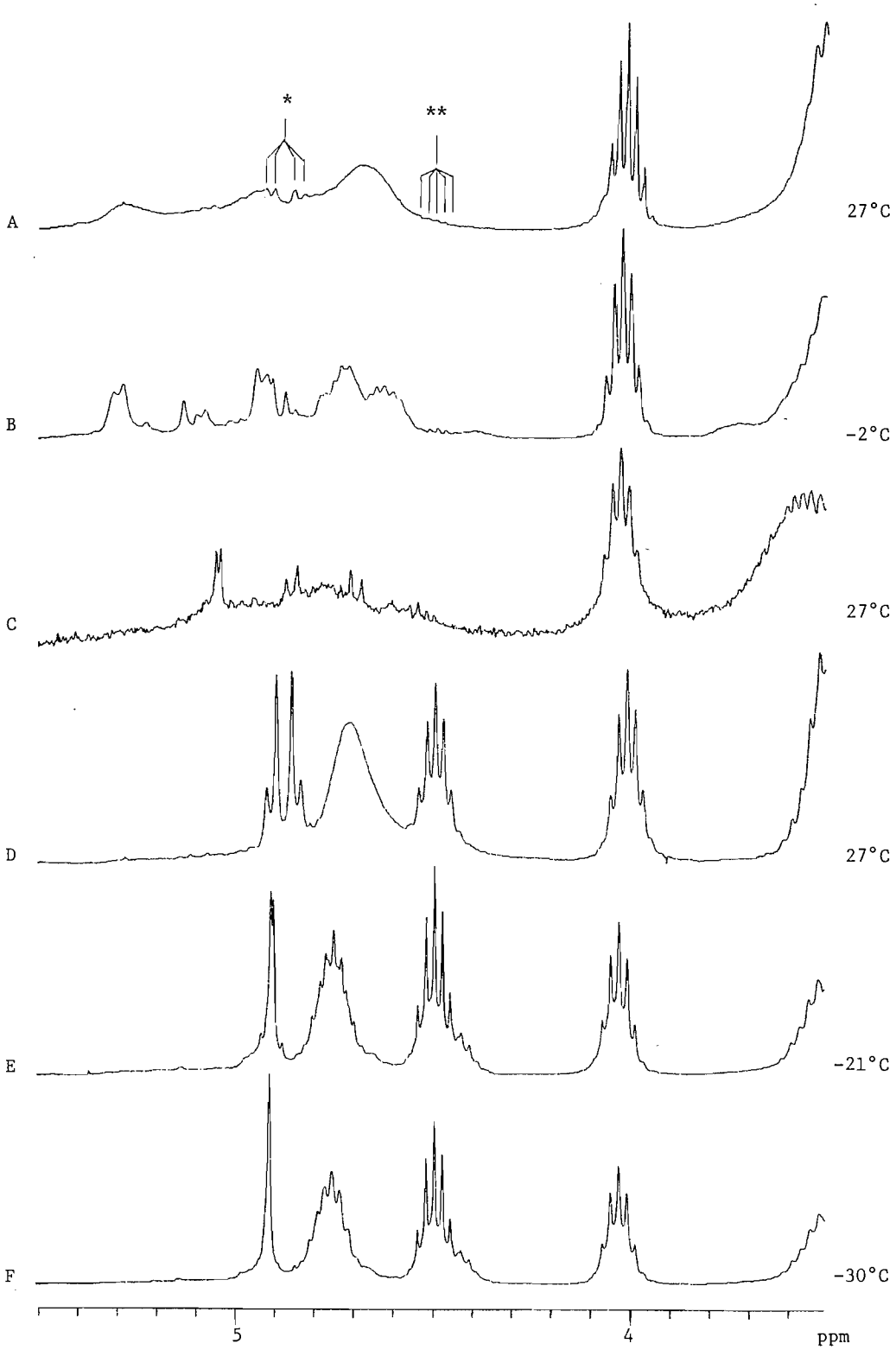
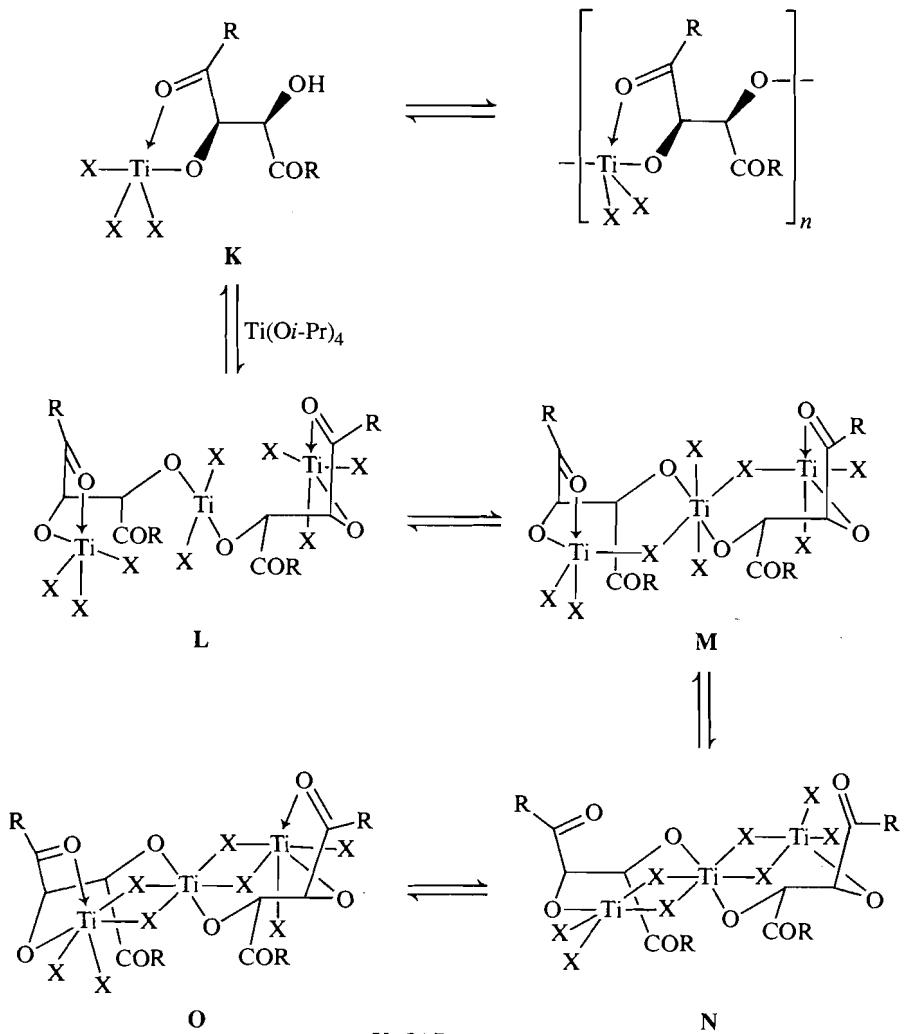


FIG. 3. OCH regions of ^{1}H nmr spectra taken at the indicated temperatures of DPET complexes with 1 (A–C) and 2 (D–F) equivalents of $Ti(O^iPr)_4$ (refer to text). Spectrum C taken approximately 15 min after tenfold dilution of the sample that gave spectrum A. Starred and double-starred patterns in spectrum A overlap with the AB pattern and the $Ti(O^iPr)_4$ heptet of spectrum D, respectively. Peaks on the far right are part of the $NHCH_2$ multiplet.

throughout, as pairs of signals were seen for all other ligand nuclei. The presence of pairs of N*H* triplets throughout indicated that no ionization of the side chains was occurring, contrary to suggestion (7). The collapse of the AB quartets was then due to a fortuitous overlap, rather than a gain in symmetry.

These observations are consistent with centro-symmetric Ti–L–Ti–L–Ti arrays that impose ligand asymmetry irrespective of the binding or nonbinding of the side chains, and support the 2:3 ligand–Ti stoichiometry deduced from signal integration. The changes observed upon cooling were suggestive of a step-



wise reorganization in which the loss of side-chain binding at an intermediate step was compensated by the formation of an O^{i}Pr bridge, as was postulated to occur in the 2:2 tartrate complex, and supported by upfield TiO*C*HMe$_2$ and TiOC*H*Me$_2$ signals.

Species **L***a*, *b*, containing tetracoordinate Ti, can explain why well-defined complexes are formed only in the presence of excess Ti(O^{i}Pr)$_4$, by the "trapping" of putative acyclic 1:1 complexes **K***a*, *b*. Tetracoordination at room temperature was suggested because an equilibrium (eq. [5]) was operative, and the formation of the 2:3 species was evidently not favoured by a strong chelate effect. Species **K** are possible components of the 1:1 mixtures because the strong side-chain binding in tartramides can kinetically and thermodynamically stabilize monomeric species like **K** relative to higher molecularities, and acyclic forms relative to cyclic ones. Upon cooling, O^{i}Pr bridges offer stabilization, forming rigid structures **M***a*, *b* by −10°C. These are formulated by analogy to the warm 1:2 *R*,*R*-DIPT complex **G**/**G**′ and the cold 2:2 complex **E**/**E**′, and involve slightly unstable seven-membered rings, as with **G**/**G**′. Upon further cooling, two-step loss of side-chain binding occurs, with new bridges forming in intermediates **N***a*, *b*, but the fortuitous overlap of central OC*H* may occur somewhat earlier on the path from **M** to **N**. Finally, further cooling of the DBT complex affords **O***a*, also in two steps.

Discussion

Prior to this work, some nmr studies on Ti^{4+} alkoxides had been published. Generally, tetraalkoxides can aggregate when the alkoxides are primary (28, 29), either in solution or neat. Secondary alkoxides remain monomeric, at least in benzene solution (30), but solid 1:1 adducts with netural electron donors are known (31–33). Dilution of a decalin solution of Ti(O^{i}Pr)$_4$ caused the OC*H* signal to shift upfield. This was interpreted in terms of a fast dimer–monomer equilibrium with rapid terminal-bridging exchange. The dimer, with a higher average coordination number, would have the more downfield position (28). An earlier study with ethanolamine complexes confirmed this (34). Opposite concentration-dependent displacements occurred in aromatic solvents (35). The ^{13}C signals of Ti(O^{i}Pr)$_4$ did not change with temperature in $CDCl_3$ (36), but the bridging-terminal exchange was frozen at −90°C in methylcyclohexane-d_{14}, whence the signal for bridging O^{i}Pr was upfield of the terminal one (37).[5] The bridging OCH_3 signals of Ti(OCH$_3$)$_4$ were found upfield (in $CDCl_3$) of those for terminal OCH$_3$ but downfield in benzene-d_6 (11), but solvent impurities may have been responsible for both the dissolution of the normally insoluble (and polymeric) Ti(OCH$_3$)$_4$ and the effects on the chemical

[5]Also, M. Marsi, personal communication.

Can. J. Chem. Downloaded from www.nrcresearchpress.com by 194.225.253.170 on 09/07/12
For personal use only.

Can. J. Chem. Downloaded from www.nrcresearchpress.com by 194.225.253.170 on 09/07/12
For personal use only.

shift (35). Although this should alert us to possible interference by liberated HO^{i}Pr, we found no displacement of its OC*H* or O*C*H signals, only broadening indicative of its participation in exchanges with Ti-bound and ester O^{i}Pr. With some exceptions, the TiOC*H*Me$_2$ and TiO*C*HMe$_2$ signals observed in all our complexes were downfield of those in Ti(O^{i}Pr)$_4$, indicating an increase in average coordination number in each case (28, 34). Upfield TiO*C*HMe$_2$ signals were taken to indicate bridging O^{i}Pr in slow or frozen exchange with terminal O^{i}Pr.

In assigning structures in this study, the most telling data concern the chiral ligands, but little could be inferred with as much certainty about the geometries at the metal centres or about the O^{i}Pr ligands. However incomplete, the structural picture emerging from our analysis of the available nmr, ir, and ms data can account for the existence of equilibria [2] and [5] and for the lack of well-defined complexes in the 1:1 tartramide mixtures, and is consistent with the different side-chain binding abilities expected from the three classes of ligand.

Certain generalizations could then be made about chiral alkoxides as a result: (a) with mannitol skeletons, secondary ether groups bind in preference to primary ones; (b) with tartaric acid skeletons, only one side chain can bind at a time; (c) the effect on diolate shifts due to side-chain binding is small compared to that due to binding a second metal centre in forming a diolate bridge; and (d) isopropoxide bridging affords greater stabilization than does side-chain binding. Overall, the complexes studied fall into two broad categories: those that gave strongly asymmetric ligand signals, and those whose spectra were symmetrical or slightly asymmetric. Some effects on structure might be anticipated from differences in the nature of the side chains. Certainly, the steric bulk in the tertiary amides might be at the source of their reluctance to form single, well-defined, and soluble complexes at any stoichiometry. Poor side-chain binding in the sugar complexes (**A**) may explain their need to form strong diolate bridges and hexacoordinate metal centres at 1:1 stoichiometry, as well as their reluctance to form 1:2 complexes as the side chains compete poorly with the alkoxide bridges. Moderate side-chain binding by tartrates can apparently stabilize pentacoordinate Ti in a cyclic dimer, but O^{i}Pr bridging apparently affords greater stabilization at lower temperatures (**D** → **E**). It can be argued that such bridging was preferred in the 1:2 *R*,*R*-DIPT complex as well: where there was an opportunity to bind both ester side chains at two pentacoordinate Ti centres, a bridged cyclic form seemed to have formed instead with only one side-chain binding at a time (**G**). Such bridging was also preferred in the 2:3 secondary tartramide complexes, where, in addition, a second bridge seemed to form at lower temperatures to replace side-chain binding (**M** → **N**). As related above, the 1:1 tartramide mixtures may have consisted of many slowly equilibrating acyclic or cyclic structures. The insolubility and the presumed oligomeric nature of the TIPT complex and the reluctance of TBM to complex suggest that [L–Ti]$_n$ arrays may have formed with all tartramides, consistent with Ti–L–Ti–L–Ti arrays predominating with the secondary tartramides in the presence of excess Ti(O^{i}Pr)$_4$. Slowly evolving side-chain binding, with little difference in stability between the isomers, could account for the unresolved spectra. We are currently testing the hypothesis that these ligands may nevertheless form well-defined 1:1 or 2:2 complexes under conditions of kinetic control.

Some important lessons can be drawn from this work. Comparisons between complexes with similar ligands are important, because solution data can be mistakenly interpreted as being in agreement with crystal structure data (2, 3). We were fortunate in that the sugar complexes provided the spectra expected from the crystal data while the tartrate complex did not, and thereby piqued our curiosity. As well, the examination of more than one stoichiometry and of temperature dependence proved valuable in arriving at structures integrating with all of the data. More cursory study led to an erroneous conclusion (12). As well, molecular weight determinations can be misleading, as demonstrated with the 1:2 *R*,*R*-DIPT and tartramide mixtures. We therefore consider spectroscopic tools more valuable than crystal structures and molecular weight measurements.

These considerations are especially valid if mechanistic postulates concerning homogeneous catalysis are to be formulated. While this study cannot directly address the mechanism of the Sharpless reaction, especially since the structure of the active catalysts may change in the presence of the substrate and the oxidant, the current hypotheses concerning both 2:2 (3, 20) and 1:2 (7) ligand–Ti mixtures have been thrown into question. The results of epoxidations with the non-tartrate ligands and the implications of the nmr results on the mechanisms of Sharpless epoxidations will be dealt with elsewhere. Finally, the existence of mixtures of complexes in temperature-, concentration-, and time-dependent ratios, as demonstrated in 1:2 *R*,*R*-DIPT and in 2:2 tartramide complexes, clearly points to strong influences of reaction conditions and catalyst aging times on the stereochemical course.

With respect to our design goal, the sugar complexes do not reproduce the successful chiral environment of tartrate complexes. New base- and nucleophile-stable ligands are currently being studied for this purpose. Further work is also underway using mixed ligand complexes and with dichloro complexes to study the effect of electronegative substituents.

Acknowledgements

We thank the Natural Sciences and Engineering Research Council of Canada for financial support and for the award of a University Research Fellowship to P.G.P. We thank Prof. Michael Brook for continuing helpful discussions and a referee for useful suggestions.

1. T. Katsuki and K. B. Sharpless. J. Am. Chem. Soc. **102**, 5974 (1980).
2. K. B. Sharpless, S. S. Woodard, and M. G. Finn. Pure Appl. Chem. **55**, 1823 (1983).
3. M. G. Finn and K. B. Sharpless. *In* Asymmetric synthesis. Vol. 5. *Edited by* J. D. Morrison. Academic Press, New York. 1985. Chap 8.
4. P. Pitchen, E. Duñach, M. N. Deshmukh, and H. B. Kagan. J. Am. Chem. Soc. **106**, 8188 (1984).
5. F. Di Furia, G. Modena, and R. Seraglia. Synthesis, 345 (1984).
6. S. Miyano, L. D. L. Lu, S. M. Viti, and K. B. Sharpless. J. Org. Chem. **48**, 3608 (1983).
7. L. D. L. Lu, R. A. Johnson, M. G. Finn, and K. B. Sharpless. J. Org. Chem. **49**, 728 (1984).
8. K. Narasaka, M. Inoue, and N. Okada. Chem. Lett. 1109 (1986).
9. K. Mikami, M. Terada, and T. Nakai. J. Am. Chem. Soc. **111**, 1940 (1989).
10. I. D. Williams, S. F. Pedersen, K. B. Sharpless, and S. J. Lippard. J. Am. Chem. Soc. **106**, 6430 (1984).
11. H. Weingarten and J. R. Van Wazer. J. Am. Chem. Soc. **87**, 724 (1965).
12. P. G. Potvin, P. C. C. Kwong, and M. A. Brook. J. Chem. Soc. Chem. Commun. 773 (1988).

13. L. F. WIGGINS. J. Chem. Soc. 13 (1946).
14. J. C. IRVINE and B. M. PATERSON. J. Chem. Soc. **105**, 898 (1914).
15. G. KOHAN and G. JUST. Synthesis, 192 (1974).
16. S. CZERNECKI, C. GEORGOULIS, and C. PROVELENGHIOU. Tetrahedron. Lett. 3535 (1976).
17. P. NANASI and A. LIPTAK. Carbohydr. Res. **29**, 201 (1973).
18. D. SEEBACH, H. O. KALINOWSKI, B. BASTINI, G. CRASS, H. DAUM, H. DOERR, N. P. DUPREEZ, V. EHRIG, and W. LANGER. Helv. Chim. Acta, **60**, 301 (1977).
19. A. H. HAINES and C. S. P. JENKINS. J. Chem. Soc. Perkin Trans. 1, 273 (1972).
20. K. A. JORGENSEN, R. A. WHEELER, and R. HOFFMAN. J. Am. Chem. Soc. **109**, 3240 (1987).
21. C. B. REESE. *In* Protective groups in organic chemistry. *Edited by* J. F. W. McOmie. Plenum Press, London. 1973. Chap. 3.
22. C. B. REESE. Tetrahedron, **34**, 3143 (1978).
23. A. H. HAINES. Adv. Carbohydr. Chem. Biochem. **33**, 11 (1976).
24. M. L. WOLFRAM, A. BEATTIE, S. S. BHATTACHARJEE, and G. G. PAREKH. J. Org. Chem. **33**, 3990 (1968).
25. A. N. DEBELDER, P. J. GAREGG, B. LINDBERG, G. PETROPAVLOVSKII, and O. THEANDER. Acta Chim. Scand. **16**, 623 (1962).
26. O. KENNARD, W. D. S. MOTHERWELL, J. C. COPPOLA, B. E. GRIFFIN, C. B. REESE, and A. C. LARSON. J. Chem. Soc. B, 1940 (1971).
27. S.-I. HAKOMORI. J. Biochem. (Tokyo), **55**, 205 (1964).
28. D. C. BRADLEY and C. E. HOLLOWAY. J. Chem. Soc. A, 1316 (1968).
29. W. R. RUSSO and W. H. NELSON. J. Am. Chem. Soc. **92**, 1521 (1970).
30. L. H. THOMAS and G. H. DAVIES. J. Chem. Soc. A, 1271 (1969).
31. C. M. COOK. J. Am. Chem. Soc. **81**, 3828 (1959).
32. M. S. BAINS and D. C. BRADLEY. Can. J. Chem. **40**, 1350 (1962).
33. S. A. IMAN. Nature, **206**, 1146 (1965).
34. K. NAKAMOTO and A. MARTELL. J. Chem. Phys. **32**, 588 (1960).
35. C. E. HOLLOWAY. Ph.D. Thesis, University of Western Ontario, 1966.
36. C. E. HOLLOWAY. J. Chem. Soc. Dalton Trans. 1050 (1976).
37. M. MARSI and D. C. ROE. Presented at the ACS National Meeting, Los Angeles, Sept. 1988.

Can. J. Chem. Downloaded from www.nrcresearchpress.com by 194.225.253.170 on 09/07/12
For personal use only.

Alkaloids of *Lycopodium selago*. On the identity of selagine with huperzine A and the structure of a related alkaloid[1]

WILLIAM A. AYER, LOIS M. BROWNE, AND HELENA ORSZANSKA
Department of Chemistry, University of Alberta, Edmonton, Alta., Canada T6G 2G2

ZDENEK VALENTA
Department of Chemistry, University of New Brunswick, Fredericton, N.B., Canada E3B 6E2

AND

JIA-SEN LIU
Shanghai Institute of Materia Medica, Academia Sinica, Shanghai 200031, People's Republic of China

Received April 5, 1989

WILLIAM A. AYER, LOIS M. BROWNE, HELENA ORSZANSKA, ZDENEK VALENTA, and JIA-SEN LIU. Can. J. Chem. **67**, 1538 (1989).

Selagine, an alkaloid of *Lycopodium selago*, is shown to be identical with huperzine A (**2**). A minor alkaloid, $C_{15}H_{18}N_2O_2$, isolated from *L. selago* is found to be 6β-hydroxyhuperzine A (**4**).

Key words: huperzine A, selagine, Lycopodium alkaloids, Alzheimer's disease, acetylcholine esterase inhibitor.

WILLIAM A. AYER, LOIS M. BROWNE, HELENA ORSZANSKA, ZDENEK VALENTA et JIA-SEN LIU. Can. J. Chem. **67**, 1538 (1989).

On a démontré que la sélagine, un alcaloïde du *Lycopodium selago*, est identique à l'huperzine A (**2**). On a trouvé qu'un alcaloïde mineur, $C_{15}H_{18}N_2O_2$, isolé du *L. selago* est la 6β-hydroxyhuperzine A (**4**).

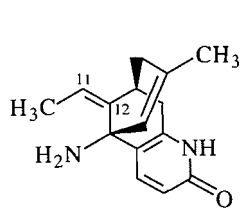
Mots clés : huperzine A, selagine, alcaloïdes Lycopodium, maladie d'Alzhéimer, agent inhibiteur d'acétylcholine estérase.
[Traduit par la revue]

Introduction

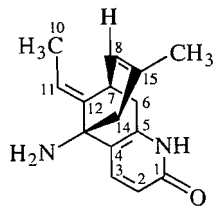
In 1960, Wiesner and co-workers proposed structure **1** for selagine, an alkaloid isolated from *Lycopodium selago* L. (1, 2). In 1986, Liu *et al.* reported the structure of huperzine A (**2**), an alkaloid isolated from *Lycopodium serratum* Thunb. (= *Huperzia serrata* (Thunb.) Trev.), a plant used in Chinese folk medicine (3). Huperzine A (**2**) shows very strong anticholinesterase activity and markedly increases efficiency for learning and memory in animals (3). The use of huperzine A (**2**) in the treatment of myasthenia gravis and Alzheimer's disease is currently under clinical investigation in China (4). Because of the structural similarity of selagine (**1**) and huperzine A (**2**), the Alberta group has reinvestigated the alkaloids of *L. selago* to obtain selagine in order to determine its anticholinesterase activity. We report herein the isolation of selagine and the finding that selagine is identical with huperzine A (**2**). The structure of a hydroxy derivative of huperzine A, originally isolated by the New Brunswick group in 1960, is also reported.

Results and discussion

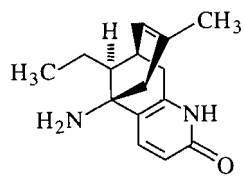
Lycopodium selago was collected near Grovelsjon and near Tarna in Sweden,[2] in the Tonquin valley near Jasper, Alberta, and near Summit Lake in northern British Columbia.[3] The dried plant material was extracted with 2% aqueous tartaric acid. The crude alkaloid fraction was dissolved in chloroform and the pyridone (hydroxypyridine) alkaloids were extracted into dilute aqueous sodium hydroxide. Separation of the crude phenolic alkaloids was achieved by preparative thin-layer chromatography over silica gel. Crystallization from acetone provided a pure compound, mp 214–215°C, $[\alpha]_D$ −147°, identical with an authentic sample of selagine *and identical with* an authentic sample of huperzine A (**2**). A nuclear Overhauser enhancement (nOe) experiment confirmed the proximity of the C-10 methyl (δ 1.70) to the allylic C-7 hydrogen (δ 3.60) and spin decoupling experiments revealed that this allylic hydrogen was coupled (J = 5 Hz) to the C-8 alkenic hydrogen. This coupling was not



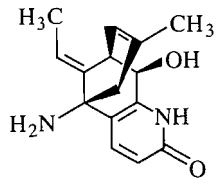
1



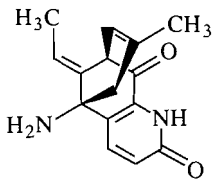
2



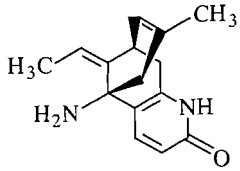
3



4



5



6

[1]This paper is dedicated to the memory of Professor Karel Wiesner, a pioneer in the field of Lycopodium alkaloids.

[2]We thank Dr. O. Martinsson, Swedish University of Agricultural Studies, Umea, Sweden, for this collection.

[3]A voucher specimen from each of the collections is deposited in the University of Alberta Herbarium, voucher numbers 93010, 93018, 93019, and 93020.

Printed in Canada / Imprimé au Canada

Can. J. Chem. Downloaded from www.nrcresearchpress.com by 194.225.253.170 on 09/07/12
For personal use only.

Can. J. Chem. Downloaded from www.nrcresearchpress.com by 194.225.253.170 on 09/07/12
For personal use only.

detected in the 60-MHz spectrum of selagine recorded by the earlier workers (1, 2). The stereochemistry at C-11 was not proposed in the original papers on selagine (1, 2) but was assigned as shown in **1** on the basis of a study of the rate of methiodide formation (5). Catalytic hydrogenation (over PtO_2) of the "selagine" isolated from *L. selago* provided the dihydro derivative **3**, identical in spectroscopic properties with 11,12-dihydrohuperzine A (**3**) (3). Observation of an nOe effect between the hydrogen at C-12 and the α-hydrogen at C-6 allows the assignment of stereochemistry at C-12.

During the search for an authentic sample of selagine among the late Prof. Wiesner's Lycopodium alkaloid samples we discovered a sample code named selagine-II.[4] High resolution mass spectrometry (hrms) indicated a molecular formula of $C_{15}H_{18}N_2O_2$ and the ultraviolet (uv) spectrum (λ_{max} 238, 302, 331 nm) was very similar to that of huperzine A (**2**). The infrared (ir) spectrum showed characteristic α-pyridone absorption (ν_{max} 1664, 1643, 1605, 1544 cm^{-1}). The ^1H nmr and ^{13}C nmr spectra indicate that this alkaloid is 6-β-hydroxyhuperzine A (**4**). The ^1H nmr spectrum shows the presence of the two alkenic methyls (doublet at δ 1.66 (J = 7 Hz), singlet at δ 1.56), the two α-pyridone hydrogens (δ 7.88 and 6.40, J = 9 Hz), the C-8 alkenic hydrogen (δ 5.56, d, J = 5 Hz), and the C-11 alkenic hydrogen (δ 5.52, q, J = 7 Hz), all with chemical shifts and couplings similar to those observed with huperzine A (3). The nOe experiments demonstrated the proximity of the C-10 methyl group to the allylic C-7 hydrogen (δ 3.74, dd, J = 5 and 5.5 Hz). The C-7 hydrogen is also coupled to a signal at δ 4.68 (d, J = 5.5 Hz), which is assigned to the benzylic carbinyl hydrogen at C-6. This result locates the position of the hydroxyl group in this alkaloid. The size of the coupling between H-6 and H-7 (5.5 Hz) indicates that the hydroxyl group has the β orientation (3). Oxidation of **4** with Jones' reagent *or* manganese dioxide provided the ketone **5** (ν_{max} 1694, 1662, 1600 cm^{-1}; λ_{max} 238, 260, 353 nm). The signal for the hydrogen at C-7 now appears as a doublet (J = 5.0 Hz) at δ 4.24. The coupling to the C-8 (δ 5.42, J = 5.0 Hz) hydrogen was confirmed by spin decoupling, confirming the position of the endocyclic double bond.

A compound assigned structure **6** and named isoselagine has been reported from *L. serratum* Thunb. var. *longipetiolatum* Spring (7). We have compared infrared, ^1H nmr, and ^{13}C nmr spectra of this alkaloid[5] with those of huperzine A and find that they are virtually identical. In veiw of this we suggest that isoselagine (lit. (7) mp 228–229°C; $[\alpha]_D$ −96°) may also be identical with huperzine A.

In view of the identity of selagine with huperzine A, we suggest that the name huperzine A be retained for the alkaloid possessing structure **2**.

Experimental

General

High resolution electron impact mass spectra (hrms) were recorded on an AEI MS-50 mass spectrometer. Unless diagnostically significant, only those peaks with an intensity of >20% of the base peak are recorded. Chemical ionization mass spectra (cims) were obtained using an AEI MS-12 mass spectrometer with ammonia as the reagent gas. The data were processed using DS-55 software and a Nova-4 computer. Fourier transform infrared (Ftir) spectra were recorded on a Nicolet 7199 FTIR interferometer. Nuclear magnetic resonance (nmr) spectra (^1H and ^{13}C) were obtained on Bruker WP-80, WH-300, and WM-360 spectrometers with either Aspect 2000 or Aspect 3000 computer systems. ^1H chemical shifts and coupling constants are reported as if they are first order. Tetramethylsilane was used as an internal standard. Ultraviolet (uv) spectra were obtained on a Hewlett Packard 8450A Diode Array spectrophotometer and optical rotations on a Perkin Elmer 241 polarimeter. Melting points are uncorrected and were determined on a Leitz Wetzler melting point apparatus. Preparative thin-layer chromatography (ptlc) was performed on E. Merck precoated 20 × 20 glass plates of silica gel 60 F-254. Analytical thin-layer chromatography (tlc) was carried out on cut sections of E. Merck precoated aluminum sheets of silica gel 60 F-254. Ultraviolet active materials were detected by visualization under a uv lamp (254 nm). All solvents were distilled prior to use.

Isolation of huperzine A (2)

Ground, dried *L. selago* (1.43 kg), collected near Summit Lake, B.C., was suspended in 2% aqueous tartaric acid (6 L) and the suspension stirred for 12 h, then filtered (cheese cloth). The process was repeated twice more. The combined extracts were filtered (Buchner funnel), concentrated to ca. one tenth volume, and extracted with chloroform (discarded). The aqueous layer was basified (aqueous ammonia) and extracted (5×) with chloroform, dried (Na_2SO_4), and concentrated to provide the crude alkaloids (8.4 g). These were dissolved in $CHCl_3$ and extracted with 1% aqueous NaOH (3×). The combined aqueous extracts were acidified (concentrated HCl) to pH ~2 and then basified with aqueous ammonia to pH ~12, then extracted with $CHCl_3$ (3×). This provided the crude phenolic alkaloids (1.77 g). Purification by ptlc afforded *huperzine A* (262 mg), which after crystallization from acetone melted at 214–215°C (lit. (3,6) mp 230°C, (1) 224–226°C); $[\alpha]_D$ −147° (*c* 0.36, CH_3OH) (lit. (3,6) $[\alpha]_D$ −150.4°, (1) −99°). The alkaloid isolated in this way was identical (^1H nmr and ^{13}C nmr, ir, tlc) with an authentic sample of huperzine A (3, 6), and with an authentic sample of selagine (^1H nmr, tlc).[6] The plant material collected near Jasper and that obtained from Sweden gave similar results.

Catalytic hydrogenation of huperzine A

Huperzine A (50 mg) in ethyl alcohol (7 mL) was stirred under hydrogen in the presence of Adams' catalyst (20 mg) at room temperature and atmospheric pressure for 2 h. The crude product was purified by ptlc over silica gel (eluent $CHCl_3$–CH_3OH (3:3)) to give a tacky oil (27 mg), which crystallized from methanol–acetone, mp 265°C (lit. (3,6) mp 269–270°C). The spectroscopic properties (ir, ^1H nmr, ^{13}C nmr, ms) are identical with those of dihydrohuperzine A (**3**) (6).

Isolation of 6β-hydroxyhuperzine A (4)[7]

The crude phenolic alkaloids (30 g) of *L. selago* (ca. 10 kg) were chromatographed over Florisil (500 g). Elution with $CHCl_3$ and $CHCl_3$–CH_3OH (up to 2% CH_3OH) provide huperzine A (as selagine, 8.6 g). Elution with $CHCl_3$–CH_3OH (19:1) gave material (3.2 g) that on crystallation from acetone provides 6β-hydroxyhuperzine A (as selagine-II, 0.58 g), mp 207–210°C after recrystallization from acetone–methanol. *Anal.* calcd. for $C_{15}H_{18}N_2O_2$: C 69.74, H 7.02, N 10.84, O 12.39%. found: C 69.88, H, 7.15, N 10.46, O 12.29%.

6β-Hydroxyhuperzine A (4): $[\alpha]_D$ −206° (*c* 0.37, CH_3OH); uv (CH_3OH) λ_{max} (log ε): 238 (3.83), 302 (3.74) nm; Ftir (KBr) ν_{max}: 3380, 1664, 1643, 1605, 1545 cm^{-1}; ^1H nmr ($CDCl_3$) δ: 7.88 (1H, d, J = 9 Hz, H-3), 6.40 (1H, d, J = 9 Hz, H-2), 5.56 (1H, d, J = 5 Hz, H-8), 5.52 (1H, q, J = 7 Hz, H-1), 4.68 (1H, d, J = 5.5 Hz, H-6), 3.74

[4]The isolation of the compound, which is presented in the Experimental, is well described in the lab book of H. Yoshimura, a post-doctoral fellow with Prof. Wiesner in 1959–1960. This compound was not isolated from the *L. selago* examined in this study.

[5]Kindly provided by S. S. Lee, National Taiwan University.

[6]The only sample of selagine remaining in Prof. Wiesner's collection was in the form of a KBr pellet used for an infrared spectrum. The pellet was ground and the ground material was exhaustively washed with CH_2Cl_2. Evaporation provided sufficient material for a 360-MHz ^1H nmr spectrum. The spectrum thus obtained was identical with a spectrum of huperzine A determined on the same instrument.

[7]This is taken from the lab book of H. Yoshimura. See footnote 4.

(1H, dd, J = 5, 5.5 Hz, H-7), 2.12 (2H, bs, H-14), 1.66 (3H, d, J = 7 Hz, H-10), 1.56 (3H, s, H-16); ^{13}C nmr ($CDCl_3$) δ: 12.5 (C-10, signals assigned by multiplicity and by analogy with huperzine A (3, 6)), 22.9 (C-16), 39.9 (C-7), 49.7 (C-14), 54.9 (C-13), 71.1 (C-6), 113.5 (C-11), 118.3 (C-2), 120.3 (C-8), 123.0 (C-4), 135.7 (C-15), 140.5 (C-3), 141.3 (C-5), 145.5 (C-12), 164.8 (C-1); hrms (probe), m/z calcd. for $C_{15}H_{18}N_2O_2$ (M^+): 258.1369; found: 258.1366 (83), 243 (51), 241 (77), 212 (100, $C_{14}H_{14}NO$), 199 (25), 197 (26).

Oxidation of 6β-hydroxyhuperzine A

6β-Hydroxyhuperzine A (5 mg) was dissolved in acetone (2.5 mL), and Jones' reagent (3 drops) was added at room temperature. After 20 min the reaction mixture was diluted with water, basified with aqueous ammonia, and extracted with chloroform. Purification by ptlc (chloroform–methanol, 3:1) gave ketone **5** (2.4 mg) as a viscous oil. Ftir (film cast from $CHCl_3$) ν_{max}: 3360–3200, 1694, 1662, 1600 cm^{-1}; uv (CH_3OH) λ_{max} (log ε): 238 (3.42), 260 (3.41), 353 (3.37) nm; ^{1}H nmr ($CDCl_3$) δ: 7.98 (1H, d, J = 9 Hz), 6.76 (1H, d, J = 9 Hz), 5.64 (1H, q, J = 7 Hz), 5.42 (1H, d, J = Hz), 4.24 (1H, d, J = 5 Hz), 2.24 (2H, bs), 1.68 (3H, d, J = 7 Hz), 1.62 (3H, s); hrms (probe), m/z calcd. for $C_{15}H_{16}N_2O_2$: 256.1213; found: 256.1216 (100), 241 (48), 227 (22), 201 (18).

The same product was obtained, albeit in lower yield, when the oxidation was performed using manganese dioxide in chloroform.

Acknowledgements

We gratefully acknowledge the financial support of the Natural Sciences and Engineering Research Council of Canada and the Alberta Mental Health Research Fund. We thank Dr. Y. Hiratsuka, Dr. K. Nozawa, Mr. J. F. Clarke, and Mrs. Dorothy Ayer for their help in locating and collecting *Lycopodium selago*, and Mr. Y. T. Ma and Mr. R. Andrade for determining the nmr spectra. We also acknowledge with thanks the earlier work of H. Yoshimura.

1. Z. Valenta, H. Yoshimura, E. F. Rogers, M. Ternbah, and K. Wiesner. Tetrahedron Lett. No. 10, 26 (1960).
2. H. Yoshimura, Z. Valenta, and K. Wiesner. Tetrahedron Lett. No. 12, 14 (1960).
3. J. S. Liu, Y. L. Zhu, C. M. Yu, Y. Z. Zhou, Y. Y. Han, F. W. Wu, and B. F. Qi. Can. J. Chem. **64**, 837 (1986).
4. Drugs of the Future, **13**, 575 (1988).
5. M. Shamma, C. D. Jones, and J. A. Weiss. Tetrahedron, **25**, 4347 (1969).
6. J. S. Liu, C. M. Yu, Y. Z. Zhou, Y. Y. Han, F. W. Wu, B. F. Qi, and Y. L. Zhu. Acta Chim. Sin. **44**, 1035 (1986).
7. C. H. Chen and S. S. Lee. J. Taiwan Pharm. Assoc. **36**, 1 (1984).

Can. J. Chem. Downloaded from www.nrcresearchpress.com by 194.225.253.170 on 09/07/12
For personal use only.

Rate constants for abstraction of hydrogen from benzene, toluene, and cyclopentane by methyl and ethyl radicals over the temperature range 650–770 K

H.-X. ZHANG,[1] S. I. AHONKHAI,[2] AND M. H. BACK
Ottawa–Carleton Chemistry Institute, Department of Chemistry, University of Ottawa, Ottawa, Ont., Canada K1N 6N5

Received March 17, 1989

H.-X. ZHANG, S. I. AHONKHAI, and M. H. BACK. Can. J. Chem. **67**, 1541 (1989).

Rate constants for the abstraction of hydrogen from benzene, toluene, and cyclopentane by methyl and ethyl radicals have been measured relative to the corresponding abstraction reaction from ethylene. The method is based on the effect on the rates of formation of methane and ethane of the addition of small quantities of the reactants to the thermal chain reactions of ethylene in the temperature range 650–770 K. Taking the following values of the rate constants for the reference reactions (R = 8.314 J mol^{-1} K^{-1}):

[3] $CH_3 + C_2H_4 \rightarrow CH_4 + C_2H_3$; $\log k_3$ (L mol^{-1} s^{-1}) = 8.7 ± 0.2 − (63000 ± 3000)/2.3RT

[4] $C_2H_5 + C_2H_4 \rightarrow C_2H_6 + C_2H_3$; $\log k_4$ (L mol^{-1} s^{-1}) = 8.2 ± 0.2 − (62200 ± 3000)/2.3RT

the following rate constants were measured:

[7] $CH_3 + C_6H_6 \rightarrow CH_4 + C_6H_5$; $\log k_7$ (L mol^{-1} s^{-1}) = 9.3 ± 0.3 − (63000 ± 5000)/2.3RT

[8] $C_2H_5 + C_6H_6 \rightarrow C_2H_6 + C_6H_5$; $\log k_8$ (L mol^{-1} s^{-1}) = 8.8 ± 0.3 − (62200 ± 5000)/2.3RT

[11] $CH_3 + C_7H_8 \rightarrow CH_4 + C_7H_7$; $\log k_{11}$ (L mol^{-1} s^{-1}) = 7.4 ± 0.5 − (29000 ± 7000)/2.3RT

[12] $C_2H_5 + C_7H_8 \rightarrow C_2H_6 + C_7H_7$; $\log k_{12}$ (L mol^{-1} s^{-1}) = 7.7 ± 0.5 − (37000 ± 7000)/2.3RT

[15] $CH_3 + c\text{-}C_5H_{10} \rightarrow CH_4 + c\text{-}C_5H_9$; $\log k_{15}$ (L mol^{-1} s^{-1}) = 8.3 ± 0.5 ± (36000 ± 7000)/2.3RT

[16] $C_2H_5 + c\text{-}C_5H_{10} \rightarrow C_2H_6 + c\text{-}C_5H_9$; $\log k_{16}$ (L mol^{-1} s^{-1}) = 8.2 ± 0.5 − (40000 ± 7000)/2.3RT

The values of the activation energies are discussed in relation to the dissociation energies of the C—H bonds in the reactants.

Key words: kinetics, abstraction, methyl, ethyl, benzene, toluene.

H.-X. ZHANG, S. I. AHONKHAI et M. H. BACK. Can. J. Chem. **67**, 1541 (1989).

On a mesuré les constantes de vitesse d'enlèvement d'hydrogène du benzène, du toluène et du cyclopentane par des radicaux méthyle et éthyle relatives à la réaction correspondante d'enlèvement à partir de l'éthylène. La méthode est basée sur l'effet, sur les vitesses de formation du méthane et de l'éthane, de l'addition de faibles quantités de réactifs à des réactions thermiques en chaîne de l'éthylène, à des températures allant de 650 à 770 K. En prenant les valeurs suivantes comme constantes de (R = 8,314 J mol^{-1} K^{-1}) :

[3] $CH_3 + C_2H_4 \rightarrow CH_4 + C_2H_3$; $\log k_3$ (L mol^{-1} s^{-1}) = 8,7 ± 0,2 − (63000 ± 3000)/2,3RT

[4] $C_2H_5 + C_2H_4 \rightarrow C_2H_6 + C_2H_3$; $\log k_4$ (L mol^{-1} s^{-1}) = 8,2 ± 0,2 − (62200 ± 3000)/2,3RT

on a mesuré les constantes de réaction suivantes :

[7] $CH_3 + C_6H_6 \rightarrow CH_4 + C_6H_5$; $\log k_7$ (L mol^{-1} s^{-1}) = 9,3 ± 0,3 − (63000 ± 5000)/2,3RT

[8] $C_2H_5 + C_6H_6 \rightarrow C_2H_6 + C_6H_5$; $\log k_8$ (L mol^{-1} s^{-1}) = 8,8 ± 0,3 − (62200 ± 5000)/2,3RT

[11] $CH_3 + C_7H_8 \rightarrow CH_4 + C_7H_7$; $\log k_{11}$ (L mol^{-1} s^{-1}) = 7,4 ± 0,5 − (29000 ± 7000)/2,3RT

[12] $C_2H_5 + C_7H_8 \rightarrow C_2H_6 + C_7H_7$; $\log k_{12}$ (L mol^{-1} s^{-1}) = 7,7 ± 0,5 − (37000 ± 7000)/2,3RT

[15] $CH_3 + c\text{-}C_5H_{10} \rightarrow CH_4 + c\text{-}C_5H_9$; $\log k_{15}$ (L mol^{-1} s^{-1}) = 8,3 ± 0,5 ± (36000 ± 7000)/2,3RT

[16] $C_2H_5 + c\text{-}C_5H_{10} \rightarrow C_2H_6 + c\text{-}C_5H_9$; $\log k_{16}$ (L mol^{-1} s^{-1}) = 8,2 ± 0,5 − (40000 ± 7000)/2,3RT

On discute des valeurs des énergies d'activation en relation avec les énergies de dissociation des liaisons C—H des réactifs.

Mots clés : cinétique, enlèvement, méthyle, éthyle, benzène, toluène.

[Traduit par la revue]

Introduction

Methods for the measurement of rate constants for hydrogen-transfer reactions for small radicals, represented for methyl and ethyl radicals by the following reactions,

[1] $CH_3 + RH \rightarrow CH_4 + R$

[2] $C_2H_5 + RH \rightarrow C_2H_6 + R$

have been developed and applied to a wide variety of systems during the past several decades (1, 2). Accurate and reliable values for such rate constants are important both for a fundamental understanding of the reaction and for use in the development of reaction mechanisms. For methyl and ethyl radicals in the low temperature region, <700 K, these rate

[1]Present address: Department of Chemistry, Peking University, Beijing, People's Republic of China.

[2]Present address: Department of Chemistry, University of Benin, Benin City, Nigeria.

Can. J. Chem. Downloaded from www.nrcresearchpress.com by 194.225.253.170 on 09/07/12
For personal use only.

Can. J. Chem. Downloaded from www.nrcresearchpress.com by 194.225.253.170 on 09/07/12
For personal use only.

constants are generally measured relative to the rate of radical combination. In the high temperature region, >1000 K, methods for measurements of absolute values have been reported (3), but most measurements are made relative to a reference reaction, which may be a radical combination (4) or other radical reaction (5), or a thermal dissociation process (6). Values measured in these two regions are not always in agreement with an extrapolation of a simple Arrhenius expression and this problem has been discussed from different points of view (7–9). There is as yet little agreement on the most satisfactory functional form to describe the change in the rate constant with temperature or indeed whether the simple Arrhenius expression is inadequate, but all agree that more measurements are required, preferably in the range of temperature between the high and low regions. The present paper describes results that are a small step in this direction.

The method used involves the perturbation of the thermal chain reaction mechanism of ethylene by small quantities of additives at temperatures in the range 650–770 K. The method has been described previously for the systems involving ethylene with the additives hydrogen (10), ethane (11), propane, and isobutane (12) and will be only briefly summarized here. In this temperature region ethylene reacts by a complex series of chain reactions giving methane, ethane, propylene, and butene-1 as the main low molecular weight products. Studies of the kinetics of the reaction (13) showed that the saturated products, methane and ethane, were formed by the hydrogen transfer reactions,

[3] $CH_3 + C_2H_4 \rightarrow CH_4 + C_2H_3$

[4] $C_2H_5 + C_2H_4 \rightarrow C_2H_6 + C_2H_3$

while the unsaturated products, propylene and butene-1, as well as butadiene and other higher molecular weight unsaturated products, were formed by isomerization and decomposition reactions following addition of radicals to ethylene. Addition of small quantities of a saturated hydrocarbon, such as those mentioned earlier, introduced new hydrogen transfer reactions, described by eqs. [1] and [2], and increased the rates of formation of methane and ethane, but did not affect the rates of formation of propylene and butene-1 and other products formed through addition of radicals to ethylene. On the assumption that the additive did not undergo thermal dissociation and hence increase the total radical concentration in the system, the ratio of the initial rates of formation of methane and ethane in the presence and absence of the additive were given by the following expressions:

$$[5] \quad \frac{(R^0_{CH_4})_a}{R^0_{CH_4}} = 1 + \frac{k_1[RH]}{k_3[C_2H_4]}$$

$$[6] \quad \frac{(R^0_{C_2H_6})_a}{R^0_{C_2H_6}} = 1 + \frac{k_2[RH]}{k_4[C_2H_4]}$$

It was also assumed that the additive did not alter the relative concentration of the main chain-carrying radicals or the termination steps. This is a reasonable assumption since the amount of additive was usually less than 10% and no new products were introduced.

From the measurements with the additives mentioned, ratios of k_1/k_3 and k_2/k_4 were obtained and, using the values of k_1 and k_2 corresponding to the particular additive, values for k_3 and k_4 were calculated. The present study has made use of these measurements for k_3 and k_4 to obtain values for rate constants for abstraction reactions using additives for which, particularly in this region of temperature, fewer, or, in the case of the ethyl radicals, no data have been reported. The additives used were benzene, toluene, and cyclopentane.

Experimental

The thermal reactions were performed in a conventional static pyrolysis system, similar to that described previously (14). The quartz reaction vessel (volume 0.21 L, S/V 1 cm^{-1}) was enclosed in a stainless steel cylinder and heated by a three-zone Lindberg cylindrical furnace. The temperature gradient along the length of the vessel was less than one degree and temperatures were controlled to within one degree. Mixtures of gases were prepared by admitting first a low pressure of additive followed by a high pressure of ethylene. In the spherical mixing flasks with minimum connecting tubing this procedure induced good mixing currents. Reactants were thoroughly degased in small quantities before mixing and were not condensed after mixing.

For the purpose of the present experiments analysis of only the four major products, methane, ethane, propylene, and butene-1, was necessary. Measurements of the relative rates of formation of methane and ethane in the presence and absence of the additive gave values for the ratios k_1/k_3 and k_2/k_4, while measurements of the yields of propylene and butene-1 served to show that no new initiation processes occurred in the presence of the additive. The products were analyzed by a gas chromatography using a Durapak column (phenylisocyanate on Porasil C) 3.4 m × 4 mm maintained at 30°C. Both benzene and toluene are retained for long periods of time on this column and the carrier gas was allowed to flow overnight to clean the column. Cyclopentane was eluted at the same time as butene-1 and this product was therefore not analyzed in experiments with cyclopentane as additive.

Ethylene was Research Grade reagent from Matheson Co., Whitby, Ont., L1N 5R9, and was thoroughly degassed before each experiment. The only measurable impurity was about 50 ppm ethane (amounts too small to affect the chain reaction mechanism) but correction was made to the yield of ethane produced in the reaction. Benzene and toluene were "assured ACS" grade, low in sulphur-containing compounds, purchased from BDH, Toronto, Ont. An impurity of cyclopentane, 0.3% was detected by gas chromatographic analysis in the benzene. No comparable impurities were detected in the toluene. Cyclopentane was obtained from two sources. Preliminary experiments were performed with reagent of purity 99.5% from Tridom/Fluka (Mandel Scientific, Montreal, P.Q.) while for most experiments cyclopentane of purity 99.9% from Wiley Organics, Coshocton, Ohio, was used. Impurities of concern in these reagents were compounds with an easily abstractable hydrogen atom, so that small quantities could compete with the reactant in the hydrogen transfer reactions. In the case of toluene, hydrogen transfer is very rapid and hydrocarbon impurities in small quantities should not affect the results. For benzene, the cyclopentane impurity was too low to compete significantly for reactions with methyl and ethyl radicals, although other impurities (not detected) could have contributed to the formation of methane or ethane. Such an error would yield a rate constant too large and an activation energy too low. As seen later, this does not appear to be a problem with the present results. In cyclopentane, the impurity of cyclopentene was a cause for concern, since abstraction from cyclopentene may be 50 times faster than from cyclopentane. With amounts of cyclopentene not greater than 0.1%, however, its effect on the rate of formation of methane or ethane should have been unimportant.

Results

As evident from eqs. [5] and [6] the important measurement for the determination of the ratio of rate constants is the ratio of rates in the presence and absence of the additive. Two approaches to this measurement have been adopted and have been described in previous studies (10–12). In the first method a single measurement of the rate of formation of products in pure ethylene was followed by a similar measurement on the mixture

Can. J. Chem. Downloaded from www.nrcresearchpress.com by 194.225.253.170 on 09/07/12
For personal use only.

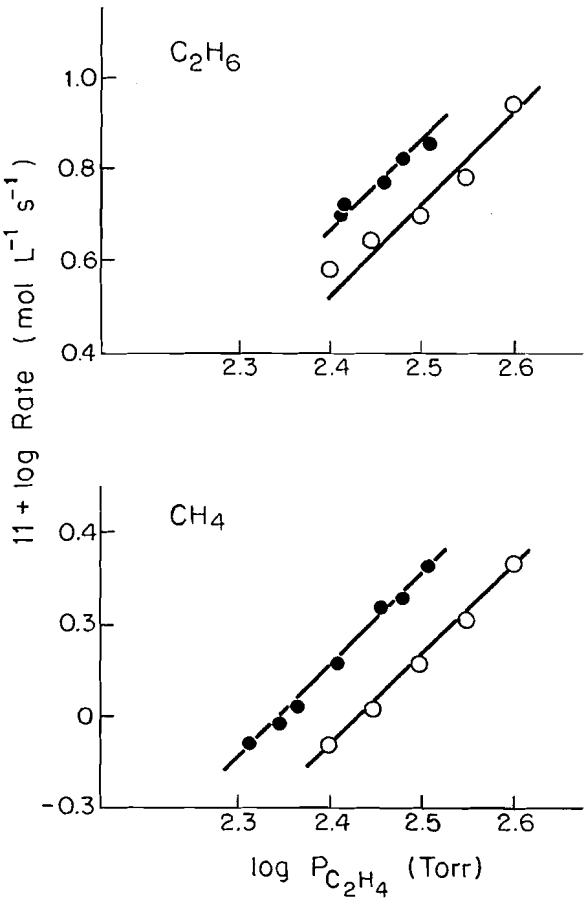


FIG. 1. Double logarithmic plots of the rates of formation of methane and ethane as a function of the initial pressure of ethylene at 683 K in the presence and absence of benzene. Lines have been drawn with slope = 2. ○: pure ethylene; ●: 12% C_6H_6.

under identical conditions of temperature and pressure of ethylene. A number of ratios were measured to obtain a final average value. This approach was used in the studies using ethane, propane, and isobutane as additives (11, 12). The second method involved a series of measurements of the initial rate of formation of products from the reaction of pure ethylene over a range of pressure, followed by a similar series with a mixture of ethylene with additive. Since the order of the rates of formation of methane and ethane was the same in the presence and absence of the additive, the ratio of rates was the same at all pressures and was obtained by interpolation. Thus several measurements were made with one mixture without the constraint of adjusting the pressure of ethylene to a particular value. This method was used with hydrogen as additive (10). In both methods measurements were made at each temperature of the yield of products as a function of time to establish the reaction time within which initial rates were measurable, before the onset of auto-catalysis. In the studies reported here the second method was used with the additives benzene and toluene, while the first method was used with cyclopentane as additive.

A. Benzene

An example of the results of measurements of the rates of formation of methane and ethane in the presence and absence of benzene as a function of pressure of ethylene are shown as double logarithmic plots in Fig. 1. Average ratios of rates were obtained for each mixture from such plots and the results are summarized in Table 1. Each ratio was obtained from a series of experiments over the approximate range of pressure of 230–380 Torr (1 Torr = 133.3 Pa). The rates of formation of propylene and butene-1 were unaffected by the addition of benzene. An example of the measurements of these products is given later for the additive toluene.

For the additive benzene, reactions [1] and [2] are expressed as follows,

[7] $CH_3 + C_6H_6 \rightarrow CH_4 + C_6H_5$

[8] $C_2H_5 + C_6H_6 \rightarrow C_2H_6 + C_6H_5$

and eqs. [5] and [6] become

$$[9] \quad \frac{(R^0_{CH_4})_a}{R^0_{CH_4}} = 1 + \frac{k_7[C_6H_6]}{k_3[C_2H_4]}$$

$$[10] \quad \frac{(R^0_{C_2H_6})_a}{R^0_{C_2H_6}} = 1 + \frac{k_8[C_6H_6]}{k_4[C_2H_4]}$$

The linearity of eqs. [9] and [10] for the rates of formation of methane and ethane is illustrated in Fig. 2A. The ratios of rate constants, k_7/k_3 and k_8/k_4, were obtained from the slopes of these plots and are included in Table 1. The Arrhenius plots for k_7/k_3 and k_8/k_4 are given in Fig. 3. Although there is some scatter in these ratios, it appears that there is no measurable difference in activation energy between reactions [7] and [3] or between [8] and [4] and the ratio of frequency factors is the same for both ratios of rate constants. The ratios of rate constants may be expressed as follows:

$$\log(k_7/k_3) = 0.60 \pm 0.01$$

$$\log(k_8/k_4) = 0.60 \pm 0.1$$

Taking the values for k_3 and k_4 reported previously (10) (R = 8.314 J mol^{-1} K^{-1}),

$$\log k_3\,(\mathrm{L\,mol^{-1}\,s^{-1}}) = 8.7 \pm 0.2 - \frac{63000 \pm 3000}{2.3RT}$$

$$\log k_4\,(\mathrm{L\,mol^{-1}\,s^{-1}}) = 8.2 \pm 0.2 - \frac{62200 \pm 3000}{2.3RT}$$

the following values were calculated for k_7 and k_8:

$$\log k_7\,(\mathrm{L\,mol^{-1}\,s^{-1}}) = 9.3 \pm 0.3 - \frac{63000 \pm 5000}{2.3RT}$$

$$\log k_8\,(\mathrm{L\,mol^{-1}\,s^{-1}}) = 8.8 \pm 0.3 - \frac{62200 \pm 5000}{2.3RT}$$

The present measurements for k_7 are shown together with previous measurements in Fig. 4. The present measurements to some extent span the measurements from the low and high temperature regions, but indicate an activation energy considerably higher than the other two values, 38.9 kJ mol^{-1} (15) and 43.1 kJ mol^{-1} (16), and also greater than the value of 46 kJ mol^{-1} recommended by Kerr and Parsonage (1). These values will be discussed later in relation to the bond dissociation energies of ethylene and the additives. No values were found in the literature for k_8.

B. Toluene

The effect of addition of toluene on the rates of formation of methane and ethane as a function of pressure of ethylene are shown as double logarithmic plots in Fig. 5. Average ratios of rates of formation of methane and ethane in the presence and absence of toluene for each mixture, obtained from these plots,

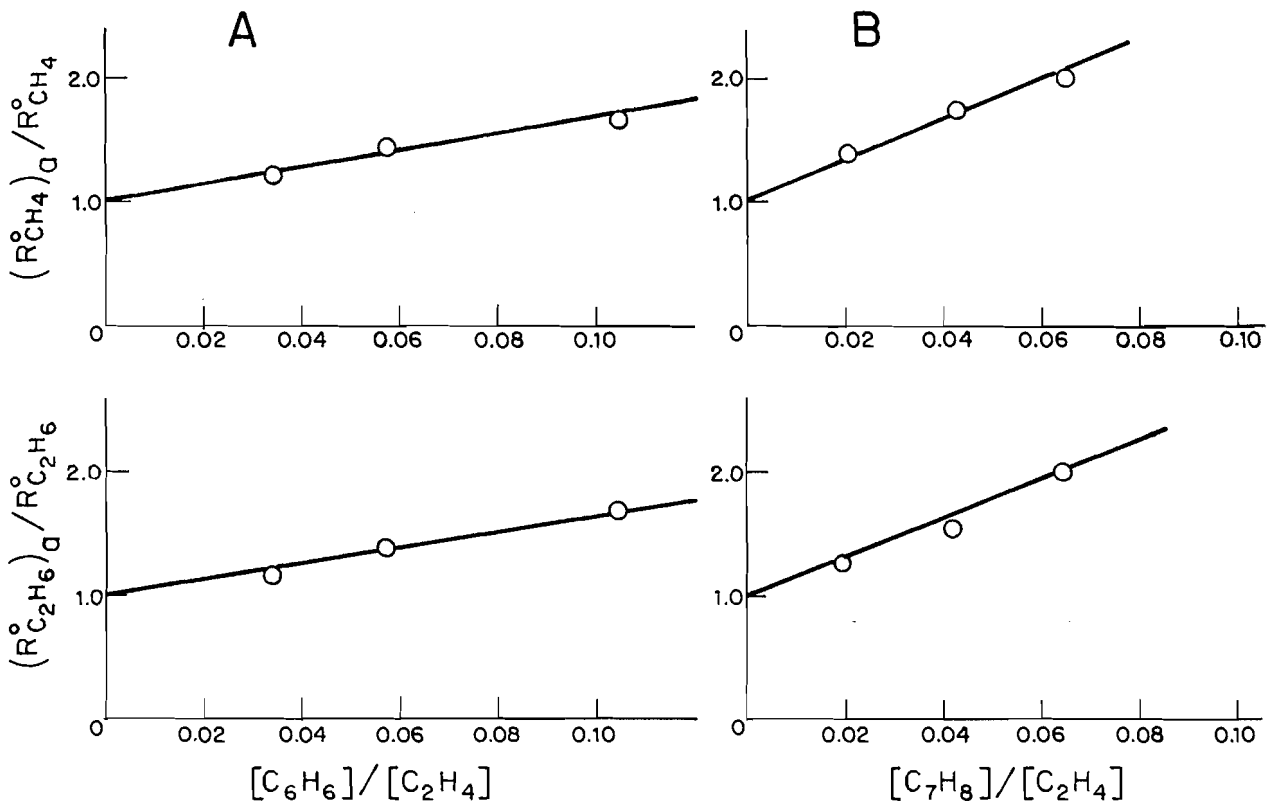


FIG. 2. Relative rates of product formation in the presence and absence of additive as a function of the ratio of additive to ethylene. A. benzene, 743 K; B. toluene, 723 K.

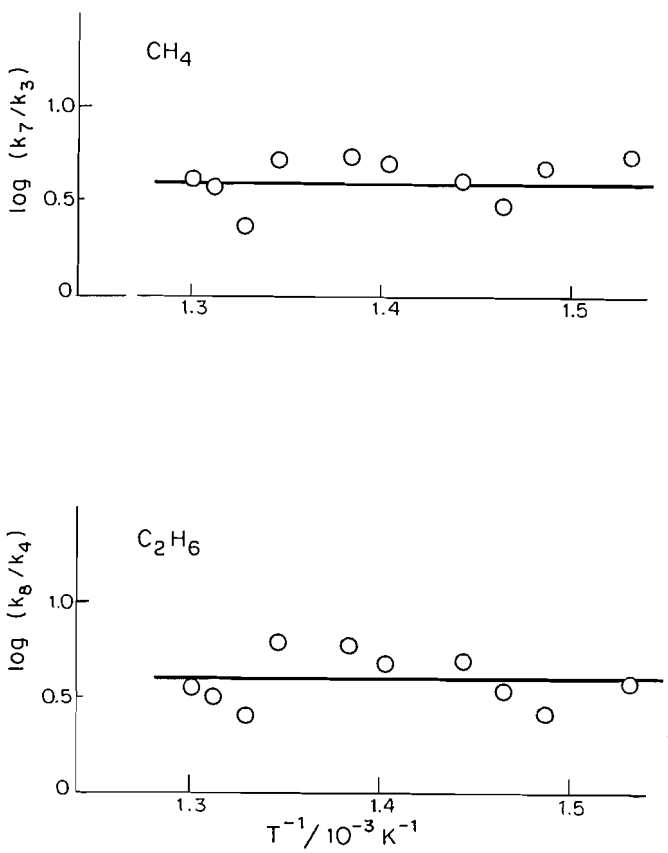


FIG. 3. Arrhenius plot of the ratios k_7/k_3 and k_8/k_4.

are summarized in Table 2. For each ratio a series of experiments was made covering a pressure range of approximately 220–360 Torr. Toluene had, within the error in the measurements, no effect on the rates of formation of either propylene or butene-1, as illustrated in Fig. 6 by the results at 743 K. Thus no new initiation processes were introduced by the addition of toluene.

In the presence of toluene, methane, and ethane are formed by the following reactions, in addition to reactions [3] and [4]:

[11] $CH_3 + C_7H_8 \rightarrow CH_4 + C_7H_7$

[12] $C_2H_5 + C_7H_8 \rightarrow C_2H_6 + C_7H_7$

In the presence of toluene, eqs. [5] and [6] become

$$[13]\quad \frac{(R^0_{CH_4})_a}{R^0_{CH_4}} = 1 + \frac{k_{11}[C_7H_8]}{k_3[C_2H_4]}$$

$$[14]\quad \frac{(R^0_{C_2H_6})_a}{R^0_{C_2H_6}} = 1 + \frac{k_{12}[C_7H_8]}{k_4[C_2H_4]}$$

Plots of the results according to these equations are shown in Fig. 2B and the ratios of rate constants k_{11}/k_3 and k_{12}/k_4 obtained from these plots are included in Table 2. Arrhenius plots for these ratios of rate constants are shown in Fig. 7. The dependence on temperature of the ratios may be expressed as follows ($R = 8.314$ J mol^{-1} K^{-1}):

$$\log (k_{11}/k_3) = -1.3 \pm 0.3 + \frac{34000 \pm 4000}{2.3RT}$$

$$\log (k_{12}/k_4) = -0.50 \pm 0.3 + \frac{25000 \pm 4000}{2.3RT}$$

Can. J. Chem. Downloaded from www.nrcresearchpress.com by 194.225.253.170 on 09/07/12
For personal use only.

Can. J. Chem. Downloaded from www.nrcresearchpress.com by 194.225.253.170 on 09/07/12
For personal use only.

TABLE 1. Ratios of rate constants for abstraction from benzene to abstraction from ethylene for methyl and ethyl radicals

T/K	$\frac{C_6H_6}{C_2H_4}$	$\frac{(R^0_{CH_4})_a}{R^0_{CH_4}}$	$\frac{k_7}{k_3}$	$\frac{(R^0_{C_2H_6})_a}{R^0_{C_2H_6}}$	$\frac{k_8}{k_4}$
770	0.030	1.12		1.13	
	0.053	1.23	4.2	1.18	3.7
763	0.100	1.38	3.8	1.32	3.2
753	0.051	1.12		1.12	
	0.111	1.25	2.3	1.28	2.5
743	0.034	1.20		1.19	
	0.057	1.41		1.38	
	0.104	1.64	5.2	1.68	6.2
723	0.036	1.15			
	0.065	1.29		1.48	
	0.105	1.62	5.5	1.58	6.0
713	0.053			1.17	
	0.099	1.51	5.2	1.50	4.8
693	0.065	1.28		1.30	
	0.107	1.44	4.2	1.55	5.0
683	0.136	1.48	3.5	1.41	3.0
673	0.111	1.55	4.9	1.29	2.6
653	0.083	1.48	5.8	1.32	3.8

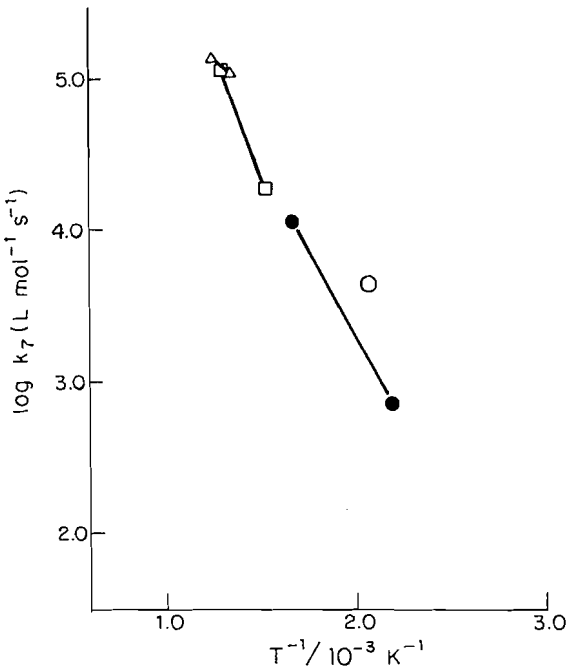


FIG. 4. Arrhenius plot of k_7. ●: ref. 16; ○: ref. 26; △: ref. 15; □: present work.

With the values for k_3 and k_4 mentioned earlier the following expressions were obtained for k_{11} and k_{12}:

$$\log k_{11}(\mathrm{L\,mol^{-1}\,s^{-1}}) = 7.4 \pm 0.5 - \frac{29000 \pm 7000}{2.3RT}$$

$$\log k_{12}(\mathrm{L\,mol^{-1}\,s^{-1}}) = 7.7 \pm 0.5 - \frac{37000 \pm 7000}{2.3RT}$$

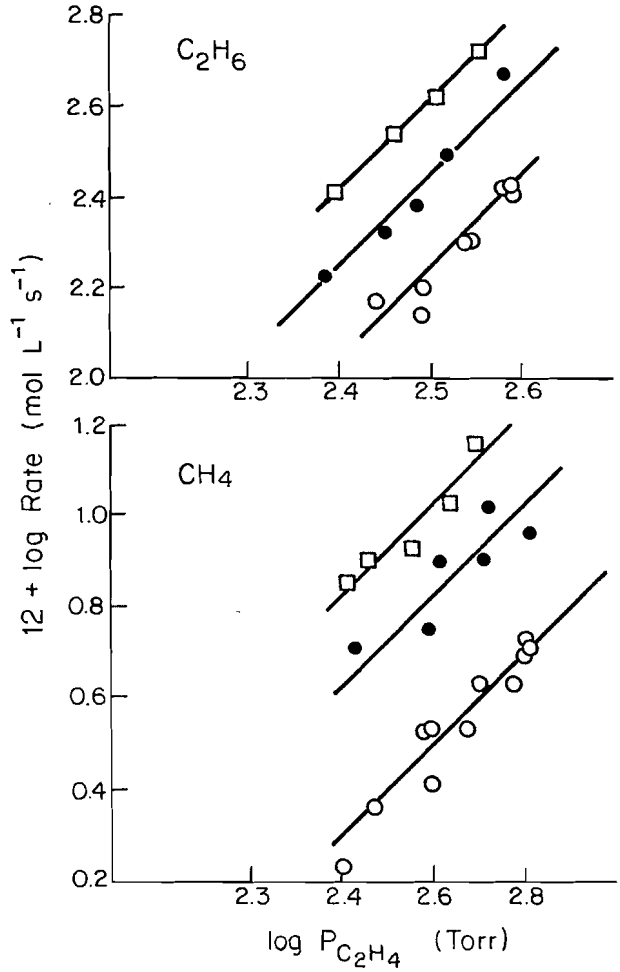


FIG. 5. Double logarithmic plots of the rates of formation of methane and ethane as a function of the initial pressure of ethylene in the presence and absence of toluene; Lines have been drawn with slope = 2. Methane: 653 K; ○: pure ethylene; ●: 3.1% toluene; □: 5.6% toluene. Ethane: 713 K; ○: pure ethylene ●: 2.5% toluene □: 4.1% toluene.

Measurements reported for k_{11} are shown together with the present results in Fig. 8. The present measurements are in agreement with the measurements of Dunlop, Kominar, and Price (17) made over a similar range of temperature but the rate constants are significantly lower than those measured at higher temperatures. The activation energy measured in the present work is also considerably lower than those values obtained at higher temperatures and lower than the value recommended by Kerr and Parsonage (1). The significance of the activation energy for this reaction will be discussed later.

The activation energy and frequency factor for reaction [12] are in good agreement with the values obtained by Price and co-workers (18, 19, 32, 33) from their studies of the thermal decomposition of alkyl metal compounds in the presence of toluene. Their activation energies were in the range 41 ± 4 kJ mol^{-1} with corresponding frequency factors in the range, and log A (L mol^{-1} s^{-1}) = 8.1 ± 0.2, the measurements covering the temperature range 465–833 K. It is interesting that the rate constants at 653 K from the present method and from the four studies of Price and co-workers lie within 15% of an average value. This is remarkable agreement between two very different methods.

Can. J. Chem. Downloaded from www.nrcresearchpress.com by 194.225.253.170 on 09/07/12
For personal use only.

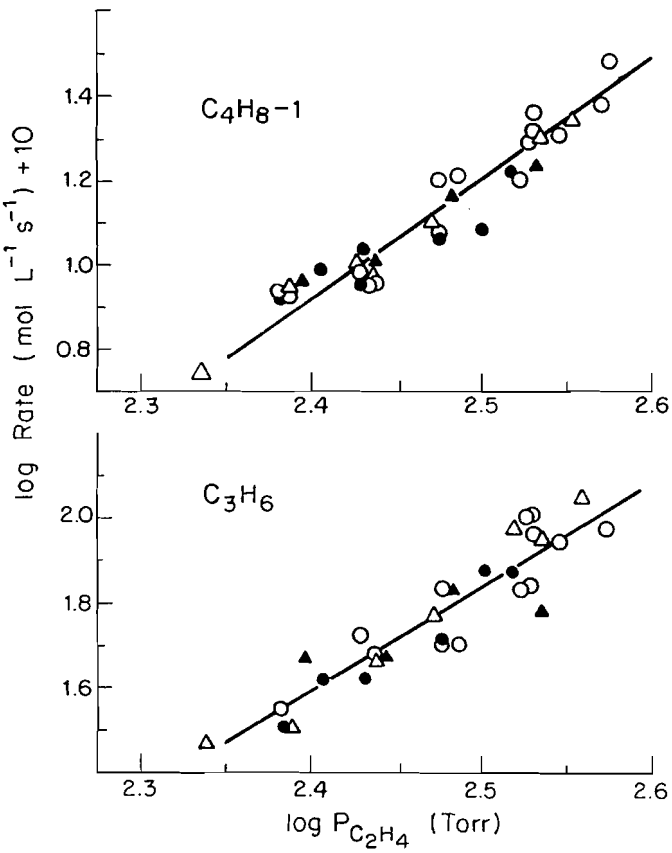


FIG. 6. Double logarithmic plots of the rates of formation of propylene and butene-1 as a function of the initial pressure of ethylene in the presence and absence of toluene at 743 K. ○: pure ethylene; ▲: 2.1% toluene; △: 3.1% toluene; ●: 5.3% toluene.

TABLE 2. Ratios of rate constants for abstraction from toluene to abstraction from ethylene for methyl and ethyl radicals

T/K	$\frac{C_7H_8}{C_2H_4}$	$\frac{(R^0_{CH_4})_a}{R^0_{CH_4}}$	$\frac{k_{11}}{k_3}$	$\frac{(R^0_{C_2H_6})_a}{R^0_{C_2H_6}}$	$\frac{k_{12}}{k_4}$
770	0.025	1.25		1.41	
	0.043	1.50		1.77	
	0.066	1.68	11	1.99	17
763	0.059	1.82	14		
743	0.021	1.41		1.58	
	0.032	1.58		1.74	
	0.056	1.82	15	2.00	20
723	0.020	1.38		1.26	
	0.042	1.73		1.55	
	0.064	2.00	17	2.00	17
713	0.025	1.41		1.58	
	0.042	2.04	22	2.23	26
693	0.016	1.26		1.26	
	0.039	1.51			
	0.066	2.30	20	2.45	24
673	0.037			1.78	
	0.064	2.75	30	2.51	23
653	0.032	2.0		1.95	
	0.059	2.96	32	2.75	30

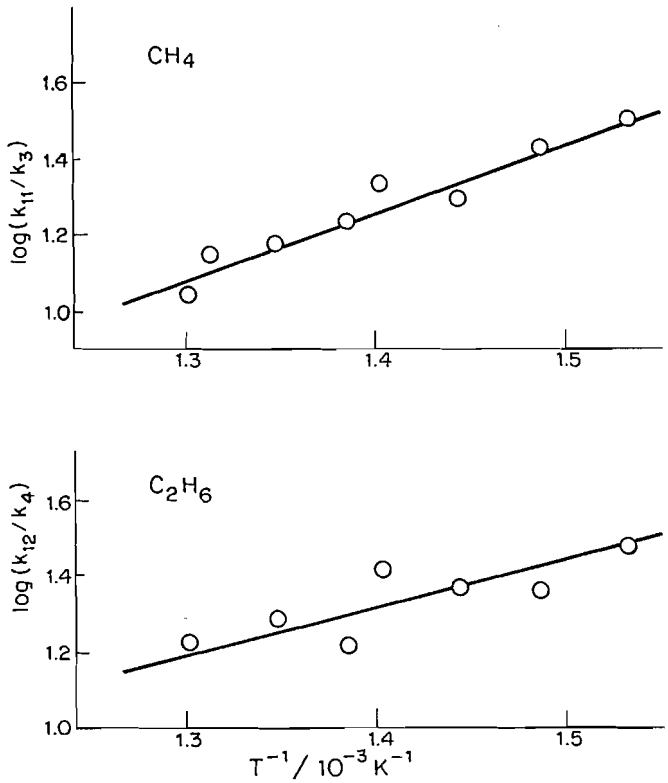


FIG. 7. Arrhenius plots of the ratios k_{11}/k_3 and k_{12}/k_4.

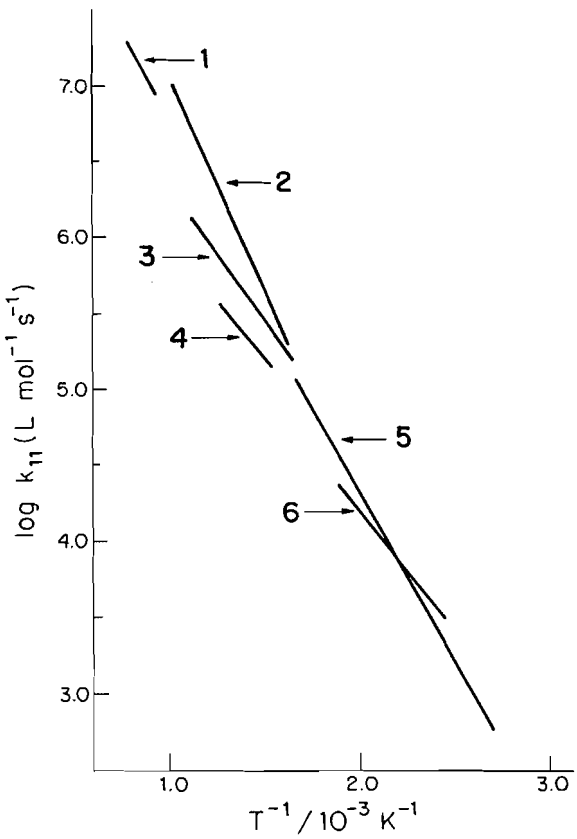


FIG. 8. Arrhenius plot for k_{11}. 1. ref. 6; 2. ref. 27; 3. ref. 17; 4. present work; 5. recommended by Kerr and Parsonage (1), average of refs. 26, 28, and 29; 6. average of refs. 30 and 31.

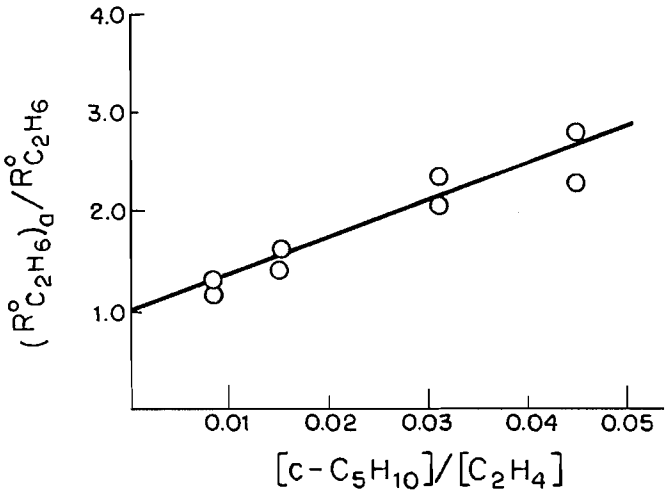


FIG. 9. Relative rates of formation of ethane in the presence and absence of cyclopentane as a function of the ratio of cyclopentane to ethylene at 718 K.

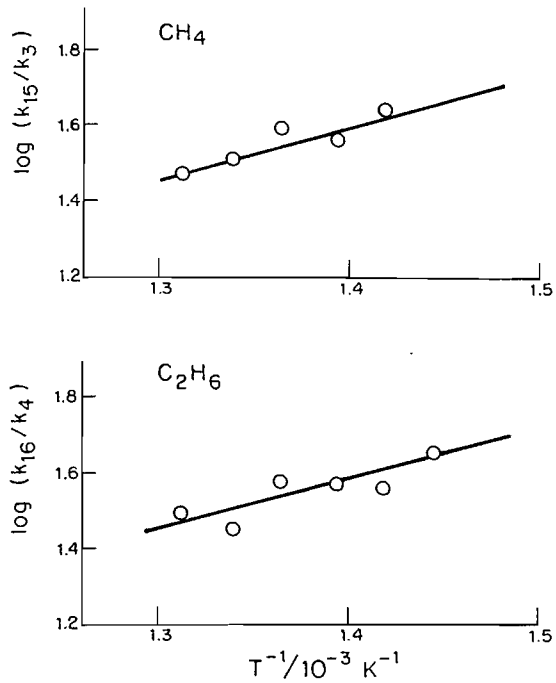


FIG. 10. Arrhenius plots of the ratios k_{15}/k_3 and k_{16}/k_4.

C. Cyclopentane

Experiments with the additive cyclopentane were performed by the first method described earlier. Initial pressures of ethylene ranged from 190 to 377 Torr. The relatively large quantities of cyclopentane obscured the peak due to butene-1 in the analysis and prevented a reliable measurement of its rate of formation. The cyclopentane had no effect on the rate of formation of propylene and it may be concluded that no new initiation processes were occurring in the presence of this additive. The rates of formation of methane and ethane were increased in the presence of cyclopentane due to the occurrence of the following abstraction reactions:

[15] $CH_3 + c\text{-}C_5H_{10} \rightarrow CH_4 + c\text{-}C_5H_9$

[16] $C_2H_5 + c\text{-}C_5H_{10} \rightarrow C_2H_6 + c\text{-}C_5H_9$

TABLE 3. Ratios of rate constants for abstraction from cyclopentane to abstraction from ethylene for methyl and ethyl radicals

T/K	$P_{C_2H_4}$/Torr	$\frac{c\text{-}C_5H_{10}}{C_2H_4}$	$\frac{(R^0_{CH_4})_a}{R^0_{CH_4}}$	$\frac{k_{15}}{k_3}$	$\frac{(R^0_{C_2H_6})_a}{R^0_{C_2H_6}}$	$\frac{k_{16}}{k_4}$
763	260	0.015	1.34		1.41	
	211	0.015	1.52		1.64	
	287	0.031	1.89		2.03	
	260	0.031	1.68	29	1.90	31
747	208	0.0082	1.27		1.11	
	211	0.014	1.60		1.52	
	328	0.014	1.42		1.46	
	211	0.031	2.02		1.97	
	327	0.031		33	1.68	28
733	246	0.0083	1.49		1.39	
	284	0.0082	1.49		1.40	
	285	0.031	2.30			
	246	0.031	2.21	39	2.15	37
718	328	0.0082	1.31		1.15	
	371	0.0082	1.46		1.30	
	200	0.015			1.41	
	311	0.015			1.61	
	289	0.031	2.24		2.06	
	201	0.031	2.03		2.36	
	201	0.045			2.29	
	310	0.045		37	2.79	37
705	203	0.015			1.71	
	308	0.015	1.90		1.58	
	205	0.045	2.85	47	2.69	36
	308	0.045	3.37			
692	199	0.015			1.53	
	348	0.015			1.58	
	377	0.015			1.71	
	193	0.045			3.05	
	377	0.045			2.93	44

and the ratios of the rates of formation of these products in the presence and absence of cyclopentane may be written as follows:

$$[17] \quad \frac{(R^0_{CH_4})_a}{R^0_{CH_4}} = 1 + \frac{k_{15}[c\text{-}C_5H_{10}]}{k_3[C_2H_4]}$$

$$[18] \quad \frac{(R^0_{C_2H_6})_a}{R^0_{C_2H_6}} = 1 + \frac{k_{16}[c\text{-}C_5H_{10}]}{k_4[C_2H_4]}$$

A plot of the results at 718 K according to eq. [18] is shown in Fig. 9 and the measurements are summarized in Table 3, which includes the ratios of rate constants k_{15}/k_3 and k_{16}/k_4 obtained from eqs. [17] and [18]. The Arrhenius plots for k_{15}/k_3 and k_{16}/k_4 are shown in Fig. 10, from which were derived the following expressions ($R = 8.314$ J mol^{-1} K^{-1}):

$$\log(k_{15}/k_3) = -0.4 \pm 0.3 + \frac{27000 \pm 4000}{2.3RT}$$

$$\log(k_{16}/k_4) = 0 \pm 0.3 + \frac{22000 \pm 4000}{2.3RT}$$

Using the expressions for k_3 and k_4 as in Sect. A, the following expressions for k_{15} and k_{16} were calculated.

Can. J. Chem. Downloaded from www.nrcresearchpress.com by 194.225.253.170 on 09/07/12
For personal use only.

TABLE 4. Relation of activation energies for hydrogen-transfer reactions to bond dissociation energies of the reactants

Reaction	Reference 1		Present method		Literature values	
	E, kJ mol^{-1}	D(R—H), kJ mol^{-1}	E, kJ mol^{-1}	D(R—H), kJ mol^{-1}	D(R—H), kJ mol^{-1}	Ref.
$CH_3 + C_2H_4$	45.6	426	63	445	460	25
$CH_3 + H_2$	45.8	425	55	433	435	25
$CH_3 + C_2H_6$	48.7	421			418	34
$CH_3 + C_3H_8$	40.3	408			402	34
$CH_3 + i\text{-}C_4H_{10}$	33.6	396			393	34
$CH_3 + C_6H_6$	46.2	417	63	445	464	25
$CH_3 + C_7H_8$	39.7	407	29	389	368	25
$CH_3 + c\text{-}C_5H_{10}$	39.3	406	36	401	400	34

$$\log k_{15}\,(\mathrm{L\,mol^{-1}\,s^{-1}}) = 8.3 \pm 0.5 - \frac{36000 \pm 7000}{2.3RT}$$

$$\log k_{16}\,(\mathrm{L\,mol^{-1}\,s^{-1}}) = 8.2 \pm 0.5 - \frac{40000 \pm 7000}{2.3RT}$$

Four of the five measurements reported for k_{15} (20–23) give values for the activation energy in the range 38 ± 2 kJ mol^{-1} with log A (L mol^{-1} s^{-1}) = 8.7 ± 0.3, and the present measurement falls within the range. No values for k_{16} were found in the literature.

Discussion

It is of interest to examine the activation energies for the hydrogen transfer reactions measured by the method described here, and by other methods, in relation to the bond dissociation energy of the compound RH of eq. [1]. Relations between such activation energies and bond dissociation energies have often been discussed and were recently examined in detail for small radicals such as methyl (24). The authors developed a semi-empirical procedure to calculate activation barriers for hydrogen-abstraction reactions and showed that these barriers were related to the overall energy change in the reaction. For reactions of methyl radicals of the type

$$CH_3 + RH \rightarrow CH_4 + R$$

the following relation was proposed,

[19] $$E = 0.609\,D_1 - 0.473\,D_2$$

where D_1 and D_2 are the C—H bond dissociation energies for RH and CH_4 respectively and E is the activation barrier for the reaction. Although the activation barrier is not necessarily equivalent to the experimental activation energy it will be close enough that this equation may be used to test the correlation of the measured activation energies with the bond dissociation energies of the reactants, RH. Taking the activation energies recommended by Kerr and Parsonage (1) and the values measured using the present technique, values of D_1 were calculated from this equation for several RH molecules. These are shown in Table 4 together with values from the literature (25, 34).

For the reactions with the saturated hydrocarbons ethane, propane, isobutane, and cyclopentane, the activation energies recommended by Kerr and Parsonage predict dissociation energies in reasonable agreement with the values discussed by McMillen and Golden (25). On the other hand, for the reactions with the unsaturated hydrocarbons ethylene, benzene, and toluene, the activation energies measured by the present method provide better correlation with the bond dissociation energies. For example, the C—H bond dissociation energy in ethylene is considerably stronger than that in ethane, but the activation energy for abstraction from ethylene recommended by Kerr and Parsonage is smaller than that for abstraction from ethane. Benzene and toluene provide a contrasting situation. The activation energy for abstraction from benzene measured by the present technique is considerably higher than the value recommended by Kerr and Parsonage, while the reverse is the case for toluene. In both cases the present method gives values that are more realistically related to the C—H bond dissociation energy in these molecules. The activation energies recommended by Kerr and Parsonage for these two abstraction reactions appear too close. The difference of about 6 kJ mol^{-1} suggests that the C—H bond dissociation energies in benzene and toluene are similar. In fact, the difference, according to the values recommended by McMillen and Golden, is almost 100 kJ mol^{-1}.

It should be mentioned that for the case of toluene the measured activation energy has been related to the bond dissociation energy of the C—H bond in the methyl group. In fact, the measurements do not distinguish between abstraction from the ring and from the side chain. Because the dissociation energy of the C—H bond in the methyl group is considerably less than that of the ring hydrogens, abstraction from the methyl group will be dominant at moderate temperatures. With increasing temperature, abstraction from the ring will assume increasing importance with a consequent increase in the apparent activation energy. As is evident from Fig. 8, this effect does not account for the difference in activation energy between the present results and that recommended by Kerr and Parsonage (1). Nevertheless, because of the uncertainty in the position of the abstraction, the comparison presented in Table 4 for toluene should be regarded as qualitative.

We have included in Table 4 an activation energy of 55 kJ mol^{-1} for abstraction from hydrogen. This value was not measured by the present method but was used as a reasonable average value in the temperature range of the experiments where hydrogen was the additive (10). In fact it is close to an average of the value recommended by Kerr and Parsonage, 45.8 kJ mol^{-1}, and the value proposed by Moller, Mozzhukhin, and Wagner (3), 60 kJ mol^{-1}, based on experiments in the temperature range 1200–2000 K. Use of the value of 55 kJ mol^{-1} led to a value for the activation energy for abstraction from ethylene the same as that obtained from results using ethane as additive. Thus, indirectly, the present method using measure-

Can. J. Chem. Downloaded from www.nrcresearchpress.com by 194.225.253.170 on 09/07/12
For personal use only.

ments of relative rates strongly suggests that the activation energy for abstraction from hydrogen is at least 6 kJ mol^{-1} greater than that for abstraction from ethane, and not less, as recommended by Kerr and Parsonage. This conclusion is also in accord with the difference in bond dissociation energy between the two reactants.

In conclusion, Table 4 shows that even though the relation expressed in eq. [19] is approximate when applied to the measured activation energies, an examination of the qualitative relation between activation energy and bond dissociation energy for a particular elementary reaction may offer new insights into the results. In particular, the activation energies measured in the present study for abstraction from unsaturated hydrocarbons appear more realistic in relation to the dissociation energies of the reactants than the values recommended by Kerr and Parsonage.

Acknowledgments

The authors thank the Natural Sciences and Engineering Research Council of Canada for financial support of this research. H.-X.Z. thanks the NSFC of the People's Republic of China for financial support during her visit to Canada.

1. J. A. KERR and M. J. PARSONAGE. Evaluated kinetic data on gas-phase hydrogen transfer reactions of methyl radicals. Butterworths, London. 1976.
2. J. A. KERR and S. J. MOSS. CRC Handbook of bimolecular and termolecular gas reactions. Vol 1. CRC Press, Boca Raton, FL. 1981.
3. W. MÖLLER, E. MOZZHUKHIN, and H. GG. WAGNER. Ber. Bunsenges. Phys. Chem. **90**, 854 (1986).
4. P. C. KOBRINSKY and P. D. PACEY. Can. J. Chem. **52**, 3665 (1974).
5. C.-J. CHEN, M. H. BACK, and R. A. BACK. Can. J. Chem. **55**, 1624 (1977).
6. J. DZARNOSKI, M. A. RING, and H. E. O'NEAL. Int. J. Chem. Kinet. **14**, 279 (1982).
7. T. C. CLARK and J. E. DOVE. Can. J. Chem. **51**, 2147 (1973).
8. W. C. GARDINER. Acc. Chem. Res. **10**, 326 (1977).
9. H. FURUE and P. D. PACEY. J. Phys. Chem. **90**, 397 (1986).
10. H.-X. ZHANG and M. H. BACK. Int. J. Chem. Kinet. In press.
11. S. I. AHONKHAI and M. H. BACK. Can. J. Chem. **66**, 578 (1988).
12. S. I. AHONKHAI, X.-H. LIN, and M. H. BACK. Int. J. Chem. Kinet. **21**, 1 (1989).
13. M. H. BACK and R. MARTIN. Int. J. Chem. Kinet. **11**, 757 (1979).
14. G. AYRANCI and M. H. BACK. Int. J. Chem. Kinet. **13**, 897 (1981).
15. M. KRECH and S. J. W. PRICE. Can. J. Chem. **45**, 157 (1976).
16. A. F. TROTMAN-DICKENSON and E. W. R. STEACIE. J. Chem. Phys. **19**, 169 (1951).
17. A. N. DUNLOP, R. J. KOMINAR, and S. J. W. PRICE. Can. J. Chem. **48**, 1269 (1970).
18. A. C. LALONDE and S. J. W. PRICE. Can. J. Chem. **49**, 3367 (1971).
19. A. A. KOSKI, S. J. W. PRICE, and B. C. TRUDELL. Can. J. Chem. **54**, 482 (1976).
20. A. F. TROTMAN-DICKENSON and E. W. R. STEACIE. Can. J. Chem. **32**, 40 (1954).
21. J. R. MCNESBY and A. S. GORDON. J. Am. Chem. Soc. **79**, 825 (1957).
22. A. S. GORDON, S. R. SMITH, and J. R. MCNESBY. 7th Int. Symp. Combustion, Butterworths, London. 1959. p. 317.
23. A. S. GORDON. Can. J. Chem. **43**, 570 (1965).
24. G. LEROY, M. SANA, and A. TINANT. Can. J. Chem. **63**, 1447 (1985).
25. D. F. MCMILLEN and D. M. GOLDEN. Ann. Rev. Phys. Chem. **33**, 493 (1982).
26. M. F. R. MULCAHY, D. J. WILLIAMS, and J. R. WILMHURST. Aust. J. Chem. **17**, 1329 (1964).
27. S. J. W. PRICE and A. F. TROTMAN-DICKENSON. J. Chem. Soc. 4025 (1958).
28. M. CHER, C. S. HOLLINGSWORTH, and F. SICILIO. J. Phys. Chem. **70**, 877 (1966).
29. A. F. TROTMAN-DICKENSON and E. W. R. STEACIE. J. Chem. Phys. **19**, 329 (1951).
30. R. E. REBBERT and E. W. R. STEACIE. J. Chem. Phys. **21**, 1723 (1953).
31. I. B. BURKLEY and R. E. REBBERT. J. Phys. Chem. **67**, 168 (1963).
32. M. DALY and S. J. W. PRICE. Can. J. Chem. **54**, 1814 (1976).
33. M. C. PAPUTA and S. J. W. PRICE. Can. J. Chem. **57**, 3178 (1979).
34. A. L. CASTELHANO and D. GRILLER. J. Am. Chem. Soc. **104**, 3655 (1982).

Can. J. Chem. Downloaded from www.nrcresearchpress.com by 194.225.253.170 on 09/07/12
For personal use only.

Solution inclusion complexes of cyclodextrins with sodium perfluorooctanoate

RAMAMURTHY PALEPU
Department of Chemistry, University College of Cape Breton, Sydney, N.S., Canada B1P 6L2

AND

VINCENT C. REINSBOROUGH
Department of Chemistry, Mount Allison University, Sackville, N.B., Canada E0A 3C0

Received April 4, 1989

RAMAMURTHY PALEPU and VINCENT C. REINSBOROUGH. Can. J. Chem. **67**, 1550 (1989).

Pre-micellar and micellar sodium perfluorooctanoate solutions (SPFO) were examined conductometrically with added α-cyclodextrin (α-CD), β-cyclodextrin (β-CD), and γ-cyclodextrin (γ-CD). The order of stability of the 1:1 inclusion complex was β-CD > γ-CD > α-CD determined largely by the goodness of fit of the fluorocarbon chain in the CD cavity. Sodium ion electrode studies revealed that some Na^+ ion is associated with the β-CD/SPFO complex. As shown by fluorine-19 nmr, β-CD girds the SPFO molecule snugly amidship with the terminal CF_3 group still in solution. On the other hand, SPFO manages only a weak penetration of the fluorocarbon chain into the smaller α-CD cavity.

Key words: perflurooctanoate, cyclodextrin complexes, fluorocarbon surfactant, ^{19}F nmr.

RAMAMURTHY PALEPU et VINCENT C. REINSBOROUGH. Can. J. Chem. **67**, 1550 (1989).

Faisant appel à la conductimétrie, on a étudié des solutions pré-micellaires et micellaires de perfluorooctanoate de sodium (PFOS) auxquelles on a ajouté des α- (α-CD), β- (β-CD) et γ-cyclodextrines (γ-CD). L'ordre de stabilité des complexes d'inclusion 1:1 (β-C > γ-CD > α-CD) est fortement déterminé par la facilité de la chaîne fluorocarbonée à s'adapter dans la cavité de la CD. Des études à l'aide d'une électrode sélective pour l'ion sodium ont révélé que quelques ions Na^+ sont associés avec le complexe β-CD/PFOS. La rmn du ^{19}F a permis de montrer que la β-CD entoure le milieu de la molécule de PFOS alors que le groupement CF_3 est encore en solution. Par ailleurs, la pénétration de la chaîne fluorocarbonée de la molécule de PFOS dans la cavité de l'α-CD est faible.

Mots clès : perfluorooctanoate, complexes cyclodextrines, surfactant fluorocarbone, rmn du ^{19}F.

[Traduit par la revue]

Introduction

In the inclusion of ligands by cyclodextrins in solutions, a major factor in the stability of the resultant complex is thought to be the closeness of fit of the guest molecule within the cyclodextrin cavity. Thus, for example, the binding constant for adamantanecarboxylate is 10^5 dm^3 mol^{-1} in β-cyclodextrin (β-CD) but only 10^2 dm^3 mol^{-1} in α-cyclodextrin (α-CD) and 10^3 dm^3 mol^{-1} in γ-cyclodextrin (γ-CD) (1) because the adamantane moiety with diameter 7 Å fits most snugly into the cavity of β-CD which has the same diameter. Adamantane cannot deeply penetrate α-CD of cavity diameter 5 Å and has room to spare inside γ-CD of cavity diameter 8.5 Å. Another hydrophobic entity that may demonstrate similar behavior is the fluorocarbon tail with cross-sectional diameter of 6 Å which should fit more snugly into the β-CD cavity than the α-CD cavity. Recent work has shown that fluorocarbon surfactants bind very strongly with β-CD (2, 3) with little tendency to form inclusates with α-CD (2). However, surfactant hydrocarbon chains of diameter 4.5 Å apparently are readily accommodated within the α-CD cavity because stable complexes are formed with both α-CD and β-CD (3–8). A complicating feature in the hydrocarbon chain situation is that α-CD/surfactant complexation appears to favour 2:1 complexes while 1:1 complexes predominate with β-CD (4, 8). A detailed, multi-faceted study of the inclusion of a perfluorinated surfactant by the cyclodextrins in solution was deemed appropriate to shed light on the importance of size parameters in the strength and position of binding. Binding constants and related thermodynamic data for sodium perfluorooctanoate (SPFO) inclusions with CDs were obtained through conductance measurements. Sodium ion activities were monitored by ion selection electrode techniques while environmental changes to the fluorine atoms was tracked by fluorine-19 nmr.

Experimental

Conductance measurements were performed with a Radiometer CDM83 Bridge at 25.0°C. Potentiometric and sodium ion activity measurements were peformed with an Orion Research microprocessor ion analyzer/901 with 0.1 mV sensitivity. The sodium selective electrode was an Orion 90-02 double junction electrode with the out chamber filling of KNO_3 solution replaced by 5 *M* NH_4NO_3 solution to prevent leaking of potassium ions into the test solutions. With this electrochemical cell, the response of the electrode against aqueous NaCl was linear in the concentration range investigated (10^{-3} to 5×10^{-1} mol dm^{-3}) with a slope equal to 56 mV.

Fluorine-19 nmr spectra were obtained in SPFO solutions on a Nicolet 360NB spectrometer at the Atlantic Region Magnetic Resonance Centre (Dalhousie University) with CCl_3F as reference. The cyclodextrins (Sigma) were previously dried before use while sodium perfluorooctanoate (SPFO) was obtained from the acid (Aldrich).

Results and discussion

The dependence of the conductance of SPFO on cyclodextrin concentration for α-CD, β-CD, and γ-CD is shown in Fig. 1 for some pre-micellar SPFO solutions. Clearly, the order of binding with SPFO is β-CD > γ-CD > α-CD with the last showing very little association at all. The intersection of the linear portions of the curves for the three cyclodextrins gives the stoichiometry of the main complex formed as 1:1 in agreement with findings from other surfactant systems (3–8). All pre-micellar SPFO solutions displayed the same behavior. From the change in conductivity and with reasonable assumptions about the ionic contributions to the conductivity, it is possible to derive the binding constants for the inclusion complex. A number of these relationships exists in the literature but perhaps the most versatile and computer compatible is that due to Zollinger *et al.* (9) which generates binding constants for both the 1:1 and 2:1 β-CD/inclusate

Can. J. Chem. Downloaded from www.nrcresearchpress.com by 194.225.253.170 on 09/07/12
For personal use only.

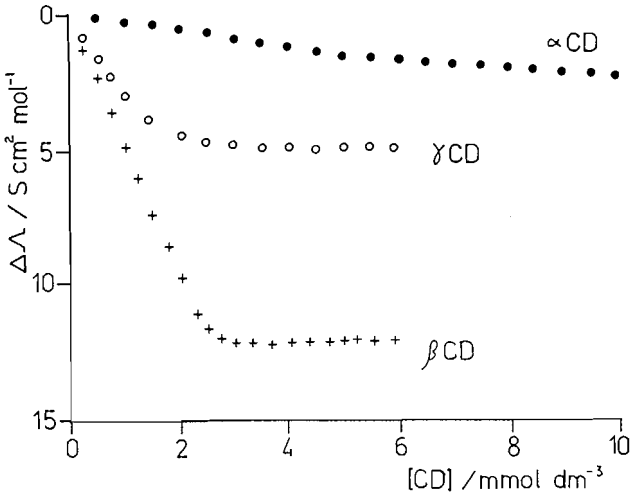


FIG. 1. Conductance decrease of SPFO solutions with added cyclodextrins. Concentration of SPFO is 5.00 mmol dm^{-3} in α-CD solutions and 2.00 mmol dm^{-3} in β-CD and γ-CD solutions.

complexes. Both complexes are generally recognized as coexisting in solution systems of this sort although one complex usually predominates. From this relationship, the value of the binding constant for the β-CD/SPFO complex was found to be 4500 dm^3 mol^{-1}, 640 dm^3 mol^{-1} for the γ-CD/SPFO complex, and essentially zero for α-CD/SPFO. The analysis revealed that no significant amounts of 2:1 complexes were present in any of the systems.

In micellar solution, the conductance of SPFO was initially little affected by additions of β-CD but beyond a certain concentration decreased rapidly (Fig. 2). With micellized hydrocarbon surfactants, the conductance behavior had been similar in concentrated β-CD solutions but in dilute β-CD solutions rose to a maximum which was identified as the amount of β-CD required to initiate micelle formation at this particular surfactant concentration (8). In other words, the latter concentration was the critical micelle concentration of SPFO in the presence of β-CD the concentration of which corresponded to the maximum in the conductivity curve. The sudden sharp drop in conductivity beyond the maximum that was common to both hydrocarbon and fluorocarbon surfactant systems is consistent with the micelles having been destroyed and with surfactant ion and perhaps also Na^+ ion being sequestered by β-CD (8, 10). One reason for the initially flat portion of the curve for micellar NaPFO solution may be that Na^+ ion was assimilated into the NaPFO complex almost as rapidly as it was released from the micellar surface region so that little net increase in the overall solution conductivity was registered. Once the micelles have been totally destroyed by β-CD addition (at the end of the flat portion of the curve), further addition of β-CD serves to bind the remaining perfluorooctanoate monomers in 1:1 complexes which in turn partly assimilate Na^+ ions from solution.

Direct evidence for the binding of Na^+ ions from solution by the β-CD/SPFO complex was provided by Na^+ ion activities measured by selective ion electrodes. Figure 3 shows the electrode potential of a Na^+ ion electrode in 5.00 mmol dm^{-3} SPFO solutions with various amounts of β-CD added. A marked drop in Na^+ ion activity acompanied β-CD addition but for stoichiometric ratios of β-CD to SPFO of unity or greater the decrease was approximately the same. Similar separate additions of β-CD or of SPFO to 5 mmol dm^{-3} NaCl solutions did not

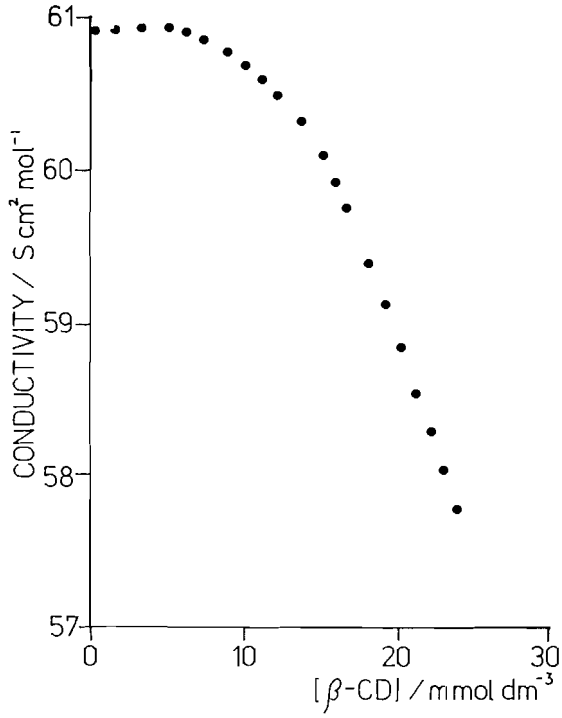


FIG. 2. Conductance of 4.00 × 10^{-2} mol dm^{-3} SPFO in β-CD solutions.

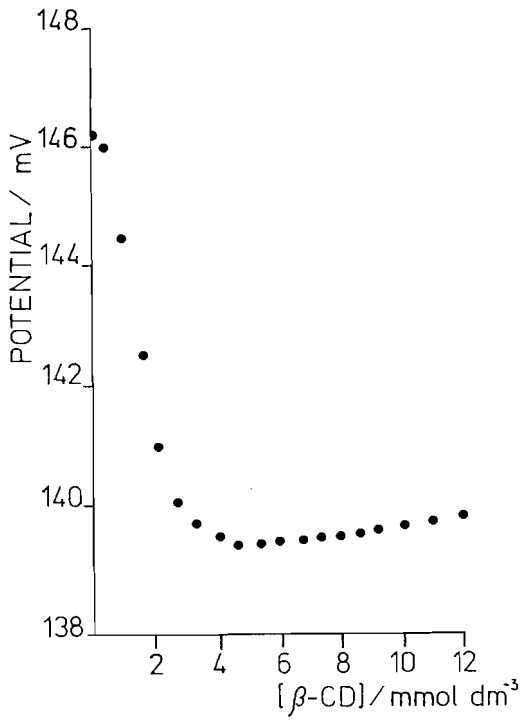


FIG. 3. Sodium ion potentials in 5.00 mmol dm^{-3} SPFO with added β-CD.

alter the observed Na^+ ion activity. Thus, it would appear that Na^+ ion was removed from solution by β-CD only when the latter was bound with SPFO. This apparent Na^+ ion association with β-CD/surfactant complexes in solution had been noted previously from our laboratory with other anionic surfactants (8) and is now being investigated more thoroughly. At this stage, the most reasonable explanation is that ion-pairing between Na^+

Can. J. Chem. Downloaded from www.nrcresearchpress.com by 194.225.253.170 on 09/07/12
For personal use only.

ion and included SPFO is abetted by the hydrophilic β-CD exterior.

The molar conductivities of SPFO in several pre-micellar β-CD solutions were measured at four different temperatures to obtain estimates of ΔH^0 and ΔS^0 for the associative process. From the expansion of ΔG as a polynomial and by a plot of $\ln K$ versus $1/T$, an average value of ΔH^0 and ΔS^0 could be obtained. It was found that $\Delta H^0 = -12 \pm 1$ kJ mol^{-1} and $\Delta S^0 = 70 \pm 5$ J mol^{-1} K^{-1} for the formation of the β-CD/SPFO complex and 32 ± 3 kJ mol^{-1} and 200 ± 25 J mol^{-1} K^{-1}, respectively, for the γ-CD/SPFO complex.

Similar temperature dependence studies were conducted in sodium dodecylsulfate solutions (SDS) to obtain comparison thermodynamic data for β-CD/SDS inclusion complexes. In 2.0 mmol dm^{-3} SDS solution, ΔH^0 was endothermic at 10.5 ± 0.3 kJ mol^{-1} and ΔS^0 was 139 ± 1 J mol^{-1} K^{-1}. Measurements in three other pre-micellar SDS solutions gave similar results. It is clear from these numbers that, both for the inclusion of the hydrocarbon chain and that of the fluorocarbon chain, entropy is the significant driving force which might be expected with the solvent elimination from the cavity and the subsequent internal binding occurring with the insertion process.

Fluorine-19 nmr spectra for three 0.020 mol dm^{-3} SPFO solutions, one with only SPFO, one together with 0.020 mol dm^{-3} β-CD and one together with 0.020 mol dm^{-3} α-CD, gave rise to seven peaks as shown in Fig. 4 and Table 1. These were assigned to the fluorines of the seven carbons of the surfactant chain following the usual convention of beginning the numbering with the fluorine-less carbon of the polar head (C1). Peak assignments were taken from Muller and Simsohn (11) who, however, had relegated the fluorines of C_3, C_4, C_5, and C_6 to one complex peak. In this same region, with the better resolution possible in the present work, four peaks were easily distinguished and these have been tentatively assigned to specific carbons. The placement of peaks C_3, C_4, C_5, and C_6 may not be correct relative to each other but this is not important to the present argument.

No new peaks appeared when cyclodextrins were added to the SPFO solutions but several of the peaks underwent appreciable chemical shifts. Thus the exchange between the fluorine atoms in SPFO in solution and in the inclusion complex must be rapid. All the observed shifts in both CD systems were downfield, indicating probably a loosening of the restrictive environment fluorine atoms experience in water as compared to the situation within the CD cavity. The theoretical background for both the direction and magnitude of chemical shifts is far from resolved at the moment and the environmental constraint is but one of several factors deemed important in the relative movement of peaks. However, the situation with the strongly polarizing fluorine atoms in aqueous media may not be so complex. The association of perfluorinated surfactant monomers in aqueous solution into micelles results in upfield shifts in F-19 nmr (12). The close packing of fluorine atoms to fluorine atoms in the micelle is envisaged as being more restrictive to the observed resonant frequency than in the aqeous situation. It is well known that upfield shifts for fluorine peaks are recorded for movement from a hydrocarbon environment into a fluorocarbon one and thus passage from aqueous to fluorocarbon medium should be similarly disposed. It would appear from the present results that fluorine atoms in passing from the aqueous solution situation into the hydrophobic CD interior enter into a less constrained environment.

The pattern of the chemical shifts in both CD systems was entirely different. With β-CD, only C_2–C_6 showed noticeable shifts (peaks for C_4 and C_5 essentially coalesced and thus could be pinpointed less accurately) while peak movement was only noted with C_5–C_8 when α-CD was the complexing agent. Moreover, the most pronounced shifts with β-CD occurred with the fluorines of the middle carbons while with α-CD the fluorines of the terminal group experienced the greatest peak displacement. It is clear from this nmr study that the binding sites of the two cyclodextrins on the surfactant chain differ markedly: β-CD girds the fluorocarbon chain over the region C_3 to C_6 while α-CD is impaled on the surfactant tail. Simple geometry dictates the difference: the cavity size of β-CD allows for a snug fit over the fluorocarbon chain but the interior of α-CD is not large enough for this. Only the terminal group of the chain and a few further carbons experience environmental or conformational changes on binding with α-CD. The C_6 and C_5 peaks were assigned on the basis of diminishing chemical shift from the tail in the α-CD/SPFO spectrum and the C_3 and C_4 peaks were decided from symmetry considerations in the chemical shift pattern in the β-CD/SPFO spectrum. These assignments are clearly tentative but receive some support in their self-consistency.

The conductivity data would indicate that the inclusion of the SPFO by β-CD is much stronger than with α-CD where the binding constant could not be measured accurately by this

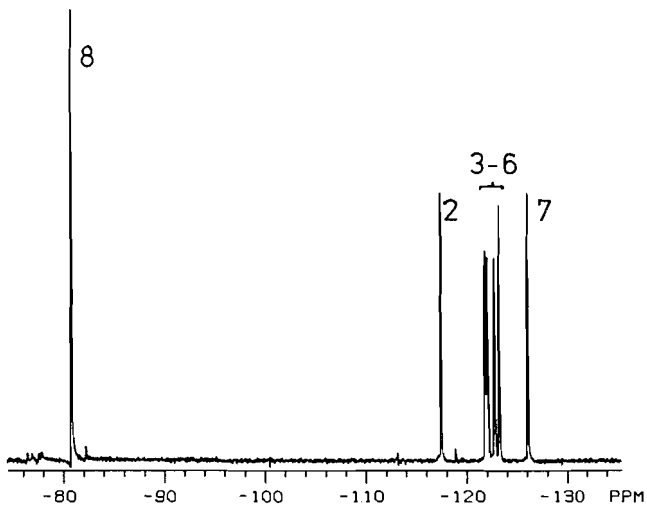


FIG. 4. Fluorine-19 nmr of 2.00 mmol dm^{-3} SPFO. Numbering refers to the carbon atom to which the fluorines are bound.

TABLE 1. ^{19}F nmr data*

	δ(ppm)		
Carbon	Pure SPFO	SPFO/β-CD	SPFO/α-CD
2	−117.55	−117.36 (0.19)	−117.50
3	−121.94	−121.54 (0.40)	−121.95
4	−123.31	−122.6 (0.7)	−123.24
5	−122.17	−121.75 (0.42)	−121.90 (0.27)
6	−122.88	−122.6 (0.3)	−122.67 (0.21)
7	−126.17	−126.17	−125.81 (0.36)
8	−80.88	−80.88	−80.34 (0.54)

*Fluorine-19 nmr chemical shifts in 0.020 mol dm^{-3} sodium perfluorooctanoate (SPFO) solutions containing equimolar α-CD and β-CD.

All shifts are in ppm. Values in parentheses report the down-field shifts where they are greater than 0.1 ppm from the pure solution values.

Can. J. Chem. Downloaded from www.nrcresearchpress.com by 194.225.253.170 on 09/07/12
For personal use only.

method. The nmr picture is entirely consistent with this in that the smaller internal diameter of the α-CD torus allows only partial penetration by the end of the fluorocarbon tail in probably loose fashion while β-CD sits tightly amidship relatively close to the polar head of the surfactant. The two configurations also would not give rise to the same loss in ion mobility when the surfactant ion was complexed and this may be the reason why the conductivity measurements failed to indicate any appreciable concentration of α-CD/SPFO complex when the F-19 nmr gave results of a different nature.

Acknowledgement

We wish to thank the Natural Sciences and Engineering Research Council of Canada for support through grants.

1. W. C. Cromwell, K. Bystrom, and M. R. Eftink. J. Phys. Chem. **89**, 326 (1985).
2. X.-K. Jiang, J.-H. Gu, X.-E. Cheng, and Y.-Z. Hui. Acta Chim. Sin. **45**, 159 (1987).
3. R. Palepu, J. M. Richardson, and V. C. Reinsborough. Langmuir, **5**, 218 (1989).
4. A. Hersey, B. H. Robinson, and H. C. Kelly. J. Chem. Soc. Faraday Trans. 1, **82**, 1271 (1986).
5. T. Okubo, H. Kitano, and N. Ise. J. Phys. Chem. **80**, 2661 (1976).
6. I. Satake, T. Ikenoue, T. Takeshita, K. Hayakawa, and T. Maeda. Bull. Chem. Soc. Jpn. **58**, 2746 (1985).
7. I. Satake, S. Yoshida, K. Hayakawa, T. Maeda, and Y. Kusumoto. Bull. Chem. Soc. Jpn. **59**, 3991 (1986).
8. R. Palepu and V. C. Reinsborough. Can. J. Chem. **66**, 325 (1988).
9. D. P. Zollinger, E. Bulten, A. Christenhusz, M. Bos, and W. E. van der Linden. Anal. Chim. Acta, **198**, 207 (1987).
10. R. Palepu and V. C. Reinsborough. Unpublished results.
11. N. Muller and H. Simsohn. J. Phys. Chem. **75**, 942 (1971).
12. B. M. Fung, D. L. Mamrosh, E. A. O'Rear, C. B. Frech, and J. Afzal. J. Phys. Chem. **92**, 4405 (1988).

Can. J. Chem. Downloaded from www.nrcresearchpress.com by 194.225.253.170 on 09/07/12
For personal use only.

Infrared spectroscopic studies of surfactant micelles: the behaviour of aliphatic ketones as guests[1]

HECTOR L. CASAL AND ADÈLE MARTIN

Division of Chemistry, National Research Council of Canada, Ottawa, Ont., Canada K1A 0R6

Received February 20, 1989

HECTOR L. CASAL and ADÈLE MARTIN. Can. J. Chem. **67**, 1554 (1989).

Aliphatic ketones were incorporated into micelles and bilayers formed by various surfactant molecules. These ketones are used as "probe" molecules; hydrogen bonding to their carbonyl groups is easily detected by means of infrared spectroscopy. The extent of hydrogen bonding between the C=O groups and the solvent (D_2O) is monitored by a parameter which gives a relative (qualitative) measure of the volumes of different micellar environments. It is also shown that structural changes may induce translocation of the ketone probes and that there are subtle structural differences between cooling-induced and ion-induced coagels.

Key words: infrared, micelles, water penetration, bilayers, surfactants.

HECTOR L. CASAL et ADÈLE MARTIN. Can. J. Chem. **67**, 1554 (1989).

On a incorporé des cétones aliphatiques dans des micelles et dans des bicouches formées par divers agents tensioactifs. On a utilisé ces cétones comme «sondes»; grâce à la spectroscopie infrarouge, on peut facilement détecter la formation de ponts hydrogènes avec leurs groupements carbonyles. Utilisant un paramètre qui donne une mesure relative (qualitative) des volumes des divers environnements micellaires, on a évalué l'importance de la liaison hydrogène entre les groupements C=O et le solvant (D_2O). On montre que les changements structuraux peuvent induire une translocation des «sondes» cétoniques et qu'il existe des différences structurales subtiles entre des coagels induits par le froid ou par les ions.

Mots clés : infrarouge, micelles, penetration d'eau, bicouches, tensioactifs.

[Traduit par la revue]

Can. J. Chem. Downloaded from www.nrcresearchpress.com by 194.225.253.170 on 09/07/12
For personal use only.

Introduction

The structure of micelles and other mesomorphs formed by surfactant molecules continues to be a subject of considerable interest. Recently, we investigated micelles and bilayers by using keto surfactants and aliphatic ketones as "probes" (1, 2). The infrared spectra of keto-surfactants as guests in micelles demonstrated that the extent of contact between the solvent (water) and the surfactant aliphatic chains is considerable. In fact, in the case of a short keto surfactant molecule (sodium 7-oxooctanoate) in micelles of sodium octanoate, there do not appear to be C=O groups at positions free from contact with the solvent (D_2O). However, when 5-nonanone was used as the guest, the infrared spectra demonstrated that this molecule coexists in two environments; in one there is extensive ketone:water contact while in the other there is no such contact. Therefore, from that comparison, two micellar environments were found (1).

In the work reported here, we explore the possibility of using aliphatic ketones as probes of micellar structure with particular emphasis on determining changes in the extent of contact between the solvent and the surfactant aliphatic chains. We use the infrared spectra of the guest ketones to measure the extent of hydrogen bonding to their C=O groups. In the systems studied the only source of hydrogen bond donors is the solvent (D_2O). Several different surfactant systems (forming micelles and bilayers) have been measured and the results indicate that the infrared spectra of guest ketones yield a qualitative comparison of different mesomorphs.

Aliphatic ketones such as those used in this study are incorporated into micelles and at the concentrations used here do not bring about gross structural changes (3). Malliaris (4) has determined several micellar properties of SDS[2] in the presence of ketones. For example, the cmc of SDS goes from 8 m*M* in the absence of ketones to 7 m*M* in the presence of 9.9 m*M* 6-undecanone, while the aggregation number changes from 67 to 61 (the SDS concentration was 0.04 *M*, i.e. samples of 4:1 molar ratio SDS:ketone). These results give us some confidence that the information derived from guest ketones does not come from systems grossly distorted by the probe.

Experimental

The aliphatic ketones used in this study were obtained from Aldrich or Wiley Organics and used without further purification. SDS was from BDH (especially pure grade); sodium octyl sulfate, sodium decyl sulfate, sodium tetradecyl sulfate, and sodium hexadecyl sulfate were from Lancaster Synthesis and purified by recrystallization from methanol. Triton X-100 was from Sigma. DTAC, CTAB (Eastman Kodak), and DODAC (Shelex Chemical Co.) were purified by repeated recrystallization from acetone. Sodium octanoate and sodium dodecanoate were from Nu-Check Chemical Co. and used as received.

In all cases, the mixtures of the ketones with the surfactants were prepared by adding the desired amount of ketone to a ready made solution of the detergent prepared in D_2O. After addition of the ketones, the samples were warmed to 40°C and vortexed. They were left at room temperature for 24 h prior to measurement. In all cases, the molar ratios detergent:ketone were higher than 14:1. Specific concentrations are found in the captions to the figures. D_2O was used throughout as the solvent for two reasons: H_2O has a strong absorption band at 1640 cm^{-1} which overlaps the ketone C=O stretching bands and, hydrogen bonds to D_2O induce larger frequency shifts of the C=O stretching vibration.

Infrared spectra at 2 cm^{-1} resolution were recorded on a Digilab FTS-60 Fourier transform spectrometer equipped with a DTGS detector. Curve-fitting of the C=O stretching bands was carried out with an iterative procedure, the estimated error in the band areas determined from band fitted spectra is ±10%.

Results and discussion

The C=O stretching vibrational mode, $\nu_{C=O}$, gives intense bands in the 1750 to 1650 cm^{-1} region, characteristic of carbonyl-containing compounds. When a C=O group is

[1]NRCC No. 30207.

[2]Abbreviations used: SDS: sodium dodecyl sulfate; DTAC: dodecyltrimethylammonium chloride; CTAB: cetyltrimethylammonium bromide; DODAC: dioctadecyldimethylammonium chloride.

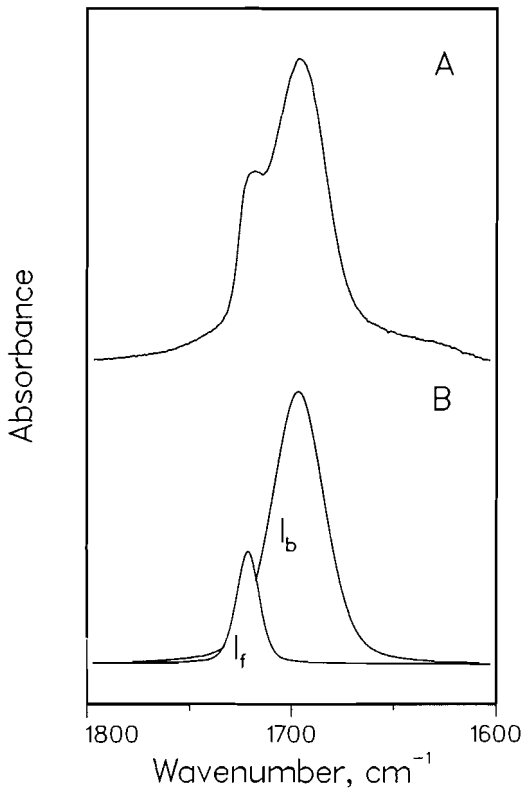


FIG. 1. Infrared spectrum of 6-undecanone (0.018 *M*) in SDS (0.25 *M*) (*A*). The bottom traces are the result of curve-fitting (*B*).

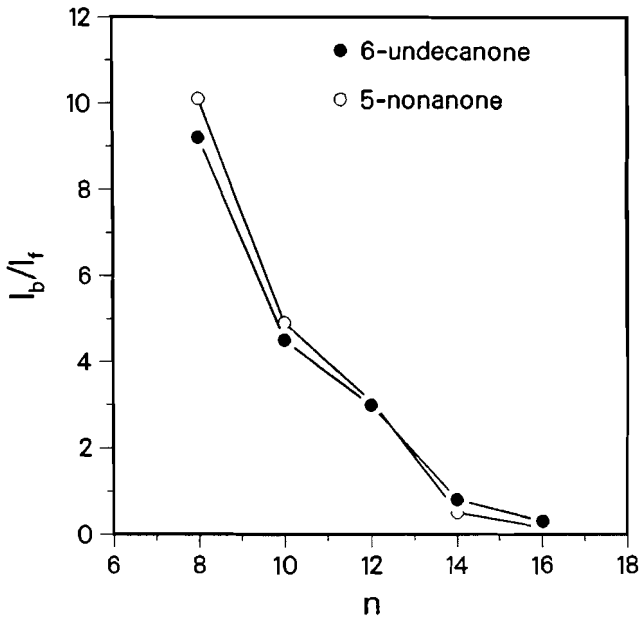


FIG. 2. The parameter I_b/I_f as a function of n, the number of methylene groups in a series of sodium alkyl sulfates. ●, values obtained from spectra of 6-undecanone, and ○, values obtained from spectra of 5-nonanone.

engaged in hydrogen bonding, the C=O frequency decreases (5–8); this well known effect is easily and readily detected in the infrared spectra. Symons and co-workers (9–11) have investigated in detail hydrogen bonding to esters and ketones. In the particular case of acetone (9), they found three C=O stretching bands depending on the extent of hydrogen bonding to the C=O group. A band at 1717 cm^{-1} is due to the non-bonded species and bands at 1707 and 1697 cm^{-1} are due to the mono- and dihydrogen-bonded species, respectively. Thus, the different C=O stretching frequencies may be assigned to specific species. Our own experiments with ketones longer than acetone (e.g. 3-pentanone and 4-heptanone) reproduce the frequencies for the three species described for acetone. The different C=O stretching frequencies are used in this work to detect hydrogen bonding to ketones mixed with surfactants and to determine which particular species are formed.

Ketones in micelles

As an example, a typical spectrum is shown in Fig. 1*A*. In this case, the ketone is 6-undecanone and the micelles are those of SDS. There are two C=O stretching bands from the ketone at 1720 and 1698 cm^{-1}. These two bands are assigned to the "free C=O" and the "hydrogen-bonded C=O" group, respectively. These two bands arise from the ketone residing, respectively, in a micellar region completely devoid of water (D_2O in this case) and in a region where contact with the solvent is possible. The intensities of these two bands are related to the number of ketone molecules in each of these micellar regions. However, the absorptivities of these two bands are not known and without them it is not possible to use band intensities in a quantitative manner. The individual band intensities (integrated areas) are obtained by curve fitting the observed spectra, as depicted in Fig. 1*B*. While the ratio I_b/I_f gives only a qualitative idea of the relative volumes of the two micellar regions, variations in its value reflect structural micellar changes that modify the extent of contact between the solvent and the surfactant hydrocarbon chains.

Figure 2 shows a plot of I_b/I_f values obtained from spectra of 6-undecanone and 5-nonanone as guests in micelles of a series of sodium alkyl sulfates. The chain length of the surfactant molecules varies from 8 to 16. The results of this plot show that the values of I_b/I_f measured are the same for the two ketones used and that I_b/I_f decreases as the surfactant chain length increases. Since I_b/I_f decreases as the extent of ketone:solvent contact decreases, we may conclude that as the surfactant chain length increases the volume of the micellar region completely devoid of solvent increases. This observation also implies that the ketones are not located preferentially in a polar environment or that they reside outside the micelle or exclusively at the Stern layer. The decrease in the values of I_b/I_f as the micelles grow shows that the extent of hydrogen bonding to the ketones depends on the medium in which they reside, and not exclusively on the polarity of the C=O group. The plot of Fig. 2 illustrates that the infrared spectra of guest ketones gives a measure (qualitative at the moment) of the relative volumes of the two micellar regions in coexistence. Previous ^{13}C-NMR work on ketones as guest in micelles detected only one environment (highly polar) for the guest ketone (12). As pointed out earlier (1) this is due to the time scale of the NMR experiment; in the presence of "fast" chemical exchange only one "average" NMR signal is observed. In the infrared, the two environments are observed separately because the ketone signals arising from the two environments are sufficiently different and the exchange rate is "slow" compared to the infrared time scale. Nevertheless, this comparison of the results from infrared and NMR spectra shows that the guest ketones are exchanging between the two environments; and, therefore it also shows that the hydrogen bonds formed between the ketone C=O group and the solvent dissociate once the ketone migrates to a micellar region devoid of solvent.

Can. J. Chem. Downloaded from www.nrcresearchpress.com by 194.225.253.170 on 09/07/12
For personal use only.

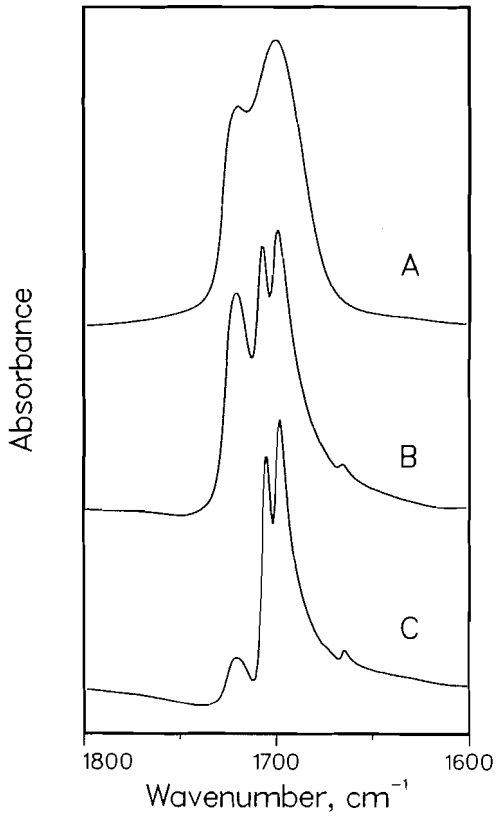


FIG. 3. Infrared spectra of 7-tridecanone (*A*); 9-heptadecanone (*B*), and 10-nonadecanone (*C*) as guests in SDS. Molar ratios SDS:ketones were 14:1 and the concentration of SDS was 0.28 *M*.

The fact that the I_b/I_f values obtained from spectra of 5-nonanone and 6-undecanone are practically identical (Fig. 2) indicates that the results are related to the micellar properties and not to some particular property of the individual ketones. However, the chain lengths of these two ketones are comparable to or less than the chain lengths of the surfactant molecules. Quite different results are obtained when the guest ketone is much longer than the surfactant molecules. Figure 3 shows spectra of 7-tridecanone, 9-heptadecanone, and 10-nonadecanone as guests in SDS micelles. The spectrum of 7-tridecanone (Fig. 3*A*) is practically the same as that of 6-undecanone (Fig. 1) and the value of I_b/I_f (≈ 3) coincides with that for 6-undecanone (Fig. 2). The spectra of 9-heptadecanone and 10-nonadecanone (Fig. 3, *B* and *C*) are completely different from those of 5-nonanone, 6-undecanone, and 7-tridecanone. In these cases, there are three C=O stretching bands instead of two. The band at 1720 cm^{-1} is clearly due to a free C=O group (i.e. not hydrogen bonded), showing that these ketones may also occupy the dry micellar region. The other two bands at 1705 and 1698 cm^{-1} are due to hydrogen-bonded C=O groups. As pointed out above these two bands are due to 1:1 and 1:2 C=O$\cdots$D$_2$O hydrogen bonds, respectively. It is interesting to note that the half widths (~ 10 cm^{-1}) of these two bands are much less than the half width of the C=O hydrogen-bonded band in the spectrum of 6-undecanone (~ 30 cm^{-1}). Two bands due to a hydrogen-bonded C=O group appear when the ketone is in direct contact with water (or D$_2$O), for example, a ketone dissolved in acetonitrile and in the presence of a large excess of water (cf. Fig. 1, ref. 2). The appearance of these two narrow bands due to hydrogen bonded C=O groups in the spectra of 9-heptadecanone and 10-nonadecanone as guests in SDS indicates that the C=O groups are in direct contact with D$_2$O. It appears that when the ketone chain length is much longer than the surfactant chain length, the ketones adopt a conformation which favours direct contact with the solvent. Furthermore, the small width of the "bound" bands suggests that in such a situation the C=O groups are restricted motionally with respect to the other cases. Therefore, in these cases where the mismatch in chain length is very pronounced, there appears to be a third micellar environment, one in which the ketone adopts a ∩ conformation and the C=O group is anchored at the Stern layer. Such a conformation has been proposed for ketones in gel phases (13) and may also be present in other lamellar phases (see below). These results, obtained with ketones much longer than the surfactant chain length, serve as a caveat for studies of micellar systems with probe molecules of greatly differing chain length.

TABLE 1. I_b/I_f values obtained from the infrared spectra of various ketones in micelles of different surfactants

Surfactant	Ketone	I_b/I_f
Na-C$_8$	5-Nonanone	8.0
SDS	5-Nonanone	3.0
NaC$_{12}$	7-Tridecanone	2.0
SDS	7-Tridecanone	3.0
SDS	6-Undecanone	3.0
CTAB	6-Undecanone	<1.0
DTAC	6-Undecanone	7.0
Triton X-100	6-Undecanone	0.8

A comparison of the I_b/I_f values determined from spectra of ketones in different surfactant systems is presented in Table 1. The values for 5-nonanone, 6-undecanone, and 7-tridecanone are the same within experimental error as already mentioned. The value of I_b/I_f for 7-tridecanone in sodium dodecanoate is smaller than that for 7-tridecanone in SDS. This demonstrates that the extent of contact between the solvent and the guest ketone is dependent on the nature of the polar group of the surfactant molecules. Menger *et al.* (14) found differences in the conformational order of the chains in these two surfactant molecules. In the case of DTAC and CTAB, I_b/I_f (determined from guest 6-undecanone) decreases as the surfactant chain length increases, the same as in the case of the series of alkyl sulfates (Fig. 2). The value of I_b/I_f for 6-undecanone in DTAC is 7 while it is only 3 for 6-undecanone in SDS. Thus, there is a pronounced difference between anionic and cationic surfactants of the same chain length. At the moment there is not enough information to conclude that this difference is a general phenomenon. But, as the extent of contact between the ketone and the solvent can be monitored by I_b/I_f, which as shown above is dependent on the "order" of the surfactant chains, these different I_b/I_f values are probably a reflection of packing differences and/or differences in the extent of solvent penetration. The value of I_b/I_f measured from the spectrum of 5-nonanone in sodium octanoate is large (8.0) compared to the others. This is undoubtedly a reflection of a very disordered micelle, one in which the water-chain contact is extensive (15). In the case of Triton X-100, the value of I_b/I_f measured from the spectrum of 6-undecanone is 0.8. This low value reflects a limited surfactant-water contact, probably a consequence of a more ordered micellar structure (16).

Can. J. Chem. Downloaded from www.nrcresearchpress.com by 194.225.253.170 on 09/07/12
For personal use only.

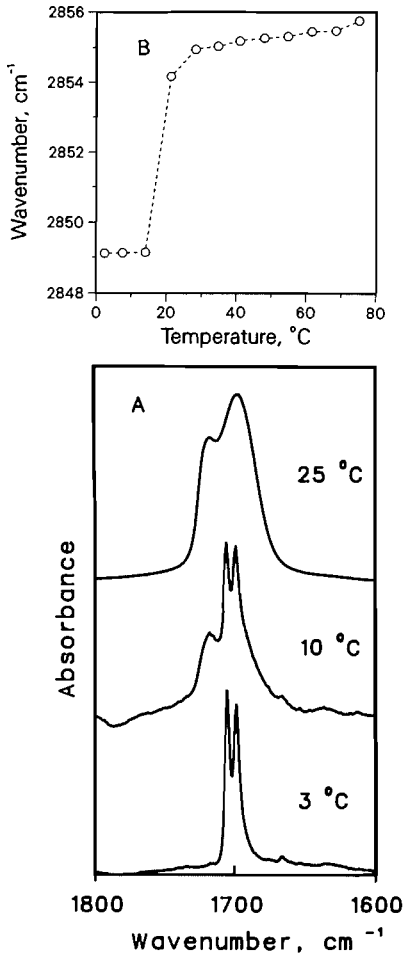


FIG. 4. *A*: Infrared spectra of 7-tridecanone (0.02 *M*) in SDS (0.28 *M*) at the indicated temperatures. *B*: temperature dependence of the wavenumber of the symmetric stretching from the methylene groups of SDS.

Effect of structural changes

One important question in this type of study is the precise location of the probe. So far, we have not addressed this question and have simply used the I_b/I_f value as a qualitative parameter to monitor the extent of contact between the solvent and guest ketones. The structure of micelles may be changed by external agents such as temperature. In the case of SDS it is well known that upon cooling a clear micellar solution, a poorly hydrated lamellar phase (coagel) forms. Several studies have determined the critical temperature of this phase transition (17–19). It is accepted that in the coagel phase the SDS alkyl chains are fully extended in the all *trans* conformation. Such changes may be easily followed by infrared spectroscopy, by monitoring the temperature dependence of the wavenumber of the methylene symmetric stretching mode, $\nu_s(CH_2)$, for example.

The C=O stretching bands of 7-tridecanone as a guest in SDS micelles at various temperatures are shown in Fig. 4*A*. The temperature dependence of the $\nu_s(CH_2)$ wavenumber of the SDS alkyl chains in the same sample is presented in Fig. 4*B*. In accord with previous work, the coagelization temperature is centered at 15°C, characterized by a large shift in the $\nu_s(CH_2)$ wavenumber. The micelle to coagel transition is complete in ≈2°C. The C=O stretching bands of the guest 7-tridecanone do change with temperature, but only below the coagelization temperature, and even then the changes are not as distinct as those of the $\nu_s(CH_2)$ mode. The C=O bands in the spectrum recorded at 25°C are those characteristic of a micellar system; there are two bands at 1718 and 1698 cm^{-1} representing the "free" and the "bound" C=O groups, respectively. The same is observed in the spectrum recorded at 14°C; that is at a temperature slightly below the coagelization temperature, the ketone C=O stretching bands have not changed.

The ketone C=O stretching bands change dramatically at lower temperatures as demonstrated in the spectra recorded at 10 and 3°C. In the 10°C spectrum there are three C=O stretching bands at 1718, 1705, and 1698 cm^{-1} while only two at 1705 and 1698 cm^{-1} are observed in the 3°C spectrum. These spectra demonstrate that as the coagel forms, there are structural changes that modify the extent of contact between the solvent and the guest ketone. The formation of the coagel seems to be complete in a narrow temperature range (≈2°C), but the changes in the ketone spectra occur in a progressive manner covering a wider temperature range. These spectral effects are a reflection of a change in location of the guest ketone. The characteristics of the ketone C=O stretching bands in the low temperature spectrum (3°C) are those expected for direct contact between D_2O and the C=O group, and as explained above, they imply that the ketone is immobilized in a region forming 1:1 and 1:2 C=O···D_2O hydrogen bonds. We propose that in the coagel, the ketone adopts the ∩ conformation exposing the C=O group. The same conformation was proposed for the long chain ketones above and also proposed by Weiss *et al.* (13) in studies of ketones in interdigitated gel phases. In such a conformation, the ketone should also serve to stabilize the lamellar coagel phase acting as a charge "separator".

In the spectrum recorded at 3°C (Fig. 4) there are no bands due to "free" C=O groups indicating that no ketone molecules remain free from contact with the solvent.

The spectral changes induced by cooling (Fig. 4) are entirely reversible but the C=O bands show some hysteresis in following the structural changes. That is, when a sample is heated from 3 to 30°C, the coagel reverts to micelles at ≈16°C but the C=O stretching bands do not change until the system is micellar. At all temperatures below 20°C there appear only two bands at 1705 and 1698 cm^{-1}. At temperatures above 18°C, the "free" C=O band at 1718 cm^{-1} appears, and its intensity grows with time such that after 2 h, the spectrum is that typical of the micellar phase.

These spectra show that the guest ketone translocates as a consequence of structural changes and that these changes are reversible. The ketone changes from a situation in which it coexists between two environments in the micelle, to one in which there is only one in the coagel. Furthermore, in the latter case it is immobilized, forming strong hydrogen bonds. On increasing the temperature and upon reformation of the micelles, the ketone C=O stretching bands indicate that it is again exchanging between the two coexisting micellar environments. This emphasizes that the C=O···D_2O hydrogen bonds may dissociate when the ketone occupies a dry micellar region.

The structure of micelles may also be changed in the presence of a large excess of added ions (20–22). In some cases there is micellar growth, while in others there are specific ion–micelle interactions such as direct association and precipitation. The values of I_b/I_f obtained from spectra of 6-undecanone in SDS in the presence of increasing quantities of several ions are shown in Fig. 5. These results point to some contrasting effects with no ready explanation.

Can. J. Chem. Downloaded from www.nrcresearchpress.com by 194.225.253.170 on 09/07/12
For personal use only.

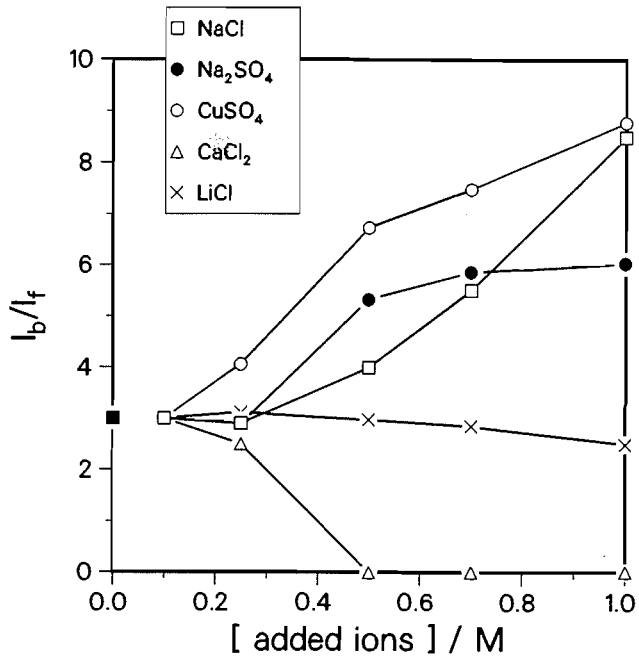


FIG. 5. The parameter I_b/I_f obtained from spectra of 6-undecanone (0.018 *M*) as guest in SDS (0.25 *M*) as a function of the concentration of added ions.

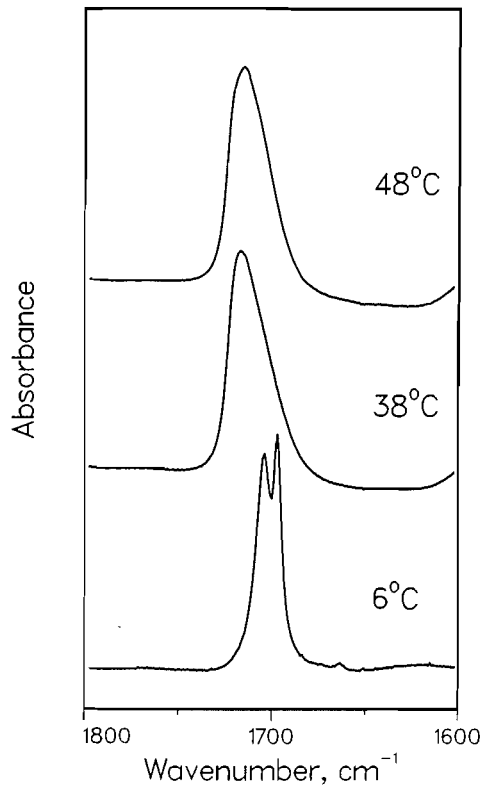


FIG. 6. Infrared spectra of 6-undecanone (0.018 *M*) mixed with DODAC (0.25 *M*) at the indicated temperatures.

Addition of increasing quantities of Ca^{2+} ions results in the disappearance of the "bound" C=O bands and therefore the I_b/I_f values decrease and tend to zero. Addition of Cu^{2+} ions has the opposite effect to that of Ca^{2+}, the I_b/I_f values increase. Both Ca^{2+} and Cu^{2+} ions associate strongly to SDS and, at the concentrations used here induce precipitation possibly forming lamellar (coagel) structures (20, 21, 23). However, there is a distinct difference between the C=O bands of the ion-induced and the cooling-induced coagels. It appears that in the ion-induced precipitation, the ketone does not adopt the ∩ conformation which allows it to come in direct contact with the solvent.

In the presence of excess Na_2SO_4, the I_b/I_f values increase slightly. Excess Na_2SO_4 induces a large increase in the aggregation number of SDS micelles (24) and in these larger micelles there is increased possibility of contact between the solvent and the probe ketones. Excess NaCl induces increases in I_b/I_f in a similar manner as with Na_2SO_4. Addition of excess LiCl does not induce significant changes in the I_b/I_f values, even though Li^+ ions interact with these surfactants inducing a lower coagelization temperature (18).

As pointed out above, there is, at present, no ready explanation for these observations at the molecular level. However, these data show that the interaction of each of these ions with micelles can alter significantly the location and/or conformation of the guest ketone, thereby affecting its ability to sample the extent of contact with the solvent.

Ketones in bilayers

In a previous report (2) of the infrared spectra of guest ketones in lipid bilayers, it was found that the I_b/I_f parameter from those spectra was lower than in the case of micelles studied here. This is a manifestation of less water penetration in bilayers as compared to micelles (25). Spectra of 6-undecanone in DODAC (21 wt.% in D_2O) at different temperatures are shown in Fig. 6. At this concentration, DODAC bilayers undergo two transitions: at room temperature it forms a coagel which transforms to a gel at 35.5°C. The gel forms a liquid crystalline phase at 45.5°C. These phase transitions have been well characterized by infrared spectroscopy (26). The C=O stretching bands of the guest 6-undecanone are at 1705 and 1698 cm^{-1} at temperatures characteristic of the coagel phase. These bands are those typical of the immobilized ketone in direct contact with the solvent. Upon formation of the gel phase (see spectrum at 38°C) the C=O bands change dramatically. The main band is at 1718 cm^{-1} with a weak shoulder at 1700 cm^{-1}; these features do not change appreciably on transition to the liquid-crystalline phase. The values of I_b/I_f measured from the spectra recorded at 38 and 48°C are 1.5 and 0.7, respectively. These spectral changes are entirely reversible; after cooling the sample back to 16°C, the C=O bands are the same as those obtained before heating.

In the coagel phase of DODAC, the alkyl chains are fully extended in the all-*trans* conformation and the polar groups are poorly hydrated (26). In this case, the ketone adopts the ∩ conformation and comes into direct contact with the solvent, possibly serving as "charge separator". Thus the DODAC coagel induces the same type of ketone location and immobilization as in the cooling-induced coagel formed by the single chain SDS. In the gel phase, the DODAC alkyl chains are also fully extended but the polar groups are hydrated (26); it is apparent that in this case the ketone is not immobilized at the solvent interface and migrates to a hydrophobic region with no possibility of contact with D_2O. The same holds for the liquid crystalline phase of DODAC. From the values of I_b/I_f it appears that in passing from the gel phase to the liquid-crystalline phase of DODAC the extent of chain–water contact decreases; a similar result was found in the case of lipid bilayers (2).

Can. J. Chem. Downloaded from www.nrcresearchpress.com by 194.225.253.170 on 09/07/12
For personal use only.

Concluding remarks

In this work, we have explored the possibility of using the infrared spectra of aliphatic ketones to study micellar properties. The approach uses ketones as probes and is based on the sensitivity of the C=O stretching vibration to hydrogen bonding. Therefore, the extent of contact between the guest ketones and the solvent (water) is readily followed. In the infrared spectra (cf. Fig. 1), there are C=O stretching bands characteristic of hydrogen-bonded C=O groups as well as bands due to non-bonded or "free" C=O groups. Thus, the guest ketones occupy at least two different micellar environments. One environment offers the possibility of contact between the ketone and water, while the other does not. The relative intensity of the "bound" and "free" C=O bands, I_b/I_f, is used as a parameter to monitor the extent of contact between water and the surfactant chains. This parameter gives a qualitative measure of the relative volumes of these two micellar environments. Variations in this parameter are used to compare different systems. It is shown that as the volume of micelles increases, I_b/I_f decreases (cf. Fig. 2) demonstrating that the volume of the micellar region devoid of solvent increases. Formation of lamellar phases of SDS induced by cooling induces a reversible translocation of the guest ketones. It is proposed that in these coagels the ketones adopt a bent conformation. A similar conformation is proposed for guest ketones in micelles when there is a pronounced mismatch between the ketone chain length and the surfactant chain length (cf. Fig. 3).

In summary, the infrared spectra of carbonyl-containing compounds dissolved in various mesomorphs yield a qualitative comparison of different systems regarding the water–chain contacts. The determination of the absorptivities of the individual C=O stretching bands coupled with "locking" of the probe molecules at known locations will help to quantitate the effects observed and to remove the uncertainties derived from probe translocations. Such work is in progress.

1. H. L. Casal. J. Am. Chem. Soc. **110**, 5203 (1988).
2. H. L. Casal. J. Phys. Chem. **93**, 4328 (1989).
3. G. P. Spada, G. Lesa, G. Gottarelli, P. de Maria, and P. Mariani. Liq. Cryst. **3**, 1031 (1988).
4. A. Malliaris. J. Photochem. Photobiol. A: Chem. **40**, 79 (1987).
5. L. J. Bellamy. Advances in infrared group frequencies. Methuen and Company, London. 1968.
6. G. C. Pimentel and A. L. McClellan. The hydrogen bond. W. H. Freeman, San Francisco. 1960.
7. M. D. Joesten and L. J. Schaad. Hydrogen bonding. Marcel Dekker, New York. 1974.
8. H. E. Hallam. *In* Infrared spectroscopy and molecular structure. *Edited by* M. Davies. Elsevier, Amsterdam. 1963.
9. M. C. R. Symons and G. Eaton. J. Chem. Soc. Faraday Trans. 1, **81**, 1963 (1985).
10. K. B. Patel, G. Eaton, and M. C. R. Symons. J. Chem. Soc. Faraday Trans. 1, **81**, 2775 (1985).
11. M. C. R. Symons. Pure Appl. Chem. **58**, 1121 (1986).
12. F. M. Menger, J. M. Jerkunica, and J. C. Johnston. J. Am. Chem. Soc. **100**, 4676 (1978).
13. R. L. Treanor and R. G. Weiss. J. Am. Chem. Soc. **110**, 2170 (1988).
14. F. M. Menger, M. A. Dulany, D. W. Carnahan, and L. H. Lee. J. Am. Chem. Soc. **109**, 6899 (1987).
15. K. Watanabe, M. Ferrario, and M. L. Klein. J. Phys. Chem. **92**, 819 (1988).
16. J. Villalaín, J. C. Gomez-Fernandez, and M. J. E. Prieto. J. Colloid Interface Sci. **124**, 233 (1988).
17. P. W. Yang and H. H. Mantsch. J. Colloid Interface Sci. **113**, 218 (1986).
18. H. H. Mantsch, V. B. Kartha, and D. G. Cameron. *In* Surfactants in solution. Vol. 1. *Edited by* K. L. Mittal and B. Lindman. Plenum, New York. 1984. pp. 673–690.
19. T. Kawai, J. Umemura, and T. Takenaka. Bull. Inst. Chem. Res. Kyoto Univ. **61**, 314 (1983).
20. M. Baviere, B. Bazin, and R. Aude. J. Colloid Interface Sci. **92**, 580 (1983).
21. M. Hato and K. Shinoda. Bull. Chem. Soc. Jpn. **46**, 3889 (1973).
22. W. Baumuller, H. Hoffmann, W. Ulbricht, C. Tondre, and R. Zana. J. Colloid Interface Sci. **64**, 418 (1978).
23. J. Jay, L. J. Johnston, and J. C. Scaiano. Chem. Phys. Lett. **148**, 517 (1988).
24. D. J. Miller, U. K. A. Klein, and M. Hauser. Ber. Bunsenges. Phys. Chem. **84**, 1135 (1980).
25. F. M. Menger, P. Aikens, and M. Wood, Jr. J. Chem. Soc. Chem. Commun. 180 (1988).
26. J. Umemura, T. Kawai, T. Takenaka, M. Kodama, Y. Ogawa, and S. Seki. Mol. Cryst. Liq. Cryst. **112**, 293 (1984).

Can. J. Chem. Downloaded from www.nrcresearchpress.com by 194.225.253.170 on 09/07/12
For personal use only.

Reactions of α-phenylglycinamide with some carbonyl compounds. Formation of 5,7-diisopropyl-8,8-dimethyl-2-oxo-3-phenylimidazolidino-[1,2-*c*]-tetrahydro-[1,3]-oxazine, and determination of structure and stereochemistry by nuclear Overhauser effect difference measurements

NING QING AND LAWRENCE D. COLEBROOK[1]

Department of Chemistry and Biochemistry, Concordia University, 1455 de Maisonneuve Blvd. W., Montreal, P.Q., Canada H3G 1M8

AND

JOHN T. EDWARD, ALLAN KON, AND FRANCIS L. CHUBB

Department of Chemistry, McGill University, 801 Sherbrooke St. W., Montreal, P.Q., Canada H3A 2K6

Received January 17, 1989

NING QING, LAWRENCE D. COLEBROOK, JOHN T. EDWARD, ALLAN KON, and FRANCIS L. CHUBB. Can. J. Chem. **67**, 1560 (1989).

α-Phenylglycinamide **5** reacts with ketones to give either the Schiff base **3** or the 4-imidazolidone **4**, but reacts with boiling isobutyraldehyde to give the bicyclic compond **6**. The structure and stereochemistry of **6** have been established by ^{1}H nuclear Overhauser effect difference measurements, supported by molecular mechanics calculations.

Key words: structure, stereochemistry, nuclear Overhauser effect, molecular mechanics, α-phenylglycinamide reactions.

NING QING, LAWRENCE D. COLEBROOK, JOHN T. EDWARD, ALLAN KON et FRANCIS L. CHUBB. Can. J. Chem. **67**, 1560 (1989).

L'α-phénylglycinamide (**5**) réagit avec les cétones pour fournir soit les bases de Schiff **3** soit les 4-imidazolinones **4**; toutefois, il réagit avec l'isobutyraldéhyde bouillant pour conduire au composé bicyclique **6**. On a déterminé la structure et la stéréochimie du composé **6** à l'aide de mesures de différences d'effet Overhauser nucléaire du ^{1}H ainsi que par des calculs de mécanique moléculaire.

Mots clés : structure, stéréochimie, effet Overhauser nucléaire, mécanique moléculaire, α-phénylglycinamide.

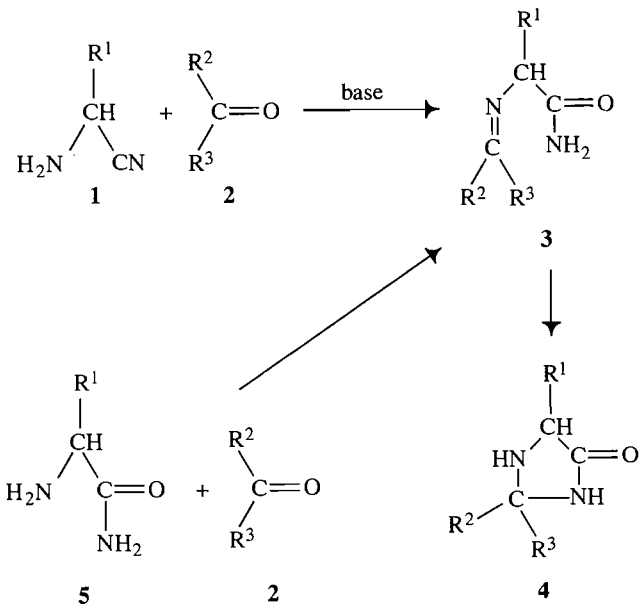
[Traduit par la revue]

Can. J. Chem. Downloaded from www.nrcresearchpress.com by 194.225.253.170 on 09/07/12
For personal use only.

Under basic conditions, α-aminonitriles **1** react with neat acetone (**2**; $R^2 = R^3 =$ Me) to give sometimes the Schiff bases **3** ($R^2 = R^3 =$ Me) (1–4), and sometimes the isomeric 4-imidazolidones **4** ($R^2 = R^3 =$ Me) (5); on the other hand, they are reported to react with cyclohexanone (**2**; $R^2R^3 = (CH_2)_5$) to give only the imidazolidones **4** ($R^2R^3 = (CH_2)_5$) (4, 5). The isomers **3** and **4** may be distinguished by their characteristic infrared and nuclear magnetic resonance spectra (6, 7), and by differing chemistries. Thus, while the imidazolidones are sufficiently basic and sufficiently stable to form stable picrates, the Schiff bases are readily hydrolyzed and with picric acid give picrates of the α-aminoamides **5** (4).

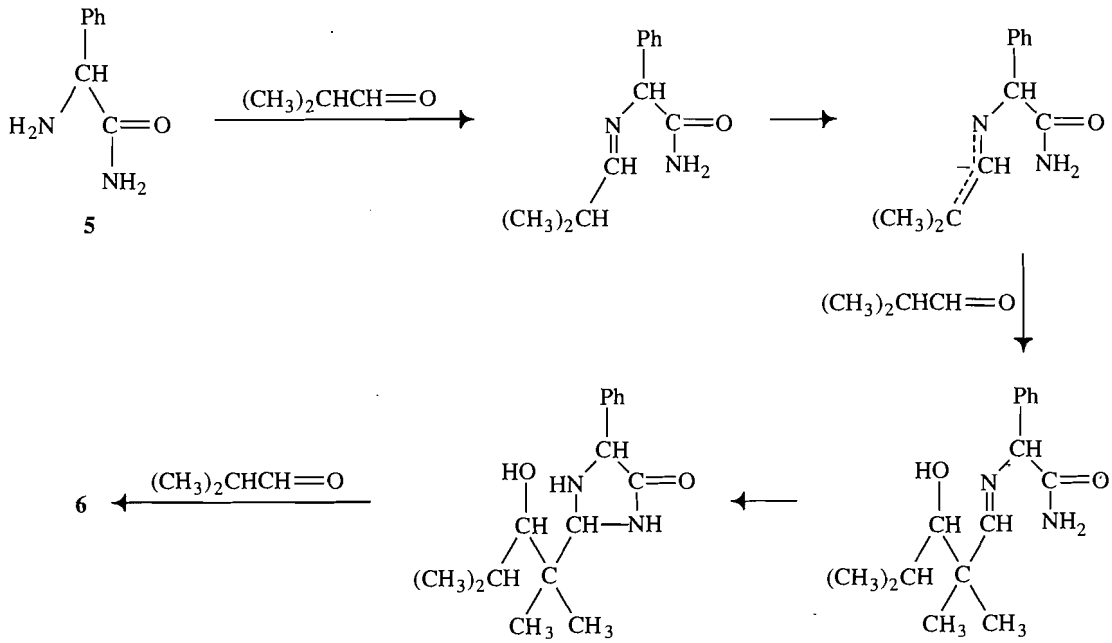
On mechanistic grounds (6–9) it seems likely that in all the reactions cited above the Schiff bases are first formed, but that in basic solution some are readily cyclized to the imidazolidones (cf. ref. 4). To study the differing cyclization tendencies, we attempted to prepare various Schiff bases by reaction of α-amido-α-phenylacetamide (**5**; R^1 = Ph) with ketones or aldehydes in neutral solution. While acetone yielded the Schiff base **3** (R^1 = Ph, $R^2 = R^3$ = Me), cyclopentanone in refluxing absolute alcohol yielded the imidazolidone **4** (R^1 = Ph, $R^2R^3 = (CH_2)_4$), and cyclohexanone the imidazolidone **4** (R^1 = Ph, $R^2R^3 = (CH_2)_5$). However, in refluxing benzene, cyclopentanone and cyclohexanone formed the corresponding Schiff bases, which then cyclized to the imidazolidones in refluxing absolute alcohol. The order of reactivity of the Schiff bases in forming the cyclic product (**3**, R^1 = Ph, $R^2R^3 = (CH_2)_5$ > **3**, R^1 = Ph, $R^2R^3 = (CH_2)_4$ > **3**, R^1 = Ph, $R^2 = R^3$ = Me) accords with the order of reactivity of the parent ketones (10).

Commeyras and co-workers (9) found isobutyraldehyde (**2**; R^2 = *i*-Pr, R^3 = H) very effective in catalyzing the hydrolysis of α-aminopropionitrile (**1**; R^1 = Me) in basic aqueous solution to the amide **5** (R^1 = Me), and concluded that the Schiff base **3** (R^1 = Me, R^2 = *i*-Pr, R^3 = H) was first formed but readily hydrolyzed. We attempted to obtain the Schiff base **3** (R^1 = Ph, R^2 = *i*-Pr, R^3 = H) by reaction of **5** (R^1 = Ph) with boiling neat isobutyraldehyde, but obtained instead a compound shown by analysis to be formed by condensation of one molecule of α-phenylglycinamide with three molecules of isobutyraldehy-



SCHEME 1

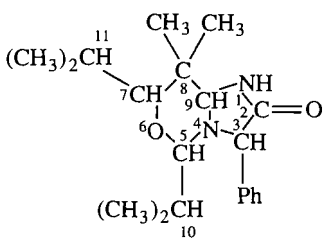
[1]Author to whom correspondence may be addressed.



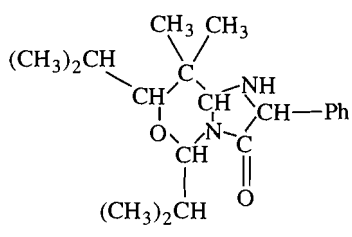
SCHEME 2

de, with the elimination of two molecules of water. Two possible structures for this compound are **6**, formed by the route of Scheme 2 or some equivalent route, or **7**.

This structural problem presents an interesting challenge, because both **6** and **7** contain four chiral centres. Since these chiral centres form isolated spin systems, scalar ^1H–^1H coupling information that might have related them is not available. Hence their relative stereochemistry was determined using dipolar (through-space) coupling via ^1H nuclear Overhauser effect difference (NOED) spectroscopy (11–13).



6



7

The 400-MHz (C_6D_6 solution) ^1H nmr spectrum shows well-resolved aromatic proton signals, which were assigned on the basis of their multiplicities and intensities (Table 1). The NH proton shows a broad singlet at δ 8.47.

The ring protons give rise to two singlets (H-3 and H-9), and two doublets due to spin coupling to the isopropyl groups (H-5 and H-7). The singlet at δ 4.12 was broadened due to unresolved long range coupling, and hence was assigned to the benzylic proton at C-3. The remaining (sharp) singlet (δ 4.25) in this region must be due to H-9.

The geminal methyl groups at C-8 are diastereotopic since the molecule is chiral, and give rise to singlets at δ 1.04 and δ 0.82.

Similarly, the isopropyl methyl groups are diastereotopic, and give rise to four doublets, those at δ 0.85 and 0.88 being incompletely resolved. Spin-decoupling experiments identified and established the spin connectivities of the complete isopropyl and associated ring proton spin systems. Thus H-5 (δ 3.94, J = 1.5 Hz), H-10 (δ 1.44), the δ 1.14 and δ 0.88 methyl groups

TABLE 1. ^1H and ^{13}C chemical shifts of **6**

Carbon atom	$^{13}C^a$	$^1H^b$	$^1H^c$
(NH)		8.47	
C=O	179.01		
Phenyl-1′	135.52		
m-Phenyl	128.96	7.25	7.28
p-Phenyl	127.93	7.13	7.17
o-Phenyl	127.66	7.96	7.92
C-5	93.02	3.94(J = 1.5 Hz)	3.99
C-7	81.92	3.14(J = 5.0 Hz)	3.06
C-9	80.36	4.25	4.35
C-3	66.58	4.12	4.09
C-8	35.30		
C-10	31.65	1.44	1.50
C-11	28.66	1.70	1.68
C-10-Me	23.21[d]	0.88	0.90
C-11-Me	22.98[d]	0.85	0.89
C-8-Me	21.06	1.04	1.07
C-11-Me	19.04	0.94	0.93
C-8-Me	18.97[d]	0.82	0.85
C-10-Me	14.97	1.14	1.12

[a]Measured at 20.1 MHz, C_6D_6 solution.
[b]Measured at 400.13 MHz, C_6D_6 solution.
[c]Calculated from ^{13}C data using the CHORTLE method.
[d]Assignment uncertain because of small ^1H chemical shift range.

form one isolated spin system, while H-7 (δ 3.14, J = 5.0 Hz), H-11 (δ 1.70), the δ 0.94 and δ 0.85 methyl groups form the other.

The relative stereochemistry at the chiral centres was established by NOED experiments. Irradiation of the benzylic ring proton (H-3) led to intensity enhancement of the signals from the *ortho* aromatic protons, H-5, H-10, but not for the NH proton signal. This demonstrates the close proximity of H-3 to H-5 and H-10, so that H-5 and H-3 must be on the same face of the ring system. The proximity of H-3 to H-5 and H-10 is consistent with structure **6**, but not **7**. Further, an NOE between the benzylic

Can. J. Chem. Downloaded from www.nrcresearchpress.com by 194.225.253.170 on 09/07/12
For personal use only.

Can. J. Chem. Downloaded from www.nrcresearchpress.com by 194.225.253.170 on 09/07/12
For personal use only.

ring proton and the NH proton would have been expected for structure **7**.

Irradiation of H-9, which produces the other ring proton singlet, enhances the signals of the *ortho* aromatic protons, the NH proton, and the δ 1.04 geminal methyl group. There is no detectable enhancement of signals from the other ring protons, indicating that H-9 is not in close proximity, and suggesting that H-9 is on the opposite side of the ring from H-3 and H-5. Detection of a relaxation pathway between H-9 and the *ortho* protons indicates that H-9 and the phenyl group are on the same face of the ring system.

Irradiation of H-5 strongly enhances the signals of H-3, H-7, and weakly enhances the signal of H-10, its vicinal neighbour. This indicates that H-5 and H-7 are in close proximity, i.e., on the same side of the molecule.

Irradiation of H-7 strongly enhances the signal of H-5 (verifying the steric relationship of H-5 and H-7), and weakly enhances the signal of H-11, its vicinal neighbour.

We note that irradiation of H-5 enhances the signals of *both* H-3 and H-7, but that the only ring proton affected by irradiation of H-3 and H-7 is H-5. This suggests that H-5 is close to both H-7 and H-3, but that H-7 and H-3 are distant from each other. Examination of a molecular model of the assigned structure shows that H-3, H-5, and H-7 have an approximately linear relationship, such that a significant NOE pathway between H-3 and H-7 is not expected.

The NOE pathway between H-3 and H-10 indicates that H-3 is close to the isopropyl group containing H-10, and that this group is in a conformation with H-10 close to H-3. A study of molecular models suggests that H-10 would be close to H-3 in the preferred conformation of the C-5 isopropyl group.

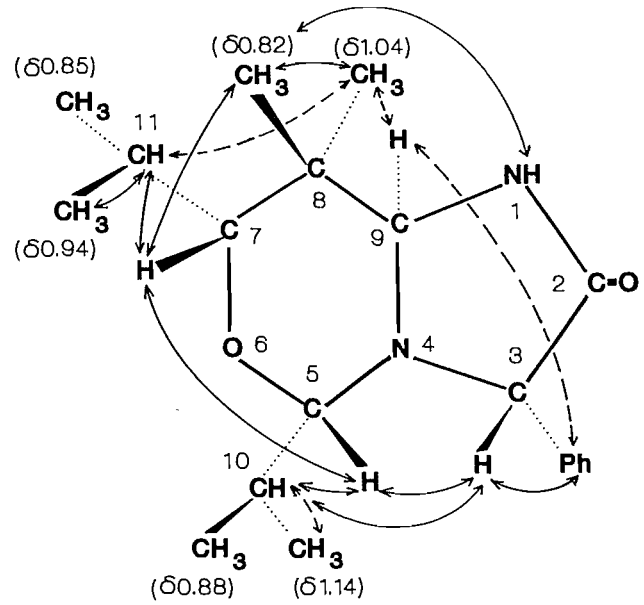
Irradiation of H-11 affects only the signal of its vicinal neighbour, H-7, and methyl groups, indicating that H-11 is remote from other ring protons.

Irradiation of the δ 1.14 isopropyl methyl group enhances the signals of H-10 and the δ 0.88 isopropyl methyl group, i.e., within the same isopropyl group, and also the *ortho* aromatic proton signals. Hence the δ 1.14 isopropyl methyl group is on the same face of the molecule as the phenyl group. Irradiation of the δ 0.94 isopropyl methyl group enhances the signals of H-11 and H-7. Hence the δ 0.94 isopropyl methyl group is on the same face of the molecule as H-7.

The NOED experiments on the geminal methyl groups permit assignment of their signals. Thus irradiation of the δ 1.04 methyl produces an enhancement of the signal of its geminal neighbour, of H-11, and of H-9. Irradiation of the δ 0.82 methyl produces enhancement of H-9, H-11, the δ 1.04 geminal methyl, the NH, and the H-7 signals. It may be inferred that the geminal methyl groups lie between C-7 (and C-11) and C-9, that the δ 0.82 methyl is on the same face of the molecule as H-7, and is close to NH, and that the δ 1.04 methyl group is on the same face as H-9. The C-7 isopropyl group must have a low energy conformation with H-11 facing the *gem*-dimethyl groups.

The ^{13}C spectrum, which shows 18 resolved signals, was assigned with the aid of the DEPT (ref. 11, Chap. 8) spectral editing sequence to classify the signals of the carbons according to the numbers of attached protons. Thus, the six signals in the range 14–24 ppm were identified as arising from methyl groups (all geminal methyl groups are diastereotopic), and nine signals (three of which were characterized by their chemical shifts as aromatic) were shown to arise from CH units. Correlation of the carbon signals with the chemical shifts of directly attached, previously assigned, protons was achieved using the CHORTLE method (14). Unequivocal assignment of all carbon signals except those at 23.21, 22.98, and 18.97 ppm was possible by this method. There is some uncertainty in the assignment of these three signals because of the small chemical shift differences of the attached protons.

Thus, the NOED data indicate that the structure of the molecule is:



(plus its enantiomer). In the preferred conformations of the isopropyl groups, H-10 faces towards H-3, while H-11 faces the *gem*-dimethyl system. The major NOE (relaxation) pathways are indicated.

Other spectral properties (e.g., ir) are in agreement with the structure **6** but of no particular value in establishing structure.

Further insight into the geometry of the molecule was obtained from molecular mechanics calculations, using an implementation of the Allinger MMP2 algorithm (15), with provision for π-electrons. The lowest energy optimized structure, based on the configuration established by the NOED measurements, was predicted with the six-membered ring in a chair conformation, with both isopropyl groups equatorial, the N-4—C-3 bond pseudo-equatorial, and the C-9—NH bond pseudo-axial (Fig. 1). Molecular mechanics calculations in which rotation about the C-5—C-10 bond is driven indicated an overall energy minimum for the conformation with H-10 facing towards the phenyl group. The three-bond $^1H-^1H$ coupling constant calculated using the Karplus equation (16) for the predicted H-5—C—C—H-10 dihedral angle (about 60°) for this conformation is consistent with the observed value of 1.5 Hz.

Similarly, energy calculations for rotation of the other isopropyl group about the C-7—C-11 bond indicated a broad low energy region centred on a H-7—C—C—H-11 dihedral angle of about 122°, with H-11 facing towards the *gem*-dimethyl group. The calculated three-bond coupling constant for this angle is consistent with the observed 5.0-Hz coupling constant.

The H-9—C—N—H dihedral angle in the calculated minimum energy conformation is 87°, corresponding to a near minimum three-bond coupling constant predicted from a Karplus-type relationship (17). This is consistent with the absence of observable coupling in the H-9 and NH signals.

This molecular conformation (Fig. 1), deduced from molecular mechanics calculations, is completely consistent with the NOED measurements.

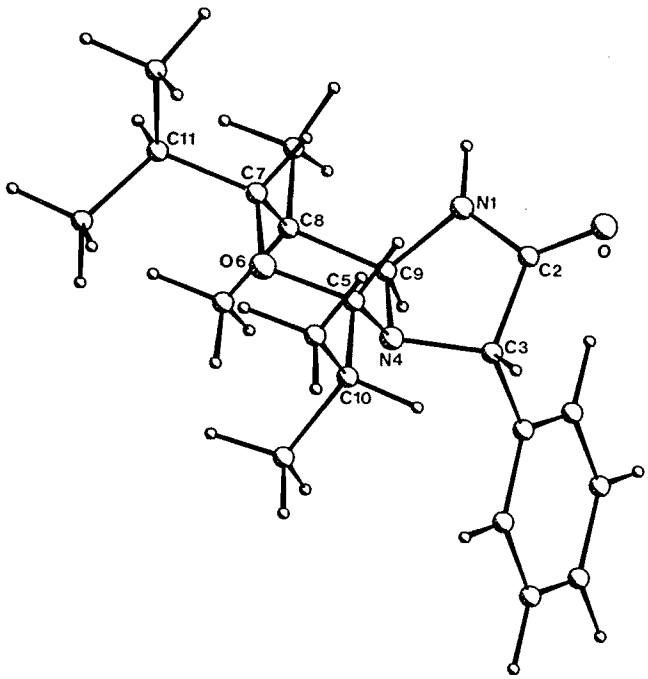


FIG. 1. Lowest energy conformation of **6**, predicted by molecular mechanics calculations for the configuration established by NOED measurements.

Experimental

The ^1H nmr spectra were recorded at 60 MHz unless otherwise noted. The ^1H nmr spectra of **6** were determined at 400.13 MHz using $CDCl_3$ and C_6D_6 solutions on a Bruker WH-400 spectrometer located at the Montreal Regional High Field NMR Laboratory. The spectra obtained in C_6D_6 solution showed better signal dispersion, so this solvent was used for spin-decoupling and NOED (11–13) measurements. The method of successive multiple irradiation of the components of multiplets described by Kinns and Sanders (13) was used for NOED experiments, with the sample not spinning. The NOED assignments were verified by the reverse irradiation experiments.

The ^{13}C nmr spectra were measured at 20.1 MHz on C_6D_6 solutions using a Bruker WP-80SY spectrometer equipped with a 10-mm broadband probe. The DEPT (ref. 11, Chap. 8) spectral editing pulse sequence was used to identify the numbers of attached protons associated with each carbon signal. The carbon signals were correlated with the previously assigned attached proton signals using the CHORTLE (14) method, with evolution times of 0.4, 1.0, 2.4, and 3.2 ms, and data processing using the program CHFIT (14) on an Olivetti M24 microcomputer. CHORTLE, which is a one-dimensional technique, has the advantage over the two-dimensional heteronuclear ($^{13}C-^1H$) method of identifying the chemical shifts of protons attached to carbon atoms with high accuracy, and so is equivalent to a two-dimensional experiment that uses a very large data matrix. It is also suitable for use with a low field ^{13}C instrument, provided that a high field ^1H spectrum, with good chemical shift dispersion, is available for signal assignment, and the ^1H spectra are approximately first order.

Molecular mechanics and coupling constant calculations were carried out on an Olivetti M24 microcomputer using the programs MMPMI and PCMODEL, obtained from Serena Software, Bloomington, Indiana, U.S.A. MMPMI is an implementation of the Allinger program MMP2 (15), which includes π calculations, and has been modified to run on IBM-compatible microcomputers. Three-bond coupling constants for the appropriate low energy geometries were calculated within PCMODEL, which uses the parameters of Haasnoot *et al.* (18). The program PCDISPLAY (Serena Software) was used for molecular graphics display.

Synthetic procedures

N-Isopropylidenephenylglycinamide

Phenylglycinamide (1 g) was heated with 50 mL acetone under reflux for 2 h. Concentration yielded 0.9 g (71%) of crude product, mp 135–139°C. A sample recrystallized from acetone had mp 142–144°C (lit. (4) mp 144°).

N-*Cyclopentylidenephenylglycinamide*

A solution of 1.5 g phenylglycinamide and 2 mL cyclopentanone in 25 mL benzene was heated under reflux with a Dean Stark trap. Separation of water occurred during 1 h. After 2.5 h the solvent was evaporated and the residue was washed with petroleum ether and filtered to yield 2.1 g (97%), mp 143–145°C, of *N*-cyclopentylidenephenylglycinamide. This was recrystallized from benzene (20 mL) and petroleum ether (20 mL) to yield 1.9 g, mp 145–147°C; ir ν_{max} (KBr): 3272 (NH_2), 3098 (aromatic CH), 2956 (aliphatic CH), 1674 (CO), 1653 (N=C); ^1H nmr ($CDCl_3$) δ: 1.55–2.58 (m, 8H, aliphatic CH), 4.73 (s, 1H, aliphatic CH), 6.25 (br s, 1H, amide H, D_2O exchangeable), 7.28 (m, 6H, reduced to 5H by D_2O, 5 aromatic CH, 1 amide H). *Anal.* calcd. for $C_{13}H_{16}N_2O$: C 72.19, H 7.46; found: C 72.35, H 7.54.

2,2-Tetramethylene-5-phenylimidazolidone-4

Procedure A: A solution of 1.5 g phenylglycinamide and 2.0 mL of cyclopentanone in 25 mL absolute alcohol was heated under reflux for 3 h. After evaporation of solvent the residue was washed with petroleum ether and filtered to yield 1.97 g (91%) of crude product, mp 128–142°C. Recrystallization from water and alcohol raised the mp to 150–153°C. An analytical sample melted at 155–157°C; ir ν_{max} (KBr): 3260, 3172 (NH_2), 3073, 3032 (aromatic CH), 2935, 2853 (aliphatic CH), 1710 (CO) 1687 (C=N); ^1H nmr ($CDCl_3$) δ: 1.33–2.00 (m, 8H, aliphatic CH), 2.22 (s, 1H, NH, exchangeable with D_2O), 4.67 (s, 1H, aliphatic CH), 7.00–7.63 (m, 5H, aromatic CH), 8.15 (s, 1H, CONH, exchangeable with D_2O). *Anal.* calcd. for $C_{13}N_{16}N_2O$: C 72.19, H 7.46; found: C 72.42, H 7.42.

Procedure B: When 1 g of *N*-cyclopentylidenephenylglycinamide was heated to reflux in 20 mL absolute alcohol for 3 h it was converted to the cyclic compound in 60% yield.

Picrate of 2,2-tetramethylene-5-phenylimidazolidone-4

The picrate was prepared by dissolving 0.22 g of the above compound and 0.23 g of picric acid in 5 mL of alcohol. On dilution with 5 mL water, 0.27 g (61%) of the picrate separated, mp 146–147°C. *Anal.* calcd. for $C_{19}H_{19}N_5O_8$: C 51.23, H 4.30; found: C 51.29, H 4.34.

N-*Cyclohexylidenephenylglycinamide*

A mixture of 3.0 g phenylglycinamide and 4 mL of redistilled cyclohexanone in 50 mL benzene was heated to reflux under a Dean Stark trap. Heating was continued until water ceased coming over (about 15 min). Evaporation of solvent left a solid residue, which was washed with petroleum ether and filtered to yield 4.3 g (93.5%) of crude product, mp 104–107°C; ir ν_{max} (KBr): 3398, 3229, 3164 (NH_2), 3085, 3071, 3027 (aromatic CH), 2947, 2933, 2857 (aliphatic CH), 1639 (CO), 1659 (C=N); ^1H nmr ($CDCl_3$) δ: 1.30–1.90 (m, 6H, aliphatic CH_2), 1.90–2.5 (m, 4H, aliphatic CH_2), 4.78 (s, 1H, aliphatic CH), 6.00 (br s, amide NH, exchangeable with D_2O), 6.73–7.40 (m, 6H, 5 aromatic CH, 1 amide NH, reduces to 5H with D_2O). *Anal.* calcd. for $C_{14}H_{18}N_2O$: C 73.01, H 7.88; found: C 73.10, H 7.86.

2,2-Pentamethylene-5-phenylimidazolidone-4

Procedure A: A solution of 2.5 g phenylglycinamide and 2.0 mL of cyclohexanone in 17 mL of absolute alcohol was heated to reflux for 2.5 h. Concentration of the solution yielded 3.1 g (81%) of the product, mp 168–171°C. Recrystallization from alcohol raised the mp to 174–176°C; ir ν_{max} (KBr): 3170, 3070 (NH), 3040 (aromatic CH), 2940, 2860 (aliphatic CH_2), 1695 (CO); ^1H nmr ($CDCl_3$) δ: 1.16–1.96 (m, 1OH, aliphatic CH_2), 2.16 (s, 1H, NH, exchangeable with D_2O), 4.71 (s, 1H, aliphatic CH), 7.20–7.68 (m, 5H, aromatic CH), 7.85 (s, amide NH, exchangeable with D_2O). *Anal.* calcd. for $C_{14}H_{18}N_2O$: C 73.01, H 7.88; found: C 72.92, H 8.02.

Procedure B: When 1.0 g of *N*-cyclohexylidenephenylglycinamide in 40 mL absolute alcohol was heated under reflux for 2.5 h, concentra-

Can. J. Chem. Downloaded from www.nrcresearchpress.com by 194.225.253.170 on 09/07/12
For personal use only.

tion and crystallization of the residue from alcohol–water yielded 0.71 g (71%), mp 172–174°C, of the cyclic amide (structure confirmed by ir).

Picrate of 2,2-pentamethylene-5-phenylimidazolidone-4

2,2-Pentamethylene-5-phenylimidazolidone-4 (0.1 g) and 0.1 g picric acid were dissolved in 1 mL absolute alcohol. Dilution with petroleum ether yielded 0.16 g (80%) of the picrate, mp 146–148°C. *Anal.* calcd. for $C_{20}H_{21}N_5O_8$: C 52.29, H 4.60; found: 52.31, H 4.54.

5,7-Diisopropyl-8,8-dimethyl-2-oxo-3-phenylimidazolidino-[1,2-c]-tetrahydro-[1,3]-oxazine, 6

A solution of 2.5 g phenylglycinamide in 40 mL isobutyraldehyde was heated under reflux for 6 h. Cooling and filtering the solution yielded a crop of white crystals, which were recrystallized from ethanol to yield 1 g (18%) of product, mp 192–194°C; ir ν_{max} (Nujol): 3175 (NH), 1700 (CO). *Anal.* calcd. for $C_{20}H_{30}N_2O_2$: C 72.69, H 9.15, N 8.48; found: C 72.26, H 9.41, N 8.22.

Alternative procedure: Phenylglycinamide (2.5 g) in 40 mL isobutyraldehyde was heated under reflux for 7 h. After diluting with petroleum ether, 1.2 g of product, mp 197–199°C, crystallized from the solution. When the filtrate was extracted with 4 N HCl and the extract made basic with NaOH an additional 0.54 g of product separated, mp 187–193°C. The total yield of crude product was 1.74 g (32%). When recrystallized from alcohol, it melted at 196–198°C.

Acknowledgments

This work was supported by operating grants from the Natural Sciences and Engineering Research Council of Canada (NSERC), who also provided funding towards the purchase of the NMR spectrometers. We wish to thank Dr. G. A. Pearson for providing copies of the CHCORR pulse program for the Bruker spectrometer and the CHFIT program for data reduction.

1. A. H. Cook, I. Heilbron, and A. L. Levy. J. Chem. Soc. 201 (1948).
2. A. H. Cook, I. Heilbron, and A. Mahadevan. J. Chem. Soc. 1061 (1949).
3. A. H. Cook and A. L. Levy. J. Chem. Soc. 642 (1950).
4. A. C. Davis and A. L. Levy. J. Chem. Soc. 3479 (1951).
5. T. Toda, S. Morihura, Z. Mori, H. Horiuchi, and K. Murayama. Bull. Soc. Chem. Jpn. **44**, 3445 (1971).
6. R. Pascal, J. Taillades, and A. Commeyras. Bull. Soc. Chim. Fr. II, 177 (1978).
7. J. T. Edward and F. L. Chubb. Proc. R. Ir. Acad. Sect. B: **83B**, 57 (1983).
8. R. Pascal, J. Taillades, and A. Commeyras. Tetrahedron, **34**, 2275 (1978).
9. R. Pascal, J. Taillades, and A. Commeyras. Tetrahedron, **36**, 2999 (1980).
10. T. H. Lowry and K. S. Richardson. Mechanism and theory in organic chemistry. Harper and Row, New York. 1976. p. 417.
11. J. K. M. Sanders and B. K. Hunter. Modern NMR spectroscopy. A guide for chemists. Oxford University Press, Oxford. 1987. Chap. 6.
12. W. J. Chazin, L. D. Colebrook, and J. T. Edward. Can. J. Chem. **61**, 1749 (1983); W. J. Chazin, L. D. Colebrook, B. R. Davis, I. R. N. McCormick, and S. J. Johnson. Can. J. Chem. **63**, 2332 (1985); W. J. Chazin and L. D. Colebrook. J. Org. Chem. **51**, 1243 (1986).
13. M. Kinns and J. K. M. Sanders. J. Magn. Reson. **56**, 518 (1984).
14. G. A. Pearson. J. Magn. Reson. **64**, 487 (1985).
15. N. L. Allinger and J. T. Sprague. J. Am. Chem. Soc. **95**, 3893 (1973); J. Kao and N. L. Allinger. J. Am. Chem. Soc. **99**, 975 (1977).
16. M. Karplus. J. Chem. Phys. **30**, 11 (1959); J. Am. Chem. Soc. **85**, 2870 (1963).
17. M. Barfield and H. L. Gearhart. J. Am. Chem. Soc. **95**, 641 (1973).
18. C. A. G. Haasnoot, F. A. M. M. Deleeuw, and C. Altona. Tetrahedron, **36**, 2783 (1980).

Can. J. Chem. Downloaded from www.nrcresearchpress.com by 194.225.253.170 on 09/07/12
For personal use only.

Photophysics of bis(*p*-*N*,*N*-dimethylamino)benzylidene acetone: Does photoinduced electron transfer occur from a twisted excited state?[1]

R. J. DeVoe, M. R. V. Sahyun[2], and E. Schmidt[3]
3M Science Research Laboratory, St. Paul, MN 55144, U.S.A.

Mahin Sadrai[4]
3M Graphic Research Laboratory, St. Paul, MN 55144, U.S.A.

and

N. Serpone and D. K. Sharma
Canadian Centre for Picosecond Laser Flash Spectroscopy, Concordia University, Montreal, P.Q., Canada H3G 1M8

Received February 1, 1989

R. J. DeVoe, M. R. V. Sahyun, E. Schmidt, Mahin Sadrai, N. Serpone, and D. K. Sharma. Can. J. Chem. **67**, 1565 (1989).

Photoexcitation of the title compound (DMBA) in polar solvents leads to sequential formation of at least three excited species as detected by laser transient absorption spectroscopy: the lowest Franck–Condon singlet, a twisted singlet (*P*-state), and the lowest triplet states. Only the initially formed, localized singlet is emissive under our conditions. Interystem crossing to triplet occurs primarily from the twisted *P*-state in acetonitrile and in methanol. Photo-CIDNP and quantum yield measurements indicate that electron transfer occurs exclusively from the triplet in acetonitrile or methanol to sensitize decomposition of diphenyliodonium cation and to bleach DMBA. Analysis of the photochemistry is complicated by formation of a charge transfer complex of enhanced photolability. Using tris(trichloromethyl)-*sym*-triazine as the electron acceptor in hydrocarbon solvent, bleaching of DMBA again occurs, somewhat more efficiently than with the 'onium salt in polar solvent. We infer that under these conditions electron transfer occurs from the *P*-state.

Key words: photochemistry, fluorescence, electron transfer, TICT, chalcone.

R. J. DeVoe, M. R. V. Sahyun, E. Schmidt, Mahin Sadrai, N. Serpone et D. K. Sharma. Can. J. Chem. **67**, 1565 (1989).

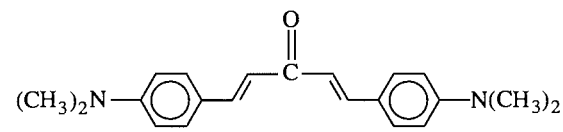
La photoexcitation du composé mentionné dans le titre (DMBA), dans des solvants polaries, conduit à la formation en série d'au moins trois espèces excitées que l'on a détectées par spectroscopie d'absorption au laser des espèces transitoires : l'état singulet Franck–Condon le plus bas, un état singulet déformé (état-*P*) et l'état triplet le plus bas. Dans les conditions utilisées, le seul état à émettre est le singulet localisé qui se forme initialement. Dans l'acétonitrile ou le méthanol, il se produit un passage intersystème de l'état-*P* déformé vers l'état triplet. Des études de photo-CIDNP et des mesures de rendement quantique effectuées dans l'acétonitrile ou dans le méthanol indiquent que le transfert d'électron se produit exclusivement à partir du triplet, qu'il sensibilise la décomposition du cation diphényliodonium et qu'il décolore le DMBA. L'analyse de la photochimie est compliquée par la formation d'un complexe de transfert de charge de photolabilité accrue. Lorsqu'on utilise de la tris(trichlorométhyl)-*sym*-triazine comme accepteur d'électron dans un solvant hydrocarboné, il se produit encore de la décoloration du DMBA dont l'efficacité est plus grande qu'avec le «sel onium» dans un solvant polarie. On en déduit que dans ces conditions le transfert d'électron se produit à partir de l'état-*P*.

Mots clés : photochimie, fluorescence, transfert d'électron, TICT, chalcone.

[Traduit par la revue]

Introduction

The spectroscopic properties of bis(*p*-*N*,*N*-dimethylaminobenzylidene)acetone (DMBA) have been studied by Eisenhart and Ellis (1), who also reported its photodimerization. These investigators report a sub-ns lifetime for the fluorescent singlet excited state of DMBA, but find evidence in the dimerization kinetics for the existence of a second, longer-lived "phantom" singlet state. Given the structural relationship between DMBA and other molecules, e.g., Michler's Ketone, in which the formation of twisted internal intramolecular charge transfer (TICT) excited states have been confirmed (2), we anticipated



DMBA

that this phantom state of DMBA might be of a similar nature. Fluorescence spectroscopy (1), however, provided no evidence for a TICT state; TICT states are usually emissive (2).

One purpose of this study, therefore, was the characterization of the excited states of this interesting molecule; detailed description of the excited state dynamics is, furthermore, prerequisite to interpretation of the behaviour of DMBA as a sensitizer of electron transfer photoreactions.

Electrochemical studies[5] suggested that DMBA, $E_{ox} = +1.0$ V vs. SCE in acetonitrile, should be capable in one or more of its

[1]Presented in part at the SPSE Summer Symposium, "Photochemistry for Imaging," White Bear Lake, MN, U.S.A., June 1988.

[2]Author to whom correspondence may be addressed at 3M Center, 201-3N-05, St. Paul, MN 55144, U.S.A. This paper comprises contributions no. 1630A and 1661 from 3M Corporate Research Laboratories.

[3]Present address: Department of Chemistry, Michigan State University, E. Lansing, MI 48824, U.S.A.

[4]Present address: Department of Photo Science and Technology, St. Cloud State University, St. Cloud, MN 56301, U.S.A.

[5]We thank Dr. M. C. Palazzotto of these laboratories for the electrochemical measurements by cyclic voltammetry in acetonitrile. The electrochemical properties of DMBA do not differ significantly from those of molecules composed of only one aminophenylvinylcarbonyl chromophore (3).

Can. J. Chem. Downloaded from www.nrcresearchpress.com by 194.225.253.170 on 09/07/12
For personal use only.

Can. J. Chem. Downloaded from www.nrcresearchpress.com by 194.225.253.170 on 09/07/12
For personal use only.

excited states (4) of donating an electron to a relatively oxidizable, photolabile species, such as tris(trichloromethyl)-*sym*-triazine, $E_{ox} = -0.7$ V vs. SCE (5), or diphenyliodonium cation, $E_{red} = -0.7$ V vs. SCE,[6]. The chemistry of the latter cation has been under extensive investigation in other laboratories (7–9) as well as our own (10), especially with respect to electron transfer sensitized photolysis. We are presently interested in the question of participation of a nonlocalized excited state, either of the TICT (2) or the *P* (11) type, in such electron transfer sensitization.

As with our previous study (10) of anthracene sensitized photolysis of the diphenyliodonium cation, several lines of investigation have proved fruitful in elucidating the pathways responsible for electron transfer sensitization with DMBA: photo-CIDNP experiments; quantum yield measurements for the photobleaching of the DMBA chromophore; picosecond-resolved transient absorption spectroscopy; and kinetic analysis of the results obtained in these and the steady-state irradiations. It is thus a further intent of this paper to correlate these observations with the photophysical insights.

Experimental

Materials and methods

Bis(*trans-p-N,N*-dimethylaminobenzylidene)acetone, mp 191–192°C, was prepared according to the method of Olomucki and LeGall (12) and recrystallized from toluene.[7] Diphenyliodonium hexafluorophosphate (Aldrich), mp 136°C, was purified by recrystallization from isopropanol. The tris(trichloromethyl)-*sym*-triazine, mp 93–95°C, was prepared as previously described (13). Spectral quality, glass distilled acetonitrile (EM OmniSolv^R) was used for solution preparation. Other solvents were likewise spectral quality. Most solutions were prepared directly; solutions of DMBA in cyclohexane were prepared by appropriate dilution of aliquots of a *freshly sonicated* dispersion of DMBA, 0.0010 M in cyclohexane.

Fluorescence intensities were recorded on a Perkin Elmer MPF-44B fluorescence spectrophotometer. The data for the fluorescence quantum yields were based on emission intensities of 5×10^{-7} M solutions of DMBA, excited at λ_{max} where the optical density was accordingly ca. 0.2. Spectra for absolute quantum yield measurements were recorded in the "ratio" mode of the spectophotometer to provide correction of the data for wavelength-dependent lamp output. The quantum yields were estimated by comparison at the integrated emission intensities to that of an anthracene standard (14).

Laser flash photolyses

The instrumentation used for these experiments has already been described in detail (15). The double beam, mode-locked, Nd-YAG laser system employed a silicon intensified target Vidicon detector. Light pulses at 355 nm were obtained by frequency-stripling; typical irradiances were ca. 2 mJ per pulse focused to a 2 mm diameter spot on the face of a 2-mm quartz sample curvette. The pulse width was 30 ps (FWHM). As in the quantum yield experiments, below, the solutions were deoxygenated by dry argon purge prior to irradiation. The fluorescence lifetime of DMBA in cyclohexane was measured on a similarly excited sample; fluorescence was detected with a Hamamatsu streak camera (16). Other fluorescence lifetimes were measured on a PRA time-resolved single photon counting apparatus with Xe flash excitation.

Photo-CIDNP

The photo-CIDNP spectra were obtained using the proton probe on a Varian XL-100 magnetic resonance spectrometer, with the probe modified to allow direct irradiation of the sample at the receiver coil. Typical sample composition was 0.05 M 'onium salt and ca. 0.01 M DMBA. The light source, a 300-W Xe arc operating at full power, was focused on the receiver coil using quartz optics on an optical rail. Heating of the sample was a problem, as infrared filtration decreased the light intensity too much to observe CIDNP. Consequently, photo-CIDNP spectra were recorded in the Fourier transform mode of the XL-100, collecting two transients over ca. 5 s exposure time, during which heating was minimal. Samples (2 mL volume) were deoxygenated by nitrogen purge, and dark spectra were taken before and after irradiation. Thermal instability of the solutions of the requisite concentration precluded the photo-CIDNP experiment on DMBA with the triazine acceptor in deuterocarbon solvent.

Quantum yields

Quantum yields were measured with no more than 10% conversion of DMBA as described in the text; loss of DMBA was followed spectrophotometrically at 450 nm in AN and at 425 nm in hexane. The solutions were deoxygenated by dry argon purge, as required. Aliquots (3 mL) in a 1-cm quartz spectrophotometer cell were irradiated at 405 or 450 nm on an optical bench with light from the Xe arc lamp, passed through a monochromator with the slits adjusted to allow a 20–30 nm bandpass. The output of the source was calibrated by means of potassium ferrioxalate actinometry (17) and continuously monitored with a radiometer. Typical fluxes of 1×10^{-6} einstein min^{-1} required 2–5 min irradiation to yield ca. 10% conversion with the iodonium salt. Correspondingly shorter times were required with the triazine acceptor. Ultraviolet–visible absorption spectra were recorded on the samples in the reaction cuvette before and after irradiation.

Photophysics of DMBA

As the absorption and fluorescence spectra of DMBA are not dissimilar to those of singly chromophoric *p*-aminophenyl carbonyl compounds (2, 18, 19), we consider the molecule to comprise two identical cross-conjugated chromophores; excitation may thus reside in either aminophenylvinylcarbonyl segment of the molecule. Intramolecular rotation to convert the vertical first singlet excited state to a TICT state would accordingly occur about the C—N single bond (2); alternatively this localized singlet may decay by twisting of the vinylic double bond, to form a *P*-state, according to Hochstrasser's (11) nomenclature. This state may be either charge transfer or biradicaloid in nature. A potential energy diagram incorporating the *P*-state is shown in Fig. 1.

Studies in acetonitrile

We determined the fluorescence lifetime of DMBA in acetonitrile (AN) by time-correlated single photon counting. The emission decays as a single exponential with time constant, τ, 0.7 ns. Based on the oscillator strength of 0.89, calculated by integration of the DMBA absorption spectrum in acetonitrile, we estimated (20) the first-order fluorescence rate constant, k_f, to be 4.8×10^8 s^{-1}, consistent with the directly measured value (see below):

$$[1] \quad \phi f = k_f(k_f + k_d)$$

and

$$[1a] \quad \tau = 1/(k_f + k_d)$$

where ϕ_f is the fluorescence quantum yield and k_d is a rate constant for radiationless decay. The radiationless decay process, responsible for the deactivation of the initially formed, fluorescent, singlet excited state then occurs with a first-order rate constant, k_d, of ca. 1×10^9 s^{-1} in AN.

[6]A commonly cited reference (6) for the reduction potential of diphenyliodonium cation in this solvent has proved unreproducible in our laboratories, although the value cited in this earlier work has recently been reproduced in Prof. Timpe's laboratory (8). We thank Prof. Timpe for bringing this reference to our attention and for providing a reprint.

[7]We thank Dr. M. Z. Ali of the Graphics Research Laboratory, 3M, for the sample used in these experiments.

Can. J. Chem. Downloaded from www.nrcresearchpress.com by 194.225.253.170 on 09/07/12
For personal use only.

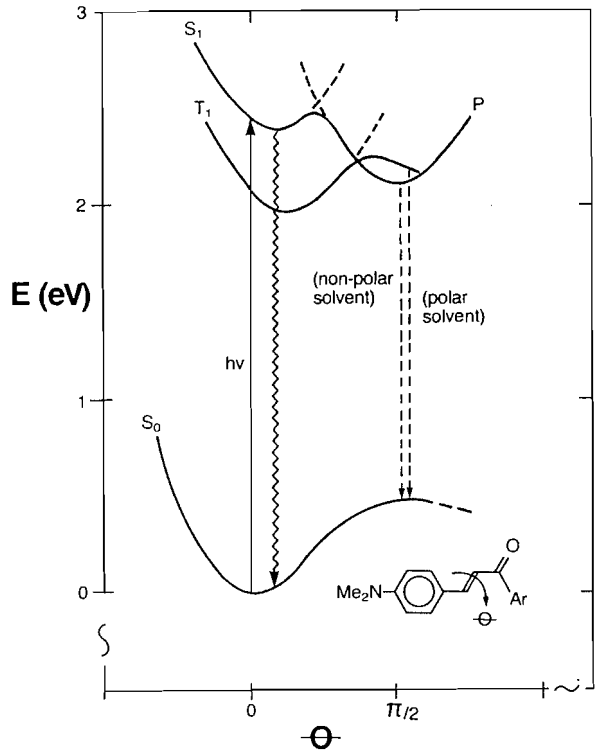


FIG. 1. Potential energy surfaces for S_0, S_1, P, and T states of DMBA as a function of torsional angle about the vinylic C—C bond.

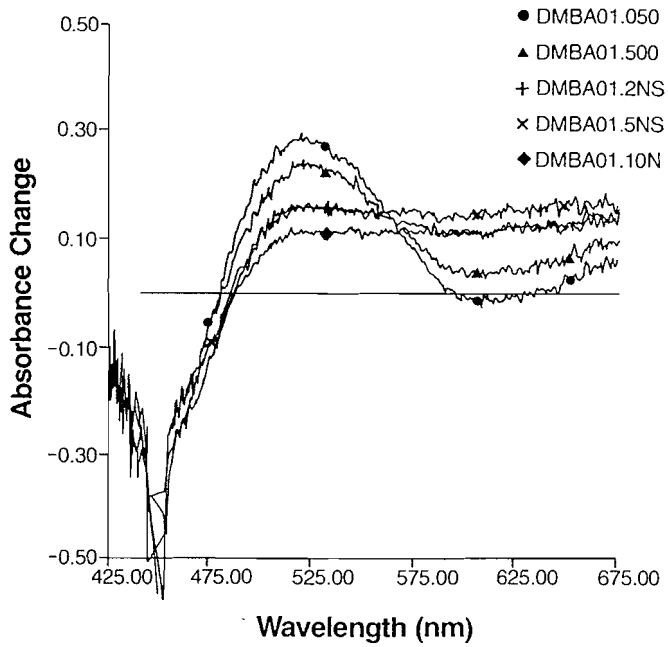


FIG. 2. Transient absorption spectra of DMBA (8×10^{-5} M in AN): (●) 50 ps, (▲) 500 ps, (+) 2 ns, (×) 5ns, and (◆) 10 ns delays after excitation with a 30-ps (FWHM) 355-nm laser pulse.

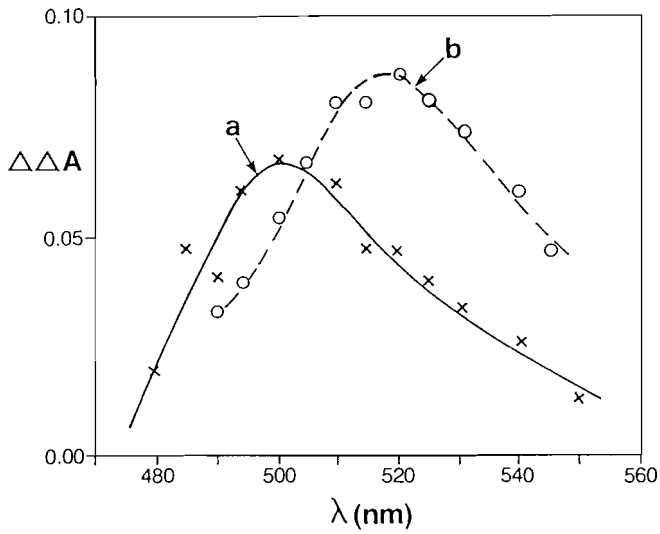


FIG. 3. Difference spectra obtained by subtracting (a) the 500-ps trace of Fig. 2 from the 50-ps trace, and (b) the 5-ns trace from the 500-ps trace.

To elucidate the nature of the radiationless decay process associated with k_d, we looked for light absorbing transients on laser irradiation at 355 nm of 8×10^{-5} M solutions of DMBA in AN. Such laser flash exposures led to transient bleaching of the 440-nm DMBA absorption, assigned by Eisenhart and Ellis (1) to the π–π^* electronic transition; no permanent changes in the absorption spectrum resulted, however. At this concentration dimerization is unimportant (raman-shifted pump radiation at 450 nm, characteristic of such experiments in acetonitrile, interferes with observation of the bleaching.) With ca. 2 mJ per excitation pulse, nearly 50% of the DMBA, 3.5×10^{-5} M, was converted to S_1, based on the intensity of bleaching.

Consequent to excitation, a new absorption occurs, apparently centered on 517 nm, assigned to an S_n–S_1 transition, with extinction coeffient 3.5×10^4 M^{-1} cm^{-1}, estimated by comparison with the extent of bleaching of the S_1–S_0 transition of known extinction coefficient (see Fig. 1). Over the lifetime of the experiment, this absorption exhibits biphasic decay, from which we infer that the S_1 state exists in two isomeric forms. Based on the time-resolved Vidicon response at 517 nm, we estimate that photo-excited DMBA surviving more than 1 ns after excitation has a lifetime in this second, phantom state of ca. 19 ± 3 ns; it represents about two-thirds of the originally excited species. This value compares with the 40-ns lifetime estimate of Eisenhart and Ellis in methylene chloride (1), based on the dimerization kinetics. The faster decaying component of the DMBA excitation corresponds to the sub-ns lifetime fluorescent species.

We illustrate that the initially formed transient of Fig. 2 actually comprises two species by taking the difference spectra between (a) the transients recorded 50 and 500 ps after the exciting pulse, and (b) the transients recorded 500 ps and 5 ns thereafter. As shown in Fig. 3, the initially formed transient has an absorption maximum at 500 nm, which subsequently red-shifts to 519 nm, characteristic of the longer-lived isomeric form of the singlet.

In AN, the ca. 20-ns lifetime state converts cleanly to a species absorbing in the red (Fig. 2). The extinction coefficient of the new transient is ca. 4.5×10^4 M^{-1}, assuming complete conversion of the first phantom state to this product. We assign it to triplet excited DMBA. In addition to the photo-CIDNP evidence, below, the rate constant for formation of this species is comparable to other intersystem crossing rate constants reported for aromatic and carbonyl compounds (20, 21).[8] Some decay of the transient is observed at 10-ns delay, despite purging with dry

[8]We thank Dr. T. S. Godfrey, Minnesota 3M Research, Harlow, England for bringing ref. 21 to our attention.

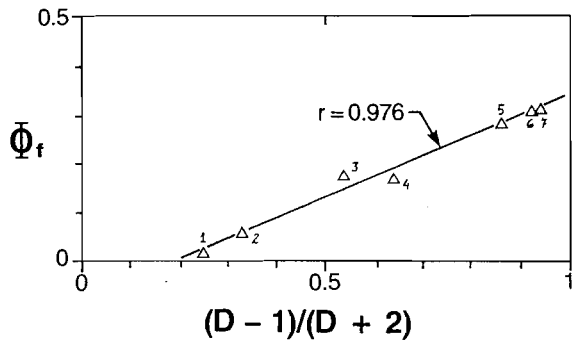


FIG. 4. DMBA fluorescence quantum yield as a function of the Debye solvent polarizability function: solvents are (1) cyclohexane (ref. 1), (2) toluene (this work and ref. 1), (3) methylene chloride (ref. 1), (4) tetrahydrofuran, (5) acetone, (6) *N*,*N*-dimethylformamide, and (7) acetonitrile (AN).

argon, suggestive again of a short triplet lifetime, which may be rationalized by the facility of isomerization about the vinylic C—C bond to provide a diabatic deactivation pathway. Sub-μs triplet lifetimes for substituted stilbenes possessing polar excited states have recently been reported (22), as well as for nitro-substituted azobenzenes (23). Similar lifetimes have also been reported for a variety of alkene triplets (24).

Solvent polarity effects

Additional experiments were accordingly undertaken to establish the nature of the secondary singlet state and elucidate the pathways for radiationless decay. The fluorescence quantum yield for DMBA correlates in non-hydroxylic solvents with the Debye solvent polarizability function $(D - 1)/(D + 2)$ (25), where D is the solvent (static) dielectric constant, as shown in Fig. 4. The plot includes data both from this work and from that of Eisenhardt and Ellis (1). The spectral energy corresponding to maximum fluorescence intensity also correlates with the same function, indicative of significant charge separation in the lowest Franck–Condon singlet.

Fluorescence rate constants, k_f, calculated as above, differ by less than a factor of two among the solvents studied; by eq. [1], k_d must therefore increase with decreasing solvent polarity. This is the opposite dependence than expected for a process that forms a charge-separated, e.g., TICT, state (28) and suggests an assignment of the non-emissive, longer-lived, singlet state as a biradicaloid *P*-state. This assignemnt is consistent with intersystem crossing therefrom, insofar as pyramidalization of the ethylenic carbons can be expected (27) to give rise to modest, but significant, spin-orbit coupling. In further support of this assignment, singlet excited 7-aminocoumarins, which contain the same chromophore as DMBA, but in which the rotation about the vinylic bond is precluded, decay (a) monoexponentially, and (b) with fluorescence as the exclusive deactivation pathway (18). That the *P*-state is biradicaloid in character is also consistent with its participation in DMBA photodimerization (1), which is accordingly orbital symmetry allowed. The biradicaloid character of the *P*-state might be expected to contribute toward the facility of intersystem crossing therefrom, as well: Caldwell *et al.* (24) have shown that pyramidalization of ethylenic carbon atoms leads to small, but significant, enhancement of spin-orbit coupling.

In cyclohexane, the least polar solvent in the series shown in Fig. 4, k_d must reach ca. 10^{12} s^{-1}, from eq. [1] and k_f, estimated as above, as 4.2×10^8 s^{-1}. Depopulation of the Franck–Condon

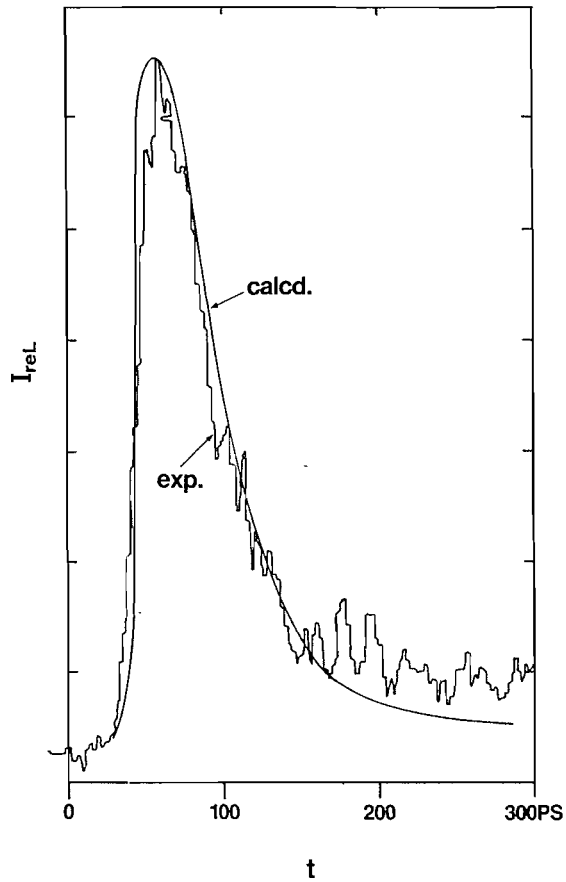


FIG. 5. Determination of fluorescence lifetime for DMBA in cyclohexane: stepped line is the trace of the streak camera as recorded, 2.2 ps per channel; smooth curve is simulation of the experimental data for 30-ps laser pulse width and 25-ps decay of fluorescence.

S_1 state on this time scale in nonpolar media was confirmed by direct measurement of the fluorescence lifetime using the 355-nm pulsed laser excitation and time-resolved fluorescence detection with a streak camera. The trace from this experiment, Fig. 5, is consistent with a ca. 25-ps lifetime for the emissive state. We also repeated the transient absorption laser flash photolysis experiment on 8×10^{-5} M DMBA dissolved in cyclohexane, as shown in Fig. 6. Despite intense bleaching of the DMBA absorption at 430 nm, no significant transient corresponding to S_2–S_1 absorption between 500 and 550 nm was observed even within the duration of the laser pulse. Ground state DMBA was, however, regenerated only to the extent of ca. 30% in 10 ns, the maximum time available in the experiment, indicating that a phantom state of up to 30-ns lifetime is, indeed, intermediate between the localized S_1 and the ground state in the nonpolar solvent, even though it is transparent to the experiment. The monotonic dependence of the relationship of Fig. 4 suggests, furthermore, that the same phantom state is involved in all solvents studied.

Solvent viscosity effects

In addition, DMBA fluorescence intensity exhibits a viscosity dependence, as shown in Fig. 7 for measurements made in a series of methanol–glycerol mixtures[9] (among which the polarizability function varied only trivially, from 0.919 to 0.936).

[9]We thank Dr. Colleen C. Nagel of these laboratories for recommending this solvent system.

Can. J. Chem. Downloaded from www.nrcresearchpress.com by 194.225.253.170 on 09/07/12
For personal use only.

Can. J. Chem. Downloaded from www.nrcresearchpress.com by 194.225.253.170 on 09/07/12
For personal use only.

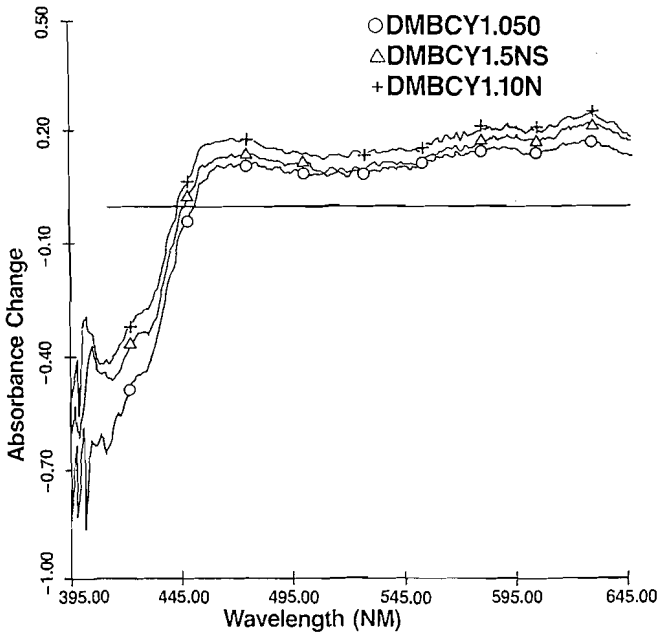


FIG. 6. As Fig. 2, in cyclohexane. Traces correspond to 50 ps (○), 5 ns (△), and 10 ns (+) after the initial 355-nm pump pulse.

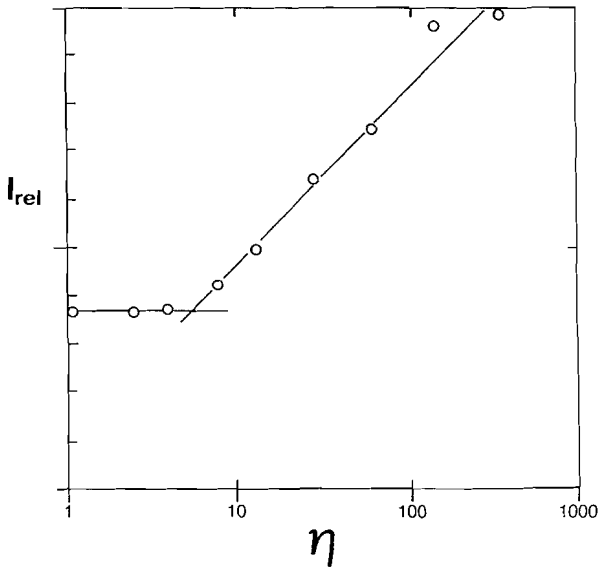


FIG. 7. DMBA fluorescence intensity as a function of solvent viscosity (cP): methanol–glycerol mixtures.

We assign the viscosity dependent radiationless decay process as isomerization to the phantom singlet state, occurring with k_d = ca. 1×10^9 s^{-1} in AN and ca. 5×10^9 s^{-1} in methanol. From Fig. 7, the rotational correlation time apparently becomes rate limiting at a viscosity of ca. 7.5 cP; at this viscosity we would then expect the correlation time to be of the order of 1 ns. At lower viscosities, the rate of formation of the phantom state is apparently limited by some intrinsic activation barrier.

The Debye formula (28) for rotational relaxation time,

$$[2] \quad t = \eta V / k_b T$$

where η is the medium viscosity, has been demonstrated to be applicable to barrierless isomerizations (2, 29). From the estimate for t when $\eta \geq 7.5$ cP and eq. [2], we estimate the sweep

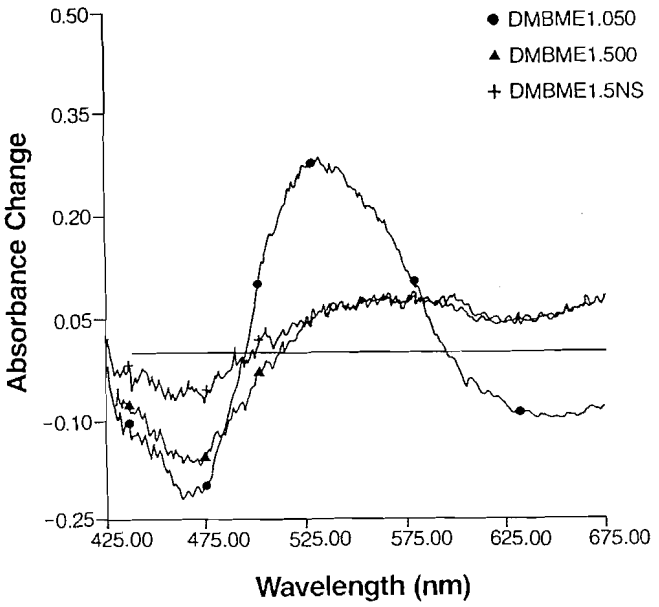


FIG. 8. As Fig. 2, in methanol. Traces shown correspond to 50 ps (●), 500 ps (▲), and 5 ns (+) after excitation; traces for intermediate delay times, used in kinetic analysis, are omitted for sake of clarity.

volume, V, of the rotating fragment to be 225 Å^3, in reasonable agreement with the volume of rotation through 90° of the *p*-dimethylaminobenzyl radical, calculated from molecular models, 192 Å^3. This correspondence is consistent with an assignment of the phantom state as a *P*-state, derived by twisting about the (ground state) vinylic double bond from a predominantly charge transfer, directly excited singlet state of DMBA, as shown in Fig. 1.

Studies in methanol

In methanol the quantum yield for fluorescence was lower, 0.06, than in aprotic solvents of comparable polarity. The fluorescence lifetime for DMBA in this solvent, measured by single photon counting, was 0.12 ns, consistent with this quantum yield and eq. [1]. Coupling of the vibrational modes of hydrogen bonded solvent is the most likely loss pathway (30); actual protonation of the carbonyl carbon is unlikely under these conditions (31).

Representative transient absorption spectra obtained following 355-nm laser flash excitation of 8×10^{-5} M DMBA in methanol are shown in Fig. 8. There are, in comparison to the AN result, several new features. First, the absorptions are slightly red-shifted in this solvent; the light absorbing transients corresponding to the initially populated localized singlet and its decay product, hypothesized to the the *P*-state, are clearly distinguishable. Second, the fluorescence is also red-shifted, so significantly negative A's are observed for wavelengths beyond 590 nm at the shortest delay times (<100 ps). Third, there is no light absorbing transient, within the wavelength regime of the experiment, that appears to be associated with the decay product of the *P*-state.

As in AN, the transient absorption assigned to S_1, with λ_{max} ca. 530 nm, decays more rapidly than the ground state is repopulated. Kinetics for the disappearance of absorption at 530 and 575 nm and its reappearance at 460 nm, obtained at 11 delay increments including those shown in Fig. 8, are plotted in Fig. 9. The rate of ground state regeneration from fluorescent singlet after pulse excitation is given by

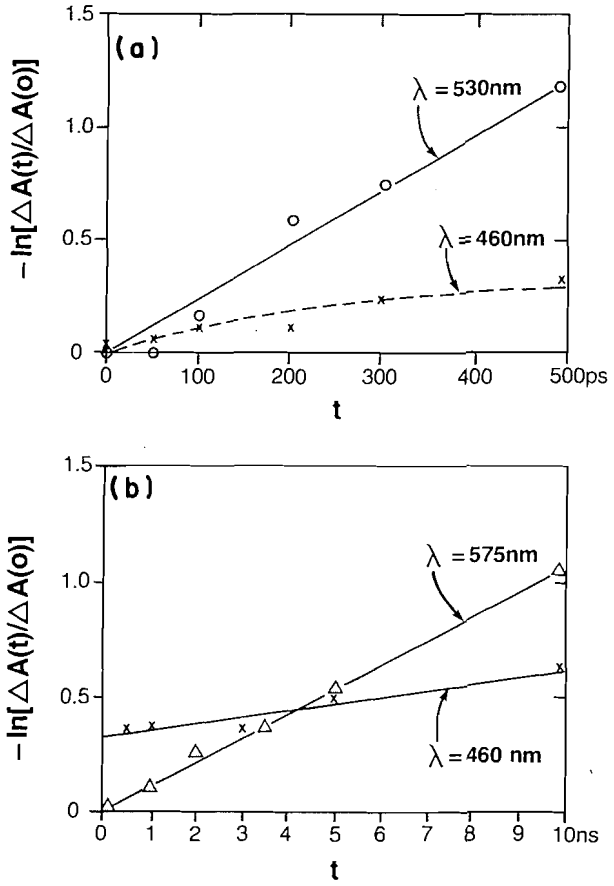


FIG. 9. First-order kinetic plots for (a) decay of 530-nm transient absorption and recovery of 460-nm absorption over the interval 0–500 ps after laser excitation, and (b) decay of 575-nm absorption and recovery of 460-nm absorption over the interval 0.5–10 ns after excitation, in the experiment of Fig. 8. Dashed line in Fig. 9a represents eq. [3] with $(k_f + k_r)$ equal to 3.3×10^9 s^{-1}.

$$[3] \quad d[DMBA]/dt = (k_f + k_r)\,[^1DMBA]_0 \cdot \exp(-t/\tau_1)$$

where $[^1DMBA]_0$ is the concentration of DMBA converted to the localized singlet state by the pump laser (3×10^{-5} M in our experiment), k_r is the rate constant for the radiationless processes *not* leading to the *P*-state, so that

$$[4] \quad \tau_1^{-1} = k_f + k_r + k_d + \ldots$$

Given our estimate of τ_1, 0.12 ns, the data for recovery of DMBA ground state could be fit by eq. [3] with $(k_f + k_r)$ equal to $(3.3 \pm 1.0) \times 10^9$ s^{-1}, as shown in Fig. 9a.

Formation of the *P*-state occurs to an extent of ca. 60% of the initially excited DMBA, based on (a) the maximum observed absorption at 575 nm, assuming the same extinction coefficient for the *P*-state as estimated in AN, and (b) the extent of recovery of ground state DMBA at 1 ns after excitation. As the quantum yield for *P*-state formation is given by $k_d\tau_1$, we estimate its formation rate constant, $k_d = (5 \pm 0.7) \times 10^9$ s^{-1}. Note that this is about fivefold faster than in the non-hydrogen bonding solvent of comparable polarizability and viscosity (AN). The sum of k_d and $(k_f + k_r)$ is then $(8.3 \pm 1.2) \times 10^9$ s^{-1}, in good agreement with the measured value (8×10^9 s^{-1}) for the disappearance of the localized singlet; no additional decay pathways need be postulated.

TABLE 1. Rate constants for interconversion of excited states of DMBA in various solvents

	Rate constant ($\times 10^{-9}$ s^{-1})		
Process	AN	Hexane	Methanol
k_f	0.48[a]	0.42[a]	0.50
k_r	—	—	2.8±1.0
k_d	1.0	1×10^3	5.0±0.7
k_{isc}	0.5	—	0.10
1/3	ca. 0.02	—	0.025

[a]Estimated from transition probabilities calculated from DMBA absorption spectra in the indicated solvents.

The species absorbing at 575 nm decays (Fig. 9b) with a first-order rate constant of 1×10^8 s^{-1}, while ground state DMBA recovers more slowly on this time scale, at ca. 2.5×10^7 s^{-1}. The *P*-state must therefore decay to a species of ca. 40 ns lifetime, which is transparent to the experiment. By analogy to the results obtained in AN (above) we assign this species as triplet DMBA. The reason for the transparency of ^{3}DMBA in methanol is not directly apparent: the transition active in AN may involve excitation of an oxygen *n*-orbital electron, which becomes involved in hydrogen bonding in methanol; alternatively the geometry of the triplet states obtaining in these two solvents may be different, planar in one case and twisted in the other. The observed and calculated rate constants for interconversion of the excited states of DMBA are summarized in Table 1.

Electron transfer photochemistry

Photolysis of DMBA in either methanol or acetonitrile, AN, in the presence of diphenyliodonium hexafluorophosphate leads both to bleaching of the DMBA and decomposition of the iodonium cation (to iodobenzene, benzene, and other minor products). The electron transfer sensitization mechanism has considerable precedent in the sensitized photochemistry of 'onium salts (8–10, 19).

A similar bleaching is observed with the triazine acceptor, in nonpolar solvents, such as toluene or cyclohexane, as well as in polar solvents. By analogy to the electron transfer photochemistry of benzyl halides (32), haloforms (8), and carbon tetrahalides (33), one-electron reduction of the triazine is expected to liberate chloride ion, leaving a neutral radical whose recombination with the DMBA radical cation results in the observed bleaching.

When the reaction is carried out with either acceptor to, e.g., 50% conversion, a ca. 10-nm blue shift in the DMBA absorption maximum is observed. This suggests that the two more-or-less independent chromophores in DMBA are bleached sequentially, and that two electron transfer events are required for the complete bleaching of the ketone.

Photo-CIDNP

Photochemically Induced Dynamic Nuclear Polarization experiments (Fig. 10) show that benzene, presumably formed by H-abstraction by the phenyl radical product of cleavage of the diphenyliodo radical, has a triplet radical pair precursor, when the iodonium salt is photolyzed in perdeutero-AN. Our inference is based on application of Kaptein's Rules (34), as embodied in the equation

Can. J. Chem. Downloaded from www.nrcresearchpress.com by 194.225.253.170 on 09/07/12
For personal use only.

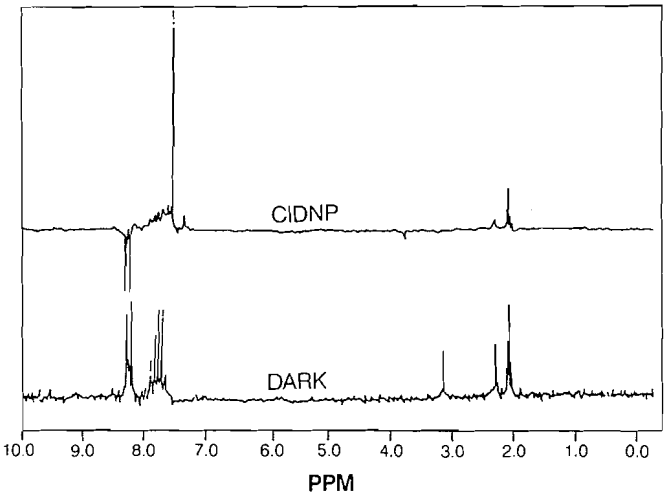


FIG. 10. Photo-CIDNP and dark proton nmr spectra of DMBA (0.01 M) with diphenyliodonium hexafluorophosphate (0.05 M) in acetonitrile.

$$[5] \quad G = \mu\epsilon\cdot\Delta g\cdot a$$

where $G < 0$ corresponds to emission and $G > 0$ corresponds to absorption in the magnetic resonance spectrum of a given product of a photoreaction. The absolute signs of three parameters in eq. [5] must be known in order to assign the fourth: the hyperfine coupling constant, a, and the difference between the g-factors of the two radicals, Δg, are experimentally measured; the other two are assigned by convention, with $\mu > 0$ for in-cage products and $\mu < 0$ for cage-escape products, and $\epsilon < 0$ or > 0 for singlet and triplet radical pair precursors of the product, respectively.

We have already established, in similar photolyses with aromatic hydrocarbon sensitizers, that benzene (emission at 7.55 ppm) is a cage-escpae product ($\mu < 0$) (10). The sign of the product, $\Delta g\cdot a$, was inferred from a similar experiment with the structurally related Michler's Ketone as the sensitizer. Owing to its high intersystem crossing quantum yield, Michler's Ketone sensitizes only by a triplet pathway ($\epsilon > 0$) (35); the observation in this case of enhanced absorption, $G > 0$, then requires $\Delta g\cdot a < 0$. Since DMBA also yields essentially an amine-centered cation radical, we infer that $\Delta g\cdot a$ is also < 0 for its photoreaction. The enhanced absorption at 7.55 ppm observed in Fig. 1 then requires that the benzene product results from a triplet radical pair precursor in this case as well.

The diphenyliodonium polarization (8.2 ppm) shows the characteristics of a special CIDNP effect, magnetic field induced $T_- - S_0$ mixing (ref. 20, pp. 273–288). In this kind of spin-sorting mechanism, only emission is observed and radical pair dissociation (hence cage-escape) is not necessary: Zeeman splitting of the triplet sublevels causes the lowest energy triplet sublevel (T_-) to become degenerate with the singlet ground state at a finite interradical distance, thus enhancing the rate of intersystem crossing from the T_- sublevel. Conservation of angular momentum requires a concomitant nuclear spin inversion from spin states aligned with the magnetic field, hence emission of *all* diphenyliodonium protons is characteristic of this effect. It is, furthermore, obtained *only* when the initial radical pair is a triplet.

Charge transfer complexation

DMBA and the diphenyliodonium cation form a one-to-one charge transfer complex reversibly in solution. No spectroscopic evidence was obtained, on the other hand, for an analogous complex with the triazine acceptor, even in the nonpolar solvents. The iodonium salt complex can be detected by optical absorption between 520 and 550 nm, along with a corresponding decrease in absorption at λ_{max}, 430 nm. These changes are illustrated by the spectra of Fig. 11. Similar spectral changes are reportedly observed for *p*-dimethylaminobenzoyl chromophores in acrylic polymers on incorporation of iodonium salts therein (19). A Benesi–Hildebrand analysis (36) of the absorptivity changes in AN at λ_{max} leads to an estimate of the formation constant for the complex in this solvent as $6 \pm 2\ M^{-1}$.

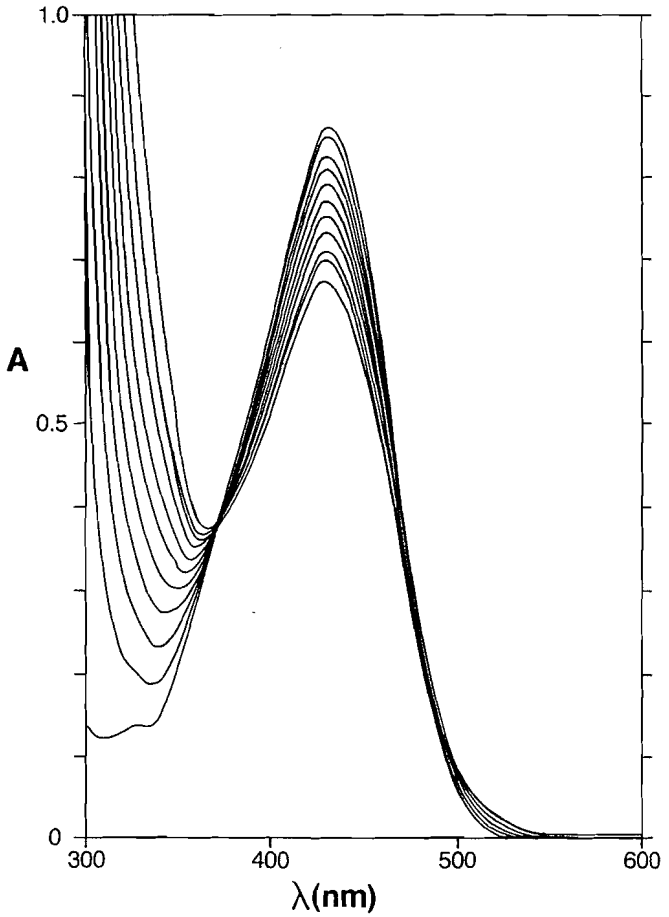


FIG. 11. Spectra changes observed on addition of diphenyliodonium hexafluorophosphate to 2×10^{-5} M DMBA in acetonitrile. Iodonium salt concentrations range from 0.001 to 0.04 M.

Electron transfer quenching of photoexcited DMBA in either a twisted singlet (P) or the triplet excited state represents a case of gated electron transfer. Statistically significant quenching of DMBA fluorescence by added diphenyliodonium hexafluorophosphate was not detectable in AN after correction of the observed emission intensity for formation of the fluorescence-inactive charge transfer complex. The fluorescent excited singlet of DMBA is too short-lived for collisional deactivation, so the electron transfer quenching is "gated" by the rotational relaxation about the vinylic C—C bond (37).

Transient absorption spectroscopy

The results of pulsed laser irradiation at 355 nm of an AN solution 8×10^{-5} M in DMBA and 0.045 M in diphenyliodonium hexafluorophosphate are shown in Fig. 12. Comparison

Can. J. Chem. Downloaded from www.nrcresearchpress.com by 194.225.253.170 on 09/07/12
For personal use only.

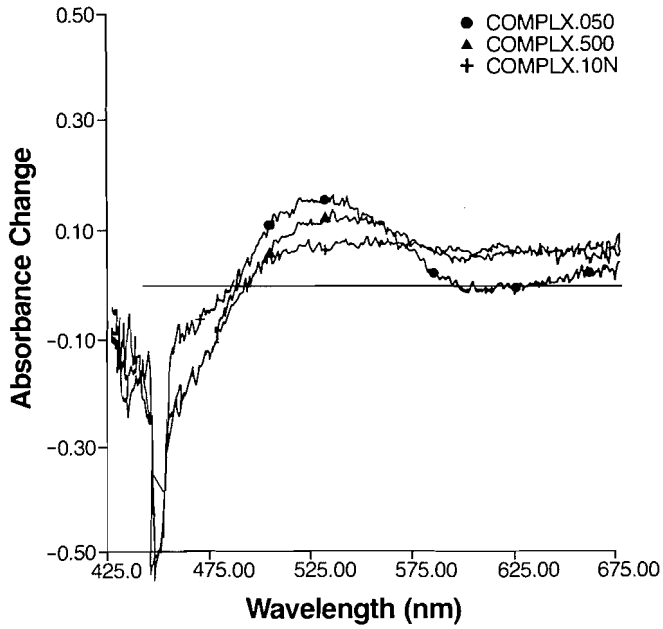


FIG. 12. Transient absorption spectra, recorded 50 ps (●), 500 ps (▲), and 10 ns (+) after initial 355-nm laser pulse excitation of DMBA in the presence of 0.045 M diphenyliodonium salt.

with Fig. 2 reveals that addition of the iodonium salt does not significantly affect the bleaching of the 430-nm transition. The 517-nm absorption was, however, significantly attenuated. Based on our estimates of the extinction coefficients for the transitions, above, 3.2×10^{-5} M DMBA was excited in the experiment, but only 2.2×10^{-5} M of the lowest singlet was formed. We relate this observation to formation of the ground state charge transfer complex, which absorbs light in the same spectral region as uncomplexed DMBA, but does not generate the light absorbing transient; 31% of the DMBA is thus inactivated, compared to a prediction of 27 ± 9% based on the experimental formation constant for the complex. The 430-nm absorption is regenerated to a comparable extent within 10 ns in this experiment, indicative of decay of the charge transfer complex to ground state on this time scale.

Intensity of the 610-nm transient indicates that the quantum yield for triplet DMBA (based on photoexcited, uncomplexed DMBA) is ca. 0.45 after 10 ns, compared with 0.42 in the absence of the iodonium salt. Thus little or none of the DMBA appears to be diverted to a photoproduct from the biradicaloid *P*-state, consistent with the photo-CIDNP observations.

Electron transfer from the *P*-state to the iodonium cation must be thermodynamically allowed insofar as we expect it to be more reducing than the electron transfer active triplet DMBA. At the same time electron transfer from the *P*-state must be strongly disfavored kinetically, since the *P*-state is not quenched by the added iodonium cation. We attribute the kinetic barrier to electron transfer from DMBA in part to a large intramolecular contribution to the reorganization energy (38); unlike the *P*-state, the minimum energy conformation of $DMBA^{\cdot+}$ ought to be planar, so as to maximize charge *delocalization*. This hypothesis implies that triplet DMBA, at least in AN, approximates the ground state conformation.

Mechanistic inferences: quantum yields

The combination of deactivation processes can be accommodated most economically by a reaction scheme comprising the following steps. Photochemical reaction, leading to decomposition of the 'onium cation and bleaching of DMBA, is presumed *a priori* to occur from both complexed and uncomplexed sensitizer. The quantum yield for formation of triplet DMBA in AN, ϕ_3, is given by $(1 - \phi_f)$, ca. 0.7 (see eq. [1]), and K is the formation constant for the ground state charge transfer complex, ca. 6 M^{-1} (above). The quantum yield of any photoproduct, ϕ_r, is then

$$\text{DMBA} + \text{Ph}_2\text{I}^+ \rightleftharpoons [\text{DMBA/Ph}_2\text{I}^+] \qquad K$$
$$[\text{DMBA/Ph}_2\text{I}^+] + h\nu \longrightarrow {}^{CT}[\text{DMBA/Ph}_2\text{I}^+]$$
$${}^{CT}[\text{DMBA/Ph}_2\text{I}^+] \longrightarrow \text{DMBA}^{\cdot+} + \text{PhI} + \text{Ph}^{\cdot} \qquad \phi_c$$
$$\text{DMBA} + h\nu \longrightarrow {}^{P}\text{DMBA}$$
$${}^{P}\text{DMBA} \longrightarrow {}^{3}\text{DMBA} \qquad k_{isc}$$
$${}^{3}\text{DMBA} \longrightarrow \text{DMBA} \qquad 1/\tau$$
$${}^{3}\text{DMBA} + \text{Ph}_2\text{I}^+ \longrightarrow {}^{3}\{\text{DMBA/Ph}_2\text{I}^+\} \qquad k_{diff}[\text{Ph}_2\text{I}^+]$$
$${}^{3}\{\text{DMBA/Ph}_2\text{I}^+\} \longrightarrow \text{DMBA}^{\cdot+} + \text{PhI} + \text{Ph}^{\cdot} \qquad \phi_p$$

SCHEME 1. Electron transfer sensitization.

$$[6] \quad \phi_r = \phi_3\phi_p f_r \cdot k_{diff}\tau\,[\text{Ph}_2\text{I}^+]/(1 + k_{diff}\tau\,[\text{Ph}_2\text{I}^+])$$

where f_r is the fraction of the products of the last step in the scheme converted to the detected photoproduct. If the observable quantum yield, ϕ_{obs}, also includes a contribution from the photoreaction of complexed DMBA, ϕ_c, then

$$[7] \quad \phi_{obs} = f_c\phi_c + (1 - f_c)\phi_r$$

where $f_c = K[\text{Ph}_2\text{I}^+]$.

The analysis was tested experimentally by observing the spectrophotometric disappearance of DMBA, ϕ_{obs}, in nitrogen-purged samples of DMBA (4×10^{-6} M) irradiated at 405 and 450 nm. The relevant data are reported in Table 2. The dependence of the quantum yield on iodonium cation concentration is represented in the form of a double reciprocal plot in Fig. 13. At 0.008 M iodonium salt, the quantum yield for DMBA disappearance was ca. 0.6 that of iodobenzene formation, estimated by quantitative gas chromatography of the reaction mixtures; iodobenzene is presumably formed in every event described by ϕ_r. This ratio, 0.6, then corresponds to f_r for DMBA disappearance, and agrees reasonably with the value of 0.5 expected on the basis of our hypothesis, above, that two electron transfer events are required for the complete bleaching of DMBA. (The two events may not occur with exactly equal probabilities.)

There are two regimes in the concentration dependence of the quantum yield in Fig. 13. At lower concentrations, at both wavelengths the plot is essentially linear, with an intercept-to-slope ratio of 1.2×10^3 M^{-1}. This ratio should be equal to $k_{diff}\tau$, if each encounter leads to electron transfer;[10] as k_{diff}, the second-order diffusional encounter rate constant in AN, is ca. 2×10^{10} s^{-1}, we estimate the lower limit lifetime of the photoactive excited state, τ, to be ca. 60 ns. This value is consistent with involvement of a short-lived triplet state of DMBA, cf. the 40-ns triplet lifetime estimated in methanol on the basis of the observed rate of ground state recovery. Quantum yields in this concentration regime decreased by ca. 30% on admission of air, also consistent with the intervention of a short-lived triplet state of the sensitizer.

The dimensionless intercept of the plot, numerically 15 ± 1 at

[10]The triplet state of Michler's Ketone is quenched by diphenyliodonium cation at much less than the diffusion controlled rate, ca. 10^7 M^{-1} s^{-1}, despite the exergonicity of the electron transfer (8).

Can. J. Chem. Downloaded from www.nrcresearchpress.com by 194.225.253.170 on 09/07/12
For personal use only.

TABLE 2. quantum yields for DMBA disappearance in AN

$[Ph_2I^+]$ (M)	$\phi_{obs}(405)$	$\phi_{obs}(405)$	$f_{complex}$	$\phi_c(405)^a$	$\phi_c(405)^a$
0.08	0.14	0.13	0.48	0.22	0.21
0.025	0.098	0.080	0.15	0.28	0.20
0.008	0.064	0.059	0.05	0.14	0.14
0.0025	0.052	0.047	0.01	0.20	0.20
0.0008	0.035	0.032	—	—	—
0.0004	0.028	0.021	—	—	—
0.00025	0.016	0.015	—	—	—

[a]Calculated from eq. [7].

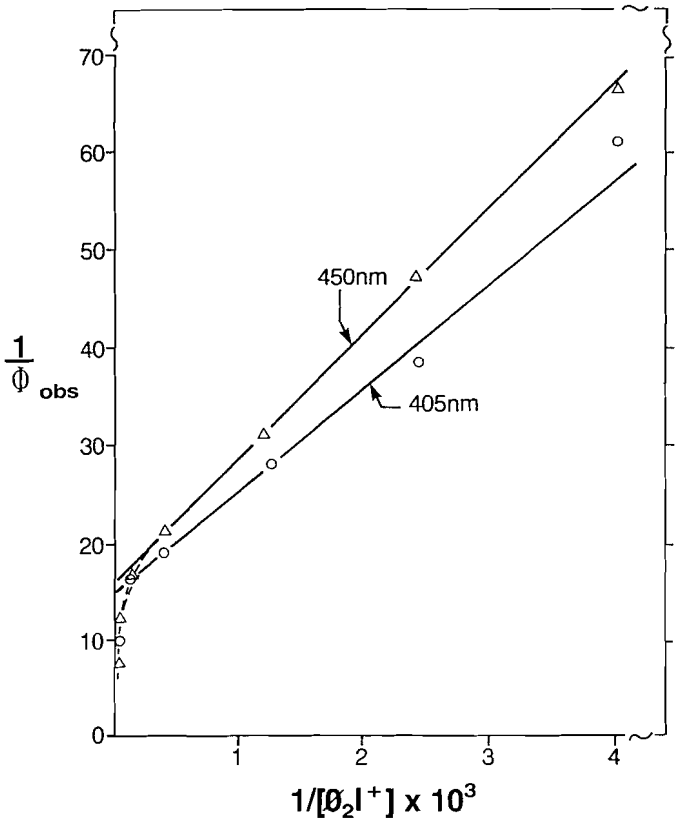


FIG. 13. Double reciprocal plot for DMBA bleaching at 405 and 450 nm in the presence of diphenyliodonium hexafluorophosphate.

both wavelengths, corresponds to $1/\phi_0$, where

[8] $\phi_0 = \phi_3 f_r \phi_p$

i.e., 0.067 ± 0.04, for $\phi_p = 0.16$. At the higher concentrations of iodonium salt, the quantum yield for disappearance of DMBA is higher than expected from extrapolation of the linear portion of the double reciprocal plot. We infer that the additional contribution to photoreaction arises from the DMBA-iodonium cation charge transfer complex, whose concentration becomes significant at these iodonium concentrations (see Table 2). Analysis according to eq. [7] allows us to estimate ϕ_c as 0.20 ± 0.03 for $\phi_p = 0.32$ from the complex.

On the basis of these quantum yield estimates, the charge transfer complex is twice as reactive as the encounter complex. This reactivity difference does not likely have an energetic basis, although electron transfer from the ^{3}DMBA is inevitably slightly less exergonic than from the complex. As Gould *et al.*

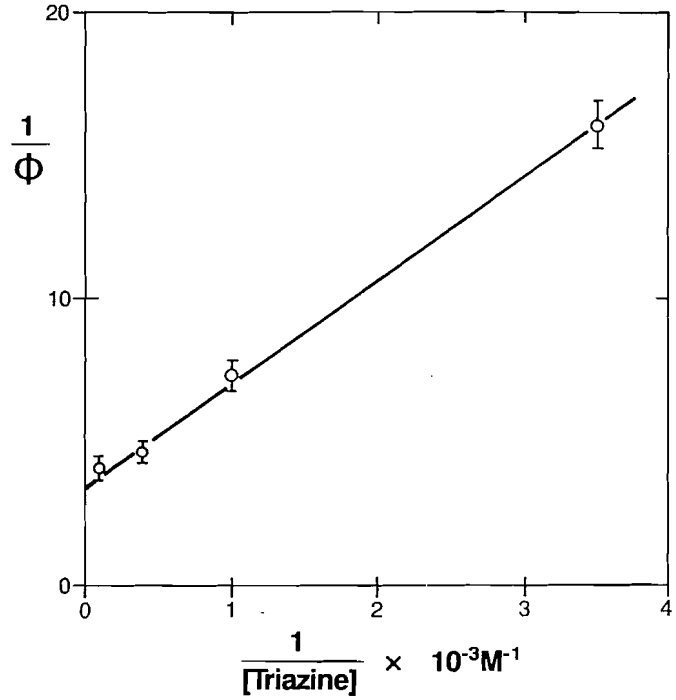


FIG. 14. As Fig. 13, for DMBA bleaching at 420 nm in cyclohexane in the presence of tris(trichloromethyl)-*sym*-triazine.

(40) have recently shown, back electron transfer may be significantly slower in the radical pair produced by photoexcitation of a charge transfer complex, than in the corresponding solvent-separated radical pair formed from an encounter complex. This interpretation is consistent with the ca. 2-ns lifetime of the excited state of the DMBA-iodonium cation charge transfer complex (see. Fig. 12). If the quantum yield for photolysis via the encounter complex reflects the competition between decomposition of the diphenyliodo radical (which occurs in ca. 250 ps (10)) and back electron transfer in the radical pair, the latter process would have to occur with a rate constant of ca. 4×10^{10} s^{-1}, i.e., in 25 ps.

The observed quantum yields for disappearance of 7×10^{-5} M DMBA in the presence of the triazine acceptor in cyclohexane (420-nm irradiation) are also presented in the form of a double reciprocal plot in Fig. 14. These data were obtained on argon-purged samples, but were entirely reproducible when the samples were exposed to air. We accordingly exclude intervention of triplet DMBA in this experiment, consistent with the abence of spectroscopic evidence for intersystem crossing from the *P*-state in this solvent. The quantum yields in cyclohexane were also unaffected by added hydroquinone (saturated, ca. 0.001 M): we thus exclude a radical chain process, such as has been proposed with other halocarbon acceptors (8). By contrast, the quantum yield for DMBA disappearance in the presence of 0.005 triazine in argon-purged AN, 0.016, drops to 0.009 on admission of air. We infer that electron transfer to the triazine in AN, like that to the iodonium cation, occurs from ^{3}DMBA; the extent of oxygen quenching is consistent with a DMBA triplet lifetime of ca. 40 ns in this solvent (see above).

The intercept of Fig. 14 indicates a limiting quantum yield, ϕ_0, of 0.28, corresponding to a quantum yield for electron transfer under these conditions of 0.56, insofar as bleaching of one DMBA molecule requires two photoinduced electron transfer events (see above). The intercept-to-slope ratio, i.e., Stern–

Can. J. Chem. Downloaded from www.nrcresearchpress.com by 194.225.253.170 on 09/07/12
For personal use only.

Volmer slope, derived from Fig. 14 is 1.0×10^3 M^{-1}. This value requires an excited state lifetime of 50 ns, if it is quenched by the acceptor at a diffusion limited rate. The estimate is in reasonable agreement with the rate of repopulation of the ground state observed in the transient absorption experiments. We infer that the biradicaloid *P*-state is not significantly inhibited from undergoing electron transfer photochemistry in relatively nonpolar media: in the conventional dielectric continuum approximation (39) we expect the medium reorganization contribution to the activation barrier for electron transfer to be substantially reduced in a nonpolar solvent compared to, e.g., AN; at the same time the solvatochromism of DMBA suggests that its excited states may be somewhat more reducing in hydrocarbon solvent than in AN. Both of these arguments are consistent with the higher quantum yield for DMBA bleaching observed in cyclohexane compared to AN.

Conclusions

DMBA is characterized by more than one singlet excited state accessible by excitation of its lowest energy electronic transition. The shorter-lived charge transfer state is efficiently fluorescent; the longer-lived twisted *P*-state undergoes intersystem crossing in either AN or methanol, but apparently decays to ground state in cyclohexane.

The *P*-state is essentially unreactive towards diphenyliodonium cation in polar solvent, while its principal product, the DMBA triplet, reacts, albeit somewhat inefficiently, on encounter with the cation in solution. We attribute the unreactivity of the *P*-state to association of a large reorganization energy with electron transfer therefrom.

Photoreaction from triplet DMBA is an example of so-called gated electron transfer. That only the encounters with triplet DMBA yield detectable photochemistry with the iodonium cation in AN is in agreement with photo-CIDNP observations. DMBA also forms a ground state charge transfer complex with diphenyliodonium cation. Photoexcitation of this complex leads, at least twice as efficiently, to products as does capture of triplet DMBA by iodonium cation. Differences in back electron transfer rates may be responsible for the enhanced photoreactivity of the complex.

The phantom *P*-state is, however, efficiently reactive towards another electron acceptor, tris(trichloromethyl)-*sym*-triazine in hydrocarbon solvent. No evidence was obtained to suggest that either a DMBA triplet or a charge transfer complex might be involved under these conditions. The observation of oxygen quenching implicates the involvement of triplet DMBA in the photoreduction of this acceptor in AN, however.

Acknowledgments

This work was supported *in part* by the Natural Sciences and Engineering Research Council of Canada and *in part* by 3M Canada, Ltd. We thank J. R. Hill, 3M Analytical and Properties Research Laboratory, for assistance with the photo-CIDNP work, along with Mr. Reza Danesh and Ms. Gwen Crooks, who provided able technical assistance at Concordia and 3M, respectively.

1. J. M. Eisenhart and A. B. Ellis. J. Org. Chem. **50**, 4108 (1983).
2. W. Rettig. Angew. Chem. **98**, 969 (1986); Appl. Phys. B: **B45**, 145 (1988).
3. G. Jones, Jr., S. F. Griffin, C.-y. Choi, and W. R. Bergmark. J. Org. Chem. **49**, 2705 (1984).
4. D. Rehm and A. Weller. Ber. Bunsen-ges. Phys. Chem. **73**, 834 (1969); Isr. J. Chem. **8**, 259 (1970); A. Weller. Pure Appl. Chem. **54**, 1885 (1982).
5. G. H. Smith. U.S. Patent 3,729,313 (1973); R. B. Hartman and G. H. Smith. U.S. Patent 3,617,288 (1971).
6. H. E. Bachofner, F. M. Beringer, and L. Meites. J. Am. Chem. Soc. **80**, 4269 (1958).
7. R. Billing, D. Rehorek, J. Salvetter, and H. Hennig. Z. Anorg. Allg. Chem. **557**, 234 (1988).
8. H.-J. Timpe. Sitzungsber. Akad. Wiss. DDR, Math. Naturwiss. Tech. 13N, 3 (1986).
9. S. P. Pappas. J. Imaging Technol. **11**, 146 (1985); S. P. Pappas, B. C. Pappas, L. R. Gatechair, and W. R. Schnabel. J. Polym. Sci. Polym. Chem. Ed. **22**, 69 (1984); S. P. Pappas, L. R. Gatechair, and J. H. Jilek. J. Polym. Sci. Polym. Chem. Ed. **22**, 77 (1984); H. Baumann and H.-J. Timpe. Acta Polymer. **37**, 309 (1986); H.-J. Timpe and A. Bah. Makromol. Chem. Rapid Commun. **6**, 353 (1987); S. M. Linden and D. C. Neckers. J. Am. Chem. Soc. **110**, 1257 (1988).
10. R. J. DeVoe, M. R. V. Sahyun, E. Schmidt, N. Serpone, and D. K. Sharma. Can. J. Chem. **66**, 319 (1988).
11. F. E. Doany, E. J. Heilweil, R. Moore, and R. Hochstrasser. J. Chem. Phys. **80**, 201 (1980).
12. M. Olomucki and J.-Y. LeGall. Bull. Soc. Chim. Fr. 1467 (1976).
13. T. R. Norton. J. Am. Chem. Soc. **72**, 3527 (1950).
14. I. B. Berlman. Handbook of fluorescence spectra of aromatic molecules. Academic Press, New York. 1971. p. 356.
15. G. Ponterini, N. Serpone, M. A. Bergkamp, and T. L. Netzel. J. Am. Chem. Soc. **105**, 4639 (1983); N. Serpone, T. L. Netzel, and M. Gouterman. J. Am. Chem. Soc. **104**, 246 (1982); N. Serpone, D. K. Sharma, J. Moser, and M. Graetzel. Chem. Phys. Lett. **136**, 47 (1987).
16. W. Yu. *In* Picosecond phenomena. *Edited by* C. V. Shank, E. P. Ippen, and S. L. Shapiro. Springer, Berlin, 1978. pp. 346ff; K. L. Sala, R. W. Yip, and R. LeSage. Appl. Spectrosc. **37**, 273 (1983).
17. J. G. Calvert and J. N. Pitts, Jr. Photochemistry, John Wiley, New York. 1966. p. 785ff.
18. M. A. Kahlow, T.-J. Kang, and P. F. Barbara. J. Chem. Phys. **88**, 2372 (1988).
19. K. Ichimura, A. Kameyama, and K. Hayashi. J. Appl. Polym. Sci. **34**, 2747 (1987).
20. N. J. Turro. Modern molecular photochemistry. Benjamin-Cummings, Don Mills, Ont. 1978. pp. 87ff.
21. G. Porter and P. Suppan. Pure Appl. Chem. **9**, 499 (1964); Trans. Faraday Soc. **62**, 3375 (1966).
22. H. Görner, F. Elisei, U. Mazzucato, and G. Galiazzo. Photochem. Photobiol. A**43**, 139 (1988); H. Görner and D. Schulte-Frohlinde. J. Phys. Chem. **83**, 1307 (1979).
23. H. Görner, H. Gruen, and D. Schulte-Frohlinde. J. Phys. Chem. **84**, 3031 (1980).
24. R. A. Caldwell. Pure Appl. Chem. **56**, 1196 (1984); R. A. Caldwell and C. V. Cao. J. Am. Chem. Soc. **104**, 6174 (1982).
25. P. Debye. Polar molecules. Dover, New York. 1945.
26. J. M. Hicks, M. T. Vandersall, E. V. Sitzmann, and K. B. Eisenthal. Chem. Phys. Lett. **135**, 413 (1987).
27. R. A. Caldwell, L. Carlacci, C. E. Doubleday, Jr., T. R. Furlani, H. F. King, and J. W. McIver, Jr. J. Am. Chem. Soc. **110**, 6901 (1988).
28. E. M. Kosower. Physical organic chemistry. John Wiley, New York. 1968. p. 279.
29. S.-B. Zhu, J. Lee, and G. W. Robinson. J. Phys. Chem. **92**, 2401 (1988).
30. H. E. A. Kramer. Chimia, **40**, 160 (1986).
31. L. G. Arnaut and S. J. Formoshinho. J. Phys. Chem. **92**, 685 (1988).
32. D. R. Eaton. Pure Appl. Chem. **56**, 1191 (1984).

Can. J. Chem. Downloaded from www.nrcresearchpress.com by 194.225.253.170 on 09/07/12
For personal use only.

33. J. KOSAR. Light sensitive systems. John Wiley, New York. 1975. Chap. 8.
34. R. KAPTEIN. Adv. Free Radical Chem. **5**, 319 (1975); R. G. LAWLER. Acc. Chem. Res. **5**, 25 (1972).
35. S. L. MUROV. Handbook of photochemistry. Marcel Dekker, New York. 1973.
36. R. FOSTER. Organic charge transfer complexes. Academic Press, New York. 1969. pp. 133ff.
37. B. M. HOFFMAN and M. A. RATNER. J. Am. Chem. Soc. **109**, 6237 (1987).
38. M. D. NEWTON and N. SUTIN. Adv. Phys. Chem. **35**, 437 (1984), and references cited therein.
39. I. R. GOULD, J. E. MOSER, D. EGE, R. MOODY, B. ARMITAGE, and S. FARID. *In* Photochemistry for imaging. *Edited by* A. J. Herbert. SPSE, Washington, DC. 1988. pp. 62ff; J. Imaging Sci. **33**, 44 (1989).

Can. J. Chem. Downloaded from www.nrcresearchpress.com by 194.225.253.170 on 09/07/12
For personal use only.

Gas-phase measurements of the kinetics of BF_2^+-induced polymerization of olefinic monomers

LEONARD FORTE, MIN H. LIEN, ALAN C. HOPKINSON, AND DIETHARD K. BOHME
Department of Chemistry, York University, Downsview, Ont., Canada M3J 1P3

Received February 9, 1989

LEONARD FORTE, MIN H. LIEN, ALAN C. HOPKINSON, and DIETHARD K. BOHME. Can. J. Chem. **67**, 1576 (1989).

The initial steps in the BF_2^+-induced polymerization of the monomers of ethylene, propylene, *cis*-2-butene, isobutene, and styrene have been observed in the gas phase at room temperature using the Selected-Ion Flow Tube (SIFT) technique. Rate constants and product distributions have been determined for the initiation of the polymerization in each case. All five initiation reactions were found to be rapid ($k \geq 5.0 \times 10^{-10}$ cm^3 molecule^{-1} s^{-1}). The primary product ions that propagate polymerization have been identified and sequential addition reactions have been followed in all five systems. For ethylene the energetics of the initial steps have been followed using *ab initio* molecular orbital theory. Reactions of BF_2^+ with the vapours of water and benzene have also been characterized.

Key words: ion-induced polymerization, alkenes, kinetics, gas phase ion chemistry.

LEONARD FORTE, MIN H. LIEN, ALAN C. HOPKINSON et DIETHARD K. BOHME. Can. J. Chem. **67**, 1576 (1989).

Opérant en phase gazeuse, à la température ambiante et faisant appel à la technique du tube à écoulement sélectif d'ion (SIFT), on a observé les étapes initiales de la polymérisation, induite par le BF_2^+, de monomères de l'éthylène, du propylène, du *cis*-but-2-ène, de l'isobutène et du styrène. Dans chacun des cas, on a déterminé les constantes de vitesse ainsi que les distributions des produits obtenus pour l'initiation de la polymérisation. On a trouvé que chacune de ces cinq initiations est rapide ($k < 5{,}0 \times 10^{-10}$ cm^3 molécule^{-1} s^{-1}). Dans chacun des cinq systèmes, on a identifié les ions des produits primaires qui propagent la polymérisation et on a suivi les réactions subséquentes d'addition. Dans le cas de l'éthylène, on a déterminé les énergies impliquées dans les étapes initiales en faisant appel à la théorie des orbitales moléculaires *ab initio*. On a aussi caractérisé les réactions du BF_2^+ avec les vapeurs d'eau et de benzène.

Mots clés : polymérisation induit par les ions, alkènes, cinétique, chimie des ions en phase gazeuse.

[Traduit par la revue]

Can. J. Chem. Downloaded from www.nrcresearchpress.com by 194.225.253.170 on 09/07/12
For personal use only.

Introduction

Friedel–Crafts or Lewis acid catalysts such as the halides BF_3, $AlCl_3$, and $TiCl_4$ are widely used to initiate carbocationic polymerization in solution (1). In industry, polymerizations designed to yield high-molecular-weight polymers invariably involve Friedel–Crafts catalysts in the presence of protogenic cocatalysts. At one time cocatalysts were thought to be essential for the initiation of cationic polymerization (2), but the number of systems in which cationic polymerization has been shown to occur without the purposeful addition of a cocatalyst has grown. Compilations of such systems have recently appeared in the literature (3, 4). We note here that the mechanism of direct initiation and the nature of the species involved in the initiation remain a matter of speculation (5–7). One theory attributes initiation to the ionized form of the initiator, which becomes available in solution by self-dissociation of the initiator (8). For example, in the polymerization of isobutene by $AlCl_3$, the $AlCl_2^+$ cation formed by self-dissociation would immediately add to the double bond to give an equivalent concentration of carbenium ions (8, 9). Indirect evidence for such a mechanism based on conductivity measurements has been given by Grattan and Plesch, but direct identification of the initiating and propagating species is lacking (9, 10). The initial steps are difficult to isolate for study in solution. We show here that this is not the case in the gas phase, as we address the intrinsic features of such a mechanism with gas-phase measurements designed to mimic the initiation of cation-induced polymerization in solution (11).

We have chosen to investigate the initiation of the polymerization of ethylene, propylene, *cis*-2-butene, isobutene, and styrene by the BF_2^+ cation in the gas phase. The experiments provide both the specific rate and the product distribution of the initial step, as well as insight into the ensuing steps that propagate the polymerization. For the reaction with ethylene, quantum-chemical calculations that follow the energetics of the initial steps of polymerization are also reported. Such a combined experimental and theoretical approach can provide a detailed understanding of the intrinsic features of the initial steps in cationic polymerization.

Experimental

The experiments were performed with the selected-ion flow tube/flowing afterglow apparatus in the Ion Chemistry Laboratory at York University. The apparatus and technique have been described in detail elsewhere (12, 13). The range of the downstream mass spectrometer was ca. 260 amu. The BF_2^+ cation was generated from either pure BF_3 (Matheson, C.P. grade) or mixtures of BF_3 in helium by electron impact at energies in the range 55–80 eV. The BF_2^+ was selected from the ionized gas using a quadrupole mass filter and injected into a flow tube containing helium at ca. 0.3 Torr (1 Torr = 133.3 Pa). A typical spectrum of BF_2^+ in helium, observed downstream using a second quadrupole mass filter, is shown in Fig. 1. The ion at m/z 47 ($FBOH^+$) arises from reaction with water impurity in the helium and the ion at m/z 30 (BF^+) arises from collisional dissociation of BF_2^+. Low ion injection energies (nominally 18–24 V) were used to minimize collisional dissociation.

Ethylene, isobutene, propylene (all Matheson, C.P. grade), and *cis*-2-butene (Phillips, research grade) were used as reagent gases while styrene and benzene (both Aldrich) were used as their vapours, diluted with helium as 5 mol% and 10 mol% mixtures, respectively.

All measurements were done at a room temperature of 296 ± 2 K and a total pressure of 0.34 Torr. Helium (Matheson, high purity 99.995%) was used as carrier gas.

Theory

Closed shell *ab initio* molecular orbital calculations were carried out with the MONSTERGAUSS program (14). Geometry optimization on the ions $C_2H_4BF_2^+$ and on all smaller species was performed at the 6-31G* level (15), while the 3-21G basis

Can. J. Chem. Downloaded from www.nrcresearchpress.com by 194.225.253.170 on 09/07/12
For personal use only.

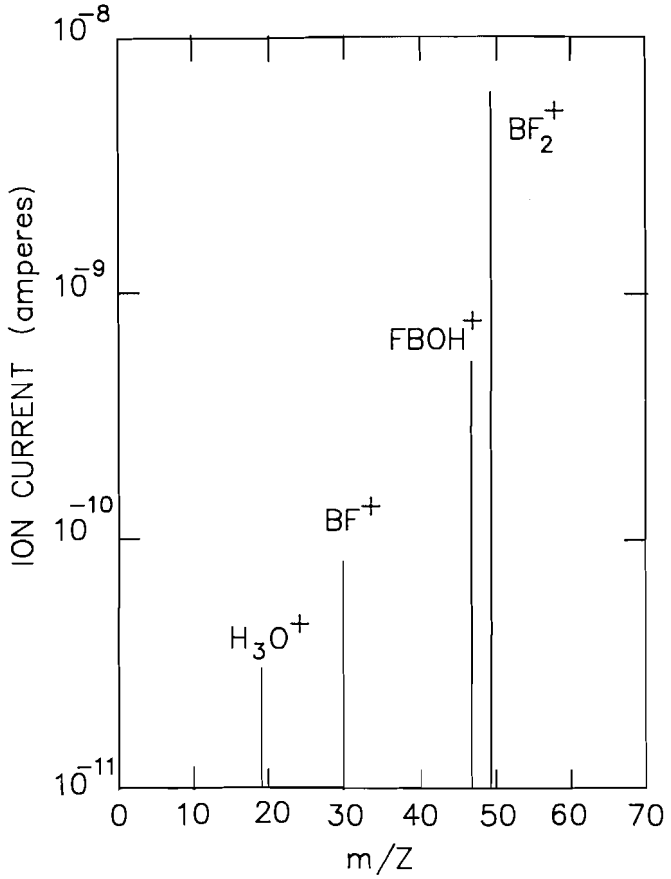


FIG. 1. Downstream SIFT spectrum for BF_2^+ derived from a mixture of BF_3 in He by electron ionization at 51 eV. The buffer gas is helium at 0.33 Torr and the ion injection energy is ca. 24 V. The background "chemical noise" arises from the collisional dissociation of BF_2^+ and from reactions with water vapour impurity in the buffer gas.

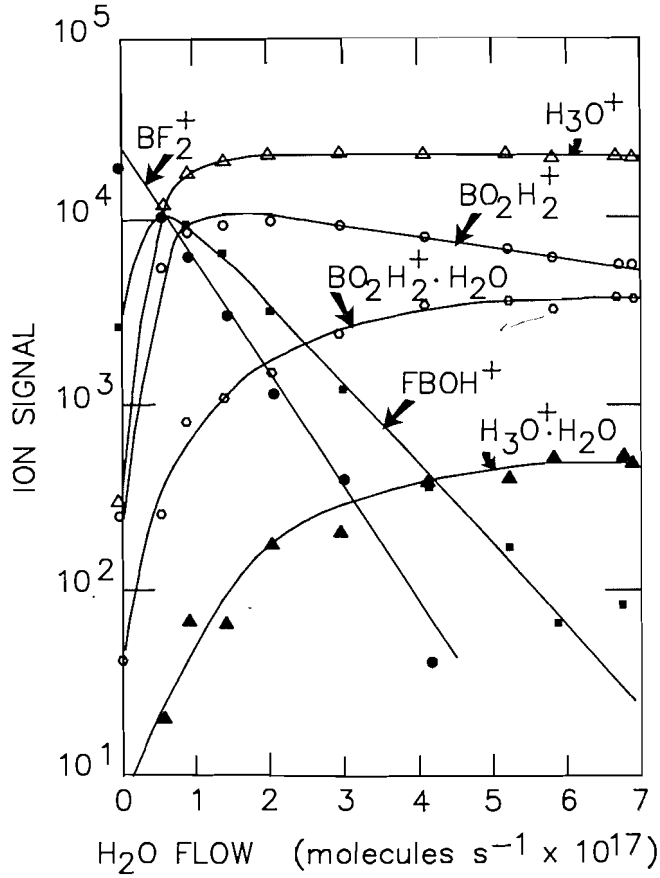


FIG. 2. The variation in ion signals observed for the addition of water vapour into the reaction region of the SIFT apparatus in which the BF_2^+ ion is initially established in helium buffer gas. P = 0.35 Torr, [He] = 1.1×10^{16} atoms cm^{-3}, $\bar{v} = 7.1 \times 10^3$ cm s^{-1}, L = 46 cm, and T = 296 K.

set (16) was used for preliminary work and for optimization of the ion $C_4H_7BF^+$. For the ion $C_4H_7BF^+$, single point 6-31G* calculations were performed at the 3-21G structure (these calculations are denoted as 6-31G*//3-21G).

Results and discussion

Table 1 provides a summary of the reaction rate constants and product distributions obtained in this study and a comparison with specific rates for collision. Standard enthalpy changes are also indicated for those reactions for which the required enthalpies of formation were available.

Water

The reaction of BF_2^+ with water vapour was investigated in order to elucidate the contribution to the ion spectrum observed downstream of ion–molecule reactions with the water vapour impurities in the helium carrier gas. When water vapour was deliberately added into the reaction region in which BF_2^+ was established as a dominant ion, $FBOH^+$ was observed to be produced according to reaction [1].

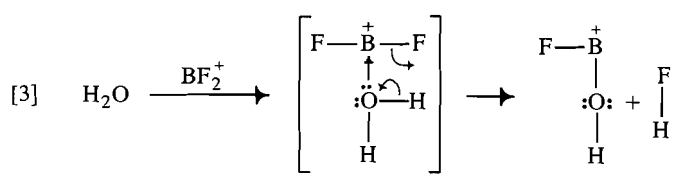
$$[1] \quad BF_2^+ + H_2O \longrightarrow FBOH^+ + HF$$

The $FBOH^+$ ion reacted further with H_2O by proton transfer and condensation according to reaction [2]. Both H_3O^+ and $BO_2H_2^+$

$$[2] \quad FBOH^+ + H_2O \xrightarrow{0.75} H_3O^+ + FBO$$
$$\xrightarrow{0.25} BO_2H_2^+ + HF$$

were observed to react further by adding a water molecule in what are presumed to be termolecular reactions with He as the third molecule. The observed reaction sequence initiated by BF_2^+ in H_2O is shown in Fig. 2. The semilogarithmic decay of BF_2^+ provides a measure of the rate constant for reaction [1], which was found to be $(1.5 \pm 0.5) \times 10^{-9}$ cm^3 $molecule^{-1}$ s^{-1}. The rate constant for reaction [2] was determined to be 1.3×10^{-9} cm^3 $molecule^{-1}$ s^{-1} from a computer fit to the growth and decay of the $FBOH^+$ ion.

Mechanistic considerations suggest that the $FBOH^+$ ion produced in reaction [1] is FB=O protonated at the oxygen, F—B^+—O—H, which may be formed directly by electrophilic attack on the oxygen of water with elimination of HF as shown in reaction [3]. The isomers F—B(H)—O^+ and H—B^+—O—F would require more bond redisposition for their formation. The secondary reaction of F—B^+—O—H with H_2O can proceed similarly to eliminate HF and produce HO—B^+—OH rather than, say, H—B^+—OOH.



The assignment of F—B^+—O—H is consistent with results of molecular orbital calculations. Calculations at the 6-31G*

TABLE 1. Summary of rate constants (in units of 10^9 cm^3 molecule^{-1} s^{-1}) and product distributions measured at 296 ± 2 K for reactions of BF_2^+ with selected olefinic monomers, with benzene, and with water vapour

Monomer	Products	Branching ratio[a]	k_{exp}[b]	k_{ADO}[c]	ΔH^0_{298}[d] (kJ mol^{-1})
$H_2C{=}CH_2$	$C_2H_3BF^+ + HF$	1.0	0.73 (0.66)	1.1	
$H_2C{=}CH(CH_3)$	$C_3H_5^+ + HBF_2$	0.80	0.50 (0.38)	1.3	−130 to −92
	$C_2H_2BF_2^+ + CH_4$	0.20			
$H_2C{=}C(CH_3)_2$	$C_2H_5^+ + C_2H_3BF_2$	0.35	0.81 (0.58)	1.4	−146
	$C_4H_7^+ + HBF_2$	0.25			−225
	$C_2H_4BF_2^+ + C_2H_4$	0.25			
	$C_3H_4BF_2^+ + CH_4$ $C_3H_5^+ + CH_3BF_2$ $C_4H_8{\cdot}BF_2^+$ (He)	0.15			
cis-2-C_4H_8	$C_2H_5^+ + C_2H_3BF_2$	0.20	0.78 (6.60)	1.3	−156
	$C_4H_7^+ + HBF_2$	0.40			−225
	$C_2H_4BF_2^+ + C_2H_4$	0.25			
	$C_3H_4BF_2^+ + CH_4$ $C_3H_5^+ + CH_3BF_2$ $C_4H_8{\cdot}BF_2^+$ (He)	0.15			
$C_6H_5CHCH_2$	$C_8H_8{\cdot}BF_2^+$ (He)	0.95	0.82 (0.43)	1.9	
	$C_8H_7BF^+ + HF$ $C_6H_7^+ + C_2HBF_2$	0.05			−74
C_6H_6 (benzene)	$C_6H_6{\cdot}BF_2^+$ (He)	0.80	0.74 (0.53)	1.4	
	$C_6H_5BF^+ + HF$	0.20			
H_2O	$FBOH^+ + HF$	1.0	1.5 (0.75)	2.0	

[a]Primary product ions that contribute 5% or more to the total product ions observed are listed. The branching ratio is rounded off to the nearest 5%.

[b]The apparent bimolecular rate constant is given in each case. All measurements were taken in helium buffer gas at a total pressure of 0.34 Torr and a number density of 1.1×10^{16} atoms cm^{-3}. The accuracy of the rate constants is estimated to be ±30%. The value given in parentheses represents the reaction efficiency, k_{exp}/k_{ADO}.

[c]Collision rate constants were derived with the combined variational transition-state theory/calculated trajectory approach of Su and Chesnavich (29).

[d]Enthalpies of formation were derived from ref. 30.

level indicated an energy for F—B=O 184 kcal mol^{-1} lower than that for B—O—F, compared to a difference of 146 kcal mol^{-1} based on calculations at the STO-4G* level reported previously (17). Protonation of FBO was also investigated at the 6-31G* level. The proton affinity of the oxygen site was found to be 90 kcal mol^{-1} higher than the proton affinity at the fluorine site. Protonation on the boron atom did not give rise to a minimum and gave rise to H-atom migration to the oxygen site in the structure optimization procedure.

Due to the presence of water vapour impurities in the helium buffer, $FBOH^+$ ions were always present in the reaction tube when BF_2^+ was selected upstream (in spite of the depletion of its precursor ion, BF_2^+, in the reaction region). The $FBOH^+$ was observed to react rapidly with benzene and with all of the olefins investigated in this study. The predominant channel in each case was proton transfer. In each case the observed decay of $FBOH^+$ was rate-limited by the depletion of its precurser ion, BF_2^+, so that only a lower limit of the rate constant equal to the rate constant for the reaction of BF_2^+ can be derived from these observations. The protonated ethylene was observed to react rapidly with ethylene to form $C_3H_5^+$ and the adduct ion, as reported previously (18). Protonated propylene produced only the adduct ion with propylene with a rate constant of 2.3×10^{-10} cm^3 molecule^{-1} s^{-1}. The two butenes, styrene, and benzene reacted only slowly with their protonated parent molecules to form adduct ions. Rate constants of 3×10^{-11}, 8×10^{-11}, $\leq 4 \times 10^{-11}$, and $\leq 1 \times 10^{-12}$ cm^3 molecule^{-1} s^{-1} were obtained for the reactions with *cis*-2-butene, isobutene, styrene, and benzene, respectively. In the case of the reaction with isobutene there is good agreement with a previous determination of 7×10^{-11} cm^3 molecule^{-1} s^{-1} using high-pressure mass spectrometry at 450 K (19).

Ethylene

BF_2^+ was found to react rapidly with ethylene in a bimolecular fashion with a rate constant of $(7.3 \pm 2.2) \times 10^{-10}$ cm^3 molecule^{-1} s^{-1} to form the $C_2H_3BF^+$ cation as shown in reaction [4].

[4] $BF_2^+ + H_2C{=}CH_2 \longrightarrow C_2H_3BF^+ + HF$

Figure 3 shows the further occurrence of several propagation steps. In total, the sequential addition of four molecules of ethylene was observed as expressed in reaction [5].

Can. J. Chem. Downloaded from www.nrcresearchpress.com by 194.225.253.170 on 09/07/12
For personal use only.

Can. J. Chem. Downloaded from www.nrcresearchpress.com by 194.225.253.170 on 09/07/12
For personal use only.

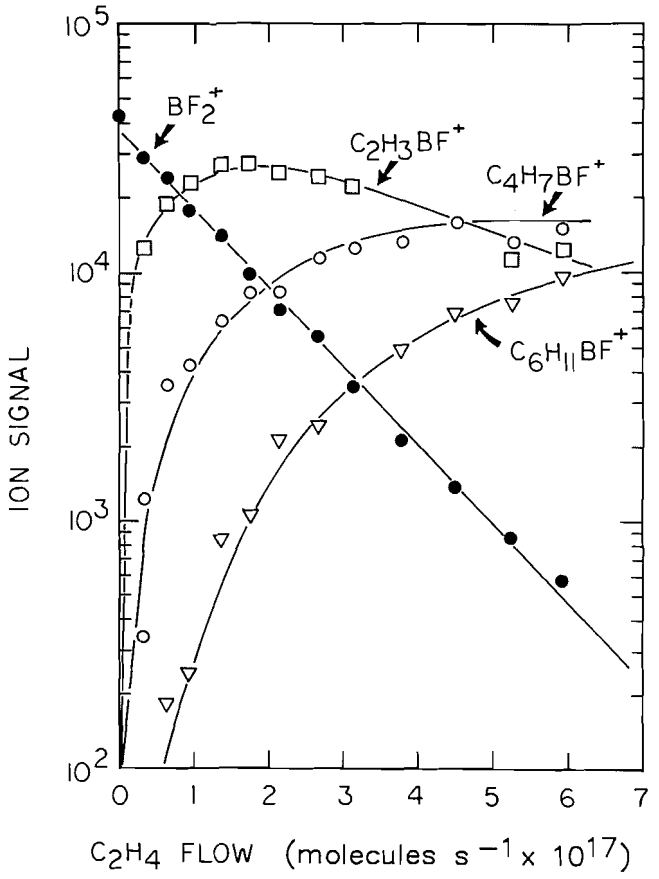


FIG. 3. SIFT measurements of the sequential ion chemistry initiated by BF_2^+ in ethylene and helium buffer gas. $P = 0.349$ Torr, [He] = 1.15×10^{16} atoms cm^{-3}, $\bar{v} = 6.5 \times 10^3$ cm s^{-1}, $L = 46$ cm, and $T = 294$ K. The solid lines represent a computer fit by the method of least squares.

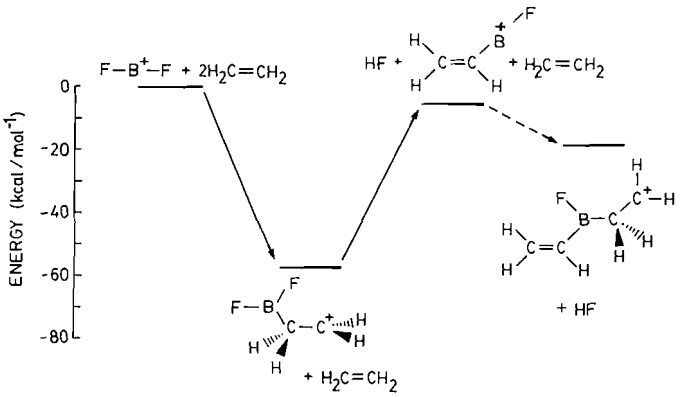


FIG. 4. Relative energies (in kcal mol^{-1}) computed at the 6-31G*//6-31G* level (**4** is at the 6-31G*//3-21G level) for combinations of BF_2^+ and two ethylene molecules.

[5] $C_2H_3BF^+ \xrightarrow{C_2H_4} C_4H_7BF^+ \xrightarrow{C_2H_4} C_6H_{11}BF^+ \xrightarrow{C_2H_4}$

$C_8H_{15}BF^+ \xrightarrow{C_2H_4} C_{10}H_{19}BF^+$

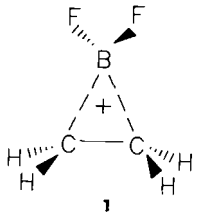
The sequential additions of ethylene proceed with slightly decreasing specific rates. Rate constants were determined with a computer fit to the ion profiles using the method of least squares. One such fit is shown in Fig. 3 and it provides effective bimolecular rate constants for the first three steps in reaction [4] of 1.6, 1.3, and 1.3×10^{-10} cm^3 $molecule^{-1}$ s^{-1}. The individual steps are likely to be termolecular with helium acting as the stabilizing third body.

TABLE 2. Total energies (in hartrees) computed for the open and cyclic isomers of the adduct formed from BF_2^+ and ethylene[a]

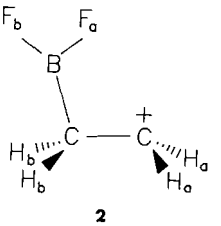
Structure	3-21G	6-31G*	MP2/6-31G*
Cyclic	−299.78534 (10.6)	−301.43044 (2.4)	−302.08957 (0)
Open	−299.80229 (0)	−301.43424 (0)	−302.07991 (6.1)

[a]Numbers in parentheses indicate relative energies (in kcal mol^{-1}).

The reaction profile for the addition of BF_2^+ to ethylene was examined using molecular orbital theory and is shown schematically in Fig. 4. At the level of theory indicated in Fig. 4 (HF 6-31G*), the most stable form of the intermediate adduct ion $BF_2^+.C_2H_4$ has an open structure, but the cyclic structure is more stable when correlation energy is included. Preliminary calculations at the 3-21G//3-21G level of theory showed the cyclic ion with structure **1** to be 10.6 kcal mol^{-1} higher in energy than the open ion with structure **2**. At the 6-31G* level of theory the energy of the cyclic ion was found to be only 2.4 kcal mol^{-1} higher, but at the MP2/6-31G* level of theory it became lower by 6.1 kcal mol^{-1}. Table 2 summarizes the energies obtained for the cyclic and open $C_2H_4BF_2^+$ isomers at the different levels of theory. Structural parameters for the 6-31G* optimized structures of the cyclic and open ions shown as **1** and **2** are given in Table 3. One structural feature is worthy of note. In **1** the C—B



1



2

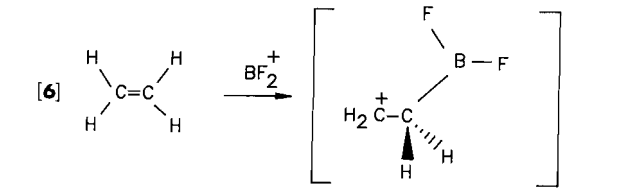
distance of 1.967 Å is extremely long and compares with a formal single-bond distance of 1.533 Å in borirane (20). The 6-31G* calculated charge distribution for **1** has a charge of +0.45 on the BF_2 group and +0.55 on the ethylene fragment. The bonding between ethylene and BF_2^+ then is best described as π donation from $H_2C{=}CH_2$ to the vacant p orbital on BF_2^+ with little or no back-donation from BF_2^+ to the π^* orbital on ethylene, i.e., only two electrons are formally involved in the bonding and **1** should be considered to be a π complex and not a three-membered ring.

The addition of ethylene to BF_2^+, which is shown mechanistically in eq. [6], is computed to be exothermic by 58 kcal mol^{-1} at the 6-31G*//6-31G* level of theory and so provides sufficient energy to eliminate HF, leaving the observed ion $C_2H_3BF^+$, which can be drawn in the two resonance forms ***3a*** and ***3b***. A Mulliken population analysis showed the boron atom to carry most of the positive charge. Nucleophilic attack by another ethylene molecule may then occur, in principle, at either the terminal carbon or the boron atom, with the latter being indicated by the charge distribution. Calculations at the STO-3G level (21) showed the product of attack at boron (structure **4**) to be lower in energy (by 38 kcal mol^{-1}) than that formed by attack on carbon (structure **5**). The primary carbenium ions **4** and **5** are both at local minima in C_s symmetry. However, the barrier to rearrangement of primary carbenium ions to secondary ions by 1,2-hydride shifts is, in general, very low and it is likely that these ions will rearrange prior to reacting further with another

Can. J. Chem. Downloaded from www.nrcresearchpress.com by 194.225.253.170 on 09/07/12
For personal use only.

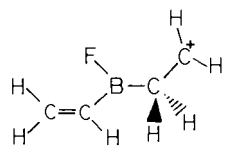
TABLE 3. Structural parameters optimized at 6-31G* for the cyclic (I) and open (II) isomers of the adduct formed from BF_2^+ and ethylene. Bond lengths are in angstroms and angles in degrees

Parameter	I(C_{2v})	II(C_s)
r(CC)	1.356	1.410
r(CH)	1.078	
r(CH_a)		1.078
r(CH_b)		1.086
r(CB)	1.967	1.667
r(BF)	1.270	
r(BF_a)		1.292
r(BF_b)		1.279
∠CCH	120.9	
∠CCH_a		121.7
∠CCH_b		114.5
∠CCB		105.6
∠FBF	129.4	
∠CBF_a		120.4
∠CBF_b		115.5
∠HCCB	92.8	
∠H_aCCB		87.9
∠H_bCCB		113.7

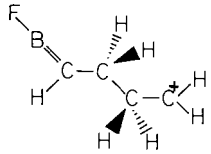
[6] 

3*a* **3***b*

ethylene molecule. Therefore it is uncertain whether polymerization occurs by repeated ethylene addition at the end of the newly formed primary carbenium ion, or whether ethylene adds at secondary carbenium sites to form polymers with ($CHCH_3$) repeating units.



4



5

Propylene

A rapid reaction was observed between BF_2^+ and propylene, $k = (5.0 \pm 1.6) \times 10^{-10}$ cm^3 molecule^{-1} s^{-1}. The following primary products were identified:

[7*a*] $BF_2 + C_3H_6 \xrightarrow{0.80} C_3H_5^+ + HBF_2$

[7*b*] $\xrightarrow{0.20} C_2H_2BF_2^+ + CH_4$

The preferred channel [7*a*] corresponds to hydride abstraction, which results in the formation of the $C_3H_5^+$ ion. This latter ion has several possible structures including the allyl, propenyl, and cyclopropyl structures, which decrease in thermodynamic stanbility in the order presented. The formation of all three isomers is exothermic. Channel [7*b*], which corresponds to the elimination of methane, proceeds in one of every five reactive collisions of BF_2^+ with propylene. The occurrence of a minor (≃5%) channel corresponding to the elimination of HF could not be excluded. The ion $C_3H_5BF^+$ was observed as a product but could not be attributed unambiguously to the reaction of BF_2^+. An alternative or additional source for this ion at the operating conditions of the experiment was the reaction of the impurity ion $FBOH^+$ with propylene.

Secondary and higher-order reactions were also observed. The $C_3H_5^+$ was seen to react rapidly with propylene according to reaction [8] in approximately the following proportions:

[8*a*] $C_3H_5^+ + C_3H_6 \xrightarrow{0.6} C_4H_7^+ + C_2H_4$

[8*b*] $\xrightarrow{0.4} C_6H_{11}^+$

A fit to the rise and decay of the $C_3H_5^+$ signal led to a rate constant of 5.0×10^{-10} cm^3 molecule^{-1} s^{-1} for the overall reaction. Both $C_4H_7^+$ and $C_6H_{11}^+$ were observed to add one molecule of propylene to form the adduct ions $C_7H_{13}^+$ and $C_9H_{17}^+$, respectively, presumably in a termolecular fashion by collisional stabilization. The addition reaction with $C_4H_7^+$ was rapid, $k \geq 10^{-10}$ cm^3 molecule^{-1} s^{-1}, while that with $C_6H_{11}^+$ was much slower, $k \leq 3 \times 10^{-12}$ cm^3 molecule^{-1} s^{-1}. The propylene adduct of $C_7H_{13}^+$, $C_{10}H_{19}^+$, was also observed but was formed again in a slow reaction, $k \leq 2 \times 10^{-12}$ cm^3 molecule^{-1} s^{-1}. In the absence of further work the mechanisms of reactions [8*a*] and [8*b*] are necessarily a matter of conjecture, but it is interesting to note that the $2\pi_s + 2\pi_s$ cycloaddition of allyl cations and alkenes is thermally forbidden by the Woodward–Hoffman orbital symmetry rules, so that the rapid addition of propene to the allyl cation may best be viewed as electrophilic attack by a terminal carbon of the cation on the double bond of propene, forming a secondary cation that may ring-close to the methylcyclopentyl cation. This latter ion can eliminate ethylene to form a methylcyclopropyl cation, which will ring-open without barrier to form the 1-methylallyl cation, $C_4H_7^+$. Alternatively the adduct $C_6H_{11}^+$ may be stabilized by collision. The further reaction of the methylcyclopentyl cation, $C_6H_{11}^+$, with propene is likely to be slower than the further reaction of the 1-methylallyl cation, $C_4H_7^+$, with propene as the latter can be expected to proceed with a similar mechanism and probably similar rate as the initial allyl cation.

The secondary reaction of $C_2H_2BF_2^+$ with propylene was seen to be fast, $k = 8.0 \times 10^{-11}$ cm^3 molecule^{-1} s^{-1}. While the propylene adduct ion was observed in small amounts, the main product appeared to be $C_5H_7^+$:

[9] $C_2H_2BF_2^+ + C_3H_6 \longrightarrow C_5H_7^+ + HBF_2$

The $C_5H_7^+$ did not react further, $k \leq 3 \times 10^{-12}$ cm^3 molecule^{-1} s^{-1}.

Isomeric butenes

The reaction of BF_2^+ with the isomeric butenes, *cis*-2-butene and isobutene, proved to be more complex than the others. Both reactions were equally rapid, $k = (7.8 \pm 2.4) \times 10^{-10}$ cm^3 molecule^{-1} s^{-1}, and led to product ions with identical m/z as indicated by reaction [10].

[10*a*] $BF_2^+ + C_4H_8 \longrightarrow C_4H_7^+ + HBF_2$

[10*b*] $\longrightarrow C_2H_4BF_2^+ + C_2H_4$

[10*c*] $\longrightarrow C_2H_5^+ + C_2H_3BF_2$

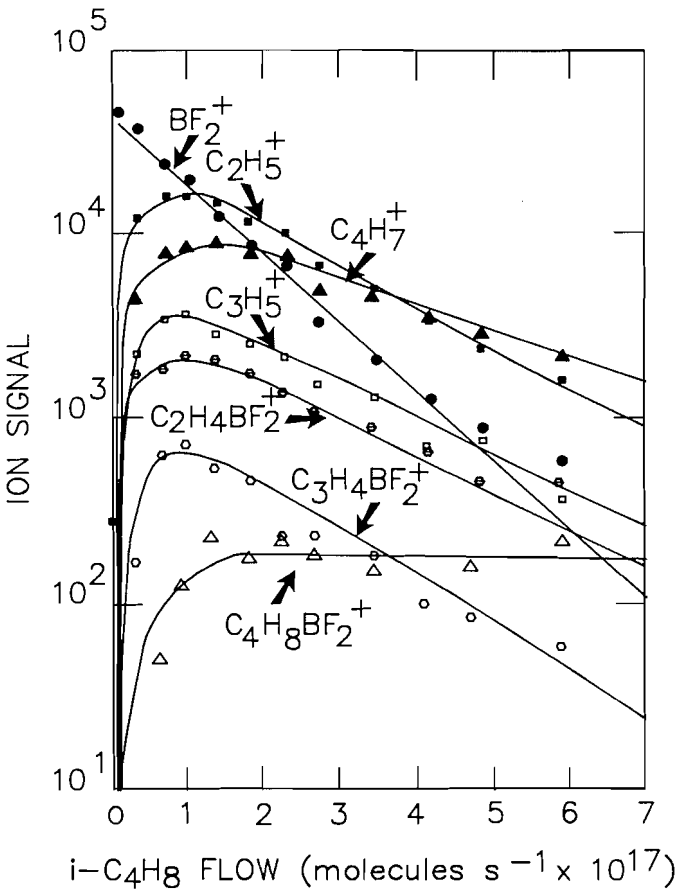


FIG. 5. The variation in ion signals observed for the addition of isobutene into the reaction region of the SIFT apparatus in which BF_2^+ is initially established in helium buffer gas. $P = 0.35$ Torr, [He] = 1.1×10^{16} atoms cm^{-3}, $\bar{v} = 6.9 \times 10^3$ cm s^{-1}, $L = 46$ cm, and $T = 294$ K. Only primary products are indicated.

$$[10d] \longrightarrow C_3H_5^+ + CH_3BF_2$$

$$[10e] \longrightarrow C_3H_4BF_2^+ + CH_4$$

$$[10f] \longrightarrow C_4H_8BF_2^+$$

Channel [10*a*] corresponds to H^- abstraction. Channel [10*b*] leads to elimination of C_2H_4 and will be preempted by channel [10*c*] if a proton is transferred before the products separate. Channel [10*d*] corresponds to CH_3^- abstraction, which may leave the allyl cation $C_3H_5^+$. Channel [10*e*] leads to elimination of methane while [10*f*] corresponds to adduct formation.

Figure 5 shows the semilogarithmic decay of BF_2^+ upon addition of isobutene, and the appearance of the product ions indicated in reaction [10]. All of the primary product ions in reaction [10], with the exception of the adduct, were observed to react further with isobutene. Several of the primary product ions were active in propagating additions of isobutene molecules, which presumably occur in a termolecular fashion. For example, the $C_4H_7^+$ cation formed primarily by H-abstraction from the isobutene, and, to some extent, by secondary reactions of $C_2H_5^+$ and $C_3H_5^+$ with isobutene, was observed to add two molecules of isobutene in sequential reactions. Other isobutene adducts observed were those of $C_3H_4BF_2^+$, $C_4H_9^+$, which is a derivative of the chemistry initiated by $C_2H_5^+$, and $C_5H_{11}^+$, which is a derivative of $C_4H_9^+$ (22). $C_4H_9^+$ is also produced by proton transfer from the impurity $FBOH^+$ to the isobutene.

Slightly different product distributions were observed for the two butene isomers. Channels [10*a*]–[10*c*] account for about

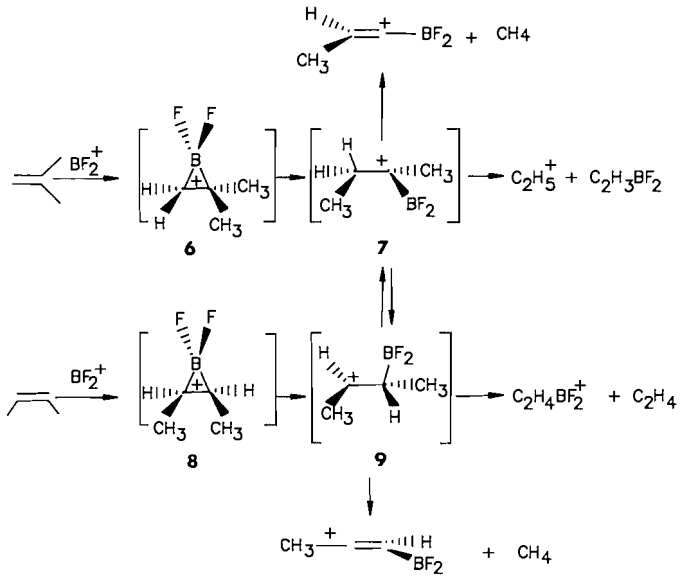


FIG. 6. Possible mechanism for the formation of the primary product ions $C_2H_5^+$, $C_2H_4BF_2^+$, and $C_3H_4BF_2^+$ from the reaction of BF_2^+ with *cis*-2-butene and isobutene.

85% of the total reaction in both cases. Formation of $C_4H_7^+$ by hydride abstraction constitutes a larger channel than does formation of $C_2H_5^+$ in the case of *cis*-2-butene. The reverse is true in the case of isobutene. This may reflect differences in stabilities of the two isomeric $C_4H_7^+$ ions. Hydride abstraction from *cis*-2-butene forms the 1-methylallyl cation, whereas abstraction from isobutene yields the 2-methylallyl cation. Allyl cations are stabilized by π-electron-donating substituents on a terminal carbon, but substitution at the central carbon has little effect. The methyl group is a weak π donor and *ab initio* molecular orbitals at the HF 6-31G*//3-21G level indicate the 1-methylallyl cation to be 11.3 kcal mol^{-1} lower in energy than the 2-methylallyl cation (23). Thus when the 1-methylallyl cation is the product, hydride abstraction competes more effectively with other channels.

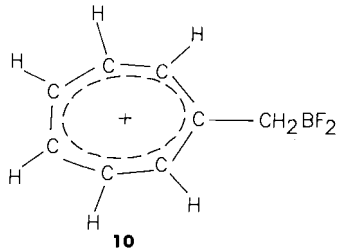
A mechanism for the formation of the primary products $C_2H_5^+$, $C_2H_4BF_2^+$, and $C_3H_4BF_2^+$ is proposed in Fig. 6. The reactions of the two isomeric butenes are likely to involve similar intermediates since their observed products are the same and the product distributions are not radically different. BF_2^+ and isobutene are likely to form the cyclic π complex indicated by structure **6**. Rearrangements of the type shown in Fig. 6 may then lead to structure **9**. These rearrangements involve the migration of the BF_2 group with a concomitant transfer of CH_3^- to leave structure **7**, which may undergo a 1,2 hydride transfer to leave structure **9**. Addition of BF_2^+ to *cis*-2-butene should give the cyclic π complex indicated by structure **8**, which can open to yield structure **9**. Structures **7** and **9** may decompose by 1,2 CH_4 elimination to form the vinyl cations shown in Fig. 6 or by C—C bond scission as indicated.

Styrene

The major primary product ion observed in the reaction of BF_2^+ with styrene was the adduct ion, possibly a termolecular product at our operating pressure. The observed effective bimolecular rate constant is quite large so that chemical bonding in the adduct ion is indicated. One could assume the structure of the adduct to be benzylic ($C_6H_5C^+HCH_2BF_2$) in which the positive charge is delocalized onto the phenyl group. However, other experimental evidence indicates that benzylic-type ions can rearrange to form tropylium-type ions (24, 25). It is there-

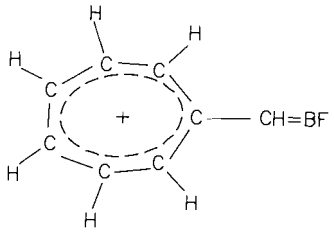
Can. J. Chem. Downloaded from www.nrcresearchpress.com by 194.225.253.170 on 09/07/12
For personal use only.

fore possible that the structure of the adduct ion observed in this case is that of the tropylium-like ion shown in **10**. The other



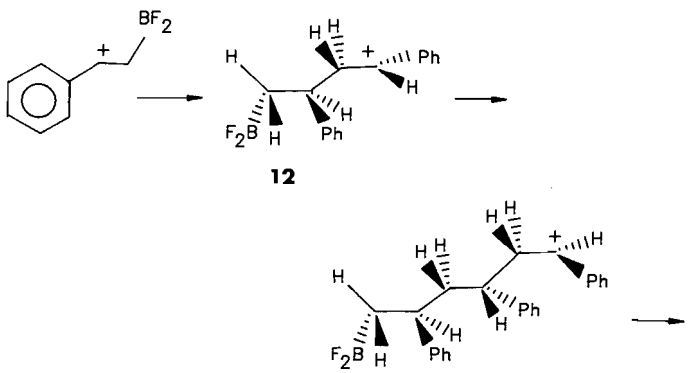
10

minor primary product ions that were observed may arise from the elimination of HF or C_2HBF_2 from the intermediate adduct ion, which is likely to leave an ion with structure **11** or protonated benzene, respectively. The identification of the source for the $C_8H_7BF^+$ ion observed at m/e 133 as the reaction of BF_2^+ with styrene and the elimination of HF was not unequivocal. Another possible source for this ion was the reaction of $FBOH^+$ with styrene and the elimination of H_2O.



11

One other styrene molecule was observed to add to the primary adduct ion. The specific rate for this addition was one half that for the primary addition, having an effective bimolecular value of 4.7×10^{-10} cm^3 molecule^{-1} s^{-1} at our operating conditions. Further additions could not be observed due to the low vapour pressure of styrene that permitted the introduction of only a limited flow of styrene molecules into the reaction region. The high specific rate of addition of the second styrene molecule is suggestive of further chemical bonding. Such bonding seems more probable if the primary adduct ion has a benzylic rather than tropylium-like structure. In the former case the second addition of styrene could occur on the benzylic carbon to yield the structure indicated in reaction [11] as **12**. Reaction [11] shows how polymerization would then be achieved by repeated styrene addition to the cationic carbon of the benzyl cations.



12

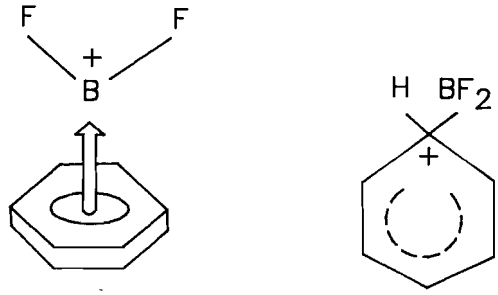
Benzene

For the reaction of BF_2^+ with styrene the question arose as to whether BF_2^+ could be adding to the benzene ring of styrene. Thus we decided to carry out the reaction of BF_2^+ with benzene. It was found to be rapid, $k = (7.4 \pm 2.2) \times 10^{-10}$ cm^3 molecule^{-1} s^{-1}, and to produce two primary species according to reaction [12].

$$[12] \quad BF_2^+ + C_6H_6 \xrightarrow{0.80} BF_2^+.C_6H_6$$

$$\xrightarrow{0.20} C_6H_5BF^+ + HF$$

Adduct formation was the major channel observed. The high efficiency of this channel is again suggestive of chemical bonding. Several structures can be envisaged for a chemically bonded adduct, including a complex in which BF_2 sits on top of the benzene π cloud (structure **13***a*) as well as the σ complex **13***b*.



13*a* **13***b*

Conclusions

The results of the experiments reported in this study characterize the intrinsic chemistry that the BF_2^+ ion initiates by reacting with the olefinic monomers of ethylene, propylene, isobutene, *cis*-2-butene, and styrene, and with benzene and H_2O. They provide values for the specific rates and product distributions of the initiation steps and the early propagating steps that lead to the build-up or polymerization of the ions.

All of the initiation reactions of BF_2^+ are rapid, $k \geq 5.0 \times 10^{-10}$ cm^3 molecule^{-1} s^{-1}, and efficient, and they show an interesting range in the nature of their reaction products. The major reaction pathways for the monomers selected for study are elimination of HF, CH_4, C_2H_4, or $C_2H_3BF_2$, hydride transfer, and adduct formation. HF elimination is unique to the reaction with ethylene. It is not observed with the butenes and constitutes only a very small channel with styrene and possibly propylene. Hydride transfer is an important channel in the reactions with monomers containing an allylic hydrogen. For instance, hydride transfer was observed to compete effectively with other channels in the reactions of BF_2^+ with propylene and the butenes from which stable allylic cations can be formed. Styrene and ethylene do not contain an allylic hydrogen and were not observed to react with BF_2^+ by hydride transfer. The implication of these results is that other monomers having an allylic hydrogen such as, for example, α-methylstyrene and cyclopentadiene, can also be expected to react with BF_2^+ by hydride transfer to form allylic cations that may propagate polymerization.

The results indicate that ethylene, styrene, *cis*-2-butene, and isobutene can all be polymerized in the gas phase by propagating species formed in reactions with BF_2^+. The BF or BF_2 group may or may not be retained in the propagating ion. The former (e.g., $C_2H_3BF^+$, $C_8H_8BF_2^+$) appear more reactive in propagating monomer additions and are predominant in the polymerization observed with ethylene and styrene. Carbocations are the main propagating ions produced in the initiation reactions of BF_2^+ with the two butenes.

Propylene appears to be an exception in that propagation is terminated early in the reaction sequence. A possible explanation is illustrated in Fig. 7. If an allylic structure is assumed for $C_3H_5^+$, addition of propylene should lead to the 1-methylallyl

Can. J. Chem. Downloaded from www.nrcresearchpress.com by 194.225.253.170 on 09/07/12
For personal use only.

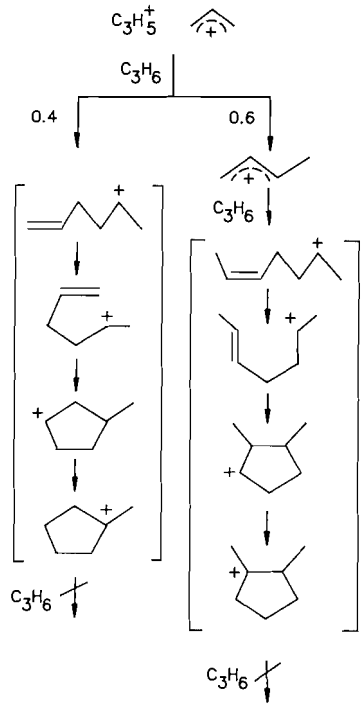


FIG. 7. Possible mechanism for the termination of the polymerization of propylene initiated by allylic $C_3H_5^+$ in the gas phase.

cation and a secondary methylcyclopentyl cation, which might undergo a 1,3 hydride shift to form the thermodynamically more stable tertiary methylcyclopentyl cation. If the further reaction of the 1-methylallyl cation with propene proceeds with a mechanism and rate similar to the initial allyl cation, we can expect the intramolecular cyclization to produce the tertiary 1,2-methylcyclooentyl cation shown in Fig. 7. Both of the methyl-substituted tertiary cyclopentyl cations should be less reactive because the attack by another propylene molecule is hindered. This is consistent with our experimental observations, which indicate further propylene additions to the tertiary cyclic cations, which proceed with rate constants that are much smaller, $k \leq 3 \times 10^{-12}$ cm^3 molecule^{-1} s^{-1}, than those for the addition of propylene to the acyclic precursor cations, $k \geq 10^{-10}$ cm^3 molecule^{-1} s^{-1}. The polymerization of propylene therefore appears to be impeded in the gas phase by intramolecular cyclization. In contrast, if solvent molecules act to hinder the cyclization, we can expect the analogous polymerization to be allowed in solution.

It is interesting to compare the cocatalytic role of water in the gas phase and solution. Water is known to act as a coinitiator in many polymerization systems in solution, including BF_3/isobutene (26), BCl_3/isobutene (27), and $TiCl_4$/diphenylethylene (28). Our gas-phase measurements indicate that water vapour acts in a cocatalytic fashion by leading to the protonated monomers $C_2H_4^+$, $C_3H_7^+$, $C_4H_9^+$, and $C_8H_9^+$ via the $FBOH^+$ ion formed by reaction of BF_2^+ with water vapour. $FBOH^+$ was observed to transfer a proton to all of the monomers investigated and also to water vapour. The latter implies that H_3O^+ may be an intermediate when $FBOH^+$ is formed in solution in the presence of water.

The interaction between other Lewis acid cations and olefinic monomers remains to be examined in the gas phase. Of special interest is the reaction of olefinic monomers with $AlCl_2^+$ derived from $AlCl_3$, perhaps the best known and most popular initiator. Gas-phase measurements of the reaction of $AlCl_2^+$ with isobutene may allow some insight into one of the oldest and most studied cationic polymerizations.

Acknowledgment

We thank the Natural Sciences and Engineering Research Council of Canada for financial support.

1. J. P. KENNEDY and E. MARECHAL. Carbocationic polymerizations. John Wiley – Interscience, New York. 1982.
2. (*a*) A. G. EVANS and M. POLANYI. J. Chem. Soc. 252 (1947); (*b*) P. H. PLESCH, M. POLANYI, and H. A. SKINNER. J. Chem. Soc. 257 (1947); (*c*) A. G. EVANS and G. W. MEADOWS. Trans. Faraday Soc. **46**, 327 (1950).
3. J. P. KENNEDY. J. Macromol. Sci-Chem. **A6**, 329 (1972).
4. A. GRANDINI and H. CHERADAME. Adv. Polym. Sci. **34/35**, 1 (1980).
5. P. SIGWALT. Makromol. Chem. **175**, 1017 (1974).
6. K. E. RUSSEL. Cationic polymerizations. *In* High polymers. Vol 29. *Edited by* C. E. Schildknecht and I. Skeist. John Wiley & Sons, New York. 1977. p. 306.
7. P. SIGWALT. *In* Recent progress in carbocationic polymerizations. 6th Conv. Ital. Sci. Macromol. Atti, (1983). p. 125.
8. P. H. PLESCH. Makromol. Chem. **175**, 1065 (1974).
9. D. W. GRATTAN and P. H. PLESCH. Makromol. Chem. **181**, 751 (1980).
10. D. W. GRATTAN and P. H. PLESCH. J. Chem. Soc. Dalton Trans. 1734 (1977).
11. L. FORTE, M. H. LIEN, A. C. HOPKINSON, and D. K. BOHME. Makromol. Chem. Rapid Commun. **8**, 87 (1987).
12. G. I. MACKAY, G. D. VLACHOS, and D. K. BOHME. Int. J. Mass Spectrom. Ion Phys. **36**, 259 (1980).
13. A. B. RAKSIT and D. K. BOHME. Int. J. Mass Spectrom. Ion Phys. **55**, 69 (1983).
14. M. R. PETERSON and R. A. PORIER. Monstergauss, University of Toronto. 1980.
15. P. C. HARIHARAN and J. A. POPLE. Theor. Chim. Acta, **28**, 218 (1973).
16. J. S. BRINKLEY, J. A. POPLE, and W. J. HEHRE. J. Am. Chem. Soc. **102**, 939 (1980).
17. SUK PING SO. J. Mol. Struc. (Theochem), **122**, 311 (1985).
18. J. A. BURT, J. L. DUNN, M. J. MCEWEN, M. M. SUTTON, A. E. ROCHE, and H. I. SCHIFF. J. Chem. Phys. **52**, 6062 (1970).
19. M. S. B. MUNSON. J. Am. Chem. Soc. **90**, 83 (1968).
20. K. KROGH-JESPERSEN, D. CREMER, J. D. DILL, J. A. POPLE, and P. v. R. SCHLEYER. J. Am. Chem. Soc. **103**, 2589 (1981).
21. W. J. HEHRE, R. F. STEWART, and J. A. POPLE. J. Chem. Phys. **51**, 2657 (1969).
22. F. P. ABRAMSON and J. H. FUTRELL. J. Phys. Chem. **72**, 1994 (1968).
23. M. H. LIEN and A. C. HOPKINSON. J. Phys. Chem. **88**, 1513 (1984).
24. J. M. S. TAIT, T. W. SHANNON, and A. G. HARRISON. J. Am. Chem. Soc. **84**, 4 (1962).
25. F. MEYER and A. G. HARRISON. J. Am. Chem. Soc. **84**, 4757 (1964).
26. M. CHMELIN, M. MAREK, and O. WICHTERLE. J. Polym. Sci. Part C: **16**, 833 (1967).
27. J. P. KENNEDY and F. J.-Y. CHEN. Polym. Bull. **15**, 203 (1980).
28. G. SAUVET, J. P. VARION, and P. SIGWALT. J. Polym. Sci. Polym. Chem. Ed. **16**, 3047 (1978).
29. T. SU and W. J. CHESNAVICH. J. Chem. Phys. **76**, 5183 (1982).
30. H. M. ROSENSTOCK, K. DRAXL, B. W. STEINER, and J. T. HERRON. J. Phys. Chem. Ref. Data, **6**, Suppl. 1 (1977); J. G. ANICICH, G. A. BLAKE, K. J. KIM, M. J. MCEWAN, and W. T. HUNTRESS. J. Phys. Chem. **88**, 4614 (1984); F. P. LOSSING. Can. J. Chem. **50**, 3973 (1972); M. J. S. DEWAR and H. S. RZEPA. J. Am. Chem. Soc. **100**, 59 (1978).

Can. J. Chem. Downloaded from www.nrcresearchpress.com by 194.225.253.170 on 09/07/12
For personal use only.

Diphosphido bridged early/late heterobimetallic complexes: synthesis and molecular structure of $Cp_2Zr(\mu\text{-}PPh_2)_2ReH(CO)_3$

PEI YAO ZHENG and DOUGLAS W. STEPHAN[1]

Department of Chemistry and Biochemistry, University of Windsor, Windsor, Ont., Canada N9B 3P4

Received February 28, 1989

PEI YAO ZHENG and DOUGLAS W. STEPHAN. Can. J. Chem. **67**, 1584 (1989).

The reaction of the metal–metal bonded complex $Re_2(CO)_{10}$ with $Cp_2Zr(PPh_2)_2$ results in formation of the diphosphido bridged heterobimetallic species, $Cp_2Zr(\mu\text{-}PPh_2)_2ReH(CO)_3$, **1**. Complex **1** crystallizes in the space group $P2_1/c$ with a = 17.393(3) Å, b = 14.348(7) Å, c = 13.036(3) Å, β = 92.35(2)°, Z = 4, and V = 3250(2) Å^3. The crystallographic study confirmed that complex **1** contains two phosphido bridges between the Zr and Re centres. The Zr—P bond distances are 2.629(3) and 2.615(3) Å, while the Re—P bonds are 2.498(3) and 2.474(3) Å. The Zr—Re separation is 3.274(1) Å. The details of the geometry of the ZrP_2Re core are discussed in relation to that of other diphosphido bridged early/late heterobimetallics. The possibility of dative bonding between the electron-rich, late metal and the electron-deficient early metal centre is discussed. The data indicate that if such dative bond is present in the d^0–d^6 complex **1**, it is very weak.

Key words: rhenium, zirconium, heterobimetallic, crystal structure.

PEI YAO ZHENG et DOUGLAS W. STEPHAN. Can. J. Chem. **67**, 1584 (1989).

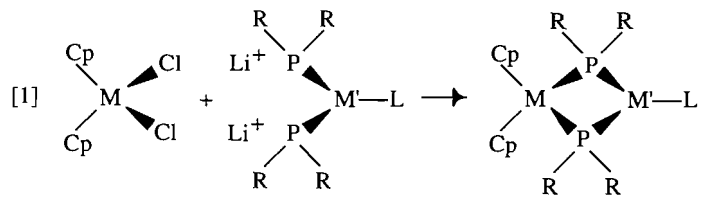
La réaction du complexe $Re_2(CO)_{10}$, comportant une liaison métal–métal, avec le $Cp_2Zr(PPh_2)_2$ conduit à la formation de l'espèce diphosphido hétérobimétallique pontée, $Cp_2Zr(\mu\text{-}PPh_2)_2ReH(CO)_3$, **1**. Le composé **1** cristallise dans le groupe d'espace $P2_1/c$ avec a = 17,393(3), b = 14,348(7), c = 13,036(3) Å, β = 92,35(2)°, Z = 4, et V = 3250(2) Å^3. L'étude cristallographique confirme que le complexe **1** contient deux ponts phosphido entre les centres Zr et Re. Les longueurs des liaisons Zr—P sont égales à 2,629(3) et 2,615 (3) Å alors que celles des liaisons Re—P sont égales à 2,498(3) et 2,474(3) Å. La distance entre le Zr et le Re est de 3,274(1) Å. On discute des détails de la géométrie du noyau ZrP_2Re en relation avec ceux d'autres diphospido hétérobimétalliques pontés. On discute de la possibilité de l'existence d'une liaison dative entre le métal de la fin, riche en électrons, et le centre métallique du début, déficient en électron. Les données indiquent que si une telle liaison est présente dans le complexe **1**, d^0–d^6 elle est très faible.

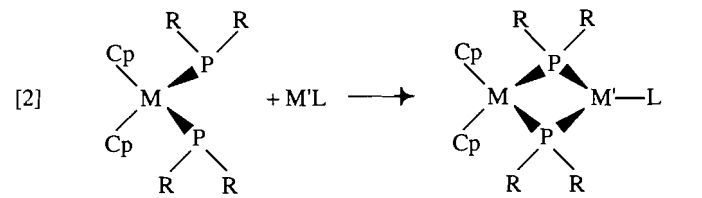
Mots clés : rhénium, zirconium, hétérobimétallique, structure cristalline.

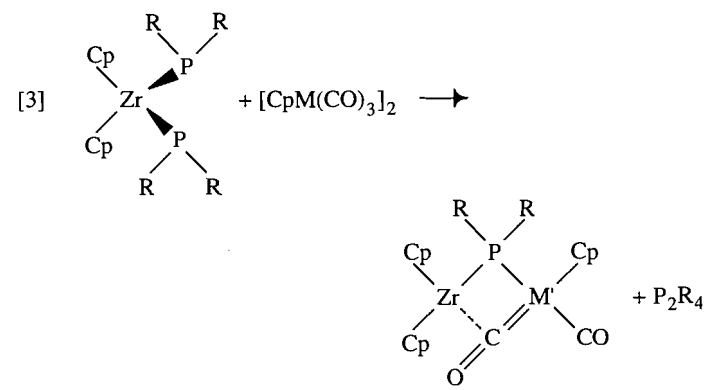
[Traduit par la revue]

Introduction

Complexes containing both early, oxophilic and late, electron-rich metal centres have been the subject of numerous studies and have been recently reviewed (1). Interest in such species is spurred by the potential applications in carbon oxide reduction chemistry. Such early/late heterobimetallic complexes combine the Lewis acidity of the early metals with the known abilities of the late metals for hydrogen activation. Interest is also prompted by the observation of strong metal–support interactions (SMSI) in heterogeneous catalytic systems (2). Direct electronic communication between the late metal centres and the early metals of the supports is presumed to be responsible for unique reactivity arising from these catalyst systems. Attempts to understand the nature of such interactions and their effects on the chemistry of the constituent metals have led to the development of numerous synthetic routes to compounds containing such early/late metal combinations. A variety of bridging ligands including thiolates (3–20) and pendent chelates (21–49) have been employed to link such metal pairs. In addition, we (50–53) and others (54–62) have described early/late heterobimetallics in which phosphido groups link early and late metal centres. For example, complexes of the form $Cp_2M(\mu\text{-}PR_2)_2M'L_n$ have been prepared via one of two synthetic routes; reaction of late metal phosphide dianions with early metal halides (54–56) ([1]) or reaction of early metal phosphides with labile late metal species (50–53, 57–61) ([2]). More recently, we have described the formation of monophosphido bridged early/late heterobimetallics from the redox reaction of $Cp_2Zr(PR_2)_2$ with $[CpM(CO)_3]_2$ [(3]) (63). In the course







[1]To whom correspondence should be addressed.

Can. J. Chem. Downloaded from www.nrcresearchpress.com by 194.225.253.170 on 09/07/12
For personal use only.

Can. J. Chem. Downloaded from www.nrcresearchpress.com by 194.225.253.170 on 09/07/12
For personal use only.

of investigating other reactions of $Cp_2Zr(PPh_2)_2$ with metal–metal bonded species, we have prepared and structurally characterized the complex $Cp_2Zr(\mu\text{-}PPh_2)_2ReH(CO)_3$, **1**. This paper presents the results of our study. The structure of **1** is described and the implications of metal–metal interactions are discussed.

Experimental section

General data

The preparation was done under an atmosphere of dry O_2-free N_2. Solvents were reagent grade, distilled from the appropriate drying agents under N_2, and degassed by the freeze–thaw method at least three times prior to use. ^1H NMR spectra were recorded on a Bruker AC-300 spectrometer operating at 300 MHz. Trace amounts of protonated solvents were used as references and chemical shifts are reported relative to $SiMe_4$. $^{31}P\{^1H\}$ NMR spectra were recorded using a Bruker AC-200 NMR spectrometer operating at 81 MHz and are reported relative to external 85% H_3PO_4. Infrared absorption data were recorded on a Nicolet 5DX Fourier Transform IR spectrometer. Cp_2ZrCl_2, $Re_2(CO)_{10}$ were purchased from the Aldrich Chemical Co. $Cp_2Zr(PPh_2)_2$ was prepared by the literature method (50, 57).

Synthesis of $Cp_2Zr(\mu\text{-}PPh_2)_2ReH(CO)_3$, 1

To a solution of $Cp_2Zr(PPh_2)_2$ (0.100 g, 0.17 mmol) in 35 mL of THF was added a solution of $Re_2(CO)_{10}$ (0.055 g, 0.09 mmol) in 10 mL of THF. The mixture was stirred for 12 h. The volume of the solvent was reduced to about 10 mL under vacuum. Slow addition of *n*-hexane (50 mL) caused the precipitation of a yellow solid. The solid **1** was isolated by filtration and washed with an additional 50 mL of *n*-hexane. (Yield 0.025 g, 17%.) Crystals of **1** were obtained by slow diffusion of pentane into a THF solution of **1**. ^1H NMR (C_6D_6, δ, ppm): 4.99 (s, Cp), 4.81 (s, Cp), 8.3–8.0, 7.2–6.9 (m, Ph), −9.52 (t, H, $|J_{P-H}| = 29$ Hz). $^{31}P\{^1H\}$ NMR (C_6D_6, δ, ppm): 154.2 (s). IR (KBr, cm^{-1}): 1996, 1939, 1911, 1869.

X-ray data collection and reduction

Diffraction experiments were performed on a four-circle Syntex $P2_1$ diffractometer with graphite-monochromatized Mo Kα radiation. The initial orientation matrix was obtained from 15 machine-centred reflections selected from a rotation photograph. These data were used to determine the crystal system. Partial rotation photographs around each axis were consistent with a monoclinic crystal system. Ultimately, 35 reflections ($20° < 2\theta < 25°$) were used to obtain the final lattice parameters and the orientation matrix. Machine parameters, crystal data, and data collection parameters are summarized in Table 1. The observed extinctions were consistent with the space group $P2_1/c$. $\pm h$, $+k$, $+l$ data were collected in one shell ($4.5° < 2\theta < 45.0°$) and three standard reflections were recorded every 197 reflections. Their intensities showed no statistically significant change over the duration of the data collection. The data were processed using the SHELX-76 program package on the computing facilities at the University of Windsor. A total of 3118 reflections with $F_o^2 > 3\sigma F_o^2$ were used in the refinement. An empirical absorption correction was applied to the data based on two sets of Ψ scan data.

Structure solution and refinement

Non-hydrogen atomic scattering factors were taken from the literature tabulations (64–66). The Zr and Re atom positions were determined using direct methods. The remaining non-hydrogen atoms were located from successive difference Fourier map calculations. The refinements were carried out by using full-matrix least squares techniques on F, minimizing the function $w(|F_o| - |F_c|)^2$ where the weight, w, is defined as $4F_o^2/2\sigma(F_o^2)$ and F_o and F_c are the observed and calculated structure factor amplitudes. In the final cycles of refinement all the non-hydrogen atoms were assigned anisotropic temperature factors. Hydrogen atom positions were calculated and allowed to ride on the carbon to which they are bonded assuming a C—H bond length of 0.95 Å. Hydrogen atom temperature factors were fixed at 1.10 times the isotropic temperature factor of the carbon atom to which they are bonded. In the case of the carbon bound hydrogen atoms, contributions were calculated, but not refined. The hydride was not located and its contribution was omitted in the final cycles of least squares. The final values of R and R_w are given in Table 1. The maximum Δ/σ on any of the parameters in the final cycles of the refinement and the location of the largest peaks in the final difference Fourier map calculation are also given in Table 1. The residual electron densities were of no chemical significance. The following data are tabulated: positional parameters (Table 2) and selected bond distances and angles (Table 3). Thermal parameters (Table S1), hydrogen atom parameters (Table S2), and values of 10 $|F_o|$ and 10 $|F_c|$ (Tables S3) have been deposited as supplementary material.[2]

TABLE 1. Crystallographic parameters

Formula	$C_{37}H_{31}O_3P_2ReZr$
Crystal colour, form	Yellow blocks
a (Å)	17.393(3)
b (Å)	14.348(7)
c (Å)	13.036(3)
β (deg)	92.35(2)
Crystal system	Monoclinic
Space group	$P2_1/c$
Volume (Å^3)	3250(2)
Density (g cm^{-3}) calcd.	1.76
Z	4
Crystal dimensions (mm)	0.31 × 0.42 × 0.21
Absorption coefficient, μ(cm^{-1})	39.54
Radiation, λ(Å)	Mo Kα (0.71069)
Temperature (°C)	24
Scan speed (deg/min)	2.0–5.0 (θ/2θ scan)
Scan range (deg)	1.0 below Kα1 1.0 above Kα2
Background scan time ratio	0.5
Data collected	4476
No. of unique data $F_o^2 > 3\sigma(F_o^2)$	3118
No. of variables	349
R (%)	5.23
R_w (%)	5.33
Largest Δ/σ in the final least-squares cycle	0.010
Maximum residual electron density (e/A^3)	2.5
Atom associated	Re

Results and discussion

The reaction of two equivalents of $Cp_2Zr(PPh_2)_2$ with $Re_2(CO)_{10}$ in THF results in a gradual colour change from red–black to yellow over a 12 h period. Monitoring of the reaction by $^{31}P\{^1H\}$ NMR spectroscopy implies the formation of numerous phosphorus containing products including the species **1** that exhibits a single resonance at 154.2 ppm. In addition, chemical shifts indicate that other products include P_2Ph_4, PPh_2H, and several uncharacterized species containing coordinated phosphine or phosphido moieties. Fractionation of the products with pentane and fractional crystallization of the pentane insoluble residue from THF/pentane led to isolation of yellow crystals of the complex **1**, in relatively low yield (17%). The $^{31}P\{^1H\}$ NMR spectrum of **1** shows a resonance at 154 ppm. The similarity of this chemical shift to that seen for $Cp_2Zr(\mu\text{-}PPh_2)_2W(CO)_4$ (56) suggests the presence of bridging phosphido groups between Zr and Re. ^1H NMR data for **1** show reso-

[2]Tables of thermal and hydrogen atom parameters, bond distances and angles, and values of $10F_o$ and $10F_c$ (15 pages) have been deposited. A complete set of the deposited material may be purchased from the Depository of Unpublished Material, CISTI, National Research Council of Canada, Ottawa, Ont., Canada K1A 052.

TABLE 2. Positional parameters*

Atom	x	y	z	Atom	x	y	z
Re	2968(1)	−143(1)	2072(1)	Zr	2549(1)	1885(1)	2864(1)
P1	4229(2)	1138(2)	2348(2)	P2	1375(2)	423(2)	2642(2)
O1	4866(8)	−1323(7)	1747(6)	O2	2513(7)	654(7)	426(5)
O3	1676(9)	−1944(8)	1872(7)	C1	214(6)	505(6)	1999(4)
C41	4168(10)	−839(9)	1845(7)	C2	−580(6)	1103(6)	2191(4)
C42	2664(8)	343(9)	1030(8)	C3	−1462(6)	1168(6)	1712(4)
C43	2160(10)	−1266(9)	1943(8)	C4	−1551(6)	635(6)	1042(4)
C5	−757(6)	38(6)	850(4)	C6	126(6)	−27(6)	1328(4)
C11	915(5)	−335(6)	3434(5)	C12	−92(5)	−256(6)	3669(5)
C13	−430(5)	−816(6)	4264(5)	C14	239(5)	−1454(6)	4624(5)
C15	1246(5)	−1533(6)	4389(5)	C16	1584(5)	−974(6)	3794(5)
C21	5313(5)	831(5)	3019(4)	C22	6201(5)	1374(5)	3038(4)
C23	6989(5)	1194(5)	3585(4)	C24	6888(5)	471(5)	4113(4)
C25	6000(5)	−72(5)	4093(4)	C26	5212(5)	108(5)	3546(4)
C31	4933(6)	1549(4)	1515(4)	C32	5206(6)	2486(4)	1459(4)
C33	5733(6)	2799(4)	826(4)	C34	5988(6)	2174(4)	250(4)
C35	5715(6)	1237(4)	305(4)	C36	5187(6)	925(4)	938(4)
C51	2038(11)	1539(10)	4200(7)	C52	3062(12)	1219(10)	4148(6)
C53	3697(11)	1991(10)	4047(7)	C54	3105(10)	2782(10)	4048(7)
C55	2052(10)	2495(9)	4132(7)	C61	1894(12)	3467(10)	2529(8)
C62	2820(11)	3341(9)	2130(8)	C63	2578(10)	2637(9)	1556(7)
C64	1564(10)	2350(9)	1640(8)	C65	1170(10)	2857(10)	2251(8)

*Parameters reported multiplied by 10^4.

TABLE 3. Selected bond distances and angles

Bond	Distance (Å)	Bond	Distances (Å)	Bond	Distance (Å)
Re...Zr	3.274(1)	Re—P1	2498(3)	Re—P2	2.474(3)
Re—C41	1.91(1)	Re—C42	1.97(2)	Re—C43	1.93(2)
Zr—P1	2.629(3)	Zr—P2	2.615(3)	Zr—C51	2.49(1)
Zr—C52	2.50(1)	Zr—C53	2.50(1)	Zr—C54	2.51(1)
Zr—C55	2.48(1)	Zr—C61	2.49(1)	Zr—C62	2.48(1)
Zr—C63	2.52(1)	Zr—C64	2.53(1)	Zr—C65	2.48(1)
C21—P1	1.848(7)	C31—P1	1.843(7)	C1—P2	1.848(8)
C11—P2	1.874(8)	C51—C52	1.42(2)	C52—C53	1.40(2)
C53—C54	1.37(2)	C51—C55	1.38(2)	C54—C55	1.45(2)
C61—C62	1.43(2)	C62—C63	1.45(2)	C63—C64	1.40(2)
C61—C65	1.36(2)	C64—C65	1.40(2)	C41—O1	1.16(1)
C42—O2	1.15(2)	C43—O3	1.16(2)		

Bonds	Angle (deg)	Bonds	Angle (deg)
P2—Re—P1	103.8(1)	C41—Re—Zr	134.7(4)
C41—Re—P1	83.5(4)	C41—Re—P2	164.2(4)
C42—Re—Zr	92.4(3)	C42—Re—P1	91.3(3)
C42—Re—P2	96.4(3)	C42—Re—C41	97.5(5)
C43—Re—Zr	133.6(4)	C43—Re—P1	170.5(4)
C43—Re—P2	81.8(4)	C43—Re—C41	89.3(5)
C43—Re—C42	95.7(5)	P2—Zr—P1	96.5(1)
Zr—P1—Re	79.3(1)	C21—P1—Re	115.2(2)
C21—P1—Zr	120.5(3)	C31—P1—Re	115.4(2)
C31—P1—Zr	125.9(3)	C31—P1—C21	100.4(4)
Zr—P2—Re	80.0(1)	C1—P2—Re	117.3(2)
C1—P2—Zr	129.8(3)	C11—P2—Re	113.8(2)
C11—P2—Zr	124.1(3)	C11—P2—C1	101.7(4)
C55—C51—C52	108(1)	C53—C52—C51	108(1)
C54—C53—C52	109(1)	C55—C54—C53	108(1)
C54—C55—C51	108(1)	C65—C61—C62	110(1)
C63—C62—C61	105(1)	C64—C63—C62	108(1)
C65—C64—C63	108(1)	C64—C65—C61	109(1)
O1—C41—Re	174(1)	O2—C42—Re	177(1)
O3—C43—Re	179(1)		

Can. J. Chem. Downloaded from www.nrcresearchpress.com by 194.225.253.170 on 09/07/12
For personal use only.

TABLE 4. Structural parameters for diphosphido bridged early/late heterobimetallics†

Compound	P—M—P	P—M′—P	M—P—M	M—M′	M—P	M′—P	Reference
$Cp_2Zr(\mu\text{-}PPh_2)_2Mo(CO)_4$	98.5(1)	103.1(1)	79.2(1)	3.299(1)	2631(1)	2.547(1)	50
			79.1(1)		2.630(1)	2.543(1)	
$Cp_2Zr(\mu\text{-}PPh_2)_2W(CO)_4$	98.3(1)	103.3(1)	79.2(1)	3.289(1)	2.619(3)	2.537(3)	56
			79.3(1)		2.631(3)	2.529(3)	
$Cp_2Hf(\mu\text{-}PEt_2)_2Mo(CO)_4$	95.3(1)	98.2(1)	83.0(1)	3.400(1)	2.592(1)	2.538(1)	57
			83.0(1)		2.596(1)	2.534(1)	
$Cp_2Zr(\mu\text{-}PPh_2)_2ReH(CO)_3$	96.5(1)	103.8(1)	79.3(1)	3.274(1)	2.629(3)	2.498(3)	This
			80.1(1)		2.615(3)	2.474(3)	work
$Cp_2Zr(\mu\text{-}PPh_2)_2RhH(CO)PPh_3$	95.6(1)	118.3(1)	72.4(1)	2.9801(1)	2.698(2)	2.320(2)	53
			73.0(1)		2.671(2)	2.313(2)	
$Cp_2Zr(\mu\text{-}PPh_2)_2Rh(indenyl)$	92.0(1)	110.7(1)	78.7(1)	3.088(1)	2.590(1)	2.264(1)	59
$Cp_2Hf(\mu\text{-}PPh_2)_2RhH(CO)PPh_3$	96.4(1)	117.4(1)	72.4(1)	2.964(1)	2.672(2)	2.325(2)	53
			73.2(1)		2.640(2)	2.309(2)	
$Cp^*_2Th(\mu\text{-}PPh_2)_2Ni(CO)_2$	83.7	117.9	76.6	3.206	2.869	2.242	60
			75.8		2.900	2.251	
$Cp^*_2Th(\mu\text{-}PPh_2)_2PtPMe_3$‡	88.3(2)		69.1(1)	2.984(1)	2.891(6)		61
			67.8(2)		2.953(6)		

†Distances are given in Å, angles in degrees.
‡Report is prelinminary and thus full details are not available.

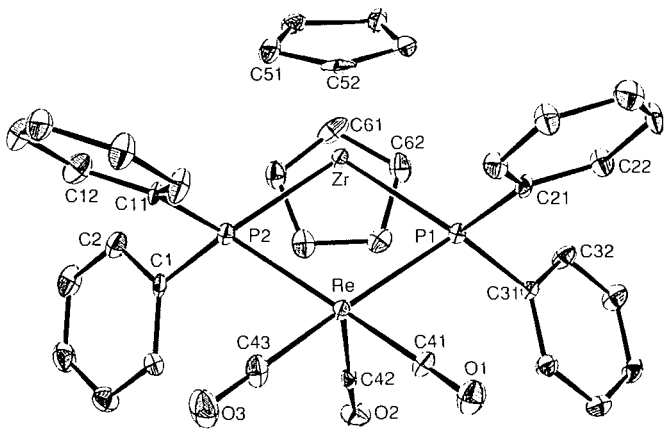


FIG. 1. ORTEP drawing of molecule **1**, 20% thermal ellipsoids are shown. Hydrogen atom are omitted for clarity.

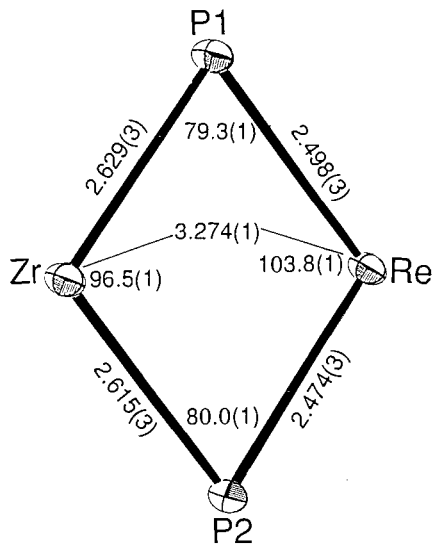


FIG. 2. Structural details of the core of **1**.

nances attributable to the phenyl rings of the phosphido groups, as well as, two inequivalent cyclopentadienyl groups. A triplet at −9.52 ppm is attributable to a Re bound hydride. The $|J_{P—H}|$ value suggests the coordination of a hydride *cis* to two equivalent phosphorus atoms. Infrared data are consistent with the presence of carbonyl groups and a hydride bound to Re. Thus, these spectroscopic data suggest the formulation of **1** as $Cp_2Zr(\mu\text{-}PPh_2)_2ReH(CO)_3$. This formulation was confirmed by X-ray crystallography (*vide infra*).

As mentioned above, numerous species appear to form during the course of the reaction, consequently, the mechanism of **1** formation is not understood. One might speculate that substitution reactions and heterolytic cleavage of the Re—Re bond gives an intermediate of the form $[Cp_2Zr(\mu\text{-}PPh_2)_2Re(CO)_3]^-$. Related heterobimetallic anions are known to be efficient proton scavengers (67), and thus the formation of this proposed intermediate would readily lead to the formation of **1** in the presence of a proton source. As it is necessary to perform the synthesis of **1** in the strict absence of H_2O, the source of proton in the present reaction is unknown, but is the subject of ongoing research.

Crystals of **1** are made up of unit cells each containing four discrete molecules. The closest non-bonding distance between molecules in the unit cell is 2.327 Å (H33—H26). Selected interatomic distances and angles are given in Table 3. An ORTEP drawing of the molecule is shown in Fig. 1. The study confirmed the general formulation of **1** as given above. The coordination sphere of Zr is best described as pseudo-tetrahedral. Two π-bonded cyclopentadienyl rings are bound to Zr with two diphenylphosphido groups completing the Zr coordination sphere and bridging to Re. Three terminal carbonyl moieties are also bonded to Re. Two of the carbonyl moieties are *trans* to the phosphido group, while the third cabonyl is *cis* to the phosphides. Although not located in the X-ray study, the geometry of the Re coordination shell is consistent with the location of a hydride *cis* to the phosphido groups. Thus, the coordination shell of Re is best described as pseudo-octahedral. The M—C bond distances in the Cp_2Zr fragments average to a typical value of 2.50(1) Å (50), while the Re—C distances range

Can. J. Chem. Downloaded from www.nrcresearchpress.com by 194.225.253.170 on 09/07/12
For personal use only.

from 1.91(1)–1.97(2) Å. The slightly longer Re—C42 bond length is consistent with the proposed location of the hydride *trans* to C42. The C—O bond distances average 1.16(2) Å and are typical of terminal carbonyl moieties (50, 56, 57). The bond distances and angles within the PPh_2 and Cp fragments are also typical (50, 57) and thus warrant no further comment.

The structural details of the ZrP_2Re core are shown in Fig. 2. The four atoms are essentially coplanar. The Zr—P distances of 2.615(3) and 2.629(3) Å, the Zr—P—Re angles of 79.3(1) and 80.0(1)° and the P—Re—P angle of 103.8(1)° are similar to corresponding values found in $Cp_2Zr(\mu\text{-}PPh_2)_2M(CO)_4$(M = Mo, W) (50, 56). The P—Zr—P angle of 96.5(1)° is substantially smaller than the angle found in the Zr/Mo or Zr/W heterobimetallics, while it is greater than the P—Zr—P angle found in the Zr/Rh heterobimetallic, $Cp_2Zr(\mu\text{-}PPh_2)_2RhH(CO)PPh_3$ (53). In a similar trend, the Re—P distances of 2.498(3) and 2.474(3) Å and the Re—Zr distance of 3.271(1) Å are intermediate between the corresponding values for $Cp_2Zr(\mu\text{-}PPh_2)_2M(CO)_4$ (M = Mo, W) (50, 56) and $Cp_2Zr(\mu\text{-}PPh_2)_2RhH(CO)PPh_3$ (53). The trend in the M—P distances for this series of Mo, Re, and Rh species corresponds to that expected on the basis of decreasing covalent radii. These trends suggest that increased electron density on the late metal centre enhances back bonding, resulting in stronger M—P bonds. As the M—P shortens, the angle subtended at Zr decreases, as does the Zr—M separation.

The question of dative bonding between the electron-rich, late metal centre and electron-deficient, early metal centre has been previously discussed for other early/late heterobimetallics (13–16, 50–53, 60–62, 69). Table 4 lists the pertinent structural parameters for all of the crystallographically characterized diphosphido bridged early/late heterobimetallics. These data show that the complexes that contain d^8 and d^{10} metal centres exhibit angles at P (i.e., M—P—M′) that are significantly less than 80°. This has been previously cited (13–16, 50–53, 61, 62) as a criterion indicative of metal–metal bonding. The P—M′—P angles in the d^8 and d^{10} complexes exceed 110°, indicative of dative donation to the early metal centre. The relatively long M—P (M = Zr, Hf, Th) bond lengths and relatively short M—M′ distances are further evidence of acceptance of electron density from the late metal centre by the early metal centre. For the d^6 complexes of the form, $Cp_2M(\mu\text{-}PR_2)_2M(CO)_4$ as well as complex **1**, the angles at P are only slightly less than 80°, while the P—M′—P angles are less than 103.8(1)°. The M—P bond distances are relatively short and the metal–metal separation exceeds 3.271(1) Å. Furthermore, the planarity of the ZrP_2M cores in the d^6 complexes suggests little perturbation of the bonding involving the metal centres. This is in contrast to that seen for $Cp_2M(\mu\text{-}PPh_2)_2RhH(CO)PPh_3$ and $Cp^*_2Th(\mu\text{-}PPh_2)_2PtPMe_3$[3] where a "butterfly" distortion of the core atoms accommodates a shorter metal–metal separation. Although the cause of such distortions is not clear, metal–metal interactions and crystal packing effects have been suggested (53, 61). Thus, the structural data for these species support the notion that direct dative bonding between the late and early metal centres is present for d^0–d^8 and d^0–d^{10} heterobimetallics. This conclusion is also supported by molecular orbital calculations (62, 68). However, the structural data also suggest that if such metal–metal bonding is present in d^0–d^6 species, it is at best very weak.

[3]Report is preliminary and thus full structural details are not available.

Acknowledgements

Financial support from NSERC of Canada is gratefully acknowledged.

1. D. W. Stephan. Coord. Chem. Rev. **95**, 41 (1989).
2. R. T. K. Baker, S. J. Tauster, and J. A. Dumesic (*Editors*). Strong metal-support interactions. Am. Chem. Soc. Washington, DC. 1986.
3. H. Kopf and K. H. Rathlein. Angew. Chem. Internat. Edit. Eng. **8**, 980 (1969).
4. P. S. Braterman, V. A. Wilson, and K. K. Joshi. J. Chem. Soc. (A), 191 (1971).
5. C. J. Ruffing and T. B. Rauchfuss. Organometallics,, 524 (1985).
6. T. S. Cameron, K. C. Prout, G. V. Rees, M. L. H. Green, K. K. Joshi, G. R. Davies, and B. T. Kilbourn. J. Chem. Soc. Chem. Commun. 14 (1971).
7. P. S. Braterman, V. A. Wilson, and K. K. Joshi. J. Organomet. Chem. **31**, 123 (1971).
8. G. R. Davies and B. T. Kilbourn. J. Chem. Soc. (A), 87 (1971).
9. J. C. Kotz, W. Vining, W. Coco, R. Rosen, A. R. Dias, and M. H. Garcia. Organometallics, **2**, 68 (1983).
10. W. E. Douglas and M. L. H. Green. J. Chem. Soc. D, 1796 (1972).
11. H. Werner, B. Ulrich, U. Schubert, P. Hofmann, and B. Zimmer-gasser. J. Organomet. Chem. **297**, 27 (1985).
12. P. S. Braterman and V. A. Wilson. J. Organomet. Chem. **31**, 131 (1971).
13. G. S. White and D. W. Stephan. Inorg. Chem. **24**, 1499 (1985).
14. T. A. Wark and D. W. Stephan. Inorg. Chem. **26**, 363 (1987).
15. G. S. White and D. W. Stephan. Organometallics, **6**, 2169 (1987).
16. G. S. White and D. W. Stephan. Organometallics, **7**, 903 (1988).
17. W. E. Douglas, M. L. H. Green, K. C. Prout, and G. V. Rees. J. Chem. Soc. Chem. Commun. 896 (1971).
18. K. C. Prout, S. R. Critchley, and G. V. Rees. Acta Crystallogr. B, **30**, 2305 (1974).
19. K. K. Joshi, R. Wardle, and V. A. Wilson. Inorg. Nucl. Chem. Lett. **6**, 49 (1970).
20. J. C. Daran, B. Meunier, and K. Prout. Acta Crystallogr. B, **35**, 1709 (1979).
21. V. H. Burger and C. J. Kluess. Organomet. Chem. **56**, 269 (1973).
22. A. G. Osborne and R. H. Whiteley. J. Organomet. Chem. **181**, 425 (1979).
23. A. A. Pasynskii, Y. V. Skripkin, V. T. Kalinnikov, M. A. Porai-Koshits, A. S. Antsyshkina, G. G. Sadikov, and V. N. Ostrikova. J. Organomet. Chem. **165**, 49 (1979).
24. M. Etienne, R. Choukroun, and D. Gervais. J. Chem. Soc. (D), 915 (1984).
25. H. Burger and C. Z. Kluess. Anorg. Allge. Chem. **432**, 112 (1976).
26. G. A. Razuvaev, G. A. Domrachev, V. V. Sharutin, and O. N. Suvorova. J. Organomet. Chem. **141**, 313 (1977).
27. N. E. Schore. J. Am. Chem. Soc. **101**, 7410 (1979).
28. D. R. Tuetin, S. R. Iyer and N. E. Schore. J. Organomet. Chem. **320**, 349 (1987).
29. J. C. Leblanc, C. Moise, A. Maisonnat, R. Poilblanc, C. Charrier, and F. Mathey. J. Organomet. Chem. **231**, C43 (1982).
30. M. D. Rausch, B. H. Edwards, R. D. Rogers, and J. L. Atwood. J. Am. Chem. Soc. **105**, 3882 (1983).
31. C. P. Casey and F. Nief. Organometallics, **4**, 1219 (1985).
32. W. Tikkanen, Y. Fujita, and J. L. Petersen. Organometallics, **5**, 888 (1986).

Can. J. Chem. Downloaded from www.nrcresearchpress.com by 194.225.253.170 on 09/07/12
For personal use only.

33. B. DEMERSEMAN, P. H. DIXNEUF, J. DOUGLADE, and R. MERCIER. Inorg. Chem. **21**, 3942 (1982).
34. N. E. SHORE, S. J. YOUNG, M. M. OLMSTEAD, and P. HOFMANN. Organometallics, **2**, 1769 (1983).
35. R. CHOUKROUN and D. GERVAIS. J. Organomet. Chem. **266**, C37 (1984).
36. F. SENOCQ, M. BASSO-BERT, R. CHOUKROUN, and D. GERVAIS. J. Organomet. Chem. **297**, 155 (1985).
37. M. ETIENNE, R. COUKROUN, M. BASSO-BERT, F. DAHAN, and D. GERVAIS. Nouv. J. Chem. **8**, 531 (1984).
38. H. H. KARSCH, G. MULLER, and C. KRUGER. J. Organomet. Chem. **273**, 195 (1984).
39. R. CHOUKROUN, A. IRAQI, and D. GERVAIS. J. Organomet. Chem. **311**, C60 (1986).
40. R. CHOUKROUN, A. IRAQI, D. GERVAIS, J. C. DARAN, and Y. JEANNIN. Organometallics, **6**, 1197 (1987).
41. F. SENOCQ, C. RANDRIANLIMANANA, A. THOREZ, P. KALCK, R. CHOUKROUN, and D. GERVAIS. J. Chem. Soc. Chem. Commun. 1376 (1984).
42. R. COUKROUN, D. GERVAIS, J. JAUD, P. KALCK, and F. SENOCQ. Organometallics, **5**, 67 (1986).
43. F. SENOCQ, C. RADRIANLIMANANA, A. THOREZ, and P. KALCK. J. Mol. Catal. **35**, 213 (1986).
44. G. S. FERGUSON and P. T. WOLCZANSKI. Organometallics, **4**, 1601 (1985).
45. G. S. FERGUSON and P. T. WOLCZANSKI. J. Am. Chem. Soc. **108**, 8293 (1986).
46. U. THEWALT and D. SCHOMBERG. Z. Naturforsch. Teil. B, **30**, 636 (1975).
47. N. E. SCHORE and H. HOPE. J. Am. Chem. Soc. **102**, 4251 (1980).
48. R. CHOUKROUN and D. GERVAIS. J. Chem. Soc. Chem. Commun. 1300 (1982).
49. R. J. DORODA, G. WILKINSON, M. H. HURSTHOUSE, K. M. A. MALIK, and M. THORNTON-PETT. J. Chem. Soc. (D), 2315 (1980).
50. L. GELMINI, L. C. MATASSA, and D. W. STEPHAN. Inorg. Chem. **24**, 2585 (1985).
51. L. GELMINI and D. W. STEPHAN. Inorg. Chim. Acta, **111**, L17 (1986).
52. L. GELMINI and D. W. STEPHAN. Inorg. Chem. **25**, 1222 (1986).
53. L. GELMINI and D. W. STEPHAN. Organometallics, **7**, 849 (1988).
54. G. JOHANNSEN and O. STELZER. Chem. Ber. **110**, 3448 (1977).
55. O. STELZER, E. UNGER, and V. WRAY. Chem. Ber. **110**, 3430 (1977).
56. T. S. TARGOS, R. P. ROSEN, R. R. WHITTLE, and G. L. GEOFFROY. Inorg. Chem. **24**, 1375 (1985).
57. R. T. BAKER, T. H. TULIP, and S. S. WREFORD. Inorg. Chem. **24**, 1379 (1985).
58. M. G. B. DREW, S. R. WADE, M. G. H. WALLBRIDGE, and G. R. WILLEY. J. Chem. Soc. (D), 714 (1986).
59. R. T. BAKER and T. H. TULIP. Organometallics, **5**, 839 (1986).
60. J. M. RITCHEY, A. J. ZOZULIN, D. A. WROBLESKI, R. R. RYAN, H. J. WASSERMAN, D. C. MOODY, and R. T. PAINE. J. Am. Chem. Soc. **107**, 501 (1985).
61. P. J. HAY, R. R. RYAN, K. V. SALAZAR, D. A. WROBLESKI, and A. P. SATTELBERGER.J. Am. Chem. Soc. **108**, 313 (1986).
62. J. V. ORTIZ. J. Am. Chem. Soc. **108**, 550 (1986).
63. P. Y. ZHENG, T. T. NADASDI, and D. W. STEPHAN. Organometallics. **8**, 1393 (1989).
64. D. T. CROMER and J. B. MANN. Acta Crystallogr. A**24**, 324 (1968).
65. D. T. CROMER and J. B. MANN. Acta Crystallogr.
66. D. T. CROMER and J. T. WABER. International tables for X-ray crystallography. Kynoch Press, Birmingham, England. 1974.
67. L. GELMINI, D. G. DICK, and D. W. STEPHAN. Unpublished results.
68. G. S. WHITE, T. A. WARK, J. S. TSE, and D. W. STEPHAN. Unpublished results.
69. G. S. FERGUSON, P. T. WOLCZANSKI, L. PARKANYI, and M. C. ZONNEVYLLE. Organometallics, **7**, 1967 (1988).

Can. J. Chem. Downloaded from www.nrcresearchpress.com by 194.225.253.170 on 09/07/12
For personal use only.

Stereochemistry of hydrogen loss during C-21 dehydroxylation of tetrahydrodeoxycorticosterone by *Eubacterium lentum*

HERBERT L. HOLLAND, RONALD W. NINNISS, AND FRANCES M. BROWN
Department of Chemistry, Brock University, St. Catharines, Ont., Canada L2S 1Y3

Received April 5, 1989

HERBERT L. HOLLAND, RONALD W. NINNISS, and FRANCES M. BROWN. Can. J. Chem. **67**, 1590 (1989).

The loss of hydrogen from the C-21 position of 5β-pregnane-3α,21-diol-20-one (tetrahydrodeoxycorticosterone, THDOC) during reductive removal of the 21-hydroxy group by the anaerobic bacterium *Eubacterium lentum* has been shown to be selective for the pro-*S* position by the use of THDOC labelled with deuterium at the C-21 pro-*S* and C-21 pro-*R* positions. The labelled substrates were obtained by using the bacterium *Clostridium paraputrificum* to reduce chemically prepared C-21 labelled samples of pregn-4-en-21-ol-3,20-dione (deoxycorticosterone, DOC) at C-3 and C-4 (5). The stereochemistry of deuterium label introduced by chemical means at C-21 of DOC was determined by comparison with a sample of 21-(*R*)-DOC-21-d_1 produced by reduction of the corresponding aldehyde pregn-4-en-21-al-3,20-dione, 21-*d* by the enzyme 21-hydroxysteroid NAD oxidoreductase from beef liver.

Key words: *Eubacterium*, *Clostridium*, steroids, tetrahydrodeoxycorticosteroids.

HERBERT L. HOLLAND, RONALD W. NINNISS et FRANCES M. BROWN. Can. J. Chem. **67**, 1590 (1989).

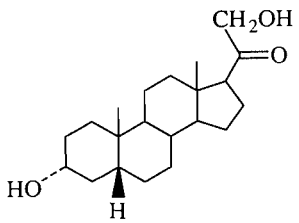
Utilisant des THDOC marquées aux deutérium dans les positions C-21-pro-*S* et C-21-pro-*R*, on a démontré que la perte d'un hydrogène de la position C-21 de la 5β-pregnane-3α,21-diol-20-one (tétrahydrodésoxycorticostérone, THDOC) au cours de l'enlèvement réducteur du groupement 21-hydroxy par la bactérie anaérobique *Eubacterium lentum* est sélective pour la position pro-*S*. On a obtenu les substrats marqués en réduisant, à l'aide de la bactérie *Clostridium paraputrificum*, les positions C-3 et C-4(5) d'échantillons de pregn-4-en-21-ol-3,20-dione marqués en C-21 et préparés d'une façon chimique. On a déterminé la stéréochimie du deutérium introduit en C-21 par des méthodes chimiques en procédant à une comparaison avec un échantillon de 21-(*R*)-DOC-21-d_1, préparé par réduction de l'aldéhyde correspondant pregn-4-en-21-al-3,20-dione, 21-*d* par l'enzyme oxydoréductase 21-hydroxystéroïde NAD provenant du foie de boeuf.

Mots clés : *Eubacterium*, *Clostridium*, stéroïdes, tétrahydrodésoxycorticostérones.

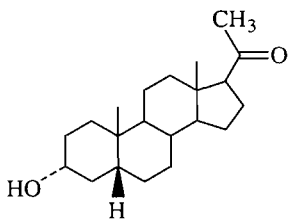
[Traduit par la revue]

Those 21-hydroxycorticosteroids that are reabsorbed into the liver after passage through the intestines can be excreted as derivatives in which the hydroxyl group at C-21 has been replaced by hydrogen (1). This process is performed by the anaerobic bacterium, *Eubacterium lentum*, present in the intestines (2).

In an earlier paper (3) we examined the conversion of the 21-hydroxycorticosteroid 5β-pregnane-3α,21-diol-20-one (tetrahydrodeoxycorticosterone, THDOC, **6**) to 5β-pregnan-3α-ol-20-one (**7**) by *E. lentum*, and determined that the enzymic



6

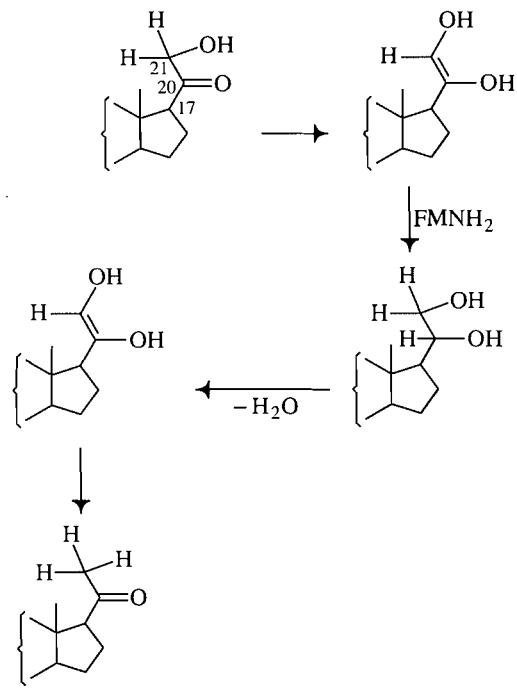


7

removal of the C-21 hydroxy group proceeds with retention of hydrogen at C-17, but with loss of one of the two hydrogen atoms originally present at C-21. A consideration of the cofactor (2, 4) and substrate (1) requirements for the 21-dehydroxylase enzyme, together with the primary kinetic hydrogen/deuterium isotope effect at C-21 (3), led us to propose the mechanism for the action of this enzyme shown in Scheme 1.

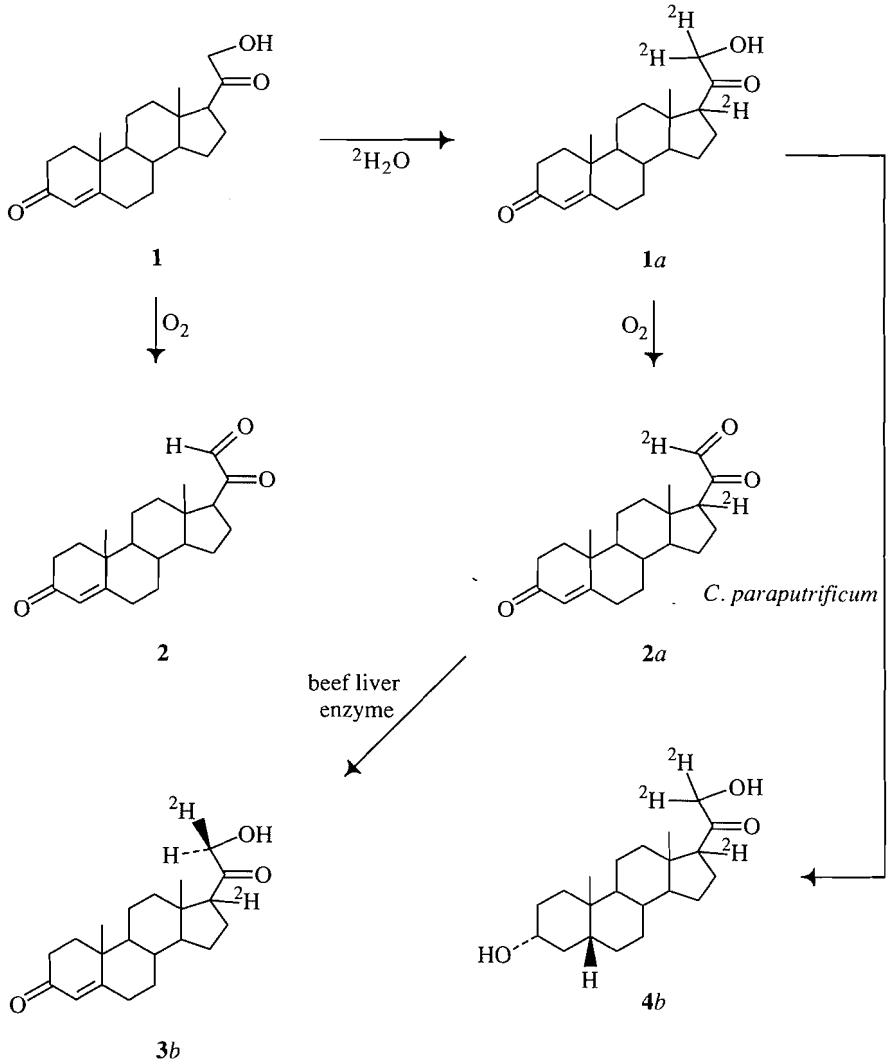
We have now extended our study of this enzyme by the use of substrates with asymmetric deuterium labelling at C-21, and report that the loss of hydrogen from C-21 in the first step of Scheme 1 is specific for the pro-*S* position.

The substrates required for our study were the 21-(*S*) and 21-(*R*) deuterium labelled tetrahydrodeoxycorticosteroids, **4** and **4***a*, respectively. In view of the high cost of THDOC as a starting material for synthetic procedures, the stereoselective introduction of deuterium label at C-21 was carried out by reduction of the readily available 21-aldehydes **2** and **2***a*, the 4-ene-3-keto functionality of ring A being subsequently reduced by *Clostridium paraputrificum* (5) to the 3α-ol-5β stereochemistry required by *E. lentum* (3).



SCHEME 1. Proposed route for C-21 dehydroxylation by *E. lentum*.

Can. J. Chem. Downloaded from www.nrcresearchpress.com by 194.225.253.170 on 09/07/12
For personal use only.



SCHEME 2

In two parallel synthetic routes, pregn-4-ene-3,20-dion-21-ol (deoxycorticosterone, DOC, **1**), and its analogue labelled at C-17 and -21 (**1***a*), were first converted by copper catalysed air oxidation (6–8) to the corresponding 21-aldehydes **2** and **2***a* (Scheme 2). To facilitate the analysis of the stereochemistry of reduction of **2** and **2***a*, the labelled aldehyde **2***a* was reduced at C-21 by the enzyme 21-hydroxysteroid NAD oxidoreductase, isolated from beef liver (9). This enzyme is specific for delivery of hydrogen to the pro-*S* position at C-21 (8, 10), giving in the present case the 21-(*R*) labelled DOC **3***b* (Scheme 2).

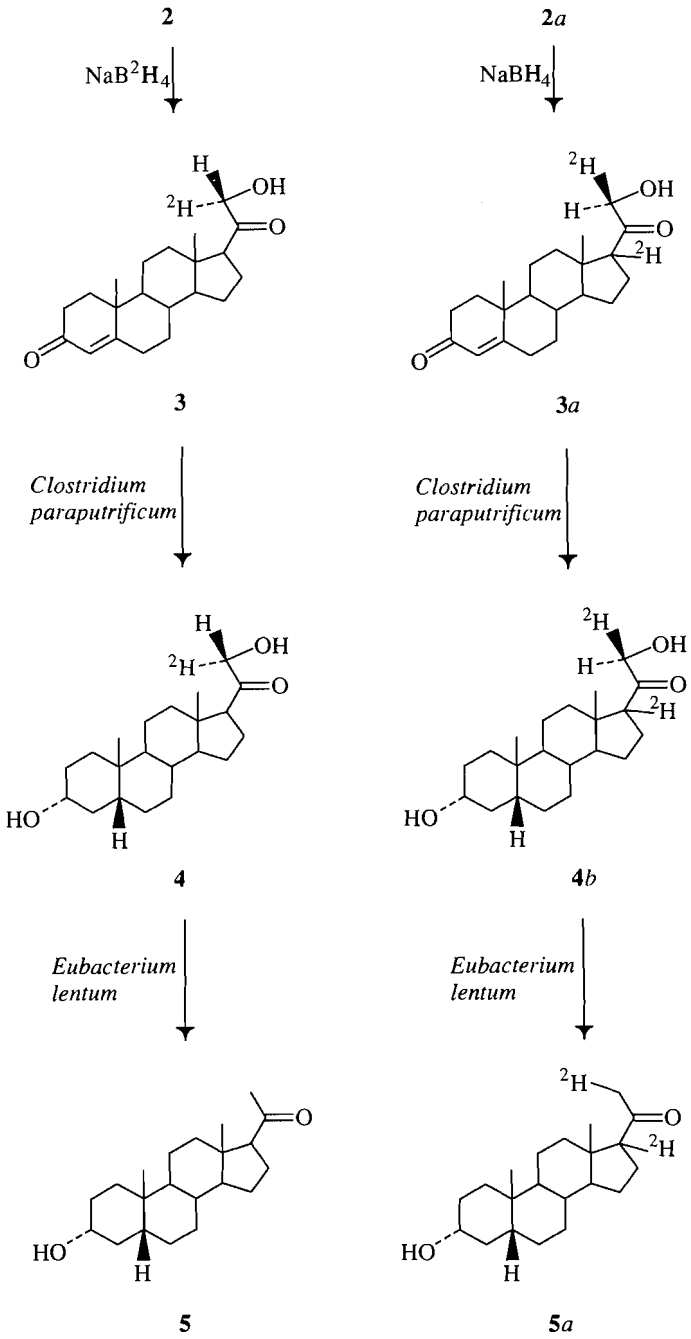
At 500 MHz the proton nmr spectrum of DOC shows the prochiral hydrogens at C-21 as a well-resolved AB quartet centered at δ 4.12 and 4.18 ppm, and in the C-21 deuterium labelled samples these signals are shifted to 4.10 and 4.16 ppm (see Experimental). The ^1H nmr spectrum of **3***b* derived from enzymic reduction of **2***a* shows a large singlet at δ 4.10 ppm, with a very minor peak at δ 4.16, confirming the assignment of the prochiral C-21 hydrogen absorptions as pro-*S*: upfield at δ 4.10/4.12; pro-*R*: downfield at δ 4.16/4.18 ppm. Using these assignments it is possible to assign the stereochemistry of the products resulting from the sodium borodeuteride reduction of the aldehyde **2** and the sodium borohydride reduction of the deuterium labelled aldehyde **2***a* (Scheme 3) as 21-(*S*) and 21-(*R*) respectively. The same stereoselectivity has been observed in the hydride reduction of 21-aldehydes in 17α-hydroxysteroids (8). The stereochemistry of chemical reduction at the C-21 aldehyde group therefore parallels the enzymic reduction, with preferential delivery of hydride or deuteride at the pro-*S* position.

Analysis of the 500-MHz proton nmr spectra of the C-21 chirally labelled DOC samples **3** and **3***a* was performed as outlined above and in the experimental section to determine the stereochemical integrity of labelling: the 21-(*S*) isomer **3** was found to be a 3:1 mixture of the (*S*) and (*R*) configurations at C-21, while the 21-(*R*) isomer was a 2:1 mixture of (*R*) to (*S*). Both samples were essentially completely labelled at C-21, as evidenced by the virtual absence of the AB quartet at δ 4.12 and 4.18 characteristic of C-21 unlabelled material.

Accurate estimation of the deuterium content of the side chain in 21-hydroxy-20-ketopregnanes by mass spectrometry is difficult: electron impact spectra show very weak molecular ions, fragmentation of which invariably occurs by loss of the side chain, and FAB spectra are difficult to use for precise deuterium determination in view of the presence of M + H and M − H ions. However, the FAB mass spectra of **3** and **3***a* were recorded (see Experimental) and qualitatively confirm the results of the high resolution nmr analysis.

To establish that reduction of ring A could be carried out by

Can. J. Chem. Downloaded from www.nrcresearchpress.com by 194.225.253.170 on 09/07/12
For personal use only.



SCHEME 3

Clostridium paraputrificum without the loss of stereochemical integrity at C-21, the C-21 labelled DOC **1***a* was converted to the labelled 3α-hydroxy-5β-steroid **4***b* (Scheme 2). Some loss of label from C-21 was observed, the product containing 0.2 hydrogens at C-21 by ^{1}H nmr analysis compared with 0.05 hydrogens present in **1***a*. However, integration of the resulting signals at δ 4.10 and 4.16 ppm showed that this loss did not occur in a stereoselective manner. This was confirmed following analysis of the labelled THDOC samples **4** and **4***a* derived from reduction of **3** and **3***a* respectively using *C. paraputrificum* (Scheme 3). As determined by high resolution ^{1}H nmr analysis and outlined in the experimental section, these products had the same *R*:*S* ratios at C-21 as the starting materials from which they were derived.

The labelled THDOC samples **4** and **4***a* were then converted to 5β-pregnan-3α-ol-20-one (**5** and **5***a* respectively) by *E. lentum* as outlined in Scheme 3. The analysis of these experiments is presented in Tables 1 and 2. Table 1 predicts the deuterium content at C-21 that would result from loss of hydrogen/deuterium from the pro-*R* or the pro-*S* positions of THDOC, while Table 2 presents the experimentally determined values.

TABLE 1. Predictions of deuterium content arising from loss of the pro-*R* or pro-*S* hydrogen/deuterium atoms of THDOC on conversion to 5β-pregnan-3α-ol-20-one by *Eubacterium lentum*

		Predicted D content of product			
		pro-*R* loss		pro-*S* loss	
Substrate	Composition (%)	C21-*d*	ΣD	C21-*d*	ΣD
4	21-*S* (63) 21-*R* (21) 21-unlabelled (16) Total D = 0.84 C-21-D = 0.84	0.73	0.73	0.34	0.34
4*a*	21-*S* (30) 21-*R* (58) 21-unlabelled (12) Total D = 1.55 C-21-D = 0.88	0.46	1.13	0.71	1.38

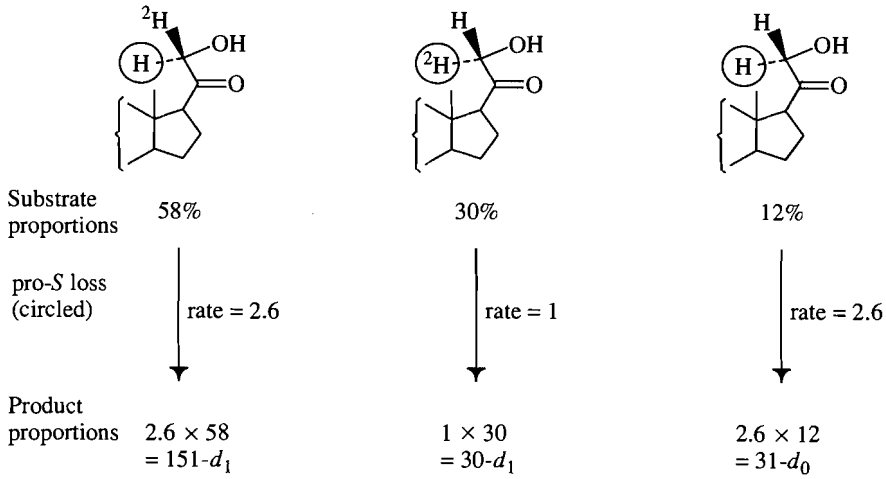
TABLE 2. Deuterium content of 5β-pregnan-3α-ol-20-one arising from C-21 dehydroxylation of 21-(*R*)- and 21-(*S*)-THDOC by *Eubacterium lentum*

		Deuterium at C-21		Total deuterium	
Substrate	Product	MS	NMR	MS	NMR
4	**5**	0.30	0.38	0.30	0.38
4*a*	**5***a*	—	0.78	1.42	—

The values in Table 1 were calculated starting from the isotopic compositions of the substrates **4** and **4***a*, as determined by 500-MHz ^{1}H nmr and FAB MS analysis (see Experimental for details), with the assumption of a primary kinetic isotope effect, k_H/k_D, of 2.6 for the conversion to **5** and **5***a* (3). The calculation for substrate **4***a* is detailed in Scheme 4. To avoid complications arising from changes in isotopic composition of substrate as the reactions proceeded, incubations with *E. lentum* were carried out only to the point of 10% conversion to product. Recovered starting material at this stage was essentially identical to isotopic content and stereochemistry with starting material analysed before exposure to *E. lentum*.

The values for isotopic content of the products **5** and **5***a* are presented in Table 2. The deuterium contents at C-21 in both **5** and **5***a* were estimated by integration of the signal from the C-21 methyl group in their 500-MHz ^{1}H nmr spectra, in which the signals from all three methyl groups of the product are cleanly resolved to the baseline. The values obtained (**5** = 38%, **5***a* = 78% d_1; predicted for pro-*S* loss **5** = 34%, **5***a* = 71% d_1) clearly indicate that loss has occurred from the pro-*S* position. In the case of **5**, the deuterium content at C-21 could also be obtained directly from mass spectral analysis, as the method of synthesis ensured that any label present must be located at the

Can. J. Chem. Downloaded from www.nrcresearchpress.com by 194.225.253.170 on 09/07/12
For personal use only.



Therefore total product $d_0 = 30 + 31 = 61$
total product $d_1 = 151$
deuterium content of **5***a* = 151/212 = 0.71

Substrate total *d* content at C-21 = 0.58 + 0.30 = 0.88
Product total *d* content at C-21 = 0.71
Predicted loss from C-21 = 0.88 − 0.71 = 0.17*d*

SCHEME 4. Calculations used to predict the deuterium content in **5***a* resulting from pro-(*S*) loss of hydrogen or deuterium from 21-(*R*)-THDOC **4***a*.

C-21 position. The value obtained (d_1 = 30%) also supports a loss from the pro-*S* position of **4** (predicted deuterium content for pro-*S* loss = 34%).

In the case of **5***a*, however, the presence of deuterium elsewhere in the molecule precluded direct determination of the deuterium content at C-21 by mass spectrometry. Mass spectral analysis of **5***a* nevertheless indicated the presence of a total of 1.42 deuteriums per molecule (see Experimental and Table 2), thus permitting the deuterium loss for the conversion of **4***a* to **5***a* to be estimated by comparison with the total deuterium content of **4***a* (1.55 deuteriums) as 0.13 deuterium atoms per molecule, a value in reasonable agreement with the loss of 0.17 deuteriums per molecule predicted for loss of the pro-*S* atom from C-21 of **4***a*. The ms data are thus supportive of the conclusions reached from nmr analysis, namely that conversion of 5β-pregnane-3α,21-diol-20-one (**6**) into 5β-pregnan-3α-ol-20-one (**7**) by *Eubacterium lentum* proceeds with stereospecific loss of the pro-*S* hydrogen from C-21.

This finding now opens possibilities for the synthesis of C-21 pro-*S* substituted deoxycorticosteroids whose metabolic deactivation by anaerobic C-21 dehydroxylation may be blocked.

Experimental

Apparatus, materials, and methods

Melting points were determined on a Kofler heating stage and are uncorrected. Proton nmr spectra were determined at 80 MHz on a Bruker WP80CW, at 200 MHz on a Bruker AC200, or at 500 MHz on the Bruker AM500 at McMaster University, using deuterochloroform as solvent and chloroform as internal standard. Deuterium nmr spectra were obtained at 30.7 MHz using the Bruker AC200 instrument with chloroform as solvent and deuterochloroform as internal standard. Electron impact (EI) mass spectra were obtained with an AEI MS30 interfaced to a Kratos DS55 data system, and fast atom bombardment (FAB) spectra were obtained with the same machine fitted with an Ion Tech saddle field gun operating at 7 keV using a glycerol matrix. Deuterium content was estimated following repetitive analyses and application of the appropriate corrections for natural isotopic abundances, and is accurate to ± 2% (EI) or ± 5% (FAB). Centrifugation was done using either a Sorvall RC5 with a GSA head or an IEC B20A with an IEC 870 head. Liver homogenates were obtained from fresh commercial beef liver using a Waring blender. Flash column chromatography was performed on silica gel (Merck 230–400 mesh or equivalent), thin-layer chromatography on Merck silica gel 60F-254 (0.2 mm), and preparative layer chromatography on 2.0-mm Merck F-254 silica gel plates.

Maintenance of micro-organisms

Eubacterium lentum ATCC 25559 was maintained on a medium of cysteine supplemented brain heart infusion broth (sBHIB) as previously described (3). *Clostridium paraputrificum* ATCC 25780 was also maintained on sBHIB using identical techniques. Cultures were maintained by transfers to fresh medium at intervals of 7 days.

Isolation of 21-hydroxysteroid NAD oxidoreductase

This enzyme was isolated from fresh commercial beef liver using the published procedure (9) to the point of the supernatant fluid from the 55°C heat treatment. The resulting preparation was stored at 4°C and used within 2 weeks.

Reduction of **2**a *with 21-hydroxysteroid NAD oxidoreductase*

The above enzyme preparation (5 mL) was diluted to 100 mL with 0.1 M phosphate buffer, pH 7.4, and NADH (50 mg) dissolved in this solution. A solution of pregn-4-en-21-al-3,20-dione, 17,21-d_2 (25 mg) in 95% ethanol (1.5 mL) was then added, and the mixture stirred at room temperature for 2 h. The aqueous solution was then extracted with ethyl acetate, and the extract dried and evaporated to give a residue (20 mg). Crystallization from ethyl acetate/hexane afforded 21-(*R*)-pregn-4-ene-3,20-dion-21-ol, 17,21-d_2 (**3***b*), identified by comparison with an authentic sample of unlabelled material. The ^{1}H nmr included δ 4.12 (s, C-21 pro-*S* H) and 4.16 (s, C-21 pro-*R* H) ppm in the ratio 25:1.

Synthesis of substrates

Pregn-4-ene-3,20-dion-21-ol, 17,21,21-d_3 *(DOC-*d_3*,* **1***a*)

This was prepared from unlabelled material using the method previously described for the preparation of 5β-pregnane-3α,21-diol-20-one, 17,21,21-d_3 (3). A solution of unlabelled **1** (1.5 g) in methanol-OD (15 mL) was added to a solution of Tris base (3.15 g,

Can. J. Chem. Downloaded from www.nrcresearchpress.com by 194.225.253.170 on 09/07/12
For personal use only.

Can. J. Chem. Downloaded from www.nrcresearchpress.com by 194.225.253.170 on 09/07/12
For personal use only.

previously exchanged with deuterium oxide and vacuum dried) in methanol-OD (50 mL) and deuterium oxide (50 mL). Following exchange and work-up of the reaction mixture, the residue (1.63 g) was resubmitted to the exchange procedure, and the resulting material purified by chromatography to give **1***a* (1.2 g), identical in physical properties (mp, tlc) to unlabelled starting material. Using the C-4 ^{1}H nmr signal at δ 5.68 ppm as an internal standard of 1.0 hydrogens allowed the residual ^{1}H content at C-21 (δ 4.15 ppm) to be estimated as 0.05H; ^{2}H nmr: δ 2.4, 4.14 ppm (no detectable signal at δ 5.68 ppm). Using the C-21 ^{2}H signal at δ 4.14 ppm as an internal standard of 1.94 deuteriums, the total signal at δ 2.4 ppm corresponded to 1.59 deuteriums. FAB MS showed a molecular ion cluster at *m/e* 330–336.

Pregn-4-en-21-al-3,20-dione (2)

Following the procedure outlined (6), a solution of cupric acetate in dry methanol (100 mL, 0.005 M) was added to a solution of **1** (1.2 g) in dry methanol (100 mL), and the resulting mixture stirred with aeration at the rate of one bubble per second for 45 min. A solution of disodium EDTA (200 mg) in water (12 mL) was then added, and stirring continued for a further 15 min. The solvent was then removed by evaporation, water (200 mL) added, and the resulting mixture extracted with methylene chloride (3 × 50 mL). The yellow extract was washed with 5% aqueous sodium bicarbonate and water, then dried and evaporated to give a residue (1.2 g), which was used directly in the preparation of **3**. As noted by others (7, 8) this product is a mixture of the aldehyde **2** (^{1}H nmr including signals at δ 0.65 (C-18H), 1.18 (C-19H), 5.68 (C-4H), and 9.1 (C-21H) ppm), and the 21 hydrate (^{1}H nmr including a signal at δ 4.70 (C-21H)). FAB MS showed ions at *m/e* 347 (M^+ hydrate + H, 15) and 329 (M^+ aldehyde + H, 64) relative to 307 (M − CHO or $CH(OH)_2$, 100).

*Pregn-4-en-21-al-3,20-dione, 17,21,21-*d$_3$ *(2*a*)*

This was prepared from DOC-d_3 (**1***a*) (1.2 g) by the method described above for the preparation of **2**, with extension of the reaction time to 105 min as a consequence of tlc monitoring. Work-up as described above gave the title compound (1.19 g) as a yellow solid, identical on tlc with unlabelled material; ^{2}H nmr: δ 2.4 (C-17 ^{2}H), 4.82 (C-21 $C^2H(OH)_2$), and 9.2 (C-21 C^2H) ppm.

*21-(*S*)-Pregn-4-ene-3,20-dion-21-ol, 21-*d *(3)*

Sodium borodeuteride (38 mg) was added in one portion to a stirred solution of pregn-4-en-21-al-3,20-dione (**2**) (1.2 g) in dry pyridine (24 mL) at −5°C. Stirring was continued for 15 min, and the solution then poured into water (50 mL) and extracted with ethyl acetate (4 × 100 mL). The extract was washed with 2 M tartaric acid (3 × 50 mL) and water, and then dried and evaporated to give a residue (1.0 g) that was purified by chromatography (benzene/ether gradient elution) to give the title compound (0.76 g), crystallized from ethyl acetate/hexane. The product showed physical and spectral data identical with those of authentic unlabelled material with the following exceptions: ^{13}C nmr: triplet at δ 69.0, J = 21 Hz (C-21); ^{1}H nmr (500 MHz): included δ 4.12 (s, C-21 pro-*S* H) and 4.16 (s, C-21 pro-*R* H) ppm in the ratio 1:3.1. FAB MS: *m/e* (%) 332 (100), 331 (24). Comparison with unlabelled material indicated the presence of >90% d_1 labelled material.

*21-(*R*)-Pregn-4-ene-3,20-dion-21-ol, 17,21-*d$_2$ *(3*a*)*

This was prepared by the procedure described for compound **3**, using sodium borohydride (35 mg) and the labelled aldehyde **2***a* (1.2 g). The crude product (0.93 g) was purified as described above to give a total of 0.2 g of the desired product, identical on spectral analysis with authentic unlabelled material, with the following exceptions: ^{1}H nmr (500 MHz): included δ 4.12 (s, C-21 pro-*S* H) and 4.16 (s, C-21 pro-*R* H) ppm in the ratio 2.0:1. FAB MS: *m/e* (%) 333–335, comparison with unlabelled material indicating approximately equal amounts of d_2 and d_3 labelled material.

Incubations with Clostridium paraputrificum *ATCC 25780*

Pregn-4-ene-3,20-dion-21-ol (DOC, 1)

To 1.5 L of sBHIB growth medium, prepared as described (3), was added 10 mL of an overnight culture of *C. paraputrificum*, followed by a solution of DOC (150 mg) in 95% ethanol (7.5 mL). The culture was maintained at 37°C for 7 days, and then worked up as described (3) to give a residue (1.13 g) that, following chromatography, afforded 0.12 g of 5β-pregnane-3α,21-diol-20-one (THDOC, **6**), identical in all respects with an authentic sample.

*Pregn-4-ene-3,20-dion-21-ol, 17,21,21-*d$_3$ *(DOC-*d$_3$*, 1*a*)*

Using the procedure described above, incubation of **1***a* (25 mg) with *C. paraputrificum* gave, after purification, 17.5 mg of 5β-pregnane-3α,21-diol-20-one, 17,21,21-d_3 (**4***b*). The ^{1}H nmr (200 MHz) showed the presence of a signal at δ 4.13 (0.20H) in addition to the signals expected for THDOC-d_3. At 500 MHz, signals at δ 4.10 (0.1H, C-21 pro-*S* H) and 4.16 (0.1H, C-21 pro-*R* H) ppm were observed; ^{2}H nmr: δ 2.90 (C-17 ^{2}H), 4.10 (C-21 ^{2}H) ppm.

*21-(*S*)-Pregn-4-ene-3,20-dion-21-ol, 21-*d *(3)*

Incubation of **3** (200 mg) with *C. paraputrificum* (2 L culture) as described above gave, following chromatography of the extract, 21-(*S*)-5β-pregnane-3α,21-diol-20-one, 21-*d* (**4**) (120 mg), identical in all respects with authentic unlabelled material **6** with the following exceptions: ^{1}H nmr (500 MHz) included δ 4.10 (s, C-21 pro-*S* H) and 4.16 (s, C-21 pro-*R* H) ppm in the ratio 1:3.0, together with 4.12, 4.18 ppm (ABq, total 0.32H, unlabelled C-21H). FAB MS *m/e* (%) 336 (74), 335 (34) relative to 318 (100). Comparison with the spectrum of unlabelled material indicated the isotopic composition to be d_0 22%, d_1 78%.

*21-(*R*)-Pregn-4-ene-3,20-dion-21-ol, 17,21-*d$_2$ *(3*a*)*

Incubation of **3***a* (200 mg) with *C. paraputrificum* as described above gave, following chromatography, 21-(*R*)-5β-pregnane-3α,21-diol-20-one, 17,21-d_2 (**4***a*) (95 mg), identical in all respects with an authentic sample of unlabelled material **6** with the following exceptions: ^{1}H nmr (500 MHz) included signals at δ 4.10 (s, C-21 pro-*S* H) and 4.16 (s, C-21 pro-*R* H) in the ratio 1.9:1, together with 4.12, 4.18 (ABq, total 0.25H, unlabelled C-21H). FAB MS *m/e* 335–338: comparison with the spectrum of unlabelled material indicated the isotopic composition to be d_0 19%, d_1 26%, d_2 36%, d_3 19%, corresponding to a total of 1.55 deuteriums per molecule (0.26 + 0.36 × 2 + 0.19 × 3).

Incubations with Eubacterium lentum *ATCC 25559*

Incubations with *E. lentum* were performed exactly as described (3), using an incubation period of 140 h.

*21-(*S*)-5β-Pregnane-3α,21-diol-20-one, 21-*d *(21-(*S*)-THDOC-21-*d*, 4)*

Incubation of **4** (100 mg) with a mixed *E. lentum/E. coli* culture gave, following extraction and chromatography, 5β-pregnan-3α-ol-20-one (**5**, 9 mg), identified by comparison of spectral properties with those of an authentic sample of unlabelled material. The ^{1}H nmr (500 MHz) included signals at δ 0.56 (3H, s, C-18H), 0.89 (3H, s, C-19H), and 2.09 (2.62H, s, C-21H) ppm. EIMS *m/e* (%) 319 (21), 318 (44) relative to 301 (100); *d* content d_0 71.3%, d_1 29.7%. Also obtained was recovered substrate **4** (77 mg) identical in all respects with the sample of **4** described above.

*21-(*R*)-5β-Pregnane-3α,21-diol-20-one, 17,21-*d$_2$ *(21-(*R*)-THDOC-17,21-*d$_2$*, 4*a*)*

Incubation of **4***a* with *E. lentum/E. coli* gave an extract that, following chromatography, afforded 5β-pregnan-3α-ol-20-one (**5***a*, 11 mg), identified as described above for **5**; ^{1}H nmr (500 MHz) included signals at δ 0.56 (3H, s, C-18H), 0.89 (3H, s, C-19H), and 2.09 (2.22H, s, C-21H) ppm. EIMS *m/e* 318–321, indicating the isotopic composition to be d_0 20%, d_1 35%, d_2 28%, d_3 17% for a total of 1.42 deuteriums (0.35 + 0.28 × 2 + 0.17 × 3). Also obtained was recovered substrate (75 mg) identical in all respects with the initial substrate **4***a*.

Acknowledgements

This research was funded by the Natural Sciences and Engineering Research Council of Canada. We are grateful to Mr. T. Jones (Brock) and Dr. D. Hughes (McMaster) for their assistance in the acquisition of spectral data.

1. J. WINTER and V. D. BOKKENHEUSER. J. Steroid Biochem. **9**, 379 (1978).
2. V. D. BOKKENHEUSER, J. WINTER, P. DEHAZYA, and W. J. KELLY. Appl. Environ. Microbiol. **34**, 571 (1977).
3. H. L. HOLLAND and E. RIEMLAND. Can. J. Chem. **63**, 981 (1985).
4. S. D. FEIGNER, V. D. BOKKENHEUSER, J. WINTER, and P. B. HYLEMAN. Biochem. Biophys. Acta, **574**, 154 (1979).
5. V. D. BOKKENHEUSER, J. WINTER, P. DEHAZYA, O. DE LION, and W. G. KELLY. J. Steroid Biochem. **7**, 837 (1976).
6. M. L. LEWBART and V. R. MATTOX. J. Org. Chem. **28**, 2001 (1963).
7. P. GREENZAID, Z. LUZ, and D. SAMUEL. J. Am. Chem. Soc. **89**, 749 (1967).
8. J. C. ORR and C. MONDER. J. Biol. Chem. **250**, 7547 (1975).
9. C. MONDER and A. WHITE. J. Biol. Chem. **238**, 767 (1963).
10. C. MONDER and H. L. BRADLOW. Recent Prog. Horm. Res. **36**, 345 (1980).

Can. J. Chem. Downloaded from www.nrcresearchpress.com by 194.225.253.170 on 09/07/12
For personal use only.

The dissociation constant and acid hydrolysis rate of hydroxysulfamic acid

DAVID LITTLEJOHN, ABIGAIL R. WIZANSKY, and S. G. CHANG[1]

Lawrence Berkeley Laboratory, University of California, Berkeley, California 94720, U.S.A.

Received August 29, 1988

DAVID LITTLEJOHN, ABIGAIL R. WIZANSKY, and S. G. CHANG. Can. J. Chem. **67**, 1596 (1989).

The acid dissociation constant and hydrolysis rate of hydroxysulfamic acid (HSA) in acid aqueous solutions have been studied. The acid dissociation constant was determined to be $K = 1.5 \pm 0.5\ M$ at 298 K. The hydrolysis rate, R, was found to be $R = k[H^+][HSA]$, where $k = 6.2 \times 10^{12} \exp(-26\,300/RT)\ M^{-1}\ s^{-1}$ at $\mu = 1.0\ M$ and [HSA] is the concentration of all forms of hydroxysulfamic acid.

Key words: hydroxysulfamic acid, hydrolysis, acid dissociation.

DAVID LITTLEJOHN, ABIGAIL R. WIZANSKY et S. G. CHANG. Can. J. Chem. **67**, 1596 (1989).

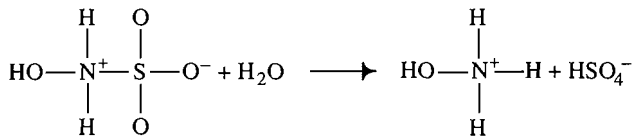
On a étudié la constante de dissociation acide et la vitesse d'hydrolyse de l'acide hydroxysulfamique (AHS) dans des solutions diluées d'acides aqueux. A 298 K, on a déterminé que la constante de dissociation acide est $K = 1{,}5 \pm 0{,}5\ M$. On a trouvé que, à une valeur de $\mu = 1.0\ M$, la vitesse d'hydrolyse $R = k[H^+][AHS]$, dans laquelle $k = 6{,}2 \times 10^{12} \exp(-26\,3000/RT)\ M^{-1}\ s^{-1}$ et [AHS] est la concentration de toutes les formes de l'acide hydroxysulfamique.

Mots clés : acide hydroxysulfamique, hydrolyse, dissociation acide.

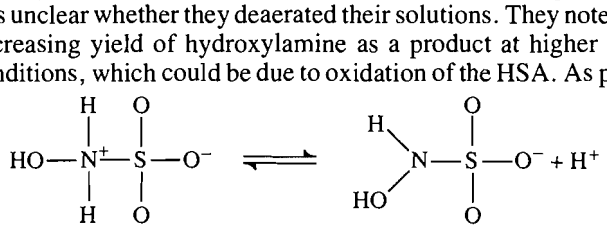
[Traduit par la revue]

Introduction

Reactions between nitrite ions and bisulfite ions occur in aqueous solutions and may be involved in the acid rain formation from SO_2 and NO_x in aqueous aerosols. These reactions can also be important in solution-based flue gas scrubbing systems. Knowledge of the chemistry of these compounds is needed to predict their behavior in aqueous solutions. Most of the chemistry associated with the nitrogen sulfonate products of these reactions is fairly well understood (1). An exception is the



decomposition of hydroxysulfamic acid (HSA) in acidic conditions. Ackermann and Powell (2, 3) have investigated the akaline hydrolysis and oxidation by oxygen of HSA. The only quantitative study of the acid hydrolysis of HSA was done by Candlin and Wilkins (4), who performed a limited number of hydrolysis runs in their studies of nitrogen–sulfur compounds. It is unclear whether they deaerated their solutions. They noted a decreasing yield of hydroxylamine as a product at higher pH conditions, which could be due to oxidation of the HSA. As part



of our studies of the chemistry of nitrogen–sulfur compounds (5–7), we have investigated the acid dissociation constant of HSA. While working with HSA it was decided to make a determination of the acid hydrolysis rate.

Experimental

HSA was prepared in aqueous solution by hydrolyzing dissolved potassium hydroxyimidodisulfate (HIDS). HIDS is prepared by reacting nitrite ion with bisulfite ion at 0°C (8). The synthesis of potassium HIDS is more straightforward than for HSA (8, 9), and higher yields and purity can be obtained. HIDS hydrolyzes much more quickly than HSA, and did not interfere in the studies. The potassium IDS was stored in a refrigerated dessicator to retard decomposition. Reagent grade compounds were used in the HIDS synthesis and in the solutions used for this study.

The acid dissociation constant for HSA was determined by observing solutions of HSA with varying concentrations of perchloric acid using Raman spectroscopy. Quantitative measurements of the concentrations of compounds above about 0.01 M in solution by Raman spectroscopy can be obtained by use of a reference compound. At higher concentrations (about 0.5 M or higher), scan-to-scan reproducibility is generally better than ±5% when the peaks are free of interference. Raman spectra of the HSA – perchloric acid solutions were obtained immediately after preparation to avoid problems with the hydrolysis of HSA. The solutions were prepared under a nitrogen atmosphere. The heights of the Raman peaks for the two forms of HSA were compared with each other and the ClO_4^- peak to determine the dissociation constant. Since the peaks of the two forms of HSA overlap, reference spectra of the two forms were scaled to yield a flat baseline on subtraction to determine the concentrations. The spectra were corrected for the presence of HSO_4^-, which slightly overlapped the HSA peaks. These corrections introduced some uncertainty into the results. All measurements were made with deaerated solution.

The hydrolysis of HSA was studied using ion chromatography to monitor the decay of HSA and the growth of the sulfate product (10). Solutions were prepared by adding the HIDS salt to a deaerated perchloric acid solution. The solutions were kept under a nitrogen atmosphere in a water bath of the desired temperature. The ionic strength of the solutions was adjusted with sodium perchlorate when necessary. When the HIDS had completely hydrolyzed, as determined by Raman spectra of the solution, it was placed in a controlled-temperature bath. Aliquots were then taken periodically and diluted for analysis by ion chromatography. The ion chromatograph has a linear response to HSA and sulfate at concentrations up to $10^{-4}\ M$, so solutions were diluted to ensure that the HSA and sulfate ions were below this level.

Results and discussion

For the determination of the acid dissociation constant of HSA, Raman spectra were obtained of 0.01 M HSA solutions with perchloric acid concentrations ranging from 0.001–5.1 M over a temperature range of 288–338 K. The spectra obtained at the lowest acid concentrations had only the deprotonated form of HSA present, with a Raman peak at 1056 cm^{-1}. These spectra were used to determine the amount of deprotonated HSA in other solutions and correct their spectra, so that the peak due to

[1]Author to whom all correspondence should be addressed.

Can. J. Chem. Downloaded from www.nrcresearchpress.com by 194.225.253.170 on 09/07/12
For personal use only.

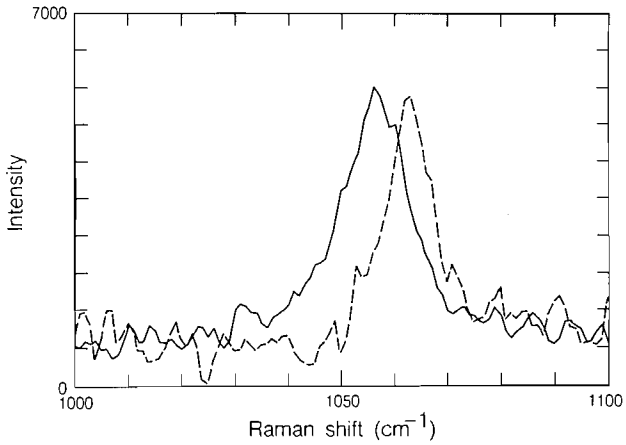


FIG. 1. Raman spectra of the anion (1056 cm^{-1}) and the acid (1063 cm^{-1}) forms of HSA.

protonated HSA at 1063 cm^{-1} could be measured. From these measurements, it was found that the HSA acid and the HSA anion had Raman scattering efficiencies of 0.50 and 0.48 respectively, compared to the 980 cm^{-1} sulfate peak at 298 K. Raman spectra of the two peaks are shown in Fig. 1. These Raman peaks are due to the SO_3 stretch in the molecules (11). The small shift in the stretch frequency observed on protonation suggests that the hydrogen ion is attaching to the nitrogen (structure **I**) rather than the SO_3 group (structure **II**).



I

II

There was a significant amount of HSA anion present in the 5.1 *M* perchloric acid solution. From the measured concentrations of the two forms of HSA and the hydrogen ion concentration, the acid dissociation constant was calculated. The average value obtained was $K = 1.5 \pm 0.5\ M$ at 298 K. The uncertainty is due largely to the noise in the Raman spectra. Within the uncertainty, no significant temperature dependence of the dissociation constant was observed over a temperature range of 288–338 K. Work done by Hall and Sprinkle (12) suggests that there should be a relatively small change in the equilibrium constant with temperature. The ionic strengths of the solutions studied were not controlled. Most of the solutions were in the range of $\mu = 1$ to 5 *M*.

To determine the hydrolysis rate of HSA, measurements were made on HSA solutions over a range of conditions. Perchloric acid concentrations varied from 0.03 to 2.0 *M* and HSA concentrations varied from 3×10^{-4} to $3 \times 10^{-2}\ M$. Ionic strengths of these solutions ranged from 0.03 to 2.1 *M*. The hydrolysis was studied over a temperature range of 298 to 358 K. Most of the hydrolysis runs were done at perchloric acid concentrations of 0.10 and 1.0 *M*.

The dependence of the hydrolysis rate on hydrogen ion concentration was determined with a series of runs at 348 K in which $[H^+]$ was varied from 0.03 to 1.0 *M* at [HSA] = 0.01 *M* and $\mu = 1.0\ M$. The effective rate exhibited first order dependence on $[H^+]$. A run done at $[H^+] = 2.0\ M$ was corrected for ionic strength and its rate was found to be in agreement with the results obtained at lower acidities. The hydrolysis rate dependence on HSA concentration was determined from runs done with 0.1 *M* $HClO_4$ at 348 K and $\mu = 0.13$–$0.18\ M$. The rate showed first order dependence on [HSA] for concentrations from 1×10^{-3} to $3 \times 10^{-2}\ M$.

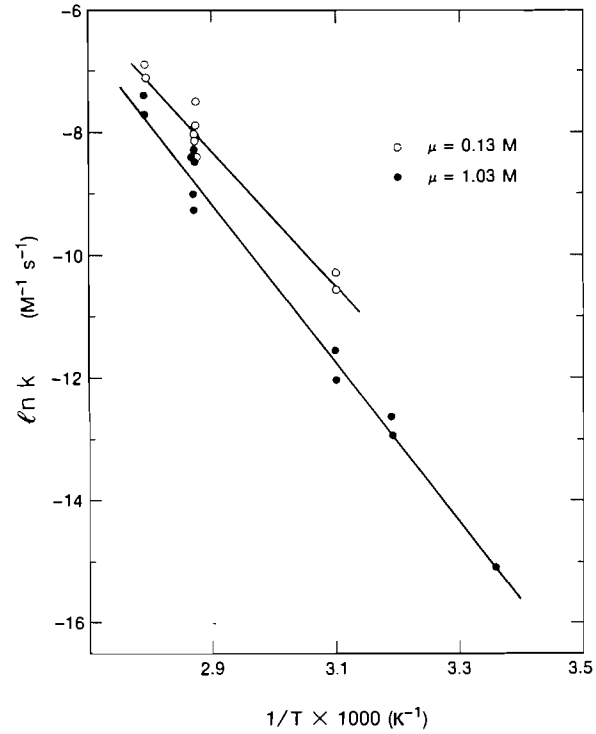


FIG. 2. Arrhenius plot of the rate constant for the hydrolysis of HSA at $\mu = 0.13\ M$ ($[H^+] = 0.1\ M$) and $\mu = 1.03\ M$ ($[H^+] = 1.0\ M$). [HSA] = 0.01 *M* for both conditions.

The rate constants were calculated from the experimental results using the expression of rate = $k[H^+][HSA]$, where [HSA] is the sum of the concentrations of the protonated and deprotonated forms of HSA. The ionic strength dependence was determined from a plot of log *k* vs. $\mu^{1/2}/(1 + \mu^{1/2})$ for runs at 348 and 358 K. At both temperatures, the results yielded a slope of −1, within the uncertainty of the data. This is what would be expected for a reaction of HSA with a 1− charge with H^+. Candlin and Wilkins obtained a slightly lower slope, possibly due to interference by oxygen. Extrapolating the 358 K data to $\mu = 0$ leads to a value of $k = 1.63 \times 10^{-3}\ M^{-1}\ s^{-1}$, close to the value of $1.75 \times 10^{-3}\ M^{-1}\ s^{-1}$ obtained by Candlin and Wilkins. The temperature dependence of the rate constant can be expressed as $k = A \exp(-E_a/RT)$, where *A* is the pre-exponential factor, E_a is the activation energy, *R* is the gas constant and *T* is the absolute temperature. Plots of ln *k* vs. $1/T$ for $\mu = 0.13\ M$ and $\mu = 1.03\ M$ are shown in Fig. 2. The lines are least-squares fits to the data, which give $A = 1.3 \times 10^{10}$ ($\ln A = 23.3 \pm 2.5$) and $E_a = 21.7 \pm 0.7$ kcal mol^{-1} for $\mu = 0.13\ M$, and $A = 6.2 \times 10^{12}$ ($\ln A = 29.5 \pm 1.4$) and $E_a = 26.3 \pm 1.0$ kcal mol^{-1} for $\mu = 1.03\ M$. Candlin and Wilkins obtained a rate expression of $k = 3.2 \times 10^{10} \exp(22\ 800/RT)\ M^{-1}\ s^{-1}$ at 1 *M* H^+. Both expressions for the rate constant at $\mu = 1\ M$ give similar values of the rate constant in the temperature range of 323 to 358 K.

The results indicate that HSA is fairly stable in moderately acid solutions (pH 2–4) where other nitrogen–sulfur compounds hydrolyze. The results indicate that significant amounts of HSA could accumulate in aqueous aerosols exposed to SO_2 and NO_x. In an acidic environment, oxidation by O_2 is fairly

Can. J. Chem. Downloaded from www.nrcresearchpress.com by 194.225.253.170 on 09/07/12
For personal use only.

slow (3). Since the acid hydrolysis is also slow, except under highly acidic conditions, the oxidation and acid hydrolysis pathways will be competitive. Under these conditions, HSA may have time to react to form other compounds if other reactive species are present.

Acknowledgement

This work was supported by the Assistant Secretary for Fossil Energy, Office of Coal Utilization Systems, U.S. Department of Energy under Contract No. DE-AC03-76SF00098 through the Pittsburgh Energy Technology Center, Pittsburgh, PA.

1. S. G. CHANG, D. LITTLEJOHN, and N. H. LIN. Am. Chem. Soc. Symp. Ser. No. 188, 127, 1982.
2. M. N. ACKERMANN and R. E. POWELL. Inorg Chem. **5**, 1334 (1966).
3. M. N. ACKERMANN and R. E. POWELL. Inorg. Chem. **6**, 1718 (1967).
4. J. P. CANDLIN and R. G. WILKINS. J. Am. Chem. Soc. **87**, 1490 (1965).
5. S. B. OBLATH, S. S. MARKOWITZ, T. NOVAKOV, and S. G. CHANG. J. Phys. Chem. **85**, 1017 (1981).
6. D. LITTLEJOHN, K. Y. HU, and S. G. CHANG. Inorg. Chem. **25**, 3131 (1986).
7. D. LITTLEJOHN, A. R. WIZANSKY, and S. G. CHANG. Inorg. Chem. **25**, 4160 (1986).
8. G. K. ROLLEFSON and C. F. OLDERSHAW. J. Am. Chem. Soc. **54**, 977 (1932).
9. R. NAST, K. NYUL, and E. GRZIWOK. Z. anorg. allg. Chem. **267**, 304 (1952).
10. D. LITTLEJOHN and S. G. CHANG. Anal. Chem. **58**, 158 (1986).
11. J. R. HALL and R. A. JOHNSON. Raman Spectrosc. **11**, 279 (1981).
12. N. F. HALL and M. R. SPRINKLE. J. Am. Chem. Soc. **54**, 3469 (1932).

Can. J. Chem. Downloaded from www.nrcresearchpress.com by 194.225.253.170 on 09/07/12
For personal use only.

Spectrophotometric determination of sulfanilic acid and sulfonamides in pharmaceutical samples with potassium 1,2-naphthoquinone-4-sulfonate

A. PUNTA CORDERO, F. J. BARRAGÁN DE LA ROSA, and A. GUIRAUM

Department of Analytical Chemistry, Faculty of Chemistry, University of Sevilla, 41012-Sevilla, Spain

Received February 1, 1989

A. PUNTA CORDERO, F. J. BARRAGÁN DE LA ROSA, and A. GUIRAUM. Can. J. Chem. **67**, 1599 (1989).

An accurate and simple method is proposed for the determination of sulfanilic acid in the presence of sulfonamides. This method is based on measuring the intensity of the red colour that develops when sulfanilic acid is allowed to react with potassium 1,2-naphthoquinone-4-sulphonate (NS) in a chloroaceticchloroacetate buffer at pH 3.4. Colour development reaches completion after 2 h, allowing sulfanilic acid to be quantified spectrophotometrically at 470 nm ($\epsilon = 4.7 \times 10^3$ L mol^{-1} cm^{-1}). The main product causing colour formation, potassium 1,2-naphthoquinone-4-(N-aminophenylen-4-sulphonate) (NSSA), was isolated and characterized. When samples also contain sulfonamides an extraction into chloroform must be performed. Sulfanilic acid in binary mixtures with sulfanilamide, sulfacetamide, or sulfathiazole can be determined either by direct measurement of the aqueous phase after extraction at 470 nm or by subtracting from the absorbance of the aqueous phase before extraction the absorbance of sulfonamide as determined by measuring the extracted chloroform phase at 345 nm. Sulfadiazine, sulfamethoxipyridazine, and sulfamethoxazole interferences are prevented by their extraction into chloroform at pH 7.2; these species cannot be determined. The effects of pH, reagent concentration, time, and temperature on colour formation were investigated. In all cases the standard addition method gave more accurate results. The method was applied to several pharmaceutical samples.

Key words: spectrophotometry, sulfanilic acid, sulfonamides, potassium 1,2-naphthoquinone-4-sulphonate.

A. PUNTA CORDERO, F. J. BARRAGÁN DE LA ROSA et A. GUIRAUM. Can. J. Chem. **67**, 1599 (1989).

On propose une méthode précise et simple pour déterminer l'acide sulfanilique en présence de sulfonamides. La méthode est basée sur la mesure de l'intensité de la couleur rouge qui se développe lorsqu'on fait réagir de l'acide sulfanilique avec le 1,2-naphtoquinone-4-sulfonate de potassium (NS) dans un tampon d'acide chloroacétique-chloroacétate, à un pH de 3,4. La couleur est complètement développée après deux heures et l'on peut alors quantifier l'acide sulfanilique d'une façon spectrophotométrique à 470 nm ($\epsilon = 4{,}7 \times 10^3$ L mol^{-1} cm^{-1}). On a isolé et caractérisé le produit principal responsable de la couleur, le 1,2-naphtoquinone-4-(N-aminophénylène-4-sulfonate) de potassium (NSSA). Lorsque les échantillons contiennent aussi des sulfonamides, on doit procéder à une extraction au chloroforme. L'acide sulfanilique en mélanges binaires avec la sulfanilamide, la sulfacétamide ou le sulfathiazole peut être déterminée soit par une mesure directe de la phase aqueuse à 470 nm après extraction soit en soustrayant l'absorbance de la sulfonamide, telle que déterminée par une mesure à 345 nm de la phase chloroformique extraite, de l'absorbance de la phase aqueuse avant extraction. On peut prévenir les interférences de la part de la sulfadiazine, de la sulfaméthoxipyridazine et du sulfaméthoxazole en procédant à leur extraction dans le chloroforme à un pH de 7,2; on ne peut déterminer ces espèces. On a examiné les effets du pH, de la concentration des réactifs, du temps et de la température sur la formation de la couleur. Dans tous les cas, la méthode standard d'addition a fourni les meilleurs résultats. On a appliqué la méthode à de nombreux échantillions pharmaceutiques.

Mots clés : spectrophotométrie, acide sulfanilique, sulfonamides, 1,2-naphtoquinone-4-sulfonate.

[Traduit par la revue]

Introduction

Sulfonamides are pharmaceuticals used extensively as antibacterial compounds. They have, in general, very high chemotherapeutic coefficients, so that overdosage can cause digestive or renal accidents. Sulfonamides can rupture under the action of mineral acids at the S—N bond, producing sulfanilic acid (1). Sulfanilic acid exhibits a still greater toxicity than sulfonamides. It is therefore of interest to detect its presence in drugs.

The voltammetric behaviour of sulfanilic acid and sulfonamides has been studied, and selected mixtures have been analyzed by differential pulse voltammetry (2). It is difficult to obtain quantitative results using this approach, however, since the peaks of different compounds are not well resolved. Therefore, the method is proposed only for detection after high-performance liquid chromatography. On the other hand, the spectrophotometric determination of primary arylamines, including sulfonamides, sulfanilic acid, and aniline derivatives, with metol in the presence of *N*-bromosuccinimide has been proposed (3). Nevertheless, these compounds are usually determined by colourimetry based on the Bratton–Marshal procedure (4), which involves diazotation of the amine and coupling to a coloured dye. Since these methods are tedious, it is of interest to find less complicated procedures.

The present study is a method for the determination of sulfanilic acid, sulfonamides, and binary mixtures of the two based on condensation with potassium 1,2-naphthoquinone-4-sulphonate (NS) and separation of the resulting sulfonamide adducts by extraction into chloroform. The derivative of sulfanilic acid remains in the aqueous phase owing to its higher polarity. A few publications on the use of NS for detecting sulfonamides have appeared (5–7), but the proposed methods have been applied only to the pure amines, with no attempt to resolve mixtures in real samples.

In this paper we also report a study of the pure derivative of sulfanilic acid with NS (NSSA) (8) by UV–visible, IR, ^{1}H- and ^{13}C-NMR, and mass spectroscopy including the determination of its acid dissociation contant.

Experimental

Apparatus

Perkin Elmer 1310 and Varian XL 200 spectrometers were used for recording IR and NMR spectra. A Perkin Elmer 554-UV–visible spectrophotometer with matched glass cells of 1.00 cm path was employed. The mass spectrum was obtained with a Kratos MS8RFA apparatus under 70 eV as ionisation voltage and 300°C as the temperature of the source. A Beckman model-70 pH-meter was used.

Chemicals and pharmaceuticals

Amberlite CG-50 I cation exchange resin (Merck) was digested with

Printed in Canada / Imprimé au Canada

Can. J. Chem. Downloaded from www.nrcresearchpress.com by 194.225.253.170 on 09/07/12
For personal use only.

TABLE 1. Infrared spectral data for NSSA*

Bands (cm^{-1})	Assignments
3450 s	ν_{O-H}
3330 m	$\nu_{as\ N-H}$
1670 m	$\nu_{C=O}$ (quinone)
1620 vs	$\nu_{C=N}$
1185 s	ν_{C-O} (phenol)
1155 m	$\nu_{as\ SO_2}$
1010 m	$\nu_{s\ SO_2}$
810–750 w	δ_{Ph-H} (out-of-plane)

*Abbreviations: s, strong; m, medium; w, weak; v, very.

1 *M* KOH, and then placed in a 1-cm diameter ion exchange column to a depth of 10 cm. The column was washed with water until the pH of the eluate was 5 to 6. Sulfanilic acid was analytical grade (Merck-Schuchard), and 1,2-naphthoquinone-4-sulfonic acid, potassium salt (NS) was technical grade (Ega-Chemie). Sulfamethoxazole, sulfamethoxipirydazine, sulfadiazine, sulfanilamide (sodium salt), sulfacetamide, and sulfathiazole were pharmaceutical grade (Acofarma Tarrasa, Barcelona), and were utilized as working standards as received. Distilled-deionised water and spectroscopic grade chloroform were used throughout. Abactrim was an antibacterial chemotherapeutic suspension (Roche) containing 40 mg of trimetoprime and 200 mg of sulfamethoxazole per 5 mL; Bio Exazol Simple was an antibacterial tablet (Andreu–Barcelona) containing 125 mg of erythromycine base, 125 mg of sulfamethoxipyridazine total, and 150 mg of dimethylchlorotetracycline chlorhydrate per tablet; Amidrin was an antibacterial antiseptic solution (Fardi–Barcelona) containing 4 mg of sulfanilamide, 8 mg chlorhydrate of efedrine, and 5 mg of chlorobutanol per mL; and colirio Oculos was a sedative antiseptic solution (Frumtost-Zyma S.A. Barcelona) containing 100 mg of sulfacetamide sodium salt, 4 mg of tetracaine chlorhydrate, 6 mg of carbamide, and 0.4 mg of naphazoline per mL.

Synthesis and purification of NSSA

A solution of sulfanilic acid (0.7 g) in 60% ethanol–water (v:v) was added to an aqueous solution of 1,2-naphtoquinone-4-sulphonate (NS) (1.0 g). The mixture was refluxed for 30 min, then cooled and passed through an Amberlite CG-50 I column at a rate not exceeding 3 mL min^{-1}. The resin was washed with 200 mL of water and the eluates (about 400 mL) concentrated to approximately 40 mL. The solution upon cooling yielded a deep red violet product. The product when recrystallized from water showed only one spot in TLC tests on silica gel (R_f = 0.72 for chloroform–ethanol 75:25 and R_f = 0.30 for acetone–methanol 90:10). Melting point >300°C. *Anal.* Calcd. for $C_{16}H_{10}NSO_5K$: C 52.30, H 2.74, N 3.81, S 8.72; found: C 51.89, H 2.78, N 3.76, S 8.45. The assignments made for the IR, ^1H- and ^{13}C-NMR spectra of the product are showed in Tables 1 to 3. The calculated values of the ionization constant of the product are collected in Table 4. The molecular peak in the mass spectrum at m/z 368 is close to the calculated molecular weight of the compound (367.1 g mol^{-1}).

Reagent solutions

Sulfanilic acid and sulfonamide stock solutions

Dissolve in 250 mL of water an accurately weighed each of the following: for sulfanilic acid about 39.5 mg, sulfanilamide sodium salt about 44 mg, sulfacetamide about 49 mg, sulfathiazole about 49 mg, sulfamethoxipyridazine about 49 mg, sulfamethoxazole about 231 mg, and sulfadiazine about 200 mg. Working standard solutions are prepared by diluting with water as necessary.

NS stock solution

Dissolve 0.2012 g of potassium 1,2-naphthoquinone-4-sulphonate (Ega-Chemie) in 50 mL of water and dilute to 100 mL with water. This NS solution must be prepared daily.

Chloroacetic acid – chloroacetate (sodium salt) buffer, 0.1 *M* (total concentration), pH = 3.42.

Imidazole – hydrochloric acid buffer, 0.1 *M* (total concentration), pH = 7.20.

Prepared pharmaceutical samples

To accurately weighed amounts of Abactrim, Bio Exazol Simple, Amidrin, and Colirio Oculos an accurately weighed amount of sulfanilic acid was added. The samples were then dissolved in water and diluted to give the compositions shown in Table 5. The samples so prepared were starting materials for the analyses.

Assay procedure

Transfer 5 mL of a prepared pharmaceutical sample solution into a 25-mL calibrated flask and add 0, 1, 3, or 5 mL of sulfanilic acid or sulfonamide working standard solution to construct a standard additions graph (see Table 6). Add 5 mL of chloroaceticchloroacetate solution buffer and 5 mL of NS solution. Mix thoroughly and dilute to volume with water. Let stand for 2 h, then measure the absorbance at 470 nm (A_0) in a 1-cm cell against a blank. Subsequently carry out the separation of sulfonamides into chloroform using either technique A or B.

(A) For samples containing sulfamethoxipyridazine, sulfamethoxazole, or sulfadiazine

Adjust the pH of a 10-mL aliquot of prepared solution to 7.2 by adding 10 mL of imidazole–HCl buffer. Transfer 10 mL of this sample into a separatory funnel and extract twice for 2 min each time with 5 mL of chloroform. Discard the extracts and measure the absorbance of the aqueous phase at 470 nm (A_a) against blanks prepared under the same conditions, but using 5 mL of water instead of sample solution.

The intercept value in a plot of A_a vs. mg of added sulfanilic acid gives the sulfanilic acid concentration in the prepared pharmaceutical sample.

(B) For samples containing sulfanilamide, sulfacetamide or sulfathiazole

Place a 5-mL aliquot of prepared solution from the 25-mL calibrated flask in a separatory funnel and extract twice for 2 min each time with 5 mL of chloroform. Collect the extracts and measure the absorbance of the chloroform phase at 345 nm (A_b) against a blank.

The intercept value of a plot of $(A_0 - \epsilon_{470}/\epsilon_{345} \times A_b)$ vs. mg of added sulfanilic acid gives the sulfanilic acid concentration in the pharmaceutical sample. In the above expression ϵ_{470} and ϵ_{345} are the apparent molar absorptivities for the sulfonamide in the aqueous phase (λ_{max} 470 nm) and chloroform phase (λ_{max} 345 nm), respectively.

The intercept value of the graphic representation of A_b vs. mg of added sulfonamides gives the sulfonamide concentration in the prepared pharmaceutical sample.

Construction of calibration graphs

The calibration graphs to determine the molar absorptivities were not prepared from pure substances, but with binary mixtures of sulfanilic acid and sulfonamides, prepared by diluting and mixing aliquots of the stock solutions to give a series of suitable concentrations. Linearity is maintained over the range 7 to 28 μg mL^{-1} for sulfanilic acid; 7 to 15 μg mL^{-1} for sulfanilamide, sulfacetamide, or sulfathiazole; and 0 to 45 μg mL^{-1} for sulfamethoxipyridazine, sulfamethoxazole, or sulfadiazine. Sulfamethoxipyridazine, sulfamethoxazole, and sulfadiazine are not determinable because they develop little colour in the organic phase; their interference with the sulfanilic acid determination is eliminated by extraction at pH 7.20.

Determination of the stoichiometry of the sulfanilic acid – NS species

Job's method of continuous variations in equimolar (9) and in non-equimolar (10) conditions was employed. Standard aqueous solutions of sulfanilic acid (1.09×10^{-3} *M* to 2.30×10^{-3} *M*) and NS (2.20×10^{-3} *M* to 0.82×10^{-3} *M*) were used. A series of standard solutions of sulfanilic acid and NS in complementary proportions totalling 12 mL (from 0 to 12 and 12 to 0 inclusive) were prepared in 25-mL calibrated flasks. To each was added 5 mL of chloroacetic acid – sodium chloroacetate solution buffer. After 2 h the absorbance of each solution was measured at 470 nm against blanks prepared under the same conditions, but replacing the sulfanilic acid with an equal volume of water.

Yoe and Jones' method of molar ratios was also applied (11). Into a

Can. J. Chem. Downloaded from www.nrcresearchpress.com by 194.225.253.170 on 09/07/12
For personal use only.

Can. J. Chem. Downloaded from www.nrcresearchpress.com by 194.225.253.170 on 09/07/12
For personal use only.

TABLE 2. ^{1}H-nmr spectral data[a] (δ ppm)

Proton number	Sulfanilic acid	Compound III	Compound IV	NSSA Signal	NSSA Integration
3	—	5.87(s)	[b]	6.18(s)	1
5	—	8.06(m)	8.09(m)	7.96(m)	
6	—	7.76(m)	7.88(m)	7.81(m)	
7	—	7.82(m)	7.88(m)	7.86(m)	4
8	—	8.33(m)	8.05(m)	8.10(m)	
2′, 6′	7.30(m)[c]	7.24(m)	—	7.39(m)	4
3′, 5′	7.76(m)[c]	7.32(m)	—	7.65(m)	
4′	—	7.51(m)	—	—	
2(—OH)	—	—	11.50(s)	9.29	1
4(—NH—)	—	8.50(s)	—		

[a]Concentration of the compounds about 40 mg mL^{-1} in d_6-dimethylsulfoxyde, s = singlet, m = multiplet.
[b]Not comparable chemical environment.
[c]Assignments may be reversed.

TABLE 3. ^{13}C-nmr spectra[a] (δ ppm)

Carbon number	Sulfanilic acid	Compound IV	NSSA
1	—	181.3[c]	182.6[c]
2	—	159.7	152.6[c]
3	—	111.1	102.4
4	—	84.7[b,c]	168.4[c]
5	—	133.3	132.6
6	—	126.0	126.1
7	—	125.5	125.3
8	—	134.5	134.9
9	—	130.6[c]	130.4[c]
10	—	131.9[c]	132.5[c]
1′	147.0	—	—
2′, 6′	122.3	—	—
3′, 5′	127.0	—	—
4′	132.0	—	—

[a]Concentration of the compounds about 40 mg mL^{-1} in d_6-dimethylsulfoxide.
[b]Chemical environment of carbon not comparable.
[c]Quaternary carbon atom confirmed by Attached Proton Test (APT).

TABLE 4. Determination of pK_{a2}

Method	pK_{a2}[a,b]	ϵ_{HR^-}(470 nm)[c] (L mol^{-1} cm^{-1})	$\epsilon_{R^{2-}}$(530 nm)[b] (L mol^{-1} cm^{-1})
Maroni–Calmon			
Parallel straight lines	11.31	4480	3680
Concurrent straight lines	11.31	4480	3700
Romain–Colleter	11.26	4480	—
Potentiometric	11.62	—	—

[a]Mean value, 11.37.
[b]Obtained by corresponding method.
[c]Experimental value.

series of 25-mL calibrated flasks were placed 5 mL of chloroacetic acid – sodium chloroacetate solution buffer, 4 mL of sulfanilic acid (1.09×10^{-3} *M*) and variable amounts of NS solution (6.20×10^{-3} *M*). After 2 h the absorbances at 470 nm were measured against blanks.

Results and discussion

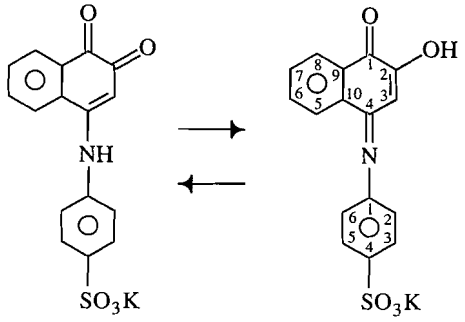
(A) Study of the NSSA adduct

Infrared, NMR, and UV–visible spectra

The use of several spectroscopic techniques permits one to establish the nature of the adduct formed between sulfanilic acid and 1,2-naphthoquinone-4-sulphonate (potassium salt). Two tautomers could be present (**I**, 4-arylamino-1,2-naphthoquinone; and **II**, 4-arylamino-2-hydroxy-naphthoquinone).

The infrared spectrum of the derivative (potassium bromide disk) is complicated; the main bands and their assignments are given in Table 1. The characteristic strong C=N band at 1620 cm^{-1} and the presence of a C=O band at 1670 cm^{-1} confirm the coupling of sulfanilic acid at position 4 of the NS molecule.

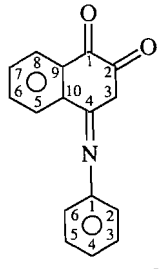
The most relevant features of ^{1}H- and ^{13}C-NMR spectra in d_6-dimethylsulphoxide are summarized in Tables 2 and 3. For



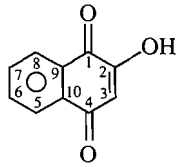
Tautomer I Tautomer II

comparison we synthesized substances **III** and **IV** by the method of Fieser (12, 13).

The most characteristic signal for this type of substance in the ^{1}H-NMR spectrum (Table 2) is a singlet at δ = 6.2 ppm



Compound III



Compound IV

TALE 5. Composition of synthetic pharmaceutical samples

Pharmaceutical sample	Sulfonamide contained	Concentration in sample solutions (mg mL^{-1}) Sulfonamide content	Sulfanilic acid added
Abactrim	Sulfamethoxazole	400	73
Bio exazol simple	Sulfamethoxipyridazine	415	73
Amidrin	Sulfanilamide	40	73
Colirio oculos	Sulfacetamide (sodium salt)	36	55

TABLE 6. Concentration of used working standard solutions to be added to the prepared pharmaceutical samples in the standard addition graph

Sample	Concentration of sulfonamides ($\mu g\ mL^{-1}$)	Concentration of sulfanilic acid ($\mu g\ mL^{-1}$)
Abactrim	—	111
Bio exazol simple	—	55
Amidrin	39 (sulfanilamide) (sodium salt)	55
Colirio oculos	132 (sulfacetamide)	111

corresponding to the proton attached at C_3. The peak at 9.29 ppm disappears on deuteration. The δ-value lies between those of —NH in **III** and —OH in **IV**, suggesting the tautomeric character of this proton.

The number of ^{13}C-NMR signals, Table 3, are 16 as expected and their positions agree well with those of corresponding carbons in the comparison compounds. The APT technique (14) shows no inversion for the C_1, C_2, and C_4 signals, in accordance with the quaternary character of these atoms. The presence in the NSSA spectrum of a single signal around 182 ppm (assigned to C=O) and one signal for C=N at 168.4 ppm is consistent with the tautomer **II** structure. On the other hand, for product **IV** two signals for C=O (C_1 and C_4) appear but the C=N signal is not present.

Ultraviolet–visible spectra at various pH values in water (Fig. 1) show a band at 270 nm and a shoulder at 340 nm, both assigned to $\pi \rightarrow \pi^*$ transitions, and a wide band with a maximum at 470 nm characteristic of 1,2-naphthoquinone nuclei bounded with arylamines at position 4. The chromophoric system changes beyond pH 11 and the maximum at 470 nm shifts to 525 nm. This may be explained by considering that in alkaline medium the 2-keto group is converted to a —OH group (transformation of form **I** to form **II**, producing maxima at 253 and 280 nm, typical for 1,4-naphthoquinones) which then deprotonates go give the corresponding anion. An analogous change in the molecular structure of other NS arylamine derivatives does not appear in alkaline media, but only in strong acids (pH ≤ 0.8) due to protonation of the 2-keto group (15). Weakly acidic or alkaline solutions contain 4-arylamino-1,2-naphthoquinone as the more important form. The fact that NSSA in strong acids does not undergo transformation from form **I** to form **II** could be attributable to the presence of the $-SO_3^-$ group, which precludes protonation of the 2-keto group.

Equilibria of NSSA with protons

The spectra of aqueous solutions of NSSA are pH-dependent

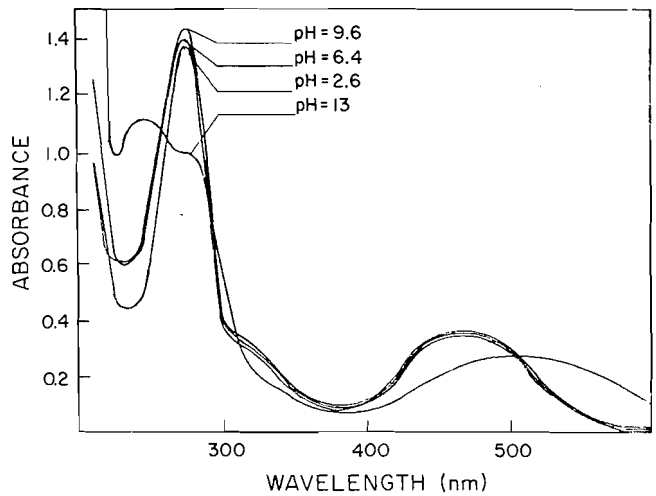


FIG. 1. Ultraviolet absorption spectra of NSSA ($c = 6.4 \times 10^{-5}$ mol L^{-1}) at different pH values.

(Fig. 2). The NSSA spectrum over pH 1 to 11 is attributed to the charged species RH^-, with an absorption maximum in the visible region at 470 nm which in strong acids may be converted to a fully protonated species (RH_2). We did not study this pK_a because we found that protonation of the $-SO_3^-$ group, if it occurs, is not reflected by any change in the spectrum of NSSA when a large amount of acid is present. Moreover, this pK_a lacks practical interest. The major species above pH 11 is the anion R^{2-}, which has an absorption maximum in the visible region at 525 nm.

Graphical analysis of A vs. pH curves (Fig. 2*A*) over the appropriate wavelengths yielded a pK_{a2} value. The Maroni–Calmon and Romain–Colleter methods were used. Deprotonation is shown by the absorbance step that appears for each wavelength in the basic region, with an inflection point dividing the steep part of the graph into two sections.

Maroni and Calmon (15) developed two techniques which permit one to obtain the pK_{a2} value and the molar absorptivity $\epsilon_{R^{2-}}$. In the first technique (method of parallel straight lines) A vs. $|A_{HR^-} - A|[H^+] \times 10^{12}$ is plotted (Fig. 2*B*); in the second one $1/|A - A_{HR^-}|$ vs. $[H^+] \times 10^{12}$ is plotted (Fig. 2*C*). In both cases the inverse of the slope yields the pK_{a2} value.

The Romain–Colleter method (16) was started with an initial pK_{a2} value of 10.3 (estimated from Maroni–Calmon's method) to obtain a more refined value. Budesinky's technique (17) to calculate the number of protons implicated in the ionization reaction was applied to the A vs. pH curves. It was found that only one proton participated in the reaction.

Potentiometric titration of a NSSA solution (0.0016 mol / L)

Can. J. Chem. Downloaded from www.nrcresearchpress.com by 194.225.253.170 on 09/07/12
For personal use only.

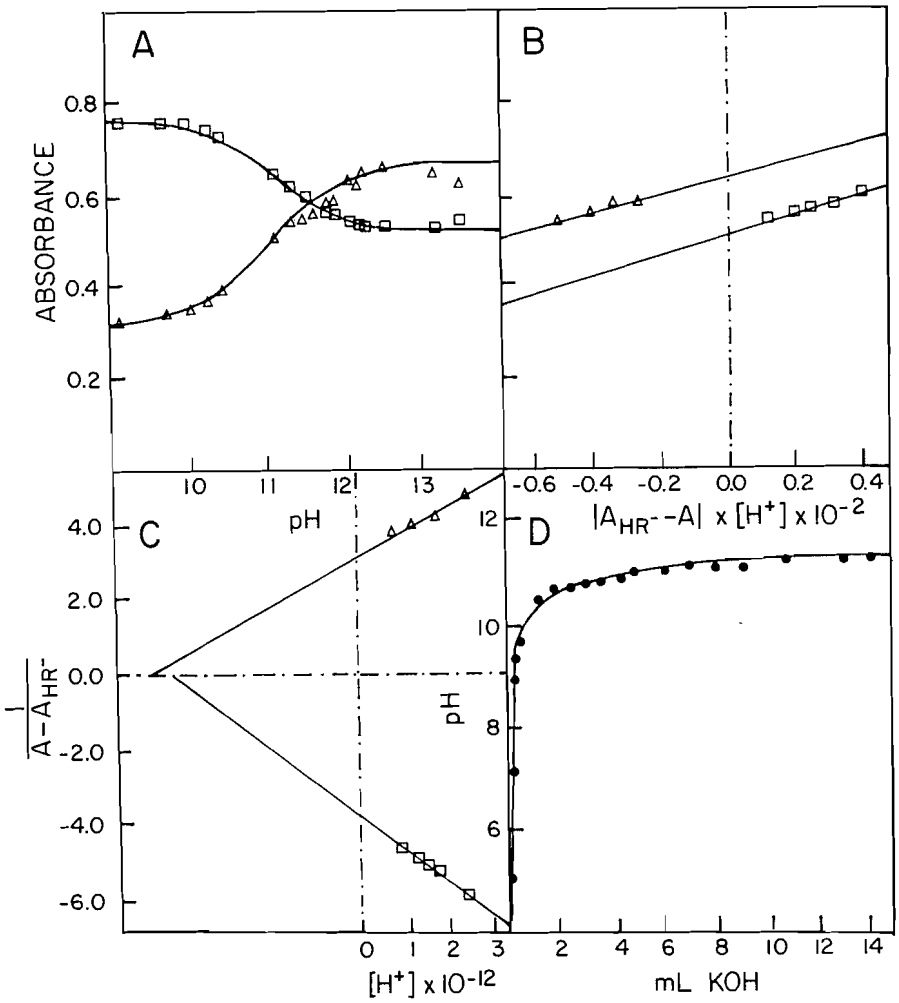


FIG. 2. Determination of pK_{a2} of NSSA: (*A*) absorbance vs. pH curves; (*B*) parallel straight lines method; (*C*) concurrent straight lines method; (*D*) potentiometric method.

with 0.0185 mol / L KOH in water under nitrogen while keeping temperature and ionic strength constant was also carried out (Fig. 2*D*). A pK_{a2} determination from the potentiometric measurements was made using Schwarzenbach's method (18).

The pK_{a2} and arithmetic mean values obtained by all these methods are summarized in Table 4.

Stability and behaviour against reducing and oxidizing agents

NSSA is very stable in the pH 4 to 9 range, but out of this range it suffers rapid decomposition. Both reducing and oxidizing agents at 1% (w / v) concentration alter the absorption spectra of NSSA in water, the material being more unstable against oxidizing than reducing agents. The decomposition products were not identified.

(B) Reaction of sulfanilic acid with NS and determination of sulfanilic acid and sulfonamides

A characteristic red colour with an absorption maximum at 470 nm develops when sulfanilic acid reacts with NS in the chloroacetic acid – chloroacetate (sodium salt) buffer. The reaction can be used to determine this acid. NS is yellow in aqueous solution, but its color does not affect sulfanilic acid determintions if blanks with the same concentration of NS are used.

The reaction of NS with six sulfonamides was studied. Sulfanilamide, sulfacetamide, and sulfathiazole also show intense red colouration when treated with NS in the presence of chloroaceticchloroacetate buffer, both in aqueous medium and after extraction into chloroform. In chloroform quantitative measurements can be undertaken.

Preliminary studies revealed the additivity of the absorbance caused by sulfanilic acid and by the other sulfonamides studied. Hence, we attempted to resolve the several binary mixtures by mathematical analysis of the spectroscopic data, as well as by derivative spectroscopy. The results were not satisfactory, however, because the absorption maxima and molar absorptivities were very close. Extraction into chloroform to prevent the interference of sulfanilamide, sulfacetamide, and sulfathiazole with the sulfanilic acid determination was, however, successful. Moreover, simultaneous determinations are possible. To determine sulfanilic acid in these mixtures a simple absorbance measurement of the aqueous layer at 470 nm can be employed, but results are more precise if the equation described under the Assay Procedure is used. This equation corrects the total absorbance of the aqueous phase before extraction by subtracting the sulfonamide contribution (obtained from measurement of the chloroform phase at 345 nm). Sulfamethoxiazole, sulfamethoxipyridazine, and sulfadiazine form so little colour with NS that they cannot be quantitatively determined; instead they are extracted into chloroform from an imidazole buffer to eliminate their slight interference in the aqueous phase.

Can. J. Chem. Downloaded from www.nrcresearchpress.com by 194.225.253.170 on 09/07/12
For personal use only.

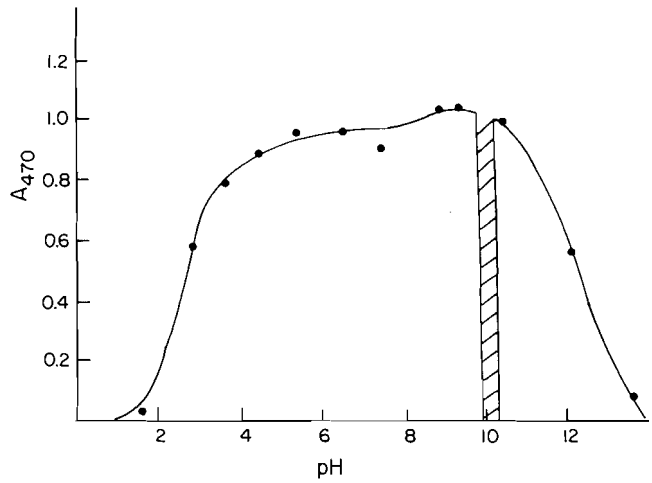


FIG. 3. Absorption intensity of the chromogen as a function of pH. Concentration of sulfanilic acid 43 μg mL^{-1}. The cross-hatched zone represents precipitation of NS in the samples.

Optimisation of variables

The optimisation of several variables influencing the reaction between sulfanilic acid and NS was studied. Maximum colour intensity was obtained after 90 min at 20 ± 5°C. The colour was stable for a further 24 h. The optimum pH range using an equimolar solution of both compounds is 3.3 to 8.0 (Fig. 3). A pH value of 3.5, adjusted with chloroacetic acid – sodium chloroacetate buffer, is recommended. The optimum concentration of NS leading to maximum intensity of colour was found to be 15-fold that of the sulfanilic acid concentration in the final solution. The amount of buffer solution, ionic strength, addition order, and temperature did not affect the results. A modified simplex method (19) was used to optimize pH and relative amount of NS reagent to sulfanilic acid in addition to the classical approach for optimisation. The result obtained by the simplex method was the same as that obtained by the classical one.

Quantification, linearity of Beer's law plot, accuracy, and precision

A linear correlation ($r = 0.9997$) was found between absorbance at 470 nm and concentration of sulfanilic acid in the range 3.1 to 31.0 μg mL^{-1}. The apparent molar absorptivity was found to be 4.7×10^3 L mol^{-1} cm^{-1}. The reproducibility of the procedure was determined by running replicate samples, each containing 15.8 μg mL^{-1} of sulfanilic acid in the final test solution. At this concentration level the relative standard deviation did not exceed 0.4% for twelve separate samples.

Sensitivity and specificity

The optimum range for measurement of sulfanilic acid with NS was determined by Ringbom's method (20) to be in the range from 8 to 25 μg mL^{-1}. This indicates good sensitivity for the reaction, and thus the present method can be recommended for the detection of trace amounts of sulfanilic acid in drugs. The influence of numerous cations and some amines on sulfanilic acid quantification was tested. Cations do not interfere except for Cu(II) and Al(III) at molar ratios higher than 1:10 (sulfanilic acid:cation). Hydrazides, semicarbazides, and some aminopyridines interfer by forming precipitates with NS. Aniline and sulfonamides give coloured products with NS in aqueous medium, but can be separated by extraction into organic solvents.

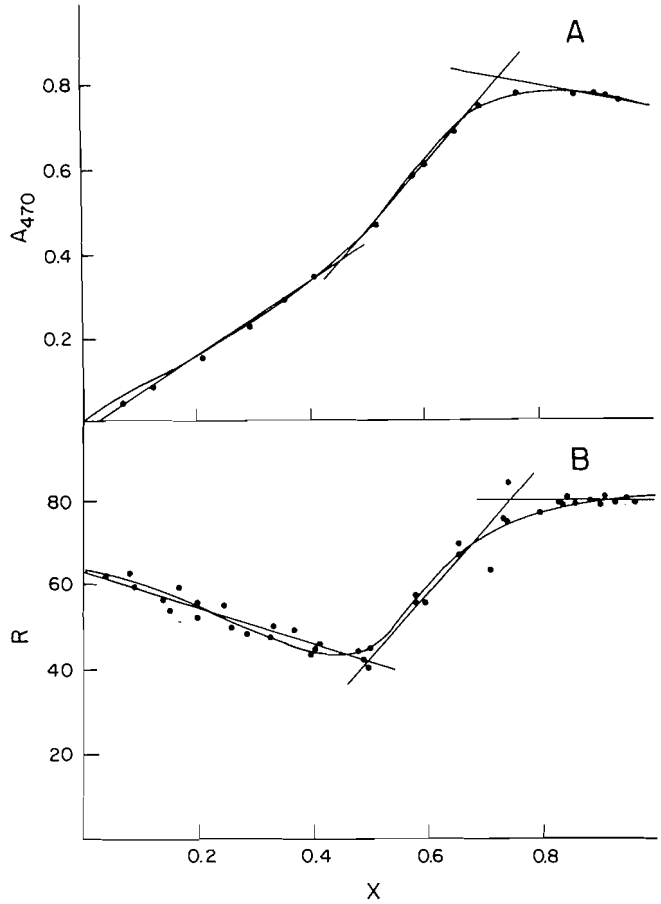


FIG. 4. Sulfanilic acid to NS ratio in the chromogen: (*A*) molar ratio method; (*B*) plot of data from investigation in non-equimolar conditions. *X* is the molar fraction of NS $C_{NS} / (C_{NS} + C_S)$.

Sulfanilic acid to NS ratio in the chromogen

A continuous molar variation study of sulfanilic acid and NS showed that interaction between them does not occur on a equimolar basis. Hence we applied the continuous variation method in non-equimolecular solutions according to Ramanathan and Walvekar (10) to a set of experimental curves obtained at different molarities of the reactants. This study suggested the possible presence of more than a single complex if a large excess of NS is present, even though the isolated adduct obtained under experimental conditions of equal molar amounts of both reactants corresponds clearly to a 1:1 stoichiometry.

To evaluate more precisely the combining ratios of sulfanilic acid and NS, we used the molar ratio method (11) with a fixed amount of sulfanilic acid (Fig. 4*A*), and also the data from an investigation under non-equimolar conditions (Fig. 4*B*).

Plots of *R* (relative percentage of adduct to total amount of minor component in sulfanilic–NS mixtures) against *X* (molar fraction of NS in the sulfanilic acid – NS mixtures) are shown in Fig. 4*B*. *R* is calculated on the assumption that the absorbance limit at each end of the studied range corresponds to different species involving sulfanilic acid and NS. If these species are called **I** and **II**, $C_{\mathbf{I}}$ and $C_{\mathbf{II}}$ are calculated from $\epsilon_{\mathbf{I}}$ and $\epsilon_{\mathbf{II}}$ at each point and thus situation (*A*) occurs when $C_S \geq C_{NS}$, $R = (C_{\mathbf{I}} / C_{NS}) \times 100$, and (*B*) when $C_S \leq C_{NS}$, $R = (C_{\mathbf{II}} / C_S) \times 100$. In the above expressions C_S and C_{NS} are the concentrations of sulfanilic acid and NS in the samples. Situation *A* reflects predominance of sulfanilic acid, and *B* when NS predominates.

Can. J. Chem. Downloaded from www.nrcresearchpress.com by 194.225.253.170 on 09/07/12
For personal use only.

TABLE 7. Assay of sulfanilic acid and some sulfonamides in pharmaceuticals by the NS method

Sample	Sulfonamide assay: Amount present (mg mL^{-1}) I[b]	II[c]	Recovery, %[a] I	II	Sulfanilic acid spike recovery: Amount added (mg mL^{-1})	Recovery, %[a]
Abactrim	—	—	—	—	7	93±1.5
Bio exazol simple	—	—	—	—	22[d]	109±1.3
Amidrin	4	—	98±2.1	—	7	96±1.3
Colirio oculos	—	100	—	89±2.0	152	113±1.2

[a]All averages are based on the three determinations; uncertainties are one standard deviation. Theoretical recovery is 100%.
[b]**I** = sulfanilamide.
[c]**II** = sulfacetamide.
[d]In mg/tablet.

The graph R vs. X should be monotonic if only one complex is involved, but the presence of two points of discontinuity demonstrates that, in agreement with the molar ratio method, there is an initial combining ratio of 1:1 (sulfanilic acid – NS) and a second above a 1:3 ratio.

The first ratio indicates formation of the equimolar adduct that was isolated and characterised in this work. The second inflection point is not easy to interpret. We conclude that the red colour produced when sulfanilic acid reacts with a large excess of NS is due to a mixture of a 1:1 complex and a second complex of undefined higher stoichiometry.

Application to pharmaceuticals

The suggested method was applied to the quantitative determination of spiked sulfanilic acid, and to sulfonamides in pharmaceuticals. The data in Table 7 indicate the suitability of the method for routine quality control analysis.

Conclusions

The nature of the species formed between sulfanilic acid and 1,2-naphthoquinone-4-sulphonate has been established by elemental and spectroscopic analysis. The adduct has two tautomers: 4-arylamino-1,2-naphthoquinone (form **I**) and 4-arylimine-1,4-naphtoquinone (form **II**). Form **I** is present in acidic and slightly basic aqueous solutions. Deprotonation of this form leads to form **II** (pK_a = 11.3).

Although several methods are described in the literature for the determination of sulfonamides, all have serious limitations. The photometric Bratton–Marshal method for amines, which uses diazotation and coupling of the formed azo dye, is tedious. Acid–base titrimetry in dimethylformamide with tetramethylammonium hydroxide of the sulfonamide group (—SO_2—NH—) presents problems from interferences by other substances in the sample. Moreover, relatively high concentrations are needed. In this study we propose a new simple procedure for the determination of sulfanilic acid and sulfonamides. Furthermore, binary mixtures can be resolved. Sulfanilic acid can be determined in the presence of a two-fold molar excess of sulfanilamide, sulfacetamide, and sulfathiazole and vice versa. The method also tolerates sulfamethoxazole, sulfamethoxipyridazine, and sulfadiazine at molar concentrations five- to eight-fold greater than sulfanilic acid, but these sulfonamides could not be quantified in the mixtures.

Although direct analysis is feasible, use of a standard additions method is recommended to obtain more precise results. When the amines are alone the direct procedure is more advantageous.

Results of application of the method to several samples are in general satisfactory and deviations from theoretical recovery of 100.0% are minimal (Table 7).

Acknowledgement

The authors thank the Comisión Asesora de Investigación Científica y Técnica del Ministerio de Educación y Ciencia de España for supporting this study (Project No. 1024-84).

1. H. J. ROTH, K. EGER, and R. TROSHUTZ. Pharmazeutische Chemie II Arzneistoffanalyse. Thieme Verlag, Stuttgart. **336** (1985).
2. A. MOMBERG, M. E. CARRERA, D. VON BAER, and C. BRUHN. Anal. Chim. Acta, **159**, 119 (1984).
3. C. S. P. SASTRY, B. G. RAO, B. S. REDDY, and S. S. N. MURTHY. J. Indian Chem. Soc. **58**, 655 (1981).
4. A. C. BRATTON and E. K. MARSHAL JR. J. Biol. Chem. **128**, 537 (1939).
5. E. G. SCHMIDT. J. Biol. Chem. **122**, 757 (1938).
6. R. TULUS and A. GURAN. J. Fac. Sci. Univ. Instanbul, Serie C, **28**, 108 (1963).
7. H. AMAL and S. DEMIR. J. Fac. Pharm. Instanbul. **4**, 28 (1968).
8. Beilstein. H (14) 701.
9. P. JOB. Ann. Chim. **10**, 9 (1928).
10. P. S. RAMANATHAN and A. P. WALVEKAR. Z. Phys. Chemie. Leipzig. **257**, 801 (1976).
11. J. M. YOE and A. L. JONES. Ind. Eng. Chem. **16**, 111 (1944).
12. L. F. FIESER. J. Am. Chem. Soc. **48**, 2922 (1926).
13. L. F. FIESER and M. FIESER. J. Am. Chem. Soc. **57**, 491 (1935).
14. S. L. PATT and J. M. SCHOOLERY. J. Magn. Reson. **46**, 536 (1982).
15. P. MARONI and J. P. CALMON. Bull. Soc. Chim. Fr. 519 (1935).
16. P. ROMAIN and J. C. COLLETER. Compt. Rend. 1456 (1958).
17. B. BUDESINSKY. Talanta, **16**, 1277 (1969).
18. G. SCHWARZENBACK, A. WILLI, and R. BACH. Helv. Chim. Acta, **39**, 1303 (1947).
19. J. A. NELDER and R. MEAD. Computer, **7**, 308 (1965).
20. A. RINGBOM. Z. Anal. Chem. **115**, 332 (1938/1939).

Can. J. Chem. Downloaded from www.nrcresearchpress.com by 194.225.253.170 on 09/07/12
For personal use only.

New method for the determination of permeation coefficients of functional chemical groups using membrane model vesicles

JEAN-LOUIS KRAUS, SOPHIE MICHEAU, AND PHILIPPE PERNICE

Laboratoire de Chimie Biomoléculaire, Faculté des Sciences de Luminy, Case 901, 13288 Marseille Cedex 9, France

AND

MADELEINE CASTAING

Collège de France – Chimie des Interactions Moléculaires 75231 Paris Cedex 05, France

Received March 10, 1989

JEAN-LOUIS KRAUS, SOPHIE MICHEAU, PHILIPPE PERNICE, and MADELEINE CASTAING. Can. J. Chem. **67**, 1606 (1989).

New substituent constants π_p, derived from permeation coefficients, of membrane model vesicles have been evaluated for fifteen functional groups. The excellent correlation found between the new substituent constants and the values derived from partition coefficients in octanol–water system leads one to consider this new parameter and the technique used for its evaluation as new promising tools for quantitative structure–activity relationship studies and for hydrophobic properties measurement.

Key words: permeation coefficients, model membrane, dihexadecyl-phosphate vesicles.

JEAN-LOUIS KRAUS, SOPHIE MICHEAU, PHILIPPE PERNICE et MADELEINE CASTAING. Can. J. Chem. **67**, 1606 (1989).

Les coefficients de perméation π_p de quinze groupements chimiques fonctionnels ont été évalués à l'aide de membranes de vésicules de dihexadecyl phosphate. L'excellente corrélation trouvée entre ces coefficients de perméation π_p et les coefficients de partition π mesurés dans le système octanol–eau d'une part et la simplicité de la nouvelle technique d'évaluation de π_p d'autre part, permettent d'envisager leur utilisation dans des études de relation structure-activité et pour des mesures d'hydrophobicité.

Mots clés : coefficients de perméation, modèle membrane, vésicules de dihexadecyl phosphate.

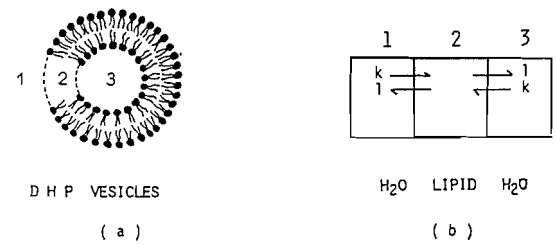
[Traduit par la revue]

Introduction

For a drug to be absorbed from the intestine to the interior of a cell, it has to penetrate cell membranes. The factors that determine the permeability of cell membranes to drugs are of interest to medicinal chemists and biochemists (1–7).

In attempting to rationalize the correlation between the chemical structure of a drug and its biological activity, Hansch and co-workers focused on the hydrophobic character of drugs (refs. 8, 9 and references therein). They used, for an operational representation of the capacity of molecules to form hydrophobic bonding, the values for the octanol–water partition coefficient of drugs, expressed as log P (P is the octanol–water partition coefficient of the unionized molecule) (10), and showed good correlation between the hydrophobic character of the drugs and various biological responses (9, 11). The fundamental basis underlying these results was the assumption that the rather orderly shell of water molecules surrounding an organic compound in an aqueous solution would disintegrate when this compound is transferred into a non-polar phase. The entropic change associated with this process appears to be one of the most important contributing factors to "hydrophobic bonding".

Following the considerable work of Hansch and co-workers, other substituent constants for organic compounds were proposed in the field of structure-activity relationship, the most widely used being the Hammett constants (12), and their extension by Taft, Brown, and Charton (13). In this work we proposed a new method for the determination of a new substituent parameter which can be easily determined whatever the chemical structure of a drug. This constant was derived from permeation coefficient of dihexadecyl phosphate vesicles. Indeed, using a model membrane made of dihexadecyl phosphate bilayers, it has been possible to determine permeation values which directly reflect the hydrophobic character of the organic molecules. As is well known, single compartment vesicles made of dihexadecyl phosphate (DHP) offer a realistic model for permeability investigations, as like living cells, their membrane is made of bilayers.



SCHEME 1

Scheme 1 shows that the DHP vesicle (*a*) can be visualized as a lipid barrier separating two aqueous compartments (*b*). Let k be the rate constant for the passive movement of a given marker from the aqueous phase towards the lipid phase, and l the same but for the reverse process, the value for the partition coefficient P of this marker is equal to the ratio of the rate constants ($P = k/l$). In the present study the marker encapsulated in the vesicle cavity (compartment 3) was the tris(2,2′-bipyridyl)ruthenium(II) chloride hexahydrate ($Ru(bpy)_3^{2+}$).

The magnitude of the leakage of $Ru(bpy)_3^{2+}$ ions through the membrane of DHP vesicles, when induced by various organic molecules, was quantified. The permeation properties of these drugs were determined by monitoring the outflux of $Ru(bpy)_3^{2+}$ ions from the vesicles (compartment 3 to compartment 1) using electronic absorption. Defining $PD50_H$ and $PD50_X$ as the respective concentrations of $CH_3(CH_2)_4CH_3$ and $CH_3(CH_2)_4CH_2X$ required to decrease the $Ru(bpy)_3^{2+}$ content of the vesicles to 50% of its initial value, a new substituent constant expressed by the equation $\pi_p = \log PD50_X - \log PD50_H$ can be calculated. The purpose of this work was therefore to evaluate π_p values of various compounds of the hexane series using a model membrane of bilayers and to establish a correlation between these π_p values and those derived from Hansch's partition coefficients.

Can. J. Chem. Downloaded from www.nrcresearchpress.com by 194.225.253.170 on 09/07/12
For personal use only.

TABLE 1. Substituent parameter values derived from permeation coefficients in the hexane series $CH_3(CH_2)_4$—CH_2X

Compound	X	PD50 $M\,L^{-1}$	π_p[e,f]	π according to Hansch (17)[a]
Hexane, $CH_3(CH_2)_4CH_3$	—H[b]	0.83×10^{-2}	0	0
1-Chlorohexane, $CH_3(CH_2)_5Cl$	—Cl	0.30×10^{-2}	−0.48±0.05	+0.71±0.03
1-Bromohexane, $CH_3(CH_2)_5Br$	—Br	0.18×10^{-2}	−0.66±0.03	+0.86±0.02
1-Iodohexane, $CH_3(CH_2)_5I$	—I	0.14×10^{-2}	−0.76±0.05	+1.01±0.01
Heptane, $CH_3(CH_2)_5CH_3$	—CH_3[b]	0.30×10^{-2}	−0.45±0.02	+0.56±0.02
Octane, $CH_3(CH_2)_6CH_3$	—CH_2CH_3[b]	0.325×10^{-2}	−0.40±0.02	+1.02±0.02
Heptanoic acid, $CH_3(CH_2)_5CO_2H$	—COOH	4.4×10^{-2}	+0.72±0.04	−0.28±0.02
Heptanoamide, $CH_3(CH_2)_5CONH_2$	—$CONH_2$	29.2×10^{-2}	+1.61±0.04	−1.49±0.02
Hexylcyanide, $CH_3(CH_2)_5CN$	—CN	7.8×10^{-2}	+0.96±0.03	−0.57±0.02
Hexylamine, $CH_3(CH_2)_5NH_2$	—NH_2[c]	0.19×10^{-2}	−0.64±0.04	−1.23±0.02
1-Nitrohexane, $CH_3(CH_2)_5NO_2$	—NO_2	1.50×10^{-2}	+0.26±0.07	−0.28±0.02
Hexanal, $CH_3(CH_2)_4CHO$	—CHO[d]	2.30×10^{-2}	+0.44±0.11	−0.65±0.02
1-Hexyltetrazole, $CH_3(CH_2)_4CN_4H$	—CN_4H[d]	7.20×10^{-2}	+0.94±0.03	—
Hexyl alcohol, $CH_3(CH_2)_5OH$	—OH	3.95×10^{-2}	+0.68±0.02	−0.67±0.01
1-Hexanethiol, $CH_3(CH_2)_5SH$	—SH	0.31×10^{-2}	−0.43±0.03	+0.39±0.02

[a]The values reported in this column correspond to those reported by Hansch (17) in the case of benzene system. The function X is placed in position 4 of the aromatic ring.
[b]The following values for PD50 have been determined in using DMSO as indicated in the Materials and Methods section.
[c]This value does not verify the linear relationship shown in Fig. 1 (see Discussion).
[d]The π values for these substituents were not available in the benzene system reported by Hansch (ref. 17).
[e]The error values refer to the standard deviation.
[f]π_p was calculated according to the equation $\pi_p = \log PD50_X - \log PD50_H$.

Experimental

Most of the tested compounds used in this work were stated to be 99% pure or more, manufactured by Aldrich Chemicals. Hexyltetrazole has already been described in a previous paper (14). The other chemicals dimethylsulfoxide (DMSO), $Ru(bpy)_3Cl_26H_2O$ were purchased from Aldrich Chemicals. The analytical grade cation exchange resin AG 50W-X2 (100–200 mesh, hydrogen form) was purchased from Biorad Laboratories.

Preparation of DHP vesicles

The present experiments were performed on vesicles made of DHP since they are known to be highly stable (a few months). The entrapment of $Ru(bpy)_3Cl_26H_2O$ ions into such vesicles has been extensively studied by Tricot *et al.* (15). Based on their data, the optimal concentration of DHP was estimated to be $2 \times 10^{-3}\,M\,L^{-1}$, while that of $Ru(bpy)_3Cl_26H_2O$ ions would reach $3.3 \times 10^{-4}\,M\,L^{-1}$, and the pH at sonication a value of 5.7.

Vesicles were prepared by heating the required amount of DHP dissolved in double distilled deionized water for 60 min at 80°C. The solution was then alkalinized to the required pH by NaOH addition and the $Ru(bpy)_3Cl_26H_2O$ injected to the mixture. A sonication was then performed for approximately 45 min at 80°C. After cooling, the vesicle suspension was filtered to remove the titanium particles released by the sonicating probe. The suspension contained single-compartment vesicles with $Ru(bpy)_3Cl_26H_2O$ ions adsorbed within the outer and inner surfaces of their membrane. Further details on DHP vesicles preparation are available in the data reported by Tricot and Fendler (16).

PD50 calculation

The optical density (OD) of $Ru(bpy)_3Cl_26H_2O$, at approximately 455 nm, was determined by recording the visible absorption spectra of the samples with a 860 KONTRON Spectrometer (KONTRON/Instrument Division). The experimental procedure was as follows. First, the DHP vesicles suspension was passed over a cation-exchange resin, and therefore, the free $Ru(bpy)_3Cl_26H_2O$ ions of the sample, as well as those adsorbed at the outer surface of the membranes, were exchanged with the H^+ ions of the resin. The OD value of this suspension, when corrected from the contribution of vesicles with no entrapped marker molecules, was taken to be "standard OD" (OD_S). Secondly, the perturbing agent was added to the eluted vesicles suspension. This induced a membrane perturbation and $Ru(bpy)_3Cl_26H_2O$ leakage from the inside of the vesicles. These ions were removed from the sample, as explained above, using a cation-exchange resin, and the absorption spectrum was recorded. The OD value determined now, when corrected from vesicles contribution, was taken to be the "measured OD" (OD_M). The value of the OD_M/OD_S ratio was then equal to the percentage of $Ru(bpy)_3Cl_26H_2O$ ions remaining entrapped in the vesicles after the action of a given perturbing agent, at a given concentration. The permeation dose at 50%, i.e. PD50 was defined as the concentration of the perturbing agent required to induce a 50% decrease in the value of the initial $Ru(bpy)_3Cl_26H_2O$ ion concentration. In other words, PD50 corresponds to a OD_M/OD_S ratio equal to 0.50. This provided a useful means to compare the action of the various perturbing agents.

It must be emphasized that because of their low hydrophilicity, the perturbing agents were dissolved in DMSO. An equivalent amount of DMSO was added to the standard vesicles suspensions previous to the recording of their absorption spectra allowing the calculation of the standard OD_S. In addition we ascertained that the perturbing effect of DMSO on the vesicles membranes could be neglected as the PD50 determined for this solvent was higher than 7 *M*.

All experiments were carried out at 25°C. We ensured that the incubation time was long enough to reach the equilibrium state which corresponds to the maximum leakage of $Ru(bpy)_3^{2+}$ from the inner to the outer surface of the vesicles.

Results and discussion

The results reported in Table 1 show that the hexane congeneric compounds behave as perturbing agents of DHP vesicles. Their PD50 values are within the range 10^{-3} to $0.5\,M\,L^{-1}$. The new substituent parameter has been calculated from the equation

$$\pi_p = \log PD50_X - \log PD50_H.$$

Figure 1 illustrates the correlation between the new substituent parameter π_p and Hansch's substituent constant derived from partition coefficients. The correlation equation is as follows:

$$[1]\quad \pi_p = -0.99\pi(\pm 0.08) + 0.17(\pm 0.07)$$
$$r = 0.9189 \qquad n = 12 \qquad p < 0.001$$

Can. J. Chem. Downloaded from www.nrcresearchpress.com by 194.225.253.170 on 09/07/12
For personal use only.

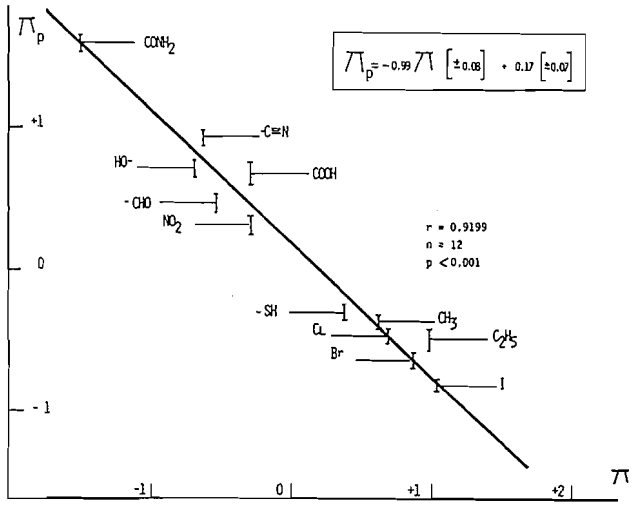


FIG. 1. Correlation between π_p values derived from permeation coefficients of model membrane vesicles and π values derived from partition coefficients according to Hansch (17).

In eq. [1] π is the partition coefficient constant according to Hansch's data (17); π_p is the permeation coefficient derived from the present experimental data, r is the correlation coefficient, n represents the number of data points used and this linear regression was highly significant: $p < 0.001$. S.E.M. values are given in parentheses.

Let us start by pointing out the selection of the hexane series for this study, because of our recent results (14). In this work, we have showed that carboxylic acids having a carbon chain length from 5 to 8 carbon atoms induced vesicle membrane perturbations the magnitude of which is controlled by two parameters — carbon chain length and the carboxylic function while for carboxylic acids having a carbon chain length of more than 10 carbon atoms, the perturbing effect is mainly under the control of the carbon chain length, the contribution of the functional group to the perturbing effect is very low and not suitable for the purpose of this work.

Our second question is that: are partition coefficients representative enough in quantitative structure–activity relationships? As stated in the Experimental section, PD50 values reported are easy to determine and are available for all types of chemical functions using DMSO to overcome eventual solubility problems. Moreover, single-compartment vesicles represent a more realistic model for the study of membrane permeability than the partition coefficients in octanol–water, since like real membranes, single-compartment vesicles are made from bilayers. Finally, a point of concern to us is that the determination of partition coefficients in the octanol–water system requires the presence of an aromatic moiety in the chemical structure of the drug. This aromatic part could interact with the rest of the molecule bearing the chemical group. Such an interaction of the side-chain dipole with the electrons of the aromatic ring could result in a folding of the molecule that can modify the intramolecular hydrophobic bonding (for comprehensive examples see ref. 10). On the other hand, permeation coefficients as determined in this study exclude the participation of π electrons as a governing factor in the permeability properties.

In the case of the primary amino group, whose co-ordinates do not significantly verify the linear relationship shown in Fig. 1, a possible explanation could be found in considering the electrical effects of an amino group in an anilin system which are widely different from that of a primary aliphatic amine such as hexylamine. This point is illustrated in comparing the pK_a of the two compounds.

The permeation induced by the hexane congeners is a very fast kinetic process, the mechanism of which remains unclear. It is possible that the interaction between the permeant molecules and the lipid head groups of the outer interface of the vesicles would slightly affect the bridging of the water molecules within the membrane, allowing therefore, the formation of pores and the release of $Ru(bpy)_3^{2+}$ ions.

Since Hansch and co-workers have provided powerful tools of physical organic chemistry in introducing hydrophobic substituent constants which represent the linkage between the dynamic effects of substituent (hydrogen bonding power, degree of polarization, and Van der Waals forces) and the biological response for a set of congeners, biological chemical structure–activity problems have made remarkable improvements. Related to these problems we believe that the introduction of new substituent constants π_p derived from permeation coefficients of membrane model vesicles could be of interest, since the latter are closely representative of the hydrophobic properties of substituents.

Moreover, the fact that no aromatic ring is involved in the determination of π_p made the use of this new substituent parameter a very attractive one. Finally if one considers that π_p values can be determined for any type of function, we can postulate the permeation coefficients could be used for numerical analysis of biochemical structure–activity studies.

Acknowledgements

We gratefully acknowledge Dr. P. Jelasko for statistical treatment of the data. We are indebted to Dr. P. Menassa (Concordia University, Montreal) for some helpful comments.

1. S. W. DIETRICH, J. M. BLANEY, M. A. REYNOLDS, P. Y. C. JOW, and C. HANSCH. J. Med. Chem. **23**, 1205 (1980).
2. C. HANSCH, R. L. LI, J. M. BLANEY, and R. LANGRIDGE. J. Med. Chem. **25**, 777 (1982).
3. R. L. LI, C. HANSCH, D. MATTHEWS, J. M. BLANEY, R. LANGDRIDGE, T. J. DELCAMP, S. S. SUSTEN, and J. H. FREISCHEIM. Quant. Struct.-Act. Relat. Pharmacol. Chem. Biol. **1**, 1 (1982).
4. J. M. BLANEY, S. W. DIETRICH, A. R. MARK, and C. HANSCH, J. Med. Chem. **22**, 614 (1979).
5. R. L. LI, S. W. DIETRICH, and C. HANSCH. J. Med. Chem. **24**, 538 (1981).
6. R. L. LI, C. HANSCH, and B. T. KAUFMAN. J. Med. Chem. **25**, 435 (1982).
7. R. L. LI and M. Poe. J. Med. Chem. **31**, 366 (1988).
8. C. HANSCH. Acc. Chem. Res. **2**, 232 (1969).
9. C. HANSCH and A. LEA. Substituent constants for correlation analysis in chemistry and biology. Wiley Intersciences, New York. 1979.
10. C. HANSCH and S. M. ANDERSON. J. Org. Chem. **32**, 2583 (1967).
11. C. HANSCH, J. E. QUINLAN, and G. L. LAWRENCE. J. Org. Chem. **33**, 347 (1968).
12. H. H. JAFFE. Chem. Rev. **53**, 191 (1953).
13. M. CHARTON. J. Am. Chem. Soc. **91**, 624 (1969).
14. P. PERNICE, M. CASTAING, P. MENASSA, and J. L. KRAUS. Biophys. Chem. **32**, 15 (1988).
15. M. TRICOT, D. N. FURLONG, A. W. H. MAU, and W. H. F. SASSE. Aust. J. Chem. **38**, 527 (1985).
16. Y. M. TRICOT and J. H. FENDLER. J. Am. Chem. Soc. **106**, 735 (1984).
17. T. FUJITA, J. ISAWA, and C. HANSCH. J. Am. Chem. Soc. **86**, 5175 (1964).

Can. J. Chem. Downloaded from www.nrcresearchpress.com by 194.225.253.170 on 09/07/12
For personal use only.

Synthesis and transannular Diels–Alder reaction of a *cis–trans–trans* and a *trans–cis–cis* 13-membered macrocyclic trienone

ANNE MARINIER,[1] KURT BAETTIG, CAROL DALLAIRE,[1] RITA PITTELOUD, AND PIERRE DESLONGCHAMPS[2]

Laboratoire de synthèse organique, Département de chimie, Faculté des sciences, Université de Sherbrooke, Sherbrooke (Qué.), Canada J1K 2R1

Received April 25, 1989

ANNE MARINIER, KURT BAETTIG, CAROL DALLAIRE, RITA PITTELOUD, and PIERRE DESLONGCHAMPS. Can. J. Chem. **67**, 1609 (1989).

The synthesis of the *cis–trans–trans* **5** and *trans–cis–cis* **6** macrocyclic trienones from cyclohexene is described. Upon heating at 300°C, trienone **5** underwent 1,5-H shift and transannular Diels–Alder reaction to give adducts **33**, **34**, and **35** while trienone **6** provided tricyclic ketone **37**.

Key words: transannular Diels–Alder reaction.

ANNE MARINIER, KURT BAETTIG, CAROL DALLAIRE, RITA PITTELOUD et PIERRE DESLONGCHAMPS. Can. J. Chem. **67**, 1609 (1989).

La synthèse des triénones macrocycliques *cis–trans–trans* **5** et *trans–cis–cis* **6** à partir du cyclohexène est décrite. En chauffant à 300°C, la triénone **5** subit un réarrangement sigmatropique-1,5 et une réaction Diels–Alder transannulaire pour donner les adduits **33**, **34** et **35**, alors que la triénone **6** conduit à la cétone tricyclique **37**.

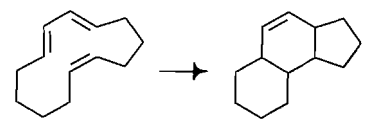
Mots clés : réaction Diels–Alder transannulaire.

Can. J. Chem. Downloaded from www.nrcresearchpress.com by 194.225.253.170 on 09/07/12
For personal use only.

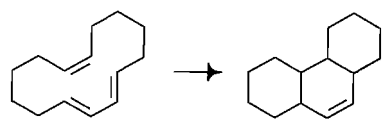
During the last decade, chemists have become increasingly interested in the synthesis of macrocarbocyclic molecules. Many naturally occurring compounds contain medium or large rings (1) and their syntheses require good methods for the preparation of these rings. The cyclization of long chains of carbons was first shown to be possible by direct processes (2). It was also recently demonstrated through a systematic study that the introduction of unsaturation in the carbon chain greatly helped the cyclization process by improving the yields considerably (3).

The reactivity of macrocarbocycles has also been studied. Chemists have shown that intermolecular reactions of these molecules can be carried out with high chemo-, regio-, and stereoselectivity (4, 5). Some examples of the transannular reactions of macrocycles have also been reported (6), demonstrating the facility with which these processes can take place. Transannular reactions, however, have rarely been used as cornerstones in specific syntheses.[3] In 1984, we pointed out (8) that transannular processes of macrocycles[4] represent a powerful approach for the development of new strategies for the construction of complex polycyclic molecules. From this perspective, the transannular Diels–Alder reaction of macrocycles, i.e., **1** → **2** or **3** → **4** has the potential to be a good synthetic approach to polycyclic systems. Recent communications from our laboratory (10) and from Takahashi *et al.* (11) demonstrate promise for the synthesis of diterpenes, triterpenes, steroids, etc., by the transannular Diels–Alder methodology.

We wish to report here our first detailed preliminary studies on the transannular Diels–Alder methodology. We describe the synthesis and the Diels–Alder reactivity of two 13-membered macrocyclic trienones, i.e., the *cis–trans–trans* (CTT) **5** and *trans–cis–cis* (TCC) **6** trienones.



1 **2**



3 **4**

Synthesis of trienones 5 and 6

Dimethoxy acetal aldehyde **7** prepared from cyclohexene by the method of Schreiber *et al.* (12) was used as starting material for the synthesis of the two trienones **5** (Scheme 1) and **6** (Scheme 2). Horner–Emmons condensation (13) of **7** with trimethyl phosphonoacetate provided unsaturated *trans* ester **8** (69%), which was reduced with diisobutylaluminium hydride (89%). The resulting dimethoxyalcohol **9** was hydrolyzed under acidic conditions to liberate the aldehyde moiety and protected (14) with dihydropyran to give aldehyde **11** in 55% overall yield. Condensation (15) with the lithium dienolate of isopropyl tiglate **12** produced the *trans–trans*-γ-coupling aldol product **13** (67%), which was converted into the methoxyethoxymethyl (MEM) ether derivative **14** (16) (88%).

Basic hydrolysis of **14** with lithium hydroxide (60% to **15**) followed by treatment with carbonyldiimidazole and reaction with the magnesium salt of monomethylmalonic acid (17) provided the β-ketoester **16**. Removal of the tetrahydropyrannyl protecting group afforded **17** (81% from **15**) from which subsequent halogenation gave the allylic chloride **18** in 89% yield.

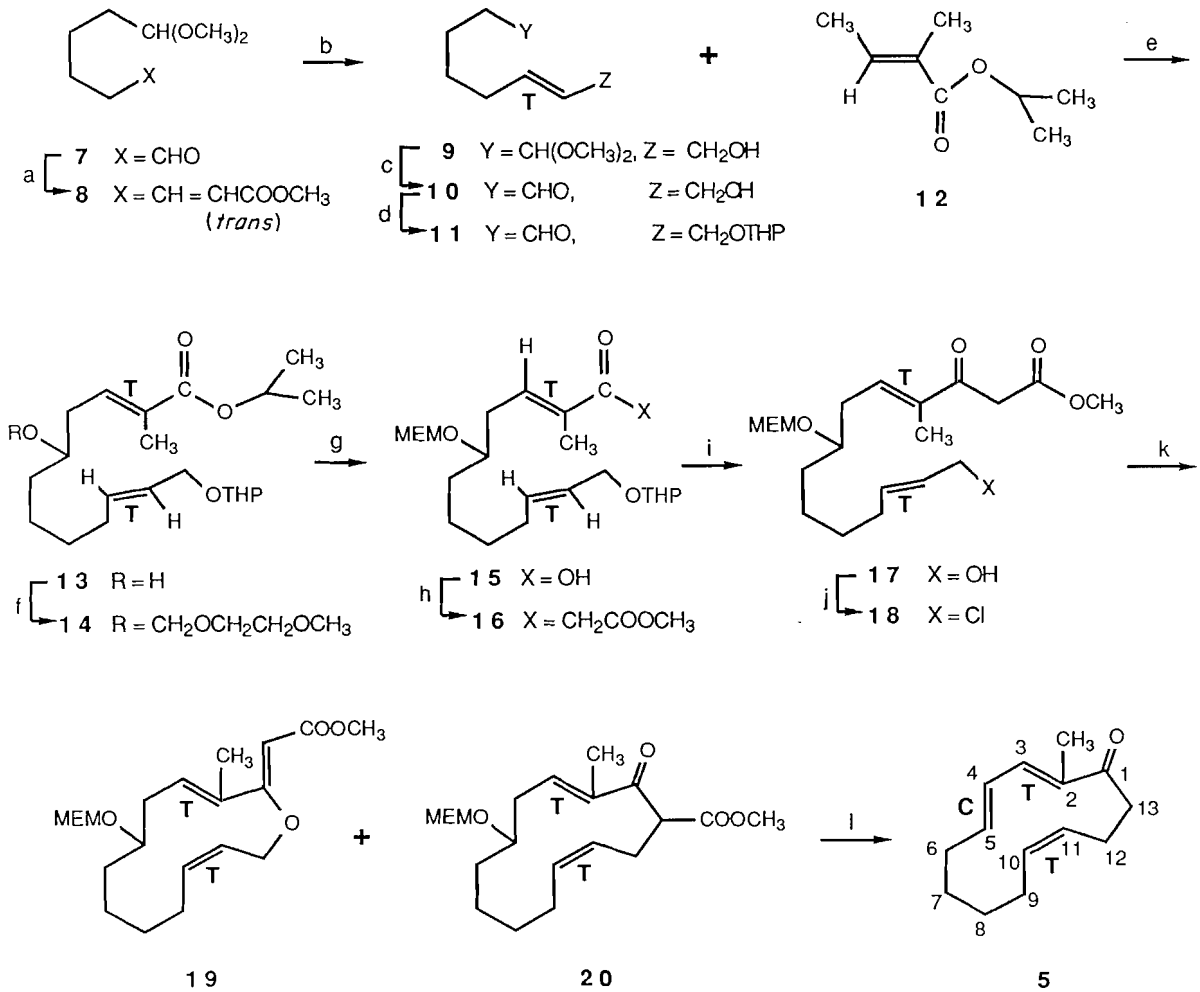
Macrocyclization was carried out by slow addition of allylic chloride **18** to a suspension of cesium carbonate (18) in tetrahydrofuran-*N*,*N*-dimethylformamide and produced macrocycles **19** and **20** in 9% and 77% isolated yields respectively after

[1]NSERCC and FCAR predoctoral fellows, 1985–1987.

[2]Author to whom correspondence maybe addressed.

[3]For example, two transannular key steps were used in our work on the total synthesis of ryanodol (cf. steps **25** → **26** and **46** → **48** in ref. 7).

[4]For other examples of synthetically useful transannular reactions, see ref. 9.



(a) $(MeO)_2POCH_2CO_2Me$, NaH, THF, −78°C to r.t., chromatography (*trans* ester = 69%, *cis* ester = 15%); (b) Dibal-H, cyclohexane, CH_2Cl_2, 20 min, −70°C (89%); (c) HCl 5%, ether, 18 h, r.t. (d) DHP, PPTS, CH_2Cl_2, 2 h, r.t. (55% from **5**) (ref. 13); (e) LDA, THF, HMPA, **12**, 20 min, −78°C; add **11**, 30 min, 0°C (67%); (f) $MeOCH_2CH_2OCH_2Cl$, diisopropylethylamine, CH_2Cl_2, 4 h, 0°C (88%); (g) LiOH, DME–H_2O (15:85), reflux, 12 h (60%); (h) **15**, carbonyldiimidazole, THF, 1 h, 50°C; add to a solution of $MeO_2CCH_2CO_2H$, $Me_2CHMgCl$, THF–CH_2Cl_2 (1:1), 10 min, −10°C and 15 min, r.t.; (i) PPTS, MeOH–H_2O (95:5), reflux, 4 h (81% from **15**); (j) $MeSO_2Cl$, $(C_2H_5)_3N$, CH_2Cl_2, 10 min, 0°C; LiCl, HMPA, 1 h, r.t. (89%); (k) Slow addition of **18** in THF to Cs_2CO_3, DMF–THF (1:1), 26 h, chromatography (**19** = 9%, **20** = 77%); (l) KOH (0.26 N), *tert*-butanol–H_2O (9:1), reflux, 12 h (59%)

SCHEME 1

chromatography. Subsequent treatment of **20** with potassium hydroxide in *tert*-butanol and water provided the CTT macrocyclic trienone **5** (59%). The CTT olefin geometries were assigned on the basis of spectroscopic data of **5** ($J_{5,4}$ = 11.6 Hz, $J_{10,11}$ = 15.2 Hz, $J_{3,4}$ = 10.8 Hz, and $J_{3,Me}$ = −1.3 Hz)[5] and that of its acyclic precursors.

Dimethoxyacetal aldehyde **7** was condensed with methyl-bis(trifluoroethyl)phosphonoacetate following Still's procedure (19) to give unsaturated *cis* ester **21** in 79% isolated yield. Reduction with diisobutylaluminum hydride (72% to **22**), silylation (20) (95% to **23**), and acidic hydrolysis gave aldehyde **24** (88%), which was treated with (formylmethylene)triphenylphosphorane (21). The resulting *trans* unsaturated aldehyde **25** (65% from **24**) underwent aldol condensation (22) with the lithium dianion of methyl 3-oxo-pentanoate to provide β-ketoester **26** as a diastereoisomeric mixture in 72% yield. The alcohol moiety of **26** was immediately converted into its tetrahydropyranyl ether derivative (14) **27** (88%). Removal of the silyl protecting group (23) (88% to **28**) followed by halogenation provided a diastereoisomeric mixture of allylic chlorides **29** (87%).

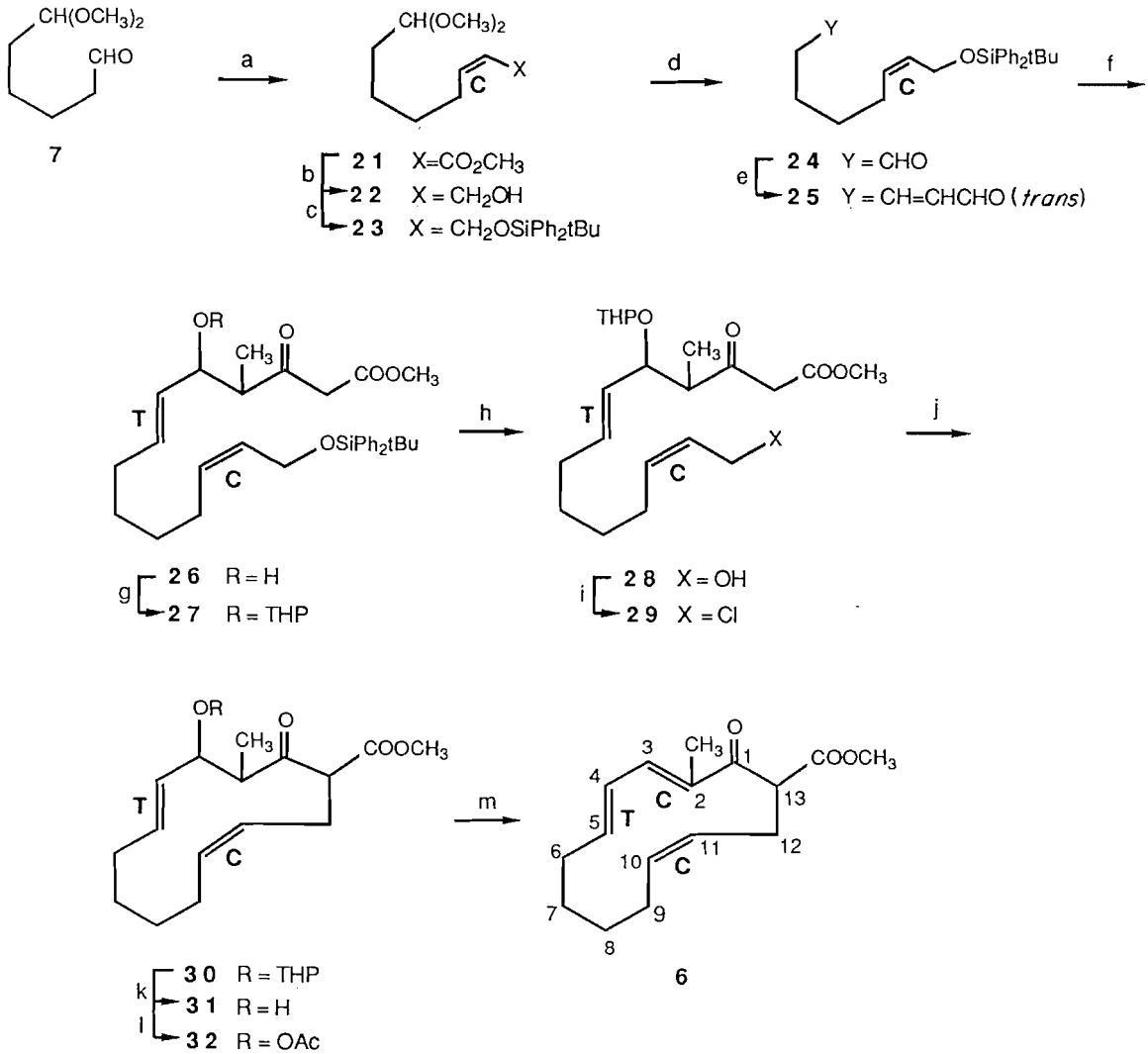
Macrocyclization in refluxing acetone with sodium iodide and potassium carbonate produced *trans–cis* macrocycle **30** as a diastereoisomeric mixture in 74% yield. Deprotection (90%) followed by transformation of the resulting alcohols **31** into acetates (93% to **32**) provided, after treatment with 1,8-diazabicycloundecene in refluxing benzene, the macrocyclic trienone **6** in 50% yield. The olefin geometries were again assigned on the basis of spectroscopic data of **6** ($J_{5,4}$ = 15.4 Hz, $J_{4,3}$ = 10.5 Hz, and $J_{3,Me}$ = 1.2 Hz)[5] and that of its acyclic precursors. Furthermore, a nuclear Overhauser effect was noted between H-C3 and CH_3-C2 by an nOe difference experiment, proving the *cis* geometry of the olefin formed.

Diels–Alder reactivity of 5

On heating at 300°C in toluene (sealed tube) for 4.5 h,

[5]For numbering see structures **5** and **6** in Schemes 1 and 2.

Can. J. Chem. Downloaded from www.nrcresearchpress.com by 194.225.253.170 on 09/07/12
For personal use only.



(a) HMDSK, toluene, THF, $(CF_3CH_2O)_2POCH_2CO_2Me$, 0.5 h, −78°C, chromatography (*cis* ester = 79%, *trans* ester = 15%); (b) Dibal-H, cyclohexane, CH_2Cl_2, 15 min, −78°C (72%); (c) imidazole, *t*-$BuPh_2SiCl$, DMF, 2 h, 0°C to r.t. (85%); (d) HCl 5%, THF (1:1), 24 h, r.t. (88%); (e) $Ph_3PCHCHO$, benzene, CH_2Cl_2 (7.5:3) reflux, 40 h (65%); (f) NaH, methyl 3-oxopentanoate, THF, 30 min, *n*-BuLi, hexane, 30 min, −50°C; add **25** in THF, 5 min, −5°C (72%); (g) DHP, PPTS, CH_2Cl_2, 2 h, r.t. (88%); (h) $(Bu)_4NF$, THF, 2 h, r.t. (88%); (i) $MeSO_2Cl$, $(C_2H_5)_3N$, CH_2Cl_2, 0.5 h, 0°C; LiCl, HMPA, 1.5 h, r.t. (87%); (j) K_2CO_3, NaI, acetone, reflux, 72 h (74%); (k) PPTS, MeOH–H_2O (9.5:0.5), reflux, 1.5 h, (90%); (l) $(MeCO)_2O$, $(C_2H_5)_3N$, dimethylaminopyridine, CH_2Cl_2, 9 h, 0°C, (93%); (m) DBU, benzene, reflux, 12 h (50% after crystallization)

SCHEME 2

macrocyclic trienone **5** was transformed into a mixture of three products **33**, **34**, and **35** (Scheme 3) in a ratio of 1.8:2:1 respectively (90% yield). These compounds were separated by chromatography and were converted into their 2,4-dinitrophenylhydrazone (2,4-DNP) derivatives.[6]

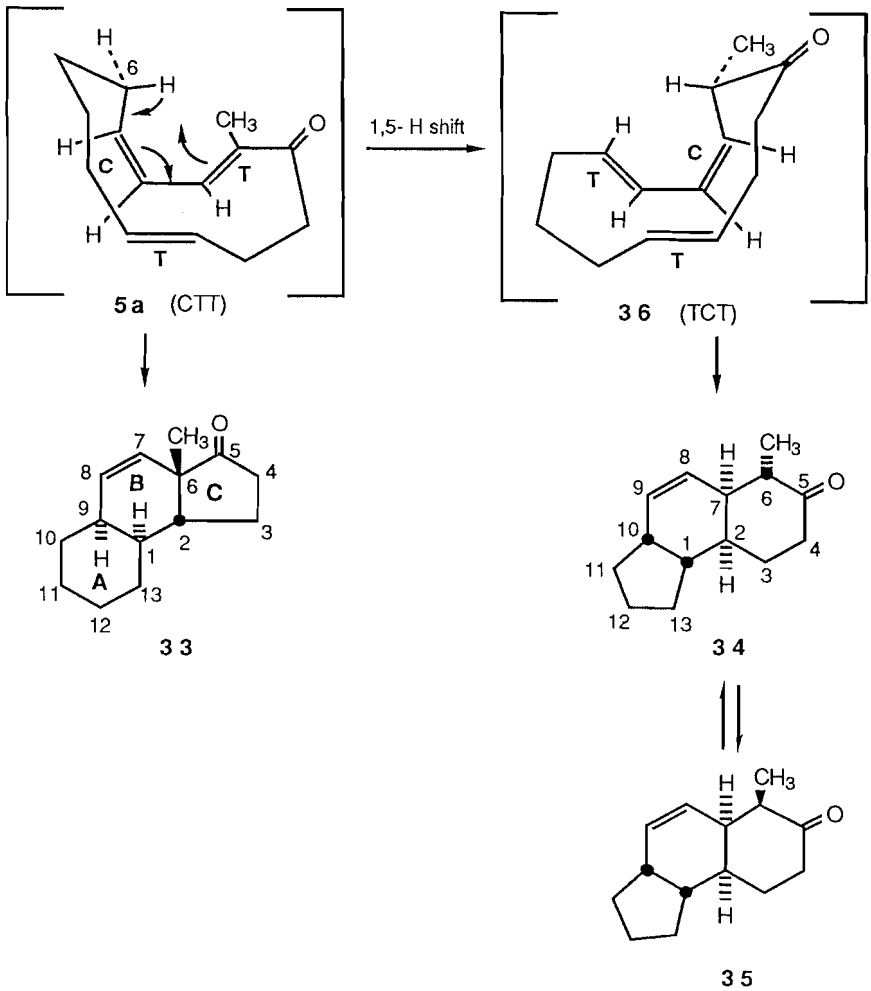
The structure of the minor adduct **35** was rigorously established by X-ray crystallography of its 2,4-DNP derivative. Similarities in the spectral data of **34** and **35** suggested that the former was simply the epimer of the latter. This assumption was confirmed by the interconversion of compounds **34** and **35** in the presence of sodium methoxide in methanol. It was further demonstrated that tricycles **34** and **35** can be thermally isomerized at 300°C, suggesting that one isomer might have been formed selectively in the course of the cycloaddition process.

The formation of these three tricyclic products can be explained in the following way. The Diels–Alder reaction must take place via a boat-like transition state (10*d*). With this requirement in mind, molecular models show that CTT trienone **5** can undergo Diels–Alder reaction only via conformer **5***a* (Scheme 3) to produce a tricycle having the *cis–anti–cis* (CAC) relative stereochemistry. However, the planar cisoid conformation that the diene moiety must take up is quite hindered because the C6 methylene and the methyl group are very close to each other (cf. **5***a*). The steric repulsion generated must raise considerably the energy of the transition state for the Diels–Alder reaction. To relieve this stress, a competing suprafacial 1,5-sigmatropic hydrogen shift could take place. This would produce the nonconjugated trienone **36** having *trans–cis–trans* (TCT) olefin geometry, which could then give the CAC tricycle **34** via a transannular Diels–Alder reaction. Compound **34** could then undergo thermally induced equilibration with its less stable epimer **35** via the formation of an enol.

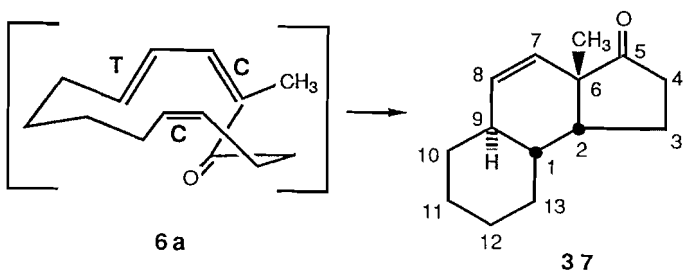
The structure of tricycle **33** was deduced on the basis of its spectroscopic data. However, the CAC relative stereochemistry

[6]F. Brisse, Université de Montréal. Unpublished results.

Can. J. Chem. Downloaded from www.nrcresearchpress.com by 194.225.253.170 on 09/07/12
For personal use only.



SCHEME 3



SCHEME 4

was not rigorously established. By chemical shift comparison of the C18 methyl ^{1}H nmr signal in steroids (24) (0.86 ppm for the 14-α steroids and 1.08 ppm for the 14-β steroids) with that of **33** (1.18 ppm), it was supposed that the junction between ring B and ring C was *cis*. As **4***a* is the sole possible transition state conformer of macrocycle **5**, there should be only one Diels–Alder adduct of CAC relative stereochemistry (10*d*). However, it is also conceivable that CTT trienone **5** could undergo a thermally induced isomerization of the *cis* olefin to produce a *trans–trans* (TTT) macrocyclic trienone. For this trienone, molecular models predict the formation of two Diels–Alder products, i.e., a *cis–anti–trans* (CAT) and (or) a *trans–anti–cis* (TAC) tricycle (10*d*).

Diels–Alder reactivity of **6**

On heating at 300°C for 2.5 h, macrocycle **6** was transformed into tricyclic ketone **36** by transannular Diels–Alder reaction with concomitant decarbomethoxylation (90%) (Scheme 4). The chemical structure and the *trans–syn–cis* (TSC) relative stereochemistry of **37** was established spectroscopically and by X-ray diffraction analysis of its 2,4-dinitrophenylhydrazone derivative.[7] This result is readily explained since molecular models indicate that trienone **6** can only produce TSC tricycle **37** by Diels–Alder reaction of conformer **6***a*.

In conclusion, this preliminary investigation demonstrates that transannular Diels–Alder reaction of macrocycles is possible, and in some cases is a high yield process, even with nonactivated dienes and dienophiles. This reaction shows good promise for the synthesis of natural products. Work in this direction is currently underway in our laboratory.

Experimental

All reactions were carried out under an argon atmosphere. The infrared spectra (ir) were taken on a Perkin–Elmer 681 spectrophotometer. Proton nmr spectra were recorded on a Bruker WM-250 instrument. Chemical shifts are reported in δ values relative to chloroform as internal standard. Abbreviations used are m: multiplet, s: singlet, t: triplet, d: doublet, q: quartet, sp: septuplet. Mass spectral assays (ms *m*/*e*) and peak matching were obtained using a VG Micromass ZAB-1F spectrometer. Chromatographic separations were done using Merck silica gel 230–400 mesh ASTM. High pressure liquid chromatography was carried out on a Waters instrument using μPorasil Waters column of 7.8 mm by 30 cm.

[7]M. Proulx, G. Boulay, and A. Michel, Université de Sherbrooke. Unpublished results.

Can. J. Chem. Downloaded from www.nrcresearchpress.com by 194.225.253.170 on 09/07/12
For personal use only.

Can. J. Chem. Downloaded from www.nrcresearchpress.com by 194.225.253.170 on 09/07/12
For personal use only.

α,β-*Unsaturated* trans *ester* ***8***

To a stirred suspension of sodium hydride (3.36 g, 140 mmol, 1.4 equiv.) in tetrahydrofuran (600 mL) was added dropwise at −78°C trimethylphosphonoacetate (22.8 mL, 141 mmol, 1.41 equiv.). After the addition, the resulting mixture was allowed to warm to room temperature and then stirred for 20 min. A solution of aldehyde **7** (16.0 g, 100 mmol) in tetrahydrofuran was added to the cooled (−78°C) reaction mixture. After stirring at −78°C for 15 min, the resulting mixture was allowed to warm to room temperature, poured over a saturated solution of ammonium chloride, and extracted three times with ether. The combined organic layers were dried over magnesium sulfate, filtered, and concentrated to give an oily residue that was purified by column chromatography (5% to 15% ethyl acetate in hexane) affording ester **8** (14.8 g, 69%); ir (neat): 2990, 2950, 2830, 1725, 1628, 1440 cm^{-1}; nmr ($CDCl_3$) δ: 7.0 (1H, dt, J = 15.6 Hz and 7Hz, $-CH_2-CH{=}CH-$), 5.8 (1H, dt, J = 15.6 Hz and −1.6 Hz, $-CH_2-CH{=}CH-$), 4.35 (1H, t, J = 5.7, $-CH_2-CH(OCH_3)_2$), 3.7 (3H, s, $-CO_2CH_3$), 3.3 (6H, s, $-CH-(OCH_3)_2$), 2.2 (2H, dtd, J = 7.0 Hz, and −1.6 Hz, $-CH_2-CH_2-CH{=}CH-$), 1.25–1.55 and 1.55–1.65 (6H, m, $-CH_2-CH_2-CH_2-CH(OCH_3)_2$).

Allylic alcohol ***9***

To a stirred solution of ester **8** (16.4 g, 76 mmol) in dichloromethane at −78°C was added dropwise a solution of diisobutylaluminium hydride in cyclohexane (1 M, 167 mL, 167 mmol, 2.2 equiv.). After stirring for 20 min at −78°C, sodium sulfate decahydrate (17.9 g, 56 mmol, 0.73 equiv.) was added and the resulting stirred mixture was allowed to warm to room temperature. The mixture was then filtered and the solid was rinsed with acetone several times. After concentration of the filtrate the resulting residue was purified by column chromatography (20% to 40% ethyl acetate in hexane) giving alcohol **9** (12.7 g, 89%); ir (neat): 3420, 1227, 2940 cm^{-1}; nmr ($CDCl_3$) δ: 5.65 (2H, m, $-CH{=}CH-$), 4.35 (1H, t, J = 5.7 Hz, $-CH(OCH_3)_2$), 4.1 (2H, m, $-CH{=}CH-CH_2OH$), 3.3 (6H, s, $-CH(OCH_3)_2$), 2.05 (2H, m, $-CH_2-CH_2-CH{=}CH-$), 1.65–1.55 and 1.5–1.3 (7H, m, $-CH_2-CH_2CH_2-CH-(OCH_3)_2$ and -OH)); ms m/e (70 eV): 188 (M^+), 171 (M^+-OH), 157 ($M^+ - OCH_3$).

Aldehyde ***11***

To a stirred solution of dimethoxyalcohol **9** (12.7 g, 67.6 mmol) in ether was added a 5% aqueous solution of hydrochloric acid (120 mL). The two-phase solution was vigorously stirred at room temperature for 18 h. The organic layer was then separated and the aqueous layer was extracted three times with ether. The combined organic layers were washed with an aqueous solution of sodium bicarbonate (10%), dried with magnesium sulfate, filtered, and concentrated to provide crude aldehyde-alcohol **10** (9.1 g).

Without any purification this oily residue was dissolved in dichloromethane (250 mL), and dihydropyran (18.5 mL, 3 equiv.) followed by pyridinium *para*-toluenesulfonate (200 mg) were added. After stirring for 2 h, the resulting mixture was poured over water and extracted three times with dichloromethane. The combined organic layers were dried with magnesium sulfate, filtered, and concentrated to give an oily residue that was purified by column chromatography (5% to 20% ethyl acetate in hexane) affording aldehyde **11** (8.4 g, 55%); ir CH_2Cl_2): 3060–3000, 3000–2800, 2730, 2660, 1740, 1460, 1030 cm^{-1}; nmr ($CDCl)_3$ δ: 9.76 (1H, t, J = 1.8 Hz, $-CHO$), 5.78–5.53 (2H, m, $-CH{=}CH-$), 4.63 (1H, dd, J = 4.2 Hz and 2.7 Hz, -O-CH-O-), 4.25–4.15 and 3.97–3.85 (2H, m, $-CH{=}CH-CH-CH_2-O$), 3.95–3.83 and 3.55–3.45 (2H, m), 2.43 (2H, dt, J = 1.8 Hz, 7.3 Hz, $-CH_2-CH_2-CH_2-CHO$), 2.1 (2H, dt, J = 6.5 Hz and 6.5 Hz, $-CH_2-CH_2-CH{=}CH-$), 1.9–1.4 (10H, m); ms m/e (70 eV): 227 (MH^+).

δ-*Hydroxy-ester* ***13***

To a stirred solution of diisopropylamine (2.62 mL, 18.7 mmol, 1.1 equiv.) in tetrahydrofuran at 0°C was added a 1.6 M solution of butyllithium in hexane (11.7 mL, 18.7 mmol, 1.1 equiv.). The solution was stirred for 10 min and was cooled to −78°C. Hexamethylphosphoramide (3.3 mL) was added and, after stirring for 10 min, a solution of isopropyltiglate **12** (2.66 g, 18.7 mmol, 1.1 equiv.) in tetrahydrofuran (2 mL) was added. Additional stirring was continued for 20 min at −78°C and a solution of aldehyde **11** (3.83 g, 17 mmol) in tetrahydrofuran (2 mL) was added to the resulting solution. After stirring for 30 min at 0°C, the mixture was treated with a saturated aqueous solution of ammonium chloride and extracted 3 times with ether. The combined organic layers were washed with water, dried with magnesium sulfate, filtered, and concentrated to give a residue that was purified by column chromatography (10% to 14% of ethyl acetate in hexane) affording ester **13** (4.21 g, 67%); ir ($CHCl_3$): 3610, 3460, 3008, 2940, 2870, 1700, 1650, 1270, 1110 cm^{-1}; nmr ($CDCl_3$) δ: 6.8 (1H, tq, J = 7.5 Hz and −1.5 Hz, H-C3), 5.8–5.5 (2H, m, H-C10 and H-C11, 5.05 (1H, sp, J = 6.3 Hz, $-O-CH(CH_3)_2$), 4.63 (1H, dd, J = 4.0 Hz and 2.5 Hz, -O—CH—O-), 4.2 and 3.9 (2H, m, H-C12), 3.9–3.8 and 3.55–3.45 (2H, m), 3.8–3.7 (1H, m, H-.C5), 2.4–2.3 (2H, m, H-C4), 2.1–2.0 (2H, m, H-C9), 1.84 (3H, d, J = −1.5 Hz, CH_3-C3), 1.7–1.3 (15H, m), 1.2 (6H, d, J = 6.3 Hz, $-O-CH(CH_3)_2$; ms m/e (70 eV): 368 (M^+), 285 (MH^+ − DHP).

Methoxyethoxymethyl ether ***14***

To a stirred solution of δ-hydroxy-ester **13** (2.50 g, 6.79 mmol) in dichloromethane (20 mL) was added dropwise at 0°C *N,N*-diisopropylethylamine (2.6 mL, 13.6 mmol, 2.2 equiv.) followed by methoxyethoxymethyl chloride (1.6 mL, 13.6 mmol, 2 equiv.). After stirring for 4 h at −40°C, the resulting solution was poured over water and extracted 3 times with dichloromethane. The combined organic layers were washed with brine, dried with magnesium sulfate, filtered, and concentrated to give a residue that was purified by column chromatography (10% to 20% ethyl acetate in hexane) affording ether **14** (2.72 g, 88%); ir ($CHCl_3$): 2935, 1708, 1650, 1110, 1025 cm^{-1}; nmr ($CDCl_3$) δ: 6.75 (1H, tq, J = 6.6 Hz and −1.5 Hz, H-C3), 5.65 (2H, m, H-C10 and H-C11), 5.05 (1H, sp, J = 6.3 Hz, $-O-CH-(CH_3)_2$), 4.75 (2H, s, -O-CH_2-O-), 4.6 (1H, dd, J = 4.1 Hz and 2.7 Hz, -O—CH—O-), 4.2 and 3.9 (2H, m, H-C12), 3.9–3.5 (7H, m, H-C5, $-O-CH_2-CH_2-O-$ and $-CH_2-CH_2-O-$ cyclic), 3.4 (3H, s, $-CH_2-OCH_3$), 2.4 (2H, dd, J = 6.6 Hz and 6.6 Hz, H-C4), 2.4 (2H, m, H-C9), 1.83 (3H, s, CH_3-C2), 1.6–1.3 (13H, m), 1.25 (6H, d, J = 6.3 Hz, $-O-CH(CH_3)_2$; ms m/e (70 eV): 457 (MH^+).

Carboxylic acid ***15***

To a stirred solution of ester **14** (1.54 g, 3.38 mmol) in 85% aqueous dimethoxyethane (100 mL) was added lithium hydroxide (275 mg, 11.8 mmol, 3.5 equiv.). The resulting mixture was heated under reflux for 12 h and then allowed to cool to room temperature. The solution was neutralized and concentrated to give a residue that was poured over water, acidified to pH 2, and extracted 3 times with dichloromethane. The combined organic layers were washed with water, dried with magnesium sulfate, filtered, and concentrated to give a residue that was purified by column chromatography (20% to 30% ethyl acetate in hexane) affording acid **15** (855 mg, 61%); ir ($CHCl_3$): 3600–2420, 2930, 1688, 1645 cm^{-1}; nmr ($CDCl_3$) δ: 6.94 (1H, tq, J = 6 Hz and −1.1 Hz, H-C3, 5.8–5.5 (2H, m, H-C16 and H-C10), 4.75 (2H, s, -O-CH_2-O-), 4.63 (1H, dd, J = 4.2 Hz and 2.7 Hz, -O—CH—O-), 4.2 and 3.9 (2H, m, H-C12), 3.9–3.5 (7H, m, H-C5, $-O-CH_2-CH_2-O-$ and $-CH_2-CH_2-O-$ and $-CH_2-CH_2-O-$ cyclic), 3.4 (3H, s, $-CH_2-OCH_3$), 2.44 (2H, dd, J = 6 Hz and 6Hz, H-C4), 2.05 (2H, m, H-C9), 1.85 (3H, d, J = −1.1 Hz, CH_3-C2), 1.7–1.3 (14H, m); ms m/e (70 eV): 415 (MH^+), 331 (MH^+ −DHP).

β-*Ketoester* ***17***

To a stirred solution of carboxylic acid **15** (2.12 g, 5.12 mmol) in tetrahydrofuran (20 mL) was added carbonyldiimidazole (1.1 g, 6.8 mmol, 1.33 equiv.). The resulting clear solution was stirred for 1 h at 50°C. A solution of monomethylmalonic acid (1.21 g, 10.24 mmol, 2 equiv.) in dichloromethane (20 mL) was placed in a second two-necked flask. A solution of isopropylmagnesium chloride 1.15 N in tetrahydrofuran (17.8 mL, 20.48 mmol, 4 equiv.) was added to this ice-cooled solution. After stirring for 10 min at 0°C, the solution was allowed to cool to −10°C. To this solution, the previously prepared imidazolide solution was added dropwise and the resulting mixture was stirred for 15 min at −10°C and an additional 15 min at room temperature. This mixture was poured over a 1N aqueous solution of hydrochloric acid and extracted 3 times with dichloromethane. The combined organic

Can. J. Chem. Downloaded from www.nrcresearchpress.com by 194.225.253.170 on 09/07/12
For personal use only.

layers were washed with a saturated aqueous solution of sodium bicarbonate, dried with magnesium sulfate, filtered, and concentrated to give crude β-ketoester **16** (2.36 g).

Without any purification, the crude β-ketoester **16** was dissolved in 95% aqueous methanol (100 mL) and pyridinium *para*-toluenesulfonate (400 mg) was added. The resulting solution was heated under reflux during 3 h. After cooling, the solution was concentrated and the resulting residue was poured over water and extracted 3 times with dichloromethane. The combined organic layers were washed with brine, dried with magnesium sulfate, filtered, and concentrated to give a residue that was purified by column chromatography (25% to 50% of ethyl acetate in hexane) affording alcohol **17** (1.6 g, 81%); ir ($CHCl_3$): 3460, 2930, 1745, 1670, 1642 cm^{-1}; nmr ($CDCl_3$) δ: 6.7 (1H, tq, J = 6 Hz and −1.1 Hz, H-C3), 5.65 (2H, m, H-C10 and H-C11), 4.75 (2H, s, -O-CH_2-O-), 4.1 (2H, dd, J = 4.5 Hz and −1.1 Hz, H-C12), 3.75 (2H, s, H-C13), 3.7 (3H, s, -COOCH_3), 3.8–3.5 (5H, m, H-C5, -O-CH_2-CH_2-O-), 3.4 (3H, s, -CH_2-OCH_3), 2.5 (2H, dd, J = 6 Hz and 6 Hz, H-C4), 2.05 (2H, m, H-C9), 1.8 (3H, d, J = −1.1 Hz, CH_3-C2), 1.6–1.3 (6H, m, H-C6, H-C7, and H-C8); ms m/e (70 eV): 279 (M^+ − $MEMOH_2$).

*Allylic chloride **18***

To a stirred solution of alcohol **17** (1.55 g, 4 mmol) in dichloromethane (15 mL) at −10°C were added triethylamine (0.84 mL, 6 mmol, 1.5 equiv.) and methanesulfonyl chloride (0.48 mL, 4.8 mmol, 1.2 equiv.). The resulting mixture was allowed to warm to 0°C and stirred for 10 min. Hexamethylphosphoramide (1.4 mL, 8 mmol, 2 equiv.) and dry lithium chloride (0.51 g, 12 mmol, 3 equiv.) were then added and the mixture, warmed to room temperature, was stirred for 1 h. The solution was poured over water and extracted 3 times with dichloromethane. The combined organic layers were washed with brine, dried with magnesium sulfate, filtered, and concentrated to give a residue that was purified by column chromatography (10% and 25% ethyl acetate in hexane) affording chloride **18** (1.45 g, 89%); ir ($CHCl_3$): 2930, 1745, 1670, 1640 cm^1; nmr ($CDCl_3$) δ: 6.6 (1H, tq, J = 6 Hz and −1 Hz, H-C3), 5.85–5.55 (2H, m, H-C10 and H-C11), 4.75 (2H, s, -O-CH_2-O-), 4.02 (2H, d, J = 6.8 Hz, H-C12), 3.75 (2H, s, H-C13), 3.7 (3H, s, -COOCH_3), 3.8–3.5 (5H, m, H-C_5 and -O-CH_2-CH_2-O-), 3.4 (3H, s, -CH_2-OCH_3), 2.5 (dd, J = 6 Hz and 6.2 Hz, H-C_4), 2.05 (2H, m, H-C9), 1.8 (3H, d, J = −1 Hz, CH_3-C2), 1.6–1.25 (6H, m, H-C6 and H-C8); ms m/e (70 eV): 331 (M^+ − CH_2COOCH_3), 329 (M^+ − $OCH_2CH_2OCH_3$).

*Macrocycles **19** and **20***

To a stirred mixture of cesium carbonate (537 mg, 1.65 mmol, 1.3 equiv.) in *N*,*N*-dimethylformamide (200 mL) and tetrahydrofuran (200 mL) was added a solution of allylic chloride **18** (513 mg, 1.27 mmol) in tetrahydrofuran (15 mL) over 26 h. After the addition, the resulting mixture was stirred for an additional 14 h. A saturated aqueous solution of ammonium chloride was then added and the solvants were evaporated. The resulting residue was extracted 3 times with ether and the combined organic layers were dried with magnesium sulfate, filtered, and concentrated to give a residue. After purification by column chromatography, this residue afforded macrocycles **19** (49 mg, 9%) and **20** (361 mg, 77%); ir $CHCl_3$) **20**: 2938. 1750, 1660, 1650, 1040 cm^{-1}; nmr ($CDCl_3$) δ **19**: 6.3 (1H, tq, J = 7 Hz and −1 Hz, H-C3), 5.75–5.4 (2H, m, H-C10 and H-C11), 5.4 (1H, s, -C═CH-CO_2CH_3), 4.8 (2H, s, -O-CH_2-O-), 4.7–4.55 (2H, m, H-C12), 3.85 (1H, m, H-C5), 3.7 (3H, s, -COOCH_3), 3.75–3.55 (4H, A_2B_2, -O-CH_2-CH_2-O-), 3.4 (3H, s, -CH_2-OCH_3), 2.55–2.3 (2H, m, H-C4), 2.1 (2H, m, H-C9), 1.75 (3H, d, J = −1 Hz, CH_3-C2), 1.6–1.2 (6H, m); nmr ($CDCl_3$) δ **20**: 6.8–6.5 (1H, m, H-C3), 5.4–5.2 (2H, m, H-C10 and H-C11), 4.78 (2H, s, -O-CH_2-O-), 4.25 (1H, t, J = 11.1 Hz, 11.5 Hz, H-C13), 3.95 (1H, m, H-C5), 3.7 (3H, s, -COOCH_3), 3.55 (4H, A_2B_2, -O-CH_2-CH_2-O-), 3.4 (3H, s, -CH_2-OCH_3), 2.8–2.4 (4H, m, H-C4 and H-C12), 2.1–1.95 (2H, m, H-C9), 1.85 (3H, d, J = −1.2 Hz, CH_3-C2), 1.6–1.1 (6H, m); ms m/e **19**: 368 (M^+); ms m/e (70 eV) **20**: 368 (M^+).

*Trienone **5***

The macrocycle **20** (210 mg, 0.57 mmol) was dissolved in a solution of 0.26 N potassium hydroxide in 90% aqueous *tert*-butanol (68 mL). The resulting stirred mixture was heated under reflux for 12 h. Then the mixture was poured over water, neutralized with an aqueous solution of hydrochloric acid 10%, and extracted 3 times with ether. The combined organic layers were washed with water, dried with magnesium sulfate, filtered, and concentrated to give a residue that was purified by column chromatography (3% to 10% ethyl acetate in hexane) affording trienone **5** (68 mg, 59%); mp 19–20°C; ir ($CHCl_3$): 3030, 2930, 2855, 1650, 1628 cm^{-1}; nmr ($CDCl_3$) δ: 7.35 (1H, ddq, $J_{3,4}$ = 10.8 Hz, $J_{3,5}$ = −1.4 Hz, $J_{3,Me}$ = −1.3 Hz, H-C3), 6.35 (1H, ddt, $J_{4,5}$ = 10.6 Hz, $J_{4,3}$ = 10.8 Hz, $J_{4,6}$ = −1 Hz, H-C4), 6.05 (1H, dtd, $J_{5,6}$ = 8.3 Hz, $J_{5,4}$ = 10.6 Hz, $J_{5,3}$ = −1.4 Hz, H-C5), 5.65–5.35 (2H, m, $J_{10,11}$ = 15.2 Hz, $J_{9,10}$ = 7.3 Hz, $J_{11,12}$ = 7.4 Hz, $J_{10,12}$ = −1.3 Hz, $J_{9,11}$ = −1.4 Hz, H-C10 and H-C11), 2.7 (2H, m, H-C13) 2.4 (2H, m, H-C12), 2.2 (4H, m, H-C6, H-C9), 1.8 (3H, d, $J_{3,Me}$ = −1.3 Hz, CH_3-C2), 1.55–1.3 (4H, m, H-C7 and H-C8); ms m/e (70 eV): 204 (M^+).

*Tricycles **33**, **34**, and **35***

Trienone **5** (30 mg, 0.14 mmol) was dissolved in anhydrous toluene (2 mL) and was heated in a sealed tube for 4.5 h. After cooling, the resulting solution was concentrated to give a residue that was analyzed by capillary gc affording 35% of tricycle **33**, 42% of **34**, and 20% of **35**. This residue was then purified by column chromatography (1% to 4% ethyl acetate in hexane) to afford tricycles **33** (9.5 mg, 32%), **34** (3.4 mg), and a mixture of **34** and **35** (14 mg, 58%); ir (neat) **33**: 3017, 2955, 2855, 1740, 1447 cm^{-1}; ir (CH_2Cl_2) **34**: 3020, 2970, 2945, 2930, 1705 cm^{-1}; nmr ($CDCl_3$) **33** δ: 5.6 (1H, dtd, $J_{8,7}$ = 9.9 Hz, $J_{8,9}$ = 3.4 Hz, H-C8), 5.47 (1H, dd, $J_{7,8}$ = 9.9 Hz, $J_{7,9}$ = −2.1 Hz, H-C7), 2.35–2.25 (3H, m, H-C9 and H-C4), 2.15 (1H, q apparent, J = 7 Hz), 2.05–1.85 (2H, m, H-C3), 1.85–1.7 (2H, m), 1.7–1.3 (7H, m), 1.18 (3H, s, -CH_3); nmr ($CDCl_3$) **34** δ: 5.8–5.6 (2H, m, H-C7 and H-C8), 2.5–2.2 (4H, m, H-C9, H-C10), and H-C11), 2.15 (1H, m, H-C6), 2.1–1.6 (6H, m), 1.55–1.2 (4H, m), 1.1 (3H, d, $J_{10,Me}$ = −6.6 Hz, CH_3-C10); ms m/e (70 eV) **33**: 204 (M^+); ms m/w (70 eV) **34**: 204 (M^+).

Partial epimerization of a 1:4 mixture of compounds **34** and **35** using a 0.45 M solution of sodium methoxide in methanol afforded a mixture of **34** and **35** in 2:1 ratio after 23 h. Evidence was established by thermally induced isomerization of heating in a sealed tube over 2 h at 300°C; the ratio of **34**:**35** changed from 89.11 to 72.28 and from 34:66 to 58:42 in separate experiments.

*2,4-Dinitrophenylhydrazone derivative of **33***

To a stirred solution of tricycle **33** (2 mg, 0.01 mmol) in ethanol (1.5 mL) and *N*,*N*-dimethylformamide (0.5 mL) were added 2,4-dinitrophenylhydrazine (4 mg, 0.029 mmol, 3 equiv.) and a drop of dilute hydrochloric acid. When the reaction was completed (≈ 2 h), the resulting mixture was filtered on silica gel with dichloromethane as eluant and the filtrate was concentrated to give a residue that was purified by preparative chromatography (15% ethyl acetate in hexane). Despite considerable effort, crystallization of the resulting derivative (1.5 mg) was not possible, attempts giving powder and (or) flakes; nmr ($CDCl_3$) δ: 10.8 (1H, s, -NH-), 9.1 (1H, d, J = 2.6 Hz, >C═C(NO_2)-CH═C(NO_2)-), 8.28 (1H, dd, J = 9.6 Hz, 2.6 Hz, >C═CH-CH═C(NO_2)-), 7.95 (1H, d, J = 9.6 Hz, >C═CH-CH═(NO_2)-), 5.75 (1H, dd, J = 9.9 Hz and 1.4 Hz, H-C7), 5.65 (1H, dd, J = 9.9 Hz and 4.0 Hz, H-C8), 5.6–5.5 (2H, m, H-C4), 2.25–1.95 (4H, m, H-C3, H-C2, and H-C9), 1.85–1.75 (1H, m), 1.7–1.2 (7H, m), 1.34 (3H, s, CH_3-C5).

*2,4-Dinitrophenylhydrazone derivative of **34** and **35***

To a stirred solution of mixture of epimers **34** and **35** in ethanol (2 mL) and *N*,*N*-dimethylformamide (1 mL) were added 2,4-dinitrohenylhydrazine (10.8 mg, 0.055 mmol, 1.1 equiv.) and a drop of dilute hydrochloric acid. When the reaction was completed (≈ 15 min), the resulting mixture was filtered on silica gel with hexane – ethyl acetate (3:1) as eluant and the filtrate was concentrated to give a residue that was purified by successive recrystallizations from dichloromethane and hexane. The derivative of **35** was the first to crystallize and later the derivative of **34** was obtained (20 mg, 100%); mp, derivative of **35**: 204–205°C; nmr $CDCl_3$) derivative of **34** δ: 11.2 (1H, -NH-), 9.1 (1H, d, J = 2.6 Hz, -C(NO_2)═CH-C(NO_2)═CH-), 8.15

Can. J. Chem. Downloaded from www.nrcresearchpress.com by 194.225.253.170 on 09/07/12
For personal use only.

(1H, dd, J = 9.6 Hz, 2.6 Hz, >C=CH-C*H*=C(NO_2)-), 8.0 (1H, d, J = 9.6 Hz, =C-C*H*=CH-C(NO_2)<), 5.6 (2H, m, H-C7 and H-C8), 2.6–2.45 (3H, m, H-C10 and H-C12), 2.27–2.1 (2H, m), 2.0–1.6 (6H, m), 1.55–1.3 (4H, m), 1.3 (3H, d, J = 6.9 Hz, CH_3-C10); nmr $CDCl_3$) derivative of **35** δ: 11.2 (1H, -N*H*-), 9.1 (1H, d, J = 2.6 Hz, -C(NO_2)=C*H*-C(NO_2)-), 8.3 (1H, dd, J = 9.6 Hz and 2.6 Hz, >C=CH-C*H*=C(NO_2)-), 8.0 (1H, d, J = 9.6 Hz, >C=C*H*-CH=C(NO_2)-), 5.5 (2H, m, H-C7 and H-C8), 2.8 (1H, ddd, J = 14.2 Hz, 4.2 Hz, and 3.1 Hz), 2.7–2.6 (2H, m, H-C10), 2.55–2.45 (1H, m), 2.15–2.0 (3H, m), 1.85–1.6 (3H, m), 1.55–1.25 (3H, m), 1.3 (3H, d, J = 6.5 Hz, CH_3-C10).

α,β-*Unsaturated* cis *ester* ***21***

To a stirred solution of methylbis(trifluoroethyl)phosphonoacetate (4.220 g, 13.3 mmol, 1.2 equiv.) in tetrahydrofuran (72 mL) was added dropwise a solution of potassium bis(trimethylsilyl)amide in toluene (0.657 M, 20.2 mL, 13.3 mL, 1.2 equiv.) at −78°C. The resulting solution was stirred for 15 min and a solution of aldehyde **7** (1.771 g, 11.1 mmol) in tetrahydrofuran (3 mL) was then added. After stirring for an additional 15 min, the mixture was allowed to warm to room temperature, poured over a saturated aqueous solution of ammonium chloride, and extracted 3 times with ether. The combined organic layers were washed with brine, dried with magnesium sulfate, filtered, and concentrated to afford an oily residue that was purified by column chromatography (5% to 25% ethyl acetate in hexane) affording *cis* ester **21** (1.874 g, 79%); ir ($CHCl_3$): 3005, 2945, 1718, 1645, 1440, 1200, 1137 cm^{-1}; nmr ($CDCl_3$) δ: 1.34–1.55 and 1.57–1.67 (6H, m, -CH_2-CH_2-CH_2-CH(OCH_3)$_2$, 2.66 (2H, tdd, J = 7.5 Hz, 7.5 Hz, and 1.7 Hz, -CH_2-CH_2-CH=CH-), 3.31 (6H, s, -CH(OCH_3)$_2$), 3.70 (3H, s, -CO_2CH_3), 4.35 (1H, t, J = 5.7 Hz, -CH_2-CH(OCH_3)$_2$), 5.77 (1H, dt, J = 11.5 Hz and 1.7 Hz, -CH_2-CH=C*H*-), 6.22 (1H, dt, J = 11.5 Hz, 7.5 Hz, -CH_2-C*H*=CH-); ms m/e (70 eV): 215 (M^+ −H), 185 (M^+ −OCH_3).

Allylic alcohol ***22***

To a stirred solution of ester **21** (14.044 g, 65.0 mmol) in dichloromethane (200 mL) at −78°C was added dropwise a solution of diisobutylaluminum hydride in cyclohexane (1 M, 143 mL, 143.0 mmol, 2.2 equiv.). The resulting mixture was stirred for 15 min and methanol, followed by a saturated aqueous solution of ammonium chloride, was added. The mixture was then allowed to warm to room temperature, stirred for 2 h, and extracted 4 times with dichloromethane. The combined organic layers were washed with brine, dried with sodium sulfate, filtered, and concentrated to give a residue that was purified by column chromatography (10% to 25% ethyl acetate in hexane) affording alcohol **22** (7.936 g, 65%); ir ($CHCl_3$): 3610, 3450, 3005, 2940, 1450, 1383, 1363, 1128, 1050 cm^{-1}; nmr ($CDCl_3$) δ: 1.29–1.48 and 1.55–1.68 (6H, m, -CH_2-CH_2-CH_2-CH(OCH_3)$_2$), 2.02–2.26 (2H, m, -CH_2-CH=CH-), 3.31 (6H, s, -CH(OCH_3)$_2$), 4.00–4.11 (1H, m, -CH_2OH), 4.18 (2H, d, J = 6.3 Hz, -CH_2OH), 4.34 (1H, t, J = 5.7 Hz, -CH_2-CH(OCH_3)$_2$), 5.45–5.67 (2H, m, -CH=CH-).

Silyl ether ***23***

To a stirred ice-cooled solution of alcohol **22** (442 mg, 2.3 mmol) in *N*,*N*-dimethylformamide (1.7 mL), were added imidazole (240 mg, 3.5 mmol, 1.5 equiv.) and *tert*-butylchlorodiphenylsilane (730 μL, 2.8 mmol, 1.2 equiv.). The resulting solution was allowed to warm to room temperature, stirred for 2 h, poured over a 10% aqueous solution of hydrochloric acid and extracted 3 times with ether. The combined organic layers were washed with brine, dried with sodium sulfate, filtered, and concentrated to give a residue that was purified by column chromatography (10% ethyl acetate in hexane) affording silyl ether **23** (851 mg, 85%); ir ($CHCl_3$): 3075, 3010, 2930, 2860, 1471, 1462, 1428, 1110, 1080 cm^{-1}; nmr ($CDCl_3$) δ: 1.04 (9H, s, -OSiC(CH_3)$_3$$Ph_2$), 1.23–1.34 and 1.49–1.59 (6H, m, -CH_2-CH_2-CH_2-CH(OCH_3)$_2$), 1.81–1.92 (2H, m, -CH_2-CH=CH-), 3.29 (6H, s, -CH(OCH_3)$_2$), 4.24 (2H, dd, J = 6.1 Hz and 1.5 Hz, -CH=CH-CH_2-), 5.34–5.41 and 5.54–5.66 (2H, m, -CH=CH-), 7.34–7.45 and 7.67–7.75 (10H, m, -OSiPh_2C(CH_3)$_3$).

Aldehyde ***24***

To a stirred solution of silyl ether **23** (708 mg, 1.7 mmol) in tetrahydrofuran (3.5 mL) was added a 5% aqueous solution of hydrochloric acid (3.5 mL). The resulting solution was stirred for 24 h at room temperature, then diluted in water and extracted 3 times with ether. The combined organic layers were washed with brine, dried with sodium sulfate, filtered, and concentrated to give a residue that was purified by column chromatography (hexane to 50% ethyl acetate in hexane) affording aldehyde **24** (557 mg, 88%); ir ($CHCl_3$): 3010, 2930, 2860, 2725, 1472, 1462, 1428, 1110, 1080 cm^{-1}; nmr ($CDCl_3$) δ: 1.04 (9H, s, -OSiPh_2C(CH_3)$_3$), 1.21–1.37 and 1.49–1.52 (4H, m, -CH_2-CH_2-CH_2-CHO), 1.88 (2H, td, J = 7.3 Hz and 7.3 Hz, -CH_2-CH=CH-), 2.35 (2H, td, J = 7.4 Hz and 1.8 Hz, -CH_2-CHO), 4.24 (2H, dd, J = 6.1 Hz and 1.5 Hz, -CH=CH-CH_2-), 5.33–5.45 and 5.58–5.69 (2H, m, -CH=CH-), 7.34–7.44 and 7.64–7.72 (10H, m, -OSiPh_2C(CH_3)$_3$), 9.71 (1H, t, 1.8 Hz, -CHO).

α,β-*Unsaturated* trans *aldehyde* ***25***

To aldehyde **24** (453 mg, 1.19 mmol) was added a solution of (formylmethylene)triphenylphosphorane (600 mg, 1.97 mmol, 1.7 equiv.) in benzene (7.5 mL) and dichlormethane (3 mL). The resulting mixture was heated under reflux for about 40 h. After cooling, the solution was concentrated and the resulting residue was purified by column chromatography (2.5% ethyl acetate in hexane) to afford aldehyde **25** (316 mg, 65%); ir ($CHCl_3$): 3005, 2930, 2860, 2740, 1687, 1637, 1470, 1428, 1110 cm^{-1}; nmr ($CDCl_3$) δ: 1.04 (9H, s, -OSiPh_2C(CH_3)$_3$), 1.19–1.50 (4H, m, -CH_2-CH_2-CH=CH-CHO), 1.88 (2H, td, J = 7.0 Hz, and 7.0 Hz, -CH_2-CH=CH=CH_2OSiPh_2*t*-Bu), 2.40 (2H, tdd, J = 7.4 Hz, 7.4 Hz and 1.1 Hz, -CH_2-CH=CH-CHO), 4.24 (2H, dd, J = 6.1 Hz and 1.5 Hz, -CH_2OSiPh_2*t*-Bu), 5.33–5.45 and 5.58–5.70 (2H, m, -CH=CH_2OSiPh_2*t*-Bu), 6.08 (1H, ddt, J = 16.3 Hz, 8.0 Hz, 1.2 Hz, -CH=C*H*-CHO), 6.79 (1H, dt, J = 16.3 Hz, 7.5 Hz, -CH=CH-CHO), 7.34–7.45 and 7.66–7.72 (10H, m, -OSiPh_2C(CH_3)$_3$), 9.48 (1H, d, J = 7.9 Hz, -CHO); ms m/e (70 eV): 349 (M^+ −*t*-Bu).

β-*Ketoester* ***26***

To a stirred suspension of sodium hydride (61 mg, 1.52 mmol, 3.1 equiv.) in tetrahydrofuran (1.5 mL) was added methyl 3-oxopentanoate (185 μL, 1.474 mmol, 3 equiv.) at −5°C. After stirring for 30 min, a solution of butyllithium in hexane (1.68 M, 821 μL, 1.38 mmol, 2.8 equiv.) was added and the resulting solution was stirred for an additional 30 min at −5°C. A solution of aldehyde **25** (198 mg, 0.49 mmol) in tetrahydrofuran (0.5 mL) was finally added to the mixture, which was then allowed to stir for 5 min, poured over an aqueous saturated solution of ammonium chloride, and extracted 3 times with dichloromethane. The combined organic layers were dried with magnesium sulfate, filtered, and concentrated to give a residue that was rapidly purified by column chromatography (25% ethyl acetate in hexane) affording β-ketoester **26** (188 mg, 72%). The product was immediately converted into its tetrahydropyranyl derivative; ir ($CHCl_3$): 3592, 3005, 2930, 2860, 1740, 1710, 1438, 1428, 1111 cm^{-1}; nmr ($CDCl_3$) δ: 1.04 (9H, s, -OSiPh_2C(CH_3)$_3$), 1.11 (3H, d, J = 7.1 Hz, -CHOH-CHCH_3-CO-), 1.17–1.37 (4H, m, -CH_2-CH_2-CH_2-CH=CH-CH_2-OSiPh_2*t*-Bu), 1.76–1.91 and 1.92–2.08 (4H, m, -CH=CH-CH_2-(CH_2)$_2$-CH_2-CH=CH-), 2.70–2.86 (1H, m, -CHOH-CHCH$_3$-CO-), 3.56 (2H, s, -CO-CH_2-CO_2Me), 3.73 (3H, s, -CO_2CH_3), 4.23 (2H, d, J = 6.2 Hz, -CH_2-OSiPh_2*t*-Bu), 4.33–4.44 (1H, m, -CHOH-CHCH$_3$-), 5.33–5.46 (2H, m, -CH=CH-CH_2OSiPh_2*t*-Bu), 5.53–5.65 (2H, m, -CH=CH-CHOH-), 7.33–7.44 and 7.65–7.73 (10H, m, -OSiPh_2C(CH_3)); ms m/e (70 eV): 461 (M^+ −H_2O−*t*-Bu).

Tetrahydropyrannyl ether ***27***

To a stirred solution of alcohol **26** (1.86 g, 3.47 mmol) in dichloromethane (35 mL) were added dihydropyran (3.16 mL, 34.6 mmol, 10 equiv.) and pyridinium *para*-toluenesulfonate (37 mg, 0.147 mmol, 0.04 equiv.) After stirring for 2 h, the resulting mixture was poured over water and extracted 3 times with dichloromethane. The combined organic layers were washed with brine, dried with sodium sulfate, filtered, and concentrated to give a residue that was purified by column chromatography (10% to 25% ethyl acetate in hexane) affording ether

Can. J. Chem. Downloaded from www.nrcresearchpress.com by 194.225.253.170 on 09/07/12
For personal use only.

27 (1.901 g, 88%); ir $CHCl_3$): 3005, 2930, 2860, 1745, 1712, 1425, 1111 cm^{-1}; nmr ($CDCl_3$) δ: 0.84–1.11 (3H, m, -CHOTHP-CHCH_3), 1.04 (9H, s, -OSiPh_2C(CH_3)$_3$), 1.18–1.38 (4H, m, -(CH_2)$_2$-CH_2-CH=CH-CH_2OSiPh_2*t*-Bu), 1.41–1.64 (6H, m, -(CH_2)$_3$-CH_2-O-), 1.77–1.91 and 1.92–2.05 (4H, m, -CH=CH-CH_2-(CH_2)$_2$-CH_2-CH=CH-),2.77–3.02 (1H, m, -CHOTHP-C*H*CH$_3$-CO-), 3.34–3.87 (4H, m,-CH_2-CH_2-O- and -CO-CH_2-CO_2CH_3), 3.71, 3.72, 3.73, 3.74 (3H, s, -COOCH_3), 3.91–4.20 (1H, m, -C*H*OTHP-CHCH$_3$-), 4.24 (2H, d, J = 6.2 Hz, -CH_2OSiPh_2*t*-Bu), 4.54, 4.62, 4.70 (1H, t, J = 3.8 Hz, -O-C*H*-O-), 4.98–5.45 and 5.54–5.74 (4H, m, -C*H*=C*H*-(CH_2)$_4$-C*H*=C*H*-), 7.34–7.45 and 7.66–7.73 (10H, m, -OSi*Ph*$_2$*t*-Bu); ms *m/e* (70 eV): 563 (M^+ − *t*-Bu).

Allylic alcohol ***28***

To an ice-cooled stirred solution of silyl ether **27** (2.30 g, 3.71 mmol) in tetrahydrofuran (45 mL) was added a solution of tetrabutylammonium fluoride in tetrahydrofuran (1 M, 4.45 mL, 4.45 mmol, 1.2 equiv.). After stirring for 2 h at room temperature, the resulting mixture was poured over water and extracted 3 times with dichloromethane. The combined organic layers were washed with brine, dried and sodium sulfate, filtered, and concentrated to give a residue that was purified by column chromatography (25% ethyl acetate in hexane) to afford alcohol **28** (1.200 g, 88%); ir ($CHCl_3$): 3610, 3450, 3010, 2935, 2855, 1745, 1712, 1652, 1629, 1452, 1438, 1020, 1008 cm^{-1}; nmr ($CDCl_3$) δ: 0.96, 0.99, 1.06, 1.09 (3H, d, J = 7.1 Hz, 7.0 Hz, 6.9 Hz, and 6.9 Hz, -CHOTHP-CHCH_3-CO-), 1.29–1.44 (4H, m, -(CH_2)$_2$-CH_2-CH=CH-CH_2OH), 1.44–1.86 (6H, m, -(CH_2)$_3$-CH_2-O-), 1.96–2.13 (4H, m, -CH=CH-CH_2-(CH_2)$_2$-CH_2-CH=CH-), 2.76–3.06 (1H, m, -CHOTHP-C*H*CH$_3$-CO-), 3.34–3.88 (4H, m, -CH_2-C*H*-O- and -CO-CH_2-CO_2CH_3), 3.71, 3.72, 3.73, 3.74 (3H, s, -COOCH_3), 3.91–4.24 (1H, m, -C*H*OTHP-CHCH$_3$-), 4.12–4.22 (2H, m, -CH=CH-CH_2OH), 4.51–4.56, 4.61–4.65 and 4.68–4.75 (1H, m, -O—C*H*-O-), 4.98–5.76 (4H, m, -C*H*=C*H*-(CH_2)$_4$-C*H*=C*H*-); ms *m/e* (70 eV): 383 (M^+).

Allylic chloride ***29***

To a stirred solution of alcohol **28** (201 mg, 0.526 mmol) in dichloromethane (3 mL) were added triethylamine (110 μL, 0.789 mmol, 1.5 equiv.) and methanesulfonyl chloride (49 μL, 0.633 mmol, 1.2 equiv.) at −10°C. The resulting mixture was allowed to warm to 0°C and stirred for 30 min. Hexamethylphosphoramide (201 μL, 1.161 mmol, 2.2 equiv.) and lithium chloride (49 mg, 1.156 mmol, 2.2 equiv.) were added to the ice-cooled mixture, which was then allowed to warm to room temperature, stirred for 1.5 h, poured over brine, and extracted 3 times with ether. The combined organic layers were dried with sodium sulfate, filtered, and concentrated to give a residue that was purified by column chromatography (5% ethyl acetate in hexane) affording chloride **29** (183 mg, 87%); ir ($CHCl_3$): 3015, 3005, 2852, 1745, 1712, 1650, 1480, 1452, 1440, 1020, 1008 cm^{-1}; nmr ($CDCl_3$) δ: 0.95, 0.98, 1.07 and 1.09 (3H, d, J = 7.6 Hz, 7.1 Hz, 6.9 Hz, and 6.9 Hz, -CHOTHP-CHCH_3-), 1.30–1.44 (4H, m, -(CH_2)$_2$-CH_2-CH=CH-CH_2Cl), 1.44–1.90 (6H, m, -(CH_2)$_3$-CH_2-O-), 1.97–2.20 (4H, m, -CH=CH-CH_2-(CH_2)$_2$-CH_2-CH=CH-), 2.79–3.03 (1H, m, -CHOTHP-C*H*CH$_3$-), 3.34–3.90 (4H, m, -CH_2-CH_2-O- and -CO-CH_2-COOCH$_3$), 3.71 and 3.72 (3H, s, -COOCH_3), 3.91–4.26 (1H, m, -C*H*OTHP-CHCH$_3$-), 4.05–4.12 (2H, m, -CH_2Cl), 4.51–4.57, 4.60–4.66, and 4.67–4.75 (1H, m, -O-C*H*-O-), 4.98–5.45 and 5.53–5.76 (4H, m, -C*H*=C*H*-(CH_2)$_4$-C*H*=C*H*-); ms *m/e* (70 eV): 369 (M^+ −OCH$_3$), 365 (M^+ − Cl). *Exact Mass* (M^+ − Cl) calcd.: 365.2335; found: 365.2335.

Macrocycle ***30***

To a stirred solution of chloride **30** (104 mg, 0.260 mmol) in dry acetone (120 mL) were added potassium carbonate (107 mg, 0.774 mmol, 3 equiv.) and sodium iodide (116 mg, 0.774 mmol, 3 equiv.). The heterogeneous mixture was heated under reflux for 72 h. After cooling, the mixture was poured over a saturated aqueous solution of ammonium chloride and concentrated. The resulting residue was then poured over a 1:1 mixture of dichloromethane and water and extracted **3** times with dichloromethane. The combined organic layers were washed with brine, dried with sodium sulfate, filtered, and concentrated to give a residue that was purified by column chromatography (5% to 10% of ethyl acetate in hexane) to afford macrocycle **30** (69 mg, 74%); spectra of one diastereoisomer only: ir ($CHCl_3$): 2922, 2855, 1742, 1712, 1455, 1447 cm^{-1}; nmr ($CDCl_3$) δ: 1.27 (3H, d, J = 6.7 Hz, CH$_3$-C2), 1.01–2.27 (14H, m, H-C6, H-C7, H-C8, H-C9, and -(CH_2)$_3$-CH_2-O-), 2.29–2.43 and 2.51–2.64 (2H, m, H-C12), 3.09 (1H, dq, J = 10.0 Hz, 6.7 Hz, H-C2), 3.45–3.56 and 3.79–3.90 (2H, m, -(CH_2)$_3$-CH_2-O-), 3.73 (3H, s, -COOCH_3), 3.55 (1H, dd, J = 9.9 Hz, 3.6 Hz, H-C13), 4.03 (1H, dd, J = 10.0 Hz, 7.5 Hz, H-C3), 4.68 (1H, t, J = 3.1 Hz, -O—C*H*-O-), 5.21 (1H, ddt, J = 15.0 Hz, 7.5 Hz, 1.8 Hz, H-C4), 5.44–5.69 (3H, m, H-C5, H-C9, and H-C11); ms *m/e* (70 eV): (M^+). *Exact Mass* (M^+) calcd.: 364.2250; found: 364.2253.

Alcohol ***31***

To a stirred solution of macrocycle **30** (71 mg, 0.195 mmol) in 95% methanol (10 mL) was added pyridinium *para*-toluenesulfonate (37 mg, 0.147 mmol, 0.75 equiv.). The mixture was heated under reflux for 1.5 h, then poured over brine and extracted 3 times with dichloromethane. The combined organic layers were dried with sodium sulfate, filtered, and concentrated to give a residue that was purified by column chromatography (10% to 25% ethyl acetate in hexane) affording alcohol **31** (49 mg, 90%); spectra of one diastereoisomer only: ir ($CHCl_3$): 3525, 3020, 2930, 2855, 1747, 1702, 1455, 1438, 1261 cm^{-1}; nmr ($CDCl_3$) δ: 1.24 (3H, d, J = 6.6 Hz, CH$_3$-C2), 1.04–2.23 (8H, m, H-C6, H-C7, H-C8, and H-C9), 2.33–2.61 (2H, m, H-C12), 2.97 (1H, dq, J = 9.4 Hz and 6.7 Hz, H-C2), 3.56 (1H, dd, J = 10.0 Hz and 3.7 Hz, H-C13), 3.74 (3H, s, -COOCH_3), 4.02 (1H, dd, J = 9.8 Hz and 6.8 Hz, H-C3), 5.42-5.75 (4H, m, H-C4, H-C5, H-C10, and H-C11); ms *m/e* (70 eV): 280 (M^+), 262 (M^+ − H_2O). *Exact Mass* (M^+) calcd.: 280.1674; found: 280.1673.

Acetate ***32***

To an ice-cooled stirred solution of alcohol **31** (43 mg, 0.154 mmol) in dichloromethane (3.5 mL) were added triethylamine (42 μL, 0.30 mmol, 2 equiv.) acetic anhydride (29 μL, 0.307 mmol, 2 equiv.), and dimethylaminopyridine (1 crystal). The resulting mixture was stirred for 9 h, then poured over a 5% aqueous solution of hydrochloric acid and extracted 3 times with dichloromethane. The combined organic layers were washed with a saturated aqueous solution of sodium bicarbonate, dried with magnesium sulfate, filtered, and concentrated to give a residue that was purified by column chromatography (25% ethyl acetate in hexane) affording acetate **32** (46 mg, 93%); spectrum of one diastereoisomer only: nmr ($CDCl_3$) δ: 1.14 (3H, d, J = 6.7 Hz, CH$_3$-C2), 1.05–1.24 (8H, m, H-C6, H-C7, H-C8, and H-C9), 2.07 (3H, s, -OCOCH_3), 2.33–2.66 (2H, m, H-C12), 3.14 (1H, dq, J = 9.8 Hz and 6.7 Hz, H-C2), 3.57 (1H, dd, J = 9.5 Hz and 4.0 Hz, H-C13), 3.74 (3H, s, -COOCH_3), 5.18 (1H, dd, J = 9.8 Hz and 7.0 Hz, H-C3), 5.32–5.76 (4H, m, H-C4, H-C5, H-C10, and H-C11).

Trienone ***6***

To an ice-cooled stirred solution of acetate **32** (46 mg, 0.143 mmol) in benzene (11 mL) was added 1,8-diazabicyclo[5.4.0]undec-7-ene (63 μL, 0.421 mmol, 3 equiv.). The resulting solution was heated under reflux for 12 h, then poured over a 5% aqueous solution of hydrochloric acid and extracted 3 times with ether. The combined organic layers were washed with a saturated aqueous solution of sodium bicarbonate, dried with sodium sulfate, filtered, and concentrated to give a residue that was purified by column chromatography (5% to 10% ethyl acetate in hexane) affording impure trienone **6** (27 mg, 72%). The product was recrystallized from a mixture of hexane–dichloromethane at −20°C to afford pure trienone **6** (17.1 mg, 46%); mp 68–70°C; ir (CH_2Cl_2): 3010, 2925, 2885, 1745, 1685, 1432, 1222 cm^{-1}; nmr ($CDCl_3$) δ: 1.12–2.45 (8H, m, H-C6, H-C7, H-C8, and H-C9), 1.91 (3H, d, J = 1.2 Hz, CH$_3$-C2), 2.58–2.65 (2H, m, H-C12), 3.71 (3H, s, -COOCH_3), 3.94 (1H, dd, J = 7.5 Hz, 7.5 Hz, H-C13), 5.60–5.66 (2H, m, H-C11 and H-C12), 5.83 (1H, dt, $J_{5,4}$ = 15.4 Hz, $J_{5,6}$ = 7.6 Hz, H-C5), 6.15 (1H, dd, $J_{4,5}$ = 15.2 Hz, $J_{4,3}$ = 10.5 Hz, H-C4), 6.37 (1H, d, J = 10.3 Hz, H-C3); ms *m/e* (70 eV): 262 (M^+), 247 (M^+ − CH_3), 244 (M^+ − H_2O), 231 (M^+ − OMe). *Exact Mass* (M^+) calcd: 262.1569; found: 262.1567.

Can. J. Chem. Downloaded from www.nrcresearchpress.com by 194.225.253.170 on 09/07/12
For personal use only.

Tricycle 37

A solution of trienone **6** (8.3 mg, 0.032 mmol) in toluene (0.5 mL) was heated in a sealed tube at 300°C for 1.25 h. After evaporation of the solvent, the residue was purified by column chromatography (10% ethyl acetate in hexane) to give tricycle **37** (3.9 mg, 60%) and non-reacted trienone **6** (2.7 mg, 33% recovered). The trienone **6** in toluene (0.5 mL) was heated again in a sealed tube at 300°C for 2.5 h. After evaporation of the solvant and column chromatography, tricycle **37** was obtained (2.1 mg, 100%, total yield = 93%); mp 88–89°C; ir (CH_2Cl_2): 3030, 2920, 2850, 1732, 1477, 1454 cm^{-1}; nmr ($CDCl_3$) δ: 1.12 (3H, s, CH_3-C6), 1.15–2.49 (15H, m, H-C1, H-C2, H-C3, H-C4, H-C9, H-C10, H-C11, H-C12, and H-C13), 5.20 (1H, ddd, J = 10.0 Hz, 2.5 Hz, and 1.3 Hz, H-C7), 5.50 (1H, dd, J = 10.0 Hz and 1.7 Hz, H-C8); ms m/e (70 eV): 204 (M^+), 189 ($M^+ - CH_3$). *Exact Mass* (M^+) calcd.: 204.1514; found: 204.1514.

2,4-Dinitrophenylhydrazone derivative of 37

To a stirred solution of impure tricycle **37** (5.1 mg, 0.025 mmol) in ethanol (3.8 mL) and *N*,*N*,-dimethylformamide (1.2 mL) were added 2,4-dinitrophenylhydrazine (25 mg, 0.126 mmol, 5 equiv.) and a drop of 5% aqueous solution of hydrochloric acid. When the reaction was completed (≈ 0.5 h), the resulting mixture was filtered on silica gel with dichloromethane as eluant and the filtrate was concentrated to give a residue that was purified by preparative chromatography (10% ethyl acetate in hexane) and by high pressure liquid chromatography (0.75% of tetrahydrofuran in hexane) to afford derivative of **37** (2.9 mg, 30%); mp 172–177°C (dec.); ir (CH_2Cl_2): 3050, 2930, 2880, 1615, 1590, 1520, 1420, 1340, 1320, 1160 cm^{-1}; nmr ($CDCl_3$) δ: 1.34 (3H, s, CH_3-C6), 1.13–2.12 (12H, m), 2.23–2.46 (2H, m), 2.69 (1H, dd, J = 8.4 Hz and 17.6 Hz), 5.33 (1H, d, J_{AB} = 9.5 Hz, H-C7), 5.44 (1H, d, J_{AB} = 9.5 Hz, H-C8), 7.99 (1H, d, J = 9.7 Hz, >C=C*H*-CH=C(NO_2)-), 8.30 (1H, dd, J = 9.7 Hz and 2.6 Hz, >C=CH-C*H*=C(NO_2)-), 9.13 (1H, d, J = 2.5 Hz, >C=C(NO_2)-C*H*=C(NO_2)-), 10.83 (1H, s, =N-N*H*-Ar); ms m/e (70 eV): 384 (M^+). *Exact Mass* (M^+) calcd.: 384.1797, found: 384.1793.

Acknowledgements

This research was supported by the Natural Sciences and Engineering Research Council of Canada (NSERCC, Ottawa) and by the "Ministère de l'Éducation" (FCAR, Québec).

1. (*a*) T. K. Devon and A. I. Scott. Handbook of naturally occurring compounds. Vol. II: Terpenes. Academic Press, New York. 1972; (*b*) T. Kametani (*Editor*). Heterocycles, **20**, Suppl. no. 2. June (1983).
2. (*a*) J. Tsuji, T. Yamada, M. Kaito, and T. Mandai. Tetrahedron Lett. 2257 (1979); (*b*) J. Tsuji and T. Mandai. Tetrahedron Lett. 3285 (1977); (*c*) J. Tsuji and S. Hashiguchi. Tetrahedron Lett. **21**, 2955 (1980); (*d*) J. P. Schaeffer and J. J. Bloomfield. Org. React. **15**, 1 (1967); (*e*) G. Stork and E. Nakamura. J. Org. Chem. **44**, 4010 (1979); (*f*) K. C. Nicolaou, S. P. Seitz, M. R. Pavia, and N. A. Petasis. J. Org. Chem. **44**, 4011 (1979); (*g*) J. E. McMurry, K. L. Kees, M. P. Flemming, and L. R. Krebski. J. Org. Chem. **43**, 3255 (1978); (*h*) B. M. Trost and T. R. Verhoeven. J. Am. Chem. Soc. **102**, 4743 (1980); (*i*) T. Takahashi, H. Nemoto, and J. Tsuji. Tetrahedron Lett. **24**, 2005 (1983); **24**, 3485 (1983); (*j*) T. Takahashi, K. Kitamura, and J. Tsuji. Tetrahedron Lett. **24**, 4695 (1983); (*k*) M. A. Casadei, C. Gailli, and L. Mandolini. J. Org. Chem. **46**, 3127 (1983); (*l*) M. Kodama, S.-I. Yokoo, H. Yamada, and S. Itô. Tetrahedron, **34**, 3121 (1978); (*m*) W. C. Still and D. Mobilio. J. Org. Chem. **48**, 4786 (1983); (*n*) J. A. Marshall and D. G. Cleary. J. Org. Chem. **51**, 858 (1986); (*o*) T. Kitahara and K. Mori. J. Org. Chem. **49**, 3281 (1984).
3. (*a*) P. Deslongchamps, S. Lamothe, and H.-S. Lin. Can. J. Chem. **65**, 1298 (1987); (*b*) D. Brillon and P. Deslongchamps. Can. J. Chem. **65**, 43 (1987); **65**, 56 (1987).
4. W. C. Still and I. Galynker. Tetrahedron, **37**, 3981 (1981).
5. E. Neeland, J. P. Ounsworth, R. J. Sims, and L. Weiler. Tetrahedron Lett. **28**, 35 (1987), and references therein.
6. (*a*) A. C. Cope, M. M. Martin, and M. A. McKervey. Q. Rev. Chem. Soc. **20**, 119 (1966); (*b*) N.-J. Leonard. Acc. Chem. Res. **12**, 423 (1979); (*c*) H. H. Wasserman and A. R. Doumaux, Jr. J. Am. Chem. Soc. **84**, 4611 (1962); (*d*) D. J. Cram, C. S. Montgomery, and C. R. Knox. J. Am. Chem. Soc. **88**, 515 (1966); (*e*) W. E. Minter, G. J. Fonken, and F. T. Cook. Tetrahedron Lett. 711 (1979); (*f*) W. E. Dauben, D. M. Michno, and E. G. Olsen. J. Org. Chem. **46**, 687 (1981). (*g*) E. Vogel, H.-J. Altenbach, and D. Cremer. Angew. Chem. Int. Ed. Engl. **11**, 935 (1972); (*h*) H. Prinzbach, D. Stusche, M. Breuninger, and J. Markert. Chem. Ber. **109**, 2823 (1976); (*i*) G. Kaupp and K. Rösch. Angew. Chem. Int. Ed. Engl. **15**, 163 (1976).
7. A. Bélanger, D. J. F. Berney, H.-J. Broschberg, R. Brousseau, A. Doutheau, R. Durand, H. Katayama, R. Lapalme, D. M. Leturc. C.-C. Liao, F. N. MacLachlan, J.-P. Maffrand, F. Marazza, R. Martino, C. Moreau, L. St-Laurent, R. Saintonge, P. Soucy, L. Ruest, and P. Deslongchamps. Can. J. Chem. **57**, 3348 (1979).
8. (*a*) P. Deslongchamps. Aldrichimica Acta, **17**, 59 (1984); (*b*) Bull. Soc. Chim. Fr. II, **9–10**, 349 (1984).
9. (*a*) T. Takahashi, H. Nemoto, Y. Kanda, J. Tsuji, Y. Fukazawa, T. Okajima, and Y. Fujise. Tetrahedron, **43**, 5499 (1987); (*b*) J. A. Marshall and J. Lebreton. J. Am. Chem. Soc. **110**, 2925 (1988).
10. (*a*) K. Baettig, C. Dallaire, R. Pitteloud, and P. Deslongchamps. Tetrahedron Lett. **28**, 5249 (1987); (*b*) K. Baettig, A. Marinier, R. Pitteloud, and P. Deslongchamps. Tetrahedron Lett. **28**, 5253 (1987); (*c*) G. Bérubé and P. Deslongchamps. Tetrahedron Lett. **28**, 5255 (1987); (*d*) S. Lamothe, A. Ndibwami, and P. Deslongchamps. Tetrahedron Lett. **29**, 1639 (1988); (*e*) S. Lamothe, A. Ndibwami, and P. Deslongchamps. Tetrahedron Lett. **29**, 1641 (1988); (*f*) A. Marinier and P. Deslongchamps. Tetrahedron Lett. **29**, 6215 (1988).
11. T. Takahashi, K. Shimizu, T. Doi, and J. Tsuji. J. Am. Chem. Soc. **110**, 2674 (1988).
12. S. L. Schreiber, R. E. Claus, and J. Reagan. Tetrahedron Lett. **23**, 3867 (1982).
13. W. S. Wadsworth, Jr. and W. D. Emmons. J. Am. Chem. Soc. **83**, 1733 (1961).
14. N. Miyashita, A. Yoshikoshi, and P. A. Grieco. J. Org. Chem. **42**, 3772 (1977).
15. (*a*) A. Kajikawa, M. Morisaki, and N. Ikekawa. Tetrahedron Lett. 4135 (1975); (*b*) D. M. Savu and J. A. Katzenhellenbogen. J. Org. Chem. **46**, 239 (1981).
16. E. J. Corey, J.-L. Gras, and P. Ulrich. Tetrahedron Lett. 809 (1976).
17. (*a*) G. Bram and M. Vilkas. Bull. Soc. Chim. Fr. 945 (1964); (*b*) D. Pollet and S. Gelin. Synthesis, 142 (1978); (*c*) D. W. Brooks, L. D. L. Lu, and S. Masamune. Angew. Chem. Int. Ed. Engl. **18**, 72 (1979).
18. J. Buter and R. M. Kellogg. J. Chem. Soc. Chem. Commun. 466 (1980).
19. C. Still and C. Gennari. Tetrahedron Lett. **24**, 4405 (1983).
20. S. Hanessian and P. Lavallée. Can. J. Chem. **53**, 2975 (1975).
21. S. Trippett and D. M. Walker. J. Chem. Soc. 1266 (1961).
22. S. N. Huckin and L. Weiler. Can. J. Chem. **52**, 2157 (1974).
23. E. J. Corey and A. Venkateswarlu. J. Am. Chem. Soc. **94**, 6190 (1972).
24. L. M. Jackman and S. Sternhell. Application of NMR spectroscopy in organic chemistry. 2nd ed. Pergamon Press, Oxford. 1969. p. 243.

Studies on some selective and competitive substitution reactions of cyclopentadienyliron complexed chloronitrobenzenes with amines as nucleophiles

ALAA S. ABD-EL-AZIZ,[1] ADAM PIÓRKO, CHOI CHUCK LEE, AND RONALD G. SUTHERLAND
Department of Chemistry, University of Saskatchewan, Saskatoon, Sask., Canada S7N 0W0

Received April 5, 1989

ALAA S. ABD-EL-AZIZ, ADAM PIÓRKO, CHOI CHUCK LEE, and RONALD G. SUTHERLAND. Can. J. Chem. **67**, 1618 (1989).

Nucleophilic substitution reactions of the (η^6-*o*-, -*m*-, or -*p*-chloronitrobenzene)(η^5-cyclopentadienyl)iron cation (**2***a*, **2***b*, or **2***c*, respectively) with aniline, *n*-butylamine, or pyrrolidine as nucleophile were investigated. It was found that only selective displacement of the nitro group occurred for reactions with aniline. For reaction with *n*-butylamine or pyrrolidine, *o*-isomer **2***a* resulted in the selective displacement of only the chloro group, giving rise to the (η^6-*o*-*n*-butylaminonitrobenzene)(η^5-cyclopentadienyl)iron cation (**5***a*) or the (η^6-*o*-nitro-*N*-pyrrolidinylbenzene)(η^5-cyclopentadienyl)iron cation (**7***a*), respectively. With the *m*- or *p*-isomer **2***b* or **2***c*, reaction with *n*-butylamine or pyrrolidine gave a mixture of substitution products from competitive displacements of both chloro and nitro groups, the major product from the *m*-isomer being derived from displacement of the chloro group while the major product from the *p*-isomer resulted from displacement of the nitro group. Possible interpretations of these results on the basis that the basicity of the nucleophile and the combined inductive effects of the nitro and chloro substituents would play important roles are presented.

Key words: (η^6-*o*-, -*m*-, and -*p*-chloronitrobenzene)(η^5-cyclopentadienyl)iron cations, nucleophilic substitution reactions, aniline, *n*-butylamine, pyrrolidine.

ALAA S. ABD-EL-AZIZ, ADAM PIÓRKO, CHOI CHUCK LEE et RONALD G. SUTHERLAND. Can. J. Chem. **67**, 1618 (1989).

On a étudié les réactions de substitutions nucléophiles des cations (η^6-*o*-, -*m*- ou -*p*-chloronitrobenzène)(η^5-cyclopentadiényl)fer (respectivement **2***a*, **2***b* ou **2***c*) avec l'aniline, la *n*-butylamine ou la pyrrolidine. On a trouvé que, avec l'aniline, il ne se produit qu'un déplacement sélectif du groupement nitro. Pour les réactions de la *n*-butylamine ou de la pyrrolidine avec l'isomère *ortho*, **2***a*, on n'observe que le déplacement sélectif du groupement chloro conduisant respectivement aux cations (η^6-*o*-*n*-butylaminonitrobenzène)(η^5-cyclopentadiényl)fer (**5***a*) ou (η^6-*o*-*n*-nitro-*N*-pyrrolidinylbenzène)(η^5-cyclopentadiényl)fer (**7***a*). Avec les isomères *méta* ou *para* (**2***b* ou **2***c*), les réactions avec la *n*-butylamine ou la pyrrolidine conduisent à des mélanges de produits de substitution provenant des réactions de substitutions compétitives des groupements chloro et nitro; le produit majeur obtenu à partir de l'isomère *méta* provient de la substitution du groupement chloro alors que le produit majeur obtenu à partir de l'isomère *para* provient de la substitution du groupement nitro. On présente des interprétations possibles de ces résultats qui sont basées sur les basicités relatives des nucléophiles et sur l'hypothèse que les effets inductifs combinés des substituants nitro et chloro joueraient un rôle important.

Mots clés : cations (η^6-*o*-, -*m*- ou -*p*-chloronitrobenzène)(η^5-cyclopentadiényl)fer, réactions de substitutions nucléophiles, aniline, *n*-butylamine, pyrrolidine.

[Traduit par la revue]

The displacement of the chloro group in the (η^6-chlorobenzene)(η^5-cyclopentadienyl)iron cation (**1***a*) by a number of nucleophiles was first reported by Nesmeyanov *et al.* in 1967 (1) and it was estimated that the "mobility" of the chloro group in **1***a* was similar to that in 2,4-dinitrochlorobenzene (2). Similar displacement reactions with **1***a* were carried out with the hydroxide or hydrosulfide ion as nucleophile in 1979 (3), and with the azide ion to give the cyclopentadienyliron (CpFe) complexed azidobenzene in 1981 (4). Subsequently, nucleophilic substitution reactions with **1***a* and related systems, such as the CpFe complexed *o*-, *m*-, and *p*-chlorotoluenes and *o*-, *m*-, and *p*-dichlorobenzenes, with a variety of nucleophiles, were studied in our laboratory (5–11) and by a former colleague, U. S. Gill, in his post-doctoral work (12–14). We have also shown that CpFe complexes of nitroarenes, as those of chloroarenes, could undergo nucleophilic substitution reactions (7, 15). In the present work, substitution reactions of the (η^6-*o*-, -*m*-, or -*p*-chloronitrobenzene)(η^5-cyclopentadienyl)-iron cation (**2***a*, **2***b*, or **2***c*, respectively), as its hexafluorophosphate, with aniline, *n*-butylamine, or pyrrolidine as nucleophile, were investigated to determine whether a selective displacement of either the chloro or nitro group would take place or if competitive substitutions of both chloro and nitro groups would occur.

Cations **2***a*, **2***b*, and **2***c*, isolated as their hexafluorophosphate salts, were prepared from the oxidation of the corresponding CpFe complexed *o*-, *m*-, and *p*-chloroanilines (**3***a*, **3***b*, and **3***c*) with H_2O_2 in CF_3COOH (5), while the aniline complexes, **3***a*, **3***b*, and **3***c*, were obtained from reaction of the CpFe complexed *o*-, *m*-, and *p*-dichlorobenzenes (16) with NH_3 as previously described for the same reaction with the *o*-isomer to give **3***a* (8). The ^1H and ^{13}C nmr data for **2***a–c* and for **3***b* and **3***c*, which have not been prepared previously, are given in Tables 1 and 2.

Reaction of **2***a*, **2***b*, or **2***c* with aniline resulted solely in the selective displacement of the nitro group, giving rise to **4***a*, **4***b*, or **4***c*, respectively, as its hexafluorophosphate. It has been reported (17) that chlorobenzene complex **1***a* did not give a nucleophilic substitution reaction with aniline. On the other hand, we have found in the present work that the (η^6-nitrobenzene)(η^5-cyclopentadienyl)iron cation (**1***b*) readily reacted with aniline to give a 70% yield of substitution product **4***d*, also obtained as its hexafluorophosphate. It is, therefore, not surprising that reactions of chloronitrobenzene complexes **2***a*, **2***b*, and **2***c* with aniline resulted only in the displacement of the nitro group to give **4***a*, **4***b*, and **4***c*. Incidentally, diphenylamine complex **4***d* was prepared previously by a ligand exchange reaction between diphenylamine and ferrocene (18), but the yield was only 6%.

In contrast to the results obtained for reactions with aniline, *o*-isomer **2***a* reacted with *n*-butylamine or pyrrolidine solely by selective displacement of the chloro group, giving rise to

[1]Currently a post-doctoral fellow, Department of Chemistry, University of Toronto.

Can. J. Chem. Downloaded from www.nrcresearchpress.com by 194.225.253.170 on 09/07/12
For personal use only.

Can. J. Chem. Downloaded from www.nrcresearchpress.com by 194.225.253.170 on 09/07/12
For personal use only.

TABLE 1. The ^{1}H nmr data for (η^6-*o*-, -*m*-, and -*p*-chloronitrobenzene)(η^5-cyclopentadienyl)iron cations (**2***a*, **2***b*, and **2***c*, respectively) and precursors (η^6-*o*-, -*m*-, and -*p*-chloroaniline)(η^5-cyclopentadienyl)iron cations (**3***a*, **3***b*, and **3***c*, respectively)

	δ(acetone-d_6)(ppm from TMS)		
Cation[a]	Cp[b]	Complexed Ar[c]	Others
2*a*	5.62	6.73–7.00 (m, 2H, H3,4) 7.10–7.26 (m, 1H, H5) 7.43–7.60 (m, 1H, H6)	—
2*b*	5.60	7.04–7.23 (m, 3H, H2,4,5) 7.50–7.73 (m, 1H, H6)	—
2*c*	5.42	6.75 (d, J = 6.4, 2H, H3,5) 7.72 (d, J = 6.4, 2H, H2,6)	—
3*a*[d]	5.03	6.00–6.35 (m, 4H)	6.50–6.70 (m, 2H, NH_2)
3*b*	5.08	6.20–6.50 (m, 4H)	5.86–6.06 (m, 2H, NH_2)
3*c*	5.06	6.00 (d, J = 6.8, 2H, H2,6) 6.40 (d, J = 6.8, 2H, H3,5)	6.30 (br s, 2H, NH_2)

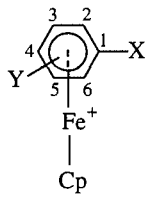
[a]As the hexafluorophosphate.
[b]All Cp absorptions are 5H singlets.
[c]J values are in Hz.
[d]From ref. 8.

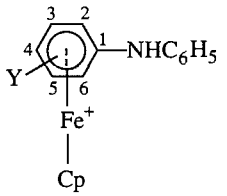
TABLE 2. The ^{13}C nmr data for **2***a*, **2***b*, and **2***c* and precursors **3***a*, **3***b*, and **3***c*

	δ(acetone-d_6) (ppm from TMS)	
Cation[a]	Cp	Complexed Ar[b]
2*a*	83.5	85.9, 88.2, 90.1, 91.2, 102.1*, 119.2*
2*b*	83.5	84.7, 85.9, 89.3, 92.6, 108.5*, 114.7*
2*c*	83.4	85.4 (2C), 89.8 (2C), 110.5*, 119.0*
3*a*[c]	78.9	71.4, 81.4, 86.5, 87.4, 90.6*, 124.5*
3*b*	79.1	70.1, 72.4, 81.8, 86.6, 107.1*, 127.0*
3*c*	79.2	70.2 (2C), 87.2 (2C), 101.9*, 126.3*

[a]As the hexafluorophosphate.
[b]Asterisks denote quaternary carbons.
[c]From ref. 8.

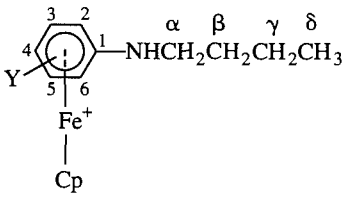
the hexafluorophosphate of **5***a* or **7***a*, respectively. On the other hand, reactions with **2***b* or **2***c* resulted in competitive displacements of both the chloro and the nitro groups. *m*-Isomer **2***b* gave a 4:1 mixture of **5***b* and **6***b* from reaction with *n*-butylamine, and a 3:1 mixture of **7***b* and **8***b* from reaction with pyrrolidine; in both of these reactions, displacement of the chloro group predominated over displacement of the nitro group. For similar reactions with *p*-isomer **2***c*, however, the major products were derived from displacement of the nitro group, a 2:3 mixture of **5***c* and **6***c* being obtained from reaction with *n*-butylamine and a 1:2 mixture of **7***c* and **8***c* from reaction with pyrrolidine.

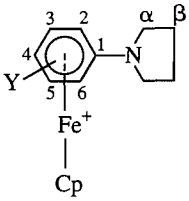




1*a*, X = Cl, Y = H
1*b*, X = NO_2, Y = H
2*a*, X = NO_2, Y = *o*-Cl
2*b*, X = NO_2, Y = *m*-Cl
2*c*, X = NO_2, Y = *p*-Cl
3*a*, X = NH_2, Y = *o*-Cl
3*b*, X = NH_2, Y = *m*-Cl
3*c*, X = NH_2, Y = *p*-Cl

4*a*, Y = *o*-Cl
4*b*, Y = *m*-Cl
4*c*, Y = *p*-Cl
4*d*, Y = H





5*a*, Y = *o*-NO_2
5*b*, Y = *m*-NO_2
5*c*, Y = *p*-NO_2
6*b*, Y = *m*-Cl
6*c*, Y = *p*-Cl

7*a*, Y = *o*-NO_2
7*b*, Y = *m*-NO_2
7*c*, Y = *p*-NO_2
8*b*, Y = *m*-Cl
8*c*, Y = *p*-Cl

The ^{1}H and ^{13}C nmr spectral data in support of the structures assigned to all of the above substitution products are summarized in Tables 3 and 4. It may be pointed out that in the reactions that gave mixtures of products, **5***b* and **6***b* or **5***c* and **6***c* from reaction of **2***b* or **2***c* with *n*-butylamine, and **7***b* and **8***b* or **7***c* and **8***c* from reaction with pyrrolidine, one component of each product mixture, namely, **6***b*, **6***c*, **8***b*, or **8***c*, was previously prepared from reactions of the CpFe complexed *m*- or *p*-dichlorobenzene with *n*-butylamine and with pyrrolidine (11). The spectral data of these known compounds together with those for the product mixtures allowed the nmr spectra of **5***b*, **5***c*, **7***b*, and **7***c* to be deduced and the relative ratios of the two components in the product mixtures to be estimated.

In nucleophilic aromatic substitutions following the S_NAr mechanism as depicted in eq. [1] (19), both inductive and resonance effects of substituent Y would each exert its influence (20). In a 1978 review on nucleophilic displacement of aromatic nitro groups (21), examples were cited that under different experimental conditions for various substrates, selective displacement of the nitro or chloro group, or competitive displacement of both nitro and chloro groups, could take place, but

TABLE 3. The ^{1}H nmr data for substitution products from reactions with **2***a*, **2***b*, and **2***c*

Product cation[a]	δ (acetone-d_6) (ppm from TMS)		
	Cp[b]	Complexed Ar[c]	Others[c]
4*d*	5.06	6.13–6.18 (m, 3H, H2,4,6) 6.31 (t, J = 5.8, 2H, H3,5)	7.31 (t, J = 7.7, 1H, H4 of Ph) 7.40 (d, J = 7.7, 2H, H2,6 of Ph) 7.51 (t, J = 7.7, 2H, H3,5 of Ph) 8.21 (br s, 1H, NH)
4*a*	5.24	6.29 (d, J = 5.1, 1H, H6) 6.50–6.55 (m, 3H, H3,4,5)	7.37–7.61 (m, 5H, Ph) 9.04 (br s, 1H, NH)
4*b*	5.14	6.31 (s, 1H, H2) 6.55 (t, J = 6.5, 1H, H5) 6.64 (d, J = 6.5, 2H, H4,6)	6.90–7.30 (m, 5H, Ph) 8.10 (br s, 1H, NH)
4*c*	5.22	6.37 (br s, 2H, H2,6) 7.36 (br s, 2H, H3,5)	7.40–7.55 (m, 5H, Ph) 8.55 (br s, 1H, NH)
5*a*	5.18	6.38 (d, J = 6.2, 1H, H6) 6.48 (t, J = 6.2, 1H, H4) 6.62 (t, J = 6.2, 1H, H5) 7.30 (d, J = 6.2, 1H, H3)	1.00 (t, J = 7.4, 3H, CH_3) 1.50 (sextet, J = 7.4, 2H, γ-CH_2) 1.79–1.85 (m, 2H, β-CH_2) 3.54–3.64 (m, 2H, α-CH_2) 6.15 (br s, 1H, NH)
5*b*	5.21	6.15 (d, J = 6.3, 1H, H6) 6.58 (t, J = 6.3, 1H, H5) 6.79 (br s, 1H, H2) 7.22 (d, J = 6.3, 1H, H4)	0.99 (t, J = 7.2, 3H, CH_3) 1.50 (sextet, J = 7.2, 2H, γ-CH_2) 1.70–1.80 (m, 2H, β-CH_2) 3.45–3.56 (m, 2H, α-CH_2) 6.80 (br s, overlap with H2, 1H, NH)
5*c*	5.18	6.17 (d, J = 7.2, 2H, H2,6) 7.29 (d, J = 7.2, 2H, H3,5)	0.93 (t, J = 7.5, 3H, CH_3) 1.37 (sextet, J = 7.5, 2H, γ-CH_2) 1.56 (quintet, J = 7.5, 2H, β-CH_2) 3.41–3.48 (m, 2H, α-CH_2) 6.72 (br s, 1H, NH)
6*b*	5.08	5.84 (d, J = 6.3, 1H, H6) 6.22 (br s, 1H, H2) 6.26 (t, J = 6.3, 1H, H5) 6.40 (d, J = 6.3, 1H, H4)	0.97 (t, J = 7.4, 3H, CH_3) 3.35–3.41 (m, 2H, α-CH_2) 6.34 (br s, 1H, NH) [d]
6*c*	5.08	5.89 (d, J = 6.9, 2H, H2,6) 6.50 (d, J = 6.9, 2H, H3,5)	0.96 (t, J = 7.4, 3H, CH_3) 1.45 (sextet, J = 7.4, 2H, α-CH_2) 1.68 (quintet, J = 7.4, 2H, β-CH_2) 3.26–3.34 (m, 2H, α-CH_2) 6.16 (br s, 1H, NH)
7*a*	5.24	6.21 (d, J = 6.2, 1H, H6) 6.35 (t, J = 6.0, 1H, H4) 6.51 (t, J = 6.2, 1H, H5) 6.93 (d, J = 6.0, 1H, H3)	2.00–2.05 (m, 4H, β-CH_2) 3.45–3.55 (m, 4H, α-CH_2)
7*b*	5.24	5.74 (d, J = 6.4, 1H, H6) 6.57 (t, J = 6.4, 1H, H5) 6.60 (br s, 1H, H2) 7.23 (d, J = 6.4, 1H, H4)	2.06–2.15 (m, 4H, β-CH_2) 3.44–3.53 (m, 4H, α-CH_2)
7*c*	5.21	6.05 (d, J = 7.3, 2H, H2,6) 7.27 (d, J = 7.3, 2H, H3,5)	2.04–2.11 (m, 4H, β-CH_2) 3.48–3.54 (m, 4H, α-CH_2)
8*b*	5.11	5.72 (1H, H6, overlap with H6 of **7***b*) 6.10 (br s, 1H, H2) 6.28 (t, J = 6.4, 1H, H5) 6.42 (d, J = 6.4, 1H, H4)	[e]
8*c*	5.12	5.78 (d, J = 7.0, 2H, H2,6) 6.51 (d, J = 7.0, 2H, H3,5)	2.04–2.11 (m, 4H, β-CH_2) 3.48–3.54 (m, 4H, α-CH_2)

[a]Cations **4***d*, **4***a*, **4***b*, **4***c* are the CpFe complexes of diphenylamine, and *o*-, *m*-, and *p*-chlorodiphenylamines, respectively; **5***a*, **5***b*, and **5***c* are the CpFe complexes of *o*-, *m*-, and *p*-*n*-butylaminonitrobenzenes; **6***b* and **6***c* are the previously reported (11) CpFe complexes of *m*- and *p*-*n*-butylaminochlorobenzenes; **7***a*, **7***b*, and **7***c* are the CpFe complexes of *o*-, *m*-, and *p*-nitro-*N*-pyrrolidinylbenzenes; and **8***b* and **8***c* are the previously reported (11) CpFe complexes of *m*- and *p*-chloro-*N*-pyrrolidinylbenzenes. All these cations were obtained as their hexafluorophosphates.

[b]All Cp absorptions are 5H singlets.

[c]J values are in Hz.

[d]α- and β-CH_2 obscured by other peaks in the 4:1 mixture of **5***b* and **6***b*.

[e]α- and β-CH_2 obscured by other peaks in the 3:1 mixture of **7***b* and **8***b*.

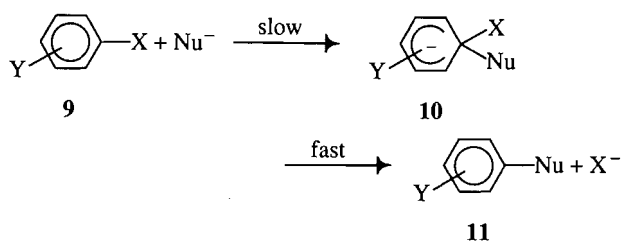
Can. J. Chem. Downloaded from www.nrcresearchpress.com by 194.225.253.170 on 09/07/12
For personal use only.

TABLE 4. The ^{13}C nmr data for substitution products from reactions with **2***a*, **2***b*, and **2***c*

Product cation[a]	δ (acetone-d_6) (ppm from TMS)		
	Cp	Complexed Ar[b]	Others[b]
4*d*[c]	75.4	70.1 (2C), 81.2, 85.6 (2C), 121.6*	122.6 (2C), 125.0, 129.5 (2C), 137.9* (Ph)
4*a*	79.5	71.2, 82.8, 83.2, 89.8, 95.2*, 123.2*	126.2 (2C), 128.1, 130.7 (2C), 137.2* (Ph)
4*b*	79.1	65.7, 68.9, 87.1, 87.8, 113.3*, 129.0*	123.4 (2C), 127.5, 131.6 (2C), 137.6* (Ph)
4*c*	79.4	69.8 (2C), 83.8 (2C), 107.5*, 126.9*	124.3 (2C), 127.0, 130.7 (2C), 138.1* (Ph)
5*a*	79.3	66.7, 82.1, 83.9, 90.1, 94.1*, 126.8*	13.9 (CH_3), 20.5 (γ-CH_2), 30.8 (β-CH_2), 43.8 (α-CH_2)
5*b*	79.5	61.6, 69.4, 77.1, 86.3, 111.5*, 129.0*	13.6 (CH_3), 20.2 (γ-CH_2), 30.6 (β-CH_2), 43.3 (α-CH_2)
5*c*	78.7	77.0 (2C), 88.1 (2C), 113.0*, 130.5*	13.5 (CH_3), 20.3 (γ-CH_2), 30.8 (β-CH_2), 43.6 (α-CH_2)
6*b*	78.1	66.5, 69.0, 81.1, 85.6, 106.6*, 127.3*	13.8 (CH_3), 20.3 (γ-CH_2), 30.8 (β-CH_2), 43.1 (α-CH_2)
6*c*	78.4	66.9 (2C), 86.7 (2C), 101.4*, 127.0*	13.8 (CH_3), 20.4 (γ-CH_2), 31.0 (β-CH_2), 43.4 (α-CH_2)
7*a*	79.2	65.7, 80.7, 82.4, 88.5, 104.2, 125.9*	25.8 (2C, β-CH_2), 51.0 (2C, α-CH_2)
7*b*	78.4	67.2, 68.4, 76.8, 86.0, 110.8*, 126.6*	24.9 (2C, β-CH_2), 48.1 (2C, α-CH_2)
7*c*	78.3	75.4 (2C), 86.2 (2C), 106.2*, 128.7*	25.4 (2C, β-CH_2), 49.0 (2C, α-CH_2)
8*b*	77.9	66.8, 69.0, 81.1, 85.7, 106.9*, 126.1*	25.5 (2C, β-CH_2), 48.8 (2C, α-CH_2)
8*c*	77.9	66.8 (2C), 86.5 (2C), 101.4*, 125.5*	25.6 (2C, β-CH_2), 48.7 (2C, α-CH_2)

[a]As the hexafluorophosphate.
[b]Asterisks denote quaternary carbons.
[c]The solvent was CD_3CN instead of acetone-d_6.

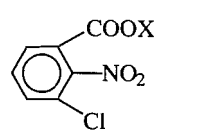
Can. J. Chem. Downloaded from www.nrcresearchpress.com by 194.225.253.170 on 09/07/12
For personal use only.

[1] 

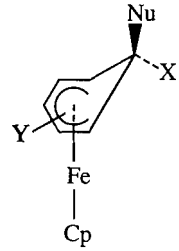
9 **10** **11**

no detailed mechanistic explanations were presented. More recently, it was reported that under appropriate conditions, reaction of the methyl ester of 3-chloro-2-nitrobenzoic acid (**12***a*) with benzylamine resulted in the selective displacement of only the nitro group (22, 23), while a similar reaction with amide derivative **12***b* gave selective displacement of the chloro group (23), and it was suggested that conjugative effects involving the lone pair of electrons on the amide N of **12***b* could play an important role (23). The results from the present studies on complexed cations **2***a*, **2***b*, and **2***c*, however, appear to indicate that conjugative or resonance effects may be of lesser importance. Possibly because adduct **13**, analogous to **10** of eq. [1], is a neutral species with no negative charge to be delocalized by Y, there would be a relatively minor role for the resonance effect.

Utilizing the addition–elimination mechanism of the S_NAr reaction and assuming that inductive effects would be the major factor in governing the course of reaction of **2***a–c*, the present results could be qualitatively interpreted. With aniline, a weak base (pK_b = 9.4 (24)), as nucleophile, *ipso* addition could take place only at the carbon bearing the strongly electron-withdrawing nitro group, and subsequent elimination of the nitro group would give the overall substitution product. No *ipso*



12*a*, X = CH_3
12*b*, X = $N(CH_3)_2$



13

Can. J. Chem. Downloaded from www.nrcresearchpress.com by 194.225.253.170 on 09/07/12
For personal use only.

addition with aniline was possible at the carbon containing the less electron-withdrawing chloro substituent. Hence there was no S_NAr reaction between aniline and chlorobenzene complex **1***a*, but such a reaction occurred readily with nitrobenzene complex **1***b* to give **4***d*, and with **2***a*, **2***b*, and **2***c* to give **4***a*, **4***b*, and **4***c*, respectively, from selective displacement of the nitro group.

With a stronger base, *n*-butylamine (pK_b = 3.3 (24)) or pyrrolidine (pK_b = 2.7 (24)), nucleophilic addition with *o*-isomer **2***a* took place solely at the *ipso* position containing the chloro substituent and *ortho* to the strongly electron-withdrawing nitro group, thus leading to the selective displacement of the chloro group to give substitution product **5***a* or **7***a*. It may be of interest to note that in a study on product distributions in the nucleophilic addition of the hydride ion to 15 CpFe complexed substituted benzenes (25), only the nitrobenzene complex **1***b*, with its strongly electron-withdrawing nitro substituent (σ_{para} = +0.78 (26)), gave rise exclusively to the *ortho*-addition product, while the other complexed substituted benzenes containing a substituent ranging from dimethylamino (σ_{para} = −0.83 (26)) to cyano (σ_{para} = +0.66 (26)) all gave various mixtures of *o*-, *m*-, *p*-, and (or) *ipso*-adducts. Apparently, the combined electron-withdrawing inductive effects of the chloro and the *o*-nitro groups in **2***a* led to the addition of *n*-butylamine or pyrrolidine at the carbon containing the chloro group and *ortho* to the nitro group, thus leading to the observed selective displacement of the chloro group in the formation of **5***a* or **7***a* from **2***a*.

With *m*-isomer **2***b*, the strongly electron-withdrawing effect of the nitro group would be less pronounced on the *m*-chloro position than the analogous effect on the *o*-chloro position of **2***a*. Thus *ipso* addition of the nucleophile occurred at both positions containing the chloro and the nitro substituents, giving rise to a mixture of products from competitive displacement of the chloro as well as the nitro groups. Apparently, the combined inductive effects of the chloro group and the *m*-nitro group led to a greater extent of *ipso* addition at the position containing the chloro substituent, giving rise to the formation of **5***b* or **7***b* as major product.

For the reaction of *p*-isomer **2***c* with *n*-butylamine or pyrrolidine, however, the major product obtained was **6***c* or **8***c*, respectively, derived from displacement of the nitro group. These results again would fit in with the suggestion that inductive effects played a dominant role. For **2***c*, the nitro group would exert the least inductive effect on the *p*-position in comparison to the *m*- and *o*-positions, thus leading to more *ipso* addition at the site containing the strongly electron-withdrawing nitro group, giving rise to **6***c* or **8***c* as major product. It may also be pointed out that if resonance effects were to play an important role, one would anticipate similar behavior for the *o*- and *p*-isomers **2***a* and **2***c*, but this was not the case, with **2***a* giving rise solely to the selective displacement of the chloro group, while **2***c* resulted in a competitive displacement of both nitro and chloro groups with the minor product derived from displacement of the chloro group.

Experimental

*(η^6-m- and -p-Chloroaniline)(η^5-cyclopentadienyl)iron hexafluorophosphate (**3**b-PF_6 and **3**c-PF_6, respectively)*

Using the same procedure as previously described for the reaction of (η^6-*o*-dichlorobenzene)(η^5-cyclopentadienyl)iron hexafluorophosphate with concentrated NH_4OH to give (η^6-*o*-chloroaniline)(η^5-cyclopentadienyl)iron hexafluorophosphate (**3***a*-PF_6) (8), reaction of the CpFe complexed *m*- or *p*-dichlorobenzene with concentrated NH_4OH gave the *m*- or *p*-chloroaniline complex as the hexafluorophosphate (**3***b*-PF_6 or **3***c*-PF_6) in 76 or 81% yield, respectively. Their ^1H and ^{13}C nmr data are summarized in Tables 1 and 2. *Anal.* calcd. for $C_{11}H_{11}NClFePF_6$: C 33.58, H 2.82, N 3.56; found: C 33.17, H 2.85, N 3.60 for **3***b*-PF_6 and C 33.20, H 2.88, N 3.47 for **3***c*-PF_6. For these and other compounds reported in the present work, the nmr data were obtained using a Bruker AM300 spectrometer. The elemental analyses were done in the analytical laboratory of the University of Saskatchewan.

*(η^6-o-, -m-, and -p-Chloronitrobenzene)(η^5-cyclopentadienyl)iron hexafluorophosphates (2*a*-PF_6, 2*b*-PF_6, and 2*c*-PF_6)*

Oxidation of *o*-, *m*-, or *p*-chloroaniline complex **3***a*-PF_6, **3***b*-PF_6, or **3***c*-PF_6 with H_2O_2 in CF_3COOH as previously described for the preparation of nitrobenzene complex **1***b* from the CpFe complexed aniline (5) gave the hexafluorophosphate of **2***a*, **2***b*, or **2***c* with a yield of 50, 56, or 57%, respectively. *Anal.* calcd. for $C_{11}H_9O_2NClFePF_6$: C 31.20, H 2.14, N 3.31; found: C 31.35, H 2.17, N 3.54 for **2***a*-PF_6, C 31.37, H 2.20, N 3.42 for **2***b*-PF_6, and C 31.20, H 2.10, N 3.35 for **2***c*-PF_6.

Reactions with aniline

A mixture of 1.0 mmol of the hexafluorophosphate of nitrobenzene complex **1***b* or the *o*-, *m*-, or *p*-chloronitrobenzene complex **2***a*, **2***b*, or **2***c*, 102 mg (1.1 mmol) of aniline, and 345 mg (2.5 mmol) of K_2CO_3 in 10 mL of THF was heated under reflux and under N_2 for 6 h. The resulting material was filtered into 10 mL of 10% HCl and a solution of 163 mg (1.0 mmol) of NH_4PF_6 in 20 mL of H_2O was added. The product was recovered by extraction with CH_2Cl_2 (3 × 20 mL). The combined extract was dried over $MgSO_4$ and, after removal of the solvent, the residue was washed with ether and then crystallized from CH_2Cl_2–ether to give a 70% yield of the hexafluorophosphate of diphenylamine complex **4***d* from **1***b*, or the hexafluorophosphate of the *o*-, *m*-, or *p*-chlorodiphenylamine complex **4***a*, **4***b*, or **4***c* with a yield of 70, 40, or 70%, respectively, from **2***a*, **2***b*, or **2***c*. *Anal.* calcd. for $C_{17}H_{15}NClFePF_6$: C 43.48, H 3.22, N 2.98; found: C 43.58, H 3.40, N 2.92 for **4***a*-PF_6, C 43.62, H 3.37, N 3.09 for **4***b*-PF_6, and C 43.40, H 3.43, N 2.87 for **4***c*-PF_6.

Reactions with n-butylamine and with pyrrolidine

A mixture of 423 mg (1.0 mmol) of **2***a*-PF_6, **2***b*-PF_6, or **2***c*-PF_6, 73 mg (1.0 mmol) of *n*-butylamine or 71 mg (1.0 mmol) of pyrrolidine, and 345 mg (2.5 mmol) of K_2CO_3 in 10 mL of a 1:1 mixture of THF–DMSO was heated under reflux and under N_2 for 6 h. The resulting material was worked up as described above for the reactions with aniline except that in the final stages most of the solvent was removed from the dried CH_2Cl_2 extract and the product was precipitated upon addition of ether. For the reaction of *o*-isomer **2***a*-PF_6 with *n*-butylamine, a 73% yield of the hexafluorophosphate of *o*-*n*-butylaminonitrobenzene complex **5***a* was obtained. *Anal.* calcd. for $C_{15}H_{19}O_2N_2FePF_6$: C 39.50, H 4.20, N 5.26; found: C 39.15, H 4.16, N 5.29. Similarly, the reaction of **2***a*-PF_6 with pyrrolidine gave a 75% yield of the hexafluorophosphate of *o*-nitro-*N*-pyrrolidinylbenzene complex **7***a*. *Anal.* calcd. for $C_{15}H_{17}O_2N_2FePF_6$: C 39.67, H 3.77, N 5.29; found: C 39.45, H 3.87, N 5.23.

From the reaction of *m*-isomer **2***b*-PF_6 with *n*-butylamine or pyrrolidine, respectively, the products obtained were a 61% yield of a 4:1 mixture of the hexafluorophosphate of *m*-*n*-butylaminonitrobenzene complex **5***b* and the known hexafluorophosphate of *m*-*n*-butylaminochlorobenzene complex **6***b* (11) or a 52% yield of a 3:1 mixture of the hexafluorophosphate of *m*-nitro-*N*-pyrrolidinylbenzene complex **7***b* and the known hexafluorophosphate of *m*-chloro-*N*-pyrrolidinylbenzene complex **8***b* (11), the product ratios being obtained from the ^1H nmr spectra of these mixtures.

In the reactions with *p*-isomer **2***c*-PF_6, a 58% yield of a 2:3 mixture of the hexafluorophosphate of *p*-*n*-butylaminonitrobenzene complex **5***c* and the known hexafluorophosphate of *p*-*n*-butylaminochlorobenzene complex **6***c* (11) was obtained from reaction with *n*-butylamine, while reaction with pyrrolidine gave a 63% yield of a 1:2

mixture of the hexafluorophosphate of *p*-nitro-*N*-pyrrolidinylbenzene complex **7***c* and the known hexafluorophosphate of *p*-chloro-*N*-pyrrolidinylbenzene **8***c* (11). Again the product ratios were determined from the ^{1}H nmr spectra.

Acknowledgment

The financial support given by the Natural Sciences and Engineering Research Council of Canada is sincerely acknowledged.

1. A. N. NESMEYANOV, N. A. VOL'KENAU, and I. N. BOLESOVA. Dokl. Akad. Nauk SSSR, **175**, 606 (1967).
2. A. N. NESMEYANOV, N. A. VOL'KENAU, I. S. ISAEVA, and I. N. BOLESOVA. Dokl. Akad. Nauk SSSR, **183**, 834 (1968).
3. J. F. HELLING and W. A. HENDRICKSON. J. Organomet. Chem. **168**, 87 (1979).
4. C. C. LEE, C. I. AZOGU, P. C. CHANG, and R. G. SUTHERLAND. J. Organomet. Chem. **220**, 181 (1981).
5. C. C. LEE, U. S. GILL, M. IQBAL, C. I. AZOGU, and R. G. SUTHERLAND. J. Organomet. Chem. **231**, 151 (1982).
6. R. G. SUTHERLAND, A. PIÓRKO, U. S. GILL, and C. C. LEE. J. Heterocycl. Chem. **19**, 801 (1982).
7. C. C. LEE, A. S. ABD-EL-AZIZ, R. L. CHOWDHURY, A. PIÓRKO, and R. G. SUTHERLAND. Synth. React. Inorg. Met.-Org. Chem. **16**, 541 (1986).
8. C. C. LEE, A. S. ABD-EL-AZIZ, R. L. CHOWDHURY, U. S. GILL, A. PIÓRKO, and R. G. SUTHERLAND. J. Organomet. Chem. **315**, 79 (1986).
9. A. S. ABD-EL-AZIZ, C. C. LEE, A. PIÓRKO, and R. G. SUTHERLAND. Synth. Commun. **18**, 291 (1988).
10. A. S. ABD-EL-AZIZ, C. C. LEE, A. PIÓRKO, and R. G. SUTHERLAND. J. Organomet. Chem. **348**, 95 (1988).
11. C. C. LEE, C. H. ZHANG, A. S. ABD-EL-AZIZ, A. PIÓRKO, and R. G. SUTHERLAND. J. Organomet. Chem. **364**, 217 (1989).
12. R. M. MORIARTY and U. S. GILL. Organometallics, **5**, 253 (1986).
13. U. S. GILL and R. M. MORIARTY. Synth. React. Inorg. Met.-Org. Chem. **16**, 485 (1986).
14. U. S. GILL and R. M. MORIARTY. Synth. React. Inorg. Met.-Org. Chem. **16**, 1103 (1986).
15. R. L. CHOWDHURY, C. C. LEE, A. PIÓRKO, and R. G. SUTHERLAND. Synth. React. Inorg. Met.-Org. Chem. **15**, 1237 (1985).
16. I. U. KHAND, P. L. PAUSON, and W. E. WATTS. J. Chem. Soc. C, 2261 (1968).
17. P. L. PAUSON and J. A. SEGAL. J. Chem. Soc. Dalton Trans. 1677 (1975).
18. J. F. HELLING and W. A. HENDRICKSON. J. Organomet. Chem. **141**, 99 (1977).
19. J. MARCH. Advanced organic chemistry. 3rd ed. John Wiley and Sons, New York, NY. 1985. pp. 576–578.
20. P. BUCK. Angew. Chem. Internat. Ed. Engl. **8**, 120 (1969).
21. J. R. BECK. Tetrahedron, **34**, 2057 (1978).
22. C. W. BIRD and M. LATIF. Chem. Ind. (London), 795 (1987).
23. T.-L. HO and A. BERGMANIS. Chem. Ind. (London), 529 (1988).
24. L. G. WADE, JR. Organic chemistry. Prentice–Hall, Englewood Cliffs, NJ. 1987. p. 923.
25. R. G. SUTHERLAND, C. H. ZHANG, R. L. CHOWDHURY, A. PIÓRKO, and C. C. LEE. J. Organomet. Chem. **333**, 367 (1987).
26. J. HINE. Physical organic chemistry. 2nd ed. McGraw–Hill, New York, NY. 1962. pp. 85–88.

Can. J. Chem. Downloaded from www.nrcresearchpress.com by 194.225.253.170 on 09/07/12
For personal use only.

The conductance behaviour of $NaBPh_4$ in acetonitrile–toluene mixtures at 15, 25, and 35°C

N. PAPADOPOULOS

Laboratory of Physical Chemistry, Department of Chemistry, Aristotelian University of Thessaloniki, Greece

Received August 29, 1988[1]

N. PAPADOPOULOS. Can. J. Chem. **67**, 1624 (1989).

The limiting molar conductances and association constants for $NaBPh_4$ have been evaluated in acentonitrile–toluene mixtures at 15, 25, and 35°C. Experimental data have been analysed by the Lee–Wheaton conductance equation. The thermodynamic parameters of the non-coulombic interaction have been evaluated.

Key words: conductance, association constant, Lee–Wheaton equation, acetonitrile–toulene.

N. PAPADOPOULOS. Can. J. Chem. **67**, 1624 (1989).

Opérant a 15, 25 et 35°C, dans des mélanges d'acétonitrile–toluène, on a évalué les conductivités et les constantes d'association molaires limites du $NaBPh_4$. On a analysé les données expérimentales à l'aide de l'équation de conductance de Lee–Wheaton. On a évalué les paramètres thermodynamiques de l'interaction non-coulombique.

Mots clés : conductivitès, constant d'association, l'équation de Lee–Wheaton, acétonitrile–toulène.

[Traduit par la revue]

Introduction

A complete theory of the phenomena of solution chemistry will become a reality only when solute–solvent interactions are completely elucidated. Theoretical treatments of these processes have been hampered by incomplete knowledge of the electrostatic forces in the immediate vicinity of solvated ions.

Various similar but not identical equations have been published in the literature (1, 2) trying to correlate the association constant of an electrolyte in a solution to parameters such as the size of the ions and the dielectric constant of the solvent. However, in addition to the electrostatic forces, solvation forces also exist which are completely system-specific and their contribution to association cannot be predicted.

Conductimetry is one of the most direct methods to study the behaviour of ions in solution. In this work, the conductances of $NaBPh_4$ in toluene–acetonitrile mixtures are reported at 15, 25, and 35°C.

Experimental

Sodium tetraphenyl boride (Merck p.a. 99.5%) was recrystallized from acetone and dried under vacuum over P_2O_5. The purification of the solvent was carried out as described previously (3). Details of the experimental procedure have been reported elsewhere (4). The physical constants of acetonitrile–toluene mixtures have been reported previously (3).

Results and discussion

The measured molar conductivities at various concentrations are given in Table 1. The experimental results have been analysed according to the method of Pethybridge and Taba (5) who use the Lee–Wheaton conductance equation (6, 7). This equation is different from the previous conductance equations, most of which are based on the "primitive" model (8).

Lee and Wheaton envisage three regions around the ion itself which is treated as a rigid, conducting sphere. In region 1, all the solvent molecules are aligned by the ion's field and there is dielectric saturation. In region 2 the solvent's structure is still modified by the ion's field though to a lesser extent, and in region 3 the solvent retains its bulk properties. The resulting equation is complicated in the general case of a single, associated symmetrical electrolyte. Details for the analysis of the experimental results have been given previously (9).

The analysis of conductivity data can provide three parameters: the value of equivalent conductance at infinite dilution Λ_0, the value of the association constant K_A, and the distance of the closest approach of the ions R. The values of Λ_0 and K_A calculated from the experimental results are given in Table 2. In all cases a sharp minimum was observed in the $\sigma\%-R$ plot (Fig. 1) at 11 ± 1 Å. The minimum was sharper the higher the proportion of toluene in the toluene–acetonitrile solvent mixture. The center-to-center distance of $NaBPh_4$ is about 6 Å (10, 11). The diameter of the acetonitrile molecule was calculated from the formula $d = 1.183\ (m/\rho)^{1/3}$ (12) and was found to be equal to 4.4 Å. The value of 11 ± 1 Å suggests that the ions that are formed in this solvent mixture are solvent-separated ion pairs. It is reasonable to accept that each ion pair is separated by one molecule of acetonitrile because acetonitrile is a much more polar solvent than toluene.

The conductance of solutions of $NaBPh_4$ in acetonitrile at 25°C has also been measured by Kay *et al.* (14) who obtained $\Lambda_0 = 134.1$ and $K_A = 0$. They analysed their experimental data with a conductance equation based on the primitive model. Conductance data of sufficient precision with the exception of the work of Kay *et al.* do not exist in the literature. Consequently, direct comparison for this electrolyte between the values of Λ_0 and K_A calculated from the equations based on the "primitive" model are not possible. In two previous papers (14, 15), conductance data for many other systems from the literature have been analysed with the Lee–Wheaton conductance equation. In all cases a much better fit of the conductance data to the Lee–Wheaton equation than to the equations based on the "primitive" model has been observed. The values of Λ_0 calculated from the previous conductance equations do not differ significantly from the value of Λ_0 calculated from the Lee–Wheaton conductance equation. The values of K_A calculated with the Lee and Wheaton equation are generally higher. The older conductance equations gave a distance of a closest approach that was very low. The experimental data of Kay *et al.* were reanalysed with the Lee–Wheaton conductance equation and the results $\Lambda_0 = 134.4$ and $K_A = 8.3$ were obtained. These values are in good agreement with our results. The association constant of a pure electrolyte is largely influenced by the radius

[1]Revision received June 12, 1989.

Printed in Canada / Imprimé au Canada

Can. J. Chem. Downloaded from www.nrcresearchpress.com by 194.225.253.170 on 09/07/12
For personal use only.

TABLE 1. Equivalent conductance of $NaBPh_4$ in acetonitrile–toluene mixtures at 15, 25, and 35°C (ΔS cm_2 mol^{-1} cm mol L^{-1})

0% toluene		20% toluene		40% toluene		50% toluene		60% tuluene		70% toluene		80% toluene	
$c \times 10^4$	Λ	$c \times 10^4$	Λ	$c \times 10^4$	Λ	$c \times 10^4$	Λ	$c \times 10^4$	Λ	$c \times 10^4$	Λ	$c \times 10^4$	Λ
						15°C							
3.0342	116.19	2.2379	108.06	3.0103	95.89	1.5159	90.67	1.1881	83.74	2.1640	70.28	2.8400	44.557
5.6592	114.55	4.6193	105.97	4.9146	94.06	3.1334	88.32	2.2392	81.30	4.5728	64.62	6.5900	36.460
8.2045	113.33	6.6455	104.66	6.4836	92.88	4.7773	86.60	3.4242	79.30	6.8853	61.22	8.8671	33.913
10.394	112.45	8.6455	103.62	9.1161	91.33	5.3496	85.25	4.6477	77.63	9.0404	58.92	11.156	32.052
13.684	111.33	12.150	102.22	11.771	90.06	9.5196	83.07	6.1413	76.01	11.860	56.95	14.041	30.299
17.291	110.27	16.396	100.78	14.360	88.97	12.362	81.56	8.2906	74.08	13.740	55.34	16.208	29.282
20.339	109.55	19.515	99.86			14.913	80.40	10.090	72.76	15.779	54.18	18.851	28.241
23.304	108.90	22.682	99.09			17.671	79.34	12.484	71.29				
						25°C							
1.9593	130.82	2.3769	120.42	3.1974	111.62	3.4809	98.89	1.1101	95.45	1.3122	82.07	3.4498	48.001
7.0108	127.04	4.4226	118.54	4.7777	109.98	5.4642	96.66	2.1355	92.41	3.9994	74.07	6.3661	41.443
9.5981	125.79	6.4445	117.11	6.2501	108.67	7.2230	95.01	3.3761	89.84	5.3994	71.33	9.5861	37.499
13.273	124.33	8.3482	116.02	10.425	105.78	10.219	92.81	5.1574	87.10	7.2057	68.57	12.839	34.892
17.258	123.02	12.599	114.02	15.548	103.20	13.414	90.97	7.3945	84.52	9.5598	65.84	15.586	33.296
21.179	121.91	15.857	112.76	17.535	102.37	16.163	89.62	9.7238	82.45	11.864	63.75	18.624	31.914
24.841	121.01	19.429	111.56			18.835	88.49	11.983	80.80	14.008	62.15	21.586	30.835
		22.745	110.61					14.221	79.42			24.568	29.931
						35°C							
2.7976	114.09	2.0432	134.89	1.6901	121.94	1.3482	114.67	1.1560	106.48	3.2116	85.04	2.3454	58.067
4.9207	142.38	4.0976	132.61	3.3612	119.48	2.6828	112.08	2.1667	103.15	5.7637	79.14	4.5586	49.911
8.2986	140.12	5.9785	131.05	4.8502	117.78	4.0694	109.96	3.2805	100.51	8.5875	74.87	7.3466	44.444
10.905	138.86	8.3782	129.45	6.3810	116.37	5.3161	108.45	4.2991	98.60	10.898	72.28	9.9001	41.305
15.064	137.16	12.132	127.45	9.1873	114.40	8.3308	105.54	8.3662	93.26	13.429	69.99	12.740	38.825
18.326	136.03	15.990	125.75	11.958	112.67	10.615	103.86	12.674	89.52	15.649	68.33	15.274	37.159
22.059	134.87	19.740	124.38	14.388	111.44					17.733	66.98	17.742	35.852
25.671	133.82	23.299	123.22	15.783	110.79					19.592	65.92	20.134	34.796

TABLE 2. Conductance parameters and ΔG^0 values of the non-coulombic interaction

	15°C			35°C		
% toluene	Λ_0	K_A	σ_Λ%	Λ_0	K_A	σ_Λ%
0	121.00	7.7	0.02	150.18	8.6	0.03
20	112.90	13.6	0.02	141.03	13.2	0.02
40	102.70	37.2	0.03	128.58	39.3	0.02
50	96.54	72.2	0.04	121.72	79.7	0.04
60	90.52	190.0	0.07	114.80	228.0	0.08
70	85.30	832.0	0.08	108.30	858.0	0.09
80	85.56	10036.0	0.09	109.71	10983.0	0.10

	25°C			
% toluene	Λ_0	K_A	σ_Λ%	ΔG^0(kJ)
0	135.33	8.5	0.015	1.4
20	126.23	13.3	0.02	1.2
40	117.88	40.3	0.02	0.6
50	108.78	76.2	0.04	0.5
60	102.82	212.8	0.08	0.2
70	95.32	840.0	0.08	0.1
80	96.01	10801.0	0.09	0.0

of the compound under investigation and the dielectric constant of the solvent. There is, however, considerable evidence that the ions are solvated (1), i.e. that each ion is surrounded on the average by a number of solvent molecules which accompany the ion in solution. Consequently the value of the association constant will also depend on the non-electrostatic interaction between the solvent medium and the electrolyte. In solvent media of medium and low dielectric constant, the attractive electrostatic forces between the ions become large and ion pairs that will be reasonably stable will tend to form. There exists a number of equations that have been proposed in order to predict the non-coulombic part (16–18) of the free energy of association. In this work the "Fuoss 75" (18) equation has been used for the evaluation of the nonelectrostatic free energy in the form:

$$K_A = (4\pi n/1000) \exp(-\Delta G^0/RT) \int_a^R r^2 \exp(\beta/r) dr$$

where $\beta = e/DkT$ and a = the center-to-center distance of an ion pair.

The non-Coulombic forces are taken into account in this equation by the factor $\exp(-\Delta G^0/RT)$ where ΔG^0 is the non-electrostatic free energy of association. The ΔG^0 values at 25°C calculated from the above equation are given in Table 2. The ΔH^0 value was found to be equal to about zero for all the compositions of the solvent system. Thus ΔG^0 arises solely to

Can. J. Chem. Downloaded from www.nrcresearchpress.com by 194.225.253.170 on 09/07/12
For personal use only.

Can. J. Chem. Downloaded from www.nrcresearchpress.com by 194.225.253.170 on 09/07/12
For personal use only.

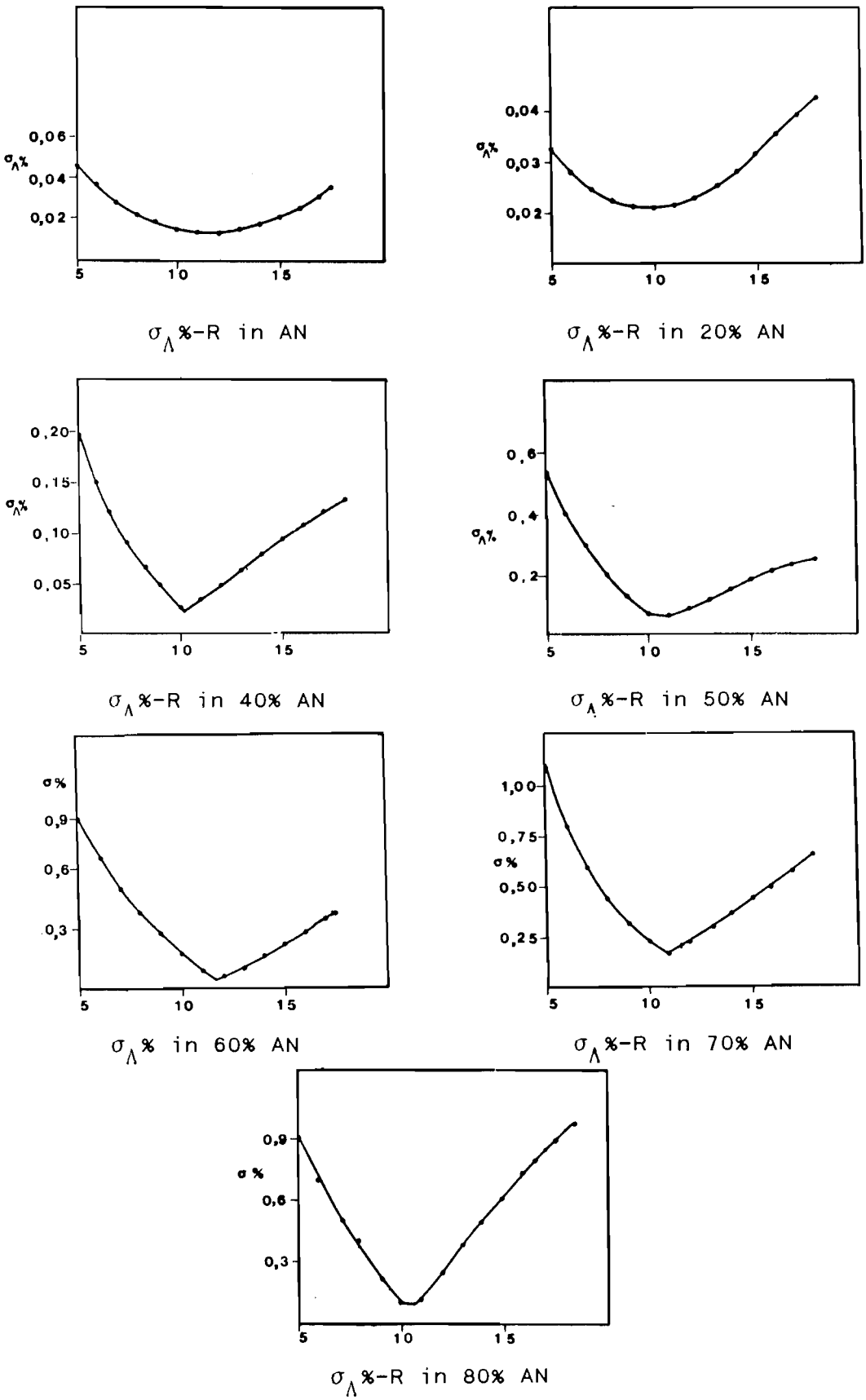


FIG. 1. σ_Λ%–R plots for $NaBPh_4$ in % w/w acetonitrile(AN)–toluene mixtures at 25°C

entropic effects. It can be concluded that the ion pairs that are formed are solvated with acetonitrile molecules in their vicinity better than the ions with a resultant lowering of the entropy of the system. As the solvent is enriched in toluene, the ΔG^0 values of the non-electrostatic interaction are lower, indicating that the bulk competes with the ion pairs for the acetonitrile molecules. The inverse behaviour has been observed for Bu_4NI and Pr_4NI in the same solvent system. For these electrolytes desolvation of the ion pair occurred as the solvent mixture was enriched in toluene (14, 15).

1. J. GORDON. The organic chemistry of electrolyte solutions. John Wiley & Sons, New York. 1975.
2. J. PRUE. J. Chem. Educ. **46**, 12 (1969).
3. G. RITZOULIS, N. PAPADOPOULOS, and D. JANNAKOUDAKIS. J. Chem. Eng. Data, **31**, 146 (1986).
4. G. RITZOULIS, N. PAPADOPOULOS, V. GALIATSATOS, D. CHRISTODOULOU, and D. JANNAKOUDAKIS. Z. Naturforsch. **38***a*, 579 (1983.
5. A. PETHYBRIDGE and S. TABA. J. Chem. Soc. Faraday I, **76**, 368 (1980).
6. W. LEE and R. WHEATON. J. Chem. Soc. Faraday II, **74**, 743 (1978).
7. W. LEE and R. WHEATON. J. Chem. Soc. Faraday II, **74**, 1456 (1978).
8. R. FERNADÉZ-PRINI. *In* Conductance. *Edited by* A. Convington and T. Dickinson. Plenum Press, London, 1973.
9. N. PAPADOPOULOS and G. RITZOULIS. Chim. Chron. New Ser. **15**, 193 (1986).
10. S. BOILEAU and P. HEMERY. Electrochim. Acta, **21**, 647 (1976).
11. J. COMYN, S. DAINTON, and K. IVIN. Electrochim. Acta, **13**, 1851 (1968).
12. R. FUOSS. J. Phys. Chem. **80**, 2427 (1978).
13. R. KAY, B. HALES, and G. CUNNINGHAM. J. Phys. Chem. **71**, 3925 (1967).
14. N. PAPADOPOULOS and G. RITZOULIS. J. Sol. Chem. **16**, 31 (1987).
15. N. PAPADOPOULOS and G. RITZOULIS. Ann. Chim. (Rome), **76**, 307 (1986).
16. J. BARTHEL. Chemn. Ing. Tech. **50**, 259 (1978).
17. R. WACHTER and J. BARTHEL. Ber. Buns. Phys. Chem. **83**, 252 (1979).
18. R. FUOSS. J. Phys. Chem. **79**, 525 (1975).

Can. J. Chem. Downloaded from www.nrcresearchpress.com by 194.225.253.170 on 09/07/12
For personal use only.

Electron affinities of aza-substituted polycyclic aromatic hydrocarbons

GLEN W. DILLOW AND P. KEBARLE
Chemistry Department, University of Alberta, Edmonton, Alta., Canada T6G 2G2

Received April 7, 1989

GLEN W. DILLOW and P. KEBARLE. Can. J. Chem. **67**, 1628 (1989).

Electron affinities for aza-substituted polycyclic aromatics were determined from measurements of electron transfer equilibria in the dilute gas phase with a pulsed electron high pressure mass spectrometer (PHPMS). These are (in kcal / mol): quinazoline (12.7), quinoxaline (15.8), cinnoline (16.0), acridine (20.3), benzo[*c*]cinnoline (20.6), pyrido[2,3-*b*]pyrazine (22.5), phenazine (29.5). Solvation energies of the corresponding radical anions in acetonitrile and dimethylformamide are derived from the gas phase data and literature on electron reduction potentials in solution. An observed linear relationship between the electron affinities and the reduction potentials allows estimates of electron affinities to be made for 12 aza compounds whose EA's are too low to be measured with the present method.

Key words: aza-substituted aromatic hydrocarbons, electron affinities, electron transfer, radical anions, reduction potentials, solvation energies of radical anions, stabilities of radical anions.

GLEN W. DILLOW et P. KEBARLE. Can. J. Chem. **67**, 1628 (1989).

En se basant sur des mesures d'équilibre de transfert d'électron en phase gazeuse diluée et effectuées à l'aide d'une spectromètre de masse à haute pression et à électrons pulsés, on a déterminé les affinités électroniques de dérivés aromatiques polycycliques dans lesquels on a remplacé des carbones par des azotes. Les valeurs obtenues sont les suivantes (en kcal / mol) : quinazoline (12,7), quinoxaline (15,8), cinnoline (16,0), acridine (20,3), benzo]*c*]cinnoline (20,6), pyrido[2,3-*b*]pyrazine (22,5) et phénazine (29,5). En se basant sur des données en phase gazeuse et des données de la littérature relatives aux potentiels de réduction électronique en solution, on a obtenu les énergies de solvatation des radicaux anions correspondants dans l'acétonitrile ainsi que dans le diméthylformamide. Sur la base de la relation linéaire qui a été observée pour les affinités électroniques et les potentiels de réduction, on peut évaluer les affinités électroniques de 12 autres composés aza dont les affinités électroniques sont trop faibles pour être mesurées par la méthode actuelle.

Mots clés : hydrocarbures aromatiques substitués par de l'azote, affinités électroniques, transfert d'électron, radicaux anions, potentiels de réduction, énergies de solvatation de radicaux anions, stabilités de radicaux anions.

[Traduit par la revue]

Introduction

We have recently used pulsed high pressure mass spectrometry (PHPMS) (1) to determine equilibrium constants of electron transfer equilibria [1] in the dilute gas phase. With these one can obtain gas phase electron affinities (EA's) of organic molecules (2–4). The method is applicable only when stable negative ions are formed, i.e., when the EA's are positive. The previous work included a few unsubstituted polycyclic aromatic hydrocarbons (2*b*), but no aza-substituted aromatics.

[1] $A^- + B = A + B^-$

It was determined previously (5), by electron transmission spectroscopy, that aza-substitution of benzene to yield pyridine stabilizes the LUMO and thus increases the EA by ~12 kcal/mol. The LUMO energies for benzene and pyridine are relatively high, so that no stable negative ions are formed in the gas phase; i.e., the EA's are negative, $EA(C_6H_6) \approx -26.4$ kcal/mol and $EA(C_5H_5N) \approx -14.1$ kcal/mol) (5, 6). A stabilization of the aromatic LUMO and the valence electron MO's by replacement of C with N is expected, due to the greater electronegativity of the nitrogen atom. Therefore, for example, in simple Hückel MO theory the value of the coulomb integral α is taken to be lower when heteroatoms of higher electronegativity are part of the aromatic system. Successful predictions of the EA of a number of aza-substituted aromatics have been obtained by Compton and co-workers (7) on the basis of LUMO energies evaluated with the Pariser–Parr–Pople approximation to the Hartree–Fock equation, where variable β–γ were used to empirically account for the different electronegativities of heteroatoms. Compton and co-workers (7) compared their results with EA's from electron transmission spectroscopy, when the EA's were negative, but essentially no experimental data for aza-substituted aromatics with *positive* EA's were available at the time.

Indirect information on electron affinities is available from one-electron reduction potentials measured in solution. Since solvation stabilizes the ion very significantly, stable radical anions in solution can be formed even when the gas phase EA is negative. Reduction potentials for a number of aza-substituted aromatics are available (8, 9) and these include compounds whose EA's are both negative and positive. The present work, which provides electron affinities for seven aza-substituted di- and tri-cyclic aromatics, is thus of significance not only to disciplines where gas phase negative ions occur, such as the electron capture detector, chemical ionization mass spectrometry, and gas phase ion chemistry, but also provides numerical data for comparison with results of future quantum chemical calculations as well as a cross-check to the assumed reversibility of the one-electron reductions in solution. Furthermore, when the reduction potentials are reversible, the gas phase electron affinities can be combined with the solution reduction potentials to obtain solvation energies of the radical anions in the given solvents.

Results and discussion

Results

Values for: $\Delta G_1^0 = -RT \ln K_1$ were determined from the electron transfer equilibria, see reaction [1]. These measurements were made under conditions similar to those used in previous work (1–4): ion-source temperature 150°C, total ion source pressure 5 Torr (1 Torr = 133.3 Pa), mTorr pressures of the neutral reactants. The ΔG_1^0 values obtained are shown in Fig. 1. The reference compounds whose electron attachment free energies, see eq. [2], were determined in earlier work (2) are shown on the left side of Fig. 1.

Can. J. Chem. Downloaded from www.nrcresearchpress.com by 194.225.253.170 on 09/07/12
For personal use only.

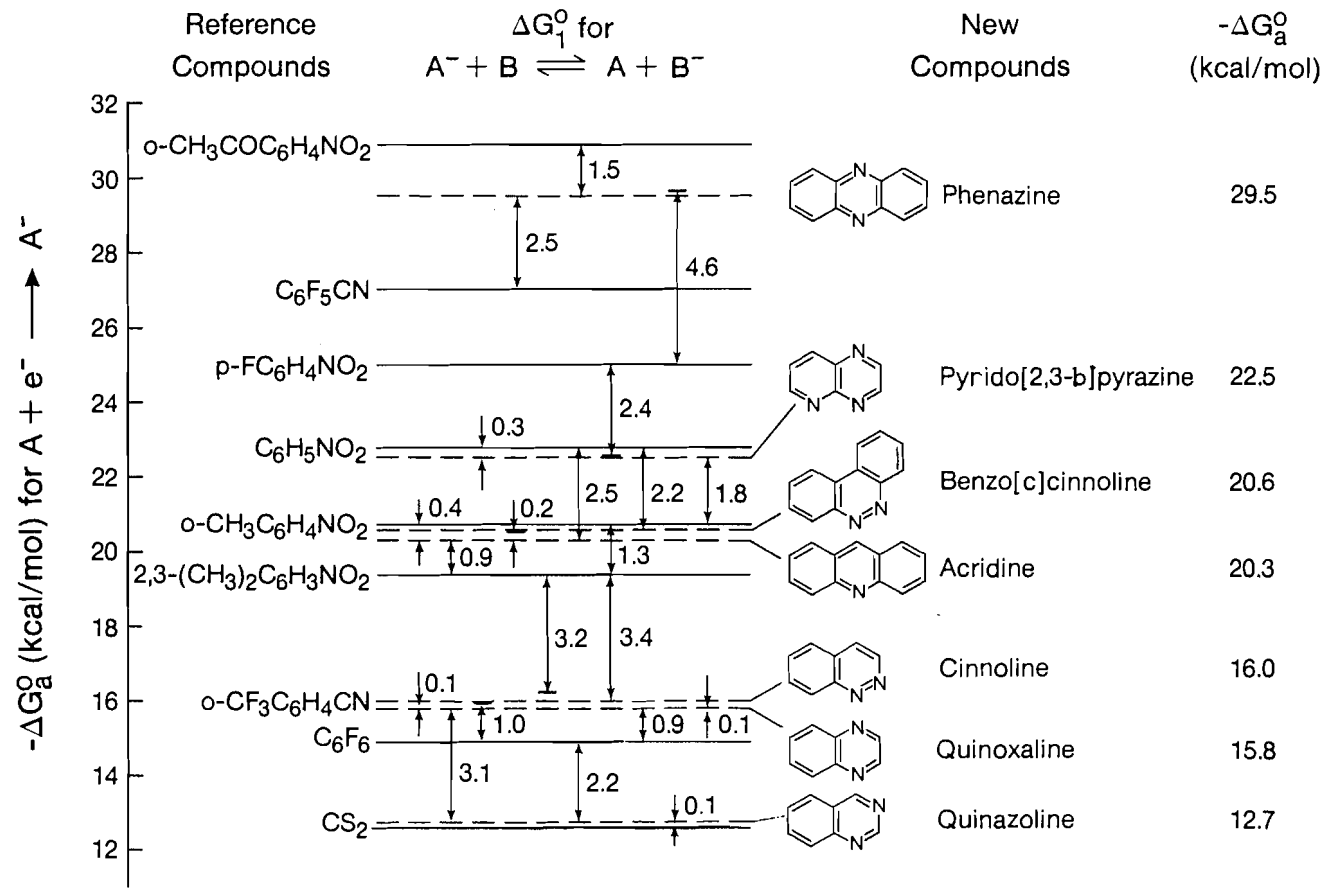


FIG. 1. Scale constructed from experimentally determined $\Delta G_1^0 = -RT \ln K_1$, obtained for electron transfer equilibria [1]: $A^- + B = A + B^-$. Scale is converted to electron capture free energies $\Delta G_a^0(B)$ by calibrating scale to known $\Delta G_a^0(A)$ of reference compounds (temperature 150°C).

[2] $e + A = A^-$ $\Delta G_a^0(A)$

Combination of the ΔG_1^0 with the known $\Delta G_a^0(A)$ of the reference compounds leads to the attachment free energies for the aza compounds shown in Fig. 1 and given in Table 1. In earlier work (*2a*) it was shown that the ΔG_a^0 values are close to the ΔH_a^0 values and that $-\Delta H_a^0 \approx$ EA. The relative values for the ΔG_a^0 of the polycyclic aromatics used should be particularly close to the relative electron affinities, since the LUMO's for these systems are delocalized over the whole molecule and, therefore, only minimal changes of geometry are to be expected between the neutral and negatively charged molecule.

Discussion of EA of aza compounds

The electron affinities of the aza-substituted benzenes, naphthalenes, and anthracenes are shown in Fig. 2, plotted versus the number of nitrogen atoms. The values for benzene, pyridine, and naphthalene are from electron transmission spectroscopy (5, 6), while that for quinoline was estimated from the electrochemical data as discussed later. Two trends are evident in Fig. 2.

1. The increase in EA, in a given series, with increasing number of nitrogens is approximately additive. This trend is particularly evident for the naphthalene series, for which most data are available. Overall, the addition of N to any of the molecules in the benzene, naphthalene, and anthracene series causes an increase of EA of ~10 kcal/mol per nitrogen atom.

2. The effect on the EA's of added nitrogens is attenuated only slightly as the size of the aromatic system increases, i.e., from benzene to anthracene.

TABLE 1. Free energy change for electron attachment to the aza-substituted polycyclic aromatic hydrocarbons

$M + e^- \rightleftharpoons M^-$ $\Delta G^0 = \Delta G_a^0$

Compound	$-\Delta G_a^0$ (kcal/mol)[a]
Quinazoline	12.7
Quinoxaline	15.8
Cinnoline	16.0
Acridine	20.3
Benzo[*c*]cinnoline	20.6
Pyrido[2,3-*b*]pyrazine	22.5
Phenazine	29.5

[a]Data from Fig. 1.

Both of the above effects are very similar to the field effects of substituents added onto, rather than into, the aromatic system. It was observed in earlier work that the field effects on the EA's are approximately additive in multiple substitution and attenuate only slowly with increasing molecular size (*2b*, 3, 4).

Comparison of electron affinities with reduction potentials in solution

The electrochemical reduction potentials of a variety of aza-substituted PAH's in solution have been reported (8, 9). These

Can. J. Chem. Downloaded from www.nrcresearchpress.com by 194.225.253.170 on 09/07/12
For personal use only.

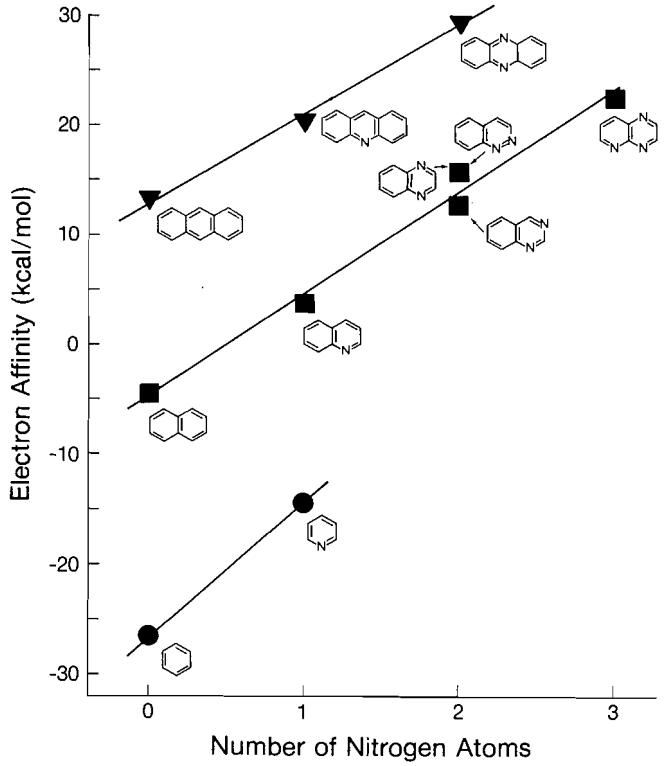


FIG. 2. Plots of electron affinities for aza-substituted polycyclic aromatics. EA for benzene, pyridine, and naphthalene from electron transmission spectroscopy (5, 6). EA for quinoline (1-azanaphthalene) estimated, see Table 2 and text. Remaining data from Fig. 1.

studies included most of the compounds used in the present study. Typically, the first reduction step in solution involves the reversible addition of an electron (from the electrode) to the molecule and is thus the solution equivalent of electron attachment.

Shown in Fig. 3 is a plot of the gas phase attachment free energies ΔG_a^0 versus reduction potentials in acetonitrile solution (8). The reduction potentials used are actually the polarographic halfwave potentials $E_{1/2}$, which for reversible processes are close to the reduction potentials. A similar plot is shown in Fig. 4 where now the $E_{1/2}$ are for dimethylformamide solution (9). In both plots, pyridine was included to extend the range of the data. Both sets of solution data were obtained with 0.1 M tetraethylammonium perchlorate as supporting electrolyte, and were measured versus the SCE reference electrode.

A very good linear correlation is obtained in Fig. 3, correlation coefficient 0.997, while the correlation in Fig. 4 has somewhat more scatter, correlation coefficient 0.985. The very good correlations indicate that all the reduction potentials involved are due to reversible one-electron reduction reactions.

From the plots in Figs. 3 and 4 one can estimate $-\Delta G_a^0$ for a number of molecules for which reduction potentials are available (8, 9) but ΔG_a^0 are difficult to measure. Measurements with the PHPMS electron transfer equilibrium method are difficult for molecules whose $-G_a^0$ are less than ~12 kcal/mol. For such systems thermal electron detachment (10) occurs above 100°C. Furthermore, often minor impurities with higher $-\Delta G_a^0$ become the dominant ions. Table 2 lists $-\Delta G_a^0$ for 12 aza compounds estimated on the basis of the linear plots of Figs. 3 and 4.

The slopes in Figs. 3 and 4 are similar, 0.72 for acetonitrile

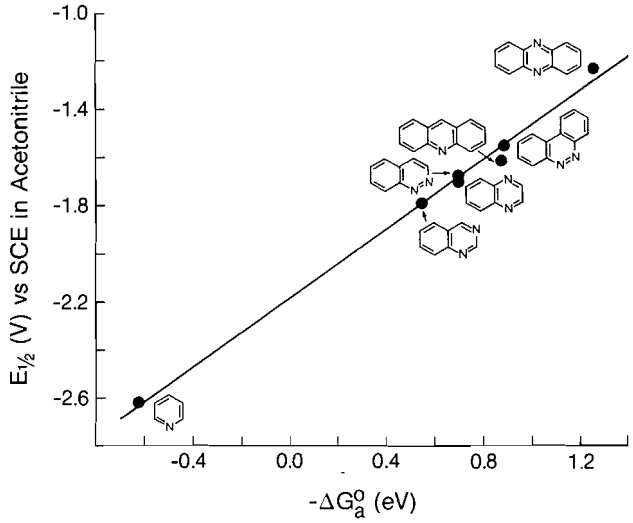


FIG. 3. Plots of $-\Delta G_a^0$ (gas phase) versus polarographic halfwave reduction potentials in acetonitrile from ref. 8. $-\Delta G_a^0$ (pyridine) based on EA of Nenner and Schulz (5).

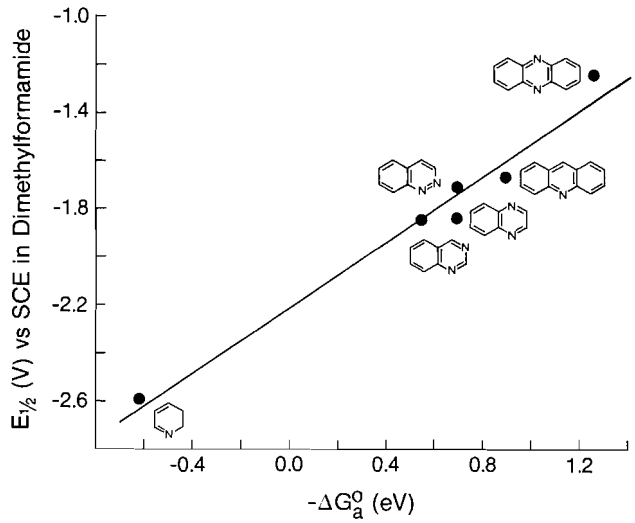


FIG. 4. Same as in Fig. 3 but $E_{1/2}$ for dimethylformamide (9).

and 0.69 for dimethylformamide. Less than unit slopes were observed in earlier comparisons (2–4) of reduction potentials with $-\Delta G_a^0$ values and are attributed to an approximately linear decrease of solvation exoergicity of the negative ions with increasing electron affinities ($-\Delta G_a^0$). The same explanation should hold also in the present cases. Increases in the electron affinities of the aza systems used are achieved by increasing delocalization of the negative charge and charge delocalization leads to decreasing exoergicity for the solvation of the ion.

In earlier work (2*d*, 2*c*, 11) approximate solvation free energies were evaluated with eq. [3]. For the origin of the equation and numerical constants see ref. 2*d*.

$$[3]\quad \Delta G_{sol}^0(B^-) - \Delta G_{sol}^0(B) = -108.6 - 23.06\,E_{1/2}(B) - \Delta G_a^0(B)$$

The numerical constant −108.6 is adjusted for answers in kcal/mol when $E_{1/2}$ is introduced in volts and ΔG_a^0 in kcal/mol. The reference electrode (SCE) potential is included in the constant. Substitution of available ΔG_a^0 and $E_{1/2}$, from ref. 8, for the

Can. J. Chem. Downloaded from www.nrcresearchpress.com by 194.225.253.170 on 09/07/12
For personal use only.

TABLE 2. $-\Delta G_a^0$ values estimated from reduction potentials, $E_{1/2}$, in DMF[a] and acetonitrile[b]

Compound	$-E_{1/2}$ (V) in DMF	Estimated[c] $-\Delta G_a^0$ (eV)	$-E_{1/2}$ (V) in acetonitrile	Estimated[c] $-\Delta G_a^0$ (eV)
Pyrazine	2.07	0.22	2.080	0.16
Pyridazine	2.30	−0.10	2.120	0.10
Pyrimidine	2.55	−0.46	2.340	−0.20
Triazine	2.02	0.29	—	—
Quinoline	2.10	0.18	2.105	0.12
Isoquinoline	2.19	0.05	2.220	−0.04
Phthalazine	2.06	0.24	1.976	0.30
Phenanthridine	—	—	2.118	0.10
1,4-Phenanthroline	—	—	1.744	0.62
1,7-Phenanthroline	—	—	2.092	0.14
1,10-Phenanthroline	—	—	2.053	0.19
4,7-Phenanthroline	—	—	2.044	0.21

[a]Reduction potentials from Millefiori (8).
[b]Reduction potentials from Maruyama *et al.* (9).
[c]Estimated error ±0.1 eV.

TABLE 3. Evaluated solvation energies: $\Delta G_{sol}^0(B^-) - \Delta G_{sol}^0(B) = \Delta\Delta G_{sol}^0$, for aza-substituted compounds

Compound	ΔG_a^0(B) (kcal/mol)	$E_{1/2}(CH_3CN)$ (V)	$\Delta\Delta G_{sol}^0$ (kcal/mol)	$E_{1/2}$(DMF) (V)	$\Delta\Delta G_{sol}^0$ (kcal/mol)
Pyridine	14.3	−2.622	−62.4	−1.60	−62.9
Quinazoline	−12.7	−1.799	−54.3	−1.85	−53.2
Quinoxaline	−15.8	−1.702	−53.5	−1.89	−50.4
Cinnoline	−16.0	−1.686	−53.8	−1.71	−53.2
Acridine	−20.3	−1.620	51.0	−1.68	−49.5
Benz[c]cinnoline	−20.6	−1.554	−52.0	—	—
Phenazine	−29.5	−1.227	−50.7	−1.24	−50.5

$E_{1/2}$ for CH_3CN from Millefiori (8), DMF from Maruyama *et al.* (9).

aza compounds leads to the solvation free energies in acetonitrile and dimethylformamide given in Table 3. Since the solvation energies of the neutral compounds, $-\Delta G^0$(B), are relatively much smaller than those for the negative ions, $-\Delta G^0(B^-)$ (2*d*, 2*e*, 11), it can be assumed that the $\Delta\Delta G^0$ data in Table 3 correspond largely to the solvation energies of the negative ions. The energies for acetonitrile and DMF are quite similar, a result that conforms to previous observations (2*d*, 2*e*, 11). The smallest ion, pyridine$^-$, has the highest solvation exothermicity (−63 kcal/mol). On the other hand the tricyclic phenzaine, for which the charge is also partially dispersed over two nitrogens, has the lowest solvation energy (−50 kcal/mol). These results can be compared with $\Delta\Delta G^0$ data for other radical anions: −59 kcal/mol (nitrobenzene) versus −48 kcal/mol (1,4-dinitrobenzene) in acetonitrile (11) and −54 kcal/mol (1,4-benzoquinone) versus −52 kcal/mol (9,10-anthraquinone) in acetonitrile (2*d*). The much smaller spread for the quinones can be attributed to the facts that most of the charge is expected to be on the electronegative oxygens and that the number of oxygens does not increase for this pair.

Acknowledgement

This reasearch was supported by the Natural Sciences and Engineering Research Council of Canada.

1. P. KEBARLE. Pulsed electron high pressure mass spectrometer in techniques for the study of ion molecule reactions. *Edited by* J. M. Farrar and W. Saunders, Jr. John Wiley, New York. 1988.
2. (*a*) P. KEBARLE and S. CHOWDHURY. Chem. Rev. **87**, 513 (1987); (*b*) S. CHOWDHURY, T. HEINIS, and P. KEBARLE. J. Am. Chem. Soc. **108**, 4662 (1986); (*c*) S. CHOWDHURY and P. KEBARLE. J. Am. Chem. Soc. **108**, 5453 (1986); (*d*) T. HEINIS, S. CHOWDHURY, S. L. SCOTT, and P. KEBARLE. J. Am. Chem. Soc. **110**, 400 (1988); (*e*) G. PAUL and P. KEBARLE. J. Am. Chem. Soc. **111**, 464 (1989).
3. S. CHOWDHURY, H. KISHI, G. W. DILLOW, and P. KEBARLE. Can. J. Chem. **67**, 603 (1989).
4. (*a*) S. CHOWDHURY, E. P. GRIMSRUD, T. HEINIS, and P. KEBARLE. J. Am. Chem. Soc. **108**, 3630 (1986); (*b*) G. W. DILLOW and P. KEBARLE. J. Am. Chem. Soc. **111**, 5592 (1989).
5. I. NENNER and G. J. SCHULTZ. J. Chem. Phys. **62**, 1747 (1975).
6. K. D. JORDAN and B. P. BURROW. Acc. Chem. Res. **11**, 341 (1978); J. Chem. Phys. **71**, 5384 (1979).
7. J. M. YOUNKIN, L. J. SMITH, and R. N. COMPTON. Theor. Chim. Acta, **41**, 157 (1976).
8. S. MILLEFIORI. J. Heterocycl. Chem. **7**, 145 (1970).
9. M. MARUYAMA and K. MURAKAMI. J. Electroanal. Chem. **102**, 221 (1979).
10. E. P. GRIMSRUD, S. CHOWDHURY, and P. KEBARLE. J. Chem. Phys. **83**, 3983 (1983).
11. P. KEBARLE, G. W. DILLOW, K. HIRAO, and S. CHOWDHURY. Faraday Discuss. Chem. Soc. **85**, 23 (1988).

Can. J. Chem. Downloaded from www.nrcresearchpress.com by 194.225.253.170 on 09/07/12
For personal use only.

Spectroelectrochemical behaviour of the trinuclear $[Ru_3O(O_2CCH_3)_6(isonicotinamide)_3]$ cluster

HENRIQUE E. TOMA[1] AND CARLOS J. CUNHA

Instituto de Quimica, Universidade de São Paulo Caixa Postal 20780, São Paulo, SP, Brazil

Received January 19, 1989

HENRIQUE E. TOMA and CARLOS J. CUNHA. Can. J. Chem. **67**, 1632 (1989).

The $[Ru_3O(OOCCH_3)_6(isonicotinamide)_3]$ cluster exhibits reversible electrochemical and spectroelectrochemical behaviour in acetonitrile solutions, associated with a series of successive μ-oxo $Ru^{IV}Ru^{IV}Ru^{III}/Ru^{IV}Ru^{III}Ru^{III}/.../Ru^{II}Ru^{II}Ru^{II}$ redox couples with E^0 = 2.16, 1.21, 0.19, −0.98, and −1.4 V versus SHE. The metal-isonicotinamide and metal–metal charge-transfer transitions shift to lower energies as the oxidation states of the ruthenium ions decrease. In alkaline aqueous solution, the μ-oxo $Ru^{III}Ru^{III}Ru^{II}$ cluster can be reversibly reduced to the μ-oxo $Ru^{III}Ru^{II}Ru^{II}$ product (E^0 = −0.85 V); however, below pH 4, the reduction proceeds according to two successive steps, yielding $Ru^{II}Ru^{II}Ru^{II}$ species with loss of the central oxygen ion. These species can be reoxidized in the reverse potential scan, regenerating the μ-oxo $Ru^{III}Ru^{III}Ru^{II}$ complex.

Key words: ruthenium–acetate clusters, cluster spectroelectrochemistry, cluster electrochemistry, ruthenium–isonicotinamide complex, trinuclear cluster.

HENRIQUE E. TOMA et CARLOS J. CUNHA. Can. J. Chem. **67**, 1632 (1989).

En solutions dans l'acétonitrile, l'agrégat de $[Ru_3O(OOCCH_3)_6(isonicotinamide)_3]$ présente un comportement électrochimique et spectroélectrochimique réversible associé avec une série de couples rédox successifs μ-oxo $Ru^{IV}Ru^{IV}Ru^{III}/Ru^{IV}Ru^{III}Ru^{III}/.../Ru^{II}Ru^{II}Ru^{II}$ avec des E^0 = 2,16, 1,21, 0,19, −0,98 et −1,4 V vs SHE. Les transitions des transferts de charge métal–isonicotinamide et métal–métal se déplacent vers les énergies plus basses avec une diminution des états d'oxydation des ions ruthénium. En solution alcaline aqueuse, on peut réduire réversiblement l'agrégat μ-oxo $Ru^{III}Ru^{III}Ru^{II}$ en produit μ-oxo $Ru^{III}Ru^{II}Ru^{II}$ (E^0 = −0,85 V); toutefois, à des pH inférieur à 4, la réduction se produit par le biais de deux étapes successives et elle fournit des espèces $Ru^{II}Ru^{II}Ru^{II}$ avec une perte de l'ion oxygène central. Un balayage de potentiel inverse permet de réoxyder ces espèces et de régénérer le complexe μ-oxo $Ru^{III}Ru^{III}Ru^{II}$.

Mots clés : agrégats d'acétate de ruthénium, spectroélectrochimie des agrégats, électrochimie des agrégats, complexe de ruthénium–isonicotinamide, agrégats trinucléaires.

[Traduit par la revue]

Introduction

This work deals with the electrochemical and spectroelectrochemical behaviour of the $[Ru_3O(OOCCH_3)_6(isonic)_3]$ cluster (isonic = isonicotinamide) in aqueous and acetonitrile solutions. This complex is a typical example of ruthenium trinuclear cluster exhibiting a triangular structure strongly held by acetate bridges and a central μ-oxo bridge (1–6), as well as by extended metal–metal bonds (Fig. 1). A large number of oxidation states is accessible for this type of trinuclear cluster; however, detailed spectroelectrochemical studies have never been reported up to the present time.

Experimental section

The $[Ru_3O(OOCCH_3)_6(isonic)_3]A$ (A = PF_6^- or BF_4^-) cluster was synthesized according to the procedure previously reported in the literature for the 2-methyl pyrazine analogue (4). *Anal.* calcd. for $Ru_3C_{30}H_{36}N_6O_{16}PF_6$: C 30.4, H 3.1, N 7.1; found: C 28.9, H 3.1, N 7.4. *Anal.* calcd. for $Ru_3C_{30}H_{36}N_6O_{16}BF_4$: C 31.9, H 3.3, N 7.5; found: C 30.1, H 3.6, N 7.6.

Cyclic voltammetry was carried out with a Princeton Applied Research (PAR) instrument, consisting of a model 173 potentiostat and a model 175 universal programmer. Platinum (A = 0.09 cm^2) or glassy carbon electrodes (A = 0.23 cm^2) were employed for the measurements, using the conventional Luggin capillary arrangement with the Ag/AgCl (I = 1 mol dm^{-3} KCl) reference electrode (E^0 = 0.222 V vs, SHE) in aqueous solution (0.5 mol dm^{-3} KCl), or the $Ag/AgNO_3$ (0.01 mol dm^{-3}) reference electrode (E^0 = 0.503 V vs, SHE) (7) in acetonitrile solution containing 0.100 mol dm^{-3} tetraethylammonium perchlorate. A platinum wire was used as the auxiliary electrode.

The electronic spectra of the complexes were recorded on a Cary 17, or a Hewlett–Packard model HP 8451-A diode-array spectrophotometer. Spectral deconvolution was carried out using a local variation of the SPECSOLV (8) program. For the spectroelectrochemical measurements, the PAR-173 potentiostat was used in parallel with the Cary 17 or HP 8451-A spectrophotometers. A three-electrode system was designed for a rectangular quartz cell of 0.020 cm internal optical pathlength. A gold minigrid was used as a transparent working electrode, in the presence of a small Ag/AgCl reference electrode and a platinum auxiliary electrode.

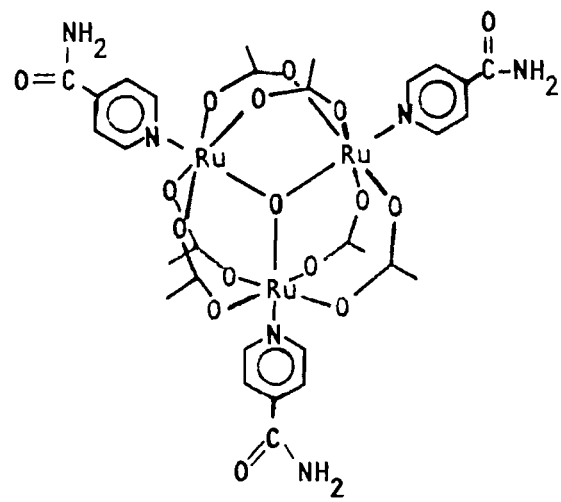


FIG. 1. The $[Ru_3O(OOCCH_3)_6(isonicotinamide)_3]$ cluster employed in this work.

Results and discussion

Cyclic voltammentry in acetonitrile solution

The cyclic voltammograms for the $[Ru_3O(OOCCH_3)_6(isonic)_3]$ cluster in acetonitrile exhibited five sucessive redox waves in the range of potentials from −1.5 to 2.3 V (Fig. 2). The electro-

[1]To whom correspondence should be addressed.

Can. J. Chem. Downloaded from www.nrcresearchpress.com by 194.225.253.170 on 09/07/12
For personal use only.

Can. J. Chem. Downloaded from www.nrcresearchpress.com by 194.225.253.170 on 09/07/12
For personal use only.

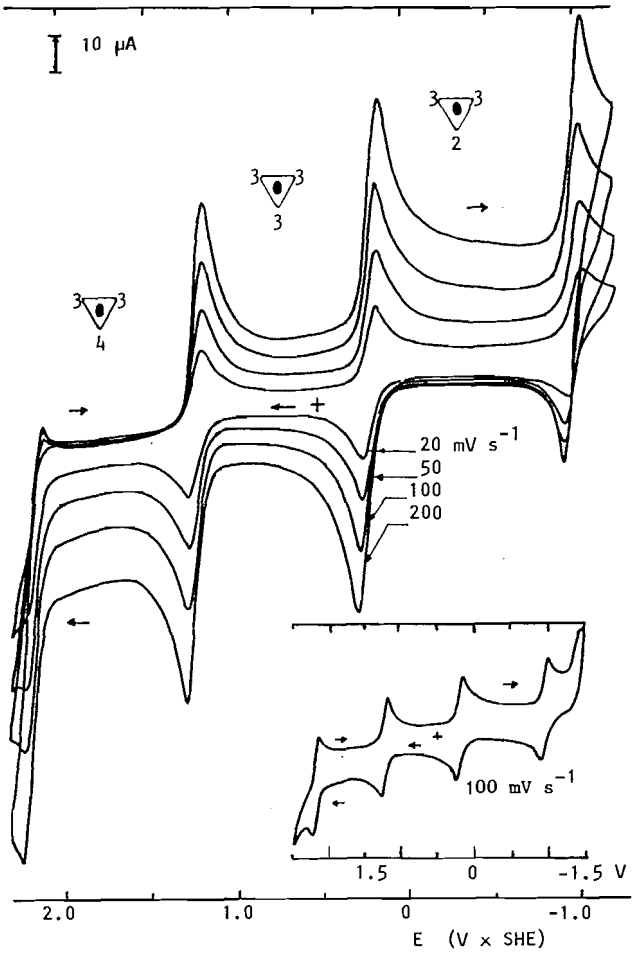


FIG. 2. Cyclic voltammograms of the $[Ru_3O(OOCCH_3)_6(isonic)_3]$ cluster (2 mmol dm^{-3}) obtained at several potential scan rates, in acentonitrile, $[NEt_4ClO_4] = 0.100$ mol dm^{-3}, 298 K, using a platinum working electrode; a fifth wave is shown at -1.4 V in the inserted voltammogram.

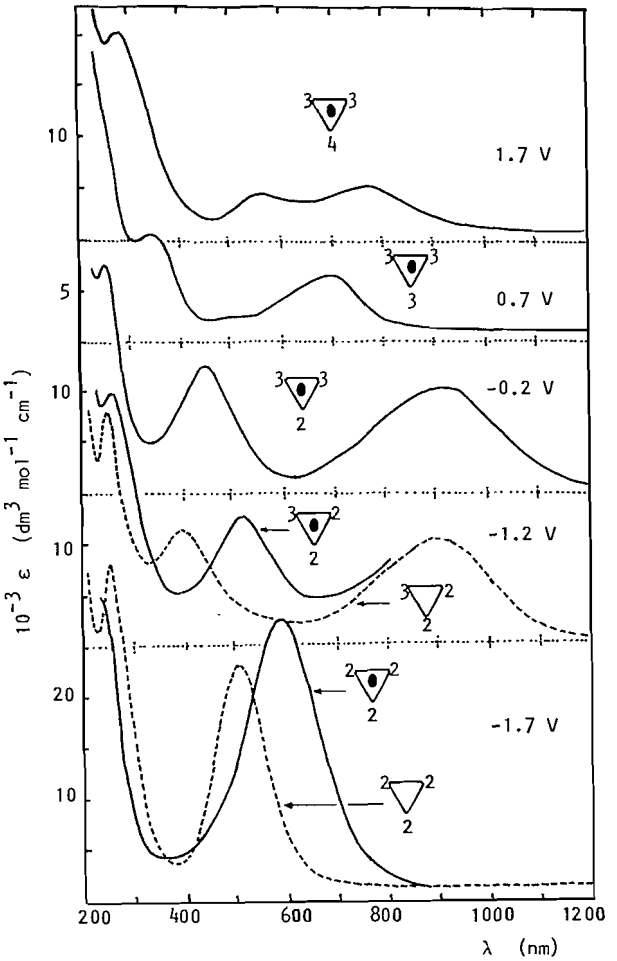


FIG. 3. Spectroelectrochemical behaviour of the $[Ru_3O(OOCCH_3)_6(isonic)_3]$ cluster in acetonitrile at several applied potentials (V versus SHE), $[NEt_4ClO_4] = 0.100$ mol dm^{-3} (acetonitrile), 298 K, showing the μ-oxo species (solid lines) before the loss of the central oxygen ion (---) which occurs below -1 V.

chemical behaviour was practically reversible (9), with the ratio of the anodic and cathodic peak currents very close to unity. The separation between the anodic and cathodic peak potentials was approximately 60 mV at low potential scan rates (e.g. 20 mV s^{-1}), increasing up to 70 mV at 200 mV s^{-1}. The assignment of the formal redox couples was proposed based on related examples from the literature (4):

$E^0(Ru^{IV}Ru^{IV}Ru^{III}/Ru^{IV}Ru^{III}Ru^{III}) = 2.16$ V vs. SHE
$E^0(Ru^{IV}Ru^{III}Ru^{III}/Ru^{III}Ru^{III}Ru^{III}) = 1.21$ V
$E^0(Ru^{III}Ru^{III}Ru^{III}/Ru^{III}Ru^{III}Ru^{II}) = 0.19$ V
$E^0(Ru^{III}Ru^{III}Ru^{II}/Ru^{III}Ru^{II}Ru^{II}) = -0.98$ V
$E^0(Ru^{III}Ru^{II}Ru^{II}/Ru^{II}Ru^{II}Ru^{II}) = -1.4$ V

The difference between the redox potentials of the $Ru^{IV}Ru^{IV}Ru^{III}/Ru^{IV}Ru^{III}Ru^{III}/.../Ru^{III}Ru^{II}Ru^{II}$ redox couples is as large as 1 V, indicating that the changes in the oxidation states of each metal ion have a pronounced influence on the electrochemical behaviour of the neighboring ions. This fact is consistent with a strong interaction between the ruthenium ions in the trinuclear centre.

Spectroelectrochemistry in acetonitrile solution

In order to characterize the chemical species involved in the electrochemical processes, spectroelectrochemical measurements were carried out for the $[Ru_3O(OOCCH_3)_6(isonic)_3]$ cluster in acetonitrile solutions, as illustrated in Fig. 3. The spectroelectrochemical behaviour was typically reversible, except for the μ-oxo $Ru^{III}Ru^{II}Ru^{II}$ and $Ru^{II}Ru^{II}Ru^{II}$ clusters, which can only be detected as transient species using a diode-array spectrophotometer. These species react with trace amounts of water, converting into the corresponding products without the oxygen bridge, as previously reported by Spencer and Wilkinson for the pyridine analogue (1, 2).

The assignment of the electronic transitions can be discussed based on the qualitative molecular orbital scheme proposed by Cotton and Norman (3) and by Baumann *et al.* (4) for the triangular Ru_3O centre, as shown in Fig. 4. The symmetry assumed is D_{3h}. The central oxygen atom is considered to be sp^2 hybridized leaving a single p orbital to interact with the d_{yz} orbitals of the three ruthenium ions, in order to generate one e'' and two a_2'' molecular orbitals. Metal–metal bonding involving the combination of the neighboring $Ru(d_{xz})$ orbitals leads to the $1e'$ and a_2' molecular orbitals. The remaining $d_{x^2-y^2}$ orbitals are separated by a considerable distance, but can interact weakly via a through-space interaction, giving rise to the $2e'$ and a_1' molecular orbitals.

According to the molecualr orbital scheme, the $[Ru_3O(OOCCH_3)_6(isonic)_3]^+$ complex can be formally de-

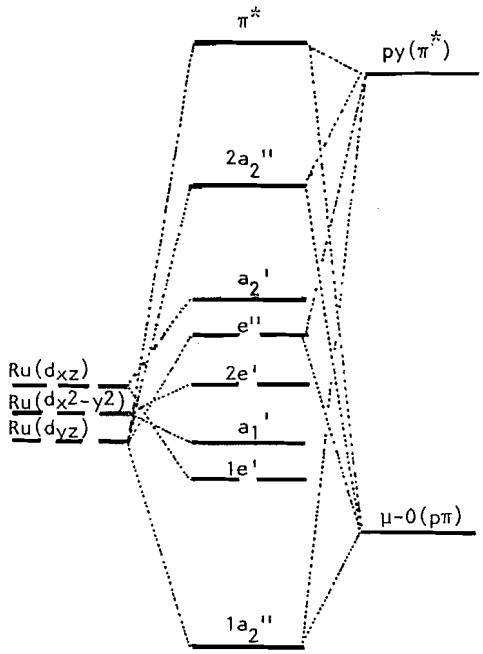


FIG. 4. Qualitative molecular orbital scheme for the $[Ru_3O(OOCCH_3)_6(isonic)_3]$ cluster in D_{3h} symmetry.

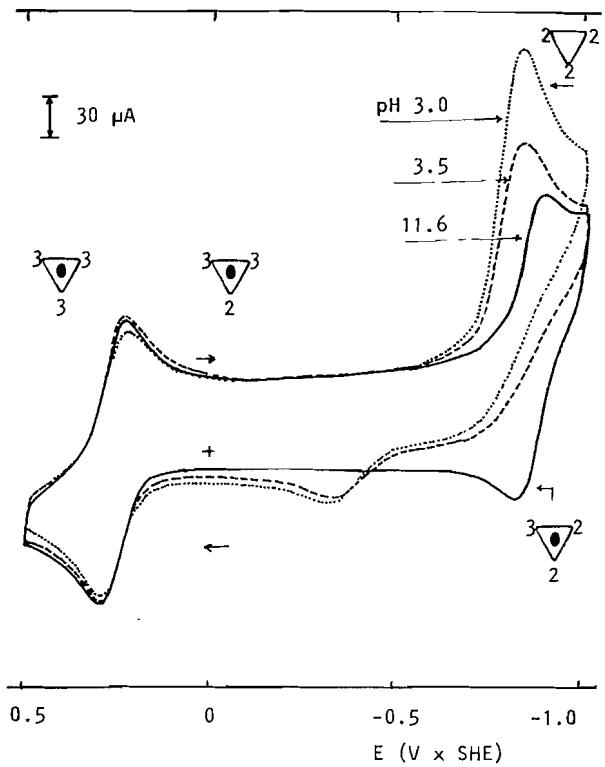


FIG. 5. Cyclic voltammogram of the $[Ru_3O(OOCCH_3)_6(isonic)_3]$ cluster (2.4 mmol dm^{-3}) in aqueous solution, obtained at several pHs, 100 mV s^{-1} KCl = 0.100 mol dm^{-3}, 298 K, using a glassy carbon working electrode.

scribed as $Ru^{III}Ru^{III}Ru^{III}$, exhibiting the electronic configuration $(1a_2'')^2(1e')^4(a_1')^2(2e')^4(e'')^4(a_2')$, leaving an empty $2a_2''$ orbital. Deconvolution of the absorption band at 710 nm leads to three Gaussian components at 707, 614, and 481 nm, ascribed to the symmetry-allowed $e'' \rightarrow a_2''$ and $a_1' \rightarrow a_2''$ transitions, and to the e' (1) $\rightarrow a_2''$ electric dipole-forbidden transition, as in the anaogous pyridine complex (4). The corresponding transitins in the $Ru^{IV}Ru^{III}Ru^{III}$, and $Ru^{III}Ru^{III}Ru^{II}$ clusters were located at 588, 481, 420 and 943, 797, and 632 nm, respectively. The optical energies display a linear correlation with the oxidation states, indicating a gradual increase of energy of the occupied metal d_π levels with the increasing number of electrons. In the case of the $Ru^{II}Ru^{II}Ru^{II}$ clusters, the d_π orbitals are completely filled and no metal–metal band is observed. In contrast, the $Ru^{IV}Ru^{III}Ru^{III}$ cluster exhibits three vacant levels, and an additional metal–metal band is observed at 778 nm, arising probably from the $1e' \rightarrow a_2'$ transition.

The isonicotinamide ligands have π^* orbitals of appropriate symmetry to interact with the ruthenium d_π molecular orbitals, particularly those of e'' and a_2'' symmetry if one assumes a planar configuration. The absorption band in the ultraviolet region, around 260 nm, is also observed in the free isonicotinamide ligand, and can be ascribed to π–π^* transitions in the aromatic ring. The band of intermediate energy is strongly sensitive to the oxidation states, moving from 310 nm in the $Ru^{IV}Ru^{III}Ru^{III}$ complex to 600 nm in the completely reduced $Ru^{II}Ru^{II}Ru^{II}$ form, with a great increase of intensity (Fig. 3). This band can be ascribed to a charge-transfer transition from occupied ruthenium(II) d_π orbitals of e'' symmetry, to the lowest unoccupied π^* orbitals of the isonicotinamide ligands.

Cyclic voltammetry in aqueous solution

Above pH 8, the waves associated with the μ-oxo $Ru^{IV}Ru^{III}Ru^{III}/Ru^{III}Ru^{III}/Ru^{III}Ru^{III}Ru^{II}/Ru^{III}Ru^{II}Ru^{II}$ redox couples are typically reversible (Fig. 5), with $E_{1/2}$ = 1.22, 0.27, and −0.85 V, respectively. The reduction of the $Ru^{III}Ru^{III}Ru^{II}$ cluster is pH dependent. Below pH 4, as one can see in Fig. 5, the cathodic peak moves from −0.88 to −0.84 V and becomes broader. The net charge involved is two times that observed above pH 4, being consistent with the transfer of two electrons, in a successive way, involving intermediarily a proton-dependent step. By reversing the potential scan, the starting μ-oxo bridged $Ru^{III}Ru^{III}Ru^{II}$ complex is regenerated. The electrochemical process can be repeated many times, in a cyclic way, with no evidence of decomposition of the trinuclear cluster.

Spencer and Wilkinson (1, 2) have shown that the $[Ru^{III}Ru^{III}Ru^{III}O(OOCCH_3)_6(pyridine)_3]^+$ cluster can be reduced by hydrogen at 2 atm pressure, in aqueous solution, in the presence of platinum oxide catalyst yielding the corresponding $Ru^{II}Ru^{II}Ru^{II}$ end product with loss of the central μ-oxo ion. This species can be oxidized, in a reversible way, without changing the overall structure of the triangular cluster.

Considering the elecrochemical behaviour in acetonitrile solutions, and the results reported by Spencer and Wilkinson (1), the pH-dependent step observed in aqueous solution can be associated with the elimination of the central oxygen ion in the μ-oxo $Ru^{III}Ru^{II}Ru^{II}$ species. Above pH 4 these μ-oxo bridged species are stable. However, as the pH decreases, the elimination of the central oxygen ion is favored, leading to an $Ru^{III}Ru^{II}Ru^{II}$ intermediate which undergoes further reduction to the $Ru^{II}Ru^{II}Ru^{II}$ end product, at the applied potentials. The overall process is illustrated in the scheme of Fig. 6. In the reverse scan, below pH 4, the reoxidation of the $Ru^{III}Ru^{II}Ru^{II}$ intermediate can be detected at approximately −0.3 V (Fig. 5). Scan rate dependence studies for the peak currents at −0.3 V were carried out at pH 4.20. The plots of the logarithm of the peak currents divided by $v^{1/2}$ (v = scan rate) against time were linear, leading to an observed rate constant of 0.02 s^{-1}. This

Can. J. Chem. Downloaded from www.nrcresearchpress.com by 194.225.253.170 on 09/07/12
For personal use only.

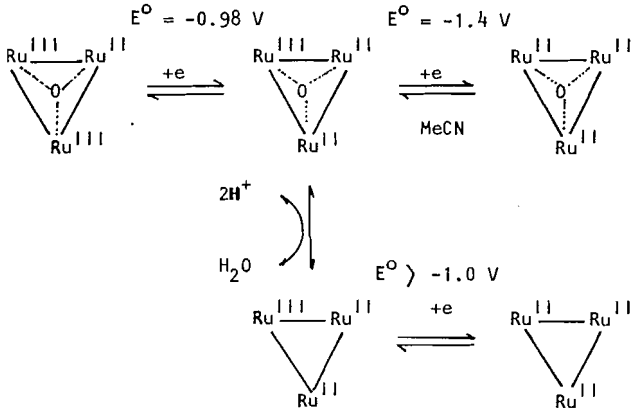


FIG. 6. Mechanistic scheme proposed for the electrochemical reduction of the $[Ru_3O(OOCCH_3)_6(isonic)_3]$ cluster in aqueous and acetonitrile solutions.

value provides a relative time scale for simple reoxidation versus oxide loss in the μ-oxo $Ru^{III}Ru^{II}Ru^{II}$ cluster.

According to the molecular orbital diagram of Fig. 4 the central oxygen ion plays an important role in the stabilization of the ruthenium(III) or (IV) species, by donating π-eletrons to the empty d_{yz} orbitals. When the cluster is completely reduced, the d_{yz} orbitals become saturated and this type of interaction is no more possible, facilitating the transfer of the oxygen ion to the proton donor species in the solvent.

Acknowledgements

We thank CNPq, FAPESP, and FINEP for financial support, and Professor Albert Haim for his invaluable help at the beginning of this work.

1. A. SPENCER and G. WILKINSON. J. Chem. Soc. Dalton Trans. 1570 (1972).
2. A. SPENCER and G. WILKINSON. J. Chem. Soc. Dalton Trans. 786 (1974).
3. F. A. COTTON and J. G. NORMAN. Inorg. Chim. Acta, **6**, 411 (1972).
4. J. A. BAUMANN, D. J. SALMON, S. T. WILSON, T. J. MEYER and W. E. HATFIELD. Inorg. Chem. **17**, 3342 (1978).
5. J. A. BAUMANN, D. J. SALMON, S. T. WILSON, and T. J. MEYER. Inorg. Chem. **18**, 2472 (1979).
6. J. A. BAUMANN, S. T. WILSON, D. J. SALMON, P. L. HOOD, and T. J. MEYER. J. Am. Chem. Soc. **101**, 2916 (1979).
7. B. KRATOCHVIL, E. LORAH, and C. GARBER. Anal. Chem. **41**, 1793 (1969).
8. H. GOLD, C. E. RECHSTEINER, and R. P. BUCK. Anal. Chem. **48**, 1540 (1976).
9. R. S. NICHOLSON and I. SHAIN. Anal. Chem. **36**, 706 (1964).

Can. J. Chem. Downloaded from www.nrcresearchpress.com by 194.225.253.170 on 09/07/12
For personal use only.

Structural studies of organoboron compounds. XXXIV.[1] 4-(*N*-Methoxymethylimino)-2,2-diphenyl-1,3-dioxa-2-borata-1,2,3,4-tetrahydronaphthalene and 4-diethylimino-2,2-diphenyl-1,3-dioxa-2-borata-1,2,3,4-tetrahydronaphthalene

WOLFGANG KLIEGEL and MAHMOOD TAJERBASHI

Institut für Pharmazeutische Chemie, der Technischen Universität Braunschweig, Beethovenstraße 55, 3300 Braunschweig, Bundesrepublik Deutschland

AND

STEVEN J. RETTIG and JAMES TROTTER

Department of Chemistry, University of British Columbia, 2036 Main Mall, Vancouver, B.C., Canada V6T 1Y6

Received December 14, 1988[2]

WOLFGANG KLIEGEL, MAHMOOD TAJERBASHI, STEVEN J. RETTIG, and JAMES TROTTER. Can. J. Chem. **67**, 1636 (1989).

Details of the syntheses, physical properties, and crystal structures of the title compounds are reported. Crystals of 4-(*N*-methoxymethylimino)-2,2-diphenyl-1,3-dioxa-2-borata-1,2,3,4-tetrahydronaphthalene, **4**, are monoclinic, a = 9.8072(5), b = 9.6217(7), c = 19.6793(12) Å, β = 94.871(5)°, Z = 4, space group $P2_1/c$, and those of 4-diethylimino-2,2-diphenyl-1,3-dioxa-2-borata-1,2,3,4-tetrahydronaphthalene, **9**, are orthorhombic, a = 17.0593(7), b = 16.1372(6), c = 14.3753(5) Å, Z = 8, space group *Pbca*. Both structures were solved by direct methods and were refined by full-matrix least-squares procedures to R = 0.046 and 0.038 for 2198 and 2969 reflections with $I \geq 3\sigma(I)$, respectively. In both structures the *N*,*N*-dialkylsalicylamidate ligands coordinate the diphenylboron moieties via the phenolate oxygen and amide oxygen atoms, forming six-membered O—B—O chelate rings. The O(ar)—B, O(amide)—B, and mean C—B bond lengths (corrected for libration) are as follows: 1.490(3), 1.549(4), and 1.612 Å for **4** and 1.494(2), 1.550(2), and 1.612 Å for **9**.

Key words: crystal structures, boron compounds, organoboron compounds.

WOLFGANG KLIEGEL, MAHMOOD TAJERBASHI, STEVEN J. RETTIG et JAMES TROTTER. Can. J. Chem. **67**, 1636 (1989).

On rapporte les détails relatifs à la synthèse, à la détermination des propriétés physiques et aux structures cristallines des composés mentionnés dans le titre. Les cristaux du 4-(*N*-méthoxyméthylimino)-2,2-diphényl-1,3-dioxa-2-borata-1,2,3,4-tétrahydronaphtalène, **4**, sont monocliniques, groupe d'espace $P2_1/c$ avec a = 9,8072(5), b = 9,6217(7) et c = 19,6793(12) Å, β = 94,871(5)° et Z = 4 alors que ceux du 4-diméthylimino-2,2-diphényl-1,3-dioxa-2-borata-1,2,3,4-tétrahydronaphtalène, **9**, sont orthorhombiques, groupe d'espace *Pbca*, avec a = 17,0593(7), b = 16,1372(6) et c = 14,3753(5) Å et Z = 8. On a résolu les deux structures par des méthodes directes et on les a affinées par la méthode des moindres carrés (matrice entière) jusqu'à des valeurs de R respectives de 0,046 et 0,038 pour 2198 et 2969 réflexions avec $I \geq 3\sigma(I)$. Dans chacune de ces structures, les ligands *N*,*N*-dialkyl-salicylamidates effectuent des coordinations avec les portions diphénylbores par le biais des atomes d'oxygène du phénolate et de l'amide en donnant lieu à la formation de cycles de chélates O—B—O à six chaînons. Les longueurs moyennes des longueurs des liaisons O(ar)—B, O(amide)—B et C—B (corrigées pour la libration) sont les suivantes: 1,490(3), 1,549(4) et 1,612 Å pour le compsé **4** et 1,494(2), 1,550(2) et 1,612 Å pour le composé **9**.

Mots clés : structures cristallines, composés du bore, composés du organobore.

[Traduit par la revue]

Introduction

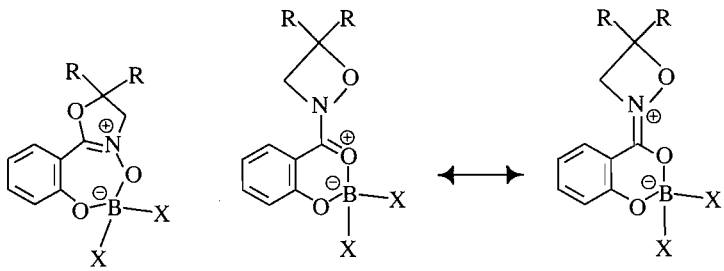
In the course of the analysis of the boron chelates **1** (X = C_6H_5 or F) an isomeric compound **2** was included in the discussion as a possible result from an intramolecular cyclization of a particular salicylhydroxamic acid derivative (1). Structure **2** would represent an example of the O—B—O boron chelate structure of an *N*,*O*-bisalkylated salicylhydroxamic acid. To obtain more information about this hitherto unknown type of compound, *N*-methoxy-*N*-methylsalicylamide **3** has been synthesized and reacted with oxybis(diphenylborane) to yield a crystalline product with the elemental composition indicating the expected diphenylboron chelate **4**, or the isomeric compounds **5** and **6**. Chelate **5**, with the hydroxylamine oxygen atom serving as ligand, would have the same ring size and sequence of ring-member atoms as found in **1** (1), whereas **6** would be an equal ring size "rotamer" of **4** having the hydroxylamine nitrogen atom bonded to boron. General considerations, in particular the well-known (2) predominant coordination of the carbonyl oxygen atom of amide groups to Lewis acids, favor the structure **4** with the carbonyl oxygen atom bonded to boron. Infrared and ^{1}H nmr spectra, however, did not allow for an unambiguous decision betwen the structures **4**, **5**, and **6**. Thus an X-ray crystallographic study was undertaken to resolve this ambiguity.

By replacing the weakly basic (pK_a = 4.75) (3) *N*,*O*-dimethylhydroxylamine component in **6** by the strong base (pK_a = 11.04) (3) diethylamine leading to **7**, the possibility of realizing such a N—B coordinated ring system via increasing the ligand basicity at the nitrogen site could be explored. Reaction of *N*,*N*-diethylsalicylamide **8** with oxybis(diphenylborane) gave crystals which show an elemental composition consistent with the structures **7** or **9**. N—B coordination as in **7** has already been discussed for products or intermediates in the reaction of *N*,*N*-dimethylsalicylamide with boric acid in a spectrophotometric study of complexing ability and ester formation of boric acid with different salicylamide derivatives (4). The alternative possibility of coordination with the amide carbonyl group, as formulated in structure **9**, was also mentioned in that work. N→B coordination has been suggested for derivatives of *o*-boronophenylacetamide (5). Some dialkylboron chelates of *N*,*N*-dimethyl- and *N*,*N*-diphenylamides of 3-oxobutyric acid

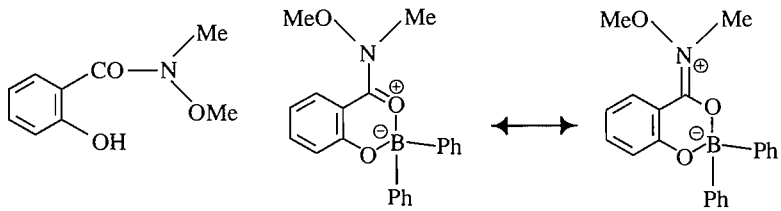
[1]For Part XXXIII, see ref. 36.

[2]Revision received May 13, 1989.

Can. J. Chem. Downloaded from www.nrcresearchpress.com by 194.225.253.170 on 09/07/12
For personal use only.

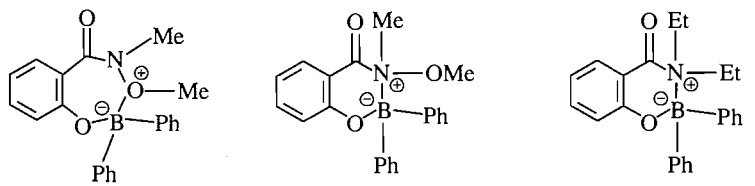


1 2

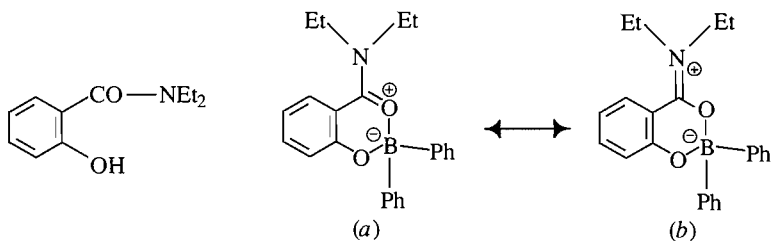


(a) (b)

3 4

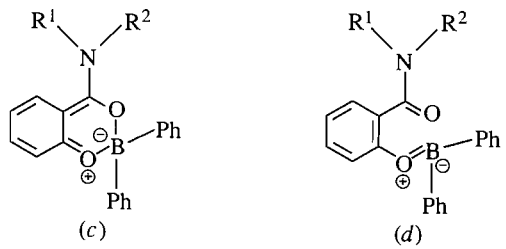


5 6 7

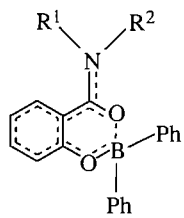


(a) (b)

8 9



(c) (d)



(a–d)

9

Can. J. Chem. Downloaded from www.nrcresearchpress.com by 194.225.253.170 on 09/07/12
For personal use only.

Can. J. Chem. Downloaded from www.nrcresearchpress.com by 194.225.253.170 on 09/07/12
For personal use only.

TABLE 1. Crystallographic data[a]

Compound	**4**	**9**
Formula	$C_{21}H_{20}BNO_3$	$C_{23}H_{24}BNO_2$
fw	345.20	357.26
Crstal system	Monoclinic	Orthorhombic
Space group	$P2_1/c$	*Pbca*
a (Å)	9.8072(5)	17.0593(7)
b (Å)	9.6217(7)	16.1372(6)
c (Å)	19.6793(12)	14.3753(5)
β (deg)	94.871(5)	—
V (Å^3)	1850.2(2)	3957.3(3)
Z	4	8
ρ_c (g/cm^3)	1.239	1.199
F (000)	728	1520
μ (Cu-K_α) (cm^{-1})	6.19	5.54
Crystal dimensions (mm)	0.18 × 0.25 × 0.45	0.38 × 0.45 × 0.53
Transmission factors	0.781–0.898	0.748–0.840
Scan type	ω–2θ	ω–2θ
Scan range (deg in ω)	0.80 + 0.14 tan θ	0.70 + 0.14 tan θ
Scan speed (deg/min)	0.8–6.7	1.2–10.0
Data collected	$+h, -k, \pm l$	$+h, +k, +l$
$2\theta_{max}$ (deg)	150	150
Crystal decay	Nonuniform (16–56%)	Negligible
Unique reflections	3787	4053
Reflections with $I \geq 3\sigma(I)$	2198	2969
Number of variables	316	341
R	0.046	0.038
R_w	0.052	0.043
S	0.993	0.846
Mean Δ/σ (final cycle)	0.013	0.007
Max Δ/σ (final cycle)	0.159	0.084
Residual density (e/Å^3)	−0.19 to +0.20	−0.20 to +0.20

[a]Temperature 294 K, Enraf-Nonius CAD4-F diffractometer, Cu-K_α radiation ($\lambda_{K\alpha_1}$ = 1.540562, $\lambda_{K\alpha_2}$ = 1.544390 Å), nickel filter, takeoff angle 2.7°, aperture (2.0 + tan θ) × 4.0 mm at a distance of 173 mm from the crystal, scan range extended by 25% on both sides for background measurement, $\sigma^2(I) = C + 2B + [0.04(C - B)]^2$ (C = scan count, B = normalized background count), function minimized: $\Sigma w(|F_o| - |F_c|)^2$ where $w = 1/\sigma^2(F)$, $R = \Sigma||F_o| - |F_c||/\Sigma|F_o|$, $R_w = (\Sigma w(|F_o| - |F_c|)^2/\Sigma w|F_o|^2)^{1/2}$, $S = (\Sigma w(|F_o| - |F_c|)^2/(m - n))^{1/2}$. Values given for R, R_w, and S are based on those reflections with $I \geq 3\sigma(I)$.

have been reported to form N—B bonds, and in one case an O—B bond between the amide group and boron (6). The diphenylboron chelate of (*N*-unsubstituted) salicylamide has been synthesized and studied by mass spectrometry (7), but the structure could not be assigned by this method.

Scale models of **7** demonstrate some steric strain (F-strain) between the dimethylamino and diphenylboron groups, but do not rule out a N—B bond for steric reasons. The ethyl groups, however, would each be fixed in a different neighborhood, which would appear in the ^{1}H nmr spectrum as separate ethyl signals. The free rotation of the diethylamino group about the N—C(O) bond in **9** should be hindered by the amide resonance ($a \leftrightarrow b$) and also could cause the two ethyl signals in the ^{1}H nmr spectrum to be inequivalent. There are some examples in the literature of boron chelates with *N*,*N*-dialkylamide groups displaying two different *N*-alkyl signals in their ^{1}H nmr spectra. This has been associated with the barrier to rotation about the amide C—N bond and therefore complexation through the amide oxygen atom (7–10). The signal separation appears at room temperature and has even been observed at temperatures ranging from 50 to 120°C (9). Compound **7**/**9**, dissolved in $CDCl_3$, produces only one sharp triplet (at 1.32 ppm) for both methyl groups, and one slightly broadened quartet (at 3.64 ppm) for both N—CH_2—groups at room temperature. The signals separate into two triplets and two quartets upon cooling to 3°C, indicating magnetically inequivalent *N*-ethyl groups. This temperature dependence is consistent with the structure **9** which would allow full rotation of the diethylamino group without breaking the N—B bond; but not conclusive because of the possibility of fast N—B bond breaking, *N*-inversion, rotation of the diethylamino group, and reformation of the N—B bond in **7**, similar to the processes believed to occur in cyclic N—B complexes of amines (11, 12). For clarification of this general problem, an X-ray crystallographic study was undertaken.

Experimental

4-(N-Methoxymethylimino)-2,2-diphenyl-1,3-dioxa-2-borata-1,2,3,4-tetrahydronaphthalene, ***4***

N-Methoxy-*N*-methylsalicylamide, prepared by acylation of *N*,*O*-dimethylhydroxylamine (13) (0.36 g, 2 mmol), is dissolved in ethanol, oxybis(diphenylborane) (0.35 g, 1 mmol) added, and the mixture heated for 10 min under reflux. Crystallization occurs upon concentration of the solution *in vacuo*. Colorless crystals (0.61 g, 88%) were collected, mp 133–134°C (from ethanol). Infrared (KBr): 1615 cm^{-1} (C=O / C=N$^+$). ^{1}H nmr (90 MHz, $CDCl_3$ / TMS): δ (ppm) = 3.41 (s, NCH_3), 3.43 (s, OCH_3), 6.44–7.91 (m, BPh_2 and C_6H_4). Mass spectrum (70 eV, 80°C): m/e (relative intensity) = 268 (100, M − C_6H_5),

Can. J. Chem. Downloaded from www.nrcresearchpress.com by 194.225.253.170 on 09/07/12
For personal use only.

236 (30), 133 (23). *Anal.* calcd. for $C_{21}H_{20}BNO_3$: C 73.07, H 5.84, N 4.06; found: C 73.03, H 5.85, N 3.97. Crystals suitable for X-ray analysis were obtained by recrystallization from absolute ethanol.

4-Diethylimino-2,2-diphenyl-1,3-dioxa-2-borata-1,2,3,4-tetrahydronaphthalene, 9

N,N-Diethylsalicylamide (0.57 g, 3 mmol) and oxybis(diphenylborane) (0.51 g, 1.5 mmol) are dissolved in ethanol and refluxed for 10 min. During concentration of the solution *in vacuo* crystallization occurs. Yield: 0.92 g (86%). mp 183°C (from ethanol). Infrared (KBr): 1615 cm^{-1} (C═O / C═N^+). ^1H nmr (90 MHz, $CDCl_3$ / TMS, 36°C): δ (ppm) = 1.32 (t, J = 7 Hz, 2 CH_3), 3.64 (q, J = 7 Hz, 2 NCH_2), 6.50–7.95 (m, BPh_2 and C_6H_4); ($CDCl_3$ / TMS, 3°C): δ (ppm) = 1.35 and 1.37 (2 t, J = 7 Hz, 2 CH_3), 3.59 and 3.67 (2 q, J = 7 Hz, 2 NCH_2), 6.50–7.92 (m, BPh_2 and C_6H_4). Mass spectrum (70 eV, 100°C): m/e (relative intensity) = 280 (100, M − C_6H_5), 121 (14). *Anal.* calcd. for $C_{23}H_{24}BNO_2$: C 77.33, H 6.77, B 3.03, N 3.92; found: C 77.54, H 6.81, B 3.13, N 3.81. Crystals suitable for X-ray analysis were obtained by recrystallization from absolute ethanol.

X-ray crystallographic analyses of 4 and 9

Crystallographic data for the two compounds appear in Table 1. Unit-cell parameters were refined by least-squares on 2 sin θ / λ values for 25 reflections (2θ = 60–91° for **4** and 80–92° for **9**) measured with Cu-$K\alpha_1$ radiation. Data were corrected[3] for Lp, absorption, and, for **4**, non-uniform decay (14). Both structures were solved by direct methods, the coordinates of the non-hydrogen atoms being determined from *E*-maps and those of the hydrogen atoms from subsequent difference Fourier syntheses. Non-hydrogen atoms were refined with anisotropic thermal parameters and hydrogen atoms with isotropic thermal parameters; neutral atom scattering factors and anomalous dispersion corrections were taken from ref. 15. Isotropic Type I extinction corrections (Thornley-Nelmes definition of mosaic anisotropy with a Lorentzian distribution) were applied in both cases (16–18), the final values of g being 0.25(8) × 10^4 for **4** and 3.27(12) × 10^4 for **9**. Final positional and anisotropic thermal parameters for the non-hydrogen atoms are given in Tables 2 and 7[4], respectively. Measured and calculated structure factors have been placed in the Depository of Unpublished Data[4].

The thermal motion for both structures has been analysed in terms of the TLS model (19). The rms errors in the temperature factors σU_{ij} (derived from the least-squares analyses) are 0.0019 and 0.0011 Å^2 for **4** and **9**, respectively. The structural subunits PhB and the fused-ring system plus O(3) and N were separately analysed for **4** (rms ΔU_{ij} = 0.0025–0.0026 Å^2); PhB and the fused-ring system plus N, C(8), and C(10) for **9** (rms ΔU_{ij} = 0.0016–0.0022 Å^2). The appropriate bond lengths have been corrected for libration (19, 20). Bond lengths, bond angles, and intra-annular torsion angles are listed in Tables 3–5, respectively. Hydrogen atom parameters (Table 6), bond lengths and angles involving hydrogen, and a complete listing of torsion angles (Tables 8–10) have been deposited.[4]

Results and discussion

Both diphenylboron chelates (Fig. 1) show O—B coordination involving the amide carbonyl oxygen atom as depicted by canonical formulae **4** and **9**. The molecular geometries of the two compounds are very similar, thus there are no significant structural differences which would indicate amide groups of different basicity in the two boron complexes. The crystal structure of **4** consists of well-separated molecules, the only intermolecular contact between non-hydrogen atoms shorter than 3.6

TABLE 2. Final positional (fractional × 10^4 for **4**, × 10^5 for **9**) and isotropic thermal parameters (U × 10^3 Å^2) with estimated standard deviations in parentheses

Atom	x	y	z	U_{eq}
		4		
O(1)	3318(2)	278(2)	1423(1)	51
O(2)	4197(2)	1713(2)	2375(1)	51
O(3)	2575(2)	1265(2)	3861(1)	71
N	3419(3)	1735(2)	3380(1)	57
C(1)	3254(3)	1287(3)	2744(1)	47
C(2)	2164(3)	391(3)	2452(1)	48
C(3)	1009(3)	−36(3)	2778(2)	61
C(4)	49(4)	−896(4)	2464(2)	68
C(5)	193(4)	−1385(3)	1815(2)	66
C(6)	1294(3)	−983(3)	1473(2)	58
C(7)	2278(3)	−92(3)	1783(2)	48
C(8)	4390(6)	2823(5)	3626(3)	80
C(9)	3266(7)	188(5)	4280(3)	95
C(10)	3028(3)	2926(3)	1336(1)	46
C(11)	3318(3)	4267(3)	1581(2)	60
C(12)	2499(4)	5400(3)	1375(2)	69
C(13)	1388(4)	5227(4)	924(2)	69
C(14)	1064(4)	3929(4)	673(2)	74
C(15)	1887(4)	2792(3)	876(2)	63
C(16)	5465(3)	1614(3)	1293(1)	46
C(17)	6707(3)	1702(3)	1682(2)	60
C(18)	7943(4)	1586(4)	1389(2)	73
C(19)	7960(4)	1379(4)	703(2)	77
C(20)	6752(4)	1294(4)	303(2)	73
C(21)	5521(3)	1430(3)	598(2)	60
B	3991(3)	1636(3)	1588(2)	47
		9		
O(1)	13110(7)	12061(7)	21735(8)	47
O(2)	21753(7)	10298(7)	8555(8)	44
N	23104(8)	−1931(8)	1771(10)	44
C(1)	18693(10)	3137(9)	6759(11)	40
C(2)	10991(9)	1108(9)	10741(12)	42
C(3)	5824(11)	−4967(11)	7426(15)	52
C(4)	−863(12)	−6970(13)	12242(18)	63
C(5)	−2497(13)	−3023(13)	20532(18)	66
C(6)	2247(12)	3227(12)	23771(15)	59
C(7)	8852(10)	5582(10)	18761(12)	44
C(8)	21693(13)	−10893(11)	401(15)	55
C(9)	19183(20)	−12907(19)	−9434(19)	79
C(10)	30821(12)	947(13)	−1578(15)	57
C(11)	37226(16)	−602(18)	5469(24)	80
C(12)	10875(9)	21256(9)	7275(12)	41
C(13)	13096(11)	23769(10)	−1646(12)	45
C(14)	8191(13)	28336(12)	−7356(15)	56
C(15)	832(13)	30466(13)	−4343(18)	66
C(16)	−1601(14)	28050(15)	4351(19)	73
C(17)	3361(12)	23502(13)	10078(16)	59
C(18)	23144(10)	23241(9)	18574(11)	41
C(19)	31226(11)	22430(12)	18051(14)	51
C(20)	36266(13)	28249(14)	21947(15)	62
C(21)	33303(15)	35029(14)	26480(14)	63
C(22)	25369(15)	36021(13)	27120(16)	66
C(23)	20358(13)	30241(12)	23197(14)	55
B	17044(11)	16795(11)	14154(13)	40

[3]The computer programs used include locally written programs for data processing and locally modified versions of the following: MULTAN 80, multisolution program by P. Main, S. J. Fiske, S. E. Hull, L. Lessinger, G. Germain, J. P. Declercq, and M. M. Woolfson; AGNOST, absorption corrections, by J. A. Ibers; ORFLS, full-matrix least-squares, and ORFFE, function and errors, by W. R. Busing, K. O. Martin and H. A. Levy; FORDAP, Patterson and Fourier syntheses, by A. Zalkin; ORTEP II, illustrations, by C. K. Johnson.

[4]*Supplementary material mentioned in the text may be purchased from the Depository of Unpublished Data, CISTI, National Research Council of Canada, Ottawa, Ont., Canada K1A 0S2.*

TABLE 3. Bond lengths (Å) with estimated standard deviations in parentheses

Bond	Length		Bond	Length	
	Uncorr.	Corr.		Uncorr.	Corr.
			4		
O(1)—(7)	1.339(3)	1.342	C(10)—C(11)	1.339(4)	1.410
O(1)—B	1.487(3)	1.490	C(10)—C(15)	1.383(4)	1.395
O(2)—C(1)	1.291(3)	1.294	C(10)—B	1.612(4)	1.616
O(2)—B	1.545(4)	1.549	C(11)—C(12)	1.394(4)	1.399
O(3)—N	1.386(3)	1.389	C(12)—C(13)	1.355(5)	1.366
O(3)—C(9)	1.456(5)	1.458	C(13)—C(14)	1.370(5)	1.381
N—C(1)	1.320(4)	1.323	C(14)—C(15)	1.398(5)	1.402
N—C(8)	1.469(4)	1.470	C(16)—C(17)	1.385(4)	1.395
C(1)—C(2)	1.454(4)	1.457	C(16)—C(21)	1.386(4)	1.396
C(2)—C(3)	1.410(4)	1.413	C(16)—B	1.603(4)	1.607
C(2)—C(7)	1.409(4)	1.412	C(17)—C(18)	1.390(5)	1.396
C(3)—C(4)	1.362(5)	1.369	C(18)—C(19)	1.367(5)	1.377
C(4)—C(5)	1.380(5)	1.383	C(19)—C(20)	1.368(5)	1.377
C(5)—C(6)	1.375(4)	1.378	C(20)—C(21)	1.390(4)	1.395
C(6)—C(7)	1.392(4)	1.395			
			9		
O(1)—C(7)	1.343(2)	1.346	C(10)—C(11)	1.511(3)	1.513
O(1)—B	1.491(2)	1.494	C(12)—C(13)	1.397(2)	1.406
O(2)—C(1)	1.294(2)	1.297	C(12)—C(17)	1.392(2)	1.401
O(2)—B	1.547)2)	1.550	C(12)—B	1.614(3)	1.618
N—C(1)	1.322(2)	1.325	C(13)—C(14)	1.385(3)	1.389
N—C(8)	1.479(2)	1.482	C(14)—C(15)	1.372(3)	1.381
N—C(10)	1.477(2)	1.479	C(15)—C(16)	1.373(3)	1.381
C(1)—C(2)	1.470(2)	1.474	C(16)—C(17)	1.390(3)	1.395
C(2)—C(3)	1.402(2)	1.405	C(18)—C(19)	1.387(3)	1.396
C(2)—C(7)	1.408(2)	1.412	C(18)—C(23)	1.394(2)	1.403
C(3)—C(4)	1.373(3)	1.376	C(18)—B	1.603(2)	1.606
C(4)—C(5)	1.380(3)	1.383	C(19)—C(20)	1.391(3)	1.394
C(5)—C(6)	1.375(3)	1.378	C(20)—C(21)	1.370(3)	1.379
C(6)—C(7)	1.390(2)	1.393	C(21)—C(22)	1.366(3)	1.375
C(8)—C(9)	1.513(3)	1.514	C(22)—C(23)	1.385(3)	1.389

Å being O(1)···C(8) ($1 - x$, $1/2 + y$, $1/2 - z$) = 3.268(5) Å. The shortest intermolecular contacts between non-hydrogen atoms in the structure of **9** are C(3)···C(3) ($-x$, $-y$, $-z$) = 3.328(4) Å and C(14)···O(1) (x, $1/2 - y$, $z - 1/2$) = 3.484(2) Å, the latter possibly representing a weak C—H···O interaction (H···O = 2.53(2) Å, C—H···O = 163(2)°). Each of the structures also contains intramolecular C—H···O interactions (for **4**: C(3)—H(3)···O(3), C(8)—H(8a)···O(2), and C(8)—H(8b)···O(2); C···O = 2.813(5), 2.677(5), and 2.677(5) Å; H···O = 2.17(3), 2.36(5), and 2.38(4) Å; C—H···O = 125(2), 98(4), and 80(3)°; respectively; and for **9**: C(10)—H(10b)···O(2) and C(19)—H(19)···O(2), C···O = 2.606(2) and 2.882(4) Å, H···O = 2.26(2) and 2.47(2) Å, C—H···O = 97(1) and 106(2)°, respectively).

The four substituents about the amide C—N bond are qualitatively coplanar in both compounds (mean and maximum deviations from the six-atom mean planes are 0.067 and 0.215(5) Å for **4**, 0.054 and 0.133(2) Å for **9**), consistent with a reasonable degree of double bond character for the C—N bond. The π-bond order of the amide C—N bonds in both **4** and **9** can be estimated as 0.75 (21) or 0.65 (22) from plots of bond length vs. MO π-bond order. The double bond character of the amide C—O bonds is reduced to about 50% in both **4** and **9** (1.294(3) and 1.297(2) Å, respectively)[5], as derived from the plot of C—O bond length vs. π-bond order reported for compounds having NC/CO π-systems (22). The resonance structures **4**(*b*) and **9**(*b*), therefore, are the most important contributors to the overall mesomeric systems. The nomenclature employed for these compounds reflects this point.

Another resonance structure (*c*) for both compounds **4** and **9** must also be considered on the basis of the observed molecular geometry. The C(3)—C(4) and C(5)—C(6) bonds (1.369–1.378 Å) are shorter than the C(2)—C(3), C(2)—C(7), and C(6)—C(7) bonds (1.395–1.413 Å) within the aromatic ring systems. The C(7)—O(1) phenolate bonds (1.342 and 1.346 Å) are relatively short when compared to average C(ar)—O bond lengths of 1.364 Å in phenols, 1.370–1.381 Å in phenolate ethers, and 1.401 Å in phenolate esters (23); and the C(1)—C(2), C(ar)—C(amide) bonds (1.457 and 1.474 Å) are shorter than the average value of 1.503 Å reported for this type of bond (23).

[5]Libration corrected bond lengths (esd's assumed equal to those of the uncorrected values) are employed in the discussion and those involving the boron atom are compared with similarly treated (19) distances unless otherwise stated.

Can. J. Chem. Downloaded from www.nrcresearchpress.com by 194.225.253.170 on 09/07/12
For personal use only.

TABLE 4. Bond angles (deg) with estimated standard deviations in parentheses

Bonds	Angle (deg)	Bonds	Angle (deg)
	4		
C(7)—O(1)—B	117.5(2)	C(15)—C(10)—B	123.4(3)
C(1)—O(2)—B	120.7(2)	C(10)—C(11)—C(12)	121.7(3)
N—O(3)—C(9)	110.0(3)	C(11)—C(12)—C(13)	120.4(3)
O(3)—N—C(1)	120.6(2)	C(12)—C(13)—C(14)	119.8(3)
O(3)—N—C(8)	114.5(3)	C(13)—C(14)—C(15)	120.0(4)
C(1)—N—C(8)	124.7(3)	C(10)—C(15)—C(14)	122.0(3)
O(2)—C(1)—N	113.2(3)	C(17)—C(16)—C(21)	116.5(3)
O(2)—C(1)—C(2)	120.2(3)	C(17)—C(16)—B	125.3(3)
N—C(1)—C(2)	126.6(3)	C(21)—C(16)—B	118.2(3)
C(1)—C(2)—C(3)	125.8(3)	C(16)—C(17)—C(18)	121.6(3)
C(1)—C(2)—C(7)	116.8(2)	C(17)—C(18)—C(19)	120.3(4)
C(3)—C(2)—C(7)	117.4(3)	C(18)—C(19)—C(20)	119.7(4)
C(2)—C(3)—C(4)	121.4(4)	C(19)—C(20)—C(21)	119.6(4)
C(3)—C(4)—C(5)	120.4(3)	C(16)—C(21)—C(20)	122.2(3)
C(4)—C(5)—C(6)	120.2(3)	O(1)—B—O(2)	106.2(2)
C(5)—C(6)—C(7)	120.2(3)	O(1)—B—C(10)	111.8(2)
O(1)—C(7)—C(2)	122.1(3)	O(1)—B—C(16)	107.9(2)
O(1)—C(7)—C(6)	117.6(3)	O(2)—B—C(10)	107.2(2)
C(2)—C(7)—C(6)	120.3(3)	O(2)—B—C(16)	108.5(2)
C(11)—C(10)—C(15)	116.2(3)	C(10)—B—C(16)	114.9(2)
C(11)—C(10)—B	120.5(3)		
	8		
C(7)—O(1)—B	114.19(13)	C(13)—C(12)—B	121.01(15)
C(1)—O(2)—B	119.97(13)	C(17)—C(12)—B	122.6(2)
C(1)—N—C(8)	125.75(15)	C(12)—C(13)—C(14)	122.3(2)
C(1)—N—C(10)	119.30(15)	C(13)—C(14)—C(15)	119.9(2)
C(8)—N—C(10)	114.15(15)	C(14)—C(15)—C(16)	119.5(2)
O(2)—C(1)—N	115.52(15)	C(15)—C(16)—C(17)	120.3(2)
O(2)—C(1)—C(2)	118.80(14)	C(12)—C(17)—C(16)	121.8(2)
N—C(1)—C(2)	125.58(15)	C(19)—C(18)—C(23)	116.2(2)
C(1)—C(2)—C(3)	125.8(2)	C(19)—C(18)—B	124.24(15)
C(1)—C(2)—C(7)	115.86(14)	C(23)—C(18)—B	119.6(2)
C(3)—C(2)—C(7)	118.3(2)	C(18)—C(19)—C(20)	121.9(2)
C(2)—C(3)—C(4)	121.0(2)	C(19)—C(20)—C(21)	120.2(2)
C(3)—C(4)—C(5)	119.7(2)	C(20)—C(21)—C(22)	119.4(2)
C(4)—C(5)—C(6)	120.8(2)	C(21)—C(22)—C(23)	120.3(2)
C(5)—C(6)—C(7)	120.2(2)	C(18)—C(23)—C(22)	122.0(2)
O(1)—C(7)—C(2)	121.29(15)	O(1)—B—O(2)	105.48(12)
O(1)—C(7)—C(6)	119.1(2)	O(1)—B—C(12)	112.52(14)
C(2)—C(7)—C(6)	119.6(2)	O(1)—B—C(18)	109.58(14)
N—C(8)—C(9)	112.4(2)	O(2)—B—C(12)	108.80(13)
N—C(10)—C(11)	112.0(2)	O(2)—B—C(18)	108.00(14)
C(13)—C(12)—C(17)	116.1(2)	C(12)—B—C(18)	112.14(13)

The contribution of the resonance structures (*c*) to the overall structures of **4** and **9** could also explain the results of the variable temperature ^{1}H nmr spectra of **9** which show a lower barrier to rotation about the amide C—N bond than observed for other boron-chelated *N*,*N*-dialkylamide functions (7–12). A similar lowering of the rotational barrier about the amide C—N bond has been reported for both *N*,*N*-dimethyl- (24) and *N*,*N*-diethylsalicylamide (25). This has been attributed to the effect of an intramolecular hydrogen bond in a hydrogen-bridged chelate structurally comparable to **4** and **9**. In these boron chelates the diphenylborenium ion (Ph_2B^+) replaces H^+ in the intramolecular hydrogen bridge which is generally believed to exist in solutions of *N*,*N*-dialkylsalicylamides (26). It is not known whether any *N*,*N*-dialkylsalicylamides contain intramolecular hydrogen bonds in the solid state. The structure of salicylamide itself (27) does contain an intramolecular hydrogen bond from the phenolic OH group to the amide carbonyl oxygen atom, whereas crystalline salicylhydroxamic acid (28) and other *N*-monosubstituted salicylamides (29) have the reverse conformation with intramolecular N—H···O hydrogen bonds between the amide NH and phenol oxygen atoms. The amide C—N bond is shortest in salicylamide (27), 1.309 Å; compared with corresponding distances of 1.316 Å in salicylhydroxamic acid (28), 1.344 Å in salicylanilide (29*a*), and 1.359 Å in a substituted salicylhydrazide (29*b*).

In each compound, **4** and **9**, the O—B bond from the carbonyl oxygen atom to boron is about 0.06 Å longer than that from the phenolate oxygen atom. This is consistent with a corresponding

Can. J. Chem. Downloaded from www.nrcresearchpress.com by 194.225.253.170 on 09/07/12
For personal use only.

Can. J. Chem. Downloaded from www.nrcresearchpress.com by 194.225.253.170 on 09/07/12
For personal use only.

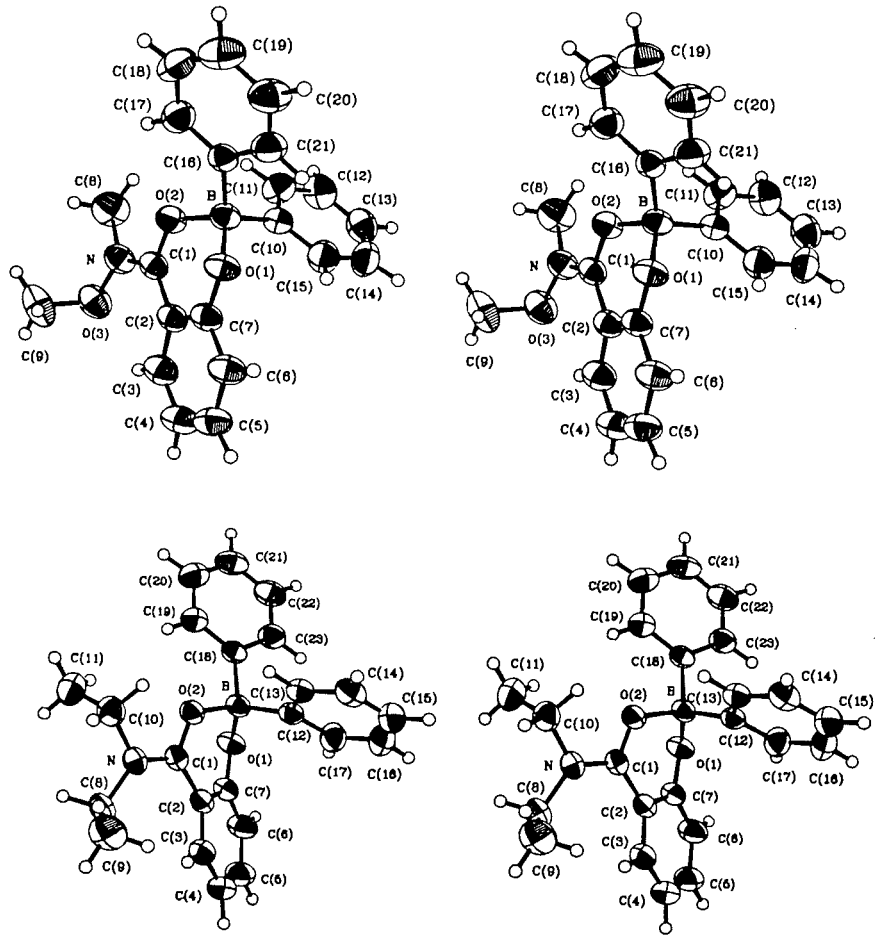


FIG. 1. Stereoscopic views of **4** (top) and **9** (bottom); 50% probability thermal ellipsoids are shown for the non-hydrogen atoms.

TABLE 5. Intra-annular torsion angles (deg) standard deviations in parentheses

Atoms	Value (deg)
4	
C(7)—O(1)—B—O(2)	44.7(3)
C(1)—O(2)—B—O(1)	−40.9(3)
B—O(2)—C(1)—C(2)	17.0(4)
O(2)—C(1)—C(2)—C(7)	6.6(4)
C(1)—C(2)—C(7)—O(1)	−1.7(4)
B—O(1)—C(7)—C(2)	−26.9(4)
9	
C(7)—O(1)—B—O(2)	−53.6(2)
C(1)—O(2)—B—O(1)	41.3(2)
B—O(2)—C(1)—C(2)	−4.7(2)
O(2)—C(1)—C(2)—C(7)	−22.9(2)
C(1)—C(2)—C(7)—O(1)	9.0(2)
B—O(1)—C(7)—C(2)	31.4(2)

difference of 0.07 Å observed in the structure of the diphenylboron chelate of salicylaldehyde (30). The difference between the O—B distances suggests stronger donation from the phenolate oxygen atom, possibly by O—B $pp(\pi)$ interaction as symbolized by the resonance form (*d*). In consideration of these observations, the delocalization of electron density in **4** and **9** is best summarized by the overall mesomeric general formulae (*a*–*d*) (ignoring interactions between the boron atom and the *B*-phenyl groups). The B—C(phenyl) distances are similar to those reported for other diphenylboron O—B—O chelates. The small differences between the B—C distances in **4** and **9** (0.009 and 0.012 Å, respectively) are typical for Ph_2B chelates having (pseudo)axial and (pseudo)equatorial *B*-phenyl substituents (30–36) and were also observed in the structure of **1** (X = Ph) (1). As observed in every case, the pseudo-axial B—C bond is longer than the pseudo-equatorial B—C bond. The mean C—B / mean O—B bond length ratios of 1.061 for **4** and 1.059 for **9** are near the average value of 1.059 observed for other "Ph_2BO_2" chelates containing six-membered chelate rings (refs. 36, 37, and references therein), indicating an intermediate overall binding strength of the *O,O*-chelating ligand to the Ph_2B moiety.

Acknowledgements

We thank the Natural Sciences and Engineering Research Council of Canada and the Fonds der Chemischen Industrie, Frankfurt am Main, for financial support, and the University of British Columbia Computing Centre for assistance. We are also grateful to Dr. L. Preu for running the low temperature nmr spectra.

1. W. KLIEGEL, M. TAJERBASHI, S. RETTIG, and J. TROTTER. Can. J. Chem. **66**, 2621 (1988).
2. (*a*) W. E. STEWART and T. H. SIDDALL. Chem. Rev. **70**, 517 (1970); (*b*) R. B. HOMER and C. D. JOHNSON. *In* The chemistry of amides. *Edited by* J. Zabicky. London. 1970. p. 187; (*c*) B. C. CHALLIS and J. A. CHALLIS. *In* Comprehensive organic chemis-

try. Vol. 2. *Edited by* D. Barton and W. D. Ollis. Oxford. 1979. p. 994.
3. D. D. PERRIN. Dissociation constants of organic bases in aqueous solution. London. 1965.
4. D. W. TANNER and T. C. BRUICE. J. Am. Chem. Soc. **89**, 6954 (1967).
5. J. C. CATLIN and H. R. SNYDER. J. Org. Chem. **34**, 1660 (1969).
6. P. PAETZOLD and S. KOSMA. Chem. Ber. **112**, 654 (1979).
7. J. R. HORDER and M. F. LAPPERT. J. Chem. Soc. Chem. Commun. 485 (1967); J. Chem. Soc. Sect. A, 173 (1969).
8. P. PAETZOLD and M. LASCH. Chem. Ber. **112**, 663 (1979).
9. A. S. FLETCHER, W. E. PAGET, and K. SMITH. Heterocycles, **18**, 107 (1982).
10. K. HARTKE, B. KRUG, and R. HOFFMANN. Liebigs Ann. Chem. 370 (1984).
11. H. KESSLER, G. ZIMMERMANN, H. FIETZE, and H. MOHRLE. Chem. Ber. **111**, 2605 (1978).
12. T. BURGEMEISTER, R. GROBE-EINSLER, R. GROTSTOLLEN, A. MANNSCHRECK, and G. WULFF. Chem. Ber. **114**, 3403 (1981).
13. W. KLIEGEL and M. TAJERBASHI. In preparation.
14. J. A. IBERS. Acta Crystallogr. Sect. B, **25**, 1667 (1969).
15. International tables for X-ray crystallography. Vol. IV. Kynoch press, Birmingham. 1974. pp. 99–102 and 149.
16. P. J. BECKER and P. COPPENS. Acta Crystallogr. Sect. A, **30**, 129 (1974); **30**, 148 (1974); **31**, 417 (1975).
17. P. COPPENS and W. C. HAMILTON. Acta Crystallogr. Sect. A, **26**, 71 (1970).
18. F. R. THORNLEY and R. J. NELMES. Acta Crystallogr. Sect. A, **30**, 748 (1974).
19. V. SCHOMAKER and K. N. TRUEBLOOD. Acta Crystallogr. Sect. B, **24**, 63 (1968).
20. D. W. J. CRUICKSHANK. Acta Crystallogr. **9**, 747 (1956); **9**, 754 (1956); **14**, 896 (1961).
21. L. M. TREFONAS, R. L. FLURRY, R. MAJESTE, E. A. MEYERS, and R. F. COPELAND. J. Am. Chem. Soc. **88**, 2145 (1966).
22. G. HAFELINGER. Chem. Ber. **103**, 2941 (1970).
23. F. H. ALLEN, O. KENNARD, D. G. WATSON, L. BRAMMER, A. G. ORPEN, and R. TAYLOR. J. Chem. Soc. Perkin II, S1 (1987).
24. M. HIROTA and K. TODOKORO. Chem. Lett. 777 (1974).
25. A. GRYFF-KELLER, J. TERPINSKI, and E. ZAJACZKOWSKA-TERPINSKA. Pol. J. Chem. **57**, 429 (1983).
26. (*a*) A. H. LEVIN and M. FRUCHT. Tetrahedron Lett. 1079 (1970); (*b*) M. KONDO. Bull. Chem. Soc. Jpn. **52**, 521 (1979); (*c*) C. W. FONG. Aust. J. Chem. **33**, 1285 (1980); (*d*) W. B. JENNINGS, D. RANDALL, and B. M. SAKET. J. Chem. Soc. Chem. Commun. 508 (1982).
27. Y. SASADA, T. TAKANO, and M. KAKUDO. Bull. Chem. Soc. Jpn. **37**, 940 (1964).
28. I. K. LARSEN. Acta Crystallogr. Sect. B, **34**, 962 (1978).
29. (*a*) S. KASHINO, T. MATSUSHITA, T. IWAMOTO, K. YAMAGUCHI, and M. HAISA. Acta Crystallogr. Sect. C. **42**, 457 (1986) and references therein; (*b*) P. DOMIANO, A. MUSATTI, C. PELIZZI, and G. PREDIERI. Cryst. Struct. Commun. **3**, 531 (1974).
30. S. J. RETTIG and J. TROTTER. Can. J. Chem. **54**, 1168 (1976).
31. S. J. RETTIG and J. TROTTER. Can. J. Chem. **60**, 2957 (1982).
32. B. A. ARBUZOV, O. A. ERASTOV, G. N. NIKONOV, A. A. ESPENBETOV, A. I. YANOVSKII, and YU. T. STRUCHKOV. Bull. Acad. Sci. USSR, Div. Chem. Sci. 1243 (1981).
33. W. KLIEGEL, H.-W. MOTZKUS, S. J. RETTIG, and J. TROTTER. Can. J. Chem. **64**, 507 (1986).
34. W. KLIEGEL, S. J. RETTIG, and J. TROTTER. Can. J. Chem. **66**, 377 (1988).
35. W. KLIEGEL, S. J. RETTIG, and J. TROTTER. Can. J. Chem. **66**, 1091 (1988).
36. E. EBELING, W. KLIEGEL, S. J. RETTIG, and J. TROTTER. Can. J. Chem. **67**, 933 (1989).
37. W. R. CULLEN, S. J. RETTIG, J. TROTTER, and E. B. WICKENHEISER. Can. J. Chem. **66**, 2007 (1988).

Can. J. Chem. Downloaded from www.nrcresearchpress.com by 194.225.253.170 on 09/07/12
For personal use only.

Structural studies of organoboron compounds. XXXV.[1] 4,8-Diethyl-2,2,6,6-tetraphenyl-1,3,5,7-tetraoxa-4,8-diazonia-2,6-diborata-1,2,3,5,6,7-hexahydronaphthalene

WOLFGANG KLIEGEL and MAHMOOD TAJERBASHI

Institut für Pharmazeutische Chemie, der Technischen Universität Braunschweig, Beethovenstraße 55, 3300 Braunschweig, Bundesrepublik Deutschland

AND

STEVEN J. RETTIG and JAMES TROTTER

Department of Chemistry, University of British Columbia, 2036 Main Mall, Vancouver, B.C., Canada V6T 1Y6

Received December 14, 1988[2]

WOLFGANG KLIEGEL, MAHMOOD TAJERBASHI, STEVEN J. RETTIG, and JAMES TROTTER. Can. J. Chem. **67**, 1644 (1989).

The reaction of *N,N'*-diethyloxalohydroxamic acid with oxybis(diphenylborane) yields the title compound. Crystals of 4,8-diethyl-2,2,6,6-tetraphenyl-1,3,5,7-tetraoxa-4,8-diazonia-2,6-diborata-1,2,3,5,6,7-hexahydronaphthalene are monoclinic, $a = 14.3405(9)$, $b = 14.3053(5)$, $c = 14.9301(8)$ Å, $\beta = 116.136(4)°$, $Z = 4$, space group $P2_1/n$. The structure was solved by direct methods and was refined by full-matrix least-squares procedures to $R = 0.038$ and $R_w = 0.038$ for 3501 reflections with $I \geq 3\sigma(I)$. The molecule has a novel bis-six-membered binuclear chelate structure, the Ph_2B moieties each being coordinated by (N)O and (C=)O oxygen atoms from different hydroxamate groups. The mean libration-corrected bond distances (C=)O—B, 1.587 Å, (N)O—B, 1.511 Å, and B—C, 1.602 Å, represent the weakest overall binding strength of an *O,O*-chelating ligand with respect to the Ph_2B moiety yet observed for a six-membered O—B—O chelate.

Key words: crystal structure, boron compound, organoboron compound.

WOLFGANG KLIEGEL, MAHMOOD TAJERBASHI, STEVEN J. RETTIG et JAMES TROTTER. Can. J. Chem. **67**, 1644 (1989).

La réaction de l'acide *N,N'*-diéthyloxalohydroxamique avec l'oxybis(diphénylborane) fournit le composé mentionné dans le titre. Les cristaux du 4,8-diéthyl-2,2,6,6,-tétraphényl-1,3,5,7-tétraoxa-4,8-diazonia-2,6-diborata-1,2,3,5,6,7-hexahydronaphtalène sont monocliniques, groupe d'espace $P2_1/n$, avec $a = 14,3405(9)$, $b = 14,3053(5)$ et $c = 14,9301(8)$ Å, $\beta = 116,136(4)°$ et $Z = 4$. On a résolu la structure par des méthodes directes et on l'a affinée par la méthode des moindres carrés (matrice complète) jusqu'à des valeurs de $R = 0,038$ et $R_w = 0,038$ pour 3501 réflexions avec $I \geq 3\sigma(I)$. La molécule possède une nouvelle structure de chélate binucléaire à deux cycles à six chaînons dans laquelle les portions Ph_2B sont toutes les deux coordonnées à des atomes d'oxygène (N)O et (C=)O de groupements hydroxamates différents. Les longueurs moyennes, corrigées pour la libration, des liaisons (C=)O—B, 1,587 Å, (N)O—B, 1,511 Å et B—C, 1,602 Å correspondent à la plus faible force globale observée jusqu'à maintenant pour la liaison d'un ligand chélatant-*O,O* par rapport à la portion Ph_2B d'un chélate à six chaînons O—B—O.

Mots clés : structure cristalline, composés du bore, composé du organobore.

[Traduit par la revue]

Introduction

In the course of our investigation of hydroxamic acids as bidentate ligands in the formation of boron chelates (1–5), the general structures **1** and **2** have been established by X-ray structure analysis and support the *B,N*-betaine formulation as rationale for these five-membered chelate rings. Blocking of the carbonyl oxygen atom of the hydroxamate function by alkylation, in addition to offering an intramolecular phenolate ligand, led us to the seven-membered chelate type **3** (R + R = —$(CH_2)_5$—), the structure of which has been established by an X-ray crystallographic analysis (6). The simplest bishydroxamic acids are derived from oxalic acid and are of interest because of the two neighbouring hydroxamate functions. The literature reports some *N,N*-diaryloxalohydroxamic acids as coordinating ligands for organotin (7) and ruthenium compounds (8). *N,N*-Dialkyloxalohydroxamic acids and chelates thereof, to our knowledge, have not been reported.

From a series of newly synthesized (9) *N,N*-dialkyloxalohydroxamic acids, we chose the *N,N*-diethyl derivative **4** and reacted it with oxybis(diphenylborane). The crystalline reaction product has the elemental composition of a bis(diphenylboron) chelate. Infrared and ^1H nmr spectra are consistent with a two-fold chelate formation, but cannot differentiate between structure **5**, having the "normal" hydroxamate complex arrangement (10), and structure **6**, displaying an alternative binuclear chelate system with both hydroxamate groups mutually contributing one oxygen donor to each of the adjacent six-membered chelate rings.

Structure **5** is derived from the well-established (1–5) formula **1** for boron chelates and is consistent with the formulation of the binuclear ruthenium complex of *N,N*-diphenyloxalohydroxamic acid (8) which, however, is not based on solid evidence. Structure **6** would be the very first example of this type of hydroxamate complex formation. The third possible isomer, **7**, incorporates a five-membered boron chelate of the type well known from the reaction of ethanediamides with bromodimethylborane (11), and a seven-membered ring resembling that in **3**. Although **7** seems unlikely on the basis of symmetry arguments, it cannot be definitively excluded from consideration. In order to resolve any ambiguities, an X-ray crystallographic analysis was undertaken.

Experimental

*4,8-Diethyl-2,2,6,6-tetraphenyl-1,3,5,7-tetraoxa-4,8-diazonia-2,6-diborata-1,2,3,5,6,7-hexahydronaphthalene, **6***

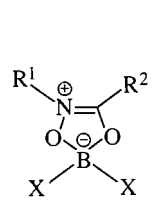
N,N'-Diethyl-*N,N'*-dihydroxyethanediamide, **4** (9) (0.18 g, 1 mmol), and oxybis(diphenylborane) (0.35 g, 1 mmol) are dissolved in ethanol and refluxed for 20 min. Crystallization starts during concentration of the reaction mixture *in vacuo*. After complete crystallization,

[1]For Part XXXIV, see ref. 34.

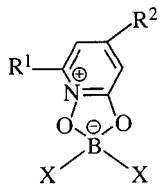
[2]Revision received May 1, 1989.

Can. J. Chem. Downloaded from www.nrcresearchpress.com by 194.225.253.170 on 09/07/12
For personal use only.

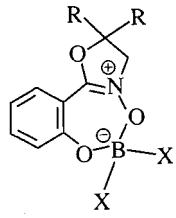
Can. J. Chem. Downloaded from www.nrcresearchpress.com by 194.225.253.170 on 09/07/12
For personal use only.



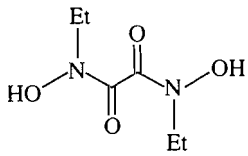
1
(X = F or C_6H_5)



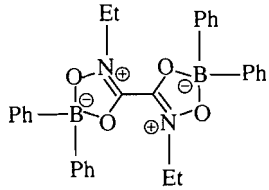
2



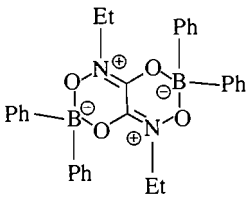
3



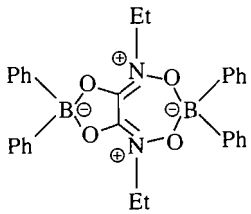
4



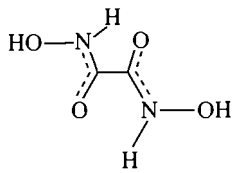
5



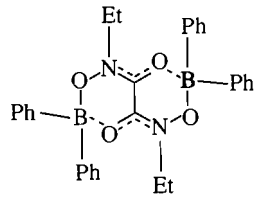
6



7



8



9

0.44 g (86%) of colorless crystals are obtained; mp 173–174°C (from ethanol). Infrared (KBr): 1625 cm^{-1} (C=O / C=N$^+$). ^{1}H nmr (90 MHz, $CDCl_3$ / TMS): δ (ppm) = 1.31 (t, J = 6 Hz, 2 CH_3), 3.92 (q, J = 6 Hz, 2 NCH_2), 7.20–7.90 (m, 2 BPh_2). *Anal.* calcd. for **6**: C 71.47, H 6.00, N 5.55; found: C 71.25, H 5.94, N 5.36. Crystals suitable for X-ray analysis were obtained by stepwise (approximately 0.5°C / h over 2–3 days) cooling of a saturated ethanol solution from 50°C to 10–20°C using a cryostat with electronic temperature control.

X-Ray crystallographic analysis

A crystal bounded by the six faces (followed by the distances in mm between parallel faces): {0 1 1}, 0.28–0.37, and {2 0 −1}, 0.37, was mounted in a general orientation. Unit-cell parameters were refined by least-squares on 2 sin θ / λ values for 25 reflections (2θ = 55–80°) measured on a diffractometer with Cu-$K\alpha$ radiation (λ($K\alpha_1$) = 1.540562, λ($K\alpha_2$) = 1.544390 Å). Crystal data at 22°C are:

$C_{30}H_{30}B_2N_2O_4$ fw = 504.20

Monoclinic, a = 14.3405(9), b = 14.3053(5), c = 14.9301(8) Å, β = 116.136(4)°, V = 2749.6(3) Å^3, Z = 4, ρ_c = 1.218 Mg m^{-3}, F(000) = 1064, μ(Cu-$K\alpha$) = 6.0 cm^{-1}. Absent reflections: $h0l$, $h + l$ odd, and $0k0$, k odd, uniquely indicate the space group $P2_1/n$ (C_{2h}^5, No. 14).

Intensities were measured with nickel-filtered Cu-$K\alpha$ radiation on an Enraf-Nonius CAD4-F diffractometer. An ω–2θ scan at 1.2–10.0° min^{-1} over a range of (0.80 + 0.14 tan θ) degrees in ω (extended by 25% on both sides for background measurement) was employed. Data were measured to 2θ = 150°. The intensities of three check reflections, measured every 3600 s throughout the data collection, showed only small (<3.5%) random variations. Of the 5642 independent reflections measured and processed,[3] 3501 (62.1%) had intensities greater than or equal to 3σ(I) above background where $\sigma^2(I) = S + 2B + (0.03(S - B))^2$ with S = scan count and B = normalized background count.

The structure was solved by direct methods, the coordinates of all 38 non-hydrogen atoms being determined from an E-map. After refinement of the non-hydrogen atoms with anisotropic thermal parameters, the hydrogen atoms were positioned from a difference Fourier synthesis and were subsequently refined with isotropic thermal parameters. Scattering factors for all atoms and anomalous dispersion corrections for the non-hydrogen atoms were taken from ref. 12. The weighting scheme $w = 1/\sigma^2(F)$, where $\sigma^2(F)$ is derived from the previously defined $\sigma^2(I)$, gave uniform average values of $w(|F_o| - |F_c|)^2$ over

TABLE 1. Final positional (fractional × 10^4) and isotropic thermal parameters (U × 10^3 Å^2) with estimated standard deviations in parentheses

Atom	x	y	z	U_{eq}
O(1)	5408(1)	1446(1)	4918(1)	50
O(2)	7150(1)	1065(1)	6166(1)	48
O(3)	8326(1)	331(1)	4661(1)	47
O(4)	7129(1)	1604(1)	3833(1)	46
N(1)	5794(1)	1644(1)	4242(1)	45
N(2)	8135(1)	442(1)	5485(1)	44
C(1)	7374(2)	970(2)	5425(2)	41
C(2)	6753(2)	1441(1)	4455(2)	41
C(3)	5039(2)	2031(2)	3289(2)	62
C(4)	4849(6)	3037(3)	3367(4)	138
C(5)	8771(2)	−156(2)	6338(2)	58
C(6)	8416(5)	−1147(3)	6146(4)	104
C(7)	6472(2)	2765(2)	6096(2)	44
C(8)	7428(2)	3142(2)	6278(2)	60
C(9)	7613(3)	4101(2)	6376(2)	75
C(10)	6834(3)	4706(2)	6287(2)	67
C(11)	5877(2)	4357(2)	6100(2)	65
C(12)	5703(2)	3406(2)	6008(2)	60
C(13)	5676(2)	1314(2)	6683(2)	49
C(14)	6144(2)	1527(2)	7695(2)	58
C(15)	5703(3)	1270(2)	8324(3)	70
C(16)	4777(3)	801(2)	7946(3)	76
C(17)	4300(3)	576(2)	6957(3)	86
C(18)	4752(2)	822(2)	6338(2)	74
C(19)	9081(2)	1996(2)	4852(2)	45
C(20)	8858(2)	2937(2)	4831(2)	62
C(21)	9603(3)	3586(2)	5403(3)	74
C(22)	10587(3)	3308(3)	6022(2)	73
C(23)	10831(3)	2381(3)	6065(2)	81
C(24)	10090(2)	1735(2)	5489(2)	64
C(25)	8327(2)	1019(2)	3113(2)	47
C(26)	8537(2)	1736(2)	2599(2)	64
C(27)	8507(3)	1607(3)	1674(3)	87
C(28)	8292(3)	745(3)	1247(3)	92
C(29)	8093(2)	17(3)	1721(3)	84
C(30)	8106(2)	156(2)	2654(2)	62
B(1)	6169(2)	1681(2)	5976(2)	46
B(2)	8277(2)	1239(2)	4138(2)	44

[3]The computer programs used include locally written programs for data processing and locally modified versions of the following: MULTAN 80, multisolution program by P. Main, S. J. Fiske, S. E. Hull, L. Lessinger, G. Germain, J. P. Declercq, and M. M. Woolfson; ORFLS, full-matrix least-squares, and ORFFE, function and errors, by W. R. Busing, K. O. Martin and H. A. Levy; FORDAP, Patterson, and Fourier syntheses, by A. Zalkin; ORTEP II, illustrations, by C. K. Johnson.

Can. J. Chem. Downloaded from www.nrcresearchpress.com by 194.225.253.170 on 09/07/12
For personal use only.

TABLE 2. Bond lengths (Å) with estimated standard deviations in parentheses

Bond	Length		Bond	Length	
	Uncorr.	Corr.		Uncorr.	Corr.
O(1)—N(1)	1.376(2)	1.380	C(13)—C(14)	1.390(3)	1.403
O(1)—B(1)	1.510(3)	1.515	C(13)—C(18)	1.383(3)	1.396
O(2)—C(1)	1.288(2)	1.290	C(13)—B(1)	1.596(3)	1.600
O(2)—B(1)	1.577(3)	1.580	C(14)—C(15)	1.392(4)	1.396
O(3)—N(2)	1.383(2)	1.385	C(15)—C(16)	1.368(4)	1.380
O(3)—B(2)	1.501(3)	1.506	C(16)—C(17)	1.364(4)	1.376
O(4)—C(2)	1.284(2)	1.286	C(17)—C(18)	1.388(4)	1.392
O(4)—B(2)	1.590(3)	1.593	C(19)—C(20)	1.381(3)	1.393
N(1)—C(2)	1.301(3)	1.303	C(19)—C(24)	1.388(3)	1.404
N(1)—C(3)	1.465(3)	1.468	C(19)—B(2)	1.600(3)	1.604
N(2)—C(1)	1.296(2)	1.299	C(20)—C(21)	1.389(4)	1.393
N(2)—C(5)	1.471(3)	1.474	C(21)—C(22)	1.362(4)	1.377
C(1)—C(2)	1.487(3)	1.492	C(22)—C(23)	1.366(4)	1.377
C(3)—C(4)	1.479(5)	1.480	C(23)—C(24)	1.385(4)	1.389
C(5)—C(6)	1.491(5)	1.493	C(25)—C(26)	1.391(3)	1.403
C(7)—C(8)	1.383(3)	1.397	C(25)—C(30)	1.380(3)	1.391
C(7)—C(12)	1.395(3)	1.404	C(25)—B(2)	1.594(3)	1.600
C(7)—B(1)	1.600(3)	1.605	C(26)—C(27)	1.376(4)	1.382
C(8)—C(9)	1.393(4)	1.397	C(27)—C(28)	1.361(5)	1.371
C(9)—C(10)	1.373(4)	1.381	C(28)—C(29)	1.358(5)	1.369
C(10)—C(11)	1.369(4)	1.384	C(29)—C(30)	1.399(4)	1.405
C(11)—C(12)	1.379(4)	1.383			

ranges of both $|F_o|$ and $\sin\theta/\lambda$ and was employed in the final stages of full-matrix refinement of 464 variables. Reflections with $I < 3\sigma(I)$ were not included in the refinement. An isotropic Type 1 extinction correction (Thornley-Nelmes definition of mosaic anisotropy with a Lorentzian distribution) was applied (13–15). The final value of g was $1.42(6) \times 10^4$. Convergence was reached at $R = 0.038$ and $R_w = 0.038$ for 3501 reflections with $I \geq 3\sigma(I)$. The function minimized was $\Sigma w(|F_o| - |F_c|)^2$, $R = \Sigma||F_o| - |F_c||/\Sigma|F_o|$ and $R_w = (\Sigma w(|F_o| - |F_c|)^2/\Sigma w|F_o|^2)^{1/2}$.

On the final cycle of refinement the mean and maximum parameter shifts corresponded to 0.016 and 0.35σ respectively. The mean error in an observation of unit weight was 0.852. A final difference map showed maximum fluctuations of −0.17 to +0.18 e Å^{-3}. The final positional and thermal parameters appear in Tables 1 and 6,[4] respectively. Measured and calculated structure factors have been placed in the Depository of Unpublished Data.[4]

The ellipsoids of thermal motion for the non-hydrogen atoms are shown in Fig. 1. The thermal motion has been analysed in terms of the rigid-body modes of translation, libration, and screw motion (16). The rms standard error in the temperature factors σU_{ij} (derived from the least-squares analysis) is 0.0018 Å^2. The structural subunits PhB and the central fused-ring system plus the α-carbons of the *N*-ethyl groups were separately analysed (rms ΔU_{ij} = 0.0019–0.0029 Å^2). The appropriate bond distances have been corrected for libration (16, 17), using shape parameters q^2 of 0.08 for all atoms involved. Corrected bond lengths appear in Table 2 along with the uncorrected values; bond angles appear in Table 3 and intra-annula torsion angles in Table 4. Hydrogen atom parameters (Table 5), bond lengths and angles involving hydrogen and a complete listing of torsion angles (Tables 7–9) have been deposited.[4]

Results and discussion

The crystal structure of 4,8-diethyl-2,2,6,6-tetraphenyl-1,3,5,7-tetraoxa-4,8-diazonia-2,6-diborata-1,2,3,5,6,7-hexahydronaphthalene consists of well-separated molecules, the shortest intermolecular distances between non-hydrogen atoms being C(2)···C(17) $(1 - x, -y, 1 - z)$ = 3.497(4) Å. The molecule (Fig. 1) has the bis-six-membered binuclear chelate structure **6** rather than the "normal" bishydroxamate structure **5**. To the best of our knowledge, this is the first fully characterized example of this type of hydroxamate complex, involving a neighboring hydroxamate ligand in chelate formation. Other examples of metal complexes of hydroxamic acids with a second ligand function adjacent to the hydroxamic acid group involve *N*-unsubstituted hydroxamate derivatives: Ni(II) (18) and Cu(II) complexes (19) of glycinehydroxamic acid exhibit chelation by the amide nitrogen and α-amino nitrogen atoms while other metal chelates of glycinehydroxamic acid form "normal" hydroxamate complexes (20).

In structure **6** the conformation of the oxalohydroxamic acid moiety differs from that of free oxalohydroxamic acid in the crystalline state (21), which has the *N*-hydroxy group and the carbonyl oxygen in a *cis* orientation with respect to the HO—N—C—O segment of the molecule **8**. The formulation of **6** as a cyclic *B*,*N*-betaine is justified by the considerable double bond character of the C=N bond. The mean C=N distance[5] of 1.301 Å is very similar to the uncorrected value of 1.302 Å in the alkylidene iminium ion $Me_2C{=}NMe_2^+$ (22). From plots of bond lengths vs. π-bond order, the MO π-bond order of the C=N bonds is estimated as 0.8 (22) or 0.75 (23). The hydroxamate C=N bond lengths in **1** (X = F), 1.298 Å, **1** (X = C_6H_5), 1.300 Å, **3** (X = F), 1.294 Å, and **3** (X = C_6H_5), 1.306 Å, are very similar to that in **6**. Compared with uncorrected C=N bond lengths of 1.328 Å (24), 1.332 Å (25), and 1.374 Å (26) reported for free *N*-alkylhydroxamic acids, the shorter C=N bonds observed for **6** and **1** (1, 2) are indicative of increased

[4]The structure factor table, Table 6 (anisotropic thermal parameters), and other material mentioned in the text may be purchased from the Depository of Unpublished Data, CISTI, National Research Council of Canada, Ottawa, Ont., Canada K1A 0S2.

[5]Libration corrected bond lengths (esd's assumed equal to those of the uncorrected values) are employed in the discussion and are compared with similarly treated (16) distances unless otherwise stated.

TABLE 3. Bond angles (deg) with estimated standard deviations in parentheses

Bonds	Angle (deg)	Bonds	Angle (deg)
N(1)—O(1)—B(1)	112.5(2)	C(15)—C(16)—C(17)	119.7(3)
C(1)—O(2)—B(1)	116.5(2)	C(16)—C(17)—C(18)	120.1(3)
N(2)—O(3)—B(2)	112.4(2)	C(13)—C(18)—C(17)	122.2(3)
C(2)—O(4)—B(2)	116.5(2)	C(20)—C(19)—C(24)	116.0(2)
O(1)—N(1)—C(2)	119.9(2)	C(20)—C(19)—B(2)	123.7(2)
O(1)—N(1)—C(3)	115.2(2)	C(24)—C(19)—B(2)	120.1(2)
C(2)—N(1)—C(3)	124.8(2)	C(19)—C(20)—C(21)	122.1(3)
O(3)—N(2)—C(1)	119.8(2)	C(20)—C(21)—C(22)	120.5(3)
O(3)—N(2)—C(5)	114.4(2)	C(21)—C(22)—C(23)	118.9(3)
C(1)—N(2)—C(5)	125.4(2)	C(22)—C(23)—C(24)	120.6(3)
O(2)—C(1)—N(2)	121.6(2)	C(19)—C(24)—C(23)	121.9(3)
O(2)—C(1)—C(2)	121.3(2)	C(26)—C(25)—C(30)	116.3(2)
N(2)—C(1)—C(2)	117.1(2)	C(26)—C(25)—B(2)	119.8(2)
O(4)—C(2)—N(1)	121.3(2)	C(30)—C(25)—B(2)	123.8(2)
O(4)—C(2)—C(1)	121.6(2)	C(25)—C(26)—C(27)	122.5(3)
N(1)—C(2)—C(1)	117.0(2)	C(26)—C(27)—C(28)	119.5(4)
N(1)—C(3)—C(4)	112.0(3)	C(27)—C(28)—C(29)	120.5(3)
N(2)—C(5)—C(6)	111.0(3)	C(28)—C(29)—C(30)	119.8(3)
C(8)—C(7)—C(12)	115.9(2)	C(25)—C(30)—C(29)	121.4(3)
C(8)—C(7)—B(1)	126.6(2)	O(1)—B(1)—O(2)	103.9(2)
C(12)—C(7)—B(1)	117.5(2)	O(1)—B(1)—C(7)	111.6(2)
C(7)—C(8)—C(9)	122.0(3)	O(1)—B(1)—C(13)	107.0(2)
C(8)—C(9)—C(10)	120.1(3)	O(2)—B(1)—C(7)	110.1(2)
C(9)—C(10)—C(11)	119.4(3)	O(2)—B(1)—C(13)	108.5(2)
C(10)—C(11)—C(12)	120.1(3)	C(7)—B(1)—C(13)	115.0(2)
C(7)—C(12)—C(11)	122.6(3)	O(3)—B(2)—O(4)	103.8(2)
C(14)—C(13)—C(18)	116.1(2)	O(3)—B(2)—C(19)	112.6(2)
C(14)—C(13)—B(1)	120.3(2)	O(3)—B(2)—C(25)	108.5(2)
C(18)—C(13)—B(1)	123.5(2)	O(4)—B(2)—C(19)	108.6(2)
C(13)—C(14)—C(15)	122.0(3)	O(4)—B(2)—C(25)	105.6(2)
C(14)—C(15)—C(16)	119.9(3)	C(19)—B(2)—C(25)	116.7(2)

TABLE 4. Intra-annular torsion angles (deg) standard deviations in parentheses

Atoms	Torsion angle (deg)
B(1)—O(1)—N(1)—C(2)	42.1(3)
O(1)—N(1)—C(2)—C(1)	1.9(3)
O(2)—C(1)—C(2)—N(1)	−25.4(3)
B(1)—O(2)—C(1)—C(2)	1.7(3)
C(1)—O(2)—B(1)—O(1)	37.4(2)
N(1)—O(1)—B(1)—O(2)	−59.2(2)
B(2)—O(3)—N(2)—C(1)	44.4(3)
O(3)—N(2)—C(1)—C(2)	−0.9(3)
N(2)—C(1)—C(2)—O(4)	−24.0(3)
B(2)—O(4)—C(2)—C(1)	2.4(3)
C(2)—O(4)—B(2)—O(3)	36.2(2)
N(2)—O(3)—B(2)—O(4)	−59.1(2)

double bond character in the boron chelates. The nitrogen lone pair delocalization into the carbonyl function, increasing the negative charge density at the carbonyl oxygen atom, has also been discussed for Fe(III) complexes of *N*-alkylhydroxamic acids (27).

The carbonyl C=O bond, however, still retains appreciable double bond character. The π-bond order of the C=O bond in **6** (mean 1.288 Å) can be estimated as 0.55 from a plot of π-bond order vs. C=O bond length for N—C/C—O containing π-systems (23). This is less double bond character than found in the C=O bonds of free *N*-alkylhydroxamic acids with uncorrected C—O bond lengths of 1.241 Å (24) and 1.246 Å (25). The unsubstituted oxalohydroxamic acid **8** has uncorrected C—O bond lengths of 1.232 Å (21). The C—N and C—O bond distances in **6** are similar to those reported for dimethylboron O—B—N and O—B—O chelates of *N*-substituted diamides of oxalic acid (11). The short C—N and C—O bonds in these compounds were also ascribed to significant double bond character. The shorter and stronger C—N bond in amide functions has recently been discussed in terms of a higher electron population at the nitrogen atom, and a more ionic character of the C—N bond in the planar conformers, deduced from calculations of the structures and energies of formamide rotamers (27).

The nearly planar arrangement of both hydroxamate moieties in **6**, having partial double bond character in both the C—N and C—O bonds, allows an overall formulation **9** for the mesomeric structure of **6**. This is consistent with the central C(1)—C(2) bond length of 1.492 Å, corresponding to a C(sp^2)—C(sp^2) single bond. This distance is comparable to the sample median of 1.491 Å for *o*-substituted biphenyls (28) but shorter than the corresponding uncorrected distances of 1.526 Å in oxalohydroxamic acid (21) and 1.542 Å in oxalic acid (29). In spite of the shorter C—C bond in **6**, the two amide groups are not coplanar (angle between normals to the mean amide planes = 27.9°). This represents a twisting of the hydroxamate moieties with respect to the C(1)—C(2) bond, the mean O—C—C—N torsion angle being −24.7°.

The relatively weak donation from the carbonyl oxygen atom to boron, symbolized in formula **9** by a dotted line, gives rise to an unusually long O—B bond (mean 1.587 Å). This is the

Can. J. Chem. Downloaded from www.nrcresearchpress.com by 194.225.253.170 on 09/07/12
For personal use only.

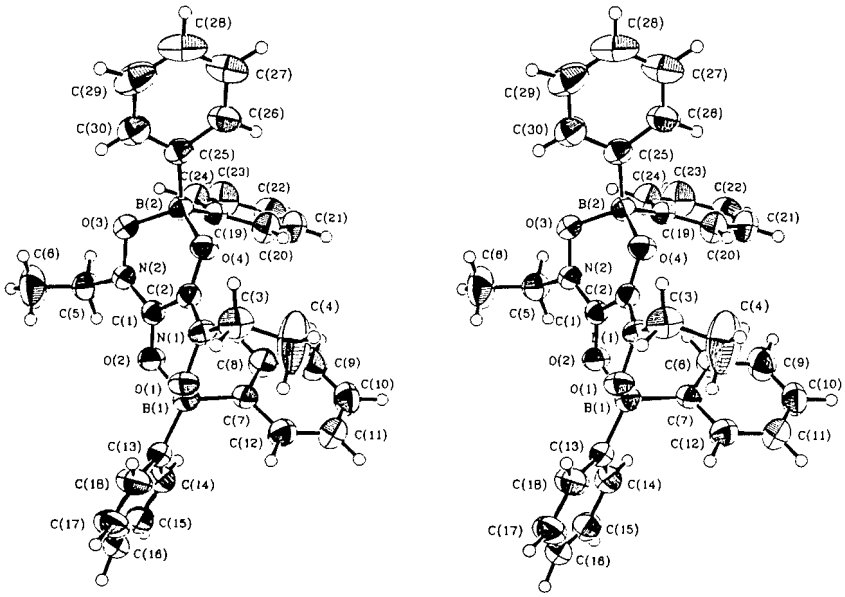


FIG. 1. Stereoscopic view of 4,8-diethyl-2,2,6,6-tetraphenyl-1,3,5,7-tetraoxa-4,8-diazonia-2,6-diborata-1,2,3,5,6,7-hexahydronaphthalene; 50% probability thermal ellipsoids are shown for the non-hydrogen atoms.

longest O—B distance yet observed for a six-membered diphenylboron chelate; however, longer O—B distances of the type (C=)O—B have been reported for the five-membered diphenylboron chelates (maltolato)diphenylboron (30), 1.600 Å, and (3-hydroxy-2-methyl-4-pyridinonato)diphenylboron (31), 1.650 Å. The other O—B bond in **6**, (N)O—B (mean 1.511 Å), is shorter by an average of 0.076 Å. Differences between O—B bond lengths in O—B—O chelates of Ph_2B where one of the bonds is of the type (C=)O—B range from 0.067 to 0.153 Å (30–32). The mean C—B / mean O—B bond length ratio of 1.035 for **6** is the smallest yet reported for a six-membered O—B—O chelate of diphenylboron (33), thus the overall binding strength of the *O,O*-chelating ligand with respect to the Ph_2B moiety is the weakest yet observed. The mean N—O distance in **6** (1.383 Å) is longer than the corresponding distances of 1.331–1.343 Å in the five-membered chelates **1** (1, 2) and **2** (5), and 1.369 Å in the seven-membered chelate **3** (6), but shorter than the uncorrected distance of 1.388 Å in free oxalohydroxamic acid (21). The two six-membered chelate rings in **6** have slightly distorted 1,3-diplanar ("twist-envelope") conformations (see Table 4).

Based on the ease of preparation of five-membered boron chelates of *N*-substituted hydroxamic acids (**1** and **2**) (1–5), the formation of **6** (instead of **5**) could be due to steric factors. From molecular scale models it can be seen that there is less strain in the six-membered ring isomer. Thus **6** would be the thermodynamically preferred structure, compared with both **5** and **7**, the latter showing some strain in the five-membered ring but none in the seven-membered ring.

Acknowledgments

We thank the Natural Sciences and Engineering Research Council of Canada and the Fonds der Chemischen Industrie, Frankfurt am Main, for financial support and the University of British Columbia Computing Centre for assistance.

1. S. J. RETTIG, J. TROTTER, W. KLIEGEL, and D. NANNINGA. Can. J. Chem. **55**, 1 (1977).
2. S. J. RETTIG, J. TROTTER, W. KLIEGEL, and D. NANNINGA. Can. J. Chem. **56**, 1676 (1978).
3. W. KLIEGEL and D. NANNINGA. Pharmazie, **38**, 131 (1983).
4. W. KLIEGEL and D. NANNINGA. Chem. Ber. **116**, 2616 (1983).
5. W. KLIEGEL, D. NANNINGA, S. J. RETTIG, and J. TROTTER. Can. J. Chem. **61**, 2493 (1983).
6. W. KLIEGEL, M. TAJERBASHI, S. J. RETTIG, and J. TROTTER. Can. J. Chem. **66**, 2621 (1988).
7. S. K. CHAUDHURI, P. S. ROY, and A. K. GHOSH. Indian J. Chem. Sect. A, **23**, 917 (1984).
8. P. GHOSH and A. CHAKRAVORTY. J. Chem. Soc. Dalton Trans. 361 (1985).
9. W. KLIEGEL and M. TAJERBASHI. To be published.
10. Y. K. AGRAWAL. Russ. Chem. Rev. **48**, 948 (1979).
11. W. MARINGGELE, G. M. SHELDRICK, A. MELLER, and M. NOLTEMEYER. Chem. Ber. **117**, 2112 (1984).
12. International tables for X-ray crystallography. Vol. IV. Kynoch press, Birmingham. 1974. pp. 99–102 and 149.
13. P. J. BECKER and P. COPPENS. Acta Crystallogr. Sect. A, **30**, 129 (1974); **30**, 148 (1974); **31**, 417 (1975).
14. P. COPPENS and W. C. HAMILTON. Acta Crystallogr. Sect. A, **26**, 71 (1970).
15. F. R. THORNLEY and R. J. NELMES. Acta Crystallogr. Sect. A, **30**, 748 (1974).
16. V. SCHOMAKER and K. N. TRUEBLOOD. Acta Crystallogr. Sect. B, **24**, 63 (1968).
17. D. W. J. CRUICKSHANK. Acta Crystallogr. **9**, 747 (1956); **9**, 754 (1956); **14**, 896 (1961).
18. (*a*) D. A. BROWN, A. I. ROCHE, T. A. PAKKANEN, T. T. PAKKANEN, and K. SMOLANDER. J. Chem. Soc. Chem. Commun. 676 (1982); (*b*) M. JULIEN-POUZOL, S. JAULMES, P. LARUELLE, S. CARVALHO, and E. B. PANIAGO. Acta Crystallogr. Sect. C, **41**, 712 (1985).
19. C. O. B. DE MIRANDA-PINTO, E. B. PANIAGO, S. CARVALHO, M. TABAK, and Y. P. MASCARENHAS. Inorg. Chim. Acta, **137**, 145 (1987).
20. E. B. PANIAGO and S. CARVALHO. Inorg. Chim. Acta, **136**, 159 (1987).
21. C. K. LOWE-MA and D. L. DECKER. Acta Crystallogr. Sect. C, **42**, 1648 (1986).
22. L. M. TREFONAS, R. L. FLURRY, R. MAJESTE, E. A. MEYERS, and R. F. COPELAND. J. Am. Chem. Soc. **88**, 2145 (1966).
23. G. HAFELINGER. Chem. Ber. **103**, 2941 (1970).
24. W. L. SMITH and K. N. RAYMOND. J. Am. Chem. Soc. **102**, 1252 (1980).

Can. J. Chem. Downloaded from www.nrcresearchpress.com by 194.225.253.170 on 09/07/12
For personal use only.

25. V. N. KALININ, M. YU. ANTIPIN, V. M. YURCHENKO, and YU. T. STRUCHKOV. J. Struct. Chem. **23**, 723 (1982).
26. H. G. AURICH, H. GRIGAT, W. MASSA, K. D. MOGENDORF, and G. ZINNER. Chem. Ber. **119**, 1441 (1986).
27. K. B. WIBERG and K. E. LAIDIG. J. Am. Chem. Soc. **109**, 5935 (1987).
28. F. A. ALLEN, O. KENNARD, D. G. WATSON, L. BRAMMER, A. G. ORPEN and R. TAYLOR. J. Chem. Soc. Perkin Trans. II, S1 (1987).
29. E. M. AYERST and J. R. C. DUKE. Acta Crystallogr. **7**, 588 (1954).
30. C. ORVIG, S. J. RETTIG, and J. TROTTER. Can. J. Chem. **65**, 590 (1987).
31. W. O. NELSON, C. ORVIG, S. J. RETTIG, and J. TROTTER. Can. J. Chem. **66**, 132 (1988).
32. W. KLIEGEL, H.-W. MOTZKUS, D. NANNINGA, S. J. RETTIG, and J. TROTTER. Can. J. Chem. **64**, 507 (1986).
33. W. R. CULLEN, S. J. RETTIG, J. TROTTER, and E. B. WICKENHEISER. Can. J. Chem. **66**, 2007 (1988).
34. W. KLIEGEL, M. TAJERBASHI, S. J. RETTIG, and J. TROTTER. Can. J. Chem. **67**, 1636 (1989).

Can. J. Chem. Downloaded from www.nrcresearchpress.com by 194.225.253.170 on 09/07/12
For personal use only.

FOR ERRATA SEE
69 1991 p.1038

Synthesis and crystal structure of an octahedral nickel(II) complex derived from pentaerythrityl tetraamine

A. McAuley,[1] S. Subramanian, and T. W. Whitcombe
Department of Chemistry, University of Victoria, P.O. Box 1700, Victoria, B.C., Canada V8W 2Y2

Received July 25, 1988[2]

A. McAuley, S. Subramanian, and T. W. Whitcombe. Can. J. Chem. **67**, 1650 (1989).

The Ni(II) complex, $Ni(Htam)_2^{4+}$ (tam = pentaerythrityl tetraamine), has been prepared under controlled conditions. In this ion, three of the four amino groups of each ligand are coordinated to yield an octahedral structure which shows tetragonal and trigonal distortion. The fourth amino group is protonated in each case and binds strongly to the counter ion SO_4^{2-}. The crystal structure (triclinic, $P\bar{1}$, a = 8.913(3), b = 9.775(2), c = 7.505(3), α = 102.61(4)°, β = 106.28(4)°, γ = 96.40(3)°) has been refined, converging to final values of R = 0.0347 and R_w = 0.0386. The three dimensional nature of the hydrogen bonding in the crystal structure has been described. Differences in Ni—N bond lengths are observed. A transient nickel(III) species is generated chemically or electrochemically. The esr spectrum is consistent with a low spin d^7 centre and is axial in nature.

Key words: nickel, pentaerythrityl tetraamine, hydrogen bonding, oxidation.

A. McAuley, S. Subramanian et T. W. Whitcombe. Can. J. Chem. **67**, 1650 (1989).

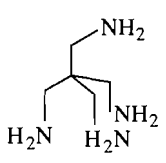
Opérant dans des conditions contrôlées, on a préparé le complexe de Ni(II), $Ni(Htam)_2^{4+}$ (tam = pentaérythrityl tétraamine). Dans cet ion, trois des quatre groupements aminés de chacun des ligands sont coordonnés pour donner une structure octaédrique qui présente une distorsion tétragonale et trigonale. Dans chaque cas, le quatrième groupement aminé est protoné et il se lie fortement au contre-ion SO_4^{2+}. On a affiné la structure cristalline (triclinique, $P\bar{1}$, a = 8,913(3), b = 9,775(2) et c = 7,505(3) Å, α = 102,61(4), β = 106,28(4) et γ = 96,40(3)°) jusqu'à des valeurs finales de R = 0,0347 et R_w = 0,0386. On décrit la nature tridimensionnelle des liaisons hydrogènes dans la structure cristalline. On a observé des différences dans les longueurs des liaisons Ni—N. Il y a génération chimique ou électrochimique d'une espèce transitoire de Ni(III). Le spectre rpe est en accord avec un centre d^7 de faible spin et de nature exiale.

Mots clés : nickel, pentaérythrityl tétraamine, liaison hydrogène, oxydation.

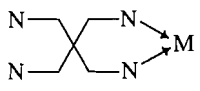
[Traduit par la revue]

Introduction

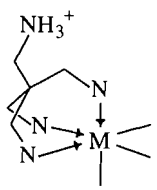
Although the ligand 2,2-bis(aminomethyl)-1,3-diaminopropane (**I**) (tam), was first prepared fifty years ago (1), there have been relatively few reports on its coordination chemistry. This is surprising, since several coordination geometries are possible and have been postulated. In the case of complexes involving nickel(II) and copper(II), the potential binucleating ability of the ligand has been described (2), leading to the formation of polymeric entities with extended square planar arrays. In such arrangements, two primary amines would be coordinated to each metal centre (**II**). In general, such species are rather ill characterised (2). For example, complexes of the metals described are viewed as isostructural from powder patterns and the polymeric species $\{[Ni(tam)_{1.5}]Cl_2\}_x$ was considered as exhibiting a three dimensional array of octahedral nickel(II) centers. The magnetic moment was consistent with such an observation. However, preparation of an aquated form provided a species with a significantly different uv–visible spectrum. An alternate perspective suggests that three of the four amine groups be disposed such that three primary nitrogens could occupy the face of an octahedron, leading to six-coordinate bis-complexes $M(HL_2)^{n+}$ in which one of the amine moieties is protonated (**III**). Such a configuration has been proposed from solution studies (3). Free ligands of this type are "globular" and in the case of the fully protonated amines, $(H_4tam)^{4+}$, crystallographic studies have been made for both the chloride and sulfate salts (4) in an investigation of hydrogen bonding associated with a compact, quadruply charged cation.



I



II



III

Our interest in such ligands stems from their possible use as building blocks for octaamines (5, 6) and C-spiro macrocycles (7) where the tetraaza systems are joined at a single quaternary carbon. Elaborations lead to dinuclear complexes (e.g. with $(H_2NCH_2CH_2NHCH_2)_4C$) which may be viewed as extended forms of the ligand 2,3,2-tet, $(H_2N(CH_2)_2NH(CH_2)_3NH(CH_2)_2NH_2)$, a species well studied in its interaction with metal ions (8, 9).

In this paper, we report a ready synthesis, under controlled conditions, of a hexa-coordinate nickel(II) ion related to some of the polymeric species described previously. The complex is of interest in that the X-ray structure provides evidence for different Ni—N bond lengths. Also, electrochemical and chemical oxidations are consistent with a transient Ni(III) complex. This is believed to be the first example of a species of this type generated from six primary amines in the inner coordination sphere.

Experimental

Synthesis

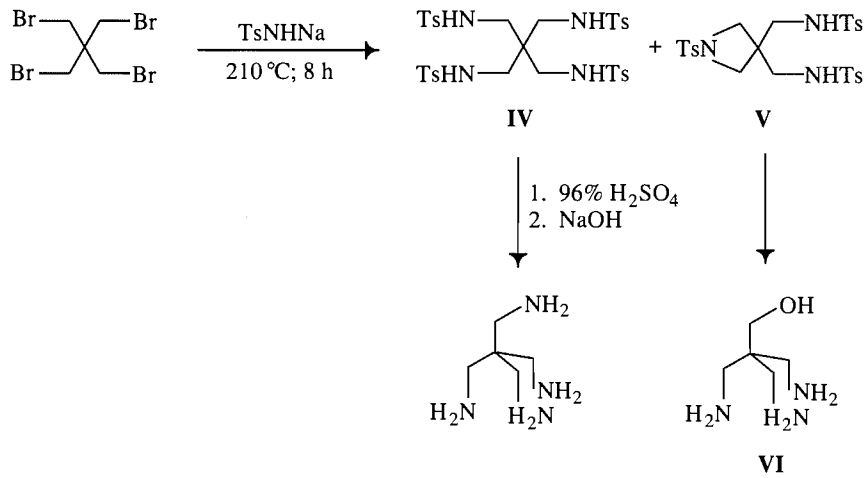
Pentaerythrityl tetrabromide was prepared by literature methods (10). The tam tetratosylate was prepared by a modification of the procedure described by Litherland and Mann (1).

*Preparation of tam tetratosylate (**IV**)*

A 500 mL three-necked reaction flask, equipped with a mechanical stirrer and a thermometer, was heated in an oil bath to 210°C. Pentaerythrityl tetrabromide (38.8 g 0.1 mol) was ground well with 95.0 g 0.5 mol) of the sodium salt of *p*-toluene sulphonamide and added in four (equal) amounts to the pre-heated reaction vessel while stirring. The reaction mixture formed a viscous melt within 40 min. The melt

[1]To whom correspondence should be addressed.
[2]Revision received June 19, 1989.

Can. J. Chem. Downloaded from www.nrcresearchpress.com by 194.225.253.170 on 09/07/12
For personal use only.



SCHEME 1

was maintained under stirring at 210°C for 8 h. Pentaerythrityl tetrabromide subliming on the cooler parts of the reaction flask was melted down occasionally by pumping hot oil or blowing hot air. The reaction mixture was cooled to 180°C under stirring and then allowed to cool to room temperature. Acetic acid (150 mL, 70% V / V) was added to the reaction flask equipped with a reflux condensor and the contents refluxed until the hard reaction mixture disintegrated into a fine white suspension. The mixture was filtered while hot and the filtrate was set aside to recover the tritosylate (**V**) (Scheme 1). The residue was washed several times with hot water to remove sodium bromide and *p*-toluene sulphonamide. The resulting white crystalline powder weighed 50 g and was found to be pure tetratosylate of tam. Melting point: 248°C (lit. 248°C). ^{1}H nmr in $CDCl_3$: 7.25–7.99 (m) aromatic protons, 5.8 (5) —NH— protons, 2.75 (d) C—CH_2—N protons, 2.4 (s) CH_3—Ar— protons. Mass spectroscopy (methane chemical ionisation) $M^+ = 748$.

Isolation of tritosylate (V)

The mother liquor obtained after the removal of tetratosylate of tam was processed as described (1) to recover the tritosylate. Yield: 25 g. Melting point: 214°C (lit. 214°C). ^{1}H nmr in $CDCl_3$: 7.25–7.99 (m) aromatic protons, 5.08 (t) —NH— protons, 3.36 (s) —CH_2— protons of the azetidine ring, 2.86 (d) —CH_2—NHTs protons, 2.5 (s) and 2.4 (s) CH_3—Ar— protons. Mass spectrometry (methane chemical ionisation) $M^+ = 577$. This species may be detosylated with ring opening to yield the tripodal ligand (**VI**).

Detosylation of tetratosylate of tam

Concentrated sulphuric acid (150 mL) was taken in a three-necked flask equipped with a mechanical stirrer and heated to 160°C in an oil bath. Powdered tosylate (82 g, 0.108 mol) was added in small lots over 40 min. The tosylate dissolved immediately to form a clear solution and the temperature rose to 180°C. The reaction mixture was maintained at 180°C for 30 min. After cooling to room temperature and pouring into 30% V / V ethanol, the white crystalline solid formed was allowed to settle. The supernatant was decanted off and the precipitate recovered by filtration under suction. This precipitate was dissolved in minimum amount of 10% sodium hydroxide and filtered to remove any insoluble material. The filtrate was neutralized and made just acidic with 50% sulfuric acid. On standing, pure white crystals of the sulfate salt of protonated 2,2′-bis(aminomethyl)-1,3-diaminopropane were deposited. Yield: 28.6 g, approximately 80%. Melting point: 303°C (lit. 303°C), melted into a clear liquid and charred at 306°C.

A sample of free anhydrous amine was prepared by neutralising the sulfate salt of tam in 40% sodium hydroxide and extracting with pyridine. The extract was dried over potassium hydroxide and pyridine distilled off under vacuum to yield the anhydrous amine, soluble in chloroform. ^{1}H nmr in $CDCl_3$: 2.5 —CH_2— protons, 1.07 —NH_2 protons. ^{13}C nmr in $CDCl_3$: 44.60 —CH_2— carbon, 43.8 quarternary carbon.

Preparation of $[Ni(tamH)_2]\cdot(SO_4)_2\cdot 4H_2O$

Amine sulphate (0.328 g, 0.001 mol) was suspended in 10 mL of water containing 0.131 g (0.0005 mol) of $NiSO_4\cdot 6H_2O$. Anhydrous sodium carbonate (0.159 g, 3 mole equivalents) was added, and the solution warmed to 40°C. Reaction produced a clear pink-coloured solution. On standing, pink crystals suitable for X-ray structure determination were formed. Yield: 0.244 g, 83%. A second crop of crystals could be octained on concentrating the mother liquor. *Anal.* calcd.: C 19.69, H 7.09, N 18.6, Ni 10.3: found: C 20.38, H 7.1, N 19.0, Ni 9.9. 3500–3000, br; 2080, m; 1600, br; 1465, s; 1180–1100, br; 950, m; 770, s; 610, m.

Infrared spectra were obtained as KBr discs using a Perkin Elmer 283 grating spectrometer. High field ^{1}H and ^{13}C nmr spectra were obtained using a Bruker WM 250 instrument. All chemical shifts are reported relative to tetramethylsilane (TMS).

Electron spin resonance spectra were measured using a Varian E6S spectrometer (77 K) with dpph (diphenylpicrylhydrazyl, g = 2.0037) as reference standard.

Ultraviolet–visible spectra were run on either a Cary 17 or a Perkin Elmer Lambda 4B dual beam spectrophotometer.

Elemental analyses were performed by Canadian Microanalytical Services, Vancouver, B.C.

Electrochemical measurements were made using a Princeton Applied Research Model 273 Potentiostat / Galvanostat. Pt working and counter electrodes were used while the reference electrode was a saturated calomel linked to the cell via a saturated KCl bridge.

Structure determination

Crystals were obtained by slow growth from aqueous SO_4^{2-} media. The crystal was mounted inside a Lindemann tube and photographed using Weissenberg and precession cameras. The final lattice parameters were obtained from a least-squares refinement of 15 accurately centred reflections over the range 14–48° in 2θ. The data were collected on a Picker four circle diffractometer, automated with a PDP11 / 10 computer. Intensity measurements were made using Zr-filtered Mo radiation, λ = 0.71069 Å by scanning in the 2θ mode by using 152 steps of 0.01° in 2θ counting for 0.25 s per step. Background counting was for 19 s at each end of the scan. A set of three standard reflections preceded each batch of 50 measurements. Pertinent crystallographic data are given in Table 1. Solution of the phase problem was achieved using the direct methods package of SHELX (11). Neutral atom scattering factors were taken from the compilation of Cromer and Mann (12*a*), and correction for the real component of anomalous dispersion was taken from the table of Cromer and Libermann (12*b*). The Ni *f* curve was from the International tables (13). The absorption correction was made by numerical integration using an 8 × 8 × 8 Gaussian grid. The program (14) was modified locally for the axis system of the monochromator. The nickel was located on a special position and other

Can. J. Chem. Downloaded from www.nrcresearchpress.com by 194.225.253.170 on 09/07/12
For personal use only.

Can. J. Chem. Downloaded from www.nrcresearchpress.com by 194.225.253.170 on 09/07/12
For personal use only.

TABLE 1. Crystallographic parameters for $Ni(tamH)_2(SO_4)\cdot 4H_2O$

Formula	$C_{10}H_{42}N_8NiS_2O_8$
Molecular weight	589.32
Space group	Triclinic, $P\bar{1}$
Unit cell: a	8.913(3) Å
b	9.775(2) Å
c	7.505(3) Å
α	102.61(4)°
β	106.28(4)°
γ	96.40(3)°
Volume	602.01 Å^3
Z	1
D_{calc}	1.625 g/cm^3
Crystal dimensions	0.42 × 0.11 × 0.51 mm
μ	10.38 cm^{-1}
Transmission range	0.684–0.890
Radiation	Mo K_α, 0.71069 Å
Scan width	1.52°
2θ	2–50.0°
Reflections collected	2264
Reflections used	2113
No. of parameters	235
Standards: (no decay)	003, 400, 020
Residual electron density	0.3 e/Å^3
Maximum final shift/error	0.08
R, R_w	0.0347, 0.0386

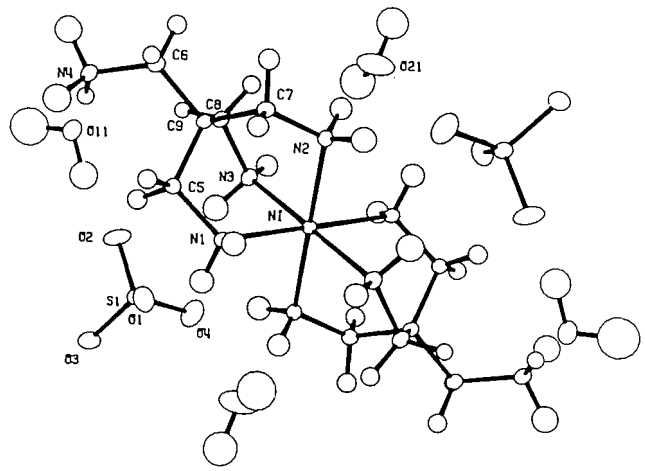


FIG. 1. ORTEP diagram of $Ni(Htam)_2(SO_4)_2(H_2O)_4$ complex, showing 25% thermal ellipsoids.

atoms were obtained from the Fourier difference maps following least-squares refinement. The hydrogen atoms were locatable from the difference map after all other atoms had been found and were included in the final stages of refinement. With this procedure the reported N—H distances were in the range 0.79–0.85 Å with an unacceptably low O—H value at 0.67 Å. The N—H and O—H distances were therefore constrained to 1.02 Å (DFIX) and the refinement repeated. All non-hydrogen atoms were refined anisotropically. A weighting scheme was employed in the latter stages of refinement, with $R_w = (\Sigma w(|F_o| - |F_c|)^2 / \Sigma w|F_o|^2)^{1/2}$ where $w = 0.0606/(\sigma^2|F| + 0.001F^2)$. The refinement converged with $R = 0.0347$ and $R_w = 0.0386$. The ORTEP diagram is shown in Fig. 1, together with the atomic labelling scheme for all the atoms except the hydrogens. The hydrogen atoms are labelled in the following manner: N_1 has associated H_{11}, H_{12}, N_2 with H_{21}, H_{22}, etc., N_4, H_{41}, H_{42}, H_{43}. O_{11} has associated H_{111} and H_{112}.

Results and discussion

Preparation of ligands

There are only two relevant methods for the preparation of tam available in the literature (1, 15). The drastic experimental conditions and the tedious nature of the preparatory method of Litherland and Mann (1) often yield products of poor quality even though it is the reasonable method for the preparation of substantial amounts of the tetratosylate. Fleischer's method (15) is not generally advisable considering the explosive nature of the tetraazide intermediate. In the present investigation, it was found that many of the problems associated with the former procedure can be overcome conveniently by very slight modification. Under the experimental conditions suggested previously, the reaction mixture often charred and non-homogenity of the reaction mixture led to lower yields of products. In our procedure, homogeneity of the reactions mixture was maintained by mechanical stirring and occasionally melting down the subliming starting materials. Reaction time was shorter and hence yielded products of good quality and quantity. Also, 5, not 4 moles, of sodium salt of *p*-toluene sulfonamide were used to minimize the formation of by-product aminetosylate (**V**). Although the yield was found to be variable in the range of 40–60%, the procedure was reliable for large scale preparations.

Preparation of the nickel(II) complex

Previous authors (2) used the free amine to form complexes with metal ions. This procedure leads to polymeric products. In the present method the Ni^{2+} complex was prepared by reacting the metal ion and the ligand salt in 1:2 ratio and neutralizing only 3 equiv. of the amine, thereby preventing the formation of polymers. Under basic conditions (pH greater than 10) on refluxing, only an insoluble polymeric complex of nickel is obtained as described by Bailar and Oekhme (2).

Crystallography

The crystal structure of $[Ni(tamH)_2](SO_4)_2(H_2O)_4$ is shown in Fig. 1 together with the atomic labelling scheme for all of the atoms except the hydrogens. The fractional coordinates, bond lengths and bond angles are given in Tables 2–5, respectively. All other tables are available as supplemental material (S1–S4).[3]

The nickel atom occupies an inversion centre in the unit cell giving half the molecule as the asymmetric unit. The molecule is thus symmetric with respect to nickel. However, the molecular geometry is not perfectly octahedral. The coordination environment has three of the four primary animes of each ligand coordinated to the metal, and may be described as both tetragonally distorted owing to the elongation of the Ni—N bonds, and, as trigonally distorted due to the closing of the chelate angles. The Ni—N1 bond is significantly longer (2.140(2) Å) than the remaining two bonds (2.121(2) Å; 2.120(2) Å). It is of interest to compare the present system with other NiN_6 systems. Somewhat greater differences in axial and equatorial bond lengths (2.12 and 2.22 Å, respectively) are observed for the *bis* triamine complex of 3-axapentane-1,5-diamine where the three nitrogens of each ligand are disposed meridionally about the distorted octahedron (16). For the cyclic triamine complex (17) with a facially disposed N_3 system, $Ni([9]\text{-aneN}_3)_2^{2+}$, ([9]-aneN$_3$: 1,4,7-triazacyclononane) all bond lengths are equivalent within experimental error at 2.10 Å, slightly shorter than in the present system. An identical value has been reported (18) in the case of

[3]Tables S1 through S4 contain fractional atomic coordinates, anisotropic temperature parameters, interatomic distances, and bond angles involving the hydrogen atoms; Tables 5 list calculated and observed structure factors. A complete set of material may be purchased from the Depository of Unpublished Data, CISTI, National Research Council of Canada, Ottawa, Ont., Canada K1A 0S2.

Can. J. Chem. Downloaded from www.nrcresearchpress.com by 194.225.253.170 on 09/07/12
For personal use only.

TABLE 2. Fractional atomic coordinates and temperature parameters[a]

Atom	x/a	y/b	z/c	U_{eq}
Ni	0( )	50000( )	0( )	190(1)
N(1)	−379( )	2760( )	−1302(3)	24(1)
N(2)	2196(2)	5237(2)	−575(3)	25(1)
N(3)	1234(2)	4448(2)	2517(2)	25(1)
N(4)	3616(2)	845(2)	1419(3)	27(1)
C(5)	881(2)	1973(2)	−551(3)	25(1)
C(6)	3848(2)	2068(2)	568(3)	28(1)
C(7)	2821(2)	3908(2)	−911(3)	26(1)
C(8)	2680(2)	3861(2)	2428(3)	27(1)
C(9)	2516(2)	2955(2)	394(3)	22(1)
S(1)	−20015(6)	19408(5)	32812(6)	249(2)
O(1)	−(2)	1654(2)	1295(2)	42(1)
O(2)	−448(2)	1908(2)	4573(3)	53(1)
O(3)	−3205(2)	851(2)	3426(3)	52(1)
O(4)	−2428(3)	3342(2)	3816(3)	57(1)
O(11)	2325(2)	1058(2)	4470(3)	44(1)
O(21)	4293(3)	7548(3)	3216(3)	77(1)

[a]Estimated standard deviations are given in parentheses; coordinates $\times 10^n$ where n = 5,5,4,4,4 for Ni,S,O,N,C temperature parameters $\times 10^n$ where n = 4,4,3,3,3 for Ni,S,O,N,C; U_{eq} = the equivalent isotropic temperature parameter; $U_{eq} = (1/3)\Sigma_i\Sigma_j U_{ij} a_i^* a_j^* (a_i \cdot a_j)$; $T = \exp -(8\pi^2 U_{iso} \sin^2\theta/\lambda^2)$; hydrogen atom fractional atomic coordinates and isotropic temperature parameters are presented in Table S1.

TABLE 3. Interatomic distances (Å)[a]

Atoms	Distance	Atoms	Distance
N(1)—Ni	2.140(2)	C(9)—C(5)	1.537(3)
N(2)—Ni	2.117(2)	C(9)—C(6)	1.540(3)
N(3)—Ni	2.118(2)	C(9)—C(7)	1.546(3)
C(5)—N(1)	1.483(2)	C(9)—C(8)	1.546(3)
C(7)—N(2)	1.469(2)	O(1)—S(1)	1.457(2)
C(8)—N(3)	1.480(3)	O(2)—S(1)	1.460(2)
C(6)—N(4)	1.493(3)	O(3)—S(1)	1.469(2)
		O(4)—S(1)	1.463(2)

[a]Estimated standard deviations are given in parentheses.

TABLE 4. Bond angles (deg)[a]

Atoms	Angle	Atoms	Angle
N(2)—Ni —Ni(1)	89.0(1)	C(7)—C(9)—C(5)	110.2(2)
N(3)—Ni —N(1)	83.9(1)	C(7)—C(9)—C(6)	104.8(1)
N(3)—Ni —N(2)	86.7(1)	C(8)—C(9)—C(5)	111.7(2)
C(5)—N(1)—Ni	117.5(1)	C(8)—C(0)—C(6)	108.3(2)
C(7)—N(2)—Ni	113.9(1)	C(8)—C(9)—C(7)	111.3(1)
C(8)—N(3)—Ni	114.9(1)	O(2)—S(1)—O(1)	110.9(1)
C(9)—C(5)—N(1)	111.9(1)	O(3)—S(1)—O(1)	108.8(1)
C(9)—C(6)—N(4)	114.8(2)	O(3)—S(1)—O(2)	109.3(1)
C(9)—C(7)—N(2)	113.0(2)	O(4)—S(1)—O(1)	108.8(1)
C(9)—C(8)—N(3)	112.7(2)	O(4)—S(1)—O(2)	110.1(1)
C(6)—C(9)—C(5)	110.3(2)	O(4)—S(1)—O(3)	108.9(1)

[a]Estimated standard deviations are given in parentheses.

TABLE 5. Selected intermolecular distances (Å)[a]

Atoms	Distance	Symmetry	T_x	T_y	T_z
O(1)...N(1)	3.032	1	0	0	0
O(2)...N(1)	3.002	1	0	0	1
N(2)...N(1)	3.035	−1	0	1	0
N(3)...N(1)	3.165	−1	0	1	0
O(21)...N(1)	3.328	−1	0	1	0
N(3)...N(2)	3.079	−1	0	1	0
S(1)...N(2)	3.754	−1	0	1	0
O(1)...N(2)	3.213	−1	0	1	0
O(4)...N(2)	3.093	−1	0	1	0
O(21)...N(2)	3.156	1	0	0	0
O(4)...N(3)	2.932	−1	0	1	0
S(1)...N(4)	3.701	1	−1	0	0
O(3)...N(4)	2.806	1	−1	0	0
S(1)...N(4)	3.749	−1	0	0	0
O(1)...N(4)	2.757	−1	0	0	0
O(3)...N(4)	3.556	−1	0	0	0
O(11)...N(4)	2.817	1	0	0	0
O(2)...C(5)	3.500	1	0	0	1
S(1)...C(6)	3.719	1	−1	0	0
O(3)...C(6)	3.403	1	−1	0	0
O(4)...C(6)	3.428	1	−1	0	0
O(1)...C(6)	3.612	−1	0	0	0
O(3)...C(6)	3.518	−1	0	0	0
O(4)...C(9)	3.550	−1	0	1	1
O(11)...S(1)	3.703	−1	0	0	1
O(21)...S(1)	3.736	−1	0	1	1
O(11)...O(2)	3.488	−1	0	0	1
O(11)...O(3)	2.731	−1	0	0	1
O(21)...O(3)	3.100	−1	0	1	1
O(21)...O(4)	3.339	−1	0	1	1
O(21)...O(11)	3.002	−1	1	1	1
O(2)...O(11)	2.714	1	0	0	0

[a]The symmetry positions are for the second atom; they are defined: 1 = X, Y, Z. A negative symmetry position denotes inversion. The translations (T) are applied after any symmetry operation has been applied.

the Ni(sepulchrate)$^{2+}$ ion (sepulchrate = 1,3,6,8,10,13,16,19-octa-azabicyclo-[6.6.6]eicosane), and for the Ni(en)$_3^{2+}$ (en = ethylenediamine) (19) the length is 2.12 Å. The trigonal distortion observed in the present complex is confirmed by the N—Ni—N angles where the six-membered chelating rings are smaller than the 90° angle anticipated for a regular octahedron. The average angle observed is 86.5° and is typical of the N—Ni—N angle for six-membered chelating rings as exemplified by nickel trispropylenediamine, Ni(pn)$_3^{2+}$ where an average of 87.5° is observed (20). In Ni(non)$_2^{2+}$ these angles (17) at 82.6° represent a significant distortion. Deviations from trigonal symmetry may be observed with one Ni—N bond shorter than the others. However, the magnitude of the distortion is much less in the present complex in keeping with the more tightly bound ring. Unlike a number of other hexacoordinated amine complexes (21, 22) there is no significant twist to the structure around the nominal C_3 axis.

The crystal structure also describes a number of hydrogen bonding interactions between the cation, the anion, and the waters of crystallization. There are present 13 H atom donors (nine from amines and two each from the waters). All N—H and O—H hydrogen atoms are used in the bonding with the exception of one hydrogen on N3 where contacts are considered very long for bonding. The number of acceptor positions is 12 on the sulfate oxygens and two each of O11 and O21. All interactions may be accounted for by strong (O11—O2, 2.714 Å and O11—O3, 2.731 Å) and weaker bonding (e.g., O11—O2, 3.488 Å and O21—O4, 3.339 Å). In other instances the bond lengths are significantly less than 3.0 Å. The longest bond required for complete description was O3—N4 at 3.556 Å. The depiction of the hydrogen bonding scheme requires a minimum of six complete molecules. Interactions extend through the crystal structure in the x, y, and z directions. A stereo projections of the hydrogen bonding arrangement is provided in Fig. 2. There is a

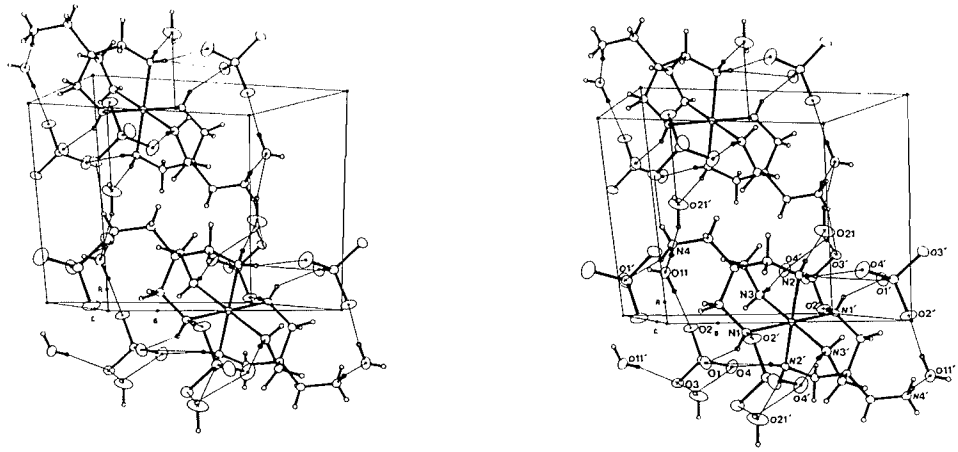


FIG. 2. Stereo projection of the hydrogen bonding arrangement.

ribbon of hydrogen bonding which links together the sulfate and water fragments. Oxygen atoms O2 and O3 of one SO_4^{2-} group bind to centrosymmetrically related O11 molecules which link back to the O2 and O3 atoms of a related sulfate. Also, O3 links a similar pair of O21 water molecules back to a symmetrically related SO_4^{2-}. The weak bonds (i.e., O3—H211 = 2.30 Å) provides linking for the crystal lattice. The short distance (1.78 Å) between O2 and H111 is indicative of a very strong interactions, and indeed, this is seen through the distension of this hydrogen from O11. Presumably this interaction tends to neutralize the positive charge present on the protonated amine through dipolar interactions. The sulfate also interacts with H112 of an adjacent molecular through O3 (1.75 Å).

The protonated nitrogen, N4, interacts with one of the waters of crystallisation (O11) through a strong hydrogen bond. This is seen in the close N4—O11 distance (2.81 Å) and the shorter O11—H43 distance (2.00 Å). There are also attachments to O1 and O3, thus providing the linking for the crystalline lattice, with additional bonding between N2 and O4, N2, and O21 and N1—O1.

The positioning of the sulfate allows for a strong interaction between this anion and all the amines through hydrogen bonding interactions with the oxygens. Short bonds are observed (<2.2 Å) between O1—H41, O2—H11, O3—H42, and O4—H31. It can be seen from these distances that the sulfate is situated over one of the "faces" of the octahedral cation and forms links between adjacent cations within the crystalline structure. It is also of interest to note that the sulfate does not interact more strongly with N1 than with the remaining nitrogens and is thus not the source for the distortion of the Ni—N1 bond length. However, among the chelated nitrogen atoms, N1 forms two of the three shortest N—O contacts. This could be the source of the elongation of the Ni—N bond.

Ultraviolet–visible studies

Owing to the protonated amines, the overall 4+ charge on the nickel complex leads to ion-pair formation and imparts poor solubility to the species. In water, the uv–visible spectrum is consistent with the maintenance of the pseudo-octahedral structure in solution. The principal features at λ = 331.7 nm (ϵ = 8.5 M^{-1} cm^{-1}), 519.0 nm (ϵ = 6.9 M^{-1} cm^{-1}), 795 nm (sh) and 850 nm (ϵ = 7.0 M^{-1} cm^{-1}) are typical of six-coordinate Ni(II). It is of interest that these wavelengths are close (335 nm (ϵ = 16.6) and 522 nm (ϵ = 14.2) to those described previously (2) under similar conditions. Owing to the differences in preparation, there may be a mixture of species present in the latter study since the extinction coefficients are significantly higher than those anticipated for species of this type. For $Ni(en)_3Cl_2$ (23) features at 345 and 545 nm have ϵ = 8.6 and 6.7 M^{-1} cm^{-1}, respectively. The more symmetrical $Ni(sep)^{2+}$ exhibits features (18) at 316 and 510 nm (ϵ = 11.2 and 8.0 M^{-1} cm^{-1} respectively) which may be due to the macrocyclic nature of the ion. The value of 10 Dq deduced for the present complex (11 695 cm^{-1}) indicates a strong field for the tricoordinate system which is only slightly weaker than the facially coordinated bis(1,4,7-triazacyclononane) nickel(II) ion (10 Dq = 12 500 cm^{-1}) (24). The present complex retains its integrity in the pH range 6–10. At higher pH's, precipitation of $Ni(OH)_2$ is observed and below pH 3 and the H_4tam^{4+} salt is formed, leaving Ni(II) in solution.

Addition of sodium persulfate at low temperature (≈0°C) leads to the formation of a green Ni(III) complex. The features of this ion are similar to those observed previously (25, 26) with an absorption band centred at 540 nm and overlapping features at 341 and 305 nm. Owing to the unstable nature of the complex, extinction coefficients could not be measured with any reasonable accuracy.

Electrochemical studies

Cyclic voltammetric studies of the complex were made in 1 M Li_2SO_4 solutions at various pH's. At pH ≈7 a quasi-reversible wave was observed for the Ni(II) / (III) couple with a peak–peak separation consistent with a $1e^-$ process. The observed $E_{1/2}$ = 0.89 V against NHE. At pH ≈10 there appears to be partial deprotonation of the terminal ammonium ion, leading to the formation of two species with features at 0.84 and 0.99 V respectively with respect to NHE.

$$[Ni(tamH)_2]^{4+} \overset{OH^-}{\rightleftharpoons} [Ni(tam)_2]^{2+}$$

However, these waves are much less well defined and, as identified earlier, rearragnements to polymeric entities are also possible.

It is of interest to note that the $E_{1/2}$ value for $Ni(tamH)_2^{5+/4+}$

Can. J. Chem. Downloaded from www.nrcresearchpress.com by 194.225.253.170 on 09/07/12
For personal use only.

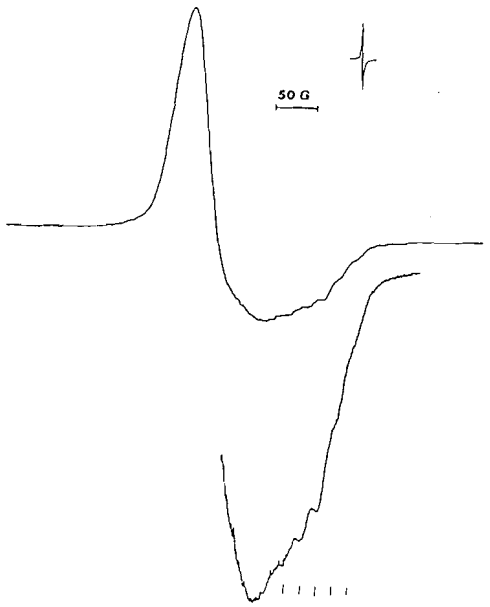


FIG. 3. Frozen solution esr spectrum of $[Ni(III)(Htam)_2]^{5+}$ ion at 77 K in aqueous media. Oxidation carried out using persulfate ion at 273 K.

is less than that observed for $Ni([9]aneN_3)_2^{3+/2+}$. The structural differences between the two molecules around the Ni(II) cation are not very great and hence, the lower $E_{1/2}$ value is presumably a result of the primary amines in the coordination sphere.

Electron spin resonance of Ni(III) species

Confirmation of the Ni(III) centre in the oxidation by persulfate is provided by the esr spectrum (Fig. 3). This is characteristic of a low spin d^7 ion $g_\perp = 2.13$, $g_\parallel = 2.028$ ($A_\parallel = 20$ G) (77 K). The spectrum shows significant tetragonal distortion with hyperfine coupling in the parallel feature consistent with the maintenance of axial *N*-coordination. There was little change observed over the pH range 6–9. However, outside these values the Ni(III) species was not stable.

This complex is of interest in that it is considered to be the first example of a Ni(III) ion with a NiN_6 chromophore involving primary amine coordination of sufficient stability to permit identification at room temperature. Previous examples, e.g. $Ni(en)_3^{3+}$, have been monitored only under pulse radiolytic conditions (27). The ion $Ni(en)_2Cl_2^+$ has been identified previously (28) and is stable only in acidic media, pH = 1, probably as a result of the axially coordinated chlorides. At pH > 2, the decay of Ni(III) is rapid. This ion, on exposure to moisture, gradually changes in the solid state to a black mixed-valence Ni(II)—Ni(IV) chloro-bridged dimer (29). The present finding of a more stable Ni(III) species in solution at pH ~6, may be due to the tripodal nature of the ligand resulting in facial coordination. In sulfate media, there is evidence for ion-pairing which is partly responsible for the non-isotropic nature of the esr spectrum. An NiN_6^{3+} chromophore of high symmetry would be expected to show features with $g_\perp$ close to $g_\parallel$, but where ion pairs are formed (30), the asymmetry imparted to the ion is such as to produce a more axial spectrum. The hyperfine coupling constant $A_\parallel$ (≈20 G) is similar to that observed where secondary amine coordination is involved. For $Ni(9\text{-}aneN_3)_2^{3+}$ (30, 31) $A_\parallel$ = 23.7 G and with $Ni(bipy)_3^{3+}$, the corresponding value is 18.6G (32). There appears to be little difference between primary and secondary amines on the residence time of the electron on the N-donor atom.

Conclusion

The tetraamine tam forms an octahedral complex with Ni^{2+} ion in which three of the four nitrogen atoms from each tam moiety are involved. Axial elongation consistent with Jahn–Teller distortion is seen in the crystal structure of the Ni^{2+} species. Electron spin resonance spectra of the oxidised ion are consistent with a low spin d^7 Ni(III) centre which shows extensive ion-pairing. The quasi-reversible nature of the $Ni^{2+/3+}$ redox couple is in keeping with retention of the primary coordination sphere upon electron transfer.

Acknowledgements

We thank NSERC and the University of Victoria for support. T.W.W. acknowledges the receipt of a NSERC Postgraduate Scholarship and S.S. the award of a University of Victoria Fellowship. We wish to thank Mrs. K. Beveridge for assistance with the X-ray studies, and Dr. G.W. Bushnell for advice. The comments of one referee are especially appreciated.

1. A. LITHERLAND and F. G. MANN. J. Chem Soc. 1588 (1938).
2. R. W. OEKHME and J. C. BAILAR JR. J. Inorg. Nucl. Chem. **27**, 2199 (1965).
3. L. J. ZOMPA and R. F. BOGUCKI. J. Am. Chem. Soc. **88**, 5186 (1966).
4. T. S. CAMERON, W. J. CHUTE, and O. KNOP. Can. J. Chem. **63**, 586 (1985).
5. A. T. PHILLIP. Aust. J. Chem. **21**, 2301 (1968).
6. L. R. GAHAN, H. E. HART, C. H. L. KENNARD, M. A. KINGSTON, G. SMITH, and T. C. W. MAK. Inorg. Chim. Acta, **5**, 116 (1986).
7. A. McAULEY, S. SUBRAMANIAN, and T. W. WHITCOMBE. J. Chem. Soc. Chem. Commun. 539 (1987).
8. D. K. CABBINESS and D. W. MARGERUM. J. Am. Chem. Soc. **91**, 6540 (1969).
9. B. BOSNICH, R. D. GILLARD, E. D. McKENZIE, and G. A. WEBB. J. Chem. Soc.(A) 1331 (1966).
10. R. RIEMSCHNEIDER, O. GOEHRING, P. GROSS, A. ROUK, K. BRENDL, and C. FARIA. Monatsch. Chem. **96**, 147 (1965).
11. G. M. SHELDRICK. SHELX76, Program for crystal structure refinement. University of Cambridge, UK. 1976.
12. (*a*) D. T. CROMER and J. B. MANN. Acta Crystallogr Sec. A, **24**, 321 (1968); (*b*) D. T. CROMER and D. A. LIBERMANN. J. Chem. Phys. **53**, 1891 (1970).
13. International tables for X-ray crystallography. Vol. IV. Kynoch, Birmingham, U.K. 1974.
14. Program written originally by P. Coppens, L. Leiserowitz and R. Rabinovitch, modified locally by G. W. Bushnell.
15. E. B. FLEISCHER, A. E. CREBALA, A. LEVEY, and P. A. TASKER. J. Org. Chem. **36**, 3042 (1971).
16. S. BIAGINI and M. CANNAS. J. Chem. Soc. (A), 2398 (1970).
17. R. YANG and L. J. ZOMPA. Inorg. Chem. **15**, 1499 (1976); L. J. Zompa and T. N. MARGULIS. Inorg. Chim. Acta, **28**, L157 (1978).
18. M. P. SUH, W. SHIN, D. KIM, and S. KIM. Inorg. Chem. **23**, 618 (1984).
19. L. N. SWINK and M. ATOJI. Acta Crystallogr. B**13**, 639 (1960).
20. G. D. ANDREETTI, L. CAVALCA, and P. SGARABOTTO. Gazzetta, **101**, 494 (1971).
21. G. W. BUSHNELL, D. FORTIER, and A. McAULEY. Inorg. Chem. **27**, 2626 (1988).
22. L. CHRISTIANSEN, D. N. HENDRICKSON, H. TOFTLUND, S. R. WILSON, and C. L. XIE. Inorg. Chem. **25**, 2813 (1986).

Can. J. Chem. Downloaded from www.nrcresearchpress.com by 194.225.253.170 on 09/07/12
For personal use only.

23. W. MANCH and W. C. FERNELIUS. J. Chem. Educ. **38**, 192 (1961).
24. S. M. HART, J. C. A. BOEYENS, and R. D. HANCOCK. Inorg. Chem. **22**, 982 (1983).
25. R. I. HAINES and A. MCAULEY. Coord. Chem. Rev. **39**, 77 (1981).
26. K. WIEGHARDT, W. SCHMIDT, W. HERRMANN, and H. J. KUPPERS. Inorg. Chem. **22**, 2953 (1983).
27. J. LATI and D. MEYERSTEIN. Inorg. Chem. **11**, 2397 (1972).
28. W. SHEN and J. H. LUNSFORD. Inorg. Chim. Acta, **102**, 199 (1985).
29. M. YAMASHITA and I. MURASE. Inorg. Chim. Acta, **97**, L43 (1985).
30. A. MCAULEY, P. R. NORMAN, and O. OLUBUYIDE. Inorg. Chem. **23**, 1939 (1984).
31. K. WIEGHARDT, W. WALZ, B. NUBER, J. WEISS, A. OZAROWSKI, H. STRATEMEIER, and D. REINEN. Inorg. Chem. **25**, 1650 (1986).
32. J. C. BRODOVITCH and A. MCAULEY. Can. J. Chem. **59**, 1610 (1981).

Can. J. Chem. Downloaded from www.nrcresearchpress.com by 194.225.253.170 on 09/07/12
For personal use only.

Isolation and characterization of polydentate ligands derived from the reaction of pentaerythrityltetrabromide and ethylenediamine

A. McAuley,[1] K. Beveridge, S. Subramanian, and T. W. Whitcombe
Department of Chemistry, University of Victoria, Victoria, B.C., Canada V8W 2Y2

Received August 29, 1988[2]

A. McAuley, K. Beveridge, S. Subramanian, and T. W. Whitcombe. Can. J. Chem. **67**, 1657 (1989).

Reaction of pentaerythrityltetrabromide with ethylenediamine yields three product amines. These have been isolated by separation of the corresponding Ni^{2+} complexes. The free amine hydrochlorides have been obtained by acid hydrolysis of the Ni^{2+} species and have been characterized by nuclear magnetic resonance and mass spectroscopy. The crystal structures have been determined for the hexahydrochloride salt of polyamine ligand L_1, $[H_6(L_1)]Cl_6 \cdot 4H_2O$ ($L_1 = C_{11}H_{28}N_6$, 6,6-bis(4-amino-2-azabutyl)-1,4-diazacycloheptane) ($C2/c$, $a = 15.975$) Å, $b = 10.723$ (1) Å, $c = 14.686$(1) Å, $\beta = 99.40(1)°$, $Z = 4$), and for the octahydrochloride salt of L_2, $[H_2(L_2)]Cl_8 \cdot 2H_2O$ (L_2 = 5,5-bis(4-amino-2-azabutyl)-1,9-diamino-3,7-diazanonane) ($Pccn$, $a = 12.834(2)$ Å, $b = 16.691(1)$ Å, $c = 14.167(1)$ Å, $Z = 4$). Both crystals exhibit strong N—H...Cl,O,N bonding, although in the latter compound the waters of crystallization do not participate in the apparent hydrogen bonding interaction. Both these species are of interest since they represent the precursors to square planar Ni^{2+} complexes that incorporate the MN_4 chromophore. Ring closure of both the free amines L_1 and L_2 by reaction with diethyl malonate leads to cyclized products that are related to the cyclam ([14-aneN_4) tetraaza macrocylic ligands.

Key words: pentaerythrityl, amine, spiro ligand hydrochlorides.

A. McAuley, K. Beveridge, S. Subramanian et T. W. Whitcombe. Can. J. Chem. **67**, 1657 (1989).

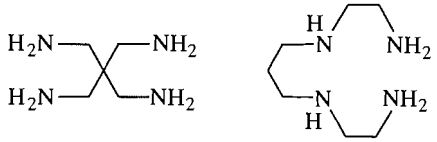
La réaction du tétrabromure de pentaérythrityle avec l'éthylènediamine fournit trois produits aminés. On les a séparés sous la forme des complexes correspondants du Ni^{2+}. On a obtenu les chlorhydrates des amines libres par hydrolyse acide des complexes de Ni^{2+} et on les a caractérisés par spectroscopies de résonance magnétique nucléaire et de masse. On a déterminé les structures cristallines de l'hexachlorohydrate du ligand polyamine L_1, $[H_6(L_1)]Cl_6 \cdot 4H_2O$ ($L_1 = C_{11}H_{28}N_6$, 6,6-bis(4-amino-2-azabutyl)1,4-diazacycloheptane) ($C2/c$, $a = 15,975(1)$, $b = 10,723(1)$ et $c = 14,686(1)$ Å, $\beta = 99,40(1)°$ et $Z = 4$), et de l'octachlorhydrate du ligand L_2, $[H_8(L_2)]Cl_8 \cdot 2H_2O$ (L_2 = 5,5-bis(4-amino-2-azabutyl)-1,9-diamino-3,7-diazanonane) ($Pcnn$, $a = 12,834(2)$, $b = 16,691(1)$ et $c = 14,167(1)$ Å et $Z = 4$). Les deux cristaux présentent de fortes liaisons N—H...Cl,O,N même si, dans le dernier composé, les molécules d'eau de cristallisation ne participent pas aux interactions hydrogènes apparentes. Ces deux espèces sont intéressantes parce qu'elles représentent les précurseurs des complexes plans carrés du Ni^{2+} qui comprennent le chromophore MN_4. La cyclisation des deux amines libres L_1 et L_2, par réaction avec le malonate de diéthyle, conduit à des produits qui sont reliés aux ligands tétraaza macrocycliques ([14-aneN_4).

Mots clés : pentaérythrityle, amine, chlorohydrates du ligand spiro.

[Traduit par la revue]

Introduction

The mode of formation of tetrasubstituted pentaerythritol species and their use as starting materials in synthesis has been an ongoing theme in organic chemistry. Several studies have been made in characterizing extended molecules in which all of the hydroxy groups are replaced (1). The convenient large scale synthesis of the tetraamine, tetrakis(aminomethyl)methane (tam), was first achieved by Litherland and Mann (2). However, crystallographic characterization of the molecule as a tetraammonium salt was reported only recently by Cameron *et al.* (3). This structural investigation revealed $[H_4tam]^{4+}$ to exist as a



tam

2,3,2-tet

highly compact quadruply charged cation with extensive hydrogen bonding interactions in the solid state. The utilization of tam in the complexation of metal ions has been examined by Bailar and Oehmke (4) and Zompa and Bogucki (5). A recent study[3] in our laboratory has shown that tam may form a bis-monoprotonated complex ion with Ni^{2+}, $[Ni(Htam)_2]^{4+}$, in which three of the four primary amines are coordinated onto the faces of an octahedral complex (NiN_6 chromophore) whilst the fourth amino group is protonated. However, because of the presence of the coordinated primary amino groups, this species is of limited stability in acidic media.

An ongoing theme in our research is the extension of the pentaerythrityl moiety to provide a synthetic route into bicyclo-macrocyclic complexes (6), where the cyclic ligands are fused at a spiro or quaternary carbon. This paper describes the synthesis and characterization of the precursor amines, which may be viewed as structural extensions of 1,9-diamino-3,7-diazanonane (2,3,2-tet), a ligand that has been examined extensively (7) in its metal complexes.

Investigation of the crystal structures of the amine hydrochlorides has shown evidence of extensive hydrogen bonding in the solid state and the present studies provide an extension of such data. In addition, characterization of the ligands forms a basis for the comparison of structural changes occurring in the organic framework upon complexation by metal ions. This latter aspect will be discussed elsewhere.[4]

Experimental

Pentaerythrityltetratosylate, tetrabromide and tetraiodide were prepared by literature methods (8). Ethylenediamine (anhydrous) from

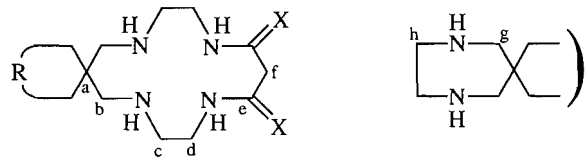
[1]Author to whom correspondence may be addressed.

[2]Revision received April 18, 1989.

[3]A. McAuley, S. Subramanian, and T. W. Whitcombe. Accompanying paper.

[4]A. McAuley, S. Subramanian, and T. W. Whitcombe. Unpublished results.

Can. J. Chem. Downloaded from www.nrcresearchpress.com by 194.225.253.170 on 09/07/12
For personal use only.



R = -NHCH$_2$CH$_2$NH-; X = O = L_4
X = H_2 = L_5
R = -NH(CH$_2$)$_2$NH(CH$_2$)$_3$NH(CH$_2$)$_2$NH-; X = O = L_6
X = H_2 = L_7

CHART 1. Alphabetic representation of carbon atoms in ligands (see Scheme 2 for structure).

either Fisher Scientific Co. or Aldrich Chemical Co. was used as received. All other chemicals used were of reagent grade.

The uv–vis were recorded on a Perkin–Elmer Lambda 4 spectrometer at 25°C in H_2O. The ir spectra of complexes were obtained as KBr discs using a Perkin–Elmer 283 grating spectrometer. The ^1H and ^{13}C nmr spectra were obtained using a Bruker WM 250(FT) instrument. ^{13}C chemical shifts in D_2O were monitored relative to the nitrile group of CH_3CN used as internal reference (*C*N = 118.2 ppm relative to TMS). ^{13}C and ^1H chemical shifts in $CDCl_3$ were measured relative to TMS as internal standard. The nmr resonances were assigned on the basis of comparison with known systems such as pentaerythrityl tetraamine and related amines. The various ^1H and ^{13}C resonances are described alphabetically as shown in Chart 1.

The labelling starts from the quaternary carbon (spiro carbon) and proceeds towards the middle methylene carbon in the propylene chain of the tetraaza unit in cyclic ligands L_4, L_5, L_6, and L_7 and towards the carbon bearing the primary amino group in the open chain ligands L_1, L_2, and L_3. In the diazacycloheptyl rings in ligands L_1, L_4, and L_6, the methylene carbon bonded to the quaternary carbon is denoted by C_g and the methylene carbon of the ethylene bridge by C_h respectively. In ligand L_3 the carbons in the chain —CH_2—NH—CH_2—CH_2—NH—CH_2—, bridging the two hexaaza units —C—(—CH_2—NH—CH_2—CH_2—NH_2)$_3$, do not differ distinctly from the rest of the carbons in the molecule.

The mass spectra of free amines were recorded with a Finnegan 330 gc–ms instrument by electron impact or by methane / isobutane chemical ionization methods as indicated. Ligands (oils) that proved difficult to purify or crystallize were complexed with Ni^{2+} ions, recrystallized, and the complexes analysed. Elemental analyses were performed by Canadian Microanalytical Services, Vancouver, B.C., Canada.

Structure determination

The crystals were mounted with epoxy resin inside Lindemann tubes and photographed using Weissenberg and precession cameras. The final lattice parameters were obtained from the accurate centering of 25 high angle reflections on an Enraf–Nonius CAD4 diffractometer, prior to the collection of the data set. For $[H_6(L_1)]Cl_6 \cdot 4H_2O$, the range of 2θ values of reflections for centering was 28°–50° and for $[H_8(L_2)]Cl_8 \cdot 2H_2O$, 8°–29°. The corresponding crystal sizes were 0.40 × 0.47 × 0.76 mm (μ = 7.4 cm^{-1}) for $[H_6(L_1)]Cl_6 \cdot 4H_2O$ and 0.50 × 0.08 × 0.05 mm (μ = 7.64 cm^{-1}) for $[H_2(L_2)]Cl_8 \cdot 2H_2O$ respectively. Three intensity standards were measured after each hour of exposure time, with no significant loss in intensity observed. Following corrections for absorption effects, based on the CAD4 EMPABS absorption curve, both structures were solved using the direct methods package in SHELX (9). The chlorine atoms were obtained initially, with the remaining atoms being located from subsequent Fourier difference maps. A unit weighing scheme was used and the least-squares refinement with all non-hydrogen atoms anisotropic gave the *R* values shown in Table 1. The hydrogen atoms were not found from the final difference maps. For both compounds, the maximum residual peak height was 0.5 e / Å^3. The neutral atom scattering factors were obtained from the usual source (10).

Synthesis

The ligands L_1, L_2, and L_3 prepared by reaction of pentaerythrityltetrabromide with anhydrous ethylenediamine were separated via Ni^{2+} complexation (see Scheme 1) and cyclized using the methods outlined in Scheme 2. This approach involves modification of the methods reported by Philip (11) and Gahan *et al.* (12) for the preparation of ligand L_2.

Preparation and isolation of ligands L_1, L_2, and L_3

Pentaerythrityltetrabromide (38.8 g, 0.1 mol) suspended in anhydrous ethylenediamine (500 g, 8.0 mol) was refluxed (72 h) with stirring at 145°C in a CO_2- and moisture-free N_2 atmosphere. After cooling the reaction mixture, most of the excess ethylenediamine was removed under vacuum. The resulting viscous oil, containing residual ethylenediamine and the product amines, weighed approximately 95 g.

Excess ethylenediamine was removed in the following manner: 60 g of this mixture, dissolved in 1 L H_2O, was adsorbed onto a pre-acid-washed Dowex 50X8 cation exchange resin (100–200 mesh) (500 g, column dimensions: 60 × 5 cm). the column was eluted with 2 L H_2O to remove all the hydrobromic acid liberated during the adsorption onto the column. Subsequent elution with 8–10 L of 2.25 M HCl yielded, on concentration, ethylenediamine dihydrochloride (65 g) (equivalent weight 79–81). Further elution with 8–10 L of 4.0 M HCl yielded, on concentration, 46 g of a mixture containing the hydrochloride salts of L_1, L_2, and L_3 (equivalent weight 85–86) (87% yield based on the pentaerythrityltetrabromide). Pentaerythrityltetratosylate and tetraiodide gave products with approximately the same composition but in lower yields (see discussion). The only method for satisfactory separation of the individual amines was via complexation using Ni^{2+}.

Preparation of Ni^{2+} complexes

Twenty grams of the amine hydrochloride mixture was dissolved in 250 mL H_2O and a solution of NaOH (10 g in 100 mL) was added. Following the addition of a solution of 16 g $NiCl_2 \cdot 6H_2O$ in 150 mL H_2O, the mixture was heated to nearly boiling and then diluted to 1 L. The complexes formed were adsorbed onto a Sephadex CM C-25 cation exchange column (60 g Sephadex, column dimension: 60 × 5 cm) to form a dark violet band. Gradient elution with 0.25–0.7 M NaCl yielded four distinct bands.

Elution of the first fraction with 0.25 M NaCl (2–3 L), followed by evaporation of the fractions to dryness and successive washing with 90% ethanol to remove the sodium chloride, resulted in a violet coloured ethanolic solution that yielded crystals (5.4 g) of the complex $[Ni(H(L_1))]Cl_3$ (where $H(L_1)$ is the monoprotonated (one N of the diazacycloheptyl ring) form of the amine L_1); ir: 3300(br), N—H; 1600(sh); 1455(sh); 965(sh); 640(m); uv–vis (in H_2O) (λ_{max} in nm (ε(M^{-1} cm^{-1}) at 25°C)): 384.7(7.1), 448.4(2.5), 537(3.8), 746.8(3.5), 790.3(3.3). *Anal.* calcd. (found) for $C_{11}H_{29}N_6NiCl_3$: C 32.18(31.9), H 7.07(7.29), N 20.48(19.98), Cl 25.94(25.36)%. A somewhat better analysis is provided if the complex is considered a hemihydrate, i.e., $[Ni(H(L_1))]Cl_3 \cdot 1/2H_2O$ yield C 31.5, H 7.16, N 20.04, Cl = 25.40%.

The second band eluted with 0.4 M NaCl (1–2 L) was identified as $[Ni(H_2O)_6]^{2+}$.

The third major band, pale violet in colour, was eluted with 0.45–0.5 M NaCl (4–5 L), concentrated, and sodium chloride removed as described previously. To the concentrated ethanolic solution was added, saturated aqueous $NaClO_4$ and the solution allowed to stand overnight, yielding yellow crystals of the perchlorate salt of $[Ni_2(L_2)]^{4+}$ (12.6 g); ir: 3250(br), N—H; 1600(sh), 1450(br), 1100(br), ClO_4; 620(sh); uv–vis (in H_2O) (λ_{max} in nm(ε(M^{-1} cm^{-1}) at 25°C)): 345.2(17.4), 448.4(9.2), 537.0(9.9), 741.9(8.2), 787.1(7.5). *Anal.* calcd. (found) for $C_{13}H_{36}N_8Ni_2Cl_4O_{16}$: C 19.8(19.6), H 4.41(4.39), N 13.87(13.9)%.

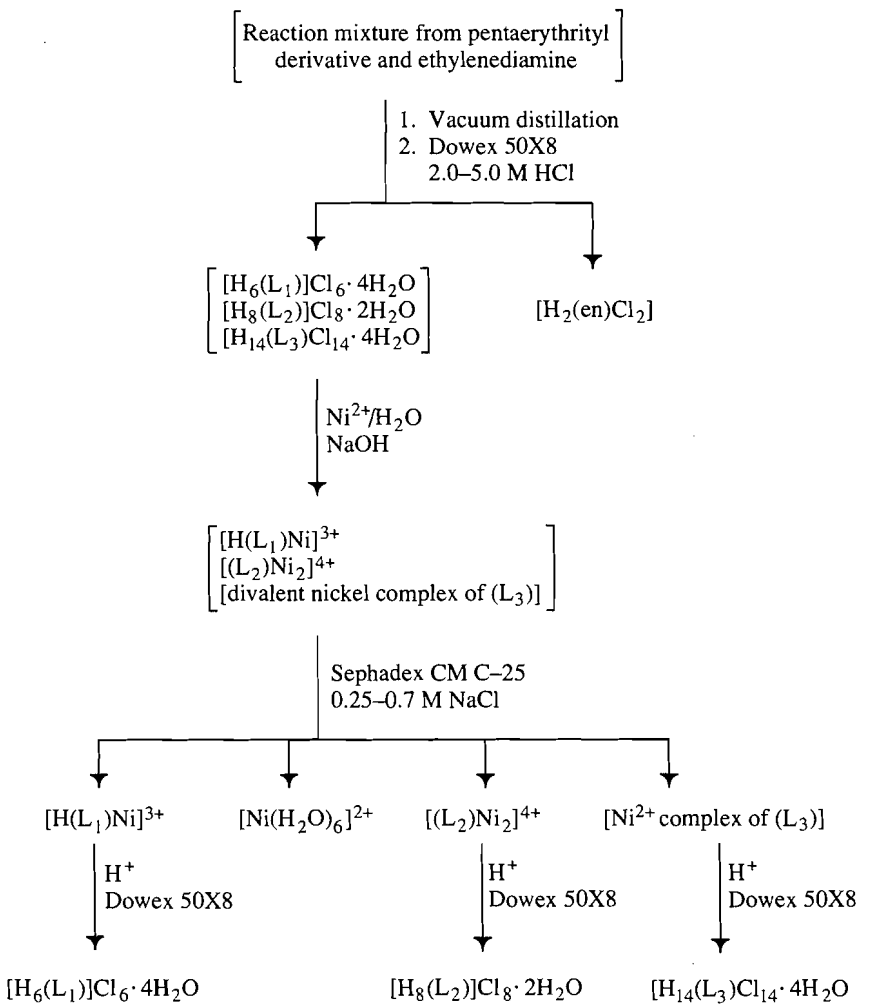
On prolonged standing the mother liquor deposited dark brown crystals of composition [(Ni) (Ni(Cl) (H_2O)) (L_2)] $(ClO_4)_3 \cdot 3H_2O$ (*vide infra*).

Small amounts of a final violet band were derived after elution with 0.5–0.7 M NaCl. A violet ethanolic solution was obtained but, owing to insufficient quantities available, the Ni(II) complex of L_3 was not isolated. However, nmr characterization of the amine hydrochloride was achieved (*vide infra*).

Can. J. Chem. Downloaded from www.nrcresearchpress.com by 194.225.253.170 on 09/07/12
For personal use only.

TABLE 1. Crystallographic parameters

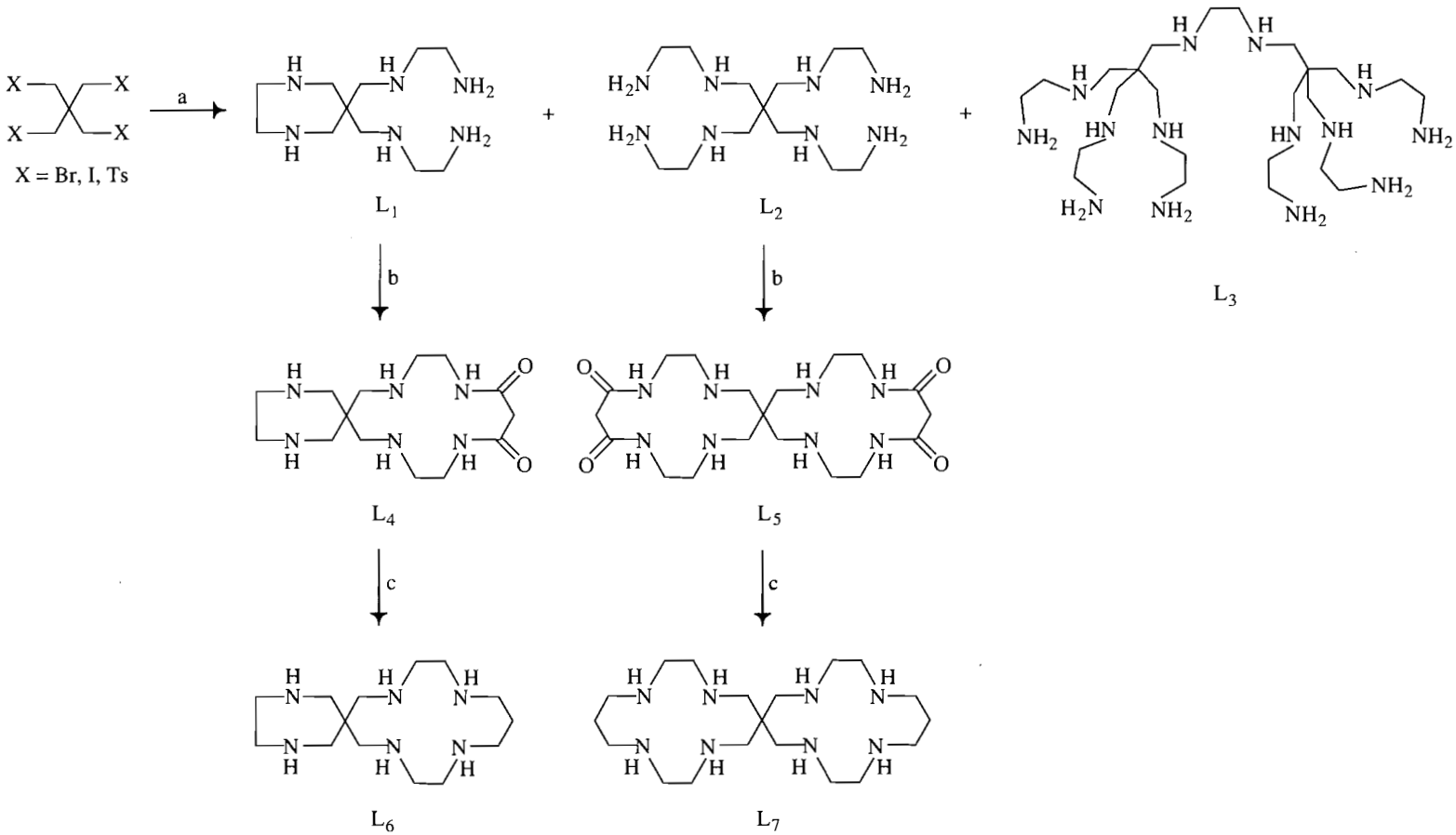
Compound:	$[H_6(L_1)]Cl_6 \cdot 4H_2O$	$[H_8(L_2)]Cl_8 \cdot 2H_2O$
Molecular formula:	$C_{11}H_{42}N_6Cl_6O_4$	$C_{13}H_{48}N_8Cl_8O_2$
Crystal system:	Monoclinic	Orthorhombic
Space group:	$C\,2/c$ (No. 15)	*Pccn* (No. 56)
Unit cell:	*a*: 15.975(1) Å	$a = 12.834(2)$ Å
	b: 10.723 (1) Å	$b = 16.691(1)$ Å
	c: 14.686(1) Å	$c = 14.167(2)$ Å
	β: 99.40(1)°	
Volume:	2482 Å^3	3035 Å^3
Z	4	4
Density measured:	1.43(2) g/cm^3	1.38(1) g/cm^3
calculated:	1.470 g/cm^3	1.383 g/cm^3
μ:	7.4 cm^{-1}	7.64 cm^{-1}
Radiation: MoKα ($\lambda = 0.71069$ Å used for both the crystals)		
Scan width: (variable for both; given by $1.5(0.80 + 0.34 \tan\theta)$ where $\theta = \omega/2$)		
Octants measured	$-h +k +l$, $+h$, $+k$, $+l$	$+h$, $+k$, $+l$
2θ	2°–50°	2°–50°
Reflections collected:	1962	2667
Reflections used: $I > 5\sigma(I)$	1444	$I > 3\sigma(I)$ 778
No. of parameters:	123	141
Standards:	12,0,0	4,0,0
	0,8,0	0,8,0
	0,0,8	0,3,4
$R = \Sigma(\|\|F_o\| - \|F_c\|)/\Sigma\|F_o\|$	0.088	0.085



SCHEME 1. Separation of amines L_1, L_2, and L_3 via Ni^{2+} complexation.

Can. J. Chem. Downloaded from www.nrcresearchpress.com by 194.225.253.170 on 09/07/12
For personal use only.

Can. J. Chem. Downloaded from www.nrcresearchpress.com by 194.225.253.170 on 09/07/12
For personal use only.



SCHEME 2. Reaction conditions: a. 8 moles of ethylenediamine, 140°C / 72 h / N_2 atmosphere. b. EtOH / diethylmalonate / 82°C / N_2 / 7 days. c. BH_3 / THF / reflux / 20 h.

Can. J. Chem. Downloaded from www.nrcresearchpress.com by 194.225.253.170 on 09/07/12
For personal use only.

Decomplexation and isolation of ligand hydrochlorides

Isolation of $[H_6(L_1)]Cl_6 \cdot 4H_2O$

$[Ni(H(L_1))]Cl_3$ (4.1 g) was dissolved in 250 mL of water. Addition of 25 mL concentrated HCl induced acid hydrolysis of the Ni^{2+} complex. The solution was charged onto a Dowex 50 × 8 cation exchange column. The $[Ni(H_2O)_6]^{2+}$ was removed using a 2 M HCl and the ligand hydrochloride eluted with 5 M HCl (2–3 L). After concentration of the eluate to 50 mL, ethanol was added until the solution turned just cloudy. On standing, the hydrochloride salt crystallized in near quantitative yield (5.3 g) as the tetrahydrate; ^{1}H nmr (amine L_1 in $CDCl_3$): H_h = 2.84(s), H_g = 2.72(s), H_b = 2.46(s), H_c = 2.76(m), H_d = 2.63(t), N—H = 1.4(br); ^{13}C nmr ($(H_6(L_1))]Cl_6$ in D_2O): C_a = 38.2(s), C_b = 45.2(t), C_c = 44.5(t), C_d = 35.2(t), C_g = 50.6(t), C_h = 49.0(t); (amine L_1 in $CDCl_3$): C_a = 44.4(s), C_b = 53.5(t), C_c = 54.8(t), C_d = 41.6(t), C_g = 55.9(t), C_h = 54.2(t); ms of free amine(methane chemical ionisation), *m / e*: 244. *Anal.* calcd. (found) for the hydrochloride salt $C_{11}H_{42}N_6O_4Cl_6$: C 24.68(23.99), H 7.8(7.56), N 15.7(15.2), Cl 39.78(39.16).

Isolation of $[H_8(L_2)]Cl_8 \cdot 2H_2O$

$[Ni_2(L_2)](ClO_4)_4$ (6.0 g) was dissolved in 500 mL of water and 50 mL concentrated HCl was added to hydrolyse the complex. Separation of the $[Ni(H_2O)_6]^{2+}$ (2 L of 2 M HCl) and isolation of hydrochloride (4 L of 5 M HCl) was achieved as outlined above (yield 4.3 g); ^{1}H nmr (amine L_2 in $CDCl_3$): H_b = 2.57(s), H_c = 2.76(m), H_d = 2.62(t), N—H = 1.4(br); ^{13}C nmr ($[H_8(L_2)]Cl_3$ in D_2O): C_a = 37.8(s), C_b = 49.1(t), C_c = 44.8(t), C_d = 34.9(t); (amine L_2 in $CDCl_3$): C_a = 41.5(s), C_b = 54.5(t), C_c = 53.3(t), C_d = 41.3(t); ms of free amine (isobutane chemical ionization), *m / e* (relative intensity): 306(58), 307(92), 308(100), 309(83), 310(47), 311(22) (Mol. wt. 304). *Anal.* calcd. (found) for the hydrochloride salt $C_{13}H_{48}N_8O_2Cl_8$: C 24.7(25.01), H 7.65(7.52), N 17.72(17.67), Cl 44.86(45.37).

Isolation of $[H_{14}(L_3)]Cl_{14} \cdot 4H_2O$

Using the procedure as above, white microcrystals of the hydrochloride were obtained from the final band eluted from the Sephadex column; ^{13}C nmr ($[H_{14}(L_3)]Cl_{14}$ in D_2O): C_a = 37.9(s), C_b = 49.6(t), C_c = 45.0(t), C_d = 35.2(t); ms of free amine (isobutane chemical ionization): $(M + 1)^+$ = 549.

Preparation of anhydrous amines L_1, L_2, and L_3

In a typical experiment, the octahydrochloride of amine L_2 (6.0 g) was dissolved in 150 mL of 40% NaOH. The free amine liberated as an oil was extracted into pyridine (3 × 50 mL) and the combined extracts were allowed to stand over KOH pellets. The viscous aqueous layer was removed and the pyridine solution again allowed to stand over KOH pellets for 24 h. After removal of any residual aqueous phase, the pyridine extract was roto-evacuated to dryness. Final traces of pyridine were removed under vacuum overnight. The resulting viscous oil (3.0 g) was completely soluble in chloroform without any cloudiness. Satisfactory ^{13}C nmr and mass spectroscopic data were obtained on the free amines (see isolation of aminehydrochlorides). However, for ease of storage, the hydrochloride salts were preferred.

Cyclization of L_1 and L_2

Cyclization of these amines was carried out according to the method of Tabushi *et al.* (13). Excess diethylmalonate was used and the unreacted ester was removed under high vacuum at room temperature. The products obtained were characterized by ^{13}C nmr and mass spectroscopy and were reduced without further purification.

Preparation of L_5

The anhydrous amine L_2 (3.0 g, 0.0098 mol) dissolved in 2.5 L 100% ethanol was mixed under stirring with significant excess of diethylmalonate (4.5 g, 0.028 mol) present in 500 mL of 100% ethanol. The reaction mixture was refluxed with stirring in a CO_2- and moisture-free N_2 atmosphere at 82°C for 7 days. The outlet of the condensor was protected with a NaOH pellet trap. On completion of the reaction, the mixture was concentrated to a viscous oil. Most of the unreacted ester was removed under vacuum and the residual sticky solid was digested in 100 mL of dry THF for about 30 min. A colourless microcrystalline solid was obtained. This was filtered and washed with ether and dried under vacuum. Yield 3.0–3.2 g (70%); mp 248–250°C; ^{13}C nmr (L_5 in D_2O): C_a = 37.3(s), C_b = 47.2(t), C_c = 38.9(t), C_d = 44.3(t), C_e = 168.5(s), C_f = 51.5(t); ms, *m / e* (relative intensity): 441(100) (isobutane chemical ionization).

Preparation of L_4

In an experiment similar to the above, amine L_1 (1.5 g, 0.006 mol) in 1.0 L of ethanol containing 1.5 g diethylmalonate was refluxed gently for 7 days under N_2 atmosphere. The reaction mixture was processed as before to get a hygroscopic white solid. Yield 0.2 g (23% see discussion); ^{13}C nmr (L_4 in D_2O): C_a = 37.1(t), C_b = 47.6(t), C_c = 41.6(t), C_d = 50.7(t), C_e = 168.6(s), C_f = 53.5(s), C_g = 52.8(t), C_h = 52.2; ms (methane chemical ionization), *m / e* (relative intensity): 313(90).

Reduction of cyclic lactams L_4 and L_5

Both compounds were reduced to the saturated macrocyclic ligand in a similar manner using BH_3 / THF as reducing agent. In a typical experiment a well-dried sample of L_5 (2.2 g, 0.005 mol) was treated with an appropriate amount of the reagent (8.0 mol equivalent of BH_3 / THF per mol of lactam) and refluxed for 24 h. Excess reductant was destroyed by dropwise addition of water and any white sublimate from the inner walls of the condensor was washed into the round-bottom flask with a minimum amount of 10% NaOH. The reaction mixture was taken to dryness in a rotary evaporator. This solid was suspended in 100 mL of 10% HCl and refluxed for 30 min. The resulting mixture was neutralized, the pH adjusted to 12–13, and the mixture then extracted with $CHCl_3$ in a continuous liquid–liquid extractor for 6 h. The chloroform layer was dried over anhydrous sodium sulfate and concentrated to dryness. Traces of chloroform were removed under vacuum and the resulting oil (1.34 g, approximately 70% yield), on standing, slowly solidified to a semisolid; ^{1}H nmr: H_b = 2.55(s), H_c, H_d, H_e = 2.63(m), H_f = 1.67(m), N—H = 2.4(br); ^{13}C nmr (L_7 in $CDCl_3$): C_a = 40.7(s), C_b = 55.4(t), C_c = 50.1(t), C_d = 49.4(t), C_e = 48.8(t), C_f = 29.2(t); ms (methane chemical ionization), *m / e* (relative intensity): 384 (electron impact); $M + 1$ = 385(100%), $(M - 1)$ = 383(91%).

Material obtained from amine L_1 did not lead to pure products (see discussion). The crude ligand was used for metal complexation and the metal complex purified on a Sephadex CM C-25 column. The isolation and characterization of the Ni^{2+} and Ni^{3+} complexes will be reported in a forthcoming publication.[5]

Results and discussion

Synthesis

In similar earlier studies, Philip (11) first reported the isolation of amine L_2 together with its Cu^{2+}, Ni^{2+}, and Pd^{2+} complexes. Recently Gahan *et al.* (12) have extended the reaction to prepare derivatives of propylenediamine and have characterized the Cu^{2+} complex of L_2 by X-ray crystallography. No detailed account has been given of the complete isolation and characterization of all the reaction products. In this study an attempt has been made to separate and isolate the product amines, providing a complete mass balance of the products.

The isolation method described herein does not involve conditions such as fractional distillation under vacuum at high temperatures, which often leads to decomposition and charring of polyamines. Hence the method described here has been found to be readily reproducible and accounts for the overall composition of the products obtained. Better yields of the amine L_2 have been identified together with significant amounts of the hitherto unreported amine L_1.

Pentaerythrityltetratosylate and tetraiodide were used as substrates in the place of pentaerythrityltetrabromide. Identical conditions were maintained and the reaction mixture processed in a similar manner. Comparison of results indicated that the

[5]A. McAuley and S. Subramanian. Unpublished results.

Can. J. Chem. Downloaded from www.nrcresearchpress.com by 194.225.253.170 on 09/07/12
For personal use only.

relative ratios of products obtained from all the three substrates did not vary significantly. The tetraiodide was not stable under reaction conditions and evolved iodine on prolonged heating. In the case of the tetratosylate the reaction was sluggish, presumably due to steric effects, and complete conversion of the tetratosylate to the amines did not occur. About 10–20% of unreacted tetratosylate was recovered. Hence, the overall conversion of the pentaerythrityl moiety into product amines was much higher in the case of pentaerythrityltetrabromide (up to 87%) compared to the tetratosylate and tetraiodide, where only 60% conversion was observed. Varying the mole ratio of ethylenediamine in the range of 4–10 moles per mole of pentaerythrityl derivative did not affect the ratio of products significantly. In all these experiments the products varied in the range of 30–40% for L_1, 50–60% for L_2, and 2–5% for L_3.

In the present procedure, the excess ethylenediamine was separated from the products by cation exchange resin chromatography. The presence of this diamine often leads to formation of mixed ligand amine species. Also the formation of large quantities of $[Ni(en)_3]^{2+}$ complicates the efficiency of separation of the nickel complexes. The isolation of the amines L_1–L_3 on a Dowex cation exchange resin column by gradient elution with 0.25–0.5 M HCl solutions often gives only mixtures of the products, as is evident from the ^{13}C nmr spectra of the different fractions. A similar method has been used effectively by Geue and Searle (14) for other polydentate ligands.

The amines under consideration may be compared with 2,3,2-tet. All form a sequence of 5,6,6-membered metal chelate rings around the metal ion and this arrangement of chelate rings has been shown to impart significant thermodynamic stability (15) as measured by the equilibrium constant (for example, log $K[Ni(2,3,2\text{-tet})]^{2+} = 15.9$). As a result, the structural integrity of metal complexes such as those of Ni^{2+} renders the species suitable for separation. Also, the noncyclic amine complexes containing primary amines that undergo protonation are readily hydrolysed by mineral acids to provide the ligand salts, which may then be separated from the metal ions (14). Products derived from propylenediamine and pentaerythrityl derivatives are comparable with 3,3,3-tet (3,3,3-tet: 1,5,9,13-tetraazatridecane). These form a sequence of 6,6,6-membered chelate rings, which are thermodynamically much less stable. Studies carried out in our laboratory aimed at separating such amine products using Ni^{2+} ions failed to provide pure amine hydrochlorides. Recrystallization of Ni^{2+} amine complexes of L_1–L_3 represents a good route to the amine salts, which are analytically pure.

The ^{13}C nmr spectra of the amine hydrochlorides are shown in Fig. 1(a–c). In amines L_1 and L_2 all the carbons are distinctly different in their environment, with six and four carbon resonances respectively. In the case of amine L_3, owing to the symmetry and identical chemical environment of some of the carbon centres, only four carbon signals were observed. However, comparison of the spectra of hydrochlorides of amines L_2 and L_3 showed only very slightly different chemical shifts and relative intensities (see Fig. 1). Mass spectra of the free amines confirm the identity of the products. For L_3, apart from the $(M + 1)$ ion observed at $m/e = 549$, the major fragment observed had an $e/e = 304$ corresponding to the amine fragment L_2, which could arise through loss of an N_6-containing fragment from amine L_3.

Equivalent weights of the amine hydrochlorides were determined by elution of a known amount of the solution of amine hydrochlorides through a Dowex 50 × 8 analytical column and determination of the liberated acid. By this method the equivalent weights of the hydrochlorides of amines were found to be 81.2 for amines L_2 and L_3 and 88.2 for amine L_1. Equivalent weights thus obtained compared well with the composition of the hydrochlorides of the amines and provided a quick assay of the products before their cyclization. Similar determination of equivalent weights of pure ethylenediamine dihydrochloride and the crude amine hydrochlorides obtained after the removal of ethylenediamine gave values of 79–81 and 85–86 respectively. Even though the values obtained for the hydrochlorides of

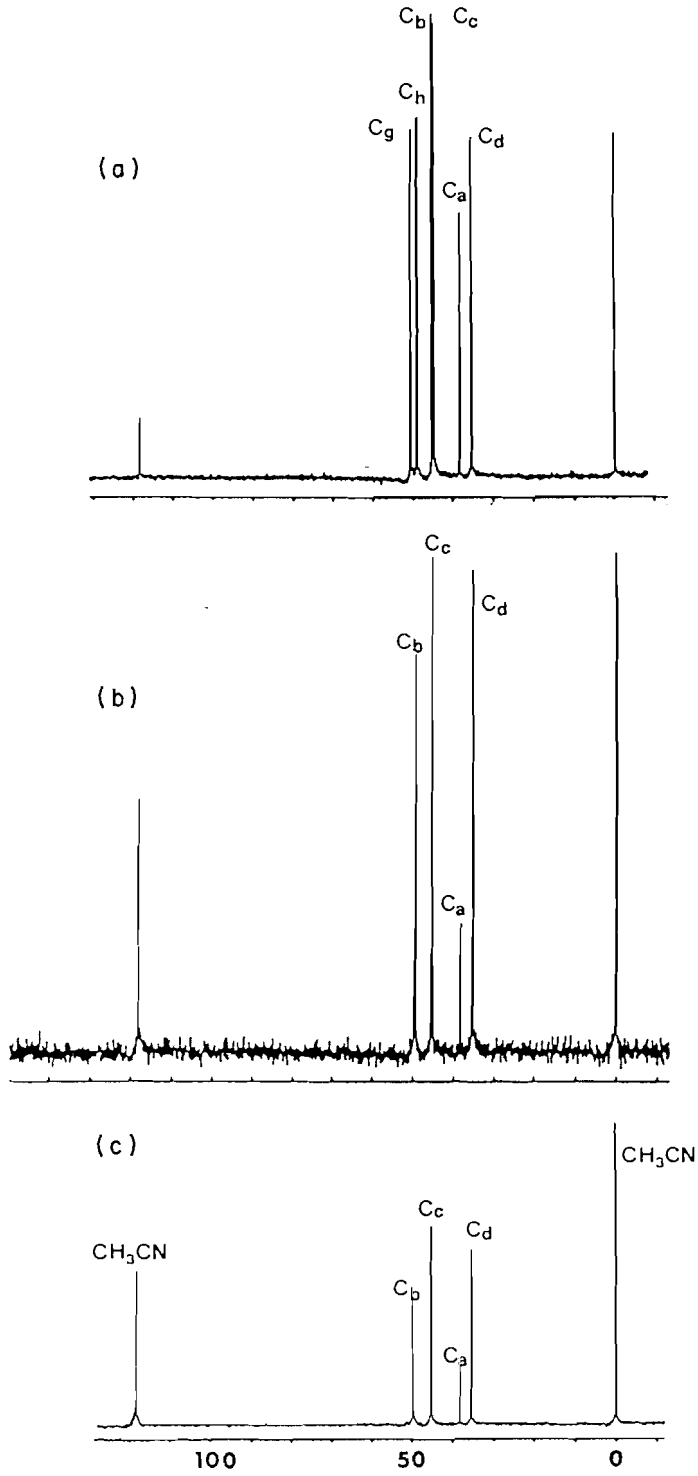
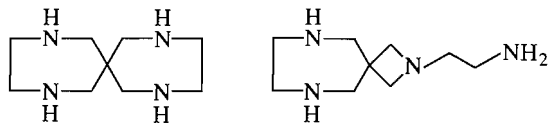


FIG. 1. The ^{13}C nmr spectra of hydrochloride salts of amines (a) L_1, (b) L_2, and (c) L_3 in D_2O with CH_3CN as internal reference.

Can. J. Chem. Downloaded from www.nrcresearchpress.com by 194.225.253.170 on 09/07/12
For personal use only.

amines L_1, L_3, and ethylenediamine are not too distinctly different, the observed values were found to be consistent when the reaction was repeated several times. However, the anhydrous amine salts gave distinctly different values.

The amine hydrochlorides were quite stable and could be stored indefinitely without any deterioration. The amine L_2, refluxed in concentrated HCl, and at pH 14, did not show any sign of decomposition, as indicated by the ^{13}C nmr spectrum. The amine L_1 was quite stable in acidic conditions but the free amine in nonaqueous media (for example in ethanol) showed signs of decomposition. The major decomposition product identified showed a m/e = 184, indicating the loss of an ethylenediamine moiety. The ^{13}C nmr spectra indicated this decomposition product to be **II** rather than **I**. This finding explains the impure product mixture obtained during cyclization and subsequent reduction of the lactam obtained in the case of amine L_1. Cyclization of amine L_1 carried out at room temperature over long periods of standing has provided better yields of the products.



I II

Crystal structures

Although there were limitations in the data sets, the basic structural features of the molecules were exhibited and confirmed. Both $[H_6(L_1)Cl_6]\cdot 4H_2O$ and $[H_8(L_2)Cl_8]\cdot 2H_2O$ provided weak data sets with somewhat poor residuals. However, the X-ray results are complementary to the other chemical observations reported. The structures of ions $[H_8(L_2)]^{8+}$ and $[H_6(L_1)]^{6+}$ are shown with the atomic labelling scheme in Figs. 2 and 3 respectively. The fractional coordinates are provided in Tables 2 and 3 respectively. Details of bond lengths and angles and intermolecular distances are given in Supplementary Tables S1–S6.[6]

The quaternary or "spiro" carbon, C(4), of the ion $[H_8(L_2)]^{8+}$ occupies a special position in the unit cell, lying on a twofold axis. Thus, the asymmetric unit consists of one half of the molecular or two of the arms. The bond lengths from C(4) to C(3) and C(5) are typical of C—C single bonds but one of the two sets of internal angles is slightly larger than the tetrahedral value (114(2)° vs. 109.4°), as has been seen in fully extended aliphatic chains. As can be seen from Fig. 2, the ion is essentially shaped like a flat cross with two of the arms above and below the plane containing the C(4). The distension in the C(3)—C(4)—C(5) (114(2)°) angle serves to move the arms further away from this plane than would be dictated by tetrahedral geometry. This is reflected in the C(5)—C(4)—C(5)′ (101(2)°) and C(3)—C(4)—C(3)′ (99(2)°) angles, which are less than the tetrahedral value. Presumably this distortion serves to lengthen the distance between the secondary amines, N(2) and N(3), and lessen any electrostatic interactions.

A structurally related ion is the protonated amine, tetrakis-(aminomethyl)methane $[H_4(tam)]^{4+}$, reported by Cameron *et al.* (3). This cation is described as adopting a planar rather than globular geometry, with the cation and anions occupying narrow "slabs" within the unit cell. In both the structure of $[H_4(tam)]^{4+}$ and $[H_8(L_2)]^{8+}$, the pentaerythrityltetraamine fragment adopts a very similar geometry. In $[H_8(L_2)]^{8+}$, the aminoethyl groups provide a further extension of this type of geometrical arrangement, lying essentially in the same plane as the central core. The unit cell for $[H_8(L_2)]Cl_8\cdot 2H_2O$ is provided in Fig. 4 and may be viewed as the stacking of flat cations along the twofold axes with the chloride and water molecules dispersed interstitially.

The crystal packing forces arise from the interactions in an

[6]These tables may be purchased from the Depository of Unpublished Data, CISTI, National Research Council of Canada, Ottawa, Ont., Canada K1A 0S2.

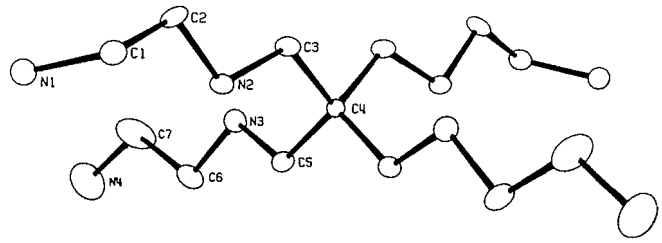


FIG. 2. ORTEP diagram of cation $[H_2(L_2)]^{8+}$ with atomic labelling (25% thermal ellipsoids are shown).

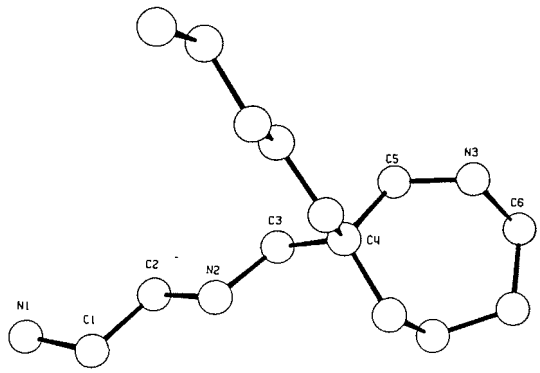


FIG. 3. ORTEP diagram of cation $[H_6(L_1)]^{6+}$ with atomic labelling.

TABLE 2. Fractional atomic coordinates and temperature parameters for $[H_8(L_2)]Cl_8\cdot 2H_2O$

Atom	x/a	y/b	z/c	U_{eq}
Cl(1)	7665(5)	4455(4)	665(4)	44(2)
Cl(2)	−522(5)	6371(4)	453(5)	43(2)
Cl(3)	3933(6)	5082(4)	1546(5)	48(2)
Cl(4)	−80(7)	7729(4)	2835(5)	71(3)
N(1)	−59(15)	4644(12)	1432(13)	40(7)
N(2)	1658(14)	6121(10)	1315(12)	29(7)
N(3)	723(13)	8181(11)	844(13)	32(7)
N(4)	−1941(19)	8818(17)	−1(19)	83(12)
C(1)	1068(19)	4699(13)	1660(16)	33(9)
C(2)	1364(18)	5516(14)	2093(15)	30(8)
C(3)	2153(17)	6852(13)	1773(15)	27(8)
C(4)	2500	7500	1066(19)	16(10)
C(5)	1639(18)	7760(13)	380(16)	29(8)
C(6)	−64(21)	8398(15)	94(17)	38(9)
C(7)	−1057(23)	8683(23)	643(2)	94(15)
O(1)	2060)21)	1520(22)	2679(3)	19(2)

Estimated standard deviations are given in parentheses.
Coordinates $\times 10^n$ where $n = 4$ for Cl,O,N,C.
Temperature parameters $\times 10^n$ where $n = 3$ for Cl,O,N,C.
U_{eq} = the equivalent isotropic temperature parameter.
$U_{eq} = 1/3\,\Sigma_i\Sigma_j U_{ij} a_i^* a_j^* (a_i \cdot a_j)$.

TABLE 3. Fractional atomic coordinates and temperature parameters for $[H_6(L_1)]Cl_6 \cdot 4H_2O$

Atom	x/a	y/b	z/c	U_{eq}
Cl(1)	3816(2)	3758(3)	−209(2)	264(10)
Cl(2)	3002(2)	−1378(3)	2573(2)	306(11)
Cl(3)	3861(2)	−2490(3)	−325(2)	328(11)
O1)	2029(6)	821(10)	333(3)	37(3)
O)2)	4460(6)	446(10)	345(4)	42(4)
N(1)	2778(6)	468(10)	49(7)	25(3)
N(2)	4236(6)	2148(9)	148(7)	16(3)
N(3)	5306(6)	5808(10)	353(7)	20(3)
C(1)	3481(8)	490(14)	52(9)	31(4)
C(2)	3413(7)	1401(12)	131(4)	20(4)
C(3)	4179(7)	3102(11)	221(3)	16(4)
C(4)	5000	3855(14)	250	9(4)
C(5)	4770(7)	4699(10)	330(7)	14(4)
C(6)	4938(8)	6977(11)	300(4)	20(4)

Estimated standard deviations are given in parentheses.
Coordinates $\times 10^4$ for Cl,O,N,C.
Temperature parameters $\times 10^n$ where $n = 4,3,3,3$, for Cl,O,N,C.
U_{eq} = the equivalent isotropic temperature parameter.
$U_{eq} = 1/3\Sigma_i\Sigma_j U_{ij} a_i^* a_j^* (a_i a_j)$.

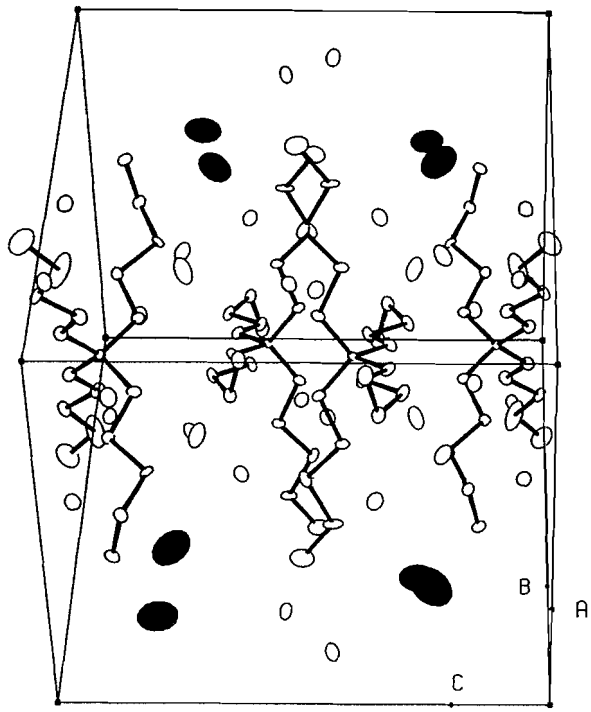


FIG. 4. Unit cell diagram of $[H_8(L_2)]Cl_8 \cdot 2H_2O$ showing stacks of cations and anions in layers. Filled and open ellipses represent oxygen and chlorine atoms respectively.

extensive array of hydrogen bonds. The absence of locatable hydrogens from the crystal structure necessitates that the information on hydrogen bonding be derived from the distances between the atoms (A--B) rather than the distance between the proton and the donor atom (H--B) (16).

Within the lattice, there are a number of short intermolecular contacts. Of particular note are the distances N(2)--Cl(1) (3.09(2) Å), N(2)--Cl(2) (3.08(3) Å), N(3)--Cl(3) (3.10(3) Å), and N(3)---Cl(4) (3.09(3) Å), which are significantly shorter than the sum of the van der Waals (17) radii (3.3 Å) for N and Cl. These distances are typical of hydrogen bonding interactions in $[H_4(tam)]Cl_4$ where the shortest N—H--Cl distance is 3.15 Å and in Et_3N—H---Cl with a distance of 3.10 Å (18). Indeed, the distances are considerably shorter than the 3.2 Å observed in $NH_2OH \cdot HCl$ (19). Several other slightly longer N---Cl distances linking the remaining amines are listed in Supplementary Table S2.

Of particular note in this structure is the absence of hydrogen bonding between the water of crystallization and the nitrogens of the cation. The O(1) atom has only very long interactions with the chlorides, the shortest of which is to Cl(2) with a distance of 3.31(2) Å. This is in contrast to the crystal structure of $[H_6(L_1)]Cl_6 \cdot 4H_2O$ (*vide infra*).

The structure of $[H_6(L_1)]^{6+}$ is shown in Fig. 3. The quaternary carbon is located on a twofold axis within the unit cell that bisects the seven-membered ring, and thus the asymmetric unit is one-half of the cations and anions. The cations are oriented within the unit cell into planes with a head-to-tail arrangement. That is, within the planes of cations, the arms of one cation are overlapped with the rings of the adjacent molecular ions. In addition, the different planes are staggered to provide the head-to-tail overlap. Also, the anions and waters of crystallization occupy sites within the planes rather than being dispersed interstitially. A diagram of the unit cell is provided in Fig. 5.

The quaternary carbon has essentially the same distorted tetrahedral structure in both the ions $[H_6(L_1)]^{6+}$ and $[H_4tam]^{4+}$, with the interior angle separating the two arms being slightly larger than the ideal tetrahedral angle (116.7(1.3)° vs. 109.4°). This distortion serves to increase the distance between N(2) and N(2)′, decreasing electrostatic interactions. Within the seven-membered ring, the C(5)—C(4)—C(5)′ angle is 110.2(1.2)°, which is typical of the value expected for a cyclic compound and indicates very little distortion of the bonding within the ring. This is to be anticipated since the rigidity of the cyclic structure would prevent large distortions in the bonding. Further evidence for the distortion of the tetrahedral structure is provided by the C(3)—C(4)—C(5) angle, which is 102.4(6)°. Essentially, the geometry of the spiro carbon implies a close similarity of structure between the three cations $[H_6(L_1)]^{6+}$, $[H_8(L_2)]^{8+}$, and $[H_4(tam)]^{4+}$.

The crystal packing forces are provided by an extensive network of hydrogen bonding interactions within the lattice. Information on hydrogen bonding was derived from the interatomic distances as given above, with distances of 2.9 Å for the N--O and 3.2 Å for the Cl--O interactions (16).

Within the lattice, there are a number of short intermolecular contacts. The positioning of the O(2) atom is of particular interest as it serves to bridge N(2) with its symmetry generated partner N(2)′. The bridge is asymmetric with one N(2)--O(2) distance being 2.76(3) Å and the other 3.40(3) Å. The latter distance is slightly longer than might be anticipated but the positioning of the water molecule would certainly suggest that it interacts with both nitrogens. Also, N(2) has a very short contact distance (3.00(3) Å) with Cl(1).

In addition to the binding of O(2), the water molecule incorporating O(1) is bound to N(3) (2.81(3) Å) and to N(1) (3.22(3) Å) of a different cation. This arrangement is facilitated by the head-to-tail arrangement of the cations within the planes. A number of other close contacts are observable within the unit cell and these are included in the intermolecular distances given in Supplementary Table S5.

Of particular interest in this structure is the absence of strong interactions between the adjacent planes of cations / anions. The closest approach is a long interaction between N(3) and Cl(1) at 3.43(3) Å. This suggests that the planes within the unit cell are

Can. J. Chem. Downloaded from www.nrcresearchpress.com by 194.225.253.170 on 09/07/12
For personal use only.

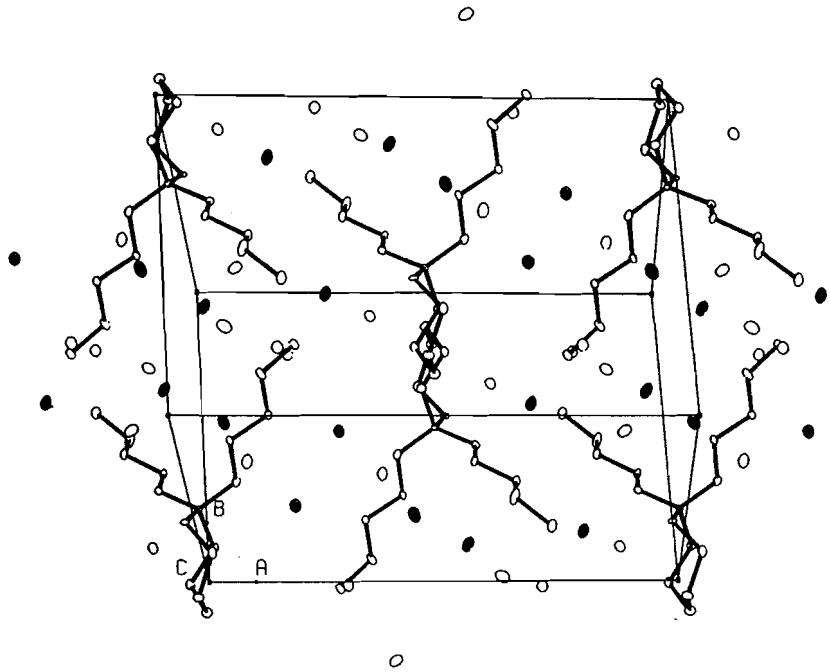


FIG. 5. Unit cell diagram of $[H_6(L_1)]Cl_6 \cdot 4H_2O$. Head-to-tail arrangement of cations is shown. Filled and open ellipses represent oxygen and chlorine atoms respectively.

predominantly internally bonded and the stacking of the planes is a result of other interactive forces, with the closest approach being the van der Waals surfaces.

Conclusion

Interest in these polydentate amine ligands comes from their preparation and characterization prior to their use in the synthesis of metal complexes.

The amine L_1 and its cyclized derivatives form mononuclear complexes with transition metal ions. In the seven-membered ring of the ligand L_1, one of the nitrogen atoms is protonated while the metal complexes are formed. This cationic moiety acts as an anion binding site close to the metal centre. Redox reactions involving perchlorate anion and divalent nickel complexes have been reported recently by Fabbrizzi and co-workers (20) in the case of *N*-aminoethylcyclam. Ni^{2+} complexes of amines L_1 and L_2 have been found to exhibit such redox activity, and the trivalent nickel complex has been isolated in the case of ligand L_6 and characterized crystallographically[5].

Ligands L_3, L_5, and L_7 are binucleating. Homo- and heterobinuclear complexes of ligand L_7 have been prepared and characterized (21). The binuclear Ni^{2+} complex of ligand L_2 crystallizes in several forms depending upon the counteranion. X-ray crystallographic studies have shown that both Ni^{2+} centres can exist either in low spin square planar form or as a mixed low spin – high spin form depending upon the nature of the counteranion. Recently, in a polyketo system (biacetylacetone) of a binuclear nickel complex, Fukuda and Mafune (22) have shown the geometry around the nickel centres to be variable. Crystal structures and detailed reactivity studies of the complexes of the ligands L_1–L_7 have been made and will be reported elsewhere.

Acknowledgements

We would like to thank NSERC and the University of Victoria for financial support. The award of Fellowships (T.W.W., NSERC; S.S., University of Victoria) is also acknowledged. Helpful comments from referees are appreciated.

1. G. R. NEWKOME, Z. YAO, G. R. BAELER, and V. K. GUPTA. J. Org. Chem. **50**, 2003 (1985).
2. A. LITHERLAND and F. G. MANN. J. Chem. Soc. 1588 (1938).
3. T. S. CAMERON, W. J. CHUTE, and O. KNOP. Can. J. Chem. **63**, 586 (1985).
4. R. W. OEHMKE and J. C. BAILAR, JR. J. Inorg. Nucl. Chem. **27**, 2199 (1965).
5. L. J. ZOMPA and R. F. BOGUCKI. J. Am. Chem. Soc. **88**, 5186 (1966).
6. A. MCAULEY, S. SUBRAMANIAN, and T. W. WHITCOMBE. J. Chem. Soc. Chem. Commun. 539 (1987).
7. B. BOSNICH, R. D. GILLARD, E. D. MCKENZIE, and G. A. WEBB. J. Chem. Soc. (A), 1331 (1966).
8. R. RIEMSCHNEIDER, O. GOEHRING, P. GROSS, A. ROOK, K. BRENDL, and C. FARIA. Monatsch. Chem. **96**, 147 (1965).
9. G. M. SHELDRICK. SHELX76, Programme for crystal structure refinement. University of Cambridge, UK. 1976.
10. D. T. CROMER and J. B. MANN. Acta. Crystallogr. Sect. A: Cryst. Phys. Diffr. Theor. Gen. Crystallogr. **24**, 321 (1968).
11. A. T. PHILIP. Aust. J. Chem. **21**, 2301 (1968).
12. L. R. GAHAN, H. E. HART, C. H. L. KENNARD, M. A. KINGSTON, G. SMITH, and T. C. W. MAK. Inorg. Chim. Acta, **5**, 116 (1986).
13. I. TABUSHI, Y. TANIGUCHI, and H. KATO. Tetrahedron Lett. 1049 (1977).
14. R. J. GEUE and G. H. SEARLE. Aust. J. Chem. **36**, 927 (1983).
15. L. FABBRIZZI, P. PAOLETTI, and R. BARBUCCI. Inorg. Chem. **12**, 1961 (1973).
16. S. N. VINOGRADOV and R. H. LINNELL. Hydrogen Bonding. Van Nostrand Reinhold, Toronto, Ont. 1971.
17. H. BONDI. J. Phys. Chem. **68**, 441 (1964).
18. F. GENET. Bull. Soc. Fr. Min. Crist. **88**, 463 (1965).
19. J. A. IBERS. Ann. Rev. Phys. Chem. **16**, 375 (1965).
20. P. S. PALLAVIANI, A. PAOLETTI, A. POGGI, B. SEGHI, and L. FABBRIZZI. J. Am. Chem. Soc. **109**, 5139 (1987).
21. A. MCAULEY and S. SUBRAMANIAN. 70th Canadian Chemical Conference, Québec, P.Q. 1987. Abstracts no. ING-66-G2.
22. Y. FUKUDA and K. MAFUNE. Chem. Lett. 697 (1988).

Can. J. Chem. Downloaded from www.nrcresearchpress.com by 194.225.253.170 on 09/07/12
For personal use only.

Molecular structure and relative proton and electron affinities of isomeric nitroimidazoles

SALIM F. FARAH, ROBERT A. MCCLELLAND, MICHAEL R. PETERSON, AND IMRE G. CSIZMADIA
Department of Chemistry, University of Toronto, Toronto, Ont., Canada M5S 1A1

Received February 21, 1989

SALIM F. FARAH, ROBERT A. MCCLELLAND, MICHAEL R. PETERSON, and IMRE G. CSIZMADIA. Can. J. Chem. **67**, 1666 (1989).

The isomeric 2-nitro, 4-nitro, and 5-nitroimidazoles have been studied in their planar ground state, C—NO_2 rotational transition state, 3-H protonated conjugate acid and radical anion forms, with *ab initio* computations at the split-valence 3-21G basis set level. The stabilities of the parent compounds follow the order 5-NO_2 ~ 4-NO_2 > 2-NO_2. In solution 4-nitro is more stable than 5-nitro; the calculations suggest that this is a solvation effect, since the 4-nitro isomer has a considerably higher dipole moment. Barriers for nitro group rotation range from 10 to 16 kcal/mol. However, the relative change in dipole moment during the rotation is small, suggesting that dipole moments of nitroimidazoles are determined mainly by inductive effects, with resonance interactions being relatively unimportant. This conclusion is supported by calculations of molecular electrostatic potentials of the planar and rotated forms. Electron affinities follow the order 2-NO_2 > 5-NO_2 >> 4-NO_2, closely matching the order of biological effectiveness of nitroimidazole radiosensitizers. This is consistent with suggestions that the "nitro:nitro radical anion" redox cycle is an important determinant of biological activity.

Key words: nitroimidazole, *ab initio* computation, rotational barrier, proton affinity, electron affinity.

SALIM F. FARAH, ROBERT A. MCCLELLAND, MICHAEL R. PETERSON et IMRE G. CSIZMADIA. Can. J. Chem. **67**, 1666 (1989).

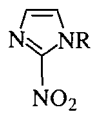
Opérant au niveau de l'ensemble de base 3-21G, on a effectué des calculs *ab initio* sur les 2-nitro, 4-nitro et 5-nitroimidazoles dans leur état fondamental pla, dans leur état de transition de rotation du C-NO_2 ainsi que sous les formes acide conjugué et radical anionique de la forme protonée en 3-H. Les stabilités relatives des composés de base suivent l'ordre suivant : 5-NO_2 ~ 4-NO_2 > 2-NO_2. En solution, le 4-nitro est plus stable que le 5-NO_2; les calculs indiquent que cette situation est le résultat d'un effet de solvatation dû au moment dipolaire beaucoup plus élevé du 4-nitro. Les barrières à la rotation du groupement nitro varient de 10 à 16 kcal/mol. Toutefois, le changement relatif du moment dipolaire au cours de la rotation est faible; ce résultat suggère que les moments dipolaires des nitroimidazoles sont principalement déterminés par des effets inductifs alors que les interactions de résonance ne sont pas très importantes. Cette conclusion est supportée par des calculs de potentiels électrostatiques moléculaires des formes planes et celles ayant subi une rotation. Les affinités électroniques sont dans l'ordre 2-NO_2 > 5-NO_2 >> 4-NO_2; cet ordre ressemble beaucoup l'ordre observé pour l'efficacité biologique des nitroimidazoles comme radiosensibilisateurs. Cette conclusion est en accord avec les suggestions suivant lesquelles le cycle rédox de l' «anion radical nitro:nitro» est un déterminant important de l'activité biologique.

Mots clés : nitroimidazole, calcul *ab initio*, barrière à la rotation, affinité protonique, affinité électronique.

[Traduit par la revue]

Can. J. Chem. Downloaded from www.nrcresearchpress.com by 194.225.253.170 on 09/07/12
For personal use only.

A class of drugs which has seen active investigation over the past few years is the nitroaromatics. Solid tumors develop regions where the cells are hypoxic (deficient in oxygen), and because of this are resistant to radiation therapy. Nitroaromatics function as sensitizers (1–4), selectively enhancing the response of these hypoxic cells to radiation, and the 2-nitroimidazoles misonidazole (5) and SR-2508 (6) are currently in clinical trial in this respect.

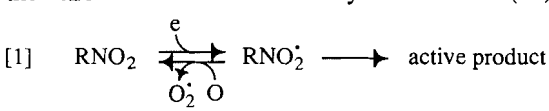


R = $CH_2CHOHCH_2OCH_3$ (Misonidazole)

R = $CH_2CONHCH_2CH_2OH$ (SR-2508)

The development of these particular drugs arose from observations that more powerful oxidizing agents were more efficient sensitizers (7). The sensitizing effect is believed to be related to an interaction of the nitro compound with electron excess or free radical centers on DNA with the concomitant formation of nitro radical anions (8). Thus there is a direct correlation between radiosensitizing ability of nitroaromatics and their one-electron reduction potential (9).

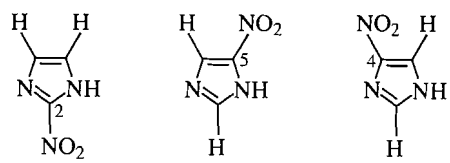
The 2-nitroimidazoles have also been found to be selectively toxic towards hypoxic tumor cells, that is, preferentially killing cells which are oxygen deficient (10). The model for this has the nitro radical anion as the key intermediate (11).



[1] $RNO_2 \underset{O_2\ O}{\overset{e}{\rightleftharpoons}} RNO_2^{\cdot} \longrightarrow$ active product

In this case, the radical anion species is produced in the cell by electron transfer to the nitro compound from cellular nitroreductase enzymes. When high concentrations of oxygen are present, the radical anion simply transfers its extra electron to the more electron affinic oxygen, a process known as "futile reduction" (3) which regenerates the parent nitro compound. At low concentrations of oxygen further reduction can occur. The toxicity observed under these conditions is believed to arise from the action of one or more of these further reduction products (active product), and indeed a synthetic 2-nitrosoimidazole has recently been found to be very biologically active (12).

In this paper we address at the theoretical level the question of the geometry, conformation, electron affinity, and proton affinity of the parent 2-, 4-, and 5-nitroimidazoles.

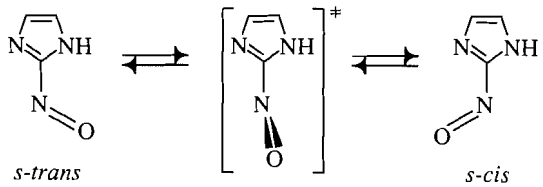


An understanding of various aspects of the chemistry and related biological effects were the objectives of this research. For example, the experimental electron affinity decreases in the order 2-NO_2 > 5-NO_2 > 4-NO_2, which also represents the order of biological activity (3). Additionally some nitroimidazoles show enhanced radiosensitization when there is also present a group which is protonated at physiological pH (13,

TABLE 1. Total energies in hartrees of nitroimidazole isomers

Parameter	Value		
	2-NO_2	4-NO_2	5-NO_2
Total energy (3-21G)	−425.83174	−425.83714	−425.83725
Total energy (6-31G*)	−428.26876	−428.27441	−428.27410
E(6-31G*) − E(3-21G)	−2.43702	−2.43727	−2.43685

14). On their own, nitroimidazoles are, however, weak bases with pK_a values (for the conjugate acids of 1-methyl derivatives) of −0.5, +0.6, and +2.3 for 2-nitro, 4-nitro, and 5-nitro, respectively (15). Finally, in a previous communication (16) 2-nitrosoimidazole was examined at the theoretical level, the calculations revealing that planar *s-cis* and *s-trans* forms were stable minima, with the *s-trans* 2.5 kcal/mol lower in energy. The transition state for rotation of the C—NO bond was found to have a twisting angle of 93.3°, with the barrier to rotation from the *s-trans* form of 13.0 kcal/mol.

[2] 

Methods

The internal coordinates (bond lengths and bond angles) of the nitroimidazoles, and the transition states for rotation of the nitro group were geometry optimized using the split-valence 3-21G basis set within the Restricted Hartree–Fock formalism (17–19) (Unrestricted Hartree–Fock in the case of the anions) using the analytic gradient of the SCF energy with respect to the internal geometrical parameters. The optimally conditioned (OC) algorithm (20) was employed to determine the optimal geometry. Geometries were regarded as converged when the internal coordinate derivatives of the parameters were less than 0.001 Å for bond lengths or 0.01° for bond angles, and the parameter gradient lengths fell below 5×10^{-4} mdyn. This is generally sufficient to give bond lengths within 0.0001 Å and bond angles within 0.01° of the true minimum. Once a converged geometry had been obtained for a given conformation, it was determined by finite differences of gradients using the minimization of the sums of squares algorithm VAO5AD (21) whether or not this structure represented a minimum on the potential energy surface. The order of minima must be zero, while transition states must have an order of one. All computations were performed on the Gould 32/9705 computer system at the University of Toronto using the MONSTERGAUSS *ab initio* programme (22).[1]

Results and discussion

Computations in this study were generally performed at the 3-21G basis set level. This sees wide applicability to molecules of moderate size, and while it has the same number of primitives as the minimal STO-3G basis set (23), it contains nearly twice the number of contracted basis set functions per atom. The 3-21G basis set has been shown to be superior to STO-3G as a means for determining equilibrium geometries and force constants, for comparing geometries with experimental studies and for assessing relative molecular energies (24). Energies of the three parent neutral compounds were also calculated using the more extensive 6-31G* basis set, using the planar optimal geometries obtained at the 3-21G level. As shown in Table 1 the differences in the total energies of the parent nitroimidazoles were nearly the same in the two basis sets.

Geometry and conformation of nitroimidazoles

The initial estimate for the geometry of 2-nitroimidazole was based upon a previously optimized geometry for 2-nitrosoimidazole (16). However, the SCF failed to converge at the 3-21G basis set level, both in the planar ground state and in the torsional transition state. Thus the conformations were first optimized at the STO-3G basis set level, the molecular coefficients were extracted from these geometries, and these were employed via coefficient matrix projection to initiate the optimizations in the 3-21G basis set. In the case of the 4- and 5-nitroimidazoles, initial guesses were based upon the optimized geometries for the 2-nitroimidazole obtained in the 3-21G basis set and no problems were encountered in the SCF convergence. All optimized geometries were order-checked using the minimization of the sum of squares VAO5AD (21). Within this programme, there exists the option of determining second derivatives for all parameters or only for those of particular interest, such as parameters whose perturbation would break the symmetry of the molecule. In this study, the second option was chosen since all molecules possess a plane of symmetry allowing optimization within the C_S symmetry. For the torsional transition state structures, all orders were found to be equal to unity, while for the other structures orders were found to be zero.

The bond lengths and angles obtained with the planar ground states and the transitions state for carbon—nitro group rotation are shown in Fig. 1, with the rotational barriers and torsion angles in the transition state given in Table 2. The latter is very close to 90° in case of the 2-nitro isomer, and is about 7° off the perpendicular for the other two. One interesting feature of the data for the 2-nitroimidazole is that the barrier, 12.4 kcal/mol, is very similar to that previously obtained, 13.0 kcal/mol for the 2-nitrosoimidazole analog (16). These barriers arise through the interaction in the fully planar forms of the electron-rich π electrons of the imidazole ring and the π electrons of the nitro and nitroso substituents. The conclusion is that these two substituents are affected in a very similar way. It is also interesting to note that the barrier to rotation calculated for nitrobenzene, 8.5 kcal/mol (6-31G basis set) (25), is not that much smaller than those obtained here.

Dipole moments

Table 3 lists dipole moments for the three isomers obtained

[1]This program uses the integral and derivative routines from Gaussian 80, J. A. Pople, Department of Chemistry, Carnegie-Mellon University.

Can. J. Chem. Downloaded from www.nrcresearchpress.com by 194.225.253.170 on 09/07/12
For personal use only.

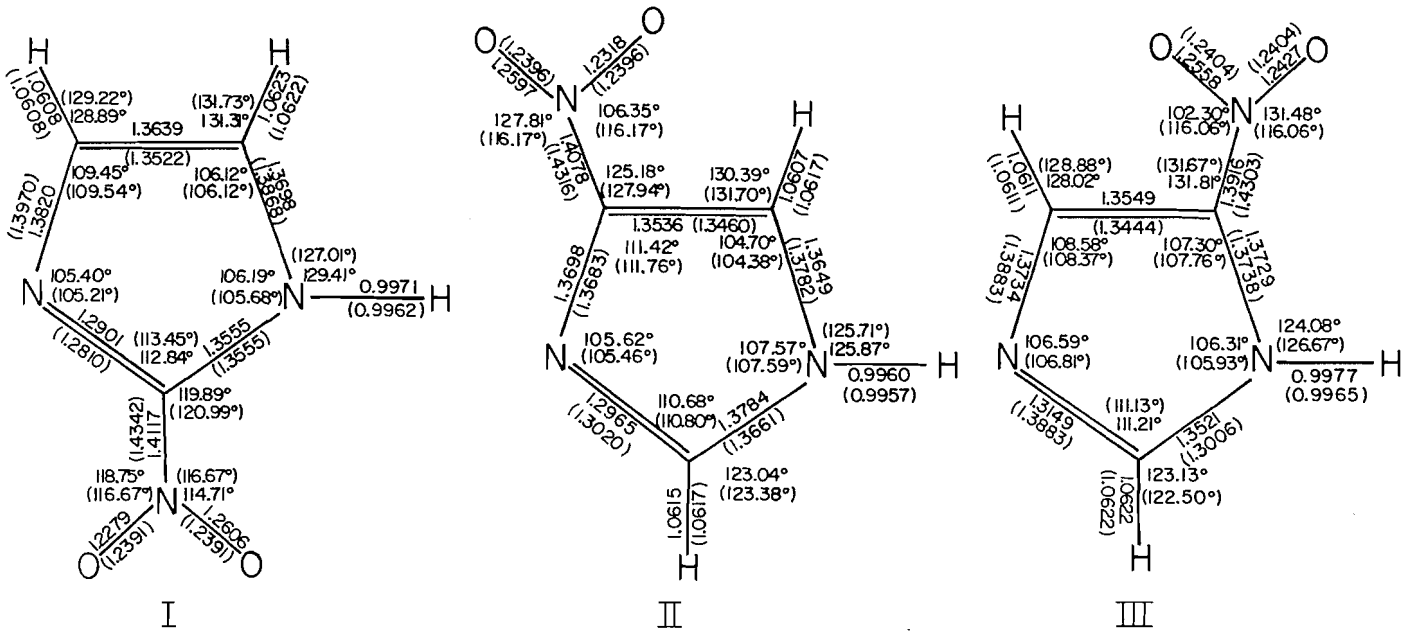


FIG. 1. Bond lengths and bond angles of nitroimidazoles. Numbers in parentheses represent the torsional transition states (3-21G calculations).

TABLE 2. Barriers (kcal/mol) for nitro group rotation in 2-nitro-, 4-nitro-, and 5-nitroimidazoles calculated with the 3-21G basis set

Parameter	Value		
	2-NO_2	4-NO_2	5-NO_2
E(TS) − E(PC)[a]	12.4	10.6	15.5
TAU[b]	90.77	82.82	97.52

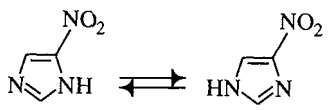
[a]TS = transition state for nitro group rotation. PC = planar ground state.
[b]Torsion angle in degrees of the nitro group in the transition state.

TABLE 3. Melting points and calculated dipole moments (3-21G basis set) of nitroimidazoles

Parameter	Value		
	2-NO_2	4-NO_2	5-NO_2
Melting point (1-H)[a]	284(dec)[b]	308(dec)[c]	—[d]
Melting point (1-Me)	102[e]	133[f]	51[g]
Dipole moment[h] (GS)	6.00	8.23	3.88
Dipole moment[h] (TS)	5.93	7.94	3.54

[a]Parent nitro compound.
[b]Reference 26.
[c]Reference 27.
[d]Unknown. 4-Nitroimidazole is stable tautomeric form.
[e]Reference 15.
[f]Reference 28.
[g]Reference 29.
[h]Dipole moments in Debyes calculated for parent 2-nitroimidazoles planar ground state (GS) and torsional transition state (TS) forms.

from the 3-21G calculations. For both the planar and torsional forms, these show an order 5-NO_2 < 2-NO_2 < 4-NO_2. This order does not match that observed for biological effects of nitroimidazoles, with the implication that with this class of agents the polarity of the parent drug is a relatively unimportant factor in determining its efficiency. The order does, however, correctly predict the experimental order of melting points. In general, as the dipole moment of a series of isomers increases, the melting point increases, and this is the case here as well. The pattern is most clearly seen with the melting points for the 1-methyl substituted nitroimidazoles. The parent 2-nitro- and 4-nitroimidazoles also show the correct order, but there is no experimental number for the 5-nitroimidazole. This is due to the fact that in condensed phases 5-nitroimidazole spontaneously tautomerizes to its 4-nitro isomer (30).



The usual argument is that the 4-nitro isomer is more stable because it has better resonance interactions between the nitro group and the aromatic ring. Our calculations, however, indicate that there is very little difference in energy between 4-nitroimidazole and 5-nitroimidazole, the 5-nitro isomer being 0.07 kcal/mol lower in energy at the 3-21G level and 0.19 kcal/mol higher in energy at the 6-31G* level (Table 1). These calculations of course can only be directly compared to gas phase experimental results, while in fact the above conclusion about the position of equilibrium refers to condensed phases, in particular polar solvents. We suggest that the favoring of the 4-nitro tautomer observed in the latter case is principally a solvation phenomenon. The calculated dipole moments (Table 3) indicate that the 4-nitroimidazole is considerably more polar, and thus will be more strongly solvated in polar solvents. There are in fact a number of heterocyclic tautomerizations with dramatic changes in the position of equilibrium between the gas phase and solution associated with polarity differences between the two isomers (31).

With each nitroimidazole the dipole moment is seen to decrease on proceeding from the planar ground state to the torsional transition state (Table 3). This is expected since rotating the nitro group out of the plane of the ring prevents the conjugation of the type shown below for the 2-nitro isomer.

Can. J. Chem. Downloaded from www.nrcresearchpress.com by 194.225.253.170 on 09/07/12
For personal use only.

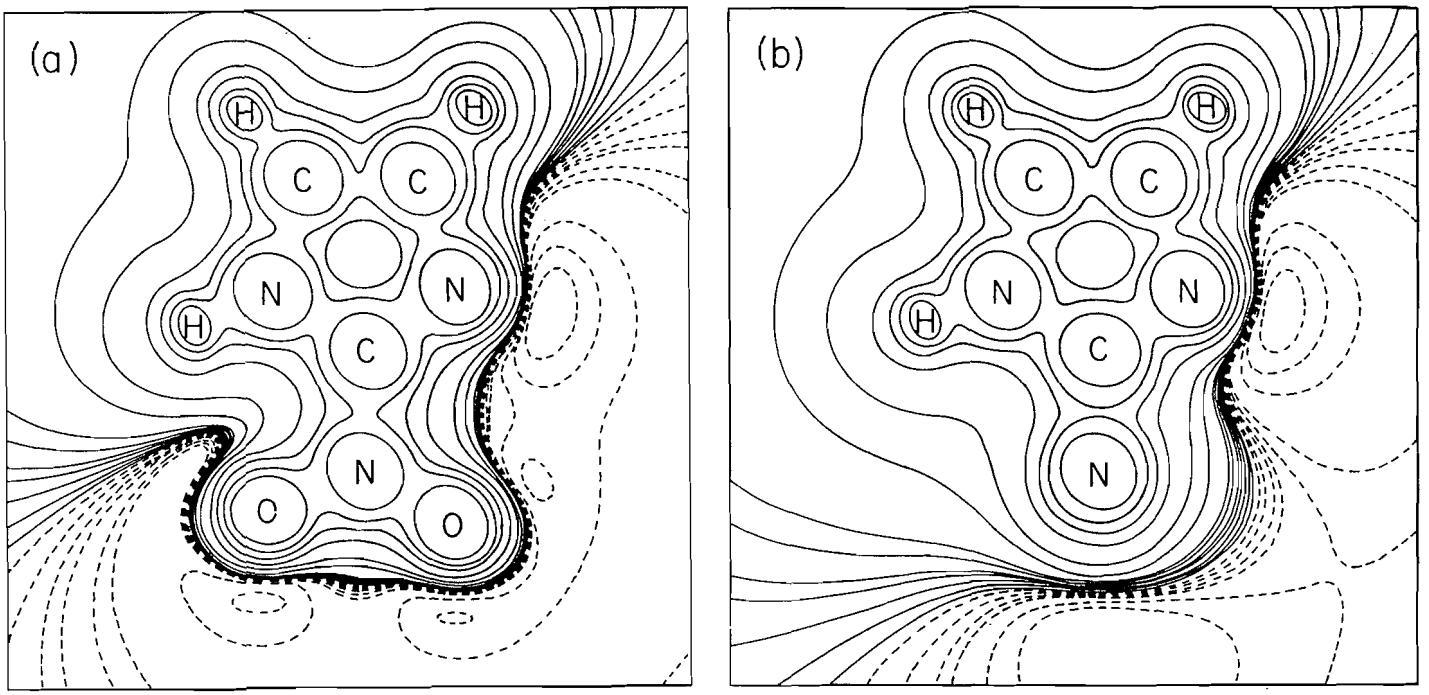
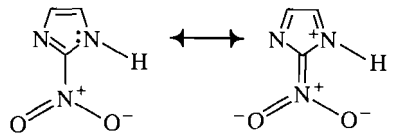


FIG. 2. Calculated electrostatic potentials of the planar (*a*) and rotated (*b*) forms of 2-nitroimidazole in the plane of the imidazole ring. Dashed contours correspond to negative potentials.



Consistent with this idea, it is observed that with each nitroimidazole a small increase in the length of the carbon—nitro bond in the transition state as compared to the ground state (Table 4). Interestingly, however, the changes in both the dipole moments and the bond lengths for each nitroimidazole are rather small. This would suggest that the resonance interaction has a minor effect, and that the principal contribution of the nitro group to the dipole moment is inductive, that is an interaction which is not affected by the loss of conjugation in the rotated form. The relative unimportance of the resonance interaction of nitro groups attached to benzene rings has been noted previously, nitro for example having a large value for its σ_I substituent constant but a small σ_R (32). What is somewhat surprising in the present case is that the imidazole ring is a π electron-rich system, capable, for example, of interacting with adjacent carbenium ion centers more strongly than a *p*-methoxyphenyl ring (33). However, even the imidazole–nitro combination does not apparently result in a greater resonance effect. This lack of importance of resonance would also explain why the barriers of rotation in nitroimidazoles and nitrobenzene are similar. Strong resonance interactions would predict greater barriers in the former.

Electrostatic potentials

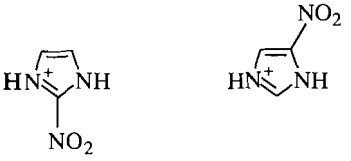
The relatively small degree of conjugation in nitrobenzene has also recently been established by Politzer and co-workers, through a computational analysis of the planar and rotated forms (25). One indicator used by these authors was the similarity in the electrostatic potentials of the two forms. We have carried out similar calculations for the nitroimidazoles. The results for the 2-nitro derivative are presented in Fig. 2; similar profiles are found with the other isomers. In the molecular planes of the planar forms there are apparent large regions of negative potential which can be attributed to the lone pairs of the oxygens of the nitro group and the ring nitrogen σ lone pair of electrons. The most negative values (local minima) of the potential are −83.6, −86.7, and −86.5 kcal/mole for the 2-nitro-, 4-nitro-, and 5-nitroimidazole, respectively. In the transition state when the nitro is ~90° rotated, these large negative regions remain associated with the lone pairs, and there is little change in the absolute magnitude of the potential, the most negative values being −81.7, −83.9, and −87.6, respectively. These relatively small changes are further indicators of the unimportance of the resonance interaction.

TABLE 4. Carbon–nitrogen (NO_2) bond lengths (Å) of planar and torsional transition state nitroimidazoles (3-21G basis set)

	Bond length (Å)		
Form	2-Nitro	4-Nitro	5-Nitro
Planar form	1.4117	1.4079	1.3916
Transition state	1.4342	1.4316	1.4303

Relative proton affinities

Geometry optimization of the N-3 protonated nitroimidazoles was achieved at the 3-21G basis set level. The protonated forms were in each case about 220 kcal/mol more stable than their neutral conjugate base. (Note that 4-nitroimidazole and 5-nitroimidazole have the same conjugate acid.) The additional stability of the protonated forms is due to the extra N—H bond created during protonation.



Can. J. Chem. Downloaded from www.nrcresearchpress.com by 194.225.253.170 on 09/07/12
For personal use only.

TABLE 5. Total energies of nitroimidazoles and their N-3 protonated conjugate acids (3-21G basis set level)

Parameter	Value		
	2-Nitro	4-Nitro	5-Nitro
$E(\text{Im})^{a,b}$	−425.83174	−425.83714	−425.83725
$E(\text{3-HIm}^+)^{b,c}$	−426.18657	−426.19825	−426.19825
$(E(\text{Im}) - E(\text{3-HIm}^+))^d$	−222.7	−226.6	−226.5
pK_a (3-H-1MeIm$^+$)^e	−0.4	0.6	2.3

[a]Total energy in Hartrees.
[b]Neutral parent imidazole.
[c]N-3 protonated imidazolium ion.
[d]kcal/mol.
[e]Aqueous pK_a values for 1-methyl-*X*-nitroimidazolium ions, from ref. 15.

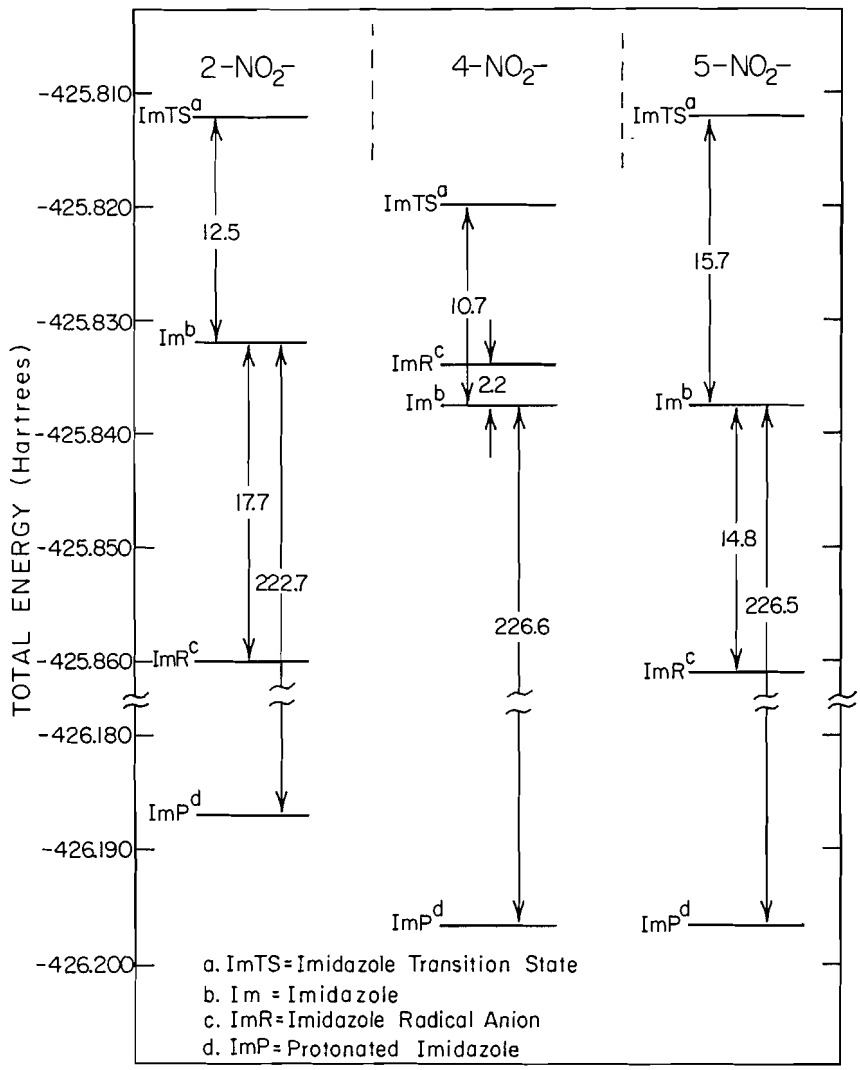


FIG. 3. Total energies of nitroimidazoles (Im), torsional transition states (ImTS), radical anions (ImR), and 3-H protonated conjugate acids (ImP).

Energies of the neutral and conjugate acid forms are compared in Table 5. The 4(5)-nitroimidazolium ion is calculated to be about 7 kcal/mol more stable than the 2-nitroimidazolium isomer, while the relative gas phase proton affinities of the neutral nitroimidazoles follow the order 4-NO_2 ~ 5-NO_2 > 2-NO_2. As illustrated in the last row of Table 5 in aqueous solution the basicity order is 5-NO_2 > 4-NO_2 > 2-NO_2. We have previously suggested that there may be solvation differences on the neutral nitroimidazoles, and this could be behind the differences between gas phase and solution.

Relative electron affinities

The radical anions of the three nitroimidazoles have been SCF geometry optimized in the 3-21G basis set within the

Can. J. Chem. Downloaded from www.nrcresearchpress.com by 194.225.253.170 on 09/07/12
For personal use only.

TABLE 6. Total energies in Hartrees and energy differences in kcal/mol of nitroimidazoles and their anions

Parameter	Value		
	2-Nitro	4-Nitro	5-Nitro
$E(ImNO_2)$	−425.8317	−425.8371	−425.8372
$E(ImNO_2^-)$	−425.8599	−425.8336	−425.8608
$E(ImNO_2^-) - E(ImNO_2)$	−18.69	+2.23	−14.80

(UHF/RHF) formalism. The energies are summarized in Table 6. Recognizing that without Configuration Interaction calculations, the absolute electron affinities must be regarded as being uncertain, the relative electron affinities are probably reasonably accurate as no electron pairs are formed or destroyed during the process of electron capture. These follow the order 2-NO_2 > 5-NO_2 > 4-NO_2, with a particularly large gap between 5-NO_2 and 4-NO_2. These numbers do correlate with the relative biological activities of differently substituted nitroimidazoles, which follow an order in both radiosensitization and hypoxic cytotoxicity of 2-NO_2 slightly more effective than 5-NO_2, with both significantly better than 4-NO_2. As discussed in the Introduction, the biological effects of nitroimidazoles are believed to be closely related to the "nitro:nitro radical anion" redox cycle, and the relationship of biological activity with theoretical electron affinity is therefore not surprising. This excellent correlation does suggest, however, that theory might provide useful new information in predicting biological effects to aid in the design of new drugs. A neurotoxic side reaction is limiting the clinical effectiveness of nitroimidazoles as radiation sensitizers, and there is considerable interest in finding new molecules of similar electron affinity but lacking the nitro group.

Summary

Figure 3 graphically compares the total energies of the species calculated in this work. The relative stability of the parent planar nitroimidazoles is 5-NO_2 ~ 4-NO_2 > 2-NO_2, and this is independent of the basis set (3-21 versus 6-31G*). The similar energy of the 5-NO_2 and 4-NO_2 isomers in the gas phase does not extend to solution, where the 4-NO_2 is more stable. The calculations, however, indicate that this isomer has a significantly higher dipole moment, and it is suggested that a solvation effect is behind the solution order. A comparison of the relative dipole moments of the planar compounds and the torsional transition states indicates that the dipole moments are largely determined by inductive effects, with resonance interactions between the nitro group and the imidazole ring being relatively unimportant. The same conclusion is reached through the analysis of bond angle and electrostatic potential differences between the two forms. The relative electron affinities correlate well with the order of biological activities (2-NO_2 > 5-NO_2 > 4-NO_2). This is consistent with suggestions that the relative stability of the radical anion is an important factor in determining the biological effectiveness of nitroimidazole drugs.

Acknowledgements

This work was supported from grants from the Natural Sciences and Engineering Research Council of Canada and from the National Cancer Institute of Canada.

1. G. E. ADAMS, J. DENEKAMP, and J. F. FOWLER. Chemotherapy, **7**, 187 (1976).
2. J. F. FOWLER, G. E. ADAMS, and J. DENEKAMP. Cancer Treat. Rev. **3**, 227 (1976).
3. P. WARDMAN. Curr. Topics Radiat. Res. **11**, 347 (1977).
4. G. E. ADAMS, J. F. FOWLER, and P. WARDMAN (*Editors*). Br. J. Cancer **37**, Suppl. III (1978).
5. S. DISCHE. Radiother. Oncology, **3**, 97 (1985).
6. C. N. COLEMAN, T. H. WASSERMAN, R. C. URTASUN, J. HALSEY, V. K. HIRST, S. HANCOCK, and T. L. PHILLIPS. Int. J. Radiat. Oncol. Biol. Phys. **12**, 1105 (1986).
7. G. E. ADAMS and M. S. COOKE. Int. J. Radiat. Biol. **15**, 457 (1969).
8. R. L. WILSON, W. A. CRAMP, and R. M. J. INGS. Int. J. Radiat. Biol. **26**, 557 (1974).
9. G. E. ADAMS, E. D. CLARKE, I. R. FLOCKHART, R. S. JACOBS, D. S. SEHMI, I. J. STRATTFORD, P. WARDMAN, and M. E. WATTS. Int. J. Radiat. Biol. **35**, 133 (1979).
10. J. M. BROWN. Int. J. Radiat. Oncol. Biol. Phys. **8**, 1491 (1982).
11. A. M. RAUTH. Int. J. Radiat. Oncol. Biol. Phys. **10**, 1293 (1984).
12. M. NOSS, A. M. RAUTH, R. PANICUCCI, and R. A. MCCLELLAND. Biochem. Pharmac. **37**, 2585 (1988).
13. P. WARDMAN and E. D. CLARKE. J. Chem. Soc. Faraday Trans. **72**, 1377 (1976).
14. R. F. ANDERSON, K. B. PATEL, and C. E. SMITHEN. Int. J. Radiat. Biol. **32**, 471 (1977).
15. G. G. GALLO, C. R. PASQUALUCCI, C. R. RADAELLI, and G. C. LANCINI. J. Org. Chem. **29**, 862 (1964).
16. J. L. BOLTON, R. A. MCCLELLAND, and M. R. PETERSON. Can. J. Chem. **66**, 3044 (1988).
17. D. R. HARTREE. Proc. Cambridge Phil. Soc. **24**, 89 (1928); **24**, 111 (1928).
18. V. FOCK. Z. Physik. **61**, 126 (1930).
19. J. C. SLATER. Phys. Rev. **35**, 210 (1930).
20. W. C. DAVIDSON and L. NAZARETH. Technical Memos 303 and 306, Argonne National Laboratories, Argonne, IL. 1977.
21. M. J. D. POWELL. Numerical methods for nonlinear algebraic equations. *Edited by* P. Rabinowitz. Gordon and Breach, London. 1970. p. 87.
22. M. R. PETERSON and R. A. POIRIER. MONSTERGAUSS, Department of Chemistry, University of Toronto, Toronto, Ont. Canada M5S 1A1. 1981.
23. W. J. HEHRE, R. F. STEWART, and J. A. POPLE. J. Chem. Phys. **51**, 2567 (1969).
24. J. S. BINKLEY, J. A. POPLE, and W. J. HEHRE. J. Am. Chem. Soc. **102**, 939 (1980).
25. P. POLITZER, P. LANE, K. JAYASURIYA, and L. N. DOMELSMITH. J. Am. Chem. Soc. **109**, 1899 (1987).
26. G. C. LANCINI, N. MAGGI, and P. SENIS. Farmaco (Pavia) Ed. Sci. **18**, 390 (1963).
27. R. G. FARGHER and F. L. PYMAN. J. Chem. Soc. **115**, 217 (1919).
28. W. G. FORSYTH and F. L. PYMAN. J. Chem. Soc. **127**, 573 (1925).
29. C. E. HAZELTINE, F. L. PYMAN, and J. WINCHESTER. J. Chem. Soc. **125**, 1431 (1924).
30. B. CAVALLERI. Nitroimidazole chemistry, pharmacology and clinical application. *Edited by* A. Breccia, B. Cavalleri, and G. E. Adams. Plenum Press, London. 1982.
31. P. BEAK, F. S. FRY, J. LEE, and F. STEELE. J. Am. Chem. Soc. **98**, 171 (1976).
32. T. H. LOWRY and K. S. RICHARDSON. Mechanism and theory in organic chemistry. 2nd ed. Harper and Row, New York. 1981. p. 131.
33. D. S. NOYCE and G. T. STONE. J. Org. Chem. **38**, 3762 (1973).

Can. J. Chem. Downloaded from www.nrcresearchpress.com by 194.225.253.170 on 09/07/12
For personal use only.

Volumetric studies on binary mixtures of some furan derivatives with benzene, chlorobenzene, and bromobenzene at 298.15 K

HOMENDRA NAOREM AND S. K. SURI[1]

Department of Chemistry, Indian Institute of Technology, Delhi, New Delhi – 110016, India

Received February 3, 1989

HOMENDRA NAOREM and S. K. SURI. Can. J. Chem. **67**, 1672 (1989).

Molar excess volumes for the binary mixtures of tetrahydrofuran, furan, furfural, and furfuryl alcohol with benzene, chlorobenzene, and bromobenzene have been calculated from precise experimental density data at 298.15 K over the entire composition range. The results have been discussed in light of unlike n–π interactions between the π-electron cloud of the aromatic ring and the oxygen atom of the heterocyclic ring. The substitution of a halogen atom in the aromatic ring activates the molecule for n–π interactions in tetrahydrofuran and furan solutions and deactivates the molecule in furfural and furfuryl alcohol solutions.

Key words: furan derivatives, binary mixtures, excess volumes, n–π interactions, π–π interactions.

HOMENDRA NAOREM et S. K. SURI. Can. J. Chem. **67**, 1672 (1989).

Utilisant des données expérimentales précises relatives aux densités de mélanges à 298,15 K, on a calculé les volumes molaires en excès pour des mélanges binaires formés d'une part de tétrahydrofurane, de furane, de furfural et d'alcool furfurylique et d'autre part de benzène, de chlorobenzène et de bromobenzène. On discute des résultats à la lumière d'interactions différentes n–π entre le nuage d'électrons π du noyau aromatique et l'atome d'oxygène du noyau hétérocyclique. La substitution du noyau aromatique par un halogène active la molécule pour les interactions n–π dans les solutions de tétrahydrofurane et de furane et désactive la molécule dans les solutions de furfural et d'alcool furfurylique.

Mots clés : dérivés du furane, mélanges binaires, volumes en excès, interactions n–π, interactions π–π.

[Traduit par la revue]

Can. J. Chem. Downloaded from www.nrcresearchpress.com by 194.225.253.170 on 09/07/12
For personal use only.

Introduction

Our recent studies on binary mixtures of tetrahydrofuran (1–3), furan (4), furfural (5, 6), and furfuryl alcohol (7) with a variety of organic liquids revealed a strong n–π interaction between the π-electron cloud of the aromatic ring and the oxygen atom of the heterocyclic ring in tetrahydrofuran (THF) and furan. These interactions were found to be highly influenced by geometric factors and exhibited a significant change on going from furan to furfural to furfuryl alcohol (FA). As an extension of these studies, it was considered worthwhile to examine the effect of electronegative halogen atoms in the aromatic ring on the solution properties of the binary mixtures. In this paper we report the results of our studies on the excess molar volumes for binary mixtures of THF, furan, furfural, and FA with benzene, chlorobenzene, and bromobenzene at 298.15 K.

Experimental

Analytical reagent grade sample of THF (E. Merck, India) was refluxed over stannous chloride for about 8 h, filtered, stored over anhydrous calcium chloride for about 48 h, and then distilled. The sample of furan (Ferak, Germany) was refluxed over potassium hydroxide and distilled over sodium. Laboratory reagent grade samples of furfural and FA (SRL, India) were distilled under reduced pressure and the middle fractions collected (5, 6). The samples of the chlorobenzene and bromobenzene (AG-Fluka) were purified by shaking repeatedly with portions of sulfuric acid until the acid was no longer colored. It was washed with water and then with dilute potassium carbonate solution. The decanted liquid was dried over calcium chloride for 24 h before the sample was finally subjected to fractional distillation (8). Spectroscopic grade sample of benzene (Fluka) was used as such without further purification. All liquids were stored in brown bottles and fractionally distilled immediately before use. The densities of THF, furan, furfural, FA, benzene, chlorobenzene, and bromobenzene samples purified by us were 0.88193, 0.93163, 1.15473, 1.12499, 0.87352, 1.10069, and 1.48811 g cm^{-3}, respectively, at 298.15 K. These values are in close agreement with the reported literature values 0.88195, 0.93095, 1.15450, 1.12615, 0.87370, 1.10090, and 1.48820 of the liquids, respectively (8, 9).

The excess molar volumes of mixing, V^E, have been computed from the experimental density data. The solutions for the measurement of densities were prepared by weight and corrections for buoyancy were applied. The details of the experimental technique for the preparation of solutions have been described elsewhere (10).

The densities were measured with a vibrating tube digital density meter Model DMA 602/DMA 60 (Anton Paar, Austria). Water from a thermostated bath was circulated through the metal block of the density meter at a flow rate of ~3 dm^3 min^{-1}. The temperature of the water bath was controlled to $\pm 1 \times 10^{-3}$ K using a Tronac PTC-40 proportional temperature controller. The density meter was calibrated with dried air and degassed ion-exchanged water. The density of water was taken to be 0.9970429 g cm^{-3} at 298.15 K (11). Duplicate densities of liquids and liquid mixtures studied agreed to within 5×10^{-5} g cm^{-3}. This propagates a maximum uncertainty of about ± 0.005 cm^3 mol^{-1} in the V^E values. For solutions containing furan experimental uncertainties were slightly higher. However, the reported V^E values for these mixtures are expected to be uncertain by not more than ± 0.008 cm^3 mol^{-1}.

Results and discussion

The V^E values for the binary mixtures at 298.15 K are recorded in Table 1 and plotted as a function of solution composition in Fig. 1. Each set of the results were fitted into a polynomial of the type:

$$[1] \quad V^E = x(1-x)[A_0 + A_1(2x-1) + A_2(2x-1)^2 + A_3(2x-1)^3]$$

where x is the mole fraction of THF, furan, furfural, or FA in the binary mixture and A_i's are constants. The values of the constants as determined by the least-squares method (unweighted) along with the standard deviation $\sigma(V^E)$ of the fit are listed in Table 2. Since the $\sigma(V^E)$ values for all the systems

[1]To whom all correspondence should be addressed.

Printed in Canada / Imprimé au Canada

Can. J. Chem. Downloaded from www.nrcresearchpress.com by 194.225.253.170 on 09/07/12
For personal use only.

TABLE 1. Molar excess volumes, V^E ($cm^3\ mol^{-1}$), for the binary mixtures at 308.15 K

x	V^E	x	V^E
	xTHF + (1 − x)benzene		
0.0984	−0.078	0.5951	−0.262
0.2029	−0.157	0.7049	−0.208
0.2979	−0.226	0.8029	−0.149
0.3939	−0.256	0.8979	−0.075
0.4955	−0.279		
	xTHF + (1 − x)chlorobenzene		
0.0912	−0.135	0.6436	−0.507
0.2064	−0.290	0.6891	−0.487
0.3480	−0.438	0.8301	−0.323
0.4511	−0.503	0.9113	−0.194
0.5537	−0.531		
	xTHF + (1 − x)bromobenzene		
0.1621	−0.288	0.6237	−0.581
0.2821	−0.437	0.7102	−0.514
0.3668	−0.532	0.7932	−0.417
0.4350	−0.578	0.8863	−0.263
0.5595	−0.598		
	$x$furan + (1 − x)benzene		
0.1007	0.016	0.5417	0.058
0.2711	0.044	0.5854	0.059
0.2895	0.037	0.7345	0.041
0.3601	0.050	0.8204	0.028
0.4413	0.051		
	$x$furan + (1 − x)chlorobenzene		
0.0846	−0.085	0.6650	−0.195
0.2195	−0.167	0.7582	−0.137
0.3013	−0.199	0.8603	−0.083
0.4349	−0.242	0.9428	−0.038
0.5375	−0.234		
	$x$furan + (1 − x)bromobenzene		
0.1004	−0.115	0.5260	−0.348
0.1796	−0.197	0.6688	−0.286
0.2971	−0.291	0.7646	−0.228
0.3190	−0.303	0.8824	−0.118
0.4462	−0.347		
	$x$furfural + (1 − x)benzene		
0.1978	−0.057	0.6677	−0.086
0.3278	−0.089	0.7553	−0.066
0.3783	−0.088	0.8447	−0.042
0.4881	−0.098	0.9214	−0.023
0.5349	−0.102		
	$x$furfural + (1 − x)chlorobenzene		
0.0847	0.026	0.4911	0.077
0.1471	0.049	0.5697	0.065
0.2345	0.062	0.6685	0.058
0.3086	0.074	0.7655	0.043
0.3864	0.079		
	$x$furfural + (1 − x)bromobenzene		
0.1103	0.042	0.6085	0.098
0.2217	0.075	0.7035	0.083
0.3710	0.098	0.7852	0.069
0.4874	0.104	0.8579	0.042
0.5286	0.107		

TABLE 1 (*concluded*)

x	V^E	x	V^E
	xFA + (1 − x)benzene		
0.0926	−0.025	0.5799	−0.090
0.2002	−0.054	0.6560	−0.081
0.2786	−0.073	0.8086	−0.052
0.3955	−0.089	0.9127	−0.022
0.4864	−0.093		
	xFA + (1 − x)chlorobenzene		
0.0796	0.054	0.4748	0.119
0.1763	0.104	0.6003	0.098
0.2537	0.126	0.7614	0.063
0.3037	0.132	0.8869	0.028
0.3465	0.130		
	xFA + (1 − x)bromobenzene		
0.0943	0.075	0.5438	0.143
0.1552	0.112	0.6592	0.117
0.2413	0.145	0.7724	0.080
0.3104	0.164	0.9276	0.024
0.3961	0.163		

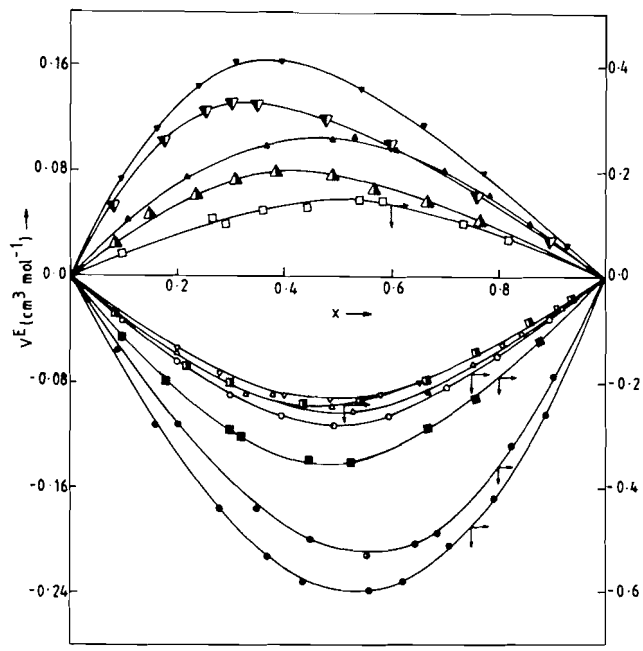


FIG. 1. Molar excess volumes, V^E, as a function of composition for the binary mixtures at 298.15 K. THF + benzene, ○; THF + chlorobenzene, ◐; THF + bromobenzene, ●; furan + benzene, □; furan + chlorobenzene, ◨; furan + bromobenzene, ■; furfural + benzene, △; furfural + chlorobenzene, ◭; furfural + bromobenzene, ▲; FA + benzene, ▽; FA + chlorobenzene, ▼; FA + bromobenzene, ▼.

are less than the experimental uncertainty, the constants in eq. [1] may be considered representative of the experimental V^E values.

It is observed from Fig. 1 that V^E varies almost symmetrically with x for all the binary mixtures studied. The V^E values for mixtures containing THF or furan (except for the binary mixtures of furan and benzene) are negative and those containing furfural

TABLE 2. Values of the parameters in eq. [1] along with the standard deviation $\sigma(V^E)$ ($cm^3\ mol^{-1}$)

System	A_0	A_1	A_2	A_3	$\sigma(V^E)$
THF + benzene	−1.1036	0.0488	0.4009	−0.0179	0.004
THF + chlorobenzene	−2.1887	−0.4692	0.1310	0.0164	0.004
THF + bromobenzene	−2.3792	−0.3637	0.0851	0.0269	0.005
Furan + benzene	0.2297	0.0396	−0.1012	−0.0905	0.003
Furan + chlorobenzene	−0.9418	0.2373	0.2354	−0.1851	0.006
Furan + bromobenzene	−1.3928	0.1330	0.3035	−0.0628	0.004
Furfural + benzene	−0.4029	0.0194	0.1245	−0.0258	0.003
Furfural + chlorobenzene	0.2972	−0.1559	0.0177	0.1565	0.003
Furfural + bromobenzene	0.4222	0.0038	−0.0615	−0.1026	0.002
FA + benzene	−0.3770	0.0079	0.1272	1.0023	0.002
FA + chlorobenzene	0.4775	−0.3529	0.0576	0.1096	0.003
FA + bromobenzene	0.6208	−0.3389	0.0117	0.0354	0.002

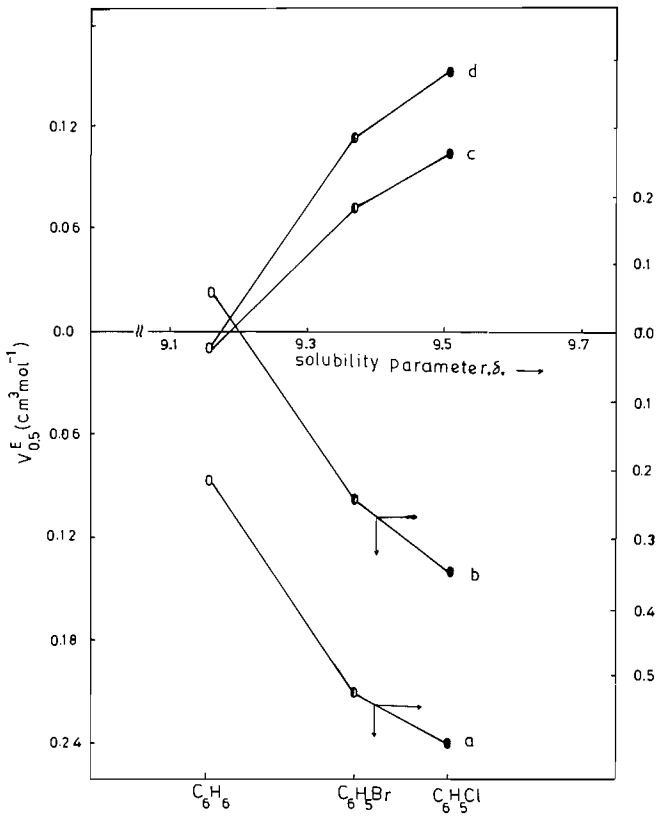


FIG. 2. Plot of $V^E_{0.5}$ against Hildebrand's solubility parameter, δ, for the binary mixtures containing (*a*), THF; (*b*), furan; (*c*), furfural, and (*d*), FA.

or FA (except for the mixtures containing benzene) were found to be positive over the entire composition range. The binary mixtures containing furan and benzene exhibited a positive V^E and those containing furfural or FA and benzene exhibited negative V^E. Our V^E values for the binary mixtures containing THF and benzene are in good agreement with those reported by Meyer and co-workers (12), the maximum difference being $\sim 0.009\ cm^3\ mol^{-1}$ over the composition range $x \approx 0.4$ to 0.6. To the best of our knowledge, no V^E data at 298.15 K have been reported in the literature for other binary mixtures considered in this paper.

For the binary mixtures containing THF or furan the molar excess volumes at equimolar concentration $V^E_{0.5}$ was found to follow the order benzene > chlorobenzene > bromobenzene. When a halogen atom is introduced into the aromatic ring, it brings about a change in the π-electron density around the aromatic ring and also a change in the shape and size of the resultant molecule. Both these factors are likely to contribute to the overall volumetric effects in the mixtures. Bromobenzene makes the molecule more asymmetric, resulting into a higher free volume in solution and in view thereof a relatively larger positive contribution to V^E is expected as compared to the mixtures containing chlorobenzene. However, it is observed that V^E for the binary mixtures containing bromobenzene are more negative than those containing chlorobenzene, whereby indicating the presence of strong intermolecular interactions. The decrease in V^E on going from benzene to chlorobenzene to bromobenzene appears to be a consequence of increased polarizability of the molecule due to the introduction of a halogen atom in the aromatic ring. For the binary mixtures of cyclohexane with benzene, chlorobenzene and bromobenzene a similar behavior has been reported (13–15).

The V^E values for the binary mixtures containing furan are observed to be consistently larger than those containing THF (Fig. 1). This may be ascribed to the presence of strong π–π interactions in furan molecules (16). Breaking this π–π interactions on addition of a hydrocarbon would lead to a positive contribution to V^E. The presence of π-electron clouds in furan molecule is also likely to restrict the participation of n-electron of the oxygen atom of furan molecule for the n–π interactions in the mixtures and hence a smaller contribution to volumetric effects arising from intermolecular interactions are anticipated (4). The $V^E_{0.5}$ for the binary mixtures containing furfural and FA follow the order benzene < chlorobenzene < bromobenzene. In pure state, the molecules of furfural are known to be associated through dipole–dipole interactions (17, 18). Also, the unusually higher viscosity value of FA (4.63 cps at 298.15 K) is indicative of the fact that the molecules of FA, like aliphatic alcohols, are self associated through hydrogen bonding in the pure state. The addition of a liquid to furfural or FA would, therefore, tend to break the molecular aggregates in pure furfural or FA resulting in an increase in V^E. These effects would, however, be counteracted by the unlike n–π interactions which would lead to a decrease in V^E. In view of the observed V^E for the mixtures, it is apparent that with the introduction of a halogen atom in the benzene ring, the "structure breaking" effects becomes more predominating in the mixtures. The relatively larger V^E values for mixtures containing FA as compared to those containing furfural (Fig. 1) suggest that the molecules of FA are associated to a larger extent

Can. J. Chem. Downloaded from www.nrcresearchpress.com by 194.225.253.170 on 09/07/12
For personal use only.

than the furfural molecules. Strictly speaking, more work is required to be done to reach a definite conclusion in this regard.

It is interesting to observe that $V^E_{0.5}$ for these mixtures varies almost linearly with the Hildebrand solubility parameter, δ (Fig. 2). A similar behavior has been observed for the binary mixtures of cyclohexanone with substituted benzenes (19) and is attributed to the presence of dipoles in the mixtures.

1. S. K. SURI and H. NAOREM. J. Chem. Eng. Data, **32**, 462 (1987).
2. S. K. SURI. Can. J. Chem. **59**, 2839 (1981).
3. S. K. SURI and B. CHAWLA. J. Chem. Eng. Data, **26**, 268 (1981).
4. H. NAOREM and S. K. SURI. J. Soln. Chem. In press.
5. H. NAOREM and S. K. SURI. Can. J. Chem. **66**, 1295 (1988).
6. H. NAOREM, N. KISHORE, and S. K. SURI. Can. J. Chem. **67**, 648 (1989).
7. H. NAOREM and S. K. SURI. To be published.
8. J. A. RIDDICK and W. B. BUNGER. Organic solvents. Wiley Interscience, New York. 1970.
9. J. TIMMERMANS (*Editor*). Physicochemical constants of pure organic compounds. Elsevier, Amsterdam. 1965.
10. R. C. MAHESWARI, S. K. SURI, and U. S. TEWARI. J. Chem. Eng. Data, **24**, 239 (1979).
11. H. WAGENBRETH and H. BLANKE. PTB-Mitt. **6**, 412 (1971).
12. R. MEYER, G. GUISTI, M. MEYER, and E. J. VINCENT. Thermochim. Acta, **13**, 379 (1975).
13. R. H. STOKES, B. J. LEVIEN, and K. N. MARSH. J. Chem. Thermodyn. **2**, 43 (1970).
14. T. M. LETCHER. J. Chem. Thermodyn. **4**, 59 (1972).
15. F. KOHLER and F. ROTT. Monatsh. **85**, 703 (1954).
16. M. D. GUILLEN and C. G. LOSA. J. Chem. Thermodyn. **10**, 567 (1978).
17. Y. M. SHAPIRO and V. G. KULNEVICH. Zh. Fig. Khim. **45**, 981 (1971).
18. V. G. KULNEVICH and Y. M. SHAPIRO. Khim. Geter. Soedinenii, **12**, 1594 (1972).
19. B. CHAWLA, S. K. MEHTA, R. V. JASRA, and S. K. SURI. Can. J. Chem. **61**, 2147 (1983).

Can. J. Chem. Downloaded from www.nrcresearchpress.com by 194.225.253.170 on 09/07/12
For personal use only.

The nitrous acid catalysed nitration of naphthalene. Evidence for a kinetic term that is second order with respect to the aromatic compound

J. RAMÓN LEIS,[1] M. ELENA PEÑA,[1] AND JOHN H. RIDD[2]

Chemistry Department, University College, 20 Gordon Street, London WC1H 0AJ, England

Received January 23, 1989

This paper is dedicated to Professor Ronald J. Gillespie on the occasion of his 65th birthday

J. RAMÓN LEIS, M. ELENA PEÑA, and JOHN H. RIDD. Can. J. Chem. **67**, 1677 (1989).

The kinetic equation for the nitrous acid catalysed nitration of naphthalene in aqueous mixtures of sulphuric acid and acetic acid has at least two kinetic terms: one first order with respect to naphthalene and one second order with respect to naphthalene. The orders with respect to nitrous acid and nitric acid vary with the conditions in the way characteristic of the electron transfer mechanism of this reaction. The second-order term with respect to naphthalene is considered to derive from the formation of the dimeric radical cation $(ArH)_2^{+\bullet}$. The acidity dependence of the rate coefficients and the absence of a normal isotope effect in the reaction of naphthalene-d_8 are consistent with this interpretation.

Key words: naphthalene, nitration, nitrous acid.

J. RAMÓN LEIS, M. ELENA PEÑA et JOHN H. RIDD. Can. J. Chem. **67**, 1677 (1989).

L'équation cinétique de la réaction de nitration du naphtalène, réalisée dans des mélanges aqueux d'acides sulfurique ou acétique et catalysée par l'acide nitreux, comporte au moins deux termes cinétiques : un du premier ordre par rapport au naphtalène et un autre du deuxième ordre par rapport au naphtalène. Les ordres par rapport à l'acide nitreux et à l'acide nitrique varient suivant les conditions de la réaction et ils sont caractéristiques du mécanisme de transfert d'électron de cette réaction. On considère que le terme du deuxième ordre par rapport au naphtalène provient de la formation d'un cation radicalaire dimère $(ArH)_2^{+\bullet}$. La relation entre les coefficients de vitesse et l'acidité ainsi que l'absence d'effet isotopique normal dans la réaction du naphtalène-d_8 sont en accord avec cette interprétation.

Mots clés : naphtalène, nitration, acide nitreux.

[Traduit par la revue]

Introduction

A considerable amount of evidence has appeared in recent years to show that the nitrous acid catalysed nitration of many substrates is a radical reaction initiated by the oxidation of the aromatic compound to a cation radical or, with phenols, to a phenoxy radical. The unusual kinetic forms observed in the nitration of *para*-nitrophenol (1) have been interpreted in this way (2) and the conclusion is supported by the observation of ^{15}N CIDNP (chemically induced dynamic nuclear polarisation) effects in the nitrous acid nitration of *para*-nitrophenol (3), mesitylene (4), and durene (5). The nitrous acid catalysed nitration of *para*-methylphenol also shows ^{13}C CIDNP effects (6). The nitrous acid catalysed nitration of phenol shows the kinetic forms characteristic of this radical reaction but there also appears to be a small contribution from the "classical" mechanism involving nitrosation followed by oxidation (7).

Kinetic studies are not available on all of the above reactions but in those that have been carried out the order with respect to the aromatic compound is unity. However, in 1983, Ross, Moran, and Malhotra showed that the nitrous acid catalysed nitration of naphthalene in aqueous sulphuric acid appeared to have an order of 1.5 in the aromatic compound (8). They showed that the reaction gave a quantitative yield of nitronaphthalenes with an α/β ratio of 25. They did not provide a detailed interpretation of their results but suggested that a chain reaction involving electron transfer could explain the unusual order. The use of aqueous sulphuric acid severely limits the range of concentrations that can be used because of the low solubility of naphthalene. In the present work, we have reinvestigated this reaction using aqueous mixtures of sulphuric acid and acetic acid since naphthalene is more soluble in these media; the results support those published in the preliminary account of this work (9).

Results

The reaction has been followed by the same method (uv spectroscopy) as used previously (8) and, as before, a large excess of nitric acid has been used so that, providing the concentration of nitrous acid can be taken as constant, the observed order of the reaction is that with respect to the naphthalene. However, probably because some of our studies have used considerably greater concentrations of naphthalene, our work indicates that the order with respect to naphthalene changes from one to about two as the concentration of naphthalene is increased. This change in the form of the kinetic runs is shown in Fig. 1 for two runs carried out with very different concentrations of naphthalene: at low concentrations, good first-order kinetics are obtained but, when the initial concentration of naphthalene is high, the second-order plot is more nearly linear.

The change in the kinetic order from first to second also leads to an increase in the rate of reaction above that expected for the first-order form. The change has therefore been represented as the incursion of an additional kinetic term as shown in eq. [1]:

$$[1] \quad \text{Rate} = k_1[\text{ArH}] + k_2[\text{ArH}]^2$$

A number of kinetic runs have been carried out using intermediate concentrations of naphthalene and many of these have been fitted to eq. [1] using a computer program. For this calculation to yield reasonably accurate results for both rate coefficients, it is necessary that the two kinetic terms should be of approximately similar magnitude; almost all the values quoted refer therefore to runs in which the contribution of the first-order term at the start of the reaction is between 17 and 70% of the total rate. These percentages are given in the final columns of the tables. The runs are grouped into sets depending

[1]Present address: Departamento de Química Fisíca, Universidad de Santiago, E-Santiago de Compostela, Spain.

[2]Author to whom correspondence may be addressed.

Printed in Canada / Imprimé au Canada

Can. J. Chem. Downloaded from www.nrcresearchpress.com by 186.148.149.217 on 09/07/12
For personal use only.

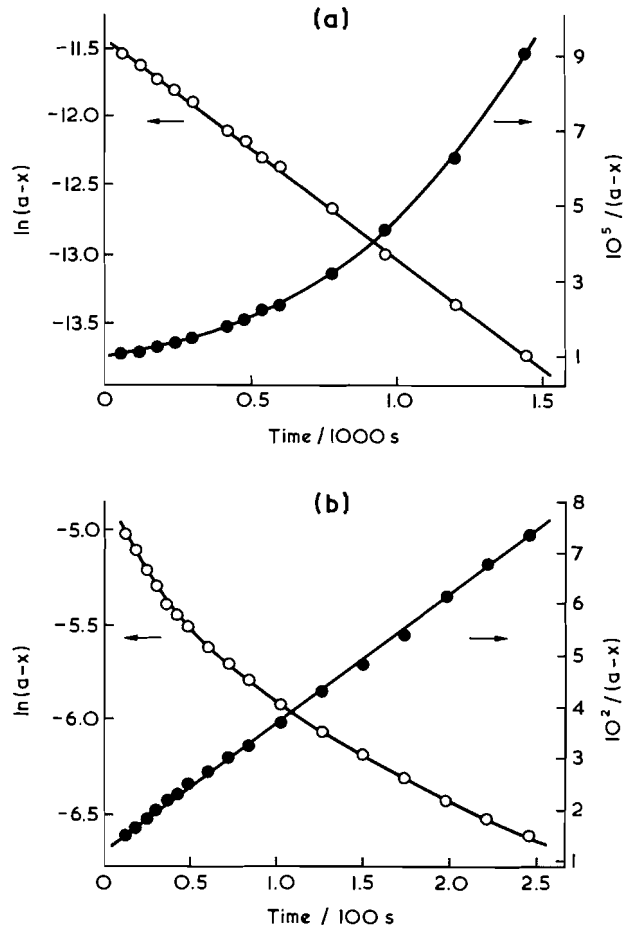


FIG. 1. First-order (open circles) and second-order (dots) plots for two kinetic runs carried out with very different concentrations of naphthalene. (a) [ArH] = 1.17×10^{-5} mol dm^{-3}; other conditions as shown in Table 1. (b) [ArH] = 7.8×10^{-3} mol dm^{-3}; other conditions as shown in Table 2.

on the other conditions used and the resulting rate coefficients and half-lives are shown in Tables 1–3. The first-order rate coefficients obtained in this way accord well with those obtained by applying a first-order equation to the runs with very low concentrations of naphthalene (Table 1) but the second-order rate coefficients from eq. [1] are significantly lower than those obtained by applying a second-order equation to the runs with high concentrations of naphthalene (Tables 2 and 3). This is presumably because the relative importance of the first-order component in eq. [1] increases during a kinetic run as the concentration of naphthalene falls.

The different sets of runs in Tables 1–3 differ in the concentrations of the other components, and it is necessary to consider whether these changes influence the apparent order with respect to naphthalene. Evidence on this is provided by the logarithmic plot of the half-lives against the concentration of naphthalene in Fig. 2. The solid lines indicate the experimental results; the broken line indicates the consequence of displacing the plobs (b) and (c) so as to form a continuous curve with plot (a). Since the curve produced has no sharp changes of slope, it would appear that the effective order with respect to naphthalene is determined primarily by the concentration of naphthalene, as implied by eq. [1]. The broken curve is drawn to have a final slope of -1; the results therefore accord with the transition between first-order and second-order kinetics.

TABLE 1. The effect of varying the concentration of naphthalene in nitration by nitric acid (0.01 mol dm^{-3}) and nitrous acid (2.3×10^{-4} mol dm^{-3}) in 52.2% sulphuric acid containing 4.9% acetic acid at 25°C

10^5[ArH] (mol dm^{-3})	$t_{1/2}$ (s)	$10^3 k_1$ (s^{-1})	k_2 (mol^{-1} s^{-1} dm^3)	1st order (%)$_{t=0}$
1.17	377	(1.56)[a]	—	—
1.17	396	(1.6)[a]	—	—
1.95	348	1.53	—	74
3.9	315	1.6	19	69
5.85	307	1.47	16	60.6
7.8	290	1.53	14	58
15.7	238	1.27	16	34
23.5	192	1.52	11.4	36
31.3	166	1.32	13	25

[a]Calculated assuming first-order kinetics.

TABLE 2. The effect of varying the concentration of naphthalene in nitration by nitric acid (0.084 mol dm^{-3}) and nitrous acid (2.39×10^{-4} mol dm^{-3}) in 46.5% sulphuric acid containing 27.8% acetic acid at 25°C

10^3[ArH] (mol dm^{-3})	$t_{1/2}$ (s)	$10^4 k_1$ (s^{-1})	k_2 (mol^{-1} s^{-1} dm^3)	1st order (%)$_{t=0}$
0.313	513	8.3	1.87	59
0.548	418	8.6	1.74	47.5
0.793	355	7.4	1.99	32
1.11	306	8.4	1.71	31
1.59	229	6.5	1.98	17
2.38	183	—	1.45	25
3.17	138	—	(2.55)[a]	—
3.97	112	—	(1.82)[a]	—
4.76	77.9	—	(3.27)[a]	—
6.34	63.4	—	(2.61)[a]	—
7.93	50.6	—	(2.46)[a]	—
9.52	37.7	—	(3.46)[a]	—

[a]Calculated assuming pure second-order kinetics.

TABLE 3. The effect of varying the concentration of naphthalene in nitration by nitric acid (8.34×10^{-2} mol dm^{-3}) and nitrous acid (1.22×10^{-4} mol dm^{-3}) in 47% sulphuric acid containing 29% acetic acid at 25°C

10^3[ArH] (mol dm^{-3})	$t_{1/2}$ (s)	$10^4 k_1$ (s^{-1})	k_2 (mol^{-1} s^{-1} dm^3)	1st order (%)$_{t=0}$
0.313	956	5.1	0.84	66
0.793	660	6.3	0.7	53
1.59	416	8.1	0.7	43
4.76	160	—	0.84	25
6.34	119.5	—	0.91	23
7.93	88.2	—	(1.74)[a]	—

[a]Calculated assuming pure second-order kinetics.

In principle, the kinetic form of these reactions could be markedly influenced by any side reactions that led to an increase or decrease in the amount of nitrous acid present. We have therefore checked the above conclusions by a study of how the instantaneous rate at a point near the start of reaction varies with the concentration of naphthalene. If eq. [1] is correct, then a plot of Rate/[ArH] against [ArH] should be linear with an intercept equal to k_1 and a slope equal to k_2. The complete set of these

Can. J. Chem. Downloaded from www.nrcresearchpress.com by 186.148.149.217 on 09/07/12
For personal use only.

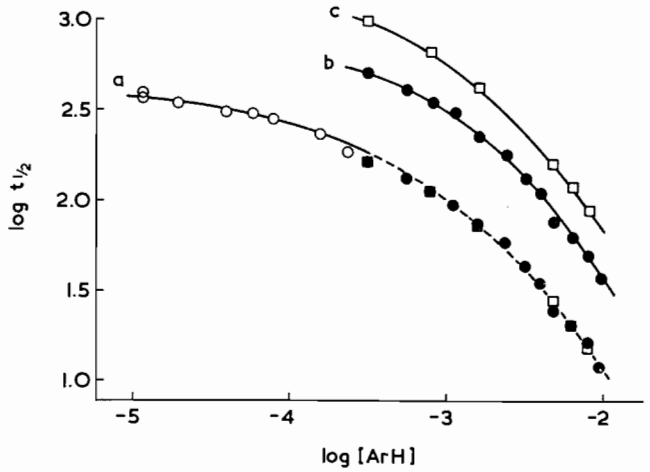


FIG. 2. Logarithmic plots of the half-life against the concentration of naphthalene for the kinetic runs in (a) Table 1; (b) Table 2; and (c) Table 3. The broken line indicates the plot obtained by displacing sets (b) and (c) to form a continuous curve with the points in set (a).

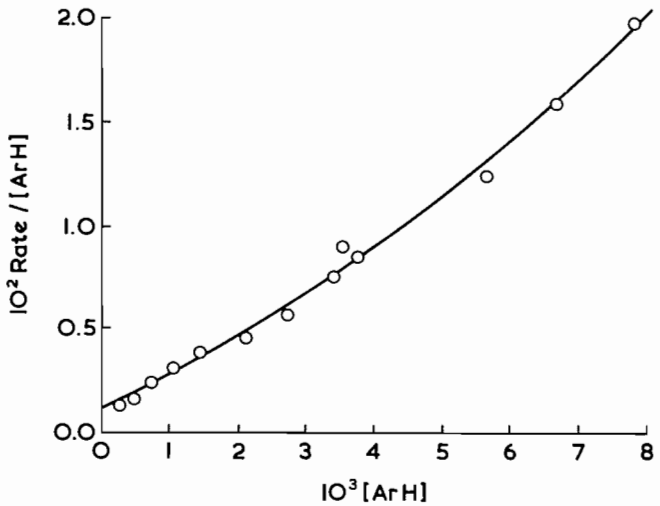


FIG. 3. A plot of the instantaneous rate of reaction divided by the concentration of the aromatic compound against the concentration of the aromatic compound. The data derive from the initial points of the kinetic runs in Table 2.

results and two related figures are given in the Supplementary Data Section (Tables 1S–3S, Figs. 1S and 2S)[3] but the results for the most extensive set of data are shown in Fig. 3. Rather unexpectedly, the plot shows slight upward curvature and accords with the presence of a third-order term in the rate equation as shown in eq. [2].

$$[2] \quad \text{Rate} = k_1[\text{ArH}] + k_2[\text{ArH}]^2 + k_3[\text{ArH}]^3$$

From the fit of the plot in Fig. 3 to a quadratic equation, the values of the rate coefficients in eq. [2] are k_1, 1.15×10^{-3} s^{-1}; k_2, 1.54 mol^{-1} s^{-1} dm^3; k_3, 1.03×10^{-2} mol^{-2} s^{-1} dm^6. However, if the last three points in Fig. 3 are omitted, the remainder give a good approximation to a linear plot and the corresponding values of the rate coefficients become k_1, 7.6×10^{-4} s^{-1}; k_2, 2.1 mol^{-1} s^{-1} dm^3. These values are very close

[3]This material may be purchased from the Depository of Unpublished Data, CISTI, National Research Council of Canada, Ottawa, Ont., Canada K1A 0S2.

TABLE 4. Variation of the concentration of nitrous acid in the nitration of naphthalene (3.13×10^{-4} mol dm^{-3}) by nitric acid (1.0×10^{-2} mol dm^{-3}) in 52.2% sulphuric acid containing 4.8% acetic acid at 25°C

10^3[ArH] (mol dm^{-3})	$t_{1/2}$ (s)	$10^4 k_1$ (s^{-1})	k_2 (mol^{-1} s^{-1} dm^3)	1st order $(\%)_{t=0}$
0.69	502	5.14	3.89	30
1.15	286	8.93	6.66	30
2.3	168	13.2	12.6	25
3.83	112	18.0	19.2	23
6.38	83.0	27.5	22.5	28
12.8	63.7	34.2	27.9	28

TABLE 5. Variation of the concentration of nitric acid in the nitration of naphthalene (7.83×10^{-5} mol dm^{-3}) in 54.1% sulphuric acid containing nitrous acid (1.15×10^{-4} mol dm^{-3}) and acetic acid (1.3%) at 25°C

10^3[ArH] (mol dm^{-3})	$t_{1/2}$ (s)	$10^4 k_1$ (s^{-1})	k_2 (mol^{-1} s^{-1} dm^3)	1st order $(\%)_{t=0}$
1.45	394	9.67	12.6	50
2.89	275	12.0	22.8	40
5.79	196	14.0	38.3	32
10.3	184	19.3	36.1	41
15.5	195	16.3	33.1	39
20.7	180	18.6	34.3	41
60.0	170	18.6	38.8	38

TABLE 6. Variation of the acidity in the nitration of naphthalene (3.13×10^{-4} mol dm^{-3}) by nitric acid (1.0×10^{-2} mol dm^{-3}) and nitrous acid (1.15×10^{-4} mol dm^{-3}) in sulphuric acid containing 4.8% acetic acid at 25°C

H_2SO_4 (%)	$t_{1/2}$ (s)	$10^4 k_1$ (s^{-1})	k_2 (mol^{-1} s^{-1} dm^3)	1st order $(\%)_{t=0}$
50.7	569	4.47	3.43	29
52.2	286	8.93	6.66	30
52.9	206	7.59	12.1	17
54.0	120	16.3	17.1	23
55.1	86.5	18.7	29.3	17
56.4	56.7	21.9	46.5	13
58.7	33.9	64.6	75.0	22

to those obtained from the analysis of the individual kinetic runs under the same conditions (Table 2).

Some work has been done on the variation of the first-order and second-order rate coefficients with the concentrations of nitrous acid and nitric acid. The results for nitrous acid are in Table 4 and those for nitric acid are in Table 5; both sets of data are shown as logarithmic plots in Fig. 4. The variation of these rate coefficients with acidity has also been studied (Table 6); a comparison of the results with the variation of the concentration of the nitrosonium ion with acidity[4] is shown in Fig. 5.

The deuterium isotope effect has also been measured (Table 7). A small inverse isotope effect appears to be present in k_1, k_2, and the half-life of the reaction.

[4]Based on a new investigation of this equilibrium: R. B. Moodie and S. W. Richards, personal communication.

Can. J. Chem. Downloaded from www.nrcresearchpress.com by 186.148.149.217 on 09/07/12
For personal use only.

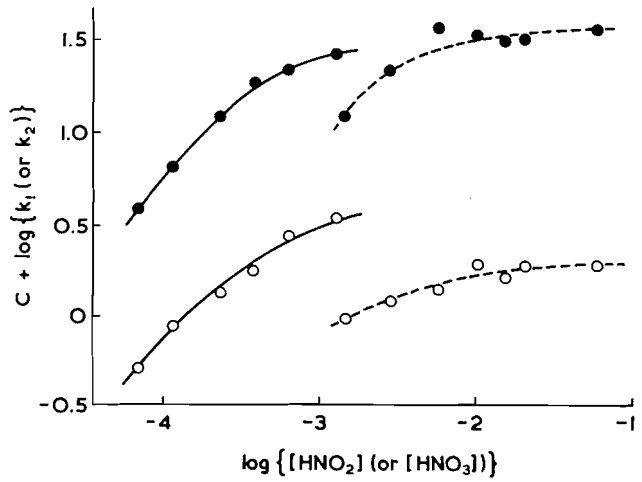


FIG. 4. A logarithmic plot of the variation of k_1 (open circles) and k_2 (dots) with the concentration of nitrous acid (solid line) and nitric acid (broken line). For k_1, $C = 3$; for k_2, $C = 0$.

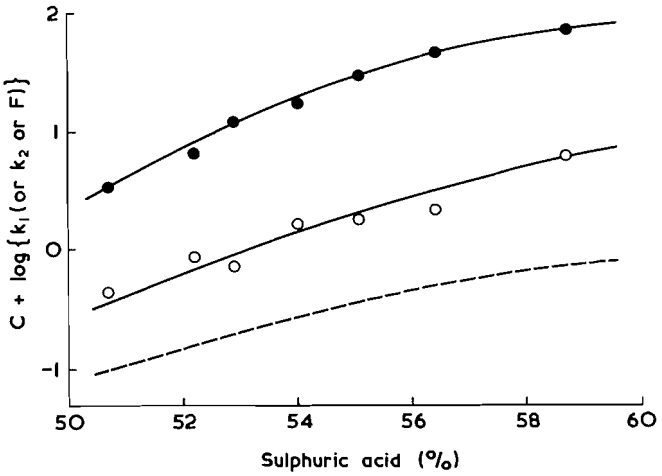


FIG. 5. A comparison of the acidity dependence of log k_1 (open circles) and log k_2 (dots) with the logarithm of the fraction (F) of nitrous acid present as the nitrosonium ion (broken line). For k_1, $C = 3$; for k_2 and F, $C = 0$.

TABLE 7. A comparison of naphthalene and naphthalene-d_8 in nitration by nitric acid (1.0×10^{-2} mol dm^{-3}) and nitrous acid (3.29×10^{-4} mol dm^{-3}) in 51.1% sulphuric acid containing 5.23% acetic acid at 25°C

ArH	10^4[ArH] (mol dm^{-3})	$t_{1/2}$ (s)	$10^4 k_1$ (s^{-1})	k_2 (mol^{-1} s^{-1} dm^3)
$C_{10}H_8$	1.84	353	8.28	8.49
$C_{10}D_8$	1.84	327	8.82	9.39
$C_{10}H_8$	0.92	398	9.95	10.4
$C_{10}D_8$	0.92	374	11.0	10.7
Mean values	$k_1^H/k_1^D = 0.92$	$k_2^H/k_2^D = 0.94$	$t_{1/2}^H/t_{1/2}^D = 1.07$	

Discussion

The studies described above have concentrated mainly on the order with respect to naphthalene, partly because this is the first example of such a second-order process in aromatic nitration and partly because this is also the area of our partial disagreement with the earlier work (where the order was believed to be 1.5 (8)). There is no doubt over the high order with respect to naphthalene: the decrease in the half-life by a factor of 13 when the concentration of naphthalene is increased by a factor of 30 (Table 2) cannot be missed. There is some doubt over whether eq. [1] is satisfactory representation of this kinetic form. The complete logarithmic plot of the half-lives in Fig. 2 is drawn to have a final slope of -1 but the fit of the points to a quadratic equation gives a slightly greater final slope (-1.3) and this hint of an order greater than 2 is supported by the slight curvature of the instantaneous rate plot in Fig. 3. However, even the kinetic runs corresponding to the last three points in Fig. 3 fit the integrated form of eq. [1] (see Experimental) with correlation coefficients >0.999 and so eq. [1] appears to be a good approximation to the kinetic form observed.

Under the conditions listed in Table 4, the order with respect to nitrous acid as calculated from the values of k_1 is 0.83 when $[HNO_2] = 1 \times 10^{-4}$ mol dm^{-3}, decreasing to 0.43 when $[HNO_2] = 1 \times 10^{-3}$ mol dm^{-3}. The corresponding values calculated from the variation of k_2 are 1.09 and 0.22 (see Fig. 4). The results for the order with respect to nitric acid (Table 5) show considerably more scatter (Fig. 4) but, from the variation of k_1, the order appears to change from 0.3 to 0 as the concentration of nitric acid is increased. From the variation of k_2, the corresponding change is from 0.5 to 0.

Such changes in the orders with respect to nitrous acid and nitric acid (as calculated from the variation of k_1) have been observed previously in nitrous acid catalysed nitration (2, 7) and have been ascribed to the electron transfer pathway shown in Scheme 1. The initial electron transfer may occur through the intermediate formation of a Wheland intermediate. The middle reaction of this scheme is shown within brackets because it is considered to represent only the stoichiometry of the process; the mechanism must be more complex (2). Provided that the electron transfers involved in the middle reaction are considered to be fast, this scheme leads to the kinetic form shown in eq. [3] (2).

$$[3] \quad \text{Rate} = \frac{b[\text{ArH}][HNO_2]}{c + d([HNO_2]/[HNO_3])}$$

In this equation, the concentration terms are considered to be the stoichiometric concentrations and the terms b, c, and d should be constant at a given acidity. This equation has two limiting forms: one first order with respect to nitrous acid and zero order with respect to nitric acid and the other first order with respect to nitric acid and zero order with respect to nitrous acid. These two forms correspond to the rate-determining electron transfer and the rate-determining formation of the Wheland intermediate (Scheme 1, stages 1 and 3). The variation of k_1 in Fig. 4 shows that the present work provides examples of runs near the first limiting form and covers part of the range towards the second limiting form.

The mechanism shown in Scheme 1 provides a basis for an explanation of the high order with respect to naphthalene observed in the present work, for naphthalene radical cations are known to be stabilised by complex formation with another naphthalene molecule (10) and the esr spectrum of the dimeric radical cation has been observed following the oxidation of naphthalene by nitrosonium ions (11). The resulting equilibrium (eq. [4]) has been studied in acetone solution (10) and an extrapolation of the results obtained then gives an equilibrium constant of 326 mol^{-1} dm^3 at 25°C. However, it is not sufficient merely to introduce this equilibrium since the mixed order

Can. J. Chem. Downloaded from www.nrcresearchpress.com by 186.148.149.217 on 09/07/12
For personal use only.

$$ArH + NO^+ \rightleftharpoons ArH^{+\bullet} + NO^\bullet$$

$$(NO^\bullet + NO_2^+ \rightleftharpoons NO^+ + NO_2^\bullet)$$

$$ArH^{+\bullet} + NO_2^\bullet \longrightarrow ArNO_2 + H^+$$

SCHEME 1

$$ArH + NO^+ \rightleftharpoons (ArH...NO)^+$$

$$(ArH...NO)^+ + ArH \rightleftharpoons (ArH)_2^{+\bullet} + NO^\bullet$$

$$(NO^\bullet + NO_2^+ \rightleftharpoons NO^+ + NO_2^\bullet)$$

$$(ArH)_2^{+\bullet} + NO_2^\bullet \longrightarrow ArNO_2 + ArH + H^+$$

SCHEME 2

kinetics with respect to the aromatic compound are also observed under conditions where the initial electron transfer appears to be rate determining. The results can be explained if the second naphthalene molecule is considered to facilitate the initial electron transfer as shown in Scheme 2. In this scheme, the reactants are considered to be brought together by initial π-complex formation between a nitrosonium ion and a naphthalene molecule followed by reaction with another naphthalene molecule. An alternative pathway in which the nitrosonium ion reacts with a pair of naphthalene molecules cannot be excluded but is considered less probable since we agree with the previous workers (8) that there is no evidence from Beer's Law for the association of naphthalene molecules in these solutions.

[4] $ArH^{+\bullet} + ArH \rightleftharpoons (ArH)_2^{+\bullet}$

If the reaction paths in Schemes 1 and 2 could be considered to be independent, the full kinetic equation for reaction at a given acidity would have the additional term shown in eq. [5].

$$[5]\quad \text{Rate} = \frac{b[ArH][HNO_2]}{c + d([HNO_2]/[HNO_3])} + \frac{e[ArH]^2[HNO_2]}{f + g([HNO_2]/[HNO_3])}$$

However, this is almost certainly an oversimplification because of the equilibrium shown in eq. [4]. A more complete analysis of the expected kinetic form has been carried out but it is unnecessary to consider this in detail since most of the kinetic runs described here refer to conditions where the initial oxidation stage appears to be essentially rate determining. Under these conditions and at a given acidity, both the complete kinetic analysis and eq. [5] reduce to the form of eq. [1] and hence accord with the experimental results.

The comparison of the acidity dependence of k_1 and k_2 with the fraction of nitrous acid present as the nitrosonium ion (Fig. 5) is consistent with the representation of the nitrosonium ion as the oxidising agent in Schemes 1 and 2. Exact agreement between the slopes of the logarithmic plots cannot be expected because the studies of the nitrosonium ion equilibria refer to aqueous sulphuric acid without the presence of acetic acid. Comparison with studies of the nitration of naphthalene by the nitronium ion (12) shows that this reaction cannot contribute significantly, even at the highest acidity used.

Nitrosation reactions normally give rise to conventional deuterium isotope effects (13) and when nitrous acid catalysed nitration occurs through nitrosation followed by oxidation such isotope effects remain in the overall reaction (7). The absence of such isotope effects in the present reaction (Table 7) suggests therefore that the classical mechanism for nitrous acid catalysed nitration makes no significant contribution to the reaction considered here.

Experimental

Kinetic studies

The sulphuric acid, acetic acid, sodium nitrite, sodium nitrate, and naphthalene were AnalaR or "Gold Label" reagents and were used without further purification. Naphthalene-d_8 (98+ atom% D) was from Aldrich. The naphthalene was initially dissolved in acetic acid. Mixtures of this solution with aqueous sulphuric acid and, where necessary, water and further acetic acid were prepared and brought to 25°C. Reaction was started by the addition of small volumes (50–100 μL) of aqueous solutions of sodium nitrate and then sodium nitrite. The small amount of sulphuric acid involved in the liberation of nitrous acid and nitric acid from these salts was ignored in the specification of the percentage composition by weight of these solutions.

The amount of naphthalene remaining $(a - x)$ at time t was calculated from the change in the absorbance (A_t) with time (eq. [6]) using a Perkin–Elmer 554 UV–VIS spectrometer with the cells maintained at 25°C. The initial reading (A_0) was taken from equivalent solutions not containing nitric acid. The final reading (A_∞) was taken when no further change could be detected. For a number of runs, the absorbance was also checked on the following day but no further change was found.

$$[6]\quad (a - x) = a(A_\infty - A_t)/(A_\infty - A_0)$$

For concentrations of naphthalene below 4×10^{-4} mol dm^{-3}, the wavelength used was 350 nm; for concentrations above this value, the wavelength used was in the range 410–430 nm. The final absorbance ($\epsilon(ArNO_2)_{350} = 4000$) agreed with that observed previously (8) for the mixture of nitronaphthalenes formed.

The earlier observation (8) that both nitric acid and nitrous acid needed to be present for a detectable amount of reaction to occur within the time intervals considered was confirmed. Passing nitrogen through the solutions before reaction to remove any dissolved oxygen does not appear to change the reaction rate.

Analysis of the results

The calculations of the rate coefficients k_1 and k_2 were based on the integrated form of eq. [1] (14), which may be written as eq. [7] (where $r = k_1/k_2$).

$$[7]\quad \ln \frac{(ra + a(a - x))}{((r + a)(a - x))} = k_1 t$$

The values of r and k_1 giving the best (least-squares) fit to a straight line were determined by a computer program. The values of the instantaneous rates were calculated by fitting the first 4–6 points of each kinetic run to a quadratic equation and determining the slope at the time of the first point. The half-life was determined by a similar procedure using the 4–6 points about this time and solving for $x = a/2$.

Acknowledgement

Two of us (J.R.L. and M.E.P.) thank the Rectorado of the University of Santiago for financial support.

1. A. P. GOSNEY and M. I. PAGE. J. Chem. Soc. Perkin Trans. 2, 1783 (1980).
2. M. ALI and J. H. RIDD. J. Chem. Soc. Perkin Trans. 2, 327 (1986).

Can. J. Chem. Downloaded from www.nrcresearchpress.com by 186.148.149.217 on 09/07/12
For personal use only.

3. A. H. CLEMENS, J. H. RIDD, and J. P. B. SANDALL. J. Chem. Soc. Perkin Trans. 2, 1667 (1984).
4. A. H. CLEMENS, J. H. RIDD, and J. P. B. SANDALL. J. Chem. Soc. Perkin Trans. 2, 1659 (1984).
5. A. H. CLEMENS, J. H. RIDD, and J. P. B. SANDALL. J. Chem. Soc. Perkin Trans. 2, 1227 (1985).
6. M. ALI, J. H. RIDD, J. P. B. SANDALL, and S. TREVELLICK. J. Chem. Soc. Chem. Commun. 1168 (1987).
7. U. AL-OBAIDI and R. B. MOODIE. J. Chem. Soc. Perkin Trans. 2, 467 (1985).
8. D. S. ROSS, K. D. MORAN, and R. MALHOTRA. J. Org. Chem. **48**, 2118 (1983).
9. J. R. LEIS, M. E. PEÑA, and J. H. RIDD. J. Chem. Soc. Chem. Commun. 670 (1988).
10. M. A. J. RODGERS. J. Chem. Soc. Faraday Trans. 1, **68**, 1278 (1972).
11. A. S. MORKOVNIK and O. YU. OKHLOBYSTIN. Zh. Obshch. Khim. **55**, 692 (1985).
12. R. G. COOMBES, R. B. MOODIE, and K. SCHOFIELD. J. Chem. Soc. Perkin Trans. 2, 800 (1968).
13. B. C. CHALLIS and A. J. LAWSON. J. Chem. Soc. B, 770 (1971).
14. R. WEGSCHNEIDER. Z. Phys. Chem. **41**, 52 (1902).

Can. J. Chem. Downloaded from www.nrcresearchpress.com by 186.148.149.217 on 09/07/12
For personal use only.

A point-charge representation of nonbonding electron pairs: model derived from the ability of the hydrogen bond to act as a probe of electron density

A. C. LEGON
Department of Chemistry, University of Exeter, Stocker Road, Exeter EX4 4QD, England
AND
D. J. MILLEN
Christopher Ingold Laboratories, Department of Chemistry, University College London, 20 Gordon Street, London WC1H 0AJ, England

Received March 5, 1989

This paper is dedicated to Professor Ronald J. Gillespie on the occasion of his 65th birthday

A. C. LEGON and D. J. MILLEN. Can. J. Chem. **67**, 1683 (1989).

A simple point-charge model is presented for some molecules B which assigns charges to atom centres and to nonbonding pairs, those for the latter placed at distances r along directions α as conventionally envisaged. The magnitude δ of the charge assigned to the nonbonding pairs is chosen so that the variation of the electrostatic interaction energy between B and HF with the angular position of HF agrees with that calculated on the basis of a more complete description (DMA) of the electrostatic charge distribution of B. The charges δ in the three molecules explored (B = H_2O, H_2CO, and H_2S) prove to be only a few hundredths of an electron at distances r comparable with bond distances in B.

Key words: nonbonding pairs, point-charge model, hydrogen bond, Gillespie–Nyholm model, electron localization.

A. C. LEGON et D. J. MILLEN. Can. J. Chem. **67**, 1683 (1989).

On présente un modèle de charge ponctuelle simple, pour quelques molécules B, qui attribue des charges aux atomes centraux et aux paires non liées, dont les atomes sont placés à des distances r selon des directions α conventionnelles. On a choisi l'ordre de grandeur δ de la charge attribuée aux paires non liées de telle sorte que la variation d'énergie électrostatique entre B et HF avec la position angulaire de HF s'accorde avec celle calculée à partir d'une description plus complète (DMA) de la distribution de charge électrostatique de B. Les charges δ dans les trois molécules étudiées (B = H_2O, H_2CO et H_2S) s'avèrent être seulement qu'une centaine d'électrons situés aux distances r comparable aux distances de liaison dans B.

Mots clés: paires non liées, modèle de charge ponctuelle, liaison hydrogène, modèle Gillespie–Nyholm, localisation d'électron.

[Traduit par la revue]

Can. J. Chem. Downloaded from www.nrcresearchpress.com by 186.148.149.217 on 09/07/12
For personal use only.

Introduction

We have discussed recently (1) a set of rules for predicting the angular geometries of a wide range of hydrogen-bonded dimers B···HX. As originally presented, these rules were generalizations from some observations made on a carefully selected but limited subset of dimers. Subsequent expansion of the experimental observations further established the validity of the rules (2), which are as follows:

(*i*) *The axis of the HX molecule coincides with the supposed axis of a nonbonding electron pair on the acceptor atom of B as conventionally envisaged,*

or, if B has no nonbonding electron pairs but does have π-bonding pairs,

(*ii*) *the axis of the HX molecule intersects the symmetry axis of the atoms forming the π-bond and is perpendicular to the plane of symmetry of the π-bond.*

Rule (*i*) is definitive when B has both nonbonding and π-bonding electron pairs. These rules appear to apply quite generally when only a single hydrogen bond occurs, and even when two hydrogen bonds occur in a given dimer (as in H_2CO, HCCH (3)) the geometry appears to be determined in a manner that can still be rationalized in terms of the rules.

The rules are readily understood on the basis of a simple electrostatic model (2) in which the angular variation of the potential at appropriate distances from B is considered. As a result of examining the electrostatic potential due to B it was possible to enunciate the following:

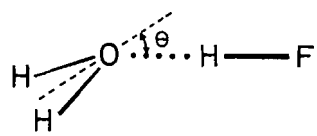


FIG. 1. Definition of the angle θ in the dimer $H_2O\cdots HF$.

(*iii*) *A corollary to rules (i) and (ii): as long as the hydrogen bond in B···HF is sufficiently weak that the electric charge distributions of B and HF are essentially unperturbed, the HF axis acts as a probe for the direction of a nonbonding (or π-bonding) pair on B.*

The explanation underlying this corollary is that the electric charge distribution of HF can be represented in good approximation by a simple extended dipole $\overset{\delta^+}{H}—\overset{\delta^-}{F}$, where $\delta^+ = 0.54e$ and $\delta^- = -0.54e$ (e is the proton charge). Starting, for example, with this model of the HF molecule lying along the C_2 axis of H_2O ($\theta = 0°$, where θ is defined in Fig. 1) and allowing the HF molecule to roll around the oxygen atom in the vertical symmetry plane of H_2O (i.e., θ increases from zero, see Fig. 1), the angular variations of the potential energies $V_H(\theta)$, $V_F(\theta)$, and $V_H(\theta) + V_F(\theta)$ are as shown in Fig. 2. These potential energies have been calculated using the distributed multipole analysis (4) of the electric charge distribution of water given by Buckingham and Fowler (5) and are being used with the implicit assumption that the dominant term in describing the angular variation of the potential energy is the electrostatic one (6, 7). The important

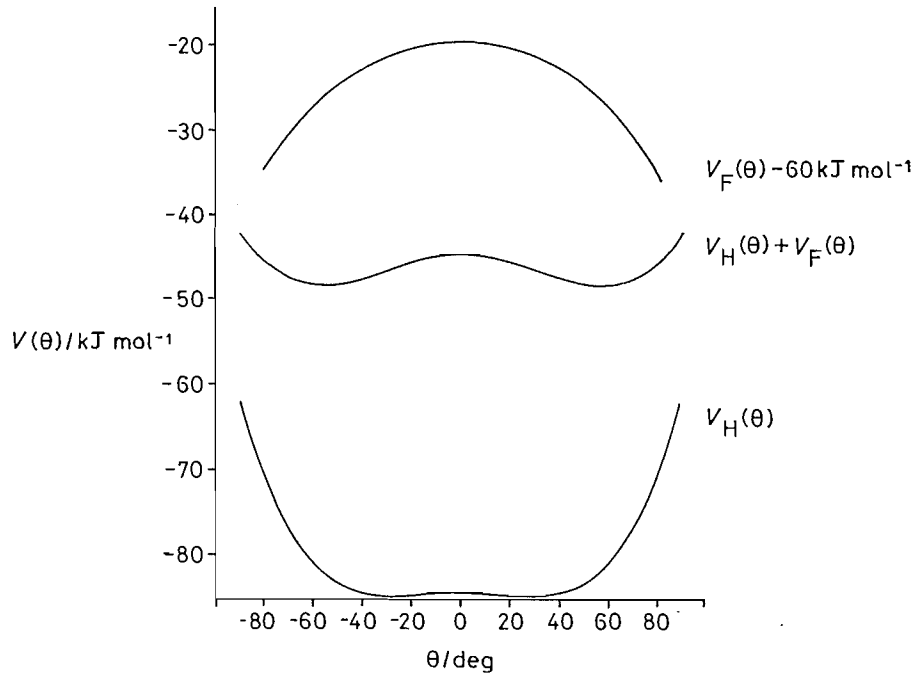


FIG. 2. Variation of the potential energy $V_H(\theta)$ and $V_F(\theta)$ of point charges $0.54e$ at H and $-0.54e$ at F, respectively, with the angle θ in $H_2O\cdots HF$ calculated using the full DMA description of the H_2O charge distribution. The total potential energy of interaction $V_H(\theta) + V_F(\theta)$, which is then that of the extended dipole model of HF with H_2O, is also shown. For convenience the curve for $V_F(\theta)$ is displaced downwards by 60 kJ mol^{-1}.

result is that the potential energy $V_H(\theta) + V_F(\theta)$ of the above extended dipole model of HF in the vicinity of B at the correct distance has a shape and barrier height in satisfactory agreement with experiment (8). Similar agreement with experiment (9) is obtained when such a model is applied to $H_2CO\cdots HF$.[1]

In this paper, we seek to interpret the rules in the simplest possible manner, i.e., a point-charge representation of the electric charge distribution of B together with the extended dipole model of HF. In particular, we show that, to obtain agreement with experiment and with calculations based on more detailed charge distributions for B, it is necessary to place only small fractional electronic charges at physically reasonable distances along the directions of nonbonding pairs as conventionally envisaged. This model has obvious parallels with the valence-shell-electron-pair repulsion model of Gillespie and Nyholm (10) and the partial localization of electron density along nonbonding pair directions discussed by Bader, Gillespie, and MacDougall (11). It is therefore a pleasure to be able to contribute such a relevant paper to this special issue of the Canadian Journal of Chemistry in honour of Professor R. J. Gillespie.

The model

Several electrostatic descriptions of the interaction between molecules B and, e.g., HF have been discussed (5, 12). The most important contribution to the electrostatic energy is the interaction between the distributed charges assigned to B by the model with those of HF. Thus, the simplest possible model consists of point charges placed on atoms and implies a spherical charge distribution centred on each nucleus. Such a model is quite good for obtaining the electrostatic interaction energy but fails completely to predict the correct angular geometry of dimers such as $H_2O\cdots HF$, $H_2CO\cdots HF$, and $H_2S\cdots HF$. The latter can be reproduced by, for example, placing in addition point dipoles and quadrupoles on the atoms according to the distributed multipole analysis (DMA) of B due to Stone (4). This approach has been used successfully by Buckingham and Fowler (5) to calculate electrostatic energies and find their minima with respect to the angular variations of HX about the molecule B. An alternative model, which is developed here, leaves the DMA point charges on the atoms but accounts for the deviations from sphericity about atom centres by translating small fractions of the point charge on the acceptor atom of B away from the atom centre and along directions conventionally associated with nonbonding pairs.

The procedure for constructing the model is to begin with point charges on the atoms of, for example, H_2O, which for convenience are taken from the DMA given in ref. 5 but could be generated in other ways, such as use of the molecular electric dipole moment (12). Small fractional point charges δ are then removed from the DMA charge on the acceptor atom (e.g., O in H_2O) and translated through a distance r along the directions α normally associated with the axes of nonbonding electron pairs in, for example, the Gillespie–Nyholm VSEPR model, as shown in Fig. 3. The point charges q_i appropriate to the DMA's of H_2O and HF are recorded in Table 1, which also includes those for H_2CO and H_2S to be used in the discussion later. Then the potential energy $V(\theta) = V_H(\theta) + V_F(\theta)$ of the HF molecule is calculated at the experimental (8) distance $r(O\cdots F) = 2.662$ Å for the range of angle $\theta = 0$–$90°$ (see Fig. 1). This procedure is repeated for various sets of values δ, r, α and that set chosen which best reproduces the potential energy barrier calculated by using the full DMA of B (see Fig. 2).

We find that physically reasonable solutions are obtained for only a limited range of values of δ and r in the region of $0.04e$ and 1 Å, respectively. Indeed, for $r \approx 0.5$ Å the double

[1]A. C. Legon and D.J. Millen, unpublished calculations.

Can. J. Chem. Downloaded from www.nrcresearchpress.com by 186.148.149.217 on 09/07/12
For personal use only.

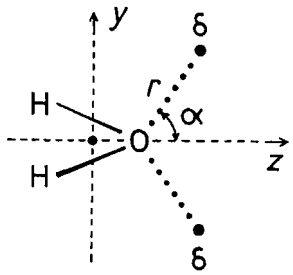


FIG. 3. Definition of the parameters δ, r, α describing the point-charge model of nonbonding electron pairs in H_2O.

TABLE 1. Distributed point charges and their coordinates for H_2O, H_2CO, H_2S, and HF[a]

Molecule	Atom	x	z	q
H_2O	O	0	0.123	−0.802
	H	1.432	−0.986	0.401
H_2CO	O	0	1.135	−0.542
	C	0	−1.138	0.679
	H	1.766	−2.231	−0.068
H_2S	S	0	0.103	0.033
	H	1.808	−1.637	−0.016
HF	F	—	0.087	−0.540
	H	—	−1.645	0.540

[a]Coordinates x, z and charges q are in atomic units and are taken from ref. 5.

TABLE 2. Position (r, α) and magnitude (δ) of point negative charges representing nonbonding pairs in acceptor molecules B and barrier heights (h) calculated for B···HF[a]

Quantity		H_2O···HF	H_2CO···HF	H_2S···HF
r(Å)		1.0	1.0	1.75
δ(au)		0.038	0.05	0.025
α(deg)		54.0	60	90
h(kJ mol^{-1})	This model:	6.9	12	35
	Full DMA:	6.6	11	36
θ_{min}(deg)	This model:	45	50	90
	Full DMA:	55	65	80

[a]See Figs. 3–5 and text for definition of r, α, and δ. h is the height of the potential energy barrier $V(\theta_{max}) - V(\theta_{min})$ calculated by the present model (see text) and also using the full DMA for B. θ is defined in Fig. 1.

minimum apparent in the full calculation (Fig. 2) is not obtained from our model and when r is in the region of 1.5 Å, the barrier height becomes very large for even very small δ. Physical acceptability therefore constrains r to be in the region of 1 Å, which we note is similar to the O—H bond length in H_2O. The important conclusion is that δ is found to be a relatively small fraction of the electronic charge. The results for δ and α when r = 1 Å, which reproduce the barrier height and θ_{min} of the full DMA, are given in Table 2.

We have also carried out a similar analysis for H_2CO···HF

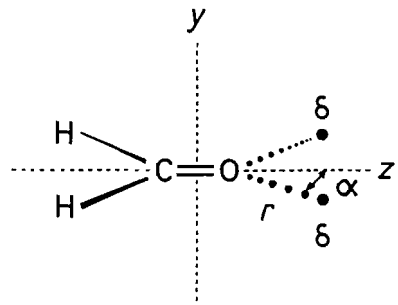


FIG. 4. Definition of the parameters δ, r, α describing the point-charge model of nonbonding electron pairs in H_2CO.

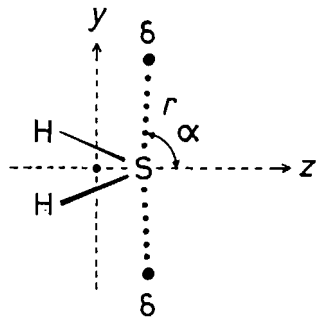


FIG. 5. Definition of the parameters δ, r, α describing the point-charge model of nonbonding electron pairs in H_2S.

(see Fig. 4) and H_2S···HF (see Fig. 5) at the appropriate experimental distances (13, 14) with the results shown in Table 2. For H_2CO···HF the angles α and θ are defined in a similar way but lie in the molecular plane rather than the perpendicular plane. We note that again reasonable solutions are obtained only when $\delta \approx 0.04e$ and $r \approx 1$ Å for H_2CO···HF, while for H_2S···HF longer distances r of δ from the S atom are required. This is not inconsistent with the notion that the H_2S molecule is generally more extensive than the H_2O molecule. Again for both H_2S and H_2CO, δ is found to be only a few per cent of the full electronic charge.

Discussion

We have presented in this paper a very simple model for the electric charge distributions of a few prototype molecules, which not only allows the electrostatic interaction within pairs such as H_2O···HF, H_2CO···HF, and H_2S···HF to be calculated very easily but also leads to observed angular geometries and reasonable angular variation of the potential energy of interaction. The main advantages of this model are that it is easily visualized and is consonant with the valence-shell–electron-pair repulsion model and the convention of nonbonding pairs. The difference from many earlier methods of representing nonbonding pairs with point charges is that our model requires relatively tiny charges (e.g., a few hundredths of an electron) at reasonable distances ($r \approx 1$ Å). These small charges arise quite naturally from the requirement that the "observed" barrier heights (e.g., those from the full DMA calculation or from experiment in the case of H_2O···HF and H_2CO···HF) are reproduced. In fact, similar 5-point charge models were discussed for H_2O and H_2S by Kollman (15) but were deduced without the advantage of the recent experimental or theoretical estimates of the barrier heights in the intermolecular potential energy functions of H_2O···HF, H_2CO···HF, and H_2S···HF.

Can. J. Chem. Downloaded from www.nrcresearchpress.com by 186.148.149.217 on 09/07/12
For personal use only.

Another advantage of the model introduced here is that it is consistent with the generally accepted nearly spherical nature of the electronic charge distribution in H_2O (16) in which there are only very small deviations from hemisphericity at oxygen. Moreover, such a model is very easy to use in situations where large clusters are being discussed, for the electrostatic calculations involve only point charges rather than higher poles. Finally, we note that the model accords well with the ideas recently advanced by Bader, Gillespie, and MacDougall (11), who show that a small localization of electron density along the VSEPR nonbonding pair directions results from the ligand field operating in concert with the Pauli exclusion principle. Geometries of hydrogen-bonded dimers prove to be strongly dependent on these local concentrations of charge and our model gives a measure of such local concentrations.

1. A. C. LEGON and D. J. MILLEN. Discuss. Faraday Soc. **73**, 71 (1982).
2. A. C. LEGON and D. J. MILLEN. Chem. Soc. Rev. **16**, 467 (1987).
3. N. W. HOWARD and A. C. LEGON. J. Chem. Phys. **88**, 6793 (1988).
4. A. J. STONE. Chem. Phys. Lett. **83**, 233 (1981).
5. A. D. BUCKINGHAM and P. W. FOWLER. Can. J. Chem. **63**, 2018 (1985).
6. H. UMEYAMA and K. MOROKUMA. J. Am. Chem. Soc. **99**, 1316 (1977).
7. G. J. B. HURST, P. W. FOWLER, A. J. STONE, and A. D. BUCKINGHAM. Int. J. Quantum Chem. **29**, 1223 (1986).
8. Z. KISIEL, A. C. LEGON, D. J. MILLEN, and S. C. ROGERS. Proc. R. Soc. London, A, **372**, 441 (1980); Z. KISIEL, A. C. LEGON, and D. J. MILLEN. Proc. R. Soc. London, A, **381**, 419 (1982).
9. F. J. LOVAS, R. D. SUENRAM, S. ROSS, and M. KLOBUKOWSKI. J. Mol. Spectrosc. **123**, 167 (1987).
10. R. J. GILLESPIE and R. S. NYHOLM. Q. Rev. Chem. Soc. **11**, 339 (1957).
11. R. F. W. BADER, R. J. GILLESPIE, and P. J. MACDOUGALL, J. Am. Chem. Soc. **110**, 7329 (1988).
12. J. M. BROBJER and J. N. MURRELL. J. Chem. Soc. Faraday Trans. 2, **78**, 1853 (1982).
13. F. A. BAIOCCHI and W. KLEMPERER. J. Chem. Phys. **78**, 3509 (1983).
14. R. VISWANATHAN and T. R. DYKE. J. Chem. Phys. **77**, 1166 (1982).
15. P. A. KOLLMAN. Acc. Chem. Res. **10**, 365 (1977).
16. J. BICERANO, D. S. MARYNICK, and W. N. LIPSCOMB. J. Am. Chem. Soc. **100**, 732 (1978).

Can. J. Chem. Downloaded from www.nrcresearchpress.com by 186.148.149.217 on 09/07/12
For personal use only.

The preparation and X-ray crystal structure of $Te(N_3)_3SbF_6$ containing the triazidotellurium(IV) cation, $Te(N_3)_3^+$

JAMES P. JOHNSON, GREGORY K. MACLEAN, JACK PASSMORE,[1] AND PETER S. WHITE[1]

Department of Chemistry, University of New Brunswick, Bag Service No. 45222, Fredericton, N.B., Canada E3B 6E2

Received October 31, 1988

This paper is dedicated to Professor Ronald J. Gillespie on the occasion of his 65th birthday

JAMES P. JOHNSON, GREGORY K. MACLEAN, JACK PASSMORE, and PETER S. WHITE. Can. J. Chem. **67**, 1687 (1989).

The crystal structure of $Te(N_3)_3SbF_6$ containing the first binary tellurium–nitrogen cation, triazidotellurium(IV) ($Te(N_3)_3^+$), has been determined by X-ray crystallography. Single crystals of $Te(N_3)_3SbF_6$ are monoclinic, space group $P2_1/c$ with a = 9.201(6), b = 8.445(4), c = 13.582(7) Å, β = 100.36(5)°, Z = 4, final R_1 = 0.036 for 1286 observed reflections. The structure consists of discrete $Te(N_3)_3^+$ cations and distorted octahedral SbF_6^- anions, with some cation–anion interactions. The average Te—N_α—N_β—N_γ bond distances in $Te(N_3)_3^+$ are Te—N_α, 1.994(7); N_α—N_β, 1.237(11); and N_β—N_γ, 1.116(12) Å. The average bond angles about the Te, N_α, and N_β atoms are 94.1(3)°, 116.5(6)°, and 173.7(9)°. Structural correlations with other TeX_3^+ species have yielded an estimate of the electronegativity of the N_3^- group to be 3.1 ± 0.1.

Key words: tetratellurium (2+) cation, triazidotellurium(IV) cation, electronegativity, azide.

JAMES P. JOHNSON, GREGORY K. MACLEAN, JACK PASSMORE et PETER S. WHITE. Can. J. Chem. **67**, 1687 (1989).

Faisant appel à la diffraction des rayons-X, on a déterminé la structure cristalline du $Te(N_3)_3SbF_6$ qui est le premier complexe contenant le cation binaire du tellure et de l'azote, le triazidotellure(IV) ($Te(N_3)_3^+$). Les cristaux uniques du $Te(N_3)_3SbF_6$ sont monocliniques et ils cristallisent dans le groupe d'espace $P2_1/c$ avec a = 9,201(6), b = 8,445(4) et c = 13,582(7) Å, β = 100,36°, Z = 4 et une valeur finale de R_1 de 0,036 pour 1286 réflexions observées. La structure comporte des cations $Te(N_3)_3^+$ individuels, des anions SbF_6^- de forme octaédrique déformée et quelques interactions cation–anion. Les longueurs moyennes des liaisons Te—N_α—N_β—N_γ dans le cation $Te(N_3)_3^+$ sont TeN_α, 1,994(7); N_α—N_β, 1,237(11) et N_β—N_γ, 1,116(12) Å. Les angles moyens de liaisons des atomes de Te, N_α et N_β sont 94,1(3)°, 116,5(6)° et 173,7(9)°. En se basant sur des corrélations de structure avec d'autres espèces TeX_3^+, on a pu évaluer que l'électronégativité du groupement N_3^- est égale à 3,1 ± 0,1.

Mots clés : cation du tétratellure (2+), cation triazidotellure(IV), électronégativité, azoture.

[Traduit par la revue]

Introduction

The S_2N^+ cation, in S_2NAsF_6 (1) has a rich chemistry, and is an important building block in the systematic synthesis of other sulfur–nitrogen-containing compounds (2–9). It would be of interest to prepare the selenium and tellurium analogues, Se_2NAsF_6 and Te_2NAsF_6, as they should also have extensive chemistries, because they are of interest in their own right and because very few isolated selenium–nitrogen or tellurium–nitrogen species exist. These include Se_4N_4 (10), Te_4N_4 (11), and Te_3N_4 (12). Binary anionic or cationic species have not been characterized. The most convenient preparation of S_2NAsF_6 (1) is given in eq. [1].

$$[1]\quad S_4N_4 + \tfrac{1}{2}S_8 + 6AsF_5 \xrightarrow[\text{Trace } Br_2]{\text{Liquid } SO_2} 4S_2NAsF_6 + 2AsF_3$$

The analogous reactions leading to Se_2NAsF_6 and Te_2NAsF_6 would involve the use of explosive Se_4N_4 (10) and Te_4N_4 (11), which we wished to avoid. An alternative synthesis of S_2NAsF_6, but in lower yield, is that of $S_8(AsF_6)_2$ and NaN_3 in liquid SO_2 (1). We therefore attempted analogous reactions of azides and homopolyatomic cations of selenium, Se_4^{2+} (13), Se_{10}^{2+} (14), and tellurium, Te_4^{2+} (13, 15). Subsequently, the reaction between $Te_4(SbF_6)_2$ and KN_3 yielded, as one of the products, the compound $Te(N_3)_3SbF_6$, which was identified from its infrared spectrum and by X-ray crystallography. The compound $Te(N_3)_3SbF_6$ contains the triazidotellurium(IV) cation, $Te(N_3)_3^+$, and contains the first example of a binary tellurium–nitrogen cation. An account of this work is given below.

[1]Authors to whom correspondence may be addressed.

Experimental

Reagents and general procedures

Except where stated, the apparatus and chemicals were as previously described (16). The $Te_4(AsF_6)_2$ (13, 15, 17), $Te_4(SbF_6)_2$ (15), and $Se_{10}(AsF_6)_2$ (14) salts were prepared as described in the literature. The $Se_4(AsF_6)_2$ was prepared using a trace of bromine at room temperature (18). The salts NaN_3 (Fisher) and KN_3 (Pfaltz and Bauer) were vacuum dried before use. The SO_2 (Matheson) was dried and stored over CaH_2.

The glass reaction vessels either (A) consisted of two bulbs separated by a coarse or medium glass frit and equipped with a Teflon-in-glass J. Young Valve (15), or (B) consisted of a similar vessel with the valve attached to an evacuable condenser containing a coarse or medium glass frit and a pressure-equalizing tube (a drawing of such a vessel is given in ref. 19). Infrared spectra of Nujol mulls between KBr plates were obtained on a Perkin–Elmer model 683 grating spectrometer. Spectra were calibrated using indene (20). Mass spectra were obtained via the direct inlet port at 110°C on a Hitachi Perkin–Elmer RMU6D mass spectrometer with an ionizing voltage of 70 eV.

Reaction of $Te_4(SbF_6)_2$ with KN_3[2]

In a typical reaction, an excess of KN_3 (0.41 g, 5.05 mmol) was

[2]A 1:1 reaction between $Te_4(SbF_6)_2$ and NaN_3 in one bulb of a two-bulb glass vessel (A) yielded a colorless solid and a small amount of a yellow species. Attempted removal of the product with a nickel spatula resulted in an explosion.

We believe that $Te(N_3)_3SbF_6$ is not itself explosive but, if care is not taken in its preparation, other products that are yellow or orange in color are also formed. These materials are highly shock and friction sensitive. They may be neutral or anionic tellurium–nitrogen-containing compounds and, if formed, should be considered dangerous and highly explosive and disposed of appropriately. The method reported here successfully yielded $Te(N_3)_3SbF_6$, without the explosive impurities.

Can. J. Chem. Downloaded from www.nrcresearchpress.com by 194.225.253.170 on 09/07/12
For personal use only.

Can. J. Chem. Downloaded from www.nrcresearchpress.com by 194.225.253.170 on 09/07/12
For personal use only.

TABLE 1. Infrared and Raman spectra (cm^{-1}) of the colorless crystals from the $Te_4(SbF_6)_2/KN_3$ reaction

Infrared (bulk material, mull)	Raman (single crystal)	Tentative[a] assignments
3330w 3280w		$\nu_{as} + \nu_s N_3^-$
2425w 2410w 2390w 2360mw		$2\nu_s N_3^-$
	2165(3)	
2145s	2149(11)	
2130s	2128(8)	$\nu_{as} N_3^-$
	2114(6)	
2100s	2102(4)	
1299m 1217m 1197s 1175m	1196(1)	$\nu_s N_3^-$
1093w		$2\gamma N_3^-$
1028w		?
728mw		νTe—F or νTe=N? (in impurity)
685mw	680(1)	δN_3^-
659s	656(8)	$\nu_3 SbF_6^-$
636mw	638(11)	$\nu_1 SbF_6^-$
584mw	566(1)	$\nu_2 SbF_6^-$
549ms		γN_3^-
460w	456(100)	ν_sTe—N + νSb—N?
440m 426ms	432(41)	ν_{as}Te—N + νSb—N?
390sh[b]		$\nu_4 SbF_6^-$
	266(1)	δN—Te—N or $\nu_5 SbF_6^-$

[a]Tentative assignments were made by comparison of species such as N_3^- (25), SbF_6^- (21*a*), $TeCl_3N_3$ and $TeCl_2(N_3)_2$ (26), TeF_3^+ (27, 28), $SbCl_5N_3^-$ (29, 30), and $SbCl_4(N_3)_2^-$ (31). Standard definitions (21*b*) of abbreviations (s, as, ν, α, δ).

[b]Shoulder on KBr cutoff.

placed onto the coarse sintered glass frit in the refluxing condenser of vessel B and the $Te_4(SbF_6)_2$ (6.00 g, 6.11 mmol) was added into the bulb of the two-bulb glass vessel below the refluxing condenser. The SO_2 (25.00 g, 390.2 mmol) was then condensed onto the $Te_4(SbF_6)_2$. The stirred $Te_4(SbF_6)_2/SO_2$ slurry was held at ~30°C, which caused SO_2 to condense on the inside walls of the water-cooled condenser and to slowly dissolve the KN_3 and thus wash down slowly into the reaction bulb holding the $Te_4(SbF_6)/SO_2$ solution. This slow addition of KN_3 to the $Te_4(SbF_6)_2$ was continued until the initial red coloration of the $Te_4(SbF_6)_2/SO_2$ solution had just disappeared (approximately 9 days). The yellowish solution was then filtered into the second bulb and the brown-gray insoluble solids (4.77 g) were washed twice with liquid SO_2. The SO_2 was slowly condensed back into the first bulb by placing it in a cold water bath. This produced colorless crystals (<0.5 g) suitable for X-ray analyses in the second bulb. The SO_2, and a noncondensible gas, were then removed by evacuation. The infrared spectrum of the brown-grey insoluble solids showed only peaks attributable to the SbF_6^- anion (21*a*). The infrared spectrum of the bulk crystals is given in Table 1. The Raman spectrum of a single colorless crystal is also given in Table 1. The mass spectrum of the colorless crystals gave peaks only attributable to HN_3^+ (rel. int. = 59) and N_2^+ (rel. int. = 100).

A colorless oil was sublimed from a mixture of pale-yellow-colored products obtained from a similar reaction to that in footnote 2, but between $Te_4(AsF_6)_2$ and NaN_3. The mass spectrum of this oil gave peaks at (*m/e* (rel. int.) assigned species) 233(<1) $TeF(N_3)_2^+$, 220(1) $AsF(N_3)_3^+$, 210(3) $TeF_2N_3^+$, 197(8) $AsF_2(N_3)_2^+$, 187(31) TeF_3^+, 174(16) $AsF_3N_3^+$, 168(6) TeF_2^+, 155(4) $AsF_2N_3^+$, 151(8) AsF_4^+, 149(2) TeF^+, 146(2) AsF_3N^+, 136(3) $AsFN_3^+$, 132(5) AsF_3^+, 130(2) Te^+, 113(22) AsF_2^+, 108(2) $AsFN^+$, 94(6) AsF^+, 89(1) AsN^+, 75(3) As^+, 47(1) N_2F^+, 43(71) HN_3^+, 42(13) N_3^+, 28(100) N_2^+. Only the ion fragments containing the ^{130}Te isotope are included above. Ion fragments containing the other tellurium isotopes were observed in their appropriate abundances.

X-ray crystal structure crystal data

$Te(N_3)_3SbF_6$ $M = 489.4$

Monoclinic, space group $P2_1/c$, $a = 9.201(6)$, $b = 8.445(4)$, $c = 13.582(7)$ Å, $\beta = 100.36(5)°$, $U = 1038$ Å^3, $Z = 4$, $D_c = 3.13$ Mg m^{-3}, $F(000) = 880$, $\mu = 5.48$ mm^{-1}, λ(MoKα) = 0.71073 Å, crystal size = 0.5 × 0.3 × 0.2 mm, $T = 293$ K.

A suitable crystal was mounted under dry nitrogen in a rigorously dried (evacuated at 250°C) capillary tube. Preliminary precession photographs provided space group information and approximate unit cell dimensions, after which the crystal was mounted on a Picker FACS-I diffractometer equipped with graphite monochromated MoKα radiation. Unit cell parameters and an orientation matrix were refined by least squares using the centered coordinates of 27 reflections with $30° \leqq 2\theta \leqq 37°$. Intensity data were collected using an ω–2θ at a scan rate of 2°(2θ) min^{-1}. Backgrounds were estimated by standing counts of 1/10 scan time at each end of the scan. If the reflection had a significant intensity ($I \geqq 3\sigma(I)$) the profile of the peak was analyzed and those portions of the scan that were not part of the peak were included in the background estimate. Data were collected in the range $5 \leqq 2\theta \leqq 50°$, resulting in 1805 unique reflections of which 1286 were considered observed ($I \geqq 3\sigma(I)$) and included in the subsequent calculations. Three standard reflections, monitored every 150 reflections throughout the data collection, showed no significant deviations from their mean values.

The structure was solved by locating the position of the Te and Sb atoms from inspection of the three-dimensional Patterson function. Least-squares refinement using SHELX-76 (22) of the scale, positional, and isotropic thermal parameters gave an R_1 of 0.26. The Te positional parameters were assumed to be correct and a least-squares refinement followed by difference Fourier synthesis revealed the correct Sb positional parameters, which were shifted by 0.2 Å along *b*. Refinement of scale, positional, and isotropic thermal parameters gave an R_1 of 0.20, indicating a significant improvement over the original solution. The remaining atoms were located from a subsequent difference Fourier synthesis. A DIFABS (23) absorption correction was applied. Anisotropic thermal parameters were used for all the atoms and the function minimized was $\Sigma(w)(\Delta F)^2$ with $w = [\sigma(F)^2 + kF_o^2]^{-1}$ where $k = 0.0023$ and $\sigma(F)$ was derived from counter statistics. The final refinement resulted in $R_1 = \Sigma|\Delta F|/\Sigma|F| = 0.036$ and $R_2 = \Sigma w|\Delta F|^2/\Sigma w|F|^2 = 0.039$ (0.064 and 0.050, respectively, when all reflections are included). Scattering factors for neutral atoms were taken from the International tables for X-ray crystallography (24) and corrected for anomalous dispersion. Table 2 gives the final atomic coordinates.[3]

Results and discussion

The reaction of $Te_4(SbF_6)_2$ and KN_3 leading to $Te(N_3)_3SbF_6$

The reaction of a 1:1 mixture of $Te_4(SbF_6)_2$ and NaN_3 in SO_2 led to the formation of both a colorless and a yellow solid, which exploded on attempted removal using a nickel spatula. It is possible, in view of the identification of $Te(N_3)_3SbF_6$ in a similar reaction, that the explosive component was the unknown

[3]Listings of calculated and observed structure factors, as well as anisotropic thermal parameters for the $Te(N_3)_3SbF_6$ structure have been deposited, and may be purchased from the Depository of Unpublished Data, CISTI, National Research Council of Canada, Ottawa, Ont., Canada K1A 0S2.

Can. J. Chem. Downloaded from www.nrcresearchpress.com by 194.225.253.170 on 09/07/12
For personal use only.

TABLE 2. Fractional atomic coordinates with standard deviations in parentheses for $Te(N_3)_3SbF_6$

Atom	x/a	y/b	z/c
Te	0.11646(6)	0.23063(6)	0.20821(4)
N(1)	0.1628(8)	0.0595(8)	0.3095(6)
N(2)	0.2924(9)	0.0216(9)	0.3323(6)
N(3)	0.4075(10)	−0.0220(13)	0.3583(8)
N(4)	0.1553(8)	0.4143(8)	0.3029(5)
N(5)	0.2826(8)	0.4695(8)	0.3161(5)
N(6)	0.3913(10)	0.5287(12)	0.3316(7)
N(7)	0.3217(7)	0.2363(7)	0.1814(6)
N(8)	0.3374(7)	0.2275(8)	0.0921(6)
N(9)	0.3673(11)	0.2234(11)	0.0153(7)
Sb	0.83098(6)	0.24743(5)	0.92322(4)
F(1)	0.6390(7)	0.2198(7)	0.8567(5)
F(2)	1.0258(6)	0.2703(5)	0.9860(4)
F(3)	0.8893(6)	0.2636(5)	0.7972(4)
F(4)	0.8607(6)	0.0293(6)	0.9167(4)
F(5)	0.8060(7)	0.4648(6)	0.9206(4)
F(6)	0.7824(9)	0.2297(6)	1.0473(5)

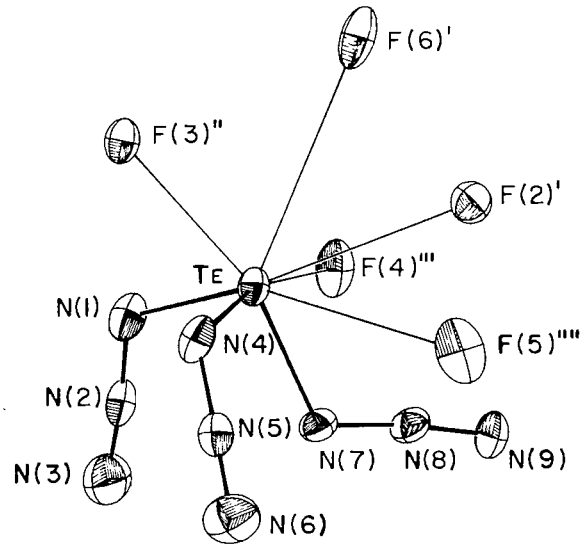


FIG. 1. Stereoscopic views of the $Te(N_3)_3SbF_6$ unit cell.

$Te(N_3)_4$ or alternatively Te_4N_4 (11) or Te_3N_4 (12). To minimize the chance of the formation of $Te(N_3)_4$, a related reaction was carried out such that the red Te_4^{2+} was always present. This was done by washing the sparingly soluble KN_3 into $Te_4(SbF_6)_2$, and stopping the reaction as soon as the solution became colorless. This in effect is a titration of the red Te_4^{2+} by N_3^-. Several single crystals of the soluble product were shown to be $Te(N_3)_3SbF_6$ by single crystal X-ray diffraction. In addition, the Raman spectrum (Table 1) of a single crystal is consistent with the presence of $Te(N_3)_3SbF_6$. The infrared spectrum of the bulk material (Table 1) appears to be more complex but it certainly contains $Te(N_3)_3[SbF_6]$. It possibly also contains other species (e.g., $Te(N_3)_2F[SbF_6]$). This suggestion is supported by the results of the related reaction of $Te_4(AsF_6)_2$ and NaN_3 in a 1:1 ratio in liquid SO_2. A yellowish oil was produced on removal of SO_2, from which was condensed a colorless oil. The mass spectrum of this oil (see experimental section) showed peaks attributable to $Te(N_3)_{3-x}F_x^+$ ($x = 1$–3) and $As(N_3)_xF_{4-x}^+$ ($x = 0$–3) arising from the dissociation of $Te(N_3)_{3-x}F_x^+$ $As(N_3)_xF_{6-x}^-$ by fluoride ion transfer from the anion to the cation, and loss of F^- from the neutral fragments on ionization. This clearly shows some ligand scrambling has occurred in the $Te_4(AsF_6)_2/NaN_3$ reaction. The infrared spectrum of the colorless oil from the $Te_4(AsF_6)_2/KN_3$ reaction is similar to that of the solid from the $Te_4(SbF_6)_2/KN_3$ but is more complex with some overlapping bands suggesting the presence of a mixture of related species. This is further evidence that fluoride–azide exchange is more extensive in the AsF_6^- reaction. The greater simplicity of the $Te_4(SbF_6)_2$ system may relate to the manner in which it was carried out, and (or) to the greater Lewis basicity of the AsF_6^- anion, leading to greater cation–anion interaction and greater azide–fluoride cation–anion exchange. The mass spectrum of $Te(N_3)_3SbF_6$ showed peaks only attributable to N_2 (and HN_3 presumably given by hydrolysis), indicating that decomposition is occurring preferentially to fluoride ion transfer.

The reaction of $Te_4(SbF_6)_2$ and KN_3 is very different from that of $S_8(AsF_6)_2$ and NaN_3 leading to ca. 30% yield of S_2NAsF_6 (1). Presumably the tellurium reaction proceeds as indicated by eq. [2], leading to the formation of the unstable azide derivative of Te_4^{2+}, $Te_4N_3^+$, which may disproportionate as indicated by eq. [3]. The unstable intermediate $Te_{11}(SbF_6)_2$ may then disproportionate according to eq. [4].

[2] $Te_4(SbF_6)_2 + KN_3 \rightarrow KSbF_6\downarrow + \text{“}Te_4N_3SbF_6\text{”}$

[3] $3Te_4N_3SbF_6 \rightarrow Te(N_3)_3SbF_6 + \text{“}Te_{11}(SbF_6)_2\text{”}$

[4] $\text{“}Te_{11}(SbF_6)_2\text{”} \rightarrow Te_6(SbF_6)_2\downarrow + 5Te\downarrow$

The insoluble dark brown $Te_6(SbF_6)_2$ (32) may be one of the observed products, or may further react with KN_3 by related reactions leading to elemental tellurium and $Te(N_3)_3SbF_6$.

The reactions of the homopolyatomic cations $Se_4(AsF_6)_2$ and $Se_{10}(AsF_6)_2$ with alkali azides were also attempted but yielded no evidence for the formation of a Se–N containing species in either the soluble or insoluble products (ir). A brown product was observed in the Se_4^{2+}/N_3^- reaction, which appeared to be $CsAsF_6$ (ir) mixed with $Se_{10}(AsF_6)_2$ (14) (solubility and color of the material). A much darker brown product was formed in the Se_{10}^{2+}/N_3^- reaction, which appeared to be unreacted $Se_{10}(AsF_6)_2$ mixed with elemental selenium (black) and $NaAsF_6$ (ir). All of these selenium reactions yielded nearly quantitative amounts of nitrogen gas.

The lack of success at preparing a new selenium–nitrogen cation may relate to the instability of the selenium–nitrogen bond. Thus, although a large number of thermally stable =N—TeF_5 compounds are known (33–37), attempts to prepare the analogous selenium compounds have been unsuccessful (38). The analogous Se(IV) compounds containing the —N=SeX_2 (X = F, Cl) (34, 39) and —N=Se=N— (40) groups, as well as compounds of the type Cl_2ArSe—N=SeArCl (Ar = aryl) (41), are thermally unstable under ambient conditions. On the other hand, cations containing selenium–nitrogen bonds have been prepared of salts that are stable at room temperature. These include $(Se_2N_2S)_2(AsF_6)_2$ (42), $Se_3N_2(AsF_6)_2$, $Se_3N_2(AsF_6)$ (43), and $Se_2N_2S(AsF_6)_2$ (43, 44) containing the $\overline{NSeSeNS}^+$, $\overline{NSeSeNSe}^+$, $\overline{NSeSeNSe}^{2+}$, and $\overline{NSeSeNS}^{2+}$ rings respectively.

The X-ray crystal structure of $Te(N_3)_3SbF_6$

The structure of $Te(N_3)_3SbF_6$ consists of discrete $Te(N_3)_3^+$ and SbF_6^- ions, with some cation–anion interactions. The contents of a unit cell are illustrated in Fig. 1. The $Te(N_3)_3^+$

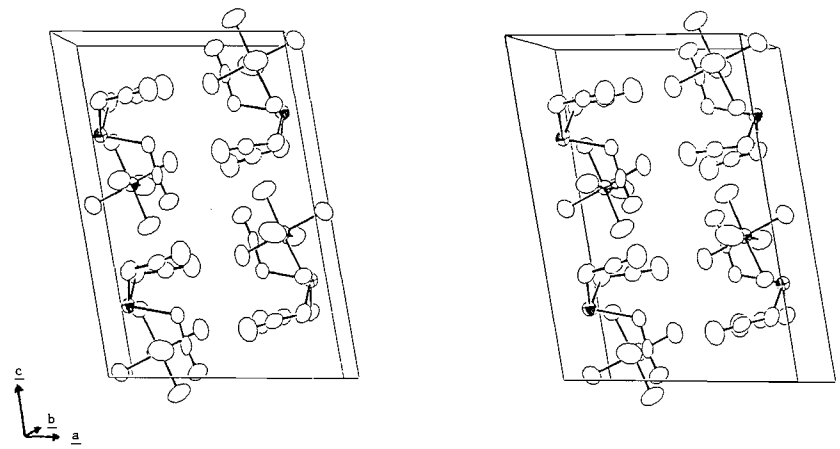


FIG. 2. The $Te(N_3)_3^+$ cation, with tellurium–fluorine contacts.

cation, with contacts to antimony fluorine atoms, is shown in Fig. 2. The bond distances and angles, within the $Te(N_3)_3^+$ cation, and the interionic contacts are given in Table 3 (a and b), and bond distances and angles within the SbF_6^- anion are given in Table 4.

The triazidotellurium(IV) cation, $Te(N_3)_3^+$, is the first binary tellurium–nitrogen cation to be prepared and structurally characterized. The related species, $TeCl_3N_3$ and $TeCl_2(N_3)_2$, have however, been reported (26). The average Te—N bond distance in $Te(N_3)_3^+$ is 1.994(7) Å, which is approximately equal to the single bond distance (1.99 Å) calculated by the Schomaker–Stevenson equation (45) (eq. [5]), where r_{AB} is the calculated single bond distance (Å), r_A and r_B are the covalent single bond radii (Å) for the elements (Te = 1.37 Å, N = 0.70 Å (46)), and χ_A and χ_B are their respective Pauling's (47) electronegativities for nitrogen (3.0) and tellurium (2.1). The electronegativity of the azide group has been estimated (2.95 ± 0.09) (48) to be very similar to that of nitrogen itself (3.0) (47), which was used in our estimate of the tellurium–nitrogen distance.

$$[5] \quad r_{AB} = r_A + r_B - 0.09|\chi_A - \chi_B|$$

The observed bond distances in all MX_3^+ cations (M = chalcogen, X = Cl, Br, I) are also very similar (within 0.01 Å) to values estimated by the Schomaker–Stevenson equation (49). As far as we are aware, the only other Te^{IV}—N bond distance reported is that in $(p\text{-}CH_3OC_6H_4)_2Te—NSO_2C_6H_4CH_3\text{-}p$ (1.980(3) Å) (50), rather similar to that in $Te(N_3)_3^+$. The compounds $(C_6H_5)_3Te(NCS)$ (51), $(C_6H_5)_3Te(NCO)$ (52), and $[(C_6H_5)_2Te(NCS)]_2O$ (53) have tellurium–nitrogen distances of 3.099(7), 2.986(10), and 2.400(10) Å respectively; these species are largely ionic. A relatively large number of other tellurium(IV) nitrogen-containing compounds have been prepared (26, 54) but their structures have not been determined. The tellurium(VI)–nitrogen distances in $F_5TeNWCl_4$ (34) (1.98(3) Å) and in $Hg[N(CF_3)TeF_5]_2$ (36) (2.01(3) Å) are not significantly different from that (1.994(7) Å) in $Te(N_3)_3^+$. However, the tellurium–nitrogen distance in F_5TeNCO (35) (1.859(21) Å) is significantly shorter, which may possibly be due to some π bonding.

The overall shape of $Te(N_3)_3^+$ is similar to one half of the $Sn(N_3)_6^{2-}$ anion (55). The N—N bond distances (average of $N_\alpha—N_\beta$ = 1.237(11) Å and $N_\beta—N_\gamma$ = 1.116(12) Å) and near linearity (average $N_\alpha—N_\beta—N_\gamma$ = 173.7(9)°) of the azide groups in $Te(N_3)_3^+$ are similar to those found in other azide species (56), and in HN_3 ($N_\gamma—N_\beta$ = 1.237(2) Å, $N_\beta—N_\gamma$ = 1.133(2) Å, $N_\alpha—N_\beta—N_\gamma$ = 180°) (57). This implies that the bonding in the TeN_3 fragments is covalent and similar to that in HN_3. The average Te—N_α—N_β bond angle (116.5(6)°) is also similar to the corresponding angle in related species (56) and HN_3 (114.1(5)°) (57).

The average XTeX angles in TeX_3^+ (X = F, Cl, Br, I) for a

TABLE 3. Bond distances and angles, including interionic contacts, for the $Te(N_3)_3^+$ cation, with estimated standard deviations in parentheses

(a) Bond distances and angles

Bond	Distance (Å)	Bonds	Angle (deg)
Te—N(1)	1.988(7)	N(1)—Te—N(4)	97.3(3)
N(1)—N(2)	1.219(11)	N(1)—Te—N(7)	93.0(3)
N(2)—N(3)	1.117(12)	N(4)—Te—N(7)	91.9(3)
Te—N(4)	2.006(7)	Te—N(1)—N(2)	116.4(6)
N(4)—N(5)	1.243(10)	Te—N(4)—N(5)	115.9(6)
N(5)—N(6)	1.104(11)	Te—N(7)—N(8)	117.2(5)
Te—N(7)	1.987(7)	N(1)—N(2)—N(3)	174.3(10)
N(7)—N(8)	1.248(12)	N(4)—N(5)—N(6)	174.3(9)
N(8)—N(9)	1.127(14)	N(7)—N(8)—N(9)	172.5(8)

(b) Interionic contacts[a]

Contact	Distance (Å)	Contacts	Angle (deg)[b]
Te—F(2)	3.001(6)	F(2)—Te—N(1)	139.8(2)
Te—F(3)	2.596(6)	F(2)—Te—N(4)	122.8(2)
Te—F(4)	2.805(5)	F(2)—Te—N(7)	85.1(2)
Te—F(5)	3.261(6)	F(3)—Te—N(1)	77.4(3)
Te—F(6)	3.436(7)	F(3)—Te—N(4)	75.7(2)
N(1)—F(3)	2.905(9)	F(3)—Te—N(7)	163.0(2)
N(4)—F(3)	2.861(9)	F(4)—Te—N(1)	79.6(3)
N(4)—F(3′)	3.035(9)	F(4)—Te—N(4)	165.7(2)
N(5)—F(3)	3.012(8)	F(4)—Te—N(7)	74.4(2)
N(5)—F(6)	3.004(10)	F(5)—Te—N(1)	154.7(2)
N(6)—F(6)	3.014(13)	F(5)—Te—N(4)	72.6(2)
N(7)—F(5)	3.014(8)	F(5)—Te—N(7)	65.0(2)
N(8)—F(2)	2.991(8)	F(6)—Te—N(1)	119.6(2)
N(8)—F(4)	2.821(9)	F(6)—Te—N(4)	116.4(2)
N(8)—F(5)	2.906(9)	F(6)—Te—N(7)	130.9(3)

[a]All interionic contacts shown for Te---F ≦ 3.55 Å, and N---F ≦ 3.05 Å (vdW Te---F = 3.53 Å, and N---F = 3.02 Å (61)).

[b]Only the interionic contact angles about the tellurium atom are given.

Can. J. Chem. Downloaded from www.nrcresearchpress.com by 194.225.253.170 on 09/07/12
For personal use only.

TABLE 4. Bond distances and angles for the SbF_6^- anion of $Te(N_3)_3SbF_6$, with estimated standard deviations in parentheses

Bond	Distance (Å)	Bonds	Angle (deg)
Sb—F(1)	1.848(6)	F(2)—Sb—F(1)	177.8(3)
Sb—F(2)	1.851(5)	F(3)—Sb—F(1)	88.2(3)
Sb—F(3)	1.889(6)	F(3)—Sb—F(2)	90.1(2)
Sb—F(4)	1.867(5)	F(4)—Sb—F(1)	89.3(3)
Sb—F(5)	1.850(5)	F(4)—Sb—F(2)	89.2(2)
Sb—F(6)	1.826(7)	F(4)—Sb—F(3)	87.7(2)
		F(5)—Sb—F(1)	90.7(3)
		F(5)—Sb—F(2)	90.2(2)
		F(5)—Sb—F(3)	88.0(2)
		F(5)—Sb—F(4)	175.7(3)
		F(6)—Sb—F(1)	94.0(3)
		F(6)—Sb—F(2)	87.7(3)
		F(6)—Sb—F(3)	177.7(3)
		F(6)—Sb—F(4)	91.4(2)
		F(6)—Sb—F(5)	92.8(3)

related series of weakly basic AsF_6^- and $Sb_2F_{11}^-$ salts decrease as the electronegativity of X increases, as expected by a V.S.E.P.R. model (58). In fact a plot of the electronegativity of the X atom against the X—Te—X bond angle (X = Cl, Br, I) falls on a reasonably straight line (correlation coefficient $r = 0.990$). The corresponding average N_α—Te_α—N_α angle (94.1(3)°) in $Te(N_3)_3^+$ then gives an electronegativity for N_3^- as 3.23 on the Pauling scale (47). This value is higher than the corresponding values for chlorine (3.0), nitrogen (3.0), and an older estimated value (2.95 ± 0.09), Pauling scale (48), for N_3^-. The strength of the tellurium–fluorine cation–anion contacts increases as the electronegativity of the halogen in TeX_3^+ increases (49). The extent of this interaction can be estimated by summing the Te---F bond valences as defined by Brown (59), in all TeX_3^+ salts. A plot of the sum of the Te---F bond valences (0.85 valence units in $Te(N_3)_3SbF_6$) against the electronegativity of the X atom (X = Cl, Br, I) also yields a reasonably straight line (correlation coefficient $r = 0.998$). This plot gives the electronegativity for N_3^- as 3.03 on the Pauling scale (47). Therefore we estimate the electronegativity of the N_3^- group to be 3.1 ± 0.1. Incorporation of this value for N_3^- in eq. [5] yields a calculated Te—N bond distance of 1.98 Å, again not significantly different than that found in $Te(N_3)_3^+$.

There are three tellurium–fluorine contacts with F(3), F(4), and F(5) that are approximately *trans* to tellurium–nitrogen bonds (163.0(2), 165.7(2), 154.7(2)° respectively), giving the tellurium atom a distorted octahedral AX_3Y_3E geometry (60). The contact Te—F(3) is significantly stronger (2·596(6) Å) than the other two (2·805(5), 3·261(6) Å) and presumably cation–anion exchange would proceed by donation of F(3) to tellurium. The strongest of the cation–anion contacts, Te—F(3), also affects the observed bond distances in the SbF_6^- anion, with the Sb—F(3) bond (1·889(6) Å) being the longest, and the opposite Sb—F(6) bond (1·826(7) Å) being the shortest. The Sb—F(4) bond (1·867(5) Å) is also lengthened due to the relatively strong Te—F(4) contact. In addition, the contacts Te—F(2) (3·001(6) Å) and Te—F(6) (3·436(7) Å) are also less than the sums of the corresponding van der Waals radii (3·53 Å) (61) and each cap a face of the octahedron, with the longer Te—F(6) contact approaching the anticipated position of the lone pair, giving an overall $AX_3Y_3Y'_2E$ geometry (60) about the tellurium atom. There are also a large number of anionic fluorine contacts to the nitrogen atoms of $Te(N_3)_3^+$ (see Table 3) but no significant correlation can be made between the number or the strength of these contacts and the observed N—N bond distances.

Acknowledgements

We thank the Natural Sciences and Engineering Research Council of Canada and the University of New Brunswick for financial support.

1. A. J. BANISTER, R. G. HEY, G. K. MACLEAN, and J. PASSMORE. Inorg. Chem. **21**, 1679 (1982).
2. F. A. KENNETT, G. K. MACLEAN, J. PASSMORE, and M. N. S. RAO. J. Chem. Soc. Dalton Trans. 851 (1982).
3. W. V. F. BROOKS, G. K. MACLEAN, J. PASSMORE, P. S. WHITE, and C.-M. WONG. J. Chem. Soc. Dalton Trans. 1961 (1983).
4. G. K. MACLEAN, J. PASSMORE, and P. S. WHITE. J. Chem. Soc. Dalton Trans. 211 (1984).
5. G. K. MACLEAN, J. PASSMORE, M. J. SCHRIVER, P. S. WHITE, D. BETHELL, R. S. PILKINGTON, and L. H. SUTCLIFFE. J. Chem. Soc. Dalton Trans. 1405 (1985).
6. N. BURFORD, J. P. JOHNSON, J. PASSMORE, M. J. SCHRIVER, and P. S. WHITE. J. Chem. Soc. Chem. Commun. 966 (1986).
7. N. BURFORD, J. PASSMORE, and M. J. SCHRIVER. J. Chem. Soc. Chem. Commun. 140 (1986).
8. E. G. AWERE, N. BURFORD, C. MAILER, J. PASSMORE, M. J. SCHRIVER, P. S. WHITE, A. J. BANISTER, H. OBERHAMMER, and L. H. SUTCLIFFE. J. Chem. Soc. Chem. Commun. 66 (1987).
9. W. V. F. BROOKS, N. BURFORD, J. PASSMORE, M. J. SCHRIVER, and L. H. SUTCLIFFE. J. Chem. Soc. Chem. Commun. 69 (1987).
10. H. BARNIGHAUSEN, T. VON VOLKMANN, and J. JANDER. Acta Crystallogr. **21**, 571 (1966); G. WOLMERHÄUSER, C. R. BRULET, and G. B. STREET. Inorg. Chem. **17**, 3586 (1978).
11. H. GARCIA-FERNANDEZ. Bull. Soc. Chim. Fr. 1210 (1973).
12. O. SCHMITZ-DUMONT and B. ROSS. Angew. Chem. Int. Ed. Engl. **6**, 1071 (1967).
13. P. A. W. DEAN, R. J. GILLESPIE, and P. K. UMMAT. Inorg. Synth. **15**, 213 (1974).
14. R. C. BURNS, W.-L. CHAN, R. J. GILLESPIE, W.-C. LUK, J. F. SAWYER, and D. R. SLIM. Inorg. Chem. **19**, 1432 (1980).
15. G. CARDINAL, R. J. GILLESPIE, J. F. SAWYER, and J. E. VEKRIS. J. Chem. Soc. Dalton Trans. 765 (1982).
16. M. MURCHIE and J. PASSMORE. Inorg. Synth. **24**, 76 (1986).
17. R. J. GILLESPIE and J. PASSMORE. Adv. Inorg. Radiochem. **17**, 49 (1975), and references therein.
18. J. PASSMORE, G. SUTHERLAND, and P. S. WHITE. J. Chem. Soc. Chem. Commun. 330 (1980).
19. R. W. H. SMALL, A. J. BANISTER, and Z. V. HAUPTMAN. J. Chem. Soc. Dalton Trans. 1377 (1984).
20. R. N. JONES and A. NADEAU. Can. J. Spectrosc. **20**, 33 (1975).
21. (*a*) G. M. BEGUN and A. C. RUTENBERG. Inorg. Chem. **6**, 2212 (1967); (*b*) K. NAKAMOTO. Infrared and Raman of inorganic and coordination. 4th ed. J. Wiley & Son, New York. 1986.
22. G. M. SHELDRICK. SHELX-76, Cambridge University. 1976.
23. N. WALKER and D. STUART. Acta Crystallogr. Sect. A: Found. Crystallogr. **A39**, 158 (1983).
24. International tables for X-ray crystallography. Vol. IV. Kynoch Press, Birmingham. 1974.
25. J. I. BRYANT. J. Chem. Phys. **45**, 689 (1966).
26. N. WIBERG, G. SCHWENK, and K. H. SCHMID. Chem. Ber. **105**, 1209 (1972).
27. J. A. EVANS and D. A. LONG. J. Chem. Soc. A, 1688 (1968).
28. G. W. SUTHERLAND. Ph.D. Thesis, University of New Brunswick, Fredericton, N.B. 1981.
29. A. SCHMIDT. Chem. Ber. **101**, 4015 (1968).
30. U. MÜLLER. Z. Anorg. Allg. Chem. **396**, 187 (1973).
31. J. PEBLER, K. SCHMIDT, and K. DEHNICKE. Z. Anorg. Allg. Chem. **440**, 269 (1978).

Can. J. Chem. Downloaded from www.nrcresearchpress.com by 194.225.253.170 on 09/07/12
For personal use only.

32. J. BARR, R. J. GILLESPIE, G. P. PEZ, P. K. UMMAT, and O. C. VAIDYA. Inorg. Chem. **10**, 362 (1971).
33. J. S. THRASHER and K. SEPPELT. Angew. Chem. Int. Ed. Engl. **22**, 789 (1983).
34. H. HARTL, P. HUPPMANN, D. LENTZ, and K. SEPPELT. Inorg. Chem. **22**, 2183 (1983); **23**, 510 (1984).
35. H. OBERHAMMER, K. SEPPELT, and R. MEWS. J. Mol. Struct. **101**, 325 (1983).
36. J. S. THRASHER, J. B. NIELSEN, S. G. BOTT, D. J. MCCLURE, S. A. MORRIS, and J. L. ATWOOD. Inorg. Chem. **27**, 570 (1988).
37. G. W. FRASER, R. D. PEACOCK, and P. M. WATKINS. J. Chem. Soc. A, 1125 (1971); K. SEPPELT. Inorg. Chem. **12**, 2837 (1973); P. HUPPMANN, G. KLÖTER, J. S. THRASHER, K. SEPPELT, and D. D. DESMARTEAU. Inorg. Chem. **23**, 2217 (1984); J. S. THRASHER and K. SEPPELT. Inorg. Chem. **24**, 4171 (1985); R. HOPPENHEIT and R. MEWS. Chem. Ber. **118**, 4276 (1985); P. HUPPMANN and K. SEPPELT. Chem. Ber. **118**, 457 (1985).
38. K. SEPPELT and H. OBERHAMMER. Inorg. Chem. **24**, 1227 (1985).
39. YA. G. BOL'ON and E. S. LEVCHENKO. Zh. Org. Khim. **3**, 777 (1967); N. YA. DERKACH and N. A. PASMURTSEVA. J. Org. Chem. USSR, **9**, 1443 (1973); J. S. THRASHER and K. SEPPELT. Z. Anorg. Allg. Chem. **507**, 7 (1983); J. S. THRASHER, C. W. BAUKNIGHT, JR., and D. D. DESMARTEAU. Inorg. Chem. **24**, 1598 (1985).
40. N. YA. DERKACH and G. G. BARASHENKOV. J. Org. Chem. USSR, **12**, 2408 (1976); M. HERBERHOLD and W. JELLEN. Z. Naturforsch. B: Anorg. Chem. Org. Chem. **41B**, 144 (1986); F. FOCKENBERG and A. HAAS. Z. Naturforsch. B: Anorg. Chem. Org. Chem. **41B**, 413 (1986); K. B. SHARPLESS, T. HORI, L. K. TRUESDALE, and C. O. DIETRICH. J. Am. Chem. Soc. **98**, 269 (1976).
41. N. YA. DERKACH, T. V. LYAPINA, and E. S. LEVCHENKO. J. Org. Chem. USSR, **17**, 536 (1981).
42. R. J. GILLESPIE, J. P. KENT, and J. F. SAWYER. Inorg. Chem. **20**, 4053 (1981).
43. E. G. AWERE, J. PASSMORE, P. S. WHITE, and T. KLAPÖTKE. J. Chem. Soc. Chem. Commun. In press.
44. E. G. AWERE, J. PASSMORE, K. F. PRESTON, and L. H. SUTCLIFFE. Can. J. Chem. **66**, 1776 (1988).
45. V. SCHOMAKER and D. P. STEVENSON. J. Am. Chem. Soc. **63**, 37 (1941).
46. F. A. COTTON and G. WILKINSON. Advanced inorganic chemistry. 3rd ed. Interscience, New York, NY. 1972.
47. L. PAULING. The nature of the chemical bond. 3rd ed. Cornell University Press, Ithaca, NY. 1960.
48. A. F. CLIFFORD. J. Phys. Chem. **63**, 1227 (1959).
49. J. P. JOHNSON, M. P. MURCHIE, J. PASSMORE, M. TAJIK, P. S. WHITE, and C.-M. WONG. Can. J. Chem. **65**, 2744 (1987), and references therein.
50. N. G. FURMANOVA, V. I. NADDAKA, and V. P. KRASNOVA. Zh. Strukt. Khim. **22**, 118 (1981); V. I. NADDAKA. J. Org. Chem. USSR, **21**, 648 (1985).
51. J.-S. LEE, D. D. TITUS, and R. F. ZIOLO. Inorg. Chem. **16**, 2487 (1977).
52. D. D. TITUS, J.-S. LEE, and R. F. ZIOLO. J. Organomet. Chem. **120**, 381 (1976).
53. C. S. MANCINELLI, D. D. TITUS, and R. F. ZIOLO. J. Organomet. Chem. **140**, 113 (1977).
54. R. F. ZIOLO and K. PRITCHETT. J. Organomet. Chem. **116**, 211 (1976); R. F. ZIOLO and D. D. TITUS. J. Appl. Crystallogr. **9**, 506 (1976); L. N. MARKOVSKII, E. A. STUKALO, and G. P. KUNITSKAYA. J. Org. Chem. USSR, **13**, 2337 (1977); E. A. STUKALO, E. M. YUR'EVA, and L. N. MARKOVSKII. J. Org. Chem. USSR, **20**, 2305 (1984); L. N. MARKOVSKII, E. A. STUKALO, and G. P. KUNITSKAYA. J. Org. Chem. USSR, **13**, 1911 (1977); V. I. NADDAKA, V. P. GAR'KIN, I. D. SADEKOV, and V. I. MINKIN. J. Org. Chem. USSR, **13**, 202 (1977); V. I. NADDAKA, V. P. GAR'KIN, I. D. SADEKOV, V. P. KRASNOV, and V. I. MINKIN. J. Org. Chem. USSR, **15**, 804 (1979); V. I. NADDAKA, V. P. GAR'KIN, A. A. MAKSIMENKO, and I. D. SADEKOV. J. Org. Chem. USSR, **16**, 2210 (1980); V. I. NADDAKA and V. P. GAR'KIN. J. Org. Chem. USSR, **17**, 341 (1981); A. K. SHIRYAEV, V. P. GAR'KIN, I. D. SADEKOV, and V. I. NADDAKA. J. Org. Chem. USSR, **21**, 750 (1985); V. BERTINI, F. LUCCHESINI, and A. DEMUNNO. Synthesis, 681 (1982).
55. D. FENSKE, H.-D. DÖRNER, and K. DEHNICKE. Z. Naturforsch. B: Anorg. Chem. Org. Chem. **38B**, 1301 (1983).
56. Z. DORI and R. F. ZIOLO. Chem. Rev. **73**, 247 (1973), and references therein.
57. M. WINNEWISSER and R. L. COOK. J. Chem. Phys. **41**, 999 (1964).
58. R. J. GILLESPIE. Molecular geometry. Van Nostrand Reinhold, London. 1972.
59. I. D. BROWN. *In* Structure and bonding in crystals. Vol. II. *Edited by* M. O'Keefe and A. Navrotsky. Academic Press, London. 1981. p. 1.
60. J. F. SAWYER and R. J. GILLESPIE. Prog. Inorg. Chem. **34**, 65 (1986).
61. A. BONDI. J. Phys. Chem. **68**, 441 (1964).

Can. J. Chem. Downloaded from www.nrcresearchpress.com by 194.225.253.170 on 09/07/12
For personal use only.

La base faible ClO_4^- et la chimie du ligand perchlorato. Synthèse et analyse structurale de complexes de germanium(IV) : $GeCl_3ClO_4$, $GeCl_2(ClO_4)_2$ et $(ClO_2)_2Ge(ClO_4)_6$

MOHIEDDINE FOURATI ET MONCEF CHAABOUNI

École nationale d'ingénieurs de Sfax, Laboratoire de chimie physique et inorganique, B.P. W, 3038 Sfax, Tunisie

ET

JEAN LOUIS PASCAL[1] ET JACQUELINE POTIER

Université des sciences et techniques du Languedoc Laboratoire des agrégats moléculaires et matériaux inorganiques, Unité de recherche associée n° 79 du Centre national de la recherche scientifique, 2, Place Eugène Bataillon, 34060 Montpellier CEDEX, France

Reçu le 27 janvier 1989

Cet article est dédié au Professeur Ronald J. Gillespie à l'occasion de son 65e anniversaire

MOHIEDDINE FOURATI, MONCEF CHAABOUNI, JEAN LOUIS PASCAL et JACQUELINE POTIER. Can. J. Chem. **67**, 1693 (1989).

La réaction de Cl_2O_6 avec un excès de $GeCl_4$ conduit, à température ambiante, à un liquide incolore, mélange complexe. Par distillation fractionnée on peut séparer $GeCl_3ClO_4$ et $GeCl_2(ClO_4)_2$. Avec un défaut de $GeCl_4$ on prépare $(ClO_2)_2Ge(ClO_4)_6$, un solide jaune orange, qui se sublime dès 32°C pour donner des cristaux très instables. La spectroscopie de vibration montre que, dans tous ces complexes, le ligand ClO_4 est monodenté et fortement lié au métal. Ge est dans un environnement tétraédrique dans $GeCl_3ClO_4$ et octaédrique dans les deux autres composés. $GeCl_3ClO_4$ et $(ClO_2)_2Ge(ClO_4)_6$ forment des entités discrètes tandis que $GeCl_2(ClO_4)_2$ est un polymère avec des ponts Ge–Cl–Ge. $(ClO_2)_2Ge(ClO_4)_6$ a une structure analogue à celle de $(ClO_2)_2Sn(ClO_4)_6$: des groupements ClO_4 monodentés entourent l'atome central, certains d'entre eux interagissent avec ClO_2^+ définissant ainsi un nouveau mode de coordination pour le groupement ClO_4.

Mots clés : germanium, trioxyde de chlore, synthèse, perchlorato, spectroscopie de vibration.

MOHIEDDINE FOURATI, MONCEF CHAABOUNI, JEAN LOUIS PASCAL, and JACQUELINE POTIER. Can. J. Chem. **67**, 1693 (1989).

Reaction of Cl_2O_6 with an excess of $GeCl_4$ at room temperature yields a colorless liquid, a complex mixture. Fractional distillation leads to $GeCl_3ClO_4$ and $GeCl_2(ClO_4)_2$. $(ClO_2)_2Ge(ClO_4)_6$, a yellow-orange solid, is obtained by reacting excess Cl_2O_6 with $GeCl_4$. It sublimes into unstable crystals above 32°C. Vibrational spectroscopy shows mainly unidentate perchlorato groups strongly bonded to Ge in the three compounds characterized. Ge is tetrahedrally surrounded in $GeCl_3ClO_4$ while it is octahedrally surrounded in the other complexes. $GeCl_2(ClO_4)_2$ and $(ClO_2)_2Ge(ClO_4)_6$ are individual entities while $GeCl_2(ClO_4)_2$ has a polymeric structure with Ge–Cl–Ge bridges. The structure of $(ClO_2)_2Ge(ClO_4)_6$ is analogous to that found for $(ClO_2)_2Sn(ClO_4)_6$. Six unidentate perchlorato groups surround the core atom; some of them interact with ClO_2^+, defining a new mode of coordination for ClO_4 groups.

Key words: germanium, chlorine trioxide, perchlorato, syntheses, vibrational spectroscopy.

Introduction

Depuis ces dernières années la chimie du ligand ClO_4, base faible conjuguée de l'acide très fort $HClO_4$, s'est largement développée (1), cependant parmi les éléments du bloc p, seuls les complexes de la colonne IIIB [13] ont été bien caractérisés (2). Il est donc apparu important de poursuivre ces travaux en préparant des complexes des éléments de la colonne IVB [14]. On a abordé, en premier lieu, l'étude des complexes du germanium, élément frontière entre la chimie organique et inorganique. Les agents perchloratants se comportent essentiellement comme des oxydants vis à vis de C(3) et Si(4) (pour ce dernier seul est bien connu Ph_3SiClO_4 (5)). Il semblait également intéressant d'identifier les complexes pouvant être formés avec le germanium afin de les comparer avec ceux de la famille du titane(IV). Ces derniers présentent la particularité de stabiliser des entités monomères où le ligand ClO_4 est bidenté et chelatant; est ce une propriété générale pour les éléments M(IV) ou est-elle limitée à Ti(IV) (3), Zr(IV) (6) ou Hf(IV) (7) ? C'est en partie pour répondre à cette question qu'a été entrepris ce travail.

Jusqu'à maintenant la connaissance des complexes perchlorato non solvatés du germanium(IV) était limitée aux synthèses : (*i*) d'un produit cristallisé obtenu par réaction de $HClO_4$ à 72% sur $GeCl_4$ à haute température (8); (*ii*) de $Ge(CH_3)_3ClO_4$ (9).

Dans les lignes suivantes sont présentées la synthèse et l'analyse structurale par spectroscopie de vibration ir et Raman de trois complexes perchlorato du germanium(IV), $GeCl_3ClO_4$, $GeCl_2(ClO_4)_2$ et $(ClO_2)_2Ge(ClO_4)_6$.

Partie expérimentale

Attention : le trioxyde de chlore et les composés préparés au cours de ce travail sont des réactifs très puissants, plus particulièrement $(ClO_2)_2Ge(ClO_4)_6$. Les consignes de manipulation déjà signalées doivent être rigoureusement respectées (1).

Produits de base

Cl_2O_6 est préparé et purifié suivant des méthodes déjà décrites (1). $GeCl_4$ (Merck pour la synthèse >99%) est stocké sous azote U (<5 ppm en H_2O ou O_2) dans des ampoules munies de robinets Rotaflo; il est distillé, sous vide, dans les réacteurs de synthèse.

Analyses chimiques

Les ions ClO_4^- sont dosés par potentiométrie à l'aide d'une électrode spécifique à perchlorate Orion (1). Les ions ClO_2^+ s'hydrolysent en solution en donnant des ions ClO_3^- qui sont réduits en Cl^- par Fe^{2+}, l'excès de Fe^{2+} est déterminé par manganimétrie (1). Le germanium(IV) est dosé par le Service d'analyse du CNRS (Vernaison, Rhône). Remarquons que l'analyse du sel de chloryle est délicate; on

1. Auteur à qui adresser toute correspondance.

Printed in Canada / Imprimé au Canada

Can. J. Chem. Downloaded from www.nrcresearchpress.com by 194.225.253.170 on 09/07/12
For personal use only.

doit tenir compte de la dismutation de ClO_3^- et de la décomposition de ClO_4^- (13).

Analyses structurales

Les appareils d'analyses ir, Raman ainsi que leur étalonnage ont été présentés par ailleurs (2*a*). Les spectres Raman de $GeCl_3ClO_4$ et de $GeCl_2(ClO_4)_2$ sont enregistrés à température ambiante. Ces composés sont contenus dans des tubes en Pyrex de 5 mm de diamètre scellés sous vide. Il en est de même pour $(ClO_2)_2Ge(ClO_4)_6$. Pour ce dernier, afin d'éviter toute décomposition, on effectue les enregistrements à −160°C.

Les échantillons ir de $GeCl_3ClO_4$, sous forme de verre, sont obtenus par projection du liquide sur une face en Si refroidie à −180°C et supportée par une cellule déjà décrite (10).

Synthèse

(a) $GeCl_3ClO_4$ et $GeCl_2(ClO_4)_2$

L'action de Cl_2O_6 (2 g) sur un excès de $GeCl_4$ (6 g) sous agitation, suivie d'une élimination sous vide des gaz de décomposition (Cl_2, ClO_2) et de l'excès de $GeCl_4$, conduit à un liquide incolore dont l'analyse chimique et la spectroscopie Raman montrent qu'il est constitué d'un mélange de chloro et d'oxochloroperchlorato complexes.

Placé sous vide dynamique (ca. 1,33 Pa), à température ambiante, ce mélange laisse distiller, en premier lieu, un liquide incolore ayant une forte tension de vapeur et dont l'analyse chimique est en accord avec la stœchiométrie $GeCl_3ClO_4$ (Ge 26,85 (26,07); ClO_4 34,90 (35,72); Cl 37,60 (38,20)).

Le résidu liquide après élimination de Cl_3GeClO_4, sous contrôle Raman, à une stœchiométrie proche de $GeCl_2(ClO_4)_2$ (Ge 22,64 (21,20); ClO_4 56,85 (58,09); Cl 20,51 (20,71)). La présence, sur le spectre Raman, d'une raie à 447 cm^{-1}, proche de ν_s GeO_2 (11), indique la formation, par oxydation, soit de GeO_2, soit d'un oxochlorogermanium.

Les tentatives de purification de $GeCl_2(ClO_4)_2$, par entrainement sous vide, conduisent à l'oxyder. Il se forme des complexes de compositions variables mais pouvant s'écrire : $Ge_6O_4Cl_x(ClO_4)_{16-x}\cdot nGeO_2$. La constitution de ponts Ge–O–Ge s'accompagne de la libération de Cl_2O_7 comme l'indiquent les spectres Raman (raies caractéristiques à 287 (ρ_r), 709 (ν ClO_p) et 1058 cm^{-1} (ν_s ClO_t) (12)).

(b) $(ClO_2)_2Ge(ClO_4)_6$

Obtenu par réaction d'un excès de Cl_2O_6 sur $GeCl_4$, il n'est pas très stable. À température ambiante, il se décompose, au bout de 10 h, en donnant un mélange d'oxoperchlorates et de GeO_2. Il est, de plus, oxydé par un contact prolongé avec Cl_2O_6. Cette dernière remarque conduit à proposer le protocole de synthèse suivant :

À 10°C sous agitation, on ajoute Cl_2O_6 à $GeCl_4$ par petites fractions successives. Les temps de contact sont limités à 4 min. Après élimination, sous vide, des gaz de décomposition et de l'excès de Cl_2O_6, on obtient une poudre homogène, jaune orange, dont la composition est celle de $(ClO_2)_2Ge(ClO_4)_6$ (Ge 9,01 (9,02); ClO_4^- 75,05 (74,21); ClO_2^+ 15,93 (16,77)).

$(ClO_2)_2Ge(ClO_4)_6$ se sublime sous vide dynamique (1,33 Pa) dès 25°C. Il est possible d'obtenir de beaux cristaux à 32°C, mais leur instabilité a rendu toute analyse aux rayons X impossible. À pression atmosphérique et à 59°C il y a décomposition totale et brutale en GeO_2.

NOTE : Il n'a pas été possible, dans le cadre de ce travail, d'isoler $Ge(ClO_4)_4$. La dégradation thermique du sel de chloryle n'obéit pas aux règles classiques (14). Les réactions, en quantités stœchiométriques, de $GeCl_4$ avec $(ClO_2)_2Ge(ClO_4)_6$ ou Cl_2O_6 conduisent à des oxochloroperchlorate et à GeO_2. Par ailleurs, il est impossible d'extraire Cl_2O_6 de $(ClO_2)_2Ge(ClO_4)_6$ avec $HClO_4$ anhydre. De plus avec $GeCl_4$, cet acide donne une démixtion. Elle disparait vers 60°C mais, à cette température, $HClO_4$ se décompose rapidement. $AgClO_4$ est peu actif; tout au plus donne-t'il $GeCl_3ClO_4$ en solution dans $GeCl_4$.

Résultats et discussion

Approche structurale par spectroscopie de vibration

L'influence des modes de coordination sur le ligand ClO_4

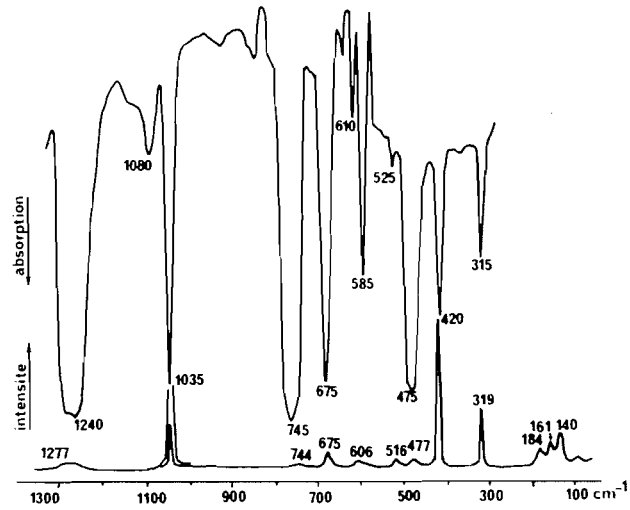


FIG. 1. Spectres infrarouge (a) et Raman (b) de $GeCl_3ClO_4$.

a fait l'objet, ces dernières années, d'études systématiques par rayons X (3), Extended X-ray Absorption Fine Structure (EXAFS) (2*c*) et spectroscopie de vibration ir et Raman (1). L'analyse des spectres obtenus, au cours de ce travail, reposera donc sur ce faisceau de connaissances.

(a) $GeCl_3ClO_4$

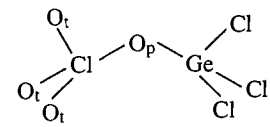
Les spectres sont reproduits sur la figure 1.

(*i*) La présence de trois bandes et raies à 1250, 1035 et 745 cm^{-1}, fréquences voisines de celles notées pour $HClO_4$ anhydre (15), est compatible avec l'existence de groupements ClO_4 monodentés.

(*ii*) La raie intense à 420 cm^{-1}, à une fréquence proche de celle observée pour ν_s GeCl dans le composé $GeCl_4$ (397 cm^{-1}) (16), est l'indication de liaisons GeCl terminales.

Ces faits conduisent à proposer une structure monomère dans laquelle Ge est dans un environnement tétraédrique. Elle diffère de la structure polymère trouvée pour $GaCl_2ClO_4$ dans laquelle les groupements ClO_4 sont bidentés pontants (10).

$GeCl_3ClO_4$, représenté selon le schéma suivant,



a une symétrie maximum C_s. Il s'apparente aux composés de types X_2Y_7 tels Cl_2O_7, $Ga_2X_7^-$ (X = Cl, Br), $P_2O_7^{4-}$, $S_2O_7^{2-}$, $Cr_2O_7^{2-}$ et Mn_2O_7.

On attend 21 vibrations actives en ir et Raman, leur description s'effectuera par analogie avec ce qui a été trouvé par ailleurs (12). Mis à part les 2 torsions de faible intensité et de faible énergie (<100 cm^{-1}), les 19 autres vibrations attendues se répartiront dans les 15 groupes de bandes ou raies observées (tableau 1).

Les attributions, données dans le tableau 1, sont effectuées sans problème pour les groupements ($OClO_3$) et ($GeCl_3$). Pour le premier, on tient compte de celles notées pour différents perchlorato complexes (1) et, pour le second, des observations effectuées pour $GeCl_4$ (16) ou $HGeCl_3$ (11). Il est, par contre, délicat de localiser la vibration de valence ν GeO.

Si l'on se réfère aux corrélations $dMO = f(R)$ où R est le rayon ionique effectif (1), on remarque que, avec un environnement tétraédrique pour Ge, la liaison Ge—O peut adopter une longueur voisine de celles signalées dans GeO_2 (≈1,88 Å) (17).

Can. J. Chem. Downloaded from www.nrcresearchpress.com by 194.225.253.170 on 09/07/12
For personal use only.

Can. J. Chem. Downloaded from www.nrcresearchpress.com by 194.225.253.170 on 09/07/12
For personal use only.

TABLEAU 1. Attributions des bandes infrarouge et des raies Raman relevées pour $GeCl_3ClO_4$

Raman	Infrarouge	Attributions
1277 (2) 1249	1265 (s) 1240 (s)	ν_{as} ClO_3 (A′ + A″)
1035 (30)	1030 (s)	ν_s ClO_3 (A′)
744 (2) 736	745 (s)	ν ClO_p (A′)
675 (10)	675 (s)	ν GeO_p (A′)
606 (5) 588 (sh)	585 (m)	δ_{as} ClO_3 (A′ + A″)
516 (6)	525 (w)	δ_s ClO_3 (A′)
477 (6)	475 (s)	ν_{as} $GeCl_3$ (A′ + A″)
420 (100)	418 (m)	ν_s $GeCl_3$ (A′)
319 (40)	315 (m)	ρ_r $OClO_3$ (A′ + A″)
184 (12)		δ_{as} $GeCl_3$ (A′ + A″)
162 (17)		ρ_r $GeCl_3$ (A′ + A″)
141 (25)		δ_s $GeCl_3$ (A′)
100 (5)		δ GeOCl (A′)

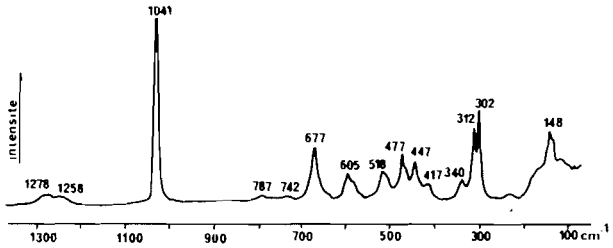


FIG. 2. Spectre Raman de $GeCl_2(ClO_4)_2$.

ν GeO doit être attendu à une fréquence proche de celle observée pour ν moyen Ge—O dans GeO_2 : 656 cm^{-1}.

Sur le spectre ir apparait, dans le domaine des vibrations de déformation ClO_4, une bande intense vers 670 cm^{-1}, fréquence convenable pour ν Ge—O(ClO_3). Elle diffère de celle donnée pour ν GeO dans $(CH_3)_3GeNO_3$ (18) mais est voisine de celle trouvée dans $(CH_3)_3GeOH$ (19).

NOTE : dans le tableau 1 ne figurent pas un certain nombre de bandes ir de faible intensité à 1125, 1080, 950, 830, 640 et 570 cm^{-1}. Elles correspondent à des harmoniques ou des combinaisons facilement détectables sur un spectre ir d'un composé vitreux.

(b) $GeCl_2(ClO_4)_2$

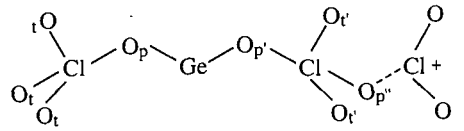
On remarque la grande similitude de son spectre Raman (fig. 2) et de celui de $GeCl_3ClO_4$ dans le domaine des modes de vibrations internes de ClO_4. En particulier, la présence d'une raie intense à 1041 cm^{-1}, due à ν_s ClO_3, conduit à admettre, dans ce complexe, la présence de groupes ClO_4 monodentés. La fréquence moyenne ν ClO_p (765 cm^{-1}) révèle que ClO_4 est moins fortement lié à Ge que dans $GeCl_3ClO_4$ (741 cm^{-1}).

Par ailleurs, on note : (*i*) l'absence de la raie très intense à 420 cm^{-1} due à ν_s GeCl dans $GeCl_3ClO_4$; (*ii*) l'apparition autour de 322 cm^{-1} de deux nouvelles composantes (340 cm^{-1} et 302 cm^{-1}). Ceci indique que, dans $GeCl_2(ClO_4)_2$, les atomes de chlore sont donc des atomes pontants avec ν_{as} $GeCl_p$: 340 cm^{-1} et ν_s $GeCl_p$ soit 312 soit 302 cm^{-1} (l'une de ces raies correspondant à ρ_r ClO_3).

Ces observations permettent d'envisager, pour $GeCl_2(ClO_4)_2$, une forme polymère comme pour $SnCl_2(ClO_4)_2$ (20). Dans ces complexes, l'élément central est dans un environnement octaédrique : cependant, avec le germanium, ce sont les atomes de chlore qui sont pontants alors que, avec l'étain, ce sont les groupes perchlorate. Les attributions principales sont analogues à celles données pour $GeCl_3ClO_4$. Les deux nouvelles raies à 447 et 417 cm^{-1} (fig. 2), bien que proches respectivement de ν_s GeO dans GeO_2 et ν_s GeCl dans $GeCl_3ClO_4$, pourraient correspondre aux vibrations ν GeO(ClO_3).

(c) $(ClO_2)_2Ge(ClO_4)_6$

Ce sel est comparable à $(ClO_2)_2Sn(ClO_4)_6$ déjà caractérisé (20). Par rayons X, il a été montré que $Sn(ClO_4)_6^{2-}$ est un anion discret où 6 groupements monodentés ClO_4 entourent l'atome d'étain; cependant certains de ces groupements sont en forte interaction avec ClO_2^+. Un tel phénomène a déjà été observé dans $ClO_2^+ClO_4^-$ (10, 21). Cette interaction anion–cation assure un environnement pseudo tétraédrique à l'atome de chlore de ClO_2^+ et confère aux groupements ClO_4 correspondants un caractère pseudo bidenté. Les différents modes de coordination des groupements ClO_4 sont schématisés ci-dessous.



Sur la figure 3 sont reproduits les spectres ir et Raman des sels d'étain et de germanium; on constate une très grande similitude. On peut donc faire, pour le complexe du germanium, une analyse sur la base d'une structure similaire de celle observée pour $(ClO_2)_2Sn(ClO_4)_6$.

Les attributions sont reportées dans le tableau 2. Comme pour le complexe de l'étain (20), les vibrations des deux types de ClO_4 sont nettement individualisées. Celles relatives au groupement ClO_4 monodenté classique $O_{3t}ClO_p$ sont observées aux fréquences habituelles (1). Celles correspondant au groupement ClO_4 interagissant avec ClO_2^+ sont plus proches d'un groupement ClO_4 bidenté pontant. La fréquence moyenne ν ClO_p (745 cm^{-1}) est de 31 cm^{-1} plus basse que celle relevée pour le complexe de l'étain (776 cm^{-1}). Ceci traduit une interaction métal–$OClO_3$ plus grande pour le germanium que pour l'étain; cette différence pourrait être due aux rayons ioniques respectifs de ces deux éléments.

Le domaine de basse fréquence (<400 cm^{-1}) où apparaissent les vibrations du squelette GeO_6, le balancement (ρ_r) de $O_{3t}ClO_p$ et la vibration de valence de la liaison longue, $ClO_{p''}\cdots ClO_2^+$, méritent quelques commentaires.

Par analogie avec les fréquences observées pour des squelettes MO_n dans des complexes perchlorato (1), on attribue la raie à 284 cm^{-1} et le doublet à 266 cm^{-1}, en Raman, et la bande en ir à 320 cm^{-1}, aux modes ν GeO_6. La fréquence moyenne (298 cm^{-1}) traduit un affaiblissement de la liaison métal–oxygène, par rapport à l'interaction observée dans $GeCl_3ClO_4$. On note, aussi, un renforcement de la liaison M—O par rapport à celle du complexe de l'étain ($\bar{\nu}$ 273 cm^{-1}). À ρ_r $OClO_3$ correspond logiquement le doublet à 210 et 219 cm^{-1}. L'évolution des fréquences de ce mode de vibration en fonction du composé : 319 cm^{-1} : $GeCl_3ClO_4$; 279 cm^{-1} : Cl_2O_7; est assez délicate à expliquer.

La vibration de valence ν $(ClO_3)O\cdots ClO_2^+$ correspondant à l'interaction anion–cation peut être assimilée à une vibration de réseau; elle doit donc apparaître à basse fréquence. La comparaison des spectres Raman de $ClO_2^+ClO_4^-$ (21) et de $(ClO_2^+)_2Ge(ClO_4)_6^{2-}$ montre que, dans le premier, existe

Can. J. Chem. Downloaded from www.nrcresearchpress.com by 194.225.253.170 on 09/07/12
For personal use only.

TABLEAU 2. Attributions des bandes infrarouge et des raies Raman relevées pour $(ClO_2)_2Ge(ClO_4)_6$

Raman	Infrarouge	Attributions
1310 (1) 1297 (w)	1295 (sh)	$\nu_{as}\ ClO_2^+$
1276 (sh) 1264 (5)	1270 (sh) 1250 (s)	$\nu_{as}\ ClO_{3t}$
1217 (w) 1187 (25) 1178 (sh)	1195 (s) 1175 (s)	$\nu_{as}\ ClO_{t'}$
1059 (100)	1050 (ww)	$\nu_s\ ClO_2^+$
1052 (95)	1030 (sh)	$\nu_s\ ClO_{3t}$
1018 (25) 1007 (20)	1018 (s) 1010 (s)	$\nu_s\ ClO_{t'}$
890 (3)	915 (sh)	$\nu\ ClO_{p''}$
761 (6)	785 (s)	$\nu\ ClO_{p'}$
751 (w)		
739 (15) 722 (25)	760 (s,br)	$\nu\ ClO_p$
664 (6) 622 (5)	670 (m)	ρ_r, ρ_w[a]
606 (6)	600 (s)	$\delta\ ClO_{2t'}$
591 (5)	575 (sh)	$\delta_{as}\ ClO_{3t}$
520 (10)	515 (w)	$\delta\ ClO_2^+$
504 (5) 491 (5)		$\delta_s\ ClO_{3t}$
464 (3)		ρ_t[a]
433 428 (5)	440	$\delta\ O_{p'}ClO_{p''}$
	320 (s)	$\nu_{as}\ GeO_6$
284 (10) 266 (3)		$\nu_s\ GeO_6$
248 (w)		
219 (sh) 210 (25)	210 (s)	$\rho\ O_pClO_{3t}$
190 183 (5)		$\nu\ O_{p''}\cdots Cl$[b]
159 151 (10) 136 (20) 124 (22)		$\delta\ GeO_6$
113 (20) 96 (22) 77 (20)		Reseau
64 (15) 53 (25) 40 (5)		

[a] $O_{p'}ClO_{2t'}O''$.
[b] Cf. texte.

une raie à 227 cm^{-1} absente dans le second; corrélativement apparaissent, dans ce dernier, deux raies à 190 et 183 cm^{-1}. Il semble logique de les attribuer à $\nu\ (ClO_3)O\cdots ClO_2^+$. Le déplacement vers les basses fréquence est dû à la différence de masse entre les deux anions.

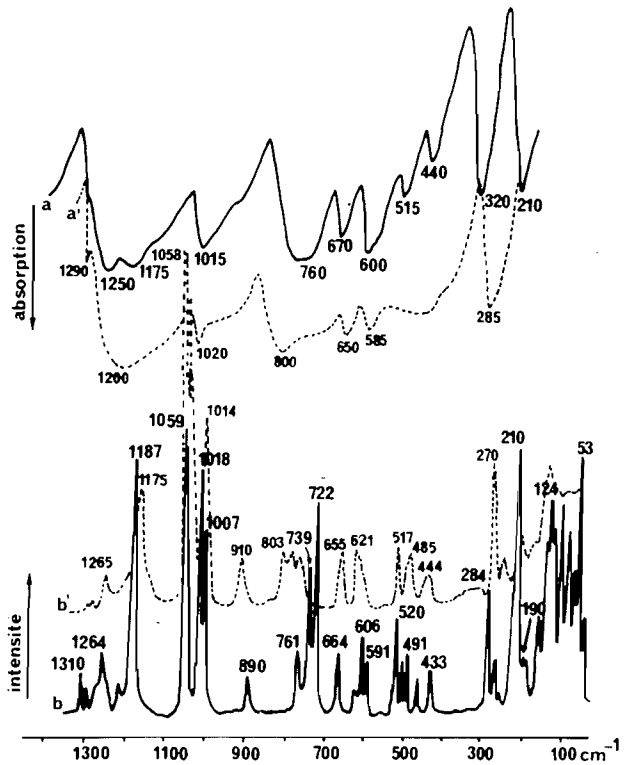


FIG. 3. Spectre infrarouge (a) et Raman (b) de $(ClO_2)_2Ge(ClO_4)_6$ en traits pleins, comparés a ceux de $(ClO_2)_2Sn(ClO_4)_6$ en traits pointillés.

Conclusion

Au cours de ce travail, il a été montré que Ge(IV), comme Ti(IV) et Sn(IV), conduit à des chloroperchlorato complexes, des oxochloroperchlorato complexes et à un sel de chloryle. Cependant, à la différence de Ti ou Sn, il n'a pas été possible d'isoler le perchlorato complexe neutre : $M(ClO_4)_4$.

Aux rares perchlorates covalents stables, liquides à température ambiante, $HClO_4$ (15), Cl_2O_7 (15), $ClOClO_3$ (22), $BCl_2(ClO_4)$ (2*a*), $GaCl_2ClO_4$ (23), $CrO_2(ClO_4)_2$ (24) sont venus s'ajouter $GeCl_3ClO_4$ et $GeCl_2(ClO_4)_2$.

Remarquons que, pour le germanium comme pour le bore ou le gallium, la substitution d'un seul atome de chlore par un groupe ClO_4 conduit à un environnement de l'élément central analogue à celui qu'il y a dans MCl_x (x = 3, 4). Dès la substitution d'un second atome de chlore, le germanium comme le gallium adopte un environnement octaédrique. Cet environnement se retrouve dans le sel de chloryle.

Par ailleurs il faut souligner que, à la différence de l'étain et du titane, le germanium a tendance à stabiliser des ligands ClO_4 monodentés.

On peut se demander pourquoi il n'a pas été possible d'isoler $Ge(ClO_4)_4$; c'est encore un des mystères de la chimie des perchlorato complexes.

Remerciements

À l'occasion de la célébration du 65e anniversaire du Professeur R. J. Gillespie, les auteurs sont heureux de lui adresser leurs sincères félicitations pour sa contribution au développement des connaissances de la Chimie.

Les aides matérielles du CNRS (France) et de la DRST (Tunisie) ont permis aux auteurs d'effectuer les recherches décrites dans cet article. Ils remercient ces organismes.

1. M. FOURATI, M. CHAABOUNI, J. L. PASCAL et J. POTIER. Can. J. Chem. **65**, 2783 (1987) et références citées.
2. (*a*) T. CHAUSSE, J. L. PASCAL, A. POTIER et J. POTIER. Nouv. J. Chim. **5**, 261 (1981); (*b*) M. FOURATI, M. CHAABOUNI, H. F. AYEDI, J. L. PASCAL et J. POTIER. Can. J. Chem. **63**, 3499 (1985); (*c*) J. POTIER, J. ROZIERE, A. SEIGNEURIN, D. J. JONES, J. L. PASCAL et A. MICHALOWICZ. Nouv. J. Chim. **11**, 641 (1987).
3. M. FOURATI, M. CHAABOUNI, C. BELIN, M. CHARBONNEL, J. L. PASCAL et J. POTIER. Inorg. Chem. **25**, 1386 (1986).
4. M. SCHMEISSER et K. BRANDLE. Adv. Inorg. Chem. Radiochem. **5**, 41 (1963).
5. G. K. S. PRAKASH, S. KEYANIYAN, R. ANISZFELD, L. HEILIGER, G. A. OLAH, R. C. STEVENS, H. K. CHOI et R. BAU. J. Am. Chem. Soc. **109**, 5123 (1987).
6. E. A. GENKINA, V. P. BABAEVA et V. YA. ROSOLOVSKII. Koord. Khim. **10**, 1415 (1984).
7. E. A. GENKINA, V. P. BABAEVA et V. YA. ROSOLOVSKII. Koord. Khim. **11**, 1221 (1985).
8. T. OSTERUD et M. PRYTZ. Arch. Math. Naturvidensk. **47**, 107 (1943).
9. I. RUIDISCH et M. SCHMIDT. Z. Naturforsch. B: Anorg. Chem. Org. Chem. Biochem. Biophys. Biol. **18B**, 508 (1963).
10. J. L. PASCAL. Thèse, Université des sciences et techniques du Languedoc. Montpellier, France (1978).
11. H. SIEBERT. Anwendungen der Schwingungsspektroskopie in der Anorganischen Chemie. Springer Verlag, Berlin. 1966.
12. (*a*) J. ROZIERE, J. L. PASCAL et A. POTIER. Spectrochim. Acta, Part A: **29A**, 169 (1973); (*b*) J. D. WITT et R. M. HAMMAKER. J. Chem. Phys. **58**, 303 (1973).
13. J. L. PASCAL et M. FOURATI. C.R. Acad. Sci. Paris. Serie II, **308**, 281 (1989).
14. J. L. PASCAL, J. POTIER et C. S. ZHANG. J. Chem. Soc. Dalton Trans. 297 (1985).
15. A. C. PAVIA. Rev. Chim. Miner. **7**, 471 (1970).
16. K. NAKAMOTO. Infrared and Raman spectra of inorganic and coordination compounds. 4^{e} ed. John Wiley and Sons, New York. 1986.
17. A. F. WELLS. Structural inorganic chemistry. 4^{e} ed. Oxford University Press, Londres. 1975.
18. D. POTTS et A. WALKER. Can. J. Chem. **49**, 2171 (1971).
19. E. MASLOWSKY, JR. Vibrational spectra of organometallic compounds. John Wiley and Sons, New York. 1977.
20. M. FOURATI, M. CHAABOUNI, C. BELIN, J. L. PASCAL et J. POTIER. Inorg. Chem. Sous presse.
21. M. JANSEN et K. M. TOBIAS. Z. Anorg. Allg. Chem. **16**, 550 (1987).
22. C. S. SCHACK et D. PILIPOVICH. Inorg. Chem. **9**, 1589 (1970).
23. M. CHAABOUNI, J. L. PASCAL, A. POTIER et J. POTIER. J. Chem. Res. 80 (1977); J. Chim. Phys. **74**, 1083 (1977).
24. C. J. SCHACK, D. PILIPOVICH et K. O. CHRISTE. J. Inorg. Nucl. Chem. Supp. **76**, 207 (1976).

Can. J. Chem. Downloaded from www.nrcresearchpress.com by 194.225.253.170 on 09/07/12
For personal use only.

The conversion of a divinyldi-μ-methylene-dirhodium complex into a μ-ethylidene-μ-methylene-dirhodium complex

JESUS MARTINEZ, JOHN B. GILL, HARRY ADAMS, NEIL A. BAILEY, ISABEL M. SAEZ, AND PETER M. MAITLIS[1]
Department of Chemistry, The University, Sheffield, S3 7HF, U.K.

Received February 22, 1989

This paper is dedicated to Professor Ronald J. Gillespie on the occasion of his 65th birthday

JESUS MARTINEZ, JOHN B. GILL, HARRY ADAMS, NEIL A. BAILEY, ISABEL M. SAEZ, and PETER M. MAITLIS. Can. J. Chem. **67**, 1698 (1989).

The dichloro-μ-ethylidene-μ-methylene-dirhodium complex, $[(C_5Me_5Rh)_2(\mu\text{-CHMe})(\mu\text{-}CH_2)Cl_2]$ (**2**) was the main product of the reaction of the divinyl-di-μ-methylene-dirhodium complex $[(C_5Me_5Rh\text{-}\mu\text{-}CH_2)_2(CH{=}CH_2)_2]$ (**1**), with HCl in toluene at −78°C. It was identified by an X-ray crystal structure determination and spectroscopically.

Key words: vinyl, μ-methylene, μ-ethylidene, rhodium, X-ray.

JESUS MARTINEZ, JOHN B. GILL, HARRY ADAMS, NEIL A. BAILEY, ISABEL M. SAEZ et PETER M. MAITLIS. Can. J. Chem. **67**, 1698 (1989).

Le complexe dichloro-μ-éthylidène-μ-méthylène-dirhodium $[(C_5Me_5Rh)_2(\mu\text{-CHMe})(\mu\text{-}CH_2)Cl_2]$ (**2**) est le produit majoritaire de la réaction du complexe divinyl-di-μ-méthylène-dirhodium $[(C_5Me_5Rh\text{-}\mu\text{-}CH_2)_2(CH{=}CH_2)_2]$ (**1**), avec HCl dans le toluène à −78°C. On a identifié le complexe **1** par détermination de structure cristalline aux rayons X et par spectroscopie.

Mots clés : vinyl, μ-méthylène, μ-éthylidène, rhodium, rayons-X.

[Traduit par la revue]

Can. J. Chem. Downloaded from www.nrcresearchpress.com by 186.148.149.217 on 09/07/12
For personal use only.

Although many μ-methylene-dimetal complexes have now been made (for useful recent references, see ref. 1), an almost unique feature of the rhodium systems, $[(C_5Me_5Rh\text{-}\mu\text{-}CH_2)_2(R)_2]$ (2), is the facility with which the coupling of the R and one or two CH_2 ligands takes place to give organic products (3). Expansion of this chemistry has so far been hampered by a lack of success in making μ-homologues of such complexes. However, we now report the conversion of the divinyl-di-μ-methylene-dirhodium complex (**1**) (4) into the dichloro-μ-ethylidene-μ-methylene complex (**2**, 65% yield), by reaction with HCl (3:1 molar ratio) in toluene at −78°C. The major organic product from this reaction is propene. The dibromo analogue of **2** was formed (50% yield) when **1** was reacted with HBr in pentane.

$$[(C_5Me_5Rh\text{—}\mu\text{—}CH_2)_2(CH{=}CH_2)_2] + HX =$$

1

$$[(C_5Me_5Rh)_2(\mu\text{—}CHMe)(\mu\text{—}CH_2)X_2]$$

2

The new complex was identified as the *trans*-dichloro-μ-ethylidene-μ-methylene (**2**) by a single crystal X-ray structure determination,[2] and by nmr spectroscopy.[3] The molecule of complex **2** (Fig. 1) comprises two inequivalent rhodium atoms, each bearing an η^5-C_5Me_5 ring and a Cl, and joined by one μ-CH_2 and one μ-CHMe. The Rh—Rh distance, 2.678(3) Å, is a little greater than in other complexes of this series, (cf. 2.659(1) Å in $[(C_5Me_5Rh\text{-}\mu\text{-}CH_2)_2(CO)_2]^{2+}$ and 2.588(2) Å in $[(C_5Me_5Rh)_2(\mu\text{-}CH_2)_2(CH{=}CH_2)_2]$), but is still well within bonding range, as required for a diamagnetic complex of Rh(IV). The bridging ligands are disordered across the crystallographic inversion centre, and thus no detailed comparison can be made between their bridging geometries, but they appear very similar to those in the di-μ-methylene complexes. The ^{1}H nmr spectrum is consistent with the X-ray results, and the absence of a centre of symmetry in a single molecule is shown in particular by two different signals for the two μ-CH_2 hydrogens.

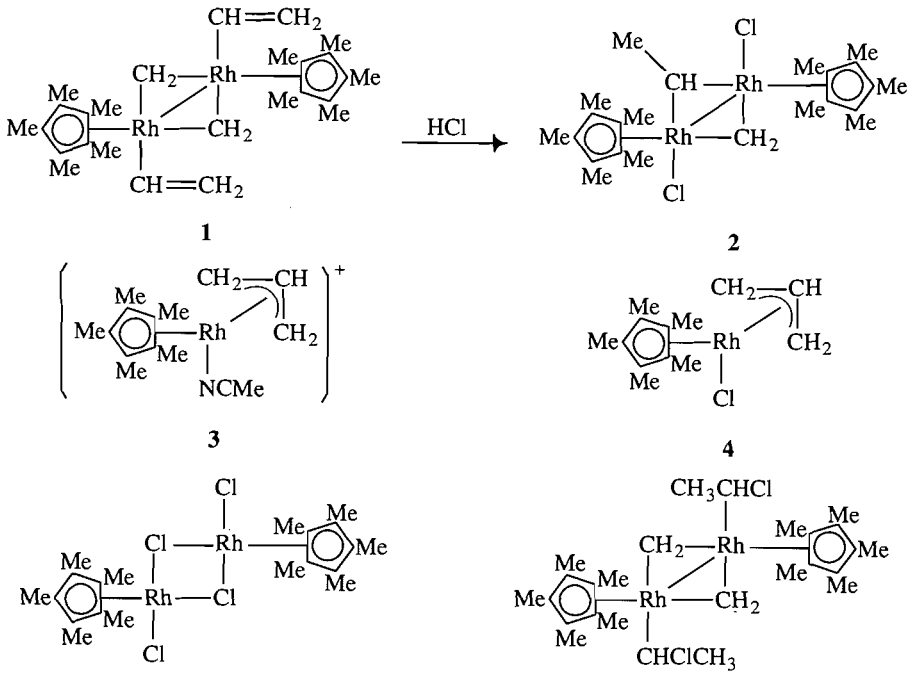
The reactions of **1** with acids are very complex and depend on the precise conditions. Thus, treatment of **1** with *p*-toluenesulphonic acid in acetonitrile, in the presence of KPF_6, gave the η^3-allyl cation **3**, which was also formed by reaction of **1** with $AgPF_6$. Reaction of **1** with low molar proportions of HCl in chloroform gave the η^3-allyl chloro complex **4**, but this readily

[1]Author to whom correspondence may be addressed.

[2]*X-ray structure determination.*
Crystal data:
$C_{23}H_{36}Cl_2Rh_2$ $M = 589.25$
Orthorhombic, space group *Pccn* (D_{2h}^{10}, No. 56), $a = 18.485(19)$, $b = 14.357(17)$, $c = 9.233(6)$ Å, $U = 2451(4)$ Å^3, $D_c = 1.597$ g cm^{-3}, $Z = 4$, Mo-K_α radiation ($\lambda = 0.71069$ Å; $\mu = 15.53$ cm^{-1}), crystal dimensions 0.30 × 0.25 × 0.175 mm. X-ray data $3.5 < 2\theta < 50°$ on Nicolet R3 four-circle diffractometer to give 1571 independent reflections, $|F|/\sigma(|F|) > 3.0$, corrected for Lorentz and polarisation effects, and for absorption by analysis of azimuthal scans. The structure was solved by Patterson and Fourier techniques and refined by blocked cascade least-squares methods. The two bridging ligands are disordered between their centrosymmetrically related sites; thus the composite model was refined with constrained geometry with C(11) common to the two ligands. Hydrogen atoms were placed in predicted positions with isotropic thermal parameters related to those of the supporting atom. Refinement converged at a final R 0.0750, with allowance for the thermal anisotropy of all non-hydrogen atoms with the exception of the half-occupancy C(12). The atomic coordinates are being filed with the Director of the Cambridge Crystallographic Centre, University Chemical Laboratory, Lensfield Road, Cambridge CB2 1EW, England. Any request should be accompanied by the full literature citation for this communication. This table may also be purchased from the Depository of Unpublished Data, CISTI, National Research Council of Canada, Ottawa, Ont., Canada K1A 0S2.

[3]Values for ^{1}H nmr, in C_6D_6, δ: 1.43, 1.47 (2 × C_5Me_5; d, J(Rh) = 1 Hz), 3.00 (μ-*Me*CH, dt, J(H–H) = 7.5, J(Rh–H) = 1.2 Hz), 10.40, 10.82 (μ-CH_2; 2 × ddd, J(H–H) = 4, J(Rh^1–H) = 3, J(Rh^2–H) = 2 Hz), and 11.65 (μ-C*H*Me, qt, J(H–H) = 7, J(Rh^{1,2}–H) = 2.5 Hz); ^{13}C nmr, in $CDCl_3$, δ: 9.7, 9.4 (2 × C_5Me_5), 34.7 (μ-CH*Me*), 102.1, 103.2 (2 × C_5Me_5; d, J(Rh–C) = 5.0 Hz), 186.1 (μ-CH_2, t, J(Rh–C) = 26 Hz), 207.3 (μ-*C*HMe, t, J(Rh–C) = 25 Hz).

Can. J. Chem. Downloaded from www.nrcresearchpress.com by 186.148.149.217 on 09/07/12
For personal use only.



1 2 3 4 5 6

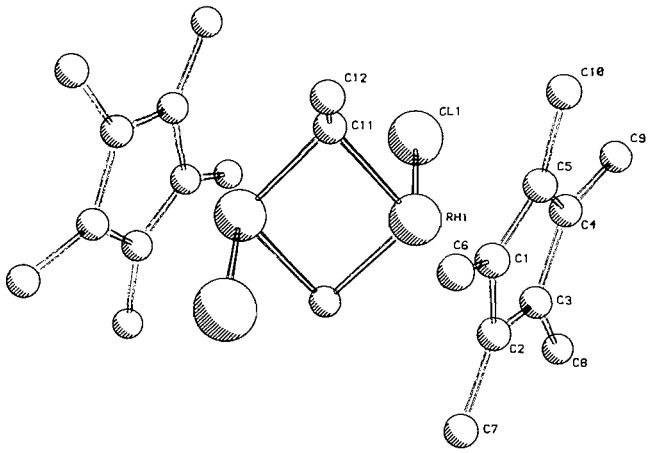


FIG. 1. The structure of complex **2**. (Because of disorder C11 and C11′ are equivalent crystallographically.)

reacted further with more HCl to give $[(C_5Me_5RhCl_2)_2]$ (**5**) (72%) and propene (71%).

While reactions of a number of cationic η^1, η^2 (i.e., bridging) vinyl complexes with hydride to yield μ-ethylidene complexes are known (5), there does not appear to have been any report of the transformation of terminal vinyls, and by protonation, into μ-ethylidene ligands. We suggest that the reaction of **1** to **2** proceeds via primary protonation of the terminal vinylic carbons, and that the intermediate terminal ethylidene so formed migrates to a bridging position (or possibly exchanges with the μ-CH_2). In support of this, a sparingly soluble orange solid, **6**, with analysis corresponding to $[(C_5Me_5Rh(\mu\text{-}CH_2)(CHClMe))]_2$, was obtained from reaction of **1** with HCl gas in pentane. The ir ν(C=C) at 1559 cm^{-1}, characteristic of the vinyls in **1**, had disappeared and we suggest that **6** has two chloroethylrhodiums (Rh—$CHClCH_3$) arising from addition of HCl to the double bonds. The solid **6** was converted into a 1:1 mixture of **2** and **5** on reaction with HCl in C_6D_6 at 20°C.

This work shows that vinyl–transition metal compounds have much potential in synthesis.

Acknowledgements

We thank the SERC for support, Johnson Matthey for the loan of rhodium salts, and Dr. B. F. Taylor for nmr spectra.

1. W. A. HERRMANN. Angew. Chem. Int. Ed. Engl. **21**, 117 (1982); C. ZHENG, Y. APELOIG, and R. HOFFMANN. J. Am. Chem. Soc. **110**, 749 (1988); R. J. PUDDEPHATT. Polyhedron, **7**, 767 (1988); R. M. BULLOCK, R. T. HEMBRE, and J. R. NORTON. J. Am. Chem. Soc. **110**, 7868 (1988).
2. K. ISOBE, A. VÁZQUEZ DE MIGUEL, P. M. BAILEY, S. OKEYA, and P. M. MAITLIS. J. Chem. Soc. Dalton Trans. 1441 (1983); K. ISOBE, S. OKEYA, N. J. MEANWELL, A. J. SMITH, H. ADAMS, and P. M. MAITLIS. J. Chem. Soc. Dalton Trans. 1215 (1984); S. OKEYA, N. J. MEANWELL, B. F. TAYLOR, K. ISOBE, A. VÁZQUEZ DE MIGUEL, and P. M. MAITLIS. J. Chem. Soc. Dalton Trans. 1453 (1984).
3. I. M. SAEZ, N. J. MEANWELL, A. NUTTON, K. ISOBE, A. VÁZQUEZ DE MIGUEL, D. W. BRUCE, S. OKEYA, D. G. ANDREWS, P. R. ASHTON, I. R. JOHNSTONE, and P. M. MAITLIS. J. Chem. Soc. Dalton Trans. 1565 (1986); I. M. SAEZ, N. J. MEANWELL, B. F. TAYLOR, B. E. MANN, and P. M. MAITLIS. J. Chem. Soc. Chem. Commun. 361 (1987); I. M. SAEZ, D. G. ANDREWS, and P. M. MAITLIS. Polyhedron, **7**, 827 (1988).
4. J. MARTINEZ, H. ADAMS, N. A. BAILEY, and P. M. MAITLIS. J. Chem. Soc. Chem. Commun. 286 (1989); P. M. MAITLIS, I. M. SAEZ, N. J. MEANWELL, J. MARTINEZ, K. ISOBE, A. VÁZQUEZ DE MIGUEL, and A. NUTTON. Pure Appl. Chem. In press.
5. A. F. DYKE, S. A. R. KNOX, P. J. NAISH, and A. G. ORPEN. J. Chem. Soc. Chem. Commun. 440 (1980); A. F. DYKE, S. A. R. KNOX, M. J. MORRIS, and P. J. NAISH. J. Chem. Soc. Dalton Trans. 1417 (1983); D. L. DAVIES, S. A. R. KNOX, K. A. MEAD, M. J. MORRIS, and P. WOODWARD. J. Chem. Soc. Dalton Trans. 2293 (1984); A. F. DYKE, S. A. R. KNOX, and P. J. NAISH. J. Organomet. Chem. **199**, C47 (1980); R. E. COLBORN, A. F. DYKE, S. A. R. KNOX, K. A. MEAD, and P. WOODWARD. J. Chem. Soc. Dalton Trans. 2099 (1983).

Hexafluoro antimonates(V) of divalent metals, synthesis and properties

M. S. R. CADER AND F. AUBKE[1]

Department of Chemistry, The University of British Columbia, Vancouver, B.C., Canada V6T 1Y6

Received February 8, 1989

This paper is dedicated to Professor Ronald J. Gillespie on the occasion of his 65th birthday

M. S. R. CADER and F. AUBKE. Can. J. Chem. **67**, 1700 (1989).

Solvolysis of metal(II) fluorosulfates in liquid antimony(V) fluoride according to:

$$M(SO_3F)_2 + 6SbF_5 \xrightarrow{25-60°C} M(SbF_6)_2 + 2Sb_2F_9SO_3F$$

with M = Sn, Ni, Pd, Cu, or Ag, is found to be a clean, efficient route to the hexafluoro antimonates of the corresponding metals. Two of the compounds reported here display unusual features: $Pd(SbF_6)_2$ is, like its fluorosulfate precursor, paramagnetic with the Pd^{2+} ion in a $^3A_{2g}$ ground state, and an analysis of the ligand field spectrum is presented; $Ag(SbF_6)_2$ is, unlike a recently reported paramagnetic, blue, valence isomer, diamagnetic and nearly white in color. Formulation as a mixed valency compound $Ag(I)Ag(III)(SbF_6)_4$ is suggested. Low temperature magnetic susceptibility measurements (where appropriate), Raman, and IR data are reported. The hexafluoro antimonates of Ni, Pd, and Cu show antiferromagnetic exchange at very low temperatures. $Pd(SbF_6)_2$ shows very weak ferromagnetism below 10 K.

Key words: fluoroantimonates of divalent metals, synthesis and solvolysis in SbF_5, vibrational spectra, magnetic susceptibility measurements.

M. S. R. CADER et F. AUBKE. Can. J. Chem. **67**, 1700 (1989).

On a trouvé que la solvolyse de fluorosulfonates de métal(II) dans le fluorure d'antimoine(V) liquide, suivant la réaction :

$$M(SO_3F)_2 + 6SbF_5 \xrightarrow{25-60°C} M(SbF_6)_2 + 2Sb_2F_9SO_3F$$

et dans laquelle M = Sn, Ni, Pd, Cu ou Ag, est une méthode propre et efficace de préparer les hexafluoro antimonates des métaux correspondants. Deux des composés ainsi préparés présentent des caractéristiques particulières : comme son précurseur fluorosulfonate, le $Pd(SbF_6)_2$ est paramagnétique avec l'ion Pd^{2+} dans un état fondamental $^3A_{2g}$ et on présente une analyse du spectre de champ de ligand; par ailleurs, contrairement à ce qui a été rapportée récemment pour un isomère de valence, bleu et paramagnétique, le $Ag(SbF_6)_2$ est diamagnétique et d'une couleur pratiquement blanche. On propose que sa formule correspond à celle d'un composé de valence mixte $Ag(I)Ag(III)(SbF_6)_4$. On rapporte des données relatives à l'IR, au Raman et à des mesures de susceptibilité magnétique à basse température (lorsque c'est approprié). À des températures très basses, les hexafluoro antimonates de Ni, de Pd et de Cu présentent des échanges antiferromagnétiques. À des températures inférieures à 10 K, le $Pd(SbF_6)_2$ présente un très faible ferromagnétisme.

Mots clés : fluoroantimonates de métaux divalents, synthèse et solvolyse dans le SbF_5, spectres de vibration, mesures de susceptibilité magnétique.

[Traduit par la revue]

Introduction

Antimony(V) fluoride, SbF_5, is commonly regarded as the strongest molecular Lewis acid (1). Conversely the anions SbF_6^- and the related $Sb_2F_{11}^-$ are extremely weak nucleophiles (2), capable of stabilizing a wide range of electrophilic cations, both in solid compounds or in HF–SbF_5 superacid solution (3, and references therein).

The objective of this study is the synthesis and characterization of SbF_6^- salts formed by divalent metal cations. The synthetic route chosen is the solvolysis of metal fluorosulfates in liquid SbF_5 according to the general route:

[1] $$M(SO_3F)_2 + 6SbF_5 \rightarrow M(SbF_6)_2 + 2Sb_2F_9SO_3F$$

with M = Sn, Ni, Pd, Cu, *or* Ag.

Early work by Gillespie and Rothenbury (4) and a subsequent investigation by us (5) into the antimony–fluoride–fluorosulfate system form the basis of this reaction, focussing attention on $Sb_2F_9SO_3F$ as the most volatile component in this system, which allows ready removal of the SO_3F group from the reaction mixture. Initial uses of the solvolysis reaction in SbF_5 have involved the stabilization of nonmetallic cations, such as ClO_2^+ (6), a series of triatomic interhalogen cations (7), or the dihalogen cations Br_2^+ and I_2^+ (8) in solid compounds. Use of this method in the synthesis of the first stage graphite salt C_8SbF_6 (9) and stabilization of the dimethyltin(IV) cation as $(CH_3)_2Sn(Sb_2F_{11})_2$ (10) illustrate its versatility.

There have been a variety of alternative methods used for the synthesis of hexafluoro antimonates of divalent metals, and some of the compounds discussed here (e.g., $Ni(SbF_6)_2$ (11, 12) and $Sn(SbF_6)_2$ (13)) had been prepared when this study was started. All methods have the use of SbF_5 in common, even though the routes vary. Metal oxidation by either elemental fluorine or by SbF_5 in SO_2 solution has allowed the synthesis of $Ni(SbF_6)_2$ (11, 12) as well as of $Fe(SbF_6)_2$ and $Mn(SbF_6)_2$ (12). There are obvious limitations to this approach. Where higher oxidation states are accessible, direct fluorination may result in oxidation beyond the +2 state, unless the reaction conditions are well understood and carefully controlled. Oxidation by SbF_5 fails for metals, with higher oxidation potentials than provided for by the Sb(V)/Sb(III) couple. Quantitative separation of the reduced product, solid $SbF_3 \cdot SbF_5$, may prove difficult, and finally mixed fluoride–hexafluoro antimonates like $CoF(SbF_6)$ (12) may form instead.

Fluoride abstraction from MF_2 by SbF_5 in SO_2 or anhydrous HF may be more versatile (13, 14), but here another problem surfaces: the MF_2 lattice may be incompletely broken up under the reaction conditions. With $MF(Sb_2F_{11})$, a structural isomer

[1]Author to whom correspondence may be addressed.

Can. J. Chem. Downloaded from www.nrcresearchpress.com by 186.148.149.217 on 09/07/12
For personal use only.

Can. J. Chem. Downloaded from www.nrcresearchpress.com by 186.148.149.217 on 09/07/12
For personal use only.

of $M(SbF_6)_2$, chemical analysis becomes inconclusive. When moving from ionic SbF_6^- to coordinated SbF_6^- in these compounds, vibrational spectra become more complex and are less readily interpreted. As a consequence, in a recent publication, formulation as $MF_2 \cdot 2SbF_5$ is employed for materials obtained in this manner (14).

There has been a fair amount of evidence for cations of the type $[MF]^+$, $[M_2F_3]^+$, and $[MF^+]_n$ when AsF_6^- is used as a counteranion (15, 16), and a crystal structure obtained on $AgF_2 \cdot AsF_5$ (17) had shown a chain-type cation $[AgF^+]_n$ with AsF_6^- as counteranion. In $AgF_2 \cdot 2SbF_5$, however, a true Ag^{2+} appears to be present and the crystal structure supports formulation as $Ag(SbF_6)_2$ (14).

The advantages of the $M(SO_3F)_2$ solvolysis in excess SbF_5 are: (*i*) $M(SO_3F)_2$ precursors are readily available either from the solvolysis of $SnCl_2$ or $NiCl_2$, or the corresponding Ni(II) or Cu(II) benzoates in HSO_3F (18), or by the use of $S_2O_6F_2$ in case of $Pd(SO_3F)_2$ (19) and $Ag(SO_3F)_2$ (20); (*ii*) in all instances further oxidation by SbF_5 appears unlikely; (*iii*) vibrational spectra allow monitoring of the reaction by probing the absence of SO_3F vibrations; and (*iv*) reactions may be carried out in glass and followed by weight.

Our reasons for selecting these five $M(SbF_6)_2$ compounds for our study, with M = Sn, Ni, Pd, Cu, or Ag, are twofold: (*i*) To avoid structural ambiguities of the type observed above, it became necessary to obtain a ^{119}Sn Mössbauer spectrum on a sample of $Sn(SbF_6)_2$ prepared by a different route and compare it to the spectrum reported previously (13). (*ii*) We had recently (21) observed significant ferromagnetism in the fluorosulfates of Pd^{2+} and Ag^{2+} with a weaker manifestation of this interesting coupling phenomenon in the Ni^{2+} and Cu^{2+} analogues. It became interesting to study the magnetic properties of the four transition-metal SbF_6^- derivatives at temperatures below 80 K. Since $Ni(SbF_6)_2$ had been obtained previously by all three methods (11, 12, 14) discussed above, its formation by solvolysis in liquid SbF_5 is viewed as a test case. A final point of interest concerns the palladium(II) compound. Pd^{2+} in the fluorosulfate is found in an unusual octahedral coordination environment, resulting in a paramagnetic $^3A_{2g}$ ion ground state. It was hoped a $Pd(SbF_6)_2$ would exhibit parmagnetism as well.

Experimental

Chemicals

The fluorosulfates $Ni(SO_3F)_2$ (18), $Cu(SO_3F)_2$ (18), $Sn(SO_3F)_2$ (18), $Pd(SO_3F)_2$ (19), and $Ag(SO_3F)_2$ (20) were all synthesized according to published methods. Antimony(V) fluoride (Ozark Mahoning) was purified by repeated distillation as described (5, 8) and transferred *in vacuo* into the reaction vessels. $AgSbF_6$ and AgF_2 were obtained from Aldrich Chemicals.

Instrumentation

Infrared spectra were obtained with a Nicolet 5DX FT-IR instrument, internally calibrated with a He/Ne laser. Samples were pressed between AgCl or AgBr windows and run as thin films without a mulling agent. Raman spectra were obtained with a Spex Ramalog-5 spectrophotometer, equipped with an argon ion laser. The 514.5-nm line was used for excitation. UV–VIS–NIR spectra were recorded on a Cary 14 spectrophotometer. Samples were run as mulls in either SbF_5 or Fluorolube oil (Halocarbon Corp.) as mulling agent in a cell fitted with quartz windows. The Mössbauer spectrometer and details regarding the recording and calibration of ^{119}Sn Mössbauer spectra have been described before (22). A P.A.R. model 155 vibrating sample magnetometer was used to obtain magnetic susceptibilities between ~2.0 and 82 K. Again, details on the instrument have been published (23). Magnetic fields of 7501 and 9225 G were used, and diamagnetic corrections were made using Pascal constants. Samples were packed into Kel-F (Fluoro-chlorocarbon polymer) capsules.

All moisture-sensitive solids were handled in a Vacuum Atmospheres Corp. Dri-Lab model no. He-493, filled with purified dry nitrogen and equipped with a Dri-Train circulating unit. The reactions were performed in Pyrex reaction vessels of about 50-mL capacity made from round-bottom flasks fitted with Kontes Teflon stem valves and equipped with Teflon-coated spin bars. The reactions were monitored by weight. Chemical analysis was carried out by the Analytische Laboratorium, Gummersbach, West Germany. Differential scanning calorimetry (DSC) studies were made by using a Mettler DSC 20 cell and a Mettler TC 10 TA processor.

Synthetic reactions

A general reaction scheme was applied to the solvolysis reactions in liquid SbF_5. Approximately 500 mg of the $M(SO_3F)_2$ compound was transferred inside the inert-atmosphere box into a preweighed reaction vessel. Approximately 10 mL of freshly purified SbF_5 was added subsequently by vacuum distillation. The reaction vessel was warmed up, initially to room temperature, and subsequently to 50–60°C in an oil bath. Detailed temperatures and reaction times are given below. Only the reactions of $Pd(SO_3F)_2$ (purple → light-grey) and $Ag(SO_3F)_2$ (black-brown → yellow-green → off-white) involved perceptible color changes of the solid reactant and the mixture remained heterogeneous throughout. The initially very viscous antimony(V) fluoride became somewhat more mobile after about 24 h and the mixture could be stirred effectively with a magnetic stirrer. Volatiles were removed in a dynamic vacuum.

Physical properties and analyses

Both $Ni(SbF_6)_2$ (11, 12, 14) and $Sn(SbF_6)_2$ (13) are known compounds. Their identity is ascertained by weight and by infrared spectroscopy. Formation of both $Ni(SbF_6)_2$ and $Sn(SbF_6)_2$ requires reaction times of 14 and 2 days at 60 and 50°C, respectively. The IR frequencies observed for $Ni(SbF_6)_2$ are listed in Table 1. For $Sn(SbF_6)_2$ the following IR bands are found (estimated intensities are in parentheses): 700 (s, sh), 678 (s), 648 (s), 620 (m), 595 (ms), 571 (ms), 520 (m, sh), 477 (m), 432 (w).

$Cu(SbF_6)_2$, reaction time 10 days, reaction temperature 50°C, white hygroscopic solid that is thermally stable up to 210°C. *Anal.* calcd. for $CuSb_2F_{12}$: Cu 11.88, Sb 45.51, F 42.61; found: Cu 11.65, Sb 45.75, F 42.47. Total: 99.87.

$Pd(SbF_6)_2$, reaction time 14 days, reaction temperature 50°C, light-grey solid, very hygroscopic and thermally stable up to 250°C. *Anal.* calcd. for $PdSb_2F_{12}$: Pd 18.62, Sb 42.14, F 39.45; found: Pd 18.35, Sb 41.90, F 39.18. Total: 99.43.

β-$Ag(SbF_6)_2$, reaction time 10 days, reaction temperature 25°C, creamy white, hygroscopic solid, melts at 180–182°C to clear liquid. *Anal.* calcd. for $AgSb_2F_{11}$: Ag 19.25, F 37.25, Sb 43.45; calcd. for $AgSb_2F_{12}$: Ag 18.62, F 39.35, Sb 42.03; found: Ag 18.65, F 39.06, Sb 42.30. Total: 100.01.

Alternate routes to β-$Ag(SbF_6)_2$: (a) 0.323 g of $AgSbF_6$ is allowed to react with an excess of $S_2O_6F_2$ at room temperature. The white color of $AgSbF_6$ changes immediately to black-brown. The $S_2O_6F_2$ is removed *in vacuo* and subsequently replaced by an excess of SbF_5. The mixture is kept at room temperature for 2 days, then heated at 60°C for 2 h. β-$Ag(SbF_6)_2$ is isolated by removing the excess SbF_5 *in vacuo* and is identified by its IR spectrum. (b) 0.436 g of AgF_2 is loaded inside the dry box into a Kel-F reactor together with 4.5 g of SbF_5. About 6.5 mL anhydrous HF is distilled onto this mixture *in vacuo*. After warming to room temperature under magnetic stirring, a light-yellow solid forms immediately. The solution's initial color, which fades quickly, is light blue. Removal of all volatiles yields pure β-$Ag(SbF_6)_2$ as a cream-colored solid.

Results and discussion

Synthesis

As noted previously (6–10), solvolysis reactions of fluorosulfates in a large excess of SbF_5 proceed smoothly and

TABLE 1. Vibrational spectra of $Ni(SbF_6)_2$, $Pd(SbF_6)_2$, and $Cu(SbF_6)_2$

$Ni(SbF_6)_2$[a] Ra[b] $\Delta\nu(cm^{-1})$ Int.[c]	$Ni(SbF_6)_2$ IR $\nu(cm^{-1})$ Int.	$Pd(SbF_6)_2$ IR $\nu(cm^{-1})$ Int.	$Cu(SbF_6)_2$ IR $\nu(cm^{-1})$ Int.	$Cu(SbF_6)_2$ Ra $\Delta\nu(cm^{-1})$ Int.	Approximate band description for $M(SbF_6)_2$; M = Ni, Pd or Cu
742 (1)	738 vs	730 s, sh	729 s	725 (65)	$\nu_{as}SbF_3^t$ out of phase
717 (12)	721 s, sh	716 vs	707 vs, b	721 (70)	$\nu_{as}SbF_3^t$ in phase
710 (44)	710 vs	698 s	672 s	709 (18)	$\nu_{sym}SbF_3^t$ out of phase
674 (100)	672 m	667 ms	665 m	671 (100) 657 (22)	$\nu_{sym}SbF_3^t$ in phase
	631 m	630 m	633 m		$\nu_{as}SbF_3^b$ out of phase
618 (5)	621 m, sh	615 ms	617 m	620 (4)	$\nu_{sym}SbF_3^b$ out of phase
568 (2)	573 s 560 w, sh	570 m 550 w, sh	556 ms	592 (8)	$\nu_{as}SbF_3^b$ in phase
511 (2)	521 mw	522 ms	496 m 465 m	450 (8)	$\nu_{sym}SbF_3^b$ in phase
348 (0+)	350 w, sh	345 m		395 (7)	M···F–Sb stretching
322 (5) 308 (24) 299 (25) 272 (3)	330 w 310 w 295 w	335 m, sh ~300 w 285 w		335 (11) 305 (19) 295 (26) 270 (29)	Sb–F deformation modes

[a]Additional bands at 246, 220, and 198 cm^{-1} and shoulders at 172, 146, and 130 cm^{-1}.
[b]Denotes ref. 14.
[c]Values in parentheses are relative intensity.
Abbreviations: s = strong, m = medium, w = weak, v = very, sh = shoulder, b = broad, as = asymmetric, sym = symmetric, t = terminal, b = bridging.

Can. J. Chem. Downloaded from www.nrcresearchpress.com by 186.148.149.217 on 09/07/12
For personal use only.

frequently without any colour change of the solid reactant. Hence, rather long reaction times are chosen to ensure complete conversion. Two indications that a reaction takes place are a noticeable decrease in the viscosity of SbF_5 after about 1 day, and a slight increase in vapour pressure above the reaction mixture. Both observations may be attributed to the formation of $Sb_2F_9SO_3F$ (7).

To reduce the viscosity even further in order to stir the heterogeneous mixture more effectively, slightly elevated reaction temperatures are chosen. Removal of all volatiles proceeds easily in a dynamic vacuum, with the reaction flask at room temperature.

It is noteworthy that, after pumping overnight, the correct weight for $M(SbF_6)_2$ is obtained. Previous use of this synthetic method by us (6–8, 10) had in all instances led to products where molecular cations are stabilized by $Sb_2F_{11}^-$, and in one case (8) even by $Sb_3F_{16}^-$. For the spherical, less electrophilic M^{2+} cations, SbF_6^- appears to be the more suitable counteranion, allowing formation of layered materials as discussed below. In any event, neither product weights on isolation, nor chemical analyses, nor vibrational spectra give any indication of $Sb_2F_{11}^-$ containing intermediates or by-products.

Of the resulting compounds, $Ni(SbF_6)_2$ (11) and $Sn(SbF_6)_2$ (13) are identified by their weights and their previously reported IR spectra. The ^{119}Sn Mössbauer spectrum of $Sn(SbF_6)_2$ shows a single broad line (Γ = 1.35 mm s^{-1}) caused by unresolved quadrupole splitting. The isomer shift is found at 4.39 mm s^{-1} relative to SnO_2, in excellent agreement with the previously reported value (13). This poses an interesting problem: we had previously concluded, based on ^{119}Sn Mössbauer parameters, that both SbF_6^- and $Sb_2F_{11}^-$ are extremely weakly basic and the least nucleophilic anions when stabilizing the cation $(CH_3)_2Sn^{2+}$ with a linear C—Sn—C group (2). We had expected the SbF_6^- anion to be ideally suited to stabilize the "bare" Sn^{2+} ion equally well. For such a species with a stereochemically inactive, spherically distributed $5s^2$ pair, a single line is expected and calculations suggest a value of 4.84 mm s^{-1} relative to SnO_2 for the isomer shift (24). The results, with identical ^{119}Sn Mössbauer parameters regardless of methods of preparation, and an isomer shift about 0.45 mm s^{-1} lower than suggested by calculations for Sn^{2+}, indicate that steric factors rather than low nucleophilicity of the counteranion may be important. The list of stannous compounds with single-line ^{119}Sn Mössbauer spectra and isomer shifts higher than the ones observed for $Sn(SbF_6)_2$ provides a clue. $Sn[Sn(SO_3F)_6]$, 4.48 (25); $Sn(ClO_4)_2$(15-crown-5)$_2$, 4.53 (26); $Sn(SbF_6)_2 \cdot 2AsF_3$, 4.66 (27); and $Sn[Sn(SO_3CF_3)_6]$ 4.69 mm s^{-1} relative to SnO_2 (28) all approach a true Sn^{2+} more closely than $Sn(SbF_6)_2$ and all involve sterically more demanding ligands than SbF_6^-. A crystal structure for $Sn(SbF_6)_2 \cdot 2AsF_3$ (27), where the Lewis base AsF_3 is coordinated as well to tin, indicates 9-coordinate tin. The use of crown ether ligands (26) also supports the view that steric factors play an important role in stabilizing the bare Sn^{2+} ion.

The solvolysis of $Ag(SO_3F)_2$ is expected to lead to the recently reported blue $Ag(SbF_6)_2$. The X-ray diffraction study had revealed a true Ag^{2+} ion in a distorted octahedral environment (14). However, the course of the solvolysis and the final product are surprising. The initial black-brown color of $Ag(SO_3F)_2$ quickly disappears and a greenish-blue solid slowly changes color to yellow. Ultimately a cream-colored, diamagnetic solid is isolated, which melts at ~180°C, without decomposition, to a clear, colorless liquid. The magnetic behavior, the color, and the observed lack of solubility in anhydrous HF (29) suggest the possible presence of univalent silver. An alternative formulation of the reaction product as

Can. J. Chem. Downloaded from www.nrcresearchpress.com by 186.148.149.217 on 09/07/12
For personal use only.

$AgSb_2F_{11}$ is, however, not supported by the weight change during reaction, a complete chemical analysis (see experimental section), the vibrational spectrum, or the chemical behavior of the material. Besides, with paramagnetic divalent silver well established in $Ag(SO_3F)_2$ (20), the other reactant, SbF_5, can hardly be regarded as a reducing agent. A possible reductive decomposition of the reaction product appears unlikely since, besides excess SbF_5, $Sb_2F_9SO_3F$ is the only volatile reaction product obtained.

The chemical behavior of $Ag(SbF_6)_2$ is not consistent with the presence of Ag^+ in the reaction product. Unlike other silver(I) salts, the material will not undergo further oxidation by $S_2O_6F_2$ in the presence or the absence of HSO_3F. On the other hand, $AgSbF_6$ is immediately oxidized by $S_2O_6F_2$ alone, to give a black-brown solid, with the increase in weight consistent with the composition $Ag(SbF_6)(SO_3F)$. Subsequent solvolysis of this material in SbF_5 proceeds in an identical manner to the solvolysis of $Ag(SO_3F)_2$, suggesting a viable alternative synthetic route to $Ag(SbF_6)_2$.

Strong evidence for the presence of silver in an oxidation state higher than +1 comes from the hydrolysis of $Ag(SbF_6)_2$ in aqueous KI solution. The reaction proceeds very vigorously and I_2 and O_2 are produced. Formation of I_2 may in part be due to oxidation by Sb(V) in an acidic environment (30), but evolution of O_2 can only be caused by Ag(II) or Ag(III) (31) in our product.

In summary, all evidence suggests that the material obtained in the solvolysis of $Ag(SO_3F)_2$ in SbF_5 is β-$Ag(SbF_6)_2$, a valence isomer of the previously reported α-$Ag(SbF_6)_2$ (14).

Attempts to synthesize this α form using the published method (14)

$$[2]\quad AgF_2 + 2SbF_5 \xrightarrow{HF} Ag(SbF_6)_2$$

are only partially successful if a slight excess of SbF_5 (ratio SbF_5:AgF_2 = 2.32) over the stoichiometric amount is used. Even here a fair amount of solid β-$Ag(SbF_6)_2$ forms in addition to a blue solution, from which crystalline α-$Ag(SbF_6)_2$ is obtained by slow evaporation of the volatiles. When a larger excess of SbF_5 is used (SbF_5:AgF_2 = 6.01), β-$Ag(SbF_6)_2$ is the only product. The blue color of the HF solution quickly fades within an hour. Removal of HF and the excess SbF_5 yields pure β-$Ag(SbF_6)_2$.

It appears that formation of α-$Ag(SbF_6)_2$ in HF represents an acid–base titration with both the cation $Ag^{2+}_{(solv)}$ and the final product α-$Ag(SbF_6)_2$ stable in, and isolable from, anhydrous HF. Similar behavior is reported for all other transition-metal hexafluoro antimonates of the $M(SbF_6)_2$ or $MF_2 \cdot 2SbF_5$ type (14). On the other hand, β-$Ag(SbF_6)_2$ is insoluble in anhydrous HF, suggesting structural differences.

The observed diamagnetism is best explained by assuming a mixed-oxidation-state compound of the composition Ag(I)-Ag(III)$(SbF_6)_4$. To account for the diamagnetism, Ag^{3+} should be in a square planar, or at least in a tetragonally elongated, octahedral environment. Argentic oxide, AgO, represents a precedent, according to neutron diffraction studies on this compound (31). The black-brown color, also found for the recently reported oxides Ag_2O_3 (32) and Ag_3O_4 (33), is seemingly common to binary oxides and oxy salts of di- or trivalent silver, e.g., the sulfonates $Ag(SO_3F)_2$ (20) or $Ag(SO_3CF_3)_2$ (34), and may possibly be due to a charge transfer transition (35). On the other hand, alkali metal salts containing the $[AgF_4]^-$ ion are reported to be yellow (31, 36), while AgF_2 and many Ag(II) fluoro derivatives are blue (37), just like α-$Ag(SbF_6)_2$ (14).

It appears, then, that all our observations support formulation of the β form as Ag(I)Ag(III)$(SbF_6)_4$; however, our inability to oxidize Ag^+ further is not consistent with an ionic formulation as silver(I) tetrakis(hexafluoroantimonato)argentate(III), Ag^+-$[Ag(SbF_6)_4]^-$.

We are not aware of any other valence isomeric pair of the Ag(II) vs. Ag(I)Ag(III) type. The above mentioned AgO is reported to be Ag(I)Ag(III)O_2 (31), but a true Ag(II)O appears to be still missing. The crystal structure of Ag_3O_4 (33) shows both Ag(II) and Ag(III) in square planar coordination sites, however, and mixed-oxidation-state compounds of the type Pd(II)Pd(IV)X_6, with X = F (38) or SO_3F (19), are known for palladium, the neighboring element in the 4*d* series, with Pd(III)X_3 so far unknown.

Observations made during the course of this study suggest that α-$Ag(SbF_6)_2$ may be irreversibly converted to the β-valence isomer. This conversion occurs at room temperature, if SbF_5 is present in an excess, either in the presence or absence of HF. It is therefore not surprising that all our attempts to synthesize pure α-$Ag(SbF_6)_2$ from AgF_2 and SbF_5 in anhydrous HF (14) produce β-$Ag(SbF_6)_2$ as well, as an insoluble precipitate in addition to the blue solution. Removal of the solvent at −78°C in a dynamic vacuum affords a mixture of the two valence isomers.

Heating the isomeric mixture allows transformation to the pure β form. Following this conversion by differential scanning calorimetry indicates two endothermic events, a sharp peak at 100°C, and a broad peak at 139–140°C. The latter peak coincides with the melting point, where a colorless liquid forms. The β form melts at ~180°C, consistent with differential scanning calorimetry. Absence of the peak at 100°C suggests interpretation of this thermal event as a phase transition from α-$Ag(SbF_6)_2$ to β-$Ag(SbF_6)_2$.

It appears that electron transfer between two Ag^{2+} ions to give Ag^+ and Ag^{3+} is mediated by an antimony(V) fluoro species (SbF_5 or SbF_6^-). Considering our observations regarding the relative stability of the two valence isomers, it is surprising that β-$Ag(SbF_6)_2$ has not been reported while the α form has.

The solvolysis of $Pd(SO_3F)_2$ in SbF_5, on the other hand, does not appear to involve a change in the electronic structure of the Pd^{2+} ion. The resulting material of the composition $Pd(SbF_6)_2$ is paramagnetic. The electronic spectrum of the mull exhibits three broad bands: ν_1 at 840 nm ($^3A_{2g} \rightarrow {}^3T_{2g}$), ν_2 at 550 nm ($^3A_{2g} \rightarrow {}^3T_{1g}(F)$), and ν_3 at 375 nm ($^3A_{2g} \rightarrow {}^3T_{1g}(P)$). Analysis of the observed ligand-field spectrum according to Figgis (39) suggests a $10Dq$ value of 12 400 cm^{-1}, B = 587 cm^{-1} and B/B_0 = 0.707. Very similar parameters are reported for $Pd(SO_3F)_2$ with $10Dq$ = 11 770 and B = 633 cm^{-1} (19). This in turn suggests a structural similarity between both compounds. For $Pd(SO_3F)_2$ (19), as for most fluorosulfates of divalent metals (18), a layer structure based on the $CdCl_2$ prototype is postulated. The same structural type is reported for α-$Ag(SbF_6)_2$ (14) and implicitly also for $Ni(SbF_6)_2$ (11). From a comparison of the Dq and B values for the two Pd(II) compounds, it appears that in this case the tridentate SbF_6^- group ranks slightly higher in both the spectrochemical and nephelauxetic ligand series (34) than does the O-tridentate fluorosulfate group.

TABLE 2. Vibrational spectra of the two valence isomers of $Ag(SbF_6)_2$

β-$Ag(SbF_6)_2$ Ra $\Delta\nu(cm^{-1})$ Int.	β-$Ag(SbF_6)_2$ IR $\nu(cm^{-1})$ Int.	α-$Ag(SbF_6)_2$ Ra[a] $\Delta\nu(cm^{-1})$ Int.	α-$Ag(SbF_6)_2$ IR[a] $\nu(cm^{-1})$ Int.	Approximate band description
720 sh (12)	719 s, sh			
700 sh (33)	692 vs		692 vs	
682 (100)	673 s			SbF^t stretching
659 (93)	654 s	668 (100)	668 ms	
651 sh (30)		658 (75)	640 m	
600 (16)	602 m	600 (37)		
		580 (31)	583 w	
526 (4)	515 vw	552 (20)	554 w	SbF^b stretching
	490 ms		496 w	
365 (1)	368 mw			M···FSb stretching
	357 w, sh			
312 sh (13)				
303 (32)	301 sh			
290 (18)	283 s	290 (37)		SbF deformation
	278 s			

[a]Denotes ref. 14.

Paramagnetic Pd^{2+} complexes with fluorometallate anions have precedents. Complexes of the general type $Pd[MF_6]$, with M = Pd, Pt, Ge, or Sn, have been known for almost 25 years (38), and their magnetic susceptibility measurements have been reported down to 80 K. The presence of MF_6^{2-} anion would suggest a different structural type, but the coordination environment of Pd^{2+} should again be octahedral.

Vibrational spectra

The infrared spectra obtained for $Ni(SbF_6)_2$, $Pd(SbF_6)_2$, $Cu(SbF_6)_2$, and β-$Ag(SbF_6)_2$, together with the Raman spectra for the latter two compounds, are summarized in Tables 1 and 2. Also included are the previously reported Raman spectra for $Ni(SbF_6)_2$ (11) and α-$Ag(SbF_6)_2$ (14) as well as an approximate band description, also proposed previously (11). However, this description pertains only to the Ni^{2+}, Pd^{2+}, and Cu^{2+} compounds in Table 1. The Raman spectrum of β-$Ag(SbF_6)_2$ is illustrated in Fig. 1. Attempts to obtain a Raman spectrum of $Pd(SbF_6)_2$ result in partial sample decomposition. Apparently the excitation line of the Ar^+ laser falls within ν_2 of the electronic spectrum of $Pd(SbF_6)_2$.

Agreement with the previously reported IR and Raman spectra for $Ni(SbF_6)_2$ (11) is very good with only a minor exception: we do not observe an IR band at 583 cm^{-1} attributed to ν_{as} out of phase for the bridging SbF_3 group. This band does not have a counterpart in the Raman spectrum, and may be spurious. We have amended the band description in Table 1 slightly. There is only a partial comparison possible with the vibrational spectra reported for $NiF_2 \cdot 2SbF_5$ (14). The limited number of bands listed, six Raman and four IR bands with five non-coincidences, suggests an incomplete listing. Nevertheless, the Raman bands reported for $NiF_2 \cdot 2SbF_5$ (14) are all observed with similar relative intensities in the Raman spectrum of $Ni(SbF_6)_2$ (11). Since the reported X-ray powder data have the principle lines in common (11, 14), it is reasonable to conclude that both compounds are identical.

This is possibly not the case for $Cu(SbF_6)_2$ reported here, or for $CuF_2 \cdot 2SbF_5$ (14). Very intense Raman and IR bands at ~725 cm^{-1} (see Table 1) are apparently not observed for $CuF_2 \cdot 2SbF_5$ (14). However, the case for polymorphism is by no means as strong as in the case of the two forms of $Ag(SbF_6)_2$.

The available structural information on $M(SbF_6)_2$ compounds facilitates a discussion of the vibrational data shown in Table 1. A common $CdCl_2$-type layer strucure is proposed for $Ni(SbF_6)_2$, based on X-ray powder diffraction data (11), and evident for α-$Ag(SbF_6)_2$ from the X-ray single crystal diffraction study (14). The structure for $Ni(SbF_6)_2$ is deduced, starting from the well-known $LiSbF_6$ structure (40) by placing Ni^{2+} into every second, nearly octahedral Li^+ site (11). In α-$Ag(SbF_6)_2$, Ag^{2+} is situated in a tetragonally elongated octahedral site, resulting almost in square planar coordination, similar to the coordination in AgF_2 (41). SbF_6^- acts as a tridentate bridging group, with the bridging fluorines, F^b, and the terminal fluorines, F^t, in *fac*-octahedral positions. Unlike the SbF_3^b unit, the corresponding SbF_3^t-trigonal pyramid is remarkably regular with two $d_{Sb-F^t} \approx 1.836$ Å and one slightly longer at 1.846 Å. The vibrational assignment for $Ni(SbF_6)_2$ by Christe *et al.* (11), adopted by us in this study, suggests a useful subdivision into $Sb-F_3^t$ stretching modes found above ~660 cm^{-1} and $\nu_{Sb-F_3^b}$ below ~635 cm^{-1}. Each set is further divided into symmetric and asymmetric in-phase and out-of-phase modes. The basic difference between both sets, SbF_3^b and

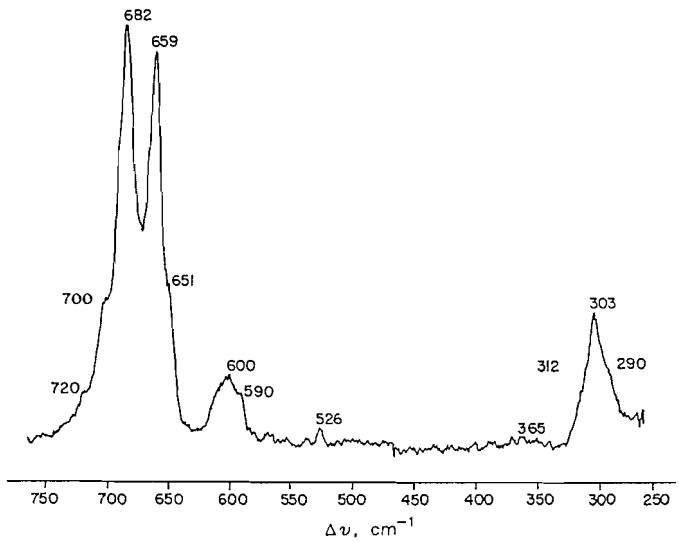


FIG. 1. Raman spectrum of $Ag(SbF_6)_2$.

Can. J. Chem. Downloaded from www.nrcresearchpress.com by 186.148.149.217 on 09/07/12
For personal use only.

Can. J. Chem. Downloaded from www.nrcresearchpress.com by 186.148.149.217 on 09/07/12
For personal use only.

SbF_3^t, is that the former belong to a filled, and the latter to an unoccupied, octahedral hole in the $M(SbF_6)_2$-layer structure.

The data summarized in Table 1 for $M(SbF_6)_2$, with M = Ni, Pd, and Cu, indeed show a common group of four strong vibrations, some small band splittings for $Cu(SbF_6)_2$ notwithstanding, which are assigned as ν_{Sb-F^t} vibrations. Most prominent among them is a Raman band at ~670 cm^{-1}, which is clearly the strongest band in the respective spectra. Interestingly, this band is found as well for a number of additional $M(SbF_6)_2$ compounds with M = Mg, Zn, Fe, Co, and Cu (14), in the same position, and always of the highest intensity. This is altogether not too surprising, since the reported X-ray powder diffraction data had indicated the existence of two structurally related triads, consisting of the hexafluoro antimonates of Mg, Zn, and Ni, and those of Fe, Co, and Cu (14). However, the structural differences between the two triads appear to be so small that they do not seriously affect the positions of the $\nu_{Sb-F_3^t}$ bands. In the Raman data, the 670-cm^{-1} band is attributed to a symmetric in-phase $Sb-F_3^t$ stretching mode, which suggests a common SbF_3^t grouping in both triads as well as in $Cu(SbF_6)_2$ reported by us. A corresponding IR band of medium intensity is observed in all instances as well. This band is found for $Pd(SbF_6)_2$ at 667 cm^{-1}. In addition, there is a rather close correspondence between $Ni(SbF_6)_2$ and $Pd(SbF_6)_2$, in both IR band positions and intensities, to suggest isostructural compounds.

The remaining $M(SbF_6)_2$ compounds reported by Gantar *et al.* (14), with M = Cr, Pb, and Cd, differ slightly in both vibrational spectra and X-ray powder diffraction data. The highest intensity Raman band is now found at about 650 cm^{-1}. Even for these compounds, as for all the others (14), formulation as $M(SbF_6)_2$ is suggested. None of the vibrational data reported here or published previously (11, 14) suggest the presence of the anion $Sb_2F_{11}^-$, by comparison to published precedents (13, 42, 43).

The vibrational data for both forms of $Ag(SbF_6)_2$ in Table 2 show interesting differences. Both have two very intense Raman bands, rather than one, in the $\nu_{Sb-F_3^t}$ region, at 668 and 658 cm^{-1} for α-$Ag(SbF_6)_2$ and at 682 and 659 cm^{-1} for the β form (see Fig. 1). In each case the band with the largest Raman shift also has the highest intensity, and yet in spite of the incomplete band listing for α-$Ag(SbF_6)_2$, there appears to be some structural similarity between the two forms. Only a rather general band description is suggested because there may be some band overlap for β-$Ag(SbF_6)_2$, while the listing for the α form appears, as stated above, to be incomplete.

The distorted layer structure formed for α-$Ag(SbF_6)_2$, with all tetragonally elongated octahedral holes occupied by Ag^{2+} and concomitant tetragonally compressed vacant sites (14), provides a suitable model for the valence isomer as well. Regular occupation of half of the compressed holes by Ag^+ and half of the elongated holes by Ag^{3+} would allow retention of the layer structure, where Ag^+ achieves linear and Ag^{3+} square planar coordination. Conversely, two types of vacant sites are formed, with two sets of $Sb-F^t$ vibrations and different band positions for the $Sb-F^b$ stretching modes as well, consistent with observations.

Ultimately, structural proof will have to come from a single-crystal X-ray diffraction study, and our efforts are currently aimed in this direction. The lack of solubility in HF and the high reactivity of β-$Ag(SbF_6)_2$ present obstacles.

Low temperature magnetic susceptibility measurements

Magnetic susceptibilities over the temperature range of ~2 to 80 K are recorded for $Ni(SbF_6)_2$, $Pd(SbF_6)_2$, and $Cu(SbF_6)_2$ on a P.A.R. vibrating sample magnetometer. Relevant data are summarized in Table 3 and the plot of the magnetic moments vs. temperature for all three compounds is shown in Fig. 2.

As discussed in the experimental section, we have not been able to obtain pure α-$Ag(SbF_6)_2$ in quantities large enough for a bulk magnetic measurement. The results of measurements made, on what is obviously a mixture of the two valence isomeric forms, allow only limited conclusions, since the small amount of paramagnetic material in the sample did not permit us to extend the measurements to temperatures higher than 65 K. Usually, for paramagnetic materials with one or two unpaired electrons, the vibrating sample magnetometer is useful to ~90 K. In the temperature range of 65–3 K the magnetic moment calculated for α-$Ag(SbF_6)_2$ appears to be independent of temperature with a shallow maximum at ~6 K before falling off. It is unclear whether the observed dilute magnetic behavior is due to α-$Ag(SbF_6)_2$, or is caused by β-$Ag(SbF_6)_2$ acting as a dilutant.

The diamagnetism of β-$Ag(SbF_6)_2$ is confirmed by measurements made at room temperature, using the Gouy technique. The measured susceptibility of -68×10^{-6} cm^3 mol^{-1} is less than the sum of Pascal constants of -128×10^{-6} cm^3 mol^{-1}; however, the Gouy balance used is insufficiently sensitive for a more accurate determination of diamagnetic susceptibilities. In addition, a trace amount of α-$Ag(SbF_6)_2$ could be responsible for the slight discrepancy, as well as some temperature independent paramagnetism (TIP).

Of the remaining three compounds, $Ni(SbF_6)_2$ presents the clearest picture. As seen in Fig. 2, the magnetic moment decreases gradually before a steep decline becomes apparent at ~10 K, indicative of strong antiferromagnetic ordering. Both $Pd(SbF_6)_2$ and $Cu(SbF_6)_2$ also show strong antiferromagnetic coupling when approaching 4 K, but in both instances, most noticeably for $Pd(SbF_6)_2$, a very slight increase of the magnetic moment is observed, just before antiferromagnetic ordering dominates. This increase is rather small for $Cu(SbF_6)_2$ and the discussion will concentrate on the palladium(II) case. The observed weak effect is reproducible and two possible interpretations are suggested: (a) a phase transition occurs at ~10 K, and (b) very weak ferromagnetism is responsible for the small effect.

We tend to favor the latter explanation because there are a number of precedents for simultaneous ferromagnetic and antiferromagnetic ordering in fluoro derivatives of palladium(II). Very weak ferromagnetism is observed for PdF_2 (44), which has a rutile structure (45), and for the ternary fluorides $Pd(II)Pd(IV)F_6$ and $Pd(II)Pt(IV)F_6$ (46). According to a recent crystal structure reported for the latter compound (47), there may even be a close structural relationship: $Pd(II)Pt(IV)F_6$ has a $LiSbF_6$ structure. For $Pd(II)(SbF_6)_2$ a layer structure is suggested, which, as discussed above, is also derived from the $LiSbF_6$ prototype, with half of the octahedral holes occupied by Pd^{2+} compared to all holes filled for $Pd(II)Pt(IV)F_6$ (47).

Some similarity in magnetic behavior is also evident from the μ_{eff}^{80} values, which are for the ternary palladium(II) fluorides in the range of 2.7–~3.0 μ_B for the series $Pd(II)M(IV)F_6$, with M = Pd, Pt, Ge or Sn (38*a*), while 3.09 μ_B are found for $Pd(SbF_6)_2$, where Pd^{2+} is slightly more dilute.

Substantially higher magnetic moments (3.30–3.60 μ_B) are found for the corresponding fluorosulfato complexes of palladium(II) (19*b*), where the bulkier fluorosulfate groups appear to prevent antiferromagnetic exchange. It is interesting to note that

TABLE 3. Magnetic properties of $M(SbF_6)_2$ compounds, M = Ni, Cu, Pd

$Ni(SbF_6)_2$			$Cu(SbF_6)_2$			$Pd(SbF_6)_2$		
Temp. (K)	$\chi_m^{corr} \times 10^5$ ($cm^3\ mol^{-1}$)	μ_{eff} (μ_B)	Temp. (K)	$\chi_m^{corr} \times 10^5$ ($cm^3\ mol^{-1}$)	μ_{eff} (μ_B)	Temp. (K)	$\chi_m^{corr} \times 10^5$ ($cm^3\ mol^{-1}$)	μ_{eff} (μ_B)
81.67	745	2.21	81.83	372	1.56	81.50	1462	3.09
77.78	781	2.20	78.06	390	1.56	77.55	1530	3.08
74.08	820	2.20	74.24	413	1.57	73.91	1597	3.07
69.72	867	2.20	70.11	440	1.57	69.77	1676	3.06
65.31	916	2.19	65.65	469	1.57	65.19	1774	3.04
60.15	995	2.19	60.44	510	1.57	60.03	1901	3.02
54.20	1095	2.18	54.45	562	1.56	54.00	2063	2.99
47.60	1237	2.17	51.40	594	1.56	47.15	2299	2.95
40.05	1447	2.15	47.95	636	1.56	39.80	2626	2.89
30.80	1850	2.14	40.55	749	1.56	31.10	3208	2.83
26.28	2149	2.13	30.70	977	1.55	30.45	3257	2.82
21.17	2609	2.10	26.00	1151	1.55	26.55	3621	2.77
16.20	3282	2.06	21.22	1410	1.55	21.60	4199	2.69
11.00	4561	2.00	16.25	1818	1.54	20.80	4315	2.68
7.72	6061	1.93	11.00	2689	1.54	16.50	5216	2.62
5.34	8020	1.85	7.46	3975	1.54	10.80	8412	2.70
4.78	8665	1.82	5.56	5421	1.55	9.94	9166	2.70
4.32	8986	1.76	4.24	7293	1.57	7.12	11269	2.53
3.70	9769	1.70	4.04	7248	1.49	5.84	11719	2.34
2.99	10339	1.57	3.02	8895	1.47	5.26	11832	2.23
2.50	10731	1.47	2.40	10745	1.44	4.76	11911	2.13
2.00	11159	1.34	1.97	12482	1.40	4.36	11911	2.04
			1.86	13226	1.40	4.00	11948	1.96
						3.64	11948	1.87
						3.37	11986	1.80
						2.99	11986	1.69
						2.20	11986	1.45
						2.10	12023	1.42

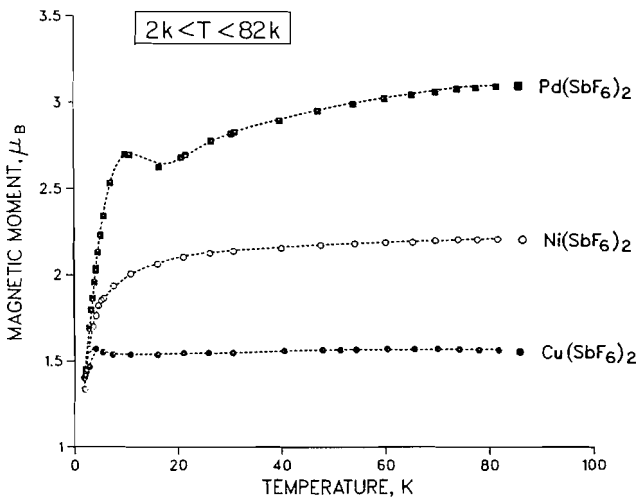


FIG. 2. Magnetic moment vs. temperature of $M(SbF_6)_2$ (M = Ni, Cu, Pd).

at low temperatures (~20 K) significant ferromagnetism has been observed for two members of this group, $Pd(SO_3F)_2$ and $Pd(II)Pd(IV)(SO_3F)_6$. The former, like $Pd(SbF_6)_2$, has a layer structure, derived from the $CdCl_2$ type, and both appear to have the Pd^{2+} ion in very similar electronic environments at room temperature, as reflected in their respective electronic mull spectra discussed above.

Finally it should be pointed out that the magnetic moments obtained for $Cu(SbF_6)_2$ are unusually low for Cu^{2+} (48) with values well below the spin-only value of 1.73 μ_B, and for the most part down to ~4 K, invariant with temperature. This behavior clearly rules out antiferromagnetic coupling as a possible cause for the low moments. With the composition of the material well established by a complete analysis, the possible presence of a diamagnetic mixed valency compound $Cu(I)Cu(III)(SbF_6)_4$ must be considered likely. A number of square-planar diamagnetic complexes of Cu(III) have been studied (48); however, the only fluorocomplex $K_3[CuF_6]$ is paramagnetic, with $\mu_{eff} = 2.80\ \mu_B$ (49). The unusual Raman spectrum of $Cu(SbF_6)_2$ has been discussed above, and it seems that a further, more detailed investigation into a possible second, perhaps less pronounced, case of valence isomerism, affecting again with $Cu^{2+}(d^9)$ a "Jahn-Teller ion", is indicated.

Conclusions

Even though a number of seemingly simpler synthetic routes to compounds of the type $M(SbF_6)_2$ are known, the solvolysis of metal fluorosulfates in excess SbF_5 is found to be a very useful addition. This is evidenced by $Pd(SbF_6)_2$ with interesting spectroscopic and magnetic properties and more so by the new diamagnetic valence isomer β-$Ag(SbF_6)_2$. Since a fair number of transition-metal fluorosulfates are known, there appears to be a wide synthetic potential for this route.

Acknowledgements

Financial support by the Natural Sciences and Engineering

Can. J. Chem. Downloaded from www.nrcresearchpress.com by 186.148.149.217 on 09/07/12
For personal use only.

Research Council of Canada is gratefully acknowledged. Professor R. C. Thompson is thanked for much helpful advice and valuable assistance during the course of this work.

1. P. L. FABRE, J. DEVYNCK, and B. TREMILLON. Chem. Rev. **82**, 591 (1982), and references therein.
2. S. P. MALLELA, S. YAP, J. R. SAMS, and F. AUBKE. Inorg. Chem. **25**, 4327 (1986).
3. G. A. OLAH, G. K. S. PRAKASH, and J. SOMMER. Superacids. Wiley, New York. 1985.
4. R. J. GILLESPIE and R. A. ROTHENBURY. Can. J. Chem. **42**, 416 (1964).
5. W. W. WILSON and F. AUBKE. J. Fluorine Chem. **13**, 431 (1979).
6. P. A. YEATS and F. AUBKE. J. Fluorine Chem. **4**, 243 (1974).
7. W. W. WILSON, J. R. DALZIEL, and F. AUBKE. J. Inorg. Nucl. Chem. **37**, 665 (1975).
8. W. W. WILSON, R. C. THOMPSON, and F. AUBKE. Inorg. Chem. **19**, 1489 (1980).
9. S. KARUNANITHY and F. AUBKE. J. Fluorine Chem. **23**, 541 (1983).
10. S. P. MALLELA, S. YAP, J. R. SAMS, and F. AUBKE. Rev. Chim. Miner. **23**, 572 (1986).
11. K. O. CHRISTE, W. W. WILSON, R. BOUGON, and P. CHARPIN. J. Fluorine Chem. **34**, 287 (1987).
12. P. A. W. DEAN. J. Fluorine Chem. **5**, 499 (1975).
13. T. BIRCHALL, P. A. W. DEAN, and R. J. GILLESPIE. J. Chem. Soc. A, 1777 (1971).
14. D. GANTAR, I. LEBAN, B. FRLEC, and J. H. HOLLOWAY. J. Chem. Soc. Dalton Trans. 2379 (1987).
15. B. FRLEC, D. GANTAR, and J. H. HOLLOWAY. J. Fluorine Chem. **20**, 385 (1982).
16. B. FRLEC, D. GANTAR, and J. H. HOLLOWAY. J. Fluorine Chem. **19**, 485 (1982).
17. D. GANTAR, B. FRLEC, D. R. RUSSELL, and J. H. HOLLOWAY. Acta Crystallogr. Sect. C: Cryst. Struct. Commun. **C43**, 618 (1987).
18. C. A. ALLEYNE, K. O'SULLIVAN-MAILER, and R. C. THOMPSON. Can. J. Chem. **52**, 336 (1974).
19. (*a*) K. C. LEE and F. AUBKE. Can. J. Chem. **55**, 2473 (1977); (*b*) **57**, 2058 (1979).
20. P. C. LEUNG and F. AUBKE. Inorg. Chem. **17**, 1765 (1978).
21. M. S. R. CADER, R. C. THOMPSON, and F. AUBKE. Chem. Phys. Lett. Submitted.
22. S. P. MALLELA, K. LEE, P. F. GEHRS, J. I. CHRISTENSEN, J. R. SAMS, and F. AUBKE. Can. J. Chem. **65**, 2649 (1987).
23. J. S. HAYNES, K. W. OLIVER, S. J. RETTIG, R. C. THOMPSON, and J. TROTTER. Can. J. Chem. **62**, 891 (1984).
24. (*a*) J. K. LEES and P. A. FLINN. Phys. Lett. **19**, 186 (1965); J. Chem. Phys. **48**, 882 (1968); (*b*) P. A. FLINN, G. K. SHENNOY, F. E. WAGNER (*Editors*). Mössbauer isomer shifts. North-Holland, Amsterdam. 1978. p. 593ff.
25. S. P. MALLELA, S. T. TOMIC, K. LEE, J. R. SAMS, and F. AUBKE. Inorg. Chem. **25**, 2939 (1986).
26. R. H. HERBER and G. CARRASQUILLO. Inorg. Chem. **20**, 3693 (1981).
27. A. J. EDWARDS and K. I. KHALLOW. J. Chem. Soc. Chem. Commun. 50 (1984).
28. R. J. BATCHELOR, J. N. R. RUDDICK, J. R. SAMS, and F. AUBKE. Inorg. Chem. **16**, 1414 (1977).
29. A. F. CLIFFORD, H. C. BEACHELL, and W. M. JACK. J. Inorg. Nuclear Chem. **5**, 57 (1957).
30. A. I. VOGEL. Quantitative inorganic analysis. 3rd ed. John Wiley and Sons, New York. 1961.
31. J. A. MCMILLAN. Chem. Rev. **62**, 65 (1962), and references therein.
32. B. STANDKE and M. JANSEN. Angew. Chem. Int. Ed. Engl. **24**, 118 (1985).
33. B. STANDKE and M. JANSEN. Angew. Chem. Int. Ed. Engl. **25**, 77 (1986).
34. P. C. LEUNG, K. C. LEE, and F. AUBKE. Can. J. Chem. **57**, 326 (1979).
35. L. HELMHOLTZ and R. LEVINE. J. Am. Chem. Soc. **64**, 354 (1942).
36. W. KLEMM. Angew. Chem. **66**, 468 (1954).
37. B. G. MÜLLER. Z. Anorg. Allg. Chem. **553**, 196 (1987), and references therein.
38. (*a*) N. BARTLETT and R. P. RAO. Proc. Chem. Soc. London, 393 (1964); (*b*) R. P. RAO. Ph.D. Thesis, University of British Columbia, 1965.
39. B. N. FIGGIS. Introduction to ligand fields. John Wiley and Sons, New York. 1966. p. 220.
40. J. H. BURNS. Acta Crystallogr. **15**, 1098 (1962).
41. P. FISCHER, G. ROULT, and D. SCHWARZENBACH. J. Phys. Chem. Solids, **32**, 1641 (1971).
42. B. FRLEC and J. H. HOLLOWAY. J. Chem. Soc. Dalton Trans. 535 (1975).
43. J. FAWCETT, J. H. HOLLOWAY, D. LAYCOCK, and D. R. RUSSELL. J. Chem. Soc. Dalton Trans. 1355 (1982).
44. R. P. RAO, R. C. SHERWOOD, and N. BARTLETT. J. Chem. Phys. **49**, 3728 (1988).
45. N. BARTLETT and R. MAITLAND. Acta Crystallogr. **10**, 63 (1957).
46. J.-M. DANCE and A. TRESSAUD. *In* Inorganic solid fluorides. *Edited by* P. Hagenmuller. Academic Press, New York. 1985. p. 380, and references therein.
47. B. G. MÜLLER. Z. Anorg. Allg. Chem. **556**, 79 (1988).
48. Landolt–Börnstein. Numerical data and functional relationships in science and technology. Vol. 2. Magnetic properties of coordination and organometallic transition metal compounds. Springer Verlag, Berlin. 1966.
49. B. G. MÜLLER. Angew. Chem. Int. Ed. Engl. **26**, 1081 (1987).

Can. J. Chem. Downloaded from www.nrcresearchpress.com by 186.148.149.217 on 09/07/12
For personal use only.

One-pot synthesis of *N*-substituted-3-hydroxy-4-pyridinone chelate complexes of aluminum, gallium, and indium

ZAIHUI ZHANG, T. L. THOMAS HUI, AND CHRIS ORVIG[1]

Department of Chemistry, University of British Columbia, 2036 Main Mall, Vancouver, BC, Canada V6T 1Y6

Received January 24, 1989

This paper is dedicated to Professor Ronald J. Gillespie on the occasion of his 65th birthday

ZAIHUI ZHANG, T. L. THOMAS HUI, and CHRIS ORVIG. Can. J. Chem. **67**, 1708 (1989).

A series of tris(3-hydroxy-2-methyl-4-pyridinonato)metal(III) and tris(3-hydroxy-6-hydroxymethyl-4-pyridinonato)-metal(III) complexes have been prepared in water by one-pot synthesis directly from maltol and kojic acid, respectively, and the metal ion (M = Al, Ga, In) with an appropriate amine. The pyridinones have substituents at the ring nitrogen atom (CH_3, C_2H_5). The tris(3-hydroxy-4-pyronato)metal(III) complexes are formed *in situ* and these undergo nucleophilic attack by the primary amine; the appropriate tris(3-hydroxy-4-pyridinonato)metal(III) complexes are obtained. This method bypasses the sequential syntheses of ligand and metal complex, and has improved the yields of the tris(ligand)metal complexes, in particular by making them much more easily accessible. The electronic effects of binding the pyrone to the metal ions and of the substituents on the pyrone ring on the reactivity are discussed.

Key words: 3-hydroxy-4 pyridinone complexes, group 13 metal ions, one-pot synthesis.

ZAIHUI ZHANG, T. L. THOMAS HUI et CHRIS ORVIG. Can. J. Chem. **67**, 1708 (1989).

Utilisant des réactions de type «pot au feu» impliquant respectivement du maltol et de l'acide kojique, l'ion métallique (M = Al, Ga et In) et une amine appropriée, on a préparé une série de complexes tris(hydroxy-3 hydroxyméthyl-6 pyridinato-4)métal(III) dans l'eau. Les pyridinones portent des substituants sur l'atome d'azote du cycle (CH_3, C_2H_5). Les complexes tris(hydroxy-3 pyronato-4)métal(III) se forment *in situ* et ceux-ci subissent une attaque nucléophile par l'amine primaire; on obtient les complexes tris(hydroxy-3 pyridinonato-4(métal(III) appropriés. La méthode évite de passer par les synthèses en série du ligand et du complexe et conduit à de meilleurs rendements des complexes tris(ligand)métal, en particulier en les rendant beaucoup plus accessibles. On discute de l'influence que les effets électroniques de la liaison de la pyrone aux ions métalliques et des substituants présents sur le cycle pyrone peuvent avoir sur la réactivité.

Mots clés : complexes hydroxy-3 pyridinone-4, ions métallique du groupe 13, synthèse de type « pot au feu ».

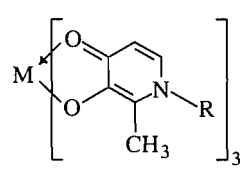
[Traduit par la revue]

Introduction

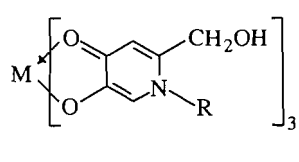
Group IIIA (13) metal complexes of certain 3-hydroxy-4-pyrones and *N*-substituted-3-hydroxy-4-pyridinones are neutral, water-soluble, and lipophilic (1–5). The pyridinone complexes are thermodynamically stable (overall formation constants β_3 of 10^{32} to 10^{37}) and they strongly resist hydrolysis because the tris(ligand) species predominate between pH 4 and pH 9 (6, 7). Burgeoning interest in the bioinorganic chemistry of Al, Ga, and In has necessitated the investigation of compounds of these elements (such as those with the *N*-substituted-3-hydroxy-4-pyridinone ligands) that are soluble and stable under physiological conditions (6).[2]

The syntheses of these complexes have been reported previously (2, 4, 5); however, in these reports the metal complexes were prepared from the ligands, which were synthesized separately in other work (9). It has become obvious that the development of simple methods to synthesize the pyridinone ligand complexes is of considerable importance. 3-Hydroxy-4-pyridinones are usually prepared by amination of the analogous 3-hydroxy-4-pyrone (5, 9–16). Two common methods have been used to achieve this conversion process. The oldest method uses methyl-, benzyl-, or glucosyl-protected pyrones (9–15) as the precursors; recently, in a second procedure, workers have found that the hydroxypyrone can be converted directly (5, 16). Three steps are involved in the former method: protection of the ring hydroxyl group with methyl, benzyl, or glucosyl groups, conversion via the amine insertion reaction, and deprotection to give the pyridinone. The multistep reactions are, of course, time consuming and rigorous. Control of the pH is vital to success with the second method (5). A suitable and more general method was sought that would allow the direct preparation of tris(3-hydroxy-4-pyridinonato)metal(III) complexes; this is reported here.

Reactions of ligands coordinated to metal ions have been used frequently in the synthesis of organic compounds and, more frequently, in the preparation of their metal complexes (17–21). The preparation of macrocyclic metal complexes in high yield via the metal template effect is but one application of reactions of coordinated ligands. This knowledge of previous work on the reactions of coordinated ligands stimulated an interest in prepared tris(3-hydroxy-4-pyridinonato)metal(III) complexes by this simple route. We report the one-pot synthesis of group IIIA (complexes **1** and **2** pyridinones derived from maltol (3-hydroxy-2-methyl-4-pyrone) and kojic acid (5-hydroxy-2-hydroxymethyl-4-pyrone), respectively.



1



2

Experimental

Materials and methods

The materials used were as previously detailed (3, 9); maltol (Aldrich) and kojic acid (Sigma) were used as received. ^{1}H NMR spectra were recorded with a Bruker WH-80; infrared spectra were obtained on a Perkin–Elmer PE 783 spectrometer and were referenced to polystyrene. Characterization of the products was accomplished by

[1]Author to whom correspondence may be addressed.

[2]Also, D. R. McLachlan. Work in progress.

Can. J. Chem. Downloaded from www.nrcresearchpress.com by 186.148.149.217 on 09/07/12
For personal use only.

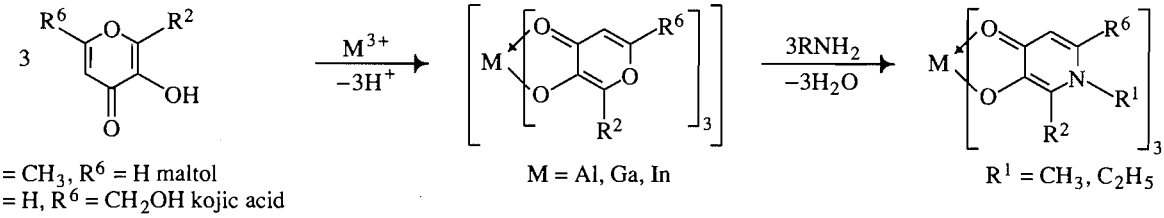


FIG. 1. Scheme for the one-pot synthesis of tris(3-hydroxy-4-pyridinonato)metal(III) complexes.

comparing infrared and ^1H NMR spectral data with those for authentic samples prepared by literature methods (2, 4, 5),[3] as well as by elemental analysis where necessary. Representative preparative details are given below and yields are presented in Table 1.

Tris(3-hydroxy-1,2-dimethyl-4-pyridinonato)aluminum(III), Al(dpp)$_3$

Maltol (2.51 g, 19.9 mmol) and $AlCl_3 \cdot 6H_2O$ (1.64 g, 6.8 mmol) were dissolved in 25 mL distilled deionized water, and methylamine (40% aqueous, 25 mL) was added. The pH of this solution was adjusted to 11.0 and the reaction mixture was transferred to a 100-mL flask in which it was refluxed for 6.5 h. The excess amine was removed under reduced pressure and the volume of the solution was reduced to 5 mL. The solution was stored in the refrigerator overnight; the light pink crystals that formed were collected by filtration and recrystallized in hot water. The recrystallized product was dried *in vacuo*, giving 2.63 g of product (90% yield based on maltol).

Tris(6-hydroxymethyl-3-hydroxy-1-methyl-4-pyridinonato)-aluminum(III), Al(hmp)$_3$

Kojic acid (1.98 g, 13.9 mmol) was dissolved in 60 mL distilled deionized water, and methylamine (40% aqueous, 10.8 mL) was added. $AlCl_3 \cdot 6H_2O$ (1.05 g, 4.35 mmol) was then added to this solution. The pH was adjusted to 11.0 and monitored regularly during 2 days of refluxing. The reaction mixture was subsequently cooled to room temperature, its volume was reduced *in vacuo*, and it was then cooled in the refrigerator overnight. A yellowish solid precipitated from the solution; it was collected by filtration, recrystallized from hot water, and dried *in vacuo*, giving 1.27 g of product (57% based on Al).

Results and discussion

A series of *N*-substituted tris(3-hydroxy-4-pyridinonato)- and tris(6-hydroxymethyl-3-hydroxy-4-pyridinonato) complexes of aluminum(III), gallium(III), and indium(III) are prepared in good yield by the one-pot synthesis method from commercially available starting materials. In this preparation, the metal–pyrone complex is first formed *in situ* and then undergoes the insertion of the primary amine into the pyrone ring to form the appropriate 3-hydroxy-4-pyridinone complex under pH control. The general synthetic scheme is outlined in Fig. 1. Neither the metal–pyrone complexes nor the product ligands were isolated because the aim of this work is the *direct* preparation; however, the conditions are completely compatible with those used in their formation (3, 4).[3]

The accepted mechanism for the preparation of a 4-pyridinone by conversion of an appropriate 4-pyrone is nucleophilic attack by a primary amine, followed by ring opening, elimination of water, and ring closure to give the 4-pyridinone (23). The nucleophilic attack is an important step in this process. Any factor that affects the electron density on the pyrone ring (especially next to the in-ring oxygen atom at C2 or C6) influences the nucleophilic attack step and therefore the whole conversion reaction. The reactivity of the pyrone ring towards the entering nucleophile varies with the substituents on the ring as well. Electron-withdrawing groups should enhance the reactivity of the ring while electron-donating groups should have the opposite effect.

TABLE 1. The yields of tris(ligand)-metal(III) complexes via the one-pot synthesis reaction

	R^1	1	2
Al	CH_3	90	57
	C_2H_5	46	21
Ga	CH_3	85	49
	C_2H_5	61	32
In	CH_3	82	54
	C_2H_5	63	63

Complex formation between a trivalent metal and the pyrone enhances the reactivity of the coordinated pyrone in two ways. In the pyrone amination reaction, the charge localization on the ring plays a crucial role in determining the effectiveness of the reaction. Deprotonation of the hydroxyl group on the pyrone ring gives an anionic hydroxyl oxygen, which hinders the formation of the 4-pyrone reasonance hybrid most susceptible to nucleophilic attack. As well, protonation of the primary amine will stop the nucleophilic attack. Complexation of the hydroxyketone oxygen atom prevents the undesired deprotonation process; in addition, the metal ion causes polarization of the ligand through an electron-withdrawing effect. This phenomenon results in increased acidity of the coordinated ligands upon conjugation and the coordinated pyrone will be more susceptible to the nucleophilic attack than the uncoordinated pyrone. Conversion reactions of the coordinated pyrones to the appropriate pyridinones should be easier. Group IIIA(13) metals are strong Lewis acids and they form stable complexes with maltol and kojic acid (1, 3, 4, 24). They should strongly polarize the coordinated pyrone and make the nucleophilic attack by a primary amine much easier. The conditions of conversion reactions should then be improved and the yield of the tris-ligand complexes should be increased.

The results (Table 1) show that the yields of the complexes are quite reasonable by this one-pot synthesis method, verifying the hypotheses as outlined. The yields for the metal complexes **1** where $R^1 = CH_3$ compare very favorably with literature results for the ligand (51% in three steps via protection (9); 70% (5) or 50% (16) directly) followed by complex preparation (79% for Al, Ga (2)). For **1** ($R^1 = C_2H_5$), the one-pot synthesis compares less favorably (ligand, 58% (5, 8) or 24% (16) directly; complex >80% (5, 8)); however, the ease of the one-pot method is not factored into the yield results, naturally.

Maltol and kojic acid were compared to investigate the effect of different substituents on the pyrone ring. Substituents

[3]Also, T. L. T. Hui, Z. Zhang, and C. Orvig. Unpublished results.

Can. J. Chem. Downloaded from www.nrcresearchpress.com by 186.148.149.217 on 09/07/12
For personal use only.

influence the reactivity by changing the electron density on the pyrone ring and, consequently, the basicity of pyrones (22). Electron-donating groups, such as the methyl group on maltol, increase the electron density on the pyrone ring and hinder the nucleophilic attack while increasing the basicity of the pyrone. Accordingly, more stable complexes with metal ions are formed. Electron-withdrawing groups, like the hydroxymethyl group on kojic acid, decrease the electron density on the pyrone ring, facilitating nucleophilic attack. This decreased electron density decreases the basicity of the pyrone, however. That kojic acid ($pK_a = 7.6$) is a stronger acid than maltol ($pK_a = 8.4$ (22, 24) illustrates these arguments. These two effects are seen to compete during the reaction process. Upon complexation, the electron-withdrawing effect of the positively charged metal ions should be much more drastic than that of the ring substituents. The relative stability of the complexes would be important in determining which effect is dominating during the reaction. The more stable the complex, the more pronounced the effect on the electron density should be. Even though electron-donating groups could impede the nucleophilic attack process, the enhanced stability of the metal complexes would compensate for this negative effect. The conversion reaction would be easier for the electron-donating substituted pyrones than for the electron-withdrawing substituted ones. The results in Table 1 show that the conversion reaction of maltol is a higher yield process than that of kojic acid.

In conclusion, the one-pot synthesis of tris(3-hydroxy-4-pyridinonato)metal(III) has proven to be a useful example of the reaction of a coordinated pyrone, and its general applicability to all R^1N substituents is currently under study.

Acknowledgement

Acknowledgement is made to the British Columbia Health Care Research Foundation and the Natural Sciences and Engineering Research Council of Canada for operating grants. The authors also thank NSERC for a University Research Fellowship (C.O.) and an Undergraduate Student Research Award (T.L.T.H.), and U.B.C. for a University Graduate Fellowship (Z.Z.).

1. D. G. Tuck and M. K. Yang. J. Chem. Soc. A, 3100 (1971).
2. W. O. Nelson, T. B. Karpishin, S. J. Rettig, and C. Orvig. Inorg. Chem. **27**, 1045 (1988).
3. M. M. Finnegan, T. G. Lutz, W. O. Nelson, A. Smith, and C. Orvig. Inorg. Chem. **26**, 2171 (1987).
4. C. A. Matsuba, W. O. Nelson, S. J. Rettig, and C. Orvig. Inorg. Chem. **27**, 3935 (1988).
5. W. O. Nelson. Ph.D. Thesis, the University of British Columbia, 1988.
6. D. J. Clevette, D. M. Lyster, W. O. Nelson, T. Rihela, G. A. Webb, and C. Orvig. Inorg. Chem. Submitted.
7. D. J. Clevette, W. O. Nelson, A. Nordin, C. Orvig, and S. Sjöberg. Inorg. Chem. **28**, 2079 (1989).
8. W. O. Nelson, S. J. Rettig, and C. Orvig. Inorg. Chem. In press.
9. W. O. Nelson, T. B. Karpishin, S. J. Rettig, and C. Orvig. Can. J. Chem. **66**, 123 (1988).
10. A. Peratoner. Gazz. Chim. Ital. **36**, I, 52 (1906).
11. V. Ettel and J. Hebky. Collect Czech. Chem. Commun. **15**, 356 (1950); **15**, 639 (1950).
12. M. Yasue, N. Kawamura, and J. Sakakibara. Yakugaku Zasshi, **90**, 1222 (1970).
13. R. L. N. Harris. Aust. J. Chem. **29**, 1329 (1976).
14. J. H. Looker, R. J. Prokop, W. E. Serbousek, and M. D. Cliffton. J. Org. Chem. **44**, 3408 (1979).
15. J. H. Looker and M. D. Cliffton. J. Heterocycl. Chem. **23**, 5 (1986).
16. G. J. Kontoghiorghes and L. Sheppard. Inorg. Chim. Acta, **136**, L11 (1987).
17. L. F. Lindoy and D. H. Busch. Prep. Inorg. React. **6**, 1 (1971).
18. L. F. Lindoy. Chem. Soc. Rev. **4**, 421 (1975).
19. M. De S. Healy and A. J. Rest. Adv. Inorg. Chem. Radiochem. **21**, 1 (1978).
20. D. H. Busch. Acc. Chem. Res. **11**, 392 (1978).
21. D. St C. Black. *In* Comprehensive coordination chemistry. Vol. 1. *Edited by* G. Wilkinson, R. D. Gillard, and J. A. McCleverty. Pergamon, Oxford. 1987. pp. 415–462.
22. G. Choux and R. L. Benoit. J. Org. Chem. **32**, 3974 (1967).
23. M. A-F. Elkaschef and M. H. Nosseir. J. Am. Chem. Soc. **82**, 4344 (1960).
24. T. Hedlund and L.-O. Öhman. Acta. Chem. Scand. Ser. A: **A42**, 702 (1988).

Can. J. Chem. Downloaded from www.nrcresearchpress.com by 186.148.149.217 on 09/07/12
For personal use only.

Bis(tertiary amine)dihaloboron cations and related species: nuclear magnetic resonance and fast atom bombardment mass spectrometry studies

MELVIN J. FARQUHARSON AND J. STEPHEN HARTMAN[1]

Department of Chemistry, Brock University, St. Catharines, Ont., Canada L2S 3A1

Received January 31, 1989

This paper is dedicated to Professor Ronald J. Gillespie on the occasion of his 65th birthday

MELVIN J. FARQUHARSON and J. STEPHEN HARTMAN. Can. J. Chem. **67**, 1711 (1989).

The formation of four-coordinate haloboron cations from aliphatic tertiary amine adducts of the mixed boron trihalides by heavy halogen displacement has been systematically studied by ^{19}F and ^{11}B nuclear magnetic resonance and positive ion fast atom bombardment mass spectrometry (FAB). Low-steric-hindrance donor molecules readily displace bromide ion from tertiary amine – bromodifluoroborane adducts, $D \cdot BF_2Br$, to form difluoroboron cations $D_2BF_2^+$ and $DD'BF_2^+$, but the corresponding dibromofluoroborane and tribromoborane adducts are highly resistant to bromide ion displacement. Bis(tertiary amine)dichloroboron and -chloroiodoboron cations can be obtained by selective iodide displacement from $D \cdot BCl_2I$ and $D \cdot BClI_2$. Fast atom bombardment mass spectrometry selectively detects the haloboron cations in preference to the neutral adducts in mixtures, and is a valuable complement to nmr in monitoring formation of the haloboron cations as well as any ionic by-products.

Key words: difluoroboron cations, dihaloboron cations, NMR, ^{11}B, ^{19}F, fast atom bombardment (FAB), ligand substitution, redistribution reactions.

MELVIN J. FARQUHARSON et J. STEPHEN HARTMAN. Can. J. Chem. **67**, 1711 (1989).

Faisant appel à la résonance magnétique nucléaire du ^{19}F et du ^{11}B ainsi qu'à la spectrométrie de masse des ions positifs par bombardement avec des atomes rapides (FAB), on a étudié d'une façon systématique la formation des cations halogénobores tétra-coordonnés à partir d'adduits d'amines tertiaires aliphatiques sur des trihalogénures mixtes du bore par déplacement des halogènes lourds. Des molécules de faible empêchement stérique pouvant agir comme donneur déplacant facilement l'ion brome d'adduits amine tertiaire – bromodifluoroborane, $D \cdot BF_2Br$, pour conduire à la formation de cations difluorobore, $D_2BF_2^+$ et $DD'BF_2^+$; toutefois, les adduits correspondants du dibromofluoroborane et tribromoborane sont très résistants à tous déplacements de l'ion bromure. On peut obtenir les cations bis(amine tertiaire) dichlorobore et chloroiodobore par déplacement sélectif de l'iodure des composés $D \cdot BCl_2I$ et $D \cdot BClI_2$. La spectrométrie de masse par bombardement avec des atomes rapides détecte les cations halogénobores d'une façon sélective par rapport aux adduits neutres présents dans les mélanges; cette méthode s'avère utile comme complément à la rmn pour détecter la formation des cations halogénobores ainsi que de leurs sous-produits ioniques.

Mots clés : cations difluorobores, cations dihalogénobores, RMN, ^{11}B, ^{19}F, bombardement avec des atomes rapides (FAB), substitution de ligands, réactions de redistribution.

[Traduit par la revue]

Introduction

Following original studies in Gillespie's laboratory (1), halogen redistribution about four-coordinate boron has been under study in this laboratory since 1968, and has been shown to give rise to mixed boron trihalide adducts (2, 3) and mixed tetrahaloborate anions (4). Rates and equilibria of halogen redistribution are highly dependent on the donor ligand and the halogen atoms present. It is well known that boron–halogen bond strengths decrease in the order $F \gg Cl > Br > I$ (5), and thus not surprising that boron–halogen bonds involving the heaviest halogens are the most easily displaced. However, one intriguing observation from our earlier studies is that the presence of fluorine on the same boron atom makes heavier halogens far more labile than they would otherwise be (3, 4). The effect is increased as more fluorines are present, and the BF_3X^- ions (X = Cl and especially Br) are particularly susceptible to rapid chemical exchange involving breaking and re-forming of the boron – heavy halogen bond (4).

The effect of fluorine in selectively labilizing boron – heavy halogen bonds provides a systematic route to formation of fluoroboron cations by displacement of heavy halide ion from mixed boron trihalide adducts of tertiary amines by neutral donors:

[1] $D \cdot BF_2X + D' \longrightarrow DD'BF_2^+ + X^-$

[2] $D \cdot BFX_2 + D' \longrightarrow DD'BFX^+ + X^-$

$\downarrow D'$

$DD'_2BF^{2+} + X^-$

In a preliminary report (6) we noted that reaction [1] occurs readily, provided that D' is a tertiary amine of sufficiently low steric hindrance, and that the reactions [2] do not occur to any appreciable extent under the same conditions. We now report our detailed studies of these systems.

Cationic boron species are a topic of current interest and a number of 3-coordinate and even 2-coordinate (7) boron cations have been reported in recent years (8), as have polyboron complex cations (9). Tetrahedral four-coordinate boron cations $D_2BH_2^+ \cdot X^-$ (where D represents the donor ligand) are well known (10), but relatively few fluoroboron cations have been reported. Hydrogen substitution in already formed $D_2BH_2^+$ gives a range of products, but the use of elemental fluorine is required to obtain difluoroboron cations by this route (11). A few chelating ligands LL give $(LL)BF_2^+ \cdot BF_4^-$ directly on reaction with BF_3 (12), but others do not (13). In solution, tetramethylurea$\cdot BF_3$ and hexamethylphosphoramide$\cdot BF_3$ are in equilibrium with a small proportion of the ionic

[1]Author to whom correspondence may be addressed.

Can. J. Chem. Downloaded from www.nrcresearchpress.com by 186.148.149.217 on 09/07/12
For personal use only.

Can. J. Chem. Downloaded from www.nrcresearchpress.com by 186.148.149.217 on 09/07/12
For personal use only.

form of the adduct $D_2BF_2^+ \cdot BF_4^-$ (14), but few BF_3 adducts behave in this way.

Experimental

Materials

Moisture-sensitive materials were normally handled under dry nitrogen using glove bag and Schlenk line methods. Boron trifluoride and boron trichloride (Matheson) were used directly from lecture bottles with no further purification. Boron tribromide (Alfa Inorganics) was treated with metallic mercury to remove bromine (orange discoloration), and trap-to-trap distilled into glass ampoules. The sealed ampoules, containing 0.5–3 mL of colorless liquid, were stored in the dark. Boron triiodide (Alfa Inorganics) was used without further purification; some iodine (pink discoloration) was evident. Solutions (0.5–2.5 M) of boron tribromide and boron triiodide were prepared in solvents such as $CDCl_3$ and stored at temperatures below −20°C to minimize decomposition.

Quinuclidine (Aldrich) was recrystallized from acetone. Me_3N (Matheson), Me_2NEt, $MeNEt_2$, and *i*-Pr_2NEt (Aldrich), Et_3N (British Drug Houses), and *n*-Pr_3N (Eastman) were used as supplied, as were a number of other reagent grade Lewis bases. Pyridine and 2-methylpyridine were stored over NaOH following fractional distillation. Methyl benzoate (Eastman), $(Me_2N)_3P{=}O$ (Aldrich), and $(Me_2N)_3P$ (BDH) were distilled before use. Deuterated chloroform (Norell) and reagent grade chloroform (BDH) were stored over Linde 4A molecular sieves before use. Methylene chloride (BDH), 1,1,2,2-tetrachloroethane (Eastman), and methylene bromide (BDH) were purified by fractional distillation and stored over Linde 13X molecular sieves, Linde 4A molecular sieves, and in the dark, respectively. Reagent grade 1,1,2,2-tetrabromoethane (BDH) was used without further purification. Hexane was dried over sodium wire.

Hexafluorobenzene (Whittaker) was used without further purification as an internal secondary ^{19}F reference. $BF_3 \cdot OEt_2$, the external primary ^{11}B reference, was prepared by reaction of BF_3 with diethyl ether and fractional distillation of the liquid adduct.

Amine – boron trihalide adducts

BF_3 or BCl_3 gas was bubbled through a mechanically stirred 0.3 M solution of the amine in dry hexane, while cooling in an ice bath and maintaining positive nitrogen pressure. The adduct precipitated from the hexane solvent, and normally the solvent was removed using syringe/septum methods. Fine precipitates that formed an emulsion-like slurry were separated using a Schlenk vessel containing a fritted glass filter. The precipitated adducts, many of which are very hygroscopic, were washed twice with dry hexane and stored under nitrogen.

In a few cases oils were obtained instead of precipitates of BF_3 adducts. Lowering the donor concentration and slowing the rate of Lewis acid addition eliminated most, but not all, oiling problems. The few oils that could not be crystallized were subjected to vacuum to remove traces of hexane. The ^{19}F nmr spectra of the oils indicated a small proportion of BF_4^- impurity. Reactions initiated with the oils were not noticeably different from those using BF_3 adducts that were crystalline white precipitates.

Difluoroboron cation formation in solution

The preparation of difluoroboron cations requires $D \cdot BF_2X$ intermediates, which form readily by halogen redistribution between $D \cdot BF_3$ (or $D \cdot BCl_3$) and an uncomplexed boron trihalide BX_3. Equilibration at room temperature for 30 min of a mixture of 0.5–1.0 M solutions of $D \cdot BF_3$ adducts with 0.5–2.5 M BX_3 (X = Br or I), both in $CDCl_3$, gave equilibrated mixtures containing all of the possible $D \cdot BF_nX_{3-n}$ and BF_nX_{3-n} (n = 0–3) species (2). To maximize the proportion of the $D \cdot BF_2Br$ adduct relative to the other adducts in the $D \cdot BF_3 + BBr_3$ system, about 0.5 mmol of BBr_3 should be added per mmol of $D \cdot BF_3$. $D \cdot BF_nCl_{3-n}$ adducts were formed by direct addition of gaseous boron trichloride to solutions containing $D \cdot BF_3$.

Reaction occurs similarly in other chlorinated and brominated solvents, but lower solubility and (or) greater ease of decomposition can be problems. Chlorinated solvents (chloroform, methylene chloride, and 1,1,2,2-tetrachloroethane) give adequate adduct solubility but allow Cl/Br exchange. Brominated solvents eliminate this problem but generate others. Decomposition occurs readily in methylene bromide. Adduct solubilities are low in 1,1,2,2-tetrabromoethane. Bromoform is a fairly good solvent and its use should be further explored. Typically though, fluoroboron cation formation reactions that do not succeed in chloroform also do not succeed in bromoform. Although solubilities are low in toluene, difluoroboron cations do form and may precipitate, facilitating isolation as their bromide salts. Elimination of solvent, i.e., placing $D \cdot BF_nBr_{3-n}$ adducts directly in liquid amines (e.g., Me_2NEt) was ineffective.

The solutions of mixed boron trihalide adducts plus uncomplexed Lewis acids were transferred to 5-mm nmr tubes and cooled to 0°C or below, and uncomplexed donor was added by syringe. Initially the donor quenches the rapid halogen exchange reactions by complexation with the uncomplexed boron trihalide, as can be monitored by ^{19}F nmr. Further donor (which can be either the same species D or a different Lewis base D′) may attack the $D \cdot BF_2X$ species, displacing X^- to form a cation of type $D_2BF_2^+$ or $DD'BF_2^+$.

Most halide displacement reactions were carried out directly in nmr tubes at temperatures up to 100°C using a constant temperature oil bath. Typically the tubes were capped and wrapped with Parafilm rather than sealed, so temperatures above 70°C required solvents of higher boiling point than $CDCl_3$, such as $CHBr_3$ or toluene. Stronger heating of a few samples of $D \cdot BF_nBr_{3-n}$ systems in $CHBr_3$, sealed in medium-wall nmr tubes, was also carried out; in these the reactions occur at pressures considerably greater than atmospheric. Reaction with water can cause major contamination if capped nmr tubes are allowed to stand over long periods of time. This gives rise to $DH^+ \cdot X^-$ (X = Cl, Br, BF_4), which is readily detected by FAB peaks corresponding to D_2H^+, $(DH)_2X^+$, and sometimes $(D_2BF_2)(DH)X^+$.

Where the initial donor D in the $D \cdot BF_nX_{3-n}$ adducts and the further donor added are not the same species, mixed boron trihalide adducts of the second donor D′ are also formed. To minimize these, the solutions containing $D \cdot BF_nX_{3-n}$ and BF_nX_{3-n} were reacted with sufficient of the initial donor to complex with most of the free boron trihalide. Therefore little of the second donor is consumed by reaction with uncomplexed boron trihalides, and almost all is available to displace heavy halide ion.

Isolation of $D_2BF_2^+$ salts

Precipitation conditions differ considerably for each type of $D_2BF_2^+$ and counterion. The best procedures follow. The "mother solution" referred to is the solution (normally in $CHCl_3$ solvent) containing the difluoroboron cation and the various boron trihalide adducts. To determine the amounts of precipitating reagents required, the amounts of difluoroboron cation present were determined from ^{19}F nmr peak areas. Elemental analyses for carbon, hydrogen, and nitrogen were consistently satisfactory but those for fluorine were erratic, some being satisfactory and others being in error by several percent, perhaps due to interference by boron. Only the satisfactory fluorine analyses are given.

(Quinuclidine)$_2BF_2 \cdot Br$

Method A: Extraction of the mother solution with water removed the ionic species, leaving the covalent adducts behind. The water was removed under vacuum and the residue of crude $Q_2BF_2 \cdot Br$ redissolved in chloroform. Benzene was slowly added down the wall of a narrow tube, so that two layers of solvent were present. Slow diffusion of benzene into chloroform led to crystallization of the salt, which is stable in water, ethanol, and dimethylformamide.

Method B: Hexane or petroleum ether was added to the mother solution to precipitate all the adducts as well as the ionic species. In most cases an oil rather than a solid precipitate formed. This was separated and residual solvent removed under vacuum, leaving a solid residue that was dissolved in absolute ethanol by gentle heating. Cooling to below 0°C led to precipitation of $Q_2BF_2 \cdot Br$, while the covalent adducts remained in solution. A second recrystallization in absolute ethanol was then carried out.

(Quinuclidine)$_2BF_2 \cdot BPh_4$

The mother solution was diluted with an equal volume of absolute ethanol, and 1.5 equivalents of $NaBPh_4$ in a saturated solution

Can. J. Chem. Downloaded from www.nrcresearchpress.com by 186.148.149.217 on 09/07/12
For personal use only.

in ethanol were slowly added while vigorously stirring. White $Q_2BF_2 \cdot BPh_4$ precipitated immediately. The precipitate was filtered, washed with water to remove sodium salts, washed with chloroform to remove adducts and excess donor, and recrystallized from 1:1 acetone/ethanol. *Anal.* calcd.: C 77.38, H 7.86, N 4.75, F 6.44; found: C 77.21, H 8.19, N 4.82, F 6.72.

(Quinuclidine)$_2BF_2 \cdot PF_6$

The mother solution was evaporated to dryness under vacuum. Water was added, and the residue not dissolving at 50°C was removed by filtration. To the filtrate was added 1.5 equivalents of $NH_4 \cdot PF_6$ as a saturated aqueous solution. White $Q_2BF_2 \cdot PF_6$ precipitated immediately. The precipitate was recrystallized from 1:1 acetone/water by allowing the acetone to evaporate on standing. *Anal.* calcd.: C 40.41, H 6.30, N 6.73, F 36.53; found: C 40.65, H 6.27, N 6.60, F 36.90.

(Quinuclidine)$_2BF_2 \cdot BF_4$

Shaking the mother solution with two portions of saturated aqueous NH_4BF_4, followed by addition of hexane in a 1:1 ratio, precipitated the compound, which was recrystallized from 1:1 chloroform/hexane. *Anal.* calcd.: C 46.97, H 7.32, N 7.83; found: C 47.10, H 7.39, N 8.07.

$(Me_3N)_2BF_2 \cdot Br$

The mother solution was diluted with an equal volume of toluene and cooled to 0°C. The white $(Me_3N)_2BF_2 \cdot Br$ that precipitated was filtered and washed with toluene. $Me_3N \cdot BF_3$ was a minor contaminant in this precipitate; it was removed by dissolution in chloroform, followed by reprecipitation by addition of toluene. This salt is extremely hygroscopic, and is slowly decomposed by ethanol. It has not been obtained pure. *Anal.* calcd.: C 29.18, H 7.38, N 11.34, Br 32.36; found: C 27.47, H 7.31, N 10.84, Br 34.10.

$(Me_3N)_2BF_2 \cdot BPh_4$

The bromide salt described above was dissolved in CH_3CN, and 1.5 equivalents of $NaBPh_4$, as a saturated solution in CH_3CN, was then added. The resulting white precipitate was washed with toluene. The salt is soluble in water and insoluble in CH_3CN, acetone, and toluene.

$(Me_3N)_2BF_2 \cdot PF_6$

The isolation technique was identical to that for $Q_2BF_2 \cdot PF_6$. *Anal.* calcd.: C 28.10, H 5.81, N 8.98; found: C 28.16, H 5.76, N 8.76.

$(Me_2NEt)_2BF_2 \cdot BPh_4$

The isolation technique was identical to that for $Q_2BF_2 \cdot BPh_4$. *Anal.* calcd.: C 74.58, H 8.22, N 5.44, F 7.57; found: C 75.33, H 8.69, N 5.33, F 8.80.

Chloroboron cations

The formation of the non-fluorine-containing boron cations $D_2BCl_2^+$ and D_2BClI^+ as their I^- salts from $D \cdot BCl_3$ adducts (D = trimethylamine, quinuclidine) and BI_3 was carried out in methylene chloride solvent, by a procedure essentially identical to that described above. Iodide ion displacement is less favoured in $D \cdot BClI_2$ than in $D \cdot BCl_2I$. Salts of these cations have not yet been isolated in pure form.

Nuclear magnetic resonance instrumentation

^{19}F spectra were obtained at 56.45 MHz on a Bruker WP-60 FT nmr spectrometer, using a fixed frequency probe and quadrature detection. Typically a spectral width of 3800 Hz with a 1.08-s acquisition time was used to obtain an 8K FID. Fifty to 2000 scans were accumulated using 30° pulses and the PAPS sequence, and transformed using 0.5-Hz line broadening into 4K spectra. ^{19}F chemical shifts are accurate to ±0.1 ppm and were internally referenced to C_6F_6 as a secondary standard (−162.7 ppm from $CFCl_3$). $^{11}B-^{19}F$ coupling constants are accurate to within ±1 Hz. Most spectra were obtained at ambient temperature.

^{11}B spectra were obtained from three instruments, but primarily from a Bruker WH-400 multinuclear Fourier Transform nmr spectrometer operating at 128.38 MHz. A spectral width of 10 000 Hz was used to obtain an 8K FID. The FIDs with 8K of zero filling were transformed with 0.5 Hz of line broadening into 8K spectra. ^{11}B chemical shifts are accurate to ±0.1 ppm and were referenced to external $Et_2O \cdot BF_3$. ^{11}B spectra were also obtained on the WP-60 FT instrument operating at 19.25 MHz, using a fixed-frequency probe. However, peak overlap, especially of multiplets due to coupling to ^{19}F, made interpretation difficult. A Bruker CXP-200 instrument operating at 64.27 MHz gave intermediate chemical shift dispersion, so that most multiplets were distinguishable. 8K FIDs were accumulated by 200–1000 30° pulses covering a 5000-Hz range. These were transformed with 8K of zero filling and 0–1 Hz of line broadening into 8K spectra. The ^{27}Al nmr spectra were obtained at 104.18 MHz on the Bruker WH-400 instrument.

"Pairwise interaction" parameters (15, 16) for chemical shifts and coupling constants were calculated on a Burroughs B7900 computer, using a least-squares fitting program written by J. M. Miller and modified by A. G. Basile. The pairwise parameters were calculated from a data set including all available nmr data for boron trihalide adducts and haloboron cations involving only Q, Me_3N, pyridine, and 2-methylpyridine as donors, and the tetrahaloborate anions. The halogen,halogen and Me_3N,halogen pairwise terms ($\eta_{i,j}$) calculated from this data set are very similar to those reported previously (16). Chemical shifts calculated from the pairwise interaction parameters agreed well with experimental values, and were helpful in assigning haloboron cation resonances.

Fast atom bombardment mass spectrometry (17)

FAB analyses were carried out on an AEI MS-30 (Kratos Ltd., Manchester, U.K.) mass spectrometer fitted with a saddle field atom gun (Ion Tech Ltd.) and a Kratos FAB source with a rear entry probe. Samples were run at 4-kV accelerating voltage, 1000 resolving power, xenon gas (7–8 kV energy), and using glycerol as a matrix. Data were stored and worked up on a DS-55 Kratos data system. Spectra and mass intensity data were plotted on a Hewlett–Packard 2631G printer. Each spectrum is an average of five or more scans. Subtraction of peaks due to glycerol was automatically done for all spectra except where these peaks were of minimal intensity. The BMASROS program, written by D. Rosenburg and modified by D. Hoskins, J. M. Miller, and T. R. B. Jones to run on the Kratos, was utilized for calculation of isotope cluster patterns.

Results

(Quinuclidine)$_2BF_2^+$: reactions of $Q \cdot BF_nX_{3-n}$ (X = Cl, Br, I)

$Q \cdot BF_2Br$ (Q = quinuclidine, 1-azabicyclo[2.2.2]octane]), incorporating a low steric hindrance donor of high basicity, undergoes reaction [1] with no major side reactions, and was chosen for detailed study. Figure 1 shows ^{11}B nmr spectra of a $CDCl_3$ solution of the $Q \cdot BF_nBr_{3-n}$ (n = 0–3) adducts in the presence of excess Q. At ambient temperature or above, the 1:2:1 triplet of $Q \cdot BF_2Br$ disappears and is replaced by a new triplet assigned to $Q_2BF_2^+$. The total peak area of these two triplets remains constant as one grows at the expense of the other, and the multiplets of the other adducts remain unaffected. In the ^{19}F spectrum (Fig. 2) a new 1:1:1:1 quartet at −161.5 ppm grows at the expense of the $Q \cdot BF_2Br$ quartet. $Q_2BF_2^+$ has been isolated as its bromide, tetraphenylborate, hexafluorophosphate, and tetrafluoroborate salts and is stable in water, ethanol, and dimethylformamide as well as in chloroform.

The positive ion Fast Atom Bombardment (FAB) mass spectrum of $Q_2BF_2^+Br^-$, obtained in a glycerol matrix, is shown in Fig. 3. Its high-abundance peaks at m/z 271 ($Q_2BF_2^+$), 160 ($Q \cdot BF_2^+$), 112 (QH^+), and 111 (Q^+) confirm the difluoroboron cation structure. All other peaks are of much lower intensity. (Peaks at m/z greater than 280 in Fig. 3 are enhanced by a factor of ten.) Note the ion cluster peak at m/z 621, which corresponds to two cations and an anion. This was not readily detectable at lower ion current, such as was used to obtain the spectrum reported in our preliminary communication (6). Such peaks allow identification of the anion as well as the cation in positive ion FAB spectra of ionic compounds. The identity of the $Q_2BF_2^+$ and $[(Q_2BF_2)_2Br]^+$ peaks has been confirmed by analysis of these ions' isotope cluster patterns.

Attempts to form Q_2BFBr^+ and (or) Q_3BF^{2+} from $Q \cdot BFBr_2$

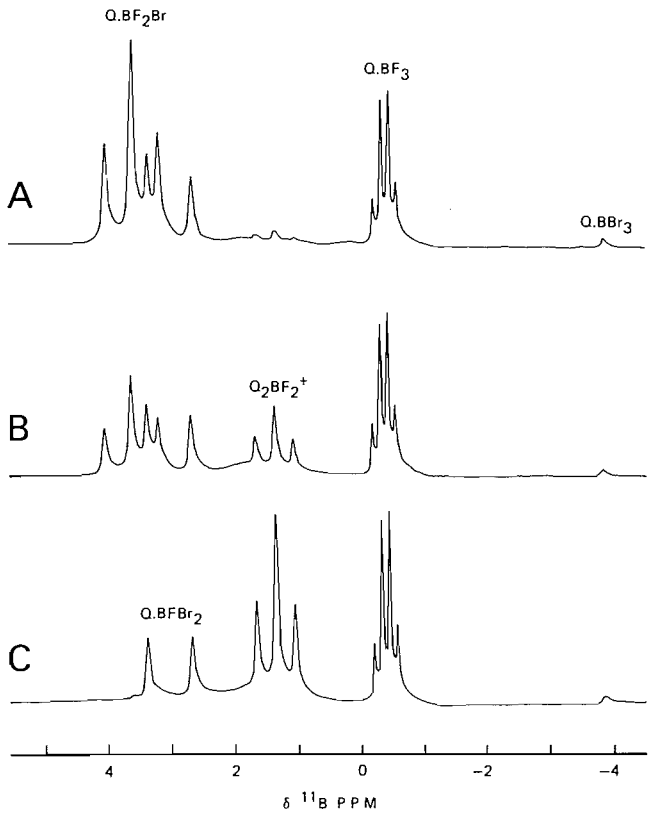


FIG. 1. 128.4 MHz ^{11}B nmr spectra of the quinuclidine·BF_nBr_{3-n} adduct system in $CDCl_3$. A, freshly prepared; B, after 14 min at 50°C; C, plus 18 h at 25°C.

according to eq. [2] have been unsuccessful under a range of conditions including large excess of quinuclidine, high temperatures, and (or) changing the solvent from chloroform to toluene or bromoform. In one sample that gave a broad ^{19}F impurity peak at −152 ppm after sufficient standing at 35°C to react all of the Q·BF_2Br (Fig. 4A), heating at 55°C for 3 days led to shrinkage of the Q·$BFBr_2$ ^{19}F quartet and appearance of Q·BFClBr and Q·BF_2Cl quartets and further unidentified broad peaks (Fig. 4B), as well as some precipitate formation. The Q·BF_3 and $Q_2BF_2^+$ signals remained essentially unchanged. Q·BFClBr no doubt arises from Cl/Br exchange with the solvent, but the source of Q·BF_2Cl is less clear; it could not arise from halogen exchange with Q·BF_2Br, which had long since been converted to $Q_2BF_2^+$, but might perhaps arise from attack of solvent-derived chloride on $Q_2BF_2^+$.

When water was added to the Q·BF_nBr_{3-n} system in $CDCl_3$, two broad unidentified peaks at −147 and −140 ppm and a BF_4^- peak appeared at the expense of Q·BF_2Br (Fig. 5). On further reaction the BF_4^- peak remained small while the broad peaks increased in intensity. Changes in chemical shift of these peaks between Figs. 5A and 5B may indicate a solvent shift due to extraction of the hydrolysis products into a minor water-rich phase. Although all B—Br bonds are highly susceptible to hydrolysis, water reacts selectively with Q·BF_2Br rather than with the other adducts (Fig. 5B).

Relative rates for halide ion displacement in Q·BF_2X in eq. [1] are I >> Br >> Cl. Less than 10% of Q·BF_2Cl reacts after a month at 48°C. The reactivity of Q·BF_2I is far greater than that of Q·BF_2Br but this species is difficult to obtain, due to the low yield of D·BF_2I (and D·BFI_2) in the halogen redistribution reaction of tertiary amine adducts D·BF_3 with BI_3, as a result of an unfavourable equilibrium (2, 3). Also, BI_3 adducts are less soluble. Neither of the mixed Q·BF_nI_{3-n} adducts could be observed by ^{19}F nmr in $CDCl_3$ solution, perhaps due to their small proportions and (or) rapid fluorine exchange among the adducts. The poor resolution of the Q·BF_3 peak was consistent with rapid fluorine exchange. After the addition of uncomplexed Q a small amount of $Q_2BF_2^+$ could be detected by ^{19}F nmr, providing indirect evidence for the intermediate existence of Q·BF_2I. With toluene as solvent it was possible to observe very low intensity ^{19}F signals for these adducts: Q·BF_2I, −119.8 ppm, J_{BF} 66.1 Hz; Q·BFI_2, −108.8 ppm, J_{BF} 114.3 Hz, consistent with nmr parameters of other tertiary amine·BF_nI_{3-n} adducts (2). Bromide displacement from R_3N·BF_2Br is clearly the most suitable route to difluoroboron cations containing aliphatic tertiary amines.

The high reactivity of D·BF_nI_{3-n} systems led to hopes for Q_2BFI^+ and (or) Q_3BF^{2+} formation from the reaction of Q·BFI_2 with excess Q (eq. [2]). Instead only a broad ^{19}F singlet at −152 ppm was observed (a frequently observed decomposition product; see Fig. 4) in addition to the $Q_2BF_2^+$ and Q·BF_3 quartets, and some precipitate appeared.

In attempts to facilitate formation of $Q_2BF_2^+$ or possibly the three-coordinate Q·BF_2^+ cation from Q·BF_2Br, Al_2Br_6 was added to extract bromide ion. Instead of cation formation this gave rapid Cl/Br exchange with the solvent, leading to all of the possible F,Cl,Br-containing boron trihalide adducts of quinuclidine. ^{11}B (Fig. 6A) and ^{19}F nmr peaks of Q·BF_2Br, Q·BF_2Cl, and Q·BF_3 were broad, indicative of rapid chemical exchange. These narrowed at temperatures below ambient, the Q·BF_2Cl peaks sharpening first, consistent with chemical exchange involving this species being slower than chemical exchange involving Q·BF_2Br. Addition of sufficient quinuclidine to complex with the Al_2Br_6 stopped the ambient-temperature chemical exchange and gave sharp ^{11}B (Fig. 6B) and ^{19}F peaks. The involvement of Al_2Br_6 in halogen exchange was confirmed by ^{27}Al nmr, which showed the presence of the known species $AlCl_2Br_2^-$ and $AlClBr_3^-$ in addition to $AlBr_4^-$ (18).

Other $(R_3N)_2BF_2^+$ species

In addition to Q, Me_3N and Me_2NEt are the only aliphatic tertiary amines that have formed $(R_3N)_2BF_2^+$ (i.e., both R_3N groups the same) from R_3N·BF_nBr_{3-n} under our conditions. The nmr parameters are given in Table 1. $(Me_3N)_2BF_2^+$ forms at ambient temperature somewhat more slowly than $Q_2BF_2^+$, whereas $(Me_2NEt)_2BF_2^+$ forms only on prolonged heating at 60°C. More sterically hindered systems (D = $MeNEt_2$, Et_3N, *n*-Pr_3N, *i*-Pr_2NEt) have undergone prolonged heating, in the presence of large excesses of the uncomplexed amine, to no avail. Instead, on heating, D·BF_2Br exchanges halogen with chlorinated solvents to form D·BF_2Cl, and D·$BFBr_2$ forms D·BFClBr. In brominated or non-halogenated solvents halogen exchange cannot give rise to chlorine-containing species, but solubility tends to be less, and no additional bis(tertiary amine)difluoroboron cations were formed. Tertiary amine·BF_nI_{3-n} systems, which have the potential to force difluoroboron cation formation in reluctant systems involving higher-steric-hindrance amines (2), are more difficult to work with and have not yet been studied systematically.

The behaviour of the (diisopropylethylamine)·BF_nBr_{3-n} system is unique. Immediately after addition of sufficient free amine to stop rapid halogen redistribution and allow well-resolved ^{19}F spectra, about half of both mixed-halogen adducts had already been converted to the chlorinated analogues.

Can. J. Chem. Downloaded from www.nrcresearchpress.com by 186.148.149.217 on 09/07/12
For personal use only.

Can. J. Chem. Downloaded from www.nrcresearchpress.com by 186.148.149.217 on 09/07/12
For personal use only.

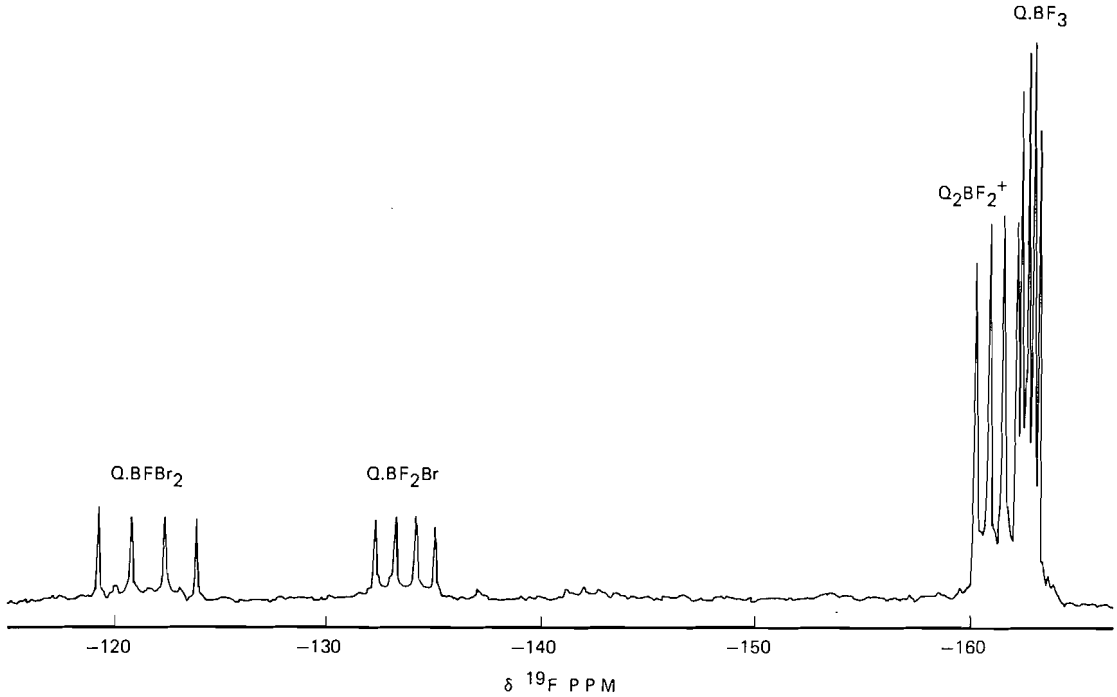


FIG. 2. 56.4 MHz ^{19}F nmr spectrum of the quinuclidine·BF_nBr_{3-n} adduct system in $CDCl_3$.

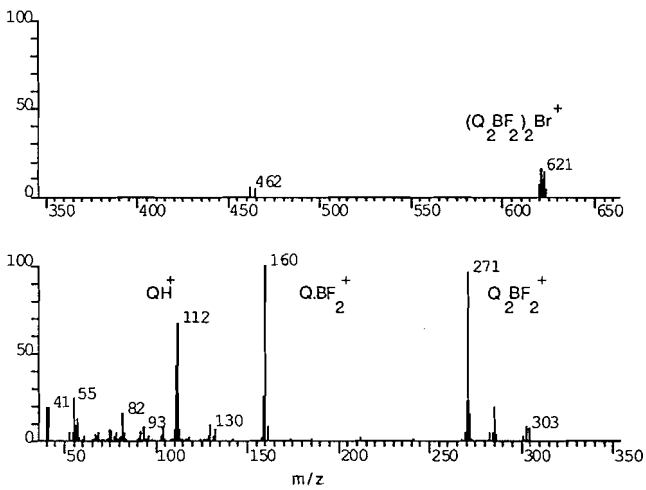


FIG. 3. Positive ion fast atom bombardment mass spectrum of $(quinuclidine)_2BF_2^+$. Peaks at m/z greater than 280 are enhanced by a factor of 10.

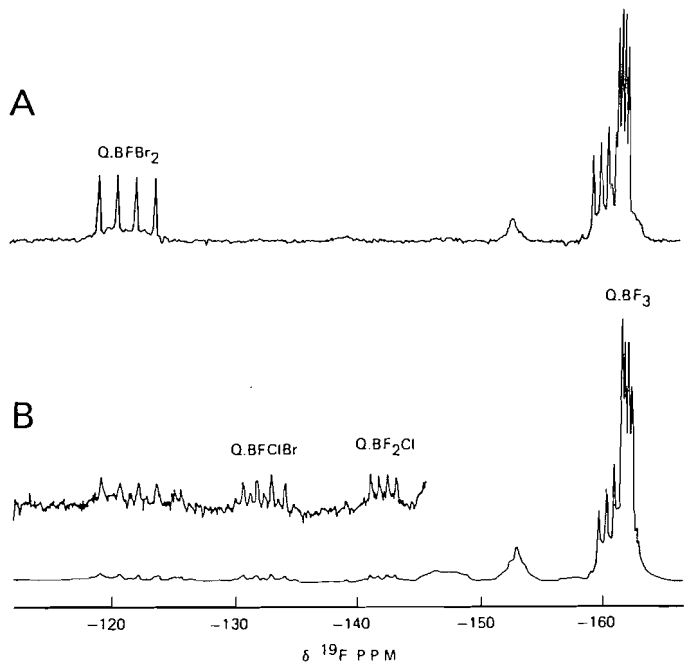


FIG. 4. 56.4 MHz ^{19}F spectra showing reaction of Q·$BFBr_2$ in $CDCl_3$ on prolonged heating. A, after complete reaction of Q·BF_2Br at 35°C; B, after 3 days at 55°C.

Anomalous behaviour of this adduct system has been attributed to very high amine steric hindrance (2).

$D_2BF_2^+$ formation by bromide displacement, when it occurs, normally goes essentially to completion if sufficient time is allowed. However, the reaction can be reversed under forcing conditions. Following completion of $(Me_2NEt)_2BF_2^+$ formation from $Me_2NEt·BF_2Br$ at 60°C in chloroform, the sample was heated to 160°C, evaporating solvent and excess Me_2NEt. Addition of fresh solvent gave a ^{19}F spectrum with no $D_2BF_2^+$ quartet and a large $D·BF_2Br$ quartet. This is consistent with Me_2NEt displacement from $(Me_2NEt)_2BF_2^+$ by bromide counterion and loss of the displaced Me_2NEt by volatilization at high temperature.

Non-fluorine-containing $D_2BX_2^+$ ions from $D·BCl_nI_{3-n}$ (D = Q, Me_3N)

$D·BCl_nBr_{3-n}$ adduct systems in chloroform and methylene chloride were unreactive to halide displacement by excess donor. No adduct ^{11}B nmr peaks changed in intensity, and no new peaks were evident, after 8 h at 30°C. In contrast, $D·BCl_nI_{3-n}$ systems (D = Q, Me_3N) underwent iodide displacement under these conditions, as shown by disappearance

Can. J. Chem. Downloaded from www.nrcresearchpress.com by 186.148.149.217 on 09/07/12
For personal use only.

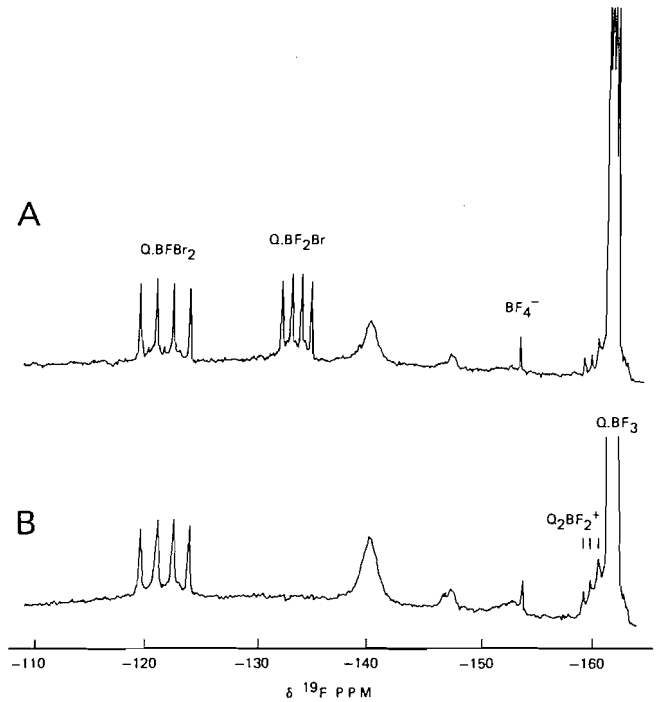


FIG. 5. 56.4 MHz ^{19}F nmr spectra of the $Q \cdot BF_nBr_{3-n}$ system in $CDCl_3$, in the presence of water. A, 30 min at 22°C; B, plus 7 h at 40°C.

of the ^{11}B signal of $D \cdot BCl_2I$ and the appearance of a new peak close to the $D \cdot BCl_3$ peak, which we assign to $D_2BCl_2^+$ (Fig. 7). Also a small singlet appeared, which we assign to D_2BClI^+. ^{11}B chemical shifts of the non-fluorinated bis(tertiary amine)haloboron cations and of the corresponding $D \cdot BCl_nI_{3-n}$ adducts are given in Table 2, along with values calculated from pairwise interaction nmr parameters (16) that support our assignments.

FAB spectra confirm the existence of the $D_2BCl_2^+$ ions but show that they are not the major ionic product. Figure 8 shows the FAB spectrum of material obtained from reaction of the $Me_3N \cdot BCl_nI_{3-n}$ adducts with excess Me_3N in methylene chloride. The assignment of the isotope cluster pattern at m/z 199 in Fig. 8 to $(Me_3N)_2BCl_2^+$ has been confirmed by calculation using the BMASROS program. However, the most intense peak in Fig. 8, at m/z 108, arises from $Me_3NCH_2Cl^+$ formed by Me_3N attack on the methylene chloride solvent. This is not too surprising in view of the extreme reactivity of systems containing B—I bonds, and emphasizes the value of FAB in identifying unexpected ionic products. Perhaps CH_2ClI, formed by halogen exchange, is an intermediate. Note the factor of 10 increases in the vertical scale of Fig. 8 above m/z 150; the dichloroboron cation parent-ion cluster has only about 5% of the intensity of the most abundant species. FAB also shows the presence of cluster ions (two cations and a chloride ion) of both $(Me_3N)_2BCl_2^+$ and $Me_3NCH_2Cl^+$, and the mixed cluster including both of these. (Note the further factor of two increase in vertical scale above m/z 300 in Fig. 8.) The counterion is chloride rather than iodide, consistent with the predominance of chloride displacement from solvent over iodide displacement from $Me_3N \cdot BCl_2I$. This predominance of a side reaction illustrates the difficulties of working with highly reactive BI_3-containing adduct systems, which often give precipitates on standing (2).

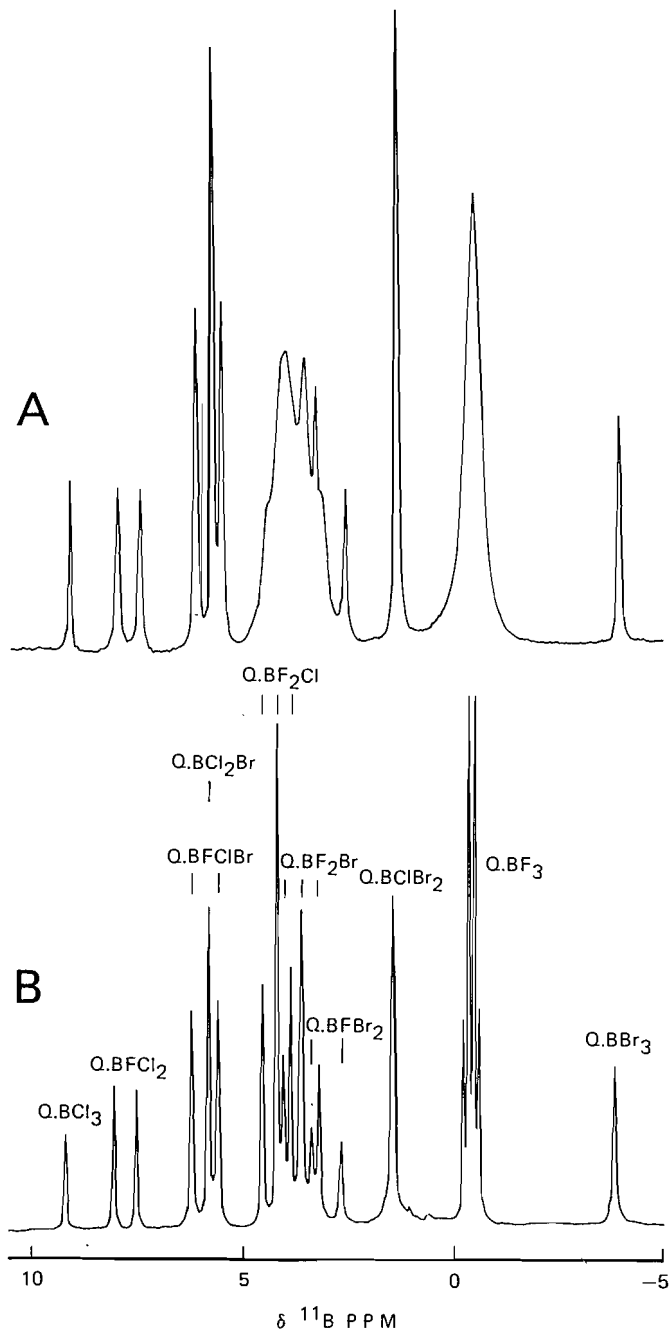


FIG. 6. 128.4 MHz ^{11}B nmr spectrum of $Q \cdot BF_nBr_{3-n}$ with Al_2Br_6 in $CDCl_3$, before (A) and after (B) addition of uncomplexed Q to react with the excess Lewis acid. Peaks of all the possible $Q \cdot B(F,Cl,Br)_3$ adducts are present.

Interestingly, D_2BClI^+ formed from $D \cdot BClI_2$ before all of the $D \cdot BCl_2I$ was converted into $D_2BCl_2^+$. Thus there is not as great a selectivity, for loss of the heaviest halogen from the adduct containing two of the lightest halogens, as occurs in the F/Br adducts. It may be possible to obtain D_3BCl^{2+} from D_2BClI^+ by further iodide displacement.

Attempts to prepare $D_2BBr_2^+$ species from $Q \cdot BBr_3$ were unsuccessful. Only the $Q \cdot BBr_3$ ^{11}B nmr peak could be detected after refluxing in toluene with an excess of either quinuclidine or trimethylamine. Perhaps $D_2BI_2^+$ cations could be obtained from $Q \cdot BI_3$ by this method.

Can. J. Chem. Downloaded from www.nrcresearchpress.com by 186.148.149.217 on 09/07/12
For personal use only.

TABLE 1. Nuclear magnetic resonance parameters of $(R_3N)_2BF_2^+$ and $(R_3N)D'BF_2^+$ cations[a]

Donors		Chemical shifts (ppm)[b]		
D	D'	^{19}F	^{11}B	$J_{^{11}B-^{19}F}$ (Hz)
Quinuclidine	Quinuclidine	−161.5	1.5	39.5
	Me_3N	−163.7	1.7	38.1
	Me_2NEt	−159.9	1.8	38.8
	$MeNEt_2$	−155.2	1.9	40.5
	Et_3N	−148.4	2.2	43.0
	n-Pr_3N	−149.3	2.1	42.3
	MeNEtBz[c]	−154.1		42
	Pyridine	−161.5	1.6	28.5
	2-Mepyr	−151.8	2.4	30.3
	2-Etpyr	−151.9	2.4	30.5
	2,4-Me_2pyr	−151.8	2.2	29.7
	3,5-Me_2pyr	−161.1	1.5	28.8
	4-Mepyr	−162.3	1.6	28.3
	4-Phpyr	−161.7	1.7	29.7
	Quinoline	−150.1		29.7
	TMU	−156.0	0.3	27.3
	MeBenzoate	−160.5	0.8	26.6
	DMAC	−156.8	0.7	24.8
	DMSO	−157.8	0.6	26.5
	HMPA	−156.4	−0.3	24.4
	Me_3PO	−156.2	0.0	26.3
	t-BuNC	−159.6	−1.8	38.1
	MeCN[c]	−162.1		29.6
Me_3N	Me_3N	−165.4	1.9	36.2
	Me_2NEt	−162.5	2.2	37.8
	$MeNEt_2$	−157.6	2.3	40.2
	Et_3N	−150.6	2.5	42.4
	n-Pr_3N	−150.2		41.9
	Pyridine	−162.5	2.0	28.5
	2-Mepyr	−152.8	2.4	31.2
	2,4-Me_2pyr	−153.7	2.4	30.3
	3,5-Me_2pyr	−162.5	2.0	28.5
	4-Mepyr	−163.0	1.9	28.6
	TMU	−157.0	0.7	27.7
	MeBenzoate	−162.7	1.2	26.6
	HMPA	−157.4	0.1	24.8
	DMAC	−158.0	1.2	26
Me_2NEt	Me_2NEt	−158.9	2.3	39.3
	$MeNEt_2$	−153.8	2.3	40.8
	n-Pr_3N[d]	−147.0	1.7	42.2
	Pyridine	−160.4		29.7
	2-Mepyr	−150.5	2.6	30.6
	2,4-Me_2pyr	−151.1		30.7
	4-Mepyr	−160.9		29.3
Et_3N	Pyridine	−150.4		33.0
n-Pr_3N	TMU	−144.6		29.4
N-MePiperidine	Pyridine	−162.7		27.9
$PhMe_2N$	$PhMe_2N$[e]	−155.1		37.4
MeEtBzN	MeEtBzN[e,f]	−147.8[d]	2.4	42.6

[a] In $CDCl_3$ or $CHCl_3$ unless otherwise noted.
[b] ^{19}F, ppm to low field of $CFCl_3$; ^{11}B, ppm to low field of $Et_2O \cdot BF_3$.
[c] In toluene.
[d] In bromoform.
[e] Reference 2.
[f] Chiral donor; *meso* and optically active isomers.

Formation of mixed-donor difluoroboron cations $DD'BF_2^+$, and competing exchange reactions

A wide range of mixed-donor difluoroboron cations $(R_3N)D'BF_2^+$ have been prepared in solution through bromide displacement by low-steric-hindrance donors D'. The nmr parameters are included in Table 1. Of the aliphatic tertiary amines, only Q, Me_3N, and Me_2NEt are effective as attacking groups D', but many other low-steric-hindrance donors are effective as well, e.g., pyridines, *N,N*-dialkylamides, dimethylsulfoxide, etc. Steric hindrance is the dominant factor in determining the effectiveness of D'; no correlation of reactivity with D' base strength is evident.

Steric effects for the already attached amine in $D \cdot BF_2Br$ are much less stringent. Even tertiary amines such as Et_3N that are too bulky to displace Br^- can be incorporated into difluoroboron cations if present in the $D \cdot BF_2Br$ precursor and reacted with a low-steric-hindrance D'. However, amine exchange prevented the formation of certain mixed-donor cations, e.g., in the case of $Me_2NPh \cdot BF_2Br$ with Q or Me_3N. Substitution of the D' amine for Me_2NPh in the BF_2Br adduct was so much more effective than bromide displacement that only the $D'_2BF_2^+$ cation could be detected. *i*-Pr_2NEt as well was too readily displaced from its BF_2Br adduct.

Reaction of a $D \cdot BF_nX_{3-n}$ system with a second donor D' led to the additional complexity of D' for D exchange as well as halogen exchange with the solvent, giving a mixture of cations and adducts involving both donors. This is illustrated by the ^{19}F spectrum of the *n*-$Pr_3N \cdot BF_nBr_{3-n}$ + quinuclidine system (Fig. 9). The desired mixed-donor $Q(n\text{-}Pr_3N)BF_2^+$ quartet is present. In addition, however, quinuclidine had displaced *n*-Pr_3N from practically all of its BF_3 adduct and from much of its BF_2Br adduct, but not from its $BFBr_2$ adduct. Also *n*-$Pr_3N \cdot BF_2Cl$ and $Q \cdot BF_2Cl$ had formed by halogen exchange with the solvent. There is also a $Q_2BF_2^+$ quartet. On further standing for several weeks at ambient temperature with excess Q, *n*-Pr_3N was displaced entirely from the mixed-donor cation leaving $Q_2BF_2^+$ as the only difluoroboron cation present. Even then there was no evidence for Q displacement of *n*-Pr_3N in the $BFBr_2$ adduct. This example illustrates the complexities of redistribution reactions about boron (3). Reaction rates are difficult to reproduce and may be affected by traces of moisture, but the relative reactivities of the different adduct types remain as described.

FAB spectra of mixed-donor difluoroboron cations include major peaks corresponding to DH^+, $D'H^+$, DBF_2^+, $D'BF_2^+$, and $DD'BF_2^+$ and there is normally a dication cluster peak of much lower intensity. This is illustrated in Fig. 10 for $(Me_3N)(2\text{-}MePyr)BF_2^+$. The peak at m/z 489 corresponds to $[(Me_3N)(2\text{-}MePyr)BF_2]_2BF_4^+$.

Neutral and negatively charged donors of a range of structural types displace bromide to give cationic and neutral $(R_3N)D'BF_2$ species, respectively. Table 1 includes nmr parameters of various mixed-donor $(R_3N)(D')BF_2^+$ species. As when low-steric-hindrance tertiary amines are the D' species, the original D may be displaced giving $D'_2BF_2^+$. The ^{19}F spectrum of the $Q \cdot BF_nBr_{3-n}$ system after reaction with dimethylsulfoxide (DMSO; Fig. 11) illustrates this. Not only $(Q)(DMSO)BF_2^+$ but also $(DMSO)_2BF_2^+$ appears to be present. Previous attempts in this laboratory to obtain $(DMSO)_2BF_2^+$ directly from $DMSO \cdot BF_nX_{3-n}$ adducts were unsuccessful due to insolubility of all $DMSO \cdot BX_3$ adducts except $DMSO \cdot BF_3$ in the usual solvents.

Can. J. Chem. Downloaded from www.nrcresearchpress.com by 186.148.149.217 on 09/07/12
For personal use only.

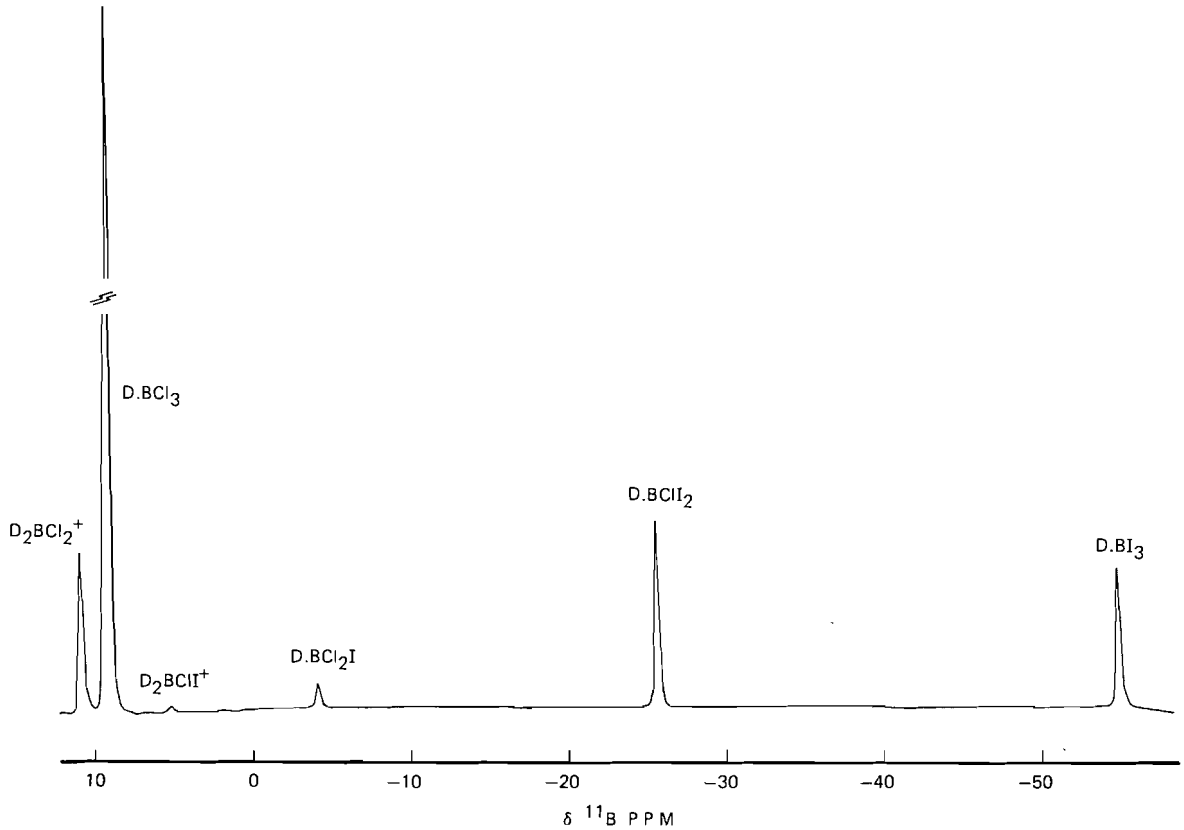


FIG. 7. 128.4 MHz ^{11}B nmr spectrum of a solution of $Me_3N \cdot BCl_nI_{3-n}$ adducts in CH_2Cl_2, to which Me_3N was added, after standing at 30°C (D = Me_3N).

TABLE 2. ^{11}B chemical shifts of $(R_3N)_2BCl_2^+$ and $(R_3N)_2BClI^+$ ions, and $R_3N \cdot BCl_nI_{3-n}$ adducts[a]

	Observed	Calculated[b]	Difference
$Q_2BCl_2^+$	10.7	10.1	−0.6
$Q(Me_3N)BCl_2^+$	10.8	10.5	−0.3
$(Me_3N)_2BCl_2^+$	11.0	11.2	0.2
Q_2BClI^+	5.9	6.1	0.2
$Q(Me_3N)BClI^+$	5.4	5.8	0.4
$(Me_3N)_2BClI^+$	6.1	5.7	−0.4
$Q \cdot BCl_3$	9.2[c]	9.3	0.1
$Q \cdot BCl_2I$	−3.7	−3.4	0.3
$Q \cdot BClI_2$	−24.4	−24.3	0.1
$Q \cdot BI_3$	−53.1[c]	−53.6	−0.5
$Me_3N \cdot BCl_3$	9.6	9.7	0.1
$Me_3N \cdot BCl_2I$	−4.0	−3.0	1.0
$Me_3N \cdot BClI_2$	−25.7	−24.6	1.1
$Me_3N \cdot BI_3$	−55.0	−54.5	0.5

[a]In ppm to low field of external $Et_2O \cdot BF_3$; CH_2Cl_2 solvent.
[b]From pairwise interaction nmr parameters.
[c]Reference 2.

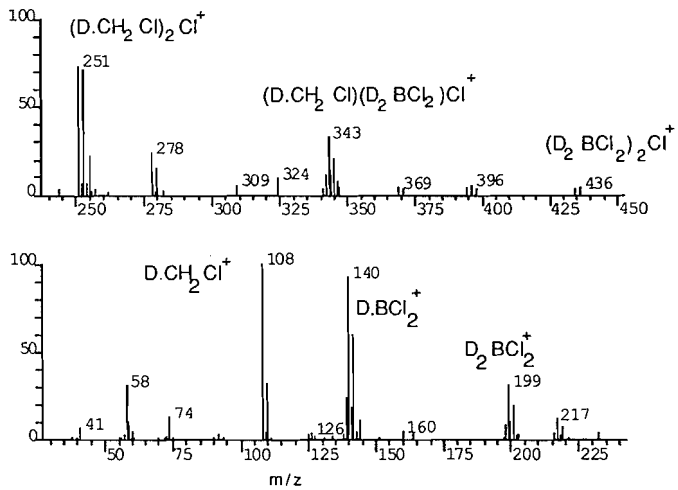


FIG. 8. Positive ion FAB mass spectrum of ionic material obtained from a CH_2Cl_2 solution of the $Me_3N \cdot BCl_nI_{3-n}$ adduct system. Peaks at m/z greater than 150 are enhanced by a factor of 10, and peaks at m/z greater than 300 are enhanced by a further factor of 2 (D = Me_3N).

Not all attempts to prepare $(R_3N)(D')BF_2^+$ ions with non-amine donors were successful. Et_2O and dihydrofuran as well as the "soft" sulfur donors Me_3PS and Me_2S did not displace Br^- from $Q \cdot BF_2Br$. (However, the soft isonitrile *t*-BuNC was successful in displacing Br^-.) Me_2O caused decomposition, not surprisingly in view of its reactivity in the presence of B—Br bonds (19). In contrast, hexamethylphosphoramide (HMPA) was such a good donor and so reactive that donor-for-donor exchange occurred in many $D \cdot BF_nBF_{3-n}$ systems (D = MeEtNBz, pyr, and 2-Mepyr) resulting in $(HMPA)_2BF_2^+$ formation exclusively. We have previously reported the formation of this species by disproportionation of $HMPA \cdot BF_3$ (14*b*). The nmr spectra of systems with HMPA and tetramethylurea (TMU) as D′ are complex and suggest that D_2BFX^+ (X = Cl, Br) and D_3BF^{2+} ions may be formed in these systems.

Addition of the potentially chelating 2:2′-bipyridyl to $D \cdot BF_2Br$ (D = Q, Me_3N) solutions gave some precipitate but no new nmr signals. Addition of acetylacetone to $Q \cdot BF_nBr_{3-n}$

Can. J. Chem. Downloaded from www.nrcresearchpress.com by 186.148.149.217 on 09/07/12
For personal use only.

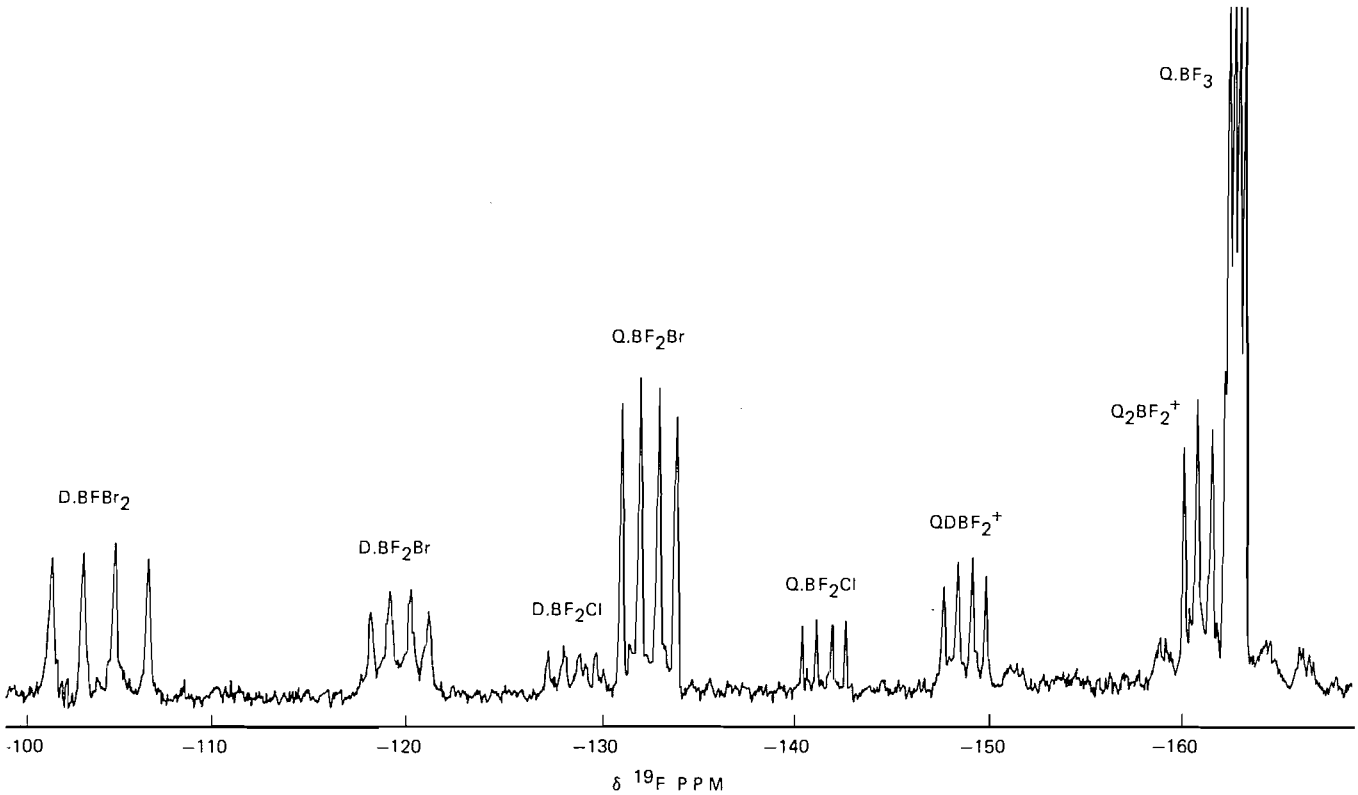


FIG. 9. 56.4 MHz ^{19}F nmr spectrum of the n-$Pr_3N \cdot BF_nBr_{3-n}$ adduct system in $CDCl_3$, following the addition of quinuclidine (D = n-Pr_3N).

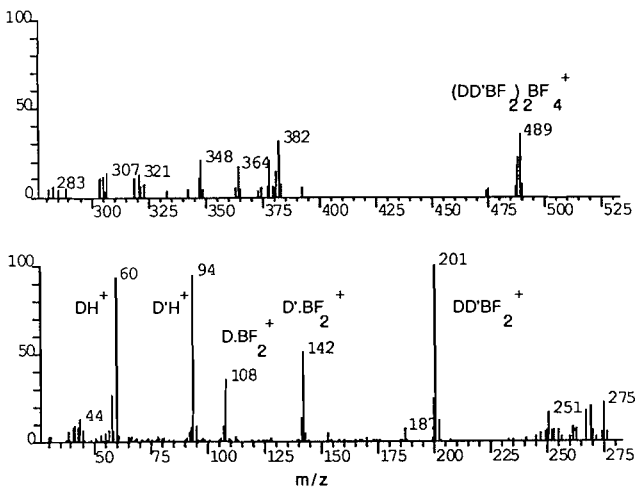


FIG. 10. Positive ion FAB mass spectrum of (Me_3N)(2-methylpyridine)$BF_2^+ \cdot BF_4^-$. Peaks at m/z greater than 250 are enhanced by a factor of 20 (D = Me_3N; D′ = 2-methylpyridine).

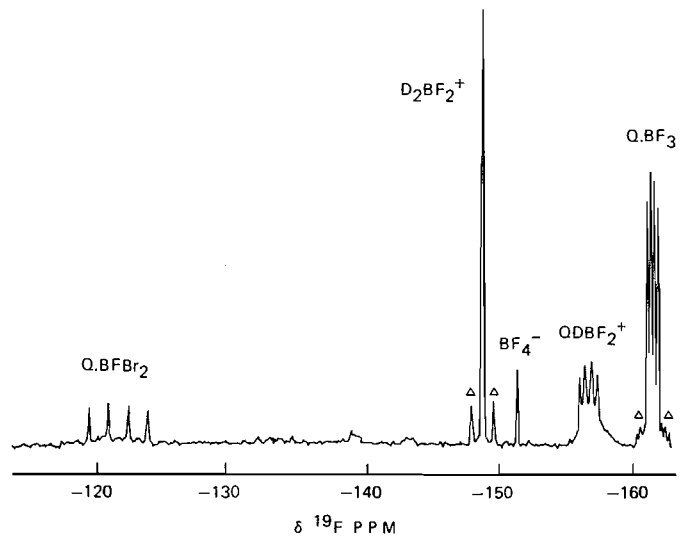


FIG. 11. 56.4 MHz ^{19}F nmr spectrum of the quinuclidine$\cdot BF_nBr_{3-n}$ adduct system in $CDCl_3$, following the addition of DMSO. The peaks marked △ are spinning sidebands (D = DMSO).

gave a large ^{19}F singlet at −139.4 ppm, consistent with the formation of (acac)BF_2 (lit. (20) −139.1 ppm). Neutral chelated LL$\cdot BF_2$ species such as this are well known (20, 21).

The displacement of X^- from D$\cdot BF_2X$ by an anion Y^- to form D$\cdot BF_2Y$ is no different in principle than displacement by a neutral D′ to form $DD'BF_2^+$, and it is not surprising that D$\cdot BF_2Br$ reacts readily with many anions, notably oxoanions, to give products that are apparently neutral D$\cdot BF_2Y$ species (Table 3). Their ^{19}F nmr parameters are consistent with those of other (R_3N)(O-donor)BF_2 species (Table 1). Addition of OH^- to D$\cdot BF_2Br$ (D = both Me_3N and Q) resulted in the same ^{19}F nmr quartet (−153.1 ppm; J_{BF} 12.1 Hz) in both cases. Instead of the intended D$\cdot BF_2OH$, this species is apparently BF_3OH^- (22). Cyanide, iodide, and acetate could not displace bromide but chloride could, giving Q$\cdot BF_2Cl$. This is consistent with earlier work (23) showing that heavier-halogen $R_3N \cdot BX_3$ adducts form mixed boron trihalide adducts by reaction with lighter-halogen tetraalkylammonium halide salts.

TABLE 3. Nuclear magnetic resonance parameters of $D \cdot BF_2Y$ species from $R_3N \cdot BF_2Br$ and Y^- [a]

D	Y	Chemical shifts (ppm)[b] ^{19}F	^{11}B	$^1J_{^{11}B-^{19}F}$ (Hz)
Quinuclidine	MnO_4^-	−153.5		30.6
	NO_3^-	−164.1	0.6	24.1
	ClO_4^-	−160.1	0.8	21.2
	SO_4^{2-}	−159.8		22.5
	Cl^-	−141.9	4.1	43.5
	CN^-, OAc^-, I^- [c]			
Me_3N	NO_3^-	−165.0	1.0	24.1
Pyridine	NO_3^-	−163.3		27.3

[a] In $CDCl_3$ or $CHCl_3$.
[b] ^{19}F, ppm to low field of $CFCl_3$; ^{11}B, ppm to low field of $Et_2O \cdot BF_3$.
[c] No reaction.

TABLE 4. Variations in ^{19}F chemical shift and $^{11}B-^{19}F$ coupling constant over selected $Q_nD'_{2-n}BF_2^+$ (n = 2–0) systems

	D'			
	TMU	DMAC	HMPA	Methyl benzoate
^{19}F chemical shifts				
$Q_2BF_2^+$	−161.5	−161.5	−161.5	−161.5
$QD'BF_2^+$	−156.0	−156.8	−156.4	−160.5
$D'_2BF_2^+$	−146.0[a]	−144.2[a]	−141.8[b]	−145.2[c]
$^{11}B-^{19}F$ coupling constants				
$Q_2BF_2^+$	39.5	39.5	39.5	39.5
$QD'BF_2^+$	27.3	24.8	24.4	26.6
$D'_2BF_2^+$	19[a]	—[a]	12[b]	—[c]

[a] Reference 14*a*.
[b] Reference 14*b*.
[c] Reference 31.

Discussion

General

This is the first systematic study of the simple but elusive bis(amine)difluoroboron cations, and the first easy method of preparation. It is remarkable that, in spite of extensive continuing studies of amine – boron trihalide adducts (24), these simple derivatives have been missed. They may occur more widely than is currently recognized, and their existence might explain a number of anomalies in the literature. There are a number of adduct studies in which their existence has been postulated but not confirmed (see for example ref. 25). Amine·BF_3 adducts are important catalysts, in for example epoxy resin curing (26, 27). Happe *et al.* conclude that an unidentified highly reactive species in commercial $EtNH_2 \cdot BF_3$ is probably $(EtNH_2)_2BF_2^+ \cdot BF_4^-$ (26). Primary- and secondary-amine difluoroboron cations would be expected to be far more reactive than our tertiary-amine cations because they can also function as Bronsted acids, and thus could be highly effective catalysts. Preparation of primary- and secondary-amine difluoroboron cations by methods similar to ours would be of interest, but complications could arise due to reactivity of N—H and B—Br bonds, splitting off HBr.

The mode of initiation of cationic polymerization by Lewis acids such as Al_2Cl_6 and BF_3 remains an active and controversial area of investigation (28). Some investigators, but not all, believe that a key step of Al_2Cl_6-catalysed initiation requires that Al_2Cl_6 dissociate to give $AlCl_2^+$ and $AlCl_4^-$. Characterization of difluoroboron cations may help to support an analogous mode of action of BF_3 in catalysing cationic polymerization. Three-coordinate BF_2 cations, a logical further development of our work that might be accessible by using highly hindered donors, would be highly relevant.

This work illustrates the value of using fast atom bombardment mass spectrometry in tandem with nmr to confirm the identity of the haloboron cations and to monitor cation synthesis. Nuclear magnetic resonance and FAB are complementary techniques. The haloboron cations volatilize readily in the FAB source and give well-defined spectra. FAB spectra of mixtures of haloboron cations and neutral adducts strongly discriminate against the neutral adducts (which give no parent ion peaks) and allow monitoring of haloboron cation formation in the presence of many neutral adducts, without the need for separation. Application of FAB to studies of catalysis by BF_3 adducts (26, 27) could be very fruitful.

A problem with FAB has recently been recognized: significant ion–molecule reactions can take place in the gas phase (29), so that some FAB peaks might not correspond to species present in the original sample. Recent work in this laboratory has shown that a protic matrix liquid, 3-nitrobenzyl alcohol, inhibits gas phase ligand substitution reactions involving difluoroboron cations (30). Since glycerol, which is an even more effective proton donor than 3-nitrobenzyl alcohol in FAB, was the matrix liquid for all FAB spectra reported in this work, we can discount the occurrence of appreciable gas phase reactions.

Increased D and D′ steric hindrance shifts the difluoroboron cation ^{19}F resonances to lower field and increases the magnitude of the $^{11}B-^{19}F$ coupling constant (Table 1), the same trends as observed previously for mixed boron trihalide adducts of trialkylamines (2). There is no evident relationship of these parameters to amine base strength. ^{11}B chemical shifts vary only slightly. $^{11}B-^{19}F$ coupling constants diminish in magnitude when an oxygen donor is present, consistent with the low steric hindrance of the carbonyl donors involved. Comparison of nmr parameters across the series $Q_2BF_2^+$, $QD'BF_2^+$, $D'_2BF_2^+$ (Table 4) is possible since several of the $D'_2BF_2^+$ ions have been reported previously (14, 31). The variations are fairly regular. Extrapolation predicts fairly small but non-zero $J_{^{11}B-^{19}F}$ values in $(O\text{-donor})_2BF_2^+$ cations, and often the ^{19}F signals of such species do not show splittings due to $^{11}B-^{19}F$ coupling. This is probably a result of rapid ^{11}B quadrupole relaxation as well as small J values. Similar trends in coupling constants are observed in neutral chelated BF_2 complexes as the donor atoms change from nitrogen to oxygen, and here too most $(O\text{-donor})_2BF_2$ species give unsplit ^{19}F signals (20). The absence of splittings renders peak identification less certain (e.g., the proposed $(DMSO)_2BF_2^+$ peak at −149.5 ppm in Fig. 11). A number of unsplit ^{19}F signals have been observed in Q/acetone, Q/MeO^-, Q/*i*-PrO^-, Me_3N/MeO^-, etc. systems. These probably arise from $QD'BF_2$ and D'_2BF_2 species, but await confirmation. FAB spectra should be conclusive in identifying the cationic species such as $Q(acetone)BF_2^+$.

The neutral $Q \cdot BF_2Y$ species, where Y is a range of oxyanions and Y^- must donate through an oxygen atom, have ^{19}F chemical shifts and $^{11}B-^{19}F$ coupling constants (Table 3) consistent with those of the oxygen-donor $QD'BF_2^+$ cations.

Can. J. Chem. Downloaded from www.nrcresearchpress.com by 186.148.149.217 on 09/07/12
For personal use only.

Can. J. Chem. Downloaded from www.nrcresearchpress.com by 186.148.149.217 on 09/07/12
For personal use only.

Chemical shifts of various nuclei, which are not linearly additive with respect to the substituent groups, have been shown to be "pairwise additive" in a number of cases, and the same can be true for coupling constants between directly bonded atoms (15). In other words, chemical shift or coupling constant can be expressed as a sum of pairwise terms $\eta_{i,j}$, associated with substituents i and j and independent of all other substituents. The sum is taken over all possible pairs of substituents about the central atom, excluding the nucleus being observed in the nmr experiment. We have previously shown that pairwise additivity applies to chemical shifts and coupling constants of the mixed tetrahaloborate anions (4), and extended this to a wide range of mixed boron trihalide adducts (16). This empirical relationship is useful in predicting chemical shifts of unknown species including (with the addition of donor,donor $\eta_{i,j}$ terms) haloboron cations. Sets of ^{19}F and ^{11}B chemical shift and $J_{^{11}B-^{19}F}$ pairwise interaction parameters based on all adduct and cation nmr data for Q, Me_3N, pyridine, and 2-methylpyridine together with tetrahaloborate anion data gave halogen–halogen pairwise terms very similar to those determined previously (16). Calculated and observed values are compared in Table 2 for the $D{\cdot}BCl_nI_{3-n}$ (D = Q, Me_3N) adducts and the dichloroboron and chloroiodoboron cations derived from these donors. Agreement for the cations is as good on average as for the neutral boron trihalide adducts, and confirms our chemical shift assignments.

Selectivity of bromide displacement

The high selectivity of bromide displacement from $R_3N{\cdot}BF_n{\cdot}Br_{3-n}$, with displacement occurring only for $n = 2$ and not for $n = 1$ or 0, could be rationalized in thermodynamic or kinetic terms. Some reactions can be very slow (e.g., displacement of chloride from $Q{\cdot}BF_2Cl$) and we cannot be sure that our unreactive adducts are in fact at equilibrium. Complete substitution of bromine even in a BBr_3 adduct to give D_4B^{3+} is possible, but only under forcing conditions with a low-steric-hindrance pyridine donor (32). We cannot disentangle thermodynamic and kinetic factors without kinetic studies on rigorously dry systems. We discuss here two rationalizations for the high selectivity observed, which apply if based on assumptions that we are observing (*i*) near-equilibrium systems, or (*ii*) kinetic effects favouring certain reactions in systems that may be far from equilibrium. Both aspects may come into play in specific cases, so elements of both explanations may be valid. Rates of halogen redistribution about boron can be extremely variable, and where rates are known to be rapid, equilibria of halogen redistribution can be far from statistical (3, 33).

Reactivity of $R_3N{\cdot}BF_2Br$ with "hard" donors to lose Br^- should be thermodynamically favourable, provided steric hindrance is low, according to the "Symbiotic Principle" of Pearson and Songstad (34): hard bases tend to cluster together on a central atom, as do soft bases, whereas a system with both hard and soft ligands is less stable. Major deviations from statistical redistribution equilibria do occur in, for example, $Me_2S{\cdot}BF_nX_{3-n}$ (X = Cl, Br, I) adduct systems, with the mixed F,Br and F,I adducts not being detectable although equilibration is rapid (33). These are precisely the halogen pairs that would be predicted to be the least compatible according to the Symbiotic Principle. Against this explanation we must note that the rapid $R_3N{\cdot}BF_3 + BBr_3$ halogen redistribution reaction that forms the mixed boron trihalide adducts does give large amounts of the BF_2Br and $BFBr_2$ adducts. Nitrogen and oxygen donors would, however, be more compatible with the fluorine substituents than would bromine, according to the Symbiotic Principle, and displacement of the single bromine by such donors should be thermodynamically favoured.

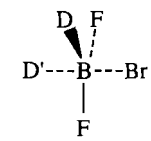
Kinetic factors must, however, be important since higher-steric-hindrance amines such as Et_3N cannot attack $D{\cdot}BF_2Br$, but the desired $DD'BF_2^+$ complex is readily formed by attacking $Et_3N{\cdot}BF_2Br$ with the low-steric-hindrance amine. We now consider possible mechanisms.

A dissociative mechanism, $D{\cdot}BF_2Br$ giving $D{\cdot}BF_2^+$ and Br^-, would have the advantage of maximizing F—B π bonding in the trigonal planar intermediate, stabilizing the intermediate. (This is analogous to bond stabilization in BF_3 by fluorine-to-boron π bonding, which makes BF_3 the weakest Lewis acid of the BX_3 series (5).) This should selectively lower the activation energy when fluorine is present, and to a greater extent when two fluorines rather than one are present.

However, we can probably discount a dissociative mechanism for a number of reasons. (*i*) The highly reactive three-coordinate cation should react readily with D′ amines such as Et_3N, and reaction rates should not depend much on D′ steric hindrance. (*ii*) Although no systematic study has yet been carried out, reaction rates in at least some systems increase when D′ concentrations increase. (*iii*) There is no evidence for the presence of appreciable amounts of any three-coordinate boron species, which would be expected to cause rapid halogen redistribution in all species including the solvent. (*iv*) The ability of iodine-containing boron trihalide adducts of Me_3N to form three-coordinate ionic complexes was proposed by some (35, 36), but has been questioned by others (23, 37); loss of bromide seems far less likely than loss of iodide.

We should note, however, the special case of $i\text{-}Pr_2NEt{\cdot}BF_n{\cdot}Br_{3-n}$ adducts. Especially rapid halogen exchange with the solvent occurs with this highly hindered system, consistent with dissociation to give either $D{\cdot}BX_2^+$ or BX_3. We have not, however, been able to form any fluoroboron cations containing $i\text{-}Pr_2NEt$.

Thus the evidence seems strong against dissociation to give a three-coordinate reactive intermediate in our typical adduct systems. A typical S_N2 transition state (trigonal bipyramidal) seems more plausible, provided that this is lowered in energy by a maximization of fluorine-to-boron π bonding when the $D{\cdot}BF_2$ unit becomes planar:



As in the three-coordinate intermediate, the effect would be greater as the number of fluorines increases, and could account for the high selectivity.

Trialkylamines, being already four-coordinate when bonded to boron as D, cannot contribute to the stabilization of the transition state by π bonding to boron, but pyridines could, and would further stabilize the structure. In accord with this possibility, the formation of the mixed $(R_3N)(pyr)BF_2^+$ ions occurs more rapidly when R_3N is added to the $pyr{\cdot}BF_nBr_{3-n}$ system, than when pyr is added to the $R_3N{\cdot}BF_nBr_{3-n}$ system. The enhancement of these reactions when D is pyridine rather than R_3N is dramatic, and our work on the formation of haloboron cations in $pyr{\cdot}BF_nX_{3-n}$ (X = Cl, Br) systems will be reported separately (38).[2]

[2]Also, M. J. Farquharson and J. S. Hartman. Manuscript in preparation.

Can. J. Chem. Downloaded from www.nrcresearchpress.com by 186.148.149.217 on 09/07/12
For personal use only.

Our mixed-donor systems are complicated by D′ for D exchange. These reactions too are highly selective, and the selectivity could be related to a similar transition state to the above. D for D′ exchange is faster when at least two fluorines are present (Fig. 9).

Once formed, $D_2BF_2^+$ ions are stable even in water. This is likely a kinetic rather than a thermodynamic effect, similar to the stability of BF_4^- to hydrolysis. The stability of the bulky $D_2BF_2^+$ cations suggests their use as large cations for precipitating large anions, much as cobalticinium ion is used.

The reactions of the non-fluorine-containing cations have not yet been studied. $DD'BClI^+$ may undergo replacement of the second iodine to give doubly charged cations of type $DD'D''BCl^{2+}$. Bis(R_3N)haloboron cations of the types D_2BFX^+ (X = Cl, Br, I) and D_3BF^{2+} have not been reported in the literature, but we have observed cations of these types in the more reactive pyridine (38) and *N*,*N*,*N*′-trialkylamidine (39)[3] systems.

There have been a number of recent observations of cation formation from neutral main group halide compounds via displacement of halide by a neutral donor: e.g., about aluminum (40), tin (41), titanium (42), and tantalum (43), as well as additional examples about boron, in some cases leading to three-coordinate cations (44). HMPA, which we find to be exceptionally effective in displacing other donors, is the only one of a wide range of donors that gives cationic complexes $D_3TiX_3^+ \cdot X^-$ (X = Cl, Br); all the rest give only neutral complexes D_2TiX_4 under the same conditions (42). Much remains to be learned about such reactions. Fluoride abstraction from *mer*-Ph_3TeF_3 by PF_5 gives $Ph_3TeF_2^+ \cdot PF_6^-$ (45), from which it might be possible to prepare $D \cdot TePh_3F_2^+$ cations. Fluoro- and chlorosilicon cations $(bipyridyl)_2SiX_2^{2+}$ can be obtained by a different route (46). $(THF)_2AlCl_3$ can exist as the molecular complex but can also be isolated as the ionic isomer $(THF)_4AlCl_2^+ \cdot AlCl_4^-$ (47), just as our $D_2BF_2^+ \cdot BF_4^-$ compounds are ionization isomers of the corresponding molecular $D \cdot BF_3$ complexes.

Conclusions

The wide range of R_3N-containing dihaloboron cations described here demonstrates their ready availability under mild conditions from simple starting materials. Particularly striking is the need for one heavy and two light halogens (normally fluorine) on boron, to maximize the ease of displacement of the heavy halogen. The most plausible explanation for this involves stabilization of the transition state or reactive intermediate by π bonding from fluorine to boron. Positive ion FAB mass spectrometry is shown to be a potent technique, in tandem with nmr spectroscopy, in monitoring dihaloboron cation formation and identifying the ions. Continuing work has shown that mixed boron trihalide adducts of pyridines and amidines are even more reactive than those of aliphatic tertiary amines and give a wider variety of cationic haloboron species; these systems will be described elsewhere.

Acknowledgements

We thank Mr. T. R. B. Jones for technical assistance, Dr. J. M. Miller for helpful discussions and for suggesting the use of FAB in this work, Mr. A. G. Basile for modifications to the computer program for calculating pairwise interaction parameters, Mr. J. Nye, Ms. C. L. MacLaurin, and Mr. R. Théberge for running FAB spectra, and the Natural Sciences and Engineering Research Council of Canada for financial support. We also thank Prof. A. F. Janzen and Prof. K. E. Russell for helpful discussions, on reaction mechanisms and cationic polymerization respectively. High-field nmr spectra were obtained with the assistance of Dr. R. E. Lenkinski and Mr. W. Klimstra at the South Western Ontario High Field NMR Centre, funded by a Major Installation Grant from NSERC.

[3]Also, J. S. Hartman and Z. Yuan. Manuscript in preparation.

1. R. J. Gillespie and J. S. Hartman. Can. J. Chem. **46**, 2147 (1968); R. J. Gillespie, J. S. Hartman, and M. Parekh. Can. J. Chem. **46**, 1601 (1968).
2. A. Fox, J. S. Hartman, and R. E. Humphries. J. Chem. Soc. Dalton Trans. 1275 (1982).
3. J. S. Hartman and J. M. Miller. Adv. Inorg. Chem. Radiochem. **21**, 147 (1978).
4. J. S. Hartman and G. J. Schrobilgen. Inorg. Chem. **11**, 940 (1972).
5. A. G. Massey. Adv. Inorg. Chem. Radiochem. **10**, 1 (1967).
6. M. J. Farquharson and J. S. Hartman. J. Chem. Soc. Chem. Commun. 256 (1984).
7. H. Nöth, R. Staudigl, and H.-U. Wagner. Inorg. Chem. **21**, 706 (1982); J. Higashi, A. D. Eastman, and R. W. Parry. Inorg. Chem. **21**, 716 (1982); H. Nöth. Angew. Chem. Int. Ed. Engl. **27**, 1603 (1988).
8. B. Wrackmeyer. Annu. Rep. NMR Spectrosc. **20**, 61 (1988).
9. M. Kameda, R. E. DePoy, and G. Kodama. 6th International Meeting on Boron Chemistry. Proceedings. *Edited by* S. Hermanek. 1987. pp. 104–117.
10. G. E. Ryschkewitsch. *In* Boron hydride chemistry. *Edited by* E. L. Muetterties. Academic Press, New York. 1975. Chap. 6; H. Nöth. Prog. Boron Chem. **3**, 211 (1970); M. A. Mathur and G. E. Ryschkewitsch. Inorg. Chem. **19**, 3054 (1980).
11. N. E. Miller and E. L. Muetterties. J. Am. Chem. Soc. **86**, 1033 (1964).
12. N. Wiberg and J. W. Buchler. Chem. Ber. **96**, 3000 (1963); D. D. Axtell, A. C. Campbell, P. C. Keller, and J. V. Rund. J. Coord. Chem. **5**, 129 (1976); D. Mukhopadhyay, S. Roychoudhury, B. Sur, and R. G. Bhattacharyya. Ind. J. Chem. **22A**, 333 (1983).
13. H. C. Brown, B. Singaram, and J. R. Schwier. Inorg. Chem. **18**, 51 (1979); H. C. Brown and B. Singaram. Inorg. Chem. **18**, 53 (1979).
14. (*a*) J. S. Hartman and G. J. Schrobilgen. Inorg. Chem. **13**, 874 (1974); (*b*) J. S. Hartman and P. Stilbs. J. Chem. Soc. Dalton Trans. 1142 (1980).
15. T. Vladimiroff and E. R. Malinowski. J. Chem. Phys. **46**, 1830 (1967).
16. J. S. Hartman and J. M. Miller. Inorg. Chem. **13**, 1467 (1974).
17. M. I. Bruce and M. J. Liddell. Appl. Organomet. Chem. **1**, 196 (1987); J. M. Miller. Adv. Inorg. Chem. Radiochem. **28**, 1 (1984); M. Barber, R. S. Bordoli, G. J. Elliott, R. D. Sedgwick, and A. N. Tyler. Anal. Chem. **54**, 645A (1983).
18. R. G. Kidd and D. R. Truax. J. Am. Chem. Soc. **90**, 6867 (1968).
19. M. J. Bula, D. E. Hamilton, and J. S. Hartman. J. Chem. Soc. Dalton Trans. 1405 (1972).
20. N. M. D. Brown and P. Bladon. J. Chem. Soc. A, 526 (1969).
21. G. Klebe and D. Tranqui. Inorg. Chim. Acta, **81**, 1 (1984); N. N. Shapetko, L. N. Kurkovskaya, V. G. Medvedeva, A. P. Skoldinov, and L. K. Vasyanina. J. Struct. Chem. **10**, 5 (1969).
22. K. Kuhlmann and D. M. Grant. J. Phys. Chem. **68**, 3208 (1964).
23. B. W. Benton and J. M. Miller. Can. J. Chem. **52**, 2866 (1974).
24. K. Niedenzu (*Editor*). Gmelin handbook of inorganic chemistry, boron compounds. 2nd Suppl. Vol. 2: Boron and halogens,

chalcogens, carboranes. Springer-Verlag, Berlin, Heidelberg, and New York. 1982. pp. 26–29, 88–90, 129–130, 147.
25. D. R. MARTIN, J. U. MONDAL, R. D. WILLIAMS, J. B. IWAMOTO, N. C. MASSEY, D. M. NUSS, and P. L. SCOTT. Inorg. Chim. Acta, **70**, 47 (1983).
26. J. A. HAPPE, R. J. MORGAN, and C. M. WALKUP. Polymer, **26**, 827 (1985).
27. R. E. SMITH and C. H. SMITH. J. Appl. Polym. Sci. **31**, 929 (1986).
28. D. W. GRATTAN and P. H. PLESCH. J. Chem. Soc. Dalton Trans. 1734 (1977); M. MASURE and P. SIGWALT. Makromol. Chem. Rapid Commun. **4**, 269 (1983).
29. J. A. SUNNER, R. KULATUNGA, and P. KEBARLE. Anal. Chem. **58**, 1312 (1986); J. A. SUNNER, A. MORALES, and P. KEBARLE. Anal. Chem. **60**, 98 (1988); H. MUNSTER, F. THEOBALD, H. BUDZIKIEWICZ, and E. SCHROEDER. Int. J. Mass Spectrom. Ion Processes, **79**, 73 (1987); J. M. MILLER, K. BALASANMUGAM, and A. FULCHER. Org. Mass Spectrom. In press.
30. K. BALASANMUGAM, J. S. HARTMAN, J. M. MILLER, and Z. YUAN. Can. J. Chem. **67**, 685 (1989).
31. J. S. HARTMAN, B. D. MCGARVEY, and C. V. RAMAN. Inorg. Chim. Acta, **49**, 63 (1981).
32. C. W. MAKOSKY, G. L. GALLOWAY, and G. E. RYSCHKEWITSCH. Inorg. Chem. **6**, 1972 (1967); Inorg. Synth. **12**, 141 (1970).
33. M. J. BULA and J. S. HARTMAN. J. Chem. Soc. Dalton Trans. 1047 (1973).
34. R. G. PEARSON and J. SONGSTAD. J. Am. Chem. Soc. **89**, 1827 (1967).
35. J. R. BLACKBOROW. J. Chem. Soc. Dalton Trans. 2139 (1973).
36. S. S. KRISHNAMURTHY and M. F. LAPPERT. Inorg. Nucl. Chem. Lett. **7**, 919 (1971).
37. B. BENTON-JONES and J. M. MILLER. Inorg. Nucl. Chem. Lett. **8**, 485 (1972).
38. M. J. FARQUHARSON and J. S. HARTMAN. Paper IN 12-3, 67th Annual Canadian Chemical Conference, Montreal, June 3–6, 1984; M. J. FARQUHARSON. M.Sc. thesis, Brock University, 1985.
39. J. S. HARTMAN and Z. YUAN. Paper INOR-507, Third Chemical Conference of North America, Toronto, June 5–10, 1988; Z. YUAN. M.Sc. thesis, Brock University, 1988.
40. J. LEWINSKI and S. PASYNKIEWICZ. Inorg. Chim. Acta, **143**, 39 (1988).
41. R. COLTON and D. DAKTERNIEKS. Inorg. Chim. Acta, **148**, 31 (1988).
42. E. TURIN, R. M. NIELSON, and A. E. MERBACH. Inorg. Chim. Acta, **134**, 67 (1987).
43. J. PAULI, W. STOREK, and L. RIESEL. Z. Chem. **28**, 226 (1988).
44. P. JUTZI, B. KRATO, M. HURSTHOUSE, and A. J. HOWES. Chem. Ber. **120**, 1091 (1987).
45. A. S. SECCO, K. ALAM, B. J. BLACKBURN, and A. F. JANZEN. Inorg. Chem. **25**, 2125 (1986).
46. D. KUMMER and T. SESHADRI. Z. Anorg. Allgem. Chem. **428**, 129 (1977).
47. N. C. MEANS, C. M. MEANS, S. G. BOTT, and J. L. ATWOOD. Inorg. Chem. **26**, 1466 (1987).

Can. J. Chem. Downloaded from www.nrcresearchpress.com by 186.148.149.217 on 09/07/12
For personal use only.

Superacid-induced ring-opening reactions of fluorinated heterocycles[1]

STEFAN P. KOTUN AND DARRYL D. DESMARTEAU[2]

Department of Chemistry, Howard L. Hunter Laboratory, Clemson University, Clemson, SC 29634-1905, U.S.A.

Received March 15, 1989

This paper is dedicated to Professor Ronald J. Gillespie on the occasion of his 65th birthday

STEFAN P. KOTUN and DARRYL D. DESMARTEAU. Can. J. Chem. **67**, 1724 (1989).

HF/AsF_5 and HF/SbF_5 superacid mixtures react with fluorinated small-ring heterocycles such as 1,2-oxazetidines and oxetanes with consequent addition of HF to give alcohol and amine ring-opened products in high yield. Excess HF serves as solvent and reactant. Ring compounds containing both nitrogen and oxygen as heteroatoms protonate predominantly on nitrogen; a case with competing O-protonation arises in the case of a chloro-substituted oxazetidine. In general, rings containing two heteroatoms retain the heteroatom–heteroatom bond and it is a carbon–heteroatom bond that opens. The resulting OH and NH functional groups are not protonated and lost in the superacid medium due to the instability of the highly fluorinated cations that would be left behind. Most of the heterocycles react at or below room temperature, although the very weakly basic 2,2-bis(trifluoromethyl)-3,3,4,4-tetrafluorooxetane requires the stronger HF/SbF_5 superacid system and more severe conditions.

Key words: superacids, hydrogen fluoride, ring opening, fluorinated oxazetidines, fluorinated oxetanes.

STEFAN P. KOTUN et DARRYL D. DESMARTEAU. Can. J. Chem. **67**, 1724 (1989).

Les mélanges de superacides HF/AsF_5 et HF/SbF_5, réagissent avec les petits hétérocycles fluorés, comme les 1,2-oxazétidines et oxétanes, par additions de HF qui conduisent à des alcools et à des amines en chaîne ouverte avec d'excellente rendements. Le HF en excès sert de solvant et de réactif. Les composés cycliques contenant de l'azote ainsi que de l'oxygène comme hétéroatomes se protonent principalement sur l'azote; dans le cas des oxazétidines substituées par un chlore, on observe aussi une protonation sur l'oxygène. En général, avec les cycles contenant deux hétéroatomes, la liaison hétéroatome–hétéroatome est conservée alors que la liaison carbone–hétéroatome s'ouvre. Les groupements fonctionnels OH et NH qui en résultent ne sont pas protonés, ainsi ils ne sont pas perdus, dans le milieu superacide à cause de l'instabilité des cations hautement fluorés qui seraient laissés en arrière. La plupart des hétérocycles réagissent à la température ambiante ou à des températures plus basses; toutefois, pour faire réagir le 2,2-bis(trifluorométhyl)-3,3,4,4-tétrafluorooxétane qui est très faiblement basique, on doit utiliser le système de superacide HF/SbF_5 qui est plus fort ainsi que des conditions plus vigoureuses.

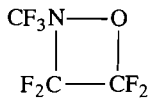
Mots clés : superacides, fluorure d'hydrogène, ouverture de cycle, oxazétidines fluorées, oxétanes fluorés.

[Traduit par la revue]

Introduction

Superacid chemistry has achieved a position of high visibility in the past several years (1). Mixtures of anhydrous hydrogen fluoride and Lewis acids such as NbF_5, BF_3, TaF_5, AsF_5, or SbF_5 constitute an important class of superacids. Among the more recent reports are those of O'Donnell on the acidity of HF (2) and on the equilibria of the HF/AsF_5 system (3) while Gillespie and Liang's particularly definitive measurements (4) now establish HF itself as one of the most acidic single-component systems known and show HF/SbF_5 mixtures to have the highest acidity values ever observed, with HF/AsF_5 about 1.3 orders of magnitude behind. X-ray crystal structures of the active protonating species, H_2F^+ and $H_3F_2^+$, have also recently been determined (5).

We wish to report here synthetic uses of HF/AsF_5 and HF/SbF_5 superacid mixtures with excess HF as solvent in the preparation of fluorinated amines and alcohols. Our initial goal in this area involved insertion of tetrafluoroethylene into the N—O bond of the 2-trifluoromethyl-3,3,4,4-tetrafluoro-1,2-oxazetidine **1** for possible conversion to polymers in which the



1

N—O bond, which limits the thermal applications of nitroso rubbers (6), would no longer be present. One part of this investigation consisted of superacid protonation in the expectation of obtaining a stable cyclic ammonium salt in analogy to previous open-chain cases such as H_2O (7), H_2S (8), HNF_2 (9), $(CF_3)_2NCF{=}NCF_3$ (10), and the more closely related conversion of $CF_3N(H)—OCF_3$ to $CF_3N^+(H)(H)—OCF_3\ AsF_6^-$ (11).

The volatile product from **1**, however, is $CF_3N(H)—OCF_2CF_3$, isolated in excellent yield and arising via opening of the N—C bond and formal addition of HF. We here show this to be a synthetically useful transformation for several fluorinated small-ring heterocycles.

Experimental

Caution! We have not encountered any difficulties with the starting materials, reagents, or products in this work; users should, however, familiarize themselves with their properties and hazards. HF and SbF_5 are very corrosive toward tissue and materials of construction; AsF_5 is, in addition, very toxic and a strong oxidizer. Some of the reactions occur at elevated pressures. The reactants and products containing N—O bonds seem to be quite thermally stable, but adequate shielding is advisable.

Manipulation of volatile materials

Volatile compounds were handled in vacuum lines constructed of Pyrex with glass/Teflon® valves and of types 304 and 316 stainless steel. Amounts of volatiles were determined by PVT techniques, assuming ideal gas behavior, using a Wallace & Tiernan series 1500 differential pressure gauge. Materials with significant nonideality (anhydrous HF) or low vapor pressure (SbF_5) were vacuum-transferred but determined by direct weighing. Low-temperature trap-to-trap distillations were performed under dynamic vacuum. AsF_5 may be handled in glass vacuum systems under sufficiently dry conditions. SbF_5,

[1]Presented in part in ref. 24.

[2]Author to whom correspondence may be addressed.

Printed in Canada / Imprimé au Canada

Can. J. Chem. Downloaded from www.nrcresearchpress.com by 186.148.149.217 on 09/07/12
For personal use only.

Can. J. Chem. Downloaded from www.nrcresearchpress.com by 186.148.149.217 on 09/07/12
For personal use only.

while also safe in dry glass, was generally vacuum-transferred through a short stainless steel connector external to the metal line, as was HF.

Reagent and starting materials

SbF_5 (PCR), BF_3 and octafluorocyclobutane (Matheson), and NaF (Aldrich) were used as received. Anhydrous HF (Air Products) was usually dried in an FEP reactor (see below) with SbF_5; dry HF was removed by vacuum transfer at −40°C (7). Arsenic pentafluoride was used for this purpose in some early work, but this produces uncertainties in reaction stoichiometries due to subsequent vacuum transfer of unreacted AsF_5 with the dry HF. Christie *et al.* have pointed out (12) that BiF_5 should be the most convenient drying agent in this regard. $H_3O^+AsF_6^-$ (7), $CF_3\overline{N—O—CFXCF_2}$ where X = F (13), Cl (14), and H (15), and $\overline{C(CF_3)_2—O—CF_2CF_2}$ (16, 17) were prepared by literature methods. AsF_5 was prepared from As_2O_5 and F_2 (18, 19).

Reaction vessels

Reactors for superacid ring-openings were constructed from Teflon® -FEP tubing of $\frac{1}{16}$ in. wall thickness and either $\frac{1}{2}$ in. or $\frac{5}{8}$ in. o.d. The tube was heat-sealed at one end, fitted with a 316 stainless insert at the other, and connected to a Nupro SS-4JBR valve by means of Swagelok 316 SS tube fittings and Teflon® ferrules. Neutralizations of the superacid mixtures with NaF were conducted in 75- or 150-mL 304 SS Hoke bombs, also with the above Nupro valve.

Instrumentation

Infrared spectra were recorded in the gas phase on a Perkin–Elmer 1430 instrument equipped with a P–E 7500 data station. IR cells were 10 cm in length with KCl plates secured using Halocarbon 1500 wax. ^1H and ^{19}F NMR spectra were obtained on an IBM NR/200AF spectrometer at 200.13 and 188.31 MHz, respectively, and were referenced to internal $Si(CH_3)_4$ and $CFCl_3$. Chemical shifts upfield from these are reported as negative. Mass spectra were run on a Hewlett–Packard 5985A at 70 eV. CH_4 was the CI gas. Samples were introduced by direct gas insertion.

*Reaction of $CF_3\overline{N—O—CF_2CF_2}$, **1**, with HF/AsF_5*

An FEP reactor of internal volume 39.5 mL was evacuated, weighed, and cooled to −196°C. Anhydrous HF (0.97 g, 48 mmol) was condensed in by vacuum transfer on the steel vacuum line. The reactor was weighed, cooled again, and 10.00 mmol AsF_5 condensed in. The mixture was warmed to room temperature with a water bath to form a homogeneous solution and then frozen again in liquid nitrogen. Oxazetidine **1** (5.00 mmol) was condensed in and the reactor was warmed with agitation under a stream of running water. A vigorous reaction began as soon as the mixture began to melt (mp HF = −83°C). The reactor was allowed to stand at 23°C for 18 h. After degassing (freeze–pump–thaw) on the metal line the contents of the reactor were vacuum-transferred into a 150-mL bomb cooled to −196°C, containing several steel balls and 12.22 g (291 mmol) NaF powder to remove HF and AsF_5. A solid began to form as the volatiles were removed from the FEP reactor; this solid was somewhat volatile and with some heating and agitation nearly all of it could be transferred to the NaF bomb. The crude product was allowed to stand over the NaF for 2.5 h at 23°C with occasional shaking; it was then pumped into a glass U-trap cooled with liquid nitrogen and purified by trap-to-trap distillation using traps at −70, −95, and −196°C. The −95°C trap retained the product **1***a*, $CF_3N(H)—OCF_2CF_3$ (4.84 mmol, 97% yield).

1*a* was characterized as follows: mp −66.8°C; vapor pressure curve measured from −33.4 to +18.4°C: $\log_{10}P$ (Torr; 1 Torr = 133.3 Pa) = 6.544 − 724.735/T − 121255.969/T^2, ΔH = 6942.07 cal/mol, ΔS = 22.68 eu, extrapolated bp +32.9°C; IR (3 Torr): 3342 ($\nu_{N—H}$, m), 1483 (sh, w), 1453 (s), 1399 (w), 1313 (vs), 1275 (sh, m), 1236 (vs), 1197 (vs), 1170 (vs), 1107 (vs), 1028 (w), 969 (w), 919 (m), 863 (m), 814 (w), 741 (m), 679 (w), 620 (w), 569 (w) cm^{-1}; NMR $CF_3^AN(H)—OCF_2^BCF_3^C$, δ ^1H ($CDCl_3$): 6.56 (br q); δ ^{19}F ($CDCl_3$): A, −70.6 (3F, dt); B, −95.3 (2F, qq); C, −84.9 (3F, t) ppm; J_{HA} = 8.6, J_{AB} = 3.8, J_{BC} = 1.7, J_{HB} = J_{HC} = J_{AC} = 0 Hz; MS, major *m/z* [EI]: 219 (M^+), 200 ($M - F^+$), 180 ($M - F - HF^+$), 130 ($M - HF - CF_3^+$), 119 ($CF_3CF_2^+$), 69 (CF_3^+); major *m/z* [CI]: 220 (MH^+), 200 ($MH - HF^+$), 180 ($MH - 2HF^+$), 130 ($M - HF - CF_3^+$), 119 ($CF_3CF_2^+$).

*Reaction of $CF_3\overline{N—O—CFClCF_2}$, **2**, with HF/AsF_5*

The procedure of compound **1** was followed using a 40-mL FEP reactor, 1.45 g (72.5 mmol) dried HF, 10.00 mmol AsF_5, and 5.00 mmol oxazetidine **2**. The reaction, less energetic than for **1**, stood for 16 h at 24°C and was then vacuum-transferred with heating and agitation onto 15.22 g (362 mmol) NaF powder in a 150-mL bomb containing several steel balls. After 3.5 h at 24°C the product was pumped out and fractionated through traps cooled to −58, −80, and −196°C. The −80°C trap contained 4.12 mmol of crude **2***a*, $CF_3N(H)—OCFClCF_3$, with some AsF_3. The yield of **2***a* was determined by ^{19}F NMR to be 45 mol% of the sample or 1.86 mmol of pure compound (37% yield). The −58°C trap contained 1.34 mmol (27% yield) of the known (20, 21) hydroxylamine **2***b*, $CF_3N(OH)—CF_2CF_2Cl$.

2*a* was characterized as follows: IR (4 Torr): 3333 ($\nu_{N—H}$, m), 1489 (sh, w), 1450 (s), 1336 (s), 1308 (vs), 1279 (sh, m), 1228 (vs), 1206 (sh, s), 1149 (s), 1126 (s), 1093 (vs), 1022 (m), 993 (s), 918 (m), 874 (w), 839 (m), 654 (w), 604 (w), 563 (w) cm^{-1}; NMR $CF_3^AN(H)—OCF^BClCF_3^C$, δ ^1H ($CDCl_3$): 6.63 (br q); δ ^{19}F ($CDCl_3$): A, −69.9 (3F, dd); B, −81.3 (1F, qq); C, −83.1 (3F, d) ppm; J_{HA} = 8.5, J_{AB} = 4.1, J_{BC} = 2.4, J_{HB} = J_{HC} = J_{AC} = 0 Hz; MS, major *m/z* [EI]: 200 ($M - Cl^+$), 180 ($M - Cl - HF^+$), 135/137 ($CFClCF_3^+$), 85/87 (CF_2Cl^+), 69 (CF_3^+); major *m/z* [CI]: 236/238 (MH^+), 216/218 ($MH - HF^+$), 200 ($M - Cl^+$), 180 ($M - Cl - HF^+$), 135/137 ($CFClCF_3^+$).

The previously reported compound **2***b* was not well examined in the original publication (20); we report its characterization as follows: IR (4 Torr): 3600 ($\nu_{O—H}$, sharp, m), 1390 (m), 1320 (s), 1277 (vs), 1250 (vs), 1211 (vs), 1185 (vs), 1115 (s), 1043 (m), 984 (s), 873 (s), 833 (s), 753 (m), 683 (m), 661 (w), 630 (w), 585 (w) cm^{-1}; NMR $CF_3^AN(OH)—CF_2^BCF_2^CCl$, δ ^1H ($CDCl_3$): 5.88 (s); δ ^{19}F ($CDCl_3$): A, −67.2 (3F, br t); B, −106.0 (2F, qt); C, −69.0 (2F, tq) ppm; J_{AB} = 12.9, J_{AC} = 1.4, J_{BC} = 2.8, J_{HA} = J_{HB} = J_{HC} = 0 Hz; MS, major *m/z* [EI]: 200 ($M - Cl^+$), 180 ($M - Cl - HF^+$), 150 ($M - CF_2Cl^+$), 135/137 ($CF_2CF_2Cl^+$), 85/87 (CF_2Cl^+), 69 (CF_3^+), 50 (CF_2^+); major *m/z* [CI]: 236/238 (MH^+), 216/218 ($MH - HF^+$), 200 ($M - Cl^+$), 150 ($M - CF_2Cl^+$).

*Reaction of $CF_3\overline{N—O—CHFCF_2}$, **3**, with HF/AsF_5*

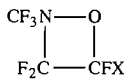
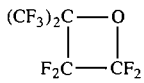
The same procedure was followed as for compound **1**, using an FEP reactor of 35 mL volume. Amounts of reactants were 1.73 g (86 mmol) HF, 10.00 mmol AsF_5, and 5.00 mmol oxazetidine **3**. The initially exothermic reaction was allowed to stand at 23°C for 24 h and was then vacuum-transferred with heating and agitation onto 18.16 g (432 mmol) NaF powder in a 150-mL bomb containing several steel balls, where it was allowed to remain for 36 h at 23°C with occasional shaking. Trap-to-trap fractionation through traps cooled to −65, −90, and −196°C gave 3.20 mmol (64% yield) of $CF_3N(H)—OCHFCF_3$, **3***a*, in the −90°C trap.

3*a* was characterized as follows: IR (3 Torr): 3335 ($\nu_{N—H}$, m), 2989 ($\nu_{C—H}$, w), 1478 (sh, w), 1433 (s), 1409 (w), 1344 (w), 1291 (vs), 1214 (vs), 1191 (vs), 1127 (vs), 1088 (s), 1021 (w), 989 (sh, w), 923 (m), 904 (m), 830 (w), 725 (m), 700 (m), 609 (w), 563 (w) cm^{-1}; NMR $CF_3^AN(H^B)—OCH^CF^DCF_3^E$, δ ^1H ($CDCl_3$): B, 6.75 (1H, br q); C, 5.66 (1H, dq); δ ^{19}F ($CDCl_3$): A, −71.2 (3F, dd); D, −144.8 (1F, dqq); E, −82.6 (3F, dd) ppm; J_{AB} = 8.4, J_{AD} = 2.2, J_{CD} = 57.6, J_{CE} = 3.2, J_{DE} = 5.9, J_{AC} = J_{AE} = J_{BC} = J_{BD} = J_{BE} = 0 Hz; MS, major *m/z* [EI]: 201 (M^+), 182 ($M - F^+$), 162 ($M - F - HF^+$), 132 ($M - CF_3^+$), 112 ($M - CF_3 - HF^+$), 101 (CF_3CHF^+), 100 (CF_3CF^+), 69 (CF_3^+); major *m/z* [CI]: 202 (MH^+), 182 ($MH - HF^+$).

*Reaction of $\overline{C(CF_3)_2—O—CF_2CF_2}$, **4**, with HF/SbF_5*

Into a 12-mL FEP reactor was vacuum-transferred 2.07 g (9.55 mmol) SbF_5 followed by 2.21 g (110 mmol) dried HF. The superacid mixture was then warmed to room temperature and agitated to form a homoge-

TABLE 1. Summary of superacid ring-opening reactions

Reactant	Lewis acid	Lewis acid: heterocycle[a]	Product	Yield (%)
				
X = F (**1**)	AsF_5	2:1	$CF_3N(H)—OCF_2CF_3$ (**1***a*)	97
		1.5:1	**1***a*	88
		1:1	**1***a*	77
		1:2	**1***a*	50
	SbF_5	1.5:1	**1***a*	31
		1:1	**1***a*	54
		1:2	**1***a*	40
	BF_3[b]	1:2	**1***a*	2
X = Cl (**2**)	AsF_5	2:1	$CF_3N(H)—OCFClCF_3$ (**2***a*)	37
			$CF_3N(OH)—CF_2CF_2Cl$ (**2***b*)	27
X = H (**3**)	AsF_5	2:1	$CF_3N(H)—OCHFCF_3$ (**3***a*)	64
				
(**4**)	SbF_5[c]	1:1	$CF_3CF_2C(CF_3)_2—OH$ (**4***a*)	96
	SbF_5[d]	1:1	**4***a*	11
	AsF_5[e]	1:1	**4***a*	0

All reactions used excess HF and were quenched with NaF. Conditions were ambient temperature and 12–24 h unless otherwise specified.
[a]Molar ratio.
[b]23°C, 3 days.
[c]55°C, 17 h.
[d]23°C, 36 h.
[e]23°C, 40 h.

neous solution. Oxetane **4** (9.55 mmol) was then condensed in; upon warming, the reactants formed two liquid phases and did not appear to react. The reactor was placed in an oil bath and heated to 55°C (**Caution! High pressure!**) for 17 h, by which time the reaction mixture had become homogeneous. Nearly all the material was vacuum-transferred with heating (no solid formation was observed) onto 23.19 g (553 mmol) NaF powder in a 150-mL bomb containing several steel balls. After 4 h at 23°C with occasional shaking, the product was pumped out and fractionated through traps cooled to −40, −80, and −196°C; the product, 9.20 mmol (96% yield) of the known (22, 23) $CF_3CF_2C(CF_3)_2—OH$, **4***a*, collected in the −80°C trap.

Only the boiling point and ^{19}F NMR chemical shifts have been reported (22) for **4***a*; we report additional characterization as follows: IR (1 Torr): 3620 ($\nu_{O—H}$, m), 1376 (sh, w), 1342 (w), 1274 (s), 1249 (vs), 1227 (s), 1142 (m), 1071 (w), 966 (m), 955 (sh, w), 880 (m), 736/725 (d, m), 660 (w), 621 (w) cm^{-1}; NMR $CF_3^ACF_2^BC(CF_3^C)_2—OH$, δ ^1H ($CDCl_3$): 3.56 (s); δ ^{19}F ($CDCl_3$): A, −80.5 (3F, sept); B, −119.6 (2F, sept); C, −73.3 (6F, tq) ppm; J_{AC} = 5.7, J_{BC} = 10.9, J_{AB} = J_{HA} = J_{HB} = J_{HC} = 0 Hz; MS, major *m/z* [EI]: 247 ($M - F - HF^+$), 217 ($M - CF_3^+$), 197 ($M - CF_3 - HF^+$), 167 ($M - C_2F_5^+$), 147 ($M - C_2F_5 - HF^+$), 119 ($C_2F_5^+$), 100 (CF_3CF^+), 97 (CF_3CO^+), 69 (CF_3^+); major *m/z* [CI]: 305 ($MH + H_2O^+$), 287 (MH^+), 267 ($MH - HF^+$), 247 ($MH - 2HF^+$), 217 ($M - CF_3^+$), 197 ($M - HF - CF_3^+$), 167 ($M - C_2F_5^+$), 150 ($CF_3CCF_3^+$), 147 ($M - HF - C_2F_5^+$), 119 (C_2F_5), 100 (CF_3CF^+).

Results and discussion

Synthetic results of this investigation are summarized in Table 1. The ring-opening reactions reported here exhibit several noteworthy, although completely reasonable, features. The first is that for **1**–**3** the normally fragile N—O bond remains intact; these reaction systems do not involve radicals and, even if the N—O bond were to cleave through a more ionic mechanism, the result would be a thermodynamically unfavorable N—F or O—F compound.

The other feature is that the >NH and —OH functional groups of these highly fluorinated products are not "protonated off" (protonated and removed as initially neutral leaving groups) in the superacid media to give cations, as is often observed in hydrocarbon superacid chemistry, for example, the cleavage of secondary oxonium ions (protonated ethers) to give alkyl cations (ref. 1, pp. 82, 182–184). The product **4***a*, for instance, would produce the corresponding carbocation $CF_3CF_2C^+(CF_3)_2$, the perfluoroalkyl substituents of which would be very destabilizing (25), even relative to fluorine substituents, since inductive withdrawal is still present but resonance stabilization of the type in eq. [1] is lacking.

[1] $>C^+—F \leftrightarrow >C{=}F^+$

These reactions are similar to the use of $(HF)_x\cdot$ pyridine or trialkylamine complexes in the ring opening of cyclopropane (26), hydrocarbon epoxides (27), aziridines (28–31), and azirines (28, 29); X-ray structures of $(HF)_x\cdot$py have recently been determined (32). The fluorinated heterocycles in this work, however, should be much less basic than the above examples and it is unlikely that $(HF)_x\cdot$py would be sufficiently acidic to protonate them. The oxetane **4**, in fact, requires the strongest system available to produce good yields. Recent work has also

Can. J. Chem. Downloaded from www.nrcresearchpress.com by 186.148.149.217 on 09/07/12
For personal use only.

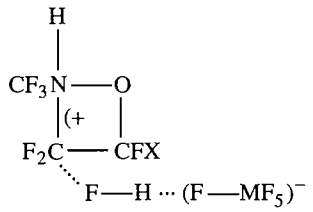


FIG. 1. Proposed solvent interaction leading to ring opening of a protonated 1,2-oxazetidine.

appeared (33) concerning the ring-opening of partially fluorinated oxetanes with $AlCl_3$. Likewise, others in our laboratory have found (34) that a Lewis acid alone (SbF_5) converts **1–3** to dimers and trimers, presumably through a fluoride-ion abstraction mechanism; this should not contribute in the current Brönsted–Lowry acid work since the amount of molecular SbF_5 in an HF mixture is negligible (4). A significant, temperature-dependent concentration of AsF_5 exists in HF solution, however, as free AsF_5 (3).

Since the reagent in this work is a protic superacid it seems reasonable to assume that the reaction is initiated by protonation of the most basic site of the substrate. Highly fluorinated, weakly basic molecules such as these require a heteroatom to provide sufficient basicity; otherwise, even a superacid will not react. An attempted reaction of octafluorocyclobutane with HF/AsF_5 at room temperature resulted in quantitative recovery of the starting material. We have not checked the stronger HF/SbF_5. The "weak" superacid HF/BF_3 undergoes only a trace of reaction with **1** (see Table 1). Possible catalytic effects from water (wet HF) were excluded by testing **1** with a sample of $H_3O^+AsF_6^-$ (7) (the result of wet HF plus AsF_5) alone; no reaction was observed.

We have not looked for discrete carbocation intermediates of the form $CF_3N(H)—OCF_2CF_2^+$, for example, which could be involved in the opening of the ring after protonation. A lower-energy "solvent-assisted" pathway seems more reasonable, where an interaction of the type shown in Fig. 1, for instance, leads to $CF_3N(H)—OCFXCF_3$. Competing protonation on oxygen would lead to fluoride-ion donation to the other ring carbon, giving a hydroxylamine as observed for **2**. The reason for this pattern of product variation with substituent X is not entirely clear. It cannot be an inductive (electronegativity) effect, because if the appropriate hydroxylamine is not observed for X = F (**1**) but is for X = Cl (**2**), then X = H (**3**) would be expected to yield even more hydroxylamine; instead, none is found. This implies a resonance effect and suggests, in the limit of the free carbocations $CF_3N(OH)—CF_2—FXC^+$, that X = Cl is more stabilizing than X = F, perhaps through the resonance form $CF_3N(OH)—CF_2—FC{=}X^+$, a contributor that is not possible for X = H. This goes against the well-known ability of α-fluorine to stabilize carbocations by back-donation of lone-pair electrons (refs. 1, p. 114, and 25) and also contradicts the known trend of Lewis acidities of the isoelectronic boron halides: $BBr_3 > BCl_3 > BF_3$. The trifluoride is the weakest Lewis acid precisely because the $2p$–p overlap is *more* effective for fluorine than for the other halogens. That is, resonance structures of the form $X_2B^-{=}X^+$ are more significant for X = F with the accompanying stronger negative charge on boron acting to reduce the acidity of BF_3 relative to the other trihalides.

Hine and Lee, however, have reported kinetic data (35, 36) for solvolysis reactions of side-chain halogenated toluenes; their rate constants, when interpreted in terms of a primarily S_N1 (carbocation) mechanism, show a superior tendency for α-chlorine relative to α-hydrogen or -fluorine to activate the departure of a chloride leaving group. Solvolysis in 50% aqueous acetone of $PhCF_2—Cl$, $PhCH_2—Cl$, and $PhCCl_2—Cl$, for example, gave rate constants in a ratio of 1:5.3:2600 respectively. While this situation is clouded by probable deviations from the extreme S_N1 case and by ground state stability differences, the trend matches the observation that in the current oxazetidine ring-opening work only the chloro-substituted **2** produces any hydroxylamine. As discussed above in the S_N1 limit, the oxygen functionality would be considered a leaving group whose departure is not sufficiently activated by X = H or F substituents. Although useful as a formalism, the purely dissociative mechanism cannot, of course, represent the initiation of the ring-opening reaction itself to a significant degree since this would predict complete reaction using HF alone without the benefit of added Lewis acid. It does, however, provide a viewpoint for following the course of the ring opening subsequent to or simultaneous with protonation.

The ring opening of oxetane **4** is regiospecific since the only product is ***4a*** and no $C(CF_3)_2F—CF_2C(O)F$ is observed. The acid fluoride would arise from spontaneous dehydrofluorination of $C(CF_3)_2F—CF_2CF_2OH$, the other possible ring-opening product. Again, in the limit of free carbocations derived from HO^+—C bond cleavage, the positive charge would prefer to develop on a carbon with substituents of F, F, R_f[3] ($HOC(CF_3)_2$-$CF_2CF_2^+$) rather than on a carbon bearing two CF_3 and one longer perfluoroalkyl group ($C^+(CF_3)_2CF_2CF_2OH$), as mentioned previously and implied by the failure of hexafluoroacetone to protonate in $HOSO_2F/SbF_5$ ("Magic Acid") (25).

An important consequence of the heteroatom basicity is that if the ring protonates and opens, then the resulting product may also be protonated. This could explain the formation of volatile solids as the superacid mixture evaporates and is vacuum-transferred onto NaF following ring-opening reactions with the nitrogen heterocycles. That is, products of the form $CF_3N(H)—OCFXCF_3$ are likely to be protonated to $CF_3N^+(H)(H)—OCFXCF_3$. Precedent for this resides in the independent synthesis of $CF_3N^+(H)(H)—OCF_3$ AsF_6^- and $CF_3N^+(H)(H)—OCF(CF_3)_2$, which exhibit dissociation pressures of 50 and 10 Torr, respectively, at 22°C (11). While the ring-opening reactions should in principle be catalytic in Lewis acid, examination of the yields of ***1a*** in Table 1 as a function of equivalents of AsF_5 used also suggests that much of the AsF_5 becomes unavailable for further reaction. The 2:1 molar ratio of AsF_5: ring necessary for optimum yields under these conditions means that most of the counterion associated with the protonated product should be $As_2F_{11}^-$. The existence of equilibria in the HF/AsF_5–AsF_6^-–$As_2F_{11}^-$ system (3) and between protonated and unprotonated product (11), however, makes the observed yield dependence somewhat surprising. Another possible answer is that the solid is the salt of the protonated unopened ring, which was an original goal of this research, and that ring opening occurs mostly upon heating via donation of fluoride from the anion to the protonated ring. The observed yield data, when interpreted in the light of such a hypothesis, would indicate that $As_2F_{11}^-$ is more effective in donating fluoride to open the ring than is AsF_6^-. Occasionally, when an FEP reactor is allowed to stand for a few days after vacuum-transferring most of its contents onto NaF, colorless crystals will sublime onto

[3] R_f is a perfluoroalkyl group.

Can. J. Chem. Downloaded from www.nrcresearchpress.com by 186.148.149.217 on 09/07/12
For personal use only.

the sides of the FEP tube. These crystals sublime away when the reactor is cut open in a drybox, and fume in moist air. An X-ray diffraction and Raman study would help to answer these mechanistic and structural questions. Standard elemental analyses on such corrosive samples would present formidable challenges and were not attempted. It should be possible, however, to determine arsenic and antimony in aqueous solution using X-ray fluorescence spectroscopy.

Yields of **1***a* using SbF_5 are lower, due, we feel, to difficulties in removing the much more strongly protonated product from the viscous SbF_5 matrix using the current experimental technique. For the less basic oxygen in oxetane **4** the HF/AsF_5 system is simply not strong enough and the use of SbF_5 is necessary. At 55°C the reaction is still slow but the use of equimolar SbF_5:**4** gives an excellent yield, indicating that product protonation is easily reversible and not a problem. No solids are observed as the reaction mixture is transferred out of the FEP reactor, so **4***a* is formed before the heating/transfer step. That is, the protonated oxetane cannot wait until being heated for the counterion to donate F^-, opening the ring as described in the second scenario for the oxazetidines. If this second mechanism were true for **4** there would probably be volatile solid formed during the transfer. The fact that there is none means either that the protonated ring–counterion pair collapses very easily or that it no longer exists at that time, lending credence to the belief that the oxazetidine solids are protonated product and not protonated starting material.

Synthetic chemistry using superacids should be capable of producing many more interesting and unusual compounds. Fluorinated oxazetidines (37, 38) and oxetanes (ref. 33 and references therein) can be made in large variety. We are investigating other ring systems, especially with regard to size, and exploring the chemistry of the amine products reported here.

Acknowledgement

The authors thank Montefluos S.p.A. of Italy for financial support.

1. G. A. Olah, G. K. S. Prakash, and J. Sommer. Superacids. John Wiley & Sons, New York. 1985.
2. T. A. O'Donnell. J. Fluorine Chem. **25**, 75 (1984).
3. C. G. Barraclough, J. Besida, P. G. Davies, and T. A. O'Donnell. J. Fluorine Chem. **38**, 405 (1988).
4. R. J. Gillespie and J. Liang. J. Am. Chem. Soc. **110**, 6053 (1988).
5. D. Mootz and K. Bartmann. Angew. Chem. Int. Ed. Engl. **27**, 391 (1988).
6. M. C. Henry, C. B. Griffis, and E. C. Stump. Fluorine Chem. Rev. **1**, 1 (1967).
7. K. O. Christe, C. J. Schack, and R. D. Wilson. Inorg. Chem. **14**, 2224 (1975).
8. K. O. Christe. Inorg. Chem. **14**, 2230 (1975).
9. K. O. Christe. Inorg. Chem. **14**, 2821 (1975).
10. R. Minkwitz, R. Kerbachi, R. Nass, D. Bernstein, and H. Preut. J. Fluorine Chem. **37**, 259 (1987).
11. D. D. DesMarteau, W. L. Lam, B. A. O'Brien, and S.-C. Chang. J. Fluorine Chem. **25**, 387 (1984).
12. K. O. Christe, W. W. Wilson, and C. J. Schack. J. Fluorine Chem. **11**, 71 (1978).
13. D. A. Barr and R. N. Haszeldine. J. Chem. Soc. 1881 (1955).
14. D. A. Barr, R. N. Haszeldine, and C. J. Willis. J. Chem. Soc. 1351 (1961).
15. R. E. Banks, R. N. Haszeldine, H. Sutcliffe, and C. J. Willis. J. Chem. Soc. 2506 (1965).
16. M. M. Schlechter and C. Woolf. Fr. Patent 1,391,493 (1965); Chem Abstr. **63**, 8317g (1965).
17. Allied Chemical Corp. Neth. Patent Appl. 6,404,593 (1964); Chem. Abstr. **62**, 11782g (1965).
18. G. Mitra. J. Am. Chem. Soc. **80**, 5639 (1958).
19. S.-C. Chang. Ph.D. Dissertation. Kansas State University, Manhattan, KS. 1982.
20. V. A. Ginsburg, L. L. Martynova, M. F. Lebedeva, B. I. Tetel'baum, and A. N. Medvedev. Zh. Obshch. Khim. **37**, 1077 (1967).
21. V. A. Ginsburg and M. F. Lebedeva. U.S.S.R. Patent 210,127 (1968); Chem. Abstr. **69**, 51560q (1968).
22. D. P. Graham and W. Viktor. J. Org. Chem. **31**, 957 (1966).
23. D. P. Graham. U.S. Patent 3,317,615 (1967); Chem. Abstr. **67**, 53654f (1967).
24. (*a*) D. D. DesMarteau and S. P. Kotun. 12th International Symposium on Fluorine Chemistry, Santa Cruz, CA. Abstract P233, August 1988; (*b*) D. D. DesMarteau, S. P. Kotun, and A. Malacrida. Ital. Patent Appl. 21615 A/88, August 2, 1988.
25. R. D. Chambers. Fluorine in organic chemistry. John Wiley & Sons, New York. 1973. pp. 73–84.
26. G. A. Olah, M. Nojima, and I. Kerekes. Synthesis, 779 (1973).
27. G. A. Olah and D. Meidar. Israel J. Chem. **17**, 148 (1978).
28. T. N. Wade and R. Guedj. Tetrahedron Lett. 3251 (1978).
29. G. Alvernhe, E. Kozlowska-Gramsz, S. Lacombe-Bar, and A. Laurent. Tetrahedron Lett. 5203 (1978).
30. T. N. Wade, F. Gaymard, and R. Guedj. Tetrahedron Lett. 2681 (1979).
31. G. Alvernhe, S. Lacombe, and A. Laurent. Tetrahedron Lett. **21**, 289 (1980).
32. D. Boenigk and D. Mootz. J. Am. Chem. Soc. **110**, 2135 (1988).
33. P. Tarrant and R. N. Bull. J. Fluorine Chem. **40**, 201 (1988).
34. D. D. DesMarteau and A. Malacrida. Ital. Patent Appl. 21266 A/88 (1988).
35. J. Hine and D. E. Lee. J. Am. Chem. Soc. **73**, 22 (1951).
36. J. Hine and D. E. Lee. J. Am. Chem. Soc. **74**, 3182 (1952).
37. A. Haas. *In* Gmelin Handbuch der Anorganischen Chemie. 8th ed. Syst.-No. 5, Teil 5. *Edited by* D. Koschel. Springer-Verlag, New York. 1978. pp. 29–50.
38. A. Haas. *In* Gmelin Handbuch der Anorganischen Chemie. 8th ed. Syst.-No. 5, Teil 7. *Edited by* D. Koschel. Springer-Verlag, New York. 1979. pp. 161–173, 193–195.

Can. J. Chem. Downloaded from www.nrcresearchpress.com by 186.148.149.217 on 09/07/12
For personal use only.

Reaction of RuO_4 with KrF_2: A clear-cut method to prepare ruthenium oxide tetrafluoride

LAURENT MEUBLAT, MONIQUE LANCE, AND ROLAND BOUGON[1]

Département d'étude des lasers et de la physico-chimie, Service de chimie moléculaire — Unité de recherche associée n° 331, Centre national de la recherche scientifique, Commissariat à l'énergie atomique — Centre d'études nucléaires de Saclay, 91191 Gif sur Yvette CÉDEX, France

Received January 10, 1989

This paper is dedicated to Professor Ronald J. Gillespie on the occasion of his 65th birthday

LAURENT MEUBLAT, MONIQUE LANCE, and ROLAND BOUGON. Can. J. Chem. **67**, 1729 (1989).

The fluorination of ruthenium tetroxide RuO_4 was attempted by using either fluorine or krypton difluoride KrF_2 in HF solution. Of the two fluorinating agents, only KrF_2 was found to be powerful enough to react with RuO_4 and to transform it into ruthenium oxide tetrafluoride $RuOF_4$. This oxide fluoride of ruthenium VI was characterized by elemental analysis, X-ray powder diffraction, and infrared absorption spectroscopy.

Key words: ruthenium tetroxide, ruthenium oxide tetrafluoride, krypton difluoride, fluorination.

LAURENT MEUBLAT, MONIQUE LANCE et ROLAND BOUGON. Can. J. Chem. **67**, 1729 (1989).

La fluoration du tétroxyde de ruthénium RuO_4 a été recherchée en utilisant le fluor ou le difluorure de krypton en solution HF. Des deux agents fluorants, seul KrF_2 s'est révélé suffisamment puissant pour réagir avec RuO_4 et le transformer en oxytétrafluorure de ruthénium $RuOF_4$. Cet oxyfluorure de ruthénium VI ainsi préparé a été caractérisé par l'analyse élémentaire, la diffraction des rayons X sur poudre et la spectroscopie d'absorption infrarouge.

Mots clés : tétroxyde de ruthénium, oxytétrafluorure de ruthénium, difluorure de krypton, fluoration.

Introduction

Studies on the volatile species of ruthenium are of interest both for academic research and for the nuclear industry, for the latter especially because of problems caused by the radioactive ^{106}Ru element.

The volatile species may include, in particular, the two oxide fluorides $RuOF_3$ and $RuOF_4$, for which there have been few properties reported.

Ruthenium oxide trifluoride $RuOF_3$ was reported quite recently (1) as being obtained from the reaction of ruthenium dioxide RuO_2 with F_2 at 300–320°C. The first mention of the synthesis of $RuOF_4$ appeared in 1963, when the compound was reported (2) to have been obtained by the reaction of an equimolar mixture of bromine and bromine trifluoride on ruthenium metal. The nature of the reactor, made of Pyrex glass (3), probably accounted for the assumed presence of oxygen in the final product. The suggestion (4) that an oxide film on the metal was the source of oxygen has to be ruled out since the authors (2) had treated the ruthenium metal with hydrogen at a dull-red heat before use. The F and Ru contents of the compound were in agreement with those expected for $RuOF_4$, and several properties were given. However, the X-ray powder pattern was reported to be complex and different from that of RuF_5. The presence of oxygen in the stable, pale, otherwise colorless solid so prepared, containing a small amount of green impurity, was inferred mainly from its vapor pressure and magnetic susceptibility, which were both found to be in agreement with those expected for an oxide tetrafluoride. Later on, a yellowish-green $RuOF_4$ was reported (5, 6) to have been obtained from the reaction of RuO_2 with F_2 at temperatures higher than 400°C. The compound was characterized by its mass spectrum, which displayed the molecular ion $RuOF_4^+$ as the heaviest species; chemical analysis, which gave a value of 4.0 ± 0.1 for the F/Ru molar ratio; and the release of oxygen identified by mass spectrometry. An infrared spectrum of the material was also given; however, the properties of this product differed from those reported by the first authors (2). In particular, the compound prepared by Sakuraï and Takahashi (5, 6) was reported to be unstable at room temperature and to decompose into ruthenium tetrafluoride and oxygen.

The work reported in the present paper, which was initially aimed at preparing new oxide fluorides of ruthenium in its high oxidation states, led in fact to a new and clear-cut method of preparation of $RuOF_4$.

Experimental

Materials

Commercial fluorine (from Union Carbide), helium (from l'Air Liquide), and ruthenium oxide hydrate, $RuO_2 \cdot xH_2O$, containing 60% of ruthenium by weight (from Merck) were used as received. The synthesis of RuO_4 was made according to the method described in the literature (7, 8), which consists of treating $RuO_2 \cdot xH_2O$ alternately with F_2 and a stream of helium saturated with water. These treatments were repeated until 90% of the black starting material was volatilized and condensed in a trap at −196°C. The ruthenium tetroxide was purified by fractional vaporization to remove SiF_4, and by passage through P_2O_5 and NaF to remove H_2O and HF, respectively. Ruthenium tetroxide was identified by the visible and infrared absorption spectra of its vapor, which were found to be identical with those published (7, 9–11). The solubility of RuO_4 in anhydrous HF was found to be 0.1 mol L^{-1} at room temperature, and the Raman spectrum of the solution showed three characteristic bands at 884, 920, and 320 cm^{-1}, assigned to $\nu_1(A_1)$, $\nu_3(F_2)$, and $\nu_2(E)$ and (or) $\nu_4(F_2)$, respectively (7).

The fluorine used for the preparation of KrF_2 was passed over NaF to remove HF, and krypton (from l'Air Liquide) was used without purification. The synthesis of KrF_2 was as previously described (12). Anhydrous HF (from Union Carbide) was dehydrated on bismuth pentafluoride before use (13). The sample of ruthenium pentafluoride used for comparison of the X-ray powder pattern of $RuOF_4$ with that of RuF_5 was prepared as described in the literature (2) using commercial fluorine and ruthenium powder (from Union Carbide and Cie des métaux Précieux, respectively).

Apparatus

Volatile materials used in this work were manipulated in a Monel Teflon–FEP vacuum system. Prior to handling of the moisture-

[1]Author to whom correspondence may be addressed.

Printed in Canada / Imprimé au Canada

Can. J. Chem. Downloaded from www.nrcresearchpress.com by 186.148.149.217 on 09/07/12
For personal use only.

TABLE 1. Room-temperature X-ray powder data[a] for $RuOF_4$ and RuF_5

$RuOF_4$		RuF_5			
d_{obsd}, Å	Intensity	d_{obsd}, Å	d_{calcd}, Å[b]	Intensity	$h\ k\ l$
7.70	w	7.70	7.76	vw	1 1 0
5.60	w				
5.35	w	5.37	5.34	w	0 0 1
5.14	w				
4.62	m	4.64	4.64	mw	$\bar{1}$ 1 1, 120
4.37	ms	4.436	4.421	ms	$\bar{2}$ 0 1
4.177	m	4.187	4.193	m	1 1 1
3.863	s	3.847	3.880	s	2 2 0
3.667	ms	3.630	3.652	m	0 2 1
3.287	vvw				
		3.066	3.072	vw	4 0 0
2.986	mw	2.976	2.989	mw	$\bar{2}$ 2 1
2.838	w	2.882	2.884	vw	$\bar{4}$ 0 1, 311
2.712	vw	2.795	2.814	vw	$\bar{1}$ 3 1
		2.688	2.670	vw	0 0 2
2.597	w	2.634	2.618	vw	4 2 0
2.447	ms(double)	2.486	2.486	m	$\bar{2}$ 3 1, 401
2.354	w	2.372	2.366	m	$\bar{3}$ 1 2
2.325	w				
2.225	mw	2.194	2.200	m	$\bar{1}$ 4 1
2.174	m	2.169	2.178	vw	$\bar{2}$ 4 1
		2.036	2.037	vvw(br)	3 1 2
		1.971	1.976	w	1 5 0
1.932	vw	1.932	1.937	w	5 2 1
1.773	vw				
1.757	vw	1.754	1.753	m	5 4 0
1.732	vw				
1.682	m(br)	1.699	1.699	s	$\bar{1}$ 2 3
1.649	w				
1.619	w(br)				
1.552	w(br)	1.576	1.577	w	$\bar{6}$ 4 1
1.445	mw	1.435	1.435	w	7 3 1

[a]Abbreviations used: br, broad; (v)w or (m)w, (very or middle) weak; m, medium; s, strong.
[b]Calculated from the crystal structure parameters given in ref. 16.

sensitive compounds, the part of the system used was passivated with ClF_3 and (or) hot fluorine. The syntheses were achieved either in Monel vessels equipped with CaF_2 or sapphire windows, or in Teflon–FEP or sapphire tubes equipped with Monel or Teflon–FEP valves. It was noticed that cracks rapidly developed when Kel-F valves were used for handling mixtures of KrF_2, HF, and RuO_4, so that the use of this chlorofluoropolymer had to be ruled out. Moisture-sensitive nonvolatile materials were handled in the dry nitrogen atmosphere of a glove box.

X-ray diffraction patterns, spectra, and analyses

The Debye–Scherrer powder patterns of the samples sealed in 0.3 mm o.d. glass or quartz capillaries were obtained by using a Phillips camera (diameter 11.46 cm) using Ni-filtered CuKα radiation. Infrared spectra were recorded in the range 4000–200 cm^{-1} on a Perkin Elmer model 283 spectrophotometer. Spectra of solids were obtained by using dry powders pressed between AgCl or AgBr windows in an Econo press (Barnes Engineering Co). Spectra of gases were obtained by using a Monel cell of 10-cm path length equipped with AgCl or polyethylene windows. Raman spectra were recorded on a Coderg model T 800 spectrophotometer using the 514.5-nm exciting line of an Ar ion model 165 Spectra-Physics laser filtered with a Coderg premonochromator. Solutions were examined in a Teflon–FEP or sapphire reaction tube. The electronic absorption spectrum of RuO_4 in the gaseous phase was recorded on a Beckman model UV 5270 spectrophotometer. The cell was identical with that used for the IR spectra except for the windows, which consisted of CaF_2 discs. Elemental analyses were performed by Mikroanalytische Laboratorien Elbach, West Germany.

Reaction of RuO_4 with F_2 in HF solution

An amount of hydrogen fluoride (0.87 g) saturated with RuO_4 (ca. 0.08 mmol) was condensed at liquid nitrogen temperature into a Teflon–FEP tube. Fluorine was then admitted to the tube kept at liquid nitrogen temperature so that the partial pressure of F_2 over the HF solution was calculated to be 2 atm (1 atm = 101.3 kPa) at room temperature, and to correspond to ca. 0.22 mmol.

The mixture was stirred and allowed to react for 1 day at room temperature. The resulting solution remained yellow and its Raman spectrum showed only the three characteristic signals mentioned above for RuO_4 in HF solution.

Reaction of RuO_4 with KrF_2 in HF solution

Hydrogen fluoride (7.527 g) was distilled into a sapphire reaction tube, then 0.1275 g of RuO_4 (0.772 mmol) and 0.4453 g of KrF_2 (3.656 mmol) were condensed at liquid nitrogen temperature into the reactor. The mixture was left at room temperature for a few hours during which the solution, initially yellow colored, turned dark orange and a brown orange solid was formed. The Raman spectrum of the slightly orange colored solution over the precipitate showed only the characteristic ν_1 line of KrF_2 at 464 cm^{-1} (14); the lines associated with RuO_4 had disappeared. The mixture was cooled to −196°C and the volatile materials put in contact with silicon powder contained in a Monel reactor in liquid nitrogen. Fluorine is known (15) to react with

Can. J. Chem. Downloaded from www.nrcresearchpress.com by 186.148.149.217 on 09/07/12
For personal use only.

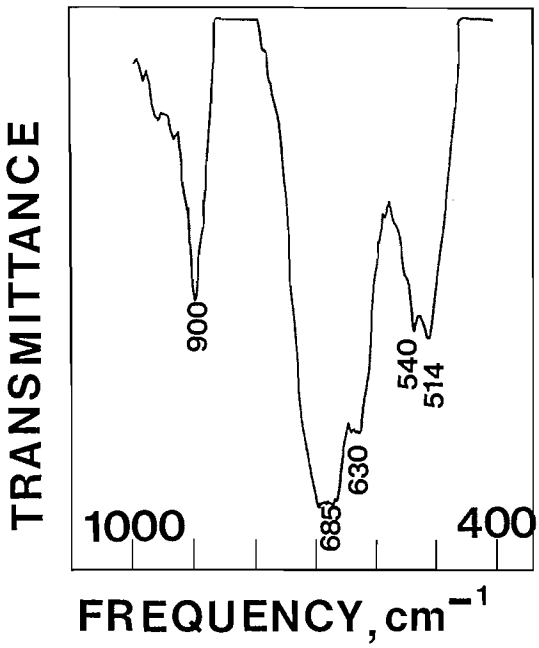


FIG. 1. Infrared spectrum of $RuOF_4$ between AgCl discs at room temperature. Ordinate expansion 5.

silicon at temperatures as low as −196°C to yield SiF_4, which is nonvolatile at these temperatures, so that F_2 is thus normally easily removed from a gaseous mixture. However, due to the diluting effect of the other gases (Kr and O_2), several cycles of condensation and warming up were necessary to convert all the fluorine into SiF_4. The amount of F_2 in the initial gaseous mixture was deduced from the decrease of pressure measured at room temperature in the same volume. The O_2, Kr, SiF_4 mixture was then trapped at −210°C with a liquid nitrogen slush, and the oxygen pumped off. Its amount was deduced from the decrease of pressure measured at room temperature in the same volume and was found to correspond to 2.9 ± 0.2 oxygen atoms per initial Ru atom, indicating that one oxygen atom per Ru atom remained in the solid residue. The determination of the amounts of Kr and F_2 was not accurate enough to distinguish between the KrF_2 that had just been decomposed (with or without intermediary reaction with RuO_4) and that which had effectively fluorinated RuO_4. The excess of KrF_2 and HF was pumped off at −30°C, and the brown residue analysed for its Ru and F contents. *Anal.* calcd. for $RuOF_4$: Ru 52.35, F 39.36; found: Ru 52.35, F 39.15%.

Results and discussion

Fluorine was found to be not powerful enough to fluorinate RuO_4 at room temperature in HF solution, and a fluorinating agent as strong as KrF_2 had to be used.

The composition of the solid obtained was clearly identified as being $RuOF_4$. The compound is brown and very moisture sensitive. No significant rate of decomposition was observed after storage for a few hours at room temperature in a sapphire tube. The compound is not volatile at 0°C, and only slightly volatile at 20°C.

As expected, the X-ray powder pattern of $RuOF_4$ was found to be closely related to that of RuF_5 and the patterns of the two compounds are listed in Table 1.

The infrared spectrum of solid $RuOF_4$ was recorded and the region of the fundamental vibrations is shown in Fig. 1. Contrary to the spectrum reported by previous authors (5), a strong band appears at 900 cm^{-1} and is assigned to the Ru–O stretching vibration. The strong bands at 685 and 630 cm^{-1} are assigned to $Ru–F_{terminal}$ stretching vibrations, and the two bands at 540 and 514 cm^{-1} to $Ru–F_{bridged}$ stretching vibrations. Probably owing to the color of the compound, its Raman spectrum could not be recorded.

The structural unit of RuF_5 was shown (16) to consist of $(RuF_5)_4$ tetramers with the Ru ions occupying the corners of a rhombus. It may be inferred from the present observations that $RuOF_4$ has the same type of tetrameric unit. The ruthenium–oxygen stretching vibration, which is in the range expected (17) for a double bond, favors a fluorine-bridged type of arrangement in the tetramer.

In conclusion, the reaction between RuO_4 and KrF_2 in HF solution led to a compound that was unambiguously identified as $RuOF_4$. It should be stressed that both the X-ray powder pattern and the infrared spectrum of $RuOF_4$ were found to be different enough from those of RuF_5 to rule out the assumption that the product of the reaction consisted of a mixture of crystalline RuF_5 and noncrystalline RuO_4. Furthermore, as attested by the Raman spectra, the reaction, which was achieved in the presence of an excess of KrF_2, went to completion as far as RuO_4 is concerned, and no RuF_5 or RuF_6 derivatives such as $KrF^+RuF_6^-$, or $KrF^+Ru_2F_{11}^-$ (18) were observed. The formal reduction of ruthenium from the oxidation states +8 to +6 probably implies some intermediary ruthenium oxide fluoride in the oxidation states +8 or +7. Further studies on the system, especially regarding the reaction mechanism and the properties of $RuOF_4$, are now in progress.

1. E. G. RAKOV and A. V. DZHALAVYAN. Zh. Neorg. Khim. **32**, 853 (1987).
2. J. H. HOLLOWAY and R. D. PEACOCK. J. Chem. Soc. 527 (1963).
3. J. H. HOLLOWAY and D. LAYCOCK. *Quoted* (p. 84) *in* Adv. Inorg. Chem. Radiochem. **28**, 73 (1984).
4. E. A. SEDDON and K. R. SEDDON. *In* The chemistry of ruthenium. Topics in inorganic and general chemistry. Monograph 19. *Edited by* R. J. H. Clark. Elsevier, Amsterdam, New York, Tokyo. 1984. pp. 63–64.
5. T. SAKURAÏ and A. TAKAHASHI. J. Inorg. Nucl. Chem. **39**, 427 (1977).
6. T. SAKURAÏ and A. TAKAHASHI. J. Phys. Chem. **82**, 780 (1978).
7. R. S. MCDOWELL, L. B. ASPREY, and L. C. HOSKINS. J. Chem. Phys. **56**, 5712 (1972).
8. T. SAKURAÏ and A. TAKAHASHI. J. Inorg. Nucl. Chem. **41**, 681 (1979).
9. G. B. BARTON. Spectrochem. Acta, **19**, 1619 (1963).
10. E. J. WELLS, A. D. JORDAN, D. S. ALDERDICE, and I. G. ROSS. Aust. J. Chem. **20**, 2315 (1967).
11. I. W. LEVIN and S. ABRAMOWITZ. J. Chem. Phys. **50**, 4860 (1969).
12. R. BOUGON and M. LANCE. C.R. Acad. Sci. Sér. 2, **297**, 117 (1983).
13. K. O. CHRISTE, W. W. WILSON, and C. J. SCHACK. J. Fluorine Chem. **11**, 71 (1978).
14. H. H. CLAASEN, G. L. GOODMAN, J. G. MALM, and F. SCHREINER. J. Chem. Phys. **42**, 1229 (1965).
15. Y. MACHETEAU. Thesis, Conservatoire national des arts et métiers, Paris (1969).
16. J. H. HOLLOWAY, R. D. PEACOCK, and R. W. H. SMALL. J. Chem. Soc. 644 (1964).
17. C. G. BARRACLOUGH, J. LEWIS, and R. S. NYHOLM. J. Chem. Soc. 3552 (1959).
18. V. B. SOKOLOV, YU. V. DROBYSCHEVSKII, V. N. PRUSAKOV, A. V. RYZHKOV, and S. S. KHOROSHEV. Dokl. Chem. **229**, 503 (1976).

Can. J. Chem. Downloaded from www.nrcresearchpress.com by 186.148.149.217 on 09/07/12
For personal use only.

A comparative study of the conversion of ethanol and of ethylene over the "Mobil" zeolite catalyst, H-ZSM-5. An application of the Benzene Sequestration Test

DESMOND V. DASS AND ALLAN L. ODELL[1]

Urey Radiochemical Laboratory, Department of Chemistry, University of Auckland, Private Bag, Auckland, New Zealand

Received December 27, 1988

This paper is dedicated to Professor Ronald J. Gillespie on the occasion of his 65th birthday

DESMOND V. DASS and ALLAN L. ODELL. Can. J. Chem. **67**, 1732 (1989).

Ethanol and ethylene both convert to gasoline over the pentasil zeolite catalyst, H-ZSM-5, at 250°C, but yields are lower for ethanol. Adding benzene produces different arrays of alkylbenzenes for the two feeds, propylbenzene being absent using ethanol feed but present using ethylene feed. Neither feed gives rise to toluene or xylene yield increments on adding benzene, showing methylating intermediates to be absent. Hence methylation of C_2 species is ruled out as a route to C_3 intermediate production, and cracking of built-up molecules must be invoked. These results may be understood by postulating stronger sorption of ethanol than of ethylene on the catalyst surface, blocking both carbon chain lengthening sites and cracking sites.

Key words: conversion, ethanol, ethylene, sequestration by benzene, H-ZSM-5.

DESMOND V. DASS et ALLAN L. ODELL. Can. J. Chem. **67**, 1732 (1989).

L'éthanol et l'éthylène se transforment en essence par passage sur un catalyseur zéolite pentasile H-ZSM-5 à 250°C, mais les rendements sont plus faibles dans le cas de l'éthanol. L'addition de benzène produit différents types d'alkylbenzènes dans les deux cas; il se forme du propylbenzène avec l'éthylène mais pas avec l'éthanol. Dans les deux cas, l'addition de benzène provoque une augmentation des rendements en toluène ou en xylène, prouvant ainsi l'absence d'une méthylation des intermédiaires. On a alors écarté la possibilité d'une méthylation des espèces en C_2 comme moyen d'accès aux composés intermédiaires en C_3, et on doit envisager le cracking des molécules formées. On peut comprendre ces résultats en envisageant une sorption plus forte de l'éthanol que de l'éthylène à la surface du catalyseur, bloquant à la fois les sites d'élongation des chaînes carbonées et les sites de cracking.

Mots clés : conversion, éthanol, éthylène, séquestration par le benzène, H-ZSM-5.

[Traduit par la revue]

Can. J. Chem. Downloaded from www.nrcresearchpress.com by 186.148.149.217 on 09/07/12
For personal use only.

Introduction

Since 1986 synthetic gasoline has been produced on an industrial scale in New Zealand using the "Mobil" process. This process utilizes a synthetic pentasil zeolite catalyst, H-ZSM-5, which catalyses the conversion of methanol to a high octane gasoline in one process. The study of the steps in this complex reaction has given rise to an extensive literature. An exhaustive review (1) up to 1982 and a more recent survey in the form of Proceedings of a Symposium in Methane Conversion (2) (1988) provide an introduction to this field, which includes conversion studies on a variety of small molecules over H-ZSM-5.

Fort and Davis have shown (3) that when ethanol is converted over H-ZSM-5 in the presence of added benzene there is a large increase in the yield of ethylbenzene compared to the yield without benzene. They state "... benzene serves as an excellent trap for one or more precursors for chain growth." Our studies on the effect of adding benzene to converting systems led us to similar conclusions, and we have developed this method into the Benzene Sequestration Test (4) for reactive intermediates.

Novakova *et al.* (5, 6) have also utilized sequestration effects of benzene, as well as ethane, propane, and ethylene, to trap reactive intermediates in their temperature programmed desorption studies of methanol and ethanol transformations over zeolite catalysts.

While using the Benzene Sequestration Test to study conversion of C_2 feeds, we noticed interesting differences in product distributions when changing from ethylene feed to ethanol feed.

[1]Author to whom correspondence may be addressed.

Experimental

Mixtures of ethylene (MHSV 0.4 h^{-1}) and benzene (MHSV 0.1 h^{-1}) and of ethanol (MHSV 0.4 h^{-1}) and benzene (MHSV 0.1 h^{-1}) were converted over H-ZSM-5 using a range of temperatures in an apparatus previously described (7, 9).[2]

Yields of the major components in the resulting gasolines were measured by gas–liquid chromatography, and yields of alkylbenzenes with and without added benzene were recorded.

Results

Results, expressed as Δ_B values (increase in wt.% yield of various alkylbenzenes on adding benzene) are shown in Fig. 1 for ethylene feed and in Fig. 2 for ethanol feed, and yields of other products are reported in the text. All wt.% data exclude benzene. Results may be summarized as follows.

1. Conversion

Ethylene converts in the absence of benzene at 250°C to yield a typical gasoline mixture with a yield of 51.3 wt.% (excluding ethylene) leaving residual ethylene 48.7 wt.%.

Ethanol, under similar conditions, gives a smaller gasoline yield of 23.5% (excluding ethylene), an ethylene yield of 76.5 wt.%, and zero residue of ethanol.

2. Effect of adding benzene

(a) Ethylene feed

Little change was found in the yield of gasoline except for

[2]MHSV = Mass Hourly Space Velocity in grams of feed per gram of catalyst per hour.

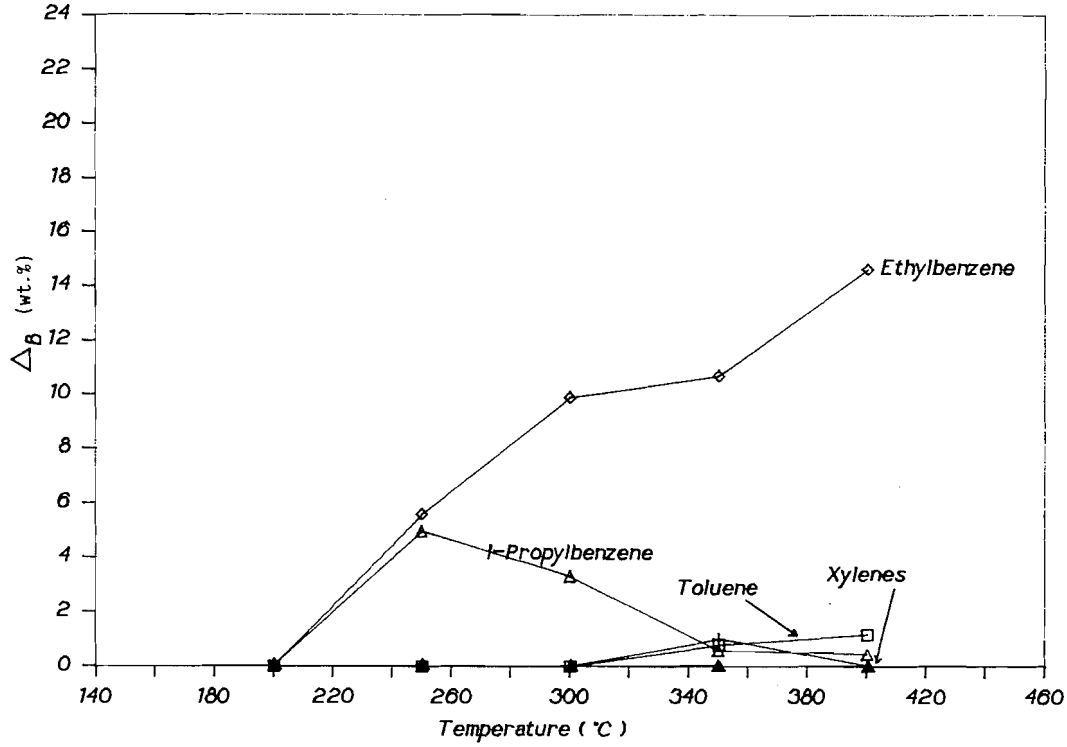


FIG. 1. Ethylene conversion with added benzene: aromatic yield increase vs. temperature.

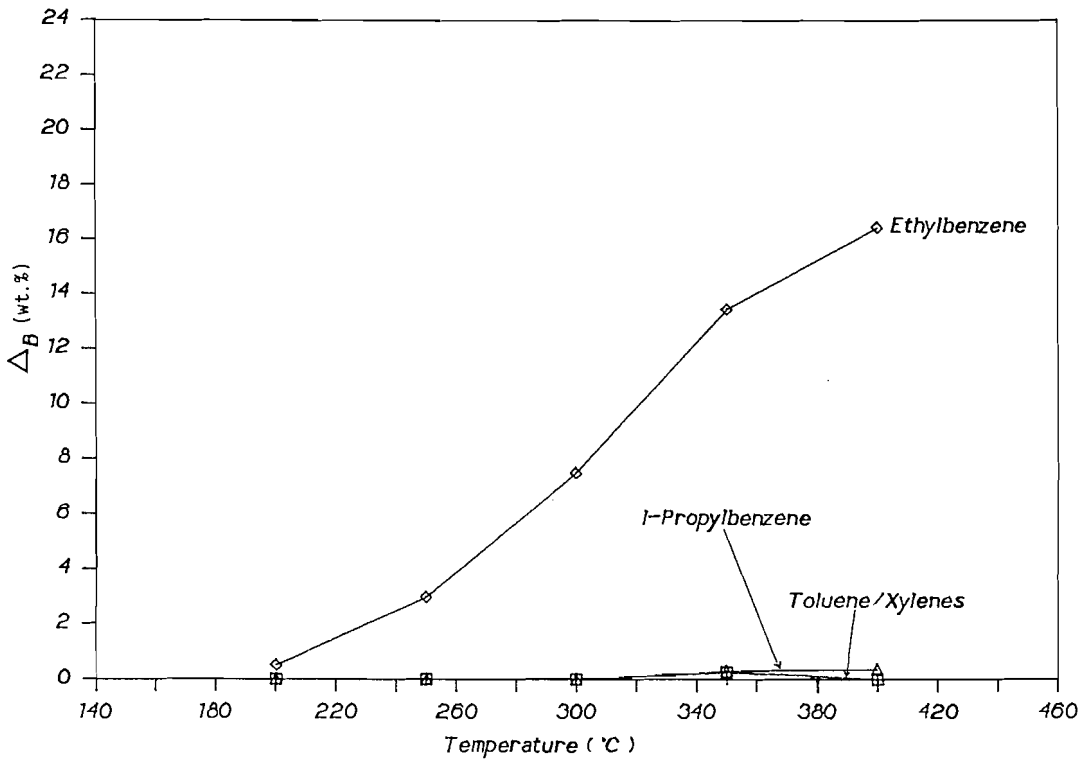


FIG. 2. Ethanol conversion with added benzene: aromatic yield increase vs. temperature.

the two components ethylbenzene and *i*-propylbenzene (see 3 below). Small changes were found in relative selectivities of other components of the resulting gasoline.

(b) Ethanol feed

A lowering of yields of gasoline components to between one half and two thirds of the yields found from benzene-free feed, except for ethylbenzene and *i*-propylbenzene (see 3 below). Small changes were found in relative selectivities of other components of the resulting gasoline.

3. Benzene Sequestration Test

(a) Ethylene feed

Large increments in yields of ethylbenzene and *i*-propylben-

Can. J. Chem. Downloaded from www.nrcresearchpress.com by 186.148.149.217 on 09/07/12
For personal use only.

zene, i.e., large values for Δ_B (ethylbenzene) and Δ_B (*i*-propylbenzene).

(b) Ethanol feed

Large values for Δ_B (ethylbenzene) but Δ_B (*i*-propylbenzene) = 0. Small but measurable values for Δ_B (diethylbenzene).

These studies were extended to cover a range of temperatures from 140 to 400°C and results are shown in Figs. 1 and 2.

Discussion

Important features of these results are (*i*) the large value of Δ_B (ethylbenzene) found for both ethylene and ethanol feeds, showing abundance of a reactive C_2 intermediate, which increases with temperature. We shall refer to this species as C_2*; (*ii*) the contrast between the high values observed for Δ_B (*i*-propylbenzene) from ethylene feed and the zero values observed using ethanol feed.

As usual (4), Δ_B (*i*-propylbenzene) values fall off sharply above 300°C due to the instability of *i*-propylbenzene in the presence of the catalyst at such temperatures. Clearly, a C_3* type intermediate is abundant in the conversion of ethylene at least below 300°C, and possibly above this temperature also. Such a species is absent during the conversion of ethanol.

Another interesting feature is the absence of any "one carbon" reactive intermediate, C_1*, as shown by the fact that Δ_B values for toluene and for xylenes are zero at temperatures up to 300°C for both ethylene and ethanol feeds and very small above this temperature for both feeds. We conclude that methylation is absent in this system and that the C_3* intermediate found in ethylene conversion is not produced by methylation of C_2* or of any other C_2 species. Indeed, the increase in yield of *i*-propylbenzene observed on adding benzene to converting ethylene must be attributed to the production of C_3* by the cracking of larger molecules in the product mixture (10), rather than to methylation of C_2 species, since methylation is absent.

While yields of such built-up products are certainly lowered when benzene is added to converting ethanol (see 2(*b*) above), they are not lowered to zero. Hence some C_3* would be expected from cracking of these products. None is found.

Furthermore, high yields of ethylene found in converting ethanol (74 wt.% at 250°C) would be expected to give products obtained from the conversion of ethylene, including *i*-propylbenzene after the addition of benzene. That this species is not seen calls for a more specific explanation than a small general lowering of yields when benzene is added to converting ethanol.

We suggest that these effects may be accounted for by supposing that the more polar ethanol blocks sites on the catalyst used for chain lengthening or those used for cracking larger molecules in a manner not found in the conversion of ethylene. This blocking of chain lengthening sites must be partial since, in the case of ethanol feed, yields of gasoline components are lowered to only about one half of those found for ethylene conversion. Blocking of cracking sites, however, appears to be virtually complete if the zero values for Δ_B (*i*-propylbenzene) in ethanol conversion are to be understood. Above 300°C, however, some small amount of cracking appears.

It is interesting to recall that it has been argued (8) that information concerning reaction paths utilized by converting alkenes may be obtained working from experiments carried out on the corresponding alcohols. In the case of ethylene, at least, it is now clear that it is not safe to assume (8) that the alcohol is instantly dehydrated to the corresponding alkene and that all features of ethylene conversion will be the same as those of ethanol conversion. Not only are yields different, but some reactive intermediates, revealed by the Benzene Sequestration Test in conversion of the alkene, are entirely absent in the case of the converting alcohol. This principle may well apply to the higher alcohols.

These results illustrate something of the usefulness of the Benzene Sequestration Test.

1. C. D. CHANG. Hydrocarbons from methanol. Catal. Rev.–Sci. Eng. **25**, 1 (1982).
2. D. M. BIBBY, C. D. CHANG, R. F. HOWE, and S. YURCHAK (*Editors*). Methane conversion: Proceedings of a Symposium on Production of Fuels and Chemicals from Natural Gas. Stud. Surf. Sci. Catal. Vol. 36. Elsevier, New York. 1988.
3. A. W. FORT and B. H. DAVIS. J. Catal. **96**, 357 (1985).
4. D. V. DASS and A. L. ODELL. J. Catal. **110**, 310 (1988).
5. J. NOVAKOVA, L. KUBELKOVA, and Z. DOLEJSEK. J. Catal. **108**, 208 (1987).
6. J. NOVAKOVA, L. KUBELKOVA, and Z. DOLEJSEK. J. Mol. Catal. **45**, 365 (1988).
7. D. V. DASS, R. W. MARTIN, A. L. ODELL, and A. J. WERNHAM. J. Chromatogr. **387**, 410 (1987).
8. T. MOLE. J. Catal. **84**, 423 (1983); **103**, 524 (1987).
9. D. V. DASS, R. W. MARTIN, and A. L. ODELL. J. Catal. **108**, 153 (1987).
10. R. M. DESSAU. J. Catal. **99**, 111 (1986).

Can. J. Chem. Downloaded from www.nrcresearchpress.com by 186.148.149.217 on 09/07/12
For personal use only.

Preparation and characterization of diphenylbis(*N*,*N*-dialkyldithiocarbamato)tellurium(IV) and chlorodiphenyl(*N*,*N*-dialkyldithiocarbamato)tellurium(IV). Crystal structures of $Ph_2Te[S_2CNMe_2]_2$, $Ph_2TeCl[S_2CNEt_2]$, and $Ph_2TeCl[S_2CN(i\text{-}Pr)_2]$

JANE H. E. BAILEY, JOHN E. DRAKE,[1] ANIL B. SARKAR, AND MARIA L. Y. WONG
Department of Chemistry and Biochemistry, University of Windsor, Windsor, Ont., Canada N9B 3P4

Received December 19, 1988

This paper is dedicated to Professor Ronald J. Gillespie on the occasion of his 65th birthday

JANE H. E. BAILEY, JOHN E. DRAKE, ANIL B. SARKAR, and MARIA L. Y. WONG. Can. J. Chem. **67**, 1735 (1989).

A number of dithiocarbamate derivatives $Ph_2Te[S_2CNR_2]_2$, where R = Me, Et, and $Ph_2TeCl[S_2CNR_2]$, where R = Me, Et, *i*-Pr, have been prepared and characterized initially by analysis and vibrational spectroscopy. Three crystal structures have been completed that allow for comparisons of the effect of the change in the nature of R and of the presence of a chlorine atom. The dithiocarbamate groups are monodentate (or anisobidentate) and the geometry about tellurium is consistently that of a distorted sawhorse structure. Examples of both inter- and intra-molecular Te...S interactions are observed as well as an intermolecular Te...Cl interaction. The crystal structures of $Ph_2Te[S_2CNMe_2]_2$ **1**, $Ph_2TeCl[S_2CNEt_2]\cdot\frac{1}{2}CS_2$ **4** and $Ph_2TeCl[S_2CN(i\text{-}Pr)_2]$ **5** were determined. The cell parameters for **1** are a = 20.158(5) Å, b = 8.632(2) Å, c = 12.727(4) Å, β = 92.70(2)°, V = 2212(1) Å^3, Z = 4, R = 0.0221, and R_w = 0.0243; for **4** are a = 11.198(4) Å, b = 13.974(4) Å, c = 13.812(5) Å, α = 99.56(2)°, β = 103.08(3)°, γ = 87.39(3)°, V = 2076(1) Å^3, Z = 4, R = 0.0363, and R_w = 0.0398; and for **5** are a = 12.736(3) Å, b = 8.397(1) Å, c = 21.961(1) Å, β = 117.36(1)°, V = 2086(7) Å^3, Z = 4, R = 0.0266, and R_w = 0.0312. NMR spectra are not simple and indicate that several species are present in solution.

Key words: structure, tellurium, chloro, diphenyl, dialkyldithiocarbamato.

JANE H. E. BAILEY, JOHN E. DRAKE, ANIL B. SARKAR et MARIA L. Y. WONG. Can. J. Chem. **67**, 1735 (1989).

On a préparé une série de dérivés dithiocarbamates $Ph_2Te[S_2CNR_2]_2$, où R = Me, Et et $Ph_2TeCl[S_2CNR_2]$, où R = Me, Et, *i*-Pr, et on les a caractérisés initialement par analyse et par spectroscopie vibrationnelle. On a complété trois structures cristallines qui tiennent compte de l'effet des changements dans la nature de R et de la présence d'un atome de chlore. Les groupes dithiocarbamates sont monodentates (ou anisobidentates) et la géométrie autour du tellure est essentiellement celle d'une structure déformée de type chevalet. On a relevé des exemples d'interactions inter et intramoléculaires Te...S aussi bien que des interactions intermoléculaires Te...Cl. On a déterminé les structures cristallines du $Ph_2Te[S_2CNMe_2]_2$ **1**, $Ph_2TeCl[S_2CNEt_2]\cdot\frac{1}{2}CS_2$ **4** et du $Ph_2TeCl[S_2CN(i\text{-}Pr)_2]$ **5**. Le composé **1** a les paramètres de maille suivants : a = 20,158(5) Å, b = 8,632(2) Å, c = 12,727(4) Å, β = 92,70(2)°, V = 2212(1) Å^3, Z = 4, R = 0,0221 et R_w = 0,0243; le composé **4** a les paramètres suivants : a = 11,198(4) Å, b = 13,974(4) Å, c = 13,812(5) Å, α = 99,56(2)°, β = 103,08(3)°, γ = 87,39(3)°, V = 2076(1) Å^3, Z = 4, R = 0,0363 et R_w = 0,0398; les paramètres du composé **5** sont a = 12,736(3) Å, b = 8,397(1) Å, c = 21,961(1) Å, β = 117,36(1)°, V = 2086(7) Å^3, Z = 4, R = 0,0266 et R_w = 0,0312. Les spectres de RMN ne sont pas simples et indiquent la présence de plusieurs espèces en solution.

Mots clés : structure, tellure, chloro, diphényl, dialkyldithiocarbamato.

[Traduit par la revue]

Introduction

Dithiocarbamate complexes have been extensively studied (1–7). The dithiocarbamate group frequently acts in a bidentate fashion (3–7), and examples can be cited both for transition metals such as cobalt in $Co[S_2CNMe_2]NO$ (8), and copper in $Cu_4[S_2CNEt_2]_4$ (9), as well as for main group elements such as tin in $C_4H_9Sn[S_2CNEt_2]_2$ (10). Examples of monodentate dithiocarbamates are relatively fewer in transition metal chemistry, where they usually occur in mixed ligand complexes such as $Pt[S_2CN(i\text{-}Bu)_2]_2[P(Me_2)Ph]_2$ (11). We have reported on several dithiocarbamates of germanium in which monodentate (or anisobidentate) bonding is consistently found (12–15). In some instances changes in mode of attachment have been noted with variation of the alkyl group of the dithiocarbamate, as illustrated by $Zn[S_2CNMe_2]_2$ in which the dithiocarbamate groups are both bidentate and bridging (16), and $Zn[S_2CNEt_2]_2$ where both of the dithiocarbamate groups are bidentate and the molecule is monomeric (17).

We have prepared the tellurium dithiocarbamate derivatives $Ph_2Te[S_2CNR_2]_2$, where R = Me, Et, and $Ph_2TeCl[S_2CNR_2]$, where R = Me, Et, *i*-Pr. All compounds were characterized by elemental analysis and vibrational spectroscopy and several structural determinations were completed by X-ray crystallography.

[1]Author to whom correspondence may be addressed.

Experimental

Materials

$TeCl_4$, Ph_4Sn, NaS_2CNMe_2, NaS_2CNEt_2, diisopropylamine, toluene, diethyl ether, and petroleum ether were obtained from Aldrich. All but toluene, which was distilled, were used as supplied. Carbon disulfide (BDH) was distilled from P_4O_{10} prior to use, whereas ethanol and methylene chloride were used as supplied by BDH.

Synthesis of $NaS_2CN(i\text{-}Pr)_2$

Sodium hydroxide (3.96 g) was dissolved in ethanol (15 mL) followed by the addition of distilled CS_2 (3.67 g). Diisopropylamine (9.61 g) was introduced slowly at the rate of 2 drops/s, while nitrogen gas was bubbled through the mixture at a rate of 3 bubbles/s. The system was heated at 20°C for 1 h. The desired product, sodium *N*,*N*-diisopropyldithiocarbamate (8.47 g; 42.56%) was filtered, washed with cold diethyl ether, and dried in vacuum (1).

Synthesis of Ph_2TeCl_2

An equimolar mixture of tetraphenyltin (4.56 g) and tellurium tetrachloride (2.87 g) in toluene (20 mL) was refluxed at 60°C for 12 h and worked up in the manner previously described (18).

Can. J. Chem. Downloaded from www.nrcresearchpress.com by 186.148.149.217 on 09/07/12
For personal use only.

Can. J. Chem. Downloaded from www.nrcresearchpress.com by 186.148.149.217 on 09/07/12
For personal use only.

TABLE 1. Summary of crystal data, intensity collection, and structural refinement for $Ph_2Te[S_2CNMe_2]_2$ **1**, $Ph_2TeCl[S_2CNEt_2]\cdot\frac{1}{2}CS_2$ **4**, and $Ph_2TeCl[S_2CN(i\text{-}Pr)_2]$ **5**

Parameter		$C_{18}H_{22}N_2S_4Te$ **1**	$C_{17.5}H_{20}ClNS_3Te$ **4**	$C_{19}H_{24}ClNS_2Te$ **5**
Cell constants	a (Å)	20.158(5)	11.198(4)	12.736(3)
	b (Å)	8.632(2)	13.974(4)	8.397(1)
	c (Å)	12.727(4)	13.812(5)	21.961(4)
	α (deg)	90.0	99.56(2)	90.0
	β (deg)	92.70(2)	103.08(3)	117.36(1)
	γ (deg)	90.0	87.39(3)	90.0
Cell volume	Å^3	2212(1)	2076(1)	2086(1)
Crystal system		Monoclinic	Triclinic	Monoclinic
Space group		$C2/c$	$P\bar{1}$	$P2_1/c$
Mol. wt. g mol^{-1}		522.2	503.6	493.6
Z		4	4	4
ρ obsd., ρ calcd., g cm^{-3}		1.51, 1.57	1.59, 1.61	1.60, 1.57
Crystal dimensions, mm		0.19 × 0.23 × 0.42	0.27 × 0.42 × 0.46	0.58 × 0.31 × 0.25
Abs. coeff. μ, cm^{-1}		15.76	16.31	16.22
Temperature, °C		24 ± 1	21 ± 1	24 ± 1
Radiation		MoK$_\alpha$ 0.71069 Å		
Monochromator		Highly oriented graphite		
2θ angle, deg		4–40	4–45	4–40
Scan method		Coupled θ(crystal)/2θ(counter)		
Scan width		Kα$_1$ −1° to Kα$_2$ +1°		
Background time/scan time		0.5		
Scan speed, deg min^{-1}		variable, 2.02–4.88		
Total reflections measured		2188 ($\pm h$, $+k$, $+l$)	5438 ($+h$, $\pm k$, $\pm l$)	2203 ($\pm h$, $+k$, $+l$)
Unique data used		776 ($I > 3\sigma(I)$)	4372	1632
No. of parameters (NP)		84	300	157
$R = (\Sigma\|\|F_o\| - \|F_c\|\|/\Sigma\|F_o\|)$		0.0221	0.0363	0.0266
$R_w = [\Sigma w(\|F_o\| - \|F_c\|)^2/\Sigma w\|F_o\|^2]^{1/2}$		0.0243	0.0398	0.0312
Largest Δρ e Å^{-3} shift/error max.		0.0001	0.004	0.002
Largest residual electron density, e Å^{-3}		0.29	0.93 1.05	0.37
Atom assoc. with residual density		Te	Te(1) Te(2)	C12

*Synthesis of diphenylbis(*N,N*-dialkyldithiocarbamato)tellurium(IV)*

Typically, sodium *N,N*-dimethyldithiocarbamate (0.25 g), which had been previously well dried *in vacuo* for 3–4 days, was added to an excess of carbon disulfide (approximately 12 mL). Diphenyltellurium dichloride (0.62 g) was added to the solution, which was then refluxed at 45°C for 3 h while nitrogen gas bubbled through at a rate of 3 bubbles/s. The solution was filtered to remove sodium chloride and any unreacted materials. A few drops of petroleum ether were added to the solution before it was left in the refrigerator to crystallize. After approximately 3 days, the product, $Ph_2Te[S_2CNMe_2]_2$, was filtered, washed with cold *n*-hexane, and dried in vacuum; 0.73 g; 79% yield; yellow crystals; mp 132°C. *Anal.* calcd. for $C_{18}H_{22}N_2S_4Te$: C 41.40, H 4.25, N 5.36; found: C 41.99, H 4.35, N 5.96%. Similarly was formed $Ph_2Te[S_2CNEt_2]_2$, pale yellow crystals; mp 140°C. *Anal.* calcd. for $C_{22}H_{30}N_2S_4Te$: C 45.69, H 5.25, N 4.84; found: C 45.56, H 5.25, N 4.93%).

*Synthesis of chlorodiphenyl(*N,N*-dialkyldithiocarbamato)tellurium(IV)*

Typically, an equimolar mixture of sodium *N,N*-dimethyldithiocarbamate (0.13 g), which had been previously dried as described above, and diphenyltellurium dichloride (0.62 g) was refluxed in excess of methylene chloride or carbon disulfide (approximately 10 mL) at 41°C for 3 h. Nitrogen gas was bubbled through at a rate of 3 bubbles/s during the reflux. The solution was then filtered to remove any excess material and placed in the refrigerator to crystallize. The ethyl and isopropyl derivatives were obtained in a similar manner: $Ph_2TeCl[S_2CNMe_2]$, pale green crystals, mp 124°C. *Anal.* calcd. for $C_{15}H_{16}ClNS_2Te$: C 41.18, H 3.69, N 3.20; found: C 41.07, H 3.60, N 3.17%; $Ph_2TeCl[S_2CNEt_2]\cdot\frac{1}{2}CS_2$, pale green crystals; mp 95°C. *Anal.* calcd. for $C_{17.5}H_{20}ClNS_3Te$: C 41.74, H 4.00, N 2.78; found: C 42.03, H 3.98, N 2.98%; and $Ph_2TeCl[S_2CN(i\text{-}Pr)_2]$, yellow crystals: mp 144°C. *Anal.* calcd. for $C_{19}H_{24}ClNS_2Te$: C 46.24, H 4.90, N 2.84; found: C 46.21, H 4.71, N 3.05%.

Physical measurements

All solvents were dried and distilled prior to use. The elemental analyses were performed by Guelph Chemical Laboratories, Guelph, Ontario. Density measurements were performed by the flotation method in CCl_4/CH_3I. The infrared spectra were recorded on a Nicolet 5DX FT spectrometer as CsI pellets. Samples for Raman spectrometry were sealed in capillary tubes and the spectra recorded on a Ramanor U-1000 spectrometer using the 4880 Å exciting line. The ^{1}H NMR spectra were recorded on a Bruker AC 300 spectrometer in CS_2 or $CDCl_3$ solutions using tetramethylsilane as internal standard. The same instrument was used to record the $^{13}C\{^1H\}$ NMR spectra. The melting points were determined on a Fisher–Johns apparatus.

X-ray crystallographic analysis

X-ray diffraction data were collected on a Syntex $P2_1$ diffractometer by the procedure already described in detail (13). In each case the crystal was sealed in a capillary and mounted along the largest dimension. The least-squares refinement of the setting angles of 35 high-angle reflections ($15° > 2\theta > 30°$) led to the cell dimensions given in Table 1. The appropriate space group was used in each case and later assumed correct because of successful refinement of the data. During data collection, the intensities of three monitor reflections measured after 200 reflections decreased in the range of approximately 2–4% and the appropriate scaling factor was applied. Each set of data was corrected for Lorentz and polarization effects, and an empirical absorption correction was applied but resulted in no significant changes

TABLE 2. Final fractional coordinates for non-hydrogen atoms of $Ph_2Te[S_2CNMe_2]_2$ **1**

Atom	*x*	*y*	*z*	Atom	*x*	*y*	*z*
Te	0.0	0.1076(5)	0.25	C4	0.0409(2)	0.2677(5)	0.3638(3)
S1	0.1056(1)	0.1286(1)	0.1382(1)	C5	0.0648(3)	0.4125(6)	0.3362(4)
S2	0.1286(1)	−0.0889(2)	0.3190(1)	C6	0.0914(3)	0.5095(7)	0.4142(4)
N	0.2056(2)	−0.0645(6)	0.1587(4)	C7	0.0939(3)	0.4633(7)	0.5161(4)
C1	0.1516(3)	−0.0144(6)	0.2045(4)	C8	0.0711(2)	0.3203(7)	0.5447(4)
C2	0.2251(3)	−0.006(1)	0.0595(5)	C9	0.0444(3)	0.2214(6)	0.4667(4)
C3	0.2487(4)	−0.184(1)	0.2082(6)				

TABLE 3. Final fractional coordinates for non-hydrogen atoms of $Ph_2TeCl[S_2CNEt_2]\cdot\frac{1}{2}CS_2$ **4**

Atom	*x*	*y*	*z*	Atom	*x*	*y*	*z*
Te1	−0.02278(2)	0.96357(2)	0.30622(2)	Te2	0.46996(3)	0.49083(2)	0.17257(2)
Cl1	−0.2156(1)	1.0215(1)	0.1804(1)	Cl2	0.4957(2)	0.3238(1)	0.2376(1)
S1	0.1783(1)	0.9141(1)	0.4096(1)	S3	0.4632(1)	0.6648(1)	0.1455(1)
S2	−0.0317(1)	0.8325(1)	0.4661(1)	S4	0.2929(1)	0.5459(1)	−0.0258(1)
N1	0.2001(5)	0.8174(4)	0.5613(4)	N2	0.3338(4)	0.7337(3)	−0.0114(3)
C1	0.1193(5)	0.8496(4)	0.4877(4)	C18	0.3577(5)	0.6534(4)	0.0282(4)
C2	0.1621(7)	0.7619(4)	0.6300(5)	C19	0.2513(6)	0.7355(5)	−0.1102(5)
C3	0.1534(7)	0.6548(5)	0.5937(6)	C20	0.1219(6)	0.7621(6)	−0.1006(5)
C4	0.3331(7)	0.8424(5)	0.5847(5)	C21	0.3877(7)	0.8303(4)	0.0382(5)
C5	0.4037(8)	0.7727(6)	0.5271(6)	C22	0.5015(7)	0.8504(6)	0.0083(7)
C6	0.0903(5)	1.0378(4)	0.2365(4)	C23	0.3075(5)	0.5075(4)	0.2291(4)
C7	0.1570(5)	1.1152(4)	0.2941(4)	C24	0.2252(6)	0.4323(5)	0.2006(5)
C8	0.2278(6)	1.1668(5)	0.2519(5)	C25	0.1189(8)	0.4420(6)	0.2371(6)
C9	0.2321(6)	1.1402(5)	0.1528(5)	C26	0.0954(8)	0.5244(6)	0.2977(6)
C10	0.1662(6)	1.0628(4)	0.0940(5)	C27	0.1746(6)	0.5982(5)	0.3237(5)
C11	0.0932(5)	1.0118(4)	0.1360(4)	C28	0.2838(6)	0.5915(5)	0.2896(5)
C12	−0.0389(5)	0.8290(4)	0.2055(4)	C29	0.5980(5)	0.5455(4)	0.3083(4)
C13	−0.1552(6)	0.7898(4)	0.1686(4)	C30	0.7066(5)	0.5801(4)	0.2988(5)
C14	−0.1670(6)	0.7009(5)	0.1062(5)	C31	0.7935(6)	0.6171(5)	0.3840(5)
C15	−0.0682(6)	0.6531(5)	0.0797(5)	C32	0.7699(6)	0.6186(5)	0.4775(5)
C16	0.0467(6)	0.6919(5)	0.1159(5)	C33	0.6625(6)	0.5837(5)	0.4871(5)
C17	0.0623(4)	0.7816(4)	0.1810(5)	C34	0.5759(6)	0.5458(4)	0.4008(5)
S5	0.6466(3)	0.8478(2)	0.3832(3)				
S6	0.4283(3)	0.9692(2)	0.3013(3)				
C35	0.5380(8)	0.9074(6)	0.3443(6)				

in refinement. The ranges of absorption correction factors were 0.945–0.993 for **1** and 0.937–0.957 for **5**. A summary of crystal and refinement data is given in Table 1.

The position of the tellurium atom was determined by a sharpened Patterson synthesis using SHELX, and difference maps revealed the remaining atoms. Tellurium, sulfur, nitrogen, and, where appropriate, chlorine atoms were refined anisotropically. Limitations on data in two cases allowed the anisotropic refinement of carbon atoms other than those in the phenyl rings. Hydrogen atoms were included at the idealized positions (C—H = 0.95 Å; HCH and CCH (for ethyl and isopropyl) = 109.5°; CCH = 120° (for phenyl rings)) with isotropic U values set at approximately 0.01 Å^2 greater than the corresponding carbon atom. Complete refinement by full-matrix least-squares methods minimizing the function $\Sigma w(|F_o| - |F_c|)^2$ converged satisfactorily in all three cases at $R = 0.0221$ and $R_w = 0.0243$ for **1**; $R = 0.0363$ and $R_w = 0.0398$ for **4**; and $R = 0.0266$ and $R_w = 0.0312$ for **5**. A weighting scheme of the form $w = 1/\Sigma[\sigma^2(F) + pF_2]$ was employed with final p values of 0.00048 for **1**; 0.00036 for **4**; and 0.00001 for **5** respectively. No evidence was found of reflections being affected by secondary extinctions.

The final fractional coordinates for non-hydrogen atoms of **1**, **4**, and **5** are listed in Tables 2, 3, and 4 respectively. Anisotropic (Te, S, N, Cl, and all C atoms not in the phenyl ring) and isotropic (C) thermal parameters for non-hydrogen atoms are listed in Tables 5, 6, and 7 respectively for **1**, **4**, and **5**. All molecules were thus subjected to the same degree of refinement and in all cases NP/P was greater than 9. Important bond lengths and angles are given in Tables 8 and 9. The molecular structures of each of the compounds are given in Figs. 1–3. Tables of final fractional coordinates and thermal parameters of hydrogen atoms as well as tables of observed and calculated structure factors have been deposited.[2]

Results and discussion

The diphenyltellurium(IV) derivatives are made by the reaction of diphenyltellurium dichloride with the sodium salt of the appropriate *N*,*N*-dialkyldithiocarbamic acid.

$$Ph_2TeCl_2 + NaS_2CNR_2 \rightarrow Ph_2TeCl[S_2CNR_2] + NaCl$$

(R = Me, Et, *i*-Pr)

$$Ph_2TeCl_2 + 2NaS_2CNR_2 \rightarrow Ph_2Te[S_2CNR_2]_2 + 2NaCl$$

(R = Me, Et)

[2]A complete set of these data may be purchased from the Depository of Unpublished Data, CISTI, National Research Council of Canada, Ottawa, Ont., Canada K1A 0S2.

Can. J. Chem. Downloaded from www.nrcresearchpress.com by 186.148.149.217 on 09/07/12
For personal use only.

TABLE 4. Final fractional coordinates for non-hydrogen atoms of $Ph_2TeCl[S_2CN(i\text{-}Pr)_2]$ **5**

Atom	*x*	*y*	*z*	Atom	*x*	*y*	*z*
Te	0.16489(2)	0.26422(4)	0.28369(2)	C8	0.3176(5)	0.1331(6)	0.2965(3)
Cl	0.0393(2)	0.0338(2)	0.1979(1)	C9	0.4119(5)	0.2094(7)	0.2973(3)
S1	0.2866(2)	0.4912(2)	0.3526(1)	C10	0.5129(6)	0.1186(8)	0.3077(3)
S2	0.2486(2)	0.2619(2)	0.4428(1)	C11	0.5131(6)	−0.0389(8)	0.3178(3)
N	0.2829(4)	0.5746(5)	0.4678(2)	C12	0.4186(6)	−0.1163(9)	0.3177(3)
Cl	0.2722(5)	0.4494(7)	0.4283(3)	C13	0.3181(6)	−0.0280(7)	0.3063(3)
C2	0.2985(6)	0.7420(6)	0.4487(4)	C14	0.1468(4)	0.3973(6)	0.1966(3)
C3	0.4113(7)	0.8155(9)	0.5023(4)	C15	0.1657(5)	0.3293(7)	0.1463(3)
C4	0.1887(6)	0.8418(7)	0.4289(4)	C16	0.1475(5)	0.4187(7)	0.0882(3)
C5	0.2701(6)	0.5629(8)	0.5320(3)	C17	0.1094(6)	0.5739(8)	0.0823(4)
C6	0.1452(5)	0.5159(8)	0.5173(3)	C18	0.0908(6)	0.6409(8)	0.1332(8)
C7	0.3651(6)	0.4658(8)	0.5882(3)	C19	0.0944(5)	0.5996(7)	0.2253(3)

TABLE 5. Final thermal parameters ($Å^2 \times 10^3$) of non-hydrogen atoms of $Ph_2Te[S_2CNMe_2]_2$ **1**

Atom	U_{11}	U_{22}	U_{33}	U_{12}	U_{13}	U_{23}
Te	48.1(3)	35.5(3)	48.6(4)	0	−1.4(2)	0
S1	56.3(9)	49.8(8)	54.3(9)	7.3(6)	3.1(7)	7.2(6)
S2	91(1)	64(1)	63(1)	13(1)	−6(1)	16(1)
N	60(3)	93(4)	71(4)	27(3)	−2(3)	18(3)
C1	53(1)	55(3)	52(3)	4(3)	−6(3)	−10(3)
C2	85(5)	148(7)	101(6)	31(5)	15(4)	13(6)
C3	98(6)	155(7)	111(6)	51(6)	−4(5)	29(6)
C4	46(1)					
C5	57(1)					
C6	68(2)					
C7	65(2)					
C8	64(2)					
C9	59(1)					

With the sodium salt added in equimolar amounts, the chlorodiphenyl(*N*,*N*-dialkyldithiocarbamato)tellurium(IV) derivatives can be isolated in yields of up to 75%. The methyl and ethyl derivatives form pale green crystals, while those of the isopropyl derivative have a more yellow tinge. With an excess of sodium salt the diphenylbis(*N*,*N*-dialkyldithiocarbamato)tellurium(IV) compounds are also prepared in up to 75% yields for the methyl and ethyl derivatives, whose crystals are best described as yellowish. Attempts to prepare pure samples of the bis isopropyl derivative were not successful even with larger excesses of the sodium salt.

The crystal structure of $Ph_2Te[S_2CNMe_2]_2$ *1*

This compound crystallizes as discrete molecular units in the space group $C2/c$, containing a crystallographic twofold axis (Fig. 1). The geometry about tellurium can be described as being that of a distorted sawhorse structure based on a distorted trigonal bipyramid in which a lone pair occupies an equatorial position. The structure bears a strong resemblance to that of $Ph_2Te[S_2P(OMe)_2]_2$ (19), in that the sulfur-containing groups are monodentate with the bonding sulfur atoms occupying the axial positions. The S1—Te—S1′ angle in **1** is 172.0(1)°, comparable to 171.8(1)° in the dithiophosphate. In **1**, the Te—S bond length of 2.621(1) Å is essentially the same as those reported for the dithiophosphate (19). The carbon atoms of the two phenyl groups attached to tellurium occupy two of the equatorial positions with a C—Te—C angle of 99.4(1)° and a Te—C distance of 2.140(5) Å in **1**, again comparable to the angle of 98.5(2)° and length of 2.133(5) and 2.136(5) Å in the dithiophosphate.

The two dithiocarbamate groups are positioned in such a way that the nonbonded sulfur atoms approach the tellurium atom at a distance of 3.186(2) Å. This distance is shorter than the previously reported Te—S distances of a similar type such as 3.383(2) and 3.362(2) Å in $Ph_2Te[S_2P(OMe)_2]_2$ (19), 3.225(3) Å in $(PhN_2C_6H_4)Te(S_2CNMe_2)$ (20), and 3.228(4) Å in $PhTe[S_2CNEt_2]_3$ (21), and is also considerably shorter than the sum of the van der Waals distances of 4.05 Å. This type of linkage is probably better described as being anisobidentate rather than simply monodentate. However, as with $Ph_2Te[S_2P(OMe)_2]_2$, the suggestion that these secondary interactions complete a distorted octahedral geometry around the tellurium atom is less attractive when it is noted that these secondary sulfur atoms are considerably above and below the plane formed by the two carbon atoms and the tellurium atom by approximately 1.86 Å. Thus, the secondary bonds appear to be formed in positions to allow them to avoid a stereochemically active lone pair.

The similarities to a Ph_2TeL_2 species with a different sulfur ligand are striking when comparisons are drawn with $PhTe[S_2CNEt_2]_3$ with the same family of ligands (21). In $PhTe[S_2CNEt_2]_3$, the tellurium atom is described as being bonded to all six sulfur atoms, leading to a distorted pentagonal bipyramidal configuration (21). Two dithiocarbamate groups are bidentate with all four sulfur atoms in the equatorial plane, giving similar Te—S bond lengths of 2.701(3), 2.797(3),

Can. J. Chem. Downloaded from www.nrcresearchpress.com by 186.148.149.217 on 09/07/12
For personal use only.

TABLE 6. Final thermal parameters ($Å^2 \times 10^3$) of non-hydrogen atoms of $Ph_2TeCl[S_2CNEt_2]\cdot\frac{1}{2}CS_2$ **4**

Atom	U_{11}	U_{22}	U_{33}	U_{12}	U_{13}	U_{23}
Te1	43.1(2)	38.3(1)	34.3(2)	−2.0(2)	7.2(2)	6.5(2)
Te2	42.7(2)	40.5(2)	41.1(2)	−0.3(2)	10.1(2)	9.4(2)
Cl1	55.1(9)	52.1(9)	58.7(9)	5.5(7)	1.7(7)	12.9(7)
Cl2	62(1)	48.0(9)	93(1)	2.9(7)	10.9(9)	23.8(8)
S1	44.8(8)	60.7(9)	50.0(9)	−7.1(7)	2.6(7)	21.3(7)
S2	56.0(8)	62.7(8)	52.6(8)	−8.4(6)	16.1(6)	15.0(6)
S3	66(1)	45.4(8)	44.1(8)	−9.2(7)	−3.0(7)	13.1(7)
S4	60(1)	46.8(8)	44.0(8)	−7.7(7)	9.6(7)	3.5(7)
S5	106(2)	124(2)	161(3)	29(2)	13(2)	15(2)
S6	81(2)	153(3)	165(3)	26(2)	10(2)	−1(2)
N1	63(3)	57(3)	44(3)	−1(3)	1(3)	17(2)
N2	59(3)	46(3)	44(3)	1(2)	5(2)	13(2)
C1	58(4)	39(3)	32(3)	2(3)	−1(3)	6(2)
C2	98(6)	59(4)	48(4)	2(4)	16(4)	18(3)
C3	92(6)	68(5)	84(5)	−1(4)	23(4)	26(4)
C4	87(6)	83(5)	57(4)	6(4)	−3(4)	20(4)
C5	100(7)	104(6)	78(6)	6(5)	18(5)	10(5)
C18	44(3)	43(3)	34(3)	−1(2)	11(2)	8(3)
C19	74(5)	65(4)	43(4)	−1(3)	2(3)	19(3)
C20	67(5)	94(6)	69(5)	−3(4)	8(4)	31(4)
C21	94(6)	47(4)	57(4)	−1(4)	−1(4)	15(3)
C22	90(6)	83(6)	112(7)	−29(5)	−4(5)	23(5)

Atom	U_{11}	Atom	U_{11}	Atom	U_{11}
C6	41(1)	C7	47(1)	C8	63(2)
C9	65(2)	C10	60(2)	C11	53(2)
C12	41(1)	C13	54(2)	C14	65(2)
C15	65(2)	C16	63(2)	C17	56(2)
C23	38(1)	C24	59(2)	C25	83(2)
C26	84(2)	C27	72(2)	C28	60(2)
C29	42(1)	C30	53(2)	C31	67(2)
C32	65(2)	C33	69(2)	C34	60(2)
C35	87(2)				

TABLE 7. Final thermal parameters ($Å^2 \times 10^3$) of non-hydrogen atoms of $Ph_2TeCl[S_2Cn(i\text{-}Pr)_2]$ **5**

Atom	U_{11}	U_{22}	U_{33}	U_{12}	U_{13}	U_{23}
Te	37.8(3)	34.0(3)	43.7(3)	−1.8(2)	22.4(2)	−2.8(2)
Cl	57(1)	56(1)	75(1)	−18(1)	31(1)	−21(1)
S1	60(1)	46(1)	56(1)	−16(1)	37(1)	13(1)
S2	81(1)	36(1)	65(1)	−3(1)	37(1)	2(1)
N	49(3)	39(3)	47(3)	−4(2)	26(3)	−4(3)
Cl	42(4)	37(4)	52(4)	−1(3)	19(3)	−2(3)
C2	74(5)	40(4)	61(4)	−14(4)	39(4)	−1(3)
C3	86(6)	79(5)	108(7)	−51(5)	31(6)	−4(5)
C4	85(5)	39(4)	103(6)	6(4)	48(5)	13(4)
C5	67(5)	54(4)	51(4)	−11(4)	31(4)	−7(4)
C6	66(5)	59(5)	88(5)	−7(4)	47(4)	4(4)
C7	74(5)	66(5)	57(5)	−13(4)	11(4)	11(4)

Atom	U_{11}	Atom	U_{11}	Atom	U_{11}
C8	38(1)	C9	50(2)	C10	68(2)
C11	73(2)	C12	73(2)	C13	60(2)
C14	38(1)	C15	48(2)	C16	60(2)
C17	63(2)	C18	61(2)	C19	53(2)

Can. J. Chem. Downloaded from www.nrcresearchpress.com by 186.148.149.217 on 09/07/12
For personal use only.

TABLE 8. Interatomic distances (Å) in compounds **1**, **4**, and **5**

$Ph_2Te[S_2CNMe_2]_2$ **1**		$Ph_2TeCl[S_2CNEt_2]\cdot\frac{1}{2}CS_2$ **4**[a]				$Ph_2TeCl[S_2CN(i\text{-}Pr)_2]$ **5**[b]	
Te—S1	2.621(1)	Te1—Cl1	2.638(1)	Te2—Cl2	2.616(2)	Te—Cl	2.661(2)
		Te1—S1	2.516(1)	Te2—S3	2.513(2)	Te—S1	2.484(2)
Te—S2	3.186(2)	Te1—S2	3.112(2)	Te2—S4	3.184(1)	Te—S2	3.149(2)
Te—C4	2.140(5)	Te1—C6	2.114(6)	Te2—C23	2.124(6)	Te—C8	2.137(5)
		Te1—C12	2.129(5)	Te2—C29	2.133(5)	Te—C14	2.134(5)
S1—C1	1.738(5)	S1—C1	1.760(6)	S3—C18	1.763(5)	S1—C1	1.788(6)
S2—C1	1.678(5)	S2—C1	1.669(6)	S4—C18	1.675(5)	S2—C1	1.660(6)
N—C1	1.333(6)	N1—C1	1.325(7)	N2—C18	1.319(7)	N—C1	1.329(7)
N—C2	1.432(7)	N1—C2	1.461(9)	N2—C19	1.467(7)	N—C2	1.505(7)
N—C3	1.471(8)	N1—C4	1.494(9)	N2—C21	1.491(7)	N—C5	1.494(7)
Ring C4–C9		C2—C3	1.495(9)	C19—C20	1.51(1)	C2—C3	1.510(9)
						C2—C4	1.512(9)
Mean C—C	1.38(2)[c]	C4—C5	1.47(1)	C21—C22	1.48(1)	C5—C6	1.523(8)
						C5—C7	1.509(8)
		Ring C6–C11		Ring C23–C28		Ring C8–C13	
		Mean C—C	1.373(6)	Mean C—C	1.37(2)	Mean C—C	1.38(3)
		Ring C12–C17		Ring C29–C34		Ring C14–C19	
		Mean C—C	1.38(2)	Mean C—C	1.37(2)	Mean C—C	1.38(2)
		S5—C35	1.492(9)				
		S6—C35	1.535(9)				
		Te1...Te1″	5.185(2)	Te2...Te2″	5.005(2)		
		Te1...S2″	3.825(2)	Te2...S4″	3.656(2)	Te...Cl″	3.607(2)

[a]Symmetry-equivalent position: the double prime indicates $1 - x, 1 - y, 1 - z$.
[b]Symmetry-equivalent position: the double prime indicates $-x, y - 0.5, 0.5 - z$.
[c]The esd's on mean values have been calculated with the use of the Scatter formula $\sigma = [\Sigma(d_i - d)^2/(N - 1)]^{1/2}$, where d_i is the ith and d is the mean of N equal measurements.

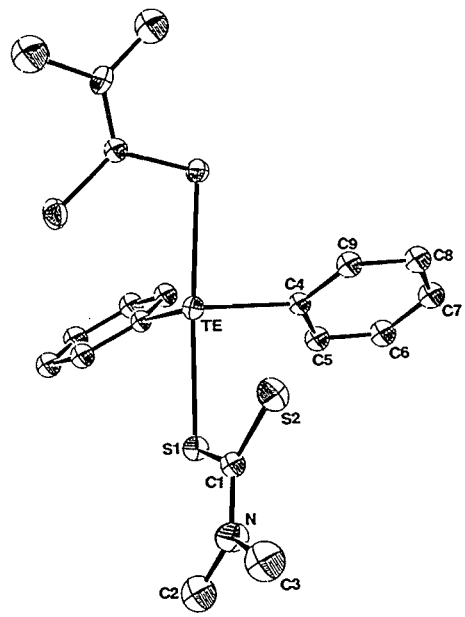


FIG. 1. ORTEP plot of the molecule $Ph_2Te[S_2CNMe_2]_2$ **1**. The atoms are drawn with 20% probability ellipsoids. Hydrogen atoms are omitted for clarity.

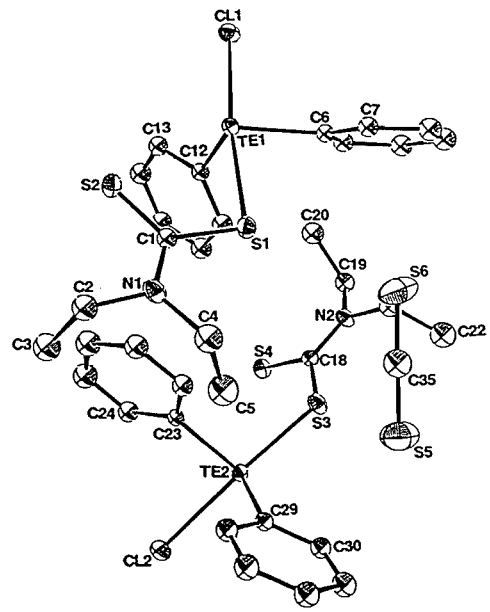


FIG. 2. ORTEP plot of the molecule $Ph_2TeCl[S_2CNEt_2]$ **4** showing the two independent molecules and CS_2. The atoms are drawn with 20% probability ellipsoids. Hydrogen atoms are omitted for clarity.

2.816(3), and 2.657(3) Å. The shortest of these is longer, but not considerably longer, than the Te—S distances of 2.621(1) Å for the axial bonds in **1**. There is a fifth sulfur atom in the equatorial plane of $PhTe[S_2CNEt_2]_3$ giving the shortest Te—S bond of 2.606(3) Å. The second sulfur atom of this third ligand lies in an approximately axial position with a Te—S distance of 3.228(4) Å, which is longer than, but of the same order as, the secondary bonding distance of 3.186(2) Å in the anisobidentate ligands of **1**. Interestingly, the C—Te—S angle to the secondary bonded sulfur atom in $PhTe[S_2CNEt_2]_3$ is 144.6(2)°, which is very similar to the corresponding angle in **1** of 144.4(1)°. Similarly, the C—Te—S angles to the bonded sulfur atoms in **1** are 83.3(1) and 91.5(1)°, values that are close to those in $PhTe[S_2CNEt_2]_3$, which range from 84.2(2) to 93.7(3)°.

Can. J. Chem. Downloaded from www.nrcresearchpress.com by 186.148.149.217 on 09/07/12
For personal use only.

TABLE 9. Bond angles (deg) in compounds **1**, **4**, and **5** with standard deviations in parentheses

$Ph_2Te[S_2NCMe_2]_2$ **1**[a]		$Ph_2TeCl[S_2CNEt_2]\cdot\frac{1}{2}CS_2$ **4**[b]				$Ph_2TeCl[S_2CN(i\text{-}Pr)_2]$ **5**[c]	
S1—Te—S1′	172.0(1)	S1—Te1—Cl1	172.0(1)	S3—Te2—Cl2	168.7(1)	S1—Te—Cl	173.2(1)
S1—Te—C4	91.5(1)	Cl1—Te1—C6	88.2(1)	Cl2—Te2—C23	85.8(1)	Cl—Te—C8	86.2(1)
S1′—Te—C4	83.3(1)	S1—Te1—C6	84.2(1)	S3—Te2—C23	92.4(1)	S1—Te—C14	85.7(1)
S1—Te—C4′	83.3(1)	Cl1—Te1—C12	86.5(1)	Cl2—Te2—C29	86.0(2)	Cl—Te—C14	87.9(1)
S1′—Te—C4′	91.5(1)	S1—Te1—C12	92.3(1)	S3—Te2—C29	83.2(2)	S1—Te—C8	92.2(1)
C4—Te—C4′	99.4(1)	C6—Te1—C12	98.2(2)	C23—Te2—C29	98.5(2)	C8—Te—C14	96.0(2)
S1—Te—S2	61.0(1)	S1—Te1—S2	62.5(1)	S3—Te2—S4	61.8(1)	S1—Te—S2	62.0(1)
Te—S1—C1	96.6(2)	Te1—S1—C1	97.9(2)	Te2—S3—C18	99.1(2)	Te—S1—C1	96.6(2)
C1—N—C2	122.3(5)	C1—N1—C2	121.5(5)	C18—N2—C19	122.4(4)	C1—N—C2	122.9(5)
C1—N—C3	121.2(5)	C1—N1—C4	122.4(6)	C18—N2—C21	123.9(4)	C1—N—C5	122.7(5)
C2—N—C3	116.4(5)	C2—N1—C4	115.9(5)	C19—N2—C21	113.6(5)	C2—N—C5	114.2(5)
S1—C1—S2	122.1(3)	S1—C1—S2	119.5(3)	S3—C18—S4	120.4(3)	S1—C1—S2	117.9(3)
S1—C1—N	116.5(4)	S1—C1—N1	116.6(5)	S3—C18—N2	115.8(4)	S1—C1—N	115.3(4)
S2—C1—N	121.5(5)	S2—C1—N1	123.9(5)	S4—C18—N2	123.8(4)	S2—C1—N	126.8(5)
		N1—C2—C3	114.4(6)	N2—C19—C20	111.7(5)	N—C2—C3	111.4(6)
						N—C2—C4	112.0(5)
						C3—C2—C4	114.9(6)
		N1—C4—C5	112.5(6)	N2—C21—C22	113.1(6)	N—C5—C6	111.8(5)
						N—C5—C7	114.4(5)
						C6—C5—C7	113.6(5)
Te—C4—C5	122.5(4)	Te1—C6—C7	117.7(4)	Te2—C23—C24	117.6(4)	Te—C8—C9	120.4(4)
Te—C4—C9	117.4(4)	Te1—C6—C11	121.9(4)	Te2—C23—C28	121.2(4)	Te—C8—C13	117.9(4)
		Te1—C12—C13	117.5(4)	Te2—C29—C30	117.1(4)	Te—C14—C15	121.5(4)
		Te1—C12—C17	121.1(4)	Te2—C29—C34	122.7(4)	Te—C14—C19	118.2(4)
Ring C4–C9		Ring C6–C11		Ring C23–C28		Ring C8–C13	
Mean C—C—C	120.0(9)[d]	Mean C—C—C	120.0(7)	Mean C—C—C	120(1)	Mean C—C—C	120(2)
		Ring C12—C17		Ring C29—C34		Ring C14—C19	
		Mean C—C—C	120(1)	Mean C—C—C	120.0(4)	Mean C—C—C	120.0(2)
		Te1—S2—Te1″	96.2(2)	Te2—S4—Te2″(2)	93.8	Te—Cl—Te″	127.3(1)
		S2—Te1—S2″	83.8(1)	S4—Te2—S4″(1)	86.2	Cl—Te—Cl″	107.8(1)

[a]Symmetry-equivalent positions: prime indicates $-x, y, 0.5 - z$.
[b]Symmetry-equivalent positions: double prime indicates $1 - x, 1 - y, 1 - z$.
[c]Symmetry-equivalent positions: double prime indicates $-x, y - 0.5, 0.5 - z$.
[d]The esd's on mean values have been calculated with the use of the Scatter formula $\sigma = [\Sigma(d_i - d)^2/(N - 1)]^{1/2}$, where d_i is the ith and d is the mean of N equal measurements.

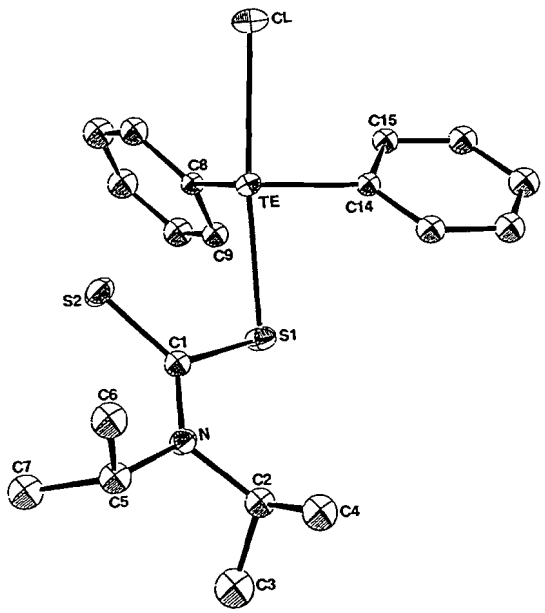


FIG. 3. ORTEP plot of the molecule $Ph_2TeCl[S_2CN(i\text{-}Pr)_2]$ **5**. The atoms are drawn with 20% probability ellipsoids. Hydrogen atoms are omitted for clarity.

The structure of a tellurium(II) compound, $(PhN_2C_6H_4)Te(S_2CNMe_2)$, that contains a dimethyldithiocarbamate group has been reported (20). The dimethyldithiocarbamate group is again anisobidentate with Te—S distances of 2.568(2) and 3.225(3) Å. The sums of the two Te—S linkages of this type are thus 5.807 Å in **1**, 5.834 Å in $PhTe[SCNEt_2]_3$, and 5.793 Å in $C_6H_4N_2PhTeS_2CNMe_2$. The S—Te—S bite angle is 61.0(1)° in **1**, which is similar to the corresponding angle of 60.9(1)° in the tellurium(II) compound and that of the anisobidentate ligand in the tris compound of 60.5(1)°. All the bite angles are larger in the fully bidentate ligands in $PhTe[S_2CNEt_2]_3$, being 64.76(9) and 65.04(8)° (21).

The C1—S1 and C1—S2 distances of 1.738(5) and 1.678(5) Å respectively in **1** are as expected for an anisobidentate or monodentate ligand and are comparable to the values of 1.73(2) and 1.67(1) Å for the anisobidentate ligand in $PhTe[S_2CNEt_2]_3$ (21) and of 1.736(9) and 1.679(9) Å in the tellurium(II) compound (20). However, the two different C—S bond lengths are also observed in one of the bidentate ligands in $PhTe[S_2CNEt_2]_3$ where values of 1.748(9) and 1.69(1) Å were reported, although in the other bidentate ligand the two C—S distances are essentially identical at 1.721(9) and 1.722(9) Å (21). The same lack of clear differential between monodentate and bidentate ligand appears to extend to the partially double

Can. J. Chem. Downloaded from www.nrcresearchpress.com by 186.148.149.217 on 09/07/12
For personal use only.

TABLE 10. Selected features in the vibrational spectra (cm^{-1}) of compounds **1–5**[a]

	ν(C···NR$_2$)		ν(C—STe)		ν(Te—S)		ν(Te—Cl)
	IR	Raman	IR	Raman	IR	Raman	Raman
$Ph_2Te[S_2CNMe_2]_2$ **1**	1490vs.br[b]	1483(7)[b]	971vs[c]	973(34)	352s[d]	365(100)	
$Ph_2TeCl[S_2CNMe_2]$ **2**	1509vs.br	1510(5)	967s	961(30)	375s	376(66)	212(70)
$Ph_2Te[S_2CNEt_2]_2$ **3**	1476vs.br	1471(20)	983s	978(40)	341s	353(55)	
$Ph_2TeCl[S_2CNEt_2]$ **4**	1510vs.br	1505(6)	989s	980(20)	377m	375(65)	199(100)
$Ph_2TeCl[S_2CN(i\text{-}Pr)_2]$ **5**	1519s	1520(6)	951s	949(20)	386m	389(80)	189(50)

[a]Parentheses denote relative intensities in Raman; in the infrared s = strong, m = medium, br = broad, v = very.
[b]Probably overlapping with the phenyl vibration (m).
[c]Probably overlapping with the phenyl ring vibration (p).
[d]For the "bis" species, there are both *sym* and *asym* modes.

C···N bond. In all cases it is of course shorter than the single C—N bond. In the anisobidentate ligands in **1**, the tellurium(II) compound, and $PhTe[S_2CNEt_2]_3$ the C···N bond is 1.333(6), 1.34(1) Å (20), and 1.39(1) Å (21) respectively with the C—N single bonds being 1.432(7) and 1.471(8) Å, 1.46(1) and 1.47(1) Å (20), 1.49(2) and 1.61(2) Å (21) respectively. However, the bidentate ligand bond lengths in $PhTe[S_2CNEt_2]_3$ are very similar, being 1.34(1) and 1.33(1) Å for N···C and 1.48(1), 1.52(2), 1.49(1), and 1.48(1) Å for the C—N single bonds (21).

*The crystal structures of $Ph_2TeCl[S_2CNEt_2]\cdot\frac{1}{2}CS_2$ **4** and $Ph_2TeCl[S_2CN(i\text{-}Pr)_2]$ **5***

The ethyl derivative crystallizes out with CS_2 contained in the lattice so that the two derivatives are in different crystal systems and space groups, triclinic and $P\bar{1}$ for **4** and monoclinic and $P2_1/c$ for **5**. However, the two independent molecules in **4** and the molecular unit of **5** have the same distorted sawhorse structure about tellurium described for **1** with a Te—Cl bond replacing an axial Te—S bond. The Te—Cl bond is considerably longer than the Te—S bond in these molecules. The Te—Cl bonds, 2.638(1) and 2.616(2) Å in the two independent molecules in **4** and 2.661(2) Å in **5**, are also considerably longer than has been generally observed in R_2TeCl_2 species (22), where for seven species with six different R groups the shortest Te—Cl bond was 2.47(1) and the longest was 2.576(3) Å (22).

In **4** the molecules are packed together in such a way that there is no secondary Te···Cl interaction with an adjacent molecule. However, in **5** the chlorine atom is only 3.305 Å from the tellurium atom of an adjacent molecule and this may account for the longer Te—Cl primary bond. The Cl—Te—S bond angles of 172.0(1), 168.7(1)° in **4** and 173.2(1) in **5** compare well with the corresponding S—Te—S angle of 172.0(1)° in **1**.

In both compounds the dithiocarbamate groups are anisobidentate as they are in **1**. The Te—S bond distances of 2.516(1) and 2.513(2) Å in **4** and 2.484(2) Å in **5** are considerably shorter than those observed in **1**, $PhTe[S_2CNEt_2]_3$, or the tellurium(II) compound. The shorter bond is not unexpected when comparing a Te(IV) to a Te(II) compound (20), and the closer approach compared to the tris compound could be associated with the relative crowding in the latter where the five Te—S bonds are essentially in one plane and two of the ligands are bidentate (21). The association of the longer Te—Cl bond with the shorter Te—S bond in **5** could be a reflection of the degree to which the compounds are approaching a structure of the form $[Ph_2Te(S_2CNR_2)]^+Cl^-$.

The Te—C bond lengths of 2.114(6) and 2.124(6) Å in **4** and 2.137(5) Å in **5** are also slightly shorter than in **1**. The C—Te—C angles of 98.2(2) and 98.5(2)° in **4** and 96.0(2)° in **5** are comparable to that of **1**. The secondary Te···S interactions at 3.112(2) and 3.184(1) Å for **4** and 3.149(2) Å for **5** are similar to those in **1**. The sum of the Te—S and Te···S distances for each linkage is 5.628 and 5.697 Å for **4** and 5.633 Å for **5**, which is less than, but of the same order as, that noted for **1**, so that the bonding, around tellurium as a whole, does appear to be slightly tighter in the chlorinated derivatives. The bite angles of each of the anisobidentate ligands are similar, being 62.5(1) and 61.8(1)° for **4**, 62.0(1)° for **5**, and 61.0(1)° for **1**. In addition, the C—Te···S angles, which were noted in **1** to be 144.4(1)°, are 146.7(1), 145.1(2)° in **4** and 147.1(1)° in **5**. The secondary S atom is again well out of the plane formed by tellurium and the two carbon atoms attached to it by approximately 1.71 and 1.82 Å in **4** and 1.67 Å in **5** comparable to 1.86 Å in **1**. The position occupied by the second secondary-bonded S atom in **1** is approximately the position taken up by a secondary-bonded S atom of an *adjacent* molecule in **4** at a distance of 3.825(2) and 3.656(2) Å respectively for the two independent molecules. The four atoms Te1—S2—Te1″—S2″ or Te2—S4—Te2″—S4″ form planes with S2—Te1—S2″ or S4—Te2—S4″ angles of 83.8(1)° or 86.2(1)° respectively and Te1—S2—Te1″ or Te2—S4—TeS2″ angles of 96.2(2)° or 93.8(2)° respectively. By contrast, in **5**, as mentioned above, the closest interaction between molecules involves the chlorine atoms rather than a sulfur atom.

The C—S (bonded) distances in the two chlorinated derivatives of 1.760(6), 1.763(5) Å for **4** and 1.788(6) Å for **5** are all longer than found in **1** or in the anisobidentate and bidentate ligands in $PhTe(S_2CNEt_2)_3$ (21), or the tellurium(II) compound (20). However, the C—S (secondary-bonded) distances are very similar to those reported for the other compounds, being close to the value of 1.68 ± 1 at 1.669(6), 1.675(5) Å for **4** and 1.660(6) Å for **5**, the C···N bond lengths of 1.325(7), 1.319(7) Å in **4** and 1.329(7) Å in **5** are slightly shorter than those in **1** and previously reported compounds, reflecting the tighter bonding associated with the chloro derivatives. Indeed, the presence of chlorine indicates some sort of trend whereas changing R groups in the dithiocarbamate does not.

Vibrational spectra

Features that are considered characteristic of dithiocarbamate derivatives are listed in Table 10. The well-known phenyl vibrations (23) are of course excluded from the table but their presence makes the spectra very "busy". The N···C stretching vibration is typically assigned to a feature in the region of

Can. J. Chem. Downloaded from www.nrcresearchpress.com by 186.148.149.217 on 09/07/12
For personal use only.

TABLE 11. ^1H and ^{13}C chemical shifts in the NMR spectra of compounds **1–5**[a]

	C_6H_5	N–C*H*	C–CH_3	C_6H_5	N–*C*H	C–*C*H$_3$
$Ph_2Te[S_2CNMe_2]_2$ **1**	8.0,7.4m(10H)	3.5b(12H)	—	135.8,130.0,129.6	43.9	—
$Ph_2TeCl[S_2CNMe_2]$ **2**	8.2,7.7m(10H)	3.8b(6H)	—	133.0,130.6,129.0	44.8	—
$Ph_2Te[S_2CNEt_2]_2$ **3**	7.8,7.3m(10H)	3.7b(8H)	1.2m(12H)	135.6,130.0,129.8	48.7	13.0
$Ph_2TeCl[S_2CNEt_2]$ **4**	7.9,7.4m(10H)	3.7b(4H)	1.2m(6H)	135.0,130.8,129.8	49.1	12.9
$Ph_2TeCl[S_2CN(i\text{-}Pr)_2]$ **5**	7.9,7.3m(10H)	n.o.[b](2H)	1.4b(12H)	134.9,130.6,129.6	n.o.	20.5

[a]Number of hydrogen atoms given in parentheses; m = multiplet, b = broad.
[b]n.o. = not observed.

1450–1550 cm^{-1}. It appears that the compounds containing a Te—Cl bond generally show the band at a higher wave number than the related bis compound. This is consistent with the shorter C···N bond being found in **4** and **5**. There is no obvious dependence in any of the characteristic features in the spectra on the nature of R in the R_2NCS_2 group. Any shifts in the positions of ν(C—S) are more probably associated with vibrational interactions than with structural effects. The ν(Te—S) region is very distinctive, as is typical for many metal–sulfur bonds, and well separated from other vibrations. The values of ν(Te—S) in the Raman effect at 365, 375, and 389 cm^{-1} respectively for **1**, **4**, and **5** correspond to Te—S bond lengths of 2.621(1) Å in **1**, 2.516(1) and 2.513(2) Å in **4**, and 2.484(2) Å in **5**. The assignment of the Te—Cl stretching vibration to 212, 199, and 189 cm^{-1} in **2**, **4**, and **5** respectively is at an unusually low wave-number region but is consistent with the presence of the very long Te—Cl bonds of 2.638(1) and 2.616(2) Å in **4** and 2.661(2) Å in **5**. These results can be compared to the assignments of the ν(Te—Cl) symmetric and asymmetric modes in Me_2TeCl_2 at 281 and 248 cm^{-1} (24), and Ph_2TeCl_2 at 287 and 267 cm^{-1} (25), where the Te—Cl bond lengths are reported to be much shorter, within the range of 2.48–2.54 Å (23).

The NMR spectra of all compounds gave results inconsistent with the existence of one compound in solution. The compounds are not particularly soluble but attempts were made to record the spectra in $CDCl_3$ and CS_2. The latter solvent seemed more appropriate because this was the medium from which the pure crystals were recrystallized. Typically for the $Ph_2Te[S_2CNR_2]_2$ species, the predominant peaks in the ^1H and ^{13}C NMR spectra were consistent with the presence of Ph_2Te and the dimer of the ligand, $[S_2CNR_2]_2$, rather than the complex $Ph_2Te[S_2CNR_2]_2$, particularly if there was any time lapse between making up the solution and recording the spectra. However, it was possible to also identify the peaks attributable to $Ph_2Te[S_2CNR_2]_2$ species, particularly when the spectra were recorded immediately after they were made up. While it is clear that the $Ph_2Te[S_2CNR_2]_2$ species ultimately decompose to form Ph_2Te and $[S_2CNR_2]_2$, the spectra suggest that a second isomeric form of the bis-ligated compound could be an intermediate. For the $Ph_2TeCl[S_2CNR_2]_2$ species, the NMR spectra are even more complex because disproportionation to Ph_2TeCl_2 and $Ph_2Te[S_2CNR_2]_2$ is obviously also taking place, along with the subsequent decomposition of the bis-ligand compound.

Acknowledgements

We thank the Natural Sciences and Engineering Research Council of Canada and the Ministry of Colleges and Universities of Ontario for financial support.

1. G. D. THORN and R. A. LUDWIG. The dithiocarbamates and related compounds. Elsevier, Amsterdam. 1962.
2. D. COUCOUVANIS. Prog. Inorg. Chem. **11**, 233 (1970).
3. J. WILLIAMS, J. A. CRAS, J. J. STEGGERDA, and C. P. KEIJZERS. Struct. Bonding (Berlin), **28**, 83 (1976).
4. J. L. TEMPLETON and B. C. WARD. Inorg. Chem. **19**, 1753 (1980).
5. M. G. KANATZIDIS, D. COUCOUVANIS, A. SIMOPOULOS, A. KOSHKAS, and V. J. PAPAEFTHYMIOU. J. Am. Chem. Soc. **107**, 4925 (1985).
6. (*a*) M. G. B. DREW, D. A. RICE, and D. M. WILLIAMS. J. Chem. Soc. Dalton Trans. 1821 (1985); (*b*) E. J. PETERSON, R. B. VON DREELE, and T. M. BROWN. Inorg. Chem. **17**, 1410 (1978).
7. (*a*) S. J. M. BURGMAYER and J. L. TEMPLETON. Inorg. Chem. **24**, 2224 (1985); (*b*) T. C. W. MAK, K. S. JASIM, and C. CHIEH. Inorg. Chem. **24**, 1587 (1985); (*c*) C. D. GARNER, N. C. HOWLADER, F. E. MABBS, A. T. MCPHAIL, R. W. MILLER, and K. D. ONAN. J. Chem. Soc. Dalton Trans. 1582 (1978).
8. P. R. H. ALDERMAN, P. G. OWSTON, and J. M. ROWE. J. Chem. Soc. 668 (1962).
9. R. HESSE. Ark. Kemi, **20**, 481 (1963).
10. J. S. MORRIS and E. D. SCHLEMPER. J. Cryst. Mol. Struct. **9**, 1 (1979).
11. I. J. B. LIN, H. W. CHEN, and J. P. FACKLER, JR. Inorg. Chem. **17**, 394 (1978).
12. R. K. CHADHA, J. E. DRAKE, and A. B. SARKAR. Inorg. Chem. **23**, 4769 (1984).
13. R. K. CHADHA, J. E. DRAKE, and A. B. SARKAR. Inorg. Chem. **25**, 2201 (1986).
14. R. K. CHADHA, J. E. DRAKE, and A. B. SARKAR. Inorg. Chimica Acta, **143**, 31 (1988).
15. R. K. CHADHA, J. E. DRAKE, A. B. SARKAR, and M. L. Y. WONG. Acta Crystallogr. Sect. C: Cryst. Struct. Commun. **C45**, 37 (1989).
16. H. P. KLUG. Acta Crystallogr. **21**, 536 (1966).
17. M. BONAMICO, G. MAZZONE, A. VACIAGO, and L. ZAMBONELLI. Acta Crystallogr. **19**, 898 (1965).
18. R. C. PAUL, K. K. BHASIN, and R. K. CHADHA. J. Inorg. Nucl. Chem. **37**, 2337 (1975).
19. R. K. CHADHA, J. E. DRAKE, N. T. MCMANUS, B. A. QUINLAN, and A. B. SARKAR. Organometallics, **6**, 813 (1987).
20. M. A. K. AHMED, A. E. MCCARTHY, and W. R. MCWHINNIE. J. Chem. Soc. Dalton Trans. 771 (1986).
21. S. ESPERAS and S. HUSEBYE. Acta Chem. Scand. **26**, 3293 (1972).
22. R. K. CHADHA, J. E. DRAKE, and J. L. HENCHER. Can. J. Chem. **61**, 1222 (1983).
23. D. H. WHIFFEN. J. Chem. Soc. 1350 (1956).
24. G. C. HAYWARD and P. J. HENDRA. J. Chem. Soc. (A), 1760 (1969).
25. W. R. MCWHINNIE and G. P. PATEL. J. Chem. Soc. Dalton Trans. 199 (1972).

Can. J. Chem. Downloaded from www.nrcresearchpress.com by 186.148.149.217 on 09/07/12
For personal use only.

Protium–deuterium exchange of alkylated benzenes in dilute acid at elevated temperatures

NICK HENRY WERSTIUK AND GEORGE TIMMINS
Department of Chemistry, McMaster University, Hamilton, Ont., Canada L8S 4M1

Received March 16, 1989

This paper is dedicated to Professor Ronald J. Gillespie on the occasion of his 65th birthday

NICK HENRY WERSTIUK and GEORGE TIMMINS. Can. J. Chem. **67**, 1744 (1989).

Benzene (**1**), toluene (**2**), *o*-xylene (**3**), *m*-xylene (**4**), *p*-xylene (**5**), 1,2,3-trimethylbenzene (**6**), 1,2,4-trimethylbenzene (**7**), 1,3,5-trimethylbenzene (**8**), 1,2,3,4-tetramethylbenzene (**9**), 1,2,3,5-tetramethylbenzene (**10**), 1,2,4,5-tetramethylbenzene (**11**), pentamethylbenzene (**12**), hexamethylbenzene (**13**), hexaethylbenzene (**14**), ethylbenzene (**15**), and tetralin (**16**) have been labelled with deuterium by the high temperature – dilute acid (HTDA) method. In dilute DCl/D_2O (0.14–0.27 M) at temperatures of 250–285°C, the ring hydrogens of these compounds equilibrate with the deuterium pool. At temperatures above 250°C the methyl groups of **3**, **4**, **5**, **6** and **11** undergo slow H/D exchange; the methyl groups of **8**, **9**, **10**, and **13** undergo exchange much more readily and hexamethylbenzene (**13**) can be readily perlabelled. Hexamethylbenzene exhibits a lower reactivity than **13** at the benzylic sites.

Key words: deuterium, exchange, alkyl groups, benzenes, acid-catalyzed.

NICK HENRY WERSTIUK et GEORGE TIMMINS. Can. J. Chem. **67**, 1744 (1989).

Utilisant la méthode faisant appel à un acide dilué et à une température élevée (ADTE), on a marqué les molécules suivantes avec du deutérium : la benzène (**1**), la toluène (**2**), les *o*- (**3**), *m*- (**4**) et *p*- (**5**) xylènes, les 1,2,3- (**6**), 1,2,4- (**7**) et 1,3,5- (**8**) triméthylbenzènes, les 1,2,3,4- (**9**), 1,2,3,5- (**10**) et 1,2,4,5- (**11**) tétraméthylbenzènes, le pentaméthylbenzène (**12**), l'hexaméthylbenzène (**13**), l'hexaéthylbenzène (**14**), l'éthylbenzène (**15**) et la tétraline (**16**). À des températures allant de 250 à 285°C, dans du DCl/D_2O (0,14–0,27 M), les hydrogènes des cycles de ces composés s'équilibrent avec le bassin de deutérium. À des températures supérieures à 250°C, les hydrogènes des groupements méthyles des composés **3**, **4**, **5**, **6** et **11** subissent un échange lent des H/D; les groupements méthyles des composés **8**, **9**, **10** et **13** subissent des échanges beaucoup plus rapides et l'hexaméthylbenzène (**13**) peut facilement être perdeutéré. Les sites benzyliques de l'hexaméthylbenzène présentent une réactivité qui est plus faible que celle du composé **13**.

Mots clés : deutérium, échange, groupements alkyles, benzènes, catalyse acide.

[Traduit par la revue]

Introduction

In our continuing investigation of hydrogen isotope exchange by the high temperature – dilute acid (HTDA) method, we undertook a study of a group of alkylated benzenes to establish its scope and limitations (1–9). Our goal was to determine whether the HTDA method can be used to label alkyl substituents with deuterium (or tritium). In this paper, we document the results of this study; it is clear that the HTDA method is useful for labelling alkyl groups of substituted benzenes with deuterium (or tritium).

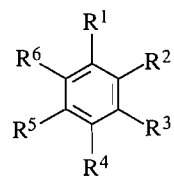
Results

The deuterium incorporations for each substrate including benzene are listed in Table 1. In all cases, the ring hydrogens equilibrate with the deuterium pool. At temperatures above 250°C, the methyl groups of **2**–**13** and the benzylic methylene groups of **14**, **15**, and **16** undergo H–D exchange to varying degrees. While the methyl groups of the xylenes **3**, **4**, and **5** incorporate only a small amount of deuterium, the methyl groups of **13** are equilibrated with the deuterium pool at 285°C. H–D exchange β to the aromatic ring in **15** and **16** occurs much more slowly than exchange at the benzylic sites.

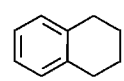
Discussion

H–D exchange of methyl-substituted benzenes

The ease of exchange of the methyl groups depends on the degree of substitution of the benzene ring, the position of the methyl groups, and on statistical factors for deprotonation of the intermediate cyclohexadienyl cations. For example, deuteronation of *m*-xylene (**4**) at C2 or C4 yields cyclohexadienyl



1 $R^{1-6} = H$
2 $R^{1} = CH_3, R^{2-6} = H$
3 $R^{1,2} = CH_3, R^{3-6} = H$
4 $R^{1,3} = CH_3, R^{2,4-6} = H$
5 $R^{1,4} = CH_3, R^{2,3,5,6} = H$
6 $R^{1-3} = CH_3, R^{4-6} = H$
7 $R^{1,2,4} = CH_3, R^{3,5,6} = H$
8 $R^{1,3,5} = CH_3, R^{2,4,6} = H$
9 $R^{1-4} = CH_3, R^{5,6} = H$
10 $R^{1,2,3,5} = CH_3, R^{4,6} = H$
11 $R^{1,2,4,5} = CH_3, R^{3,6} = H$
12 $R^{1-5} = CH_3, R^{6} = H$
13 $R^{1-6} = CH_3$
14 $R^{1-6} = Ch_2CH_3$
15 $R^{1} = CH_2CH_3, R^{2-6} = H$



16

cations **17** and **18**, which are inductively and hyperconjugatively stabilized by two methyl groups. In the case of the cyclohexadienyl cations generated from **3** and **5**, only one methyl group is positioned to provide maximal hyperconjugative stabilization. Also, while cations **17** and **18** can be deprotonated at either methyl group, the cations derived from **3** and **5** can only be deprotonated at a single methyl. On the basis of these factors, **4** is expected to undergo H–D exchange of the methyls faster than **3** or **5**. In fact, the exchange rates roughly correlate with the pK_b's of **3**, **4** and **5** (−5.3, −3.2, and −5.7, respectively) obtained at low temperatures (10).

Can. J. Chem. Downloaded from www.nrcresearchpress.com by 186.148.149.217 on 09/07/12
For personal use only.

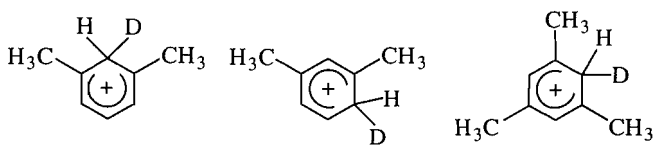
TABLE 1. Protium–deuterium exchange of alkylbenzenes

			Deuterium incorporation[d]					
			Ring		Side chain		Total	
Entry	Substrate	Conditions[a,b,c]	D atoms	%	D atoms	%	D atoms	%
1	**1**	0.24 M, 250°C, 24 h	5,94	99.0				
3	**2**	0.24 M, 250°C, 24 h	4.95	99.0				
4	**3**	0.27 M, 270°C, 43 h	3.84	96.0	0.24	4.0	4.08	40.4
5	**4**	0.27 M, 270°C, 43 h	3.84	96.0	0.50	5.0	4.34	43.4
6	**5**	0.27 M, 270°C, 43 h	3.84	96.0	0.12	3.0	3.96	39.6
7	**6**	0.27 M, 270°C, 44 h	2.87	95.8	0.56	6.2	3.43	28.6
8	**7**	0.27 M, 270°C, 44 h	2.87	95.8	0.57	6.3	3.44	28.7
9	**8**	0.27 M, 270°C, 44 h	2.87	95.8	2.92	32.4	5.79	48.3
10	**8**	0.27 M, 285°C, 48 h	2.87	95.8	6.93	77.0	9.80	81.6
11	**9**	0.27 M, 270°C, 44 h	1.91	95.6	1.72	14.3	3.63	25.9
12	**10**	0.27 M, 270°C, 44 h	1.91	95.6	2.67	29.7	4.58	32.7
13	**11**	0.27 M, 270°C, 44 h	1.91	95.6	.49	5.4	2.40	17.1
14	**12**	0.27 M, 270°C, 43 h	0.95	95.4	4.17	27.8	5.12	32.0
15	**12**	0.27 M, 285°C, 48 h	0.95	95.4	12.16	81.1	13.11	81.9
16	**13**	0.27 M, 270°C, 43 h			15.42	85.7	15.42	85.7
17	**13**	0.27 M, 285°C, 48 h			17.22	95.7	17.22	95.7
18	**14**	0.27 M, 270°C, 44 h			4.05	13.5[f]	4.05	13.5
19	**15**	0.14 M, 280°C, 72 h	4.78	95.6	0.37	18.5[f]	5.15	73.6
20	**16**	0.14 M, 280°C, 72 h[e]	3.83	95.8	2.03	50.8[g]		
					0.20	5.0[h]	6.06	50.5

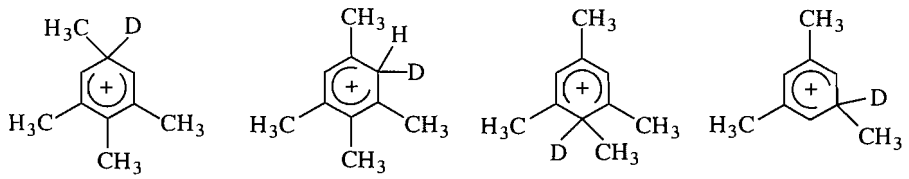
[a]DCl in D_2O.
[b]The recoveries of deuteriated compounds were generally greater than 90%. Incorporations of ≥95% correspond to equilibration with the deuterium pool.
[c]Temperatures are ±5°C.
[d]Deuterium content was determined by mass spectrometry at low ionizing voltage (10–15 eV).
[e]The reaction was agitated and decalin was used as a cosolvent.
[f]Value is for methylene; trace of D in methyl.
[g]Value is for α-CH_2s.
[h]Value is for β-CH_2s.

The same rationale can be used to account for the fact that the methyl groups of 1,3,5-trimethylbenzene (**8**) undergo exchange faster than the methyl groups of its isomers **6** and **7**. Deuteronation of **8** can occur at either of three identical sites to yield a cyclohexadienyl cation (**19**) maximally stabilized by three methyl groups. In the case of **19**, deprotonation can occur from either of three methyls to form a triene, in competition with deprotonation (dedeuteronation) to form **8**; in the case of the cations derived from **6** and **7**, deprotonation can occur from two methyl groups. Consequently, **8** should undergo exchange approximately 1.3 times faster than **6** due to a statistical factor. This coupled with the fact that **8** is more basic than **6** or **7** (pK_b: **6** (−2.9), **7** (−2.8), **8** (−0.4) (ref. 10)), accounts for the enhanced rate of exchange of the methyls of **8** relative to **6** and **7**. It should be possible to perlabel **8** simply by increasing the reaction time.

That 1,2,3,5-tetramethylbenzene (**10**) undergoes exchange of the methyl groups faster than its isomers **9** and **11** is again in accord with the relative basicities of these compounds (pK_b: **9** (−1.9), **10** (0.1), **11** (−2.2) (ref. 10)). It is not exactly clear why **10** incorporates less deuterium than **8** even though **10** is slightly more basic than **8**. This may be due to the fact that the solubility of the substrates in D_2O decreases as the number of alkyl substituents increases. At 270°C, **10** incorporates 2.67



17 **18** **19**



20 **21** **22** **23**

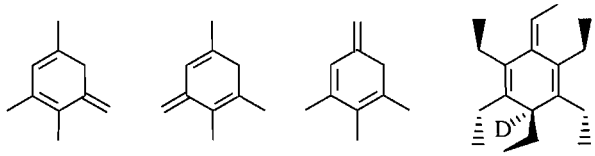
Can. J. Chem. Downloaded from www.nrcresearchpress.com by 186.148.149.217 on 09/07/12
For personal use only.

TABLE 2. Heats of formation of cations and trienes calculated by AM1

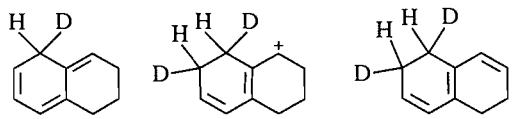
Substrate	ΔH_f (kcal/mol)[a]
20	174.0
21	165.8
22	168.5
23	179.4
24	17.8
25	18.8
26	18.6

[a]Calculations were carried out on the protio species and the geometries were fully optimized.

deuterium atoms in the methyl groups. Analysis of the 73.4-MHz ^2H nmr spectrum of the deuteriated sample obtained using enhanced resolution established that the C1 and C3 methyls undergo H–D exchange slightly faster than the other methyls. To gain information on the source of this selectivity, AM1 (11) calculations were carried out on the isomeric cyclohexadienyl cations **20**, **21**, **22**, and **23** and the heats of formation are given in Table 2. According to AM1, **21** is the most stable cation; this is in accord with low temperature protonation studies, which established that protonation at carbons bearing hydrogens in benzene derivatives is preferred over protonation at alkylated carbons by a factor of 10–20 (10). In an attempt to predict which methyl of **21** deprotonates preferentially, AM1 calculations were also carried out on isomeric trienes **24**, **25**, and **26** derivable from **21**; the heats of formation are given in Table 2. On the basis of these computational studies, and on the assumption that there are no differential kinetic effects, deprotonation should occur preferentially at the C1 and C3 methyls; this prediction is in accord with the experimental results.



24 **25** **26** **27**



28 **29** **30**

Pentamethylbenzene (**12**) undergoes exchange of the methyls at a rate comparable to **10** and the methyls equilibrate with the deuterium pool after 48 h at 285°C. That hexamethylbenzene (**13**) can be perlabelled in good yield in a single reaction is remarkable (entry 17, Table 1).

H–D exchange of hexamethylbenzene

As seen from the data in entries 16 and 18 of Table 1, **14** undergoes exchange at the benzylic sites more slowly than **13**. There are two reasons for this. In comparison with the cation formed from **13**, there is a statistical factor of 0.66 for the deprotonation at a methylene group relative to ring deprotonation of the cyclohexadienyl cation derived from **14**. More importantly, the activation energy for formation of **27** by deprotonation at a methylene of the hexaethylcyclohexadienyl cation is expected to be higher than the activation energy for the analogous deprotonation of the cation derived from **13**. A steric interaction between the incipient vinyl methyl and ethyl groups precludes optimal alignment of the methylene C-Hs with the π system of the hexaethyl cyclohexadienyl cation.

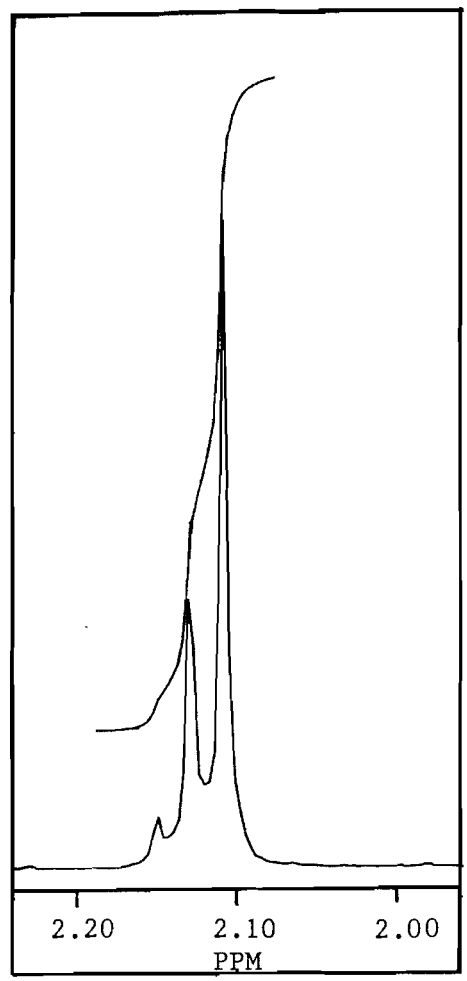


FIG. 1. The ^2H nmr spectrum (76.77 MHz, CCl_4) of deuteriated **13**.

H–D exchange of ethylbenzene and tetralin

Exchange of ethylbenzene (**15**) and tetralin (**16**) was also carried out under forcing conditions. While considerable deuteriation of the methylene of **15** (entry 19) is observed, only a trace of deuterium is incorporated in the methyl group. Tetralin (**16**) incorporates more deuterium in the α-methylene positions and a significant amount in the β-methylene positions (entry 20). A small amount of exchange at the β-methylene indicates that triene **28** (assuming that deuteronation of **16** occurs initially at C5) is deuteronated at C6 to yield cation **29**, which can return to **28** or **28**-*d* or deprotonate at C3 to yield **30**. A similar scheme is possible if **16** is deuteronated initially at C6. That exchange occurs to a greater degree in **16** than in **15** may be due to a number of factors: tetralin (**16**) is expected to be more basic than **15**; deprotonation of the α-methylene group of the first-formed cyclohexadienyl cation is expected to compete more effectively with deprotonation at C5 for **16** than for **15**. This is so because a more highly substituted double bond is formed in the former case; deprotonation of **29** at C3, which is β to the

Can. J. Chem. Downloaded from www.nrcresearchpress.com by 186.148.149.217 on 09/07/12
For personal use only.

incipient aromatic ring, competes more effectively with deprotonation at C6 because a more highly substituted double bond is formed than is the case for **15**.

^2H nuclear magnetic resonance studies

We have shown previously (12) that geminal deuterium isotope effects on deuterium chemical shifts can be determined by obtaining high field ^2H nmr spectra. In this study, for certain cases, separate resonances were observed for methyls bearing one, two, or three deuterium atoms. For example, the high field portion of the 73.4-MHz ^2H spectrum of **13**-$d_{15.42}$ (entry 16, Table 1) is shown in Fig. 1. The resonances at 2.110, 2.131, and 2.153 ppm correspond to the CD_3 (63.5%), CHD_2 (31.1%), and CH_2D (5.4%) groups respectively. The geminal deuterium isotope shifts on the deuterium resonances are 21.0 ppb. In the case of **13**-$d_{17.22}$ (entry 17, Table 1), based on the analysis of the ^2H nmr spectrum, the methyls are dideuteriated (14.9%) and trideuteriated (85.9%).

Experimental

The ^1H and ^2H nmr spectra were recorded on a Bruker AM500 spectrometer using CCl_4 as solvent and TMS as the standard. Mass spectra were performed on a VG Micromass 7070 spectrometer at low ionizing voltage (9–12 eV) to minimize fragmentation. Gas chromatographic analyses were done on a 6 ft × ⅛ in. stainless steel 3% OV-1 on Chromosorb W column in a Tracor 560 chromatograph. Preparative chromatography was carried out on a 6 ft × ¼ in. stainless steel 15% SE-30 on Chromosorb W column in a Varian Aerograph 200 chromatograph.

General exchange procedure

The substrate (0.02 g) and 0.27 M DCl/D_2O (5 mL) were sealed under vacuum in a medium-walled glass tube after degassing via three freeze–pump–thaw cycles. The tube was then heated for the prescribed time and temperature in a Parr high pressure autoclave containing water to equalize pressure. Solid products were filtered from the reaction mixture and liquids were extracted with ether (3 × 5 mL). Yields were generally quantitative; however, the gas chromatogram of 1,2,3,4-tetramethylbenzene (**9**) showed several side product peaks (12.9, 2.0, 1.0%) and after collection by preparative gc the yield was 52%.

A modification of this procedure was used for ethylbenzene (**15**) and tetralin (**16**); these reactions were run using decalin as an inert cosolvent and the mixing of the reagents was achieved through a rocking motion of the autoclave.

Acknowledgement

We thank the Natural Sciences and Engineering Research Council of Canada for financial support.

1. N. H. WERSTIUK and T. KADAI. Can. J. Chem. **51**, 1485 (1973).
2. N. H. WERSTIUK and T. KADAI. Can. J. Chem. **52**, 2169 (1974).
3. N. H. WERSTIUK and T. KADAI. U.S. Patent No. 3,989,705 (1976).
4. N. H. WERSTIUK and T. KADAI. Can. Patent No. 1048556 (1979).
5. N. H. WERSTIUK and T. KADAI. Can. J. Chem. **59**, 1022 (1981).
6. N. H. WERSTIUK and T. KADAI. Can. J. Chem. **59**, 3218 (1981).
7. N. H. WERSTIUK and T. KADAI. Can. J. Chem. **63**, 530 (1985).
8. N. H. WERSTIUK. *In* Isotopes in physical and biomedical sciences. *Edited by* J. R. Jones and E. Buncel. Elsevier, New York. 1987.
9. N. H. WERSTIUK and G. TIMMINS. Can. J. Chem. **66**, 2309 (1988).
10. D. M. BROUWER, E. L. MACKOR, and C. MACLEAN. *In* Carbonium ions. Vol. II. *Edited by* G. A. Olah and P. von R. Schleyer. Wiley–Interscience, New York. 1970. Chap. 20.
11. AMPAC; Austin Method 1 Package (QCPE 506). Dewar Research and J. P. Stewart. QCPE Bull. **6**, 2 (1986).
12. N. H. WERSTIUK, G. TIMMINS, and B. SAYER. Can. J. Chem. **64**, 465 (1986).

Can. J. Chem. Downloaded from www.nrcresearchpress.com by 186.148.149.217 on 09/07/12
For personal use only.

The electron spin resonance spectra of dioxene radical cations

ALWYN G. DAVIES[1] AND CHARLES J. SHIELDS
Chemistry Department, University College London, 20 Gordon Street, London WC1 OAJ U.K.

AND

JEFFREY C. EVANS AND CHRISTOPHER C. ROWLANDS
Chemistry Department, University College, Cardiff CF1 1XL U.K.

Received March 16, 1989

This paper is dedicated to Professor Ronald J. Gillespie on the occasion of his 65th birthday

ALWYN G. DAVIES, CHARLES J. SHIELDS, JEFFREY C. EVANS, and CHRISTOPHER C. ROWLANDS. Can. J. Chem. **67**, 1748 (1989).

The electron spin resonance spectra of the radical cations of dioxene (**1***a*), 2,3-dimethyldioxene (**1***b*), 2,3-diphenyldioxene (**1***c*), and benzodioxane (**2**) in fluid solution have been observed and analysed, with the help of ENDOR spectroscopy in the case of **1***c*. It is concluded that in **1***c* the molecule has overall C_2 molecular symmetry. In all four compounds, the pseudo-axial and pseudo-equatorial protons of the methylene groups in the half-chair dioxene rings are distinguished by different hyperfine coupling constants, and simulation of the spectra over a range of temperatures has given the Arrhenius parameters for the ring inversion of **1***a*, **1***b*, and **2**.

Key words: ESR spectra, radical cation, 1,4-dioxene, inversion barrier.

ALWYN G. DAVIES, CHARLES J. SHIELDS, JEFFREY C. EVANS et CHRISTOPHER C. ROWLANDS. Can. J. Chem. **67**, 1748 (1989).

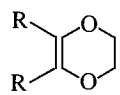
On a déterminé les spectres en résonance paramagnétique électronique des radicaux cations du dioxène (**1***a*), du 2,3-diméthyldioxène (**1***b*), du 2,3-diphényldioxène (**1***c*) et du benzodioxane (**2**) en solutions fluides et, dans le cas du composé **1***c*, on a aussi analysé le spectre à l'aide de la spectroscopie ENDOR. On en conclut que le composé **1***c* possède une symétrie moléculaire globale C_2. Dans les quatre composés, des constantes de couplage hyperfin différentes permettent de distinguer les protons pseudo-axiaux et pseudo-équatoriaux des groupements méthylènes des cycles demi-chaises du dioxène; de plus, une simulation des spectres sur une plage importante de températures a permis d'évaluer les paramètres d'Arrhénius pour les inversions des cycles **1***a*, **1***b* et **2**.

Mots clés : spectres RPE, cation radical, 1,4-dioxène, barrière à l'inversion.

[Traduit par la revue]

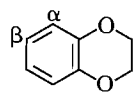
Can. J. Chem. Downloaded from www.nrcresearchpress.com by 186.148.149.217 on 09/07/12
For personal use only.

The electron spin resonance (esr) spectra of some acyclic alkoxyalkene (vinyl ether) radical cations have recently been identified (1), but there appear to be no reports in the literature of the esr spectra of the related dioxene radical cations ($\mathbf{1}^{+\cdot}$).



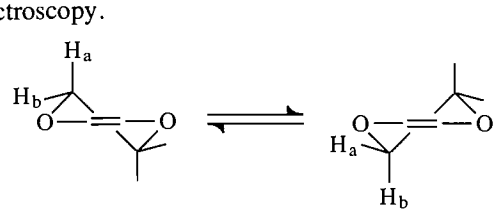
1

a R = H
b R = Me
c R = Ph



2

These species are interesting because in the half-chair conformation of the parent dioxenes, the axial and equatorial protons of the methylene groups can be distinguished in the nmr spectra by different chemical shifts (2, 3). Similarly in the esr spectra of the radical cations, H_{ax} and H_{eq} should be distinguished by different hyperfine coupling constants, and in principle it should be possible to examine the effect of one-electron oxidation on the conformational inversion (4) illustrated in eq. [1], by variable temperature nmr and esr spectroscopy.

[1] 

[1]Author to whom correspondence may be addressed.

Indeed the esr spectrum of the 2,3-benzodioxane radical cation $\mathbf{2}^{+\cdot}$ (which is better regarded as a 1,2-dialkoxybenzene than a dioxene) was recorded at room temperature in 1976 by Dixon and Murphy (5), and it showed an alternating line width effect characteristic of conformational inversion.

We report here the generation of the radical cations of dioxene (**1***a*), 2,3-dimethyldioxene (**1***b*), 2,3-diphenyldioxene (**1***c*), and benzodioxane (**2**) in fluid solution, and a study of their esr spectra at varying temperatures (for a preliminary note, see ref. 6).

Results

The dioxenes **1***a*, **1***b*, and **1***c* (7) were prepared by condensation of the appropriate diol and acyloin under acid conditions. This is analogous to the method used by Gelas and Petrequin (8) for preparing **1***b*, and provides a more convenient route to **1***a*, which is usually prepared by dehydrogenation/dehydration of bis(2-hydroxyethyl)ether over a copper chromite/potassium hydrogen sulphate catalyst at 230–250°C (9).

The esr spectrum of $\mathbf{1}b^{+\cdot}$ could readily be observed without photolysis when 2,3-dimethyldioxene (**1***b*) was dissolved in concentrated sulphuric acid, or in trifluoroacetic acid containing mercury trifluoroacetate, or in liquid sulphur dioxide containing fluorosulphonic acid. At 296 K, the spectrum consisted of a septet of quintets with some alternating line width effect (Fig. 1c); hyperfine coupling constants are listed in Table 1.

In SO_2/FSO_3H (10), the spectrum could be studied at low temperatures. At around 230 K, the second and fourth lines of the quintets were lost (Fig. 1b), then at near 200 K the couplings to the methylene protons resolved into a triplet of triplets

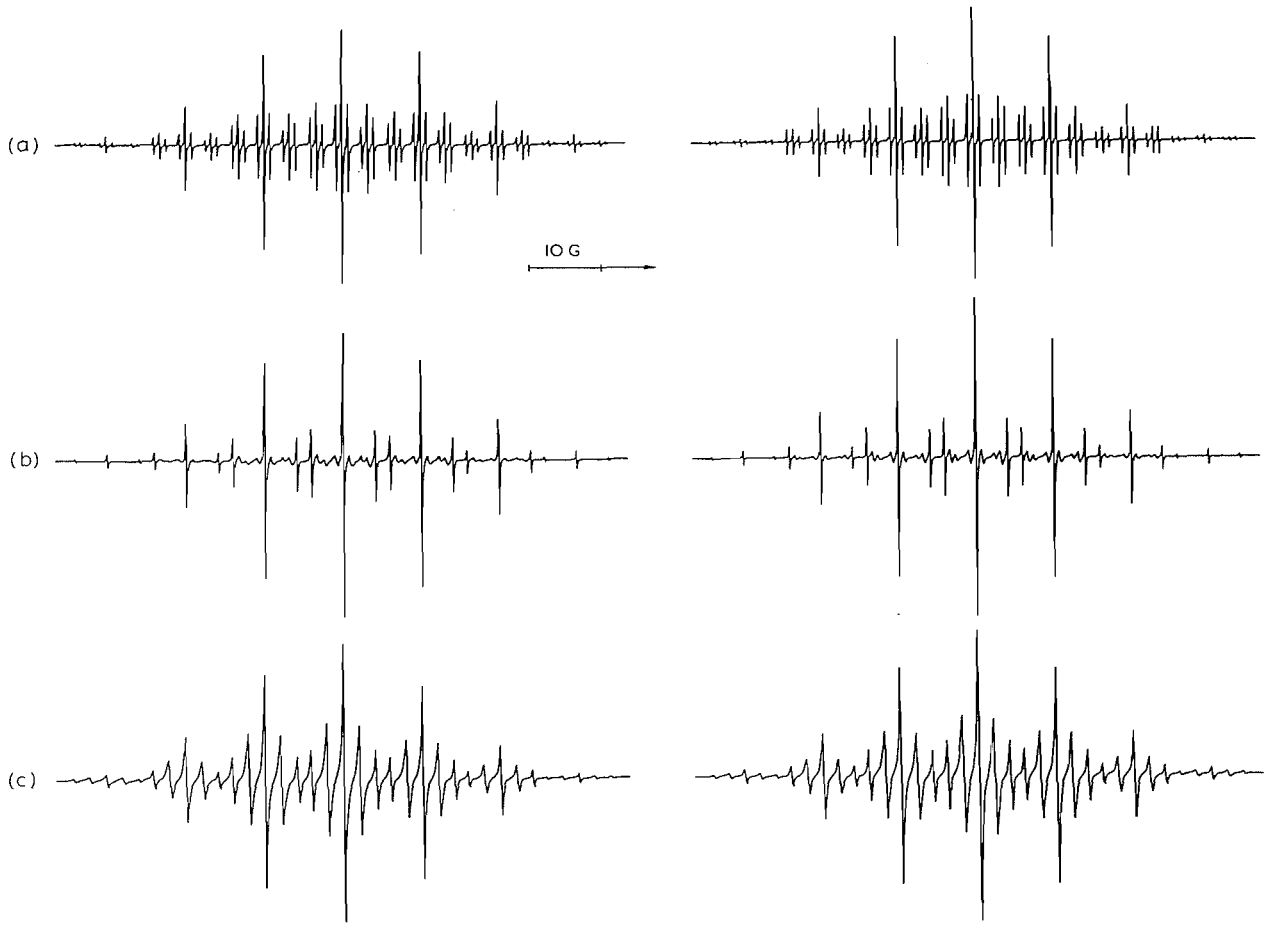


FIG. 1. The esr spectra (left) and simulations (right) of the 2,3-dimethyldioxene radical cation $\mathbf{1}b^{\dot{+}}$ in SO_2/FSO_3H at (a) 200 K, (b) 230 K, and (c) 296 K.

TABLE 1. The esr spectra of dioxenes

	a(G)			
	$2H_{ax}$	$2H_{eq}$	Others	g
$\mathbf{1}a^{\dot{+}}$	4.70	1.11	9.10(2H)	2.0040
$\mathbf{1}b^{\dot{+}}$	3.55	0.85	10.80(6H)	2.0036
$\mathbf{1}c^{\dot{+}}$ [a]	2.58	0.61	1.94($2H_p$) 1.66($2H_o$) 1.54($2H'_o$) 1.04($2H_m$) 0.67($2H'_m$)	2.0034
$\mathbf{2}^{\dot{+}}$	4.01	0.95	0.4 ($2H_\alpha$) 4.57($2H_\beta$)	2.0038

[a]For labelling of positions, see **3**.

(Fig. 1a and Table 1), resulting from nonequivalent axial and equatorial methylene protons. Simulation of the spectra over the temperature range 175–300 K gave the Arrhenius plot shown in Fig. 2, and the values of A and E for the conformational equilibrium (eq. [1]) that are given in Table 2.

Dixon and Murphy oxidized benzodioxane (**2**) using cerium(IV) and concentrated sulphuric acid in a flow system (5). We found it difficult to obtain satisfactory spectra in a static system. In trifluoroacetic acid containing thallium(III) trifluoroacetate at 263 K, **2** showed a spectrum similar to that reported by Dixon and Murphy, superimposed on a second weaker spectrum. In

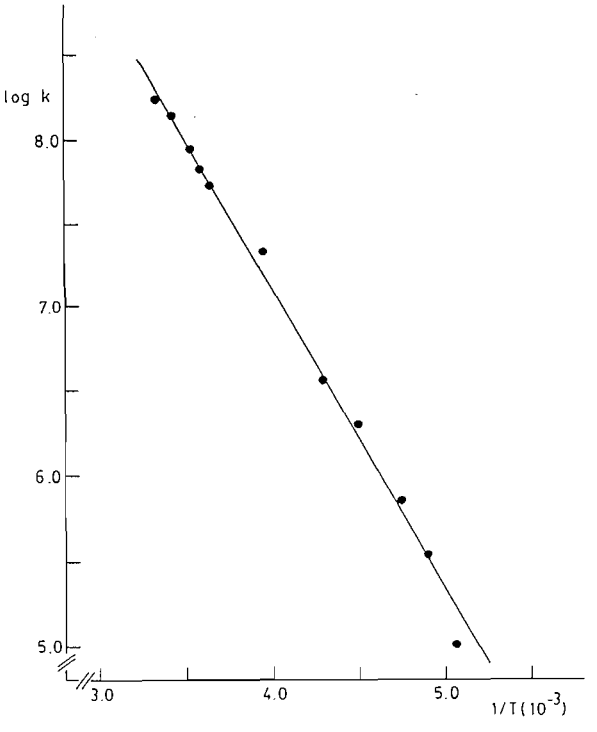


FIG. 2. Arrhenius plot for the conformational inversion of $\mathbf{1}b^{\dot{+}}$.

Can. J. Chem. Downloaded from www.nrcresearchpress.com by 186.148.149.217 on 09/07/12
For personal use only.



FIG. 3. The esr spectra and simulations of the benzodioxane radical cation $\mathbf{2}^{\dot{+}}$ (a) in SO_2/FSO_3H at 175 K, and (b) the wing lines, in SO_2ClF/FSO_3H at 205 K.

TABLE 2. Arrhenius parameters for reaction [1]

	log A	E (kJ mol^{-1})
$\mathbf{1}a^{\dot{+}}$	12.8±0.7	22.6±2.2
$\mathbf{1}b^{\dot{+}}$	13.7±0.7	31.4±2.5
$\mathbf{2}^{\dot{+}}$	15.1	34.7

dichloromethane containing aluminium chloride at 189 K it showed this second spectrum, which became much stronger when oxygen was admitted; a similar but weaker spectrum was obtained in the dark below 193 K with SO_2/FSO_3H. This spectrum could be simulated using the coupling constants a(4H) 2.15, a(2H) 0.875, a(2H) 0.26 G, g 2.0038, but the origin of the spectrum is not obvious.

However, photolysis with Pyrex-filtered light of a solution of **2** in SO_2/FSO_3H at 175 K showed a strong spectrum (Fig. 3), with the hyperfine coupling constants given in Table 1. Dixon and Murphy reported a(2H) 0.40, a(2H) 4.65 G, and from the illustration of their spectrum the sum of $a(H_{ax})$ and $a(H_{eq})$ can be estimated to be 5.13 G, in line with our figures.

Above 203 K, the spectrum of $\mathbf{2}^{\dot{+}}$ became contaminated in the centre with that of another radical, but the wing multiplets remained clear and could be simulated for determining the kinetics of the inversion process (Fig. 3). A rather more stable spectrum at higher temperatures was obtained by photolysis of a solution of SO_2ClF/FSO_3H, and by using these two solvents the Arrhenius plot shown in Fig. 4 could be obtained over the range 175–215 K, giving the values of A and E in Table 2.

As only the ring multiplets are being considered in the simulation, the probable errors in A and E are likely to be larger than they are for $\mathbf{1}a^{\dot{+}}$ and $\mathbf{1}b^{\dot{+}}$.

Simulation of the spectrum illustrated in Dixon and Murphy's paper gives a rate constant, at an assumed 290 K (their room temperature), that is within 5% of that given by our Arrhenius plot.

We found it much more difficult to oxidize dioxene itself ($\mathbf{1}a$) than 2,3-dimethyldioxene ($\mathbf{1}b$), and satisfactory spectra could be obtained only over the range 252–309 K in $CF_3CO_2H/Hg(OCOF_3)_2$ (Fig. 5). A low enough temperature could not be reached to measure $a(H_{ax})$ and $a(H_{eq})$ directly, but their average (2.91 G) could be obtained at the higher temperatures. The ratio of $a(H_{ax})/a(H_{eq})$ is the same in $\mathbf{1}b^{\dot{+}}$ (4.226) and $\mathbf{2}^{\dot{+}}$ (4.221) and we assumed this ratio would also be 4.22 in $\mathbf{1}a^{\dot{+}}$. From this we calculate $a(H_{ax})$ to be 4.70 G, and $a(H_{eq})$ 1.11 G.

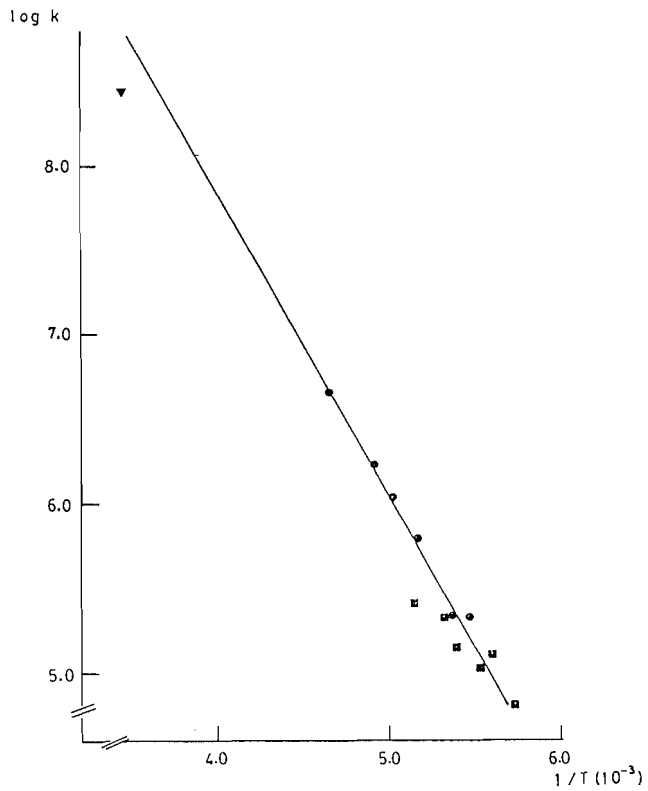


FIG. 4. Arrhenius plot for the conformational inversion of $\mathbf{2}^{\dot{+}}$, ■ in SO_2/FSO_3H, ● in SO_2ClF/FSO_3H, ▼ taken from ref. 5.

Using these values good simulations of the spectra were obtained (Fig. 5), giving the Arrhenius plot illustrated in Fig. 6, and the values of A and E listed in Table 1.

Strong esr spectra were obtained in the dark from a solution of 2,3-diphenyldioxene ($\mathbf{1}c$) in $CF_3CO_2H/Hg(OCOCF_3)_2$, or by photolysis of a solution of $\mathbf{1}c$ in $CH_2Cl_2/AlCl_3$, and under these second conditions the spectrum persisted indefinitely in the dark at 193 K. Schaap *et al.* (1) have reported detecting esr signals of some 2,3-diaryldioxenes by electrochemical oxidation or by oxidation with tris(*p*-bromophenyl)aminium tetrafluoroborate, but details of the spectra have not been published.

Our spectrum (Fig. 7) was too complicated to be analysed by inspection, but the ENDOR spectrum at 188 K provided the hyperfine coupling constants given in Table 1, which gave a good simulation of the esr spectrum.

The observation of seven different hyperfine coupling con-

Can. J. Chem. Downloaded from www.nrcresearchpress.com by 186.148.149.217 on 09/07/12
For personal use only.

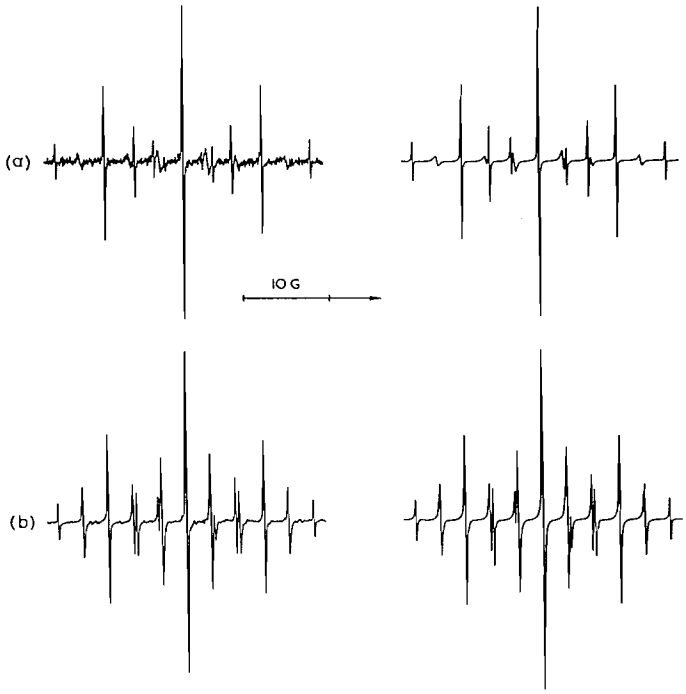


FIG. 5. The esr spectra (left) and simulations (right) of the dioxene radical cation $\mathbf{1}a^{+\cdot}$ in $CF_3CO_2H/Hg(OCOCF_3)_2$ at (a) 252 K, and (b) 309 K.

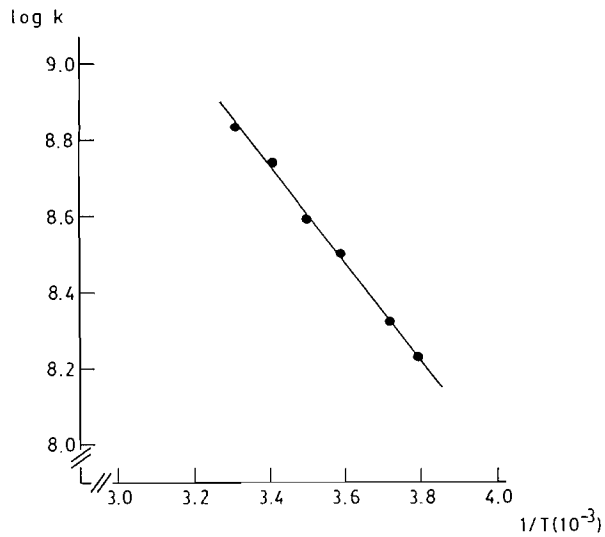


FIG. 6. Arrhenius plot for the conformational inversion of $\mathbf{1}a^{+\cdot}$.

stants (which would give 2187 lines in the esr spectrum) implies that the two *ortho* and the two *meta* protons in each phenyl ring are nonequivalent, that is, that the phenyl groups are not freely rotating, nor coplanar with, nor orthogonal to the dioxene ring, but twisted as illustrated in **3**, as they are in other compounds related to *cis*-stilbene (12–14).

Presumably this twisted conformation results from a compromise between maximization of the π-overlap and minimization of *ortho* interactions. Gerson has observed the same phenomenon in the esr spectra of various radical anions containing the π-system of *cis*-stilbene (e.g., *cis*-stilbene itself (12), and 1,2-diphenyl-cyclobutene (12), -cyclopentene (13), and -cyclohexene ($\mathbf{4}^{-\cdot}$) (14); this last compound is conformationally closely related to our diphenyldioxene $\mathbf{1}c^{+\cdot}$). A similar

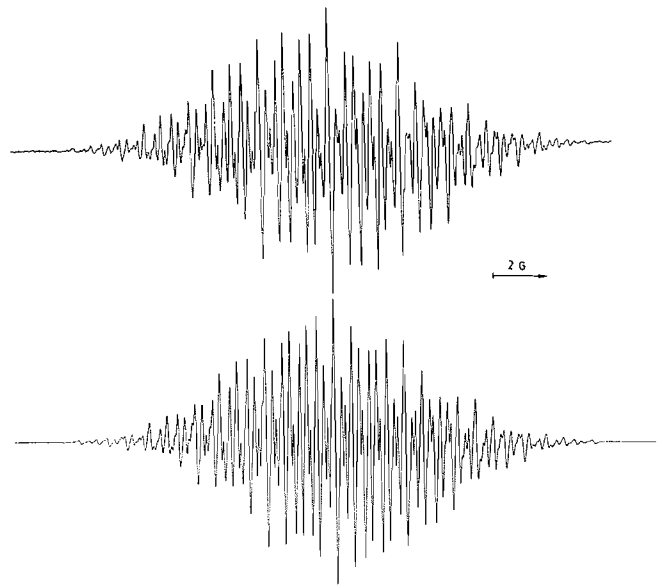
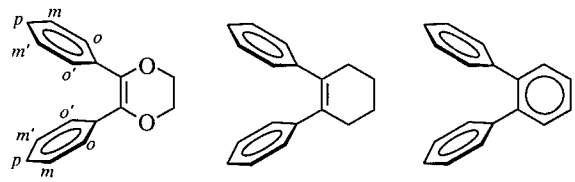


FIG. 7. The esr spectrum (top) and simulation (bottom) of the diphenyldioxene radical cation $\mathbf{1}c^{+\cdot}$ in SO_2/FSO_3H at 188 K.

effect is observed in the *ortho*-triphenyl radical anion $\mathbf{5}^{-\cdot}$ (4, 15), and we have recently identified it also in the corresponding radical cation $\mathbf{5}^{+\cdot}$.[2]



3 **4** **5**

The tentative assignment of the hyperfine coupling constants in $\mathbf{1}c^{+\cdot}$ is based on the assumption that $a(H_{ax})/a(H_{eq}) =$ ca. 4.2 (here it is 4.2), and on Gerson's analysis of the spectra of the radical anions related to *cis*-stilbene, particularly his argument that, in this context, steric hindrance leads to a reduction in the absolute value of an α-proton coupling constant (12–14).

We were unable to determine the inversion barrier (eq. [1]) for the 1,2-diphenyldioxene radical cation $\mathbf{1}c^{+\cdot}$ because variation of the temperature caused a change not only in the hyperfine coupling constants of the axial and equatorial methylene protons, but also in those of the protons of the phenyl groups. Gerson and Martin studied the esr and ENDOR spectrum of the 1,2-diphenylcyclohexene radical anion $\mathbf{4}^{-\cdot}$ over the temperature range 173–293 K (14), but even at the highest temperature they could not observe exchange between the axial and equatorial protons, and they concluded that the inversion barrier was considerably raised by the introduction of the two phenyl groups.

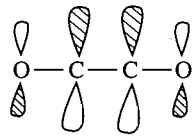
Discussion

The Hückel model predicts that the HOMO of 1,4-dioxene and of its radical cation should have a node between the terminal atoms of the O—C=C—O system, with the electron density concentrated on the carbon atoms as shown in **3**.

This is supported by an *ab initio* (STO-3G) calculation, which predicts also a low ionization potential of 8.43 eV, close

[2]A. G. Davies and D. C. McGuchan, unpublished work.

Can. J. Chem. Downloaded from www.nrcresearchpress.com by 186.148.149.217 on 09/07/12
For personal use only.



3

to the value of 8.48 ± 0.02 eV that is found by photoelectron spectroscopy (16).

On the basis of infrared and Raman spectroscopy, two transition states were identified for the inversion of 1,4-dioxene (**1***a*). The first (31.99 ± 2.51, or 34.59 kJ mol^{-1}) (17, 18) had a bent half-chair conformation, and the second (78.09 ± 9.04, or 81.65 kJ mol^{-1}) (17, 18) was planar. Larkin and Lord (2) studied the ring inversion by variable temperature (−150°C to room temperature) proton nmr and found an activation energy to inversion of 31.90 ± 0.63 kJ mol^{-1}.

Allinger and co-workers (19) calculated the barrier to ring inversion in **1***a* by the molecular mechanics (MM2) method. They were unable to locate the nonplanar transition state, and for the planar structure they calculated a barrier of 25.04 kJ mol^{-1}. They proposed that the situation could best be interpreted in terms of the existence of only one barrier represented by the planar structure, and although the calculation may have too low a value, the errors in the experiments were thought to have been underestimated.

The ready formation of the radical cations $\mathbf{1}a^{\dot{+}}$ and $\mathbf{1}b^{\dot{+}}$, and the hyperfine coupling constants that we observe, are in accord with the MO calculations. Particularly noticeable is the substantial coupling at the central carbon atoms (e.g., *a*(2Me) 10.80 G in $\mathbf{1}b^{\dot{+}}$) compared with that in butadiene radical cations (e.g., *a*(2Me) 4.2 G in hexamethylbutadiene (20)), reflecting the different orbital occupancy. These hyperfine coupling constants, and the *g*-values that we observe in the dioxene radical cations $\mathbf{1}a^{\dot{+}}$ and $\mathbf{1}b^{\dot{+}}$ are close to those we reported for the acyclic 1,2-di-*tert*-butoxyalkene radical cations (e.g., *E*/*Z*-Bu^{t}OCH=CHOBu^t$^{\dot{+}}$, *a*(2H) 8.25 G, *g* 2.0049; *Z*-Bu^{t}OCMe=CMeOBu^t$^{\dot{+}}$, *a*(2Me) 9.69 G, *g* 2.0040) (1).

The barrier to inversion (eq. [1]) that we find in the dioxene radical cation $\mathbf{1}a^{\dot{+}}$ (22.6 ± 2.2 kJ mol^{-1}) is smaller than that measured by Larkin and Lord (2) by nmr for the parent molecule **1***a* (though it is close to that (25.04 kJ mol^{-1}) calculated by Allinger (19) for a planar transition state). If the transition state is planar, the inversion process involves twisting about the terminal O—C bonds where the wave function (**3**) is locally antibonding, and also about the central C—C bond where the wave function is locally bonding. The former element would increase the activation energy for achieving the transition state, and the latter element would reduce it. If we accept Larkin and Lord's results, removal of an electron from the orbital apparently reduces the activation energy, and this would be consistent with the sum of the π-bond orders in the two O—C bonds being greater than the bond order in the C—C bond. Any changes in bond lengths and bond angles, and in solvation, which will accompany ionization, however, may of course also contribute to changes in activation energy. The introduction of the two methyl groups in $\mathbf{1}b^{\dot{+}}$ increases the inversion barrier, and fusion of the dioxene and benzene rings in $\mathbf{2}^{\dot{+}}$ similarly increases the rigidity of the dioxene ring.

Experimental

The esr spectra were obtained using a Varian E109 spectrometer fitted with a 500-W high pressure mercury arc focussed on the cavity. Temperatures were measured with a calibrated thermocouple placed alongside the esr tube, and are corrected for the heating effect of the uv light on the sample. Spectra were simulated using the ESRXN programme.

*1,4-Dioxene (**1**a)*

Glycolaldehyde dimer (Aldrich; 1.5 g) was converted into the monomer by heating it in ethylene glycol (65 cm^3) at 100°C for 15 min. *p*-Toluenesulphonic acid was then added, and a mixture (ca. 1:1) of the dioxene and 2-methyl-1,3-dioxolane was distilled off through a reflux air condenser (30 min). Purification by preparative glc gave 1,4-dioxene as a colorless liquid, ^{1}H nmr ($CDCl_3$): 4.15 (s, 4H, CH_2) and 5.9 (s, 2H, =CH—).

*2,3-Dimethyl-1,4-dioxene (**1**b)*

Acetoin dimer (Aldrich; 4.4 g) was converted into the monomer by heating it in ethylene glycol (120 cm^3) for 15 min. *p*-Toluenesulphonic acid (0.1 g) was then added, and the product was distilled off through a reflux air condenser (100 min). Redistillation gave the dioxene (4.2 g, 74%) as a yellow liquid, bp 74°C/80 Torr; 1 Torr = 133.3 Pa); ^{1}H nmr ($CDCl_3$): 1.75 (s, 6H, Me), 4.0 (s, 4H, CH_2). A small sample was purified by preparative glc, giving the dioxene as a colourless liquid that turned yellow again within ca. 2 h. Both the colourless and the yellow samples showed the same nmr and esr spectra.

2,3-Diphenyl-1,4-dioxene (**1***c*) was prepared from benzoin and ethylene glycol by Summerbell and Berger's method (7), and benzo-1,4-dioxane (**2**) was a commercial product (Aldrich).

Acknowledgements

We are grateful to Dr. B. P. Roberts for assistance with the kinetic simulations, and to Mr. S. Corker for carrying out the preparative glc. This work was supported by the S.E.R.C.

1. A. J. Bloodworth, A. G. Davies, and R. S. Hay-Motherwell. J. Chem. Soc. Chem. Commun. 862 (1988).
2. D. H. Larkin and R. C. Lord. J. Am. Chem. Soc. **95**, 5129 (1973).
3. D. M. Fatheree, G. L. Deeg, D. B. Matthews, and J. G. Russel. Org. Magn. Reson. **18**, 92 (1982).
4. W. Huber and K. Mullen. Acc. Chem. Res. **19**, 300 (1986).
5. W. T. Dixon and D. Murphy. J. Chem. Soc. Perkin Trans. 2, 1823 (1976).
6. A. G. Davies and C. J. Shields. Organic free radicals. *Edited by* H. Fischer and H. Heimgartner. Springer, Berlin. 1988. p. 195.
7. R. K. Summerbell and D. R. Berger. J. Am. Chem. Soc. **81**, 633 (1959).
8. J. Gelas and D. Petrequin. Bull. Soc. Chim. Fr. 1101 (1972).
9. R. D. Moss and J. Paige. J. Chem. Eng. Data, **12**, 452 (1967).
10. A. G. Davies and C. J. Shields. J. Chem. Soc. Perkin Trans. 2. In press.
11. A. P. Schaap, K. A. Zaklika, B. Kaskar, and L. W.-M. Fung. J. Am. Chem. Soc. **102**, 389 (1980).
12. F. Gerson, H. Ohya-Nishiguchi, M. Szwarc, and G. Levin. Chem. Phys. Lett. **52**, 587 (1977).
13. F. Gerson, W. B. Martin, and C. Wydler. Helv. Chim. Acta, **62**, 2517 (1979).
14. F. Gerson and W. B. Martin. Helv. Chim. Acta, **70**, 1558 (1987).
15. M. Plato, R. Biehl, K. Mobius, and K. P. Dinse. Z. Naturforsch. A: Phys. Phys. Chem. Kosmophys. **31A**, 169 (1976).
16. M. Block, F. Brogli, E. Heilbronner, T. B. Jones, H. Prinzbach, and O. Schweikert. Helv. Chim. Acta, **61**, 1388 (1978).
17. J. R. Durig, R. O. Carter, and L. A. Carreira. J. Chem. Phys. **60**, 3098 (1974).
18. R. C. Lord, T. C. Rounds, and T. Ueda. J. Chem. Phys. **57**, 2572 (1972).
19. H. Dodziuk, H. vom Voithenberg, and N. L. Allinger. Tetrahedron, **38**, 2811 (1982).
20. J. L. Courtneidge and A. G. Davies. J. Chem. Soc. Chem. Commun. 136 (1984).

Can. J. Chem. Downloaded from www.nrcresearchpress.com by 186.148.149.217 on 09/07/12
For personal use only.

Thermolysis of 2-acyloxy-Δ^3-1,3,4-oxadiazolines. Evidence for a preferred sense of cycloreversion to carbonyl ylides and for fast 1,4-sigmatropic ylide rearrangement

MICHAEL W. MAJCHRZAK AND JOHN WARKENTIN[1]

Department of Chemistry, McMaster University, Hamilton, Ont., Canada L8S 4M1

Received February 27, 1989

This paper is dedicated to Professor Ronald J. Gillespie on the occasion of his 65th birthday

MICHAEL W. MAJCHRZAK and JOHN WARKENTIN. Can. J. Chem. **67**, 1753 (1989).

Thermolysis of 2-acyloxy-2,5,5-trialkyl-Δ^3-1,3,4-oxadiazolines in benzene solution at 80°C furnishes acyloxy-substituted enol ethers (hemiacylals) in high yield. Mixtures of *cis*:*trans* isomers of such oxadiazolines afford mixtures of isomeric hemiacylals in nearly the same ratio. Those and other results are rationalized in terms of cycloreversion of the oxadiazolines to carbonyl ylides that are not equilibrated during their lifetimes and undergo primarily 1,4-sigmatropic H-migration. Some fragmentation of the ylides to anhydrides and carbenes was also observed. A consistent mechanistic account includes concerted suprafacial ($4\pi + 2\pi$) cycloreversion in the sense that places a large ylide substituent at C-1 or at C-3, preferentially *exo*. A smaller preference for the cycloreversion that places the acetoxy group at C-1 in the *endo* position, when the steric effect of the alkyl group at C-1 is small, can be inferred. The possibility that the overall 1,4-H shift is the result of sequential 1,7-antarafacial and 1,4-suprafacial shifts, in some cases, is considered.

Key words: carbonyl ylide; 1,4-sigmatropic rearrangement; cycloreversion, thermal, of oxadiazolines; ylide, carbonyl; oxadiazoline, thermolysis of.

MICHAEL W. MAJCHRZAK et JOHN WARKENTIN. Can. J. Chem. **67**, 1753 (1989).

La thermolyse des 2-acyloxy-2,5,5-alkyl-Δ^3-1,3,4-oxadiazolines, en solution dans le benzène à 80°C, fournit des éthers énoliques substitués par des groupements acyloxy (hémiacylals) avec un excellent rendement. Les mélanges *cis*:*trans* de telles oxadiazolines fournissent des mélanges d'hémiacylals isomères qui sont dans le même rapport. On rationalise ces résultats ainsi que d'autres en fonction d'une cycloréversion des oxadiazolines en ylures de carbonyles qui ne s'équilibrent pas durant leur existence et qui subissent principalement des migrations sigmatropiques-1,4 d'hydrogène. On a aussi observé quelques fragmentations des ylures en anhydrides et en carbènes. Un mécanisme cohérent comporte une cycloréversion ($4\pi + 2\pi$) suprafaciale concertée dans le sens qui permet de placer un substituant ylure volumineux en positions C-1 ou C-3, d'une façon préférentielle *exo*. On peut supposer qu'il existe aussi une préférence plus faible pour la cycloréversion qui place le groupement acétoxy en position *endo* en C-1, où l'effet stérique du groupement alkyle en C-1 est faible. On considère qu'il est possible, dans quelques cas, que le déplacement global 1,4 d'hydrogène puisse être le résultat des déplacements successifs antérafacial-1,7 et suprafacial-1,4.

Mots clés : carbonyle ylure; transposition sigmatropique-1,4; cycloréversion, thermique, d'oxadiazolines; ylure, carbonyle; oxadiazoline, thermolyse de.

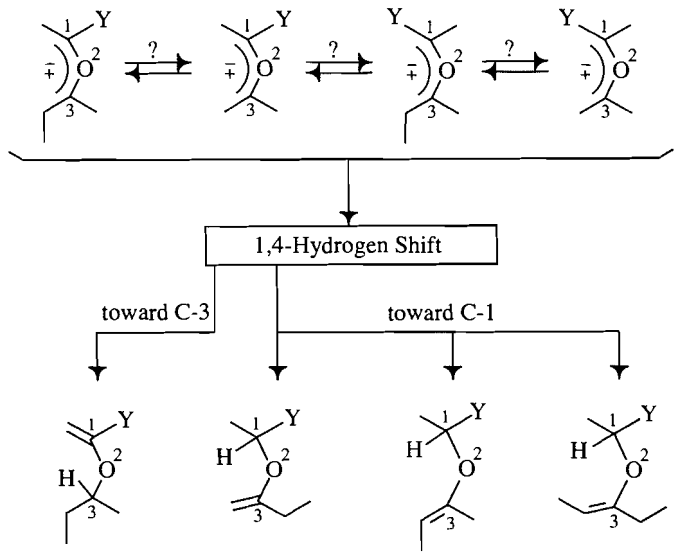
[Traduit par la revue]

Introduction

1,4-Sigmatropic H-migrations (1) in ylides, including azomethine ylides (2–4) and carbonyl ylides (5–7), are well known. Many details of those rearrangements, however, are poorly understood. First, there is the question of whether ylide equilibration, by rotation about one or both carbon–heteroatom bonds, is faster or slower than sigmatropic rearrangement. Second, the preferred geometry (*E* or *Z*) about the newly formed double bond of the product of H-migration is not known. Third, the sense of sigmatropic rearrangement (toward C-1 or C-3) in unsymmetric systems is not established for a variety of cases. Finally, there is little information in the literature concerning substitution patterns that cause suppression of the sigmatropic rearrangement in favour of alternative unimolecular processes such as fragmentations to carbonyl compounds and carbenes.

These questions are illustrated in Scheme 1 for a simple carbonyl ylide to which they would apply.

We now report the synthesis and thermolysis of a series of 2-acetoxy-2,5,5-trialkyl-Δ^3-1,3,4-oxadiazolines (**2** and **5**). Systematic changes of the alkyl substituents and a study of *cis*/*trans* mixtures provided information concerning some of the questions posed above.



SCHEME 1

Methods and results

Oxadiazolines **2** were prepared by oxidation of acyl hydrazones (**1**) of ketones with lead tetraacetate (LTA) in methylene chloride (1), eq. [1]. That method afforded *cis*:*trans* mixtures

[1]Author to whom correspondence may be addressed.

Can. J. Chem. Downloaded from www.nrcresearchpress.com by 186.148.149.217 on 09/07/12
For personal use only.

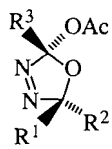
TABLE 1. Substrate ratios and product yields[a–d]

Substrate	R^1	R^2	R^3	Isomer ratio *trans*:*cis*	Products (yields)
2*b*	Me	Et	Me	2.2:1.0	**7**(62), **8**(28)
2*b*				1.0:1.9	**7**(35), **8**(55)
2*c*	Et	Et	Me		**20**(88)
2*d*	Me	*i*-Pr	Me	3.0:1.0	**10**(69), **12**(17)
2*d*				1.0:2.6	**10**(37), **12**(45)
2*e*	*i*-Pr	*i*-Pr	Me		**17**(11), **16**(60)
2*f*	Me	*t*-Bu	Me	14.5:1.0	**24**(~95)
2*g*	Me	Et	*i*-Pr	2.5:1.0	**18**(57), **19**(28)
2*h*	Me	*i*-Pr	*i*-Pr	2.4:1.0	**26**(60), **12**(30)
5	See eq. [4]				**28**(91)

[a]All isomer ratios were estimated by integration of the ^{1}H nmr spectra.
[b]Yields were estimated by analysis of the nmr spectra of the crude pyrolysates after identification of the major components, and are not subject to losses incurred during separations.
[c]Errors in the isomer ratios were estimated to be no more than 5%. Errors in product yields were estimated to range from about 5% to 20% of the values quoted, depending on their actual magnitude.
[d]Additional products, usually minor, are mentioned in the Experimental.

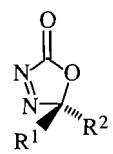
of **2***b*, **2***d*, and **2***f* in which the *trans* isomer predominated (Table 1). Oxadiazolines **2***b* and **2***d* were also obtained from 2-oxooxadiazolines **3**, by the alkylation/acylation sequence of eq. [2]. Compounds **3** were prepared by the oxidative cyclization/hydrolysis sequence of eq. [3], from semicarbazones **4**. The procedure of eq. [2] afforded *cis*/*trans* mixtures of **2** in which the *cis* isomer predominated. These two synthetic approaches permitted the assignment of the *trans* structure to the major product of the synthesis according to eq. [1] and of the *cis* structure to the major product of the synthesis according to eq. [2]. Finally the oxadiazoline **5** was prepared from **2***c* by the deacylation/reacylation sequence illustrated with eq. [4].

[1] $R^1R^2C{=}NNHCOR^3 \xrightarrow{LTA}$ **1**



2

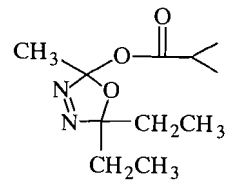
2*a*: $R^1 = R^2 = R^3 = CH_3$
2*b*: $R^1 = R^3 = CH_3$, $R^2 = CH_2CH_3$
2*c*: $R^1 = R^2 = CH_2CH_3$, $R^3 = CH_3$
2*d*: $R^1 = R^3 = CH_3$, $R^2 = CH(CH_3)_2$
2*e*: $R^1 = R^2 = CH(CH_3)_2$, $R^3 = CH_3$
2*f*: $R^1 = R^3 = CH_3$, $R^2 = C(CH_3)_3$
2*g*: $R^1 = CH_3$, $R^2 = CH_2CH_3$, $R^3 = CH(CH_3)_2$
2*h*: $R^1 = CH_3$, $R^2 = R^3 = CH(CH_3)_2$

[2]  $\xrightarrow[(2)\ CH_3COCl]{(1)\ CH_3Li}$ **2**

3

b: $R^1 = CH_3$, $R^2 = CH_2CH_3$; *d*: $R^1 = CH_3$, $R^2 = CH(CH_3)_2$

[3] $R^1R^2C{=}NNHCONH_2$ **4** $\xrightarrow[(2)\ H_3O^+]{(1)\ LTA,\ CH_2Cl_2}$ **3**

[4] **2***c* $\xrightarrow[(2)\ Me_2CHCOCl]{(1)\ MeLi(-30\ to\ 0\,°C)}$ 

5

Separation of the geometric isomers of the oxadiazolines by hplc was not successful and they are too unstable to survive glpc conditions. Selective deacylation of one of the isomers by treatment of the mixture **2***b* (*trans*:*cis* = 2.3:1) with half an equivalent of methyllithium at −78°C was not promising. The *trans*:*cis* ratio in recovered **2***b* was only slightly different from that in the starting material. It was therefore necessary to use the different mixtures of isomers of **2***b* and of **2***d*, from the two synthetic approaches (eqs. [1], [2]), to infer the selectivities of the cycloreversion step and of the subsequent 1,4-sigmatropic hydrogen atom shifts, illustrated for the case of **2***b* with Scheme 2.

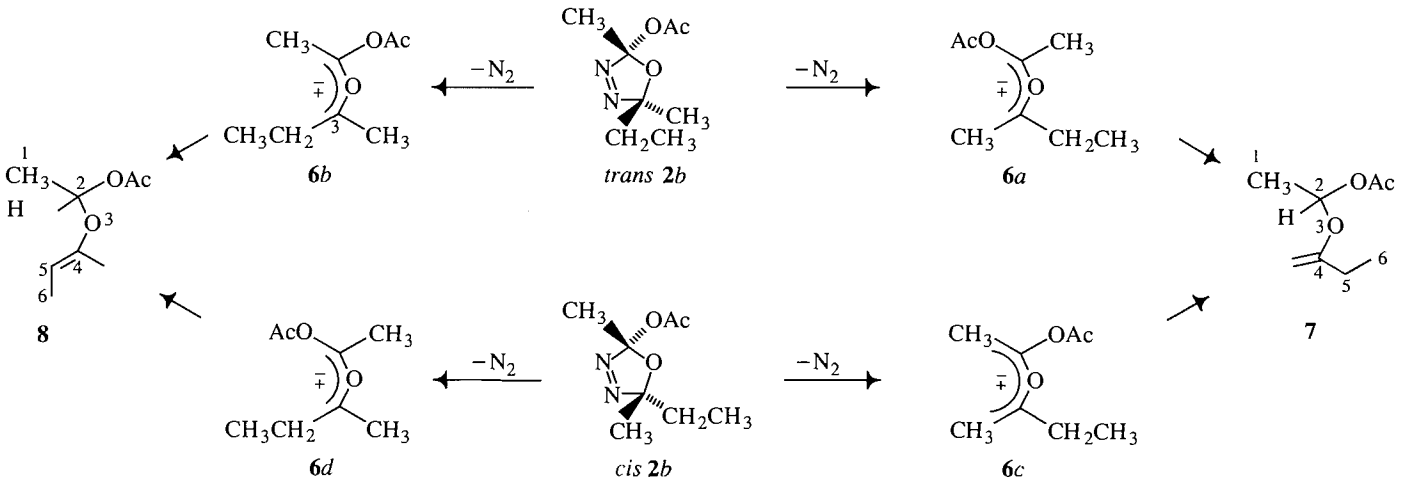
A striking result is the fact that a mixture (*trans*:*cis* = 2.3:1) of the isomers **2***b* afforded a product mixture in which the ratio **7**:**8** was 2.2:1. Similarly, when the isomer ratio for **2***b* was *trans*:*cis* = 1:1.9, the product ratio was **7**:**8** = 1:1.6, suggesting a substantial overall memory effect. An immediate conclusion from those results is that the geometric isomers (**6***a*–*d*) of the carbonyl ylide intermediate are not equilibrated by rotation about the bonds to the central oxygen atom during their lifetimes. Equilibration would require a product ratio independent of the ratio of isomers in the starting material.

The fact that carbonyl ylides **6***a*–**6***d* are not equilibrated during their lifetimes means that it is possible, in principle, to discover which ones are formed preferentially by the cycloreversions of *trans*- and *cis*-**2***b*. Because stereochemical information is lost in the 1,4-hydrogen atom shifts that convert the transient ylides to stable products, it was necessary to use an indirect probe. The probe chosen relies on the assumption that the cycloreversion transition states are sufficiently productlike to reflect steric effects on product stability. That is, a transition state leading to an ylide with the larger substituents *endo* will, other factors being equal, be of higher energy than a transition state leading to an isomeric ylide with the larger substituents *exo*, Scheme 3.

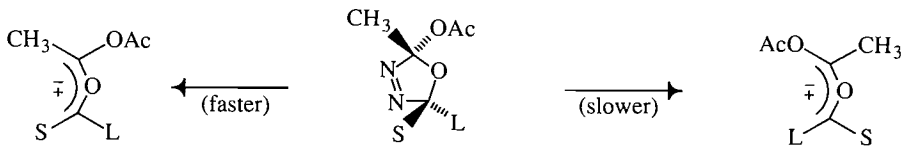
The assumption that large groups cannot be accommodated well in the *endo* position of a planar carbonyl ylide received strong support from the results of thermolysis of **2***d* (Scheme 4). A sample of **2***d* (*trans*:*cis* = 3:1) gave **10** and **12** in 4:1 ratio. Isomer **11** was not formed. Similarly, a sample of **2***d* (*trans*:*cis* = 1:2.6) gave **10** and **12** in 1.2:1 ratio and, again, **11** could not be detected. In both cases the combined yields of **10** and **12** accounted for more than 90% of the original isopropyl groups. Although there was a preference for formation of **12** in each case, the carbonyl ylides from **2***d* are clearly only partially equilibrated during their lifetimes and the sense of equilibration is most likely to be **9***b* → **9***c* and **9***d* → **9***a* (Scheme 4). Fragmentation presumably competes quite effectively with those rotational equilibrations, to afford **12** and 1-acetoxyethylidene (**13**), which rearranges to biacetyl **14**.

Further support for the presumed crowding experienced by *endo* isopropyl substituents of carbonyl ylides came from the

Can. J. Chem. Downloaded from www.nrcresearchpress.com by 186.148.149.217 on 09/07/12
For personal use only.

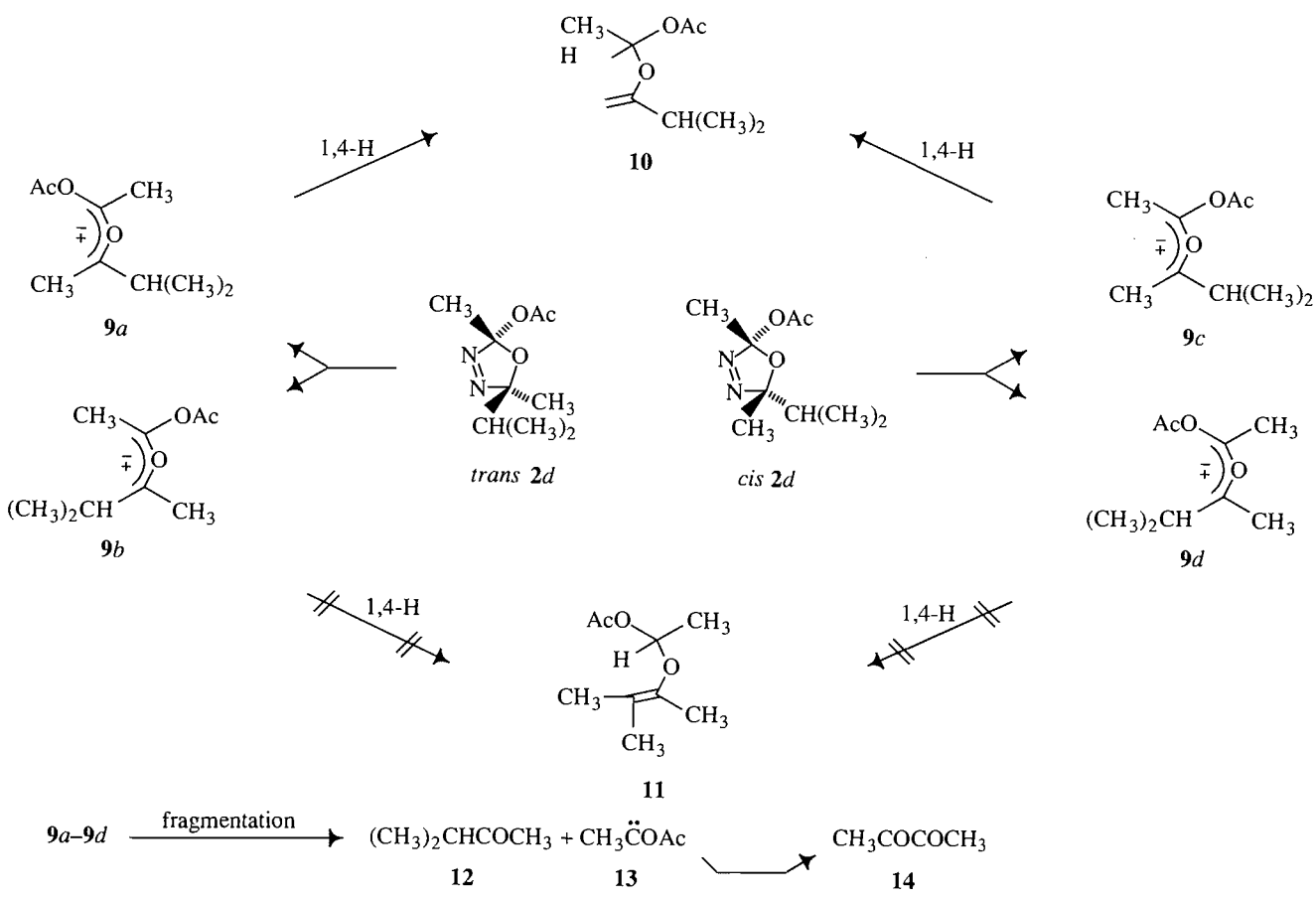


SCHEME 2



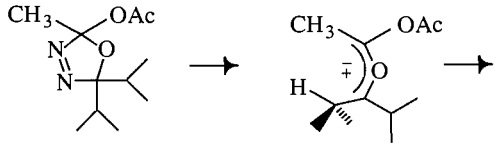
(L = larger: S = smaller)

SCHEME 3

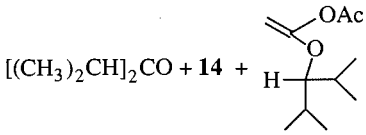


SCHEME 4

Can. J. Chem. Downloaded from www.nrcresearchpress.com by 186.148.149.217 on 09/07/12
For personal use only.

[5] 

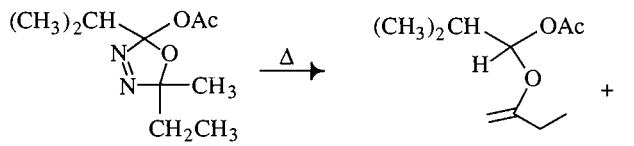
2e 15



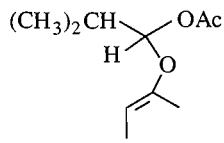
16 17

finding that **2***e* afforded none of the product of 1,4-sigmatropic rearrangement in the normal sense but only products from fragmentation (**14** and **16**) and, in approximately 10% yield, the product (**17**) of 1,4-sigmatropic rearrangement from the methyl group at C-1 (eq. [5]). Presumably the ylide **15** cannot readily adopt the conformation (8) required for sigmatropic migration of methine hydrogen and is constrained instead to a conformation in which the methine hydrogen of the *endo* isopropyl group lies in the ylide plane, or to nonplanar conformations of the ylide. The alternative migration, toward C-3, which is not competitive in other 1-acetoxy or 1-alkoxy carbonyl ylides, therefore becomes observable.

The evidence that *endo* isopropyl conformations of carbonyl ylides are probably unstable, presumably because they cannot adopt the 0°,0° geometry that is the ground state (9), was used to prepare a carbonyl ylide with an *endo* acetoxy substituent. Oxadiazoline **2***g* (*trans*:*cis* = 2.5:1) gave **18** and **19** in the ratio 2.0:1 in good yield (85%) on thermolysis, eq. [6]. Again

[6] 

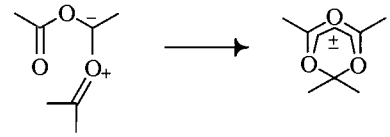
2g 18



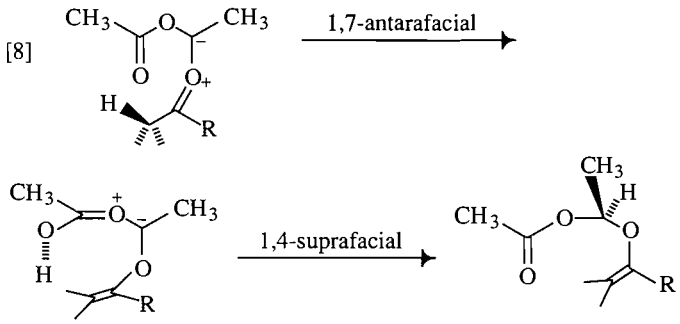
19

only partial equilibration of ylides occurred and the overall 1,4-hydrogen atom transfer took place efficiently from the "acetoxy *endo*" conformation, the "isopropyl *endo*" geometry presumably being too hindered, as was discussed above.

From the evidence that the *endo* acetoxy conformation is sufficient for sigmatropic rearrangement toward C-1 to occur, it does not follow that *endo* acetoxy is the kinetically preferred mode of cycloreversion. It also does not follow that the sigmatropic rearrangement toward C-1 is particularly facile if the acetoxy group is in the *endo* position. Nevertheless, there are reasons for believing that both of the preferences referred to above may be real. First, a carbonyl ylide must have a considerable net dipole bisecting the ylide COC angle and having the negative end in the *endo* region. Stabilizing dipole–dipole and dipole – induced dipole interactions between a substituent and the ylide framework can therefore be expected to be largest if the substituent is close to the main dipole by lying in an *endo* position. An extreme representation of internal solvation is the imagined cyclization shown in eq. [7].

[7] 

Second, a sigmatropic rearrangement in an *endo* acetoxy carbonyl ylide *could* be unusually easy because an initial 1,7-antarafacial sigmatropic shift, from carbon to oxygen to form a new ylide with a strong O—H bond, is possible. The new ylide could then undergo a suprafacial 1,4-shift (eq. [8]).

[8] 

Although the two-step process is stereochemically different from a one-step rearrangement, there is no simple test available for distinguishing between the mechanisms. We mention the hypothesis of a 1,7-antarafacial initial step as an intriguing possibility. The fact that acetoxy carbonyl ylides such as **2***b* afford products of 1,4-sigmatropic rearrangement in good yield whereas corresponding methoxy carbonyl ylides afford analogous products in low yield, except in the case of gas phase thermolysis (10), may be used to support the hypothesis.

In summary, many acyloxy-substituted carbonyl ylides undergo 1,4-sigmatropic H-migrations faster than ylide isomerization by rotations. The calculated rotational barrier[2] for the parent (unsubstituted) carbonyl ylide is 14 kcal mol^{-1} and experimental barriers of 8–13 kcal mol^{-1} have been reported for 1-cyano-1,3-diphenyl carbonyl ylide (11). It is very likely then that the free energy of activation for the observed sigmatropic rearrangement is less than 14 kcal mol^{-1}. Conformations of 1-acetoxy carbonyl ylides in which the acetoxy group is *endo* may actually rearrange by sequential 1,7-antarafacial and 1,4-suprafacial H-shifts, but the evidence for two steps is not compelling.

In those cases where sigmatropic rearrangement generated a trisubstituted double bond, the *E* isomer was formed, as predicted from a consideration of steric factors in the transition structure for the rearrangement. Sigmatropic migration of methine hydrogen from an isopropyl group was not observed. Fragmentation is the major fate of those ylides that would have to place an isopropyl group *endo* in order to be planar.

Experimental

General

Melting points were determined on a Thomas Hoover capillary melting point apparatus and are uncorrected. Proton NMR spectra were recorded on a Bruker AM-500 or an EM-390 spectrometer using TMS or residual ^1H signals from $CDCl_3$ or C_6D_6 as internal standards. ^{13}C NMR spectra were recorded with the Bruker AM-500 machine. Centrifugal chromatography was carried out on silica (Merck Kieselgel $60PF_{254}$) coated plates (coating 2 mm thick) spinning in a Chromatotron model 17924T apparatus. Plastic-backed, Merck Kieselgel $60F_{254}$, 0.2-mm silica plates were used for analytical thin-layer chromatography (TLC). Commercially available solvents and reagents were purified by standard procedures.

[2]Calculation by W. J. Hehre, quoted in ref. 11.

Can. J. Chem. Downloaded from www.nrcresearchpress.com by 186.148.149.217 on 09/07/12
For personal use only.

Can. J. Chem. Downloaded from www.nrcresearchpress.com by 186.148.149.217 on 09/07/12
For personal use only.

Acetylhydrazones of ketones (1)

Most of these were prepared by refluxing solutions of equimolar amounts of acetylhydrazine and of the appropriate ketone in benzene until all water was removed (Dean–Stark trap, 5–15 h). The solvent was removed under vacuum and the residue was recrystallized. The acetyl hydrazone of pinacolone (**1***e*) was obtained by refluxing a solution of acetylhydrazine in excess pinacolone for 20 h. Excess pinacolone was distilled off and the residue was recrystallized (12). New acetylhydrazones are reported below.

*1-Acetyl-2-(2,4-dimethyl-3-pentylidene)hydrazine (1*e*)*

The yield of **1***e* was 75%, mp 75–77°C (Et_2O/petroleum); ^{1}H NMR (90 MHz, $CDCl_3$) δ: 8.85 (br s, 1H, NH), 2.87 (sept, J = 6.9 Hz, 1H), 2.62 (sept, J = 6.9 Hz, 1H), 2.22 (s, 3H), 1.06 (d, J = 6.9 Hz, 6H), 1.04 (d, J = 6.9 Hz, 6H).

*1-(2-Methylpropanoyl)-2-(2-butylidene)hydrazine (1*g*)*

The general procedure afforded **1***g* in 70% yield, mp 60–68°C (Et_2O/EtOH); ^{1}H NMR (90 MHz, $CDCl_3$) δ: 8.62 (br s, 1H, NH), 3.42 (sept, J = 6.9 Hz, 1H), 2.37 (q, J = 7.5 Hz, 2H), 1.84 (s, 3H), 1.18 (d, J = 6.9 Hz, 6H), 1.12 (t, J = 7.5 Hz, 3H).

*1-(2-Methylpropanoyl)-2-(3-methyl-2-butylidene)hydrazine (1*h*)*

Yield 75%, mp 85–87°C (petroleum ether/benzene); ^{1}H NMR (90 MHz, $CDCl_3$) δ: 8.40 (br s, 1H, NH), 3.38 (sept, J = 6.9 Hz, 1H), 2.51 (sept, J = 6.9 Hz, 1H), 1.82 (s, 3H), 1.23 (d, J = 6.9 Hz, 6H), 1.17 (d, J = 6.9 Hz, 6H).

2-Acetoxy-2,5,5-trialkyl-Δ^3-1,3,4-oxadiazolines (2) by the route of eq. [1]

The lead tetraacetate oxidation of acylhydrazones of ketones was carried out as described previously (13). The products, purified by vacuum distillation, are described below. Some chemical shift assignments of methyl signals in ^{13}C NMR spectra are tentative.

*2-Acetoxy-5-ethyl-2,5-dimethyl-Δ^3-1,3,4-oxadiazoline (2*b*)*

The *trans*:*cis* ratio was 2.2:1; bp 44–45°C (0.5 Torr; 1 Torr = 133.3 Pa); ^{1}H NMR of *trans* isomer (500 MHz, C_6D_6) δ: 1.88 (s, 3H, Ac), 1.67–1.58 (m, 2H), 1.57 (s, 3H), 1.31 (s, 3H), 0.64 (t, J = 7.5 Hz, 3H); ^{1}H NMR of *cis* isomer (500 MHz, C_6D_6) δ: 1.82 (s, 3H, Ac), 1.76–1.67 (m, 2H), 1.58 (s, 3H), 1.19 (s, 3H), 0.77 (t, J = 7.5 Hz, 3H); ^{13}C NMR of *trans* isomer (125.76 MHz, C_6D_6) δ: 167.10 (CO), 130.19 (C-2), 126.27 (C-5), 30.90 (CH_2), 23.15 (Me at C-5), 22.24 (CH_3CO), 21.27 (Me), 7.62 (Me); ^{13}C NMR of *cis* isomer (125.76 MHz, C_6D_6) δ = 167.06 (CO), 130.49 (C-2), 126.66 (C-5), 30.39 (CH_2), 22.28 (CH_3CO), 22.21 (Me), 21.17 (Me), 8.08 (Me).

*2-Acetoxy-5,5-diethyl-1-methyl-Δ^3-1,3,4-oxadiazoline (2*c*)*

This compound was obtained in 75% yield, bp 53–54°C (0.4 Torr); ^{1}H NMR (90 MHz, $CDCl_3$) δ: 2.25–1.55 (m, 10H), 0.90 (t, J = 7.5 Hz, 3H), 0.77 (t, J = 7.5 Hz, 3H).

*2-Acetoxy-5-(1-methylethyl)-2,5-dimethyl-Δ^3-1,3,4-oxadiazoline (2*d*)*

The product, obtained in 75% yield, was a mixture, *trans*:*cis* ratio = 3:1; bp 53–55°C (0.5 Torr); ^{1}H NMR of *trans* isomer (500 MHz, C_6D_6) δ: 1.90–1.81 (m), 1.87 (s, 3H), 1.68 (s, 3H), 1.25 (s, 3H), 0.84 (d, J = 6.9 Hz, 3H), 0.73 (d, J = 6.9 Hz, 3H); ^{1}H NMR of *cis* isomer (500 MHz, C_6D_6) δ: 1.90–1.81 (m), 1.80 (s, 3H), 1.70 (s, 3H), 1.18 (s, 3H), 0.92 (d, J = 6.9 Hz, 3H), 0.76 (d, J = 6.9 Hz, 3H). The total integral for the overlapping signals in the region δ 1.90–1.81 was satisfactory. ^{13}C NMR of *trans* isomer (125.76 MHz, C_6D_6) δ: 167.11 (CO), 129.81 (C-2), 128.52 (C-5), 35.41 (CH), 21.81 (CH_3CO), 21.42 (2-CH_3), 20.04 (5-CH_3), 17.18 (CH_3), 16.93 (CH_3); ^{13}C NMR of *cis* isomer (125.26 MHz, C_6D_6) δ: 167.01 (CO), 130.37 (C-2), 129.21 (C-5), 35.27 (CH), 23.01 (CH_3CO), 21.29 (2-CH_3), 19.28 (5-CH_3), 17.77 (CH_3), 17.21 (CH_3).

*2-Acetoxy-5,5-di-(1-methylethyl)-2-methyl-Δ^3-1,3,4-oxadiazoline (2*e*)*

Oxadiazoline **2***e* was obtained in 72% yield; bp 58–60°C (0.1 Torr); ^{1}H NMR (90 MHz, C_6D_6) δ: 2.42–2.00 (m, 2H, CH), 1.98 (s, 3H, Ac), 1.62 (s, 3H), 0.97–0.59 (m, 12H).

*2-Acetoxy-5-(1,1-dimethylethyl)-2,5-dimethyl-Δ^3-1,3,4-oxadiazoline (2*f*)*

Mixture **2***f* was obtained in 70% yield; *trans*:*cis* ratio = 14.5:1; bp 53–55°C (0.3 Torr); mp 36–37°C (petroleum ether); ^{1}H NMR of *trans* isomer (500 MHz, C_6D_6) δ: 2.04 (s, 3H, Ac), 1.54 (s, 3H), 1.23 (s, 3H), 0.87 (s, 9H); ^{1}H NMR of *cis* isomer (500 MHz, C_6D_6) δ: 1.89 (s, 3H, Ac), 1.60 (s, 3H), 1.12 (s, 3H), 0.91 (s, 9H); ^{13}C NMR of *trans* isomer (125.76 MHz, C_6D_6) δ: 167.07 (CO), 130.68 (C-2), 129.89 (C-5), 37.27 (CMe_3), 25.45 (2-Me), 21.31 (CH_3CO or 5-Me), 21.06 ((CH_3)$_3$), 19.11 (5-Me or CH_3CO).

*2-Acetoxy-5-ethyl-2-(1-methylethyl)-5-methyl-Δ^3-1,3,4-oxadiazoline (2*g*)*

The yield was 60%, bp 65–66°C (0.3 Torr); *trans*:*cis* ratio 2.5:1; ^{1}H NMR of *trans* isomer (500 MHz, $CDCl_3$) δ: 2.84 (sept, J = 6.9 Hz, 1H), 2.05 (s, sum of two Ac integrals), 1.77–1.66 (m, 2H, CH_2), 1.52 (s, 3H), 1.12 (d, J = 6.9 Hz, 3H), 1.10 (t, J = 7.5 Hz, 3H), 1.02 (d, J = 6.9 Hz, 3H); ^{1}H NMR of *cis* isomer (500 MHz, $CDCl_3$) δ: 3.02 (sept, J = 6.9 Hz, 1H), 2.05 (s, sum of two Ac integrals), 2.00–1.90 (m, 2H, CH_2), 1.55 (s, 3H), 1.15 (d, J = 6.9 Hz, 3H), 1.00 (t, J = 7.5 Hz, 3H), 0.93 (d, J = 6.3 Hz, 3H); ^{13}C NMR of *trans* isomer (125.76 MHz, $CDCl_3$) δ: 167.39 (CO), 133.21 (C-2), 125.52 (C-5), 32.70 (CH), 30.48 (CH_2), 21.46 (5-Me), 20.70 (CH_3CO), 16.62 (CH_3), 16.32 (CH_3), 8.05 (CH_3); ^{13}C NMR of *cis* isomer (125.76 MHz, $CDCl_3$) δ: 167.39 (CO), 133.68 (C-2), 126.20 (C-5), 31.87 (CH), 30.55 (CH_2), 21.42 (5-Me), 20.83 (CH_3CO), 16.77 (CH_3), 16.08 (CH_3), 8.05 (CH_3). This last signal was assigned by analogy because one CH_3 signal of one isomer is superimposed on a CH_3 signal of the other isomer.

*2-Acetoxy-2,5-di-(1-methylethyl)-5-methyl-Δ^3-1,3,4-oxadiazoline (2*h*)*

Mixture **2***h* was formed in 65% yield; bp 66–68°C (0.3 Torr); *trans*:*cis* ratio = 2.4:1; ^{1}H NMR of *trans* isomer (500 MHz, $CDCl_3$) δ: 2.84 (sept, J = 6.9 Hz, 1H), 2.04 (s, 3H, Ac), 1.78 (sept, J = 6.9 Hz, 1H), 1.42 (s, 3H), 1.24 (d, J = 6.9 Hz, 3H), 1.10 (d, J = 6.9 Hz, 3H), 1.05 (d, J = 6.9 Hz, 3H), 1.04 (d, J = 6.9 Hz, 3H); ^{1}H NMR of *cis* isomer (500 MHz, $CDCl_3$) δ: 3.08 (sept, J = 6.9 Hz, 1H), 2.05 (s, 3H, Ac), 1.89 (sept, J = 6.9 Hz, 1H), 1.47 (s, 3H), 1.17 (d, J = 6.9 Hz, 3H), 1.16 (d, J = 6.9 Hz, 3H), 0.95 (d, J = 6.9 Hz, 3H), 0.90 (d, J = 6.9 Hz, 3H); ^{13}C NMR of *trans* isomer (125.76 MHz, $CDCl_3$) δ: 167.24 (CO), 133.04 (C-2), 127.86 (C-5), 35.44 (CH), 32.72 (CH), 18.10 (CH_3CO), 17.19 (CH_3), 16.90 (CH_3), 16.64 (CH_3), 16.39 (CH_3); ^{13}C NMR of *cis* isomer (125.76 MHz, $CDCl_3$) δ: 169.24 (CO), 133.50 (C-2), 128.76 (C-5), 35.66 (CH), 31.61 (CH), 21.39 (CH_3CO), 17.93 (CH_3), 17.10 (CH_3), 16.85 (CH_3), 16.02 (CH_3).

*2-Acetoxy-2,5,5-trialkyl-Δ^3-1,3,4-oxadiazolines, 2*b *and 2*d*, by the route of eq. [2]*

The reaction of **3***b* or **3***d* with methyllithium was carried out as described previously (14). Acetyl chloride in ethyl ether was used at the end of the reaction to trap the lithium alkoxide. The temperature during addition was kept at −40°C; then the cooling bath was removed and, while stirring, the reaction mixture was allowed to come to room temperature (2 h). Next it was quenched with water and extracted with ethyl ether (3 × 50 mL). The ether extracts were washed with 5% sodium bicarbonate solution (3 × 10 mL) and dried ($MgSO_4$). The drying agent was filtered off, and the filtrate was concentrated under vacuum and distilled. The oxadiazoline **2***b* obtained by this method was a 1.9:1 (*cis*:*trans*) mixture of isomers. The isomer ratio (*cis*:*trans*) of oxadiazoline **2***d* was 2.7:1.

*5-Ethyl-5-methyl-2-oxo-Δ^3-1,3,4-oxadiazoline (2*b*)*

This compound was prepared as described in the literature (14); ^{1}H NMR (90 MHz, $CDCl_3$) δ: 2.16 (q, J = 7.5 Hz, 2H), 1.72 (s, 3H), 0.80 (t, J = 7.5 Hz, 3H).

*5-(1-Methylethyl)-5-methyl-2-oxo-Δ^3-1,3,4-oxadiazoline (2*d*)*

This compound was prepared as described earlier (14); ^{1}H NMR (90 MHz, $CDCl_3$) δ: 2.27 (sept, J = 6.9 Hz, 1H), 1.69 (s, 3H), 1.10 (d, J = 6.9 Hz, 3H), 0.90 (d, J = 6.9 Hz, 3H).

5,5-Diethyl-2-(2-methylpropanoyloxy)-2-methyl-Δ^3-1,3,4-oxadiazoline (5)

To a stirred solution of 2-acetoxy-5,5-diethyl-2-methyl-Δ^3-1,3,4-oxadiazoline **2***c* (5 g, 0.025 mol) in THF (35.0 mL) under argon was added, dropwise at −50°C, methyllithium (0.055 mol, 37 mL of 1.5 M

Can. J. Chem. Downloaded from www.nrcresearchpress.com by 186.148.149.217 on 09/07/12
For personal use only.

solution). The reaction mixture was stirred at this temperature for 0.5 h and then for 1 h at −20°C before it was recooled to −60°C. At this temperature isobutyryl chloride (5.33 g, 0.05 mol) in THF (10 mL) was added dropwise. The cooling bath was removed and stirring was continued for another 3 h. After this time the solvent was removed under vacuum, the residue was dissolved in methylene chloride (50 mL), washed with saturated NaCl (2 × 10 mL), and dried ($MgSO_4$). The drying agent was filtered off, the solvent was evaporated under vacuum, and the residue was distilled to afford 3 g (53% yield) of **7**, bp 54–56°C (0.7 Torr); ^{1}H NMR (90 MHz, $CDCl_3$) δ: 2.57 (sept, J = 6.9 Hz, 1H), 2.17 (s, 3H), 2.18–1.68 (m, 4H), 1.21 (d, J = 6.9 Hz, 3H), 1.19 (d, J = 6.9 Hz, 3H), 0.95 (t, J = 7.5 Hz, 3H), 0.82 (t, J = 7.5 Hz, 3H).

Thermolysis of oxadiazolines

An oxadiazoline (40 mg) dissolved in benzene-d_6 (0.5 mL) was placed in a thick-walled NMR tube, which was put through three freeze–pump–thaw cycles (vacuum line pressure 10^{-2} Torr) prior to sealing. Thermolysis at 80.0 ± 0.2°C was monitored by taking the NMR spectrum, and was completed after 3 days. The tubes were opened after freezing in liquid nitrogen and the reaction mixture was analysed by gc, ms, and by nmr spectroscopy.

*Thermolysis of 2-acetoxy-5-ethyl-2,5-dimethyl-Δ^3-1,3,4-oxadiazoline (**2**b)*

The mixture of **2***b* (*trans*:*cis* ratio 2.2:1) gave in 90% yield a 2.2:1 mixture of 2-acetoxy-4-methylene-3-oxahexane (**7**) and *E*-2-acetoxy-4-methyl-3-oxahex-4-ene (**8**), respectively. A 1.9:1 (*cis*:*trans*) mixture of the isomers of **2***b* gave upon thermolysis, in 90% yield, a 1.6:1 mixture of **8** and **7**, respectively. ^{1}H NMR of **7** (500 MHz, C_6D_6) δ: 6.45 (q, J = 5.2 Hz, 1H, H-2), 4.13 (d, J = 2.5 Hz, 1H, *E*-methylene), 4.04–4.00 (m, 1H, *Z*-methylene), 2.03 (J = 7.5 Hz, 2H, H-5), 1.63 (s, 3H, Ac), 1.30 (d, J = 5.2 Hz, 3H, H-1), 0.96 (t, J = 7.5 Hz, 3H, H-6); ^{13}C NMR (125.76 MHz, C_6D_6) δ: 169.21 (CO), 162.21 (C-4), 91.79 (C-2), 83.62 (sp^2-methylene), 28.05 (C-5), 20.47 (C-1), 20.21 (CH_3CO), 11.38 (C-6); MS (ci, NH_3), *m*/*e*: 159; calcd. for $(C_8H_{14}O_3 + H)^+$: 159. ^{1}H NMR of **8** (500 MHz, C_6D_6) δ: 6.40 (q, J = 5.2 Hz, 1H, H-2), 4.76 (q, J = 6.8 Hz, 1H, H-5), 1.67–1.65 (m, 3H, 4-*Me*), 1.64 (s, 3H, Ac), 1.40 (d of q, J = 6.8 Hz and 0.9 Hz, 3H, H-6), 1.32 (d, J = 5.2 Hz, 3H, H-1); ^{13}C NMR (125.76 MHz, C_6D_6) δ: 169.22 (CO), 150.43 (C-4), 97.72 (C-5), 91.94 (C-2), 20.68 (CH_3CO), 20.58 (C-6), 15.29 (4-Me), 11.89 (C-1); MS (ci, NH_3), *m*/*e*: 159; calcd. for $(C_8H_{14}O_3 + H)^+$; 159.

*Thermolysis of 2-acetoxy-5,5-diethyl-2-methyl-Δ^3-1,3,4-oxadiazoline (**2**c)*

Thermolysis of **2***c* furnished, in 88% yield, *E*-2-acetoxy-4-ethyl-3-oxahex-4-ene (**20**). Diethyl ketone (**21**), butane-2,3-dione (**14**), and acetic anhydride (**22**) were detected as minor products.

E-*2-Acetoxy-4-ethyl-3-oxahex-4-ene (**20**)*: ^{1}H NMR (500 MHz, C_6D_6) δ: 6.26 (q, J = 5.2 Hz, 1H, H-2), 4.59 (q, J = 6.9 Hz, 1H, H-5), 2.14–2.08 (q, J = 7.5 Hz, 2H, CH_2), 1.91 (s, 3H, Ac), 1.51 (d, J = 6.9 Hz, 3H, H-6), 1.41 (d, J = 5.2 Hz, 2H, H-1), 1.02 (t, J = 7.5 Hz, 3H); ^{13}C NMR (125.76 MHz, C_6D_6) δ: 170.01 (CO), 155.50 (C-4), 96.79 (C-2), 92.64 (C-5), 22.81 (CH_2), 21.13 (CH_3CO), 20.71 (C-6), 11.93 (C-1), 11.63 (Me); MS (ci, NH_3), *m*/*e*: 173; calcd. for $(C_9H_{16}O_3 + H)^+$: 173.

*Thermolysis of 2-acetoxy-5-(1-methylethyl)-2,5-dimethyl-Δ^3-1,3,4-oxadiazoline (**2**d)*

Thermolysis of a 3:1 mixture (*trans*:*cis*) of **2***d* furnished a 4:1 mixture of 2-acetoxy-5-methyl-4-methylene-3-oxahexane (**10**) and 3-methylbutan-2-one (**12**) in 86% yield. A 2.6:1 mixture (*cis*:*trans*) of **2***d* gave a 1.2:1 mixture of **12** and **10**, respectively, in 82% yield. 1,1-Diacetoxyethane (**23**), acetic anhydride (**22**), and biacetyl (**14**) were detected as minor products. ^{1}H NMR of **10** (500 MHz, C_6D_6) δ: 6.43 (q, J = 5.2 Hz, 1H, H-2), 4.04 (d, J = 2.6 Hz, 1H, vinyl), 4.00 (d, J = 2.6 Hz, 1H, vinyl), 2.24 (sept, J = 6.9 Hz, 1H, H-5), 1.65 (s, 3H, Ac), 1.29 (d, J = 5.2 Hz, 3H, H-1), 1.02 (d, J = 6.9 Hz, 3H, H-6), 1.00 (d, J = 6.9 Hz, 3H, H-6); ^{13}C NMR (125.76 MHz, C_6D_6) δ: 169.18 (CO), 165.84 (C-4), 91.88 (C-2), 82.28 (sp^2-methylene), 33.54 (C-5), 20.79 (C-6), 20.68 (CH_3CO), 20.43 (CH_3), 20.21 (C-1).

*Thermolysis of 2-acetoxy-5,5-di-(1-methylethyl)-2-methyl-Δ^3-1,3,4-oxadiazoline (**2**e)*

The crude pyrolysate showed, in the ^{1}H nmr spectrum (C_6D_6), a pair of doublets at δ 4.52 and 4.14 (J = 2.2 Hz) attributed to the terminal methylene group of **17**. The ^{13}C spin-sort spectrum gave a positive signal at δ 81.61 (H_2C=C of the enediol system). Analysis by gc/ms gave *m*/*e* 199.1332; calcd. for $C_{11}H_{19}O_3$: 199.1329 $(M - H)^+$.

*Thermolysis of 2-acetoxy-5-(1,1-dimethylethyl)-2,5-dimethyl-Δ^3-1,3,4-oxadiazoline (**2**f)*

Thermolysis of a 14.5:1 mixture (*trans*:*cis*) of **2***f* furnished almost exclusively 2-acetoxy-5,5-dimethyl-4-methylene-3-oxahexane **24**. Minor products were 1,1-diacetoxyethane (**23**) and pinacolone (**25**) in less than 5% yield. ^{1}H NMR of **24** (500 MHz, C_6D_6) δ: 6.43 (q, J = 5.2 Hz, 1H, H-2), 4.15 (d, J = 2.9 Hz, 1H, vinyl), 4.10 (d, J = 2.9 Hz, 1H, vinyl), 1.62 (s, 3H, Ac), 1.25 (d, J = 5.2 Hz, 3H, H-1), 1.10 (s, 9H); ^{13}C NMR (125.76 MHz, C_6D_6) δ: 169.17 (CO), 168.10 (C-4), 92.14 (C-2), 81.67 (CH_2), 35.79 (C-5), 28.30 (C-6), 20.40 (CH_3CO), 20.18 (C-1).

*Thermolysis of 2-acetoxy-5-ethyl-5-methyl-2-(1-methylethyl)-Δ^3-1,3,4-oxadiazoline (**2**g)*

A 2.5:1 mixture (*trans*:*cis*) of **2***g* furnished a 2:1 mixture of 3-acetoxy-2-methyl-5-methylene-4-oxaheptane (**18**) and *E*-3-acetoxy-2,5-dimethyl-4-oxahept-5-ene (**19**), respectively.

*3-Acetoxy-2-methyl-5-methylene-4-oxaheptane (**18**)*: ^{1}H NMR (500 MHz, C_6D_6) δ: 6.29 (d, J = 4.9 Hz, 1H, H-3), 4.30 (d, J = 2.3 Hz, 1H, vinyl), 4.01 (d, J = 2.3 Hz, 1H, vinyl), 2.02 (q, J = 7.5 Hz, 2H, C-6), 1.99–1.92 (m, H-2; superimposed on the same multiplet from **19**), 1.66 (s, 3H, Ac), 0.99–0.87 (m, ~9H, CH_3; superimposed on the Me signals of **19**); ^{13}C NMR (125.76 MHz, (C_6D_6) δ: 170.12 (CO), 162.89 (C-5), 97.10 (C-3), 84.35 (=CH_2), 33.51 (C-2), 28.68 (C-6), 20.92 (CH_3CO), 17.32 (CH_3), 17.10 (CH_3), 12.50 (C-7).

E-*3-Acetoxy-2,5-dimethyl-4-oxahept-5-ene (**19**)*: ^{1}H NMR (500 MHz, C_6D_6) δ: 6.20 (d, J = 4.9 Hz, 1H, H-3), 4.91 (q, J = 6.9 Hz, 1H, H-6), 1.95–1.92 (m, 1H, H-2), 1.68 (s, 3H, Ac), 1.62 (s, 3H, 5-Me), 1.41 (d, J = 6.9 Hz, 3H, H-7), 0.99–0.87 (m, 6H, CH_3); ^{13}C NMR (125.76 MHz, C_6D_6) δ: 170.19 (CO), 151.17 (C-5), 99.08 (C-3), 97.32 (C-6), 21.09 (C-2), 20.93 (CH_3-CO), 17.47 (C-7), 17.23 (CH_3), 16.93 (CH_3), 15.66 (CH_3).

*Thermolysis of 2-acetoxy-2,5-di-(1-methylethyl)-5-methyl-Δ^3-1,3,4-oxadiazoline (**2**h)*

A 2.4:1 mixture (*trans*:*cis*) of isomers of **2***h* furnished, after thermolysis, 3-acetoxy-2,6-dimethyl-5-methylene-4-oxaheptane (**26**) and methyl isopropyl ketone (**12**) in 2:1 ratio. The yield of these products was 90%. 4-Methylpentane-2,3-dione (**27**) as detected as a minor product.

*3-Acetoxy-2,6-dimethyl-5-methylene-4-oxaheptane (**26**)*: ^{1}H NMR (500 MHz, C_6D_6) δ: 6.23 (d, J = 4.9 Hz, 1H, H-3), 4.19 (d, J = 2.6 Hz, 1H, vinyl), 4.00 (d, J = 2.6 Hz, vinyl), 2.24 (sept, J = 6.9 Hz, 1H, methine), 1.95 (d of sept, J = 6.9 and 4.9 Hz, 1H, H-2), 1.69 (s, 3H, Ac), 1.02 (d, J = 6.9 Hz, 3H, Me), 1.01 (d, J = 6.9 Hz, 3H, Me), 0.90 (d, J = 6.9 Hz, 3H, Me), 0.89 (d, J = 6.9 Hz, 3H, Me); ^{13}C NMR (125.76 MHz, C_6D_6) δ: 169.48 (CO), 165.78 (C-5), 96.38 (C-3), 82.24 (=CH_2), 32.74 (C-6), 32.97 (C-2), 20.79 (CH_3CO), 20.75 (CH_3), 20.35 (CH_3), 16.79 (CH_3), 16.46 (CH_3).

*Thermolysis of 5,5-diethyl-2-(2-methylpropanoyloxy)-2-methyl-Δ^3-1,3,4-oxadiazoline (**5**)*

Thermolysis of this oxadiazoline gave the 2-(2-methylpropanoyloxy)-4-ethyl-3-oxahex-4-ene, presumably the *E* isomer (**28**), in 91% yield; ^{1}H NMR (500 MHz, C_6D_6) δ: 6.43 (q, J = 5.2 Hz, 1H, H-2), 4.66 (q, J = 6.8 Hz, 1H, H-5), 2.34 (sept, J = 6.9 Hz, 1H, CH-CO), 2.07 (q, J = 7.5 Hz, 2H, CH_2), 1.42 (d, J = 6.8 Hz, 3H, H-6), 1.33 (d, J = 5.2 Hz, 3H, H-1), 1.04–0.98 (m, 9H, CH_3); ^{13}C NMR (125.76 Hz, C_6D_6) δ: 175.88 (CO), 155.86 (C-4), 96.53 (C-2), 92.38 (C-5), 34.70 (*C*HCO), 23.31 (CH_2), 21.00 (CH_3), 19.36 (CH_3), 19.14 (CH_3), 12.36 (CH_3), 11.85 (CH_3).

Acknowledgements

The authors are grateful to the Natural Sciences and Engineering Research Council of Canada for financial support.

1. I. FLEMING. Frontier orbitals and organic chemical reactions. Wiley, New York. 1976.
2. R. SMITH and T. LIVINGHOUSE. Tetrahedron, **41**, 3559 (1985).
3. (*a*) A. A. LEONE and P. S. MARIANO. Rev. Chem. Intermed. **4**, 81 (1981); (*b*) O. L. CHAPMAN, G. L. EIAN, A. BLOOM, and J. CLARDY. J. Am. Chem. Soc. **93**, 2918 (1971).
4. A. G. SCHULZ. Acc. Chem. Res. **16**, 210 (1983).
5. J. A. LANDGREBE and H. IRANMANESH. J. Org. Chem. **43**, 1244 (1978).
6. M. BÉKHAZI and J. WARKENTIN. J. Org. Chem. **47**, 4870 (1982).
7. M. SHIMIZU and P. D. BARTLETT. J. Am. Chem. Soc. **100**, 4260 (1987).
8. F. JENSEN and K. N. HOUK. J. Am. Chem. Soc. **109**, 3139 (1987).
9. K. N. HOUK, N. G. RONDAN, C. SANTIAGO, C. J. GALLO, R. W. GANDOUR, and G. W. GRIFFIN. J. Am. Chem. Soc. **102**, 1504 (1980).
10. A. P. HITCHCOCK, S. SWEEP, T. STEEL, M. BÉKHAZI, and J. WARKENTIN. Can. J. Chem. **60**, 2914 (1982).
11. R. HUISGEN. Angew. Chem. Int. Ed. Engl. **16**, 572 (1977).
12. M. W. MAJCHRZAK, M. BÉKHAZI, I. TSE-SHEEPY, and J. WARKENTIN. J. Org. Chem. **54**, 1842 (1989).
13. (*a*) R. N. BUTLER, F. L. SCOTT, and T. A. F. O'MAHONY. Chem. Rev. **73**, 93 (1973); (*b*) J. WARKENTIN. Synthesis, 279 (1970).
14. A. J. PAINE and J. WARKENTIN. Can. J. Chem. **57**, 2681 (1979).

Can. J. Chem. Downloaded from www.nrcresearchpress.com by 186.148.149.217 on 09/07/12
For personal use only.

Preparation, reactions, and characterization of trichloroselenium(IV) and trichlorotellurium(IV) sulfonates: $SeCl_3(XSO_3)$ and $TeCl_3(XSO_3)$ with X = CF_3, CH_3, and p-$CH_3C_6H_4$

RAMESH KAPOOR, POONAM WADHAWAN, VANDANA KATYAL, VIJAY RANI SOOD, AND PRATIBHA KAPOOR
Chemistry Department, Panjab University, Chandigarh-160 014, India

Received March 4, 1989

This paper is dedicated to Professor Ronald J. Gillespie on the occasion of his 65th birthday

RAMESH KAPOOR, POONAM WADHAWAN, VANDANA KATYAL, VIJAY RANI SOOD, and PRATIBHA KAPOOR. Can. J. Chem. **67**, 1760 (1989).

The compounds trichloroselenium(IV) and trichlorotellurium(IV) sulfonates, $MCl_3(XSO_3)$ (M = Se and Te; X = CF_3, CH_3, and p-$CH_3C_6H_4$), have been prepared and characterized by elemental analysis and infrared spectroscopy. Infrared spectra suggest that the XSO_3^- group acts as a monodentate ligand in the Se compounds and as a tridentate ligand in the Te compounds. $MCl_3(CF_3SO_3)$ (M = Se and Te) are found to act as $CF_3SO_3^-$ ion acceptors, and compounds $(C_2H_5)_4N[MCl_3(CF_3SO_3)_2]$ have been isolated. Some other reactions involving ligand substitution and complex formation have also been investigated. Reactions of potassium tellurate(IV) with trifluoromethane-, methane-, and paratoluenesulfonic acids are seen to yield $K_2[Te(CF_3SO_3)_6]$, $K_2[Te(CH_3SO_3)_6]$ and $K_2[TeO(p\text{-}CH_3C_6H_4SO_3)_4]$, respectively.

Key words: trichloroselenium(IV) sulfonates, trichlorotellurium(IV) sulfonates, tetraethylammonium trichlorobis(trifluoromethanesulfonato)selenate(IV), tetraethylammonium trichlorobis(trifluoromethanesulfonato)tellurate(IV), IR spectra.

RAMESH KAPOOR, POONAM WADHAWAN, VANDANA KATYAL, VIJAY RANI SOOD et PRATIBHA KAPOOR. Can. J. Chem. **67**, 1760 (1989).

On a préparé les sulphonates de trichlorosélénium(IV) et de trichlorotellure(IV), $MCl_3(XSO_3)$ (M = Se et Te; X = CF_3, CH_3 et p-$CH_3C_6H_4$) et on les a caractérisés en faisant appel à l'analyse élémentaire et à la spectroscopie infrarouge. Les spectres infrarouges suggèrent que le groupe XSO_3^- agit comme un ligand monodentate dans le composé du sélénium et comme un ligand tridentate dans le dérivé du tellure. On a trouvé que les composés $MCl_3(CF_3SO_3)$ (M = Se et Te) agissent comme accepteurs d'ions $CF_3SO_3^-$ et on a isolé les composés $(C_2H_5)_4N[MCl_3(CF_3SO_3)_2]$. On a également étudié quelques autres réactions impliquant une substitution et une formation de complexes. Les réactions du tellurate(IV) de potassium avec les acides trifluorométhanesulfonique, méthanesulfonique et paratoluènesulfonique semblent donner respectivement les complexes suivants : $K_2[Te(CF_3SO_3)_6]$, $K_2[Te(CH_3SO_3)_6]$ et $K_2[TeO(p\text{-}CH_3C_6H_4SO_3)_4]$.

Mots clés : sulphonates de trichlorosélénium(IV) et de trichlorotellure(IV), tétraéthylammonium trichlorobis(trifluorométhanesulphonato)sélénate(IV), tétraéthylammonium trichlorobis(trifluorométhanesulfonato)tellurate(IV), spectres IR.

[Traduit par la revue]

Introduction

There are no previous reports in the literature on the synthesis of selenium(IV) and tellurium(IV) salts of sulfonic acids (1, 2). Seleninyl bis(trifluoromethanesulfonate), $SeO(CF_3SO_3)_2$, has been shown by X-ray crystallography to contain a 9-coordinated Se (3). In this paper we report the preparation and characterization of $MCl_3(XSO_3)$, $(C_2H_5)_4N[MCl_3(CF_3SO_3)_2]$ (M = Se and Te; X = CF_3, CH_3, and p-$CH_3C_6H_4$), $K_2[Te(CF_3SO_3)_6]$, $K_2[Te(CH_3SO_3)_6]$, and $K_2[TeO(p\text{-}CH_3C_6H_4SO_3)_4]$, and some reactions of the $MCl_3(XSO_3)$ compounds.

Experimental

Both metal(IV) chlorides were prepared by methods reported in the literature (4). Potassium tellurate(IV) (BDH) was dried at ≃100°C *in vacuo* for several hours before use. Trifluoromethanesulfonic acid (Fluka AG) was fractionally distilled through a glass column packed with small glass rings and the fraction distilling at 161–162°C was collected (5). Methanesulfonic acid (Fluka AG, 98%) was made anhydrous by equilibrating with methanesulfonic acid anhydride for about 4–6 h at 70°C and then distilling it under reduced pressure (bp 165°C at 2 Torr; 1 Torr = 133.3 Pa). Paratoluenesulfonic acid monohydrate was made anhydrous by removing water as the toluene–water azeotrope (6). Trifluoromethane- and methanesulfonic acid anhydrides were prepared by mixing P_4O_{10} with the appropriate acid in equimolar amounts. Trifluoromethanesulfonic acid anhydride was obtained by distilling the equilibrated mixture at 81–82°C (745 Torr) and methanesulfonic acid anhydride was obtained as a white crystalline solid, mp 68–70°C, by distilling the equilibrated mixture at 110°C (10^{-2} Torr). Silver sulfonates, $Ag^I(XSO_3^-)$ (X = CF_3, CH_3, and p-$CH_3C_6H_4$) were prepared by the reaction of Ag_2O (BDH) with an aqueous solution of the appropriate acid. All solvents were distilled before use. Tetramethylammonium bromide and tetraethylammonium trifluoromethanesulfonate were dried at ≃100°C *in vacuo*.

Preparations

All the compounds discussed in this paper are sensitive to moisture and thus required handling in dry nitrogen atmosphere, dry box, or *in vacuo*.

Trichloroselenium(IV) and trichlorotellurium(IV) sulfonates, $MCl_3(XSO_3)$ (M = Se and Te; X = CF_3, CH_3, and p-$CH_3C_6H_4$)

These compounds were obtained when equimolar amounts of the metal(IV) chloride and the appropriate silver sulfonate, in carbon tetrachloride for the selenium derivatives and in nitromethane for the tellurium derivatives, were magnetically stirred for 8–10 h at room temperature. Silver chloride was filtered off, and pale-yellow Se and light-grey Te compounds recovered by distilling off the solvent *in vacuo* at room temperature. $TeCl_3(CF_3SO_3)$ and $TeCl_3(CH_3SO_3)$ were also prepared by the solvolyses at $TeCl_4$ in trifluoromethane- and methanesulfonic acids, respectively. Reactions of $TeCl_4$ with acid anhydrides, i.e., $(CF_3)_2S_2O_5$ and $(CH_3)_2S_2O_5$, also gave the monosubstituted products.[1] Any unreacted CF_3SO_3H or $(CF_3)_2S_2O_5$ was distilled off by keeping the compound *in vacuo* for several hours. Methanesulfonic acid or its anhydride was removed by washing the compound with an 80:20 mixture of *n*-hexane and diethyl ether. The compounds did not undergo any further substitution, even under drastic conditions (i.e., use of a large excess of the acid or its anhydride and heating the contents to about 100°C).

[1]Report of $SeCl_4$ with CF_3SO_3H or $(CF_3)_2S_2O_5$ did not yield any definite compound.

Can. J. Chem. Downloaded from www.nrcresearchpress.com by 186.148.149.217 on 09/07/12
For personal use only.

TABLE 1. Analytical data of sulfonate derivatives of selenium(IV) and tellurium(IV)

Compound		Elemental analysis*					
		M	S	Cl	C	H	N
$SeCl_3(CF_3SO_3)$	(1)	23.4	9.3	31.7	3.42	—	—
		(23.6)	(9.6)	(31.8)	(3.59)		
$SeCl_3(CH_3SO_3)$	(2)	28.0	11.0	37.7	4.12	1.21	—
		(28.2)	(11.4)	(38.0)	(4.28)	(1.07)	
$SeCl_3(p\text{-}CH_3C_6H_4SO_3)$	(3)	21.6	8.6	29.7	23.32	2.08	—
		(22.2)	(9.0)	(29.9)	(23.57)	(1.96)	
$TeCl_3(CF_3SO_3)$	(4)	33.7	8.1	27.3	3.10	—	—
		(33.3)	(8.4)	(27.8)	(3.13)		
$TeCl_3(CH_3SO_3)$	(5)	38.5	9.5	32.2	3.89	1.03	—
		(38.8)	(9.7)	(32.4)	(3.65)	(0.91)	
$TeCl_3(p\text{-}CH_3C_6H_4SO_3)$	(6)	30.9	8.0	26.0	20.93	1.82	—
		(31.5)	(7.9)	(26.3)	(20.74)	(1.73)	
$(C_2H_5)_4N[SeCl_3(CF_3SO_3)_2]$	(7)	13.0	9.9	17.1	19.32	3.34	2.15
		(12.9)	(10.4)	(17.4)	(19.56)	(3.26)	(2.28)
$(C_2H_5)_4N[TeCl_3(CF_3SO_3)_2]$	(8)	18.9	9.3	16.0	18.00	3.17	2.02
		(19.3)	(9.7)	(16.1)	(18.12)	(3.02)	(2.11)
$SeCl_3(CF_3SO_3)\cdot 2C_5H_5N$	(9)	15.5	6.2	21.3	26.34	1.96	5.42
		(16.0)	(6.5)	(21.6)	(26.80)	(2.03)	(5.69)
$TeCl_3(CF_3SO_3)\cdot 2C_5H_5N$	(10)	22.9	5.7	19.4	24.62	1.97	5.21
		(23.5)	(5.9)	(19.7)	(24.39)	(1.85)	(5.17)
$[(CH_3)_4N]_2[SeCl_3Br_3]$	(11)	13.4	—	—	16.61	4.10	4.62
		(13.8)			(16.74)	(4.19)	(4.88)
$[(CH_3)_4N]_2[TeCl_3Br_3]$	(12)	20.1	—	—	15.53	3.95	4.81
		(20.5)			(15.44)	(3.86)	(4.50)
$(NH_4)_2[TeCl_3(CF_3SO_3)(NCS)_2]$	(13)	23.6	17.7	20.1	6.37	1.57	10.51
		(23.9)	(17.9)	(19.9)	(6.73)	(1.50)	(10.47)
$(NH_4)_2[TeCl_3(CH_3SO_3)(NCS)_2]$	(14)	27.1	19.9	21.8	7.47	2.57	11.29
		(26.6)	(20.0)	(22.1)	(7.48)	(2.29)	(11.64)
$K_2[Te(CF_3SO_3)_6]$	(15)	11.3	17.5	—	6.64	—	—
		(11.6)	(17.5)		(6.55)		
$K_2[Te(CH_3SO_3)_6]$	(16)	16.0	24.7	—	9.50	2.53	—
		(16.4)	(25.0)		(9.28)	(2.32)	
$K_2[TeO(p\text{-}CH_3C_6H_4SO_3)_4]$	(17)	13.8	14.3	—	37.42	3.17	—
		(14.1)	(14.1)		(37.10)	(3.09)	

*Required values are given in parentheses.

Tetraethylammonium trichlorobis(trifluoromethanesulfonato)selenate(IV)/tellurate(IV), $(C_2H_5)_4N[MCl_3(CF_3SO_3)_2]$ (M = Se and Te)

To a solution of 0.37–0.42 g (1.1 mmol) of $MCl_3(CF_3SO_3)$ in carbon tetrachloride was added 0.65 g (≈2.2 mmol) of $(C_2H_5)_4N^+$-$(CF_3SO_3^-)$. The mixture was stirred for 4–6 h at room temperature. Any unreacted tetraethylammonium trifluoromethanesulfonate was removed by filtration and the white products were recovered by distilling off the solvent *in vacuo*.

Tetramethylammonium tribromotrichloroselenate(IV)/tellurate(IV), $[(CH_3)_4N]_2[MCl_3Br_3]$ (M = Se or Te)

To a solution of ≈0.3–0.4 g (1 mmol) of $MCl_3(XSO_3)$ in methanol (10 mL) was added a solution of 0.9 g (≈6 mmol) of $(CH_3)_4NBr$ in 20 mL of the same solvent. A yellow-coloured compound immediately precipitated out. The mixture was magnetically stirred for about 3 h and then filtered. The precipitates were washed with methanol and dried *in vacuo*. The products were air stable.

Ammonium trichlorobis(isothiocyanato)trifluoromethane/methanesulfonatotellurate(IV), $(NH_4)_2[TeCl_3(XSO_3)(NCS)_2]$ (X = CF_3, CH_3)

To a solution of 0.38 g (1 mmol) of $TeCl_3(CF_3SO_3)$ in 1,2-dimethoxyethane (10 mL) was added a solution of 0.3 g (4 mmol) of NH_4CNS in 25 mL of the same solvent. A white precipitate immediately appeared. The mixture was stirred for 2–3 h, and the product was filtered and dried *in vacuo*. Reaction with $TeCl_3(CH_3SO_3)$ was carried out in a similar fashion.

Pyridine complexes

Addition compounds of $MCl_3(CF_3SO_3)$ (M = Se and Te) with pyridine were prepared by adding an excess of pyridine to an ice-cold solution of the sulfonate derivative in CCl_4, with constant stirring. The voluminous precipitate was filtered, washed several times with CCl_4, and finally dried *in vacuo*.

Analyses

Selenium and tellurium in these compounds were determined gravimetrically as elemental selenium and tellurium by reducing a known weight of the compound with hydrazine hydrate and a saturated solution of SO_2. Sulfur and chlorine were determined gravimetrically as $BaSO_4$ and AgCl, respectively. Carbon, hydrogen, and nitrogen were determined microanalytically on a Carlo Erba Strumentazione elemental analyzer model 1106. Table 1 summarizes the analytical results of the complexes prepared above.

Infrared spectra were recorded on a Perkin–Elmer 1430 ratio recording spectrophotometer in Nujol and hexachlorobutadiene mulls between NaCl/KBr and polyethylene plates. The ^{19}F nmr spectra were recorded on a Varian EM 390 instrument with reference to $CFCl_3$ as external standard. Thermal analysis was carried out on a Paulik, Paulik and Erdey type MOM Budapest Derivatograph.

Results and discussion

Metathetical reactions between $SeCl_4$ (or $TeCl_4$) and silver sulfonates in 1:1 stoichiometry yield $MCl_3(XSO_3)$ salts (M =

Can. J. Chem. Downloaded from www.nrcresearchpress.com by 186.148.149.217 on 09/07/12
For personal use only.

TABLE 2. Infrared spectra

Assignments* (C_s symmetry for XSO_3 part)	Infrared frequencies (cm^{-1})									
	1†	**2**	**3**	**7**	**8**	**13**	**14**	**15**	**16**	**17**
(SO_2) asym. stretch	1395s	1260m	1255s, 1220sh	1400m	1400s	1370s	1240m	1390m	1200s	1270m, 1240sh
(SO_2) sym. stretch	1205s	1165m	1160s	1210s	1300s	1220s	1160m	1200s	1125m	1140s
(S—O*) stretch	1020s	1090s	1100m	1020s	1030s	1030m	1050s	1030s	1065m	1080m
S—X stretch	795s	795m	690m	785s	790m	830m	780s	790m	760s	700m
(SO_2) bend	635m	550m	580m	630m	645m	640m	554m	645m	560m	590w
(SO_2) rock	615m	530m	565m	610m	585m	610w	530w	610m	525w	560m
(S—O*) wag		515w	500w			510w	510m		495w	490m
S—X torsion	360m	380m	360m	370sh	353w	350m	350w	360m	370w	340m
S—X wag	310w	360m	325w	350m	322w	320w	335w	325w	350w	310w
CF_3, CH_3, and $CH_3C_6H_4$ internal vibrations	1240m, 1150m, 1100w	720m	1020m, 810w, 720w	1245m, 1145m, 1090m	1240m, 1145m, 1100w	1245m, 1130m,	725m	1230m, 1185m, 805w	720m	1020m, 840w, 725m

*Coordinating oxygen atom of the sulfonate group.
†See Table 1 for identification of compounds.

TABLE 3. Infrared spectra

C_{3v} assignment for XSO_3 part	Infrared frequencies (cm^{-1})				
	4*	**5**	**6**	**9**	**10**
$\nu_4(E)$ SO_3 asym. stretch	1260s	1200s	1240s	1285s	1265s
$\nu_1(A_1)$ SO_3 sym. stretch	1028s	1040m	1110m	1030s	1035s
$\nu_2(A_1)$ SX stretch	765m	780m	700m	754s	760m
$\nu_5(E)$ SO_3 asym. defn.	635s	550m	590m	640m	640m
$\nu_3(A_1)$ SO_3 sym. defn.	520m	525w	500w	528m	520m
$\nu_6(E)$ SX defn. CF_3, CH_3, and $CH_3C_6H_4$ internal vibrations	1230m, 1180m, 810w, 720w, 705w, 350m	720m	1080m, 1055w, 815m, 630w, 340m	1240m, 1160m, 1100w	1230m, 1180m, 810w

*See Table 1 for identification of compounds.

Se or Te; X = CF_3, CH_3, and p-$CH_3C_6H_4$). Solvolysis of tellurium(IV) chloride in trifluoromethane- and methanesulfonic acids or their anhydrides also yield the monosubstituted compounds, $TeCl_3(XSO_3)$ (X = CF_3 and CH_3). Further substitution of chlorine by XSO_3^- in $TeCl_3(XSO_3)$ could not be effected even when drastic conditions were used. Salts of $SeCl_3^+$ and $TeCl_3^+$ in the presence of chloride ion acceptors or donor solvents are quite well known (7).

All six sulfonates, $MCl_3(XSO_3)$ (M = Se and Te; X = CF_3, CH_3, and p-$CH_3C_6H_4$) are highly sensitive to moisture, and fume in moist air. The $SeCl_3(XSO_3)$ salts are reduced to elemental selenium, and are soluble in common organic solvents such as CCl_4, C_6H_6, CH_2Cl_2, CH_3NO_2, $C_6H_5NO_2$, CH_3CN, etc. The analogous tellurium compounds dissolve only in polar organic solvents such as CH_2Cl_2, CH_3NO_2, CH_3CN, etc. Millimolar solutions of all six compounds in CH_3NO_2 and CH_3CN are nonconducting, thus suggesting that the XSO_3^- group is covalently bonded to the metal atom. The ^{19}F nmr spectra of $SeCl_3(CF_3SO_3)$ and $TeCl_3(CF_3SO_3)$ show single peaks at −74 and −80 ppm, respectively, from $CFCl_3$. This resonance occurs in a region characteristic for trifluoromethanesulfonates (8). TG-DTG studies of $TeCl_3(CF_3SO_3)$ and $TeCl_3(CH_3SO_3)$ show that both compounds on heating decompose at 50°C and in a single step lose their entire mass to give TeO_2 as the final residue. The weight loss values, 57.9% for $TeO_2/TeCl_3(CF_3SO_3)$ and 51.2% for $TeO_2/TeCl_3(CH_3SO_3)$, are in good agreement with the expected values, 58.3 and 51.5%, respectively. $TeCl_3(CF_3SO_3)$ and $TeCl_3(CH_3SO_3)$ melt at 145 and 90°C, respectively. The molecular weight of $TeCl_3(CH_3SO_3)$ could not be determined by the freezing point method since an elevation, rather than a lowering, of the freezing point of nitrobenzene was observed on addition of the compound. This unusual behaviour has been observed for compounds that can interact chemically with the solvent and are salted out on freezing along with the solvent (9).

The ir data for $MCl_3(XSO_3)$ salts (M = Se and Te; X = CF_3, CH_3, and p-$CH_3C_6H_4$) are reported in Tables 2 and 3. Earlier vibrational studies on sulfonate ligands provided information on ionic XSO_3^- groups (10–12), covalently bonded monodentate -OSO_2X groups (13–15), and bidentate bridging and tridentate XSO_3 groups (16–18). Band assignments have been made assuming that the C_{3v} local symmetry for the CSO_3 moiety (or tridentate XSO_3^- group), which would be responsible for six fundamentals, three E ($\nu_{as}(SO_3)$, $\delta_{as}(SO_3)$, and $\rho_r(SO_3)$) and three A ($\nu_s(SO_3)$, ν(S—C), and $\delta_s(SO_3)$) modes of ir-active vibrations, is lowered to local C_s (or C_1) on monodentate type

Can. J. Chem. Downloaded from www.nrcresearchpress.com by 186.148.149.217 on 09/07/12
For personal use only.

Can. J. Chem. Downloaded from www.nrcresearchpress.com by 186.148.149.217 on 09/07/12
For personal use only.

of coordination. With this lowering of symmetry the three E modes are split to give six bands, and a total of nine ir active bands may be expected.

The ir spectra of the $SeCl_3(XSO_3)$ compounds are quite identical, indicating strong structural similarity between them. The number and the position of the sulfur–oxygen stretching bands suggest that the XSO_3^- group in these compounds is acting as a monodentate ligand. Bands at 1395, 1205, and 795 cm^{-1} for $SeCl_3(CF_3SO_3)$ may be assigned to sulfur–oxygen stretching modes of a monodentate trifluoromethanesulfonate group, primarily on the basis of their similarity to the corresponding bands for this group in $Rb[I(CF_3SO_3)_4]$ (14). The remaining bands in this region at 1240, 1150, and 1100 cm^{-1} may be assigned to CF_3 stretching modes. The ir spectra of the $TeCl_3(XSO_3)$ compounds (Table 3) are quite simple and are distinctly different from those obtained for the $SeCl_3(XSO_3)$ compounds. Band positions are very close to the observed frequencies for ionic XSO_3^- ions (10–12), suggesting C_{3v} local symmetry for the CSO_3 moiety in these compounds. The presence of the ionic XSO_3^- group is, however, ruled out on the basis of molar conductance values. The ir data may be interpreted in terms of XSO_3^- ions acting as tridentate bridging ligands in which the three oxygens are involved in coordination to the central tellurium atom.

Complexes of $MCl_3(CF_3SO_3)$ (M = Se and Te) with $(C_2H_5)_4N^+(CF_3SO_3^-)$

The interaction of $SeCl_3(CF_3SO_3)$ and $TeCl_3(CF_3SO_3)$ with $(C_2H_5)_4N^+(CF_3SO_3^-)$ yields 1:1 salts of the type $(C_2H_5)_4N[MCl_3(CF_3SO_3)_2]$. The evidence that these products are not simple mixtures of $(C_2H_5)_4N^+(CF_3SO_3^-)$ and $MCl_3(CF_3SO_3)$, but definite compounds, is evident from their preparation and vibrational spectra (Table 2). The observed frequencies for $(C_2H_5)_4N[TeCl_3(SO_3CF_3)_2]$ are distinctly different from those seen for $TeCl_3(CF_3SO_3)$ (Table 3) and the $CF_3SO_3^-$ ion (10). The ir spectra of $TeCl_3(CF_3SO_3)$ and $CF_3SO_3^-$ are interpreted in terms of local C_{3v} symmetry for the CSO_3 moiety. The CSO_3 group in $(C_2H_5)_4N[TeCl_3(CF_3SO_3)_2]$ has symmetry reduced below C_{3v} as suggested by a splitting of both ν_4 and ν_5 bands. This reduction in symmetry results from a change of coordination of the $CF_3SO_3^-$ group from tridentate (C_{3v}) in $TeCl_3(CF_3SO_3)$ to monodentate (C_s) in $(C_2H_5)_4N[TeCl_3(CF_3SO_3)_2]$. As expected, the ir spectrum of $(C_2H_5)_4N[SeCl_3(CF_3SO_3)_2]$ does not show any significant change in the S—O stretching region from the corresponding bands for $SeCl_3(CF_3SO_3)$ since the $CF_3SO_3^-$ group retains the same functionality in both the compounds.

Complexes of $MCl_3(XSO_3)$ (M = Se and Te; X = CF_3, CH_3, and p-$CH_3C_6H_4$) with $(CH_3)_4N^+Br^-$

Tetramethylammonium bromide reacts instantaneously with $MCl_3(XSO_3)$ compounds to give salts of the type $[(CH_3)_4N]_2[MCl_3Br_3]$ in which the sulfonate groups have been replaced by bromo groups. Their ir spectra do not show any band in the S—O stretching region.

Complexes of $MCl_3(SO_3CF_3)$ (M = Se and Te) with pyridine

Both $SeCl_4$ and $TeCl_4$ are known to form complexes with donor molecules, and on the basis of electrical conductivity and vibrational spectra these complexes have been suggested to have the structure $[L_2MCl_3]^+Cl^-$ (7). It was of interest to find out whether or not the metal atom in these compounds is coordinately saturated. Both $SeCl_3(CF_3SO_3)$ and $TeCl_3(CF_3SO_3)$ form 1:2 addition compounds with pyridine. These complexes are insoluble in all common organic solvents. Their ir spectra are very complex due to a large number of bands for coordinated pyridine (19). However, bands at 1285, 1030, and 640 cm^{-1} and 1240 and 1160 cm^{-1}, which are present in the spectrum of $SeCl_3(CF_3SO_3)\cdot 2C_5H_5N$ (Table 3) and assigned to S—O and C—F stretching modes respectively, are in close agreement with the corresponding bands observed for ionic $CF_3SO_3^-$ (10, 11). The $CF_3SO_3^-$ ion had a monodentate mode of coordination in the parent compound, $SeCl_3(CF_3SO_3)$ (Table 2). The ir spectrum of $TeCl_3(CF_3SO_3)\cdot 2C_5H_5N$ does not exhibit any change in the S—O and C—F stretching region with the corresponding bands for $TeCl_3(CF_3SO_3)$ (Table 3). The CSO_3 groups in both these compounds have C_{3v} local symmetry, although the $CF_3SO_3^-$ group has different functionality in the two compounds. It acts as a tridentate ligand in $TeCl_3(CF_3SO_3)$ but is probably present in ionic form in the pyridine complex. The findings agree with the presence of an ionic $CF_3SO_3^-$ ion in the two pyridine complexes and may be represented as $[MCl_3(Py)_2]^+CF_3SO_3^-$.

Complexes of $TeCl_3(XSO_3)$ (X = CF_3 and CH_3) with NH_4CNS

Ammonium thiocyanate reacts with $TeCl_3(XSO_3)$ to give mixed ligand complexes of the type $(NH_4)_2[TeCl_3(NCS)_2(XSO_3)]$ (X = CF_3 and CH_3). Bands at ≃2070 (C—N stretch), ≃780 (C—S stretch), and ≃470 cm^{-1} (N—C—S bending modes) in these complexes suggest that the thiocyanate ligand binds to the Te through the N atoms (20). The presence of bands at 1370, 1220, and 830 cm^{-1} for the S—O stretching modes in the compound $(NH_4)_2[TeCl_3(NCS)_2(CF_3SO_3)]$ suggests a monodentate mode of coordination for the $CF_3SO_3^-$ ion (14) (Table 2). Both ν_4 and ν_5 bands are split for the complex $(NH_4)_2[TeCl_3(NCS)_2(CH_3SO_3)]$ (Table 2), indicating a lowering of the symmetry of the CSO_3 moiety from C_{3v} in $TeCl_3(CH_3SO_3)$ to C_s in the complex.

Potassium hexakis(trifluoromethane)/methanesulfonatotellurate(IV), $K_2[Te(XSO_3)_6]$ (X = CF_3 and CH_3), and potassium oxotetrakis(paratoluenesulfonato)tellurate(IV), $K_2[TeO(p\text{-}CH_3C_6H_4SO_3)_4]$

Potassium tellurate(IV) reacts with trifluoromethane-, methane-, and paratoluene-sulfonic acids to yield $K_2[Te(CF_3SO_3)_6]$, $K_2[Te(CH_3SO_3)_6]$, and $K_2[TeO(p\text{-}CH_3C_6H_4SO_3)_4]$, respectively. These compounds are insoluble in all common organic solvents. Their ir spectra (Table 2) show split ν_4 and ν_5 modes and are assigned to the presence of monocoordinated sulfonate groups in these salts. The incomplete solvolysis of potassium tellurate(IV) by paratoluenesulfonic acid may be attributed to the lower acidity of paratoluenesulfonic acid vis-à-vis the other two sulfonic acids considered here.

1. R. D. Howells and J. D. McCown. Chem. Rev. 77, 69 (1977).
2. G. A. Lawrance. Chem. Rev. **86**, 17 (1986).
3. R. Kapoor, P. Wadhawan, P. Kapoor, and J. F. Sawyer. Can. J. Chem. **66**, 2367 (1988).
4. G. Brauer. Handbook of preparative inorganic chemistry. 2nd ed. Academic Press, New York. 1963.
5. (*a*) G. M. Kramer. J. Org. Chem. **40**, 298 (1975); (*b*) J. Org. Chem. **40**, 302 (1975).
6. R. Feld. J. Chem. Soc. 3963 (1964).
7. N. N. Greenwood and A. Earnshaw. Chemistry of the elements. Pergamon Press, Toronto. 1984. p. 906.
8. C. H. Dungon and J. R. Van Wazer. Compilation of reported ^{19}F chemical shifts 1951–67. Wiley–Interscience, New York. 1970.

9. S. H. MARRON and C. F. PRUTTON. Principles of physical chemistry. 4th ed. Macmillan, New York. 1966. p. 325.
10. M. G. MILES, G. DOYLE, R. P. COONEY, and R. S. TOBIAS. Spectrochim. Acta, Part A: **25A**, 1515 (1969).
11. H. BURGER, K. BURCZYK, and A. BLASCHETTE. Monatsh. Chem. **101**, 102 (1970).
12. R. J. GILLESPIE and E. A. ROBINSON. Can. J. Chem. **40**, 644 (1962).
13. M. WECHSBERG, P. A. BULLINER, F. O. SLADKY, R. MEWS, and N. BARTLETT. Inorg. Chem. **11**, 3063 (1972).
14. J. R. DALZIEL and F. AUBKE. Inorg. Chem. **12**, 2707 (1973).
15. S. K. SHARMA, R. K. MAHAJAN, B. KAPILA, and V. P. KAPILA. Polyhedron, **2**, 973 (1983).
16. P. A. YEATS, J. R. SAMS, and F. AUBKE. Inorg. Chem. **11**, 2634 (1972).
17. A. L. ARDUINI, M. GARNETT, R. C. THOMPSON, and C. T. C. WONG. Can. J. Chem. **53**, 3812 (1975).
18. J. S. HAYNES, J. R. SAMS, and R. C. THOMPSON. Can. J. Chem. **59**, 669 (1981).
19. N. N. GREENWOOD and K. WADE. J. Chem. Soc. 1130 (1960).
20. R. A. BAILEY, S. L. KOZAK, T. W. MICHELSEN, and W. N. MILLS. Coord. Chem. Rev. **6**, 407 (1971).

Can. J. Chem. Downloaded from www.nrcresearchpress.com by 186.148.149.217 on 09/07/12
For personal use only.

An NMR study of the Lycopodium alkaloids, annotinine and annotine: verification of the annotine structure

DONALD W. HUGHES,[1] ROBERT V. GERARD, AND DAVID B. MACLEAN[1]
Department of Chemistry, McMaster University, Hamilton, Ont., Canada L8S 4M1

Received March 17, 1989

This paper is dedicated to Professor Ronald J. Gillespie on the occasion of his 65th birthday

DONALD W. HUGHES, ROBERT V. GERARD, and DAVID B. MACLEAN. Can. J. Chem. **67**, 1765 (1989).

The Lycopodium alkaloids, annotinine and annotine, were examined by ^{1}H and ^{13}C NMR spectroscopy. Proton spectra were assigned by the application of double-quantum filtered phase-sensitive COSY and nuclear Overhauser enhancement difference spectra. These and other data confirmed the structure previously assigned to annotine. The ^{13}C chemical shifts were consistent with the structural data derived from the proton spectra. The NMR data showed a good correlation with structures determined from molecular mechanics (MMX) calculations.

Key words: Lycopodium alkaloids ^{1}H and ^{13}C NMR, annotinine, annotine, structure of Lycopodium alkaloids, NMR alkaloids.

DONALD W. HUGHES, ROBERT V. GERARD et DAVID B. MACLEAN. Can. J. Chem. **67**, 1765 (1989).

On a étudié des alcaloïdes du Lycopodium, l'annotinine et l'annotine, par RMN du ^{1}H et du ^{13}C. On a attribué les raies des spectres du proton par l'application de spectres de différence eOn et COSY, sensibles à la phase et doublement filtrés d'un point de vue quantique. Ces données ainsi que d'autres confirment la structure attribuée antérieurement à l'annotine. Les déplacements chimiques du ^{13}C sont en accord avec les données structurales obtenues à partir des spectres du proton. Les données de la RMN présentent une bonne corrélation avec les structures déterminées à l'aide de calculs MMX basés sur la mécanique moléculaire.

Mots clés : RMN ^{1}H et ^{13}C des alcaloïdes du Lycopodium, annotinine, annotine, structure des alcaloïdes du Lycopodium, RMN d'alcaloïdes.

[Traduit par la revue]

Introduction

The structure assigned to annotine (1, 2) (Fig. 1), a minor component of the alkaloids of *Lycopodium annotinium L.*, is unique among the more than 100 alkaloids of established structure of the Lycopodium family (3). The structural elucidation was based upon degradation experiments, spectroscopic examination (IR, ^{1}H NMR, and MS) of annotine and a number of its derivatives, and on biogenetic considerations. In the latter context, annotine and a related alkaloid, lyconnotine (4, 5), are the only members of the family isolated thus far that cannot be directly accommodated into the biogenetic schemes that apply consistently to the other members of the family (3). Because of this biogenetic anomaly and because the structure was assigned tentatively in the initial investigation, a reexamination of the structure of the alkaloid was undertaken. Here we report an NMR investigation of annotine using refinements of previously used procedures and new methods that were not available at the time of the original study.

In a parallel study we have reexamined the NMR spectra of annotinine (Fig. 1), another member of this family of alkaloids bearing a lactone function, whose structure and stereochemistry had been verified by an X-ray analysis of its bromohydrin derivative (6). Rings A and C of annotine and annotinine were expected to be conformationally similar, despite the different functionality of ring A in the two systems. Accordingly, we undertook a comprehensive examination of the ^{1}H and ^{13}C NMR spectra of annotinine and used the information so obtained as a model to interpret the annotine spectra and thereby to test the structure previously assigned.

Experimental

All NMR spectra were recorded on a Bruker AM-500 spectrometer. Proton spectra were acquired at 500.135 MHz using a 5 mm dual frequency $^{1}H/^{13}C$ probe. Spectra were obtained in 48 scans in 32K data points over a 2.000 kHz spectral width (8.192 s acquisition time) for annotinine and a 2.747 kHz spectral width (5.964 s acquisition time) for annotine. Sample temperature was maintained at 30°C by a Bruker BVT-1000 variable temperature unit. The free induction decays were processed using Gaussian multiplication for resolution enhancement and were zero-filled to 64K before Fourier transformation.

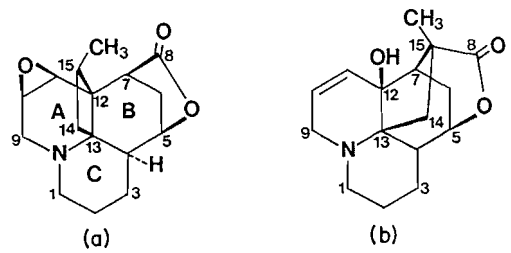


FIG. 1. Structure and numbering of (a) annotinine and (b) annotine.

The inversion–recovery experiments used the standard pulse sequence 180°–τ–90°–ACQ in which the delay τ was adjusted to selectively invert methine proton signals. The 90° ^{1}H pulse width was 18.6 μs. The relaxation delay was 5.0 s and the delay τ was 1.05 s for annotinine and 0.8 s for annotine. Free induction decays were acquired in 16 scans and processed with exponential multiplication (line broadening: 0.2 Hz) before Fourier transformation.

Nuclear Overhauser enhancement (nOe) difference spectra were obtained by subtraction of the off-resonance control FID from the on-resonance FID. The signal of interest was selectively saturated for 5.0 s and the decoupler was gated off during acquisition. This saturation period also served as the relaxation delay. Either 8 or 16 scans were acquired for each irradiation with the cycle of irradiations repeated 4–10 times. Free induction decays were processed using exponential multiplication (line broadening: 4–5 Hz) before Fourier transformation. Samples were not degassed.

Double-quantum filtered COSY 2-D NMR spectra were acquired in the phase-sensitive mode using the pulse sequence: 90°–t_1–90°–τ–90°–ACQ. Phase-sensitive data were obtained using time-proportional

[1]Authors to whom correspondence may be addressed.

Can. J. Chem. Downloaded from www.nrcresearchpress.com by 194.225.253.170 on 09/07/12
For personal use only.

Can. J. Chem. Downloaded from www.nrcresearchpress.com by 194.225.253.170 on 09/07/12
For personal use only.

phase incrementation (TPPI) (7, 8). The fixed delay τ was 3.0 μs. In the F2 dimension 4K data points were used during the acquisition of the 512 FIDs. The annotinine spectra were acquired in 48 scans over a 2.000 kHz spectral width using a 2.0 s relaxation delay while the annotine data were recorded in 64 scans over a 2.747 kHz spectral width using a 1.5 s relaxation delay. Zero-filling in the F1 dimension produced a 2K × 512 data matrix after 2-D Fourier transformation of the phase-sensitive data. This resulted in an F2 digital resolution of 0.977 Hz/point for annotinine and 1.341 Hz/point for annotine. During the 2-D Fourier transformation a sine-bell window function shifted by $\pi/2$ was applied to both dimensions. The transformed data was not symmetrized. The digital resolution of the F2 cross sections was improved by performing an inverse Fourier transform to regenerate the FID of the particular row. This was followed by zero-filling to 32K and then Fourier transformation.

COSY 2-D NMR spectra optimized for long-range couplings were recorded in the absolute value mode using the pulse sequence: $90°-t_1-90°-\tau-$ACQ. The fixed delay τ was set to 0.278 s and was determined from the calculation of $1/4J$ with J = 0.9 Hz. A 1.0 s relaxation delay was used for both samples. Spectra were acquired in 96 scans for annotinine and 128 scans for annotine for each of the 256 FIDs that contained 2K data points in F2 over the previously mentioned spectral widths. Zero-filling in F1 produced a 1K × 1K data matrix with a digital resolution of 1.953 Hz/point for annotinine and 2.683 Hz/point for annotine in both dimensions. During 2-D Fourier transformation a sine-bell squared window function was applied to both dimensions. The transformed data was then symmetrized.

Carbon-13 spectra were recorded at 125.759 MHz using the 5-mm dual frequency $^1H/^{13}C$ probe. The spectra were acquired over a 30.0 kHz spectral width in 32K data points (0.557 s acquisition time) using the standard J-modulated spin sort or DEPT pulse sequences for editing. The ^{13}C 90° pulse width was 6.4 μs while the ^1H 90° pulse width through the decoupler channel was 18.8 μs. A 1.0 s relaxation delay was used. The FIDs were processed using exponential multiplication (line broadening: 2.0 Hz).

The $^{13}C-^1H$ 2-D chemical shift correlation spectra were acquired using the standard pulse sequence incorporating the BIRD pulse during the evolution period for $^1H-^1H$ decoupling in F1 (9–11). The spectra in F2 were recorded over the aliphatic carbon spectral range of 8.0–9.5 kHz in 4K data points. The 256 FIDs in F1 were obtained over the ^1H spectral widths stated above. The fixed delays in the pulse sequence were a 1.0 s relaxation delay, BIRD pulse and polarization transfer delays ($1/2\,^1J_{CH}$) of 0.003571 s, and a refocussing delay ($1/4\,^1J_{CH}$) of 0.001786 s. The data were processed using exponential multiplication (line broadening: 4.0 Hz) in F2 and unshifted sine bell in F1. Zero-filling in F1 resulted in a 2048 × 512 data matrix.

Spectra simulations were performed using the commercially available Bruker Aspect 3000 PANIC program.

Energy-minimized structures were generated using MMX force field calculations derived from MM2 (available from Quantum Chemistry Program Exchange, Chemistry Department, Indiana University, Bloomington, IN 47405, U.S.A.). The calculations were carried out using the program PCMODEL (available from Dr. K. Gilbert, Serena Software, P.O. Box 3076, Bloomington, IN 47402-3076, U.S.A.). Vicinal coupling constants measured from these structures were calculated using a modified Karplus equation that takes into account substituent electronegativity (12).

The compounds used in this study were isolated and purified according to the procedures given in ref. 1. Samples were dissolved in C_6D_6 (MSD Isotopes) to an average concentration of 0.14 M. Chemical shifts for the ^1H and ^{13}C spectra are reported in ppm relative to TMS using the residual solvent signals at 7.15 and 128.0 ppm as internal references.

Results and discussion

NMR experiments were initially performed on annotinine since the stereochemistry of this molecule had been previously established (6). The proton chemical shifts and coupling constants are presented in Tables 1 and 2, respectively. Assignment of the annotinine ^1H spectrum shown in Fig. 2a was accomplished by a combination of one- and two-dimensional NMR methods. Protons that could be assigned in this spectrum included H-5 at 3.811 ppm, H-15 at 3.304 ppm, since the signal from this proton contained a quartet component within its multiplet structure, and the CH_3 doublet at 1.492 ppm. The remaining proton resonances were found in two sections of the spectrum. Between 2.0 and 3.0 ppm the methylene protons on C-1, C-9, and C-14 were located as well as the epoxide ring protons H-10 and H-11. The region from 0.8 to 1.6 ppm contained signals from the C-2, C-3, and C-6 methylene protons and the ring junction methine H-4.

TABLE 1. ^1H chemical shifts for annotinine and annotine in C_6D_6

Proton	Annotinine	Annotine
1α	2.022	2.171
1β	2.921	2.409
2α	1.179	1.439
2β	0.842	0.828
3α	1.085	1.089
3β	1.263	1.540
4	1.004	1.164
5	3.811	3.608
6α	0.961	1.180
6β	1.607	1.415
7	2.289	1.816
9α	2.540	2.876
9β	2.676	2.686
10	2.683	5.204
11	2.252	5.656
14*t*	1.911	2.182
14*c*	2.059	1.899
15	3.304	
16-CH_3	1.492	1.693

Following this preliminary analysis a series of inversion–recovery experiments were carried out to differentiate methylene from methine resonances. These experiments exploit the fact that the methine protons should have a longer spin-lattice relaxation time. Multiplets that remained inverted after the application of the inversion–recovery pulse sequence were at 3.811, 3.304, 2.683, 2.252, 2.289, and 1.004 ppm. The results confirmed the assignment of the lowest field resonances as the methine protons H-5 and H-15. The three signals between 2.2 and 2.7 ppm were considered to arise from H-10, H-11, and H-7 but could not be specifically assigned. Based on its high field position, the multiplet at 1.004 ppm was tentatively assigned to H-4.

Most of the chemical shift assignments in Table 1 were obtained from a double-quantum filtered phase-sensitive COSY 2-D NMR spectrum. This version of the COSY pulse sequence was used because it not only reduced diagonal peak intensity but also produced pure 2-D absorption lineshapes, which resolved spin couplings within cross-peaks and provided more accurate measurement of chemical shifts (13–16). Correlations among the annotinine protons were established by examining the connectivities to the methine protons and the CH_3 group. The A-ring epoxide methine protons H-10 and H-11 and the C-9 methylene protons were difficult to analyze because of the overlap of the signals at 2.683 and 2.676 ppm (Fig. 2).

Upon completing the analysis of the connectivities in the COSY spectrum it was then necessary to determine the individual chemical shift assignments of the nonequivalent methylene protons. These protons are designated using the α,β

TABLE 2. ^1H coupling constants (Hz) for annotinine and annotine in C_6D_6

	Annotinine	Annotine
Geminal couplings		
1α,β	−14.6	−14.0
2α,β	−12.7	−13.5
3α,β	−11.9	−13.0
6α,β	−11.8	−14.2
9α,β	−13.7	−18.9
14*c*,*t*	−11.4	−12.3
Vicinal couplings		
1α,2α	4.9	4.8
1α,2β	1.5	1.6
1β,2α	12.8	13.7
1β,2β	4.0	3.8
2α,3α	3.8	5.1
2α,3β	12.5	13.0
2β,3α	2.4	1.7
2β,3β	3.4	5.2
3α,4	1.5	3.6
3β,4	12.0	12.6
4,5	1.5	3.6
6α,5		2.7
6β,5	5.8	2.7
6α,7		1.1
6β,7	5.7	6.0
9α,10	1.5	2.8
9β,10	1.6	3.5
10,11	4.0	10.0
14*t*,15	8.8	
14*c*,15	11.1	
16-CH_3,15	7.5	
Long-range couplings		
1α,3α	1.5	1.6
4,14*c*		2.1
5,7	0.7	1.7
1α,9α	[a]	[a]
1β,9β	[a]	
1β,10	0.6	0.7
11,9α	0.7	2.8
11,9β		2.2
11,14*t*	[a]	0.8
15,6β	[a]	
15,7	[a]	

[a]Coupling was not observed in the 1-D ^1H spectrum but was detected by the long-range COSY experiment.

terminology. A β proton, for example H-1β in Fig. 3a, is located on the same side of the molecule as the lactone ring. The C-14 methylene protons are designated as H-14*c* and H-14*t*, which indicated that they are *cis* or *trans*, respectively, to the CH_3 group.

The nOe difference experiments were the most effective technique for providing both methylene proton chemical shift assignments and structural data. The information derived from these experiments was examined in relation to an energy-minimized structure determined from molecular mechanics (MMX) calculations (Fig. 3a). Proton internuclear distances, measured from the calculated structure, were found to agree favourably with the spatial relationships indicated in the nOe difference spectra.

The nOe experiments began with the saturation of H-15, which produced an enhancement of the CH_3 doublet and the C-14 proton resonance at 1.911 ppm. This H-14 multiplet was assigned to the proton *trans* to the CH_3. Assignment of H-14*t* also aided in the discrimination of the C-1 methylene protons because irradiation of the C-1 proton at 2.921 ppm resulted in an nOe of the H-14*t* signal. The 2.921 ppm multiplet was therefore assigned to H-1β. This result was consistent with the 2.3 Å distance between the H-1β and H-14*t* in the energy-minimized structure. Other signals enhanced during this experiment were identified as H-1α (2.022 ppm) and H-2β (0.842 ppm). Methylene protons on C-6 and C-3 were also assigned by nOe difference spectra when H-7 and H-5, respectively, were saturated.

The nOe difference spectra that provided key structural data involved the irradiation of the protons on C-11 and C-9. Prior to this experiment the doublet of doublets at 2.252 ppm could not be unambiguously assigned to either H-10 or H-11. Saturation of the resonance at 2.252 ppm not only produced the expected enhancement of the adjacent epoxide proton at 2.683 ppm but also resulted in an nOe being observed on the H-6α doublet at 0.961 ppm. Examination of the annotinine structure in Fig. 3a revealed that the only epoxide proton capable of producing an nOe on the axial H-6α was H-11. The internuclear distance from H-11 to H-6α in the calculated structure was found to be 2.8 Å. Proton 11 was therefore assigned to 2.252 ppm. This particular experiment provides a means of characterizing the geometry of the C-12 substituents because the observed nOe between H-11 and H-6α can only result if the C-11 to C-12 bond is axial to ring B. This observation should prove useful in the examination of other alkaloids in this series.

The final nOe experiment on annotinine involved the saturation of the C-9 proton at 2.540 ppm. As expected, there was an enhancement of the H-9 signal at 2.676 ppm. The most surprising result was the nOe observed on H-4. From Fig. 3a it is evident that the C-9 proton labelled H-9α is directed underneath ring C toward H-4, which must have an axial geometry for the nOe to be observed. In fact the internuclear distance between these protons in the minimized structure was 2.0 Å. This particular nOe experiment may be used to probe the stereochemistry at C-4 provided that the N—C9 bond is axial to ring C in other Lycopodium alkaloids.

The coupling constants in Table 2 were indicative of the distinct conformations for each of the rings of annotinine. A considerable distortion of the B-ring conformation (Fig. 3a) was evident from the absence of any observable coupling between H-6α and H-7 and H-5. To accommodate the five-membered lactone, C-6 must be puckered well below the plane formed by carbons 1, 2, 4, and 13. Because of this distortion, the dihedral angles between H-6α and H-5 and H-7 lie in the range 80°–90°. A small coupling between H-6α and H-5 and H-7 was detected by the observation of cross-peaks between these protons in a COSY experiment optimized for long-range couplings. The COSY experiment also detected a four-bond coupling between H-5 and H-7, indicating that the intervening bonds must be in planar W structure.

The C-ring protons displayed couplings that were characteristic of a chair conformation (Table 2). Signals from H-2α,β and H-3α,β were the most difficult to interpret because of the numerous vicinal as well as long-range couplings contributing to their multiplet structure and the partial overlap of H-2α and H-3β (Fig. 1a). Some of these couplings were resolved by examining cross sections in the F2 dimension through the cross-peaks in the phase-sensitive COSY spectrum, while others were obtained by spin decoupling or computer simulation.

Can. J. Chem. Downloaded from www.nrcresearchpress.com by 194.225.253.170 on 09/07/12
For personal use only.

Can. J. Chem. Downloaded from www.nrcresearchpress.com by 194.225.253.170 on 09/07/12
For personal use only.

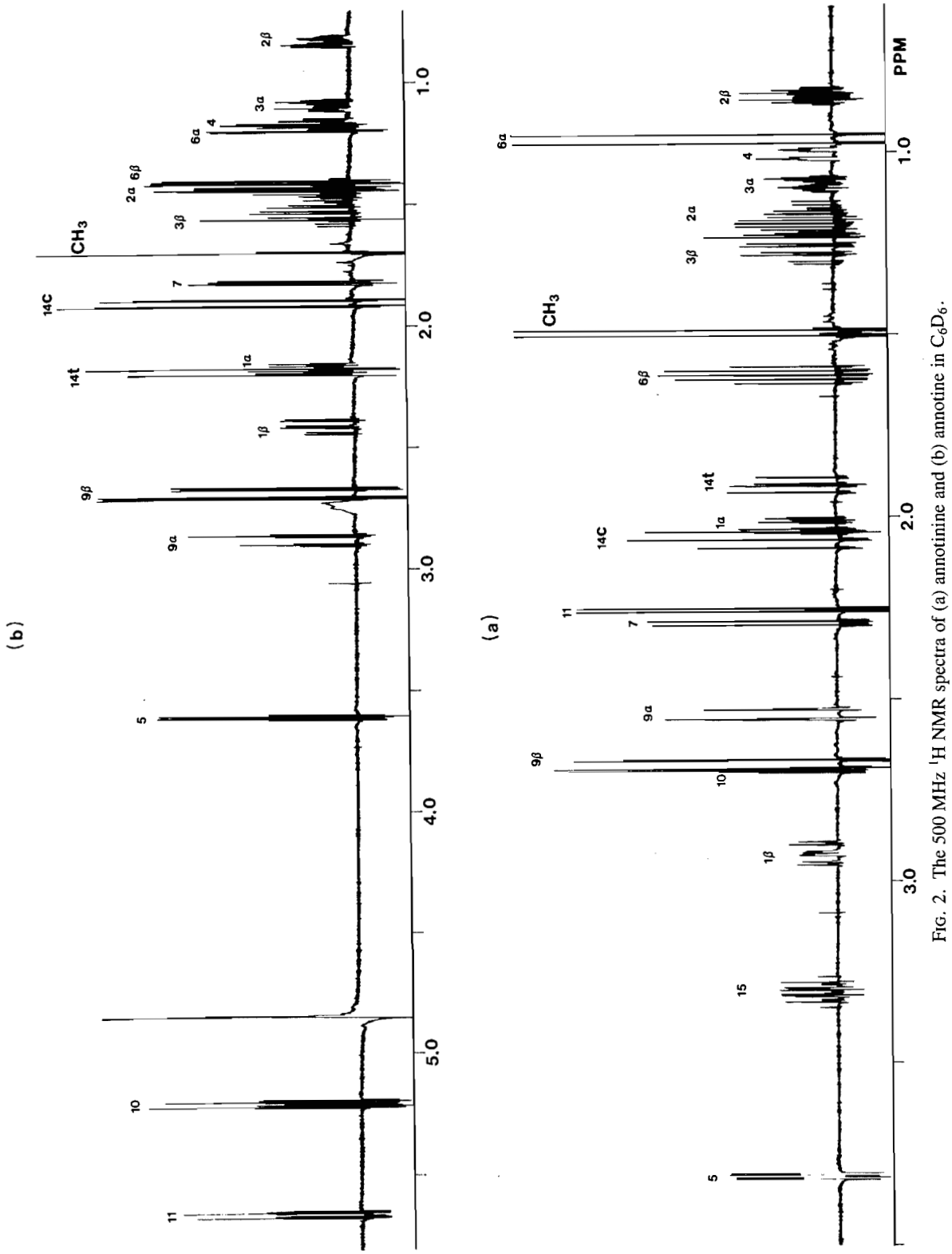


FIG. 2. The 500 MHz ^{1}H NMR spectra of (a) annotinine and (b) annotine in C_6D_6.

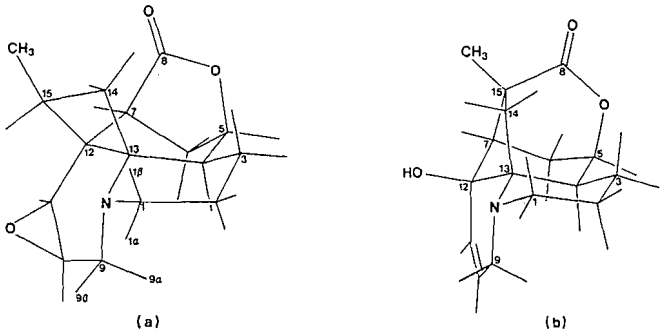


FIG. 3. Energy-minimized structures of (a) annotinine and (b) annotine obtained from MMX force field calculations.

Long-range couplings were also detected between the C-ring protons. In particular, a four-bond coupling of 1.5 Hz was observed between the equatorial protons H-1α and H-3α, indicating the planar W arrangement of the bonds in the coupling pathway.

The A-ring protons 10 and 11 displayed a 4.0 Hz vicinal coupling typical of *cis* protons in an epoxide structure (17). The C-9 protons had nearly identical couplings with H-10 (Table 2), suggesting similar dihedral angles. Molecular modelling indicated that the A ring could best accommodate the cyclobutyl and epoxide rings if it adopted a boatlike conformation (Fig. 3a). When viewed along the C-9 to C-10 bond, H-10 in this conformation appears equidistant between H-9α and H-9β and this would account for the similar vicinal couplings. Several unresolved long-range couplings were detected on the A-ring protons during the long-ranged COSY experiment. These included four-bond coupling between the C-9 protons and both H-11 and H-1β, and five-bond couplings between H-11 and H-14*t*, and H-9β and H-14*c*.

The vicinal coupling constants for H-15 and the C-14 protons (Table 2) were in the range reported for cyclobutyl compounds (17). Proton 15 was long-range coupled through four and five bonds to H-7 and H-6β, respectively.

The annotinine vicinal coupling constants measured from the ^{1}H NMR spectra corresponded to within 1–3 Hz of those calculated from the energy-minimized structure. These results, along with the nOe data and the structural constraints imposed by the long-range couplings, indicated that the calculated structure in Fig. 3a was a reasonable representation of the annotinine structure in solution.

With the analysis of the annotinine data completed, we then applied the same techniques to assign the ^{1}H spectrum of annotine to determine whether the structure and relative stereochemistry previously assigned were correct. The most obvious changes in the annotine ^{1}H spectrum (Fig. 2b) relative to that of annotinine were the presence of the olefinic protons 10 and 11, the absence of H-15, and the appearance of a singlet for the CH_3 at 1.693 ppm. Tentative assignments were made for some methine and methylene protons on the basis that their chemical shifts and multiplet patterns were similar to the corresponding annotinine protons. However, several annotine ^{1}H signals were shifted upfield and in two cases there was a reversal in position of the resonances for the α and β protons of a methylene group. An additional complication in the annotine spectrum was the overlap of the multiplets in the 1.1–1.5 ppm region (Fig. 2b). The methine signal (H-4) at 1.164 ppm was obscured by an overlapping H-6 resonance and could only be resolved by the use of the inversion–recovery pulse sequence. This experiment also resulted in the selective inversion of the olefinic protons, the H-5 multiplet at 3.608 ppm and the methine signal from H-7 at 1.816 ppm, which had undergone a 0.5 ppm upfield shift relative to annotinine. The remaining chemical shift assignments (Table 1) were determined from the COSY and nOe difference spectra.

The contour plot of the annotine double-quantum filtered phase-sensitive COSY experiment could not be used to distinguish between olefinic protons 10 and 11 since they both showed correlations to the C-9 protons at 2.876 and 2.686 ppm. The H-5 signal had cross-peaks to the H-6 proton at 1.415 ppm and the overlapped H-4 and H-6 protons near 1.1 ppm. A cross-peak between H-5 and H-7 was also observed. The multiplet at 2.409 ppm was tentatively assigned to H-1β because of the similarity in both chemical shift and multiplet structure to the corresponding proton in annotinine. This proton was correlated with H-1α at 2.171 ppm and the C-2 methylene protons at 0.828 and 1.439 ppm. By comparison with the annotinine spectrum, the H-2 multiplet at 0.828 ppm was assigned to H-2β. Proton 2β displayed other cross-peaks to H-2α (1.439 ppm) and the H-3 proton at 1.540 ppm while the cross-peaks to H-1α and the H-3 proton at 1.089 ppm were of lower intensity. Finally, a correlation was detected between the geminal coupled C-14 methylene protons at 1.899 and 2.182 ppm. A result that provided the first indication of the geometry of the C—H bond at position 4 was the cross-peak between the H-14 proton at 1.899 ppm and H-4.

In addition to the connectivity data, the phase-sensitive COSY experiment provided a means for obtaining coupling constants from overlapping multiplets. As stated in the annotinine discussion, the analysis of the protons of ring C, H-2α,β and H-3α,β, was difficult because of the large number of coupling interactions. The annotine spectrum was further complicated by the overlap of H-2α with both H-3β and H-6β (Fig. 2b). The problem of measuring the coupling constants for H-2α was solved by examining the cross-peaks in the phase-sensitive COSY spectrum. To illustrate this procedure, Fig. 4 presents a section of the contour plot containing the diagonal peak of H-1β and the cross-peaks to H-1α, H-2α, and H-2β. The cross section at the bottom of the diagram was selected from the row in the F2 dimension indicated by the arrow. It can be readily seen that the H-2α multiplet is completely resolved without the interference of other overlapping resonances.

The other advantage of the technique is that the active coupling that gives rise to the cross-peak can be identified by the antiphase transitions (13–16). All other couplings to H-2α, designated as the passive couplings, appear in-phase superimposed on the antiphase transitions (Fig. 4). The active coupling between H-1β and H-2α was measured from the point at the centre of the pair of inverted or in-phase triplets to the centre of the multiplet where the phase change occurs. The reason for this is that the geminal and *trans* diaxial couplings were nearly identical (Table 2). In the absence of all other couplings H-2α would appear as a doublet of doublets overlapped at the central transition. This pseudo triplet in the phase-sensitive COSY spectrum would have its central transition cancelled because the transition intensities of an antiphase triplet must be −1, 0, and +1 (13–16). A more straightforward example is the H-1α cross-peak in which the antiphase transitions are separated by the geminal coupling.

These examples demonstrated that cross-peaks arising from multiplets with large geminal and *trans* diaxial couplings could be readily analyzed because the individual transitions were well

Can. J. Chem. Downloaded from www.nrcresearchpress.com by 194.225.253.170 on 09/07/12
For personal use only.

Can. J. Chem. Downloaded from www.nrcresearchpress.com by 194.225.253.170 on 09/07/12
For personal use only.

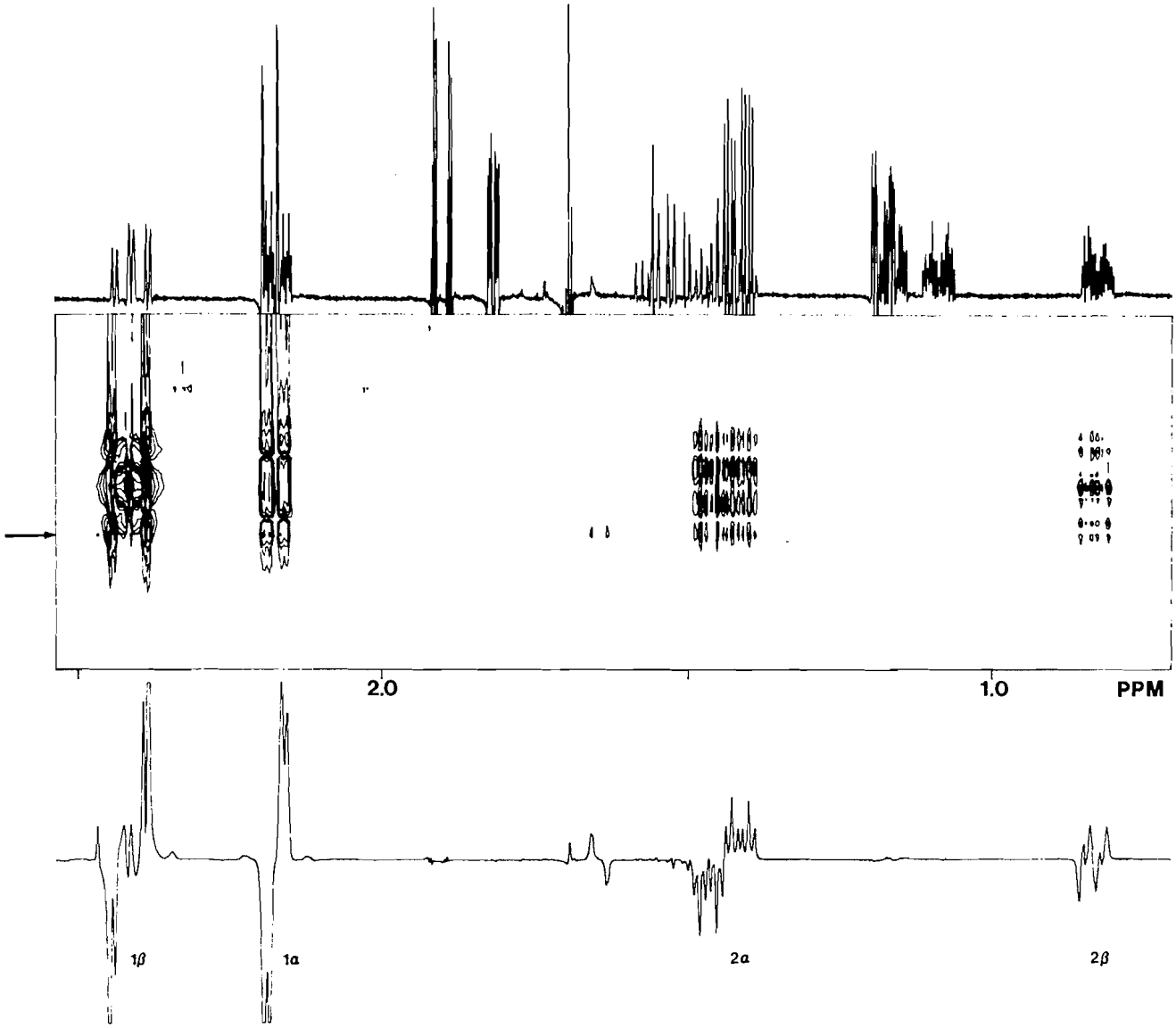


FIG. 4. Contour plot and cross section of the H-1β diagonal peak and cross-peaks to H-1α, H-2α, and H-2β of annotine.

separated. This technique was less effective for protons such as the equatorial H-2β. The H-2β multiplet was composed of many closely spaced transitions that could only be resolved in the higher resolution 1-D spectrum. In the COSY spectrum these transitions would cancel each other when they became antiphase, resulting in the loss of coupling information and lower intensity cross-peaks. Other techniques such as spin decoupling and heteronuclear shift correlation were applied to obtain the coupling information.

The nOe difference spectra were then recorded to assign the methylene protons and to examine the relative stereochemistry at C-4 and C-12. The nOe data were also compared with the ^1H distances measured from an energy-minimized structure of annotine (Fig. 3b). These experiments began by saturating the CH_3 singlet, which produced an enhancement of H-14*c* at 1.899 ppm and the H-7 signal. Irradiation of H-14*t* enhanced both H-14*c* and the H-3 multiplet at 1.540 ppm. This C-3 proton was therefore assigned to H-3β, which was separated by 2.2 Å from H-14*t* in the calculated structure. A reverse experiment in which H-3β was saturated confirmed the H-14*t* result and also produced an nOe at H-3α (1.087 ppm) and H-2β (0.828 ppm). This experimental verification of the H-2β resonance enabled us to confirm the assignment of H-1β by irradiating the 2.409 ppm multiplet. An enhancement of both H-1α (2.171 ppm) and H-2β was observed. In ring B the methylene protons at C-6 were differentiated by irradiation of H-7. The signal at 1.415 ppm experienced the nOe and was assigned to the equatorial H-6β. An additional result of this experiment was the enhancement of the lowest field olefinic proton at 5.656 ppm. On the basis of interproton distances this signal was assigned to H-11.

With the assignment of H-11 confirmed it was now possible to probe the geometry of the C-11,C-12 bond. Saturation of H-11 enhanced the *cis* olefinic proton H-10 as well as H-7. The definitive result was the nOe observed on the 1.180 ppm multiplet assigned to H-6α (Fig. 5b). This nOe to the axial C-6 proton indicated an axial orientation of the bond between carbons 11 and 12 with the C-12 hydroxyl group being equatorial. Therefore the relative stereochemistry at C-12 was identical with that of annotinine and the majority of other Lycopodium alkaloids (3). The internuclear distance from H-11 to H-6α in the calculated structure was 2.4 Å, which was smaller than the annotinine separation. This result implied that

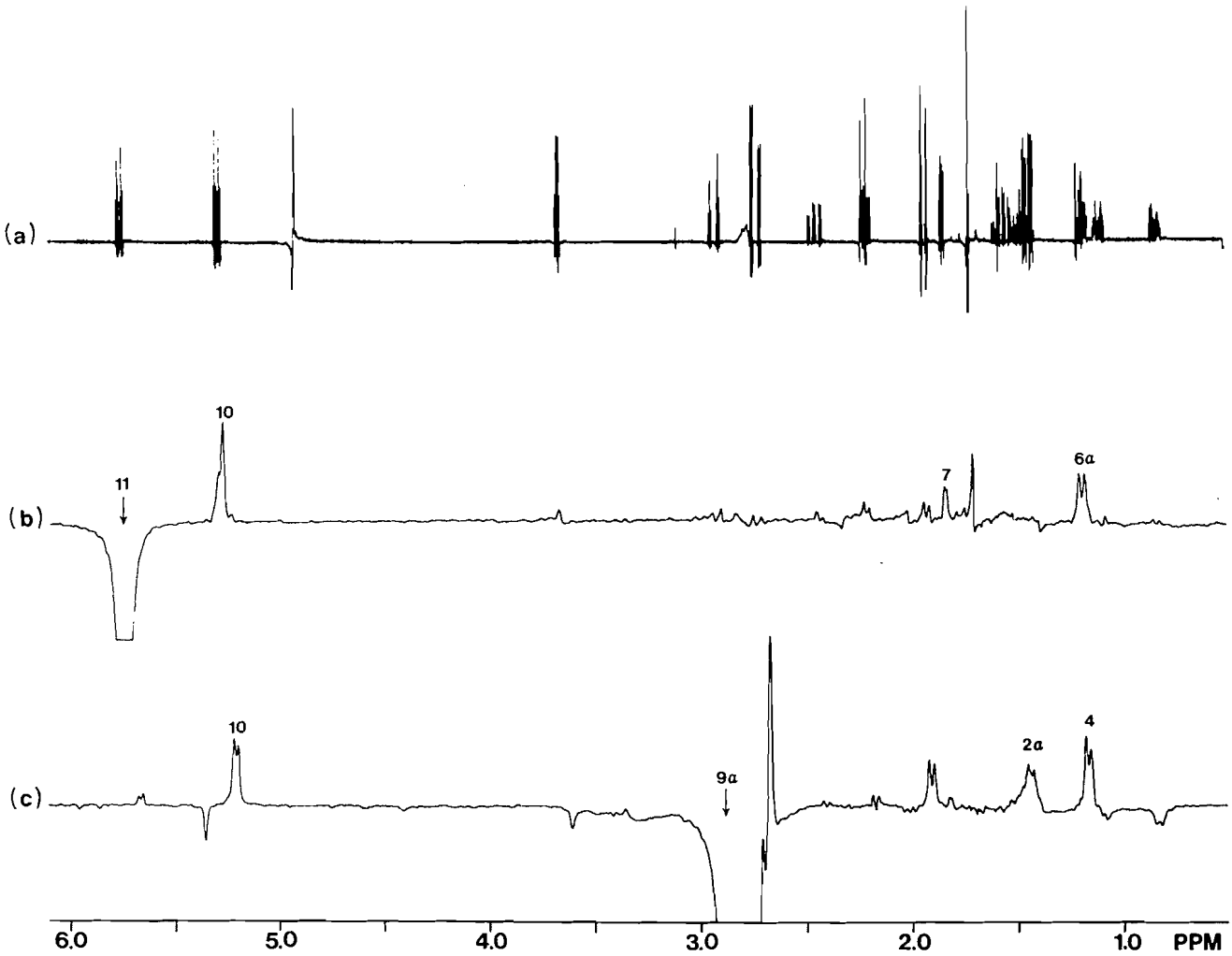


FIG. 5. Comparison of the (a) 500 MHz ^{1}H spectrum with the nOe difference spectra obtained by saturation of (b) H-11 and (c) H-9α of annotine.

changes in the conformations of the A and B rings relative to annotinine, such as those shown in Fig. 3b, would bring H-11 closer to both H-7 and H-6α.

The relative stereochemistry of the C—H bond at position 4 of annotine was determined by irradiating the C-9 protons. Saturation of the lower field H-9 proton at 2.876 ppm resulted in the enhancement of H-4 (Fig. 5c) and therefore confirmed the axial geometry of the C—H bond at carbon 4. Thus the relative stereochemistry of annotine at C-4 is also the same as annotinine. The interproton distance between H-9α and H-4 in the calculated structure was 2.5 Å, which was larger than the annotinine distance. This nOe experiment also produced an enhancement of H-2α, H-9β, and H-10.

With the spatial relationships of the annotine protons determined by the nOe experiments, the ring conformations were then examined using the ^{1}H–^{1}H coupling constants (Table 2). In contrast to annotinine, the axial H-6α in ring B of annotine showed couplings of 2.7 and 1.1 Hz to H-5 and H-7, respectively. This indicated that the B ring was adopting a more chairlike conformation (Fig. 3b) than in annotinine since the dihedral angles from these coupling constants would be in the range of 50°–70°. There is less distortion of the B ring since the lactone forms a six-membered ring and the two-carbon unit bridging C-7 and C-13 is accommodated within a five-membered ring structure involving carbons 7, 12, 13, 14, and 15. The conformation of ring B was further defined by the 1.7 Hz four-bond coupling between H-5 and H-7.

The chair conformation of ring C remained similar to that of annotinine. There were minor changes in the dihedral angles about the C—C bonds that were reflected in the variation in some of the vicinal coupling constants (Table 2). Long-range coupling was observed between H-1α and H-3α. The four-bond coupling between H-14*c* and H-4 also defined the orientation of the C—H bond at C-4. The structure in Fig. 3b shows that with an axial H-4 the bonds to H-14*c* form the planar W pathway required for the four-bond coupling.

Ring A underwent a change in conformation relative to annotinine owing to the presence of the double bond between carbons 10 and 11. This was first indicated by the substantial increase in magnitude of the H-9α,β geminal coupling constant (Table 2). The change in geminal coupling was caused by the nodal plane of the π system being oriented such that it bisects the angle between the C-9 methylene protons (17–19). Carbons 9, 10, and 11 must have a planar geometry for this to occur. From the energy-minimized structure (Fig. 3b) it can be seen that the nitrogen and all the carbon atoms except C-13 were planar, resulting in a sofa conformation.

The A-ring protons also displayed long-range couplings. A four-bond coupling was detected between H-9α and H-1β in the long-range COSY spectrum. Five-bond couplings were

Can. J. Chem. Downloaded from www.nrcresearchpress.com by 194.225.253.170 on 09/07/12
For personal use only.

Can. J. Chem. Downloaded from www.nrcresearchpress.com by 194.225.253.170 on 09/07/12
For personal use only.

TABLE 3. ^{13}C chemical shifts of annotinine and annotine in C_6D_6

Carbon	Annotinine	Annotine
1	46.6	47.1
2	22.7	17.4
3	25.4	22.3
4	35.7	35.2
5	79.9	76.8
6	34.9	30.9
7	43.9	47.0
9	43.9	46.2
10	51.0	127.7
11	52.1	128.1
12	44.6	77.9
13	58.2	66.3
14	35.2	41.8
15	32.1	46.3
16-CH_3	12.7	25.0
C=O	177.9	176.4

observed between H-11 and H-14*t*, and H-10 and H-1β (Table 2). The ^1H NMR data derived from the nOe experiments and the coupling constants showed a good correlation with the energy-minimized structure in Fig. 3b.

This study concluded with an examination of the ^{13}C NMR spectra of annotinine and annotine. The ^{13}C chemical shifts are presented in Table 3. Assignment of the chemical shifts initially involved the identification of carbon types from the *J*-modulated spin sort spectra. In the case of annotine, DEPT spectra were required to suppress the benzene solvent signal in order to observe the olefinic carbon resonances at 127.7 and 128.1 ppm. These signals were assigned to carbons 10 and 11, respectively, by performing selective ^1H decoupling during the acquisition of the DEPT spectra. Some preliminary assignments for the aliphatic carbons were made by combining the results of the edited spectra with ^{13}C data reported for other Lycopodium alkaloids (20). The lowest field methine signal near 80 ppm was assigned to C-5. Methine carbon signals from the epoxide group in annotinine appeared near 50 ppm. The methylene carbons adjacent to the nitrogen were located in the region 44–48 ppm. The highest field methylene carbon resonances were attributed to carbons 2 and 3. Assignment of the quaternary carbons, 12 and 13, was made on the basis of their chemical shifts. In the annotinine spectrum C-13 (58.2 ppm) was deshielded relative to C-12 (44.6 ppm) because C-13 was bonded to the nitrogen. These carbon resonances were reversed in annotine since C-12 (77.9 ppm) was directly bonded to the hydroxyl group. Carbon 13 was also deshielded in annotine relative to annotinine due to the change in ring size as well as to the β substituent effect of the hydroxyl group at C-12.

The definite assignment of the protonated carbon chemical shifts relied on the ^1H–^{13}C chemical shift correlation experiment. The pulse sequence used the BIRD pulse (21) during the evolution period to remove homonuclear ^1H couplings in the F1 dimension. Carbon atoms directly bonded to nonequivalent methylene protons produced two signals that still retained their geminal coupling. This feature of the shift correlation spectrum was especially useful for resolving the overlapping methylene proton resonances H-3β, H-2α, and H-6β of annotine. From the F1 cross sections through carbons 2, 3, and 6 a good estimate was obtained for the methylene proton chemical shifts and geminal coupling constants. These results helped to confirm the analysis of the ^1H spectrum. In the ^{13}C spectra it was difficult to distinguish C-1 and C-9 because of their similar chemical shifts. Assignment of these carbons was achieved by their correlation with the directly bonded protons H-1α,β and H-9α,β, which appeared as well-resolved multiplets in the ^1H spectra.

A comparison of the ^{13}C data of these two alkaloids indicated that the methyl resonance of annotinine had a high field chemical shift of 12.7 ppm. Similar results were also reported for the methyl groups of *cis*-1,2-dimethylcyclobutane (22). The shielding of the annotinine methyl was caused primarily by steric interactions with C-7, which is both *cis* and γ relative to the methyl. In the X-ray structure the methyl was found to be pointed in the direction of the carbonyl oxygen (6). This additional steric interaction would also contribute to the shielding of the methyl carbon. The chemical shift of C-4 in both alkaloids was essentially the same, indicating no significant difference in the structure around this carbon. Carbons 2 and 6 were both shielded in annotine relative to annotinine (Table 3). This was due to the γ steric effect of carbons 9 and 11. The change in the A-ring conformation to the sofa form shown in Fig. 3b forces the bonds between the nitrogen and C-9, and between C-11 and C-12 to become completely axial to ring B. This factor, combined with the reduced distortion of the B- and C-ring chair conformations, resulted in more effective γ interactions.

Conclusions

The application of both high field NMR and one- and two-dimensional techniques has permitted the complete assignment of the ^1H and ^{13}C NMR spectra of the Lycopodium alkaloids, annotinine and annotine. The nOe difference spectra established that the relative stereochemistry at C-4 and C-12 of annotine was identical with that of annotinine. The double-quantum filtered phase-sensitive COSY experiment has been shown to be an effective method for analyzing natural products spectra. This pulse sequence was able to provide both connectivity and coupling constant information in regions of the ^1H spectrum containing complicated overlapping multiplets. Both the ^1H and ^{13}C data indicated that the A ring of annotine has a sofa conformation. The complete assignment of both the annotinine and annotine ^{13}C spectra will be useful to those engaged in biosynthetic studies on these alkaloids.

Acknowledgments

We thank Monica Fischer for preparing the annotine sample and the Natural Sciences and Engineering Research Council of Canada for financial support.

1. W. A. SZAREK, K. A. H. ADAMS, M. CURCUMELLI-RODOSTAMO, and D. B. MACLEAN. Can. J. Chem. **42**, 2584 (1964).
2. D. B. MACLEAN and M. CURCUMELLI-RODOSTAMO. Can. J. Chem. **44**, 611 (1966).
3. D. B. MACLEAN. *In* The alkaloids. Vol. 26. *Edited by* A. Brossi. Academic Press, New York. 1985. p. 241.
4. F. A. L. ANET, M. Z. HAQ, N. H. KHAN, W. A. AYER, R. HAYASTU, S. VALVERDE-LOPEZ, P. DESLONGCHAMPS, W. RIESS, M. TERNBAH, Z. VALENTA, and K. WIESNER. Tetrahedron Lett. 751 (1964).
5. Z. VALENTA, P. DESLONGCHAMPS, R. A. ELLISON, and K. WIESNER. J. Am. Chem. Soc. **86**, 2533 (1964).
6. M. PRZYBYLSKA and L. MARION. Can. J. Chem. **35**, 1075 (1957).
7. D. MARION and K. WUTHRICH. Biochem. Biophys. Res. Commun. **113**, 967 (1983).
8. G. BODENHAUSEN, H. KOGLER, and R. R. ERNST. J. Magn. Reson. **58**, 370 (1984).
9. A. BAX. J. Magn. Reson. **53**, 517 (1983).

10. V. RUTAR. J. Magn. Reson. **58**, 306 (1984).
11. J. A. WILDE and P. H. BOLTON. J. Magn. Reson. **59**, 343 (1984).
12. C. A. G. HAASNOOT, F. A. A. M. DE LEEUW, and C. ALTONA. Tetrahedron, **36**, 2783 (1980).
13. K. WUTHRICH. NMR of proteins and nucleic acids. J. Wiley and Sons, New York. 1986.
14. R. R. ERNST, G. BODENHAUSEN, and A. WOKAUN. Principles of magnetic resonance in one and two dimensions. Claredon Press, Oxford. 1987.
15. A. E. DEROME. Modern NMR techniques for chemistry research. Pergamon Press, Oxford. 1987.
16. H. KESSLER, M. GEHRKE, and C. GRIESINGER. Angew. Chem. Intl. Ed. Engl. **27**, 490 (1988).
17. H. BOOTH. Prog. NMR Spectrosc. **5**, 149 (1969).
18. M. BARFIELD and D. M. GRANT. J. Am. Chem. Soc. **85**, 1899 (1963).
19. A. A. BOTHNER-BY. *In* Advances in magnetic resonance. Vol. 1. *Edited by* J. S. Waugh. Academic Press, New York. 1965. p. 195.
20. T. T. NAKASHIMA, P. P. SINGER, L. M. BROWNE, and W. A. AYER. Can. J. Chem. **53**, 1936 (1975).
21. J. R. GARBOW, D. P. WEITEKAMP, and A. PINES. Chem. Phys. Lett. **93**, 504 (1982).
22. E. L. ELIEL and K. M. PIETRASIEWICZ. Org. Magn. Reson. **13**, 193 (1980).

Can. J. Chem. Downloaded from www.nrcresearchpress.com by 194.225.253.170 on 09/07/12
For personal use only.

Ligand substitution reactions of pentacyanoferrate(II) complexes with *N*-heterocyclic cations in aqueous solution

DONAL HUGH MACARTNEY[1] AND LAUREN JEAN WARRACK
Department of Chemistry, Queen's University, Kingston, Ont., Canada K7L 3N6

Received January 31, 1989

This paper is dedicated to Professor Ronald J. Gillespie on the occasion of his 65th birthday

DONAL HUGH MACARTNEY and LAUREN JEAN WARRACK. Can. J. Chem. **67**, 1774 (1989).

Kinetic and spectroscopic studies have been carried out in aqueous solution on the formation (from $Fe(CN)_5OH_2^{3-}$) and dissociation of pentacyanoferrate(II) complexes containing 1-(4-pyridyl)pyridinium and the neutral, protonated, and *N*-methylated forms of 4,4′-bipyridine (BPY), 1,2-bis(4-pyridyl)ethane (BPA), and *trans*-1,2-bis(4-pyridyl)ethylene (BPE). The pH dependences of the formation kinetics have been analyzed in terms of the specific rate and acid dissociation constants for these ligands. The rate constants (25.0°C, $I = 0.10$ M) for the formation of the dinuclear complexes $(NC)_5FeLFe(CN)_5^{6-}$ have been determined for BPY (50 M^{-1} s^{-1}), BPA (66 M^{-1} s^{-1}), BPE (95 M^{-1} s^{-1}), and pyrazine (10 M^{-1} s^{-1}), and are compared with the respective rate constants for the formation of $(NC)_5FeLCo(NH_3)_5$. The relationships between the formation rate constants and the size of the ligand, the number of donor sites, and the magnitude and position of charges on the ligand are discussed in terms of an ion-pair dissociative mechanism.

Key words: pentacyanoferrate(II) complexes, *N*-heterocycles, ligand substitution, kinetics.

DONAL HUGH MACARTNEY et LAUREN JEAN WARRACK. Can. J. Chem. **67**, 1774 (1989).

Opérant en milieu aqueux, on a effectué des études cinétiques et spectroscopiques sur la formation (à partir de $Fe(CN)_5OH_2^{3-}$) et sur la dissociation de complexes de pentacyanoferrate(II) contenant du (pyridyl-4)-1 pyridinium ainsi que les formes neutres, protonées et *N*-méthylées de la bipyridine-4,4′ (BPY), du bis(pyridyl-4)-1,2 éthane (BPA) et du bis(pyridyl-4)-1,2 éthylène-*trans* (BPE). La relation qui existe entre le pH et la cinétique de formation a été analysée en fonction de la vitesse spécifique et des constantes de dissociation acide de ces ligands. On a déterminé les constantes de vitesse (25,0°C, $I = 0{,}10$ M) de formation des complexes dinucléaires $(NC)_5FeLFe(CN)_5^{6-}$ du BPY (50 M^{-1} s^{-1}), du BPA (66 M^{-1} s^{-1}), du BPE (95 M^{-1} s^{-1}) et de la pyrazine (10 M^{-1} s^{-1}) et on les a comparées avec les constantes de vitesse respectives pour la formation des complexes $(NC)_5FeLCo(NH_3)_5$. Pour discuter des relations qui existent entre les constantes de vitesse de formation et le volume du ligand, le nombre de sites du donneur et l'importance et la position des charges sur le ligand, on fait appel à un mécanisme dissociatif de paires d'ion.

Mots clés : complexes de pentacyanoferrate(II), *N*-hétérocycles, substitution du ligand, cinétique.

[Traduit par la revue]

Introduction

The properties and reactions of substituted pentacyanoferrate(II) complexes have been of considerable interest in the past 15 years (1). The formation of substituted $Fe(CN)_5L^{3-}$ complexes from the aqua species (eq. [1]) has been shown to follow an ion-pair dissociative mechanism (2–5), with a dependence of k_f on the charge of the entering ligand.

$$[1] \quad Fe(CN)_5OH_2^{3-} + L^{n+} \underset{k_d}{\overset{k_f}{\rightleftharpoons}} Fe(CN)_5L^{(3-n)-} + H_2O$$

An interesting aspect of the dependences of k_f on the nature of the entering ligand has been the effects of the position(s) of the charge(s) within the ligand with respect to the available coordination sites. Using a series of amino acid derivatives as entering ligands in the substitution of water on $Fe(CN)_5OH_2^{3-}$, Toma *et al.* (5) observed an increase of ≈ 30 M^{-1} s^{-1} with every additional C—C bond (≈ 1.3 Å) separating the coordination site from the carboxylate group. The rate constants for the reactions of $Fe(CN)_5OH_2^{3-}$ with a series of $Co(NH_3)_5L^{3+}$ complexes (L is a bridging *N*-heterocycle) depend on the distance between the free nitrogen site and the Co(III) metal center (6–10).

In this paper the results of kinetic and spectroscopic studies on the ligand substitution reactions of pentacyanoferrate(II) complexes with a series of *N*-heterocyclic cationic ligands in aqueous solution are reported. The ligands employed in this study include the neutral, protonated, and *N*-methylated forms of 4,4′-bipyridine (BPY), 1,2-bis(4-pyridyl)ethane (BPA), and *trans*-1,2-bis(4-pyridyl)ethylene (BPE). These species have been used frequently as bridging ligands in homo- and heterobinuclear complexes containing $Fe(CN)_5^{n-}$ (11, 12), $M(NH_3)_5^{n+}$ (M = Co(III) (9), Rh(III) (13), Ru(II) and (III) (14)), and $M(CO)_5$ (M = Mo, W (15)) centers. The kinetics of the formation and dissociation of $Fe(CN)_5(L—X)^{n-}$, where L is BPY, BPE, or BPA and X is a lone pair, H^+, CH_3^+, or $Fe(CN)_5^{3-}$, have not, however, been reported in detail previously. The rate and activation parameters determined in this study are discussed in relation to the magnitude and distribution of charges on the entering ligand, in terms of an ion-pair dissociative mechanism.

Experimental

Materials

Sodium amminepentacyanoferrate(II), $Na_3[Fe(CN)_5NH_3]\cdot 3H_2O$, was prepared by a reported procedure (16) and recrystallized from concentrated ammonia. Solutions of the aquapentacyanoferrate(II) ion ($\lambda_{max} = 444$ nm, $\varepsilon = 660$ M^{-1} cm^{-1} (5)) were produced by dissolving the solid $Na_3[Fe(CN)_5NH_3)]\cdot 3H_2O$ in nitrogen-saturated distilled water containing a slight excess of ascorbic acid. Low concentrations of the ion ($< 2 \times 10^{-5}$ M) were generally used to minimize dimerization. The ligands pyrazine (pyz), 4,4′-bipyridine (BPY), 1-(4-pyridyl)pyridinium chloride hydrochloride ($pyrpyr^+$), 1,2-bis(4-pyridyl)ethane (BPA), and *trans*-1,2-bis(4-pyridyl)ethylene (BPE) were used as received (Aldrich). The quaternary salts 1-methyl-4-(4′-pyridinyl)pyridinium iodide (CH_3BPY^+), 1-methyl-4-[2-4′-pyridinyl)ethyl]pyridinium iodide (CH_3BPA^+), and 1-methyl-4-[*trans*-2-4′-pyridinyl)ethenyl]pyridinium iodide (CH_3BPE^+) were prepared by treating the appropriate ligand with methyl iodide in benzene (17). The

[1]Author to whom correspondence may be addressed.

Can. J. Chem. Downloaded from www.nrcresearchpress.com by 186.148.149.217 on 09/07/12
For personal use only.

TABLE 1. Band maxima in the visible spectra of $Fe^{II}(CN)_5(L—X)^{n-}$ complexes in aqueous solution

	Lone pair		H^+		CH_3^+		$Fe(CN)_5^{3-}$	
L	λ_{max} (nm)	$10^{-3}\varepsilon$ (M^{-1} cm^{-1})	λ_{max} (nm)	$10^{-3}\varepsilon$ (M^{-1} cm^{-1})	λ_{max} (nm)	$10^{-3}\varepsilon$ (M^{-1} cm^{-1})	λ_{max} (nm)	$10^{-3}\varepsilon$ (M^{-1} cm^{-1})
pyz	452[a]	5.01[a]	≈625[c]		655[a]	12.0[a]	508[e]	13.2[e]
BPY	432[a]	5.62[a]	515[d]	4.7[d]	520[a]	5.62[a]	452[e]	12.9[e]
BPA	365	4.66	368	4.2	368	4.34	365	9.2
BPE	460[b]	7.2[b]	520	7.0	533	6.92	472[e]	14.1[e]

[a]Reference 19.
[b]Reference 9.
[c]Reference 20.
[d]Reference 6.
[e]Reference 12.

melting points and ^1H nmr spectra of $[CH_3BPY]I$ and $[CH_3BPE]I$ were in agreement with reported data (11, 18). The ^1H nmr spectrum (Varian HX-60) of $[CH_3BPA]I$ in D_2O displayed peaks at (δ vs. TSP) 3.03 (m 4H), 4.06 (s 3H), 6.80 (d 2H), 7.03 (m 2H), 7.83 (m 2H), and 8.06 (d 2H). Solutions of the substituted pentacyanoferrate(II) complexes were prepared by adding an excess of the ligand (10^{-3} M) to a nitrogen-saturated solution of aquated $Fe(CN)_5NH_3^{3-}$ (10^{-4} M).

Kinetic measurements

Kinetic measurements were performed using both stopped-flow and conventional mixing techniques. The formation reactions were carried out using a TDI Model IIA (Cantech Scientific) stopped-flow apparatus and data acquisition system interfaced to a Zenith ZF-151 microcomputer. Pseudo-first-order conditions of excess ligand were employed and plots of ln $(A_\infty - A_t)$ against time were linear for at least three half-lives. The first-order rate constants were determined from the average of four to six replicate experiments. The kinetics of the ligand dissociation reactions, along with uv–visible spectra of the substituted pentacyanoferrate(II) complexes, were measured using Bausch and Lomb Spectronic 2000 and Hewlett–Packard 8452A diode–array spectrophotometers, with cell blocks thermostatted by means of an external water bath.

The ionic strength of the reaction solutions was maintained at 0.10 M with added sodium chloride. The pH of the solutions was controlled using phthalate, acetate, or phosphate buffers, or by additions of appropriate amounts of hydrochloric acid.

Results

The reactions of the $Fe(CN)_5OH_2^{3-}$ ion with an excess of an *N*-heterocyclic ligand (L^{n+}), such as 4,4′-bipyridine, result in substitution of the aqua ligand, and the formation of highly coloured $Fe(CN)_5L^{(3-n)-}$ species in solution. The absorption maxima ($t_{2g} \rightarrow L\pi^*$ metal-to-ligand charge transfer (MLCT) band) and molar absorptivity coefficients (Table 1) for a number of the complexes in this study have been reported previously (9, 12, 19, 20). The shift in λ_{max} upon protonation or methylation of the remote pyridine nitrogen depends on the extent of conjugation to the coordinated pyridine ring. In the BPY and BPE ligands (as also seen for pyrazine) a bathochromic shift is oberved, while for the BPA ligand, where the pyridine rings are insulated from each other by the saturated $-CH_2CH_2-$ linkage, little change in the MLCT energy is observed.

The acid dissociation constant for the protonated complex $Fe(CN)_5(HBPE)^{2-}$ was determined by a spectrophotometric pH titration. The λ_{max} shifts from 466 nm to 520 nm when the solution is acidified below a pH of 6.5, and a pK_a of 5.1 ± 0.1 was determined at 25°C and I = 0.10 M. Gaswick and Haim (6) report a pK_a of ≈5.3 (ionic strength not stated) for the $Fe(CN)_5(HBPY)^{2-}$ complex. The pK_a for the $Fe(CN)_5(HBPA)^{2-}$ complex is assumed to be very similar to that for the free ligand (H_2BPA^{2+}). At lower pH these complexes may be protonated at a cyanide ligand (pK_a of $(HNC)(NC)_4Fe(L)^{2-}$ is ≈2 (19, 20)), resulting in an increase in the MLCT energies.

TABLE 2. Rate and activation parameters for the ligand substitution of the $Fe(CN)_5OH_2^{3-}$ ion by L^{n+}

Ligand L^{n+}	$10^{-3}k_f$[a] (M^{-1} s^{-1})	$\Delta H_f^{\ddagger}$ (kcal mol^{-1})	$\Delta S_f^{\ddagger}$ (cal K^{-1} mol^{-1})	Ref.
BPY	0.586±0.020	15.2±0.6	5.1±1.8	b
$HBPY^+$	1.61 ±0.10			b
CH_3BPY^+	2.82 ±0.11	16.3±1.0	11.9±3.0	b
BPE	0.683±0.023	15.6±1.1	6.7±3.3	b
$HBPE^+$	1.86 ±0.12			b
CH_3BPE^+	2.71 ±0.11	14.3±0.6	5.2±1.9	b
BPA	0.780±0.015	16.4±0.5	9.7±1.4	b
$HBPA^+$	1.48 ±0.05			b
CH_3BPA^+	1.58 ±0.08	16.0±0.6	9.9±1.7	b
pyr	0.38	16.1±0.5	7±2	c
$pyrpyr^+$	2.56 ±0.20	15.2±0.3	8.2±0.9	b
pyz	0.38[d]	15.4±0.5	5±2	c
CH_3pyz^+	2.35 ±0.10			e
	2.41	16.8±0.5	10±2	c

[a]At 25.0°C, I = 0.10 M.
[b]This work.
[c]Reference 2, k_f at I = 0.10 M, $\Delta H_f^{\ddagger}$ and $\Delta S_f^{\ddagger}$ at I = 0.50 M.
[d]k_f at I = 0.50 M.
[e]Reference 21.

Kinetic studies

The kinetics of the ligand substitution reactions of $Fe(CN)_5OH_2^{3-}$ with a series of *N*-heterocyclic L^{n+} ligands were investigated in aqueous solution (I = 0.10 M, pH 7) at 25.0°C. The reactions were carried out under pseudo-first-order conditions of excess ligand concentrations ($[L^{n+}] = (1–10) \times 10^{-4}$ M, $[Fe(CN)_5OH_2^{3-}] = 1 \times 10^{-5}$ M) by following the formation of the $Fe(CN)_5L^{(3-n)-}$ product at its visible maximum (Table 1). The rate of formation may be expressed as in eq. [2]

$$[2] \quad \frac{d[Fe(CN)_5L^{(3-n)-}]}{dt} = k_f[Fe(CN)_5OH_2^{3-}][L^{n+}]$$

with $k_{obs} = k_f[L^{n+}]$. Linear plots of k_{obs} against $[L^{n+}]$ were observed for each ligand employed in the study. The second-order rate constants, k_f, and the corresponding activation parameters are presented in Table 2.

Can. J. Chem. Downloaded from www.nrcresearchpress.com by 186.148.149.217 on 09/07/12
For personal use only.

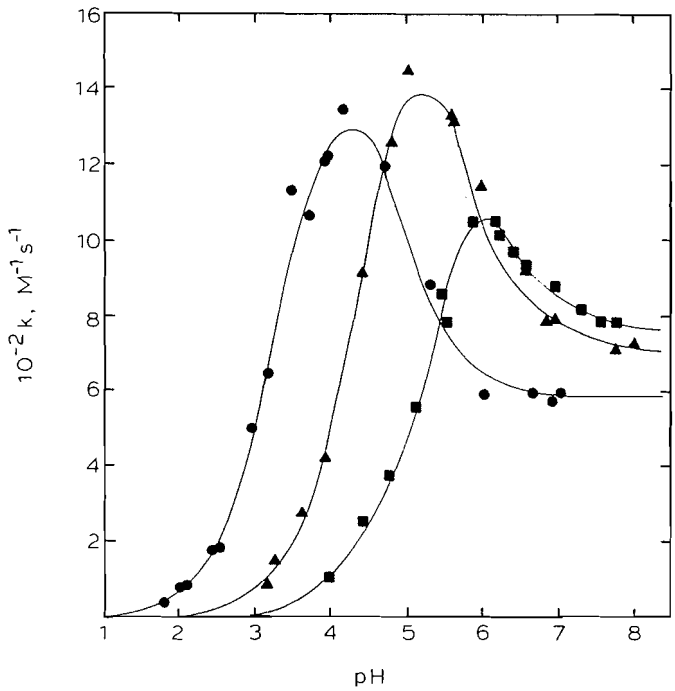


FIG. 1. The dependences of k on pH for the ligand substitution reactions of the $Fe(CN)_5OH_2^{3-}$ ion with the ligands BPY (●), BPE (▲), and BPA (■) at 25.0°C, I = 0.10 M. The solid curves represent the fits of the data to eq. [8].

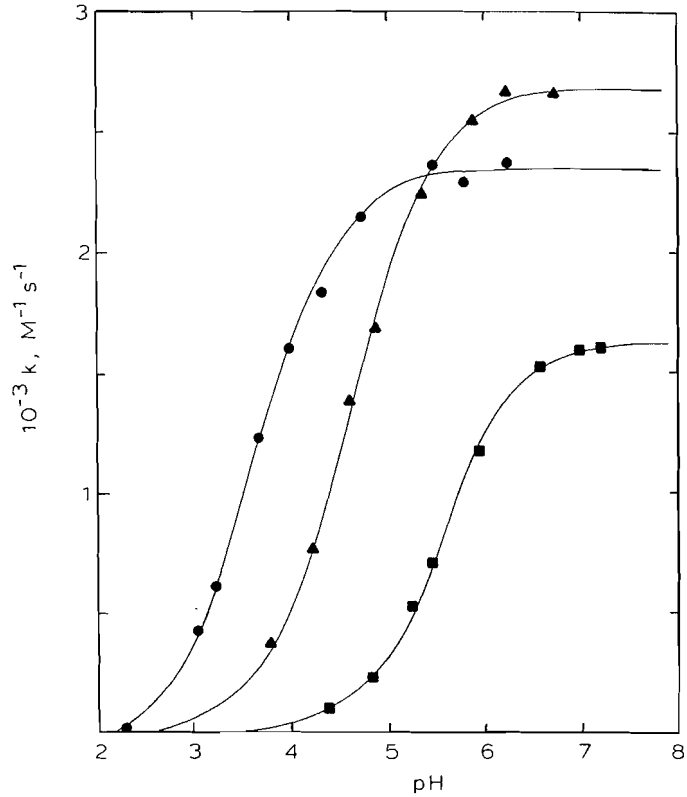


FIG. 2. The dependences of k on pH for the ligand substitution reactions of the $Fe(CN)_5OH_2^{3-}$ ions with the ligands CH_3BPY^+ (●), CH_3BPE^+ (▲), and CH_3BPA^+ (■) at 25.0°C, I = 0.10 M. The solid curves represent the fits of the data to eq. [9].

The pH dependences of the kinetics of the substitution reactions of the $Fe(CN)_5OH_2^{3-}$ ion with the BPY, BPE, and BPA ligands were investigated at 25.0°C and an ionic strength of 0.10 M (NaCl). Substantial decreases in the formation rate constants at low pH have been observed in a number of studies (4, 21, 22) and have been attributed to the greatly reduced lability of the aqua ligand in the protonated species $(HNC)Fe(CN)_4OH_2^{2-}$ (pK_m = 2.63, I = 0.10 M (21)). The rate of formation of the substituted complexes is also affected by the degree of protonation of the entering ligand. Addition of the first proton to produce HL^+ is expected to change its formation rate constant in two opposing ways: an increase owing to the increased charge on the ligand, and a decrease resulting from the loss of one potential coordination site. Protonation of both nitrogens to give H_2L^{2+} will render the ligand unreactive towards substitution on $Fe(CN)_5OH_2^{3-}$.

The acid dissociation constants K_1 (H_2L^{2+}) and K_2 (HL^+) have been reported for BPY (pK_1 = 2.69 (23) (3.31 in ref. 24) and pK_2 = 4.77 (23) (4.85 in ref. 24)) and BPE (pK_1 = 4.49 ± 0.04 and pK_2 = 5.92 ± 0.02 (25)) at 25.0°C and an ionic strength of 0.10 M. The pK values for the BPA ligand have not been determined but the pK_2 value is likely to be about 6, by comparison with analogous 4-methyl- (pK_a = 6.04) and 4-ethylpyridine (pK_a = 6.06) compounds (26). The dependences of the second-order rate constants k_H on pH for the three ligands are illustrated in Fig. 1. Each of the curves shows an increase in the rate constant as the pH is lowered below pH 8, followed by a decrease at lower pH. The positions of the maximum rate constants and the decreases in rate constant for the three ligands in Fig. 1 may be related to the acid–base equilibria of the entering species as depicted in the reaction scheme in eqs. [3]–[7].

$$[3] \quad (HNC)Fe(CN)_4OH_2^{2-} \overset{K_m}{\rightleftharpoons} Fe(CN)_5OH_2^{3-} + H^+$$

$$[4] \quad H_2L^{2+} \overset{K_1}{\rightleftharpoons} HL^+ + H^+$$

$$[5] \quad HL^+ \overset{K_2}{\rightleftharpoons} L + H^+$$

$$[6] \quad Fe(CN)_5OH_2^{3-} + HL^+ \xrightarrow{k_1} Fe(CN)_5(HL)^{2-} + H_2O$$

$$[7] \quad Fe(CN)_5OH_2^{3-} + L \xrightarrow{k_2} Fe(CN)_5L^{3-} + H_2O$$

The extent of protonation of the $Fe(CN)_5L^{n-}$ products has been determined by spectrophotometric pH titrations (see above). The observed second-order rate constant, k_f, may be expressed in terms of the specific rate constants and acid-dissociation constants in eq. [8].

$$[8] \quad k_H = \frac{k_1K_1K_m/[H^+]^2 + k_2K_1K_2K_m/[H^+]^3}{(1 + K_1/[H^+] + K_1K_2/[H^+]^2)(1 + K_m/[H^+])}$$

A non-linear least-squares fit (Simplex optimization program (27)) of the experimental data to eq. [8] produced the rate parameters and acid dissociation constants for the three systems. The k_1 and k_2 values are presented (k_f) in Table 2. The pK_1 value for BPY (pK_2 = 4.77) and the values of pK_1 and pK_2 for BPA were allowed to float, as the literature values are absent or uncertain. A pK_1 value of 3.07 was found for BPY, in good agreement with the reported values. The derived pK_1 value of 5.31 (pK_2 = 6.05) for BPA is 0.74 pK units lower than the pK_2 value, only a slightly larger difference than 0.60 based solely on statistical factors (K_1/K_2 = 4). This is also an indication of the lack of electronic communication between the two heterocyclic N-donor sites on the BPA ligand (ΔpK_a = 1.7 for BPY, 1.4 for BPE).

Can. J. Chem. Downloaded from www.nrcresearchpress.com by 186.148.149.217 on 09/07/12
For personal use only.

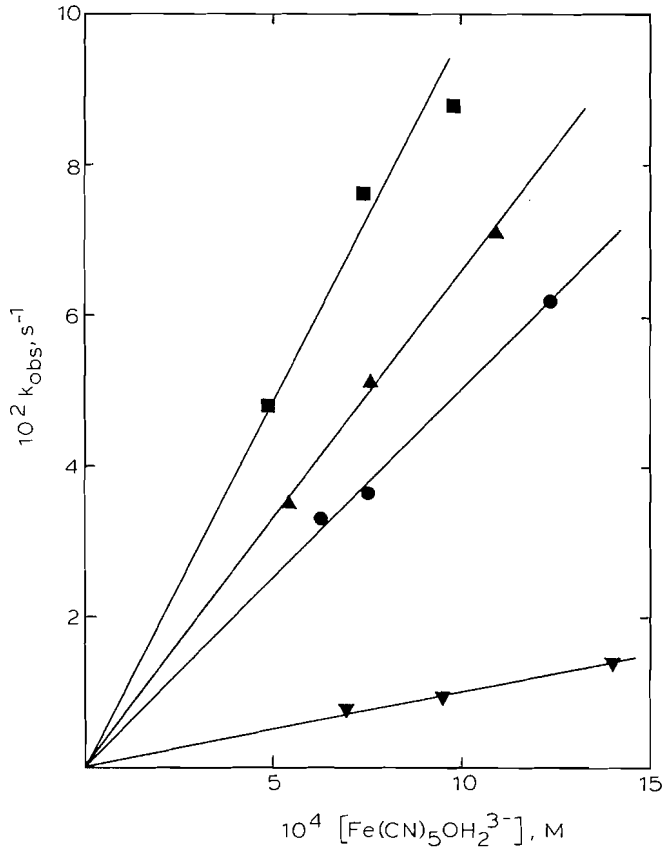


FIG. 3. The dependences of k_{obs} on $[Fe(CN)_5OH_2^{3-}]$ for the formation of $(NC)_5FeLFe(CN)_5^{6-}$ at 25.0°C, pH 7.0, and $I = 0.10$ M, where L = BPE (■), BPA (▲), BPY (●), and pyrazine (▼) ($[Fe(CN)_5L^{3-}] = 5 \times 10^{-5}$ M).

The pH dependence of the kinetics of the formation reactions of CH_3BPY^+, CH_3BPE^+, and CH_3BPA^+ were also investigated at 25.0°C ($I = 0.10$ M). In these reactions protonation of the free *N*-donor atom would render the ligands unreactive towards substitution on $Fe(CN)_5OH_2^{3-}$, and a study of the pH rate dependence would permit the determination of the pK_a values for the $(H)CH_3L^{2+}$ species. The pK_a for $(H)CH_3BPY^{2+}$ has been reported (28) to be 3.5 ± 0.1 at 25.0°C ($I = 0.10$ M), while analogous values have not been reported for $(H)CH_3BPE^{2+}$ or $(H)CH_3BPA^{2+}$. The dependences of k_H on pH are depicted in Fig. 2 for these three ligands. A fit of the data to eq. [9]

$$[9] \quad k_H = \frac{k_3 K_3 K_m/[H^+]^2}{(1 + K_3/[H^+])(1 + K_m/[H^+])}$$

yielded pK_3 values of 3.6 ± 0.1 for $(H)CH_3BPY^{2+}$, 4.6 ± 0.2 for $(H)CH_3BPE^{2+}$, and 5.6 ± 0.1 for $(H)CH_3BPA^{2+}$. The differences between pK_3 and pK_1 (H_2L^{2+}) for the three species are found to be in the range of 0.1–0.3. A slight increase (≈0.3 pK units) in pK_3 with respect to pK_1 is expected purely on statistical grounds as there are two sites of deprotonation on H_2L^{2+} and only one site on $(H)CH_3L^{2+}$.

With the potential bridging ligands BPY, BPE, BPA, and pyrazine, the addition of an excess of $Fe(CN)_5OH_2^{3-}$ to a solution of $Fe(CN)_5L^{3-}$ results in the coordination of the remote nitrogen and the formation of a bimetallic species, $(NC)_5FeLFe(CN)_5^{6-}$ (12).

$$[10] \quad Fe(CN)_5L^{3-} + Fe(CN)_5OH_2^{3-} \rightarrow (NC)_5FeLFe(CN)_5^{6-}$$

TABLE 3. Rate constants for the ligand substitution reactions of $Fe(CN)_5OH_2^{3-}$ with $Fe(CN)_5L^{3-}$ and $Co(NH_3)_5L^{3+}$ at 25°C and $I = 0.10$ M

L	k_f (M^{-1} s^{-1})	
	$Fe(CN)_5L^{3-}$	$Co(NH_3)_5L^{3+}$
pyz	10 ± 1	10800 ± 500[a]
BPY	50 ± 2	5500 ± 300[b]
BPA	66 ± 3	4540 ± 170[c]
BPE	95 ± 8	2050 ± 40[c]

[a]Extrapolated to $I = 0.10$ M (eq. [14]), from data in ref. 8.
[b]Reference 6.
[c]Reference 9.

TABLE 4. Rate and activation parameters for the dissociation of L^{n+} from $Fe(CN)_5L^{(3-n)-}$

Ligand L^{n+}	$10^3 k_d$[a] (s^{-1})	$\Delta H_d^{\ddagger}$ (kcal mol^{-1})	$\Delta S_d^{\ddagger}$ (cal K^{-1} mol^{-1})	Ref.
BPY	0.62	26.5 ± 0.5	16 ± 2	b
CH_3BPY^+	2.64	26.4 ± 0.6	18.1 ± 1.8	c
BPE	1.12	24.4 ± 0.1	9.9 ± 0.3	c
	0.74			d
$HBPE^+$	2.84			c
CH_3BPE^+	2.44	24.7 ± 0.1	12.4 ± 0.3	c
BPA	1.61	24.3 ± 0.7	10.2 ± 0.3	c
	1.42			d
CH_3BPA^+	2.75	26.0 ± 0.9	17.0 ± 2.6	c
pyr	1.10	24.8 ± 0.5	11 ± 2	b
$pyrpyr^+$	3.27	24.8 ± 0.2	13.1 ± 0.6	c
pyz	0.42	26.4 ± 0.5	14 ± 2	b
CH_3pyz^+	0.28	27.5 ± 0.5	18 ± 2	b,e

[a]At 25.0°C, $I = 0.10$ M.
[b]Reference 19, $I = 0.50$ M.
[c]This work.
[d]Reference 6.
[e]$I = 1.0$ M.

The MLCT bands of the dimer display bathochromic shifts with respect to the monomer, with energy shifts decreasing in the order pyrazine > BPY > BPE > BPA (Table 1). This trend follows the order observed for protonation or methylation of the remote nitrogen on $Fe(CN)_5L^{3-}$.

The kinetics of the formation of the dimer species were studied by reacting the monomer (prepared in solution by the addition of a slight excess of $Fe(CN)_5OH_2^{3-}$ to the ligand) with a pseudo-first-order excess of a freshly prepared $Fe(CN)_5OH_2^{3-}$ solution. The first-order dependences of k_{obs} on $[Fe(CN)_5OH_2^{3-}]$ at 25.0°C ($I = 0.10$ M, pH 7) are displayed in Fig. 3 and the second-order rate constants are presented in Table 3.

The rate and activation parameters for the dissociation of L^{n+} from $Fe(CN)_5L^{(3-n)-}$ were determined in the presence of 0.1–0.2 M dimethylsulphoxide at an ionic strength of 0.10 M. The ligand DMSO is employed in the role of the entering species as it forms a very stable, colourless $Fe(CN)_5(DMSO)^{3-}$ complex (29). At these high concentrations, the limiting dissociation rate constant, k_d, is measured (3, 5, 20). The rate and activation parameters for the ligand dissociation reactions of $Fe(CN)_5L^{(3-n)-}$ are presented in Table 4.

Can. J. Chem. Downloaded from www.nrcresearchpress.com by 186.148.149.217 on 09/07/12
For personal use only.

Can. J. Chem. Downloaded from www.nrcresearchpress.com by 186.148.149.217 on 09/07/12
For personal use only.

Discussion

The kinetic and activation parameters determined for the formation of $Fe(CN)_5L^{(3-n)-}$ complexes in this study (Table 2) support a dissociatively activated ligand substitution process, as postulated previously for the reactions of the $Fe(CN)_5OH_2^{3-}$ ion (1). The neutral ligands BPY, BPE, and BPA form complexes with rate constants in the range of 580–780 $M^{-1}\,s^{-1}$, while the values for the protonated and methylated derivatives, along with pyrpyr$^+$ and CH_3pyz^+, fall in the range of 1500–2800 $M^{-1}\,s^{-1}$. The rate constants for the reactions with BPY, BPE, and BPA are about twice the value determined for pyridine, due to the presence of two coordination sites on the ligands. The trend in the formation rate constants, pyz < BPY < BPE < BPA, reflects the separation distance between the two donor sites, with BPA behaving kinetically as if it were two pyr molecules. The enthalpies and entropies of activation for the ligands in this study also fall in relatively narrow ranges of 14–17 kcal mol^{-1} and 5–12 cal $K^{-1}\,mol^{-1}$, respectively.

The dependence of the rate of complexation of $Fe(CN)_5OH_2^{3-}$ by L^{n+} on the charge of the entering ligand is consistent with an ion-pair dissociative mechanism (eqs. [11]–[13]).

$$[11]\quad Fe(CN)_5OH_2^{3-} + L^{n+} \underset{}{\overset{K_{OS}}{\rightleftharpoons}} [Fe(CN)_5OH_2,L]^{(3-n)-}$$

$$[12]\quad [Fe(CN)_5OH_2,L]^{(3-n)-} \xrightarrow{k_{-w}} [Fe(CN)_5,L]^{(3-n)-} + H_2O$$

$$[13]\quad [Fe(CN)_5,L]^{(3-n)-} \xrightarrow{\text{fast}} Fe(CN)_5L^{(3-n)-}$$

The rate-determining loss of the coordinated water molecule (k_{-w}) is preceded by an outer-sphere ion-pair association, for which K_{OS} is dependent on the size and charge of L^{n+} and on the ionic strength of the reaction medium. The expression for the observed formation rate constant reduces to $k_f = k_{-w}K_{OS}$ in this study as $K_{OS}[L^{n+}] \ll 1$ and the rate of ligand dissociation from $Fe(CN)_5L^{(3-n)-}$ is very small (Table 3).

The value of the association constant is frequently calculated using the Eigen–Fuoss expression (5)

$$[14]\quad K_{OS} = (4\pi N\sigma^3/3000)\exp(-\omega(\sigma)/RT)$$

where

$$[15]\quad \omega(\sigma) = \frac{Z_M Z_L e^2}{D_s\sigma(1 + \beta\sigma I^{1/2})}$$

In these expressions σ is the sum of the radii of the reactants, Z_M and Z_L are the charges on the reactants, D_s is the solvent dielectric constant, and $\beta = (8\pi Ne^2/1000D_skT)^{1/2}$. Toma (17) has determined the outer-sphere ion-pair association constants for the interactions of the substitution inert $Fe(CN)_6^{4-}$ ion with *N*-heterocyclic cations, such as CH_3pyz^+ (K_{OS} = 10–13 M^{-1}), and dications such as *N*,*N*′-dimethyl-4,4′-bipyridine (K_{OS} = 30–40 M^{-1}). The K_{OS} values for the ion pairs between $Fe(CN)_5OH_2^{3-}$ and the HL^+ and CH_3L^+ ligands in this study are likely to be similar in magnitude, with the effects of reducing Z_M and increasing σ cancelling each other out to some extent. If k_{-w} is taken to be 300 s^{-1} (an average value from k_f/K_{OS} for neutral ligands for which $K_{OS} \approx 1\,M^{-1}$ (1)), values of K_{OS} in the range of 5–10 M^{-1} are suggested by the k_f parameters for HL^+ and CH_3L^+. The use of σ = 6.5–12.0 Å in eqs. [14] and [15] yields ion-pair constants in this range and, with a radius of 4.5 Å for the $Fe(CN)_5OH_2^{3-}$ ion (5), an effective radius of 2–7 Å is calculated for the cationic ligands. This is a reasonable range of values for these ligands (17), which vary in size from the small CH_3pyz^+ ion to large CH_3BPE^+ or CH_3BPA^+ species.

For substitution reactions of $[Fe(CN)_5OH_2]^{3-}$ it has been observed that in addition to the total charge on the ligand, the positions of the charge(s) have an effect on the complexation rate constant (4, 5). The rate constants for the formations of the bimetallic complexes, $(NC)_5FeLFe(CN)_5^{6-}$, fall in the range of 10–95 $M^{-1}\,s^{-1}$, depending on the nature of the bridging ligand L (Table 4). The smallest value was observed for pyrazine, with the rate constants increasing with the increase in the distance between the iron center and the free *N*-donor atom on the $Fe(CN)_5L^{3-}$ ligand. The observed range of formation rate constants is comparable to the values reported for a number of monoanionic ligands, such as the cysteinate (4) and glycinate (3) anions. A similar trend has been reported (13) using $Co(CN)_5L^{2-}$ as the entering ligand, with k_f = 0.5 $M^{-1}\,s^{-1}$ for L = pyz and 3.0 $M^{-1}\,s^{-1}$ for L = BPY (I = 0.50 M). The trend in the rate constants for the $Fe(CN)_5L^{3-}$ ligands is opposite to that found for the same ligands in the set of $Co(NH_3)_5L^{3+}$ complexes (Table 4). In the former complexes the rate constants increase as the distance between the 3− center and the available *N*-donor atom increases, reducing the electrostatic repulsions. As the distance between the 3+ center and the available *N*-donor atom increases in the latter complexes the electrostatic attraction towards $Fe(CN)_5OH_2^{3-}$ decreases, as does the rate constant of formation of the bimetallic complex. The results of this study suggest that the most favourable ion-pair conformation may not be the most appropriate for ligand substitution, if it places the ligand donor atom at some distance from the site of eventual coordination on the metal. Kinetic and spectroscopic studies on the substitution reactions of $Fe(CN)_5OH_2^{3-}$ with novel bis(*N*-heterocyclic) dications of the types $pyz(CH_2)_npyz^{2+}$ (30), $BPY(CH_2)_nBPY^{2+}$, and $BPE(CH_2)_nBPE^{2+}$ (n = 1–10) are in progress in this laboratory to further investigate the nature and stabilities of the ion-pair precursor conformations.

The ligand dissociation rate constants for the $Fe(CN)_5L^{(3-n)-}$ complexes in this study (Table 4) are found in the relatively narrow range of (0.6–3.3) × $10^{-3}\,s^{-1}$. The complexes containing the protonated or methylated ligands displayed somewhat larger values of k_d than were observed for the corresponding neutral ligand complexes. An increase in the rate of dissociation upon ligand protonation has also been reported for $Fe(CN)_5L^{(3-n)-}$ complexes containing alkane-α,ω-diamines (31), nicotinic acid and isonicotinohydrazine (32), amino acid derivatives (4), and anions such as cyanide and sulphite (33). This observation has been attributed to the relative basicities of the leaving ligands and the greater ease of transfer of the protonated (or *N*-methylated) ligands to the bulk solvent, with the effect ($k_d(L^+)/k_d(L)$) becoming more pronounced when the positive charge on the terminal nitrogen is closer to the $Fe(CN)_5^{3-}$ center (31). The solvation and basicity effects would be offset to varying degrees by the attraction of the cationic ligand to the negatively charged metal center and, in the case of the *N*-heterocycles, by the increase in the Fe–L π-back bonding (as reflected in the MLCT energies) upon protonation or *N*-methylation. These effects are evident in the smaller value of k_d found for CH_3pyz^+ compared with that for pyrazine. For the ligands in this study the rate constants and activation parameters for the dissociations of neutral and cationic species would likely be affected by each of these factors. The similarities and uncertainties in the values, however, do not readily allow for a dissection of the differences in terms of the offsetting effects.

Acknowledgements

Financial support from the Natural Sciences and Engineering Research Council of Canada in the form of operating and

equipment grants to D.H.M. and an Undergraduate Research Award to L.J.W. is gratefully acknowledged. We thank Queen's University for support of this work through a grant from its Advisory Research Committee, and Mr. G. Sluggett for the preparation and characterization of [CH_3BPA]I.

1. D. H. MACARTNEY. Rev. Inorg. Chem. **9**, 101 (1988), and references therein.
2. H. E. TOMA and J. M. MALIN. Inorg. Chem. **12**, 2080 (1973).
3. H. E. TOMA, J. M. MARTINS, and E. GIESBRECHT. J. Chem. Soc. Dalton Trans. 1610 (1978).
4. D. H. MACARTNEY and A. MCAULEY. J. Chem. Soc. Dalton Trans. 1780 (1981).
5. H. E. TOMA, A. A. BATISTA, and H. B. GRAY. J. Am. Chem. Soc. **104**, 7509 (1982).
6. D. GASWICK and A. HAIM. J. Am. Chem. Soc. **96**, 7845 (1974).
7. L. A. A. OLIVEIRA, H. E. TOMA, and E. GIESBRECHT. Inorg. Chim. Acta, **22**, 269 (1977).
8. J. M. MALIN, D. A. RYAN, and T. V. O'HALLORAN. J. Am. Chem. Soc. **100**, 2097 (1978).
9. J.-J. JWO, P. L. GAUS, and A. HAIM. J. Am. Chem. Soc. **101**, 6189 (1979).
10. A. P. SZECSY and A. HAIM. J. Am. Chem. Soc. **103**, 1679 (1981); **104**, 3063 (1982).
11. J. E. FIGARD, P. V. PAUKSTELIS, E. R. BYRNE, and J. D. PETERSEN. J. Am. Chem. Soc. **99**, 8417 (1977).
12. F. FELIX and A. LUDI. Inorg. Chem. **17**, 1782 (1977).
13. K. J. PFENNING, L. LEE, H. D. WOHLERS, and J. D. PETERSEN. Inorg. Chem. **21**, 2477 (1982).
14. C. CREUTZ. Prog. Inorg. Chem. **30**, 1 (1983), and references therein.
15. M. M. ZULU and A. J. LEES. Inorg. Chem. **27**, 1139 (1988); **28**, 85 (1989), and references therein.
16. G. BRAUER. Handbook of preparative inorganic chemistry. 2nd ed. Academic Press, New York. 1975. p. 1511.
17. H. E. TOMA. Can. J. Chem. **57**, 2079 (1979).
18. J. VANSANT, G. SMETS, J. P. DECLERCQ, G. GERMAIN, and M. VAN MEERSSCHE. J. Org. Chem. **45**, 1557 (1980).
19. H. E. TOMA and J. M. MALIN. Inorg. Chem. **12**, 1039 (1973).
20. C. R. JOHNSON and R. E. SHEPHERD. Inorg. Chem. **22**, 1117 (1983).
21. J. M. MALIN and R. C. KOCH. Inorg. Chem. **17**, 752 (1978).
22. D. H. MACARTNEY and A. MCAULEY. Inorg. Chem. **20**, 748 (1981).
23. J. ULSTRUP. Acta Chem. Scand. **25**, 3397 (1971).
24. T. R. MUSGRAVE and C. E. MATSON. Inorg. Chem. **7**, 1433 (1968).
25. D. K. LAVALLEE and E. B. FLEISHER. J. Am. Chem. Soc. **94**, 2583 (1972).
26. R. M. SMITH and A. E. MARTELL. Critical stability constants. Vol. 2. Plenum Press, New York. 1975. pp. 169, 170.
27. C. L. SHAVERS, M. L. PARSONS, and S. N. DEMING. J. Chem. Educ. **56**, 307 (1979).
28. K. R. LEOPOLD and A. HAIM. Inorg. Chem. **17**, 1753 (1978).
29. H. E. TOMA, J. M. MALIN, and E. GIESBRECHT. Inorg. Chem. **12**, 2084 (1973).
30. D. A. FOUCHER, S. FORTIER, and D. H. MACARTNEY. Acta Crystallogr. Sect. C: Cryst. Struct. Commun. **C45**, 112 (1989).
31. N. E. KATZ, M. A. BLESA, J. A. OLABE, and P. J. AYMONINO. J. Chem. Soc. Dalton Trans. 1603 (1978).
32. M. A. BLESA, I. A. FUNAI, P. J. MORANDO, and J. A. OLABE. J. Chem. Soc. Dalton Trans. 2092 (1977).
33. J. LEGROS. J. Chim. Phys. **61**, 909 (1964); **61**, 923 (1964).

Can. J. Chem. Downloaded from www.nrcresearchpress.com by 186.148.149.217 on 09/07/12
For personal use only.

The oxidation of dimethyl sulphide, trimethylamine, and trimethylphosphine by solvated copper(II) or thallium(III) hexafluorometallates in acetonitrile

RANA M. SIDDIQUE AND JOHN M. WINFIELD[1]

Department of Chemistry, University of Glasgow, Glasgow G12 8QQ, Scotland, U.K.

Received February 2, 1989

This article is dedicated to Professor Ronald J. Gillespie on the occasion of his 65th birthday

RANA M. SIDDIQUE and JOHN M. WINFIELD. Can. J. Chem. **67**, 1780 (1989).

Dimethyl sulphide, trimethylamine, and trimethylphosphine are oxidized by solvated copper(II) hexafluorophosphate or solvated thallium(III) hexafluorouranate(V) in acetonitrile at room temperature. The reactions are all very similar and spectroscopic studies suggest that the oxidized products are the dinuclear, non-metal cations $[Me_2SSMe]^+$, $[Me_3NNMe_2]^+$, and $[Me_3PPMe_3]^{2+}$. The compound $[Me_3PPMe_3][PF_6]_2$ is obtained from the oxidation of PMe_3 by diiodine in MeCN, followed by treatment with nitrosonium hexafluorophosphate. Coloured intermediates observed in the reactions of solvated Cu^{II} are formulated as redox-active cations $[CuL_x(NCMe)_y]^{2+}$, L = SMe_2, NMe_3, or PMe_3, and a generalized reaction scheme is proposed.

Key words: copper(II), thallium(III), acetonitrile, oxidation, fluorometallate.

RANA M. SIDDIQUE et JOHN M. WINFIELD. Can. J. Chem. **67**, 1780 (1989).

On a oxydé le sulfure de diméthyle, le triéthylamine et la triméthylphosphine avec l'hexafluorophosphate de cuivre(II) solvaté ou avec l'hexafluorouranate(V) de thallium(III) solvaté dans l'acétonitrile à la température ambiante. Les réactions sont très voisines et les études spectroscopiques suggèrent que les produits d'oxydation sont les cations non métalliques dinucléaires : $[Me_2SSMe]^+$, $[Me_3NNMe_2]^+$ et $[Me_3PPMe_3]^{2+}$. L'oxydation du composé PMe_3 par l'iode dans le MeCN, suivie de la réaction avec l'hexafluorophosphate de nitrosonium conduit au composé $[Me_3PPMe_3][PF_6]_2$. On considère les intermédiaires colorés, observés dans les réactions du cuivre(II) comme étant des cations $[CuL_x(NCMe)_y]^{2+}$, L = SMe_2, NMe_3 ou PMe_3 actifs dans des réactions d'oxydo-réduction et on propose un mécanisme général de réaction.

Mots clés : cuivre(II), thallium(III), acétonitrile, oxydation, fluorométallate.

[Traduit par la revue]

Introduction

Mononuclear cations, solvated by acetonitrile, of several elements can be prepared readily under anhydrous conditions by taking advantage of the good oxidizing and Lewis acid abilities that many hexa- and penta-fluorides have in acetonitrile (1). The cations are ideal starting points for investigation of the coordination chemistry of the elements involved and we have recently reported the behaviour of simple N- and P-donor ligands towards iron(II) in this solvent (2). An extension of this work to a study of reactions occurring between dimethyl sulphide, trimethylamine, or trimethylphosphine and solvated copper(II) or thallium(III) cations is now reported.

There is abundant evidence that the copper(I) cation is effectively solvated by MeCN (3), consequently the solvated copper(II) cation is a moderately strong oxidizing agent in MeCN (4). The thallium(III) cation appears to be more effectively solvated by MeCN than is the thallium(I) cation (5), nevertheless electrochemical measurements indicate that solvated Tl^{III} is a stronger oxidizing agent than Cu^{II} in MeCN (4). Redox reactions between Cu^{II} and thiourea derivatives (6, 7) or tertiary phosphines (8) in several solvents are well documented and similar behaviour was expected for reactions involving SMe_2 and PMe_3. A redox reaction between anhydrous $CuCl_2$ and NMe_3 at 348 K has been reported (9) as has the spontaneous reduction of Cu^{II} to Cu^{I} in the presence of 3,6-bis(2-pyridylthio)pyridazine (10).

A great advantage of carrying out the reactions under rigorously anhydrous conditions is that it has been possible to obtain evidence for cations containing S—S, P—P, or N—N bonds, which are formed as a result of the redox reactions. In two cases evidence for the formation of redox-active Cu^{II}–ligand complexes has been obtained.

[1]Author to whom correspondence may be addressed.

Results

Oxidation of dimethyl sulphide by solvated copper(II) or thallium(III) cations

Neither solvated copper(I) nor thallium(I) cations, counter-anions hexafluorophosphate and hexafluorouranate(V) respectively, reacted with dimethyl sulphide in acetonitrile at room temperature but the copper(II) and thallium(III) cations reacted readily. Addition of SMe_2 to a solution of copper(II) hexafluorophosphate in MeCN at room temperature led to the immediate formation of a dark-green solution, $\tilde{\nu}_{max}$ 14 300 and 24 300 cm^{-1}. Both bands decayed rapidly when a large excess, tenfold, of SMe_2 was used but spectral changes could be followed by conventional means providing the concentration ratio $[Cu^{II}]$:$[SMe_2]$ was less than 1:5. With the concentration ratio $[Cu^{II}]$:$[SMe_2]$ = 1:4 and with initial $[Cu^{II}]$ = 5.0×10^{-4} mol dm^{-3} the low energy band was unobservable after 0.5 h but 3 h were required for the high energy band to become unobservable.

Mixing solutions of SMe_2 and thallium(III) hexafluorouranate(V) at room temperature resulted in a transient yellow colour but otherwise the solutions were pale green, characteristic of the UF_6^- anion. When the concentration ratio $[Tl^{III}]$:$[SMe_2]$ was 1:1, ^{205}Tl nmr resonances due to both Tl^{III} and Tl^{I} were observed after mixing but only a Tl^{I} resonance was observed when the ratio used was 1:4.

Small quantities of ethane were produced from both reactions. Colourless or pale-green solids isolated from reactions that employed a large molar excess of SMe_2 were identified from their ^1H nmr and ir spectra as mixtures of $[Me_2SSMe][MF_6]$, M = P or U, and $[Cu(NCMe)_4][PF_6]$ or $TlUF_6$. Salts of the dimethyl(thiomethyl)sulphonium cation are well known and the crystal structure of the $SbCl_6^-$ salt has been described (11). The compound $[Me_2SSMe][BF_4]$ was prepared by methylation of dimethyl disulphide with trimethyloxonium tetrafluoroborate

Can. J. Chem. Downloaded from www.nrcresearchpress.com by 186.148.149.217 on 09/07/12
For personal use only.

Can. J. Chem. Downloaded from www.nrcresearchpress.com by 186.148.149.217 on 09/07/12
For personal use only.

TABLE 1. The ^1H nmr chemical shifts of $[Me_2SSMe]^+$ and $[Me_3NNMe_2]^+$ cations

Product	Chemical shift δ(ppm)	Relative intensity ratio
$[Me_2SSMe][BF_4]$	3.20, 2.80	2:1
$[Me_2SSMe][BF_4]$ + Me_2S (1:1)	2.65, 2.80	4:1
Involatile product, solvated Cu^{II} + Me_2S in CD_3CN	2.95, 2.35	2:1
Involatile product, solvated Tl^{III} + Me_2S in CD_3CN	2.80, 3.10	2:1
Tl^{III} product + Me_2S (1:1)	2.40, 2.70	4:1
Involatile product, solvated Cu^{II} + Me_3N in CD_3CN	2.45, 1.90	3:2
$[Me_3NNMe_2][UF_6]$[a]	1.95, 2.25	3:2

[a] δ(^{13}C) 31.7 and 27.5 ppm.

(12) and its ^1H nmr spectrum (Table 1) consisted of two singlets, relative intensity 2:1, rapid exchange being observed between the Me_2S moiety and added Me_2S as reported previously (12). Very similar behaviour was observed in the ^1H nmr spectra of the products from reactions between SMe_2 and fully deuteriated solvated Cu^{II} or Tl^{III} cations (Table 1) although the exact chemical shift values depended on the nature of the anion.

The ir spectrum of solid $[Me_2SSMe][BF_4]$ (Table 2) was very similar to that of the Tl^{III} reaction product. The spectrum of the Cu^{II} product contained bands due to the cation $[Cu(NCMe)_4]^+$ and those attributable to $[Me_2SSMe]^+$, in particular a band, $\tilde{\nu}_{max}$ 280 cm^{-1}, cf. Table 2. The assignment proposed for ν(SS) in the $[Me_2SSMe]^+$ cation is not unreasonable in view of the value of 276 cm^{-1} suggested for ν(SS) in the transient radical cation $[Me_2SSMe_2]^{\cdot+}$ (13).

The behaviour observed is consistent with reactions described by

[1] $2Cu^{2+}_{(solv.)} + 4SMe_2 \rightarrow 2Cu^{+}_{(solv.)} + 2[Me_2SSMe]^{+}_{(solv.)} + C_2H_6$

[2] $Tl^{3+}_{(solv.)} + 4SMe_2 \rightarrow Tl^{+}_{(solv.)} + 2[Me_2SSMe]^{+}_{(solv.)} + C_2H_6$

Oxidation of trimethylamine by solvated copper(II) or thallium(III) cations

In both cases ethane was produced and reduction of solvated Cu^{II} or Tl^{III} to Cu^{I} or Tl^{I} occurred at room temperature. The decay of the dark-green intermediate, $\tilde{\nu}_{max}$ 14 400 and 24 400 cm^{-1}, formed in the Cu^{II} reaction was similar to that in the reaction with SMe_2 and could be followed spectroscopically when the ratio $[Cu^{II}]$:$[NMe_3]$ was 1:4 and the initial $[Cu^{II}]$ was 5.0×10^{-4} mol dm^{-3}. The behaviour observed with a 1:3 ratio was similar, but using lower ratios, 1:1 or 1:2, reduction of Cu^{II} was incomplete even after 12 h. Reduction was complete within the time of mixing when $[Cu^{II}]$:$[NMe_3]$ was 1:10.

Two products were isolated from the Tl^{III} reaction, pale-green, insoluble $[Tl(NMe_3)_2][UF_6]$, which was also prepared from NMe_3 and $TlUF_6$ in MeCN, and a pale-green, soluble solid that decomposed readily on standing at room temperature. Its electronic spectrum in MeCN indicated the presence of UF_6^-, and from this and its ^1H nmr spectrum it was formulated as pentamethylhydrazinium(+1) hexafluorouranate(V), $[Me_3NNMe_2][UF_6]$. Tentative assignments of the bands in its ir spectrum (Table 3) were made by comparison with the spectra of the $N_2H_5^+$ cation (14).

Complexation of Cu^{I} by NMe_3 in MeCN was not observed and the ir spectrum of the colourless solid obtained from the

TABLE 2. The ir spectra of solid $[Me_2SSMe]^+$ salts

$\tilde{\nu}_{max}$ (cm^{-1})		
$[Me_2SSMe][BF_4]$ solid	Reaction product Tl^{III} + Me_2S	Suggested assignments
3040 (m)	3030 (m)	C—H str.
2940 (m)	2940 (m)	C—H str.
1425 (s)		C—H def.
1348 (m)	1315 (m)	C—H def.
1085 (m)	1050 (m)	CH_3 rock (+ BF_4^- ν_3)
980 (s)	995 (s)	CH_3 rock
765 (m)		BF_4^- (ν_1)
690 (m)	690 (m)	C—S str.
670 (m)		C—S str.
520 (s)		BF_4^- (ν_4)
	510 (s)	UF_6^- (ν_3)
300 (m)	285 (m)	S—S str.

TABLE 3. The ir spectrum of solid $[Me_3NNMe_2][UF_6]$

$\tilde{\nu}_{max}$ (cm^{-1})	Suggested assignments
3215 (m)	C—H str.
1470 (s)	C—H def.
1250 (m)	CH_3 rock
1050 (s)	C—N str.
980 (m)	N—N str.
520 (s)	UF_6^- (ν_3)
320 (m)	N—N def.

reaction between solvated Cu^{II} and NMe_3 was consistent with it being a mixture of $[Cu(NCMe)_4][PF_6]$ and $[Me_3NNMe_2][PF_6]$, $\tilde{\nu}_{max}$ 980 and 315 cm^{-1}, cf. Table 3. Similarly the ^1H nmr spectrum of the product from NMe_3 and deuteriated, solvated Cu^{II} was consistent with the presence of the $[Me_3NNMe_2]^+$ cation (Table 1). The reactions observed therefore appear to be

[3] $2Cu^{2+}_{(solv.)} + 4NMe_3 \rightarrow 2Cu^{+}_{(solv.)} + 2[Me_3NNMe_2]^{+}_{(solv.)} + C_2H_6$

[4] $Tl^{3+}_{(solv.)} + UF_6^- + 6NMe_3 \rightarrow [Tl(NMe_3)_2][UF_6] + 2[Me_3NNMe_2]^{+}_{(solv.)} + C_2H_6$

Oxidation of trimethylphosphine by solvated copper(II) or thallium(III) cations

The reaction between solvated Cu^{II} and trimethylphosphine in MeCN at room temperature involved the formation and very rapid decay of a pink intermediate. Ethane was not detected and the product was an off-white, involatile solid. Comparison with the $^{31}P\{^1H\}$ nmr and ir spectra of the compound $[Cu(PMe_3)_4][PF_6]$, obtained by reaction between PMe_3 and $[Cu(NCMe)_4][PF_6]$ in MeCN, indicated that this was a component of the mixture. The other component was shown to be hexamethylbis(phosphonium) hexafluorophosphate, $[Me_3PPMe_3][PF_6]_2$, by comparison with an independently synthesized and characterized sample.

Although the bis(phosphonium), $\equiv\overset{+}{P}—\overset{+}{P}\equiv$, moiety is probably best stabilized by the use of bridging groups (15), the compounds $[R_3PPR_3][I_3]_2$, R = alkyl, have been reported as the products from the alkylation of red phosphorus by alkyl iodides or from the oxidation of trialkylphosphines with I_2, molar ratio = 2:3, in refluxing MeCN (16). Using the latter route, but at room temperature and with an excess of PMe_3, led

TABLE 4. The ir spectra (1400–300 cm^{-1}) of solid $[Me_3PPMe_3]^{2+}$ salts

$\tilde{\nu}_{max}$ (cm^{-1})		
$[Me_3PPMe_3][PF_6]_2$	$[Me_3PPMe_3][I]_2$	Suggested assignments
1310 (s)	1308 (s)	C—H def.
975 (m)	975 (m)	CH_3 rock
945 (m)	945 (m)	CH_3 rock
840 (vs)		PF_6^- (ν_3)
775 (s)	775 (s)	C—P str.
650 (s)	650 (s)	C—P str.
560 (m)		PF_6^- (ν_4)
325 (m)	325 (m)	P—P def.?

to a colourless involatile solid formulated as $[Me_3PPMe_3][I]_2$, the iodide anion of which was oxidized to I_2 by $NOPF_6$ in MeCN to leave colourless, soluble $[Me_3PPMe_3][PF_6]_2$. The $^{31}P\{^1H\}$ nmr spectrum due to the cation was a singlet, $\delta(^{31}P)$ 27.8 ppm; the coupled spectrum was a complex multiplet that was not analysed. Details of the ir spectra of the two salts, together with tentative band assignments, are given in Table 4. In comparison, the $^{31}P\{^1H\}$ nmr spectrum of the solvated Cu^{II} reaction product contained a singlet $\delta(^{31}P)$ 27.5 ppm and its ir spectrum contained a band $\tilde{\nu}_{max}$ 330 cm^{-1}, cf. Table 4.

The course of the reaction between solvated Tl^{III} and PMe_3 was very similar to that with NMe_3 except that ethane was not detected. The pale-green, insoluble product was formulated as $[Tl(PMe_3)_2][UF_6]$ and the soluble product, which decomposed readily at room temperature, as $[Me_3PPMe_3][UF_6]$, in both cases on the basis of their spectra. The ^{31}P nmr chemical shift of the latter compound was $\delta(^{31}P)$ 65.0 ppm, possibly a result of the paramagnetic anion. Pronounced concentration effects on the ^{205}Tl nmr chemical shifts in MeCN solutions of Tl^I hexafluoromolybdate(V) or hexafluorouranate(V) have been interpreted on the basis of ion pairing involving the paramagnetic anions (5). The ^{31}P chemical shift in $[Me_3PPMe_3][I_3]_2$ is $\delta(^{31}P)$ 46.3 ppm (17), possibly also an indication of some degree of cation–anion interaction.

The reactions between the solvated cations and PMe_3 are formulated as

$$[5]\quad 2Cu^{2+}_{(solv.)} + 10PMe_3 \rightarrow 2[Cu(PMe_3)_4]^+_{(solv.)} + [Me_3PPMe_3]^{2+}_{(solv.)}$$

$$[6]\quad Tl^{3+}_{(solv.)} + UF_6^- + 4PMe_3 \rightarrow [Tl(PMe_3)_2][UF_6] + [Me_3PPMe_3]^{2+}_{(solv.)}$$

Discussion

The reactions reported are all very similar and a number of generalizations can be made. The use of acetonitrile as the solvent and weakly basic hexafluorometallates as counter-anions favours the formation of mononuclear copper(I) cations, although only trimethylphosphine is a good enough ligand to compete with MeCN. Coordination of organic bases to thallium(I) is characteristically weak (18), and the isolation of Tl^I salts containing ligated trimethylamine or PMe_3 probably owes more to the low solubilities of the compounds than to any other reason. In both cases the ligands are lost readily from the solids on pumping at room temperature.

Reactions between solvated copper(II) and SMe_2, NMe_3, or PMe_3 involve the formation of coloured intermediates whose lifetimes depend on the nature of the ligand used. Precedents for this type of behaviour in MeCN are the reactions between Cu^{II} and trimethyl phosphite (19) or tetramethylthiourea (tmtu) (20), which give rise to short-lived and long-lived Cu^{II}–ligand complexes respectively. Using water as solvent it has been possible to isolate and structurally characterize the intermediate $CuCl_2(tmtu)_2$ (6). The electronic spectra of the intermediates in MeCN are compared with those of Cu^{II} redox-inactive complexes in Table 5.

The spectra of the redox-active systems are all very similar but show a trend to increasing energy with the expected order of increasing ligand strength. Both bands in a given system are considered to be due to Cu^{II} d–d transitions on the basis of their intensities estimated immediately after mixing. In all cases the intensity of the high frequency band is the greater and it is possible that in some cases its strength is due to intensity-borrowing from an adjacent charge transfer band (19). That the higher energy band arises from a purely organic species is inconsistent with its absence in the spectra of the Tl^{III} reactions. In addition the electronic spectrum of $[Me_2SSMe_2]^{\cdot+}$, $\tilde{\nu}_{max}$ 21 500 cm^{-1} (21), which might be a possible intermediate in the SMe_2 reaction, is significantly different from the bands observed (Table 5).

Electronic spectra of redox-inactive systems are characterized by a single band in each case, which occurs at higher energy with increasing $[Cu^{II}]$:[L] up to a limiting value, for example 1:4 for Cu^{II} versus pyridine (py) or NH_3 in MeCN (22) or 1:2 versus NMe_3 in methanol (23). Formation constants for $[Cu(NMe_3)]^{2+}$ and $[Cu(NMe_3)_2]^{2+}$ have been determined in MeOH (23) and, assuming that the values are similar in MeCN, the major species in solution under the conditions used will be di- and mono-ligand complexes, $[Cu(NCMe)_6]^{2+}$ and free NMe_3. We tentatively suggest that the lower energy band, whose $\tilde{\nu}_{max}$ is little different from that of $[Cu(NCMe)_6]^{2+}$, $\tilde{\nu}_{max}$ 13 500 cm^{-1}, arises from species $[Cu(NMe_3)_x(NCMe)_{6-x}]^{2+}$, where $x \leqslant 2$. These species are in equilibrium with the redox-active complexes for which $x > 2$. The concentration of the latter will be very small but its spectrum is observable possibly due to intensity-borrowing from the nearby charge transfer band. Similar arguments can be made for solvated Cu^{II} reacting with SMe_2 and possibly also with tmtu. A redox-active Cu^{II}—$P(OMe)_3$ cation has been proposed previously to account for the redox behaviour observed in this system (19). Precise descriptions of the individual species present in each case cannot be given on the basis of the available data, neither can any inferences be drawn as to their structures.

It is suggested that the primary oxidation products from the reactions are the monomeric radical cations $Me_2S^{\cdot+}$, $Me_3N^{\cdot+}$, and $Me_3P^{\cdot+}$, formed, at least in the Cu^{II} reactions, by an inner sphere electron transfer, and that these species undergo further reactions to give the observed products. Dimeric radical cations, $R_2SSR_2^{\cdot+}$, derived from dialkyl sulphides and identified by epr spectroscopy, have been widely reported and are believed to be the result of reactions between $R_2S^{\cdot+}$ and SR_2 (13, 21, 24). The loss of C_2H_6 from $Me_2SSMe_2^{\cdot+}$ has not been reported previously but the decomposition pathway of this radical cation in protic media may be more complex than that in an aprotic solvent. The formation of $[Me_3NNMe_2]^+$ is suggested to occur by an analogous route from $Me_3N^{\cdot+}$. Alkyliminium radical cations, $R_3N^{\cdot+}$, have been observed or inferred as transient intermediates in a number of redox reactions (25), but normally undergo further reactions to give $[R_2N{=}CR_2']^+$ or R_3NH^+ cations. The previous studies of NMe_3 oxidation by VCl_4 (26) or $CuCl_2$ (9) reported the

Can. J. Chem. Downloaded from www.nrcresearchpress.com by 186.148.149.217 on 09/07/12
For personal use only.

TABLE 5. Electronic spectra of Cu^{II}–ligand mixtures in acetonitrile

Ligand (L)	$[Cu^{II}]:[L]$	$\tilde{\nu}_{max}$ (cm^{-1})	(ε (mol^{-1} dm^3 cm^{-1}))	Reference
SMe_2	1:4	14 300 (22)	24 300 (280)[a]	this work
NMe_3	1:4	14 400 (27)	24 400 (70)[a]	This work
tmtu	1:5[b]	19 600	25 000	20
$P(OMe)_3$	1:10	[c]	29 000 (3000)	19
py	1:4	17 200 (70)		22
NH_3	1:4	17 000 (69)		22
NMe_3[d]	1:2	13 900		23

[a]Values of ε are estimates from the first spectrum after mixing.
[b]Conditions used in the present work at 243 K. Reaction was too fast for estimation of ε.
[c]Spectrum not obtained in this region.
[d]In MeOH as solvent.

formation of Me_3NH^+ and $[Me_2N{=}CH_2]^+$ rather than the $[Me_3NNMe_2]^+$ cation obtained here.

The formation of the $[Me_3PPMe_3]^{2+}$ cation from the oxidation of PMe_3 implies that dimerization of the short-lived $Me_3P^{\cdot+}$ radical cation (27) is more favoured than a reaction between $Me_3P^{\cdot+}$ and PMe_3. This is not unreasonable, since the concentration of free ligand in solution would be expected to be smaller than is the case for the weaker ligands SMe_2 and NMe_3. The available evidence indicates that the behaviour of PMe_3 towards Cu^{II} is very like that of tmtu (6).

Experimental

All operations were performed in a Pyrex vacuum line or N_2-atmosphere glove box ($H_2O < 5$ ppm) using techniques, instrumentation, and reagent purification procedures that have been described elsewhere (1, 2, 5). The solvated metal cation, fluoroanion salts $[Cu(NCMe)_5][PF_6]_2$, $[Cu(NCMe)_4][PF_6]$ (28), $[Tl(NCMe)_5][UF_6]_3$, and $TlUF_6$ (4, 5) were prepared as described previously. The ^1H and ^{13}C nmr chemical shifts are with respect to Me_4Si and ^{31}P with respect to 85% H_3PO_4, low field shifts being positive.

Reactions of [Cu(NCMe)$_4$][PF$_6$]

A mixture of $[Cu(NCMe)_4][PF_6]$ (0.5 mmol), PMe_3 (2.5 mmol), and MeCN (5 cm^3) was allowed to warm from 77 K to room temperature and gave a colourless solution from which an off-white solid was isolated on removal of volatile material. The solid was identified as tetrakis(trimethylphosphine)copper(I) hexafluorophosphate. *Anal.* calcd. for $C_{12}H_{36}CuF_6P_5$: C 28.1, H 7.0, Cu 12.5, F 22.2, P 30.2%; found: C 28.1, H 6.9, Cu 12.6, F 22.1, P. 30.0. $^{31}P\{^1H\}$ nmr spectrum: $\delta(^{31}P)$ −41.5 and −144.9 ppm; $^1J(^{31}P{-}^{63}Cu)$ 795, $^1J(^{31}P{-}^{65}Cu)$ 851, $^1J(^{19}F{-}^{31}P)$ 707 Hz. The ir spectrum of the solid is given in Table 6.

The salt $[Cu(NCMe)_4][PF_6]$ was recovered unchanged after reactions with SMe_2 or NMe_3 under similar conditions.

Reactions of [Cu(NCMe)$_5$][PF$_6$]$_2$ in MeCN

Mixtures of $[Cu(NCMe)_5][PF_6]_2$ (0.3 mmol), SMe_2 or NMe_3 (3.0 mmol), and MeCN (5 cm^3) were allowed to warm slowly from 77 K. A deep-green colour developed as SMe_2 or NMe_3 melted and flowed into the frozen solution. The colour faded slowly but disappeared rapidly if the mixture was agitated. The fraction volatile at 183 K was identified by gas chromatography as ethane. Removal of the remaining volatile material at room temperature left a colourless solid, which was identified as described in the Results section.

The reactions were also studied by electronic spectroscopy with $[Cu^{II}] = 5.0 \times 10^{-4}$ mol dm^{-3} and $[SMe_2]$ or $[NMe_3]$ varied between 5.0×10^{-4} and 5.0×10^{-3} mol dm^{-3}. Copper(II) solutions were loaded in the glove box into reaction vessels that were sealed to 10-mm Spectrosil cells. A frangible ampoule containing the appropriate quantity of ligand was added to each vessel, the solutions were degassed, and a spectrum of the Cu^{II} solution recorded after equilibrating the solution at 298 K. The ampoules were broken, the solutions allowed to mix, and spectra of the mixtures obtained over a period of several hours using a thermostated cell holder.

TABLE 6. The ir spectrum of solid $[Cu(PMe_3)_4][PF_6]$

$\tilde{\nu}_{max}$ (cm^{-1})	Suggested assignments
2960 (m)	C—H as. str.
2870 (m)	C—H sym. str.
1305 (s)	C—H def.
1290 (s)	C—H def.
950 (vs)	CH_3 rock
880 (s)	CH_3 rock
840 (vs)	PF_6^- (ν_3)
726 (vs)	C—P as. str.
665 (m)	C—P sym. str.
560 (vs)	PF_6^- (ν_4)

A mixture of $[Cu(NCMe)_5][PF_6]_2$ (0.3 mmol), PMe_3 (3.0 mmol), and MeCN (5 cm^3) developed a pink colouration as it was allowed to warm from 77 K. This decreased rapidly even below 230 K and an off-white solid was isolated after removal of volatile material at room temperature. The identification of the solid is described in the Results section.

Similar behaviour was observed from the reaction between $[Cu(NCMe)_5][PF_6]_2$ and tetramethylthiourea, tmtu, under identical conditions. In this case, however, it was possible to record the electronic spectrum of the intermediate at 233 K by injecting a solution of tmtu into the Cu^{II} solution via a septum cap. $[Cu^{II}]$ was 0.5×10^{-2} and [tmtu] was 2.5×10^{-2} mol dm^{-3}. In a separate experiment coordination of tmtu to Cu^I in MeCN was demonstrated by isolation of a solid complex and recording its ir and ^1H nmr spectra.

Reactions of TlUF$_6$ in MeCN

Addition of NMe_3 (5.0 mmol) to a solution of $TlUF_6$ (0.5 mmol) in MeCN (5 cm^3) at room temperature resulted in the formation of a pale-green precipitate. The solid was identified as bis(trimethylamine)-thallium(I) hexafluorouranate(V). *Anal.* calcd. for $C_6H_{18}F_6N_2TlU$: C 10.6, H 2.6, N 4.1%; found: C 10.3, H 2.4, N 3.8. On pumping the solid at room temperature NMe_3 was evolved. The ir spectrum of the solid contained bands due to coordinated NMe_3, $\tilde{\nu}_{max}$ 3220, 1475, and 1055 cm^{-1} (2), and to UF_6^-, $\tilde{\nu}_{max}$ 520 cm^{-1} (4).

Similar behaviour was observed between $TlUF_6$ and PMe_3 under identical conditions and led to the isolation of an insoluble blue-green solid that readily lost PMe_3 *in vacuo* and was formulated as $[Tl(PMe_3)_2][UF_6]$; ir, $\tilde{\nu}_{max}$: 1305, 950, 726, and 665 cm^{-1} due to coordinated PMe_3 (cf. Table 6 and ref. 2) and 520 cm^{-1} due to UF_6^-.

The salt $TlUF_6$ was recovered unchanged from a reaction with SMe_2 under identical conditions.

Reactions of [Tl(NCMe)$_5$][UF$_6$]$_3$ in MeCN

A mixture of $[Tl(NCMe)_5][UF_6]_3$ (0.5 mmol), SMe_2 (5.0 mmol),

Can. J. Chem. Downloaded from www.nrcresearchpress.com by 186.148.149.217 on 09/07/12
For personal use only.

and MeCN (5 cm^3) had a lemon-yellow colour when it was allowed to warm to room temperature but this rapidly faded to give a pale-green solution. A product volatile at 183 K was identified by gas chromatography as C_2H_6 and a pale-green solid isolated after removal of the remaining volatile material at room temperature was identified by its ^1H, $^{13}C\{^1H\}$, and ^{205}Tl nmr, electronic, and ir spectra as a mixture of $TlUF_6$ and $[Me_2SSMe][UF_6]$. The ^{205}Tl nmr chemical shifts obtained were similar to those reported previously for Tl^I and Tl^{III} UF_6^- salts in MeCN (5).

The reaction between $[Tl(NCMe)_5][UF_6]_3$ and NMe_3 in MeCN, carried out under identical conditions, was similar except that insoluble $[Tl(NMe_3)_2][UF_6]$ precipitated from solution and could be separated from soluble $[Me_3NNMe_2][UF_6]$. Similarly insoluble $[Tl(PMe_3)_2][UF_6]$ and soluble $[Me_3PPMe_3][UF_6]_2$ were identified by their spectra from the reaction between $[Tl(NCMe)_5][UF_6]_3$ (0.5 mmol) and PMe_3 (5.0 mmol) in MeCN (5 cm^3) at room temperature. No transient colour was observed in this reaction and C_2H_6 was not detected.

Preparation of $[Me_2SSMe][BF_4]$ (12)

The reaction between trimethyloxonium tetrafluoroborate (0.2 mmol) and dimethyl disulphide (0.6 mmol) in MeCN (5 cm^3) at room temperature for 0.25 h led to a colourless solid after removal of volatile material. The solid was identified by its ^1H nmr spectrum and reaction with SMe_2 (Table 1). The data obtained were in good agreement with those reported previously (12). Its ir spectrum is given in Table 2.

Preparation of $[Me_3PPMe_3][PF_6]_2$

A solution of I_2 (0.2 mmol) in MeCN (5 cm^3) was prepared *in vacuo* and PMe_3 (0.6 mmol) was added to the frozen solution. On warming the mixture to room temperature, a colourless precipitate formed, which was identified as hexamethyldiphosphonium diiodide. *Anal.* calcd. for $C_6H_{18}I_2P_2$: C 17.6, H 4.4, I 62.6, P 15.4%; found: C 17.4, H 4.5, I 62.9, P 15.3. Its ir spectrum is given in Table 4.

A solution of $NOPF_6$ (0.2 mmol) in MeCN was added to a portion of solid $[Me_3PPMe_3][I]_2$ at room temperature. A colourless gas, presumed to be NO, was immediately evolved and the solid dissolved giving a brown solution. An off-white solid was isolated on removal of MeCN and I_2 and was identified as hexamethyldiphosphonium hexafluorophosphate. *Anal.* calcd. for $C_6H_{18}F_{12}P_4$: C 16.3, H 4.1, P 28.0%; found: C 16.1, H 4.3, P 27.9. Its $^{31}P\{^1H\}$ nmr spectrum consisted of a signal due to PF_6^- and a singlet $\delta(^{31}P)$ 27.8 ppm. Its ir spectrum is given in Table 4.

Acknowledgements

We thank Professor W. McFarlane and colleagues, City of London Polytechnic, for obtaining the ^{205}Tl nmr spectra under the auspices of the SERC nmr service, and Dr. D. S. Rycroft and Mr. J. Gall for help in obtaining the other nmr spectra. The award of a Government of Pakistan scholarship to R.M.S. is gratefully acknowledged.

1. J. M. Winfield. J. Fluorine Chem. **25**, 91 (1984); G. M. Anderson and J. M. Winfield. J. Chem. Soc. Dalton Trans. 337 (1986).
2. L. McGhee, R. M. Siddique, and J. M. Winfield. J. Chem. Soc. Dalton Trans. 1309 (1988).
3. J. D. MacLeod, D. M. Muir, A. J. Parker, and P. Singh. Aust. J. Chem. **30**, 1423 (1977); V. V. Giridhar and C. Kalidas. J. Solution Chem. **11**, 539 (1982); S. Ahrland, K. Nilsson, and B. Tagesson. Acta Chem. Scand. Ser. A, **A37**, 193 (1983); D. S. Gill, N. Kumari, and M. S. Chauhan. J. Chem. Soc. Faraday Trans. 1, **81**, 687 (1985).
4. G. M. Anderson, J. Iqbal, D. W. A. Sharp, J. M. Winfield, J. H. Cameron, and A. G. McLeod. J. Fluorine Chem. **24**, 303 (1984).
5. R. M. Siddique and J. M. Winfield. J. Fluorine Chem. **40**, 71 (1988).
6. E. A. H. Griffith, W. A. Spofford III, and E. L. Amma. Inorg. Chem. **17**, 1913 (1978), and references therein.
7. G. Davies and D. J. Loose. Inorg. Chem. **15**, 694 (1976).
8. F. H. Jardine. Adv. Inorg. Chem. Radiochem. **17**, 115 (1975); D. J. Gulliver, W. Levason, and M. Webster. Inorg. Chim. Acta, **52**, 153 (1981).
9. T. A. Lane and J. T. Yoke. Inorg. Chem. **15**, 484 (1976).
10. S. K. Mandal, L. K. Thompson, E. J. Gabe, F. L. Lee, and J.-P. Charland. Inorg. Chem. **26**, 2384 (1987).
11. R. Laitinen, R. Steudel, and R. Weiss. J. Chem. Soc. Dalton Trans. 1095 (1986), and references therein.
12. S. H. Smallcombe and M. C. Caserio. J. Am. Chem. Soc. **93**, 5826 (1971).
13. R. Wilbrandt, N. H. Jensen, P. Pagsberg, A. H. Sillesen, K. B. Hansen, and R. E. Hester. J. Raman Spectrosc. **11**, 24 (1981).
14. A. Nieuwpoort and R. Reedijk. Inorg. Chim. Acta, **7**, 323 (1973); R. Savoie and M. Guay. Can. J. Chem. **53**, 1387 (1975).
15. D. Schomburg, G. Bettermann, L. Ernst, and R. Schmutzler. Angew. Chem. Int. Ed. Engl. **24**, 975 (1985).
16. Yu. P. Makovetskii, N. G. Feshchenko, V. V. Malovik, V. Ya. Semenii, I. E. Boldeskul, V. A. Bondar, and N. P. Chernukho. J. Gen. Chem. USSR (Engl. Transl.), **50**, 1967 (1980).
17. Yu. P. Makovetskii, V. E. Lidkovskii, I. E. Boldeskul, N. G. Feshchenko, and N. N. Kalibabchuk. J. Gen. Chem. USSR (Engl. Transl.), **52**, 1989 (1982).
18. H. Schmidbauer, W. Bublak, J. Riede, and G. Müller. Angew. Chem. Int. Ed. Engl. **24**, 414 (1985); H. Schmidbauer. Angew. Chem. Int. Ed. Engl. **24**, 893 (1985).
19. G. M. Anderson, J. H. Cameron, A. G. Lappin, J. M. Winfield, and A. McAuley. Polyhedron, **1**, 467 (1982).
20. D. A. Zatko and B. Kratochvil. Anal. Chem. **40**, 2120 (1968).
21. J. Mönig, M. Göbl, and K. D. Asmus. J. Chem. Soc. Perkin Trans. 2, 647 (1985).
22. J. Iqbal. Ph.D. Thesis, University of Glasgow. 1985.
23. A. P. Sakharov. J. Gen. Chem. USSR (Engl. Transl.), **41**, 2145 (1971)
24. R. L. Peterson, D. J. Nelson, and M. C. R. Symons. J. Chem. Soc. Perkin Trans. 2, 225 (1978); W. B. Gara, J. R. M. Giles, and B. P. Roberts. J. Chem. Soc. Perkin Trans. 2, 1444 (1979); M. J. Davies, B. C. Gilbert, and R. O. C. Norman. J. Chem. Soc. Perkin Trans. 2, 503 (1984).
25. Y. L. Chow, W. C. Danen, S. F. Nelsen, and D. H. Rosenblatt. Chem. Rev. **78**, 243 (1978).
26. R. Kiesel and E. P. Schram. Inorg. Chem. **12**, 1090 (1973).
27. A. Hasegawa, G. D. G. McConnachie, and M. C. R. Symons. J. Chem. Soc. Faraday Trans. 1, 1005 (1984).
28. A. C. Baxter, J. H. Cameron, A. McAuley, F. M. McLaren, and J. M. Winfield. J. Fluorine Chem. **10**, 289 (1977).

Can. J. Chem. Downloaded from www.nrcresearchpress.com by 186.148.149.217 on 09/07/12
For personal use only.

Synthesis of a new unsaturated 16-membered heterocycle with alternating CC and NS building blocks

JÖRG SUNDERMEYER, HERBERT W. ROESKY,[1] AND MATHIAS NOLTEMEYER

Institut für Anorganische Chemie der Universität, Tammannstrasse 4, 3400 Göttingen, Federal Republic of Germany

Received January 19, 1989

This paper is dedicated to Professor Ronald J. Gillespie on the occasion of his 65th birthday

JÖRG SUNDERMEYER, HERBERT W. ROESKY, and MATHIAS NOLTEMEYER. Can. J. Chem. **67**, 1785 (1989).

The reaction between $C_6H_4(SCl)_2$ **3** and $(PhC{=}NSiMe_3)_2$ **4** leads to the 16-membered heterocycle $(SC_6H_4SN{=}CPhCPh{=}N)_2$ **5**. The X-ray structure analysis of **5** shows a nonplanar macrocyclic system with alternating CC and NS units.

Key words: 16-membered heterocycle, X-ray structure, sulfur–nitrogen.

JÖRG SUNDERMEYER, HERBERT W. ROESKY et MATHIAS NOLTEMEYER. Can. J. Chem. **67**, 1785 (1989).

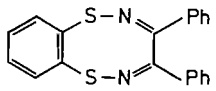
La réaction du $C_6H_4(SCl)_2$ **3** avec le $(PhC{=}NSiMe_3)_2$ **4** donne l'hétérocycle à 16 chaînons $(SC_6H_4SN{=}CPhCPh{=}N)_2$ **5**. L'analyse de la structure de **5** à l'aide de rayons-X montre un système macrocyclique que n'est pas plan avec des unités de construction CC et NS alternates.

Mots clés : hétérocycle à 16 chaînons, structure à l'aide de rayons-X, soufre–azote.

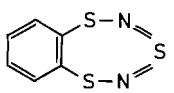
Introduction

The synthesis and electronic structure of planar carbon–sulfur–nitrogen rings continue to attract the attention of research groups (1). Many of the novel 10π- and 14π-aromatic CNS heterocycles discovered recently can formally be derived from the well-known planar dication $S_4N_4^{2+}$ (2) by substitution of sulfur or thiazyl units by isoelectronic carbocyclic fragments (3).

In this context we were interested in the target molecule **1** since, if planar, this 1,4,5,8-benzodithiadiazocine is expected to show properties of a 14π electron system, similar to the known 1,3,5,2,4-benzotrithiadiazepine **2** (4).



1



2

As a possible synthetic approach, we studied the reaction between the two bifunctional reagents 1,2-bis(chlorothio)-benzene **3** and benzil-bis(trimethylsilyl)imine **4** in dilute CH_2Cl_2 solution, and obtained (by elimination of trimethylchlorosilane) and air-stable yellow crystalline precipitate in good yield. This was separated by filtration and recrystallized from hot 1,1,2,2-tetrachloroethane (TCE) or boiling dioxane.

Experimental

The reaction was carried out under an atmosphere of nitrogen using dried solvents. The following spectrometers were used: ir spectra: Perkin Elmer 180; ^1H and ^{13}C nmr spectra: Bruker AM250; mass spectra: Finnigan MAT System 8230. Elemental analysis: Mikroanalytisches Laboratorium Beller, Göttingen. 1,2-Bis(chlorothio)benzene (5) and benzil-bis(trimethylsilyl)imine (6) were prepared by literature methods.

Preparation of the macrocycle **5**

The solutions of **3** (6.33 g, 30 mmol) in CH_2Cl_2 (100 mL) and **4** (10.56 g, 30 mmol) in CH_2Cl_2 (100 mL) were simultaneously dropped into refluxing CH_2Cl_2 (150 mL) over a period of 3 h. After 1 h a yellow crystalline material began to precipitate. After another 24 h of stirring at room temperature it was isolated by filtration and washed with CH_2Cl_2 (80 mL) to give pure **5** (yield: 7.8 g, 75%), mp 288°C. **5** can be recrystallized from boiling dioxane or hot TCE; ir (Nujol): 3050, 1570, 1495, 1440, 1430, 1320, 1300, 1255, 1230, 1182, 1025, 925, 910, 795, 770, 750, 740, 715, 705, 685, 580, and 495 cm^{-1}; ^1H nmr (250 MHz, $CDCl_3$) δ: 7.23–7.89 m; ^{13}C nmr (63 MHz, $CDCl_3$) δ: 161.6, 139.4, 134.4, 130.3, 129.4, 128.9, 127.6, and 126.6 ppm; FD–MS *m/z*: 692 (M, 100%); EI–MS *m/z*: 692 (M, 10%), 346 ($\frac{1}{2}$M, 15%), 314 ($\frac{1}{2}$M − S, 10%), 238 ($\frac{1}{2}$M − C_6H_4S, 25%), 192 ($\frac{1}{2}$M − $C_6H_4S_2N$, 100%). *Anal.* calcd. for $C_{40}H_{28}N_4S_4$: C 69.3, H 4.1, N 8.1; found: C 68.9, H 4.2, N 7.9.

Single crystals suitable for X-ray analysis were obtained by slow diffusion of pentane vapour into a saturated solution of **5** in TCE. The crystals contained half a mole of TCE per mole of **5**. The space group is $C2/c$ with cell constants a = 2389.4(9); b = 1064.9(7); c = 2992.0(9) pm; β = 102.2(1)°; V = 7.4413 nm^3, Z = 8, d_{calc} = 1.387 g/cm^3. 6165 reflections ($2\theta < 45°$) were measured on a STOE four-circle diffractometer with MoK_α radiation; 4847 reflections were independent but only 2759 observed with $F > 3\sigma(F)$. The poor quality of the data set results from the weakly diffracting crystal of size 0.2 × 0.2 × 0.5 mm^3 with strongly anisotropic reflection profiles. The structure was solved by SHELXS86 and refined by SHELX76. Because of the bad reflection-to-parameter ratio and to keep the refinement stable, rigid phenyl groups were introduced (391 parameters). From difference syntheses during the later refinement cycles, disorder of a solvent molecule TCE about the twofold axis, 0, y, $\frac{1}{4}$ was evident. Only two general peaks for chlorine appeared in the map, and weak indications for carbon atoms C(71) and C(72) lying 52 and 47 pm away from the axis. These peaks satisfied the geometrical requirements for TCE (excluding hydrogen atoms). Refinement of these locations was, however, unstable, so that thermal ellipsoids fixed on the axis with occupancies equal to 0.5 represent a dynamic inversion of the C atoms between relatively well-defined chlorine atoms, which also obey the twofold symmetry. $wR = [\Sigma w\Delta F^2/\Sigma wF_o^2]^{1/2}$ converged at 0.082 and $R = \Sigma\Delta F/\Sigma F_o$ at 0.11 ($w = [\sigma^2(F_o) + 0.0004F_o^2]^{-1}$).[2] Fractional atom coordinates are given in Table 1 and selected bond lengths and angles in Table 2.[3]

[1]Author to whom correspondence may be addressed.

[2]Further details of the crystal structure investigations may be obtained from the Fachinformationszentrum Energie, Physik, Mathematik GmbH, D-7514 Eggenstein–Leopoldshafen 2 (F.R.G.), on quoting the depository number CSD 53935, the names of the authors, and the journal citation.

[3]Supplementary data may be purchased from the Depository of Unpublished Data, CISTI, National Research Council of Canada, Ottawa, Ont., Canada K1A 0R6.

Can. J. Chem. Downloaded from www.nrcresearchpress.com by 186.148.149.217 on 09/07/12
For personal use only.

Can. J. Chem. Downloaded from www.nrcresearchpress.com by 186.148.149.217 on 09/07/12
For personal use only.

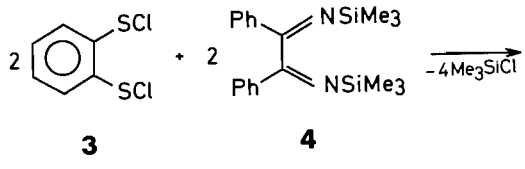
TABLE 1. Atomic coordinates ($\times 10^4$) and equivalent isotropic displacement parameters ($pm^2 \times 10^{-1}$)

Atom	x	y	z	U^*(eq)
S(1)	3400(1)	597(3)	3965(1)	52(1)
N(1)	3284(3)	−488(9)	3541(3)	46(4)
C(1)	3541(4)	−1561(12)	3621(4)	45(5)
C(2)	3905(4)	−1906(10)	4076(4)	43(5)
N(2)	3706(3)	−2505(8)	4382(3)	51(4)
S(2)	2986(1)	−2713(3)	4248(1)	61(1)
S(3)	1801(1)	−3091(3)	4493(1)	58(1)
N(3)	1700(3)	−3377(9)	3922(3)	49(4)
C(3)	1398(4)	−2586(11)	3642(4)	47(5)
C(4)	1168(4)	−1338(11)	3805(4)	45(5)
N(4)	1454(3)	−299(8)	3818(3)	43(3)
S(4)	2092(1)	−355(3)	3670(1)	53(1)
C(12)	3722(3)	−3700(11)	3359(3)	75(6)
C(13)	3621	−4661	3035	98(8)
C(14)	3247	−4465	2615	113(10)
C(15)	2973	−3309	2520	115(9)
C(16)	3074	−2348	2844	71(6)
C(11)	3448	−2544	3264	50(5)
C(22)	4854(4)	−1669(8)	4616(3)	86(7)
C(23)	5438	−1401	4698	105(8)
C(24)	5690	−1026	4339	95(8)
C(25)	5357	−918	3898	88(7)
C(26)	4772	−1185	3815	67(6)
C(21)	4521	−1561	4174	52(5)
C(32)	1650(3)	−3611(7)	2966(3)	69(6)
C(33)	1543	−3830	2496	76(6)
C(34)	1085	−3233	2207	74(6)
C(35)	735	−2416	2389	91(7)
C(36)	842	−2196	2859	77(6)
C(31)	1299	−2793	3147	43(5)
C(42)	316(3)	−2465(6)	3946(3)	68(6)
C(43)	−192	−2486	4104	82(6)
C(44)	−388	−1396	4281	76(6)
C(45)	−74	−286	4299	71(6)
C(46)	435	−265	4140	59(5)
C(41)	630	−1355	3964	49(5)
C(52)	1823(2)	2167(8)	3615(2)	64(6)
C(53)	1963	3440	3626	63(6)
C(54)	2536	3809	3710	68(6)
C(55)	2968	2905	3783	65(6)
C(56)	2828	1632	3772	45(5)
C(51)	2255	1263	3688	45(4)
C(62)	3357(3)	−4776(8)	4799(3)	58(5)
C(63)	3260	−5772	5076	77(7)
C(64)	2716	−5964	5163	80(7)
C(65)	2268	−5160	4973	61(5)
C(66)	2364	−4165	4696	55(5)
C(61)	2908	−3973	4609	51(5)
Cl(1)	−227(2)	1092(7)	2000(2)	184(3)
Cl(2)	622(3)	3607(8)	2625(2)	228(4)
C(71)	0	1837(34)	2500	291(54)
C(72)	0	3068(51)	2500	289(32)

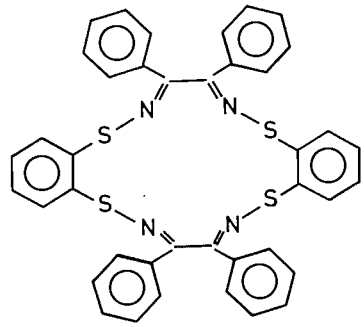
*Equivalent isotropic U defined as one third of the trace of the orthogonalized U_{ij} tensor.

Discussion

The room temperature ^{13}C nmr of a saturated $CDCl_3$ solution of the yellow crystalline material showed eight signals. This result is consistent with the assumed structure **1** or any higher symmetric oligomer. Signals of a second oligomer could not be detected. FD mass spectroscopic experiments showed a molecular ion $M^{+\bullet}$ with m/z 692 as the only detectable peak



3 **4**



5

under these conditions. This result is consistent with a 2:2 macrocyclic oligomer **5**.

The X-ray analysis (Fig. 1) confirmed the conclusions from the ^{13}C nmr and mass spectroscopic results. Furthermore we found that the macrocycle is not planar (Fig. 2). The conformation of **5** is mainly determined by the two rigid *o*-dimercaptophenylene units, which are close to planar. The torsion angles are 12.0° (S4—C51—C56—S1) and 5.2° (S2—C61—C66—S3). The remarkably high values for the torsion angles in the α-diimino units (93.1° (N3—C3—C4—N4) and 94.6°

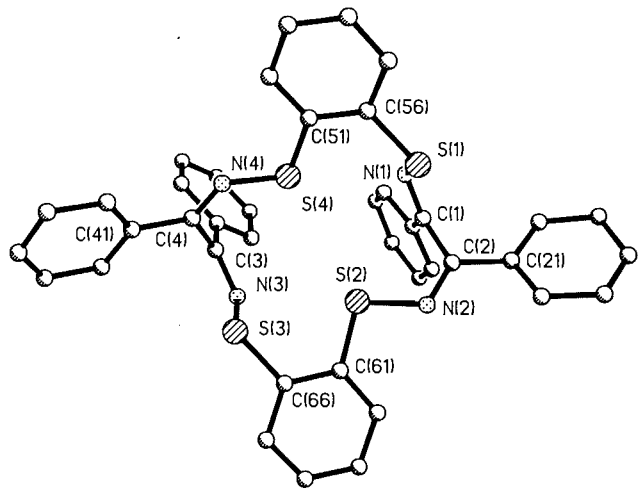


FIG. 1. **5** viewed perpendicular to the least-squares plane.

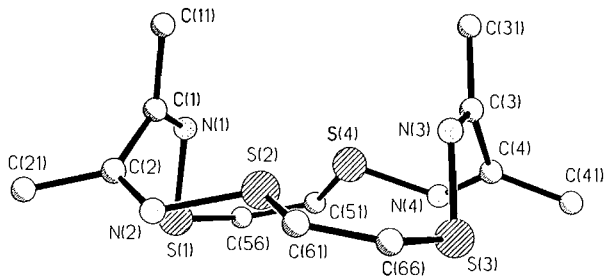


FIG. 2. The macrocyclic skeleton of **5** viewed along the least-squares plane. The fused six-membered rings (not shown) are inclined to each other at 38°, whereas the phenyl rings (also not shown) fill space irregularly.

TABLE 2. Selected bond lengths (pm) and angles (deg)

Atoms	Length	Atoms	Length
S(1)—N(1)	169.5(10)	S(1)—C(56)	175.6(7)
N(1)—C(1)	129.5(15)	C(1)—C(2)	149.7(15)
C(1)—C(11)	148.0(16)	C(2)—N(2)	128.6(15)
C(2)—C(21)	148.5(13)	N(2)—S(2)	169.7(8)
S(2)—C(61)	175.7(9)	S(3)—N(3)	170.2(10)
S(3)—C(66)	177.3(8)	N(3)—C(3)	129.4(14)
N(4)—S(4)	167.4(9)	S(4)—C(51)	176.6(9)

Atoms	Angle	Atoms	Angle
N(1)—S(1)—C(56)	100.9(4)	S(1)—N(1)—C(1)	117.8(7)
N(1)—C(1)—C(2)	123.1(10)	N(1)—C(1)—C(11)	119.8(9)
C(2)—C(1)—C(11)	116.9(10)	C(1)—C(2)—N(2)	122.5(9)
C(1)—C(2)—C(21)	118.8(10)	N(2)—C(2)—C(21)	118.7(9)
C(2)—N(2)—S(2)	113.9(7)	N(2)—S(2)—C(61)	100.8(4)
N(3)—S(3)—C(66)	99.5(4)	S(3)—N(3)—C(3)	118.3(9)
N(3)—C(3)—C(4)	122.6(11)	N(3)—C(3)—C(31)	120.2(10)
C(4)—C(3)—C(31)	116.9(9)	C(3)—C(4)—N(4)	121.4(9)
C(3)—C(4)—C(41)	118.9(9)	N(4)—C(4)—C(41)	119.7(9)
C(4)—N(4)—S(4)	117.7(8)	N(4)—S(4)—C(51)	99.5(4)
S(1)—C(56)—C(55)	115.8(3)	S(1)—C(56)—C(51)	123.2(3)
S(4)—C(51)—C(52)	121.1(2)	S(4)—C(51)—C(56)	118.9(2)
S(3)—C(66)—C(65)	119.0(3)	S(3)—C(66)—C(61)	120.8(3)
S(2)—C(61)—C(62)	123.2(2)	S(2)—C(61)—C(66)	116.8(2)

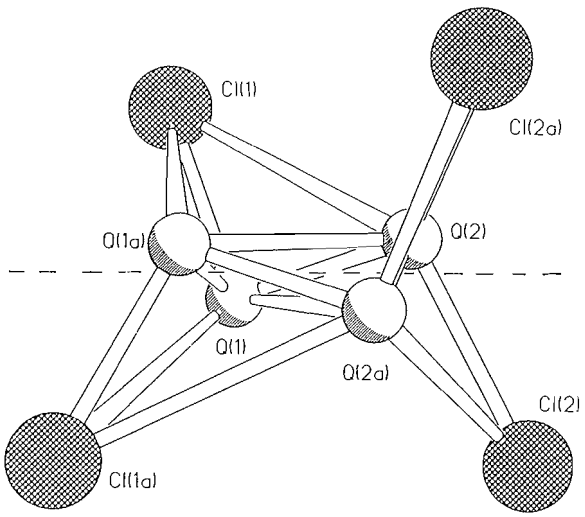


FIG. 3. Disorder of TCE shown in a difference Fourier synthesis calculated without the listed fixed positions C(71) and C(72): the peaks Q1 and Q2 are 52 and 47 pm away from the axis 0, y, $\frac{1}{4}$ ("a" refers to symmetry equivalent positions and dashes represent axis).

(N1—C1—C2—N2)) rule out *p*-conjugation, as also observed in the 2,1,3-benzothiadiazole (7). The average bond lengths for the SN bonds (169.2 pm) and CN bonds (129.3 pm) are typical for SN single and CN double bonds in nonaromatic heterocycles (see, for example, ref. 8). Due to the poor quality of the available crystals a more detailed discussion of the structure is inappropriate.

The macrocycle **5** does not possess C_1 crystallographic symmetry in the solid state conformation. However, as mentioned before, the ^{13}C nmr in $CDCl_3$ solution shows only signals for eight equivalent carbon atoms. This result is indicative of a facile change of conformation in solution.

We believe that steric factors (ring torsion) are mainly responsible for our not being able to detect any of the 1:1 ring compound **1** (Fig. 3).

A future research project should show whether **5** can be oxidized to a dicationic species, which then may be a planar 18π electron system.

1. H. W. ROESKY, P. SCHÄFER, M. NOLTEMEYER, and G. M. SHELDRICK. Z. Naturforsch. B: **38**, 347 (1983); T. CHIVERS, F. EDELMANN, J. F. RICHARDSON, N. M. R. SMITH, O. TREU, and M. TRSIC. Inorg. Chem. **25**, 2119 (1986); A. W. CORDES, M. HOJO, H. KOENIG, M. C. NOBLE, R. T. OAKLEY, and W. T. PENNINGTON. Inorg. Chem. **25**, 1137 (1986); S. T. A. K. DALEY, C. W. REES, and D. J. WILLIAMS. J. Chem. Soc. Chem. Commun. 55 (1984); J. L. MORRIS and C. W. REES. Pure Appl. Chem. **58**, 197 (1986), and refs. cited.
2. R. J. GILLESPIE, J. P. KENT, J. F. SAWYER, D. R. SLIM, and J. D. TYRER. Inorg. Chem. **20**, 3799 (1981).
3. H. U. HÖFS, G. HARTMANN, R. MEWS, and G. M. SHELDRICK. Angew. Chem. Int. Ed. Engl. **23**, 988 (1984); I. ERNEST, W. HOLICK, G. RIHS, D. SCHOMBURG, G. SHOHAM, D. WENKERT, and R. B. WOODWARD. J. Am. Chem. Soc. **103**, 1540 (1981).
4. J. L. MORRIS, C. W. REES, and D. J. WILLIAMS. J. Chem. Soc. Chem. Commun. 396 (1985); J. L. MORRIS and C. W. REES. J. Chem. Soc. Perkin Trans. 211 (1987).
5. F. FEHRER, F. MALCHAREK, and K. GLINKA. Z. Naturforsch. B: **26**, 67 (1971).
6. G. TUCHTENHAGEN and K. RÜHLMANN. Liebigs Ann. Chem. 174 (1968).
7. V. LUZZATI. Acta Crystallogr. **4**, 193 (1951).
8. S. T. A. K. DALEY, C. W. REES, and D. J. WILLIAMS. J. Chem. Soc. Chem. Commun. 57 (1984).

Can. J. Chem. Downloaded from www.nrcresearchpress.com by 186.148.149.217 on 09/07/12
For personal use only.

Spectroscopic studies of N–S–O anions: The reactions of NSO^- with elemental sulphur and with S_4N_4

TRISTRAM CHIVERS[1] AND KENNETH J. SCHMIDT
Department of Chemistry, The University of Calgary, Calgary, Alta., Canada T2N 1N4

AND

DEANE D. MCINTYRE AND HANS J. VOGEL
Department of Biological Sciences, The University of Calgary, Calgary, Alta., Canada T2N 1N4

Received February 3, 1989

This paper is dedicated to Professor Ronald J. Gillespie on the occasion of his 65th birthday

TRISTRAM CHIVERS, KENNETH J. SCHMIDT, DEANE D. MCINTYRE, and HANS J. VOGEL. Can. J. Chem. **67**, 1788 (1989).

The reaction of $(Me_2N)_3S^+NSO^-$ with sulphur has been investigated by ultraviolet–visible, infrared, Raman, and ^{14}N, ^{17}O, and ^{33}S nuclear magnetic resonance spectroscopies. The red species (λ_{max} 501 nm) formed initially is tentatively identified as $SSNSO^-$. This anion is thermally unstable with respect to the formation of S_4N^- and sulphur oxyanions. Previously reported salts of the "NSO_2^-" ion have been reinvestigated by infrared, Raman, and ^{14}N nmr spectroscopies, which indicate that the major component of these salts is the NSO^- ion. The reaction of $(Me_2N)_3S^+NSO^-$ with S_4N_4 is shown by ^{14}N nmr spectroscopy to produce both $S_3N_3O^-$, the major product, and $S_3N_3^-$.

Key words: nitrogen–sulphur–oxygen (N–S–O) anions, ^{14}N NMR spectroscopy.

TRISTRAM CHIVERS, KENNETH J. SCHMIDT, DEANE D. MCINTYRE et HANS J. VOGEL. Can. J. Chem. **67**, 1788 (1989).

Faisant appel aux méthodes spectroscopiques ultraviolet–visible, infrarouge, Raman et résonance magnétique nucléaire du ^{14}N, ^{17}O et ^{33}S, on a étudié la réaction du $(Me_2N)_3S^+NSO^-$ avec le soufre. En première approximation, on a attribué la structure $SSNSO^-$ aux espèces rouges (λ_{max} de 501 nm) qui se forment initialement. Cet anion est thermiquement stable par rapport à la formation d'ions S_4N^- et d'oxyanions du soufre. Utilisant les méthodes spectroscopiques ir, Raman et rmn du ^{14}N, on a réexaminé la structure de l'ion «NSO_2^-» dont la formation avait été rapportée antérieurement; ces résultats indiquent que la composante principale de ces sels est l'ion NSO^-. En se basant sur la rmn du ^{14}N, on démontre que la réaction du $(Me_2N)_3^+NSO^-$ avec le S_4N_4 conduit à la formation tant de $S_3N_3O^-$, le produit principal, que de $S_3N_3^-$.

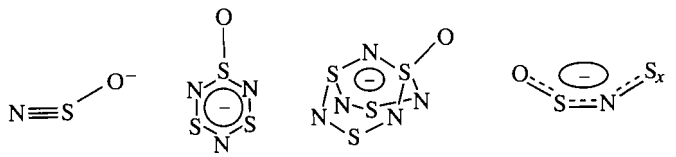
Mots clés : anions de nitrogène–soufre–oxygène (N–S–O), spectroscopie RMN du ^{14}N.

[Traduit par la revue]

Introduction

Several nitrogen–sulphur–oxygen (N–S–O) anions that contain a sulphoxy group have been characterized. These include the acyclic species NSO^-, **1** (1–3), the ring system $S_3N_3O^-$, **2** (4), and the cage anion $S_4N_5O^-$, **3** (5). Recently we discovered that electrochemically generated solutions of **1** in acetonitrile (ca. 0.3 mM) react with elemental sulphur to give a red anion (λ_{max} 496 nm) tentatively identified as S_xNSO^- (**4***a*, $x = 1$; **4***b*, $x = 2$) (6). This species is an oxy analogue of the known binary anions $SNSS^-$ ($x = 1$) (7) or $SSNSS^-$ ($x = 2$) (8) in which a terminal sulphur is replaced by oxygen. In this investigation, the reaction of NSO^- with *cyclo*-S_8 has been carried out on a preparative scale and monitored by uv–visible, ^{14}N, ^{17}O, and ^{33}S nmr, and vibrational spectroscopies to elucidate the course of the reaction and the identities of the final products. In addition, the previously reported salts of the "NSO_2^-" anion (9) have been reinvestigated by ^{14}N nmr, ir, and Raman spectroscopies. The spectra of such salts, prepared by following the literature procedure (9), indicate the presence of **1** as the predominant anion.

Electrochemically generated solutions of **1** (ca. 0.3 mM) react with S_4N_4 to give **2** (6), which may also be prepared in ca. 40% yield by the controlled aerial oxidation of $S_3N_3^-$ (4). The latter synthesis also produces the cage anions **3** and $S_4N_5^-$. Consequently, the reaction of NSO^- with S_4N_4 has been performed on a preparative scale to evaluate this route as a specific, high-yield synthesis of **2**.



1 **2** **3** **4***a*, $x = 1$; **4***b*, $x = 2$

Experimental

Reagents and general procedures

Solvents were dried and distilled before use: CH_3CN ($CaH_2/P_4O_{10}/CaH_2$), CH_2Cl_2 (P_4O_{10}), THF (Na/benzophenone), diethyl ether (Na/benzophenone). Anhydrous DMSO (Aldrich gold label) was used without purification. All manipulations were carried out under an atmosphere of dry N_2. The following reagents were prepared by the literature procedures: S_4N_4 (10), $Cs^+NSO_2^-$ (9), $PPN^+NSO_2^-$-[PPN^+=$(Ph_3P)_2N^+$] (9), PPN^+Cl^- (11), $PPN^+S_4N^-$ (8), $[PPN]_2S_2O_3$ (12), $[PPN]_2SO_4$ (12), $PPN^+S_4N_5O^-$ (4, 5) K^+NSO^- (1), TAS^+-NSO^- [TAS^+=$(Me_2N)_3S^+$] (3). 18-Crown-6 (Aldrich) was dried by recrystallization from CH_3CN and then twice dissolved in THF and pumped to dryness to remove residual CH_3CN. S_8 (sublimed, Fisher) was used without further purification.

Instrumentation

The ir spectra of solids were recorded as Nujol mulls (CsI windows) on a Nicolet 5-DX FTIR spectrometer (4000–400 cm^{-1}) and on a Perkin–Elmer model 457 grating spectrometer (400–250 cm^{-1}). Subtractive ir spectra were obtained on CH_3CN solutions ((3–4) × 10^{-2} M) in a specially designed 303 stainless steel cell (13), using KBr windows (0.5 mm pathlength) and Viton O-rings, on a Nicolet 8000A FTIR spectrometer using an MCT (HgCdTe) liquid nitrogen-cooled detector (4000–400 cm^{-1}). The reaction of TAS^+NSO^- with sulphur

[1]Author to whom correspondence may be addressed.

Can. J. Chem. Downloaded from www.nrcresearchpress.com by 186.148.149.217 on 09/07/12
For personal use only.

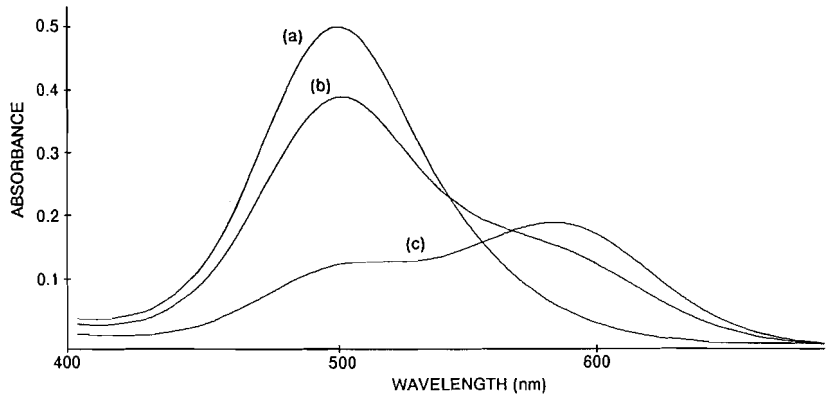


FIG. 1. Ultraviolet–visible spectra of the reaction of TAS^+NSO^- with sulphur in CH_3CN after (a) 5 min; (b) 3 h; (c) 14 h.

was performed directly in the ir cell. An ir spectrum of TAS^+NSO^- in CH_3CN was subtracted from the spectra so obtained. This procedure removed the bands due to TAS^+ and the weaker CH_3CN vibrations. The bands due to reaction products appear as positive peaks while bands attributable to reagents that are being consumed show up as negative peaks.

Raman spectra (1500–100 cm^{-1}) were recorded on a Jarrel–Ash model 25-100 double monochromator calibrated with CCl_4. The monochromator was interfaced to an IBM-PC microcomputer to permit multiple scanning and data manipulation. A Coherent Radiation CR4 argon ion laser fitted with an Innova plasma tube was used to obtain exciting radiation at 488 and 514.5 nm and to pump a Coherent Radiation model 590-03 dye laser to obtain exciting radiation at 600 nm. Low temperature Raman spectra were obtained by using sealed 5-mm glass tubes, which contained a fine frit to suspend solid S_8 near the top of the reaction solution (ca. 2×10^{-1} M) and to keep the solid out of the laser beam. A laser power of 400 mW was used. The tubes were cooled to −45°C in a thermostatted glass Dewar by the evaporation of liquid nitrogen. The laser beam was directed through the bottom of the glass Dewar and up through the bottom of the 5-mm tube into the cooled solutions to give Raman scattering that was collected through the Dewar walls at 90° to the incident beam. Raman spectra of air-sensitive solids were obtained on pressed pellets (1 cm diameter) mounted in a push-top glass vial sealed with epoxy glue. Samples were spun at ca. 1000 rpm to prevent thermal decomposition, and laser powers of 250 mW were used.

Ultraviolet–visible spectra were obtained on a Cary 219 spectrophotometer using either 0.01, 0.1, or 1 cm pathlength quartz cells. The reaction of TAS^+NSO^- (5×10^{-3} to 1.5×10^{-2} M) with elemental sulphur in CH_3CN was carried out in the uv–visible cells, which were fitted with rubber septa to exclude air.

All nmr experiments were performed on Bruker AM-400 nmr spectrometers operating at 28.915 MHz for ^{14}N, 54.244 MHz for ^{17}O, and 30.690 MHz for ^{33}S. Both a 10-mm broad-band probe and a 15-mm solenoidal coil probe were used to obtain the ^{14}N spectra, while only the former was used for ^{17}O and ^{33}S experiments. Typical parameters for ^{14}N were an acquisition time (AQ) of 0.07 s, a relaxation delay (RD) of zero, a sweep width (SW) of 30 000 Hz, and a data collection size (TD) of 4K, which was zero-filled to 16K before transformation. At least 3000 scans were collected. The signal from dissolved N_2 gas was used as an internal standard for all ^{14}N nmr spectra (15). For ^{17}O, AQ = 0.025 s, RD = 0 s, SW = 84 000 Hz, TD = 4K. For ^{33}S, AQ = 0.02 s, SW = 50 000 Hz, TD = 2K. In both cases the FIDs were zero-filled to 16K before transforming and at least 100 000 scans were collected. The RIDE (14) pulse sequence was used to reduce the effect of probe ringing for ^{33}S spectra. All reactions that were monitored by nmr spectroscopy were carried out directly in the nmr tubes using at least 1 M concentrations of reagents.

Reaction of TAS^+NSO^- with sulphur

A mixture of TAS^+NSO^- (0.55 g, 2.4 mmol) and S_8 (0.15 g, 0.59 mmol) in acetonitrile (10 mL) was stirred at 23°C. The solution became bright red immediately, then purple after 1 h and finally dark blue after 24 h. The volume of the solution was reduced to 2 mL under vacuum and then the addition of cold diethyl ether (30 mL) produced a sticky blue solid, which was recrystallized from CH_3CN/diethyl ether to give $TAS^+S_4N^-$ identified by ir, Raman, visible, and ^{14}N nmr spectra (8) (see Results and discussion for details).

Reaction of TAS^+NSO^- with S_4N_4

A solution of TAS^+NSO^- (1.25 g, 5.52 mmol) in CH_3CN (10 mL) was added dropwise to a stirred slurry of S_4N_4 (0.50 g, 2.71 mmol) in CH_3CN (30 mL) at −35°C. The solution became red within 1 min. The mixture was stirred at −35°C for 16 h and then solvent was removed under vacuum to give a red solid (1.45 g), which was shown by ^{14}N nmr, uv–visible, and ir spectra to be a mixture of $TAS^+S_3N_3O^-$ (4) and $TAS^+S_3N_3^-$ (16, 17) (see Results and discussion for details).

Results and discussion

Reaction of NSO^- with sulphur

The reaction of the soluble salt TAS^+NSO^- with elemental sulphur in acetonitrile produces a series of colour changes. The initially bright yellow solution of TAS^+NSO^- turns intensely red immediately upon the addition of sulphur. The solution then becomes purple after ca. 1 h and finally turns dark blue within a day. This transformation was followed by uv–visible spectroscopy (Fig. 1), which showed that the red species was associated with a visible absorption band at 501 nm (cf. λ_{max} 496 nm for S_xNSO^- (6)) and the blue species had an absorption band at 582 nm (cf. λ_{max} 582 nm for S_4N^- (8)). The absence of an isosbestic point indicates the involvement of an intermediate in the conversion of S_xNSO^- to S_4N^-. The red anion $SSNO^-$, a linkage isomer of **4***a*, has λ_{max} 448 nm (18) and therefore can be ruled out as a possible candidate for the red species. Attempts to isolate the red species by carrying out the reaction at low temperatures always gave a mixture of the red and blue products. When the reaction was allowed to go to completion at 23°C the final blue product was isolated and identified as $TAS^+S_4N^-$ by ir, Raman, and ^{14}N nmr spectra (*vide supra*).

Further characterization of the 501-nm species was achieved by ^{14}N nmr and vibrational spectra. The ^{14}N nmr spectra of the reaction of TAS^+NSO^- with 2 equivalents of sulphur are illustrated in Fig. 2 and the nmr parameters for relevant species are summarized in Table 1. Several recent publications have demonstrated the value of ^{14}N nmr spectroscopy for monitoring the solution behaviour of small S–N molecules (14, 19, 20), and N–S–O anions fall into this category. The ^{14}N nmr spectrum of NSO^- exhibits a relatively sharp peak at +139 ppm. Upon addition of sulphur to a solution of TAS^+NSO^- in acetonitrile a new signal appears at +45 ppm, which is attributed to the

Can. J. Chem. Downloaded from www.nrcresearchpress.com by 186.148.149.217 on 09/07/12
For personal use only.

Can. J. Chem. Downloaded from www.nrcresearchpress.com by 186.148.149.217 on 09/07/12
For personal use only.

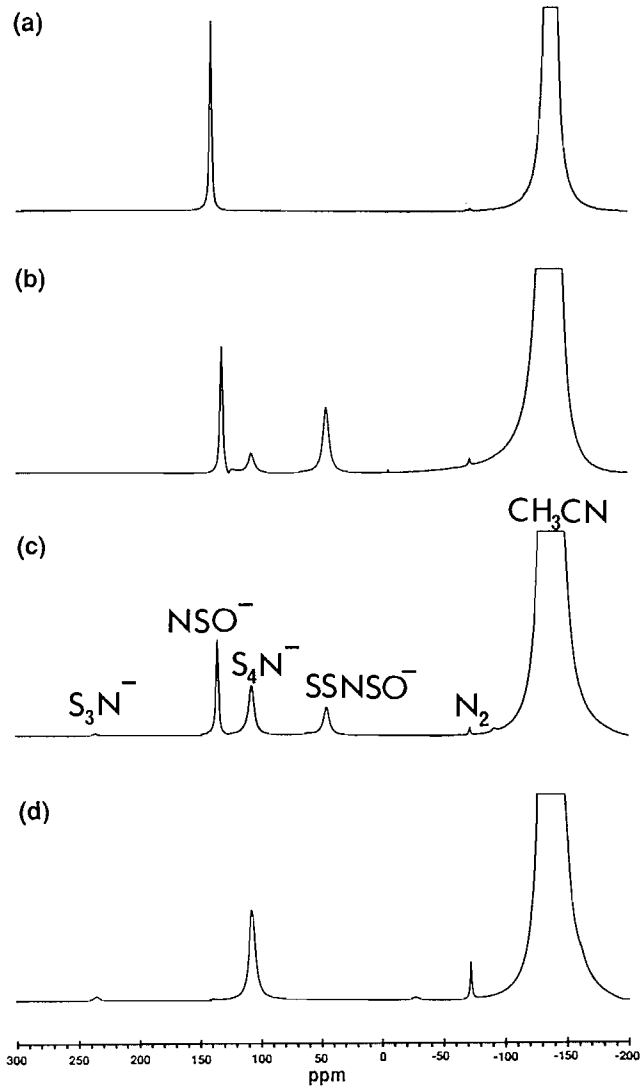


FIG. 2. The ^{14}N nmr spectra of the reaction of TAS^+NSO^- with sulphur in CH_3CN: (a) TAS^+ NSO^-; (b) after 40 min; (c) after 11 h; (d) after 16 weeks. The intensities of the signals in spectra (b), (c), and (d) are three times those of spectrum (a).

501-nm species. The new signal grows gradually at the expense of the signal due to NSO^-, which is shifted to higher field by ca. 10 ppm during the course of the reaction, and after ca. 40 min a third peak is evident at +107 ppm. This resonance was shown to be due to the S_4N^- ion by comparison with the chemical shift of an authentic sample of PPN^+ S_4N^- (Table 1). The transformation of NSO^- to the 501-nm species and the subsequent disproportionation of the red species to give S_4N^- continues over a period of several weeks until only the peak due to S_4N^- is observed (Fig. 2d). Apart from a very small amount of S_3N^-, which is known to be in photochemical equilibrium with S_4N^- (21, 22), and $S_3N_3^-$, no other nitrogen-containing products are evident from the ^{14}N nmr spectra. To rule out the possibility that peak(s) due to other nitrogen-containing product(s) are obscured by the broad CH_3CN signal, the $TAS^+NSO^-/2S$ reaction was also carried out in DMF and the reaction of KNSO with two equivalents of sulphur in the presence of 18-crown-6 was performed in THF. Both of these reactions gave S_4N^- as the only detectable nitrogen-containing species among the final products. If the TAS^+NSO^-/S reaction is carried out using a 1:1 stoichiometry, unreacted NSO^- remains even after 22 weeks. Thus 2 equivalents of S are necessary to ensure complete consumption of NSO^-, indicating that the red species is $SSNSO^-$ rather than $SNSO^-$ (cf. the rapid reaction of $SNSS^-$ with sulphur to give $SSNSS^-$ (7)).

Vibrational spectra provide some support for this conclusion (see Table 2). The blue species is clearly identified as S_4N^- by comparison of the ir and Raman spectra of the isolated product with those of $PPN^+S_4N^-$ (8). The bands at ca. 570 and ca. 595 cm^{-1} are attributed to S–S stretching vibrations and the weak band at ca. 890 cm^{-1} and the very strong band at ca. 710 cm^{-1} in the Raman spectra are assigned to ν_{as}(SNS) and ν_s(SNS), respectively (8). By analogy with the spectral assignments for $SSNSS^-$, the strong bands at 575 cm^{-1} in the Raman spectrum and at 574 cm^{-1} in the ir spectrum of red solutions of $TAS^+NSO^-/2S$ are tentatively attributed to an S–S stretching vibration and the Raman bands at ca. 705 vs and 815 w cm^{-1} are assigned to ν_{as}(SNS) and ν_s(SNS), respectively. Thus the vibrational spectra also indicate that the red species is $SSNSO^-$ rather than $SNSO^-$.

The $SSNSO^-$ can be viewed as a thionylimide derivative and such compounds are known to eliminate SO_2 readily in the presence of a base (23). Although evidence for the formation of SO_2 was not apparent from ir spectra, bands that might be attributed to sulphur oxyanions were observed for the final blue solutions. Consequently, the $TAS^+NSO^-/2S$ reaction was monitored by ^{17}O and ^{33}S nmr spectroscopies in an attempt to identify the sulphur oxyanion(s) formed. Table 3 gives the ^{17}O and ^{33}S nmr chemical shifts for NSO^- and the more common sulphur oxyanions. An ^{17}O signal at ca. 300 ppm, which is observed in the early stages of the reaction and disappears after 24 h, is attributed to $SSNSO^-$. A signal at 194 ppm, which appears after 7 h, is tentatively assigned to SO_3^{2-} (see Table 3). However, this signal also disappears after 24 h and two new peaks are observed at 178 and 220 ppm. Although these chemical shifts are in the range observed for sulphur oxyanions, we have been unable to identify the species responsible for them. The ^{33}S nmr spectra were less informative, since the signals for the intermediates were too broad to be detected. The final blue solution did, however, give a ^{33}S nmr signal at ca. 0 ppm. The width of this peak ($\Delta\nu_{1/2} \sim 1000$ Hz) is much greater than that of SO_4^{2-} (see Table 3), so it is likely due to a closely related sulphur oxyanion of lower symmetry. The $S_2O_3^{2-}$ ion is a possible candidate for the species that gives rise to the 220-ppm signal in the ^{17}O nmr spectrum, but no evidence for the formation of $S_2O_3^{2-}$ is provided by the ^{33}S nmr spectrum.

Spectroscopic characterization of the "NSO_2^-" ion

The "NSO_2^-" ion has been obtained as a cesium salt by the reaction of wet CsF with $Me_3SiNSNSiMe_3$ (9). This anion was characterized primarily on the basis of field desorption mass spectra of the Ph_4P^+ and PPN^+ salts, which exhibited molecular ion peaks with 1% of the intensity of the base peaks. The X-ray structure of the Ph_4P^+ salt could not be solved due to disorder (9*b*, 24).

We have repeated the literature preparation of "$Cs^+NSO_2^-$" to determine whether the NSO_2^- ion was one of the products of the decomposition of $SSNSO^-$. However, $Cs^+NSO_2^-$ shows ir and Raman bands characteristic of the NSO^- ion (see Table 4). We note that the strong bands at 1260–1270 and ca. 990 cm^{-1} are also present in the published ir spectra of "$PPN^+NSO_2^-$" and "$Ph_4P^+NSO_2^-$". Additional bands are apparent in the ir

Can. J. Chem. Downloaded from www.nrcresearchpress.com by 186.148.149.217 on 09/07/12
For personal use only.

TABLE 1. The ^{14}N nmr chemical shifts and line widths for N–S–O and S–N anions

Compound[a]	Solvent	δ(ppm)[b]	$\Delta\nu_{1/2}$ (Hz)
$PPN^+S_3N^-$	CH_3CN	235	120
$(Me_2N)_3S^+NSO^-$	CH_3CN	139	55
$K(18\text{-crown-6})^+NSO^-$	THF	134	760
$PPN^+S_4N^-$	CH_3CN	106[c]	130
$(Me_2N)_3S^+SSNSO^-$	CH_3CN	45	170
$PPN^+S_3N_3O_2^-$ [e]	CH_2Cl_2	−28, −165	[f]
N_2	CH_3CN	−71.4[d]	30
$PPN^+S_3N_3O^-$ [e]	CH_2Cl_2	−92, −155	[f]
CH_3CN	—	−136	100
$PPN^+S_3N_3^-$ [g]	$CHCl_3$	−232	[f]
$Ph_4P^+S_3N_3^-$ [h]	CH_2Cl_2	−234	[f]
DMF	—	−275	200
$PPN^+S_4N_5O^-$	CH_2Cl_2	−225, −251, −276[i]	770, 770, 1000
$(Me_2N)_3S^+NSO^-$	CH_3CN	−325	900

[a]This work unless otherwise indicated.
[b]Relative to $MeNO_2$.
[c]Incorrectly given as −136 ppm (relative to $MeNO_2$) in ref. 7.
[d]Data from ref. 15.
[e]^{15}N values from ref. 4.
[f]Not reported.
[g]Data from ref. 17.
[h]Data from ref. 20.
[i]Literature values: −232, −251, −276 (4).

TABLE 2. Infrared and Raman bands for TAS^+SSNSO^- and S_4N^- salts

Sample	Raman bands (cm^{-1})[a]	Infrared bands (cm^{-1})	Assignment
$PPN^+S_4N^-$ [b]		416 w (415 w)	δ(NSS)
	570 s	567 vs (562 vs)	ν(S–S)
	592 s	594 s (592 m)	ν(S–S)
	710 vs	711 m (709 m)	ν_s(SNS)
	892 w	893 w (892 w)	ν_{as}(SNS)
$TAS^+S_4N^-$ [c]	574 s	568 m	[f]
	592 m	595 s	[f]
	706 vs	[d]	[f]
	893 w	[e]	[f]
TAS^+SSNSO^- [g]	438 w		δ(NSS)
	505 vw	494 m	δ(NSO)
		550 s	?
	575 s	574 vs	ν(S–S)
	704 vs		ν(SNS)
	815 w		ν(SNS)
	982 vw		ν(NSO)

[a]Laser wavelength 514.5 nm, unless otherwise indicated.
[b]Data taken from ref. 8; ir bands in parentheses are for a solution in CH_3CN.
[c]Blue solid isolated from the TAS^+NSO^-/2S reaction.
[d]Obscured by Nujol.
[e]Obscured by TAS^+ band.
[f]As for S_4N^-.
[g]Red solution in CH_3CN. Infrared data recorded at room temperature, Raman data recorded with both 488 and 514.5 nm excitation at −45°C.

and Raman spectra of $Cs^+NSO_2^-$ that can be attributed to the presence of $Cs^+S_3N_3^-$ (16). The ^{14}N nmr spectrum of $Cs^+NSO_2^-$ in a variety of solvents shows a strong signal at 138–140 ppm (cf. 139 ppm for NSO^-). A signal was also observed for $S_3N_3^-$ at −232 ppm (see Table 1) and minor peaks at −92 and −155 ppm can be attributed to a small amount of $S_3N_3O^-$ (formed by the air oxidation of $S_3N_3^-$ (4)). The PPN^+ salt of NSO_2^- was prepared from $Cs^+NSO_2^-$ and PPN^+Cl^- and

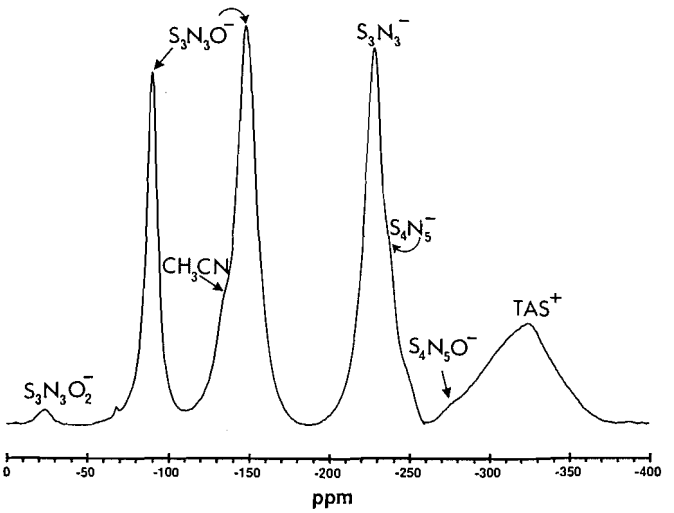


FIG. 3. The ^{14}N nmr spectrum of a DMSO solution of the products from the reaction of TAS^+NSO^- with S_4N_4 in CH_3N.

the ^{14}N nmr spectrum of the crude product revealed the presence of $S_3N_3^-$ in addition to the major signal at 138 ppm attributed to NSO^-. A recrystallized sample of $PPN^+NSO_2^-$ showed only the NSO^- peak. Thus we conclude that the major component of the product from the reaction of $Me_3SiNSNSiMe_3$ with wet CsF is Cs^+NSO^- rather than $Cs^+NSO_2^-$ as previously claimed (9). We note that the published analytical data (C, H, N, and S) for the Ph_4P^+ and PPN^+ salts are not sufficiently accurate to distinguish between NSO_2^- and NSO^- salts (9). This finding may also explain the unexpected conversion of NSO_2^- to the NSO^- ligand in the reaction of $Cs^+NSO_2^-$ with $RhH(CO)(PPh_3)_3$ to give *trans*-$Rh(CO)(NSO)(PPh_3)_2$ (25).

Reaction of NSO^- with S_4N_4

The reaction of S_4N_4 with nucleophiles, e.g., N_3^-, S^{2-}, is known to promote ring contraction to give $S_3N_3^-$ (26) probably via a 1,3-nitrogen shift (27). Six-membered rings may also

TABLE 3. The ^{17}O and ^{33}S nmr chemical shifts and line widths of N–S–O and S–O anions

Compound	Solvent	$\delta\ ^{17}O$(ppm)[a]	$\Delta\nu_{1/2}$(Hz)	$\delta\ ^{33}S$(ppm)[b]	$\Delta\nu_{1/2}$(Hz)
$(Me_2N)_3S^+NSO^-$ [c]	CH_3CN	449	55	282	275
$PPN^+S_4N_5O^-$	CH_2Cl_2	167	165	−36	650
$[PPN]_2S_2O_3$	CH_3CN	234	140	33[d]	60
$Na_2S_2O_3$	H_2O	224	180	33[d]	50
$[PPN]_2SO_4$	CH_3CN	171	140	2	100
Na_2SO_4	H_2O	165	110	0	20
$[PPN]_2SO_3$	CH_3CN	193	280	[e]	
Na_2SO_3	NaOH(aq) pH 12	208	180	[e]	

[a]Relative to H_2O.
[b]Relative to SO_4^{2-}(aq).
[c]$\delta(^{33}S)$ 400 ppm, $\Delta\nu_{1/2}$ 12 000 Hz for $(Me_2N)_3S^+$ in THF.
[d]Only the central S atom is observed.
[e]No signal observed.

TABLE 4. Infrared and Raman spectra (cm^{-1}) of salts of the NSO^- and "NSO_2^-" anions

K^+NSO^-		TAS^+NSO^- [a]		$Cs^+NSO_2^-$ [b]		
Infrared[c]	Raman[d]	Infrared	Raman[d]	Infrared	Raman[e]	Assignments
1275 vs	1276 s	1261 vs	1264 m	1267 vs	1266 s	ν_{as}(NSO)
				1197 m		[f]
991 s	992 vs	991 s	989 m	989 s	988 s	ν_s(NSO)
				943 m		[f]
				920 m	920 s	[g]
					894 vs	[f]
					862 s	[f]
					714 s	[f]
				649 w		[g]
					584 s	[g]
517 m	520 m	493 m	494 m	509 m		δ(NSO)
					436 br,s	[f]

[a]Cation bands are not included.
[b]Crude product from the reaction of $Me_3SiNSNSiMe_3$ with wet CsF.
[c]Literature values: 1270 vs, 990 vs, 515 vs (ref. 1).
[d]Laser wavelength 600 nm.
[e]Laser wavelength 514.5 nm.
[f]Unassigned bands.
[g]Bands attributed to $S_3N_3^-$ (ref. 16).

be obtained in high yields from S_4N_4 by 1,4-cycloaddition reactions, e.g., with P═N— bonds (28). The formation of **2** from the reaction of electrochemically generated NSO^- with S_4N_4 (6) may also result from the latter reaction pathway. We have, therefore, performed this reaction on a preparative scale in the hope that it would provide a specific, high-yield synthesis of **2**.

The reaction of TAS^+NSO^- with S_4N_4 in acetonitrile at −35°C occurs rapidly to give a dark red solution. However, the ^{14}N nmr spectrum of this solution (see Fig. 3) shows that $S_3N_3^-$ is formed in significant amounts, in addition to the major product, **2**. From the integrated intensities of the nmr signals the approximate ratio $S_3N_3O^-$:$S_3N_3^-$ is 3:2 and very small amounts of $S_4N_5^-$, $S_4N_5O^-$, and $S_3N_3O_2^-$ are also present. The presence of $S_4N_5O^-$, which was difficult to ascertain from the ^{14}N nmr spectrum due to overlap with the signals for $S_3N_3^-$, $S_4N_5^-$, and $(Me_2N)_3S^+$, was confirmed by both ^{17}O and ^{33}S nmr spectra (see Table 3). Thus the reaction of NSO^- with S_4N_4 occurs predominantly via 1,4-cycloaddition to give **2**, but, even at low temperatures, a significant amount of ring contraction to produce $S_3N_3^-$, via a 1,3-nitrogen shift (27), also takes place (see Fig. 4).

Thermolysis of $S_3N_3O^-$

The thermolysis of $S_3N_3^-$ in CH_3CN at reflux produces $SSNSS^-$ (8). The formation of the latter ion is thought to occur via initial loss of N_2S from $S_3N_3^-$ to give SNS^-, which reacts rapidly with sulphur to give S_4N^-. By analogy, the thermolysis of $S_3N_3O^-$ might be expected to give $SSNSO^-$ (via $SNSO^-$). In the context of the present study of the reaction of NSO^- with sulphur (*vide infra*), it is significant that an investigation of the thermolysis of $PPN^+S_3N_3O^-$ revealed $PPN^+S_4N^-$ as the only identifiable product (29).[2] The results described here indicate that, under the conditions of the thermolysis, $SSNSO^-$ would disproportionate rapidly to give S_4N^- and sulphur oxyanions.

[2]We are grateful to Professor R. T. Oakley (University of Guelph) for this unpublished information.

Can. J. Chem. Downloaded from www.nrcresearchpress.com by 186.148.149.217 on 09/07/12
For personal use only.

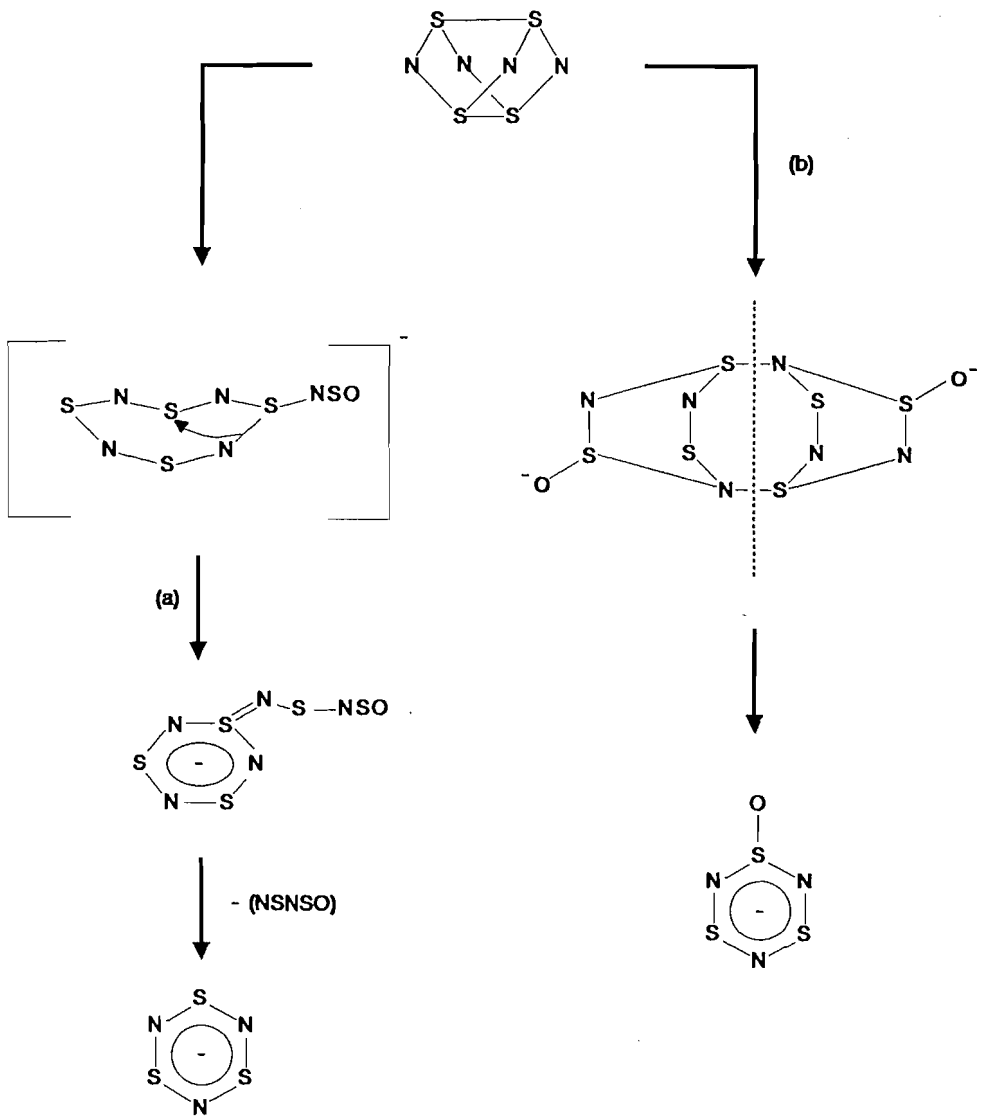


FIG. 4. Pathways for the reaction of NSO^- with S_4N_4: (a) 1,3-nitrogen shift; (b) 1,4-cycloaddition.

Conclusions

This study of the reactivity of NSO^- has demonstrated the usefulness of ^{14}N nmr spectroscopy for the analysis of solutions containing complex mixtures of N–S–O (and N–S) anions. The formation of $SSNSO^-$, rather than $SNSO^-$, from NSO^- and sulphur is consistent with the rapid conversion of $SNSS^-$ into $SSNSS^-$ via reaction with itself (or another source of sulphur). The low thermal stability of $SSNSO^-$ was unexpected and may be related to the ease of intramolecular elimination of SO_2. The formation of both $S_3N_3O^-$ and $S_3N_3^-$ from NSO^- and S_4N_4 provides a unique example of a dual reaction pathway for the cleavage of S_4N_4 by nucleophiles. The treatment of $Me_3SiNSNSiMe_3$ with wet CsF gives Cs^+NSO^- as the major product, rather than $Cs^+NSO_2^-$ as previously claimed, and alternative routes to the NSO_2^- ion should be considered.

Acknowledgements

The financial support of NSERC (Canada) in the form of operating grants (to T.C. and H.J.V.) and a postgraduate scholarship to K.J.S. is gratefully acknowledged. We also wish to thank Dr. K. S. Dhathathreyan for the initial investigation of the reaction of NSO^- with S_4N_4, Dr. F. Edelmann for a generous gift of $TAS^+Me_3SiF_2^-$, Dr. R. Kydd for use of the Raman and FTIR spectrometers, Dr. R. A. Shaw, Mr. E. Villeneuve, and Mr. T. Eggimann for assistance with the FTIR spectra, and Canadian Tool Engineering Ltd. (Montreal) for the manufacture of the subtractive infrared cell. We also acknowledge helpful correspondence from Professor H. W. Roesky regarding the NSO_2^- ion. H.J.V. is a scholar of the Alberta Heritage Foundation for Medical Research (AHFMR). The NMR spectrometers were purchased with funds provided by NSERC and the AHFMR.

1. D. A. ARMITAGE and J. C. BRAND. J. Chem. Soc. Chem. Commun. 1078 (1979).
2. W. HEILEMANN and R. MEWS. Chem. Ber. **121**, 461 (1988).
3. T. CHIVERS, K. S. DHATHATHREYAN, C. LENSINK, and J. F. RICHARDSON. Inorg. Chem. **27**, 1570 (1988).
4. T. CHIVERS, A. W. CORDES, R. T. OAKLEY, and W. T. PENNINGTON. Inorg. Chem. **22**. 2429 (1983).
5. (*a*) R. STEUDEL, P. LUGER, and H. BRADACZEK. Angew. Chem. Int. Ed. Engl. **12**, 316 (1973); (*b*) P. LUGER, H. BRADACZEK, and R. STEUDEL. Chem. Ber. **109**, 3441 (1976).
6. T. CHIVERS and M. HOJO. Inorg. Chem. **23**, 4088 (1984).

Can. J. Chem. Downloaded from www.nrcresearchpress.com by 186.148.149.217 on 09/07/12
For personal use only.

7. J. BOJES, T. CHIVERS, W. G. LAIDLAW, and M. TRSIC. J. Am. Chem. Soc. **104**, 4837 (1982).
8. T. CHIVERS, W. G. LAIDLAW, R. T. OAKLEY, and M. TRSIC. J. Am. Chem. Soc. **102**, 5773 (1980).
9. (*a*) H. W. ROESKY, W. SCHMIEDER, W. ISENBERG, D. BOHLER, and G. M. SHELDRICK. Angew. Chem. Int. Ed. Engl. **21**, 153 (1982); (*b*) H. W. ROESKY, W. SCHMIEDER, W. ISENBERG, W. S. SHELDRICK, and G. M. SHELDRICK. Chem. Ber. **115**, 2714 (1982).
10. M. VILLENA-BLANCO and W. L. JOLLY. Inorg. Synth. **9**, 98 (1967).
11. J. F. RUFF and W. J. SCHLIENTZ. Inorg. Synth. **15**, 84 (1974).
12. A. MARTINSEN and J. SONGSTAD. Acta Chem. Scand. A, **31**, 645 (1977).
13. R. A. KYDD. Appl. Spectrosc. **32**, 250 (1978).
14. P. S. BELTON and J. D. WOOLLINS. Magn. Reson. Chem. **24**, 1080 (1986).
15. D. D. MCINTYRE, A. W. APBLETT, P. LUNDBERG, K. J. SCHMIDT, and H. J. VOGEL. J. Magn. Reson. **83**, 377 (1989), and references therein.
16. J. BOJES, T. CHIVERS, W. G. LAIDLAW, and M. TRSIC. J. Am. Chem. Soc. **101**, 4517 (1979).
17. T. CHIVERS, R. T. OAKLEY, O. J. SCHERER, and G. WOLMERSHAUSER. Inorg. Chem. **20**, 914 (1981).
18. F. SEEL, R. KUHN, G. SIMON, M. WAGNER, B. KREBS, and M. DARTMANN. Z. Naturforsch. B: Anorg. Chem. Org. Chem. **40B**, 1607 (1985).
19. J. PASSMORE and M. SCHRIVER. Inorg. Chem. **27**, 2749 (1988).
20. P. S. BELTON, I. P. PARKIN, D. J. WILLIAMS, and J. D. WOOLLINS. J. Chem. Soc. Chem. Commun. 1479 (1988).
21. L. BERNARD, J. P. LELIEUR, and G. LEPOUTRE. Nouv. J. Chim. **9**, 199 (1985).
22. H. PRESTEL and U. SCHINDEWOLF. Z. Anorg. Allg. Chem. **551**, 21 (1987).
23. T. CHIVERS, C. LENSINK, and J. F. RICHARDSON. Organometallics, **6**, 1904 (1987), and references therein.
24. W. SCHMIEDER. Ph.D. Thesis, Universität Göttingen, 1982.
25. H. W. ROESKY, K. K. PANDEY, B. KREBS, and M. DARTMANN. J. Chem. Soc. Dalton Trans. 2271 (1984).
26. J. BOJES, T. CHIVERS, I. DRUMMOND, and G. MACLEAN. Inorg. Chem. **17**, 3668 (1978).
27. R. T. OAKLEY. Prog. Inorg. Chem. **36**, 299 (1988).
28. T. CHIVERS, K. S. DHATHATHREYAN, S. W. LIBLONG, and T. PARKS. Inorg. Chem. **27**, 1305 (1988).
29. M. SHEVALIER. B.Sc. Thesis, The University of Calgary, 1981.

Can. J. Chem. Downloaded from www.nrcresearchpress.com by 186.148.149.217 on 09/07/12
For personal use only.

Synthesis of fluorinated phosphonic, sulfonic, and mixed phosphonic/sulfonic acids

DEBAO SU, WENBIAO CEN, ROBERT L. KIRCHMEIER, AND JEAN'NE M. SHREEVE[1]
Department of Chemistry, University of Idaho, Moscow, ID 83843, U.S.A.

Received February 3, 1989

This article is dedicated to Professor Ronald J. Gillespie on the occasion of his 65th birthday

DEBAO SU, WENBIAO CEN, ROBERT L. KIRCHMEIER, and JEAN'NE M. SHREEVE. Can. J. Chem. **67**, 1795 (1989).

The acids $(HO)_2P(O)CFHSO_3H$, $(HO)_2P(O)(CF_2)_4O(CF_2)_2SO_3H$, $H(CF_2)_2O(CF_2)_2P(O)(OH)_2$, $H(CF_2)_2O(CF_2)_4P(O)(OH)_2$, $(HO)_2P(O)(CF_2)_2O(CF_2)_4H$, and the acid precursor $(C_2H_5O)_2P(O)CF(SO_3Na)_2$ have been synthesized. Elemental analysis, ^{19}F, ^1H, and ^{31}P NMR, and mass spectroscopy were used for characterization of these materials. They are very strong acids, and exhibit a high degree of stability in aqueous solution at elevated temperature, which makes them attractive candidates for use as electrolytes in fuel cells.

Key words: fluorinated phosphonic acids; fluorinated sulfonic acids; ^1H, ^{19}F, ^{31}P NMR.

DEBAO SU, WENBIAO CEN, ROBERT L. KIRCHMEIER et JEAN'NE M. SHREEVE. Can. J. Chem. **67**, 1795 (1989).

On a synthétisé les acides $(HO)_2P(O)CFHSO_3H$, $(HO)_2P(O)(CF_2)_4O(CF_2)_2SO_3H$, $H(CF_2)_2O(CF_2)_2P(O)(OH)_2$, $H(CF_2)_2O(CF_2)_4P(O)(OH)_2$, $(HO)_2P(O)(CF_2)_2O(CF_2)_4H$ ainsi que de leur précurseur acide $(C_2H_5O)_2P(O)CF(SO_3Na)_2$. Pour la caractérisation de ces composés, on a fait appel à l'analyse élémentaire, à la RMN du ^{19}F, du ^1H et du ^{31}P ainsi qu'à la spectrométrie de masse. Ces composés sont des acides très forts et ils sont très stables en solution aqueuse, à température élevée; ces caractéristiques en font d'excellents candidats comme électrolytes dans des cellules à combustible.

Mots clés : acides phosphoniques fluorés; acides sulfoniques fluorés; RMN du ^1H, du ^{19}F et du ^{31}P.

[Traduit par la revue]

Can. J. Chem. Downloaded from www.nrcresearchpress.com by 186.148.149.217 on 09/07/12
For personal use only.

Introduction

Many fluorinated sulfonic and phosphonic acids exhibit properties that make them potentially useful as electrolytes in fuel cells. They are much stronger acids than their nonfluorinated analogues, and are generally more stable. In addition, oxygen solubility is greatly enhanced, and volatility at elevated temperatures may be lower. In fuel cell applications, these factors combine to provide increased conductivity, enhanced oxygen reduction kinetics, and longer term system stability when compared to phosphoric acid as the electrolyte.

The primary acid used in fuel cells today is H_3PO_4. However, it has many drawbacks, including low oxygen solubility and anion adsorption on the catalyst surface. There is a need to develop new compounds that have the desirable properties of H_3PO_4 but fewer of the less desirable ones, in order to enhance the usefulness of fuel cells as alternative energy sources.

Fluorocarbon electrolytes have the ability to lower the surface tension of water. This effect is in part due to several structural factors: (1) terminal grouping; (2) chain-length; and (3) the presence of heteroatoms in the chain. For example, a CF_3 terminal group attached to a CF_2 chain will have a greater surface tension lowering effect than a HCF_2 terminal group attached to a similar chain. The solubility of oxygen in fluorocarbon systems is dependent on the boiling point, density, molecular weight, and viscosity of the fluorocarbon. These properties in turn are dependent in part on the structural factors and composition mentioned above.

At low temperature trifluoromethanesulfonic acid has been found to be superior to H_3PO_4 with respect to electrode kinetics. However, the acid hydrate is too volatile for extended use at the operating temperature of fuel cells (>100°C), and in addition it tends to wet the Teflon surface of the electrodes used (1). A variety of other partially fluorinated or perfluoroalkylsulfonic and disulfonic acids (1–5) as well as phosphonic acids (6–8), mixed sulfonic or phosphonic/carboxylic acids (9), and a mixed sulfonic/phosphonic acid (10) have been synthesized for evaluation as potential fuel cell electrolytes.

To further the evaluation of structure and composition factors effective for fuel cell electrolytes, we have prepared a number of additional partially fluorinated and perfluoro mixed sulfonic/phosphonic, and phosphonic acids. Electrochemical testing of these acids in model fuel cells should provide valuable information in this regard.

Results and discussion

The starting material for the preparation of the mixed acid $(HO)_2P(O)(CF_2)_4O(CF_2)_2SO_3H$ is the iodide $I(CF_2)_4O(CF_2)_2SO_2F$, which was prepared by the literature method (11).

$$I(CF_2)_4O(CF_2)_2SO_2F + (C_2H_5O)_2POP(OC_2H_5)_2 + (CH_3)_3COOC(CH_3)_3 \xrightarrow[120\,^\circ C,\ 3\ h]{CF_2ClCFCl_2}$$

$$(C_2H_5O)_2P(CF_2)_4O(CF_2)_2SO_2F \xrightarrow[-10 \rightarrow -5\,^\circ C,\ 2\ h]{(CH_3)_3COOH/CH_3OH}$$

$$(C_2H_5O)_2P(O)(CF_2)_4O(CF_2)_2SO_2F \xrightarrow[N_2,\ 85\,^\circ C,\ 2\ h]{Na_2S_2O_4/NaHCO_3,\ H_2O/CH_3CN}$$

$$(C_2H_5O)_2P(O)(CF_2)_4O(CF_2)_2SO_2Na \xrightarrow[25\,^\circ C,\ 12\ h]{30\%\ H_2O_2} \mathbf{1}\ (90\%)$$

$$(C_2H_5O)_2P(O)(CF_2)_4O(CF_2)_2SO_3Na \xrightarrow[120\,^\circ C,\ 6\ h]{HCl} \mathbf{2}\ (93\%)$$

$$(HO)_2P(O)(CF_2)_4O(CF_2)_2SO_3Na \xrightarrow[resin]{acid} \mathbf{3}\ (88\%)$$

$$(HO)_2P(O)(CF_2)_4O(CF_2)_2SO_3H \quad \mathbf{4}\ (76\%)$$

[1]Author to whom correspondence may be addressed.

Can. J. Chem. Downloaded from www.nrcresearchpress.com by 186.148.149.217 on 09/07/12
For personal use only.

Removal of inorganic impurities from **1** was found to be necessary for the successful synthesis of **2**, **3**, and **4**. Compound **3** is converted to **4** by passing an aqueous solution of **3** through a 20 mm × 30 cm long column packed with Amberlite IR-120 resin at an approximate flow rate of 2 mL/min. Purification was accomplished by repetitive dissolution of **1** in acetonitrile, followed by filtration. Attempts to simplify the synthesis of **4** by replacing the starting material $I(CF_2)_4O(CF_2)_2SO_2F$ with $I(CF_2)_4O(CF_2)_2SO_2Cl$ or $I(CF_2)_4O(CF_2)_2SO_3Na$ were unsuccessful. The sulfonyl chloride reacted vigorously with tetraethylpyrophosphite in the absence of di-*tert*-butylperoxide to give a complex mixture. No suitable solvent for the reaction of the sodium sulfonate with tetraethylpyrophosphite could be found.

Conversion of $I(CF_2)_4O(CF_2)_2SO_2F$ or $I(CF_2)_2O(CF_2)_2SO_2F$ to the respective diiodide

$$I(CF_2)_nO(CF_2)_2SO_2F \xrightarrow[H_2O/CH_3CN,\ 25\,^\circ C,\ 8\ h]{K_2SO_3} I(CF_2)_nO(CF_2)_2SO_2K \quad \begin{matrix} n=2 & (80\%) \\ n=4 & (71\%) \end{matrix}$$

$$\xrightarrow[CH_3CN\ 80\,^\circ C,\ 7\ h]{I_2} I(CF_2)_nO(CF_2)_2I \quad \mathbf{5}\,(n=2)\ (39\%) \text{ and } \mathbf{6}\,(n=4)\ (37\%)$$

provided the starting materials for the synthesis of $H(CF_2)_2O(CF_2)_4P(O)(OH)_2$, $(HO)_2P(O)(CF_2)_2O(CF_2)_4H$, and $H(CF_2)_2O(CF_2)_2P(O)(OH)_2$.

$$I(CF_2)_2O(CF_2)_2I + (C_2H_5O)_2P{-}O{-}P(OC_2H_5)_2$$
5

$$\xrightarrow{(CH_3)_3COOC(CH_3)_3} H(CF_2)_2O(CF_2)_2P(OC_2H_5)_2$$

$$\xrightarrow[MeOH]{(CH_3)_3COOH} H(CF_2)_2O(CF_2)_2P(O)(OC_2H_5)_2$$
7

$$\mathbf{7} + BrSi(CH_3)_3 \xrightarrow[2d]{25\,^\circ C} H(CF_2)_2O(CF_2)_2P(O)[OSi(CH_3)_3]_2$$
8

$$\mathbf{8} + H_2O \longrightarrow H(CF_2)_2O(CF_2)_2P(O)(OH)_2$$
9

However, the product of the tetraethylpyrophosphite reaction with **6** is a mixture of $H(CF_2)_4O(CF_2)_2P(OC_2H_5)_2$ and $(C_2H_5O)_2P(CF_2)_4O(CF_2)_2H$. This intermediate mixture was separated by distillation under reduced pressure prior to conversion to the corresponding acids $H(CF_2)_4O(CF_2)_2P(O)(OH)_2$ **10** and $(HO)_2P(O)(CF_2)_4O(CF_2)_2H$ **11**. No evidence for the formation of any other products, i.e., ether-containing diphosphonic acids, was obtained.

(Sulfomonofluoromethyl)phosphonic acid, $(HO)_2P(O)CFHSO_3H$, was prepared as described below from triethylphosphite and tribromofluoromethane.

$$(C_2H_5O)_3P + CFBr_3 \xrightarrow[4\ h]{0\,^\circ C} (C_2H_5O)_2P(O)CFBr_2$$
12 (77%)

$$\mathbf{12} + Na_2S_2O_4 \xrightarrow[25\,^\circ C,\ 4\ h]{NaHCO_3} (C_2H_5O)_2P(O)CFBrSO_2Na$$
13 (64%)

$$\mathbf{13} + H_2O_2 \xrightarrow[5\ h]{0 \rightarrow 25\,^\circ C} (C_2H_5O)_2P(O)CFBrSO_3Na$$
14 (75%)

$$\mathbf{14} + Zn \xrightarrow[(2)\ H_2O]{(1)\ 60\,^\circ C,\ 6\ h,\ THF} (C_2H_5O)_2P(O)CFHSO_3Na$$
15 (49%)

$$\mathbf{15} + HCl \xrightarrow[10\ h]{125\,^\circ C} (HO)_2P(O)CFHSO_3Na$$
16 (59%)

Compound **16** was then converted to the final acid product utilizing Amberlite IR-120 acid resin.

$$\mathbf{16} \xrightarrow[resin]{acid} (HO)_2P(O)CFHSO_3H$$
17 (80%)

Alternatively, treatment of **14** with sodium dithionite results in the formation of the disodium salt **18**.

$$\mathbf{14} \xrightarrow[NaHCO_3\ 0\,^\circ C,\ 4\ h]{Na_2S_2O_4} (C_2H_5O)_2P(O)CF(SO_3Na)(SO_2Na)$$
18 (80%)

The corresponding di(sodium sulfonate) is then obtained by oxidation with hydrogen peroxide.

$$\mathbf{18} \xrightarrow[-15\,^\circ C,\ 1\ h]{H_2O_2} (C_2H_5O)_2P(O)CF(SO_3Na)_2$$
19 (32%)

It was not possible to convert this salt to the acid by using HCl_{aq}. Other methods for conversion to this interesting disulfonic/phosphonic acid are under study.

Titration of aqueous solutions of either **17** or **4** with sodium hydroxide (0.0508 N) gave rise to two inflection points, one for 2 equivalents (the sulfonic acid proton and one phosphonic acid proton) and one for 1 equivalent (the second phosphonic acid proton) of the acid. The total titre for **17** gives 97% of a tribasic acid based on an anhydrous molecular weight of 194 g/mol. For **4** the total titre gives 100% of a tribasic acid based on an anhydrous molecular weight of 478 g/mol.

When **4** is dissolved in isopropyl alcohol and titrated with a toluene/methanol solution of tetrabutylammonium hydroxide (TBAH, 0.0392 N), two equivalence points are observed at approximately equal volumes of titrant. Addition of a slight excess (~10%) of TBAH after the second inflection point was followed by the addition of 10 mL (~15%) of H_2O. When the electrode had stabilized, the titration with TBAH was continued to a third inflection point. The three acid protons are easily resolved by this combination of nonaqueous/aqueous titration.

In summary, successful routes to a variety of mixed phosphonic/sulfonic acids, and partially fluorinated phosphonic acids have been developed. Study of several of these acids in

fuel cell systems should provide valuable insights regarding the effects of particular structural moieties on the performance of fluorinated *electrolytes*.

Experimental

Materials

The literature method was used to prepare $I(CF_2)_4O(CF_2)_2SO_2F$ (11). Other chemicals were obtained as follows: $Na_2S_2O_4$, CH_3CN, and HCl (Merck); $NaHCO_3$, H_2O_2 (30%), and K_2SO_3 (J. T. Baker); charcoal (activated "Norit" SGII) (MCB).

General procedures

The ^{19}F NMR spectra were obtained on a JEOL FX-90Q Fourier transform NMR spectrometer operating at 84.26 MHz. Chloroform-*d*, D_2O, CD_3CN, or DMSO-d_6 was used as solvent with $CFCl_3$ as external reference. ^{31}P NMR spectra were obtained at an operating frequency of 36.20 MHz with H_3PO_4 as an external reference. ^1H NMR spectra were recorded at 89.56 MHz. Mass spectra were recorded with a VG 7070HS mass spectrometer with FAB at 3.9, 4.8, or 10 V. Elemental analyses were performed by Beller Mikroanalytisches Laboratorium, Göttingen, Federal Republic of Germany.

Preparation of $(C_2H_5O)_2P(O)(CF_2)_4O(CF_2)_2SO_2F$

A mixture of $I(CF_2)_4O(CF_2)_2SO_2F$ (20.3 g, 38 mmol) and tetraethyl pyrophosphite (9.55 g, 57 mmol) in $CF_2ClCFCl_2$ (83 mL) with di-*tert*-butylperoxide (2.8 g, 19 mmol) was heated at 120°C for 3 h in a 150-mL autoclave. After reaction the mixture was placed in a glass flask fitted with a dropping funnel. The flask was cooled to −10°C under nitrogen and a solution of *tert*-butylhydroperoxide (138 mmol) in methanol (46 mL) was added slowly via the dropping funnel. After addition was complete at −10 to −5°C, stirring was continued at 0°C for 1 h.

The solution was washed with water (50 mL × 3) and volatile materials were removed *in vacuo*. The residue was distilled under reduced pressure to give 9.83 g of $(C_2H_5O)_2P(O)(CF_2)_4O(CF_2)_2SO_2F$ (yield 48%); bp 133°C/1.1 Torr (1 Torr = 133.3 Pa). Spectral data are ^{19}F NMR, Φ: 44.48m SO_2F, −82.99m CF_2, −83.92m CF_2, −113.05m CF_2, −121.80m CF_2, −123.45dt CF_2 (J_{P-F} = 83.58 Hz, J_{F-F} = 14.6 Hz), −126.08t CF_2; ^{31}P NMR, δ: −1.58t; ^1H NMR, δ: 1.19t CH_3 (J_{H-H} = 6.96 Hz), 4.18m CH_2; MS (CI, *m/e* (species) %): 537 ($M^+ + 1$) 64, 509 ($M^+ + 1 - C_2H_4$) 40, 495 ($M^+ + 1 - C_3H_6$) 36, 481 ($M^+ + 1 - C_4H_8$) 83, 397 ($(CF_2)_2O(CF_2)_4(O)(OH)_2P^+$) 25, 137 ($(C_2H_5O)_2(O)P^+$) 60, 109 ($C_2H_5O(O)(OH)P^+$) 100, 81 ($(HO)_2(O)P^+$) 46. *Anal.* calcd. for $C_{10}H_{10}F_{13}O_6PS$: C 22.40, H 1.88, F 46.06, P 5.78, S 5.98; found: C 22.38, H 1.71, F 46.4, P 5.88, S 6.03.

Preparation of $(C_2H_5O)_2P(O)(CF_2)_4O(CF_2)_2SO_2Na$, 1

In a 50-mL three-necked round-bottomed flask were placed 9.3 mmol $(C_2H_5O)_2P(O)(CF_2)_4O(CF_2)_2SO_2F$, 18.6 mmol $Na_2S_2O_4$, 18.6 mmol $NaHCO_3$, 8 mL H_2O, and 4 mL of CH_3CN. Under a stream of nitrogen, the contents were stirred vigorously at 85°C for 2 h. After cooling, the reaction mixture was filtered. The filtrate was evaporated to dryness under reduced pressure to give a white solid that was purified by repetitive extraction with CH_3CN. Finally 4.5 g (8.3 mmol) of **1** was obtained in 90% yield. Spectral data are ^{19}F NMR, Φ: −82.53m CF_2, −82.99m CF_2, −120.70m CF_2, −121.57dt CF_2 (J_{P-F} = 74.78 Hz, J_{F-F} = 14.01 Hz), −125.22t CF_2, −133.26s CF_2; ^{31}P NMR, δ: −4.73t; ^1H NMR, δ: −1.13t CH_3 (J_{H-H} = 6.97 Hz), 3.87m CH_2.

Preparation of $(C_2H_5O)_2P(O)(CF_2)_4O(CF_2)_2SO_3Na$, 2

Into a 30-mL flask were placed 8.3 mmol of $(C_2H_5O)_2P(O)(CF_2)_4O(CF_2)_2SO_2Na$ and 5 mL of water. At 0°C, a 3:1 mole ratio of hydrogen peroxide (30%) was added dropwise. The mixture was then stirred at room temperature for 12 h. After reaction, solvent was removed under reduced pressure, and the residue was dried to give 4.3 g of **2** (93% yield). Spectral data are ^{19}F NMR, Φ: −82.06m CF_2, −83.17m CF_2, −118.03s CF_2, −120.81m CF_2, −121.83dt CF_2 (J_{P-F} = 73.24 Hz, J_{F-F} = 14.6 Hz), −125.16t CF_2; ^{31}P NMR, δ: −4.61t; ^1H NMR, δ: 1.15t CH_3 (J_{H-H} = 7.33 Hz), 3.93m CH_2.

Preparation of $(HO)_2P(O)(CF_2)_4O(CF_2)_2SO_3Na$, 3

A mixture of 4.3 g of $(C_2H_5O)_2P(O)(CF_2)_4O(CF_2)_2SO_3Na$ (7.7 mmol) and 4.5 g of hydrochloric acid (12 N) were stirred vigorously at 120°C for 6 h and the reaction mixture was filtered. The filtrate was evaporated to dryness under vacuum to give 3.4 g (6.8 mmol) of **3** in 88% yield. Spectral data are ^{19}F NMR, Φ: −83.28m CF_2, −84.09m CF_2, −118.85s CF_2, −121.51m CF_2, −124.12d CF_2 (J_{P-F} = 79.18 Hz), −126.14m CF_2; ^{31}P NMR, δ: −3.27.

Preparation of $(HO)_2P(O)(CF_2)_4O(CF_2)_2SO_3H$, 4

An aqueous solution of 2.3 g of $(HO)_2P(O)(CF_2)_4O(CF_2)_2SO_3Na$ (4.6 mmol) was passed through an Amberlite IR-120 ion exchange resin at an approximate flow rate of 2 mL/min. The resulting solution was evaporated to dryness under reduced pressure. The crude product was dissolved in water and 0.15 g charcoal was added. The mixture was stirred at room temperature for 2 h. After the charcoal was removed by filtration, the filtrate was evaporated at reduced pressure at a temperature of 100°C to give 1.7 g **4** (3.5 mmol, 76% yield). The acid is a white solid, mp 91–92°C, and is very hygroscopic. Spectral data are ^{19}F NMR, Φ: −81.89m CF_2, −82.99m CF_2, −118.03s CF_2, −120.70m CF_2, −123.16dt CF_2 (J_{P-F} = 79.18 Hz, J_{F-F} = 14.01 Hz), −125.16t CF_2; ^{31}P NMR, δ: −3.76t; ^1H NMR, δ: 9.62s; MS (CI, *m/e* (species) %): 479 ($M^+ + 1$) 16, 281 ($(HO)_2P(O)CF_2CF_2CF_2CF_2^+$) 16, 231 ($(HO)_2P(O)CF_2CF_2CF_2^+$) 11, 181 ($(HO)_2P(O)CF_2CF_2^+$) 8, 131 ($(HO)_2P(O)CF_2^+$) 38, 111 ($HO_3PCF^+$) 11, 100 ($C_2F_4^+$) 68, 81 ($(HO)_2P(O)^+$) 46, 65 ($(HO)_2P^+$) 100. *Anal.* calcd. for $C_6H_3F_{12}O_7PS \cdot H_2O$: C 14.52, H 1.02, F 46.0, P 6.24, S 6.46; found: C 14.79, H 1.02, F 45.4, P 6.25, S 6.37.

Preparation of $I(CF_2)_4O(CF_2)_2SO_2K$

In a 250-mL three-necked round-bottomed flask were placed 15 g of $I(CF_2)_4O(CF_2)_2SO_2F$ (28.5 mmol), 13.6 g of K_2SO_3 (86 mmol), 60 mL water, and 40 mL CH_3CN. Under a stream of nitrogen the contents were stirred vigorously at room temperature for 10 h. The reaction mixture was filtered and the filtrate was evaporated to dryness under reduced pressure to give a white residue. Inorganic impurities were removed by repetitive extraction with CH_3CN. Finally, the solid was dried under vacuum at 70°C for 4 h to give 11.1 g (71% yield) of $I(CF_2)_4O(CF_2)_2SO_2K$ (20.3 mmol). Spectral data are ^{19}F NMR, Φ: −64.29m CF_2, −83.24m CF_2, −83.86m CF_2, −114.44m CF_2, −125.22m CF_2, −134.36s CF_2.

Preparation of $I(CF_2)_4O(CF_2)_2I$, 6

Under a stream of nitrogen, a mixture of 11.1 g $I(CF_2)_4O(CF_2)_2SO_2K$ (20.3 mmol), 6.8 g I_2 (26.8 mmol), and 30 mL of CH_3CN was stirred vigorously at 80°C for 7 h. A saturated $NaHSO_3$ aqueous solution was added to the reaction mixture to remove excess I_2 at room temperature. The mixture was filtered and the filtrate was dissolved in 50 mL of ether. The ether solution was washed with water repeatedly. After drying, 4.3 g of colorless liquid **6** (7.5 mmol) was obtained and purified by distillation (bp 60°C/10 Torr). The yield is 37%. Spectral data are ^{19}F NMR, Φ: −64.64m CF_2, −70.13s CF_2, −84.61m CF_2, −86.64m CF_2, −114.50m CF_2, −125.33m CF_2.

Preparation of $H(CF_2)_4O(CF_2)_2P(O)(OC_2H_5)_2$ and $H(CF_2)_2O(CF_2)_4P(O)(OC_2H_5)_2$

A mixture of 4.3 g of $I(CF_2)_4O(CF_2)_2I$ (7.5 mmol) and 5.8 g of tetraethylpyrophosphite (22.5 mmol) in 20 mL of $CF_2ClCFCl_2$ with 1.1 g of di-*tert*-butylperoxide (7.5 mmol) was heated at 120°C for 3 h in a 75-mL autoclave. After reaction, the mixture was placed into a glass flask fitted with a dropping funnel. The flask was cooled to −10°C under a nitrogen atmosphere and a solution of *tert*-butylhydroperoxide (60 mmol) in 20 mL of methanol was slowly added via the dropping funnel. After complete addition at −10 to −5°C, stirring was continued at 0°C for 1 h. The solution was washed with water (15 mL × 3) and volatile materials were removed *in vacuo*. The residue was distilled under reduced pressure to give 0.75 g of $H(CF_2)_4O(CF_2)_2P(O)(OC_2H_5)_2$ (1.65 mmol) and 0.25 g of $H(CF_2)_2O(CF_2)_4P(O)(OC_2H_5)_2$ (0.55 mmol). The combined yield is 29%. Spectral data for $HCF_2CF_2CF_2CF_2OCF_2CF_2P(O)(OC_2H_5)_2$ (bp 97°C/0.5 Torr) are ^{19}F NMR,

Can. J. Chem. Downloaded from www.nrcresearchpress.com by 186.148.149.217 on 09/07/12
For personal use only.

Can. J. Chem. Downloaded from www.nrcresearchpress.com by 186.148.149.217 on 09/07/12
For personal use only.

Φ: −83.45m OCF_2, −124.64d CF_2 (J_{P-F} = 87.97 Hz), −127.07m CF_2, −129.79m CF_2, −137.11d CF_2H (J_{F-H} = 53.71 Hz); ^{13}P NMR, δ: −0.36t; ^1H NMR, δ: 1.40t CH_3 (J_{H-H} = 6.96 Hz), 4.34m CH_2, 6.16tt CF_2H (J_{F-H} = 53.71 Hz, J_{F-H} = 5.5 Hz). Spectral data for $HCF_2CF_2OCF_2CF_2CF_2CF_2P(O)(OC_2H_5)_2$ (bp 126°C/0.5 Torr) are ^{19}F NMR, Φ: −84.27m CF_2, −84.79m CF_2, −123.94d CF_2 (J_{P-F} = 87.97 Hz), −126.61m CF_2, −130.77m CF_2, −139.75d CF_2H (J_{F-H} = 48.83 Hz); ^{31}P NMR, δ: −1.09t.

Preparation of $H(CF_2)_2O(CF_2)_2P(O)(OC_2H_5)_2$, 7

The method of preparation is the same as that described for $HCF_2CF_2CF_2CF_2OCF_2CF_2P(O)(OC_2H_5)_2$ and $HCF_2CF_2OCF_2CF_2$-$CF_2CF_2P(O)(OC_2H_5)_2$ above. The overall yield is 16%. Spectral data are ^{19}F NMR, Φ: −83.80m CF_2, −88.44m CF_2, −124.87d CF_2 (J_{P-F} = 87.89 Hz), −137.49d CF_2H (J_{F-H} = 52.40 Hz); ^{13}P NMR, δ: 0.12t (J_{P-F} = 87.89 Hz); ^1H NMR, δ: 1.33t CH_3 (J_{H-H} = 7.15 Hz), 4.37m CH_2, 5.83tt CF_2H (J_{F-H} = 2.94 Hz); MS (CI, *m/e* (species) %): 355 ($M^+ + 1$) 84, 335 ($M^+ - F$) 12, 327 ($M^+ + 1 - C_2H_4$) 82, 299 ($M^+ + 1 - C_4H_8$) 100, 279 ($M^+ + 1 - C_4H_9F$) 60, 137 ($(C_2H_5O)_2(O)P^+$) 50, 109 ($(HO)(O)P(OC_2H_5)^+$) 71.

Preparation of $H(CF_2)_4O(CF_2)_2P(O)(OH)_2$, 10

A mixture of 0.30 g $H(CF_2)_4O(CF_2)_2P(O)(OC_2H_5)_2$ (0.66 mmol) and 1.0 g Me_3SiBr (6.5 mmol) was stirred vigorously at room temperature for 24 h and at 50°C for 8 h. After reaction all volatiles were removed under vacuum. One millilitre of water was added, and the mixture was stirred vigorously at room temperature for 16 h followed by extraction with ether. Excess water was removed *in vacuo* to give the crude product. The product was dissolved in water and stirred with a small amount of charcoal at room temperature for 2 h to remove color. Finally, the solution was filtered, and evaporated *in vacuo* at 70°C to give 0.21 g of colorless viscous oil **10** (0.38 mmol). The yield is 58%. Spectral data are ^{19}F NMR, Φ: −84.32m OCF_2, −127.36d CF_2 (J_{P-F} = 79.17 Hz), −127.88m CF_2, −130.77m CF_2, −139.31d CF_2H (J_{F-H} = 53.71 Hz); ^{31}P NMR, δ: −4.00t; ^1H NMR, δ: −6.48tt CF_2H (J_{F-H} = 5.31 Hz), 8.61s $P(O)(OH)_2$; MS (CI, *m/e* (species) %): 399 ($M^+ + 1$) 100, 379 ($M^+ - F$) 33, 181 ($(OH)_2P(O)CF_2CF_2^+$) 71, 81 ($(HO)_2P(O)^+$) 57.

Preparation of $H(CF_2)_2O(CF_2)_4P(O)(OH)_2$, 11, and $H(CF_2)_2O$-$(CF_2)_2P(O)(OH)_2$, 9

The method of preparation is the same as that described above for **10**. Spectral data for **11** are ^{19}F NMR, Φ: −82.47m OCF_2, −122.47d CF_2 (J_{P-F} = 79.18 Hz), −124.81m CF_2, −128.69m CF_2, −138.18d CF_2H (J_{F-H} = 48.83 Hz); ^{31}P NMR, δ: −4.61t; ^1H NMR, δ: 7.13tt CF_2H (J_{F-H} = 5.50 Hz), 9.15s $P(O)(OH)_2$; MS (CI, *m/e* (species) %): 399 ($M^+ + 1$) 63, 181 ($(HO)_2P(O)CF_2CF_2^+$) 31, 81 ($(HO)_2P(O)^+$) 100. Spectral data for **9** are ^{19}F NMR, Φ: −84.44m CF_2, −89.42m CF_2, −127.30d CF_2 (J_{P-F} = 87.89 Hz), −139.46d CF_2H (J_{F-H} = 48.83 Hz); ^{31}P NMR, δ: −1.82t; ^1H NMR, δ: 6.21tt CF_2H (J_{H-F} = 2.94 Hz), 11.03s $P(O)(OH)_2$; MS (CI, *m/e* (species) %): 299 ($M^+ + 1$) 100, 279 ($M^+ - F$) 50, 181 ($(HO)_2P(O)CF_2CF_2^+$) 90, 81 ($(HO)_2P(O)^+$) 51.

Preparation of $(C_2H_5O)_2P(O)CFBr_2$, 12

Tribromofluoromethane (27.1 g, 0.1 mol) was slowly added to triethylphosphite (16.6 g, 0.1 mol) at 0°C under a nitrogen atmosphere and then stirred continuously at 0°C for 4 h. The reaction mixture was distilled under reduced pressure to yield 25.24 g (76.9%) of diethyl-dibromofluoromethylphosphonate (bp 86–87°C/0.7 Torr). Spectral data are ^{19}F NMR, Φ: −75.98d (J_{F-P} = 78.12 Hz); $^{13}P\{H\}$ NMR, δ: 1.51d; ^1H NMR, δ: 1.38t (3H, J_{H-H} = 6.96 Hz), 4.32q (1H), 4.41q (1H) (J_{H-P} = 8.03 Hz); MS (FB^+, solv. glycerol, *m/e* (species) %): 331 ($M^{81+} + 1$) 5.4, 329 ($M^{81}M^{79+} + 1$) 10.5, 327 ($M^{79+} + 1$) 6.02, 250 ($M^{81+} + 1 - Br^{81}$) 1.83, 248 ($M^{79+} + 1 - Br^{79}$) 1.5, 193 ($CFBr_2^{81+}$) 6.9, 189 ($CFBr_2^{79+}$) 6.9, 168 ($(C_2H_5O)P(O)CF^+$) 1.1, 149 ($(C_2H_5O)_2P(O)C^+$) 6.7, 137 ($(C_2H_5O)_2P(O)^+$) 29.4, 112 ($CFBr^{81+}$) 2.4, 110 ($CFBr^{79+}$) 3.0, 65 ($H_2O_2P^+$) 100, 63 (PO_2^+) 4.9. All other fragments are consistent with the isotope ratio expected for **12**.

Preparation of $(C_2H_5O)_2P(O)CFBrSO_2Na$, 13

In a 50-mL three-necked round-bottomed flask were placed 10.04 g (57.6 mmol) of $Na_2S_2O_4$, 4.84 g (57.6 mmol) of $NaHCO_3$, and 16 g (48 mmol) of $(C_2H_5O)_2P(O)CFBr_2$. Ten millilitres of water and 10 mL of CH_3CN were added. Under a stream of nitrogen, the contents were stirred vigorously at room temperature for 4 h. The reaction mixture was evaporated to dryness under reduced pressure to give a white product that was extracted with acetonitrile. The extract was filtered to remove solids, and the filtrate was evaporated to dryness under reduced pressure to give 13.8 g (84.4% yield) of **13**. Spectral data are ^{19}F NMR, Φ: −136.36d (J_{F-P} = 83.01 Hz); $^{31}P\{H\}$ NMR, δ: 9.76d; ^1H NMR, δ: 1.43t (3H, J_{H-H} = 6.96 Hz), 4.37q (1H), 4.46q (1H) (J_{H-P} = 8.03 Hz); MS (FB^+, solv. H_2O, *m/e* (species) %): 354 ($M^{81+} + H_2O$) 0.7, 353 ($M^{81}M^{79+} + H_2O$) 7.2, 352 ($M^{79+} + H_2O$) 0.4, 336 (M^{81+}) 0.5, 334 (M^{79+}) 0.3, 249 ($M^{81+} - SO_2Na$) 2.0, 247 ($M^{79+} - SO_2Na$) 1.7, 149 ($(C_2H_5O)_2P(O)C^+$) 13.9, 137 ($(C_2H_5O)_2P(O)^+$) 5.3, 87 ((SO_2Na^+) 1.9, 65 ($PO_2H_2^+$) 100, 63 (PO_2^+) 13.7. All other fragments are consistent with the isotope ratio expected for **13**.

Preparation of $(C_2H_5O)_2P(O)CFBrSO_3Na$, 14

A sample of 5 g (14.9 mmol) of $(C_2H_5O)_2P(O)CFBrSO_2N$ and 5 mL of water were placed in a 25-mL flask. Then 2.95 g of hydrogen peroxide (30%) (molar ratio $(C_2H_5O)_2P(O)CFBrSO_2Na:H_2O_2$ = 1:1.75) was added at 0°C. The mixture was stirred at room temperature for 5 h and then filtered. The filtrate was evaporated under reduced pressure to give the crude product. After repetitive extraction with acetonitrile and filtering to remove small amounts of solids, the filtrate was evaporated to dryness under reduced pressure to give 3.92 g of $(C_2H_5O)_2P(O)CFBrSO_3Na$ (74.8% yield). Spectral data are ^{19}F NMR, Φ: −128.46d (J_{F-P} = 78.13 Hz); $^{31}P\{H\}$, δ: 6.30d; ^1H NMR, δ: 1.43t (3H, J_{H-H} = 6.96 Hz), 4.41q (1H), 4.49q (1H) (J_{H-P} = 7.14 Hz); MS (FB^+, solv. glycerol, *m/e* (species) %): 375 (M^{81+} + Na) 66.6, 374 ($M^{81}M^{79+}$ + Na) 4.5, 373 (M^{79+} + Na) 66.3, 149 ($(C_2H_5O)_2P(O)C^+$) 10.3, 137 ($(C_2H_5O)_2P(O)^+$) 5.5, 121 ($SO_3Na\cdot H_2O^+$) 2.0, 109 ($C_2H_6O_3P^+$) 10.2, 103 (SO_3Na^+) 2.0, 65 ($PO_2H_2^+$) 100, 63 (PO_2^+) 17.3.

Preparation of $(C_2H_5O)_2P(O)CFHSO_3Na$, 15

Activated zinc dust and 5.95 g of **14** (16.9 mmol) were reacted in dry tetrahydrofuran for 6 h at 60°C under dry nitrogen. After THF was removed from the reaction mixture under reduced pressure, the residue was hydrolyzed with water at room temperature for 4 h. An aqueous solution of **15** was obtained. The solvent was evaporated under reduced pressure to give a white solid. After washing with acetonitrile and acetone, the white solid was dried under vacuum at 70°C for 2 h to yield 2.24 g of **15** (48.6% yield). Spectral data are ^{19}F NMR, Φ: −197.96dd (J_{F-P} = 73.24 Hz, J_{F-H} = 43.94 Hz); $^{31}P\{H\}$, δ: 10.43d; ^1H NMR, δ: 1.42t (6H, J_{H-H} = 7.15 Hz), 4.32q (2H), 4.41q (2H) (J_{H-P} = 7.85 Hz), 5.72dd (1H) (J_{H-P} = 5.5 Hz); MS (FB^+, solv. glycerol H_2O, *m/e* (species) %): 295 (M^+ + Na) 100, 289 ($M^+ + H_2O$ − 1) 1.5, 273 ($M^+ + 1$) 16.8, 149 ($(C_2H_5O)_2P(O)C^+$) 1.9, 137 ($(C_2H_5O)_2P(O)^+$) 4.6, 65 ($PO_2H_2^+$) 14.7, 63 (PO_2^+) 3.9.

Preparation of $(HO)_2P(O)CFHSO_3Na$, 16

A mixture of 2.24 g of $(C_2H_5O)_2P(O)CFHSO_3Na$ (8.2 mmol) and 5 g of hydrochloric acid (12 N) were stirred vigorously at 120°C for 10 h. The reaction mixture was filtered and the filtrate was evaporated to dryness under vacuum to obtain a crude product that was taken up in CH_3CN. A small quantity of solid was removed by filtration. After removal of the solvent under vacuum, a white solid was obtained. This process was repeated twice. The product was taken up in water, and methylene chloride was added. The mixture was stirred vigorously for 1 h. The water phase was collected and evaporated under reduced pressure at 80°C to yield 1.07 g of **16** (59.4% yield). Spectral data are ^{19}F NMR, Φ: −194.25dd (J_{F-P} = 68.85 Hz, J_{F-H} = 48.82 Hz); $^{31}P\{H\}$ NMR, δ: 6.91d; ^1H NMR, δ: 4.90dd CH (J_{H-P} = 5.13 Hz), 8.58s OH; MS (FB^+, glycerol, *m/e* (species) %): 215 ($M^+ - 1$) 19.9, 193 ($M^+ - Na$) 79.9, 175 ($M^+ - Na - H_2O$) 29.3, 113 ($M^+ - SO_3Na$) 9.1, 112 ($(HO)_2P(O)CF^+$) 1.5, 111 ($CHFPO_3^+$) 4.4, 91 (CPO_3^+)

46.2, 81 ($PO_3H_2^+$) 18.5, 64 (PO_2H^+) 12.0, 63 (PO_2^+) 33.1, 59 ($P(O)C^+$) 100.

*Preparation of $(HO)_2P(O)CFHSO_3H$, **17***

An aqueous solution of 0.8 g of $(HO)_2P(O)CFHSO_3Na$ (3.7 mmol) was passed through an Amberlite IR-120 ion exchange resin at a flow rate of approximately 2 mL/min. The volume of the aqueous acid was reduced by evaporation, and the crude product was dried under reduced pressure at 50–80°C for 4 h. The product was dissolved in water and 0.1 g of charcoal was added. The mixture was stirred at 50°C for 2 h. Charcoal was removed by filtration, and the filtrate was evaporated under vacuum at 80°C for 4 h to yield 0.57 g of $(HO)_2P(O)CFHSO_3H$ (79.2% yield). The solid melts at 115–116°C, and is very hygroscopic. Spectral data are ^{19}F NMR, Φ: −193.67dd (J_{F-P} = 68.36 Hz, J_{F-H} = 48.83 Hz); $^{31}P\{H\}$ NMR, δ: 6.55d; ^1H NMR, δ: 4.89dd CH (J_{H-P} = 5.13 Hz), 12.18(s) OH; MS (CI^+, *m/e* (species) %): 213 ($M^+ + H_2O + 1$) 0.3, 113 ($M^+ - SO_3H$) 1.0, 81 (SO_3H^+ or $(HO)_2P(O)^+$) 52.7, 80 (PO_3H^+) 1.5, 79 (PO_3^+) 3.1, 65 ($PO_2H_2^+$) 100, 64 (PO_2H^+) 4.1, 59 ($P(O)C^+$) 1.5. *Anal.* calcd. for CH_4FO_6PS: C 6.19, H 2.06, F 9.79, S 16.52; found: C 6.20, H 2.10, F 9.90, S 16.36.

*Preparation of $(C_2H_5O)_2P(O)CF(SO_3Na)(SO_2Na)$, **18**, and $(C_2H_5O)_2P(O)CF(SO_3Na)_2$, **19***

In a 25-mL three-necked, round-bottomed flask were placed 1.49 g of $Na_2S_2O_4$ (8.6 mmol), 0.72 g of $NaHCO_3$ (8.6 mmol), 2 g of $(C_2H_5O)_2P(O)CFBrSO_3Na$ (5.7 mmol), 6 mL of water, and 6 mL of CH_3CN. Under a stream of nitrogen, the contents were stirred vigorously at 0°C for 4 h. The reaction mixture was filtered and the filtrate was evaporated to dryness under reduced pressure to give crude $(C_2H_5O)_2P(O)CF(SO_3Na)(SO_2Na)$. Spectral data are ^{19}F NMR, Φ: −165.78d (J_{F-P} = 73.24 Hz); $^{31}P\{H\}$, δ: 9.76d; ^1H NMR, δ: 1.41t (3H, J_{H-H} = 6.96 Hz), 4.32q (1H), 4.40q (1H) (J_{H-P} = 7.23 Hz); MS (FAB, solv. glycerol, *m/e* (species) %): 395 ($M^+ + 1 + 2H_2O$) 1.3, 376 ($M^+ + H_2O$) 1.6, 330 ($M^+ + 1 - C_2H_5$) 3.3, 313 ($M^+ + 1 - 2Na$) 4.1, 271 ($M^+ - SO_2Na$) 4.1, 255 ($M^+ - SO_3Na$) 0.9, 168 ($((C_2H_5O)_2P(O)CF^+$) 5.3, 149 ($((C_2H_5O)_2P(O)C^+$) 29.2, 137 ($((C_2H_5O)_2P(O)^+$) 18.9, 108 ($C_2H_5O_3P^+$) 8.3, 105 ($SO_2Na\cdot H_2O^+$) 13.1, 103 (SO_3Na^+) 2.2, 64 (PO_2H^+) 100, 63 (PO_2^+) 36.2.

Crude $(C_2H_5O)_2P(O)CF(SO_3Na)(SO_2Na)$ and 5 mL of water were placed in a 25-mL flask. Then hydrogen peroxide (30%) (molar ratio **18**:H_2O_2 = 1:1) was added at −15°C, and the mixture was stirred for 1 h. After concentrating and cooling, the inorganic solid impurities were removed by filtration. The filtrate was evaporated under reduced pressure to give crude **19**. The crude product was extracted with acetone three times. The acetone extract was collected and evaporated at reduced pressure to give 0.71 g (32%) of pure $(C_2H_5O)_2P(O)CF(SO_3Na)_2$. Spectral data are ^{19}F NMR, Φ: −151.82d (J_{F-P} = 73.24 Hz); $^{31}P\{H\}$ NMR, δ: 7.82d; ^1H NMR, δ: 1.39t (3H, J_{H-H} = 6.97 Hz), 4.32q (1H), 4.41q (1H) (J_{H-P} = 8.04 Hz); MS (FAB, solv. glycerol, *m/e* (species) %): 410 ($M^+ + 2H_2O$) 3.0, 330 ($M^+ + 1 - OC_2H_5$) 8.1, 271 ($M^+ - SO_3Na$) 2.5, 168 ($M^+ - 2SO_3Na$) 4.0, 149 ($(C_2H_5O)_2P(O)C^+$) 24.9, 137 ($((C_2H_5O)_2P(O)^+$) 14.5, 121 ($SO_3Na^+ + H_2O$) 2.2, 109 ($C_2H_6O_3P^+$) 14.3, 103 (SO_3Na^+) 3.1, 65 ($PO_2H_2^+$) 1.4, 64 (PO_2H^+) 100, 63 (PO_2^+) 55.3.

Titration

Titration of the acids was monitored utilizing an Orion model 701A digital Ionalyzer and Corning combination pH electrode. Sodium hydroxide was standardized with primary standard potassium acid phthalate. Tetrabutylammonium hydroxide in toluene/methanol solution was prepared from tetrabutylammonium iodide (12) and standardized against primary standard benzoic acid in dimethyl formamide.

Acknowledgments

Acknowledgment is made to the donors of the Petroleum Research Fund administered by the American Chemical Society, to NSF CHE-8703790, to AFOSR 87-0067, and to the Gas Research Institute for support of this work.

1. C. Bunyagldj, H. Piotrowska, and M. H. Aldridge. J. Chem. Eng. Data, **26**, 344 (1981).
2. D. B. Su, J. Y. Chen, R. X. Zhu, and H. P. Hu. Huaxue Xuebao, **41**, 946 (1983).
3. W. Y. Huang, B. N. Huang, and C. M. Hu. J. Fluorine Chem. **23**, 193 (1983).
4. R. D. Howells and J. D. McCown. Chem. Rev. **77**, 69 (1977).
5. W. B. Cen, Z. X. Dong, T. J. Huang, D. B. Su, and J. M. Shreeve. Inorg. Chem. **27**, 1376 (1988).
6. T. Mahmood and J. M. Shreeve. Inorg. Chem. **25**, 3830 (1986).
7. T. Mahmood and J. M. Shreeve. Inorg. Chem. **25**, 4081 (1986).
8. T. Mahmood and J. M. Shreeve. Synth. Commun. **17**, 71 (1987).
9. D. J. Burton, L. G. Sprague, D. J. Pietrzyk, and S. H. Edelmuth. J. Org. Chem. **49**, 3437 (1984); **53**, 1523 (1988).
10. D. J. Burton, A. S. Modak, R. Guneratne, D. Su, W. Cen, R. L. Kirchmeier, and J. M. Shreeve. J. Am. Chem. Soc. **111**, 1773 (1989).
11. Perfluoro Sulfonic Acid Group, Shanghai Institute of Organic Chemistry. Acad. Sin. Sci. Sin. (Engl. Ed.) **21**, 773 (1978).
12. United States Pharmacopeial Convention. United States Pharmacopeia/National Formulary XX(XV) 1980. p. 1113.

Can. J. Chem. Downloaded from www.nrcresearchpress.com by 186.148.149.217 on 09/07/12
For personal use only.

A route to trinuclear platinum–gold clusters

G. J. ARSENAULT AND R. J. PUDDEPHATT[1]

Department of Chemistry, University of Western Ontario, London, Ont., Canada N6A 5B7

Received January 17, 1989

This paper is dedicated to Professor Ronald J. Gillespie on the occasion of his 65th birthday

G. J. ARSENAULT and R. J. PUDDEPHATT. Can. J. Chem. **67**, 1800 (1989).

New A-frame cluster complexes have been prepared by addition of electrophilic gold fragments to the Pt—Pt bond of $[Pt_2Cl_2(\mu\text{-dppm})_2]$, dppm = $Ph_2PCH_2PPh_2$. For example, $[AuCl(SMe_2)]$ gave $[Pt_2Cl_2(\mu\text{-AuCl})(\mu\text{-dppm})_2]$ and $[Au(NO_3)(PPh_3)]$ gave $[Pt_2Cl_2(\mu\text{-AuPPh}_3)(\mu\text{-dppm})_2]NO_3$. The complexes $[(CH_2)_n(PPh_2AuBF_4)_2]$ reacted with $[Pt_2Cl_2(\mu\text{-dppm})_2]$ to give $[Pt_2Cl_2(\mu\text{-AuPPh}_2(CH_2)_nPPh_2AuCl)(\mu\text{-dppm})_2]BF_4$ when $n = 1$ or 2, but the bridged bis(A-frame) cluster complex $[\{Pt_2Cl_2(\mu\text{-dppm})_2(\mu\text{-AuPPh}_2CH_2)\}_2CH_2](BF_4)_2$ when $n = 3$. In contrast, CuCl reacted with $[Pt_2Cl_2(\mu\text{-dppm})_2]$ to give $[Pt_2Cl(CuCl_2)(\mu\text{-dppm})_2]$. Attempts to synthesize A-frame clusters containing Pt_2Ag, Pt_2Cu, Pd_2Au, or PdPtAu units were unsuccessful, and it is concluded that these units are considerably weaker than the analogous 3-center 2-electron bond of the Pt_2Au unit. The AuCl unit is displaced from $[Pt_2Cl_2(\mu\text{-AuCl})(\mu\text{-dppm})_2]$ on reaction with diazomethane, with formation of $[Pt_2Cl_2(\mu\text{-CH}_2)(\mu\text{-dppm})_2]$.

Key words: platinum, gold, cluster, copper, silver.

G. J. ARSENAULT et R. J. PUDDEPHATT. Can. J. Chem. **67**, 1800 (1989).

On a préparé un nouveau cadre-À de complexes agglomérés, en ajoutant des fragments d'or électrophiles à la liaison Pt—Pt du complexe $[Pt_2Cl_2(\mu\text{-dppm})_2]$, dppm = $Ph_2PCH_2PPh_2$. Par exemple le composé $[AuCl(SMe_2)]$ donne le complexe $[Pt_2Cl_2(\mu\text{-AuCl})(\mu\text{-dppm})_2]$ et le composé $[Au(NO_3)(PPh_3)]$ donne le complexe $[Pt_2Cl_2(\mu\text{-AuPPh}_3)(\mu\text{-dppm})_2]NO_3$. Les complexes $[(CH_2)_n(PPh_2AuBF_4)_2]$ réagissent avec le $[Pt_2Cl_2(\mu\text{-dppm})_2]$ pour donner le complexe $[Pt_2Cl_2(\mu\text{-AuPPh}_2(CH_2)_nPPh_2AuCl)(\mu\text{-dppm})_2]BF_4$ lorsque $n = 1$ ou 2, mais donne le complexe aggloméré bis(cadre-À) ponté : $[\{Pt_2Cl_2(\mu\text{-dppm})_2(\mu\text{-AuPPh}_2CH_2)\}_2CH_2](BF_4)_2$ lorsque $n = 3$. Le CuCl au contraire réagit avec le $[Pt_2Cl_2(\mu\text{-dppm})_2]$ pour donner le complexe $[Pt_2Cl(CuCl_2)(\mu\text{-dppm})_2]$. On a essayé sans succès de préparer des groupements de cadre-À contenant du Pt_2Ag, du Pt_2Cu, du Pd_2Au ou du PdPtAu, et on en arrive à conclure que ces unités sont considérablement plus faibles que leur analogue Pt_2Au ayant une liaison à trois centres et deux électrons. La réaction du complexe $[Pt_2Cl_2(\mu\text{-AuCl})(\mu\text{-dppm})_2]$ avec le diazométhane déplace le AuCl en donnant le complexe $[Pt_2Cl_2(\mu\text{-CH}_2)(\mu\text{-dppm})_2]$.

Mots clés : platine, or, agglomérat, cuivre, argent.

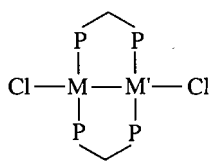
[Traduit par la revue]

Can. J. Chem. Downloaded from www.nrcresearchpress.com by 186.148.149.217 on 09/07/12
For personal use only.

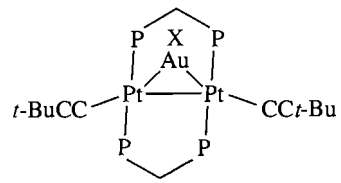
Heteronuclear cluster compounds containing the coinage metals are currently attracting considerable interest (1–9) and now constitute a well-established class of compounds, especially when the coinage metal is gold. However, relatively few reports have appeared on mixed-metal cluster complexes containing platinum and one of the coinage metals (4, 5).

The reactivity of the metal–metal bond of $[Pt_2Cl_2(\mu\text{-dppm})_2]$, **1***a*, to insertion reactions with small organic molecules and to addition of electrophilic reagents has been studied (6). These reactions often give "A-frame" complexes, such as $[Pt_2Cl_2(\mu\text{-CH}_2)(\mu\text{-dppm})_2]$ by reaction with CH_2N_2 and $[Pt_2Cl_2(\mu\text{-H})(\mu\text{-dppm})_2]^+$ by reaction with H^+. However, there has been less work on the reactions of **1** with metal moieties that are isolobal to CH_2 or H^+. $SnCl_2$ does not add to the Pt—Pt bond but inserts into the Pt—Cl bond to give $[Pt_2Cl(SnCl_3)(\mu\text{-dppm})_2]$ (7). Reaction with the nucleophilic metal carbonyl anion $[Fe(CO)_4]^{2-}$ disrupts the skeleton of **1** to give a triangulo-Pt_2Fe complex (8) and other carbonylmetallates may behave similarly. Thus, prior to the initiation of this work (11) no A-frame cluster complexes had been synthesized directly by addition of a metal fragment to the Pt—Pt bond of **1***a*. Such complexes appear to have good stability since two examples, **2** (9) and **3** (10), have been prepared indirectly, and the complex $[Pt_2Cl_2(\mu\text{-HgCl}_2)(\mu\text{-dppm})_2]$ was prepared recently by direct addition of $HgCl_2$ to **1***a* (12).

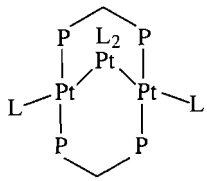
Herein, we report the reactions of complexes **1** with several electrophilic gold fragments that are isolobal with H^+. Complex **1***a* gives A-frame complexes containing Pt_2Au units by addition of the gold moeity across the Pt—Pt bond of **1***a*. However, **1***b* and **1***c* fail to give the corresponding A-frame complexes containing Pd_2Au or PdPtAu units. Reaction of **1***a* with similar copper or silver fragments also does not give A-frame complexes.



	M	M'
1*a*	Pt	Pt
1*b*	Pd	Pd
1*c*	Pd	Pt



	X
2*a*	Cl
2*b*	I
2*c*	CC*t*-Bu



3

L = 2,6-$Me_2C_6H_3NC$

Results and discussion

Synthesis and characterization of Pt_2Au A-frame complexes

The reaction of equimolar amounts of **1***a* and $[Au(NO_3)(PPh_3)]$

[1]Author to whom correspondence may be addressed.

Can. J. Chem. Downloaded from www.nrcresearchpress.com by 186.148.149.217 on 09/07/12
For personal use only.

TABLE 1. Analytical[a] and physical data of the new complexes

Complex	Analysis[a] C	H	N	Melting point [b](°C)
4*a*	46.25 (46.65)	3.50 (3.40)	0.70 (0.80)	182–223
4*b*	46.45 (46.00)	3.55 (3.35)		205–210
4*c*	43.30 (42.80)	3.50 (3.15)	0.45 (0.65)	233–245
4*e*	43.10 (42.55)	3.30 (3.20)		201–212
5	41.20 (41.05)	3.05 (3.05)		235–245
7*b*	47.15 (47.25)	3.70 (3.60)	0.95 (1.05)	185–280
8	46.65 (45.85)	3.95 (3.55)	1.65 (2.00)	170–225
9	44.80 (45.20)	3.70 (3.35)		195–240
10	44.90 (44.35)	3.90 (3.35)		225–240

[a]Calculated values are given in parentheses.
[b]Decomposes.

TABLE 2. ^{1}H NMR data[a] of new complexes

Complex	$[Pt_2(\mu\text{-dppm})_2]$ δCH_2	^2J(HH)	^2J(PH)	^3J(PtH)	Other Resonances
4*a*, **4***b*	5.02	14	—	112	
	3.56	14	5.5	20	
4*c*	4.89	12.5	—	108	3.22[b]
	4.07	12.5	5.5	25	
4*d*, **4***e*	5.00	14	—	108	2.10[c,d]
	3.83[c]	14	—[e]	25	2.35[c,d]
4*f*	5.40	13	—	112	2.05–2.65[c,f]
	3.60[c]	13	—[e]	—	
5	4.69	14	2	112	
	4.10	14	5.5	20	
7*a*	4.3	—	—	—	
	4.8				
7*b*	4.43	—	3.5	62	1.75[g]
8	4.61	—	4	58	2.11[g]
9	4.65	—	3.8	62	
9[h]	4.2[c]	—[e]	—	—	
	4.8[c]	—[e]	—	—	
10	4.94	14	—	112	1.64[f]
	3.56[c]	14	—[e]	—	1.80[f]

[a]Chemical shifts (δ) in ppm, coupling constants in Hz. Measurements at ambient temperature in CD_2Cl_2 with Me_4Si as internal reference unless otherwise stated.
[b]CH_2P; ^2J(PH) = 8 Hz and 10 Hz.
[c]Broad hump.
[d]Methylenes of dppe.
[e]Unresolved.
[f]Methylenes of dppp.
[g]Resonance due to coordinated H_3CCN.
[h]Measured at 203 K.

in dichloromethane solution gave $[Pt_2Cl_2(\mu\text{-}AuPPh_3)(\mu\text{-dppm})_2]NO_3$, as an air-stable yellow solid in analytically pure form (Table 1). The structure of **4***a* was readily deduced from its ^{1}H, ^{31}P, and ^{195}Pt NMR spectra (Tables 2, 3, and 4).

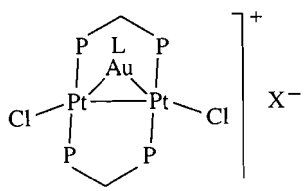
The ^{31}P NMR spectrum of **4***a* contains only two resonances, which are attributable to the $[Pt_2Cl_2(\mu\text{-dppm})_2]$ and Ph_3PAu phosphorus atoms respectively (Fig. 1). The dppm resonance had the typical appearance of a symmetrical A-frame complex (6–9) and the Ph_3PAu resonance appeared as 1:8:18:8:1 quintet, due to ^2J(PtP) coupling, indicating that the gold fragment is coordinated symmetrically to the Pt—Pt bond of **1***a*. Further evidence for a symmetrical structure is shown in the ^{195}Pt NMR spectrum, in which a single resonance is observed with the expected multiplicity due to ^{31}P coupling. In the ^{1}H NMR spectrum of **4***a*, the methylene protons of the dppm ligand appear as an AB spin system, as anticipated for an A-frame structure. The isolobally related complex $[Pt_2Cl_2(\mu\text{-H})(\mu\text{-dppm})_2]^+$ undergoes an easy A-frame inversion process (14) since an intermediate with a linear ClPtHPtCl unit is readily accessible. No such inversion process occurs for **4***a* or related complexes since it is obviously not possible for the bulky $AuPPh_3$ unit to pass between the platinum atoms.

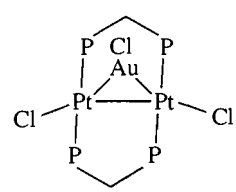
The spectroscopic data for **4***a* do not prove that the nitrate ion is not coordinated. The corresponding complex **4***b* was therefore prepared from Ph_3PAuBF_4, and the ^{1}H and ^{31}P NMR spectra were shown to be identical to those of **4***a*. Since the BF_4^- ion does not coordinate, the nitrate group in **4***a* is also not coordinated. The structures of **4***a* and **4***b* are like that for **2***b*, which has been established crystallographically (9, 11).

When a solution of **1***a* in CD_2Cl_2 was treated with two equivalents of $[Ph_3PAuNO_3]$, the ^{31}P NMR spectrum of the reaction mixture showed resonances attributable to **4***a* and to $[Ph_3PAuNO_3]$. This shows, as expected, that only one mole of gold(I) can add to **1***a* and that an exchange of Ph_3PAu units between **4***a* and $[Ph_3PAuNO_3]$ either does not occur or is at least very slow on the NMR time scale.

The reaction of **1***a* and $[AuCl(SMe_2)]$ gave the A-frame cluster $[Pt_2Cl_2(\mu\text{-AuCl})(\mu\text{-dppm})_2]$, **5**, which could be isolated as air-stable red crystals, and free SMe_2 was also formed. The structure of **5** was assigned on the basis of its ^{1}H, ^{31}P, and ^{195}Pt NMR spectra, which are very similar to those of **4**.

It is interesting to compare the magnitudes of the coupling constants ^1J(PtPt) for the cluster complexes with that of the parent complex, **1***a* (Table 5). The magnitude of ^1J(PtPt) can be determined from the ^{31}P or ^{195}Pt NMR spectra by analysis of the





5

	L	X
4*a*	PPh_3	NO_3
4*b*	PPh_3	BF_4
4*c*	$Ph_2PCH_2PPh_2AuCl$	NO_3
4*d*	$Ph_2P(CH_2)_2PPh_2AuCl$	NO_3
4*e*	$Ph_2P(CH_2)_2PPh_2AuCl$	BF_4
4*f*	$Ph_2P(CH_2)_3PPh_2AuCl$	BF_4

TABLE 3. ^{31}P NMR data[a] of the complexes

Complex	[$Pt_2(\mu$-dppm)$_2$] δ(P)	[$Pt_2(\mu$-dppm)$_2$] ^1J(PtP)	[PAu] δ(P)	[PAu] ^2J(PtP)
4*a*, **4***b*	8.3[b]	2400	36.5	600
4*c*	7.8[c]	2390	19.1[d]	—[e]
			35.3[g]	600
4*d*, **4***e*	7.7[f]	2390	35.3[g]	600
			31.6[g]	—
4*f*	8.5[h]	2365	33.0	590
			26.7	—
5	9.1[i]	2410	—	
6*a*	9.9	3040	—	
	−2.0	2860		
7*b*	6.9	2885	—	
	−4.1	2785		
8	−1.0	2700	—	
9[j]	11.9	2860	—	
	−4.3	2760		
10	7.8[k]	2395	31.4	590

[a]Chemical shifts (δ) in ppm, coupling constants in Hz. Measurement at ambient temperature in CD_2Cl_2 with trimethylphosphate as external reference unless otherwise stated.
[b]^2J(PtP) = −100 Hz, $^2J(P^AP^{A\prime\prime})$ = 62 Hz, $^4J(P^AP^{A\prime\prime\prime})$ = 26 Hz.
[c]^2J(PtP) = −91 Hz, $^2J(P^AP^{A\prime\prime})$ = 63 Hz, $^4J(P^AP^{A\prime\prime\prime})$ = 36 Hz.
[d]^2J(PP) = 16 Hz.
[e]^4J(PtP) = 25 Hz.
[f]^2J(PtP) = −92 Hz, $^2J(P^AP^{A\prime\prime})$ = 64 Hz, $^4J(P^AP^{A\prime\prime\prime})$ = 29 Hz.
[g]^2J(PP) = 49 Hz.
[h]^2J(PtP) = −60 Hz, $^2J(P^AP^{A\prime\prime})$ = 60 Hz, $^4J(P^AP^{A\prime\prime\prime})$ = 30 Hz.
[i]^2J(PtP) = −78 Hz, $^2J(P^AP^{A\prime\prime})$ = 59 Hz, $^4J(P^AP^{A\prime\prime\prime})$ = 25 Hz.
[j]Measured at 203 K.
[k]^2J(PtP) = −91 Hz, $^2J(P^AP^{A\prime\prime})$ = 64 Hz, $^4J(P^AP^{A\prime\prime\prime})$ = 29 Hz.

TABLE 4. ^{195}Pt NMR data[a] of the complexes

Complex	δ(Pt)	^1J(PtP)	^2J(PtP)	^1J(PtPt)[b]
4*a*[c]	912	2396	−77	6730
5	684	2419	−72	6290
9[d]	653	2770[e]	−105[e]	10334
	315	2860[e]	−153[e]	
11*b*	861	2890	—	—
		4670		

[a]Chemical shifts (δ) in ppm, coupling constants in Hz. Measurement at ambient temperature in CD_2Cl_2 with aqueous K_2PtCl_4 as external reference unless otherwise stated.
[b]Estimated error ±100 Hz.
[c]^2J(PtAuP) = 604 Hz.
[d]Measured at 203 K.
[e]Measured from the AA'BB'X isotopomer.

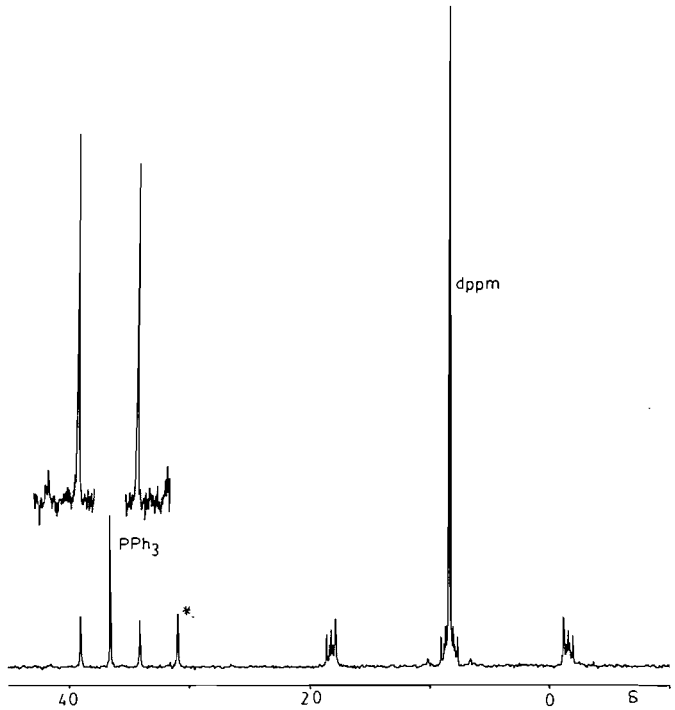


FIG. 1. The ^{31}P NMR spectrum (121 MHz) of [$Pt_2Cl_2(\mu$-$AuPPh_3)(\mu$-dppm$)_2]^+$, **4***a*. The expansion shows the weak outer ^{195}Pt satellites of the Ph_3PAu resonance; the multiplet has relative intensities of 1:8:18:8:1.

TABLE 5. Platinum–platinum coupling constants[a] for the complexes

Complex	^1J(PtPt)
[$Pt_2Cl_2(\mu$-dppm$)_2$], **1***a*	8145[b]
[$Pt_2Cl_2(\mu$-AuCl$)(\mu$-dppm$)_2$], **5**	6100[c]
[$Pt_2Cl_2(\mu$-$AuPPh_3)(\mu$-dppm$)_2]^+$, **4***a*	6980[c]
[$Pt_2Cl_2(\mu$-$AuPPh_2CH_2PPh_2AuCl)(\mu$-dppm$)_2]^+$, **4***c*	6520[c]
[$Pt_2Cl_2(\mu$-$AuPPh_2(CH_2)_2PPh_2AuCl)(\mu$-dppm$)_2]^+$, **4***d*	6710[c]
[$Pt_2Cl_2(\mu$-$AuPPh_2(CH_2)_3PPh_2AuCl)(\mu$-dppm$)_2]^+$, **4***f*	5580[c]
[$(Pt_2Cl_2)_2((\mu$-$AuPPh_2CH_2)_2CH_2)(\mu$-dppm$)_4]^{2+}$, **10**	7380[c]
[$Pt_2Br_2(\mu$-H$)(\mu$-dppm$)_2]^+$	5585[b]
[$Pt_2(CC$*t*-Bu$)_2(\mu$-AuCC*t*-Bu$)(\mu$-dppm$)_2$], **2***c*	2450[c]
[$Pt_2(CC$t-Bu$)_2(\mu$-AuI$)(\mu$-dppm$)_2$], **2***b*	2060[c]

[a]Coupling constants in Hz, obtained from ^{31}P NMR spectra.
[b]Reference 13.
[c]This work, estimated error ±100 Hz.

weak peaks arising from the $^{195}Pt_2$ isotopomers (13). The A-frame complexes all have lower ^1J(PtPt) values than in the parent complex **1***a*. This is not surprising since a lengthening of the Pt—Pt distance is expected and found on formation of A-frame complexes by addition of electrophiles such as H^+ or isolobal species such as AuCl or $AuPPh_3^+$. Increasing the *trans* influence of the terminal ligands on platinum leads to a great decrease in ^1J(PtPt) as expected (compare ^1J(PtPt) values of 6200 and 2060 Hz for **5** and **2***b* respectively). In contrast, increasing the *trans* influence of the ligand on gold leads to an increase in the magnitude of ^1J(PtPt) ((compare values of ^1J(PtPt) = 6100 and 6980 Hz for **5** and **4***a* respectively). We suggest that a ligand on gold having a strong *trans* influence weakens the AuPt interactions and hence leads to a stronger Pt—Pt interaction. This conclusion is tentative at this stage, since it is based only on the NMR parameters, and further X-ray studies are needed to confirm the effect.

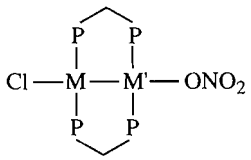
Although the Pt_2Au cluster complexes have good thermal stability, the gold fragment can be displaced. For example, reaction of **5** with diazomethane gave [$Pt_2Cl_2(\mu$-$CH_2)(\mu$-dppm$)_2$] and "AuCl".

Attempted synthesis of Pt_2Ag and Pt_2Cu A-frame clusters

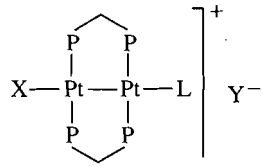
Since the above Pt_2Au complexes were very stable, attempts were made to synthesize A-frame complexes with the other coinage metals. However, in contrast to the ease of formation of the Pt_2Au complexes, it has not yet been possible to prepare similar derivatives of copper and silver.

For example, the reaction of **1***a* with Ph_3PAgNO_3 gave a

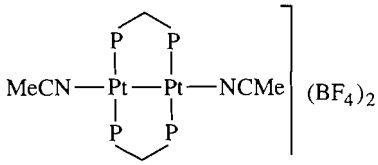
Can. J. Chem. Downloaded from www.nrcresearchpress.com by 186.148.149.217 on 09/07/12
For personal use only.



	M	M'
6*a*	Pt	Pt
6*b*	Pd	Pd
6*c*	Pd	Pt



	X	L	Y
7*a*	Cl	PPh_3	NO_3
7*b*	Cl	MeCN	BF_4
7*c*	H	MeCN	PF_6

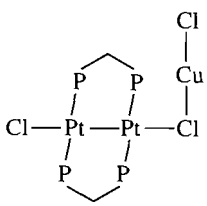


8

precipitate of AgCl and a yellow solid, characterized as $[Pt_2Cl(PPh_3)(\mu\text{-dppm})_2]NO_3$, **7***a*, by the ^1H and ^{31}P NMR data, which were identical to those of the known hexafluorophosphate salt (15). Pt—Ag complexes have only been isolated when no halides were present (16) or when unusual stabilization of the heteronuclear complex prevented the precipitation of AgCl (4).

Similarly, attempts to prepare Pt_2Cu A-frame clusters were unsuccessful. Reaction of **1***a* with $Cu(PPh_3)_2NO_3$ gave complex **7***a*, while reaction with one or two equivalents of $[Cu(MeCN)_4]BF_4$ gave CuCl and **7***b* or **8** respectively. The similar complex **7***c* had been characterized previously (17), and the characterization of the new compounds **7***b* and **8** was therefore straightforward.

A 1:1 adduct of complex **1***a* and CuCl was prepared by stirring the reagents together, using excess copper(I) chloride in dichloromethane. The adduct was thermally stable in the solid state but a solution in acetone slowly deposited CuCl and complex **1***a* was regenerated. This slow decomposition in solution has frustrated attempts to grow single crystals suitable for X-ray structure determination (crystals could be grown but all were twinned), and so the structure was deduced from NMR studies. At low temperature (−70°C), two resonances were observed in both the ^{195}Pt and the ^{31}P NMR spectra, and so the symmetrical A-frame structure analogous to complex **5** is immediately ruled out. The coupling constant $^1J(PtPt)$ from the ^{195}Pt NMR spectrum was 10 330 Hz, a value *higher* than for the parent **1***a*. Again this is inconsistent with an A-frame structure and indicates that a strong Pt—Pt bond is present. The CH_2P_2 resonance in the ^1H NMR spectrum at low temperature appeared as an AB quartet due to $^2J(HH)$ coupling, showing that there was no plane of symmetry containing the $Pt_2(\mu\text{-dppm})_2$ unit. At room temperature, a single CH_2P_2 resonance was observed in the ^1H NMR and a single ^{31}P resonance was also observed. The activation energy obtained from either ^1H or ^{31}P NMR spectra was 55 ± 4 kJ mol^{-1}, indicating a single fluxional process. We tentatively suggest that the structure of the complex is **9**, with a weakly coordinated $CuCl_2^-$ ligand and a strong Pt—Pt bond, and that the fluxional process involves exchange between $CuCl_2^-$ and Cl^- ligands on platinum, though the mechanism of this process cannot be determined. The "AB" pattern for the $CH^aH^bP_2$ protons of the dppm ligands is expected only if the $CuCl_2^-$ ligand is bound as shown in **9** and is unable to rotate about the Pt—Cl axis due to steric hindrance by the phenyl substituents.

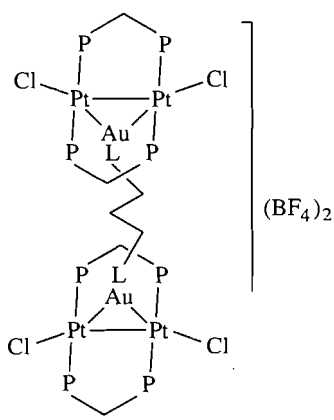


9

Synthesis and characterization of bridged bis(A-frame) cluster complexes

Attempts were made to prepare bis(A-frame) cluster complexes by using the digold reagents $[(AuNO_3)_2\{\mu\text{-}Ph_2P(CH_2)_n\text{-}PPh_2\}]$ or $[(AuBF_4)_2\{\mu\text{-}Ph_2P(CH_2)_nPPh_2\}]$ with two equivallents of **1***a*. When n = 1 or 2, only the complexes **4***c*–**4***e* were formed and, for the nitrate derivatives, complex **6***a*. Complex **4***d* was an oil, which was characterized only spectroscopically, but **4***c* and **4***e* were solids obtained in analytically pure form. It seems that the first electrophilic gold atom can add to the Pt—Pt bond of **1***a* to give an A-frame cluster but then the second gold atom abstracts chloride from the second equivalent of **1***a* to give **4***c* or **4***d* and **6***a*. The complexes **4***c* and **4***d* could also be prepared by reaction of $[NO_3AuPPh_2(CH_2)_nPPh_2AuCl]$ with an equimolar amount of **1***a*, and in this case no side product **6***a* is formed. Complex **4***f*, n = 3, was prepared in the same way.

It was considered that, after addition of the first gold atom of the digold reagents to the Pt—Pt bond of **1***a*, the bulky A-frame substituent probably prevented approach of the second gold atom of the reagents to the Pt—Pt bond of the second equivalent of **1***a*, and so halogen abstraction took place instead to give **4***c*–**4***e*. The reaction of two molar equivalents of **1***a* with the longer chain diphosphine derivative $[BF_4AuPPh_2(CH_2)_3PPh_2AuBF_4]$ was therefore attempted, since the above type of steric hindrance should decrease with chain length. The bis(A-frame) complex **10** was obtained in high yield and was readily characterized by NMR spectroscopy. Thus in the ^{31}P NMR spectrum, single resonances, with the expected multiplicities, were observed in a 4:1 intensity ratio for the dppm and $Ph_2P(CH_2)_3PPh_2$, dppp, ligands as expected for a symmetrical bridged bis(A-frame) cluster complex. In the ^1H NMR spectrum, the expected "AB" resonance due to $CH^aH^bP_2$ protons of the dppm ligands and two resonances in a 2:1 ratio for the CH_2 protons of the bridging dppp ligand were observed. Complex **10** appears to be the first bis(A-frame) complex of any kind to be reported.



10

Attempted synthesis of Pd_2Au and PdPtAu A-frame complexes

To our knowledge, no examples of PdAu bonded complexes have been reported, and it was therefore of interest to attempt the synthesis of the dipalladium analogues of complexes **4** and **5**.

Can. J. Chem. Downloaded from www.nrcresearchpress.com by 186.148.149.217 on 09/07/12
For personal use only.

TABLE 6. ^{31}P and ^{1}H NMR data[a] of complexes **11***a* and **11***b*

	^{31}P NMR								^{1}H NMR	
Complex	$\delta(P^1)$	$\delta(P^2)$	$\delta(P^3)$	$\delta(P^4)$	$J(P^1P^2)$	$J(P^2P^3)$	$J(P^2P^4)$	$J(P^3P^4)$	$\delta(CH_2)$	$J(PH)$
11*a*	21.5	−7.9	4.0	−15.2	86	94	67	29	4.15[b]	11
11*a*[c]	23.1	−1.6	4.3	−6.6	75	98	66	29	—	
11*b*	20.7[d]	1.2[d,e]	6.4[f]	−20.2[d]	—[g]	96	—[g]	17	3.4[d]	—[g]
									5.2[h]	12
11*b*[c]	21.3	1.7	6.9	−17.5	53	99	30	17	—	

[a]δ in ppm, *J* in Hz. Measurements at ambient temperature in CD_2Cl_2 with trimethylphosphate as external reference unless otherwise stated.
[b]Broad triplet.
[c]At 210 K.
[d]Broad resonance.
[e] $^1J(PtP) = 2755$ Hz.
[f] $^1J(PtP) = 4760$ Hz.
[g]Unresolved.
[h] $^3J(PtH) = 94$ Hz.

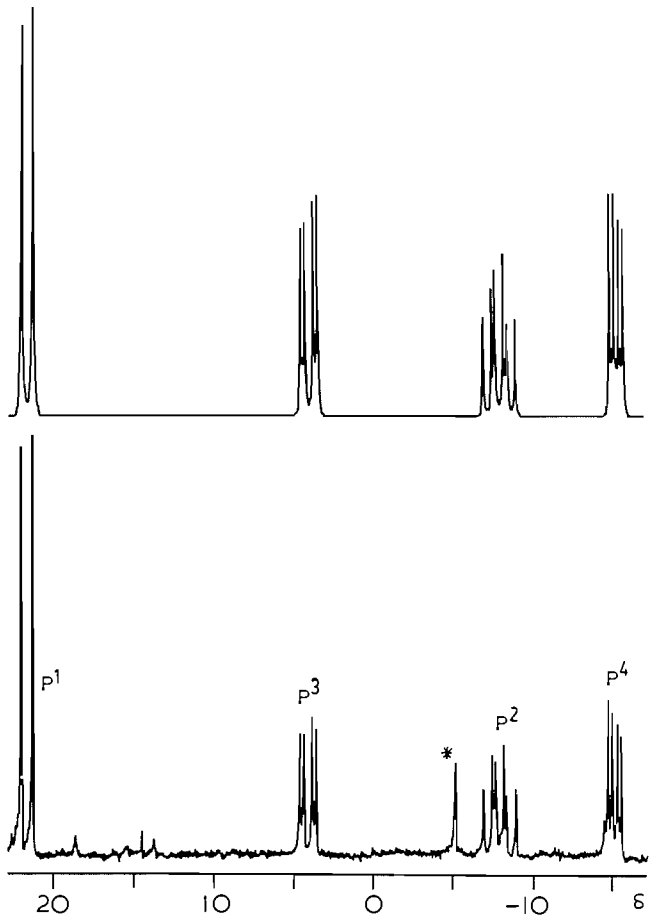
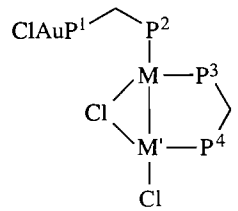


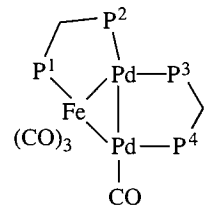
FIG. 2. The ^{31}P NMR spectrum (121 MHz) of **11***a*. The observed spectrum is shown below and the simulated spectrum above.

Reaction of $[Pt_2Cl_2(\mu\text{-dppm})_2]$, **16**, with $[AuCl(SMe)_2]$ in dichloromethane at −80°C gave a red solution. The ^{31}P NMR spectrum (Fig. 2, Table 6) at this temperature contained four equal intensity resonances. The spectral parameters resemble those for **12** (8), except for the absence of long range P^1P^3 and P^1P^4 couplings, and suggest an analogous metal–phosphorus skeleton but without PdAu bonds. We tentatively suggest structure **11***a*, though only the metal–phosphorus skeleton is characterized with confidence.

The coupling $^2J(P^2P^3)$ is less than 100 Hz and so indicates that these phosphorus atoms are mutually *cis* as shown in **11***a*. The CH_2P_2 protons of each dppm ligand gave a separate broad triplet resonance on the ^1H NMR spectrum. Braunstein *et al.* have independently studied the reaction of $[Pd_2Cl_2(\mu\text{-dppm})_2]$ with $[AuCl(SEt_2)]$ and have observed this same complex, but they too have not been able to obtain X-ray quality crystals (18). The complex decomposed to $[PdCl_2(dppm)]$ and $[Au_2Cl_2(\mu\text{-dppm})]$ and other unidentified complexes at room temperature or on attempted crystallization at low temperature. Reaction of **11***a* with PPh_3 gave $[AuCl(PPh_3)]$ and **1***b* in almost quantitative yield, as monitored by ^{31}P NMR spectroscopy.



11*a*, M = Pd, M' = Pd
11*b*, M = Pt, M' = Pd
11*c*, M = Pd, M' = Pt



12

Reaction of **1***b* with $[Au(NO_3)(PPh_3)]$ gave only $[AuCl(PPh_3)]$ and complex **6***b*. Thus, no evidence for A-frame cluster formation was obtained in any of the reactions of **1***b*, a result which has been independently obtained by Braunstein *et al.* (18).

Very similar results were obtained on reaction of the Pd—Pt bonded dimer **1***c*. Thus reaction with $[AuCl(SMe_2)]$ gave **11***b*, formed by selective cleavage of a Pd—P rather than a Pt—P bond (17). The latter reaction would have given **11***c*, which was not consistent with the spectroscopic data (Tables 4 and 6). Thus, both the ^{31}P NMR and the ^{195}Pt NMR spectra show that platinum remains bonded to two phosphorus atoms. Again it is emphasized that structure **11** is tentative. The complex decomposed rapidly at room temperature to give $[PdCl_2(dppm)_2]$, $[PtCl_2(dppm)]$, and $[Au_2Cl_2(\mu\text{-dppm})]$ and reacted cleanly with PPh_3 to give $[AuCl(PPh_3)]$ and **1***c*. Similarly, reaction of **1***c* with $[Au(NO_3)(PPh_3)]$ gave only halogen abstraction with formation of $[AuCl(PPh_3)]$ and **6***c* (19).

Conclusions

The addition of electrophilic gold fragments to metal–metal bonds is now a well-established reaction, especially with

Can. J. Chem. Downloaded from www.nrcresearchpress.com by 186.148.149.217 on 09/07/12
For personal use only.

Can. J. Chem. Downloaded from www.nrcresearchpress.com by 186.148.149.217 on 09/07/12
For personal use only.

Ph_3PAu^+ units adding to metal cluster complexes. The reactions lead to 3-centre 2-electron $[M_2AuPPh_3]^+$ units analogous to $[M_2(\mu\text{-}H)]^+$ units formed by addition of a proton to the metal–metal bond. This work has shown that such reactions occur readily with the diplatinum(I) complex **1***a* to give the A-frame cluster complexes **4***a* and **4***b*. Further, it is shown that $[AuCl(SMe_2)]$ can act as a precursor to the neutral fragment AuCl, which is also isolobal with H^+. From this reagent, the neutral A-frame cluster complex **5** was prepared and it is probable that many neutral cluster complexes containing AuCl units could be prepared by reaction of $[AuCl(SMe_2)]$ with metal–metal bonded complexes.

There is clearly a fine balance between whether an electrophilic metal fragment will add to the metal–metal bond of the complexes **1** or give other reactions. Indeed A-frame cluster formation is restricted to the case of the diplatinum(I) complex **1***a* and electrophilic gold fragments. Similar copper or silver fragments do not give A-frame clusters, but usually give halogen abstraction instead, yielding only the substituted diplatinum(I) complexes **6** or **7**. Reaction of electrophilic gold fragments with **1***b* or **1***c* also failed to give Pd_2Au or PdPtAu A-frame cluster complexes, but addition of gold to a dppm ligand occurred instead. The Pt_2Au A-frame complexes thus appear to have unique stability.

Experimental

Elemental analyses were performed by Guelph Chemical Laboratories Limited, Guelph, Ontario. NMR spectra were recorded on Varian XL-200 (^1H) and Varian XL-300 (^{31}P and ^{195}Pt) spectrometers. Chemical shifts are quoted with respect to $Me_4Si(^1H)$, trimethylphosphate (^{31}P), and K_2PtCl_4 (^{195}Pt).

Published methods were used to prepare the compounds: $[Pt_2Cl_2(\mu\text{-}dppm)_2]$ (13), $[Pd_2Cl_2(\mu\text{-}dppm)_2]$ (20), $[PdPt_2Cl_2(\mu\text{-}dppm)_2]$ (20), Ph_3PAuNO_3 (21), $(SMe_2)AuCl$ (22), $[Au_2Cl_2(\mu\text{-}dppm)_2]$ (22), $(Ph_3P)_2CuNO_3$ (23), $[Cu(CH_3CN)_4]BF_4$ (24), and $[Pt_2Cl_2(\mu\text{-}CH_2)(\mu\text{-}dppm)_2]$ (25, 26).

Synthetic routes to Pt_2Au A-frame complexes

$[Pt_2Cl_2(\mu\text{-}AuPPh_3)(\mu\text{-}dppm)_2]NO_3$, **4**a

To a solution of **1***a* (29.7 mg, 0.0241 mmol) in CH_2Cl_2 (10 mL) was added a solution of Ph_3PAuNO_3 (14.0 mg, 0.0269 mmol) in CH_2Cl_2 (5 mL) and the mixture was stirred for 14 h at ambient temperature. The resulting solution was concentrated to 1 mL and addition of hexane (5 mL) gave an air-stable yellow precipitate. The solvent was decanted and the solid product **4***a* was washed with hexane and dried *in vacuo* (36.1 mg, 86% based on **1***a*).

In a similar experiment, 2 equivalents of Ph_3PAuNO_3 were added to a solution of **1***a* in dichloromethane. The ^{31}P NMR spectrum of the reaction mixture at ambient temperature showed resonances due to **4***a* and to free Ph_3PAuNO_3 (δ 29.0).

$[Pt_2Cl_2(\mu\text{-}AuPPh_3)(\mu\text{-}dppm)_2]BF_4$, **4**b

In a similar way, 1 equivalent of Ph_3PAuBF_4 was added to a solution of **1***a*. After stirring for 30 min, the resulting solution was concentrated and addition of excess hexane gave an air-stable yellow solid that was identified as **4***b*.

$[Pt_2Cl_2(\mu\text{-}AuCl)(\mu\text{-}dppm)_2]$, **5**

To a solution of **1***a* (49.0 mg, 0.0398 mmol) in CH_2Cl_2 (20 mL) was added a solution of $(SMe_2)AuCl$ (11.8 mg, 0.0401 mmol) in CH_2Cl_2 (2 mL) and the mixture was stirred for 16 h at ambient temperature. The solvent was removed to give a red solid, which was then crystallized from dichloromethane/diethyl ether to give red microcrystalline needles and plates. These were dried under vacuum (50.1 mg, 86%) and identified as **5**.

Reaction of **5** *with CH_2N_2*

To a solution of **5** (8 mg, 0.005 mmol) in CH_2Cl_2 (10 mL) at 0°C was added CH_2N_2 (0.1 mmol, ether solution). An immediate reaction occurred and metallic gold was precipitated. After 10 min, the solution was filtered, the solvents evaporated, and the product was identified as $[Pt_2Cl_2(\mu\text{-}CH_2)(\mu\text{-}dppm)_2]$ by its ^1H and ^{31}P NMR spectra (25).

$[Pt_2Cl_2(\mu\text{-}AudppmAuCl)(\mu\text{-}dppm)_2][NO_3]$, **4**c

To a solution of $dppm(AuCl)_2$ (14.8 mg, 0.0174 mmol) in CH_2Cl_2 (20 L) was added a solution of $AgNO_3$ (2 equiv.) in aqueous ethanol. The mixture was stirred for 1 h, the white precipitate was filtered off, and the solvent was removed to give $dppm(AuNO_3)_2$. This was immediately dissolved in CH_2Cl_2 (5 mL), and the solution was filtered and added to a solution of **1***a* (42.8 mg, 0.0340 mmol) in CH_2Cl_2 (15 mL). After stirring for 16 h, the solvent was removed to give an orange-red solid. The ^{31}P NMR spectrum of this solid showed resonances attributable to **4***c* and **6***a*. Crystallization from dichloromethane/hexane gave clusters of red needles. These were dried under vacuum (30.0 mg, 42%) and identified as **4***c*.

The above experiment was repeated except that only 1 equivalent of $AgNO_3$ was used. Crystallization of the reaction mixture from dichloromethane/diethyl ether gave red needles (28 mg, 50%) identified as **4***c*.

$[Pt_2Cl_2(\mu\text{-}AudppeAuCl)(\mu\text{-}dppm)_2]NO_3$, **4**d

This was prepared similarly from $dppe(AuCl)_2$ (19.4 mg, 0.0225 nmol) and 2 equivalent $AgNO_3$. Thus, after $dppe(AuNO_3)_2$ and **1***a* (55.5 mg, 0.0451 mmol) were combined and stirred for 18 h in dichloromethane (30 mL), the solvent was removed to give a yellow-orange solid. The ^{31}P NMR spectrum of the reaction mixture, in$CDCl_3$, gave resonances attributable to **4***d*, **6***a*, and $dppe(AuCl)_2$ (δ 29.1). This reaction mixture could not be induced to crystallize.

In a similar experiment, $dppe(AuCl)_2$ (44.6 mg, 0.0517 mmol) was treated with 1 equivalent $AgNO_3$ to give $dppeAu_2ClNO_3$, which was combined with **1***a* (61.7 mg, 0.0502 mmol) and stirred for 30 min in dichloromethane (30 mL). The solvent was removed to give a yellowish-red solid. The ^{31}P NMR spectrum of the reaction mixture gave resonances attributable to one major component, **4***c*, with trace amounts of $dppe(AuCl)_2$ and unreacted **1***a*. Complex **4***c* could not be induced to crystallize.

$[Pt_2Cl_2(\mu\text{-}AudppeAuCl)(\mu\text{-}dppm)_2]BF_4$, **4**e

This was prepared similarly except that $dppeAu_2ClBF_4$ (30.7 mg, 0.0356 mmol) was prepared instead of $dppeAu_2ClNO_3$. The digold reagent was stirred in dichloromethane (35 mL) in the presence of **1***a* (42.1 mg, 0.0342 mmol) for 30 min at ambient temperature. Evaporation of the solvent gave a yellow solid that was identified as **4***e* and was contaminated with small amounts of $dppe(AuCl)_2$ as evidenced by NMR spectroscopy. Complex **4***e* was purified by precipitation out of a dichloromethane solution with diethyl ether. Complex **4***f* was prepared similarly.

$[\{Pt_2Cl_2(\mu\text{-}dppm)_2(\mu\text{-}AuPPh_2CH_2)\}_2CH_2][BF_4]_2$, **10**

To a solution of $dppp(AuCl)_2$ (16.9 mg, 0.0193 mmol) in 20 mL of dichloromethane were added 2 equivalents of $AgBF_4$ in 95% aqueous ethanol (2 mL). This solution was stirred for 5 min, the white precipitate (AgCl) was filtered off and then immediately added to a solution of **1***a* (47.0 mg, 0.0382 mmol) in dichloromethane (15 mL). After stirring for 15 min, the solvent was removed to give a yellow solid, which was redissolved in a minimum amount of dichloromethane and excess hexane was added to precipitate complex **10** (54.9 mg, 85%) as a yellow solid.

Reaction of **1**a *with Ag(I) and Cu(I) complexes*

$AgNO_3$: To a solution of **1***a* (33.2 mg, 0.0270 mmol) in 15 mL CH_2Cl_2 was added a solution of $AgNO_3$ (4.5 mg, 0.0265 mmol) in aqueous ethanol. After stirring for 30 min, the solution was filtered and the solvent removed to give a yellow solid that was identified as **6***a* by ^{31}P NMR spectroscopy.

Ph_3PAgNO_3: Triphenylphosphine (11.6 mg, 0.0442 mmol) and $AgNO_3$ (6.9 mg, 0.0406 mmol) were dissolved in dichloromethane/95% ethanol and stirred for 20 min at ambient temperature. The solvent was removed to give a clear oil that was redissolved in CH_2Cl_2 (4 mL). To this solution was added **1***a* (51.5 mg, 0.0419 mmol) dissolved in CH_2Cl_2 (10 mL). After stirring for 1 h, the reaction mixture was filtered and the solvent removed to give a yellow solid (57.9 mg, 91%) that was identified as **7***a* by NMR spectroscopy.

$(Ph_3P)_2CuNO_3$: To a solution of **1***a* (66.6 mg, 0.0542 mmol) in 15 mL CH_2Cl_2 was added a solution of $(Ph_3P)_2CuNO_3$ (36.3 mg, 0.0558

mmol) in CH_2Cl_2 (3 mL). After stirring for 19 h, the solvent was removed to give a yellow solid (77.4 mg, 94%) that was identified as **7***a* by NMR spectroscopy.

$Cu(CH_3CN)_4BF_4$: To a solution of **1***a* (85.8 mg, 0.0698 mmol) in CH_2Cl_2 (30 mL) was added $Cu(CH_3CN)_4BF_4$ (22.2 mg, 0.0706 mmol), which dissolved and was immediately replaced by a fine white precipitate (CuCl). After stirring for 18 h, the solvent was removed and the residue was crystallized from dichloromethane/hexane to give a light yellow cluster of crystals, which was dried *in vacuo* for 3 h (86.7 mg, 94%) and identified as **7***b* (IR(Nujol)ν(MeCN): 2328 cm^{-1}).

Copper(I) chloride: To a solution of **1***a* (31 mg) in CH_2Cl_2 (10 mL) was added CuCl (4.5 mg). The mixture was stirred at ambient temperature for 20 h, then filtered and the solvent evaporated to give the product **9** (30 mg). Good crystals could be grown from CH_2Cl_2/ether by diffusion, but all crystals examined were twinned.

Reaction of **1**b *with gold reagents*

To a solution of **1***b* (68.6 mg, 0.0652 mmol) in CH_2Cl_2 (5 mL) at 0°C was added $(SMe_2)AuCl$ (22.7 mg, 0.771 mmol) in CH_2Cl_2 (5 mL). An immediate color change from light to dark red was observed. The solvent was removed after stirring for 1 h, giving a dark red solid. Examination of this reaction mixture by NMR spectroscopy in $CDCl_3$ indicated that one major compound **11***a* (see Table 6) was present along with trace amounts of $dppm(AuCl)_2$ (^{31}P NMR δ: 24.1 ppm), and other unidentified compounds. Attempted crystallization of **11***a* in CH_2Cl_2/hexane resulted in the decomposition of **11***a* to give a metal mirror (Pd° and (or) Au°), $dppm(AuCl)_2$, $dppmPdCl_2$, and other identifiable products as observed by NMR spectroscopy. This experiment, with minor changes, was repeated several times and gave similar results.

Reaction of **1**c *with gold reagents*

To a solution of **1***c* (39.2 mg, 0.0321 mmol) in CH_2Cl_2 (25 mL) was added $(SMe_2)AuCl$ (15.2 mg, 0.0516 mmol). As the gold reagent dissolved, an immediate color change from orange to dark red was observed. After stirring for 5 min at ambient temperature, the solvent was removed giving a dark red oil. This residue was dissolved in CD_2Cl_2 and the ^1H, ^{31}P, and ^{195}Pt NMR spectra were determined and gave resonances attributable to **11***b* (see Table 6), and to small amounts of dppm(AuCl). Attempted crystallization from several solvents resulted in the decomposition of **11***b* to metal, $dppm(AuCl)_2$, $dppmPdCl_2$, $dppmPtCl_2$ (δ −69.7 ppm), and other unidentified species as determined by ^{31}P NMR spectroscopy.

A solution of **11***b* was prepared as above, from **1***c* (39.2 mg, 0.0321 mmol) with $(SMe_2)AuCl$ (9.7 mg, 0.0329 mmol) in CH_2Cl_2 (20 mL) at 0°C for 10 min. Triphenylphosphine (8.6 mg, 0.0328 mmol) was added and an immediate color change from dark red to yellow was observed. The solvent was removed after stirring for 15 min and the ^1H and ^{31}P NMR spectra of the dark red residue in $CDCl_3$ gave resonances due to **1***c* and Ph_3PAuCl.

Acknowledgments

We thank NSERC (Canada) for financial support.

1. S. S. D. Brown, P. J. McCarthy, and I. D. Salter. J. Organomet. Chem. **306**, C27 (1986).
2. P. A. Bates, S. S. D. Brown, A. J. Dent, M. B. Hursthouse, G. F. M. Kitchen, A. G. Orpen, I. D. Salter, and V. Sik. J. Chem. Soc. Chem. Commun. 600 (1986).
3. T. Beringhelli, G. Ciani, G. D'Alfonso, V. De Malde, and M. Freni. J. Chem. Soc. Chem. Commun. 735 (1986); M.I. Bruce, E. Horn, J. G. Matisons, and M. R. Snow. J. Organomet. Chem. **286**, 271 (1985); I.D. Salter and F. G. A. Stone. J. Organomet. Chem. **260**, C71 (1984).
4. R. Uson, J. Fornies, M. Tomas, J. M. Casas, F. A. Cotton, and L. R. Falvello. Polyhedron, **5**, 901 (1986); M. Ghedini, F. Neve, F. Morazzini, and C. Oliva. Polyhedron, **4**, 497 (1985).
5. D. I. Gilmour and D. M. P. Mingos. J. Organomet. Chem. **302**, 127 (1986); P. Braunstein and J. Rose. Gold Bull. **18**, 17 (1985); R. Uson. Pure Appl. Chem. **58**, 647 (1986); A. J. Deeming, S. Donovan-Mtunzi, and H. Hardcastle. J. Chem. Soc. Dalton Trans. 543 (1986); P. Braunstein, J. Rose, A. Dedieu, Y. Dusausay, J.-P. Mangeot, A. Tiripicchio, and M. Tiripicchio-Camelline. J. Chem. Soc. Dalton Trans. 225 (1986); F. G. A. Stone. Angew. Chem. Int. Ed. Engl. **23**, 89 (1984).
6. R.J. Puddephatt. Chem. Soc. Rev. 99 (1983); B. Chaudret, B. Delavaux, and R. Poilblanc. Coord. Chem. Rev. **86**, 191 (1988); M. L. Kullberg and C. P. Kubiak. Inorg. Chem. **25**, 26 (1986).
7. M. C. Grossel, R. P. Moulding, and K. R. Seddon. Inorg. Chim. Acta, **64**, L275 (1975).
8. M. C. Grossel, R. P. Moulding, and K. R. Seddon. J. Organomet. Chem. **253**, C50 (1983).
9. LJ. Manojlovic-Muir, K. W. Muir, I. Treurnicht, and R. J. Puddephatt. Inorg. Chem. **26**, 2418 (1987).
10. Y. Yamamoto, K. Takahashi, and H. Yamazaki. J. Am. Chem. Soc. **108**, 2458 (1986).
11. G. J. Arsenhault, LJ. Manojlovic-Muir, K. W. Muir, R. J. Puddephatt, and I. Treurnicht. Agnew Chem. Int. Ed. Engl. **26**, 86 (1987).
12. P. R. Sharp. Inorg. Chem. **25**, 4185 (1986).
13. M. C. Grossel, J. R. Batson, R. P. Moulding, and K. R. Seddon. J. Organomet. Chem. **304**, 391 (1986).
14. R. J. Puddephatt, K. A. Azam, R. H. Hill, M. P. Brown, C. D. Nelson, R. P. Moulding, K. R. Seddon, and M. C. Grossel. J. Am. Chem. Soc. **105**, 5642 (1983); R. Uson, J. Fornies, P. Espinet, and C. Fortuno. J. Chem. Soc. Dalton Trans. 1849 (1986); S. J. Higgins and B. L. Shaw. J. Chem. Soc. Dalton Trans. 457 (1988).
15. R. J. Blau, J. H. Espenson, S. Kim, and R. A. Jacobson. Inorg. Chem. **25**, 757 (1986).
16. R. Uson, J. Fornies, M. Tomas, J. M. Casas, F. A. Cotton, and L. R. Falvello. J. Am. Chem. Soc. **107**, 2556 (1985); R. Uson, J. Fornies, M. Tomas, J. M. Casas, F. A. Cotton, L. R. Falvello, and R. Llusar. Organometallics, **7**, 2279 (1988).
17. H. C. Foley, R. H. Morris, T. S. Targos, and G. L. Geoffroy. J. Am. Chem. Soc. **103**, 7337 (1981).
18. P. Braunstein, M. A. Luke, A. Tiripicchio, and M. T. Camellini. Nouv. J. Chem. **12**, 429 (1988); Angew. Chem. Int. Ed. Engl. **26**, 768 (1987).
19. J. M. Wisner, T. J. Bartczak, and J. A. Ibers. Organometallics, **5**, 2044 (1986).
20. P. G. Pringle and B. L. Shaw. J. Chem. Soc. Dalton Trans. 895 (1983).
21. L. Malatesta, L. Naldini, G. Simonetta, and F. Cariati. Coord. Chem. Rev. **1**, 255 (1966).
22. R. J. Puddephatt. The chemistry of gold. Elsevier, Oxford. 1978. pp. 56–60.
23. H. J. Gysling. Inorg. Synth. **19**, 92 (1979).
24. G. J. Kubas. Inorg. Synth. **19**, 90 (1979).
25. K. A. Azam, A. A. Frew, B. R. Lloyd, LJ. Manojlovic-Muir, K. W. Muir, and R. J. Puddephatt. Organometallics, **4**, 1400 (1985).
26. M. P. Brown, R. J. Puddephatt, M. Rashidi, and K. R. Seddon. J. Chem. Soc. Dalton Trans. 951 (1977).

Can. J. Chem. Downloaded from www.nrcresearchpress.com by 186.148.149.217 on 09/07/12
For personal use only.

One-electron transfer processes in the reaction of elemental gallium, indium, and tin with tetrahalogeno-*ortho*-benzoquinones

THEODORE A. ANNAN AND DENNIS G. TUCK[1]

Department of Chemistry and Biochemistry, University of Windsor, Windsor, Ont., Canada N9B 3P4

Received February 8, 1989

This paper is dedicated to Professor Ronald J. Gillespie on the occasion of his 65th birthday

THEODORE A. ANNAN and DENNIS G. TUCK. Can. J. Chem. **67**, 1807 (1989).

Tin reacts with tetrahalogeno-*o*-benzoquinones $X_4C_6O_2$ (X = Cl, Br) in refluxing toluene to give the tin(IV) catecholato species $Sn(O_2C_6X_4)_2$, and neutral and anionic derivatives have also been obtained. A mixture of Sn + $X_4C_6O_2$-*o* + I_2 + 1,10-phenanthroline (phen) yields $SnI_2(O_2C_6X_4)$phen. With gallium or indium (= M), the corresponding experiments give derivatives of M^{II} (e.g., $[M(O_2C_6X_4)phen]_2$), or M^{III} (e.g., $MI(O_2C_6X_4)$phen). Intermediate paramagnetic species were detected in the case of In/$Cl_4C_6O_2$-*o*/$\frac{1}{2}I_2$, and a reaction mechanism involving one-electron transfer processes is proposed on the basis of these results. Solvated crystals of the compound $InCl(O_2C_6Cl_4)(C_6H_7N)_3$ were obtained from CH_2Cl_2 solution, and the structure of this molecule has been determined by X-ray crystallographic methods.

Key words: gallium, indium, tin, benzoquinones, oxidation.

THEODORE A. ANNAN et DENNIS G. TUCK. Can. J. Chem. **67**, 1807 (1989).

En solution dans le toluène au reflux, l'étain réagit avec les tétrahalogéno *o*-benzoquinones ($X_4C_6O_2$ (X = Cl, Br) pour donner des espèces catécholato-étain(IV) $Sn(O_2C_6X_4)_2$ ainsi que des dérivés neutres et anioniques. Un mélange de Sn + *o*-$X_4C_6O_2$ + phénanthroline-1,10 (phen) fournit du $SnI_2(O_2C_6X_4)$phen. Lorsqu'on réalise la même expérience avec du gallium ou de l'indium (= M), on obtient les dérivés correspondants du M^{II} (e.g., le $[M(O_2C_6X_4)phen]_2$) ou du M^{III} (e.g., $MI(O_2C_6X_4)$phen). Dans le cas de la réaction du In/*o*-$Cl_4C_6O_2$/$\frac{1}{2}I_2$, on a détecté la présence d'intermédiaires paramagnétiques et, sur la base de ces résultats, on propose un mécanisme réactionnel impliquant des processus de transfert par un électron. En utilisant une solution de CH_2Cl_2, on a isolé des cristaux solvatés du $InCl(O_2C_6Cl_4)(C_6H_7N)_3$ et, faisant appel à des méthodes de diffraction des rayons-X, on a déterminé la structure de cette molécule.

Mots clés : gallium, indium, étain, benzoquinones, oxydation.

[Traduit par la revue]

Introduction

Recent papers from this laboratory have described the reactions between *ortho*-quinones and the halides of tin(II) or indium(I), processes which correspond formally to oxidative addition. In the case of the tetrahalogeno-*o*-benzoquinones $X_4C_6O_2$ (X = Cl, Br), the products are the corresponding tin(IV) or indium(III) catecholato compounds, as has been established by a variety of preparative, spectroscopic, and structural investigations (1, 2). More detailed mechanistic studies were possible when the oxidant was 3,5-di-*tert*-butyl-*ortho*-benzoquinone (TBQ), since the use of electron spin resonance spectroscopy demonstrated the importance of the appropriate semi-quinonate complexes as intermediates (ref. 3 and footnote 2). The general conclusion is that these reactions involve two successive one-electron transfer processes, rather than the two-electron transfer reactions generally assumed to occur in Main Group redox chemistry.

In a related study, we have shown that indium metal reacts with TBQ in refluxing toluene to give a solution of the indium(I)-semiquinone complex (TBSQ·)In, whose chemistry has been investigated (5). We have now carried out analogous studies of the oxidation of elemental gallium, indium, and tin by tetrahalogeno-*o*-benzoquinones, and find significant differences between the present results for indium and those reported earlier for TBQ. It is worth noting that direct oxidation of indium and tin can also be achieved by reaction with nonaqueous solutions of diphenyl disulphide or diselenide to give the appropriate $M(EPh)_n$ species (E = S, Se) (6), and it may well be that such simple reactions are of wider application than has been generally believed to be the case.

[1]Author to whom correspondence may be addressed.

[2]T. A. Annan, R. K. Chadha, D. H. McConville, B. R. McGarvey, A. Ozarowski, and D. G. Tuck. Unpublished results.

Experimental

General

Tin, indium, and gallium metals, tetrahalogeno-*o*-benzoquinones, 1,10-phenanthroline (phen), and 2,2′-bipyridine (bpy) (Aldrich) were used as supplied; 4-methyl pyridine (γ-picoline) (Aldrich) was stored over molecular sieves. Solvents were dried by conventional methods, and stored over drying agents. All reactions were carried out in an atmosphere of dry nitrogen.

Metal analysis was carried out by using atomic absorption spectrophotometry, with an IL 151/251 instrument and samples decomposed by aqueous nitric acid; microanalysis was by Guelph Chemical Laboratory Ltd. Halogen analysis by the Volhard method proved to be unreliable due to the presence of the strongly coloured *o*-quinone in the acidified aqueous solution. The ^1H and ^{13}C nmr spectra were recorded on a Bruker AC 300L instrument. Infrared spectroscopy involved the use of samples in KBr pellets with a Nicolet 5DX spectrometer. Conductivities were measured in a standard platinum electrode cell, standardized with 1 M aqueous KNO_3. Mass spectra of samples dissolved in 3-nitrobenzyl alcohol were recorded on a VG-ZAB-HF instrument, operating in the FAB mode, and electron spin resonance (esr) studies on a Varian E12 spectrometer, which was calibrated with an nmr gaussmeter.

Preparative

1. In the synthesis of substituted catecholato complexes of tin(IV), indium(II), and gallium(II), the general method used involved refluxing the finely divided metal (ca. 1 g) with a toluene solution of the *o*-quinone in a 1:1 (M = In, Ga) or 1:2 (M = Sn) molar ratio for 24 h. The mixture obtained at the end of this period was filtered, and any unreacted metal was collected, washed, dried, and weighed, which allowed the amount of metal consumed, typically ca. 85%, to be measured. The calculated equimolar amount of neutral donor ligand

Can. J. Chem. Downloaded from www.nrcresearchpress.com by 194.225.253.170 on 09/07/12
For personal use only.

TABLE 1. Analytical results

Compound[a]	Found/calcd. (%) M	C	H	N
$Sn(O_2C_6Cl_4)_2$bipy·0.5 tol	14.3(14.6)			
$SnI_2(O_2C_6Cl_4)$phen·0.25 tol	14.5(14.4)			
$Et_4N[SnBr(O_2C_6Cl_4)_2]$	14.0(14.5)			
$Ph_4P[SnCl(O_2C_6Cl_4)_2]$	12.0(12.1)			
$Ga(O_2C_6Cl_4)$phen·0.5 tol	12.9(12.9)			
$GaI(O_2C_6Cl_4)$phen·0.25 tol	10.4(10.8)	35.9(36.7)	1.71(1.56)	4.99(4.34)
$Ga(O_2C_6Br_4)$phen·0.5 tol	10.3(10.3)			
$GaI(O_2C_6Br_4)$phen·0.5 tol	8.15(8.23)			
$In(O_2C_6Cl_4)$phen·0.25 tol	20.0(20.4)	42.2(42.1)	2.09(1.78)	4.73(4.97)
$In(O_2C_6Br_4)$phen·0.5 tol	15.0(15.0)			
$In(O_2C_6Cl_4)$pic·0.25 tol	24.2(24.1)	34.4(34.6)	2.15(1.90)	2.93(2.94)
$In(O_2C_6Br_4)$pic·0.5 tol	17.0(16.9)			
$InI(O_2C_6Cl_4)$phen·DMF	15.9(15.5)	34.1(34.2)	2.04(2.30)	5.70(5.60)
$InI(O_2C_6Br_4)$phen·0.5 tol	13.2(13.6)			
$InCl(O_2C_6Cl_4)(pic)_3$·0.5 CH_2Cl_2	16.8(16.0)	41.7(41.0)	2.87(3.09)	5.99(5.85)

[a]bipy = 2,2′-bipyridine; phen = 1,10-phenanthroline; pic = 4-$CH_3C_5H_4N$; tol = toluene.

(phen, bpy) was dissolved in toluene and added to the filtrate. Precipitation of the product occurred upon complete addition of the ligand; the resultant mixture was stirred at room temperature for 2 h, after which the precipitate was collected by filtration, washed with petroleum ether (2 × 20 mL), and dried *in vacuo*. Addition of petroleum ether to the filtrate caused further precipitation of the product, which was isolated in a similar manner; the two products were found to be identical on the basis of elemental and spectroscopic analyses. When γ-picoline was used as the neutral donor, the product only precipitated when the volume of the solution was reduced by 50%, followed by the addition of petroleum ether (50 mL), yielding a brown product that was washed with petroleum ether and dried *in vacuo*. Analytical results are presented in Table 1. Yields were typically ca. 90%, based on the quantity of metal consumed.

2. The compounds $MI(O_2C_6Cl_4)$·phen (M = Ga, I) were prepared by either of two related procedures. In the first, a suspension of $M(O_2C_6Cl_4)$·phen in toluene was treated with a half-molar quantity of iodine in the same solvent, added over 30 min; the mixture was stirred at room temperature for 2 h, by which time the colour of iodine had completely discharged, and the product that precipitated on the slow addition of petroleum ether (ca. 20 mL) was collected and dried *in vacuo*. In the second method, gram quantities of the metal, *o*-quinone, and iodine (I_2), in the molar ratio 2:2:1, were refluxed in toluene for 24 h; addition of 1,10-phenanthroline in toluene then led to the precipitation of the product in the form of the brown phenanthroline adduct. The isolation procedure was that described above. A DMF-solvate was obtained when $InI(O_2C_6Cl_4)$·phen was recrystallized from this solvent. In the case of indium, a deep blue colour developed in the solution after about 2 h, and the mixture became red only on complete consumption of the metal. A sample of this blue solution exhibited a very strong esr signal (see below).

3. The compound $SnI_2(O_2C_6Cl_4)$·phen was prepared by refluxing tin metal (0.40 g, 2.4 mmol), iodine (0.86 g, 3.4 mmol, calculated as I_2), and quinone (0.83 g, 3.4 mmol) in toluene for 3 h, by which time the tin had dissolved completely. An equimolar amount of 1,10-phenanthroline was added to the resultant pale-green solution, and refluxing stopped. The mixture was stirred for 1 h as it cooled to room temperature, and the orange solid which deposited was collected by filtration and isolated as above.

4. The compound $In(O_2C_6Cl_4)$·pic·0.25 toluene was obtained when a twofold excess of γ-picoline was used in the reaction described in 1. The resultant solution was slowly evaporated *in vacuo* to give colourless crystals, which were collected and redissolved in hot methylene chloride; X-ray quality crystals were formed as this solution slowly cooled. Spectroscopic and elemental analysis, and a subsequent X-ray crystallographic study, showed that this product was the methylene chloride solvate $InCl(O_2C_6Cl_4)(C_6H_7N)_3 \cdot nCH_2Cl_2$; the material submitted for elemental analysis appears to have corresponded to the hemisolvate, whereas that used in the X-ray studies in the presence of excess CH_2Cl_2 (see below) proved to be the monosolvate. The source of the chloride ligand in this molecule is discussed below.

5. Salts containing the anionic complexes $[SnX(O_2C_6Cl_4)_2]^-$ were made by the dropwise addition of one equivalent of Et_4NBr or Ph_4PCl, dissolved in the minimum amount of acetonitrile, to a toluene solution of $Sn(O_2C_6Cl_4)_2$ (see 1). As the halide solution was added, a light-brown material began to deposit. After complete addition, the reaction mixture was stirred at room temperature for 2 h; addition of diethyl ether (20 mL) precipitated a solid, which was collected by filtration and dried *in vacuo*. The yield was almost quantitative. The molar conductivities (millimolar solution) of $Ph_4P[SnCl(O_2C_6Cl_4)_2]$ and $Et_4N[SnBr(O_2C_6Cl_4)_2]$ in DMF are 72 and 85 $ohm^{-1}\,cm^2$ respectively, to be compared with the normally accepted value of 70–90 $ohm^{-1}\,cm^2\,mol^{-1}$ (7) for 1:1 electrolytes in this solvent.

X-ray crystallographic analysis

A single crystal of $InCl(O_2C_6Cl_4)(C_6H_7N)_3 \cdot CH_2Cl_2$ was sealed in a capillary tube containing a drop of methylene chloride; experience showed that in the absence of this solvent, loss of crystallinity occurred and the solid turned to a powder. The crystal was mounted along its largest dimension, and the cell parameters were obtained from 15 strong reflections in the range $15° < 2\theta < 25°$. Data were collected on a Syntex $P2_1$ diffractometer following the procedures described previously (8). The intensities of three monitored reflections did not change significantly during data collection. The data were corrected for Lorentz and polarization effects; no absorption correction was deemed necessary because of low absorption coefficient. The space group $P\bar{1}$ was used and later assumed to be correct due to successful refinement. Details of the X-ray data collection are given in Table 2.

The position of the indium atom was obtained from a sharpened Patterson synthesis using SHELX-76. Fourier synthesis gave positions for the remaining non-hydrogen atoms, including one molecule of methylene chloride per $InCl(O_2C_6Cl_4)(C_6H_7N_3)_3$. Refinement was carried out by using full-matrix least-squares methods, with scattering factors taken from ref. 9. In the final cycles of least-squares refinement, the In, Cl, O, and N atoms were refined with anisotropic thermal coefficients, while the remaining atoms were refined with isotropic coefficients. This refinement converged at $R = 0.0726$ and $R_w = 0.0782$. All hydrogen atoms were included in idealized positions

Can. J. Chem. Downloaded from www.nrcresearchpress.com by 194.225.253.170 on 09/07/12
For personal use only.

Can. J. Chem. Downloaded from www.nrcresearchpress.com by 194.225.253.170 on 09/07/12
For personal use only.

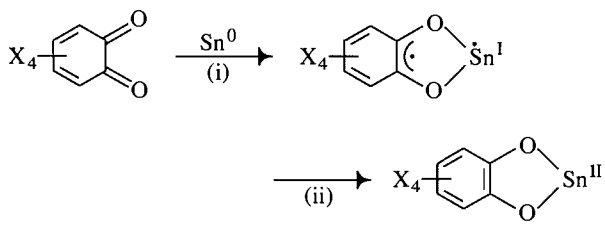
(C—H = 0.95 Å and CCH = 109.5°). Isotropic thermal parameters were assigned values 0.01 U (Å^2) greater than those for the adjacent (bonded) carbon atoms. After six more cycles of refinement, convergence was achieved with the final R = 0.0632 and R_w = 0.0678 and 2226 unique "observed ($I > 3\sigma(I)$)" reflections. The solvated methylene chloride molecule was found to be slightly disordered, and the C—Cl bond distances were therefore constrained at 1.760 Å. The quantity $\Sigma_w(|F_o| - |F_c|)^2$ was minimized during the least-squares refinement; in the final cycles a weighting scheme of the form $w = 1/[\sigma^2(F) + \rho F^2]$ was employed, with a final ρ-value of 0.00001. Final difference Fourier map calculations did not reveal any peaks of chemical significance. There was no evidence of any secondary extinction.

The final atomic coordinates for non-hydrogen atoms are given in Table 2, and important bond distances and angles in Table 3. Tables of structure factors, anisotropic thermal parameters, and fractional coordinates for hydrogen atoms are available as supplementary material.[3] The structure is shown in Fig. 1.

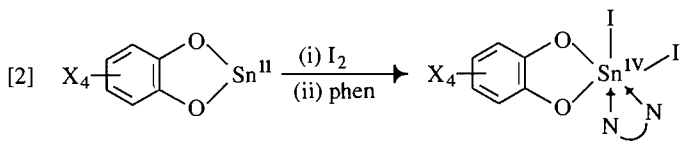
Results and discussion

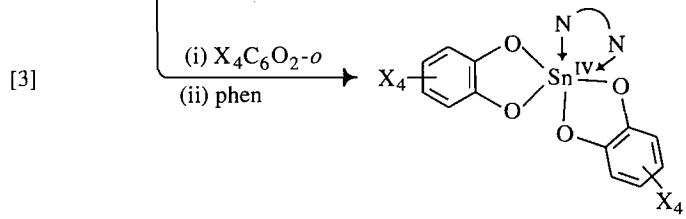
The reaction of $X_2C_6O_2$-o with tin

The reaction of metallic tin with the substituted *o*-quinones can be understood in terms of reactions already reported in other papers from this laboratory. Both $Cl_4C_6O_2$-*o* and $Br_4C_6O_2$-*o* are strongly oxidizing species, and the initial reaction involves two successive one-electron transfer processes, giving a tin(II) species as the primary product:

[1] 

The justification for step (i) lies in the analogous reaction between indium metal and TBQ (5), which has been shown to give rise to a stable (TBSQ·)In^I species in solution. The internal one-electron transfer (ii) depends on the fact that the compounds $X_4C_6O_2$-*o* are stronger oxidizing agents than TBQ (10); it is reasonable to conclude that the $X_4C_6O_2$· semiquinones are similarly more strongly oxidizing than is TBSQ·, and it follows that the reaction of tin with $X_4C_6O_2$-*o* will yield the tin(II) species rather than a derivative of the unknown tin(I)-semiquinone. We return to the difference between indium and tin in the next section. The formation of the tin(II)-catecholato compound in this reaction is in keeping with the known stability of such substances, which can be conveniently synthesized by the one-step electrochemical oxidation of tin anodes in nonaqueous solutions of aromatic diols (11). These latter compounds are stable in the solid state but can be oxidized, and it is especially appropriate that oxidation of (say) $Sn(O_2C_6H_4)$ by I_2 gives $SnI_2(O_2C_6H_4)$, and that reaction with $Br_4C_6O_2$-*o* yields $Sn(O_2C_6H_4)(O_2C_6Br_4)$. In both cases, these tin(IV) compounds were isolated as stable 1:1 adducts with 2,2′-bipyridine, so that the previous results are congruent with the one-step syntheses reported in paragraphs 1 and 3 of the preparative work in the experimental section. These latter experiments then involve the *in situ* oxidation of $Sn^{II}(O_2C_6X_4$-*o*) formed in reaction [1] via eqs. [2] and [3]:

[2] 

[3] 

In summary, the mechanism of the reaction of metallic tin with $X_4C_6O_2$-*o* can be readily understood in the context of previous work. The infrared and nmr spectra, which were essentially identical to those of the indium and gallium products discussed below, confirm the presence of tetrahalogenocatecholate and 1,10-phenanthroline in the final products.

The reactions of $X_4C_6O_2$-o with gallium or indium

As noted above, the reaction of indium metal with TBQ in refluxing toluene gives the indium(I)-semiquinone compound (TBSQ·)In, whose chemistry includes both the formation of adducts, and oxidation by reagents such as I_2, Ph_2S_2, or $Cl_4C_6O_2$-*o* to the appropriate indium(III)-semiquinone product. These oxidation reactions bring about substantial changes in the

TABLE 2. Summary of crystal data, intensity collection, and structural refinement for $InCl(O_2C_6Cl_4)(C_6H_7N)_3$, CH_2Cl_2 solvate

Parameter	Value
a (Å)	15.437(4)
b (Å)	10.810(3)
c (Å)	10.387(3)
α (°)	91.05(2)
β (°)	117.26(3)
γ (°)	95.53(2)
V (Å^3)	1529.81(5)
Crystal system	Triclinic
Space group	$P\bar{1}$
Mol. wt.	760.59
Z	2
ρ_c (g cm^{-3})	1.67
ρ_0 (g cm^{-3})	1.68
Crystal dimensions (mm)	0.15 × 0.02 × 0.46
Radiation	Mo-K_α, 0.71069 Å
Monochromator	Highly oriented graphite
Temperature (°C)	21
Abs. coeff., μ (cm^{-1})	12.99
2θ angle (°)	4–45°
Scan type	Coupled θ(crystal)/2θ(counter)
Scan width	$K\alpha_1$ − 1° to $K\alpha_2$ + 1°
Scan speed (deg min^{-1})	Variable, 2.02–4.88
Background time/scan time	0.5
Total reflections measured	2616
Unique data used	2226
No. of parameters (NP)	223
R	0.0632
R_{wF}	0.0678

[3]This material may be purchased from the Depository of Unpublished Data, CISTI, National Research Council of Canada, Ottawa, Ont., Canada K1A 0S2.

Can. J. Chem. Downloaded from www.nrcresearchpress.com by 194.225.253.170 on 09/07/12
For personal use only.

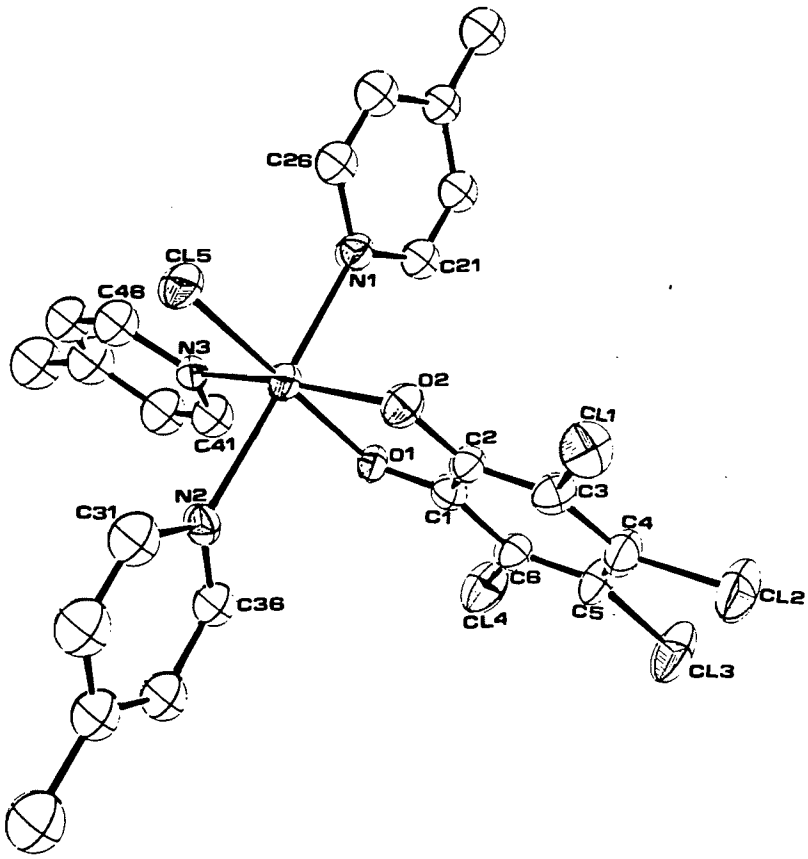
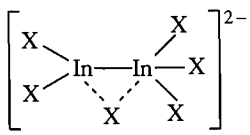


FIG. 1. Molecular structure of $InCl(O_2C_6Cl_4)(C_6H_7N)_3$, showing the atomic numbering scheme; ORTEP diagram, with 50% probability ellipsoids. Hydrogen atoms have been omitted for the sake of clarity.

esr hyperfine coupling constant A_{In}, which is ca. 9–11 G for indium(I) compounds, and 6–7 G for the indium(III) derivatives (5). In the present case, the products of the reaction of either gallium or indium metal with $X_4C_6O_2$-*o* are identified as the M(II)-catecholato derivatives, prepared as the neutral adducts. When iodine is present in the reaction mixture, one obtains adducts of the M(III) compounds $MI(O_2C_6X_4)$, in keeping with the known oxidation $L_nM^{II} + \frac{1}{2}I_2 \rightarrow L_nM^{III}I$, a characteristic reaction in indium(II) chemistry (12).

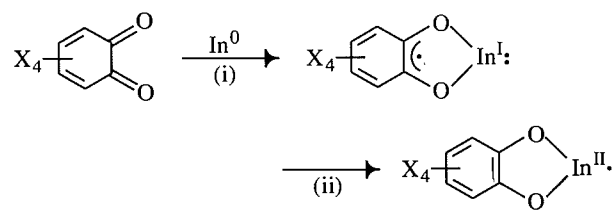
It is well established that the M^{II} compounds of gallium and indium, as exemplified by the halides, may be either the mixed oxidation state dimers $M^I[MX_4]$ or the M—M bonded species X_2MMX_2. While no simple halides are in fact known in this latter form, a number of neutral ($M_2X_4L_2$) and anionic ($M_2X_6^{2-}$) complexes are known, and in some cases crystal structure determinations have confirmed the formulation (13, 14). An important reaction of such molecules is disproportionation to indium(I) + indium(III), a process that can be seen as an internal halide transfer, e.g.,

[4] $X_3InInX_3^{2-} \rightleftharpoons$ 

[5] $In^IX_2^- + In^{III}X_4^-$

The arguments in favour of this mechanism, which is equally applicable in its reverse mode to the formation of indium(II) halide derivatives by the oxidative insertion of InX into an In—X bond of InX_3, have been discussed elsewhere (15). Similar behaviour has been identified for the corresponding gallium(II) halides (14).

On the basis of these previous results, we propose the following reaction scheme, set out here in the case of indium. The initial reaction between the metal and $X_4C_6O_2$-*o* is presumed to give the indium(I)-semiquinone by analogy with the In/TBQ system (5), but one must also accept the possibility of a further internal electron transfer process to yield the indium(II)-catecholate monomer

[6] 

Given the electrophilic nature of the X_4C_6 group, it seems reasonable to assume that the catecholato-indium(I) form may indeed make a significant contribution. Scheme 1 shows a set of reactions that then readily explain the preparative and spectroscopic results obtained. Treatment of the semiquinone $(X_4C_6O_2\cdot)In^I$: with a strong bidentate base such as 1,10-phenanthroline (eq. [7]) produces the adduct of the indium(II)

TABLE 3. Final fractional coordinates and thermal parameters for non-hydrogen atoms of $InCl(O_2C_6Cl_4)(C_6H_7N)_3$, CH_2Cl_2 solvate, with standard deviations in parentheses

Atom	x	y	z	U_{eq}/U ($Å^2 \times 10^3$)
In	0.34528(1)	0.20799(1)	0.17343(1)	54(1)
Cl(1)	0.00076(2)	0.16577(4)	0.11577(4)	66(2)
Cl(2)	−0.01179(3)	0.26889(4)	0.39167(4)	90(2)
Cl(3)	0.17641(3)	0.38082(4)	0.65632(4)	82(2)
Cl(4)	0.37576(2)	0.38714(4)	0.64604(3)	53(2)
Cl(5)	0.51757(2)	0.21873(3)	0.23187(4)	67(2)
O(1)	0.36275(5)	0.28376(8)	0.37537(8)	43(4)
O(2)	0.19702(5)	0.19622(7)	0.13716(7)	42(4)
N(1)	0.32378(6)	0.39996(9)	0.07406(9)	44(4)
N(2)	0.35279(6)	0.00478(9)	0.24448(10)	42(4)
C(11)	0.27734(7)	0.28447(10)	0.37909(11)	40(6)
C(12)	0.19134(7)	0.23602(10)	0.25688(10)	35(5)
C(13)	0.10123(8)	0.23212(11)	0.25842(12)	25(6)
C(14)	0.09712(8)	0.27668(13)	0.38216(13)	56(8)
C(15)	0.18312(9)	0.32514(14)	0.50437(13)	54(7)
C(16)	0.27323(8)	0.32904(12)	0.50283(11)	38(6)
C(21)	0.39683(10)	0.47201(14)	0.06960(14)	73(3)
C(22)	0.38426(11)	0.58507(16)	0.01598(16)	80(3)
C(23)	0.29728(9)	0.63693(13)	−0.03975(13)	65(3)
C(24)	0.28306(11)	0.75976(17)	−0.10016(17)	88(4)
C(25)	0.22031(11)	0.56418(13)	−0.03655(13)	68(3)
C(26)	0.23696(8)	0.45314(13)	0.01921(13)	65(3)
C(31)	0.27001(9)	−0.06831(13)	0.21170(13)	65(3)
C(32)	0.27289(10)	−0.18517(15)	0.25337(14)	73(3)
C(33)	0.36352(10)	−0.24203(15)	0.33439(16)	80(3)
C(34)	0.37327(13)	−0.36754(21)	0.38669(20)	107(5)
C(35)	0.44826(13)	−0.16223(19)	0.37069(18)	100(5)
C(36)	0.44004(10)	−0.04944(16)	0.32376(15)	78(3)
C(41)	0.19411(10)	0.09682(14)	−0.14150(14)	72(3)
C(42)	0.16203(13)	0.04638(19)	−0.27683(18)	94(4)
C(43)	0.22217(10)	0.03478(18)	−0.34037(14)	95(6)
C(44)	0.19542(16)	−0.02570(24)	−0.48429(19)	135(6)
C(45)	0.30860(10)	0.05457(19)	−0.26026(15)	93(4)
C(46)	0.35043(11)	0.10673(16)	−0.11290(15)	83(4)
C(01)	0.92617(12)	0.42729(17)	0.67716(18)	105(9)
Cl(6)	0.82308(9)	0.35569(15)	0.52195(14)	162(4)
Cl(7)	0.97958(9)	0.30477(15)	0.78668(14)	130(3)

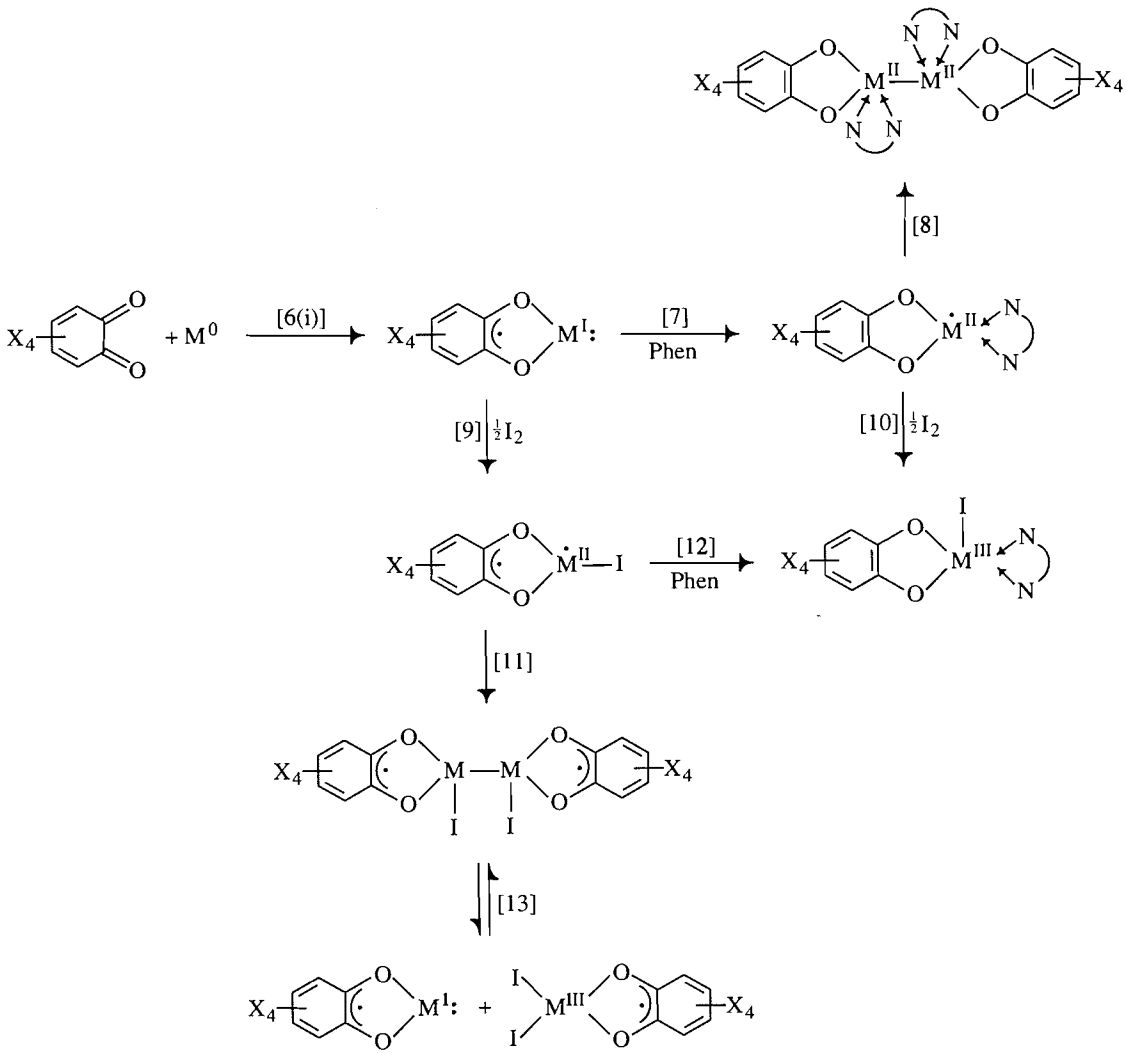
U_{eq} for all non-carbon atoms except C(11)–C(16) is calculated from the refined anisotropic thermal parameters ($U_{eq} = \frac{1}{3}\Sigma_i\Sigma_j u_{ij} a_i^* a_j^* \cdot a_i a_j$). The remaining carbon atoms are refined isotropically.

catecholate $(X_4C_6O_2)In\cdot phen$, by a process that parallels that observed in the SnX_2/TBQ system. The driving forces for this process are twofold; the addition of electron density by coordination tends to make the indium atom electron-rich, and the electrophilic nature of the $X_4C_6O_2\cdot$ ligand aids the internal electron transfer. Dimerization of this monomer then obviously gives the In—In bonded species, which was obtained in this work as the appropriate neutral adduct $[(X_4C_6O_2)In\cdot phen]_2$ (eq. [8]), which cannot undergo internal ligand transfer (cf. eq. [4]) since there is no labile monodentate ligand. The infrared and nmr spectroscopic evidence summarized below confirm this structure, but unfortunately we were not able to identify the diagnostic ν(In—In) mode in the Raman spectrum because of high fluorescent emission from each of these compounds. An additional piece of evidence was provided by the mass spectrum of $[Ga(O_2C_6Cl_4)phen]_2$; this showed prominent ions identified as $[Ga(O_2C_6Cl_4)phen]^+$ (m/e = 675) and $[Ga(O_2C_6Cl_4)]^+$ (m/e = 495) and, in the latter case, the experimental and computer-simulated isotopic distribution patterns were in good agreement. Given that the products are diamagnetic, there is little doubt that these are indeed the M^{II}–M^{II} bonded catecholates as formulated in Scheme 1. The coordination at the indium centre in such molecules gives an InO_2N_2In' kernel, similar to the InX_2N_2In' core identified in other indium(II) dimeric species (16).

When the reaction mixture involves $X_4C_6O_2$-*o* + M + $\frac{1}{2}I_2$, the products obtained are the $MI(O_2C_6X_4)$ species, again stabilized against ligand redistribution reaction by adducts with neutral nitrogen donors (see Table 1). These molecules are clearly identical with, or related to, those obtained previously from the reaction of $X_4C_6O_2$-*o* + InX (2), as demonstrated by the spectroscopic results (see below).

The present system gives additional information not available in the earlier work, in that we were able to obtain and analyze the esr spectrum of an intermediate species. The reaction mixture $Cl_4C_6O_2$-*o* + $In_{(s)}$ + $\frac{1}{2}I_2$ is initially dark red, becomes deep blue as the reaction proceeds, and finally shows the red-wine colour of the indium(III) product. A sample of the blue solution was

Can. J. Chem. Downloaded from www.nrcresearchpress.com by 194.225.253.170 on 09/07/12
For personal use only.



SCHEME 1

abstracted, so as to remove any unreacted metal, and the esr spectrum recorded (Fig. 2). Computer simulation showed that this is the spectrum of a mixture of two species, each involving a semiquinone radical bonded to an indium atom. There is no evidence of an interaction between the unpaired electron and the chlorine atoms of the ring. The hyperfine coupling constants derived from Fig. 1, 9.8 and 7.2 G, established the presence of indium(I) and indium(III) species, and the reaction pathway by which these could arise is shown in Scheme 1. We propose that the reaction proceeds via a monomeric indium(II) $(X_4C_6O_2\cdot)In\cdot I$ molecule, which dimerizes (eq. [11]) to the corresponding In—In bonded species. This can disproportionate by halide transfer (eq. [13]), parallel to the process described above (eqs. [4] and [5]), to give an equimolar mixture of $(X_4C_6O_2\cdot)In^{I}$ and $(X_4C_6O_2\cdot)In^{III}I_2$, whose hyperfine coupling constants are those quoted above. This mechanism of dimerization and disproportionation is parallel to that proposed for the reaction of TBQ with both SnX_2 (3) and InX.[2] Similarly, the reaction of the $(X_4C_6O_2\cdot)In\cdot I$ species with a strong neutral donor stabilizes the adduct in the indium(III) form $(X_4C_6O_2)In^{III}I\cdot phen$, and the arguments in favour of this have been set out elsewhere (2, 3, and footnote 2).

The hyperfine constants for these species can be compared with the values of 9.83 and 6.44 G derived for $(TBSQ\cdot)In^{I}$ and $(TBSQ\cdot)InI_2$ in toluene. The difference between these values and those found in the present work indicates a lower electron density at the metal centre, which can be readily related to the change of ring substituents from $Bu^t_2H_2$ to Cl_4, a change that increases the electrophilic nature of the ring system.

Spectroscopic results

None of the complexes prepared show the infrared active ν(C=O) bond stretching frequency observed at ~1700 cm^{-1} in the parent tetrahalogeno-*o*-quinones, and instead ν(C—O) modes appear at ~1450 cm^{-1} in the catecholato derivatives. These changes are identical with those observed in studies of the reaction of the same *o*-quinones with SnX_2 (1) and InX (2). The ir spectra also confirmed the presence of coordinated bipy, phen, and γ-picoline in the appropriate compounds.

These compounds have appreciable solubility in DMSO, and hence the ^1H and ^{13}C nmr spectra were recorded at room temperature. The ^1H nmr spectra complemented the ir spectra by confirming the presence of the donor ligands in the appropriate region of the spectra. The ^{13}C nmr spectra on the

Can. J. Chem. Downloaded from www.nrcresearchpress.com by 194.225.253.170 on 09/07/12
For personal use only.

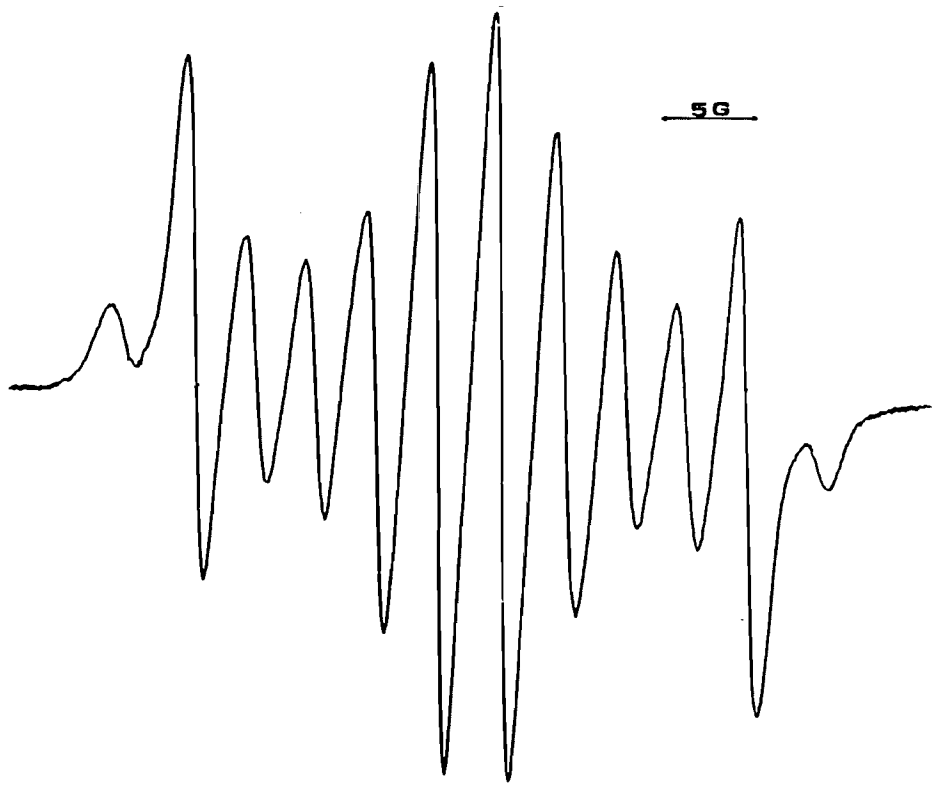


FIG. 2. Electron spin resonance spectrum of a solution obtained during the reaction of $Cl_4C_6O_2$-*o* + In + $\frac{1}{2}I_2$ in toluene.

TABLE 4. Interatomic distances (Å) and angles (deg) for $InCl(O_2C_6Cl_4)(C_6H_7N)_3$, CH_2Cl_2 solvate

Atoms	Distance	Atoms	Angle
In—O(1)	2.127(7)	O(1)—In—O(2)	78.2(3)
In—O(2)	2.130(6)	O(1)—In—N(1)	92.3(3)
In—Cl(5)	2.430(3)	O(1)—In—N(2)	93.5(3)
In—N(1)	2.322(12)	O(1)—In—Cl(5)	98.6(2)
In—N(2)	2.325(11)	O(2)—In—Cl(5)	176.1(2)
In—N(3)	2.265(9)	O(2)—In—N(1)	87.5(3)
Cl(1)—C(13)	1.660(6)	O(2)—In—N(2)	89.7(3)
Cl(2)—C(14)	1.723(5)	O(2)—In—N(3)	88.5(3)
Cl(3)—C(15)	1.729(6)	O(1)—In—N(3)	166.5(3)
Cl(4)—C(16)	1.652(6)	N(2)—In—Cl(5)	88.5(2)
O(1)—C(11)	1.337(8)	N(2)—In—N(1)	172.9(3)
O(2)—C(12)	1.351(8)	N(3)—In—N(2)	88.5(4)
N(1)—C(21)	1.327(15)	N(1)—In—N(3)	84.9(4)
N(1)—C(26)	1.382(21)	C(12)—O(2)—In	111.7(5)
N(2)—C(31)	1.332(14)	C(11)—O(1)—In	112.7(5)
N(2)—C(36)	1.410(22)	C(21)—N(1)—In	122.0(9)
N(3)—C(41)	1.319(16)	C(26)—N(1)—In	124.7(8)
N(3)—C(46)	1.350(15)	C(26)—N(1)—C(21)	113.3(13)
γ-pic C(21)—C(25)		Ring C(11)—C(15)	
mean C—C	1.360(2)	mean C—C	1.389(2)
C(23)—C(24)	1.475(2)		
γ-pic C(31)—C(35)			
mean C—C	1.377(2)		
C(33)—C(34)	1.464(2)		
γ-pic C(41)—C(45)			
mean C—C	1.347(2)		
C(44)—C(45)	1.51(3)		

other hand also showed the significant shift of the resonance observed at ~170 ppm and assigned to *C*=O in the parent quinone, to ~150 ppm, assignable to *C*—O in the catecholato derivative. The numerical values were essentially identical with those reported earlier (1, 2). Finally, we may note that the sharpness of the spectral lines for the $[(X_4C_6O_2)InL]_2$ compounds confirms that these compounds are diamagnetic, and hence must be dimeric.

Crystallographic studies

As reported in the experimental section, an attempt to recrystallize $[In(O_2C_6Cl_4)pic]_2$ from hot CH_2Cl_2 gave crystals subsequently identified as $InCl(O_2C_6Cl_4)(pic)_3$, CH_2Cl_2 solvate. This indium(III) species is clearly the result of an oxidation reaction, with the chloride ligand being derived from the solvent. There is little experimental evidence on which to discuss the mechanism of such a reaction, except to note earlier and continuing studies of the reactions of indium halide molecules with dihalogenomethanes (17).

The crystallographic results confirm that the compound is indeed an indium(III)-catecholate derivative, and are therefore important in supporting the formulations given above. The In—Cl bond length of 2.430(3) Å is in good agreement with the distances reported previously for other six-coordinate indium(III) complexes, for which values between 2.538(5) and 2.394(1) Å are known. The factors that can affect the length of this bond, and the actual experimental results, have been reviewed elsewhere (18). The In—O distance, average 2.128(7) Å, is best compared with those in $InCl_2(acac)(bipy)$, for which the values are 2.124(3) Å *cis* to chlorine, and 2.164(3) Å *trans* to chlorine (4), although in the present case there is no discernible difference in the two In—O bonds. For

Can. J. Chem. Downloaded from www.nrcresearchpress.com by 194.225.253.170 on 09/07/12
For personal use only.

the In—N bonds, that *trans* to oxygen (In—N3) is substantially shorter (2.265(9) Å) than the other two, which are virtually identical (average 2.324(12) Å), and these distances are again close to those reported for other complexes in which an indium(III) ion is coordinated to neutral heterocyclic *N*-donor ligands (cf. ref. 18). The bond angles are those expected in an octahedral complex with distortion due to the presence of a bidentate ligand, for which the O—In—O bite angle of 78.2(3)° is close to that in other catecholato complexes (cf. refs. 1 and 3).

From the mean plane calculations (set out in the supplementary material), we found all the rings in the compound to be planar, with negligible deviations from planarity. The plane through the atoms Cl(1), Cl(2), Cl(3), Cl(4), C(11)–C(16) had an average deviation of 0.025 Å; that through the atoms N(1), C(21)–C(26) had a deviation of ±0.005 Å; for N(2), C(31)–C(36) the value was 0.022 Å; and that through N(3), C(41)–C(46) had an average deviation of 0.05 Å. The angles between the normal to these planes show that the *trans*-picoline ligands are almost perpendicular to each other, and the same relationship exists between the equatorial picoline and the two apical (*trans*) ligands.

The other bond lengths and angles call for little comment, except for the significant C—O bonds of the tetrachlorocatecholato ligand, for which the average value of 1.34(1) Å is typical of that in catecholato rather than semiquinone or *o*-quinone ligands, in complete agreement with the conclusions of the spectroscopic studies.

Acknowledgment

This work was supported in part by an Operating Grant (to D.G.T.) from the Natural Sciences and Engineering Research Council of Canada. We thank Drs. B. R. McGarvey and A. Ozarowski for helpful discussions of the esr results.

1. T. A. Annan, R. K. Chadha, D. G. Tuck, and K. D. Watson. Can. J. Chem. **65**, 2670 (1987).
2. T. A. Annan and D. G. Tuck. Can. J. Chem. **66**, 2935 (1988).
3. T. A. Annan, R. K. Chadha, B. R. McGarvey, A. Ozarowski, and D. G. Tuck. J. Chem. Soc. Dalton Trans. 439 (1989).
4. J. G. Contreras, F. W. B. Einstein, and D. G. Tuck. Can. J. Chem. **52**, 3793 (1974).
5. T. A. Annan, D. H. McConville, B. R. McGarvey, A. Ozarowski, and D. G. Tuck. Inorg. Chem. **28**, 1644 (1989).
6. H. E. Mabrouk, R. Kumar, and D. G. Tuck. J. Chem. Soc. Dalton Trans. 1045 (1988).
7. W. J. Geary. Coord. Chem. Rev. **7**, 81 (1971).
8. M. A. Khan, R. C. Steevensz, D. G. Tuck, J. G. Noltes, and P. W. R. Corfield. Inorg. Chem. **19**, 3407 (1980).
9. D. T. Cromer and J. T. Waber. International tables for X-ray crystallography. Vol. IV. Kynoch Press, Birmingham, UK. 1974.
10. O. Ryba, J. Pilar, and J. Petránek. Collect. Czech. Chem. Commun. **33**, 26 (1968).
11. H. E. Mabrouk and D. G. Tuck. J. Chem. Soc. Dalton Trans. 2539 (1988).
12. D. G. Tuck. *In* Comprehensive coordination chemistry. Vol. 3. *Edited by* G. Wilkinson, R. D. Gillard, and J. A. McCleverty. Pergamon Press; Oxford. 1987. Chap. 25.2.
13. M. J. Taylor. *In* Comprehensive coordination chemistry. Vol. 3. *Edited by* G. Wilkinson, R. D. Gillard, and J. A. McCleverty. Pergamon Press, Oxford. 1987. Chap. 25.1.
14. M. J. Taylor. Metal-to-metal bonded states of the main group elements. Academic Press, London. 1975. Chap. 3.
15. C. Peppe and D. G. Tuck. Can. J. Chem. **62**, 2793 (1984).
16. M. A. Khan, C. Peppe, and D. G. Tuck. Can. J. Chem. **62**, 601 (1984).
17. M. A. Khan, C. Peppe, and D. G. Tuck. Organometallics, **5**, 525 (1986), and unpublished work.
18. M. A. Khan, C. Peppe, and D. G. Tuck. Acta Crystallogr. Sect. C: Cryst. Struct. Commun. **C39**, 1339 (1983).

Can. J. Chem. Downloaded from www.nrcresearchpress.com by 194.225.253.170 on 09/07/12
For personal use only.

Synthesis and thermal study of tris(ammonium) hexafluoro metallates(III) of some rare earths

S. J. PATWE, B. N. WANI, U. R. K. RAO,[1] AND K. S. VENKATESWARLU
Water Chemistry Division, Bhabha Atomic Research Centre, Trombay, Bombay 400 085, India

Received January 31, 1989

This paper is dedicated to Professor Ronald J. Gillespie on the occasion of his 65th birthday

S. J. PATWE, B. N. WANI, U. R. K. RAO, and K. S. VENKATESWARLU. Can. J. Chem. **67**, 1815 (1989).

Fluorination of oxides of rare earths using ammonium hydrogen fluoride at room temperature gave new compounds $[NH_4]_3MF_6 \cdot nH_2O$, where M = Y, La, Nd, and Pr. In the case of cerium, $[NH_4]_4CeF_8$ is formed. The course of thermal decomposition of all these compounds is studied by thermogravimetry/differential thermal analysis (TG/DTA) and X-ray powder diffraction (XRD).

Key words: hexafluoro metallates, rare earths, ammonium hydrogen fluoride, thermal decomposition, X-ray diffraction.

S. J. PATWE, B. N. WANI, U. R. K. RAO et K. S. VENKATESWARLU. Can. J. Chem. **67**, 1815 (1989).

La fluoration d'oxydes de terres rares à l'aide du fluorure d'ammonium, à la température ambiante, fournit de nouveaux composés, du type $[NH_4]_3MF_6 \cdot nH_2O$ dans lesquels M = Y, La, Nd et Pr. Dans le cas du cérium, il se forme du $[NH_4]_4CeF_8$. On a étudié la décomposition thermique de ces composés à l'aide de la TG/DTA et de la diffraction de rayons-X sur des poudres.

Mots clés : métallates hexafluoro, terres rares, fluorure d'ammonium, décomposition thermique, diffraction des rayons-X.
[Traduit par la revue]

Can. J. Chem. Downloaded from www.nrcresearchpress.com by 186.148.149.217 on 09/07/12
For personal use only.

Ammonium ytterbium/yttrium fluoride was believed to be an intermediate compound in the formation of ytterbium/yttrium trifluoride (1, 2). Bukhalov and Babaeva (1) prepared the ammonium complex by dissolving ytterbium nitrate in 48% HF in the presence of ammonium carbonate. This complex gave ytterbium trifluoride on heating. According to Thoma *et al.* (2), by heating a mixture of Y_2O_3 and NH_4HF_2 in a 1:6 mole ratio to 150°C an ammonium complex was formed, which on further heating at 300–400°C gave YF_3. In the first case 48% HF was used as fluorinating agent whereas in the second case ammonium hydrogen fluoride was used, but in neither case was the ammonium complex isolated or characterized. In this communication, we describe the synthesis and characterization of ammonium hexafluoro metallates(III) of rare earths and their pyrolytic behaviour.

In our earlier communications (3–6), ammonium hydrogen fluoride was used to fluorinate the corresponding oxides to prepare several oxyfluoride compounds such as $NH_4VO_2F_2$, $[NH_4]_3NbOF_6$, $[NH_4]_3VF_6$, $[NH_4]_4UF_8$, $[NH_4]_4ThF_8$, and $[NH_4]_3UO_2F_5$. By physical mixing of the oxide and ammonium hydrogen fluoride together at room temperature or close to room temperature, one gets the above oxyfluoride complexes. Fluoride was believed to be incorporated in the complex superconducting oxide $YBa_2Cu_3O_{6+\delta}$ by using ammonium hydrogen fluoride (7, 8) as fluorinating agent. It was our aim to prepare the title compounds starting from ammonium hydrogen fluoride and M_2O_3 (M = Y, La, Ce, Nd, Pr, and Gd) according to the following scheme:

[1] $M_2O_3 + 6NH_4HF_2 \rightarrow 2[NH_4]_3MF_6 \cdot 1.5H_2O$

Experimental

The rare earth oxides used in this study, viz., Y_2O_3, La_2O_3, Nd_2O_3, $PrO_{1.83}$, Gd_2O_3, and CeO_2 were preheated to ≈700°C to remove absorbed moisture. Ammonium hydrogen fluoride used was of BDH LR grade dried at 80–100°C prior to mixing. All the metal oxides except CeO_2 were of BARC make with purity of 99.9%. The CeO_2 used was from EMERC.

The reactants (a few hundred milligrams) in the stoichiometric ratio as given in eq. [1] were ground together for half an hour inside a polythene bag instead of in a mortar and pestle to avoid the reaction of ammonium hydrogen fluoride with the mortar and pestle. The powder X-ray diffraction (XRD) pattern of the resultant mixture showed the presence of oxide along with the ammonium hydrogen fluoride. Some additional new reflections were also seen in the XRD pattern. The mixture was kept in a polythene bag at room temperature in a desiccator over $CaCl_2$. After keeping for 3 days, completion of reaction was ascertained from the absence of reflections due to reactants in the X-ray powder pattern. Compared to the reaction with oxides of vanadium, thorium, and uranium, this reaction was very slow. The reaction can be completed within 10 min if the mixture is heated at 100°C with a slight excess of ammonium hydrogen fluoride. The final product was characterized using the powder XRD technique. The instrument used was a Philips PW-1050 wide-angle goniometer mounted on a Philips PW-1009 X-ray generator with Ni-filtered Cu-Kα radiation (λ = 1.5418 Å). In the cases of Y, La, Nd, and Pr, the reaction proceeded according to eq. [1]. In case of CeO_2, when it was mixed with ammonium hydrogen fluoride in 1:3 mole ratio the reaction did not go to completion, as was seen from the XRD pattern, which showed some new lines in addition to those of unreacted CeO_2. These new lines were those characteristic (9) of $[NH_4]_4CeF_8$. Hence a new mixture was prepared by mixing CeO_2 and ammonium hydrogen fluoride in 1:4 mole ratio just as in the case of UO_2 studied by us (6) recently.

[2] $CeO_2 + 4NH_4HF_2 \rightarrow [NH_4]_4CeF_8 + 2H_2O$

The XRD pattern of the product matches well with that reported (9) for the octafluoro compound. The above complex had been prepared earlier by Penneman and Rosenzweig (10) using 48% HF as a solvent. If the physical mixture is heated at 100°C, the reaction proceeds more quickly.

In the case of gadolinium oxide, even at the end of 4 days after mixing, the reaction did not go to completion and the XRD pattern of the product showed lines due to unreacted Gd_2O_3 along with the new lines. Heating the mixture at 100°C did not hasten the reaction.

The simultaneous TG/DTA instrument was an Ulvac Sinku Riko TGD model 7000 RHP. The heating/cooling rate was 8°C/min. The atmosphere used was static air and the sample size ≈35 mg.

Results and discussion

Powder XRD

The XRD patterns of tris(ammonium) hexafluoro metallates-(III) of all rare earths except cerium are identical. They are

[1]Author to whom correspondence may be addressed.

Can. J. Chem. Downloaded from www.nrcresearchpress.com by 186.148.149.217 on 09/07/12
For personal use only.

TABLE 1. XRD powder pattern of $[NH_4]_3LaF_6 \cdot 1.5H_2O$[a]

Ser. no.	*h k l*	d_{obsd}	d_{calcd}	I/I_0
1	1 2 0	5.828	5.838	18
2	2 0 1	5.644	5.640	100
3	3 0 1	4.291	4.293	18
4	1 1 2	3.969	3.970	38
5	4 1 1	3.290	3.289	36
6	2 2 2	3.232	3.232	48
7	1 0 3	2.849	2.850	36
8	4 0 2	2.823	2.820	90
9	3 5 0	2.259	2.259	25
10	3 0 4	1.993	1.993	18
11	7 1 2	1.881	1.881	15

[a]Orthorhombic. $a = 14.798 \pm 0.006$ Å; $b = 12.706 \pm 0.004$ Å; $c = 8.713 \pm 0.002$ Å.

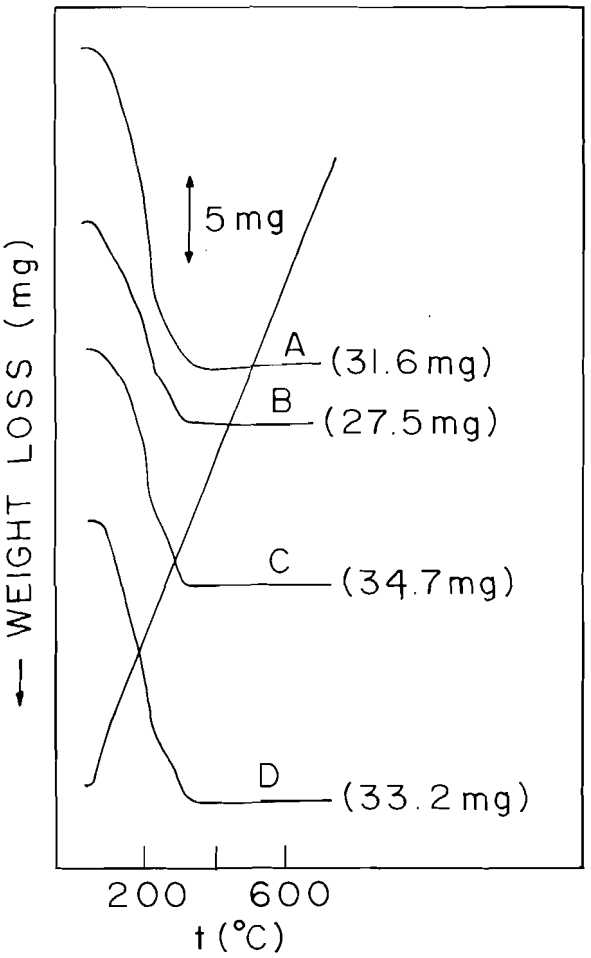


FIG. 1. TG curves of (a) $[NH_4]_3YF_6 \cdot nH_2O$, (b) $[NH_4]_3LaF_6 \cdot 1.5H_2O$, (c) $[NH_4]_3PrF_6$, and (d) $(NH_4)_3NdF_6 \cdot 2H_2O$ in air.

isostructural in the case of Y, La, Pr, and Nd. Since the nature of preparation involves reaction by physical mixing of two powdered components, the product could only be polycrystalline material. The question of obtaining a single crystal does not arise in this method. Table 1 gives a fit of the XRD powder pattern of the lanthanum compound based on an orthorhombic unit cell along with the cell dimensions. The

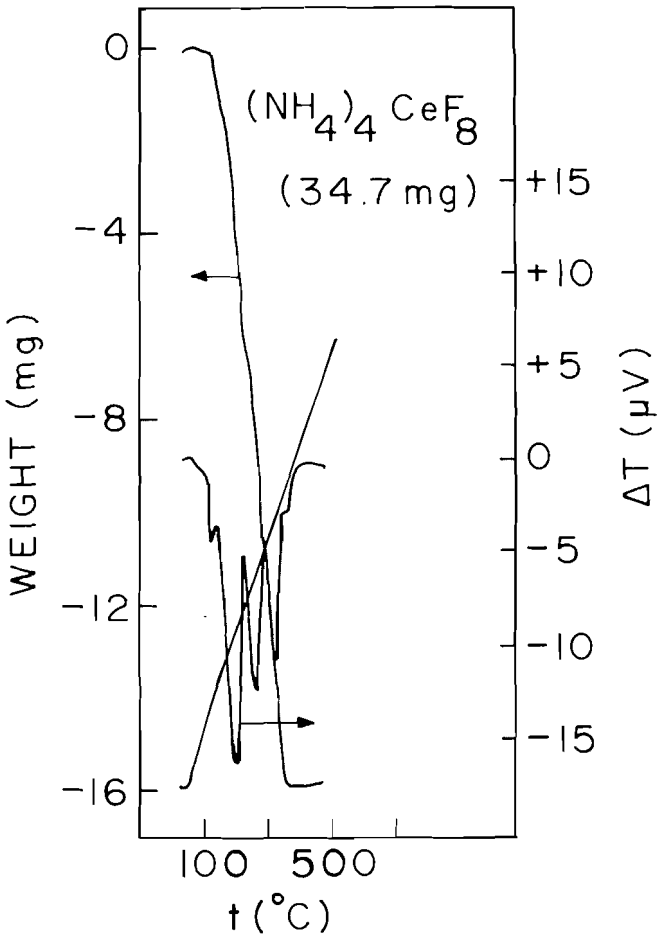


FIG. 2. Simultaneous TG/DTA curves of $[NH_4]_4CeF_8$ in air.

XRD of the complex of cerium matches well with that reported for $(NH_4)_4CeF_8$.

Thermogravimetry

TG curves of $[NH_4]_3MF_6 \cdot nH_2O$ (M = Y, La, Pr, and Nd) and $[NH_4]_4CeF_8$ are shown in Figs. 1 and 2. In all cases weight loss commences at 70°C and levels off at 320°C. The residues obtained at 320°C were the respective trifluorides, identified by XRD. The weight loss in the TG curves is consistent with the formation of MF_3 (Table 2). These TG curves indicate a single-step loss but exhibit change in slope at one or two temperatures. Since the steps overlap, one has to take recourse to simultaneous DTG or DTA to get the stepwise information. The overall decomposition is as follows:

[3] $[NH_4]_3MF_6 \cdot nH_2O \rightarrow MF_3 + 3NH_4F + nH_2O$

[4] $[NH_4]_4CeF_8 \rightarrow CeF_3 + 4NH_4F + \frac{1}{2}F_2$

Differential thermal analysis

Figure 3 shows DTA curves of the above ammonium fluoro complexes. Even though TG curves show one single-step loss in weight in all cases, the DTA shows multistep decomposition (Table 2). Similar behaviour was earlier observed in case of $[NH_4]_3VO_2F_4$ and, by a DTA analysis of different possible intermediates, the detailed thermal degradation path was delineated (3). Going from the Y to the Nd complexes, even though the TG and XRD patterns are the same, the nature of

TABLE 2. Summary of TG/DTA data

Compound	TG				DTA
	Temperature range (°C)	% Weight loss		Molecule lost	Peak temperature endotherm (°C)
		Obsd.	Calcd.		
$[NH_4]_3YF_6 \cdot 1.5H_2O$	80–320	58.0	51.0	nH_2O, $3NH_4F$	205
$[NH_4]_3LaF_6 \cdot 1.5H_2O$	70–150	7.1	8.0	$1.5H_2O$	120
	150–225	24.9	22.0	$2NH_4F$	195
	225–320	9.8	11.0	NH_4F	280
$[NH_4]_4CeF_8$	70–220	19.6	20.3	$2NH_4F$	200
	220–290	10.95	10.16	NH_4F	260
	290–370	14.98	15.38	NH_4F, $1/2F_2$	320
$[NH_4]_3PrF_6$	110–230	23.07	23.95	$2NH_4F$	195
	230–320	11.53	11.97	NH_4F	265
$[NH_4]_3NdF_6 \cdot 2H_2O$	70–150	10.36	10.32	$2H_2O$	100, 140
	150–225	21.32	21.23	$2NH_4F$	195
	225–320	10.95	10.60	NH_4F	275

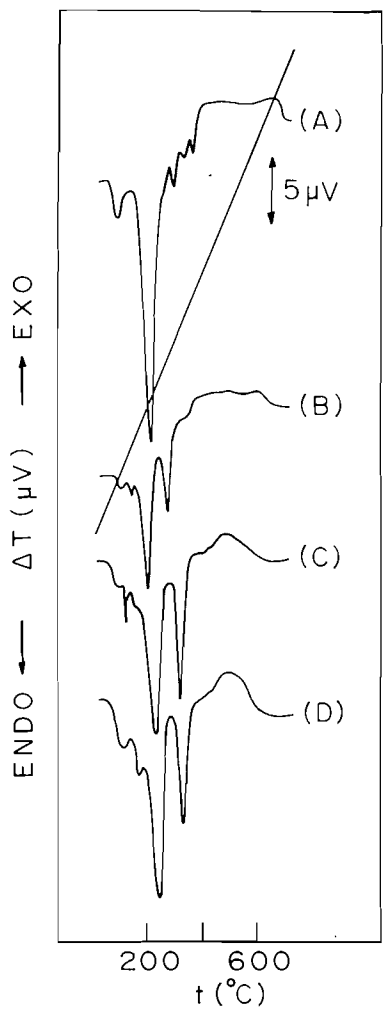


FIG. 3. DTA curves of (a) $[NH_4]_3YF_6 \cdot nH_2O$, (b) $[NH_4]_3LaF_6 \cdot 1.5H_2O$, (c) $[NH_4]_3PrF_6$, and (d) $(NH_4)_3NdF_6 \cdot 2H_2O$ in air.

decomposition is different. The first endotherm at 80°C in all cases is attributed to the removal of water of reaction.

In the case of yttrium all three ammonium fluorides are lost in one single step, as indicated by one endotherm in its DTA. In the case of lanthanum the DTA exhibits two endotherms of relative intensities 2 and 1, suggesting that two molecules of ammonium fluoride are lost in the first step and one more in the second step. This is further corroborated by the weight loss considerations as well as temperatures of inflection in the TG (Table 2). The thermal degradation of the octafluoro complex of cerium proceeds in three distinct steps, as seen in three DTA peaks with area ratio of 2:1:1 and a residue of CeF_3 above 270°C. In the case of Pr and Nd complexes, just as in the case of lanthanum, ammonium fluoride is lost in two steps. In the first step two molecules are lost, and in the second one molecule. The course of decomposition of each compound may thus be shown as follows:

$$1.\ [NH_4]_3YF_6 \cdot nH_2O \xrightarrow{80\text{–}320^\circ C} YF_3 + 3NH_4F + nH_2O$$

$$2.\ [NH_4]_3LaF_6 \cdot 1.5H_2O \xrightarrow{70\text{–}150^\circ C} [NH_4]_3LaF_6 + 1.5H_2O$$

$$[NH_4]_3LaF_6 \xrightarrow{150\text{–}225^\circ C} NH_4LaF_4 + 2NH_4F$$

$$NH_4LaF_4 \xrightarrow{225\text{–}320^\circ C} LaF_3 + NH_4F$$

$$3.\ [NH_4]_4CeF_8 \xrightarrow{70\text{–}220^\circ C} [NH_4]_2CeF_6 + 2NH_4F$$

$$[NH_4]_2CeF_6 \xrightarrow{220\text{–}290^\circ C} NH_4CeF_5 + NH_4F$$

$$NH_4CeF_5 \xrightarrow{290\text{–}370^\circ C} CeF_3 + NH_4F + \tfrac{1}{2}F_2$$

The cerium compound, when formed at room temperature, has two molecules of water as product of reaction occluded by the solid octafluoride. The fluorine evolved during decomposition of the octafluoride can thus react with water to yield HF and O_2. Analysis for the gaseous products was not attempted.

Can. J. Chem. Downloaded from www.nrcresearchpress.com by 186.148.149.217 on 09/07/12
For personal use only.

The ammonium complexes of Pr and Nd follow the course given above for lanthanum.

Acknowledgement

We are grateful to Dr. Satya Brat and Shri Z. A. Khan of the Process Engineering Division of this Centre for the TG/DTA data.

1. G. A. BUKHALOV and E. P. BABAEVA. Russ. J. Inorg. Chem. **11**, 337 (1966).
2. R. G. THOMA, C. F. WEAVER, H. A. FRIEDMAN, H. INSLEY, L. A. HARRIS, and H. A. YAKEL, JR. J. Phys. Chem. **65**, 1096 (1961).
3. U. R. K. RAO, K. S. VENKATESWARLU, and B. N. WANI. Thermochim. Acta, **81**, 23 (1984).
4. U. R. K. RAO, K. S. VENKATESWARLU, and B. N. WANI. J. Fluorine Chem. **31**, 29 (1986).
5. B. N. WANI, U. R. K. RAO, and K. S. VENKATESWARLU. National Symposium on Unusual Valency States in coordination compounds. Bombay, India. 1987.
6. B. N. WANI, S. J. PATWE, U. R. K. RAO, and K. S. VENKATESWARLU. J. Fluorine Chem. **44**, 177 (1989).
7. U. R. K. RAO, A. K. TYAGI, S. J. PATWE, and R. M. IYER. Pramana, **31**, L79 (1988).
8. U. R. K. RAO, A. K. TYAGI, S. J. PATWE, R. M. IYER, M. D. SASTRY, R. M. KADAM, Y. BABU, and A. G. I. DALVI. Solid State Commun. **67**, 385 (1988).
9. X-ray powder diffraction file. ASTM card number 23-6.
10. R. A. PENNEMAN and A. ROSENZWEIG. Inorg. Chem. **8**, 627 (1969).

Can. J. Chem. Downloaded from www.nrcresearchpress.com by 186.148.149.217 on 09/07/12
For personal use only.

Inner-shell excitation studies of conducting organic polymers: selenophene, 3-methyl selenophene, and their polymers

A. P. HITCHCOCK
Institute for Materials Research, McMaster University, Hamilton, Ont., Canada L8S 4M1

G. TOURILLON
Laboratoire pour l'utilisation de rayonnement électromagnétique, Laboratoire CNRS, CEA et MEN, Université Paris-Sud, Orsay, F-91405, France

AND

W. BRAUN
BESSY GmbH, Lentzeallee 100, D-1000 Berlin, 33, W. Germany

Received February 27, 1989

This article is dedicated to Professor Ronald J. Gillespie on the occasion of his 65th birthday

A. P. HITCHCOCK, G. TOURILLON, and W. BRAUN. Can. J. Chem. **67**, 1819 (1989).

Inner-shell electron energy loss spectra (ISEELS) of gaseous selenophene and 3-methylselenophene in the regions of Se 3*d*, Se 3*p*, Se 3*s*, and C 1*s* are presented and analyzed. The ISEELS spectra are compared to the C 1*s* near-edge X-ray absorption fine structure (NEXAFS) spectra of the corresponding polymers deposited electrochemically onto Pt, both with and without doping, to form the electrically conducting state. Methyl substitution at the 3-position of the selenophene ring is found to have little effect on the intensity of the C $1s \rightarrow \pi^*$ transition, suggesting that the π manifold is relatively unaffected. The C 1*s* NEXAFS of thin polyselenophene and poly-3-methylselenophene films confirms that (1) the polymeric chain is composed of the same structural units as the monomers and (2) doping enhances electrical conductivity via a narrowing of the $\pi-\pi^*$ band gap.

Key words: core excitation, ISEELS, NEXAFS, conducting polymers.

A. P. HITCHCOCK, G. TOURILLON et W. BRAUN. Can. J. Chem. **67**, 1819 (1989).

Les spectres de perte d'énergie d'électrons en couches internes (ISEELS) du sélénophène et du 3-méthyl sélénophène en phase gaz et aux seuils Se 3*d*, Se 3*p*, Se 1*s* et C 1*s* sont présentés. Ces spectres ISEELS sont comparés aux spectres d'absorption X (NEXAFS) obtenus avec les polymères correspondants déposés électrochimiquement en films minces sur une surface de Pt. La substitution en position 3 d'un hydrogène par un groupement méthyl affecte très peu l'intensité de la transition C $1s \rightarrow \pi^*$, suggérant que les orbitales π et π^* ne sont pas modifiées. Les spectres NEXAFS des films minces polymériques confirment que (1) les chaînes polymériques sont composées des mêmes unités structurales que les monomères et que (2) le dopage de ces films vers l'état conducteur s'accompagne d'un rétrécissement de la bande interdite $\pi-\pi^*$.

Mots clés : excitation de coeur, ISEELS, NEXAFS, polymères conductant.

1. Introduction

Polymers of unsaturated heterocyclic compounds such as pyrrole, thiophene, and selenophene can be doped to form conducting materials (1). The magnitude and mechanism of conduction, the stability and mechanisms of decomposition, and the control of processibility all need to be better understood to develop practical applications of these materials. Recent studies of polythiophene by near-edge and extended X-ray absorption fine structure (NEXAFS, EXAFS) and by inverse photoemission (2) have shown that the ring structures are not changed by doping but that the π and π^* levels shift with doping such that the $\pi-\pi^*$ gap decreases considerably. The influence on the electrical properties and electronic structure of methyl substitution at the 3-position of the thiophene ring has also been studied (1). Companion studies of the core edge spectra of both gas phase monomer and thin film polymer specimens of a series of alkyl-substituted thiophenes have recently been carried out (3, 4).

It is useful to derive spectral assignments from comparison of free and condensed monomer spectra in order to take advantage of the individual strengths of the two inner-shell excitation spectroscopies we have employed. These are inner-shell electron energy loss spectroscopy (ISEELS) (5), which examines, with good energy resolution, the unoccupied electronic structure of monomers of known molecular structure in the gas phase; and NEXAFS (6), which examines doped and undoped thin film polymers and can provide additional information toward spectral assignments through polarization dependence in the case of oriented films. The combination of the two spectroscopies constitutes a powerful probe of both the electronic and geometric structures of materials such as conducting organic polymers. Studies of this nature have been carried out for polythiophene (2, 7) and polypyrrole (8) but not as yet for polyselenophene. In recent NEXAFS studies of 3-alkyl polythiophenes (3) the spectra were interpreted to indicate that the intensity of the C $1s \rightarrow \pi^*$ transition decreases with increasing length of the alkyl side chain, suggesting that the electron distribution in the π and π^* orbitals is modified by the alkyl substitution. However, the ISEEL spectra of the gas phase monomers, along with a reanalysis of the polymer NEXAFS (4), suggest that the C $1s \rightarrow \pi^*$ intensity is essentially independent of the length of a 3-alkyl side chain. Thus a motivation of the present study was to examine the effect of alkyl substitution on the π-electronic structure of heterocyclic rings in a different system, namely selenophene and 3-methylselenophene. All core excitations below 350 eV are reported

Can. J. Chem. Downloaded from www.nrcresearchpress.com by 186.148.149.217 on 09/07/12
For personal use only.

Can. J. Chem. Downloaded from www.nrcresearchpress.com by 186.148.149.217 on 09/07/12
For personal use only.

for the gas phase monomers, which have not been studied previously to our knowledge. The C 1*s* NEXAFS spectra of the doped and undoped polymers are compared to the gas phase monomer C 1*s* ISEEL spectra. Information relating to the conduction mechanism of doped heterocyclic polymers is derived.

Selenophene is a planar molecule with C_{2v} symmetry and a high degree of aromaticity. The selenium atom provides two $p\pi$ electrons, which, in addition to the four $p\pi$ electrons from the carbon atoms, makes a six-electron aromatic system. In an LCAO-MO description these five p_z atomic orbitals combine to produce five molecular orbitals, three of which ($1b_1\pi$, $2b_1\pi$, and $1a_2\pi$) are occupied and two of which ($3b_1\pi^*$ and $2a_2\pi^*$) are unoccupied in the neutral ground state (9). The highest occupied level ($1a_2\pi$) and the lowest unoccupied level ($3b_1\pi^*$) both have pure carbon character. There are no theoretical calculations available for the energies of π-bonding and π^*-antibonding orbitals formed upon polymerization of selenophene. However, we expect, as for polythiophene (10), a broadening and shift toward the Fermi level E_f of the π and the π^* bands associated with the coupling of the monomers. The polymer has a band gap of 2.5 eV, as determined by UV–visible spectroscopy (11). In addition to the π bands, there are unoccupied levels of σ symmetry associated with both the C—Se and C—C bonds [7].

2. Experimental

2.1. ISEELS

The electron energy loss spectra were recorded at McMaster with an ISEEL spectrometer using 2.5 keV final electron energy, 2° scattering angle, and 0.7 eV FWHM resolution. Under these experimental conditions electric dipole transitions dominate the inelastic scattering and thus the spectra are similar to the corresponding X-ray absorption spectra, aside from kinematic factors that, relative to photoabsorption, produce a gradual downward tilt in the spectra towards higher energy loss. The procedures used to synthesize the selenophene and 3-methylselenophene samples have been published elsewhere (12). The energy loss spectra were calibrated in the C 1*s* region relative to the C $1s \rightarrow \pi^*$ transition in CO at 287.40 eV (13), while the other spectral regions were calibrated internally relative to the calibrated C $1s \rightarrow \pi^*$ feature of the selenophene species. The C 1*s* spectra were converted to absolute oscillator strength scales by kinematic correction and normalization at 315 eV to $n \times 0.0078\ \text{eV}^{-1}$, where n is the number of carbon atoms per molecule and $0.0078\ \text{eV}^{-1}$ is the oscillator strength of a single carbon atom at 25 eV above the ionization threshold. This procedure of normalizing to atomic values in the far continuum has been developed and tested previously (14).

2.2. NEXAFS of polymer films

Films of polyselenophene and poly-3-methylselenophene were electrochemically deposited onto a Pt electrode immersed in an acetonitrile medium composed of 0.5 M $LiClO_4$ – 0.5 M monomer (11). The electrode was first polarized at +1.35 V/SCE (saturated calomel electrode) for the 3-methylselenophene and at +1.85 V for selenophene to obtain doped films and then at −0.2 V/SCE to obtain the films in the undoped state. Film thicknesses were in the range of 500 Å. The deposited films were rinsed in acetone, dried in air, and then inserted into a vacuum chamber at 10^{-8} Torr (1 Torr = 133.3 Pa). NEXAFS experiments were carried out at the electron storage ring BESSY-Berlin using the high energy TGM1 beam line with a resolution of 0.5 eV at the C K-edge (15). The incident photon beam I_0 was monitored by measuring the total electron yield from a high transmission metal grid freshly coated with gold. The total electron yield from the sample (I) was then normalized with respect to I_0. The background at the C K-edge was estimated from the yield of a clean Pt surface in the C K-edge region. Spectra recorded at grazing and normal incidence were found to be identical, indicating random orientation of the polymer at these film thicknesses. The NEXAFS spectra presented were recorded with X-rays incident at 40° relative to the surface.

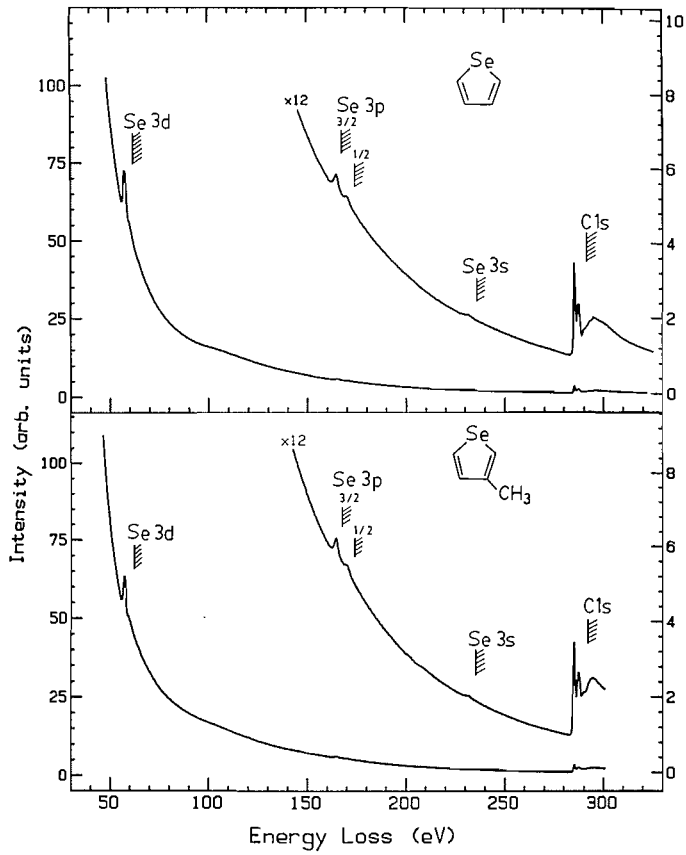


FIG. 1. Long range electron energy loss spectra of gas phase selenophene and 3-methylselenophene showing the Se 3*d*, Se 3*p*, Se 3*s*, and C 1*s* edges. Each spectrum is a composite of two spectra matched at 130 eV. All of the ISEEL spectra were recorded using 2.5 keV final electron energy, 2° scattering angle, and 0.7 eV FWHM resolution. The hatched lines indicate the estimated locations of the ionization potentials (IPs).

3. Results and discussion

A. Gas-phase ISEELS of selenophene and 3-methylselenophene

Long range spectra of selenophene and 3-methylselenophene throughout the energy loss region studied are shown in Fig. 1. As in all of the spectra presented throughout this paper, the hatched lines indicate the onset of the inner-shell ionization continua as deduced from the IPs of related species determined by X-ray photoelectron spectroscopy (16). The rapid decline in intensity with increasing energy loss arises partly because of the intrinsic falloff in photoionization cross section with increasing transition energy and partly because of additional damping of large energy-loss inelastic scattering processes relative to photoabsorption. The Se 3*p* and Se 3*s* signals are particularly weak. For each spectral region the pre-edge continuum was least-squares fitted to $a(E - b)^c$, where a, b, and c were adjusted for best fit, in order to extrapolate the background and isolate the signal associated with each core edge. The background subtracted spectra of selenophene and 3-methylselenophene in the region of each core-excitation edge are shown in Figs. 2, 3, and 4 for the C 1*s*, Se 3*d*, and Se 3*p*/3*s* respectively. The Se 3*d*, Se 3*p*, and C 1*s* spectra of selenophene are compared in Fig. 5 on a common term value scale by aligning the spectra at the ⟨Se $3d$⟩, Se $3p_{3/2}$, and C 1*s* estimated

Can. J. Chem. Downloaded from www.nrcresearchpress.com by 186.148.149.217 on 09/07/12
For personal use only.

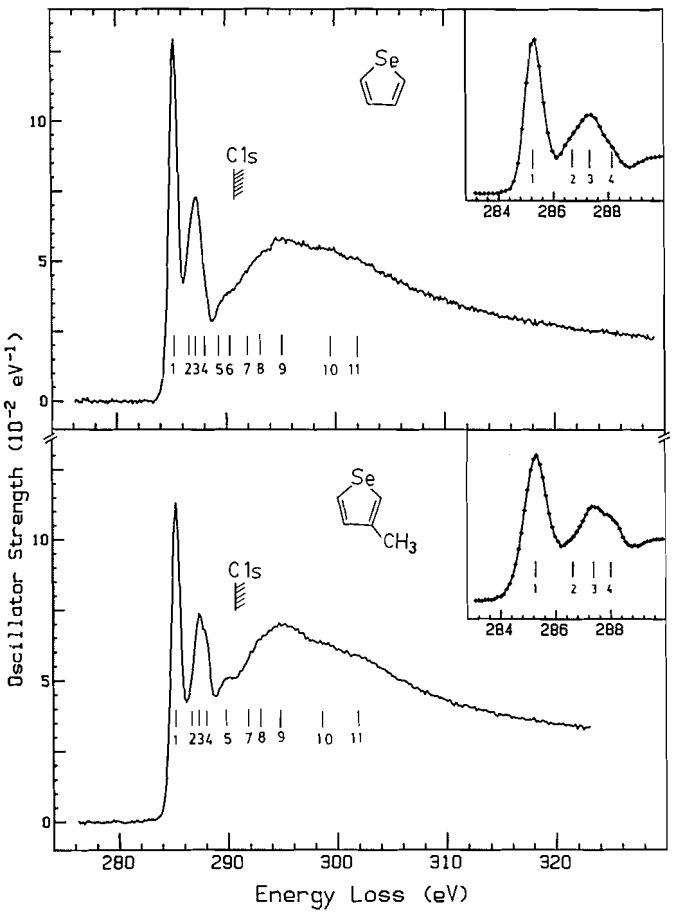


FIG. 2. The oscillator strengths for C 1*s* excitation in selenophene and 3-methylselenophene derived from dipole regime ISEELS. The insert is an expansion that shows the shoulders of the second band more clearly.

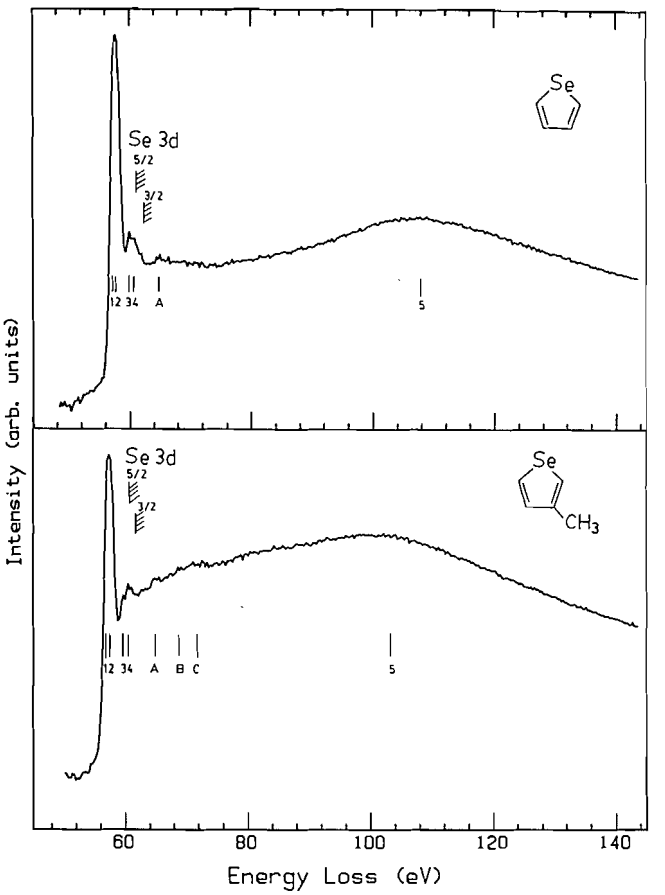


FIG. 3. The Se 3*d* ISEEL spectra of selenophene and 3-methylselenophene, after background subtraction. Features A, B, and C are Br 3*d* signals from an impurity.

IPs, where ⟨Se 3*d*⟩ is the average of the Se $3d_{5/2}$ and Se $3d_{3/2}$ IPs. Within a frozen orbital approximation, excitations to the same upper orbital from different core orbitals should have the same term value. A similar comparison for 3-methylselenophene is presented in Fig. 6. The spectral features, confirmed by observation in several independently recorded spectra, are indicated by numbered tics. Their energies, estimated term values, and proposed assignments are listed in Table 1 (C 1*s*), Table 2 (Se 3*d*), and Table 3 (Se 3*p*, 3*s*).

A.1. C 1s spectra

The C 1*s* ionization potentials (IPs), which are useful in detailed spectral analysis, were estimated by considering the following: the C 1*s* IP of $(CH_3)_2Se$ (290.9 eV (16)); extrapolation of the C 1*s* IPs of furan and thiophene, which indicates a C 1*s* IP of 290.3 eV for the ring carbons in selenophene; and the addition of 6.5 eV to the XPS value for solid thiophene (17), giving 290.7 eV. We have used 290.7 eV, an average of these estimates for the C 1*s* IP of the ring carbons and 290.3 eV as an estimate of the methyl carbon IP in 3-methylselenophene. The assignments of the spectral features in selenophene (Table 1) are guided by comparison to the C 1*s* spectrum of thiophene, where the assignments are supported by MS-Xα calculations and by comparison of solid, oriented monolayer, and gas phase spectra (7). The assignment of the C 1*s* spectrum of 3-methylselenophene is guided by comparison to the C 1*s* spectra of the 3-alkyl thiophenes (4).

The most intense peak, that at lowest energy, is clearly the C $1s \rightarrow \pi^*(3b_1)$ transition. The broad band centred at 287 eV is attributed to overlap of the C $1s \rightarrow \pi^*(2a_2)$, C $1s \rightarrow \sigma^*$(C—Se), C $1s \rightarrow \sigma^*$(C—H), and C $1s \rightarrow 3s$ Rydberg transitions. There are low and high energy shoulders on this band, which are most clearly seen in the spectrum of 3-methylselenophene (see inserts to Fig. 2). Proposed assignments of these shoulders are given in Table 1. A third low-intensity broad band around 290 eV likely arises from the overlap of unresolved Rydberg transitions leading up to the IP. The C 1*s* continuum exhibits several broad structures, with rather poorly defined low- and high-energy shoulders. The occurrence of several C $1s \rightarrow \sigma^*$(C—C) shape resonances in the near continuum of aromatic ring systems has been noted in several recent studies (7, 8, 18, 19). In the ISEEL spectra of the selenophenes these overlap to form a rather ill-defined structure. We note that the near continuum region is somewhat sharper in the NEXAFS spectra of the corresponding polymers (Fig. 7). This has been observed in several recent comparisons of gas phase ISEELS and condensed phase NEXAFS of related systems. It may be associated with preferential enhancement of continuum shape resonances in partially oriented materials because of the strong polarization dependence of X-ray absorption.

The C 1*s* spectra of selenophene and 3-methylselenophene (Fig. 2) are generally very similar. The main modifications associated with addition of the methyl group are an increase of the continuum intensity relative to that of the π^* peak, an increased intensity around 288 eV (associated with σ^*(C—H)

Can. J. Chem. Downloaded from www.nrcresearchpress.com by 186.148.149.217 on 09/07/12
For personal use only.

TABLE 1. Energies (E, eV), estimated term values (T, eV), and proposed assignments of features in the C 1s spectra of selenophene and 3-methylselenophene

	Selenophene		3-Methylselenophene		Assignment	
No.	E (±0.1 eV)	T	E (±0.1 eV)	T	C_{25}[a]	C_{34}[a]
1	285.3[b]	5.4	285.3[b]	5.4	$\pi^*(3b_1)$	$\pi^*(3b_1)$
2	286.7	4.0	286.7	4.0	σ^*(C—Se)	
3	287.3	3.4	287.4	3.5	$\pi^*(2a_2)$	
4 sh	288.1	2.6	288.0	2.7	5p	$\pi^*(2a_2)$
5 sh	289.5	1.2	289.9	1.2		6p
6	290.4	0.3	—	—		7p
IP	290.7[c]		290.7[c]			
7 sh	292.0	−1.3	292.0	−1.3	Double excitation	
8	293.2	−2.5	292.8	−2.1	σ^*(C—C)	
9	295.0	−4.3	295.0	−4.3	σ^*(C—C)′	
10 br	299.5(8)	−8.8	298.8(8)	−8.1	σ^*(C=C)	
11 br	302(1)	−11	302(1)	−11	Shake-up	

[a]C_{25} refers to the ring carbons adjacent to the S atom while C_{34} refers to the ring carbons most distant from the S atom (i.e., S-atom is labelled 1).

[b]Calibration: selenophene: −2.13(5) eV; 3-methylselenophene: −2.12(4) eV relative to C 1s → π^* in CO (287.4 (ref. 13)).

[c]The C 1s IP is taken to be the average of that of $(CH_3)_2Se$ (290.9 eV (ref. 16)), and the extrapolation of the C 1s IPs of furan and thiophene (290.3 eV). In thiophene the C_{25} and C_{34} IPs are separated by less than 0.4 eV (ref. 16). The methyl C 1s IP should be 290.3 ± 0.2 eV.

TABLE 2. Energies (E, eV), estimated term values (T, eV), and proposed assignments of features in the Se 3d spectra of selenophene and 3-methylselenophene

	Selenophene			3-Methylselenophene			Assignment	
No.	E	T(5/2)	T(3/2)	E	T(5/2)	T(3/2)	5/2	3/2
1 sh	57.1	4.0		57.1	4.0		$\pi^*(2a_2)$	
2	57.7[a]	3.3	4.4	57.7[a]	3.3	4.4	σ^*(C—Se)	$\pi^*(2a_2)$, σ^*(C—Se)
3	60.0	1.1	2.1	59.7	1.4	2.4	6p	5p
4	60.8	0.3	1.3	60.6	0.5	1.5	7p	6p
$3d_{5/2}$	61.1[b]			61.1[b]			IP	
$3d_{3/2}$	62.1[b]			62.1[b]				IP
5	108(3)	46		103(3)	42		εf shape resonance	
A	65.0(5)			65.0			Br 3d impurity	
B				68.9			Br 3d impurity	
C				72.			Br 3d impurity	

[a]Calibration: selenophene: −227.6(2) eV; 3-methylselenophene: −227.6(2) eV relative to first C 1s peak.

[b]The Se 3d IP were obtained by adding 6.5 eV to the tabulated IP of solid Se (17). This estimate is in good agreement with the average value reported for the Se 3d IP of $(CH_3)_2Se$ (61.5 eV (16)).

levels), and an increase and shift to lower energy of the principal σ^*(C—C) continuum maximum (that around 295 eV). These modifications are those expected from consideration of the C 1s spectra of alkanes (20). Similar but more pronounced changes are observed in the C 1s spectra of the 3-alkyl thiophene series (R = methyl to decyl) (4). Of perhaps greater interest in the context of the conduction mechanism of polyselenophenes is the question of the relative energies and intensities of the C 1s → π^* transitions in these two molecules. There is no detectable shift in position (<0.05 eV) and the integrated oscillator strengths are very similar. On visual inspection it appears that there is a considerable reduction in intensity since the peak oscillator strength of the C 1s → π^* feature falls from 0.123 to 0.111 with alkylation. However, there is a simultaneous increase in the peak width, from 0.92 to 0.98 eV, according to least-squares fits to Gaussian lines. Thus the integrated peak intensity decreases by only 5%, from 0.118(3) to 0.112(5), a smaller amount than suggested by a simple visual inspection of Fig. 2. It is perhaps inappropriate to make conclusions with regard to the effect of 3-alkyl substitution on the π manifold on the basis of this comparison alone. However, the absence of any significant effect of alkylation on the π^* oscillator strength is consistent with the recent results for the 3-alkyl thiophenes, where the examination of species with much longer alkyl side chains led to the conclusion that the ring π and π^* electronic structure is not significantly affected by alkylation, at least in the monomers (4).

*A.2. Se 3*d *spectra*

The Se 3d spectra of selenophene and 3-methylselenophene (Fig. 3) are very similar. The difference in the ratio of the main discrete peak to the continuum intensity is most likely

Can. J. Chem. Downloaded from www.nrcresearchpress.com by 186.148.149.217 on 09/07/12
For personal use only.

an artefact of the background subtractions rather than a real difference in the cross sections. The difficulties of deriving a unique extrapolated background can be appreciated in view of the very steep decline of the underlying valence ionization continuum (Fig. 1). The Se 3*d* signal in these two compounds is expected to be very similar since the methyl group is remote from the Se atom. The only likely influence of methyl substitution, via modification of the π-system, is indicated to be small by the C 1*s* results. In any case the main peak in each Se 3*d* spectrum is attributed mainly to Se $3d \rightarrow \sigma^*$(C—Se) transitions with, at most, only minor contribution from Se $3d \rightarrow \pi^*(2a_2)$ transitions. The Se $3d_{5/2}$ and Se $3d_{3/2}$ IPs are separated by only 1.0 eV (6) and thus it is difficult to resolve excitations associated with each ionization limit at our experimental resolution. Since the intrinsic Se 3*d* natural linewidth is small, additional structure may be revealed at higher resolution. However, it is also possible that the dominant Se $3d \rightarrow \sigma^*$(C—Se) transitions are broad due to a dissociative potential curve of the excited state, in which case higher resolution spectra would turn out to be rather similar to those presented in Fig. 3. On the basis of the orbital spatial distributions, the Se $3d \rightarrow \sigma^*$(C—Se) excitation should be more intense while the Se $3d \rightarrow \pi^*$ transition should be much weaker, relative to their intensity in the C 1*s* spectra. Comparison of the Se 3*d* and C 1*s* edge structure on a common term value scale (Figs. 5 and 6) shows that the main Se 3*d* peak is aligned with the *second* band in the C 1*s* spectra, consistent with its assignment to a σ*(C—Se) resonance. Our assignments of the pre-edge features to Se 3*d* excitations to σ*(C—Se) and *np* Rydberg orbitals are supported by the similarity of the Se 3*d* term values to those of corresponding C 1*s* transitions.

The near-edge Se 3*d* spectrum of 3-methylselenophene is very similar to that of selenophene. The dominant peak at 58 eV is attributed to Se $3d \rightarrow \sigma^*$(C—Se) transitions, broadened by spin-orbit interaction. Weaker features above this peak are assigned as higher energy Se $3d \rightarrow np$ Rydberg transitions. Although the lower energy structure in the Se 3*d* spectrum of 3-methylselenophene is very similar to that of selenophene, additional peaks (labelled A, B, C) and continuum intensity are found between 68 and 95 eV. These are Br 3*d* excitation features from a Br-containing organic impurity, probably CH_3Br, which was used in the synthesis (9).

Although it is not very visible in Fig. 1, the background subtraction (Fig. 3) reveals a broad maximum (feature 5) in the Se 3*d* continuum of each species, peaking around 105(3) eV. This broad maximum is a Se $3d \rightarrow \varepsilon f$ atomic-like shape resonance, which is associated with the energy at which the photoelectron final state exceeds the $l = 3$ centrifugal barrier and penetrates into the inner-well region where the Se 3*d* orbital is localized. Similar features are well known in the 3*d* spectrum of atomic Kr (21) and are calculated to occur in the 3*d* continua of neighbouring atoms (22). Connerade and Mansfield (23) have reported that the Se 3*d* spectrum of molecular Se_2 contains only a continual rise to higher energies up to 160 eV. We believe this result is an artefact, possibly associated with an inadequate correction for the incident photon flux. Morin and Nenner have studied the Br 3*d* spectra of HBr and CH_3Br (24) and found continuum shapes very similar to those reported for Kr (21) and expected for atomic Br (25). Careful comparison of atomic and molecular 3*d* continuum shapes is of interest with regard to possible molecular effects on "atomic-like" shape resonances (25).

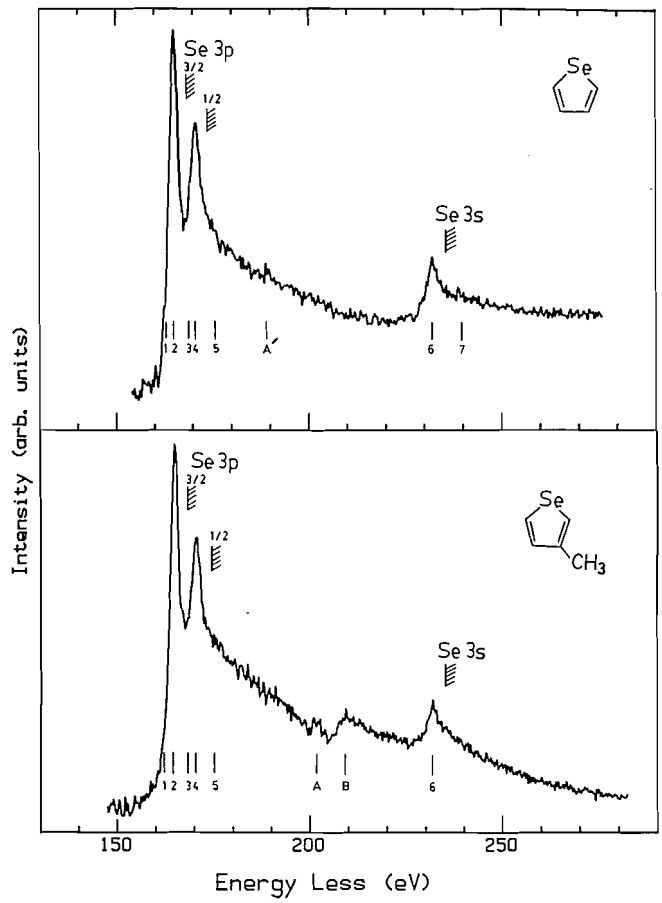


FIG. 4. The background-subtracted ISEEL spectra of selenophene and 3-methylselenophene in the Se 3*p* and Se 3*s* region. Features A and B in the spectrum of 3-methylselenophene are Cl 2*p* signals from an impurity.

A.3. Se 3p and Se 3s spectra

Although the noise level is somewhat high on account of the very weak signal, the Se 3*p* and Se 3*s* spectra of selenophene and 3-methylselenophene are readily detected (Fig. 4). The spectra are consistent with the expectation that the strongest features will correspond to excitations to orbitals localized on Se, i.e., weak Se $3p \rightarrow \pi^*$ and strong Se $3p \rightarrow \sigma^*$(C—Se) transitions. The main peaks at 165.0 and 170.6 eV are assigned to excitations to (Se $3p_{3/2}$, σ*(C—Se)) and (Se $3p_{1/2}$, σ*(C—Se)) states, since they have similar term values to those of the features attributed to Se $3d \rightarrow \sigma^*$(C—Se) and Se $3d \rightarrow$ σ*(C—Se) excitations. Weak Se $3p \rightarrow \pi^*$ transitions also appear to contribute as low energy shoulders to the 165 and 170.6 eV peaks. Se $3p \rightarrow 5s$ Rydberg transitions may also contribute to the breadth of these peaks (see Figs. 5 and 6). The Se 3*p* assignments are somewhat less certain than those for the C 1*s* and Se 3*d* features, partly because of the poor definition of the spectrum, but also because the Se 3*p* IPs are difficult to estimate accurately. Adding 6.5 eV to the tabulated value for solid Se (17) gives Se 3*p* IPs that are 1.1 eV below those derived from combining the estimated Se 3*p* IP of SeF_6 (26) with the difference in the S 2*p* IPs of SF_6 and thiophene. This latter procedure is very indirect but it was selected since it gives term values that provide a good alignment of the Se $3p_{3/2} \rightarrow$ σ*(C—Se) feature with the Se 3*d* and C 1*s* excitations to σ*(C—Se) (Figs. 5 and 6).

TABLE 3. Energies (E, eV), estimated term values (T, eV), and proposed assignments of features in the Se $3p$ and Se $3s$ spectra of selenophene and 3-methylselenophene

(a) Se $3p$

	Selenophene			3-Methylselenophene			Assignment	
No.	E	$T(3/2)$	$T(1/2)$	E	$T(3/2)$	$T(1/2)$	3/2	1/2
1 sh	162.8	5.5	—	162.4	5.9	—	$\pi^*(3b_1)$	
2	165.0[a]	3.3	—	165.0[a]	3.3	—	σ^*(C—Se)	
$3p_{3/2}$	168.3(5)[b]			168.3(5)[b]			IP	
3 sh	169.1	—	5.0	168.4	—	5.7		$\pi^*(3b_1)$
4	170.6	—	2.9	170.6	—	2.9		σ^*(C—Se)
$3p_{1/2}$	174.1(5)[b]			174.1(5)[b]				IP
5 wk	175.3		1	175.4		1		
A′	189.3		7				Impurity?	
A				201.3			Cl $2p$ impurity	
B				209.2			Cl $2p$ impurity	

(b) Se $3s$

	Selenophene		3-Methylselenophene		
No.	E	T	E	T	Assignment
6	232.0	4.2	231.8	4.4	σ^*(C—Se), $\pi^*(2a_2)$
3s	236.2[c]		236.2[c]		IP
7	240	−4			σ^*(C—C)

[a]Calibration: selenophene (Se $3p$): −120.3(3) eV; 3-methylselenophene (Se $3p$): −120.3(2) eV relative to the first C $1s$ peak.

[b]The Se $3p$ IPs were obtained from the estimated Se $3p_{3/2}$ IP of SeF_6 (179.1 eV (ref. 26)) minus the difference between the S $2p$ IPs of SF_6 and thiophene (10.8 eV (ref. 16)).

[c]The Se $3s$ IP was obtained by adding 6.5 eV to the tabulated value for solid Se (17).

Although Se $3p \rightarrow 4d$ resonances might be expected to be prominent features by analogy to the prominent $2p \rightarrow 3d$ resonances in the S $2p$ spectra of many compounds, the Se $3p$ continuum does not appear to contain features of this character. This point was made recently in a dramatic fashion through comparison of the Se $3p$ spectrum of SeF_6 with the S $2p$ spectra of SF_6 and SF_5Cl (26). The weakness of the Se $3d \rightarrow 4d$ resonances was attributed to changes of the nodal pattern between the $3d$ and $4d$ orbitals, which apparently leads to much poorer $\langle 3p|\mu|4d\rangle$ than $\langle 2p|\mu|3d\rangle$ dipole overlap.

The relative prominence of the Se $3p \rightarrow \sigma^*$(C—Se) features and limited contributions from Se $3p \rightarrow \pi^*$ transitions suggest that the Se $2p_{3/2}$ edge (1440 eV) may be a more sensitive probe than the C $1s$, Se ns, or Se $3d$ edges for studying possible changes in the C—Se bond length with polymer formation or doping. However, the energies of σ^*(S—X) (X = C, O, F) orbitals as probed from S $1s$ excitation are much less sensitive to bond length changes than the energies of σ^*(O—X) orbitals (27), suggesting that the σ^*(C—Se) orbital energy, accessed by C $1s$, Se $3d$, or Se np core excitation, may also be a rather insensitive probe of C—Se bond length.

As with the Se $3d$ region, the Se $3p$ near-edge features of 3-methylselenophene are essentially identical to those of selenophene. This is not surprising, given that excitation from the Se core levels is localized at the Se atom, and thus the Se core excitation features can only be modified by second-order changes in the optical orbitals resulting from shifts in the electron density at Se as a result of methyl substitution at a relatively distant site. In contrast to the Se $3d$ spectra, the continuum shape (aside from the impurity signals marked with letters) is very similar in these two compounds. The difference between the Se $3p$ and Se $3d$ edges in this regard is the more gentle slope of the background in the $3p$ region (Fig. 1). The additional features (A, B) observed around 200–210 eV in the Se $3p$ continuum of 3-methylselenophene are most likely Cl $2p$ features of an impurity. Given the intrinsically weak intensity of Se $3p$ excitation (Fig. 1) as compared to Cl $2p$ excitation, the amount of Cl-containing impurity is very small.

The Se $3s$ spectra (Figs. 1, 4) are very weak, in part because of the large Coster–Kronig broadening of this edge. The single broad peak below the estimated Se $3s$ IP has a term value consistent with contributions from Se $3s$ excitations to both $\pi^*(2a_2)$ and σ^*(C—Se) orbitals. A similar conclusion was drawn with regard to the single, broad peak observed in the S $2s$ and S $1s$ spectra of thiophene (7).

B. NEXAFS of polymer thin films of selenophene and 3-methylselenophene

B.1. C 1s spectra of undoped polymers

The C K-edge NEXAFS spectra of 500 Å thick films of undoped polyselenophene and poly-3-methylselenophene grafted onto Pt (Fig. 7) exhibit very similar features to those observed in the ISEEL spectra of the gas phase monomer (Fig. 2). This confirms that the subunits of the polymeric chains have the same basic structure as the monomer. All of the NEXAFS spectra have had the underlying valence continuum subtracted and are normalized to the same relative intensity at 325 eV since the nonresonant continuum at this energy should be "atomic-like". We note that, although this normalization is valid if there are the same number of carbon atoms in the depth of the polymer film

Can. J. Chem. Downloaded from www.nrcresearchpress.com by 186.148.149.217 on 09/07/12
For personal use only.

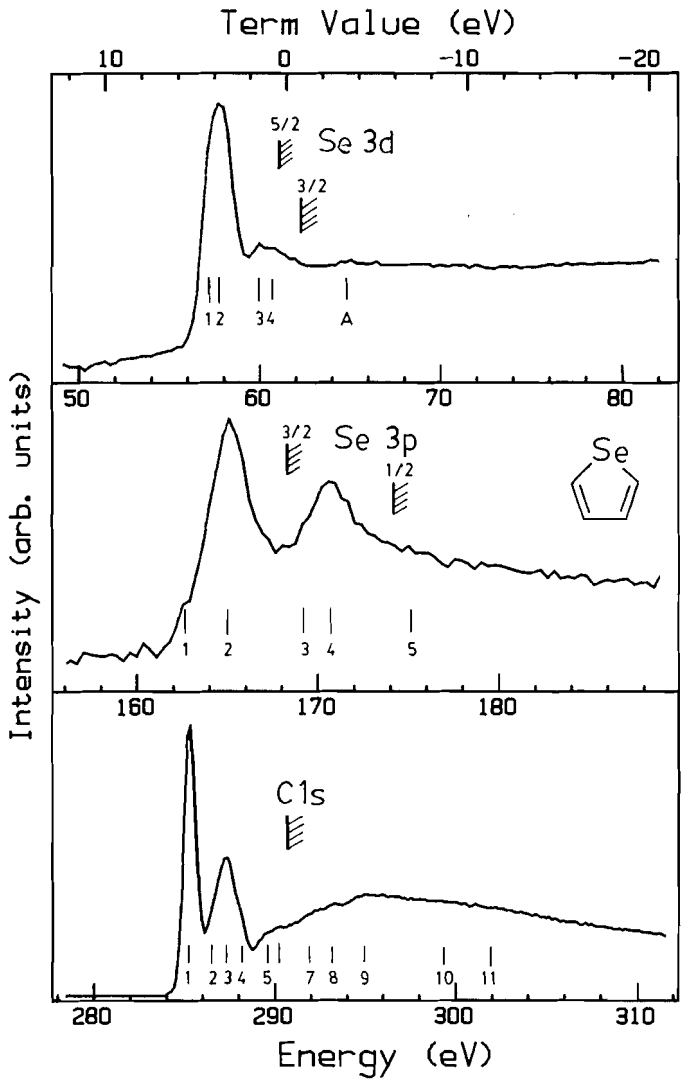


FIG. 5. Comparison of the Se $3d$, Se $3p$, and C $1s$ spectra of selenophene on a common term value scale. The spectra are aligned at the estimated ⟨Se $3d$⟩, Se $3p_{3/2}$, and C $1s$ IPs.

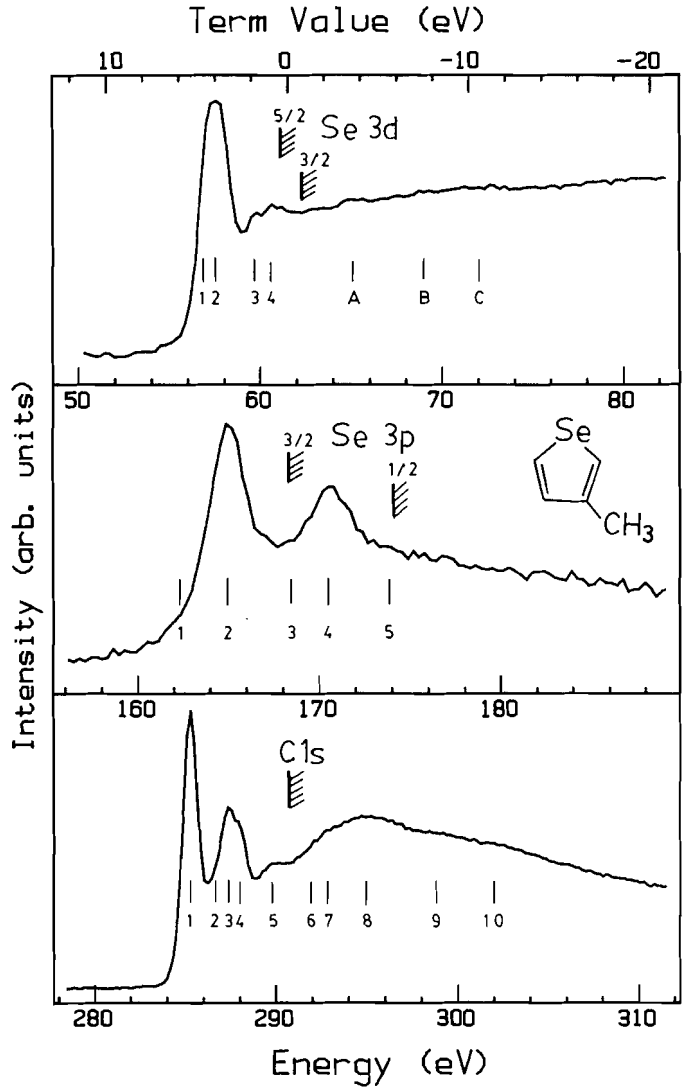


FIG. 6. Comparison of the Se $3d$, Se $3p$, and C $1s$ spectra of 3-methylselenophene on a common term value scale. The spectra are aligned at the estimated ⟨Se $3d$⟩, Se $3p_{3/2}$, and C $1s$ IPs.

sampled by the electron yield detection scheme used, it does not give spectra directly comparable to the gas phase monomer results since it does not correct for the additional methyl carbon atom in 3-methylselenophene. The normalization to constant continuum intensity explains why the C $1s \rightarrow \pi^*(3b_1)$ peak appears smaller in 3-methylselenophene than in selenophene. The consequences of different normalization treatments of the gas and surface data have been discussed in detail in connection with the 3-alkyl thiophene study (4).

Six transitions are clearly observed in the C $1s$ NEXAFS spectra of the polymers. Their energies and proposed assignments are summarized in Table 4. With reference to polythiophene (3), selenophene in the gas phase, and the Xα computations of selenophene reported by Modelli *et al.* (28), we assign the first transition to the $1s \rightarrow \pi^*(3b_1)$ bound state transition. The Xα results also predict the existence of a second $\pi^*(2a_2)$ orbital, 1.8 eV higher in energy. This is in good agreement with assignment of feature 3 (288.4 eV) to C $1s \rightarrow \pi^*(2a_2)$ transitions. Peak 2 at 287.1 eV is associated with the σ*(C—Se) shape resonance, which is consistent with observation of an opposite angular dependence for the first and the second peaks in oriented thin films of polyselenophene (29). Peaks 4 and 5 are attributed to σ*(C—C) shape resonances, in agreement with the C $1s$ ISEEL spectra of gas phase selenophene, thiophene (7), and the NEXAFS of polythiophene (3). The origin of the last transition at 302 eV, observed in essentially all aliphatic compounds (20, 30), is not well understood but may arise from a higher energy σ*(C—C) resonance or from multiple scattering of the outgoing photoelectron by several C atoms (which may be alternate descriptions of the same physical process).

B.2. C 1s NEXAFS of doped polyselenophene and poly-3-methylselenophene

When polyselenophene and poly-3-methylselenophene are doped into the conducting state with ClO_4^-, the σ*(C—Se) and σ*(C—C) shape resonances are observed at the same energy as in the spectra of the undoped polymer films (Fig. 8), suggesting that the bond lengths are not modified during the doping process. However, the C $1s \rightarrow \pi^*$ band in the polymer NEXAFS is greatly affected as evidenced by the decrease in intensity and shift in the $\pi^*(3b_1)$ band by 0.3 eV to lower energy. Additionally, a new transition, denoted 1′, appears at low energy, with an onset at 283 eV. (Note that the onset of 1′ is considered the characteristic energy of interest for this feature

Can. J. Chem. Downloaded from www.nrcresearchpress.com by 186.148.149.217 on 09/07/12
For personal use only.

TABLE 4. Assignments of features in the C 1*s* NEXAFS spectra of doped and undoped thin films of polyselenophene and poly-3-methylselenophene

	Energy (±0.3 eV)				
	Polyselenophene		Poly-3-methylselenophene		
Peak	Undoped	Doped	Undoped	Doped	Assignment
1′ onset	—	283.1	—	283.0	New empty states
1	285.3	284.8	285.2	284.9	$3b_1$ π*
IP	285.7[a]		285.7[a]		IP
2	286.9	286.7	287.1	286.8	σ*(C—Se)
3	288.6	288.3	288.1	288.3	$2a_2$ π*
4 sh	293.5	295.2(5)	293.5	293.4(5)	σ*(C—C)
5	296.8(5)		296.1(5)	296(1)	σ*(C—C)
6	302(1)	—	302(1)	—	σ*(C—C)′

[a]From XPS (34).

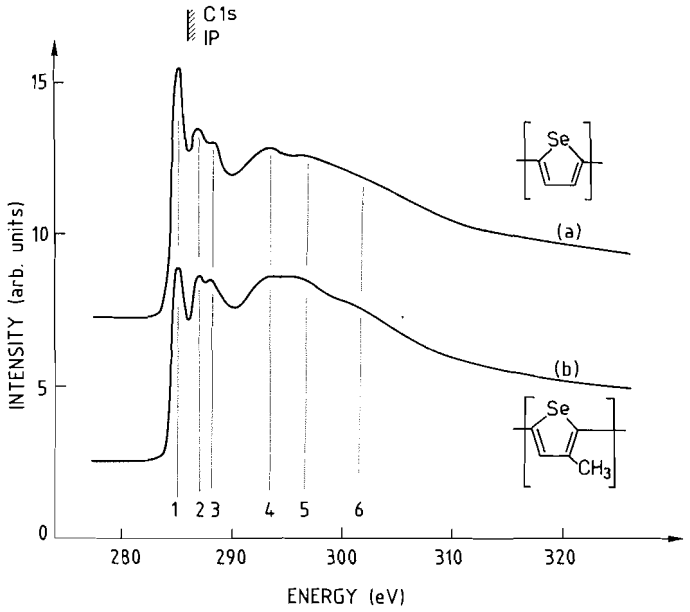


FIG. 7. C 1*s* edge NEXAFS spectra recorded at 40° X-ray incidence for 500 Å thick undoped films electrochemically deposited on a Pt surface: (a) polyselenophene; (b) poly-3-methylselenophene. The spectra do not depend on the angle of X-ray incidence.

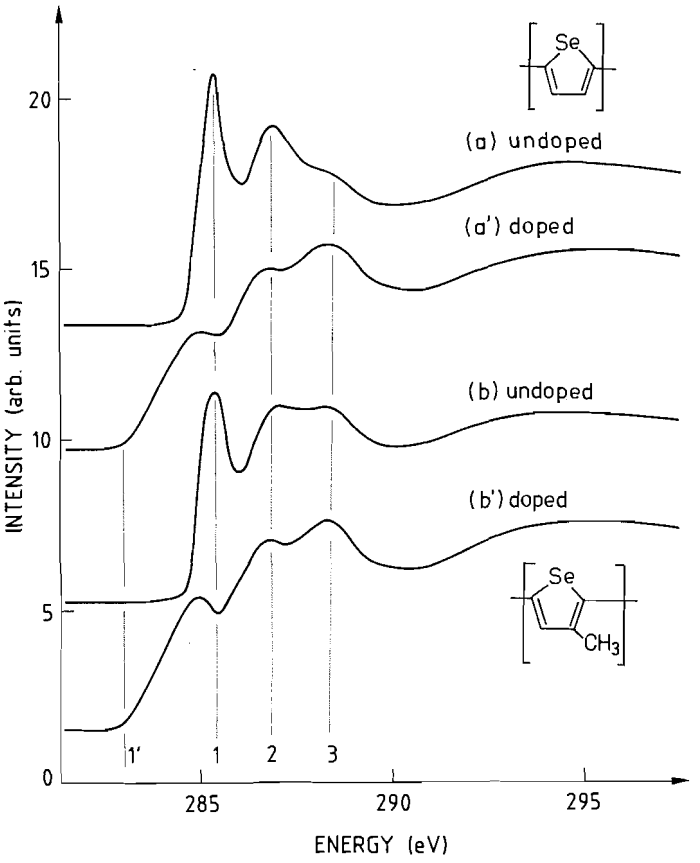


FIG. 8. C 1*s* edge NEXAFS spectra of 500 Å thick films recorded at 40° X-ray incidence: (a) and (a′) are the NEXAFS spectra of the undoped and doped states of polyselenophene respectively while (b) and (b′) are NEXAFS spectra characteristic of the undoped and doped forms of poly-3-methylselenophene.

since the edge of the "π*-conduction band" as sampled by C 1*s* excitation is defined by the onset rather than the peak. An underestimate of the band edge by about 0.3 eV will then arise because of the finite instrumental resolution.) The intensity of 1′ increases with the doping level. These additional empty states are observed in doped polyselenophenes, independent of the nature of the dopant (ClO_4^-, BF_4^-, or $SO_3CF_3^-$). Moreover, similar changes in the C 1*s* NEXAFS have been observed on doping polythiophene and poly-3-methylthiophene (3). This suggests that there is a common conduction mechanism for these polymers of five-membered heterocycles.

Several models have been proposed to explain the large increase of conductivity during the electrochemical oxidation of these polymers:

(*i*) Formation of a degenerate semiconductor associated with extraction of electrons from the π bonding band and a shift of the Fermi level below the valence band (31). With this scheme, the C K-edge NEXAFS spectra would exhibit a peak followed by a sharp threshold 2.5 eV higher in energy (the band gap of polyselenophene) due to transitions to the π* conduction band. Moreover, the intensity of this last transition should be constant during the doping process since the π* antibonding density of states would not be affected. Evidently the NEXAFS characteristics do not agree with this model.

(*ii*) Formation of local distortions in the polymeric chain around localized charges associated with the evolution of the ring system from an aromatic to a quinoid structure. In the bipolaron model (32) doping should lead to the development of *two* localized empty levels in the band gap. Structural

Can. J. Chem. Downloaded from www.nrcresearchpress.com by 186.148.149.217 on 09/07/12
For personal use only.

Can. J. Chem. Downloaded from www.nrcresearchpress.com by 186.148.149.217 on 09/07/12
For personal use only.

modifications are thus expected, especially in the C—C bond lengths of the polymeric backbone, so energy variations of peaks 5, 6, and possibly 2 should be observed (33). This is not the case experimentally. Moreover, the NEXAFS spectra would show two new peaks at low energy corresponding to the C 1*s* excitations to the bipolaron bands. The evolution of the C K-edge NEXAFS characteristics, combined with Se K-edge dispersive-EXAFS results obtained during an *in situ* doping–undoping electrochemical cycle that again do not reveal any modification in the C—Se bond length (34), are not in agreement with the bipolaron predictions.

(*iii*) Finally, if the conducting state corresponds to a metal-like behaviour, a simple step-like absorption edge would be observed 1.3 eV below the π^* band edge (mid-gap value) (31). In the fully doped state, the C 1*s* $\rightarrow$ π^* resonance observed in the undoped form of polyselenophene or poly-3-methylselenophene has almost vanished and the absorption threshold has shifted 3.4 eV to lower energy. Thus the NEXAFS characteristics suggest a closed-gap metallic state.

As with the conduction mechanism deduced for polythiophene (3), we conclude that dopant oxidation of polyselenophene and poly-3-methylselenophene proceeds through extraction of electrons from the π bonding band and a narrowing of the π–π^* gap. XPS and UPS experiments are underway which seek to confirm this scheme.

Summary

The electron energy loss spectra of selenophene and 3-methylselenophene in the regions of Se 3*d*, Se 3*p*, Se 3*s*, and C 1*s* have been recorded and analyzed. The C 1*s* spectra have been compared to the C 1*s* NEXAFS results of the corresponding polymers. The spectra of these two speices are very similar at all inner-shell edges. Only the C 1*s* spectra show minor differences that are consistent with additional σ^*(C—H) and σ^*(C—C) intensity in 3-methylselenophene, which occur at expected energies (33).

The similarity of the C 1*s* spectra of the monomers and their corresponding polymers strongly suggests that the polymer subunits have essentially the same structure as the monomers. The effect of doping on the NEXAFS of the polymer thin films is consistent with a narrowing of the band gap and the development of metal-like behaviour. Finally, doping produces modifications of the C 1*s* NEXAFS similar to those observed upon doping polythiophene (3). This indicates that the conduction mechanism is similar for these two poly-penta-heterocycles.

Acknowledgements

This research is supported financially by the Natural Sciences and Engineering Research Council of Canada (NSERC) and by the Bundersministerium für Forschung und Technologie (grant 05390FXB2TP4). A.P.H. acknowledges the support of an NSERC university research fellowship. We thank C. Mahatsekake and C. Andrieu at the Laboratoire des Thioorganiques, Université de Caen, France for their synthesis of selenophene and 3-methylselenophene. We want to thank A. M. Bradshaw for making available the HE-TGM1 of the Fritz-Haber Institute.

1. T. Skotheim and M. Dekker (*Editors*). Handbook of conducting polymers. Vols. 1 and 2. Academic, New York. 1986.
2. G. Tourillon, A. Fontaine, M. Sagurton, R. Garrett, and G. P. Williams. J. Phys. **47**, C8-579 (1986); G. Tourillon, A. Fontaine, R. Garrett, M. Sagurton, P. Xu, and G. P. Williams. Phys. Rev. B: Condens. Matter, **35**, 9863 (1987); G. Tourillon, A. Fontaine, Y. Jugnet, Tran Minh Duc, W. Braun, J. Feldhaus, and E. HolubKrappe. Phys. Rev. B: Condens. Matter, **36**, 3483 (1987); G. Tourillon, A. M. Flanck, and P. Legarde. J. Phys. Chem. **92**, 4397 (1988).
3. G. Tourillon, C. Mahatsekake, C. Andrieu, G. P. Williams, R. Garrett, and W. Braun. Surf. Sci. **201**, 171 (1988).
4. A. P. Hitchcock, G. Tourillon, R. Garrett, G. P. Williams, C. Mahatsekake, and C. Andrieu. J. Phys. Chem. Submitted.
5. C. E. Brion, S. Daviel, R. N. S. Sodhi, and A. P. Hitchcock. Am. Inst. Phys. Conf. Proc. Ser. **94**, 429 (1982).
6. J. Stöhr and D. A. Outka. Springer Series in Surface Science. *Edited by* R. Vanselow and R. Howe. 1989. In press.
7. A. P. Hitchcock, J. A. Horsley, and J. Stöhr. J. Chem. Phys. **85**, 4835 (1986).
8. D. C. Newbury, I. Ishii, and A. P. Hitchcock. Can. J. Chem. **64**, 1145 (1986); G. Tourillon, S. Raaen, T. Skotheim, M. Sagurton, R. Garrett, and G. P. Williams. Surf. Sci. **184**, L345 (1987).
9. C. B. Duke, A. Paton, and W. R. Salaneck. J. Chem. Phys. **77**, 5030 (1982).
10. C. B. Duke, A. Paton, and W. R. Salaneck. Mol. Cryst. Liq. Cryst. **83**, 177 (1982).
11. C. Mahatsekake, C. Andrieu, G. Lecoustumer, and G. Tourillon. Phosphorus Sulfur Lett. In press.
12. D. Guay, C. Bovy, C. Mahatsekake, C. Andrieu, and G. Tourillon. J. Electrochem. Soc. Submitted.
13. R. N. S. Sodhi and C. E. Brion. J. Electron Spectrosc. Relat. Phenom. **34**, 363 (1984).
14. R. McLaren, S. A. C. Clark, I. Ishii, and A. P. Hitchcock. Phys. Rev. A: **36**, 1683 (1987).
15. E. Dietz, W. Braun, A. M. Bradshaw, and R. L. Johnson. Nucl. Instrum. Methods Phys. Res. Sect. A: **239**, 359 (1985).
16. W. L. Jolly, K. D. Bomben, and C. J. Eyermann. At. Data Nucl. Data Tables, **31**, 433 (1984).
17. G. P. Williams. Table of X-ray energies, X-ray data booklet. Lawrence Berkeley Laboratory publication no. 490. Berkeley, CA. 1986.
18. A. P. Hitchcock, P. Fischer, A. Gedanken, and M. B. Robin. J. Phys. Chem. **91**, 531 (1987).
19. E. Rühl and A. P. Hitchcock. J. Am. Chem. Soc. **111**, 5069 (1989).
20. I. Ishii and A. P. Hitchcock. J. Electron Spectrosc. Relat. Phenom. **42**, 11 (1987).
21. J. P. Connerade and M. W. D. Mansfield. Proc. R. Soc. London, A: **343**, 415 (1975).
22. S. T. Manson and J. W. Cooper. Phys. Rev. **165**, 126 (1968).
23. J. P. Connerade and M. W. D. Mansfield. Proc. R. Soc. London, A: **356**, 135 (1977).
24. P. Morin and I. Nenner. Phys. Scr. **T17**, 171 (1987), and unpublished work.
25. F. Keller and H. Levebvre-Brion. Z. Phys. D: At. Mol. Clusters, **4**, 15 (1986).
26. B. M. Addison, K. H. Tan, G. M. Bancroft, and F. Cerrina. Chem. Phys. Lett. **129**, 468 (1986).
27. A. P. Hitchcock and M. Tronc. Chem. Phys. **121**, 265 (1988).
28. A. Modelli, M. Guerra, D. Jones, G. Distefano, K. J. Irgolic, K. French, and G. C. Pappalardo. Chem. Phys. **88**, 455 (1984).
29. G. Tourillon, E. Dartyge, C. Mahatsekake, C. Andrieu, and W. Braun. J. Phys. Chem. Submitted.
30. J. Stöhr, D. A. Outka, K. Baberschke, D. Arvanitis, and J. A. Horsley. Phys. Rev. B: Condens. Matter, **36**, 2976 (1987).
31. J. J. Ritsko. Phys. Rev. Lett. **46**, 849 (1981).
32. J. L. Bredas, B. Themans, J. G. Fripiat, J. M. Andre, and R. R. Chance. Phys. Rev. B: Condens. Matter, **29**, 6761 (1984).
33. F. Sette, J. Stöhr, and A. P. Hitchcock. J. Chem. Phys. **81**, 4906 (1984).
34. G. Tourillon, E. Dartyge, A. Fontaine, A. Jucha, and C. Andrieu. J. Phys. **47**, C8-551 (1986).

Disproportionation of chlorine in hydrogen fluoride and related media

MARIO GAMBARDELLA,[1] SANTAD KONGPRICHA,[2] JAMES J. PITTS,[3] AND ALBERT W. JACHE[4]
Department of Chemistry, Marquette University, Milwaukee, WI 53233, U.S.A.

Received February 2, 1989

This paper is dedicated to Professor Ronald J. Gillespie on the occasion of his 65th birthday.

MARIO GAMBARDELLA, SANTAD KONGPRICHA, JAMES J. PITTS, and ALBERT W. JACHE. Can. J. Chem. **67**, 1828 (1989).

Chlorine can be made to disproportionate to chlorine monofluoride and chloride, taking advantage of Le Chatelier's principle in several different ways. It will disproportionate to form insoluble silver chloride and chlorine monofluoride when silver fluoride is present. It will disproportionate in a melt of alkali metal fluorides to form alkali metal chlorides and chlorine monofluoride. The alkali metal chlorides will react with hydrogen fluoride to regenerate the metal fluorides and hydrogen chloride. Chlorine will also disproportionate in hydrogen fluoride containing antimony pentafluoride to yield antimony pentafluoride adducts of chlorine monofluoride and of hydrogen chloride. These adducts are readily decomposed to yield the disproportionation products and the original antimony pentafluoride.

Key words: hydrogen fluoride, disproportionation, chlorine, waterlike, solvent system.

MARIO GAMBARDELLA, SANTAD KONGPRICHA, JAMES J. PITTS et ALBERT W. JACHE. Can. J. Chem. **67**, 1828 (1989).

En mettant à profit le principle de Le Chatelier, on peut amener le chlore à donner une réaction de dismutation conduisant au monofluorure et au chlorure de chlore. En présence de fluorure d'argent, il donne une réaction de disproportionation conduisant à la formation de chlorure d'argent insoluble. Dans des fluorures de métaux alcalins fondus, la réaction conduit à la formation de chlorures de métaux alcalins et de monofluorure de chlore. Les chlorures de métaux alcalins réagissent avec le fluorure d'hydrogène pour régénérer les fluorures métalliques et le chlorure d'hydrogène. En présence de fluorure d'hydrogène contenant du pentafluorure d'antimoine, la réaction de disproportionation du chlore fournit des adduits de pentafluorure d'antimoine avec soit du monofluorure de chlore ou de chlorure d'hydrogène. Ces adduits se décomposent facilement pour donner les produits de disproportionation et le pentafluorure d'antimoine original.

Mots clés : fluorure d'hydrogène, dismutation, chlore, semblable à l'eau, septème de solvant.

[Traduit par la revue]

Introduction

Over two decades ago, a program investigating chemistry in and of anhydrous hydrogen fluoride and interhalogen fluorides was undertaken in the research laboratories of Olin Mathieson Chemical Corporation, now Olin Corp. Part of the work involved investigations of the parallels between chemistry in water and that in hydrogen fluoride.

During the course of the work, it was shown that the relationship between IO_2^+, IO_2F, and $IO_2F_2^-$ could be explained on the basis of amphoterism (1). The concentration of fluoride controls the loss or gain of fluoride in a manner analogous to the manner in which the loss of gain of isoelectronic hydroxide in the aqueous chemistry of Al^{3+} is controlled by hydroxide ion concentration or pH.

$$[1] \quad \begin{aligned} IO_2^+ + F^- &= IO_2F \\ IO_2F + F^- &= IO_2F_2^- \end{aligned}$$

Investigations involving the chemistry of phosphorus in hydrogen fluoride showed that parallels with water chemistry exist here also (2). Phosphorus at temperatures above 280°C behaves as a metal in its reaction with water (for primary references, see ref. 3).

$$[2] \quad P_4 + 16H_2O(g) \rightarrow 10H_2 + 4H_3PO_4\ (OP(OH)_3)$$

In boiling basic aqueous solution it undergoes disproportionation.

$$[3] \quad P_4 + 3OH^- + 3H_2O \rightarrow PH_3 + 3H_2PO_2^-$$

It was shown that in the absence of intentionally added metal fluorides phosphorus reacts as a metal with hydrogen fluoride to form hydrogen and phosphorus trifluoride

$$[4] \quad P_4 + 12HF \rightarrow 6H_2 + 4PF_3$$

Small amounts of alkali or alkaline earth fluorides catalyze the reaction. The metal fluorides are generally ultimately converted to metal hexafluorophosphates. When larger amounts of fluoride are added, given sufficient time, much of the phosphorus is found as metal hexafluorophosphate. Apparently, disproportionation of the trifluoride to phosphorus (which may undergo further reaction) and phosphorus pentafluoride occurs. The phosphorus pentafluoride is tied up with the metal fluoride as a hexafluorophosphate, thus, in accordance with Le Chatelier's principle, shifting the position of equilibrium.

$$[5] \quad 10PF_3 + 6MF \rightarrow P_4 + 6MPF_6$$

The efficacy of catalysis of reaction [4] by metal fluorides and of bringing about reaction [5] can be correlated with properties that can be correlated with charge/size ratio of the metal ion (e.g., radii, lattice energy of fluoride, solubility of fluoride in HF).

While chlorine will slowly liberate oxygen from water, it primarily disproportionates in water. The degree of disproportionation is enhanced by increased basicity. Although the equilibria involved are complicated and are much influenced by kinetics (4), under ordinary conditions one sees primarily

$$[6] \quad Cl_2 + H_2O \rightarrow HOCl + HCl$$

The analogous reaction in hydrogen fluoride is

$$[7] \quad Cl_2 + HF \rightarrow FCl\ (ClF) + HCl$$

Since the heat and free energy of formation of chlorine monofluoride (negative) is much less than the (negative) difference between the heats and free energies of formation of hydrogen chloride and hydrogen fluoride, one would not expect reaction

[1]Present address: 259 Currier Dr., Orange, CT 06477, U.S.A.
[2]Present address: Olin Research Center, Cheshire, CT 06410, U.S.A.
[3]Present address: Olin Corp., Joliet, IL 60434, U.S.A.
[4]Author to whom correspondence may be addressed.

Printed in Canada / Imprimé au Canada

Can. J. Chem. Downloaded from www.nrcresearchpress.com by 186.148.149.217 on 09/07/12
For personal use only.

Can. J. Chem. Downloaded from www.nrcresearchpress.com by 186.148.149.217 on 09/07/12
For personal use only.

[7] to go spontaneously as written. Indeed, the reverse reaction goes spontaneously, even in hydrogen fluoride solutions saturated with cesium fluoride. However, it seemed worthwhile to attempt to accomplish disproportionation by taking advantage of Le Chatelier's principle. Success in this endeavour was reported only in the patent literature (5) at the time, since there was then some interest in potential commercial applications. Although a decade later much of this information was presented at the 8th International Symposium on Fluorine Chemistry (6), it seems particularly appropriate to publish this work now in a journal issue honoring Professor Gillespie, whose many accomplishments include exciting work in highly acidic, fluorine-containing media.

Experimental

General

Infrared spectra were generally obtained with a Perkin–Elmer model 137 Infracord spectrometer using a 10-cm AgCl-window gas cell with a Monel body. Vapor phase chromatography was performed using an all-metal (Monel and nickel) unit at room temperature. The column was packed with Kel-F No. 1 oil on Fluor-Pak. A gas density balance was used as a detector. The AgF was obtained from Harshaw Chemical Co. and the $AgBF_4$ from the Ozark-Mahoning Co., while the SbF_5 was an Allied Chemical Corp. product.

Reactions involving antimony pentafluoride

Reactions were, in general, carried out in a Kel-F reaction vessel, which could be sealed and attached to an all-metal (copper and Monel) vacuum manifold. The reaction vessel contained a Teflon-covered magnetic stirring bar.

Antimony pentafluoride (18.5 g; 85 mmol) was poured, under a dry nitrogen blanket, into the reaction vessel, which was then evacuated on the vacuum manifold. When chlorine monofluoride (12 g; 220 mmol) was bled slowly into the system, the solution first became yellow-green, then orange-red, and finally dark maroon as the ClF was absorbed over a period of 6 h. At this time the total pressure was about 1 atm at room temperature (1 atm = 101.3 kPa). A trichloroethylene – Dry Ice bath was placed around the reaction vessel. The vapor pressure dropped to about 300 Torr (1 Torr = 133.3 Pa) and a tan-yellow solid formed. Gaseous ClF was taken from the system. The solid product exhibited no appreciable vapor pressure until, on warming, the temperature reached −40°C. The solid darkened and melted to a maroon liquid between −20 and −15°C. Extrapolated vapor pressure indicated that the vapor pressure of ClF would be 1 atm at 25°C. Elemental analysis of the solid showed a chlorine content of 16.3%. Theoretical content for Cl_2FSbF_6 is 21.8%; for $Cl_2FSb_2F_{11}$ or $ClSbF_6$ is 13.1%.

When ClF was introduced over a solution of SbF_5 (15 g; 69 mmol) in 20 mL of liquid HF at −78°C the ClF was taken up by the solution and a yellow precipitate appeared. After 12 g (22 mmol) of ClF had been added the system was closed and the pressure in the system remained constant at 1 atm. The system was then opened to a liquid nitrogen-cooled Monel cylinder until the vapor pressure in the −78°C vessel was essentially zero. When the vessel containing the solution and precipitate was warmed toward room temperature the solution started to turn red, the solid slowly disappearing at approximately −20°C. At 0°C there was no solid, the solution was orange-red, and the vapor pressure above the solution was 150 Torr. At room temperature the pressure was close to atmospheric. A sample of the vapor was collected in a liquid nitrogen-cooled Monel cylinder. Vapor pressure chromatography showed the presence of ClF and HF.

Antimony pentafluoride (30 g; 138 mmol), under a blanket of dry nitrogen, was placed in the Kel-F reactor, along with the stirring bar attached to the vacuum system, and evacuated. The SbF_5 froze when the vessel was cooled to −78°C. After HF (32 g; 1.62 mol) was distilled into the reactor the SbF_5 dissolved to give a colorless solution at −78°C. Chlorine (7 g; 99 mmol) was slowly condensed into the reactor solution with stirring, the temperature being maintained with the trichloroethylene – Dry Ice bath. A yellow solution with some droplets of liquid chlorine and a yellow precipitate resulted. Stirring was continued and the vessel warmed to −35°C. The pressure was 1 atm. The vessel was opened to a liquid nitrogen-cooled Monel cylinder and the gaseous products condensed in the cylinder until the vapor pressure in the vessel was reduced to zero. Two grams of gas were collected (condensed) in the cylinder. Vapor phase chromatography showed that the gas which had been condensed in the cylinder contained Cl_2, HF, and ClF. The reaction vessel and contents were then allowed to warm further. The yellow solid dissolved at about −20°C. The vapor coming off was condensed into a liquid nitrogen-cooled Monel cylinder as the vessel temperature was between 0 and 15°C. Vapor phase chromatography showed a large amount of ClF along with some HF and Cl_2.

Reactions involving silver salts

Silver fluoride (41 g; 0.32 mol) was placed in a 150-mL Monel cylinder equipped with a 1/4-in. Monel dip tube and outlet. The outlet was connected to a copper trap maintained at Dry Ice temperature. The outlet of the trap was connected to a 10-cm Monel body cell for the purpose of "on-stream" infrared spectrometric analysis of gaseous products. The outlet of the cell led to a Kel-F oil bubbler and an anhydrous calcium sulfate filled drying tube. The infrared cell could be bypassed. The reactor was heated by a vertical tube furnace. After the system was evacuated, Cl_2 was passed through the AgF, heated to 220°C, for 9 h. On-stream infrared analysis of the gaseous stream showed the presence of ClF. The solid residue in the reaction vessel consisted of AgCl and unreacted AgF.

A 240-mL Monel autoclave, previously passivated with chlorine trifluoride, was charged with AgF (45 g; 0.359 mol), Cl_2 (23 g; 0.324 mol), and HF (16 g; 0.80 mol), heated to 200°C, and shaken. A pressure of 49.9 atm gradually developed and remained constant throughout the heating period of 5 h. The autoclave was cooled and the gaseous products were removed to a Monel cylinder. Only 28.5 g was recovered. Vapor phase chromatography retention time and oxidizing power identified HF, Cl_2, and ClF in the gaseous products. The solid residue left in the autoclave contained 20.5% AgCl, consistent with about an 18.5% conversion of Cl_2 to ClF.

Silver tetrafluoroborate was loosely packed into 3/8-in. o.d. copper tubing connected to traps and an on-line infrared cell. After the system was evacuated, Cl_2 was passed through the $AgBF_4$ heated to 150°C. After 3 h of reaction time ClF and some ClF_3 were seen by infrared spectroscopy. They were also formed at 200 and at 250°C. Boron trifluoride was also seen. The solid residue in the copper tubing consisted of unreacted $AgBF_4$, AgF, and AgCl.

Reaction with alkali metal fluorides

A well-mixed mixture of NaF (5 g), LiF (10 g), and KHF_2 (60 g) was placed in a 150-mL Monel cylinder having a 1/4-in. o.d. nickel dip tube and outlet for gaseous products. The outlet was connected to three copper traps maintained at Dry Ice temperature, liquid nitrogen temperature, and room temperature, respectively. The system was protected from the atmosphere by a mercury seal at the end of the train. The reactor was heated, with an electric furnace, to 725°C while nitrogen was bubbled through the molten salt for about an hour. Then a stream of Cl_2 was bubbled through the molten salt for 5 h, consuming 32 g of Cl_2. The contents of the liquid nitrogen-cooled trap, about 20 g, was transferred into a Monel cylinder. Infrared spectroscopic analysis showed the presence of ClF along with some ClF_3. The solid residue in the reactor contained chloride, as evidenced by the precipitation of silver chloride upon the addition of silver ion. The aqueous filtrate from the precipitated silver chloride oxidized starch iodide solution.

Discussion and results

At the time this work was done the existence of an adduct of ClF with SbF_5 had not been established. When this work led to the conclusion that such an adduct could be made by reacting SbF_5 with ClF either neat or in HF solution, we initially and tentatively considered it to be $ClSbF_6$ admixed with $ClSb_2F_{11}$. We were uncomfortable with this since it suggested a bare positive chlorine, and the chlorine content did not fit well. When

other workers (7–9) identified and characterized Cl_2FAsF_6 and Cl_2FBF_4, we realized that our adduct must have been a Cl_2F^+ compound. Hence the likely reactions were

[8] $2ClF + SbF_5 \rightarrow Cl_2FSbF_6$

and

[9] $2ClF + 2SbF_5 \rightarrow Cl_2FSb_2F_{11}$

While it is clear that chlorine will not, by itself, disproportionate in hydrogen fluoride to a significant extent, this work shows that disproportionation can be brought about by tying up one or both disproportionation products. Both products are tied up when Cl_2 disproportionates in HF solution containing SbF_5, the ClF as the adduct discussed above, and HCl as $HSbF_5Cl$.

[10] $2Cl_2 + 3SbF_5 + 2HF \rightarrow Cl_2FSbF_5 + 2HSbF_6Cl$

Upon warming to about −20°C the ClF adduct decomposes, yielding ClF and SbF_5.

[11] $Cl_2FSbF_6 \rightarrow 2ClF + SbF_5$

At higher temperature the HCl (10) is liberated.

[12] $2HSbF_5Cl \rightarrow 2HCl + 2SbF_5$

The starting SbF_5 is regenerated. Equations [10], [11], and [12] combine to give twice eq. [7]. Overlap of the reactions shown in eqs. [11] and [12] will lead to the reverse of [7], thus accounting for some of what appeared to be unreacted chlorine. That HF is necessary for the disproportionation to occur (eq. [10]) is attested by nonreaction of Cl_2 with SbF_5 when reactions were attempted.

The low solubility of AgCl in HF (and water), contrasted with the high solubility of AgF in these solvents, might lead one to expect that the presence of Ag^+ would shift equilibria involving Cl^- in the direction of formation of Cl^- since AgCl would precipitate in the presence of significant, but low, concentrations of Cl^- and Ag^+. Hence it is not completely unexpected to note that Cl_2 will react with silver fluoride under a variety of conditions to give chloride, which is tied up as the silver salt. The other product has to be something formally oxidized. Hence ClF (and ClF_3) are likely products. Probably one of the factors that limit extent of reaction with solid AgF is a coating of chloride, which inhibits the attack of Cl_2.

[13] $Cl_2 + AgF \rightarrow ClF + AgCl$

Reactions involving $AgBF_4$ probably occur according to reaction [13] since loss of BF_3 results in AgF. One is tempted to invoke tying up of the interhalogen as a BF_3 adduct (BF_4^- species) when one speculates about intermediates, especially since some ClF_3 is observed when $AgBF_4$ is used. However, the temptation is resisted upon observation that reaction temperatures are above the decomposition temperature of the ClF_3 adduct.

Were reaction [13] a general one, where any metal (Li, Na, K, etc.) could substitute for Ag,

[14] $MF + Cl_2 \rightarrow ClF + MCl$

one could consider a scheme whereby the metal fluoride could be regenerated by reaction with HF

[15] $MCl + HF \rightarrow MF + HCl$

since this reaction, [15], occurs with most metal chlorides. Unfortunately it does not with silver chloride, probably for the same reason that [13] does. The net reaction (sum of [14] and [15] would be [7] were they to occur. In all cases where M is an alkali metal, the standard free energy (also enthalpy change) for the reaction is quite positive since the free energy of formation of ClF is not more negative than the difference between that of the metal fluoride and that of the metal chloride. However, the differences between the free energies of formation of the fluoride and chloride of given metals become less as one goes down the periodic table. This is a reflection of lattice energies showing less sensitivity to identity of the halide as the cation radius increases. Upon subtraction of lattice energies from the free energies or heats of formation one gets what might be called residual free energies or residual heats. These are the free energies or heats of formation were the metal halides liquid in their standard states. Obviously they are not liquids in their standard states and their melting points are well above room temperature. However, it was hoped that these data might give some guidance with respect to experiments in molten fluorides. It turns out that in all cases considered, the difference between the residual free energies (or enthalpies) of formation of the fluoride and chloride and the free energy of formation of ClF were less negative than is the free energy (or enthalpy) of formation of ClF. The difference in free energy of formation for the lithium halides is −204.6 kJ/mol; for the sodium halides, −161.0 kJ/mol; for the potassium halides, −130.2 kJ/mol; and for the cesium fluorides, −110.0 kJ/mol, while the difference in lattice energy of the halides is, for the lithium salts, 196 kJ/mol; sodium salts, 145 kJ/mol; potassium salts, 109 kJ/mol; and for the cesium salts, 100 kJ/mol. The residual free energy differences (negative) are then Li, 8.6 kJ/mol; Na, 16.0 kJ/mol; K, 21.2 kJ/mol; and Cs 11.0 kJ/mol. In all cases this is less than the free energy of formation of ClF, −57.7 kJ/mol, thus leading to a negative free energy change for the desired reaction were the salts liquid at room temperature. This encouraged the possibility that one could carry out the reaction by passing Cl_2 into a molten Group I halide melt, allowing the gaseous ClF product to escape from the melt (Le Chatelier's principle). Of course these conditions are far from the standard state. The fact that, when Cl_2 was bubbled through molten LiF–NaF–KF, ClF exited and chloride was formed in the melt demonstrates that, at least in this case, imprecise use of thermodynamic data gives useful guidance. It is unfortunate that the work was inadvertantly carried out at as high a temperature as it was, since it probably would have worked at temperatures down to the melting point of the mixture and thus minimized the corrosion of the apparatus that occurred.

That some ClF_3 is observed along with the ClF in some cases may be explained by the known equilibrium between ClF, ClF_3, and Cl_2 or by further disproportionation of ClF.

[16] $3ClF = ClF_3 + Cl_2$

Several years after this work was completed a study of Br_2 reactions in HF solutions containing AgF and of I_2 reactions in the same kind of medium was carried out and reported (11). While thermodynamic considerations predict that the halogen would disproportionate to halide (silver halide) and halogen monofluoride, further considerations underline the likely recovery of BrF_3 and IF_5, since these monofluorides are unstable with respect to disproportionation to halogen and the trifluoride and, in the case of iodine, to the pentafluoride. This is, except in the case of sufficient excess of Br_2, what is experimentally observed.

The trend, then, as one goes down the halogen group is to find primarily ClF, BrF_3, and IF_5 in the disproportionation products. This is pleasing to those of us who take pleasure in noting trends in the periodic table.

Can. J. Chem. Downloaded from www.nrcresearchpress.com by 186.148.149.217 on 09/07/12
For personal use only.

Chlorine, then, in ionic fluorine-containing media can be caused to undergo disproportionation when one or both of the products is tied up. The reduced product ends up in basic media as chloride and in acidic media as SbF_5Cl^-. The oxidized product is Cl_2F^+ in acidic media and as volatile ClF in basic media.

Examples exist of other kinds of waterlike behaviour (12) in hydrogen fluoride media. Drawing analogies with aqueous chemistry continues to be useful.

Acknowledgement

The authors wish to thank Olin Corp. for permission to publish this work at this time.

1. J. J. PITTS, S. KONGPRICHA, and A. W. JACHE. Inorg. Chem. **4**, 257 (1965).
2. S. KONGPRICHA and A. W. JACHE. J. Fluorine Chem. **1**, 79 (1971/72).
3. J. R. VAN WAZER. Phosphorus and its compounds. Vol 1. Interscience Publishers, Inc., New York. 1958. pp. 99–100.
4. F. A. COTTON and G. WILKINSON. Advanced inorganic chemistry. John Wiley and Son, New York. 1988. pp. 563–567.
5. A. W. JACHE, S. KONGPRICHA, and J. J. PITTS. U.S. Patent 3,451,775, 24 Jun 1969; Chem. Abstr. **71**, P40878q (1969); M. GAMBARDELLA, A. W. JACHE and S. KONGPRICHA. U.S. Patent 3,446,592, 27 May 1969; Chem. Abstr. **71**, P23371b (1969).
6. A. W. JACHE, M. GAMBARDELLA, S. KONGPRICHA and J. J. PITTS. Abstracts of Papers: 8th International Symposium on Fluorine Chemistry, Kyoto, Japan, August 22–27, 1976.
7. K. O. CHRISTIE and W. SAWODNY. Inorg. Chem. **8**, 212 (1969).
8. R. J. GILLESPIE and M. J. MORTON. Inorg. Chem. **9**, 811 (1970).
9. B. D. JOSHI and K. MOROKUMA. J. Am. Chem. Soc. **101**, 1714 (1979).
10. L. KOLDITZ and H. Z. DAUNICHT. Anorg. Allgem. Chem. **302**, 230 (1959).
11. J. L. RUSSELL and A. W. JACHE. Inorg. Nucl. Chem. – Herbert H. Hyman Mem. Vol. Supplement, 81 (1976).
12. A. W. JACHE. *In* Fluorine-containing molecules: structure, reactivity, synthesis and applications. *Edited by* J.F. Liebman and A. Greenberg. Doblier, W.R. Jr. VCH Publishers, Inc., New York. 1988. Chap. 9.

Can. J. Chem. Downloaded from www.nrcresearchpress.com by 186.148.149.217 on 09/07/12
For personal use only.

Synthesis and X-ray structure determination of the Ir–Ag–Ir donor–acceptor metal–metal bonded complex $[\{(\eta^5\text{-}C_5Me_5)(CO)_2Ir\}_2Ag][BF_4]$

FREDERICK W. B. EINSTEIN, RICHARD H. JONES, XIAOHENG ZHANG,[1] AND DEREK SUTTON[2]

Department of Chemistry, Simon Fraser University, Burnaby, B.C., Canada V5A 1S6

Received March 1, 1989

This paper is dedicated to Professor Ronald J. Gillespie on the occasion of his 65th birthday

FREDERICK W. B. EINSTEIN, RICHARD H. JONES, XIAOHENG ZHANG, and DEREK SUTTON. Can. J. Chem. **67**, 1832 (1989).

The title complex (**2**) has been synthesized from the reaction of $(\eta^5\text{-}C_5Me_5)Ir(CO)_2$ (**1**) with $AgBF_4$. Complex **2** crystallizes in the monoclinic space group $P2_1/c$ with a = 12.355(2) Å, b = 13.713(2) Å, c = 16.672(3) Å, β = 97.70(1)°, and Z = 4. The structure was solved by using 3131 observed reflections ($I \geq 2.5\sigma(I)$) in the range $0° < 2\theta < 50°$ to final discrepancy indices of R_F = 0.032 and R_{wF} = 0.038. The cation may be described as consisting of two molecules of **1** bound to Ag^+ by donor–acceptor Ir → Ag bonds. The Ir—Ag—Ir skeleton is nearly linear (angle 173.67(6)°). The Ag—Ir bond lengths are equal (2.659(1) Å), and the two molecules of **1** are disposed mutually *trans*, to give the cation approximate (noncrystallographic) C_{2h} symmetry.

Key words: complex, iridium, silver, metal-metal bond, X-ray, crystal, structure, carbonyl, donor-acceptor, pentamethylcyclopentadienyl.

FREDERICK W. B. EINSTEIN, RICHARD H. JONES, XIAOHENG ZHANG et DEREK SUTTON. Can. J. Chem. **67**, 1832 (1989).

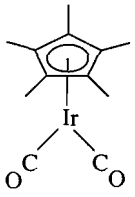
On a préparé le composé $[\{(\eta^5\text{-}C_5Me_5)(CO)_2Ir\}_2Ag][BF_4]$ (2) en faisant réagir le composé $(\eta^5\text{-}C_5Me_5)Ir(CO)_2$ (**1**) avec $AgBF_4$. Le complexe **2** cristallise dans le groupe d'espace monoclinique $P2/c$ avec a = 12,355(2) Å, b = 13,713(2) Å, c = 16,672(3) Å, β = 97,70(1)° et Z = 4. On a résolu la structure en faisant appel à 3131 réflexions observées ($I \geq 2{,}52\sigma(I)$ dans l'intervalle $0° < 2\theta < 50°$ jusqu'à des valeurs finales de R_F = 0,032 et de R_{wF} = 0,038. On peut décrire le cation comme étant constitué de deux molécules du composé **1** liées à l'ion Ag^+ par la liaison Ag → Ir donneur–accepteur. Le squelette Ir—Ag—Ir est quasi linéaire (angle 173,67(6)°). Les longueurs de liaison Ir—Ag sont de 2,659(1) Å, et les deux molécules du composé **1** sont mutuellement en position *trans*, pour donner le cation de symmétrie approximative (non cristallographique) C_{2h}.

Mots clés : complexe, iridium, argent, liaison métal–métal, rayons X, cristal, structure, carbonyle, donneur–accepteur, pentaméthylcyclopentadiényle.

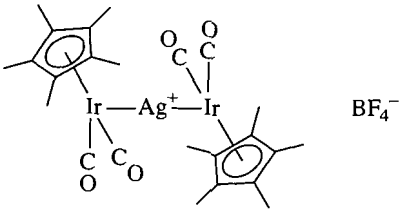
[Traduit par la revue]

Introduction

There is considerable current interest in heteronuclear metal–metal bonded complexes (1), and one subset includes those which can be formulated in a simplistic way to contain a heteropolar (or dative), metal–metal bond that is not "supported" by the presence of concurrent bridging ligands (i.e., M → M′) (see, for example, ref. 2). Recently, two X-ray structures have been published involving complexes with unbridged Ir → Ag bonds (3), and in this paper we describe the synthesis and X-ray structure of a further example, $[\{(\eta^5\text{-}C_5Me_5)(CO)_2Ir\}_2Ag][BF_4]$ (**2**).



1



2

Results

Synthesis and characterization

The addition of $AgBF_4$ to the iridium complex $(\eta^5\text{-}C_5Me_5)Ir(CO)_2$ (**1**) in acetone solution in 1:2 ratio readily affords $[\{(\eta^5\text{-}C_5Me_5)(CO)_2Ir\}_2Ag][BF_4]$ (**2**), which is isolated as a pale yellow, air-stable crystalline solid. Compound **2** is soluble in common polar solvents such as acetone, chloroform, or dichloromethane to give stable solutions, but is insoluble in benzene, hexane, and diethyl ether. The crystals decompose above 220°C.

The infrared spectrum (acetone) exhibits two ν(CO) absorptions, at 2033 and 1984 cm^{-1}. This is consistent with a C_{2h} structure for the cation with *trans* $\eta^5\text{-}C_5Me_5$ groups (where only the A_u and B_u ν(CO) modes are infrared active) but not with a *cis* structure of C_{2v} symmetry. However, two infrared active ν(CO) bands would also be anticipated if the two $(\eta^5\text{-}C_5Me_5)Ir(CO)_2$ moieties are not vibrationally coupled, and only the local ν(CO) vibrations of this unit are effective. As expected, both ν(CO) absorptions are shifted to higher wavenumber by comparison with $(\eta^5\text{-}C_5Me_5)Ir(CO)_2$ (**1**) itself. In the ^1H NMR spectrum, the $\eta^5\text{-}C_5Me_5$ resonance is at δ 2.37 ppm, shifted downfield by comparison with **1**. Both effects are consistent with the withdrawal of electron density from Ir as a result of the formation of formal Ir → Ag^+ donor–acceptor bonds.

The fast-atom-bombardment (FAB) technique employing a thioglycerol matrix and xenon bombardment gave an excellent mass spectrum (FABMS) of the parent cation (Fig. 1) with the appropriate isotopic cluster for the presence of one Ag and two Ir atoms; some fragmentation of the trimetallic cation occurred under these conditions, giving ions $[(\eta^5\text{-}C_5Me_5)(CO)_2IrAg]^+$, $[(\eta^5\text{-}C_5Me_5)(CO)IrAg]^+$, and $[(\eta^5\text{-}C_5Me_5)Ir(CO)_2]^+$.

X-ray structure

The structure consists of discrete $[\{(\eta^5\text{-}C_5Me_5)(CO)_2Ir\}_2Ag]^+$ cations and $[BF_4]^-$ anions with no unusually short interionic contacts. A view of the structure of the cation is given in Fig. 2. The cation features two crystallographically distinct $(\eta^5\text{-}C_5Me_5)Ir(CO)_2$ moieties bound to Ag^+ such that the

[1] Visiting scientist. Permanent address: Instrumentation and Analysis Research Centre, Zhongshan University, Guangzhou, People's Republic of China.

[2] Author to whom correspondence may be addressed.

Can. J. Chem. Downloaded from www.nrcresearchpress.com by 186.148.149.217 on 09/07/12
For personal use only.

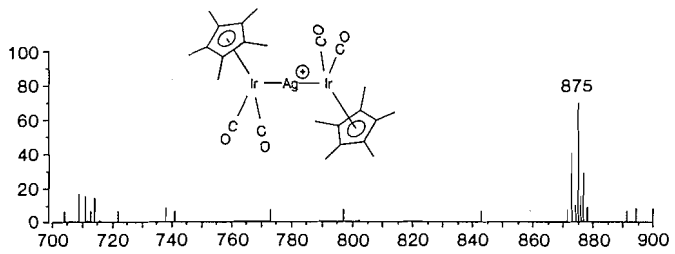


FIG. 1. Fast-atom bombardment mass spectrum (xenon gas, thioglycerol matrix) for the parent cation of **2**. Abscissa, m/z; ordinate, arbitrary intensity.

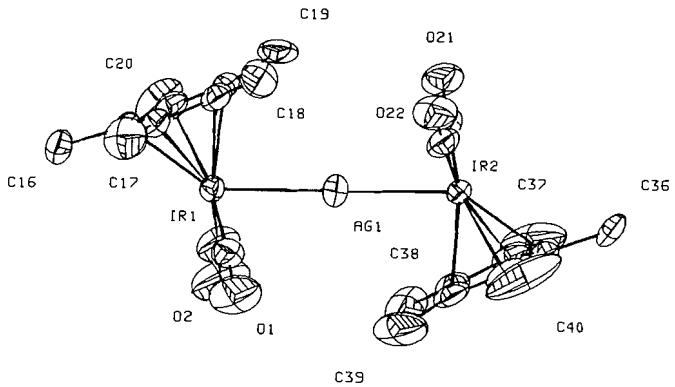


FIG. 2. View of the structure of the cation in **2** with atom numbering.

Ir—Ag—Ir skeleton is near linear (angle = 173.67(6)°) and the set of ligands on one Ir atom is disposed mutually *trans* to the set on the other Ir to give a noncrystallographic centrosymmetric (C_{2h}) ideal structure. The torsion angle Cp(1)—Ir(1)—Ir(2)—Cp(2) is 178.4° (where Cp(1) and Cp(2) are the centroids of the η^5-C_5Me_5 rings. The two Ag—Ir bond lengths are equal at 2.659(1) Å. This value may be compared with a previously determined Ag—Ir bond length of 2.683(1) Å in $IrCl(CO)(PPh_3)_2 \cdot Ag(B_{11}CH_{12})$, which also has an unbridged Ag—Ir bond and is therefore a good comparison (3*a*), and with bond lengths of 2.808(4) Å and 2.764(4) Å in $[(Ph_3P)_3Ir(\mu_3\text{-}H)(\mu\text{-}H)_2Ag_2(OSO_2CF_3)(H_2O)][CF_3SO_3]$ where, however, the Ag—Ir bonds have hydrogen bridges (3*b*). A somewhat larger value (2.87 Å) was observed for the Ag—Ir bond in a triazenide-bridged compound (4). The sum of empirical covalent radii of Ir and Ag may be estimated at 2.61 Å (5).

A notable feature of the structure is the acute angle Ag—Ir—C formed between the Ag—Ir and Ir—CO bonds in each case, ranging from 81°–83°. Thus, the CO groups appear to lean over the Ag—Ir bond toward the Ag to some extent; however, the observed Ir—C—O skeletons are close to linear, and there are no short contacts from Ag to carbonyl group carbon or oxygen atoms. This leaning is evident because each $(\eta^5\text{-}C_5Me_5)Ir(CO)_2$ group is minimally distorted from the regular structure that **1** itself is expected to possess, by comparison with the structure of $(\eta^5\text{-}C_5Me_5)Co(CO)_2$ (6*a*). (Note, however, that no determination of the X-ray structure of **1** has been reported.) Thus, the sum of the angles Cp(1)—Ir(1)—C(1), Cp(1)—Ir(1)—C(2), and C(1)—Ir(1)—C(2) is 358°, as is the sum of the corresponding angles around Ir(2). So, it appears that the presence of the Ir—Ag bond seems to be accompanied by little reorganization of each $(\eta^5\text{-}C_5Me_5)Ir(CO)_2$ moiety; the carbonyl groups have not moved away from this bond to generate the more regular three-legged piano-stool geometry typical of $(\eta^5\text{-}C_5Me_5)ML_3$ structures. Whether the CO groups assume these positions in **2** on account of some bonding interaction with the Ag^+ we cannot say at this time. Recently determined structures of related derivatives of $(\eta^5\text{-}C_5Me_5)Ir(CO)_2$ such as $(\eta^5\text{-}C_5Me_5)(CO)_2\text{-}IrW(CO)_5$ (6*b*) and $[(\eta^5\text{-}C_5Me_5)(CO)_2IrCH_2Cl]^+$ (6*c*) show somewhat greater reorganization of the carbonyl groups, to accommodate the extra ligand, than is observed here.

Discussion

The ability to form direct covalent metal–metal bonds between silver and transition metals has been known for over 50 years. Indeed a compound formulated as $[AgCo(CO)_4 \cdot xH_2O]$ was reportedly the first heteronuclear metal–metal bonded complex to be synthesized (refs. 1, p. 765, and 7*a*, *b*). In a study of the reactions of nucleophilic organometallic anions such as $[CpM(CO)_3]^-$ (M = Cr, Mo, W; Cp = η^5-C_5H_5) with $AgNO_3$, Hackett and Manning (7*c*) synthesized a series of anionic complexes $[\{Cp(CO)_3M\}_2Ag]^-$ that presumably have linear structures with two-coordinated Ag, related to the present example. The closest structural parallel that we can find to the one presented here (i.e., a discrete cationic complex of Ag with a cobalt-group metal) is the complex $[\{Cp(CO)(PPh_3)Rh\}_2Ag][PF_6]$ (**3**) synthesized by Connelly *et al.* (8). Several related mixed-metal silver complexes are known that are of different structure (4, 9).

The structure of complex **3** and that of **2** have many common features despite the different metal atom and the presence of PPh_3 ligands in the former. Thus the Ag—M distances are comparable (Ag—Ir = 2.659(1) Å in **2**, Ag—Rh = 2.651(1) and 2.636(1) Å in **3**); the M—Ag—M framework is close to linear (angle = 173.7(1)° in **2** and 171.0° in **3**); the structure adopted is *transoid* in both cases; and the M—C—O groups lean toward the Ag atom resulting in acute Ag—M—(CO) angles (80.6(4)°–83.0(5)° in **2** and 77.1(2)°, 84.3(2)° in **3**). These add further examples of carbonyl groups leaning toward metal–metal bonds to those observed previously in similar unbridged systems (2, 10).

The iridium complex **1** exhibits basic properties as, for example, in its ability to be protonated (11) to give $[(\eta^5\text{-}C_5Me_5)IrH(CO)_2]^+$. It is therefore convenient to view complex **2** as a complex with donor–acceptor $Ir \rightarrow Ag^+$ bonds, formed directly from the reaction of the Lewis base **1** with the Lewis acid Ag^+, though undoubtedly this is a gross oversimplification of the charge distribution in the final complex. For complex **3**, Connelly (8) has suggested that an alternative description as a silver(0)-stabilized source of the radical cation $[(\eta\text{-}C_5H_5)Rh(CO)(PPh_3)]^+$ provides a rationalization of the reactions of **3** with NO and NO_2. While we have not examined this possibility in detail for complex **2**, there may indeed be a parallel. Thus, we have found that addition of $AgBF_4$ and **1** to the dinuclear complex $[(\eta^5\text{-}C_5Me_5)_2Ir_2(CO)_3Cl][BF_4]$ does not yield any tri-iridium species that might be anticipated from simple chloride abstraction and coordination of a further $(\eta^5\text{-}C_5Me_5)Ir(CO)_2$; instead, the product is $[(\eta^5\text{-}C_5Me_4\overline{CH_2})(CO)_2Ir—Ir(CO)(\eta^5\text{-}C_5Me_5)][BF_4]$ where possibly the dehydrochlorination and metal–carbon bridge-bond formation occurs by a radical process. The details of this chemistry will be the subject of a future publication.[3]

[3]X. Zhang, R. Nagelkerke, and D. Sutton, unpublished results.

Can. J. Chem. Downloaded from www.nrcresearchpress.com by 186.148.149.217 on 09/07/12
For personal use only.

Can. J. Chem. Downloaded from www.nrcresearchpress.com by 186.148.149.217 on 09/07/12
For personal use only.

TABLE 1. Crystallographic and experimental data for **2**

(a) Crystal data

Parameter	Value
Compound	$[Ag\{Ir(CO)_2Cp^*\}_2]^+[BF_4]^-$
Formula	$AgIr_2C_{24}H_{30}O_4BF_4$
Molecular weight	931.37
Crystal system	Monoclinic
Space group	$P2_1/c$
a, Å	12.355(2)
b, Å	13.713(2)
c, Å	16.672(3)
β, deg	97.70(1)
V, Å^3	2799.2
Z	4
λ, Å	0.71069
μ (Mo-K$_\alpha$), mm^{-1}	10.19
D_{calc}, Mg m^{-3}	2.282

(b) Data collection and refinement

Parameter	Value
Crystal dimensions, mm	0.33 × 0.06 × 0.09
Temperature, K	295
Radiation	Mo-K$_\alpha$ graphite monochromated
Transmission factors	0.423–0.595
Scan mode	Coupled ω–2θ
Scan speed range, deg min^{-1}	0.78–2.75
Scan width, deg	0.70 + 0.35 tan θ
θ limits, deg	$0 < 2\theta \leq 50$
Data collection range	$h, k, \pm l$
Unique reflections	4906
Observed reflections ($I \geq 2.5\sigma(I)$)	3131
Number of variables	313
R_F[a]	0.032
R_{wF}[b]	0.038
Goodness of fit[c]	1.070

[a] $R_F = \Sigma||F_o| - |F_c||/\Sigma|F_o|$.
[b] $R_{wF} = [\Sigma w(|F_o| - |F_c|)^2/\Sigma F_o^2]^{1/2}$.
[c] G.O.F. = $[\Sigma w(|F_o| - |F_c|)^2/(\text{no. of degrees of freedom})]^{1/2}$.

TABLE 2. Atomic coordinates (×10^4) with esd's and U_{iso}/U_{eq} (Å^2 × 10^4) with esd's in parentheses for the non-hydrogen atoms of **2**

Atom	x/a	y/b	z/c	U_{iso}/U_{eq}
Ag(1)	2119.5(8)	2672.7(8)	1296.6(8)	561
Ir(1)	4072.7(4)	1846.0(3)	1644.7(3)	349
Ir(2)	181.9(3)	3454.4(3)	778.3(3)	331
O(1)	2898(11)	152(9)	790(8)	797
O(2)	3185(11)	1183(11)	3140(7)	845
O(21)	1308(9)	5249(7)	1500(7)	658
O(22)	1207(9)	3801(8)	−743(6)	685
C(1)	3335(12)	822(10)	1107(10)	578
C(2)	3518(12)	1450(12)	2555(8)	598
C(11)	5897(9)	2114(9)	1776(8)	427
C(12)	5494(9)	2081(9)	973(8)	457
C(13)	4745(10)	2860(10)	777(8)	467
C(14)	4678(9)	3391(9)	1509(8)	420
C(15)	5356(10)	2910(10)	2129(8)	452
C(16)	6786(10)	1455(11)	2240(10)	600
C(17)	5854(14)	1363(13)	355(10)	760
C(18)	4239(13)	3144(12)	−58(9)	673
C(19)	4122(13)	4349(9)	1592(12)	609
C(20)	5568(13)	3242(13)	3016(9)	695
C(21)	885(10)	4542(10)	1244(9)	522
C(22)	834(10)	3660(10)	−163(9)	505
C(31)	−1651(10)	3258(11)	720(9)	486
C(32)	−1162(11)	3235(10)	1512(8)	496
C(33)	−472(10)	2390(10)	1642(9)	500
C(34)	−505(11)	1948(10)	876(10)	477
C(35)	−1188(11)	2460(12)	306(9)	522
C(36)	−2516(11)	3971(15)	338(15)	730
C(37)	−1413(18)	3917(15)	2185(13)	896
C(38)	70(15)	2027(17)	2462(12)	832
C(39)	25(17)	979(11)	739(17)	905
C(40)	−1470(18)	2212(20)	−582(10)	813
B(1)	2271(10)	3894(20)	3681(8)	804(56)
F(1)	1560(23)	3384(10)	4073(17)	1418(36)
F(2)	2161(22)	3696(24)	2879(14)	1418(36)
F(3)	3322(19)	3786(24)	4028(16)	1418(36)
F(4)	2037(25)	4877(18)	3785(19)	1418(36)
F(5)	1963(24)	3378(20)	4326(16)	1418(36)
F(6)	1558(23)	4593(21)	3359(18)	1418(36)
F(7)	3276(20)	4283(23)	3928(17)	1418(36)
F(8)	2424(24)	3230(21)	3080(16)	1418(36)

Experimental

General procedures

Reactions were carried out under dry nitrogen using standard Schlenk techniques. Infrared spectra were recorded on a Perkin–Elmer 983G spectrometer, NMR spectra on Bruker WM-400 (at 400 MHz) and 100-SY (at 100 MHz) spectrometers, and mass spectra were recorded on a Hewlett–Packard HP 5985 instrument equipped with a Phrasor Scientific Inc. fast atom bombardment accessory. Microanalyses were performed by M. K. Yang of the SFU microanalysis laboratory. $(\eta^5\text{-}C_5Me_5)Ir(CO)_2$ was synthesized by a modification of the published procedure (12).[4]

Synthesis of $[\{(\eta^5\text{-}C_5Me_5)(CO)_2Ir\}_2Ag][BF_4]$ (2)

$AgBF_4$ (15 mg, 0.078 mmol) was added to a stirred bright-yellow solution of $(\eta^5\text{-}C_5Me_5)Ir(CO)_2$ (**1**) (60 mg; 0.157 mmol) in dry acetone, under nitrogen. The colour became pale yellow and the reaction was followed by IR spectroscopy until absorptions from **1** were no longer present. The solvent was removed under vacuum and **2** was recrystallized from acetone–ether as a yellow solid, mp above 220°C (dec.). Yield (recrystallized) 60.6 mg; 80.8%. IR (acetone, cm^{-1}): 2033 s, 1984 s (ν(CO)); ^{1}H NMR ($CDCl_3$) δ: 2.37 (C_5Me_5); FABMS (xenon–thioglycerol) m/z (cation): 875 (M^+), 491 (M^+ − $Cp^*Ir(CO)_2$), 463 (M^+ − $Cp^*Ir(CO)_2$ − CO), 384 ($Cp^*Ir(CO)_2^+$) (values are for the most abundant mass in the isotopic pattern). *Anal.* calcd. for **2**: C 29.97, H 3.12; found: C 30.02, H 3.08%.

X-ray structure determination for 2

A suitable crystal of **2** was mounted on the end of a glass fibre and transferred to an Enraf–Nonius CAD4F diffractometer equipped with graphite monochromated Mo-K$_\alpha$ radiation. The unit cell was obtained from the accurate setting angles of 25 reflections ($25 < 2\theta < 35°$). Three standard reflections measured every two hours showed no appreciable variation with time (1.25%). The data were corrected for Lorentz polarization and analytically for absorption effects (13). Pertinent crystallographic and experimental parameters are given in Table 1.

The structure was solved by heavy atom methods, and refined by full-matrix least squares. During the course of the refinement it became apparent that the tetrafluoroborate anion was disordered and two orientations of this group were included in the refinement. Restraints were applied to the B—F bond lengths and the F—B—F bond angles (14). In addition, the sum of the occupation numbers of the two disordered sites were constrained to unity. The locations of most of the hydrogen atoms were found in difference Fourier maps but it was

[4] W. A. G. Graham and J. K. Hoyano, personal communication.

TABLE 3. (a) Bond lengths (Å) and (b) angles (deg) for **2**, with esd's in parentheses

(a)

Bond	Length	Bond	Length
Ag(1)—Ir(1)	2.659(1)	C(12)—C(17)	1.533(19)
Ag(1)—Ir(2)	2.659(1)	C(13)—C(14)	1.432(18)
Ir(1)—C(1)	1.840(16)	C(13)—C(18)	1.499(17)
Ir(1)—C(2)	1.829(14)	C(14)—C(15)	1.405(17)
Ir(1)—C(11)	2.265(11)	C(14)—C(19)	1.498(17)
Ir(1)—C(12)	2.228(12)	C(15)—C(20)	1.537(18)
Ir(1)—C(13)	2.245(12)	C(31)—C(32)	1.376(19)
Ir(1)—C(14)	2.268(12)	C(31)—C(35)	1.452(21)
Ir(1)—C(15)	2.225(12)	C(31)—C(36)	1.523(20)
Ir(2)—C(21)	1.845(14)	C(32)—C(33)	1.437(20)
Ir(2)—C(22)	1.878(15)	C(32)—C(37)	1.525(21)
Ir(2)—C(31)	2.269(12)	C(33)—C(34)	1.410(20)
Ir(2)—C(32)	2.211(12)	C(33)—C(38)	1.523(20)
Ir(2)—C(33)	2.273(12)	C(34)—C(35)	1.375(20)
Ir(2)—C(34)	2.247(12)	C(34)—C(39)	1.512(20)
Ir(2)—C(35)	2.234(12)	C(35)—C(40)	1.514(20)
O(1)—C(1)	1.158(17)	B(1)—F(1)	1.357*
O(2)—C(2)	1.168(16)	B(1)—F(2)	1.353*
O(21)—C(21)	1.155(15)	B(1)—F(3)	1.357*
O(22)—C(22)	1.142(16)	B(1)—F(4)	1.395*
C(11)—C(12)	1.364(17)	B(1)—F(5)	1.382*
C(11)—C(15)	1.445(18)	B(1)—F(6)	1.363*
C(11)—C(16)	1.547(17)	B(1)—F(7)	1.364*
C(12)—C(13)	1.423(18)	B(1)—F(8)	1.385*

*Denotes that a restraint was applied to this bond.

(b)

Bonds	Angle	Bonds	Angle
Ir(2)—Ag(1)—Ir(1)	173.67(6)	C(20)—C(15)—C(14)	125.3(13)
C(1)—Ir(1)—Ag(1)	81.0(4)	O(21)—C(21)—Ir(2)	176.5(13)
C(1)—Ir(1)—Cp(1)	134.6	O(22)—C(22)—Ir(2)	178.2(13)
C(2)—Ir(1)—Ag(1)	83.0(5)	C(35)—C(31)—C(32)	106.8(12)
C(2)—Ir(1)—Cp(1)	135.1	C(36)—C(31)—C(32)	127.5(17)
C(2)—Ir(1)—C(1)	87.8(7)	C(36)—C(31)—C(35)	125.7(16)
Cp(1)—Ir(1)—Ag	113.1	C(33)—C(32)—C(31)	109.8(13)
C(21)—Ir(2)—Ag(1)	80.6(4)	C(37)—C(32)—C(31)	125.8(17)
C(21)—Ir(2)—Cp(2)	135.2	C(37)—C(32)—C(33)	124.0(16)
C(22)—Ir(2)—Ag(1)	82.2(4)	C(34)—C(33)—C(32)	105.4(12)
C(22)—Ir(2)—Cp(2)	133.0	C(38)—C(33)—C(32)	125.4(16)
C(22)—Ir(2)—C(21)	90.0(6)	C(38)—C(33)—C(34)	128.9(16)
Cp(2)—Ir(2)—Ag(1)	112.5	C(35)—C(34)—C(33)	110.3(13)
O(1)—C(1)—Ir(1)	177.2(14)	C(39)—C(34)—C(33)	123.6(17)
O(2)—C(2)—Ir(1)	178.4(16)	C(39)—C(34)—C(35)	125.6(17)
C(15)—C(11)—C(12)	107.2(11)	C(34)—C(35)—C(31)	107.5(12)
C(16)—C(11)—C(12)	127.8(13)	C(40)—C(35)—C(31)	125.5(18)
C(16)—C(11)—C(15)	125.0(13)	C(40)—C(35)—C(34)	126.9(18)
C(13)—C(12)—C(11)	110.0(12)	F(2)—B(1)—F(1)	112.8*
C(17)—C(12)—C(11)	125.4(12)	F(3)—B(1)—F(1)	112.5*
C(17)—C(12)—C(13)	124.5(13)	F(3)—B(1)—F(2)	111.3*
C(14)—C(13)—C(12)	107.2(11)	F(4)—B(1)—F(1)	106.2*
C(18)—C(13)—C(12)	125.9(13)	F(4)—B(1)—F(2)	108.8*
C(18)—C(13)—C(14)	126.5(13)	F(4)—B(1)—F(3)	104.8*
C(15)—C(14)—C(13)	107.0(11)	F(6)—B(1)—F(5)	115.9*
C(19)—C(14)—C(13)	127.2(13)	F(7)—B(1)—F(5)	107.4*
C(19)—C(14)—C(15)	125.4(13)	F(7)—B(1)—F(6)	111.0*
C(14)—C(15)—C(11)	108.5(11)	F(8)—B(1)—F(5)	107.7*
C(20)—C(15)—C(11)	126.0(13)	F(8)—B(1)—F(6)	108.7*
		F(8)—B(1)—F(7)	105.6*

Cp is the centroid of the η^5-C_5Me_5 ring.
*Denotes that a restraint was applied to this bond angle.

Can. J. Chem. Downloaded from www.nrcresearchpress.com by 186.148.149.217 on 09/07/12
For personal use only.

decided to geometrically place these and allow them to "ride" on the carbon atoms to which they were bonded. The variables included in the final cycles of refinement were scale, extinction, positional and anisotropic thermal parameters for the silver, iridium, carbon, and oxygen atoms, positional parameters of the boron atom and fluorine atoms, one occupation parameter for the disordered site ($F(1,\text{occ}) = 0.499(22)$), an isotropic thermal parameter for the boron atoms, one overall isotropic thermal parameter for the fluorine atoms, and two overall thermal parameters for the hydrogen atoms (one for each ring).

The final residuals were $R = 0.032$, $R_w = 0.038$, and the goodness of fit was 1.070. Refinement was by full-matrix least squares minimizing the function $\Sigma w(|F_o| - |F_c|)^2$, where w was calculated from a three-term Chebyshev series so that $w = [1.709t_0(x) + 2.239t_1(x) + 0.898t_2(x)]^{-1}$, where $x = F_o - F_{max}$ (15). The refinement was considered complete when the ratio of all shifts to esd's was less than 0.1. The highest peak in the final difference map was 1.06(3) e $Å^{-3}$ and was situated 1.183 Å from Ir(1). Complex neutral atom scattering factors were taken from International Tables for Crystallography (16). Calculations were carried out on a Microvax II computer with use of the NRC VAX Crystal Structure System (17) and the CRYSTALS suite of programs (18). Positional parameters are given in Table 2. Selected bond distances and angles are listed in Table 3. Anisotropic thermal parameters, hydrogen atom coordinates, and tables of calculated and observed structure factors are available as supplementary material.[5]

Acknowledgements

This work was supported by N.S.E.R.C. through operating and infrastructure grants to D.S. and F.W.B.E. We thank Johnson-Matthey Co. for a generous loan of iridium trichloride, Zhongshan University for providing leave of absence for X.Z., and Xiaoqian Yan for experimental assistance.

1. G. L. GEOFFROY and D. A. ROBERTS. *In* Comprehensive organometallic chemistry. Vol. 6. *Edited by* G. Wilkinson, F. G. A. Stone, and E. W. Abel. Pergamon Press, Oxford. 1982. Chap. 40, pp. 763–878.
2. (*a*) A. A. DEL PAGGIO, E. L. MUETTERTIES, D. M. HEINEKEY, V. W. DAY, and C. S. DAY. Organometallics, **5**, 575 (1986), and references therein; (*b*) F. W. B. EINSTEIN, M. C. JENNINGS, R. KRENTZ, R. K. POMEROY, P. RUSHMAN, and A. C. WILLIS. Inorg. Chem. **26**, 1341 (1987); (*c*) R. USÓN, J. FORNIÉS, P. ESPINET, C. FORTUÑO, M. TOMAS, and A. J. WELCH. J. Chem. Soc. Dalton Trans. 3005 (1988).
3. (*a*) D. J. LISTON, C. A. REED, C. W. EIGENBROT, and W. R. SCHEIDT. Inorg. Chem. **26**, 2739 (1987); (*b*) P. BRAUNSTEIN, T. M. GOMES CARNEIRO, D. MATT, A. TIRIPICCHIO, and M. TIRIPICCHIO CAMELLINI. Angew. Chem. Int. Ed. Engl. **25**, 748 (1986).
4. (*a*) J. KUYPER, P. I. VAN VLIET, and K. VRIEZE. J. Organomet. Chem. **105**, 379 (1976); (*b*) J. KUYPER, K. VRIEZE, and K. OLIE. Cryst. Struct. Commun. **5**, 179 (1976).
5. R. J. PUDDEPHATT and P. K. MONAGHAN. The periodic table of the elements. 2nd ed. Clarendon Press, Oxford. 1986.
6. (*a*) L. R. BYERS and L. F. DAHL. Inorg. Chem. **19**, 277 (1980); (*b*) F. W. B. EINSTEIN, R. K. POMEROY, P. RUSHMAN, and A. C. WILLIS. Organometallics, **4**, 250 (1985); (*c*) F. W. B. EINSTEIN, P. G. GLAVINA, R. K. POMEROY, P. RUSHMAN, and A. C. WILLIS. J. Organomet. Chem. **317**, 255 (1986).
7. (*a*) M. I. BRUCE. J. Organomet. Chem. **44**, 209 (1972); (*b*) M. P. SCHUBERT. J. Am. Chem. Soc. **55**, 4563 (1933); (*c*) P. HACKETT and A. R. MANNING. J. Chem. Soc. Dalton Trans. 1606 (1975); J. Chem. Soc. Chem. Commun. 71 (1973).
8. N. G. CONNELLY, A. R. LUCY, J. D. PAYNE, A. M. R. GALAS, and W. E. GEIGER. J. Chem. Soc. Dalton Trans. 1879 (1983); N. G. CONNELLY, A. R. LUCY, and A. M. R. GALAS. J. Chem. Soc. Chem. Commun. 43 (1981).
9. (*a*) B. D. ALEXANDER, B. J. JOHNSON, S. M. JOHNSON, P. D. BOYLE, N. C. KANN, A. M. MEUTING, and L. H. PIGNOLET. Inorg. Chem. **26**, 3506 (1987), and references therein; (*b*) P. I. VAN VLIET, G. VAN KOTEN, and K. VRIEZE. J. Organomet. Chem. **182**, 105 (1979).
10. T. L. BLUNDELL and H. M. POWELL. J. Chem. Soc. (A), 1685 (1971).
11. W. A. HERRMANN, J. PLANK, C. BAUER, M. L. ZIEGLER, E. GUGGOLZ, and R. ALT. Z. Anorg. Allg. Chem. **487**, 85 (1982).
12. P. M. MAITLIS, J. W. KANG, and K. J. MOSELEY. J. Am. Chem. Soc. **91**, 5970 (1969).
13. N. W. ALCOCK. *In* Crystallographic computing. *Edited by* F. R. Ahmed. Munksgaard, Copenhagen, Denmark. 1969. p. 271.
14. J. WASER. Acta Crystallogr. **16**, 1091 (1963); J. S. ROLLET. *In* Crystallographic computing. *Edited by* F. R. Ahmed. Munksgaard, Copenhagen, Denmark. 1969. p. 169.
15. J. R. CARRUTHERS and D. J. WATKIN. Acta Crystallogr. Sect. A: Cryst. Phys. Diffr. Theor. Gen. Crystallogr. **A35**, 698 (1979).
16. International Tables for Crystallography. Vol. IV. Kynoch, Birmingham, England, 1974. Tables 2.2b and 2.3.1.
17. E. J. GABE, A. C. LARSON, F. L. LEE, and Y. LE PAGE. NRC Crystal Structure System, National Research Council of Canada, Ottawa. 1984.
18. D. J. WATKIN, J. R. CARRUTHERS, and P. W. BETTERIDGE. CRYSTALS user guide. Chemical Crystallography Laboratory, University of Oxford, Oxford, England. 1985.

[5]Supplementary material may be purchased from the Depository of Unpublished Data, CISTI, National Research Council of Canada, Ottawa, Ont., Canada K1A 0S2.

Tables of bond lengths and angles involving hydrogen, and atomic coordinates for hydrogen atoms of **2** have been deposited with the Cambridge Crystallographic Data Centre, University Chemical Laboratory, Lensfield Road, Cambridge CB2 1EW, U.K.

Can. J. Chem. Downloaded from www.nrcresearchpress.com by 186.148.149.217 on 09/07/12
For personal use only.

Polyfluoroaralkyl amines. Further studies on the reactivity of 4,5,6,7-tetrafluoroindole

ROBERT FILLER, SARAH M. WOODS, AND WILLIAM L. WHITE
Department of Chemistry, Illinois Institute of Technology, Chicago, IL 60616, U.S.A.

Received February 20, 1989

This paper is dedicated to Professor Ronald J. Gillespie on the occasion of his 65th birthday

ROBERT FILLER, SARAH M. WOODS, and WILLIAM L. WHITE. Can. J. Chem. **67**, 1837 (1989).

4,5,6,7-Tetrafluoroindole **1** undergoes electrophilic formylation and aminoalkylation at C-3 to give compounds that can be readily converted to a variety of products, including the skatole, tryptamine, and tryptophan. **1** reacts with ethyl diazoacetate to yield 4,5,6,7-tetrafluoroethyl-3-indole acetate. The Grignard reagent of **1** offers a direct route to the versatile substituted acetonitrile **10** via C-3 alkylation with chloroacetonitrile.

Key words: tetrafluoroindole, tetrafluorotryptamine, tetrafluoroindolyl magnesium bromide, tetrafluorotryptophan.

ROBERT FILLER, SARAH M. WOODS et WILLIAM L. WHITE. Can. J. Chem. **67**, 1837 (1989).

Le 4,5,6,7-tétrafluoroindole (**1**) subit des formylation et des aminoalkylation en C-3 qui fournissent des produits qui peuvent facilement être transformés en une variété de composés comprenant le skatole, la tryptamine et le tryptophane. Le composé **1** réagit avec le diazoacétate d'éthyle pour conduire au 4,5,6,7-tétrafluoroindole-3-acétate d'éthyle. Le réactif de Grignard du composé **1**, par le biais d'une alkylation en C-3 à l'aide du chloroacétonitrile, offre une voie d'accès directe vers l'acétonitrile substitué **10** qui est très versatile.

Mots clés : tétrafluoroindole, tétrafluorotryptamine, bromure de tétrafluoroindylmagnésium, tétrafluorotryptophane.
[Traduit par la revue]

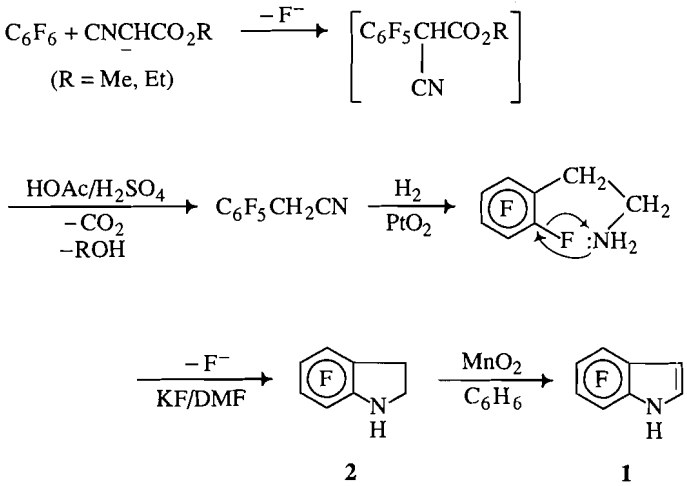
Can. J. Chem. Downloaded from www.nrcresearchpress.com by 186.148.149.217 on 09/07/12
For personal use only.

In previous papers (1–3), we reported the chemistry of polyfluoroaralkyl amines, including the facile synthesis of 4,5,6,7-tetrafluoroindole **1** (3). This compound and other fluorine-containing amines are of interest as potential bioactive molecules, especially as central nervous system agents. Although Yakobson and co-workers (4–7) and Fujita and Ojima (8) have previously described some reactions of **1** and substituted analogs, we wish to report new observations that extend the chemistry of this heterocyclic system. Compound **1** was readily prepared by aromatization of the indoline **2**, which was obtained by fluoride-catalyzed nucleophilic cyclization of 2-pentafluorophenylethylamine (Scheme 1) (3).

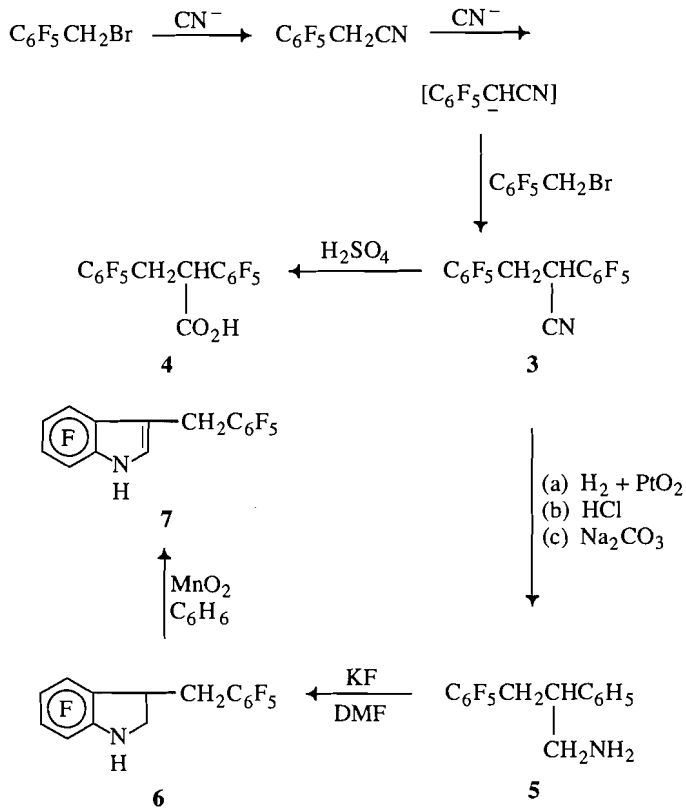
The 3-substituted tetrafluoroindole **7** was similarly obtained (Scheme 2). A by-product of this synthesis was the previously unreported carboxylic acid **4**.

Electrophilic reactions of 4,5,6,7-tetrafluoroindole

The Mannich reaction of **1** afforded the gramine **8**, which readily formed the methiodide **9**. The 3-cyanomethyl compound **10** was obtained on reaction of **9** with NaCN. Sodiodiethylacetamidomalonate and **9** gave **11**, which we were unable to convert to the tetrafluorotryptophan (Scheme 3).



SCHEME 1

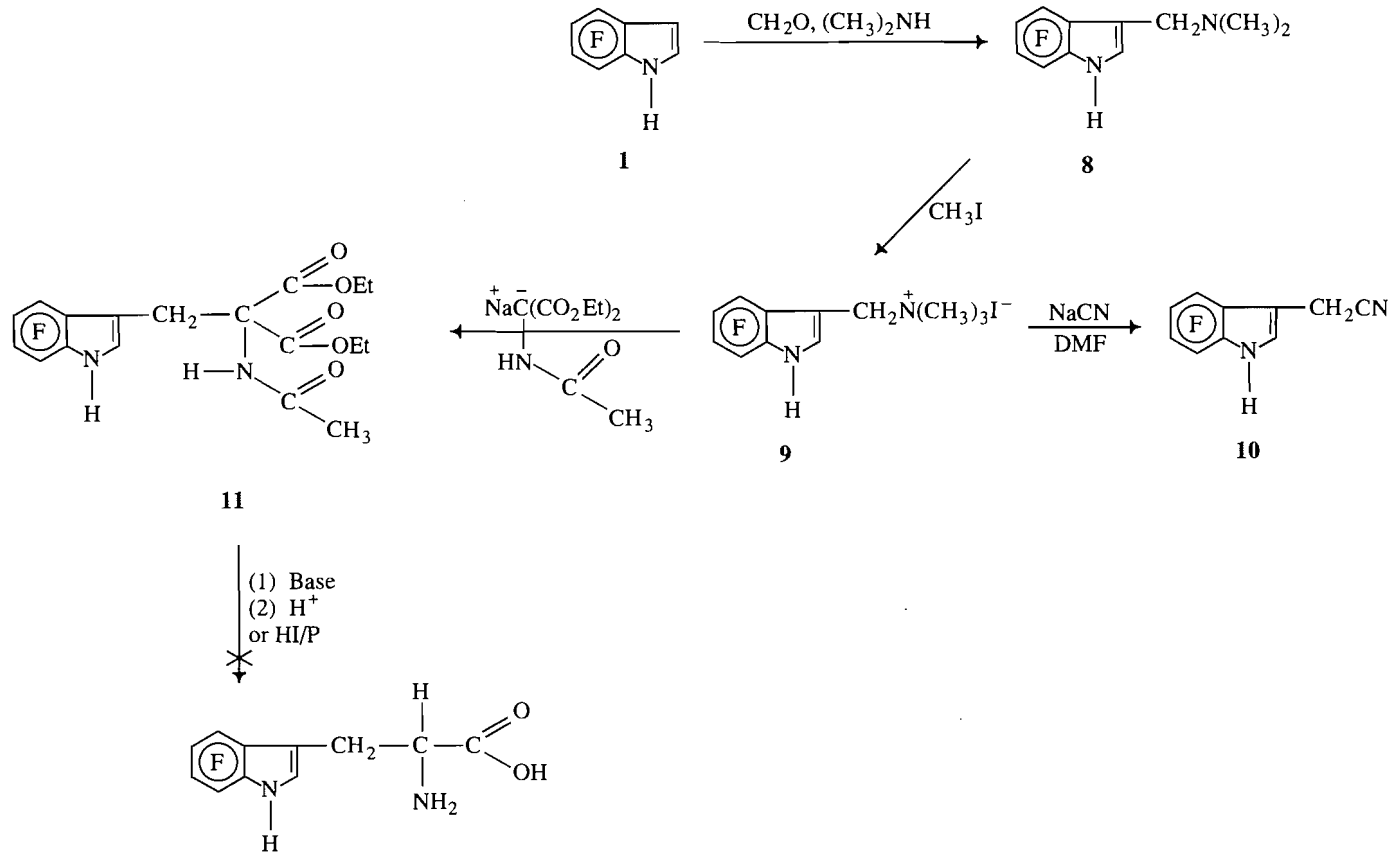


SCHEME 2

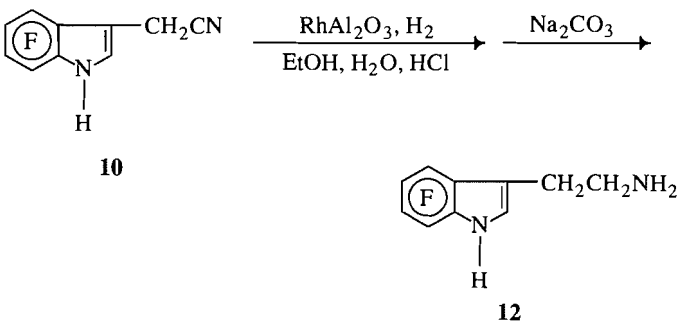
Catalytic hydrogenation of **10** afforded a low yield of the tryptamine **12**, which was unstable on standing, probably owing to intermolecular displacement of fluoride by the free amine.

Vilsmeier formylation of **1** readily yielded the 3-carboxaldehyde **13**, from which the skatole **14**, carboxylic acid **15**, and *N*-acetylazlactone **16** were easily prepared (Scheme 4). A small quantity of tetrafluorotryptophan **17** was obtained via compound **16**.

Printed in Canada / Imprimé au Canada



SCHEME 3



The reaction of **1** with an electrophilic carbenoid species is illustrated by the facile formation, using ethyl diazoacetate, of the corresponding ethyl 3-indole acetate **18**.

The Grignard reagent derived from **1** was easily prepared by reaction with ethyl magnesium bromide in tetrahydrofuran solvent. C-3 alkylation with chloroacetonitrile then gave a 50% yield of **10** as the sole isolable product. This method offers a much more direct route to **10** than the nucleophilic displacement reaction.

Experimental

2-Cyanodecafluorodibenzyl (3)

A mixture of 53.0 g (0.203 mol) of 2,3,4,5,6,-pentafluorobenzyl bromide (9) and 14.1 g (0.21 mol) of potassium cyanide in 140 mL of ethanol was heated with stirring at 75–80°C for 45 min. Work-up and fractionation of the residual oil through a 10-cm Vigreux column gave 32.47 g (78% yield) of 2,3,4,5,6-pentafluorophenylacetonitrile, bp 98–101°C (13 Torr; 1 Torr = 133.3 Pa) and 7.5 g (19% yield) of the dibenzyl. The dibenzyl compound appeared as a white sublimate in the Vigreux column as soon as the boiling point began to drop. Heating was continued, with warm water flowing through the condenser, until about 3.5 g of this material was collected. The dark solid remaining in the flask was dissolved in hot 95% ethanol and treated with decolorizing carbon. Light tan prisms were isolated, mp 125°C. The crystallized material was combined with the sublimate and all of the material was sublimed at 120°C/6 Torr to give a purified sample, mp 132°C; ir (hexachlorobutadiene mull): 2825, 2920 (s, CH_2 and CH_3), 2250 (s, CN), 1500 and 1140 (s, CF), 1610 and 1570 (s, aromatic); ^{1}Hmr (acetone-d_6) δ: 3.78 (d, fine structure, 2, CH_2), 5.13 (t, fine structure, 1, CH); mass spectrum (70 eV) *m/e*: 387 (M^+); calcd.: 387. *Anal.* calcd. for $C_{15}H_3F_{10}N$: C 46.53, H 0.77, N 3.62; found: C 46.18, H 0.71, N 3.42.

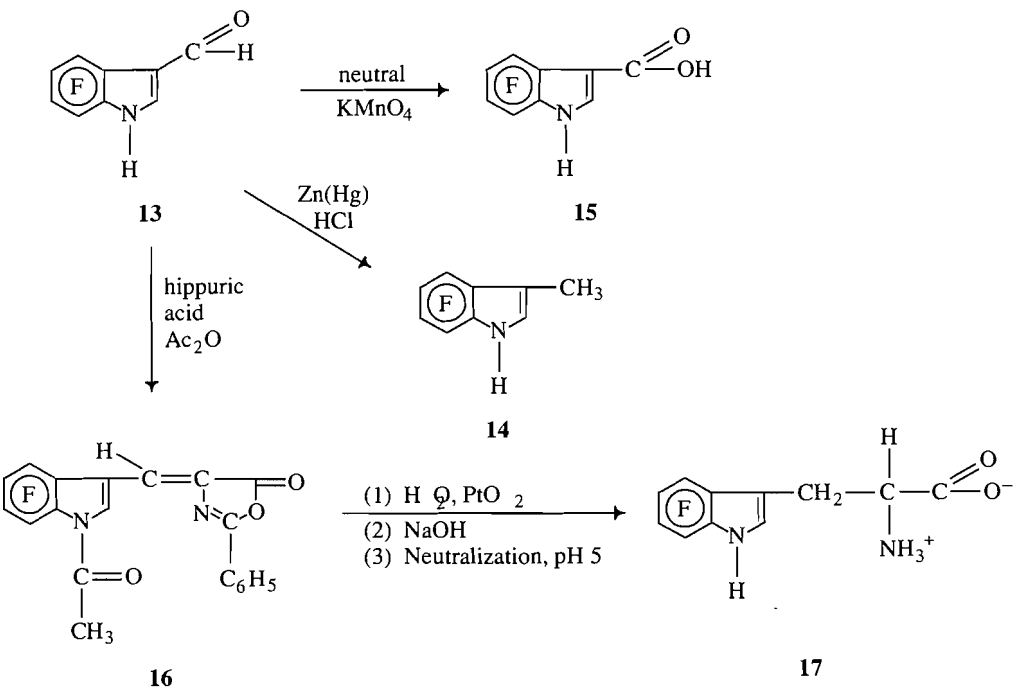
2,3-Bis(pentafluorophenyl) propionic acid (4)

2-Cyanodecafluorodibenzyl (1.0 g, 2.57 mmol) was placed in a 50-mL round-bottom flask and wet thoroughly with a chilled mixture of 2.4 g concentrated H_2SO_4 (25 mmol) and 1.8 mL of water. The mixture was heated rapidly, using a bunsen burner through a small (ca. 2 cm) hole in an asbestos sheet. The boiling was continued for 5 min. After allowing the mixture to cool to room temperature, it was diluted with ice-cold water. The precipitate was filtered on a Buchner funnel and washed several times with cold water. The yield of this crude material was 1.06 g (100%). After several recrystallizations from acetone using decolorizing carbon, a white crystalline substance was obtained, mp 167°C; ir (hexachlorobutadiene mull): 3540–3000 (br, OH), 2920, 2844 (CH), 1730 (s, C=O), 1640, 1520, 1450 (aromatic), 1500, 1150 (CF) cm^{-1}; mass spectrum (70 eV) *m/e*: 406 (M^+); calcd.: 406. *Anal.* calcd. for $C_{15}H_4F_{10}O_2$: C 44.17, H 0.99, N 0.00; found: C 44.18, H 0.78, N trace.

2-Pentafluorophenyl-2-pentafluorobenzylethylamine (5)

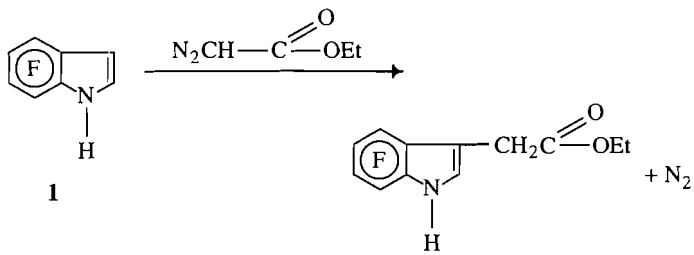
2-Cyanodecafluorodibenzyl (**3**) (7.74 g, 20 mmol) was dissolved in 150 mL of ethyl acetate in a 500-mL Parr flask. To this solution was added 50 mL of water containing 7 mL of concentrated hydrochloric acid and 0.10 g of platinum oxide. The two-phase mixture was cooled below 20°C and shaken on a Parr hydrogenation apparatus until hy-

Can. J. Chem. Downloaded from www.nrcresearchpress.com by 186.148.149.217 on 09/07/12
For personal use only.



13 15 14 16 17

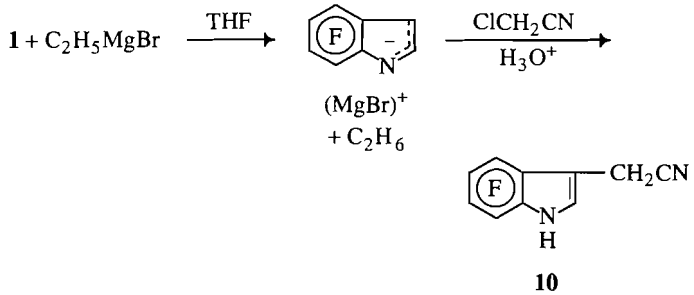
SCHEME 4



1 18

drogen uptake ceased. The light tan crystals that precipitated during the hydrogenation were collected on a filter. The filtrate, after concentration on a rotary evaporator, yielded 0.5 g of additional product. The solids were combined and washed on the filter with anhydrous ether, then with acetone, and dried. The combined mass was 7.0 g (82%), mp 220°C (dec.); mass spectrum (70 eV) *m/e*: 392, 427 (M^+); calcd.: 427. *Anal.* calcd. for $C_{15}H_8F_{10}NCl$: C 42.13, H 1.87, N 3.27; found: C 42.06, H 1.64, N 3.27.

Six grams (14 mmol) of the amine hydrochloride were dissolved in a chilled solution of sodium carbonate. The basic aqueous cold solution was extracted with several portions of ether. The combined ethereal layers were washed with water and dried over anhydrous $MgSO_4$. A white solid remained after evaporation of the ether *in vacuo*. The yield was 3.0 g (55%). The solid was recrystallized from CCl_4, using Norite as a decolorizing agent, and dried. The material was light-sensitive and reddened rapidly; ir (CCl_4): 3500–3000 (br, NH), 2940, 2800 (CH), 1650 (s, NH), 1540, 1450 (aromatic), 1500, 1130 (vs, CF) cm^{-1}; ^{1}Hmr



10

(CCl_4–acetone-d_6) δ: 4.73 (m, 1, C*H*), 3.66 (m, 4 C*H*), 2.2 (s, 2, N*H*). *Anal.* calcd. for $C_{15}H_7F_{10}N$: C 45.90, H 1.79, N 3.58; found: C 45.54, H 1.29, N 3.43.

3-Pentafluorobenzyl-4,5,6,7-tetrafluoroindoline (6)

For this preparation, the amine formed from 3.35 g (10 mmol) of **3** was not isolated. The ethereal layer was stripped *in vacuo*, until about 10 mL of solution remained. A 250-mL one-necked flask was fitted with an adapter for condenser, carrying a calcium chloride tube and nitrogen inlet tube. After the addition of 150 mL of dry DMF and 1.5 g of anhydrous potassium fluoride, the contents were stirred magnetically and refluxed for 3 h. The DMF was removed by distillation at 10 Torr. The residue remaining was transferred to a sublimator and sublimed at 60°C (0.5–1.5 Torr). After 4 days, 1.5 g of a white solid had sublimed, melting range 72–110°C; ^{1}Hmr δ: 3.3 (m), 3.6 (m); mass spectrum (70 eV) *m/e*: 419 (very small) M^+; base peak 372, which is the molecular mass of the indoline **6**; *Anal.* calcd. for $C_{15}H_6F_9N$: C 48.30, H 1.44, N 4.02; found: C 46.61, H 1.07, N 3.67.

Pentafluorobenzyl-4,5,6,7-tetrafluoroindole (7)

Several batches of impure indoline were combined to total 1.8 g (5 mmol). Seven grams of MnO_2 and 50 mL of dry benzene were added to it in a 125-mL round-bottom flask. The mixture was cooled to 20°C and placed on a wrist-action shaker for 24 h. After filtration through a Celite filter and on a Buchner funnel, the solid was extracted in a Soxhlet for 7 h. Solvent was removed from the combined solutions by vacuum distillation. The addition of water to the residue in the flask caused the formation of white crystals. The crystals were filtered, dried, and sublimed twice at 80°C, 0.7–1.0 Torr. One gram (60%) of this material was obtained, mp 115°C; ^{1}Hmr (acetone-d_6) δ: 8.75 (br, m, 1, N*H*), 6.90 (m, 1, C*H*), 4.20 (s, 2, CH_2); mass spectrum (70 eV) *m/e*: 369 (M^+); calcd.: 369. *Anal.* calcd. for $C_{15}H_4F_9N$: C 48.80, H 1.08, N 3.79; found: C 48.74, H 1.02, N 3.68.

3-Dimethylaminomethyl-4,5,6,7-tetrafluoroindole (4,5,6,7-tetrafluorogramine) (8)

To 0.85 mL of 5.2 N aqueous dimethylamine (ca. 0.25% solution, 4.42 mmol), cooled in an ice bath, was added first 0.60 g (10.0 mmol) of cold glacial acetic acid and, secondly, 0.34 g of cold 37% aqueous formaldehyde (6.3 mmol). To the resulting solution was added 0.75 g (3.98 mmol) of 4,5,6,7-tetrafluoroindole (**1**). After the indole had partially dissolved, the mixture was allowed to warm to room tempera-

Can. J. Chem. Downloaded from www.nrcresearchpress.com by 186.148.149.217 on 09/07/12
For personal use only.

Can. J. Chem. Downloaded from www.nrcresearchpress.com by 186.148.149.217 on 09/07/12
For personal use only.

ture and stirred magnetically overnight or placed on a wrist-action shaker. A solution of 0.55 g of sodium hydroxide in 10 mL of water, cooled to 0°C, was added with vigorous stirring and, after the mixture was cooled for about 2 h in an ice bath, the resulting precipitate was broken up, filtered, washed with three 10-mL portions of cold water, and dried to constant weight *in vacuo* at 50°C. The yields of crude material were suitable for subsequent reactions. An analytical sample was prepared by three recrystalliztions from $CHCl_3$, mp 133°C; ir ($CHCl_3$): 3460 (s, NH_2), 2942, 2860, 2820, 2790 (br, CH), 1600, 1530, 1480, 1420 (aromatic), 1010 (CF) cm^{-1}; ^{1}Hmr (acetone-d_6-DMSO-d_6) δ: 9.03 (b, 1, N*H*), 7.33 (s, 1, C*H*) 3.5 (s, 2, CH_2), 2.17 (s, 6, N-(CH_3); mass spectrum (70 eV) *m/e*: 246 (M^+); calcd.: 246. *Anal.* calcd. for $C_{11}H_{10}F_4N_2$: C 53.63, N 3.71, N 11.07; found: C 53.41, H 3.82, N 11.22.

*4,5,6,7-Tetrafluorogramine methiodide (**9**)*

To 18.0 g (0.127 mmol) of purified CH_3I, contained in a glass bottle chilled in ice, was added slowly 0.71 g (2.9 mmol) of 4,5,6,7-tetrafluorogramine. The mixture was stirred magnetically during the addition, and for 45 min afterwards. The solid gramine did not dissolve completely. The container was capped and placed in a refrigerator at 10°C for 6 h, then shaken on a wrist-action shaker for 24 h. The resulting solid was filtered, air-dried, and desiccated over $CaCl_2$. The crude material weighed 1.00 g (99.0% yield) and was recrystallized by dissolving in 8 mL of warm methanol, cooling, and adding hexane until a slight turbidity was observed. This suspension was placed in a refrigerator until crystallization occurred. After three recrystallizations, the material was dried in an Abderhalden flask with refluxing acetone at 2 Torr. The yellowish crystals melted at approximately 270°C; ir (hexachlorobutadiene mull): 3400, 3320 (m, br. NH), 3120 (s), 3020, 2980, 2840, 1580, 1500, 1450 (aromatic), 1010 (CF) cm^{-1}; ^{1}Hmr (DMSO-d_6) δ: 8.33 (m, ~1, N*H*), 7.6 (m, 1, C*H*), 5.1 (m, 2, CH_2), 3.2 (m, 9, N(CH_3)$_3$); mass spectrum (70 eV) *m/e*: 388 (M^+); calcd.: 388. *Anal.* calcd. for $C_{12}H_{13}F_4N_2I$: C 37.13, H 3.75, N 7.16; found: C 37.78, H 3.54, N 6.88.

*3-Cyanomethyl-4,5,6,7-tetrafluoroindole (**10**)*

To 0.393 g (10 mmol) of 4,5,6,7-tetrafluorogramine methiodide, in a 50-mL three-necked flask fitted with a reflux condenser, nitrogen inlet tube, and stopper, were added 25 mL of DMF and 9.8 mg (2.0 mmol) of reagent grade sodium cyanide, with magnetic stirring. The gramine methiodide did not dissolve entirely in this amount of solvent. The mixture was refluxed for 2 h, cooled, reduced to a volume of about 10 mL by vacuum distillation, transferred to a 50-mL separatory funnel, and extracted with three 8-mL portions of ether. The ethereal extracts were dried over anhydrous $MgSO_4$, filtered, and evaporated to dryness on a rotary evaporator. The 13 mg of solid (60% yield) was transferred to the sublimation apparatus and the purified material collected at 95°C and 0.7 Torr. After three sublimations the material melted at 133°C (lit. (4) mp 134°C); ir (hexachlorobutadiene mull): 3400–3120 (br, but sharp, NH), 3120, 3080, 2940, 2900 (w, CH), 2260 (s, CN), 1580, 1490, 1440 (aromatic), 1000 (CF) cm^{-1}; ^{1}Hmr (CCl_4) δ: 11.8 (s, 1, N*H*), 7.62 (m, 1, C*H*), 4.05 (m, 2, CH_2).

*Reaction of **9** with sodiodiethylacetamidomalonate*

A three-necked round-bottom flask fitted with a condenser, a nitrogen inlet tube, and a pressure equalizing dropping funnel was flamed and continuously purged with a positive nitrogen pressure. In this apparatus was placed 5.0 g (22 mol) of sodiodiethylacetamidomalonate, 17 mL of purified dry DMF, and 1.0 g (3 mmol) of 4,5,6,7-tetrafluorogramine methiodide. By use of an oil bath, the mixture was kept at 55°C for 22 h, by which time the reaction mixture had become maroon in color. The solution was poured into 40 mL of water at 0°C with stirring. The resulting crystals were filtered off and recrystallized from 80% ethanol to give 0.58 g of product (41%), mp 200°C becoming mp 205°C, after repeated recrystallizations and sublimation at ca. 180°C (0.7–2 Torr); ^{1}Hmr (acetone-d_6, CCl_4) δ: 7.7 (m, 1, N*H*), 7.12 (m, 1, C*H*), 5.2 (s, 1, N*H*), 4.17 (q, 4, CH_2), 3.73 (s, 3, CH_2) 3.4 (s, 2, CH_2), 1.21 (t, 6, CH_3). *Anal.* calcd. for $C_{18}H_{18}O_4F_4N_2$: C 51.37, H 4.53, N 6.67; found: C 51.37, H 4.28, N 6.47.

4,5,6,7-Tetrafluorotryptamine hydrochloride

To 0.85 g (3.72 mmol) of 3-cyanomethyl-4,5,6,7-tetrafluoroindole dissolved in 100 mL absolute ethanol was added 20 mL of water containing 4 mL of 12 N HCl and 0.2 g of Rh–Al_2O_3 catalyst. The mixture was reduced on a Parr apparatus. Only one half of the theoretical amount of hydrogen reacted. The mixture was filtered and concentrated on a rotary evaporator until yellow needles precipitated. These were filtered, washed with anhydrous ether, and dried to give 0.29 g (32%), mp 240°C; ^{1}Hmr (D_2O) δ: 7.60 (m), 3.50 (complex multiplet).

*4,5,6,7-Tetrafluorotryptamine (**12**)*

To 10 mL of a chilled aqueous solution of sodium carbonate was added 0.29 g (1.1 mmol) of the tryptamine hydrochloride. The resulting solution was extracted with several portions of ether and the combined ethereal extracts were washed with water and dried over anhydrous $MgSO_4$. The ether was removed *in vacuo* to give 100 mg (49%) of white solid, mp 125–130°C. Chromatography on 5 g of neutral alumina yielded a white substance. Before a melting point was determined, the material began to turn blue.

*3-Formyl-4,5,6,7-tetrafluoroindole (**13**)*

In a 150-mL round-bottom three-necked flask fitted with a nitrogen inlet tube, a drying tube containing calcium chloride, and a 50-mL dropping funnel was placed 7.24 g (10.2 mmol) of freshly distilled dimethylformamide. The flask and contents were cooled in an ice–salt bath and stirred magnetically for about half an hour. Freshly distilled phosphorus oxychloride (4.5 g, 23 mmol) was added dropwise over a period of 15 min. The mixture turned yellow. The first dropping funnel was replaced with a second charged with 1.0 g (5.3 mmol) of 4,5,6,7-tetrafluoroindole dissolved in 7.24 g (10.2 mmol) of DMF. The mixture was added dropwise over a period of 0.5 h and the temperature not allowed to rise above 10°C during the addition. The mixture was heated with stirring to 35°C and maintained at this temperature for 3 h. Crushed ice (30 g) was added and a solution of 2.2 g NaOH in 6 mL water was added dropwise to the reaction mixture. The mixture was then heated rapidly to boiling and the flask placed in the refrigerator overnight. The precipiate was collected, suspended in water, filtered, and washed. The precipitate was air-dried and sublimed twice at 110°C and 0.7 Torr; 1.02 g (89%); ir ((KBr): 3040 (s, NH), 3180 (s), 3140, 2920, 2820, 2770 (CH), 1680–1640 (br, sharp, C=O), 1550, 1480 (aromatic), 1500, 1000 (CF) cm^{-1}; mass spectrum (70 eV) *m/e*: 217 (M^+); calcd.: 217. *Anal.* calcd. for $C_9H_3F_4ON$: C 49.79, H 1.38, N 6.45; found: C 49.63, H 1.42, N 6.33.

*3-Methyl-4,5,6,7-tetrafluoroindole (**14**)*

In a three-necked 100-mL flask fitted with a 50-mL dropping funnel and reflux condenser was placed 1.0 g of freshly prepared amalgamated zinc. Concentrated hydrochloric acid (5 mL) was added dropwise. The contents were stirred magnetically and heated to gentle reflux. 95% Ethanol (15 mL) containing 0.3 g (1.5 mmol) of 4,5,6,7-indole-3-carboxaldehyde was added dropwise and the mixture refluxed for 30 min. The cooled mixture was decanted from the unreacted zinc, taken up in carbon tetrachloride, and neutralized with sodium bicarbonate. The organic layer was washed with water, dried over anhydrous $MgSO_4$, filtered, and concentrated *in vacuo* to give white crystals, which were purified by sublimation at 35°C and 0.8 Torr, mp 94–95°C; ^{1}Hmr (CCl_4) δ: 7.67 (very broad, 1, N*H*), 6.83 (m, 1, C*H*), 2.40 (s, 3, fine structure, CH_3). *Anal.* calcd. for $C_9H_5F_4N$: C 53.20, H 2.41, N 6.89; found: C 53.60, H 2.49, N 6.72.

*4,5,6,7-Tetrafluoroindole-3-carboxylic acid (**15**)*

A solution of 0.503 g (3.08 mmol) of potassium permanganate in 15 mL of water was added with stirring to 0.5 g (2.5 mmol) of the aldehyde **13** dissolved in 15 mL of acetone. The temperature was maintained between 30 and 40°C. After 5 min the purple color of potassium permanganate disappeared and the brown precipitate of MnO_2 formed. The mixture was filtered on a Buchner funnel using Celite filter aid. The filtrate was concentrated on a steam bath and a white precipitate formed after addition of six drops of 6 N hydrochloric acid. The precipitate was dissolved in sodium bicarbonate, reprecipitated with a few drops of 6 N HCl, and dried, mp 233°C, 0.537 g (90%); ir (hexachlorobutadiene

mull): 3400 (s, NH), 3260 (w), 2920, 2840 (CH), 1720–1650 (s, C═O), 1580, 1540, 1440 (aromatic), 1500, 1000 (CF) cm^{-1}; ^{1}Hmr (acetone-d_6) δ: 8.33, 8.15, 6.67; mass spectrum (70 eV) *m/e*: 233 (M^+); calcd.: 233. *Anal.* calcd. for $C_9H_3F_4O_2N$: C 46.33, H 1.29, N 6.49; found: C 46.07, H 1.11, N 6.29.

*Azlactone of 4,5,6,7-tetrafluoroindole-3-carboxaldehyde (**16**)*

A mixture of 0.35 g (2.4 mmol) of hippuric acid and 0.20 g (2.5 mmol) of anhydrous sodium acetate, 0.5 g (2.4 mmol) of 4,5,6,7-tetrafluoroindole-3-carboxaldehyde, and 6.12 g (9.2 mmol) of freshly distilled acetic anhydride was warmed in a loosely corked 25-mL Erlenmeyer flask with magnetic stirring until solution was complete. A deep orange suspension formed immediately. After filtration, the material was recrystallized from benzene and dried, mp 254–256°C, yield 89%; mass spectrum (70 eV) *m/e*: 402 (M^+); calcd.: 402. *Anal.* calcd. for (N-acetylated compound) $C_{20}H_{10}N_2O_2F_4$: C 59.72 H 2.45, N 6.98; found: C 59.56, H 2.42, N 6.95. After hydrolysis in dilute sodium hydroxide a white solid formed and was removed by filtration. The filtrate was concentrated *in vacuo* and the total solid (0.42 g, 50% yield) was taken up in 25 mL of ethyl acetate, 3 drops of concentrated HCl added, and 0.1 g platinum dioxide added to the mixture. The mixture was reduced on a Parr apparatus until hydrogen uptake ceased. The mixture was neutralized, separated from the water phase, and the ethyl acetate removed on a rotary evaporator. Infrared analysis suggests that the substance is 4,5,6,7-tetrafluorotryptophan, **17**; ir (hexachlorobutadiene mull): 3450 (s, NH), 3300 (br, OH in CO_2H), 2960, 2840 (CH), 1770–1670 (br, C═O, 1600, 1540, 1440 (aromatic), 1500, 1000 (CF) cm^{-1}.

*Ethyl-3-(4,5,6,7-tetrafluoroindolyl) acetate (**18**)*

In a 50-mL three-necked flask fitted with a 125-mL pressure equalizing dropping funnel, a condenser carrying a calcium chloride drying tube at the top, and a nitrogen inlet tube was placed 1.0 g (5.7 mmol) of 4,5,6,7-tetrafluoroindole and 2.62 g (22.8 mmol) of ethyl diazoacetate (10). The mixture was stirred magnetically and heated for 5 h at 140°C, using an oil bath. The contents of the flask were then dissolved in ether, washed with water, dried, and sublimed at 60°C and 0.7 Torr to give 0.50 g of a crystalline material, mp 91°C. This material was unreacted indole. The remainder of the material, 1.50 g (80% yield), was transferred to a 50-mL flask fitted with a condenser and refluxed with a mixture of 0.74 g (1.0 mmol) of methanesulfonic acid and 1.0 g (22 mmol) of formic acid for 5 h to give a bright red mixture. This mixture was extracted with several portions of ether and aqueous Na_2CO_3. The aqueous layer yielded no crystals when acidified. The combined ethereal layers were washed with water and dried over anhydrous $MgSO_4$. Concentration *in vacuo* left a red viscous oil. Chromatography on 5 g of Al_2O_3 using ether–hexane provided no separation. Spectral characterization showed no hydrolysis had occurred; ir (neat): 3460 (w, NH), 3300 (s, NH), 2980, 2940, 2860 (s, CH), 1780, 1670, 1550, 1480, 1440 (aromatic), 1490, 1000 (CF) cm^{-1}; ^{1}Hmr (CCl_4) δ: 9.4 (1, N*H*), 7.10 (m, 1, C*H*), (q, 2, CH_2), 3.80 (s, 2, CH_2), 1.3 (t, 3, CH_3).

Preparation of the 4,5,6,7-tetrafluoroindole Grignard reagent

Two grams (10.6 mmol) of 4,5,6,7-tetrafluoroindole dissolved in 20 mL of anhydrous THF was added dropwise to a 100-mL 3-necked flask containing ethyl bromide (0.952 g, 8.9 mmol) dissolved in 40 mL of THF, and magnesium turnings (0.312 g, 13 mmol), in a nitrogen atmosphere. The mixture was allowed to reflux for 0.5 h.

Reaction of 4,5,6,7-tetrafluoroindole Grignard reagent with chloroacetonitrile

Chloroacetonitrile (0.09 g, 13.24 mmol) was dissolved in 5 mL of dry THF and added dropwise to the Grignard reagent. The mixture was heated, using an oil bath, for 0.5 h. After cooling, the material in the flask was worked up. Crystals formed, mp 132°C. The product was 4,5,6,7-tetrafluoroindolylacetonitrile, obtained in 50% yield. Its ^{1}Hmr was superimposable with that of **10**.

1. W. L. WHITE and R. FILLER. J. Chem. Soc. (C), 2062 (1971).
2. R. FILLER and R. C. RICKERT. J. Fluorine Chem. **18**, 483 (1981).
3. R. FILLER, S. M. WOODS, and A. F. FREUDENTHAL. J. Org. Chem. **38**, 811 (1973).
4. T. D. PETROVA, T. I. SAVCHENKO, L. N. SHCHEGOLEVA, T. F. ARDYUKOVA, and G. G. YAKOBSON. Khim. Geterotsikl. Soedin. 1344 (1970): Chem. Abstr. **74**, 76257n (1971).
5. T. D. PETROVA, T. I. SAVCHENKO, T. F. ARDYUKOVA, and G. G. YAKOBSON. Khim. Geterotsikl. Soedin. 213 (1971); Chem. Abstr. **75**, 48812s (1971).
6. T. D. PETROVA, T. I. SAVCHENKO, T. F. ARDYUKOVA, and G. G. YAKOBSON. Russ. Pat. 289,088 (1970); Chem. Abstr. **74**, P141528t (1971).
7. T. D. PETROVA, T. I. SAVCHENKO, T. F. ARDYUKOVA, and G. G. YAKOBSON. Russ. Pat. 299,507 (1970); Chem. Abstr. **75**, P63606w (1971).
8. M. FUJITA and I. OJIMA. Tetrahedron Lett. **24**, 4573 (1983).
9. J. M. BIRCHALL and R. N. HASZELDINE. J. Chem. Soc. 3719 (1961).
10. E. B. WOMACK and A. B. NELSON. Org. Synth., Coll. Vol. III, John Wiley and Sons, Inc., New York. 1955. p. 392.

Can. J. Chem. Downloaded from www.nrcresearchpress.com by 186.148.149.217 on 09/07/12
For personal use only.

Extending the VSEPR model through the properties of the Laplacian of the charge density

PRESTON J. MACDOUGALL[1] AND MICHAEL B. HALL
Department of Chemistry, Texas A&M University, College Station, TX 77843, U.S.A.

AND

RICHARD F. W. BADER AND JAMES R. CHEESEMAN
Department of Chemistry, McMaster University, Hamilton, Ont., Canada L8S 4M1

Received April 3, 1989

This paper is dedicated to Professor Ronald J. Gillespie on the occasion of his 65th birthday

PRESTON J. MACDOUGALL, MICHAEL B. HALL, RICHARD F. W. BADER, and JAMES R. CHEESEMAN. Can. J. Chem. **67**, 1842 (1989).

The Laplacian of the electronic charge density demonstrates the presence of local concentrations of charge in the valence shell of an atom in a molecule. These local maxima faithfully duplicate in number, location, and size the spatially localized electron pairs of the VSEPR model. Thus the Laplacian of the charge density provides a physical basis for the Lewis and VSEPR models. The VSEPR model can fail to predict the observed geometry when a transition metal is the central atom in the system. In such a case there is no basis within the model itself to predict the existence of the nonbonded pair or pairs of electrons whose presence would account for the observed geometry. By appealing to the Laplacian of the charge density in one such system, namely $VOCl_3$, one observes that the penultimate shell of charge concentration of this transition metal atom exhibits nonbonded concentrations of charge with the locations and properties required to account for the observed geometry of the molecule. Thus the properties of the Laplacian distribution, which are model independent, can be used to extend the applicability of the VSEPR model to those cases where the usual arguments fail to account for the number and type of charge concentrations that exist within the outer shell of an atom.

Key words: Laplacian of the charge density, VSEPR model, transition metal.

PRESTON J. MACDOUGALL, MICHAEL B. HALL, RICHARD F. W. BADER et JAMES R. CHEESEMAN. Can. J. Chem. **67**, 1842 (1989).

La distribution de Laplace de la densité de la charge électronique démontre qu'il existe des concentrations locales de charges dans la couche de valence d'un atome d'une molécule. Ces maxima locaux sont une réplique exacte du nombre, de la position et de la grandeur des paires d'électrons localisées dans l'espace du modèle VSEPR. La distribution de Laplace de la densité de charge fournit donc une base physique pour les modèles de Lewis et VSEPR. Lorsque l'atome central d'un système est un élément de transition, il existe des cas où le modèle VSEPR ne permet pas de prédire la géométrie observée. Dans un tel cas, il n'existe pas de base dans le modèle pour prédire l'existence de la paire non-liée ou des paires d'électrons dont la présence pourrait expliquer la géométrie observée. En faisant appel à la distribution de Laplace de la densité de charge d'un tel système, à savoir le $VOCl_3$, on peut observer que l'avant-dernière couche de la concentration de charge de cet élément de transition présent des concentrations de charge non-liées dont les positions et les propriétés correspondent à celles requises par la géométrie observée pour la molécule. Les propriétés de la distribution de Laplace, qui sont indépendantes du modèle, peuvent donc être utilisées pour permettre d'appliquer le modèle VSEPR aux cas où les arguments usuels ne permettent pas d'expliquer le nombre ou le type de concentrations de charge qui existent dans la couche extérieure d'un atome.

Mots clés : distribution de Laplace de la densité de la charge, modèle VSEPR, élément de transition.

[Traduit par la revue]

Introduction

The valence-shell electron pair repulsion or VSEPR model (1) is a natural extension of the localized electron pair model of Lewis (2). It has become the most successful and widely used model for the prediction of the geometries of closed-shell molecules AX_n. The VSEPR model has two basic assumptions: (1) the valence charge density of the central atom A is spatially localized into pairs of electrons, and (2) the geometrical arrangement of the ligands X about atom A is that which maximizes the separations between the pairs, assuming the pairs to be on the surface of a sphere centred on the A nucleus. In general, not all the pairs are equivalent and three subsidiary postulates are required to determine the relative sizes of the electron pair domains: (a) nonbonding pairs have larger domains than bonding pairs; (b) bonding pair domains decrease in size with increasing electronegativity of the ligand, and increase in size with increasing electronegativity of the central atom; (c) double and triple bond domains are larger than single bond electron pair domains.

The Laplacian distribution of the electronic charge density, the quantity $\nabla^2\rho$, has been shown to provide the physical basis for the Lewis and VSEPR models (3). It does this by demonstrating the presence of local concentrations of charge in the valence shell of an atom in a molecule. These local charge concentrations, local maxima in $-\nabla^2\rho$, faithfully duplicate in number, location, and size the spatially localized electron pairs of the VSEPR model (3, 4), recovering all of the properties ascribed to them as put forth in the postulates of the model. The existence and the arrangement of the local charge concentrations within the valence shell of an atom are a consequence of the partial condensation of the valence electrons into pairs (3*b*, 4). The condensation is caused by a corresponding spatial localization of the Fermi hole, a localization that arises from the ligand field acting in concert with the Pauli exclusion principle. Because of this linking of the concepts of the VSEPR model to a physical property of a system, the model is reduced to but a

[1]Author to whom correspondence may be addressed.

Printed in Canada / Imprimé au Canada

Can. J. Chem. Downloaded from www.nrcresearchpress.com by 186.148.149.217 on 09/07/12
For personal use only.

TABLE 1. Structural data of oxyhalides[a]

Compound		Bond lengths and bond angles[b]	Compound		Bond lengths and bond angles[b]
POF_3	P—F	1.524	$VOCl_3$	V—O	1.57
	P—O	1.436		V—Cl	2.14
	∠FPF	101.3		∠OVCl	108
				∠ClVCl	111
$POCl_3$	P—Cl	1.993			
	P—O	1.449	CrO_2Cl_2	Cr—O	1.57
	∠ClPCl	103.3		Cr—Cl	2.12
				∠OCrCl	109.5
SO_2F_2	S—F	1.53		∠OCrO	105
	S—O	1.40		∠ClCrCl	113
	∠FSF	97			
	∠OSO	123	CrO_2F_2	Cr—O	1.58
				Cr—F	1.74
SO_2Cl_2	S—Cl	1.99		∠OCrO	102
	S—O	1.43		∠FCrF	119
	∠ClSCl	111			
	∠OSO	120			

[a]Reference 8.
[b]Values in angstroms and degrees.

single postulate. This postulate is that the most stable molecular geometry of a molecule AX_n corresponds to maximally separating, according to size and magnitude, the local maxima in the valence shell of charge concentration (VSCC) of the atom A as defined by the Laplacian of the charge density.

An advantage of finding a physical basis for a model is that one can then investigate those cases that are perhaps of greatest interest in providing a deeper understanding of the phenomena covered by the model, namely, the exceptions to the model. The VSEPR model does not fail for closed-shell systems composed of main group elements. Exceptions to the model can be found, however, for systems containing transition group elements. This brief note is an initial study of one such exception, as provided by the molecule $VOCl_3$.

The basic tetrahedral geometries of main group compounds such as POF_3 and $POCl_3$ are explained on the basis of the presence of four electron domains in the valence shell of phosphorus, three containing singly bonded pairs and one containing the two bonded pairs of the double bond. The subsidiary postulate regarding the relative sizes of single and double bond domains then correctly predicts the XPO angle to be greater than the XPX angle and for this latter angle to be less than tetrahedral in these molecules. In agreement with these predictions, the XPX angle is 101.3° in the fluoride and 103.3° in the chloride. Table 1 gives the geometrical parameters for these and other related molecules. In the compounds SO_2X_2, the XSX angle is smaller than the OSO angle. Also given in this table are data for transition metal compounds that exhibit contrasting behaviour. In the CrO_2X_2 systems, the XCrX angle is greater than the OCrO angle. In the molecule $VOCl_3$, the OVCl angle is actually slightly less than tetrahedral, being equal to 108°, thereby yielding a value of 111° for the ClVCl angle. This opening of the ClVCl angle to a value greater than the tetrahedral value cannot be explained by the VSEPR model if one assumes, as is correct for the corresponding main group compounds, that the valence shell of the central atom has but four electron domains. The model is saved if one could argue that five electron domains exist in the outermost electron shell of a transition element, with the fifth domain being located in the nonbonded position along the threefold axis, that is, opposite the oxygen atom. It is shown here that the Laplacian of the charge density for the vanadium atom in $VOCl_3$ does indeed exhibit five local maxima or local charge concentrations in its outermost shell of charge concentration, with the largest of these concentrations being found in the nonbonded position along the threefold axis. The positions of the three "bonded maxima" associated with the chlorine atoms are, however, not as anticipated on the basis of analogous behaviour with the main group compounds. A corresponding polarization of the outermost shell of charge concentration is shown to be present in the molecule VCl_3. The properties of the Laplacian distribution, which link the tenets of the model to observed properties of the charge distribution, do more than simply extend the domain of application of the model. In addition, the Laplacian of ρ delineates the differences in the properties of the electronic charge distributions that exist between main group and transition metal atoms, differences that are responsible for their differing chemical behaviour. Gillespie *et al.* (5) have stated that "the 3*d* electrons cannot be clearly identified as either valence shell electrons or as core electrons. This special nature of the 3*d* electrons is responsible for most of the unusual properties of the transition metals."

Calculations

The RHF SCF calculations for VCl_3 and $VOCl_3$ were caried out using the Huzinaga basis sets (6): V(532121*s*/5211*p*/221*d*), O(5211*s*/321*p*/1*d*), Cl(53211*s*/5211*p*/1*d*).[2] The calculations included an optimization of the geometries. The calculated geometrical parameters for $VOCl_3$ are R(V—O) = 1.501 Å, R(V—Cl) = 2.147 Å, ∠ClVCl = 110.5°, ∠OVCl = 108.4°. The agreement with the experimental values is good (see Table

[2]A single polarization function was added to each atom's basis (*d* for O, Cl and *p* for V). The V basis was that optimized for the $(3d)^4(4s)^1$ atomic state. To satisfactorily describe the diffuse charge on the ligands, diffuse *s* and *p* functions were added to their bases (exp. = 0.08 for O, 0.05 for Cl).

Can. J. Chem. Downloaded from www.nrcresearchpress.com by 186.148.149.217 on 09/07/12
For personal use only.

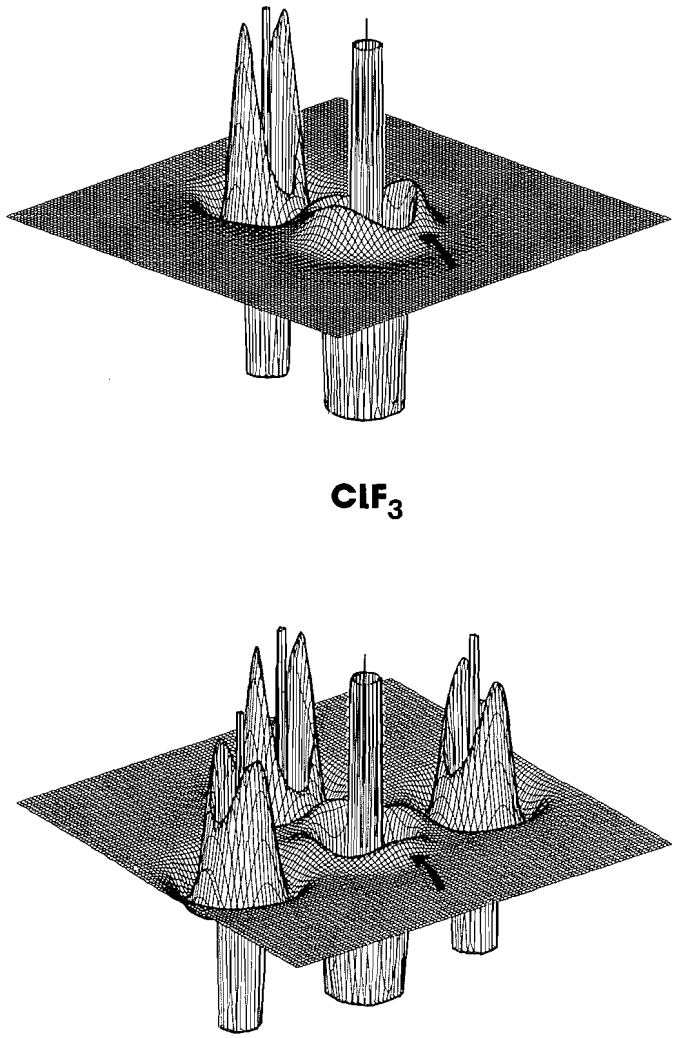


FIG. 1. Relief maps of $-\nabla^2\rho$ for the equatorial (upper) and the axial (lower) planes of ClF_3. The chlorine atom exhibits three shells of charge concentration. The equatorial plane shows the presence of two nonbonded and one smaller bonded charge concentration. In the axial plane there are three bonded charge concentrations and a fourth apparent maximum indicated by an arrow. This peak is actually another view of the (3, −1) critical point between the two nonbonded maxima, which is also denoted by an arrow. The VSCC of Cl possesses five local charge concentrations, three bonded and two larger nonbonded maxima in $-\nabla^2\rho$.

1), particularly the bond angles. The theoretical model certainly recovers the angular behaviour that is the topic of discussion. The calculated parameters for VCl_3 are R(V—Cl) = 2.184 Å, ∠ClVCl = 120.0°. The calculated energies are $E(VOCl_3)$ = −2395.66771 au, $E(VCl_3)$ = −2320.89293 au.

The VSEPR model and the local charge concentrations of the Laplacian of ρ

The spherical surface on which the electron pairs are assumed to be localized in the VSEPR model is identified with the sphere of maximum charge concentration found in the valence shell charge concentration, the VSCC, of the central atom (3), and the localized pairs of electrons are identified with the local concentrations of charge present on the surface of this sphere. This is illustrated for the chlorine atom in the molecule ClF_3 in Fig. 1. Since a local charge concentration corresponds to a maximum in $-\nabla^2\rho$, this and other relief diagrams illustrate the negative of the Laplacian of ρ, a maximum in this function being a maximum in charge concentration. There are pairs of regions, one negative, one positive, for each quantum shell, with the innermost region being a spike-like maximum in charge concentration. This shell structure is evident in the figure, with three shells being present on chlorine and two on fluorine.

The extrema in ρ or $-\nabla^2\rho$ are points where the first derivative of the scalar field vanishes. Whether such a point is a maximum, minimum, or a saddle is determined by the signs of the associated curvatures of the function at the critical point, i.e., by the eigenvalues of the Hessian of the function. If all three eigenvalues or curvatures are negative, the function exhibits a local maximum at that point, a (3,−3) critical point. If all three curvatures are positive, the function exhibits a local minimum, a (3,+3) critical point. The other two possible critical points with three nonzero curvatures are correspondingly labelled as (3,−1) and (3,+1). The outer or valence shell of charge concentration of Cl exhibits five maxima in $-\nabla^2\rho$, or local charge concentrations. There are two nonbonded and three bonded concentrations, with the size and magnitude of these maxima decreasing in the following order: nonbonded > equatorial bonded > axial bonded. The angle between the two nonbonded maxima is relatively large and equal to 148°, while the axial bonded–nonbonded angle is opened to 97°. In higher energy geometries of this molecule, the angles between the bonded and nonbonded maxima are all smaller than those found for this favoured geometry. Similar results are obtained for other molecules containing third-row elements such as ClF_3O, SF_4, SF_4O, and ClF_5 (3*a*, 4).

The Laplacian distribution of the vanadium atom is first investigated in the simpler, more symmetrical compound VCl_3. This molecule is known experimentally only in its polymeric form. The Laplacian distribution of this molecule is shown in Fig. 2. Also shown in this figure are the intersections of the interatomic surfaces as defined by the zero flux boundary condition that defines a quantum subsystem, the basis of the theory of atoms in molecules (7). All properties of such a subsystem, which is identified with an atom in a molecule, are defined by quantum mechanics. In this brief account we shall refer to only the average electron population. This is obtained by an integration of ρ over the basin of the atom. The charge on the Cl atom in ClF_3 for example is +1.56*e*. In VCl_3, the charge on the vanadium atom is +1.992*e*, 0.664*e* having been transferred to each Cl atom. The vanadium atom has the electron configuration $[Ar]4s^23d^3$ and two of the five valence electrons of V have been transferred to the ligands in VCl_3. Because of this charge transfer, the vanadium nuclear-electron attractive force increases in dominance within the atomic basin and the orbital ordering approaches more closely the true one-electron case. Thus the 3*d* orbitals are closer in spatial extent and *energy* to the *s* and *p* orbitals of the third quantum shell in the bound than they are in the free vanadium atom. This ordering of the orbital levels and the transfer of valence density are in agreement with the presence of three quantum shells on the vanadium atom (Fig. 2). As is discussed below, still stronger evidence for the mixing of the 3*d* orbitals with the 3*s* and 3*p* orbitals of the bound vanadium atom is provided by the polarizations of this shell.

Each Cl atom exhibits the anticipated three complete quantum shells, Fig. 2. The polarization of the VSCC of each of these atoms towards the positively charged vanadium atom is evident from the contour diagram of the Laplacian and there is a bonded charge concentration in the VSCC of each Cl atom of magnitude

Can. J. Chem. Downloaded from www.nrcresearchpress.com by 186.148.149.217 on 09/07/12
For personal use only.

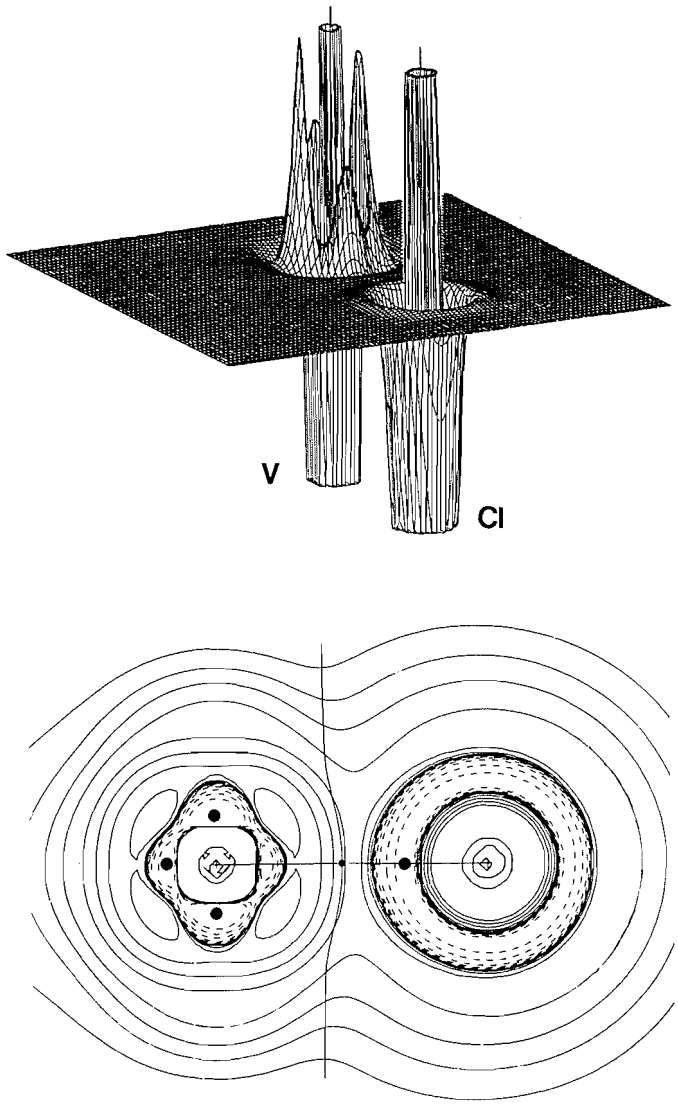


FIG. 2. Contour and relief maps of the Laplacian of ρ for VCl_3. The plane shown contains the vanadium nucleus and one of the chlorine nuclei. The dashed contours denote negative, the solid contours positive values of $\nabla^2\rho$. The interatomic surfaces and the bond paths are also shown, the bond critical points being indicated by the small dots. The large dots indicate the positions of maxima in the i-VSCC of vanadium and in the VSCC's of the ligands. Note the extreme polarization of the i-VSCC of the vanadium atom. The relief map shows that the vanadium atom does not possess a fourth or valence shell of charge concentration. The peak in the i-VSCC of vanadium nearest the Cl is a (3, −1) critical point. Directly behind it is the nonbonded maximum induced in the i-VSCC by the negatively charged Cl ligand. The two remaining and largest of the peaks in the i-VSCC are the axial nonbonded charge concentrations.

0.63 au; 1 au = 1 atomic unit = e/a_0^5. Because of its small relative magnitude, its presence is not evident in the relief map. Since vanadium does not possess a fourth shell of charge concentration, there are no bonded charge concentrations on vanadium. However, the shell of charge concentration associated with the third quantum shell of vanadium exhibits very marked polarizations. It is the thrusting of this inner shell of charge concentration of a transition metal atom into the forefront of chemical interaction with the ligands that accounts for the differing behaviour of a transition metal atom from main group elements.

The third shell of charge concentration on V shall be referred to as the inner-valence shell charge concentration, or i-VSCC. There are cases where a first-row transition metal atom still possesses a fourth shell of charge concentration, an example being $Mn_2(CO)_{10}$ (3*b*). In such a case, where the bonding to the transition metal atom involves two quantum shells, the second shell is distinguished by referring to it as the outer or o-VSCC. The i-VSCC of vanadium exhibits a (3,−1) critical point on each of the V—Cl bond paths (with a magnitude of 17 au), with its unique positive curvature lying in the plane of the nuclei. Thus this critical point appears as a two-dimensional maximum in the display shown in Fig. 2, since its two negative curvatures lie in the plane of the diagram. On the side of the i-VSCC opposite each such (3,−1) critical point is a (3,−3) critical point, or local charge concentration of magnitude 22 au. The i-VSCC is clearly very susceptible to polarization by the negatively charged ligands, and a local charge concentration is induced in this shell opposite each of the chlorine atoms. Two more maxima are present in the i-VSCC on the threefold axis on each side of the molecular plane. They are by far the largest of the local charge concentrations found in this shell, with a magnitude of 39 au. The existence of concentrations of electronic charge along distinct spatial axes indicates that the electrons in the third shell of vanadium possess significant angular momentum, and they cannot be described as occupying a closed, albeit slightly polarized, inner shell. Thus the charge concentrations in the i-VSCC of vanadium form a trigonal bipyramid, reminiscent of the set of sp^3d hybrid orbitals of the valence bond model. In agreement with the observation that the o-VSCC of vanadium is absent and that the 3*d* orbitals have reverted to the third quantum shell, the i-VSCC of vanadium can be described as possessing the configuration $3s^23p^63d^2$. There are five pairs of electrons in the third quantum shell of the vandium atom and, correspondingly, its i-VSCC exhibits five local concentrations of charge.

Figure 3 shows corresponding diagrams of the Laplacian distribution for $VOCl_3$. The vanadium atom in this molecule possess a charge of $+2.405e$, with each chlorine bearing a charge of $-0.554e$ and the oxygen one of $-0.743e$. The VSCC of oxygen exhibits a bonded charge concentration with a magnitude of 2.64 au and a single, slightly larger, nonbonded maximum of magnitude 3.09 au. The bonded charge concentration present in the VSCC of each Cl is slightly reduced from its value in VCl_3, to 0.60 au. The i-VSCC of vanadium is topologically equivalent to that found in VCl_3 — the same number and type of critical points are present in each case — but their relative magnitudes have changed in significant ways. The extent of charge concentration in the i-VSCC of vanadium is decreased relative to that found in VCl_3 because of the further loss of charge to the oxygen atom. The magnitude of the (3, −1) critical point along the bond path to each of the chlorines is decreased to 10 au and the opposing maximum induced in the i-VSCC by the presence of the negatively charged ligand is reduced in magnitude to 19 au. It is the axial charge concentrations, however, that undergo the largest changes. The magnitude of the axial charge concentration lying on the bond path to the oxygen, now a bonded charge concentration in the i-VSCC of vanadium, is reduced from 39 au to 9.5 au while the magnitude of the remaining axial concentration, a nonbonded charge concentration, is reduced by a lesser amount, to 21 au. Thus the charge concentration along the threefold axis, while reduced in magnitude from that present in VCl_3, is strongly polarized away from the oxygen into the corresponding nonbonded region.

One anticipates that the addition of oxygen to the ligand

Can. J. Chem. Downloaded from www.nrcresearchpress.com by 186.148.149.217 on 09/07/12
For personal use only.

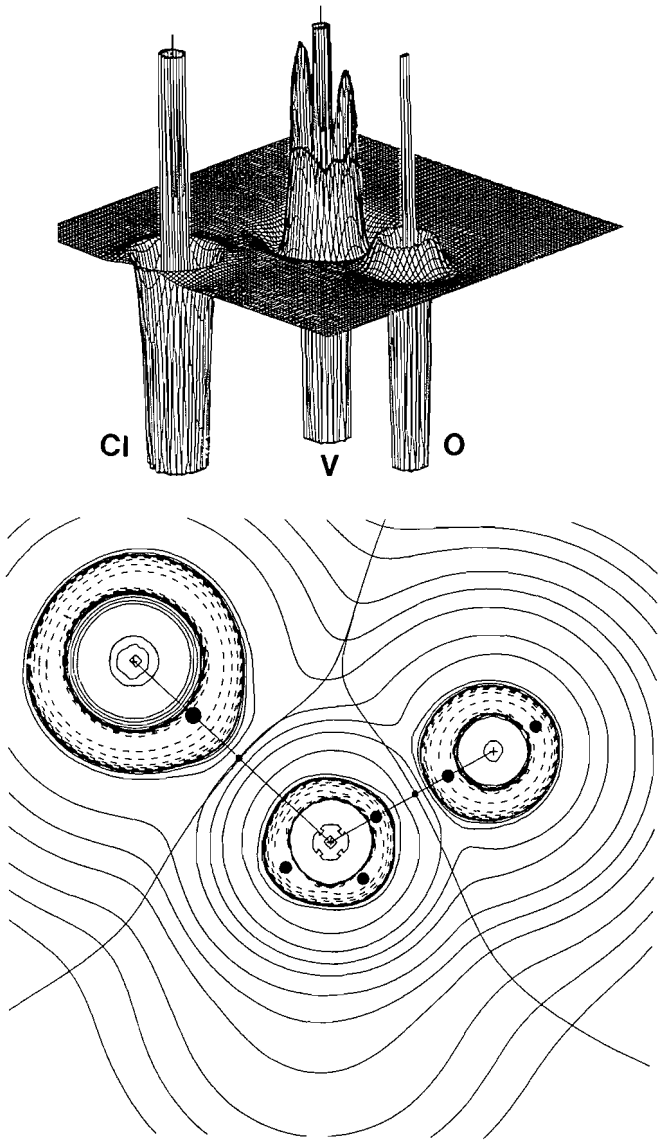


FIG. 3. Contour and relief maps of $VOCl_3$ for a plane containing the vanadium, the oxygen, and one of the chlorine nuclei. Details as for Fig. 2. Note the increase in the angle between the axial nonbonded and one of the nonbonded maxima opposite a Cl from the value of 90° found in VCl_3. The i-VSCC of vanadium in this plane exhibits three local charge concentrations — the bonded maximum nearest oxygen and the larger axial nonbonded maximum directly behind it with the nonbonded induced maximum lying between them. The peak nearest the Cl corresponds to a (3, −1) critical point.

sphere with its double-bonded domain will cause the ClVCl angle to decrease from its value of 120° in VCl_3. However, it is clear from the polarization of the i-VSCC of the vanadium that the ClVCl angle will not be reduced to less than the tetrahedral value, as would be found for a main group element, because of the presence of the axial nonbonded charge concentration, the largest of all the charge concentrations in the i-VSCC of vanadium. Because of the dominance of the nonbonded charge concentration in the i-VSCC of vanadium, the angle between it and the nonbonded charge concentration opposite each of the chlorine atoms is increased from the value of 90° in VCl_3 to 106.1°. This upward shift in these critical points away from the axial nonbonded concentration is coupled to the downward motion of the Cl ligands that are responsible for their presence. This downward motion is equilibrated for a ClVCl angle greater than tetrahedral by the approach of the bonded maxima on the chlorine ligands to the axial nonbonded maximum on the metal and by the approach of the nonbonded maxima associated with the chlorines towards the bonded maximum opposite oxygen within the i-VSCC of vanadium.

Conclusions

It has been suggested (*3b*, 4) that a modified VSEPR model be given in terms of the Laplacian of the charge density, one which is free of the assumptions regarding the existence of some number and arrangement of localized pairs of electrons with prescribed sets of properties. In the modified version of the model, this information is provided by the Laplacian of ρ, an observable and physical property of a system. The prediction of a molecular geometry then requires but a single postulate, that the minimum energy geometry is the one that maximizes the separations between the local concentrations of charge in the outer shell of charge concentration of the central atom. It is possible in some systems, particularly those involving transition metal atoms, that charge concentrations in both the o-VSCC and i-VSCC play a role in determining the geometry. The domain of applicability of the model is then extended to all systems, since the Laplacian distribution has a definable set of properties in every system. What remains to be done is to continue to categorize the properties of the Laplacian of the charge density and discover in what ways it can deviate from our models of localized electron pairs. The vanadium systems that have been discussed in this brief note illustrate how this can be done. With these examples, there can be no doubt as to the fundamental nature of the basic assumption underlying the VSEPR model, that the most stable molecular geometry is in some manner determined by maximizing the separations between local concentrations of electronic charge. The Laplacian of ρ extends the physical basis of the model and removes the constraints of its range of applicability, but Gillespie's basic assumption remains true.

Acknowledgement

The authors wish to thank Professor Gillespie for suggesting the problem addressed in this paper. They also wish to dedicate the paper to him and to his ideas. P.J.M. and M.B.H. thank the National Science Foundation (U.S.A.) for partial support of this work. P.J.M. thanks N.S.E.R.C. of Canada for the award of a postdoctoral fellowship.

1. R. J. GILLESPIE. Molecular geometry. Van Nostrand Reinhold, London. 1972; R. J. GILLESPIE and R. S. NYHOLM. Q. Rev. Chem. Soc. **11**, 239 (1957).
2. G. N. LEWIS. J. Am. Chem. Soc. **38**, 762 (1916).
3. (*a*) R. F. W. BADER, P. J. MACDOUGALL, and C. D. H. LAU. J. Am. Chem. Soc. **106**, 1594 (1984); (*b*) P. J. MACDOUGALL. The Laplacian of the electronic charge distribution. Ph.D. Thesis, McMaster University, Hamilton, Ont. 1989.
4. R. F. W. BADER, R. J. GILLESPIE, and P. J. MACDOUGALL. J. Am. Chem. Soc. **110**, 7329 (1988).
5. R. J. GILLESPIE, D. A. HUMPHREYS, N. C. BAIRD, and E. A. ROBINSON. Chemistry. Allyn and Bacon, Boston. 1986. p. 763.
6. S. HUZINAGA. Gaussian basis sets for molecular calculations. Elsevier, Amsterdam. 1984.
7. R. F. W. BADER and T. T. NGUYEN-DANG. Adv. Quantum Chem. **14**, 63 (1981).
8. A. F. WELLS. Structural inorganic chemistry. 5th ed. Oxford University Press, London. 1984.

Can. J. Chem. Downloaded from www.nrcresearchpress.com by 186.148.149.217 on 09/07/12
For personal use only.

"Through-space" spin–spin coupling between thallium and fluorine in fluorophenylthallium compounds

GERALD NORMAN PECKSEN AND RAYMOND FREDERICK MARTIN WHITE
Department of Chemistry, City of London Polytechnic, Jewry Street, London, England EC3N 2EY

Received January 24, 1989

This paper is dedicated to Professor Ronald J. Gillespie on the occasion of his 65th birthday

GERALD NORMAN PECKSEN and RAYMOND FREDERICK MARTIN WHITE. Can. J. Chem. **67**, 1847 (1989).

Thallium to fluorine spin–spin coupling constants have been measured for a number of fluoro- and trifluoro-methyl-substituted mono- and di-arylthallium derivatives. The results provide evidence of "through-space" coupling in the diaryl derivatives when the fluoro- or trifluoro-methyl group is *ortho* to the thallium atom.

Key words: thallium, fluorine, NMR, through-space coupling.

GERALD NORMAN PECKSEN et RAYMOND FREDERICK MARTIN WHITE. Can. J. Chem. **67**, 1847 (1989).

On a mesuré les constantes de couplage spin–spin du thallium au fluor pour un certain nombre de dérivés mono- et di-arylthallium substitués par des groupements fluoro- et trifluoro-méthyles. Les résultats obtenus confirment que, dans les dérivés diaryles portant une groupement fluoro- ou trifluoro-méthyl en *ortho* de l'atome de thallium, il existe un couplage «à travers l'espace».

Mots clés : thallium, fluor, RMN, couplage à travers l'espace.

[Traduit par la revue]

Introduction

"Through-space" spin–spin coupling can occur when the internuclear distance between a pair of nuclei is abnormally small (1, 2). Observation of a coupling constant that is larger than might be otherwise expected is frequently taken to be indicative of a through-space mechanism (3–6). Examples of through-space coupling involving nuclei other than hydrogen or fluorine are few, but recent examples include $^{13}C-^{77}Se$ coupling in *cis*-selenoimidates (7) and $^{13}C-^{31}P$ coupling in phosphorus-substituted alkenes (8). McFarlane (9) has suggested that van der Waals penetration and concomitant through-space coupling are likely between fluorine and the magnetic nuclei of elements larger than helium, in their *o*-trifluoromethyl derivatives. Mercury and phosphorus(III) are favourable in this respect and evidence for through-space coupling in *o*-trifluoromethylphenyl derivatives of these nuclei have been reported (9, 10). A study of the thallium-to-hydrogen side-chain coupling constants for mono- and di-arylthallium derivatives in which a series of alkyl groups (CH_3-, C_2H_5-, *i*-C_3H_7-, *t*-C_4H_9-) are *ortho* and *para* to the thallium atom has provided evidence of through-space coupling between thallium and hydrogen in some of the *o*-alkylphenylthallium compounds (11).

Values of J_{Tl-H} for arylthallium compounds were first reported by Maher and Evans (12), who proposed Fermi contact as the dominant mechanism of spin–spin coupling in these compounds. The observed increase in the magnitude of J_{Tl-H} in the series R_3Tl, R_2Tl^+, and RTl^{2+} (where R is aryl) was qualitatively (12, 13) interpreted on the basis of the Fermi contact term increasing with both the effective nuclear charge (Z_{eff}) of the thallium atom and the *s*-character of the thallium valence electrons, an interpretation supported by other workers (14, 15). McKillop *et al.* (16) have measured J_{Tl-H} and J_{Tl-CH_3} for a range of arylthalliumtrifluoroacetates obtained by the direct thallation technique, and the results of their studies are in agreement with those of Maher and Evans (12, 13). The large differences in the coupling constants for Tl–*o*H, Tl–*m*H, and Tl–*p*H make possible the unambiguous determination of the orientation of any substituent with respect to the thallium atom and to distinguish among mono-, di-, and tri-arylthallium compounds.

From homonuclear double resonance (H–{H}) experiments Maher and Evans (12) were able to show that in any one of the compound types R_3Tl, R_2TlX, or $RTlX_2$ the couplings $^3J_{Tl-H}$, $^4J_{Tl-H}$, and $^5J_{Tl-H}$ all had the same *relative* sign. Hildenbrand and Dreeskamp (15) used heteronuclear double resonance to determine signs of coupling constants relative to $^1J_{C-H}$ and $^3J_{H-H}$ (experimental evidence (17) has shown that the absolute sign of $^3J_{H-H}$ in *p*-nitrotoluene is positive) for a number of organometallic compounds. Their measurements on a liquid ammonia solution of diphenylthallium chloride showed that all thallium-to-hydrogen coupling constants are positive for this compound.

Although the nmr spectra of arylthallium compounds have been extensively studied, little has been reported on the nmr spectra of fluorophenylthallium derivatives (ref. 18, and references therein). Deacon *et al.* have reported parameters, including signs of some coupling constants, for a number of polyfluorophenylthallium derivatives (18). They find that the general pattern of thallium-to-fluorine constants $^3J > {}^4J > {}^5J$ and $^nJ_{R_2TlX} > {}^nJ_{R_3Tl\cdot dioxane}$ parallels the behaviour of thallium-to-hydrogen coupling constants and they conclude that thallium-to-fluorine coupling is probably dominated by the Fermi contact term.

The aim of the present work was to investigate the possibility of through-space coupling between thallium and fluorine in suitable compounds and evidence is presented for the occurrence of this coupling mechanism in *o*-fluoro- and *o*-trifluoromethylphenylthallium derivatives. To detect the effects of through-space coupling it is necessary to compare coupling constants in structurally similar compounds that differ only in the proximities of possibly interacting groups. In this study mono- and di-aryl compounds in which the groups of interest are *ortho*, *meta*, and *para* to the thallium atom are compared, and where possible the signs as well as the magnitudes of the coupling constants have been determined. Through-space coupling might be possible for the *ortho*-substituted derivatives whereas *meta* and *para* substitution offers no opportunity of a through-space contribution to the coupling constant because of the greater distance separating the coupled nuclei. In addition it would be expected (11) that the through-space effect would be less

Can. J. Chem. Downloaded from www.nrcresearchpress.com by 186.148.149.217 on 09/07/12
For personal use only.

TABLE 1. Tl to ring F coupling constants in $RTlX_2$ and R_2TlX derivatives

Substituents	X	Solvent*	Coupling	Coupling constant (Hz) $RTlX_2$	Coupling constant (Hz) R_2TlX
2-F, 5-CH_3	$OCOCF_3$	P	^3J	+1241	+1347
2-F, 5-CH_3	$OCOCF_3$	A	^3J	—	+1268
2-F, 3-CH_3, 4-CH_3	$OCOCF_3$	P	^3J	+1273	+1430
2-F, 4-CH_3	$OCOCF_3$	P	^3J	+1221	+1281
2-F, 4-F	$OCOCF_3$	P	^3J	+1124	+1272
			^5J	+68	+18
2-F, 4-F	$OCOCF_3$	A	^3J	—	+1158
			^5J	—	+16
2-F, 5-F	$OCOCF_3$	P	^3J	+1049	—
			^5J	+471	—
3-F	Cl	P	^4J	+593	—
	Cl	D	^4J	+640	+319
	Cl	A	^4J	+620	+240
	Br	P	^4J	—	+310
	Br	D	^4J	—	+313
3-F, 6-CH_3	Cl	P	^4J	+602	+208
3-F, 4-CH_3	Cl	P	^4J	+546	+268
4-F, 3-CH_3	Cl	P	^5J	+121	+81
4-F, 3-CH_3	$OCOCF_3$	P	^5J	+140	+78
4-F	$OCOCF_3$	P	^5J	+242	+121

*Solvent P = C_5D_5N, A = $(CD_3)_2CO$, D = $(CD_3)_2SO$.

pronounced for monoarylthallium derivatives than for the corresponding diaryl compounds.

Results and discussion

Initial heteronuclear double irradiation experiments, interpreted on the basis that $^3J_{H-H}$ in aryl groups is positive, showed that, as expected, Tl–H coupling constants in monoarylthallium compounds are all positive.

Values of $^nJ_{Tl-F}$ (n = 3–5) for fluorophenylthallium compounds in which fluorine is directly bonded to the aromatic ring are given in Table 1; different couplings to the isotopes ^{203}Tl and ^{205}Tl were not resolved but showed up as broadening of lines. Double resonance experiments showed that all thallium-to-ring-fluorine coupling constants are positive, and these are discussed further below. The coupling constants show the same trend as $^nJ_{Tl-H}$, decreasing in the order $^3J_{Tl-F} > {}^4J_{Tl-F} > {}^5J_{Tl-F}$. The second trend followed by thallium–hydrogen couplings, $^nJ(RTlX_2) > {}^nJ(R_2TlX) > {}^nJ(R_3Tl)$, which was found to be followed by $^nJ_{Tl-F}$ in di- and tri-polyfluorophenylthallium compounds (18), is, in the present work, found to be followed by mono- and difluorophenylthallium compounds only when n = 4 or 5; when n = 3 the thallium-to-fluorine coupling constant in R_2TlX is *greater* than the corresponding coupling constant in $RTlX_2$. This anomalous result suggests that although J_{Tl-F} in these compounds is dominated by the Fermi contact term an additional mechanism can operate when thallium is *ortho* to a fluorine atom in the aromatic ring.

It is not possible to calculate accurate internuclear distances and thence the extent of penetration of van der Waals radii of nuclei in arylthallium compounds; however, reasonable approximations (11) indicate that there is steric overcrowding between *ortho* thallium and fluorine atoms, the overcrowding and associated through-space effect being more pronounced in diarylthallium derivatives than it is in monoarylthallium. The anomalously high values of $^3J_{Tl-F}$ are then interpreted as arising from a positive through-space contribution to the coupling that is greater in bis(*o*-fluorophenyl)thallium than in mono-(*o*-fluorophenyl)thallium derivatives.

Double resonance experiments have shown (12, 15) that in phenylthallium compounds all J_{Tl-H} have the same sign. Similar experiments in the present work show that for fluorine attached to the aromatic ring in mono- and di-fluorophenylthallium derivatives all J_{Tl-F} are positive. This is in contrast to the report by Deacon *et al.* (18) that $^3J_{Tl-F}$ and $^4J_{Tl-F}$ are positive while $^5J_{Tl-F}$ is negative. In their discussion of J_{Tl-H} in polyfluorophenylthallium compounds they make the point that while fluorine is strongly inductively electron withdrawing through σ bonds, it is electron donating by resonance effects through π bonds; hence multiple fluorine substitution could shift $^5J_{Tl-H}$ in the opposite direction from $^3J_{Tl-H}$ and $^4J_{Tl-H}$. If $^5J_{Tl-F}$ is transmitted via both σ and π bonds and these effects are opposed, the net result could be the small negative coupling that they observed for $^5J_{Tl-F}$. The present work provides some support for this suggestion in that $^5J_{Tl-F}$ in 4-fluorophenylthallium bis(trifluoroacetate) is +242 Hz while in 2,4-difluorophenylthallium bis(trifluoroacetate) it is only +68 Hz; in the corresponding diaryl compounds the values of $^5J_{Tl-F}$ are +121 and +18 Hz, showing a marked decrease in $^5J_{Tl-F}$ when an additional fluorine atom is attached to the aromatic ring.

In addition to the above investigation, compounds containing a trifluoromethyl substituent in the aromatic ring were studied and the thallium-to-fluorine coupling constants for these are given in Table 2; where experimental difficulties allowed (see experimental section), the signs of these coupling constants were also determined and are included in the table. In the mono-(trifluoromethylphenylthallium) halides $^nJ_{Tl-F}$ follows the same pattern of signs as $^nJ_{Tl-CH_3}$ in methylphenylthallium derivatives, with ^4J and ^6J negative and ^5J positive. Surprisingly, in bis(2-trifluoromethylphenyl)thallium bromide $^4J_{Tl-F}$ is positive. In addition, this compound shows an unusually large solvent dependence of $^4J_{Tl-F}$, which varies from 58 Hz for a solution of the compound in chloroform to being unresolvably small

Can. J. Chem. Downloaded from www.nrcresearchpress.com by 186.148.149.217 on 09/07/12
For personal use only.

TABLE 2. Tl...F side-chain couplings in $RTlX_2$ and R_2TlX derivatives

Substituent	X	Solvent*	Coupling	Coupling constant (Hz)† $RTlX_2$	R_2TlX
2-CF_3	Cl	A	^4J	−221	
	Cl	P	^4J	193	
	Cl	C	^4J	219	58
	Br	A	^4J		+42
	Br	P	^4J		0
3-CF_3	Cl	A	^5J	+86	
	Cl	P	^5J	78	
	Br	A	^5J		43
	Br	P	^5J		39
4-CF_3	Cl	A	^6J	−66	
	Br	P			38

*Solvent P = C_5D_5N, A = $(CD_3)_2CO$, C = $CDCl_3$.
†Signs of coupling constants were only obtained from solutions in acetone-d_6.

in a pyridine solution. Titration with pyridine of a chloroform solution containing a known amount of bis(2-trifluoromethylphenyl)thallium bromide gave an almost linear decrease of $^4J_{Tl-F}$ to 29 Hz at an approximately 1:1 ratio of pyridine to thallium; after this the decrease of $^4J_{Tl-F}$ with added pyridine was much slower and only in the presence of a large excess of pyridine did the coupling become undetectably small. Thallium-to-hydrogen coupling constants in this compound show no such unusual variation; $^3J_{Tl-H}$ varies only from 477 Hz (chloroform solution) to 470 Hz (pyridine solution).

Through-space coupling is to be expected for magnetic nuclei of elements larger than helium in their *o*-trifluoromethyl derivatives (9), and the through-space effect is expected to be more pronounced in diaryl- than in monoaryl-thallium compounds (11). The observed couplings observed for the trifluoromethylphenyl derivatives can then be interpreted in terms of a dominant positive through-space coupling in bis(2-trifluoromethylphenyl)thallium bromide, giving a resultant positive $^4J_{Tl-F}$, while in the mono-(2-trifluoromethylphenyl) derivative any smaller through-space contribution is dominated by a negative through-bond coupling.

The results of the titration experiment are consistent with an appreciable interaction between pyridine and thallium. If the through-space contribution to coupling depends on the extent to which fluorine lone-pair orbitals overlap empty thallium orbitals, the presence of a competing pyridine ligand coordinating to the thallium atom could reduce the availability of thallium orbitals and hence reduce the through-space contribution. If this were a major factor a similar effect would be expected for the coupling in bis(2-fluorophenyl)thallium derivatives. Table 1 contains two examples that show that a change from acetone to pyridine solvent leads to an *increase* in $^3J_{Tl-F}$, suggesting that in fact reduced availability of thallium orbitals on coordination of pyridine does not influence the through-space contribution to coupling. A second possible explanation of these results comes from McFarlane's discussion of through-space coupling between mercury and fluorine in 2-trifluoromethylphenylmercury compounds (9). Here it has been suggested that the shortest mercury–fluorine separation (on the assumption of free rotation of the trifluoromethyl group) is more significant than the mean mercury–fluorine distance, as through-space coupling will depend on $\langle r^{-n} \rangle$ rather than $\langle r \rangle^{-n}$ where r is the mercury–fluorine separation and n is fairly large. If similar considerations apply to the thallium compounds considered here, then coordination of pyridine molecules could introduce a steric hindrance to the free rotation of the trifluoromethyl group, resulting in an increase in $\langle r^{-n} \rangle$ (where r is now the thallium–fluorine separation) and consequently a decrease in the through-space contribution to the coupling. Such a steric effect might not eliminate the through-space contribution completely, for as one fluorine atom in the trifluoromethyl group is moved away from the vicinity of the thallium atom one of the other fluorine atoms of the group approaches the thallium atom, a case of "the further off from England the nearer is to France" (19). More experimental data, including information on degrees of ionization and dissociation and on possible dimer formation, are necessary for better understanding of the unusual solvent effects described above.

Experimental

Instrumentation

The nmr spectra were recorded using a JEOL C-60-H spectrometer operating at 60 MHz for ^1H and 56.45 MHz for ^{19}F. The second radiofrequency field for heteronuclear double resonance experiments was derived from a frequency synthesizer (Schlumberger FS 30 digital signal generator) and fed via a tuned amplifier to a tuned circuit with a coil within the spectrometer probe. An auxiliary stabilized 20-MHz output of the frequency synthesizer was used as the master oscillator of the spectrometer so that there were no relative frequency drifts. As the organothallium compounds studied gave rise to slightly broadened spectra, an external field/frequency lock was found to be adequate. The spectrometer could be operated in either field or frequency sweep mode, the latter being used for double resonance experiments.

Determination of the relative signs of coupling constants requires a minimum of three coupled nuclei, AMX, and an experiment in which the spectrum of A is observed while the sample is irradiated at the frequency of an M transition (A–{M} experiment) can then give the relative signs of J_{AX} and J_{MX} (ref. 20, and references therein). Magnitudes of J_{Tl-F} were determined from ^{19}F spectra, which could also be used to obtain the range of ^{19}F frequencies required for double resonance experiments. Signs of J_{Tl-F} were then obtained relative to J_{Tl-H} (shown to be positive with respect to $^3J_{H-H}$). Difficulties were encountered with the trifluoromethyl derivatives as $^4J_{H-F}$ in these compounds is small and only gives rise to a broadening of peaks in the ^1H spectrum. However, by the use of low power radiofrequency fields for double irradiation it was possible in favourable cases to detect sharpening of peaks in H–{F} experiments and hence to determine relative signs. Low solubility and peak broadening prevented sign determinations in the cases of bis(3-trifluoromethylphenyl)thallium bromide and bis(4-trifluoromethylphenyl)thallium bromide.

Preparation of compounds

As previously (11), organothallium compounds were prepared by standard methods. Direct thallation of substituted benzenes by thallic trifluoroacetate (McKillop *et al.* (21)) yields an arylthallium bis(trifluoroacetate) and addition of this to trimethyl phosphite yields the diarylthallium trifluoroacetate, McKillop *et al.* (13). Reaction of an arylboronic acid with aqueous thallic chloride gives either mono- or di-arylthallium chlorides depending on the relative quantities of the reactants (22). Substituted boronic acids are prepared by reaction of an aryl Grignard derivative with a borate ester followed by hydrolysis to produce the boronic acid (23, 24). Diarylthallium compounds were also obtained by reaction of thallic halide with the appropriate Grignard reagent at 0°C, followed by hydrolysis and extraction with pyridine (12).

1. L. PETRAKIS and C. H. SEDERHOLM. J. Chem. Phys. **35**, 1243 (1961).
2. S. NG and C. H. SEDERHOLM. J. Chem. Phys. **40**, 2090 (1964).

Can. J. Chem. Downloaded from www.nrcresearchpress.com by 186.148.149.217 on 09/07/12
For personal use only.

3. H. S. GUTOWSKY and V. D. MOCHEL. J. Chem. Phys. **39**, 1195 (1963).
4. J. JONAS, L. BOROWSKI, and H. S. GUTOWSKY. J. Chem. Phys. **47**, 2441 (1967).
5. F. J. WEIGERT and J. D. ROBERTS. J. Am. Chem. Soc. **90**, 3577 (1968).
6. K. L. SERVIS and K. N. FANG. J. Am. Chem. Soc. **90**, 6712 (1968).
7. R. H. CONTRERAS, M. C. RUIZ DE AZÚA, and C. G. GIRIBET. Magn. Reson. Chem. **24**, 675 (1986).
8. A. C. DIZ, C. G. GIRIBET, M. C. RUIZ DE AZÚA, and G. A. AUCAR. Magn. Reson. Chem. **25**, 883 (1987).
9. W. MCFARLANE. J. Chem. Soc. Chem. Commun. 609 (1971).
10. S. O. GRIM, G. R. MILLER, and A. W. YANKOWSKY. J. Chem. Phys. **51**, 3185 (1969).
11. B. V. CHEESMAN and R. F. M. WHITE. Can. J. Chem. **62**, 521 (1984).
12. J. P. MAHER and D. F. EVANS. J. Chem. Soc. 637 (1965).
13. J. P. MAHER and D. F. EVANS. Proc. Chem. Soc. London, 176 (1963).
14. J. V. HATTON. J. Chem. Phys. **40**, 933 (1964).
15. K. HILDENBRAND and H. DREESKAMP. Z. Phys. Chem. (Frankfurt/Main), **69**, 171 (1970).
16. A. MCKILLOP, J. D. HUNT, and E. C. TAYLOR. J. Organomet. Chem. **24**, 77 (1970).
17. A. D. BUCKINGHAM and K. A. MCLAUCHLAN. Proc. Chem. Soc. London, 144 (1963).
18. G. B. DEACON, R. M. SLADE, and D. G. VINCE. J. Fluorine Chem. **11**, 57 (1978).
19. C. W. DODGSON. Alice's adventures in wonderland. 1865.
20. W. MCFARLANE and R. F. M. WHITE. Techniques of high resolution nuclear magnetic resonance. Butterworth, London. 1972.
21. A. MCKILLOP, J. S. FOWLER, M. J. ZELESKO, J. D. HUNT, E. C. TAYLOR, and G. MCGILLIVRAY. Tetrahedron Lett. **29**, 2427 (1969).
22. F. CHALLENGER and B. PARKER. J. Chem. Soc. 1462 (1931).
23. W. SEAMAN and J. R. JOHNSON. J. Am. Chem. Soc. **53**, 711 (1931).
24. F. R. BEAN and J. R. JOHNSON. J. Am. Chem. Soc. **54**, 4415 (1932).

Can. J. Chem. Downloaded from www.nrcresearchpress.com by 186.148.149.217 on 09/07/12
For personal use only.

A nuclear magnetic resonance spectroscopic study of some tri-sulfide bridged ferrocenes

IAN R. BUTLER[1] AND WILLIAM R. CULLEN
The Chemistry Department, The University of British Columbia, Vancouver, B.C., Canada V6Y 1Y6

Received November 29, 1988

This paper is dedicated to Professor Ronald J. Gillespie on the occasion of his 65th birthday

IAN R. BUTLER and WILLIAM R. CULLEN. Can. J. Chem. **67**, 1851 (1989).

The synthesis of some new $[S_3]$-bridged aminoferrocenophanes is described. The ^1H nuclear magnetic resonance spectra of these compounds are completely assigned and are discussed in terms of the stereochemistry of the tri-sulfide bridge. In addition $^{13}C/^1H$ correlation spectra of one of the derivatives are presented to illustrate the complete assignment of the ^{13}C spectrum.

Key words: ferrocene derivatives, sulfur-bridged, synthesis, NMR, conformation.

IAN R. BUTLER et WILLIAM R. CULLEN. Can. J. Chem. **67**, 1851 (1989).

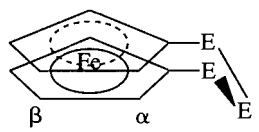
On décrit la synthèse de quelques nouveaux aminoferrocènophanes comportant des ponts de $[S]_3$. On a attribué toutes les bandes des spectres RMN du ^1H de ces composés et on les discute en fonction de la stéréochimie du pont trisulfure. Afin d'illustrer l'attribution complète des spectres du ^{13}C, présente aussi le spectre de corrélation $^{13}C/^1H$ d'un de ces dérivés.

Mots clés : dérivés du ferrocène, ponts de soufre, synthèse, RMN, conformation.

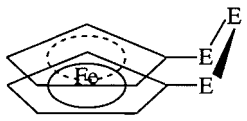
[Traduit par la revue]

Introduction

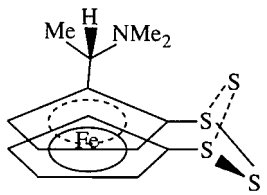
The stereochemistry of chalcogen bridged [3]-ferrocenophanes has been investigated by a number of workers (1–5) since the preparation of the first compound, **1** E = S (2), and an extensive series of such compounds now exists. Abel and coworkers (3, 5) have prepared and carried out nmr studies on a variety of these compounds. They established, by dynamic band shape fitting, that the barrier to the bridge reversal process (**1***a* ⇌ **1***b*) is relatively high, lying in the range 60–80 kJ mol^{-1}. The temperature of coalescence of the α-ferrocenyl ring protons, adjacent to the heteroatom substituent, is higher than that of the β protons. This reflects the large chemical shift differences observed between the individual α protons (compared to those of the β protons) caused by the anisotropic effect of the heteroatoms.



1*a*



1*b*



2*a,b*

Our initial interest in this class of compounds arose because the formation of [3]-ferrocenophanes, from the reaction of hetero-ring dilithiated ferrocenes, proved to be a useful method for establishing the sites of lithiation (6). We are now beginning to study the reaction chemistry of [3]-ferrocenophanes such as **2** in which a ring substituent in addition to the chalcogen atoms is available for coordination; the few reports on this topic to date (7–9) indicate that this will be a fruitful area to study in depth.

[1]Present address: Chemistry Department, University of Ottawa, Ottawa, Ont., Canada.

TABLE 1. Conformer distribution in the [3]-ferrocenophanes

Compound	Conformer (α)	Conformer (β)
2	73	27
3*a*	60	40
3*b*	>90	>10
4	54	46
5*	>90†	<10†
6	61	39

*Difficult to estimate because of the poorly resolved spectrum.
†The isomers may be **5***b* (major) and **5***a* (minor).

The present paper describes the synthesis of a number of new S_3-bridged ferrocenophanes that also have an amine function in the molecule. The nmr spectra of these products are described in relation to their assignment and the presence of diastereomers.

Experimental

The ^1H nmr spectra were recorded by using Bruker WH-400, WM-270, or Varian XL-300 spectrometers, SUPER-COSY experiments were conducted as previously described (1). Mass spectra were recorded by using a Kratos MS-50 instrument (probe temperature, 150°C). Elemental analyses were performed by Mr. Peter Borda of this department. Solvents were distilled prior to use after predrying by conventional methods. *N,N'*-dimethylaminomethylferrocene (10) was purchased from Strem Chemicals Inc. and was dried under vacuum prior to use, and *n*-butyllithium solutions were obtained from Aldrich Chemical Company. Selected spectroscopic data for new compounds are given in the tables.

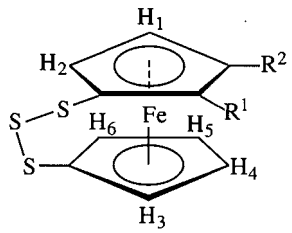
Preparation of **4**

To a solution of *N,N'*-dimethylaminomethylferrocene (2.0 g, 8.23 mmol) in diethyl ether (25 mL), was added 5.1 mL of a 1.6 M solution of *n*-butyllithium. The reaction solution was stirred for 2 h and a further 5.5 mL of *n*-butyllithium solution and TMED (1.0 g, 8.62 mmol) were added. The reaction solution was stirred overnight. Elemental sulfur (1.0 g, 3.9 mmol, S_8) was then added carefully and the reaction mixture was stirred for a further 2 h before it was hydrolyzed with a saturated solution of sodium bicarbonate (ca. 25 mL). The ether fraction was separated and the aqueous phase (and solids) was extracted with ether (3 × 40 mL). The combined ether fractions were evaporated to dryness. The solid residue was washed with hot petroleum ether (bp

Can. J. Chem. Downloaded from www.nrcresearchpress.com by 186.148.149.217 on 09/07/12
For personal use only.

Can. J. Chem. Downloaded from www.nrcresearchpress.com by 186.148.149.217 on 09/07/12
For personal use only.

TABLE 2. Nuclear magnetic resonance spectra of diastereomers



	2	**4**	**6**	***3a***	***3b***
R^1	$CH(CH_3)N(CH_3)_2$	$CH_2N(CH_3)_2$	$CH_2N(CH_3)_2$	H	$P(S)Ph_2$
R^2	H	H	$P(S)Ph_2$	$P(S)Ph_2$	H
H	4.38	4.39	—	4.66	4.32
H'*	4.47	4.57	—	4.07	—
H_1	3.79	3.80	3.83	4.16	4.07
H_1'	4.40	4.39	4.41	4.76	—
H_2	4.34	4.39	4.38	4.73	4.54
H_2'	4.33	4.32	—	4.60	—
H_3	3.82	3.85	3.72	3.78	3.77
H_3'	4.58	4.61	4.52	4.45	—
H_4	4.44	4.47	4.38	4.37	4.36
H_4'	4.38	4.43	4.47	4.24	—
H_5	4.32	4.39	5.34	4.80	4.38
H_5'	4.33	4.37	5.48	4.89	5.28
H_6	4.12	4.16	4.17	4.32	—
H_6'	3.58	3.50	3.70	3.68	—
$N(CH_3)_2$	2.08	2.20	1.77	—	—
$N(CH_3)_2'$	2.17	2.28	1.76	—	—
CH_3	1.21	*ortho* H of $P(S)Ph_2$	7.70–7.90	7.60–8.80	7.60–7.80
CH_3'	1.22				
CH	3.54	*meta* and *para* H of	7.30–7.52	7.32–7.50	7.30–7.50
CH'	3.42	$P(S)Ph_2$ groups			
CH_2	—	3.06	2.97	—	—
CH_2'	—	3.01	2.65	—	—

*Primed substituents refer to the minor isomer, i.e., the one in which the S_3-bridge points towards R^1.

TABLE 3. Selected mass spectral data (*m/e*, (rel. intensity))

4: 338(9.06); 337(48.18); M^+; 318(6.15); 294(4.90); 293(6.83); 275(31.21); 274(13.69); 232(10.99); 231(42.94); 230(100.00).

5: 548(16.49); 547(29.06); 546(85.9); M^+; 519(19.65); 503(20.33); 502(34.40): 476(7.57); 475(17.22); 460(8.04); 459(100.00); 425(9.70).

6: 555(23.03); 554(32.70); 553(10.00); M^+; 538(10.51); 521(17.63); 520(53.63); 510(20.44); 509(14.30); 508(38.72); 477(4.85); 457(17.19); 456(13.21); 424(18.53); 423(15.24); 414(27.89); 386(8.33); 305(19.09); 258(24.42); 256(66.44); 241(10.39).

30–60°C), 30 mL. The residue was next extracted with CH_2Cl_2 (15 mL). The resultant solution was filtered through a small column containing alumina (2 cm thick). A top layer of hexane (20 mL) was added to the dichloromethane solution and the mixture was cooled to −20°C for 3 days during which time crystals of **4** grew as yellow nodules (yield 65–70% including a second crop from the concentrated solutions of the supernatant). *Anal.* calcd. for $C_{13}H_{15}FeNS_3$: C 46.29, H 4.41, N 4.15; found: C 45.78, H 4.52, N 4.26.

Preparation of 5

A solution of 1,1'-bis(α-*N*,*N*'-dimethylaminobenzyl)ferrocene (11) (1.0 g, 2.2 mmol) in diethyl ether (80 mL) was treated with a solution of *n*-butyllithium in hexane (3.0 mL, 1.6 M). The reaction mixture was stirred overnight before excess sulfur (1.0 g, 3.9 mmol) was added. After the reaction mixture was stirred for a further 2 h, it was hydrolyzed and worked up as described for the preparation of **4**. Crystallization of the dichloromethane solution gave **5** (15–25%) as yellow/orange nodules. These were characterized by mass spectroscopy (Table 3), and ^1H nmr spectroscopy: major isomer δ: 2.01 (s, 6, $2N(CH_3)$), 2.06 (m, 1), 3.33 (m, 1), 3.38 (m, 1), 3.53 (m, 1), 4.37 (m, 1), 4.55 (m, 1) (ferrocenyl protons), 3.51 (s, 1, *CH*), 7.20–7.34 (m's, 10, $2C_6H_5$)).

Preparation of 6

A solution of 2-(*N*,*N*'-dimethylaminomethylferrocenyl)diphenylphosphine (12) (1.0 g, 2.34 mmol) in diethyl ether (25 mL) was treated with a solution of *n*-butyllithium in hexane (3.0 mL, 1.6 M) and TMED (0.5 g, 4.3 mmol). The reaction mixture was stirred at 20°C for 12 h and then was carefully treated with excess sulfur (1.0 g, 3.9 mmol). The remaining work-up procedure was identical with that described for the preparation of **4**. The hexane washings yielded a small quantity of **6** in addition to the bulk portion obtained from dichloromethane/hexane as golden orange crystals (total yield 45%). *Anal.* calcd. for $C_{25}H_{24}FeNPS_4$: C 54.25, H 4.37, N 2.53; found: C 54.44, H 4.45, N 2.53.

Results and discussion

The reaction of the dilithio derivative of ferrocenyldiphenylphosphine with S_8 affords two isomers ***3a*** and ***3b*** in the ratio 3:1 (1); both isomers have eclipsed cyclopentadienyl rings in the solid state like **1**, E = S (13). Because both isomers contain a disubstituted cyclopentadienyl ring, resulting in planar chiral-

Can. J. Chem. Downloaded from www.nrcresearchpress.com by 186.148.149.217 on 09/07/12
For personal use only.

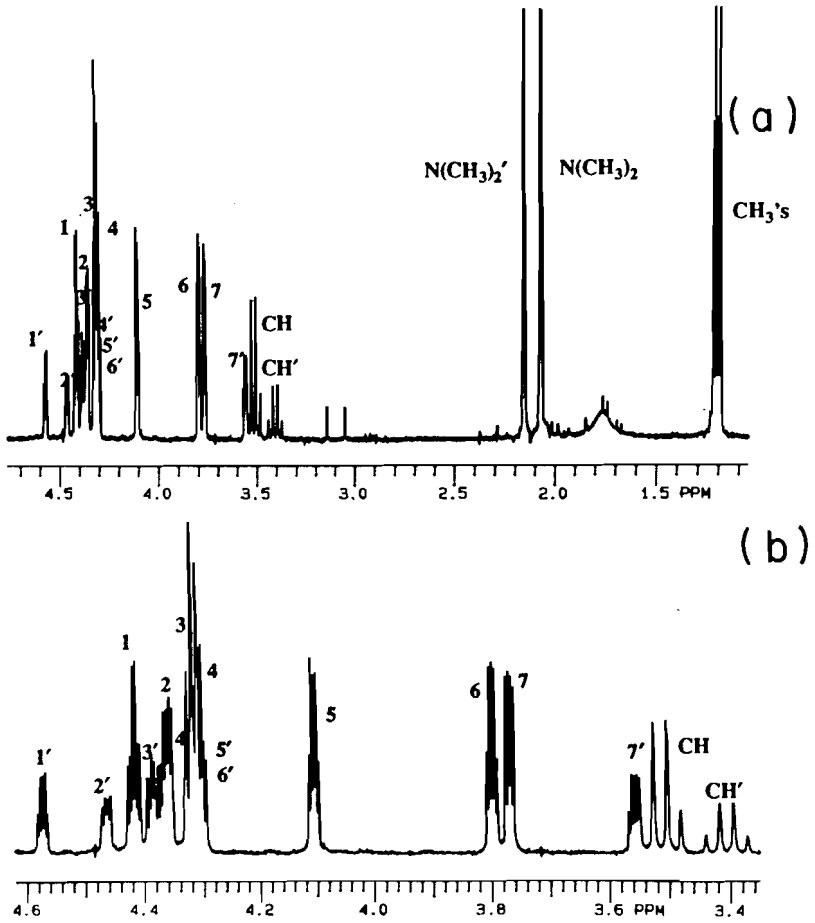
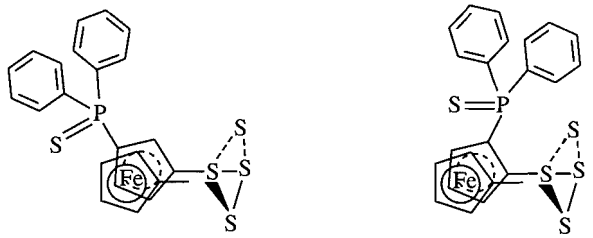


FIG. 1. (a) The ^{1}H nmr spectrum of the ferrocenyl region of **2**. (b) The ^{1}H nmr spectrum of **2**.



3a *3b*

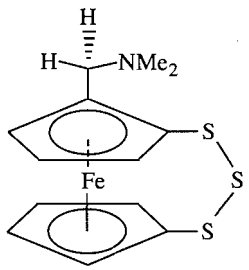
ity, and an S_3-bridge, they can exist as diastereomeric conformers defined by the conformation of the half chair. Nuclear magnetic resonance studies show that at room temperature in solution **3***a* exists as a 60:40 mixture of conformers while **3***b* exists predominantly as one diastereomer (>90%). The predominant conformers in solution are those indicated by the full lines of **3***a* and **3***b* (1).

We previously described the synthesis of **2** from the reaction of dilithiated α-*N*,*N*′-dimethylaminoethylferrocene with S_8 (6), and now report that **4**, **5**, and **6** can be prepared similarly from the appropriate starting material.

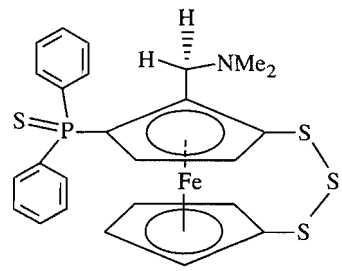
The reactions require little comment apart from noting that **5** is the product, obtained in low yield, from a crystalline precursor mixture of *rac* and *meso* 1,1′-disubstituted ferrocenes (11) and that lithiation of amino substituted ferrocenes is almost exclusively directed to the ring position adjacent to the substituent (14). Of course, lithiation of an unsubstituted cyclopentadienyl ring is random.

The ^{1}H nmr spectra of the products **2**, **4**–**6** reveal the presence of isomers in solution, as found for solutions of **3***a* and **3***b*. These new spectra can be completely assigned using a similar strategy to that used for the conformers of **3***a* and **3***b* (1). As an example, the assignment of the ^{1}H nmr spectrum of **2** is made as follows.

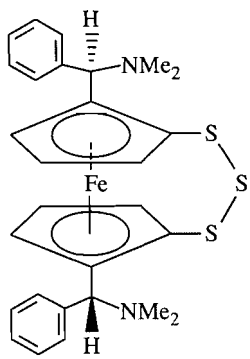
At ambient temperature the ^{1}H nmr spectrum of **2** shows two sets of resonances, Fig. 1, which are associated with the two



4



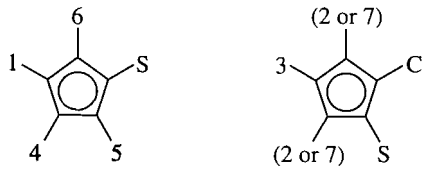
6



5

conformers **2α** and **2β**. All seven ferrocenyl protons in each conformer are magnetically inequivalent and the cyclopentadienyl region (δ 3.50–5.05) of the spectrum consists of 14 multiplets (7 major, 7 minor, Fig. 1b). Integration of the spectrum gives the ratio of **2α** to **2β** as 73:27. Considerable resonance overlap is apprent. It should also be noted that the spectra are solvent dependent and some subtle changes result on changing solvents, the most important of these being the possible transposition of resonances 3 and 4.

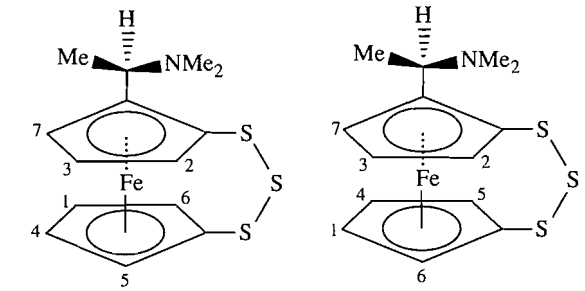
The initial proton resonance assignments for the major conformer **2α** were made following the application of homonuclear decoupling in conjunction with resonance line shape analysis. On this basis the monosubstituted ring of **2α** can be fully assigned as shown in **A**; however, there are two alternate formulations, **B**, of the disubstituted ring because protons 2 and 7, adjacent to the sulfur substituted carbon, cannot be unequivocally assigned using only this information. Previous nmr studies on



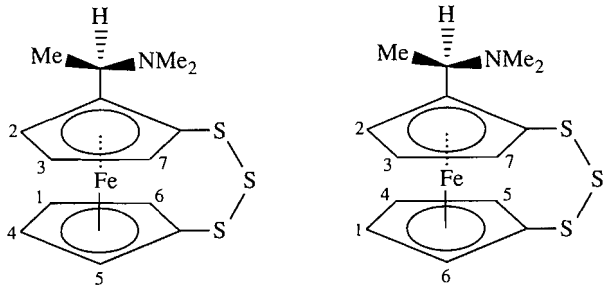
A **B**

S_3-bridged ferrocenophanes show that the chemical shift of the protons adjacent to the S_3-bridge is highly dependent on the stereochemistry of the bridge itself.

The information gained from decoupling experiments is verified on examination of the SUPER-COSY (15) spectrum of **2**, Fig. 2, which shows all the connectivities of the ferrocenyl protons; for example, the connectivities of resonances 1, 4, 5, and 6 are easily discerned in the figure. In addition, resonance 2 can be assigned tentatively to the proton adjacent to the C substituent since a cross peak is observed between resonance 2 and the α-C*H* resonance. Thus, by using the available information to this point, four possible resonance assignments of **2α** can be made, shown as **C**–**F**. There is a preference for **E** or **F**



C **D**



E **F**

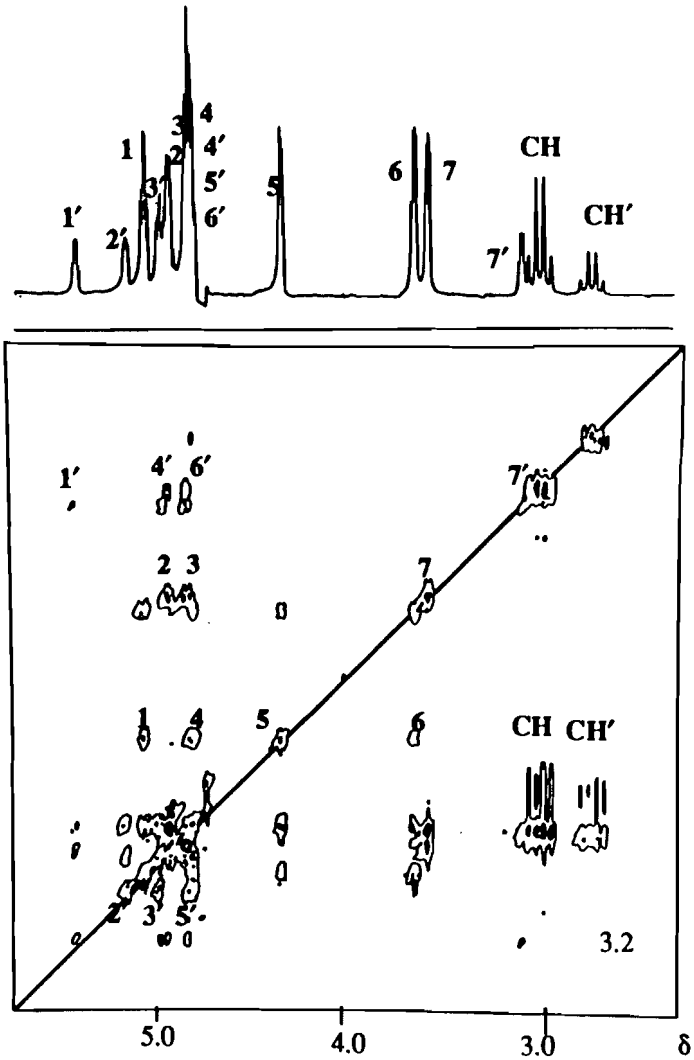


FIG. 2. The SUPER-COSY spectrum of **2** (ferrocenyl region).

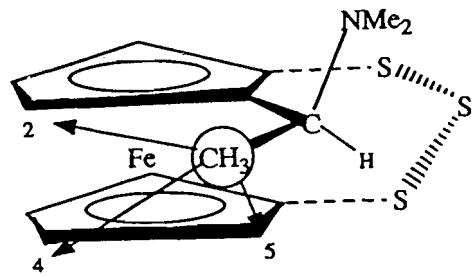


FIG. 3. Observed nOe enhancements on irradiating the C-methyl protons of **2**.

because of the assignment of resonance 2. It should be emphasized that the stereochemistry of the S-bridge is not indicated, although it is expected that the major isomer present in solution would be the one in which, for steric reasons, the middle S atom in the bridge is directed away from the ring substituent (1).

It should be noted that although many of the ferrocenyl proton resonances of the minor conformer **2β** are hidden in the normal 1-D spectrum because of overlap, the SUPER-COSY spectrum technique allows the complete positional characteriztion of all the resonances (1′–7′).

To complete the resonance assignments of **2** to specific proton

Can. J. Chem. Downloaded from www.nrcresearchpress.com by 186.148.149.217 on 09/07/12
For personal use only.

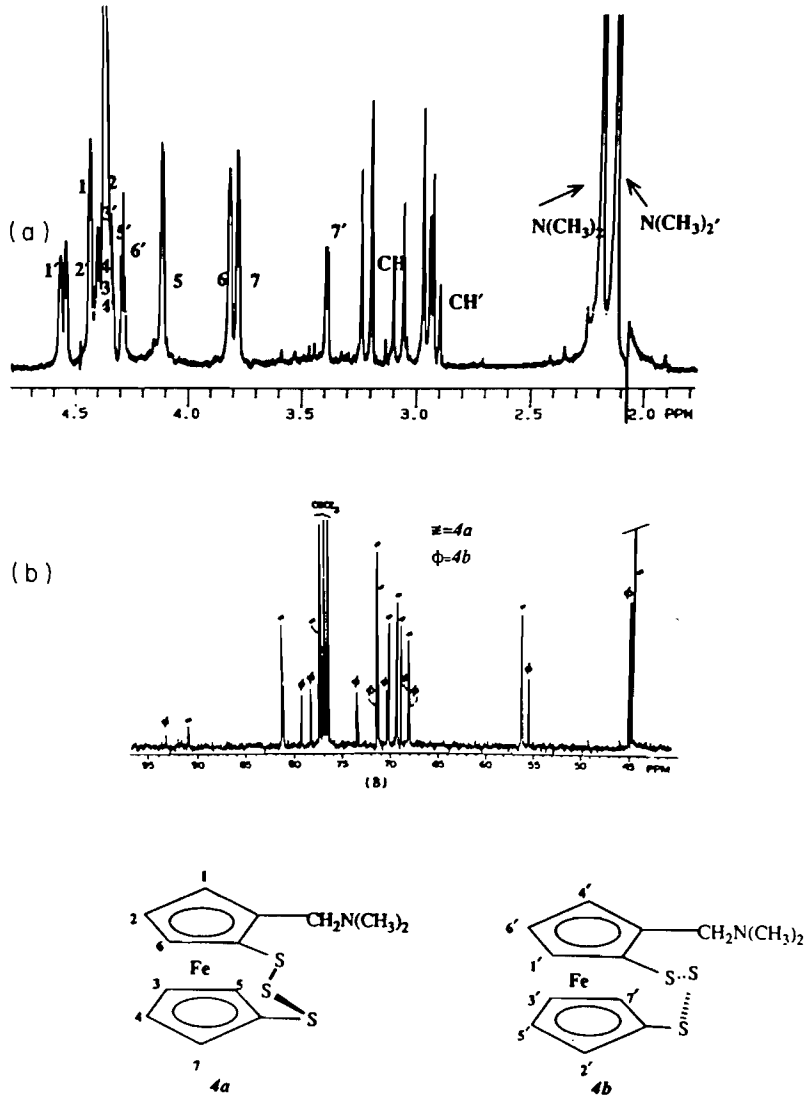
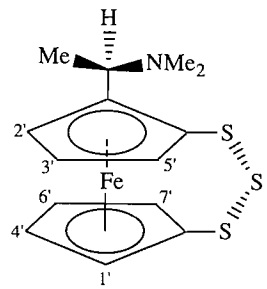


FIG. 4. (a) The ^{1}H nmr spectrum of **4**. (b) The ^{13}C nmr spectrum of **4**.

sites, the results of an nOe difference experiment were used. The C(CH_3) position was irradiated, resulting in strong positive enhancements of resonance 2 (major confomer) and 2′ (minor conformer). Simultaneously, information regarding the relative position of the lower cyclopentadienyl ring protons is garnered since positive enhancements are also observed in resonances 5 and 7′. Weak enhancements may be present for the 4 and 3′ protons but these are difficult to assign because of resonance overlap. This spatial correlation is more clearly seen in Fig. 3. Thus the correct assignment for the major conformer present in solution is given by **F**. The minor conformer is assigned as in **G**.

The ^{1}H nmr and ^{13}C nmr spectra of **4** and **6** are shown in Figs. 4 and 5 respectively. The chemical shift differences for the major and minor conformer resonances of the α-carbon atoms in **4** is 0.7 ppm (resonances near 56 ppm) and of the *N*-methyl carbons is 0.37 ppm (resonances near 45 ppm) in the opposite direction. However, the most pronounced difference (2.35 ppm) is observed for the S-substituted carbon of the lower ring (resonances near 92 ppm). A similar but less pronounced effect is found in the case of **6**. Correspondingly, in the proton nmr spectrum of **4** the α-C*H* protons are shifted downfield in the major conformer, relative to the minor conformer, by 0.14 ppm



G

and 0.05 ppm respectively. The more pronounced effect observed on one of the two CH_2 protons indicates that, for the major conformer present in solution, a strong deshielding effect is apparent on the C*H* nearest to the S_3 bridge. On bridge reversal the ferrocenyl protons experience the stronger deshielding influence. This observation is consistent with our previous findings indicating that the anisotropic effect of the exocyclic S-atom is as shown in Fig. 6. Interestingly, in the case of **2** and **4** the carbon and proton resonances of the N(CH_3)$_2$ groups in the major conformer are upfield of those of the minor.

Can. J. Chem. Downloaded from www.nrcresearchpress.com by 186.148.149.217 on 09/07/12
For personal use only.

Can. J. Chem. Downloaded from www.nrcresearchpress.com by 186.148.149.217 on 09/07/12
For personal use only.

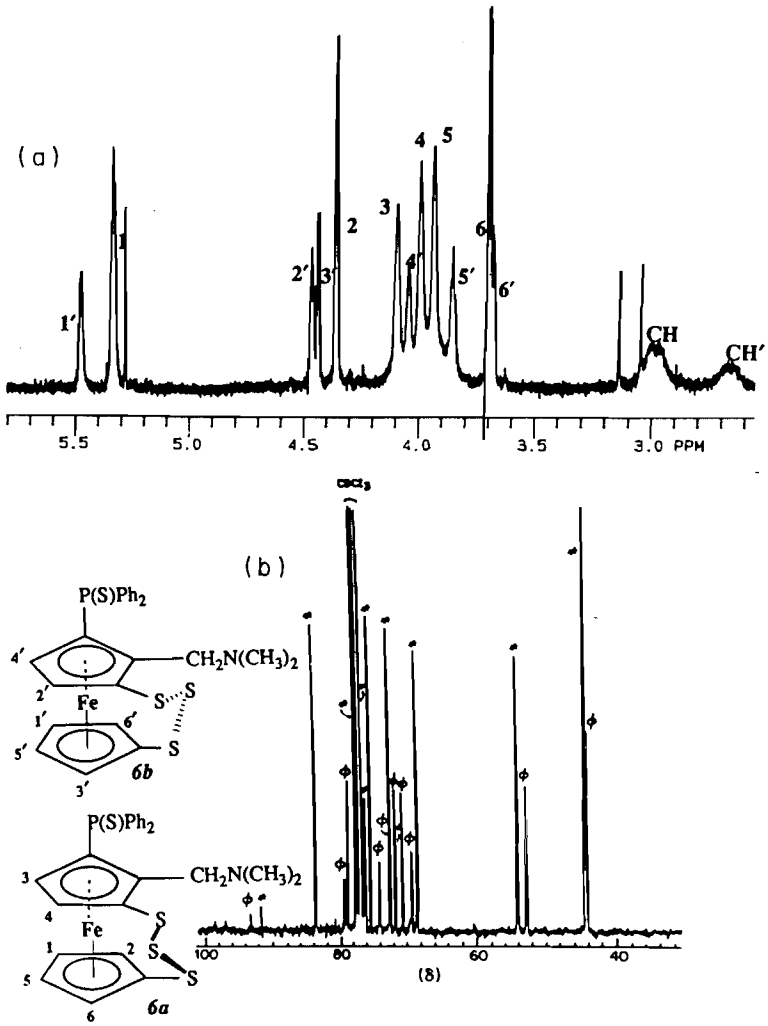


FIG. 5. (a) The ^1H nmr spectrum of **6**. (b) The ^{13}C nmr spectrum of **6**.

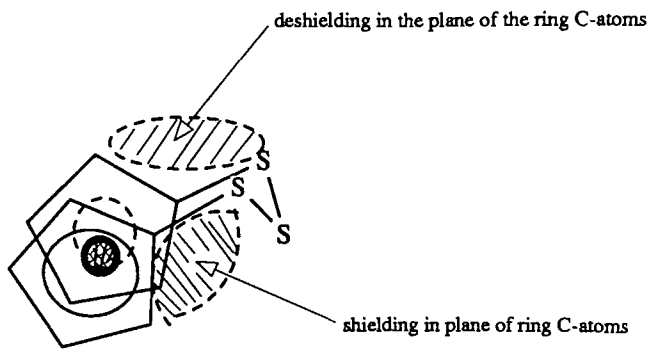


FIG. 6. The anisotropic effect of the S_3-bridge on ferrocenyl ring proton chemical shifts.

Further ^1H nmr studies on compound **4** have been made. These involve a variety of experiments including homo- and hetero-correlation, 2D-*J* and NOESY spectroscopic techniques. Some of these results are shown in Figs. 7a–7d. Of particular interest are the NOESY spectra, which enable the direct correlation of major and minor conformer resonances of **4**; they also contain the spatial information necessary for a complete structural assignment. This technique, which is complementary to the COSY experiment, leads to the unequivocal identification of all the ^{13}C resonances of **4**. On bridge reversal (major conformer–minor conformer, $4\alpha \rightleftharpoons 4\beta$, see Fig. 4), an extensive shift of the cyclopentadienyl carbon resonance lines is observed for atoms that are adjacent to the S-substituted carbons; the typical chemical shifts vary from 9.4 to 12.3 ppm. Cyclopentadienyl carbon atom resonances for carbons β to the S-bearing carbon show much smaller shifts on bridge reversal (0–2.5 ppm). This information serves as a cross-check of the original assignments for the disubstituted ring protons since the protonated carbon atoms adjacent to the sulfur should be extensively shifted in comparison to the protonated carbon adjacent to the methylene group. This is indeed found.

In addition, *inter-ring* coupling is observed between protons adjacent to the sulfur. Interestingly this phenomenon is *only* observed in the case of the major conformer **4**α and can perhaps be explained in terms of an interaction that includes the middle S atom in the bridge, which in this case lies between the coupled protons.

In compound **5**, where both the top and the bottom rings are disubstituted, two products, **5***a* and **5***b*, are possible depending on whether the starting material was the *meso* or *rac* compound (11). When the orientation of the S_3-bridge is considered, a preponderance of one conformer would be expected in the case of the *meso* compound; this conformer would have the central sulfur atom in the bridge pointing away from both ring substituents as shown in **5***a*. In the case of the ferrocenophane derived

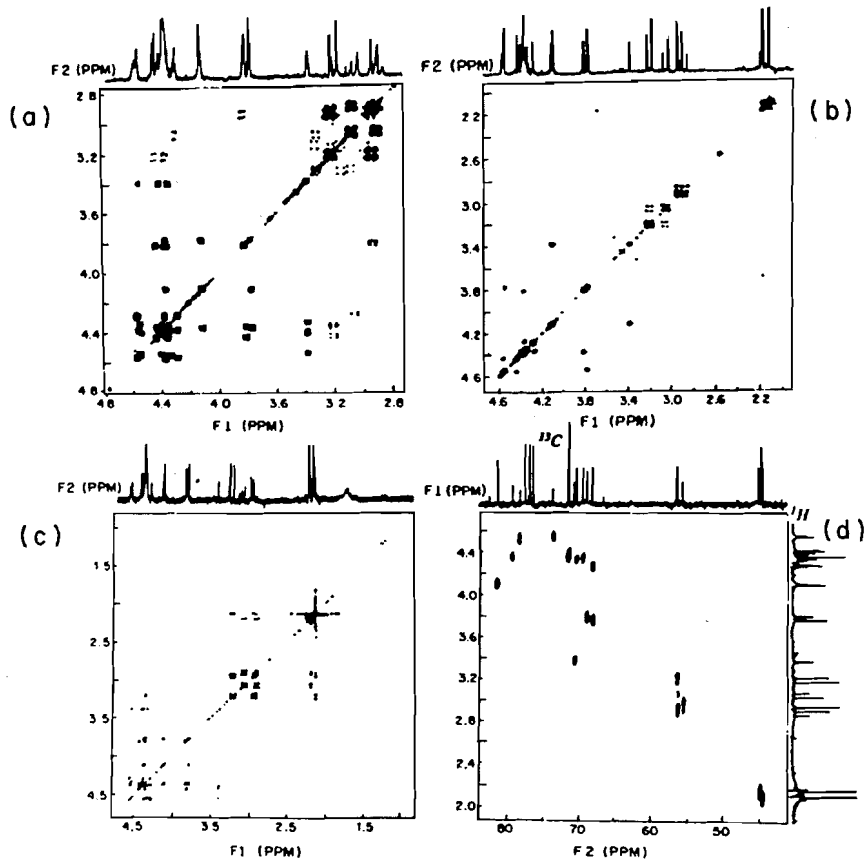
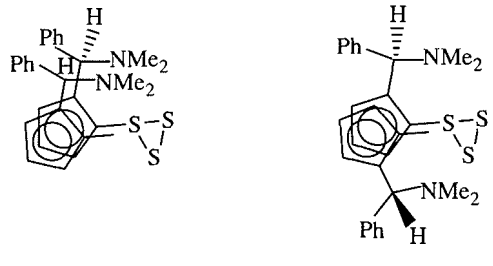


FIG. 7. (a) COSY spectrum of the ferrocenyl region of **4**. (b) NOESY spectrum of **4**. (c) Full COSY spectrum of **4**. (d) $^{13}C/^{1}H$ HETCOR spectrum of **4**.



5a *5b*

from the *rac*-derivative ***5b***, the bridge flipping process would be undetectable by ^{1}H nmr because the ferrocenophanes would be homomeric. The ^{1}H nmr spectrum of the isolated product is poorly resolved but shows a preponderance (>90%) of one isomer. The spectrum is best interpreted in terms of a mixture of ***5a*** and ***5b*** with ***5b*** predominant, because the ferrocenyl proton chemical shifts observed from the major product (δ 4.55–2.61) indicate that the central S atom points towards at least one ring substituent, as shown in ***5b***. This result essentially establishes that the starting material for the preparation was the *rac* isomer of $Fe(C_5H_4CH(Ph)NMe_2)_2$.

In the case of **6** the chemical shifts of the $N(CH_3)_2$ groups are almost identical. This shift can be attributed to an anisotropic effect of the central sulfur, which is pointing towards the $N(CH_3)_2$ groups, in the minor conformer. The ^{1}H nmr spectrum of **6** (Fig. 5a), recorded at ambient temperature, indicates a broadening of the resonances on the trisubstituted ring while the resonances on the monosubstituted ring are sharp. Although this broadening, in part, is caused by the additional phosphorus coupling, the extent seems to indicate a kinetic phenomenon, namely, a faster equilibration. This broadening is also observed in the side-chain resonances.

The conformer distribution found for compounds **2**–**6** is listed in Table 1. The conformer (α) is assigned the structure in which the central sulfur atom in the bridge is directed away from the other substituents (the solid line in the diagrams). The high ratio (α):(β) in **2** compared with **4** presumably reflects the steric effects of the extra CH_3 group in the former case. The isomer ratio found for **6** is slightly higher than **2** but much less than the diphenylphosphine sulfide ***3b*** (4). This observation affords indirect evidence that the S-substitution in **6** is α to carbon rather than to phosphorus. (This is expected as a consequence of the amine assisted lithiation of the starting materials (14).) The steric effect of the substitutent, therefore, greatly influences the ratio of the conformers (α):(β).

When a solution of **2** in DMSO is heated to 120°C, a gradual change is observed in the proton nmr spectrum, Fig. 8a. At 120°C the four proton resonances neighbouring sulfur are sharp; however, the remaining three proton resonances (i.e., 5, 6, and 7 of the major isomer) adjacent to the sulfur have completely collapsed. Further heating results in slow decomposition of **2**.

A similar experiment, conducted in nitrobenzene-d_5 to attain higher temperatures, indicates a resharpening of the broadened resonances at 3.85 ppm, Fig. 8b. After collapse, however, further heating again results in partial decomposition of the sample; unmetallated diene resonances appear in the spectrum. The ^{1}H nmr spectrum recorded after cooling these samples is identical to that of an unheated sample provided decomposition has been minimized by performing all operations as quickly as

Can. J. Chem. Downloaded from www.nrcresearchpress.com by 186.148.149.217 on 09/07/12
For personal use only.

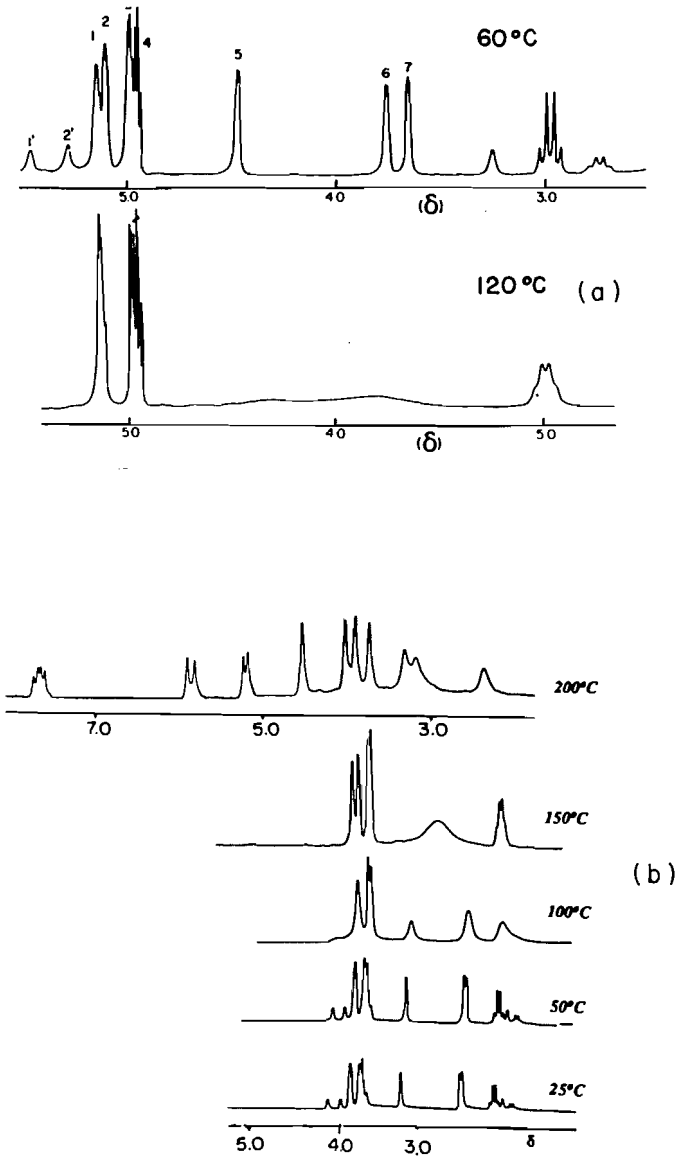


FIG. 8. The variable temperature ^1H nmr spectrum of **2**. (a) in DMSO-d_6; (b) in nitrobenzene-d_5.

possible. These results correlate with those previously described for the unsubstituted [3]-ferrocenophanes in which the coalescence temperature of the protons adjacent to the sulfur atom is higher than that of the other pair.

Acknowledgements

Funding for this project was provided by the Natural Sciences and Engineering Research Council of Canada in the form of an operating grant to W.R.C. The useful discussions with the staff of the U.B.C. nmr service and Dr. Heather Dettman from the University of Ottawa are gratefully acknowledged.

1. I. R. BUTLER, W. R. CULLEN, F. W. B. EINSTEIN, F. G. HERRING, N. R. JAGANNATHAN, and R. W. JONES. Inorg. Chem. **25**, 4534 (1986).
2. A. DAVISON and J. C. SMART. J. Organomet. Chem. **174**, 321 (1981).
3. E. W. ABEL, M. BOOTH, and K. G. ORRELL. J. Organomet. Chem. **208**, 213 (1981).
4. A. G. OSBORNE, R. E. HOLLANDS, J. A. K. HOWARD, and R. F. BRYAN. J. Organomet. Chem. **205**, 395 (1981).
5. E. W. ABEL, M. BOOTH, C. A. BROWN, K. G. ORRELL, and R. L. WOODFORD. J. Organomet. Chem. **214**, 93 (1981).
6. I. R. BUTLER and W. R. CULLEN. Organometallics, **5**, 2537 (1986).
7. D. SEYFERTH and B. W. HAMES. Inorg. Chim. Acta, **77**, L1 (1983).
8. D. SEYFERTH, B. W. HAMES, T. J. RUCKER, M. COWIE, and R. S. DICKSON. Organometallics, **2**, 472 (1983).
9. S. AKOBORI, T. KUMAGAI, T. SHIRAHIGE, S. SATO, K. KAWOZOE, and C. TAMURA. Organometallics, **6**, 2105 (1987).
10. G. R. KNOX, J. D. MUNRO, P. L. PAUSON, G. S. SMITH, and W. E. WATTS. J. Chem. Soc. 4619 (1961).
11. I. R. BUTLER and W. R. CULLEN. Synth. React. Inorg. Met.-Org. Chem. **13**, 321 (1983).
12. W. R. CULLEN, F. W. B. EINSTEIN, C.-H. HUANG, A. C. WILLIS, and E.-S. YEH. J. Am. Chem. Soc. **102**, 988 (1980), and references therein.
13. B. R. DAVIES and I. BERNAL. J. Cryst. Mol. Struct. **2**, 107 (1972).
14. I. R. BUTLER, W. R. CULLEN, F. G. HERRING, and N. R. JAGANNATHAN. Can. J. Chem. **64**, 667 (1986), and references therein.
15. A. KUMAR, R. V. HOSAR, and K. CHANDRASEKHAR. J. Magn. Reson. **60**, 143 (1984).

Can. J. Chem. Downloaded from www.nrcresearchpress.com by 186.148.149.217 on 09/07/12
For personal use only.

The far-ultraviolet photochemistry of alkylcyclopropenes in solution

BRIAN J. FAHIE AND WILLIAM J. LEIGH[1]

Department of Chemistry, McMaster University, Hamilton, Ont., Canada L8S 4M1

Received April 4, 1989

This paper is dedicated to Professor Ronald J. Gillespie on the occasion of his 65th birthday

BRIAN J. FAHIE and WILLIAM J. LEIGH. Can. J. Chem. **67**, 1859 (1989).

The photochemistry of 1,3,3-trimethylcyclopropene and 1-*tert*-butyl-3,3-dimethylcyclopropene has been investigated in hydrocarbon, methanol, and 1-hexene solution with far-ultraviolet (185–228 nm) light. Direct photolysis of the two compounds affords allene, alkyne, and 1,3-diene derivatives, formally as a result of initial bond cleavage to yield vinylcarbene intermediates. Products derived from cleavage of the most substituted (C1—C3) cyclopropene bond account for 60–80% of the observed mixture in each case. Results from the photolysis of 1,3,3-trimethylcyclopropene-1-^{13}C suggest a second pathway for formation of alkyne products in cyclopropene photochemistry, which occurs in competition with (or by exclusion of) the vinylcarbene [1,2]-hydrogen migration pathway. The data are consistent with the intermediacy of a vinylidene species, formed by [1,2]-hydrogen migration/ring opening, although attempts to chemically trap this intermediate with methanol or alkene were unsuccessful.

Key words: cyclopropene, photolysis, vinylmethylene, propenylidene, far-UV.

BRIAN J. FAHIE et WILLIAM J. LEIGH. Can. J. Chem. **67**, 1859 (1989).

Opérant dans des solutions d'hydrocarbure, de méthanol et de hex-1-ène et utilisant de la lumière ultraviolette lointaine (185–228 nm), on a étudié la photochimie des 1,3,3-triméthylcyclopropène et 1-*tert*-butyl-3,3-diméthylcyclopropène. La photolyse directe de ces deux composés fournit des dérivés allènes, alcynes et 1,3-diènes qui proviennent d'une façon formelle du bris initial d'une liaison qui fournit des intermédiaires vinylcarbènes. Dans chacun des cas, les produits qui proviennent du bris de la liaison la plus substituée (C1—C3) du cyclopropène forment de 60 à 80% du mélange observé. Les résultats obtenus lors de la photolyse du 1,3,3-triméthylcyclopropène-1-^{13}C suggèrent que, lors de la photochimie des cyclopropènes, il existe une deuxième voie de formation des alcynes qui est en compétition avec (ou à l'exclusion de) la voie impliquant la migration-[1,2] d'hydrogène du vinylcarbène. Les données sont en accord avec la présence d'intermédiaires vinylidènes qui seraient formés par une migration-[1,2] d'hydrogène/ouverture de cycle; toutefois, des essais effectués en vue de piéger cet intermédiaire avec du méthanol ou un alcène se sont avérés infructueux.

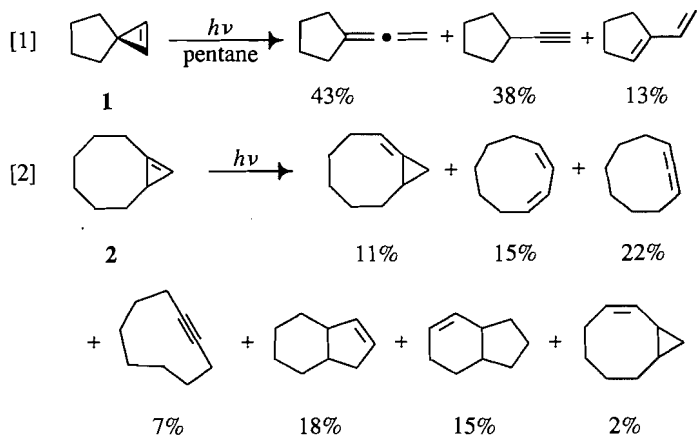
Mots clés : cyclopropène, photolyse, vinylméthylène, propénylidène, UV lointaine.

[Traduit par la revue]

Introduction

The photochemistry of cyclopropenes has received a considerable amount of attention over the past 20 years (1–3). Early studies of phenylated cyclopropenes demonstrated that the product distribution from direct photolysis is normally characteristic of reactivity associated with vinylcarbene intermediates, formed by cleavage of the C1—C3 and (or) C2—C3 cyclopropene bonds in the first excited singlet state (4–6), although other reaction pathways can intervene if the system bears appropriate substituents (1, 2, 7, 8). In addition, numerous theoretical studies have been carried out in an effort to assist in understanding the nature of the excited state(s) and intermediates involved (9–15). Considering that the majority of theoretical studies have been confined to the parent C_3H_4 system while experimental studies have mostly concentrated on phenylated systems, the agreement between the two approaches has been quite remarkable.

While the photochemistry of arylcyclopropenes has thus been extensively investigated (1–8), there have been few reported studies of simple alkyl-substituted derivatives in solution (16, 19), probably because the parent chromophore is devoid of absorption above 210 nm and hence requires the use of far-uv techniques for its investigation. Recent reports of the photochemistry of two bicyclic alkylcyclopropene derivatives (eqs. [1] (16) and [2] (19)) have demonstrated that the photochemical behaviour of alkylated systems differs in several respects from



that typical of arylcyclopropenes. These compounds afford substantial amounts of allene and alkyne products in addition to the 1,3-dienes and other products that are characteristic of vinylcarbene intermediates. The photochemistry of compounds **1** and **2** supplements the elegant studies of Steinmetz *et al.* (16–18) and Johnson and co-workers (19–21) on the photochemistry of allene derivatives. Allenes have been shown to afford cyclopropenes in both the ground and singlet excited state via vinylcarbene as well as concerted pathways (3, 16–22).

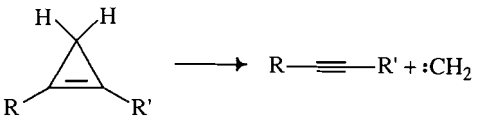
Recent *ab initio* theoretical investigations of the thermal and photochemical interconversions of the C_3H_4 hydrocarbons (14, 15) underline the need for further studies of the photochemistry of simple cyclopropene derivatives. On the basis of these calculations, at least two unknown thermal and (or)

[1]Natural Sciences and Engineering Research Council of Canada University Research Fellow (1983–1993). Author to whom correspondence may be addressed.

Can. J. Chem. Downloaded from www.nrcresearchpress.com by 186.148.149.217 on 09/07/12
For personal use only.

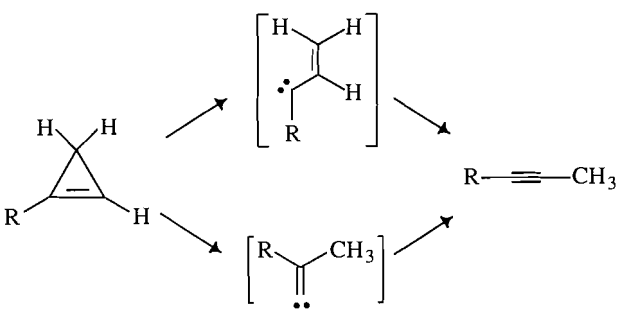
photochemical reaction pathways (in addition to vinylmethylene formation), whose efficacy may depend dramatically on substitution and the excited state energy of the chromophore, have been proposed.

The *ab initio* SCF-CI calculations of Sevin and Arnaud-Danon suggest that two-bond fragmentation leading to a carbene and an alkyne (eq. [3]) may provide an important

[3] 

photochemical decomposition pathway in simple cyclopropenes with high singlet excitation energies (14). Carbene photoextrusions are rather common in cyclopro*pane* photochemistry (23, 24) (particularly in alkyl-substituted systems) (24), but have apparently not been observed in cyclopropene systems.

More recently, Yoshimine and co-workers have proposed that the well-documented, thermal rearrangement of cyclopropene to propyne (3, 25) may proceed by *two* competitive pathways (eq. [4]), one involving [1,2]-H migration in vinylmethyl-

[4] 

ene and the other involving the intermediacy of propenylidene (15). The latter intermediate (formed by concerted[2] or stepwise [1,2]-hydrogen migration/ring opening) has been calculated to be ca. 16 kcal/mol lower in energy than either of the two lowest singlet states of vinylmethylene, and is thus a viable intermediate on both the ground and excited singlet state potential energy surfaces for the cyclopropene/propyne interconversion (26). While direct experimental evidence for this process (either thermal or photochemical) evidently does not yet exist, the reverse reaction, thermal rearrangement of vinylidene carbenes to cyclopropenes, has been documented (27).

We have undertaken a study of the photochemistry of two unsymmetrical, alkyl-substituted cyclopropenes (**3** and **4**) in hydrocarbon and methanol solution with far-uv light. These compounds afford the possibility of exploring the effects of substituent on the mode of cyclopropene bond cleavage in monocyclic, alkyl-substituted systems (i.e., the competition between ring opening to yield substituted vs. unsubstituted vinylmethylene intermediates), and could provide the basis for comparison with the analogous behaviour of phenylated cyclopropenes. Furthermore, the thermal chemistry of both compounds has been previously reported (28, 29) and is thus available for comparison with their photochemical behaviour. In addition, the possibility that the photochemical rearrangement to alkynes may proceed via propenylidene intermediates

[2]NOTE ADDED IN PROOF: More recent calculations favour a concerted mechanism for the cyclopropene to propenylidene conversion, and indicate that both *syn* and *anti* vinylmethylenes undergo ring closure to cyclopropene. See ref. 15*c*.



3 **4** **5**

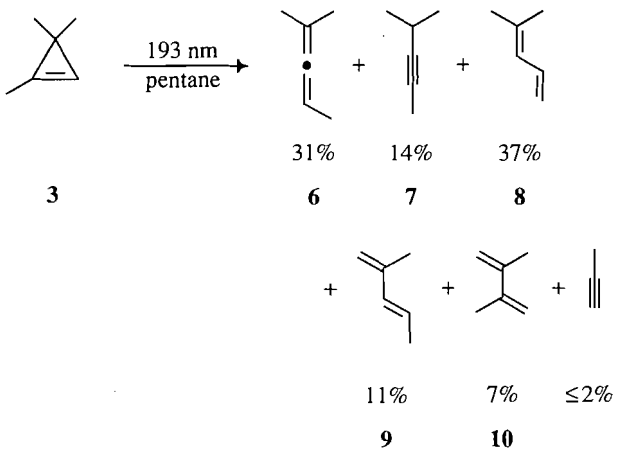
has been investigated using a ^{13}C-labelled derivative of **3** (**5**). The results of our study are reported below.

Results

1,3,3-Trimethylcyclopropene (**3**) and (1-^{13}C)-1,3,3-trimethylcyclopropene (**5**) were synthesized by base-catalysed decomposition of the tosylhydrazones of mesityl oxide and (2-^{13}C)-mesityl oxide, respectively, with only minor changes to the previously reported procedure for the preparation of **3** (30). (2-^{13}C)-Mesityl oxide was synthesized according to the reported procedure for the unlabelled compound (31), starting from (2-^{13}C)-sodium acetate. 1-*tert*-Butyl-3,3-dimethylcyclopropene (**4**) was synthesized in similar fashion from the tosylhydrazone of 2,2,5-trimethylhex-4-en-3-one.

The uv absorption spectra of **3** and **4** in deoxygenated pentane solution showed single peaks with λ_{max} = 194 ± 1 nm (ϵ = 4500) and 196 ± 1 nm (ϵ = 6800), respectively. Both spectra were devoid of absorption above ca. 235 nm.

Photolysis of a deoxygenated, 0.041 M pentane solution of **3** with the unfocussed pulses from an Ar/F_2 excimer laser (193 nm; ca. 8 ns; 20–80 mJ) produced the six primary products shown in eq. [5]. Each compound was identified by coinjection

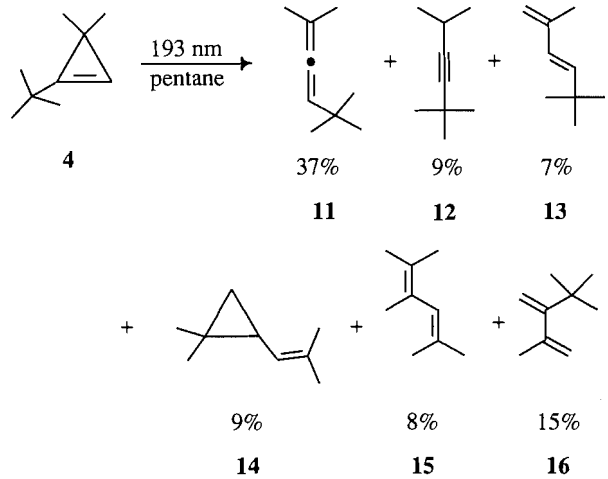
[5] 

of the photolysate and an authentic sample on at least two vpc columns. Relative product yields for **6**–**10** were determined by triplicate vpc analyses of the photolysate at several light dosages between ca. 0.5 and 5% conversion (see experimental section). *cis*-**9** could not be detected in the photolysis mixture up to ca. 10% conversion. The yield of propyne could not be accurately determined, but is estimated to be in the 0.3–2% range. Propene could *not* be found in the photolysis mixture (limit of detection <0.3%), under vpc conditions adequate to separate it from propyne.

Similarly, 193-nm photolysis of a deoxygenated, 0.018 M pentane solution of **4** produced the eight primary products shown in eq. [6]. Products **14** and **15** were identified by coinjection of the photolysate with authentic samples on two different vpc columns. Products **11**–**13** and **16** were isolated by preparative vpc from larger scale runs carried to ca. 20% conversion, and identified by ir and $^1H/^{13}C$ nmr spectroscopy and gc/ms analysis, and comparisons to literature data in the cases of **11** and **12**. Relative product yields were determined by a similar method to that used for the photolysis of **3**. The

Can. J. Chem. Downloaded from www.nrcresearchpress.com by 186.148.149.217 on 09/07/12
For personal use only.

Can. J. Chem. Downloaded from www.nrcresearchpress.com by 186.148.149.217 on 09/07/12
For personal use only.

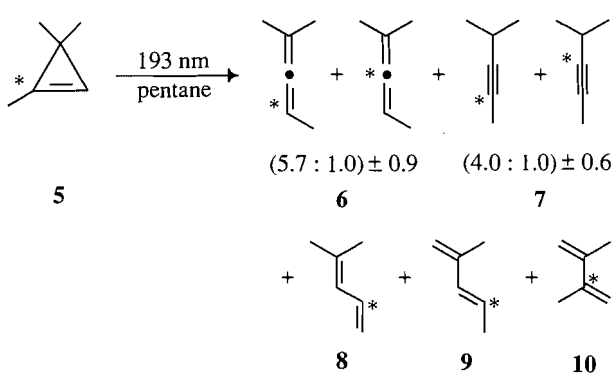
[6] 

photolysate also contained two additional, minor products (each in <8% yield) for which quantities sufficient for identification could not be obtained. 3,3-Dimethyl-1-butyne was not observed as a product of photolysis of **4** (i.e., yield ≤0.3%), as indicated by vpc analysis of the photolysate under conditions adequate for resolving this compound from the solvent or any other component of the mixture.

We have ruled out sequential two-photon excitation by the laser as contributing to the observed photochemistry for either **3** or **4** on the basis that photolysis of deoxygenated pentane solutions of the two compounds with a low pressure mercury lamp (185 + 254 nm) resulted in similar product distributions to those obtained in the 193-nm runs.

Reaction quantum yields were not determined quantitatively, but they appeared to be quite low on the basis of qualitative comparisons to other systems that we have studied under similar conditions (32). We thus estimate the upper limit for the quantum yields of disappearance of **3** and **4** to be in the range 0.01–0.1.

A deoxygenated, 0.25 M pentane solution of **5** was photolysed (193 nm) to approximately 25% conversion, and the products were isolated from the crude photolysate by semi-preparative vpc. As expected, the formal product distribution from photolysis of **5** was virtually identical to that obtained from **3**. The distribution of the ^{13}C label in each product was determined by integration of the ^{13}C nmr spectrum of a $CDCl_3$ solution containing $Cr(acac)_3$ (to shorten the ^{13}C spin-lattice relaxation time (33*a*)), and comparison to the spectrum of the corresponding unlabelled material recorded under identical conditions (see experimental section). These results are summarized in eq. [7]. For **8**–**10**, these experiments indicated that the label exists almost exclusively at a single carbon (see eq. [7]), but the error in the determinations for these

[7] 

compounds may be as high as ±30% due to the qualitative procedure that was employed for the ^{13}C integrations in these cases. More rigorous procedures were employed for **6** and **7**. In the case of **6**, the spectrum was recorded using inverse gate decoupling (in which nOe enhancement is suppressed by turning on the proton decoupler only during acquisition of the FID (33*b*)), and with a delay of $>5T_1$ between pulse sequences to ensure complete relaxation. The distribution of the label in **6** that is quoted in eq. [7] is the average of three independent determinations, and the error is quoted as a single standard deviation from the mean. In the case of **7**, the determination involved a much more rigorous approach, which has been described in detail elsewhere (34), and which affords significantly lower systematic errors compared to the more conventional method that was used for **6**.

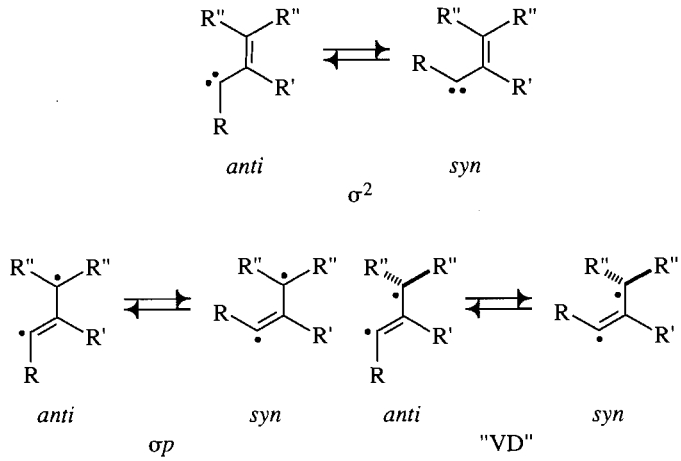
Photolysis of deoxygenated, 0.05 M pentane solutions of **3** was also carried out using Zn (214 nm) and Cd (228 nm) resonance lamps as the light sources. Product yields were determined by vpc from photolysates carried to ca. 5% conversion, and did not differ significantly from those obtained using the excimer laser (193 nm) as the light source. Photolyses of deoxygenated, 0.05 M solutions of **3** in methanol and in 1-hexene with the 214- and 228-nm light sources, respectively, afforded product distributions that were similar in all respects to those obtained in the pentane runs. In particular, no new products were formed in either case within the detection limits of our vpc method.

Discussion

It is well established that the photochemistry of cyclopropene derivatives is dominated by initial ring opening to yield vinylcarbene intermediates. In the parent (C_3H_4) system, the ground state of vinylmethylene is the planar vinyl-diradical (σp) triplet state (9–15, 35), but the two lowest excited singlet states, the carbenic σ^2 and higher energy σp (vinyl-diradical) states, are thought to be the ones normally obtained in thermal or photochemical ring opening of cyclopropenes (3). Calculations reveal that the ground state of cyclopropene correlates with the vinylmethylene σp state, while the first excited singlet state correlates with the lower energy σ^2 state (9–15). The avoided crossing of these surfaces is thought to result in σ^2 vinylcarbene being the result of thermal cyclopropene ring opening, while the excited singlet state process involves initial formation of σp vinylcarbene (14–21). Also pertinent to discussion of vinylcarbene reactivity is the bisected vinyl-diradical geometry ("VD"), which is related to singlet σp vinylcarbene by rotation (90°) about the C2—C3 bond.

The most recent calculations for the parent (C_3H_4) system indicate that (for both planar and bisected geometries of σ^2 and σp vinylmethylene) the *anti* geometric isomers are <2 kcal/mol lower in energy than the *syn* isomers, with low (<8.3 kcal/mol) barriers for their interconversion (15). This situation should clearly be expected to change with substituents, however. The bisected (VD) conformers are calculated to be ca. 1.5 and 4.5 kcal/mol higher in energy than the planar *syn* and *anti* σp states, respectively, with no barrier to interconversion between the planar and bisected geometries. In fact, the bisected geometries may represent energy *maxima* on the σp vinylcarbene potential energy surfaces (15, 21).

The predominant reaction pathway for both thermally and photochemically generated vinylcarbenes is ring closure to cyclopropene (3). This leads to a rather large component of reversibility in both thermal (36) and photochemical (37) ring

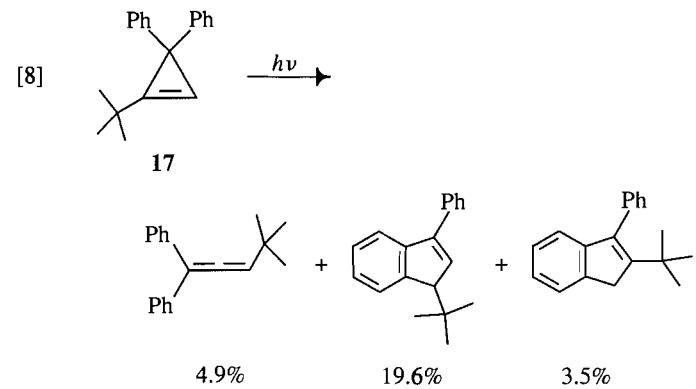


opening of cyclopropenes, and presumably ensues from the *anti* vinylcarbene isomer(s) (15*c*). From the planar vinylcarbene isomers, ring closure requires C2—C3 bond rotation, either preceding or in concert with bond formation.

Substituted 1,3-butadienes are formed via [1,2]-hydrogen (or -alkyl) migration when R = alkyl, or by [1,4]-hydrogen migration when R″ = alkyl. Presumably, the former can proceed from either the *syn* or *anti* vinylcarbene isomers, while the latter proceeds only from the *anti* isomer.

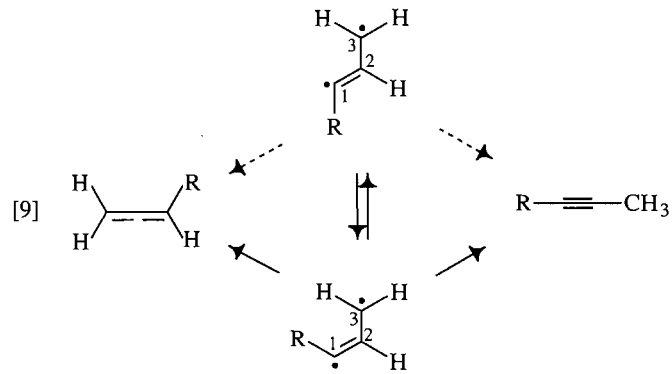
[1,4]-Hydrogen migration might thus be expected to lead to stereospecific diene formation, although numerous examples in arylcyclopropene photochemistry are nonstereospecific (1, 2). Indenes and furans are formed in systems where R″ = Ph and acyl, respectively (1, 2), presumably also from the *anti* vinylcarbene isomers. None of these reaction pathways require C2—C3 bond rotation.

Allenes and acetylenes are of particular current interest due to the fact that the generality of their formation from singlet excited cyclopropenes has only recently been established (see, for example, eqs. [1] (ref. 16), [2] (ref. 19), and [8] (ref. 18))



(3, 21). Depending on substitution, products of this type can clearly be the predominant ones from photolysis of cyclopropenes. These products can be most simply envisaged as deriving from the *syn* vinyl-diradical by [1,2]-H-migrations to either C3 or C1 (17) (eq. [9]). Both H-migrations must be accompanied (or preceded) by rotation about the C2—C3 bond. Evidently, the formation of these products is blocked (or largely so) in derivatives substituted with alkyl groups at the 2-position. Klett and Johnson have also reported the formation of allene products in low yield from photolysis of 1,3,3-triphenyl- and 1,2,3,3-tetraphenylcyclopropene, and attributed their formation to [1,2]-aryl migration in the corresponding vinylcarbenes (21). On the basis of the observation that allenes and acetylenes appear to be formed in much higher yield from photolysis of cyclopropenes than from either thermolysis of the same compound or from independently generated (presumably σ^2) vinylcarbene (18–21), the σp state is strongly implicated. Whether σp vinylcarbene affords these products directly (in state-specific fashion (17)) or indirectly, as a result of funnelling to the σ^2 state at an appropriate geometry for hydrogen migration (18, 19, 21), has been the subject of some discussion. The possibility that these products may alternatively be formed from excited cyclopropene by a concerted process has also been suggested (21).

In the present cases, ring opening of **3** and **4** can proceed in two ways: cleavage of the C1—C3 bond, to ultimately yield products formally derived from a (C1) alkyl-substituted vinylcarbene, or cleavage of the C2—C3 bond to yield products derived from an un- (i.e., H) substituted vinylcarbene. The

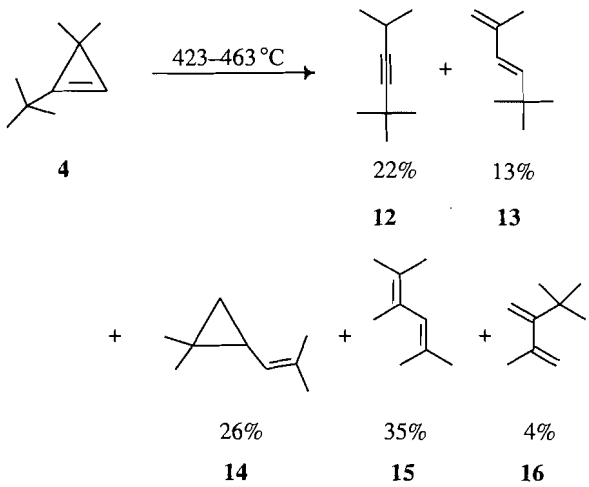


product distribution obtained from photolysis of **3** is such that 70–90% of the observed products can be formally attributed to the initial formation of the more highly substituted of the two possible vinylcarbene intermediates from ring opening of this compound. Only diene **10** is derivable from the less substituted of the two possible vinylcarbenes. This trend also holds for the behaviour of **4**, as well as that of **2** (eq. [2] (19)) and **17** (eq. [8] (18)). For example, of the seven products shown in eq. [7], only the first is attributable to the less substituted vinylcarbene formed by cleavage of the exocyclic (C8–C9) cyclopropenyl bond; the rest can be rationalized as arising from the vinylcarbene formed by cleavage of the endocyclic (C1—C8) bond. Similarly, the first two products shown in eq. [8] are both attributable to the vinylcarbene derived from cleavage of the more substituted cyclopropene σ-bond.

Similar selectivities have been observed in the thermolysis of **3** and **4**. Gas-phase thermolysis of **3** has been reported to afford **9** and **10** in yields of 71 and 21%, respectively; no other products were reported (28). Thermolysis of **4** has been reported to afford the products shown in eq. [10] (29). In both these cases, the observed product distributions are consistent with predominant (70–90%) ring opening to yield the more highly substituted vinylcarbene isomer. However, aside from this gross similarity between the ground and excited state behaviour of **3** and **4**, the more detailed aspects of these product distributions differ considerably (*vide infra*).

This general behaviour contrasts that frequently observed in phenylated cyclopropene derivatives (1–3). In 1-aryl (21) and 1-aryl-2-alkyl (6, 37, 38) systems, for example, it has been found that while thermolysis affords products associated with ring opening to yield the thermodynamically more stable vinylcarbene, photolysis yields products associated with formation of the less stable carbene. This has been explained in terms of

Can. J. Chem. Downloaded from www.nrcresearchpress.com by 186.148.149.217 on 09/07/12
For personal use only.

[10] 

the "funnel theory" of excited- to ground-state conversions (39); the thermodynamically less stable product is formed photochemically because its potential energy surface is the one that approaches the excited state potential surface for cyclopropene ring opening in closest proximity (1, 2). In the present alkyl systems, however, the differences in thermodynamic stability between the two possible carbenes are much smaller than is the case in aryl-H or aryl-alkyl systems. Since the two (sets of) vinylcarbene surfaces will approach the cyclopropene excited state surface to comparable extents, funneling to the lower energy of the two surfaces might be expected to be more facile. The result is that ring opening to the more stable carbene is favoured. Klett and Johnson have pointed out that reversal of the ground- and excited-state bond orders for the two cyclopropene σ-bonds could provide an alternative explanation for the differences observed in thermal and photochemical arylcyclopropene ring opening (21).

For both **3** and **4**, the formation of allenes and acetylenes is substantially enhanced (at the expense of dienes and intramolecular C—H insertion products) in the excited state compared to the ground state (thermal) reactions. Allenes are usually absent altogether in cyclopropene thermolysis (3), and calculations indicate that this is due to a higher activation barrier for the formation of this product from vinylmethylene compared to that for formation of alkyne (15). Photochemical activation provides a pathway to the higher energy potential energy surface, leading to allene that is essentially inaccessible from the ground state of cyclopropene, and in both cases the allene is the major product of direct photolysis.

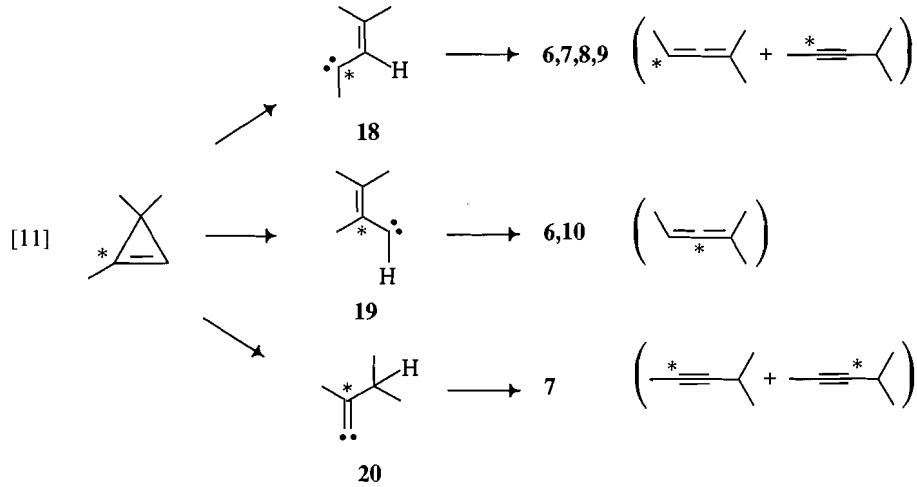
The results of the carbon-labelling experiment (photolysis of **5**; eq. [6]) indicate that the origins of allene **6**, alkyne **7**, and 1,3-dienes **8**–**10** can all be rationalized as due *predominantly* to formal [1,2]- or [1,4]-H migrations in the two possible vinylcarbene intermediates (**18** and **19**; see eq. [11]), as expected (3, 15). However, careful nmr analysis of **6*** and **7*** reveals that these products are not exclusively formed by [1,2]-H migration pathways in **18**. The result that **6*** contains ca. 15% of the label at carbon-3 indicates that the allene may be formed to a minor extent from [1,2]-methyl migration, formally involving the less substituted vinylcarbene (**19**) that is also responsible for the formation of diene **10**. While [1,2]-aryl migrations leading to allenes are known to be facile in vinylcarbene chemistry (21, and references cited therein), there have been no reports of similar migrations involving alkyl groups. The present results verifies that the process is an exceedingly minor reaction pathway for 2-alkyl substituted vinylcarbenes, though it is finite. Steinmetz *et al.* have found that [1,2]-alkyl migrations in the reverse direction (i.e., excited allene ⇒ vinylcarbene) occur in cyclic systems when the migration can substantially relieve ring strain (17). We note that diene **15**, formed in both the thermolysis (29) and photolysis of **4**, is also derived from [1,2]-methyl migration in the corresponding vinylcarbene, although this involves migration of a *tert*-butyl-methyl group to the C1 carbon.

The scrambling of the label that occurs in product **7*** is more significant. [1,2]-H migration in **18** should lead to material containing label only at C4, and the preponderance of label that exists at this position in **7*** may be due to a substantial contribution from this pathway. An attractive mechanism that would account for scrambling of the label between C3 and C4 is the propenylidene route suggested by Yoshimine and co-workers (15). Cyclopropene excited state C2—C3 bond cleavage accompanied by hydrogen migration (from C2 to C3) in **3** (**5**) would yield the vinylidene species (**20**) shown in eq. [11]. It is well known that carbenes of this type afford alkynes by [1,2]-alkyl migration (26). Thus, methyl migration would afford C3-labelled **7***, and isopropyl migration would afford the C4-labelled isomer. While the relative migratory aptitudes of alkyl groups in vinylidene carbenes is evidently unknown, it seems reasonable to suggest that the migratory aptitude of isopropyl is *at least* as large as that of methyl, given the electrophilic nature of alkylidene carbenes (26). The relative proportion of ^{13}C-label at C3 and C4 in **7*** thus indicates that at least 40% of this product must arise via the alkylidene pathway, assuming equal migratory aptitudes for methyl and isopropyl.

Attempts to obtain further evidence for the formation of this intermediate in the photochemistry of **3**, by trapping with 1-hexene or methanol, are inconclusive since no new products were observed upon photolysis in either solvent. We were initially disturbed by our failure to observe *any* new products from photolysis in methanol, since we expected to at least observe allylic ethers corresponding to trapping of the vinylcarbene intermediates by the solvent. There are numerous reports of successful alcohol-trapping experiments with vinylcarbenes derived from arylcyclopropene derivatives (1, 2, 5). Indeed, in aryl systems, alcohol trapping of vinylcarbenes appears to proceed quantitatively (5). We note, however, that Stierman and Johnson have reported similar (negative) results from the photolysis of **2** (as well as 1,2-cyclononadiene) in methanol (19). Evidently, simpler (alkyl-substituted) vinylcarbenes are substantially less reactive towards bimolecular OH insertion than their phenylated counterparts. This can probably be explained in terms of unfavourable frontier molecular orbital interactions in the alkylated systems. One example of intramolecular OH insertion in an alkyl vinylcarbene has been reported (40). Intermolecular trapping of alkylidenes by alkenes is well documented (26*b*), although direct generation of these species has traditionally been carried out by thermal methods. It is possible that the photochemical generation from cyclopropenes yields the alkylidene in an excited state, from which alkyl migration is too fast to allow bimolecular trapping to compete. It should also be recognized that, in the present case, the alkylidene is formed in fairly low (≤7%) yield, and its trapping products could have easily avoided detection under our vpc conditions. Bimolecular vinylcarbene trapping by alkenes has also been reported for a cyclic vinylcarbene derivative in which ring closure to cyclopropene (the predominant fate of acyclic vinylcarbenes) is blocked by geometric constraints (41).

The formation of propyne in low yield from photolysis of

Can. J. Chem. Downloaded from www.nrcresearchpress.com by 186.148.149.217 on 09/07/12
For personal use only.



3 is difficult to explain, since the accompanying presence of propene in the photolysate could not be verified. By a two-bond cleavage pathway, these two products should be formed together, since the latter is the expected observable product of dimethylcarbene. Solvent trapping of the carbene (by C—H insertion) should be noncompetitive with intramolecular H migration to yield propene (42), so it is unlikely that the absence of this product is due to other reaction pathways of the carbene. Two-bond cleavage products are not observed from photolysis of **2** (19), spiro[4.2]hept-6-ene (**1**; eq. [1]) (16), or **4**. We conclude that, in solution, this decomposition pathway is unimportant even for cyclopropenes with high excited singlet state energies.

Summary and conclusions

The present study represents the first investigation of the photochemistry of monocyclic, alkyl-substituted cyclopropene derivatives in solution. Photolysis of these compounds yields a variety of products, most of which are formally derived from the vinylcarbene formed by cleavage of the more highly substituted cyclopropene σ-bond in the excited singlet state. Carbon-13 labelling experiments have demonstrated that alkynes may be formed by two competitive pathways, one involving H-migration in a vinylcarbene intermediate, and the other involving alkyl migration in an alkylidene species. The latter is presumably formed by (concerted (15*c*)) [1,2]-H-migration/ring opening in the cyclopropene excited state, as suggested by recent theoretical calculations of the C_3H_4 ground state surface. Our results indicate that the alkylidene pathway accounts for at least 40% (perhaps more, depending on the relative migrative aptitudes of isopropyl vs. methyl groups in alkylidene carbenes) of the alkyne formed in direct cyclopropene photolysis. Two-bond cleavage of excited cyclopropenes to yield carbenes and alkynes is unimportant in solution, even for cyclopropenes with high excitation energies.

Experimental

The ^{1}H nmr spectra were recorded on Varian EM390 (90 MHz) or Bruker AM500 (500 MHz) spectrometers in carbon tetrachloride (or deuteriochloroform where noted). The ^{13}C nmr spectra were recorded at 62.5 or 125.6 MHz on Bruker WM250 or AM500 spectrometers, respectively. All spectra are reported in parts per million downfield from tetramethylsilane. Mass spectra were recorded on a Finnigan 4000 mass spectrometer with a model 4500 ion source. The mass spectrometer was interfaced with a Finnigan gas chromatograph, equipped with a 60 m × 1.0 μm DB1-30W (Chromatographic Specialties, Inc.) fused silica capillary column. Ultraviolet absorption spectra were recorded in deoxygenated pentane solution using a Perkin–Elmer Lambda 9 spectrometer equipped with a model 3600 data station. Infrared spectra were recorded on a Perkin–Elmer 283 spectrometer as the neat liquids or in carbon tetrachloride or chloroform solution; spectra are reported in wavenumbers, calibrated using the 1601.9 cm^{-1} polystyrene absorption.

Analytical vpc separations were carried out using a Varian 3700 gas chromatograph (injector temperature = 80°C) equipped with a flame ionization detector, a Varian CDS101 or Hewlett–Packard HP-3393a integrator, and one of the following columns: (a) 1.0 μm SPB-1 wide-bore capillary (60 m × 0.75 mm i.d. borosilicate; Supelco, Inc.); or (b) 20% β,β-oxydipropionitrile (ODPN) on 80/100 Chromosorb PNAW (14 ft × 1/8 in. stainless steel; Supelco, Inc.); or (c) 23% SP-1700 on 80/100 Chromosorb PAW (15 ft × 1/4 in. stainless steel; Supelco, Inc.). Relative detector responses toward products and starting materials from photolysis of **3** and **4** (with the exception of propyne) were verified to be approximately unity by analysis of a few standard solutions of authentic samples.

Semipreparative vpc separations employed a Hewlett–Packard 5750B gas chromatograph equipped with a thermal conductivity detector (detector temperature 160°C) and one of the following stainless steel columns: (d) 3.8% UC W982 on 80/100 PNAW (24 ft × 1/4 in.; Supelco Inc.); (e) 20% ODPN on 80/100 Chromosorb PNAW (24 ft × 1/4 in. stainless steel; Supelco Inc.).

n-Pentane (Baker Photrex) and methanol (Caledon HPLC) were used as received from the supplier. Mesityl oxide (Aldrich Chemical Co.) was distilled once before use. 1-Hexene (Aldrich) was distilled four times prior to use and had final optical densities as follows (1.0 mm path length): <210 nm (>3); 220 nm (0.74); 230 nm (0.53). *p*-Toluenesulfonhydrazide, 3,3-dimethyl-2-butanone, *trans*-2-methyl-1,3-pentadiene (**9**), 2,3-dimethyl-1,3-butadiene (**10**), 3-methyl-2-butanone, 2,5-dimethyl-2,4-hexadiene, and sodium hydride were all used as received from Aldrich. 4-Methyl-2,3-pentadiene (**6**; ICN Pharmaceuticals Inc.), 4-methyl-2-pentyne (**7**; Farchan), and (2-^{13}C)-sodium acetate (MSD Isotopes) were also used as received from the suppliers.

1,3,3-Trimethylcyclopropene (3) was synthesized by a variation of the previously published method (30). A suspension of mesityl oxide tosylhydrazone (10 g, 0.038 mol; from mesityl oxide and *p*-toluenesulfonhydrazide (30)) in *o*-dichlorobenzene (40 mL) was added over a period of 1 h to a solution of sodium hydride (1.8 g, 0.076 mol) in refluxing *o*-dichlorobenzene (150 mL), in a two-neck, round-bottom flask fitted with a small Vigreux column. The column head was connected to three sequential cold-traps, which were immersed in Dry Ice/acetone baths. The addition rate of the tosylhydrazone solution and the reaction temperature were controlled in such a manner as to prevent the condensation of any solvent vapours in the cold traps. After the addition of the tosylhydrazone was complete, the reaction flask was heated for an additional 30 min. The contents of the cold traps were combined (3.1 g, ca. 50% **3** by vpc). After bulb-to-bulb distillation,

Can. J. Chem. Downloaded from www.nrcresearchpress.com by 186.148.149.217 on 09/07/12
For personal use only.

Can. J. Chem. Downloaded from www.nrcresearchpress.com by 186.148.149.217 on 09/07/12
For personal use only.

compound **3** was purified (>99.9% purity) by semipreparative vpc (column (d), column temperature 30°C). The material exhibited spectral characteristics (ir, ^{1}H nmr) similar to those previously reported (43).

*1-*tert*-Butyl-3,3-dimethylcyclopropene (**9**)* was prepared in similar fashion from the tosylhydrazone of 2,2,5-trimethylhex-4-en-3-one (44). A solution of glacial acetic acid (25 mL), water (100 mL), and 3,3-dimethylbutanone (40 g, 0.40 mol) was placed in a 500-mL three-neck, round-bottom flask equipped with a reflux condenser, a thermometer, and an addition funnel. The solution was heated to 85°C while bromine (22 mL, 0.38 mol) was added dropwise. After addition of the bromine was complete (ca. 45 min), the solution was stirred for an additional 2 h. The resulting pale yellow mixture was then cooled to 10°C and neutralized with solid sodium carbonate. The resulting oil was separated from the aqueous layer and distilled under vacuum to give a colourless liquid (bp 73°C (25 Torr; 1 Torr = 133.3 Pa); 44 g, 0.25 mol), which was identified as 1-bromo-3,3-dimethylpropan-2-one on the basis of its ^{1}H nmr spectrum (δ($CDCl_3$): 1.25 (s, 9H), 4.23 (s, 2H)).

The bromoketone (10 g, 0.056 mol) and acetone (5 g, 0.086 mol), both dried over 4A molecular sieves, were dissolved in dioxane (100 mL; distilled from sodium) and placed in a 250-mL two-neck, round-bottom flask fitted with a reflux condenser, powder funnel, and gas inlet. A dry nitrogen atmosphere was maintained over the reactants. Freshly activated zinc (45) (5.6 g, 0.086 mol) was added slowly with stirring. After the addition of the zinc was complete, the contents of the flask were stirred for an additional hour and then cooled to room temperature. The solution was dried over anhydrous sodium sulfate and the solvent was partially removed on the rotary evaporator to yield a pale yellow dioxane solution of 2,2,5-trimethylhexan-5-ol-3-one, identified on the basis of its ^{1}H nmr spectrum (δ($CDCl_3$): 1.15 (s, 9H), 1.25 (s, 6H), 2.65 (s, 2H)).

Dehydration of this compound by the previously published method (46) yielded 2,2,5-trimethylhex-4-en-3-one (3.5 g, 0.025 mol, 45% overall yield). Identification was made on the basis of its ^{1}H nmr spectrum (δ($CDCl_3$): 1.12 (s, 9H), 1.90 (s, 3H), 2.10 (s, 3H), 6.33 (br s, 1H).

A solution of the alkenone (5 g, 0.035 mol) and *p*-toluenesulfonhydrazide (6.5 g, 0.035 mol) in methanol (50 mL) was refluxed for 6 h in a 100-mL round-bottom flask. The reflux condenser was then removed and the methanol was allowed to distill until the solution became turbid. The heat source was then removed and enough methanol was added to the solution to remove the turbidity. The solution was allowed to cool slowly to room temperature, affording crystalline 2,2,5-trimethylhex-4-en-3-one tosylhydrazone (2.3 g, 0.0074 mol, 21%, mp 108–113°C), which was identified on the basis of its ^{1}H nmr spectrum (δ($CDCl_3$): 1.40 (s, 3H), 1.80 (s, 3H), 2.40 (s, 3H), 5.30 (s, 1H), 7.25 (s, 1H), 7.35 (s, 1H), 7.78 (s, 1H), 7.88 (s, 1H)).

Base-catalysed thermal decomposition of the tosylhydrazone (4 g, 0.013 mol) by the published method (44) afforded a colourless liquid that was identified as 1-*tert*-butyl-3,3-dimethylcyclopropene (**4**; 0.24 g, 0.0019 mol). The compound was obtained in greater than 99.9% purity after bulb-to-bulb distillation and vpc purification (column (e), column temperature 85°C); ir ($CDCl_3$, cm^{-1}): 3068, 2960, 2930–2875, 1755, 1700, 1588, 1519, 1396; ^{1}H nmr δ(CCl_4): 1.08 (s, 15H), 6.55 (s, 1H) (the singlet at 1.08 ppm can be resolved at high field (250 MHz) into a singlet and a doublet, which integrate 3:2, respectively); δ(C_6D_6): 1.18 (s, 9H), 1.37 (s, 6H), 6.65 (s, 1H); ^{13}C nmr δ(C_6D_6): 28.5, 29.0, 33.0, 109.2, 143.2; ms (*m/e* (I)), 124 (2), 109 (82), 91 (15), 81 (64), 79 (40), 77 (22), 69 (27), 68 (18), 67 (100), 65 (20).

*1-^{13}C-1,3,3-Trimethylcyclopropene (**5**)* was prepared in similar fashion to **3**, from the tosylhydrazone of (2-^{13}C)-mesityl oxide, as a 10% mixture with unlabelled material (**3**). To a suspension of anhydrous sodium acetate (2.25 g, 0.027 mol), (2-^{13}C)-sodium acetate (0.25 g, 0.003 mol, 99.6 at.% ^{13}C), lithium (1 g, 0.15 mol), and glass beads in anhydrous ether (500 mL) was added a solution of 1-bromo-2-methylpropene (12 g, 0.088 mol) in anhydrous ether, dropwise over 20 min (46). A dry argon atmosphere was maintained over the reactants during the entire reaction. After vigorous stirring for 24 h, the reaction mixture was cooled in an ice bath. Excess lithium was removed from the flask and the solution was treated with an excess of saturated aqueous ammonium chloride. The organic portion was separated, dried over anhydrous sodium sulfate, and the solvent was removed carefully on a rotary evaporator while maintaining a bath temperature of ca. 0°C. The product obtained was shown to be a mixture of (2-^{13}C)-4-methyl-3-penten-2-one and 2,5-dimethyl-2,4-hexadiene (2.6 g; ca. 75% mesityl oxide by ^{1}H nmr). The product was used without further purification for the preparation of **5**, using a procedure similar to that outlined above for **3**, and was purified to >99.9% purity by semipreparative vpc (see above). The ^{13}C spectrum of the mixture (δ($CDCl_3$): **131.00**, 112.56, 27.0, 9.97), compared to that of unlabelled **3**, showed it to be approximately 10% enriched at the 1-position (δ 131.0 ppm).

*4-Methyl-1,3-pentadiene (**8**) and* cis*-2-methyl-1,3-pentadiene (*cis*-**9**)* were prepared by dehydration of 2-methyl-2,4-pentanediol according to the published method (45). Purification by semipreparative vpc (columns (d) and (e)) afforded both compounds in greater than 99% purity. *cis*-**9** exhibited the following spectral data: ir (CCl_4): 3082, 2950, 1790, 1640, 1600, 1450, 1370, 885, 665, 515; ^{1}H nmr, δ(CCl_4): 1.64 (d, 3H), 1.70 (s, 3H), 4.67 (s, 1H), 4.78 (s, 1H), 5.35 (m, 1H), 5.67 (d, 1H); ^{13}C nmr, δ(CCl_4): 140.85, 131.83, 124.78, 115.05, 23.29, 14.43.

*1-(2,2-Dimethylcyclopropyl)-2-methylpropene (**14**)* was prepared in 87% yield from 2,5-dimethyl-2,4-hexadiene, diiodomethane, and Zn/Cu couple by a previously described method for the generation of cyclopropanes from alkenes (47), with only slight modification to the general procedure. After work-up, bulb-to-bulb distillation and purification by semipreparative vpc (column (d), column temperature 80°C) afforded **14** in greater than 99% purity. The ^{1}H and ^{13}C nmr spectra of the compound agreed satisfactorily with those previously reported (47).

*2,3,5-Trimethyl-2,4-hexadiene (**15**)*

Finely chopped lithium (0.23 g, 0.033 mol) and about 50 glass beads were added to anhydrous ether (100 mL) in a two-neck round-bottom flask fitted with a reflux condenser, magnetic stirrer, and dropping funnel. A slight positive pressure of dry argon was maintained inside the reaction flask. A solution of 1-bromo-2-methyl-propene (48) (4 g, 0.03 mol) in anhydrous ether (30 mL) was added dropwise to the reaction flask with vigorous stirring, controlling the addition rate to maintain a gentle reflux. After the addition of the bromide was complete, the reaction was stirred for an additional 15 min. A solution of 3-methyl-2-butanone (2.6 g, 0.03 mol) in anhydrous ether (30 mL) was then added dropwise to the mixture. Following addition of the ketone, the reaction mixture was stirred at room temperature for an additional hour. The reaction mixture was quenched with 5% aqueous HCl, the ether layer was separated, and the remaining aqueous fraction was extracted with ether (3 × 25 mL). The combined ether extracts were washed with water and dried over anhydrous sodium sulfate. Evaporation of the solvent on the rotary evaporator afforded a pale yellow oil (3.5 g, 0.025 mol, 82%), which was identified as 2,3,5-trimethylhex-4-en-3-ol on the basis of its ^{1}H nmr spectrum. The alkenol (3.5 g, 0.025 mol) and a crystal of *p*-toluenesulfonic acid were dissolved in benzene (150 mL), and the resulting solution was refluxed for 4 h in a 250-mL round-bottom flask fitted with a small Dean–Stark trap and reflux condenser. The solution was then cooled to room temperature and the solvent was removed on the rotary evaporator, affording a yellow oil (2.7 g, 0.022 mol, 87%). Bulb-to-bulb distillation followed by semipreparative vpc (column (e), column temperature 80°C) yielded a colourless liquid in greater than 99.5% purity, which was identified as 2,3,5-trimethyl-2,4-hexadiene (**15**) by comparison of its ir and ^{1}H nmr spectra with previously reported data (49).

Photochemical experiments employed the pulses (193 nm, ca. 10 ns, 20–100 mJ, 2.0 and 0.25 Hz repetition rate for quantitative and preparative photolyses, respectively) from a Lumonics TE-861M excimer laser filled with an argon/fluorine/helium mixture, a 10-W Osram HNS 10W/U OZ low pressure mercury lamp (185 + 254 nm),

Can. J. Chem. Downloaded from www.nrcresearchpress.com by 186.148.149.217 on 09/07/12
For personal use only.

a 16-W zinc resonance lamp (Philips 93106E; 214 nm), or a 16-W cadmium spectral lamp (G. W. Gates & Co.; 228 nm). The lamps were given a 20-min warm-up period before each experiment and were cooled with a stream of dry nitrogen.

Preparative photolyses were carried out with the laser in rectangular cells constructed from 10 × 20 mm rectangular Suprasil tubing (Vitro Dynamics). The solutions were deoxygenated before irradiation with dry nitrogen, and agitated during irradiation with a small magnitude stirrer.

The products from photolysis of **3** were identified by coinjecting photolysates carried to ca. 5% conversion with authentic samples on at least two vpc columns, and by comparison of the ^{1}H nmr spectra of isolated (from preparative runs carried to 20–25% conversion; by vpc with column (e)) samples with those of the authentic samples.

Compounds **11–13** and **16** were isolated from a preparative photolysis of **4** in *n*-pentane by semipreparative vpc (column (e)). They were identified on the basis of their ir, nmr (^{1}H and ^{13}C), and gc/ms spectra, and comparisons of the ^{1}H nmr spectra with published data. Compounds **14** and **15** were identified by coinjection of authentic samples with a photolysate carried to ca. 5% conversion on two vpc columns and by gc/ms comparisons to the authentic materials.

*2,2,5-Trimethyl-2,3-hexadiene (**11**)*: ^{1}H nmr (ref. 50), δ: 1.10 (d, 6H), 1.51 (s, 9H), 2.50 (m, 1H); ms, *m/e* (I): 124 (38), 109 (42), 81 (22), 79 (17), 77 (18), 68 (35), 67 (100), 65 (15).

*2,2,5-Trimethyl-3-hexyne (**12**)*: ^{13}C nmr (ref. 51), δ: 87.64, 83.93, 31.17, 30.60, 23.27, 20.07; ms, *m/e* (I): 124 (7), 109 (39), 81 (33), 79 (19), 77 (39), 67 (100). The ^{1}H nmr spectrum of this compound agreed with that previously published (50).

trans-*2,5,5-Trimethyl-1,3-hexadiene (**13**)*: ir ($CDCl_3$): 2962, 2865, 1607, 1551, 1437, 1364, 1263, 1202, 1007; ^{1}H nmr, δ: 1.06 (s, 9H), 1.80 (s, 3H), 4.87 (s, 2H), 5.6 (d, 1H), 6.05 (d, 1H); ^{13}C nmr, δ: 18.5, 29.5, 32.7, 114.2, 127.4, 141.3, 142.0; ms, *m/e* (I): 124 (28), 109 (100), 81 (29), 79 (18), 67 (77).

*2-Methyl-(3-*tert*-butyl)-1,3-butadiene (**16**)*: ^{1}H nmr (500 MHz), δ: 1.09 (s, 9H), 1.87 (t, 3H), 4.64 (m, 1H), 4.71 (d, 1H), 4.84 (m, 1H), 4.86 (d, 1H); ^{13}C nmr, δ: 25.8, 29.8, 35.4, 108.7, 113.0, 147.4, 161.4; ms, *m/e* (I) = 124 (12), 109 (100), 81 (29), 79 (15), 68 (36), 67 (92).

Quantitative photolyses were carried out at ambient temperature (ca. 23°C) in 10 × 25 mm cylindrical Suprasil quartz cells (Hellma). In all cases, the sample was agitated during irradiation with a small magnetic stirrer or with a mechanical shaker. Solutions were deoxygenated before irradiation by bubbling dry nitrogen or argon through the cooled (to ca. 0°C) solutions for 5–15 min. Photolysis solutions were monitored between 0.25 and 5% conversion, with aliquots being withdrawn at suitable time intervals (every 50–100 laser pulses) for vpc analysis on column (b). Relative product yields were determined from triplicate vpc analysis. The yields listed in eqs. [5] and [6] for the photolyses (193 nm) of **3** and **4** in pentane represent the averages of the determinations at several conversions below 5%.

Carbene trapping experiments were attempted in deoxygenated methanol (0.1 M **3**, 214 nm) and 1-hexene (0.1 M **3**, 228 nm) solution. The pure methanol and methanol/**3** solutions had uv absorbances (1 mm pathlength) of 0.15 and >5 respectively at 214 nm. Similarly, the 1-hexene and 1-hexene/**3** solution had uv absorbances of 0.7 and >5 respectively at 228 nm. In both experiments, aliquots were taken at various irradiation times, up to 6–10% conversion, and analysed by vpc (column (a)). In both cases, the product distributions were indistinguishable from those obtained in control runs at each wavelength using deoxygenated *n*-pentane as solvent.

The ^{13}C-labelled products **6*–10*** were isolated by semipreparative vpc (column (e)) from the preparative photolysis of **5**. Their identities were verified on the basis of their ^{1}H and ^{13}C nmr spectra. Single-pulse ^{13}C nmr spectra of **8*–10*** were measured at 62.5 MHz in $CDCl_3$ in the presence of $Cr(acac)_3$, with a delay of 0.6 s between pulses. Prior to obtaining the Fourier transform, 10^4–10^5 acquisitions were signal-averaged in 16K of memory, and processed with 40-Hz line-broadening. The spectra were compared to those of the unlabelled compounds recorded under the same conditions. The positions of the ^{13}C-label in **6*–10*** are indicated below with boldface text.

*2-Methyl-2,3-pentadiene (**6***)*: ^{13}C nmr, δ: **203.43**, **93.86**, 83.57, 20.61, 14.90.

*4-Methyl-2-pentyne (**7***)*: ^{13}C nmr, δ: **84.97**, **74.37**, 23.19, 20.34, 3.29.

*4-Methyl-1,3-pentadiene (**8***)*: ^{13}C nmr, δ: 135.64, **133.35**, 125.84, 113.98, 25.74, 18.09.

trans-*2-Methyl-1,3-pentadiene (**9***)*: ^{13}C nmr, δ: 142.05, 134.07, **125.27**, 113.69, 18.56, 17.98.

*2,3-Dimethyl-1,3-butadiene (**10***)*: ^{13}C nmr, δ: **143.29**, 112.71, 20.36.

Quantitative ^{13}C nmr integrations were carried out with solutions of **6*** and **7*** (ca. 0.05 M) and $Cr(acac)_3$ (ca. 0.01 M) in $CDCl_3$ using an inverse gate decoupling pulse sequence (33*a*). Carbon T_1 measurements were carried out for **6** and **7** on the Bruker AM500, and employed a π–τ–$\pi/2$ nonselective inversion–recovery pulse sequence. In the presence of $Cr(acac)_3$, the carbon T_1 values were found to vary between 0.6 and 1.1 s for both compounds. A delay of 7 s was therefore used between acquisitions for quantitative integrations.

For **6***, 10^4 free induction decays were recorded and signal-averaged in 16K of memory, and were processed with baseline correction and 40-Hz line-broadening prior to obtaining the Fourier transform. Comparison to a spectrum of unlabelled **6** recorded under the same conditions revealed relative signal enhancements for only the peaks due to C3 (203.43 ppm) and C4 (93.86 ppm); the relative intensities of the peaks due to all other carbons in the molecule were indistinguishable from those in the unlabelled material. Enrichment factors at C3 and C4 were then calculated using the integrals for the other carbon signals as a standard. The enrichment factors for **6*** reported in eq. [7] are the average of three independent determinations, and the error is quoted as a single standard deviation of the mean.

The more rigorous procedure employed for **7*** has been described in detail elsewhere (34). Briefly, spectra were recorded for a solution of **7*** and $Cr(acac)_3$ in $CDCl_3$ in a 5-mm nmr tube in which was placed a coaxial insert containing a $CDCl_3$ solution of ethanol of accurately measured concentration. The latter functioned as an external integration standard. For **7***, 10^3 free induction decays was recorded and signal-averaged in 16K of memory, and were processed with baseline correction, 40-Hz line-broadening, and zero-filling to 64K, followed by the Fourier transform. The integrals for each carbon in the spectrum were measured as the peak heights. Ten such spectra were recorded, and the peak heights of the signals due to **7*** relative to those due to the standard were averaged. The procedure was repeated for six different concentrations of the ethanol external standard, and the results plotted against inverse ethanol concentration. The slopes of these plots are proportional to the number of ^{13}C nuclei in the sample for each carbon. Comparison to data obtained for a sample of unlabelled **7** by a similar procedure reveals that only the signals due to C3 (84.97 ppm) and C4 (74.37 ppm) are enhanced in the labelled material. Enrichment factors at C3 and C4 were then calculated using the integrals (slopes of the above plots) for the other carbon signals as a standard, and are listed in eq. [7]. The errors were calculated using the standard deviations from least-squares analysis of the intensity vs. $[\text{ethanol}]^{-1}$ plots.

Acknowledgments

We thank Professor A. D. Bain (McMaster University) for his help with the ^{13}C nmr analyses, Professor R. E. Hill (McMaster University) for the gc/ms analyses, and Mr. B. Sayer for technical assistance. The financial support of this work by the Natural Sciences and Engineering Research Council of Canada is gratefully acknowledged.

1. A. Padwa. Org. Photochem. **4**, 261 (1979).
2. A. Padwa. Acc. Chem. Res. **12**, 310 (1979).
3. M. G. Steinmetz, R. Srinivasan, and W. J. Leigh. Rev. Chem. Intermed. **5**, 57 (1984).

4. H. DURR. J. Liebigs Ann. Chem. **723**, 102 (1969).
5. J. A. PINCOCK, R. MORCHAT, and D. R. ARNOLD. J. Am. Chem. Soc. **95**, 7536 (1973).
6. A. PADWA, T. J. BLACKLOCK, D. GETMAN, N. HATANAKA, and R. LOZA. J. Org. Chem. **43**, 1481 (1978).
7. A. PADWA, T. J. BLACKLOCK, D. M. CORDOVA, and R. LOZA. J. Am. Chem. Soc. **102**, 5648 (1980).
8. H. E. ZIMMERMAN and S. A. FLEMING. J. Am. Chem. Soc. **105**, 622 (1983).
9. R. HOFFMANN, G. D. ZEISS, and W. VAN DINE. J. Am. Chem. Soc. **90**, 1485 (1968).
10. S. D. PEYERIMHOFF and R. J. BUENKER. Theor. Chem. Acta, **14**, 305 (1969).
11. L. SALEM and C. ROWLAND. Angew. Chem. Int. Ed. Engl. **11**, 92 (1972).
12. J. H. DAVIS, W. A. GODDARD III, and R. G. BERGMAN. J. Am. Chem. Soc. **98**, 4015 (1976); **99**, 2427 (1977).
13. J. A. PINCOCK and R. J. BOYD. Can. J. Chem. **55**, 2482 (1977).
14. A. SEVIN and L. ARNAUD-DANON. J. Org. Chem. **46**, 2346 (1981).
15. (*a*) W. HONJOU, J. PACANSKY, and M. YOSHIMINE. J. Am. Chem. Soc. **106**, 5361 (1984); (*b*) J. Am. Chem. Soc. **107**, 5332 (1985); (*c*) M. YOSHIMINE, J. PACANSKY, and N. HONJOU. J. Am. Chem. Soc. **111**, 2785 (1989).
16. M. G. STEINMETZ, Y. P. YEN, and G. K. POCK. J. Chem. Soc. Chem. Commun. 1504 (1983).
17. M. G. STEINMETZ, E. J. STARK, Y.-P. YEN, R. T. MAYES, and R. SRINIVASAN. J. Am. Chem. Soc. **105**, 7209 (1983).
18. M. G. STEINMETZ and R. T. MAYES. J. Am. Chem. Soc. **107**, 2111 (1985).
19. T. J. STIERMAN and R. P. JOHNSON. J. Am. Chem. Soc. **105**, 2492 (1983); **107**, 3971 (1985).
20. J. D. PRICE and R. P. JOHNSON. J. Am. Chem. Soc. **107**, 2187 (1985).
21. M. W. KLETT and R. P. JOHNSON. J. Am. Chem. Soc. **107**, 3963 (1985).
22. O. L. CHAPMAN. Pure Appl. Chem. **40**, 511 (1974).
23. G. W. GRIFFIN. Angew. Chem. Int. Ed. Engl. **10**, 537 (1971).
24. W. J. LEIGH and R. SRINIVASAN. Acc. Chem. Res. **20**, 107 (1987).
25. (*a*) R. WALSH. J. Chem. Soc. Faraday Trans. 1, **72**, 2137 (1976); (*b*) I. M. BAILEY and R. WALSH. J. Chem. Soc. Faraday Trans. 1, **74**, 1146 (1978).
26. (*a*) P. J. STANG and M. G. MANGUM. J. Am. Chem. Soc. **97**, 6478 (1975); (*b*) P. J. STANG. Acc. Chem. Res. **11**, 107 (1978).
27. J. WOLINSKY, G. W. CLARK, and P. C. THORSTENSON. J. Org. Chem. **41**, 745 (1976).
28. R. SRINIVASAN. J. Chem. Soc. Chem. Commun. 1041 (1971).
29. R. D. STREEPER and P. D. GARDNER. Tetrahedron Lett. 767 (1973).
30. G. L. CLOSS, L. E. CLOSS, and W. A. BOLL. J. Am. Chem. Soc. **85**, 3796 (1963).
31. E. A. BRAUDE and J. A. COLES. J. Chem. Soc. 2012 (1950).
32. K. B. CLARK and W. J. LEIGH. J. Am. Chem. Soc. **109**, 6086 (1987).
33. (*a*) A. E. DEROME. *In* Modern NMR techniques for chemistry research. *Edited by* J. E. Baldwin. Pergamon Press, New York. 1987; (*b*) R. FREEMAN, H. D. W. HILL, and R. KAPTEIN. J. Magn. Reson. **7**, 327 (1972).
34. A. D. BAIN, B. J. FAHIE, T. KOSLUK, and W. J. LEIGH. Magn. Reson. Chem. Submitted.
35. (*a*) R. S. HUTTON, M. L. MANION, H. D. ROTH, and E. WASSERMAN. J. Am. Chem. Soc. **96**, 4680 (1974); (*b*) O. L. CHAPMAN. Pure Appl. Chem. **6**, 1649 (1974); (*c*) D. R. ARNOLD, R. W. HUMPHREYS, W. J. LEIGH, and G. E. PALMER. J. Am. Chem. Soc. **98**, 6225 (1976).
36. E. J. YORK, W. DITTMAN, J. R. STEVENSON, and R. G. BERGMAN. J. Am. Chem. Soc. **94**, 2882 (1972); **95**, 5680 (1973).
37. (*a*) J. A. PINCOCK and A. A. MOUTSOKAPAS. Can. J. Chem. **55**, 979 (1977); (*b*) H. E. ZIMMERMAN and R. A. BUNCE. J. Org. Chem. **47**, 3377 (1982).
38. H. E. ZIMMERMAN and D. J. KREIL. J. Org. Chem. **47**, 2060 (1982).
39. J. MICHL. Mol. Photochem. **4**, 243 (1972); **4**, 257 (1972).
40. A. C. DAY and M. C. WHITING. J. Chem. Soc. C, 1719 (1966).
41. M. JONES and G. R. CHAMBERS. J. Am. Chem. Soc. **102**, 4516 (1980).
42. W. J. BARON, M. R. DECAMP, M. E. HENDRICK, M. JONES, JR., R. H. LEVIN, and M. B. SOHN. *In* Carbene chemistry. *Edited by* W. Kirmse. Academic Press, New York. 1964. Chap. 1.
43. G. L. CLOSS and L. E. CLOSS. J. Am. Chem. Soc. **83**, 1003 (1961); **85**, 7536 (1963).
44. S. MURAHASHI, K. OKUMURA, T. NAOTO, and S. NAGASE. J. Am. Chem. Soc. **104**, 2466 (1982).
45. (*a*) G. B. BACHMAN and C. G. GOEBEL. J. Am. Chem. Soc. **64**, 787 (1942); (*b*) F. A. KERDESKY, R. J. ARDECKY, M. V. LAKSHMIKANTHAM, and M. P. CAVA. J. Am. Chem. Soc. **103**, 1992 (1981).
46. J. COLONGE and J. GRENET. C.R. Acad. Sci. **234**, 1181 (1952).
47. (*a*) H. E. SIMMONS and R. D. SMITH. J. Am. Chem. Soc. **81**, 4256 (1959); (*b*) C. P. CASEY, W. H. MILES, and H. TUKADA. J. Am. Chem. Soc. **107**, 2924 (1985).
48. E. A. BRAUDE and E. A. EVANS. J. Chem. Soc. 3324 (1955).
49. (*a*) D. P. G. HAMON. Aust. J. Chem. **28**, 2641 (1975); (*b*) R. P. THUMMEL and B. RICKBORN. J. Org. Chem. **37**, 4250 (1972).
50. R. M. FANTAZIER and M. L. POUTSMA. J. Am. Chem. Soc. **90**, 5490 (1968).
51. J. M. KORNPROBST and J. P. DOUCET. J. Chim. Phys. **71**, 1129 (1974).

Can. J. Chem. Downloaded from www.nrcresearchpress.com by 186.148.149.217 on 09/07/12
For personal use only.

The reactions of nitrosoarenes with cationic cyclohexadienyl complexes of iron tricarbonyl: an ESR study

LIJUAN LI, RICHARD E. PERRIER, DONALD R. EATON,[1] AND MICHAEL J. MCGLINCHEY
Department of Chemistry, McMaster University, Hamilton, Ont., Canada L8S 4M1

Received March 31, 1989

This paper is dedicated to Professor Ronald J. Gillespie on the occasion of his 65th birthday

LIJUAN LI, RICHARD E. PERRIER, DONALD R. EATON, and MICHAEL J. MCGLINCHEY. Can. J. Chem. **67**, 1868 (1989).

The reactions of nitrosoarenes with the (cyclohexadienyl)$Fe(CO)_3$ cation have been investigated by using electron spin resonance spectroscopy. The radicals produced are nitroxides of the type $(OC)_3Fe(C_6H_7)(Ar)N—O•$ but, in some cases, disproportionation and loss of the metal carbonyl fragment leads to the corresponding $C_6H_5(Ar)N—O•$ radical. With bulky nitrosoarenes, such as C_6Me_5NO, isomers are observed in which the aryl ring rotation is slow on the ESR time scale. The analogous reactions with the cyclohexadienyl cation derived from the B ring of (ergosteryl acetate)$Fe(CO)_3$ lead to initial attack not at one of the termini of the delocalized system but rather at the central carbon, i.e., at C-7. Subsequent hydrogen migration leads to the (5,7-diene)$Fe(CO)_3$ complex bearing the arylnitroxide at the 7-position. The mechanisms of these reactions are discussed.

Key words: nitrosoarenes, iron cations, ESR.

LIJUAN LI, RICHARD E. PERRIER, DONALD R. EATON et MICHAEL J. MCGLINCHEY. Can. J. Chem. **67**, 1868 (1989).

Utilisant la spectroscopie RPE, on a étudié les réactions des nitrosoarènes avec le cation (cyclohexadiényl)$Fe(CO)_3$. Les radicaux qui sont produits sont des nitroxydes du type $(OC)_3Fe(C_6H_7)(Ar)N—O•$; toutefois, dans quelques cas, il se produit une disproportionation et la perte du fragment métallocarbonyle conduit à la formation du radical $C_6H_5(Ar)N—O•$ correspondant. Avec des nitrosoarènes encombrés, comme le C_6Me_5NO, on observe la formation d'isomères dans lesquels la rotation du noyau aryle est lente pour l'échelle de temps de la RPE. Les réactions analogues effectuées sur le cation cyclohexadiényle dérivé du cycle B de l'(acétate d'ergostéryle)$Fe(CO)_3$ conduisent à une première attaque qui s'effectue sur le carbone central, C-7, et non sur les extrémités du système délocalisé. Une migration subséquente d'hydrogène conduit au complexe (5,7-diène-$Fe(CO)_3$ portant le nitroxyde d'aryle en position 7. On discute des mécanismes de ces réactions.

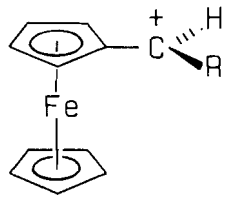
Mots clés : nitrosoarènes, cations du fer, RPE.

[Traduit par la revue]

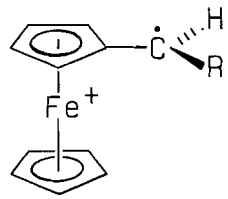
Introduction

Nitroso compounds have been used extensively for spin trapping (1). Their use for this purpose has been particularly developed by Terabe *et al.* (2–4). The chemistry involved is rather straightforward. An unstable radical R• reacts rapidly with a nitroso compound R′NO to give a stable nitroxide radical RR′N—O•. The ESR spectrum of the nitroxide radical may be examined at leisure and the structure of the short-lived radical R• inferred from the analysis. The technique has been extensively applied to the identification of free radicals generated by the photolysis of organometallic compounds (5). A number of reactions are also known in which nitroxide radicals are generated by the reactions of nitroso compounds with diamagnetic materials. In these cases, the chemistry must be rather more complex since two diamagnetic spin-paired molecules react to give an odd electron radical. The reactions with certain olefins, for which an "ene" mechanism has been suggested (6–8), are perhaps the best characterized.

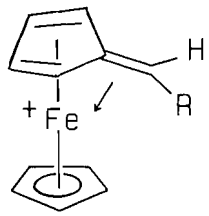
There are also several reports in which the reaction of nitroso compounds with diamagnetic organometallic complexes yields nitroxide radicals. Cais and co-workers (9, 10) studied the reactions of nitrosobenzene with cationic iron complexes with substituted cyclopentadienyl, cycloheptadienyl, and other dienyl ligands. In the first type of compound the ferrocene **1***a* had a CHR^+ substituent and it was suggested that reaction might occur via a structure **1***b* containing Fe^{3+} and CHR• moieties. Spin trapping of the latter fragment seemed a very reasonable experiment to try. Nitroxide radicals corresponding to addition at the CHR group were indeed detected but the observation that the precursor CH_2OH compounds gave the same products with



1*a*



1*b*

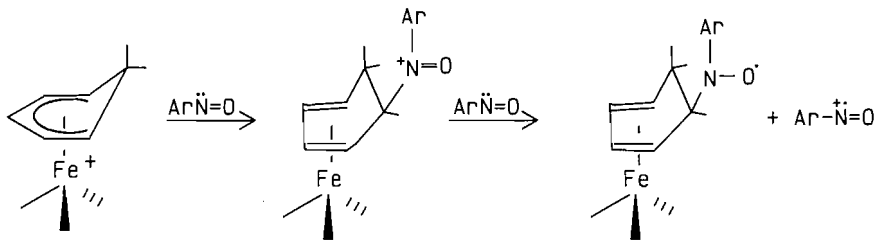


1*c*

equal ease cast doubts on the radical mechanism. An alternative mechanism involving nucleophilic attack by the nitrosobenzene was suggested. Subsequent X-ray crystallographic studies of both iron and osmium analogues of **1** reveal that the exocyclic methylene is bent towards the metal by ≈20°, and so the best representation of the ferrocenylmethyl cation may well be that shown in **1***c* (11, 12) Returning to the reactions of nitroso compounds with organometallic molecules, we note that Belousov and Kolosova have recently reported the reactions of 2-methyl-2-nitrosopropane with a number of iron carbonyls. A variety of radicals, including some nitroxides, were observed by ESR and the mechanisms of the reactions discussed in some detail (13).

[1]Author to whom correspondence may be addressed.

Can. J. Chem. Downloaded from www.nrcresearchpress.com by 194.225.253.170 on 09/07/12
For personal use only.



2

3*a* Ar = C_6H_5
b Ar = C_6Me_4H
c Ar = C_6Me_5

In the present paper, we describe initially the reactions of several nitroso compounds with the [(η^5-cyclohexadienyl)tricarbonyliron(I)]$^+$ cation, **2**. This complex, which is particularly notable for the stabilization of the organic cation brought about by complexation, should provide a site for facile nucleophilic attack by the nitroso compound. This complex is also a model for cationic derivatives of steroids, and spin labelling of the steroidal system (14) has considerable potential for structural and stereochemical studies. Thus, having established the reactivity pattern for the model system **2**, we then describe the behavior of several nitrosoarenes with the novel cation **4** in which the metal-stabilized cyclohexadienyl system is located in the steroidal B ring (15).

Results

[(η^5-Cyclohexadienyl)tricarbonyliron(I)]$^+$ tetrafluoroborate, **2**, was allowed to react with nitrosobenzene, nitroso-2,3,5,6-tetramethylbenzene (nitrosodurene), and also with nitrosopentamethylbenzene. In each case nitroxide radicals were detected by ESR spectroscopy and we describe each separately since their reactions are not identical.

Reaction of 2 with C_6H_5NO

Upon mixing a well-degassed solution of **2** in acetonitrile with nitrosobenzene at ambient temperature, an ESR spectrum appears within about 20–30 min. This spectrum (see Fig. 1a) comprises a triplet of quintets. The triplet structure is ascribed to ^{14}N hyperfine splitting (a_N = 11.2 G) and the pseudo-quintet to ^1H coupling where four protons exhibit almost equivalent hyperfine coupling (a_H = 3.0 G). The radical has a g value of 2.0067 and the spectrum remains unchanged after several days in a sealed ESR tube. The spectrum disappears if the tube is irradiated with a high pressure mercury lamp and in this case no other ESR signal is observed. The spectrum illustrated in Fig. 1a is attributed to the nitroxide radical **3***a* formed by addition of C_6H_5NO to the cationic carbon atom of the iron complex **2**.

If the above reaction is carried out in dichloromethane rather than in acetonitrile, the same ESR spectrum is initially observed. However, this radical is not stable in CH_2Cl_2 and, after 1 day, a complex spectrum develops, which eventually simplifies to that shown in Fig. 1c. This latter radical is very stable and has been identified as diphenylnitroxide. A simulated spectrum using literature hyperfine coupling constants (16) is presented as Fig. 1d. Although $(C_6H_5)_2NO\bullet$ is clearly the major product of the reaction, there are also some additional lines from a second radical. During this reaction the colour of the solution changes from yellowish-green to dark yellow and the formation of some brown precipitate is observed. The ESR parameters obtained from the above spectra are collected in Table 1.

Reaction of 2 with C_6HMe_4NO

Nitrosodurene has some advantage over nitrosobenzene as a spin trap in that the resulting ESR spectra are generally simpler and hence easier to analyse. In the solid, and also in solution, nitrosodurene exists as a colourless dimer (17). When such a solution is warmed a light green colour appears and this has been attributed to dissociation of the dimer to reactive monomer. It was found that, even at room temperature when the concentration of monomer is very small, nitrosodurene reacts with **2** and the product gives an ESR spectrum. The mixture of the cationic iron complex, **2**, and C_6HMe_4NO is not soluble in either pure acetonitrile or pure chloroform; there is, however, sufficient solubility in a 1:1 mixture of these solvents to obtain ESR spectra. The initial spectrum (Fig. 2a) is a triplet of doublets (a_N = 13.75 G, a_H = 3.6 G, g = 2.0069) as anticipated. However, over a period of several days, new and more complex spectra appear as shown in Fig. 2b. The final spectrum (Fig. 2c) corresponds to a very stable radical and no subsequent changes were observed over a further period of 4 days. Very similar spectra were obtained in CH_3CN/CH_2Cl_2 (1:1) mixtures. However, if the reaction is run in a 1:1 mixture of dimethylsulfoxide and benzene there is evidence for a second less abundant radical and the spectrum (Fig. 3a) can be simulated (Fig. 3b) as a superposition of two six-line spectra with an intensity ratio of 4:1. The parameters extracted from this analysis were a_N = 13.4 G, a_H = 3.3 G, and g = 2.0068 for the more intense species and a_N = 13.95 G, a_H = 12.3 G, g = 2.0060 for the minor component. It may be noted that the parameters for the more intense species are very similar to those obtained in $CH_3CN/CHCl_3$ mixtures. These spectra also changed with time to give initially a complex spectrum (Fig. 3c) but finally reverted to a six-line spectrum (Fig. 3d) very similar to the initial more intense spectrum. Further spectra were obtained in other mixed solvent systems containing chloroform or methylene chloride in addition to benzene and DMSO. The radicals obtained were essentially the same as those of Fig. 3, suggesting that acetonitrile is necessary to obtain the spectrum shown in Fig. 2c. Hyperfine coupling constants and g values obtained from the nitrosodurene spectra are collected in Table 2.

Reaction of 2 with C_6Me_5NO

The reaction was examined in mixtures of DMSO and benzene (1:1) and in benzene alone. The results in the two solvent systems were very similar. In both cases, the initial spectra consisted principally of two six-line patterns, which in this case were of roughly equal intensity. There are two additional lines in the wings of the spectrum that we are unable to assign. The hyperfine parameters obtained from the two six-line spectra are very similar to those obtained from the corresponding nitroso-

Can. J. Chem. Downloaded from www.nrcresearchpress.com by 194.225.253.170 on 09/07/12
For personal use only.

Can. J. Chem. Downloaded from www.nrcresearchpress.com by 194.225.253.170 on 09/07/12
For personal use only.

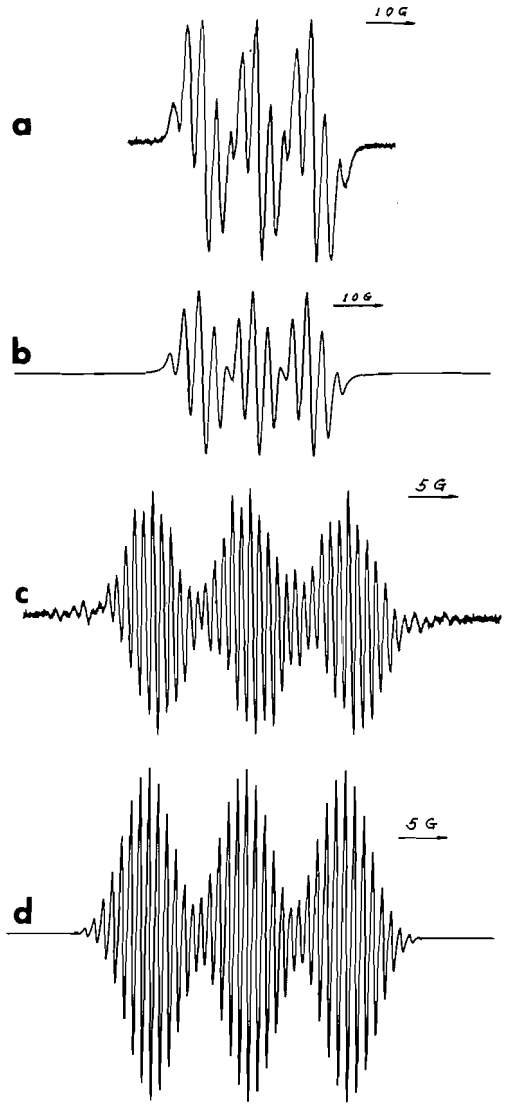


FIG. 1. ESR spectra from the reaction of **2** with C_6H_5NO (a) in CH_3CN; (b) simulation of (a) using the data in Table 1; (c) in CH_2Cl_2 after 6 days; (d) simulation of $(C_6H_5)_2N$—O• using data from ref. 20.

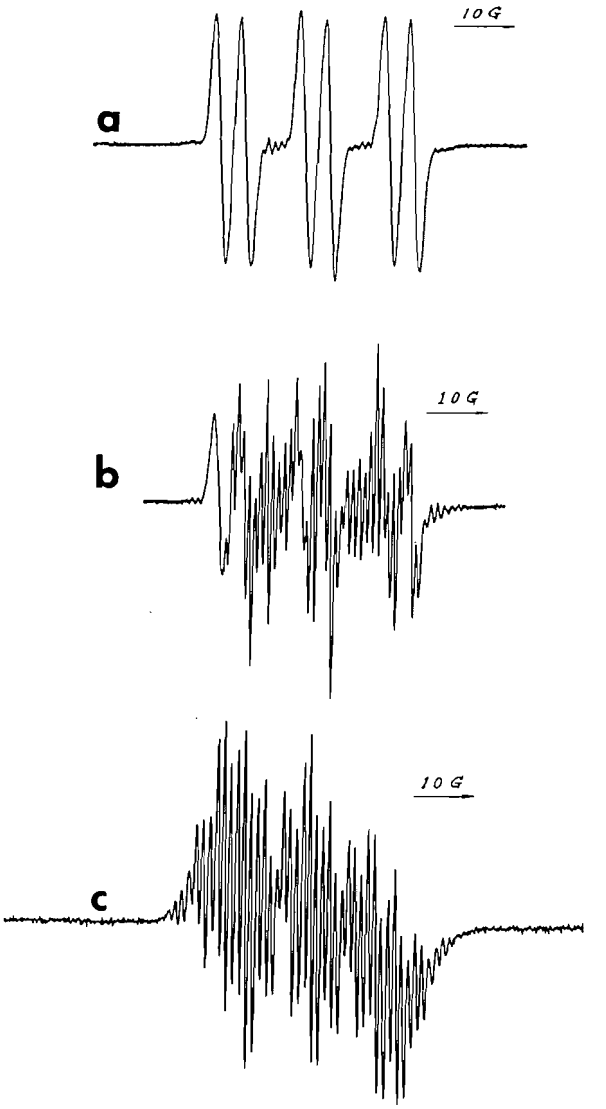


FIG. 2. ESR spectra from the reaction of **2** with C_6Me_4HNO in 1:1 $CH_3CN/CHCl_3$ (a) after 30 min; (b) after 20 h; (c) after 4 days.

durene reaction. On standing, more complex, but not analysable, spectra appear. Eventually most of the additional lines disappear and a six-line spectrum corresponding to one of the original spectra is left, as was the case for nitrosodurene in the DMSO/benzene solvent mixture. The data for this set of spectra are given in Table 2.

*Reaction of **4** with C_6H_5NO*

The steroidal cation **4** reacts with nitrosobenzene in acetonitrile solution almost immediately and causes a colour change from yellowish-green to yellow and, after a day, to red. The spectrum shown in Fig. 4a is that observed after ≈3 h and exhibits the expected triplet pattern for the nitrogen coupling as well as the hyperfine interactions with the phenyl protons. However, there is an extra and unanticipated relatively large doublet splitting (2.95 G) that, over the course of 24 h, gradually disappears. The final spectrum (Fig. 4b) still exhibits hyperfine coupling to the C_6H_5N moiety but the 2.95 G doublet splitting has disappeared. The data are collected in Table 1.

*Reaction of **4** with C_6Me_5NO*

The ESR spectrum initially produced when **4** reacts with nitrosopentamethylbenzene reveals a triplet of doublets overlapping a simple triplet (Fig. 5a); over a period of 10 h the latter feature (i.e., the triplet) gradually increases at the expense of the former. The final spectrum (after 21 h) is shown as Fig. 5d and exhibits a hyperfine interaction only with nitrogen.

*Reaction of **4** with C_6HMe_4NO*

Nitrosodurene and **4** give ESR spectra almost identical to those produced in the analogous nitrosopentamethylbenzene reaction.

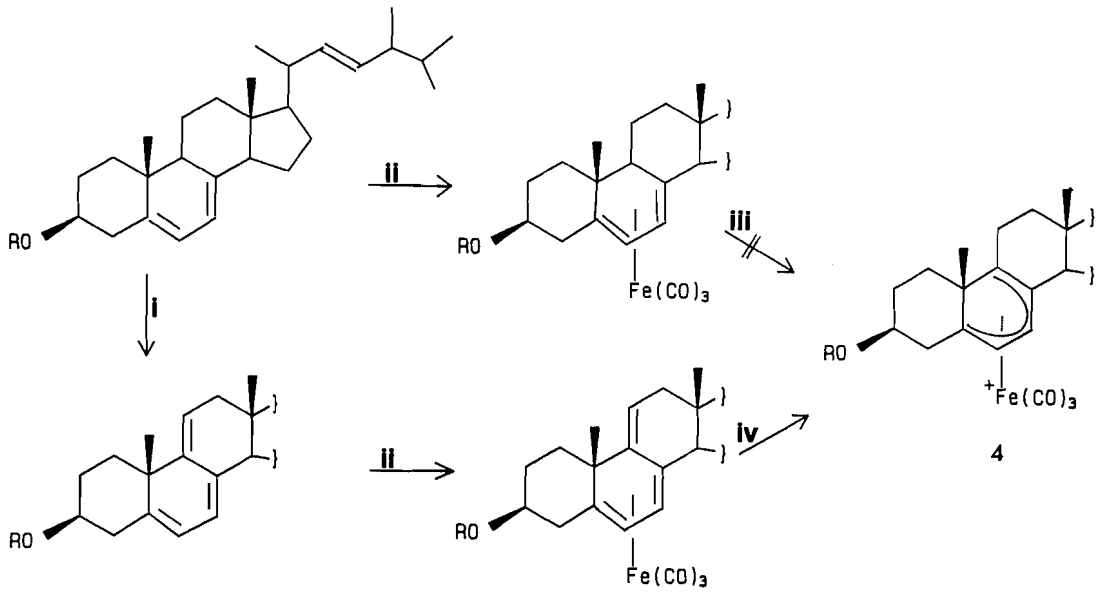
Discussion

$[(Cyclohexadienyl)Fe(CO)_3]^+$ systems such as **2** are thermally stable, air-stable cations that react readily with nucleophiles (18) and so are valuable synthetic intermediates. Steroidal analogues of **2** are also known in which the delocalized system is sited in the A ring. It is only very recently that B ring cationic systems have become available. Attempts to remove the 9α hydrogen from the iron tricarbonyl complex of ergosteryl acetate are thwarted by the bulk of the organometallic fragment, which hinders the approach of the trityl cation that is normally used as the hydride abstracting agent. Instead, a multistep route

TABLE 1. ESR parameters for phenylnitroxide radicals

Substances	Solvent	Temperature	*g* factor;	*a* value(G)	Ref.
$(CO)_3FeC_6H_7N$—Ph | O•	CH_2Cl_2	293 K	2.006$_7$	N: 11.2 H(*o*, *p*): 3.0 H(CH): 3.0	This work
	CH_3CN	293 K	2.006$_7$	N: 11.2 H(CH): 3.0 H(*o*, *p*): 3.0	This work
$(CO)_3FeC_7H_9N$—Ph | O•	CH_2Cl_2	293 K		N: 11.1 H(CH): 2.95 H(*o*, *p*): 3.0	10
$C_5H_5FeC_5H_4CH$—N—Ph | | Ph O•	CH_2Cl_2	Room temp.	2.006$_7$	N: 10.90 H(CH): 2.95 H(*o*): 2.73; 2.95 H(*p*): 2.95 H(*m*): 1.0	9
S—N—Ph[a] | O•	CH_3CN	293 K	2.006$_8$	N: 11.0 H(β-H): 2.95 H(γ-H): 0.98 H(*o*, *p*): 2.75 H(*m*): 0.98	This work
C_6H_{11}—N—Ph | O•	C_6H_{12}	300 K		N: 10.5 H(*o*, *p*): 3.0 H(CH): 3.0	34
Ph—N—Ph | O•	CH_2Cl_2 DMSO	298 K		N: 10.1 H(*o*, *p*): 1.9 H(*m*): 0.9	20

[a]S = steroidal group, see text.



SCHEME 1. Synthetic route to the steroidal cation **4**. (i) Mercuric acetate/acetic acid. (ii) (Benzylideneacetone)$Fe(CO)_3$. (iii) $[(C_6H_5)_3C]^+ BF_4^-$. (iv) HPF_6.

has been developed that involves initial oxidation of ergosterol to 9,11-dehydroergosterol; complexation of the $Fe(CO)_3$ moiety to the 5,6,7,8-diene unit and subsequent protonation at C-11 yields the required cation **4**, as shown in Scheme 1.

Nucleophilic attack on metal-complexed polyenyls generally occurs at one of the termini of the delocalized system (19); indeed, nucleophilic attack by the nitrosoarene on the [pentadienyl)$Fe(CO)_3$]$^+$ cation **5** is an entirely reasonable mechanism to account for the observations of Cais *et al.* (9, 10). They reported that the initially formed radical **6** can be reduced to the corresponding amine **7**, and the latter molecule, which is diamagnetic, was readily characterized by NMR spectroscopy.

Assignments of the ESR spectra

The ESR data we have obtained are collected in Tables 1 and 2. These tables also contain some relevant literature data. The

Can. J. Chem. Downloaded from www.nrcresearchpress.com by 194.225.253.170 on 09/07/12
For personal use only.

Can. J. Chem. Downloaded from www.nrcresearchpress.com by 194.225.253.170 on 09/07/12
For personal use only.

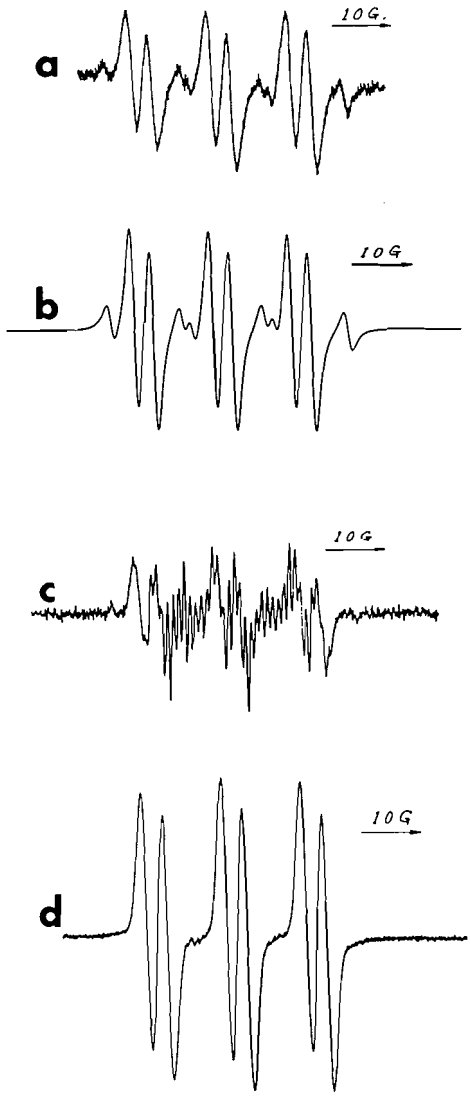


FIG. 3. ESR spectra from the reaction of **2** with C_6Me_4HNO in 1:1 benzene/dimethylsulfoxide (a) after 30 min; (b) simulation of (a) using the data in Table 2; (c) after 18 h; (d) after 5 days.

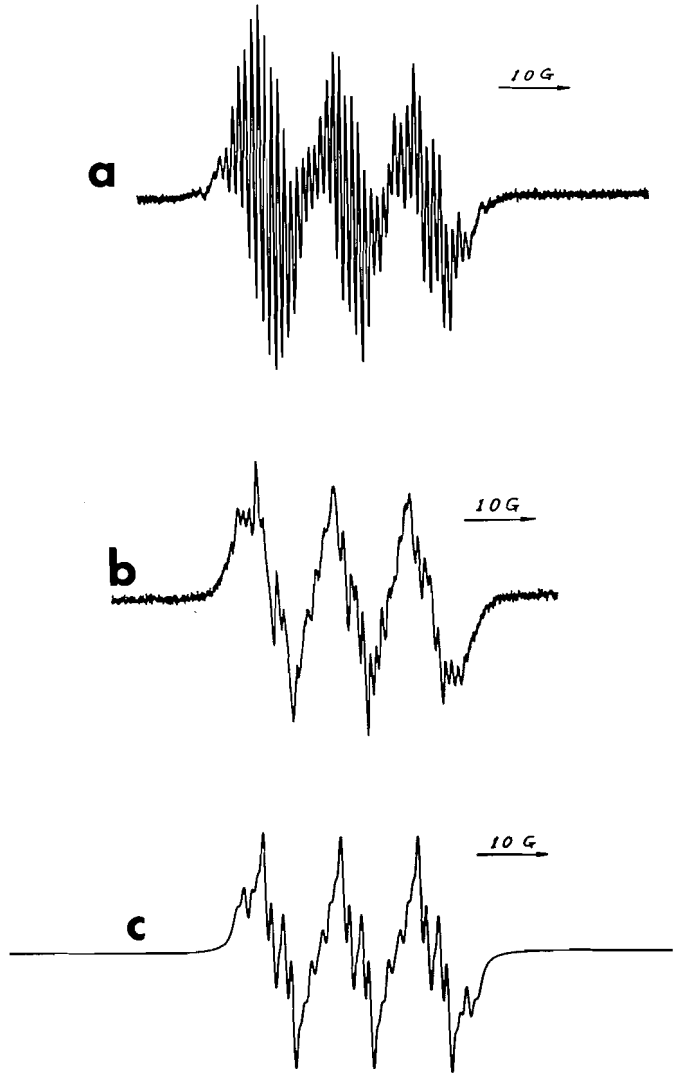
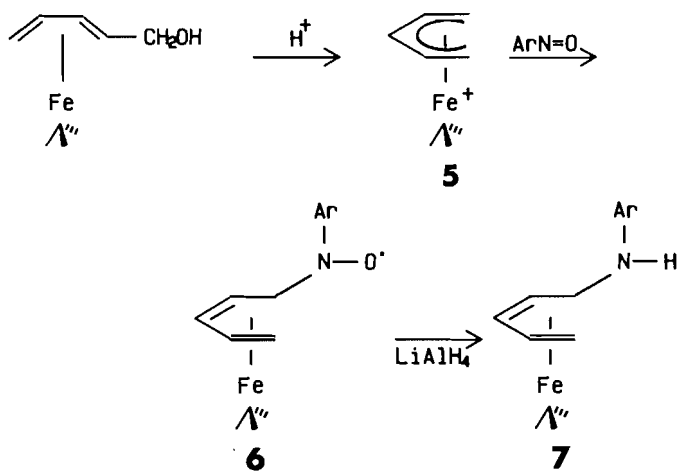


FIG. 4. ESR spectra from the reaction of **4** with C_6H_5NO in CH_3CN (a) after 3 h; (b) after 27 h; (c) simulation of (b) using the data in Table 1.

initial task is to assign the various spectra. By analogy with the results of Cais *et al.*, the radical that would be expected is that shown as **3**, that is, the cyclohexadiene iron tricarbonyl system substituted at the formerly cationic carbon by the group NOAr, where Ar varies according to the identity of the nitrosoarene



used. In Table 1 the hyperfine coupling constants obtained from the spectra resulting from the reaction of **2** with nitrosobenzene are compared with those reported by Cais and with several organic nitroxide radicals with mixed phenyl and aliphatic substituents. The hyperfine coupling constants of the initial radical from the reactions of **2** in both CH_2Cl_2 and CH_3CN agree closely with those of molecules from the literature possessing analogous structural features and there seems little doubt that the structure of the radical is **3***a*, where Ar = phenyl. As noted above, the final spectrum of the reaction in dichloromethane has been identified as the diphenylnitroxide radical.

The six-line spectrum initially obtained from the reaction of **2** with nitrosodurene is entirely consistent with a radical of structure **3***b*, with Ar = C_6Me_4H. The single proton splitting arises from the hydrogen at the point of attachment to the cyclohexadiene ring. As described above, in DMSO/benzene two six-line spectra are observed. They differ substantially in the hydrogen coupling constant: 3.3 G compared with 12.3 G. It is suggested that these two spectra arise from different rotamers of the same radical depending on the orientation of the NOAr group. There is ample precedent for slowed rotation in nitroxides containing such bulky substituents as durene or pen-

TABLE 2. ESR parameters for durene- and pentamethylbenzene nitroxide radicals

Substances	Solvent	Temperature (K)	g factor;	a value(G)	Ref.
C_6H_{11}—N(O•)—Ar[a]	C_6H_6	300	2.006_0	N: 13.57 H: 6.93	2
Ph—CH(CH_3)—N(O•)—Ar	C_6H_6	300	2.006_0	N: 13.8 H: 3.77	2
$(CO)_3FeC_6H_7$—N(O•)—Ar	CH_2Cl_2 CH_3CN	293	2.006_9	N: 13.7 H: 4.2	This work
	CH_3Cl CH_3CN	293	2.006_9	N: 13.75 H: 3.6	This work
	DMSO C_6H_6	293	$g(1) = 2.006_8$ $g(2) = 2.006_0$	N(1): 13.4 H(1): 3.3 N(2): 13.95 H(2): 12.3	This work
	DMSO C_6H_6 CH_2Cl_2 CH_3Cl (CCl_4)	293	$g(1) = 2.006_6$ $g(2) = 2.006_1$	N(1): 13.6 H(1): 3.4 N(2): 14.1 H(2): 12.5	This work
$Me_3C(C_6H_8)$—N(O•)—Ar	CD_3CN CH_2Cl_2	298		N(eq): 13.87 H(eq): 4.62 N(ax): 14.37 H(ax): 10.75	5
S—N(O•)—Ar	CH_3CN	293	2.006_0	N(t): 13.4 N(t, d): 13.9 H: 7.9	This work
	$CHCl_3$	293	2.005_6	N(t): 13.5 N(t, d): 14.5 H: 9.2	This work
$(CO)_3FeC_6H_7$—N(O•)—Ar′	DMSO C_6H_6	293	$g(1) = 2.006_9$ $g(1) = 2.006_6$	N(1): 13.7 H(1): 4.0 N(2): 13.9 H(2): 12.7	This work
	C_6H_6	293	$g(1) = 2.006_7$ $g(2) = 2.006_4$	N(1): 13.5 H(1): 3.3 N(2): 13.8 H(2): 12.3	This work
C_6H_{11}—N(O•)—Ar′	C_6H_6	300	2.005_8	N: 14.0 H(CH): 7.6	35
S—N(O•)—Ar′	CH_3CN	293	2.005_9	N(t): 13.5 N(t, d): 13.6 H: 7.7	This work

[a]Ar = durenyl; S = steroidal group; Ar′ = pentamethylphenyl.

tamethylbenzene (20). Simulation of the spectra indicates that the two isomers are present in a ratio of approximately 4:1. The angular dependence of the β-hydrogen coupling constants of nitroxide radicals has been discussed by Chapelet-Letourneux *et al.* (20). These workers examined the spectra of a variety of radicals with both alkyl and saturated ring substituents and suggested a relationship of the form $a_H = B \cos^2 \theta$ between the hyperfine coupling constant and the angle made between the C—H_β bond and the axis of the p orbital containing the unpaired electron. By calculating an average value of B from the literature data (5) we can see that a hyperfine coupling constant of 12.3 G gives an angle θ of 46° while a coupling constant of 3.3 G yields a θ value of 69°. We are currently in the process of trying to grow crystals of a closely analogous molecule with a view to obtaining X-ray data that could clarify this point.

There are data in the literature that support this assignment of the isomers. Thus Suehiro *et al.* (17) have trapped substituted 1,4-cyclohexadienyl radicals (the present results refer to the 1,3 isomer) and report a_H values of 6–8 G for the proton on the adjacent carbon atom. Kanimori *et al.* (21) report additional radicals of this type and discuss the hydrogen coupling constants in terms of the angle between the C—H bond and the p orbital on the nitrogen. It may be noted that the reported hyperfine coupling constants in these cases are close to the average of the values we find for the two isomers (1/2(3.3 + 12.3) = 7.8 G). A further paper by Konaka *et al.* (22) reports the observation of

Can. J. Chem. Downloaded from www.nrcresearchpress.com by 194.225.253.170 on 09/07/12
For personal use only.

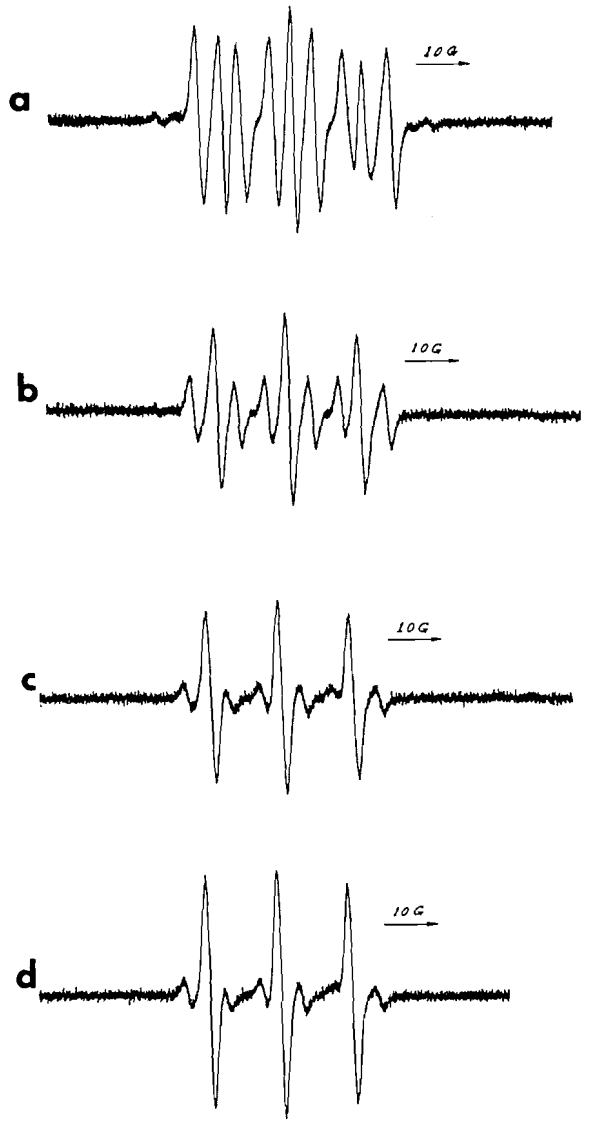


FIG. 5. ESR spectra from the reaction of **4** with C_6Me_5NO in CH_3CN (a) after 3 h; (b) after 6 h; (c) after 9 h; (d) after 21 h.

line width alternations for nitroxide spectra obtained with nitrosodurene. This observation is attributed to restricted rotation because of the bulkiness of the duryl group. The present observation is therefore consistent with more extreme steric restrictions. It may be taken as excellent proof that the iron tricarbonyl group remains attached to the nitroxide radical.

By analogy with the results with nitrosobenzene, it would have been expected that the more complex spectra that were obtained from the decomposition of the above radicals would correspond to the nitroxide radical with a phenyl group and a duryl group as substituents. However, the spectrum cannot be fitted to the hyperfine coupling constants expected for this radical. It appears more complex and we suspect that it may be a mixture of isomeric radicals differing in the relative orientations of the phenyl and duryl radicals. Again, this implies that the iron tricarbonyl group remains attached to the radical. The analysis of the spectra obtained from the reaction of **2** with nitrosopentamethylbenzene is identical to that for nitrosodurene. The angles derived from the proton coupling constants are also very similar. We have been unable to analyse the more complex spectra and similar reasons, based on mixtures of isomeric radicals, are suggested.

In a similar manner, the ESR spectra derived from the reactions of the steroidal cation **4** with the various nitrosoarenes can be assigned in a relatively straightforward manner. The initial spectrum in each case shows hyperfine couplings appropriate for the presence of the ArN fragment and also a single hydrogen on the steroidal carbon adjacent to the nitrogen. However, in each of the final spectra it is clear that the hydrogen atom is no longer bonded to the aforementioned carbon. In the nitrosopentamethylbenzene case, for example, ultimately we see merely the triplet splitting from the nitrogen.

Mechanistic considerations

The initial stages of these reactions are directly analogous to those studied by Cais, which involved the attack of nitroso compounds on pentadienyl- or cycloheptadienyl-$Fe(CO)_3$ cations. One of the suggested mechanisms involved nucleophilic attack at the cationic carbon to give an oxo-ammonium ion that suffers one-electron reduction to give the nitroxide radical. There are some variations possible on this theme — reduction may occur before addition of the nitroso moiety or the reactive species may be a triplet ferricinium complex — but the end result is the same. It is assumed that a second molecule of nitroso compound acts as the one-electron reducing agent.

The subsequent reactions are rather more speculative but a reasonable scheme can be devised based on reactions that have literature precedents. We note first that the homolytic decomposition of nitroso compounds according to eq. [1] has been shown by Chatgilialoglu and Ingold (23) to be thermodynamically improbable as a thermal reaction, although it proceeds readily photochemically. However, Bilkis and Shein (24) have demonstrated that the analogous reaction involving the radical anion occurs readily, as in eq. [2].

[1] $R—N{=}O \rightarrow R\bullet + \bullet N{=}O$

[2] $[R—N{=}O]^- \rightarrow R\bullet + [NO]^-$

More relevant, perhaps, is the report (25) that dialkylnitroxides react with $SbCl_5$ giving *N,N*-dialkyl-*N*-oxoammonium salts; these in turn yield NO^+, as in eqs. [3] and [4].

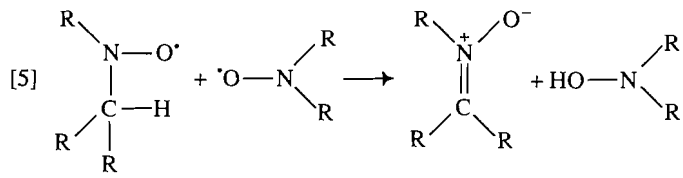
[3] $(t\text{-Bu})_2N—O\bullet + SbCl_5 \rightarrow [(t\text{-Bu})_2N{=}O]^+SbCl_6^-(+ SbCl_3)$

[4] $[(t\text{-Bu})_2N{=}O]^+SbCl_6^- \rightarrow N{\equiv}O^+SbCl_6^- + Me_2C{=}CH_2 + HCl$

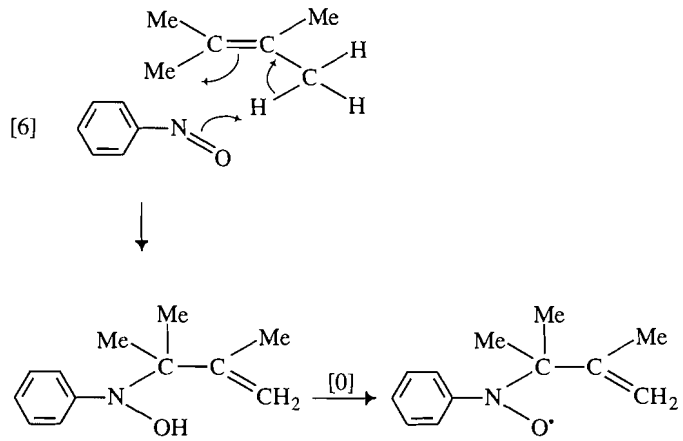
Thus, a not unreasonable initial postulate is that fragmentation of the radical cation arising from the one-electron reduction of the initially formed adduct of nitrosobenzene and **2** yields NO^+ and the phenyl radical; this in turn can be trapped by nitrosobenzene to form diphenylnitroxide. One should note, however, that analogous reactions with C_6Me_5NO and C_6HMe_4NO would then be expected to give rise to the corresponding diarylnitroxides, i.e., $(C_6Me_5)_2NO\bullet$ and $(C_6HMe_4)_2NO\bullet$, but these are not observed in reactions with **2**. In fact, there is another possible route to $Ph_2NO\bullet$ that involves dehydrogenation of the cyclohexadienyl(phenyl)nitroxide ***3a***. (We mention parenthetically that the reaction of *t*-BuNO with cation **2** yields not only the expected nitroxide but also C_6H_5—(*t*-Bu)$NO\bullet$, which must arise via dehydrogenation of a cyclohexadienyl intermediate.) In this context, we next recall information on the self-reactions of nitroxides. These have been extensively studied by Ingold and co-workers (26–28) and also by Golubev *et al.* (29). Several different products can be formed depending on the nitroxide substituents but the typical reaction involves dimerization followed by hydrogen atom transfer to give a reduced product, often a hydroxylamine, and an oxidized product, frequently a nitrone, as in eq. [5].

Furthermore, the mechanism of the ene reaction of nitroso

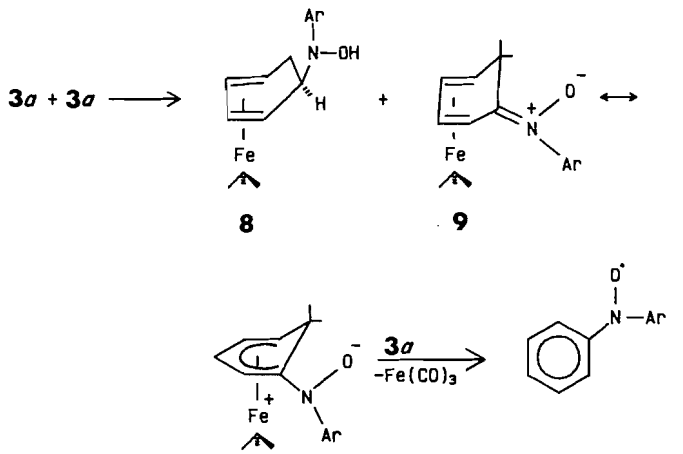
Can. J. Chem. Downloaded from www.nrcresearchpress.com by 194.225.253.170 on 09/07/12
For personal use only.



compounds with olefins involves initial formation of a C—N bond followed by hydrogen atom transfer to give a hydroxylamine; subsequently there occurs oxidation of the hydroxylamine to a nitroxide by a second molecule of nitroso compound, as in eq. [6] (7, 8, 30).



One could follow these literature precedents and postulate a disproportionation of radical **3***a* with a second nitroxide radical to give the hydroxylamine **8** and a neutral product **9**; subsequent



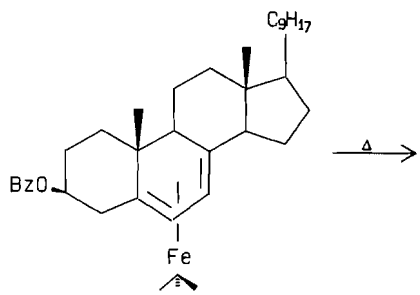
hydrogen abstraction by another molecule of **3***a* and loss of the $Fe(CO)_3$ fragment would then yield $Ph_2NO\bullet$. The formation of the aromatic ring would provide the thermodynamic driving force for such a reaction. Of course, the $Fe(CO)_3$ moiety binds strongly to diene units but is generally less firmly attached to arene rings; consequently, the radicals detected at the end of the reaction sequence are those of the noncomplexed diarylnitroxide and the metal is left as a residue at the bottom of the tube.

To summarize, therefore, the reaction of **2** with nitrosobenzene in acetonitrile yields the radical **3***a*, Ar = C_6H_5; in contrast, in dichloromethane the disproportionation reaction becomes significant. This leads to the corresponding hydroxylamine and nitrone; the latter can then suffer hydrogen atom abstraction by another molecule of **3***a* so that eventually there is complete conversion to diphenylnitroxide.

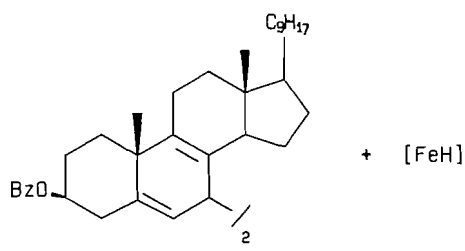
With nitrosodurene (and also with C_6Me_5NO) the initial reaction in CH_3CN/CH_2Cl_2 follows the pattern established for nitrosobenzene. Disproportionation occurs but the steric bulk of the polymethylated arene is sufficient to prevent free rotation and so a mixture of Ph(Ar)NO• isomers is detectable on the ESR time scale. In the DMSO/benzene mixtures two isomers are observed for the initial cyclohexadiene radical **3***b* (**3***c*). We speculate that these too can disproportionate but that in this solvent mixture the equilibrium favors the nitroxide radicals rather than the hydroxylamines. The existence of this equilibrium is, however, sufficient eventually to convert all of the cyclohexadienyl niroxide to the more favored isomer.

*Reactions of ArNO with the steroidal cation, **4***

By analogy with the reactivity pattern established for the unsubstituted $[(cyclohexadienyl)Fe(CO)_3]^+$ cation, **2**, one would anticipate initial nucleophilic attack by the nitrosoarene at a terminus of the delocalized system, that is at C-5 or C-9. Furthermore, in accord with the known chemistry of such iron complexes (18), the incoming nucleophile will approach from the distal side relative to the metal carbonyl unit. That is, attack will occur on the β face of the steroid. In principle, the two sites of attack are readily differentiable since binding to the C-5 position, as in **10**, should produce a radical showing weak coupling to the olefinic hydrogen at C-6 (and possibly even to the 4α and 4β protons). In contrast, if the ArNO were to attack at C-9, as in **11**, one should see essentially a simple triplet since there is no alkene hydrogen at C-8. The result of the experiment revealed that attack had occurred at neither C-5 nor C-9. The initial ESR spectrum from the reaction of C_6Me_5NO (Fig. 5a) shows the expected 1:1:1 triplet with a_N = 13.5 G and also a doublet splitting (7.7 G) clearly indicating the presence of a single hydrogen only two bonds away from the nitrogen. Apparently, the steric problems engendered by the placement of an aryl nitroso moiety at positions C-5 or C-9 render the C-7 site, as in **12**, a more attractive target (see Scheme 2). In seeking a precedent for bond formation at the 7-position, we note that the pyrolysis of ergosteryl benzoate iron tricarbonyl, **13**, is reported to yield the dimeric product **14** in which radical coupling has occurred at the 7-position (31).

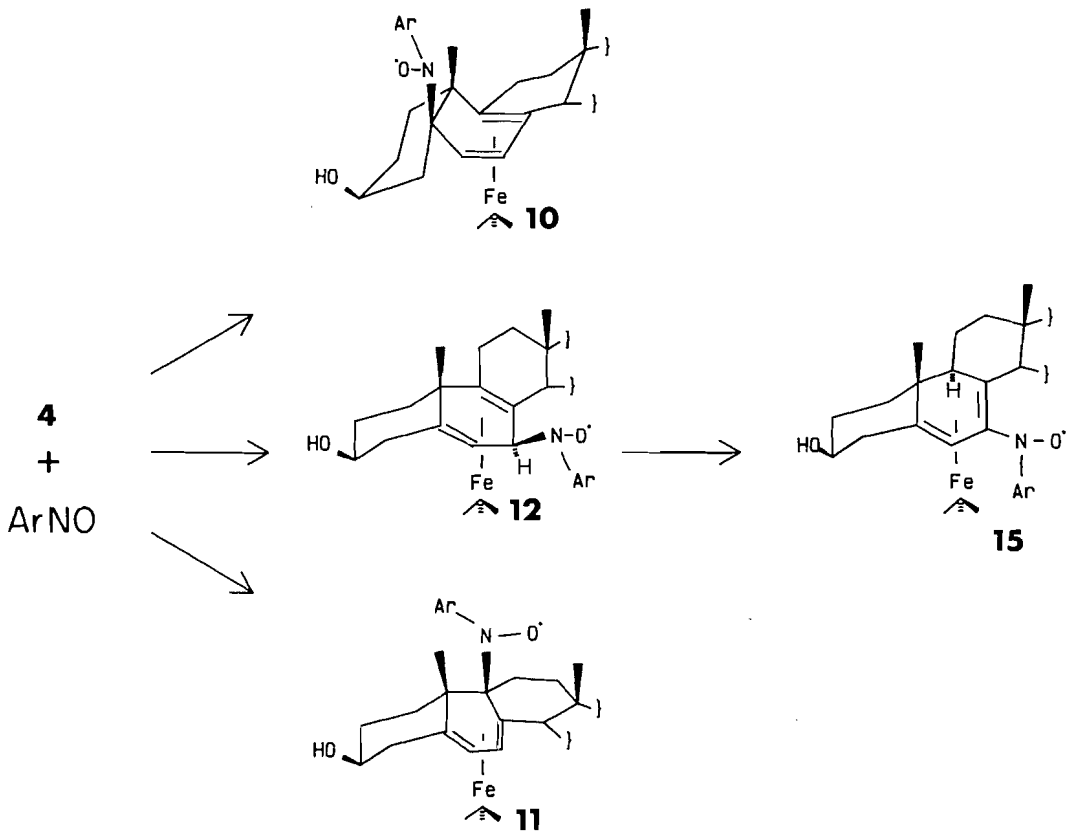


13



14

Can. J. Chem. Downloaded from www.nrcresearchpress.com by 194.225.253.170 on 09/07/12
For personal use only.



SCHEME 2. Possible sites of reaction of nitrosoarenes with the steroidal cation **4**.

In Figs. 6a, 6b, and 6c we present energy-minimized conformers that were calculated by using the program MACROMODEL (32). It is readily apparent that incorporation of the attacking nucleophile can place a bulky aryl group in rather unfavorable positions with respect to the steroidal methyl substituents at C-10 and C-13. When the nitrosoarene attacks on the β face at C-5 the A/B rings are forced into a *cis*-fusion and the methyl must bend so as to avoid the new functional group. Similarly, attack at C-9 leads to steric problems but, as shown in Fig. 6b, attachment at C-7 is relatively unencumbered. It is interesting to note that for the energy-minimized structure of the initial adduct at C-7, i.e., **12**, there is a dihedral angle of 33° between the arene ring plane and the C—H bond; this translates as a 57° angle made by the *p* orbital on nitrogen and the C—H bond. Gratifyingly, the experimental hyperfine interaction to the H-7 nucleus is 7.9 G, which corresponds to an angle of 56°.

This initial product **12** leaves the $Fe(CO)_3$ fragment attached to a 1,4-cyclohexadiene system and, as is commonly the case with such nonconjugated diene complexes (33), a subsequent 1,3-hydrogen transfer occurs to generate the favored isomer **15** in which double bond conjugation is achieved. In this latter isomer the extra hyperfine coupling from the nearby hydrogen is lost. The net result of the whole process is to introduce a functional group at the 7-position of the steroid. Future work will focus on the reduction of the nitroxide radical to the more synthetically versatile amino function.

In contrast to the behaviour described above for nitrosoarenes, the corresponding reactions with *t*-BuNO exhibit a rather novel effect. The final product of the reaction with either **2** or **4** is $(t\text{-Bu})_2NO^{\bullet}$, but the ESR spectrum of this radical exhibits fascinating behaviour in that its intensity varies in an oscillatory manner with time. We prefer not to advance mechanistic speculations at this time until we have a better understanding of the kinetic parameters involved.

Experimental

Cyclohexa-1,3-diene, nitrosobenzene, and 2-methyl-2-nitropropane were purchased from Aldrich and were used without further purification. Nitrosodurene and nitrosopentamethylbenzene were synthesized following published procedures (36, 37). All syntheses were carried out under an atmosphere of nitrogen and all solvents were dried using standard procedures.

The (cyclohexadiene)$Fe(CO)_3$ complex was prepared by heating cyclohexa-1,3-diene with an $Fe(CO)_3$ precursor, namely, (benzylideneacetone)iron tricarbonyl (36) under reflux for 24 h in toluene. The reaction mixture was cooled, filtered through Celite, and the solvent removed by rotary evaporation. Subsequent chromatographic separation on a silica column and elution with a 1:1 mixture of hexane and toluene afforded the appropriate complex (≈60% yield) as previously reported by Birch *et al.* (39). The complex was then treated with Ph_3C^+ BF_4^- in CH_2Cl_2 and the cationic complex **2** was obtained as a yellow precipitate upon addition of ether. The steroidal cation **4** was synthesized as shown in Scheme 1. The experimental details and NMR spectroscopic data on **4** are the subject of a forthcoming paper (15).

ESR spectra were recorded on a Bruker ER-100D instrument operating at X-band frequency with 100-kHz modulation. Spectral simulations were carried out using the ESR program on the Bruker ASPECT 2000 computer. The *g* values were calculated from a knowledge of the microwave frequency and the magnetic field, the latter having been calibrated by use of DPPH. The ESR samples were prepared on a vacuum line with the cationic iron complex and the nitroso compounds degassed three times separately before mixing in an ESR tube. The concentrations of the reagents used were in the range 0.005–0.02 M.

Can. J. Chem. Downloaded from www.nrcresearchpress.com by 194.225.253.170 on 09/07/12
For personal use only.

Can. J. Chem. Downloaded from www.nrcresearchpress.com by 194.225.253.170 on 09/07/12
For personal use only.

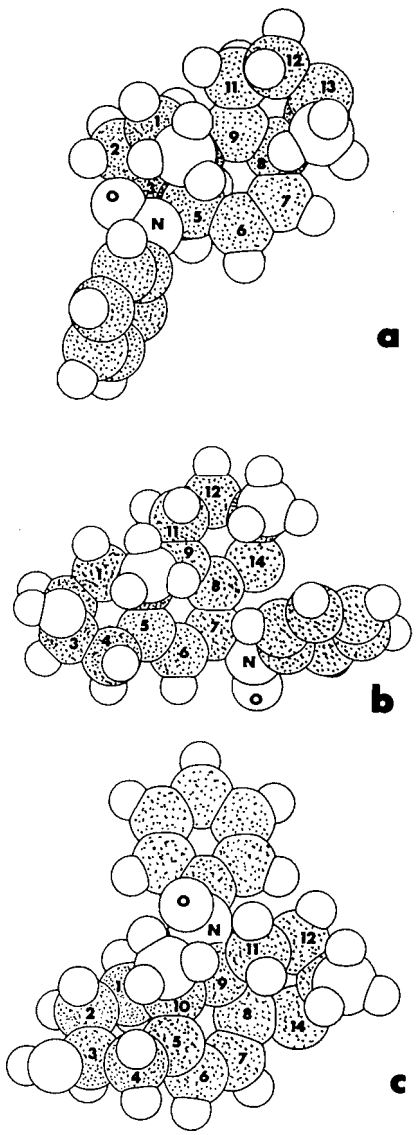


FIG. 6. (a) Space-filling model of **10** in which attachment of the ArNO fragment at C-5 causes unfavorable interaction with the methyl group at C-10. (The view is from the β face. For clarity, the α-$Fe(CO)_3$ group and the D ring of the steroid are not shown.) (b) Space-filling model of **12** in which attachment of the ArNO fragment at C-7 causes no problematic steric interactions with the methyl groups. (c) Space-filling model of **11** in which attachment of the ArNO fragment at C-9 causes unfavorable interactions with the methyl groups at C-10 and at C-13.

Acknowledgments

Financial support from the donors of the Petroleum Research Fund, administered by the American Chemical Society, and from the Natural Sciences and Engineering Research Council of Canada is gratefully acknowledged. Molecular modelling studies and energy minimizations were carried out on computers generously donated by IBM Canada Ltd.

1. (*a*) G. ROZANTSEV and V. D. SHOLLE. Synthesis, 190 (1971); (*b*) J. F. W. KEANA. Chem. Rev. **78**, 37 (1978); (*c*) E. G. JANZEN. Acc. Chem. Res. **2**, 279 (1969).
2. S. TERABE, K. KURUMA, and R. KONAKA. J. Chem. Soc. Perkin Trans. **2**, 1252 (1973).
3. S. TERABE and R. KONAKA. J. Chem. Soc. Perkin Trans. **2**, 2163 (1972).
4. S. TERABE and R. KONAKA. J. Chem. Soc. Perkin Trans. **2**, 369 (1973).
5. M. P. CROZET, J. MUZART, P. PALE, and P. TORDO. J. Organomet. Chem. **244**, 191 (1983).
6. P. SRIDHAR and R. A. FLOYD. Can. J. Chem. **60**, 1574 (1982).
7. A. B. SULLIVAN. J. Org. Chem. **31**, 2811 (1966).
8. G. T. KNIGHT and B. PEPPER. Tetrahedron, **27**, 6201 (1971).
9. M. CAIS, P. ASHKENAZI, S. DANI, and J. GOTTLIEB. J. Organomet. Chem. **124**, 49 (1977).
10. M. CAIS, P. ASHKENAZI, and J. GOTTLIEB. Rev. Roum. Chim. **22**, 545 (1977).
11. S. LUPON, M. KAPON, M. CAIS, and F. H. HERBSTEIN. Angew. Chem. Int. Ed. Engl. **11**, 1025 (1972).
12. M. I. RYBINSKAYA, A. Z. KREINDLIN, and S. S. FADEEVA. J. Organomet. Chem. **358**, 363 (1988).
13. YU. A. BELOUSOV and T. A. KOLOSOVA. Polyhedron, **6**, 1959 (1987).
14. J. F. W. KEANA, T. TAMURA, D. A. MCMILLEN, and P. C. JOST. J. Am. Chem. Soc. **103**, 4904 (1981).
15. R. E. PERRIER, C. S. FRAMPTON, R. FAGGIANI, and M. J. MCGLINCHEY. Submitted for publication.
16. E. T. STROM, A. L. BLUHM, and J. WEINSTEIN. J. Org. Chem. **32**, 3853 (1967).
17. T. SUEHIRO, M. KAMIMORI, K. TOKUMARU, and M. YOSHIDA. Chem Lett. 531 (1976).
18. A. J. PEARSON. Science, **223**, 895 (1984).
19. S. G. DAVIES, M. L. H. GREEN, and D. M. P. MINGOS. Tetrahedron, **34**, 3047 (1978).
20. G. CHAPELET-LETOURNEUX, H. LEMAIRE, R. LENK, M-A MARECHAL, and A. RASSAT. Bull. Chim. 3963 (1968).
21. M. KAMIMORI, H. SAKURAGI, T. SUEHIRO, K. TOKUMARU, and M. YOSHIDA. Bull. Chem. Soc. Jpn. **50**, 1195 (1977).
22. R. KONAKA, S. TERABE, T. MIZUTA, and S. SAKATA. Can. J. Chem. **60**, 1532 (1982).
23. C. CHATGILIALOGLU and K. U. INGOLD. J. Am. Chem. Soc. **103**, 4833 (1981).
24. R. L. BILKIS and S. M. SHEIN. Tetrahedron, **31**, 969 (1975).
25. V. A. GOLUBEV and G. N. VORONINA. Bull. Akad. Sci. USSR (Engl. Transl), **21**, 2024 (1972).
26. D. F. BOWMAN, T. GILLAN, and K. U. INGOLD. J. Am. Chem. Soc. **93**, 6555 (1971).
27. K. ADAMIC, D. F. BOWMAN, T. GILLAN, and K. U. INGOLD. J. Am. Chem. Soc. **93**, 902 (1971).
28. A. L. CASTELHANO, D. GRILLER, and K. U. INGOLD. Can. J. Chem. **60**, 1501 (1982).
29. V. A. GOLUBEV, G. N. VORONINA, and E. G. ROZANTSEV. Bull. Akad. Sci. USSR (Engl. Transl.), **21**, 146 (1972).
30. L. H. SUTCLIFFE and A. ZILNYK. J. Chem. Soc. Faraday Trans. 1, **81**, 1215 (1985).
31. A. F. MATEOS and S. G. DAVIES. Anal. Quim. **75**, 385 (1979).
32. W. C. STILL. MACROMODEL program. Columbia University, New York.
33. R. B. KING, T. A. MANUEL, and F. G. A. STONE. J. Inorg. Nucl. Chem. **16**, 233 (1961).
34. S. K.WONG and J. K. S. WAN. Can. J. Chem. **51**, 753 (1973).
35. T. DOBA, T. ICHIKAWA, and H. YOSHIDA. Bull. Chem. Soc. Jpn. **50**, 3124 (1977).
36. L. I. SMITH and F. L. TAYLOR. J. Am. Chem. Soc. **57**, 2370 (1935).
37. L. I. SMITH and F. L. TAYLOR. J. Am. Chem. Soc. **57**, 2460 (1935).
38. G. EVANS, B. F. G. JOHNSON, and J. LEWIS. J. Organomet. Chem. **102**, 507 (1975).
39. A. J. BIRCH, P. E. CROSS, J. LEWIS, D. A. WHITE, and S. B. WILD. J. Chem. Soc. (A), 332 (1968).

^{127}I Mössbauer studies of oxygen bonded iodine complexes. 2.[1] Aryliodine(III)carboxylates; the crystal and molecular structure of bis(trifluoroacetato)pentafluorophenyliodine(III), $(C_6F_5)I(O_2CCF_3)_2$

MADHUMITA BARDAN, THOMAS BIRCHALL, CHRISTOPHER S. FRAMPTON,[2] AND PRATIBHA KAPOOR[3]

The Department of Chemistry, McMaster University, 1280 Main St. West, Hamilton, Ont., Canada L8S 4M1

Received April 5, 1989

This paper is dedicated to Professor Ronald J. Gillespie on the occasion of his 65th birthday

MADHUMITA BARDAN, THOMAS BIRCHALL, CHRISTOPHER S. FRAMPTON, and PRATIBHA KAPOOR. Can. J. Chem. **67**, 1878 (1989).

The ^{127}I Mössbauer spectra of a series of mono- and diaryliodine(III) carboxylates have been recorded at 4.2 K. The observed parameters are shown to be strongly dependent on the primary bonding arrangement about iodine only and the secondary bonding interactions have little or no effect. The crystal and molecular structure of bis(trifluoroacetato)pentafluorophenyliodine(III), $(C_6F_5)I(O_2CCF_3)_2$, has been determined. Crystals are triclinic, of space group $P\bar{1}$, with a = 5.732(2) Å, b = 12.127(4) Å, c = 29.658(9) Å, α = 116.53(2)°, β = 98.02(2)°, γ = 117.09(2)°, V = 1482.0(8) Å^3, D_c = 2.33 g cm^{-3} for Z = 4, and R_1 = 0.0420 (R_2 = 0.0431) for 2722 reflections with $I > 3\sigma(I)$. The two independent molecules in the asymmetric unit have essentially the same primary geometry about the central iodine, a distorted T-shaped AX_3E_2 arrangement.

Key words: ^{127}I Mössbauer, aryliodine(III) carboxylates, crystal structure, $(C_6F_5)I(O_2CCF_3)_2$.

MADHUMITA BARDAN, THOMAS BIRCHALL, CHRISTOPHER S. FRAMPTON et PRATIBHA KAPOOR. Can. J. Chem. **67**, 1878 (1989).

Opérant à 4,2 K, on a enregistré les spectres de Mössbauer du ^{127}I d'une série de carboxyles de mono- et di-aryliode(III). On a démontré que les paramètres observés dépendent fortement et uniquement de l'arrangement de la liaison primaire autour de l'iode; les interactions secondaires de liaison n'ont que peu ou pas d'effet. On a déterminé les structures cristalline et moléculaire du bis(trifluoroacétato)pentafluorophényliode(III), $(C_6F_5)I(O_2CCF_3)_2$. Les cristaux sont triclinique et appartiennent au groupe d'espace $P\bar{1}$, avec a = 5,732(2), b = 12,127(4) et c = 29,658(9) Å et α = 116,53(2), β = 98,02(2) et γ = 117,09(2)°, V = 1482,0(8) Å^3, D_o = 2,33 g cm^{-3} et Z = 4; on a affiné la structure jusqu'à des valeurs respectives de R_1 et R_2 de 0,0420 et 0,0431 pour 2722 réflexions avec $I > 3\sigma(I)$. Les deux molécules indépendantes de l'unité asymétrique possèdent pratiquement la même géométrie primaire autour de l'iode central, un arrangement AX_3E_2 en forme de T déformé.

Mots clés : Mössbauer du ^{127}I, carboxyle d'aryliodide(III), structure cristalline, $(C_6H_5)I(O_2CCF_3)_2$.

[Traduit par la revue]

Introduction

We recently reported the ^{127}I Mössbauer parameters of some tris(carboxylato)iodine(III) complexes (1). In the course of this study the crystal and molecular structure of tris(acetato)iodine(III) was determined to gain further information regarding the nuclear environment of the iodine atom in compounds of this type and also to give an insight into any secondary bonding interactions that may be present. It was shown that the observed ^{127}I Mössbauer parameters were predominantly influenced by the strong primary bonds to the iodine nucleus, which are mainly of *p*-character, and that the secondary bonding interactions had little or no effect. This result was somewhat surprising since it has been shown by both Alcock *et al.* (2) and ourselves that there is an associated geometry change about the iodine nucleus from square-planar to pentagonal-planar coordination when going from a halogeno-iodine(III) compound to an equivalent oxo-iodine(III) compound. This change in geometry is based on the arrangement of both the primary and secondary bonds to the iodine nucleus and one would therefore expect slight changes in the observed quadrupole coupling constant and asymmetry parameter to occur.

Previous crystallographic studies on phenyliodine(III) carboxylates include compounds of the type $(C_6H_5)I(O_2CR)_2$, where R = $-CH_3$ (2, 3), $-CHCl_2$ (2), and $-CF_3$ (4) and also the μ-oxo derivative $[(C_6H_5)I(O_2CCF_3)]_2O$ (5). Inspection of the bonding in these materials reveals a variety of structural modifications, to what is nominally an AX_3E_2 trigonal-bipyramidal system. These structural modifications arise from differing secondary bonding arrangements about the central iodine nucleus.

Given the above information it was decided to extend the range of available data for these complexes and a systematic series of aryliodonium carboxylates were prepared and characterized by various techniques. In this paper, the second in a present series, we report the ^{127}I Mössbauer parameters, at 4.2 K, for a series of phenyl and diphenyliodine(III) carboxylates. The crystal and molecular structure of $(C_6F_5)I(O_2CCF_3)_2$ was determined and the ^{127}I Mössbauer data interpreted in relation to this and other available structural data.

Experimental

Materials and general procedures

Acetic acid (BDH, AnalaR) was refluxed with 2 mol% acetic anhydride (BDH) for 24 h and then distilled. The fraction distilling at 114–115°C was collected for use. Trifluoroacetic acid (Baker analyzed) was refluxed for 2 mol% of trifluoroacetic anhydride (BDH) for 8 h and then distilled. The fraction distilling at 72°C was collected for use. Mono- and dichloroacetic acids (Aldrich) were made anhydrous by the addition of their respective anhydrides. Iodine (BDH, AnalaR) was freshly sublimed before use. Iodobenzene (Aldrich, 98%), iodopentafluorobenzene (Aldrich, 99%), silver acetate (MCB, 99.5%), silver trifluoroacetate (Aldrich, 98%), and potassium iodide (reagent grade) were used without further purification.

Preparation of the compounds

The iodine absorbers used in this study were prepared using

[1]Part 1, see ref. 1.

[2]Author to whom correspondence may be addressed.

[3]On leave from Department of Chemistry, Panjab University, Chandigarh-160014, India.

Can. J. Chem. Downloaded from www.nrcresearchpress.com by 186.148.149.217 on 09/07/12
For personal use only.

Can. J. Chem. Downloaded from www.nrcresearchpress.com by 186.148.149.217 on 09/07/12
For personal use only.

TABLE 1. Crystal data for $(C_6F_5)I(O_2CCF_3)_2$

Parameter	Value
Formula	$C_{10}F_{11}O_4I$
FW	519.99
System	Triclinic
Space group	$P\bar{1}$ No-2
a, Å	5.732(2)
b, Å	12.127(4)
c, Å	29.658(9)
α, deg	116.53(2)
β, deg	98.02(2)
γ, deg	117.09(2)
V, Å^3	1482.0(8)
Z	4
D_c, g cm^{-3}	2.33
$F(000)$	973.95(976)
μ(MoKα), cm^{-1}	23.5 (21.2)
Final R_1, R_2[a,d]	0.0635, 0.0604
Weighting scheme	$w = (\sigma^2F + 0.000986F^2)^{-1}$
Error in observation of unit weight[b]	1.3116
Highest peak, e Å^{-3}; location	1.10; 0.41, 0.94, 0.54[c]
Lowest peak, e Å^{-3}	−0.97

[a] $R_1 = \Sigma||F_o| - |F_c||/\Sigma|F_o|$; $R_2 = (\Sigma w(|F_o| - |F_c|)^2/\Sigma wF_o^2)^{1/2}$.
[b] $S = (\Sigma w(|F_o| - |F_c|)^2/(m - n))^{1/2}$. m = no. of reflections, n = no. of variables.
[c] 1.06 Å from $I(1)$.
[d] R_1, R_2 for 2722 reflections with $I > 3\sigma(I)$: 0.0420, 0.0431 respectively.

established literature methods (6, 7) and their authenticity verified by X-ray crystallography and (or) analysis for iodine and acid ligand using standard procedures (8).

Synthesis of bis(trifluoroacetato)pentafluorophenyliodine(III)

This compound was prepared according to the method of Schmeisser *et al.* (9), mp 118°C. *Anal.* calcd. for $C_{10}O_4F_{11}I$: I 24.40, acid ligand 43.47; found: I 24.89, acid ligand 42.87.

Synthesis of (trifluoroacetato)diphenyliodine(III)

Diphenyliodonium bromide (10) (2.0 g; 5.54 mmol) dissolved in 100 mL of hot water was added with stirring to a solution of 1.25 g (5.66 mmol) of silver trifluoroacetate in 100 mL of hot water. The resulting precipitate of silver bromide was quickly removed by filtration. The filtrate was concentrated and (trifluoroacetato)diphenyliodine(III) precipitated as white crystals on cooling, mp 198°C. *Anal.* calcd. for $C_{14}H_{10}O_2F_3I$: I 32.20, acid ligand 28.67; found: I 32.74, acid ligand 28.13.

X-ray crystallography

Clear needle-like crystals were examined under a polarizing microscope for homogeneity and well-formed specimens were sealed in Lindemann capillaries. Unit cell parameters were obtained from a least-squares fit of χ, φ, and 2θ for 15 reflections in the range $16.1° < 2\theta < 24.5°$ recorded on a Syntex $P2_1$ diffractometer with use of graphite monochromated MoKα radiation (λ = 0.71069 Å at 22°C). Intensity data were also recorded on a Syntex $P2_1$ diffractometer with a coupled θ(crystal)–2θ(counter) scan, for 4462 reflections in the quadrant $h, \pm k, \pm l$ with $2\theta \leq 45°$. The methods of selection of scan rates and initial data treatment have been described (11, 12). Two standard reflections (0,3,5; 4.4% and −2,4,−5; 5.6% monitored every 48 reflections) showed signs of some crystal decomposition and the data were adjusted accordingly (maximum rescale factor (on I), 1.580). Corrections for Lorentz and polarization effects were applied to all reflections but not for absorption (maximum error in I, 2.28%). Symmetry-equivalent data (1081 reflections) were averaged (R_{int} = 0.0297) to give 3831 unique reflections. A summary of crystal data is given in Table 1.

Solution of the structure

The structure was solved by routine heavy atom methods. Full-matrix least-squares refinement of the coordinates of the iodine atoms followed by a three-dimensional electron density synthesis revealed all the remaining atoms and confirmed the positional assignments for the heavy ones. After refinement the temperature factors of all the atoms, which were previously isotropic, were made anisotropic and further cycles of refinement using block-matrix least squares (alternately refining molecule 1 and molecule 2), minimizing $\Sigma w(|F_o| - |F_c|)^2$, were terminated when the maximum shift/error reached 0.014. Final R_1 = 0.0420, R_2 = 0.0431 for 2722 reflections with $I > 3\sigma(I)$. Correction for secondary extinction was made by the method in SHELX-76 (13). Throughout the refinement, scattering curves were taken from ref. 14 and corrections for anomalous dispersion (15) were applied to the curve for iodine. All calculations were performed on a VAX 8650 computer. Programs used: XTAL (16), data reduction; SHELX-76 (13), structure refinement; MOLGEOM (17), molecular geometry; and SNOOPI (18), diagrams. Final atomic positional parameters are given in Table 2 and selected intra- and intermolecular bond lengths and bond angles are given in Table 3.[4]

Mössbauer spectroscopy

The source of 57.6 keV radiation was $Mg_3{}^{127m}TeO_6$. Details of the source preparation, irradiation, and Mössbauer spectrometer have been described elsewhere (1). Powdered absorber samples containing approximately 0.05 g cm^{-2} of ^{127}I were placed neat or mixed with dry Teflon powder in 20 mm i.d. threaded Kel-F Mössbauer cells under an atmosphere of rigorously dried nitrogen. Both source and absorber were immersed in liquid helium (4.2 K) in a research cryostat manufactured by the Janis Research Corp. The velocity scale was calibrated using a standard iron foil and a $^{57}Co/Rh$ source mounted on the reverse end of the transducer; calibration spectra were thus recorded without interruption of the drive sequence. The calibration spectra were computer fitted to give a linear velocity scale and folding point.

Folded ^{127}I spectra were fitted using the program GMFP (19), which incorporates full transmission integral procedures. The source linewidth was arbitrarily set at the natural linewidth 1.27 mm/s, the effective recoilless fraction was set equal to that of a previous source of $Ca_3{}^{127m}TeO_6$, 0.75 at 4.2 K, and the dimensionless absorber thickness, T_a, was made a variable parameter of the iterative fitting process. All isomer shifts were referenced to $K^{127}I$ at 4.2 K (20).

Results and discussion

Structure

From an examination of the data contained in Table 3 it can be seen that both molecules in the asymmetric unit have essentially the same geometry. A view of molecule 1 with atom numbering scheme is depicted in Fig. 1.

The primary geometry about the trivalent iodine atom can be best described as a distorted T-shaped, AX_3E_2, trigonal-bipyramidal arrangement consisting of two covalent I—O bonds to the trifluoroacetate groups in the "axial" positions and the remaining I—C covalent bond to the pentafluorophenyl group and the two nonbonding lone pairs in the "equatorial" plane. Principal bond lengths and angles about iodine are as follows. Molecule 1: I(1)—C(16), 2.078(10) Å; I(1)—O(11), 2.147(6) Å; I(1)—O(13), 2.128(6) Å; O(11)—I(1)—C(16), 81.5(3)°; O(13)—I(1)—C(16), 81.1(3)°; O(11)—I(1)—O(13), 162.6(3)°. Molecule 2: I(2)—C(12), 2.063(6) Å, I(2)—O(21), 2.145(9) Å; I(1)—O(23), 2.136(8) Å; O(21)—I(2)—C(26),

[4] Tables of full crystal data, least-squares mean planes and dihedral angles, anisotropic temperature factors, and observed and calculated structure factors may be purchased from the Depository of Unpublished Data, CISTI, National Research Council of Canada, Ottawa, Ont., Canada K1A 0S2.

Table S1, the full crystal data, has been deposited with the Cambridge Crystallographic Data Centre, and can be obtained on request from The Director, Cambridge Crystallographic Data Centre, University Chemical Laboratory, Lensfield Road, Cambridge CB2 1EW, U.K.

TABLE 2. Positional parameters ($\times 10^4$) and U_{eq} (Å^2) ($\times 10^4$) for $(C_6F_5)I(O_2CCF_3)_2$ with standard errors in parentheses

Molecule 1

Atom	x	y	z	U_{eq}
I(1)	2772.9(12)	9705.8(5)	5568.4(2)	363
C(11)	4792(18)	9755(9)	6574(4)	391
C(12)	4548(21)	9482(10)	6973(4)	446
C(13)	1886(23)	8714(10)	6961(4)	434
C(14)	−513(19)	8196(9)	6551(4)	382
C(15)	−272(17)	8450(8)	6145(3)	322
C(16)	2382(17)	9230(8)	6157(3)	308
F(11)	7428(11)	10520(6)	6600(2)	579
F(12)	6905(13)	9998(8)	7380(3)	691
F(13)	1626(15)	8476(6)	7355(2)	660
F(14)	−3141(13)	7440(6)	6539(2)	612
F(15)	−2699(11)	7927(6)	5745(2)	528
O(11)	1525(13)	7421(6)	5077(2)	418
O(12)	4725(13)	8144(6)	4736(2)	423
C(17)	2879(18)	7222(8)	4766(3)	323
C(18)	1928(23)	5553(10)	4416(4)	461
F(16)	−781(33)	4568(12)	4340(6)	904
F(17)	3820(42)	5465(20)	4577(9)	1243
F(18)	1303(37)	5013(13)	3898(5)	711
O(13)	3915(13)	11826(6)	6239(2)	434
O(14)	317(13)	11608(6)	5708(3)	480
C(19)	2278(21)	12237(9)	6133(4)	386
C(110)	3254(23)	13759(11)	6664(4)	494
F(19)	6111(25)	14812(12)	6891(4)	612
F(110)	2640(37)	13611(13)	7024(5)	876
F(111)	2169(36)	14340(15)	6508(6)	949

Molecule 2

Atom	x	y	z	U_{eq}
I(2)	124.0(12)	2920.3(5)	−582.4(2)	387
C(21)	−2196(18)	−217(10)	−1551(3)	353
C(22)	−4104(22)	−1760(10)	−1927(3)	428
C(23)	−6659(21)	−2513(9)	−1911(3)	433
C(24)	−7319(18)	−1729(10)	−1513(3)	381
C(25)	−5403(18)	−177(9)	−1135(3)	345
C(26)	−2786(17)	594(8)	−1143(3)	301
F(21)	347(12)	528(6)	−1576(2)	527
F(22)	−3437(13)	−2485(6)	−2313(2)	658
F(23)	−8514(13)	−4003(5)	−2266(2)	702
F(24)	−9889(12)	−2492(6)	−1502(3)	624
F(25)	−6135(12)	532(6)	−759(2)	552
O(21)	1131(13)	2259(6)	−65(2)	411
O(22)	5861(12)	3971(6)	231(2)	429
C(27)	3862(20)	3005(9)	228(3)	355
C(28)	4427(21)	2458(11)	583(4)	447
F(26)	5051(35)	1525(17)	370(5)	996
F(27)	6734(23)	3673(11)	1074(3)	685
F(28)	2368(25)	1898(15)	719(6)	794
O(23)	−1738(13)	2867(6)	−1274(2)	447
O(24)	−2915(15)	4382(8)	−767(3)	532
C(29)	−2855(18)	3625(9)	−1189(4)	396
C(210)	−4219(25)	3455(12)	−1722(4)	534
F(29)	−6556(23)	2130(13)	−2076(5)	866
F(210)	−4288(29)	4492(13)	−1646(5)	926
F(211)	−2549(30)	3481(17)	−2026(5)	866

$U_{eq} = \frac{1}{3}(U_{11} + U_{22} + U_{33} + 2\cos\alpha U_{23} + 2\cos\beta U_{13} + 2\cos\gamma U_{12})$.

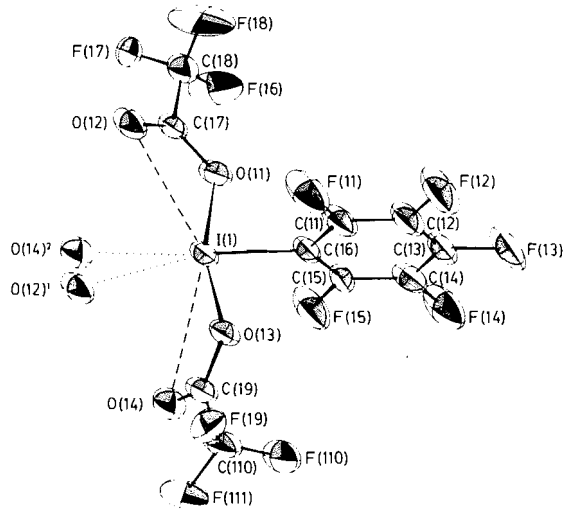


FIG. 1. View of $(C_6F_5)I(O_2CCF_3)_2$, molecule 1, showing atom numbering scheme. The intramolecular and intermolecular I···O secondary interactions are illustrated as dashed and dotted bonds respectively. The numbering scheme for molecule 2 may be inferred from the above.

80.8(3)°; O(23)—I(2)—C(26), 82.2(3)°; O(21)—I(2)—O(23), 163.0(2)°. The I—C and I—O distances found are not unusual for this type of compound although the asymmetry usually observed (2) in the I—O bonds is much less pronounced and is probably a consequence of the crystal packing (*vide infra*). This T-shaped geometry is predicted from VSEPR (21) theory and has been observed for a number of tellurium(II) (22), chlorine(III) (23), iodine(III) (1–5, 24), and xenon(IV) (25) complexes. The trifluoroacetate groups are oriented such that they are almost perpendicular to each other with a dihedral angle between the least-squares mean planes defined by the C—CO_2 atoms of 84.3(4)° and 82.5(4)° for molecules 1 and 2 respectively. As with most of these complexes the primary bonding arrangement does not describe the geometry about the central atom completely and there are further inter- or intramolecular contacts known as secondary bonds (26, 27) that complete the coordination sphere.

For $(C_6F_5)I(O_2CCF_3)_2$ there are two intramolecular contacts which bisect XE edges of the trigonal-bipyramid, I(1)···O(12), 3.075(8) Å, I(1)···O(14), 3.120(10) Å and I(2)···O(22), 3.080(7) Å, I(2)···O(24), 3.146(11) Å; these are illustrated as dashed bonds in Fig. 1. The coordination about the iodine is completed by two further intermolecular contacts. The first is an XEE face capping interaction of a centrosymmetrically related molecule forming a dimer via an I_2O_2 trapezoidal ring similar to that reported for $(C_6H_5)I(O_2CCHCl_2)_2$ (2) and $(C_6H_5)I(O_2CCF_3)_2$ (4) with I(1)···O(12),[1] 2.955(11) Å; I(2)···O(22),[3] 2.918(9) Å. These atoms lie 0.63 and 0.65 Å respectively above the plane defined by the "distorted T". The least-squares mean planes of the trifluoroacetate groups as defined above form dihedral angles with the plane of the distorted T of 40.1(4)°, 122.5(4)° for molecule 1 and 44.0(4)°, 124.8(4)° for molecule 2. These values differ from similar angles reported for $(C_6H_5)I(O_2CCHCl_2)_2$, (8.64° and 77.53°) (2), and are such that the remaining intermolecular contact caps the opposing XEE face of a centrosymmetrically related molecule, which is also translated 1 unit cell distance in *b* for molecule 1 or *a* for molecule 2, linking the dimers into chains,

Can. J. Chem. Downloaded from www.nrcresearchpress.com by 186.148.149.217 on 09/07/12
For personal use only.

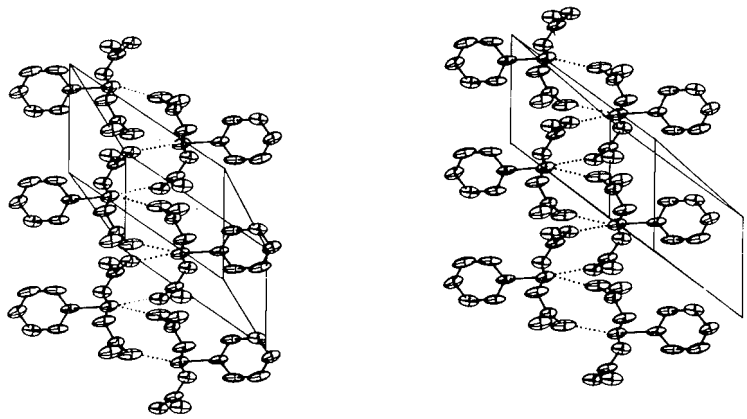


FIG. 2. Stereoscopic view of the packing of molecule 2.

Can. J. Chem. Downloaded from www.nrcresearchpress.com by 186.148.149.217 on 09/07/12
For personal use only.

I(1)···O(14),[2] 3.190(9) Å; I(2)···O(24),[4] 3.322(8) Å. O(14)[2] and O(24)[4] lie 1.35(1) and 1.31(1) Å below the plane of the distorted T and are illustrated as dotted bonds in Fig. 1. Thus it can be seen that O(12), O(14), O(22), and O(24) are inter- and intramolecularly bonded to iodine; Fig. 2 shows a stereoview of the chain formation of molecule 2. These intermolecular distances are less than the sum of the van der Waals radii (3.55 Å), and hence may still be classified as secondary bonds. The overall geometry about the iodine may be described as a distorted pentagonal $AX_3Y_2Y_2'E_2$, arrangement (for notation see ref. 27). It is worthwhile to compare the results from the present structure to those obtained for other iodine(III) complexes such as $I(O_2CCH_3)_3$ (1), and also for the related aryliodine(III) compounds $(C_6H_5)I(O_2CCH_3)_2$ (2, 3), $(C_6H_5)I(O_2CCHCl_2)_2$ (2), $(C_6H_5)I(O_2CCF_3)_2$ (4), and $[(C_6H_5)I(O_2CCF_3)]_2O$ (5). The above structures all have the same primary bonding geometry, i.e., a distorted T-shaped, AX_3E_2, arrangement based upon a trigonal-bipyramid as expected for trivalent iodine, but they differ in their arrangement of secondary bonding contacts.

$I(O_2CCH_3)_3$ (1) forms three intramolecular secondary bonding contacts. Two cap the XEE faces of the trigonal-bipyramid and are reasonably strong with lengths 2.46 and 2.52 Å, while the third is weaker (3.03 Å), and bisects an XE edge, hence the overall geometry may be described as $AX_3Y_2Y'E_2$. The case for $(C_6H_5)I(O_2CCH_3)_2$ (2, 3) is similar to that of $I(O_2CCH_3)_3$, whereby there are two intramolecular XEE face capping secondary bonds (2.817 and 2.850 Å) giving an $AX_3Y_2E_2$ geometry. Both structures are monomeric with a pentagonal planar arrangement of primary and secondary bonds. As mentioned earlier, $(C_6H_5)I(O_2CCHCl_2)_2$ (2) and the isostructural $(C_6H_5)I(O_2CCF_3)_2$ (4) dimerize in a similar manner to that of the present structure except that the dimers are stacked in columns along *b* rather than linked into chains. These complexes form one intermolecular interaction, bisecting an EE edge of an inversion equivalent molecule, and two intramolecular interactions, one bisecting an XE edge and one capping an XEE face giving an $AX_3YY'_2E_2$ arrangement. Their lengths are 2.94, 3.05, 2.94 Å and 3.00, 3.16, 3.06 Å, for the bis(dichloroacetate) and bis(trifluoroacetate) respectively.

The μ-oxo derivative, $[(C_6H_5)I(O_2CCF_3)]_2O$ (5), presents a further interesting feature in that the secondary geometry about the two unique iodine sites is different. The first site has just one intramolecular XEE face capping secondary interaction of 2.94 Å whilst the second site has an intermolecular EE edge bridging interaction of 3.08 Å from an inversion equivalent molecule, thus forming the molecules into dimers, and an intramolecular XEE face capping interaction of 3.27 Å from the same trifluoroacetate. The geometries of the two iodine sites may be described as AX_3YE_2 and $AX_3Y_2Y'E_2$ respectively.

With the variety of structural modifications displayed by the aryliodine(III)bis(carboxylate) complexes one might expect significant changes in the appearance of their ^{127}I Mössbauer spectra; this, however, does not appear to be the case.

Mössbauer spectroscopy

^{127}I Mössbauer data recorded at 4.2 K for the aryliodine(III)carboxylates are presented in Table 4 together with literature data for some related compounds for comparison purposes. The quadrupole coupling constant, $e^2q^{127}Q_g/h$, is positive for all of the complexes studied with the line from the transition, 5/2(ground)–7/2(excited), at high negative velocity (28). This is as expected for a central iodine(III) nucleus with bonds in the *xy* plane and the two nonbonding electron pairs above and below the coordination plane along the internuclear *z*-axis, the principal axis of the electric field gradient tensor. A representative spectrum of the monophenyliodine(III)bis(carboxylate) series, that of $(C_6H_5)I(O_2CCF_3)_2$, is shown in Fig. 3.

Examination of the data contained in Table 4 for the monophenyliodine(III)carboxylate series reveals, with one exception, that both the quadrupole coupling constants and the isomer shifts exhibit the expected trends with the electronegativity of the carboxylate group, i.e., an increase in carboxylate electronegativity leads to greater values of quadrupole coupling constant, $e^2q^{127}Q_g/h$, and more negative values of isomer shift; the electronegativities of the carboxylate ligands have been shown to follow the functional group order (29)

$$-CF_3 > -CCl_3 > -CHCl_2 > -CH_2Cl > -CH_3$$

This illustrates clearly the dependence of these parameters on the primary interactions at the iodine nucleus. The exception to the above is the isomer shift of the bis(trifluoroacetate) derivative. ^{127}I isomer shifts are relatively insensitive to changes in electron configuration because of the small value of $\delta R/R$ (30) and as such this result may be just an artifact. Since $\delta R/R$ is also negative for ^{127}I, the *s*-electron density at the iodine nucleus in these compounds must be greater than that of reference material, $K^{127}I$, indicating that the bonds are mainly

TABLE 3. Selected bond lengths (Å) and bond angles (deg) for $(C_6F_5)I(O_2CCF_3)_2$, with estimated standard deviations in parentheses

Molecule 1

(i) Iodine coordination					
I(1)—C(16)	2.078(10)		I(1)···O(12)	3.075(8)	
I(1)—O(11)	2.147(6)		I(1)···O(14)	3.120(10)	
I(1)—O(13)	2.128(6)		I(1)···O(12)[1]	2.955(11)	
			I(1)···O(14)[2]	3.190(9)	
O(11)—I(1)—C(16)		81.5(3)	O(13)—I(1)—C(16)		81.1(3)
O(11)—I(1)—O(13)		162.6(3)	C(16)—I(1)—O(12)[1]		151.6(3)
(ii) Pentafluorophenyl ring					
C(11)—C(12)	1.372(18)		C(11)—F(11)	1.322(11)	
C(12)—C(13)	1.363(16)		C(12)—F(12)	1.333(14)	
C(13)—C(14)	1.353(16)		C(13)—F(13)	1.334(15)	
C(14)—C(15)	1.378(16)		C(14)—F(14)	1.345(12)	
C(15)—C(16)	1.362(12)		C(15)—F(15)	1.344(11)	
C(16)—C(11)	1.364(14)				
C(12)—C(11)—C(16)		120.5(9)	C(13)—C(12)—F(12)		119.7(11)
C(11)—C(12)—C(13)		119.8(11)	C(12)—C(13)—F(13)		120.5(9)
C(12)—C(13)—C(14)		120.0(12)	C(14)—C(13)—F(13)		119.5(10)
C(13)—C(14)—C(15)		120.1(10)	C(13)—C(14)—F(14)		120.1(11)
C(14)—C(15)—C(16)		120.2(9)	C(15)—C(14)—F(14)		119.8(9)
C(15)—C(16)—C(11)		119.3(10)	C(14)—C(15)—F(15)		118.5(8)
C(12)—C(11)—F(11)		118.3(9)	C(16)—C(15)—F(15)		121.2(9)
C(16)—C(11)—F(11)		121.2(11)	C(11)—C(16)—I(1)		120.4(7)
C(11)—C(12)—F(12)		120.4(9)	C(15)—C(16)—I(1)		120.3(7)
(iii) Trifluoroacetates					
O(11)—C(17)	1.295(13)		C(18)—F(16)	1.364(19)	
O(12)—C(17)	1.191(12)		C(18)—F(17)	1.192(32)	
C(17)—C(18)	1.559(14)		C(18)—F(18)	1.286(17)	
I(1)—O(11)—C(17)		113.9(5)	C(17)—C(18)—F(17)		111.4(10)
O(11)—C(17)—O(12)		128.0(9)	C(17)—C(18)—F(18)		112.3(13)
O(11)—C(17)—C(18)		112.6(8)	F(16)—C(18)—F(17)		118.2(18)
O(12)—C(17)—C(18)		119.4(10)	F(16)—C(18)—F(18)		96.6(11)
C(17)—C(18)—F(16)		111.2(12)	F(17)—C(18)—F(18)		106.0(18)
O(13)—C(19)	1.310(17)		C(110)—F(19)	1.337(15)	
O(14)—C(19)	1.182(12)		C(110)—F(110)	1.228(23)	
C(19)—C(110)	1.554(13)		C(110)—F(111)	1.309(28)	
I(1)—O(13)—C(19)		115.5(4)	C(19)—C(110)—F(110)		112.7(12)
O(13)—C(19)—O(14)		128.2(9)	C(19)—C(110)—F(111)		107.7(10)
O(13)—C(19)—C(110)		110.1(8)	F(19)—C(110)—F(110)		108.4(12)
O(14)—C(19)—C(110)		121.7(13)	F(19)—C(110)—F(111)		102.4(13)
C(19)—C(110)—F(19)		111.5(12)	F(110)—C(110)—F(111)		113.7(18)

Symmetry operators:
[1] $1-x, 2-y, 1-z$; [2] $-x, 2-y, 1-z$

Molecule 2

(i) Iodine coordination					
I(2)—C(26)	2.063(6)		I(2)···O(22)	3.080(7)	
I(2)—O(21)	2.145(9)		I(2)···O(24)	3.146(11)	
I(2)—O(23)	2.136(8)		I(2)···O(22)[3]	2.918(9)	
			I(2)···O(24)[4]	3.322(8)	
O(21)—I(2)—C(26)		80.8(3)	O(23)—I(2)—C(26)		82.2(3)
O(21)—I(2)—O(23)		163.0(2)	C(26)—I(2)—O(22)[3]		155.9(3)
(ii) Pentafluorophenyl ring					
C(21)—C(22)	1.369(11)		C(21)—F(21)	1.355(12)	
C(22)—C(23)	1.348(16)		C(22)—F(22)	1.327(14)	
C(23)—C(24)	1.374(16)		C(23)—F(23)	1.320(8)	
C(24)—C(25)	1.377(10)		C(24)—F(24)	1.352(12)	
C(25)—C(26)	1.371(13)		C(25)—F(25)	1.328(13)	
C(26)—C(21)	1.377(14)				

Can. J. Chem. Downloaded from www.nrcresearchpress.com by 186.148.149.217 on 09/07/12
For personal use only.

TABLE 3 (*concluded*)

C(22)—C(21)—C(26)		121.4(9)	C(23)—C(22)—F(22)		121.1(7)
C(21)—C(22)—C(23)		119.9(10)	C(22)—C(23)—F(23)		120.8(10)
C(22)—C(23)—C(24)		119.9(7)	C(24)—C(23)—F(23)		119.3(9)
C(23)—C(24)—C(25)		120.4(9)	C(23)—C(24)—F(24)		119.6(7)
C(24)—C(25)—C(26)		120.1(9)	C(25)—C(24)—F(24)		120.1(9)
C(25)—C(26)—C(21)		118.3(6)	C(24)—C(25)—F(25)		118.3(8)
C(22)—C(21)—F(21)		119.3(10)	C(26)—C(25)—F(25)		121.6(6)
C(26)—C(21)—F(21)		119.3(7)	C(21)—C(26)—I(2)		120.7(6)
C(21)—C(22)—F(22)		119.0(10)	C(25)—C(26)—I(2)		121.0(7)
(iii) Trifluoroacetates					
O(21)—C(27)	1.285(11)		C(28)—F(26)	1.264(27)	
O(22)—C(27)	1.205(12)		C(28)—F(27)	1.346(10)	
C(27)—C(28)	1.542(19)		C(28)—F(28)	1.292(20)	
I(2)—O(21)—C(27)		114.3(7)	C(27)—C(28)—F(27)		108.1(10)
O(21)—C(27)—O(22)		128.0(11)	C(27)—C(28)—F(28)		114.7(14)
O(21)—C(27)—C(28)		111.5(8)	F(26)—C(28)—F(27)		106.3(13)
O(22)—C(27)—C(28)		120.4(9)	F(26)—C(28)—F(28)		108.5(15)
C(27)—C(28)—F(26)		114.1(12)	F(27)—C(28)—F(28)		104.3(10)
O(23)—C(29)	1.301(16)		C(210)—F(29)	1.272(12)	
O(24)—C(29)	1.193(13)		C(210)—F(210)	1.195(25)	
C(29)—C(210)	1.540(19)		C(210)—F(211)	1.403(22)	
I(2)—O(23)—C(29)		116.4(6)	C(29)—C(210)—F(210)		115.3(10)
O(23)—C(29)—O(24)		128.2(12)	C(29)—C(210)—F(211)		112.4(14)
O(23)—C(29)—C(210)		111.6(9)	F(29)—C(210)—F(210)		116.5(16)
O(24)—C(29)—C(210)		120.2(12)	F(29)—C(210)—F(211)		100.5(10)
C(29)—C(210)—F(29)		111.0(13)	F(210)—C(210)—F(211)		99.6(16)

Symmetry operators:
[3] $1-x, 1-y, -z$; [4] $-x, 1-y, -z$

TABLE 4. ^{127}I Mössbauer data for organoiodine(III)carboxylates and related species

Compound	$\delta^{a,b}$	$e^2q^{127}Q_g/h^c$	Γ^b	η	$T_a{}^d$	Ref.
$I(O_2CCH_3)_3$	−1.83(3)	+3419(16)	1.73(8)	0.07(3)	0.63(2)	1
$I(O_2CCF_3)_3$	−1.60(3)	+3540(18)	1.63(9)	0.00	0.87(4)	1
$(C_6H_5)I(O_2CCH_3)_2$	−0.87(1)	+2507(6)	1.53(4)	0.79(1)	na	32
$(C_6H_5)I(O_2CCF_3)_2$	−0.88(3)	+2708(15)	2.30(9)	0.82(2)	0.45(1)	e
$(C_6H_5)I(O_2CCH_2Cl)_2$	−0.93(7)	+2583(47)	1.54(22)	0.87(4)	0.18(2)	e
$(C_6H_5)I(O_2CCHCl_2)_2$	−1.09(4)	+2698(26)	1.38(10)	0.85(2)	0.78(5)	e
$(C_6F_5)I(O_2CCF_3)_2$	−1.15(4)	+2951(20)	1.87(10)	0.55(2)	1.15(5)	e
$[(C_6H_5)I(O_2CCF_3)]_2O$	−0.78(4)	+2572(19)	2.43(11)	0.65(2)	0.39(1)	e
$(C_6H_5)ICl_2$	−0.62(5)	+2525(30)	na	0.70(5)	na	33
$(C_6H_5)_2IO_2CCF_3$	−0.62(5)	+2031(20)	1.51(10)	0.36(2)	0.45(2)	e
$[(C_6H_5)_2ICl]_2$	−0.54(2)	+2044(19)	2.13(13)	0.31(2)	0.32(1)	31
$C_6H_5(o\text{-}CO_2C_6H_4)I\cdot H_2O$	−0.50(3)	+1914(6)	1.50(4)	0.50(1)	na	24
KI	0.00(6)		2.23(2)		0.28(2)	e

[a] Values relative to $K^{127}I$ at 4.2 K.
[b] Values in mm/s.
[c] Values in MHz.
[d] Dimensionless absorber thickness, see ref. 19.
[e] This work.

of *p*-character. Removal of *p*-electron density from the iodine nucleus greatly reduces the shielding effect on the 5*s* electrons, hence giving a more negative isomer shift.

The members of the above series also display large values of asymmetry parameter, η. This implies that although V_{zz} is through the nonbonded electron pairs perpendicular to the *xy* plane there exists a high degree of asymmetry within the electron density in the *x* and *y* directions. This has the effect of making the Mössbauer spectrum appear more symmetrical and as such the sign of the quadrupole coupling constant becomes harder to determine visually; the spectrum would be totally symmetrical when $\eta = 1$ (28). The high asymmetry parameter observed for these compounds is a direct consequence of the difference in the relative electronegativities of the carbon and oxygen atoms, the C—I bond contributing more electron density to the *xy* plane than the bonds to the more electronegative

Can. J. Chem. Downloaded from www.nrcresearchpress.com by 186.148.149.217 on 09/07/12
For personal use only.

Can. J. Chem. Downloaded from www.nrcresearchpress.com by 186.148.149.217 on 09/07/12
For personal use only.

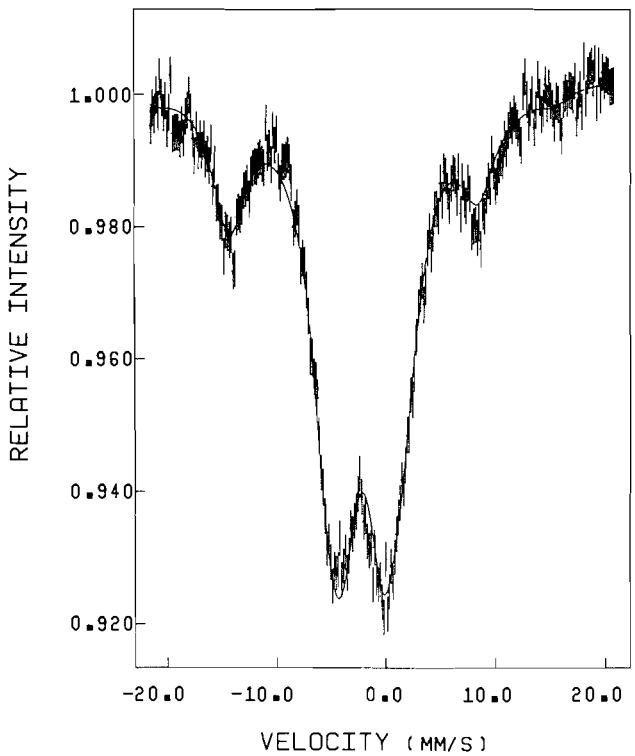


FIG. 3. ^{127}I Mössbauer spectrum of $(C_6H_5)I(O_2CCF_3)_2$ measured at 4.2 K. The solid line is the best fit to the data.

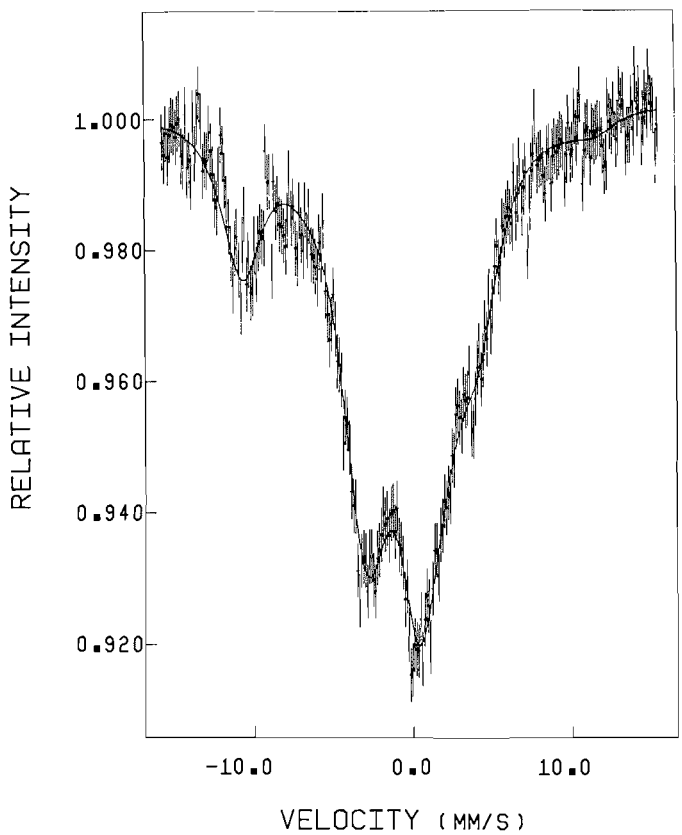


FIG. 4. ^{127}I Mössbauer spectrum of $(C_6H_5)_2I(O_2CCF_3)$ measured at 4.2 K. The solid line is the best fit to the data.

oxygens. The spectrum of $(C_6F_5)I(O_2CCF_3)_2$ bears this out in that replacement of the phenyl group with a more electronegative pentafluorophenyl group significantly reduces the asymmetry parameter from ~0.80 to 0.55. It has been shown that the asymmetry parameter is further reduced to ca. zero if the phenyl group is replaced by a trifluoroacetate (1).

The Mössbauer spectrum of the μ-oxo derivative, $[(C_6H_5)I(O_2CCF_3)]_2O$, is best fitted to just one single iodine site even though the results of the crystal structure determination show the two iodine sites to be nonequivalent through secondary bonding considerations (5). Attempts were made to fit this spectrum to two similar independent iodine sites commensurate with the findings of the crystal structure determination; however, this always yielded divergent fits. The somewhat broad linewidth (Γ = 2.43 mm/s) displayed by this material is probably a reflection of the presence of a second very similar site, although this value is still less than twice the natural linewidth ($2\Gamma_0$ = 2.54 mm/s). This result lends further weight to the conclusion that the ^{127}I Mössbauer parameters are dependent on the primary bonding arrangement about iodine only, and that the secondary bonds to the iodine nucleus have little or no effect on the Mössbauer spectrum.

The Mössbauer spectrum of $(C_6H_5)_2I(O_2CCF_3)$ is illustrated in Fig. 4. The fitted parameters for this compound are in good agreement with those observed for other diphenyliodine(III) species, e.g., $[(C_6H_5)_2IX]_2$ (31), where X = Cl, Br, I, and $C_6H_5(o\text{-}CO_2C_6H_4)I\cdot H_2O$ (24). The quadrupole coupling constant for this compound is reduced in comparison with that of the monoorganoiodine(III) species by the loss of the more electronegative carboxylate ligand. This change is also reflected in the increase in the value of the isomer shift. The decreased magnitude of η illustrates further that this parameter is dependent on both the electronegativity of the bound ligand and its position in relation to the geometry of the rest of the molecule. A full single crystal X-ray structure determination is currently in progress to determine the precise nuclear environment of the iodine in $(C_6H_5)_2I(O_2CCF_3)$.

Acknowledgements

We thank the Natural Sciences and Engineering Research Council of Canada for providing an operating grant, and R. Faggiani for technical assistance.

1. T. BIRCHALL, C. S. FRAMPTON, and P. KAPOOR. Inorg. Chem. **28**, 636 (1989).
2. N. W. ALCOCK, R. M. COUNTRYMAN, S. ESPERAS, and J. F. SAWYER. J. Chem. Soc. Dalton Trans. 854 (1979).
3. C. K. LEE, T. C. W. MAK, W. K. LI, and J. F. KIRNER. Acta Crystallogr. Sect. B: Struct. Crystallogr. Cryst. Chem. **B33**, 1620 (1977).
4. G. A. STERGIOUDIS, S. C. KOKKOU, A. P. BOZOPOULOS, and P. J. RENTZEPENIS. Acta Crystallogr. Sect. C: Cryst. Struct. Commun. **C40**, 877 (1984).
5. J. GALLOS, A. VARVOGLIS, and N. W. ALCOCK. J. Chem. Soc. Perkin Trans. 1, 757 (1985).
6. K. H. PAUSACKER. J. Chem. Soc. 107 (1953).
7. G. M. LOUDON, A. S. RADHAKRISHNA, M. R. ALMOND, J. K. BLODGETT, and R. H. BOUTIN. J. Org. Chem. **49**, 4272 (1984).
8. A. I. VOGEL. Quantitative inorganic analysis. 3rd ed. Longmans, London. 1966.
9. M. SCHMEISSER, K. DAHMEN, and P. SARTORI. Chem. Ber. **110**, 1633 (1967).
10. F. M. BERINGER, M. DREXLER, E. M. GINDLER, and C. C. LUMPKIN. J. Am. Chem. Soc. **75**, 2705 (1953).

11. B. LIPPERT, C. J. L. LOCK, B. ROSENBERG, and M. ZAVAGULIS. Inorg. Chem. **16**, 1525 (1977).
12. P. R. HUGHES, N. KRISHNAMACHARI, C. J. L. LOCK, J. POWELL, and C. T. TURNER. Inorg. Chem. **16**, 314 (1977).
13. G. M. SHELDRICK. SHELX-76, Program for crystal structure determination. University of Cambridge, England. 1976.
14. D. T. CROMER and J. B. MANN. Acta Crystallogr. Sect. A: Cryst. Phys. Diffr. Theor. Gen. Crystallogr. **A24**, 231 (1968).
15. D. T. CROMER and D. LIBERMAN. J. Chem. Phys. **53**, 1891 (1970).
16. J. M. STEWART and S. R. HALL. The XTAL system of crystallographic programs. Tech. Rept. TR-1364, University of Maryland, College Park, MD. 1983.
17. J. STEPHENS. MOLGEOM, adapted from CUDLS. McMaster University, Hamilton, Ont. 1973.
18. K. DAVIES. CHEMGRAF suite: SNOOPI. Chemical Design Ltd. Oxford, England. 1983.
19. K. RUEBENBAUER and T. BIRCHALL. Hyperfine Interact. **7**, 125 (1979).
20. R. J. BATCHELOR, T. BIRCHALL, and R. D. MYERS. J. Chem. Phys. **77**, 3383 (1982).
21. R. J. GILLESPIE. Molecular geometry. Van Nostrand Reinhold, London. 1972.
22. B. F. HOSKINS and C. D. PANNAN. Aust. J. Chem. **29**, 2337 (1976).
23. E. H. WIEBENGA, E. E. HAVINGA, and K. H. BOSWIJK. Adv. Inorg. Radiochem. **3**, 133 (1961).
24. R. J. BATCHELOR, T. BIRCHALL, and J. F. SAWYER. Inorg. Chem. **25**, 1415 (1986).
25. P. BOLDRINI, R. J. GILLESPIE, P. R. IRELAND, and G. J. SCHROBILGEN. Inorg. Chem. **13**, 1693 (1974).
26. N. W. ALCOCK. Adv. Inorg. Radiochem. **15**, 1 (1972).
27. J. F. SAWYER and R. J. GILLESPIE. Prog. Inorg. Chem. **34**, 65 (1986).
28. N. N. GREENWOOD and T. C. GIBB. Mössbauer spectroscopy. Chapman and Hall, London. 1974. pp. 464–469.
29. J. HINZE, M. A. WHITEHEAD, and H. H. JAFFÉ. J. Am. Chem. Soc. **85**, 148 (1963).
30. G. J. PERLOW and M. R. PERLOW. J. Chem. Phys. **45**, 2193 (1966).
31. T. BIRCHALL and R. D. MYERS. J. Chem. Soc. Dalton Trans. 885 (1983).
32. T. BIRCHALL, J. A. SMEGALL, and C. L. HILL. Inorg. Chem. **20**, 2207 (1981).
33. B. S. EHRLICH and M. KAPLAN. J. Chem. Phys. **54**, 612 (1971).

Can. J. Chem. Downloaded from www.nrcresearchpress.com by 186.148.149.217 on 09/07/12
For personal use only.

Momentum densities, Compton profiles, and *B* functions for the alkaline earth oxides

ARVIND KUMAR JAIN AND A. N. TRIPATHI
Department of Physics, University of Roorkee, Roorkee 247667, India

AND

VEDENE H. SMITH, JR.[1]
Department of Chemistry, Queen's University, Kingston, Ont., Canada K7L 3N6

Received May 23, 1989

This paper is dedicated to Professor Ronald J. Gillespie on the occasion of his 65th birthday

ARVIND KUMAR JAIN, A. N. TRIPATHI, and VEDENE H. SMITH, JR. Can. J. Chem. **67**, 1886 (1989).

Momentum densities $\Pi(\boldsymbol{p})$, Compton profiles $J(\boldsymbol{q})$, and internally folded densities $B(\boldsymbol{r})$ have been calculated from self-consistent field wavefunctions for the alkaline earth oxides BeO, MgO, CaO, and SrO. The results are analyzed both by means of a partial wave decomposition and by comparison with separated ionic reference moieties. The Compton profile anisotropies for these systems are shown to be quite different than those predicted on the basis of a simple scaling relation from data for the alkali fluorides.

Key words: alkaline earth oxides, Compton profiles, momentum densities, internally folded densities, *B* functions.

ARVIND KUMAR JAIN, A. N. TRIPATHI et VEDENE H. SMITH, JR. Can. J. Chem. **67**, 1886 (1989).

Utilisant des fonctions d'onde en champ auto-cohérent, on a calculé les densités des moments $\Pi(\boldsymbol{p})$, les profils de Compton $J(\boldsymbol{q})$ ainsi que les densités refermées d'une façon interne $B(\boldsymbol{r})$ des oxydes des métaux alcalino-terreux BeO, MgO, CaO et SrO. On a analysé les résultats à l'aide de la décomposition partielle des ondes ainsi que par une comparaison avec les portions de référence ioniques séparées. On a démontré que les anisotropies du profil de Compton de ces systèmes sont très différentes de celles que l'on peut prédire en se basant sur une simple relation scalaire établie à partir de données pour les fluorures alcalins.

Mots clés : métaux alcalino-terreux, profils de Compton, densités des moments, densités refermées d'une façon interne, fonctions *B*.

[Traduit par la revue]

Introduction

Compton scattering studies of atomic and molecular systems provide valuable information about the electronic structure of atoms and molecules through the analysis of Compton line shapes (1–5). In recent years a considerable amount of work (6–19) has been done relating Compton profiles and momentum densities to chemical bonding.

There are four different approaches that have been used to analyse the effect of bonding on Compton profiles. Each approach has its own special features and we shall outline them very briefly here. The first approach is essentially based on population analysis (20), which is followed routinely in position space studies. In this approach, the Compton profile (CP) is partitioned into various components ("atomic" and "overlap") stemming from the partitioning of the density matrix $\gamma(\boldsymbol{r}|\boldsymbol{r}')$, which is a bilinear form in the orbitals. The second approach (11, 12) partitions the CP into core, lone pair, and bond contributions arising from the individual localized molecular orbitals obtained from the self-consistent field procedure by one of the usual localization methods. In the third procedure, the bond difference profile (9) is constructed by subtracting from the molecular profile the sum of the profiles of the isolated atoms (reference moieties) in a promolecule condition. In the last approach, a partial wave analysis is performed to partition the profile into its various angular momentum components, thereby obtaining related chemical information (18, 19).

Among these approaches, the population analysis and bond difference profile methods have been quite popular in analyzing profiles and related anisotropies. Sharma *et al.* (17) have used these schemes to analyze the bonding effects on the isotropic Compton profile and on the momentum densities of alkaline earth oxides. In the present study we calculate the directional properties of the momentum density, Compton profile, and $B(\boldsymbol{r})$ function (internally folded density) for the alkaline earth oxides. Further, we also investigate how a study of the partial wave components reveals the changes in chemical properties and different bonding situations in this homologous series of diatomic molecules. In the analysis comparison is made with results for the appropriate separated reference moieties. They are chosen to be the singly ionized atomic ions in their ground states ($E^+(^2S) + O^-(^2P)$) where E = Be, Mg, Ca, and Sr respectively. The various other plausible choices of reference moieties and their implications have been examined by Sharma *et al.* (17). It should be noted that it is not possible to use the chemically intuitive choice of the doubly charged free ions ($E^{2+}(^1S) + O^{2-}(^1S)$) because O^{2-} is not bound (21).

Theory

Within the framework of the impulse approximation (1, 4), the directional Compton profile $J(\boldsymbol{q})$ can be expressed (3) in terms of the one-electron momentum density $\Pi(\boldsymbol{p})$ as

$$[1] \quad J(\boldsymbol{q}) = \int \Pi(\boldsymbol{p}) \delta(\boldsymbol{p}\cdot\boldsymbol{q}/q - q) \mathrm{d}\boldsymbol{p}$$

where q is the projection of the initial electron momentum $\boldsymbol{p}$ on the scattering vector of the incident particle. $\Pi(\boldsymbol{p})$ can be obtained from the electronic wavefunction ψ of the N-electron system by the prescription

$$[2] \quad \Pi(\boldsymbol{p}) = (2\pi\hbar)^{-3} \int e^{i\boldsymbol{p}\cdot(\boldsymbol{r}-\boldsymbol{r}')} \Gamma^{(1)}(\boldsymbol{r}|\boldsymbol{r}') \mathrm{d}\boldsymbol{r}\, \mathrm{d}\boldsymbol{r}'$$

where $\Gamma^{(1)}(\boldsymbol{r}|\boldsymbol{r}')$ is the spin-traced, position space one-electron reduced density matrix defined by

$$[3] \quad \Gamma^{(1)}(\boldsymbol{r}|\boldsymbol{r}') = N \int \psi^*(\boldsymbol{r}'\sigma_1, \boldsymbol{x}_2 \ldots \boldsymbol{x}_N) \psi(\boldsymbol{r}\sigma_1, \boldsymbol{x}_2 \ldots \boldsymbol{x}_N) \mathrm{d}\sigma_1 \mathrm{d}\boldsymbol{x}_2 \ldots \mathrm{d}\boldsymbol{x}_N$$

[1]Author to whom correspondence may be addressed.

Printed in Canada / Imprimé au Canada

Can. J. Chem. Downloaded from www.nrcresearchpress.com by 194.225.253.170 on 09/07/12
For personal use only.

Can. J. Chem. Downloaded from www.nrcresearchpress.com by 194.225.253.170 on 09/07/12
For personal use only.

Here $x_i = (r_i, \sigma_i)$ is the combined spin-space coordinate of electron i.

In recent years a physically meaningful quantity, the autocorrelation function $B(r)$, also known as the reciprocal form factor (internally folded density), has been introduced (22–25) for the analysis of the Compton profile. It is defined by

$$[4] \quad B(r) = \int \Gamma^{(1)}(s|s + r)ds = \int \Pi(p)e^{ip\cdot r}dp = \int J(q)e^{iq\cdot r}dq$$

In the partial wave analysis (18, 19), the $\Pi(p)$, $J(q)$, and $B(r)$ can be expressed in terms of spherical harmonics, Y_{lm}, as

$$[5a] \quad \Pi(p) = \sum_{l=0}^{\infty} \sum_{m=-l}^{l} \Pi_{lm}(p)Y_{lm}(\theta_p, \phi_p)$$

$$[5b] \quad J(q) = \sum_{l=0}^{\infty} \sum_{m=-l}^{l} J_{lm}(q)Y_{lm}(\theta_q, \phi_q)$$

and

$$[5c] \quad B(r) = \sum_{l=0}^{\infty} \sum_{m=-l}^{l} B_{lm}(r)Y_{lm}(\theta, \phi)$$

For linear molecules with the molecular axis aligned along the polar axis, which includes the alkaline earth oxide diatomics of this study, $\Pi(p)$ has $D_{\infty h}$ symmetry irrespective of whether the molecular skeleton has $C_{\infty h}$ or $D_{\infty h}$ symmetry (18, 26). Thus the expansions [5] simplify for a linear molecule as follows:

$$[6a] \quad \Pi(p) = \Pi_0(p) + \Pi_2(p)P_2(\cos\theta_p) + \Pi_4(p)P_4(\cos\theta_p) + \ldots$$

$$[6b] \quad J(q) = J_0(q) + J_2(q)P_2(\cos\theta_q) + J_4(q)P_4(\cos\theta_q) + \ldots$$

$$[6c] \quad B(r) = B_0(q) + B_2(r)P_2(\cos\theta_q) + B_4(q)P_4(\cos\theta_q) + \ldots$$

when the P_L are Legendre polynomials, $\Pi_0(p)$ is precisely equal to the spherically averaged momentum density $\overline{\Pi}(p)$, and the higher partial waves $\Pi_2(p)$, $\Pi_4(p)$, ... ($J_2(q)$, $J_4(q)$, ..., $B_2(r)$, $B_4(r)$ ...) represent the anisotropy.

The partial wave components $J_l(q)$ and $B_l(q)$ are related to the Π_l by

$$[7] \quad J_l(q) = 2\pi \int_{|q|}^{\infty} P_l(q/p)\Pi_l(p)p\,dp$$

and

$$[8] \quad B_l(r) = 4\pi(-i)^l \int_0^{\infty} \Pi_l(p)j_l(pr)p^2dp$$

In the evaluation of eqs. [7] and [8], the basic quantity of importance is $\Pi_l(p)$. Analytic formulae for these purposes are given explicitly in the paper by Kaijser and Smith (3), eqs. 129–133 and 143–147, for spherical harmonics and Cartesian Gaussian type basis functions respectively.

Equations [6] provide an alternative procedure to analyze the momentum density, Compton profile, and $B(r)$ functions into the various partial wave components, i.e., $l = 0, 2, 4, 6$, etc. This type of analysis is well suited to $\Pi(p)$, $J(q)$, and $B(r)$ because they are essentially monocentric functions (26).

In the present study self-consistent field (SCF) functions constructed (27) from basis sets of Slater type functions were employed to calculate $\Pi(p)$, $J(q)$, and $B(r)$ at the equilibrium internuclear separation (R_e) for the lowest $^1\Sigma$ state, which is the true ground state for these molecules (28). The highest occupied molecular orbitals are $(m\sigma)^2(n\pi)^4$ in BeO, CaO, and SrO with the inverted order $(n\pi)^4(m\sigma)^2$ in MgO.

These basis sets may be described as Be (6*s*, 2*p*, 1*d*, 1*f*), Mg (7*s*, 5*p*, 1*d*, 1*f*), and O (6*s*, 4*p*, 1*d*, 1*f*) in BeO and MgO, as Ca (8*s*, 5*p*, 1*d*, 1*f*) and O (4*s*, 2*p*, 1*d*, 1*f*) in CaO, and as Sr (10*s*, 7*p*, 3*d*) and O (4*s*, 2*p*, 1*d*) in SrO. The BeO and MgO wavefunctions are very close to the Hartree–Fock limit but the CaO and SrO wavefunctions are only of double zeta plus polarization quality. Of course wavefunctions including electron correlation and relativistic effects would be more appropriate, in particular for the heavier oxides (CaO, SrO). However, the qualitative trend displayed by the SCF momentum space properties should be correct to the same extent as in the case of the position space properties already calculated by Yoshimine (27).

Before we consider our results ($\Pi(p)$, $J(q)$, and $B(r)$)[2] for this homologous series, it is worthwhile to discuss the reliability and the accuracy of the partial wave expansion approach, which entirely depends upon how fast the various terms in the expansion (eqs. [5]) converge to the true value. Thakkar *et al.* (18) carried out for $\Pi(p)$ a detailed study of convergence tests on 21 linear molecules. They found that such an expansion converges very rapidly for small momentum values ($0 \leqq p \leqq 3\hbar a_0^{-1}$) and less rapidly for large momentum. Furthermore, from their study of partial wave decomposition of the momentum density, it is also evident that in the region of small momentum (the valence region) all the anisotropy of the momentum density can be understood from a chemical point of view by simply considering the first four partial waves: $l = 0$, 2, 4, and 6. Therefore, we shall pay attention to the first four partial waves in all our subsequent discussions of anisotropy for this homologous series of molecules, although the calculations have been done through $l = 10$ and for the parallel and perpendicular components directly. Fortunately, the alkaline earth oxides, which belong to the same class of linear molecules, have weakly anisotropic momentum densities ($\Pi_l(p)$) and therefore for this set of molecules a very rapidly convergent partial wave expansion is obtained. The same also holds for the case of the $J_l(q)$ and $B_l(r)$ expansions.[3] We have confirmed this by calculating $J_\perp(q)$ and $J_\parallel(q)$, $B_\perp(q)$ and $B_\parallel(q)$ directly.

Results and discussion

Momentum density: $\Pi(\mathbf{p})$

Figure 1 shows the spherically averaged momentum density $\overline{\Pi}(p) = \overline{\Pi}_0(p)$ per electron for the alkaline earth oxides EO (E = Be, Mg, Ca, Sr respectively). In view of the recent interest (29–31) in the monotonic (or otherwise?) behaviour of $\overline{\Pi}(p)$, it is seen that all the alkaline earth oxides in Fig. 1 have nonmonotonic isotropic momentum densities ordered in the sequence Mg, Be, Ca, Sr. Figures 2 and 3 show the different components of the partial waves ($l = 2$, 4, 6) for these molecules. Note that all quantities are per electron on the same scale to facilitate comparison among the molecules.

It is clearly seen from Fig. 2 that the behaviour of the $\Pi_2(p)$ and $\Pi_4(p)$ components for BeO is quite different from that

[2]Tables of the calculated values may be obtained on request from the authors.

[3]The convergence properties of the $J_l(q)$ and $B_l(r)$ expansions are discussed elsewhere (R. P. Sagar, A. M. Simas, V. H. Smith, Jr., and A. J. Thakkar. To be published).

Can. J. Chem. Downloaded from www.nrcresearchpress.com by 194.225.253.170 on 09/07/12
For personal use only.

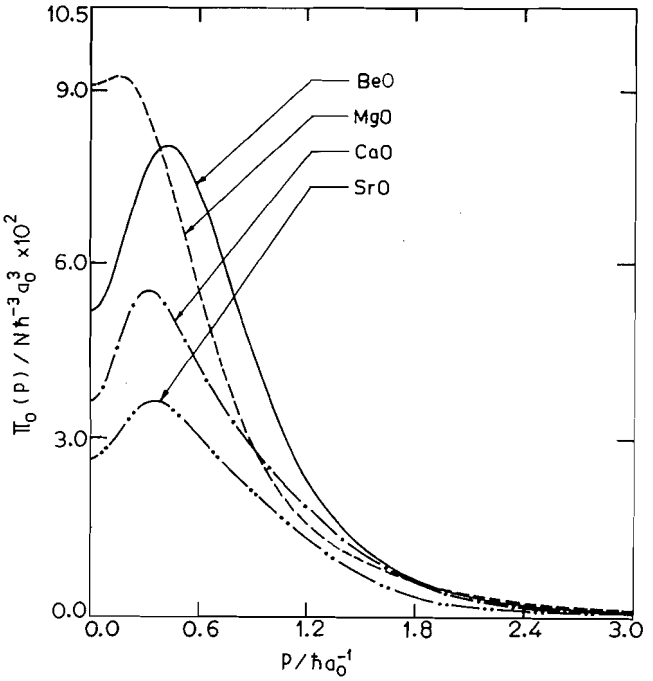


FIG. 1. Isotropic component of the momentum density (per electron) for BeO, MgO, CaO, and SrO.

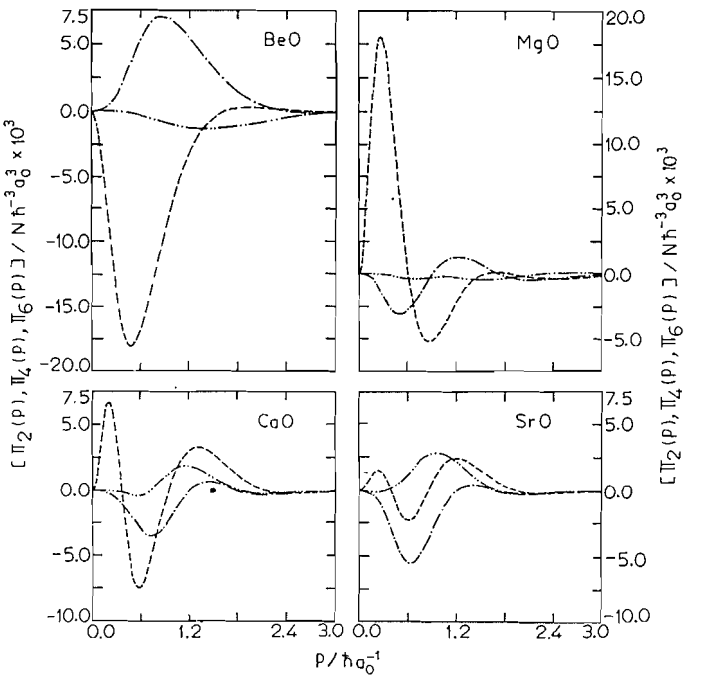


FIG. 2. Higher partial waves of the momentum density (per electron) for BeO, MgO, CaO, and SrO. (-----) $\Pi_2(p)$; (- · - · -) $\Pi_4(p)$; (- · · - · · -) $\Pi_6(p)$.

of the other oxides in the series (MgO, CaO, and SrO). On the whole, this can be rationalized by noting that $\Pi_2(p)$ is dominated by bonding contributions while $\Pi_4(p)$ and $\Pi_6(p)$ oscillate, as bonding and antibonding contributions dominate at different values of momentum p. This behaviour for $\Pi_l(p)$ is quite in agreement with the empirical rules outlined earlier (20, 21) for the prediction of the qualitative valence region behaviour of the contributions of canonical molecular orbitals (MO's) to the chemically dominant partial waves. The magnitude of the higher components, i.e., $\Pi_6(p)$, $\Pi_8(p)$, ..., is negligibly small for BeO and MgO but increases for the heavier oxides.

Our calculations of $\bar{\Pi}(p)$, $\Pi_{\parallel}(p)$, $\Pi_{\perp}(p)$, and $\Pi_{si}(p)$ at equilibrium bond length for BeO (2.4377 a_0), MgO (3.3052 a_0), CaO (3.4412 a_0), and SrO (6.283 a_0) respectively were used to construct Figs. 3(a–c). From Figs. 3 it is observed that the anisotropy ($\Pi(\boldsymbol{p}) - \Pi_{si}(p)$) of the momentum density decreases with increasing equilibrium bond length R_e in the sequence BeO, MgO, CaO, and SrO. The effects of bonding exhibited in Figs. 3(a, b) for the isotropic and parallel components of the momentum density are quite similar in nature and in both cases they follow the sequence Mg, Be, Ca, and Sr, in contrast to the sequence shown in Fig. 3(c) for the perpendicular component.

Compton profile: $J(\mathbf{q})$

Figures 4 and 5 display the isotropic Compton profile $\bar{J}(q) = J_0(q)$ and the partial wave components $J_{2l}(q)$ per electron on the same scale for all the oxides. The present calculations for $\bar{J}(q)$ are in perfect agreement with the earlier calculations of Sharma *et al.* (19) for the same wavefunctions. The $l = 0$ component ($J_0(q)$) provides the major contribution to the total profile, in particular at small q values. As q increases, there is a gradual decrease of $J_0(q)$, with the decrease more pronounced for BeO and slower for the heavier oxides in this homologous series. This reflects that the contribution from the tightly bound core electrons dominates the large q behaviour of the profile. The higher components, i.e., $l = 2$, 4, and 6, which provide the anisotropy in the various directions to the profile, are shown in Fig. 5. Note that the contributions are per electron and on the same scale.

For BeO, the $J_2(q)$ component peaks around $q = 0$ and then falls off rapidly showing a minimum around $q = 0.7$ whereas for MgO this component peaks around $q = 0.3$ and then passes through a minimum at $q = 0.7$. For CaO and SrO, the behaviour of the $J_2(q)$ component is different at smaller q (<0.5) but beyond $q > 0.5$ they exhibit a very similar pattern of variation, i.e., peaking around $q = 1.2$ and 1.1 respectively and falling rapidly thereafter.

Figures 6(a, b) show the difference between the parallel ($J_{\parallel}(q)$) and perpendicular $J_{\perp}(q)$) directional Compton profiles (DCP) and the same superposition of free moieties. From Figs. 6(a, b) it is seen that all the difference profiles are negative at small q and positive at intermediate q. This is similar to the bond difference profile ($\bar{J}(q) - \bar{J}_{si}(q)$) given in ref. 19. The lowering of $J_{\parallel}(0)$ ranges from 1 to 21% of $\bar{J}(0)$ whereas the corresponding lowering for $J_{\perp}(0)$ varies between 7 to 17% of $\bar{J}(0)$. The difference function ($J_{\perp}(0) - J_{si}(0)$) follows the sequence Mg, Be, Ca, Sr as compared to Be, Mg, Ca, and Sr for ($J_{\parallel}(0) - J_{si}(0)$) and ($\bar{J}(0) - \bar{J}_{si}(0)$). The value of $J_{\parallel}(0) - J_{si}(0)$ measures the amount of buildup of the bonding orbitals (σ, π) momentum density in a plane perpendicular to the bond and through the origin in p-space. As a consequence, the decreasing value of this difference in the sequence Be, Mg, Ca, and Sr reflects that there is an increasing concentration of the bonding orbitals in a plane orthogonal to the bond and passing through $p = 0$.

There exists in the literature an empirical relation (8, 19) used to make a crude prediction of the anisotropies of the DCP's at zero momentum, i.e., $J_{\parallel}(0) - J_{\perp}(0)$. It has been shown that this relation works moderately well for alkali halides. This empirical relation can be used to predict the anisotropies of the isoelectronic alkaline earth oxides (EO) with the help of data

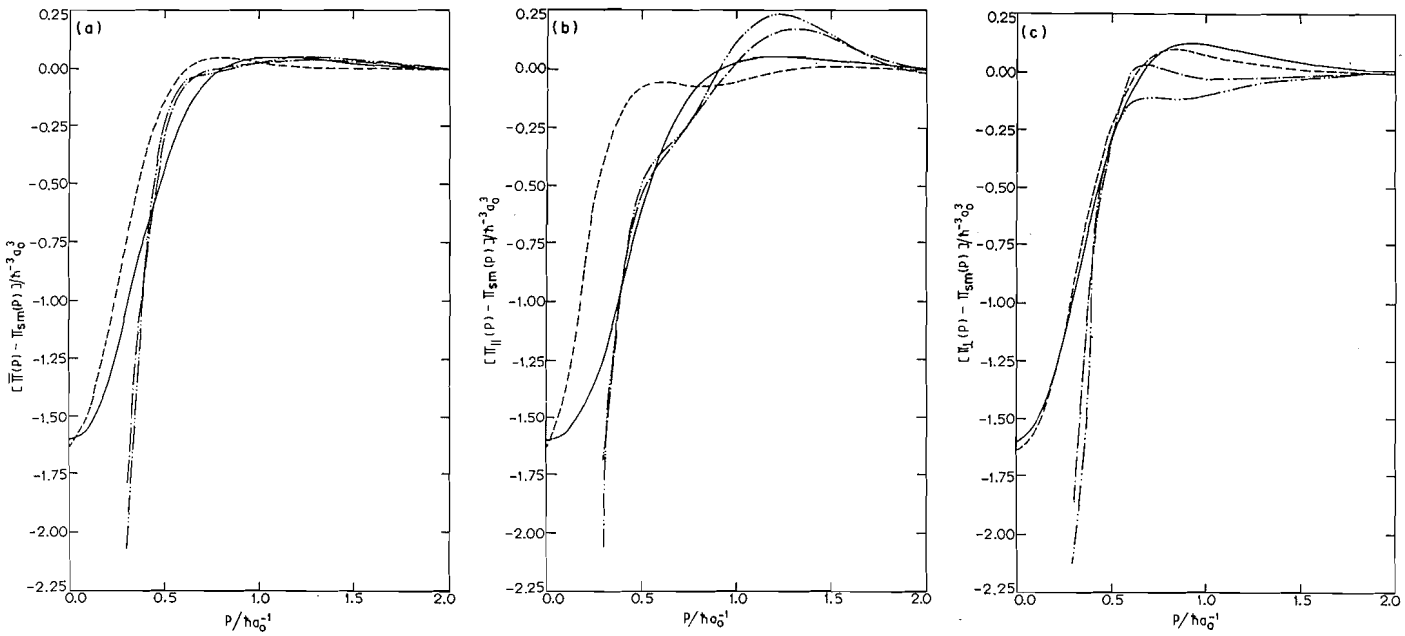


FIG. 3. (*a*) Difference curve between the molecule and superposition of free ions for the isotropic momentum density. (—) BeO; (- - -) MgO; (- · · · · ·) CaO; (- · · · · · · ·) SrO. (*b*) Difference curve for the parallel component of the momentum density. (—) BeO; (- - -) MgO; (- · · · · ·) CaO; (- · · · · · · ·) SrO. (*c*) Difference curve for the perpendicular component of the momentum density. (—) BeO; (- - -) MgO; (- · · · · ·) CaO; (- · · · · · · ·) SrO.

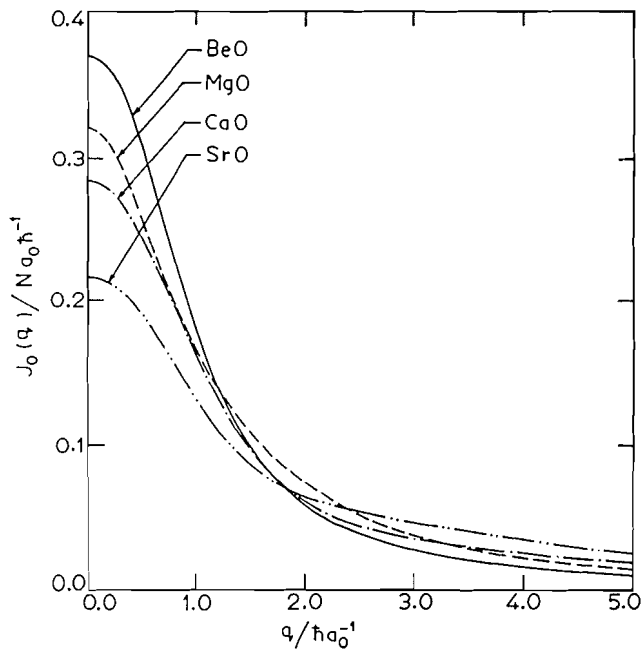


FIG. 4. Isotropic component of the Compton profile (per electron) for BeO, MgO, CaO, and SrO.

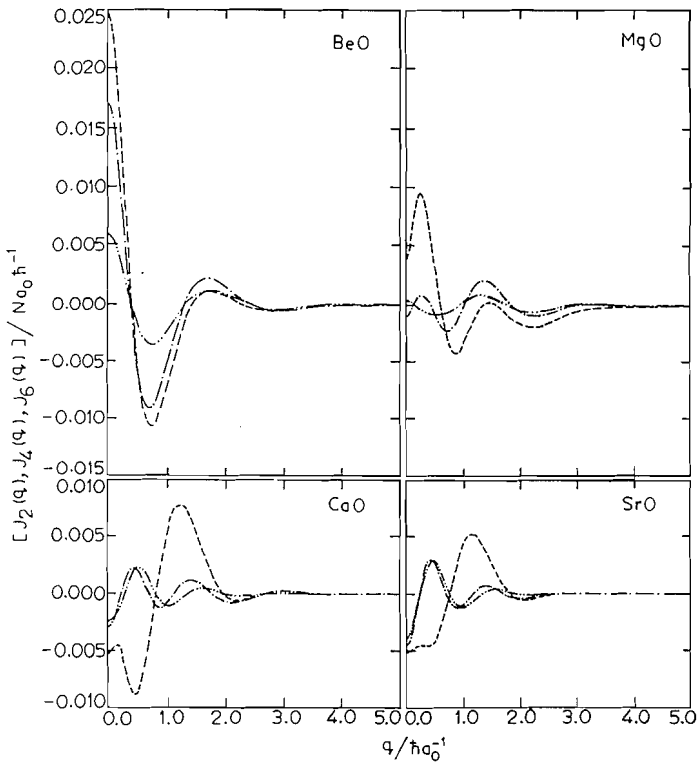


FIG. 5. Higher partial waves of the Compton profile (per electron) for BeO, MgO, CaO, and SrO. (—) BeO; (- - -) MgO; (- · · · · ·) CaO; (- · · · · · · ·) SrO.

(7) for the anisotropies of the alkali fluorides AF (A = Li, Na, K, Rb), thus assuming that

$$[9] \quad (J_\parallel(0) - J_\perp(0))_{EO} = \ln(Z_O/Z_E)[J_\parallel(0) - J_\perp(0)]_{AF}/\ln(Z_F/Z_A)$$

where Z's denote nuclear charges. Using the data for the alkaline fluorides, 3.3, −0.85, −2.0, and −2.0% of $\bar{J}(0)$ respectively in LiF, NaF, KF, and RbF, the anisotropies are predicted by eq. [9] to be −1.8, 1.5, 2.3, and 2.2% of $\bar{J}(0)$ in BeO, MgO, CaO, and SrO respectively, while the corresponding anisotropies from the present accurate molecular calculations (15.6, 1.5, −5.8, and −8.7%) are much larger and of opposite sign, except in the case of MgO where there is agreement. In addition it is seen that the DCP anisotropies of the alkaline earth oxides are larger than those of the isoelectronic alkali fluorides.

It is worth noticing that the dimensionless quantity $A = \langle p \rangle \bar{J}(0)/N^2 = 0.992, 1.143, 1.315$, and 1.566 respectively for

Can. J. Chem. Downloaded from www.nrcresearchpress.com by 194.225.253.170 on 09/07/12
For personal use only.

Can. J. Chem. Downloaded from www.nrcresearchpress.com by 194.225.253.170 on 09/07/12
For personal use only.

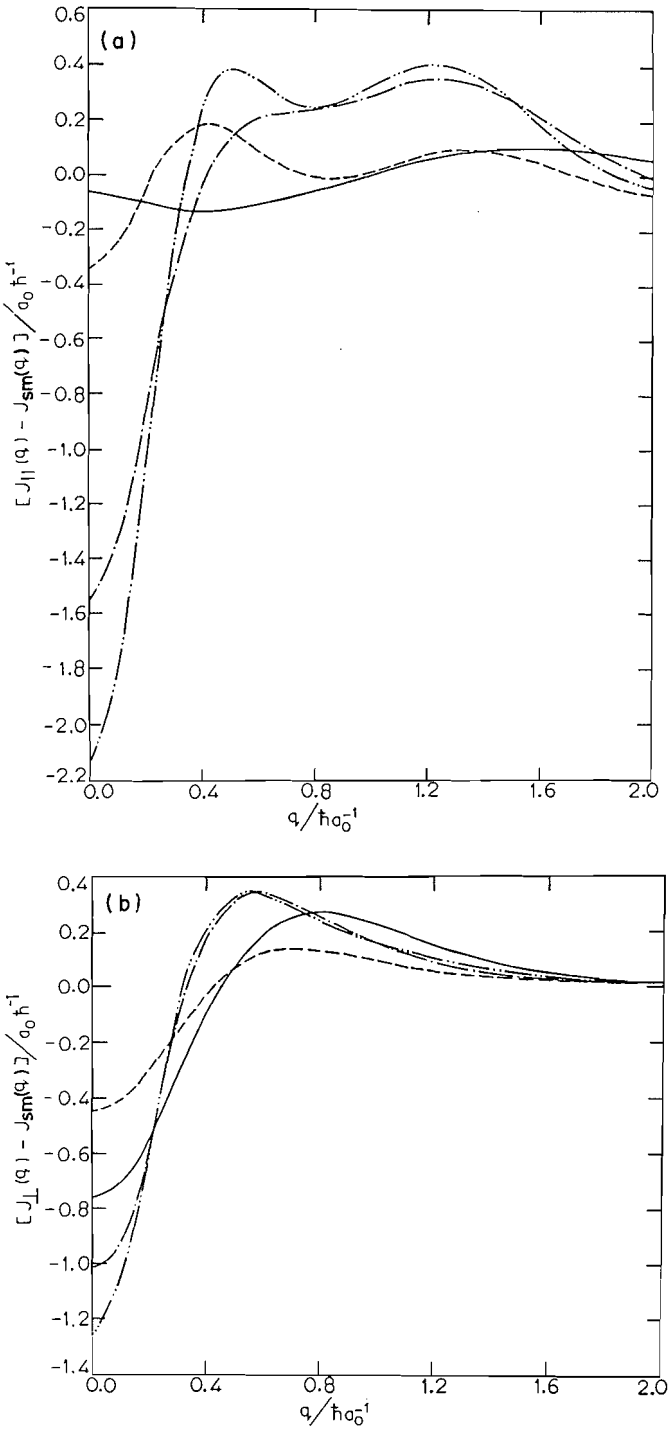


FIG. 6. (*a*) $J_{\parallel}(q) - J_{si}(q)$ of alkaline earth oxides. (—) BeO; (---) MgO; (-·-·-) CaO; (-···-) SrO. (*b*) $J_{\perp}(q) - J_{si}(q)$ of alkaline earth oxides. (—) BeO; (---) MgO; (-·-·-) CaO; (-···-) SrO.

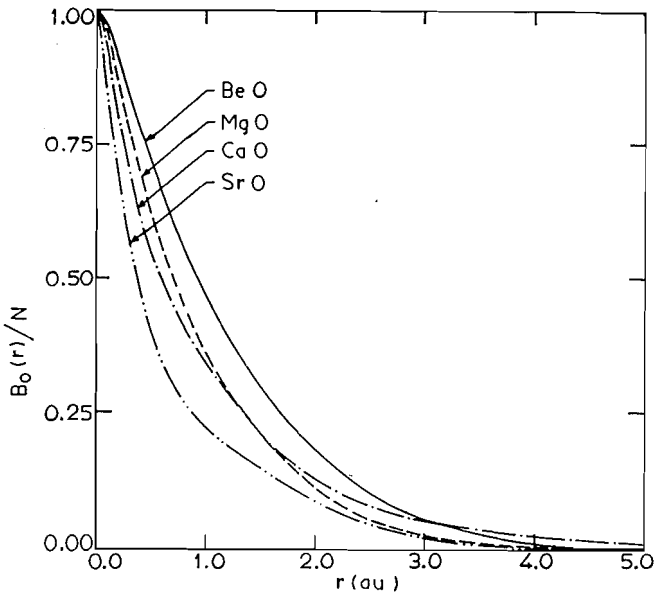


FIG. 7. Isotropic $B(r)$ function (per electron) for BeO, MgO, CaO, and SrO.

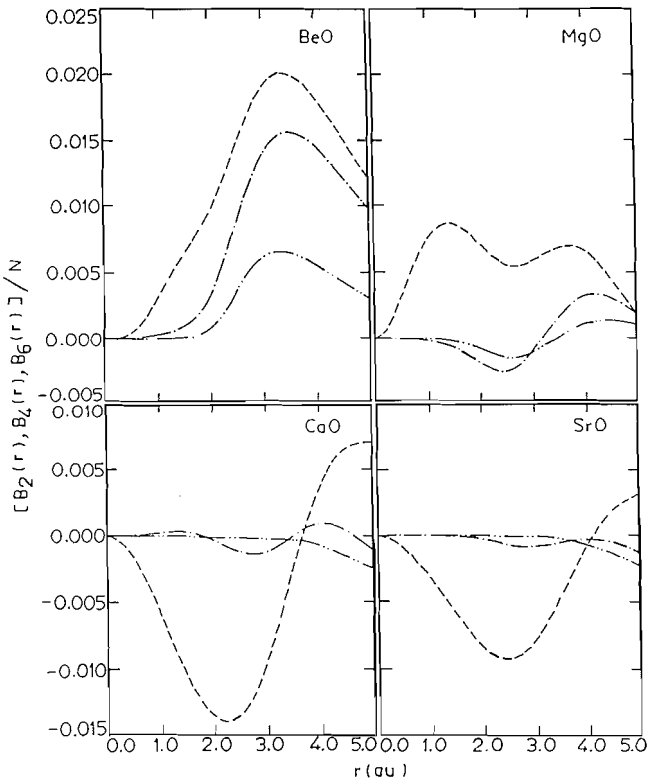


FIG. 8. Higher partial waves of $B(r)$ function (per electron) for BeO, MgO, CaO, and SrO.

BeO, MgO, CaO, and SrO. These values for the heavier oxides show that the approximation (32), $A \approx 1$, can be in error by as much as 50%.

The values of $\bar{J}(0)/a_0\hbar^{-1}$ for the alkali fluorides LiF, NaF, KF, and RbF respectively (7) are 3.99, 5.63, 7.71, and 9.80. Notice that these values are lower than those of the isoelectronic alkaline earth oxides (BeO, MgO, CaO, and SrO) calculated here, i.e., 4.47, 6.46, 8.01, 10.02, reflecting the fact (33) that the latter are less tightly bound than the alkali fluorides.

The characteristic momentum (24)

$$[10] \quad p^* = (\bar{J}(0)/2\pi\bar{\bar{\Pi}}(0))^{1/2} = (\langle p^{-1}\rangle/4\pi\bar{\bar{\Pi}}(0))^{1/2}$$

is known to increase with increasing electron sharing and number of valence electrons. Here we note that p^* for the reference moieties ($E^+ + O^-$) is fairly similar and decreases in the series, i.e., 0.6064 ($Be^+ + O^-$), 0.5544 ($Mg^+ + O^-$), 0.4797 ($Ca^+ + O^-$), and 0.4771 ($Sr^+ + O^-$); for the bound molecules (EO), p^* is large and very similar throughout the series except for MgO where it is about one-third smaller than

the others, i.e., 1.068 (BeO), 0.7510 (MgO), 1.118 (CaO), and 1.140 (SrO).

Internally folded density: B(**r**) *function*

The $B(r)$ functions have the advantage, when compared with the Compton profiles, that one is back in position space. As a result the valence electrons can be probed by studying $B(r)$ at larger values of r where the core electrons are of vanishing importance. Although a few calculations of $\bar{B}(r)$ functions have been reported, a limited amount of experience is available in interpreting the $\bar{B}(r)$ function for systems in the gaseous phase.

The isotropic internally folded density (reciprocal form factor) $\bar{B}(r) = B_0(r)$ per electron is displayed in Fig. 7 for all the alkaline earth oxides. It is seen that all the curves show an initial monotonic decrease with r and a crossing of the r-axis (zero passage) at different values of r for the various molecules. Figure 8 shows the various components $B_l(r)$. Notice that for BeO, the different components such as $B_2(r)$, $B_4(r)$, and $B_6(r)$ show a broad and positive peak in the intermediate range of r, while for the other oxides these components oscillate with both positive and negative amplitudes. $B_2(r)$ is more pronounced for the CaO and SrO molecules. The magnitude of the other components such as $B_4(r)$, $B_6(r)$ is, as usual, smaller than $B_2(r)$.

Summary and conclusions

From the foregoing analysis it is seen that partial wave analysis provides a good basis for understanding the anisotropy of these linear molecular systems. All the qualitative features of the various properties ($\Pi(p)$, $J(q)$, and $B(r)$) can be well understood in terms of the four chemically dominant partial waves (18, 19). The momentum density, Compton profiles, and the $B(r)$ functions in the parallel direction are distinctly different from the ones along the perpendicular direction.

Acknowledgements

Support of this research by the Natural Sciences and Engineering Research Council of Canada and by the University Grants Commission of India is gratefully acknowledged.

1. B. G. WILLIAMS (*Editor*). Compton scattering; the investigation of electron momentum distributions. McGraw–Hill, New York. 1977.
2. M. J. COOPER. Adv. Phys. **20**, 453 (1971); Rep. Prog. Phys. **48**, 415 (1985).
3. P. KAIJSER and V. H. SMITH, JR. Adv. Quantum Chem. **10**, 371 (1977).
4. R. BENESCH and V. H. SMITH, JR. *In* Wave mechanics — the first fifty years. *Edited by* W. C. Price *et al.* Butterworths, London. 1973. pp. 357–377; Acta Crystallogr. Sect. A: Cryst. Phys. Diffr. Theor. Gen. Crystallogr. **A26**, 579 (1970); L. MENDELSOHN and V. H. SMITH, JR. *In* Scattering; the investigation of electron momentum distributions. *Edited by* B. G. Williams. McGraw–Hill, New York. 1977.
5. B. G. WILLIAMS and J. M. THOMAS. Int. Rev. Phys. Chem. **3**, 39 (1983).
6. V. H. SMITH, JR., A. J. THAKKAR, W. H. HENNEKER, J. W. LIU, B. LIU, and R. E. BROWN. J. Chem. Phys. **67**, 3676 (1977); **73**, 4150 (1980).
7. R. L. MATCHA, B. M. PETTITT, B. I. RAMIREZ, and W. R. MCINTIRE. J. Chem. Phys. **71**, 991 (1979).
8. R. L. MATCHA and B. M. PETTITT. J. Chem. Phys. **70**, 3130 (1979).
9. P. KAIJSER, V. H. SMITH, JR., and A. J. THAKKAR. Mol. Phys. **41**, 1143 (1980).
10. A. J. THAKKAR, A. M. SIMAS, and V. H. SMITH, JR. Mol. Phys. **41**, 1153 (1980).
11. V. H. SMITH, JR. and M. H. WHANGBO. Chem. Phys. **5**, 234 (1974).
12. M. H. WHANGBO, V. H. SMITH, JR., and W. VON NIESSEN. Chem. Phys. **6**, 282 (1974).
13. B. I. RAMIREZ. J. Phys. B, **15**, 4339 (1982).
14. P. KAIJSER, V. H. SMITH, JR., A. N. TRIPATHI, and G. H. F. DIERCKSEN. Phys. Rev. A, **35**, 4074 (1987).
15. A. M. SIMAS, A. J. THAKKAR, and V. H. SMITH, JR. Int. J. Quantum Chem. **21**, 419 (1982).
16. A. ROSENDAAL and E. J. BAERENDS. Chem. Phys. **87**, 263 (1984); **95**, 57 (1985).
17. B. S. SHARMA, A. N. TRIPATHI, and A. J. THAKKAR. J. Chem. Phys. **79**, 3164 (1983); Waterloo Chem. Phys. Res. Rep. 161 (1981).
18. A. J. THAKKAR, A. M. SIMAS, and V. H. SMITH, JR. J. Chem. Phys. **81**, 2953 (1984).
19. (*a*) A. M. SIMAS, V. H. SMITH, JR., and A. J. THAKKAR. Can. J. Chem. **63**, 1412 (1985); (*b*) J. Mol. Struct. (Theochem), **123**, 221 (1985); (*c*) R. P. SAGAR, A. M. SIMAS, V. H. SMITH, JR., and A. J. THAKKAR. Ph-C2-4, 68th Canadian Chemical Conference, Kingston, Ontario. 1985.
20. E. R. DAVIDSON. Reduced density matrices in quantum chemistry. Academic, New York. 1976; R. MCWEENY and B. T. SUTCLIFFE. Methods of molecular quantum mechanics. Academic, New York. 1976.
21. D. R. HERRICK and F. H. STILLINGER. J. Chem. Phys. **62**, 4360 (1975); R. AHLRICHS. Chem. Phys. Lett. **34**, 570 (1975).
22. R. BENESCH, S. R. SINGH, and V. H. SMITH, JR. Chem. Phys. Lett. **10**, 151 (1971).
23. W. WEYRICH, P. PATTISON, and B. G. WILLIAMS. Chem. Phys. **41**, 271 (1979).
24. A. J. THAKKAR, A. M. SIMAS, and V. H. SMITH, JR. Chem. Phys. **63**, 175 (1981).
25. A. J. THAKKAR, A. C. TANNER, and V. H. SMITH, JR. *In* Density matrices and density functionals. *Edited by* R. Erdahl and V. H. Smith, Jr. Reidel, Dordrecht. 1987. pp. 327–337.
26. P. KAIJSER and V. H. SMITH, JR. *In* Methods and structure in quantum science. *Edited by* J.-L. Calais *et al.* Plenum, New York. 1976. pp. 417–426.
27. M. YOSHIMINE. J. Phys. Soc. Jpn. **25**, 1100 (1968).
28. R. W. FIELD. J. Chem. Phys. **60**, 2400 (1974).
29. A. J. THAKKAR. J. Chem. Phys. **76**, 747 (1982).
30. A. M. SIMAS, V. H. SMITH, JR., and W. M. WESTGATE. Int. J. Quantum Chem. **23**, 811 (1983).
31. W. M. WESTGATE, A. M. SIMAS, and V. H. SMITH, JR. J. Chem. Phys. **83**, 4054 (1985), and references therein.
32. S. R. GADRE and S. B. SEARS. J. Chem. Phys. **71**, 4321 (1979).
33. K. D. HUBER and G. HERZBERG. Constants of diatomic molecules. Van Nostrand, New York. 1979.

Can. J. Chem. Downloaded from www.nrcresearchpress.com by 194.225.253.170 on 09/07/12
For personal use only.

A continuing role for sulfuric acid cryoscopy. The IO_2^+ ion

J. A. LEISTEN[1]

Chancellor College, University of Malawi, P.O. Box 280, Zomba, Malawi

Received February 14, 1989

This article is dedicated to Professor Ronald J. Gillespie on the occasion of his 65th birthday

J. A. LEISTEN. Can. J. Chem. **67**, 1892 (1989).

The present state of sulphuric acid cryoscopy is discussed. A simplified technique with test results is presented for use in particular with cryoscopic solvent mixtures. Evidence is found for the existence of the iodyl ion, IO_2^+, in sulfuric acid solutions of enhanced acidity.

Key words: sulphuric acid, cryoscopy, iodyl ion.

J. A. LEISTEN. Can. J. Chem. **67**, 1892 (1989).

On discute de l'état actuel de la cryoscopie de l'acide sulfurique. On présente une technique simplifiée avec des résultats à l'appui en vue d'une utilisant dans des mélanges de solvants cryoscopiques. On prouve l'existence de l'ion iodyle IO_2^+ dans des solutions d'acide sulfurique dont l'acidité est augmentée.

Mots clés : l'acide sulfurique, la cryoscopie, l'ion iodyle.

[Traduit par la revue]

Introduction

In the first half of this century cryoscopy was a principal way of studying reactions with sulfuric acid in solvent proportions, and contributions to the dawning understanding of reaction mechanism were among its successes (1). The power of cryoscopy to solve problems of complex solute behaviour was greatly increased as a result of Gillespie's work on the sulfuric acid system (2), which led to more accuracy in the interpretation of freezing point depressions in 100% sulfuric acid (3), and to the introduction of four sulfuric acid solutions as cryoscopic solvents that enable the different types of particle produced by a solute on dissolution to be distinguished (4).

Perversely, these improvements occurred at a time when colligative methods were being overtaken by quicker and more convenient spectroscopic methods, and the use of cryoscopy therefore declined. The main purpose of the present work is to establish a simpler technique that makes sulfuric acid cryoscopy more accessible.

Four solutes of known behaviour were chosen to verify the technique. They react with sulphuric acid according to the following equations: benzoic acid (4*c*), [1]; ammonium sulfate, [2]; *o*-phenylene diamine (4*c*), [3]; and potassium nitrate (2), [4].

[1] $C_6H_5CO_2H + H_2SO_4 = C_6H_5CO_2H_2^+ + HSO_4^-$

[2] $(NH_4)_2SO_4 + H_2SO_4 = 2NH_4^+ + 2HSO_4^-$

[3] $C_6H_4(NH_2)_2 + 2H_2SO_4 = C_6H_4(NH_3)_2^{2+} + 2HSO_4^-$

[4] $KNO_3 + 3H_2SO_4 = K^+ + NO_2^+ + H_3O^+ + 3HSO_4^-$

Two other solutes were chosen for their interest.

Fernandez and Sutor found a van't Hoff *i* factor of 4.1 for bis(diethylamine)methane in aqueous sulfuric acid (5) and suggested the surprising reaction [5]; but several reactions, for example [6], could account for this result and further study seemed worthwhile.

[5] $Et_2NCH_2NEt_2 + 2H_2SO_4 = EtNH_3^+ + CH_2NEt_2^+ + 2HSO_4^-$

[6] $Et_2NCH_2NEt_2 + 3H_2SO_4 = Et_2NHCH_2NEtCH_2CH_2SO_3H^+ + H_3O^+ + 2HSO_4^-$

[1]Present address: 45 Ashleigh Drive, Loughborough LE11 3HN, England.

The final solute, potassium iodate, was first thought to react according to eq. [7] (6), but Gillespie and Senior obtained evidence instead for the formation of iodyl hydrogen sulfate (eq. [8]), and its subsequent polymerisation (7). They found no reason to believe that the iodyl ion is formed either in sulfuric acid (eq. [9]) or in oleum, although the existence of this ion in fluorosulfonic acid has been deduced from the conductivity of the solute IO_2SO_3F (8).

[7] $KIO_3 + 2H_2SO_4 = K^+ + H_2IO_3^+ + 2HSO_4^-$

[8] $KIO_3 + 3H_2SO_4 = K^+ + H_3O^+ + IO_2HSO_4 + 2HSO_4^-$

[9] $KIO_3 + 3H_2SO_4 = K^+ + H_3O^+ + IO_2^+ + 3HSO_4^-$

Results and discussion

Freezing point depressions for known molalities of the test solutes were measured in slightly aqueous sulphuric acid and four other sulphuric acid solutions, and *i* factors obtained from the results.

If water molecules or hydrogen sulfate ions are produced when a solute dissolves, the total number of foreign particles in the sulfuric acid may increase, decrease, or stay the same, depending on which of the five cryoscopic solvents is being used. Table 1 specifies this information (4*c*). Combining the information with that of eqs. [1] to [4] it is possible to calculate *i* factors that are consistent with the known behaviour of the test solutes. In Table 2 these calculated values (in italics) are compared with the experimental ones. Agreement between experimental and calculated *i* factors for the four model solutes in all five of the solvents is acceptable for the cryoscopic mixtures method, and the discrepancies can be taken into account when assessing the results for other solutes. The last set of *i* values in Table 2 shows a similar level of agreement to that in the four model sets, and this confirms eq. [5] as the reaction of bis(diethylamine)methane in sulfuric acid. (For the eq. [6] alternative the predicted *i* values in solvents A to E would be, respectively: *4*, *0*, *−1*, *0*, and *2*.)

The five solvents differ quite sharply in certain chemical properties, such as acidity and the ability to sulfate and sulfonate (4*b*), and there is always a danger when using results in the way just described for bis(diethylamine)methane that the behaviour of the solute may change from one solvent to another. In recompense, however, these differences in properties some-

Can. J. Chem. Downloaded from www.nrcresearchpress.com by 186.148.149.217 on 09/07/12
For personal use only.

TABLE 1. Changes in the number of foreign particles produced by an H_2O molecule (first row) and by an HSO_4^- ion (second row) in five sulfuric acid solutions*

A	B	C	D	E
0.1 *m* H_3O^+	0.10 *m* H_3O^+	0.10 *m* $H_2S_2O_7$	0.13 *m* $H_2S_2O_7$	0.1 *m* $HS_2O_7^-$
0.1 *m* HSO_4^-	0.13 *m* $H_3SO_4^+$	0.07 *m* $H_3SO_4^+$	0.15 *m* $HS_2O_7^-$	0.1 *m* HSO_4^-
	0.23 *m* $B(HSO_4)_4^-$	0.07 *m* $B(HSO_4)_4^-$	0.15 *m* NH_4^+	0.2 *m* NH_4^+
2	0	−1	−1	0
1	−1	−1	0	1

*The species printed in italics are inessential except as counter ions. For example, solution E would have the same properties as a cryoscopic solvent if 0.2 *m* NH_4^+ were replaced by 0.2 *m* K^+.

TABLE 2. Comparison of experimental and (in italics) calculated *i* factors

	i									
	A		B		C		D		E	
Solvent	Expt.	Calcd.	Expt.	Calcd.	Expt.	Calcd.	Expt.	Calcd.	Expt.	Calcd.
C_6H_5COOH	2.0	*2*	0.2	*0*	0.1	*0*	1.2	*1*	2.0	*2*
$(NH_4)_2SO_4$	4.0	*4*	−0.2	*0*	0.2	*0*	1.8	*2*	3.7	*4*
$C_6H_4(NH_2)_2$	3.2	*3*	−1.1	*−1*	−1.1	*−1*	0.7	*1*	2.8	*3*
KNO_3	6.1	*6*	0.2	*0*	−1.2	*−1*	1.2	*1*	4.1	*4*
$Et_2NCH_2NEt_2$	3.8	*4*	0.0	*0*	−0.1	*0*	1.8	*2*	3.8	*4*

times allow the solutions to be used for probing a solute's chemical reactivity, and this extra function is illustrated by the final set of results.

It seemed possible that in sulfuric acid solutions containing very little HSO_4^- (i.e., more strongly acid solutions) iodyl hydrogen sulfate, $IO_2.HSO_4$, might yield the IO_2^+ ion. Ionization of KIO_3 might occur according to eq. [9] rather than to eq. [8] as in 100% sulfuric acid. This solute was therefore examined in the more strongly acid solvents B and C.

For comparison potassium iodate was also examined in solvent E. In this case the polymer described by Gillespie and Senior began to deposit before the solute had all dissolved and the *i* factor changed gradually from 2.7 to 2.4, consistently with their findings and interpretation. The chemical behaviour in solvents B and C, however, was quite different. The solutions remained clear overnight, and the freezing point depressions were constant. The *i* factors shown in Table 3 and compared with the values calculated for eqs. [7], [8], and [9], point clearly to reaction [9].

The results are evidence that the iodyl ion can exist in sulfuric acid containing small concentrations of tetrahydrogensulfatoboric acid.

For a normal solute *i* factors in any three of the solvents will give all the information that the cryoscopic mixtures method can offer. Exactly the same information can be obtained (9) by a combination of conductimetric titration in oleum (10) with conductimetric (11) and cryoscopic measurements in 100% sulfuric acid. The difference in principle makes this method a valuable alternative, and it has the advantage of greater precision (12). The conductimetric titration, however, requires some 20 additions of solute, an inconvenience if the solute dissolves slowly. The method of cryoscopic mixtures is relatively quick and simple, and may still be useful in cases where slow reactions occurring after the solute has dissolved would make a conductimetric titration uncertain.

TABLE 3. Observed *i* factors for KIO_3 and (in italics) predicted *i* factors for different modes of ionization

	i			
	Experimental value	Predicted		
		eq. [7]	eq. [8]	eq. [9]
Solvent B	−0.3	*0*	*1*	*0*
Solvent C	−1.1	*0*	*0*	*−1*

For diagnosing behaviour in strong acids during recent years spectroscopic methods have been the most widely used: but spectroscopic precision is not always matched by interpretation (13), and sulfuric acid cryoscopy has a complementary function (still) that can be perilous to ignore.

Experimental

The cryoscopic technique was a much simplified modification of that previously used with the solvent mixtures (4*c*).

Re-examination of the five cryoscopic solvents showed that a significant improvement could be made by changing the composition of D to 0.13 *m* $H_2S_2O_7$, 0.15 *m* $HS_2O_7^-$. This solvent was prepared in a flask fitted with a thermometer and Teflon follower, starting with a weighed quantity of 98% sulfuric acid which was cooled in ice/water until it could be seeded. Additions of Merck 65% oleum were made, with periodic cooling to maintain the presence of sulfuric acid crystals, until the temperature, after first rising, had fallen to 8.5°C. Ammonium sulphate (0.99 g) was added for each 100 g of this oleum. Large quantities of the other solvents were similarly prepared, using the previous recipes (4*c*). A suitable composition for the slightly aqueous acid, solvent A, is 0.1 *m* H_3O^+, 0.1 *m* HSO_4^-: fp 9.4°C.

The cryoscope was a 150 mm long flat-bottomed tube of 27 mm bore, having at the top end a socket for the thermometer holder, and a cone (with socket stopper) for the addition of solutes. To allow room

Can. J. Chem. Downloaded from www.nrcresearchpress.com by 186.148.149.217 on 09/07/12
For personal use only.

for both joints the cone was at 30° to the vertical. A Teflon follower was used for stirring. Temperature was measured with a −20 to +30°C laboratory thermometer, graduated in 0.1°, and read to 0.01° by means of a cathetometer. It was fitted to the cryoscope by a standard holder with glass cone and O-ring seal.

The air jacket of controllable temperature consisted of a foam plastic box enclosing a copper cooling coil, through which water was pumped directly from and to a bath by means of a windscreen washer pump. The box was mounted on an auto-reverse magnetic stirrer plate. The bath had a stirrer, immersion heater, and constant level device, and during measurements it was adjusted by use of the heater and additions of ice to a temperature that was kept 4° (±0.1°) below the temperature in the cryoscope. (The optimal temperature difference would vary slightly with the design and ambient temperature.)

For each experiment about 70 g of the required solvent was transferred to the weighed cryoscope, which was then re-weighed and closed by the thermometer and other stopper, using chlorofluorocarbon grease. To determine the freezing point, the sulfuric acid was supercooled by dipping the cryoscope in an ice–water beaker on a stirrer plate, and then allowed to stand for a few minutes in the air jacket until a steady reading was obtained 1–2° below the freezing point. Freezing was induced and the steady temperature recorded after 6–10 min. (Longer times was sometimes needed with solvent B.) Freezing out of solid changes the concentration of dissolved species to an extent that depends on the supercooling, necessitating a small correction to the observed freezing point (14) that was read from a prepared chart.

Although platinum wire cooled in liquid nitrogen provides a more convenient way to induce freezing (1*a*) it was necessary in the present work to seed the solution with solid sulfuric acid in a loop of platinum wire. To prepare the seed the platinum loop was suspended in the surface of 100% sulfuric acid in a closed boiling tube which was stored in a freezer.

The solute, if solid, was added with a weighing bottle and funnel (both items being weighed): if liquid a weight pipette was used. The amount added must be small in relation to the solvent additives, typically 0.025 *m* but even less if the solute yields many particles per molecule. After re-determination of the freezing point the *i* factor was obtained as before (4*c*) from the equation $i = \theta/6\ m$, where *m* is the molality of the solute and θ is the associated freezing point depression. Reproducibility was checked by carrying out five separate experiments with bis(diethylamine)methane in solvent A. The mean *i* factor with standard deviation was 3.7 ± 0.1. Fernandez and Sutor quote the result 4.1 ± 0.5 for five determinations with the same solute and solvent but using a different technique (5).

The technique described is easy to set up. No way was found of reducing the 30 min or so required for each freezing point measurement, because the accuracy depends on a close approach to equilibrium, but much time and tedium is saved by recognising that the experimental error is small in relation to the general precision of the cryoscopic mixtures method and that it is not time-effective to duplicate measurements. Examination of a solute by the necessary three solvents thus requires a total of only three solute additions and six freezing point measurements.

Acknowledgments

Professor R. J. Gillespie first set me on this trail, and Professor C. C. Mjojo persuaded me to follow it in Malawi. Reference facilities were kindly granted by the Librarian, Loughborough University of Technology.

1. (*a*) R. J. GILLESPIE. Chemistry, **38**, 12 (1965); (*b*) *In* Studies on chemical structure and reactivity. *Edited by* J. H. Ridd. Methuen, London. 1966. Chap. 9.
2. R. J. GILLESPIE. *In* Inorganic sulfur chemistry. *Edited by* G. Nickless. Elsevier. Amsterdam, London, New York. 1967. Chap. 16.
3. S. J. BASS, R. J. GILLESPIE, and E. A. ROBINSON. J. Chem. Soc. 821 (1960).
4. (*a*) R. H. FLOWERS, R. J. GILLESPIE, and J. V. OUBRIDGE. J. Chem. Soc. 1925 (1956); (*b*) J. A. LEISTEN. J. Chem. Soc. 2191 (1961); (*c*) J. A. LEISTEN and K. L. WRIGHT. J. Chem. Soc. 3173 (1964); (*d*) J. A. LEISTEN and P. R. WALTON. J. Chem. Soc. 3180 (1964).
5. J. E. FERNANDEZ and R. SUTOR. J. Org. Chem. **32**, 477 (1967).
6. J. AROTSKY, H. C. MISHRA, and M. C. R. SYMONS. J. Chem. Soc. 2582 (1962).
7. R. J. GILLESPIE and J. B. SENIOR. Inorg. Chem. **3**, 440 (1964).
8. H. A. CARTER and F. AUBKE. Inorg. Chem. **10**, 2296 (1971).
9. R. J. GILLESPIE and E. A. ROBINSON. J. Am. Chem. Soc. **87**, 2428 (1965).
10. R. H. FLOWERS, R. J. GILLESPIE, and E. A. ROBINSON. Can. J. Chem. **38**, 1363 (1960).
11. R. J. GILLESPIE, J. V. OUBRIDGE, and C. SOLOMONS. J. Chem. Soc. 1804 (1957).
12. E. A. ROBINSON and S. A. A. QUADRI. Can. J. Chem. **45**, 2385 (1967).
13. J. A. LEISTEN and P. R. WALTON. Proc. Chem. Soc. 60 (1963).
14. R. J. GILLESPIE, E. D. HUGHES, and C. K. INGOLD. J. Chem. Soc. 2473 (1950).

Can. J. Chem. Downloaded from www.nrcresearchpress.com by 186.148.149.217 on 09/07/12
For personal use only.

Fluorosulfonic anhydride: a potential fluorosulfonating agent

DEBYANI G. NIYOGI, SUKHJINDER SINGH, AND R. D. VERMA
Department of Chemistry, Panjab University, Chandigarh-160014, India

Received April 12, 1989

This article is dedicated to Professor Ronald J. Gillespie on the occasion of his 65th birthday

DEBYANI G. NIYOGI, SUKHJINDER SINGH, and R. D. VERMA. Can. J. Chem. **67**, 1895 (1989).

Reactions of pyrosulfuryl fluoride, $S_2O_5F_2$, with various inorganic substrates are carried out to explore its potential and usefulness as a fluorosulfonating agent. New fluorosulfonates, viz; $\phi_3\overset{+}{P}O\overset{+}{P}\phi_3.2SO_3F^-$, $\phi_3\overset{+}{As}O\overset{+}{As}\phi_3.2SO_3F^-$, $NaBiO(SO_3F)_2$, and $Ti(OCH_3)_2(SO_3F)_2$ have been prepared by reacting ϕ_3PO, ϕ_3AsO, $NaBi(CF_3COO)_4$, and $Ti(OCH_3)_4$, respectively, with $S_2O_5F_2$. These compounds have been characterized by elemental analyses and infrared and ^{19}F nmr spectra.

Key words: new fluorosulfonates, $(C_6H_5)_3\overset{+}{P}O\overset{+}{P}(C_6H_5)_3.2SO_3F^-$, $(C_6H_5)_3\overset{+}{As}O\overset{+}{As}(C_6H_5)_3.2SO_3F^-$, $NaBiO(SO_3F)_2$, $Ti(OCH_3)_2(SO_3F)_2$.

DEBYANI G. NIYOGI, SUKHJINDER SINGH et R. D. VERMA. Can. J. Chem. **67**, 1895 (1989).

On a effectué un certain nombre de réactions du fluorure de pyrosulfuryle, $S_2O_3F_2$, avec divers substrats inorganiques afin d'évaluer son potentiel et son utilité comme agent de fluorosulfonation. En faisant réagir le $S_2O_5F_2$ successivement avec le ϕ_3PO, le ϕ_3AsO, le $NaBi(CF_3COO)_4$ et le $Ti(OCH_3)124$, on a obtenu les nouveaux fluorosulfonates suivants : $\phi_3\overset{+}{P}O\overset{+}{P}\phi_3.2SO_3F^-$, $\phi_3\overset{+}{As}O\overset{+}{As}\phi_3.2SO_3F^-$, $NaBiO(SO_3F)_2$ et $Ti(OCH_3)_2(SO_3F)_2$. On a caractérisé ces composés à l'aide d'analyses élémentaires et de spectres ir et rmn du ^{19}F.

Mots clés : nouveaux fluorosulfonates, $(C_6H_5)_3\overset{+}{P}O\overset{+}{P}(C_6H_5)_3.2SO_3F^-$, $(C_6H_5)_3\overset{+}{As}O\overset{+}{As}(C_6H_5)_3.2SO_3F^-$, $NaBiO(SO_3F)_2$, $Ti(OCH_3)_2(SO_3F)_2$.

[Traduit par la revue]

Introduction

Fluorosulfonic anhydride (pyrosulfuryl fluoride), $S_2O_5F_2$, has been known for nearly four decades (1). However, its chemistry has not been much explored. The inorganic aspects of the chemistry of $S_2O_5F_2$, its reactions with the oxides and oxide halides of nitrogen in anhydrous acetonitrile have been reported (2). Reactions of its analogue, trifluoromethanesulfonic anhydride, $(CF_3SO_2)_2O$, with various inorganic and organic substrates are known (3, 4).

In this article, we reacted $S_2O_5F_2$ with various substrates and explored its potential as a fluorosulfonating agent. We are successful in reacting $S_2O_5F_2$ with ϕ_3PO, ϕ_3AsO where ϕ = C_6H_5, $NaBi(CF_3COO)_4$, and $Ti(OCH_3)_4$ to obtain new fluorosulfonates, viz. $\phi_3\overset{+}{P}O\overset{+}{P}\phi_3.2SO_3F^-$, $\phi_3\overset{+}{As}O\overset{+}{As}\phi_3.2SO_3F^-$, $NaBiO(SO_3F)_2$, and $Ti(OCH_3)_2(SO_3F)_2$, respectively. The reaction between Bi_2O_3 and $S_2O_5F_2$ led to the formation of the previously known fluorosulfonate, $Bi(SO_3F)_3$ (5).

Experimental

Material and methods

Pyrosulfuryl fluoride (6), $NaBi(CF_3COO)_4$ (7), and $Ti(OCH_3)_4$ (8) were prepared as described in the literature. Bismuth(III) oxide (Riedel) was dried overnight in an oven at 110°C. Triphenylphosphine oxide (E. Merck) and triphenylarsine oxide (BDH) were recrystallized from benzene. Trifluoroacetic anhydride (Aldrich) and titanium(IV) chloride (Fluka) were distilled before use. Fluorosulfonic acid was prepared as reported earlier (9). The solvents were dried and distilled before use. Caution! Pyrosulfuryl fluoride is a toxic material and should be handled with care (10).

The infrared spectra of the compounds were recorded either as Nujol/hexachlorobutadiene mulls or as neat solid between AgCl or polythene plates on a Perkin Elmer 1430 infrared spectrophotometer. The ^{19}F nmr spectra were recorded on an EM 390 spectrophotometer using Freon-11 as external reference.

Sulfur and fluorine were determined as reported earlier (11, 12). Metals were analysed by standard methods (13). Carbon and hydrogen were determined microanalytically. All manipulations were carried out either in a vacuum line or in a dry box filled with nitrogen.

Preparation of $\phi_3\overset{+}{R}O\overset{+}{R}\phi_3.2SO_3F^-$, R = P or As

Triphenylphosphine oxide (1.39 g, 5 mmol) was loaded into a 50 mL Pyrex reactor fitted with a Rotaflo stopcock and evacuated for 2 h. Fluorosulfonic anhydride (1.456 g, 8 mmol) was condensed onto it via vacuum. The reaction mixture was allowed to warm slowly from −196 to +20°C and held at room temperature for 5 days. The pressure of volatiles in the reactor was checked from time to time and the reaction was terminated when no further consumption of $S_2O_5F_2$ was observed. The compound $\phi_3\overset{+}{P}O\overset{+}{P}\phi_3.2SO_3F^-$ (1.84 g, 2.5 mmol) was obtained as a white solid in quantitative yield after removal of all volatiles. *Anal.* calcd. for $C_{36}H_{30}F_2O_7P_2S_2$: C 58.54, H 4.07, F 5.15, P 8.40, S 8.67; found: C 57.9, H 3.88, F 5.20, P 8.24, S 8.81. Infrared: 1588w, 1490w, 1440m, 1340vw, 1310m, 1160w, 1125ms, 1075mw, 1040w, 998w, 940mw, 850sh, 750vw, 735bs, 690vw, 619w, 602w, 590m, 565sh, 530ms, 495w, 480w, 435vw, 415w cm^{-1} (s = strong, m = medium, w = weak, v = very, sh = shoulder, b = broad).

Similarly, $\phi_3\overset{+}{As}O\overset{+}{As}\phi_3.2SO_3F^-$ was obtained as a white solid in nearly quantitative yield by reacting ϕ_3AsO and $S_2O_5F_2$. *Anal.* calcd. for $C_{36}H_{30}As_2F_2O_7S_2$: C 52.30, H 3.63, As 18.16, F 4.60, S 7.75; found: C 51.86, H 3.55, As 18.30, F 4.52, S 8.11. Infrared: 3060w, 2925ms, 2870sh, 1580ms, 1485mw, 1475mw, 1443w, 1340ms, 1315ms, 1290m, 1265w, 1235w, 1185w, 1170sh, 1085m, 1060mb, 1025w, 1000m, 975w, 940w, 850vw, 775m, 740bs, 688w, 640m, 575mb, 520ssh, 470m, 360mb cm^{-1}.

Preparation of $Bi(SO_3F)_3$

The reaction between Bi_2O_3 (0.56 g, 1.2 mmol) and $S_2O_5F_2$ (1.456 g, 8 mmol) was carried out at ~65°C in an analogous manner as described above. However, the reaction was complete in 24 days. Removal of volatiles in vacuum gave $Bi(SO_3F)_3$ as a white solid in quantitative yield (1.218 g, 2.4 mmol). *Anal.* calcd. for $BiF_3O_9S_3$: Bi 41.30, F 11.26, S 18.97; found: Bi 40.75, F 11.08, S 19.24%. Infrared: 1300m, 1210w, 1080b, 860m, 770m, 640mw, 612w, 560m, 475w, 420sh cm^{-1}.

Preparation of $NaBiO(SO_3F)_2$

$NaBi(CF_3COO)_4$ (2.32 g, 3.4 mmol) was loaded into a 50 mL Pyrex reactor as earlier and evacuated for 6 h. An excess of $S_2O_5F_2$ (1.73 g, 9.5 mmol) was condensed onto it and the contents refluxed at ~60°C for 5 days. Final drying *in vacuo* gave a constant weight of $NaBiO(SO_3F)_2$ (1.47 g, 3.3 mmol) as a white shining powder. *Anal.*

Can. J. Chem. Downloaded from www.nrcresearchpress.com by 194.225.253.170 on 09/07/12
For personal use only.

calcd. for $BiF_2NaO_7S_2$: Bi 46.86, F 8.52, S 14.35; found: Bi 46.40, F 8.39, S 14.24%. Infrared: 1280sh, 1265s, 1090bs, 815ms, 660bs, 590s, 520wb, 475m cm^{-1}.

Preparation of $Ti(OCH_3)_2(SO_3F)_2$

Freshly sublimed $Ti(OCH_3)_4$ (0.72 g, 4.2 mmol) was transferred to a 50 mL Pyrex reactor fitted with a standard B-14 joint and $S_2O_5F_2$ (4.46 g, 24.5 mmol) was condensed onto it via vacuum transfer. The reactor was detached from the vacuum line and fitted with a reflux condenser and drying tube. The reaction mixture was heated at reflux for 50 h. The volatiles were pumped off carefully. The white solid $Ti(OCH_3)_2(SO_3F)_2$ (1.294 g, ~4.2 mmol) obtained was further treated with 0.5 mL of fresh $S_2O_5F_2$ and heated at reflux. No change in weight of product was observed after removing all volatiles. *Anal.* calcd. for $C_2H_6F_2O_8S_2Ti$: C 7.79, H 1.95, F 12.34, S 20.78, Ti 15.58; found: C 7.67, H 1.90, F 12.41, S 20.48, Ti 15.29. Infrared: 2958w, 2930m, 2858mw, 1450mw, 1405m, 1385vw, 1202s, 1155mb, 1095m, 1018w, 978vs, 818vs, 645ms, 590m, 500w, 470ssh, 390w, 368sh, 345mw, 318mw, 295w, 272m, 245m, 222m cm^{-1}.

The completion of the reactions was determined as follows: The volatile materials were removed via vacuum and change in weight of the reactor recorded from time to time. Each time these materials were condensed back into the reactor and reaction allowed to proceed under said condition. The reaction was considered to be complete when no further change in weight of reactor was observed.

Results and discussion

The reaction of triphenylphosphine oxide and triphenylarsine oxide with a slight excess of $S_2O_5F_2$ produced $\phi_3\overset{+}{M}O\overset{+}{M}\phi_3.2SO_3F^-$; M = P or As at ambient temperature. The reaction may be represented by reaction [1] or [2]:

$$[1]\quad 2\phi_3MO + S_2O_5F_2 \xrightarrow[5\text{ days}]{\text{ambient temperature}} \phi_3\overset{+}{M}O\overset{+}{M}\phi_3.2SO_3F^-$$

$$[2]\quad \phi_3MO + S_2O_5F_2 \longrightarrow \phi_3\overset{+}{M}OSO_2.SO_3F^- \xrightarrow{\phi_3MO} \phi_3\overset{+}{M}O\overset{+}{M}\phi_3.2SO_3F^- \qquad M = P \text{ or } As$$

The evidence for the formation of the salt $\phi_3\overset{+}{M}O\overset{+}{M}\phi_3.2SO_3F^-$ is based primarily on the elemental analyses (Experimental section). No change in weight of the product was noted when the reactants were allowed to react even for longer periods.

The analogous reaction between triphenylphosphine oxide and trifluoromethanesulfonic anhydride is known and the formation of monophosphonium salt, $\phi_3\overset{+}{P}OSO_2CF_3.CF_3SO_3^-$, has been reported (14). However, it was shown by a different group of workers (15) that a diphosphonium salt is obtained either by reacting ϕ_3PO or $[(CH_3)_3N]_3PO$ with trifluoromethanesulfonic anhydride. Formation of diphosphonium salt had been confirmed by X-ray crystallography (15) and P—O—P angle was found to be 180°.

The ^{19}F nmr of $\phi_3\overset{+}{M}O\overset{+}{M}\phi_3.2SO_3F^-$ shows signals (relative to $CFCl_3$) at +37.7 and +38.3 ppm for the phosphorus and arsenic compounds, respectively. Appearance of a single peak corresponding to the S—F resonance reveals the presence of only one type of fluorosulfonate group. Whilst in the case of the salt $\phi_3\overset{+}{M}OSO_2F.SO_3F^-$, two signals may be anticipated for two chemically different types of SO_3F groups. Also the chemical shift in the present compounds at ca. +38.0 ppm is comparable to that in ionic KSO_3F (+37.4 ppm).

The infrared spectra of $\phi_3\overset{+}{M}O\overset{+}{M}\phi_3.2SO_3F^-$ are given in the Experimental section. The $\nu_{P=O}$ band appears sharp and strong at 1195 cm^{-1} in pure triphenylphosphine oxide (16). No band is observed at 1195 cm^{-1} in the diphosphonium salt, $\phi_3\overset{+}{P}O\overset{+}{P}\phi_3.2SO_3F^-$. This rules out the presence of any free or unreacted ϕ_3PO in the salt. Similarly, absence of the 880 cm^{-1} band (17) in $\phi_3\overset{+}{A}sO\overset{+}{A}s\phi_3.2SO_3F^-$ rules out the possibility of a ϕ_3AsO impurity in diarsonium salt. Generally, the distinction between covalent and ionic fluorosulfonate groups is made on the basis of ν_{S-F} (800–900 cm^{-1} for covalent and 700–800 cm^{-1} for ionic) (18). Strong to medium intensity broad bands at 735 and 740 cm^{-1} in diphosphonium and diarsonium salts, respectively, reveal the presence of ionic fluorosulfonate groups in these compounds. Assignments relating to other modes of SO_3F group and ϕ_3P group are not made unambiguously as both the groups produced overlapping regions.

Fluorosulfonic anhydride, $S_2O_5F_2$, reacts with Bi_2O_3 at ~65°C for 24 days to produce the already reported (5) bismuth(III) fluorosulfonate, $Bi(SO_3F)_3$ in a facile fashion, reaction [3]:

$$[3]\quad Bi_2O_3 + 3S_2O_5F_2 \xrightarrow[24\text{ days}]{\sim 65°C} 2Bi(SO_3F)_3$$

The infrared spectrum of $Bi(SO_3F)_3$ (1300m, 1210w, 1080b, 860m, 770m, 640mw, 612w, 560m, 475w, 420sh cm^{-1}) is in good agreement with its reported spectrum (5) (1295m, 1215w, 1095m, 1075m, 865m, 770m, 635w, 610w, 540mw, 470w, 420sh cm^{-1}), where two different types of fluorosulfonate groups have been anticipated.

The reaction between $S_2O_5F_2$ and $NaBi(CF_3COO)_4$ at ~60°C for 5 days yields $NaBiO(SO_3F)_2$ in nearly quantitative yields, reaction [4]:

$$[4]\quad NaBi(CF_3COO)_4 + S_2O_5F_2 \xrightarrow[5\text{ days}]{\sim 60°C} NaBiO(SO_3F)_2 + 2(CF_3CO)_2O$$

The formation of trifluoroacetic anhydride during the reaction was confirmed by infrared spectrum of the volatile material. No attempt was made to separate $(CF_3CO)_2O$ and $S_2O_5F_2$ and determine the amount of $(CF_3CO)_2O$ formed during the reaction. The completion of the reaction was monitored as described in the Experimental section.

The salient features of the ir spectrum of $NaBiO(SO_3F)_2$ are given in Experimental section. The bands at 1265, 1090, and 815 cm^{-1} corresponding to $\nu_4(E)$, $\nu_1(A_1)$, and $\nu_2(A_1)$ modes may be attributed to a tridentate fluorosulfonate group having C_{3v} symmetry (18, 19). A band observed at 815 cm^{-1} in the 700–900 cm^{-1} region relating to ν_{S-F} supports the presence of only one type of fluorosulfonate group. A comparison of the ir spectra of $NaSO_3F$ (2590w, 2390w, 1295sb, 1165w, 1095s, 940w, 850w, 785s, 740sh, 584sb, 565sh, 425w cm^{-1}) (20) with that of $NaBiO(SO_3F)_2$ (see Experimental section) indicates that $NaBiO(SO_3F)_2$ is a definite moiety and does not contain any free $NaSO_3F$. The $\nu_{Bi=O}$ band appears at 520 cm^{-1} in BiOCl (21). It was difficult to assign the bismuth–oxygen multiple bond in $NaBiO(SO_3F)_2$ because of fluorosulfonate group bending vibrations in the same region.

The reaction between titanium(IV) methoxide and excess $S_2O_5F_2$ at reflux (~56°C) yields bis(fluorosulfonato)titanium-(IV) dimethoxide, $Ti(OCH_3)_2(SO_3F_2)$, reaction [5]:

$$[5]\quad Ti(OCH_3)_4 + 2S_2O_5F_2 \xrightarrow[50\text{ h}]{\sim 56°C} Ti(OCH_3)_2(SO_3F)_2 + 2CH_3OSO_2F$$

Can. J. Chem. Downloaded from www.nrcresearchpress.com by 194.225.253.170 on 09/07/12
For personal use only.

The completion of the reaction was monitored as before. Formation of methyl fluorosulfonate, CH_3OSO_2F, was confirmed by comparison with its reported infrared spectrum.

Titanium(IV) methoxide sublimes (8) at 243°C in vacuum (52 Torr). No sublimed product could be detected even when the product, $Ti(OCH_3)_2(SO_3F)_2$, was heated at ~230°C in vacuum (5 Torr). This observation is indicative of the fact that the product does not contain unreacted $Ti(OCH_3)_4$.

Various bands in the infrared spectrum of $Ti(OCH_3)_2(SO_3F)_2$ are given in the Experimental section. A comparison of its ir spectrum with that of $Ti(OCH_3)_4$ (2912s, 2812ms, 1456mw, 1434mw, 1142mb, 1088ms, 1044ms, 574mb, 460m, 398w, 260vs cm^{-1}: only vibrations of significant intensity are given here) reveals that $Ti(OCH_3)_2(SO_3F)_2$ is a definite entity. A careful perusal of the ir frequencies of $Ti(OCH_3)_2(SO_3F)_2$ reveals splitting of *E* modes of SO_3F group. The bands at 1405, 1202, and 978 cm^{-1} may be attributed to the monodentate SO_3F group (22). Also a strong band at 818 cm^{-1} is assigned to the covalent SO_3F group in $Ti(OCH_3)_2(SO_3F)_2$. A number of bands in the region 200–300 cm^{-1} (295, 272, 245, and 222 cm^{-1}) may be due to the metal–oxygen lattice vibrations both due to OCH_3 and SO_3F groups.

In conclusion, a potential fluorosulfonating agent is possible in $S_2O_5F_2$ as is evident from various examples described above.

Acknowledgement

One of us (D.G.N.) would like to thank the U.G.C., New Delhi for financial support.

1. E. HAYEK and W. KÖLLER. Monatsch Chem. **82**, 942 (1951).
2. J. H. HOLLOWAY and D. LAYCOCK. Adv. Inorg. Chem. Radiochem. **27**, 157 (1983) and references therein.
3. R. D. HOWELLS and J. D. MCCOWN. Chem. Rev. **77**, 69 (1977).
4. G. A. LAWRANCE. Chem. Rev. **86**, 17 (1986).
5. R. C. PAUL, S. SINGH, R. D. SHARMA, R. C. KUMAR, and R. D. VERMA. Ind. J. Chem. **17A**, 273 (1979).
6. S. KONGPRICHA, W. C. PREUSSE, and R. SCHWARER. Inorg. Synth. **11**, 151 (1968).
7. P. V. RADHESHWAR, R. D. VERMA, and G. H. CADY. J. Inorg. Nucl. Chem. **34**, 3913 (1972).
8. F. BISCHOFF and H. ADKINS. J. Am. Chem. Soc. **46**, 256 (1924).
9. S. SINGH, M. BEDI, and R. D. VERMA. J. Fluorine Chem. **20**, 107 (1982).
10. E. L. MUETTERTICS and D. D. COFFMAN. J. Am. Chem. Soc. **80**, 5914 (1958).
11. R. C. PAUL, S. SINGH, and R. D. VERMA. J. Fluorine Chem. **16**, 153 (1980).
12. R. C. PAUL, R. D. SHARMA, S. SINGH, and R. D. VERMA. J. Inorg. Nucl. Chem. **43**, 1919 (1981).
13. A. I. VOGEL. A textbook of inorganic analysis. 3rd ed. John Wiley, New York. 1961.
14. J. B. HENDRICKSON and S. M. SCHWARTZMAN. Tetrahedron Lett. 277 (1975).
15. A. AEBERG, T. GRAMSTAD, and S. HUSEBYE. Tetrahedron Lett. 2263 (1979).
16. F. A. COTTON, R. D. BURNES, and E. BANNISTER. J. Chem. Soc. 2199 (1960).
17. D. M. L. GOODGAME and F. A. COTTON. J. Chem. Soc. 2298 (1961); 3738 (1961).
18. J. GOUBEAU and J. B. MILNE. Can. J. Chem. **45**, 2321 (1967).
19. C. S. ALLYNE, K. O'SULLIVAN MAILER, and R. C. THOMPSON. Can. J. Chem. **52**, 336 (1974).
20. A. RUOFF, J. B. MILNE, G. KAUFMANN, and M. LEROY. Z. Anorg. Allgm. Chem. **372**, 119 (1970).
21. J. D. SMITH. Comprehensive inorganic chemistry. Vol. 2. *Edited by* A. F. Trotman-Dickenson. Pergamon Press. 1973. p. 600.
22. H. A. CARTER, S. P. L. JONES, and F. AUBKE. Inorg. Chem. **9**, 2485 (1970).

Can. J. Chem. Downloaded from www.nrcresearchpress.com by 194.225.253.170 on 09/07/12
For personal use only.

Tetramethylammonium bifluoride, crystal structure and vibrational spectra

WILLIAM W. WILSON AND KARL O. CHRISTE[1]

Rocketdyne, A Division of Rockwell International Corporation, Canoga Park, California 91303, U.S.A.

AND

JIN-AN FENG AND ROBERT BAU

Department of Chemistry, University of Southern California, Los Angeles, California 90007, U.S.A.

Received May 10, 1989

This paper is dedicated to Professor Ronald J. Gillespie on the occasion of his 65th birthday

WILLIAM W. WILSON, KARL O. CHRISTE, JIN-AN FENG, and ROBERT BAU. Can. J. Chem. **67**, 1898 (1989).

Single crystals of $[N(CH_3)_4]HF_2$ were obtained as a by-product during the recrystallization of $[N(CH_3)_4]ClF_4$ from CH_3CN solution. X-ray diffraction data show that $[N(CH_3)_4]HF_2$ crystallizes in the orthorhombic space group $Pmn2_1$ with $Z = 2$ and unit cell dimensions $a = 6.611(5)$, $b = 8.753(5)$, and $c = 5.386(4)$ Å. The structure was solved by direct methods and refined by least squares to a final $R = 0.055$ by using 205 independent reflections. The HF_2^- anions are symmetric, exhibit an unusually short F···F distance of 2.213(4) Å, and vibrational frequencies close to those of the free HF_2^- anion.

Key words: tetramethylammonium bifluoride, crystal structure, Raman spectrum.

WILLIAM W. WILSON, KARL O. CHRISTE, JIN-AN FENG et ROBERT BAU. Can. J. Chem. **67**, 1898 (1989).

On a obtenu des cristaux uniques de $[N(CH_3)_4]HF_2$ comme sous-produit de la recristallisation du $[N(CH_3)_4]ClF_4$ dans des solutions de CH_3CN. Les données de diffraction des rayons-X indiquent que le $[N(CH_3)_4]HF_2$ cristallise dans le groupe d'espace $Pmn2_1$, avec $Z = 2$ et $a = 6{,}611(5)$, $b = 8{,}753(5)$ et $c = 5{,}386(4)$ Å. On a résolu la structure par des méthodes directes et on l'a affinée par la méthode des moindres carrés (matrice entière) jusqu'à une valeur finale de $R = 0{,}055$ pour 205 réflexions indépendantes. Les anions HF_2^- sont symétriques; la distance F···F est relativement courte [2,213(4) Å] et les fréquences de vibration sont proches de celles de l'anion HF_2^- libre.

Mots clés : bifluorure de tétraméthylammonium, structure cristalline, spectre Raman.

[Traduit par la revue]

Introduction

During repeated recrystallization of $[N(CH_3)_4]ClF_4$ (1) from CH_3CN, some single crystals were obtained which were identified by X-ray diffraction as $[N(CH_3)_4]HF_2$. The crystals were formed by attack of some of the $[N(CH_3)_4]ClF_4$ on the solvent. Although $[N(CH_3)_4]HF_2$ is well known (2), and crystal structures have previously been reported for the higher polybifluorides containing the $H_2F_3^-$, $H_3F_4^-$, and $H_5F_6^-$ anions (3), no structural data were available for $[N(CH_3)_4]HF_2$ itself.

The HF_2^- anion is of significant structural and theoretical interest. It is a classic example for semi-ionic three centre-four electron bonding (4, 5) and exhibits the strongest known hydrogen bridge bond (6) which, depending on the symmetry of the surrounding crystal field (7), can be either symmetric or asymmetric (6, 8). Furthermore, strong oscillator coupling effects between the HF_2^- anions (9) occur in these salts which can result in very broad bands in the vibrational spectra and give rise to difficulties with their assignments. Thus, the assignment of the HF_2^- stretching modes has been in question until very recently (10–12). Since the tetramethylammonium cation is large, has a low positive charge over radius ratio, and is highly symmetrical, minimal ion–ion interactions are expected for $[N(CH_3)_4]^+HF_2^-$, and the HF_2^- anion should be relatively undisturbed. It was, therefore, interesting to compare the structure of the HF_2^- anion in $[N(CH_3)_4]HF_2$ with those of the free HF_2^- anion (12) and other HF_2^- salts.

Experimental

Single crystals of $[N(CH_3)_4]HF_2$ were obtained as a less soluble by-product during the recrystallization of $[N(CH_3)_4]ClF_4$ (1) from CH_3CN solution. They were separated from the $[N(CH_3)_4]ClF_4$ solution by decantation, followed by removal of last traces of solvent in a dynamic vacuum. Crystals were mounted in flamed out quartz capillaries in the dry nitrogen atmosphere of a glove box. A Nicolet/Syntex $P2_1$ automated four circle diffractometer, with Mo Kα radiation and a graphite crystal monochromator, was used for the intensity data collection. The unit cell parameters were determined by least-squares refinement of 15 centered reflections. Data were collected using the ω-scan technique for all reflections such that $4.0° < 2\theta < 45.0°$. Throughout the data collection, three reflections were monitored periodically, and no decay was observed. Of 206 reflections collected, 204 reflections with $I > 3\sigma(I)$ were retained for the ensuing structure analysis.

The structure was solved by direct methods using the SHELXS86 system (13) of crystallographic programs. There were two space groups that are consistent with the reflection pattern: $Pmn2_1$ (#31) and $Pmmn$ (#59). The positions of the nitrogen atom and two carbon atoms of the tetramethylammonium cation were revealed after direct method analysis of the data for both space groups. A subsequent difference-Fourier map distinctly revealed the bifluoride anion for both space groups. However, least-squares refinement of the atomic coordinates and thermal parameters in space group $Pmmn$ (#59) resulted in final agreement values of $R = 8.34\%$ and $R_w = 13.09\%$, while refinement in space group $Pmn2_1$ (#31) resulted in final agreement factors of $R = 5.52\%$ and $R_w = 7.47\%$. The ratio of agreement factors, $(8.34/5.52) = 1.51$, is sufficient (by Hamilton's R factor ratio test (14)) to state that space group $Pmn2_1$ (#31), with the lower R factor, is correct at the 99.5% confidence level. Details of the data collection parameters and other crystallographic information are given in Table 1, and the final atomic coordinates are summarized in Table 2.[2] The important bond lengths and angles are given in Tables 3 and 4, respectively, and Fig. 1 shows a packing diagram.

The Raman spectra were recorded on either a Cary Model 83 or a

[1]To whom correspondence should be addressed.

[2]Tables of anisotropic thermal parameters, and observed and calculated structure factors have been deposited and may be obtained, at a nominal charge, from the Depository of Unpublished Data, CISTI, National Research Council of Canada, Ont., Canada K1A 0S2.

Printed in Canada / Imprimé au Canada

Can. J. Chem. Downloaded from www.nrcresearchpress.com by 186.148.149.217 on 09/07/12
For personal use only.

Can. J. Chem. Downloaded from www.nrcresearchpress.com by 186.148.149.217 on 09/07/12
For personal use only.

TABLE 1. Summary of crystal data and refinement results for $[N(CH_3)_4]^+[HF_2]^-$

Space group	$Pmn2_1$ (orthorhombic)
a (Å)	6.611(3)
b (Å)	8.753(5)
c (Å)	5.386(4)
V (Å^3)	311.6(3)
Molecules/unit cell	2
Molecular weight (g)	113.0
Crystal dimensions (mm)	0.2 × 0.25 × 1.15
Calculated density (g cm^{-3})	1.203
Wavelength (Å) used for data collection	0.71069
sin θ/λ limit (Å^{-1})	0.539
Total number of reflections measured	206
Number of independent reflections	205
Number of reflections used in structural analysis $I > 3\sigma(I)$	204
Number of variable parameters	62
Final agreement factors	$R(F) = 0.0552$ $R(wF) = 0.0747$

TABLE 2. Final atomic coordinates for $[N(CH_3)_4]^+[HF_2]^-$

Atom	x	y	z	U_{eq}*	pop
N1	0.0000	0.9678(4)	0.2789	350(6)	0.5
C2	0.1837(4)	0.8091(4)	0.2825(5)	523(6)	1.0
C3	0.0000	1.1311(5)	0.4169(5)	441(6)	0.5
C4	0.0000	1.1279(5)	0.1381(5)	554(6)	0.5
F5	0.0000	0.6387(5)	0.9000(5)	899(6)	0.5
F6	0.0000	0.6428(5)	0.6471(4)	873(6)	0.5

*$U_{eq} = (1/3)\Sigma_{ij}(U_{ij} \cdot a_i^* \cdot a_j^* \cdot a_i \cdot a_j) \times 10^4$.

TABLE 3. Bond distances (Å) in $[N(CH_3)_4]^+[HF_2]^-$

Bond	Distance
N1—C2	1.485(3)
N1—C3	1.494(4)
N1—C4	1.504(4)
F5—F6	2.213(4)

TABLE 4. Bond angles (deg) in the $[N(CH_3)_4]^+$ cation

Bonds	Angle
C2—N1—C2	109.7(2)
C2—N1—C3	108.8(2)
C2—N1—C4	110.3(2)
C3—N1—C4	109.0(2)

Spex Model 1403 spectrophotometer using the 488-nm exciting line of an Ar ion laser or the 647.1-nm line of a Kr ion laser, respectively. Crushed single crystals in sealed Pyrex melting point capillaries were used as samples. The infrared spectrum was recorded as an AgCl disk on a Digilab Model FTS-45 spectrometer.

Results and discussion

Crystal structure. The structure of $[N(CH_3)_4]HF_2$ can be derived from a primitive cubic CsCl lattice which is orthorhombically distorted by the nonspherical HF_2^- anions. The packing in $[N(CH_3)_4]HF_2$ (see Fig. 1) is identical to that recently found (15) for $[N(CH_3)_4]O_3$, except for HF_2^- being linear while O_3^- is bent. For $[N(CH_3)_4]O_3$ the alternate space group *Pmmn* has been suggested in which the twofold screw axis along the ***a*** axis has been eliminated, and the only symmetry element remaining along this axis is a perpendicular symmetry plane. It should be noted, however, that the bent nature of O_3^- does not necessarily require the elimination of the twofold screw axis, and that the possibility of $Pmn2_1$ should also be tested for the ozonide.

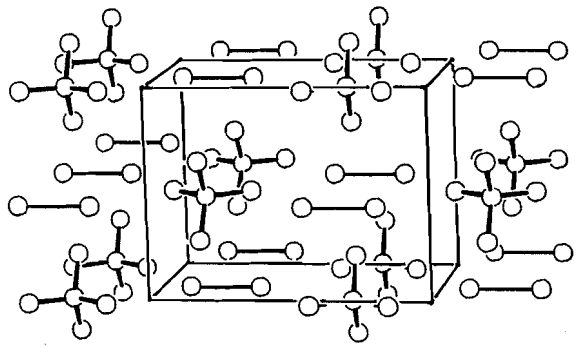


FIG. 1. Packing diagram of $[N(CH_3)_4]^+[HF_2]^-$ viewed along the ***c*** axis.

By analogy with the O_3^- salt, the large size of the $N(CH_3)_4^+$ cations minimizes the anion–anion interactions in $[N(CH_3)_4]HF_2$ and allows the HF_2^- anions to arrange in a manner (15), in which the fluorines of one HF_2^- are pointing at the fluorines of neighboring anions. In the structures of HF_2^- salts with smaller cations, such as K^+, Rb^+, or Cs^+, the negatively polarized terminal fluorine atoms of $\overset{\delta-}{F}—\overset{\delta+}{H}—\overset{\delta-}{F}$ always point at the positively polarized hydrogen atom of a neighbouring HF_2^- anion (16), as expected from Coulombic considerations. If one proceeds, however, within the family of bifluorides to salts with even smaller cations, such as Li^+ or Na^+, the HF_2^- anions are packed again in a parallel manner (16), similar to that found for the closely related linear N_3^- salts (17). It, thus, appears that for very small and very large cations, the most favorable packing conditions, i.e. a parallel arrangement of the HF_2^- anions, dominate over electrostatic dipole effects. The latter are dominant only when the cations and anions are of comparable size.

In $[N(CH_3)_4]HF_2$, all atoms, except for two methylcarbons, lie in mirror planes normal to the ***a*** axis, and the HF_2^- anions also possess a mirror plane normal to their bond line, as expected for a symmetric HF_2^- anion. Whereas the $N(CH_3)_4^+$ cation is for practical purposes an ideal tetrahedron with the expected (3, 15, 18, 19) bond lengths and angles, the F—F distance of 2.213(4) Å in HF_2^- is considerably shorter than those of 2.26–2.28 Å observed for other HF_2^- salts (16) and the free HF_2^- anion (12). This shortening is difficult to rationalize, particularly also in view of the vibrational spectrum (see below) which is very similar to that (12) of the free HF_2^- anion which has an F—F distance of 2.28 Å. It should be noted that in the alternate, but less likely (see above), *Pmmn* space group the HF_2^- anion exhibits a similarly short F—F distance of 2.22 Å. Therefore, a change in the space group of $[N(CH_3)_4]HF_2$ from $Pmn2_1$ to *Pmmn* would not result in a significant change of the F—F distance.

Vibrational spectra. The infrared and Raman spectra of

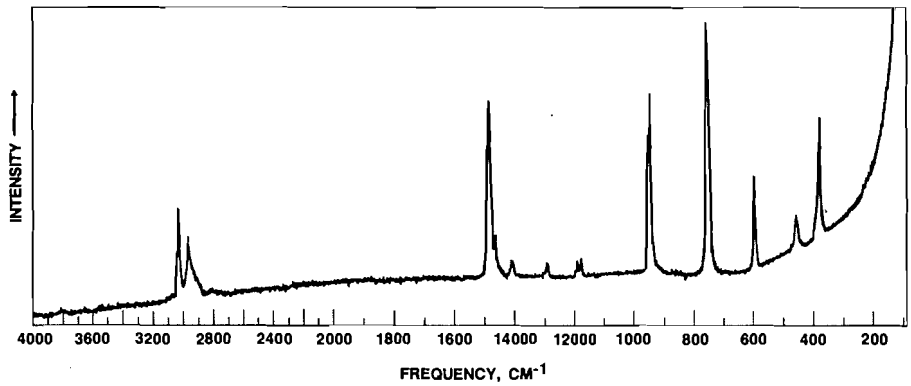


FIG. 2. Raman spectrum of solid $[N(CH_3)_4]^+[HF_2]^-$.

TABLE 5. Raman spectrum of solid $[N(CH_3)_4]^+[HF_2]^-$

Observed frequency, cm^{-1} (relative intensity)	Assignments (point group)	
	$[N(CH_3)_4]^+$ (T_d)	HF_2^- ($D_{\infty h}$)
3036 (36)	$\nu_5(E)\nu_{as}CH_3$	
2968 (24) br	$\nu_1(A_1)\nu_sCH_3$	
1481 (71)	$\nu_6(E)\delta_{as}CH_3$	
1466 (16)	$\nu_2(A_1)\delta_sCH_3$	
1409 (7)	$\nu_{16}(F_2)\delta_sCH_3$	
1292 (5)	$\nu_{17}(F_2)\delta_{rock}CH_3$	
1193 (5), 1182 (6)	$\nu_7(E)\delta_{rock}CH_3$	
956 (53), 949 (69)	$\nu_{18}(F_2)\nu_{as}CN_4$	
759 (100)	$\nu_3(A_1)\nu_sCN_4$	
596 (39)		$\nu_1(\Sigma_g^+)\nu_s$
458 (13)	$\nu_{19}(F_2)\delta CN_4$	
384, 378 (47)	$\nu_8(E)\delta NC_4$	

ground single crystals of $[N(CH_3)_4]HF_2$ were recorded. The Raman spectrum is shown in Fig. 2, and the observed frequencies together with their assignment are listed in Table 5. The bands due to the $N(CH_3)_4^+$ cation are in good agreement with previous literature data (1) and were assigned accordingly. The infrared spectrum agreed well with a previous report (2) from which the remaining frequencies for ν_3 and ν_2 of the HF_2^- anion were also taken. Table 6 gives a comparison of the frequencies of the fundamental vibrations, and the F—F and F—H distances of HF_2^- in the free ion and several salts containing either symmetric or asymmetric anions. The fundamental vibrations show the expected trends. With increasing size of the cation and better isolation of the anions, the frequencies of the symmetric HF_2^- anions approach those of the free HF_2^- anion. For the asymmetric HF_2^- anions, the frequency of ν_3 increases, and those of ν_1 and ν_2 decrease with increasing asymmetry. Therefore, the vibrational frequencies can be used for the detection of pronounced asymmetry in these anions.

The computation of standard valence force fields for HF_2^- in these salts is not rewarding in view of the uncertainties in the frequency values of ν_3, caused by their large band widths, and of the very large ionic contributions to the bonding (4, 5) which are not properly reflected by these force constants. In order to account for the strong ionic contributions to the bonding in HF_2^-, ionic force fields (20) should be used which have a stretching force constant and a force constant derived from the Coulombic force. The shortening of the F—F distance of HF_2^- in its $[N(CH_3)_4]^+$ salt is not reflected by the vibrational frequencies (see Table 6). It might, therefore, be attributed to increased Coulombic forces, but other explanations, such as possibly a slight bending of the anion caused by crystal field effects or strong librations due to loose packing of the anions, cannot be ruled out.

TABLE 6. Comparison of the vibrational frequencies (cm^{-1}) and the F—F and F—H distances of free HF_2^- with those of symmetric and asymmetric HF_2^- salts

	Vibrational frequency					
	Symmetric HF_2^-				Asymmetric HF_2^-	
	Free ion[a]	$[N(CH_3)_4]HF_2$	KHF_2[d]	$NaHF_2$[d]	$BaF(HF_2)$[e]	$CH_3C_6H_4NH_3(HF_2)$[f]
$\nu_1(\Sigma_g^+)\nu_{sym}$	583.05	596[b]	596, 603	630	587	527
$\nu_2(\Pi_u)\delta$	1286.03	1264, 1255[c]	1233	1210, 1220	1171	1108
$\nu_3(\Sigma_u^+)\nu_{as}$	1331.15	1376[c]	≈1450	≈1500	1684	1730
r_{F-F} (Å)	2.27771(7)	2.213(4)[b]	2.277(6)	2.264(3)	2.28	2.260
r_{F-H} (Å)	1.14		1.14	1.13	1.08	1.025

[a]Reference 12.
[b]This work.
[c]Reference 2.
[d]Reference 9.
[e]Reference 8.
[f]References 2 and 6.

Can. J. Chem. Downloaded from www.nrcresearchpress.com by 186.148.149.217 on 09/07/12
For personal use only.

Conclusion

The crystal structure of $[N(CH_3)_4]HF_2$ has been determined, and the vibrational spectra have been recorded. The data show that the large $[N(CH_3)_4]^+$ cations minimize the anion–anion interactions, and that the vibrational frequencies of the HF_2^- anion approach those of the free HF_2^- anion. As expected, the $[N(CH_3)_4]^+$ cations are essentially tetrahedral, and the HF_2^- anions are symmetric. The only unexpected feature which, at the present time is not fully understood and requires further investigation, is the unusually short F—F distance of 2.213(4) Å.

Acknowledgments

The authors are grateful to Dr. C. J. Schack and Mr. R. D. Wilson for their help, to Mr. S. Klee for analytical support, to Mr. L. Hill for the recording of the infrared spectrum, and to the Air Force Astronautics Laboratory for financial support.

1. W. W. Wilson and K. O. Christe. Inorg. Chem. In press.
2. K. M. Harmon and R. R. Lovelace. J. Phys. Chem. **86**, 900 (1982), and references cited therein.
3. D. Mootz and D. Boenigk. Z. Anorg. Allg. Chem. **544**, 159 (1987).
4. G. C. Pimentel. J. Chem. Phys. **19**, 466 (1951).
5. R. J. Hach and R. E. Rundle. J. Am. Chem. Soc. **73**, 4321 (1951).
6. J. M. Williams and L. F. Schneemeyer. J. Am. Chem. Soc. **95**, 5780 (1973).
7. N. S. Ostlund and L. W. Ballenger. J. Am. Chem. Soc. **97**, 1237 (1975).
8. A. Lautie, F. Romain, M.-H. Limage, A. Novak, H. Prevost-Czeskleba, and J. Moret. J. Mol. Struct. **118**, 227 (1984).
9. J. J. Rush, L. W. Schroeder, and A. J. Melveger. J. Chem. Phys. **56**, 2793 (1972).
10. K. Kawaguchi and E. Hirota. J. Chem. Phys. **84**, 2953 (1986).
11. R. D. Hunt and L. Andrews. J. Chem. Phys. **87**, 6819 (1987).
12. K. Kawaguchi and E. Hirota. J. Chem. Phys. **87**, 6838 (1987).
13. G. M. Sheldrick. SHELX system of crystallographic programs, University of Goettingen, W-Germany. 1986.
14. W. C. Hamilton. Acta Crystallogr. **18**, 502 (1965).
15. W. Hesse and M. Jansen. Angew. Chem. Int. Ed. Engl. **27**, 1341 (1988).
16. R. W. G. Wyckoff. *In* Crystal structures. Vol. II. John Wiley, New York. 1964. p. 277.
17. C. S. Choi. *In* Energetic materials. Vol. 1. *Edited by* H. D. Fair and R. F. Walker. Plenum Press, New York. 1977. p. 97.
18. Y. Wang, L. D. Calvert, and S. K. Brownstein. Acta Crystallogr. B**36**, 1523 (1980).
19. N. Buchholz, M. Leimkuehler, L. Kiriazis, and R. Mattes. Inorg. Chem. **27**, 2035 (1988).
20. Y. Matsui, K. Ezumi, and K. Iwatani. J. Chem. Phys. **84**, 4774 (1986).

Can. J. Chem. Downloaded from www.nrcresearchpress.com by 186.148.149.217 on 09/07/12
For personal use only.

The preparation of thiazyltrifluoromethane, CF_3SN, the hexachloro-3-cyclopentenylidenaminosulfides C_5Cl_6NSX ($X = CF_3$, Cl, NSO, SCF_3, C_5Cl_6N) and the crystal structures of C_5Cl_6NSX ($X = CF_3$, Cl)

ALOIS HAAS[1] AND THOMAS MISCHO

Lehrstuhl für Anorganische Chemie II, Ruhr-Universität Bochum, Postfach 10 21 48, D-4630 Bochum 1, Federal Republic of Germany

Received January 13, 1989

This article is dedicated to Professor Ronald J. Gillespie on the occasion of his 65th birthday

ALOIS HAAS and THOMAS MISCHO. Can. J. Chem. **67**, 1902 (1989).

$CF_3S(Cl)$=$NSi(CH_3)_3$ is found to undergo intermolecular decomposition to give oligomeric, possibly cyclic $(CF_3SN)_x$ rather than monomeric CF_3SN, formed by intramolecular decomposition. Monomeric thiazyltrifluoromethane, CF_3SN, is formed in the thermal decomposition of CF_3SN_3 and may be trapped before polymerizing by formation of a 1:1 adduct with hexachlorocyclopentadiene. The structure of this adduct is determined by single crystal X-ray diffraction. From the molecular structure it is evident that a (4 + 2) cycloaddition has not occurred but rather the formation of a thioketimine (**I**). The same material is formed when a suspension of CF_3SNH_2 and lead(IV) acetate in CH_2Cl_2 is refluxed and the intermediate CF_3SN is again trapped by C_5Cl_6.

By comparison ClSN and C_5Cl_6 interact in an analogous manner to give C_5Cl_6NSCl (**II**), whose structure was determined by single crystal X-ray diffraction. FSN, on the other hand, when reacted with C_5Cl_6 yields the corresponding fluoro derivative only as an intermediate. At 20°C using SO_2 as solvent C_5Cl_6NSCl (**II**) is formed. At 75°C in SO_2 the new compound C_5Cl_6N—S—NSO forms. The latter compound may also be formed from (**II**) and $Hg(NSO)_2$. In the reaction of FSN with C_5F_6 only decomposition products were observed.

Some of the reactions of C_5Cl_6NSCl (**II**) were investigated. With $Hg(SCF_3)_2$ C_5Cl_6N—$SSCF_3$ is obtained; with $SbCl_5$ in SO_2 C_5Cl_6N—S—NC_5Cl_6 forms as the main product.

Key words: synthesis of CF_3SN, preparation of C_5Cl_6NSX ($X = CF_3$, Cl, NSO, SCF_3, C_5Cl_6N), crystal structures of C_5Cl_6NSX ($X = CF_3$, Cl), chemical properties of C_5Cl_6NSCl, nmr-, ir-, ms-data.

ALOIS HAAS et THOMAS MISCHO. Can. J. Chem. **67**, 1902 (1989).

On a trouvé que le $CF_3S(Cl)$=$NSi(CH_3)_3$ subit une décomposition intermoléculaire conduisant à la formation de $(CF_3SN)_x$ oligomère et possiblement cyclique plutôt qu'une décomposition intramoléculaire conduisant au CF_3SN monomère. Le thiazyltrifluorométhane monomère, CF_3SN, se forme par la décomposition thermique du CF_3SN_3 et on peut le piéger avant sa polymérisation par la formation d'un adduit 1:1 avec l'hexachlorocyclopentadiène. On a déterminé la structure de cet adduit grâce à une étude par diffraction des rayons-X effectuée sur un cristal unique. A partir de la structure, on peut conclure qu'il ne s'est pas produit de cycloaddition (4 + 2) et qu'il y a eu formation de thiocétimine (**I**). Le même composé se forme lorsqu'on porte une suspension de CF_3SNH_2 et d'acétate de plomb(IV) dans le CH_2Cl_2 au reflux; on peut encore une fois piéger l'intermédiaire CF_3SN par le C_5Cl_6.

Par comparaison, le ClSN et le C_5Cl_6 interagissent d'une façon analogue pour donner le composé C_5Cl_6NSCl (**II**) dont la structure a été déterminée par diffraction des rayons-X sur un cristal unique. Par ailleurs, la réaction du FSN avec le C_5Cl_6 ne fournit que le dérivé fluoré correspondant comme intermédiaire. A 20°C, utilisant le SO_2 comme solvant, il se forme du C_5Cl_6NSCl (**II**). A 75°C, dans le SO_2, le nouveau composé C_5Cl_6N—S—NSO se forme. Ce dernier composé peut aussi se former à partir du produit **II** et du $Hg(NSO)_2$. Lors de la réaction du FSN avec le C_5F_6 on n'observe que la formation de produits de décomposition.

On a examiné quelques unes des réactions du C_5Cl_6NSCl. Avec le $Hg(SCF_3)_2$, on obtient du C_5Cl_6N—$SSCF_3$; avec le $SbCl_5$, dans le SO_2, le produit principal est le C_5Cl_6N—S—NC_5Cl_6.

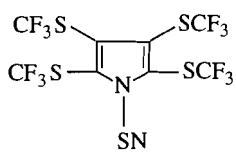
Mots clés : synthèse du CF_3SN, préparation du C_5Cl_6NSX ($X = CF_3$, Cl, NSO, SCF_3, C_5Cl_6N), structures cristallines des composés C_5Cl_6NSX ($X = CF_3$, Cl), propriétés chimiques du C_5Cl_6NSCl, données de rmn, ir et sm.

[Traduit par la revue]

Introduction

A number of monosubstituted thiazyl compounds have been prepared. These are

FSN (1), ClSN (2), BrSN (3), HOSN (4), $(CF_3)_2NOSN$ (5),



(6), and F_5TeOSN (7).

Their thermal stability and reactivity appear to depend on the size and electronegativity of the substituents.

Thiazyltrifluoromethane, another member of this group, has been mentioned twice in the literature (8, 9) as an unstable intermediate. In the present investigation an attempt is made to provide evidence for its existence. Since coordinated FSN in the form of $[Re(CO)_5(NSF)]^+[AsF_6]^-$ (10) is well known and subsequent halogen exchange reactions with SiX_4 yield $[Re(CO)_5NSX]^+[AsF_6]^-$ (X = Cl, Br) (11), initial attempts were aimed at the synthesis of $[Re(CO)_5(NSCF_3)]^+[AsF_6]^-$. As an alternate approach the trapping of intermediate CF_3SN by suitable dienes was contemplated. Similar trapping reactions with FSN and ClSN should provide a good basis for comparing these three thiazyl compounds.

Results and discussion

Reactions of $[Re(CO)_5NSF]^+[AsF_6]^-$ with $Hg(CF_3)_2$ or $(CH_3)_3SiCF_3$ in SO_2 at 20°C failed to give the anticipated

[1]Author to whom correspondence should be addressed.

Can. J. Chem. Downloaded from www.nrcresearchpress.com by 186.148.149.217 on 09/07/12
For personal use only.

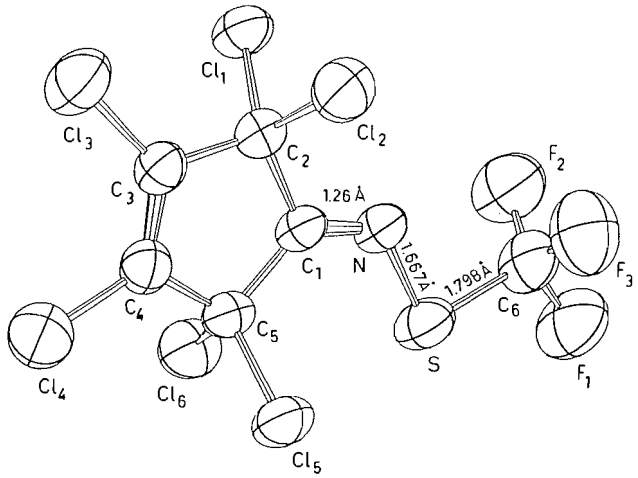


FIG. 1. Molecular structure of hexachloro-3-cyclopentenyliden-aminotrifluormethylsulfide (**I**).

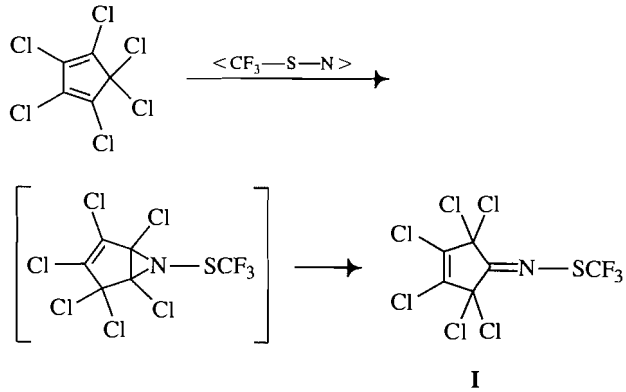
$[Re(CO)_5NSCF_3]^+[AsF_6]^-$. In both cases no F/CF_3 exchange takes place. Instead the reaction with $(CH_3)_3SiCF_3$ in CH_2Cl_2 at 20°C yields quantitatively $Re(CO)_5Cl$ and $(CH_3)_3SiF$ as well as small amounts of S_4N_4 and S_8.

The decomposition of $CF_3S(Cl)=NSi(CH_3)_3$ (8) in the presence of dienes provides a different way to detect CF_3SN. It is assumed that the final product will be oligomeric $(CF_3SN)_x$, formed via CF_3SN as a reactive intermediate.

Decomposition of $CF_3S(Cl)=NSi(CH_3)_3$ in the presence of butadiene, cyclopentadiene, hexachlorocyclopentadiene, or tetraphenylcyclopentadienone afford no addition products of CF_3SN. The only materials isolated are polymeric $(CF_3SN)_x$ and $(CH_3)_3SiCl$. The dienes are recovered quantitatively. These observations are consistent with inter- instead of intramolecular condensation. A reaction scheme, illustrating this condensation process, has been proposed in a preliminary communication (12). Because neither Cl nor $(CH_3)_3Si$, both possible end groups in a chain polymer, could be detected by elemental analysis, it is concluded that $(CF_3SN)_x$ is cyclic in nature, possibly with rings of different size.

Another method to generate CF_3SN is an *in situ* decomposition of the azide CF_3SN_3, made from CF_3SCl and $(CH_3)_3SiN_3$ (9) with $(CF_3SN)_x$ as the final product. In the presence of hexachlorocyclopentadiene a white solid is obtained in low yields, which analyses as a 1:1 adduct of C_5Cl_6 and CF_3SN. Surprisingly, the chemical shift in the ^{19}F-nmr spectrum ($\delta(CF_3) = -51.6$) appears in a region where normally trifluoromethylthioamino ($CF_3S—N=$) groups resonate. This raises some doubt whether the product obtained is formed by a (4 + 2) cycloaddition reaction. The presence of a discrete CF_3SN group is confirmed by single crystal X-ray diffraction analysis. The compound $C_5Cl_6 \cdot CF_3SN$ is found to have a thioketimine structure, shown in Fig. 1 (see crystal structure). These results prove convincingly that the intermediate CF_3SN does not react with C_5Cl_6 as a "thiazyl" but as a "nitrene", presumably via an unstable (2 + 1) cycloaddition intermediate rearranging to the final hexachloro-3-cyclopentenylidenamino-trifluoromethylsulfanide (**I**) according to reaction [1]. The low yields are caused by polymerisation of the intermediate CF_3SN to $(CF_3SN)_n$ and decomposition of the latter to the detected products CF_3SSCF_3 and N_2 (19). Alternative reaction pathways can be excluded. It could be demonstrated that under these conditions C_5Cl_6 does not react with $(CH_3)_3SiN_3$.

[1]

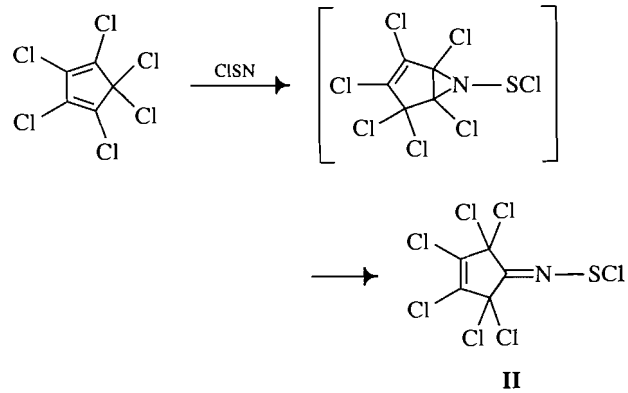


I

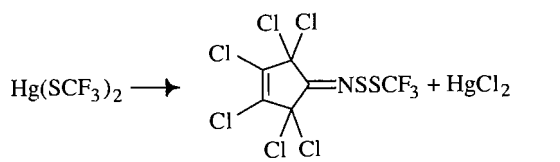
A second independent synthesis for **I** supports the proposed mechanism. Generally nitrenes are also produced by oxidation of primary amines (13). When a mixture of CF_3SNH_2, C_5Cl_6, and $Pb(CH_3COO)_4$ is refluxed in CH_2Cl_2, 5.4% **I** is formed in addition to $(CF_3S)_2NH$ and $CF_3SN{=}S{=}NSCF_3$, confirming the appearance of CF_3SN as a nitrene intermediate in the reaction.

These results raise the question of how ClSN interacts with C_5Cl_6. Generation of ClSN was accomplished by refluxing a solution of $Cl_3S_3N_3$ in toluene (14). In the presence of C_5Cl_6 the mixture turns red after 3 h and pale yellow crystals are isolated in 38% yield. They decompose slowly in moist air and are soluble in nonpolar solvents. Analytical results indicate the formation of a 1:1 adduct of the general formula $C_5Cl_6 \cdot NSCl$. A crystal structure analysis showed the compound to have an almost identical structure with **I**. Hexachloro-3-cyclopentenyl-idenaminosulfanyl chloride (**II**) is probably formed similarly to **I** according to reaction [2]. The reactivity of **II** is comparable to that of other sulfanyl chlorides. With $Hg(SCF_3)_2$ $C_5Cl_6NSSCF_3$ forms in good yields and with $SbCl_5$ in SO_2 the reaction takes place according to reaction [3]. Again it is evident that ClSN reacts as a nitrene with C_5Cl_6. The reactions of FSN with

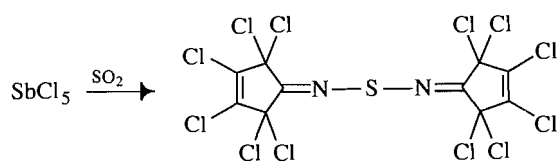
[2]



II



[3] **II** +



Can. J. Chem. Downloaded from www.nrcresearchpress.com by 186.148.149.217 on 09/07/12
For personal use only.

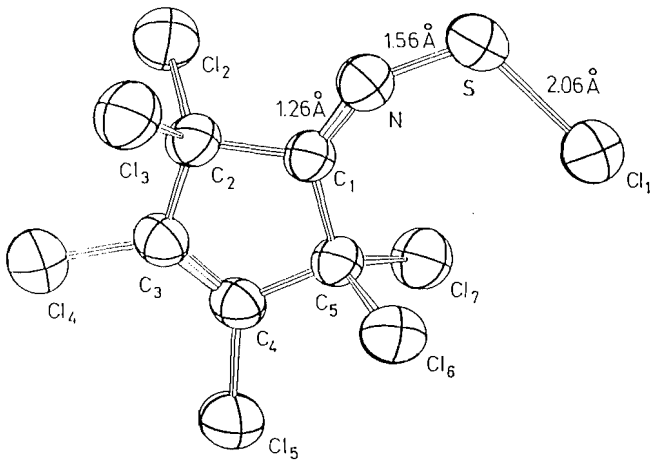
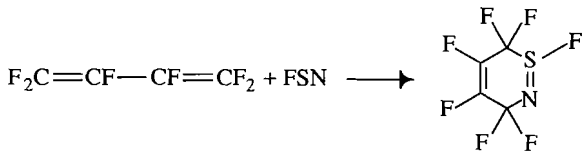


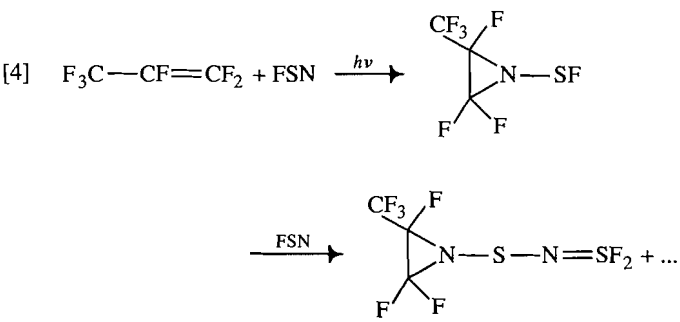
FIG. 2. Molecular structure of hexachloro-3-cyclopentenylidenaminosulfanyl chloride (**II**).

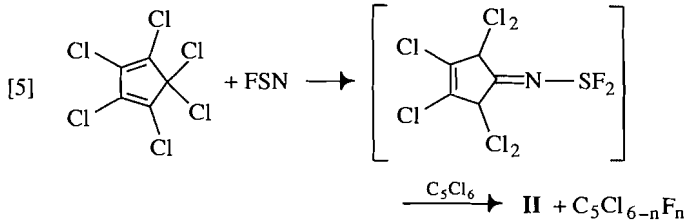
C_5Cl_6 are found to be somewhat more complicated. Analogous reactions of FSN with perfluoroolefines are reported in the literature. The products obtained are dependent on reaction conditions and the nature of the olefins. With perfluorobutadiene a (4 + 2) cycloaddition product (15) is formed and with perfluoropropene under the influence of uv-light an aziridine ring is postulated as an intermediate which adds additional FSN

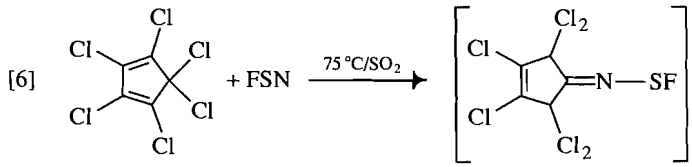


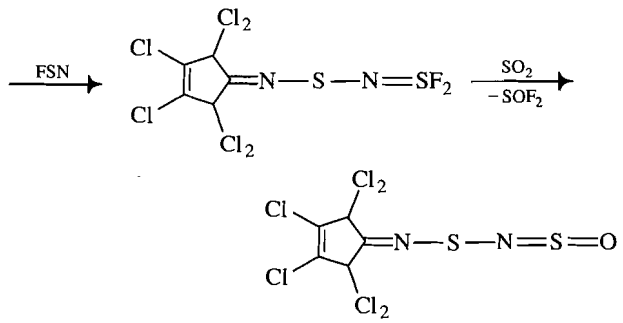
to yield the corresponding iminosulfur difluoride derivative (16) according to reaction [4].

In analogy to the chemical behaviour of CF_3SN and ClSN discussed above, it is expected that FSN forms with C_5Cl_6 the corresponding sulfanyl fluoride Cl_6C_5NSF. However, the reactivity of the known dialkylaminosulfanyl fluorides of the type $R_2N—S—F$ (R = CH_3, C_2H_5) (17) suggests that such a compound may not be isolatable. Indeed the reaction of FSN with C_5Cl_6 (molar ratio 2:1) in SO_2 at 20°C gives C_5Cl_6NSCl (**II**) in 20% yield. In addition, partially fluorinated derivatives of C_5Cl_6 are formed according to the ^{19}F nmr spectra. The formation of **II** can be explained according to eq. [5]. If this procedure is carried out at 75°C in a stainless steel autoclave (other parameters not changed) hexachlorocyclopentenylidenamino-*N*-sulfinyliminosulfide, C_5Cl_6NSNSO (**III**) is obtained according to reaction [6]. The structure of **III** was confirmed by an alternate route. Although **II** does not react with $(CH_3)_3SiNSO$, with $Hg(NSO)_2$ it forms **III** in 82% yield. Since iminosulfanyl fluorides are stabilized by perfluorinated groups





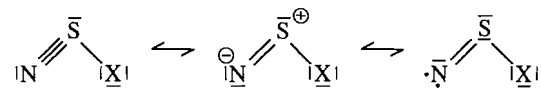




III

$((CF_3)_2C=N—S—F$ is stable at 55°C) (18), perfluorocyclopentadiene was treated with FSN. Instead of the expected reaction, decomposition occurred and S_4N_4, S_8, and SOF_2 were detected. Perfluorocyclopentadiene is not observed in the ^{19}F nmr spectrum any more and may have decomposed or polymerized.

The reactions studied so far at least with C_5Cl_6 as a reaction partner strongly suggest that XSN does not behave as a thiazyl compound but as a nitrene. Obviously the following mesomeric structures



explain the reactivity of X—SN (X = CF_3, F, Cl) best. Structural parameters are given in Table 2, X-ray structures are presented in Figs. 1 and 2. The observed differences for bond distances and angles in the groups C=N—S—CF_3 in **I** and C=N—S—Cl in **II** call for comments. The pertinent details of the two structures are shown below.



I **II**

In **I** d(N—S) = 1.66 Å is comparable to other normal N—S single bond distances, e.g., in $S_{11}N_2$ where d(S—N) = 1.67 Å (22). In contrast to this normal distance, hexachloro-3-cyclopentylidenaminosulfanyl chloride (**II**) d(N—S) is 1.56 Å, a considerable shorter distance, but such a value is not without precedents. In $[(CF_3SO_2)_2N]_2[SiF_6]$ the S—N bond length equals 1.586 (4) and 1.574 (4) Å and $\angle(S_1—N—S_2)$ = 125° (23). The shortening of d(N—S) in **II** may be explained by strong p_π–d_π interactions in the following manner.

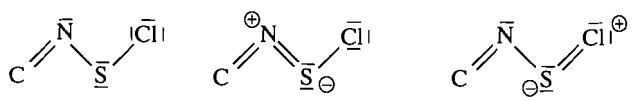
Can. J. Chem. Downloaded from www.nrcresearchpress.com by 186.148.149.217 on 09/07/12
For personal use only.

Can. J. Chem. Downloaded from www.nrcresearchpress.com by 186.148.149.217 on 09/07/12
For personal use only.

Chlorine, on account of the difference in electronegativities will act both as σ and π acceptor towards sulfur, formally in 2+ oxidation state. This is clearly different for **I** where the CF_3— group is only capable to function as a σ acceptor. As a consequence the sulfur alone in **II** will become a stronger acceptor than its counterpart in compound **I**, resulting in extensive charge delocalisation via dative $p_\pi - d_\pi$ interaction between the sp^2 hybridized nitrogen as donor and sulfur as acceptor. The C—N bonds become, for both compounds, nearly identical and are typical for normal C=N double bonds.

The proposed charge delocalisation sequence from N → S and from S → Cl is reflected not only in the trends in bond distances, but also in the observed bond angles. In **II** ∠CNS is 147.3°, considerably widened from the "ideal" angle of 120° for sp^2 nitrogen. In **I** this angle is a normal 124.3°. The same tendency is reflected in bond angles on sulfur. For **I** ∠NSC is 94.9°, very typical for a normal angle which are generally around 90° (24) for divalent sulfur compounds. For **II** this angle is again widened to 114.9°, consistent both with higher electron density in the S—N bond and some delocalisation from lone pair electron density on sulfur to chlorine. The two sets of bond angles discussed are completely consistent with expectations based on Gillespie's valence shell electron-pair repulsion theory (VSEPR) (24).

Alternatively the following mesomeric structures may be considered,



a **b** **c**

with contributions from forms ***b*** and ***c*** reflected in the observed bond parameters. For the CF_3— compound, only the mesomeric forms ***a*** and ***b*** will contribute, with ***b*** only involved to a limited extent.

Experimental

All reactions were carried out in two- or three-necked flasks or thick-walled 50 mL tubes fitted with J. Young valves. To avoid hydrolysis all equipment was dried *in vacuo* or in a stream of hot argon. Volatile compounds were handled in a standard-vacuum-line equipped with J. Young (o-ringette PTFE stopcock) valves. Solids were manipulated in a dry argon atmosphere. Solvents were dried carefully.

Literature methods were used to prepare $(CH_3)_3SiN_3$ (25), CF_3SCl (26), CF_3SNH_2 (27), $S_3N_3Cl_3$ (28), FSN (29), $Hg(NSO)_2$ (30), $Hg(SCF_3)_2$ (31), C_5F_6 (32), $Hg(CF_3)_2$ (33), $[(CO)_5Re(NSF)]^+(AsF_6)^-$ (10), $CF_3Si(CH_3)_3$ (34), $CF_3S(Cl)$=$NSi(CH_3)_3$ (8).

Mass spectra were obtained with a MAT-CH 7 spectrometer using electron impact ionisation (70 eV). Infrared spectra were recorded with a Bruker IFS 85 spectrometer using KBr pellets.

Nuclear magnetic resonance spectra were measured at room temperature on a Bruker AM 400 spectrometer using a 5-mm probe tuned to 100.618 MHz to observe ^{13}C, and on a Bruker WM 250 spectrometer using a 15-mm probe (broad band over the frequency range 11–25 MHz) tuned to 18.070 and 25.357 MHz to observe ^{14}N and ^{15}N.

^{19}F nmr spectra were obtained on a Bruker WM 250 spectrometer (10-mm probe) by using the ^1H decoupler coil retuned to 235.36 MHz as observer coil.

For ^{13}C nmr spectra, the free induction decays were accumulated in 32 k words of memory over a spectral width of 25 KHz (0.7 Hz/data point, line broadening of 1 Hz) with pulse width of 1.5 μs in 45000 scans.

For $^{14,15}N$ and ^{19}F nmr spectra, the free induction decays were accumulated in 16 k words of memory over a spectral width of 12.195 kHz (1.5 Hz/data point, line broadening of 5 Hz) with pulse width of 50 μs in 7000 scans ($^{14,15}N$ nmr spectra) and over a spectral width of 50 kHz (6.1 Hz/data point, line broadening of 1 Hz) with pulse width of 5 μs in 16 scans (^{19}F nmr spectra).

Samples were run locked (d_6-acetone for ^{13}C nmr spectra, $CDCl_3$ for $^{14,15}N$ and ^{19}F nmr spectra) and are referenced internally to TMS and $CFCl_3$ and externally to CH_3NO_2. All melting points are uncorrected.

TABLE 1. Crystal data for $C_5Cl_6NSCF_3$ and C_5Cl_6NSCl

	$C_5Cl_6NSCF_3$	C_5Cl_6NSCl
Formula		
System	Monoclinic	Triclinic
Space group	$P2_1/a$	$P\bar{1}$
a (Å)	10.999 (15)	9.566 (12)
b (Å)	8.005 (5)	9.691 (13)
c (Å)	14.885 (18)	13.67 (19) (footnote 2 in text)
α (deg)	90.0	79.51 (15)
β (deg)	99.27 (10)	89.50 (13)
τ (deg)	90.0	75.89 (12)
V (Å^3)	1293.5	1208.1
Z	4	4
λ(MoKα) (Å)	0.71069	0.71069
Crystal size (mm)	0.8 × 1.0 × 1.3	0.7 × 0.5 × 0.4
Temperature (K)	293	293
Range 2θ	0–65°	0–65°
Number of observed reflexions	4671	8710
R	0.083	0.056
R_w	0.081	0.069

X-ray crystal structure analysis of C_5Cl_6NSX ($X = CF_3$, Cl)

Data for C_5Cl_6NSCl are recorded in parentheses.

Single set of reflections 4671 (8710)

No absorption correction was applied, since $\mu = 15.04$ (17.82) cm^{-1}. The structure was solved by direct methods and refined using SHELXTL-81. The structures have been refined anisotropically to a final R-value of 0.083 (0.056), respectively. The final difference Fourier map shows maxima of 0.7 (0.5) e/Å^3. The shift of the atoms in the last "least-squares cycle" is <0.002 for the atomic and <0.005 for the thermal parameters. $R_w = 0.081$ (0.069); weighting scheme: $W = 1/\sigma^2(F) + 0.000183 \times F \times F)/K$ (K = scale factor). Atomic co-ordinates and selected bond lengths and bond angles are given in Tables 1 to 4. Thermal parameters and F_o/F_c lists are available on request from the Depository of Unpublished Data.[2] Computations are made with SHELXTL-81 (20) and Figs. 1 and 2 are prepared with ORTEP-II (21).

Reactions of $[Re(CO)_5(NSF)]^+(AsF_6)^-$

(i) With $Hg(CF_3)_2$ in SO_2

$[Re(CO)_5(NSF)]^+(AsF_6)^-$ (100 mg, 0.17 mmol) and $Hg(CF_3)_2$ (58 mg, 0.17 mmol) were dissolved in 1.5 g SO_2 in a 5-mm thick-walled nmr tube fitted with a Young valve. No reaction was observed after 5 days at 20°C by means of ^{19}F nmr spectroscopy.

(ii) With $CF_3Si(CH_3)_3$ in SO_2 or CH_2Cl_2

$[Re(CO)_5(NSF)]^+(AsF_6)^-$ (100 mg, 0.17 mmol) and $CF_3Si(CH_3)_3$ (25 mg, 0.17 mmol) were dissolved in 4 mL SO_2 in a 10-mm thick-walled nmr tube fitted with a Young valve. At 20°C no reaction took place.

When this procedure was carried out in CH_2Cl_2 at 20°C, complete decomposition of the Re-complex is observed after 1 h with formation of $Re(CO)_5Cl$, $(CH_3)_3SiF$, and minor amounts of S_4N_4 and S_8. The products were characterized by their known ir- and mass spectra.

[2]A complete set of supplementary material, comprising structure factors, final atomic positional parameters, final thermal parameters, and interatomic distances, and angles may be purchased from the Depository of Unpublished Data, CISTI, National Research Council of Canada, Ottawa, Ont., Canada K1A 0S2.

TABLE 2

(*a*) Bond distances

Bond	Distance (Å)	Bond	Distance (Å)
	$C_5Cl_6NSCF_3$		
C(1)—C(2)	1.505 (7)	C(2)—C(3)	1.497 (8)
C(1)—C(5)	1.528 (8)	C(2)—Cl(1)	1.769 (6)
C(1)—N	1.255 (7)	C(2)—Cl(2)	1.779 (5)
C(3)—C(4)	1.320 (9)	C(4)—C(5)	1.494 (8)
C(3)—Cl(3)	1.693 (6)	C(4)—Cl(4)	1.693 (6)
C(5)—Cl(5)	1.786 (6)	C(6)—F(1)	1.329 (9)
C(5)—Cl(6)	1.754 (6)	C(6)—F(2)	1.288 (10)
		C(6)—F(3)	1.321 (9)
		C(6)—S	1.798 (7)
S—N	1.667 (5)		
	C_5Cl_6NSCl		
C(1)—N	1.262 (15)	C(2)—C(3)	1.487 (18)
C(1)—C(2)	1.516 (19)	C(2)—Cl(2)	1.779 (22)
C(1)—C(5)	1.503 (18)	C(2)—Cl(3)	1.779 (22)
C(3)—C(4)	1.327 (16)	C(4)—C(5)	1.497 (18)
C(3)—Cl(4)	1.694 (20)	C(4)—Cl(5)	1.682 (20)
C(5)—Cl(6)	1.776 (22)	S—N	1.561 (19)
C(5)—Cl(7)	1.786 (22)	S—Cl(1)	2.055 (25)

(*b*) Bond angles in $C_5Cl_6NSCF_3$ and C_5Cl_6NSCl

Bonds	Angle (deg)	Bonds	Angle (deg)
	$C_5Cl_6NSCF_3$		
C(2)—C(1)—C(5)	109.3 (4)	C(1)—C(2)—C(3)	103.7 (5)
N—C(1)—C(5)	128.9 (5)	C(2)—C(3)—C(4)	111.2 (5)
C(2)—C(1)—N	121.7 (5)	C(1)—C(5)—C(4)	106.1 (4)
C(6)—S—N	94.9 (3)		
C(1)—N—S	124.3 (4)		
	C_5Cl_6NSCl		
C(5)—C(1)—C(2)	109.4 (7)	C(3)—C(2)—C(1)	102.7 (7)
C(2)—C(1)—N	120.5 (7)	C(3)—C(2)—Cl(2)	111.5 (7)
C(5)—C(1)—N	130.1 (7)		
C(4)—C(3)—C(2)	112.8 (7)	C(3)—C(4)—C(5)	112.0 (7)
Cl(4)—C(3)—C(2)	121.0 (7)	Cl(5)—C(4)—C(5)	120.8 (7)
C(4)—C(5)—C(1)	103.1 (7)		
S—N—Cl	147.2 (7)		
Cl(1)—S—N	114.9 (2)		

Pyrolysis of $CF_3S(Cl)$=$NSi(CH_3)_3$ in the presence of dienes

In a typical reaction a two-fold excess of butadiene (18 mmol) was dissolved in 150 mL toluene in a three-necked flask, equipped with a reflux condenser, cooled dropping-funnel, and gas-inlet tube. To this solution $CF_3S(Cl)$=$NSi(CH_3)_3$ (2.0 g, 9.0 mmol) dissolved in 20 mL toluene at −40°C were added dropwise. At a reaction temperature of 110°C the reaction was completed after 3 h. No addition product was detected by ^{19}F nmr and mass spectroscopy neither in solution nor in the residue, obtained after evaporation of toluene *in vacuo*. Insoluble, polymeric $(CF_3SN)_x$ (8), the principle product, decomposes under these conditions to yield CF_3SSCF_3 (characterized by ir, ^{19}F nmr and mass spectra) and nitrogen.

*Preparation of hexachloro-3-cyclopentenylidenaminotrifluoromethylsulfide (**I**)*

(i) By pyrolysis of CF_3SN_3

The reaction was carried out in a 100-mL three-necked flask equipped with condenser (−30°C), two gas inlet tubes, magnetic stirring bar, and connected via one inlet tube to a vacuum line. $(CH_3)_3SiN_3$ (8.66 g, 75 mmol), C_5Cl_6 (4.5 g, 16 mmol), and toluene (20 mL) were placed in the reaction flask and cooled to liquid nitrogen temperature. The apparatus was evacuated to 0.01 Torr. CF_3SCl (8.51 g, 62 mmol) was introduced via the gas inlet tube.

After vigorous stirring at 110°C (3 h) the formation of solid products was observed. After removing the solvent and the volatile reaction products, e.g. CF_3SSCF_3 (characterized by ^{19}F nmr and GC/MS) and N_2, formed by decomposition of $(CF_3SN)_x$, the product was sublimed at 40°C/10^{-3} Torr. Three-fold recrystallisation from CH_2Cl_2 affords analytically pure **I**. Yield: 0.40 g (6.2% based on C_5Cl_6). Subsequent sublimation at 22°C/10^{-3} Torr yields colorless single crystals suitable for X-ray diffraction studies.

(ii) By oxidation of CF_3SNH_2

In a two-necked 100-mL flask equipped with condenser a solution of CF_3SNH_2 (3.47 g, 29 mmol), dissolved in CH_2Cl_2 (10 mL) was added dropwise at 40°C (2 h) to a vigorously stirred suspension of $Pb(Ac)_4$ (7.78 g, 17 mmol) and C_5Cl_6 (3.9 g, 14 mmol) in CH_2Cl_2 (20 mL). Stirring was continued for 2 h at 40°C.

After evaporating solvent and volatile reaction products ($(CF_3S)_2NH$, CF_3SN=S=$NSCF_3$ identified by ^{19}F nmr and GS/MS) *in vacuo*, the

Can. J. Chem. Downloaded from www.nrcresearchpress.com by 186.148.149.217 on 09/07/12
For personal use only.

Can. J. Chem. Downloaded from www.nrcresearchpress.com by 186.148.149.217 on 09/07/12
For personal use only.

TABLE 3. Atomic co-ordinates for $C_5Cl_6NSCF_3$

Atom	X	Y	Z
C_1	0.10813 (52)	0.96991 (67)	0.26905 (34)
C_2	0.04443 (52)	0.12874 (67)	0.23384 (34)
C_3	0.08033 (54)	0.14948 (73)	0.14168 (34)
C_4	0.15290 (58)	0.02679 (74)	0.12359 (33)
C_5	0.18203 (52)	0.90189 (70)	0.19853 (35)
C_6	0.10536 (72)	0.74869 (102)	0.49394 (40)
Cl_1	−0.11715 (15)	0.10724 (22)	0.22464 (11)
Cl_2	0.09335 (16)	0.30470 (19)	0.30331 (10)
Cl_3	0.02888 (19)	0.31311 (22)	0.07408 (11)
Cl_4	0.21115 (19)	0.00529 (26)	0.02564 (10)
Cl_5	0.12956 (17)	0.69744 (20)	0.16316 (10)
Cl_6	0.34009 (15)	0.89568 (25)	0.24145 (12)
N	0.09940 (45)	0.91298 (60)	0.34628 (28)
S	0.16830 (18)	0.73884 (22)	0.38984 (10)
F_1	0.15040 (51)	0.61696 (62)	0.54261 (26)
F_2	−0.01320 (52)	0.74286 (77)	0.48112 (28)
F_3	0.14070 (53)	0.88512 (64)	0.50489 (24)

TABLE 4. Atomic co-ordinates for C_5Cl_6NSCl

Atom	X	Y	Z
C_1	0.26531 (37)	−0.16911 (37)	0.96408 (26)
C_2	0.26247 (40)	−0.26641 (38)	0.88932 (27)
C_3	0.22599 (41)	−0.39487 (39)	0.95130 (31)
C_4	0.21294 (42)	−0.38434 (37)	1.04652 (29)
C_5	0.23647 (38)	−0.22428 (37)	1.06563 (26)
Cl_1	0.28975 (17)	−0.10091 (14)	1.11672 (11)
Cl_2	0.13011 (17)	−0.18154 (14)	0.79228 (09)
Cl_3	0.43358 (14)	−0.31699 (14)	0.83627 (11)
Cl_4	0.20849 (16)	−0.53689 (13)	0.90044 (11)
Cl_5	0.17532 (15)	−0.50751 (13)	1.13988 (09)
Cl_6	0.38703 (13)	−0.27753 (13)	1.14930 (09)
Cl_7	0.08043 (12)	−0.14208 (12)	1.11581 (08)
N	0.29080 (36)	−0.04631 (31)	0.93675 (24)
S	0.31008 (14)	−0.09552 (11)	0.96765 (10)

residue was sublimed and purified as mentioned above. Yield: 0.27 g (5.4% based on C_5Cl_6).

Characterisation of **I**

Due to the large quadrupole moment of chlorine, the ^{13}C nmr spectra of the ring carbon atoms showed only broad singlets for all compounds.

^{13}C (ppm): 158.9 (C=N), 142.4 and 140.4 (C—Cl), 85.0 and 82.2 (CCl_2), 132.3 (q) (CF_3), $^1J_{CF}$ = 310 ± 1.9 Hz. ^{19}F (ppm): −51.6 (s). Melting point: 79°C. Infrared (cm^{-1}): 1648 (w), 1606 (m), 1211 (s), 1190 (s), 1178 (s), 1167 (s), 1118 (s), 839 (s), 818 (sh), 767 (w), 740 (m), 669 (m), 640 (m), 604 (m), 586 (vw), 503 (vw), 442 (w). Mass spectroscopy (*m/e*): 387 (M^+, 7), 352 (100), 317 (49), 248 (80), 69 (23). (CAUTION: It should be mentioned that sometimes explosions occur during mass spectroscopic examinations!) *Anal.* calcd. for $C_6Cl_6F_3NS$: C 18.6, N 3.6, S 8.3, Cl 54.8; found: C 18.6, N 3.6, S 8.3, Cl 54.9.

Reaction of ClSN with C_5Cl_6 to form **II**

In a 100-mL flask, equipped with condenser, $S_3N_3Cl_3$ (1.65 g, 20 mmol) was allowed to react at 110°C (3 h) with C_5Cl_6 (3.82 g, 14 mmol) in toluene (20 mL). The color of the reaction mixture turned from deep red to brown, and a brownish precipitate formed. After removing the solvent *in vacuo*, the residue was sublimed at 70°C/10^{-3} Torr. Recrystallisation from CH_2Cl_2 (4 times) gave analytically pure **II**. Yield: 1.9 g (38% based on C_5Cl_6). Pale yellow single crystals, suitable for X-ray structure analysis, were obtained by subsequent sublimation at 30°C/10^{-3} Torr.

Characterisation of C_5Cl_6NSCl

The compound slowly decomposes in d_6-acetone within 12 h.

^{13}C (ppm): 143.2 (C=N), 136.0 (C—Cl), 82.0 and 80.0 (CCl_2). ^{15}N (ppm): −81.0 (s). Melting point: 68°C. Infrared (cm^{-1}): 1646 (s), 1608 (s), 1205 (s), 1175 (m), 1155 (m), 1038 (m), 800 (vs), 693 (s), 636 (s), 590 (m), 582 (m), 451 (s). Mass spectroscopy (*m/e*): 355 (M^+, 12), 318 (100), 211 (40), 46 (8). *Anal.* calcd. for C_6Cl_7NS: C 17.0, N 4.0, S 9.1, Cl 70.0; found: C 17.1, N 3.9, S 9.2, Cl 69.8.

Reaction of FSN with C_5Cl_6

(i) at 20°C

In a sealed (Young valve) 50-mL glass pressure tube a mixture of C_5Cl_6 (2.73 g, 10 mmol) and FSN (1.30 g, 20 mmol) in SO_2 (14 g) was stirred for 2 days at 20°C.

Solvent and volatile reaction products were removed *in vacuo*. Sublimation of the residue at 70°C/10^{-3} Torr gave analytically pure **II**. Yield: 0.72 (20.3%). Melting point: 68°C.

(ii) at 75°C

In a 50-mL stainless steel autoclave equipped with a magnetic stirring bar FSN (0.90 g, 13.8 mmol) and SO_2 (10 g) were condensed *in vacuo* onto C_5Cl_6 (1.87 g, 6.9 mmol). The reaction mixture was vigorously stirred at 75°C for 48 h. Solvent and volatile reaction products (SOF_2) were removed *in vacuo*, leaving a red viscous oil. Sublimation at 60°C/10^{-3} Torr produced yellow crystals of analytically pure C_5Cl_6NSNSO. Yield: 0.68 g (25.9%).

Characterisation of C_5Cl_6NSNSO

^{13}C (ppm): 151.7 (C=N), 141.5 (CCl), 83.8 (CCl_2). ^{14}N (ppm): −36 (NSO), −84 (C=N). Melting point: 96°C. Infrared (cm^{-1}): 1629 (s), 1598 (s), 1214 (s), 1186 (vs), 1161 (s), 1020 (m), 985 (m), 841 (sh), 815 (vs), 750 (s), 676 (m), 659 (m), 639 (s), 601 (s), 585 (sh), 539 (w), 485 (vw). Mass spectroscopy (*m/e*): 380 (M^+, 5), 345 (25), 262 (21), 46 (100). *Anal.* calcd. for $C_5Cl_6N_2OS$: C 15.8, N 7.4, S 16.8, Cl 55.8; found: C 15.7, N 7.3, S 16.9, Cl 55.5.

Reactions of C_5Cl_6NSCl

(i) with $Hg(NSO)_2$

To a mixture of $Hg(NSO)_2$ (0.90 g, 2.8 mmol) in acetonitrile (40 mL) C_5Cl_6NSCl (0.98 g, 2.8 mmol) was added and stirred at 20°C. Reaction ceased after 10 h. After removing solvent the residue obtained was treated with dry pentane to dissolve the product. The suspension was filtered and the filtrate was evaporated to dryness *in vacuo*. Yield: 0.87 g (82%). From the residue yellow crystals of C_5Cl_6NSNSO were obtained by vacuum sublimation at 60°C/10^{-3} Torr.

(ii) with $SbCl_5$ in SO_2

In a typical reaction C_5Cl_6NSCl (0.49 g, 1.4 mmol) dissolved in SO_2 (19 g) was loaded into a Pyrex two-bulb reaction vessel (60 mL) as described previously equipped with a medium-sintered glass fritt, magnetic stirring bar, and J. Young valves. Both components were frozen at liquid nitrogen temperature and $SbCl_5$ (0.47 g, 1.6 mmol) was condensed *in vacuo* onto the mixture, forming a deep blue colored ring at the surface of the two phases. When the mixture was warmed to 20°C, precipitation of a solid takes place and the solution turns red. The soluble products were separated by filtration through the frit into the second bulb, and the white insoluble solid was washed several times with the solvent. Recrystallisation in CH_2Cl_2 yielded white needles of analytically pure $C_5Cl_6NSNC_5Cl_6$. Yield: 0.26 g (62.2% based on **II**).

(iii) with $Hg(SCF_3)_2$

C_5Cl_6NSCl (150 mg, 0.42 mmol) was treated during 48 h at 20°C with $Hg(SCF_3)_2$ (170 mg, 0.42 mmol) in CH_2Cl_2 (20 mL) in a 50-mL Schlenk tube sealed with a Young valve. Fine colorless needles of solid $HgCl_2$ form, the solution was filtered and the filtrate evaporated to dryness. Sublimation of the residue at 22°C/10^{-3} Torr yielded colorless crystals of analytically pure $C_5Cl_6NSSCF_3$. Yield: 0.152 g (86%).

Characterisation of $C_5Cl_6NSNC_5Cl_6$

Since the material showed only poor solubility in organic solvents, no ^{13}C nmr spectra could be obtained. Melting point: 263°C. Infrared (cm^{-1}): 1627 (s), 1598 (s), 1212 (vs), 1178 (m), 1158 (m), 982 (m), 841 (s), 813 (vs), 775 (s), 764 (s), 751 (sh), 731 (m), 725 (sh), 671 (s),

640 (s), 600 (s), 584 (m), 456 (w), 444 (w). Mass spectroscopy (m/e): 604 (M^+, 0.2), 569 (3.2), 318 (5.8), 248 (5.7), S_2 (100). *Anal.* calcd. for $C_{10}Cl_{12}N_2S$: C 19.8, N 4.6, S 5.3, Cl 70.2; found: C 19.7, N 4.6, S 5.4, Cl 69.9.

Characterisation of $C_5Cl_6NSSCF_3$

^{13}C (ppm): 154.9 (C=N), 137.1 (CCl), 79.0 (CCl_2), 129.2 (q) (CF_3), $^1J_{CF} = 315 \pm 0.2$ Hz. ^{19}F (ppm): −45.7 (s). Melting point: 76°C. Infrared (cm^{-1}): 1635 (m), 1603 (s), 1314 (w), 1296 (w), 1212 (s), 1170 (s), 1155 (s), 1102 (s), 983 (m), 817 (s), 753 (m), 739 (m), 693 (m), 638 (s), 602 (s), 586 (m), 451 (m). Mass spectroscopy (m/e): 419 (M^+, 24), 384 (100), 318 (10), 251 (58), 69 (68). *Anal.* calcd. for $C_5Cl_6F_3NS_2$: C 17.2, N 3.3, S 15.3, Cl 50.7; found: C 17.2, N 3.5, S 15.2, Cl 51.0.

Reaction of FSN with C_5F_6

FSN (100 mg, 1.5 mmol) and C_5F_6 (261 mg, 1.5 mmol) were condensed into a thick-walled 10-mm nmr tube sealed with a Young valve and frozen at liquid N_2 temperature together with $CFCl_3$ (3 g) as solvent. The reaction was followed by ^{19}F nmr spectroscopy. Immediately after warming up to 20°C the yellow solution turned red, forming an insoluble black precipitate. SOF_2, S_4N_4 (20 mg), and S_8 (12 mg) were isolated and characterised by infrared-, mass-, and ^{19}F nmr spectroscopy.

Acknowledgements

The authors thank Dr. W. Gebert of the Department of Geology of the Ruhr-Universität Bochum for the X-ray diffraction analysis, Professor Dr. F. Aubke for helpful discussions and the Minister für Wissenschaft und Forschung of North Rhine Westphalia for financial support.

1. O. Glemser and H. Richert. Z. Anorg. Allg. Chem. **307**, 313 (1961).
2. O. Glemser and H. Perl. Naturwissenschaften, **48**, 620 (1961).
3. S. C. Peake and H. J. Downs. J. Chem. Soc. Dalton Trans. 859 (1974).
4. P. O. Tchir and R. D. Spratley. Can. J. Chem. **53**, 2318 (1975).
5. H. J. Emeléus and R. J. Poulet. J. Fluorine Chem. **1**, 13 (1971/72).
6. A. Haas and C. Klare. Chem. Ber. **118**, 4588 (1985).
7. R. Hoppenheit and R. Mews. Chem. Ber. **118**, 4276 (1985).
8. A. Haas and R. Walz. Chem. Ber. **118**, 3248 (1985).
9. D. Bielefeldt and A. Haas. Chem. Ber. **116**, 1257 (1983).
10. R. Mews and C. Liu. Angew. Chem. **95**, 156 (1983).
11. G. Hartmann and R. Mews. Z. Naturforsch. **40B**, 343 (1985).
12. A. Haas and T. Mischo. Chimia, **41**, 344 (1987).
13. J. March. *In* Advanced organic chemistry. 3rd ed. Wiley, New York. 1985.
14. R. L. Patton and W. L. Jolly. Inorg. Chem. **9**, 1079 (1970).
15. W. Bludßus and R. Mews. J. Chem. Soc. Chem. Commun. **35** (1979).
16. W. Bludßus and R. Mews. Chem. Ber. **114**, 1539 (1981).
17. F. Seel, W. Gombler, and R. Budenz. Z. Naturforsch. **27B**, 78 (1972).
18. J. Vorwig, H. Steinbeisser, R. Mews, and O. Glemser. Z. Naturforsch. **29B**, 813 (1974); O. Glemser, R. Mews, and H. W. Roesky. Chem. Ber. **102**, 1523 (1969).
19. T. Mischo. Diplomarbeit, Bochum. 1985.
20. G. M. Sheldrick. SHELXTL-81, Program for Crystal Structure Determination. University Chemical Laboratory Cambridge, England. 1981.
21. C. K. Johnson. ORTEP-II, Report ORNL – 5138, Oak Ridge, National Laboratory, Tennessee. 1976.
22. H. G. Heal, M. S. Shahid, and H. Garcia-Fernandez. J. Inorg. Nucl. Chem. **35**, 1693 (1973).
23. F. Aubke, A. Haas, C. Klare, and P. Betz. To be published.
24. R. J. Gillespie. *In* Molekülgeometrie. Verlag Chemie, Weinheim. 1975.
25. H. R. Kricheldorf. Synthesis, 551 (1972).
26. C. W. Tullock and D. D. Coffman. J. Org. Chem. **25**, 2016 (1960).
27. H. J. Emeléus and S. N. Nabi. J. Chem. Soc. 1103 (1960).
28. W. L. Jolly and K. D. Maguire. Inorg. Synth. **9**, 107 (1967).
29. A. Haas and M. Rieland. Chimia, **42**, 67 (1988).
30. W. Verbeek and W. Sundermeyer. Angew. Chem. **81**, 330 (1969).
31. E. H. Man, D. D. Coffman, and E. L. Mutterties. J. Am. Chem. Soc. **81**, 3575 (1959).
32. G. Paprott, S. Lehmann, and K. Seppelt. Chem. Ber. **121**, 727 (1988).
33. I. L. Knunyants, Y. F. Komissarav, B. L. Dyatkin, and L. T. Lantseva. Izv. Akad. Nauk. SSR, Ser. Skim. **4**, 943 (1973).
34. I. Ruppert, K. Scheich, and W. Volbach. Tetrahedron Lett. **25**, 2195 (1984).

Can. J. Chem. Downloaded from www.nrcresearchpress.com by 186.148.149.217 on 09/07/12
For personal use only.

Phosphorus-31 NMR studies of several phosphines in the solid state

GLENN H. PENNER[1] AND RODERICK E. WASYLISHEN[2]
Department of Chemistry, Dalhousie University, Halifax, N.S., Canada B3H 4J3

Received March 29, 1989

This paper is dedicated to Professor Ronald J. Gillespie on the occasion of his 65th birthday

GLENN H. PENNER and RODERICK E. WASYLISHEN. Can. J. Chem. **67**, 1909 (1989).

Phosphorus-31 NMR powder spectra and high resolution MAS spectra have been obtained for a number of solid phosphines under conditions of high-power proton decoupling and cross-polarization. The principal components of the ^{31}P chemical shift tensor obtained from static powder spectra or slow MAS spectra are discussed in terms of the known structures of many of the phosphines. The CP/MAS ^{31}P NMR spectra are used to determine the number of crystallographically nonequivalent molecules in the unit cell. The NMR results are consistent with data available from X-ray diffraction. In one case there is evidence of polymorphism.

Key words: ^{31}P NMR of solid phosphines, principal components of ^{31}P chemical shift tensors, crystallographic nonequivalence from ^{31}P CP/MAS NMR.

GLENN H. PENNER et RODERICK E. WASYLISHEN. Can. J. Chem. **67**, 1909 (1989).

Opérant dans des conditions de découplage des protons et de polarisation croisée à haute puissance, on a examiné les spectres RMN de poudre du ^{31}P ainsi que les spectres MAS à haute résolution d'un certain nombre de phosphines solides. On discute de la nature des composantes principales du tenseur du déplacement chimique du ^{31}P et des spectres lents de MAS en fonction des structures bien connues de plusieurs de ces phosphines. On a utilisé les spectres RMN CP/MAS du ^{31}P pour déterminer le nombre de molécules non-équivalentes d'un point de vue cristallographique présentent dans la maille. Les résultats de la RMN sont en accord avec les données disponibles à partir de la diffraction des rayons-X. Dans un cas, on a des connées permettant de confirmer l'existence d'un polymorphisme.

Mots clés : RMN du ^{31}P de phosphines solides, composantes principales des tenseurs du déplacement chimique du ^{31}P, non-équivalence cristallographique à partir des spectres rmn CP/MAS du ^{31}P.

[Traduit par la revue]

Introduction

Phosphorus-31 NMR is one of the most important tools available for characterizing the structure and conformation of organophosphorus compounds (1, 2). Numerous studies have been carried out to examine the influence of electronic and molecular structure on ^{31}P chemical shifts (3–6). Although empirical rules are available for predicting isotropic chemical shifts in a series of closely related compounds such as phosphines (3, 5, 6), our understanding of the physical basis of these rules is lacking (7). The status of theoretical calculations of ^{31}P chemical shifts has recently been reviewed by Chesnut (7). There are few *ab initio* calculations of ^{31}P chemical shifts and most of the calculations have been restricted to phosphine, PH_3 (7). Recent calculations by Fleischer *et al.* (8) indicate that large basis sets including *d* functions are essential for accurate calculations of ^{31}P shift tensors. The implication is that it may be several years before reliable molecular orbital calculations of ^{31}P chemical shifts are available for organophosphines of the type investigated in this study.

A first step in improving our understanding of ^{31}P chemical shifts is to study the variation of the principal components of the chemical shift tensor, δ_{ii} ($i = 1-3$) with molecular structure. In principle, the diagonal components of the shift tensor should be more informative than the trace or isotropic shift, $\delta_{iso} = (\delta_{11} + \delta_{22} + \delta_{33})/3$. For example, there are cases where a change in molecular structure may lead to a small or negligible change in δ_{iso} while the individual principal components of the shift tensor may exhibit substantial variations in opposing directions (10).[3]

The principal components of the shift tensor, δ_{ii} ($i = 1-3$), can be obtained by studying the compound of interest in a liquid crystal system (11), from static (non-spinning) powder spectra (11–14), or from an analysis of the spectra obtained under conditions of slow MAS (15, 16). If large single crystals are available, both the principal components and their orientation in the molecular frame can be established from single crystal NMR studies (17). In this study we have measured the principal components of the ^{31}P shift tensor of a number of tertiary phosphines from static powder spectra and slow MAS spectra. As well, we have carried out MAS studies on these compounds to obtain information regarding the number of crystallographically nonequivalent molecules in the unit cell (18).

To our knowledge only a few, mostly unusual, phosphines have been studied previously by solid state ^{31}P NMR (19–22).

Experimental

All compounds were commercially available. Phosphorus-31 NMR spectra were obtained at 80.962 MHz using a Bruker MSL-200 (B_0 = 4.7 T). Powder samples (0.3 g) were packed into aluminum oxide rotors. Spectra were recorded at 21°C with high-power proton decoupling and cross-polarization using the Hartman–Hahn match. Contact and recycle times ranged from 2 to 5 ms and from 10 to 30 s, respectively.

Static spectra had acquisition times of 41–102 ms, and sensitivity enhancements corresponding to 50–100 Hz line broadening were applied before Fourier transformation.

Magic angle spinning spectra were obtained with acquisition times of 102–205 ms. Typically the MAS spinning rate was 3 kHz. The FID's were zero filled to twice their original size and the signal-to-noise was enhanced with 5–10 Hz line broadening before Fourier transformation.

Chemical shifts were referenced with respect to the ^{31}P NMR signal of external $NH_4H_2PO_4$, which has a shift of 1.00 ppm with respect to 85% H_3PO_4.

---

[1]Present address: Department of Chemistry and Biochemistry, University of Guelph, Ont., Canada N1G 2W1.

[2]Author to whom correspondence may be addressed.

[3]Also, G. H. Penner, W. P. Power, and R. E. Wasylishen, Unpublished results.

Can. J. Chem. Downloaded from www.nrcresearchpress.com by 194.225.253.170 on 09/07/12
For personal use only.

TABLE 1. Phosphosus chemical shift parameters and crystallographic data for several phosphines in the solid state[a]

Compound	R^1	R^2	R^3	δ_{11}	δ_{22}	δ_{33}	$\Delta\delta$	η^b	δ_{iso}	Space group	Z	N	Ref.
1	Phenyl	Phenyl	Phenyl	9.0	9.0	−42.0	51.0	0.0	−10.3	$P2_1/a$	4	1	24
2	*p*-Methoxyphenyl	*p*-Methoxyphenyl	*p*-Methoxyphenyl	2.0	−2.4	−39.0	41.0	0.18	−14.5	$P2_1/c$	4	1	26
3	*p*-Tolyl	*p*-Tolyl	*p*-Tolyl	2.0	2.0	−35.0	37.0	0.0	−10.4	$R\bar{3}$	6	1	27
4	*m*-Tolyl	*m*-Tolyl	*m*-Tolyl	11.0	1.5	−31.5	42.5	0.39	−7.0	$Pbca$	8	1	28
5	*o*-Tolyl	*o*-Tolyl	*o*-Tolyl	—	—	—	<15	—	−31.5	$P\bar{1}$	4	2	29
				—	—	—	<15	—	−35.5				
6	Mesityl	Mesityl	Mesityl	—	—	—	<10	—	−34.8	$P\bar{1}$	4	2	30
				—	—	—	<10	—	−35.7				
				—	—	—	<10	—	−38.0	—	—	—	
				—	—	—	<10	—	−38.0				
7	Phenyl	Phenyl	*o*-Tolyl	15.0	−28.0	−37.5	52.5	0.29	−17.4	—	—	—	
8	Phenyl	Phenyl	*o*-Methoxyphenyl[c]	15	−15	−35	50	—	−16.5	—	—	—	
								—	−13.5				
9	Phenyl	Cyclohexyl	Cyclohexyl	38.0	3.0	−31.5	69.5	0.98	2.9	—	—	—	
10	Cyclohexyl	Cyclohexyl	Cyclohexyl	34.5	17.5	−30.0	64.5	0.46	7.0	—	—	—	
11	Phenyl	Phenyl	Isopropyl	26.4	6.2	−41.2	67.6	0.52	−2.6	—	—	—	
12	CH_2CH_2CN	CH_2CH_2CN	CH_2CH_2CN[d]	−11	−39	−53	42	0.58	−35.1	$P2_1/m$	2	1	32, 33
13	1,2,5-Triphenylphosphole			29.5	−6.0	−21.5	51.0	0.54	1.0	$P2_1$	2	1	34

[a]Estimated errors in δ_{11}, δ_{22}, δ_{33}, and $\Delta\delta$ are ~1 ppm; errors in δ_{iso} are 0.1 ppm unless otherwise stated. The errors in δ_{ii} are determined by the magnitude of the intermolecular ^{31}P,^{31}P dipolar coupling,which causes the broadening of the shoulders and the discontinuities in the static powder spectra (9, 31).

[b]Following ref. 14 the asymmetry parameter is defined $\eta = (\delta_{yy} - \delta_{xx})/(\delta_{zz} - \delta_{iso})$ where the axes are labelled so that $|\delta_{zz} - \delta_{iso}| \geq |\delta_{xx} - \delta_{iso}| \geq |\delta_{yy} - \delta_{iso}|$. Note that δ_{xx}, δ_{yy}, and δ_{zz} are the principal components of the chemical shift tensor given above.

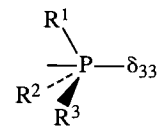
[c]Estimated errors in δ_{11}, δ_{22}, δ_{33}, and $\Delta\delta$ are ~5 ppm.

[d]Estimated errors in δ_{11}, δ_{22}, δ_{33}, and $\Delta\delta$ are ~2 ppm.

Results and discussion

The results of this study together with available crystallographic information are summarized in Table 1. The chemical shift anisotropy is simply defined as $\delta_{11} - \delta_{33}$; this provides a direct measure of the maximum width of the spectrum. More elegant definitions can be found elsewhere (13, 14). The asymmetry parameter, η, will be defined following the convention of Haeberlen (14); it is restricted to values between 0 (axial symmetry) and 1. A few general conclusions may be obtained upon examination of Table 1. First, the number of ^{31}P resonances observed in each CP/MAS spectrum agrees with the number of crystallographically nonequivalent phosphorus nuclei, N, predicted from X-ray diffraction results. Second, the chemical shift anisotropy, $\Delta\delta$, for the phosphines relative to other phosphanes (23) follows the order $\Delta\delta$ (phosphine oxides) > $\Delta\delta$ (phosphine sulphides) > $\Delta\delta$ (phosphine selenides) > $\Delta\delta$ (phosphines). Interesting exceptions to this trend are phosphirenes and phosphiranes (20, 21), three-membered cyclic systems consisting of one phosphorus and two carbon atoms. In these systems the $\Delta\delta$ values are about an order of magnitude greater than those reported here for unstrained phosphines. Third, the effects of conjugative interactions between the phosphorus lone pair and the π-systems of the phenyl rings do not seem to dominate the variation in chemical shift tensor components. Rather, overall molecular structure, in particular the conformation of the substituents, R, appears to have a greater effect. It should also be noted that the variation in δ_{33} for the phenyl and alkyl phosphines, **1–11**, is significantly smaller (by a factor of over 3) than for components δ_{11} and δ_{22}.

In this study δ_{33}, the most shielded component of the chemical shift tensor, is taken to lie along the C_3 (or pseudo C_3) axis (**14**). The orientation of δ_{11} and δ_{22}, which lie in planes perpendicular to δ_{33}, is ambiguous. When there is threefold symmetry at the phosphorus, δ_{11} and δ_{22} are degenerate, and "axially symmetric" ($\eta = 0$) powder spectra are expected.



14

Although the symmetry at the phosphorus in solid triphenylphosphine, **1**, is not C_3 (24), the ^{31}P NMR powder spectrum is consistent with an axially symmetric chemical shift tensor. There are a number of possible reasons for this: the degeneracy of δ_{11} and δ_{22} is accidental, the difference between δ_{11} and δ_{22} is below the resolution of the experiment, or δ_{11} and δ_{22} are averaged by large-amplitude motion of the phenyl rings (25).

The molecular structure of solid tris(*p*-methoxyphenyl)-phosphine, **2**, (26) has the ring planes at angles of 48°, 31°, and 46° from the pseudo C_3 axis. Therefore asymmetry in the ^{31}P shielding tensor is expected and, indeed, an η value of 0.18 is measured.

The crystal structure of tris(*p*-tolyl)-phosphine, **3** (27), shows threefold symmetry about the phosphorus and the expected axially symmetric powder spectrum is observed, as indicated in Fig. 1a.

A significant deviation from axial symmetry is observed in the powder spectrum of tris(*m*-tolyl)-phosphine, **4**. The molecular structure of crystalline **4** (28) has two of the methyl groups on the same side of the molecule as the phosphorus lone pair (*exo*) and one on the other side (*endo*). Such a conformation allows the chemical shift tensor to deviate from axial symmetry (see Fig. 1b).

The static and CP/MAS ^{31}P spectra of tris(*o*-tolyl)-phosphine, **5**, exhibit several interesting features. Two resonances are observed in the CP/MAS spectrum of solid **5**. This is consistent with the reported X-ray crystal structure (29), which indicates that there are two types of molecules in the unit cell. The separation between the two resonances is 5.5 ppm. A

Can. J. Chem. Downloaded from www.nrcresearchpress.com by 194.225.253.170 on 09/07/12
For personal use only.

Can. J. Chem. Downloaded from www.nrcresearchpress.com by 194.225.253.170 on 09/07/12
For personal use only.

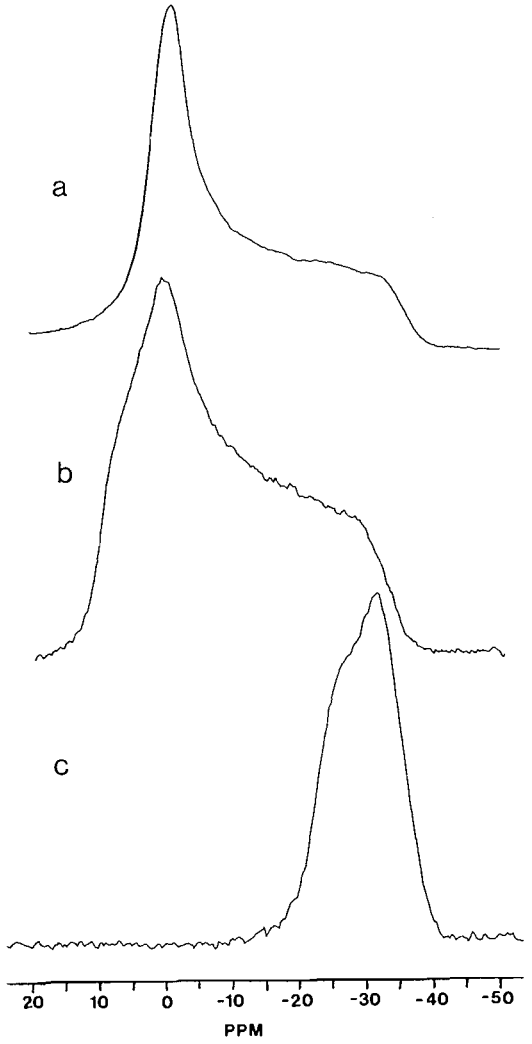


FIG. 1. Static ^{31}P NMR spectra of (a) *p*-tolyl, (b) *m*-tolyl, and (c) *o*-tolyl phosphine.

second interesting feature is the small chemical shift anisotropy, $\Delta\delta$, of the powder spectra (Fig. 1c). Although the static powder spectra for the two types of ^{31}P cannot be resolved, an upper limit of 15 ppm can be placed on their $\Delta\delta$ values. Some information on the individual shielding tensors can be obtained from slow MAS experiments. A spectrum obtained with magic angle sample spinning at 310 Hz allows the centre and spinning side bands of the two resonances to be separated while still maintaining some information on the shift tensor. Even at a MAS rate of only 310 Hz the spinning side bands are of such low intensity relative to the centre band that a reliable analysis using the Herzfeld–Berger (15) or related methods is not possible. What the experienced eye can discern from the slow MAS spectrum is that the higher frequency ^{31}P resonance has associated with it a shielding tensor of significantly higher asymmetry. An X-ray investigation of **5** shows that the major difference between the structures of the two independent molecules is in the torsion angles made by the phenyl rings with the pseudo C_3 axes. One molecule has angles of 46.8°, 40.7°, and 45.6°; the other has 36.7°, 49.0°, and 43.1°. In other words the latter molecule deviates most from C_3 symmetry and one may tentatively assign the high frequency resonance to this molecule. Obviously single crystal ^{31}P NMR measurements will be necessary to assign the ^{31}P resonances of **5**.

The CP/MAS spectrum of commercially available trimesitylphosphine, **6**, displays three resonances, which we assign as due to two closely spaced pairs (Fig. 2a). This is inconsistent with the X-ray crystal structure (30), which indicates that there are two nonequivalent molecules per unit cell. Recrystallization of **6** from chloroform/ethanol following the procedure used to prepare a single crystal for X-ray studies yielded a ^{31}P CP/MAS spectrum in which the intensity of the low frequency pair was greatly diminished (see Fig. 2b). The commercial sample was obtained by recrystallization from toluene/ethanol.[4] These results suggest that a recrystallization from toluene/ethanol yields two morphological forms of crystalline **6** in approximately equal proportions, whereas recrystallization from chloroform/ethanol yields mostly the polymorph responsible for the high frequency pair of resonances. The polymorph responsible for the high frequency resonances, and for which a crystal structure is available, will be referred to as **6*a***; the other modification, responsible for the low frequency peaks, will be referred to as **6*b***.

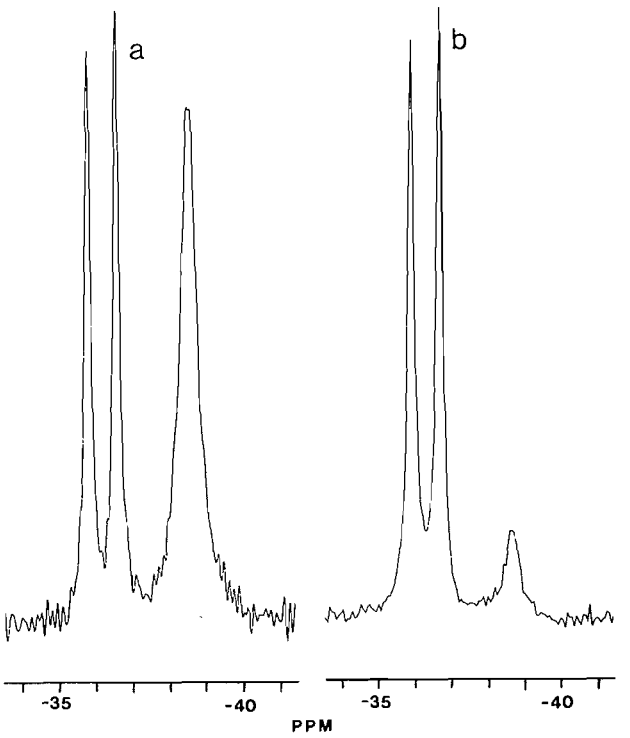


FIG. 2. MAS ^{31}P NMR spectra of trimesitylphosphine: (a) commercial sample; (b) after recrystallization from $CHCl_3$/EtOH. Only a single ^{31}P NMR resonance was observed for samples a and b in solution.

Crystalline **5** and **6*a*** are isomorphous (29, 30). The peak separations in **6*a*** and **6*b*** are 0.8 ppm and ca. 0.1 ppm (estimated from linewidth), respectively (see Fig. 2). The spectra of **6*a*** and **6*b*** share some common features with that of **5**. The rather low frequency chemical shifts of **6*a***, and **6*b***, and **5** as well as the unusually small chemical shift anisotropies are due to a large low frequency (high field) shift of the chemical shift tensor components δ_{11} and δ_{22}. The major differences in the molecular of **5** and **6** are the presence of methyl groups at the 4 and 6 positions of the phenyl rings in **6** and larger CPC bond angles for **6**. The similarities between the spectra of **5** and **6** suggest that it is the presence of the methyl groups in the *exo* position that is the major contributor towards the large low frequency shifts of δ_{11} and δ_{22}.

[4]Organometallics Inc., E. Hampstead, NH 08326, U.S.A. Private communication.

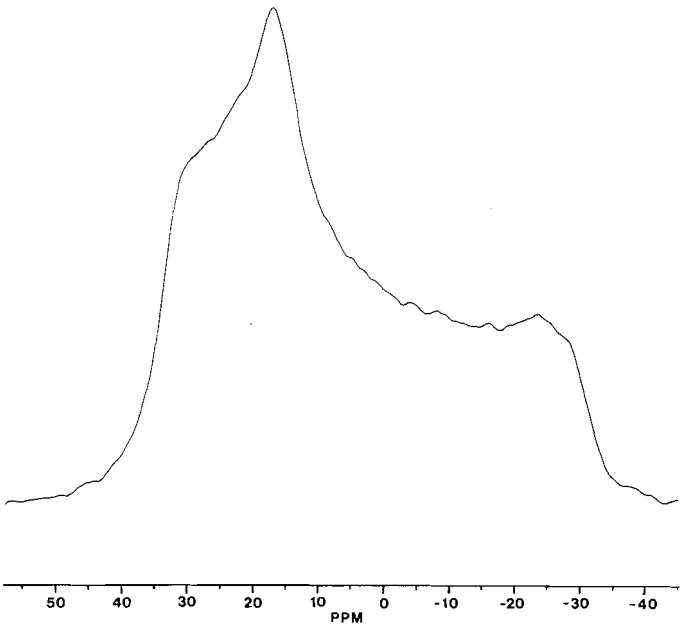


FIG. 3. Static ^{31}P NMR spectrum of tricyclohexylphosphine.

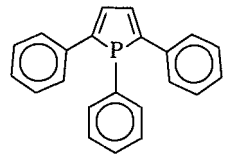
Having established the dominant contribution to the low frequency shift of δ_{11} and δ_{22} in *o*-tolylphosphine derivatives, it can be suggested that the larger low frequency shift of δ_{22} (or δ_{11}, assignment is arbitrary) in diphenyl-*o*-tolylphosphine, **7**, is due to the *o*-tolyl substituent being oriented in such a way that the *ortho* methyl group is on the same side of the molecule as the phosphorus lone pair. A crystal structure of **7** is not available in the literature.

The CP / MAS spectrum of diphenyl-2-methoxyphenylphosphine, **8**, consists of two resonances; both are broader than those for the other phosphines. The large linewidths may be a relaxation phenomenon or may be due to the presence of four, not two, nonequivalent molecules per crystal unit cell.

A common feature of the static powder spectra of compounds **9**, **10**, and **11** is the high frequency shift of δ_{11}. These three molecules have one or more alkyl substituents on the phosphorus. The asymmetries for **9** and **11** are rather large, as expected for unsymmetrically substituted phosphines. Tricyclohexylphosphine, **10**, is symmetrically substituted but, as shown in Fig. 3, the asymmetry of the chemical shift tensor is large, indicating a large deviation from C_3 symmetry in the molecule. Unfortunately an X-ray structure is not available for **10**.

X-ray studies of tri(2-cyanoethyl)phosphine, **12**, at 100 K (32) and 298 K (33) indicate a mirror plane through the molecule. The plane is defined by the heavy atoms of one of the CH_2CH_2CN substituents. The molecule is significantly distorted from C_3 symmetry; therefore a nonzero η is expected and indeed the ^{31}P powder spectrum indicates an η value of 0.64. All components of the chemical shift tensor are to lower frequency of those expected although the anisotropy, $\Delta\delta$, is typical of a phosphine. The symmetry of crystalline **12** suggests that one component of the chemcal shift tensor (δ_{33}) is along the phosphorus lone pair, another is in the mirror plane oriented at 90° to δ_{33}, and the third component is oriented perpendicular to the mirror plane. The exact assignment of the last two components to δ_{11} or δ_{22} cannot be made at present.

An X-ray diffraction investigation of the molecular structure of 1,2,5-triphenylphosphole, **13**, was undertaken by Ozbirn *et al.* (34) to assess the possibility of electron delocalization within



13

the phosphole ring. They concluded that "all the structural evidence indicates that the heterocyclic ring exhibits little if any electron delocalization." The chemical shift tensor components and the anisotropy for **13** are typical of a phosphine and provide no evidence for delocalization. Phosphine oxides, sulfides, and selenides, which exhibit resonance structure of the form $R_3P{=}X \rightleftharpoons R_3P^+{-}X^-$ (23), have ^{31}P chemical shift anisotropies in the ranges 150–200, 80–180, and 80–150 ppm, respectively. The ^{31}P NMR powder spectrum of 1,2-bis(2,4,6-tri-*tert*-butylphenyl)diphosphene (22), a system containing a formal P=P double bond, shows an exceptionally large shift anisotropy of 1239 ppm. Based on these observations, a larger value for $\Delta\delta$ would be expected if there were any significant delocalization in **13**.

Summary

The number of crystallographically nonequivalent phosphorus atoms in each solid phosphine is reflected by the number of resonances observed in the ^{31}P CP / MAS spectrum. The possibility of delocalization between the phosphorus lone pair and the ring π system is phenylphosphines does not have a significant effect on the principal components of the ^{31}P shielding tensor; rather, conformational effects dominate. One such conformational effect is the orientation of *o*-tolyl substituents with respect to the approximate C_3 axis at the phosphorus. The molecular symmetry about the phosphorus in the solid state is reflected by the symmetry of the ^{31}P powder spectrum. In general, the greater the deviation from C_3 symmetry, the larger the asymmetry, η, of the chemical shift tensor.

Finally, the principal components of the ^{31}P shielding tensor in solid 1,2,5-triphenylphosphole provide no evidence for electron delocalization in the heterocyclic five-membered ring.

Acknowledgements

We wish to thank Professor H. C. Clark and his group for supplying us with commercial samples of several phosphines and Professor E. Alyea for the commercial sample of trimesitylphosphine. We are grateful to Ron Curtis and Brian Millier for their assistance in maintaining the NMR spectrometer, and Bill Power and Professor O. Knop for several helpful suggestions. We thank Organometallics for information about compound **6**. The financial assistance of NSERC is gratefully acknowledged. G.H.P. acknowledges the award of a Killam postdoctoral fellowship by Dalhousie University.

1. D. G. GORENSTEIN (*Editor*). Phosphorus-31 NMR — Principles and applications. Academic Press, Orlando, FL. 1984.
2. J. G. VERKADE and L. D. QUIN (*Editor*). Phosphorus-31 NMR spectroscopy in stereochemical analysis. VCH Publishers, Deerfield Beach, FL. 1987.
3. D. G. GORENSTEIN. *In* Phosphorus-31 NMR — Principles and applications. *Edited by* D. G. Gorenstein. Academic Press, Orlando, FL. 1984. p. 7.
4. J. C. TEBBY. *In* Phosphorus-31 NMR spectroscopy in stereochemical analysis. *Edited by* J. G. Verkade and L. D. Quin. VCH Publishers, Deerfield Beach, FL. 1987. p. 1.

Can. J. Chem. Downloaded from www.nrcresearchpress.com by 194.225.253.170 on 09/07/12
For personal use only.

5. E. FLUCK and G. HECKMANN. *In* Phosphorus-31 NMR spectroscopy in stereochemical analysis. *Edited by* J. G. Verkade and L. D. Quin. VCH Publishers, Deerfield Beach, FL. 1987. p. 61.
6. K. R. DIXON. *In* Multinuclear NMR. *Edited by* J. Mason. Plenum Press, New York. 1987. p. 369.
7. D. B. CHESNUT. *In* Phosphorus-31 NMR spectroscopy in stereochemical analysis. *Edited by* J. G. Verkade and L. D. Quin. VCH Publishers, Deerfield Beach, FL. 1987. p. 185.
8. U. FLEISCHER, M. SCHINDLER, and W. KUTZELNIGG. J. Chem. Phys., **86**, 6337 (1987).
9. R. DIETRICH and L. TRAHMS. J. Magn. Reson. **71**, 337 (1987).
10. P. D. ELLIS. Science, **221**, 1141 (1983).
11. J. B. ROBERT and L. WIESENFELD. *In* Phosphorus-31 NMR spectroscopy in stereochemical analysis. *Edited by* J. G. Verkade and L. D. Quin. VCH Publishers, Deerfield Beach, FL. 1987. p. 151.
12. C. A. FYFE. Solid state NMR for chemists. C.F.C. Press, Guelph, Ontario. 1983.
13. M. MEHRING. High resolution NMR in solids. 2nd ed. Springer-Verlag, New York. 1983.
14. U. HAEBERLEN. *In* Advances in magnetic resonance — Supplement 1. *Edited by* J. S. Waugh. Academic Press, New York. 1976.
15. J. HERZFELD and A. E. BERGER. J. Chem. Phys. **73**, 6021 (1980).
16. N. J. CLAYDEN, C. M. DOBSON, L.-Y. LIAN, and D. J. SMITH. J. Magn. Reson. **69**, 476 (1986).
17. A. NAITO, D. L. SASTRY, and C. A. MCDOWELL. Chem. Phys. Lett. **115**, 19 (1985).
18. R. K. HARRIS, L. H. MERWIN, and G. HÄGELE. J. Chem. Soc. Faraday Trans. 1, **83**, 1055 (1987).
19. L. BEMI, H. C. CLARK, J. A. DAVIES, C. A. FYFE, and R. E. WASYLISHEN. J. Am. Chem. Soc. **104**, 438 (1982).
20. A. L. BARRA and J. B. ROBERT. Chem. Phys. Lett. **136**, 224 (1987).
21. A. L. BARRA and J. B. ROBERT. Chem. Phys. Lett. **149**, 363 (1988).
22. K. W. ZILM, G. G. WEBB, A. H. COWLEY, M. PAKULSKI, and A. ORENDT. J. Am. Chem. Soc. **110**, 2032 (1988).
23. J. B. ROBERT and L. WIESENFELD. Mol. Phys. **44**, 319 (1981).
24. J. J. DALY. J. Chem. Soc. 3799 (1964).
25. J. D. DUNITZ, E. F. MAVERICK, and K. N. TRUEBLOOD. Angew. Chem. Int. Ed. Engl. **27**, 880 (1988).
26. T. ALLMAN, R. G. GOEL, and A. L. BEAUCHAMP. Acta Crystallogr. Sect. C: Cryst. Struct. Commun. **C42**, 603 (1986).
27. A. N. SOBOLEV, V. K. BEL'SKII, I. P. ROMM, and E. N. GUR'YANOVA. Zh. Strukt. Khim. **24**, 123, (1983).
28. T. S. CAMERON, K. D. HOWLETT, and K. MILLER. Acta Crystollogr. Sect. B: Struct. Crystallogr. Cryst. Chem. **34**, 1639 (1978).
29. T. S. CAMERON and B. DAHLÈN. J. Chem. Soc. Perkin Trans. 12, 1737 (1975).
30. J. F. BLOUNT, C. A. MARYANOFF, and K. MISLOW. Tetrahedron Lett. 913 (1975).
31. R. K. HARRIS, P. JACKSON, P. J. WILKES, and P. S. BELTON. J. Magn. Reson. **73**, 178 (1987).
32. S. LARSEN, P. VINZENTS, and O. DAHL. Acta Crystallogr. Sect. C: Cryst. Struct. Commun. **C39**, 1280 (1983).
33. F. A. COTTON, D. J. DARENSBOURG, M. F. FREDRICH, W. H. ILSLEY, and J. M. TROUP. Inorg. Chem. **20**, 1869 (1981).
34. W. P. OZBIRN, R. A. JACOBSON, and J. C. CLARDY. J. Chem. Soc. Chem. Commun. 1062 (1971).

Can. J. Chem. Downloaded from www.nrcresearchpress.com by 194.225.253.170 on 09/07/12
For personal use only.

Trigonal prismatic versus octahedral coordination geometry of transition metal dithiolates: Comparison between saturated and unsaturated early transition metal tris(1,2-dithiolate) complexes

JOEL L. MARTIN[1] AND JOSEF TAKATS[2]

Department of Chemistry, University of Alberta, Edmonton, Alta., Canada T6G 2G2

Received February 20, 1989

This paper is dedicated to Professor Ronald J. Gillespie on the occasion of his 65th birthday

JOEL L. MARTIN and JOSEF TAKATS. Can. J. Chem. **67**, 1914 (1989).

Reaction of a stoichiometric amount of H_2edt/NaHedt (edt = ethane-1,2-dithiolate) with the appropriate metal amide, followed by cation exchange, gave the complexes $[NEt_4]_2[M(edt)_3]$ (M = Ti, **1**; Hf, **2**) and $[AsPh_4]$ $[Nb(edt)_3]\cdot CH_3CN$, **3**. The structure of **3** has been determined crystallographically (space group; cell dimensions; Z; unique data ($I \geq 3\sigma(I)$); R/R_w): $P\bar{1}$; a = 9.095(1), b = 14.609(3), c = 15.639(3) Å and α = 60.09(2), β = 80.07(3), γ = 89.89(2)°; z = 2; 1488; 4.3/4.5. The coordination geometry of **3** is severely distorted from the trigonal prismatic (TP) structure found in the analogous $Nb(1,2\text{-}S_2C_6H_4)_3^-$, which contains an unsaturated 1,2-dithiolate ligand system. The average twist angle between triangular faces is 33.3°. However, on the basis of VT ^{1}H NMR spectroscopy it is argued that the TP form is at most 9–10 kcal mol^{-1} less stable than the observed geometry. A comparison between the structures of tris-chelate complexes of the early transition metals containing saturated and unsaturated 1,2-dithiolates and related ligands is made, and the factors thought to be responsible for TP vs. octahedral geometry are reviewed and their relative importance assessed.

Key words: structure, trigonal prismatic, 1,2-dithiolate, early transition metals.

JOEL L. MARTIN et JOSEF TAKATS. Can. J. Chem. **67**, 1914 (1989).

La réaction d'une quantité stoechiométrique de H_2edt/NaHedt (edt = éthane-1,2-dithiolate) avec des amidures métalliques, suivie d'un échange de cation, fournit les complexes $[NEt_4]_2[Me(edt)_3]$ (M = Ti, **1**; Hf, **2**) et $[AsPh_4][Nb(edt)_3]\cdot CH_3CN$, **3**. On a déterminé la structure du composé **3** par diffraction des rayons-X. Les cristaux appartiennent au groupe d'espace $P\bar{1}$ avec a = 9,095(1), b = 14,609(3) et c = 15,639(3) Å et α = 60.09(2), β = 80,07(3) et γ = 89,89(2)° et Z = 2; on a affiné la structure jusqu'à des valeurs respectives de R et R_w de 0,043 et 0,045 pour 1488 réflexions avec $I \geq 3\sigma(I)$. La géométrie de coordination du composé **3** est fortement deformée par rapport à la structure prismatique trigonale (PT) qui a été observée antérieurement avec l'analogue $Nb(1,2\text{-}S_2C_6H_4)_3^-$ qui contient un ligand 1,2-dithiolate insaturé. L'angle moyen de déviation entre les faces triangulaires est de 33,3°. Toutefois, sur la base de la RMN du ^{1}H à température variable, on suggère que la différence de stabilité entre la forme PT et la géométrie observée ne favorise cette dernière que par 9–10 kcal mol^{-1}. On a comparé les structures des complexes tris chélates des métaux de transition du début contenant des ligands 1,2-dithiolates saturés et insaturés ainsi que d'autres ligands apparentés; on passe en revue les facteurs que l'on croit responsable des structures PT vs. les géométries octaédriques et on évalue leurs importances relatives.

Mots clés : structure, prismatique trigonal, 1,2-dithiolate, métaux de transition du début.

[Traduit par la revue]

Introduction

The possibility of trigonal prismatic (TP) geometry in highly covalent d^0 transition metal complexes was predicted as early as 1932 by Hultgren (1), based on the concept of metal orbital hybridization presenting a more favorable bonding picture for TP than for octahedral geometry. This result has been corroborated by Hoffman *et al.* (2) on the basis of extended Hückel MO calculations.

In 1965 the first observation of a discrete TP complex, $Re(1,2,\text{-}S_2C_2Ph_2)_3$ (3), rekindled interest in TP geometry and since then a host of factors, such as (a) ligand constraint (4, 5), (b) ligand field stabilization energy (2, 4, 6), (c) interdonor atom bonding (3, 7–9), (d) proper matching of ligand and metal orbital energies (1, 2, 10–12), (e) the symmetry of ligand π orbitals (2, 8, 13), and (f) the overall charge of the complex, have been suggested as important factors influencing the formation of TP, octahedral, or intermediate geometries. From experimental work of Holm and co-workers (4) and Eatough *et al.* (14) and theoretical work of Holm (4), Kepert (5), and Wentworth (6) it appears that the two most important factors involved are probably the ligand constraint (provided by cage type ligands and (or) the "bite" distance of chelating ligands) and the ligand field stabilization energy in that order. However, the ordering of factors (c) through (f) is certainly still a subject of debate. Indeed any attempts to assess the importance of subtle electronic factors in favoring TP geometry must carefully avoid the problems of ligand constraint and ligand field stabilization energy. The studies that will be considered here were directed at understanding the geometry of transition metal complexes containing unsaturated 1,2-dithiols and attempted to avoid the complications of the two overriding factors mentioned above.

The synthesis of early transition metal complexes of benzene 1,2-dithiol (15) provided the unique opportunity to study an isoelectronic series of complexes: $Mo(bdt)_3$, $Nb(bdt)_3^-$, and $Zr(bdt)_3^{2-}$ (btd = 1,2-benzenedithiolate). Although the decreasing stability of TP geometry in the order Mo > Nb > Zr suggested to Cowie and Bennett (11) that the proper matching of metal d-orbital and ligand orbital energies was an important condition for TP geometry, the study was not conclusive because the change in overall charge of the complexes should also favor the observed trend. To confirm the hypothesis of Cowie and Bennett, we undertook structural analysis of $Ta(bdt)_3^-$ and $Sb(bdt)_3^-$ complexes, which strongly resemble the Nb complex in metal size and also have the same charge (12, 16). The increasing distortion away from TP geometry in the order Nb < Ta < Sb provides substantial evidence that the stability of TP

[1]Present address: Phillips Petroleum Co., 96-G PRC, Bartlesville, OK 74004, U.S.A.

[2]Author to whom correspondence may be addressed.

Can. J. Chem. Downloaded from www.nrcresearchpress.com by 186.148.149.217 on 09/07/12
For personal use only.

$$M(NR_2)_x + (6-x)NaHedt + (x-3)H_2edt \xrightarrow{THF} Na_{(6-x)}M(edt)_3 + xHNR_2$$

M = Ti and Hf, $x = 4$; Nb, $x = 5$

$$Na_{(6-x)}M(edt)_3 \xrightarrow[Et_4NCl\ or\ Ph_4AsCl]{CH_3CN} [Et_4N]_2[M(edt)_3]/[Ph_4As][Nb(edt)_3]$$

M = Ti (**1**), Hf (**2**), Nb (**3**)

SCHEME 1

geometry hinges upon the availability of metal *d* orbitals of appropriate energy. Also, the study of the entire series of benzene-1,2-dithiolate complexes, in our mind, has cast serious doubt about the importance of interligand donor atom bonding in this regard.

However, an interesting question that remains is whether π bonding or σ bonding, as originally suggested by Hultgren (1) and later revived (10), is the factor that favors TP geometry. A possible approach to this question is to compare the behavior of analogous complexes containing unsaturated and saturated 1,2-dithiols, since the σ/π bonding capabilities of these ligand systems are expected to be different.

In this paper we present our synthesis of $M(edt)_3^{n-}$ (edta = ethane-1,2-dithiolate; M = Ti, Hf, $n = 2$; M = Nb, $n = 1$) complexes, describe the solid state structure of the niobium complex (tetraphenylarsonium salt), and comment on the relevance of these complexes to the question of TP vs. TAP coordination geometry in transition metal dithiolates. Since our initial disclosures (17), other groups have extensively investigated the chemistry and structure of transition metal complexes of ethane-1,2-dithiol (18–21). The synthesis and structure of $[NEt_4]_2[Ti(edt)_3]$ and $[NEt_4][Nb(edt)_3]$ have been reported by Holm and co-workers (20) and Tatsumi, Nakamura, *et al.* (21*a*), respectively.

Results

Synthesis and spectroscopic properties

As reported previously for the synthesis of the analogous benzene-1,2-dithiolate complexes (15), the reaction of the appropriate transition metal amide with $H_2edt/Hedt^-$, according to the stoichiometry shown in Scheme 1, gave the corresponding tris(ethane-1,2-dithiolate) complexes in moderate yield. The Ti and Nb (and Ta) complexes were also obtained from the reaction of the appropriate metal halide with Na_2edt and Li_2edt respectively, in the required 1:3 stoichiometric ratio (20, 21). It is not known whether the Hf complex also obtains from this simplified procedure.

The complexes reported are well-behaved, crystalline solids (**1** and **3** red, **2** almost colorless), but are somewhat more unstable toward hydrolysis than the corresponding benzene-1,2-dithiolate compounds. Solutions of both types of compounds are sensitive to moisture carried in the air. Under inert atmosphere, complexes **1–3** are stable in CH_3CN but, like the corresponding benzene-1,2-dithiolate complexes, the Ti and Hf derivatives decompose in CH_2Cl_2. Stability in the solid state ranges from the readily hydrolyzed Hf compound to the reasonably unreactive Ti and to the stable Nb complex. However, we note that Tatsumi, Nakamura, *et al.* (21*b*) report an interesting rearrangement of the latter compound via C—S bond cleavage, a feature not observed with the analogous unsaturated dithiol complexes.

The infrared spectra of compounds **1** and **2** show two strong bands in the metal–sulfur stretching region (**1**, 355 and 322 cm^{-1}; **2**, 297 and 268 cm^{-1}), and are tentatively thus assigned. The M–S stretching region for **3** is obscured by the tetraphenylarsonium ion bands, but Tatsumi, Nakamura, *et al.* (21*a*) report Nb–S and Ta–S stretching vibrations at 354(s), 338(s), 240(w) and 335(s), 318(s), 225(w) cm^{-1}, respectively. Once the difference in relative atomic masses between these metals is taken into account, the strength of the M–S stretch is Ti ≈ Hf < Ta ≈ Nb. The ^1H NMR spectra of the complexes at room temperature exhibit a sharp singlet for the methylene protons of the ligand. The position of the signal shifts to lower field in the order Hf, Ti, and Nb (δ: **2**, 3.23; **1**, 3.38; **3**, 3.76 ppm), which is the same order as the stability sequence of the compounds. The cause of the strong coloration of the Ti and Nb complexes is evident from Fig. 1. Charge transfer transitions, which dominate the spectra, shift to higher energy in the order Nb < Ti < Hf. Systematic blue shift of all uv–visible absorption bands on going from $Nb(edt)_3^-$ to $Ta(edt)_3^-$ was also reported by Tatsumi, Nakamura, *et al.* (21). The dependence of the lowest energy maximum upon the metal is suggestive of LMCT character of the bands. A detailed assignment of the spectra cannot be made at this time, but it must be pointed out that the same type of metal dependence was observed in the benzene-1,2-dithiolate complexes.

The chemical reactivity, infrared spectra in the ν_{M-S} region, ^1H NMR spectra, and uv–visible spectra of the ethane-1,2-

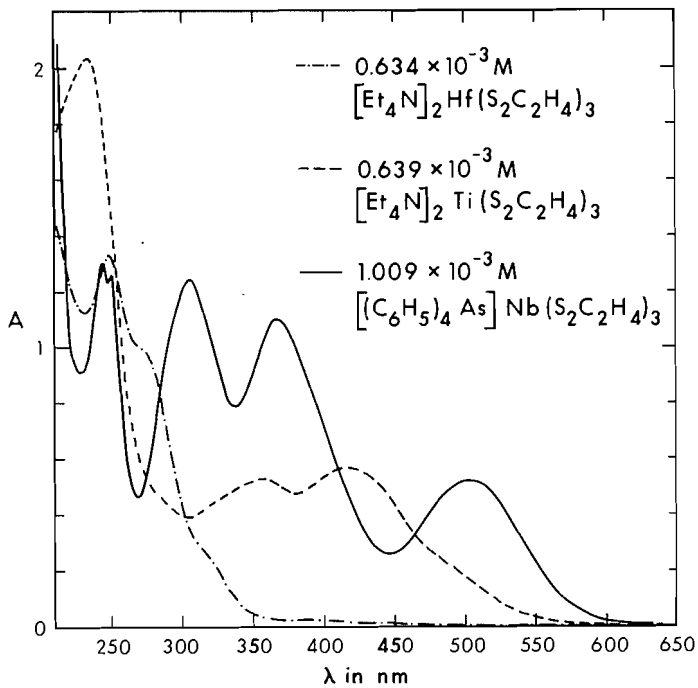


FIG. 1. Ultraviolet–visible absorption spectra of complexes **1–3** in acetonitrile.

Can. J. Chem. Downloaded from www.nrcresearchpress.com by 186.148.149.217 on 09/07/12
For personal use only.

TABLE 1. Selected distances (Å) and angles (deg) for $[Ph_4As][Nb(1,2\text{—}S_2C_2H_4)_3]\cdot CH_3CN$, **3**

Bond distances					
Nb—S(1)	2.438(3)	C(1)—S(1)	1.82(1)	C(1)—C(2)	1.50(2)
Nb—S(2)	2.432(3)	C(2)—S(2)	1.82(1)		
Nb—S(3)	2.422(4)	C(3)—S(3)	1.80(1)	C(3)—C(4)	1.49(2)
Nb—S(4)	2.435(3)	C(4)—S(4)	1.82(1)		
Nb—S(5)	2.419(3)	C(5)—S(5)	1.81(1)	C(5)—C(6)	1.52(2)
Nb—S(6)	2.438(4)	C(6)—S(6)	1.80(1)		
Intra- and inter-ligand S---S distances					
S(1)—S(2)	3.202(5)	S(1)—S(3)	3.305(5)	S(2)—S(4)	3.327(5)
S(3)—S(4)	3.178(5)	S(3)—S(5)	3.363(5)	S(4)—S(6)	3.374(5)
S(5)—S(6)	3.179(5)	S(5)—S(1)	3.287(5)	S(6)—S(2)	3.249(5)

Bond angles

"Bite"-angles		*trans*-angles	
S(1)—Nb—S(2)	82.2(1)	S(1)—Nb—S(4)	158.7(1)
S(3)—Nb—S(4)	81.7(1)	S(2)—Nb—S(5)	156.6(1)
S(5)—Nb—S(6)	81.8(1)	S(3)—Nb—S(6)	161.5(1)

Others

Nb—S(1)—C(1)	105.9(4)	S(1)—C(1)—C(2)	109.4(10)
Nb—S(2)—C(2)	105.2(4)	S(2)—C(2)—C(1)	109.6(10)
Nb—S(3)—C(3)	106.6(5)	S(3)—C(3)—C(4)	110.5(9)
Nb—S(4)—C(4)	105.8(4)	S(4)—C(4)—C(3)	109.6(10)
Nb—S(5)—C(5)	105.6(4)	S(5)—C(5)—C(6)	110.4(9)
Nb—S(6)—C(6)	107.9(5)	S(6)—C(6)—C(5)	110.1(10)

dithiolate complexes all show the trends expected for increased bond strength in the order Hf < Ti < Nb, just as in the benzene-1,2-dithiolate complexes. The rationale here, as before, is that the metal *d* orbitals are increasingly stabilized in the order Hf < Ti < Ta < Nb and as a result both σ and π donation from the ligand are enhanced. However, as yet no means other than X-ray crystallography has been developed that can answer questions regarding the exact geometry of the metal complexes. Accordingly, the single crystal X-ray structure of the Nb complex was determined.

Description of the structure of **3**

A summary of pertinent distances and angles is presented in Table 1. Numbering of the $Nb(edt)_3^-$ anion is evident from Fig. 2, which is a view down the approximate threefold axis of the complex anion. The contents of the unit cell are shown in Fig. 3 and establish that the crystal structure consists of well-separated ions and CH_3CN molecules, with no unusual interionic contacts. The disordered CH_3CN molecules are shown as five atoms, which was the model used to fit them. As may be expected for this type of disorder, the bond lengths and angles are slightly irregular and have large standard deviations. However, the C—C bond lengths, 1.35(5) and 1.40(4) Å, C≡N bond lengths, 1.17(5) and 1.18(5) Å, and C—C≡N bond angles, 174°(4) and 175°(4), are in agreement with accepted values. The geometry of the tetraphenylarsonium ion is in good agreement with previous determinations of this ion, with As—C bonds averaging 1.884(3) Å and C—As—C angles averaging 109.5(8)°.

Although there is no crystallographically imposed symmetry, it is clear from Fig. 2 that the complex anion is quite symmetrical. The six sulfur atoms are approximately equidistant from the

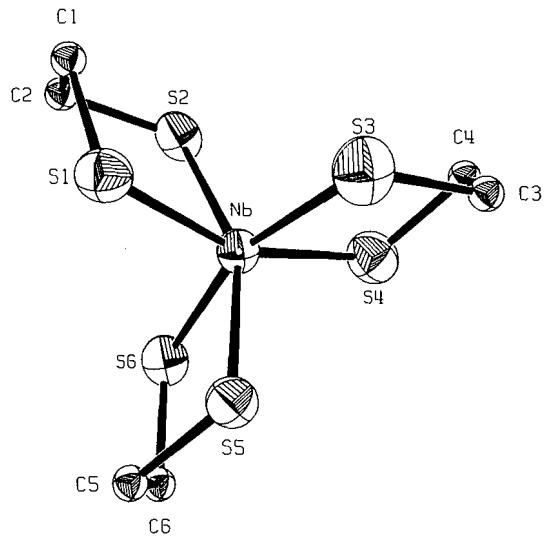


FIG. 2. A perspective view of the molecular structure of the complex anion, $Nb(edt)_3^-$, in **3**. The thermal vibrational ellipsoids for Nb and S atoms represent 50% probability, while the isotropic thermal parameters for C atoms have been reduced for clarity.

Nb center (Nb—S: 2.419(3)–2.438(3) Å, ave. 2.431(3) Å). The three five-membered chelate rings are disposed in a well-ordered propeller-like arrangement, each exhibiting the symmetric half-chain conformation. The angles also cover a fairly narrow range: S—Nb—S (bite), 81.7(1)–82.2(1)°; S—Nb—S (*trans*), 156.6(1)–161.5(1); ligand dihedral angles (SCCS), 59(1)° (S(1)—S(2)), 57(1)° (S(3)–S(4)), 55(1)° (S(5)–S(6)). The triangular faces at opposite ends of the complex anion

Can. J. Chem. Downloaded from www.nrcresearchpress.com by 186.148.149.217 on 09/07/12
For personal use only.

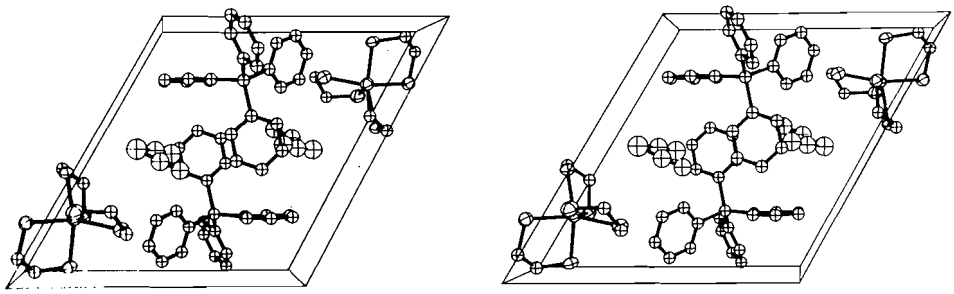


FIG. 3. A stereoview of the contents of the unit cell with *b* axis pointing to the right and *c* pointing upward.

TABLE 2. Selected distances (Å) and twist angle (deg) in tris(1,2-dithiolate) complexes

Compound	M—S	S—S(intra)	S—S(inter)	C—S	φ(ave)	φ(calcd.)[a]	Ref.
$Nb(bdt)_3^-$	2.441(11)	3.150(9)	3.23(5)	1.745(9)	0.7	48	10
$Nb(edt)_3^-$	2.431(3)	3.168(8)	3.32(2)	1.81(1)	33.3	49	This work
	2.434(1)	3.189(3)	3.30(4)	1.816(5)	30.5		19
$Ti(edt)_3^{2-}$	2.427(7)	3.213(3)		1.81(1)	38.0	51	18
$Zr(bdt)_3^{2-}$	2.543(10)	3.265(14)	3.58(14)	1.765(7)	37.0	46	10

[a]Obtained from ref. 4 and based on the normalized ligand bite distance (S—S(intra)/M—S).

(S(1,3,5) and S(2,4,6)) are tilted from being parallel by only 1°. The projected twist angles of the individual ligands (22), are $\phi_{1,2} = 32.6°$, $\phi_{3,4} = 33.3°$, and $\phi_{5,6} = 33.7°$ ($\phi_{ave} = 33.3°$) and indicate a coordination polyhedron intermediate between a trigonal prism and an octahedron. Thus the complex anion approximates D_3 molecular symmetry, the configuration shown in Fig. 2 is Δ(λλλ), and the unit cell of course contains the enantiomeric pair.

It is gratifying to note that the geometry of the complex anion in $[NEt_4]$ $[Nb(edt)_3]$ (21), **3′**, which contains a different counterion and crystallizes in a different space group, is nearly identical with the one found in **3**. The pertinent values are: Nb—$S_{(ave)}$, 2.434(7) Å; S—Nb—S (bite), 81.58(4)–82.14(4)°; S—Nb—S (*trans*), 156.29(4)–157.55(4)°. The projected twist angles (φ) are: 31.4, 30.6, and 29.4° with the average value ($\phi_{ave} = 30.5°$) being only 2.8° different from that found in **3**. The absolute configuration of **3′** was determined as Λ(δδδ). Clearly the coordination geometry of the complex anion, $Nb(edt)_3^{2-}$, is determined mainly by electronic factors between the transition metal and the coordinated ethane-1,2-dithiolate; crystal packing forces can play but a minor role in this regard.

An immediate observation that can be made concerning the structure of **3** is that it has moved away from the TP geometry of the related $Nb(bdt)_3^-$ complex, which contains unsaturated 1,2-dithiolates, yet the stereochemistry of **3** is among the closest to the TP among complexes with non-dithiolene type ligands. To properly assess the importance and the degree of this distortion it is instructive to compare the structure of **3** with those of the closely related $Ti(edt)_3^{2-}$ and $M(bdt)_3^{n-}$ (M = Nb, $n = 1$; M = Zr, $n = 2$) complexes. The relevant distances and the projected twist angles are listed in Table 2.

The C—S bond distances in **3** are typical of carbon–sulfur single bonds involving sp^3 hybridized C and S atoms (predicted value 1.81, ref. 23). These distances are significantly longer than those in $Nb(bdt)_3^-$, even after corrected for the change from sp^3 to sp^2 carbon in the latter. It is then interesting that the change in ligand character is not accompanied by a change in Nb—S bond distances, which, if anything, are marginally shorter in **3** featuring the saturated ethane-1,2-dithiolate ligand system. Thus the *strength* of the Nb—S interaction in the two complexes must be very similar even though the *nature* of the Nb—S interaction is different. A final note of interest is the very slight change in M—S distances on going to the $Ti(edt)_3^{2-}$ complex. The decrease is certainly less than anticipated from the change in ionic radii between two metal ions (0.03 Å) (24), and the longer than "predicted" distance is not inconsistent with the greater chemical reactivity of $Ti(edt)_3^{2-}$ compared to the Nb complex, and hence with the somewhat reduced Ti—S bond strength.

Reference to Table 2 shows that all the complexes listed present an average projected twist angle, ϕ_{ave}, that is smaller than the "corrected octahedral limit" imposed by the constraint of the ligand bite distance, thus indicating a real tendency of these systems to distort toward the TP geometry. The degree of distortion (measured by $\phi_{calc} - \phi_{ave}$) is $Nb(bdt)_3^-$ (47°) ≫ $Nb(edt)_3^-$ (17°) > $Ti(edt)_3^{2-}$ (13°) > $Zr(bdt)_3^{2-}$ (9°). Although it has been established that the ligand in $Zr(bdt)_3^{2-}$ is at the reduced dithiolate extreme (11), it is nevertheless noteworthy that the $Ti(edt)_3^{2-}$ and $Nb(edt)_3^-$ complexes, with saturated 1,2-dithiolate ligands, show a more severe twisting toward the prism. Clearly, unsaturation is not enough to stabilize the TP. The order of distortion toward the prismatic geometry $Nb(edt)_3^-$ > $Ti(edt)_3^{2-}$ > $Zr(bdt)_3^{2-}$ follows the progressive increase in *d*-orbital energies and further corroborates our contention that proper match between ligand and metal orbital energies is an important factor for prism stability. Yet the almost perfect TP geometry of $Nb(bdt)_3^-$ in contrast to the distorted geometry of $Nb(edt)_3^-$ also shows that unsaturated 1,2-dithiolates, and possibly related chelating ligands, have some additional property that further enhances the possibility for TP coordination geometry.

Varible temperature ^1H NMR study of 3

At ambient temperature the ^1H NMR spectrum of complex **3** shows a sharp singlet for the CH_2 hydrogen atoms.

From Fig. 2 it is evident that the methylene hydrogens of the

Can. J. Chem. Downloaded from www.nrcresearchpress.com by 186.148.149.217 on 09/07/12
For personal use only.

Can. J. Chem. Downloaded from www.nrcresearchpress.com by 186.148.149.217 on 09/07/12
For personal use only.

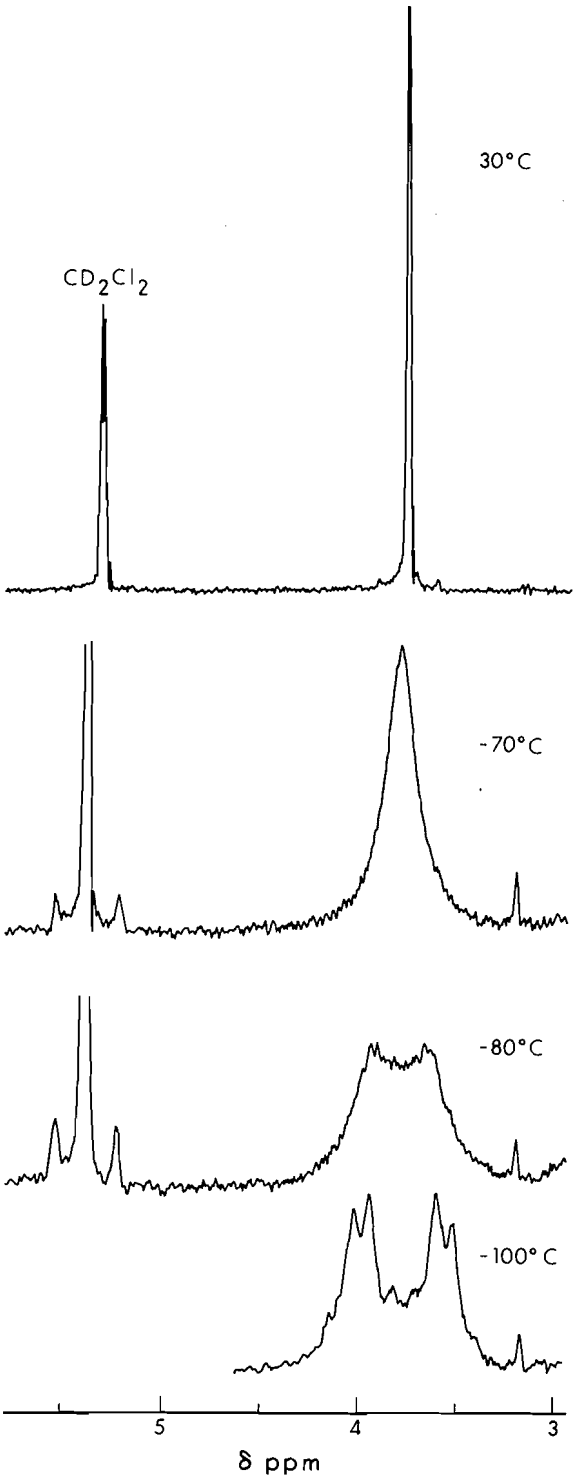


FIG. 4. Variable temperature ^1H NMR spectra of **3** in CD_2Cl_2.

ligands form two nonequivalent sets, H_{axial} and $H_{equatorial}$. As it is lucidly explained elsewhere (25), in the absence of racemization of such tris-chelate complexes the hydrogen atoms are inherently nonequivalent, even with rapid inversion of the puckered five-membered ring, and should give rise to an AA'BB' pattern. Equilibration of the two types of hydrogen atoms and observation of a single resonance is only possible by operation of both processes.

Upon cooling a solution of **3** in CD_2Cl_2, the spectral changes shown in Fig. 4 are seen. By −103°C, a well-resolved AB quartet is obtained, indicating stoppage of one of the previously mentioned processes. The $\Delta G^{\ddagger}$ associated with the process at −78°C is estimated as 9.2 kcal mol^{-1} (26). We have no direct proof that the observed fluxional behavior is intramolecular, but a dissociative process seems highly unlikely due to the reactivity of the free ligand with the solvent. Indeed the Ti and Hf complexes decompose in CH_2Cl_2. A spectrum obtained in the presence of excess of the free dithiol showed no evidence of ligand exchange.

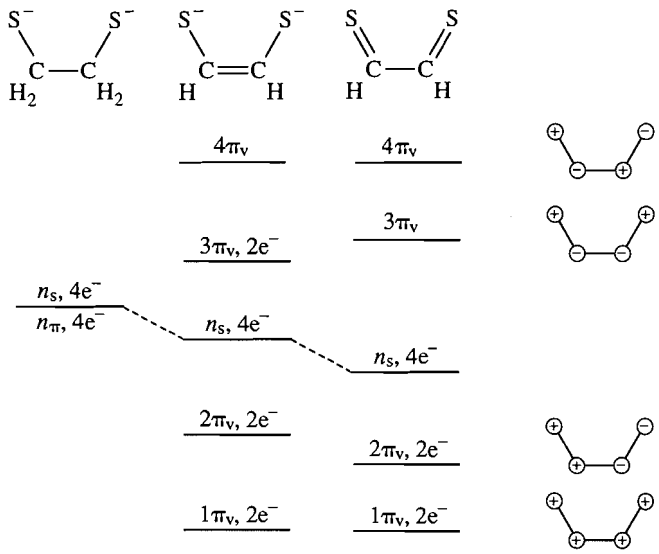
Although it is not possible to delineate which of the two previously described processes has stopped at low temperature, should the racemization go via the trigonal twist type process, the barrier observed represents an upper limit for the stabilization of the twisted form over the TP geometry in this complex.

Discussion

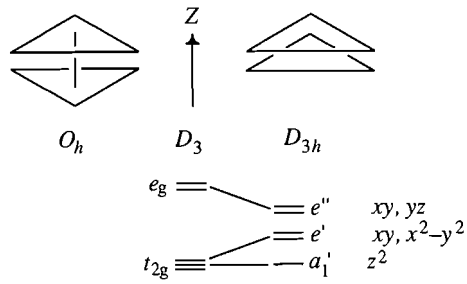
As indicated in the Introduction, the major focus of this study was to compare the structure of early transition metal tris-chelate complexes containing the saturated ethane-1,2-dithiolate ligand with those of the analogous complexes with unsaturated benzene-1,2-dithiolate moieties, with a view to establishing the electronic factors responsible for changes in coordination geometry in the complexes.

To assess the anticipated bonding changes on going from the saturated to the unsaturated 1,2-dithiolate ligand, reference to the qualitative energy level diagram is made, Scheme 2. Ethane-1,2-dithiolate can act as a σ donor donating two electrons from a lone pair on each sulfur atom for a total of four σ electrons. In principle, it can also donate additional electrons to the metal from the remaining lone pairs on the sulfur atoms through the formation of π bonds, although the orientation of these lone pairs may not contribute to this very effectively (see Fig. 2). This situation has been considerably altered in the case of unsaturated 1,2-dithiolates. These ligands can still donate the same number of electrons through σ-bonding, but two of the remaining sulfur atom lone pairs have been delocalized over the ligand π framework. Two of these electrons have gone into a bonding orbital ($2\pi_v$) and have been somewhat stabilized, and the remaining two electrons have been placed into an antibonding orbital ($3\pi_v$) and have been destabilized. This π delocalization then has two effects. First, it reduces the effective charge on the sulfur atoms and therefore stabilizes the lone pairs and, second, it causes the ligand system to become a strong π donor due to the presence of the two antibonding π electrons. The whole ligand system is then a six-electron donor. From the above reasoning an important conclusion can be drawn regarding the relative behavior of saturated and unsaturated 1,2-dithiols, namely, that the former ligand system should be a better σ but poorer π donor than the latter. Also shown in the scheme is the oxidized, dithioketone formulation of the unsaturated ligand. Under this formulation, which is the more traditional view with these "dithiolene" type ligands (7, 8, 13), the ligand presents a low-lying symmetric π-acceptor orbital ($3\pi_v$) to the metal. Although the π-donor picture is more appropriate with the anionic complexes of the early transition metals since, as detailed elsewhere (11, 12, 15), these complexes contain the more reduced form of the unsaturated 1,2-dithiolates, it is clear that to achieve a unified picture for the possible importance of π bonding in stabilizing the TP geometry with different 1,2-unsaturated ligands the π-acceptor extreme will also have to be invoked.

Returning then to the structure of $Nb(edt)_3^-$, the distortion away from the TP geometry of the analogous $Nb(bdt)_3^-$ complex



SCHEME 2

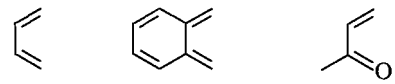


SCHEME 3

seems to imply that π bonding is responsible for, or at least contributes to, the stabilization of the TP geometry, since, according to the reasoning presented above, π bonding is expected to be less important with the saturated ethane-1,2-dithiolate than with the unsaturated benzene-1,2-dithiolate ligand system. Further support for this conclusion comes from a tris(1,2-dihydroxoethane) complex of tungsten, $W(OCH_2CH_2O)_3$ (27). This complex exhibits an average twist angle of 36.9°, once again intermediate between the TP and octahedral limits and in sharp contrast to the TP geometry observed for tris(9,10-phenanthrenequinone)molybdenum(0) (28).

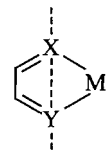
To understand how π bonding can stabilize the TP geometry, let us consider the well-known level ordering of the predominantly metal *d* character orbitals in octahedral and TP ML_6 complexes, Scheme 3 (adapted from ref. 2), and the interaction of these orbitals with the unsaturated ligands in both π-acceptor and π-donor extremes. We recall that under D_{3h} symmetry (TP geometry) the $3\pi_v$ MOs of the ligands will give rise to two group molecular orbitals of a_2' and e' symmetries.

Let us first consider the ligands in their oxidized form. This situation implies metals in low oxidation states with their full complement of valence electrons in *d*-type orbitals. It is clear from the scheme that occupation of the high-lying e' orbitals, which will happen for any d^n electronic configuration with $n > 2$, will destablize the TP in favor of the octahedral geometry. However, the 1,2-dithioketone ligands have low-lying empty orbitals of e' symmetry (see above), which can effectively stabilize the e' metal orbitals and hence lead to TP geometry. This is not a new result and had been considered by previous workers in the field (2, 8, 13). Nevertheless, it provides a natural link to other "even" type unsaturated ligands that present a symmetrical empty π-acceptor orbital to the central metal atom and properly account for the TP geometry observed in tris(buta-1,3-diene)molybdenum (29), tris(*ortho*-xylyl)tungsten (30), and tris(methylvinylketone)tungsten (31) (for the respective ligands see **a**, **b**, and **c**). Indeed recently Green, Mingos, *et al.*



a **b** **c**

(32) have used molecular orbital calculations to support the importance of π back-bonding for the observed TP rather than octahedral geometry about the metal atom in tris(buta-1,3-diene)Mo/W. It is also worthy of note that the π-bonding model provides a rationale for the often observed folding of the ligand in TP complexes about the donor–donor axis, **d**, and, in a



d

qualitative sense, for its extent. Clearly the all-carbon ligands (**a** and **b**) with no lone pair on the terminal atom(s) are the most oxidized of these unsaturated ligands and consequently elicit the largest amount of back-bonding from the metal to stabilize the e' orbital and achieve the TP geometry. This is accomplished by severe folding, to bring the $3\pi_v$ MO into maximal overlap with the metal e' orbital. Indeed all Mo—C bond distances in Mo(buta-1,3-diene)$_3$ were found equal (2.29(1) Å) (29). Replacing one CH_2 end group by an oxygen atom gives the methylvinylketone complex. Both σ donation from the oxygen lone pair and the more reduced nature of the ligand are expected to result in decreased π back-bonding and consequently to cause a smaller ligand folding. Reflecting these predictions, the terminal W—C and W—O distances (2.12(2) and 2.11(2) Å) are significantly shorter than the remaining W—C bonds (2.29(2) and 2.42(2) Å) (31). Continuing the trend toward more reduced ligands and less oxidized metal center, the situation with the unsaturated 1,2-dithiol type ligand with σ donation from two sulfur atoms, might have been expected to result in planar MS_2C_2 chelate rings. However, in most cases there is folding (11, 13). The folding of the planes within the same complex is sometimes irregular, and this is probably a consequence of crystal packing forces. Nevertheless we believe, as do Cowie and Bennett (11), that the major driving force for the ligand folding is to maximize the π bonding between $3\pi_v$ ligand molecular orbital and the metal e' (d_{xy}, $d_{x^2-y^2}$) orbitals. Ligand folding, but of an unusual type, has also been seen in the prismatic tris(9,10-phenanthrenequinone)molybdenum (28). Only one ligand is folded, the other two remain planar. However, the ligand exhibiting folding has longer C—C and Mo—O bond distances and shorter C=O bond lengths than the other two, closer to the oxidized form and hence in line with the folding arguments. We should like to close this section by mentioning that contrary to the TP geometry of the phenanthrenequinone complex, the structure of the related tetrachloro-1,2-benzoquinone derivative of chromium, Cr(1,2-

Can. J. Chem. Downloaded from www.nrcresearchpress.com by 186.148.149.217 on 09/07/12
For personal use only.

Can. J. Chem. Downloaded from www.nrcresearchpress.com by 186.148.149.217 on 09/07/12
For personal use only.

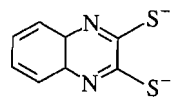
$O_2C_6Cl_4)_3$, is of the octahedral type (33). On the basis of structural parameters, Pierpont suggested that the metal center is best described as Cr(O), d^6, with only very slight contribution from the ligand empty π-acceptor orbital in the bonding. Clearly the distortion away from TP finds explanation in the orbital picture shown in Scheme 3 and the d^6 electronic configuration of the metal.

The stability of TP geometry seems not to have been discussed as fully in terms of the π-donor model as the π-acceptor property of these ligands. Yet the two points of view must ultimately lead to the same conclusion since they represent two extremes of the electronic structure of the same ligand system. The physical reality, which depends on the nature of the metal and the ligand, must lie somewhere in between. Indeed it is easily appreciated that as the metal *d* orbitals and ligand π-acceptor levels approach one another in energy, the metal is gradually oxidized and the electrons are transferred into primarily ligand-based molecular orbitals. The acceptor oribitals are full and the π acceptor has been transformed into a π donor. Even though there is this transparent link between the two extremes, we wish to present a discussion of the π-donor model because, as stated before, the ligands in the early transition metal complexes are closer to the dithiolate limit. The analysis will attempt to clarily the behavior of the saturated 1,2-dithiolates and, as we shall see, it emphasizes different aspects of the M—S interaction.

Our analysis begins by considering the unsaturated ligand at the 1,2-ditholate extreme. Since the ligand is fully reduced, the accompanying metal ion is in the high, 6+, oxidation state. In this limit of highly ionic bonding, repulsion between ligand donor atoms dominates and the octahedral geometry is favored. This again is a well-known result (1, 2). As the ligand becomes a better π donor, the energy of the $3\pi_v$ donor molecular orbital approaches that of the metal *d* levels. Under D_{3h} symmetry (TP geometry) there can be effective overlap of the full ligand *e'* MOs and empty metal *e'* orbitals; electron density now flows from ligand to metal and results in strong, delocalized bonding with concomitant decrease in ligand donor atom repulsion and stabilization, or at least movement toward the TP geometry. We recognize that it is very difficult to dissociate the contribution from, and variation in, the M—S σ bonding from the overall molecular geometry, especially in view of the results of Hultgren (1) and Hoffman (2), which show that for d^0–d^2 electronic configurations M—S σ bonding alone could result in TP geometry. Nevertheless on the basis of the structural change between $Nb(bdt)_3^-$ (TP) and $Nb(edt)_3^-$ (distorted toward octahedral), we believe that the π component is a contributor to the overall stability of the TP. This energy contribution may be quite substantial, as seen with the strongly π-acceptor ligands (butadiene, methylvinylketone), or quite small, as evidenced by the small rearrangement barrier of the $Nb(edt)_3^-$ complex (*vide supra*).

It is especially evident from the above analysis that a major role of the highly delocalized π bonding and, of course, that of the primary σ component as well is to moderate interligand repulsion, otherwise the TP geometry would be unfavorable. Thus we would argue, along with Cowie and Bennett (11), against the still sometimes held belief that interligand S---S bonding is an important factor in stablizing the TP geometry. The postulate of interligand S---S bonding rests, to a large extent, upon the observation of constant prism dimensions in the series of compounds $Re(1,2,-S_2C_2Ph_2)_3$, $Mo(1,2\text{-}S_2C_2H_2)_3$, and $V(1,2\text{-}S_2C_2Ph_2)_3$, despite the varying metal size (13). However, it can just as easily be argued that the observed interligand S---S distances in TP dithiolene complexes arise as a natural consequence of the TP geometry in complexes with M—S bond lengths on the order of 2.3–2.4 Å. The near constancy of M—S bond lengths in the previously mentioned V, Mo, and Re compounds may be a consequence of interligand donor atom repulsions tending to lengthen the M—S bonds in the smaller members rather than interligand S---S bonding determining the M—S bond length. There is some experimental support for the view that reducing interligand repulsion is important for the stability of the TP. In contrast to the distorted geometry of $Mo(mnt)_3^{2-}$ (mnt = $S_2C_2(CN)_2^{2-}$, maleonitriledithiolate) (34), the structure of $Mo(mnt)_2(dtc)^-$ (dtc = $S_2CNEt_2^-$, diethyldithiocarbamate) is TP (35).

To the best of our knowledge $Mo(mnt)_2(dtc)^-$ is the only compound containing the mnt^{2-} ligand that displays TP geometry and this may be due to an increased stabiliztion of the $3\pi_v$ orbital in this ligand and its attendant poor π-donor ability. While $Mo(mnt)_3^{2-}$ has a geometry distorted from TP, $Mo(qdt)_3^{2-}$ (qdt = quinoxaline-2,3-dithiolate, **e**) (36) and



e

$Mo(S_2C_2(COOCH_3)_2)_3^{2-}$ (37) adopt TP geometry. The Mo—S distances in both compounds average 2.393 Å and are marginally longer than in the valence isoelectronic complex $Mo(mnt)_3^{2-}$ (2.324(8) Å). The corresponding interligand S---S distances of 3.141(7) and 3.18(6) Å are nearly the same as the 3.188 Å average for $Mo(mnt)_3^{2-}$, further calling into question the interligand sulfur bonding model.

In summary, trends in the uv–visible spectra, in the M–S stretching frequencies, in the reduction potentials, and in the structural parameters for early transition metal complexes with either benzene-1,2-dithiolate, ethane-1,2-dithiolate, or the recently reported propane-1,3-dithiolates (38) point to the fact that the metal *d* orbitals lie above the ligand π orbitals in energy. Moving to the right in the periodic table, the metal *d* orbitals are stabilized. This gives rise to π bonding first from the unsaturated dithiolates, which are stronger π donors. For high valence molybdenum and rhenium, the *d* orbitals appear to be sufficiently stable that TP geometry is even observed for the weaker π-donating, saturated ligands, as seen in $Mo(SCH_2CH_2SCH_2CH_2S)_2$ (39) and $Re[(SCH_2)_3CCH_3]_2^-$ (40), although constraint imposed by the tridentate ligand may also contribute to the observed geometry. Thus, while Gray's MO scheme provides a reasonable model for interpreting the uv–visible spectra, it appears to overestimate the stability of the metal *d* orbitals, for the earliest transition metals, with respect to the ligand $3\pi_v$ level. Consequently, it is necessary in that scheme to invoke bonding with the metal d_{z^2} orbital to arrive at the correct level ordering. We propose that the metal d_{z^2} orbital is largely nonbonding, therefore the occurrence of TP geometry for d^1 and d^2 complexes is not surprising and there are numerous examples (36, 37, 39–42). We are, therefore, drawn to the conclusion that overlap of the empty metal $d_{x^2-y^2}$ and d_{xy} orbitals with filled ligand π orbitals is more crucial to the appearance of TP geometry than interdonor atom bonding and is not limited to unsaturated 1,2-dithiolates. The charge of the complex ion, although of import, may also play a secondary role

as shown by the series of TP complexes $Mo(btd)_3$, $Mo(qdt)_3^{2-}$, and $Mo(S_2C_2(COOCH_3)_2)_3^{2-}$.

The final question to address is the importance of σ bonding relative to π bonding. The occurrence of TP geometry not only in dithiolates but also in tris(butadiene)molybdenum (29), tris-(*ortho*-xylyl)tungsten (30), tris(methylvinylketone)tungsten (31), $Tc(NHC_6H_4S)_3$ (42), $Mo(NHC_6H_4S)_3$, and tris(thiobenzoyldiazene)molybdenum (43) strongly implies that π bonding, if not an essential prerequisite, plays a significant role in stablizing this interesting coordintion geometry.

Experimental

All of the procedures and techniques used here have been described previously (15) except the modifications below. Reagent grade acetonitrile was dried by distillation first from P_2O_5 and then from CaH_2. Tetrahydrofuran was distilled from Na/K alloy. Commercially available ethane-1,2-dithiol was stirred at 0°C with a small amount of $LiAlH_4$ until the vigorous reaction subsided and then distilled and stored under nitrogen. Metal dialkylamides were prepared by published methods (44–47). Tetraethylammonium chloride was used as previously described (15).

Physical measurements

Visible and uv spectra were recorded at $\sim 10^{-3}$ M in CH_3CN on a Unicam SP 1700 spectrophotometer. ^1H NMR spectra were recorded on a Varian Associates A60 or HA-100 spectrometer. Infrared spectra were recorded as KBr pellets or mineral oil and Fluorolube mulls with CsI windows, for the low energy region, on a Perkin–Elmer 467 infrared spectrometer. All analyses were performed at the analytical facilities of the University of Alberta. The sample of the Hf complex used for analysis was weighed on a Cahn electrobalance in a dry box.

Preparation of $[(C_6H_5)_4As][Nb(1,2\text{-}S_2C_2H_4)_3]\cdot CH_3CN$, 3

Sodium cyclopentadienide (2.70 mmol) in ~5 mL of THF was added to 0.60 mL (8.20 mmol) of ethane-1,2-dithiol in 50 mL of THF, resulting in the formation of a white precipitate. To this mixture 0.846 g (2.70 mmol) of pentakis(dimethylamido)niobium(V) was added in 20 mL of THF and the reaction mixture rapidly turned dark red. The mixture was stirred for ~20 h after which time a dark red precipitate was observed. Solid tetraphenylarsonium chloride (1.13 g, 2.70 mmol) was added and, after stirring 1 h, the solvent was stripped off under vacuum and replaced by 100 mL of CH_3CN. After stirring for ~20 h, most of the solid still had not dissolved so the mixture was heated to boiling and filtered hot. By cooling the filtrate overnight at ~−10°C, dark red crystals were obtained. After filtration and vacuum drying, 0.60 g (30% yield) of product was obtained. Treating the residue above with an additional 100 mL of CH_3CN produced 0.28 g of product for a total of 41% yield. The two crude products were recrystallized from 100 mL of boiling CH_3CN and, after filtration and cooling, 0.60 g of product was obtained, mp 131–138°C (dec.) uncorrected; uv–visible λ_{max} (nm) (10^{-3} ε, M^{-1} cm^{-1}): 245(12.6), 251(12.2), 307(12.1), 369(10.7), 504(5.1); ^1H NMR (CD_2Cl_2) δ: 7.5–8.0 (complex multiplet, 20H, Ph), 3.75 (s, 6H, CH_2) 1.96 (singlet, 3H, CH_3CN). *Anal.* calcd. for $C_{32}H_{35}AsNS_6Nb$: C 48.41, H 4.44, N 1.76, S 24.24; found: C 48.45, 48.25; H 4.53, 4.48; N 1.80, 1.71; S 23.65, 23.56.

Preparation of $[(C_2H_5)_4N]_2[Ti(1,2\text{-}S_2C_2H_4)_3]$, 1

Sodium cyclopentadienide (0.68 g, 7.80 mmol) in 20 mL of THF was added to 0.98 mL (11.6 mmol) of ethane-1,2-dithiol in 30 mL of THF. Tetrakis(diethylamido)titanium(IV) (3.68 mmol) in 20 mL of THF was added next, resulting in a brown solution that gradually turned orange and finally red. The sodium salt of the Ti complex is soluble, in contrast to Nb. After stirring for ~18 h, 25.8 mL of a 0.272 M solution of tetraethylammonium chloride in CH_3CN was added, resulting in formation of an orange precipitate. The solvent was stripped off under vacuum and replaced by 50 mL of CH_3CN. After stirring ~½ h the mixture was filtered to give a red solution. By alternately cooling and concentrating the solution, the product was finally obtained as large dark-red crystals. However, on occasion a yellow decomposition product was observed in small quantities and was filtered off. The yield of dark-red crystals was 0.698 g, 34%; ir ν_{Ti-S}: 355 and 332 cm^{-1}; uv–visible λ_{max} (nm) (10^{-3} ε, M^{-1} cm^{-1}): 233(33.2), 357(9.0), 414(9.6); ^1H NMR (CD_3CN) δ: 3.38 (s, 6H, CH_2 anion), 3.30 (q, 16H, CH_2N), 1.24 (tt, 24H, CH_3N). *Anal.* calcd. for $C_{22}H_{52}NS_6Ti$: C 45.17, H 8.96, N 4.79, S 32.89; found: C 45.11, 45.28, H 8.91, 9,04; N 5.12; S 32.71, 31.97.

TABLE 3. Crystal data for $[Ph_4As][Nb(edt)_3]\cdot CH_3CN$, 3

Parameter	Value
Molecular formula	$C_{32}H_{35}AsNS_6Nb$
Molecular weight	793.85
a, Å	9.095(1)
b, Å	14.609(3)
c, Å	15.639(3)
α, deg	60.09(2)
β, deg	80.07(3)
γ, deg	89.89(2)
V, Å^3	1766(1)
Z	2
Space group	$P\bar{1}$
$\rho_c(\rho_o)$, g cm^{-3}	1.495(1.49)
Crystal size, mm[a]	0.19 × 0.16 × 0.15 0.21 × 0.10 × 0.09
μ(MoKα), cm^{-1}	15.97
Transmission factors	0.89 × 0.92
Scan method	θ–2θ
Scan speed, deg min^{-1}	1.0
Scan width, deg[b]	2.0 + Δ2θ
2θ range, deg	36
Number of measured reflections	2223
Number of observed reflections $I \geq 3\sigma(I)$	1488
Number of variables	146
Goodness of fit (GOF)	1.6
Final *R*, R_w	0.043, 0.045

[a]See text for explanation for using two crystals.
[b]Δ2θ is a correction in the scan width for the dispersion of the $K_{\alpha 1}$–$K_{\alpha 2}$ doublet.

Preparation of $[(C_2H_5)_4N]_2[Hf(1,2\text{-}S_2C_2H_4)_3$, 2

This compound was prepared in the same way as the Ti compound above and was obtained as a single crystal ~1 cm long, yield 0.683 g, 23%. The product is almost colorless; ir ν_{Zr-S}: 297 and 268 cm^{-1}; uv–visible λ_{max} (nm) (10^{-3} ε, M^{-1} cm^{-1}): 249(20.4), 272 sh (15.1); ^1H NMR (CD_3CN) δ: 3.23 (s, 6H, CH_2 anion), 3.30 (q, 16H, CH_2N), 1.25 (tt, 24H, CH_3N). *Anal.* calcd. for $C_{22}H_{52}NS_6Hf$: C 36.93, H 7.32, N 3.91; found: C 36.64, 36.71; H 7.19, 7.25; N 3.88.

X-ray analysis of 3

Dark-red crystals of the compound were obtained by slow cooling of a saturated CH_3CN solution.

Details of the crystal data, intensity collection, and refinement are given in Table 3.

Weissenberg photographs using CuKα radiation and precession photographs using MoKα radiation revealed no systematic absences and 1 Laue symmetry. The intensity data were collected on a Picker FACS-1 four-circle automated diffractometer at ambient temperature using graphite monochromated MoKα radiation. Accurate cell dimensions were determined using 12 general reflections ($34° < 2\theta < 38°$). Intensity data were collected by the θ–2θ technique with background counts of 20 s at each end of the scan range. A set of three standard reflections was collected every 100 measurements, and an additional set of 10 reflections every 24 h, to test for crystal alignment and

Can. J. Chem. Downloaded from www.nrcresearchpress.com by 186.148.149.217 on 09/07/12
For personal use only.

TABLE 4. Fractional atomic coordinates and temperature factors for $[Nb(edt)_3]^-$

Atom	x	y	z	B_{eq},[a] Å^2
Nb	0.1859(1)	0.09267(8)	0.23732(8)	3.07
As	0.8294(2)	0.5917(1)	0.2362(1)	3.36
S(1)	0.1429(4)	−0.0670(2)	0.2287(2)	4.46
S(2)	0.2788(4)	0.1691(3)	0.0576(2)	4.28
S(3)	−0.0850(4)	0.0873(3)	0.2736(3)	5.07
S(4)	0.1684(4)	0.2745(2)	0.2010(3)	4.58
S(5)	0.1732(4)	−0.0283(3)	0.4150(2)	4.25
S(6)	0.4495(4)	0.1159(3)	0.2410(2)	4.17
C(1)	0.170(2)	−0.024(1)	0.096(1)	6.12
C(2)	0.305(2)	0.056(1)	0.039(1)	5.78
C(3)	−0.127(2)	0.206(1)	0.277(1)	5.58
C(4)	−0.026(2)	0.299(1)	0.193(1)	5.24
C(5)	0.365(2)	−0.057(1)	0.428(1)	5.00
C(6)	0.470(2)	0.044(1)	0.370(1)	5.68

[a]These are "equivalent" isotropic thermal parameters calculated from the anisotropic temperature factors by the program SFLS5.

stability. Approximately halfway through the collection, the intensity of the standards fell of sharply. Another crystal was mounted and collection resumed; this time no significant intensity changes were observed. The data were corrected for Lorentz and polarization effects and by an empirical absorption correction. The redundant data between the two crystals were merged.

The structure was solved by a combination of Patterson and difference Fourier maps and refined (using two scale factors) by full-matrix least-squares methods; the function minimized was $\Sigma w(|F_o| - |F_c|)^2$. Various models were attempted to describe the disordered CH_3CN molecule. Finally, use of a five-atom model, two acetonitriles with a common terminal carbon atom, seemed justified. Using occupancies of 0.45 and 0.55 for the two molecules, based upon the behavior of thermal parameters, reasonable bond distances were obtained by alternate refinement of the two molecules with all other parameters fixed. In the last two cycles of refinement the acetonitrile was not refined but the tetraphenylarsonium hydrogens were included as rigid bodies (C—H, 0.95°), also not refined. A final difference Fourier synthesis revealed peaks of 0.61, 0.56, and 0.47 e/Å^3 in the vicinity of the tetraphenylarsonium rigid bodies and a peak of 0.45 e/Å^3 near an acetonitrile carbon atom. All other features were less than 0.37 e/Å^3. The programs used in this study are those described previously (12).

Atomic coordinates and equivalent isotropic thermal parameters for the complex anion $Nb(edt)_3^{2-}$ are listed in Table 4. Anisotropic thermal parameters of the anion, atomic coordinates and thermal parameters for the rest of the complex, and structure factors are available as supplementary material in Tables S1–S3, respectively.[3]

Acknowledgement

We thank the Natural Sciences and Engineering Research Council of Canada and the University of Alberta for financial support of this work.

1. R. HULTGREN. Phys. Rev. **40**, 891 (1932).
2. R. HOFFMAN, J. M. HOWELL, and A. R. ROSSI. J. Am. Chem. Soc. **98**, 2484 (1976).
3. R. EISENBERG and J. A. IBERS. J. Am. Chem. Soc. **87**, 3776 (1965).
4. E. LARSON, G. N. LA MAR, B. E. WAGNER, J. E. PARKS, and R. H. HOLM. Inorg. Chem. **11**, 2652 (1972).
5. D. L. KEPERT. Inorg. Chem. **11**, 1561 (1972); Inorganic stereochemistry. Springer-Verlag, Berlin. 1982.
6. R. A. D. WENTWORTH. Coord. Chem. Rev. **9**, 171 (1973).
7. G. N. SCHRAUZER and V. P. MAYWEG. J. Am. Chem. Soc. **88**, 3235 (1966).
8. E. I. STIEFEL, R. EISENBERG, R. C. ROSENBERG, and H. B. GRAY. J. Am. Chem. Soc. **88**, 2956 (1966).
9. A. AVDEEF and J. P. FACKLER, JR. Inorg. Chem. **14**, 2002 (1975).
10. R. HUISMAN, R. DEJONGE, C. HAAS, and F. JELLINEK. J. Solid State Chem. **3**, 56 (1971).
11. M. COWIE and M. J. BENNETT. Inorg. Chem. **15**, 1595 (1976); **15**, 1589 (1976); **15**, 1584 (1976).
12. J. L. MARTIN and J. TAKATS. Inorg. Chem. **14**, 1358 (1975).
13. R. EISENBERG. Prog. Inorg. Chem. **12**, 295 (1970).
14. D. J. EATOUGH, J. J. CHRISTENSEN, and R. M. IZATT. Chem. Rev. **74**, 351 (1974).
15. J. L. MARTIN and J. TAKATS. Inorg. Chem. **14**, 73 (1975).
16. J. L. MARTIN and J. TAKATS. Acta Crystallogr. Submitted.
17. J. L. MARTIN and J. TAKATS. 172nd ACS National Meeting, San Francisco, CA. 1976. Abstract INOR 181.
18. J. K. MONEY, J. C. HUFFMANN, and G. CHRISTOU. Inorg. Chem. **27**, 507 (1988).
19. W. TREMEL, M. KRIEGE, B. KREBS, and G. HENKEL. Inorg. Chem. **27**, 3886 (1988).
20. R. N. MUKHERJEE, CH. PULLA RAO, and R. H. HOLM. Inorg. Chem. **25**, 2979 (1986); **25**, 428 (1986).
21. K. TATSUMI, Y. SEKIGUCHI, A. NAKAMURA, R. E. CRAMER, and J. J. RUPP. (*a*) Angew. Chem. Int. Ed. Engl. **25**, 86 (1986); (*b*) J. Am. Chem. Soc. **108**, 1358 (1986).
22. K. R. DYMOCK and G. J. PALENIK. Inorg. Chem. **14**, 1220 (1975).
23. L. PAULING. The nature of the chemical bond. Cornell University Press, Ithaca, NY. 1966. p. 224.
24. R. D. SHANNON. Acta Crystallogr. Sect. A: Cryst. Phys. diffr. Theor. Gen. Crystallogr. **32**, 751 (1976).
25. T. G. APPLETON, J. R. HALL, and C. J. HAWKINS. Inorg. Chem. **9**, 1209 (1970); C. J. HAWKINS and J. A. PALMER. Coord. Chem. Rev. **44**, 1 (1982).
26. D. KOST, E. H. CARLSON, and M. REBAN. J. Chem. Soc. Chem. Commun. 656 (1971).
27. V. J. SCHERLE and F. A. SCHRÖDER. Acta Crystallogr. Sect B: Struct. Crystallogr. Cryst. Chem. **30**, 2772 (1974).
28. C. G. PIERPONT and R. M. BUCHANAN. J. Am. Chem. Soc. **97**, 4912 (1975).
29. P. S. SKELL and M. J. MCGLINCHEY. Angew. Chem. Inter. Ed. Engl. **14**, 195 (1975).
30. M. F. LAPPERT, C. L. RALSTON, B. W. SKELTON, and A. H. WHITE. J. Chem. Soc. Chem. Commun. 485 (1981).
31. R. E. MORIARTY, R. D. ERNST, and R. BAU. J. Chem. Soc. Chem. Commun. 1242 (1972).
32. J. C. GREEN, M. R. KELLY, P. D. GREBENIK, C. F. BRIANT, N. A. MCEVOY, and D. M. P. MINGOS. J. Organomet. Chem. **228**, 239 (1982).
33. C. G. PIERPONT and H. H. DOWNS. J. Am. Chem. Soc. **98**, 4834 (1976).
34. G. F. BROWN and E. I. STIEFEL. Inorg. Chem. **12**, 2140 (1973).
35. W. P. BOSMAN and A. NIEUWPOORT. Inorg. Chem. **15**, 775 (1975).
36. (*a*) S. BOYDE, C. D. GARNER, J. H. ENEMARK, and R. B. ORTEGA. Polyhedron, **5**, 377 (1986); (*b*) S. BOYDE, C. D. GARNER, J. H. ENEMARK, M. A. BRUCK, and J. G. KRISTOFZSKI. J. Chem. Soc. Dalton Trans. 2267 (1987).
37. M. DRAGANJAC and D. COUCOUVANIS. J. Am. Chem. Soc. **105**, 139 (1983).
38. K. TATSUMI, I. MATSUBARA, Y. SEKIGUCHI, A. NAKAMURA, and C. MEALLI. Inorg. Chem. **28**, 773 (1989).
39. J. HYDE, L. MAGIN, and J. ZUBIETA. J. Chem. Soc. Chem. Commun. 204 (1980).

[3]These tables may be purchased from the Depository of Unpublished Data, CISTI, National Research Council of Canada, Ottawa, Ont., Canada K1A 0S2.

Can. J. Chem. Downloaded from www.nrcresearchpress.com by 186.148.149.217 on 09/07/12
For personal use only.

40. P. J. BLOWER, J. R. DILWORTH, J. P. HUTCHINSON, and J. ZUBIETA. Transition Met. Chem. **7**, 353 (1982).
41. S. F. COLMANET, G. A. WILLIAMS, and M. F. MACKAY. J. Chem. Soc. Dalton Trans. 2305 (1987).
42. J. BALDES, J. BOAS, J. BONNYMAN, M. F. MACKAY, and G. A. WILLIAMS. Aust. J. Chem. **35**, 2413 (1982).
43. J. R. DILWORTH, J. HYDE, P. LYFORD, P. VELLA, K. VENKATASUBRAMAN, and J. A. ZUBIETA. Inorg. Chem. **18**, 268 (1979).
44. D. C. BRADLEY and I. M. THOMAS. J. Chem. Soc. 3857 (1960).
45. D. C. BRADLEY and I. M. THOMAS. Can. J. Chem. **40**, 449 (1962); **40**, 1355 (1962).
46. D. C. BRADLEY and M. H. GITLITZ. J. Chem. Soc. A, 980, (1969).
47. G. CHANDRA and M. F. LAPPERT. J. Chem. Soc. A, 1940 (1968).

Can. J. Chem. Downloaded from www.nrcresearchpress.com by 186.148.149.217 on 09/07/12
For personal use only.

Kinetics of reactions of undecacarbonyl(triethyl phosphite)triruthenium with some P- and As-donor ligands

LEZHAN CHEN AND ANTHONY J. POË[1]

Erindale College and the Department of Chemistry, University of Toronto, Mississauga, Ont., Canada L5L 1C6

Received February 28, 1989

This paper is dedicated to Professor Ronald J. Gillespie on the occasion of his 65th birthday

LEZHAN CHEN and ANTHONY J. POË. Can. J. Chem. **67**, 1924 (1989).

The kinetics have been studied of reactions of the cluster $Ru_3(CO)_{11}(P(OEt)_3)$ with a variety of P- and As-donor nucleophiles, L, in alkane solution. Reactions proceed according to the rate equation: $k_{obsd} = k_1 + k_2[L]$ and activation parameters for the two paths have been obtained. When combined with activation parameters for $Ru_3(CO)_{12}$ and some other $Ru_3(CO)_{11}L'$ clusters the values of $\Delta H_1^{\ddagger}$ and $\Delta S_1^{\ddagger}$ are found to lie on a good isokinetic plot. The changes in the activation parameters are consistent with major and systematic changes in the nature of the $Ru_3(CO)_{10}L'$ moieties left after CO dissociation.

Analysis of the dependence of log k_2 on the electronic and steric nature of the various nucleophiles leads to the derivation of electronic and steric profiles that are characteristic of the cluster, together with values for the intrinsic or standard susceptibility of the cluster towards nucleophilic attack. These kinetic characteristics are compared with those similarly derived for $Ru_3(CO)_{12}$.

Key words: metal carbonyls, ruthenium, clusters, kinetics, mechanisms.

LEZHAN CHEN et ANTHONY J. POË. Can. J. Chem. **67**, 1924 (1989).

On a étudié la cinétique des réactions de l'agrégat $Ru_3(CO)_{11}(P(OEt)_3)$ avec une variété de nucléophiles donneurs de P et d'As, L, en solution dans les alcanes. Les réactions se produisent d'après l'équation de vitesse : $k_{obs} = k_1 + k_2[L]$ et on a obtenu les paramètres d'activation pour les deux voies. Lorsqu'on combine les paramètres d'activation des agrégats du $Ru_3(CO)_{12}$ et d'autres agrégats de formule $Ru_3(CO)_{11}L'$, on trouve que les valeurs des $\Delta H_1^{\ddagger}$ et des $\Delta S_1^{\ddagger}$ se trouvent sur une bonne droite isocinétique. Les changements dans les paramètres d'activation sont en bon accord avec les changements majeurs et systématiques dans la nature des portions $Ru_3(CO)_{10}L'$ qui restent après la dissociation d'un CO.

Une analyse de la relation entre le log k_2 et la nature électronique et stérique des divers nucléophiles permet de dériver des profils électroniques et stériques qui est caractéristique de l'agrégat effectuée en tenant compte des valeurs intrinsèques ou standard de la susceptibilité des agrégats aux attaques nucléophiles. On compare ces caractéristiques cinétiques à celles obtenues de la même manière à partir du $Ru_3(CO)_{12}$.

Mots clés : métal carbonyl, ruthénium, agrégats, cinétique, mécanismes.

[Traduit par la revue]

Introduction

Systematic studies of the reaction kinetics of metal carbonyl clusters (1) are capable of providing characteristic reactivity profiles (2). These define the nature of a particular cluster or group of clusters in a way that complements, and is of comparable importance to, the information provided by structural studies. A given cluster can be quantitatively characterized by its sensitivity to the electronic and steric nature of a series of P-donor nucleophiles (2), by its "intrinsic" reactivity towards nucleophilic attack (2), and by the distribution between substitution and fragmentation products formed as a consequence of nucleophilic attack (3). Alternatively, the S_N1 kinetics of a series of related clusters, differing only in the nature of their P-donor or similar substituents, can also lead to characteristic electronic and steric profiles (4). These studies provide an essentially new way of probing the nature of a large and significant group of organometallic compounds. They are also capable of providing some of the quantitative background necessary when assessing the environmental effects of immobilizing metal carbonyl clusters on surfaces or within zeolytic or other cavities (5), and they therefore form part of the general and continuingly hopeful search (5*b*, 5*c*, 6) for some practical use for these academically fascinating compounds. As part of an extensive study of the effects of substituents on cluster reactivity we have investigated the kinetics of some reactions of the cluster $Ru_3(CO)_{11}(P(OEt)_3)$, and our results are presented below.

[1]Author to whom correspondence may be addressed.

Experimental

General methods

Dodecacarbonyltriruthenium (Strem Chemicals) was used as received. Decalin was washed successively with 4 *M* H_2SO_4 and water, dried over $MgSO_4$, and distilled several times under reduced pressure to ensure the absence of any unsaturated impurities. It was stored over molecular sieves (Linde type 4A). THF (Aldrich) was distilled over sodium benzophenone. Liquid phosphorus ligands (triphenyl phosphite, triethyl phosphite, tri-*n*-butylphosphine, triethylphosphine, diethylphenylphosphine, diphenylethylphosphine, and tri-*t*-butylphosphine) were obtained from commercial sources and were purified by distillation under low pressures of argon or nitrogen immediately before use. Etpb, $(P(OCH_2)_3CEt)$ (Strem Chemicals), was sublimed (50°C, 0.12 mm Hg) immediately before use. Other ligands were obtained and used as described previously (7). Infrared spectra were measured with a Nicolet 10DX FTIR spectrophotometer, and ^{31}P NMR spectra with a Varian XL-200 spectrometer. Ultraviolet–visible spectra of solutions were measured with a Cary 2300 spectrophotometer, the solutions being contained in 10-mm silica cells placed in a thermostated cell holder.

Preparation of $Ru_3(CO)_{11}(P(OEt)_3)$

The cluster $Ru_3(CO)_{11}(P(OEt)_3)$ was prepared by the general method of Bruce *et al.* (8). $Ru_3(CO)_{12}$ (100 mg, 0.156 mmol) in THF (6 cm^3) was reacted with $P(OEt)_3$ (0.029 cm^3, 0.17 mmol) in the presence of a few drops of sodium ketyl in THF at 40°C until the IR band at 2060 cm^{-1} due to $Ru_3(CO)_{12}$ was no longer detectable. Solvent was removed under vacuum, the reddish oily product was dissolved in hexane, and the solution was filtered. The IR spectrum of the clear red filtrate showed bands due (Table 1) to those expected for $Ru_3(CO)_{11}(P(OEt)_3)$ by comparison with the spectrum of $Ru_3(CO)_{11}(P(OMe)_3)$ (8*c*). The cluster was purified by chromatography on

Can. J. Chem. Downloaded from www.nrcresearchpress.com by 186.148.149.217 on 09/07/12
For personal use only.

TABLE 1. Infrared spectra[a] of some ruthenium carbonyls

Complex	ν(CO), cm^{-1}
$Ru_3(CO)_{12}$	2060(s), 2029(m), 2010(w)
$Ru_3(CO)_{11}(P(OEt)_3)$	2100(w), 2045(10640), 2032(m), 2014(12670), 1996(m), 1989(m), 1978(sh), 1959(sh)
$Ru_3(CO)_{11}(P(OMe)_3)$[b]	2102(w), 2049(s), 2034(m), 2018(s), 2000(m), 1993(m), 1982(sh), 1970(sh)
$Ru_3(CO)_{10}(P(OEt)_3)_2$	2082(w), 2026(m), 2001(s)
$Ru_3(CO)_{10}(P(OMe)_3)_2$[b]	2085(w), 2030(m), 2005(s), 1985(sh)
$Ru_3(CO)_{10}(P(OEt)_3)(AsPh_3)$	2079(w), 2025(m), 1998(s), 1979(w)
$Ru_3(CO)_9(P(OEt)_3)_3$	1985(s)
$Ru_3(CO)_9(P(OMe)_3)_3$[b]	2062(vw), 1990(s), 1964(w)
$Ru(CO)_4(P(OEt)_3)$	2068(m), 1997(w), 1966(3870), 1951(5040)
$Ru(CO)_3(P(OEt)_3)_2$	1927(4420), 1915(4390)
$Ru(CO)_3(P(OEt)_3)$(etpb)[c]	1944(s), 1933(s)
$Ru(CO)_3(P(OEt)_3)(P\text{-}t\text{-}Bu_3)$[c]	1902(s), 1887(s)

[a]Spectra recorded in decalin unless otherwise indicated. Numbers in parentheses are molar absorption coefficients (M^{-1} cm^{-1}) estimated from the absorbances recorded by our spectrophotometer for solutions of known concentration. Assignments are made by reference to published data or to data for closely related clusters (8*c*).

[b]In hexane.

[c]In heptane.

a foil-wrapped 60–100 mesh Florisil column. Traces of unreacted $Ru_3(CO)_{12}$ were eluted first with a mixture of hexane and dichloromethane (ca. 2:1 by volume), followed by $Ru_3(CO)_{11}(P(OEt)_3)$, some mononuclear products remaining on the column. The $Ru_3(CO)_{11}(P(OEt)_3)$ was isolated in ca. 40% yield as a dark red oil by removal of hexane under vacuum. Attempts to obtain the cluster in crystalline form were unsuccessful.[2] It was characterized by its IR spectrum (Table 1) which is virtually identical with that of the crystallographically characterized $Ru_3(CO)_{11}(P(OMe)_3)$ (9). Its purity was demonstrated by means of its ^{31}P NMR spectrum, a single sharp peak being observed at −138.3 ppm relative to $P(OMe)_3$ and decoupled from ^1H. No peaks due to free $P(OEt)_3$ or to $Ru_3(CO)_{10}(P(OEt)_3)_2$ (4) were observed. $Ru_3(CO)_{10}(P(OEt)_3)_2$ and $Ru_3(CO)_{10}(P(OMe)_3)_2$ were prepared and purified in a similar manner (8*c*) but using ≥2 equivalents of ligand. The clusters $Ru_3(CO)_{10}(P(OEt)_3)_2$ and $Ru_3(CO)_9(P(OEt)_3)_3$ could be separated by chromatography.

Kinetic procedures

Most kinetic runs were carried out on decalin solutions prepared in Schlenk tubes wrapped with aluminium foil and equipped with rubber-septum caps to allow convenient sample removal by using a syringe with a stainless steel needle. All solutions were purged with a stream of N_2 or Ar (Canox Ltd.) for ca. 10 min before immersing the Schlenk tube in a water bath and continuing the bubbling for another 5 min. Solutions were thermostated to ±0.1°C by a Lauda Constant Temperature Bath RCS-6. Samples were withdrawn periodically, transferred to small phials, and the reaction quenched by cooling the phials in dry ice or liquid N_2. Infrared spectra of the quenched liquid samples were recorded in the absorbance mode using 1.0-mm path-length solution cells with NaCl windows. Initial concentrations of reacting complex were generally ca. 4×10^{-4} *M*.

Infrared spectra taken during the reactions followed exactly the changes expected for successive substitutions and fragmentations. The reaction of $Ru_3(CO)_{11}(P(OEt)_3)$ with PPh_3 showed that the further reaction of the initial product, $Ru_3(CO)_{10}(P(OEt)_3)(PPh_3)$, with PPh_3 was too rapid to allow accurate values of A_∞ to be obtained when employing UV–vis methods. Thus all rate measurements for this and other similar reactions had to be obtained through IR monitoring.

[2]The cluster $Ru_3(CO)_{11}(P(OMe)_3)$ has been prepared in an exactly similar manner and crystals of this cluster suitable for crystallographic investigation (9) were obtained.

Rate constants were generally obtained by monitoring the decreasing absorbances of the IR band at 2045 cm^{-1} due to $Ru_3(CO)_{11}(P(OEt)_3)$. In all cases values of A_∞ were very small and plots of ln $(A_t - A_\infty)$ were linear for ca. 80–90% reaction. The rate constants calculated instead from the decreasing absorbances at 2100, 2032, and 2014 cm^{-1} and from the increasing absorbances due to the fragmentation products (see below) were virtually the same in most of the cases tested, the differences being ca. 5%.

Infrared spectra of reactions of $Ru_3(CO)_{11}(P(OEt)_3)$ with $AsPh_3$ showed that the initial product $Ru_3(CO)_{10}(P(OEt)_3)(AsPh_3)$ (Table 1) was quite stable under the conditions used. There were very clean isosbestic points in the IR spectra and no evidence for significant further reaction of $Ru_3(CO)_{10}(P(OEt)_3)(AsPh_3)$ with $AsPh_3$ was observed. Ultraviolet–visible monitoring of this reaction was thereby shown to be satisfactory in providing good values of A_∞ and the growing band at 460 nm was monitored to obtain the rate constants. Pre-thermostated solutions were contained in 10 mm cuvettes placed in the thermostated cell holder of a Cary 2300 spectrophotometer. Solutions were purged with a stream of Ar for ca. 10 min and the cells were then sealed with Teflon stoppers. Reactions were followed by repetitive scanning of groups of up to four reacting solutions. Cell temperatures were measured with an iron–constantan thermocouple connected to a digital multimeter. In two cases reactions were instead followed using IR monitoring techniques and employing standard Schlenk tube methods.

Results

Products of reactions

The changes in the IR spectra during reactions with all nucleophiles apart from $AsPh_3$ showed initial formation of $Ru_3(CO)_{10}(P(OEt)_3)L$ followed by further reactions to form $Ru_3(CO)_9(P(OEt)_3)L_2$. The rates of these latter reactions were much faster when L = PPh_3, P-*i*-Bu_3, and P-*n*-Bu_3 than when L = $P(OPh)_3$ and $P(OEt)_3$ but no quantitative kinetic studies were performed.

In addition it was clear from the IR spectra that mononuclear $Ru(CO)_4L$ and $Ru(CO)_3L_2$ complexes were formed (Table 1) as well as the trinuclear substitution products, and the relative yields of the mononuclear products, compared with the substitution products, increased with increasing [L]. Molar absorption

Can. J. Chem. Downloaded from www.nrcresearchpress.com by 186.148.149.217 on 09/07/12
For personal use only.

TABLE 2. Rate constants for the reactions of $Ru_3(CO)_{11}(P(OEt)_3)$ with nucleophiles, L, in decalin ([complex] = ca. 4×10^{-4} M)

L (pK_a, θ°)	T (°C)	N^a	[L] (M)	$10^5 k_1$ (s^{-1})	$10^5 k_2$ ($M^{-1}\,s^{-1}$)	$\sigma(k_{obs})^b$ (%)
etpb (1.74, 101)	40.0	7	0.007–0.08	6.46±0.39[c]	175±14[c]	6.8
$P(OEt)_3$	20.0	9	0.014–0.5	0.245±0.038	66.4±1.1	
(3.31, 109)	34.0	5	0.05–0.5	4.14±0.56	173±5	3.7
	40.0	6	0.01–0.2	6.94±0.33	283±9	
	50.0	5	0.01–0.3	28.2±0.9	580±18	
$P(OPh)_3$	40.0	11	0.016–0.2	6.49±0.05	6.94±0.46	
(−2.0, 128)	50.0	5	0.024–0.3	28.1±0.3	15.7±2.0	1.5
	60.0	7	0.062–0.3	116±2	46.6±9.6	
P-n-Bu_3	30.0	9	0.05–0.45	−1.21±1.38	179±12	
(8.43, 132)	40.0	7	0.05–0.32	6.88±5.37	396±44	12.7
	50.0	4	0.04–0.23	7.85±8.85	861±103	
PPh_3	30.0	5	0.024–0.2	1.38±0.01		
(2.73, 145)	40.0	5	0.027–0.2	6.89±0.07		2.4
	50.0	6	0.049–0.2	29.7±0.9		
	60.0	5	0.029–0.2	125±2		
P-i-Bu_3	25.0	3	0.05–0.2	0.617±0.018	1.04±0.14	
(7.97, 143)	40.0	5	0.036–0.4	6.61±0.11	6.14±0.65	2.1
	60.0	3	0.067–0.2	118±3	41.4±24.7	
$AsPh_3$	20.0	1	0.0543	0.278		
(−, 142)[d]	38.9	4	0.047–0.2	6.52±0.05		
	40.0	1	0.0165	6.92		3.5
	48.4	6	0.047–0.2	25.5±0.34		
	57.1	4	0.070–0.2	88.6±0.9		
	64.0	4	0.047–0.2	216±4		

[a]Number of individual determinations of k_{obsd}; $k_{obsd} = k_1 + k_2[L]$.
[b]Probable error of an individual determination of k_{obsd} obtained by pooling data at all temperatures and then adjusting according to the number of degrees of freedom (10).
[c]Uncertainties here and below are standard deviations.
[d]The cone angle for $AsPh_3$ has been estimated as in ref. 11.

coefficients for the bands due to $Ru(CO)_4(P(OEt)_3)$ and $Ru(CO)_3(P(OEt)_3)_2$ were obtained (Table 1) from IR studies of these complexes prepared from solutions of $Ru(CO)_4(C_2H_4)$ of known concentration (11). Measurements of the growing intensities of these bands during the initial stages of the reaction of $P(OEt)_3$ with $Ru_3(CO)_{11}(P(OEt)_3)$ showed that the products $Ru(CO)_4(P(OEt)_3)$ and $Ru(CO)_3(P(OEt)_3)_2$ were formed in the constant molar ratio (2.02 ± 0.13):1, irrespective of the values of $[P(OEt)_3]$ and the temperatures. Mononuclear products, in easily detectable amounts, were also observed with L = etpb, P-n-Bu_3, and $P(OPh)_3$, but not with L = PPh_3 or P-i-Bu_3.

Kinetics of reactions of $Ru_3(CO)_{11}(P(OEt)_3)$ with L

Most reactions proceeded via a mixture of first and second order paths with the rate equation being given by $k_{obsd} = k_1 + k_2[L]$. In these cases a weighted linear least-squares analysis (10) was applied in order to obtain values for k_1 and k_2, and their probable errors. Precise values of k_1 when L = P-n-Bu_3 could not be obtained because of the high contribution from the $k_2[L]$ path. The value of k_2 at the highest temperature used for reactions with P-i-Bu_3 was very uncertain because of the high relative contribution from the k_1 path at this temperature. When L = $AsPh_3$ or PPh_3 the values of k_{obsd} showed no significant dependence on [L] and they were simply averaged to give k_1. For these, and for some other reactions when the $k_2[L]$ term was small, the values of k_{obsd} at the lower values of [L] tended to be slightly lower than expected from the rate equation. This was probably due to slight retardation of the [L]-independent path by the CO released and, when any such doubt arose, these low values were omitted from the least-squares analysis because of their tendency to lead to incorrectly high values of k_2. The values of k_1 and k_2 for all these reactions are given in Table 2.

TABLE 3. Kinetic parameters[a] for dissociative reactions of $Ru_3(CO)_{11}(P(OEt)_3)$ with nucleophiles, L

L	$\Delta H_1^{\ddagger}$ (kcal mol^{-1})	$\Delta S_1^{\ddagger}$ (cal $K^{-1}\,mol^{-1}$)	$10^5 k_1$ (40°C)[b] (s^{-1})
$AsPh_3$	29.0 ±0.2	14.9 ±0.4	7.43±0.04
$P(OEt)_3$	27.8 ±1.7	11.1 ±5.2	6.94±0.32
PPh_3	29.4 ±0.1	16.2 ±0.3	6.80±0.02
$P(OPh)_3$	29.2 ±0.3	15.4 ±0.9	6.43±0.05
P-i-Bu_3	29.0 ±0.3	15.0 ±0.8	6.68±0.01
	29.25±0.10[c]	15.70±0.23[c]	6.78±0.30

[a]Uncertainties are standard deviations (see text).
[b]Estimated from the activation parameters (to four significant figures) with uncertainties calculated by taking into account the covariance in the uncertainties of $\Delta H_1^{\ddagger}$ and $\Delta S_1^{\ddagger}$.
[c]From weighted average of individual activation parameters (to four significant figures).

Activation parameters (Tables 3 and 4) were calculated by a weighted linear least-squares analysis of the dependence of $\ln(k/T)$ on $1/T$. Since specific standard deviations were available for each value of k_1 or k_2 these could be used to calculate the standard deviations of each value of $\ln(k/T)$ so

Can. J. Chem. Downloaded from www.nrcresearchpress.com by 186.148.149.217 on 09/07/12
For personal use only.

TABLE 4. Kinetic parameters[a] for associative reactions of $Ru_3(CO)_{11}(P(OEt)_3)$ with P-donor nucleophiles, L

L	$\Delta H_2^{\ddagger}$ (kcal mol^{-1})	$\Delta S_2^{\ddagger}$ (cal K^{-1} mol^{-1})	$10^5 k_2$ (40°C)[b] (M^{-1} s^{-1})
$P(OEt)_3$	12.8±0.4	−29.4±1.4	284±5
P-*n*-Bu_3	14.5±1.3	−23.2±4.1	401±11
$P(OPh)_3$	17.7±1.9	−21.1±6.0	6.9±0.2
P-*i*-Bu_3	21.1±2.0	−10.5±6.6	6.2±0.4

[a]Uncertainties are standard deviations.
[b]Estimated from the activation parameters with uncertainties calculated by taking into account the covariance in the uncertainties of $\Delta H_2^{\ddagger}$ and $\Delta S_2^{\ddagger}$.

that each value could be weighted in the least-squares analysis according to the inverse of its variance. Two procedures could be followed. In one only relative weightings were used and absolute values for the uncertainties in the activation parameters were obtained by making use of the residuals between the calculated and experimental values of ln (k/T). Occasionally the data fitted very closely to the linear Eyring plot in spite of having relatively high individual uncertainties. This led to accidentally small residuals, and uncertainties in the activation parameters that were unreasonably low in view of the individual uncertainties in ln (k/T). In these cases the uncertainties in the activation parameters were calculated according to an equation in which the absolute uncertainties in ln (k/T) lead directly to the uncertainties in the activation parameters. However, there were cases where the internal consistency of the data at each temperature was high and the uncertainties in each value of ln (k/T) were less than the scatter of the data around the linear Eyring plot. In these cases the uncertainties in the activation parameters were unreasonably small in view of the errors involved in the actual temperature dependence and so the first method of estimating the uncertainties was used instead, i.e. in all cases the method leading to the greater uncertainties in the activation parameters was the one used. In the case of reactions with PPh_3 and $AsPh_3$, where there were no k_2[L] terms, each individual value of ln (k_{obsd}/T) was used in the analysis with equal weighting.

Derivation of electronic and steric profiles

The characterization of electronic and steric effects in associative reactions of metal carbonyls with nucleophiles has been thoroughly described elsewhere (2, 12–15). A plot of log k_2 (40°C) for reactions of $Ru_3(CO)_{11}(P(OEt)_3)$ with L against values of pK_a do not show a clear linear relationship (Fig. 1). It is obvious that steric effects are important because reactions are much slower when L = P-*i*-Bu_3 than when L = P-*n*-Bu_3. Although these nucleophiles have similar basicities (16) P-*i*-Bu_3 is bigger than P-*n*-Bu_3 (17). However, the nucleophiles $P(OPh)_3$ and P-*n*-Bu_3 have very similar cone angles (17), and their relative values of log k_2 can be taken to be determined mainly by electronic effects, making allowances (15) for the small differences in cone angle. This provides a measure of the electronic effect, for hypothetical nucleophiles of cone angle 130°, that can be quantified by the gradient, β, of the line drawn in Fig. 1. Deviations from this line of the values of log k_2 can be ascribed to steric effects. We can calculate values (2, 15) of $\log k_2^0 = \log k_2 - \beta(pK_a + 4)$ and those for reactions at 40°C are plotted in Fig. 2 against cone angles of the nucleophiles (17).

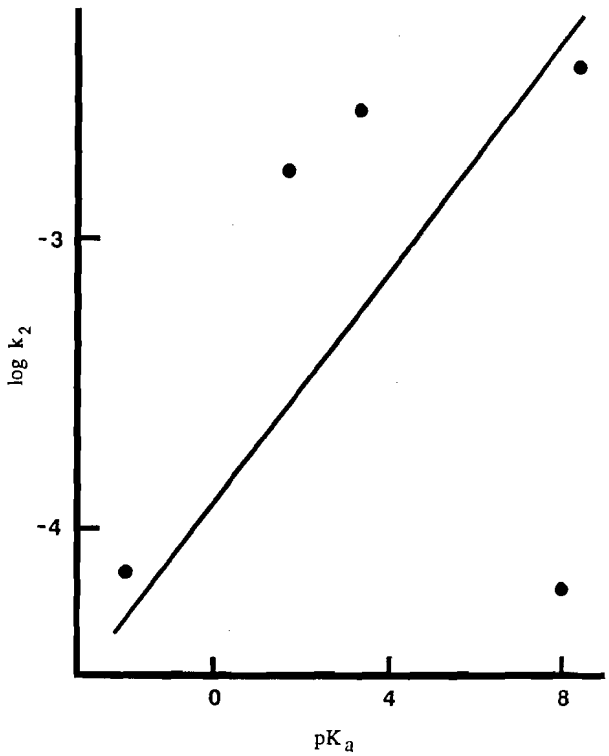


FIG. 1. Dependence of log k_2 (40°C) for reactions of $Ru_3(CO)_{11}(P(OEt)_3)$ on the σ-basicity (pK_a) of the nucleophiles. The nucleophiles are, from left to right, $P(OPh)_3$, etpb, $P(OEt)_3$, P-*i*-Bu_3, and P-*n*-Bu_3. The line is drawn for hypothetical P-donor nucleophiles of the same respective basicity as $P(OPh)_3$ and P-*n*-Bu_3 but with identical cone angles of 130°. It allows for the slightly different cone angles of $P(OPh)_3$ and P-*n*-Bu_3 (see text).

Discussion

The kinetic parameters, and their uncertainties, listed in Tables 2–4 show that the data for the reactions studied here are of very good precision. The values of k_1, $\Delta H_1^{\ddagger}$, and $\Delta S_1^{\ddagger}$ obtained by using several different entering ligands are in excellent agreement with each other (Table 3).

The [L]-independent path

The reaction governed by k_1 is normally assumed to proceed by a simple CO dissociative mechanism (18). Although other mechanisms are possible (19, 20) there is no positive evidence for them and it seems preferable therefore to continue to regard these reactions as being simply dissociative in nature. The kinetic parameters for $Ru_3(CO)_{11}(P(OEt)_3)$ can be compared (Table 5) with those reported elsewhere for $Ru_3(CO)_{11}L'$ (L′ = CO, PPh_3, or P-*n*-Bu_3). The values of k_1 fit quite well with eq. [1] (11) where $\beta_{L'}$ and $\gamma_{L'}$ represent the dependence of

$$[1] \quad \log k_1 = \alpha_{L'} + \beta_{L'}\delta + \gamma_{L'}\theta$$

the rates on the electronic parameters, δ (22)[3], and on the cone angles, θ, respectively, which are characteristic of the individual substituents, L′. Because there are only four different substituents, covering a relatively restricted range of δ and θ,

[3]The parameter δ measures the ^{13}C chemical shift of $Ni(^{13}CO)_3L$ relative to that in $Ni(^{13}CO)_4$ and is chosen (11) to represent the net electron donor capacity of L′ because, being a substituent and not a nucleophile, π-acidity of L′ will be important as well as σ-basicity (11, 22).

Can. J. Chem. Downloaded from www.nrcresearchpress.com by 186.148.149.217 on 09/07/12
For personal use only.

TABLE 5. Activation parameters for dissociative reactions of $Ru_3(CO)_{11}L'$

L' (δ)[a]	$\Delta H_1^{\ddagger}$ (kcal mol^{-1})	$\Delta S_1^{\ddagger}$ (cal K^{-1} mol^{-1})	$10^5 k_1$ (40.0°C) (s^{-1})	Reference
CO (0)	31.8±0.2	20.2±0.6	1.08±0.02	13(*a*)
$P(OEt)_3$ (3.61)	29.3±0.1	15.7±0.2	6.8±0.3	This work
PPh_3 (4.30)	25.6±0.2	9.1±0.5	86±6	20
P-*n*-Bu_3 (5.69)	22.1±0.6	−1.1±1.8	141±8	21

[a]Values of δ (ppm) from ref. 22 (see text).

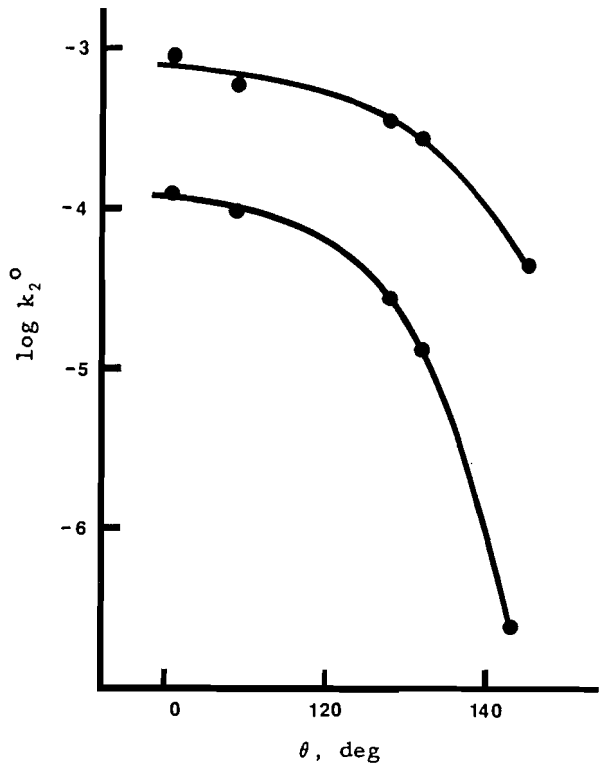
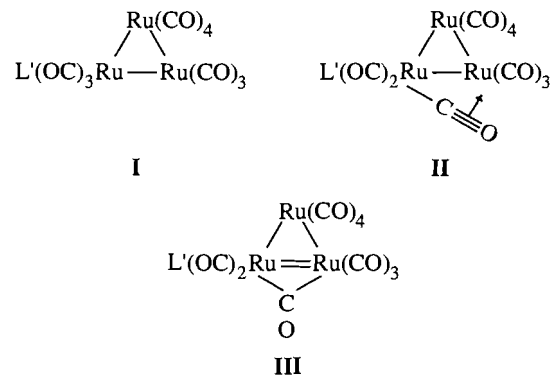


FIG. 2. Dependence of log k_2^0 at 40°C (see text) on the cone angles, θ, of the nucleophiles (upper curve for $Ru_3(CO)_{12}$; lower curve for $Ru_3(CO)_{11}(P(OEt)_3)$). The nucleophiles are, from left to right, etpb, $P(OEt)_3$, $P(OPh)_3$, P-*n*-Bu_3, and PPh_3 (upper curve) or P-*i*-Bu_3 (lower curve).

the precisions of the three parameters obtained are not very good but the values of $\beta_{L'}$ and $\gamma_{L'}$ are all positive and show a clear decrease with increasing temperature. These results will be discussed in detail elsewhere (4) together with trends in rate constants at 40°C involving a much wider range of substituents.

Apart from these trends in the rate constants we can also examine the trends in the activation parameters (Table 5). The decrease in $\Delta H_1^{\ddagger}$ is opposed, but not overcome, by a decreasingly favourable value of $\Delta S_1^{\ddagger}$ and the data fall on a good isokinetic plot[4] (Fig. 3) the gradient of which leads to an isokinetic temperature of ca. 180°C. This shows that the relative rates of the reactions are more dependent on the enthalpy of activation than on the entropy and that changes in $\Delta G_1^{\ddagger}$ are less pronounced than those of $\Delta H_1^{\ddagger}$. This also accounts for the decreasing values of $\beta_{L'}$ and $\gamma_{L'}$ with increasing temperatures because the rate constants will become completely independent of the nature of the substituent, L',at the isokinetic temperature.

The lower values of $\Delta S_1^{\ddagger}$ are not typical of those found for simple CO dissociative reactions, especially of mononuclear carbonyls (18). However, low values of this sort have been obtained several times for dissociative reactions of metal carbonyl clusters (23, 24). They can be ascribed (23) to rearrangements undergone by the residual clusters during the loss of the CO ligands. These rearrangements have the effect of maintaining the 18-electron nature of the cluster by recourse to formation of bridging carbonyls and metal–metal double bonds. The intermediates here can be envisaged (23*a*) as being of types varying from **I** (high $\Delta S_1^{\ddagger}$), **II** (intermediate $\Delta S_1^{\ddagger}$), and **III** (low $\Delta S_1^{\ddagger}$).



These correspond to increasingly tight bonding, decreasing values of $\Delta H_1^{\ddagger}$, and correspondingly decreased values of $\Delta S_1^{\ddagger}$ that result from increased strength of the bonding within the cluster (i.e. higher vibrational frequencies) and increasingly precise atomic movements to form the intermediate clusters. The values of $\Delta H_1^{\ddagger}$ decrease monotonically with increasing net electron donating capacity of L' and this correlates with the increasing tightness of bonding in the $Ru_3(CO)_{10}L'$ intermediate. The bridging nature of **II** would be expected to be encouraged by a more electron donating L', and **III** might be expected to be a logical extension of this process since this Ru_3 cluster involves four bonding electron pairs rather than the original three. Any steric effects are not sufficiently large to be rationalized at this time.

The [L]-dependent path

The procedure previously used (2, 13, 15) for separating the electronic and steric effects of different nucleophiles in associative reactions of metal carbonyl clusters is also entirely

[4]The value of $\Delta S_1^{\ddagger}$ for $Ru_3(CO)_{12}$ should probably be slightly lower than shown, compared with the values for the substituted clusters, for statistical reasons. A CO ligand can dissociate from any of the three $Ru(CO)_4$ moieties in $Ru_3(CO)_{12}$ but from only one or two of the Ru atoms in the substituted cluster. This will result in only a small adjustment to the value of $\Delta S_1^{\ddagger}$ for $Ru_3(CO)_{12}$ although it will be in the direction of making the data for $Ru_3(CO)_{12}$ fit a little less well to the isokinetic plot.

Can. J. Chem. Downloaded from www.nrcresearchpress.com by 186.148.149.217 on 09/07/12
For personal use only.

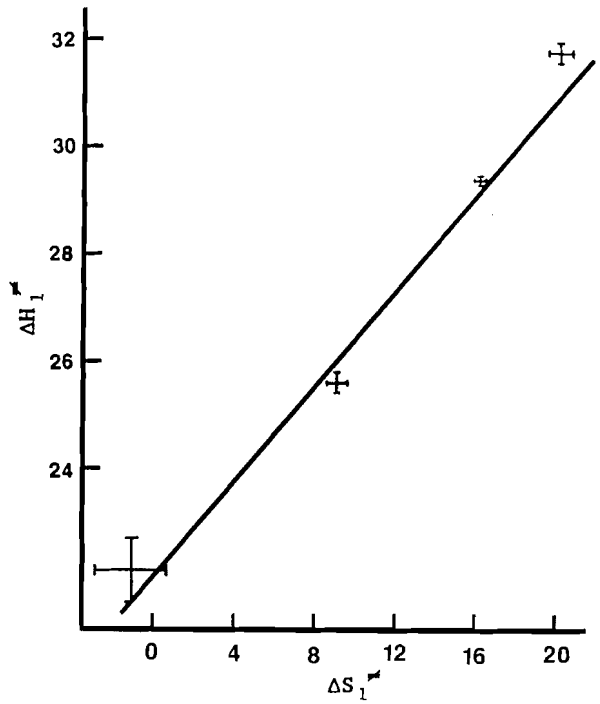


FIG. 3. Isokinetic plot of activation parameters for dissociative reactions of $Ru_3(CO)_{11}L'$ (L', from left to right, = P-*n*-Bu_3, PPh_3, $P(OEt)_3$, and CO).

successful for reactions of $Ru_3(CO)_{11}(P(OEt)_3)$ (Figs. 1 and 2). Although the gradient of the line in Fig. 1 is determined by only two points we do know that values of log k_2 depend linearly on pK_a in associative reactions of metal carbonyls for which steric effects are negligible (2, 12, 18(*b*), 25). The gradient corresponds to an electronic selectivity parameter, β, of 0.20 compared with a similarly derived value of 0.15 for $Ru_3(CO)_{12}$ (15). The slightly larger value for $Ru_3(CO)_{11}(P(OEt)_3)$ implies (2, 13) that the extent of bond making in the transition states is somewhat higher than for reactions of the unsubstituted $Ru_3(CO)_{12}$. This is counter to what might have been expected from the presumed increase of electron density on the cluster due to the presence of the electron donating P-donor substituents.

The steric profile for $Ru_3(CO)_{11}(P(OEt)_3)$ is clearly similar in form (Fig. 2) to that for $Ru_3(CO)_{12}$ but the downward curvature with increasing θ is more pronounced for the substituted cluster. This is very simply in accord both with the slightly higher degree of bond making deduced above for the reactions of $Ru_3(CO)_{11}(P(OEt)_3)$ and, more particularly, with the greater steric effect expected when a small CO is replaced by the larger $P(OEt)_3$ ligand. A similar steric effect is observed (15) for $Ru_3(CO)_{10}(\mu\text{-}Ph_2PCH_2PPh_2)$.

The steric profiles provide another kinetic parameter for the two clusters. Both steric profiles approach the horizontal as θ decreases. This means that the steric effects would decrease to zero if small enough nucleophiles were available. The value of log k_2^0 would then correspond to the value of log k_2 that would be observed for a hypothetical small and very weak nucleophile of p$K_a = -4$. This standard reactivity has been chosen so that it approaches the intrinsic reactivity of the cluster towards nucleophilic attack (2*b*, 2*c*, 15). The steric profiles coupled with the relative values of β, suggest that the substituted cluster is intrinsically less susceptible to nucleophilic attack than $Ru_3(CO)_{12}$ by ≥1 log unit or ≥1.4 kcal mol^{-1} in $\Delta G_2^{\ddagger}$ at 40°C.

The increasing yields of mononuclear products with increasing values of $[P(OEt)_3]$ show clearly that at least some of the second order reactions are proceeding by F_N2 processes (2*c*, 3). The fact that $Ru(CO)_4(P(OEt)_3)$ and $Ru(CO)_3(P(OEt)_3)_2$ are formed in the mole ratio 2:1 shows that it is mainly the $Ru_3(CO)_{11}(P(OEt)_3)$ that is undergoing direct fragmentation (3). The expansion in the Ru_3 cluster that is required during the formation of the transition state will be likely to facilitate the ultimate formation of mononuclear products, especially when this Ru_3 cluster is already expanded even in the ground state of the molecule (9, 26). The observation of substantial amounts of mononuclear products, resulting from F_N2 processes, in the reactions of $Ru_3(CO)_{11}(P(OEt)_3)$ with several other nucleophiles that show k_2 terms is therefore not unexpected but it is interesting that the proportion of F_N2 processes also depends on the nature of the nucleophiles.

Finally, it is important to note the trends in activation parameters for associative reactions of some Ru_3 clusters. The data in Table 4 show that the values of $\Delta H_2^{\ddagger}$ for attack on $Ru_3(CO)_{11}(P(OEt)_3)$ by L increase substantially in the order L = $P(OEt)_3$ < P-*n*-Bu_3 < $P(OPh)_3$ < P-*i*-Bu_3. These changes are offset by corresponding increases in $\Delta S_2^{\ddagger}$ and the data do, in fact, lie on a reasonable isokinetic plot with an isokinetic temperature of ca. 170°C. The trends in the rate constants that were discussed above are therefore clearly more dependent on $\Delta H_2^{\ddagger}$ than on $\Delta S_2^{\ddagger}$. The changes in the values of $\Delta S_2^{\ddagger}$ enable us to suggest that the expansion of the Ru_3 cluster that accompanies attack by the larger P-*i*-Bu_3 may be more pronounced than in attack by the smaller P-*n*-Bu_3. This allows for similar amounts of bond-making and must account for the higher value of $\Delta H_2^{\ddagger}$ for reaction with P-*i*-Bu_3. The greater expansion implies a more weakly bonded $Ru_3(CO)_{11}(P(OEt)_3)$ moiety in the transition state with a correspondingly less negative value of $\Delta S_2^{\ddagger}$. The low value of $\Delta H_2^{\ddagger}$ for attack by the smaller $P(OEt)_3$ can therefore be ascribed to the need for a lesser expansion of the cluster in order to have the same degree of bond making, and a corresponding more negative value of $\Delta S_2^{\ddagger}$.

The values of $\Delta H_2^{\ddagger}$ for attack by P-*n*-Bu_3 on the clusters $Ru_3(CO)_{11}L'$ increase by ca. 7 kcal mol^{-1} along the series L' = P-*n*-Bu_3 (21) < CO (13*a*) < $P(OEt)_3$ (this work). The values of $\Delta H_2^{\ddagger}$ and $\Delta S_2^{\ddagger}$ also lie on a fair isokinetic plot with an isokinetic temperature of roughly 125°C. This trend is not so easy to rationalise in view of the expected (2*b*, 2*c*) differences in extents of bond making in the transition states and the different dimensions (9, 26), and consequently different steric effects, of the clusters involved.

Acknowledgements

We are grateful to the Natural Sciences and Engineering Research Council, Ottawa, for support of this work and Tongji Medical University, P.R.C., for leave of absence for one of us (L.C.).

1. A. J. POË. *In* Metal clusters. *Edited by* M. Moskovits. Wiley, New York. 1986. Chap. 4.
2. (*a*) K. DAHLINGER, F. FALCONE, and A. J. POË. Inorg. Chem. **25**, 2654 (1986); (*b*) A. J. POË. Pure App. Chem. **60**, 1209 (1988); (*c*) N. M. J. BRODIE, L. CHEN, and A. J. POË. Int. J. Chem. Kinet. **20**, 467 (1988).
3. N. M. J. BRODIE and A. J. POË. Inorg. Chem. **27**, 3156 (1988).
4. N. M. J. BRODIE and A. J. POË. To be submitted.
5. (*a*) N. LUGAN, G. LAVIGNE, J. J. BONNET, R. REAU, D. NEIBECKER, and I. TKATCHENKO. J. Am. Chem. Soc. **110**, 5369 (1988); (*b*) P. GALLEZOT, A. BRENNER, and B. C. GATES. *In*

Can. J. Chem. Downloaded from www.nrcresearchpress.com by 186.148.149.217 on 09/07/12
For personal use only.

Metal clusters. *Edited by* M. Moskovits. Wiley, New York. 1986; (*c*) G. LAVIGNE and H. D. KAESZ. *In* Clusters and catalysis. *Edited by* Gates, Guczi, and Knozinger. Elsevier, New York. 1986. Chap. 4. pp. 43–88.
6. (*a*) N. LUGAN, J. J. BONNET, and J. A. IBERS. Organometallics, **7**, 1538 (1988); (*b*) E. L. MUETTERTIES, R. R. BURCH, and A. STOLZENBERG. Ann. Rev. Phys. Chem. **33**, 89 (1982); (*c*) G. W. PARSHALL. Homogeneous catalysis. Wiley, New York. 1980; (*d*) J. K. KOCHI. Organometallic mechanisms and catalysis. Academic Press, New York. 1978; (*e*) M. O. ALBERS and N. J. COVILLE. Coord. Chem. Rev. **53**, 227 (1984).
7. M. A. COBB, B. HUNGATE, and A. J. POË. J. Chem. Soc. Dalton Trans. 2226 (1976).
8. (*a*) M. I. BRUCE, T. W. HAMBLEY, B. K. NICHOLSON, and M. R. SNOW. J. Organomet. Chem. **235**, 83 (1982); (*b*) M. I. BRUCE, D. C. KEHOE, J. G. MATISONS, B. K. NICHOLSON, P. H. RIEGER, and M. L. WILLIAMS. J. Chem. Soc. Chem. Commun. 442 (1982); (*c*) M. I. BRUCE, J. G. MATISONS, and B. K. NICHOLSON. J. Organomet. Chem. **247**, 321 (1983).
9. N. M. J. BRODIE, L. CHEN, A. J. POË, and J. F. SAWYER. Acta Crystallogr. Part C. Cryst. Struct. Commun. In press.
10. A. J. POË and V. C. SEKHAR. Inorg. Chem. **24**, 4376 (1985).
11. L. CHEN and A. J. POË. Inorg. Chem. In press.
12. H. G. SCHUSTER-WOLDAN and F. BASOLO. J. Am. Chem. Soc. **88**, 1657 (1966); E. M. THORSTEINSON and F. BASOLO. J. Am. Chem. Soc. **88**, 3929 (1966).
13. (*a*) A. J. POË and M. V. TWIGG. J. Chem. Soc. Dalton Trans. 1860 (1974); (*b*) R. A. JACKSON, R. KANLUEN, and A. J. POË. Inorg. Chem. **23**, 523 (1984).
14. M. N. GOLOVIN, M. M. RAHMAN, J. E. BELMONTE, and W. P. GIERING. Organometallics, **4**, 1981 (1985).
15. B. AMBWANI, S. K. CHAWLA, and A. J. POË. Polyhedron, **7**, 1939 (1988).
16. M. M. RAHMAN, H. Y. LIU, A. PROCK, and W. P. GIERING. Organometallics, **6**, 650 (1987).
17. C. A. TOLMAN. Chem. Rev. **77**, 313 (1977); C. A. TOLMAN. J. Am. Chem. Soc. **92**, 2956 (1970).
18. (*a*) J. A. S. HOWELL and P. M. BIRKINSHAW. Chem. Rev. **83**, 557 (1983); (*b*) F. BASOLO and R. G. PEARSON. Mechanisms of inorganic reactions. 2nd ed. Wiley, New York. 1967.
19. S. BREITSHAFT and F. BASOLO. J. Am. Chem. Soc. **88**, 2702 (1966); L. I. B. HAINES and A. J. POË. J. Chem. Soc. (A), 2824 (1969); D. DEWIT, J. P. FAWCETT, and A. J. POË. J. Chem. Soc. Dalton Trans. 528 (1976); D. P. KEETON, S. K. MALIK, and A. J. POË. J. Chem. Soc. Dalton Trans. 233 (1977); D. TAUBE and P. FORD. Organometallics, **5**, 99 (1986); A. J. POË. Inorg. Chim. Acta, **129**, L17 (1987).
20. S. MALIK and A. J. POË. Inorg. Chem. **17**, 1484 (1978).
21. N. M. J. BRODIE, A. J. POË, and V. C. SEKHAR. J. Chem. Soc. Chem. Commun. 1090 (1985).
22. G. BODNER, M. MAY, and L. MCKINNEY. Inorg. Chem. **19**, 1951 (1980).
23. (*a*) S. K. MALIK and A. J. POË. Inorg. Chem. **18**, 1241 (1979); (*b*) A. J. POË, C. N. SAMPSON, and C. V. SEKHAR. Inorg. Chem. **26**, 1057 (1986).
24. D. J. DARENSBOURG, D. J. ZALEWSKI, and T. DELORD. Organometallics, **3**, 1210 (1984); D. J. DARENSBOURG and D. J. ZALEWSKI. Organometallics, **4**, 92 (1985).
25. F. BASOLO. Inorg. Chim. Acta, **100**, 33 (1985).
26. M. I. BRUCE, M. J. LIDDELL, C. A. HUGHES, B. W. SKELTON, and A. H. WHITE. J. Organomet. Chem. **347**, 157 (1988).

Can. J. Chem. Downloaded from www.nrcresearchpress.com by 186.148.149.217 on 09/07/12
For personal use only.

Structural features of $(C_5H_5)_2Mo_2S_6$ clusters: an EHMO study

JANICE A. CRAMER AND MICHAEL J. MCGLINCHEY
Department of Chemistry, McMaster University, Hamilton, Ont., Canada L8S 4M1

AND

JEAN-YVES SAILLARD
Laboratoire de Chimie du Solide et Inorganique Moléculaire, URA 254, Université de Rennes I, 35042 Rennes CEDEX, France

Received March 31, 1989

This paper is dedicated to Professor Ronald J. Gillespie on the occasion of his 65th birthday

JANICE A. CRAMER, MICHAEL J. MCGLINCHEY, and JEAN-YVES SAILLARD. Can. J. Chem. **67**, 1931 (1989).

Extended Hückel molecular orbital calculations on S_6 in the planar D_{6h} configuration and in the bent C_{2v} geometry reveal that the former is favored for S_6^{2+} and the latter for S_6^{4-}. It is shown that the additional six electrons would populate one π^* and two σ^* orbitals in the planar structure. In contrast, when these hexasulfur fragments are incorporated in triple-decker sandwich compounds the pseudo-D_{6h} structure is favored for $[(C_5H_5)Mo(S_6)Mo(C_5H_5)]^{6+}$ but the C_{2v} geometry is predicted for $[(C_5H_5)Mo(S_6)Mo(C_5H_5)]^{2+}$ which possesses only four more electrons. The required extra two electrons are shown to originate from a metallic δ-type molecular orbital. These EHMO calculations are in complete accord with some very recent experimental results from Gillespie's laboratory.

Key words: Molybdenum–sulfur clusters, EHMO calculations.

JANICE A. CRAMER, MICHAEL J. MCGLINCHEY et JEAN-YVES SAILLARD. Can. J. Chem. **67**, 1931 (1989).

Des calculs d'orbitales moléculaires selon la méthode de Hückel étendue sur S_6 dans la configuration plane D_{6h} ainsi que dans la géométrie C_{2v} tendue démontrent que la première est favorisée pour le cation S_6^{2+} alors que la dernière est favorisée pour l'anion S_6^{4-}. On démontre que les six électrons additionnels occuperaient une orbitale π^* et deux orbitales σ^* de la structure plane. Au contraire, lorsque ces fragments de S_6 sont incorporés dans des composés sandwich à trois étages, la structure pseudo-D_{6h} est favorisée pour le composé $[(C_5H_5)Mo(S_6)Mo(C_5H_5)]^{6+}$, mais les calculs prédisent que la géométrie C_{2v} serait favorisée pour $[(C_5H_5)Mo(S_6)Mo(C_5H_5)]^{2+}$ qui possède 4 électrons de plus. Les deux électrons supplémentaires requis proviendraient d'une orbitale moléculaire métallique de type δ. Ces calculs sont en parfait accord avec quelques résultats expérimentaux obtenus très récemment dans les laboratoires du professeur Gillespie.

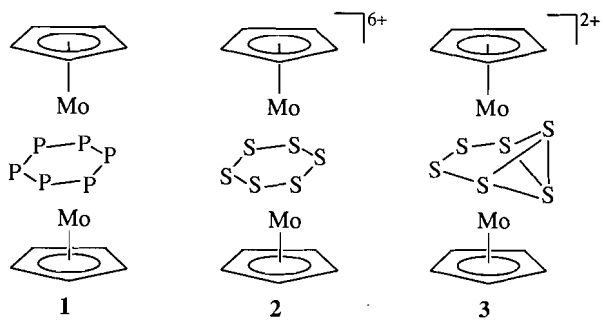
Mots clés : clusters de molybdène–soufre; calculs EHMO.

[Traduit par la revue]

Introduction

The interface of main group and transition metal cluster chemistry has attracted considerable interest in recent years and numerous synthetic and theoretical approaches have been described. Fortunately, a comprehensive overview has been provided by Whitmire (1). Among the more fascinating systems are those in which metal atoms are sandwiched between layers of organic or inorganic rings. The prototypical triple-decker, namely $[(C_5H_5)Ni(C_5H_5)Ni(C_5H_5)]^+$, which was synthesized by Werner and Salzer (2) and whose bonding patterns were rationalized by Hoffmann and co-workers (3), prompted much elegant experimental activity. One might focus particularly on the contributions of Scherer and co-workers who have prepared a series of clusters of the general type $(C_5H_5)M(P_n)M(C_5H_5)$ (4, 5). Recent extended Hückel molecular orbital calculations by Jemmis and Reddy (6) on $(C_5H_5)Mo(P_6)Mo(C_5H_5)$, **1**, and related molecules pointed out the possibility of correlating the molecular geometry, especially the metal–metal distances, with the valence electron count. Furthermore, the rich variety of structural types available for the $(C_5H_5)M(S_4)M(C_5H_5)$ system has been studied by Tremel, Hoffmann, and Kertesz (7).

Our interest in these findings was heightened as the result of a conversation with our colleague R. J. Gillespie who informed us of the synthesis and X-ray characterization of a rather novel product arising from the reaction of $(C_5H_5)_2Mo_2(CO)_6$ with S_8^{2+} (8). We have idealized the structure to the C_{2v} geometry shown in **3**. It is clear that one could construct the hypothetical molecule $[(C_5H_5)Mo(S_6)Mo(C_5H_5)]^{6+}$, **2**, which would have a 28-electron count and presumably the same structure as **1**. (In these triple-decker systems, the convention is to include only the π-electrons of the ligands in the count.) We were intrigued that the addition of four electrons took **2**, which has local D_{6h} symmetry, into **3** in which an S_2 moiety has apparently been twisted out of the central plane. To this end, we report the results of an EHMO study on the effects of distorting a planar S_6 ring by rotating a sulfur–sulfur bond through 90°; subsequently, the effects are contrasted with those observed for the corresponding clusters in which the S_6 unit (in both the D_{6h} and C_{2v} conformations) is sandwiched between two $(C_5H_5)Mo$ fragments.



1 **2** **3**

Results and discussion

We note initially that the S_6 system has been the subject of several theoretical investigations using different approaches. In their extensive treatment of the structural changes on oxidation and reduction of the sulfur species S_3, S_4, S_6, and S_8, Salahub, Foti, and Smith (9) used the SCF-Xα-SW procedure. These

Can. J. Chem. Downloaded from www.nrcresearchpress.com by 186.148.149.217 on 09/07/12
For personal use only.

Can. J. Chem. Downloaded from www.nrcresearchpress.com by 186.148.149.217 on 09/07/12
For personal use only.

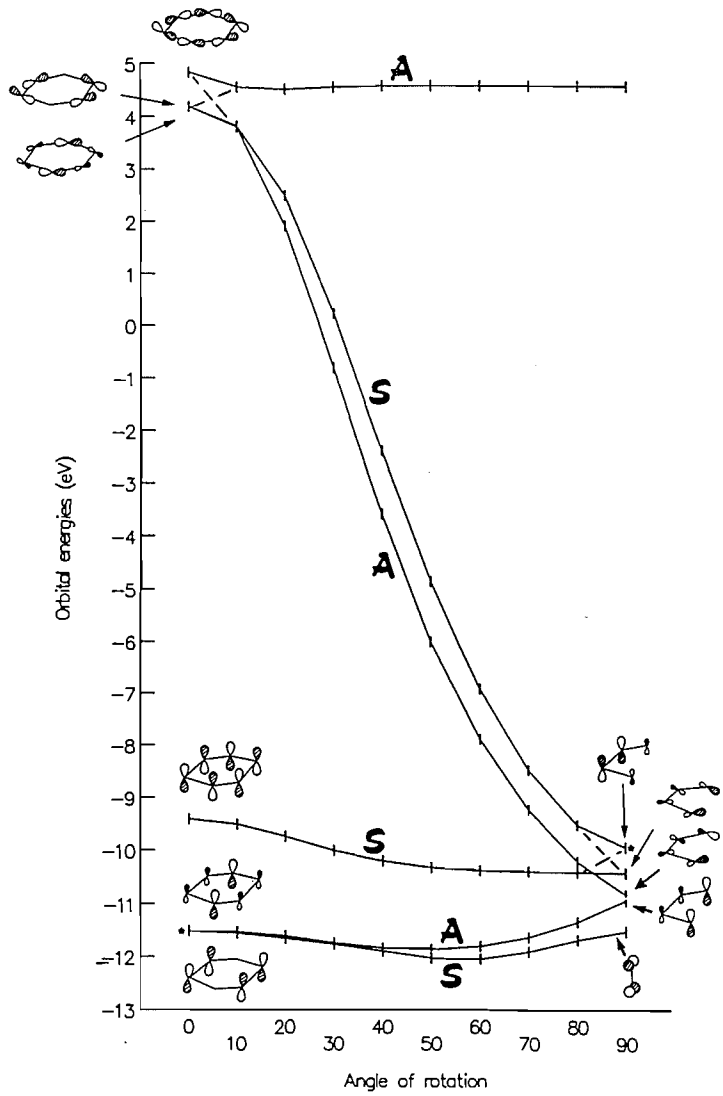


FIG. 1. Walsh diagram showing the effects of rotating a sulfur–sulfur moiety relative to the plane of the four remaining sulfur atoms. On the left hand side, $\theta = 0°$, the asterisk marks the HOMO for the D_{6h} S_6^{2+} system. On the right hand side, $\theta = 90°$, the asterisk marks the HOMO for the C_{2v} S_6^{4-} system.

results were in general accord with the EHMO calculations from this laboratory on a variety of six-atom species (10). Among the geometries which have been examined for the six-atom clusters are the octahedron (O_h), the trigonal prism (D_{3h}), the boat (C_{2v}), the flattened boat (D_{2h}), and the planar hexagon (D_{6h}). Several of these calculated geometries correspond to structurally characterized molecules: thus Te_6^{4+} is D_{3h} (11) while P_6^{4-} adopts the D_{6h} configuration (12). We are unaware of any calculations on the benzvalene-type structure, **4**, whereby a sulfur–sulfur vector has been rotated about an axis bisecting two bonds. Figure 1 depicts a Walsh diagram showing the effects on the frontier orbitals of rotating an S—S bond from $\theta = 0°$ through $\theta = 90°$. On the left hand side we see the familiar pattern for a 10π Hückel system while on the right hand side there are no longer any orbital degeneracies since we are now in the C_{2v} point group. During the transit from one structure to the other we maintain only a C_2 axis and the S and A designations reflect this lowered symmetry.

The consequence of this D_{6h} to C_{2v} isomerization in terms of structure is a replacement of two S—S bonds by four S···S loose contacts (2.38 Å). The effect of this bond breaking process on the electronic structure of the S_6 system is the generation of non-bonding MO's from bonding and antibonding σ-type levels of the planar S_6 system: two high-lying levels which are antibonding with respect to the broken bonds are strongly stabilized while several bonding MO's are destabilized. Because the sulfur–sulfur distance of 2.00 Å in the planar system is too long to provide significant overlap, the π-type levels contribute little to the S—S bonding and become even more non-bonding in the bent S_6 system.

In Fig. 1, we note that for S_6^{2+} the HOMO is a degenerate σ^* e_{2u} set and the LUMO is a single π^* orbital of b_{2g} symmetry. Of course, it is well known that the addition of two electrons to S_6^{2+} would fill the LUMO and generate S_6 itself which is not planar but adopts the D_{3d} (cyclohexane-chair) structure; however, the planar molecule yields a large HOMO/LUMO gap for S_6 itself which renders this structure *a priori* possible, if not for the free molecule, at least for S_6 as a complexed ligand (see below). We can also see from Fig. 1 that the addition of six electrons to planar S_6^{2+} to produce planar S_6^{4-} by filling not only the π^* orbital but also the high-lying e_{1u} set is evidently greatly disfavored. The Walsh diagram reveals that

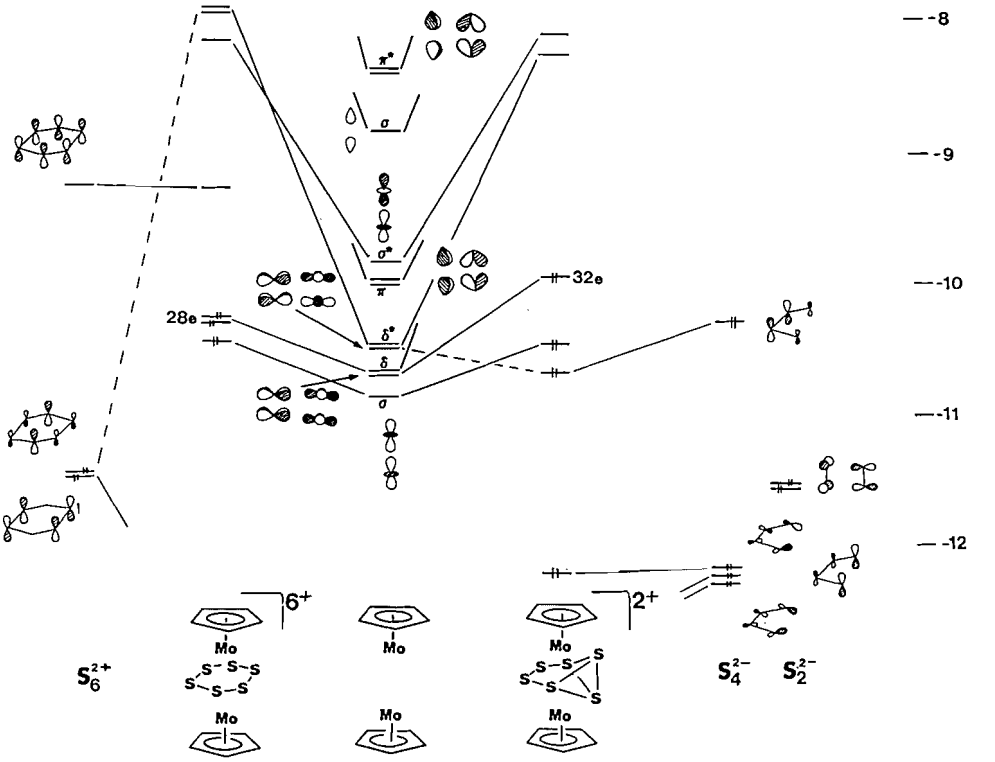
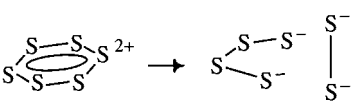


FIG. 2. Frontier orbital energy level diagram depicting the interaction of the Cp_2Mo_2 fragment with planar S_6^{2+} and with S_4^{2-} and S_2^{2-} units. The favored electron counts (28 electrons for **2**, 32 electrons for **3**) are indicated.

two high-lying orbitals of the planar molecule have undergone a precipitous drop in energy during the transformation from D_{6h} to C_{2v}; furthermore, the b_{2g} orbital (the LUMO in S_6^{2+}) correlates with a filled orbital on the right hand side of Fig. 1. It is now readily apparent that the favored count for the hexasulfur system in the C_{2v} geometry is 40 electrons, and that one has effectively generated two almost independent fragments, viz., S_4^{2-} and S_2^{2-}. A moment's thought leads to the realization that by adding six electrons to planar S_6^{2+} we have not only filled the π manifold but also populated two orbitals of strongly σ^* character. In fact, the *A* and *S* high-lying orbitals which descend so steeply are not simply the e_{1u} set; the symmetric component of this degenerate orbital does indeed fall in energy but the *A* orbital which crosses the HOMO-LUMO gap arises from a_{2g}; that is, there is an avoided level crossing at the very beginning of the transformation. Not only the electron count, but also the frontier orbital set of the S_6 system has changed during the D_{6h} to C_{2v} process. One now has two new in-phase and out-of-phase combinations of sulfur lone pairs on the termini of the S_4 fragment. On the other side, the S_2 fragment bears six frontier orbitals: the in-plane and out-of-plane π and π^* fragment orbitals, and the in-phase and out-of-phase combinations of the σ-type lone pairs on the two sulfur atoms.

To summarize, therefore, we see that rotation of a sulfur–sulfur fragment out of the S_6 plane increases the S—S distances to their former neighbours in the D_{6h} system from 2.00 to 2.38 Å. We have effectively cleaved two sulfur–sulfur σ-bonds leading ultimately to S_4^{2-} and S_2^{2-} moieties.

Turning now to the metal-complexed systems **1**, **2**, and **3**, we present in Fig. 2 the frontier molecular orbital (FMO) schemes for the well-known fragment $(C_5H_5)Mo\cdots Mo(C_5H_5)$ and for the $[(C_5H_5)Mo(S_6)Mo(C_5H_5)]^{n+}$ cluster in both its pseudo-D_{6h} and C_{2v} geometries. The metal FMO's for the



4

$(C_5H_5)Mo\cdots Mo(C_5H_5)$ moiety are labelled with their conventional σ, σ^*, π, π^*, and δ, δ^* designations. The interactions of these Cp_2Mo_2 frontier orbitals with those of planar S_6 give rise to the hypothetical molecule $[(C_5H_5)Mo(S_6)Mo(C_5H_5)]^{6+}$, **2**, possessing pseudo-D_{6h} symmetry. Analogously, the C_{2v} cluster $[(C_5H_5)Mo(S_6)Mo(C_5H_5)]^{2+}$, **3**, is derived from its Cp_2Mo_2, S_4, and S_2 constituents. As anticipated from the work of Jemmis and Reddy (6), the orbital energy level diagram for the 28-electron system $[(C_5H_5)Mo(S_6)Mo(C_5H_5)]^{6+}$ resembles qualitatively that for the isoelectronic $[(C_5H_5)Mo(P_6)Mo(C_5H_5)]$ cluster, **1**. It is further apparent that planar 30-electron triple-deckers would arise as a result of filling the vacant b_{2g} orbital, i.e., the LUMO in **1** and **2**. This possibility was raised by Hoffmann and co-workers (3) in their original paper in which they rationalized the 34-electron species $[Cp_3Ni_2]^+$. Since that time, examples of 30-electron clusters such as $(C_6H_6)Cr(C_6H_6)Cr(C_6H_6)$ or $CpFe(C_2B_2SR_4)FeCp$ have synthesized (13–15). However, it should be noted that these complexes have a somewhat different electronic structure from that of **2** or **3**.

The presence of the planar S_4 fragment situated between the two molybdenum atoms in both **2** and **3** accounts for the many similar features in the orbital energy level diagrams. The major change is the destabilization in **3** of one of the delta components (the $d_{x^2-y^2}$ combination) which now correlates with a vacant level. This situation arises because the in-phase $d_{x^2-y^2}$ orbital combination overlaps with the in-plane π orbital of S_4 and also with the in-phase combination of the S_2 lone pairs. The in-phase d_{xy} combination from Cp_2Mo_2 which yields the other

Can. J. Chem. Downloaded from www.nrcresearchpress.com by 186.148.149.217 on 09/07/12
For personal use only.

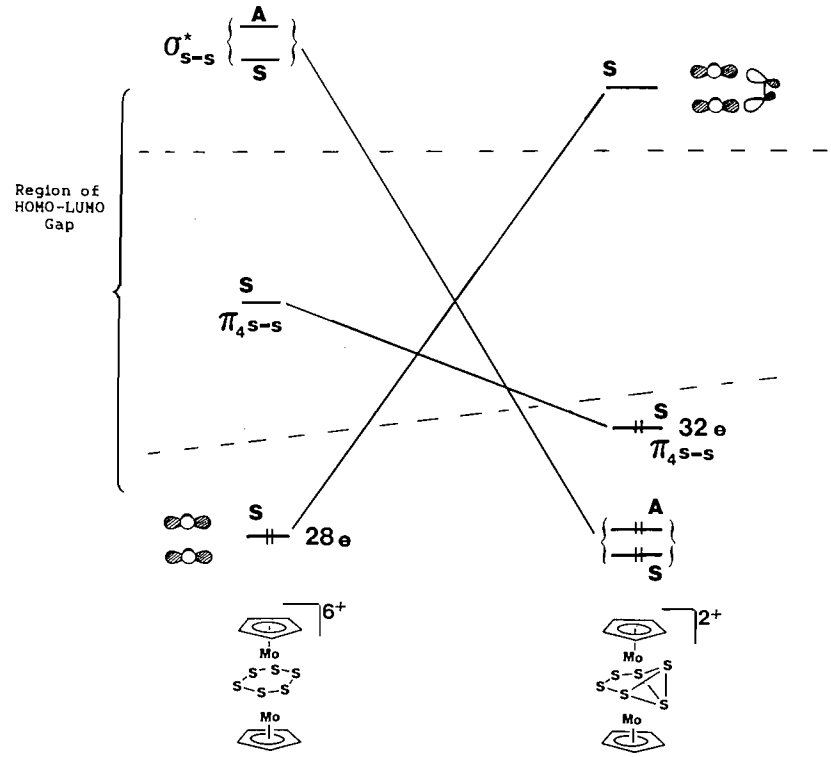


FIG. 3. Schematized correlation diagram showing how three vacant orbitals in planar $[Cp_2Mo_2S_6]^{6+}$ correlate with filled orbitals in $[Cp_2Mo_2S_6]^{2+}$; concomitantly, a δ orbital in **2** is greatly destabilized in **3**.

δ component is less affected than is its $d_{x^2-y^2}$ partner since the corresponding interaction is with the out-of-plane π orbital of S_2; the overlap integral in the d_{xy} case is smaller and consequently the δ orbital suffers only minor destabilization.

As a result of this orbital analysis, we can now explain an initially puzzling feature of the clusters **2** and **3**. It was apparent from the earlier discussion that the transformation of planar S_6^{2+} into S_4^{2-} and S_2^{2-} fragments requires a formal six-electron reduction and the population of one π* and two σ* orbitals; in contrast, this process apparently requires only a four-electron reduction to take D_{6h} $[(C_5H_5)Mo(S_6)Mo(C_5H_5)]^{6+}$, **2**, into the C_{2v} cluster $[(C_5H_5)Mo(S_6)Mo(C_5H_5)]^{2+}$, **3**. The schematized correlation diagram in Fig. 3 shows the two previously described high-lying antibonding orbitals which cross the HOMO-LUMO gap as one rotates an S_2 moiety through 90° relative to the original S_6 plane; moreover, the weakly antibonding b_{2g} orbital (the LUMO in D_{6h}) is occupied in the C_{2v} geometry. However, the destabilization of the $d_{x^2-y^2}$ component of δ symmetry results in a net increase of only two occupied orbitals and a consequent change from a 28-electron to a 32-electron cluster. If we regard the planar ring in **2** as S_6^{2+}, i.e., a 10π Hückel system, then the overall charge of 6+ tells us that the formal oxidation state of each molybdenum is 3+ (d^3); in contrast, the calculations reveal that in **3** the hexasulfur fragment has a charge of 4− which leaves each molybdenum in the 4+ (d^2) formal oxidation state. Thus the transformation from planar $[(C_5H_5)Mo(S_6)Mo(C_5H_5)]^{6+}$ into the bent $[(C_5H_5)Mo(S_6)Mo(C_5H_5)]^{2+}$ can be viewed as a six-electron superreduction of S_6^{2+} with a concomitant two-electron oxidation of $[Cp_2Mo_2]^{4+}$ to $[Cp_2Mo_2]^{6+}$. However, it should be noted that oxidation states are formal and rather different from the real atomic charges since the strong ligand-to-metal bonding implies large charge transfers: for example, the calculated charge on Mo was found to be 1.2+, a value significantly lower than 4+.

At Mo—Mo distances of about 2.6–2.8 Å, the δ-type overlap is negligible and the depopulation of one in-phase δ combination should not affect the Mo—Mo separation. In our calculations on **2** and **3**, the Mo—Mo overlap populations were found to be 0.139 and 0.159, respectively. The distances observed in $[(C_5H_5)Mo(P_6)Mo(C_5H_5)]$, **1** (2.648 Å) and $[(C_5H_5)Mo(S_6)Mo(C_5H_5)]^{2+}$, **3** (2.752 Å) may simply be attributable to the different nature and structure of the central ligand system.

The results for these 28- and 32-electron systems allow one to make some comments about other potentially viable molecules. Clearly, one would expect $[(C_5H_5)Mo(S_6)Mo(C_5H_5)]^{6+}$, **2**, to possess a planar hexasulfur ring but the rather high charge on such a cluster probably precludes its synthesis. The same structure could perhaps be obtained by taking another 28-electron system such as $[(C_5H_5)Zr(S_6)Zr(C_5H_5)]^{2+}$. Future reports will focus on experimental and calculative approaches in this general area of organometallic multiple decker compounds.

Experimental

All calculations were performed via the extended Hückel method (16) using weighted H_{ij}'s (17). Atomic parameters were taken from previous studies (18, 19). The sulfur–sulfur bond lengths in the planar hexagon were taken as 2.00 Å; the molybdenum–molybdenum distance in **3** (2.752 Å) was taken from the X-ray crystallographic data (8).

Acknowledgments

Financial support from the Donors of the Petroleum Research Fund, administered by the American Chemical Society, from the Natural Sciences and Engineering Council of Canada, and

Can. J. Chem. Downloaded from www.nrcresearchpress.com by 186.148.149.217 on 09/07/12
For personal use only.

from the CNRS (France) is gratefully acknowledged. J.A.C. thanks the Government of Ontario for a Graduate Scholarship. We particularly wish to thank Professor R. J. Gillespie and Dr. J. E. Vekris for providing us with structural data prior to publication. We also thank Professor R. Hoffmann for a preprint of the study on the $(C_5H_5)M(S_4)M(C_5H_5)$ system.

1. K. WHITMIRE. J. Coord. Chem. **17B**, 95 (1988).
2. H. WERNER and A. SALZER. Angew. Chem. **84**, 949 (1972).
3. J. W. LAUHER, M. ELIAN, R. H. SUMMERVILLE, and R. HOFFMANN. J. Am. Chem. Soc. **98**, 3219 (1976).
4. O. J. SCHERER, H. SITZMANN, and G. WOLMERSHAUSER. Angew. Chem. Int. Ed. Engl. **24**, 351 (1985).
5. O. J. SCHERER, H. SWAROWSKY, G. WOLMERSHAUSER, W. KAIM, and S. KOHLMANN. Angew. Chem. **99**, 1178 (1987), and references therein.
6. E. D. JEMMIS and A. C. REDDY. Organometallics, **7**, 1561 (1988).
7. W. TREMEL, R. HOFFMANN, and M. KERTESZ. J. Am. Chem. Soc. **111**, 2030 (1989).
8. R. J. GILLESPIE, J. E. VEKRIS, and R. FAGGIANI. To be published.
9. D. R. SALAHUB, A. E. FOTI, and V. H. SMITH. J. Am. Chem. Soc. **100**, 7847 (1978).
10. R. C. BURNS, R. J. GILLESPIE, J. A. BARNES, and M. J. MCGLINCHEY. Inorg. Chem. **21**, 799 (1982).
11. R. C. BURNS, R. J. GILLESPIE, W.-C. LUK, and D. R. SLIM. Inorg. Chem. **18**, 3086 (1979).
12. W. SCHMETTOW, A. LIPKA, and H. G. VON SCHNERING. Angew. Chem. Int. Ed. Engl. **13**, 345 (1974).
13. W. M. LAMANNA, W. B. GLEASON, and D. BRITTON. Organometallics, **6**, 1583 (1987).
14. W. SIEBERT, T. RENK, K. KINGBERGER, M. BOCHMANN, and C. KRUGER. Angew. Chem. Int. Ed. Engl. **15**, 779 (1976).
15. W. SIEBERT and W. ROTHERMEL. Angew. Chem. Int. Ed. Engl. **16**, 333 (1977).
16. R. HOFFMANN. J. Chem. Phys. **39**, 1397 (1963).
17. J. H. AMMETER, H.-B. BÜRGI, J. C. THIBEAULT, and R. HOFFMANN. J. Am. Chem. Soc. **100**, 3686 (1978).
18. M. KAMATA, T. YASHIDA, S. OTSUKA, K. HIROTSU, T. HIGUCHI, M. KIDA, K. TATSUMI, and R. HOFFMANN. Organometallics, **1**, 227 (1982).
19. J.-F. HALET, J.-Y. SAILLARD, R. LISSILLOUR, M. J. MCGLINCHEY, and G. JAOUEN. Organometallics, **5**, 139 (1986).

Can. J. Chem. Downloaded from www.nrcresearchpress.com by 186.148.149.217 on 09/07/12
For personal use only.

The disproportionation of diselenium dichloride, Se_2Cl_2, and diselenium dibromide, Se_2Br_2

MARC LAMOUREUX and JOHN MILNE
Department of Chemistry, University of Ottawa, Ottawa, Ont., Canada K1N 6N5

Received March 6, 1989

This paper is dedicated to Professor Ronald J. Gillespie on the occasion of his 65th birthday

MARC LAMOUREUX and JOHN MILNE. Can. J. Chem. **67**, 1936 (1989).

Diselenium dichloride and dibromide have been shown by Raman and ^{77}Se-nmr spectroscopy to be equilibrium mixtures of Se_2X_2 and small amounts of SeX_2 and Se_nX_2. Equilibrium constants have been estimated for the disproportionation reactions,

$$2Se_2X_2 = SeX_2 + Se_3X_2$$

$$3Se_2X_2 = SeX_2 + Se_4X_2$$

The origin of "spurious" peaks in the reported vibrational spectra of Se_2Br_2 and Se_2Cl_2, which have been variously assigned to overtone and combination bands and impurities has been clarified. Mixtures of Se_2Br_2 and Se_2Cl_2 are shown to contain Se_2BrCl in equilibrium according to

$$Se_2Br_2 + Se_2Cl_2 = 2Se_2BrCl$$

Key words: ^{77}Se nmr, Raman spectroscopy, selenium halides, diselenium dichloride, diselenium dibromide.

MARC LAMOUREUX et JOHN MILNE. Can. J. Chem. **67**, 1936 (1989).

Faisant appel aux spectroscopies Raman et rmn du ^{77}Se, on a démontré que les dichlorure et dibromure de disélénium sont des mélanges à l'équilibre de Se_2X_2 et de faibles quantités de SeX_2 et Se_2X_2. On a évalué les constantes d'équilibre pour les réactions de disproportionation suivantes:

$$2Se_2X_2 = SeX_2 + Se_3X_2$$

$$3Se_2X_2 = SeX_2 + Se_4X_2$$

On a clarifié l'origine de bandes "parasites" dont l'apparition dans les spectres de vibration avaient été rapportée antérieurement et qui avaient été attribuées à des impuretés ainsi qu'à des bandes harmoniques et de combinaison. On a démontré que les mélanges de Se_2Br_2 et de Se_2Cl_2 contiennent du Se_2BrCl formé par l'équilibre suivant:

$$Se_2Br_2 + Se_2Cl_2 = 2Se_2BrCl$$

Mots clés : rmn du ^{77}Se; spectroscopie Raman; halogénures de sélénium; dichlorure de disélénium; dibromure de disélénium.

[Traduit par la revue]

Introduction

Diselenium dichloride, Se_2Cl_2, and dibromide, Se_2Br_2, are among the oldest known compounds of selenium (1). Crystal structure determinations confirm them to be pure as solids (2). However, the vibrational spectrum of liquid Se_2Cl_2 (3–8) has weak bands, which cannot be assigned to fundamental modes and which have been variously assigned as overtones and combinations (4–8) or as due to impurities (3–6). Some vibrational bands in the spectra of the chloride and bromide have nearly identical frequencies to those exhibited by $SeCl_2$ and $SeBr_2$ (9). It appeared possible that Se_2Cl_2 and Se_2Br_2 might undergo some kind of disproportionation in the liquid phase. In order to test this hypothesis and to extend our knowledge of lower selenium halides, a study of the Raman and ^{77}Se-nmr spectra of diselenium dichloride, dibromide, and bromide chloride, as neat liquids and in solution was carried out. The work on the neat liquids is reported here.

Experimental section

Elemental selenium pellets (Aldrich, 99.99%) and chlorine (Air Products, 99.5%) were used without further purification. Bromine (Fisher Reagent) was distilled (bp 59°C) from phosphorus pentoxide. Selenium tetrachloride, diselenium dichloride and dibromide were prepared by standard methods (10, 11). Pure diselenium dichloride was also prepared from pure selenium and selenium tetrachloride in a closed container.

$$3\,Se + SeCl_4 = 2\,Se_2Cl_2$$

The reactants were weighed out with an analtyical balance and were accurate to ±1 mg. For the quantities used, the error in the 1:1 stoichiometry amounts to ±0.07%. This product will be called stoichiometric Se_2Cl_2 hereafter. Mixtures of Se and $SeCl_4$ in Se_2Cl_2 were also made up by weighing. In a typical experiment 0.443 g Se were added to 11.203 g of Se_2Cl_2. Although it has been claimed that Se is insoluble in Se_2Cl_2 (12), it was found that up to 4% by weight could be dissolved. The same method was used for Se_2Br_2 and its mixtures but in this case Se and Br_2 were used and the reaction was carried out with cooling. All manipulations were carried out in a dry box. Exclusion of oxygen was not necessary.

Raman spectra were measured with a Jobin-Yvon monochromator in conjunction with a Hamamatsu PM tube and a Princeton Applied Research photon counting system. The spectra were excited with the 647.1 nm line of a Spectra Physics Kr ion laser.

Selenium-77 nmr spectra were measured with a Varian XL-300 spectrometer operating at 57.28 MHz. The ^{77}Se reference was a saturated solution of selenous acid in distilled water made up using SeO_2 (Aldrich, 99.999%). The chemical shift for this reference is 1282 ppm to low field from selenium dimethyl (13). The probe temperature was 20°C.

Can. J. Chem. Downloaded from www.nrcresearchpress.com by 186.148.149.217 on 09/07/12
For personal use only.

Can. J. Chem. Downloaded from www.nrcresearchpress.com by 186.148.149.217 on 09/07/12
For personal use only.

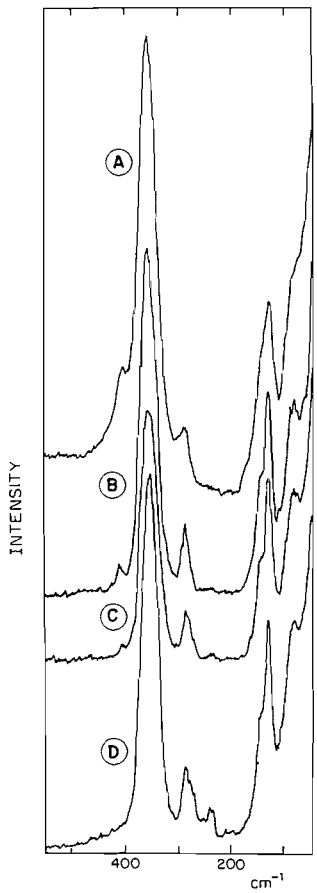


FIG. 1. The Raman spectra of Se_2Cl_2 solutions. Trace *A*: 9.5 wt.% (0.098 mole fraction) $SeCl_4$ in Se_2Cl_2; trace *B*: Se_2Cl_2, prepared by the method of Lenher and Kao (11); trace *C*: stoichiometric Se_2Cl_2; trace *D*: 3.5 wt.% (0.095 mole fraction) Se in Se_2Cl_2. Resolution: 10 cm^{-1}.

Results and discussion

Diselenium dichloride

Raman spectroscopy The Raman spectra of Se_2Cl_2, stoichiometric Se_2Cl_2 and solutions of 9.5 wt.% $SeCl_4$ (0.098 mole fraction) and 3.5 wt.% Se (0.095 mole fraction) in Se_2Cl_2 are given in Fig. 1. The spectra of Se_2Cl_2 and stoichiometric Se_2Cl_2 are in close agreement with the spectra reported earlier (3–6) and differ only in the relative intensity of the peak at 410 cm^{-1}. This peak, which has been attributed to an impurity by other workers (3, 6), corresponds to the symmetric stretching (ν_1) mode of $SeCl_2$ (9). The bending mode (ν_3) of $SeCl_2$ also appears in these spectra and those of Kiefer (6) as a weak shoulder at 166 cm^{-1}. Selenium dichloride is apparently present in Se_2Cl_2. The asymmetric stretching mode of $SeCl_2$ (ν_2) at 381 cm^{-1} is lost in the strong Se_2Cl_2 envelope (ν_1 and ν_5 of Se_2Cl_2) at 358 cm^{-1}. When $SeCl_4$ is added to Se_2Cl_2 up to 10 wt.%, homogeneous liquid mixtures are formed. The Raman spectrum of this mixture (trace *A* in Fig. 1) shows a stronger peak at 410 cm^{-1} consistent with the reaction

[1] $Se_2Cl_2 + SeCl_4 = 3\ SeCl_2$

The addition of elemental selenium to Se_2Cl_2 up to 3.5 wt.% yields a homogeneous mixture. The Raman spectrum (trace *D*) shows a barely observable peak at 410 cm^{-1} and a new peak at 240 cm^{-1} and a shoulder at 275 cm^{-1}. These new peaks have been attributed to Se_nCl_2 species present in Se/Se_2Cl_2 melts (100°C) by Volkov *et al.* (7). The additional peaks at 81 and 139 cm^{-1} reported by these authors are difficult to observe due to the presence of other strong Se_2Cl_2 bands. At the low Se concentrations studied here, these observations are consistent with the reaction

[2] $Se + Se_2Cl_2 = Se_3Cl_2$

The observations of a peak at 410 cm^{-1} in the spectrum of stoichiometric Se_2Cl_2 where the 1:1 Se / Cl mole ratio is precise to within ±0.07% indicates that Se_2Cl_2 undergoes a self-disproportionation.

[3] $2Se_2Cl_2 = SeCl_2 + Se_3Cl_2$

The very weak peak at 240 cm^{-1} in the spectrum supports the simultaneous occurrence of Se_3Cl_2 in the mixture. The simultaneous appearence of peaks due to $SeCl_2$, Se_2Cl_2, and Se_3Cl_2 species in the Se/Se_2Cl_2 solution confirms that the disproportionation [3] is taking place. The intensity of the peak at 410 cm^{-1} is stronger in the spectrum of Se_2Cl_2 prepared by the method of Lenher and Kao (11) than in the spectrum of stoichiometric Se_2Cl_2. This is attributed to the use of SeO_2 in excess of the stoichiometrically required amount in the procedure of Lenher and Kao (11).

The equilibrium constant governing [3],

$$[4]\quad K = \frac{[SeCl_2][Se_3Cl_2]}{[Se_2Cl_2]^2}$$

may be estimated from the relative intensities of the 410 cm^{-1} band in the spectra of stoichiometric Se_2Cl_2 and of the solution with 9.5 wt.% of selenium tetrachloride (0.098 mole fraction dissolved in Se_2Cl_2.

Normalized band intensities and concentrations are given in Table 1. The normalization assumption was that the 358 cm^{-1} band of Se_2Cl_2 has an area of 5 cm^2. The contribution of ν_3 of $SeCl_2$ to this band is assumed to be negligible and has been ignored. Concentrations are expressed as mol L^{-1} and the solution volume has been calculated assuming the density of Se_2Cl_2 and its mixtures to be 2.77 g mL^{-1}. Areas were determined from several spectra but as a result of the low relative intensity of the 410 cm^{-1} peak, the largest error is in the area for this peak. Two expressions for K, one for each solution, may be derived.

$$[5]\quad K = \frac{(0.038/I_{SeCl_2})^2}{(5/I_{Se_2Cl_2})^2}$$

and

$$[6]\quad K = \frac{[3c_{SeCl_4} + [Se_3Cl_2]][Se_3Cl_2]}{[c_{Se_2Cl_2} - c_{SeCl_4} - [Se_3Cl_2]]^2}$$

where

$$[7]\quad [Se_3Cl_2] = \frac{\left[\frac{0.442}{I_{SeCl_2}}\right](c_{Se_2Cl_2} - c_{SeCl_4}) - \left[\frac{15c_{SeCl_4}}{I_{Se_2Cl_2}}\right]}{5/I_{Se_2Cl_2} + 0.442/I_{SeCl_2}}$$

and I_{SeCl_2} and $I_{Se_2Cl_2}$ are the molar scattering intensities of $SeCl_2$ (410 cm^{-1}) and Se_2Cl_2 (358 cm^{-1}) in liquid Se_2Cl_2. The molar scattering intensity of Se_2Cl_2 at 358 cm^{-1} was calculated to a reasonable degree of accuracy from the stoichiometric Se_2Cl_2 spectrum and found to be 0.41 cm^2 L mol^{-1}. The contribution to this peak from Se_3Cl_2, which is expected to have SeCl stretching bands in this region but which is present at low concentration

TABLE 1. Concentrations and peak areas from Raman spectra of Se_2Cl_2 and $SeCl_4/Se_2Cl_2$ solutions

Solution	Area (cm^2) (358 cm^{-1})	Area (cm^2) (410 cm^{-1})	$c_{Se_2Cl_2}$ (mol L^{-1})	c_{SeCl_4} (mol L^{-1})
Stoichiometric Se_2Cl_2	5	0.038±0.012	12.1	—
$SeCl_4$ in Se_2Cl_2 (9.5 wt.%, 0.098 mole fraction)	5	0.442±0.046	12.1	1.2

TABLE 2. Chemical shifts and intensities for Se_2Cl_2 solutions

Solution	Chemical shift (ppm)	Observed intensity[a,b]	Assignment	Equilibrium constants
$SeCl_4$ in Se_2Cl_2	428.1	47.6(0.065)	$SeCl_2$	$K = 2(\pm0.3) \times 10^{-4}$
(3.95 wt.%;	−8.51	733	Se_2Cl_2	
0.043 mole fraction)	−11.3	—	Se_3Cl_2	
Se_2Cl_2	427.5	3.2(0.035)	$SeCl_2$	
	−9.29	90.5	Se_2Cl_2	
Stoichiometric Se_2Cl_2	424	1.7(0.010)	$SeCl_2$	$K = 4(\pm2.2) \times 10^{-4}$
	−9.81	176	Se_2Cl_2	
Se in Se_2Cl_2	425.4	6.6(0.009)	$SeCl_2$	$K = 2(\pm0.3) \times 10^{-4}$
(3.23 wt.%;	−9.74	736	Se_2Cl_2	
0.088 mole fraction)	−10.3	12(0.016)	Se_3Cl_2	$K' = 3(\pm0.6) \times 10^{-6}$
	−365.5	14(0.019)	Se_4Cl_2	

[a]The uncertainty on these intensities is ±0.5.
[b]Normalized values in parentheses are referred to Se_2Cl_2 intensity = 1.00.

and $SeCl_2$, which is also present in low concentration, is small and has been ignored. Equations [5] and [6] yield $K = 8(\pm5) \times 10^{-4}$ for $I_{SeCl_2} = 0.11$ cm^2 L mol^{-1}.

^{77}Se-nmr spectroscopy. A routine ^{77}Se nmr spectrum of stoichiometric Se_2Cl_2 consists of a single signal at −9.8 ppm, which is close to the reported value of −7.9 ppm (14). With an increase in the number of transients collected additional weak peaks are observed. The chemical shifts and peak intensities of stoichiometric Se_2Cl_2, Se_2Cl_2, and solutions of $SeCl_4$ and Se in Se_2Cl_2 are given in Table 2. The principal signal in the spectra of all of these mixtures is due to Se_2Cl_2. This signal shifts slightly to high field, −8.51 to −9.81 ppm, as the $SeCl_4$ content is decreased. The spectrum of a mixture of Se_2Cl_2 with 3.95wt.% $SeCl_4$ (0.042 mole fraction) consists of, in addition to the Se_2Cl_2 signal, a moderately strong signal at 428.1 ppm and a very weak signal at −11.3 ppm. This latter signal was discernible in this solution as a result of the large number of transients collected (2800). The nmr spectra of the Se_2Cl_2 samples showed only two signals, that of Se_2Cl_2 and the low field signal near 425 ppm which had reduced intensity compared to that in the $SeCl_4/Se_2Cl_2$ solution spectrum. The solution of 3.23wt.% (0.088 mole fraction) Se in Se_2Cl_2 gave an nmr spectrum with three signals in addition to that for Se_2Cl_2. The intensity of the signal at 425.4 ppm was further decreased while that at −10.3 ppm, just to high field of the main Se_2Cl_2 signal, increased in intensity relative to the intensity observed in the spectrum of the $SeCl_4/Se_2Cl_2$ mixture. In addition, a weak signal at −365.5 ppm was observed. The variation in relative intensity of the lowest field signal shows that it arises from $SeCl_2$ while that just to high field of the main Se_2Cl_2 signal is assigned to Se_3Cl_2. Finally in solutions to which sufficient Se had been added, Se_4Cl_2 is formed and the signal at −365.5 ppm is assigned to this species. The chemical shifts of $SeCl_2$, Se_3Cl_2, and Se_4Cl_2 are in agreement with those observed for these species in other solvents (16). The strongest nmr signals for Se_nCl_2 will arise from molecules carrying a single ^{77}Se atom in the chain and, for Se_3Cl_2 and Se_4Cl_2, these should consist of two signals for each with intensity ratios 2:1 and 1:1, respectively. These pairs of signals are observed for alkyl tri- and tetraselenides (15) and for tri- and tetraselenium chlorides and bromides dissolved in non-aqueous solvents (16). Some broadening of these signals in Se_2Cl_2 is expected due to the high viscosity of the mixtures and quadrupole relaxation of the Cl and Br nuclei (I = 3/2 for all natural isotopes) to which the ^{77}Se atoms are linked over one or two bonds. However, the appearance of a single broad peak for each species where each member of the doublet is separated by over 20 ppm (16), indicates that some intramolecular exchange is taking place.

The observation of an nmr signal for $SeCl_2$ in the stoichiometric Se_2Cl_2 spectrum confirms the conclusion of the Raman study that Se_2Cl_2 disproportionates. From the peak areas of the spectra of the mixtures studied, the disproportionation constant, K (eq. [4]), may be estimated and these are given in Table 2. In the case of the $SeCl_4/Se_2Cl_2$ mixture, peak intensities and stoichiometry were used, since the intensity of the Se_3Cl_2 peak was too weak to be measured accurately. The average values of K from the Raman spectra and the three nmr measurements is $4(\pm2) \times 10^{-4}$. Considering the relatively weak signals recorded, and the uncertainty for similar reasons, in the intensity of the Raman peak at 410 cm^{-1}, the agreement between the two methods of

Can. J. Chem. Downloaded from www.nrcresearchpress.com by 186.148.149.217 on 09/07/12
For personal use only.

TABLE 3. Chemical shifts and intensities for Se_2Br_2 solutions

Solution	Chemical shift (ppm)	Intensity[a,b]	Assignment	Equilibrium constants
Stoichiometric	164.4	4(0.025)	$SeBr_2$	$K = 1.4(\pm0.3) \times 10^{-3}$
Se_2Br_2	−110.9	163	Se_2Br_2	
	−132.9			
	−143.9	7(0.043)	Se_3Br_2	$K' = 1.8(\pm0.8) \times 10^{-6}$
	−360.7			
	−372.7	2.2(0.013)	Se_4Br_2	
Se_2Br_2	162.1	2.1(0.013)	$SeBr_2$	$K = 0.8(\pm0.2) \times 10^{-3}$
	−111.3	157	Se_2Br_2	
	−143.7	7(0.045)	Se_3Br_2	$K' = 1.5(\pm0.7) \times 10^{-6}$
	−375.1	5.8(0.037)	Se_4Br_2	
Se in Se_2Br_2	164.2	14.5(0.011)	$SeBr_2$	$K = 1.2(\pm0.1) \times 10^{-3}$
(5.8 wt.%;	−111.0	1350	Se_2Br_2	
0.199 mole fraction)	−135.2			
		114(0.084)	Se_3Br_2	
	−144.8			$K' = 1.9(\pm0.2) \times 10^{-6}$
	−361.2			
	−373.8	109(0.081)	Se_4Br_2	
	−392.5			

[a]The uncertainty on the intensities is ±0.5.
[b]Normalized values in parentheses are referred to Se_2Br_2 intensity = 1.00.

determing K is satisfactory. The lower values of K from the nmr work may well be due to masking of part of the Se_3Cl_2 signal by the strong Se_2Cl_2 signal. The greater relative intensity of the $SeCl_2$ signal in Se_2Cl_2, compared to that for stoichiometric Se_2Cl_2, confirms the earlier conclusion that the preparation of this product uses an excess of Se(IV).

The observation of an nmr signal for Se_4Cl_2, appearing simultaneously with the signal for $SeCl_2$ in the spectrum of the Se/Se_2Cl_2 solution indicates that a second equilibrium is present.

[8] $3\,Se_2Cl_2 \overset{K'}{=} 2\,SeCl_2 + Se_4Cl_2$

From the intensities of the signals for Se_2Cl_2, $SeCl_2$, and Se_4Cl_2, K' is estimated to be $3(\pm0.6) \times 10^{-6}$.

Diselenium dibromide

Raman spectroscopy. The Raman spectra of Se_2Br_2, prepared by the method of Lenher and Kao (11) and a solution of 14.1wt.% Se (0.40 mol fraction) in Se_2Br_2 are shown in Fig. 3. The peak at 286 cm^{-1}, which has been assigned to the Se—Se stretching mode, $\nu_2(A_1)$, of Se_2Br_2 (3–6) is coincident with $\nu_3(B_1)$ of $SeBr_2$ (9). With addition of elemental Se, this peak falls in intensity, indicating that there is at least some contribution to this peak from $SeBr_2$. With the addition of Se two new peaks also appear at 182 and 81 cm^{-1}, which are assigned to Se_nBr_2 species. Apparently equilibria parallel to [3] and [8] occur in these liquids.

[9] $2\,Se_2Br_2 \overset{K}{=} SeBr_2 + Se_3Br_2$

[10] $3\,Se_2Br_2 \overset{K'}{=} 2\,SeBr_2 + Se_4Br_2$

^{77}Se nmr spectroscopy. The ^{77}Se nmr chemical shifts and intensities from spectra of stoichiometric Se_2Br_2, Se_2Br_2, and a solution containing 5.8wt.% of Se (0.199 mole fraction) dissolved in Se_2Br_2 are given in Table 3. The spectrum of stoichiometric Se_2Br_2 is shown in Fig. 2. The strongest shift near −111 ppm is due to Se_2Br_2 (14). By analogy with the Se_2Cl_2 spectra, the single peak to low field near 164 ppm is

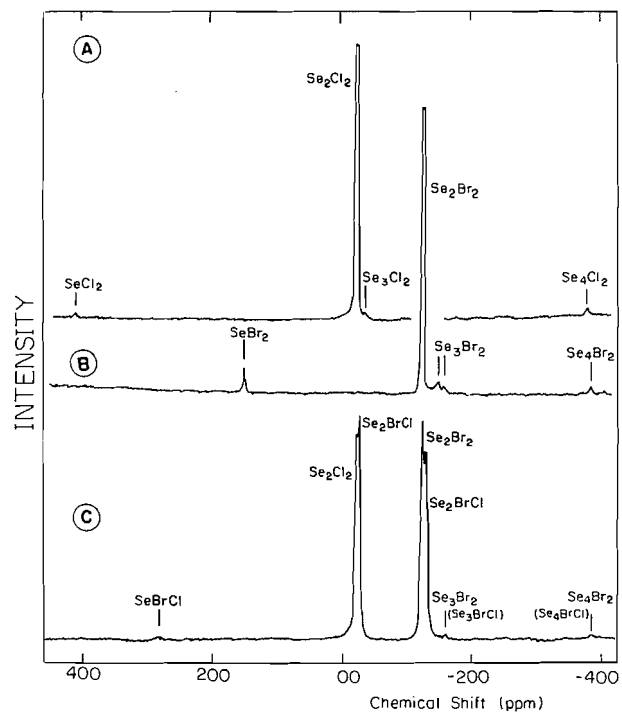


FIG. 2. The ^{77}Se-nmr spectra of Se_2X_2 solutions. Trace *A*: 3.23 wt.% (0.088 mole fraction) of Se in Se_2Cl_2: trace *B*: stoichiometric Se_2Br_2; trace *C*: 0.92:1.0:0.21 mole ratio solution of $Se_2Br_2/Se_2Cl_2/Se$.

assigned to $SeBr_2$, the two peaks just above the Se_2Br_2 shift arise from Se_3Br_2 and the set of peaks near −373 ppm are due to Se_4Br_2. This assignment is confirmed by the changes in intensities which occur when Se is added to Se_2Br_2. In the spectrum of the 5.8wt.% solution of Se in Se_2Br_2 the relative intensity of the low field peak due to $SeBr_2$, compared to that in the spectrum of pure Se_2Br_2, is lower and those of the high field peaks due to Se_3Br_2 and Se_4Br_2 are higher. Moreover, the relative intensities of the signals near −140 ppm and those near −373 ppm in the

Can. J. Chem. Downloaded from www.nrcresearchpress.com by 186.148.149.217 on 09/07/12
For personal use only.

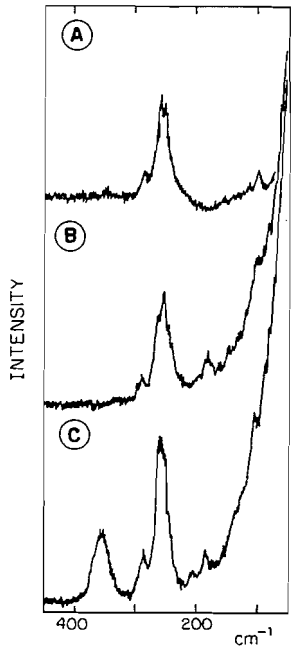


FIG. 3. The Raman spectra of Se_2Br_2 solutions. Trace *A*: Se_2Br_2, prepared by the method of Lenher and Kao (11); trace *B*: 5.8 wt.% Se (0.199 mole fraction) in Se_2Br_2; trace *C*: 0.92:1.0:0.21 mole ratio solution of $Se_2Br_2 / Se_2Cl_2 / Se$. Resolution: 10 cm^{-1}.

5.8wt.% Se solution, compared to those signals in the spectrum of stoichiometric Se_2Br_2, supports the assignment of the high field peak to Se_4Br_2. Apparently Se_2Br_2 produced by the method of Lenher and Kao contains some excess of Se and the normalized signal intensities lie between those of stoichiometric Se_2Br_2 and the 5.8wt.% solution of Se in Se_2Br_2. The nmr spectrum for Se_3Br_2 and Se_4Br_2 are expected, in the absence of exchange and considering only species with one ^{77}Se atom, to consist of doublets of 2:1 and 1:1 intensities, respectively. The envelope near −140 ppm has the appearance of a 2:1 doublet consistent with the assignment to Se_3Br_2, although the signal breadth causes the two peaks to overlap. The higher field signals appear to consist of a broad pair of peaks (−361.2 and −392.5; each intensity 1) bracketing a third peak (−373.8; intensity 4.5). Further work will be necessary to interpret the precise origin of these peaks. No evidence for Se_5Br_2 and higher homologues was found, although collection of a greater number of transients may reveal evidence for these.

All of the observations indicate that Se_2Br_2, like Se_2Cl_2, is not homomolecular but is disproportionated to a small extent according to equilibria [9] and [10]. From the intensities of the signals the disproportionation constants for these equilibria, K and K', may be estimated and these are listed in Table 3. The average values are $K = 1.1(\pm 0.2) \times 10^{-3}$ and $K' = 1.7(\pm 0.6) \times 10^{-6}$.

Diselenium bromide chloride

Raman spectroscopy. The Raman spectrum of a 0.92:1.0:0.21 mole ratio mixture of $Se_2Br_2 / Se_2Cl_2 / Se$ is shown in Fig. 3, trace *C*. The spectrum appears consistent with the sum of the individual spectra of Se_2Cl_2 and Se_2Br_2 except for the peak at 183 cm^{-1}, which corresponds to the peak assigned to the Se_nBr_2 species, and a weak band at 210 cm^{-1}. The formation of the mixed bromide chloride, according to

[11] $Se_2Cl_2 + Se_2Br_2 = 2\,Se_2BrCl$

TABLE 4. Chemical shifts and peak heights for a 0.92:1.0:0.21 mole ratio $Se_2Br_2/Se_2Cl_2/Se$ mixture

Chemical shift (ppm)	Assignment	Peak height[a]
297.4	SeBrCl	1
−9.11	Se_2Cl_2	152
−12.66	Se_2BrCl	166
−110.93	Se_2Br_2	164
−115.11	Se_2BrCl	140
−146.4	Se_3Br_2 (and Se_3BrCl ?)	2
−371.23	Se_4Br_2 (and Se_4BrCl ?)	2

[a]Peak heights are accurate to ±0.3.

is not excluded, however, since the bands expected for this product will lie very near those of Se_2Cl_2 and Se_2Br_2. No reasonable assignment of the new peak at 210 cm^{-1} to Se_2BrCl is, however, possible based upon assignments for Se_2X_2 (3–6) but this peak lies between the strong peaks of Se_nCl_2 and Se_nBr_2, 240 and 183 cm^{-1}, respectively, and probably arises from the same mode in Se_nBrCl. Similarly, the excess Se present will cause formation of Se_nBr_2, which is the origin of the peak at 183 cm^{-1}. The corresponding peak of Se_nCl_2 is masked by the strong band of Se_2Br_2 at 256 cm^{-1}.

^{77}Se nmr spectroscopy. The ^{77}Se nmr spectrum of the 0.92:1.0:0.21 mole ratio liquid mixture of $Se_2Br_2 / Se_2Cl_2 / Se$ is shown in Fig. 2 and the observed chemical shifts and peak heights are listed in Table 4. In earlier work (14) on a similar mixture, using field sweep methods, only two signals were observed and it was not possible to distinguish between a mixture of Se_2Cl_2 and Se_2Br_2 or formation of Se_2BrCl. In this work four signals were observed. The shifts at −9.11 and −110.93 ppm are readily assigned to Se_2Cl_2 and Se_2Br_2, respectively, from the shifts listed in Tables 2 and 3. The other two strong signals at −12.66 and 115.11 ppm must arise respectively from Se attached to Cl and to Br in Se_2BrCl and some halogen interchange reaction, according to

[12] $Se_2Br_2 + Se_2Cl_2 \overset{K''}{=} 2\,Se_2BrCl$

must take place. Using peak heights as a measure of concentration, K'' is estimated to be 3 but this estimate must be high, since the signal center at the base lies much loser to the Se_2Cl_2 and Se_2Br_2 peak positions than to those of Se_2BrCl, indicating that the Se_2BrCl peaks are weaker than those of the pure chloride and bromide. The apparent stronger signal for Se_2Cl_2 than for Se_2Br_2, which is the opposite of that expected from the stoichiometric ratio, is due to the differing degree of overlap with the Se_2BrCl signals. Three very weak peaks appear in the spectrum and these are assigned in Table 4 to small concentrations of disproportionation products.

Conclusion

The dihalides of selenium are regarded, for the most part, as molecules stable at high temperature in the gas phase but, more recently, $SeCl_2$ and $SeBr_2$ have been shown to be present in significant concentrations in aprotic solvents (9, 17), aqueous solution (18, 19) and now in equilibrium in diselenium dihalides. Selenium dihalide is present in higher molar concentration in Se_2Br_2 than in Se_2Cl_2, which parallels the relative stability of the dihalides in acetonitrile (9).

The presence of SeX_2 and Se_nX_2 species in pure Se_2X_2 results

Can. J. Chem. Downloaded from www.nrcresearchpress.com by 186.148.149.217 on 09/07/12
For personal use only.

in weak bands appearing in the reported spectra of these molecules (3–6), which have been assigned to vibrational modes of Se_2X_2 molecules. A reconsideration of the spectral assignment for these compounds will be necessary.

1. J. J. BERZELIUS. Ann. Chim. Phys. **9**, 225 (1818).
2. R. KNIEP, L. KORTE, and D. MOOTZ. Z. Naturforsch. **38***b*, 1 (1983).
3. P. J. HENDRA and P. J. D. PARK. J. Chem. Soc.(A), 908 (1968).
4. S. G. FRANKISS. J. Mol. Struct. **2**, 271 (1968).
5. R. FORNERIS and C. E. HENNIES. J. Mol. Struct. **5**, 449 (1970).
6. W. KIEFER. Spectrochim. Acta, **27**A, 1285 (1971).
7. S. V. VOLKOV, Z. A. FOKINA, V. F. LAPKO, V. E. POGRELOV, and G. I. SALIVON. Ukr. Khim. Zh. **48**, 899 (1982).
8. R. STEUDEL, D. JENSEN, and B. PLINKE. Z. Naturforsch. **42***b*, 163 (1987).
9. J. MILNE. Polyhedron, **4**, 65 (1985).
10. H. G. NOVAK and J. F. SUTTLE. Inorg. Synth. **5**, 125 (1957).
11. V. LENHER and C. H. KAO. J. Am. Chem. Soc. **47**, 772 (1925); F. Feher. Handbuch der Praparativen Anorganischen Chemie. 3rd ed. Vol. 1. *Edited by* G. Brauer. Enke Verlag, Stuttgart, 1975. pp. 415, 426.
12. M. LUNDQVIST and M. LELLEP. Acta Chem. Scand. **22**, 291 (1968).
13. R. K. HARRIS and B. MANN. NMR and the Periodic Table. Academic Press. 1979. p. 403.
14. T. BIRCHALL, R. J. GILLESPIE, and S. L. VEKRIS. Can. J. Chem. **43**, 1672 (1965).
15. H. EGGERT, O. NIELSEN, and L. HENRIKSEN. J. Am. Chem. Soc. **108**, 1725 (1986).
16. M. LAMOUREUX and J. MILNE. Polyhedron. In press.
17. N. KATSAROS and J. W. GEORGE. Inorg. Chem. **8**, 759 (1969).
18. M. MAHADEVAN and J. MILNE. Inorg. Chem. **22**, 1648 (1983).
19. J. MILNE. Can. J. Chem. **67**, 1056 (1989).

Can. J. Chem. Downloaded from www.nrcresearchpress.com by 186.148.149.217 on 09/07/12
For personal use only.

A low-temperature study of the magnetic properties of the molecular cations O_2^+, Br_2^+, and I_2^+

M. S. R. CADER, R. C. THOMPSON, AND F. AUBKE[1]

Department of Chemistry, University of British Columbia, Vancouver, B.C., Canada V6T 1Y6

Received May 4, 1989

This paper is dedicated to Professor Ronald J. Gillespie on the occasion of this 65th birthday

M. S. R. CADER, R. C. THOMPSON, and F. AUBKE. Can. J. Chem. **67**, 1942 (1989).

Magnetic susceptibility measurements to 4.2 K are reported for $O_2^+[AsF_6]^-$, $Br_2^+[Sb_3F_{16}]^-$, and $I_2^+[Sb_2F_{11}]^-$. The data are interpreted utilizing previous results from photoelectron spectroscopy, known crystal structures, magnetic studies on the superoxide ion and the ozonide ion, and in the case of $O_2^+[AsF_6]^-$, previous ESR studies. The magnetic properties of the three materials are quite different. $Br_2^+[Sb_3F_{16}]^-$ obeys Curie–Weiss law between 80 and 4 K: $C_m = 0.49 \pm 0.01$ cm^3 mol^{-1} K and $\theta = -0.74 \pm 0.01$ K (with TIP = 120×10^{-6} cm^3 mol^{-1}). The magnetic moment decreases slightly from 2.04 μ_B at room temperature to 1.93 μ_B at 4 K. $I_2^+[Sb_2F_{11}]^-$ exhibits relatively strong antiferromagnetic coupling with a maximum in χ_M observed at −54 K. The magnetic moment (corrected for a TIP contribution of 68×10^{-6} cm^3 mol^{-1}) decreases from 1.92 μ_B at 124 K to 0.41 μ_B at 4 K. Experimental susceptibilities for this compound over the range 300–4 K have been compared to values calculated using three different theoretical models for extended chains of antiferromagnetically coupled paramagnetic species. $O_2^+[AsF_6]^-$ exhibits Curie–Weiss behaviour over the range 60–2 K ($C_m = 0.34 \pm 0.01$ cm^3 mol^{-1} K, $\theta = -1.90 \pm 0.01$ K). The magnetic moment, uncorrected for TIP, varies from 1.63 μ_B at 80 K to 1.17 μ_B at 2 K, and the presence of weak antiferromagnetic coupling in this material is suggested.

Key words: magnetic susceptibilities, dihalogen cations, dioxygenyl cation, low temperature behaviour.

M. S. R. CADER, R. C. THOMPSON et F. AUBKE. Can. J. Chem. **67**, 1942 (1989).

On rapporte les résultats de mesures de susceptibilité magnétique, effectuées à 4,2 K sur $O_2^+[AsF_6]^-$, sur $Br_2^+[Sb_3F_{16}]^-$ et sur $I_2^+[Sb_2F_{11}]^-$. On interprète les résultats en utilisant les resultats obtenus antérieurement à l'aide de la spectroscopie photoélectronique, de la diffraction des rayons-X, d'études magnétiques sur l'ion superoxyde et sur l'ion ozonide et, dans le cas de $O_2^+[AsF_6]^-$, à l'aide d'études rpe antérieures. Les propriétés magnétiques de ces trois composés sont très différentes. Entre 80 et 4 K, le produit $Br_2^+[Sb_3F_{16}]^-$ obéit à la loi de Curie–Weiss: $C_m = 0{,}49 \pm 0{,}01$ cm^3 mol^{-1} K et $\theta = -0{,}74 \pm 0{,}01$ K (avec TIP = 120×10^{-6} cm^3 mol^{-1}). Le moment magnétique diminue un peu, de 2,04 μ_B à la température ambiante à 1,93 μ_B à 4 K. Le $I_2^+[Sb_2F_{11}]^-$ présente un couplage antiferromagnétique relativement important; le maximum de χ_M est observé à ~54 K. Le moment magnétique (corrigé pour une contribution de TIP de 68×10^{-6} cm^3 mol^{-1}) diminue de 1,92 μ_B à 124 K à 0,41 μ_B à 4 K. On a comparé les susceptibilités expérimentales de ce composé, de 300 à 4 K, avec les valeurs calculées à l'aide de trois modèles théoriques différents pour des longues chaînes d'espèces paramagnétiques couplées d'une façon antiferromagnétique. Aux températures allant de 60 à 2 K, le $O_2^+[AsF_6]^-$ présente un comportement de Curie–Weiss ($C_m = 0{,}34 \pm 0{,}01$ cm^3 mol^{-1} K, $\theta = -1{,}90 \pm 0{,}01$ K). Le moment magnétique, non-corrigé pour une contribution de TIP, varie de 1,63 μ_B à 80 K à 1,17 μ_B à 2 K; ces données suggèrent la présence d'un faible couplage antiferromagnétique dans ce composé.

Mots clés : susceptibilités magnétiques, cations de dihalogène, cation de dioxygényle, comportement à basse température.

[Traduit par la revue]

Introduction

Only a limited number of compounds with paramagnetic homonuclear ions of non-metallic main group elements are known. Of these, compounds with diatomic cations stabilized by very weakly basic fluoroanions are the subject of this study. The cations in this group consist of the dioxygenyl cation O_2^+, first discovered in $O_2^+[PtF_6]^-$ by Bartlett and Lohmann (1), and the two dihalogen cations I_2^+ and Br_2^+, first identified in strong acid and superacid solutions by Gillespie *et al.* (2, 3).

Single crystal X-ray diffraction studies were subsequently reported for $Br_2^+[Sb_3F_{16}]^-$ (4) and $I_2^+[Sb_2F_{11}]^-$ (5), while powder diffraction studies have afforded a more limited structural insight into a number of dioxygenyl salts (6). For the dihalogen cations, electronic spectra of the solvated species (2, 3), resonance Raman spectra (7), and magnetic measurements at room temperature (2, 4*a*) have allowed some information on the electronic structure, suggesting a $^2\Pi_{3/2g}$ ground state (10). In addition, a study by Herring and McLean (8) has pointed to a strong similarity between the solvated cations $I_2^+{}_{(solv)}$ and $Br_2^+{}_{(solv)}$ and their gaseous counterparts as studied by photoelectron spectroscopy (9) or molecular spectroscopy (10). This connection should permit at least an approximation of the energy separation to the nearest excited states, not only for the dihalogen cations, but also for O_2^+, where a $^2\Pi_{1/2g}$ ground state is suggested (10).

The present study involving low-temperature magnetic susceptibility measurements on suitable compounds containing the three homonuclear diatomic cations has four objectives: (*i*) To compare the magnetic behaviour of what appear to be the only three suitable paramagnetic molecular cations formed by non-metals. Structural and spectroscopic information discussed above should help in the interpretation. (*ii*) To see whether, and to what extent, van Vleck's theory of molecular paramagnetism (11), developed almost 60 years ago, can be applied to solid-state cations. So far, nitric oxide, NO, has served as the best example; however, useful experimental data for this molecule do not extend into the condensed phase. (*iii*) To examine reasons why the magnetic moments reported so far for O_2^+ salts (discussed below) fall well below the spin-only value of 1.73 μ_B. Measurement down to very low temperatures should allow detection of antiferromagnetic coupling, which is a possible cause for reduced magnetic susceptibilities. (*iv*) To compare the magnetic susceptibilities of $I_2^+[Sb_2F_{11}]^-$ and $Br_2^+[Sb_3F_{16}]^-$ below 80 K, since earlier measurements above that temperature (12) had suggested antiferromagnetic coupling for $I_2^+[Sb_2F_{11}]^-$, but not for $Br_2^+[Sb_3F_{16}]^-$.

[1]Author to whom correspondence should be addressed.

Can. J. Chem. Downloaded from www.nrcresearchpress.com by 194.225.253.170 on 09/07/12
For personal use only.

Can. J. Chem. Downloaded from www.nrcresearchpress.com by 194.225.253.170 on 09/07/12
For personal use only.

Experimental

Both $Br_2^+[Sb_3F_{16}]^-$ and $I_2^+[Sb_2F_{11}]^-$ were synthesized according to the method reported by Wilson *et al.* (12). This method involves the oxidation of previously purified Br_2 and resublimed I_2 by bis(fluorosulfuryl) peroxide, $S_2O_6F_2$, at a precise 2:1 mole ratio, and the subsequent solvolysis of the product mixture in an excess of freshly distilled antimony(V) fluoride. The reactions were followed by weight and the purity checked by melting points.

$Br_2^+[Sb_3F_{16}]^-$ (4.777 g or 5.762 mmol) was obtained from 0.924 g (5.782 mmol) of Br_2 and 0.5724 g (2.891 mmol) of $S_2O_6F_2$ after solvolysis in about 10 g of SbF_5 at room temperature and removal of all volatiles *in vacuo*. The bright red solid melted at 84 ± 1°C (lit. 85.5°C) (12).

$I_2^+[Sb_2F_{11}]^-$ (2.775 g or 3.928 mmol) was obtained from 0.9986 g (3.934 mmol) I_2 and 0.3895 g (1.967 mmol) of $S_2O_6F_2$ and subsequent solvolysis in ~12 g of SbF_5 at 50°C. The black–blue solid obtained after removal of all volatiles melted at 129 ± 1°C (lit. mp 127°C) (12).

A sample of $O_2^+[AsF_6]^-$ was obtained from Dr. Karl O. Christe of Rocketdyne. The compound was synthesized by UV photolysis of O_2, F_2, and AsF_5 in quartz. A Princeton Applied Research model 155 vibrating sample magnetometer was used to obtain magnetic susceptibilities in the 2.0–124 K range. Details on the instrument have been published previously (13). Magnetic field strengths of 7501, 9225, and 9625 G were used and temperatures lower than 4 K were achieved by pumping on the sample chamber. Samples of ~200–300 mg were loaded into Kel-F capsules. All hygroscopic solids were handled in a Vacuum Atmospheres Corp. "Dri-Lab" model No. H3-493, filled with purified dry N_2 and equipped with a Dri-Train circulating unit. Molar magnetic susceptibilities, χ_M, listed in Tables 1 and 2, are corrected for diamagnetism, with the corrections given in Table 3. For $Br_2^+[Sb_3F_{16}]^-$ and $I_2^+[Sb_2F_{11}]^-$, slightly larger χ_{dia} values are used than reported previously (12). The magnetic moments given in Tables 1 and 2 for the Br_2^+ and I_2^+ compounds are corrected for temperature-independent paramagnetism (TIP = 120 and 68 × 10^{-6} cm^3 mol^{-1}, respectively, calculated as described in the text). The Curie–Weiss law in the form $\chi_M = C_m/(T - \theta)$ is used throughout. Pertinent structural and spectroscopic features of the three compounds studied and of the three cations, O_2^+, Br_2^+, and I_2^+, either as solvated or gaseous species, are summarized in Table 3.

Results and discussion

The discussion will center around three aspects: (*i*) the selection of suitable compounds for this study in the light of previous magnetic susceptibility studies; (*ii*) the magnetic measurements on $O_2^+[AsF_6]^-$, $I_2^+[Sb_2F_{11}]^-$, and $Br_2^+[Sb_3F_{16}]^-$; and (*iii*) an attempted interpretation of these results.

Magnetic measurements in our laboratory on the compounds in the current study require ~300–500 mg of high-purity sample for duplicate measurements when the vibrating sample magnetometer is used, while the Gouy measurements require between 1–2 g. All cations are extremely reactive and only I_2^+ is sufficiently stable in HSO_3F–SbF_5 solution (2, 12), not undergoing disproportionation or further oxidation. This rules out purification by recrystallization as a general procedure for all three salts. The limited thermal stability of all materials reported so far precludes purification by sublimation. Hence, synthesis on the desired scale from highly pure starting materials, with little or no chance for side-reactions and facile product isolation, becomes the only route to materials for the intended study.

There appears to be no real choice among the Br_2^+ containing compounds, because necessary details on $Br_2^+[AsF_6]^-$ (14), the only other Br_2^+ salt, are not readily available. The original synthesis of $Br_2^+[Sb_3F_{16}]^-$ (4), from BrF_5, Br_2, and SbF_5, did produce a sample suitable for a single-crystal X-ray diffraction study, but judging by the reported physical data, in particular

TABLE 1. Magnetic data for $Br_2^+[Sb_3F_{16}]^-$

T (K)[a]	$\chi_M \times 10^6$ (cm^3 mol^{-1})	μ_{eff} (μ_B)[b]
297	1870	2.04
275	2010	2.04
255	2160	2.04
235	2330	2.03
213	2530	2.03
193	2780	2.03
172	3070	2.02
151	3430	2.00
131	3900	1.99
116	4500	2.02
104	4910	2.00
80.0	6130	1.96
81.1	6070	1.96
73.5	6720	1.97
65.7	7440	1.96
55.0	8870	1.96
43.7	10900	1.94
31.4	15000	1.93
21.4	21900	1.93
10.2	45700	1.93
9.88	45900	1.90
4.20	111300	1.93

[a]First twelve data points from ref. 12.
[b]Corrected for TIP using $\mu_{eff} = 2.828\ ((\chi_M - TIP)T)^{1/2}$ with TIP = 120 × 10^{-6} cm^3 mol^{-1}.

TABLE 2. Magnetic data for $I_2^+[Sb_2F_{11}]^-$ and $O_2^+[AsF_6]^-$

$I_2^+[Sb_2F_{11}]^-$			$O_2^+[AsF_6]^-$		
T (K)	$\chi_M \times 10^6$ (cm^3 mol^{-1})	μ_{eff}[a] (μ_B)	T (K)	$\chi_M \times 10^6$ (cm^3 mol^{-1})	μ_{eff}[b] (μ_B)
124.1	3770	1.92	80.1	4170	1.63
117.5	3860	1.89	76.3	4410	1.64
106.5	4290	1.90	72.7	4650	1.64
98.6	4510	1.87	68.5	4950	1.65
90.9	4730	1.84	64.3	5480	1.65
84.3	4900	1.81	59.2	5600	1.63
81.2	5030	1.80	53.2	6170	1.62
76.8	5120	1.76	46.5	6990	1.61
71.8	5300	1.73	42.9	7520	1.61
66.6	5380	1.68	39.1	8200	1.60
63.5	5470	1.66	30.3	10530	1.60
58.4	5560	1.60	25.3	12430	1.59
51.9	5560	1.51	20.5	15100	1.57
44.9	5090	1.34	15.3	19700	1.55
36.9	4910	1.20	10.1	28800	1.52
31.6	4700	1.08	7.12	37500	1.46
27.4	4490	0.98	5.92	44500	1.45
27.1	4520	0.98	5.28	48300	1.43
21.8	4300	0.86	4.78	52200	1.41
11.6	4270	0.62	4.62	52700	1.40
8.64	4290	0.54	4.40	54800	1.39
6.30	4490	0.47	4.04	59400	1.39
4.54	4790	0.41	2.70	70400	1.23
			2.40	75500	1.20
			2.10	81300	1.17

[a]Corrected as in Table 1 with TIP = 68 × 10^{-6} cm^3 mol^{-1}.
[b]Not corrected for TIP.

TABLE 3. Structural and spectroscopic information on $O_2^+[AsF_6]^-$, $I_2^+[Sb_2F_{11}]^-$, $Br_2^+[Sb_3F_{16}]^-$, and the corresponding ions O_2^+, Br_2^+, and I_2^+

Data, X denotes O, Br, or I	$O_2^+[AsF_6]^-$ or $O_2^+{}_{(g)}$	$Br_2^+[Sb_3F_{16}]^-$ or $Br_2^+{}_{(g)}$	$I_2^+[Sb_2F_{11}]^-$ or $I_2^+{}_{(g)}$
Shortest X···X nonbonding interaction (Å)	4 to 4.05[a] (refs. 28*b*, 30)	6.445 (refs. 12, 4*b*)	4.29 (refs. 12, 6)
van der Waals radii for X (Å) (ref. 34)	1.52	1.85	1.98
Ground state of $X_2^+{}_{(g)}$	$^2\Pi_{1/2g}$	$^2\Pi_{3/2g}$	$^2\Pi_{3/2g}$
Spin–orbit coupling constant (cm^{-1}) for $X_2^+{}_{(g)}$	185[b] 195 (ref. 10)	2820±40[c] 3141±160[d]	5125±40[c] 5081±60[e]
$\Delta E(^2\Pi_{1/2g} - {}^2\Pi_{3/2g})$			
As above for $X_2^+{}_{(solv)}$ (cm^{-1})	—	2890 (ref. 12)	5190 (ref. 2)
Diamagnetic correction[f] (10^{-6} cm^3 mol^{-1})	79	279	238

[a]Estimated from powder diffraction data.
[b]Reference 50.
[c]Reference 51.
[d]Reference 52.
[e]Reference 53.
[f]Reference 54.

the melting point and a magnetic moment of $\mu_{eff} \sim 1.6\mu_B$, the method appears to be unsuited for our purpose. Similarly, the method used for the preparation of single crystals of $I_2^+[Sb_2F_{11}]^-$ (5), the oxidation of I_2 by SbF_5 in SO_2, is not suited for preparation on a large scale, as is evident from the reported analytical data (5). The problem appears to be the quantitative separation of the by-products SbF_3 or $SbF_3 \cdot SbF_5$. Formation of anions of the type $Sb_3F_{14}^-$ becomes a possibility and, in addition, a diamagnetic compound of the composition $I_4^{2+}[(SbF_6)\text{-}(Sb_3F_{14})]^{2-}$ has recently been obtained by this synthetic route (15) with reaction conditions only slightly different. Substitution of SO_2 by AsF_3 as solvent, appears to lead to $I_2^+[Sb_2F_{11}]^-$ of higher purity, but $I_2^+[Sb_3F_{16}]^-$ may form as a by-product as well (16). Any uncertainty in the molar mass of the product will limit the usefulness of a magnetic study. Other materials not deemed suitable for our magnetic studies include the substances formulated as $(SbF_5)_2I$ (17) and the insufficiently characterized $I_2^+[TaF_6]^-$ (17).

An alternate synthetic route to both $I_2^+[Sb_2F_{11}]^-$ and $Br_2^+[Sb_3F_{16}]^-$, the oxidation of I_2 or Br_2 by stoichiometric amounts of bis(fluorosulfuryl) peroxide and subsequent solvolysis in an excess of SbF_5 according to:

$$[1]\quad 2I_2 + S_2O_6F_2 + 8SbF_5 \xrightarrow{50°C} 2I_2^+[Sb_2F_{11}]^- + 2Sb_2F_9SO_3F$$

$$[2]\quad 2Br_2 + S_2O_6F_2 + 10SbF_5 \xrightarrow{25°C} 2Br_2^+[Sb_3F_{16}]^- + 2Sb_2F_9SO_3F$$

has produced sufficiently large quantities of both compounds for a magnetic study between 298 and 80 K using the Gouy technique (12). With all starting materials readily purified and the volatile reaction product $Sb_2F_9SO_3F$ (18) easily separated from the product, this method, employed in the present study as well, is applicable to the synthesis of both $I_2^+[Sb_2F_{11}]^-$ and $Br_2^+[Sb_3F_{16}]^-$.

With well over a dozen different O_2^+ salts reported so far, this group of compounds appears to offer a wider choice, but here additional problems surface, which seem to have adversely affected earlier magnetic studies. Some of the reported compounds, $O_2^+[PtF_6]^-$ (1), $O_2^+[PdF_6]^-$ (19), $O_2^+[RuF_6]^-$ (20), or $O_2^+[RhF_6]^-$ (20) have two different paramagnetic centers in the same molecular unit. The initial approach by Bartlett and Beaton (21) involving the subtraction of the molar susceptibilities of $NO^+[PtF_6]^-$ from those obtained for $O_2^+[PtF_6]^-$ has clearly allowed identification of O_2^+ as a paramagnetic ion; however, magnetic exchange between O_2^+ and Pt(V)(d^5) is a plausible contributing cause for the observed decreasing trend of the magnetic moments attributed to O_2^+ with decreasing temperature. Magnetic ordering due to $O_2^+ \cdots Pt(V)$ exchange has subsequently been reported for this compound (23).

In addition, the high-pressure synthesis of dioxygenyl salts from O_2–F_2 mixtures and either metal fluorides or the metal itself (20, 22, 24) in metal reactors has often resulted in materials with ferromagnetic contamination (19, 23). While monel impurities can be recognized by the characteristic Curie temperature of 335 K and corrections have been attempted (23) in magnetic susceptibility studies, such materials remain suspect where the possibility of weak antiferromagnetic ordering exists.

Ultraviolet photolysis in quartz vessels (25) represents a more suitable synthetic method, but a number of the O_2^+ salts such as $O_2^+[BF_4]^-$ (26) and $O_2^+[GeF_5]^-$ (27) show rather limited thermal stability. Nevertheless, a magnetic study of $O_2^+[BF_4]^-$ between 293 and 85 K has been reported (28*a*), but only limited conclusions were reached. For the products obtained from the reaction of O_2 and F_2 with SbF_5 by either UV photolysis or high-pressure synthesis, some structural ambiguity exists. Both $O_2^+[SbF_6]^-$ and $O_2^+[Sb_2F_{11}]^-$ are well characterized (6, 24), and $O_2^+[Sb_3F_{16}]^-$ has been postulated as well (29). The problems caused by this structural ambiguity are apparent from magnetic susceptibility studies on "$O_2^+[SbF_6]^-$" reported in the Russian literature (28).

To avoid similar problems, $O_2^+[AsF_6]^-$ obtained by UV photolysis (25) was chosen for our study. An additional reason for this choice is the availability of structural information. A phase transition at 255 ± 3 K (30) results in a rhombohedral distortion of the cubic structure found at room temperature (6). This distortion is also evident from ESR studies down to 4 K (23, 31); in this work conclusions regarding the ground state of O_2^+ in this compound are useful in the interpretation of our results.

Can. J. Chem. Downloaded from www.nrcresearchpress.com by 194.225.253.170 on 09/07/12
For personal use only.

Can. J. Chem. Downloaded from www.nrcresearchpress.com by 194.225.253.170 on 09/07/12
For personal use only.

There have been two previous magnetic susceptibility studies of $O_2^+[AsF_6]^-$ down to 4 K, with rather contradictory results. In a study by Grill *et al.* (32), no ordering of the O_2^+ cations is observed down to 4 K, while weak $O_2^+ \ldots O_2^+$ exchange is suggested in another study (23) based on the small Weiss constant obtained. However, these conclusions are rendered somewhat tenuous because of ferromagnetic monel impurities in the sample, requiring correction of the susceptibility data (23).

In all previous magnetic susceptibility studies of O_2^+ salts, the magnetic moments obtained over the whole temperature range are well below the spin-only value of 1.73 μ_B, and explanations have varied from suggesting "van-Vleck behaviour" (22) in analogy to the behaviour of NO (11), to invoking the presence of 17% of an unidentified, magnetically inert impurity in $O_2^+[AsF_6]^-$ (32). Likewise in some studies down to 80 K (28), μ_{eff} values for $O_2^+[SbF_6]^-$ appear to decrease with decreasing temperature, while for the structurally related $O_2^+[AsF_6]^-$, μ_{eff} is said to be invariant with temperature to 4 K (32). It is unclear why there are so many discrepancies and contradictions in previous studies. It is felt, however, that sample identity and purity play a major role here.

The results of our magnetic susceptibility studies on $Br_2^+[Sb_3F_{16}]^-$ below 80 K, together with results obtained in our earlier study (12) at higher temperatures, are summarized in Table 1. Both sets of χ_M and μ_{eff} data have been calculated using the same diamagnetic correction and TIP values (279 and 120×10^{-6} cm^3 mol^{-1}, respectively). The agreement between the data sets in the overlap region is excellent for this compound. The data obtained here for $I_2^+[Sb_2F_{11}]^-$ and $O_2^+[AsF_6]^-$ are given in Table 2. Because of poor agreement in the 100-K region with the earlier Gouy data (12), we extended the current studies with the vibrating sample magnetometer up to 124 K for the I_2^+ compound. We also extended our studies on the O_2^+ compound down to 2 K in the hope (not realized, unfortunately) of observing a maximum in the susceptibility of this compound at very low temperatures. The contrast in the magnetic properties of the three paramagnetic cationic species studied in this work is clearly evident from the plots of magnetic moment versus temperature shown in Fig. 1. Two of the compounds, $O_2^+[AsF_6]^-$ and $Br_2^+[Sb_3F_{16}]^-$, exhibit Curie–Weiss behaviour over a wide temperature range, as is seen by the plots of χ_M^{-1} versus T given in Fig. 2.

The magnetic behaviour of $Br_2^+[Sb_3F_{16}]^-$ appears to be rather straightforward and will be discussed in detail first. The χ_M^{-1} versus T plot for this compound indicates Curie–Weiss law behaviour over the temperature range from 80–4 K ($C_m = 0.49 \pm 0.01$ cm^3 mol^{-1} K, $\theta = -0.74 \pm 0.01$ K). The magnetic moments (even when corrected for TIP) decrease slightly with temperature. A TIP correction had been arbitrarily assigned in the earlier work (12) in order to bring the magnetic moment in the high-temperature region into agreement with the value of 2.0 μ_B predicted by theory (11) for a species with a $^2\Pi_{3/2g}$ ground state and no thermally accessible excited state (see Table 3). The correction for TIP in the present study was taken as $4N\beta^2/3\Delta E$ (33), where ΔE is the energy separation between the ground $^2\Pi_{3/2g}$ and the excited $^2\Pi_{1/2g}$ state with which it is mixing. The ΔE value for Br_2^+ is the spin–orbit coupling constant, λ, for this species, estimated at 2890 cm^{-1} for the solvated ion (Table 3), and using this value a TIP of 120×10^{-6} cm^3 mol^{-1} is calculated. Magnetic moments calculated using this TIP correction are within ±2% of the theoretical value of 2.0 μ_B over the very wide temperature range of 297–55 K (Table 1). The cause of the very small drop in the moment,

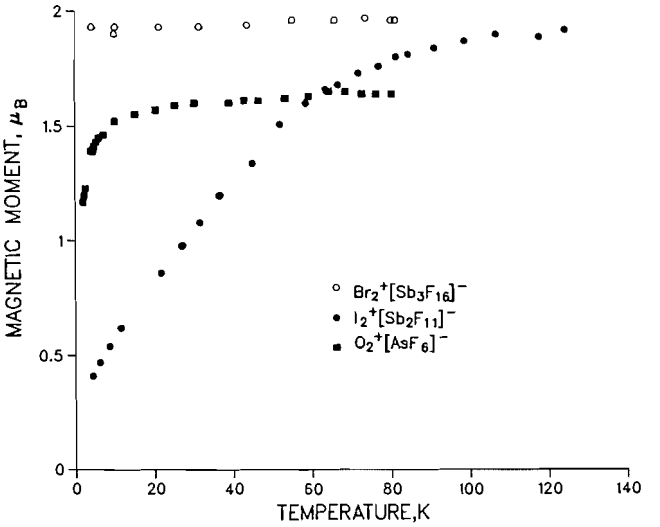


FIG. 1. Magnetic moment versus temperature plots.

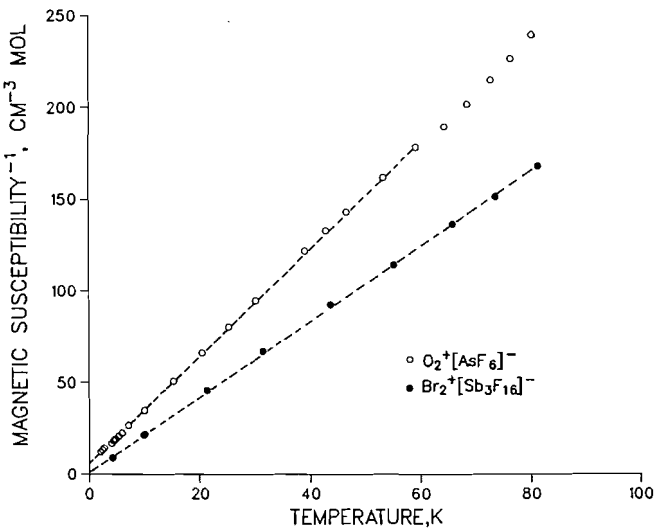


FIG. 2. Plots of inverse susceptibility versus temperature for $O_2^+[AsF]_6^-$ and $Br_2^+[Sb_3F_{16}]^-$.

particularly at the lowest temperatures (corresponding to the effect of a Curie–Weiss rather than Curie law behavior) is not certain. Although the shortest non-bonding Br···Br contact at 6.445 Å (46) is too long to invoke significant direct magnetic interaction, F···Br contacts ranging from 2.86–3.34 Å, comparable to or shorter than the sum of the van der Waals radii of 3.32 Å (34), suggest the possibility of very weak exchange via bridging anions. In any event, the effect is very minor and it is reasonable to conclude that in $Br_2^+[Sb_3F_{16}]^-$ the Br_2^+ cation is in a thermally isolated $^2\Pi_{3/2g}$ ground state and there is no conclusive evidence for any magnetic coupling between paramagnetic centers down to 4.2 K. In this regard $Br_2^+[Sb_3F_{16}]^-$ is somewhat unique, since for all other paramagnetic main group species, including O_2^- (35), the recently studied ozonides, KO_3, RbO_3, and CsO_3 (36), and solid O_2 (37), as well as I_2^+ and O_2^+ (discussed below), at least weak antiferromagnetic coupling has been suggested.

The magnetic properties of $O_2^+[AsF_6]^-$ are similar to those of the Br_2^+ compound in that Curie–Weiss law behavior is followed (Fig. 2), although over a more limited temperature range of 60–2 K. Here the Curie constant, C_m, is significantly

Can. J. Chem. Downloaded from www.nrcresearchpress.com by 194.225.253.170 on 09/07/12
For personal use only.

smaller and the absolute value of the Weiss constant, $|\theta|$, greater ($C_m = 0.34 \pm 0.01$ cm^3 mol^{-1} K, $\theta = -1.90 \pm 0.01$ K). Consequently, the effective magnetic moments are significantly smaller for $O_2^+[AsF_6]^-$ and show a stronger temperature dependence, particularly in the low temperature region (Fig. 1). We note a slight departure from linear behaviour in the Curie–Weiss plot (Fig. 2) above 60 K. This may be significant, as it coincides with the observed broadening of the ESR line (23), possibly caused by tumbling motions of O_2^+ in the crystal lattice. These findings are at variance with a previous report by Grill *et al.* (32), who first found Curie–Weiss behaviour with a positive θ value (according to our formulation of the law) of 0.7 K. Our results are in reasonable agreement with those of DiSalvo *et al.* (23), who obtained $C_m = 0.309$ cm^3 mol^{-1} K and $\theta = -0.8$ K (sign changed from ref. 23 to conform to our formulation of the law), although it must be taken into consideration that a temperature-independent paramagnetism contribution was allowed for in the earlier work and corrections for ferromagnetic impurities had to be made. In our study we chose not to correct the susceptibilities for TIP. A crystal-field analysis of ESR data for $O_2^+[AsF_6]^-$ suggests the separation between the ground and first electronic excited state is 1480 cm^{-1}, caused by both spin–orbit coupling and crystal-field splitting due to O_2^+ being in a site of orthorhombic or lower symmetry (31). In this case one is clearly not dealing with pure $^2\Pi_{1/2g}$ and $^2\Pi_{3/2g}$ states and it is not clear what the TIP correction should be. In any event, the large separation between the states means such a correction will be small, and hence ignoring it should not significantly affect our conclusions.

Turning to the question of the magnitude of the magnetic moment we observe for $O_2^+[AsF_6]^-$ in the higher temperature region, moments in the range of 1.6 μ_B agree well with values predicted using the average g values, g_{ave} of 1.89 (23) and 1.905 (31) obtained by ESR. As described by Goldberg *et al.* (31), both crystal-field splitting and spin–orbit coupling contribute to the ground state in $O_2^+[AsF_6]^-$. In a pure $^2\Pi_{1/2g}$ ground state the spin and orbital contributions cancel, and there is no first-order paramagnetism associated with this state (33). If this were the case for O_2^+ with negligible thermal population of excited states, only temperature-independent paramagnetism would be present. This is clearly not the case here. The crystal-field interactions have the effect of quenching the orbital contribution, although not completely, resulting in a μ_{eff} value slightly below the spin-only value. Quite the opposite effect is observed for the alkali metal superoxides, MO_2 with M = Na, K, Rb, Cs (35). Here the ground state is $^2\Pi_{3/2g}$ and in all instances the μ_{eff} values are well above the spin-only value of 1.73 μ_B, as was found for $I_2^+[Sb_2F_{11}]^-$ and $Br_2^+[Sb_3F_{16}]^-$ (12).

Returning to $O_2^+[AsF_6]^-$, the decrease in μ_{eff} with decreasing temperature, particularly significant below ~20 K, requires futher consideration. With a splitting of 1480 cm^{-1} separating the ground state from the nearest excited state, the variation in the effective magnetic moment with temperature observed here cannot be accounted for by the sort of van Vleck behaviour observed for gaseous NO (33). The possibility of antiferromagnetic exchange between paramagnetic centers must be considered.

The limited structural information available on $O_2^+[AsF_6]^-$ (25, 31, 38) derived from powder diffraction data does not permit an accurate determination of the shortest O···O nonbonding contact distance. Estimates of 4.00 (30*b*) and 4.05 Å (32) respectively, used to argue against O···O interaction, are simply the unit cell length a_0 divided by 2 for the room-temperature phase (25, 31, 38). The distance $a_0/2$ describes the separation between the mass centers of the O_2^+ cations, assumed to be in the most probable sites. The low-temperature phase, which is directly relevant to our study, has a powder diffraction pattern that has not been successfully indexed (30); hence the conclusion (32) that there can be no antiferromagnetic exchange in $O_2^+[AsF_6]^-$ because the O_2^+ ions are too far apart is most likely invalid.

For $O_2[Mn_2F_9]$, where a single crystal X-ray diffraction study at room temperature and at −150°C is reported (39), non-bonding O···O contacts of 3.86 Å are detected at −150°C with values of 3.98 Å observed at room temperature. However, the anion is described as a double chain of *cis*-bridged MnF_6-octahedra with O_2^+ cations between the anion layers, and the resulting structure is not comparable with that of $O_2^+[AsF_6]^-$. Moreover, studies on this material would not be suitable for our purposes as the magnetism would be complicated by the presence of Mn^{4+}, a second paramagnetic center.

With the sum of the van der Waals radius 3.02 Å for oxygen, one would reasonably expect distances of 3.2–3.3 Å as the limit for significant direct antiferromagnetic exchange. This estimate is corroborated by recent reports on the structures of the alkali metal ozonides KO_3 (40–42), RbO_3 (40, 41), and CsO_3 (43), which all exhibit more significant antiferromagnetism (34) than found for $O_2^+[AsF_6]^-$, and where O···O nonbonding contacts range between 3.01–3.15 Å for KO_3 and 3.01–3.30 Å for RbO_3, respectively. For CsO_3, where antiferromagnetic exchange is rather weak (36), only powder data are reported (43) and indexed suggesting CsO_3 to be iso-structural with RbO_3. The unit-cell dimensions indicate slightly longer O···O contacts for this compound (42). Contact distances of the order of those observed in the ozonides could be present in $O_2^+[AsF_6]^-$ and this could account for its observed magnetic properties. In summary, there appears to be weak antiferromagnetic coupling in $O_2^+[AsF_6]^-$ that may involve either super-exchange through intervening AsF_6^- anions (the smallest anion of the three encountered in this study) or even direct weak O···O interaction.

In our previous report on $I_2^+[Sb_2F_{11}]^-$ we showed that a TIP correction in excess of that assumed for the Br_2^+ compound was required to bring the experimental room-temperature moment into agreement with the value of 2.00 μ_B required by theory (12). In addition, it was suggested in the earlier work that the observed decrease in the magnetic moment on decreasing temperature to 80 K may arise from antiferromagnetic exchange between contiguous I_2^+ cations in the solid lattice. Our studies to 4.2 K reported here confirm the presence of antiferromagnetic coupling. The susceptibility rises to a maximum at ~54 K, then decreases on further cooling (Fig. 3). The rise again in susceptibility on cooling below ~10 K is probably due to trace amounts of paramagnetic structural impurity, as is often observed in antiferromagnetically coupled systems (13). In view of the clear evidence that this system is exchange-coupled, there is no justification for arbitrarily reducing the room-temperature moment to 2.00 μ_B with an appropriate TIP correction, as was done previously (12). Indeed, in view of the fact that the $^2\Pi_{3/2g}$–$^2\Pi_{1/2g}$ separation is significantly greater in the I_2^+ compound compared to Br_2^+, any TIP would be expected to be smaller in the former. TIP for I_2^+ calculated as described above for Br_2^+ is 68×10^{-6} cm^3 mol^{-1}. Magnetic moments calculated employing this value of TIP are given in Table 2. The decrease in μ_{eff} with decreasing temperature is con-

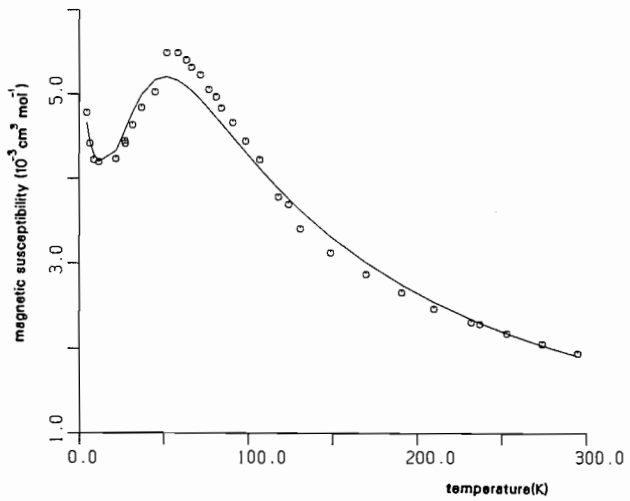


FIG. 3. Magnetic susceptibility versus temperature plot for $I_2^+[Sb_2F_{11}]^-$. Circles are experimental data. Solid line is the best fit to the Ising $S' = 1/2$ model.

sistent with antiferromagnetic coupling; interestingly though, the absolute values in the high-temperature region are in excess of the theoretically predicted value of 2.0 μ_B (11).

We have attempted to analyze our magnetic susceptibility data (including the data from 295–130 K from ref. 12) according to three theoretical models for antiferromagnetic exchange in one-dimensional systems. Considering the $^2\Pi_{3/2g}$ ground state of I_2^+ as having an effective spin, $S' = 3/2$ (44), we fitted the data to the model developed by Weng (45) employing the equations and appropriate coefficients given by Hiller *et al.* (46). The best fit of the data was with $J = -7.2$ cm^{-1}, the effective $g = 1.23$, and % paramagnetic impurity, $\%p$, = 0.35. The value of the fitting function, F (defined in ref. 47) was 0.0560. This model employs the isotropic Heisenberg Hamiltonian. In view of the molecular anisotropy of the magnetic species, the anisotropic Ising model should be examined. Unfortunately, while an exact solution exists for the parallel susceptibility of the Ising $S = 3/2$ case (48), there is no solution for the perpendicular case and hence we cannot analyze our powder data according to this model.

An alternative approach to the data analysis is to consider the possibility that the four-fold degeneracy of the ground $^2\Pi_{3/2g}$ state has been lifted by second- or higher-order interactions with excited states, leaving a thermally isolated Kramer's doublet as the only significantly thermally populated ground level. In this case one needs to consider an effective spin, $S' = 1/2$, and here both Heisenberg and Ising models are available. Employing the Weng model (45), again with appropriate coefficients taken from the paper of Hiller *et al.* (46), we obtained a best fit between theory and experiment with $J = -28$ cm^{-1}, effective $g = 2.72$ and $\%p = 0.61$ ($F = 0.0487$). Exact solutions for both the parallel and perpendicular susceptibilities for the Ising $S' = 1/2$ case are available, and we analyzed our data using the equation of Fisher (49) (assuming $\chi_{powder} = (1/3)\chi_\parallel + (2/3)\chi_\perp$), the best fit being obtained with $J = -38$ cm^{-1}, effective $g = 2.61$ and $\%p = 0.54$ ($F = 0.0368$). The agreement between experiment and theory for this Ising $S' = 1/2$ case is illustrated in Fig. 3, where the solid line is calculated from theory. The agreement between experiment and theory for the other two models is visually very similar to that shown in Fig. 3, although in both cases the agreement is slightly poorer, as is indicated by the higher F values. In all three cases, as the temperature is lowered the experimental susceptibilities rise more steeply to a higher maximum value and then decrease more steeply as compared to the calculated susceptibilities.

The analysis of the magnetic susceptibility data clearly indicates that contiguous I_2^+ ions in the lattice of $I_2^+[Sb_2F_{11}]^-$ are relatively strongly antiferromagnetically coupled, although it does not provide a clear answer to the question of whether or not the thermally occupied ground state at low temperatures is a pure $^2\Pi_{3/2g}$ state. Measurements of magnetic susceptibilities at low temperatures on suitably oriented single crystals to obtain $\chi_\parallel$ values (47) would be informative, but would require the synthesis of relatively large crystals of the materials.

The major difference in magnetic behaviour betweeen Br_2^+ and I_2^+ is due to structural differences between $Br_2^+[Sb_3F_{16}]^-$ and $I_2^+[Sb_2F_{11}]^-$. Magnetic exchange through contiguous I_2^+ ions is suggested by the crystal structure of $I_2^+[Sb_2F_{11}]^-$ (6). The shortest I...I nonbonding contact is with 4.29 Å comparable to the sum of the van der Waals radii of 3.96 Å. In $Br_2^+[Sb_3F_{16}]^-$ (4*b*) the shortest Br...Br contact is with 6.445 Å about 2.8 Å longer than the van der Waals distance, and direct magnetic exchange becomes improbable as discussed above.

Finally, it is important to note that the antiferromagnetic coupling observed here for $I_2^+[Sb_2F_{11}]^-$ is distinctly different from the dimerization process suggested for $I_2^+{}_{(solv)}$ in HSO_2F (2), just as the solid-state structure of $I_2^+[Sb_2F_{11}]^-$ differs from the structures of $I_4^{2+}[AsF_6^-]_2$ and $I_4^{2+}[(SbF_6)(Sb_3F_{14})]^{2-}$ (15) where square planar, diamagnetic I_4^{2+} cations are found.

Acknowledgement

Financial support by the Natural Sciences and Engineering Research Council of Canada is gratefully acknowledged. Dr. Karl O. Christe of Rocketdyne, Rockwell International, Canoga Park, California, is thanked for a generous gift of a sample of $O_2^+[AsF_6]^-$ and for helpful discussions.

1. N. BARTLETT and D. H. LOHMANN. (*a*) Proc. Chem. Soc. 115 (1962); (*b*) J. Chem. Soc. 5253 (1962).
2. R. J. GILLESPIE and J. B. MILNE. Inorg. Chem. **5**, 1577 (1966).
3. R. J. GILLESPIE and M. J. MORTON. (*a*) Chem. Commun. 1565 (1968); (*b*) Inorg. Chem. **11**, 586 (1972).
4. (*a*) A. J. EDWARDS, G. R. JONES, and R. J. SILLS. Chem. Commun. 1527 (1968); (*b*) A. J. EDWARDS and G. R. JONES. J. Chem. Soc. A, 2318 (1971).
5. C. G. DAVIES, R. J. GILLESPIE, P. R. IRELAND, and J. M. SOWA. Can. J. Chem. **52**, 2048 (1974).
6. R. J. GILLESPIE and J. PASSMORE. Adv. Inorg. Radiochem. **17**, 49 (1975) and references therein.
7. R. J. GILLESPIE and M. J. MORTON. J. Mol. Spectrosc. **30**, 178 (1969).
8. F. G. HERRING and R. A. N. MCLEAN. Inorg. Chem. **11**, 1667 (1972).
9. D. W. TURNER, C. BAKER, A. D. BAKER, and C. R. BRUNDLE. Molecular photoelectron spectroscopy. Wiley, New York. 1970.
10. G. HERZBERG. Spectra of diatomic molecules. van Nostrand, New York. 1950.
11. J. H. VAN VLECK. The theory of electric and magnetic susceptibilities. Oxford Press, Oxford. 1932. p. 262.
12. W. W. WILSON, R. C. THOMPSON, and F. AUBKE. Inorg. Chem. **19**, 1489 (1980).
13. J. S. HAYNES, K. W. OLIVER, S. J. RETTIG, R. C. THOMPSON, and J. TROTTER. Can. J. Chem. **62**, 891 (1984).
14. A. SMALC. Inst. Josef Stefan, I.J.S. Report. R 612, 1 (1972); Chem. Abstr. **79**, 13032t (1973).

Can. J. Chem. Downloaded from www.nrcresearchpress.com by 194.225.253.170 on 09/07/12
For personal use only.

15. R. J. GILLESPIE, R. KAPOOR, R. FAGGIANI, C. J. L. LOCK, M. J. MURCHIE, and J. PASSMORE. J. Chem. Soc. Chem. Commun. 8 (1983).
16. J. PASSMORE, E. K. RICHARDSON, and P. TAYLOR. J. Chem. Soc. Dalton Trans. 1006 (1976).
17. R. D. W. KEMMITT, M. MURRAY, V. M. MCRAY, R. D. PEACOCK, M. C. R. SYMONS, and T. A. O'DONNELL. J. Chem. Soc. A, 862 (1968).
18. W. W. WILSON and F. AUBKE. J. Fluorine Chem. **13**, 431 (1979).
19. W. E. FALCONER, F. J. DISALVO, A. J. EDWARDS, J. E. GRIFFITHS, W. A. SUNDER, and M. J. VASILE. J. Inorg. Nucl. Chem. Suppl. 59 (1976).
20. A. J. EDWARDS, W. E. FALCONER, J. E. GRIFFITHS, W. A. SUNDER, and M. J. VASILE. J. Chem. Soc. Dalton Trans. 1129 (1974).
21. N. BARTLETT and S. P. BEATON. J. Chem. Soc. Chem. Commun. 167 (1966).
22. J. B. BAAL, JR., C. PUPP, and W. E. WHITE. Inorg. Chem. **8**, 828 (1969).
23. F. J. DISALVO, W. E. FALCONER, R. S. HUTTON, A. RODRIGUEZ, and J. V. WASZCZACK. J. Chem. Phys. **62**, 2575 (1975).
24. I. V. NIKITIN and V. YA. ROSOLOVSKII. Russ. Chem. Rev. (Engl. Trans.) **40**, 889 (1971); Usp. Khim. **40**, 1913 (1971) and references therein.
25. J. SHAMIR and J. BINENBOYM. Inorg. Chim. Acta, **2**, 37 (1968); Inorg. Synth. **14**, 39 (1973).
26. J. N. KEITH, I. J. SOLOMON, I. SHEFT, and H. H. HYMAN. Inorg. Chem. **7**, 230 (1968).
27. K. O. CHRISTE, R. D. WILSON, and I. B. GOLDBERG. Inorg. Chem. **15**, 1271 (1976).
28. (*a*) V. I. BELOVA, YA.K. SYRKIN, D. V. BANTOV, and V. F. SUKHOVERKHOV. Russ. J. Inorg. Chem. (Engl. Trans.) **13**, 765 (1968); (*b*) V. I. BELOVA, V.YA. ROSOLOVSKII, and E. K. NIKITINA. Russ. J. Inorg. Chem. (Engl. Trans.) **16**, 772 (1971).
29. D. R. SLIM. Ph.D. Thesis, University of Birmingham. 1974.
30. (*a*) P. RIGNY and W. E. FALCONER. J. Chem. Phys. **62**, 2581 (1975); (*b*) C. NAULIN and R. BOUGON. J. Chem. Phys. **64**, 4155 (1976).
31. I. B. GOLDBERG, K. O. CHRISTE, and R. D. WILSON. Inorg. Chem. **14**, 152 (1975).
32. A. GRILL, M. SCHIEBER, and J. SHAMIR. Phys. Rev. Lett. **25**, 747 (1970).
33. R. J. MYERS. Molecular magnetism and magnetic resonance spectroscopy. Prentice-Hall Inc., Englewood Cliffs, NJ. 1973.
34. A. BONDI. J. Phys. Chem. **68**, 441 (1964).
35. A. ZUMSTEG, M. ZIEGLER, W. KÄNZIG, and M. BÖSCH. Phys. Cond. Matter, **17**, 267 (1974).
36. K. LUEKEN, M. DEUSSEN, M. JANSEN, W. HESSE, and W. SCHNICK. Z. Anorg. Allg. Chem. **553**, 179 (1987).
37. D. E. COX, E. J. SAMUELSON, and K. H. BECKURTS. Phys. Rev. **B7**, 3102 (1973).
38. A. R. YOUNG, II, T. HIRATA, and S. I. MORROW. J. Am. Chem. Soc. **86**, 20 (1964).
39. B. G. MUELLER. J. Fluorine Chem. **17**, 409 (1981).
40. W. SCHNICK and M. JANSEN. Angew. Chem. (Engl. Ed.) **97**, 54 (1985).
41. W. SCHNICK and M. JANSEN. Z. Anorg. Allg. Chem. **532**, 37 (1986).
42. W. SCHNICK and M. JANSEN. Rev. Chem. Miner. **24**, 446 (1987).
43. M. JANSEN and W. HESSE. Z. Anorg. Allg. Chem. **560**, 47 (1988).
44. R. L. CARLIN. Magnetochemistry. Springer-Verlag, Berlin. 1986.
45. C. H. WENG. Ph.D. Dissertation. Carnegie-Mellon University, Pittsburgh, PA. 1968.
46. W. HILLER, J. STRÄHLE, A. DATZ, M. HANACK, W. E. HATFIELD, L. W. TER HAAR, and P. GÜTLICH. J. Am. Chem. Soc. **106**, 329 (1984).
47. W. V. CICHA, J. S. HAYNES, K. W. OLIVER, S. J. RETTIG, R. C. THOMPSON, and J. TROTTER. Can. J. Chem. **63**, 1055 (1985).
48. M. SUZUKE, B. TSUJIYAMA, and S. KATSURA. J. Math. Phys. **8**, 124 (1976).
49. M. E. FISHER. J. Math. Phys. **4**, 124 (1963).
50. O. EDQUIST, E. LINDHOLM, L. E. SELIN, and L. ASBRINK. Phys. Scripta, **1**, 25 (1970).
51. A. B. CORNFORD, D. C. FROST, C. A. MCDOWELL, J. L. RAGLE, and I. A. STENHOUSE. J. Chem. Phys. **54**, 2651 (1971).
52. P. VENKATESWARLU. Can. J. Phys. **47**, 2525 (1969).
53. P. VENKATESWARLU. Can. J. Phys. **48**, 1055 (1970).
54. LANDOLT-BÖRNSTEIN. Numerical data and functional relations in science and technology. Vol. 2. Magnetic properties of coordination and organometallic transition metal compounds. Springer-Verlag, Berlin. 1966.

Can. J. Chem. Downloaded from www.nrcresearchpress.com by 194.225.253.170 on 09/07/12
For personal use only.

On pentavalent perfluoroorgano bismuth compounds

W. TYRRA AND D. NAUMANN[1]

Fachbereich Chemie, Universität Dortmund, Postfach 500 500, 4600 Dortmund 50, Federal Republic of Germany

Received December 16, 1988

This paper is dedicated to Professor Ronald J. Gillespie on the occasion of his 65th birthday

W. TYRRA and D. NAUMANN. Can. J. Chem. **67**, 1949 (1989).

The reactions of $Bi(R_f)_3$ ($R_f = CF_3$, C_6F_5) with a series of oxidizing halogenation reagents have been investigated. From the reactions of $Bi(R_f)_3$ with Cl_2, Br_2, I_2, ICl, and IF_5 no oxidation to Bi(V) compounds can be detected; in all cases the Bi(III) halides and the corresponding R_fX compounds are formed. Only the reaction of $Bi(C_6F_5)_3$ with XeF_2 yields the perfluoroorgano bismuth(V) compound $Bi(C_6F_5)_3F_2$.

Key words: bismuth perfluoroorganic compounds, polar perfluoroorganylations, oxidation with xenon difluoride.

W. TYRRA et D. NAUMANN. Can. J. Chem. **67**, 1949 (1989).

On a étudié les réactions des composés $Bi(R_f)_3$ ($R_f = CF_3$, C_6F_5) avec une série de réactifs d'halogénation oxydants. Pour les réactions des produits $Bi(R_f)_3$ avec le Cl_2, le Br_2, le ICl et le IF_5, on n'a pas détecté la formation de composés du Bi(V); dans tous les cas, il y a formation d'halogénures de Bi(III) et des composés R_fX correspondants. Seule la réaction du $Bi(C_6F_5)_3$ avec le XeF_2 conduit à un composé perfluoroorganobismuth(V), le $Bi(C_6F_5)_3F_2$.

Mots clés : composés perfluoroorganobismuth, perfluoroorganylations polaire, oxydation avec XeF_2.

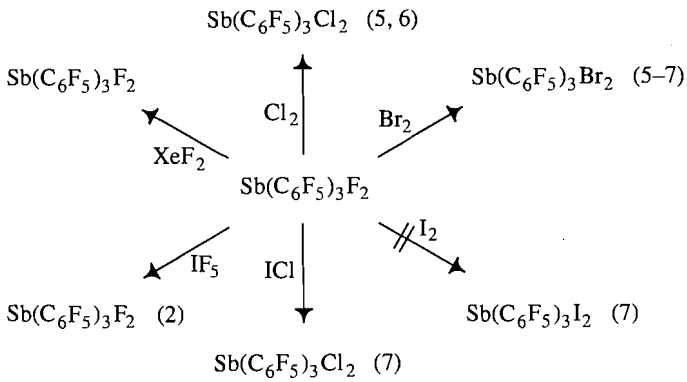
[Traduit par la revue]

Introduction

Tris(pentafluorophenyl)arsenic and -antimony difluoride can be prepared by reacting the tervalent compounds either with elemental fluorine (1) or xenon difluoride. Similar results were obtained by Frohn and Maurer (2) by reactions with iodine pentafluoride. Attempts to obtain tris(pentafluorophenyl)bismuth difluoride in a comparable way failed.

Until today only a few perfluoroorganobismuth(V) compounds could be synthesized (3). When we developed a new preparative method for the synthesis of tris(perfluoroorgano)-bismuth compounds (4) it was of interest to react tris(trifluoromethyl)bismuth and tris(pentafluorophenyl)bismuth with elemental chlorine, bromine, iodine, with iodine monochloride, iodine pentafluoride, and xenon difluoride to check their behaviour against oxidizers.

Comparable reactions with the corresponding antimony derivative have been carried out with the results given in the following scheme.



These results clearly show that tris(pentafluorophenyl)antimony can be oxidized by oxidizers stronger than iodine.

Though a great number of nonfluorinated aryl bismuth(V) compounds are known, no significant evidence has been found for alkyl or perfluoroorgano derivatives (8). The only hint for a pentavalent alkyl bismuth compound is given by Frohn and Maurer (2). Tri-*n*-butylbismuth difluoride can be detected by ^{19}F nmr spectroscopy from a reaction mixture of $(n\text{-}C_4H_9)_3Bi$ and IF_5 at −30°C in acetonitrile solution. Recently Schmuck and Seppelt reported some pentafluorophenyl bismuth(V) derivatives, e.g., $Bi(C_6F_5)_5$ (3).

Experimental

Materials

All commercially available compounds were purified by common methods. The preparations of $Bi(CF_3)_3$ and $Bi(C_6F_5)_3$ were carried out according to ref. 4, XeF_2 according to ref. 16, $[XeF][MF_6]$ according to ref. 17, and IF_5 according to ref. 18.

Nuclear magnetic resonance spectra

Bruker FT NMR spectrometer AM300; ^{19}F nmr, 282.41 MHz; ^1H nmr, 300.13 MHz; and ^{13}C nmr, 75.47 MHz.

General procedure

All reactions were carried out in a dry nitrogen atmosphere. The perfluoroorganobismuth compounds were dissolved in acetonitrile at room temperature. Before adding the corresponding reactant the solutions were cooled to −196°C and afterwards allowed to react at −30°C or room temperature, respectively; ^{19}F nmr spectroscopy was used for reaction control. The assignment of the signals was made in comparison with values given in the literature.

Tris(pentafluorophenyl)bismuth difluoride. Preparation and spectroscopic data

$Bi(C_6F_5)_3$ (1.42 g; 2 mmol) is dissolved in 10 mL CH_3CN in a Schlenk tube at room temperature and afterwards cooled to −196°C. A double excess of xenon difluoride (0.68 g; 4 mmol) is added to the frozen solution. The reaction mixture is allowed to warm to −30°C and stirred at this temperature until $Bi(C_6F_5)_3$ is no longer spectroscopically detected by ^{19}F nmr. The solvent, traces of pentafluorobenzene, and xenon difluoride are removed by vacuum condensation at 0°C. A white solid can be obtained, which contains no fluorine or hydrogen containing impurities. The yield is quantitative.

$Bi(C_6F_5)_3F_2$ is soluble in acetonitrile, chloroform, glyme, and dimethylformamide at room temperature without decomposition. It can be stored in glass flasks for several weeks at −10°C. Storage at room temperature or exposure to moisture or air leads to a decomposition of the compound.

Nuclear magnetic resonance data: ^{19}F nmr spectra, in Table 3; ^{13}C nmr (CH_3CN): δ(C1) 126.5 ppm, δ(C2,6) 139.8 ppm, δ(C3,5) 146.8 ppm, δ(C4) 146.2 ppm.

Mass spectrum (only mass fragments with $M > 160$ m/e): 748

[1]Author to whom correspondence may be addressed.

Can. J. Chem. Downloaded from www.nrcresearchpress.com by 186.148.149.217 on 09/07/12
For personal use only.

Can. J. Chem. Downloaded from www.nrcresearchpress.com by 186.148.149.217 on 09/07/12
For personal use only.

TABLE 1. Oxidation reactions of $Bi(CF_3)_3$

$Bi(CF_3)_3$		CH_3CN,	Oxidizer			Reaction temperature,	
g	mmol	mL		g	mmol	°C	Reaction products[b] (ref.)
0.44	1.06	5	Cl_2	0.29	4.10	−30	$CClF_3$, $BiCl(CF_3)_2$, $BiCl_2(CF_3)$ (4)
0.46	1.11	5	Br_2	0.59	3.67	−30	$CBrF_3$, $BiBr(CF_3)_2$, $BiBr_2(CF_3)$ (4)
0.40	0.96	5	I_2	0.86	3.38	r.t.	CF_3I, $Bi(CF_3)_2I$, $Bi(CF_3)I_2$ (4)
0.63	1.51	5	ICl	0.41	2.50	−30/r.t.	CF_3I, $BiCl(CF_3)_2$, $BiCl_2(CF_3)$ (4)
0.48	1.15	5	IF_5	0.71	3.36	−30/r.t.	CF_3IF_4 (19), $Bi(CF_3)_2F$
0.25	0.60	3	XeF_2	0.32	1.88	−30/r.t.	CF_4
0.08	0.20	1	$[XeF][TaF_6]$[a]	0.25	0.58	−30/r.t.	CF_4

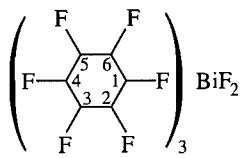
[a]**Caution!** If $[XeF][TaF_6]$ is added to the solution at temperature higher than −196°C a vigorous explosion may occur.
[b]The reaction products are identified by ^{19}F nmr spectra.

TABLE 2. Oxidation reactions of $Bi(C_6F_5)_3$

$Bi(C_6F_5)_3$		CH_3CN,	Oxidizer			Reaction temperature,	Reaction products[a]
g	mmol	mL		g	mmol	°C	(ref.)
0.81	1.14	6	Cl_2	0.30	4.23	−30/r.t.	C_6ClF_5
0.50	0.70	5	Br_2	0.45	2.80	−30/r.t.	C_6BrF_5
0.50	0.70	5	I_2	0.70	2.76	−30/r.t.	C_6F_5I
0.55	0.77	5	ICl	0.32	2.00	−30/r.t.	C_6F_5I
0.85	1.20	7	IF_5	0.70	3.35	−30/r.t.	$C_6F_5IF_4$ (10)
1.42	2.00	10	XeF_2	0.68	4.00	−30	$Bi(C_6F_5)_3F_2$
0.31	0.44	3	$[XeF][AsF_6]$[b]	0.30	0.88	−30/−20	$Bi(C_6F_5)_3F_2$

[a]The reaction products are identified by ^{19}F nmr spectra. The spectra of the product mixtures in addition show resonances of low intensity in the region of $Bi(C_6F_5)_3$, but an unambiguous assignment was not possible.
[b]**Caution!** If $[XeF][AsF_6]$ is added to the solution at temperature higher than −196°C a vigorous explosion may occur.

TABLE 3. The ^{19}F nmr data of $Bi(C_6F_5)_3F_2$[a]



Solvent	δ(F 2,6)	δ(F 4)	δ(F 3,5)	δ(BiF_2)
CD_3CN	−126.47	−143.20	−155.43	−58.02
CH_3CN	−126.87	−143.32	−155.20	−59.00
Glyme[b]	−127.65	−143.45	−156.31	−54.78
DMF-d_7	−129.88	−148.54	−158.91	−51.08
$CDCl_3$	−125.80	−141.64	−154.62	−64.07
	for comparison $Bi(C_6F_5)_3$ (ref. 4)			
CH_3CN	−117.52	−152.39	−160.37	—
C_6H_6	−118.18	−149.67	−158.55	—

[a]δ in ppm relative to external CCl_3F; the integration gives relative intensities of approximately 6:3:6:2.
[b]At −10°C.

(4.1%; $Bi(C_6F_5)_3F_2^+(M^+)$); 729 (2.3%; $Bi(C_6F_5)_3F^+$); 710 (6.5%; $Bi(C_6F_5)_3^+$); 581 (2.0%; $Bi(C_6F_5)_2F_2^+$); 562 (2.1%; $Bi(C_6F_5)_2F^+$); 543 (31.5%; $Bi(C_6F_5)_2^+$); 413 (31.5%; $Bi(C_6F_5)F_2^+$); 394 (19.1%; $Bi(C_6F_5)F^+$); 376 (52.9%; $Bi(C_6F_5)^+$); 334 (42.1%; $(C_6F_5)_2^+$); 303 (2.5%; BiF_5^+); 285 (2.1%; BiF_4^+); 266 (11.7%; BiF_3^+); 247 (14.2%; BiF_2^+); 228 (21.1%; BiF^+); 209 (53.6%; Bi^+); 187 (10.4%; $C_6F_6^+$); 168 (100%; $C_6F_5^+$).

Preparation of tris(pentafluorophenyl)antimony difluoride

To a solution of $Sb(C_6F_5)_3$ (1.93 g; 3.1 mmol) in 8 mL CH_3CN is added XeF_2 (0.56 g; 3.3 mmol) at −30°C. The reaction mixture is warmed to room temperature and allowed to react for about 2 days during which a white solid precipitates. Evaporation of the solvent and all volatile compounds left $Sb(C_6F_5)_3F_2$ as a colourless solid in quantitative yield (2.04 g; 99.6%). The spectroscopic data are identical to those in ref. 1.

Results and discussion

Reactions with elemental halogens

When we reacted $Bi(CF_3)_3$ and $Bi(C_6F_5)_3$ with elemental chlorine, bromine, or iodine, no oxidation occurred. In the case of the trifluoromethyl compound we could spectroscopically detect by ^{19}F nmr and assign the trifluorohalomethane and the intermediates $Bi(CF_3)_2X$ and $BiCF_3X_2$ (4). If tris(pentafluorophenyl)bismuth was used similar results were obtained but the intermediates could not be assigned clearly or were not observed.

$$Bi(R_f)_3 + X_2 \xrightarrow[CH_3CN]{} R_fX + Bi(R_f)_2X$$

$$Bi(R_f)_2X + X_2 \longrightarrow R_fX + BiR_fX_2$$

$$BiR_fX_2 + X_2 \longrightarrow R_fX + BiX_3$$

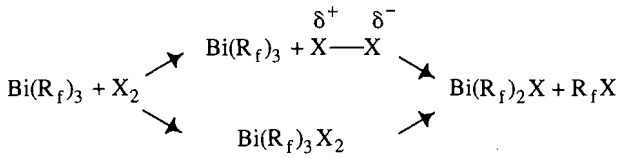
$$Bi(R_f)_3 + 3X_2 \longrightarrow 3R_fX + BiX_3$$

R_f: CF_3, C_6F_5; X: Cl, Br, I

No nmr spectroscopic evidence for bismuth(V) compounds was found. But these results do not prove unambiguously whether or not an intermediate pentavalent bismuth compound might have been formed.

The same product mixtures can be obtained either by a polar reaction of the perfluoroorgano bismuth with the halogen or a

decomposition of a bismuth(V) compound as shown below:



Reactions with interhalogens should give information about the possible reaction path.

Reactions with interhalogens

We previously described the reaction of tris(trifluoromethyl)-bismuth with iodine monochloride, forming quantitatively trifluoromethyliodide and bismuth trichloride (4). The reaction with the pentafluorophenyl derivative proceeds in the same manner, in contrast to the corresponding antimony compound (7).

$$Bi(R_f)_3 + 3ICl \rightarrow 3R_fI + BiCl_3$$

The fact that no R_fCl is formed provides evidence that these reactions proceed via a polar mechanism.

If we assume a bismuth(V) derivative, such as $Bi(C_6F_5)_3Cl_2$ or $Bi(C_6F_5)_3ClI$, subsequent decomposition will lead to the perfluoroorgano chlorine derivative.

To confirm this observation we carried out reactions of these compounds with iodine pentafluoride. Even with this strong oxidizing reagent no oxidation of the bismuth compounds was observed. The same results were obtained by Frohn und Maurer (8) using $Bi(C_6F_5)_3$ or $Bi(p\text{-}FC_6H_4)_3$. In no case was evidence found for bismuth(V) derivatives. Instead of oxidation a fluorine–aryl exchange takes place.

$$BiR_3 + 3IF_5 \rightarrow 3RIF_4 + BiF_3$$

R: CF_3; C_6F_5; $p\text{-}FC_6H_4$

These results clearly state that $Bi(R_f)_3$ is inert towards the oxidation of elemental halogens or interhalogens, but works as a powerful polar perfluoroorganylating reagent as found for perfluoroorgano cadmium complexes (4). This behaviour is proved by reactions with silver nitrate forming $[Ag(CF_3)_4]^-$, $[Ag(CF_3)_2]^-$, and CF_3NO (4, 9) as well as with $p\text{-}CH_3C_6H_4COCl$ forming the corresponding ketone.[2]

Reactions with xenon difluoride

Xenon difluoride and fluoro xenonium metallates are known to be excellent oxidizing fluorination reagents (11). It is also known that in acetonitrile solution XeF_2 dissociates into XeF^+ and F^- (12). The fluoroxenonium cation forms stable complexes with acetonitrile and other nitriles (13) as well as perfluorinated pyridine derivatives (14). These possibilities encouraged us to check the behaviour of $Bi(CF_3)_3$ and $Bi(C_6F_5)_3$ against XeF_2 and $[XeF][MF_6]$ (M: As; Sb; Ta).

If $Bi(CF_3)_3$ is used, CF_4, Xe, and BiF_3 are formed quantitatively even at −60°C according to

$$Bi(CF_3)_3 + 3XeF_2 \rightarrow BiF_3 + 3CF_4 + 3Xe$$

This reaction does not help us understand the reaction mechanism. There are two possibilities to explain these products: Firstly, polar trifluoromethylation of an intermediately formed XeF^+ cation may occur to give "CF_3XeF", which would decompose according to

$$Bi(CF_3)_3 + XeF^+F^- \rightarrow Bi(CF_3)_2F + \text{"}CF_3XeF\text{"} \rightarrow Xe + CF_4$$

[2]D. Naumann, W. Dukat, M. Finke, and W. Tyrra. Unpublished results.

Or, secondly, there may be oxidation of the bismuth compound to give "$Bi(CF_3)_3F_2$" followed by a decomposition of the bismuth derivative according to

$$Bi(CF_3)_3 + XeF_2 \rightarrow \text{"}Bi(CF_3)_3F_2\text{"} + Xe$$

$$\text{"}Bi(CF_3)_3F_2\text{"} \rightarrow Bi(CF_3)_2F + CF_4$$

and so on.

To observe one of the possible intermediates, "R_fXeF" or "$Bi(R_f)_3F_2$", we decided to carry out the reaction using the pentafluorophenyl compound.

To decide whether a polar reaction or a radical oxidation takes place, we reacted $Bi(C_6F_5)_3$ with XeF_2 and $[XeF][MF_6]$. Both reactions yield the same main product, tris(pentafluorophenyl)-bismuth difluoride, along with traces of pentafluorobenzene. Evidence for the formation of a pentafluorophenylxenon compound such as C_6F_5XeF or $[C_6F_5Xe][MF_6]$ (15) was not found.

These results show that tris(perfluoroorgano)bismuth compounds cannot easily be oxidized by common oxidizers such as elemental halogens or interhalogens. In these cases a polar reaction is favoured. Only strong fluorinating agents like xenon difluoride or fluoro xenonium metallates yield, with tris(pentafluorophenyl)bismuth, the corresponding difluoride under distinct conditions. But the oxidation of $Bi(CF_3)_3$ was never observed.

Acknowledgements

We are indebted to the Fonds der Chemischen Industrie for financial support and to the Kali-Chemie AG, Hannover, for valuable chemicals.

1. R. Kasemann and D. Naumann. J. Fluorine Chem. **41**, 321 (1988).
2. H. J. Frohn and H. Maurer. J. Fluorine Chem. **34**, 129 (1986).
3. A. Schmuck and K. Seppelt. Paper No. 6, 3. Deutscher Fluortag, Königstein. Oct. 6, 1988.
4. D. Naumann and W. Tyrra. J. Organomet. Chem. **334**, 323 (1987).
5. B. A. Nevett and A. Perry. Spectrochim. Acta, Part A: **31A**, 101 (1975).
6. A. Otero and P. Royo. J. Organomet. Chem. **154**, 13 (1978).
7. G. S. Harris, A. Khan, and I. Lennon. J. Fluorine Chem. **37**, 247 (1987).
8. Gmelins Handbuch der Anorganischen Chemie. Erg. zur 8. Aufl., Band 47. Springer Verlag, Berlin, Heidelberg, New York. 1977.
9. W. Dukat and D. Naumann. Rev. Chim. Miner. **23**, 589 (1986).
10. V. V. Bardin, G. G. Furin, and G. G. Yakobson. Zh. Org. Khim. **16**, 1256 (1980).
11. K. Alam and A. F. Janzen. J. Fluorine Chem. **36**, 179 (1987), and literature cited therein.
12. A. Zemva, A. Jesik, D. H. Templeton, A. Zalkin, A. K. Cheetham, and N. Bartlett. J. Am. Chem. Soc. **109**, 7420 (1987).
13. A. A. A. Emara and G. J. Schrobilgen. J. Chem. Soc. Chem. Commun. 1644 (1987).
14. A. A. A. Emara and G. J. Schrobilgen. J. Chem. Soc. Chem. Commun. 257 (1988).
15. D. Naumann and W. Tyrra. J. Chem. Soc. Chem. Commun. 47 (1989).
16. L. V. Streng and A. G. Streng. Inorg. Chem. **4**, 1370 (1965).
17. F. O. Sladky, P. A. Bulliner, and N. Bartlett. J. Chem. Soc. (A), 2179 (1969).
18. G. Brauer. Handbuch der Präparativen Anorganischen Chemie. Bd. 1. F. Enke Verlag, Stuttgart. 1975.
19. D. Naumann. Forschungsberichte des Landes Nordrhein–Westfalen Nr. 3115 Westdeutscher Verlag, Opladen. 1982.

Can. J. Chem. Downloaded from www.nrcresearchpress.com by 186.148.149.217 on 09/07/12
For personal use only.

On the prediction of the structures of simple and hypervalent hydrides and fluorides containing unpaired electrons

N. Colin Baird, Markus Kuhn, and Toyanne M. Lauriston
Department of Chemistry, University of Western Ontario, London, Ont., Canada N6A 5B7

Received January 9, 1989

This paper is dedicated to Professor Ronald J. Gillespie on the occasion of his 65th birthday

N. Colin Baird, Markus Kuhn, and Toyanne M. Lauriston. Can. J. Chem. **67**, 1952 (1989).

Ab initio molecular orbital calculations are reported for the optimum structures of many free radicals, including several species in which the central atom is hypervalent, and for some triplet states. Most geometries are close to those predicted by the VSEPR method for molecules with one additional electron, with the unpaired electron occupying a "lone pair" position. Deviations from the ideal geometries of hypervalent radicals can be rationalized in terms of different strengths for repulsions between electrons of different types. Alternatively the geometries can be understood by using the three-centre, four-electron bond theory for the hypervalent species and the σ-conjugation concept for the non-hypervalent molecules. The distortions from ideality of the hypervalent structure occur to allow interaction of the electron pair of the nonbonding MO of the three-center unit to interact with a lobe of the unpaired electron's orbital.

Key words: geometry of free radicals, *ab initio* MO theory for radicals, VSEPR theory for radicals, sigma conjugation for radicals.

N. Colin Baird, Markus Kuhn et Toyanne M. Lauriston. Can. J. Chem. **67**, 1952 (1989).

On rapporte les résultats de calculs d'orbitales moléculaires *ab initio* effectués sur des structures optimisées de quelques états triplets ainsi que de plusieurs radicaux libres comportant plusieurs espèces dans lesquelles l'atome central est hypervalent. Dans la plupart des cas, les géométries ressemblent à celles qui sont prédites par la méthode VSEPR pour des molécules avec un électron additionnel comportant un électron non-pairé qui occupe une position de "paire isolée". On peut rationaliser les déviations par rapport aux géométries idéales des radicaux hypervalents en fonction des forces différentes pour les répulsions entres les divers types d'électrons. On peut aussi comprendre les géométries des espèces hypervalentes en faisant appel à la théorie des liaisons à quatre électrons et à trois centres alors que celles des molécules non-hypervalentes peuvent être expliquées par le concept de conjugaison σ. Les distorsions par rapport à la structure hypervalente idéale se produisent pour permettre à la paire d'électron de l'OM non liés de l'unité à trois centres d'interagir avec un lobe de l'orbitale de l'électron non-pairé.

Mots clés : géométrie des radicaux libres, théorie *ab initio* de l'OM pour des radicaux, théorie VSEPR pour des radicaux, conjugaison σ pour des radicaux.

[Traduit par la revue]

Can. J. Chem. Downloaded from www.nrcresearchpress.com by 186.148.149.217 on 09/07/12
For personal use only.

Introduction

The geometric structure of free radicals, particularly ones which contain hypervalent atoms, and of triplet states have been largely ignored in most simple qualitative valence theories. It is known that the geometry of systems with unpaired electrons can be rationalized and predicted using delocalized MO theory, for example in the form of Walsh diagrams (see, for example, ref. 1). In this report, we consider the structure and bonding in a number of prototype radicals and triplets using variants of VSEPR theory (2), three-centre bond theory (3), and Dewar's "σ-conjugation" concept (4). We also present a series of systematic *ab initio* MO calculations of the structures of a wide series of hydrogen- and fluorine-containing radicals — particularly hypervalent ones, since generally only the shapes of these are known from experimental studies and only scattered theoretical calculations have been published to date.

Calculations

The optimized structures and total energies calculated for the systems considered herein are listed in Tables 1 through 3. Except for ClF_2 and ClF_4, all these *ab initio* MO calculations were obtained using the Unrestricted Hartree Fock (UHF) method.

The basis sets used were the 3-21G, 3-21G$^{(*)}$, 6-31G, and 6-31G* expansions of Pople and co-workers (5*a*), where * denotes the presence of *d* orbitals on all non-hydrogen atoms and $^{(*)}$ denotes *d* orbitals only on second-row atoms. We also employed a 6-31G$^{(*)}$ basis, i.e. one which corresponds to the 6-31G basis for hydrogen and first-row atoms and the 6-31G* basis for second-row atoms. The GAUSSIAN86 program was used to perform all calculations (5*b*).

As discussed previously by Hehre *et al.* (5*a*), the bond lengths and angles in first-row hydrides containing unpaired electrons are not significantly dependent upon the basis set quality (once one is beyond the STO-3G level) nor upon the inclusion of corrections for the effects of electron correlation. Our results for the non-hypervalent second-row hydride systems (Table 1) display a similar lack of dependence upon basis set, and agree well with experiment where available (as do the results for the first-row hydrides).

Pople and co-workers discovered a substantial dependence of AF bond length upon basis set for both closed-shell and open-shell molecules for first-row atoms A (5*a*). The calculated AF distances are substantially shorter at the 6-31G* level than with the 3-21G basis, particularly if A carries p_π lone pairs; the origin of this difficulty presumably is similar to that encountered for the OO bond length in H_2O_2 (5*a*). In addition, inclusion of electron correlation corrections (reported for HNF, CF, NF, and F_2^+) had a further significant effect on bond lengths, as it also does in H_2O_2.

From the calculations shown in Table 1, it can be seen that basis set quality plays a role in determining AF bond length when A is a second-row atom. Thus the 6-31G* bond lengths in AlF_2, SiF_2, and PF_2 are 0.054, 0.087, and 0.102 Å shorter than those predicted by the 6-31G basis set. The bond angles are relatively unaffected by the size of the expansion (whether 3-21G or 6-31G) and by the presence or absence of *d* orbitals.

In order to find an efficient basis set for the hypervalent

TABLE 1. Geometries for non-hypervalent radicals and triplets

Molecule	Bond angle (in degrees)					Bond distance (in Å)				
	3-21G	3-21G(*)	6-31G	6-31G*	Exptl.	3-21a	3-21a(*)	6-31G	6-31G*	Exptl.
BH_2	127.7[a]			126.5[a]	131[b]	1.185[a]			1.185[a]	1.181[b]
BF_2	119.7			120.2	bent[c]	1.332			1.301	
$CH_2(T_1)$	131.0[a]			130.4[a]	133.8[b]	1.071[a]			1.071[a]	1.075[b]
$CF_2(T_1)$	120.0[a]			118.7		1.337[a]			1.304	
NH_2	106.0[a]			104.4[a]	103.4[b]	1.026[a]			1.013[a]	1.024[b]
NF_2	102.1[a]			103.4	103.2[b]	1.396[a]			1.317	1.353[b]
CH_3	120.0[a]			120.0[a]	120.0[b]	1.072[a]			1.073[a]	1.077[b]
CF_3	111.6[a]				110.8[b]	1.329[a]				1.318[b]
AlH_2	117.8	118.1	117.7	118.0	119[b]	1.612	1.597	1.615	1.596	1.59[b]
AlF_2	112.7	116.1	115.0	117.1		1.651	1.630	1.690	1.636	
$SiH_2(T_1)$	118.6	118.0	118.7	118.0		1.482	1.471	1.488	1.472	
$SiF_2(T_1)$	113.5	112.9	115.2	114.0		1.635	1.593	1.680	1.593	
PH_2	94.2	93.4	94.3	93.5	91.7[b]	1.432	1.406	1.436	1.407	1.418[b]
PF_2	96.8	98.4	96.2	98.2		1.629	1.578	1.682	1.580	
SiH_3	111.6	110.9	111.6	110.9	pyramidal[d]	1.486	1.475	1.492	1.476	
SiF_3	106.5	107.2	106.7		pyramidal[e]	1.610	1.575	1.654		

[a]From ref. 25 or ref. 5*a* and collected here for the purpose of comparison.
[b]Reference 26.
[c]Reference 27.
[d]Reference 28.
[e]Reference 29.

fluorides, we performed a number of test calculations on the smallest of them, namely ClF_2. The ClF distance drops by 0.10 Å when *d* orbitals are added to Cl, whether in the 3-21G or the 6-31G basis set. Addition of *d* orbitals to the 6-31G basis for the fluorines shortens the bonds by an additional but smaller amount, 0.036 Å, but has almost no effect on the angle. (This behaviour is similar to that for PF_2, for which comparative results also are listed in Table 1.) The predicted FClF angles all lie in the range suggested by experiment. Sannigrahi and Peyerimhoff have reported calculations for the ground state of ClF_2 which give a similar shape to the molecule (6). They found that the FClF angle decreased only slightly (by 2.5°), and the bond length increased only slightly (by 0.02 Å), when configuration interaction was included to allow for the effects of electron correlation. Further, Pople and co-workers have established that the geometries of closed-shell hypervalent fluorides (such as PF_5, SF_4, ClF_3, and ClF_5) are well described at the SCF level, and that the 3-21G(*) results are almost identical to those at the 6-31G* level (5*a*). Since the inclusion of *d* orbitals on fluorine appears to decrease the AF length somewhat but has only a small effect on bond angles and hence upon the shape of the molecule, and since their inclusion raises enormously the running time of the calculations, we have employed the 6-31G(*) and 3-21G(*) basis sets only for the rest of the hypervalent fluorides. No attempt has been made to account for the effects of electron correlation, which appear from the ClF_2 example above and the PH_4 discussion below to be small.

The calculated structures and energies for the hypervalent radicals are given in Table 2. In all cases, there is virtually no difference between the 3-21G(*) and the 6-31G(*) results. A number of reasonable starting geometries of differing symmetries were tried using the 3-21G(*) basis set (7), but in all cases that shown in Table 2 was clearly superior energetically and the other results will not be discussed further. With the UHF method, the ClF_2 free radical under C_{2v} symmetry dissociates to free atoms (as does F_2^+), and similarly for ClF_4. There is substantial spin-contamination in the UHF wavefunctions for these systems; for example the S^2 value is 0.871 for ClF_2 in a 3-21G(*) calculation (at R = 1.707 Å, ∠FClF = 148.5°), whereas the values for the non-chlorine radicals all are close to 0.75 (see Table 2). For both ClF_2 and ClF_4, therefore, we employed the Restricted Hartree-Fock (RHF) method.

Unfortunately, there is very little structural data for hypervalent radicals with which to compare the theoretical predictions. Usually only the electron spin resonance (esr) spectrum and/or the vibrational spectrum is available, from which only the point group of the radical can be deduced.

As mentioned above, the predicted shape of ClF_2, namely bent but only to about 150°C, agrees with experiment (8).

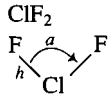
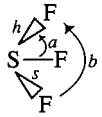
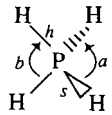
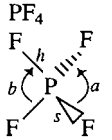
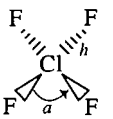
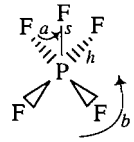
For SF_3, esr measurements (9), and *ab initio* calculations by So (10), favor a planar T shape with two types of fluorines. More elaborate *ab initio* calculations by Volatron *et al.* (11) and our own results both yield a somewhat non-planar T shape. Recently Volatron (11*b*) has shown that the pyramidal T-shape is obtained by RHF calculations even after configuration interaction is included (although the energy gain due to non-planarity becomes rather greater).

For SF_5, the infrared (12) and esr (13) spectra have been interpreted in terms of a C_{4v} structure, in agreement with our calculations. Semi-empirical INDO calculations for the C_{4v} radical by Gregory (14) also yielded a tetragonal pyramid, in contrast to the "umbrella" shape known for BrF_5.

The esr spectra of PF_4 (15), PH_4 (16), and a wide variety of phosphoranyl radicals (17) are all consistent with a "see-saw" shape, as indeed is obtained in our *ab initio* calculations for the tetrafluoro and tetrahydro systems. In contrast to the closed-shell sulfur systems, the "axial" atoms bend away from the central AX_2 unit rather than toward it. This prediction is maintained when the structure of PH_4 is re-optimized at the 6-31G* level with MP2 correction included for the effects of electron correlation; indeed none of the structural features of the

Can. J. Chem. Downloaded from www.nrcresearchpress.com by 186.148.149.217 on 09/07/12
For personal use only.

TABLE 2. Calculations for hypervalent radicals[a]

Molecule	Symmetry and state label	Parameter	Value for parameter by 6-31G(*)	3-21G(*)	Other
ClF_2 	C_{2v} $^2A_1$	h	1.716	1.707	1.680[b]
		a	148.2	148.5	149.6[b]
		E(RHF)	−658.08893	−655.01051	−658.11993
SF_3 	C_s $^2A_1$	s	1.586	1.572	
		h	1.664	1.631	
		a	87.7	87.4	
		b	154.6	152.0	
		E(UHF)	−695.63926	−692.27680	
		S^2	0.781	0.765	
PH_4 	C_{2v} $^2A_1$	s	1.395	1.395	1.406[c]
		h	1.511	1.511	1.520[c]
		a	100.8	100.2	100.2[c]
		b	169.9	170.8	171.0[c]
		E(UHF)	−342.93660	−341.30133	−343.05339
		S^2	0.777	0.778	
PF_4 	C_{2v} $^2A_1$	s	1.558	1.543	
		h	1.614	1.585	
		a	104.1	103.4	
		b	166.0	166.0	
		E(UHF)	−738.45476	−734.83035	
		S^2	0.759	0.757	
ClF_4 	C_{4v} $^2A_1$	h	1.686	1.665	1.798[d]
		a	88.7	88.8	89.6[d]
		b	163.0	163.3	170.5[d]
		E(RHF)	−856.70522	−852.59622	−856.6039
SF_5 	C_{4v} $^2A_1$	s	1.561	1.542	
		h	1.610	1.579	
		a	91.3	91.0	
		b	177.4	178.0	
		E(UHF)	−894.41432	−890.07869	
		S^2	0.767	0.761	

[a]Distances are in Å, angles are in degrees, energies are in atomic units.
[b]6-31G* basis; see text for discussion.
[c]6-31G*/MP2 result; see text for discussion.
[d]6-31G basis; see text for discussion.

radical is affected significantly by correlation (see Table 2). The same type of structure for PH_4 previously was predicted by *ab initio* calculations using the 4-31G basis set (i.e. with no *d* orbitals included) by Howell and Olsen (18).

The RHF calculations for ClF_4 clearly favor a non-planar C_{4v} rather than a planar D_{4h} structure. This same result was obtained in *ab initio* calculations by So and Richards (19) in minimal basis set (STO-3G) calculations if *d* orbitals were included, but not if they were excluded. Earlier calculations by Ungemach and Schaefer (20) using minimal and double-ζ *s*, *p* basis sets also predicted a planar radical. However, we have found that a non-planar structure, with about half the out-of-plane distortion as is obtained with 6-31G(*), is predicted by 6-31G calculations. The esr spectrum clearly shows the equivalence of all four fluorines, which is consistent with both the C_{4v} and the D_{4h} structures. On the basis of the size of the ^{35}Cl hyperfine interaction, the D_{4h} structure has been favored. The MO for the unpaired electron in our 6-31G(*) calculation for the optimum (non-planar) geometry predicts the total spin density in the *s* orbitals on chlorine amounts to be 0.161e. All the calculations for ClF_4 (by ourselves and those reported previously) agree that in the square planar geometry the unpaired electron's MO is a_{1g} in character, and corresponds to the antibonding combination of the chlorine *s* orbital with fluorine-based nonbonding MO from $3c$—$4e$ bonds. In the non-planar geometry, this MO is of the same symmetry as the doubly-occupied p_π orbital on chlorine (a_{2u} in the square planar geometry); their interaction allows the chlorine *s* orbital population to increase and presumably is the driving force for pyramidalization.

Valence-shell electron pair repulsion (VESPR) theory

Although the VSEPR theory of Gillespie and Nyholm (2) applies formally only to closed-shell species, some researchers have assumed that the geometry of a free radical containing *n* electron pairs and an unpaired electron would lie somewhere between the optimum shape for *n* pairs and that for $n + 1$ pairs (see, for example, ref. 21). Indeed Morton and Preston state that "the unpaired electron behaves very much as would a lone pair" (22).

From the idea that the geometry should lie between that for

Can. J. Chem. Downloaded from www.nrcresearchpress.com by 186.148.149.217 on 09/07/12
For personal use only.

TABLE 3. Calculated energies for newly-optimized structures of non-hypervalent systems

Molecule	Energy in atomic units by			
	3-21G	3-21G(*)	6-31G	6-31G*
BF_2		−222.41175		−223.61451
$CF_2(T_1)$				−236.60895
NF_2				−253.16069
AlH_2	−241.68547	−241.73779	−242.98939	−243.00946
AlF_2	−438.50736	−438.60155	−440.82862	−440.90055
$SiH_2(T_1)$	−288.48090	−288.55363	−289.96665	−289.99259
$SiF_2(T_1)$	−485.20298	−485.31932	−487.69893	−487.79462
PH_2	−340.11961	−340.21633	−341.81150	−341.84960
PF_2	−536.82007	−536.94873	−539.51863	−539.62264
SiH_3	−289.08054	−289.16616	−290.56692	−290.60612
SiF_3	−584.24278	−584.39393		

Can. J. Chem. Downloaded from www.nrcresearchpress.com by 186.148.149.217 on 09/07/12
For personal use only.

n and $n + 1$ pairs, we expect that the angles at boron and aluminum in their radical dihydrides and difluorides will lie between 180° (two electron pairs, as in BH_2^+) and 120° (three electron pairs, BH_2^-). The calculated 6-31G* values of 126.5° for BH_2, 120.2° for BF_2, 118.0° for AlH_2, and 117.1° for AlF_2 lie near or beneath the low end of this range. Apparently the effective VSEPR size of an unpaired electron here is about that of a shared electron pair.

The angles in the nitrogen and phosphorus dihydrides and difluorides (Table 1) are virtually identical to those in the corresponding trihydrides and trifluorides, so the structures are closer to those for four electron pairs than for three. Similarly the angles in pyramidal CF_3, SiH_3, and SiF_3 (see Table 1) are much closer to the tetrahedral value than to the 120° associated with the trigonal planar geometry; the latter shape is preferred only by CH_3, which must be considered an exception.

Unexpectedly (from the viewpoint of the VSEPR theory), the angles in the triplet states (two unpaired electrons) of CH_2, CF_2, SiH_2, and SiF_2 lie within a few degrees of those in the free radicals containing one less (unpaired) electron, i.e. BH_2, BF_2, AlH_2, and AlF_2 respectively (Table 1). It is not clear why a second unpaired electron should exert no influence over the bond angle. The lack of a significant change in angle from (singlet) CH_2 to NH_2 to H_2O (1*a*) also is problematic for VSEPR.

For ClF_2, we expect an FClF angle which lies somewhere between tetrahedral (109.5°) for four electron pairs and 180° for the axial positions in the five-pair structure. The calculated (and observed) weakly bent geometry with an angle of about 150° lies between these extremes. For SF_3, the non-planar (pyramidalized) T shape is intermediate between that for an AX_3E configuration (i.e. pyramidal, with all bond angles near 109.5°) and that for AX_3E_2 (planar T shape, with 90° and 180° angles) assuming that like a lone pair, the unpaired electron here occupies an equatorial position. However, the departure from planarity is relatively small. The free radicals PH_4 and PF_4 should also fall between structures expected for four pairs — i.e. a tetrahedron — and the "see-saw" shape expected for AX_4E molecules, again assuming the unpaired electron occupies an equatorial position. The calculated structures are closer to the latter than the former, although the axial bonds bend *away* from the equatorial PX_2 group — unlike the situation in SF_4, etc. but consistent with a transition toward a tetrahedral geometry.

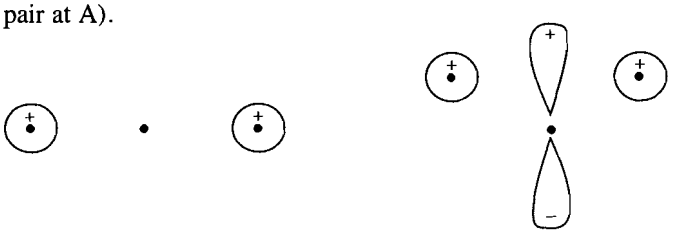
Both ClF_4 and SF_5 have five electron pairs and one unpaired electron. The square pyramidal structure for ClF_4 would be expected if the lone pair and the unpaired electron occupied *trans* positions in an octahedron, and the four in-plane bonding pairs were repelled more by the lone pair than by the unpaired electron. Similarly, the optimum structure for SF_5 is a minor distortion from the square pyramid, with the four equivalent fluorines bent slightly away from the unique fluorine (indicating that repulsion by a bonding pair is slightly more effective than by an unpaired electron), rather than one based upon the trigonal bipyramid.

Three-centre bond theory

A linear geometry usually is considered optimal for a three-centre σ bond formed by a *p* orbital, since atomic orbital overlap is greatest for the *bonding* MO at 180° (3).

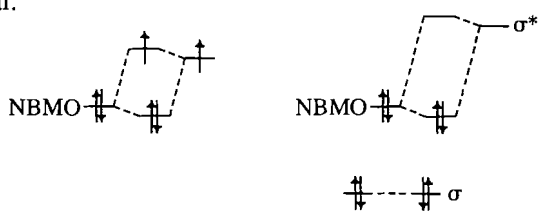


However a linear geometry precludes stabilization of the *nonbonding* MO, which to a first approximation is located only upon ligand atom orbitals, for systems in which the central atom's *s* orbital is doubly-filled (i.e. in which there is a lone pair at A).



NBMO — linear geometry NBMO — bent geometry

In such circumstances, some bending from 180° would result in stabilization of the nonbonding MO if the orbital with which it then overlaps is singly-occupied or is an empty antibonding orbital.



Analysis of the Mulliken population data indicates that the deviations from high symmetry of the geometries of the hypervalent radicals considered herein arise primarily from the stabilization of the electrons in the nonbonding MO of three-

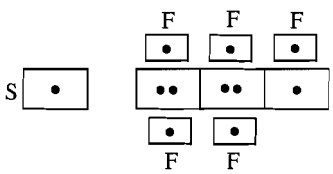
Can. J. Chem. Downloaded from www.nrcresearchpress.com by 186.148.149.217 on 09/07/12
For personal use only.

centre bonds by interaction with the singly-occupied orbital. In ClF_2 the FClF angle decreases from linearity by 30° due to the stabilization of the nonbonding MO by its overlap with one lobe of the singly-occupied *p* orbital of the chlorine; according to 6-31G(*) calculations extrapolated to an angle of 180°, the energy gain from bending amounts to about 12 kcal mol^{-1}. Thus the bonding in ClF_2 consists of a three-centre, four-electron (3c–4e) bond shared between the fluorines and stabilized by bending to yield a molecular plane which also contains the unpaired electron.

Similarly, the 3c–4e $F_{ax}SF_{ax}$ unit in T-shaped SF_3 not only is bent slightly toward the 2c–2e unique S—F bond, but it is also bent down to overlap with one lobe of the singly-occupied *p* orbital of sulfur, thus yielding a pyramidalized T shape with an axial bond angle of 154.6°. The 6-31G(*) calculated energy gain due to pyramidalization and bending of the 3c–4e unit is 3.5 kcal mol^{-1}. (A similar distortion from planarity does not occur in ClF_3 since the corresponding *p* orbital on the central atom is doubly-occupied, and net destabilization would occur if it overlapped the nonbonding MO of the three-centre bond.)

In ClF_4, all the fluorines are involved in 3c–4e bonds; both units bend in the same direction, giving a pyramidal structure with *trans* FClF angles of 163°. The energetic stabilization of the distortion from D_{4h} symmetry is 8.6 kcal mol^{-1}, according to 6-31G(*) calculations, and arises from the interaction of the doubly-occupied p_π orbital on chlorine with the singly-occupied MO which in the square planar geometry is Cl—F antibonding and at chlorine is composed entirely of *s* orbital character.

Unlike many of the hypervalent radicals discussed above, the central atom in SF_5 does not possess an *s* lone pair since, formally, one *s* electron of sulfur has been promoted to a *p* orbital in order that the atom can form two 3c–4e bonds. The valence-shell electron configuration of sulfur is conveniently displayed in the box diagram below. (The *p* orbitals which form three-centre bonds are shown with fluorine atoms above and below their boxes.)



Indeed from the population analysis it is clear that the unpaired electron here occupies an orbital with a substantial degree of sulfur 3*s* character. No significant distortion of the 3c–4e units is required in order that their nonbonding MOs overlap with that of the unpaired electron. Thus the shape of SF_4 is very nearly that of a perfect square pyramid. Similarly ClF_6 does not depart from an octahedral geometry, at least according to the interpretation of its esr spectrum (23).

In PF_4, two of the fluorines are joined to phosphorus by 2c–2e bonds, and two by a 3c–4e unit. The most stable "ideal" geometry is the see-saw shape. The unpaired electron occupies an orbital which lies in the same plane as the two (equatorial) singly-bonded fluorines and which is high in phosphorus s character. Nevertheless the *p* character of the orbital is sufficient that the axial 3c–4e bond fluorines bend toward the sp^n hybrid and away from the equatorial fluorines, though the extent of bending is only 14° compared to 30° in ClF_2, and the energetic stabilization (6-31G(*)) amounts to 4.6 kcal mol^{-1}.

The optimum structure calculated for PH_4 is very similar to that for PF_4, although the 3c–4e units bend only by 10° and the gain in energy by this distortion is only 1.5 (1.1) kcal mol^{-1}, calculated by the 6-31G(*) basis (with MP2 correction). The electronegativities of phosphorus and hydrogen are sufficiently close that a 3c–4e HPH network is feasible, whereas comparable calculations for SH_3 reveal only a potential maximum (10). (A search for a stable SiH_5 radical gave a trigonal bypyramid structure with a 3c–3e bond, which upon frequency analysis turned out to be a transition state rather than a potential minimum. A similar result was obtained in RHF calculations for ClH_2.)

σ-Conjugation

Dewar has proposed that "σ-conjugation" plays a major and often a dominant role in determining the geometries of many systems containing unpaired electrons (4). According to this hypothesis, free radicals such as BH_2 and AlH_2, and the triplet states of CH_2 and SiH_2, will be bent with a bond angle of about 120° and with sp^2 hybridization at the central atom because this allows equal sharing of *s* orbital character between the bonding orbitals and that which houses the in-plane unpaired electron, and σ-conjugation is thereby maximized (4). For the same reason, CX_3 and SiX_3 free radicals normally should be pyramidal, with bond angles close to the tetrahedral value. Deviations from these "ideal" geometries occur in some cases due to steric and/or conjugative interactions.

Dewar's hypothesis is the simplest MO-based theory for the structure of non-hypervalent systems with unpaired electrons, and can be tested by considering the *ab initio* MO calculations for the small free radicals and for molecules with low-lying triplet states in Table 1. We also studied how the optimum XAX bond angle varies over a range of chosen AX distances, since corresponding calculations for closed-shell molecules have revealed the importance of steric effects in determining bond angles, and have determined "ideal", steric-free bond angles by extrapolating the angle-versus-distance curves to longer interatomic separations (24). A limit of about 90° was obtained for the ideal angle in molecules such as H_2O, NH_3, F_2O, $(CH_3)_2O$, etc., i.e. systems which are not forced to engage in hybridization at the central atom in order to increase their valence.

Plots of the optimum HAH bond angle (determined using the 6-31G* basis set and the UHF method) as a function of the chosen AH distance for a number of AH_2 and AH_3 systems containing unpaired electron(s) are shown in Fig. 1. The form of these angle-versus-length curves is similar to that obtained previously for closed-shell hydrides (24). In particular, the angle increases substantially as the AH distance becomes very short, and the increase in angle with decrease in distance is more pronounced for second-row than first-row central atoms.

The limiting angle for the ground state electron configurations of NH_2 and PH_2 is about 90°, which corresponds to the formation of a single AH bond by each of the two (initially) singly-occupied *p* orbitals on the central atom. (Beyond about 1.7 Å, other electron configurations start to play important roles in the ground state, and lead eventually to HAH angles very different from 90° at the dissociation limits. This is irrelevant, however, since our interest is to determine the "steric-free" optimum angle for that electron configuration which dominates the ground state at or near the equilibrium distance.) The unpaired electron is localized in the π system, and thus does not become engaged in the σ bond framework at any angle; therefore σ-conjugation cannot play a role here. The optimum angle in the equilibrium geometry of NH_2 (Table 1) is rather

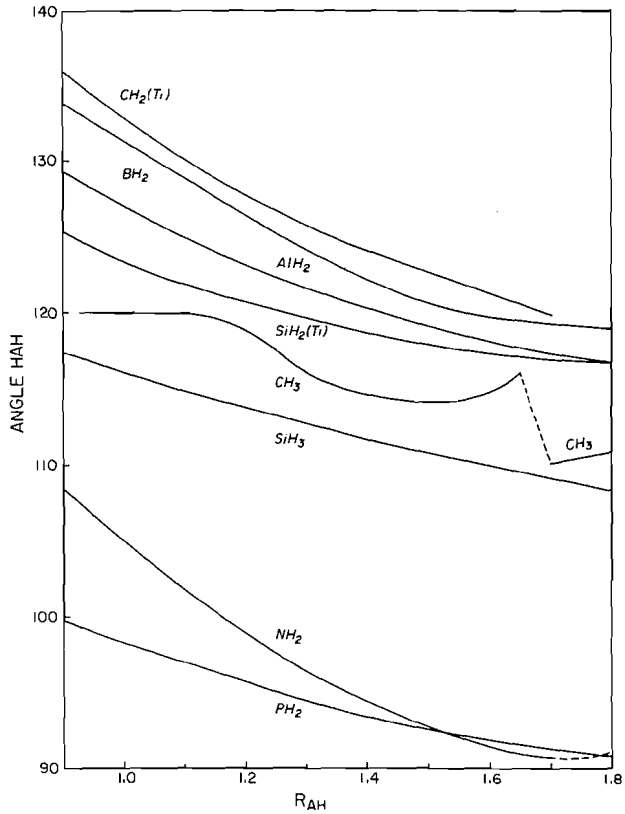


FIG. 1. Optimum angle (in deg) versus A—H bond distance (in Å) for hydrides AH_n containing unpaired electrons. Calculations use the 6-31G* basis set.

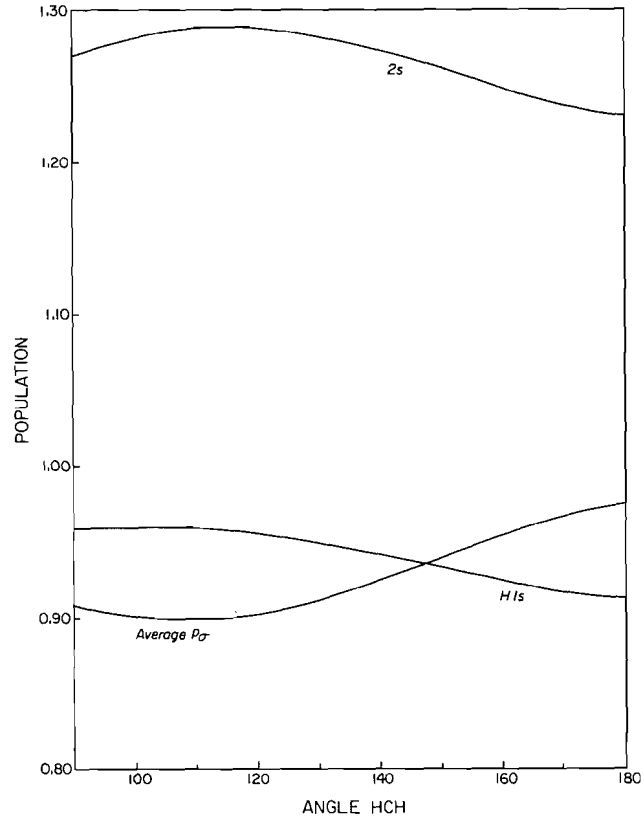


FIG. 2. Electron density in orbitals versus bond angle in triplet state of CH_2, calculated using the STO-3G basis set. The value for the p orbital is an average for the two in-plane $2p$ orbitals of carbon.

larger than that in PH_2 because the N—H bond is so short that the HNH angle opens up to relieve steric repulsion among the hydrogen atoms.

For BH_2 and AlH_2, and for the triplet state of CH_2 and SiH_2, an unpaired electron can exist in the σ framework if the molecule is bent; thus according to Dewar's theory, approximately sp^2 hybridization, with angles of 120°, should be optimum if steric and hyperconjugative factors are negligible. Although the angles at the first-row atoms exceed this value at the equilibrium geometries (Table 1), at long AH distances the optimum angle-versus-distance curves (Fig. 1) for all these cases appear to converge to just under 120°.

Dewar's theory predicts that CX_3 and SiX_3 free radicals should undergo sp^3 hybridization and have tetrahedral angles at the central atom, unless steric and/or hyperconjugative factors dominate. The angle-versus-distance curve for SiH_3 in Fig. 1 does indeed converge to a value in this region. In contrast to SiH_3, CH_3 is trigonal planar for CH distances less than 1.1 Å (which is just slightly greater than the distance in the equilibrium geometry (Table 1)) due to steric clashes among the hydrogens. The shape would be pyramidal if the optimum bond length was only a few hundredths of an angstrom larger.

The prediction that, in the absence of strong steric and/or hyperconjugative interactions, the in-plane singly-occupied orbital of a radical or triplet state should have equal hybrid character with the A—X bonding orbitals seems borne out semiquantitatively by the results for hydrides. We have also tested out Dewar's conclusion that when steric effects are absent, the superior σ-conjugation within CCC units, compared to HCH, will lead to smaller CCC and HCH angles by performing *ab initio* 6-31G* calculations on dimethylmethylene and on methylene. Indeed, the optimum CCC angle (at the optimum CC distance of 1.51 Å) of 127.2° is slightly smaller than that of 130.8° predicted for methylene.

Finally, we should like to note that the driving force behind the reduction in symmetry in molecules having unpaired electrons (i.e. from linear to bent in AX_2 systems, and from trigonal planar to pyramidal for AX_3) is the transfer of electron density from p orbitals of the central atom to its more stable s orbital. The involvement of the atomic orbital containing the unpaired electron with the MOs of the A—X bonds permits the latter to become less bonding in character since the singly-occupied orbital and its electron can take up the slack. Thus the s orbital population can increase since its density no longer needs to be shared as widely in covalent bond formation. This phenomenon is illustrated in Fig. 2, where the $2s$ electron density of the carbon atom in the triplet state of CH_2 is plotted against the chosen HAH bond angle (with the CH distance fixed at 1.10 Å in an STO-3G calculation). If the highest-occupied orbital contains two electrons rather than just one, all the bonding can be assumed by the p orbitals when the bond angles are close to 90°; the stablest valence-shell electrons then localize as a lone pair in the $2s$ orbital. This explanation of σ-conjugation seems more intuitively appealing than that derived from a localized MO basis by Dewar. The latter involves consideration of the interaction between a hybrid orbital on the central atom with the empty, antibonding MO formed by another hybrid of the same atom and an attached ligand (4). The net effect of this interaction is to introduce flexibility in the s/p ratio from that of the isolated sp^2 or sp^3 hybrids, and thus to allow an increase in the s orbital population at the expense of the p.

Can. J. Chem. Downloaded from www.nrcresearchpress.com by 186.148.149.217 on 09/07/12
For personal use only.

Can. J. Chem. Downloaded from www.nrcresearchpress.com by 186.148.149.217 on 09/07/12
For personal use only.

Conclusions

Overall, in agreement with the viewpoint expressed by Morton and Preston (22), we find that free radicals have geometries which usually are close to those predicted by VSEPR and found for closed-shell systems with one additional electron. Their generalization can be made more useful by noting that the unpaired electron in hypervalent systems occupies the same position as does a lone pair. Further, in hypervalent systems with both an unpaired electron and one or more lone pairs, the ligands distort their angles as if repulsion of a bonding pair by a lone pair exceeds its repulsion by an unpaired electron, and repulsion of a bonding pair by another bonding pair is intermediate (although this order seems inconsistent with the requirement that the unpaired electron occupies a position for a lone rather than a bonding pair):

$$\text{lone pair} - \text{bonding pair} > \text{bonding pair} - \text{bonding pair} > \text{unpaired electron} - \text{bonding pair}$$

Thus ClF_2 distorts from linearity, ClF_4 from square planarity (with all F atoms distorting in the same direction, away from the lone pair and toward the unpaired electron), PX_4 radicals distort from the see-saw shape toward the tetrahedral, and SF_5 distorts from the square planar shape toward the square pyramidal. The net distortion in SF_3 is the result of two opposing effects; the axial fluorines move in toward the equatorial fluorine due to lone pair – bond pair repulsions being greater than bond pair – bond pair, but then they leave the plane as their repulsion with the unpaired electron is less again.

The application of these modified "rules" to non-hypervalent systems containing unpaired electrons is less successful. It is not clear why the distortions from 120° angles in boron and aluminum systems should differ in sign, or why the second unpaired electron in triplet states should have no effect, or why the methyl radical should be planar.

The geometry of the hypervalent radical systems is explained equally well by the three-center bonding theory, as is the case with closed-shell hypervalent systems. The ligands of the 3c–4e units bend toward a lobe of the unpaired electron's orbital, or if the electron occurs in the 3c–4e network (e.g. ClF_4) the system bends toward one lobe of a lone pair orbital, in order to provide some net bonding energy gain (two electrons stabilized, one destabilized) to the system. When this hypothesis is combined with Dewar's σ-conjugation principle — that hybridization will include the orbital of an unpaired electron if this allows interaction with two-center bonds — and the concept that deviations of bond angles from the 120° or 109.5° or 90° values predicted by this principle occur mainly to reduce steric collisions, the geometries of almost all the systems discussed herein can be understood. The only exceptions are the bond angles of somewhat less than 120° encountered for the second-row difluorides.

Overall, it appears that the MO-based theory is marginally superior to VSEPR theory — as amended herein — in the prediction of geometries of molecules containing unpaired electrons, although as with closed-shell systems, both types of theory usually predict the same "ideal" structure.[1]

Acknowledgement

The authors are grateful to the Natural Sciences and Engineering Research Council of Canada for financial support.

[1]NOTE ADDED IN PROOF: Recently, Demolliens *et al.* (30) reported 6-31G* ab initio MO calculations for PH_4; the structural details they report agree with our results.

1. (*a*) N. C. BAIRD. J. Chem. Ed. **55**, 412 (1978); (*b*) B. M. GIMARC. Molecular structure and bonding. Academic Press, New York. 1979.
2. R. J. GILLESPIE. Molecular geometry. Van Nostrand Reinhold Co., New York. 1972.
3. (*a*) R. E. RUNDLE. Surv. Prog. Chem. **1**, 81 (1963); (*b*) G. C. PIMENTEL. J. Chem. Phys. **19**, 446 (1951); (*c*) J. I. MUSHER. Angew. Chem. Intl. Ed. Engl. **8**, 54 (1969); (*d*) E. E. HAVINGA and E. H. WIEBENGA. Rec. Trav. Chem. **78**, 724 (1959).
4. M. J. S. DEWAR. J. Am. Chem. Soc. **106**, 669 (1984) and references therein.
5. (*a*) W. J. HEHRE, L. RADOM, P. v. R. SCHLEYER, and J. A. POPLE. Ab initio molecular orbital theory. Wiley-Interscience, NY. 1986; (*b*) M. FRISCH, J. S. BINKLEY, H. B. SCHLEGEL, K. RAGHAVACHARI, R. MARTIN, J. J. P. STEWART, F. BOBROWICZ, D. DEFREES, R. SEEGER, R. WHITESIDE, D. FOX, E. FLUDER, and J. A. POPLE. GAUSSIAN 86 Release C Program. Carnegie-Mellon University, Pittsburgh. 1988.
6. A. B. SANNIGRAHI and S. D. PEYERIMHOFF. Chem. Phys. Lett. **114**, 6 (1985).
7. M. KUHN. B.Sc. Thesis. University of Western Ontario, London, Ont. 1989.
8. G. MAMANTOV, D. G. VICKROY, E. J. VASINI, T. MACKAWA, and M. C. MOULTON. J. Chem. Phys. **54**, 3419 (1971).
9. J. R. MORTON, K. F. PRESTON, and S. J. STRACH. J. Chem. Phys. **69**, 1392 (1978).
10. S. P. So. Chem. Phys. Lett. **90**, 325 (1982).
11. (*a*) F. VOLATRON, A. DEMOLLIENS, J.-M. LEFOUR, and O. EISENSTEIN. Chem. Phys. Lett. **130**, 419 (1986); (*b*) F. VOLATRON. J. Mol. Struct. (Theochem). **186**, 167 (1989).
12. R. R. SMARDZEWSKI and W. B. FOX. J. Chem. Phys. **67**, 2309 (1977).
13. J. R. MORTON and K. F. PRESTON. Chem. Phys. Lett. **18**, 98 (1973).
14. A. R. GREGORY. Chem. Phys. Lett. **28**, 552 (1974).
15. W. NELSON, G. JACKEL, and W. GORDY. J. Chem. Phys. **52**, 4572 (1970).
16. (*a*) C. A. MCDOWELL, K. A. R. MITCHELL, and P. RAGHUNATHAN. J. Chem. Phys. **57**, 1699 (1972); (*b*) K. SHIMOKOSHI, K. NAKAMURA, and S. SATO. Mol. Phys. **53**, 1239 (1984).
17. P. J. KRUSIC, W. MAHLER, and J. K. KOCHI. J. Am. Chem. Soc. **94**, 6033 (1972).
18. J. M. HOWELL and J. F. OLSEN. J. Am. Chem. Soc. **98**, 7119 (1976).
19. S. P. So and W. G. RICHARDS. J. Chem. Soc. Faraday Soc. II, 55 (1979).
20. S. R. UNGEMACH and H. F. SCHAEFER III. J. Am. Chem. Soc. **98**, 1658 (1976).
21. V. L. PERSHIN and A. I. BOLDYREV. J. Mol. Struct. (Theochem). **150**, 171 (1987).
22. J. R. MORTON and K. F. PRESTON. *In* Fluorine-containing free radical kinetics and dynamics of reactions. *Edited by* J. W. Root. Am. Chem. Soc. Symp. Ser. No. 66. 1978. p. 386.
23. A. R. BOATE, J. R. MORTON, K. F. PRESTON, and S. J. STRATCH. J. Chem. Phys. **71**, 388 (1979).
24. N. C. BAIRD. Inorg. Chem. **28**, 1224 (1989).
25. R. A. WHITESIDE, M. J. FRISCH, J. S. BINKLEY, D. J. DEFREES, H. B. SCHLEGEL, K. RAGHAVACHARI, and J. A. POPLE. Carnegie-Mellon quantum chemistry archive. 2nd ed. Carnegie-Mellon University. 1981.
26. J. H. CALLOMAN, E. HIROTA, T. IIJIMA, K. KICHITSU, and W. J. LAFFERTY. Structure data of free polyatomic molecules. Springer-Verlag, Berlin. 1987.
27. W. NELSON and W. GORDY. J. Chem. Phys. **51**, 4710 (1969).
28. G. S. JACKEL and W. GORDY. Phys. Rev. **176**, 443 (1968).
29. M. V. MERTRITT and R. W. FESSENDEN. J. Chem. Phys. **56**, 2353 (1972).
30. A. DEMOLLIENS, O. EISENSTEIN, P. C. HIBERTY, J. M. LEFOUR, G. OHANESSIAN, S. S. SHAIK, and F. VOLATRON. J. Am. Chem. Soc. **111**, 5623 (1989).

Reaction of *N,N'*-dihydroxy-*N,N'*-dimethylmethanediamine with phenylboronic acid and the crystal and molecular structure of *N,N'*-dihydroxy-*N,N'*-dimethylmethanediamine

WOLFGANG KLIEGEL

Institut für Pharmazeutische Chemie, der Technischen Universität Braunschweig, Beethovenstraße 55, 3300 Braunschweig, Bundesrepublik Deutschland

AND

STEVEN J. RETTIG AND JAMES TROTTER

Department of Chemistry, University of British Columbia, 2036 Main Mall, Vancouver, B.C., Canada V6T 1Y6

Received December 1, 1988

This paper is dedicated to Professor Ronald J. Gillespie on the occasion of his 65th birthday

WOLFGANG KLIEGEL, STEVEN J. RETTIG, and JAMES TROTTER. Can. J. Chem. **67**, 1959 (1989).

The reaction of *N,N'*-dihydroxy-*N,N'*-dimethylmethanediamine with phenylboronic acid leads to the product 1,7-dimethyl-3,5-diphenyl-2,4,6-trioxa-7-aza-1-azonia-3-bora-5-boratabicyclo[3.3.0]octane rather than the expected product 1,5-dimethyl-3-phenyl-1,5-diaza-2,4-dioxa-3-boracyclohexane. The structure of *N,N'*-dihydroxy-*N,N'*-dimethylmethanediamine has been determined and is discussed in terms of its reaction with $PhB(OH)_2$. Crystals of *N,N'*-dihydroxy-*N,N'*-dimethylmethanediamine are tetragonal, $a = 8.5346(3)$, $c = 8.4178(7)$ Å, $Z = 4$, space group $P42_1c$. The structure was solved by direct methods and was refined by full-matrix least-squares procedures to a final R of 0.036 and R_w of 0.038 for 333 reflections with $I \geq 3\sigma(I)$. The structure consists of hydrogen-bonded dimers having exact $\bar{4}$ (S_4) symmetry.

Key words: *N,N'*-dihydroxy-*N,N'*-dimethylmethanediamine, crystal structure.

WOLFGANG KLIEGEL, STEVEN J. RETTIG et JAMES TROTTER. Can. J. Chem. **67**, 1959 (1989).

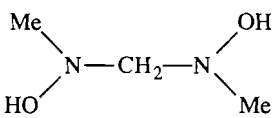
La réaction de la *N,N'*-dihydroxy *N,N'*-diméthylméthanediamine avec l'acide phénylboronique conduit à la formation du produit diméthyl-1,7 diphényl-3,5 trioxa-2,4,6 aza-7 azonia-1 bora-3 borata-5 bicyclo[3.3.0]octane plutôt que le produit attendu, le diméthyl-1,5 phényl-3 diaza-1,5 dioxa-2,4 bora-3 cyclohexane. On a déterminé la structure de la *N,N'*-dihydroxy *N,N'*-diméthylméthanediamine et on en discute en fonction de sa réaction avec le $PhB(OH)_2$. Les cristaux de la *N,N'*-dihydroxy *N,N'*-diméthylméthanediamine sont tétragonaux, avec $a = 8{,}5346(3)$ et $c = 8{,}4178(7)$ Å, $Z = 4$ et groupe d'espace $P42_1c$. On a résolu la structure par des méthodes directes et on l'a affinée par la méthode des moindres carrés jusqu'à des valeurs finales de R de 0,036 et R_w de 0,038 pour 333 réflexions avec $I \geq 3\sigma(I)$. La structure est composée de dimères liés par des ponts hydrogènes et possédant une symétrie $\bar{4}$ (S_4) exacte.

Mots clés : *N,N'*-dihydroxy *N,N'*-dimethylmethanediamine, structure cristalline.

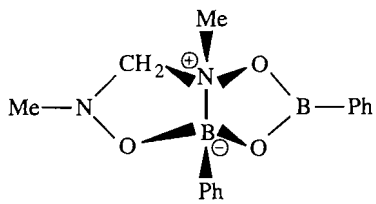
[Traduit par la revue]

Introduction

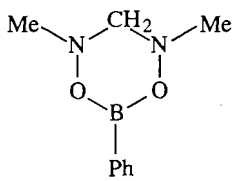
N,N'-Dihydroxy-*N,N'*-dimethylmethanediamine, **1** (1), has been employed in the synthesis of a stable pyroboronate ring system **2** (2). The crystal structure of **2** has been determined and establishes the presence of transannular N → B coordination (3). The formation of a six-membered monophenylboronate **3** should have been a favored reaction, analogous to facile



1



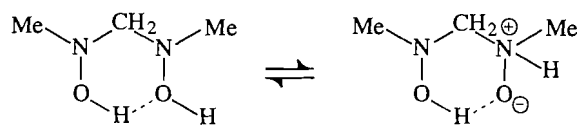
2



3

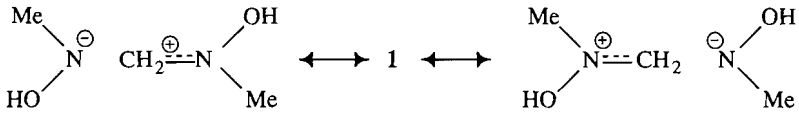
cycloboronate syntheses with 1,3-diols (4), assuming a *cis*-oriented hydrogen-bridged diol ligand **4** or its *N*-oxide tautomer **5** and also that phenylboronic acid is monomeric in solution as it is in the solid state (5). Infrared and ^1H nmr spectra of **1** (and other compounds of this type) indicate strong, and at least partial, intramolecular hydrogen bonding (2, 6, 7), but **3** could not be isolated or detected during the condensation experiments with phenylboronic acid (2). Reactions of **1** with other acylating agents (8, 9) or dipolarophiles (10), and mass spectrometric fragmentation patterns for **1**, show the tendency of **1** to dissociate at one of the central C—N bonds. This appears to be typical behavior for compounds of this type under the attack of electrophilic agents (11) and also under the conditions of the mass spectrum experiment (2).

Additional structural information about **1** is required in order to clarify the possibility of hydrogen bonding as shown in **4** and **5** and also for consideration of a possible anomeric (stereoelectronic) effect (12, 13) with respect to "double bond – no bond resonance" (13–15) or negative hyperconjugation (15). The "no bond resonance" formalism is symbolized by **6** and would require certain preferred conformations of **1** which would allow π-donation by one or both of the nitrogen lone pair electrons for $n\pi(N^1)/\sigma^*(N^2—C)$ orbital interaction. Parallelism of these orbitals would result in increased double bond character of one N—C bond and weakened single bond



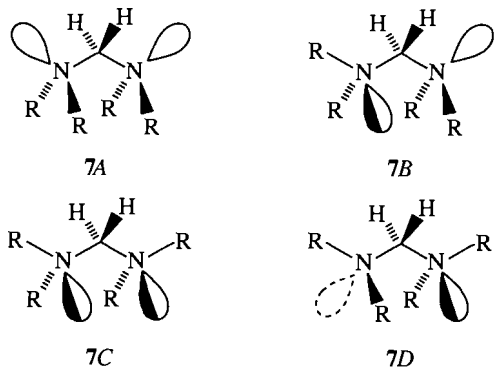
4 **5**

Can. J. Chem. Downloaded from www.nrcresearchpress.com by 186.148.149.217 on 09/07/12
For personal use only.



6 6

character for the other, causing an inequality of the N—C bond distances. Ignoring the steric and electronic influences of the substituents R = OH or CH_3, four important conformations **7A–7D** may be considered for the N^1—C—N^2 system, only the conformations *A* and *B* being stabilized by the anomeric effect. The solid state structure of **1** has been determined in order to clarify this problem.



7A 7B 7C 7D

Experimental

N,N′-*Dihydroxy*-N,N′-*dimethylmethanediamine, 1*

The title compound was prepared according to the literature (1, 6) and was recrystallized from ethanol. Melting point 113–114°C. ^{1}H nmr and mass spectral data are detailed in ref. 2.

X-ray crystallographic analysis of 1

A crystal bounded by the fourteen faces (followed by the distances in mm between parallel faces): {1 1 0}, 0.36, 6 of {1 0 1}, 0.39, ±(0 −1 2), 0.35, ±(1 −2 1), 0.40 was mounted in a general orientation. Unit-cell parameters were refined by least-squares on 2 sin θ/λ values for 25 reflections (2θ = 34–45°) measured on a diffractometer with Mo-Kα radiation ($\lambda(K\alpha_1)$ = 0.70930, $\lambda(K\alpha_2)$ = 0.71359 Å). Crystal data at 21°C are:

$C_3H_{10}N_2O_2$ f.w. = 106.12

Tetragonal, a = 8.5346(3), c = 8.4178(7) Å, V = 613.14(6) Å^3, Z = 4, ρ_c = 1.150 Mg m^{-3}, $F(000)$ = 232, μ(Mo-$K\alpha$) = 0.88 cm^{-1}. Absent reflections: *hhl*, *l* odd, 00*l*, *l* odd, and 0*k*0, *k* odd, uniquely indicate the space group $P42_1c$ (D^4_{2d}, No. 114).

Intensities were measured with graphite-monochromated Mo-$K\alpha$ radiation on an Enraf-Nonius CAD4-F diffractometer. An ω-2θ scan at 0.9–10.0° min^{-1} over a range of (0.65 + 0.35 tan θ) degrees in ω (extended by 25% on both sides for background measurement) was employed. Data were measured to 2θ = 65°. The intensities of three check reflections, measured every 4000 s throughout the data collection, showed only small random variations (<3%). Of the 653 independent reflections measured and processed,[1] 333 (51.0%) had intensities greater than or equal to 3σ(*I*) above background where

TABLE 1. Final positional (fractional × 10^4, H × 10^3) and isotropic thermal parameters (U × 10^3 Å^2) with estimated standard deviations in parentheses

Atom	x	y	z	U_{eq}/U_{iso}
O	5943(2)	2981(2)	1129(3)	55
N	6316(2)	4521(2)	1749(2)	48
C(1)	5000	5000	2728(4)	56
C(2)	7728(4)	4300(4)	2702(5)	77
H(O)	561(3)	319(4)	20(4)	71(9)
H(1)	474(3)	422(3)	343(3)	58(8)
H(2a)	764(4)	357(5)	348(5)	94(12)
H(2b)	807(5)	530(5)	320(5)	115(12)
H(2c)	859(6)	385(6)	204(5)	115(13)

$\sigma^2(I) = S + 2B + (0.04(S - B))^2$ with S = scan count and B = normalized background count.

The structure was solved by direct methods, the coordinates of the non-hydrogen atoms being determined from an *E*-map and those of the hydrogen atoms from a subsequent difference Fourier synthesis. Non-hydrogen atoms were refined with anisotropic thermal parameters and hydrogen atoms with isotropic thermal parameters. Scattering factors for all atoms were taken from ref. 16. The weighting scheme $w = 1/\sigma^2(F)$, where $\sigma^2(F)$ is derived from the previously defined $\sigma^2(I)$, gave uniform average values of $w(|F_o| - |F_c|)^2$ over ranges of both $|F_o|$ and sin θ/λ and was employed in the final stages of full-matrix refinement of 54 variables. Reflections with $I < 3\sigma(I)$ were not included in the refinement. An isotropic Type I extinction correction (Thornley–Nelmes definition of mosaic anisotropy with a Lorentzian distribution) was applied (17–19). The final value of g was 5.1(6) × 10^4. Convergence was reached at R = 0.036 and R_w of 0.038 for 333 reflections with $I \geq 3\sigma(I)$. No attempt was made to determine the polarity of the structure, anomalous scattering terms not being included in the calculations. The function minimized was $\Sigma w(|F_o| - |F_c|)^2$, $R = \Sigma||F_o| - |F_c||/\Sigma|F_o|$ and $R_w = (\Sigma w(|F_o| - |F_c|)^2/\Sigma w|F_o|^2)^{1/2}$.

On the final cycle of refinement the mean and maximum parameter shifts corresponded to 0.0004 and 0.003σ, respectively. The mean error in an observation of unit weight was 1.693. The final difference map was featureless, the largest peak being 0.16 e Å^{-3}. The final positional and thermal parameters appear in Tables 1 and 4,[2] respectively. Measured and calculated structure factors have been placed in the Depository of Unpublished Data.[2]

The ellipsoids of thermal motion for the non-hydrogen atoms are shown in Fig. 1. The thermal motion has been analysed in terms of the rigid-body modes of translation, libration, and screw motion (20). The rms standard error in the temperature factors σU_{ij} (derived from the least-squares analysis) is 0.0014 Å^2. Analysis of the entire molecule gave rms ΔU_{ij} = 0.0015 Å^2 and physically reasonable results. The appropriate bond distances have been corrected for libration (20, 21), using shape parameters q^2 of 0.08 for all atoms involved. Corrected bond lengths appear in Table 2 along with the uncorrected values; bond angles are given in Table 3. A complete listing of torsion angles (Table 5) is included as supplementary material.

[1]The computer programs used include locally written programs for data processing and locally modified versions of the following: MULTAN 80, multisolution program by P. Main, S. J. Fiske, S. E. Hull, L. Lessinger, G. Germain, J. P. Declercq, and M. M. Woolfson; ORFLS, full-matrix least-squares, and ORFFE, function and errors, by W. R. Busing, K. O. Martin, and H. A. Levy; FORDAP, Patterson and Fourier syntheses, by A. Zalkin; ORTEP II, illustrations, by C. K. Johnson.

[2]The structure factor table, Table 4 (anisotropic thermal parameters) and other material mentioned in the text may be purchased from the Depository of Unpublished Data, CISTI, National Research Council of Canada, Ottawa, Ont., Canada K1A 0S2.

Can. J. Chem. Downloaded from www.nrcresearchpress.com by 186.148.149.217 on 09/07/12
For personal use only.

TABLE 2. Bond lengths (Å) with estimated standard deviations in parentheses

Bond	Length		Bond	Length	
	Uncorr.	Corr.		Uncorr.	Corr.
O—N	1.449(2)	1.458	N—C(2)	1.460(3)	1.468
N—C(1)	1.452(3)	1.461			
O—H(O)	0.85(4)		C(2)—H(2b)	1.00(4)	
C(1)—H(1)	0.91(3)		C(2)—H(2c)	1.00(6)	
C(2)—H(2a)	0.91(4)				

TABLE 3. Bond angles (deg) with estimated standard deviations in parentheses*

Bonds	Angle (deg)	Bonds	Angle (deg)
O—N—C(1)	106.9(2)	C(1)—N—C(2)	111.3(2)
O—N—C(2)	105.2(2)	N—C(1)—N′	110.9(2)
N—O—H(O)	102(2)	N—C(2)—H(2b)	111(2)
N—C(1)—H(1)	111(2)	N—C(2)—H(2c)	110(3)
N—C(1)—H(1)′	112(2)	H(2a)—C(2)—H(2b)	108(3)
H(1)—C(1)—N′	112(2)	H(2a)—C(2)—H(2c)	101(3)
H(1)—C(1)—H(1)′	100(3)	H(2b)—C(2)—H(2c)	111(3)
N—C(2)—H(2a)	115(2)		

*Primed atoms have coordinates related to those in Table 1 by the symmetry operation: $1 - x, 1 - y, z$.

Can. J. Chem. Downloaded from www.nrcresearchpress.com by 186.148.149.217 on 09/07/12
For personal use only.

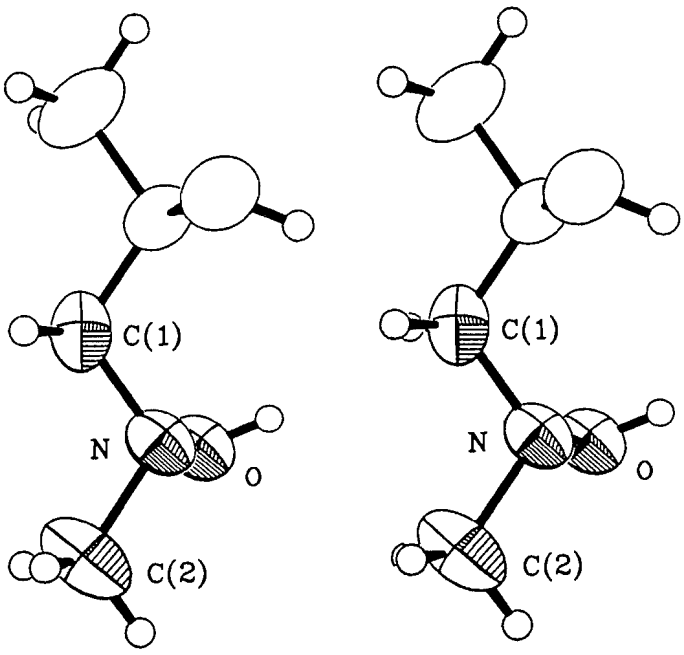
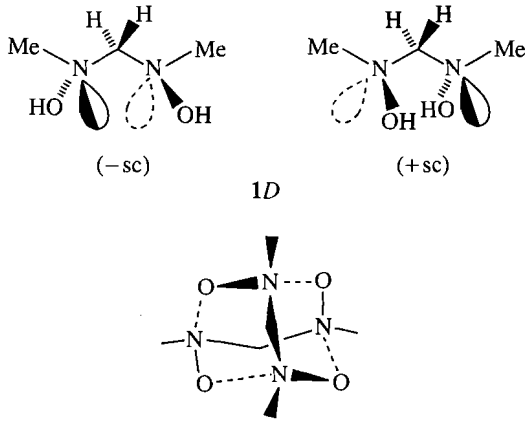


FIG. 1. Stereoscopic view of *N,N′*-dihydroxy-*N,N′*-dimethylmethanediamine; 50% probability thermal ellipsoids are shown for the non-hydrogen atoms. Shaded non-hydrogen atoms comprise the asymmetric unit.

Results and discussion

In the solid state **1** adopts the conformation **7***D*, the methyl substituents being in a fully staggered antiperiplanar orientation with respect to the geminal nitrogen substituents and with the hydroxy groups exhibiting a *trans–gauche* orientation. As a result of the *trans* positioning of the *N*-hydroxy groups, two enantiomeric conformers are possible, with both OH substituents in (+sc) or both in (−sc) arrangements. Both of these, **1***D*(+sc) and **1***D*(−sc), are realized in the crystal (Fig. 2) as hydrogen-bonded dimeric pairs having crystallographically imposed $\bar{4}$ symmetry (O—H(O)···N (y, $1 - x$, $-z$), O···N = 2.775(3), H···N = 1.93(4) Å, O—H···N = 171(2)°).



1*D*(+sc)•**1***D*(−sc)
(- - - - = H-bridge

Individual molecules of **1** (Fig. 1) have exact C_2 symmetry (lying on a crystallographic two-fold axis at ($\frac{1}{2}$, $\frac{1}{2}$, z) and are similar to molecules of *N,N,N′,N′*-tetramethylmethanediamine **8** which has a similar molecular structure and the same symmetry in the gas phase (22). The central N—C bond lengths are identical (by symmetry), and as the model **7***D* points out, no anomeric interaction is involved in this molecular conformation. The model compound **7** with R = H has been geometrically refined by *ab initio* calculations (23) and has equal N—C bond distances of 1.4653 Å in the *D* conformation, consistent with the N—C distance of 1.461(3) Å in **1**. Since the orbital interaction (anomeric effect) is of little or no importance in crystalline **1**, the associative forces of the four intermolecular O—H···N hydrogen bonds in the dimer, along with the repul-

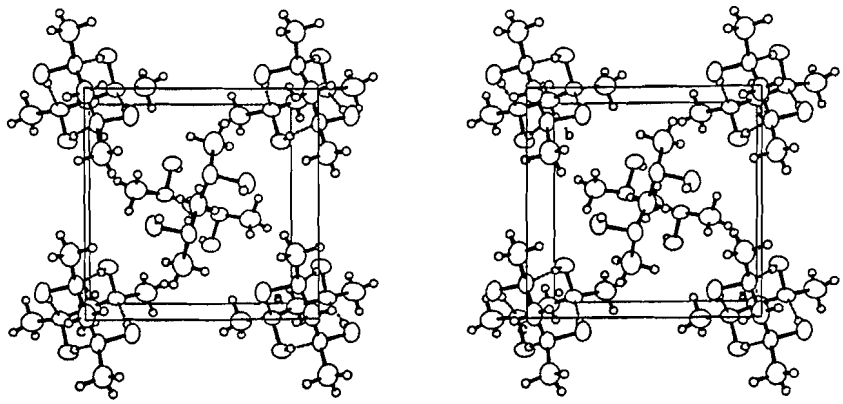
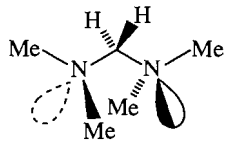


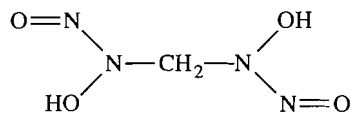
FIG. 2. Stereoscopic view of the packing arrangement of *N,N'*-dihydroxy-*N,N'*-dimethylmethanediamine.

sive interaction between the *N*-methyl groups (demonstrated by the tetramethyl derivative **8** (22)), predominate in the stabilization of **1** in the solid state.

There is one other *N,N'*-dihydroxymethanediamine derivative that has been structurally characterized, the bis-*N*-nitroso derivative **9**. In this case crystal structures have been reported for the potassium (24) and sodium (25) salts of the dianion derived from **9**. The structure of the dianion shows marked differences in both bond lengths and in conformation from, and is not directly comparable with that of **1**. The C—N(O)—NO moiety in the dianion of **9** is nearly planar and the N—C bond length of 1.512(7) Å and N—C—N angle of 104.9° observed for the dipotassium salt (24) differ from corresponding values of 1.461(3) Å and 110.9° for **1** and 1.449(4) Å and 115.8° for the gas phase structure of **8** (22).



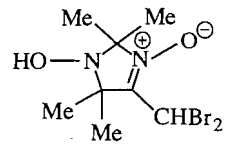
8



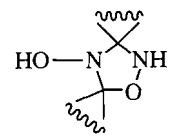
9

The geometry of the hydroxylamine moiety in **1** resembles that in MeNHOH.HCl (26) more than it does that in the free base MeNHOH as determined in the gas phase (27), since as in the H-bonded dimer of **1**, the nitrogen atom in *N*-methylhydroxylamine hydrochloride is quaternized. The N—Me and N—O bond lengths and the O—N—Me angle in **1** are 1.468(3) Å, 1.458(2) Å, and 105.2(2)°; corresponding values are 1.46 Å, 1.45 Å, and 105° for MeNHOH.HCl and 1.420 Å, 1.477 Å, and 107.7° for MeNHOH.

Infrared and ^{1}H nmr spectra indicate that the species **4** and/or **5** are present in solutions of *N,N'*-dihydroxy-*N,N'*-dimethylmethanediamine, **1**. The intramolecular hydrogen bond in **4** or **5** is not observed in the solid state which consists of stable hydrogen-bonded dimers of **1**. The intramolecular O···O distance in the *trans–gauche* conformation, 3.804(3) Å, is too large for intramolecular hydrogen bonding. *N*-oxide tautomers of **1** (such as **5**), if involved in the H-bonded dimer, would be expected to have shorter N—O bonds. The most comparable *N*-oxide, incorporated into an *N,N*-acetal structure, is that of hexamethylenetetramine *N*-oxide, hydrogen-bonded to formic acid (28) with an N—O distance of 1.388 Å and hydrogen-bonded to H_2O_2/H_2O (29) with N—O = 1.380 Å. Other related N—O distances have been reported for *N,N*-dimethyl-



10



11

2-aminoethanol *N*-oxide (30), 1.38 and 1.41 Å for intra- and intermolecular H-bonded moities, trimethylamine *N*-oxide, 1.42 Å H-bonded to HCl (31) and 1.388 Å for the free base (32). The structures of the cyclic *N,N*-acetals **10** (33) and **11** (34) (the *N,N*-acetal moiety being part of a tetracyclohexadecane system) with only one *N*-hydroxy group have been reported. The N—O(H) and (N)C—N(OH) distances in **1** of 1.458(2) and 1.468(2) Å may be compared with corresponding distances of 1.44 and 1.46 Å in **10** and 1.458(2) and 1.484(2) Å in **11**.

The *trans–gauche* orientation of the *N*-hydroxy groups of **1***D*(+sc), and also of **1***D*(−sc), is very similar to that in the phenylboronate **2** (2, 3). The torsion angles in the MeN(O)CH_2N(O)Me moiety of **2** differ by an average of 14.3° from those in **1**, the differences being greater about bonds involving the three-coordinate nitrogen atom (24.1°) than for those involving the four-coordinate nitrogen atom (4.4°). The N—C—N bond angle in **1** (110.9°) is compressed in **2** (mean 102.5°) by the formation of the fused system of five-membered rings via transannular N → B bonding. The C(1)—N—O angle of **1** (106.9°) is reduced to a mean of 101.0° at the trivalent nitrogen in **2** and remains nearly the same at the tetravalent nitrogen atom (mean 107.7°).

One significant change involves the *N,N*-acetal system: one of the N—C bonds is shortened from 1.461 Å in **1** to 1.452 Å in **2**, at the trivalent nitrogen atom, while the other is lengthened from 1.461 Å to a mean of 1.480 Å. The difference between the N—C bonds at the *N,N*-acetal function in **2** is nearly 0.03 Å, whereas in **1** both bond lengths are the same. Even though quaternization at one of the nitrogen atoms is a factor, this is interpretable in terms of a "double bond – no bond resonance" at the N—C—N segment of **2**, similar to that shown in formula **6**. Since the conformation of **2** (like that of **1**) is unfavorable for $n\pi/\sigma^*$-orbital interaction as defined by the anomeric effect (12, 13), other stabilizing forces must be active, like a more effective distribution of electrical charges (12*a*) resulting in the minimization of dipole–dipole interactions (12*c*, 13), i.e. the "reverse anomeric effect". A decrease of electron density at the trivalent nitrogen in **2** has recently been indicated by nuclear quadrupole double resonance experiments (35).

Can. J. Chem. Downloaded from www.nrcresearchpress.com by 186.148.149.217 on 09/07/12
For personal use only.

Thermodynamic factors are undoubtedly important in the reaction of **1** with phenylboronic acid. The expected product **3** would contain a sterically less favorable conformation of the ligand, but the energy difference is probably not large enough to prevent the reaction from occurring. The observed product **2**, however, is stabilized by both a transannular N → B interaction and the presence of the very stable B(sp^2)—O—B(sp^3) unit.

Acknowledgments

We thank the Natural Sciences and Engineering Research Council of Canada and the Fonds der Chemischen Industrie, Frankfurt am Main, for financial support and the University of British Columbia Computing Centre for assistance. We are also grateful to G. Lubkowitz for help in the preparation of single crystals.

1. H. Hellmann and K. Teichmann. Chem. Ber. **89**, 1134 (1956).
2. W. Kliegel. J. Organomet. Chem. **253**, 9 (1983).
3. W. Kliegel, S. J. Rettig, and J. Trotter. Can. J. Chem. **62**, 515 (1984).
4. (*a*) A. J. Hubert, B. Hargitay, and J. Dale. J. Chem. Soc. 931 (1961); (*b*) R. J. Ferrier. Adv. Carbohydr. Chem. Biochem. **35**, 31 (1978); (*c*) C. F. Poole and A. Zlatkis. J. Chromatogr. **184**, 99 (1980); (*d*) R. Koster (*Editor*). Organoborverbindungen I, Houben-Weyl Vol. XIII/3a. Stuttgart. 1982. p. 696.
5. S. J. Rettig and J. Trotter. Can. J. Chem. **55**, 3071 (1977).
6. G. Zinner and W. Kliegel. Chem. Ber. **99**, 2686 (1966).
7. M. Masui and C. Yijima. Yakugaku Zasshi, **87**, 707 (1967); **89**, 135 (1969).
8. H. Ulrich and A. A. Sayigh. J. Chem. Soc. 1089 (1963).
9. G. Zinner and W. Kliegel. Arch. Pharmaz. **299**, 977 (1966).
10. E. J. Fornefeld and A. J. Pike. J. Org. Chem. **44**, 835 (1979).
11. W. Kliegel and H.-G. Franckenstein. Leibigs Ann. Chem. 2294 (1976), and references therein.
12. (*a*) R. U. Lemieux. Pure Appl. Chem. **25**, 527 (1971); (*b*) N. S. Zefirov and N. M. Shekhtman. Russ. Chem. Rev. **40**, 315 (1971); (*c*) A. J. Kirby. The anomeric effect and related stereoelectronic effects at oxygen. Berlin. 1983; (*d*) P. Deslongchamps. Stereoelectronic effects in organic chemistry. Oxford. 1983.
13. W. F. Bailey and E. L. Eliel. J. Am. Chem. Soc. **96**, 1798 (1974).
14. J. Hine. J. Am. Chem. Soc. **85**, 3239 (1963).
15. P. v. R. Schleyer and A. J. Kos. Tetrahedron, **39**, 1141 (1983).
16. International tables for X-ray crystallography. Vol. IV. Kynoch Press, Birmingham. 1974. pp. 99–102 and 149.
17. P. J. Becker and P. Coppens. Acta Crystallogr. Sect. A, **30**, 129 (1974); **30**, 148 (1974); **31**, 417 (1975).
18. P. Coppens and W. C. Hamilton. Acta Crystallogr. Sect. A, **26**, 71 (1970).
19. F. R. Thornley and R. J. Nelmes. Acta Crystallogr. Sect. A, **30**, 748 (1974).
20. V. Schomaker and K. N. Trueblood. Acta Crystallogr. Sect. B, **24**, 63 (1968).
21. D. W. J. Cruickshank. Acta Crystallogr. **9**, 747 (1956); **9**, 754 (1956); **14**, 896 (1961).
22. H. van der Does, F. C. Mijlhoff, and G. H. Reres. J. Mol. Struct. **74**, 153 (1981).
23. L. Schäfer, C. v. Alsenoy, J. O. Williams, J. N. Scarsdale, and H. J. Geise. J. Mol. Struct. **76**, 349 (1981).
24. J. H. Bryden. Acta Crystallogr. **12**, 581 (1959).
25. V. Cherepinskii-Malov, A. S. Mukhametzyanov, V. G. Andrianov, and G. A. Marchenko. J. Struct. Chem. **24**, 157 (1983).
26. L. Toft and B. Jerslev. Acta Chem. Scand. **21**, 1388 (1967).
27. D. W. H. Rankin, M. R. Todd, F. G. Riddell, and E. S. Turner. J. Mol. Struct. **71**, 171 (1981).
28. Y. S. Lam and T. C. W. Mak. Acta Crystallogr. Sect. B, **34**, 1915 (1978).
29. T. C. W. Mak and Y. S. Lam. Acta Crystallogr. Sect. B, **34**, 1732 (1978).
30. E. R. Maia, A. Péguy, and S. Pérez. Can. J. Chem. **62**, 6 (1984).
31. (*a*) C. Rérat. Acta Crystallogr. **13**, 63 (1960); (*b*) A. Caron and J. Donohue. Acta Crystallogr. **15**, 1052 (1962).
32. A. Caron, G. J. Palenik, E. Goldish, and J. Donohue. Acta Crystallogr. **17**, 102 (1964).
33. Yu. V. Gatilov, M. M. Mitasov, I. A. Grigor'ev, and L. B. Volodarskii. J. Struct. Chem. **23**, 899 (1982).
34. H. Sato, S. Imamura, Y. Kitano, T. Kanda, and T. Ashida. Bull. Chem. Soc. Jpn. **57**, 2162 (1984).
35. A. Lötz, J. Voitländer, D. Stephenson, and J. A. S. Smith. Z. Naturforsch. Sect. A, **41**, 200 (1986).

Can. J. Chem. Downloaded from www.nrcresearchpress.com by 186.148.149.217 on 09/07/12
For personal use only.

Synthesis, structure, and vibrational spectrum of poly-μ-pyrazine(pyrazine)(trifluoromethanesulfonato-O)copper(I)

T. OTIENO, S. J. RETTIG, R. C. THOMPSON,[1] AND J. TROTTER

Department of Chemistry, University of British Columbia, 2036 Main Mall, Vancouver, B.C., Canada V6T 1Y6

Received February 10, 1989

This paper is dedicated to Professor Ronald J. Gillespie on the occasion of his 65th birthday

T. OTIENO, S. J. RETTIG, R. C. THOMPSON, and J. TROTTER. Can. J. Chem. **67**, 1964 (1989).

Orange–brown crystals of composition $Cu(pyz)_2(CF_3SO_3)$ (pyz = pyrazine, 1,4-diazine) were obtained from methanol solutions containing $Cu(CF_3SO_3)_2$ and pyrazine in approximate 1:2 mole ratio. Single crystal X-ray diffraction and infrared and Raman spectroscopy studies are reported. Crystals of the title compound are triclinic, a = 8.312(2), b = 10.903(3), c = 8.201(2) Å, α = 92.53(2), β = 113.77(2), γ = 91.40(2)°, Z = 2, space group $P\bar{1}$. The structure was solved by heavy atom methods and was refined by full-matrix least-squares to R = 0.035 and R_w = 0.044 for 2458 reflections with $I \geq 3\sigma(I)$. The compound contains chains of copper ions linked by bidentate bridging pyrazine ligands. The coordination around each copper is completed by monodentate pyrazine and trifluoromethanesulfonato groups to produce a distorted tetrahedral CuN_3O chromophore.

Key words: crystal structure, μ-pyrazine copper(I) triflate polymer, vibrational spectra.

T. OTIENO, S. J. RETTIG, R. C. THOMPSON et J. TROTTER. Can. J. Chem. **67**, 1964 (1989).

On a obtenu des cristaux bruns orangés, de composition $Cu(pyz)_2(CF_3SO_3)$ (pyz = pyrazine ou diazine-1,4), à partir de solutions méthanoliques contenant du $Cu(CF_3SO_3)_2$ et de la pyrazine dans un rapport molaire d'environ 1:2. On rapporte des études de diffraction des rayons-X sur des cristaux uniques ainsi que des études de spectroscopies infrarouge et Raman. Les cristaux mentionnés dans le titre sont tricliniques, avec a = 8,312(2), b = 10,903(3) et c = 8,201(2) Å, α = 92,53(2), β = 113,77(2) et γ = 91,40(2)°, Z = 2 et groupe d'espace $P\bar{1}$. On a résolu la structure par la méthode des atomes lourds et on l'a affinée par la méthode des moindres carrés jusqu'à des valeurs de R = 0,035 et R_w = 0,044 pour 2458 réflexions avec $I \geq 3\sigma(I)$. Le composé contient une chaîne d'ions cuivres liés par des ligands bidentates pyrazines agissant comme ponts. La coordination autour de chaque cuivre est complétée par des groupements pyrazine monodentate et trifluorométhanesulfonato qui produisent un chromophore CuN_3O tétraédrique déformé.

Mots clés : structure cristalline, polymère de μ-pyrazine cuivre(I) triflate, les spectres de vibration.

[Traduit par la revue]

Introduction

In an earlier study (1) we found that the reaction of copper(II) trifluoromethanesulfonate (copper(II) triflate) with an excess of 1,4-diazine (pyrazine, pyz) in methanol yields the molecular complex, $Cu(pyz)_4(CF_3SO_3)_2 \cdot H_2O$, and subsequent thermolysis of this compound produces the pyrazine-bridged polymeric material, $Cu(pyz)(CF_3SO_3)_2$. Subsequent attempts to prepare the bis(pyrazine) complex, the triflate analogue of $Cu(pyz)_2(CH_3SO_3)_2$ (2), by the reaction of $Cu(CF_3SO_3)_2$ with pyrazine in approximate 1:2 mole ratio in methanol failed to produce the anticipated product. Instead, on standing over a period ~3 weeks the solutions yielded orange crystals of a copper(I) complex of composition $Cu(pyz)_2(CF_3SO_3)$. We report here single crystal X-ray diffraction and vibrational spectroscopy studies on this compound.

While pyrazine-bridged complexes of copper(II) are not uncommon (1–4) examples of copper(I) compounds appear to be limited to those of composition Cu_2LX_2 (where L = pyz or a methylpyrazine and X is Cl, Br, I, or CN) reported by Lever, Lewis, and Nyholm (5, 6) in the early 1960's. The chloride and bromide pyrazine complexes were reportedly unstable and none of these materials were examined by X-ray diffraction. The compound reported in the present work is of special interest because it contains both bridging and terminal pyrazine ligands and this is the first X-ray structure determination to be reported on such a compound.

[1]Author to whom correspondence should be addressed.

Experimental

Synthesis

Copper(II) triflate was prepared as described earlier (7). In a nitrogen atmosphere glove-box, pyrazine (2.96 mmol), dissolved in 3 mL of methanol (containing about 10% v/v of 2,2-dimethoxypropane), was added to copper(II) triflate (1.45 mmol) dissolved in 4 mL of the same solvent. A green solution resulted. The reaction flask was covered with parafilm and over a period of three weeks orange–brown crystals formed. The supernatant solution was decanted and the crystals washed several times with fresh solvent then left to dry in the glove-box. It was noted that an additional product in the form of fine black particles was also present and the crystals had to be physically separated from these. The crystals were subsequently handled in the atmosphere where they showed no visible signs of decomposition. Although the microanalytical data were consistently low for carbon the composition was determined unequivocally as $Cu(C_4H_4N_2)_2(CF_3SO_3)$ from the X-ray studies. *Anal.* calcd. for $CuC_9H_8N_4F_3SO_3$: C 29.00, H 2.15, N 15.03; found: C 28.24, H 2.25, N 14.84. The analytical data suggest the possibility of some hydration (~0.5 mol water per mole of complex) as observed previously for $Cu(pyz)_2(CH_3SO_3)_2$ (2); however, the presence of water was detected by neither the X-ray nor the infrared studies. Elemental analyses were performed by P. Borda of this Department.

Vibrational spectra

The infrared spectrum of a sample mulled in Nujol and pressed between KRS-5 plates (Harshaw Chemical Co.) was recorded on a Perkin Elmer 598 spectrophotometer. Calibration was achieved using polystyrene and frequencies are considered accurate to ±3 cm^{-1}. The Raman spectrum was recorded on a Spex Ramalog 5 spectrometer

Can. J. Chem. Downloaded from www.nrcresearchpress.com by 186.148.149.217 on 09/07/12
For personal use only.

Can. J. Chem. Downloaded from www.nrcresearchpress.com by 186.148.149.217 on 09/07/12
For personal use only.

equipped with a Spectra Physics 164 argon ion laser. The green line at 514.5 nm was used for excitation. The sample was finely ground and sealed in a melting point capillary.

X-ray crystallographic analysis

A crystal ca. 0.35 × 0.40 × 0.45 mm in size was mounted in a general orientation. Unit-cell parameters were refined by least-squares on setting angles for 25 reflections (2θ = 36–42°) measured on a diffractometer with Mo-$K\alpha$ radiation (λ = 0.71069 Å). Crystal data at 21°C are as follows:

$C_9H_8CuF_3N_4O_3S$ f.w. = 372.79

Triclinic, a = 8.312(2), b = 10.903(3), c = 8.201(2) Å, α = 92.53(2), β = 113.77(2), γ = 91.40(2)°, V = 678.8(3) Å^3, Z = 2, ρ_c = 1.82 Mg m^{-3}, $F(000)$ = 372, μ(Mo-$K\alpha$) = 18.07 cm^{-1}. Absent reflections: none, space group $P\bar{1}$ (reduced cell) from structure analysis.

Intensities were measured with graphite-monochromated Mo-$K\alpha$ radiation on a Rigaku AFC6S diffractometer. An ω–2θ scan at 16° min^{-1} over a range of (1.0 + 0.30 tan θ) degrees in ω (with up to 9 rescans, background/scan time ratio = 0.5) was employed. Data were measured to 2θ = 60°. The intensities of three check reflections, measured every 150 reflections throughout the data collection, showed only small random fluctuations. After data reduction,[2] an absorption correction was applied using the analytical method (8, 9). Transmission factors ranged from 0.901 to 1.000. Of the 4428 reflections measured, 3969 were unique (R_{int} = 0.017) and 2458 (62.0%) of these had intensities greater than or equal to $3\sigma(F^2)$ above background where $\sigma^2(F^2) = (S^2(C + 4B) + (0.025(F_o^2))^2)/Lp^2$ with S = scan rate, C = scan count, B = total background count, and Lp = Lorentz-polarization factor.

The structure was solved by conventional heavy atom methods, the Cu and S atoms being positioned from the Patterson function and the remaining atoms (including hydrogen) from subsequent difference Fourier syntheses. The centrosymmetric space group $P\bar{1}$ was suggested by the Patterson function and was confirmed by successful refinement of the structure. Non-hydrogen atoms were refined with anisotropic thermal parameters and hydrogen atoms with isotropic thermal parameters. Scattering factors for all atoms and anomalous dispersion corrections for the non-hydrogen atoms were taken from ref. 10. The weighting scheme $w = 4F_o^2/\sigma^2(F_o^2)$ gave uniform average values of $w(|F_o| - |F_c|)^2$ over ranges of both $|F_o|$ and $\sin\theta/\lambda$ and was employed in the final stages of full-matrix refinement of 222 variables. Reflections with $I < 3\sigma(I)$ were not included in the refinement. Convergence was reached at R = 0.035 and R_w of 0.044 for 2458 reflections with $I \geq 3\sigma(I)$. For all 3969 reflections R = 0.087, for all 2395 reflections with $\theta \leq 25°$ R = 0.050. The function minimized was $\Sigma w(|F_o| - |F_c|)^2$, $R = \Sigma||F_o| - |F_c||/\Sigma|F_o|$ and $R_w = (\Sigma w(|F_o| - |F_c|)^2/\Sigma w|F_o|^2)^{1/2}$.

On the final cycle of refinement the maximum parameter shift corresponded to 0.03σ. The mean error in an observation of unit weight was 1.92. The final difference map showed maximum fluctuations of −0.37 to 0.44 e Å^{-3}, the latter being 0.98 Å from the Cu atom. The final positional and equivalent isotropic thermal parameters for the non-hydrogen atoms appear in Table 1. Bond lengths and angles are listed in Tables 2 and 3. Hydrogen parameters, anisotropic thermal parameters, torsion angles, intermolecular contacts, least-squares planes, and structure factors have been deposited.[3]

[2]All computations performed using the TEXSAN – TEXRAY Structure Analysis Package which includes versions of the following: AGNOST, absorption corrections, by J. A. Ibers; ORFLS, full-matrix least-squares, and ORFFE, function and errors, by W. R. Busing, K. O. Martin, and H. A. Levy; DIRDIF, phase extension and refinement of difference structures, by P. T. Beurskens; ORTEP II, illustrations, by C. K. Johnson.

[3]Supplementary material mentioned in the text may be purchased from the Depository of Unpublished Data, CISTI, National Research Council of Canada, Ottawa, Ont., Canada K1A 0S2.

TABLE 1. Final atomic coordinates (fractional) and equivalent isotropic thermal parameters with estimated standard deviations in parentheses

Atom	x	y	z	B(eq)
Cu	0.45198(5)	0.24391(3)	0.23831(5)	3.71(2)
S	0.8500(1)	0.28354(7)	0.1713(1)	3.23(3)
F(1)	0.8464(4)	0.3776(3)	−0.1151(4)	10.2(2)
F(2)	0.6057(3)	0.3884(2)	−0.0866(4)	7.7(1)
F(3)	0.6774(6)	0.2187(3)	−0.1618(4)	12.7(2)
O(1)	0.7153(3)	0.2183(2)	0.2057(3)	4.5(1)
O(2)	0.9924(3)	0.2116(2)	0.1771(4)	5.6(1)
O(3)	0.9014(4)	0.4029(2)	0.2609(4)	5.6(1)
N(1)	0.2891(3)	0.2121(2)	−0.0160(3)	3.11(8)
N(2)	0.0558(4)	0.1609(3)	−0.3701(4)	4.9(1)
N(3)	0.4812(3)	0.3981(2)	0.3842(3)	3.05(8)
N(4)	0.4794(3)	0.0968(2)	0.3885(3)	3.10(8)
C(1)	0.7388(6)	0.3163(4)	−0.0607(5)	5.5(2)
C(2)	0.2211(4)	0.3006(3)	−0.1269(4)	3.7(1)
C(3)	0.1087(5)	0.2746(3)	−0.3000(5)	4.7(1)
C(4)	0.1226(5)	0.0734(3)	−0.2584(5)	4.5(1)
C(5)	0.2382(5)	0.0973(3)	−0.0847(4)	3.9(1)
C(6)	0.6310(4)	0.4660(3)	0.4578(4)	3.6(1)
C(7)	0.6486(4)	0.5668(3)	0.5727(4)	3.6(1)
C(8)	0.3448(4)	0.0446(3)	0.4126(4)	3.8(1)
C(9)	0.3651(4)	−0.0511(3)	0.5223(4)	3.7(1)

TABLE 2. Bond lengths (Å)* with estimated standard deviation in parentheses

Atom	Atom	Distance	Atom	Atom	Distance
Cu	N(3)	1.971(2)	N(1)	C(5)	1.335(4)
Cu	N(1)	1.985(2)	N(2)	C(4)	1.322(5)
Cu	N(4)	2.027(2)	N(2)	C(3)	1.330(4)
Cu	O(1)	2.331(2)	N(3)	C(7)′	1.324(4)
S	O(2)	1.422(3)	N(3)	C(6)	1.331(4)
S	O(3)	1.432(3)	N(4)	C(9)″	1.325(4)
S	O(1)	1.440(2)	N(4)	C(8)	1.331(4)
S	C(1)	1.806(4)	C(2)	C(3)	1.361(5)
F(1)	C(1)	1.328(5)	C(4)	C(5)	1.368(5)
F(2)	C(1)	1.325(5)	C(6)	C(7)	1.381(4)
F(3)	C(1)	1.279(5)	C(8)	C(9)	1.376(4)
N(1)	C(2)	1.330(4)			

*Primed and double-primed atoms have coordinates related to those in Table 1 by symmetry operations $1 - x$, $1 - y$, $1 - z$ and $1 - x$, $-y$, $1 - z$; respectively.

Results and discussion

Synthesis

Although copper(I) triflate is known (11) there have been no reports, to our knowledge, of coordination complexes of this compound. $Cu(pyz)_2(CF_3SO_3)$ crystallized over a period of three weeks from a solution of $Cu(CF_3SO_3)_2$ and pyrazine in methanol. The isolation of a copper(I) complex of this type from a copper(II) salt in alcohol solution without added reducing agent is not without precedence. Dibromo(tetramethylpyrazine)dicopper(I) was prepared by refluxing copper(II) bromide and the ligand in ethanol (6); in this case the *o*-methyl groups on the ligand were considered to hinder sterically the formation of square planar copper(II) derivatives and thereby stabilize the linear copper(I) complex (12). In the case reported here the stabilization of the copper(I) derivative is achieved through the

TABLE 3. Bond angles (deg) with estimated standard deviations in parentheses

Atom	Atom	Atom	Angle	Atom	Atom	Atom	Angle
N(3)	Cu	N(1)	126.4(1)	C(6)	N(3)	Cu	124.1(2)
N(3)	Cu	N(4)	110.6(1)	C(9)″	N(4)	C(8)	115.6(2)
N(3)	Cu	O(1)	106.9(1)	C(9)″	N(4)	Cu	121.9(2)
N(1)	Cu	N(4)	114.0(1)	C(8)	N(4)	Cu	122.4(2)
N(1)	Cu	O(1)	97.9(1)	F(3)	C(1)	F(2)	107.5(4)
N(4)	Cu	O(1)	94.4(1)	F(3)	C(1)	F(1)	109.1(4)
O(2)	S	O(3)	114.5(2)	F(3)	C(1)	S	112.2(3)
O(2)	S	O(1)	114.7(1)	F(2)	C(1)	F(1)	105.5(3)
O(2)	S	C(1)	104.3(2)	F(2)	C(1)	S	111.5(3)
O(3)	S	O(1)	114.8(2)	F(1)	C(1)	S	110.8(3)
O(3)	S	C(1)	103.5(2)	N(1)	C(2)	C(3)	121.6(3)
O(1)	S	C(1)	102.9(2)	N(2)	C(3)	C(2)	123.3(3)
S	O(1)	Cu	142.8(1)	N(2)	C(4)	C(5)	122.9(3)
C(2)	N(1)	C(5)	115.8(3)	N(1)	C(5)	C(4)	121.6(3)
C(2)	N(1)	Cu	123.5(2)	N(3)	C(6)	C(7)	121.5(3)
C(5)	N(1)	Cu	120.6(2)	N(3)′	C(7)	C(6)	122.4(3)
C(4)	N(2)	C(3)	114.8(3)	N(4)	C(8)	C(9)	122.4(3)
C(7)′	N(3)	C(6)	116.1(2)	N(4)″	C(9)	C(8)	122.0(3)
C(7)′	N(3)	Cu	119.5(2)				

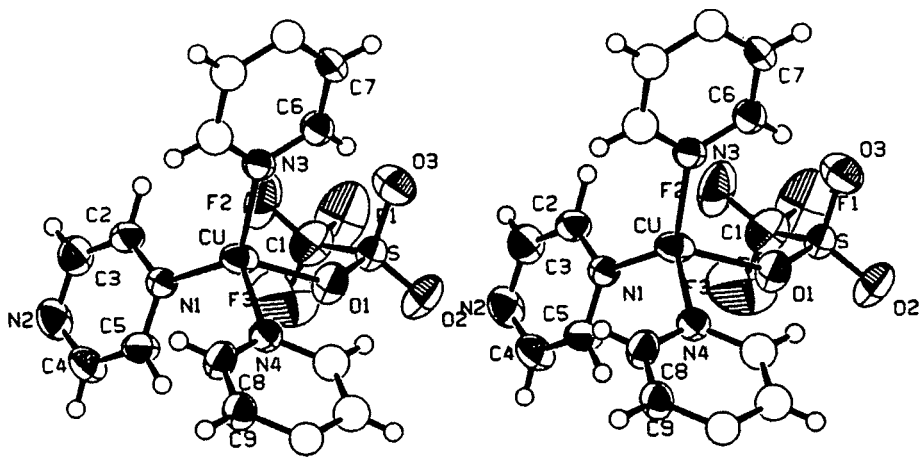


FIG. 1. View of the environment about the Cu atom in $Cu(pyz)_2(CF_3SO_3)$; 50% probability thermal ellipsoids are shown for the non-hydrogen atoms. Shaded atoms comprise the asymmetric unit.

formation of an insoluble polymer. In both cases the reducing agent is presumably the solvent.

Crystal structure analysis

The crystal structure analysis shows that the complex contains spiral chains of copper ions linked by bidentate bridging pyrazine ligands. The coordination around each copper is completed by monodentate pyrazine and triflate groups to produce a distorted tetrahedral CuN_3O chromophore. The geometry about copper together with the atom numbering scheme is shown in Fig. 1 and a stereoview of the unit cell is shown in Fig. 2. The terminal pyrazine groups and the triflate anions are both arranged syndiotactically along the polymer skeleton. The pyrazine rings are planar within experimental error, with the planes of the monodentate pyrazine rings approximately orthogonal to the planes of the bridging pyrazine ligands. This orientation minimizes repulsions between the terminal pyrazine and the triflate anion. Surprisingly, two slightly different bridging pyrazine groups alternate along the chain, one forming the shortest bonds to copper (1.971(2) Å) and the other the longest Cu—N bonds (2.027(2) Å). The Cu—N bond formed by the terminal pyrazine group is intermediate at 1.985(2) Å.

These bond lengths may be compared with published Cu(II)–pyrazine distances, keeping in mind the fact that the effective ionic radius of Cu^+ is estimated to be ~0.03 to 0.04 Å larger than that of Cu^{2+} (13). The Cu—N bond lengths in the title compound are all shorter than those found in the copper(II) pyrazine complexes, $Cu(pyz)_2(CH_3SO_3)_2$ (2.058(2) and 2.692(3) Å) (2) and $Cu(pyz)_2(ClO_4)_2$ (2.062(3) Å) (14), while only the longest of the three, at 2.027 Å, is longer than the relatively short Cu—N (pyrazine) bond found in $Cu(pyz)(NO_3)_2$ (1.984 Å) (15). This suggests relatively strong coordination by all of the pyz moieties in the compound studied here. For comparison, some representative Cu(I)—N bond lengths are: 2.05 Å in $[Cu(py)_4]ClO_4$ (16) and 2.045 Å in [Cu(phenanthroline)$_2$]ClO_4 (17). A listing of twelve copper(I) compounds containing CuN_4 chromophores in ref. 18 shows bond distances ranging from 1.985 to 2.117 Å.

The Cu—O bond length in the title compound (2.331(2) Å)

Can. J. Chem. Downloaded from www.nrcresearchpress.com by 186.148.149.217 on 09/07/12
For personal use only.

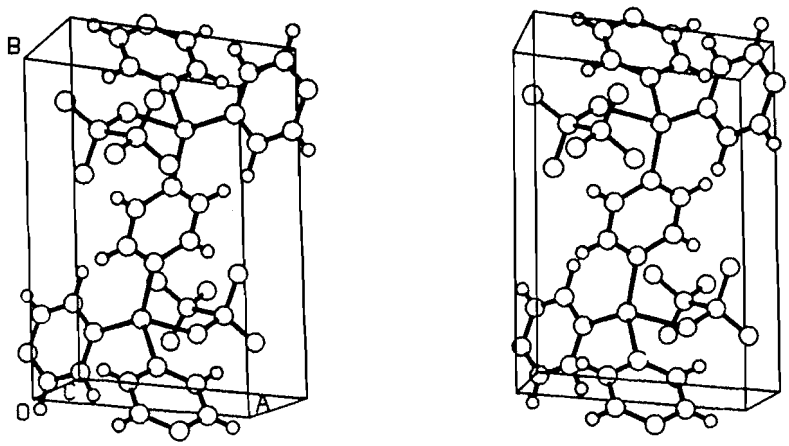


FIG. 2. Stereoview of the $Cu(pyz)_2(CF_3SO_3)$ structure.

TABLE 4. Comparison of internal bonding parameters for the triflate anion

Compound[a]		1	2	3	4	5	6
Coordination mode		Monodentate	Monodentate	Monodentate	Bidentate	Ionic	Ionic
Mean bond angles (deg)	O—S—O	114.7	114.8	114.6	114.8	114.8	115.2
	F—C—S	111.5	109.5	111.3	111.8	112.3	111.6
	C—S—O	103.6	103.4	104.5	103.4	103.4	103.0
	F—C—F	107.4	109.2	107.6	107.1	106.4	107.2
Mean bond distance (Å)	C—F	1.311	1.318	1.321	1.33	1.336	1.34
	S—O[b]	1.440	1.439	1.446	1.441	—	—
	S—O	1.427	1.425	1.424	1.422	1.417	1.430
	S—C	1.806	1.832	1.803	1.80	1.795	1.816
Reference		This work	1	25	19	19	27

[a] **1**, $Cu(pyz)_2(CF_3SO_3)$; **2**, $Cu(py)_4(CF_3SO_3)_2$; **3**, $Fe(py)_4(CF_3SO_3)_2$; **4** and **5**, $[Cu_4(OH)_4(CF_3SO_3)_2[N(C_5H_4N)_3]_4][CF_3SO_3]_2 \cdot C_3H_6O$; **6**, $[Ni(Me_4[14]hexaenato\ N_4)]_2(CF_3SO_3)_2$.
[b] Bridging.

is considerably greater than that seen in $Cu(pyz)_2(CH_3SO_3)_2$ (1.956(1) Å) (2) and, although shorter than that reported for $Cu(py)_4(CF_3SO_3)_2$ (2.425 Å) (1), is nonetheless indicative of weak coordination by the anion. In the tetranuclear cationic species $[Cu_4(OH)_4(SO_3CF_3)_2[N(C_5H_4N)_3]_4]^{2+}$ the triflates are bidentate bridging ligands (19) and here the Cu—O bonds are longer still (mean value of 2.57(4) Å). In ref. 18 thirteen Cu(I)—O bond lengths are listed for nine four-coordinate copper(I) species. They range from 2.077 to 2.278 Å, all shorter than the Cu(I)—triflate distance observed here.

Although two bridging pyrazine groups are distinguished by different Cu—N bond distances the internal bonding parameters are identical for the two species to within experimental error. Moreover, the C—C bonds (1.381(4) Å and 1.376(4) Å) and two of the C—N bonds in each (1.331(4) Å) are indistinguishable from the mean C—C and C—N bond lengths found in free pyrazine (20) (1.378 Å and 1.334 Å, respectively). The other C—N bonds at 1.324(4) Å and 1.325(4) Å are significantly shorter. The most distorted pyrazine moiety is the terminal one. It has two shortened C—C bonds at 1.361(5) Å and 1.368(5) Å and one short C—N bond at 1.322(5) Å. All three pyrazine rings in the compound studied here appear to be more distorted than those found, for example, in $Cu(pyz)_2(CH_3SO_3)_2$ (2), $Cu(pyz)(NO_3)_2$ (15), or $Cu(pyz)_2(ClO_4)_2$ (14) again consistent with relatively strong pyrazine–metal interactions in $Cu(pyz)_2(CF_3SO_3)$.

As in the previously studied $Cu(py)_4(CF_3SO_3)_2$ (1), the triflate anion in $Cu(pyz)_2(CF_3SO_3)$ adopts a staggered-ethane configuration about the C—S bond. Repulsions between adjacent oxygen atoms are apparently greater than those between the oxygen atoms and the trifluoromethyl group; consequently, the O—S—O angles are greater than, while the C—S—O angles are less than the tetrahedral angle. As expected, the S—O bond involving the oxygen coordinated to the copper is longer (1.440(2) Å) than the terminal S—O bonds (1.422(3) and 1.432(3) Å). Within experimental error these are identical to those found in $Cu(py)_4(CF_3SO_3)_2$ (1) and in the $[Cu(OH)_4(CF_3SO_3)_2[N(C_5H_4N)_3]_4]^{2+}$ cation (19). In general, the internal bonding parameters for the triflate anion in $Cu(pyz)_2(CF_3SO_3)$ are similar to those found in other triflate complexes. The mean bond distances and bond angles in $CF_3SO_3^-$ are compared with those found from some previous studies in Table 4. The relative insensitivity of these parameters to the mode of anion coordination is an indication of how "innocent" this anion is, forming only weak coordinative interactions with metals.

Vibrational spectroscopy

The use of vibrational spectroscopy to distinguish between terminal and bridging pyrazine ligands has been a matter of some interest since the first complexes of this type were characterized (6, 21, 22). $Cu(pyz)_2(CF_3SO_3)$ contains both types of pyrazine and it was of interest to see what effect this has on the vibrational spectrum of the compound. The triflate ion has also been the subject of studies directed at establishing correlations between vibrational frequencies and the mode of

Can. J. Chem. Downloaded from www.nrcresearchpress.com by 186.148.149.217 on 09/07/12
For personal use only.

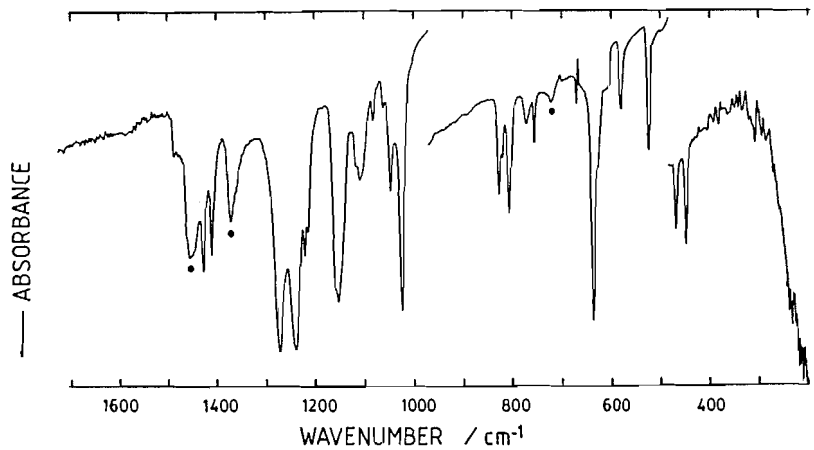


FIG. 3. Infrared spectrum of $Cu(pyz)_2(CF_3SO_3)$. Nujol peaks are identified.

coordination (1, 7, 19, 23–26). Infrared and Raman data, with assignments are given in Table 5 and the infrared spectrum is shown in Fig. 3.

The bands observed in the infrared spectrum of $Cu(pyz)_2(CF_3SO_3)$ may, for the most part, be readily separated into absorption arising either from the triflate anion vibrations or pyrazine vibrations. A pair of strong bands at 1279 and 1247 cm^{-1} is due to the antisymmetric SO_3 stretching vibration (E symmetry in C_{3v}), the splitting of the band arising from a lowering of the symmetry of the CSO_3 portion of the anion from C_{3v} to C_s due to the monodentate form of coordination. The magnitude of this splitting (32 cm^{-1}) is comparable to that observed for $Cu(py)_4(CF_3SO_3)_2$ (43 cm^{-1}) where X-ray data show a similar degree of anion distortion through coordination (1); whereas, the splitting is much smaller than that observed for $Fe(py)_4(CF_3SO_3)_2$ (~85 cm^{-1}) where X-ray studies show considerably greater anion distortion (25). We note also that the δ_{as} SO_3 (E) mode is split in the more distorted iron complex (25) but remains a single band in both of the weakly perturbed copper complexes.

It is difficult to make unambiguous assignments of the bands in the 1150 to 1230 cm^{-1} range since as indicated in Table 5 bands due to CF_3 stretching modes as well as pyrazine bands are expected in this region. Similarly, it is not possible to determine which of the two weak bands at 774 and 760 cm^{-1} is due to the C—S stretching mode and which is a neutral ligand band. The remaining bands in the infrared spectrum are readily assigned. Bands assigned to pyrazine vibrations are compared in Table 5 with those reported for $SnCl_4(pyz)_2$ (21), a compound containing non-bridging, monodentate pyrazine ligands. The doubling of these bands in $Cu(pyz)_2(CF_3SO_3)$ is clearly due to the presence of both bridging and monodentate pyrazine in this compound. In particular, we note the two medium intensity, sharp bands at 472 and 452 cm^{-1}. The lower frequency band may be assigned to the monodentate pyrazine molecules since bands at this frequency (but not at the higher frequency) and assigned to pyrazine have been observed for $SnCl_4(pyz)_2$, $SnBr_4(pyz)_2$, and $Cu(pyz)_4(CF_3SO_3)_2 \cdot H_2O$ (1, 21), all of which have monodentate pyrazine ligands only. The band at 472 cm^{-1} may be assigned to the bridging pyrazine ligand since both $SnCl_4(pyz)$ and $SnBr_4(pyz)$ (compounds containing only bridging pyz) exhibit a pyz vibration at this frequency. In $Cu(pyz)(CF_3SO_3)_2$ where, again, the pyz ligand is considered to be bridging the band appears at an even higher frequency, 504 cm^{-1} (1). This particular pyrazine band appears at 417 cm^{-1} in liquid pyrazine. Of all pyrazine vibrations observed this band is clearly the one most affected by coordination, invariably shifting to higher frequencies: to about 450 cm^{-1} in the case of monodentate coordination and to 470 cm^{-1} or higher for bidentate coordination. The position of this band would appear to be a reasonable indication of the mode of pyrazine coordina-

TABLE 5. Vibrational spectra[a]

Infrared frequency (cm^{-1})	Assignments			Raman frequency (cm^{-1})
	Anion vibration[b]	Pyz vibration[c]		
3107 wsh 3092 w		b_{1u}, b_{3u}	(3100 IR) (3040 IR)	
		a_g	(1600 R)	1608 vs
1490 wsh		b_{1u}	(1490 IR)	
1435 s		b_{3u}	(1420 IR)	
1417 s				
1279 s	$\nu_{as}SO_3$, E			1284 w
1247 s				
1228 msh	ν_sCF_3, A_1	a_g	(1228 R)	1240 m
1222 msh			(1230 IR)	
1160 sh	$\nu_{as}CF_3$, E	b_{1u}	(1160 IR)	
1156 s				
1118 sh		b_{2g}	(1125 IR)	
1112 m				
1085 w		b_{3u}	(1085 IR)	
1064 vw				
1051 m		b_{1u}	(1050 IR)	
		a_g	(1020 R)	1031 vs
1027 s	ν_sSO_3, A_1			
831 m				
823 sh		b_{2u}	(805 IR)	
811 m				
774 w	ν CS, A_1	b_{1g}	(740 IR)	
760 w				
		b_{3g}	(698 R)	669 m
641 s	δ_s SO_3, A_1		(640 IR)	
584 m	δ_{as} CF_3, E			
526 s	δ_{as} SO_3, E			
472 m				
452 m		b_{2u}	(452 IR)	

[a]v = very, s = strong, m = medium, w = weak, sh = shoulder.
[b]Assignments from ref. 24.
[c]Assignments from ref. 21. Numbers in parentheses are from the infrared (IR) and Raman (R) spectra of $SnCl_4(pyz)_2$ given in ref. 21.

Can. J. Chem. Downloaded from www.nrcresearchpress.com by 186.148.149.217 on 09/07/12
For personal use only.

tion. Like most empirical criteria of this type, however, care must be taken in its application. $Cu(pyz)_2(CH_3SO_3)_2$ exhibits two bands, corresponding to the 417 band in liquid pyrazine, at 494 and 440 cm^{-1} (2). In this case there are two types of bridging pyrazine molecules. One is involved in relatively strong interactions with copper and no doubt gives rise to the higher frequency band. The other pyrazine ligand in this molecule is involved in very weak coordination to the metal and, although bridging, gives rise to a band at 440 cm^{-1}, lower even than that normally observed for monodentate pyrazine.

Raman frequencies which we observed for $Cu(pyz)_2(CF_3SO_3)$ are recorded in Table 5. The quality of the spectrum was not particularly good due perhaps to the fairly intense orange–brown color of the sample. Nonetheless, comparison of the spectrum with those reported for the pyrazine complexes of $SnCl_4$ and for liquid pyrazine (21) shows that we are able to observe bands corresponding to the strong to very strong absorptions reported in the earlier work. As indicated in Table 5, the very strong Raman band at 1031 cm^{-1} may be assigned as either the symmetric SO_3 stretching vibration or the pyrazine a_g (1015 cm^{-1} in liquid pyrazine) vibration, or both, while the medium intensity band at 1240 cm^{-1} is likely either the symmetric CF_3 vibration or the pyrazine a_g (1232 cm^{-1} in liquid pyrazine) vibration. The bands at 1608 and 669 cm^{-1} are assignable to pyrazine vibrations while the weak absorption at 1284 cm^{-1} is tentatively assigned to an SO_3 vibration. Unfortunately, the quality of the Raman spectrum did not permit one to distinguish between bridging and monodentate pyrazine.

Acknowledgements

We thank the Natural Sciences and Engineering Research Council of Canada for financial support and the University of British Columbia Computing Centre for assistance.

1. J. S. Haynes, S. J. Rettig, J. R. Sams, J. Trotter, and R. C. Thompson. Inorg. Chem. **27**, 1237 (1988).
2. J. S. Haynes, S. J. Rettig, J. R. Sams, R. C. Thompson, and J. Trotter. Can. J. Chem. **65**, 420 (1987).
3. M. Inoue and M. Kubo. Coord. Chem. Rev. **21**, 1 (1976).
4. W. Kaim. Angew. Chem. Int. Ed. Engl. **22**, 171 (1983).
5. A. B. P. Lever, J. Lewis, and R. S. Nyholm. Nature, **189**, 58 (1961).
6. A. B. P. Lever, J. Lewis, and R. S. Nyholm. J. Chem. Soc. 3156 (1963).
7. A. L. Arduini, M. Garnett, R. C. Thompson, and T. C. T. Wong. Can. J. Chem. **53**, 3812 (1975).
8. P. Coppens, L. Leiserowitz, and D. Rabinovich. Acta Crystallogr. **18**, 1035 (1965).
9. J. De Meulenaer and H. Tompa. Acta Crystallogr. **19**, 1014 (1965).
10. International tables for X-ray crystallography. Vol. IV. Kynoch Press, Birmingham. 1974. pp. 99–102 and 149.
11. R. D. Howells and J. D. McCown. Chem. Rev. **77**, 69 (1977).
12. B. R. James and R. J. P. Williams. J. Chem. Soc. 2007 (1961).
13. R. D. Shannon. Acta Crystallogr. Sect. A, **32**, 751 (1976).
14. J. Darriet, M. S. Haddad, E. N. Duesler, and D. N. Hendrickson. Inorg. Chem. **18**, 2679 (1979).
15. A. Santoro, A. D. Mighell, and C. W. Reimann. Acta Crystallogr. Sect. B, **26**, 979 (1970).
16. A. H. Lewin, R. J. Michel, P. Ganis, U. Lepore, and G. Avitabile. Chem. Commun. 1400 (1971).
17. P. C. Healy, L. M. Englehardt, V. A. Patrik, and A. H. White. J. Chem. Soc. Dalton Trans. 2541 (1985).
18. B. J. Hathaway. *In* Comprehensive coordination chemistry. Vol. 5. *Edited by* G. Wilkinson. Pergamon, Oxford. 1987. p. 533.
19. P. L. Dedert, T. Sorrell, T. J. Marks, and J. A. Ibers. Inorg. Chem. **21**, 3506 (1982).
20. P. J. Wheatley. Acta Crystallogr. **10**, 182 (1957).
21. M. Goldstein and W. D. Unsworth. Spectrochimica Acta, **27A**, 1055 (1971).
22. M. Goldstein, F. B. Taylor, and W. D. Unsworth. J. Chem. Soc. Dalton, 418 (1972).
23. J. S. Haynes, J. R. Sams, and R. C. Thompson. Can. J. Chem. **59**, 669 (1981).
24. H. Bürger, K. Burczyk, and A. Blaschette. Monat. Chem. **101**, 102 (1970).
25. J. S. Haynes, S. J. Rettig, J. R. Sams, R. C. Thompson, and J. Trotter. Can. J. Chem. **64**, 429 (1986).
26. J. S. Haynes, J. R. Sams, and R. C. Thompson. Can. J. Chem. **66**, 2079 (1988).
27. S. M. Peng, J. A. Ibers, M. Millar, and R. H. Holm. J. Am. Chem. Soc. **98**, 8037 (1976).

Can. J. Chem. Downloaded from www.nrcresearchpress.com by 186.148.149.217 on 09/07/12
For personal use only.

Metal pyrazolate polymers. Part 1. Synthesis, structure, and magnetic properties of the $[Cu(pz)_2]_x$ polymer

M. K. EHLERT, S. J. RETTIG, A. STORR, R. C. THOMPSON, AND J. TROTTER

Department of Chemistry, University of British Columbia, 2036 Main Mall, Vancouver, B.C., Canada V6T 1Y6

Received February 10, 1989

This paper is dedicated to Professor Ronald J. Gillespie on the occasion of his 65th birthday

M. K. EHLERT, S. J. RETTIG, A. STORR, R. C. THOMPSON, and J. TROTTER. Can. J. Chem. **67**, 1970 (1989).

A novel and reliable method for the synthesis of polybis(μ-pyrazolato-*N*,*N*′)copper(II), $[Cu(pz)_2]_x$ (where pz = $N_2C_3H_3$), is presented. Single crystals of the polymer suitable for X-ray study have been grown under carefully controlled conditions. Crystals of polybis(μ-pyrazolato-*N*,*N*′)copper(II) are orthorhombic, a = 7.917(1), b = 11.491(2), c = 7.778(1) Å, Z = 4, space group *Ibam*. The structure was solved by direct methods and was refined by full-matrix least-squares procedures to R = 0.029 and R_w = 0.038 for 507 reflections with $I \geq 3\sigma(I)$. The crystal structure consists of infinite double-bridged polymeric chains. The Cu atom has a D_2 distorted tetrahedral coordination geometry with Cu—N = 1.957(2) Å and N—Cu—N = 94.3(1)–139.5(1)°. Magnetic susceptibility studies (4.2 to 299 K) on this material reveal very strong antiferromagnetic exchange between copper(II) centres in the extended linear chains. The magnetic data have been successfully analyzed according to the isotropic Heisenberg model for linear chains with $-J = 78\ cm^{-1}$ and g = 2.12.

Key words: crystal structure, copper(II) pyrazolate chain polymer, antiferromagnetic exchange.

M. K. EHLERT, S. J. RETTIG, A. STORR, R. C. THOMPSON et J. TROTTER. Can. J. Chem. **67**, 1970 (1989).

On propose une nouvelle méthode de synthèse du polybis(μ-pyrazolato-*N*,*N*′)cuivre(II), $[Cu(pz)_2]_x$, dans lequel pz = $N_2C_3H_3$. Utilisant des conditions bien contrôlées, on a fait croître des cristaux uniques du polymère qui étaient appropriés pour une étude par diffraction des rayons-X. Les cristaux de polybis(μ-pyrazolato-*N*,*N*′)cuivre(II) sont orthorhombiques avec a = 7,917(1), b = 11,491(2) et c = 7,778(1) Å, Z = 4 et groupe d'espace *Ibam*. On a résolu la structure par des méthodes directes et on l'a affinée par la méthode des moindres carrés jusqu'à des valeurs de R = 0,029 et R_w = 0,038 pour 507 réflexions avec $I \geq 3\sigma(I)$. La structure cristalline est composée de chaînes polymériques infinies à doubles ponts. L'atome de Cu possède une géométrie de coordination tétraédrique déformée D_2 avec Cu—N = 1,957(2) Å et N—Cu—N = 94,3(1)–139,5(1)°. Des études de susceptibilité magnétique effectuées sur ce matériel à des températures allant de 4,2 à 299 K révèlent l'existence d'un très puissant échange antiferromagnétique entre les centres de cuivre(II) des chaînes linéaires étendues. On a analysé avec succès les données magnétiques à l'aide du modèle isotrope d'Heisenberg pour des chaînes linéaires avec $-J = 78\ cm^{-1}$ et g = 2,12.

Mots clés : structure cristalline, chaîne polymérique de pyrazolato-cuivre(II), échange antiferromagnétique.

[Traduit par la revue]

Introduction

As part of our continuing interest in metal pyrazolate complexes and magnetic exchange effects in transition metal coordination polymers we have initiated a comprehensive study of binary transition metal pyrazolate compounds. Earlier studies in this area have been reviewed by Trofimenko (1) and the intractable nature of the polymeric species noted. Our primary interest in these materials stems from the expectation that they will provide examples of infinite-chain polymers with the bridging pyrazolate ligands acting as pathways for strong magnetic exchange between metal centres. By varying the substituents on the pz (pz = pyrazolyl) rings and studying different metal systems it should be possible to examine systematically how electronic and structural factors affect the magnetic and other properties of these materials. We present here a novel method for the synthesis of the $[Cu(pz)_2]_x$ polymer and provide evidence that the methods (2) employed in previous attempts to prepare this compound in fact yield a different product. In addition, the new route described provides excellent crystals of the binary copper(II) pyrazolate polymer enabling us to report the first X-ray crystal structure determination of this type of complex. We also describe electronic and vibrational spectroscopic, variable temperature magnetic susceptibility (4.2 to 299 K), and thermal studies on this novel material.

Experimental

Synthesis

Copper metal shot was cleaned by washing first in 12 *M* HCl, then water and finally acetone. A magnetic stir bar, 10.0 g (147 mmol) of pyrazole and 8.13 g (78.2 mmol) of cleansed copper shot were placed in a 100 mL round bottom flask fitted with a reflux condenser. The reaction mixture was heated, with stirring, to 110°C and air was bubbled into the molten pyrazole via a Pyrex tube lowered through the condenser. A green solid appeared almost immediately. The mixture was allowed to react for 18 h during which time sublimed pyrazole was periodically scraped back into the reaction mixture. The mixture, which had solidified on cooling, was then washed with 4 × 100 mL portions of CH_2Cl_2, 100 mL of high boiling petroleum ether and then suction filtered. $[Cu(pz)_2]_x$ was obtained as a bright green powder in 79% yield (based on copper shot reacted). The remaining reacted copper apparently formed a brown CH_2Cl_2 soluble material. Copper analysis was performed by gravimetry and C, H, and N analysis was performed by P. Borda of this department. *Anal.* calcd. for $C_6H_6CuN_4$: Cu 32.15, C 36.45, H 3.06, N 28.34; found: Cu 31.80, C 36.74, H 3.17, N 28.50.

Several attempts were made to prepare $[Cu(pz)_2]_x$ using the literature methods of Vos and Groeneveld (2). An insoluble black material was obtained in all cases, as described by the above authors, but the elemental composition indicated $Cu_2(pz)_3(OH)$ as the empirical formulation. *Anal.* calcd. for $C_9H_{10}Cu_2N_6O$: Cu 36.80, C 31.30, N 24.34, H 2.92, O 4.63; found: Cu 36.57, C 31.53, N 24.39, H 2.85, O 4.70.

Single crystals of $[Cu(pz)_2]_x$ suitable for X-ray analysis were synthesized in a manner similar to that described above except that only one piece of copper shot was used (~0.5 g), and the reaction mixture was not stirred. In addition, air was not bubbled through the mixture but allowed instead to slowly diffuse from the top of the reflux condenser. The reaction was allowed to proceed for 5 days after which the cooled mixture was washed with water and then acetone yielding dark green crystals.

Can. J. Chem. Downloaded from www.nrcresearchpress.com by 186.148.149.217 on 09/07/12
For personal use only.

Can. J. Chem. Downloaded from www.nrcresearchpress.com by 186.148.149.217 on 09/07/12
For personal use only.

Physical characterization

$[Cu(pz)_2]_x$ was found to be insoluble in both polar and non-polar solvents, but was solubilized with decomposition in acid. Differential scanning calorimetry measurements, obtained with a Mettler DSC 20 Standard Cell and TC10 TA Processor as described previously (3), showed the compound to decompose in air, without melting, at 270°C. $[Cu(pz)_2]_x$ exhibits thermochromism at low temperatures. The material is green at room temperature but at 77 K it is bright blue. Trofimenko, in an earlier review (4), made mention of this thermochromism in copper pyrazolate systems. At this low temperature single crystals of the polymer remain intact.

The electronic spectrum (12 200 – 31 200 cm^{-1}), obtained on a Nujol mull supported on filter paper, using a Perkin Elmer Coleman 124 spectrophotometer, showed two broad bands with maxima at 15 400 and 25 000 cm^{-1}. The infrared spectrum (4 000 – 250 cm^{-1}) was obtained on a Perkin Elmer Model 598 spectrophotometer. Samples were mulled in Nujol and pressed between KRS-5 plates (Harshaw Chemical Co.). Frequencies (cm^{-1}): 2895 s (N), 2840 s (N), 1495 m (sh), 1457 s (N), 1413 m, 1376 s (N), 1268 m, 1253 m (sh), 1181 s, 1170 s (sh), 1070 s, 974 w, 914 m, 882 m, 843 w, 770 s, 755 s, 722 m (sh) (N), 624 s, 377 m, 364 s (N = Nujol peak).

Magnetic susceptibilities over the temperature range of 4.2–100 K were measured using a P.A.R. Model 155 vibrating sample magnetometer (field = 9225 G) and over the temperature range of 80–300 K using a Gouy balance (field = 8000 G). The equipment used was as described in detail earlier (5) with the exception of the Gouy balance which has since been equipped with a Mettler AE 163 balance. Magnetic susceptibilities were corrected for diamagnetism: copper, −11; $C_3H_3N_2$, −40 (values in 10^{-6} cm^3 mol^{-1}). A correction of 60 × 10^{-6} cm^3 mol^{-1} was applied for temperature-independent paramagnetism. Values of molar magnetic susceptibilities and magnetic moments are given in Table 4.[1]

X-ray crystallographic analysis

A crystal ca. 0.10 × 0.15 × 0.20 mm in size was mounted in a general orientation. Unit-cell parameters were refined by least-squares on setting angles for 25 reflections (2θ = 26–35°) measured on a diffractometer with Mo-$K\alpha$ radiation (λ = 0.71069 Å). Crystal data at 21°C are:

$C_6H_6CuN_4$ f.w. = 197.69

Orthorhombic, a = 7.917(1), b = 11.491(2), c = 7.778(1) Å, V = 707.6(2) Å^3, Z = 4, ρ_c = 1.86 Mg m^{-3}, $F(000)$ = 396, μ(Mo-$K\alpha$) = 30.2 cm^{-1}. Absent reflections: hkl, $h + k + l$ odd, $0kl$, k and l odd, and $h0l$, h and l odd, space group *Ibam* (D_{2h}^{26}, No. 72) from structure analysis.

Intensities were measured with graphite-monochromated Mo-$K\alpha$ radiation on a Rigaku AFC6S diffractometer. An ω–2θ scan at 16° min^{-1} over a range of (1.47 + 0.35 tan θ) degrees in ω (with up to nine rescans, background/scan time ratio = 0.5) was employed. Data were measured to 2θ = 70°. The intensities of three check reflections, measured every 150 reflections throughout the data collection, remained constant to within 2%. After data reduction,[2] an empirical absorption correction, based on azimuthal scans for several reflections, was applied which resulted in transmission factors ranging from 0.907 to 1.000. Of the 832 independent reflections measured, 507 (60.9%) of these had intensities greater than or equal to $3\sigma(F^2)$ above background where $\sigma^2(F^2) = (S^2(C + 4B) + (0.045(F_o^2))^2)/Lp^2$ with S = scan rate, C = scan count, B = total background count, and Lp = Lorentz-polarization factor.

The structure was solved by direct methods in the centrosymmetric space group *Ibam* which was suggested by the E-statistics and confirmed by later calculations. The coordinates of the non-hydrogen atoms were determined from an E-map and those of the hydrogen atoms were determined from a subsequent difference Fourier synthesis. The non-hydrogen atoms were refined with anisotropic thermal parameters and the hydrogen atoms with isotropic thermal parameters. Scattering factors for all atoms and anomalous dispersion corrections for the non-hydrogen atoms were taken from ref. 6. The weighting scheme $w = 4F_o^2/\sigma^2(F_o^2)$ gave uniform average values of $w(|F_o| - |F_c|)^2$ over ranges of both $|F_o|$ and sin θ/λ and was employed in the final stages of full-matrix refinement of 35 variables. Reflections with $I < 3\sigma(I)$ were not included in the refinement. Convergence was reached at R = 0.029 and R_w = 0.038 for 507 reflections with $I \geq 3\sigma(I)$. For all 832 reflections R = 0.081. The function minimized was $\Sigma w(|F_o| - |F_c|)^2$, $R = \Sigma||F_o| - |F_c||/\Sigma|F_o|$ and $R_w = (\Sigma w(|F_o| - |F_c|)^2/\Sigma w|F_o|^2)^{1/2}$.

On the final cycle of refinement the maximum parameter shift corresponded to 0.03σ. The mean error in an observation of unit weight was 1.23. The final difference map showed maximum fluctuations of −0.34 to 0.43 e Å^{-3}. The final positional and (equivalent) isotropic thermal parameters appear in Table 1. Bond lengths and angles are listed in Tables 2 and 3. Hydrogen parameters, anisotropic thermal parameters, torsion angles, intermolecular contacts, least-squares planes, and structure factors have been deposited.[1]

TABLE 1. Final atomic coordinates (fractional) and isotropic thermal parameters with estimated standard deviations in parentheses

Atom	x	y	z	B(eq)
Cu	1/2	0	1/4	2.06(2)
N	0.3319(2)	0.0589(2)	0.0874(2)	2.21(6)
C(1)	0.2005(3)	0.1242(2)	0.1392(3)	2.81(8)
C(2)	0.1154(5)	0.1680(4)	0	3.1(1)
H(1)	0.162(4)	0.140(3)	0.262(4)	3.9(7)
H(2)	0.044(8)	0.217(5)	0	7(2)

TABLE 2. Bond lengths (Å) with estimated standard deviations in parentheses*

Atom	Atom	Distance	Atom	Atom	Distance
Cu	N	1.957(2)	C(1)	H(1)	1.02(3)
N	C(1)	1.345(3)	C(1)	C(2)	1.371(3)
N	N^i	1.359(3)	C(2)	H(2)	0.80(6)

*See footnote for Table 3.

Results and discussion

In an earlier paper by Vos and Groeneveld (2), reactions of copper salts with pyrazole in aqueous base were reported to yield black polymeric material of composition $[Cu(pz)_2]_x$. Attempts to repeat these reactions in our laboratory invariably gave a black polymeric species as reported, but of composition $[Cu_2(pz)_3(OH)]_x$ rather than the $[Cu(pz)_2]_x$ formulation stated earlier. The alternate route described here, involving the reaction of metallic copper with molten pyrazole in the presence of air, has led to the desired polymer as a green colored solid. The polymer can be obtained as X-ray quality green crystals under carefully controlled conditions. The compound is both

[1]Supplementary material mentioned in the text may be purchased from the Depository of Unpublished Data, CISTI, National Research Council of Canada, Ottawa, Ont., Canada K1A 0S2.

[2]All computations performed using the TEXSAN – TEXRAY Structure Analysis Package which includes versions of the following: MITHRIL, Integrated direct methods, by C. J. Gilmore; AGNOST, absorption corrections, by J. A. Ibers; ORFLS, full-matrix least-squares, and ORFFE, function and errors, by W. R. Busing, K. O. Martin, and H. A. Levy; DIRDIF, phase extension and refinement of difference structures, by P. T. Beurskens; ORTEP II, illustrations, by C. K. Johnson.

TABLE 3. Bond angles (deg) with estimated standard deviations in parentheses*

Atom	Atom	Atom	Angle	Atom	Atom	Atom	Angle
N	Cu	N^2	99.4(1)	H(1)	C(1)	N	128(2)
N	Cu	N^3	139.5(1)	H(1)	C(1)	C(2)	122(2)
N	Cu	N^4	94.3(1)	N	C(1)	C(2)	110.4(2)
C(1)	N	N^1	107.4(1)	H(2)	C(2)	C(1)	127.4(5)
C(1)	N	Cu	121.7(1)	C(1)	C(2)	$C(1)^1$	104.3(3)
N	N	Cu	130.28(5)				

*Superscripts refer to symmetry operations: (*1*) $x, y, -z$; (*2*) $1-x, -y, z$; (*3*) $1-x, y, \frac{1}{2}-z$; and (*4*) $x, -y, \frac{1}{2}-z$.

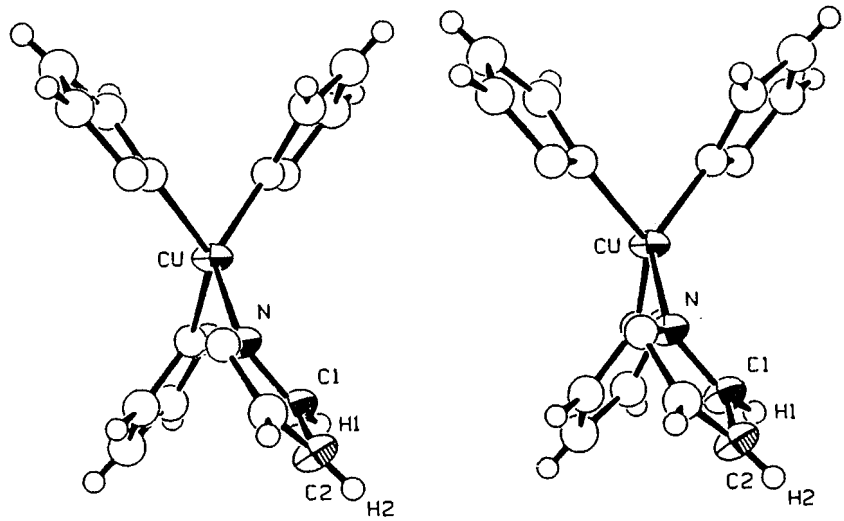


FIG. 1. Stereoscopic view of the coordination about the copper atom in polybis(μ-pyrazolato-*N,N'*)copper(II); 50% probability thermal ellipsoids are shown for the non-hydrogen atoms. Shaded non-hydrogen atoms comprise the asymmetric unit.

thermally and air-stable and, consistent with its polymeric structure, insoluble in a wide range of solvents. Interestingly the $(3,4,5\text{-}Br_3pz)_2Cu$ complex exists as a tetramer in benzene solution (4).

The crystal structure analysis confirms the polymeric nature of $[Cu(pz)_2]_x$. The coordination geometry about the Cu atom in $[Cu(pz)_2]_x$ is shown in Fig. 1, and the crystal structure of the polymer in Fig. 2. The coordination geometry about the Cu atom is that of a distorted tetrahedron having exact (crystallographic) D_2 symmetry. The Cu—N distance is 1.957(2) Å. The three unique N—Cu—N angles correspond to N atoms related to one another by the three mutually perpendicular twofold axes intersecting at the metal: that within the six-membered $Cu(N—N)_2Cu$ rings is 99.4(1)° and the others are 94.3(1) and 139.5(1)°. The pyrazolyl rings possess exact C_s symmetry, the mirror plane being perpendicular to that of the five-membered ring and containing atoms C(2) and H(2). The angle between normals to consecutive $Cu(N—N)_2Cu$ ring mean planes along the polymer chain (which extends along the *c* axis) is 53.9°. The fused pyrazolyl and $Cu(N—N)_2Cu$ rings are not strictly coplanar, the angle between normals to the mean planes being 9.1°. The Cu atoms are displaced 0.236 Å from the pyrazolyl mean planes. The shortest interchain distance between non-hydrogen atoms is $C(1)\cdots C(1) = 3.456(5)$ Å.

Obviously this material is different from that reported by Vos and Groeneveld since they predicted a square-planar Cu(II) ion from ligand field spectral data on their compound. The present structure can be compared to those of the monomeric complexes $[Me_2Gapz_2]_2Cu$ and $[Me_2Gapz''_2]_2Cu$ (pz″ = 3,5-dimethylpyrazolyl) reported earlier (7). In the former complex the Cu atom displays a square-planar coordination mode (average Cu—N = 1.987 Å) with the $Ga(N—N)_2Cu$ six-membered rings being in the boat conformation. The latter complex, containing the 3-Me and 5-Me substituents on the pyrazolyl rings, cannot adopt the same geometry about the Cu centre and the result is a distorted tetrahedrally coordinated transition metal (average Cu—N = 1.959 Å) with planar $Ga(N—N)_2Cu$ six-membered rings. From a study of molecular models a square-planar environment about the Cu atoms in the $[Cu(pz)_2]_x$ polymer should be possible but clearly the preference is for a distorted tetrahedral geometry. The dihedral angle between CuN_2 coordination planes (in different six-membered $Cu(N—N)_2Cu$ rings) is 53.9° compared to the larger value of 71.9° found in the $[Me_2Gapz''_2]_2Cu$ complex. The latter value is no doubt dictated by the steric requirement of staggering the Me groups about the three metal atoms in the molecule. The $Cu\cdots Cu$ distance of 3.8893(6) Å in $[Cu(pz)_2]_x$ is slightly longer than the $Ga\cdots Cu$ distance of 3.790 Å in $[Me_2Gapz''_2]_2Cu$, a consequence of smaller angles at the metal atoms within the six-membered $M(N—N)_2Cu$ rings (99.4° in the polymer compared with values of 104.9 and 103.4° at Cu and Ga, respectively). Other related structures include $[Me_2Gapz_2]_2Ni$ (8) which has a square-planar Ni atom and a double-boat conformation and $[H_2Bpz_2]_2Co$ (9) which has a tetrahedral Co atom and a double-boat conforma-

Can. J. Chem. Downloaded from www.nrcresearchpress.com by 186.148.149.217 on 09/07/12
For personal use only.

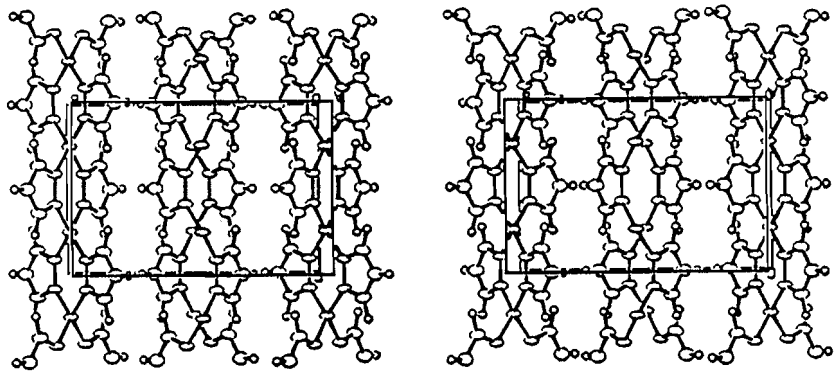


FIG. 2. Stereoscopic view down the *a* axis of the crystal structure of polybis(μ-pyrazolato-*N*,*N'*)copper(II).

tion. Spectroscopic studies of the complex $[Me_2Gapz_2]_2Co$ (10) suggest that planar $Ga(N—N)_2Co$ rings may result from steric interactions.

Electronic spectrum and magnetic properties

For Cu(II) in D_2 symmetry a total of four ligand field bands are expected (11). The $[Cu(pz)_2]_x$ polymer exhibits a single broad absorption band with a maximum at 15 400 cm^{-1}, in the frequency range expected for a CuN_4 chromophore of distorted tetrahedral symmetry (12). This band may involve all four of the *d–d* transitions, unresolved. The band at 25 000 cm^{-1} is too high in energy to be assigned to a ligand field transition and is likely charge transfer in origin.

The effective magnetic moment of $[Cu(pz)_2]_x$ varies from 1.47 BM at 299 K to a low of 0.19 BM at 4.22 K (Table 4) indicating the presence of relatively strong antiferromagnetic coupling between the copper ions. This is confirmed by the magnetic susceptibility versus temperature behaviour which shows a maximum in susceptibility at ~143 K (Fig. 3). The increase in susceptibility with decreasing temperature at the lowest temperatures studied (Fig. 3) probably arises from the presence of a very low concentration of paramagnetic structural impurity as is often observed in antiferromagnetically coupled systems (5).

The susceptibility data below 80 K were obtained using the VSM instrument and the scatter in the data points (Fig. 3) reflects the sensitivity limitations of this equipment. Because of the relatively low susceptibilities exhibited by this compound the reproducibility of the measurement at a given temperature is on the order of only ±5%. Although there is an inherent uncertainty of this order of magnitude, due to packing errors, in the absolute susceptibility determined using the Gouy apparatus, the reproducibility of the measurements of relative susceptibilities using this equipment is considerably better (on the order of ±1%); hence there is much less scatter in the data points above 80 K.

The structure of $[Cu(pz)_2]_x$ consists of infinite chains of copper(II) ions linked by double pyrazolate bridges (see above). Hence, we have analyzed the magnetic data according to the isotropic Heisenberg model for exchange coupled linear chains employing the polynomial expression for the magnetic susceptibility developed by Hall and others (13, 14). Computer fits of the experimental data to the model were obtained as described previously (3) and the best fit (solid line in Fig. 3) was obtained with values of J, g and present paramagnetic impurity of $-78 \pm 2\ cm^{-1}$, 2.12 ± 0.02, and 0.44% respectively. The value of the

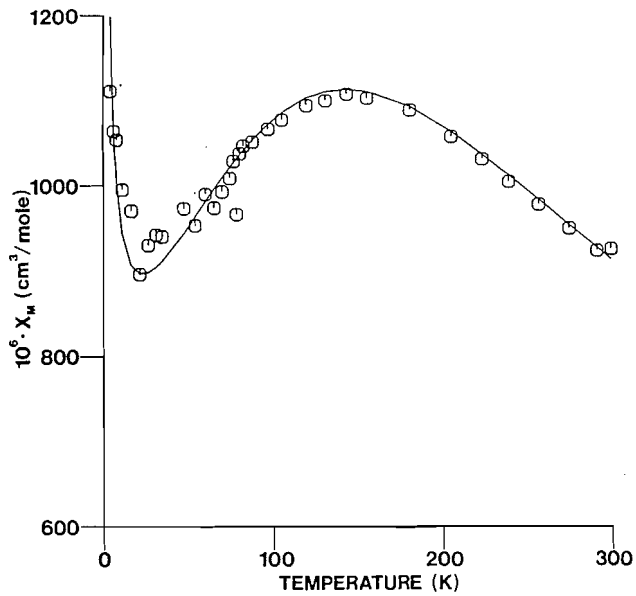


FIG. 3. Plot of the magnetic susceptibility versus temperature for polybis(μ-pyrazolato-*N*,*N'*)copper(II).

fitting function, F (defined in ref. 3), for this fit was 0.0280. The quality of fit is very good and, as expected, the amount of paramagnetic compound required to account for the increase in susceptibility at the lower temperatures is very small.

It is interesting to compare the absolute value of the exchange coupling constant, $|J|$, with values previously reported for other linear chain polymers of copper(II). Phosphinate ligands are known to form double anionic bridges between copper ions analogous to the type of bridges observed here. In the case of the phosphinates, however, the compression of the CuO_4 chromophores is greater, the O—P—O bridging system involves three bridge atoms rather than two, and while the π-system of the O—P—O is considered to contribute to the superexchange mechanism of coupling between the metal centres, it is probably considerably less effective for this purpose than is the π-system of the pz bridge. Accordingly the strongest antiferromagnetic exchange observed previously is in the α-forms of copper(II) *n*-decyl- and *n*-dodecylphosphinate where $|J|$ values of 29 cm^{-1} have been reported (3). The neutral pyrazine (1,4-diazine, $C_4H_4N_2$) ligand is also known to bridge copper centres and form linear chain polymers (15–17). An examination of the exchange coupling constants reported for

Can. J. Chem. Downloaded from www.nrcresearchpress.com by 186.148.149.217 on 09/07/12
For personal use only.

these systems show values ranging up to a maximum of 6 cm^{-1}, but not higher, in spite of the availability of the π-system in the ligand for use as an exchange pathway. Although copper(II) polymeric compounds containing bridging oxide or fluoride are known to exhibit stronger magnetic exchange than that observed here (18), the value of $|J| = 78 \pm 2$ cm^{-1} exhibited by $[Cu(pz)_2]_x$ is considerably greater than for many other chain polymers of copper(II) (14), implying a very high efficiency of the pyrazolate ligands in propagating magnetic exchange. Studies involving other pyrazolate-derived anions as well as other metal ions are currently in progress.

Acknowledgments

We thank the Natural Sciences and Engineering Research Council of Canada for financial support and the University of British Columbia Computing Centre for assistance.

1. S. TROFIMENKO. Prog. Inorg. Chem. **34**, 116 (1986).
2. J. G. VOS and W. L. GROENEVELD. Inorg. Chim. Acta, **24**, 123 (1977).
3. J. S. HAYNES, K. W. OLIVER, and R. C. THOMPSON. Can. J. Chem. **63**, 1111 (1985).
4. S. TROFIMENKO. Chem. Rev. **72**, 500 (1972).
5. J. S. HAYNES, K. W. OLIVER, S. J. RETTIG, R. C. THOMPSON, and J. TROTTER. Can. J. Chem. **62**, 891 (1984).
6. International tables for X-ray crystallography. Vol. IV. Kynoch Press, Birmingham. 1974. pp. 99–102 and 149.
7. D. J. PATMORE, D. F. RENDLE, A. STORR, and J. TROTTER. J. Chem. Soc. Dalton Trans. 718 (1975).
8. D. F. RENDLE, A. STORR, and J. TROTTER. J. Chem. Soc. Dalton Trans. 176 (1975).
9. L. J. GUGGENBERGER, C. T. PREWITT, P. MEAKIN, S. TROFIMENKO, and J. P. JESSON. Inorg. Chem. **12**, 508 (1973).
10. K. R. BREAKELL, D. J. PATMORE, and A. STORR. J. Chem. Soc. Dalton Trans. 750 (1975).
11. B. J. HATHAWAY and D. E. BILLINGS. Coord. Chem. Rev. **5**, 143 (1970).
12. B. J. HATHAWAY. J. Chem. Soc. Dalton Trans. 1196 (1972).
13. J. W. HALL. Ph.D. Thesis. University of North Carolina. 1977.
14. W. E. ESTES, W. E. HATFIELD, J. A. C. VAN OOIJEN, and J. REEDIJK. J. Chem. Soc. Dalton Trans. 2121 (1980).
15. W. E. HATFIELD, W. E. ESTES, W. E. MARSH, M. W. PICKENS, L. W. TER HAAR, and R. R. WELLER. *In* Extended linear chain compounds. Vol. 3. *Edited by* J. S. Miller. Plenum Press, New York. 1983. p. 43.
16. T. OTIENO. M.Sc. Thesis. University of British Columbia. 1988.
17. J. S. HAYNES, S. J. RETTIG, J. R. SAMS, J. TROTTER, and R. C. THOMPSON. Inorg. Chem. **27**, 1237 (1988).
18. K. SREEDHAR and P. GANGULY. Inorg. Chem. **27**, 2261 (1988).

Can. J. Chem. Downloaded from www.nrcresearchpress.com by 186.148.149.217 on 09/07/12
For personal use only.

A refined LEED structural determination for the surface designated Ni (111)–(2 × 2)–S

Y. K. Wu and K. A. R. Mitchell[1]

Department of Chemistry, University of British Columbia, 2036 Main Mall, Vancouver, B.C., Canada V6T 1Y6

Received February 10, 1989

This article is dedicated to Professor Ronald J. Gillespie on the occasion of his 65th birthday

Y. K. Wu and K. A. R. Mitchell. Can. J. Chem. **67**, 1975 (1989).

A new intensity analysis with low-energy electron diffraction is reported for the (2 × 2) surface structure obtained by the adsorption of H_2S on the (111) surface of nickel. Intensity-versus-energy curves were measured with a video LEED analyzer for 10 diffracted beams at normal incidence, and comparisons were made with intensity curves calculated with multiple-scattering methods for models in which S atoms chemisorb at three-fold coordinated adsorption sites, but with the possibilities of both lateral and vertical relaxations in the local metallic structure. Small adsorbate-induced relaxations are found, but the dominant structural feature is that the S atoms adsorb above the "expected" adsorption sites (i.e. those which continue the regular fcc packing) with a 1.50 Å spacing between the S layer and the top-most Ni layer. The S–Ni bond length of 2.10 Å agrees to within 0.02 Å of a prediction using a current bond length – bond order relation, but this value is smaller than two other recent measurements by SEXAFS and ion scattering by 0.06 and 0.10 Å, respectively. This analysis also finds the first two Ni layer spacings are expanded from the bulk value by 2 to 3%.

Key words: LEED, surface structure, S chemisorption, Ni(III) surface.

Y. K. Wu et K. A. R. Mitchell. Can. J. Chem. **67**, 1975 (1989).

On rapporte une nouvelle analyse d'intensité par diffraction d'électrons de faible énergie, pour la structure de surface (2 × 2) obtenue par adsorption de H_2S sur la surface de nickel (111). On a mesuré les courbes d'intensité en fonction de l'énergie à l'aide d'un analyseur vidéo LEED pour 10 rayons diffractés à une incidence normale, et on les a comparées aux courbes d'intensité calculées par la méthode de diffraction multiple pour les modèles dans lesquels les atomes de S absorbent chimiquement au niveau des sites d'adsorption de coordination ternaire, mais avec les possibilités de relaxations latérales et verticales dans la structure métallique locale. On a trouvé des petites relaxations induites de produit adsorbé, mais la caractéristique structurale dominante est celle à l'effet que les atomes de S adsorbent audessus des sites d'adsorption « attendus » (i.e. ceux qui continuent l'entassement régulier fcc) avec un espacement de 1.50 Å entre la couche de S et la couche de Ni la plus élevée. La longueur de liaison S–Ni de 2.10 Å s'accorde à 0.02 Å près avec celle prévue a partir de la relation courante longueur de liaison-ordre de liaison, mais cette valeur est plus faible de 0.06 et de 0.10 Å à celles mesurées récemment par SEXAFS et par diffraction d'ions respectivement. Cette analyse montre également que la distance entre les deux premières couches de nickel est de 2 à 3% supérieure à celle de la valeur totale.

Mots clés : LEED, structure de surface, absorption chimique de S, surface Ni(III).

[Traduit par la revue]

Can. J. Chem. Downloaded from www.nrcresearchpress.com by 186.148.149.217 on 09/07/12
For personal use only.

Introduction

A developing topic in structural chemistry is surface structural chemistry. Studies over the last few years with a range of experimental probes, but especially low-energy electron diffraction (LEED), are helping to establish principles for the detailed atomic arrangements in systems which involve the chemisorption of electronegative atoms or small molecules on well-characterized surfaces of transition metals (1, 2). In certain cases, substantial reconstructions of the metallic structure have been indicated (see, for example, ref. 3), although even where this is not the case relaxations can still occur (4–7), and the investigation of possible adsorbate-induced relaxations provides a topical approach to reanalysis in cases where the results of earlier surface structural studies seem at variance with expectation (2).

An early LEED study for the (2 × 2) surface structure formed by S chemisorbed on the (111) surface of nickel, which restricted to bulk distances for the metal, indicated a S–Ni chemisorption bond length equal to about 2.02 Å (8), whereas the corresponding value predicted with a current bond length – bond order relation is 2.12 Å (2). This early S–Ni distance from LEED is also short compared with subsequent determinations by other techniques, for example 2.16 Å from ion scattering (9) and 2.20 Å from a preliminary SEXAFS study (10). Taken together these observations suggest that reanalysis by LEED is needed for the Ni(111)–(2 × 2)–S surface structure, and this provides the prime objective of the present paper.

Methods used

This work used the conventional procedures of LEED crystallography; specifically intensity-versus-energy ($I(E)$) curves from experiment were compared with those from multiple-scattering calculations in order to find the geometrical model in the calculations which gave the best correspondence with the experimental data (11, 12). The experimental $I(E)$ curves used were measured for normal incidence with a video LEED analyzer following procedures which have been detailed previously (13). The starting point was the preparation of a clean, well-ordered Ni(111) surface as characterized by the cylindrical mirror analyzer showing no detectable Auger signals for impurity elements as well as by LEED showing a sharp (1 × 1) pattern (14). Such a surface at room temperature was exposed to H_2S gas at about 2×10^{-8} Torr, and the sharpness of the (2 × 2) LEED patterns was optimized with exposures held for about 2 min. $I(E)$ curves were then measured for the three integral beams designated (1 0), (0 1), and (1 1), and the seven fractional order beams designated (1/2 0), (0 1/2), (1/2 1/2), (1 1/2), (1/2 1), (3/2 0), and (0 3/2) using the beam notation detailed by Chan and Weinberg (15). Intensity measurements were made over a total energy range of about 1020 eV.

The multiple-scattering calculations of the intensity curves for the structural analysis used the combined-space method (16,

[1]To whom correspondence should be addressed.

Can. J. Chem. Downloaded from www.nrcresearchpress.com by 186.148.149.217 on 09/07/12
For personal use only.

17). Layer diffraction matrices for relaxed surfaces were calculated with up to four atoms per unit mesh, and layer stacking was done with the renormalized forward scattering method (18). The non-structural parameters used in the calculations were very similar to those used previously by Demuth *et al.* (8), and the following details for the present work. The atomic potential in the substrate was characterized by phase shifts (up to $\ell = 7$) derived from a band structure for nickel (19), and the real part of the constant potential (V_{or}) between the atomic spheres was set initially at -11 eV. For the sulphur overlayer region we used the phase shifts obtained by Demuth *et al.* from a superposition potential (20). The Debye temperatures were taken as 440 and 335 K for nickel and sulphur, respectively, while the imaginary part (V_{oi}) of the constant potential between all atomic spheres was equated to $-0.9\,E^{1/3}$ eV (where E is the electron energy in eV). Evaluations of the fit between experiment and calculation were done both visually and with LEED reliability indices, specifically R_P as introduced by Pendry (21) and R_{MZJ}, the modified form of the index introduced by Zanazzi and Jona (22) as given by Van Hove and Koestner (23).

Results and discussion

The normal-incidence LEED patterns for the (2 × 2) surface structure considered here are consistent with the diperiodic space group $p3m1$ which combines three-fold rotation axes and mirror plane symmetry, although models with lower space group symmetries could give rise to the observed LEED pattern when an averaging is taken over different patterns from the possible domains. Nevertheless, since previous evidence suggests the chemisorbed atoms occupy three-fold coordination sites, it seems most reasonable to consider the models of highest symmetry type in each case. When other metal layers of the face-centered cubic (fcc) structure are included, a distinction is needed between those three-fold adsorption sites which do not have an atom immediately below in the second metal layer (the "expected" three-fold sites for fcc packing) and the other three-fold adsorption ("unexpected") sites which do have an atom immediately below in the second layer. Figure 1 indicates the model with adsorption in the "expected" three-fold sites and lateral displacements for the topmost metal layer. The parameter Δ is used to indicate the magnitude of these displacements from the regular bulk positions; positive Δ corresponds to displacements in the directions of the arrows shown in Fig. 1.

A number of previous studies for Ni(111)–(2 × 2)–S indicated that S adsorbs at three-fold sites in this surface structure (8–10, 24, 25), although some of these studies were unable to distinguish between the two types of three-fold sites. Nevertheless, both the initial LEED study by Demuth *et al.* (8) and the ion scattering analysis by Fauster *et al.* (9) concluded that S adsorbs on the Ni(111) surface in the "expected" three-fold sites. This was independently assessed and confirmed in the present study by comparing $I(E)$ curves from experiment and calculation both visually and with LEED reliability indices. For example, without including any relaxations from the bulk metallic structure, R_{MZJ} and R_P are minimized at the values 0.123 and 0.185 respectively for the "expected" adsorption site, while the corresponding values for the "unexpected" adsorption sites are consistently larger at 0.219 and 0.311. The latter structure therefore gives the less good correspondence for the intensity curves, consequently investigations of the adsorbate-induced relaxations in the metal were only done with S chemisorbed in those three-fold sites which continue the fcc packing sequence.

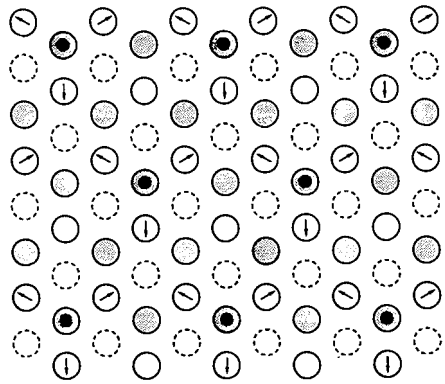


FIG. 1. Model used for the refined structural analysis of Ni(111)–(2 × 2)–S. The small filled circles represent S atoms chemisorbed in the "expected" three-fold adsorption sites; nickel atoms in the first, second, and third metal layers are represented by open circles, dashed circles, and shaded circles, respectively. The arrows define lateral displacements for nickel atoms in the first layer which correspond to positive Δ.

The structural refinement for the Ni(111)–(2 × 2)–S surface structure used the reliability index R_{MZJ}, which was minimized by iteratively varying the geometrical parameters over the ranges: $d_{01} = 1.30$ to 1.65 Å, $d_{12} = 1.903$ to 2.133 Å, $d_{23} = 2.000$ to 2.175 Å, $\Delta = -0.10$ to 0.15 Å, where the d's refer to interlayer spacings and the subscripts identify the particular layers involved. The subscripts 0, 1, 2 ... apply to the chemisorbed layer, first metal layer, second metal layer, ... respectively. At each stage in the minimization, V_{or} and one of the geometrical parameters was varied for optimal correspondence between calculation and experiment, other geometrical parameters being held constant at the optimal value from the previous iteration. The overall best match from this optimization procedure was reached with the geometrical parameters: $d_{01} = 1.50$ Å, $d_{12} = 2.09$ Å, $d_{23} = 2.08$ Å, and $\Delta = 0.03$ Å. Some indications of comparisons of $I(E)$ curves for this model, and the changes from the unrelaxed model, are shown for representative beams in Fig. 2. For the conditions of the favoured structure, R_{MZJ} and V_{or} are 0.105 and -6.0 eV, respectively, while the nearest neighbour S–Ni bond lengths equal 2.10 Å.

There is an overall improvement in the correspondence between the calculated and experimental $I(E)$ curves on including the adsorbate-induced relaxations, although for some beams the changes are relatively insignificant. The best improvement is for the (01) beam as shown in Fig. 2. For the particular calculation procedures and non-structural parameters used here, the uncertainties in the structural parameters found from the analysis appear to be around 0.02–0.03 Å, although with changes in geometrical parameters of this order, the differences in the calculated $I(E)$ curves are still relatively minor as shown in Fig. 3. These examples additionally emphasize the continuing need in LEED crystallography to test and develop improved R-factors that can quantify small changes in the $I(E)$ curve comparisons and translate them to reliable structural parameters.

The lateral displacements found here for the Ni(111)–(2 × 2)–S surface structure are small, but evidence for the (0 3/2) beam shown in Fig. 3 does suggest that Δ is slightly greater than zero. The improvement for the (0 1) beam on including the

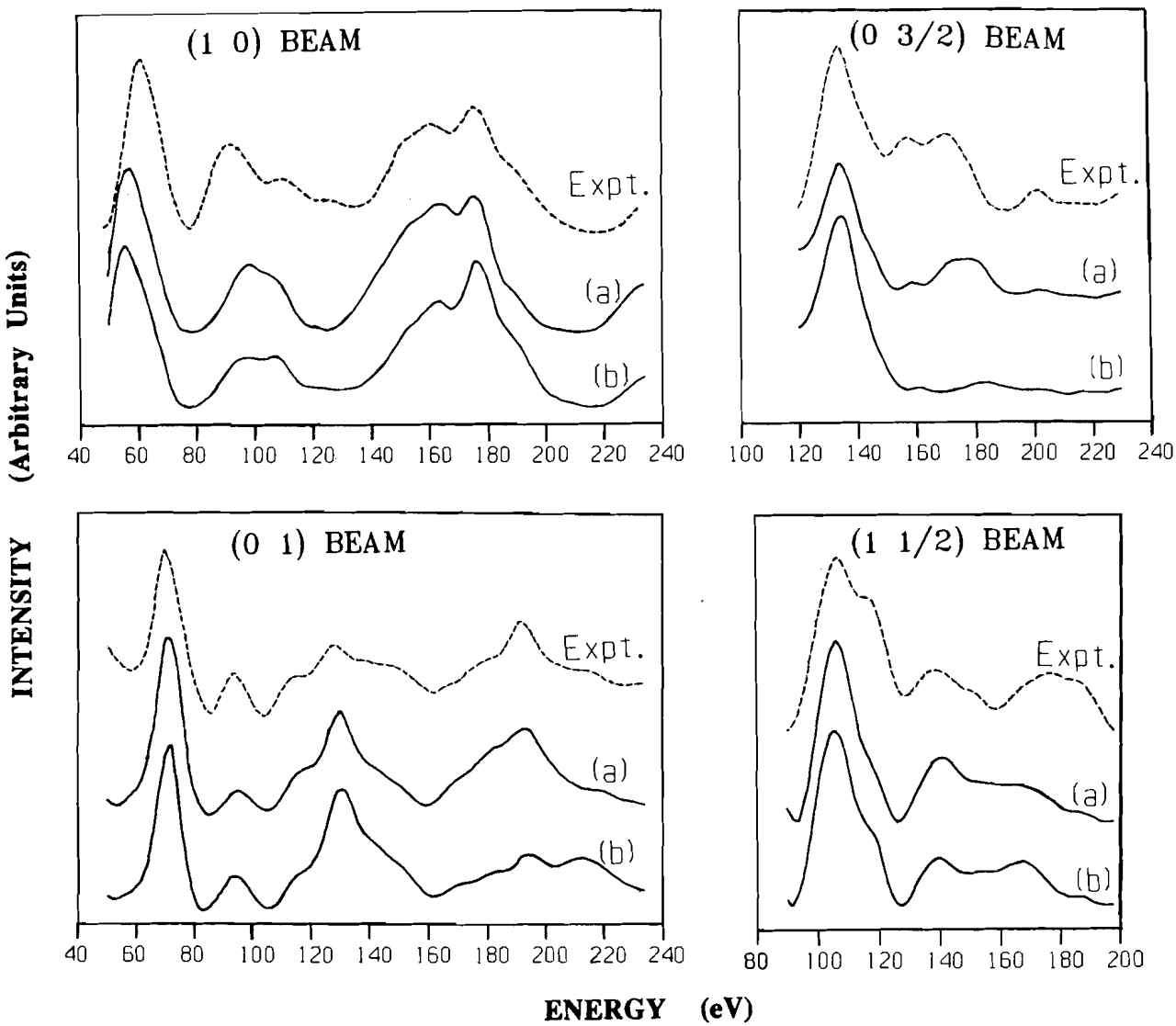


FIG. 2. Comparison of experimental $I(E)$ curves from the Ni(111)–(2 × 2)–S surface structure for the (1 0), (0 1), (0 3/2), and (1 1/2) beams at normal incidence with those calculated for S chemisorbed in the "expected" three-fold adsorption sites with d_{01} = 1.50 Å for (*a*) relaxed model with Δ = 0.03 Å, d_{12} = 2.09 Å, d_{23} = 2.08 Å; (*b*) unrelaxed model with Δ = 0.00 Å, $d_{12} = d_{23}$ = 2.03 Å.

adsorbate-induced relaxation is almost entirely due to changes in the values of d_{12} and d_{23}, the slight change occurring in Δ has a negligible effect on that experiment–calculation comparison. Nevertheless, on balance, small changes in vertical and lateral parameters seem to have an approximately equal effect on the $I(E)$ curves in this analysis, even though these intensity data are for normal incidence where LEED has often been considered less sensitive to lateral displacements than to vertical displacements of similar magnitude (26). Another feature of interest here concerns the small (2 to 3%) increase in the first two interlayer spacings for the metal (the bulk value is 2.033 Å). It is not clear at present whether this increase indicates a reduction in the bonding capability by metal atoms in the vicinity of the surface, perhaps as a consequence of the increased bonding to S, or whether there is some other cause, such as hydrogen incorporation into the metal structure.

Concluding remarks

Much modern bond length information from X-ray crystallography fits to expressions of the type

$$[1] \qquad r = r_0 - 0.85 \log s$$

which relates a particular interatomic distance of bond valence s to r_0, the corresponding distance for a bond of unit valence (27). Equation [1] has been applied to chemisorption X–M bond lengths with the assumption that the sum of bond valences at each chemisorbed atom X equals the atom valence v (e.g. 2 for S) (2). For the case that X adsorbs on a metallic surface with n equivalent neighbouring M atoms, all the bond valences equal v/n, and given r_0 that immediately enables simple predictions for the chemisorption bond length. Such comparisons of experimental and predicted bond distances are needed to assess whether structural determinations on related surface systems fit a consistent conceptual framework; also such comparisons should help note systematic differences which may identify special errors in individual determinations.

Table 1 reports structural information currently available for

Can. J. Chem. Downloaded from www.nrcresearchpress.com by 186.148.149.217 on 09/07/12
For personal use only.

Can. J. Chem. Downloaded from www.nrcresearchpress.com by 186.148.149.217 on 09/07/12
For personal use only.

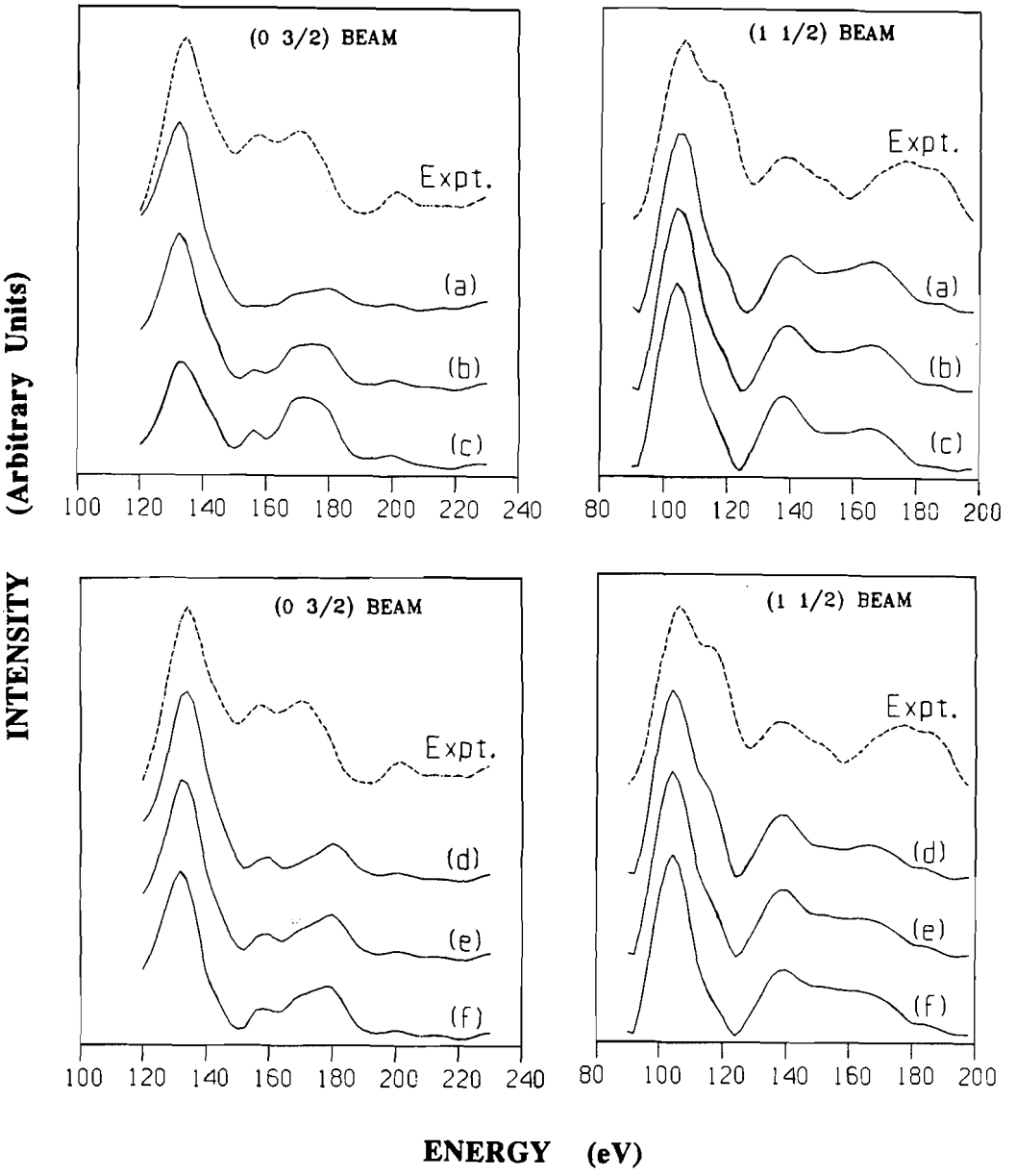


FIG. 3. Comparison of experimental $I(E)$ curves from the Ni(111)–(2 × 2)–S surface structure for the (0 3/2) and (1 1/2) beams at normal incidence with those calculated for S chemisorbed in the "expected" three-fold adsorption sites with d_{01} = 1.50 Å for (*a*) Δ = 0.00 Å, d_{12} = 2.09 Å, d_{23} = 2.08 Å; (*b*) as (*a*) but Δ = 0.03 Å, (*c*) as (*a*) but Δ = 0.06 Å; (*d*) Δ = 0.03 Å, d_{12} = 2.053 Å, d_{23} = 2.033 Å; (*e*) as (*d*) but d_{12} = 2.078 Å; (*f*) as (*d*) but d_{12} = 2.103 Å.

TABLE 1. S–Ni interatomic distances reported for S chemisorbed on the three low-index surfaces of nickel and compared with values predicted by eq. [1]

		S–Ni distances (Å)	
Surface	*n*	Eq. [1]	Surface crystallography*
Ni(100)	4	2.23	2.19 (28–30), 2.23 (31)
Ni(110)	4	2.35	2.35 (8), 2.32 (32)
	1	2.18	2.17 (8), 2.18 (32)
Ni(111)	3	2.12	2.10 (this work), 2.02 (8), 2.16 (9), 2.20 (10)

*Reference numbers in parentheses.

S chemisorbed on the three low-index crystallographic surfaces of nickel. On the (111) and (100) surfaces, S has three and four nearest neighbours respectively, but on the (110) surface there are four equal bond lengths from S to Ni atoms in the first layer and one different distance to the Ni atom directly below in the second layer. The predicted S–Ni interatomic distances given in Table 1 are determined from eq. [1] with r_0 equal to 1.97 Å (2). The information in Table 1 suggests that the bond length determined here for S chemisorbed on the Ni(111) surface, namely 2.10 Å, is consistent to within about 0.02 Å of the value that may be expected on the basis of previous structural information for S chemisorbed on the (100) and (110) surfaces. Nevertheless, this value appears significantly shorter than the

values of 2.16 Å and 2.20 Å found in the recent measurements by ion scattering and SEXAFS, respectively.

Acknowledgement

We gratefully acknowledge the support of this research provided by the Natural Sciences and Engineering Research Council of Canada.

1. K. A. R. MITCHELL. Surface Sci. **149**, 93 (1985).
2. K.A.R. MITCHELL, S.A. SCHLATTER, and R.N.S. SODHI. Can. J. Chem. **64**, 1435 (1986).
3. P. J. ESTRUP. *In* Chemistry and physics of solid surfaces. V. *Edited by* R. Vanselow and R. Howe. Springer-Verlag, Berlin. 1984. p. 205.
4. H. D. SHIH, F. JONA, D. W. JEPSEN, and P. M. MARCUS. Phys. Rev. Lett. **46**, 731 (1981).
5. J. H. ONUFERKO, D. P. WOODRUFF, and B. W. HOLLAND. Surface Sci. **87**, 357 (1979).
6. W. DAUM, S. LEHWALD, and H. IBACH. Surface Sci. **178**, 528 (1986).
7. H. C. ZENG, R. A. MCFARLANE, and K. A. R. MITCHELL. Phys. Rev. B, **39**, 8000 (1989).
8. J. E. DEMUTH, D. W. JEPSEN, and P. M. MARCUS. Phys. Rev. Lett. **32**, 1182 (1974).
9. TH. FAUSTER, H. DÜRR, and D. HARTWIG. Surface Sci. **178**, 657 (1986).
10. T. OHTA, Y. KITAJIMA, P. M. STEFAN, M. L. SHEK STEFAN, N. KOSUGI, and H. KURODA. J. Phys. (Paris) **47** *C8*, 503 (1986).
11. P. M. MARCUS and F. JONA. (*Editors*). Determination of surface structure by LEED. Plenum, New York. 1984.
12. M. A. VAN HOVE, W. H. WEINBERG, and C.M. CHAN. Low-energy electron diffraction. Springer-Verlag, Berlin. 1986.
13. P. C. WONG, M. Y. ZHOU, K. C. HUI, and K. A. R. MITCHELL. Surface Sci. **163**, 172 (1985).
14. J. E. DEMUTH and T. N. RHODIN. Surface Sci. **42**, 261 (1974).
15. C. M. CHAN and W. H. WEINBERG. J. Chem. Phys. **71**, 2788 (1979).
16. S. Y. TONG and M. A. VAN HOVE. Phys. Rev. B, **16**, 1459 (1977).
17. M. A. VAN HOVE and S. Y. TONG. Surface crystallography by LEED. Springer-Verlag, Berlin. 1974.
18. J. B. PENDRY. Low-energy electron diffraction. Academic Press, New York. 1974.
19. S. WAKOH. J. Phys. Soc. Jpn. **20**, 1984 (1965).
20. J. E. DEMUTH, D. W. JEPSEN, and P. M. MARCUS. Surface Sci. **45**, 733 (1974).
21. J. B. PENDRY. J. Phys. C, **13**, 937 (1980).
22. E. ZANAZZI and F. JONA. Surface Sci. **62**, 61 (1977).
23. M. A. VAN HOVE and R. J. KOESTNER. *In* Determination of surface structure by LEED. *Edited by* P.M. Marcus and F. JONA. Plenum, New York, 1984.
24. T. W. CAPEHART, C. W. SEABURY, G. W. GRAHAM, and T. N. RHODIN. Surface Sci. **120**, L441 (1982).
25. D. A. ANDREWS and D. P. WOODRUFF. Surface Sci. **141**, 31 (1984).
26. L. L. KESMODEL, R. C. BAETZOLD, and G. A. SOMORJAI. Surface Sci. **66**, 299 (1977).
27. I. D. BROWN and D. ALTERMATT. Acta Crystallogr. **B41**, 244 (1985).
28. J. E. DEMUTH, D. W. JEPSEN, and P. M. MARCUS. Phys. Rev. Lett. **31**, 540 (1973).
29. M. A. VAN HOVE and S. Y. TONG. J. Vacuum Sci. Technol. **12**, 230 (1975).
30. D. H. ROSENBLATT, J. G. TOBIN, M. G. MASON, R. F. DAVIS, S. D. KEVAN, D. A. SHIRLEY, C. H. LI, and S. Y. TONG. Phys. Rev. B, **23**, 3828 (1981).
31. S. BRENNAN, J. STÖHR, and R. JAEGER. Phys. Rev. B, **24**, 4871 (1981).
32. J. F. VAN DER VEEN, R. M. TROMP, R. G. SMEENK, and F. W. SARIS. Surface Sci. **82**, 468 (1979).

Can. J. Chem. Downloaded from www.nrcresearchpress.com by 186.148.149.217 on 09/07/12
For personal use only.

Reaction of transition metal carbonyls with soluble polyselenides: synthesis and structure of $[(C_6H_5)_4P]_2[Re_2(Se_4)_2(CO)_6]$

SAMUEL C. O'NEAL, WILLIAM T. PENNINGTON, AND JOSEPH W. KOLIS[1]
Department of Chemistry, Clemson University, Clemson, SC 29634, U.S.A.

Received January 31, 1989

This paper is dedicated to Professor Ronald J. Gillespie on the occasion of his 65th birthday

SAMUEL C. O'NEAL, WILLIAM T. PENNINGTON, and JOSEPH W. KOLIS. Can. J. Chem. **67**, 1980 (1989).

The reaction of rhenium decacarbonyl with polyselenide anions in DMF solution has been investigated. Two equivalents of K_2Se_3 react with $Re_2(CO)_{10}$ in DMF solution at 100°C, in the presence of excess $[(C_6H_5)_4P]Br$, to produce $[(C_6H_5)_4P]_2[Re_2(Se_4)_2(CO)_6]$. This can be isolated as an analytically pure red crystalline solid in 25% yield. The compound has been characterized crystallographically; space group $P2_1/n$, $Z = 2$, $a = 12.052(3)$ Å, $b = 14.619(5)$ Å, $c = 16.159(4)$ Å, $\beta = 98.31(2)°$, $V = 2817(1)$ Å^3, $R = 0.0583$, $R_w = 0.0653$. In addition to two well-separated tetraphenylphosphonium counterions, the compound consists of the $[Re_2(Se_4)_2(CO)_6]^{2-}$ dianion. This molecule is a rhenium dimer with each metal coordinated to three CO ligands and a Se_4^{2-} chain. One end of the chelating tetraselenide chain is bridging both rhenium atoms, completing an octahedral coordination environment around each metal atom. The bridging distances are slightly asymmetric, leading to the suggestion that the bridging selenide has some dative character.

Key words: selenides, rhenium carbonyls, Zintl ions, p-block clusters.

SAMUEL C. O'NEAL, WILLIAM T. PENNINGTON et JOSEPH W. KOLIS. Can. J. Chem. **67**, 1980 (1989).

On a étudié la réaction, en solution dans le DMF, du décacarbonyl de rhénium avec les anions polysélénures. À 100°C, dans le DMF, deux équivalents de K_2Se_3 réagissent avec le $Re_2(CO)_{10}$, en présence d'un excès de $[(C_6H_5)_4P]Br$, pour fournir du $[(C_6H_5)_4P]_2[Re_2(Se_4)_2(CO)_6]$ qui peut être isolé avec un rendement de 25% sous la forme d'un solide cristallin rouge, analytiquement pur. On a caractérisé ce composé par cristallographie; groupe d'espace $P2_1/n$, $Z = 2$, $a = 12{,}052(3)$ Å, $b = 14{,}619(5)$ Å et $c = 16{,}159(4)$ Å, $\beta = 98{,}31(2)°$, $V = 2817(1)$ Å^3, $R = 0{,}0583$ et $R_w = 0{,}0653$. En plus de deux contre-ions tétraphénylphosphonium bien séparés, le composé comporte le dianion $[Re_2(Se_4)_2(CO)_6]^{2-}$. Cette molécule est un dimère de rhénium dans laquelle chaque atome de métal est coordonnée à trois ligands CO et à une chaîne Se_4^{2-}. Une extrémité de la chaîne de tétrasélénure chélatante agit comme pont entre les deux atomes de rhénium et complète ainsi l'arrangement de coordination octaédrique de chacun de ces atomes métalliques. Les distances des ponts sont légèrement asymétriques; ceci conduit à la conclusion que le sélénure agissant comme pont possède un léger caractère datif.

Mots clés : sélénures, carbonyls de rhénium, ions Zintl, agglomérations «p-block».

[Traduit par la revue]

Can. J. Chem. Downloaded from www.nrcresearchpress.com by 186.148.149.217 on 09/07/12
For personal use only.

Introduction

The chemistry of the group 7 sulfides and selenides is considerably less well developed than their group 6 neighbors (1). There have been relatively few binary manganese and rhenium sulfides and polysulfides reported (2, 3). Several complexes containing selenide atoms coordinated to manganese (4) and rhenium (5) centers have also been described, and one has been characterized (5*a*). However, to our knowledge, there have been no soluble polyselenides or binary selenide anions of group 7 metals reported or characterized.

We have recently reported the reactions of soluble polysulfides and polyselenides with group 6 metal hexacarbonyls under anhydrous condition, to form binary metal chalcogenide anions via an oxidative decarbonylation reaction (6). This is in contrast to the reactions with polytellurides, which form coordinated polytelluride ring complexes (7). Given the synthetic utility of the binary sulfide and selenide anions (8), we have begun investigating the reaction of polychalcogenides with other metal carbonyls. We have found that binuclear metal carbonyls react cleanly with anhydrous polyselenide solution in dry DMF to form novel dimers with bridging polyselenide chelating chains. These can further react to form binary metal selenide anions.[2]

[1]Author to whom correspondence may be addressed.

[2]S. C. O'Neal and J. W. Kolis. Manuscript submitted to Inorg. Chem.

$$M_2(CO)_{10} + \text{"}Se_4^{2-}\text{"} \dashrightarrow [M_2(Se_4)_2(CO)_6]^{2-}$$

M = Mn, Re

$$[M_2(Se_4)_2(CO)_6]^{2-} \xrightarrow{90\,°C} [M(Se_4)_2]^{2-}$$

M = Mn

These reactions involve formal oxidation of the metal center and, presumably, reductive cleavage of polyselenide chains. In this paper we report the preliminary results of the reaction of rhenium carbonyl and anhydrous polyselenide solution to form $[Re_2(CO)_6(Se_4)_2]^{2-}$.

Experimental

General information

Due to the air sensitivity of the reactants, all reactions were carried out under purified argon in dried, degassed solvents using standard Schlenk techniques. Solids were manipulated in an inert atmosphere glove box under purified argon. Infrared spectra were determined as Nujol mulls. Analytical data were provided by Atlantic Microlabs. The polyselenide salt K_2Se_3, used as starting material, was prepared as previously described (6). All other reagents and solvents are commercially available and were used as received.

Preparation of $[(C_6H_5)_4P]_2[Re_2(Se_4)_2(CO)_6]$

In a typical reaction, 0.10 g (0.32 mmol) of a powder of nominal composition K_2Se_3, 0.10 g (0.15 mmol) $Re_2(CO)_{10}$, and 0.26 g (0.62 mmol) $(C_6H_5)_4PBr$ were dissolved in 5 mL DMF and stirred for 30 min at 25°C. The solution was then heated to 100°C for 30 min under

TABLE 1. Crystallographic data

Parameter	Value
Empirical formula	$C_{54}H_{40}O_6P_2Re_2Se_2$
Color; habit	Reddish-brown; parallelepiped
Size	0.38 mm × 0.28 mm × 0.10 mm
Space group	Monoclinic, $P2_1/n$ (no. 14)
Unit cell dimensions	a = 12.052(3) Å
	b = 14.619(5) Å
	c = 16.159(4) Å
	β = 98.31(2)°
Volume	2817(1) Å^3
Molecules/cell	2
Molecular weight	1850.96 g/mol
Density (calcd.)	2.18 g/cm^3
$F(000)$	1728 e$^-$
Diffractometer	Nicolet R3mV
Radiation	Mo K_α (λ = 0.71073 Å)
Temperature	21°C
Monochromator	Graphite crystal
Unit cell reflections	26 ($25.05 < 2\theta < 37.13°$)
2θ range	3.5–45.0°
Scan type	ω/2θ
Scan speed	Variable; 2.09 to 14.65°/min
Reflections collected	4106 (3708 unique; R_{int} = 0.067)
Absorption coefficient	95.72 cm^{-1}
Min./max. transmission	0.36/1.00
System used	Nicolet SHELXTL PLUS (MicroVAX II)
Solution	Direct methods
Refinement method	Full-matrix least-squares
Final residuals	R = 0.0583; R_w = 0.0653
Goodness-of-fit	1.42
Largest Δ/σ	0.01
Reflections observed	2149 ($I > 3\sigma(I)$)
Parameters refined	326
Data-to-parameter ratio	6.59:1
Max./min. difference peaks	1.42/−1.44 e$^-$/Å^3

static vacuum. The resulting cherry-red solution was allowed to cool to room temperature, filtered, and layered with 3 mL diethyl ether. The flask was stored at 4°C overnight and a white powder was deposited. The white powder was removed by filtration and 2 mL of fresh diethyl ether was added. Further storage at 4°C overnight produced lustrous red needle crystals of the product in 25% yield based on rhenium. The product was characterized by infrared spectroscopy and elemental analysis in addition to X-ray structural determination. IR (cm^{-1}, Nujol mull): 1981 (s), 1869 (s). *Anal.* calcd. for $C_{54}H_{40}O_6P_2Re_2Se_8$: C 35.03, H 2.16; found: C 34.58, H 2.17.

X-ray structure determination

A bright-red parallelepiped was sealed in epoxy and mounted on a Nicolet R3mV diffractometer. Photographs were used to determine crystal quality and obtain preliminary space group information. The unit cell was determined from 26 well-centered reflections between 25° $< 2\theta <$ 38°. The choice of space group was confirmed by axial photos and systematic absences. Data were collected in the range of 3.5° $< 2\theta <$ 45° for $0 < h < 13$, $0 < k < 16$, $-18 < l < 18$. This resulted in 4106 reflections, of which 2149 were considered observed for $I > 3\sigma(I)$. Absorption correction was performed via the psi scan technique using six intense high angle reflections. The structure was solved by direct methods (SHELXTL) and refined using standard least-squares programs in the Nicolet structure determination package. All non-hydrogen atoms were refined anisotropically and hydrogen atoms were fixed. The structure was refined to R = 0.0583, R_w = 0.0653. The largest peak remaining in the difference map was less than 1.5 electrons in the vicinity of the rhenium atom. Unit cell and structure solution information is given in Table 1. Positional and thermal parameters are given in Table 2, and bond distances and angles are given in Tables 3 and 4 respectively. Complete crystallographic data are available as supplementary material.[3]

Results and discussion

The reaction of anhydrous polyselenide solution with dirhenium decacarbonyl proceeds cleanly in dry DMF to form a dimeric species with two chelating tetraselenide chains (see Fig. 1). Although the formal composition of the selenide starting material is K_2Se_3, the solution is a complex equilibria of a variety of polyselenide species. The oxidation of the metal centers is presumably caused by reduction of a polyselenide in solution, although there is no direct experimental evidence for this.

[3]Complete tables of observed and calculated structure factors, distances and angles, anisotropic thermal parameters, and H-atom coordinates may be purchased from the Depository of Unpublished Data, CISTI, National Research Council of Canada, Ottawa, Ont., Canada K1A 0S2.

Tables of bond distances and angles and H-atom coordinates have also been deposited with the Cambridge Crystallographic Data Centre, and can be obtained on request from The Director, Cambridge Crystallographic Data Centre, University Chemical Laboratory, Lensfield Road, Cambridge CB2 1EW, U.K.

Can. J. Chem. Downloaded from www.nrcresearchpress.com by 186.148.149.217 on 09/07/12
For personal use only.

Can. J. Chem. Downloaded from www.nrcresearchpress.com by 186.148.149.217 on 09/07/12
For personal use only.

TABLE 2. Atomic coordinates ($\times 10^4$) and equivalent isotropic thermal parameters ($Å^2 \times 10^3$) for $[P(C_6H_5)_4]_2[Re_2(Se_4)_2(CO)_6]$

Atom	x	y	z	U(eq)
Re(1)	1099(1)	1008(1)	121(1)	47(1)
Se(1)	−134(2)	115(2)	−1085(2)	53(1)
Se(2)	−1648(2)	1089(3)	−1679(2)	78(1)
Se(3)	−1137(3)	2494(3)	−1068(2)	76(1)
Se(4)	−568(2)	2090(2)	317(2)	71(1)
P(1)	2060(5)	124(5)	6427(4)	50(2)
O(1)	3032(16)	−248(17)	−205(13)	95(10)
O(2)	2568(16)	1782(16)	1665(12)	86(9)
O(3)	1938(18)	2404(15)	−1031(13)	85(9)
C(1)	2303(22)	175(21)	−73(16)	63(11)
C(2)	1996(25)	1504(17)	1034(19)	73(12)
C(3)	1533(40)	1863(20)	−571(21)	134(20)
C(11)	3335(17)	206(21)	7188(14)	57(10)
C(12)	3359(24)	794(21)	7860(15)	76(12)
C(13)	4321(25)	923(26)	8409(19)	92(14)
C(14)	5236(25)	376(25)	8296(19)	84(14)
C(15)	5202(21)	−221(25)	7612(21)	85(14)
C(16)	4266(19)	−336(21)	7041(17)	67(11)
C(21)	1096(19)	−667(17)	6785(13)	50(9)
C(22)	−59(20)	−630(21)	6502(15)	69(11)
C(23)	−743(23)	−1282(22)	6753(18)	73(13)
C(24)	−307(28)	−1944(24)	7287(19)	83(14)
C(25)	803(26)	−2006(22)	7597(18)	75(13)
C(26)	1484(21)	−1372(22)	7344(16)	69(11)
C(31)	1407(21)	1217(19)	6297(16)	62(10)
C(32)	1567(24)	1729(21)	5606(20)	76(12)
C(33)	1115(24)	2598(28)	5544(19)	93(15)
C(34)	457(27)	2931(23)	6121(19)	93(14)
C(35)	336(22)	2438(19)	6785(19)	69(11)
C(36)	784(20)	1578(19)	6900(15)	56(10)
C(41)	2447(17)	−265(18)	5446(13)	44(8)
C(42)	1883(20)	−955(21)	4987(14)	64(10)
C(43)	2179(26)	−1215(26)	4250(19)	90(15)
C(44)	3011(28)	−822(31)	3958(19)	106(18)
C(45)	3622(21)	−83(23)	4390(18)	73(12)
C(46)	3322(18)	191(17)	5129(15)	54(9)

*Equivalent isotropic U defined as one third of the trace of the orthogonalized U_{ij} tensor.

TABLE 3. Selected bond distances (Å)

Bond	Distance	Bond	Distance
Re(1)—Se(1)	2.621(3)	Re(1)—Se(4)	2.612(3)
Re(1)—C(1)	1.953(29)	Re(1)—C(2)	1.847(28)
Re(1)—C(3)	1.805(35)	Re(1)—Se(1A)	2.645(3)
Se(1)—Se(2)	2.402(4)	Se(2)—Se(3)	2.322(5)
Se(3)—Se(4)	2.320(4)	O(1)—C(1)	1.121(36)
O(2)—C(2)	1.215(34)	O(3)—C(3)	1.232(43)

The structure of the molecule was determined by single crystal X-ray diffraction. It consists of two well-separated $(C_6H_5)_4P^+$ cations and the dimeric $[Re_2(CO)_6(Se_4)_2]^{2-}$ anion. The structure was solved successfully in the $P2_1/n$ space group with a crystallographic inversion center in the middle of the rhenium anionic cluster.

The Se—Se bond lengths average 2.348 Å, which is typical for metal polyselenides. In general, the structural parameters for these ligands are similar to those observed for other tetra-

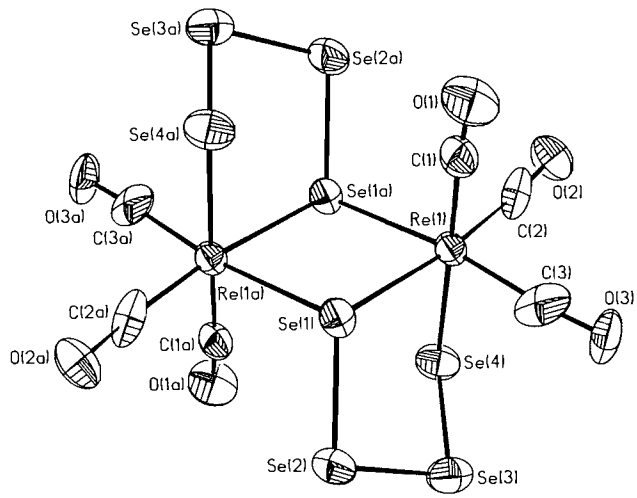


FIG. 1. ORTEP view of rhenium dianion fragment of $[(C_6H_5)_4P]_2[Re_2(Se_4)_2(CO)_6]$ with ellipsoids at 40% probability level.

chalcogen chelates. The Re—Se distances range from 2.612(3) to 2.645(3) Å with the bridging distances being longer than the terminal one (see Table 3). These can be compared to the Re—Se distances in the prototype rhenium selenide $ReSe_2$, which is a layered structure with rhenium atoms in a trigonal prismatic coordination environment with Re—Se distances ranging from 2.38 to 2.66 Å (10). The distances may also be compared to molecular complexes such as $[(Me_3P)_2(CO)_3Re]_2Se$, which contains a bridging selenide acting as a four-electron donor, and has a Re—Se distance of 2.65 Å (9). The Re—Re distance in the present molecule is 3.944(1) Å, which is out of bonding range.

The overall geometry of the molecule is unique. Each tetraselenium chain has one terminal and one bridging end. This mode of coordination has previously been observed for some complexes containing polysulfide chains such as $Cu_3(S_6)^{3-}$ (10). The bridging Se_4^{2-} group has also been observed for the first time in the chromium trimer $Cr_3Se_{24}^{3-}$ (11). Recently, a rhodium dimer containing two bridging Se_2 groups has been reported (12), as well as a complex with a pentaselenium chain terminally chelated to two vanadium centers (13). However, in general, bridging polyselenides are rare. In addition, the chemistry of polychalcogens with metal carbonyls is surprisingly undeveloped, in view of the many cyclopentadienyl polychalcogen complexes known (1, 14).

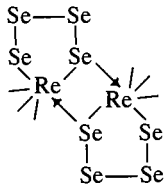
Both five-membered rings are in the envelope conformation with the metal in the base. This conformation type is well known for polychalcogen rings. The rhenium atoms are octahedrally coordinated in facial conformation by the three selenium atoms and three CO ligands. The geometry is only slightly distorted from octahedral. For example C(1)—Re(1)—Se(4) is 177.3(8)° (see Table 4). The IR spectrum shows the two stretches in the carbonyl region expected for localized C_{3v} symmetry.

Although the complex still contains coordinated carbon monoxide ligands, it has undergone oxidation at the metal centers, from 0 to 1+ upon substitution. In a formal sense, these electrons can be thought of as having been removed from the metal–metal bond. Since each metal atom is formally Re(I), each terminal selenide is a two-electron donor, and the bridging selenides are four-electron donors, the metal centers obey the 18-electron rule. It can be noticed that one of the bridging

TABLE 4. Selected bond angles (deg)

Bonds	Angle	Bonds	Angle
Se(1)—Re(1)—Se(4)	91.6(1)	Se(1)—Re(1)—C(1)	85.7(8)
Se(4)—Re(1)—C(1)	177.3(8)	Se(1)—Re(1)—C(2)	173.2(8)
Se(4)—Re(1)—C(2)	92.1(9)	C(1)—Re(1)—C(2)	90.6(12)
Se(1)—Re(1)—C(3)	93.9(11)	Se(4)—Re(1)—C(3)	87.3(14)
C(1)—Re(1)—C(3)	92.5(16)	C(2)—Re(1)—C(3)	92.0(14)
Se(1)—Re(1)—Se(1A)	83.0(1)	Se(4)—Re(1)—Se(1A)	83.9(1)
C(1)—Re(1)—Se(1A)	96.2(9)	C(2)—Re(1)—Se(1A)	91.7(9)
C(3)—Re(1)—Se(1A)	170.5(14)	Re(1)—Se(1)—Se(2)	108.6(1)
Re(1)—Se(1)—Re(1A)	97.0(1)	Se(2)—Se(1)—Re(1A)	103.3(1)
Se(1)—Se(2)—Se(3)	102.4(1)	Se(2)—Se(3)—Se(4)	102.0(2)
Re(1)—Se(4)—Se(3)	99.4(1)	Re(1)—C(1)—O(1)	174.9(26)
Re(1)—C(2)—O(2)	175.7(23)	Re(1)—C(3)—O(3)	173.2(35)

Re—Se distances is somewhat longer than the other (2.621(3) Å versus 2.645(3) Å). Thus, we can postulate a valence bond description like that shown below.



In this description, the molecule can be thought of as two 16-electron $[Re(Se_4)(CO)_3]^-$ fragments that complete their coordination environment by each sharing a lone pair of electrons on one of the terminal selenides.

Acknowledgements

This work was supported by National Science Foundation Grant CHE-8802217.

1. (*a*) H. J. GYSLING. The chemistry of organic selenium and tellurium compounds. Vol. 1. *Edited by* S. Patai and Z. Rappoport. John Wiley and Sons, New York. 1986. pp. 679–885; (*b*) M. DRAGANJAC and T. B. RAUCHFUSS. Angew. Chem. Int. Ed. Engl. **24**, 742 (1985); (*c*) A. MÜLLER and E. DIEMANN. Adv. Inorg. Chem. **31**, 89 (1987).
2. D. COUCOUVANIS, P. R. PATIL, M. G. KANATZIDIS, B. DETERING, and N. C. BAENZINGER. Inorg. Chem. **24**, 24 (1985).
3. (*a*) A. MÜLLER, E. KRICKEMEYER, and H. BÖGGE. Angew. Chem. Int. Ed. Engl. **25**, 272 (1986); (*b*) Y. DO, E. D. SIMHON, and R. H. HOLM. Inorg. Chem. **24**, 4635 (1985); (*c*) A. MÜLLER, E. KRICKEMEYER, and H. BÖGGE. Z. Anorg. Allg. Chem. **554**, 61 (1987); (*d*) F. A. COTTON, P. A. KIBALA, and M. MATUSZ. Polyhedron, **7**, 83 (1988).
4. M. HEBERHOLD, D. REINER, B. ZIMMER-GASSER, and U. SCHUBERT. Z. Naturforsch. B: Anorg. Chem. Org. Chem. **35B**, 1281 (1980).
5. (*a*) E. ROTTINGER, V. KÜLLMER, and H. VAHRENKAMP. J. Organomet. Chem. **150**, C6 (1978); (*b*) Chem. Ber. **110**, 1216 (1977).
6. S. C. O'NEAL and J. W. KOLIS. J. Am. Chem. Soc. **110**, 1971 (1988).
7. W. A. FLOMER, S. C. O'NEAL, J. W. KOLIS, D. JETER, and A. W. CORDES. Inorg. Chem. **27**, 971 (1988).
8. A. MULLER, E. DIEMANN, R. JOSTES, and H. BÖGGE. Angew. Chem. Int. Ed. Engl. **20**, 934 (1981).
9. N. W. ALCOCK and A. KJEKSHUS. Acta Chim. Scand. **19**, 75 (1965).
10. A. MULLER, F.-W. BAUMANN, H. BÖGGE, M. ROMER, E. KRICKEMEYER, and K. SCHMITZ. Angew. Chem. Int. Ed. Engl. **23**, 632 (1984).
11. W. A. FLOMER, S. C. O'NEAL, W. T. PENNINGTON, D. JETER, A. W. CORDES, and J. W. KOLIS. Angew. Chem. Int. Ed. Engl. **27**, 1702 (1988).
12. C. BIANCHINI, D. MASI, C. MEALLI, A. MELI, M. SABAT, and F. VIZZA. Inorg. Chem. **27**, 3716 (1988).
13. C.-N. CHAU, R. W. M. WARDLE, and J. A. IBERS. Inorg. Chem. **26**, 2740 (1987).
14. (*a*) B. R. DAVIS, I. BERNAL, and H. KOPF. Angew. Chem. Int. Ed. Engl. **12**, 921 (1971); (*b*) C. M. BOLINGER and T. B. RAUCHFUSS. Inorg. Chem. **21**, 3947 (1982); (*c*) A. SHAVER and J. M. MCCALL. Organometallics, **3**, 1823 (1984).

Can. J. Chem. Downloaded from www.nrcresearchpress.com by 186.148.149.217 on 09/07/12
For personal use only.

The lone electron pair and crystal packing: observations on pyramidal YEL_3^{ϵ} species, *ab initio* calculations, and the crystal structures of Me_3SOI, Et_3SI, $(Me_3S)_2SnCl_6$, $(Me_3SO)_2SnCl_6$, and $(Et_3S)_2SnCl_6$

OSVALD KNOP,[1] ANTHONY LINDEN, BEVERLY R. VINCENT,[2] S. C. CHOI, T. STANLEY CAMERON, AND RUSSELL J. BOYD

Department of Chemistry, Dalhousie University, Halifax, N.S., Canada B3H 4J3

Received March 15, 1989

This paper is dedicated to Professor Ronald J. Gillespie on the occasion of his 65th birthday

OSVALD KNOP, ANTHONY LINDEN, BEVERLY R. VINCENT, S. C. CHOI, T. STANLEY CAMERON, and RUSSELL J. BOYD. Can. J. Chem. **67**, 1984 (1989).

The results of a detailed analysis of typical situations in crystals containing trigonal-pyramidal YEL_3^{ϵ} species are used to argue that, *per se*, the lone electron pair (*E*, LP) on the Y atom determines neither the crystal structure nor the orientation of the YEL_3^{ϵ} units in the crystal. Considered as a space-filling entity, the LP has practically no effective volume of its own. Whatever space-filling or orienting properties may be associated with the presence of the LP, they are not autonomous; they arise from the intrinsic stereochemical involvement of the LP in the geometry of and the charge distribution in the *free* YEL_3^{ϵ} ion or molecule and hence from the consequences of this geometry for crystal packing. *Ab initio* (6-31G*) calculations show that the electron density in the region of the LP in an ion is only slightly perturbed by the charge on the counter ion at distances observed in crystals. There is considerable similarity in the electron density distribution in the LP region of Y between free anionic (SO_3^{2-}) and free cationic (Me_3S^+) species. The problem of the so-called stereochemical inertness of the LP in the 14-electron octahedral YEX_6^{2-} ions in crystals is examined in detail. It is concluded that the crystallographic O_h symmetry of the ion in cubic crystals is the result of dynamic averaging of possible orientations of the inherently noncubic YX_6^{2-} octahedron (cf. the *ab initio* results for $SeCl_6^{2-}$). Such averaging also appears to be responsible for the stereochemical "activation" or "inactivation" of the LP in thermally induced crystallographic transitions in the AYX_3 halide perovskites and related crystals. To provide a firmer basis for the discussion of the LP, the crystal structures of the five title compounds have been determined. The crystal chemistry of these and related compounds is discussed.

Key words: *ab initio* calculations, Me_3S^+ and $SeCl_6^{2-}$; group V trihalides; lone electron pair; trialkylsulfonium salts; VSEPR theory.

OSVALD KNOP, ANTHONY LINDEN, BEVERLY R. VINCENT, S. C. CHOI, T. STANLEY CAMERON et RUSSELL J. BOYD. Can. J. Chem. **67**, 1984 (1989).

En se basant sur les résultats d'une analyse détaillée de situations typiques dans des cristaux contenant des espèces YEL_3^{ϵ}, on suggère que la paire d'électron libre (*E*, PL) sur l'atome Y ne détermine pas *per se* la structure cristalline ou l'orientation des unités YEL_3^{ϵ} dans le cristal. Considérée comme une entité qui occupe du volume, la PL n'a pratiquement pas de volume effectif intrinsèque. Quelles que soient les propriétés associées avec la présence de la PL, elles ne sont pas autonomes; elles découlent de l'implication stéréochimique intrinsèque de la PL dans la géométrie de et de la distribution de charge dans l'ion ou la molécule YEL_3^{ϵ} *libre* et ainsi des conséquences de cette géométrie sur l'empilement cristallin. Des calculs *ab initio* (6-31G*) démontrent que, aux distances observées dans les cristaux, la densité électronique dans la région de la PL d'un ion n'est que légèrement perturbée par la charge du contre-ion. Il existe une grande similarité dans la distribution de la densité électronique dans la région de la PL de Y des espèces anionique libre (SO_3^{2-}) et cationique libre (Me_3S^+). On a procédé à un examen détaillé du problème de la soit-disant inertie stéréochimique de la PL dans les cristaux d'ions YEX_6^{2-}. On en conclut que la symétrie cristallographique O_h observée dans les cristaux cubiques est le résultat d'une moyenne dynamique des orientations possibles de l'octaèdre YX_6^{2-} qui est d'une façon inhérente non-cubique (voir les résultats de calculs *ab initio* sur le $SeCl_6^{2-}$). Il semble que de telles moyennes sont aussi responsables de l'«activation» ou de la «non-activation» stéréochimique de la PL dans des transitions cristallographiques induites par température dans des cristaux d'halogénures de perovskites (AYX_3) ainsi que dans d'autres cristaux apparentés. Afin d'asseoir la discussion des PL sur une base plus ferme, on a déterminé les structures cristallines des cinq composés mentionnés dans le titre. On discute de la chimie cristalline de ces composés ainsi que celle de composés apparentés.

Mots clés : calculs *ab initio*, Me_3S^+ et $SeCl_6^{2-}$; trihalogénures du groupe V; paire d'électrons libres; sels de trialkylsulfonium; théorie de VSEPR.

[Traduit par la revue]

The consequences of the stereochemical activity of the lone electron pair (LP, *E*) for the geometry of free molecular species are of course well known (1, 2). What is less well understood, however, is the extent to which the presence of a LP is responsible for orientational effects in crystals and, more generally, for determining the type, compactness, and symmetry of the crystal packing. In an attempt to focus attention on these problems[3] we examine, in the following, a number of situations typical of crystals containing trigonal-pyramidal YEL_3^{ϵ} ions or

[1]To whom correspondence may be addressed.

[2]Holder of NSERC (1983–1986), Killam (1984–1986), and Sumner (1986–1987) Graduate Fellowships.

[3]Galy *et al.* (3) have examined the implications of LPs for the crystal chemistry of a large number of oxides, fluorides, and oxyfluorides of elements from rows 3 to 5 of the Periodic Table. However, the aims and premises of their treatment are so different from ours that further reference to their work appears unnecessary in the present paper. We also leave out of account the infrequent *ad hoc* investigations designed to demonstrate the *existence* of the LP as a residual electron density in difference Fourier maps (e.g. refs. 4–6), for the chemistry of the available results is too random to be of much value for our stated purpose.

Can. J. Chem. Downloaded from www.nrcresearchpress.com by 194.225.253.170 on 09/07/12
For personal use only.

TABLE 1. Crystal data of Me_3SOI, Et_3SI, $(Me_3S)_2SnCl_6$ (3MSHS), $(Me_3SO)_2SnCl_6$ (3MSOHS), and $(Et_3S)_2SnCl_6$ (3ESHS)[a]

Parameter	Value				
	Me_3SOI	Et_3SI	3MSHS	3MSOHS	3ESHS
Formula	C_3H_9IOS	$C_6H_{15}IS$	$C_6H_{18}Cl_6S_2Sn$	$C_6H_{18}Cl_6O_2S_2Sn$	$C_{12}H_{30}Cl_6S_2Sn$
fw	220.07	246.15	485.75	517.75	569.91
θ-range, deg	2–30	2–30	2–23	2–25	2–25
μ_{Mo}, cm^{-1}	46.9	33.6	22.1	24.6	19.2
Max/min[b]	1.590/0.763	1.196/0.786	1.247/0.685	1.308/0.793	1.316/0.910
a, Å	11.268(2)	15.774(4)[c]	12.396(5)[d]	7.132(1)	15.736(2)
b, Å	7.686(1)	7.318(3)[c]	12.396(5)[d]	13.097(3)	10.545(2)
c, Å	8.280(1)	8.667(2)[c]	12.396(5)[d]	9.838(1)	15.430(3)
β, deg	90	90	90	90	112.42(1)
V, $Å^3$	717(1)	1000(1)	1905(3)	919(1)	2367(2)
Z	4	4	4	2	4
ρ_c, g/cm^3	2.039(3)	1.635(2)	1.694(3)	1.867(2)	1.599(1)
Space group	*Pnma* (no. 62)	$Pna2_1$ (no. 33)	$Pa3$ (no. 205)	*Pnnm* (no. 58)	$C2/c$ (no. 15)
$F(000)$, e	416	480	952	508	1144
Reflections:					
Total measured	1652[e]	1710[f]	1886[g]	1369[h]	2743[i]
Unique total	1111	1545	447	859	2085
Unique used	808[j]	800[k]	379[j]	676[j]	1744[j]
$100R_{merg}$	4.2	2.0	6.0	3.7	1.5
d/p[l]	18.8	6.0	10.5	10.2	11.0
$100R$; $100R_w$	6.18; 5.91	2.05; 2.36	3.12; 3.24	3.15; 3.42	2.42; 2.66

[a]Mo $K\alpha_1$, $\lambda = 0.70926$ Å (graphite monochromator); 22°C.
[b]Max/min empirical absorption corrections, cf. ref. 7.
[c]Reference 8: 15.81, 7.35, 8.69 Å; $\rho_o = 1.56$ g/cm^3.
[d]Reference 9: 12.41 Å; $\rho_o = 1.69$ g/cm^3. Reference 10: 12.423(2) Å.
[e]$I > 2\sigma(I)$, 1133.
[f]$I > 3\sigma(I)$, 1149.
[g]$I > 2\sigma(I)$, 1402.
[h]$I > 2\sigma(I)$, 986.
[i]$I > 2\sigma(I)$, 2186.
[j]$I > 2\sigma(I)$.
[k]$I > 3\sigma(I)$.
[l]Data to parameters of refinement.

neutral molecules (Y = mostly second-row elements, $-2 \leq \epsilon \leq 1$; L = simple ligands) and compare them with situations involving the matching tetrahedral (*sensu lato*) $YL'L_3^{\epsilon}$ species. To this end, the meager body of literature information on cationic YEL_3^+ species has been augmented by the determination of the crystal structures of the sulfonium salts Et_3SI, $(Me_3S)_2SnCl_6$ (3MSHS), and $(Et_3S)_2SnCl_6$ (3ESHS) and, for comparison, of the sulfoxonium salts Me_3SOI and $(Me_3SO)_2SnCl_6$ (3MSOHS). The crystal data of these compounds are summarized in Table 1. Details of these determinations and a discussion of the structures are relegated to the end of this paper, but the structural as well as some new *ab initio* results will be drawn upon freely in the sections that immediately follow. Detailed consideration is also given to the so-called stereochemically inert (or inactive) LP in crystals containing $YHal_6^{2-}$ ions of crystallographic O_h symmetry, and to what on the face of it appears to be conversion of an active to an inactive LP in crystallographic transitions.

Rôle of the LP in crystals

The questions we shall ask here are (*1*) Is the LP a space-filling entity? (*2*) Is the electronic charge attributed to the LP responsible for the orientation of the YEL_3^{ϵ} unit in the crystal? (*3*) Under what circumstances is a LP in a crystal stereochemically inactive, and is the inactivity real or apparent, intrinsic or associated with the particulars of the crystal structure?

These questions, with the possible exception of the last one, cannot be answered in absolute terms. Because of the elusiveness of the LP as a geometric and physical entity, the problems implicit in them can be investigated with any confidence (and without assumptions or preconceived notions) only with recourse to matched pairs of $A_m(YEL_3)_n|A_m(YL'L_3)_n$ crystals, isostructural except for L'. Very few such pairs are available. The best three we have found are $PbSO_3|PbSO_4$, $KClO_3|KClO_4$, and $PBr_3|POBr_3$, and these are examined in detail below. However, some $A_m(YEL_3)_n|A_m(YL'L_3)_n$ pairs, while not isostructural, are sufficiently similar to be informative in limited ways. Examples of these are $Me_3SI|Me_3SOI$ and the pairs listed in Table 2.

Spatial extension of the LP in crystals

The notion that a stereochemically active LP should have spatial extension implies that significant electron density is associated, locally, with the LP and that this electron density extends radially and in a particular direction from the parent atom over an appreciable portion of space in the crystal, effectively excluding other atoms from occupation of this space and thus creating a void in the crystal structure.

Effective radius. It may not be possible to establish an "effective radius" of a LP in the same way as one arrives at a self-consistent set of additive atomic or ionic radii from interatomic distances in crystals. In neutral YEL_3 molecular crystals an estimate of the upper effective length of a LP could

Can. J. Chem. Downloaded from www.nrcresearchpress.com by 194.225.253.170 on 09/07/12
For personal use only.

TABLE 2. Differences in the volume per formula unit V_1 (Å) for $A_mYEL_3|A_mYOL_3$ (m = 0–2) pairs[a]

A_mYEL_3	V_1	A_mYOL_3	V_1	ΔV_1
$NaClO_3$, $P2_13$ (13, 14)	71.1	$NaClO_4$, *Cmcm* (15)[b,c]	81.5	10.4
$KClO_3$, $P2_1/m$ (16, 17)[b,d]	87.1	$KClO_4$, *Pnma* (18)[b,c]	91.1	4.0
$RbClO_3$, $R3m$	86.8	$RbClO_4$, *Pnma*[b,c]	100.9	14.1
NH_4ClO_3, $R3m$[f]	87.3	NH_4ClO_4, *Pnma* (19, 20)[b,c]	100.0	12.7
$TlClO_3$, $R3m$	86.4	$TlClO_4$, *Pnma*[b,c]	102.1	15.7
$AgClO_3$, $I4/m$	71.1	$AgClO_4$, $I\bar{4}2m$ (21)	83.5	12.4
$KBrO_3$, $R3m$ (22)	85.0	$KBrO_4$, *Pnma* (23)	99.0	14.0
$NaIO_3$, *Pnma*	(74.1)	$NaIO_4$, $I4_1/a$	84.5	(10.4)
KIO_3, $P1$, $Z = 4$ (12, 24, 25)[g]	89.0	KIO_4, $I4_1/a$	(104.4)	(15.4)
$RbIO_3$, $R3m$ (12, 26, 27)	93.6	$RbIO_4$, $I4_1/a$	114.4	20.8
NH_4IO_3, $Pna2_1$ (12, 28)[h]	93.8	NH_4IO_4, $I4_1/a$	112.7	18.9
$CsIO_3$, *Pm*, $Z = 2$ (12, 26, 29)	102.1	$CsIO_4$, *Pnma*	(126.1)	(24.0)
$AgIO_3$, $R3m$?	79.5	$AgIO_4$, $I4_1/a$	87.3	7.8
Na_2SO_3, $P\bar{3}$ (30)	79.7	Na_2SO_4 (*I*), $P6_3/mmc$ (31)	87.5	⟨8.1⟩
		Na_2SO_4(*III*), *Cmcm* (32)	87.5	
		Na_2SO_4(*V*), *Fddd* (33)	88.5	
K_2SO_3, $P\bar{3}m1$ (34)	105.6	K_2SO_4, *Pnma* (35)[i]	108.5	2.9
Ag_2SO_3, $P2_1/c$ (36)	88.1	Ag_2SO_4, *Fddd* (12, 37)	⟨94.5⟩	⟨6.4⟩
$PbSO_3$, *Pnma* (38)	73.8	$PbSO_4$, *Pnma* (39)	79.6	5.8
PCl_3 (161 K), *Pnma* (40)	(119)	$POCl_3$, $Pn2_1a$ (41)	123.1	(4)
PBr_3 (193 K), *Pnma* (40)	130.8[j]	$POBr_3$, *Pnma* (42, 43)	145.8	15.0

[a]Where no reference is given the source is ref. 11 or ref. 12. Values in parentheses are of lower accuracy; ⟨V_1⟩ is the average of two or more literature values.

[b]Approximate transition temperatures in °C (literature values): $NaClO_4$, 308; $KClO_3$, ~250; $KClO_4$, 301; $RbClO_4$, 275; NH_4ClO_4, 238; $TlClO_4$, 267.

[c]$Fm3m$ above T_{tr}.

[d]HT-$KClO_3$, *Pnma*, V_1 = (92.2) Å^3 at 280°C (44); HP-$KClO_3$, $R3m$, V_1 = 77 Å^3 (45).

[e]$Fm3m$ at 340°C, V_1 = (104.2) Å^3.

[f]Cubic above 240°C.

[g]Monoclinic above 72.5°C, orthorhombic above 212°C. Reference 46: $R3m$ above 212°C.

[h]At 85°C transition to a nonpolar phase.

[i]At 582°C transition to $P\bar{3}m1$ (47).

[j]V_1 corrected for thermal expansion assuming $dV/dT = 0.01\%/K$.

be made from the interatomic separation of Y and the nearest coaxial L facing *E*, on the assumption that the size of L in this nonbonding Y···L contact corresponds to the van der Waals radius of L. However, molecular crystals in which there *is* an L neighbour coaxial or nearly coaxial with *E* do not appear to be known. *Ionic* crystals with YEL_3[e] as a component and containing collinear YE···counterion groupings do exist (cf. Table 3), but here the polarization of the electron density on Y in the region of the LP by the charge on the counterion renders the use of the van der Waals radii suspect.

The coaxial and the shortest lateral interatomic Y···L distances in a number of well-studied crystals are compared with the sums of the corresponding van der Waals radii (where applicable) in Table 3. The shortest lateral Y···L and Y···anion separations are all smaller than the van der Waals sums but the difference does not exceed 10%, and this is true also of the O···Br separation in $POBr_3$. However, contrary to expectation, the shortest S···I distance in Me_3SI is larger than the shortest Se···I distance in Me_3SeI, and the shortest P···Br distance in PBr_3 is larger than the shortest P···I distance in PI_3. Again, the shortest O···I distance in Me_3SOI is ~0.8 Å longer than the shortest O···Cl distance in 3MSOHS; allowing 0.4 Å for the size difference between Cl and I leaves a residue of 0.4 Å. Further, the shortest O···I distance in Me_3SOI, 4.73 Å, is much larger than the minimum S···I separation in Me_3SI, 3.95 Å. These inconsistencies suggest that the overall packing requirements in the individual structures dominate the local geometries. The same tendency is evident in the two Me_3SO^+ salts. The O···Cl distance in 3MSOHS is ~7% larger than the van der Waals sum, while in Me_3SOI the shortest non-coaxial O···I distance exceeds the sum by 30% and the axial distance by 33%.

The coaxial Y···M separations which occur in the oxyanion salts of Table 3 are, in the three halogenates, 4–19% longer than the corresponding shortest lateral Y···M separations. While it might be tempting to view this lengthening as due to the existence of directional dependence of the Y···M distance attributable to the LP, in the two sulfites the axial S···M distance is 3–4% shorter than the shortest lateral S···M distances. Furthermore, contrary to what would be expected, the axial Cl···Na distance in $NaClO_3$ is 0.16 Å *longer* than the corresponding Br···Na distance in $NaBrO_3$, in spite of the two crystals being isostructural and the Hal···Na vector coinciding with the C_3 axis of the $P2_13$ unit cell.[4] One is therefore forced to conclude that evidence from interatomic distances in crystals is not likely to lead to meaningful estimates of the effective radius of a LP, since accidents of packing appear generally to obscure whatever systematic effects may arise from the effective size of the LP.

[4]The frequency and temperature dependence of the dielectric constant of $NaClO_3$ have been interpreted (53) as involving inversion of the Cl atom through the plane of the three oxygens, i.e. twofold orientational disorder increasing with temperature. The existence of such disorder would suggest that the orientation of the anion is not determined by the interaction between the LP and the coaxial Na^+ ion at 4 Å (see below).

Can. J. Chem. Downloaded from www.nrcresearchpress.com by 194.225.253.170 on 09/07/12
For personal use only.

Can. J. Chem. Downloaded from www.nrcresearchpress.com by 194.225.253.170 on 09/07/12
For personal use only.

TABLE 3. Coaxial and shortest lateral nonbonding contacts in some crystals containing trigonal-pyramidal YEL_3^{ϵ} and $YL'L_3^{\epsilon}$ molecules[a]

Crystal	Distance Between	Coaxial	Lateral[b]	ΣvdW
$(Me_3S)_2SnCl_6$ (this work)	S···Cl	—	3.50	3.65
$(Et_3S)_2SnCl_6$ (this work)	S···Cl	—	3.57	3.65
Me_3SI (48)	S···I	—	3.95	4.00
Et_3SI (this work)	S···I	—	3.91	4.00
Me_3SeI (49)	Se···I	—	3.78	4.15
$Me_3Te^+MeTeI_4^-$ (50)[c]	Te···I	—	3.84	4.35
PBr_3 (40)	P···Br	—	3.75	3.85
PI_3 (51)	P···I	—	3.67	4.05
$(Me_3SO)_2SnCl_6$ (this work)	O···Cl	—	3.41[d]	3.20
Me_3SOI (this work)	O···I	4.87	4.73[e]	3.65
$POBr_3$ (42, 43)	O···Br	—	3.07	3.35
$NaClO_3$ (13, 14)	Cl···Na	3.98	3.35[f]	
$NaBrO_3$ (14, 22)	Br···Na	3.82	3.45[g]	
$KClO_3$ (16, 17)	Cl···K	3.97	3.82	
$KClO_4$ (18)	Cl···K	4.27		
	O···K	2.86		
K_2SO_3 (34)	S···K	3.55	3.65	
$PbSO_3$ (38)	S···Pb	3.42	3.55	
$PbSO_4$ (39)	S···Pb	4.01	3.43	
	O···Pb	2.61		
$CsSHO_3$ (52)	H···Cs	~3.5[h]	~3.7[h]	

[a]Distances in Å; ΣvdW, sum of the respective van der Waals radii (Å).
[b]Shortest non-coaxial Y···atom distance on the LP side of YEL_3^{ϵ} or $YL'L_3^{\epsilon}$.
[c]In the square-pyramidal $MeTeI_4^-$ the C—Te···I grouping is 17° off collinear, Te···I = 3.88 Å, ΣvdW = 4.35 Å.
[d]Shortest S···Cl on the LP side of S, 4.10 Å.
[e]Shortest S···I on the LP side of S, 4.60 Å; on the opposite side, 4.38 Å (cf. Table 11).
[f]Shortest Cl···Na distance on the opposite side of LP, 3.52 Å.
[g]Shortest Br···Na distance on the opposite side of LP, 3.65 Å.
[h]Assuming S—H ~ 1.30 Å. S···Cs, 4.82 Å (front), 3.89 Å (back), 3.78 Å (lateral).

Effective volume. If attempts to obtain the effective linear dimension of a LP from crystal data are disappointing, can more promise be expected from examination of crystal structures with a view to estimating the effective *volume* occupied by a LP? A space-filling LP on Y could be regarded as a ligand without a nucleus. The difference $\Delta V_1 = V_1(A_mYL'L_3) - V_1(A_mYEL_3)$ between the volumes per formula unit of the two partners in an isostructural $A_mYEL_3|A_mYL'L_3$ (m = 0–2) pair should then represent the difference between the effective volumes of L′ and the LP, provided that the molecular geometry of the YL_3 part of YEL_3^{ϵ} undergoes only small changes on conversion to $YL'L_3^{\epsilon}$ and ϵ remains the same. Since the two crystals are isostructural and have comparable unit-cell dimensions, the coordination numbers of A and YL_3 or $YL'L_3$ will be essentially unchanged and so will the effective sizes of these entities.

The relative constancy of the molecular geometry is illustrated in Table 4, which reports the equilibrium geometries of free YEL_3^{ϵ} and $YL'L_3^{\epsilon}$ resulting from 6-31G* optimizations as well as geometries obtained from the crystal structures of the isostructural pairs. For the 6-31G* optimized species the contraction of the Y—L bond on adding L′ amounts to 1.5–7% and the increase in the LYL angle to 1–12°, depending on the nature of L′ and the change in ϵ. However, for the three isostructural pairs $PBr_3|POBr_3$, $KClO_3|KClO_4$, and $PbSO_3|PbSO_4$, where the geometries derive directly from experiment, the changes in ⟨Y—L⟩ are only 1.4–3.4% and in ⟨LYL⟩, 3.1–5.0°. Changes of this order seem sufficiently small to justify the validity of comparing V_1 for the stated purpose.

The differences ΔV_1 for the three isostructural pairs as well as for a number of other, not isostructural $A_mYEL_3|A_mYOL_3$ pairs are listed in Table 2.[5] All the ΔV_1 values in this table are positive, i.e. the oxygen ligand occupies a larger effective volume than the LP. The ΔV_1 values appear to fall in two main classes, those for $YO_3^-|YO_4^-$, which average 14–15 Å^3, and those for $SO_3^{2-}|SO_4^{2-}$, for which the mean ΔV_1 is considerably smaller, about 6 Å^3. The spread of ΔV_1 in each class must be attributed to differences in packing density, especially when the $A_mYEL_3 \rightarrow A_mYL'L_3$ conversion is associated with a change of space group. The direction and magnitude of the V_1 change resulting from a change in space-group symmetry (superimposed on the ΔV_1 expected for an isostructural pair) are difficult to assess. In purely molecular organic crystals loss of symmetry is balanced by an increase in packing density (cf. ref. 57), but in ionic and other inorganic crystals containing stereochemically active LPs the trend is much less predictable (see below).

In homologous series of organic molecular crystals the average volume increments (in Å^3) are 11.1/CH(aliphatic), 14.7/CH(aromatic), 17.1/CH_2, 23.5/CH_3, 23.0/NO_2, and 23.1/COOH; the average increments per halogen atom bonded to a carbon are 9.6 for F, 19.9 for Cl, and 26.0 for Br (57). Since the average difference ΔV_1 for $YEL_3^{\epsilon}|YOL_3^{\epsilon}$ is about 15 Å^3, the effective volume V_1(O) of the oxygen ligand would be $V_1(E)$ + 15 Å^3, so that with $V_1(E)$ as small as 5 Å^3 the V_1(O) would be of the same order as V_1(Cl) and, worse still, only about 3 Å^3 smaller than the increments for NO_2 and COOH, each involving *two* oxygen atoms. This clearly is unreasonable, even if one allows for the imprecise nature of the present arguments, and one is forced to conclude that the volume effectively occupied by the LP must be (*a*) quite small and (*b*) comparable to the spread of the ΔV_1 values of Table 2. This means that either the LP has no significant volume of its own (i.e. it does not function as a space-filling ligand on Y) or that accidents of packing invalidate comparisons of V_1 values as a method for establishing $V_1(E)$ or both. Consideration of calculated electron-density distributions in the region where the LP in ClO_3^-, SO_3^{2-}, and Me_3S^+ is expected to be present (see below) tend to support the conclusion that the LP is unimportant as an autonomous space-filling entity.

For *cationic* YEL_3^{ϵ} only the pairs $Me_3SI|Me_3SOI$ and 3MSHS|3MSOHS are available (Table 5). For the iodides ΔV_1 is 8 Å^3, in the expected direction. For the hexachlorostannates, however, ΔV_1 is *negative*, −20 Å^3. This, to our knowledge the first reported case of a decrease in V_1 on $YEL_3^{\epsilon} \rightarrow YL'L_3^{\epsilon}$ conversion, is almost certainly attributable to the loss of crystal symmetry: the highly symmetric (*Pa*3) 3MSHS structure is less densely packed than the *Pnma* structure of the sulfoxonium salt (Fig. 1), and the increase in the packing density on conversion is sufficient to overcompensate the increase in V_1 expected on adding the oxygen ligand. This kind of behaviour is more likely to occur with composite than with simple L ligands and further illustrates the importance of global as opposite to local packing requirements in the crystal.

[5]Where several literature sets of crystallographic data exist for a compound, the spread on the V_1 calculated from them may amount to as much as 0.5 Å^3. Where required the V_1 was corrected for thermal expansion assuming $dV_1/dT = 0.01\%/K$.

Can. J. Chem. Downloaded from www.nrcresearchpress.com by 194.225.253.170 on 09/07/12
For personal use only.

TABLE 4. Changes in the molecular geometry resulting from conversion of a trigonal-pyramidal YEL_3^{ϵ} species to a tetrahedral $YL'L_3^{\epsilon}$ species[a]

YEL_3^{ϵ}	Y—L	LYL	$YL'L_3^{\epsilon}$	Y—L	LYL
PF_3 (54)	1.5641	97.26	PF_4^+ (55)	1.4795	109.47
			PHF_3^+	1.4912	108.03
			$PClF_3^+$ (55)	1.4925	107.06
			POF_3	1.5257	100.70
			PSF_3	1.5346	99.58
PCl_3 (54)	2.0480	100.78	$PSCl_3$	1.9003	102.23
			$PFCl_3^+$ (55)	1.9341	111.88
			PCl_4^+ (55)	1.9520	109.47
			$POCl_3$	1.9978	103.95
PBr_3[b] (40)	⟨2.213(2)⟩	⟨100.5(11)⟩	$POBr_3$[b] (42, 43)	⟨2.137(10)⟩	⟨105.5(3)⟩
ClO_3^-	1.4866	108.60	ClO_4^-	1.4503	109.47
$KClO_3$[c] (16, 17)	⟨1.477(3)⟩	⟨106.5(2)⟩	$KClO_4$[b] (18)	⟨1.457(24)⟩	⟨110.5(8)⟩
SO_3^{2-}	1.5255	107.67	$SS'O_3^{2-}$ (56)	1.4724	110.83
			SO_4^{2-}	1.4867	109.47
$PbSO_3$[b] (38)	⟨1.522(20)⟩	⟨104.7(3)⟩	$PbSO_4$[b] (39)	⟨1.492(8)⟩	⟨107.8(4)⟩

[a]Bond length Y—L in Å, bond angle LYL in deg. Where no reference is given the values refer to 6-31G* optimized molecular geometries of C_{3v} or T_d symmetry, as do the values from refs. 54–56.
[b]Space group *Pnma*, molecular symmetry C_s.
[c]Space group $P2_1/m \subset Pnma$, molecular symmetry C_s.

TABLE 5. Volume per formula unit V_1 (Å^3) of $YL'L_3^+$ onium salts

	V_1			
YL'	$Me_3YL'I$	$Et_3YL'I$	$(Me_3YL')_2SnCl_6$	$(Et_3YL')_2SnCl_6$
S*E*	171 (48)	256[a]	476[a]	592[a]
SO	179[a]		456[a]	
SeO	174 (49)			
NH	162 (58)	258 (59)	455 (60)	564 (61)
NMe	182 (11)		530 (62)	616 (11)
NEt		272 (63)	571 (11)	667 (64)

[a]This work.

LP as an orientation-determining factor

Descriptions and discussions of crystal structures often imply that the LP determines the orientation of the L_3YE^{ϵ} molecule or ion in the crystal. While a case for this can be made for molecular association or ionic interaction in solution or in the gas phase, in crystals the situation is quite different. In the liquid or gas the limit to the approach of Y to an interacting portion of another molecule or ion is ultimately set by the equilibrium interatomic distance in a properly oriented pair of the two free molecules. This distance is governed by the repulsive forces in the pair and is sufficiently small for such local concentration of electron density as may exist in the LP to interact to maximum advantage with local charge on the partner molecule in the pair. In crystals, however, the interatomic distances are determined by Coulombic and packing factors, with the result that generally the LP will be farther removed from a potentially interacting atom or ion than would be the case in the liquid or gas. Moreover, because of the actual shape and size of the L_3YE^{ϵ} unit and the relative magnitude of the crystal factors, the presumed orientation of the LP may not be in the most favourable direction possible in the isolated pair. Both circumstances would lessen the importance of the LP as a structure-determining factor in crystals, and it then becomes necessary to investigate whether the orientation of the LP is in fact the consequence of its interaction with the crystal environment. In this respect the discussion of the LP is reminiscent of the discussion of hydrogen bonding as a structure-determining factor in crystals, especially in ionic crystals.

Typical situations. A summary of the representative features of crystal structures of simple $L_3YL'^{\epsilon}$ compounds (L' = *E*, O, H, C, Br; $\epsilon = -1, 0, 1$) is presented in Figs. 1 and 2. Comparison of the orientation of the L_3YL' axis in these structures is facilitated by the tendency of the molecule to retain its C_3 or C_s skeletal symmetry, which ensures that the orientation of the Y—L' vector in the direction expected to be most effective is clearly displayed. In Fig. 2 the Y atoms and the atoms forming the quadrangular or quinquangular coordination figures (single circles) of L_3YE^{ϵ} and $L_3YL'^{\epsilon}$ are coplanar (in a mirror plane) or near-coplanar, i.e. the YL_3 axis and hence the axis of the LP and the Y—L' vector are in the same plane.[6] The following is observed (not all the structures are shown in the figures):

(*a*) In $NaClO_3$, $NaBrO_3$, $KClO_3$, and K_2SO_3 a cation facing the LP is located on the anion axis at 3.8–4 Å from the halogen and 3.55 Å from the S atom. The collinearity is consistent with the expectation that the anionic charge would reinforce the orienting effect of the LP.

(*b*) In PBr_3 and PI_3 the LP end of the molecule axis points symmetrically (C_s in PBr_3, C_3 in PI_3) between the nearest halogen neighbours at ~3.7 Å from P.

(*c*) In Me_3SI, Me_3SeI, and Et_3SI the LP end of the C_3Y axis points between the nearest I^- ions at Y···I = 3.8–4 Å. In $(CH_2)_5SMe^+I^-$ there is an I atom close to the C_3S axis but at 7.4 Å from the S atom.

(*d*) In Me_3SOI the S—O bond and an I^- neighbour are collinear (O···I ~ 4.9 Å); in $POBr_3$ the P—O bond points *between* Br neighbours of the oxygen.

(*e*) In Et_3NHI the hydrogen bond N—H···I is linear by symmetry, with an N···I separation of 3.60 Å, and in Me_3NHI the N—H···I bond is close to linear, N···I = 3.46 Å. The

[6]This is not a consequence of the LP being present but a requirement for maximizing the density of packing.

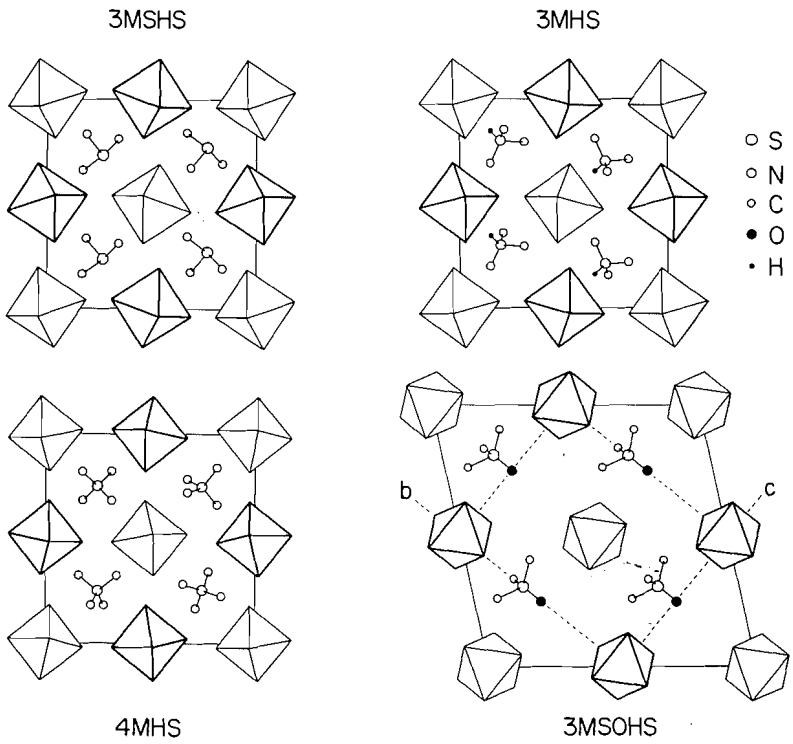


FIG. 1. Consequences of the nature of L′ for the cation orientation in *anti*-fluorite type $(Me_3YL')_2SnCl_6$ structures. Tabulated unit cells have been transformed where necessary to match as far as possible the attitudes of the $SnCl_6$ octahedra at the origin (upper left-hand corner); H_C atoms have been omitted for clarity. 3MSHS: YL′ = S*E*, lower half of the *Pa*3 unit cell; coordinates of Table 14 transformed as $x \rightarrow z$, $y \rightarrow -x$, $z \rightarrow \frac{1}{2} - y$. 3MHS: YL′ = NH, lower half of the unit cell (60). 4MHS: YL′ = NMe, lower half of the first octant of the *Fd*3*c* cell of ref. 62. 3MSOHS: YL′ = SO; solid lines, lower half of a cell related to the cell of Table 1 (broken lines) by **a**′ = **a**, **b**′ = **b** + **c**, **c**′ = −**b** + **c**.

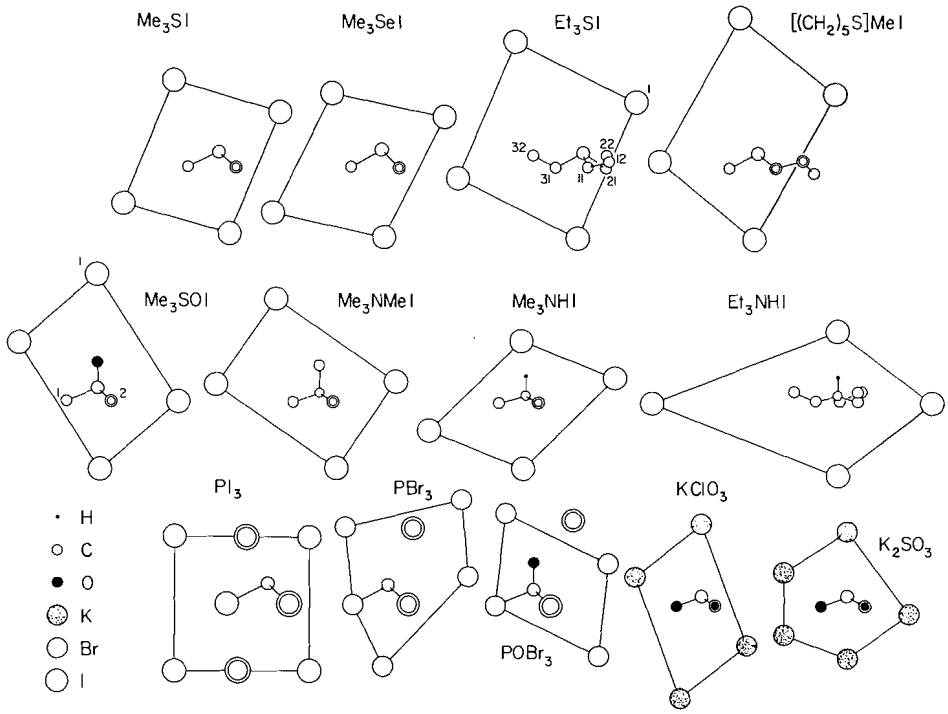


FIG. 2. Orientations of lone pairs in Me_3SI (48), Me_3SeI (49), Et_3SI (this work), $[(CH_2)_5SMe]I$ (67), PI_3 (51), PBr_3 (40), $KClO_3$ (16, 17), and K_2SO_3 (34) compared with the orientations of the SO, PO, NH, and NC bonds in Me_3SOI (this work), $POBr_3$ (42, 43), Me_3NHI (58), Et_3NHI (59), and Me_4NI (11). The central atom of the trigonal-pyramidal grouping is S, Se, N, P, or Cl; the axis is oriented vertically in the page. The central atom, the atom bonded to it on the left, and the atoms of the contour figure are coplanar or very nearly so. Double circles, pairs of mirror or pseudo-mirror images.

Can. J. Chem. Downloaded from www.nrcresearchpress.com by 194.225.253.170 on 09/07/12
For personal use only.

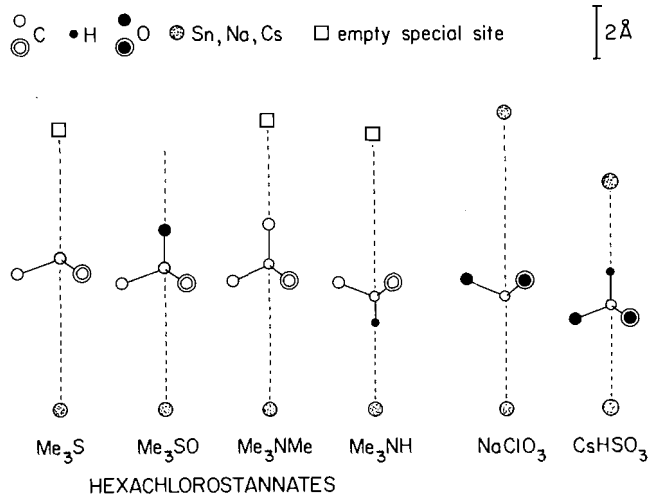


FIG. 3. Orientations of the skeletal configurations of YEL_3^{ϵ} and $YL'L_3^{\epsilon}$ ions in A_2SnCl_6 hexachlorostannates and in $NaClO_3$ and $CsSHO_3$. The ion axes are C_3 except for Me_3SO^+ which has C_s symmetry. Double circles, eclipsed ligand atoms. The Sn atom (*bottom*) is at (0, 0, 0) and the empty special site is at $(\frac{1}{2}, \frac{1}{2}, \frac{1}{2})$ of the cubic unit cells of $(Me_3S)_2SnCl_6$ and $(Me_3NH)_2SnCl_6$, and at $(\frac{1}{4}, \frac{1}{4}, \frac{1}{4})$ of the $Fd3c$ cell of $(Me_4N)_2SnCl_6$.

existence of a hydrogen-bonding interaction is corroborated from ir studies (60, 61).

(*f*) In $Cs^+HSO_3^-$ the S—H···Cs grouping is collinear by symmetry, S···Cs = 4.82 Å, H···Cs ~ 3.5 Å.

(*g*) In the 2:1 salts (Fig. 1) the Y atom is on a C_3 axis or, in 3MSOHS, in a mirror plane. If the cation orientation is disregarded, 3MSHS and $(Me_3NH)_2SnCl_6$ (3MHS) are isostructural; $(Me_4N)_2SnCl_6$ (4MHS) also is cubic, but here the doubling of the unit-cell dimensions (62) results in only one quarter of the cations being located on C_3 axes, the others have S_4 symmetry. The positioning of the cations on the C_3 axes and their orientation relative to the nearest coaxial Sn atom are shown in Fig. 3. The difference in the orientation is clearly seen. While in 3MSHS, 3MSOHS, and 4MHS the LP axis or the Y—L′ vector point at an empty site in the structure, in 3MHS the N—H bond points at the nearest $SnCl_6$ octahedron, engaging three of the Cl atoms in a symmetrically trifurcated hydrogen bond (60); the Me_3NH^+ ion is significantly displaced toward the coaxial Sn atom.

From these examples it is clear that among the interactions that could be singled out as primarily responsible for the orientation of the $YL'L_3^{\epsilon}$ molecule the least disputable is the Y—H^+···anion hydrogen bonding. For YEL_3^{ϵ}, however, it cannot generally be claimed that the orientation of the molecule is caused mainly by preferential interaction of the LP with the YEL_3^{ϵ} environment. Thus the PI_3 structure (51) consists of a hexagonal closest packing of I atoms and the P atoms, with their LPs, have no other choice but to protrude into the octahedral interstices of the hcp packing (P—I = 2.46 Å, P···I = 3.67 Å). This quasi-interstitial nature of Y is even more evident in the AsI_3 (As—I = 2.59 Å, As···I = 3.47 Å, ref. 65) and SbI_3 (Sb—I = 2.87 Å, Sb···I = 3.32 Å, ref. 66) crystals which, though not isostructural with PI_3, also consist of hcp packings of I atoms.

Matched pairs. In PBr_3 and $POBr_3$ (Fig. 2) the immediate environments of the LP and of the oxygen atom are so similar that the same explanation would have to be proposed for the orientational effect of *E and* of L′ = O. An argument based on simple charge interaction would be difficult to make here. We do not yet have *ab initio* results for the $PBr_3|POBr_3$ pair, but we can examine the almost certainly isostructural (40, 41) $PCl_3|POCl_3$ pair with the same effect. The calculated net charges (Table 6) in a free PCl_3 molecule are ϵ(P) = 0.646, ϵ(Cl) = −0.215; in a free $POCl_3$ molecule, ϵ(P) = 1.034, ϵ(Cl) = −0.151, and ϵ(O) = −0.582. If these respective charge distributions are assumed to be substantially unchanged in the two molecular crystals, the three negatively charged Cl neighbours closest to the PCl_3 or $POCl_3$ axis would see a positive net charge on the P atom in the PCl_3 crystal but a *negative* net charge on the oxygen atom in the $POCl_3$ crystal. Yet in PBr_3 in comparable circumstances the P···Br distance is practically the same as the sum of the van der Waals radii of P and Br, whereas in $POBr_3$ the O···Br distance is ~0.3 Å shorter than the corresponding van der Waals sum. Since the P^+···Br^- interaction would be expected to produce a shortening of that distance but the O^-···Br^- interaction a lengthening of the O···Br distance, it can hardly be argued that either interaction is of primary importance in determining the structure of the crystal and hence the orientation of the anion.

TABLE 6. Changes in the net charges (e) on atoms in YEL_3^{ϵ} molecules or ions resulting from addition of a fourth ligand on Y[a]

Species	ϵ(Y)	ϵ(L)	ϵ(L′)
PCl_3 (C_{3v})	0.646	−0.215	—
$POCl_3$ (C_{3v})	1.034	−0.151	−0.582
$PSCl_3$ (C_{3v})	0.541	−0.107	−0.221
$PFCl_3^+$ (C_{3v}) (55)	1.097	0.069	−0.305
PCl_4^+ (T_d) (55)	0.662	0.084	0.084
ClO_3^- (C_{3v})	1.398	−0.799	—
ClO_4^- (T_d)	1.856	−0.714	−0.714
SO_3^{2-} (C_{3v})	0.895	−0.965	—
SO_4^{2-} (T_d)	1.498	−0.875	−0.875
$SS'O_3^{2-}$ (C_{3v}) (56)	1.383	−0.823	−0.915

[a]From Mulliken population analysis on 6-31G* optimized structures. For Me_3S^+ see Table 7.

The problem of electrostatic charge interaction can be examined in more detail with reference to the $PbSO_3|PbSO_4$ and $KClO_3|KClO_4$ pairs, the two partners in each pair being isostructural if the L′ = O ligand is disregarded (Fig. 4). $PbSO_3$ and $PbSO_4$ crystallize with the same space group, *Pnma*. The ratios of their respective unit-cell dimensions are 0.932, 1.016, and 0.978, and the largest difference in their stated positional parameters of the atoms in common is only about 0.2 Å. The $KClO_3|KClO_4$ pair at room temperature is not isostructural in the strict crystallographic sense, the space groups being $P2_1/m$ and *Pnma*, respectively. However, $P2_1/m \subset Pnma$, and the difference in space-group symmetry does not affect the immediate environment of the anion in the two crystals significantly. Moreover, HT-$KClO_3$ (44) *has* the same space group as $KClO_4$ (with one dimension doubled); even though the structure determination of HT-$KClO_3$ is not accurate, comparison with $KClO_4$ reveals the essential indifference of the ClO_3^- ion in LT-$KClO_3$ and HT-$KClO_3$ to its orientation in the crystal. The ratio b(LT-$KClO_3$)/b($KClO_4$) = 0.990 and the ratio $2ac$(LT-$KClO_3$)/ac($KClO_4$) = 0.974. There also is considerable metric similarity between the *Pnma* structures of the two model compounds $KClO_4$ and $PbSO_4$, the ratios of their respective unit-cell dimensions being 1.041, 1.047, and 1.040.

Can. J. Chem. Downloaded from www.nrcresearchpress.com by 194.225.253.170 on 09/07/12
For personal use only.

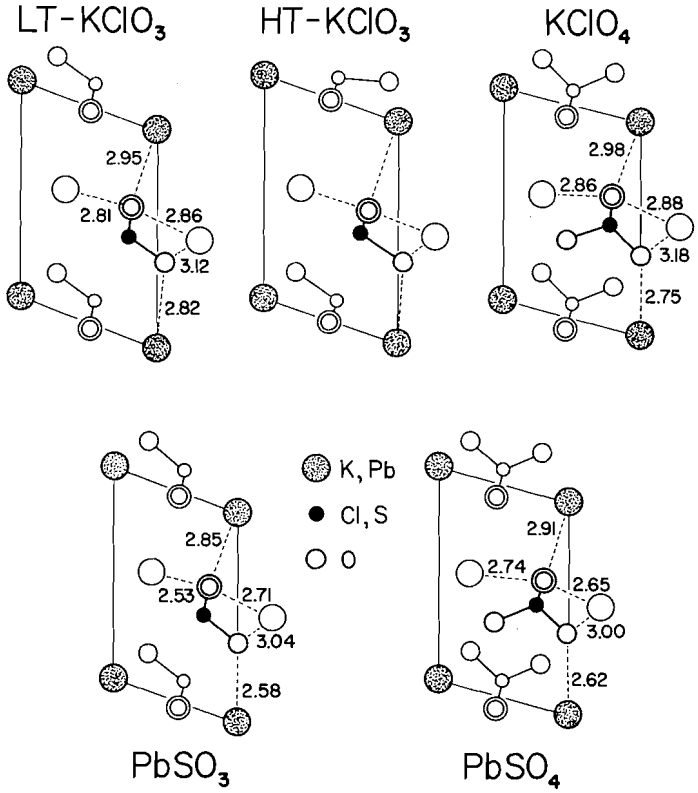


FIG. 4. Comparison of the structures of LT-$KClO_3$, HT-$KClO_3$, $KClO_4$, $PbSO_3$, and $PbSO_4$ (cf. Table 2). Heavily outlined single circles and shaded circles, atoms in m at $y = \frac{1}{4}$; heavily outlined double circles, oxygens at $\frac{1}{4} \pm y$ belonging to anions with Cl or S at $y = \frac{1}{4}$; thinly outlined double circles, oxygens at $\frac{3}{4} \pm y$ and $-\frac{1}{4} \pm y$ belonging to anions with Cl or S at $y = \frac{3}{4}$ and $-\frac{1}{4}$. O···K and O···Pb distances are in Å (broken lines). The atomic positions in HT-$KClO_3$ are too uncertain to be of value for numerical comparisons.

In $PbSO_3$ and $PbSO_4$ the distance between S and the nearest near-coaxial Pb atom is 3.42 and 4.01 Å, respectively, and the geometry of the anion environment in the two structures is quite similar (Fig. 4), i.e. the L′ = O ligand in SO_4^{2-} replaces the LP in SO_3^{2-} with relatively small changes in the crystal structure. The similarity of the anion orientation can then be interpreted in two ways: either the LP and the Y—L′ = S—O bond have much the same orientation effects, or the structure is determined by the YL_3 part of the anion, with the LP and L′ = O having little involvement in the process. The same observations are made for the $KClO_3$|$KClO_4$ pair, where the Cl···K distances are 3.97 and 4.27 Å, respectively, and the lateral O···K in the two structures match even more closely than the O···Pb distances in the Pb salts (Fig. 4).

The calculated net charges on the atoms of free SO_3^{2-}, SO_4^{2-}, ClO_3^-, and ClO_4^- are given in Table 6. In SO_3^{2-} and ClO_3^-, $\epsilon(Y) > 0$, $\epsilon(L) < 0$; in SO_4^{2-} and ClO_4^-, $\epsilon(Y) > 0$ and $\epsilon(L) = \epsilon(L') < 0$. The charges are not likely to be critically affected by the incorporation of the anion in a crystal and by the ensuing distortion of its symmetry. When SO_3^{2-} is converted to SO_4^{2-}, the $\epsilon(O)$ decreases by only ~10%, but the nearest near-coaxial Pb^{2+} ion in $PbSO_4$ now faces a net charge on the L′ = O atom of −0.88 at 2.6 Å, whereas before conversion it faced a net charge on S of +0.90 at 4.0 Å. Similarly, on converting ClO_3^- to ClO_4^-, the nearest near-coaxial K^+ ion in $KClO_4$ faces a net negative charge on L′ = O of −0.71 at ~2.9 Å, whereas before conversion it faced a net positive charge on Cl of +1.4 at ~4.3 Å. In spite of these changes in the net charge facing the coaxial or near-coaxial cation the distances from the three oxygen atoms of the SO_3^{2-} or ClO_3^- ion to other neighbouring cations are largely indifferent to the insertion of the L′ = O ligand. As Fig. 4 shows, the (uncorrected) O···K distances on conversion from $KClO_3$ to $KClO_4$ undergo a mean change of only 0.05(2) Å; for the O···Pb distances on conversion from $PbSO_3$ to $PbSO_4$ the mean change is only 0.08(6) Å. This strongly suggests that the position of the L_3YE^{ϵ} anion (and indeed the crystal structure itself) is determined by Coulombic interactions between the symmetrically disposed L atoms and their cation neighbours, and that the interaction between the LP and the coaxial cation at Y···cation separations of 4 Å or more is by itself not sufficiently strong to constitute an effective anion-orienting factor.

Lone pair on the anion: the influence of the cation. The above interpretation finds support in the magnitude of the changes which are observed in the calculated electron-density distributions in the free anion when a cation is brought coaxially in the vicinity of the LP. The anion–cation combination chosen to illustrate this point is $^-O_3Cl\cdots Na^+$, for which a calculation utilizing a 6-31G* basis set can be expected to produce an at least qualitatively reasonable result (cf. refs. 54–56). Moreover, the spatial cation–anion relationships in $NaClO_3$ are well established (cf. refs. 13 and 14; also ref. 22 for the isostructural $NaBrO_3$): the Na^+ ion is coaxial with its ClO_3^- partner by symmetry, both the Na and Cl atoms being located on a C_3 axis and about 4 Å apart; the three non-coaxial, C_3-related Na^+ ions on the LP side of the anion are at 3.35 Å from the Cl atom but the Cl···Na vector forms a 69° angle with the C_3 axis; and the three nearest Na^+ neighbours of an oxygen atom of the anion are at 2.4, 2.5, and 3.5 Å.

In the free ClO_3^- ion the local concentration of electron density ρ in the region of the LP is evident (Fig. 5*C*). The deformation of the shapes of the contour lines is not extreme but clearly present. On fixing an Na^0 atom coaxially at 4 Å from the Cl atom of ClO_3^0 and optimizing the geometry of this initial $Na^0\cdots ClO_3^0$ assembly the net charges which result are $\epsilon(Cl) = +1.328$ and $\epsilon(O) = -0.755$ compared to $\epsilon(Cl) = +1.381$ and $\epsilon(O) = -0.794$ in the free ClO_3^-, and $\epsilon(Na) = +0.938$.[7] The outermost ρ contours of the chlorine opposite the Na atom are displayed by small but significant amounts relative to free ClO_3^-. However, the contours for $\rho > 0.02$ au are shifted by no more than the thickness of a line in the plot, i.e. the polarization of ρ(Cl) in the LP region where ρ is appreciable is negligible. This is evident even more in the companion $\nabla^2\rho$ plot (Fig. 5*D*).

To see whether the magnitude of the perturbation of ρ(Cl) in the region of the LP is any different from that produced under comparable circumstances by an Na^+ ion on a Cl^- ion, i.e. in the absence of a LP, we carried out a 6-31G* calculation on an $Na^0\cdots Cl^0$ assembly at a 4 Å separation.[8] The resulting $Na^+\cdots Cl^-$ pair is less ionic ($\epsilon(Na) = +0.868$) than the $Na^+\cdots ClO_3^-$ pair (Fig. 5*F*). The shifts of the ρ contour lines between free Cl^- and the Cl^- in the $Na^+\cdots Cl^-$ pair (*A*) are appreciably larger than the corresponding shifts for the chlorate ion in $Na^+\cdots ClO_3^-$ relative to free ClO_3^- (*B*):

[7]The calculated Cl—O bond length in the $Na^+\cdots ClO_3^-$ assembly, 1.4770 Å, is ~0.01 Å shorter and the OClO angle, 109.86°, about 1.3° larger than in free ClO_3^- (Table 4).

[8]The equilibrium Na—Cl distance is 2.82 Å in NaCl crystal (RT, 1 atm), 2.361 Å in NaCl molecule (6-31G*, 2.397 Å), and 3.306 Å in tetrahedral $NaCl_4^{3-}$ (6-31G*, ref. 54).

Can. J. Chem. Downloaded from www.nrcresearchpress.com by 194.225.253.170 on 09/07/12
For personal use only.

Can. J. Chem. Downloaded from www.nrcresearchpress.com by 194.225.253.170 on 09/07/12
For personal use only.

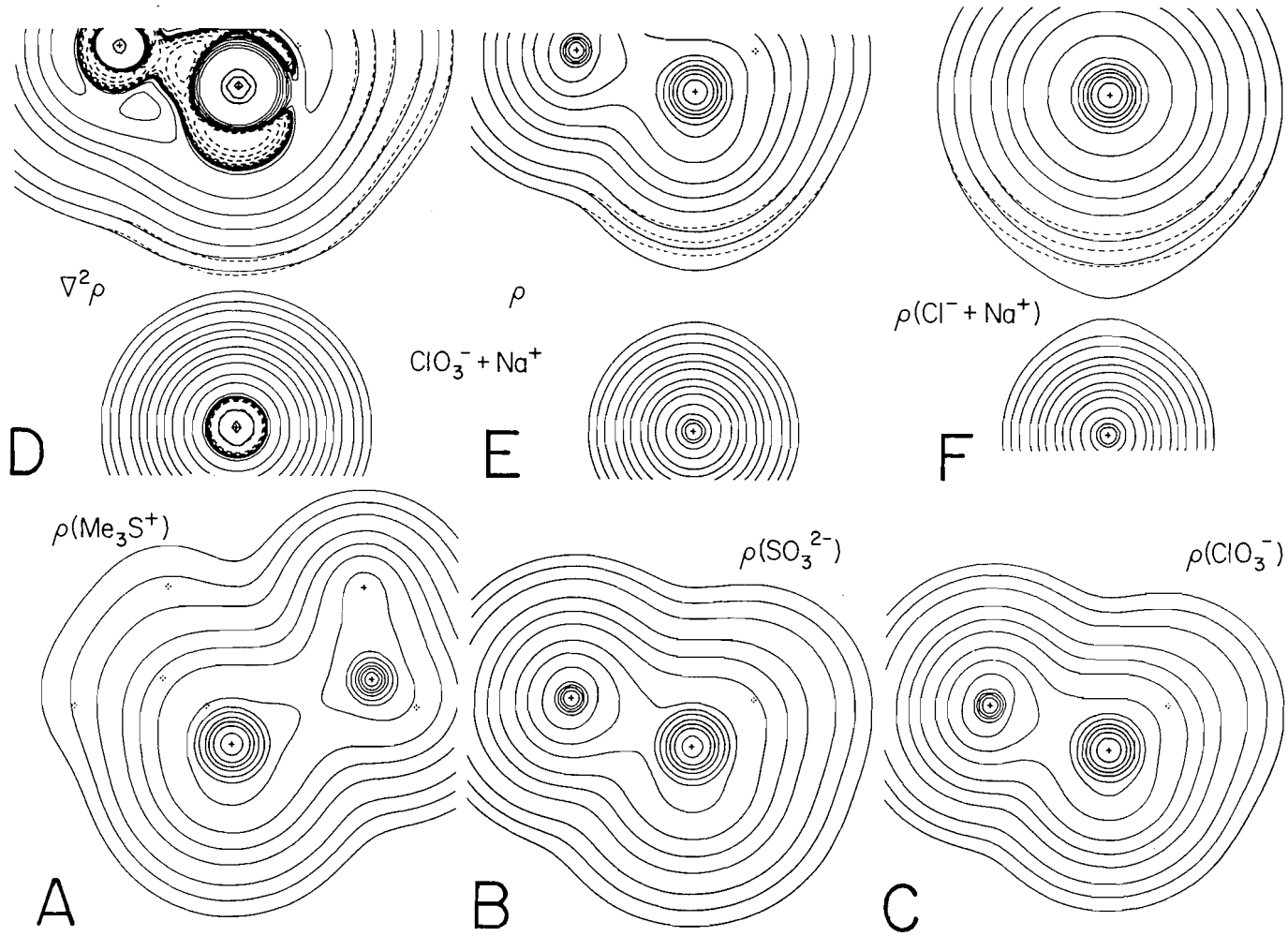


FIG. 5. Electron density (ρ) distribution in free Me_3S^+ (*A*), SO_3^{2-} (*B*), and ClO_3^- (*C*) ions and in ClO_3^- + Na^+ (*E*, ρ; *D*, $\nabla^2\rho$) and Cl^- and Na^+ (*F*) pairs (6-31G* optimization; sections coincide with an *m* of C_{3v}). The Na···Cl separation in *D* − *F*, 4 Å, matches that in $NaClO_3$ crystal. The broken lines in *E* are the ρ contours of free ClO_3^- (*C*); in *F* they are the ρ contours of a free Cl^- ion. The broken lines associated with the outer contours in *D* are the $\nabla^2\rho$ contours of free ClO_3^-. The outermost contour represents 0.002 au and is followed by the 0.004, 0.008, 0.02, 0.04, 0.08, 0.2, 0.4, and 0.8 au contours (1 au = 6.749 e/Å^3).

Contour	*A*	*B*
ρ = 0.002 au	0.36 Å	0.19 Å
ρ = 0.004 au	0.15 Å	0.10 Å
ρ = 0.008 au	0.06 Å	0.05 Å

Smaller but unmistakable displacements are observed in the ρ(Na) contours relative to free Na^+: ρ = 0.002 au, ~0.13 Å for $Na^+\cdots Cl^-$ and ~0.05 Å for $Na^+\cdots ClO_3^-$. Also, the radius of a given ρ contour in free Cl^- is larger than the radius, in the axial direction, of the corresponding contour in free ClO_3^-. The comparison of the $Na^+\cdots ClO_3^-$ with the $Na^+\cdots Cl^-$ pair can be no more than qualitative, and the cation–anion interaction in an isolated ion pair does not completely reflect the situation in a crystal. Nevertheless, it is reasonably clear that the ρ(Cl) distribution in ClO_3^- is relatively unaffected by the polarizing action of the cation and remains practically the same except in regions where ρ is quite low, perhaps ≤0.02 e/Å^3. In view of this it is unlikely that the interaction between the LP and the coaxial Na^+ in the $NaClO_3$ crystal is sufficiently strong to be orientation-determining.[4] The primary reason for the ClO_3^- orientation should be sought in the charge interaction between Na^+ and the oxygen atoms at 2.4–2.5 Å, unless one admits that lateral interaction between the LP and non-coaxial Na^+ ions at 3.35 Å from the Cl atom is sufficiently effective to be responsible for the orientation, alone or in conjunction with the O···Na interactions. Since the lateral $E\cdots Na^+$ interaction cannot be divorced from the O···Na interaction when considering the crystal as a whole, the question of the cause–effect relationship in this situation may receive only incomplete answers.

Lone pair on the cation. In the cationic YEL_3^+ species the ion as a whole carries a positive charge. A counter anion on or near the cation axis would thus face a positive charge on the Y atom in the simultaneous presence of a local electron-density concentration which constitutes the LP. In Me_3S^+, ε(S) = +0.630, ε(H) = +0.253 and +0.273 (Table 7). Comparison of the calculated ρ distributions (Fig. 5*A*) shows that the ρ contour geometry in the LP region of the free ion is quite similar to that in free SO_3^{2-} (ε(S) = +0.895), even though the ionic charges differ both as to sign and magnitude. Estimated contour radii (in Å) in the axial direction for the two ions and for ClO_3^- are

TABLE 7. 6-31G* optimization of the molecular geometry of the Me_3S^+ ion[a]

Parameter[b]	Value			
	S	C	H	H′
x, Å	0	1.6331	2.1547	1.5284
y, Å	0	0	0.8901	0
z, Å	0	0.7755	0.4542	1.8517
r_e, Å		S—C, 1.8079	C—H, 1.0805	C—H′, 1.0814
Angle		CSC, 102.9°	SCH, 108.0°	SCH′, 109.8°
			HCH, 110.9°	HCH′, 110.0°
r_c, Å	1.0294	0.7065 (C—H)		
		0.7030 (C—H′)		
ϵ, e	0.630	−0.676	0.273	0.253
$\rho(r_c)$, e/Å^3		S—C, 1.2947	C—H, 1.9279	C—H′, 1.9249

[a] $E = -516.11065$ au; $\mu = 0.968$ D.

[b] x, y, z, Cartesian coordinates, C_3 coincident with the z axis; r_c, critical radius; ϵ, net charge from Mulliken population analysis; $\rho(r_c)$, electron density at the bond critical point.

Contour	Me_3S^+	SO_3^{2-}	ClO_3^-
0.002 au	2.01	2.10	1.90
0.02 au	1.42	1.49	1.38
0.2 au	0.72	0.77	0.82
0.4 au	0.46	0.46	0.54
0.8 au	0.39	0.39	0.37

Similar arguments would therefore be valid for the lack of importance of coaxial $Me_3S^+\cdots$anion interactions as orienting factors in crystals as are set forth above for $^-L_3YE\cdots$cation interactions. Specifically, it seems unreasonable to suppose that in $(CH_2)_5SMe^+I^-$ (Fig. 2) there is sufficient interaction between S and the near-coaxial I^- at 7.4 Å, and similarly between O and the coaxial I^- at ~4.9 Å in Me_3SOI, and that the cation orientation in these structures is due to axial $E\cdots I^-$ or $O\cdots I^-$ interaction when much shorter $H^+\cdots I^-$ separations are present. It seems equally unreasonable to suppose that there can be any effective interaction between LPs in 3MSHS (Fig. 1), where two LPs face each other along a C_3 axis, across an inversion centre, at an S···S separation of ~9.9 Å; even lateral $E\cdots$Cl interactions appear unimportant in determining the cation orientation within the highly symmetric *anti*-fluorite $SnCl_6$ framework when the overall packing arrangements in Fig. 1 are compared.

In Me_3SI, Me_3SeI, and Et_3SI (Fig. 2) the LP ends of the cation axes point between coplanar I atoms while an approximately coaxial cation···I arrangement would be expected. Thus either the $E\cdots$I interaction is not sufficiently strong to overcome other tendencies in the crystal, or lateral (unsymmetric) $E\cdots$I interactions at unfavourable angles must be admitted as an orienting factor.

Similar situations exist in $SBr_3^+SbF_6^-$ (68), $SeBr_3^+SbF_6^-$ (69), $TeBr_3^+AsF_6^-$ (69) and in related salts. In SBr_3SbF_6 the S atom has on the LP side a coaxial (~10° off the cation axis) F neighbour at ~4.7 Å, i.e. too far for an effective $E\cdots$F interaction, but also three F atoms, each from a different anion, at a mean S···F distance of 2.84 Å and at a mean angle of ~49° from the cation axis. There appears to be significant interaction between the Br and F atoms, the mean Br···F separation being 2.83 Å, almost 0.5 Å smaller than the van der Waals sum of 3.3 Å.

Conclusion

As demonstrated above, and contrary to first impression, there are various reasons for believing that the rôle of LPs in determining a crystal structure or structure type is subordinate. This applies even to their rôle in determining the orientation of the LP-containing entity, especially in ionic crystals without hydrogen bonding between cations and anions. In any event, if a LP *has* an orienting effect, this effect cannot be divorced from other, equally or more important interactions in the crystal, be they ionic or dipolar or yet other in character, so that the consequences of the presence of a LP cannot be investigated in isolation. The LP of course has indirect stereochemical consequences in the crystal in the sense that it is an integral component of the molecular geometry of the free YEL_3^ϵ species and this geometry is a structure-determining factor.

The *symmetry* of a crystal containing YEL_3^ϵ is most often the result of a compromise between the tendency to attain maximum packing density and minimum lattice energy while at the same time preserving as much as possible the intrinsic geometry and symmetry of the ion or molecule. A symmetric orientation of the LP axis in a crystal is often a natural consequence of this compromise, in that high-density arrangements of units of a given symmetry (subgroups of C_{3v}) require for their realization space groups which preserve and reflect this symmetry (cf. ref. 57). This accounts, for example, for the frequent occurrence of arrangements of symmetry *Pnma* (with the LP axis in a mirror plane) and its subgroups $Pn2_1a$, $P2_12_12_1$, $P2_1/m$, $P2_1/n$, or of $R\bar{3}m$ (LP axis $\|C_3$) and its subgroups $R3m$, $R\bar{3}$, $R3$, $C2/m$. These space-group symmetries are equally frequently encountered with crystals containing $YL'L_3^\epsilon$ units, with the Y—L′ bond in a similar orientation as the LP axis in the YEL_3^ϵ species. This fact further minimizes the importance of the LP *per se* as an orienting factor.

Stereochemically inactive LP in crystals

If Y is a nontransition element of the g-th group of the Periodic Table, then a free $(2n + 2)$-electron molecule or ion YL_n^{g-n-2} with $n = g - 1$ halogen ligands (e.g. $GeCl_3^-$, $SnCl_6^{4-}$, $TeCl_6^{2-}$) will contain a stereochemically active LP on Y which will function as a $(n + 1)$-th ligand in determining the equilibrium configuration of the molecule. Provided the identity of YL_n^{g-n-2} as a mononuclear species is preserved,

Can. J. Chem. Downloaded from www.nrcresearchpress.com by 194.225.253.170 on 09/07/12
For personal use only.

Can. J. Chem. Downloaded from www.nrcresearchpress.com by 194.225.253.170 on 09/07/12
For personal use only.

the molecule will retain its geometry on incorporation in a crystal if allowance is made for distortions (usually minor) due to accidents of crystal packing. However, sometimes the molecular geometry as revealed by a crystal-structure determination will have a symmetry *higher* than observed or calculated for the free molecule; in particular, with $n = 6$ or 8 the YL_n^{g-n-2} molecule appears to assume the optimum geometry of a YL_n^{g-n} molecule (e.g. the 14-electron $TeCl_6^{2-}$ may exhibit the same symmetry as the 12-electron $SnCl_6^{2-}$, see below). These apparent exceptions to expectation from the VSEPR theory are described by saying that in the crystal the LP is stereochemically inactive or inert.[9]

14-electron species: observed geometry. Probably the most frequently quoted examples of such exceptions are the SeX_6^{2-} and TeX_6^{2-} (X = Cl, Br, I) ions. Their salts with simple cations contain discrete and, against expectation, *regular* YX_6 octahedra, often of crystallographic O_h symmetry. Where distortions occur they are quite small and do not increase significantly even when the crystal undergoes crystallographic transitions on cooling, e.g. in $(NH_4)_2TeBr_6$ (71), K_2TeBr_6 (72), and Rb_2TeBr_6 (73).[10] However, several structures have been reported (refs. 74–78 and Table V of ref. 78) in which the difference between the shortest and the longest bond in the YX_6 octahedron at room temperature amounts to as much as 10% of the mean bond length: in the triclinic $(C_{22}H_{24}N_2O_4S_4)TeCl_6$ structure (74), which contains $TeCl_6$ octahedra of C_i as well as C_1 symmetry, the first octahedron is practically undistorted, whereas in the second the $(Te—Cl)_{max} - (Te—Cl)_{min}$ difference is ~0.22 Å. Abriel (75–79) found that in contrast to the appreciably distorted $TeCl_6$ octahedron in $[H_3N(CH_2)_3NH_3]$-$TeCl_6$ the $SnCl_6$ octahedron in the corresponding hexachlorostannate(IV) is undistorted. The distortion observed in the $TeCl_6^{2-}$ and $TeBr_6^{2-}$ ions is accompanied by lifting of the degeneracy of the $\nu_3(t_{1u})$ and $\nu_4(t_{1u})$ fundamentals in the ir spectra; however, the ν_3 and ν_4 absorption bands appear to be broadened even in cubic Rb_2TeBr_6, where Te is at a site of O_h symmetry. Abriel took the static distortion of the SeX_6 and TeX_6 octahedra to be a manifestation of the expected stereochemical activity of the LP, and the lack of distortion a manifestation of dynamic averaging of instantaneous orientations of the intrinsically distorted 14-electron YX_6^{2-} ion. From his observations he concluded that the diffraction geometry of the SeX_6 or TeX_6 octahedron is imposed by the symmetry of the crystal environment (i.e. the site symmetry at Se or Te), and that the octahedron is to be expected undistorted when the Se or Te site is centrosymmetric but distorted when the site is noncentrosymmetric. An SnX_6^{2-} ion, by contrast, does not contain a LP and would therefore be insensitive to the site symmetry at Sn, although the actual geometries of all these octahedra would respond to particulars of the crystal packing.[11]

The range of values of the distortion index Δ (see footnote of Table 8) in the structures surveyed by Abriel (78) is, for centrosymmetric sites, zero (for O_h site symmetry) to 2.8 for $TeCl_6^{2-}$, 0–1.5 for $TeBr_6^{2-}$, and 0–0.1 for TeI_6^{2-}; for noncentrosymmetric sites, 2.9–187 for $TeCl_6^{2-}$ and 56–157 for $TeBr_6^{2-}$; and for $SnCl_6^{2-}$ in both types of sites, 0–5.7. However, one of the values for $TeCl_6^{2-}$ (C_2) is only 2.9, and the only Δ value for a noncentrosymmetric (C_s) $SeBr_6^{2-}$ is rather low, 7.8. Extension of Abriel's survey to discrete YX_6^{4-} (Y = Sn, Pb) and YX_6^{3-} (Y = Sb, Bi) ions (Table 8) yields Δ = 0–9.4 for centrosymmetric sites, whereas for the noncentrosymmetric sites the range is 0.2–38. For the square-antiprismatic XeF_8^{2-} ion in $(NO)_2XeF_8$ Δ is 97.

To obtain an idea of the magnitude of the distortions attributable to crystal packing we have examined 31 $SnCl_6^{2-}$ octahedra in crystal structures determined recently by Vincent (96). The choice of the organic N-containing cations (some of them quite large) in these hexachlorostannates was unrelated to the present considerations. Fifteen of the 31 octahedra are centrosymmetric (C_i), the remainder having C_1, C_2, and C_s symmetries; the anisotropic thermal parameters of the Sn and Cl atoms were unexceptionable. For the centrosymmetric octahedra, Δ = 0.1–12, with a mean of 7.2 (σ(mean) = 4.1, $\gamma_1 = 0.04$, $\gamma_2 = 1.5$); for the noncentrosymmetric octahedra, Δ = 0.1–24, with a mean of 6.6 (σ(mean) = 4.7, $\gamma_1 = 0.34$, $\gamma_2 = 1.7$); very little change results when Δ is calculated from Sn—Cl distances corrected for rigid-body motion.[12] The distortions due to factors unrelated to the LP are thus not negligible even for the centrosymmetric octahedra and can be substantial when the octahedra are noncentrosymmetric. In addition, an uncertainty of perhaps 1–2 units of Δ arising from the bond-length esd's must be included.

It would therefore seem prudent to conclude for the present that a *large* Δ value (perhaps >50) for discrete YL_n^{g-n-2} coupled with a small Δ value for the corresponding YL_n^{g-n} (e.g. in matching Te/Sn, Sb/In, Pb/Cd pairs) is evidence of static distortion attributable to the LP. For smaller Δ values and where the companion YL_n^{g-n} structure is lacking, a similar conclusion would seem much less well founded, and it is not clear from the small data set currently available whether dynamic averaging in a discrete YL_n^{g-n-2} in a crystal *is* in fact contingent on the presence or absence of an inversion centre or on some other symmetry criterion yet to be formulated.

[9]For a recent review and bibliography (with particular attention to Group IV) see ref. 70.

[10]Rb_2TeBr_6 was investigated down to 12.5 K (73).

[11]It is noteworthy that in Abriel's compounds the U_{ii} values are larger in the 14-electron anions than in $SnCl_6^{2-}$ not only in the centrosymmetric pair *a*, where this might be expected, but also (and more dramatically) in the noncentrosymmetric pair *b*, where the 14-electron anion *is* distorted and dynamic averaging not claimed; and further, that the U_{ii} and their anisotropy are large even in the cubic *d* ($Fd3c$, ref. 80), where Te occupies a centrosymmetric C_{3i} site:

Type	Symmetry	Compound pair	$\bar{U}_{ii}$(Y)	$\langle\bar{U}_{ii}(X)\rangle$*
a	Y(C_i)	$[H_3N(CH_2)_2NH_3]TeCl_6$|$[H_3N(CH_2)_2NH_3]SnCl_6$	223|166	377(16)|275(10)
b	Y(C_s)	$[H_3N(CH_2)_3NH_3]TeCl_6$|$[H_3N(CH_2)_3NH_3]SnCl_6$	477|306	809(77)|481(35)
c	Y(C_s)	$[H_3N(CH_2)_3NH_3]TeCl_6$| —	277| —	422(31)| —
d	Y(C_{3i})	$(Me_4N)_2TeBr_6$| —	521| —	716(125)| —

*All values $\times 10^4$; $\bar{U}_{ii}(Y) = \frac{1}{3}\Sigma U_{ii}(Y)$, $\langle\bar{U}_{ii}(X)\rangle = \frac{1}{8}\Sigma\bar{U}_{ii}(X)$; standard deviation of $\langle\bar{U}_{ii}(X)\rangle$ mean in parentheses.

[12]In $[H_3N(CH_2)_3NH_3]PtCl_6$ (97), Pt at C_1, Δ = 7.3.

TABLE 8. Crystallographic symmetries of discrete octahedral or square-antiprismatic YL_n^{ϵ} halogeno ions containing a lone pair on Y[a]

Ion	Compound	Symmetry	Δ	Reference
$SnCl_6^{4-}$	$[Rh(NH_3)_6][Rh(SnCl_3)_4(SnCl_4)][SnCl_6].4H_2O$	C_2	38.1	82
$SnBr_6^{4-}$	Cs_4SnBr_6	C_{3i}	0	83
PbF_6^{4-}	K_4PbF_6	C_{3i}	0	101
$PbCl_6^{4-}$	Cs_4PbCl_6	C_{3i}	0	83
$PbBr_6^{4-}$	Cs_4PbBr_6	C_{3i}	0	83
PbI_6^{4-}	$(MeNH_3)_4PbI_6.2H_2O$	C_i	2.4	84
	Cs_4PbI_6	C_{3i}	0	85
$SbCl_6^{3-}$	$Cs_2SbCl_6 = Cs_4[SbCl_6^-][SbCl_6^{3-}]$	D_{2d}	2.5	86
$SbBr_6^{3-}$	$(NH_4)_2SbBr_6 = (NH_4)_4[SbBr_6^-][SbBr_6^{3-}]$	D_{2d}	0.2	87
	$Rb_2SbBr_6 = Rb_4[SbBr_6^-][SbBr_6^{3-}]$	D_{2d}[b]	16.0	86, 113
	$Cs_2SbBr_6 = Cs_4[SbBr_6^-][SbBr_6^{3-}]$ (4.7 K)	D_{2d}	0.6	86
	$(pyH)_6[SbBr_6^-]_3[SbBr_6^{3-}]$	C_{2v}	0.2	88
$BiCl_6^{3-}$	$Cs_2(Sb_{0.5}Bi_{0.5})Cl_6 = Cs_4[SbCl_6^-][BiCl_6^{3-}]$	D_{2d}	3.0	86
	$Cs_2NaBiCl_6$	O_h	0	89, 90
	Cs_2KBiCl_6	O_h	0	91
	$Cs_3BiCl_6 = Cs_6[BiCl_6^{3-}][BiCl_6^{3-}]$ (*Pnma*)[c]			92
	$Cs_3BiCl_6 = Cs_6[BiCl_6^{3-}][BiCl_6^{3-}]$ ($C2/c$)	C_2	5.1	92
		C_i	0.3	
	$K_2CsBiCl_6 = K_4Cs_2[BiCl_6^{3-}][BiCl_6^{3-}]$	C_2	7.0	92
		C_i	4.9	
$BiBr_6^{3-}$	$Rb_3BiBr_6 = Rb_6[BiBr_6^{3-}][BiBr_6^{3-}]$	C_s	4.4	93
		C_i	9.4	
BiI_6^{3-}	$Rb_5I(I_3)[BiI_6].H_2O$	C_{2h}	0.3	94
$TeCl_6^{2-}$	$(C_{22}H_{24}N_2O_4S_4)TeCl_6$[d]	C_1	80.3	74
		C_i	1.2	
$TeBr_6^{2-}$	$(Me_4N)_2TeBr_6$[d]	C_{3i}	0	80
XeF_8^{2-}	$(NO)_2XeF_8$	C_s	97.2	95

[a]In a discrete YL_n^{ϵ} ion a ligand is not shared by other Y atoms. $\Delta = 10^5[\sigma(\bar{d})/\bar{d}]^2 = (10^5/n)\Sigma[(d_i/\bar{d}) - 1]^2$, n = number of ligands, d_i = individual bond length, $\bar{d}$ = mean bond length; this index of distortion is used for convenience of comparison with the corresponding $SnCl_6^{2-}$, $SeCl_6^{2-}$, $TeCl_6^{2-}$, $TeBr_6^{2-}$, and TeI_6^{2-} species tabulated in ref. 78.

[b]S_4 at 4.7 K (86).

[c]Isostructural with Rb_3BiBr_6 but crystal structure not determined.

[d]Not included in Table V of ref. 78.

14-electron species: "genuine" stereochemistry. The question that should perhaps be asked in the first place is, what is the "genuine" stereochemistry of a YL_n^{g-n-2} species, i.e. what is the optimized equilibrium geometry of the isolated molecule or ion. With the exception of XeF_6 (98, 99), IF_6^- and TeF_6^{2-} (99), the equilibrium geometries of the 14-electron molecules do not appear to have been investigated by *ab initio* methods. The main result of interest here of the recent all-electron SCF calculation using a large Gaussian basis set (99) is the effect of symmetry on the total electronic energy E and on Δ of XeF_6, IF_6^-, and TeF_6^{2-}. For the three configurations investigated, $E(C_{3v}) < E(C_{2v}) < E(O_h)$ for all three molecules, but the difference between the first two was not large. The distortions calculated from the optimized geometries are[13]

Species	$\Delta(C_{3v})$	$\Delta(C_{2v})$
TeF_6^{2-}	524	662
IF_6^-	234	268
XeF_6	115	113

On the assumption that these trends remain unchanged for the Cl and Br ligands, it is not unreasonable to take the C_{3v} configuration as the "genuine" geometry of YX_6^{6-n-2}. Some support for this comes from the observed geometry of $SeBr_6^{2-}$ in $[H_3N(CH_2)_3NH_3]SeBr_6$ (78) which, although at a site of C_s symmetry, closely simulates C_{3v} symmetry, and from $TeCl_6^{2-}$ (C_s) in $[H_3N(CH_2)_3NH_3]TeCl_6$ (76) which may be regarded as a distorted C_{3v} configuration. In an attempt to corroborate this assumption we have optimized the equilibrium geometry of free $SeCl_6^{2-}$ at the STO-3G* level both in O_h and C_{3v} symmetry. The result[14] is similar to that obtained for TeF_6^{2-} (99): $E(C_{3v})$

[13]These distortions seem to indicate that for SbF_6^{3-} and SnF_6^{4-} Δ would be even larger. These fluoride species may not exist as discrete ions, but for the other SbX_6^{3-} and SnX_6^{4-} ions only small distortions have been observed even at noncentrosymmetric sites (Table 8). However, the number of such ions for which structural detail is known is very small and no general conclusions can be drawn at present. It is possible that for Δ beyond a certain limit other geometries or chemistries prevail. The Mössbauer ^{129}I spectrum of $CsIF_6$ (100) indicates a significant EFG at the I atom; it has been suggested (126) that the iodine in this crystal might in fact be seven-coordinated, the increased c.n. lowering the symmetry at I and thus causing the LP to become stereochemically active.

[14]$E(O_h) = -5101.78976$ au, Se—Cl = 2.3224 Å. For the C_{3v} configuration, $E = -5101.79843$ au; the Cartesian coordinates (Å) are Se (0, 0, 0), Cl(*1*) (2.28768, 0, 0.97861), Cl(*1'*) (−1.14384, 1.98119, 0.97861), Cl(*2*) (0.86724, 1.50211, −1.33674), Cl(*2'*) (0.86724, −1.50211, −1.33674); Se—Cl(1) = 2.4882 Å, Se—Cl(2) = 2.1898 Å, Cl(*1*)SeCl(*1'*) = 105.54°, Cl(*2*)SeCl(*2'*) = 86.62°, Cl(*1*)SeCl(*2*) = 82.88°; ϵ(Se) = 0.8231, ϵ[Cl(*1*)] = −0.6378, ϵ[Cl(*2*)] = −0.3033.

Can. J. Chem. Downloaded from www.nrcresearchpress.com by 194.225.253.170 on 09/07/12
For personal use only.

Can. J. Chem. Downloaded from www.nrcresearchpress.com by 194.225.253.170 on 09/07/12
For personal use only.

is lower than $E(O_h)$ by 0.00867 au ~ 5.5 kcal/mol. The equilibrium bond length for O_h and the mean bond length for C_{3v} are both ~0.1 Å shorter than found for $SeCl_6^{2-}$ (O_h) in $(NH_4)_2SeCl_6$ at room temperature, 2.411(1) Å (125); $\Delta(C_{3v})$ = 407.

Evidence for dynamic averaging. A 14-electron YX_6^{2-} octahedron of C_{3v} symmetry consists of a larger and a smaller X_3 triangle with the LP on the C_3 axis toward the larger triangle. This configuration can be dynamically reconciled with the observed O_h symmetry at Y in the crystal by an eight-fold orientational disorder of the LP axis. The disorder cannot be static, with a random distribution of the LP orientations over the Y sites, for no quadrupole splitting has been detected in the Mössbauer ^{125}Te spectra of cubic A_2TeX_6 at 80 K (127), and nqr, Raman, and other results (cf. refs. 79 and 128) also are consistent with the cubic symmetry of the anion. However, fast reorientations of the LP resulting in dynamic averaging of the X positions would be expected to manifest themselves in the magnitude and anisotropy of the thermal parameters U_{ii}(X) of TeX_6^{2-}(O_h) relative to those in the corresponding SnX_6^{2-}(O_h).

This has been considered, for several symmetries, by Abriel and Zehnder (79), who based their examination on their U_{ii} values for cubic Rb_2TeBr_6, Cs_2TeBr_6, and Rb_2SnCl_6 at 298 and 160 K. This very small sample places them at a disadvantage in their arguments, as does the difficulty which arises from comparing the two hexa*bromotellurates* with a hexa*chloro-stannate*, i.e. YX = TeBr with YX = SnCl. When their data are combined with the U_{ii} of cubic K_2TeBr_6 at 463 K (72) and with the room-temperature thermal parameters for A_2SnCl_6 (A = K, Rb, Cs) from refs. 128 and 139–141, the following emerges from a scrutiny of the A_2SnCl_6 and A_2TeBr_6 sets: (*1*) $\bar{U}$(A) at constant temperature decreases with the increasing mass of A; (*2*) $\bar{U}$(Sn) and $\bar{U}$(Te) at constant temperature show little variation with A; (*3*) the ratio $R = U_{ii}(X)\perp / U_{ii}(X)\parallel$ for Rb_2TeBr_6 and Cs_2TeBr_6 is, within the statistics, independent of temperature;[15] (*4*) this ratio, which measures the anisotropy of the thermal motion of X, at room temperature decreases with the size of A and increases with $\bar{U}$(A) in both series (Fig. 6), and its variation with A arises essentially from the variation in the $U_{ii}\perp$ component.

The reduction of U_{ii} on cooling from room temperature to 160 K is, within the statistics, quite uniform (by a factor of 1.83(14) ~ 298/160)[16] for all the values in Table II of ref. 79. Analysis of variance (both one- and two-way) justifies rejecting the hypothesis that the variation in the reduction factor of the individual U_{ii} is not due to chance, at the 99.5% significance level. In particular, no statistically significant difference can be

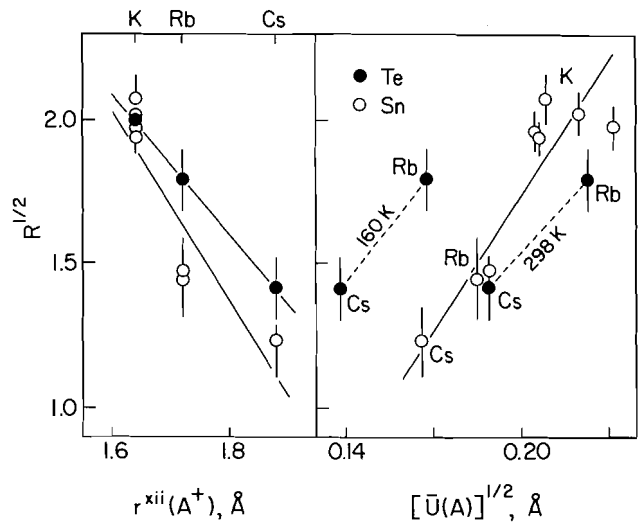


FIG. 6. Variation of the anisotropy of thermal motion of X in A_2YX_6 (Y = Sn, Te; X = Cl, Br) with the size and rms displacement of A. $r^{xii}(A^+)$, Shannon's effective ionic radius of A^+ in 12-coordination; $[\bar{U}(A)]^{1/2}$, rms displacement of A; $R^{1/2}$, ratio of the rms displacements of X ⊥ and ∥ to the Y—X bond. A_2TeBr_6 (A = Rb, Cs), 298 and 160 K (72, 79); A_2SnCl_6 (A = K, Rb, Cs) (79, 128, 139–141).

claimed to exist in this data set between the Sn and the Te compounds. This makes it especially difficult to understand the dramatic difference in the ratio $R_{TLS}(U_{ij},298)/R_{TLS}(U_{ij},160)$ of the discrepancy indices for the rigid-body motion of the $TeBr_6$ octahedron on one hand and of the $SnCl_6$ octahedron on the other: for $TeBr_6$ on cooling $R_{TLS}(U_{ij})$ increases about four-fold, whereas for $SnCl_6$ it *decreases* by a factor of ~14.[17] While increasing departure from the rigid-body character of the YX_6 motion on cooling may be expected, variation in the opposite direction is surprising, especially when the approximation to the model is, at 160 K, as close as the $R_{TLS}(U_{ij})$ = 0.2% would indicate.[18]

The quantity which *is* appreciably affected by the size *and* the vibrational displacement of the A atom (both of which in turn depend on the atomic number of A) is the anisotropy $R^{1/2}$ of the thermal motion of the X atom (Fig. 6).[19] As far as can be established from the available data, the variation of $R^{1/2}$ with $r^{xii}(A^+)$ or $[\bar{U}(A)]^{1/2}$ for A_2TeBr_6 more or less parallels that for A_2SnCl_6. In these circumstances it is difficult to know what would be the particular manifestation in the thermal parameters of a difference that might exist between the thermal motions of SnX_6^{2-} and TeX_6^{2-}.[20]

[15]The difference between $R^{1/2}$(293 K) and $R^{1/2}$(160 K) is −0.03(12) for Rb_2TeBr_6, +0.15(11) for Cs_2TeBr_6, and −0.11(8) for Rb_2SnCl_6. For the structurally related $Pm3m$ perovskite $KMgF_3 = K_2Mg\square F_6$ Muradyan *et al.* (129) found $R^{1/2}$ to fall from 1.48 at 293 K to 1.38 at 123 K, i.e. ~0.04%/K. This would correspond to a decrease of the order of −0.1 in $R^{1/2}$ of the chloro and bromo compounds, i.e. to a change comparable to the experimental uncertainty in $R^{1/2}$. In their study, which was designed to investigate the temperature variation of the thermal parameters of $Pm3m$ perovskites well away from phase transitions, Muradyan *et al.* point out that routine application of standard procedures may yield unreliable U_{ii} values.

[16]This uniformity is far greater than that observed in ref. 129 for the simple $Pm3m$ perovskite $KMgF_3$ between 293 and 123 K.[15] The F atom in $KMgF_3$ is situated between two Mg atoms, forming a symmetric Mg—F—Mg bond, in contrast to A_2YX_6, where the X atom in the Y—X bond is unattached to another Y atom.

[17]In ref. 79 it is suggested that soft modes may be present which affect the motion of the $SnCl_6$ octahedron differently from the TeX_6 octahedra, but evidence for this seems lacking.

[18]The mean amplitude of the librational motion about a C_4 axis of the YX_6 octahedron (calculated from the U_{ij} of ref. 79) is, at 298 and 160 K, respectively, 4.3° and 3.4° for Rb_2TeBr_6, 3.2° and 2.1° for Cs_2TeBr_6, and 3.3° and 2.7° for Rb_2SnCl_6; the $U_{ij}(Rb_2SnCl_6,298)$ from ref. 128 yield 3.2°, in agreement with ref. 79. The mean translational amplitude is 0.14 Å for all the 298 K data and 0.10 Å for all the 160 K data. For K_2TeBr_6 at 463 K, the U_{ij} of ref. 72 give $R_{TLS}(U_{ij})$ = 0.02% (unweighted), 8.0°, and 0.21 Å, respectively.

[19]Such anisotropy is well known from the $Pm3m$ AYX_3 perovskites, where it sometimes is very large (see below and ref. 143).

[20]Dynamic averaging would lead to an octahedron of virtual O_h symmetry even if the site symmetry (as determined by the crystal packing) were a *non*centrosymmetric cubic subgroup of O_h.

Can. J. Chem. Downloaded from www.nrcresearchpress.com by 194.225.253.170 on 09/07/12
For personal use only.

For the present one would be inclined to the view that a much more extensive investigation of the temperature dependence of U_{ij} in matching $TeX_6|SnX_6$ series would be required if evidence in support of dynamic averaging were to be extracted from analysis of the thermal motion of the YX_6 octahedra. However, while it cannot be argued conclusively from the available X-ray results that dynamic averaging is responsible for the discrepancy between the observed and the "genuine" geometry of the 14-electron YX_6^{2-} species, the observation that the ν_3 and ν_4 fundamental absorptions are well separated in the ir spectrum of Rb_2SnCl_6 but coalesced to broad unresolved bands in the spectra of Rb_2TeCl_6 and Cs_2TeBr_6 (79) suggests that such averaging in TeX_6^{2-} does occur and is present even at very low temperatures. The difference in the ir spectra is in fact the most convincing evidence in support of the averaging at present.

We shall return to the problem of dynamic averaging in a somewhat different context in the next section.

Active LP ↔ inactive LP conversion

Leaving aside the precise nature of the symmetry criterion under which dynamic averaging in discrete YX_6^{g-n-2} octahedra is quenched, we observe that crystallographic transitions in crystals where Y is at a centrosymmetric site preserve the centre of symmetry, and if the octahedron is undistorted or only weakly distorted, Δ does not increase significantly as a result of the transition (e.g. in Rb_2TeBr_6 (73) or Rb_2TeI_6 (102)).[21] The interesting problem of occurrence of temperature-induced transitions in YX_6^{g-n-2} salts where Δ is large and Y at a noncentrosymmetric site does not appear to have been investigated. However, the transitions that occur in $A^+Y^{2+}X_3$ (Y = Ge, Sn, Pb) are of considerable interest in this context in that some of them appear to affect the inversion centre at Y, i.e. on the face of it they "activate" or "inactivate" the LP. The high-temperature phases are of the cubic perovskite type ($Pm3m$, $Z = 1$), with O_h as the diffraction site symmetry at Y, so that the LP in them can be said to be stereochemically inactive. The A^+ ions are accommodated in the three-dimensional framework formed by the corner-sharing $[YX_{6/2}]$ octahedra. Although these octahedra are not discrete, their $m3m$ symmetry makes them a suitable subject for investigating the effect of the LP (Table 9).

Transitions from the $Pm3m$ to a lower-symmetry phase are basically of three types, those preserving the topology (connectivity) of the perovskite structure, those which generate structures containing discrete YX_3^- ions, and those resulting in systems of YX_6 octahedra of various connectivities. Transitions of the first type are displacive, often involving symmetry changes via tetragonal subgroups of $Pm3m$ and preserving the crystallographic inversion centre at Y. They are not of interest in the present context.

Transitions of the second type (e.g. **A** in Table 9) may also be viewed as displacive (in principle via trigonal subgroup descent from $Pm3m$), but the atomic displacements in the YX_6 octahedra are clearly dissociative, $[YX_{6/2}]^- \rightarrow [YX_3X'_3]^- \rightarrow YEX_3^-$. Breaking up the framework of the corner-sharing $[YX_{6/2}]^-$ octahedra, i.e. one half of the Y—X bonds in the $Pm3m$ structure, substantially changes the character and physical properties of the halide and leads to an essentially ionic structure. These transitions entail a loss of the centre of symmetry at Y and may be described as producing distorted X_3—Y···X_3 coordination octahedra. The mean interatomic distance $\bar{d} = \frac{1}{2}\langle Y—X\rangle + \frac{1}{2}\langle Y\cdots X\rangle$ in the low phase closely matches the Y—X distance in the YX_6 (O_h) octahedron in the $Pm3m$ phase (Fig. 7), even though the asymmetry of the X_3—Y···X_3 coordination figure (viewed as a distorted octahedron), as measured by $\sigma(\bar{d})$ and $\Delta = 10^5[\sigma(\bar{d})/\bar{d}]^2$, is considerable. The volume change also is small, $V_1(Pm3m) - V_1$(low phase) ~ 1% for $CsGeX_3$ and $CsSnCl_3$.

Transitions of the third type (**B** in Table 9) result in the formation of a low phase in which YX_6 octahedra are linked into chains. Although these octahedra (noncentrosymmetric in **B**) are distorted as a result of the inhomogeneous connectivity, Δ is remarkably small. The mean value for the **B**-type compounds of Table 9, $\langle\Delta\rangle = 154$, is only twice as large as $\langle\Delta\rangle = 66$ for the corresponding Cd compounds of this type,[22] in which there is no LP on the Y atom. The distortion due to the LP in the Ge, Sn, and Pb octahedra is thus only minor at best (cf. also ref. 84). The $\bar{d}$ values for the two **B** phases which have a known $Pm3m$ high phase, $CsSnI_3$ and $CsPbBr_3$, are about 4% larger than the Y—M distances in the $Pm3m$ phases; the volume change $V_1(Pm3m) - V_1(\mathbf{B}) \sim 7\%$ for $CsSnI_3$ and $CsPbBr_3$, i.e. larger than for transitions of the second type.

The close similarity of $\bar{d}$ in the low phase to Y—X in the $Pm3m$ phase for the compounds in Fig. 7 suggests that this similarity is due to dynamic averaging in the high phase. A feature characteristic of all cubic perovskites is the strong anisotropy R of the thermal motion of the X atom (see above). This anisotropy increases with the so-called tolerance factor t of the perovskite[23] and with the decreasing temperature difference $T - T_{tr}$ (T_{tr}, upper transition temperature; cf. Fig. 27 of ref. 143). Conventional refinement of accurate neutron data based on the ideal cubic perovskite structure gave $R = 7.6(4)$ for $CsPbCl_3$ at 331 K and 6.5(3) for $CsPbBr_3$ at 425 K; even larger R values can be obtained depending on the particulars of the model (124, 149–151).[24] The rms displacements of the atoms in $CsPbCl_3$ at ~330 K from their ideal $Pm3m$ positions were 0.29 Å for Cs, 0.17 Å for Pb, 0.44 Å for Cl perpendicular and 0.16 Å parallel to the Pb—Cl bond.[25] This shows that while a transition on cooling may not result in the appearance of a discrete YX_3^- ion, where it does the atomic displacements in the $Pm3m$ phase are such that they can accommodate, dynamically, the dimensions and geometry of the YX_3^- ion. For example, on the reasonable assumption that the rms displacements in the cubic $CsSnCl_3$ are about the same as in $CsPbCl_3$, moving the Sn and three adjacent Cl atoms in the $m3m$ $SnCl_6$ octahedron in a concerted fashion from their ideal positions by amounts corresponding to the rms displacements and in such a way that the $SnCl_3$ group shrinks symmetrically,

[21] In $[H_3N(CH_2)_2NH_3]YCl_6$ ($P\bar{1}$; Y = Pt, Sn, Pb, Te; ref. 103) only the Pt compound has a transition (T_{tr} = 357.2 K) between 77 K and the decomposition temperature.

[22] The Δ values in the $ACdX_3$ of the **B**-type are 79 for $RbCdCl_3$ (144), 65 for NH_4CdCl_3 (145), 67 for $RbCdBr_3$ (146), and 79 for $TlCdI_3$ (147); the $\sigma(\bar{d})/\bar{d}$ in these compounds is ~0.027, compared with $\langle\sigma(\bar{d})/\bar{d}\rangle = 0.037$ for the **B** compounds of Table 9.

[23] The tolerance factor in turn depends on the relative sizes of the atoms: $t = [r^{xii}(A) + r(X^-)]/[r^{vi}(Y) + r(X^-)]\sqrt{2}$.

[24] For comparison, the room-temperature R for the LT-$CsGeX_3$ perovskites (**A** of Table 9, X-ray data) are 2.9(2) for Cl, 3.2(2) for Br, and 3.8(2) for I (106).

[25] Contrary to refs. 124 and 149–151, Mair (152) considers the motion of the Cl atom *not* to be highly anharmonic: soft modes contribute significantly to the Cl vibrations and at temperatures sufficiently above T_{tr} a temperature-independent component enters into the expression for the rms displacement.

TABLE 9. $A^+Y^{2+}X_3$ (Y = Ge, Sn, Pb) halides some of which exist as cubic perovskite phases[a]

Compound	T_{tr}, K	Low phase					High phase ($Pm3m$, $Z = 1$)		
		Symmetry[b]	V_1	⟨Y—X⟩	Δ	Colour	V_1	Y—X	Colour
		YX_6 octahedra with perovskite topology in low phase							
$CsSnBr_3$ (109, 110, 142)	290	[c]					195.9	2.90	Black[d,e]
$CsPbCl_3$ (114)	321[f]	$P4/mbm$, C_{4h}					176.0[g]	2.80	Pale yellow
		Discrete YX_3^- ions in low phase[h]							
$RbGeCl_3$ (104)	[i]	$P2_1/m$, C_s	154.3	3.03(73)	5784	Colourless			
$CsGeCl_3$ (105, 106)	428[j]	**A**	160.4	2.72(37)	1870	Colourless	161.3[g]	2.73	
$CsGeBr_3$ (106)	~510[j]	**A**	178.6	2.83(29)	1061	Yellow[k]	179.6[g]	2.84	
$CsGeI_3$ (106)	~550[j]	**A**	213.8	3.01(26)	746	Black[k]	215.2[g]	3.02	
Me_4NGeCl_3 (107)	424	$Pna2_1$, C_1	264.9	3.23(94)	8486	Colourless	277.6[g]	3.276	
NH_4SnF_3 (148)		$R\bar{3}$, C_3	107.4	2.48(40)	2537	Colourless			
$CsSnCl_3$ (108–110)	390[l]	$P2_1/n$, C_1	171.5	3.00(50)	2819	White[m,n]	175	2.80	Yellow[d,l]
		Linked YX_6 octahedra in low phase							
$TlGeI_3$ (81)	[i]	**B**	181.7	3.02(11)	121	Yellow			
$CsSnI_3$ (110–112)	425[p]	**B**	217.5	3.23(11)	227	Yellow[d,q]	232[g]	3.09	Black[r]
$RbPbI_3$ (115)		**B**	213.1	3.23(11)	98				
$CsPbBr_3$ (114, 116)	403[s]	**B**	187.8	3.06(13)	187		200.3[g]	2.94	Orange
$CsPbI_3$ (114)	~581	**B**	223.1	3.24(12)	139	Yellow	(235.6)		Black[t]
$TlPbI_3$ (117)		$Cmcm$, C_{2h}[u]	204.1	3.21(2)	3.3				
Tl_4PbI_6 (117)		$Pbam$, C_{2h}[v]	433	3.22(3)	4.7				

[a] V_1 (Å^3), volume per formula unit. ⟨Y—X⟩ (Å), mean bond length, with σ(mean); for the discrete YX_3^- ions this represents the mean of the 3 (Y—X) + 3 (Y···X′) distances corresponding to the coordination $[YX_{3/2}X'_{3/2}]$, Y—X < Y···X′. For the distortion index Δ see Table 8.

[b] Space group and site symmetry at Y. (**A**) $A^+[YX_{3/1}]^-$ (or $A^+[YX_{3/2}X'_{3/2}]^-$, see footnote *a*), $R3m$. The cations and the X atoms form a trigonally distorted cubic close packing arrangement, with the Y(C_{3v}) in octahedral interstices; LP axis in C_3 and pointing between the three X′ neighbours at the larger distances from Y. (**B**) NH_4CdCl_3 type, $Pnma$, Y(C_s); double chains of distorted $[YX_{2/2}X_{3/2}X_{1/3}X_{1/1}]^-$ octahedra. These chains are preserved on hydration: $KPbBr_3 \cdot 2H_2O$ (⟨3.24(14)⟩ Å, Δ = 150), $NH_4PbBr_3 \cdot 2H_2O$ (⟨3.24(14)⟩ Å, Δ = 155), and $RbPbBr_3 \cdot 2H_2O$ are isostructural among themselves (118). $KPbBr_3 \cdot H_2O$ ($Cmc2_1$, Pb(C_s), ref. 119) contains chains of distorted $[PbBr_{2/2}Br_{2/2}Br_{1/2}Br_{1/1}]^-$ octahedra, ⟨3.06(20)⟩ Å, Δ = 436; $KSnCl_3 \cdot H_2O$ (120) at room temperature is likely to be isostructural or closely related.

[c] Probably tetragonal (142).

[d] Mössbauer QS(^{119}Sn) ~ 0.

[e] Single line in the ^{81}Br nqr spectrum (142).

[f] There are further displacive transitions on cooling (121–123), but they are not of interest in the present context.

[g] Corrected to room temperature, cf. Table 2.

[h] Or $[YX_{3/2}X'_{3/2}]^-$, see footnote *a*.

[i] No transition between room temperature and the decomposition temperature.

[j] Transition reversible, first-order in $CsGeBr_3$ and $CsGeI_3$ (106). For $CsGeCl_3$ the evidence concerning the order of the transition is contradictory (105, 106).

[k] Air- and light-sensitive.

[l] Easily supercooled down to room temperature; reversal to the LT phase very sluggish at room temperature, but ref. 109 states that the reversal is very fast at 80 K. As against this, "traces of water may catalyze the transition to the low phase; completely dry HT-$CsSnCl_3$ was stable at room temperature for at least a year and was also found stable down to 77 K" (110).

[m] The possibility cannot be excluded that the LT-$CsSnCl_3$ of ref. 108 may have been partially hydrated.

[n] Mössbauer QS(^{119}Sn) = 0.90 mm/s at 80 K.

[p] Transition to the LT phase sluggish or irreversible.

[q] Single line in the ^{127}I nqr spectrum (110).

[r] Black melt (mp 453°C) solidifies to a material black at room temperature (110).

[s] At ordinary rates of cooling the transition to **B** is irreversible. The $Pm3m$ phase undergoes transitions to a series of perovskite-derived phases ($Pm3m \rightarrow P4/mbm \rightarrow Pmbn$, refs. 121 and 124) which are not of interest in the present context. The white $CsPbBr_3$ (**B**) when dry can at room temperature be kept indefinitely, but on heating it transforms at 130°C irreversibly to the $Pm3m$ phase (116).

[t] Unstable at room temperature; monoclinic?

[u] $[PbI_{4/2}I_{2/2}]^-$ chains.

[v] $[PbI_{4/2}I_{2/1}]^-$ chains.

results in a C_{3v} $SnCl_3$ pyramid with Sn—Cl ~ 2.57 Å, in fair agreement with the bond lengths observed in the $SnCl_3^-$ ion in the low phase. It is thus clear even on this simplistic argument that the cubic phase implies dynamic averaging of all the possible orientations and positions of the YX_3^- ion under O_h symmetry. The overall result of this averaging is not necessarily representable either by conventional refinement of the ideal $Pm3m$ structure or by models in which the X atoms are offset, by amounts to be refined, from their ideal $Pm3m$ positions (e.g. with X in a *single* 12(*h*) or 12(*j*) or 12(*l*) equipoint of $Pm3m$ with fractional occupancy) and allowed to refine conventionally for thermal motion.

Solid Group V YX_3 (N to Bi; X ≠ F) halides

Most of these structures consist of clearly distinguishable YX_3 molecules, i.e. the presence of a LP is well displayed. The observed tendency of the Y atom toward c.n. ≥ 6 results from a compromise between preservation of discrete YEX_3 geometry and, especially in the $R\bar{3}$ iodides, closest packing of the halogen atoms. The YX_3 molecule is coordinated by three X atoms to form a more or less distorted X_3—Y···X_3 octahedron or trigonal prism; in the latter case additional 1–3 X atoms capping the prism on the side faces may be present at comparable or longer Y···X distances. The LP on Y points along the actual or idealized C_3 axis of the coordination polyhedron in the

Can. J. Chem. Downloaded from www.nrcresearchpress.com by 194.225.253.170 on 09/07/12
For personal use only.

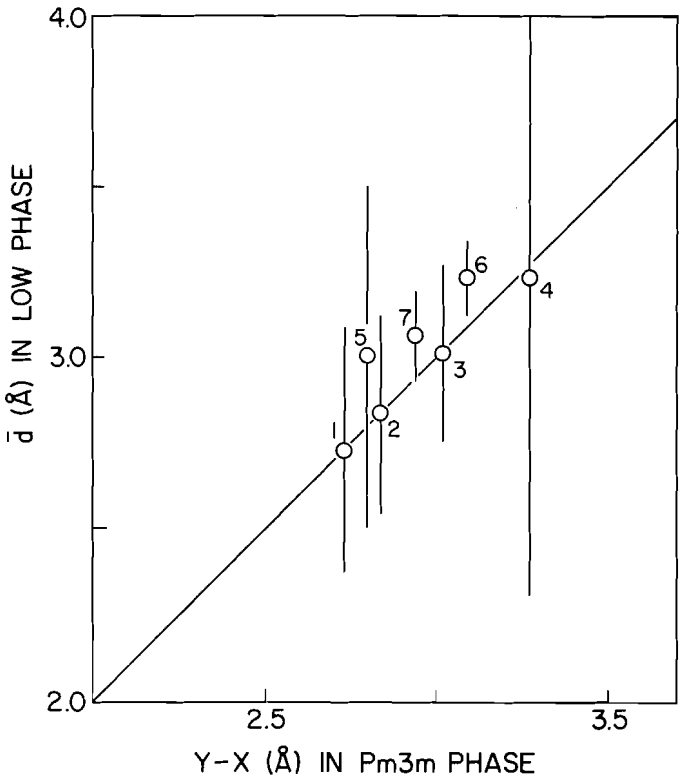


FIG. 7. Correlation of $\bar{d}$ (= mean of Y—X and Y···X distances for c.n. 6) in the low AYX_3 phase with the Y—X distance in the corresponding $Pm3m$ perovskite phase. A = Me_4N for *4*, Cs for *1–3*, *5–7*. YX: *1*, *4*, GeCl; *2*, GeBr; *3*, GeI; *5*, SnCl; *6*, SnI; *7*, PbBr. Length of vertical bar represents $\sigma(\bar{d})$. For references see Table 9.

direction of the more distant X_3 triangle. When the coordination of Y is octahedral, the situation resembles, locally, the coordination of the Ge atom in the rhombohedrally distorted $CsGeX_3$ perovskites (A compounds, Table 9). In the absence of information on the occurrence of crystallographic phase transitions in YX_3 on heating, one may ask how likely are these potentially pro-cubic X_3—Y···X_3 octahedra to undergo transitions of the second type (see above), i.e. to become metrically regular YX_6 octahedra?

Although the Y—X and Y···X distances in an YX_3 crystal may differ widely, the mean interatomic distance $\bar{d} = \frac{1}{2}[\langle Y—X\rangle + \langle Y\cdots X\rangle]$ is remarkably constant from compound to compound. It oscillates about 3 Å except in NCl_3 (this remarkable structure contains N atoms in octahedral, trigonal-prismatic as well as tetrahedral coordination (130), with $\bar{d}$ = 2.54 Å in the octahedron and 2.71 Å in the trigonal prism). In Fig. 8 the standard deviation $\sigma(\bar{d})$ is normalized to $\bar{d}$ and plotted against the mean bond length $\langle Y—X\rangle$ in the YX_3 molecule. The trend which emerges[26] is consistent even at spreads corresponding to $\sigma(\bar{d})$ ~ 30% of $\bar{d}$. The $\sigma(\bar{d})/\bar{d}$ value may be taken as an inverse measure of the density of packing in the YX_3 crystal, which ultimately depends on the relative effective sizes of the Y and X atoms and the XYX angles. In this respect $\sigma(\bar{d})/\bar{d}$ again confirms the unimportance of the spatial extension of the LP as a structure-determining factor. In the present context we take it to estimate the tendency of a YX_3 crystal to undergo conversion to a form in which the LP appears to be stereochemically inactive.

With $\sigma(\bar{d})/\bar{d} \sim 0$, the geometric condition for dynamic averaging is in fact almost satisfied in BiI_3. This $R\bar{3}$ structure is at the upper limit of packing density: the arrangement of the I atoms is very close to hcp. As a consequence the BiI_6 coordination octahedron is very nearly regular, but as its symmetry is only C_3, the averaging is not expected to be uniform.

For SbI_3, AsI_3, and PI_3 the $\sigma(\bar{d})/\bar{d}$ values fall between ~0.05 and 0.2, which corresponds to a Δ range of 250–4000. In crystals containing discrete YX_3^- ions transitions to cubic phases are known to occur even when $\Delta > 4000$ (Table 9). While this might suggest that in these triiodides the existence of transitions associated with a loss of stereochemical activity of the LP cannot be excluded, it may not be realistic to compare the molecular triiodides with the ionic AYX_3 for the present purpose, and the dimorphism that exists in $SbBr_3$ and SbI_3 is not indicative of a tendency in that direction. However, the transition at 155°C in $BiBr_3$ (apparently as yet uninvestigated) provides some grounds for optimism that transitions may yet be found and may prove to be of the averaging type, and so does the existence of polymorphism in trihalides such as $CrCl_3$ (low-$CrCl_3$, hcp BiI_3-type structure; high-$CrCl_3$, ccp YCl_3-type structure) and the variety of mutually related structure types found among the trihalides of Group III and 4*f* elements.

Structure determinations

The positional and thermal parameters for the structures described in the following and the corresponding interatomic distances and bond angles are listed in Tables 10–19.[27] The distances and angles in alkylsulfonium and alkylsulfoxonium salts are compared in Table 20 and discussed at the end of this section.

Me_3SOI

This *Pnma* structure consists of I^- anions and of Me_3S^+ cations practically of C_{3v} skeletal symmetry. The cation/anion packing is of a distorted CsCl type, as may be clearly seen from a projection of the structure on (100). The S—O bond is situated in a mirror plane and is collinear with the I atom at 4.87 Å from the oxygen (Table 11, Fig. 2). The O···I separations are all well in excess of the sum of the van der Waals radii, 3.55 Å.

Et_3SI

The unit-cell dimensions were reported by Mussgnug (8) (cf. Table 1), who also narrowed the choice of space group to *Pnma* or $Pn2_1a$, the latter group being considered the correct one because of the detection of a weak piezoelectric effect. In the present investigation the structure was refined in both space groups (in the $Pna2_1$ and *Pnam* settings).

In the $Pna2_1$ refinement, with z(I) fixed at $\frac{1}{4}$, the z coordinates of the S and C(32) atoms were found to be very close to $\frac{1}{4}$ (Table 14), but those of all the other atoms differed appreciably from $\frac{1}{4}$. The structure could be refined as completely ordered, without constraints on the bond lengths, to R = 2.05%.

In the *Pnma* refinement from the same data set (d/p = 6.2, R = 1.96%, R_w = 2.25%) z(I) and z(S) were taken as $\frac{1}{4}$ but the rest of the cation was treated as being in two-fold positional disorder with respect to the mirror plane, with no constraints

[26]The curves in Fig. 8 are quadratic regression lines: r^2 = 0.96, σ = 0.020 for c.n. 6, r^2 = 0.93, σ = 0.024 for c.n. $\geq$ 6. Inclusion of the additional X atoms in the coordination figure in $\bar{d}$ does not change the trend significantly. The only solid Group V trifluoride for which structural information appears to be available, SbF_3 (138), does not belong to the set treated in the regression.

[27]The parameters of the H atoms in Et_3SI and 3ESHS, respectively, are listed in Tables A and B (see footnote 28). The parameters for special positions ($\frac{1}{4}$, $\frac{1}{2}$) in Tables 10, 12, 14, 16 and 18 have not been multiplied by a power of ten.

Can. J. Chem. Downloaded from www.nrcresearchpress.com by 194.225.253.170 on 09/07/12
For personal use only.

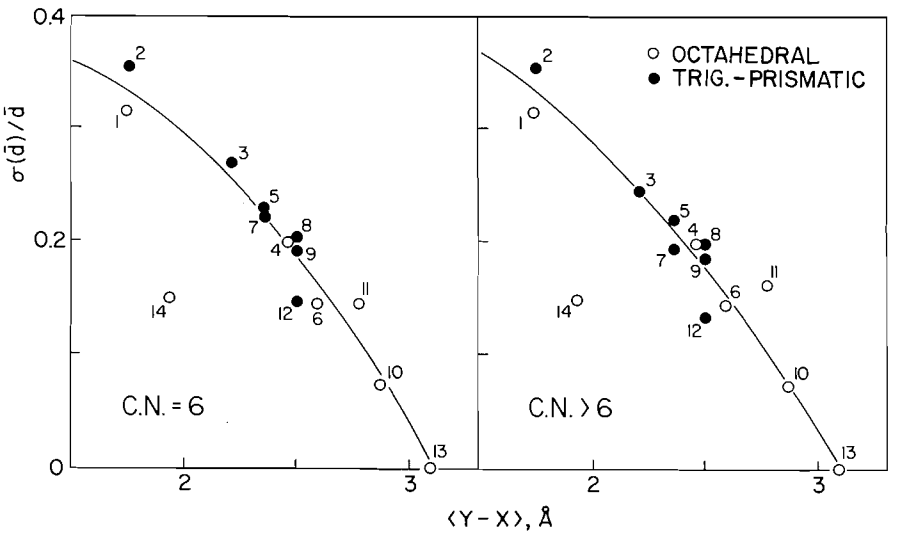


FIG. 8. Variation of the $\sigma(\bar{d})/\bar{d}$ ratio in solid YX_3 (Y = N, P, As, Sb, Bi) halides with the mean bond length ⟨Y—X⟩. $\bar{d}$, mean of Y—X and Y···X distances for c.n. 6 (*left*) or c.n. ≥ 6 (*right*; see text); $\sigma(\bar{d})$, standard deviation of $\bar{d}$; $\sigma(\bar{d})/\bar{d} \sim [\langle Y\cdots X\rangle - \langle Y—X\rangle]/[\langle Y\cdots X\rangle + \langle Y—X\rangle]$. *1*, *2*, NCl_3 (130); *3*, PBr_3 (40); *4*, PI_3 (51); *5*, $AsBr_3$ (131, 132); *6*, AsI_3 (65); *7*, $SbCl_3$ (133); *8*, α-$SbBr_3$ (134); *9*, β-$SbBr_3$ (135); *10*, SbI_3 ($R\bar{3}$) (66); *11*, SbI_3 ($P2_1/c$) (136); *12*, $BiCl_3$ (137); *13*, BiI_3 (66); *14*, SbF_3 (138) (not included in the regression).

applied. When S was allowed to refine freely, the resulting z(S) was 0.2497(3), with negligible differences in the other parameter values. Although a few of the refined parameter values differed by more than 3 esd's from those obtained in the $Pna2_1$ refinement, the structures resulting from the two refinements were scarcely distinguishable (Tables 12 and 13). No correlation coefficients larger than 0.5 were present in either refinement. We have adopted the noncentrosymmetric structure as correct solely on the strength of Mussgnug's report of the piezoelectric effect.

The Et_3SI structure consists of I^- anions and trigonal-pyramidal Et_3S^+ cations of skeletal symmetry approaching C_{3v}. The I^- ions are on a distorted fcc lattice. The cation has a fully extended, *anti–anti* configuration similar to that of the Et_3NH^+ ion in Et_3NHI (59) and related to that of the cation in $(CH_2)_5SMe^+I^-$ (67) (Fig. 2). The two shortest S···I distances, 3.96 and 4.61 Å (Table 13), are comparable to those in Me_3SI (48), 3.95 and 4.42 Å. The I atom at 4.61 Å is close to the axis of the cation on the Me_3 side, and both S···I vectors and the cation axis are in the $y = \frac{1}{4}$ plane. The orientation of the cation axis in this plane is shown in Fig. 2.[29]

On heating the iodide undergoes a transition at ~325 K. This transition probably involves a cation disordering across the pseudo-mirror of the $Pna2_1$ structure, and the *Pnam* of our centrosymmetric refinement may well be an appropriate description of the high-phase structure. While the $\exp(\Delta S_{tr}/R) \sim 6.3$ estimate from the dsc experiments is too large for a simple two-fold orientational disorder, the latter may be at least a partial feature of the transition. The reversal of the transition on cooling is remarkably sluggish (see Experimental).

[28]These tables can be purchased from the Depository of Unpublished Data, CISTI, National Research Council of Canada, Ottawa, Ont., Canada K1A 0S2.

[29]Mussgnug (153) noted a similarity in the unit-cell dimensions of Et_3SI and Et_3NHI (cf. ref. 11) when the latter is referred to an orthohexagonal setting, $a_{ohex} = a_{hex}\sqrt{3}$. However, this similarity is accidental. The cation axis on the LP side of Et_3S^+ avoids the two nearest coplanar I^- neighbours, unlike the N—H bond in Et_3NHI (59), which points directly at the nearest I^- ion and forms a N—H···I bond coincident with a crystallographic C_3 axis (Fig. 2).

$(Me_3S)_2SnCl_6$ (3MSHS)

The space group $Pa3$ suggested by Wyckoff (9) is confirmed as well as the proposed distribution of the S, Cl, and C atoms (Table 14). The equivalence of the Cl atoms is consistent with the observation of a single line in the ^{35}Cl nqr spectrum of 3MSHS (and the corresponding Pt, Se, and Te compounds) (10).

The ion packing is of the *anti*-fluorite type (Fig. 1). Each cation, of C_3 symmetry, is inside a subcube (of $\frac{1}{2}a$ edge length) the alternate corners of which are occupied by the anions. The centroid of the cation lies on a body diagonal of the subcube 0.41 Å from the centre of the subcube and 0.84 Å from the S atom. The LP end of the cation axis points at an unoccupied corner of the subcube. Each such corner (site symmetry C_{3i}) is associated with a pair of S atoms with their LPs facing each other across the centre of symmetry, S···S = 9.87 Å (Table 15).

The $SnCl_6$ octahedra, of symmetry C_{3i}, are metrically almost regular. The shortest S···Cl distance, 3.50 Å, is somewhat smaller than the sum of the van der Waals radii, 3.65 Å. Four of the H···Cl distances also are shorter than the sum of the radii, 3.0 Å (Table 15). The C(1)—H(1) bond is not far from collinear both with the Sn atom at $(0, \frac{1}{2}, 0)$ (~164°) and the centroid of the Cl—Cl(K)—Cl(L) anion face into which the bond is directed (~161°). The other two C—H bonds are oriented approximately tangentially at the nearest Cl corners of the neighbouring $SnCl_6$ octahedra.

The ion packing in 3MSHS can be characterized, and contrasted with that in 3MHS (60), if both $Pa3$ crystals are regarded as consisting of $SnCl_6^{2-}$ anions and $[Me_3S\cdots SMe_3]^{2+}$ or $[Me_3NH\cdots HNMe_3]^{2+}$ cation pairs. The Y atoms in each pair face each other across a centre of symmetry, at S···S = 9.87 Å and N···N = 8.60 Å ($H_N\cdots H_N \sim 6.6$ Å). With the centres of symmetry of the cation pairs located in equipoint 4(*a*) — 0, 0, 0 etc. of $Pa3$, the Sn atoms can be placed in 4(*b*) or in 4(*a*). In 3MSHS they are in 4(*b*) — 0, 0, ½ etc. and the ion packing is of the NaCl type, but in 3MHS they are in 4(*a*), i.e. at the centres of symmetry of the $[Me_3NH\cdots HNMe_3]^{2+}$ pairs, which results in a "molecular" fcc crystal consisting of hydrogen-bonded $[Me_3NH\cdots Cl_3SnCl_3\cdots HNMe_3]^0$ units. The 3MSHS structure

Can. J. Chem. Downloaded from www.nrcresearchpress.com by 194.225.253.170 on 09/07/12
For personal use only.

Can. J. Chem. Downloaded from www.nrcresearchpress.com by 194.225.253.170 on 09/07/12
For personal use only.

TABLE 10. Me_3SOI: positional ($\times 10^4$) and thermal ($\times 10^3$) parameters

Atom	x y z	U_{11} U_{22} U_{33}	U_{12} U_{13} U_{23}
I	−0037.8(5)	42.6(3)	0
	¼	42.8(3)	6.8(2)
	2029.8(8)	41.8(3)	0
S	3039(2)	29.1(8)	0
	¼	34.3(7)	−0.8(6)
	8380(3)	28.1(7)	0
O	2367(7)	51(4)	0
	¼	70(4)	−16(3)
	6920(8)	37(3)	0
C(1)	4556(8)	27(3)	0
	¼	44(4)	7(3)
	8018(12)	60(4)	0
H(11)	5036	68(7)[a]	
	¼		
	9147		
H(12)	4787	40(6)[a]	
	1353		
	7334		
C(2)	2757(5)	38(2)	6(2)
	4319(8)	43(3)	3(2)
	9587(8)	47(3)	−9(3)
H(21)	3270	32(6)[a]	
	4231		
	10686		
H(22)	3004	48(7)[a]	
	5482		
	8938		
H(23)	1824	66(7)[a]	
	4372		
	9883		

[a] U_{iso}.

itself may be classified as belonging to the *anti-C*2 (*anti*-pyrite) type: in FeS_2, Fe is in 4(*b*) and S in 8(*c*) — *xxx* etc., $x = 0.144$.[30] It is also related to the 3ESHS structure (see below).

$(Me_3SO)_2SnCl_6$ (3MSOHS)

The 3MSOHS structure is of an orthorhombically distorted *anti*-fluorite type and shows considerable resemblance to $(Me_2NH_2)_2SnCl_6$ (60): in the former the S—O bond is situated in the mirror plane, in the latter the mirror plane bisects the HNH angle. The structure and its relation to the other *anti*-fluorite structures of interest here are shown in Fig. 1. The $SnCl_6$ octahedron (C_{2h}) is metrically almost regular, $\Delta = 1.4$ (Tables 16 and 17).

$(Et_3S)_2SnCl_6$ (3ESHS)

Figure 9 provides an instructive comparison of the structures of 3ESHS and 3EHS (61). In the latter the ion packing is of a monoclinically distorted *anti*-fluorite type. The N—H bonds form nearly symmetrically bifurcated N—H···2Cl bonds. Each $SnCl_6^{2-}$ ion has associated with it two cations in such a way that the N—H···Sn···H—N groupings are collinear, with the Sn at a centre of symmetry. The centres of these cation pairs thus coincide with the centres at Sn, and if the structure is viewed as consisting of $[Et_3NH\cdots Cl_3SnCl_3\cdots HNEt_3]^0$ "molecules", the packing is of a distorted fcc type. By contrast, in 3ESHS the centres of cation pairs (at S···S = 4.32 Å) and the Sn atoms form a distorted lattice of the NaCl type, i.e. the structure may be regarded as consisting of $[Me_3S\cdots SMe_3]^{2+}$ and $SnCl_6^{2-}$ ions, with the cation and anion centres on separate fc lattices. In this sense the packing in 3EHS is associative (through hydrogen bonding), whereas in 3ESHS it is non-associative (cf. 3MSHS above).

[30] A distorted structure of this type occurs in β-HgO, *Pbca* ⊂ *Pa*3, Hg in 4(*b*), $x(0) = 0.075$, $y(0) = 0.062$, $z(0) = 0.095$ (11).

TABLE 11. Me_3SOI: interatomic distances (Å) and bond angles (deg)

Atoms		Atoms	Angle
S—O	1.426(5)	O—S—C(1)	112.1(3)
S—C(1)	1.735(7)	O—S—C(2)	112.9(3)
S—C(2)	1.748(7)	C(1)—S—C(2)	106.1(3)
C(1)···C(2)	2.784(9)	C(2)—S—C(2C)	106.2(3)
C(2)···C(2C)	2.796(9)	S—O—I	180.0
O···I	4.872(5)	Symmetry code:	
O···I(A)	4.387(5)	A $\frac{1}{2}+x$ $\frac{1}{4}$ $\frac{1}{2}-z$	
O···I(B)	4.734(5)	B $-x$ $\frac{3}{4}$ $1-z$	
S···I(F)	4.375(1)	C x $\frac{1}{2}-y$ z	
S···I(D)	4.593(1)	D $\frac{1}{2}-x$ $\frac{3}{4}$ $\frac{1}{2}+z$	
S···I(E)	4.599(1)	E x $\frac{1}{4}$ $1+z$	
S···I(A)	4.976(1)	F $\frac{1}{2}+x$ $\frac{1}{4}$ $\frac{3}{2}-z$	

The LP axes in the cation pairs are not collinear, which is to be attributed to packing geometry rather than to a tendency of the LPs to avoid each other. The shortest S—Cl distance, 3.57 Å (Table 19), is only slightly smaller than the sum of the van der Waals radii, 3.65 Å.

The $SnCl_6$ octahedron, of C_i symmetry, is only slightly distorted, $\Delta = 2.0$. Its thermal parameters are consistent with rigid-body motion: $R(U_{ij}) = 1.5\%$, $\text{rms}(U_{ij}) = 0.0006$.

Cation geometry

Inspection of the available data (Table 20) shows that although the ranges of the uncorrected S—C bond lengths and CSC angles are quite narrow, the S—C bonds in the sulfoxonium ions tend to be shorter and the CSC angles larger than in the sulfonium ions. The mean values are 1.80(3) Å and 102.2(14)° for the sulfonium and 1.75(1) Å and 106.1(3)° for the sulfoxonium ions. The hypothesis that the means come from the same population can be rejected, both from analysis of variance and from *t* statistics, at the 99% significance level for the bond lengths and at the 99.5% level for the angles. The S—O bond lengths average about 1.43 Å.

The observed geometry of the Me_3S^+ ion is in close agreement with the result of a 6-31G* optimization, in which the initial unconstrained configuration of C_3 symmetry ended up as a configuration of C_{3v} symmetry (Table 7). The larger CSC angle in the sulfoxonium ion is consistent with the predictions from the VSEPR theory. Indeed, as shown in Table 4, conversion of a trigonal-pyramidal YEL_3^{ϵ} species to a tetrahedral (T_d or C_{3v}) $YL'L_3^{\epsilon}$ species generally results in an opening up of the LYL angle. The increase may be quite substantial, over 10° in some instances, and is associated with a shortening of the Y—L bond. The change is particularly dramatic when it involves a change in the ionic charge, e.g. for $PF_3 \rightarrow PF_4^+$.

The shortest S···Hal distances are too few to permit generalization, but it seems that in most cases they are somewhat smaller than the respective sums of the van der Waals radii, 3.65 Å for S···Cl and 4.00 Å for S···I. This apparent shortening may be the consequence of a Coulombic interaction between the net positive charge on the S atom and the anionic charge on X^-.

Can. J. Chem. Downloaded from www.nrcresearchpress.com by 194.225.253.170 on 09/07/12
For personal use only.

TABLE 12. Et_3SI: positional and thermal parameters ($\times 10^4$) of nonhydrogen atoms (refinement in $Pna2_1$)[a]

Atom	x y z	Δ/esd	U_{11} U_{22} U_{33}	Δ/esd	U_{12} U_{13} U_{23}	Δ/esd
I	1075.4(2)	−1/2	544(2)	1/1	70(2)	−1/1
	2131.0(6)	2/5	565(2)	0/1	15(9)	−15/—
	¼	—/—	574(2)	−1/1	25(10)	−25/—
S	3408(1)	1/1	534(5)	−8/4	−6(4)	0/4
	0312(2)	0/2	380(5)	3/4	−128(12)	128/—
	2533(8)	−33/—	457(6)	−5/5	38(13)	−38/—
C(11)	3820(5)	−8/5	84(1)[b]	1/1[b]	2(1)[b]	2/1[b]
	1063(10)	9/9	69(1)[b]	0/1[b]	11(1)[b]	−1/1[b]
	0713(8)	−26/7	45(1)[b]	−1/1[b]	0(1)[b]	2/1[b]
C(12)	3306(7)	−12/6	97(1)[b]	3/1[b]	−6(1)[b]	0/1[b]
	2282(11)	32/9	87(1)[b]	−4/1[b]	−3(1)[b]	−2/1[b]
	−0222(10)	7/9	75(1)[b]	3/1[b]	18(1)[b]	0/1[b]
C(21)	3516(5)	0/4	73(1)[b]	0/1[b]	3(1)[b]	1/1[b]
	2342(8)	2/8	44(1)[b]	0/1[b]	−5(1)[b]	0/1[b]
	3719(8)	−21/7	49(1)[b]	−1/1[b]	−2(1)[b]	4/1[b]
C(22)	3146(6)	3/5	78(1)[b]	2/1[b]	2(1)[b]	2/1[b]
	2027(10)	−15/9	80(1)[b]	−3/1[b]	4(1)[b]	2/1[b]
	5280(8)	−4/7	52(1)[b]	0/1[b]	−26(1)[b]	4/1[b]
C(31)	4294(5)	−3/4	65(1)[b]	−3/1[b]	10(1)[b]	0/1[b]
	−1045(9)	0/8	54(1)[b]	−5/1[b]	−2(1)[b]	1/1[b]
	3230(8)	−28/7	61(1)[b]	−1/1[b]	4(1)[b]	1/1[b]
C(32)	4281(5)	0/5	98(1)[b]	1/1[b]	24(1)[b]	−1/1[b]
	−2894(8)	4/8	57(1)[b]	−2/1[b]	0(2)[b]	0/1[b]
	2518(14)	−15/9	89(1)[b]	3/1[b]	7(2)[b]	7/1[b]

[a]Δ/esd: $\Delta = Pnam - Pna2_1$; esd refers to refinement in *Pnam*.
[b]$\times 10^3$.

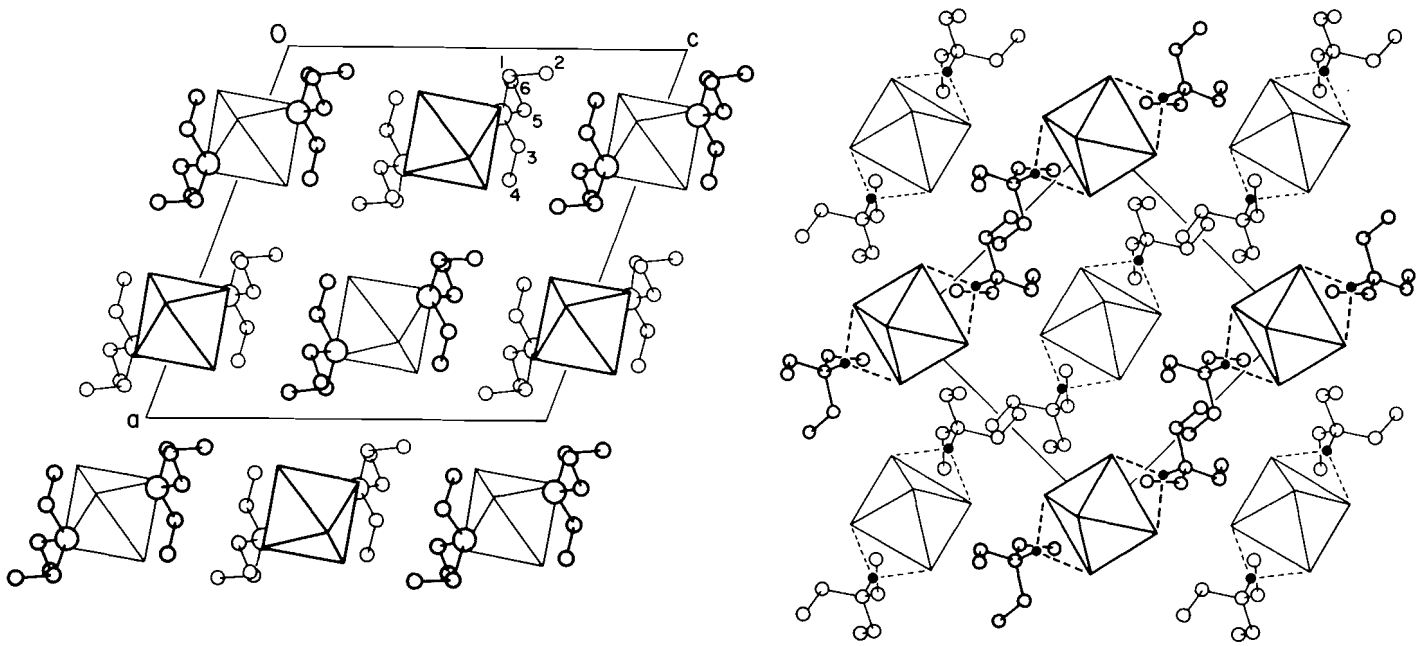


FIG. 9. Comparison of the structures of $(Et_3S)_2SnCl_6$ ($C2/c$, *left*) and $(Et_3NH)_2SnCl_6$ ($P2_1/n$, projection on (001), *right*). Broken lines, N—H···Cl bonds.

Structure type and ion packing

The space groups of trialkyl onium salts represented in Table 21 are often those which in molecular crystals consisting of neutral $YL'L_3$ (L' = *E*, O, H) units of C_{3v} subgroup symmetry would generate a closest packing ($C_1 \subset C_{3v}$) or a packing of maximum density ($C_s \subset C_{3v}$): molecular symmetry $C_1 \rightarrow P\bar{1}$, $P2_1$, $P2_1/c$, $Pca2_1$, $Pna2_1$, $P2_12_12_1$ (also $Pnnm \subset P2_1/n$); molecular symmetry $C_s \rightarrow Pmc2_1$, $Cmc2_1$, *Pnma* (cf. ref. 57). In some cases where the trigonal symmetry has not been lost, the observed space group is a supergroup of one of

Can. J. Chem. Downloaded from www.nrcresearchpress.com by 194.225.253.170 on 09/07/12
For personal use only.

TABLE 13. Et_3SI ($Pna2_1$): interatomic distances (Å) and bond angles (deg)[a]

Atoms	Distance	Atoms	Angle
S—C(11)	1.792(9)	C(11)—S—C(21)	102.3(3)
S—C(21)	1.815(7)	C(11)—S—C(31)	100.4(4)
S—C(31)	1.818(8)	C(21)—S—C(31)	100.7(4)
⟨S—C⟩	1.808(12)	⟨C—S—C⟩	101.1(8)
C(11)—C(12)	1.453(12)	S—C(11)—C(12)	118.5(6)
C(21)—C(22)	1.491(10)	S—C(21)—C(22)	110.5(5)
C(31)—C(32)	1.487(10)	S—C(31)—C(32)	110.4(6)
⟨C—C⟩	1.477(17)	⟨S—C—C⟩	113.1(38)
C(11)···C(21)	2.810(10)	Symmetry code:	
C(11)···C(31)	2.774(10)		
C(21)···C(31)	2.798(10)	A $\frac{1}{2}+x$ $\frac{1}{2}-y$ $\frac{1}{4}$	
C(12)···C(22)	4.782(12)	B $\frac{1}{2}-x$ $y-\frac{1}{2}$ $\frac{3}{4}$	
C(12)···C(32)	4.728(13)	C $\frac{1}{2}-x$ $y-\frac{1}{2}$ $-\frac{1}{4}$	
C(22)···C(32)	4.680(12)	D $\frac{1}{2}-x$ $\frac{1}{2}+y$ $\frac{3}{4}$	
S···I	3.912(3)	E $\frac{1}{2}-x$ $\frac{1}{2}+y$ $-\frac{1}{4}$	
S···I(A)	4.605(3)		
S···I(B)	4.966(3)		
S···I(C)	5.011(3)		
S···I(D)	6.641(3)		
S···I(E)	6.678(3)		

[a]The values obtained from the refinement in *Pnam* differ from the above by no more than 1.5 esd.

TABLE 14. $(Me_3S)_2SnCl_6$: positional and thermal parameters ($\times 10^4$)[a]

Atom	x y z	U_{11} U_{22} U_{33}	U_{12} U_{13} U_{23}
Sn	0	{464(3)}	−24(6)
	$\frac{1}{2}$		24(6)
	0		−24(6)
Cl	1871(1)	529(7)	−43(6)
	5428(1)	642(8)	−10(6)
	0358(1)	694(8)	−64(6)
S	{2298(1)}	{571(5)}	{−30(6)}
C	1636(5)	73(4)[b]	19(3)[b]
	3312(5)	91(4)[b]	1(3)[b]
	3053(5)	74(3)[b]	−9(3)[b]
H(1)	121(4)[b]	66(7)[b]	
	373(4)[b]		
	256(3)[b]		
H(2)	113(4)[b]	70(7)[b]	
	292(4)[b]		
	357(4)[b]		
H(3)	233(3)[b]	80(7)[b]	
	364(4)[b]		
	353(4)[b]		

[a]Values in braces: all three parameters are equal. The thermal parameters of the H atoms are U_{iso}.
[b]$\times 10^3$.

the above nine: $P6_3mc \supset Cmc2_1$ (3EHS), $Pa3 \supset (P2_12_12_1, P2_1/c)$ (3MSHS, 3MHS); this is presumably associated with some loss of economy of packing.

The fact that the above space-group symmetries do occur in onium salts is somewhat unexpected, as the requirements for high packing density are not the same when *two* dissimilar constituents are present. The rationale for the similarity of packing behaviour, at least with the hydrogen-bonded species, may be that a cation–anion or $(cation)_2$–anion pair may function and pack as a single building unit of symmetry C_1 or C_s, e.g. $Et_3NH^+\cdots X^-$ of symmetry $C_{3v} \supset C_s$.

TABLE 15. $(Me_3S)_2SnCl_6$: interatomic distances (Å) and bond angles (deg)

Atoms	Distance	Atoms	Angle
Sn—Cl	2.420(1)	Cl—Sn—Cl(A)	89.6(1)
C—S	1.769(7)	Cl—Sn—Cl(B)	90.4(1)
S···Cl(H) (3×, shortest)	3.498(2)	C—S—C(C)	101.5(3)
S···S(E) (3×, shortest)	6.218(2)	S—C—H(1)	108(3)
S···S(F) (along C_3)	9.868(2)	S—C—H(2)	106(3)
Cl···Cl(D) (between		Symmetry code:	
$SnCl_6$ octahedra)	4.798(2)	A z $\frac{1}{2}-x$ $y-\frac{1}{2}$	
(0,0,0)···Cl(G) (6×)	3.940(1)	B $-z$ $\frac{1}{2}+x$ $\frac{1}{2}-y$	
H(3)···Cl(J)	2.73(5)	C z x y	
H(2)···Cl(C)	2.81(4)	D $1-y$ $\frac{1}{2}+z$ $\frac{1}{2}-x$	
H(1)···Cl(K)	2.94(4)	E x $\frac{1}{2}-y$ $\frac{1}{2}+z$	
H(1)···Cl(L)	2.99(4)	F $-x$ $-x$ $-x$	
		G $x-\frac{1}{2}$ $y-\frac{1}{2}$ z	
		H $\frac{1}{2}-x$ $\frac{1}{2}+y$ z	
		J $\frac{1}{2}-x$ $1-y$ $\frac{1}{2}+z$	
		K $\frac{1}{2}-x$ $\frac{1}{2}+y$ z	
		L $\frac{1}{2}+z$ x $\frac{1}{2}-y$	

The 3MSHS, 3ESHS, 3MHS (60), and 3EHS (61) structures may be thought of as deriving from the *anti*-pyrite $Pa3$ aristotype. Assuming that the symmetry centres of the cation pairs occupy the $4(a)$ — 0, 0, 0 etc. equipoint and the Y atoms are in $8(c)$ — xxx etc. with $x < \frac{1}{4}$, the type of packing will be determined by the choice of equipoint adopted by the Sn atom. In the sulfonium salts the Sn atoms occupy the $4(b)$ — $\frac{1}{2}$, 0, 0 etc. positions, giving rise to a NaCl-type packing. In the ammonium salts Sn is in $4(a)$, which results in a fcc packing of internally hydrogen-bonded [cation···anion···cation]^0 units.

The *orientation* of the cation···cation pair axes in 3ESHS (Fig. 10) can be related to those in 3MSHS and 3ESHS through dichromatic subgroups of the common group *Cmca*:

$$Pa3 \supset Pbca \xleftarrow{P_Cbca} Cmca \xrightarrow{Cm'ca'} C2/c$$

3MSHS β-HgO_2 3ESHS
3MHS
FeS_2
CO_2

A similar relationship holds for 3EHS.

Experimental

Preparation

Crystals of Me_3SOI and Et_3SI suitable for single-crystal X-ray studies were obtained by recrystallizing commercial material from water and from ethanol, respectively. The hexachlorostannates were prepared by allowing an aqueous solution of the respective chloride and H_2SnCl_6 to crystallize by slow evaporation. For this purpose commercial Me_3SI and Et_3SI were converted to the chlorides by ion exchange on a resin column.

Evidence of transition in Et_3SI

Heating a ~0.1 g sample of the recrystallized material (m.p. 146–149°C) in a sealed pan of a differential scanning calorimeter (indium standard) revealed an endothermic peak at ~325 K, with an estimated thermal effect of 4.9 kJ/mol (average of three separate

Can. J. Chem. Downloaded from www.nrcresearchpress.com by 194.225.253.170 on 09/07/12
For personal use only.

TABLE 16. $(Me_3SO)_2SnCl_6$: positional and thermal parameters ($\times 10^3$)

Atom	x y z	U_{11} U_{22} U_{33}	U_{12} U_{13} U_{23}
Sn	½	29.3(3)	1.5(2)
	0	29.9(2)	0
	0	27.4(2)	0
Cl(1)	294.2(3)	41.6(9)	11.0(7)
	147.5(1)	42.0(8)	0
	0	67.6(11)	0
Cl(2)	687.8(3)	103.2(12)	10.5(8)
	079.9(1)	55.6(8)	63.5(10)
	−173.6(2)	90.5(11)	16.8(8)
S	219.6(2)	34.1(8)	3.0(6)
	107.5(1)	33.3(7)	0
	½	35.4(7)	0
O	239.7(8)	58(2)	7(2)
	−001.5(4)	35(2)	0
	½	49(2)	0
C(1)	099.5(8)	63(2)	11(2)
	151.1(4)	51(2)	11(2)
	643.4(6)	43(2)	−4(2)
H(11)	095(3)	52(3)[a]	
	227(3)		
	634(3)		
H(12)	179(3)	56(3)[a]	
	130(3)		
	720(3)		
H(13)	−030(3)	63(3)[a]	
	122(3)		
	642(3)		
C(2)	434.8(12)	33(2)	−2(3)
	171.7(8)	62(3)	0
	½	102(3)	0
H(21)	412(3)	56(3)[a]	
	248(3)		
	½		
H(22)	500(3)	50(3)[a]	
	150(3)		
	420(3)		

[a] U_{iso}.

TABLE 17. $(Me_3SO)_2SnCl_6$: interatomic distances (Å) and bond angles (deg)

Atoms	Distance	Atoms	Angle
Sn—Cl(1)	2.426(2)	Cl(1)—Sn—Cl(2)	89.38(5)
Sn—Cl(2)	2.410(2)	Cl(2)—Sn—Cl(2[a])	90.22(5)
S—O	1.435(5)	O—S—C(1)	112.0(2)
S—C(1)	1.746(5)	O—S—C(2)	113.0(4)
S—C(2)	1.750(9)	C(1)—S—C(1[a])	107.7(3)
O···Cl(2A)	3.411(4)	C(1)—S—C(2)	105.5(3)
O···Cl(1B)	4.613(4)		
O···Cl(2C)	4.654(4)		

Symmetry code: A $1-x$ $-y$ $-z$; B $\frac{1}{2}-x$ $y-\frac{1}{2}$ $\frac{1}{2}$; C x y $-z$

[a] Mirror image.

TABLE 18. $(Et_3S)_2SnCl_6$: positional ($\times 10^4$) and thermal ($\times 10^3$) parameters of nonhydrogen atoms

Atom	x y z	U_{11} U_{22} U_{33}	U_{12} U_{13} U_{23}
Sn	¼	36.2(1)	1.6(1)
	¼	36.5(5)	14.9(1)
	0	36.3(1)	2.2(1)
Cl(1)	2969.4(6)	57.1(4)	7.3(3)
	0367.8(6)	42.4(3)	24.9(3)
	0606.1(6)	58.8(4)	11.1(3)
Cl(2)	1566.3(6)	50.9(4)	4.1(3)
	2710.4(8)	54.2(4)	27.7(3)
	0938.9(5)	49.6(3)	3.9(3)
Cl(3)	3802.0(5)	44.4(3)	−4.9(3)
	3366.8(8)	62.2(4)	12.3(3)
	1274.0(6)	48.8(3)	−6.7(3)
S	1773.7(6)	51.4(4)	−3.2(3)
	2949.8(9)	54.9(4)	13.6(3)
	5899.4(5)	41.5(3)	2.4(3)
C(11)	0799(2)	53(2)	−2(1)
	3917(3)	53(2)	9(1)
	5806(2)	59(2)	5(1)
C(12)	0685(3)	62(2)	11(2)
	4246(4)	73(2)	35(2)
	6696(3)	87(2)	6(2)
C(21)	2724(2)	51(2)	−10(1)
	3780(3)	61(2)	11(1)
	6747(2)	53(2)	1(1)
C(22)	3615(3)	58(2)	−2(2)
	3215(5)	99(2)	25(2)
	6810(3)	86(2)	5(2)
C(31)	1658(2)	67(2)	8(1)
	1567(3)	46(1)	28(1)
	6527(2)	63(2)	7(1)
C(32)	0890(3)	63(2)	1(2)
	0750(3)	53(2)	42(2)
	5897(4)	122(2)	−3(2)

runs with virgin material). The sample was allowed to cool to room temperature in the calorimeter and the heating was repeated, but the endothermic peak did not reappear. In subsequent runs using new samples the transformed material was cooled to room temperature and allowed to stand (*a*) for 15 min before reheating; (*b*) overnight; (*c*) in liquid N_2 for 5 min followed by 10 min at 310 K; (*d*) in liquid N_2 for 5½ h; (*e*) in liquid N_2 overnight; (*f*) in liquid N_2 for 2 days; (*g*) at 310 K for 3 h. Reheating the *a* and *b* samples produced no recovery of the endothermic peak. For *c* the recovery was partial but small; for *d* to *g* it was larger but still not complete.

Structure determinations

The crystals were mounted on glass fibres or (3MSHS) sealed in glass capillaries (crystal dimensions, mm: Me_3SOI, 0.3 × 0.3 × 0.4; 3MSHS, 0.5 × 0.5 × 0.5; 3MSOHS, 0.1 × 0.2 × 0.4; 3ESHS, 0.3 × 0.3 × 0.6). A CAD-4 four-circle diffractometer (ω:2θ scans; 20°C) was used in the data acquisition (cf. Table 1). Lorentz, polarization, and empirical absorptions corrections (7) were applied. Scattering factors for neutral or ionized atoms and corrections for anomalous scattering were taken from ref. 154. The structures were solved as indicated below. Except where otherwise stated all calculations were performed with the SHELX-76 (155) system. After the nonhydrogen atoms had been located, full-matrix least-squares ($w\Delta|F|$ = mini-

TABLE 19. $(Et_3S)_2SnCl_6$: interatomic distances (Å) and bond angles (deg)

Atoms	Distance	Atoms	Angle
Sn—Cl(1)	2.439(1)	Cl(1)—Sn—Cl(2)	91.11(2)
Sn—Cl(2)	2.435(1)	Cl(1)—Sn—Cl(3)	89.88(2)
Sn—Cl(3)	2.414(1)	Cl(2)—Sn—Cl(3)	89.91(2)
⟨Sn—Cl⟩	2.429(13)		
		C(11)—S—C(21)	103.3(2)
S—C(11)	1.801(4)	C(11)—S—C(31)	104.1(2)
S—C(21)	1.795(3)	C(21)—S—C(31)	103.3(2)
S—C(31)	1.798(4)		
⟨S—C⟩	1.798(6)	S—C(11)—C(12)	117.1(3)
		S—C(21)—C(22)	110.7(3)
C(11)—C(12)	1.491(7)	S—C(31)—C(32)	109.8(3)
C(21)—C(22)	1.494(6)		
C(31)—C(32)	1.500(5)	C(11)—S—C(21)—C(22)	−171(4)
⟨C—C⟩	1.495(10)	C(11)—S—C(31)—C(32)	73(4)
		C(21)—S—C(11)—C(12)	−52(4)
S···Cl(1A)	3.574(1)	C(21)—S—C(31)—C(32)	−179(4)
S···Cl(1B)	4.079(1)	C(31)—S—C(11)—C(12)	55(4)
S···Cl(2C)	4.589(1)	C(31)—S—C(21)—C(22)	80(4)
S···Cl(2D)	4.626(1)		
		Symmetry code:	
S···S(D)	4.322(1)	A $\frac{1}{2}-x$ $\frac{1}{2}+y$ $\frac{1}{2}-z$	
		B x $-y$ $\frac{1}{2}+z$	
		C x $1-y$ $\frac{1}{2}+z$	
		D $\frac{1}{2}-x$ $\frac{1}{2}-y$ $1-z$	

TABLE 20. Interatomic distances (Å) and CSC angles (deg) in alkylsulfonium and alkylsulfoxonium ions[a]

Compound	S—C	S—O	S···Cl	S···I	CSC
$(Me_3S)HgCl_3$[b] (157)	⟨1.75(11)⟩	—	3.49	—	⟨102.7(13)⟩
$(Me_3S)_2SnCl_6$	1.769(7)	—	3.498(2)	—	101.5(3)
Me_3SI (48)	⟨1.83(2)⟩	—	—	3.95	⟨103(8)⟩
Me_3SOI	⟨1.744(6)⟩	1.426(5)	—	—	⟨106.1(1)⟩
$(Me_3SO)ClO_4$ (158)	⟨1.74(1)⟩	1.42	—	—	⟨105.7(1)⟩
$(Me_3SO)BF_4$ (159)	⟨1.76(1)⟩	1.44	—	—	⟨106.3(10)⟩
$(Me_3SO)_2SnCl_6$	⟨1.749(2)⟩	1.438(5)	—	—	⟨106.2(10)⟩
Et_3SI	⟨1.808(12)⟩	—	—	3.912(3)	⟨101.1(8)⟩
$(Et_3S)_2SnCl_6$	⟨1.798(6)⟩	—	3.574(1)	—	⟨103.6(4)⟩
$(CH_2)_5SMeI$[c] (67)	⟨1.80(1)⟩	—	—	4.286	⟨103.8(27)⟩
$[—(CH_2)_3S(CH_2)_3S^+—]MeI$[d] (160)	⟨1.817(19)⟩	—	—	3.748(1)	⟨100.0(27)⟩

[a]Not corrected for thermal motion. S···Cl and S···I are the shortest interatomic separations. The standard deviations for the means (in parentheses) do not include the experimental esd's.
[b]Sulfur atom in twofold disorder across the CCC plane.
[c]1-Me-1-thioniacyclohexane iodide; $S—C_{Me}$ = 1.80(2) Å.
[d]1-Me-5-thia-1-thioniacyclooctane iodide; $S—C_{Me}$ = 1.791(5) Å.

mum) refinement was carried out with isotropic temperature factors until R was reduced to a reasonably low value. The H atoms were then placed, consistent with the difference maps, and the refinement was continued with anisotropic temperature factors on the nonhydrogen atoms and isotropic factors on hydrogens. The final difference maps were featureless except as noted below. The anisotropic temperature factor is defined as $T = \exp[-2\pi^2(U_{11}h^2a^{*2} + U_{22}k^2b^{*2} + U_{33}l^2c^{*2} + 2U_{23}klb^*c^* + 2U_{13}hla^*c^* + 2U_{12}hka^*b^*)]$. The structure factors are listed in Tables C–G.[28]

Me_3SOI. Systematic absences: $hk0$, h odd; $0kl$, $k + l$ odd. Space group *Pnma* or $Pn2_1a$. There were slight changes in the crystal during data collection as witnessed by a ~20% increase in the intensity of the standard reflections over the collection period. All nonhydrogen atoms were located using the Patterson solution routine of SHELXS-86 (156). Hydrogen atoms were placed geometrically and constrained to ride on their carbon atoms. The weighting scheme was $w = 2.93/[\sigma^2(F) + 0.01366F^2]$. Seven reflections were omitted from the final refinement because of suspected extinction. The highest residual peak in the final difference map was 1.66 e/Å^3 near the I atom and the deepest trough was −2.57 e/Å^3. Satisfactory solution of the structure in *Pnma* without any indication of the presence of disorder confirmed the centrosymmetric group as the correct choice.

Et_3SI. Systematic absences: $h0l$, h odd; $0kl$, $k + l$ odd. Space group *Pnma* or $Pna2_1$. The 200 reflection contained extra intensity and was omitted from refinement. Complete refinement was carried out in both space groups; the results are compared in Table 12 (E statistics suggest centric). The I atom was located from a Patterson map and the remaining atoms from a difference map. In the $Pna2_1$ refinement z(I) was fixed at $\frac{1}{4}$. Hydrogen atoms were placed geometrically and allowed to refine. The weighting scheme (*Pnma*) was $w = 0.2344/[\sigma^2(F) + 0.005F^2]$. The highest residual peak in the final difference map was 0.4 e/Å^3.

3MSHS. Systematic absences: $hk0$, h odd; $0kl$, k odd; h, k, l not permutable. A Patterson map revealed the Sn and Cl positions. The remaining atoms were located from difference maps. The H atoms were located from a difference map and refined with the C—H distance loosely constrained; the refined positions were close to the original

Can. J. Chem. Downloaded from www.nrcresearchpress.com by 194.225.253.170 on 09/07/12
For personal use only.

TABLE 21. Ion packing types represented among $R_3YR'^+$ alkyl onium salts[a]

R_3	YR′					
	SE	Se*E*	SO[b]	NH	NMe	NEt
			$R_3YR'Cl$			
Me_3				$P2_1/m$ (153, 161)	$P4/nmm$ (11), **C**	
Et_3				$P6_3mc$ (59), **W**		$P2_1/n$[c]
			$R_3YR'I$			
Me_3	$P2_1/m$ (48, 153), **C**	*Pnma* (49), **R**[d]	*Pnma* (*), **C**	$P2_1/m$ (58)[e]	$P4/nmm$ (11), **C**	
Et_3	$Pna2_1$ (8, *)			$P6_3mc$ (59), **W**		$I\bar{4}$ (63), **Z**
$(CH_2)_5SMe$	$Pna2_1$ (67), **R**[d]					
			$(R_3YR')_2SnCl_6$			
Me_3	$Pa3$ (9, *), **A**		*Pnnm* (*), **A**	$Pa3$ (60), **A**	$Fd\bar{3}c$ (62, 162), **A**	
Me_2Et	Cubic (9), (**A**)					
Et_3	$C2/c$ (*)			$P2_1/n$ (61), **A**		$C2/c$ (64), **A**

[a]Packing types: **A**, *anti*-CaF_2; **C**, CsCl; **R**, rock salt; **W**, wurtzite; **Z**, zincblende. *, this work.
[b]$(Me_3SO)BF_4$, *Pbcn* (159), **C** (anion disorder); $(Me_3SO)ClO_4$, $P\bar{4}2_1m$ (158), **C** (anion disorder).
[c]A. Linden, T. S. Cameron, and O. Knop. To be published.
[d]Highly distorted **R**.
[e]Not isostructural with Me_3NHCl.

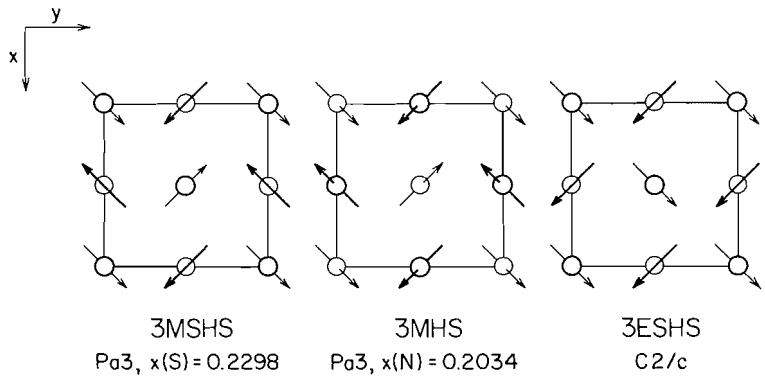


FIG. 10. Schematic representation of the relationship between the $(R_3YL')_2SnCl_6$ structures (see text). The arrow indicates the orientation of the cation–cation axis with respect to z. Light circles, Sn at $z = 0$; heavy circles, Sn at $z = \frac{1}{2}$. Light arrows, cation pair centre at $z = 0$; heavy arrows, cation pair centre at $z = \frac{1}{2}$.

positions in the difference map. A small residual peak of 0.4 e/Å^3 at (0, 0, 0) in the final difference map was initially attributed to partial occupancy of that site by H_2O, but FT-ir spectra showed no evidence of H_2O absorptions. The weighting scheme was $w = 2.235/[\sigma^2(F) + 0.000277F^2]$. Three reflections were omitted from the final refinement because of suspected extinction.

3MSOHS. Systematic absences: $h0l$, $h + l$ odd; $0kl$, $k + l$ odd. Space group *Pnnm* or *Pnn*2. Satisfactory solution of the structure in *Pnnm* without the need to invoke disorder indicated that the centrosymmetric group described the structure correctly. A Patterson map revealed the Sn position. The remaining atoms were located from difference maps. The hydrogens were located but in the refinement were placed geometrically and then allowed to refine freely. The weighting scheme was $w = 0.3211/[\sigma^2(F) + 0.005F^2]$. The highest peak in the final difference map was 0.6 e/Å^3.

3ESHS. Systematic absences: $h0l$, l odd; hkl, $h + k$ odd. Four reflections were omitted because of extinction. Structure solved by direct methods (MULTAN 80) which revealed the Sn and some Cl atoms. All remaining atoms were found from subsequent difference maps. All H atoms appeared in the difference maps and were allowed to refine. The highest peak in the final difference map was 0.4 e/Å^3. The weighting scheme was $w = [\sigma^2(F) + 0.005F^2]^{-1}$.

Ab initio *calculations*

Details of the 6-31G* optimizations and associated procedures will be found in refs. 54–56. For practical reasons the equilibrium molecular geometry of the $SeCl_6^{2-}$ in O_h and C_{3v} symmetries was optimized at a somewhat lower level, STO-3G*.

Acknowledgments

This work was supported by grants from the Natural Sciences and Engineering Research Council of Canada to O.K., T.S.C., and R.J.B. We thank Miss K. N. Robertson for most of the preparative work and Dr. M. A. White and Miss Allyson Perrott for the dsc results. We are also pleased to acknowledge the assistance provided by Randy Barkhouse, Aidan Evans, and the staff of the Dalhousie University Computing and Information Service.

1. R. J. GILLESPIE and R. S. NYHOLM. Q. Rev. Chem. Soc. **11**, 339 (1957).
2. R. J. GILLESPIE. Molecular geometry. Van Nostrand Reinhold, London. 1972.
3. J. GALY, G. MEUNIER, S. ANDERSSON, and A. ÅSTRÖM. J. Solid State Chem. **13**, 142 (1975).
4. P. COPPENS, R. BOEHME, P. F. PRICE, and E. D. STEVENS. Acta Crystallogr. A, **37**, 857 (1981).
5. F. BAERT, P. COPPENS, and E. D. STEVENS. Acta Crystallogr. A, **38**, 143 (1982).

Can. J. Chem. Downloaded from www.nrcresearchpress.com by 194.225.253.170 on 09/07/12
For personal use only.

Can. J. Chem. Downloaded from www.nrcresearchpress.com by 194.225.253.170 on 09/07/12
For personal use only.

6. J. D. DUNITZ. Bull. Chem. Soc. Jpn. **61**, 1 (1988).
7. N. WALKER and D. STUART. Acta Crystallogr. A, **39**, 158 (1983).
8. F. MUSSGNUG. Naturwiss. **28**, 366 (1940).
9. R. B. COREY and R. W. G. WYCKOFF. Radiology, **15**, 241 (1930).
10. R. IKEDA, D. NAKAMURA, R. KADEL, and A. WEISS. Ber. Bunsenges. **87**, 570 (1983).
11. R. W. G. WYCKOFF. Crystal structures. 2nd ed. Vols. 1–5. Interscience Publishers, New York. 1963–1966.
12. Natl. Bur. Stand. Monogr. 25, **1–20** (1962–1984). U.S. Dept. Commerce, Washington, D.C.
13. M. E. BURKE-LAING and K. N. TRUEBLOOD. Acta Crystallogr. B, **33**, 2698 (1977).
14. S. C. ABRAHAMS and J. L. BERNSTEIN. Acta Crystallogr. B, **33**, 3601 (1977).
15. R. WARTCHOW and H. J. BERTHOLD. Z. Kristallogr. **147**, 307 (1978).
16. J. W. BATS. Acta Crystallogr. B, **34**, 1679 (1978).
17. J. DANIELSEN, A. HAZELL, and F. K. LARSEN. Acta Crystallogr. B, **37**, 913 (1981).
18. G. B. JOHANSSON and O. LINDQVIST. Acta Crystallogr. B, **33**, 2918 (1977).
19. J.-O. LUNDGREN and R. LIMINGA. Acta Crystallogr. B, **35**, 1023 (1979).
20. J.-O. LUNDGREN. Acta Crystallogr. B, **35**, 1027 (1979).
21. H. J. BERTHOLD, W. LUDWIG, and R. WARTCHOW. Z. Kristallogr. **149**, 327 (1979).
22. D. H. TEMPLETON and L. K. TEMPLETON. Acta Crystallogr. A, **41**, 133 (1985).
23. S. SIEGEL, B. TANI, and E. APPELMAN. Inorg. Chem. **8**, 1190 (1969).
24. B. W. LUCAS. Acta Crystallogr. C, **40**, 1989 (1984).
25. B. W. LUCAS. Acta Crystallogr. C, **41**, 1388 (1985).
26. J. BOUSQUET, R. RIVIÈRE, and J.-C. REMY. C.R. **265**C, 712 (1967).
27. N. W. ALCOCK. Acta Crystallogr. B, **28**, 2783 (1972).
28. E. T. KEVE, S. C. ABRAHAMS, and J. L. BERNSTEIN. J. Chem. Phys. **54**, 2556 (1971).
29. C.-G. WANG. Huaxue Xuebao, **43**, 271 (1985).
30. L. O. LARSSON and P. KIERKEGAARD. Acta Chem. Scand. **23**, 2253 (1969).
31. W. EYSEL, H. H. HÖFER, K. L. KEESTER, and T. HAHN. Acta Crystallogr. B, **41**, 5 (1985).
32. B. N. MEHROTRA. Z. Kristallogr. **155**, 159 (1981).
33. A. G. NORD. Acta Chem. Scand. **27**, 814 (1973).
34. L. ANDERSEN and D. STRÖMBERG. Acta Chem. Scand. A, **40**, 479 (1986).
35. J. A. MCGINNETY. Acta Crystallogr. B, **28**, 2845 (1972).
36. L. O. LARSSON. Acta Chem. Scand. **23**, 2261 (1969).
37. B. N. MEHROTRA, T. HAHN, W. EYSEL, H. RÖPKE, and A. ILLGUTH. Neues Jahrb. Miner. Monatsh. [**9**], 408 (1978).
38. H. D. LUTZ, W. BUCHMEIER, and B. ENGELEN. Z. Naturforsch. **38**b, 523 (1983).
39. M. MIYAKE, I. MINATO, H. MORIKAWA, and S.-I. IWAI. Am. Mineral. **63**, 506 (1978).
40. R. ENJALBERT and J. GALY. Acta Crystallogr. B, **35**, 546 (1979).
41. K. OLIE. Acta Crystallogr. B, **27**, 1459 (1971).
42. K. OLIE and F. C. MIJLHOFF. Acta Crystallogr. B, **25**, 974 (1969).
43. L. K. TEMPLETON and D. H. TEMPLETON. Acta Crystallogr. B, **27**, 1678 (1971).
44. G. N. RAMACHANDRAN and M. A. LONAPPAN. Acta Crystallogr. **10**, 281 (1957).
45. C. W. F. T. PISTORIUS. J. Chem. Phys. **56**, 6263 (1972).
46. G. R. CRANE. Z. Kristallogr. **141**, 312 (1975).
47. L. DENIELOU, Y. FOURNIER, J.-P. PETITET, and C. TÉQUI. C.R. **270**C, 1854 (1970).
48. D. E. ZUCCARO and J. D. MCCULLOUGH. Z. Kristallogr. **112**, 401 (1959).
49. H. HOPE. Acta Crystallogr. **20**, 610 (1966).
50. F. EINSTEIN, J. TROTTER, and C. WILLISTON. J. Chem. Soc. A, 2018 (1967).
51. E. T. LANCE, J. M. HASCHKE, and D. R. PEACOR. Inorg. Chem. **15**, 780 (1976).
52. L.-G. JOHANSSON, O. LINDQVIST, and N.-G. VANNERBERG. Acta Crystallogr. B, **36**, 2523 (1980).
53. A. D. P. RAO, P. DA R. ANDRADE, and S. P. S. PORTO. Phys. Rev. B, **9**, 1077 (1974).
54. S. C. CHOI, R. J. BOYD, and O. KNOP. Can. J. Chem. **66**, 2465 (1988).
55. S. C. CHOI, R. J. BOYD, and O. KNOP. Can. J. Chem. **65**, 1109 (1987).
56. O. KNOP, R. J. BOYD, and S. C. CHOI. J. Am. Chem. Soc. **110**, 7299 (1988).
57. A. I. KITAIGORODSKY. Molecular crystals and molecules. Academic Press, New York and London. 1973.
58. G. M. SHELDRICK and W. S. SHELDRICK. Acta Crystallogr. B, **26**, 1334 (1970).
59. M. A. JAMES, T. S. CAMERON, O. KNOP, M. NEUMAN, and M. FALK. Can. J. Chem. **63**, 1750 (1985).
60. O. KNOP, T. S. CAMERON, M. A. JAMES, and M. FALK. Can. J. Chem. **61**, 1620 (1983); (errata) **62**, 1227 (1984).
61. O. KNOP, T. S. CAMERON, M. A. JAMES, and M. FALK. Can. J. Chem. **59**, 2550 (1981).
62. K. NIELSEN and R. W. BERG. Acta Chem. Scand. A, **34**, 153 (1980).
63. B. R. VINCENT, O. KNOP, A. LINDEN, T. S. CAMERON, and K. N. ROBERTSON. Can. J. Chem. **66**, 3060 (1988).
64. H. SOWA, U. DRÜCK, and A. KUTOGLU. Cryst. Struct. Commun. **10**, 699 (1981).
65. R. ENJALBERT and J. GALY. Acta Crystallogr. B, **36**, 914 (1980).
66. J. TROTTER and T. ZOBEL. Z. Kristallogr. **123**, 67 (1966).
67. R. GERDIL. Helv. Chim. Acta, **57**, 489 (1974).
68. R. MINKWITZ, R. LEKIES, and H. PREUT. Z. Naturforsch. **42**b, 1227 (1987).
69. J. PASSMORE, E. K. RICHARDSON, T. K. WHIDDEN, and P. S. WHITE. Can. J. Chem. **58**, 851 (1980).
70. S.-W. NG and J. J. ZUCKERMAN. Adv. Inorg. Chem. Radiochem. **29**, 297 (1985).
71. A. K. DAS and I. D. BROWN. Can. J. Chem. **47**, 4288 (1969).
72. W. ABRIEL. Mat. Res. Bull. **19**, 313 (1984).
73. W. ABRIEL and J. IHRINGER. J. Solid State Chem. **52**, 274 (1984).
74. K. VON DEUTEN, W. SCHNABEL, and G. KLAR. Cryst. Struct. Commun. **9**, 761 (1980).
75. W. ABRIEL and H. EHRHARDT. Angew. Chem. Int. Ed. **23**, 963 (1984).
76. W. ABRIEL and C. FRIEDRICH. Z. Naturforsch. **40**b, 1691 (1985).
77. W. ABRIEL. Acta Crystallogr. B, **42**, 449 (1986).
78. W. ABRIEL. Z. Naturforsch. **42**b, 415 (1987).
79. W. ABRIEL and E.-J. ZEHNDER. Z. Naturforsch. **42**b, 1273 (1987).
80. R. W. BERG and K. NIELSEN. Acta Chem. Scand. A, **33**, 157 (1979).
81. N. JOUINI, L. GUEN, and M. TOURNOUX. Ann. Chim. Fr. **7**, 45 (1982).
82. T. KIMURA and T. SAKURAI. J. Solid State Chem. **34**, 369 (1980).
83. R. H. ANDREWS, S. J. CLARK, J. D. DONALDSON, J. C. DEWAN, and J. SILVER. J. Chem. Soc. Dalton, 767 (1983).
84. B. R. VINCENT, K. N. ROBERTSON, T. S. CAMERON, and O. KNOP. Can. J. Chem. **65**, 1042 (1987).
85. C. K. MØLLER. Mat.-fys. Medd. Danske Vid. Selsk. **32**, no. 3 (1960).

Can. J. Chem. Downloaded from www.nrcresearchpress.com by 194.225.253.170 on 09/07/12
For personal use only.

86. K. PRASSIDES, P. DAY, and A. K. CHEETHAM. Inorg. Chem. **24**, 545 (1985).
87. S. L. LAWTON and R. A. JACOBSON. J. Am. Chem. Soc. **88**, 616 (1966).
88. S. L. LAWTON, R. A. JACOBSON, and R. S. FRYE. Inorg. Chem. **10**, 701 (1971).
89. L. R. MORSS and W. R. ROBINSON. Acta Crystallogr. B, **28**, 653 (1971).
90. F. PELLE, B. BLANZAT, and B. CHEVALIER. Solid State Commun. **49**, 1089 (1984).
91. B. V. BEZNOSIKOV and S. V. MISYUL. Sov. Phys. Cryst. **23**, 346 (1978).
92. F. BENACHENHOU, G. MAIRESSE, G. NOWOGROCKI, and D. THOMAS. J. Solid State Chem. **65**, 13 (1986).
93. F. LAZARINI. Acta Crystallogr. B, **34**, 2288 (1978).
94. F. LAZARINI. Acta Crystallogr. B, **33**, 1957 (1977).
95. S. W. PETERSON, J. H. HOLLOWAY, B. A. COYLE, and J. M. WILLIAMS. Science, **173**, 1238 (1971).
96. B. R. VINCENT. Ph.D. thesis. Dalhousie University, Halifax, N.S. 1987.
97. P. TOFFOLI, H. VÉNUMIÈRE, P. KHODADAD, N. RODIER, and R. JULIEN. Acta Crystallogr. C, **41**, 1589 (1985).
98. M. J. ROTHMAN, L. S. BARTELL, C. S. EWIG, and J. R. VAN WAZER. J. Chem. Phys. **73**, 375 (1980).
99. M. KLOBUKOWSKI, S. HUZINAGA, L. SEIJO, and Z. BARANDIARÁN. Theor. Chim. Acta, **71**, 237 (1987).
100. S. BUKSHPAN, J. SORIANO, and J. SHAMIR. Chem. Phys. Lett. **4**, 241 (1969).
101. O. SCHMITZ-DUMONT, G. BERGERHOFF, and E. HARTERT. Z. Anorg. Allg. Chem. **283**, 314 (1956).
102. W. ABRIEL. Mat. Res. Bull. **17**, 1341 (1982).
103. D. BORCHERS and A. WEISS. Ber. Bunsenges. **90**, 718 (1986).
104. D. MESSER. Z. Naturforsch. **33**b, 366 (1976).
105. A. N. CHRISTENSEN and S. E. RASMUSSEN. Acta Chem. Scand. **19**, 421 (1965).
106. G. THIELE, H. W. ROTTER, and K. D. SCHMIDT. Z. Anorg. Allg. Chem. **545**, 148 (1987).
107. W. DEPMEIER, A. MÖLLER, and K.-H. KLASKA. Acta Crystallogr. B, **36**, 803 (1980).
108. F. R. POULSEN and S. E. RASMUSSEN. Acta Chem. Scand. **24**, 150 (1970).
109. J. BARRETT, S. R. A. BIRD, J. D. DONALDSON, and J. SILVER. J. Chem. Soc. A, 3105 (1971).
110. D. E. SCAIFE, P. F. WELLER, and W. G. FISHER. J. Solid State Chem. **9**, 308 (1974).
111. P. MAUERSBERGER and F. HUBER. Acta Crystallogr. B, **36**, 683 (1980).
112. J. A. WATTS. Cited in ref. 110.
113. C. R. HUBBARD and R. A. JACOBSON. Proc. Iowa Acad. Sci. **75**, 85 (1968).
114. C. K. MØLLER. Mat.-fys. Medd. Danske Vid. Selsk. **32**, nos. 1 and 2 (1960).
115. H. J. HAUPT, F. HUBER, and H. PREUT. Z. Anorg. Allg. Chem. **408**, 209 (1974).
116. A. MARSTRANDER and C. K. MØLLER. Mat.-fys. Medd. Danske Vid. Selsk. **35**, no. 5 (1966).
117. W. STOEGER. Z. Naturforsch. **32**b, 975 (1977).
118. D. BEDLIVY and K. MEREITER. Acta Crystallogr. B, **36**, 782 (1980).
119. H.-L. KELLER and I. JESS. J. Less Common Met. **125**, 215 (1986).
120. M. FALK, C.-H. HUANG, and O. KNOP. Can. J. Chem. **52**, 2928 (1974).
121. S. HIROTSU, J. HARADA, M. IIZUMI, and K. GESI. J. Phys. Soc. Jpn. **37**, 1393 (1974).
122. Y. FUJII, S. HOSHINO, Y. YAMADA, and G. SHIRANE. Phys. Rev. B, **9**, 4549 (1974).
123. M. HIDAKA, Y. OKAMOTO, and Y. ZIKUMARU. Phys. Status Sol. (*a*) **79**, 263 (1983).
124. M. SAKATA, T. NISHIWAKI, and J. HARADA. J. Phys. Soc. Jpn. **47**, 232 (1979).
125. W. ABRIEL. Acta Crystallogr. C, **42**, 1113 (1986).
126. K. O. CHRISTE. Inorg. Chem. **11**, 1215 (1972).
127. T. C. GIBB, R. GREATREX, N. N. GREENWOOD, and A. C. SARMA. J. Chem. Soc. A, 212 (1970).
128. T. B. BRILL, R. C. GEARHART, and W. A. WELSH. J. Magn. Reson. **13**, 27 (1974).
129. L. A. MURADYAN, V. E. ZAVODNIK, I. P. MAKAROVA, K. S. ALEKSANDROV, and V. I. SIMONOV. Sov. Phys. Crystallogr. **29**, 236 (1984).
130. H. HARTL, J. SCHÖNER, J. JANDER, and H. SCHULZ. Z. Anorg. Allg. Chem. **413**, 61 (1975).
131. J. TROTTER. Z. Kristallogr. **122**, 230 (1965).
132. A. K. SINGH and S. SWAMINATHAN. Z. Kristallogr. **124**, 375 (1967).
133. A. LIPKA. Acta Crystallogr. B, **35**, 3020 (1979).
134. D. W. CUSHEN and R. HULME. J. Chem. Soc. 4163 (1964).
135. D. W. CUSHEN and R. HULME. J. Chem. Soc. 2218 (1964).
136. S. POHL and W. SAAK. Z. Kristallogr. **169**, 177 (1984).
137. S. C. NYBURG, G. A. OZIN, and J. T. SZYMAŃSKI. Acta Crystallogr. B, **27**, 2298 (1971).
138. A. J. EDWARDS. J. Chem. Soc. A, 2751 (1970).
139. J. A. LERBSCHER and J. TROTTER. Acta Crystallogr. B, **32**, 2671 (1976).
140. H. BOYSEN and A. W. HEWAT. Acta Crystallogr. B, **34**, 1412 (1978).
141. J. IHRINGER. Acta Crystallogr. A, **36**, 89 (1980).
142. K. YAMADA, S. NOSE, T. UMEHARA, T. OKUDA, and S. ICHIBA. Bull. Chem. Soc. Jpn. **61**, 4265 (1988).
143. O. KNOP, W. J. WESTERHAUS, M. FALK, and W. MASSA. Can. J. Chem. **63**, 3328 (1985).
144. M. NATARAJAN, H. E. HOWARD-LOCK, and I. D. BROWN. Can. J. Chem. **56**, 1192 (1978).
145. M. M. ROLIES and C. J. DE RANTER. Acta Crystallogr. B, **34**, 3057 (1978).
146. M. NATARAJAN IYER, R. FAGGIANI, and I. D. BROWN. Acta Crystallogr. B, **33**, 127 (1977).
147. H. W. ZANDBERGEN, G. C. VERSCHOOR, and D. J. W. IJDO. Acta Crystallogr. B, **35**, 1425 (1979).
148. G. BERGERHOFF and H. NAMGUNG. Acta Crystallogr. B, **34**, 699 (1978).
149. M. AHTEE, K. KURKI-SUONIO, A. VAHVASELKÄ, A. W. HEWAT, J. HARADA, and S. HIROTSU. Acta Crystallogr. B, **36**, 1023 (1980).
150. M. SAKATA, J. HARADA, M. J. COOPER, and K. D. ROUSE. Acta Crystallogr. A, **36**, 7 (1980).
151. J. HUTTON and R. J. NELMES. J. Phys. C: Solid State Phys. **14**, 1713 (1981).
152. S. L. MAIR. Acta Crystallogr. A, **38**, 790 (1982).
153. F. MUSSGNUG. Naturwiss. **29**, 256 (1941).
154. International tables for X-ray crystallography. Vol. IV. The Kynoch Press, Birmingham, England. 1974.
155. G. M. SHELDRICK. SHELX-76 system report. University Chemical Laboratories, Lensfield Road, Cambridge, England. 1976.
156. G. M. SHELDRICK. SHELXS-86. Program for the solution of crystal structures. Institut für Anorganische Chemie der Universität. Göttingen, FRG. 1986.
157. P. BISCARINI, L. FUSINA, G. NIVELLINI, and G. PELIZZI. J. Chem. Soc. Dalton, 664 (1977).
158. C. L. COULTER, P. K. GANTZEL, and J. D. MCCULLOUGH. Acta Crystallogr. **16**, 676 (1963).
159. I. C. ZIMMERMAN, M. BARLOW, and J. D. MCCULLOUGH. Acta Crystallogr. **16**, 883 (1963).
160. W. K. MUSKER, M. M. OLMSTEAD, and M. H. GOODROW. Acta Crystallogr. C, **39**, 887 (1983).
161. J. LINDGREN and I. OLOVSSON. Acta Crystallogr. B, **24**, 554 (1968).
162. G. A. MACKENZIE, R. W. BERG, and G. S. PAWLEY. Acta Crystallogr. B, **36**, 1001 (1980).

Mechanistic aspects of the reaction of hydrogen sulfide with dinuclear palladium(I) complexes containing bis(diphenylphosphino)methane and related ligands

A. FREDDY BARNABAS, DOMINIQUE SALLIN, and BRIAN R. JAMES
Department of Chemistry, University of British Columbia, Vancouver, B.C., Canada V6T 1Y6

Received March 1, 1989

This paper is dedicated to Professor Ronald J. Gillepsie on the occasion of his 65th birthday

A. FREDDY BARNABAS, DOMINIQUE SALLIN, and BRIAN R. JAMES. Can. J. Chem. **67**, 2009 (1989).

Kinetic and low temperature nmr data are presented for the reaction of hydrogen sulfide with $Pd_2X_2(\mu\text{-dpm})_2$ species in dichloromethane solution (X = halide, dpm = bis(diphenylphosphino)methane. The reactions form the corresponding bridged-sulfide, A-frame complex via oxidative-addition of H_2S across the Pd—Pd bond to give a hydrido(mercapto) intermediate, that subsequently liberates H_2 to give $Pd_2X_2(\mu\text{-S})$ $(\mu\text{-dpm})_2$ species. Quantitative kinetic data showing first order behaviour in both Pd_2 dimer and H_2S concentrations are given for the bromide system over the temperature range 0–35°C, as well as more limited data for the photosensitive iodide system; plausible mechanisms are discussed. Some qualitative findings are presented for related systems containing 1,1-bis(diphenylphosphino)ethane.

Key words: palladium complexes, hydrogen sulfide, bis(diphenylphosphino)methane.

A. FREDDY BARNABAS, DOMINIQUE SALLIN et BRIAN R. JAMES. Can. J. Chem. **67**, 2009 (1989).

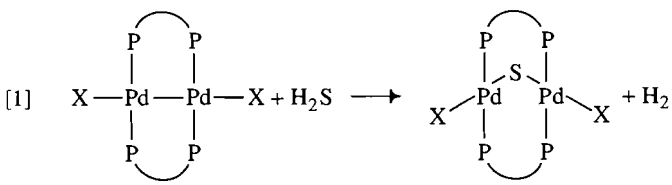
On présente des données relatives à la cinétique ainsi qu'à la rmn à basse température pour la réaction du sulfure d'hydrogène avec les espèces $Pd_2X_2(\mu\text{-dpm})_2$ (dans lesquelles X = halogénure et dpm = bis(diphénylphosphino)méthane), en solution dans le dichlorométhane. Par le biais d'une addition oxydative du H_2S à travers la liaison Pd—Pd, les réactions forment le complexe correspondant, de structure en A et comportant un pont sulfure, qui conduit à un intermédiaire hydrido(mercapto) et qui libère par la suite du H_2 pour fournir des espèces $Pd_2X_2(\mu\text{-S})$ $(\mu\text{-dpm})_2$. Des données cinétiques quantitatives démontrent que, pour le système du bromure à des températures allant de 0 à 30°C et pour des données plus limitées relatives au système photosensibilisé de l'iodure, les réactions sont du premier ordre relativement aux concentrations tant du dimère Pd_2 que du H_2S; on discute de divers mécanismes plausibles. On présente quelques données qualitatives concernant des systèmes apparentés contenant du 1,1-bis(diphénylphosphino)éthane.

Mots clés : complexes de palladium, sulfure d'hydrogène, bis(diphénylphosphino)méthane.

[Traduit par la revue]

Introduction

Work from this laboratory has reported on reaction [1], which involves (at least for the chloride and bromide systems) quantitative reduction of H_2S to H_2 and S^{2-} (1, 2):



[1] $X—Pd(P,P)—Pd—X + H_2S \rightarrow Pd_2X_2(\mu\text{-S})(\mu\text{-dpm})_2 + H_2$

1 **2**

a, X = Cl; *b*, X = Br; *c*, X = I; P P = $Ph_2PCH_2PPh_2$(dpm)

Corresponding reactions occur with H_2Se (3) and H_2Te (4), and possibly H_2O (3, 4). Oxidative-addition of H_2S to transition metal centres to give hydrido(mercapto) species is well-established (2), but reaction [1] was the first reported (1) to show generation of H_2 from H_2S; two other such systems were reported very soon after in completely independent studies, one based on zirconocene species (5) and one base on a rhodium-(triphos) species, triphos = $MeC(CH_2PPh_2)_3$ (6). Related reactivities of the zirconocene species (and titanium and hafnium analogues) toward H_2Se (7) and H_2O (8) have also been reported.

Outside of Kuehn and Taube's work on replacement of the aquo ligand of $Ru(NH_3)_5(H_2O)^{2+}$ by H_2S (9), we are unaware of any solution kinetic studies on the interaction of H_2S with transition metal centres. Reaction [1] is important in terms of possible H_2-recovery from feedstock gases (10), and thus kinetic and mechanistic information on the process is critical for any potential application, as well as for initiating a data base of kinetics for oxidative-addition type reactions of H_2S. This paper reports quantitative kinetic data for reaction [1] with X = Br, some semi-quantitative data for the iodide system, and qualitative observations on the chloride system and related systems using 1,1-bis(diphenylphosphino) ethane (dpmMe).

One suspects that kinetic studies on H_2S systems have been curtailed because of the imposed, obnoxious smell which we can verify to be more difficult to contain in kinetic versus synthetic work. Nevertheless, in contrast to the enforced and sometimes unpleasant working atmosphere, the kinetic data on the bromide systems turned out to be remarkably clean, and an account of this H_2S work dedicated to Ronald Gillespie seems particularly appropriate for an individual who has made seminal contributions to group 6 (now group 16) chemistry.

Experimental section

The materials used, synthetic procedures for the ligands and complexes, and instrumentation used for ^{31}P and ^1H nmr spectra and UV / vis spectra, have been largely described previously (2). D_2S was prepared by the action of 10 mL DCl / D_2O solution (Stohler Isotope Chemicals) on 2 g CaS; the resulting gas was bubbled through D_2O to remove any sulfur oxide impurities and HCl, and then dried over $CaCl_2$. The D_2S (4 mL at 1 atm) was added via a syringe to a CH_2Cl_2 solution of **1***a* (25 mg) in a 10 mL Schlenk tube under vacuum at room temperature (RT); the originally orange solution precipitated the μ-S product **2***a* completely after 30 min. The isolated **2***a*, redissolved in CD_2Cl_2, gave a ^1H nmr spectrum (2) showing a CH_2:phenyl integration ratio of 1:10 and thus no incorporation of deuterium at the methylene groups; consistent with this finding, analysis of the gas phase by low range mass spectroscopy, following removal of D_2S and CH_2Cl_2 at liquid-N_2 temperature, revealed only D_2.

Can. J. Chem. Downloaded from www.nrcresearchpress.com by 194.225.253.170 on 09/07/12
For personal use only.

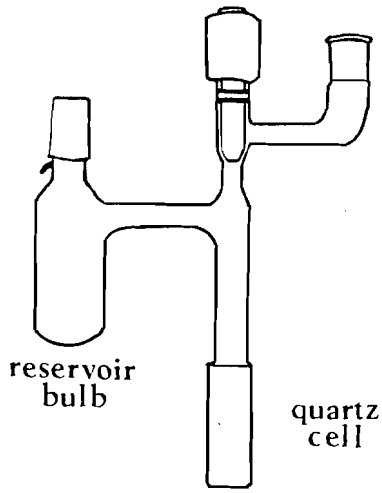


FIG. 1. Spectral cell used for anaerobic UV–visible spectroscopy; the cone on the reservoir bulb can be fitted with a stopper or a septum.

Kinetic measurements

The kinetics of reaction [1] in CH_2Cl_2 (for X = Br, I) were monitored spectrophotometrically in a thermostated Perkin-Elmer 552A instrument using anaerobic cells of the design shown in Fig. 1; cells of path lengths of 1.0 or 0.1 cm were attached by a side-arm to a reservoir bulb, and fitted with a Teflon stopcock and an O-ring joint for attachment to a vacuum/gas-handling line. For an experiment at 1 atm total pressure, a weighed amount of **1** was placed in the quartz cell and the system then evacuated and filled with H_2S gas, while a saturated solution of H_2S in CH_2Cl_2 (10 mL) was pipetted into the reservoir and thermostated at the required temperature (0–35°C); the solid and solvent were then mixed to give a homogeneous solution prior to monitoring optical density changes at some appropriate, fixed wavelength in a thermostated cell-compartment. The cell was agitated periodically to avoid any diffusion problems (e.g. from the H_2 produced). For reactions at lower partial pressures of H_2S ($p' < 1$ atm), complex was placed in the cell, and pure solvent in the reservoir was degassed by employing the freeze–thaw vacuum technique; H_2S was finally added as gas or in solution via a gas-tight syringe, after the ingredients had been mixed and thermostated. The concentrations of **1** ranged from $(0.84–22.3) \times 10^{-4}$ M, and that of H_2S from 0.07–0.53 *M* (see below); thus pseudo-first order conditions were maintained for reaction [1] and standard log (absorbance difference) vs. time plots gave excellent linearity for at least 2.5–3 half-lines, from which the pseudo-first order rate constants, k_{obs}, were readily evaluated.

H_2S solubility measurements

The H_2S solubility in CH_2Cl_2 at specific pressures at 25°C was determined using ^1H nmr spectroscopy. A known volume of CD_2Cl_2 containing either benzene (3 μL) or acetonitrile (5 μL) was degassed in an nmr tube of known volume sealed with a septum; an appropriate volume of H_2S gas was injected into the tube, which was then thoroughly shaken and the solution equilibrated at 25°C. The ^1H nmr spectrum was then run at 25°C, and from the integration intensity of the H_2S peak (δ 0.9 ppm) relative to those of benzene or acetonitrile, the H_2S solubility was determined, and the corresponding partial pressure readily calculated. The H_2S solubility was also similarly measured directly at several temperatures between 0–35°C for a solution initially saturated with H_2S at room temperature and at 1 atm.

Low temperature nmr studies

The ^1H and $^{31}P\{^1H\}$ nmr spectra of the bromide **1***b* (5 mg) in CD_2Cl_2 (0.6 mL) were run at −78°C (solid CO_2/ethanol slush bath). The yellow–orange sample was removed from the probe, and H_2S (5 mL, 1 atm) was injected into the cold, septum-sealed nmr tube via a gas-tight syringe; the H_2S (bp −65°C) condensed inside the tube, and the interface at the CD_2Cl_2 and H_2S liquid layers turned green. The nmr tube was then shaken, replaced into the −78°C probe, and the spectra

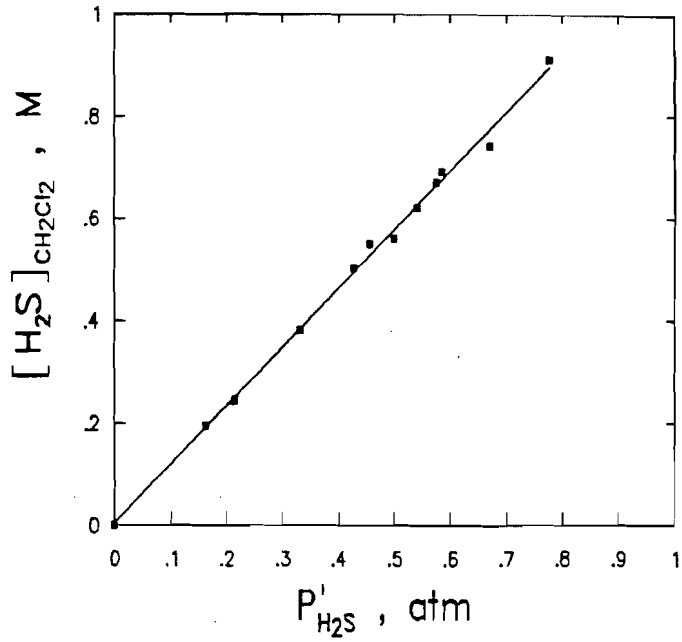


FIG. 2. Solubility of H_2S in CH_2Cl_2 at 25°C at various partial pressures; the partial pressure of CH_2Cl_2 = 0.54 atm (13).

rerun; the spectra were also taken at higher temperatures when the green intermediate disappeared. For the iodide system, **1***c*, H_2S (50 mL, 1 atm, 25°C) was administered into a Schlenk tube, containing 20 mg **1***c* dissolved in 2.5 mL degassed CD_2Cl_2; the tube was cooled to −78°C, and the initially brownish-red solution left until it turned green (10–20 h). A sample was then cannulated into an nmr tube and spectra run at different temperatures from −78 to 20°C. As discussed later, the green colour pertains to a hydrido(mercapto) intermediate; such a species was not seen in the chloride system where only **1***a* and the μ-S product **2***a* were ever detected by nmr.

Results

The rates of reaction [1] at room temperature were noticed qualitatively during synthetic procedures to be dependent on the halide X (1) and on the H_2S concentration used. The reactivity trend at 1 atm total pressure in CH_2Cl_2 (i.e. at ~0.5 atm H_2S) was Cl > Br > I, and, of these, the bromide system was chosen for detailed study because of the convenient reaction half-times for a classical spectrophotometric study at such H_2S partial pressures. Limited, semi-quantitative kinetic data only were obtained at similar conditions for the iodide system, which revealed complexities because of photosensitivity (see below). The chloride system reacts too rapidly at corresponding conditions (even for stopped-flow studies) and requires study under very different conditions, particularly at much reduced H_2S concentrations and pressures, work that is currently in progress.

It was first essential to show in reaction [1] that the evolved H_2 did originate exclusively from the H_2S. The methylene protons of dpm do have acidic character (2, 11) and involvement of the —CH_2— groups seemed at least a possibility; however, this is ruled out in that reaction of **1***a* with D_2S generates D_2 with no accompanying HD or H_2, and the **2***a* product contains only protonated dpm. In related work (12), the synthesis of $Pd_2Cl_2(\mu\text{-}PPh_2CD_2PPh_2)_2$ and its exchange with proton-containing solvents have been studied; reaction of this complex with H_2S correspondingly gives only H_2 and the —CD_2— μ-sulfide product, again showing non-involvement of the methylene protons in the H_2S reactions.

Can. J. Chem. Downloaded from www.nrcresearchpress.com by 194.225.253.170 on 09/07/12
For personal use only.

TABLE 1. Temperature dependence for the bimolecular rate constant k of the reaction of **1***b* with H_2S in CH_2Cl_2

Temp, K	$[H_2S]^a$	$k \times 10^4, M^{-1}\ s^{-1}$
273	0.50	1.59
279	0.51	3.61
288	0.525	6.53
298	0.525	17.1
298	0.525[b]	7.09
303	0.54	20.1
308	0.55	25.5

[a]The H_2S solubility was measured directly by ^1H nmr (see Experimental section); the corresponding partial pressures were not estimated.
[b]D_2S used; solubility assumed to be the same as for H_2S.

Quantitative evaluation of the kinetic data for reaction [1] depends on knowledge of the H_2S solubility in CH_2Cl_2. This was readily estimated by ^1H nmr measurements, and Henry's Law was obeyed at partial pressures (p') of H_2S at least up to 0.8 atm, the solubility being determined as 1.14 M atm^{-1} at 25°C (Fig. 2); at this temperature, $p'(CH_2Cl_2) = 0.54$ atm (13), and thus at a total pressure of 1 atm, H_2S is soluble to the extent of 0.53 M. The directly measured $[H_2S]$ values in the kinetic runs at 0–35°C are given later with some rate constant data (Table 1). We have been unable to find literature data for H_2S solubility in CH_2Cl_2; a value in $CHCl_3$ at 20°C, determined by a classical volumetric procedure (14), is 1.3 M atm^{-1}.

Kinetic data

Reaction [1] is readily monitored by solution electronic spectroscopy; species such as **1** are reddish-orange with two to three absorption maxima in the 340–590 nm region (2, 15, 16), while the μ-S products (**2**) are brown and have absorption maxima in the 325–350 and 470–485 nm regions (2, 17). Figure 3 shows spectral changes on treating a CH_2Cl_2 solution of the bromide **1***b* with H_2S at 25°C; rates for the bromide system were followed by observing the decreasing absorption at 428 nm as a function of time, and the observed isosbestic point showed a well-behaved system. The pseudo-first order rate constants, k_{obs}, obtained from the excellently linear semi-log plots (Fig. 3, inset), were strictly first order in $[H_2S]$ (Fig. 4) and were independent of the [**1***b*] from (0.84–22.3) × 10^{-4} M. Thus the rate law takes the simple form

$$[2]\quad \text{Rate} = -\frac{d}{dt}[\mathbf{1}b] = k_{obs}[\mathbf{1}b] = k[H_2S][\mathbf{1}b]$$

where k is the bimolecular rate constant for the reaction. The temperature dependence data for k were obtained at a single, directly determined $[H_2S]$, and with [**1***b*] = 1.0 × 10^{-3} M (Table 1); an Eyring plot gives a reasonably linear straight line and the activation parameters $\Delta H^{\ddagger} = 55 \pm 5$ kJ mol^{-1} and $\Delta S^{\ddagger} = -115 \pm 10$ J K^{-1} mol^{-1}.

Corresponding studies on the slower iodide system were attempted by monitoring visible absorption spectral changes around 450 nm, a region where such changes are maximal during the formation of **2***c* from **1***c*; however, it soon became obvious that the iodide system was photosensitive. An initial isosbestic point was soon lost, and the rates of spectral changes were dependent on the degree of exposure of the reaction solution to light (either laboratory light or that of the spectrophotometer light source). Even when the solution was kept in the dark,

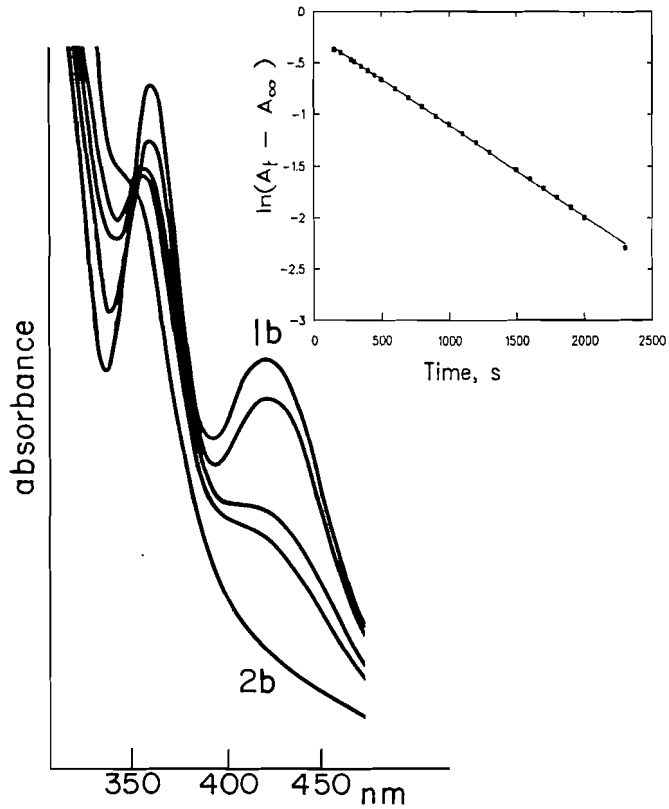


FIG. 3. Visible absorption spectral changes (350–450 nm region) for a CH_2Cl_2 solution of $Pd_2Br_2(\mu\text{-dpm})_2$ **1***b* on addition of H_2S. The inset shows a rate-plot analyzed for a first order dependence on **1***b*; initial [**1***b*] = 1.00 × 10^{-3} M, $[H_2S]$ = 0.53 M at 25°C; A_t and A_∞ represent the absorption at 428 nm at times t and ∞, respectively.

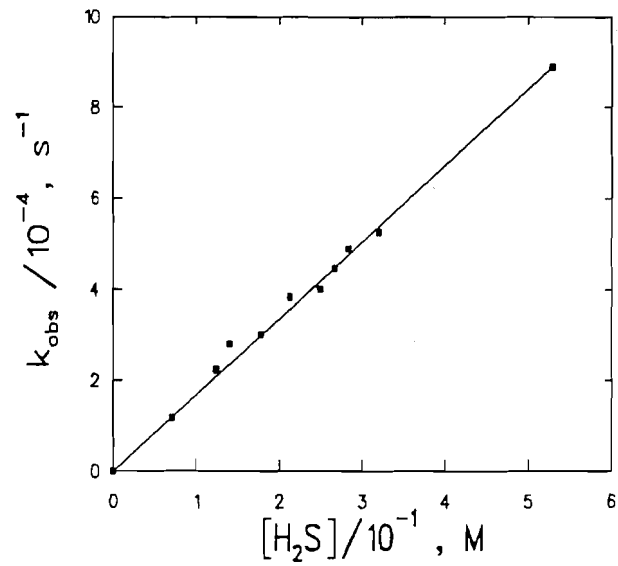


FIG. 4. The dependence of the pseudo-first order rate constants, k_{obs}, on $[H_2S]$ at [**1***b*] = 1.00 × 10^{-3} M, in CH_2Cl_2 at 25°C.

and the optical density recorded at just one wavelength (450 nm) by a sampling rather than continuous monitoring, the kinetic data were irreproducible. Complementary nmr studies at higher concentrations showed that the monomer $PdI_2(dpm)$ (18) was formed during the reaction; indeed, laboratory light readily induces formation of some monomer in solutions of $Pd_2I_2(\mu\text{-dpm})_2$. Analysis of the early visible spectral changes, using an

Can. J. Chem. Downloaded from www.nrcresearchpress.com by 194.225.253.170 on 09/07/12
For personal use only.

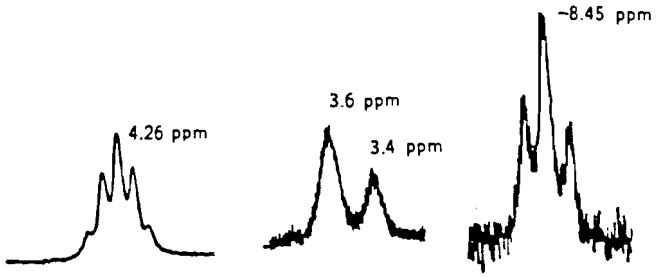


FIG. 5. The ^{1}H nmr spectrum of **1***b* + H_2S in CD_2Cl_2 ~ −78°C; the δ 4.26 quintet is unreacted **1***b*, the other peaks being assigned to **1***b*′. The peaks for **1***b*′ have been expanded.

A_∞ value from the known absorption spectrum of **2***c* (2, 17), gave $k_{obs} \sim 10^{-4}$ s^{-1} at 25°C and 1 atm total pressure; this corresponds to a bimolecular rate constant of $\sim 2 \times 10^{-4}$ M^{-1} s^{-1}, assuming the iodide system (like the bromide) obeys a first order dependence on [H_2S]. Unfortunately the data were not sufficiently reproducible to establish firmly the H_2S dependence; nevertheless, the limited data show rates about ten times slower than the bromide system under corresponding conditions (see Table 1).

Attempts to find a kinetic role for intermediate ionic or "dangling" (mondentate) phosphine species were unsuccessful. Addition of a five-fold excess of bromide as NEt_4Br to **1***b* during a reaction with H_2S generated **2***b* in only about 70% yield; several other products were evidenced by UV–visible spectroscopy and by $^{31}P\{^1H\}$ nmr (see below), especially an unidentified species with δ_p = 22.2 ppm. A five-fold excess of dpm complicated the kinetic studies by abstracting sulfur from the μ-S product **2***b*.

Nuclear magnetic resonance detection of the green reaction intermediates

The ^{1}H nmr of **1***b* at −78°C shows the characteristic dpm —CH_2— signal (δ = 4.26, quintet, J_{PH} = 4 Hz) along with the less informative phenyl signals (17); after the addition of H_2S as described in the Experimental section, in addition to the H_2S signal (δ = 0.9), two additional broad resonances at δ 3.4 and 3.6 ppm, and a high-field Pd-H 1:2:1 triplet at δ = −8.45 ppm (J_{PH} = 18 Hz) are seen (Fig. 5); this new species (**1***b*′) is formed only to the extent of ~10%, and the relative proton integrations for the methylene region: high-field region are 4:1, consistent with a monohydride intermediate. With an increase of the temperature to −65°C, the peaks of **1***b*′ decrease rapidly ($t_{1/2}$ < 30 s) in intensity and the characteristic peaks of the μ-S product **2***b* become evident, inequivalent methylene protons with virtual coupling to the remote phosphorus nuclei giving two doublets of quintets centred at δ 2.85 and 4.80 ppm (1, 17). Above −65°C, only signals of **1***b* and **2***b* are observed. The $^{31}P\{^1H\}$ nmr spectral data complement the ^{1}H nmr data and, at appropriate stages, show the singlets (1, 17) of **1***b* (δ −5.5) and **2***b* (δ 5.80), as well as four unresolved, broad peaks (δ ~ 5, 8, 19, and 23 ppm) attributed to the intermediate **1***b*′ species.

The ^{1}H and $^{31}P\{^1H\}$ nmr data for the iodide system reveal an intermediate **1***c*′ species in much the same way as the bromide system, but higher concentrations of **1***c*′ (up to 50%) can be generated. Complex **1***c* at −78°C (δ_H 4.23, quintet) reacts slowly at this temperature (see Experimental section) to generate **1***c*′ (broad singlet resonances at δ_H 5.02, and δ_H −6.05, with 4:1 integration ratios), which above −70°C converts into **2***c* (doublets of quintets centred at δ_H 3.07 and 4.97); a further weak, broad signal at δ_H 0.4 is seen accompanying the resonances for **1***c*′, the maximum intensity observed being about 1/4 that of the high-field Pd—H resonance. The corresponding ^{31}P data (Fig. 6) show the conversion of **1***c* *to* **2***c*; the **1***c*′ peaks appear as two broad resonances at −78°C, and as an averaged −4 ppm signal at −40°C. That the ^{31}P signal of **1***c* at δ −11.3 is broadened at −78°C (like the resonances of **1***c*′) suggests some inhomogeneity in the sample, perhaps resulting from the presence of both H_2S and CD_2Cl_2 liquid phases.

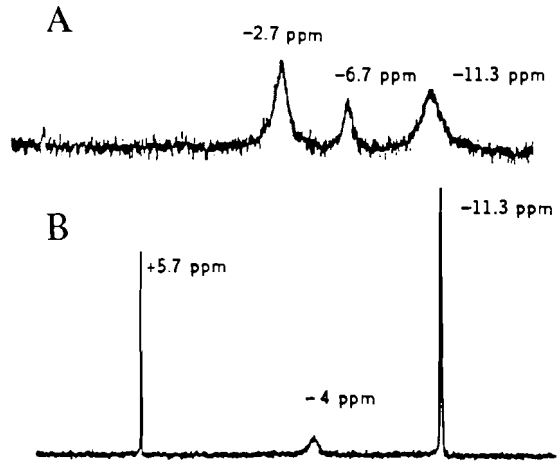
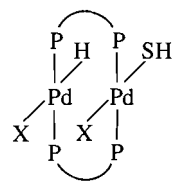


FIG. 6. The $^{31}P\{^1H\}$ spectra for the reaction of $Pd_2I_2(\mu\text{-dpm})_2$ **1***c* with H_2S in CD_2Cl_2 to give $Pd_2I_2(\mu\text{-dpm})_2(\mu\text{-S})$ **2***c* via the intermediate **1***c*′. The signals for **1***c* and **2***c* are the singlets at −11.3 and +5.7 ppm, respectively; the other signals are assigned to **1***c*′. *A* shows the −78°C spectrum measured after 8 h at this temperature; *B* shows the spectrum of the same solution warmed to −40°C, and at higher temperatures the broad −4 ppm signal disappears.

Discussion

For both the bromide and iodide systems, the low temperature ^{1}H nmr data reveal a high-field resonance attributable to a Pd—H intermediate, indicative of oxidative addition of H_2S (2). Oxidative addition reactions to the Pd_2X_2 $(\mu\text{-dpm})_2$ complexes in which the metal–metal bond acts as a nucleophile are well established (11), and such a process with H_2S would lead to an intermediate containing terminal hydrido and terminal mercapto ligands; the detected **1***b*′ and **1***c*′ species are considered to be of



X = Br, **1***b*′
X = I, **1***c*′

this type. The δ_H − 8.45, J_{PH} = 18 Hz signal for **1***b*′ is characteristic of a Pd—H *cis* to two equivalent phosphine ligands (19); The δ(Pd—SH) signal, typically at δ between 1.5 and −1.5 ppm (2), is not seen; it may be buried under the large, broad H_2S signal at ~0.9 ppm, or the SH proton which will certainly be acidic (20) may be undergoing rapid exchange with H_2S protons. The resonances of the —CH_2— protons, which are all inequivalent in a static **1***b*′ structure, appear as two unresolved peaks (δ 3.4, 3.6 ppm). The four unresolved $^{31}P\{^1H\}$ resonances presumably result from the expected AA′BB′ pattern (2). The presumed iodide intermediate **1***c* appears more "fluxional" in that only a single broad resonance is seen for the —CH_2— protons (δ 5.02) and for the Pd—H (δ −6.05), and the

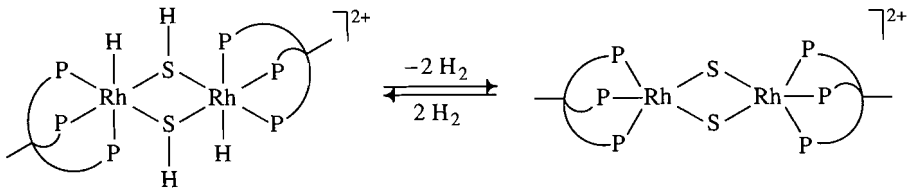
Can. J. Chem. Downloaded from www.nrcresearchpress.com by 194.225.253.170 on 09/07/12
For personal use only.

Can. J. Chem. Downloaded from www.nrcresearchpress.com by 194.225.253.170 on 09/07/12
For personal use only.

two broad $^{31}P\{^1H\}$ resonances at −78°C (δ −2.7, −6.7) collapse to a single broad resonance at −40°C (δ −4.0); the δ_H 0.4 signal could be from the —SH, although the intensity is low.

Generation of the bridged-sulfide products and H_2 via **1***b*′ (**1***c*′) is envisaged as deprotonation of the coordinated SH^- with subsequent protonation of the coordinated hydride. The chemistry has analogies in H_2S reactivity at a Pt(111) surface (21) and addition of H_2S to $Pt_3(\mu_3\text{-CO})(\mu\text{-dpm})_3^{2+}$ (20). Reaction of H_2O with zirconocene species to give a μ-oxo derivative with H_2 evolution was also presented as proceeding via oxidative addition and a subsequent proton transfer (8).

It should be noted that the spectroscopic data (and kinetic data — see below) do not rule out the possibility of the SH^- and / or H^- being bridging ligands. Several plausible alternative structures could be given for **1***b*′ and **1***c*′, because in general the nmr signals are insufficiently resolved to define the structures adequately; however, the high-field ^1H nmr triplet for the bromide system certainly demonstrates the presence of a terminal hydride. Recent work by Bianchini *et al.* (6) has shown the involvement of bridging-SH groups in the following reversible H_2-binding system (where the phosphine ligand is triphos, $MeC(CH_2PPh_2)_3$):



Solutions of the dinuclear Pd_2 (μ-S) species **2** were unreactive toward H_2 at least up to 10 atm pressure.

The kinetic data for the bromide system show simple first order dependence on both $[Pd_2{}^I]$ and $[H_2S]$, and are therefore of somewhat limited use in defining the mechanism. Direct attack by H_2S rather than by SH^- is implied, and indeed SH^- also readily displaces the halide ligands of **1** and **2** (2). The green intermediate **1***b*′ is not seen during the kinetic studies at 0–35°C and thus, assuming a steady state treatment for this species in the following mechanism,

$$[4]\quad \mathbf{1}b + H_2S \underset{k_{-1}}{\overset{k_1}{\rightleftharpoons}} \mathbf{1}b' \xrightarrow{k_2} \mathbf{2}b + H_2$$

gives the rate-law $k_1k_2[\mathbf{1}b][H_2S]/(k_{-1} + k_2)$. If $k_2 \gg k_{-1}$, the rate simplifies to $k_1[\mathbf{1}b][H_2S]$, while if $k_{-1} \gg k_2$, the rate expression becomes $k_2K_1[\mathbf{1}b][H_2S]$ where K_1 = the equilibrium constant (k_1/k_{-1}). The more complete expression for the latter case is $k_2K_1[\mathbf{1}b][H_2S]/(1 + K_1[H_2S])$, but the strictly first order dependence on $[H_2S]$ up to 0.53 *M* (Fig. 4) requires that at 25°C $K_1[H_2S] \ll 1$, as **1***b*′ is not detectable at these conditions.

An extra step with accompanying kinetic / equilibrium parameters is involved if an H_2S adduct is initially formed:

$$[5]\quad \mathbf{1}b + H_2S \underset{k_{-a}}{\overset{k_a}{\rightleftharpoons}} Pd_2Br_2(dpm)_2(H_2S) \underset{k_{-b}}{\overset{k_b}{\rightleftharpoons}} \mathbf{1}b' \xrightarrow{k_2} \mathbf{2}b + H_2$$

Consistency with the observed kinetics requires one of the following: (*a*) the k_a step is rate-determining; rate = $k_a[\mathbf{1}b][H_2S]$. (*b*) k_b governs the rate-determining step, following a rapid K_a pre-equilibrium (k_a/k_{-a}) with the H_2S adduct being undetectable; rate = $k_bK_a[\mathbf{1}b][H_2S]$. The more general case here is when a steady state treatment is applied to the H_2S adduct and $k_2 \gg k_{-b}$; rate = $k_ak_b[\mathbf{1}b][H_2S]/(k_{-a} + k_b)$. (*c*) the k_2 step is rate-determining, the two pre-equilibria K_a and K_b (k_b/k_{-b}) generating undetectable amounts of the H_2S adduct and **1***b*′; rate = $k_2K_aK_b[\mathbf{1}b'][H_2S]$.

The fact that **1***b*′ rapidly converts to **2***b* at temperatures above −65°C shows that *the* k_2 *step in mechanisms outlined in eqs. [4] and [5] cannot be rate-determining at 0–35°C*. Formation of **1***b*′ (or the H_2S adduct) must be rate-determining and this would be consistent with the non-detection of intermediates at ambient conditions. Formation of a possible H_2S adduct (the K_a equilibrium) is expected to be favoured at lower temperatures, because reactions of this type must be entropically unfavourable and therefore exothermic if they are to occur at all. A few H_2S complexes have been characterized: $Ru(NH_3)_5(SH_2)^{2+}$ (9), $W(CO)_5(SH_2)$ (22), $AlBr_3(SH_2)$ (23), and ^1H nmr spectroscopic evidence has been presented for the species $Pt(PPh_3)_2(SH_2)$ en route to formation of a more stable hydrido (mercapto) complex (24). In our Pd systems, the intermediates detected (**1***b*′, **1***c*′) are definitely mono-hydrides and not Pd—SH_2 species, as judged by the relative proton integrations and the J_{PH} value of 18 Hz recorded for **1***b*′ (three-bond coupling within a Pd—SH_2 adduct would be much less). In the recently reported species $Pd_2(CH_3)_2(\mu\text{-dpm})_2$ (μ-H), the hydride appears in the ^1H nmr at δ −7.55, as the expected quintet with J_{PH} = 15.0 Hz (19).

The activation parameters ($\Delta H^{\ddagger}$ = 55 kJ, $\Delta S^{\ddagger}$ = −115 J K^{-1}) are quite typical of those observed for oxidative addition reactions at one metal centre (25–27), but we are unaware of any useful, comparable data for dinuclear systems. For the present $Pd_2{}^I \rightarrow Pd_2{}^{II}$ system, formation of a species such as **1***b*′ necessitates breaking the Pd—Pd bond but the electronic promotional energy (25–27) is now only for a single electron at each Pd centre and will be less than that required for 2e-oxidative addition at one "comparable" metal centre; the other factors contributing to $\Delta H^{\ddagger}$ are breaking of an S—H bond and formation of the Pd—H and Pd—SH bonds. Overall, the activation parameters for the oxidative addition process for the same molecule at one or two metal centres may turn out to be similar. It is not clear from the present study if $\Delta H^{\ddagger}$ and $\Delta S^{\ddagger}$ refer to k_1 (eq. [4]), k_a or k_bK_a (eq. [5]). Corresponding ambiguities arise in oxidation addition of H_2 to give a dihydride species, now that η^2-H_2 complexes as possible intermediates have been recognized (28). Of note, the reaction of **1***b* with CO to give $Pd_2Br_2(\mu\text{-dpm})_2(\mu\text{-CO})$ in dimethylacetamide solution, with $\Delta H^{\ddagger}$ = 15 kJ, $\Delta S^{\ddagger}$ = −121 J K^{-1} (15), is some 10 times faster than the H_2S reaction in CH_2Cl_2 at comparable temperatures, and the difference is reflected entirely in the $\Delta H^{\ddagger}$ values; presumably, the higher value for the H_2S system results from energy required to break an S—H bond.

The measured isotope effect (H_2S vs. D_2S) of 2.4 appears reasonable for an oxidative addition process. Complete cleavage of an S—H versus S—D bond of $H_2S(D_2S)$ in the transition state should give a primary isotope effect of 4.8 (calculated (29)

Can. J. Chem. Downloaded from www.nrcresearchpress.com by 194.225.253.170 on 09/07/12
For personal use only.

using ν(S—H) = 2500 cm^{-1}), but this will be "offset" by formation of the Pd—H(D) bond; complete formation of a terminal or a bridged hydride (deuteride) would reduce the primary isotope effect to 1.4 or 2.0, respectively, assuming values of ν(Pd—H) = 2000 and ν(Pd—H—Pd) = 1400 cm^{-1} (30).

It would be particularly useful to have activation parameters for the other halide systems; unfortunately the iodide system was photosensitive under the kinetic conditions (indeed, even Pd_2Cl_2 (μ-dpm)$_2$ decomposes under photolysis with a tungsten lamp (31)), but at 25°C the H_2S reaction is ~10 times slower than for the bromide. The reactivity trend of **1** toward H_2S (X = Cl > Br > I) is opposite to that normally encountered for oxidative addition of gas molecules to single metal centres, where more basic auxillary ligands promote reaction (25–27). Within **1**, the Pd—Pd bond strength is expected to increase in the order I < Br < Cl (16), the reverse of the trans effect of the halides (32), and thus the reactivity trend is not dominated by differences in the metal–metal bond strength. Reactivity of **1** toward CO is also Cl > Br > I *in terms of equilibrium constants*, and this is governed by the rate of CO loss from the μ-carbonyl product that decreases in the reverse order (I > Br > Cl), the forward carbonylation reaction rates being essentially the same for the three halide species (15); it has been suggested that the strength of the metal–carbonyl bond in the product (I < Br < Cl) governs the reactivity trend (15). Such could be the case in the H_2S systems, if the k_{-1} step of the mechanism outlined in eq. [4], or the k_{-a} step of the mechanism given in eq. [5], case (*b*), becomes increasingly important (i.e. these rate constants increase in the order $k_{Cl} < k_{Br} < k_I$).

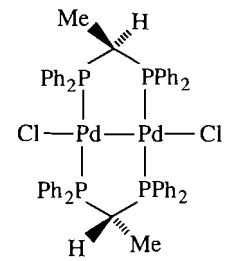
Invoking the principle of Occam's razor (33), which liberally interpreted means "rationalizing experimental data in terms of the simplest number of steps", leads to the mechanism of eq. [4] being favoured, but the existence of known transition metal – H_2S complexes suggests that the mechanism of eq. [5] is more realistic. That hydrides such as **1***b*′ and **1***c*′ are detected at low temperatures is perhaps surprising; extrapolation of the kinetic data to −78°C (using the activation parameters) shows the rate of formation of **1***b*′ is negligible at this temperature. It should be remembered that the green colour is seen only when the H_2S is present in the liquid phase and therefore in a high, localized concentration (~45 *M*). When liquid H_2S comes in contact with solid **1***b* at −78°C, a green solution is produced presumably containing **1***b*′; **2***b* is formed on warming the solution. Warming an nmr tube containing a lower frozen layer of a CH_2Cl_2 solution of **1***b* and an upper layer of frozen H_2S generated a green colour in the upper part but only in the narrow temperature range of about −78 to −60°C. The dielectric constants at −65°C (34) of CH_2Cl_2 (ϵ = 15), and of liquid H_2S (ϵ = 9), are very similar and the difference in solvent polarity is unlikely to affect the rate (oxidative addition of polar molecules are typically enhanced in more polar media (25–27)). We consider ourselves fortunate to detect the green hydrides — it appears the oxidative addition is detected, perhaps because of high [H_2S], or perhaps because a reverse rate (k_{-1} or k_{-b} step) is slowed down sufficiently at the low temperature.

Related to the H_2S additions to **1**, we have studied recently corresponding reactions with anhydrous HBr and HCl (35). The following stoichiometric, stepwise reactions have been demonstrated, including spectroscopic detection of all the species listed:

[6] **1***b* + HBr → Pd_2Br_2(μ-dpm)$_2$(H)(Br) $\xrightarrow[-H_2]{HBr}$ $Pd_2Br_4^+$(μ-dpm)$_2$ → 2$PdBr_2$(dpm)

The decomposition of the tetrabromo species, which can also be formed by oxidative addition of Br_2 to **1***b*, has been studied by Lindsay and Balch (36). Of importance to the present paper is the detection of the hydride intermediate formed by oxidative addition (δ_H −8.9 ppm, broad singlet), and the demonstration that it can be protonated, in this case by added HBr rather than by coordinated SH^-, to yield H_2 (35).

Finally, the possibility of immobilizing the Pd_2 complexes akin to **1** on a support such as polystyrene led us synthesize related complexes containing methylated dpm (dpmMe), i.e. 1,1-bis(diphenylphosphino)ethane, $Ph_2PCH(Me)PPh_2$ (2, 37). The complex Pd_2Cl_2(μ-dpmMe)$_2$ (**3**) was originally made as the



anti-**3**

anti-isomer, with the Me groups on the opposite side of the Pd—C—Pd plane (37). This species in CH_2Cl_2 is unreactive to H_2S (or CO (37)) at 1 atm; the lack of reactivity may result from a steric problem in what would be the A-frame, bridged-sulfide (or μ-CO) product. The A-frame species generally adopt a boat conformation for both of the two fused rings (11), and hence for *anti*-**3** this would necessitate the location of one Me group in the inside of the boat with consequent steric problems. Of interest, the *syn* isomer of **3** has been isolated in this laboratory by a low-temperature synthesis, and this species reacts readily and quantitatively with H_2S to generate H_2 and *syn*-Pd_2Cl_2(μ-dpmMe)$_2$(μ-S) (38); one assumes that the Me groups can now be readily accommodated, and studies are on-going in attempts to quantify the differences in reactivity btween the *syn*- and *anti*-isomers. The earlier paper (2) reports on the synthetic scale reaction of H_2S with the mixed ligand complex Pd_2Cl_2(μ-dpm)(μ-dpmMe), **4**, which does generate H_2 and a single μ-S product, although it is not known whether this is the *syn*- or *anti*-product with the μ-S and Me on the same or opposite sides of the Pd—C—Pd plane. Qualitatively, the H_2S-reactivity trend in CH_2Cl_2 at ambient conditions is **1***a* > **4** > *syn*-**3**.

Conclusions

Kinetic and mechanistic studies have been initiated on the abstraction from H_2S in solution of sulfur as sulfide by Pd_2X_2(P—P)$_2$ species where X = halide and P—P = μ-dpm and / or μ-dpmMe. The reaction type is important because it allows for recovery of the co-product, H_2. The bromide system Pd_2Br_2(μ-dpm)$_2$ shows first order kinetic dependences on both metal and H_2S concentrations, and the activation parameters and a deuterium isotope effect are consistent with oxidative addition to give a hydrido(mercapto) species en route to the μ-S product.

A hydride intermediate has been detected at low temperature within the bromide and corresponding iodide systems, although the kinetics for the H_2S / iodide system were difficult to study because of photosensitized decomposition reactions. Suitable conditions for studying the faster H_2S / chloride reactions are being sought, but it is evident that the reactivity trend is Cl > Br > I; plausible explanations are presented in terms of mechan-

isms involving oxidative addition to give the hydrido(mercapto) intermediate, perhaps, but not necessarily, via initial H_2S-adduct formation; deprotonation of the coordinated SH^- with subsequent protonation of the coordinated H^- yields H_2 and the bridged sulfide. Incorporation of a Me functionality at the methylene of dpm, for subsequent elaboration of the system to a surface-supported one, decreases reactivity toward H_2S, but efficient, quantitative H_2-generating systems are still realized.

Acknowledgements

We thank the Natural Sciences and Engineering Research Council of Canada for financial support to B.R.J. (operating grant) and D.S. (bilateral exchange program), and the University of Fribourg, Switzerland, for a Research Fellowship to D.S. Johnson Matthey Limited kindly provided a loan of palladium.

1. C. L. Lee, G. Besenyei, B. R. James, D. A. Nelson, and M. A. Lilga. J. Chem. Soc. Chem. Commun. 1175 (1985).
2. G. Besenyei, C. L. Lee, J. Gulinski, S. J. Rettig, B. R. James, D. A. Nelson, and M. A. Lilga. Inorg. Chem. **26**, 3622 (1987).
3. G. Besenyei, C. L. Lee, and B. R. James. J. Chem. Soc. Chem. Commun. 1750 (1986).
4. G. Besenyei and B. R. James. To be published.
5. F. Bottomley, D. F. Drummond, G. O. Egharevba, and P. S. White. Organometallics, **5**, 1620 (1986).
6. C. Bianchini, C. Mealli, A. Meli, and M. Sabat. Inorg. Chem. **25**, 4618 (1986).
7. F. Bottomley, T. T. Chin, G. O. Egharevba, L. M. Kane, D. A. Pataki, and P. S. White. Organometallics, **7**, 1214 (1988).
8. G. L. Hillhouse and J. E. Bercaw. J. Am. Chem. Soc. **106**, 5472 (1984).
9. G. C. Kuehn and H. Taube. J. Am. Chem. Soc. **98**, 689 (1976).
10. B. R. James, C. L. Lee, M. A. Lilga, and D. A. Nelson. U.S. Patent 4,693,875 (1987).
11. R. J. Puddephatt. Chem. Soc. Rev. **12**, 99 (1983).
12. B. R. James, J. Gulinski, and G. Besenyei. To be published.
13. Handbook of chemistry and physics. 60th ed. Chemical Rubber Co., Cleveland, OH. 1979. p. D-203.
14. P. G. T. Fogg and C. L. Young (*Editors*). Solubility data series. Vol. 32. Pergamon Press, Oxford. 1988. p. 279.
15. C. L. Lee, B. R. James, D. A. Nelson, and R. T. Hallen. Organometallics, **3**, 1360 (1984).
16. L. S. Benner and A. L. Balch. J. Am. Chem. Soc. **100**, 6099 (1978).
17. A. L. Balch, L. S. Benner, and M. M. Olmstead. Inorg. Chem. **18**, 2996 (1979).
18. C. T. Hunt and A. L. Balch. Inorg. Chem. **20**, 2267 (1981).
19. S. J. Young, B. Kellenberger, J. H. Reibenspies, S. E. Himmel, M. Manning, O. P. Anderson, and J. K. Stille. J. Am. Chem. Soc. **110**, 5744 (1988).
20. M. C. Jennings, N. C. Payne, and R. J. Puddephatt. J. Chem. Soc. Chem. Commun. 1809 (1986).
21. K. Hayek, H. Glassl, A. Gutman, H. Leonlard, M. Prutton, S. P. Tear, and M. R. Welton-Cook. Surf. Sci. **152/153**, 419 (1985).
22. M. Herberhold and G. Süss. Angew. Chem. Int. Ed. Engl. **15**, 366 (1976); J. Chem. Res. Synop. 246 (1977).
23. A. Weiss, R. Plass, and A. Weiss. Z. Anorg. Allg. Chem. **283**, 390 (1956).
24. R. Ugo, G. La Monica, S. Cenini, A. Segre, and F. Conti. J. Chem. Soc. A 522 (1971).
25. L. Vaska. Acc. Chem. Res. **1**, 335 (1968).
26. J. P. Collman and W. R. Roper. Adv. Organomet. Chem. **7**, 54 (1968).
27. J. Halpern. Pure. Appl. Chem. **20**, 59 (1969).
28. G. J. Kubas. Acc. Chem. Res. **21**, 120 (1988).
29. T. H. Lowry and K. S. Richardson. Mechanism and theory in organic chemistry. 3rd ed. Harper and Row, New York. 1987. p. 232.
30. J. P. Jesson *In* Transition metal hydrides. *Edited by* E. L. Muetterties. Marcel Dekker, New York. 1971. Ch. 4.
31. M. A. Khan and A. J. McAlees. Inorg. Chim. Acta, **104**, 109 (1985).
32. T. G. Appleton, H. C. Clark, and L. E. Manzer. Coord. Chem. Rev. **10**, 335 (1973).
33. W. M. O'Neil. Fact and theory. Sydney University Press, Sydney. 1969. Chap. 4.
34. Handbook of chemistry and physics. 60th ed. Chemical Rubber Co., Cleveland, OH. 1979. pp. E-55, 56.
35. A. F. Barnabas and B. R. James. 3rd Chem. Congress of North America, Toronto. 1988. Abstract INOR 564. To be published.
36. C. H. Lindsay and A. L. Balch. Inorg. Chem. **20**, 2267 (1981).
37. C. L. Lees, Y. P. Yang, S. J. Rettig, B. R. James, D. A. Nelson, and M. A. Lilga. Organometallics, **5**, 2220 (1986).
38. G. Besenyei, Y. Xie, and B. R. James. To be published.

Can. J. Chem. Downloaded from www.nrcresearchpress.com by 194.225.253.170 on 09/07/12
For personal use only.

Molecular geometry of M(NO)(CO) complexes. Crystal structure of acetonitrilecarbonylnitrosylbis(triphenylphosphine)iron tetrafluoroborate–dichloromethane

JEAN-LOUIS ROUSTAN[1] AND NASRIN ANSARI
Department of Chemistry, University of Ottawa, Ottawa, Ont., Canada K1N 6N5

AND

JEAN-PIERRE CHARLAND[1] AND YVON LE PAGE[1]
Division of Chemistry, National Research Council of Canada, Ottawa. Ont., Canada K1A 0R6

Received March 12, 1989

This article is dedicated to Professor Ronald J. Gillespie on the occasion of his 65th birthday

JEAN-LOUIS ROUSTAN, NASRIN ANSARI, JEAN-PIERRE CHARLAND, and YVON LE PAGE. Can. J. Chem. **67**, 2016 (1989).

$Fe(CO)_2(NO)(CH_3CN)(PPh_3)_2{}^+BF_4{}^-CH_2Cl_2$ **5** crystallizes in the triclinic system, space group $P\bar{1}$, with a = 9.7782 (7), b = 10.2832 (7), c = 20.5752 (14) Å, α = 92.903 (6), β = 99.535 (6), γ = 91.930 (6)°, V = 2035.8 (1) Å^3, Z = 2. The coordination around Fe is trigonal bipyramidal, with CH_3CN and disordered NO and CO in the equatorial plane and the PPh_3 ligands displaced from true apical positions (P—Fe—P = 170.20 (4)°). Comparison of the structure of **5** with those of the two independent molecules $\mathbf{2}_1$, and $\mathbf{2}_2$ of $Fe(CO)(NO)(H)(PPh_3)_2$ **2** shows that upon a formal H^- for CH_3CN substitution, the Fe—P bond lengths shorten by ca. 0.09 Å, the (O)C—Fe—N(O) angle opens up by ca 3° (**5** → $\mathbf{2}_1$) and 8° (**5** → $\mathbf{2}_2$), whereas the P—Fe—P angle decreases by ca. 30°. These variations are interpreted in terms of electron-pair repulsions, with those within the Fe (equatorial ligand) (axial ligand) molecular portions suggested to play a predominant role.

Key words: $D^{7+1}_{NO(Fe)}$ NO/CO complexes, bond repulsions, steric influences in phosphine complexes.

JEAN-LOUIS ROUSTAN, NASRIN ANSARI, JEAN-PIERRE CHARLAND et YVON LE PAGE. Can. J. Chem. **67**, 2016 (1989).

$Fe(CO)_2(NO)(CH_3CN)(PPh_3)_2{}^+BF_4{}^-CH_2Cl_2$ (**5**) cristallise dans le système triclinique, groupe d'espace $P\bar{1}$, avec a = 9,7782 (7) b = 10,2832 (7) et c = 20,5752 (14) Å, α = 92,903 (6), β = 99,535 (6) et γ = 91,930 (6)°, V = 2035,8 (1) Å^3, Z = 2. La coordination autour du Fe est trigonale bipyramidale, avec le CH_3CN ainsi que le NO et le CO désordonnés dans le plan équatorial et les ligands PPh_3 déplacés par rapport aux positions apicales vraies (P—Fe—P = 170,20 (4)°). Une comparaison de la structure du composé **5** avec celles des deux molécules indépendantes ($\mathbf{2}_1$ et $\mathbf{2}_2$) de $Fe(CO)(NO)(H)(PPh_3)_2$ (**2**) montre que, par une substitution formelle du CH_3CN par H^-, les longueurs de la liaison Fe—P raccourcissent par environ 0,09 Å, que l'angle (O)C—Fe—N(O) s'agrandit par environ 3° (**5** → $\mathbf{2}_1$) et 8° (**5** → $\mathbf{2}_2$) alors que l'angle P—Fe—P diminue par environ 30°. On interprète ces variations en fonction de répulsions des paires d'électrons; on suggère que celles des portions moléculaires Fe(ligand équatorial) (ligand axial) jouent un rôle prédominant.

Mots clés : complexes NO/CO du type $D^{7+1}_{NO(Fe)}$, répulsions entre liaisons, influences stériques dan des complexes phosphino.
[Traduit par la revue]

Introduction

The positive linear correlation between the Fe—P bond lengths l(Fe—P) and the degeneracy weighted CO stretching frequency $\langle\nu_{CO}\rangle$ found (1) for the set of closely structurally related pentacoordinated $D^{(8-n)+n}_{NO(Fe)}$ mononitrosyl (n = 1) and NO-free (n = 0) complexes $Fe(CO)_2(NO)(PPh_3)_2{}^+BF_4{}^-$ **1**, $Fe(CO)(NO)(H)(PPh_3)_2$ **2**, $Fe(CO)_2(N_2Ph)(PPh_3)_2{}^+BF_4{}^-$ **3**, and $Fe(CO)_4(PPh_3)$ **4**, has shown that an increase in the metal Lewis basicity does favor a shortening of the Fe—PPh_3 bond lengths.[2] In this particular set of compounds, the involvement of interligand repulsions was only reflected perceptibly in the departure of the metal coordination polyhedra from a regular geometry. This is well exemplified by the two nitrosyl complexes **1** and **2**. The geometry of complex **1** (1), with disordered CO and NO ligands and long Fe—P bonds (average[3] 2.280 [3] Å), is close to a perfect trigonal bipyramid. Alternatively, in the NO/CO disorder-free hydride **2** (3) with short Fe—P bonds (average 2.182 [7] Å), the PPh_3 ligands are severely displaced from true apical positions away from the XO ligands (X = N, C). Another member of the pentacoordinated bisphosphino $D^{7+1}_{NO(Fe)}$ subset is the title compound $Fe(CO)(NO)(NCCH_3)(PPh_3)_2{}^+BF_4{}^-$ **5** (4) with a $\langle\nu_{CO}\rangle$ about halfway between those of complexes **1** and **2**. Like in hydride **2**, the metallic center of complex **5** is expected to be more electron rich than in **1**, but unlike hydride **2**, complex **5** contains three, rather than two, nonphosphinic ligands of a comparable steric demand. This complex was therefore of interest for studying a situation where electronic and steric factors might exert antagonistic influences on the Fe—PPh_3 bond lengths, the l(Fe—P) vs. $\langle\nu_{CO}\rangle$ correlation providing a semi-quantitative basis for an estimate of the magnitude of the steric influence.[4] The X-ray structure of the acetonitrile complex **5** is reported in this paper and compared to the structure of hydride **2**.

Experimental

Single crystals of the title compound **5** (4) were grown under argon at 20°C by slow diffusion of hexane into a solution of the complex in methylene chloride. Crystals for X-ray diffraction were mounted on a glass rod and subsequently coated with a layer of epoxy resin. In the absence of such a coating the crystals slowly decayed into an amorphous yellow solid upon exposure to air.

A red–orange crystal, 0.1 × 0.1 × 0.1 mm, was selected for

[1]To whom correspondence may be addressed.

[2]For the description of transition metal complexes in terms of the D^{a+n}_{NO} notation see ref. 2.

[3]Standard deviations of mean values are calculated as $\sigma(\bar{x}) = [\Sigma^n_{i=1}(x_i - \bar{x})^2/(n-1)]^{1/2}$ and are enclosed in square brackets.

[4]l(Fe—P)(Å) = (8.742 × 10^{-4}) × $\langle\nu_{CO}\rangle$ (cm^{-1}) + 0.5124; r = 0.9999, σ = 0.0005 Å; calculated from the data of ref. 1.

Can. J. Chem. Downloaded from www.nrcresearchpress.com by 186.148.149.217 on 09/07/12
For personal use only.

Can. J. Chem. Downloaded from www.nrcresearchpress.com by 186.148.149.217 on 09/07/12
For personal use only.

TABLE 1. Crystal data and refinement indicators for $[C_{39}H_{33}FeN_2O_2P_2]BF_4 \cdot CH_2Cl_2$

fw	851.22	Radiation	Mo Kα
Crystal system	Triclinic		
Space group	$P\bar{1}$	μ, mm^{-1}	0.63
a, Å	9.7782(7)	$2\theta_{max}$, deg	45
b, Å	10.2832(7)	Measured reflections	10514
c, Å	20.5752(14)	Unmeasured reflections	5262
		Observed reflections (m)[a]	3709
α, deg	92.903(6)	Parameters varied (n)	623
β, deg	99.535(6)		
γ, deg	91.930(6)		
V, Å^3	2035.8(1)	R_F[b]	0.041
Z	2	R_w[c]	0.043
D_{calc}, g cm^{-3}	1.389	S[d]	1.67
$F(000)$	927.87	Maximum (Δ/σ)	0.33

[a] $I \geq 2.50\,(I_{net})$
[b] $R_F = \Sigma[F_o - F_c]/\Sigma F_o$.
[c] $R_w = [\Sigma w(F_o - F_c)^2/\Sigma w F_o^2]^{1/2}$.
[d] $S = [\Sigma w(F_o - F_c)^2/(m - n)]^{1/2}$.

intensity measurements at 296 K up to 45° 2-θ with graphite monochromated MoKα radiation on a Enraf-Nonius CAD-4 diffractometer controlled by the NRCCAD software (5). A total of 10514 reflections were collected which reduced to 5262 unique reflections after averaging the symmetry related ones. Among these, 3709 with $I_{net} \geq 2.5\sigma(I_{net})$ were considered observed. The data reduction comprised also corrections for Lorentz and polarisation effects but not for absorption (μ = 0.63 mm^{-1}). No statistically significant change in the intensities of the three standard reflections monitored was noted. The cell parameters (Table 1) were derived from the setting angles of 45 strong reflections in the 2-θ range $40° \leq \theta \leq 45°$ (λ(MoKα$_1$) = 0.70930 Å).

The structure was solved by direct methods and ΔF-maps techniques which disclosed all the atomic positions. The BF_4^- anion was found disordered over two positions unequally occupied (population ratio = 2) and related by a rotation of ca. 60° along a common B—F bond. In the early stage of the refinement, the NO was treated as a CO. All the non-hydrogen atoms were systematically refined anisotropically and the H atoms isotropically by least-squares block diagonal matrices minimizing $\Sigma w(|F_c| - |F_o|)^2$ with $w^{-1} = \sigma^2(F_o) + 0.00025\,F_o^2$. Once the approximate atomic positions were known, a C atom was placed on each one of the two possible positions (G1 and G2 in Fig. 1) and the occupancy factors were refined with a fixed isotropic U value of 0.05 Å^2. The shift of the occupancy factors to 1.040(7) for G1 and 1.145(7) for G2 suggested that the latter might be the actual location of the nitrosylic N atom. During the refinement of the ordered model with N on G2, some H atoms of CH_3CN, CH_2Cl_2, and phenyl rings (H134, H212, H232) displayed unreasonable geometries. Therefore, they were placed in idealized positions (C—H = 1.08 and 0.95 Å for sp^3 and sp^2 carbons, respectively) and included in all the refinement cycles performed subsequently but not refined. At convergence of this first model (R = 0.041, R_w = 0.044, S = 1.69), the Fe—G2(N) bond (1.693(4) Å) was slightly shorter than the Fe—G1(C) bond (1.714(3) Å) but the G2(N)—O2 and G1(C)—O1 bond lengths of 1.143(4) and 1.149(3) Å, respectively, were undistinguishable, contrary to what is generally found in M/NO/CO ordered structures in which the N—O bond is longer than the C—O one (3, 6–8) (with the converse for the M—N and M—C bonds). The alternate model in which N was positioned on G1 ($R = 0.042$, $R_w = 0.044$, $S = 1.70$) had to be rejected also for the Fe—G2(C) and G2(C)—O2 bond lengths of 1.678 (3) and 1.130 (4) Å, respectively, were both shorter than the Fe—G1(N) and G1(N)—O1 bond lengths of 1.734 (3) and 1.153 (4) Å, respectively. In addition, the thermal ellipsoid of G2(C) was abnormally small relative to that of G1(N) (ORTEP included in the supplementary material).[5] A disordered model was finally selected with 0.8 and 0.2 of a N atom placed on G2 and G1 respectively, as suggested by the results of the refinement on the occupancy factors. Composite scattering curves of

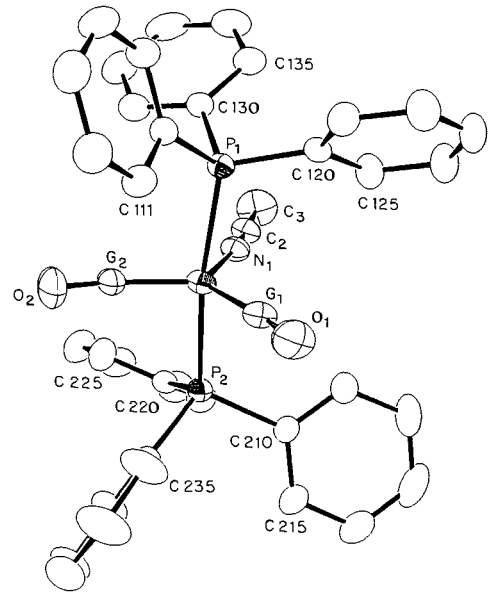


FIG. 1. Perspective view of $Fe(CO)(NO)(CH_3CN)(P(C_6H_5)_3)_2^+$ with the numbering scheme. The thermal ellipsoids have been drawn at the 50% probability level.

the form $af_N + (1 - a)f_C$(a = 0.8 (G2), 0.2 (G1)) were used. The final residuals were $R = 0.041$, $R_w = 0.043$, $S = 1.67$ with 623 parameters for 3709 reflections and $R = 0.0657$, $R_w = 0.0471$ for all reflections. In the final cycle, the maximum shift to σ ratio was 0.35 (aromatic H atom) and in the final ΔF-map the background was below 0.3 e/Å^3, except for a peak of 0.54 e/Å^3 at ca. 1 Å away from the C1 atoms. All computations were performed with the NRCVAX system of programs (9). The scattering curves and anomalous dispersion corrections were taken from ref. 10.

Apart from the variations in the bond lengths of the FeG_iO_i(i = 1, 2) moieties, no significant changes in the other bond lengths and in all the valence angles were noted from one model to another. The final atomic positions are given in Table 2. The list of calculated and observed structure amplitudes, parameters for the H atoms, U_{ij}'s for the non-hydrogen atoms have been deposited as supplementary material.[5]

Results

The crystal structure of complex **5** consists of discrete metallic cations, BF_4^- anions and CH_2Cl_2 molecules of solvent with no unusual intermolecular Van der Waals contact. The BF_4^- anions are disordered on two positions sharing the same B—F1 bond. The structure of the cation with the numbering scheme is presented in Fig. 1 and selected bond lengths and angles are listed in Table 3.

The coordination polyhedron of iron is a distorted trigonal bipyramid. As detailed in the Experimental section, none of the two possible ordered models in which the nitrosylic N atom was placed on either position G1 or position G2 (Fig. 1) led to a set of bond lengths in the FeG_iO_i moities consistent with what is usually observed in ordered M/NO/CO structures (M—N and N—O bonds respectively shorter and longer than the M—C and C—O bonds (3, 6–8). A disordered model with the (O)N and (O)C atoms unequally distributed on positions G1 and G2 was finally retained. Positions G1 and G2 together with the N1 atom of CH_3CN define the equatorial plane which contains Fe, O1, and C2, and from which O2 and C3 deviate by less than 0.02 Å.

[5] A complete set of material may be purchased from the Depository of Unpublished Data, CISTI, National Research Council of Canada, Ottawa, Ont., Canada K1A 0S2.

TABLE 2. Atomic parameters x, y, z and B_{iso} of the non-H atoms; esd refer to the last digit printed

Atom[a]	x	y	z	B_{iso}[b]
Fe	0.06385(6)	0.82764(5)	0.24528(3)	3.28(3)
P 1	0.06075(11)	0.91394(9)	0.34935(5)	2.98(4)
P 2	0.03412(10)	0.72144(10)	0.14404(5)	3.04(5)
Cl 1	0.51489(24)	0.08922(25)	0.14746(14)	14.93(18)
Cl 2	0.6683 (3)	0.32679(24)	0.16954(12)	14.68(16)
F 1	0.4238 (4)	0.5919 (3)	0.67359(19)	9.81(22)
F12*	0.3630 (6)	0.4107 (4)	0.71752(24)	9.8 (3)
F13*	0.5446 (6)	0.4229 (6)	0.6703 (3)	12.6 (4)
F14*	0.3441 (7)	0.4089 (5)	0.6110 (3)	12.8 (4)
F22**	0.2768 (10)	0.4361 (10)	0.6520 (6)	10.8 (8)
F23**	0.4475 (12)	0.4341 (13)	0.6039 (6)	12.9 (8)
F24**	0.4844 (16)	0.3961 (10)	0.7096 (6)	17.3 (10)
O 1	−0.1067 (4)	1.0323 (3)	0.19380(16)	7.16(19)
O 2	0.3430 (3)	0.9002 (4)	0.24425(18)	7.80(22)
N 1	0.0001 (3)	0.6595 (3)	0.27625(14)	3.66(15)
G 2	0.2357 (3)	0.8578 (3)	0.24815(16)	4.14(17)
G 1	−0.0468 (4)	0.9455 (4)	0.21498(18)	4.15(21)
C 2	−0.0214 (4)	0.5606 (4)	0.29496(19)	3.96(20)
C 3	−0.0454 (6)	0.4340 (5)	0.3194 (3)	7.1 (3)
C10	0.6131 (7)	0.1953 (7)	0.2065 (3)	10.7 (5)
C110	0.1760 (4)	1.0554 (3)	0.37635(18)	3.24(17)
C111	0.2071 (4)	1.1434 (4)	0.33153(20)	4.30(21)
C112	0.2915 (5)	1.2523 (4)	0.35232(23)	5.22(24)
C113	0.3449 (5)	1.2758 (4)	0.41742(24)	5.35(24)
C114	0.3141 (5)	1.1910 (4)	0.46237(21)	5.55(23)
C115	0.2318 (4)	1.0807 (4)	0.44239(20)	4.46(21)
C120	−0.1114 (4)	0.9626 (3)	0.35943(17)	3.12(17)
C121	−0.1393 (4)	1.0868 (4)	0.38072(20)	4.30(21)
C122	−0.2732 (5)	1.1204 (4)	0.38490(24)	5.74(25)
C123	−0.3808 (4)	1.0307 (5)	0.36791(24)	5.71(25)
C124	−0.3551 (4)	0.9068 (4)	0.34627(24)	5.40(25)
C125	−0.2225 (4)	0.8730 (4)	0.34163(22)	4.56(22)
C130	0.1121 (4)	0.7962 (3)	0.40977(17)	3.14(17)
C131	0.2397 (4)	0.7416 (4)	0.41167(20)	4.35(22)
C132	0.2810 (5)	0.6468 (4)	0.45492(23)	5.83(25)
C133	0.1945 (6)	0.6045 (4)	0.49612(21)	6.1 (3)
C134	0.0692 (5)	0.6572 (4)	0.49429(21)	5.5 (3)
C135	0.0264 (4)	0.7526 (4)	0.45192(19)	4.15(22)
C210	−0.1467 (4)	0.6971 (4)	0.10421(18)	3.43(18)
C211	−0.2493 (5)	0.6972 (5)	0.14184(22)	5.9 (3)
C212	−0.3860 (5)	0.6729 (6)	0.1131 (3)	8.1 (4)
C213	−0.4181 (5)	0.6507 (6)	0.0458 (3)	8.5 (3)
C214	−0.3171 (5)	0.6501 (5)	0.00769(24)	6.6 (3)
C215	−0.1814 (4)	0.6740 (4)	0.03676(21)	4.79(21)
C220	0.1005 (4)	0.5589 (3)	0.14825(17)	3.14(18)
C221	0.0177 (4)	0.4482 (4)	0.12865(21)	4.65(21)
C222	0.0703 (5)	0.3255 (4)	0.13707(23)	5.7 (3)
C223	0.2040 (5)	0.3133 (4)	0.16381(23)	5.9 (3)
C224	0.2892 (5)	0.4210 (5)	0.18357(24)	6.0 (3)
C225	0.2371 (4)	0.5437 (4)	0.17671(22)	4.77(22)
C230	0.1213 (4)	0.7996 (4)	0.08450(18)	3.52(19)
C231	0.1798 (5)	0.7306 (5)	0.03776(22)	5.9 (3)
C232	0.2395 (6)	0.7950 (6)	−0.00879(25)	7.7 (3)
C233	0.2444 (6)	0.9285 (6)	−0.0078 (3)	7.3 (3)
C234	0.1860 (7)	0.9969 (5)	0.0372 (3)	8.5 (4)
C235	0.1267 (6)	0.9332 (5)	0.08384(24)	6.7 (3)
B	0.4164 (6)	0.4592 (5)	0.6659 (3)	5.9 (3)

[a] *occupancy = 2/3, **occupancy = 1/3.

[b] B_{iso} is the mean of the principal axes of the thermal ellipsoid.

Can. J. Chem. Downloaded from www.nrcresearchpress.com by 186.148.149.217 on 09/07/12
For personal use only.

Can. J. Chem. Downloaded from www.nrcresearchpress.com by 186.148.149.217 on 09/07/12
For personal use only.

TABLE 3. Selected bond lengths (Å) and angles (deg) in $Fe(CO)(NO)(CH_3CN)(P(C_6H_5)_3)_2^+BF^-_4,CH_2Cl_2$, **5**

Bond	Distance	Bond	Distance
Fe—P1	2.281(1)	P1—C110	1.815(4)
Fe—P2	2.272(1)	P1—C120	1.813(4)
Fe—N1	1.989(3)	P1—C130	1.803(4)
Fe—G1	1.723(4)	P2—C210	1.825(4)
Fe—G2	1.689(3)	P2—C220	1.815(4)
G1—O1	1.149(5)	P2—C230	1.809(4)
G2—O2	1.140(4)	C2—C3	1.444(6)
N1—C2	1.131(5)	C10—C11	1.731(8)
C10—C12	1.700(8)		

Bonds	Angle	Bonds	Angle
P1—Fe—P2	170.20(4)	N1—C2—C3	178.6 (5)
N1—Fe—G1	123.7 (2)	N1—Fe—P1	86.85(9)
G1—Fe—G2	117.6 (2)	N1—Fe—P2	85.29(9)
G2—Fe—N1	118.8 (2)	G1—Fe—P1	90.7 (1)
Fe—G1—O1	171.9 (4)	G1—Fe—P2	90.7 (1)
Fe—G2—O2	166.3 (4)	G2—Fe—P1	94.9 (1)
Fe—N1—C2	172.5 (3)	G2—F3—P2	94.0 (1)
N1—C2—C3	178.6 (5)	C11—C10—C12	109.4 (4)
C110—P1—C120	106.0 (2)	C210—P2—C220	104.5 (2)
C120—P1—C130	107.1 (2)	C220—P2—C230	105.1 (2)
C130—P1—C110	104.5 (2)	C230—P2—C210	105.4 (2)
Fe—P1—C110	116.3 (1)	Fe—P2—C210	114.3 (1)
Fe—P1—C120	111.6 (1)	Fe—P2—C220	111.6 (1)
Fe—P1—C130	110.8 (1)	Fe—P2—C230	114.7 (1)
O1(G1)...Fe...(G2)O2[a]	108.8 (5)		

Mean values

PPh_3 ligands

	*P*1	*P*2
C—C	1.374[10]	1.373[12]
C—H	0.92 [5]	0.92 [3]
P—C—C	120.9 [20]	120.8 [16]
C—C—C	120.0 [10]	120.0 [10]
C—C—H	129.7 [18]	119.5 [23]

BF_4^-

B—F	1.338[49]	F—B—F	109[6]

Selected intramolecular Van der Waals Contacts (Å)

P1..N1	2.943(4)	G2..G1	2.918(5)
P1..G1	2.829(4)	N1..G2	3.169(4)
P1..G2	2.953(3)	N1..G1	3.275(5)
P2..N1	2.895(3)	N1..C130	3.038(5)
P2..G1	2.869(4)	N1..C220	3.102(5)
P2..G2	2.924(3)	C1..C120	3.137(5)

[a]Angle sustended at Fe by the O1 and O2 atoms.

In the equatorial plane, the Fe—G1 and Fe—G2 bond lengths of, respectively, 1.723(4) and 1.689(3) Å are shorter than the Fe—(C/N) bond lengths of $Fe(CO)_2(NO)(PPh_3)_2^+BF_4^-$ **1** (1) (range 1.756(4)–1.769(4) Å), but they compare well with the Fe—(C/N) bond lengths found in the NO/CO disordered structure of $Fe(CO)(NO)_2(PPh_3)$ **6** (11) (range 1.690(8)–1.732(8) Å). The G1—O1 and G2—O2 bonds of respectively 1.149(5) and 1.140(4) Å are also similar to the (C/N)—O ones of **6** (range 1.147(11) – 1.158(8) Å). Even if the NO/CO disorder blurs the fine details of the geometry of the Fe(NO)(CO) moiety, there is little doubt that the (O)C—Fe—N(O) angle (G1—Fe—G2) of 117.6(2)° is significantly smaller than those of 120.6(3)° and 125.8(3)° corresponding respectively to the two independent molecules $\mathbf{2}_1$ and $\mathbf{2}_2$ of $Fe(CO)(NO)(H)(PPh_3)_2$, **2** (Table 4).

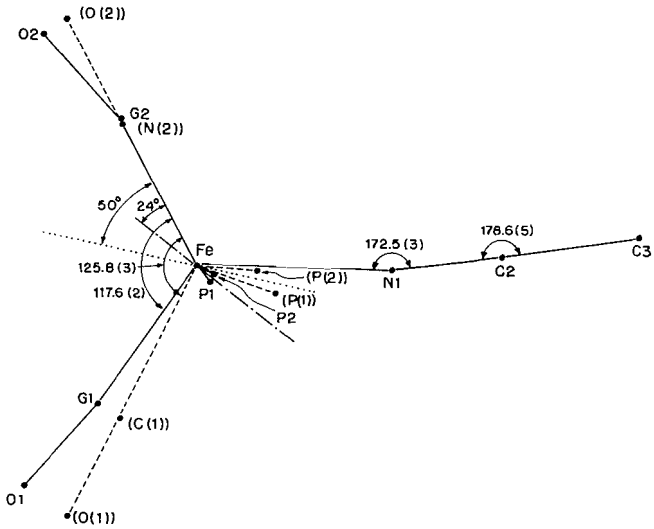


FIG. 2. Orthogonal projections of selected atoms on the G1FeG2 plane of (*a*) $Fe(CO)(NO)(CH_3CN)(P(C_6H_5)_3)_2^+$, **5**; (*b*) $Fe(CO)(NO)(H)(P(C_6H_5)_3)_2$ **2** (molecule II of ref. 3 considered, the labelling of the G_iO_i positions (i = 1, 2) as given in the original publication are enclosed in parentheses).

The structural parameters associated with the acetonitrile ligand are normal (see ref. 12*a*, *b* for other Fe/CH_3CN complexes). The Fe—N1—C2 array is nonlinear with a Fe—N1—C2 angle of 172.5 (3)°. The CH_3CN ligand is tilted towards G2, away from the PPh_3 ligands (Fig. 2), and the N1 atom is involved in the shortest intramolecular equatorial-atom/phenyl C-atom contacts of 3.038 (5) and 3.102 (5) Å with, respectively, C130 and C220.

The Fe—P bond lengths of 2.272 (1) and 2.281 (1) Å of **5** are very similar to the Fe—P distances of $Fe(CO)_2(NO)(PPh_3)_2^+BF_4^-$ **1** (1) (2.278(1) and 2.282(1) Å). Consequently, complex **5** deviates markedly from the l(Fe—P) vs. $\langle\nu_{CO}\rangle$ correlation[4] from which a l(Fe—P) bond length of 2.226 Å is calculated with the $\langle\nu_{CO}\rangle$ value of 1960 cm^{-1} associated with **5** (4). The PPh_3 ligands are displaced from the true apical positions (P—Fe—P = 170.20(4)°) away from G2, and towards the interior of the largest equatorial angle N1—Fe—G1 of 123.7(2)° (Fig. 2).

Discussion

The acetonitrile complex $Fe(CO)(NO)(CH_3CN)(PPh_3)_2^+BF_4^-$ **5** is related to $Fe(CO)_2(NO)(PPh_3)_2^+BF_4^-$, **1**, and $Fe(CO)(NO)(H)(PPh_3)_2$, **2** by the formal substitution of one equatorial ligand.

The CH_3CN for CO substitution converting **1** into **5** has no significant effect on the Fe—P bond lengths, but creates an imbalance in the influence of the XO ligands upon the PPh_3 ones. The P—Fe—P angle closes from 178.45(5)° to 170.20(4)°, and the P atoms are displaced from true apical positions away from the coordination site of the G2O2 ligand.

Interestingly, very similar deformations are observed from $Fe(CO)_2(NO)(PPh_3)_2^+BF_4^-$ to $Mn(CO)_2(NO)(PPh_3)_2$ in which the M to XO (X = C, N) retrodonation is enhanced. In the

Can. J. Chem. Downloaded from www.nrcresearchpress.com by 186.148.149.217 on 09/07/12
For personal use only.

TABLE 4. Angular parameters (deg) of selected penta and tetracoordinated M(NO)(XO) (X = N,C) complexes[a]

Complex	Reference	Compound	(O)N—M—X(O)	O(N)..M..(X)O[c]
Linear NO/linear NO or CO:				
$Fe(CO)(NO)(CH_3CN)(PPh_3)_2^{+}$[b]		**5**	117.6(2)	108.8(5)
$Fe(CO)(NO)(PPh_3)_2H$	3	**2**		
Molecule I		$\mathbf{2}_1$	120.6(3)	117.4
Molecule II		$\mathbf{2}_2$	125.8(3)	125.7
$Mn(NO)_2(L')_3^{+}(BF_4^-)$	18	**7**	116.5(5)	107.4(5)
$Mn(NO)_2L'_2Cl$	19	**8**	111.5(5)	99.0(5)
$Mn(NO)_2L'_2Cl$	21	**9**		
Molecule 2		$\mathbf{9}_1$	113.5(5)	101.9(5)
Molecule M		$\mathbf{9}_2$	112.1(5)	99.8(5)
$Fe(Gal)(NO)_2$	25	**10**	108.1(2)	90.9
$Co(NO)_2(L)_2^{+}(PF_6^-)$	22	**11**	136.7(4)	143.9
$Fe(NO)_2(L)_2$	11	**12**	123.8(4)	122.5
$Ir(NO)(CO)(L_2)$	6	**13**	128.7(4)	128.8(2)
Bent NO/linear NO or CO:				
$Ru(NO)_2(L)_2Cl^{+}(PF_6^-)$	26	**14**	102(1)	86
$Os(NO)_2(L)_2(OH)^{+}(PF_6^-)$	27	**15**	99.3(6)	82.4
$Ir(NO)(CO)(L)_2I^{+}(BF_4^-)$	28	**16**	101(2)	82
$Ir(NO)(CO)(L)_2Cl^{+}(BF_4^-)$	29	**17**	97.4(5)	77.9

[a]Abbreviations: L' = $P(OMe)_2Ph$, L = PPh_3; Gal = dimethyl (*N,N*-dimethylethanolamino)(pyrazolyl) gallate.
[b]This work.
[c]A value with a standard deviation is from the original publication. Other values have been calculated from the data given in the references quoted.

ordered model selected to describe the structure of the Mn complex (13) (P—Mn—P = 170.2 (2))°, the P atoms were found further away from the NO than from the CO ligands. In terms of electron-pair repulsions (14), this observation, and others (3, 6, 11, 15*a*), support the proposal that the repulsive influence of a M···X(O) bond is a more sensitive increasing function of the M···X bond order with a nitrosyl (X = N) than with a carbonyl (X = C) ligand.

Returning to the Fe series, it is only when CH_3CN is replaced by H^- to yield hydride **2** that the Fe—P bonds respond to the additional increase in the metal basicity and shorten to 2.182 [7] Å. Concomittantly, the closing of the P—Fe—P angle is accentuated to 140.9 (1)°, and the P atoms are moved towards the coordination site of the exchanged ligand, as shown in Fig. 2 by the sense of rotation of the trace of the PFeP plane into the G1FeG2 one. The compactness of H (and the M—H bond (14*b*)) suffices to account for these angular variations. Relating the latter with the change in the Fe—P bond lengths suggests that the H ligand, but not the CH_3CN one, allows for the angular deformations required to accommodate shorter Fe—P bonds without increasing unduly the repulsions in the $Fe(XO)(PPh_3)$ (X = N, C) molecular portions. Indeed, even if the Fe—P bonds are shorter by ca. 0.09 Å in hydride **2** than in complex **5**, the P...X intramolecular contacts are longer by ca. 0.05 to 0.11 Å (in **5**: P...G1 = 2.85 [3] Å, P...G2 = 2.94 [2] Å; in the two independent molecules $\mathbf{2}_1$ and $\mathbf{2}_2$ of **2**: P...C = 2.91 [3] Å ($\mathbf{2}_1$)/2.90 [6] Å ($\mathbf{2}_2$), P..N = 3.05 [3] Å ($\mathbf{2}_1$)/3.01 [1] Å ($\mathbf{2}_2$) (calculated from the data in ref. 3)). Consequently, this analysis suggests that in hydride **2**, the Fe—P bond lengths, which correlate well with the electronic parameter $\langle\nu_{CO}\rangle$, are under electronic control, whereas the acetonitrile complex **5** might provide an example of the predominance of steric influence on the Fe—P separations. The steric lengthening relative to the $\langle\nu_{CO}\rangle$ based value is a large 0.05 Å, about half the difference between the lowest and highest *l*(Fe—P) values reported in ref. 1.

The angular deformation of the $Fe(PPh_3)_2$ fragment might also be an important factor for allowing the (OC)—Fe—N(O) angle to expand from **5** (117.62(2)°) to **2** (120.6(3)°($\mathbf{2}_1$), 125.8(3)° ($\mathbf{2}_2$)), as suggested by considering first the variations of the (O)N—M—N(O) angle in pseudotetrahedral D_{NO}^{8+2} dinitrosyl complexes ($M(NO)_2(L)_2^x$(x = 0, +1)) which have been the subject of numerous crystallographic (16) and theoretical (17) studies. In complexes of that type, when localized bonds are considered, some of the observed variations of the (O)N—M—N(O) angle have been interpreted (11, 15) by what is essentially an electron-pair repulsion model (14), with the mutual electrostatic repulsions of the M···N bonds taken as the most influential factor. Applied to the pair of the Fe complex, **5** and **2**, this standard model would allow a straightforward interpretation of the opening of the (O)C—Fe—N(O) angle by considering solely the enhancement of the repulsions in the Fe(CO)(NO) moiety upon a H^- for CH_3CN substitution. However, when examining other triangular bipyramidal complexes, this interpretation fails to account for the closing of the (O)N—M—N(O) angle between the two equatorial NO upon an increase in the M to NO retrodonation from $Mn(NO)_2(L')_3^{+}BF_4^-$ (N—Mn—N (18) = 116.5 (5)°, ν_{NO} (19) = 1760, 1712 cm^{-1}, L' = $P(OMe)_2Ph$) to $Mn(NO)_2(L')_2Cl$ (N—Mn—N = 111.5 (5), 112.1 (5), 113.5 (5) (two crystalline forms and three independent molecules (20, 21)), ν_{NO} (19) = 1713, 1674 cm^{-1}).

We believe that such a model neglecting the bond repulsions in the M(NO)(L) molecular portions, which must also increase with the M···N(O) bond order, is not justified in every case. As shown with the D_{NO}^{8+2} pair of isoelectronic complexes $Co(NO)_2(PPh_3)_2^{+}PF_6^-$ (N—Co—N (22) = 136.7(4)°, ν_{NO} (23) = 1836, 1784 cm^{-1}) and $Fe(NO)_2(PPh_3)_2$ (N—Fe—N (11) = 123.8(4)°, ν_{NO} (24) = 1724, 1678 cm^{-1}), in which the geometry of the $M(PPh_3)_2$ fragment is little affected from one compound to the other, whereas the metal to NO retrodonation increases from the cationic complex to the uncharged one, the (O)N—M—N(O) angle decreases instead of increasing. We consider

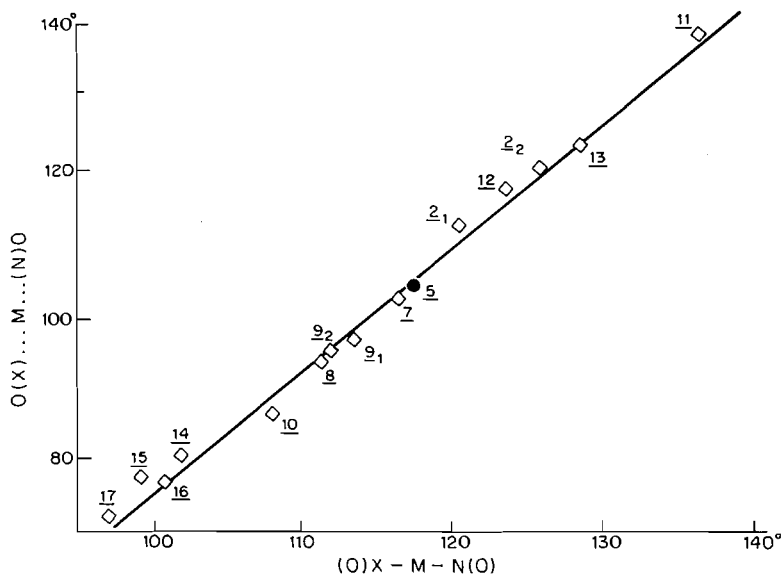


FIG. 3. O(X)...M...(N)O angle sustended at M by the two O atoms of the XO and NO ligands vs. (O)X—M—N(O) angle (X = C, N) for the complexes listed in Table 4 (r = 0.9960, σ = 1.8°, excluding the NO/CO disordered structure **5**).

that this closing is more consistent with the notion that the electrostatic repulsions in the $M(NO)(PPh_3)$ fragments, rather than those in the $M(NO)_2$ subunit, provide the most influential factor. In pentacoordination, we interpret in the same manner the closing of the (O)N—Mn—N(O) angle from the cationic Mn complex to the uncharged chloro derivative. The contrasting behavior of the pair of Fe complexes **5** and **2** could then be rationalized simply by observing that from $Fe(CO)(NO)(CH_3CN)(PPh_3)_2{}^+BF_4{}^-$ **5** to $Fe(CO)(NO)(H)(PPh_3)_2$ **2**, the magnitude of the closing of the P—Fe—P angle might allow for an opening of the (O)N—Fe—C(O) angle, as required by the standard model, while preventing detrimental excessive repulsions in the $Fe(XO)(PPh_3)$ molecular fragments, as required by the suggested modification of this model.

Finally, as shown by the plot of Fig. 3, it is worth noting that in complex **5** the (O)C—Fe—N(O) angle and the O(C)...Fe...(N)O one sustended at Fe by the oxygen atoms nicely follow the trend defined by other NO/CO disorder-free tetra and pentacoordinated complexes containing one M(XO)(NO) (x = C, N) subunit. A correlation of that type was first reported (17*b*) for a variety of tetracoordinated D_{NO}^{8+2} derivatives, and subsequently extended (18) to the pentacoordinated Mn dinitrosyl complexes listed in Table 4. The plot of Fig. 3 shows that this correlation includes also tetra and penta coordinated complexes containing one M(CO)(linear NO) moiety.[6] Unexpectedly, we have also found that some pentacoordinated complexes containing a bent-NO are part of the same correlation, as shown on Fig. 3 by the location of the representative points of the few complexes of that type listed in Table 4.

In conclusion, from $Fe(CO)(NO)(CH_3CN)(PPh_3)_2{}^+BF_4{}^-$ **5** to $Fe(CO)(NO)(H)(PPh_3)_2$, **2**, both the shortening of the Fe—P bond lengths and the opening of the (O)C—Fe—N(O) angle can be related in a simple way to the large closing of the P—Fe—P angle. A closing of this magnitude can be expediently interpreted in terms of the relative differences in the bond repulsions involving $M(PPh_3)(H)$ and $M(PPh_3)$(non-H ligand) molecular portions (14*b*). In addition, when considering an electron-pair repulsion model to account for angular variations in M(XO)(NO) complexes, it is suggested that the repulsions in both the M(XO)(NO) and M((C/N)O)(ancillary ligand) molecular portions need to be taken into account, with those of the second type possibly providing the most influential factor in several cases.

[6]For pseudotetrahedral D_{NO}^{8+2} complexes in C_{2v} symmetry, see ref. 17*b*, *c* for a possible relationship between the (O)N—M—N(O) and M—N—O angles, and consequently between the (O)N—M—N(O) and O(N)...M..(N)O ones.

Acknowledgement

The authors with to thank the Natural Sciences and Engineering Research Council of Canada for financial support to one of us (J.L.R.).

1. F. R. AHMED, J. L. ROUSTAN, and M. Y. AL-JANABI. Inorg. Chem. **24**. 2526 (1985).
2. J. L. ROUSTAN and B. A. MORROW. Inorg. Chem. **27**, 1666 (1988).
3. M. CYGLER, F. R. AHMED, A. FORGUES, and J. L. ROUSTAN. Inorg. Chem. **22**, 1026 (1983).
4. J. L. ROUSTAN, J. Y. MEROUR and J. FORGUES. J. Organomet. Chem. **184**, C13, (1980).
5. Y. LE PAGE, P. S. WHITE, and E. J. GABE. Proc. Am. Cryst. Assoc. Meeting, Hamilton. 1986. Abstract PA 23.
6. C. PRATT BROCK and J. A. IBERS. Inorg. Chem. **11**, 2812 (1972).
7. S. TOPFKE and U. BEHRENS. Acta Crystallogr. C **42**, 161 (1985).
8. C. EVRARD, R. THOMAS, B. R. DAVIS, and C. BERNAL. Inorg. Chem. **15**, 52 (1976).
9. E. J. GABE, F. L. LEE, and Y. LE PAGE. *In* Crystallographic computing III. *Edited by* G. M. Sheldrick, C. Kruger, and R. Goddard. Clarendon Press, Oxford. 1985. p. 167.
10. International tables for X-ray crystallography. Vol. IV. Birmingham. Kynoch Press, Birmingham. 1974. pp. 99, 148.
11. V. G. ALBANO, A. ARANEO, P. L. BELLON, G. CIANI, and M. J. MANASSERO. J. Organomet. Chem. **67**, 413 (1974).
12. (*a*) J. K. KOUBA, E. L. MUETTERTIES, M. R. THOMPTON, and D. W. DAY. Organometallics, **2**, 1065 (1983); (*b*) P. E. RILEY, C. E. CAPSHEW, R. PETTIT, and R. E. DAVIS. Inorg. Chem. **17**, 408 (1978).
13. J. H. ENEMARK and J. A. IBERS. Inorg. Chem. **6**, 1575 (1970).
14. (*a*) R. J. GILLESPIE. J. Chem. Ed. **47**, 18 (1970); (*b*) R. J. GILLESPIE. Molecular geometry. Van Nostrand Reinhold Publishers. 1972.
15. (*a*) V. G. ALBANO, P. L. BELLON, and G. CIANI. J. Organomet.

Can. J. Chem. Downloaded from www.nrcresearchpress.com by 186.148.149.217 on 09/07/12
For personal use only.

Chem. **38**, 155 (1972); (*b*) A. P. CAUGHAN, B. J. CORDEN, R. EISENBERG, and J. A. IBERS. Inorg. Chem. **13**, 786 (1974).
16. R. D. FELTHAM and J. H. ENEMARK. *In* Topics in inorganic and organometallic chemistry. Vol. 12. *Edited by* G. Geoffroy. Wiley, New York. 1981. p. 155.
17. (*a*) J. H. ENEMARK and R. D. FELTHAM. Coord. Chem. Rev. **13**, 335 (1974); (*b*) R. L. MARTIN and D. TAYLOR. Inorg. Chem. **15**, 2970 (1976); (*c*) R. H. SUMMERVILLE and R. J. HOFFMAN. J. Am. Chem. Soc. **98**, 7240 (1976).
18. M. LAING, R. H. REIMANN, and E. SINGLETON. Inorg. Chem. **18**, 2666 (1979).
19. R. G. COPPERTHWAITE, R. H. REIMANN, and E. SINGLETON. Inorg. Chim. Acta, **28**, 107 (1978).
20. M. LAING, R. H. REIMANN, and E. SINGLETON. Inorg. Chem. **18**, 324 (1979).
21. M. LAING, R. H. REIMANN, and E. SINGLETON. Inorg. Chem. **18**, 1648 (1979).
22. B. E. REICHERT. Acta. Crystallogr. B**32**, 1934 (1976).
23. J. A. KADUK and J. A. IBERS. Inorg. Chem. **16**, 3283 (1977).
24. D. W. MCBRIDE, S. L. STAFFORD, and F. G. A. STONE. Inorg. Chem. **1**, 386 (1962).
25. K. S. CHONG, S. J. RETTIG, A. STORR, and J. TROTTER. Can. J. Chem. **57**, 3113 (1979).
26. C. G. PIERPONT and R. EISENBERG. Inorg. Chem., **11**, 1088 (1972).
27. G. R. CLARK, J. M. WATERS, and K. R. WHITTLE. J. Chem. Soc. Dalton Trans. 463 (1975).
28. D. J. HODGSON and J. A. IBERS. Inorg. Chem. **8**, 1282 (1969).
29. D. J. HODGSON and J. A. IBERS. Inorg. Chem. Chem. **7**, 2345 (1968).

Can. J. Chem. Downloaded from www.nrcresearchpress.com by 186.148.149.217 on 09/07/12
For personal use only.

Solid-state motion of $OTeF_5^-$ compounds: detection by ^{19}F NMR and IR spectroscopy and correlation with the X-ray structure of an orthorhombic crystalline modification of $[C_{14}H_{19}N_2^+][OTeF_5^-]$ ($C_{14}H_{19}N_2^+$ = protonated 1,8-bis(dimethylamino)naphthalene)

PATTI J. KELLETT,[1] OREN P. ANDERSON, AND STEVEN H. STRAUSS[2]
Department of Chemistry, Colorado State University, Fort Collins, CO, U.S.A. 80523

AND

KENT D. ABNEY
Isotopes and Nuclear Chemistry Division (INC-4), Los Alamos National Laboratory, Los Alamos, NM, U.S.A. 87544

Received November 23, 1988

This paper is dedicated to Professor Ronald J. Gillespie on the occasion of his 65th birthday

PATTI J. KELLETT, OREN P. ANDERSON, STEVEN H. STRAUSS, and KENT D. ABNEY. Can. J. Chem. **67**, 2023 (1989).

An orthorhombic crystalline modification of $[(PS)H^+][OTeF_5^-]$ was studied by single crystal X-ray diffraction ($(PS)H^+$ = protonated 1,8-bis(dimethylamino)naphthalene): orthorhombic, space group *Cmcm*, a = 8.607(2), b = 14.048(3), c = 13.365(2) Å, Z = 4, T = −130°C. The structural parameters for the anion and cation in this modification (Mod-B) are very similar to those for the previously reported triclinic modification of this salt (Mod-A). However, variable temperature IR spectra for Mod-B suggest that the $OTeF_5^-$ anion is exhibiting a two-site O/F_{ax} interchange above −70°C. Solid-state ^{19}F NMR spectra suggest that this interchange may be as rapid as 10^4–10^5 s^{-1} at room temperature.

Key words: crystal structure of protonated 1,8-bis(dimethylamino)naphthalene)pentafluorotellurate(VI), polymorphism, solid state ^{19}F NMR.

PATTI J. KELLETT, OREN P. ANDERSON, STEVEN H. STRAUSS et KENT D. ABNEY. Can. J. Chem. **67**, 2023 (1989).

Faisant appel à la diffraction des rayons-X sur un cristal unique, on a étudié une modification cristalline orthorhombique du $[(PS)H^+][OTeF_5^-]$ ($(PS)H^+$ = bis(diméthylamino)-1,8 naphtalène) : orthorhombique, groupe d'espace *Cmcm*, a = 8,607(2), b = 14,048(3), c = 13,365(2) Å, Z = 4, T = −130°C. Les paramètres de structure de l'anion et du cation de cette modification (Mod-B) sont très semblables à ceux de la modification triclinique de ce sel (Mod-A) rapportée antérieurement. Toutefois, les spectres IR de ce sel (Mod-A) à température variable suggèrent que, à des températures supérieures à −70°C, l'anion $OTeF_5^-$ s'échange entre les deux sites O/F_{ax}. Les spectres rmn du ^{19}F à l'état solide suggèrent que la vitesse de cet échange, à la température ambiante, est de l'ordre de 10^4–10^5 s^{-1}.

Mots clés : structure cristalline du bis(diméthylamino)-1,8 naphtalène protoné, pentafluorotellurate(VI), polymorphisme, rmn du ^{19}F à l'état solide.

[Traduit par la revue]

Introduction

We have recently reported the structure and spectroscopic properties of the $OTeF_5^-$ anion (teflate) in a triclinic modification of $[(PS)H^+][OTeF_5^-]$ ($(PS)H^+$ = protonated 1,8-bis(dimethylamino)naphthalene) (1). This salt did not exhibit the O/F disorder that is characteristic of alkali metal salts of teflate (2). The Te—O distance of 1.803 Å in the pseudooctahedral $OTeF_5^-$ anion is shorter than the Te—F distances, which range from 1.862 to 1.879 Å and average 1.870 Å (1).[3] The average O—Te—F_{eq} bond angle is 95.2°. These results are in harmony with Gillespie's classic theory of molecular structure, VSEPR (3).

We now report the isolation of an orthorhombic modification of $[(PS)H^+][OTeF_5^-]$. At −130°C, X-ray diffraction results show that, like the triclinic modification (Mod-A), the orthorhombic modification (Mod-B) does not exhibit O/F disorder. However, IR spectroscopic data indicate that above −70°C the $OTeF_5^-$ anions in Mod-B are distributed between two inequivalent sites. This solid-state motion of site interchange was investigated by solid-state ^{19}F NMR spectroscopy.

[1]Formerly Patti K. Miller.

[2]Author to whom correspondence may be addressed.

[3]These distances have been corrected for the librational motion of the $OTeF_5^-$ anion.

Experimental

The general procedures and the reagents used were the same as in a previous study (1). The compounds $[N(n\text{-}Bu)_4^+][OTeF_5^-]$ and $[N(n\text{-}Bu)_4^+][H(OTeF_5)_2^-]$ were prepared by literature procedures (4).

Liquid ^{19}F NMR spectra were recorded at 188.2 MHz as previously described (1). All solid-state ^{19}F NMR spectra were recorded at 338.7 MHz on a modified Nicolet NT-360 spectrometer in the NSF Regional NMR Center at Colorado State University. The magic angle spinning (MAS) spectra were obtained at spinning speeds up to 17 kHz (5) using Torlon rotors. All spectra were recorded using a pulse (6.00 μs)–aquire (6.20 ms)–delay (1.00 s) pulse sequence. The sweep width was 125 000 Hz (369.0 ppm), and a 1 024 data point FID was collected and zero-filled to 8 192 data points before Fourier transformation. Chemical shifts (δ scale) were referred to the secondary reference poly(tetrafluoroethylene), which has a chemical shift of −122 ppm relative to $CFCl_3$.

Routine room temperature IR and Raman spectra were recorded as previously described (1). Variable temperature IR spectra were recorded on a Digilab FTS-40 spectrometer using an Air Products Displex cryostat with a Lakeshore Cryogenics silicon diode controller. Temperatures quoted are nominal cryotip temperatures; the actual sample temperatures are higher due to local heating by the incident beam. For all IR spectra peak positions are ±1 cm^{-1}.

$[(PS)H^+][OTeF_5^-]$, Mod-A and Mod-B

Equivalent amounts of Proton Sponge® (1,8-bis(dimethylamino)-naphthalene, PS) and $HOTeF_5$ were mixed in dichloromethane. Slow

Printed in Canada / Imprimé au Canada

Can. J. Chem. Downloaded from www.nrcresearchpress.com by 186.148.149.217 on 09/07/12
For personal use only.

Can. J. Chem. Downloaded from www.nrcresearchpress.com by 186.148.149.217 on 09/07/12
For personal use only.

TABLE 1. Experimental parameters for the X-ray diffraction study of $[(PS)H^+][OTeF_5^-]$, Mod-B ($(PS)H^+ = C_{14}H_{19}N_2^+$)

Formula wt, g mol^{-1}	453.9
Space group	*Cmcm*
Unit cell dimensions: *a*, Å	8.607(2)
b, Å	14.048(3)
c, Å	13.365(2)
Unit cell volume, $Å^3$	1616.0(5)
Z	4
Calcd density, g cm^{-3}	1.87
Crystal dimensions, mm	0.12 × 0.40 × 0.40
Data collection temperature, °C	−130(1)
Radiation (λ, Å)	Mo K_α (0.7107)
Monochromator	Graphite
Absorption coefficient, cm^{-1}	19.5
2θ range, deg	4–55
Reflections	$+h, +k, +l$
No. of obsd reflections	923 ($\|F_o\| > 4\sigma(F_o)$)
Total no. of reflections measured	1085
Scan type	θ–2θ
Scan speed, deg min^{-1}	variable (2–30)
Data/parameter ratio	12.5
R	0.0297
R_w	0.0418
GOF	1.84
g (refined)	4.2×10^{-4}
Slope of normal probability plot	1.43

evaporation of the solution at 22°C or cooling the solution to 4°C both resulted in crystallization of the salt, but in different crystalline modifications (ca. 90% isolated yield in either case), Mod-A and Mod-B, respectively. The oxygen-18 salts were prepared in a similar fashion using $H^{18}OTeF_5$ (1) in place of $HOTeF_5$. NMR and IR spectra and the structure of Mod-A have been reported by us in an earlier paper (1).

Crystallographic study of $[(PS)H^+][OTeF_5^-]$, Mod-B

A colorless crystal of $[(PS)H^+][OTeF_5^-]$, Mod-B was centered on a Nicolet R3m diffractometer. Centering of 25 reflections allowed least-squares calculation[4] of the cell constants given in Table 1. Other experimental parameters are also listed in Table 1.

The intensities of control reflections (800, 0 10 0, 0 0 10) monitored every 97 reflections showed no significant trend during the course of the data collection. An empirical absorption correction, based on intensity profiles for 16 reflections over a range of setting angles (ψ) for the diffraction vector, was applied to the observed data. The transmission factors ranged from 0.960 to 0.666. Lorentz and polarization corrections were applied to the data.

The structure was solved by direct methods (SOLV).[4] The cation and anion both have crystallographically imposed *mm* symmetry in the lattice. The refinements involved anisotropic thermal parameters for all non-hydrogen atoms. The hydrogen atom bridging the two nitrogen atoms was located and refined isotropically. The other hydrogen atoms were included in calculated positions (C—H = 0.96 Å, $U(H) = 1.2U_{iso}(C)$). Neutral-atom scattering factors (including anomalous scattering) were taken from ref. 6. The weighted least-squares refinements converged (weights calculated as $(\sigma^2(F_o) + |g|F_o^2)^{-1}$), with the average shift/esd < 0.010 over the last six cycles.

In the final difference Fourier synthesis, the maximum and minimum electron densities were 1.54 e $Å^{-3}$ (near Te) and −1.11 e $Å^{-3}$. Analysis of variance as a function of Bragg angle, magnitude of F_o, reflection indices, etc., showed no significant trends.

[4]Calculations for diffractometer operations were performed by using software supplied with the Nicolet R3m diffractometer. All structural calculations were performed on the Data General Eclipse S/140 computer in the X-ray laboratory at Colorado State University with the SHELXTL program library written by Professor G. M. Sheldrick and supplied by Nicolet XRD Corporation.

TABLE 2. Atomic coordinates (×10^4) and isotropic thermal parameters ($Å^2 \times 10^3$)[a] for $[(PS)H^+][OTeF_5^-]$ Mod-B

Atom	*x*	*y*	*z*	U_{iso}[b]
Te	0	2031(1)	7500	16(1)
O	0	3293(4)	7500	57(2)
F1	0	707(3)	7500	42(1)
F2	1500(2)	1866(2)	6516(2)	39(1)
C1	0	2365(2)	3445(3)	15(1)
C2	0	2861(3)	4322(3)	20(1)
C3	0	3875(3)	4305(3)	22(1)
C4	0	4351(3)	3420(3)	20(1)
C5	0	3857(3)	2500	15(1)
C6	0	2833(4)	2500	15(1)
C7	1429(3)	938(2)	3928(2)	25(1)
N	0	1319(2)	3464(2)	16(1)
H	0	−983(77)	7500	93(40)

[a]Estimated standard deviations in the least significant digits are given in parentheses.

[b]The equivalent isotropic *U* is defined as 1/3 of the trace of the U_{ij} tensor except for the refined hydrogen atom, which was refined isotropically.

Table 2 contains a list of atomic positional and isotropic thermal parameters for all unique non-hydrogen atoms of Mod-B. Complete lists of bond distances and angles (Table S-1), anisotropic thermal parameters (Table S-2), hydrogen atom parameters (Table S-3), and observed and calculated structure factors (Table S-4) are available as supplementary material.[5]

Results and discussion

Structure of the two crystalline modifications of $[(PS)H^+][OTeF_5^-]$

Crystallization from dichloromethane solutions at two different temperatures, 22 and 4°C, produced two different modifications of this salt, Mod-A and Mod-B, respectively. Both modifications are stable indefinitely at room temperature. The samples were reversibly cooled from room temperature to 60 K with no change in their respective room temperature IR and Raman spectra, but warming Mod-B to 110°C, a temperature well below the melting or decomposition temperature (170°C), caused it to convert to Mod-A.

The structure of the cation and anion in Mod-B is shown in Fig. 1. The structural results (distances, angles, and thermal parameters) leave little doubt that at −130°C the teflate anion in Mod-B has been oriented, as in Mod-A (1), by the anisotropic cation and does not exhibit the O/F disorder observed for the alkali metal salts of $OTeF_5^-$ (2). As was observed for Mod-A as well as for other $OTeF_5$ compounds (1), the oxygen and fluorine atoms in Mod-B exhibit relatively large amplitude thermal motion (see Tables 2 and S-2), despite the low temperature at which the data set was collected. A standard rigid-body librational analysis was performed (7), $R = 0.033$ for the Mod-B anion. For Mod-B, the Te—O, Te—F1, and Te—F2 distances are 1.773(5) Å, 1.861(4) Å, and 1.857(2) Å, respectively. After correction for librational motion (7), these distances are 1.801 Å, 1.890 Å, and 1.876 Å, respectively. The O—Te—F2 bond angle, which is independent of the librational correction,

[5]Supplementary Tables S-1, S-2, S-3, and S-4 may be purchased from the Depository of Unpublished Data, CISTI, National Research Council of Canada, Ottawa, Ont., Canada K1A 0S2.

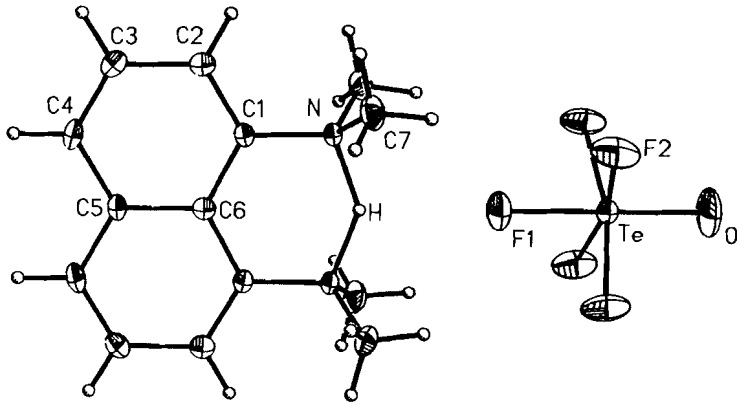


FIG. 1. A drawing of the $OTeF_5^-$ anion and the protonated Proton Sponge cation ($(PS)H^+$) in $[(PS)H^+][OTeF_5^-]$ Mod-B (50% probability ellipsoids). The separation of the ions is to scale.

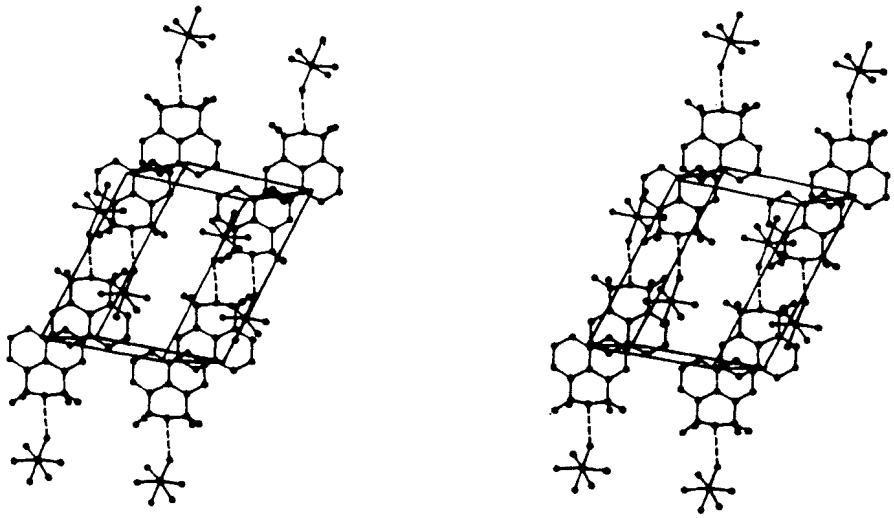


FIG. 2. A stereoview of the unit cell packing for $[(PS)H^+][OTeF_5^-]$, Mod-A.

is 97.2(1)° for Mod-B. Thus, the structure of the teflate anion in orthorhombic Mod-B is nearly the same as in triclinic Mod-A, for which the O—Te—F_{eq} bond angle is 95.2° and the Te—O and average Te—F bond distances, after correction for librational motion, are 1.803 Å and 1.870 Å, respectively.

While the bond distances and angles are nearly the same for Mod-A and Mod-B, the crystal packing of the two modifications is quite different. In Mod-A (Fig. 2), pairs of parallel $(PS)H^+$ cations, with their C5—C6 bonds oriented 180° with respect to each other, exhibit weak π–π overlap at a distance of 4.2 Å (the region of overlap is defined by C3, C4, and C5).[6] The $OTeF_5^-$ anion is in a pocket made up of four $(PS)H^+$ cations such that the librationally corrected distance between the oxygen atom and the N—H—N proton of one cation is 2.78 Å. It is easy to see why there is no O/F disorder in this modification, since O/F interchange would only allow O···H—C contacts to replace the observed O···$H(N)_2$ contact.

On the other hand, as shown in Fig. 3, each teflate anion in Mod-B is sandwiched between two $(PS)H^+$ cations whose naphthalene moieties are parallel and stacked along the x direction. Each of the four F2 atoms is only 3.032 Å from the centroid of a six-membered ring. The three closest F2···C contacts range from 3.201(2) Å to 3.315(2) Å. A distance between the teflate oxygen atom and the two N—H—N protons of these cations is 4.42 Å after correction for the librational motion of the $OTeF_5^-$ anion; the distance between F1, the axial fluorine atom, and the N—H—N proton of a third cation is 2.4 Å after librational correction. The observed crystal packing for Mod-B is also shown in the left side of Fig. 4.

Solid-state fluxional behavior of $[(PS)H^+][OTeF_5^-]$, Mod-B

At room temperature a single crystal of this salt exhibited two ν(TeO) bands in both IR and Raman spectra, at 856 and 869 cm^{-1}. The assignment was confirmed by oxygen-18 substitution, upon which both bands shifted by the appropriate amount, to 815 and 826 cm^{-1} (856/815 = 1.050, 869/826 = 1.052; for a simple TeO oscillator, $\nu(Te^{18}O)/\nu(Te^{16}O)$ = 1.053). At first, this result was surprising, since the solid-state structure of this salt at −130°C contains $OTeF_5^-$ anions in only one type of environment (see Figs. 1 and 3). It did not seem likely that the two bands were the result of coupling of the four symmetry-related TeO oscillators in the unit cell. The teflate anions are far apart and well insulated from each other by the $(PS)H^+$ cations: The closest Te···Te separation is 8.057 Å. Furthermore, the relative intensities of the two ν(TeO) bands are such that $I(856\ cm^{-1}) > I(869\ cm^{-1})$ in both IR and Raman spectra.

[6]The numbering scheme used to define atoms C3, C4, C5, and C6 in Mod-A (ref. 1) is the same used in Fig. 1 for Mod-B.

Can. J. Chem. Downloaded from www.nrcresearchpress.com by 186.148.149.217 on 09/07/12
For personal use only.

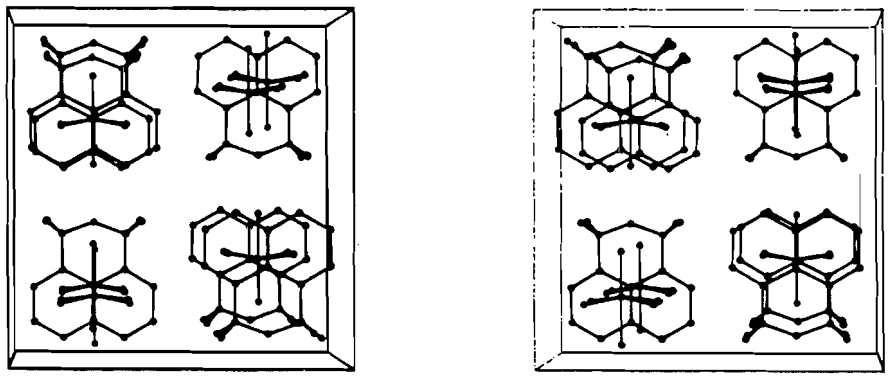


FIG. 3. A stereoview of the unit cell packing for $[(PS)H^+][OTeF_5^-]$, Mod-B.

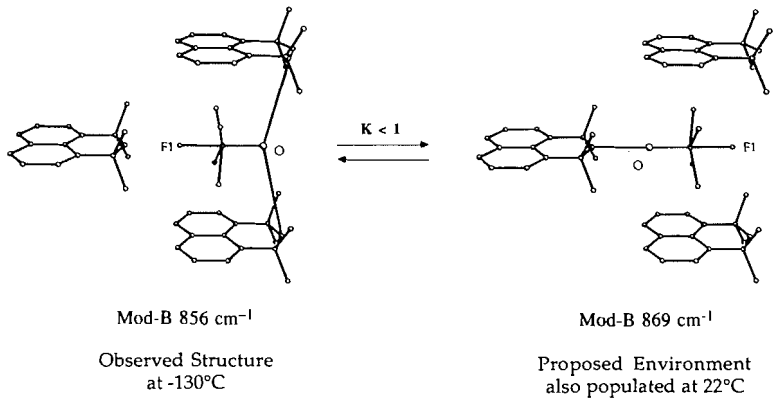


FIG. 4. A representation of the proposed solid-state equilibrium for $[(PS)H^+][OTeF_5^-]$, Mod-B. The oxygen (O) and axial fluorine (F1) atoms are labelled, and the oxygen atoms are linked to the closest N—H—N proton(s) by solid lines. The drawing on the left (the environment that gives rise to ν(TeO) = 856 cm^{-1}) shows the observed structure at −130°C, while the one on the right (the environment that gives rise to ν(TeO) = 869 cm^{-1}) depicts the proposed environment that is also populated at room temperature.

Upon further investigation, we found that the IR intensities of the two ν(TeO) bands are temperature dependent, as shown in Fig. 5. Below room temperature, the less intense 869 cm^{-1} band decreased in intensity as the 856 cm^{-1} band increased in intensity (the 832 cm^{-1} $(PS)H^+$ band served as an intensity standard since its bandwidth was relatively constant over the temperature range studied). The 869 cm^{-1} band disappeared completely below −70°C. We propose that the teflate anions in Mod-B are able to rotate about one or more axes through the tellurium atom with a low activation barrier, and that two nearly degenerate local environments exist for the $OTeF_5^-$ anions. The slightly more stable environment is the one shown in Figs. 1 and 3 and the left side of Fig. 4, which show the structure of Mod-B at −130°C; all teflate anions in Mod-B are in this environment below −70°C and have ν(TeO) = 856 cm^{-1}. The slightly less stable environment would be produced by rotating the anion so that the oxygen and axial fluorine atoms (F1) are interchanged, as shown in the right side of Fig. 4; teflate anions in this environment have ν(TeO) = 869 cm^{-1}. Figure 4 is a representation of this proposed solid-state equilibrium. Based on the intensities of the 856 and 869 cm^{-1} bands in the IR spectra of Mod-B, we conclude that the equilibrium constant $K < 1$ at room temperature and at lower temperatures.

A very simple model of nearest neighbor electrostatic attractions is in harmony with the proposal that O/F1 interchange produces two nearly degenerate environments in the structure of Mod-B. If one assumes that van der Waals and long range electrostatic contributions to the lattice energy (U) are essentially constant (C) for O/F1 interchange, that the N—H—N proton bears a full positive charge, and that the O and F1 atoms bear the amount of negative charge given by our *ab initio* calculations for the free $OTeF_5^-$ anion (1), then for the 856 cm^{-1} environment $U - C \propto [2(0.918/4.42) + (0.525/2.4)] = 0.63$ (recall that O···H = 4.42 Å and F1···H′ = 2.4 Å) while for the proposed 869 cm^{-1} environment $U - C \propto [(0.918/2.4) + 2(0.525/4.42)] = 0.62$. According to this admittedly simple model, the 856 cm^{-1} environment is predicted to be marginally more stable than the 869 cm^{-1} environment, in accord with our observations. Even allowing that the actual atom charges may differ from the values given by theoretical methods (1), it is reasonable to conclude that the two proposed environments for the teflate anion in Mod-B are nearly degenerate.

The activation barrier for the interchange of O and F1 could conceivably be very low for the nearly spherical teflate anion. Many symmetrical anions, such as BF_4^- (8), SbF_6^- (8), and PCl_6^- (9), rotate about one or more axes through the central atom. In many cases, this rotation leads to crystallographic disorder and incompletely solved structures. We decided to investigate the solid-state motion in Mod-B and other teflate salts by solid-state ^{19}F NMR spectroscopy (Figs. 6 and 7, Table 3). While several solid-state ^{19}F NMR studies have been reported since 1959 (10–18), it is only recently that magic angle spinning speeds of 18–20 kHz have allowed high-resolution spectra to be obtained (5, 19).

Can. J. Chem. Downloaded from www.nrcresearchpress.com by 186.148.149.217 on 09/07/12
For personal use only.

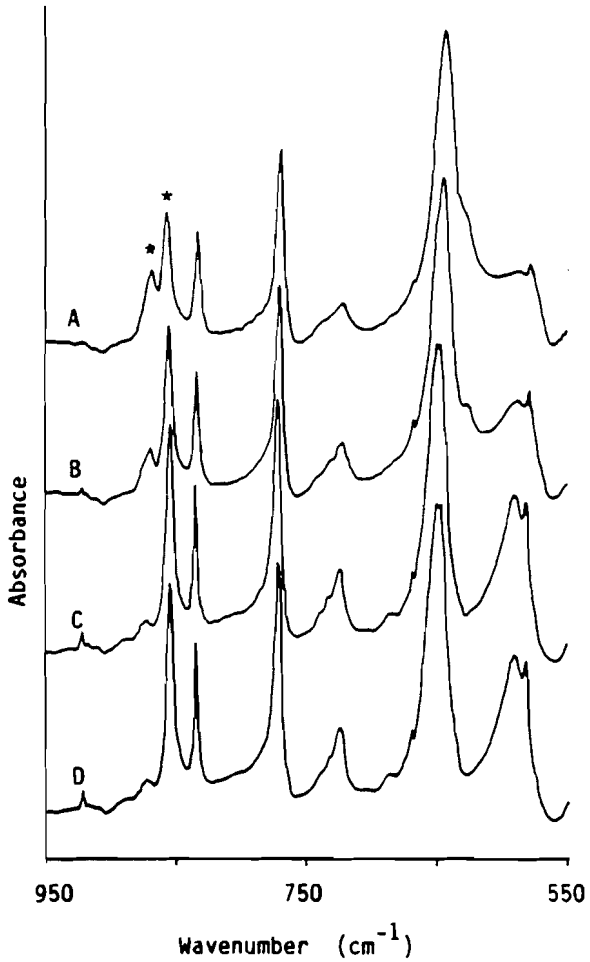


FIG. 5. Solid-state IR spectra of $[(PS)H^+][OTeF_5^-]$, Mod-B at room temperature (*A*), 250 K (*B*), 140 K (the temperature of the X-ray diffraction study of this compound) (*C*), and 60 K (*D*). The peaks at 869 and 856 cm^{-1} in the room temperature spectrum, marked with asterisks, are assigned as ν(TeO) bands based on ^{18}O substitution. Below 200 K, the weak, broad feature at ~860 cm^{-1} did not vary significantly in shape or intensity.

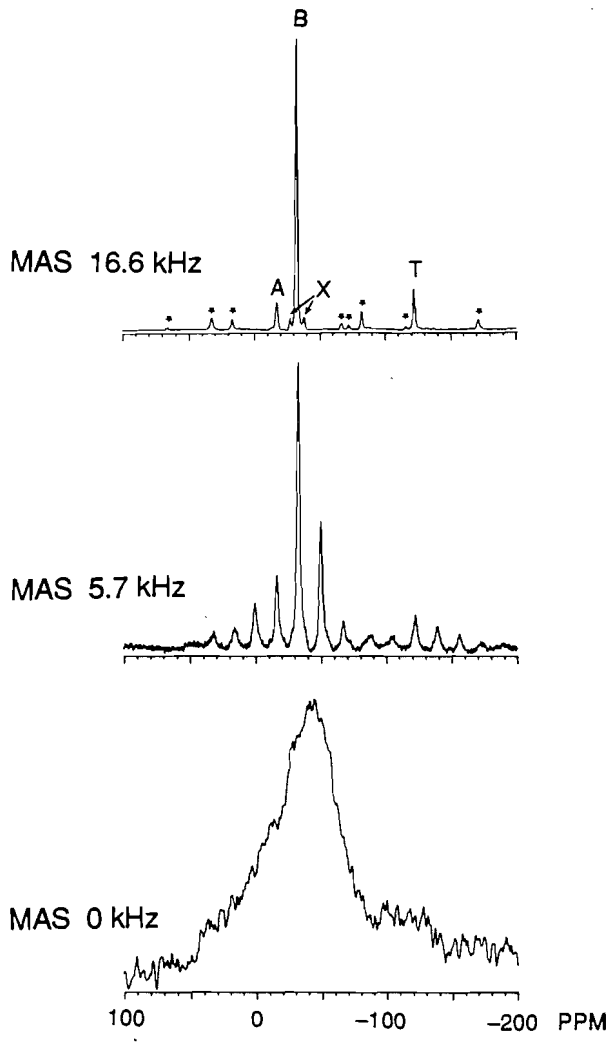


FIG. 6. Solid-state 338.7 MHz ^{19}F NMR spectra of $[(PS)H^+][OTeF_5^-]$, Mod-B as a function of MAS speed. The resonances in the 16.6 kHz spectrum are assigned as follows: axial fluorine, *A*; equatorial fluorines, *B*; ^{125}Te satellites for the equatorial fluorines, *X*; Torlon rotor, *T*. The spinning sidebands are labelled with asterisks.

The spectral lines for the four compounds we investigated, $[(PS)H^+][OTeF_5^-]$, Mod-A and Mod-B, $[N(n\text{-}Bu)_4^+][OTeF_5^-]$, and $[N(n\text{-}Bu)_4^+][H(OTeF_5)_2^-]$, were easily narrowed using high-speed magic angle spinning (MAS). However, the linewidths for each sample run at a MAS speed of about 10 kHz were essentially equal to those measured at MAS speeds greater than 16 kHz. This is evidence for the lack of strong homonuclear dipole–dipole interactions in these samples, since for strongly homonuclear dipolar coupled systems, the residual linewidth continues to decrease with increasing MAS speed until the spinning speed is much larger than the static linewidth, which for Mod-B is 18 kHz (Fig. 6). The linewidth observed in the static spectra (i.e. ~18 kHz for Mod-B) may be due to chemical shift anisotropy (CSA). However, an ^{19}F CSA of only 18 kHz seems too small, given that CSAs for fluoropolymers such as poly(tetrafluoroethylene) are ~46 kHz (19). Rapid rotation of the $OTeF_5^-$ anion, which would lead to O/F1 interchange in Mod-B, could explain the small static linewidth and the relatively low MAS speed needed to narrow the spectra, since such rotation would average, to some extent, dipolar interactions and CSA.

The two crystalline modifications of $[(PS)H^+][OTeF_5^-]$ have significantly different chemical shifts for their respective axial and equatorial fluorine atoms, both sets of which are different than the chemical shifts for $[N(n\text{-}Bu)_4^+][OTeF_5^-]$ (Table 3). Furthermore, the two crystallographically unique teflate groups in $[N(n\text{-}Bu)_4^+][H(OTeF_5)_2^-]$ also have different δ_A and δ_B values. Since the chemical shifts are so sensitive to the environment of the individual teflate groups, it is surprising that the equatorial fluorine atoms in $[(PS)H^+][OTeF_5^-]$ Mod-A, $[N(n\text{-}Bu)_4^+][OTeF_5^-]$, and in each of the two teflate groups in $[N(n\text{-}Bu)_4^+][H(OTeF_5)_2^-]$ do not display a *range* of chemical shifts: note that the δ_B linewidths for these compounds are no larger than that for Mod-B, in which the equatorial fluorine atoms are symmetry (and magnetically) equivalent. We tentatively conclude that the non-equivalent equatorial fluorine atoms in these compounds are being rendered magnetically equivalent by rapid rotation of each teflate group about, for instance, its O—Te—F_{ax} axis.

Rapid rotation of the teflate anion in Mod-B about an axis perpendicular to its O—Te—F_{ax} axis would lead to the facile room temperature interchange of O and F1 in this compound. This type of motion is supported by the observed anisotropic

Can. J. Chem. Downloaded from www.nrcresearchpress.com by 186.148.149.217 on 09/07/12
For personal use only.

Can. J. Chem. Downloaded from www.nrcresearchpress.com by 186.148.149.217 on 09/07/12
For personal use only.

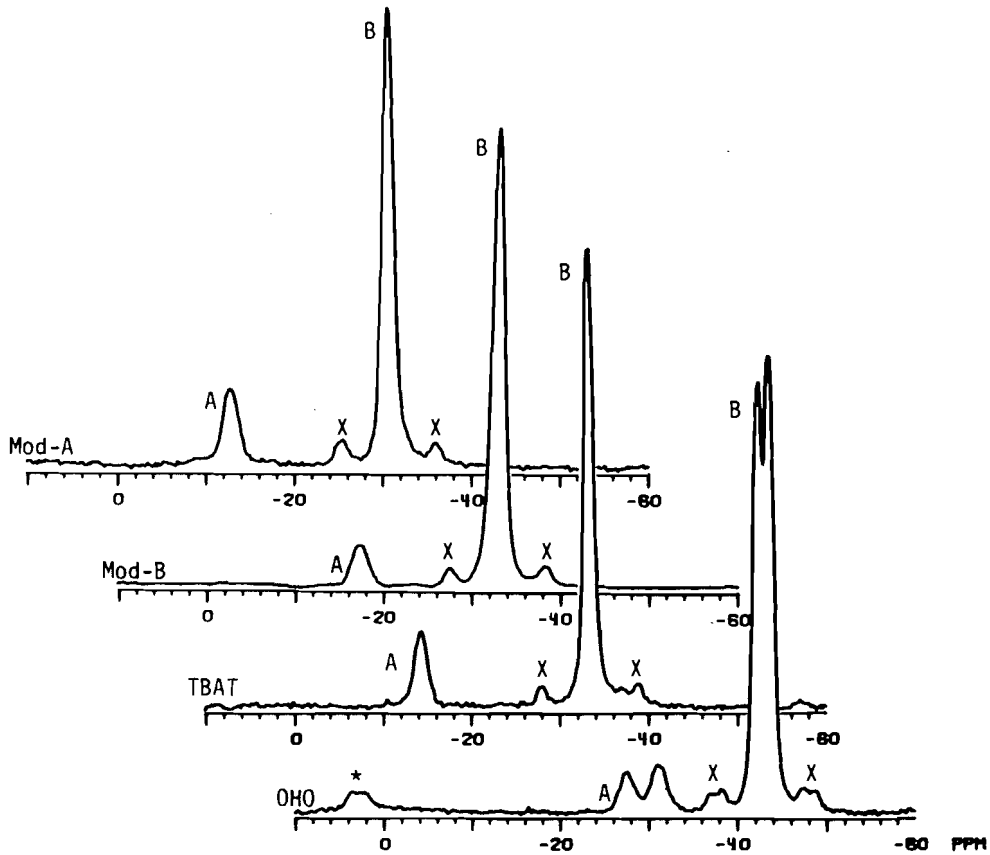


FIG. 7. Solid–state 338.7 MHz ^{19}F MAS-NMR spectra at spinning speeds of 15–17 kHz of $[(PS)H^+][OTeF_5^-]$ Mod-A, $[(PS)H^+][OTeF_5^-]$ Mod-B, $[N(n\text{-}Bu)_4^+][OTeF_5^-]$ (TBAT), and $[N(n\text{-}Bu)_4^+][H(OTeF_5)_2^-]$ (OHO).

TABLE 3. ^{19}F NMR data[a]

	$[(PS)H^+][OTeF_5^-]$			
Parameter	Mod-A	Mod-B	$[N(n\text{-}Bu)_4^+][OTeF_5^-]$	$[N(n\text{-}Bu)_4^+][H(OTeF_5)_2^-]$
δ_A ($\Delta\nu_{1/2}$)				
Solid	−12.8 (670)	−17.2 (780)	−14.3 (610)	−27.5 (700[b]), −31.1 (700[b])
Liquid	−20.0	−20.0	−19.0	−32.1
δ_B ($\Delta\nu_{1/2}$)				
Solid	−30.7 (540)	−33.1 (560)	−33.6 (440)	−42.4 (380[b]), −43.3 (410[b])
Liquid	−37.4	−37.4	−36.8	−44.8
$J_{BX'}$ Hz				
Solid	3600	3720	3690	3550,[b] 3580[b]
Liquid	3643	3643	3654	3552

[a]Chemical shifts are relative to $CFCl_3$. Liquids experiments were dichloromethane solutions. All solid chemical shifts are ±0.3 ppm. $\Delta\nu_{1/2}$ values are in Hz. The MAS spinning speeds were (compound, speed (kHz): Mod-A, 16.3; Mod-B, 16.6; $[N(n\text{-}Bu)_4^+][OTeF_5^-]$, 15.2; $[N(n\text{-}Bu)_4^+][H(OTeF_5)_2^-]$, 15.6.
[b]Determined by spectral deconvolution.

thermal parameters for F2 (Table S-2): U along the ***b*** axis (the O—Te—F1 axis), 0.070(1) Å^2, is considerably larger than U along the ***a*** and ***c*** axes, 0.022(1) and 0.024(1) Å^2, respectively. Thus, the two different δ_A resonances that might be expected for the two $OTeF_5^-$ environments in Mod-B are time averaged to yield only one observed resonance. Assuming that $\Delta\delta_A$ (for F1) would be ~3 ppm for the two $OTeF_5^-$ environments in Mod-B (this is less than $\Delta\delta_A$ for $[N(n\text{-}Bu)_4^+][H(OTeF_5)_2^-]$), then the rate of O/F1 interconversion in the solid-state may be 10^4–10^5 s^{-1}. Of course, it is possible that the δ_A chemical shifts for the two proposed teflate environments in Mod-B are accidentally equal and that the rate of exchange is slow. We have attempted to study the solid-state motion of Mod-B by ^{19}F NMR $T_{1\rho}$ measurements, which can in principle be used

to measure rates of motion on this time scale. However, correlation times could not be extracted from the observed $T_{1\rho}$ values, since a plot of $1/T_{1\rho}$ versus the excitation field strength went through a minimum. This behavior is not predicted by any known theory (20). Perhaps it is due to modulation of the experimental $T_{1\rho}$ values by the MAS, the rate of which is on the same order of magnitude as the proposed time of motion.

In principle, MAS ^{19}F NMR experiments at temperatures low enough to slow down the proposed two-site interchange would allow the two δ_A resonances for Mod-B to be observed. However, achieving low temperatures while spinning the sample fast enough to average strong ^{19}F–^{19}F dipolar coupling is difficult due to the large volume of gas which must be cooled to spin the sample (5). Once these technical problems are solved, solid-state MAS ^{19}F NMR spectroscopy will become a valuable tool for the study of dynamic processes in solids.

Acknowledgments

This research was supported by grants from the NSF (CHE-8419719 and CHE-8805788). We thank Professors J. R. Norton and A. T. Tu for the use of their IR and Raman spectrometers, respectively, and S. A. Ekberg, J. H. Reibenspies, and M. M. Miller for experimental assistance. We are grateful to Dr. S. F. Dec for his experimental assistance and for his continuing interest in the solid-state ^{19}F NMR spectroscopic behavior of $OTeF_5^-$ compounds. SHS acknowledges the A. P. Sloan Foundation for a Research Fellowship. P.J.K. thanks the Mobay Corporation for a Graduate Student Research Award. K.D.A. acknowledges the support of the Department of Energy. The Nicolet R3m/E diffractometer and computing system was purchased with NSF Grant No. CHE-8103011. The Regional NMR Center at Colorado State University is funded by NSF Grant No. CHE-8616437.

1. P. K. Miller, K. D. Abney, A. K. Rappe, O. P. Anderson, and S. H. Strauss. Inorg. Chem. **27**, 2255 (1988).
2. F. Sladky, H. Kropshofer, O. Leitzke, and P. Peringer. J. Inorg. Nucl. Chem. Suppl. 69 (1976).
3. (*a*) R. F. W. Bader, R. J. Gillespie, and P. J. Macdougall. J. Am. Chem. Soc. **110**, 7329 (1988); (*b*) R. J. Gillespie. Chem. Future, Proc. IUPAC Congr. 29th. *Edited by* H. Gruenewald. Pergamon, Oxford. 1984. p. 369; (*c*) R. J. Gillespie, D. A. Humphreys, N. C. Baird, and E. A. Robinson. Chemistry. Allyn and Bacon, Newton, MA. 1986. p. 275.
4. S. H. Strauss, K. D. Abney, and O. P. Anderson. Inorg. Chem. **25**, 2806 (1986).
5. S. F. Dec, R. A. Wind, G. E. Maciel, and F. E. Anthonio. J. Magn. Reson. **70**, 355 (1986).
6. D. T. Cromer and J. T. Waber. International tables for X-ray crystallography. Vol. IV. Kynoch Press, Birmingham, England. 1974.
7. V. Schomaker and K. N. Trueblood. Acta Crystallogr. Sect. B: Struct. Crystallogr. Chem. B**24**, 63 (1968).
8. K. O. Christe, M. D. Lind, N. Thorup, D. R. Russell, J. Fawcett, and R. Bau. Inorg. Chem. **27**, 2450 (1988).
9. H. Z. Preiss. Z. Anorg. Allg. Chem. **380**, 51 (1971).
10. I. J. Lowe. Phys. Rev. Lett. **2**, 285 (1959).
11. E. R. Andrew and D. P. Tunstall. Proc. Phys. Soc. **81**, 986 (1963).
12. E. Hunt and H. Meyer. J. Chem. Phys. **41**, 353 (1964).
13. R. Blinc, E. Pirkmajer, J. Slivnik, and I. Zupančič. J. Chem. Phys. **45**, 1488 (1966).
14. E. Fukushima and H. G. Hecht. J. Chem. Phys. **54**, 4341 (1971).
15. M. Mehring, R. G. Griffin, and J. S. Waugh. J. Chem. Phys. **55**, 746 (1971).
16. A. D. English and A. J. Vega. Macromolecules, **12**, 353 (1979).
17. J. P. Yesinowski and M. J. Mobley. J. Am. Chem. Soc. **105**, 6191 (1983).
18. A. J. Vega and A. D. English. Macromolecules, **13**, 1635 (1980).
19. S. F. Dec, R. A. Wind, and G. E. Maciel. Macromolecules, **20**, 2754 (1987).
20. D. C. Ailion. Adv. Magn. Reson. **5**, 177 (1971).

Can. J. Chem. Downloaded from www.nrcresearchpress.com by 186.148.149.217 on 09/07/12
For personal use only.

A Raman spectral study of the equilibria of zinc bromide complexes in DMSO solutions

JEFF VAN HEUMEN, TORU OZEKI,[1] AND DONALD E. IRISH[2]

Department of Chemistry, University of Waterloo, Waterloo, Ont., Canada N2L 3G1

Received March 1, 1989

This paper is dedicated to Professor Ronald J. Gillespie on the occasion of his 65th birthday

JEFF VAN HEUMEN, TORU OZEKI, and DONALD E. IRISH. Can. J. Chem. **67**, 2030 (1989).

Using Raman spectroscopy, the stepwise formation of zinc bromide complexes in dimethylsulfoxide (DMSO) solution has been investigated. The presence of four different zinc bromide complexes is suggested and their Raman spectra have been extracted. The formation constant of each reaction has been estimated by the application of factor analysis to the spectra. The usual methods of factor analysis have been extended by the introduction of constraints imposed by the equilibria.

Key words: zinc bromide complexes, solvation in DMSO, Raman spectroscopy, factor analysis.

JEFF VAN HEUMEN, TORU OZEKI et DONALD E. IRISH. Can. J. Chem. **67**, 2030 (1989).

Faisant appel à la spectroscopie Raman, on a étudié la formation par étapes de complexes du bromure de zinc en solution dans le diméthylsulfoxyde (DMSO). Ces données suggèrent la présence de quatre complexes différents du bromure de zinc et on en a extrait leurs spectres Raman. Par l'application de l'analyse factorielle aux spectres, on a pu évaluer la constante de formation de chacune des réactions. Les méthodes usuelles de l'analyse factorielle ont été étendues par l'introduction des contraintes imposées par l'équilibre.

Mots clés : complexes du bromure de zinc, solvatation dans le DMSO, spectroscopie Raman, analyse factorielle.

[Traduit par la revue]

Can. J. Chem. Downloaded from www.nrcresearchpress.com by 186.148.149.217 on 09/07/12
For personal use only.

Introduction

Professor Ronald J. Gillespie has had a long standing interest in the shapes of complexes and molecules. It is a pleasure to dedicate this article to him on the occasion of his 65th birthday.

Ahrland and co-workers have reported the results of detailed studies of metal complex formation between Group IIB metals and halide ions in the dipolar aprotic solvent, dimethylsulfoxide (DMSO) (1–9). Emphasis was placed on the thermodynamics of the stepwise equilibria and evidence for structural changes between successive complexes. The solvent, DMSO has been investigated quite extensively as a neat liquid (10–12), and as a solvent in which complex formation occurs. The complexes are more stable in DMSO than in water because the former has a lower dielectric constant (1, 3, 9). The uncomplexed metal cations — zinc, cadmium, or mercury — are believed to exist as octahedral species, the ions being solvated via oxygen by six DMSO molecules (6, 13, 14). However, evidence suggests that their coordination symmetry changes from six-coordinate octahedral to four-coordinate tetrahedral as higher halide complexes are formed. Enthalpy and entropy values for the cadmium halide system suggest that a coordination change occurs at the second step of complex formation: a step from $CdBr^+$ to $CdBr_2$ (2). For the zinc bromide complexes Ahrland *et al.* have suggested the possibility that the change occurs at the first step of complex formation in 1 *M* NH_4ClO_4 media: a step from Zn^{2+} to $ZnBr^+$ (4). In a succeeding paper (7), they reported that the step giving rise to the coordination change depends upon the co-existing salt and ionic strength of the solution, such that this change in coordination of the zinc bromide complex might occur at the second step in 0.1 *M* NH_4ClO_4 media. Several other methods such as NMR (15, 16) and X-ray diffraction (17) have also been used to study this kind of phenomenon. All reports support the view that the complex finally formed — $ZnBr_4^{2-}$ or $CdBr_4^{2-}$ — is a tetrahedral complex.

Raman spectroscopy is a useful tool for investigation of the structure of these complexes because the latter have Raman-active vibrational modes (18–21); and the technique is, in principle, capable of providing information about their geometry. From the Raman intensities information about the concentrations of each species can be obtained and hence the stability and equilibrium constants can be estimated. This work was undertaken to complement recent studies of zinc and cadmium bromide complexes in water (20, 21) and to extend those works to nonaqueous solutions. This work is focussed on zinc bromide complex formation in DMSO solutions, especially on the determination of the stepwise stability constants and the stage at which the coordination change takes place.

Experimental

Nine solutions were prepared by dissolving given amounts of zinc bromide (J. T. Baker, "Baker Analyzed") $ZnBr_2$ and different amounts of sodium bromide (BDH, Laboratory Reagent) NaBr in solvent DMSO (BDH, Analytical Reagent) $SO(CH_3)_2$. To prepare solutions with different R values (the molar ratio of total bromide to total zinc) sodium bromide was added. In the case of $R < 2.0$, zinc perchlorate (GFS Chemicals) $Zn(ClO_4)_2 \cdot 6H_2O$ was used in place of sodium bromide. The introduction of a small amount of water is not expected to introduce a serious problem as DMSO solvates zinc(II) much more strongly than water does (5, 9). R values of the sample solutions and their compositions are given in Table 1. Concentrations are given in mol kg^{-1} of DMSO.

Samples were placed in glass capillary tubes for Raman measurements. To avoid solvent evaporation the open end of the capillary was flame-sealed. All spectra were collected at a temperature of 25°C by using a thermostatted capillary tube holder.

Raman spectra were recorded using a Jarrell-Ash 25-100, 1.0 meter Czerny-Turner monochromator equipped with a digital cosecant stepping drive, an RCA 31034 selected photomultiplier tube, and an SSR model 1105/1120 photon counting system. Spectra were excited by the 514.5 nm line of a Spectra-Physics Ar^+ Laser, Model 165, operating at a power of 1400 mW. The spectrometer was interfaced to Commodore-Pet Model 2001 and 2040 computers. The digitized data were also analyzed by the DEC-PRO 380 and VAX 11/785 computers, using procedures such as spectral band fitting, exponential baseline correction, and factor analysis.

[1]Present address: Hyogo University of Teacher Education, 942-1 Shimokume, Yashiro-cho, Kato-gun, Hyogo, Japan 673-14.

[2]To whom correspondence should be addressed.

TABLE 1. Analytical compositions (mol kg^{-1}) of nine sample solutions with different R values

R	Zn^{2+}	Br^-	Na^+	ClO_4^-
1.0	0.649	0.649	0.000	0.649
1.5	0.786	1.178	0.000	0.394
2.0	0.484	0.968	0.000	0.000
2.4	0.517	1.241	0.207	0.000
2.8	0.496	1.389	0.397	0.000
3.2	0.466	1.492	0.560	0.000
3.6	0.294	1.058	0.470	0.000
4.0	0.406	1.624	0.812	0.000
6.0	0.169	1.016	0.678	0.000

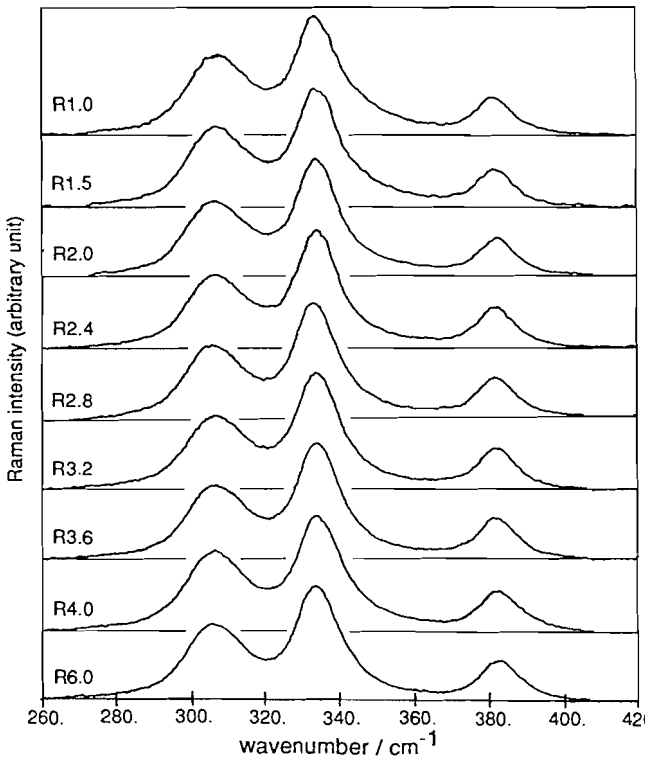


FIG. 1. The 260 to 420 cm^{-1} region of the Raman spectra of samples with the specified values of R.

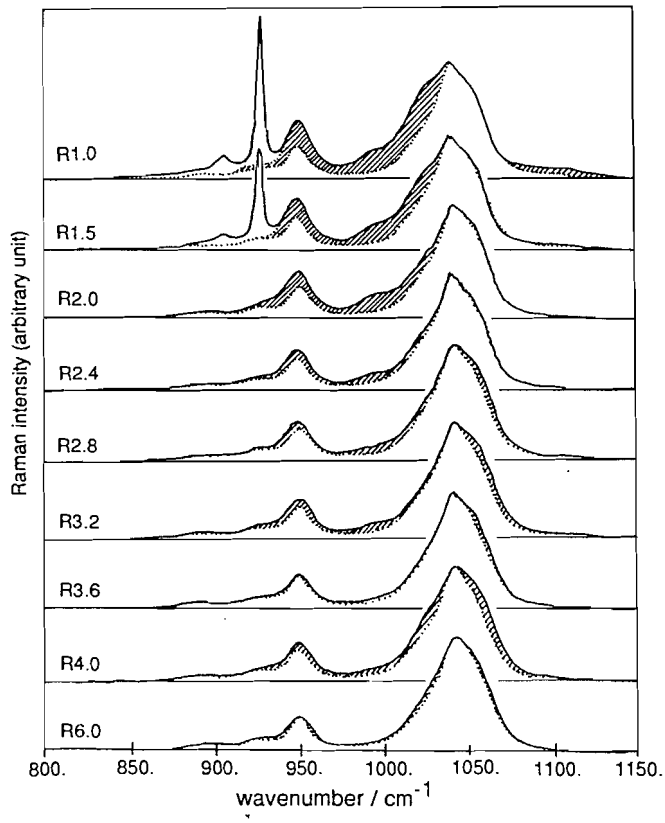


FIG. 2. The 800 to 1150 cm^{-1} region of the Raman spectra of samples with the specified values of R. Dotted lines are Raman spectra of pure DMSO solvent. The shaded part is the difference between the spectrum of the sample and that of pure DMSO.

Results and discussion

Four spectral regions: (*a*) 260 to 420 cm^{-1}, (*b*) 800 to 1150 cm^{-1}, (*c*) 600 to 750 cm^{-1}, and (*d*) 150 to 230 cm^{-1} are considered below.

(a) 260 to 420 cm^{-1} region of the Raman spectra

This region, shown in Fig. 1, contains the symmetric and the antisymmetric deformation bands of the carbon–sulfur–oxygen bond at 382 and 333 cm^{-1} respectively, as well as a carbon–sulfur–carbon deformation band at 305 cm^{-1}. No additional bands were observed and the three bands showed no significant change in band shape with the change in R value.

(b) 800 to 1150 cm^{-1} region of the Raman spectra

The bands of this region arise from the sulfur–oxygen vibration of DMSO. Figure 2 illustrates the effect of complexing on the sulfur–oxygen vibration of the DMSO molecule as the R value increases. Solid lines are the Raman spectra of each sample and dotted lines show the spectra of neat DMSO. Sharp peaks observed at 930 cm^{-1} for R = 1.0 and 1.5 samples correspond to the $\nu_1(a_1)$ symmetrical stretching vibration of perchlorate ion. The shaded area between the solid and the dotted lines indicates the difference between the spectrum of the neat solvent and that of the sample solution; it arises from the perturbed sulfur–oxygen bond, resulting from the solvation by DMSO molecules of the zinc cation (cf. ref. 6). The decrease in the shaded area suggests the decrease in the amount of DMSO solvating the zinc cation as the bromide concentration increases. The sulfur–oxygen stretching band, seen in Fig. 2 at 1042 cm^{-1}, provides indirect information for the zinc–DMSO bonding. If some interaction occurs between zinc cation and oxygen of the DMSO molecule, the metal cation will attract the electron cloud of the sulfur–oxygen bond, and as a result reduce the bond order of the sulfur–oxygen bond. Consequently, the vibrational energy will be lowered and the Raman band position will shift to a lower wavenumber. The evidence for this shift is clearly seen at R = 1.0 in Fig. 2; a new band appears at 1017 cm^{-1} (1021 cm^{-1} in the solid solvate (6)). On increasing the R value, obviously there is seen a decrease in the intensity of this new band. At R = 3.2, the new peak no longer exists. This fact is interpreted as desolvation of DMSO from the solvation sphere of the zinc cation to the free bulk state.

(c) 600 to 750 cm^{-1} region of the Raman spectra

This wavenumber region is dominated by a symmetric stretching band at 670 cm^{-1} and an antisymmetric stretching band at 700 cm^{-1}, both due to the carbon–sulfur bonding in the DMSO molecule. Figure 3 provides comparison of the

Can. J. Chem. Downloaded from www.nrcresearchpress.com by 186.148.149.217 on 09/07/12
For personal use only.

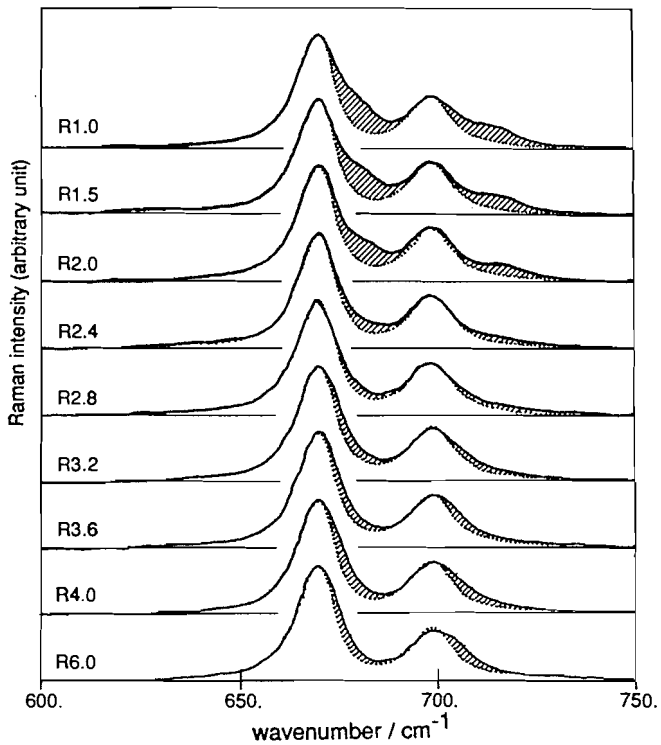


FIG. 3. The 600 to 750 cm^{-1} region of the Raman spectra of samples with the specified values of R. Dotted lines are Raman spectra of pure DMSO solvent. The shaded part is the difference between the spectrum of the sample and that of pure DMSO.

Raman spectra of the neat DMSO (dotted lines) and the DMSO/Zn^{2+}–Br^- mixtures (solid lines). The shaded area between the two spectra indicates the difference between the spectrum of the neat solvent and that of the sample solution. At the lowest R value, $R = 1.0$, two additional peaks appear at higher wavenumbers, 681 and 714 cm^{-1} (683 and 717 cm^{-1} in the solid solvate (6)). As described in the previous section the solvation of zinc ion by DMSO molecules reduces the bond order of the sulfur–oxygen bond. This may cause the adjacent carbon–sulfur bond to acquire extra electron density and its bond strength to increase. As a matter of fact, the peak wavenumber of the carbon–sulfur vibration shifts to a higher wavenumber. It is important to note that with an increasing R value the intensity of the shifted peak decreases considerably. At approximately $R = 2.8$ to $R = 3.2$ these additional bands have essentially disappeared, again. This intensity decrease seems to be consistent with the decrease in the number of DMSO molecules solvating zinc cation.

(d) 150 to 230 cm^{-1} region of the Raman spectra

The fourth region contains the vibrations due to the zinc bromide complexes as a whole (Fig. 4). These original spectra contain an exponential background due to the Rayleigh scattering. This background was subtracted by using an exponential-quadratic base-line correction program (22, 23), to give Fig. 5.

Three Raman bands at 197, 180, and 166 cm^{-1} corresponding to zinc bromide complexes are clearly seen in Fig. 5. At the low R values the presence of an additional band is also expected at 207 cm^{-1}. (A very weak shoulder at ~176 cm^{-1} for $R = 1.0$ (Fig. 4) corresponds to a band of the hexasolvate observed by Sandström *et al.* (6).) The band at 166 cm^{-1} is detected only for $R > 3.2$. These four bands seem to be related to four complexes: $ZnBr^+$, $ZnBr_2$, $ZnBr_3^-$, and $ZnBr_4^{2-}$. Ahrland *et al.* have

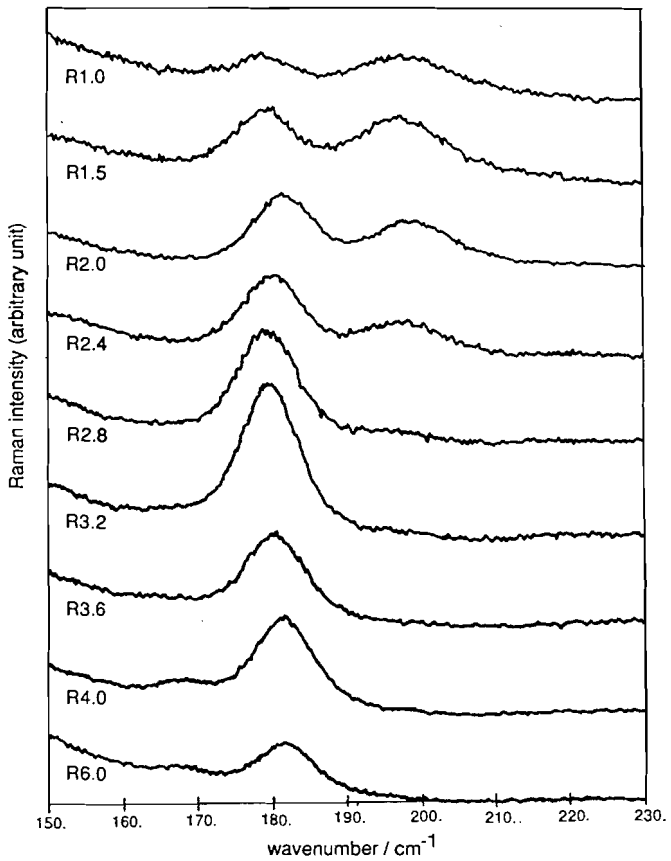


FIG. 4. The 150 to 230 cm^{-1} region of the Raman spectra of samples with the specified values of R.

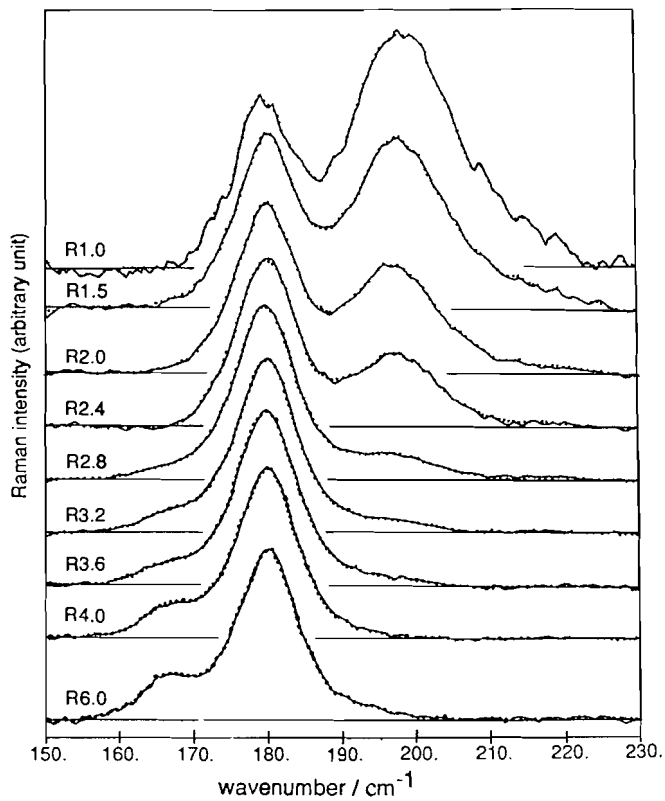


FIG. 5. Comparison of normalized Raman spectra (solid line) and reproduced spectra (dotted line) from factor analysis.

Can. J. Chem. Downloaded from www.nrcresearchpress.com by 186.148.149.217 on 09/07/12
For personal use only.

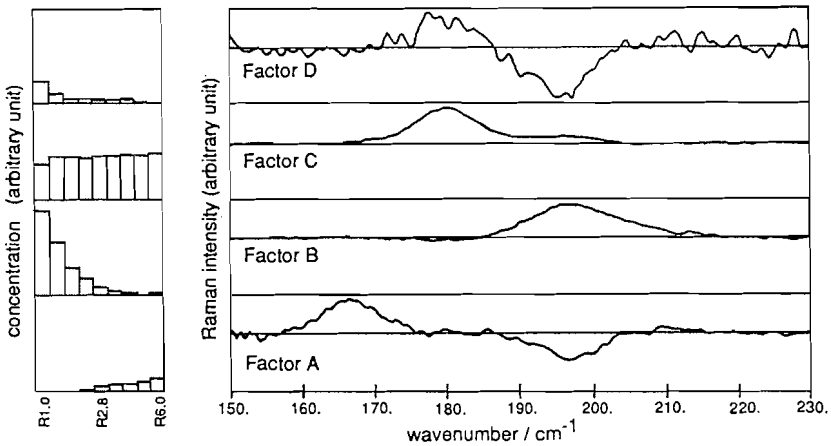


FIG. 6. The Raman spectrum of each species and its concentration distribution obtained from factor analysis.

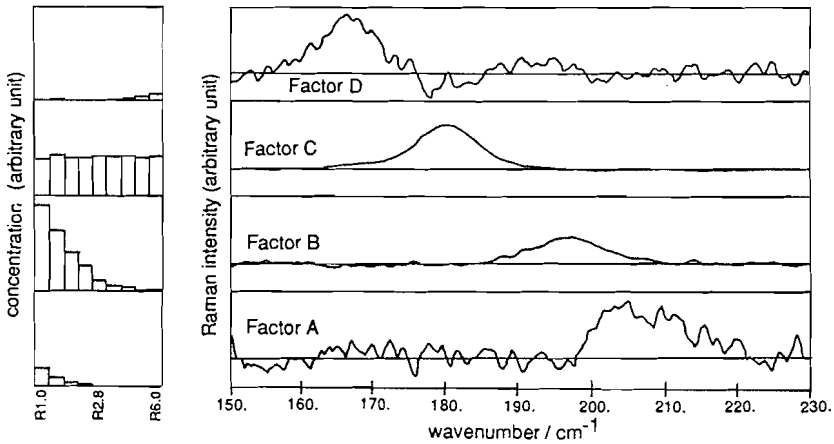


FIG. 7. The Raman spectrum of each species and its concentration distribution obtained after applying the equilibrium constraints among species.

reported the presence of three complex species — $ZnBr^+$, $ZnBr_2$, and $ZnBr_3^-$ (7, 8) — and have calculated their formation constants from calorimetric data. When the concentrations of the species are calculated using their formation constants, it is proposed that the dominant species at $R = 3.2$ is $ZnBr_3^-$; this proposal is consistent with the fact that the Raman spectrum has only one peak at 180 cm^{-1} for the $R = 3.2$ sample (Figs. 4 and 5). This fact allows an identification of the bands as follows: 207 ($ZnBr^+$), 197 ($ZnBr_2$), 180 ($ZnBr_3^-$), and 166 cm^{-1} ($ZnBr_4^{2-}$). The obvious appearance of the 166 cm^{-1} peak at $R > 3.2$ confirms the existence of the $ZnBr_4^{2-}$ complex.

In order to isolate the spectrum of each species from the overlapped spectra, factor analysis was applied to this spectral region after base-line correction. It was difficult to obtain the absolute intensities of each spectrum from experiments. Thus all spectra were normalized assuming the intensity at 180 cm^{-1} to be constant (see Fig. 5): $ZnBr_3^-$ standard. The procedure for the factor analysis is described in Appendix A. The analysis showed that three or four factors are necessary to reproduce the measured spectra. The indication of four factors (four complexes) was adopted, as this is consistent with the existence of four bands described above. In this case, the spectra shown by the dotted lines in Fig. 5 were reproduced and are in good agreement with the measured spectra as shown by solid lines in Fig. 5.

The extracted spectra of each pure species and their concentration distributions are shown in Fig. 6. The spectrum of Factor A and that of Factor D show some negative Raman intensities; and this fact indicates that this result is not necessarily correct. In factor analysis, many combinations of spectra and concentration distributions, namely **R** and **C** matrices (being introduced in Appendix A), reproduce the same spectral data (**I**). We can rotate the bases of these two matrices **R** and **C**, while keeping their product **I** constant. To carry out a meaningful rotation of the matrix, we adopted a new method, called Factor Analysis with Equilibria Constraints (FAEC) described in Appendix B, which took into account information about the equilibria among species. As a result, the spectrum of each species and its concentration change as shown in Fig. 7 were obtained. The spectra of Factors A and D still have a large contribution from the noise component, but no longer have any significant negative intensity. The formation constants were also obtained by the treatment of Appendix B and are tabulated in Table 2, together with the values determined calorimetrically (4–7). The calorimetric results suggested that the formation constants depend strongly on the ionic media; for example, in the case of 1 *M* NH_4^+, interaction between NH_4^+ and Br^- is expected. Recognizing such dependence upon the solution composition, the formation constants obtained in this work are fairly consistent with the others. Our analysis does not lead to precise estimates of the errors associated with the formation constants, other than the goodness of fit to the original spectra (Fig. 5).

Can. J. Chem. Downloaded from www.nrcresearchpress.com by 186.148.149.217 on 09/07/12
For personal use only.

TABLE 2. Stepwise stability constants of zinc bromide complexes in DMSO

Parameter	Value			
	1 *M* NH_4^+	0.1 *M* NH_4^+	1 *M* Na^+	This work
log K_1	0.85	1.86	1.56	1.6
log K_2	2.89	3.31	3.11	3.2
log K_3	1.35	1.98	2.05	2.2
log K_4	—	—	—	−0.6

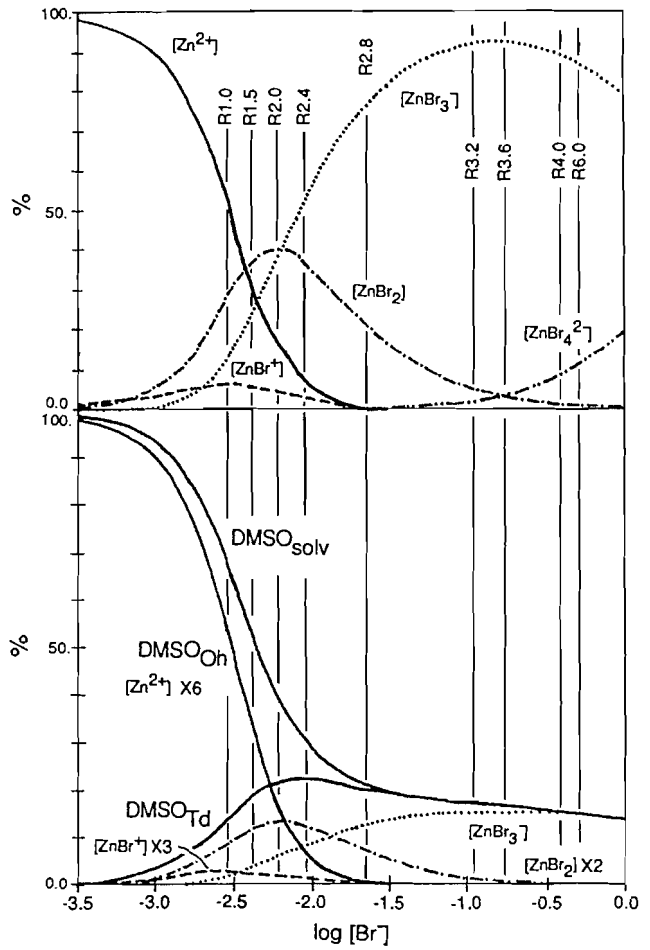


FIG. 8. The calculated concentration distribution of zinc-containing species (upper figure) and the fractions of DMSO molecules solvating the zinc-containing species (lower figure).

Considering errors in base-line construction and signal noise, uncertainties of ±10% would not be unreasonable. Raman spectroscopy is particularly valuable for identifying species and equilibria but lacks the precision available from such methods as potentiometry for quantitative analysis.

Distribution curves for each species are shown in Fig. 8. In the upper panel of Fig. 8, the fractions of each species are plotted versus logarithmic values of the free bromide concentration. Nine vertical lines show the corresponding positions of log $[Br^-]$ of the sample solutions used for this work, labelled with each R value. The figure indicates that the predominant equilibrium is between $ZnBr_2$ and $ZnBr_3^-$ in the range from $R = 2.4$ to 3.2. On the other hand, when log $[Br^-] > -1$, namely $[Br^-] > 0.1$, the contribution from the species $ZnBr_4^{2-}$ becomes important. Ahrland *et al.* reported that $ZnBr_4^{2-}$ is negligible; it was not required in the previous interpretation of the calorimetric data (7, 8). Our results, however, positively suggest the presence of $ZnBr_4^{2-}$. This ion is well characterized in aqueous solutions (20, 24).

Ahrland *et al.* have concluded that the complex with two or more bromide ions is tetrahedral; but $ZnBr^+$ might be octahedral in some ionic media (7, 8). The ~15 cm^{-1} equi-interval shift of Raman bands of successive zinc bromide complexes to lower wavenumbers, as shown in Fig. 7, may suggest that the four complex species have the same coordination; thus $ZnBr^+$ may also be a tetrahedral ion, and only the Zn^{2+} solvated ion is octahedral. The concept that $ZnBr^+$ has tetrahedral coordination is consistent with the earlier report of Ahrland, carried out in 1 *M* NH_4ClO_4 media (4).

The lower panel of Fig. 8 gives the calculated result for the fraction of DMSO molecules solvating zinc ion plotted versus log $[Br^-]$ (*i.e.*, logarithmic values of the free bromide concentration), assuming that free Zn^{2+} ion has octahedral solvation The amount of DMSO octahedrally solvating zinc ion, $DMSO_{O_h}$ of Fig. 8, rapidly decreases and becomes almost zero at $R = 2.8$. The total amount of DMSO molecules tetrahedrally solvating zinc ion, $DMSO_{T_d}$ of Fig. 8, increases with the increase of the R value. Comparing Fig. 2 and Fig. 3 with the lower panel of Fig. 8, the following picture can be imagined: the DMSO which is responsible for the shifted Raman bands, the shaded parts of Fig. 2 and Fig. 3, is octahedrally solvating the "free" zinc ion, not the tetrahedral species. Thus the shaded parts disappear at about $R = 2.8$. This opinion is still speculative, but seems to be reasonable when we consider that any zinc bromide complex has a less positive central charge due to the effect of the negative charge on the attached bromide; and an effective attraction for the electrons of DMSO by the complex becomes weaker than in the case of the di-charged free zinc ion. It is also worth noting that the hexaaquozinc ion gave a Raman signal, but not the bromide-containing complexes (20). Equilibria among Zn^{2+}, $ZnBr^+$, $ZnBr_2$, $ZnBr_3^-$, and $ZnBr_4^{2-}$ explain all the properties of the Raman spectra observed for DMSO solutions.

In conclusion, the Raman spectra of DMSO solutions containing zinc bromide complexes give information about the stepwise formation of the zinc bromide complexes as well as information about the structure arising from the solvating DMSO molecules.

Acknowledgments

This work was supported by grants from the Natural Sciences and Engineering Research Council of Canada and the Office of Naval Research. The assistance of J. Semmler is appreciated.

1. S. AHRLAND and N.-O. BJÖRK. Acta Chem. Scand. A**30**, 249 (1976).
2. S. AHRLAND and N.-O. BJÖRK. Acta Chem. Scand. A**30**, 257 (1976).
3. S. AHRLAND and N.-O. BJÖRK. Acta Chem. Scand. A**30**, 265 (1976).
4. S. AHRLAND, N.-O. BJÖRK, and R. PORTANOVA. Acta Chem. Scand. A**30**, 270 (1976).
5. S. AHRLAND, L. KULLBERG, and R. PORTANOVA. Acta Chem. Scand. A**32**, 251 (1978).
6. M. SANDSTRÖM, I. PERSSON, and S. AHRLAND. Acta Chem. Scand. A**32**, 607 (1978).

Can. J. Chem. Downloaded from www.nrcresearchpress.com by 186.148.149.217 on 09/07/12
For personal use only.

7. S. AHRLAND, N.-O. BJÖRK, and I. PERSSON. Acta Chem. Scand. A35, 67 (1981).
8. S. AHRLAND and I. PERSSON. Acta Chem. Scand. A35, 185 (1981).
9. I. PERSSON. Pure Appl. Chem. 58, 1153 (1986).
10. W. D. HORROCKS, JR. and F. A. COTTON. Spectrochim. Acta, 17, 134 (1961).
11. M.-T. FOREL and M. TRANQUILLE. Spectrochim. Acta, 26A, 1023 (1970).
12. S. ITOH and H. OHTAKI. Z. Naturforsch. 42A, 858 (1987).
13. W. BOL, G. J. A. GERRITIS, and C. L. VAN PANTHALEON VAN ECK. J. Appl. Crystallogr. 3, 486 (1970).
14. G. JOHANSSON. Acta Chem. Scand. 25, 2787 (1971).
15. G. E. MACIEL, L. SIMERAL, and J. J. H. ACKERMAN. J. Phys. Chem. 81, 263 (1977).
16. T. DRAKENBURG, N.-O. BJÖRK, and R. PORTANOVA. J. Phys. Chem. 82, 2423 (1978).
17. H. OHTAKI and G. JOHANSSON. Pure Appl. Chem. 53, 1357 (1981).
18. W. YELLIN and R. A. PLANE. J. Am. Chem. Soc. 83, 2448 (1961).
19. D. E. IRISH. *In* Ionic interactions. *Edited by* S. Petrucci. Academic Press, New York. 1971. Chap. 9. p. 187.
20. M. M. YANG, D. A. CRERAR, and D. E. IRISH. J. Solution Chem. 17, 751 (1988).
21. B. G. ANDERSON and D. E. IRISH. J. Solution Chem. 17, 763 (1988).
22. J. T. BULMER, D. E. IRISH, F. W. GROSSMAN, G. HERRIOT, M. TSENG, and A. J. WEERHEIM. Appl. Spectrosc. 29, 506 (1975).
23. K. MURATA and D. E. IRISH. Bunseki Kagaku. 36, T72 (1987).
24. P. G. GOGGIN, G. JOHANSSON, M. MAEDA, and H. WAKITA. Acta Chem. Scand. A38, 625 (1984).
25. E. R. MALINOWSKI and D. G. HOWERY. Factor analysis in chemistry. Wiley, New York. 1980.
26. T. OZEKI, H. KIHARA, and S. HIKIME. Bunseki Kagaku, 35, 885 (1986).
27. T. OZEKI, H. KIHARA, and S. HIKIME. Anal. Chem. 59, 945 (1987).
28. T. OZEKI, H. KIHARA, S. HIKIME, and S. IKEDA. Anal. Sci. 3, 285 (1987).
29. E. R. MALINOWSKI. Anal. Chem. 49, 612 (1977).
30. T. OZEKI, H. KIHARA, and S. IKEDA. Anal. Chem. 60, 2055 (1988).

Appendix A: General procedure of factor analysis

Factor analysis is a powerful procedure for the analysis of overlapped spectra (25–28). A data matrix **I** is formed from the Raman intensities; in this work nine solutions were prepared and the intensities of 80 wavenumber points were used for each spectrum. All spectra used were normalized at 180 cm^{-1} so as to have constant intensity. The data matrix **I** consists of 80 rows and 9 columns. Each column corresponds to the intensity-normalized (at 180 cm^{-1}) spectrum of each sample solution. A second-moment matrix (sometimes called covariance matrix) **Z** is obtained by multiplication of the data matrix **I** with its transposed matrix $^t\mathbf{I}$.

$$[1] \quad \mathbf{Z} = {}^t\mathbf{I}\,\mathbf{I}$$

Using the Jacobi method, an eigenvalue matrix **E** and an eigenvector matrix **Q** are obtained.

$$[2] \quad \mathbf{Z} = {}^t\mathbf{Q}\,\mathbf{E}\,\mathbf{Q}$$

The eigenvalue matrix **E** will have the same number of rows as **Z**. The number of independent components in the sample spectra, NC, can be obtained from the *IND* function introduced by Malinowski (29) or by checking the original data matrix **I** with the reproduced data matrix **I**′ assuming a proper number of NC.

In the case of NC factors, the eigenvectors corresponding to the NC largest eigenvalues can be taken out and aligned in rows to construct a new matrix **C**, known as the first expression for the concentration matrix. By multiplying the transpose of the concentration matrix **C** with the data matrix **I** a new matrix **R** is obtained, which is known as the spectral matrix.

$$[3] \quad \mathbf{R} = \mathbf{I}^t\mathbf{C}$$

When the spectral matrix **R** is multiplied with the concentration matrix **C**, a theoretical data matrix is reproduced.

$$[4] \quad \mathbf{I}' = \mathbf{R}\,\mathbf{C}$$

The reproducibility of the theoretical data matrix can be examined by calculating the error function *ER*, which is the sum of the squares of the differences of each element of two matrices **I** and **I**′ (26, 27).

$$[5] \quad ER = (\Sigma_i\Sigma_j((\mathbf{I})_{ij} - (\mathbf{I}')_{ij})^2)^{1/2}/(\Sigma_i\Sigma_j((\mathbf{I})_{ij})^2)^{1/2}$$

where $(\mathbf{I})_{ij}$ indicates the element at ith row and jth column of the matrix **I**. The optimum number of factors, NC, can be selected as the number where convergence of *ER* is observed.

In this work *IND* function proposed the presence of three factors; and *ER* function proposed three or four factors as independent factors. From the discussion of the number of complexes in the sample solutions (see text), factor number NC = 4 was adopted. The result from the *IND* function simply implies that the contribution of the peak at 207 cm^{-1} ($ZnBr^+$) to the observed Raman spectra is very small. As a result, a spectral matrix **R** of 80 rows and four columns, and a concentration matrix **C** of four rows and nine columns were obtained. Each column of **R** corresponds to the spectrum of each constituent as shown in Fig. 6, and each row of the concentration matrix **C** corresponds to a concentration distribution of this constituent.

Appendix B: Rotation of bases of R and C based on the equilibria among the species — Application of FAEC (Factor Analysis with Equilibrium Constraints)

The **R** and **C** matrices sometimes contain negative values. The result of Appendix A is such a case. Now the bases of matrices can be rotated to avoid such negative values.

$$[6] \quad \mathbf{R}^0 = \mathbf{R}\,\mathbf{T}_R$$

$$[7] \quad \mathbf{C}^0 = \mathbf{T}_C\,\mathbf{C}$$

If the square rotation matrices $\mathbf{T}_R$ and $\mathbf{T}_C$ have the following relationship,

$$[8] \quad \mathbf{T}_R\,\mathbf{T}_C = \mathbf{U}$$

where **U** is the unit matrix having unit value as diagonal elements and zero value as other elements, the product of $\mathbf{R}^0$ and $\mathbf{C}^0$ remains exactly the same as **I**′ (eq. [4]).

We assume the following equilibrium reaction for the stepwise zinc bromide complex formation:

$$[9] \quad AX_{m-1} + X = AX_m$$

Then, we can express the stepwise formation constant K_m as follows,

$$[10] \quad K_m = [AX_m]/[AX_{m-1}][X]$$

where the relation between the cumulative stability constant β and the stepwise formation constant K_m is expressed as follows,

Can. J. Chem. Downloaded from www.nrcresearchpress.com by 186.148.149.217 on 09/07/12
For personal use only.

[11] $\beta = K_1 K_2 \cdots K_m$

In this work, we assume the presence of four zinc bromide complexes; thus we have four K's. If the values of K's and the total amount of the reagents (zinc ion and bromide ion) are known, the real concentration of each species in each solution, which corresponds to the elements of the true concentration matrix $\mathbf{C}^0$, can be calculated assuming the activity coefficients are unity. The matrix obtained from factor analysis, $\mathbf{C}$, can be related to this $\mathbf{C}^0$ by using the proper rotation matrix $\mathbf{T}_C$ through eq. [7]. The elements of the rotation matrix, $\mathbf{T}_C$, can be obtained by applying the nonlinear least squares method to minimize the following function *LSM* (30).

[12] $LSM = \Sigma_i \Sigma_j ((\mathbf{C}^0)_{ij} - (\mathbf{T}_C \mathbf{C})_{ij})^2$

A set of K values gives one *LSM* value. By iterative refinement of K values so as to give a minimum *LSM* value, finally an optimum set of K's and $\mathbf{T}_C$ is obtained. Thus the optimum matrices $\mathbf{C}^0$ and $\mathbf{R}^0$ are also obtained using eqs. [6]–[8]. As a result, this procedure produced the spectra and the concentration distributions as shown in Fig. 7, as well as a set of formation constants as tabulated in Table 2. As a matter of course, the concentration of the free bromide ion used for the abscissa in Fig. 8 were also determined. For initial values of the parameters, K's, the literature values of Ahrland and Persson were used (8).

Can. J. Chem. Downloaded from www.nrcresearchpress.com by 186.148.149.217 on 09/07/12
For personal use only.

New pentafluorothio(SF_5) alkylsulfonic acids

ROBERT J. WILLENBRING, JAVID MOHTASHAM, R. WINTER, AND GARY L. GARD
Department of Chemistry, Portland State University, Portland, Oregon, U.S.A. 97207-0751

Received February 16, 1989

This paper is dedicated to Professor Ronald J. Gillespie on the occasion of his 65th birthday

ROBERT J. WILLENBRING, JAVID MOHTASHAM, R. WINTER, and GARY L. GARD. Can. J. Chem. **67**, 2037 (1989).

New pentafluorothioalkylsulfonic acids, $F_5SCXHCY_2SO_3H$ (X, Y = H, F), and the corresponding salts have been prepared from pentafluorothioalkyl bromides or olefins with sodium sulfite or sodium bisulfite. The compounds are characterized by ir, nmr (^1H, ^{19}F, ^{13}C), and mass spectra.

Key words: new pentafluorothioalkylsulfonic acids.

ROBERT J. WILLENBRING, JAVID MOHTASHAM, R. WINTER et GARY L. GARD. Can. J. Chem. **67**, 2037 (1989).

On a préparé de nouveaux acides pentafluorothioalkylsulfoniques, $F_5SCXHCY_2SO_3H$ (X, Y = H, F), ainsi que les sels correspondants à partir des bromures de pentafluorothialkyles (ou des oléfines correspondantes) et du sulfite ou du bisulfite de sodium. On a caractérisé les composés par spectroscopies ir, rmn (^1H, ^{19}F et ^{13}C) et de masse.

Mots clés : nouveaux acides pentafluorothio (SF_5) alkylsulfoniques.

[Traduit par la revue]

Introduction

In our continuing efforts in preparing new fluoroalkylsulfonic acids for use as fuel cell electrolytes we have found that pentafluorosulfur fluoroolefins can add the hydrogen sulfite ion in the presence of a free radical initiator to give β-SF_5 – fluoroethyl sulfonic acid salts in low yields. However, a more promising method involved the substitution of β-SF_5 – fluoroethyl bromides with sulfite ion.

Previously, only the pentafluorosulfur sulfonic acids $F_5SCHFSO_3H$ (1), and $F_5SCH_2SO_3H$ (2) have been reported.

Results and discussion

We have found that treatment of $F_5SCXHCY_2Br$ (X, Y = H, F) with sodium sulfite afforded the corresponding salt:

[1] $$F_5SCHXCY_2Br + Na_2SO_3 \xrightarrow{50\%\ CH_3CH_2OH} F_5SCHXCY_2SO_3Na + NaBr$$

In the case where X, Y = H, $F_5SCH{=}CH_2$ was found as a by-product; in this case the sulfite acts as a dehydrohalogenating agent.

The reaction of alkylhalides with sulfite is usually considered a nucleophilic displacement of the halogen by the sulfite ion:

[2] $$F_5SCHXCY_2Br + SO_3^{2-} \rightarrow F_5SCHXCY_2SO_3^- + Br^-$$

An alternate radical anion mechanism has been suggested for similar reactions (3). This would result in the following scheme:

[3] $$F_5SCHXCY_2Br + SO_3^{2-} \rightarrow F_5SCHXCY_2Br^{\cdot-} + SO_3^{\cdot-}$$

[4] $$F_5SCHXCY_2Br^{\cdot-} \rightarrow F_5SCHXCY_2\cdot + Br^-$$

[5] $$SO_3^{2-} + F_5SCHXCY_2\cdot \rightarrow F_5SCHXCY_2SO_3^{2\cdot-}$$

[6] $$F_5SCHXCY_2SO_3^{2\cdot-} + F_5SCHXCY_2Br \rightarrow F_5SCHXCY_2SO_3^- + F_5SCHXCY_2Br^{\cdot-}$$

Extraction of the dried residue, which contained the metal sulfite salt formed in eq. [6] ($F_5SCHXCY_2SO_3Na$) and NaBr, with 100% ethanol did not afford the pure salts, except for the compound where X, Y = H. However, when the solid residue was treated with excess aqueous hydrochloric acid only the sulfonic acids dissolved; the other by-products were removed by filtration.

[7] $$F_5SCHXCY_2SO_3Na + \text{excess } HCl_{(aq)} \rightarrow F_5SCHXCY_2SO_3H + NaCl_{(s)}$$

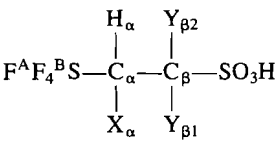
Evaporation of the filtrate left behind sulfonic acid hydrates (or in one case an acid) that were purified by sublimation. In this manner, the two acid hydrates, $F_5SCHFCF_2SO_3H\cdot H_2O$ and $F_5SCH_2CF_2SO_3H\cdot H_2O$, as well as the anhydrous $SF_5CH_2CH_2SO_3H$ were prepared. $F_5SCF_2CF_2Br$ failed to produce the corresponding sulfonic acid in sufficient yield and purity.

As a second method, metal bisulfite addition to SF_5-fluoroolefins in a buffered solution and in the presence of benzoyl peroxide was investigated:

[8] $$F_5SCX{=}CF_2 + NaHSO_3 \xrightarrow{(\phi COO)_2,\ \Delta} F_5SCHXCF_2SO_3Na \qquad X = H, F$$

The yields of these reactions were low; this pathway does not seem to be a useful method for preparing SF_5 containing sulfonic acids.

The nmr spectra of all compounds are in accord with the proposed structures:



X, Y = H, F

In the ^1H nmr spectra of the acids and their salts, it is observed that the chemical shifts of the protons are in the region expected for SF_5 hydrocarbons; the protons are found in the ~4–7 ppm range (4, 5). In three cases the couplings of the equatorial fluorines (SF_4) and the couplings of the aliphatic fluorines to the α protons could be determined; for the rest a complex multiplet was observed. These couplings are in line with the expected values. The acid protons appeared at a strongly deshielded position (>12 ppm) as somewhat broadened singlets.

In the ^{19}F nmr spectra, the SF_5 group was observed as an AB_4 system in all cases. When a CH_2 group is α to the SF_5 group, the chemical shift values are $\phi_A \sim 80$ ppm and $\phi_B \sim 70$ ppm, but with a fluorine atom substituted in the α-CH_2 group these values are shifted to $\phi_A \sim 70$ ppm and $\phi_B \sim 53$ ppm. These results are in agreement with the literature (4, 5). The coupling constants observed for the SF_5 group (J_{AB}) range from 145–150 Hz (4, 5).

Can. J. Chem. Downloaded from www.nrcresearchpress.com by 186.148.149.217 on 09/07/12
For personal use only.

Can. J. Chem. Downloaded from www.nrcresearchpress.com by 186.148.149.217 on 09/07/12
For personal use only.

In the ^{13}C spectra of the acids, the chemical shift sequence of $C_\alpha C_\beta$ in $F_5SC_\alpha C_\beta$ is inverted in going from $F_5SCH_2CH_2SO_3H$ to the two fluorinated acids. The two carbons appear as a pentet and are readily identified by the magnitude of the CB_4 coupling: $J_{C_\alpha B_4}$ = 14–23 Hz and $J_{C_\beta B_4}$ = 0–7 Hz, as established by measuring the ^{13}C spectra of SF_5 and SF_4X compounds (2, 6). In no case was coupling of the axial fluorine of the SF_5 group to either C_α or C_β observed.

The most prominent feature of the infrared spectra for the new compounds are the sulfur–fluorine symmetric and antisymmetric stretching modes in the region from 830 to 885 cm^{-1}. The other major bands are consistent with the assigned structures, with the SO_3 symmetric and antisymmetric modes from 1059 to 1100 cm^{-1} and 1180 to 1280 cm^{-1}, respectively, and the CF-stretching modes appearing at slightly higher frequencies, between 1100 and 1300 cm^{-1}. Because of this overlap, unambiguous assignment of the bands is not possible. The SO_3 scissor and wag vibrational modes are visible at 550 and 570 cm^{-1}.

The mass spectra of $F_5SCH_2CH_2SO_3H$, $F_5SCH_2CF_2SO_3H\cdot H_2O$, and $F_5SCHFCF_2SO_3H\cdot H_2O$ are similar, especially for the lower molecular weight fragments. *m/e* values of 127 (SF_5^+), 108 (SF_4^+), 89 (SF_3^+), 70 (SF_2^+), and 51 (SF^+) provide evidence for the presence of the SF_5 group in all three acids. The SF_3^+ fragment is the base peak in each case, while none of the compounds had a molecular ion. The remainder of the cracking patterns are consistent with the structures assigned to these compounds. The fast atom bombardment technique was used to obtain mass spectra of the sodium salts in a glycerol matrix. Two prominent peaks in all three salts corresponded to a composition MNa^+ and M_2Na^+. The fragmentation pattern was similar to the acids, especially for low molecular weight fragments. The peaks attributable to the SF_5-group are not as apparent, as only the SF_3^+ fragment had an appreciable intensity.

Experimental

General procedure

Gaseous materials were handled in a conventional Pyrex-glass vacuum apparatus. $F_5SC_2H_4Br$, $F_5SCH_2CF_2Br$, $F_5SCHFCF_2Br$, $F_5SCF{=}CF_2$, and $F_5SCH{=}CF_2$ were made according to the literature (7–9). Infrared spectra were obtained by using solid samples between KBr or KRS-5 disks on a Nicolet 20 DX spectrometer. The nmr spectra were recorded with a Varian model EM-390 spectrometer (90 MHz for proton, 84.67 MHz for fluorine). ^{13}C spectra were obtained on a General Electric QE-300 spectrometer operating at 75 MHz. Melting points were determined with a Mel-Temp capillary melting point apparatus and are uncorrected. Mass spectra were taken on a VG 7070 mass spectrometer at 70 eV; perfluorokerosene was the internal standard. Elemental analyses were determined by Beller Mikroanalytisches Laboratorium, Göttingen, West Germany.

1. Synthesis of $F_5SCH_2CH_2SO_3H$

1a. $F_5SCH_2CH_2SO_3Na$ from $F_5SC_2H_4Br$ and Na_2SO_3

In a 250 mL round bottomed flask, fitted with a Frederick condenser, 11.65 g (49.6 mmol) of $F_5SCH_2CH_2Br$, 6.24 g (49.5 mmol) of Na_2SO_3, and 164 mL of 50% aqueous ethanol were gently refluxed with stirring for 72 h. The solvent was removed by evaporation and the residue was transferred to a Soxhlet unit and extracted with 150 mL 100% ethanol. After evaporation of the solvent, 10.0 g of $F_5SCH_2CH_2SO_3Na$ was left behind as a white powder; dec. ≈ 260°C. Yield: 78.4%. A pure sample was obtained by first forming the free acid, subliming and titrating it, as described in Part 1*b*.

^{19}F nmr spectrum (D_2O, $CFCl_3$ ext): AB_4 system (SF_5), ϕ_A = 84.1 ppm (9 lines); ϕ_B = 65.6 ppm (d–m), J_{AB} = 144 Hz, J_{BCH_2} = 7.8 Hz. Int. A:B = 1.0:4.2.

^1H nmr (D_2O, $Si(CH_3)_4$ ext.): δ_1 = 4.58 ppm (m, $F_5SC\underline{H}_2CH_2$); δ_2 = 3.96 ppm (m, $F_5SCH_2\underline{CH}_2$). Int. δ_1:δ_2 = 1.0:1.0.

^{13}C nmr (D_2O, $Si(CH_3)_4$ ext.): δ_α = 65.4 ppm (p); δ_β = 46.9 ppm (p); J_{BC_α} = 15.86 Hz; J_{BC_β} = 4.72 Hz.

Infrared, cm^{-1}: 3040 (w); 2987 (vw); 1443 (w); 1429 (w); 1258 (m); 1226 (vs); 1193 (vs); 1072 (s); 1055 (w); 993 (m); 917 (m); 833 (vs); 809 (m); 612 (m); 574 (s); 565 (m); 550 (m); 531 (m).

Mass spectrum (FAB, *m/e*, species): 539, $(M_2Na)^+$; 537, $(M_2Na - 2H)$; 281, $(MNa)^+$; 171, $(CFHCHSO_3Na_2)^+$; 155, $F_5SC_2H_4^+$; 153, $F_5SC_2H_2^+$; 149, $F_3SCH_2CH_2S^+$; 137, $SC_2HSO_3^+$; 126, $Na_2SO_3^+$; 115, CSO_3Na^+; 105, $C_2HSO_3^+$; 89, SF_3^+; 75, C_2SF^+; 65, CH_2SF^+; 63, CSF^+; 61, $CHSO^+$; 57, C_2HS^+; 45, CHS^+; 44, CS^+.

Anal. calcd. for $C_2H_4F_5NaS_2O_3$: C 9.30, H 1.55, F 36.8, S 24.80; found: C 9.38, H 1.51, F 36.5, S 24.48.

1b Acidification of $F_5SCH_2CH_2SO_3Na$ with HCl

A 200 mL three-necked round bottomed flask containing 19.1 g of the evaporation residue from above (before Soxhlet extraction), dissolvd in ~100 mL of H_2O, was fitted with a reflux condenser and a gas bubbler. Excess HCl was bubbled into the stirred solution. A white precipitate formed and the solution turned yellow. The mixture was filtered, reduced in volume by heating, transferred to a 50 mL round bottomed flask, and dried under vacuum. Sublimation (100°C, <10 μ) left 4.3 g of $F_5SCH_2CH_2SO_3H$ as a colorless crystalline solid; mp 60°C. Yield = 13.0% (with respect to 0.077 mol of starting $SF_5CH_2CH_2Br$). The equivalent weight was 231 g/equiv. (theoretical 236 g/equiv.). The solution was clarified with activated charcoal, filtered, and brought to dryness, leaving pure $F_5SC_2H_4SO_3Na$.

^{19}F nmr (D_2O, $CFCl_3$ ext.): SF_5, ϕ_A = 82.5 ppm (9 lines), ϕ_B = 65.4 ppm (d–m), J_{AB} = 145 Hz. Int. A:B = 1.0:4.1.

^1H nmr (CD_3CN, $Si(CH_3)_4$ ext.): δ = 4.34 ppm (m, $F_5S\underline{CH}_2$), int. = 2.0; δ = 3.94 ppm (m, $F_5SCH_2\underline{CH}_2$), int. = 1.0; δ = 12.1 ppm (s, $SO_3\underline{H}$), int. = 1.0; J_{BH_α} = 7.4 Hz.

^{13}C nmr (D_2O, $Si(CH_3)_4$ ext.): δ_α = 65.4 ppm (p); δ_β = 46.9 ppm (p); J_{BC_α} = 15.9 Hz; J_{BC_β} = 4.7 Hz.

Infrared, cm^{-1}: 3400 (s, br); 2943 (s, br); 1720 (s, br); 1291 (m); 1171 (vs); 1069 (m); 1005 (s); 885 (vs); 851 (vs); 614 (m); 576 (s); 454 (m).

Mass spectrum (CI^+, *m/e*, species): 135, $F_4SC_2H_3^+$; 127, SF_5^+; 111, $FSC_2H_4S^+$; 109, $C_2H_4SO_3H^+$; 89, SF_3^+; 82, CSF_2^+; 81, SO_3H^+; 80, SO_3^+; 70, SF_2^+; 67, SOF^+; 65, SO_2H^+, CH_2SF^+; 64, SO_2^+; 51, SF^+; 48, SO^+; 47, $C_2H_4F^+$, 46, CH_2S^+; 45, CHS^+; 44, CS^+; 43, C_2F^+.

Anal. calcd. for $C_2H_5F_5O_3S_2$: C 10.17, H 2.12, F 40.3, S 27.12; found: C 10.26, H 2.32, F 39.8, S 27.44.

2. Synthesis of $F_5SCH_2CF_2SO_3H\cdot H_2O$

2a $F_5SCH_2CF_2SO_3Na$ from $F_5SCH_2CF_2Br$ and Na_2SO_3

Procedure 1*a* was employed. From 3.81 g (14.1 mmol) of $F_5SCH_2CF_2Br$ and 1.92 g (15.2 mmol) of Na_2SO_3 in 50 mL of 50% aqueous ethanol, 3.5 g of crude $F_5SCH_2CF_2SO_3Na$ was obtained after refluxing for 44 h, filtering, evaporating away the solvent, extracting the solid residue with 100% ethanol, and bringing the solution to dryness, dec. ≈ 279°C. Yield: 85%. A pure sample was obtained by titrating the corresponding acid with NaOH, as described in Part 1*b*.

^{19}F nmr (D_2O, CCl_3F ext.): ϕ_A = 80.0 ppm (9 lines); ϕ_B = 73.2 ppm (d–m), ϕ_{CF_2} = −108.6 ppm (m). Int. A:B:CF_2 = 1.0:3.9:1.9. J_{AB} = 144 Hz; J_{ACF_2} = 2.1 Hz; $J_{CH_2CF_2}$ = 15.2, 17.8 Hz (*gauche* and *anti* coupling).

^1H nmr (D_2O, $Si(CH_3)_4$ ext.): δ = 5.20 ppm.

Mass spectrum (FAB, *m/e*, species): 610, $(M_2Na - H)^+$; 317, MNa^+; 297, $(MNa - HF)^+$; 215, $C_2F_5O_2S_2^+$; 191, $F_5SCH_2CF_2^+$; 171, F_5SCHCF^+; 149, $C_2F_2NaS_2^+$; 137, $SC_2HSO_3^+$; 126, $Na_2SO_3^+$; 115, CSO_3Na^+; 107, $C_2FSO_2^+$; 105, $C_2HSO_3^+$; 89, SF_3^+; 75, C_2SF^+; 65, CH_2SF^+; 63, CSF^+; 61, $CHSO^+$; 57, C_2HS^+; 45, CHS^+; 43, C_2F^+.

Infrared, cm^{-1}: 3116 (w); 3038 (w); 2987 (w); 1656 (m); 1420 (s); 1337 (w); 1267 (vs); 1229 (vs); 1096 (s); 1049 (w); 990 (s); 915 (m);

Can. J. Chem. Downloaded from www.nrcresearchpress.com by 186.148.149.217 on 09/07/12
For personal use only.

898 (m); 856 (vs); 834 (vs); 800 (m); 675 (m); 634 (m); 613 (m); 567 (m); 552 (m); 528 (w).

Anal. calcd. for $C_2H_2F_7NaO_3S_2$: C 8.16, H 0.68, F 45.2, S 21.77; found: C 8.28, H 0.71, F 44.8, S 21.58.

2b Alternate synthesis of $F_5SCH_2CF_2SO_3Na$

Into a 75 mL stainless steel autoclave, 9.7 g (51.1 mmol) of $F_5SCH{=}CF_2$, 5.3 g (51 mmol) of $NaHSO_3$, 1.0 g (2.6 mmol) of $Na_2B_4O_7 \cdot 10H_2O$, 1.5 g (6.2 mmol) of benzoyl peroxide, and 26 mL of distilled water were added. The autoclave was closed, evacuated and heated with shaking (every 15 min) for 18 h to 115°C. The solvent was removed and the residue was extracted with hot ethanol. The extract was dried under vacuum (17 days). The resulting off-white solid (1.2 g) had the same ir spectrum as a sample prepared by method 2*a*. Yield: 7.7%.

2c Acidification of $F_5SCH_2CF_2SO_3Na$ with HCl

In a 100 mL round bottomed flask, 13.16 g (44.8 mmol) of $F_5SCH_2CF_2SO_3Na$ and 40 mL of 12 *M* HCl were added. Since no precipitate was observed, the solution was evaporated to half of its volume, transferred to a 50 mL round bottomed three-necked flask and treated with excess gaseous HCl, as described in Part 1*b*. After filtration, removal of the solvent and sublimation (100°C, $<20\mu$) 8.13 g of $F_5SCH_2CF_2SO_3H \cdot H_2O$ remained. Yield: 62.6%. ^{19}F nmr spectroscopy indicated an impurity, which was removed by treatment with 30% H_2O_2. Thus, 1.7 g of the impure material was stirred (14 days, 40–50°C) with 30% H_2O_2 (2 mL were added every 2 days), leaving after filtration and evaporation of the solvent ~1 g of pure $F_5SCH_2CF_2SO_3H \cdot H_2O$. Equivalent weight was 280 g/equiv. (calcd. 288 g/equiv.). The salt solution was purified as described in Part 1*b*.

^{19}F nmr (D_2O, CCl_3F ext.): ϕ_A = 79.0 ppm (9 lines), ϕ_B = 72.5 ppm (d–m), ϕ_{CF_2} = −110.3 ppm (m). Intensity A:B:CF_2 = 1.0:4.0:2.0; J_{AB} = 150 Hz; J_{ACF_2} = 2.2 Hz; J_{BCH_2} = 7.7 Hz; $J_{CH_2CF_2}$ = 17.4, 15.9 (*gauche* and *anti* coupling).

^1H nmr (CD_3CN, $Si(CH_3)_4$ ext.): δ_1 = 4.78 ppm (CH_2, m); δ_2 = 13.7 ppm (SO_3H, s); δ_3 = 9.2 ppm. Int. δ_1:δ_2:δ_3 = 2.0:1.0:2.0; J_{BH_α} = 8.2 Hz and J_{CF_2H} = 16.3 Hz.

^{13}C nmr (D_2O, $Si(CH_3)_4$ ext.): δ_α = 66.5 ppm (t-p); δ_β = 117.4 ppm (t-p); J_{BC_α} = 17.2 Hz; $J_{C_\alpha CF_2}$ = 20.2 Hz; J_{BC_β} = 2.1 Hz; $J_{C_\beta CF_2}$ = 281.5 Hz.

Infrared, cm^{-1}: 3490 (m, br); 3038 (w); 2988 (w); 1653 (m); 1420 (m); 1296 (m); 1285 (m); 1266 (s); 1229 (vs); 1096 (s); 1054 (m); 991 (s); 909 (m); 896 (m); 855 (s); 834 (vs); 800 (m); 675 (m); 632 (m); 605 (m); 567 (m); 553 (m).

Mass spectrum (CI^+, mass, species): 191, $F_5SCH_2CF_2^+$; 149, $CF_2SO_2H \cdot H_2O^+$; 127, SF_5^+; 89, SF_3^+; 83, F_2SCH^+; 80, SO_3^+; 70, SF_2^+; 65, CH_2SF^+; 64, $CHSF^+$; 63, CSF^+; 61, $CHSO^+$; 57, C_2HS^+; 51, SF^+; 48, SO^+; 45, CHS^+; 44, CS^+.

Anal. calcd. for $C_2H_5F_7O_4S_2$: C 8.28, H 1.72, F 45.9, S 22.07; found: C 8.37, H 1.87, F 45.3, S 22.25.

3. Synthesis of $F_5SCHFCF_2SO_3H$

3a $F_5SCHFCF_2SO_3Na$ from $F_5SCHFCF_2Br$ and Na_2SO_3

Method 1*a* was employed. Thus 23.44 g (81.1 mmol) of $F_5SCHFCF_2Br$ and 10.29 g (81.7 mmol) of Na_2SO_3 in 145 mL 50% aqueous ethanol were refluxed in a 250 mL round bottom flask for 48 h. The extraction of the residue with 100% ethanol gave 19.76 of crude $F_5SCHFCF_2SO_3Na$. Yield; 78.1%. A pure sample was obtained by titration of the free acid with NaOH, as described in Part 1*b*.

^{19}F nmr (D_2O, CCl_3F ext.): ϕ_A = 71.2 ppm; ϕ_B = 53.7 ppm, ϕF_α = −172.7 ppm; $\phi F_{\beta 1}$ = −112.5 ppm; $\phi F_{\beta 2}$ = −123.5 ppm. Int. A:B:F_α:$F_{\beta 1}$:$F_{\beta 2}$ = 1.0:4.0:0.1:0:1.1:1.0. J_{AB} = 147 Hz; J_{AF_α} = 2.6 Hz; $J_{AF_{\beta 1}}$ = 1.7 Hz; $J_{AF_{\beta 2}}$ = 1.7 Hz; J_{BH_α} = 5.1 Hz; $J_{F_\alpha H_\alpha}$ = 41.5 Hz; $J_{BF_{\beta 1}}$ = 15.2 Hz; $J_{BF_{\beta 2}}$ = 11.8 Hz; $J_{F_\alpha F_{\beta 1}}$ = 11.8 Hz; $J_{F_\alpha F_{\beta 2}}$ = 17.3 Hz; $J_{H_\alpha F_{\beta 2}}$ = 20.3 Hz; $J_{F_{\beta 1} F_{\beta 2}}$ = 266.0 Hz.

^1H nmr (D_2O, $Si(CH_3)_4$ ext.): δ = 6.79 ppm.

Infrared, cm^{-1}: 3007 (w); 1653 (m); 1635 (m); 1355 (w); 1285 (vs); 1270 (vs); 1247 (vs); 1154 (s); 1131 (s); 1098 (s); 1008 (vs); 919 (s); 859 (vs); 809 (s); 728 (w); 651 (s); 610 (s); 599 (s); 571 (s); 531 (m).

Mass spectrum (FAB, *m/e*, species): 646, $(M_2Na - H)^+$; 335, MNa^+; 207, $CFCF_2SO_3Na_2^+$; 189, $F_5SC_2F_2^+$; 171, $F_5SC_2HF^+$; 157, $C_2H_2FO_3S_2^+$; 137, $SC_2HSO_3^+$; 126, $Na_2SO_3^+$; 116, $CHSO_3Na^+$; 115, CSO_3Na^+; 114, $CF_2SO_2^+$; 105, $C_2HSO_3^+$; 93, $CHSO_3^+$; 89, SF_3^+; 73, C_2HOS^+, C_2SF^+; 61, $CHOS^+$; 57, C_2HS^+; 45, CHS^+; 44, CS^+; 43, C_2F^+.

Anal. calcd. for $C_2HF_8NaO_3S_2$: C 7.69, H 0.34, F 48.7, S 20.51; found: C 7.82, H 0.38, F 48.8, S 20.64.

3b Alternate synthesis of $F_5SCHFCF_2SO_3Na$

To a 75 mL stainless steel vessel were added 19.4 g (93.3 mmol) of $F_5SCF{=}CF_2$, 9.8 g (94.2 mmol) of $NaHSO_3$, 0.36 g (1.5 mmol) of benzoyl peroxide, 4.4 g (11.5 mmol) of $Na_2B_4O_7 \cdot 10H_2O$, and 38 mL of distilled water. The vessel was sealed with a Whitey (20 V-F4) stainless steel valve, cooled to −196°C, evacuated, and heated from 50 to 114°C (2.4 h) and kept at 114–119°C for 7.5 h. The volatile material ($F_5SCF{=}CF_2$) was removed at room temperature and the aqueous solution was filtered and dried under vacuum. The dry residue (18.9 g) was extracted with hot ethanol, leaving after removal of the solvent, 7.8 g of crude $F_5SCHFCF_2SO_3Na$. The solid was treated with 2.7 g (27.5 mmol) of 100% H_2SO_4 and distilled at reduced pressure. A clear liquid (3.7 g) and a yellow solid were collected at (100–104)°C. This product was re-distilled and gave 1.8 g of $F_5SCHFCF_2SO_3H$, bp 88°C/4μ. Yield: 6.6% (with respect to $F_5SCF{=}CF_2$).

3c Acidification with HCl

This reaction was carried out as previously described in Part 1*b*. To 19.68 g (63.1 mmol) of crude $F_5SCHFCF_2SO_3Na$ dissolved in 100 mL water excess gaseous HCl was added. After filtering and removing the solvent, sublimation (100°C, $<40\mu$) gave 7.14 g of $F_5SCHFCF_2SO_3H \cdot H_2O$. Yield: 36.8%. Equivalent weight was 298 g/equiv. (calcd. 308 g/equiv.). The salt solution was purified as described in 1*b*.

^{19}F nmr (D_2O, CCl_3F ext.): ϕ_A = 71.1 ppm; ϕ_B = 53.0 ppm; ϕF_α = −167.3 ppm; $\phi F_{\beta 1}$ = −113.9 ppm; $\phi F_{\beta 2}$ = −124.9 ppm. Integral A:B:F_α:$F_{\beta 1}$:$F_{\beta 2}$ = 1.0:4.2:1.1:1.0:1.0; J_{AB} = 144 Hz; J_{AF_α} = 2.6 Hz; $J_{AF_{\beta 1}}$ = 1.4 Hz; $J_{AF_{\beta 2}}$ = 1.6 Hz; J_{BH_α} = 5.1 Hz; $J_{BF_{\beta 1}}$ = 15.7 Hz; $J_{BF_{\beta 2}}$ = 11.9 Hz; $J_{F_\alpha H_\alpha}$ = 41.4 Hz; $J_{F_\alpha F_{\beta 1}}$ = 12.7 Hz; $J_{F_\alpha F_{\beta 2}}$ = 16.9 Hz; $J_{F_{\beta 2} H_\alpha}$ = 20.3 Hz; $J_{F_{\beta 1} F_{\beta 2}}$ = 262.0 Hz.

^1H nmr (CH_3CN, $Si(CH_3)_4$ ext.): δ_{H_α} = 6.39 ppm; δ_{SO_3H} = 13.68 ppm; J_{BH_α} = 5.1 Hz; $J_{H_\alpha F_\alpha}$ = 41.4 Hz; $J_{H_\alpha F_{\beta 1}}$ = 20.7 Hz.

^{13}C nmr (D_2O, $Si(CH_3)_4$ ext.): δ_α = 105.6 ppm (d–d–p); δ_β = 114.7 ppm (d–d–d). J_{BC_α} = 22.4 Hz; $J_{F_\alpha C_\alpha}$ = 241.9 Hz; $J_{F_{\beta 1} C_\alpha}$ = 22.2 (36.6) Hz; $J_{F_{\beta 2} C_\alpha}$ = 36.6 (22.2) Hz; J_{BC_β} = 0.0 Hz; $J_{F_\alpha C_\beta}$ = 28.0 Hz; $J_{F_{\beta 1} C_\beta}$ = 294.8 (282.0) Hz; $J_{F_{\beta 2} C_\beta}$ = 282.0 (294.8) Hz.

Infrared, cm^{-1}: 3150 (s, br); 3013 (vw); 2919 (vw); 2851 (vw); 1730 (s, br); 1356 (w); 1269 (s); 1231 (vs); 1132 (s); 1094 (m); 999 (s); 859 (vs); 812 (m); 727 (w); 645 (s); 598 (s); 568 (s); 522 (m); 479 (m); 408 (m).

Mass spectrum (CI^+, *m/e*, fragment): 191, $F_5SC_2H_2F_2^+$; 127, SF_5^+; 89, SF_3^+; 83, $CHSF_2^+$; 82, $CHFCF_2^+$; 81, $C_2F_3^+$, HSO_3^+; 80, SO_3^+; 79, $C_2HF_2O^+$; 70, SF_2^+; 65, HSO_2^+; 64, SO_2^+, $CHFS^+$; 63, $C_2HF_2^+$; 61, $CHOS^+$; 51, SF^+; 49, SOH^+; 48, SO^+; 45, CHS^+; 44, CS^+.

Anal. calcd. for $C_2H_4F_8O_4S_2$: C 7.79, H 1.30, F 49.4, S 20.78; found: C 7.87, H 1.30, F 48.9, S 20.85.

Acknowledgement

We wish to express our appreciation to the Gas Research Institute (5084-260-1085), to the Department of Energy (DE-FG21-88MC25142) for support of this research, and to Megan Lerchen for partial assistance with this project. Dr. G. D. Knerr at the University of Idaho obtained the mass spectra of Dr. D. H. Peyton (Portland State University) obtained the ^{13}C spectra.

1. J. M. Canich, M. M. Ludvig, G. L. Gard, and J. M. Shreeve. Inorg. Chem. **23**, 4403 (1984).
2. R. J. Terjeson, J. Mohtasham, and G. L. Gard. Inorg. Chem. **27**, 2916 (1988).

3. C. WAKSELMAN and C. KAZIZ. J. Fluorine Chem. **33**, 347 (1986).
4. J. M. CANICH, M. M. LUDVIG, W. W. PAUDLER, G. L. GARD, and J. M. SHREEVE. Inorg. Chem. **24**, 3668 (1985).
5. Q. C. MIR, R. DEBUHR, C. HAUG, H. F. WHITE, and G. L. GARD. J. Fluorine Chem. **16**, 373 (1980).
6. R. WINTER, D. H. PEYTON, and G. L. GARD. Inorg. Chem. To be published.
7. C. MERRILL. Ph.D. Thesis. University of Washington, Seattle, WA. 1962; U.S. Patent 3,338,685 (1967).
8. J. STEWARD, L. KEGLEY, H. F. WHITE, and G. L. GARD. J. Org. Chem. **34**, 760 (1969).
9. G. L. GARD. Research Report Sulfur–fluorine chemistry. Allied-Signal Corp. 1968; R. A. DEMARCO and W. B. FOX. J. Fluorine Chem. **12**, 137 (1978).

Can. J. Chem. Downloaded from www.nrcresearchpress.com by 186.148.149.217 on 09/07/12
For personal use only.

Preparations and the crystal structure of $3SbF_3 \cdot 4SbF_5$

JOHN FAWCETT, JOHN H. HOLLOWAY,[1] AND DAVID R. RUSSELL
Department of Chemistry, The University of Leicester, Leicester LE1 7RH, England

AND

ANTHONY J. EDWARDS AND KHALAF I. KHALLOW
Department of Chemistry, The University of Birmingham, P.O. Box 363, Birmingham B15 2TT, England

Received April 18, 1989

This paper is dedicated to Professor Ronald J. Gillespie on the occasion of his 65th birthday

JOHN FAWCETT, JOHN H. HOLLOWAY, DAVID R. RUSSELL, ANTHONY J. EDWARDS, and KHALAF I. KHALLOW. Can. J. Chem. **67**, 2041 (1989).

$3SbF_3 \cdot 4SbF_5$ has been prepared from the reaction of SbF_3 with a large excess of SbF_5 and from the reaction of WF_5 with SbF_5 in Genetron 113. An X-ray structure determination has shown that the compound crystallizes in the monoclinic space group $P2_1/c$ with $a = 8.547(10)$, $b = 13.521(8)$, $c = 19.551(12)$ Å, $\beta = 100.3(1)°$, $Z = 4$ with the final residual indices of $R = 0.0486$ and $R_w = 0.0526$ for 4274 unique reflections. If only Sb—F distances of less than 2.1 Å are considered the structure can be viewed in terms of the arrangement $(SbF^{2+})(SbF_2^+)_2(SbF_6^-)_4$. A Raman spectrum from single crystals of the compound is reported.

Key words: X-ray, structure, antimony, fluoride, Raman.

JOHN FAWCETT, JOHN H. HOLLOWAY, DAVID R. RUSSELL, ANTHONY J. EDWARDS et KHALAF I. KHALLOW. Can. J. Chem. **67**, 2041 (1989).

On a préparé le $3SbF_3 \cdot 4SbF_5$ en faisant réagir du SbF_3 avec un large excès de SbF_5 ou en faisant réagir du WF_5 avec du SbF_5 dans du Genetron 113. Faisant appel à la diffraction des rayons-X, on a démontré que le composé cristallise dans le groupe d'espace monoclinique, $P2_1/c$, avec $a = 8,547(10)$, $b = 13,521(8)$ et $c = 19,551(12)$ Å, $\beta = 100,3(1)°$ et $Z = 4$ avec des indices résiduels finals de $R = 0,0486$ et $R_w = 0,0526$ pour 4274 réflexions uniques. Si on ne considère que les distances Sb—F de moins que 2,1 Å, on peut considérer la structure en fonction de l'arrangement $(SbF^{2+})(SbF_2^+)_2(SbF_6^-)_4$. On rapporte le spectre Raman effetué sur des cristaux uniques du composé.

Mots clés : rayons-X, structure, antimoine, fluorure, Raman.

[Traduit par la revue]

Introduction

Ruff and Plato (1) reported an exothermic reaction between SbF_3 and SbF_5. Distillation of the products yielded adducts of the type $nSbF_3 \cdot SbF_5$, in which n was equal to 2 or 5 and possibly 3 or 4. No evidence for a 1:1 compound was obtained. Some years later Woolf (2) reported that SbF_3 was insoluble in SbF_5 and did not increase the conductivity of the pentafluoride, and Davies and Moss (3) were unable to repeat the work of Ruff and Plato, reporting that SbF_3 did not react with SbF_5, even on heating. More recently, Gillespie *et al.* (4) showed that SbF_5 reacts with SbF_3 or antimony metal in liquid sulphur dioxide to form two adducts with different Raman spectra which, on the basis of elemental analysis, were assigned a 1:1 stoichiometry and designated $SbF_3 \cdot SbF_5$(A) and $SbF_3 \cdot SbF_5$(B). These two adducts were not interconvertible and Raman and ^{121}Sb Mössbauer spectra suggested that they had different structures.

In 1974 Edwards and Slim (5) prepared $6SbF_3 \cdot 5SbF_5$ by the direct fluorination of elemental antimony and determined its X-ray structure. Simultaneously, Hewitt *et al.* (6) prepared the same material in a similar reaction and characterised it from the unit cell parameters obtained from single crystals. Raman spectra from single crystals were similar to those of Gillespie's $SbF_3 \cdot SbF_5$(B) and it was suggested that $SbF_3 \cdot SbF_5$(B) was, in fact, Edwards' $6SbF_3 \cdot 5SbF_5$. Very recently, in the course of a study of the reduction of $SbF_3 \cdot SbF_5$(A), Nandana *et al.* (7) obtained single crystals of an adduct whose Raman spectrum was identical to that of $SbF_3 \cdot SbF_5$(B) and similar to, but distinct from, that reported by Hewitt *et al.* (6). Determination of the single crystal structure has shown that this adduct also has the stoichiometry $6SbF_3 \cdot 5SbF_5$, hereafter called β-$6SbF_3 \cdot 5SbF_5$, with a different, but related structure to Edwards' $6SbF_3 \cdot 5SbF_5$, hereafter called α-$6SbF_3 \cdot 5SbF_5$.

In the meantime the adduct $SbF_3 \cdot SbF_5$(A) has been isolated from the products of reaction of antimony pentafluoride with S_4N_4, and the stoichiometry established as correct from an X-ray single-crystal structure determination (8). Raman spectra of the single crystals and bulk $SbF_3 \cdot SbF_5$(A) were shown to be identical.

The complexity of the SbF_3–SbF_5 system has been illustrated further by the identification of $5SbF_3 \cdot 3SbF_5$ (9), $2SbF_3 \cdot SbF_5$ (10), and $3SbF_3 \cdot SbF_5$ (11) by single crystal methods. A feature all of the adducts reported previously have in common is a stoichiometric ratio of SbF_3 to SbF_5 equal to or greater than 1.

We have now obtained the first example of an adduct containing more SbF_5 than SbF_3 by two preparative methods. An X-ray single-crystal structure determination has confirmed the $3SbF_3 \cdot 4SbF_5$ formulation and shown that the structure is best regarded as $[SbF]^{2+}[SbF_2]_2^+[SbF_6]_4^-$. A Raman spectrum of single crystals of the compound has been obtained.

Experimental

Reagents

Antimony pentafluoride was prepared by passing F_2 over antimony powder (Technical grade, BDH) in a nickel boat in a quartz system. The crude SbF_5 was purified in a Pyrex system by trap-to-trap sublimation under static vacuum. Antimony trifluoride (98%, BDH) was resublimed under dynamic vacuum prior to use. Genetron 113 (1,1,2-trichlorotrifluoroethane) (Fluka A.G.) was purified by distillation from P_2O_5.

[1]To whom correspondence should be addressed.

Can. J. Chem. Downloaded from www.nrcresearchpress.com by 186.148.149.217 on 09/07/12
For personal use only.

Can. J. Chem. Downloaded from www.nrcresearchpress.com by 186.148.149.217 on 09/07/12
For personal use only.

Preparations

$3SbF_3 \cdot 4SbF_5$ was obtained either from the solid product resulting from the removal of excess of SbF_5 from the mixture remaining after the treating of SbF_3 with a large excess of SbF_5 for at least 48 h, or from the reaction of a 2:1 molar ratio of SbF_5 and WF_5 in Genetron after the removal of volatiles and solvent. The latter reaction appears to take place according to reaction [1].

[1] $6WF_5 + 7SbF_5 \rightarrow 3SbF_3 \cdot 4SbF_5 + 6WF_6$

Characterizations

The products were characterized by single-crystal X-ray structure analysis since chemical analysis of the white powders resulting from the preparations gave total antimony ~60 and fluorine ~39.5%. These values are similar to theoretical percentages of antimony and fluorine in the adducts $SbF_3 \cdot 2SbF_5$, $3SbF_3 \cdot 5SbF_5$, and $3SbF_3 \cdot 4SbF_5$ which are Sb 59.6, F 40.4; Sb 60.2, F 39.8; and Sb 60.7, F 39.3 respectively. Raman spectra were recorded using a Coderg T800 spectrometer. The exciting radiation was the blue line (4880 Å) of a Model 52 Coherent Radiation Laboratories argon-ion laser.

X-ray crystallographic analysis

Crystal data for $F_{29}Sb_7$ are as follows:

$F_{29}Sb_7$ mw = 1403.19

Monoclinic, $P2_1/c$, $a = 8.547(10)$, $b = 13.521(8)$, $c = 19.551(12)$ Å, $\beta = 100.3(1)°$, $V = 2223.3$ Å^3, $Z = 4$, $D_x = 4.19$ g cm^{-3}, μ(Mo-K_α) = 80.05 cm^{-1}, λ(Mo-K_α) = 0.71069 Å, $F(000)$ = 2471.2.

Single crystals were obtained both from the reaction of SbF_3 with SbF_5 and the reaction of SbF_5 with WF_5. The reported structure determination was carried out on crystals from the latter preparation. Crystals were transferred in an inert atmosphere to preseasoned (ClF_3) capillaries. The crystals were colourless, air-sensitive rhomboids of dimensions (distances to faces from centre, 0.162 (1 0 0, $\bar{1}$ 0 0) × 0.093 (0 1 1, 0 $\bar{1}$ $\bar{1}$) × 0.083 (0 1 $\bar{7}$, 0 $\bar{1}$ 7) mm).

The unit cell dimensions of the crystal were determined from an oscillation photograph for the rotation axis ***a***, and from the optimized counter angles of zero and upper layer reflections on a Weissenberg camera for ***b*** and ***c***. The intensities of 5210 unique reflections ($7 \leq 2\theta \leq 60$, $+h +k \pm l$) were measured at 20°C on a Stoe STADI-2 Weissenberg diffractometer using an ω-scan technique. The data were corrected for Lorentz and polarisation effects. An absorption correction (maximum, minimum transmission factors = 0.37, 0.21) was applied to the data, giving 4274 reflections with $I \geq 3\sigma(I)$.

The structure was solved by direct methods using the program MULTAN (12) to locate the antimony atoms, and then difference Fourier techniques using the program system SHELX (13). Neutral atom scattering factors and corrections for anomalous dispersion were used as described in ref. 13. Full-matrix least-squares refinement of positional and isotropic thermal parameters for all atoms reduced R to 0.098. Final cycles, with all atoms anisotropic, employed a weighting parameter $g(0.002\ 26)\{\omega\alpha[1/\sigma^2(F) + gF^2]\}$ and gave the final residual indices R $\{= \Sigma||F_o| - |F_c||/\Sigma|F_o|\}$ 0.0486 and R' $\{= [\Sigma\omega(|F_o| - |F_c|)^2/\Sigma\omega|F_o|^2]^{1/2}\}$ 0.0526. A final difference Fourier was featureless except for peaks of ≤3*e* at ≤1.0 Å from the antimony atoms. An analysis of the weighting scheme over $|F_o|$ and $(\sin\theta)/\lambda$ was satisfactory.

Positional parameters are given in Table 1. Bond distances and angles are listed in Table 2. Thermal parameters and tables of calculated and observed structure factors have been deposited as supplementary material.[2]

TABLE 1. Fractional atomic co-ordinates for Sb_7F_{29}

Atom	*x*	*y*	*z*
Sb(1)	1.01218(9)	0.75489(5)	0.12717(4)
Sb(2)	1.44405(8)	0.76096(5)	0.25261(4)
Sb(3)	1.11366(9)	1.05941(5)	0.14033(4)
Sb(4)	1.12638(8)	0.47865(5)	0.12898(4)
Sb(5)	0.66460(8)	0.53438(5)	0.11734(4)
Sb(6)	0.65467(8)	0.97298(5)	0.11433(4)
Sb(7)	0.43602(9)	0.74980(5)	−0.00372(4)
F(1)	1.0075(9)	0.7766(6)	0.2188(4)
F(2)	1.2837(7)	0.7567(5)	0.1681(3)
F(3)	1.1029(9)	0.9192(5)	0.1239(5)
F(4)	1.0984(8)	0.6016(5)	0.1749(4)
F(5)	0.8014(7)	0.6542(5)	0.1267(4)
F(6)	0.7968(8)	0.8561(5)	0.1208(4)
F(7)	0.8850(8)	1.0447(5)	0.1421(4)
F(8)	0.8962(7)	0.4647(5)	0.1273(4)
F(9)	0.4796(8)	0.6562(5)	0.0703(3)
F(10)	0.4749(8)	0.8516(5)	0.0650(3)
F(11)	1.3373(11)	0.6580(6)	0.2864(4)
F(12)	1.5632(10)	0.6677(7)	0.2132(4)
F(13)	1.5419(11)	0.8599(7)	0.2097(5)
F(14)	1.3194(10)	0.8565(7)	0.2857(4)
F(15)	1.5968(9)	0.7697(6)	0.3327(4)
F(16)	1.3290(9)	1.0544(5)	0.1370(5)
F(17)	1.1472(10)	1.0272(7)	0.2347(5)
F(18)	1.0982(10)	1.1896(5)	0.1602(5)
F(19)	1.0583(12)	1.0816(7)	0.0460(5)
F(20)	1.3462(8)	0.5012(6)	0.1356(5)
F(21)	1.1567(9)	0.4225(6)	0.2161(4)
F(22)	1.1188(10)	0.3650(5)	0.0790(5)
F(23)	1.0790(10)	0.5599(6)	0.0522(4)
F(24)	0.6735(10)	0.5321(5)	0.0228(4)
F(25)	0.6774(10)	0.9811(5)	0.0215(4)
F(26)	0.3942(10)	0.8451(5)	−0.0741(4)
F(27)	0.2241(10)	0.7515(6)	0.0095(5)
F(28)	0.6484(9)	0.7509(5)	−0.0086(4)
F(29)	0.3947(10)	0.6462(5)	−0.0681(4)

Results and discussion

The preparation of $3SbF_3 \cdot 4SbF_5$ was achieved both by heating SbF_3 with a large excess of SbF_5 (contrary to the report of Davies and Moss (3)) in a rigorously dried Pyrex glass apparatus for 2 days and from the reaction of WF_5 with SbF_5 in Genetron 113.

The atomic arrangement in the structure of $3SbF_3 \cdot 4SbF_5$ is shown in Fig. 1. If only Sb—F distances of less than 2.1 Å are considered, then the arrangement corresponds to $(SbF^{2+})(SbF_2^+)_2(SbF_6^-)_4$. Sb(1) has a bond distance to F(1) of 1.82 Å defining the SbF^{2+} cation. This distance is shorter than those in SbF_3 (14) of 1.90 and 1.94 Å.

The two SbF_2 units are defined by Sb(5), F(5), F(24) and Sb(6), F(6), F(25). The mean Sb—F distance in both SbF_2 units (1.92 Å) is similar to that in the SbF_2 unit in the $Sb_{11}F_{43}$ adduct (5, 15*a*) (1.9 Å). Both are V-shaped as expected from VSEPR Theory (16) for two bond pairs and a lone pair of electrons around antimony. Consideration of the bond distances and bond angle, as shown in Table 3, shows that the SbF_2 units in Sb_7F_{29} adduct are comparable with those found in $6SbF_3 \cdot 5SbF_5$ (5).

The four $[SbF_6^-]$ anions, centred on Sb(2), Sb(3), Sb(4), and Sb(7), show slight angular distortion from a regular octahedral arrangement. However, the mean of the terminal Sb(V)—F distances in these octahedra is comparable with those present in the octahedral units in the $SbF_3 \cdot SbF_5$ adducts as shown in Table 4.

The octahedron [Sb(2)—F_6] possesses a bridging fluorine

[2]A complete set of data can be purchased from the Depository of Unpublished Data, CISTI, National Research Council of Canada, Ottawa, Ont., Canada K1A 0S2.

Can. J. Chem. Downloaded from www.nrcresearchpress.com by 186.148.149.217 on 09/07/12
For personal use only.

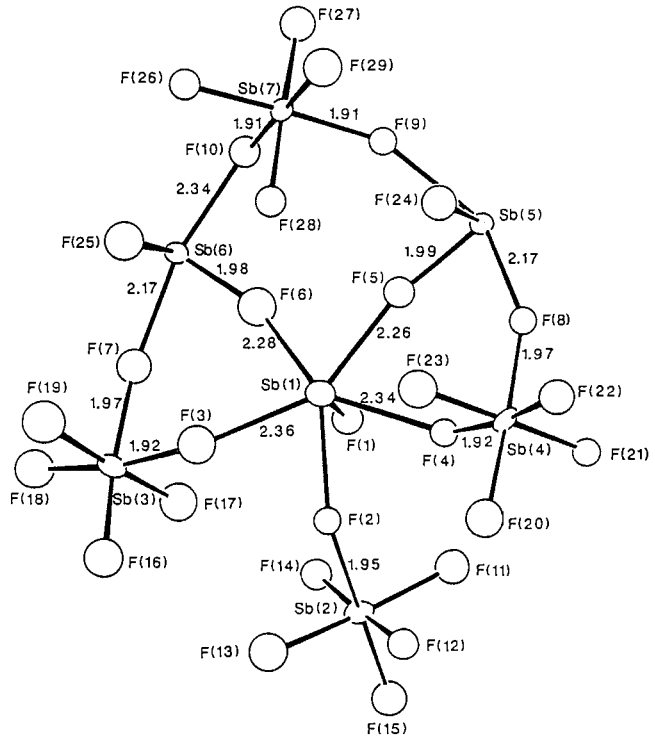


FIG. 1. The atomic arrangement in the structure of $3SbF_3 \cdot 5SbF_5$.

atom, F(2), with a distance of 1.95 Å which is significantly longer than the other Sb(2)—F distances due to the bridging interaction with the Sb(1) atom. Sb(3) and Sb(4) are both linked to the [Sb(1)—F^{2+}] ion via F(3) and F(4), respectively. The Sb(3) atom is also linked to the [Sb(6)—F_2^+] ion through the bridging fluorine atom F(7), while Sb(4) is linked to the [Sb(5)—F_2^+] ion by F(8). The bridge distances Sb(4)—F(4) of 1.92 Å and Sb(4)—F(8) of 1.97 Å are significantly longer than the other Sb(4)—F distances in the octahedra due to the bridging interactions with Sb(1) and Sb(5), respectively.

A similar phenomenon occurs with the Sb(7) atom. This has two bonds, Sb(7)—F(9) of 1.91 Å and Sb(7)—F(10) of 1.91 Å longer than the other non-bridging Sb(7)—F bonds.

All the angles F—Sb—F between *cis* fluorine atoms in the four distorted octahedral anions are in the range 80.6 to 98.9°. This is reasonably close to the 90° for a regular octahedron.

If the Sb—F distances less than 2.5 Å are now considered, no extra bonds to the SbF_6^- units are found. In addition to Sb(1)—F(1), there are five other bonds to Sb(1). These are to F(2), F(3), F(4), F(5), and F(6) which have bond lengths between 2.25 and 2.35 Å. These five atoms are coplanar with $\bar{x}$.20 Å. If the short bond is denoted by X, and the others by Y, Sb(1) can be regarded as having an AXY_5E stereochemistry in the form of a pentagonal bipyramid. F(1) and the lone pair of electrons (E) occupy the axial positions. VSEPR theory (16, 17) predicts that the bonds in the equatorial plane of a pentagonal bipyramid should be longer than the axial bonds. This is, in fact, observed in the [Sb(1)F_6] unit. The F(1)—Sb(1)—F angles are all less than 90°, as shown in Table 2, due to the greater repulsive effect of a lone pair of electrons over that of the bond pair; hence the equatorial plane is displaced towards F(1). The angles between adjacent fluorine atoms in the equatorial plane are close to 72°, which is the angle for a regular pentagon.

This arrangement has been previously recognised for one Sb atom in the [$Sb_2F_4^{2+}$] ion in the 1:1 $SbF_3 \cdot SbF_5$ adduct (8) and

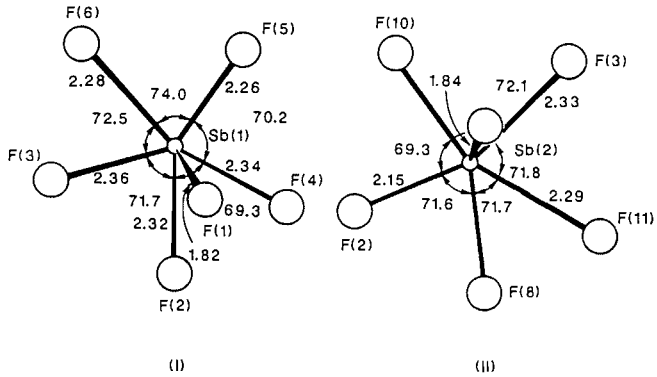


FIG. 2. (*I*) Projection of Sb(1)F_6 unit along the *c*-axis, (*II*) projection of Sb(2)F_6 unit along the *a*-axis in $(Sb_2F_4)^{2+}$ (8).

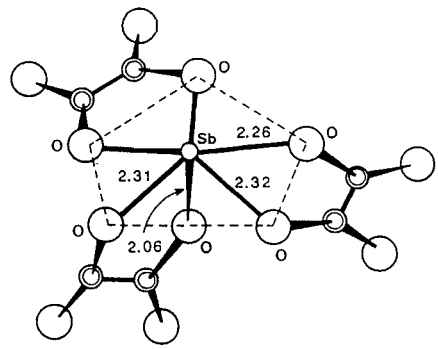


FIG. 3. A projection view of $[Sb(C_2O_4)_3]^{3-}$.

these are compared diagrammatically in Fig. 2. In Fig. 2(*II*) the axial bond length of 1.84 Å is similar to the Sb(1)—F(1) bond length of 1.82 Å in Fig. 2(*I*), while the five equatorial bonds in the range 2.10 to 2.42 Å in Fig. 2(*II*) are close to those of Sb(1)—F between 2.25 to 2.35 Å. The mean angles between the adjacent atoms in equatorial positions in both structures are the same (71.5 and 71.1°), as are the mean F(axial)—Sb—F(equatorial) angles (82.5° (Fig. 2(*I*)) and 82.3° (Fig. 2(*II*)). A similar arrangement has been observed for the $[Sb(C_2O_4)_3]^{3-}$ ion (18) which is also a pentagonal bipyramid. One oxalate group lies in the mirror plane with its two coordinated oxygen atoms bridging one equatorial and one axial site. The other two oxalate groups are mirror related and lie approximately in the equatorial plane, as shown in Fig. 3, with its vacant axial site filled by the non-bonding pair of electrons. The equatorial bond angles at antimony are all in the range 70–72° and are similar to those in Sb_7F_{29} in Fig. 2(*I*). It is interesting to note that the axial Sb—O bond length of 2.06 Å, although longer than that of Sb(1)—F(1) (1.82 Å), is still significantly shorter than the equatorial values which lie between 2.25 and 2.35 Å.

As well as 2 Sb—F distances of less than 2.1 Å, Sb(5) and Sb(6) each have two other bonds between 2.1 and 2.35 Å in length. A similar coordination is found for the iodine atom in $(IF_4^+)(Sb_2F_{11}^-)$ (19) which has two long and two short distances and a lone pair of electrons around the iodine atom. The two long bonds to Sb(5) of 2.17 and 2.35 Å, respectively, are comparable with those to Sb(6) of 2.17 and 2.34 Å, respectively. The antimony atom in these [SbF_4] units can be considered to possess a distorted trigonal bipyramidal coordination of four fluorine atoms and a lone pair of electrons. The lone-pair occupies an equatorial position in the trigonal bipyramid as is expected from VSEPR theory (16). The atoms F(8) and F(9) occupy the axial positions about Sb(5), whilst F(5)

TABLE 2. Bond lengths (Å) and bond angles (deg) for Sb_7F_{29}

Bond	Length	Bond	Length
F(1)—Sb(1)	1.822(7)	F(2)—Sb(1)	2.316(6)
F(3)—Sb(1)	2.357(7)	F(4)—Sb(1)	2.337(6)
F(5)—Sb(1)	2.257(6)	F(6)—Sb(1)	2.279(6)
F(2)—Sb(2)	1.950(6)	F(11)—Sb(2)	1.850(7)
F(12)—Sb(2)	1.872(7)	F(13)—Sb(2)	1.856(8)
F(14)—Sb(2)	1.862(7)	F(15)—Sb(2)	1.855(7)
F(3)—Sb(3)	1.923(7)	F(7)—Sb(3)	1.971(7)
F(16)—Sb(3)	1.855(7)	F(17)—Sb(3)	1.867(9)
F(18)—Sb(3)	1.813(7)	F(19)—Sb(3)	1.844(9)
F(4)—Sb(4)	1.924(7)	F(8)—Sb(4)	1.971(6)
F(20)—Sb(4)	1.885(7)	F(21)—Sb(4)	1.840(7)
F(22)—Sb(4)	1.815(8)	F(23)—Sb(4)	1.845(7)
F(5)—Sb(5)	1.987(6)	F(8)—Sb(5)	2.169(6)
F(9)—Sb(5)	2.354(6)	F(24)—Sb(5)	1.863(7)
F(6)—Sb(6)	1.984(6)	F(7)—Sb(6)	2.174(7)
F(10)—Sb(6)	2.336(6)	F(25)—Sb(6)	1.862(8)
F(9)—Sb(7)	1.908(6)	F(10)—Sb(7)	1.911(6)
F(26)—Sb(7)	1.872(7)	F(27)—Sb(7)	1.875(8)
F(28)—Sb(7)	1.835(8)	F(29)—Sb(7)	1.874(7)

Bonds	Angle	Bonds	Angle
F(2)—Sb(1)—F(1)	81.7(3)	F(3)—Sb(1)—F(1)	86.5(3)
F(3)—Sb(1)—F(2)	71.7(2)	F(4)—Sb(1)—F(1)	79.1(3)
F(4)—Sb(1)—F(2)	69.3(2)	F(4)—Sb(1)—F(3)	139.9(3)
F(5)—Sb(1)—F(1)	86.8(3)	F(5)—Sb(1)—F(2)	139.3(2)
F(5)—Sb(1)—F(3)	146.5(2)	F(5)—Sb(1)—F(4)	70.2(2)
F(6)—Sb(1)—F(1)	78.3(3)	F(6)—Sb(1)—F(2)	139.7(2)
F(6)—Sb(1)—F(3)	72.5(2)	F(6)—Sb(1)—F(4)	138.4(3)
F(6)—Sb(1)—F(5)	74.0(3)	F(11)—Sb(2)—F(2)	87.9(3)
F(12)—Sb(2)—F(2)	89.0(3)	F(12)—Sb(2)—F(11)	88.8(4)
F(13)—Sb(2)—F(2)	86.7(3)	F(13)—Sb(2)—F(11)	174.1(4)
F(13)—Sb(2)—F(12)	88.7(5)	F(14)—Sb(2)—F(2)	87.4(3)
F(14)—Sb(2)—F(11)	92.8(5)	F(14)—Sb(2)—F(12)	176.0(4)
F(14)—Sb(2)—F(13)	89.4(5)	F(15)—Sb(2)—F(2)	178.0(3)
F(15)—Sb(2)—F(11)	93.7(3)	F(15)—Sb(2)—F(12)	92.2(4)
F(15)—Sb(2)—F(13)	91.7(4)	F(15)—Sb(2)—F(14)	91.3(4)
F(7)—Sb(3)—F(3)	83.4(3)	F(16)—Sb(3)—F(3)	88.6(3)
F(16)—Sb(3)—F(7)	172.1(3)	F(17)—Sb(3)—F(3)	86.0(4)
F(17)—Sb(3)—F(7)	86.3(4)	F(17)—Sb(3)—F(16)	92.8(4)
F(18)—Sb(3)—F(3)	172.1(3)	F(18)—Sb(3)—F(7)	89.0(3)
F(18)—Sb(3)—F(16)	98.9(4)	F(18)—Sb(3)—F(17)	91.0(4)
F(19)—Sb(3)—F(3)	89.8(4)	F(19)—Sb(3)—F(7)	87.5(4)
F(19)—Sb(3)—F(16)	92.9(4)	F(19)—Sb(3)—F(17)	172.9(4)
F(19)—Sb(3)—F(18)	92.4(4)	F(8)—Sb(4)—F(4)	83.3(3)
F(20)—Sb(4)—F(4)	91.9(3)	F(20)—Sb(4)—F(8)	175.2(3)
F(21)—Sb(4)—F(4)	86.2(3)	F(21)—Sb(4)—F(8)	87.2(3)
F(21)—Sb(4)—F(20)	91.7(4)	F(22)—Sb(4)—F(4)	170.6(3)
F(22)—Sb(4)—F(8)	88.3(3)	F(22)—Sb(4)—F(20)	96.5(4)
F(22)—Sb(4)—F(21)	97.7(4)	F(23)—Sb(4)—F(4)	80.6(3)
F(23)—Sb(4)—F(8)	88.3(3)	F(23)—Sb(4)—F(20)	91.8(4)
F(23)—Sb(4)—F(21)	166.5(4)	F(23)—Sb(4)—F(22)	94.8(4)
F(8)—Sb(5)—F(5)	80.4(2)	F(9)—Sb(5)—F(5)	78.9(2)
F(9)—Sb(5)—F(8)	151.4(2)	F(24)—Sb(5)—F(5)	88.7(3)
F(24)—Sb(5)—F(8)	83.3(3)	F(24)—Sb(5)—F(9)	76.6(3)
F(7)—Sb(6)—F(6)	79.8(3)	F(10)—Sb(6)—F(6)	79.4(3)
F(10)—Sb(6)—F(7)	156.3(3)	F(25)—Sb(6)—F(6)	86.5(3)
F(25)—Sb(6)—F(7)	88.3(3)	F(25)—Sb(6)—F(10)	79.3(3)
F(10)—Sb(7)—F(9)	87.6(3)	F(26)—Sb(7)—F(9)	178.0(3)
F(26)—Sb(7)—F(10)	90.4(3)	F(27)—Sb(7)—F(9)	88.0(3)
F(27)—Sb(7)—F(10)	86.9(3)	F(27)—Sb(7)—F(26)	91.8(4)
F(28)—Sb(7)—F(9)	89.1(3)	F(28)—Sb(7)—F(10)	88.9(3)
F(28)—Sb(7)—F(26)	90.9(4)	F(28)—Sb(7)—F(27)	175.0(4)
F(29)—Sb(7)—F(9)	90.1(3)	F(29)—Sb(7)—F(10)	177.4(3)

Can. J. Chem. Downloaded from www.nrcresearchpress.com by 186.148.149.217 on 09/07/12
For personal use only.

TABLE 2 (*concluded*)

Bonds	Angle	Bonds	Angle
F(29)—Sb(7)—F(26)	91.9(3)	F(29)—Sb(7)—F(27)	91.8(4)
F(29)—Sb(7)—F(28)	92.3(4)	Sb(2)—F(2)—Sb(1)	143.3(3)
Sb(3)—F(3)—Sb(1)	158.6(4)	Sb(4)—F(4)—Sb(1)	129.5(4)
Sb(5)—F(5)—Sb(1)	161.5(4)	Sb(6)—F(6)—Sb(1)	164.0(4)
Sb(6)—F(7)—Sb(3)	153.7(4)	Sb(5)—F(8)—Sb(4)	148.4(3)
Sb(7)—F(9)—Sb(5)	141.9(3)	Sb(7)—F(10)—Sb(6)	144.6(3)

TABLE 3. Sb—F bond distances and F—Sb—F bond angles in SbF_2 units in Sb_4F_{29} and $6SbF_3 \cdot 5SbF_5$

Atom	Sb—F distance (Å)	F—Sb—F angle (deg)	Reference
Sb(5)	1.99	88.7	This work
	1.86		
Sb(6)	1.98	86.5	This work
	1.86		
Sb(2)	1.93	89.0	5, 10
	1.88		
Sb(3)	1.96		5, 10
	2.01	91.0	

TABLE 4. Sb^V—F distances in $SbF_3 \cdot SbF_5$ adducts

$SbF_3 \cdot SbF_5$	Sb^V—F (terminal) (average)	Reference
1:1	1.87	8
6:5	1.84	5, 10
2:1	1.85	10
3:1	1.87	11
3:4	1.86	This work

and F(24) are in the equatorial positions. Similarly, F(6) and F(25) are coordinated with Sb(6) in the equatorial positions with F(7) and F(10) in the axial positions.

The repulsion caused by the lone pair-bond pair interaction results in a decrease in the angles between the equatorial bonds from 120 to 88.7° for Sb(5) and 86.5° for Sb(6), and from 180 to 151.4° for Sb(5) and 156.3° for Sb(6) for the axial bonds. These are similar to the corresponding angles in the [Sb(2)F_4] unit in $Sb_{11}F_{43}$ (5, 10) the [Sb(1)F_4] unit in the $2SbF_3 \cdot SbF_5$ adduct (10), the (AsF_2^+) ion in the $AsF_3 \cdot SbF_5$ adduct (20) and the [AsF_4^-] ion in KAs_2F_7 (21).

The bridge formed by F(8) is asymmetric, Sb(4)—F(8) = 1.97 Å and Sb(5)—F(8) = 2.17 Å. Similarly, on the other side of the structure in the asymmetric bridge formed by F(7), Sb(3)—F(7) = 1.97 Å and Sb(6)—F(7) = 2.17 Å. The structural arrangement in the fragments [F_5Sb(4)—F(8)—Sb(5)] and [F_5Sb(3)—F(7)—Sb(6)] is comparable with the [F_5Sb(6)—F(19)—Sb(3)] unit in $2SbF_3 \cdot SbF_5$ in which F(19) forms an asymmetric bridge between Sb(V) and Sb(III). The Sb(V)—F(19) distance of 1.90 Å in $2SbF_3 \cdot SbF_5$ is similar to that of Sb(4)—F(8) (1.97 Å) and Sb(3)—F(7) (1.97 Å) in the two fragments (Fig. 4(*I*) and (*II*)). The Sb(III)—F(19) bond of 2.32 Å in $2SbF_3 \cdot SbF_5$ (Fig. 4(*III*)) is slightly longer than those between Sb(III) and the bridging atoms in $3SbF_3 \cdot 4SbF_5$ (Fig. 4(*I*) and (*II*)) of 2.17. The bridge angle Sb(V)—F(19)—Sb(III) of 150.0° in $2SbF_3 \cdot SbF_5$ (Fig. 4(*III*)) is similar to those of 148.4° in Fig. 4(*II*) and 153.7° in Fig. 4(*I*).

Similarity also exists between the bridging angles of Fig. 4(*I*) and (*II*) and the Sb—F—Cl angle of 143° found in (ClF_2^+)-(SbF_6^-) (22), although the latter has a *trans* bridging antimony atom. The asymmetric bridge formed by the fluorine atom in (ClF_2)$^+$(SbF_6)$^-$ (22) with an Sb—F distance of 1.88 Å and Cl—F distance of 2.33 Å is also similar to those in Fig. 4(*I*) and (*II*).

Another bridging atom is F(4), which bridges Sb(1) and Sb(4) with bond distances Sb(4)—F(4) of 1.92 Å and Sb(1)—F(4) of 2.34 Å. The bridge angle Sb(1)—F(4)—Sb(4) of 129.5° is comparable with that in $SeOCl_2 \cdot SbCl_5$ (23) of 121.5°. The atom F(3) forms the second asymmetric bridge with distances to Sb(3) of 1.92 Å and to Sb(1) of 2.36 Å. Sb(7) is linked to Sb(5) and Sb(6) through the *cis* fluorine atoms F(9) and F(10), respectively. The angles at the bridge atoms F(9), of 141.9°, and F(10), of 144.6°, are very similar to the corresponding angle Sb—F—As of 140.9° in $AsF_3 \cdot SbF_5$ (20).

In conclusion, the three octahedral units for Sb(7), Sb(3), and Sb(4) have two *cis* fluorine bridges linked to pairs of cationic species, whereas the octahedron for Sb(2) possesses one fluorine bridge atom linked to the SbF^{2+} cation. A similar arrangement has been observed in the [$Sb_3F_{16}^-$] ion, in (BrF_2^+)($Sb_3F_{16}^-$) (24) and in (O_2^+)($Sb_3F_{16}^-$) (15*b*) with a bridge angle Sb(outer)—F(bridge)—Sb(central) of 145 and 162.9°, respectively. The first of these angles is comparable with Sb(1)—F(2)—Sb(2) of 143.3°. The bridging fluorine atom in [$Sb_3F_{16}^-$] ion acts between two Sb(V) atoms. The Sb(V) atoms are considered to be more electronegative than Sb(III) atoms, and thus have more attractive forces toward the fluorine atoms. Consequently the Sb(V)—F bonds will be shorter than Sb(III)—F bonds, as is observed with Sb(III)—F(4) of 2.26 Å compared with Sb(outer)—F(bridge) of 2.10 Å in (BrF_2^+)($Sb_3F_{16}^-$) and that of 2.13 Å in (O_2^+)($Sb_3F_{16}^-$).

The overall coordination around each Sb(III) atom is completed by consideration of the longer contacts between 2.5 and 3.2 Å. Sb(6) has an overall coordination of nine, including the lone pair of electrons. The Sb(2) in the cationic species $[Sb_6F_{13}]^{5+}$ of α-$6SbF_3 \cdot 5SbF_5$ has nine coordination with inclusion of the lone pair of electrons. The geometry of Sb(6) with all contacts, including the lone electron pair, filling the ninth position, gives an asymmetric arrangement, as shown in Fig. 5.

The overall coordination number of Sb(5) is ten, including the lone pair of electrons. This also shows an irregular atom geometry, as shown in Fig. 6, similar to the potassium atom coordinated by ten fluorine atoms in KAs_2F_7 (21).

In conclusion, the asymmetric unit contains four distorted octahedral [SbF_6^-] anions, two SbF_2^+, and one SbF^{2+} cations. The Sb(1)F^{2+} cation is in the centre of the asymmetric unit with the [Sb(5)F_2^+] and [Sb(6)F_2^+] cations, together with four [SbF_6^-] anions grouped around it. Furthermore, the two sets Sb(1), Sb(4), and Sb(5), and Sb(1), Sb(3), and Sb(6) atoms form closed trimeric units with fluorine bridges. This type of

Can. J. Chem. Downloaded from www.nrcresearchpress.com by 186.148.149.217 on 09/07/12
For personal use only.

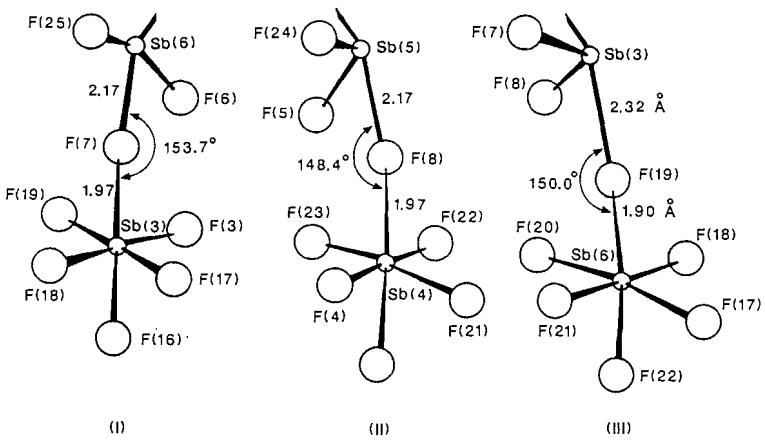


FIG. 4. (*I*) A section of Sb(3)—F(7)—Sb(6) in $3SbF_3 \cdot 4SbF_5$, (*II*) A section of Sb(4)—F(8)—Sb(5) in $3SbF_3 \cdot 4SbF_5$, (*III*) A section of Sb(6)—F(19)—Sb(3) in $2SbF_3 \cdot SbF_5$.

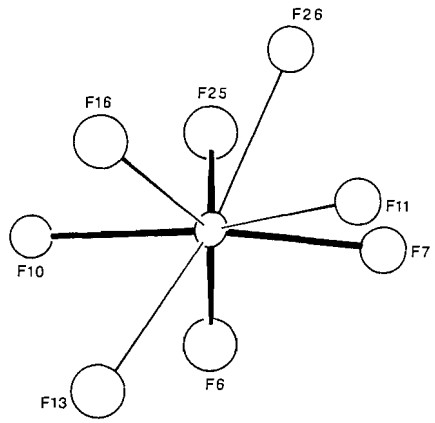


FIG. 5. The coordination of the Sb(6) atom.

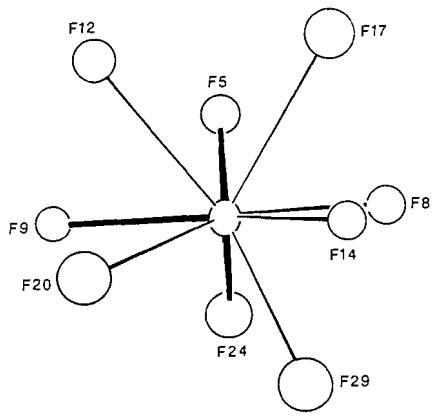


FIG. 6. The coordination of the Sb(5) atom.

arrangement is similar to that observed in $TcOF_4$ (25). The atoms Sb(1), Sb(5), Sb(6), and Sb(7), with fluorine bridges, form a closed tetrameric arrangement which has some similarities to that in pentafluorides (26).

Raman spectra were obtained on single crystals of Sb_7F_{29} in seasoned (ClF_3) Pyrex capillaries. The intensity of the bands was thus dependent upon the orientations observed. Bands were found at 200, 287, 556, 602, 638, 665, 696, and 726 cm^{-1}. The bands at 638 and 665 cm^{-1} were strong in all orientations investigated and are tentatively assigned as SbF_6^- ν_1 and ν_3 respectively. The spectra are distinct from all previously published Raman data for $n \cdot SbF_3 \cdot SbF_5$ (4, 6, 7, 9, 11).

1. O. RUFF and W. PLATO. Ber. **37**, 674 (1904).
2. A. A. WOOLF. J. Chem. Soc. 279 (1955).
3. T. K. DAVIES and K. C. MOSS. J. Chem. Soc. (A), 1054 (1970).
4. T. BIRCHALL, P. A. W. DEAN, B. DELLA VALLE, and R. J. GILLESPIE. Can. J. Chem. **51**, 667 (1973).
5. A. J. EDWARDS and D. R. SLIM. J. Chem. Soc. Chem. Commun. 178 (1974).
6. A. J. HEWITT, J. H. HOLLOWAY, and B. FRLEC. J. Fluorine Chem. **15**, 435 (1980).
7. W. A. S. NANDANA, J. PASSMORE, and P. S. WHITE. J. Chem. Soc. Dalton Trans. 1623 (1985).
8. R. J. GILLESPIE, D. R. SLIM, and J. E. VEKRIS. J. Chem. Soc. Dalton Trans. 971 (1977).
9. W. A. S. NANDANA, J. PASSMORE, P. S. WHITE, and C.-M. WONG. J. Chem. Soc. Dalton Trans. 1989 (1987).
10. A. J. EDWARDS. Private communication.
11. W. A. S. NANDANA, J. PASSMORE, D. C. N. SWINDELLS, P. TAYLOR, P. S. WHITE, and J. E. VEKRIS. J. Chem. Soc. Dalton Trans. 619 (1983).
12. P. MAIN. MULTAN-80. A system of computer programs for the automatic solution of crystal structures from X-ray diffraction data. University of York. 1980.
13. G. M. SHELDRICK. SHELX 76. Program for crystal structure determination. University of Cambridge. 1976.
14. A. J. EDWARDS. J. Chem. Soc. (A), 2751 (1970).
15. D. R. SLIM. Ph.D. Thesis, University of Birmingham. 1974. (*a*) p. 181; (*b*) p. 161.
16. R. J. GILLESPIE and R. S. NYHOLM. Chem. Soc. Quart. Rev. **11**, 195 (1957).
17. R. J. GILLESPIE. Molecular geometry. Van Nostrand Reinhold, London. 1972. pp. 74, 75.
18. M. G. POORE and D. R. RUSSELL. J. Chem. Soc. Chem. Commun. 18 (1971).
19. A. J. EDWARDS and P. TAYLOR. J. Chem. Soc. Dalton Trans. 2174 (1975).
20. A. J. EDWARDS and R. J. C. SILLS. J. Chem. Soc. (A), 942 (1971).
21. A. J. EDWARDS and S. N. PATEL. J. Chem. Soc. Dalton Trans. 1630 (1980).
22. A. J. EDWARDS and R. J. C. SILLS. J. Chem. Soc. (A), 2697 (1970).
23. Y. HERMODSSON. Acta Chem. Scand. **21**, 1313 (1967).
24. A. J. EDWARDS and G. R. JONES. J. Chem. Soc. (A), 2318 (1971).
25. A. J. EDWARDS, G. R. JONES, and R. J. C. SILLS. J. Chem. Soc. (A), 2521 (1970).
26. B. K. MORRELL, A. ZALKIN, A. TRESSAUD, and N. BARTLETT. Inorg. Chem. **12**, 2640 (1973).

Can. J. Chem. Downloaded from www.nrcresearchpress.com by 186.148.149.217 on 09/07/12
For personal use only.

Chromyl fluoride in acidic and basic hydrogen fluoride solutions

JOHN BESIDA AND THOMAS A. O'DONNELL[1]
Department of Inorganic Chemistry, University of Melbourne, Parkville, Victoria, 3052, Australia
AND
P. GARY ELLER
Isotope and Nuclear Chemistry Division, Los Alamos National Laboratory, Los Alamos, NM 87545, U.S.A.

Received March 29, 1989

This paper is dedicated to Professor Ronald J. Gillespie on the occasion of his 65th birthday

JOHN BESIDA, THOMAS A. O'DONNELL, and P. GARY ELLER. Can. J. Chem. **67**, 2047 (1989).

Chromyl fluoride provides a nonconducting solution in anhydrous hydrogen fluoride with Raman spectroscopic features indistinguishable from those of the solute in the gas phase, indicating no fluoride or proton transfer in solution. With increasing acidity in the SbF_5–HF solvent system, CrO_2F_2 forms cationic species, the nature of which is discussed. The acidity-dependence of cationic speciation in HF–TaF_5 and in HF–AsF_5 is consistent with that in HF–SbF_5.

Key words: chromyl fluoride, antimony fluoride, Lewis acid, Raman spectroscopy, hydrogen fluoride.

JOHN BESIDA, THOMAS A. O'DONNELL et P. GARY ELLER. Can. J. Chem. **67**, 2047 (1989).

Le fluorure de chromyle, dans le fluorure d'hydrogène anhydre, constitue une solution non conductrice ayant des caractéristiques spectroscopiques de Raman identiques à celles du soluté dans la phase gazeuse indiquant ainsi l'absence de transfert d'ion fluorure ou d'hydrogène en solution. Lorsqu'on augmente l'acidité du mélange SbF_5–HF utilisé comme solvant, le CRO_2F_2 forme des espèces cationiques, dont on discute ici la nature. L'influence de l'acidité sur la spéciation cationique dans les systèmes de solvent HF–TaF_5 et HF–AsF_5 s'accorde bien avec celle du système de solvant HF–SbF_5.

Mots clés : fluorure de chromyle, fluorure d'antimoine, acide de Lewis, spectroscopie de Raman, fluorure d'hydrogène.
[Traduit par la revue]

Can. J. Chem. Downloaded from www.nrcresearchpress.com by 186.148.149.217 on 09/07/12
For personal use only.

Inorganic fluorine chemists have devoted much effort to the synthesis and characterization by spectroscopic and diffraction methods of Lewis acid – Lewis base adducts involving acids like SbF_5 and BF_3 reacting with molecular fluorides of the halogens, the chalcogens, and the heavier noble gases. An early typical example was the adduct $SF_4 \cdot BF_3$, which, considerably later, was shown by X-ray crystallography to be the essentially ionic compound $SF_3^+BF_4^-$ (1). Gillespie and co-workers used conductance measurements and nmr spectroscopy to show that the adduct was completely ionized in solution in anhydrous HF (2) and Brownstein and Shamir found that the Raman spectrum of the adduct in HF was virtually identical with that of the solid (3), i.e., in both the solid and in HF solution, fluoride transfer from SF_4 to BF_3 is complete.

In similar fashion it was shown that BrF_3 and SbF_5 react to form a 1:1 adduct, and later structure determination showed that it also has an essentially ionic formulation, $BrF_2^+SbF_6^-$ (4). Surles, Quarterman, and Hyman demonstrated complete F^- transfer from BrF_3 to SbF_5 in HF solution by recording very similar Raman spectra for the solid adduct and its solution in HF (5).

There do not appear to be many other systems in which there has been the same comprehensive investigation of fluoro adducts both in the solid state and in HF solution, the solvent with which they are compatible. The ability of CrO_2F_2 to react with HF, made acidic with Lewis acids or made basic with F^-, is the subject of study in this paper.

Previously Gard and co-workers (6) prepared 1:1 and 1:2 solid adducts by direct addition of CrO_2F_2 to the Lewis acids SbF_5 and TaF_5. They showed that solid adducts, stable at room temperature, were not formed when CrO_2F_2 was interacted with the weaker, volatile Lewis acids AsF_5, PF_5, and BF_3, indicating qualitatively that CrO_2F_2 is a much weaker fluoride donor than species like SF_4 and BrF_3. Gard and co-workers used infrared and Raman spectroscopy and chemical analysis to support their formulation of the adducts as $CrO_2F \cdot SbF_6$, $CrO_2F \cdot Sb_2F_{11}$, and $CrO_2F \cdot TaF_6$, i.e., they postulated F^- transfer to the strong Lewis acids. They showed also that with very strong fluoride donors like CsF, BaF_2, and ONF solid adducts were formed, with CrO_2F_2 acting as a Lewis acid (6, 7).

It is interesting to compare the dissolution of CrO_2F_2 in acidified HF with that of the formally analogous compound UO_2F_2. By comparison of vibronic and Raman spectra of UO_2F_2 in HF–AsF_5 with those in many aqueous systems, for example $UO_2(ClO_4)_2$ in $HClO_4$, Barraclough, Cockman, and O'Donnell (8) postulated the existence of the HF-solvated cation UO_2^{2+} in acidic HF. Fawcett, Holloway, Laycock, and Russell (9) crystallized the adduct $UO_2F_2 \cdot 3SbF_5$ from HF acidified with SbF_5. An X-ray crystal structure showed UO_2^{2+} as a discrete entity in the solid. In this compound U—F distances for F atoms on bridging SbF_6^- units are 20 to 25% longer than U—F distances in typical uranium fluorides.

In this present work Raman spectroscopy has been used as the principal technique to study speciation of CrO_2F_2 in HF solution as the solvent is made basic with F^- or is made progressively more acidic by the addition of the Lewis acids SbF_5, AsF_5, and TaF_5. The chemical nature of the Lewis acid appears to have little or no effect on the spectra observed. Spectra in HF–AsF_5 and HF–TaF_5 correlate very well with those in HF–SbF_5 on the basis of relative acid strengths, as indicated by values of the Hammett Acidity Function determined by Gillespie and Liang for these solutions (10).

Experimental

Reagents

Chromyl fluoride

CrO_3 was treated with anhydrous HF according to the method described by Engelbrecht and Grosse (11).

Hydrogen fluoride

Commercial reagent (Matheson's 99%) was subjected to three trap-to-trap distillations, discarding "tails".

[1]Author to whom correspondence may be addressed.

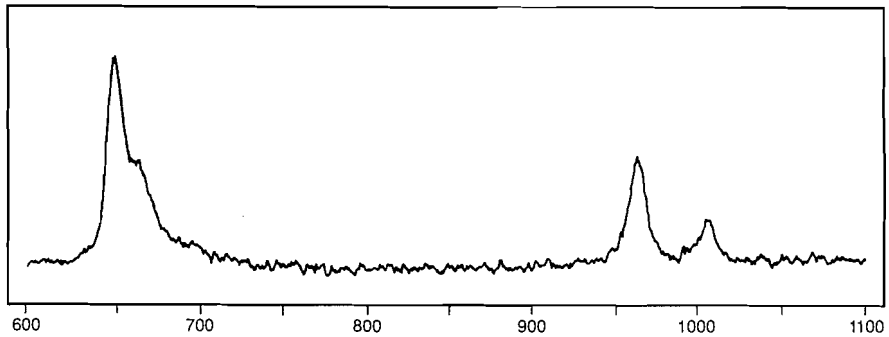


FIG. 1. Raman spectrum of HF solution 0.1 molar in CrO_2F_2 and 1 molal in SbF_5.

Antimony pentafluoride

Commercial reagent (Ozark Mahoning) was purified by distillation as previously described (12).

Arsenic pentafluoride

The commercial reagent (Ozark Mahoning) was distilled directly from the cylinder.

Tantalum pentafluoride

The commercial reagent (Ozark Mahoning) was handled under glove-box conditions.

Ammonium fluoride

Analytical reagent (B.D.H.).

Solution preparation

Concentrated solutions of SbF_5 in HF were progressively diluted with distilled HF to give more dilute solutions, solution molalities being determined by weight differences in KelF traps. Volatile AsF_5 was admitted to HF in a KelF trap via a metal and KelF vacuum line. TaF_5 and NH_4F were weighed into KelF traps under glove-box conditions, HF was added, and molalities determined by reweighing. Molalities were determined in the preparation of HF solutions of Lewis acids and of HN_4F because these could be related to mole percentages of solutes in HF — the method of expression of concentrations used by Gillespie and Liang in their determinations of H_0 values for HF solutions (10).

Solutions of CrO_2F_2 in HF, whether "neutral", acidic, or basic, were all approximately 0.1 molar in CrO_2F_2. CrO_2F_2 concentrations were based on volume of the solvent, rather than weight, because of the very great difference in density of the solvent between the extremes of "neat" HF and 20 molal (40 mol%) SbF_5.

Raman spectra

Raman spectra were recorded for HF solutions in "synthetic sapphire" tubes with a Spex Ramalog 5,14018 Spectrometer using 5145 Å irradiation and multiscan facilities. For most spectra 20 scans were accumulated and integrated.

Conductance measurements

The Kel-F cell with platinum electrodes used for conductance measurements was similar to that described previously (13).

Results and discussion

Figure 1 gives the recorded Raman spectrum for an HF solution 0.1 molar in CrO_2F_2 and 1 molal in SbF_5. Peaks in the 640–670 cm^{-1} region are characteristic of fluoro-antimonate(V) anionic species. The peak at 1007 cm^{-1}, also observed in "neat" HF (Fig. 2) where the solute is present as CrO_2F_2 as discussed below, is in the identical position to that assigned to the Cr=O stretch in gaseous CrO_2F_2 (14). The peak at 965 cm^{-1} is ascribed to a cationic species, either CrO_2F^+ or $CrO(OH)F_2^+$, for the reasons given later in this section. In the Raman spectroscopic study of gaseous CrO_2F_2 a peak at 728 cm^{-1} was assigned to the symmetric Cr—F stretch (14). No peak of sufficient intensity for diagnostic use was observed in the 720–730 cm^{-1} region in HF solutions. Raman peaks associated with metal–fluorine stretches are frequently very weak, this being attributed to the high degree of polarity of these bonds.

For these reasons, monitoring of change in speciation of the solute CrO_2F_2 as the acidity or basicity of HF solutions was changed was based on peak positions around 1000 cm^{-1}, which are associated with chromium–oxygen stretches.

Raman spectra are reproduced in Fig. 2 for HF solutions each approximately 0.1 molar in CrO_2F_2, to which SbF_5 has been added progressively. The spectrum in neat HF shows a peak at 1007 cm^{-1} in the identical position to that observed for gaseous CrO_2F_2 (14), indicating that the solute is present as the molecular entity. Although, in spectroscopy, it is common to observe significant differences between gas phase spectra and those for the same entities in solution, CrO_2F_2 behaves similarly to many other molecular fluorides in HF. MoF_6, UF_6, ReF_6, and ReF_7 have remarkably similar Raman spectra in neat HF and in the gas phase (15, 16), surprisingly, perhaps, when the highly associated state of the solvent is compared with the discrete molecularity of the solutes.

The postulation that CrO_2F_2 is present as the molecular species in neat HF is supported by the fact that addition of CrO_2F_2 to HF has little effect on the conductance of the solvent, 2.2×10^{-4} ohm^{-1} cm^{-1} for HF compared with 2.8×10^{-4} ohm^{-1} cm^{-1} for 0.48 molal CrO_2F_2 in HF. Thus CrO_2F_2 is not acting as a fluoride donor or acceptor or as a proton acceptor in HF to form cationic or anionic species.

As the concentration of SbF_5 is increased, i.e., as the acidity of the medium is increased, a new Raman peak grows in at 965 cm^{-1} at the expense of the 1007 cm^{-1} peak until, at 5 molal SbF_5, there remains little of the peak attributable to molecular CrO_2F_2. We postulate that fluoride transfer occurs from CrO_2F_2 to the HF–SbF_5 solvent system as the concentration of F^- in the solvent system decreases, i.e., as the acidity increases, and we ascribe the peak at 965 cm^{-1} to the solvated cationic species CrO_2F^+. Alternatively proton transfer could be occurring to form $CrO(OH)F_2^+$ as the acidity of the medium is increased.

It is possible to put the threshold for F^- or proton transfer between CrO_2F_2 and the acidified solution on a quantitative basis as a result of measurement by Gillespie and Liang of values of Hammett Acidity Functions (H_0) in HF containing either the base F^- or various Lewis acids, including SbF_5 (10). Reference to Fig. 2 shows no spectroscopic evidence for a cationic species in 0.025 m SbF_5 in HF (for which $H_0 = -19.53$) but there is a very small peak, ascribed to this species, observed in 0.05 m SbF_5 ($H_0 = -19.75$). Gillespie and Liang did not measure H_0 values for HF solutions more concentrated

Can. J. Chem. Downloaded from www.nrcresearchpress.com by 186.148.149.217 on 09/07/12
For personal use only.

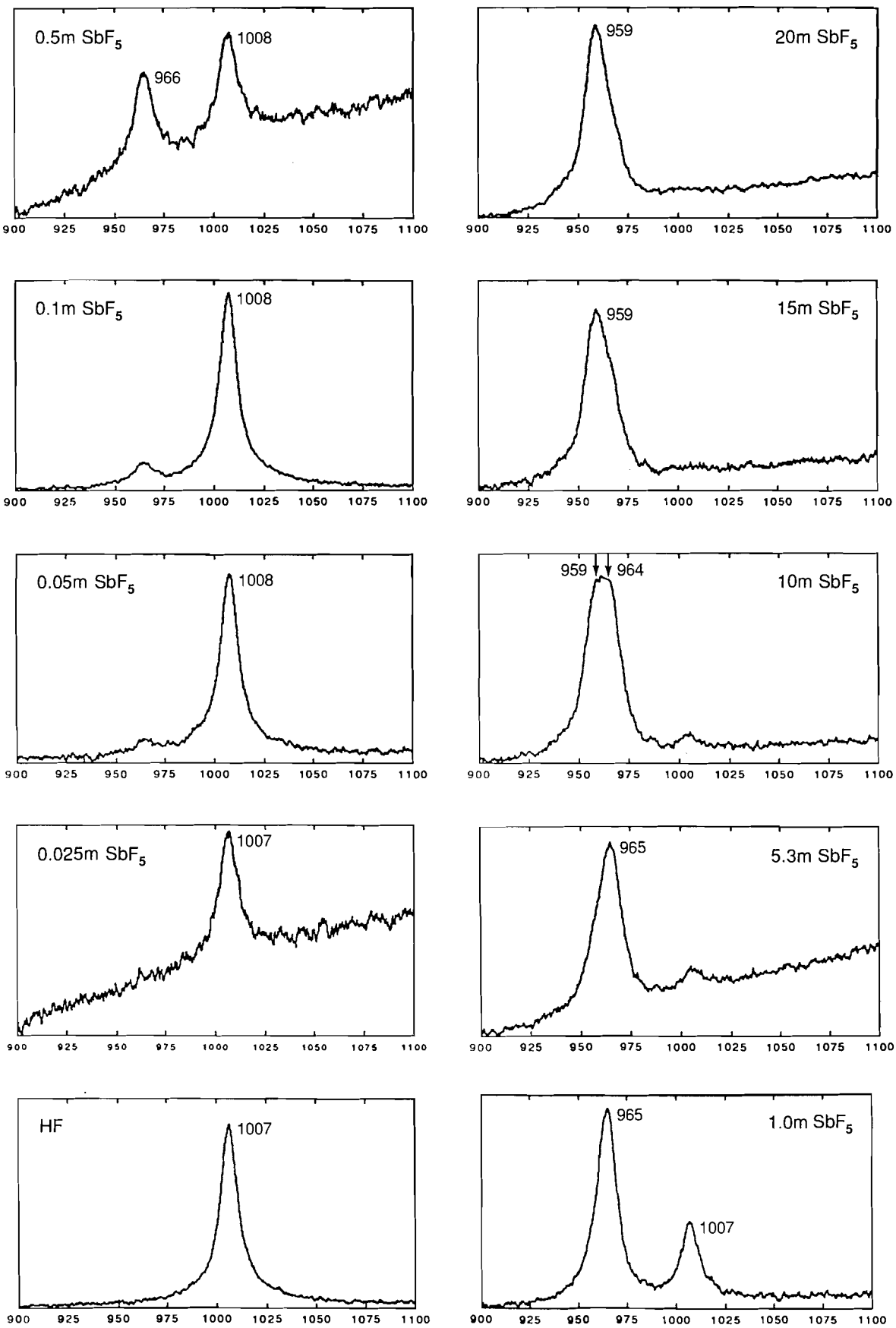


FIG. 2. Raman spectra of 0.1 M CrO_2F_2 in "neat" HF and in HF solutions containing increasing concentrations of SbF_5.

Can. J. Chem. Downloaded from www.nrcresearchpress.com by 186.148.149.217 on 09/07/12
For personal use only.

Can. J. Chem. Downloaded from www.nrcresearchpress.com by 186.148.149.217 on 09/07/12
For personal use only.

in SbF_5 than 0.3 molal, but it is known from the general chemistry of the HF–SbF_5 superacid solvent system that the acidity continues to increase with increasing SbF_5 concentration. Figure 2 also includes a Raman spectrum for CrO_2F_2 in neat HF, i.e., as purified by distillation. Gillespie and Liang estimated a value for H_0 of -15.1 ± 0.1 for absolutely pure HF, but, as they point out in their paper, the measured value of H_0 for even the best distilled HF will be about -11 because of unavoidable impurities in the distilled solvent (10).

At 10 molal SbF_5, the peak at about 960 cm^{-1} has broadened significantly. In HF solutions 15 and 20 molal in SbF_5 the peak at 1007 cm^{-1} is no longer discernible, i.e., there is no detectable amount of CrO_2F_2 in the system and the major peak narrows and shifts from 964–965 cm^{-1} (as in 0.1–5 molal SbF_5) to a new position of 959 cm^{-1} in 15 and 20 molal SbF_5. A change in speciation from CrO_2F^{2+} to CrO_2^{2+} or a change from $CrO(OH)F_2^+$ to $Cr(OH)_2F_2^{2+}$ in the strongly acidic medium seems an unlikely explanation for a shift in peak position of only 5 cm^{-1}, when it is recalled that a shift of about 40 cm^{-1} occurred for the change from CrO_2F_2 to the postulated CrO_2F^+. It is more likely a result of changes in the solvation and coordination of the cationic species. The nature of the solvent would be modified massively in moving from an SbF_5 concentration of, say, 1 molal (2 mol% SbF_5 in HF), where the SbF_5 exists almost exclusively as SbF_6^-, to 20 molal (40 mol% SbF_5), where the SbF_5 would be present largely as polymeric anions (17).

The Lewis acids TaF_5 and AsF_5 were investigated very briefly and the Raman spectra for the CrO_2F_2–HF–TaF_5 and CrO_2F_2–HF–AsF_5 solutions are shown in Fig. 3. The spectrum for a saturated solution of TaF_5 (0.4 molal), the Hammett Function for which would be -19.20 (10), gives no evidence for formation of any species except CrO_2F_2 and this is consistent with the fact that CrO_2F_2 is the only detectable species in 0.025 molal SbF_5, for which $H_0 = -19.53$.

The AsF_5 was 2–3 molal and gave the second spectrum in Fig. 3, showing the presence of both CrO_2F_2 and the cation. Gillespie and Liang did not measure H_0 values for HF–AsF_5 solutions containing concentrations of AsF_5 higher than 0.35 molal (10). Comparison with our spectra for CrO_2F_2 in HF–SbF_5 solutions suggests that the H_0 value for our HF–AsF_5 solution should be about -20.5, corresponding with that for a solution about 0.2 molal in SbF_5, and this correlates quite well with extrapolation of Gillespie and Liang's H_0 values for dilute AsF_5 solutions to higher AsF_5 concentrations.

To summarize the experimental observations in acid HF, CrO_2F_2 remains the only spectroscopically observable species until an acidity threshold between that for 0.025 molal SbF_5 ($H_0 = -19.53$) and that for 0.05 molal SbF_5 ($H_0 = -19.75$) is reached. Comparison of spectra in SbF_5, TaF_5, and AsF_5 suggests that the only role of each pentafluoride is to act as a Lewis acid in HF; at reasonable concentrations the chemical nature of the Lewis acid appears to have no effect on the coordination of the cation produced in solution.

Figure 4 gives the Raman spectrum for CrO_2F_2 dissolved in strongly basic HF, namely anhydrous HF made ca. 3 molal in NH_4F. The peak at 1007 cm^{-1} has an identical position to that for CrO_2F_2 in neat HF, indicating strongly that CrO_2F_2 is not a sufficiently strong Lewis acid in solution to accept F^- from either neutral or strongly basic HF. This postulation that CrO_2F_2 is a very weak Lewis acid in HF solution seems to present a situation different, at first sight, from that demonstrated by Gard (6, 7) where direct interaction of F^- in several fluoride donors with CrO_2F_2 led to solid involatile adducts, each of

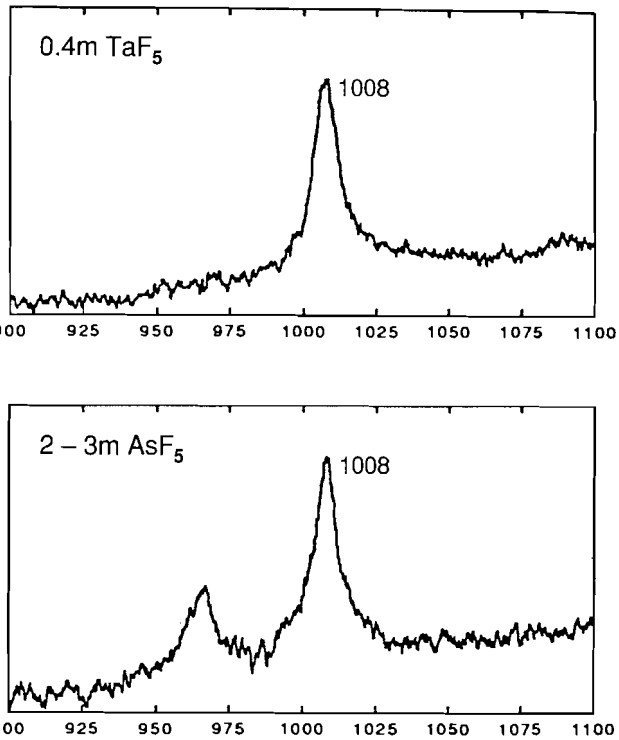


FIG. 3. Raman spectra of solutions 0.1 M in CrO_2F_2 in HF–TaF_5 and HF–AsF_5.

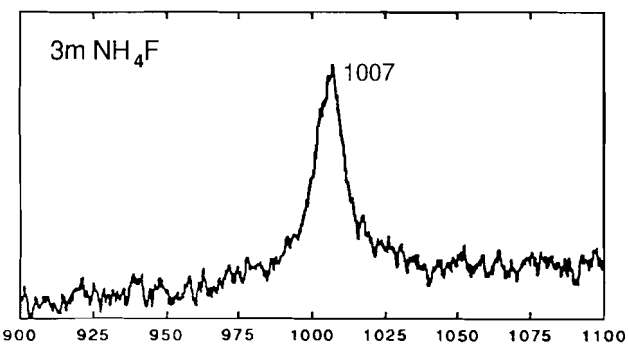


FIG. 4. Raman spectrum of 0.1 M CrO_2F_2 in HF solution 3 molal in NH_4F.

which would have had a high degree of ionic character, containing cations such as NO^+, NO_2^+, Na^+, and Ca^{2+}. However, in solution the weak Lewis acid CrO_2F_2 is competing unsuccessfully with HF for F^- whereas in Gard's systems the F^- is available from very strong fluoride donors to form ionic adducts of very low volatility.

Good experimental evidence has been developed here to show that CrO_2F_2 exists in neat HF as the molecular entity. The Cr=O stretching frequencies are virtually identical in the gas phase Raman spectrum and in the HF solution spectrum, and the addition of CrO_2F_2 to neat HF has no significant effect on the small conductance of the solvent, indicating that no ionic species are formed from the solute by fluoride transfer or by protonation.

Marked increase in the acidity of HF is required to give spectroscopic evidence of change in the nature of the molecular solute. As stated earlier the H_0 value for neat HF is usually about -11 and no new species is detected until the H_0 value is about -19.75, i.e., in 0.05 molal SbF_5. Three possible explanations

Can. J. Chem. Downloaded from www.nrcresearchpress.com by 186.148.149.217 on 09/07/12
For personal use only.

could be given for the new speciation taking into account the nature of the acidic solvent system.

The least likely of these in the light of this work, is to postulate that SbF_5 acts as an acid towards the basic oxygen site in CrO_2F_2 to form a species such as $CrF_2(O)OSbF_5$, giving rise to the new Raman peak at 965 cm^{-1}. In attempts to generate polymeric anions such as $Sb_3F_{16}^-$ by reacting stoichiometric amounts of CsF with SbF_5 in liquid SO_2, Bacon, Dean, and Gillespie found that they could isolate $Cs^+Sb_2F_{11}^-$ but that at ratios of SbF_5:CsF greater than 2:1 the complex $SO_2 \cdot SbF_5$ was formed (18). They adduced nmr spectroscopic evidence for anions of higher polymeric complexity when SO_2 was absent, i.e., the reactive matrix was SbF_5. When the available F^- concentration was initially as low as equimolar (relative to SbF_5), the next mole of SbF_5 still complexed with SbF_6^-. Beyond that point the $SO_2 \cdot SbF_5$ complex was formed. In solution, no antimony species other than SbF_6^- would form in the presence of the F^- available from solvent HF. On these grounds significant complexation of SbF_5 with an oxygen site on CrO_2F_2 dissolved in HF would be unlikely. We have shown that a solution 0.1 molar in CrO_2F_2 and 2–3 molal in AsF_5 has a spectrum with peak positions in the same position as in 0.2 molal SbF_5 and that the relative peak heights in each solution are very similar. Different peak positions would be expected for stretching frequencies for species involving Cr—O—SbF_5 and Cr—O—AsF_5 and a greater than 10-fold difference in Lewis acid concentrations would be expected to give very different relative peak heights in each solution even though AsF_5 has approximately half the Lewis acid strength of SbF_5.

It is difficult to distinguish clearly between two ways in which cationic species could be generated from CrO_2F_2 in acidic HF. The first of these would involve protonation of the oxygen site on CrO_2F_2 to give a species such as $CrF_2(O)OH^+$. On the grounds of proton availability this would be expected to occur to a similar extent in 0.2 molal SbF_5–HF and in 2–3 molal AsF_5–HF. It would also be expected to give a Raman frequency of somewhat smaller magnitude than that for the Cr=O stretch, as observed in this work.

The other possibility is that CrO_2F_2 acts like SF_4 and BrF_3 and many other molecular fluorides and also acts like UO_2F_2 in donating F^+ to the acidic, i.e., fluoride-deficient, medium HF–SbF_5, the extent of F^- transfer increasing with increasing acidity of the SbF_5–HF mixtures. This fluoride transfer and resultant formation of CrO_2F^+ would again occur approximately equally in 0.2 molal SbF_5–HF and in 2–3 molal AsF_5–HF because the fluoride level would be fixed at the same low level in each medium. The strongest evidence against this possibility is that on increase in acidity the new Raman frequency grows in at a lower wave number, not higher as would be generally expected for CrO_2F^+.

However, Gard's work on solid adducts (6) is of importance here. He added CrO_2F_2 directly to the Lewis acids SbF_5 and TaF_5. To have obtained protonated cations, there would need to have been present in each experiment an equimolar quantity of adventitious HF, i.e., to have generated solids containing the cation $CrF_2(O)OH^+$ with the anions SbF_6^-, $Sb_2F_{11}^-$, and TaF_6^-. For these compounds Gard's analytical figures for fluoride would have been 5–10% higher than the reported ones that fit the formulations $CrO_2F^+SbF_6^-$, etc. Gard also characterized his solids using infrared and Raman spectroscopy. Spectroscopic data for SbF_6^-, $Sb_2F_{11}^-$, and TaF_6^- matched those previously reported in components of known stoichiometry. He associated peaks in the 940–960 cm^{-1} region with Cr=O stretching frequencies and they correspond well with the frequencies reported in this work.

On balance, the formation of CrO_2F^+ in acidic HF is favoured here in the light of the known fluoride-donor capabilities of many fluorine-containing species including SF_4, BrF_3, and UO_2F_2 and the chemical and spectroscopic properties of the solid adducts $CrO_2F^+SbF_6^-$, $CrO_2F^+Sb_2F_{11}^-$, and $CrO_2F^+TaF_6^-$.

CrO_2F_2 is stable in HF solutions for periods of several months and this is consistent with our observations that CrO_3, CrO_4^{2-}, $Cr_2O_7^{2-}$, CrO_3F^-, and CrO_2F_2 all have the same Raman spectra when dissolved in HF or HF–SbF_5, i.e., solvolysis to CrO_2F_2 occurs for the trioxide and the oxo-anions.

Acknowledgements

We wish to acknowledge funding of this and much related work by the Australian Research Grants Scheme. We are particularly grateful to Mr. Max Beyer for his skill in recording Raman spectra and in preparing these spectra in a form suitable for publication. One of us (P.G.E.) gratefully acknowledges financial support from the University of Melbourne as a Visiting Scholar and from Los Alamos National Laboratory through Institutional Support Research funding for a period of sabbatical leave. We thank Drs. C. J. Marsden and C. G. Barraclough for very helpful discussions.

1. D. D. Gibler, C. J. Adams, M. Fischer, A. Zalkin, and N. Bartlett. Inorg. Chem. **11**, 2325 (1972).
2. M. Azeem, M. Brownstein, and R. J. Gillespie. Can. J. Chem. **47**, 4159 (1969).
3. M. Brownstein and J. Shamir. Appl. Spectrosc. **26**, 77 (1972).
4. A. J. Edwards and G. R. Jones. J. Chem. Soc. (London) A, 1467 (1969).
5. T. Surles, L. A. Quarterman, and H. H. Hyman. J. Fluorine Chem. **3**, 293 (1973/74).
6. S. D. Brown, P. J. Green, and G. L. Gard. J. Fluorine Chem. **5**, 203 (1975).
7. P. J. Green and G. L. Gard. Inorg. Nucl. Chem. Lett. **14**, 179 (1978).
8. C. G. Barraclough, R. W. Cockman, and T. A. O'Donnell. Inorg. Nucl. Chem. Lett. **17**, 83 (1981).
9. J. Fawcett, J. H. Holloway, D. Laycock, and D. R. Russell. J. Chem. Soc. Dalton Trans. 1355 (1982).
10. R. J. Gillespie and J. Liang. J. Am. Chem. Soc. **110**, 6053 (1988).
11. A. Engelbrecht and A. V. Grosse. J. Am. Chem. Soc. **74**, 5262 (1952).
12. R. J. Gillespie and T. E. Peel. J. Am. Chem. Soc. **95**, 5773 (1973).
13. J. H. Canterford and T. A. O'Donnell. *In* Technique of inorganic chemistry. Vol. VII. Wiley, New York. 1968. p. 301.
14. I. R. Beattie, C. J. Marsden, and J. S. Ogden. J. Chem. Soc. Dalton Trans. 535 (1980).
15. B. Frlec and H. H. Hyman. Inorg. Chem. **6**, 1596 (1967).
16. H. Selig and E. L. Gasner. J. Inorg. Nucl. Chem. **30**, 658 (1968).
17. R. J. Gillespie and K. C. Moss. J. Chem. Soc. 1170 (1966).
18. J. Bacon, P. A. W. Dean, and R. J. Gillespie. Can. J. Chem. **47**, 1655 (1969).

Concerning the internal rotational potential in benzal chloride. $^{37}Cl/^{35}Cl$ isotope effect on the methine ^1H NMR

TED SCHAEFER AND RUDY SEBASTIAN
Department of Chemistry, University of Manitoba, Winnipeg, Man., Canada R3T 2N2

Received April 7, 1989

TED SCHAEFER and RUDY SEBASTIAN. Can. J. Chem. **67**, 2053 (1989).

^1H NMR spectral parameters are reported for benzal chloride in CS_2/C_6D_{12}, $CDCl_3$, and acetone-d_6 solutions. The values of ^6J(H,CH), the long-range spin–spin coupling constant between the side-chain and *para* protons, are consistent with twofold barriers to rotation about the exocyclic C—C bond of 8.6(4), 8.9(4), and 10.2(6) kJ/mol, in the order of the solvents above. These numbers are somewhat smaller than the twofold barrier of 11.6 kJ/mol available from STO-3G MO computations for the free molecule. Alternatively, an internal rotational potential consisting of a twofold term of 17.0 kJ/mol and a fourfold term of −5.5 kJ/mol is also compatible with the ^6J(H,CH) measured for the $CDCl_3$ solution and with the ^{13}C spin-lattice relaxation data reported for such a solution. The ^6J(H,CH) values demonstrate that the conformer with the α C—H bond situated in the benzene plane is the most stable. A local minimum in the potential for a conformer in which this bond lies in a plane perpendicular to the phenyl group, leading to a population of about 8% for this conformer at 300 K and compatible with the magnitude of ^6J(H,CH), is represented by twofold and fourfold terms of 6.0 and 4.5 kJ/mol, respectively. The barrier height is then only 8.0 kJ/mol, however. $^{37}Cl/^{35}Cl$ isotope effects on the methine proton amount to −0.17, −0.19, and −0.22 parts per billion in CS_2, $CDCl_3$, and acetone-d_6 solutions, respectively (increased screening).

Key words: benzal chloride, internal potential, $^{37}Cl/^{35}Cl$ isotope effect on ^1H NMR.

TED SCHAEFER et RUDY SEBASTIAN. Can. J. Chem. **67**, 2053 (1989).

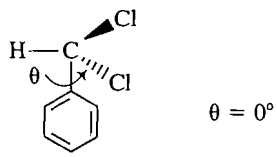
On a déterminé les paramètres des spectres RMN du ^1H du chlorure de benzal en solution dans le CS_2/C_6D_{12}, le $CDCl_3$ et l'acétone-d_6. Les valeurs des constantes de couplage spin–spin à longue distance, ^6J(H,CH), sont en accord avec des barrières binaires à la rotation autour de la liaisons exocyclique C—C de 8,6(4), 8,9(4) et 10,2(6) kJ/mol respectivement pour les solvants mentionnés plus haut. Ces valeurs sont passablement plus basses que la barrière binaire de 11,6 kJ/mol obtenue par calculs d'OM STO-3G effectués sur la molécule libre. Par ailleurs la valeur de la constante ^6J(H,CH) mesurée dans le $CDCl_3$ ainsi que les données de relaxation spin-réseau du ^{13}C obtenues pour une telle solution sont aussi compatibles avec un terme binaire de 17,0 kJ/mol et un terme quaternaire de −5,5 kJ/mol. Les valeurs des constantes ^6J(H,CH) démontrent que le conformère le plus stable est celui comportant la liaison C—H en α dans le plan du noyau benzénique. Un minimum local dans le potentiel d'un conformère dans lequel cette liaison est perpendiculaire au groupement phényle, qui correspondrait à une population de 8% de ce conformère à 300 K et qui serait compatible avec l'amplitude de la constante ^6J(H,CH), est représenté par des termes binaire et quaternaire de respectivement 6,0 et 4,5 kJ/mol. Toutefois, la hauteur de la barrière est de 8,0 kJ/mol. Les effets isotopiques des $^{37}Cl/^{35}Cl$ sur la position du proton méthine (augmentation de la constante d'écran) sont respectivement −0,17, −0,19 et −0,22 ppm dans les solutions de CS_2, de $CDCl_3$ et d'acétone-d_6.

Mots clés : chlorure de benzal, potentiel interne, effet isotopique des $^{37}Cl/^{35}Cl$ sur la RMN du ^1H.

[Traduit par la revue]

Introduction

The study of the internal rotational potential in benzal chloride, **1**, has a curious history.



θ = 0°

1

An early application (1) of the *J* method (2) gave limits of 2.9–10 kJ/mol for an assumed twofold potential for **1** dissolved in CS_2. This method depends on the relationship, $^6J/\text{Hz} = {}^6J_{90}\langle\sin^2\theta\rangle$, where ^6J is the spin–spin coupling constant over six bonds between the *para* and side-chain protons and $^6J_{90}$ is that at θ = 90° in **1**. The expectation value of $\sin^2\theta$ can be related to the internal barrier to rotation by a hindered rotor model or by a classical averaging procedure. The magnitude of $^6J_{90}$ depends on the electronegativity of the substituents on the side chain. The large uncertainty in $^6J_{90}$ at that time (1) led to the range of barriers quoted above, although a value of 9.2 ± 1.3 kJ/mol was assessed with a lesser degree of confidence (1). The measured value of ^6J suggested that **1** was the conformation of lowest energy in CS_2 solution.

Vibrational data for the phenyl ring of 4-fluorobenzal chloride (3) could be interpreted as consistent with C_1 molecular symmetry, whereas those for the $CHCl_2$ group were consistent with C_s symmetry (3). Again, the temperature dependence of the Raman spectra of liquid **1** was analyzed (4) to yield an enthalpy difference of 4.2 ± 1.3 kJ/mol between two conformers. CNDO/2 MO computations gave an internal barrier of 8.7 kJ/mol, with a single minimum at θ = 90° in **1** (4). These results were discounted for a number of reasons (4); a molecular mechanics approach (4) delivered two minima in the internal rotational potential, the lower one at θ = 0°. The upshot of these studies, together with solvent effects indicating hydrogen bonding between the methine proton and molecules like acetone, was that the internal barrier amounted to 4–6 kJ/mol and that the second minimum in the barrier lay 2–4 kJ/mol above the first. In this connection, it is pertinent that the overtone vibrational spectra (5) of liquid **1** are consistent with the presence of a second conformer to the extent of about 10%.

Another Raman and infrared study of liquid **1** (6) came to the conclusion that the internal barrier had an upper limit of 16 kJ/mol, derived on the basis of its assumed sixfoldedness.

By way of contrast, if the carbon atoms of the phenyl group are constrained to a planar hexagon, but other bond lengths and angles are optimized during the SCF cycles, then STO-3G MO computations yield a twofold internal rotational potential of

Can. J. Chem. Downloaded from www.nrcresearchpress.com by 186.148.149.217 on 09/07/12
For personal use only.

Can. J. Chem. Downloaded from www.nrcresearchpress.com by 186.148.149.217 on 09/07/12
For personal use only.

11.6 ± 0.1 kJ/mol (7). The conformer with θ as 0° is most stable. Removal of the hexagonal constraint lowers the barrier to 11.4 kJ/mol (7). Furthermore, this constraint gives a barrier of 11.0 kJ/mol in a computation with the 4-31G basis set (5). For the free molecule, at least, these calculations yield no local minimum at θ = 90°.

In $CDCl_3$ solution, the correlation times extracted from the ^{13}C spin-lattice relaxation times, the latter measured as a function of temperature, have been used (8) to find an internal barrier of 17.3 kJ/mol for **1**. This number is 1.3–3.6 kJ/mol larger than the activation energies deduced for the rotational diffusion of the whole molecule about different axes (8).

In principle, the spin-lattice relaxation times yield the height of the internal barrier because an Arrhenius dependence on temperature is assumed; they do not establish the shape of the internal rotational potential. The torsional frequencies, for a barrier substantial in magnitude compared to kT, test the bottom of the potential assumed to consist of sinusoidal components, as do the spin–spin coupling constants. The molecular orbital computations must be corrected for differences in zero-point energies between conformers in order to make comparisons with spectroscopic data; these are unlikely (9) to amount to more than about 0.5 kJ/mol in the present instance. The enthalpy differences between conformers, derived from the temperature dependence of vibrational bands assigned to the conformers, may be compared with the energies computed for the conformers if these energies are corrected for the changes in enthalpy between absolute zero and the temperatures in question. For benzal chloride the MO calculations yield an essentially twofold internal rotational potential (7), so that only one stable conformer is predicted, that with θ = 0° in **1**. Solvent effects on conformer stabilities are also possible, of course.

The purpose of the present work is to extract ^6J for benzal chloride, with a precision considerably higher than that attainable at the time of the original spectral work (1), for solutions in a nonpolar solvent mixture, in a polar solvent, and in $CDCl_3$, the solvent used for the ^{13}C spin-lattice relaxation measurements. More reliable estimates of $^6J_{90}$ are now also available. The internal rotational potentials compatible with the ^6J values are then compared with the theoretical and experimental data in the literature.

As a by-product of the spectral analysis, $^{37}Cl/^{35}Cl$ isotope shifts are found for the methine proton. They are solvent dependent.

Results and discussion

Table 1 presents the ^1H NMR spectral parameters for benzal chloride in three solvents. The somewhat larger magnitudes of the intraring coupling constants in the more polar solutions is a general result in this laboratory and is therefore unlikely to be an artefact of the spectral analyses.

$^6J(H,CH)$ and the internal barrier

$^6J(H,CH) \equiv {}^6J$ yields $\langle \sin^2 \theta \rangle$ if $^6J_{90}$ is known (2, 10–12). In toluene, $^6J_{90}$ is −1.20 Hz (13). An electronegative substituent on the side chain polarizes the C—H bond, decreases the magnitude of the σ–π interaction, and hence lowers the magnitude of $^6J_{90}$. As discussed previously for benzyl chloride (12), the values of $^6J_{90}$ of −1.02 Hz for a CH_2OR group (14, 15) and of −0.95 Hz for CH_2F (16), together with the assumption of a linear dependence of $^6J_{90}$ on the electronegativity of the α substituent, lead to a value of −1.06 Hz for $^6J_{90}$ in benzyl chloride. If a second chlorine substituent is as effective as the first in reducing the magnitude of $^6J_{90}$, intuitively rather unlikely, then $^6J_{90}$ is −0.92 Hz in benzal chloride.

Actually, the apparent twofold barrier in benzal chloride is not very sensitive to the magnitude of $^6J_{90}$. Thus, if $^6J_{90}$ is −0.98 ± 0.06 Hz, then $\langle \sin^2 \theta \rangle$ at 300 K follows as 0.18(1), 0.17(1), and 0.15(1) from the ^6J values of −0.176(2), −0.170(2), and −0.147(2) Hz in CS_2, $CDCl_3$, and acetone-d_6 solutions, respectively (Table 1). These numbers correspond to twofold barriers of 8.6(4), 8.9(4), and 10.2(6) kJ/mol for the three solvents. A very conservative approach then has it that the internal barrier to rotation in benzal chloride is 9.2 ± 1.6 kJ/mol.

Solvent dependence of the barrier

A less pessimistic attitude considers the possibility of a higher internal barrier in acetone-d_6, possibly caused by significant stabilization of the ground state by electrostatic interactions. A similar stabilization of the ground state appears to occur for benzyl chloride (12). In contrast, $^6J(H,CH)$ is independent of solvent for ethylbenzene (10) and isopropylbenzene (11). Of course, the latter are relatively nonpolar molecules. The STO-3G MO calculations (7) on benzyl chloride yield a negligible difference between the dipole moments of the conformers defined by θ = 0° and 90° (the minimal basis set in general yields dipole moments nearly as close to experiment as are 6-31G* results (17)). Therefore simple dielectric continuum models will not account for an increased barrier in acetone-d_6 solution.

Now, it is conceivable that hydrogen bonding of the polar C—H bond of the side chain in benzal chloride with acetone-d_6 molecules (note the relatively large deshielding of the α proton in acetone-d_6 solution in Table 1) causes a decrease in the magnitude of ^6J. An intrinsic solvent effect of more than 16% of its magnitude in CS_2 solution does seem unlikely, however (18).

Solvent perturbations of vicinal or longer range coupling constants between protons are more likely (18) of a size displayed for the intraring coupling constants in Table 1. $^5J_{25}$ increases by 2.4% when benzal chloride is transferred from CS_2 to acetone-d_6 solution. Yet, the same change also occurs for isopropylbenzene (11), in which ^6J is invariant to solvent. It is probable, therefore, that the internal barrier in benzal chloride is somewhat higher in the more polar medium.

The size and shape of the barrier

The apparent twofold barrier of 8.9(4) kJ/mol in $CDCl_3$ solution is smaller than the twofold barrier of 11.6 kJ/mol computed for the free molecule with the minimal basis set (7) and the barrier of 11.0 kJ/mol calculated with the 4-31G basis (5). A twofold barrier with a magnitude of 17.3 kJ/mol, as obtained from spin-lattice relaxation measurements on the $CDCl_3$ solution, requires a $\langle \sin^2 \theta \rangle$ of 0.082 at 300 K. Three possibilities present themselves.

One is that $^6J_{90}$ is very different from that used above. A ^6J of −0.170(2) Hz in the $CDCl_3$ solution will correspond to a $\langle \sin^2 \theta \rangle$ of 0.082 if $^6J_{90}$ is −2.07 Hz. In toluene, $^6J_{90}$ is −1.20 Hz (13). A larger magnitude of $^6J_{90}$ in benzal chloride than in toluene is physically unlikely, is in general contraindicated by INDO MO FPT computations (19) in our laboratory, and is rejected.

A second possibility involves the existence of an angle-independent term in the relationship, $^6J = {}^6J_0 + {}^6J_{90} \sin^2 \theta$, analogous to the equation for β-hyperfine interactions in radicals (20). This matter was recently investigated in some detail (21) for benzylidene diacetate, its 2,6-dibromo derivative, and for 2,6-dichlorobenzalchloride. For the diacetate, a maximum magnitude of 0.02 Hz for $^6J_0$ was derived, although a vanishing

TABLE 1. ^{1}H NMR spectral parameters for benzal chloride in various solvents at 300 K

Parameter	Value		
	CS_2/C_6D_{12}[a]	$CDCl_3$[b]	Acetone-d_6[b]
ν_{CH}	1972.488(1)[c,d,e]	2012.294(1)[c,f]	2163.380(1)[c,g]
ν_2	2239.682(1)	2271.114(1)	2303.522(1)
ν_3	2193.415(1)	2220.725(1)	2241.344(1)
ν_4	2186.660(1)	2214.241(2)	2243.053(1)
$^3J_{23}$	7.866(1)	7.879(1)	7.882(1)
$^3J_{34}$	7.486(1)	7.498(1)	7.501(1)
$^4J_{26}$	2.092(1)	2.113(2)	2.097(1)
$^4J_{24}$	1.211(1)	1.210(2)	1.209(1)
$^4J_{35}$	1.379(1)	1.387(2)	1.387(1)
$^5J_{25}$	0.576(1)	0.582(1)	0.590(1)
^4J(H,CH)	−0.439(1)	−0.432(1)	−0.410(1)
^5J(H,CH)	0.278(1)	0.277(2)	0.277(1)
^6J(H,CH)	−0.176(2)	−0.170(2)	−0.147(2)
Calculated transitions	186	183	179
Assigned transitions	163	164	159
Peaks	142	143	145
Largest difference	0.016	0.021	0.015
Root-mean-square deviation	0.006	0.008	0.005

[a]As a 2.5 mol% solution in CS_2, containing also 10.0 mol% of C_6D_{12} and 0.5 mol% TMS.
[b]As a 2.5 mol% solution with 0.5 mol% TMS.
[c]In Hz at 300.135$_2$ MHz to high frequency of the peak due to internal TMS.
[d]Numbers in parentheses are the standard deviations in the last significant figure.
[e]The $^{35}Cl/^{37}Cl$ isotope shift (two bonds) is 0.052(4) Hz or 0.173(4) ppb, the heavier atom causing a shift to low frequency.
[f]The $^{35}Cl/^{37}Cl$ isotope shift is 0.058(4) Hz or 0.193(4) ppb.
[g]The $^{35}Cl/^{37}Cl$ isotope shift is 0.066(5) Hz or 0.220(5) ppb.

$^6J_0$ was also compatible with experiment. In 2,6-dichlorobenzal chloride, no evidence could be adduced for other than a negligibly small $^6J_0$ (21). Nevertheless, assume a $^6J_0$ of −0.02 Hz for benzal chloride. Then $\langle \sin^2 \theta \rangle$ becomes 0.15(1) for the $CDCl_3$ solution and the apparent V_2 rises to 10.2(6) kJ/mol only.

Finally, although not supported by the MO calculations, consider the possible presence of a fourfold component in the internal rotational potential. If V_4 is of opposite sign to V_2, then a V_2 of 17.0 kJ/mol and a V_4 of −5.5 kJ/mol correspond to a $\langle \sin^2 \theta \rangle$ of 0.170 at 300 K; the barrier *height* is then 17.0 kJ/mol (V_4 does not contribute at $\theta = 90°$) and is compatible with the relaxation measurements, but not with the existence of a local minimum at $\theta = 90°$. For isopropylbenzene, STO-3G and 6-31G MO computations (11) yield V_2 and V_4 components of opposite sign for the internal rotation about the C_{sp^2}—C_{sp^3} bond, with V_4 amounting to about 20% of the magnitude of V_2. Similar computations for ethylbenzene (10) also have a negative ratio, V_2/V_4. As the length of the C_{sp^2}—C_{sp^3} is increased, the computed magnitude of V_4 decreases markedly relative to that of V_2, possibly implying that where the distance between the methyl group and the *ortho* C—H bond is sufficiently large, the latter "sees" the methyl group as an "atomic entity" and no longer distinguishes among its individual C—H bonds (10). The computed barrier for benzyl chloride is twofold (12), in agreement with such a rationalization, as is that for benzal chloride.

Of course, the MO computations for the latter might simply be wrong, or the solvent may induce a large negative V_4. Yet, the computed potentials for ethylbenzene, isopropylbenzene, and benzyl chloride are consistent with the ^6J values for these molecules in solution, so that benzal chloride would represent an exception.

A local minimum at $\theta = 90°$ can be had with a positive ratio, V_2/V_4. If V_2 is 6.0 kJ/mol and V_4 is 4.5 kJ/mol, then $\langle \sin^2 \theta \rangle$ is again 0.170 at 300 K and the population (simple two-site approximation) of the conformer at a θ of 90° is about 8%. However, the *height* of the barrier is then very near 8 kJ/mol, incompatible with the spin-lattice relaxation data.

Figure 1 displays four internal potentials for benzal chloride and the figure caption represents a summary of the preceding discussion.

$^{37}Cl/^{35}Cl$ isotope effects

These effects over two bonds have been measured for the ^{1}H NMR spectra of CH_3Cl, CH_2Cl_2, $CHCl_3$, and benzyl chloride (22, 23). Substitution of ^{37}Cl for ^{35}Cl causes an increase in screening of the proton and, in Gombler's notation (24), a negative shift. In the chlorinated methanes these effects decrease in magnitude as the number of chlorine atoms increases and are additive for $CHDCl_2$ and $CDCl_3$ (22). They are also additive for benzyl chloride (23) and are −0.20 and −0.25 ppb for CS_2/C_6D_{12} and acetone-d_6 solution, respectively. For benzal chloride (footnotes to Table 1), the isotope effects are −0.17, −0.19, and −0.22 ppb for the CS_2/C_6D_{12}, $CDCl_3$, and acetone-d_6 solutions, respectively. These numbers are not dramatically different from those for $CHDCl_2$ or $CHCl_3$ (22, 23), but do display a significant solvent dependence.

Solvent-induced changes in isotope effects on nuclear shielding are apparently important (25) when intermolecular hydrogen bonding occurs. The shielding of the methine proton in benzal chloride decreases by 0.64 ppm when the latter is transferred from CS_2 to acetone-d_2 (Table 1), considerably more than the average decrease of 0.18 ppm for the ring protons. However, for benzyl chloride (12) the decreased shielding of the side-chain protons amounts only to 0.24 ppm for the solvent pair in

Can. J. Chem. Downloaded from www.nrcresearchpress.com by 186.148.149.217 on 09/07/12
For personal use only.

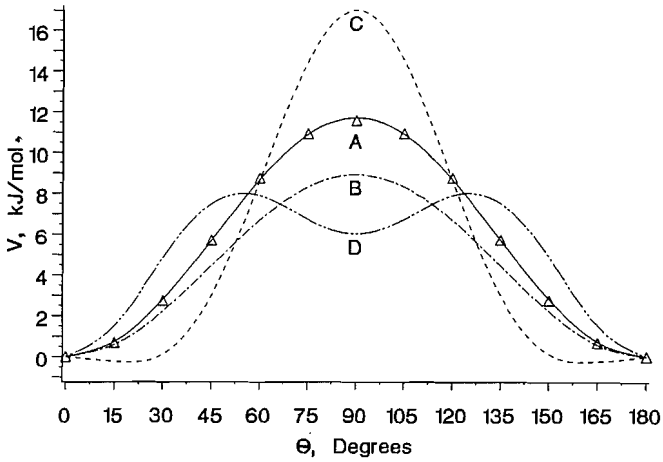


FIG. 1. In A the STO-3G MO potential (7) for rotation about the C_{sp^2}—C_{sp^3} bond in benzal chloride is shown. The computed energies are fit by the equation, $V(\text{kJ mol}^{-1}) = 11.7\sin^2\theta - 0.1\sin^2 2\theta$. In B the twofold potential, $8.9\sin^2\theta$, is compatible with the ^6J measured in $CDCl_3$ solution, θ being zero for the conformer in which the α C—H bond lies in the benzene plane. In C the potential, $V(\text{kJ mol}^{-1}) = 17.0\sin^2\theta - 5.5\sin^2 2\theta$, is displayed. It is consistent with the ^6J and with the ^{13}C spin-lattice relaxation times in $CDCl_3$ solutions; note the negative sign of V_4. In D, the potential, $V(\text{kJ mol}^{-1}) = 6.0\sin^2\theta + 4.5\sin^2 2\theta$, is compatible with a $\langle\sin^2\theta\rangle$ of 0.170 at 300 K and with a population of about 8% for the perpendicular conformer, that with θ = 90°. The height of the barrier, however, is only 8.0 kJ mol^{-1}.

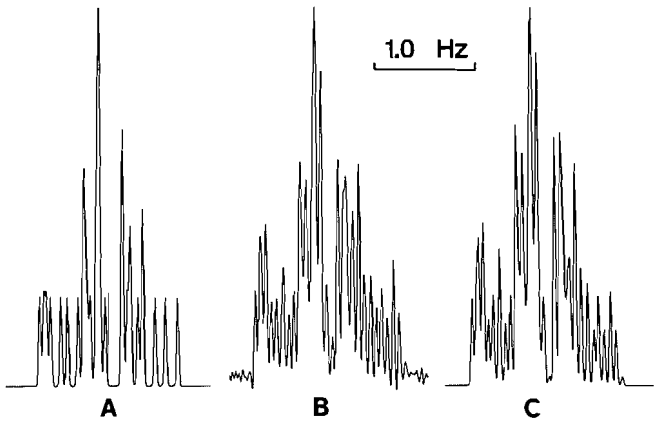


FIG. 2. The ^1H NMR spectrum of the methine proton of benzal chloride, as a 2.5 mol% solution in $CDCl_3$, is shown as B at 300 MHz and 300 K. On the left, A, the spectrum is computed with the spectral parameters in Table 1, but in the absence of $^{37}Cl/^{35}Cl$ isotope effects on the shift of the methine proton. On the right, C, the theoretical spectrum assumes an isotope shift of −0.19 ppb. The agreement with the measured spectrum is not exact, but is clearly better than in A. The ring proton spectrum does not suffer from isotope shifts, so that the long-range coupling constants are obtainable with high precision (Table 1).

question, yet the solvent dependence of the isotope effect is as large for benzyl chloride as for benzal chloride. Hence the perturbations of the electron distribution in the C—H bond by the solvent, as indicated by the observed shifts, are not simply related to those causing the changes in the isotope effect. In fact, significant solvent-induced changes in $^2H/^1H$ isotope effects on ^{13}C shielding have been recently measured for a nonpolar molecule, toluene-α-d_3 (26). In this molecule, however, the isotope effect over two bonds is *smaller* in acetone-d_6 than in $CDCl_3$ solution (26).

Experimental

Dilute solutions of benzal chloride (Aldrich) in CS_2/C_6D_{12}, $CDCl_3$, and acetone-d_6 were transferred to 5 mm o.d. NMR sample tubes. These were degassed by the freeze–pump–thaw procedure and were then flame-sealed to provide symmetrical tops. The ^1H NMR spectra derived from a Bruker AM300 spectrometer in the manner previously described (16). The spectra were analyzed with the computer program NUMARIT (27), as modified in this laboratory by R. Sebastian. The ensuing spectral data are presented in Table 1. Figure 2 illustrates the quality of the spectra, noting also that the presence of $^{37}Cl/^{35}Cl$ isotope effects on the chemical shift of the methine proton leads to complications not present for the ring proton region.

Acknowledgements

We are grateful to the Natural Sciences and Engineering Research Council of Canada for a grant-in-aid of research.

1. T. SCHAEFER, W. DANCHURA, and W. NIEMCZURA. Can. J. Chem. **56**, 36 (1978).
2. W. J. E. PARR and T. SCHAEFER. Acc. Chem. Res. **13**, 400 (1980).
3. S. TARIQ and P. K. VERMA. Spectrochim. Acta, Part A, **39**, 1027 (1983).
4. P. J. A. RIBEIRO-CLARO and J. J. C. TEIXEIRA-DIAS. J. Raman Spectrosc. **15**, 224 (1984).
5. M. K. AHMED, D. J. SWANTON, and B. R. HENRY. J. Phys. Chem. **91**, 293 (1987).
6. P. J. A. RIBEIRO-CLARO, A. M. D'A. ROCHA GONSALVES, and J. J. C. TEIXEIRA-DIAS. Spectrochim. Acta, Part A, **41**, 1055 (1985).
7. T. SCHAEFER and G. H. PENNER. J. Raman Spectrosc. **16**, 353 (1985).
8. P. J. A. RIBEIRO-CLARO, C. F. G. C. GERALDES, and J. J. C. TEIXEIRA-DIAS. J. Magn. Reson. **71**, 132 (1987).
9. K. B. WIBERG and M. A. MURCKO. J. Am. Chem. Soc. **110**, 8029 (1988).
10. T. SCHAEFER, G. H. PENNER, and R. SEBASTIAN. Can. J. Chem. **65**, 873 (1987).
11. T. SCHAEFER, R. SEBASTIAN, and G. H. PENNER. Can. J. Chem. **66**, 1495 (1988).
12. T. SCHAEFER, R. SEBASTIAN, and G. H. PENNER. **64**, 1372 (1986).
13. T. SCHAEFER, R. SEBASTIAN, and G. H. PENNER. Can. J. Chem. **63**, 2597 (1985).
14. R. LAATIKAINEN. Magn. Reson. Chem. **24**, 588 (1986).
15. R. LAATIKAINEN and K. TUPPURAINEN. J. Chem. Soc. Perkin Trans. **2**, 121 (1987).
16. T. SCHAEFER, J. PEELING, and R. SEBASTIAN. Can. J. Chem. **63**, 3219 (1985).
17. J. SAUER. Chem. Rev. **89**, 199 (1989).
18. M. BARFIELD and M. D. JOHNSTON. Chem. Rev. **73**, 53 (1973).
19. J. A. POPLE, J. W. MCIVER, and N. S. OSTLUUND. J. Chem. Phys. **49**, 2960 (1968); **49**, 2965 (1968).
20. C. HELLER and H. M. MCCONNELL. J. Chem. Phys. **32**, 1535 (1960).
21. T. SCHAEFER and C. S. TAKEUCHI. Can. J. Chem. **67**, 827 (1989).
22. F. A. L. ANET and M. KOPELEVICH. J. Am. Chem. Soc. **109**, 5870 (1987).
23. T. SCHAEFER and R. SEBASTIAN. J. Am. Chem. Soc. **109**, 6508 (1987).
24. W. GOMBLER. J. Am. Chem. Soc. **104**, 6616 (1982).
25. P. E. HANSEN. Annu. Rep. NMR Spectrosc. **8**, 1 (1979).
26. T. SCHAEFER, J. PEELING, and R. SEBASTIAN. Can. J. Chem. **65**, 534 (1987).
27. J. S. MARTIN, A. R. QUIRT, and K. E. WORVILL. The NMR program library, Daresbury Laboratory, Daresbury, U.K.

Can. J. Chem. Downloaded from www.nrcresearchpress.com by 186.148.149.217 on 09/07/12
For personal use only.

Photochemistry of cyclobutanones with nitrogen acids. A potential nucleoside synthesis

IVY E. E. HAYES, LINDA JANDRISITS, AND EDWARD LEE-RUFF[1]
Department of Chemistry, York University, Toronto, Ont., Canada M3J 1P3

Received September 8, 1988[2]

IVY E. E. HAYES, LINDA JANDRISITS, and EDWARD LEE-RUFF. Can. J. Chem. **67**, 2057 (1989).

Irradiation of 3-methylene-2,2,4,4-tetramethylcyclobutanone with nitrogen acids such as succinimide, phthalimide, imidazole, 3,5-dimethylpyrazole, purine, and benzimidazole gives 1:1 adducts that were identified as cyclic α-aminoacetals structurally related to nucleosides.

Key words: photochemistry of cyclobutanones, oxacarbene, nucleoside analogs.

IVY E. E. HAYES, LINDA JANDRISITS et EDWARD LEE-RUFF. Can. J. Chem. **67**, 2057 (1989).

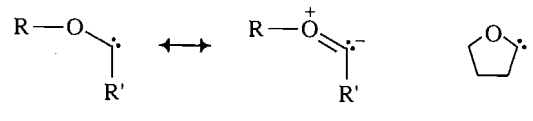
L'irradiation de la 3-méthylène-2,2,4,4-tétraméthylcyclobutanone en présence d'acides azotés comme la succinimide, la phtalimide, l'imidazole, la 3,5-diméthylpyrazole, la purine et la benzimidazole fournit des adduits 1:1 que l'on a identifiés comme étant des α-aminoacétals cycliques reliés d'un point de vue structural à des nucléosides.

Mots clés : photochimie de cyclobutanones, oxacarbène, analogues nucléoside.

[Traduit par la revue]

The strain associated with small ring systems promotes reactivity that contrasts that of larger ring strain-free molecules. Cyclobutanones undergo a variety of regio and stereoselective ring expansion reactions useful in the preparation of medicinally important compounds (1). Photochemical ring expansion to furanyl derivatives has also been reported to occur stereoselectively (2).

The photochemistry of cyclobutanones proceeds by three competitive pathways, decarbonylation, cycloelimination, and ring expansion to an oxacarbene **3** (3). The distribution of the photoproducts is largely dependent on the nature of the ring substituent and recently we have shown that it is also dependent on solvent effects (4). To date, the cyclic oxacarbene has been trapped by intra or intermolecular reactions with OH functional groups (5, 6).[3] In one case of a related cyclic oxacarbene generated photochemically, a small amount of product derived from olefin insertion was observed (8). Recent studies by Kesselmayer and Sheridan (9) on acyclic oxacarbenes indicate that these can be represented by zwitterionic resonance contributors such as **2** to account for their somewhat unusual reactivity when compared to dialkylmethylenes. The nucleophilic character of such oxacarbenes can readily account for the commonly observed OH insertion products and the lack of olefin insertion, in contrast to the behavior of dialkylmethylenes. We were interested whether oxacarbenes **3** generated from cyclobutanones would be sufficiently basic to insert into N—H bonds. Such a reaction would be of synthetic use in the direct preparation of α-aminofuranosides related to nucleosides. Pirrung and DeAmicis recently reported that N—H insertion of selected acidic amines occurs with an oxacarbene generated from a cyclobutanone (10). Preliminary investigation with cyclobutanone and ketone **4** showed that mixtures with aniline, diethylamine, and cyclohexylamine were photostable under uv irradiation based on gc and ^{1}H nmr analysis of reaction mixtures.[4] On the other hand, more acidic nitrogen acids with pK_a values comparable to, or smaller than, those of alcohols form 1:1 adducts with **4** under uv irradiation. Ketone **4** was chosen since ring expansion to oxacarbene **5** represents the dominant pathway in its photoreaction with alcohols (3). Both photodecarbonylation and cycloelimination are insignificant for **4**.



1 **2** **3**

SCHEME 1

Results and discussion

Mixtures of **4** (0.01–0.20 M) and the nitrogen acid (succinimide, phthalimide, imidazole, 3,5-dimethylpyrazole, purine, and benzimidazole) in dry tetrahydrofuran, dichloromethane, or acetonitrile were irradiated using a high pressure mercury lamp for 17.5–78 h. In most cases a single product was obtained and identified as the 1:1 photoadduct(s) **6***a–f* by spectroscopic and analytical data. The proton nmr spectra of **6** were characteristic in the separation of all four methyl protons, the observation of an acetal proton (δ 5.5–6.2 ppm), an almost equivalent AB pattern for the methylene protons (4.8–5.0 ppm), and signals associated with the nitrogen acid. In some cases, when the solvent was not rigorously dried, a 2:1 adduct of ketone **4** with water was obtained and identified as the bis-acetal **7**. This product most likely arises from the photoreaction of the water adduct **6** (X = OH) with oxacarbene **5**. Confirmation of this was obtained by photolysis of **5** in a solution containing 1 equivalent of **6** (X = OH) and the observation of **7** as a major product. Further confirmation of **6***a* was obtained from its acid methanolysis using saturated HCl solutions to give acetal **6** (X = OCH_3), identical in all respects to the photoadduct obtained when **4** was irradiated in methanol solution.

The absence of photocarbene insertion into N—H bonds of simple amines suggests that the basicity of the carbene may be a factor in such reactions. Although C—H insertion by aryl and alkyl carbenes is a common reaction (11), these proceed by

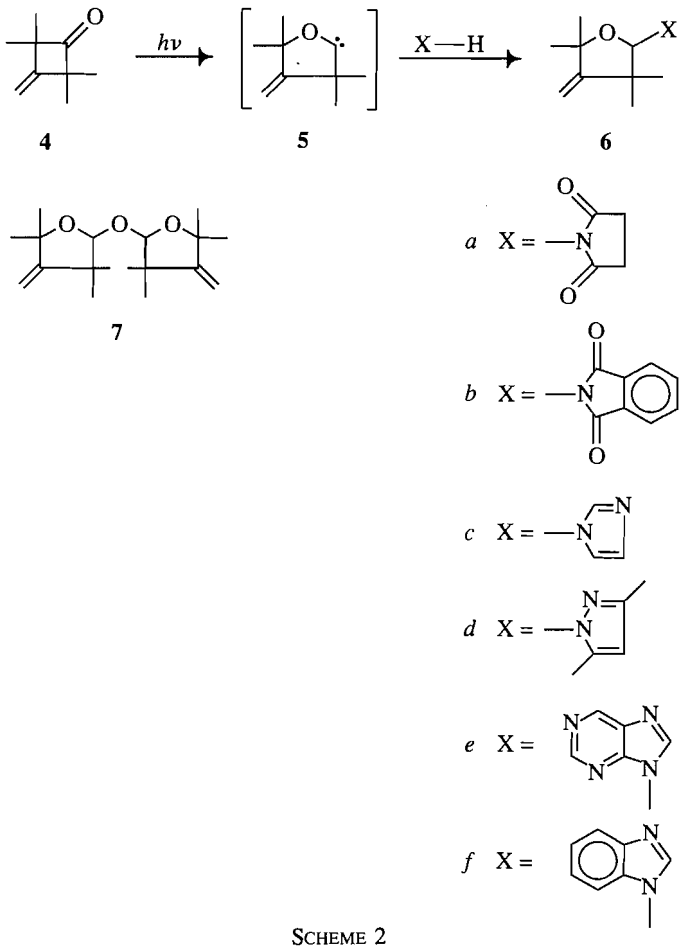
[1]Author to whom correspondence may be addressed.

[2]Revision received June 9, 1989.

[3]There are some examples of 1,2-hydrogen shifts leading to enol ethers. See, for example, ref. 7.

[4]Solutions containing 0.1 g of ketone **4** in 25 mL of CH_2Cl_2 with 5 equivalents of amine were irradiated for 17–20 h. Unreacted cyclobutanone and amine were detected by gc and nmr. Some photodecomposition of **4** to volatile products occurred (presumably 1,1,2,2-tetramethyl-3-methylenecyclopropane and 1,1-dimethyl-2-isopropylidenecyclopropane (19)) but these could not be isolated. However, no reaction products with the amines could be detected.

Can. J. Chem. Downloaded from www.nrcresearchpress.com by 186.148.149.217 on 09/07/12
For personal use only.



SCHEME 2

mechanisms not involving proton transfer. Evidence for proton transfer reactions to aryl carbenes has been obtained for the O—H insertions of these species at temperatures slightly below ambient (12). Although oxacarbenes are considered to be nucleophilic carbenes relative to alkyl and aryl carbenes, the proton affinities of methoxylmethylene are about 10 kcal/mol lower than those of methylmethylene (13). This would suggest that if the proton transfer mechanism is involved in the formation of X—H insertion photoproducts, then the X—H acidity would have to be a contributing factor in the efficiency of this reaction. An alternate mechanism for X—H insertion involving electrophilic attack by the carbene at X and formation of an ylide (14) can be ruled out in our case since the more nucleophilic aniline, diethylamine, and cyclohexylamine did not undergo photoreaction with **4**. Although it has been reported that simple amines undergo N—H insertions with a photocarbene generated from a cyclobutanone (10), these photoadducts were not unambiguously characterized and could have been misinterpreted, with their actual structures being the hemiacetal produced from cyclobutanone photolysis with adventitious water present. The nmr data and gc retention times of the amine adducts and the hemiacetal are quite similar.

The possibility of using chiral, stereospecifically substituted cyclobutanones (15) with appropriate substituents in such a photoreaction in the preparation of nucleoside analogues is under investigation. It is known that photolysis of unsymmetric cyclobutanones proceeds in a stereoselective manner (2). The question of stereochemistry at the anomeric center in unsymmetrically substituted furanosides will be investigated.

Experimental

Melting points (mp) were determined on a Reichert melting point apparatus and were uncorrected. Infrared (ir) spectra were recorded on Pye Unicam SP-1000 and SP3-200 spectrophotometers as thin films or KBr pellets. Nuclear magnetic resonance (nmr) spectra were recorded on a Bruker AM-300 (300 MHz) spectrometer using samples dissolved in $CDCl_3$ containing 1% Me_4Si as internal standard. All nmr values are reported as chemical shift δ in ppm downfield from Me_4Si. Mass spectra were recorded on a VG Micromass 16F spectrometer. High resolution mass spectrometry was performed at the McMaster Regional Centre for Mass Spectrometry using a VG ZAB-E instrument in the EI mode at 70 eV. Elemental analyses were performed by Guelph Chemical Laboratories Limited. Photolyses were carried out using a Hanovia 450-W high pressure mercury arc lamp in a water cooled quartz immersion well with a Pyrex filter. The quartz sample tube was strapped around this well and immersed in an ice–water bath. Reaction mixtures were degassed with N_2 for 1 h prior to photolyses. Column chromatography utilized Terochem silica gel (flash chromatography type, 20–45 μm) or Merck silica gel 60 (70–270 mesh). Analytical thin-layer chromatography (tlc) was conducted on precoated plastic sheets (silica gel 60 F_{254}, layer thickness 0.2 mm) manufactured by E. Merck and Co. The sheets were visualized by examination with ultraviolet light (254 nm) or by dipping with a phosphomolybdic acid solution (20% in ethanol) followed by heating the sheet to 75°C. Anhydrous ether was obtained from Fisher Scientific Ltd. Reagent grade tetrahydrofuran (Fisher) was dried over NaOH and distilled from Na before use. Gold label acetonitrile was distilled from CaH_2 and stored over molecular sieves. Glass distilled hexane and dichloromethane were obtained from BDH Chemicals and used without distillation. Nitrogen acids were obtained from Aldrich Chemical Co., Inc. and not further purified unless otherwise stated.

3-Methylene-2,2,4,4-tetramethylcyclobutanone **4**

This ketone was prepared by a modification of the method of Hamon (16) and Lee-Ruff (17). The monophenylimine of 2,2,4,4-tetramethylcyclobutane-1,3-dione (24.2 g) (18) in 121 mL ether was added in one lot to a stirred suspension of dry triphenylphosphonium methyl iodide (50.9 g) and potassium *tert*-butoxide (14.5 g) in ether (606 mL) under an atmosphere of nitrogen. The canary-yellow coloured mixture was stirred overnight. After filtration of the triphenylphosphine oxide, the filtrate was diluted with water and extracted with ether. The ether layer was then dried over anhydrous magnesium sulfate and the ether distilled using a short Vigreux column. The crude imine of **4** (16.1 g) was stirred and refluxed with 50% acetic acid (100 mL). A solid collected in the reflux condenser in a few minutes. This was washed back into the solution and refluxing continued for 1 h. After cooling, the excess acetic acid was destroyed by addition of solid bicarbonate. The mixture was then extracted with ether and the ether layer was washed with water until neutral, dried over anhydrous magnesium sulfate, and distilled through a short column to give an oil. The oil mixture was sublimed at room temperature at 25 Torr (1 Torr = 133.3 Pa) pressure to give a crystalline material **4**, mp 43–44°C (lit. (16) mp 42–43°C) (6.3 g, 40%; 2 steps).

2-Succinimidyl-3,5-tetramethyl-4-methylene tetrahydrofuran **6**a

A solution of 0.25 g (1.81 mmol) of ketone **4** and 0.90 g (9.08 mmol) of succinimide (recrystallized from EtOH) in 150 mL of CH_2Cl_2 was irradiated for 25.25 h. Removal of the CH_2Cl_2 by rotary evaporation and flash chromatography on silica gel (10% tetrahydrofuran/hexane) gave 0.11 g (26%) of **6***a* (recrystallized from pentane); mp 48–49°C; ir (KBr), cm^{-1}: 3090 (=C—H), 2980 (CH), 1790, 1710 (C=O), 1090 (C—O); ^1H nmr δ: 5.68 (s, acetal H), 4.84 (AB *exo* CH_2), 2.67 (s, CH_2 of succinimidyl), 1.51, 1.38, 1.31, 1.10 (s, methyl H's); ^{13}C nmr δ: 176.1 (CO), 163.1 (quat. C of C=C), 101.6 (*exo* CH_2), 88.9 (acetal C), 83.8 (quat. C α to O), 45.7 (quat. C), 30.5, 30.2, 27.8, 23.3 (CH_3's), 27.5 (CH_2 of succinimidyl); ms, *m/e*: 237 (M^+), 222 ($M^+ - C_{12}H_{16}NO_3$), 139 ($M^+ - C_4H_4NO_2$), 123 ($M^+ - C_9H_{15}$). *Anal.* calcd. for $C_{13}H_{19}NO_3$: C 65.80, H 8.07, N 5.90; found: C 65.76, H 8.04, N 5.68.

Can. J. Chem. Downloaded from www.nrcresearchpress.com by 186.148.149.217 on 09/07/12
For personal use only.

Can. J. Chem. Downloaded from www.nrcresearchpress.com by 186.148.149.217 on 09/07/12
For personal use only.

2-Phthalimidyl-3,5-tetramethyl-4-methylene tetrahydrofuran **6**b

A solution of 0.50 g (3.62 mmol) of ketone **4** and 0.48 g (3.26 mmol) of phthalimide in 20 mL of tetrahydrofuran was irradiated for 62 h. Solvent evaporation by rotary evaporation and column chromatography (10% tetrahydrofuran/hexane) gave 0.13 g (14%) of **6***b* (recrystallized from hexane); mp 114–115°C; ir (thin film), cm^{-1}: 3070 (=C—H), 2970 (C—H), 1775, 1720 (C=O), 1610 (C=C), 1050 (C—O); ^1H nmr δ: 7.65 (dd, J = 5.5 Hz, 3.0 Hz, CH of phthalimidyl), 7.77 (dd, J = 5.5 Hz, 3.0 Hz, CH of phthalimidyl), 5.84 (s, acetal H), 4.91 (AB *exo* CH_2), 1.57, 1.42, 1.36, 1.17 (s, methyl H's); ^{13}C nmr δ: 168.0 (CO), 160.1 (quat. C of C=C), 134.3 (phthalimide C-5, C-6), 132.5 (phthalimide C-3a, C-7a), 123.5 (phthalimide C-4, C-7), 105.7 (*exo* CH_2), 89.1 (acetal C), 85.2 (quat. C α to O), 43.3 (quat. C), 29.8, 29.6, 29.5, 29.4 (CH_3's); *m/e*: 286 $(M + H)^+$, 139 $(M^+ - C_8H_4NO_2)$; high resolution ms, *m/e* calcd.: 286.1444; found: 286.1438. *Anal.* calcd. for $C_{17}H_{19}NO_3$: C 71.56, H 6.71, N 4.91; found: C 71.29, H 7.14, N 4.46.

2-Imidazolyl-3,5-tetramethyl-4-methylene tetrahydrofuran **6**c

A solution of 0.23 g (1.66 mmol) of ketone **4** and 0.066 g (0.97 mmol) of imidazole (recrystallized from benzene) in 10 mL of tetrahydrofuran was irradiated for 26.5 h. Solvent removal by rotary evaporation, followed by two flash columns (15% tetrahydrofuran/hexane) gave 0.19 g (95%) of white crystalline **6***c* (recrystallized from hexane); mp 64.5–65.5°C; ir (KBr), cm^{-1}: 3120 (=C—H), 2990 (C—H), 1805 ($R_2C{=}CH_2$), 1520, 1490, 1465, 1378 (azole), 1080 (C—O); ^1H nmr δ: 7.66 (s, H of C-2 of imidazole), (7.04, 7.07) (s, H of C-4 and C-5 of imidazole), 5.48 (s, acetal H), 4.94 (AB *exo* CH_2), 1.53, 1.39, 1.22, 0.80 (s, methyl H's); ^{13}C nmr δ: 162.8 (quat. C of C=C), 135.7 (imidazole C-2), (129.0, 117.1) (imidazole C-4, C-5), 104.5 (*exo* CH_2), 93.1 (acetal C), 82.4 (quat. C α to O), 46.7 (quat. C), 29.9, 28.7, 24.9, 24.1 (CH_3's); ms, *m/e*: 206 (M^+), 139 $(M^+ - C_3H_3N_2)$. *Anal.* calcd. for $C_{12}H_{18}N_2O$: C 69.87, H 8.79, N 13.58; found: C 70.22, H 8.93, N 13.76.

3,5-Dimethylpyrazole adduct **6**d

A solution of 0.50 g (3.62 mmol) of ketone **4** and 1.74 g (18.1 mmol) of 3,5-dimethylpyrazole (recrystallized from EtOH) in 30 mL of CH_2Cl_2 was irradiated for 20.5 h. Removal of the CH_2Cl_2 by rotary evaporation followed by flash column chromatography (10% tetrahydrofuran/hexane) yielded 0.36 g (43%) of a colourless oil **6***d*; ir (thin film), cm^{-1}: 3070 (=C—H), 2960 (C—H), 1655 (C=C), 1555, 1465, 1365 (azole), 1065 (C—O); ^1H nmr δ: 5.73 (s, pyrazole H-4), 5.58 (s, acetal H), 4.85 (AB *exo* CH_2), (2.28, 2.16) (s, pyrazole CH_3's), 1.61, 1.41, 1.32, 0.89 (s, methyl H's); ^{13}C nmr δ: 163.8 (quat. C of C=C), (147, 139.5) (C-3 and C-5 of pyrazole), 105.5 (C-4 of pyrazole), 102.3 (*exo* CH_2), 94.0 (acetal C), 83.8 (quat. C α to O), 47.5 (quat. C), (30.3, 29.3) (pyrazole CH_3's), 29.2, 22.9, 13.5, 11.6 (CH_3's); ms, *m/e*: 234 (M^+), 139 $(M^+ - C_5H_7N_2)$; high resolution ms, *m/e* calcd.: 234.1734; found: 234.1742.

Purine adduct **6**e

A solution of 1.05 g (7.60 mmol) of ketone **4** and 0.52 g (4.33 mmol) of purine in 500 mL of acetonitrile was irradiated for 78 h. Solvent removal by rotary evaporation and column chromatography (20% tetrahydrofuran/hexane) gave 0.35 g (31%) of a yellow oil **6***e*; ir (thin film), cm^{-1}: 2960 (C—H), 1660 (C=C), 1593, 1580, 1495, 1410, 1370 (purine), 1060 (C—O); ^1H nmr δ: 9.16 (s, H-6 of purine), 8.98 (s, H-2 of purine), 8.37 (s, H-8 of purine), 6.23 (s, acetal H), 5.00 (AB *exo* CH_2), 1.59, 1.46, 1.39, 0.88 (s, methyl H's); ^{13}C nmr δ: 162.5 (quat. C of C=C), 152.3 (C-2 of purine), 151.0 (C-4 of purine), 148.3 (C-8 of purine), 143.6 (C-6 of purine), 128.0 (C-5 of purine), 104.6 (*exo* CH_2), 90.0 (acetal C), 82.9 (quat. C α to O), 46.7 (quat. C), 29.6, 28.4, 25.1, 24.4 (CH_3's); ms, *m/e*: 258 (M^+), 139 $(M^+ - C_5H_3N_4)$; high resolution ms, *m/e* calcd.: 258.1482; found: 258.1493.

2-Benzimidazolyl-3,5-tetramethyl-4-methylene tetrahydrofuran **6**f

A solution of 0.56 g (4.05 mmol) of ketone **1** and 0.46 g (3.89 mmol) of benzimidazole in 45 mL of tetrahydrofuran was irradiated for 17.5 h. Solvent removal by rotary evaporation and flash column chromatography gave 0.93 g (93%) of crystalline **6***f* (recrystallized from hexane); mp 138–139°C; ir (KBr), cm^{-1}: 3060 (=C—H), 2980 (C—H), 1662 (C=C), 1615, 1490, 1468, 1370, 1320 (azole), 1060 (C—O); ^1H nmr δ: 8.18 (s, H-2 of benzimidazole), (7.45, 7.82) (m, H-7, H-4 of benzimidazole), 7.28 (m, H-5, H-6 of benzimidazole), 5.89 (s, acetal H), 4.98 (AB *exo* CH_2), 1.60, 1.45, 1.32, 0.87 (s, methyl H's); ^{13}C nmr δ: 163.0 (quat. C of C=C), (143.6, 133.2) (quat. C's of benzimidazole), 141.3 (benzimidazole C-2), (123.0, 122.3) (benzimidazole C-5, C-6), (120.3, 110.5) (benzimidazole C-4, C-7), 104.5 (*exo* CH_2), 91.7 (acetal C), 82.4 (quat. C α to O), 47.2 (quat. C), 29.8, 28.4, 25.3, 24.5 (CH_3's); ms, *m/e*: 256 (M^+), 139 $(M^+ - C_7H_5N_2)$. *Anal.* calcd. for $C_{16}H_{20}N_2O$: C 74.97, H 7.86, N 10.93; found: C 74.61, H 7.92, N 11.10.

*3,3,5,5-Tetramethyl-4-methylene-2-methoxytetrahydrofuran (***6***) (X = OCH_3)*

A solution of 0.64 g (4.63 mmol) of ketone **4** in 20 mL of methanol was irradiated for 24 h. Solvent evaporation and column chromatography (5% tetrahydrofuran/hexane) gave **6** (X = OCH_3), whose ^1H nmr spectrum was similar to the literature (19): ^1H nmr δ: 4.82 (s, 1), 4.78 (s, 1), 4.54 (s, 1), 3.34 (s, 3), 1.37 (s, 6), 1.14 (s, 3), 1.11 (s, 3).

A solution of 0.28 g (2.03 mmol) of **6***a* in 2 mL of a saturated HCl/MeOH solution was stirred under N_2 for 1 h. The product obtained was identical to **6** (X = OCH_3).

*3,3,5,5-Tetramethyl-4-methylene-2-hydroxytetrahydrofuran (***6***) (X = OH)*

A solution of 0.50 g (3.63 mmol) of ketone **4** in 20 mL of tetrahydrofuran and 1 mL of water was irradiated for 12 h. Solvent evaporation was followed by addition of ether (50 mL) to the crude oil. The ether fraction was washed with water (2 × 50 mL), dried with magnesium sulfate, and concentrated by rotary evaporation to give 0.33 g (58%) of a yellow oil; ir (thin film), cm^{-1}: 3390 (OH), 2970 (C—H), 1665 (C=C), 1380, 1365 (*gem* dimethyls), 1080, 1035 (C—O); ^1H nmr δ: 5.06 (s, acetal H), 4.83, 4.78 (AB *exo* CH_2), 4.20 (bs, OH), 1.42, 1.32, 1.11, 1.10 (s, methyl H's); ^{13}C nmr δ: 164.0 (quat. C of C=C), 103.9 (acetal C), 102.8 (*exo* CH_2), 83.3 (quat. C α to O), 47.2 (quat. C), 31.6, 30.5, 28.1, 21.5 (CH_3's); ms, *m/e*: 139 $(M^+ - OH)$.

Bis-acetal **7**

A solution of 0.33 g (2.11 mmol) of the crude alcohol **6** (X = OH) and 0.24 g (1.74 mmol) of ketone **4** in 20 mL of tetrahydrofuran was irradiated for 7 h. Solvent evaporation and column chromatography (5% ethyl acetate/hexane) gave 0.12 g (24%) of a colourless oil **7**; ir (thin film), cm^{-1}: 2960 (C—H), 1375, 1360 (*gem* dimethyls), 1060 (C—O); ^1H nmr δ: 4.87 (s, acetal H), 4.79, 4.76 (AB *exo* CH_2), 1.41, 1.36, 1.14, 1.10 (s, methyl H's); ^{13}C nmr δ: 164.6 (quat. C of C=C), 108.9 (acetal C), 101.8 (*exo* CH_2), 83.8 (quat. C α to O), 47.7 (quat. C), 31.1, 30.6, 29.2, 22.1 (CH_3's); ms, *m/e*: 294 $(M^+$, 8%), 279 $(M^+ - CH_3$, 18%), 139 $(M^+ - C_9H_{15}O$, 100%).

Acknowledgments

We would like to thank NSERC of Canada for financial support of this project and Miss Lorna Dahl for technical assistance.

1. D. Bellus and B. Ernst. Angew. Chem. Int. Ed. Engl. **27**, 797 (1988).
2. N. J. Turro, D. Bauer, V. Ramamurthy, and F. Warren. Tetrahedron Lett. **22**, 611 (1981).
3. D. R. Morton and N. J. Turro. Adv. Photochem. **9**, 197 (1974).
4. E. Lee-Ruff, A. C. Hopkinson, and H. Kazarians-Moghaddam. Tetrahedron Lett. **24**, 2067 (1983).
5. M. Pirrung. Angew. Chem. Int. Ed. Engl. **24**, 1043 (1985).
6. D. R. Morton, E. Lee-Ruff, R. M. Southam, and N. J. Turro. J. Am. Chem. Soc. **92**, 4349 (1970).

7. S. AYRAL-KALOUSTIAN and W. C. AGOSTA. J. Org. Chem. **47**, 284 (1982).
8. P. YATES and R. O. LOUTFY. Acc. Chem. Res. **8**, 209 (1975).
9. M. A. KESSELMAYER and R. S. SHERIDAN. J. Am. Chem. Soc. **108**, 99 (1986).
10. M. C. PIRRUNG and C. V. DEAMICIS. Heterocycles, **25**, 189 (1987).
11. C. WENTRUP. Reactive molecules. J. Wiley & Sons, New York. 1984. p. 162.
12. H. TOMIOKA, S. SUZUKI, and Y. IZAWA. J. Am. Chem. Soc. **104**, 3156 (1982).
13. A. C. HOPKINSON and M. H. LIEN. Can. J. Chem. **63**, 3582 (1985).
14. W. KIRMSE, K. LOOSEN, and H. D. SLUMA. J. Am. Chem. Soc. **103**, 5935 (1981).
15. A. E. GREENE and F. CHARBONNIER. Tetrahedron Lett. **26**, 5525 (1985).
16. D. P. G. HAMON. J. Am. Chem. Soc. **90**, 4513 (1968).
17. E. LEE-RUFF. Can. J. Chem. **50**, 952 (1972).
18. R. H. HASEK, E. U. ELAN, and J. C. MARTIN. J. Org. Chem. **26**, 4340 (1961).
19. D. R. MORTON and N. J. TURRO. J. Am. Chem. Soc. **95**, 3947 (1973).

Can. J. Chem. Downloaded from www.nrcresearchpress.com by 186.148.149.217 on 09/07/12
For personal use only.

Bromation régiosélective en série aromatique. I : Monobromation en position *para* de phénols et d'amines aromatiques par le tribromure de tétrabutylammonium

JACQUES BERTHELOT,[1] CATHERINE GUETTE, PAUL-LOUIS DESBÈNE ET JEAN-JACQUES BASSELIER
Laboratoire de chimie organique structurale, Unité associée n° 455, Université Pierre et Marie Curie, Bâtiment F, 4 place Jussieu, 75252 Paris CEDEX 05, France

ET

PATRICK CHAQUIN ET DANIEL MASURE
Laboratoire de chimie organique théorique, Unité associée n° 506, Université Pierre et Marie Curie, Bâtiment F, 4 place Jussieu, 75252 Paris CEDEX 05, France

Reçu le 16 février 1989

JACQUES BERTHELOT, CATHERINE GUETTE, PAUL-LOUIS DESBÈNE, JEAN-JACQUES BASSELIER, PATRICK CHAQUIN et DANIEL MASURE. Can. J. Chem. **67**, 2061 (1989).

L'action du tribromure de tétrabutylammonium ($TBABr_3$) sur les phénols et les amines aromatiques conduit exclusivement aux composés monobromés en *para* correspondants. Cette réaction est effectuée à température ambiante dans les solvants aprotiques non basiques. Les rendements en produits isolés et purs sont très élevés. Un mécanisme faisant appel à une substitution électrophile par l'anion Br_3^- est postulé, permettant l'interprétation de cette réaction de bromation régiosélective.

Mots clés : bromation, tribromure de tétrabutylammonium, phénols, amines aromatiques.

JACQUES BERTHELOT, CATHERINE GUETTE, PAUL-LOUIS DESBÈNE, JEAN-JACQUES BASSELIER, PATRICK CHAQUIN, and DANIEL MASURE. Can. J. Chem. **67**, 2061 (1989).

The reaction of tetrabutylammonium tribromide ($TBABr_3$) with phenols and aromatic amines in aprotic and non-basic solvents at 20°C gives exclusively the corresponding *para*-brominated compounds in high yields. A mechanism involving electrophilic substitution by the tribromide anion Br_3^- itself is suggested to account for the results, especially the regioselective *para* bromination.

Key words: bromination, tetrabutylammonium tribromide, phenols, aromatic amines.

La monobromation régiosélective de noyaux aromatiques pose encore des problèmes (1) : en effet, il reste difficile de contrôler le nombre et la position des atomes de brome introduits sur des composés aromatiques activés tels que phénols et amines aromatiques. La bromation par les méthodes classiques conduit le plus souvent à un mélange de composés monobromés en *ortho* et *para* accompagnés de dérivés polybromés (1, 2). Si la bromation effectuée à l'aide des réactifs tels que le bromure d'iode (3), le bromure cuivrique (4), le perbromure de dioxanne (5) et le *N*-bromosuccinimide (6) a permis de limiter le nombre d'atomes de brome introduits, par contre le contrôle de la régiosélectivité de la substitution n'est réalisée que dans des cas limités (7). Pour éviter les inconvénients d'emploi du brome, on a eu recours à des tribromures : de pyridinium (8), de diamino-2,4 thiazole (9), de triméthylphénylammonium (10) et de triméthylbenzylammonium (11). Ils conduisent souvent à une halogénation sélective mais présentent toutefois l'inconvénient d'être soit instables soit faiblement solubles. Le rôle de l'anion Br_3^- et son mécanisme d'action dans ces réactions de bromation sont encore discutés.

Nous avons eu l'opportunité d'utiliser le tribromure de tétrabutylammonium ($TBABr_3$) pour fixer du brome sur des doubles liaisons éthyléniques (12) et des triples liaisons acétyléniques (13) ou pour substituer sélectivement en α des acétals (12). $TBABr_3$ est un solide orangé, stable, non hygroscopique, à degré de brome actif constant et facilement utilisable dans des conditions douces. Il est également employé avec succès dans un milieu aussi complexe que la matrice pétrolière où il permet enfin la mesure d'un indice de brome (14). Des résultats expérimentaux récemment publiés (15) ont montré son efficacité pour bromer très sélectivement des dérivés aromatiques. Nous désirons préciser le rôle et le mécanisme d'action de l'ion Br_3^- dans ces réactions. Dans le présent mémoire, nous montrerons l'intérêt d'utiliser le $TBABr_3$ pour bromer sélectivement des carbures aromatiques et l'importance du solvant employé, et nous proposerons une explication sur la nature de l'agent bromant.

$$C_6H_5\text{-}A + TBABr_3 \longrightarrow p\text{-}BrC_6H_4\text{-}A + TBABr + HBr$$

A : OH, NH_2, NHR, NR_2

SCHÉMA 1

Résultats

Un équivalent de $TBABr_3$ dissous dans le chloroforme ($CHCl_3$) brome un équivalent de phénol (tableau 1) ou d'amine aromatique (tableau 2) d'une façon presque quantitative à température ambiante. La solution initialement orangée devient incolore quand $TBABr_3$ a totalement réagi et indique que la réaction est terminée (schéma 1).

Cette monobromation s'effectue d'une manière très régiosélective en position *para* puisque le rendement en produit secondaire ne dépasse jamais 3%, sauf dans le cas de l'aniline (tableau 2). Quand le sommet *para* est déjà substitué par un groupement alkyle la bromation a lieu en *ortho*, avec d'excellents rendements, mais elle est ralentie. Dans tous les cas les dérivés polybromés sont totalement absents. L'action de $TBABr_3$ sur les naphtols permet d'éviter la formation de produits de désaromatisation du noyau naphtalénique et de composés polybromés qui sont obtenus avec les agents de bromation classiques (2).

$TBABr_3$ se différencie nettement de Br_2 dans son comporte-

1. Auteur à qui adresser toute correspondance.

Printed in Canada / Imprimé au Canada

Can. J. Chem. Downloaded from www.nrcresearchpress.com by 186.148.149.217 on 09/07/12
For personal use only.

Can. J. Chem. Downloaded from www.nrcresearchpress.com by 186.148.149.217 on 09/07/12
For personal use only.

TABLEAU 1. Bromation de phénols par $TBABr_3$ à 20°C dans $CHCl_3$

Composé	Temps (min)[a]	Produit	R (%)[b]
Phénol	2	*p*-Bromophénol	95
Me-2 phénol	2	Bromo-4 Me-2 phénol	96
*t*Bu-2 phénol	2	Bromo-4 *t*Bu-2 phénol	96
Thymol	2	*p*-Bromothymol	96
Me-4 phénol	14	Bromo-2 Me-4 phénol	93
*t*Bu-4 phénol	12	Bromo-2 *t*Bu-4 phénol	94
Me-4 *t*Bu-2 phénol	8	Bromo-6 Me-4 *t*Bu-2 phénol	95
Naphtol-1	2	Bromo-4 naphtol-1	95
Naphtol-2	4	Bromo-1 naphtol-2	95

[a]Durée de la réaction considérée comme terminée quand la solution, initialement orangée, est devenue incolore.
[b]Rendement en produits isolés et purs.

TABLEAU 2. Bromation d'amines aromatiques par $TBABr_3$ dans $CHCl_3$ à 20°C

Composé	Temps (min)[a]	Produits	R (%)[b]	R (%)[c]
$C_6H_5NH_2$	3	*p*-$BrC_6H_4NH_2$	84	14
$C_6H_5NHCH_3$	2	*p*-$BrC_6H_4NHCH_3$	94	5
$C_6H_5NHC_6H_{11}$	2	*p*-$BrC_6H_4NHC_6H_{11}$	95	3
$C_6H_5NEt_2$	2	*p*-$BrC_6H_4NEt_2$	99	1
$(C_6H_5)_2NH$[d]	2	$(p\text{-}BrC_6H_4)_2NH$	99	1
NH_2-2 pyridine	2	NH_2-2 Br-5 pyridine	98	2

[a]Durée de la réaction considérée comme terminée quand la solution, initialement orangée, est devenue incolore.
[b]Rendements en produits isolés et purs.
[c]Rendements en composé dibromé-2,4 correspondant.
[d]Avec 2 équivalents de $TBABr_3$.

TABLEAU 3. Action de $TBABr_3$ dans $CHCl_3$ à 20°C sur divers composés aromatiques

Composé	Durée (min)	Produit	R (%)
Anisole	1500	Composés initiaux intégralement récupérés, même en prolongeant la durée de la réaction (8 jours)	
Acétate de phényle	1500		
β-Méthoxynaphtalène	1500		
Acétanilide	1500		
Mésitylène	1500		
	450(reflux)		
Pyridine	1500		
NH_2 pyridine	2	NH_2-2 Br-5 pyridine	98
Méthoxy-2 phénol	200	Br-4 MeO-2 phénol	95

ment vis à vis de certains carbures aromatiques. Ainsi le mésitylène facilement bromé par Br_2 ne réagit pas en présence de $TBABr_3$ même à l'ébullition du solvant. La substitution électrophile par le dibrome est aisée quand les fonctions phénol et amine sont protégées respectivement sous forme d'ether ou d'anilide. Dans ce dernier cas c'est même la façon la plus simple d'obtenir une amine aromatique monobromée en *para*, après déblocage en milieu basique (1, 2). $TBABr_3$ ne brome ni l'anisole, ni l'acétanilide (tableau 3). Cette différence de réactivité peut être mise à profit en synthèse; ainsi le méthoxy-2 phénol (guaiacol) réagit avec le tribromure dans $CHCl_3$ pour donner presque quantitativement le bromo-4 méthoxy-2 phénol. La pyridine, même en très large excès, dans le chloroforme, ne réagit pas avec $TBABr_3$. Par contre une pyridine substituée par un groupement amino comme l'amino-2 pyridine est bromée rapidement pour donner exclusivement l'amino-2 bromo-5 pyridine.

Influence de différent facteurs

Nous avons pris comme modèle d'étude la bromation d'un équivalent de phénol par un équivalent de $TBABr_3$.

(A) Température

La réaction effectuée à différentes températures (de −3°C à 75°C) dans $CHCl_3$ et CCl_4 ne conduit, dans tous les cas, qu'au *para*-bromophénol avec un rendement voisin de 95%, même si on augmente la durée de bromation (tableau 4).

TABLEAU 4. Evolution de l'action de $TBABr_3$ sur le phénol en fonction de la température[a]

T (°C)	Durée (min)	*p*-Bromophénol (%)
−3	5	95
20	2	95
60	2	95
76	2	94

[a]Ces essais sont effectués sur 4 mmol de phénol, 4 mmol de $TBABr_3$ dans 10 mL de solvant ($CHCl_3$ et CCl_4 pour l'éssai à 76°C). Les rendements sont ceux des produits isolés et purs. La durée indiquée correspond au moment où la solution initialement orangée est devenue incolore. Si on prolonge cette durée de réaction (15 min) pour les différents essais ci-dessus, aucune modification n'a lieu dans la nature et le rendement du produit bromé obtenu.

(B) Dilution

La dilution n'est pas un facteur modifiant la nature et le rendement de la réaction. Des essais, effectués tous avec les mêmes quantités de phénol et de $TBABr_3$ (3 mmol), à température ambiante et respectivement dans 7, 10, 20, 50 et 75 mL de $CHCl_3$, conduisent tous au même composé monobromé en *para* avec un rendement d'environ 95% en produit isolé et pur.

(C) Solvant

Tous les essais ont été effectués à température ambiante :

Dans les solvants aprotiques, peu polaires tels que CCl_4, $CHCl_3$ et CH_2Cl_2 ou plus polaires comme CH_3CN, seul l'isomère *para*-bromé est obtenu avec d'excellents rendements. La bromation en *ortho* et les polybromations sont presque totalement inhibées.

Dans les solvants basiques aprotiques, peu polaire comme le THF ou polaire comme le DMF, la réaction ne livre un mélange de *para*-bromophénol (75%) accompagné d'*ortho* et de polybromophénols qu'après 8 jours.

Dans l'éthanol absolu, milieu protique et moyennement polaire, la bromation donne après 30 min un mélange de 85% de *para*-bromophénol et de 15% d'*ortho*-bromophénol, sans polybromation.

Dans un mélange éthanol–eau (1 : 1) plus protique et plus polaire le pourcentage d'*ortho*-bromophénol atteint 25%, la durée de la réaction étant inchangée.

Ce dernier résultat nous a incité à utiliser un milieu biphasique où $TBABr_3$ est dissous dans $CHCl_3$ et le phénol dans l'eau (le pH est de 4,5). Après 20 min, 90% de *para*-bromophénol sont recueillis accompagnés de 9% de l'isomère *ortho*.

(D) Effet de sel

Le milieu biphasique décrit ci-dessus nous a permis d'examiner l'effet de sels peu solubles en phase organique. L'addition de LiBr à la solution aqueuse du phénol ne modifie pratiquement pas son pH mais induit la formation d'*ortho*-bromophénol (22%) aux dépens de l'isomère *para* (76%) mais sans polybromation. La réaction dure alors 100 min.

Si un excès de $LiClO_4$ (5 équivalents) est ajouté à la phase aqueuse la bromation est terminée au bout de 5 min et ne conduit qu'au seul *para*-bromophénol avec un rendement de 98%.

(E) Modification du pH du milieu réactionnel

Si la réaction est conduite en milieu chloroformique acidifié (par HCl ou H_2SO_4) ou basique (par KOH, ou en présence de butylamine), le phénol par action de $TBABr_3$ conduit au même mélange d'*ortho*, de *para* et de polybromophénols. Ce résultat est analogue à celui observé par action du dibrome sur le phénol.

L'ensemble de ces résultats est rassemblé dans le tableau 5.

Discussion

Le rôle de l'anion Br_3^- comme réactif de bromation et agent électrophile reste encore controversé. Diverses opinions contradictoires ont été formulées sur sa réactivité en la comparant toujours à celle du dibrome. Il est par exemple postulé que Br_3^- n'interviendrait pas lui même dans l'attaque électrophile (17), sa réactivité serait soit supérieure à celle du dibrome pour la bromation d'alkylphénols (18), soit inférieure pour bromer des anisoles (19), soit égale vis à vis d'hydroxy-8 quinoléïne (20). Enfin, certains auteurs ne se prononcent pas sur la réactivité de Br_3^- comme entité électrophile (21). Mais récemment il a été établi (22) qu'un tribromure dans un milieu peu polaire aprotique bromait les alcènes et que le mécanisme d'action de Br_3^- était différent de celui de Br_2.

On sait que l'ion tribromure donne lieu à l'équilibre :

$$Br_3^- \rightleftarrows Br_2 + Br^-$$

et que la position de cet équilibre est fortement influencée par la nature du solvant (tableau 6).

On constate que la proportion de dibrome est faible surtout dans les solvants aprotiques. Si, néanmoins, le Br_2 formé était l'agent bromant dans les réactions décrites précédemment, les bromations par $TBABr_3$ devraient conduire à la formation du mélange d'*ortho*, de *para* et de polybromophénols, par substitution électrophile analogue à celle du dibrome sur un composé aromatique. Un certain nombre d'arguments fondés sur les résultats expérimentaux nous paraissent apporter la preuve que l'ion Br_3^- est bien l'agent bromant quand $TBABr_3$ réagit avec le phénol dans un milieu aprotique : la grande stéréosélectivité observée sur le sommet *para*, l'absence totale de polybromations et la non réactivité avec certains composés aromatiques (anisole ou acétanilide par exemple) facilement bromés par Br_2.

Nous rappelons en outre que dans un précédent mémoire (13) nous avions établi que l'ion Br_3^- pouvait être rendu responsable de la formation stéréosélective d'alcènes dibromés (*E*) quand $TBABr_3$ agit sur un alcyne (schéma 2).

Un facteur important de ces réactions de bromation par $TBABr_3$ est le rôle du solvant qui peut changer la nature du contre-ion. Dans les solvants peu polaires aprotiques, $TBABr_3$ se trouve sous forme de paire d'ions, TAB^+ étant le cation associé à l'anion Br_3^-. Par contre, dans les solvants polaires et protiques, $TBABr_3$ est dissocié et il est connu que les ions trihalogénés de type X_3^- se lient au solvant par liaison hydrogène (25) ce qui revient à changer la nature du réactif. Les paires d'ions sont également modifiées dans les solvants basiques, où en outre il a été établi (26) qu'il se forme une liaison entre l'hydrogène de l'hydroxyle phénolique et le solvant, ce qui modifie la structure du réactif qui se trouve en partie sous forme phénoxyde.

L'eau en plus de son pouvoir dissociant peut avoir un triple rôle : atténuer la réactivité de Br_3^- par création de liaisons hydrogène, augmenter la dissociation de Br_3^- en Br_2 et, comme il a été prouvé (27), accélérer l'addition électrophile du dibrome formé.

L'effet de sel, notamment quand $LiClO_4$ est additionné en excès à la solution, en modifiant la nature du contre-ion permet d'annihiler le rôle de l'eau et on retrouve alors la formation régiosélective presque quantitative de l'isomère *para*. Cet effet de sel se manifeste différemment avec LiBr puisque à la

Can. J. Chem. Downloaded from www.nrcresearchpress.com by 186.148.149.217 on 09/07/12
For personal use only.

Can. J. Chem. Downloaded from www.nrcresearchpress.com by 186.148.149.217 on 09/07/12
For personal use only.

TABLEAU 5. Action de $TBABr_3$ sur le phénol, à 20°C, dans différentes conditions

Solvants	ε^d	E_T^d (kJ/mol)	Isomère *para*[a] (%)	Isomère *ortho*[a] (%)	Durée de la réaction (min)
$CHCl_3$	4,6	163,4	95	3	2
CH_2Cl_2	9	171,8	95	3	2
CCl_4	2,2	135,8	95	3	2
CH_3CN	37,5	192	95	3	1200
EtOH	24	217	85	15	30
THF[b]	7,4	156	75	12	8 jours
DMF[b]	37	183	75	12	8 jours
$EtOH–H_2O$ (1 : 1)			75	25	30
$CHCl_3–H_2O$[c]			90	9	20
$CHCl_3–H_2O$ (+ 5 équiv. LiBr[c])			76	22	100
$CHCl_3–H_2O$ (+ 5 équiv. $LiClO_4$[c])			98		5

[a]Rendements en produits purs et isolés, calculés par rapport au phénol.
[b]Dans ces deux solvants le mélange d'isomères monobromés est accompagné d'environ 10% de composés polybromés.
[c]Milieu biphasique.
[d]Référence 16.

TABLEAU 6. Constantes de dissociation de Br_3^- dans différents solvants, à 25°C

Solvant	$CHCl_3$, CH_3CN	EtOH	H_2O	AcOH
K_D	$(8–9) \times 10^{-6}$	$5,8 \times 10^{-3}$	$6,6 \times 10^{-2}$	$1,8 \times 10^{-2}$
Référence	22, 23	24	24	10

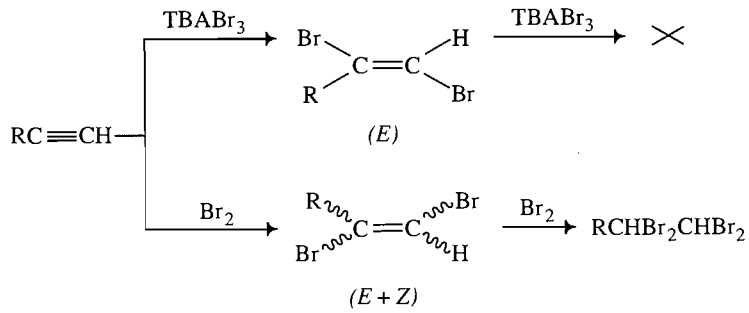


SCHÉMA 2

modification due au cation se superpose l'action de Br^-. Il en résulte la formation d'*ortho*-bromophénol aux dépens de l'isomère *para*. Une explication de ce résultat sera proposée ultérieurement (28).

Enfin nous rappelons que l'acidification du milieu permet la bromation de l'anisole par $TBABr_3$ pour donner le même mélange de produits mono- et poly-bromés que celui obtenu avec Br_2. Ce résultat nous parait normal car d'une part les hydracides solvatent fortement les anions par liaison hydrogène (29) et d'autre part les composés trihalogénés ne sont pas stables dans les milieux acidifiés et se dissocient facilement selon (25) :

$$Br_3^- + H^+ \rightarrow Br_2 + HBr$$

On peut donc envisager qu'en milieu acide Br_3^- est à la fois fortement dissocié en dibrome qui devient l'espèce réactive et que le proton se fixant comme contre-ion modifie l'aptitude électrophile des anions Br_3^- restants.

Au terme de cette discussion il est manifeste que si la température et la dilution n'apparaissent pas comme des facteurs déterminants, le solvant et les contre-ions jouent un rôle essentiel dans ces réactions de bromation par $TBABr_3$. L'anion tribromure est incontestablement l'agent responsable de ces substitutions électrophiles, comme en témoignant par exemple la grande régiosélectivité avec des rendements élevés, l'inhibition totale des polybromations et la bromation des alcynes. Toutefois le mécanisme de la réaction de l'anion Br_3^- impliquant la sélectivité sur le sommet *para* appelle des études complémentaires (28). Une confirmation de ces premières conclusions est recherchée dans des mesures cinétiques ainsi que dans une étude systématique de l'effet du contre-ion et enfin dans un essai d'approche théorique du mécanisme (28).

Partie expérimentale

Remarques générales

Tous les solvants et les réactifs ont été purifiés selon les procédés courants. Les points de fusion (*F*) ont été déterminés au banc de

Can. J. Chem. Downloaded from www.nrcresearchpress.com by 186.148.149.217 on 09/07/12
For personal use only.

Köfler. Le $TABBr_3$ et les produits utilisés proviennent de Janssen Chimica. Les spectres infra-rouges ont été enregistrés à l'aide d'un spectrophotomètre Pye Unicam SP3-200, ceux de rmn ^1H sur un appareil Bruker SY80 (80 MHz, dans $CDCl_3$ avec le TMS comme référence interne, les déplacements étant exprimés en ppm) et les spectres de masse (sm) avec un spectromètre magnétique MS 30 (à 70 eV). La chromatographie en phase gazeuse a été réalisée sur un chromatographe Hewlett Packard 5880 équipé d'un détecteur de flamme (FID) et d'une colonne capillaire Chrompack CP SIL 5 (longueur = 25 m; d_i = 0,22 mm; température de l'injecteur, 200°C). La programmation du four est de 70°C (pendant 5 min) à 200°C en 3°C/min. La pureté des produits a été vérifiée par chromatographie sur couche mince (ccm) sur gel de silice fluorescente (éluant mélange éther – éther de pétrole, de proportions diverses). La purification a été obtenue par chromatographie préparative (cp) sur gel de silice fluorescente Merck PF-254 (plaque 20 × 20 cm et e = 0,1 cm) avec un éluant composé d'un mélange ether – ether de pétrole (en général 20 : 80).

Bromation des composés phénoliques et des amines aromatiques — mode opératoire général : 2×10^{-3} mol de composé aromatique est dissoute dans 10 mL de $CHCl_3$. Sous agitation 2×10^{-3} mol de $TABBr_3$ en solution dans 10 mL de $CHCl_3$ est ajoutée rapidement à température ambiante. Le mélange, de couleur orange, devient rapidement incolore. On ajoute 20 mL d'une solution aqueuse de thiosulfate de sodium à 5% en continuant l'agitation. La phase organique est décantée, lavée à l'eau jusqu'à pH 7, puis évaporée. L'huile restante est reprise par un mélange éther–eau. Après décantation, la phase éthérée est séchée et l'éther est évaporé. Le produit aromatique bromé est ensuite purifié par cp.

Résultats

Produits monobromés obtenus : les rendements sont indiqués en produits isolés et purs.

para-*Bromophénol* : *R* % (95); *F* : 64°C (litt. (9) 65°C); ir : 3500; rmn : 5,1 (s, 1H), 6,5 (d) et 7 (d) (4H); sm : 174–172 ($M^{+\bullet}$, 100), 93 [$(M - Br)^+$, 40], 65 [$(M - Br - Co)^+$, 50].

Bromo-2 méthyl-4 phénol : *R* % (93), huile identifiée par comparaison avec un échantillon authentique (30); ir : 3500; rmn : 2,1 (s, 3H), 5,2 (s, 1H), 7 (m, 3H); sm : 188–186 ($M^{+\bullet}$, 30), 173–171 [$(M - CH_3)^+$, 100], 92 [$(M - CH_3 - Br)^+$, 70].

Bromo-2 tert-*butyl-4 phénol* : *R* % (94); *F*: 51–52°C (litt. (31) 52°C); ir : 3600; rmn : 1,6 (s, 9H), 4,8 (s, 1H), 7,4 (m, 3H); sm : 230–228 ($M^{+\bullet}$, 30), 215–213 [$(M - CH_3)^+$, 100], 134 [$(M - CH_3 - Br)^+$, 65].

Bromo-2 tert-*butyl-2 méthyl-4 phénol* : *R* % (95), huile identifiée par comparaison avec un échantillon authentique (30); ir : 3500; rmn : 1,5 (s, 9H), 2,1 (s, 3H), 5,4 (s, 1H), 6,9 (m, 2H); sm : 244–242 ($M^{+\bullet}$, 40), 229–227 [$(M - CH_3)^+$, 100], 148 [$(M - CH_3 - Br)^+$, 50].

para-*Bromothymol* : *R* % (96); *F* : 55°C (litt. (31) 55°C); ir : 3600; rmn : 1,2 (d, 6H), 1,8 (m, 1H), 2,1 (s, 3H), 5,2 (s, 1H), 6,6 (s, 1H), 7 (s, 1H); sm : 230–228 ($M^{+\bullet}$, 40), 173–171 [$(M - CH_3)^+$, 100], 92 [$(M - CH_3)^+$, 100], 134 [$(M - CH_3 - Br)^+$, 85].

Bromo-4 méthyl-2 phénol : *R* % (96); *F* : 64–65°C (litt. (32) 64°C); ir : 3500; rmn : 2,1 (s, 3H), 5,1 (s, 1H), 7 (m, 3H); sm : 188–186 ($M^{+\bullet}$, 40), 173–171 [$(M - CH_3)^+$, 100], 92 [$(M - CH_3 - Br)^+$, 40].

Bromo-1 naphtol-2 : *R* % (95); *F* : 82°C (litt. (9) 79–81°C); ir : 3500; rmn : 5,8 (s, 1H), 7,5 (m, 6H); sm : 224–222 ($M^{+\bullet}$, 80), 114 [$(M - Br - 29)^+$, 50].

Bromo-4 méthoxy-2 phénol : *R* % (95), huile identifiée avec un échantillon authentique (32); ir : 3500; rmn : 3,6 (s, 3H), 5,6 (s, 1H), 6,8 (m, 3H); sm : 204–202 ($M^{+\bullet}$, 40), 189–187 [$(M - CH_3)^+$, 100].

para-*Bromoaniline* : *R* % (84); *F* : 66°C (litt. (32) 66°C; rmn : 3,5 (s, 2H), 6,8 (2d, 4H); sm (100 eV, ICIN(N_2), 0,05 Torr) : 172–170 [$(M - H)^-$, 100], 81–79 (Br^-, 60).

Bromo-4 N-*méthylaniline* : *R* % (94), huile identifiée par comparaison avec un échantillon authentique (33); rmn : 2,6 (s, 3H), 3,7 (s, 1H), 6,6 (2d, 4H); sm (100 eV, ICIN(N_2) 0,05 Torr) : 186–184 [$(M - H)^-$, 100], 81–79 (Br^-, 60).

Bromo-4 diéthylaniline : *R* % (99), huile identifiée par comparaison avec un échantillon authentique (33); rmn : 1,5 (t, 6H), 3,1 (q, 4H), 6,6 (2d, 4H); sm : 229–227 ($M^{+\bullet}$, 60), 200–198 [$(M - C_2H_5)^+$, 100], 119 [$(M - C_2H_5 - Br)^-$, 60].

Di(bromo-4 N-*phényl)aniline* : *R* % (99); *F* : 107°C (litt. (33) 106°C); rmn (DMSO-d_6) : 7 (2d, 8H), 8,1 (s, 1H); sm : 329–327–325 ($M^{+\bullet}$, 100), 248–246 [$(M - Br)^+$, 60].

Bromo-4 N-*cyclohexylamine* : *R* % (95), huile identifiée par comparaison avec un échantillon authentique (34); rmn : 1,5 (m, 11H), 6,2 (s, 1H), 6,6 (2d, 4H); sm : 255–253 ($M^{+\bullet}$, 40), 172–170 [$(M - C_6H_{11})^+$, 100].

Amino-2 bromo-5 pyridine : *R* % (98), huile identifiée par comparaison avec un échantillon authentique (35); rmn : 5,9 (s, 2H), 7 (m, 3H); sm : 174–172 ($M^{+\bullet}$, 50), 93 [$(M - Br)^+$, 100].

Réaction de bromation du phénol en milieu biphasique : 2×10^{-3} mol de phénol est dissous dans 10 mL d'eau déminéralisée. Quand la réaction a lieu en présence d'un sel, celui-ci est ajouté à la phase aqueuse et la solution est agitée jusqu'à dissolution complète. $TABBr_3$ (2×10^{-3} mol) dissous dans 10 mL de $CHCl_3$ est ajoutée rapidement à la solution aqueuse. Le mélange est agité et la réaction est considérée comme terminée quand la phase chloroformique est décolorée. Après séparation la phase aqueuse est reprise par trois fois 15 mL de $CHCl_3$. Les phases chloroformiques sont rassemblées, séchées, puis évaporées. La purification est conduite comme il est décrit précédemment.

Remerciements

Nous remercions vivement le Docteur Claude Agami pour les fructueuses discussions et l'intérêt qu'il a porté à ce travail.

1. P. B. D. de la Mare. Electrophilic halogenation. Cambridge University Press, London. 1976.
2. R. D. C. Norman et R. Taylor. Electrophilic substitution in benzenoïd compounds. Elsevier, New York. 1965.
3. A. G. Sharpe. J. Chem. Soc. 3713 (1953).
4. E. M. Kosower, W. J. Cole, G. S. Wu, D. E. Cardy et G. Meisters. J. Org. Chem. **28**, 650 (1963).
5. G. M. Kosolappoff. J. Am. Chem. Soc. **75**, 3596 (1953).
6. H. Winkelmann, L. Horner, K. H. Knapp et W. Ludwig. Chem. Ber. **92**, 288 (1959).
7. F. Xu et Q. Wang. Huaxu Shiji, **8**, 374 (1986).
8. S. Sharma, J. Rajaram et J. C. Kuriacose. Indian J. Chem. **15B**, 274 (1977).
9. L. Forlani. Synthesis, 487 (1980).
10. A. Marquet, J. Jacques et B. Tchoubar. Bull. Soc. Chim. Fr. 511 (1965).
11. S. Kajigashi, T. Kakinami, H. Tokijama et T. Okamoto. Chem. Lett. 617 (1987).
12. M. Fournier, F. Fournier et J. Berthelot. Bull. Soc. Chim. Belg. **15**, 157 (1984).
13. J. Berthelot et M. Fournier. Can. J. Chem. **64**, 603 (1986).
14. P. L. Desbene, J. Berthelot, M. Ouchefoun, C. Guette, J. J. Basselier, A. Boulez et A. Desbene-Monvernay. Talanta, **34**, 645 (1987).
15. J. Berthelot, C. Guette, M. Essayeh, P. L. Desbene et J. J. Basselier. Synth. Commun. **16**, 1641 (1986); J. Berthelot, C. Guette, M. Ouchefoun, P. L. Desbene et J. J. Basselier. J. Chem. Res. S, 381 (1986).
16. C. Reichardt. Angew. Chem. Int. Ed. Engl. **18**, 98 (1979).
17. L. Altschuler et E. Berliner. J. Am. Chem. Soc. **88**, 5837 (1966).
18. A. E. Alexander. J. Chem. Soc. 3376 (1954).
19. J. E. Dubois et J. J. Aaron. J. Chim. Phys. 1354 (1964).
20. G. S. Kozak, Q. Fernando et H. Freiser. Anal. Chem. **36**, 296 (1964).
21. E. Berliner et M. C. Beckett. J. Am. Chem. Soc. **79**, 1425 (1957).
22. R. LeGoaller, H. Haudle, P. Labbe et J. L. Pierre. J. Am. Chem. Soc. **106**, 1694 (1984); G. Belluci, R. Bianchini et S. Vecciani. J. Org. Chem. **51**, 4224 (1986).

23. G. BELLUCI, R. BIANCHINI, R. AMBROSETTI et G. INGROSSO. J. Org. Chem. **50**, 3313 (1985).
24. G. BELLUCI, R. BIANCHINI, R. AMBROSETTI et G. INGROSSO. J. Am. Chem. Soc. **102**, 7480 (1980).
25. J. DESBARRES. Bull. Soc. Chim. Fr. 502 (1961).
26. M. G. IVANOV, V. G. GOLOV et Y. I. DERGUNOV. Kinet. Katal. **27**, 499 (1986).
27. I. D. MORTON et P. W. ROBERTSON. J. Chem. Soc. 129 (1945).
28. J. BERTHELOT, C. GUETTE, P. L. DESBENE, J. J. BASSELIER, P. CHAQUIN et D. MASURE. Can. J. Chem. Soumis.
29. A. J. PARKER. Q. Rev. **16**, 163 (1962).
30. A. CARPENTER et J. EASTER. J. Org. Chem. **20**, 401 (1955).
31. B. JONES. J. Chem. Soc. 358 (1941).
32. P. KLARMANN. J. Am. Chem. Soc. **55**, 4657 (1933).
33. O. FISCHER. Chem. Ber. **45**, 1103 (1912).
34. K. NOZAKIE et R. A. OGG. J. Chem. Soc. 697 (1942).
35. A. SLATOR. J. Chem. Soc. 424 (1933).

Can. J. Chem. Downloaded from www.nrcresearchpress.com by 186.148.149.217 on 09/07/12
For personal use only.

A dynamic NMR study of the nitrogen lone pair orientation in 2-benzoyl-5-methyl-5-aza-1,3-dithiacyclohexane

B. Mario Pinto,[1] Blair D. Johnston, and Ruby Nagelkerke
Department of Chemistry, Simon Fraser University, Burnaby, B.C., Canada V5A 1S6
and
Eusebio Juaristi[1] and Eduardo A. González
Departamento de Química, Centro de Investigación y de Estudios Avanzados del Instituto Polytécnico Nacional, México D.F., México 07000
Received June 14, 1989

B. Mario Pinto, Blair D. Johnston, and Ruby Nagelkerke. Can. J. Chem. **67**, 2067 (1989).

Nuclear Overhauser enhancement difference experiments and magnetization transfer experiments on 2-benzoyl-5-methyl-5-aza-1,3-dithiacyclohexane **1** at 186 K show conclusively that the *N*-methyl group adopts a preferred axial orientation. The result has implications for evaluation of the origin of the anomeric effect in this and related compounds. The free energy of activation for ring interconversion in **1** is estimated by spin saturation transfer experiments to be 10.7 ± 0.4 kcal mol^{-1}.
Key words: D NMR, conformational analysis, nuclear Overhauser enhancement, saturation transfer.

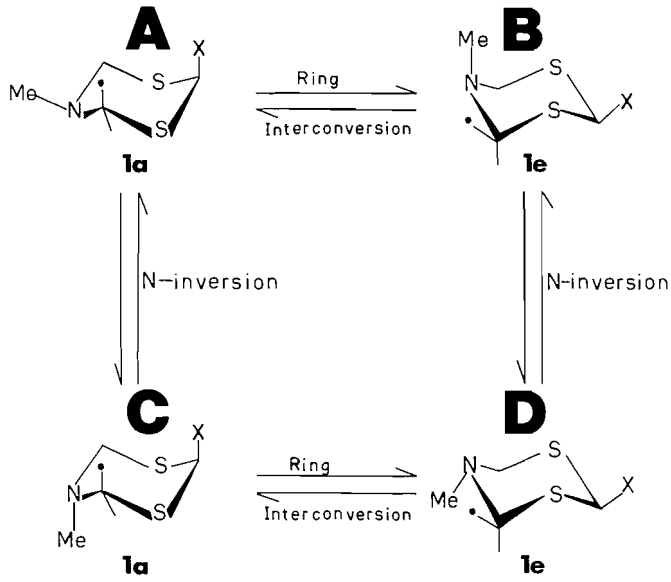
B. Mario Pinto, Blair D. Johnston et Ruby Nagelkerke. Can. J. Chem. **67**, 2067 (1989).

Des expériences d'effets Overhauser nucléaire et de transfert de magnétisation conduites sur le benzoyl-2 méthyl-5 aza-5 dithia-1,3 cyclohexane **1** à 186 K montrent de façon concluante que ie groupe *N*-méthyle adopte préférentiellement une orientation axiale. les résultats influencent l'évaluation de l'origine des effets anomériques dans ce composé et dans les composés apparentés. Faisant appel à des expériences de transfert de saturation de spin, on a évalué à 10,7 ± 0,4 kcal mol^{-1} l'énergie libre d'activation de l'interconversion du cycle dans le composé **1**.
Mots clés : RMN D, analyse de conformation, effet Overhauser nucléaire, transfert de saturation.

[Traduit par la revue]

Introduction

We recently reported (1) a study of second-row anomeric interactions in 2-substituted 5-methyl-5-aza-1,3-dithiacyclohexanes. The conformational processes of interest in these systems are those of ring interconversion and nitrogen inversion (see Scheme 1). Examination of the ^{1}H NMR spectra at 173 K indicated two sets of signals for each of the H-4$_{eq}$, H-4$_{ax}$, H-2, and N-Me protons. Upon heating, each of these sets coalesced to give averaged signals, and time-averaged spectra were observed at about 300 K. This dynamic behaviour was attributed (1) to one conformational process, namely that of ring interconversion, the barriers for nitrogen inversion being substantially lower (2). Since only two conformers predominated at low temperature, it was of some interest to assign the preponderant orientation of the *N*-alkyl group. Angiolini *et al.* and Katritzky (3) have assigned the *N*-alkyl group in *N*-alkyl-5-aza-1,3-dithiacyclohexanes a preferred axial orientation, based on a comparison of dipole moments of these compounds with those of 1,3-dithiane and *N*-alkyl piperidines. We found it preferable to deduce the orientation of the *N*-methyl group in our compounds by more direct means and present herein the results of nOe difference experiments and magnetization transfer experiments for one of the candidates, namely the 2-benzoyl derivative. The results show conclusively that the *N*-methyl group adopts a preferred axial orientation.



Scheme 1

Experimental

Acetone-d_6 was purchased from Merck Sharpe Dohme Isotopes. ^{1}H NMR spectra were recorded at 400.13 MHz on a Bruker WM-400 NMR spectrometer. Chemical shifts are given in ppm downfield from Me_4Si. The probe thermocouple was used for temperature measurement, after calibration. Temperatures are believed to be accurate to within ±2 K. The sample of 2-benzoyl-5-methyl-5-aza-1,3-dithiacyclohexane **1** (1) in $(CD_3)_2CO$ was degassed using the freeze–pump–thaw technique. The tube was sealed under vacuum. All experiments were performed at 186 K. ^{1}H NMR, **1a** δ: 2.65 (NMe), 3.94 (H-4, 6$_e$), 5.27 (H-4, 6$_a$), 5.84 (H-2); **1e** δ: 2.49 (NMe), 4.32 (H-4, 6$_e$), 5.17 (H-4, 6$_a$), 6.75 (H-2); ^{13}C NMR, **1a** δ: 36.8 (NMe), 41.6 (C-2), 55.5 (C-4, 6); **1e** δ: 36.9 (NMe), 55.9 (C-2), 60.4 (C-4, 6).

Difference nOe experiments

The selected signals were individually irradiated at the centres of the signals with a second rf field at saturating power levels for 4 s. The intensities of the affected signals were obtained by direct integration of the peaks and were calculated as percentages of the irradiated signals (Table 1).

[1]Authors to whom correspondence may be addressed.

Printed in Canada / Imprimé au Canada

Can. J. Chem. Downloaded from www.nrcresearchpress.com by 186.148.149.217 on 09/07/12
For personal use only.

TABLE 1. Summary of nOe difference and magnetization transfer experiments on **1** in $(CD_3)_2CO$ at 186 K

Entry	Irradiated signal	Affected signal	Effect	Approx. % of Irradiated signal
1	CH_3, maj	CH_3, min	Saturation transfer	13
		$H4_a$, min	Saturation transfer	Trace[a]
		$H4_e$, maj	nOe	4
2	CH_3, min	CH_3, maj	Saturation transfer	20
		$H4_a$, maj	Saturation transfer	Trace
		$H4_e$, min	nOe	3
3	$H4_e$, maj	$H4_a$, min	Saturation transfer	16
		$H4_e$, min	Saturation transfer + relayed nOe	11
		CH_3, min	Saturation transfer	Trace
		$H4_a$, maj	nOe	27
		CH_3, maj	nOe	Trace
		H2, maj	nOe	Trace
4	$H4_e$, min	$H4_a$, maj	Saturation transfer	29
		$H4_e$, maj	Saturation transfer + relayed nOe	16
		CH_3, maj	Saturation transfer	Trace
		$H4_a$, min	nOe	29
		CH_3, maj	nOe	Trace
		H2, min	nOe	Trace
5	$H4_a$, maj	$H4_e$, min	Saturation transfer	17
		$H4_a$, min	Saturation transfer + relayed nOe	5
		H2, min	Saturation Transfer	Trace
		$H4_e$, maj	nOe	28
		H2, maj	nOe	7
		CH_3, maj	Relayed nOe	Trace
6	$H4_a$, min	$H4_e$, maj	Saturation transfer	32
		$H4_a$, maj	Saturation transfer + relayed nOe	6
		$H4_e$, min	nOe	26
7	H2, maj	H2, min	Saturation transfer	29
		$H4_a$, maj	nOe	8
8	H2, min	H2, maj	Saturation transfer	42
		$H4_a$, maj	Saturation transfer + relayed nOe	Trace

[a]Trace indicates <~3% of irradiated signal.

Spin saturation transfer difference experiment

This was based on the Forsén–Hoffman method for measuring rates of exchange (4, 5). The methyl signal of the major isomer **1e** was saturated by irradiation with a second rf field; the irradiation times were 0.025, 0.05, 0.25, 0.5, 1, and 2 s. The complete saturation of the methyl signal of **1e** was verified. Equilibrium magnetization was reached after about 1 s, as judged by the constant normalized area of the methyl signal of **1a** after about 1 s of irradiation. A semilogarithmic least-squares plot of $\log(MzA - MzA_\infty)$ against irradiation time t (5) gave a straight line with slope of $-1.74 \pm 0.12\,s^{-1} = -\tau_{1A}^{-1}$. The value of MzA ($t = 0$)/MzA ($t = \infty$) was then used to evaluate τ_{1A}/T_{1A} (0.38 ± 0.04) and hence, τ_A, the pre-exchange lifetime of the site in **1a** (5). The free energy of activation, $\Delta G^\ddagger$, was then calculated by means of the Eyring equation (5).

The IR spectrum of **1** was recorded in KBr on a Perkin–Elmer 983G spectrophotometer.

Results and Discussion

The spectra were assigned in the following manner. Consideration of the γ-*gauche* effect (6) in the ^{13}C NMR spectrum permitted assignment of the respective signals to the axial and equatorial conformers. Specifically, C-4, 6 in the axial conformer is shielded (4.9 ppm) relative to that in the equatorial conformer. Once the major (COPh equatorial) and minor (COPh axial) isomers had been assigned, the signals in the low

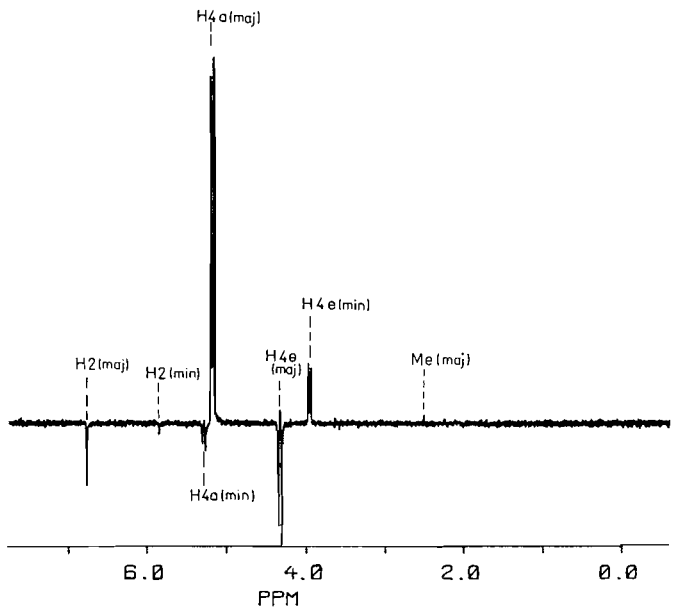


FIG. 1. Difference ^1H NMR spectrum of **1a** ⇆ **1e** in $(CD_3)_2CO$ at 186 K illustrating nOe and saturation transfer effects upon irradiation of the H4a (maj) resonance.

Can. J. Chem. Downloaded from www.nrcresearchpress.com by 186.148.149.217 on 09/07/12
For personal use only.

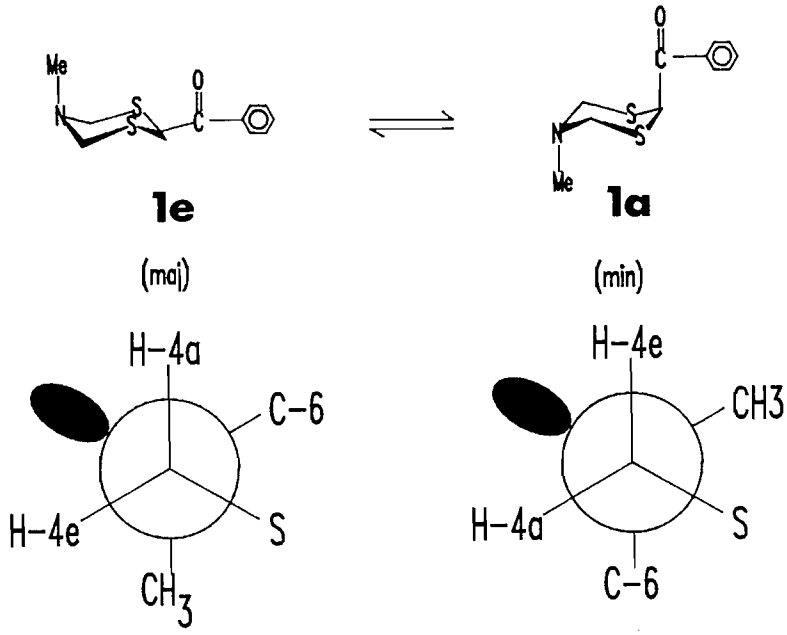


FIG. 2. Newman projections along the C-4—N bond in the preferred conformations of **1e** (B) and **1a** (C).

temperature ^{1}H NMR spectrum were assigned. For example, the signals for H-4_a and H-4_e in the minor isomer were distinguished on the basis of the long range coupling (2 Hz) between H-2_e and H-4_e (3*a*, 7). We note also that a value of $^4J_{2e,4e}$ of 2 Hz corroborates the assignment of the minor conformer to that in which the C-2 substituent is axially oriented (3*a*, 7). The distinction of the H-4_e and H-4_a signals in the spectrum of the major isomer followed from the observation of nOe effects between H-2_a and H-4_a (see below).

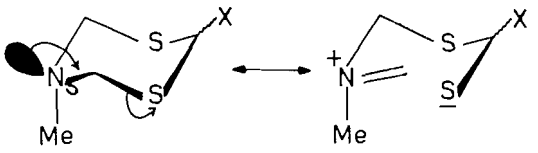
We initially envisaged that the results of nOe difference experiments would be straightforward, and would be diagnostic of the preferred orientation of the *N*-methyl group in **1**. However, it soon became evident that even though exchange was slow on the chemical-shift time scale at 186 K, it was still faster than the rates of relaxation for sets of protons in the axial and equatorial conformers **1a** and **1e**, respectively; the observed relaxation rate then represents a weighted average of the two contributing relaxation rates. The consequence of the latter effect is that this fast exchange on the relaxation time scale allows transfer of magnetization and population information from one of the resonances in **1a** to its exchange-related counterpart in **1e** (8). Thus, saturation of one of the resonances in **1a** by steady-state irradiation could be transferred to the corresponding resonance in **1e** by exchange. Indeed, nOe effects created in a particular resonance of **1a** were transferred to its counterpart in **1e**, and vice versa, by exchange. The results are summarized in Table 1 and a representative case is illustrated in Fig. 1.

Inspection of the data in Table 1 indicates the following salient features with respect to nOe effects. (1) Irradiation of an *N*-methyl resonance in either conformer (entries 1, 2) resulted in nOe effects only on H-4_e and not on H-4_a. The results are consistent only with a preponderance of conformations in which the *N*-methyl group is axially oriented (conformations B and C in Scheme 1) since otherwise an nOe effect on H-4_a would also have been expected (see Fig. 2). (2) Irradiation of the H-4_e signals of either conformer (entries 3, 4) gave a major nOe effect on H-4_a and a minor effect on the H-2 and *N*-methyl signals. (3) Irradiation of the H-4_a signal in the spectrum of the minor conformer **1a** (entry 6) gave an nOe effect only on H-4_e, as expected for a preferred axial orientation of the *N*-methyl group. (4) Irradiation of the H-4_a signal in the spectrum of the major conformer **1e** (entry 5) gave nOe effects on H-4_e and H-2, as expected. The latter effect derives from the 1,3-diaxial relationship of H-2 and H-4_a, and is also supported by the converse experiment in which H-2 is irradiated (entry 7). The results corroborate the previous assignment (1) of the equatorial orientation of the 2-benzoyl group in the major conformer.

In addition to the nOe effects described above, the effects of magnetization transfer via exchange were also detected. Thus, saturation of the *N*-methyl resonance of the major isomer **1e** (entry 1) resulted in saturation transfer to the *N*-methyl and H-4_a resonances of the minor isomer **1a**. Similarly, irradiation of the *N*-methyl resonance of the minor isomer **1a** (entry 2) gave saturation transfer effects on the H-4_a and *N*-methyl signals of **1e**. A combination of nOe and magnetization transfer effects was also observed upon irradiation of the H-4_e and H-4_a signals in the spectra of both **1a** and **1e**. Thus, saturation of H-4_e in the spectrum of **1e** (entry 3) resulted in magnetization transfer to H-4_a and H-4_e (via a relayed nOe effect) of **1a** and, similarly, saturation of H-4_e in the spectrum of **1a** (entry 4) gave magnetization transfer to H-4_a and to H-4_e (via a relayed nOe effect) of **1e**. Analogous effects were observed upon irradiation of the H-4_a signals of either conformer (entries 5, 6). Saturation transfer effects between H-2's of the two conformers (entries 7, 8) were also observed; in addition, irradiation of H-2 in the spectrum of the minor conformer **1a** also resulted in detectable magnetization transfer effects on H-4_a of the major isomer **1e**. The latter effect results from magnetization transfer via exchange of H-2_e in **1a** with H-2_a in **1e**, coupled with a relayed nOe effect between H-2_a and H-4_a in **1e**. The percentage of saturation transfer from irradiation of a signal attributable to the minor conformer (e.g., H-4_a in **1a**) to the inversion-related signal of the major conformer (e.g., H-4_e in **1e**) was always greater than in the converse experiment (major→minor). This is expected since the ground state population distribution of **1a** and **1e** dictates a lower barrier for ring interconversion in **1a** than in **1e**.

The results presented in Table 1 are consistent only with a

Can. J. Chem. Downloaded from www.nrcresearchpress.com by 186.148.149.217 on 09/07/12
For personal use only.



SCHEME 2

preponderance of conformations B and C (see Scheme 1), at 186 K, in which the *N*-methyl group is axially oriented. The conclusion is also corroborated by the IR spectrum, which indicated the absence of the Bohlmann bands (9) in the C—H stretching region; the bands would only be present if the N lone pair were antiperiplanar to the C-4, 6 axial hydrogens, that is, in the *N*-methyl equatorial conformation. Angiolini *et al.* (3) have suggested that the preference for the axial orientation of the *N*-alkyl groups in *N*-alkyl-5-aza-1,3-dithiacyclohexanes may result from destabilizing N lone pair – S lone pair repulsions in the alkyl-equatorial conformers and the stabilization of the alkyl-axial conformers by easy deformation at nitrogen. We propose further the role of $n_N \rightarrow \sigma^*_{c-s}$ stabilizing orbital interactions in stabilizing the *N*-methyl axial conformation in compounds of this type (see Scheme 2). The N lone pair orientation has implications for the evaluation of the origin of the anomeric effect in such derivatives (1).

As a final point of interest, we comment on the barrier to ring interconversion in **1**. The system was amenable to study using spin saturation transfer techniques since the pre-exchange lifetime τ_A (0.92 s) and the spin-lattice relaxation time T_{1A} (1.53 s) of the spins in the methyl site of **1a** (Site A) are of the same order of magnitude. Instantaneous saturation of the methyl signal of **1e** (Site E) for various times, t, thus leads to a decay of the intensity of the signal at site A to a new equilibrium value, permitting measurement of the rate constant for exchange (4, 5). A free energy of activation, $\Delta G^{\ddagger} = 10.7 \pm 0.4$ kcal mol^{-1}, for interconversion of **1e** to **1a**, was calculated. The value compares favorably with that ($\Delta G^{\ddagger} = 11.0 \pm 0.2$ kcal mol^{-1}) reported (3) for 5-methyl-5-aza-1,3-dithiacyclohexane.

Acknowledgement

We thank the Natural Sciences and Engineering Research Council of Canada for financial support in the form of an Operating Grant (to B.M.P.) and an International Collaborative Research Grant (to B.M.P. and E.J.).

1. E. JUARISTI, E. A. GONZALEZ, B. M. PINTO, B. D. JOHNSTON, and R. NAGELKERKE. J. Am. Chem. Soc. **111**, 6745 (1989).
2. F. G. RIDDELL and H. LABAZIEWICZ. J. Chem. Soc. Chem. Commun. 766 (1975).
3. (*a*) L. ANGIOLINI, R. P. DUKE, R. A. Y. JONES, and A. R. KATRITZKY. J. Chem Soc. Perkin Trans. 2, 674 (1972); (*b*) A. R. KATRITZKY. Adv. Heterocycl. Chem. **36**, 1 (1984).
4. S. FORSÉN and R. A. HOFFMAN. J. Chem. Phys. **40**, 1189 (1964).
5. J. SANDSTRÖM. Dynamic NMR spectroscopy. Academic Press, New York. 1982.
6. D. M. GRANT and B. V. CHENEY. J. Am. Chem. Soc. **89**, 5315 (1967); N. K. WILSON and J. B. STOTHERS. Top. Stereochem. **8**, 1 (1973).
7. E. L. ELIEL and R. O. HUTCHINS. J. Am. Chem. Soc. **91**, 2703 (1969).
8. J. K. M. SANDERS and B. K. HUNTER. Modern NMR spectroscopy. Oxford University Press, New York. 1988. Chap. 7.
9. F. BOHLMANN. ANGEW. CHEM. **69**, 641 (1957); Chem. Ber. **91**, 2157 (1958).

Can. J. Chem. Downloaded from www.nrcresearchpress.com by 186.148.149.217 on 09/07/12
For personal use only.

Structure of a pentacyclic triterpenyl angelate from *Loeselia mexicana*. ^{1}H 2D-NMR data and stereochemistry

M. JIMÉNEZ E., K. VELÁZQUEZ, A. LIRA-ROCHA, A. ORTEGA, AND E. DÍAZ

Instituto de Química, Universidad Nacional Autónoma de México, Circuito Exterior, Ciudad Universitaria, Coyoacán 04510, México, D.F.

AND

A. AUMELAS AND K. JANKOWSKI[1]

Faculté des études supérieures et de la recherche, Université de Moncton, Moncton, N.B., Canada E1A 3E9

Received April 19, 1989

M. JIMÉNEZ E., K. VELÁZQUEZ, A. LIRA-ROCHA, A. ORTEGA, E. DÍAZ, A. AUMELAS, and K. JANKOWSKI. Can. J. Chem. **67**, 2071 (1989).

The total assignment of ^{1}H NMR spectra of a pentacyclic triterpene from *Loeselia mexicana* was performed using selected 2D-NMR experiments (COSY, NOE). X-ray diffraction data were obtained from the parent compound as supplemental information to the NMR investigations. The data allowed for the unambiguous assignment of the structure and the stereochemistry of the title compound.

Key words: pentacyclic triterpene NMR, 2D NMR of terpenes, X-ray of triterpenes, triterpenyl angelate NMR, X-ray – 2D NMR structure determination.

M. JIMÉNEZ E., K. VELÁZQUEZ, A. LIRA-ROCHA, A. ORTEGA, E. DÍAZ, A. AUMELAS et K. JANKOWSKI. Can. J. Chem. **67**, 2071 (1989).

Faisant appel à des expériences de RMN en 2D (COSY, NOE), on a attribué les signaux du spectre RMN du ^{1}H d'un triterpène pentacyclique obtenu à partir du *Loeselia mexicana*. On a aussi obtenu des données de diffraction des rayons-X du composé parent. Les données permettent de faire une attribution non-ambiguë de la structure et de la stéréochimie du composé titre.

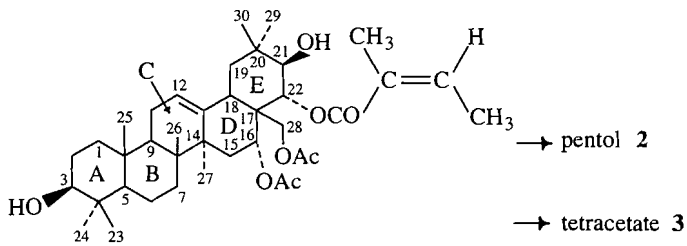
Mots clés : RMN d'un triterpène pentacyclique, RMN en 2D de terpènes, rayons-X de triterpènes, RMN d'angelate triterpényle, attribution de la structure par rayons X – RMN en 2D.

[Traduit par la revue]

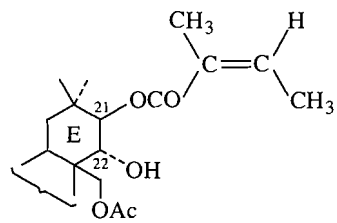
Introduction

Triterpenoids are among the most common natural products isolated from plant material (1). In spite of their simple nature, they are quite difficult to characterize because of the similarities observed for the physical and spectral properties of their different isomeric structures. Mass spectrometry, for instance, allows for the assignment of the triterpenic skeleton but fails to locate the functional groups and the unsaturation sites. As such, mass spectrometry is not a reliable technique for unambiguous structure elucidation of triterpenes (2). Two-dimensional NMR correlation experiments along with other pulsing techniques based on establishing long range couplings (3, 4) provide a more reliable method for the total assignment of triterpene structures (5). In this paper we would like to present an example of work where the use of these techniques led to the assignment of the molecular structure of one uncommon triterpenoid derivative from *Loeselia mexicana* (**1**). The parent compound, whose structure was deduced entirely from NMR spectra, was then subjected to X-ray analysis for comparison purposes. This comparison was made necessary because of the number of discrepancies found in the literature on NMR chemical shift assignments, especially for the D and E rings of pentacyclic triterpenes. In this respect, the spectra of several terpene model compounds should be used with great care as incorrect assignments as well as insufficient similarity have often led to major structure reassignments.

The following NMR spectra of the *Loeselia mexicana* triterpenic compound were interpreted: (i) high resolution (500 MHz), (ii) COSY together with COSY relayed, and (iii) NOESY.



1



4

SCHEME 1

A triterpenic fraction of *Loeselia mexicana*, an important plant of the Polemoneacea family, is widely used in Mexican native medicine because of its diuretic, purgative, emetic, or sudorific properties. This popular shrub, widely spread in the Valley of Mexico, is up to 90 cm high and the extraction of its aerial part produces ca. 1% (w/w; dry) of an amorphous solid residue, which under work-up conditions yields 0.05% of triterpenes. In a previous report (6) we tentatively assigned the structure of [olean-12-en-3β,16α,21α,22α,28-pentol]-yl-16,28-diacetate-22α-angelate (**1**) to the major component (80%) of that fraction. The white crystalline triterpene was first transformed into barringtongenol C (**2**) or into its 3β,16α,21α,28-

[1]Author to whom correspondence may be addressed.

Printed in Canada / Imprimé au Canada

Can. J. Chem. Downloaded from www.nrcresearchpress.com by 186.148.149.217 on 09/07/12
For personal use only.

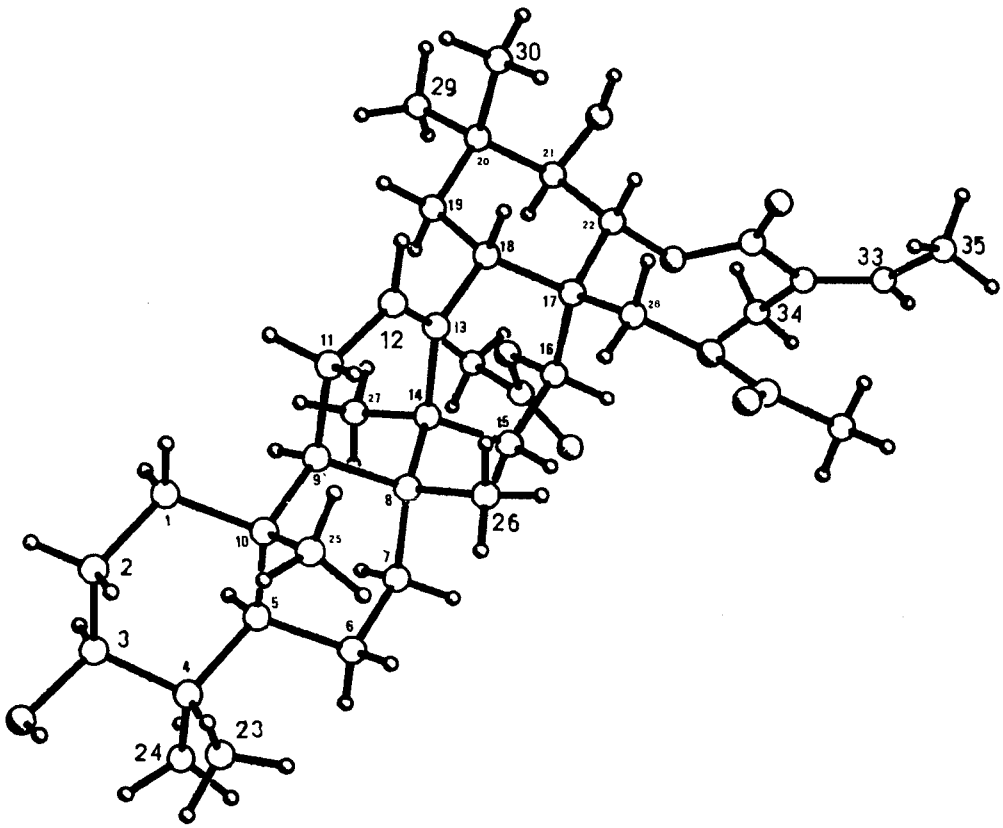


FIG. 1. ORTEP view of the molecular structure of **1**, all atoms of compound **1**.

tetraacetate, (**3**). The 2D-NMR experiments of this study were performed on the diacetate **1**. The major difficulty with this compound was the establishment of the positions of the angelic ester residue on the E ring as well as the assignment of the acetate group (Scheme 1).

X-ray of triterpene 1

The crystal structure of **1**, shown in Fig. 1, displays a few peculiarities. The E ring is in a chair conformation with its two major substituents, namely 21β-hydroxyl and the angelic acid residue at C-22, being *trans* diequatorial. The β-CH_2OCOCH_3 moiety at C-28 and the α-acetate at C-16 are also *trans*, the D–E ring junction being in the *cis* configuration. Looking at the A–E rings, we observe that the C ring shows a slight distortion and that, because of the *trans–anti–trans* steroidal configuration of the A–C rings, the 27-methyl and 19-methylene of the E ring are subjected to some form of 1,3-diaxial interaction. Consequently, the E ring is also deformed, to prevent these two substituents from falling into a 1,3-diaxial conformation.

NMR studies

High-resolution assignments

To assign the proton signals obtained from the high-resolution spectrum of **1** (Table 1) we have divided the 64 triterpene protons into eight regions with 25 non-methyl protons, seven methyls, two acetate methyls, and two vinylic methyls of the angelate residue.

The first system was that of the angelate residue. It was easily assigned using the multiplicity of the observed signals and their respective chemical shifts as criteria.

A second system consisted of protons of the C_9, C_{11}, and C_{12} carbon sequence. It was more difficult to unscramble because of the fact that H_9, in particular, is shifted to the very crowded 1.3–1.7 ppm area. The positive assignment of this proton was made after the recording of 2D experiments. However, at this stage of the identification, it was possible to assign both C_{11} protons at 1.87 and 1.92 ppm.

The third system, made up of three protons on C-18 and C-19, was assigned at 2.33 and 2.44 ppm for the two C-19 protons (the first one being axial, distinctive doublets) and 1.36 ppm for the C-18 proton.

The next system consisted of five protons on C-1, C-2, and C-3. Only the H-3 proton was easily identified at 3.20 ppm with two apparent ^3J couplings indicating an axial position.

The three protons on C-15 and C-16 were identified at 5.28, 1.53, and 1.78 ppm, respectively, as the C-16 equatorial proton and the two C-15 protons displaying a characteristic geminal coupling.

The C-28 methylene moiety was assigned to the bands at 3.75 and 3.82 ppm, related by a large geminal coupling constant (^2J = 11.4 Hz). Their chemical shifts show a characteristic shift (of 0.5 ppm) for the esterification of primary alcohols.

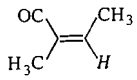
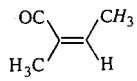
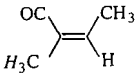
For the next group of protons, namely those on the A and B rings at C-5, C-6, and C-7, the high resolution one-dimensional spectrum does not allow for a direct positive assignment. As discussed below, the upfield protons can be assigned as shown in Table 1 from the 2D COSY spectra in particular.

Finally, the last group of protons, the C-21 and C-22 methines, show a large ^3J diaxial coupling (10.0 Hz).

The seven methyls directly attached to the triterpene skeleton are difficult to assign even with COSY and NOE spectra. From this group of seven singlets only the signals at 1.27 (C-27 methyl) and 0.92 ppm (angular C-25 methyl) can be easily assigned. In the spectrum of compound **1**, the two acetate

Can. J. Chem. Downloaded from www.nrcresearchpress.com by 186.148.149.217 on 09/07/12
For personal use only.

TABLE 1. Assignment of ^1H peaks for **3**

Region	Proton	δ_H (ppm)	Multiplicity	^nJ(Hz)	
1. Angelate		6.08	qq	7.2	1.5
		1.96	qd	7.2	1.6
		1.85	Quintet	1.6	
2. C_9—C_{11}—C_{12}	H-12	5.40	t	3.6	3.6
	H-11 eq	1.92			
	H-11 ax	1.87			
	H-9	1.53			
3. C_{18}—C_{19}	H-18	1.36	m	11.3	14.2
	H-19 eq	2.44	dd	14.2	3.8
	H-19 ax	2.33	dd	13	14.2
4. C_1—C_2—C_3	H-1	0.94			
	H-1	1.00			
	H-2	1.55			
	H-2	1.60			
	H-3	3.20	dd	4.7	10.5
5. C_{15}—C_{16}	H-15	1.53			
	H-15	1.78		4.1	16
	H-16	5.28	m	4.1	
6. C_{28}	H_{28}	3.82	d	11.4	
	$H_{28'}$	3.75	d	11.4	
7. C_5—C_6—C_7	H_5	0.67	d(?)		
	H_6	1.38			
	$H_{6'}$	1.30			
	H_7	1.44			
	$H_{7'}$	1.50			
8. C_{21}—C_{22}	H_{21}	3.74	d	10.0	
	H_{22}	5.26	d	10.0	
Methyls	C_{27}	1.27			
	C_{25}	0.92			
	C_{29}	0.04 eq			
	C_{30}	1.01 ax			
	C_{23}	0.76 ax			
	C_{24}	0.96 eq			
	C_{26}	0.88			
Acetate methyls	C_{28}	1.99	s	—	
	C_{16}	2.08	s	—	
	C_3 or C_{21}	2.15	s	—	
	C_{21} or C_3	2.15	s	—	

methyls at C-28 and C-16 are observed at 1.99 and 2.08 ppm; however, their assignment is still uncertain at this stage.

Apart from these uncertainties, the high resolution one-dimensional NMR spectrum already allows the direct, unambiguous assignment of several protons. A more detailed analysis of the structure, as well as definitive assignments, was carried out using COSY, COSY DELAYED (30 ms), and NOESY (τ_m = 280 ms) experiments as described below.

COSY[2]

Individual proton assignments are presented in Figs. 2*a*–*c*. The eight previously defined systems of protons were analyzed and the resulting additional assignments were added to Table 1. The C-1, C-2, C-3, the C-15, C-16, and the more complex C-5, C-6, C-7 sequences were all positively assigned. COSY experiments allowed further advance in the total proton assignment without, however, providing definitive answers as to the identity of the methyl moieties and the net distinction between *axial* and *equatorial* methylene protons of the skeleton.

COSY DELAYED[2]

This type of experiment allows for the assignment of axial methyls from the ^4J couplings, particularly when both methyls and protons form the W arrangement or are in axial positions. Three additional assignments were made. Taking the C-15eq

[2]The originals of all spectra are available on request from K. Jankowski.

Can. J. Chem. Downloaded from www.nrcresearchpress.com by 186.148.149.217 on 09/07/12
For personal use only.

Can. J. Chem. Downloaded from www.nrcresearchpress.com by 186.148.149.217 on 09/07/12
For personal use only.

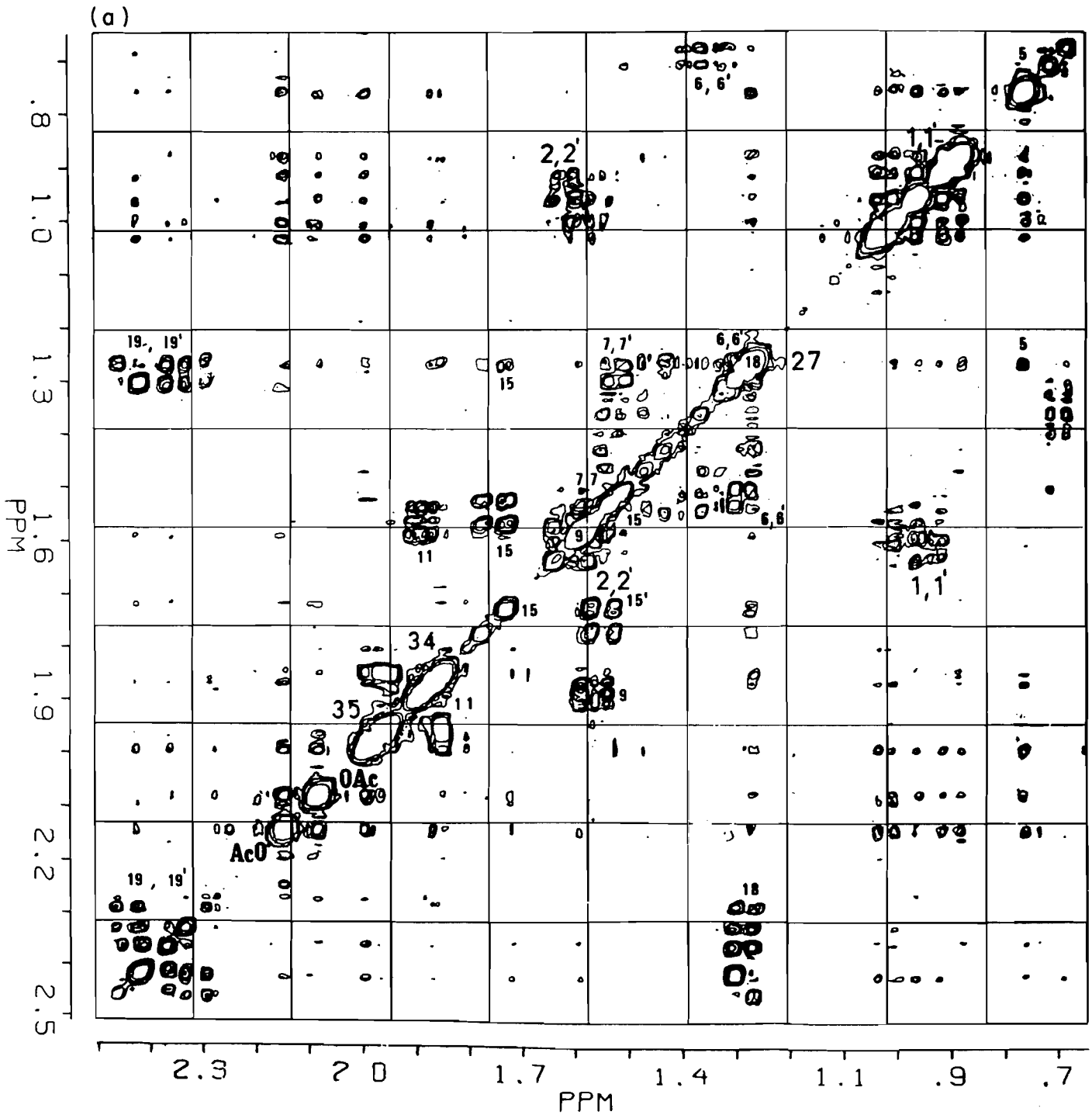


FIG. 2. (a) COSY, 0.7–2.5 ppm area of **1**.

proton as starting point, the C-27 methyl was assigned at 1.27 ppm. A second ^4J system allowed for the assignment of the two protons at C-7ax and C-9 as well as the C-26 methyl. The last sequence of protons at C-19ax and C-21ax and the axial methyl of the non *gem*-dimethyl system at C-20 were assigned and the remaining axial C-30 methyl was finally identified. At the same time we were able to observe a correlation between CH_3-24 and H-3, and between CH_3-25 and H-9 (Fig. 3).

NOESY[2]

A large number of nuclear Overhauser enhancements (NOEs) can be observed via the 2D NOE technique (NOESY). In spite of the fact that the 0.5–2.0 ppm area is very crowded, several dipolar interactions were identified.

The NOE between the vinylic proton at C-12 and the equatorial one at C-19 is particularly strong (δ = 1.90). The expected NOE effect between the C-22 and C-18 protons is not observed, probably due to the deformation of the E ring. The presence of two large substituents on C-21 and C-22 is a logical justification of this explanation.

Important correlation peaks were detected, and circled spots on the spectra connecting lines enabled us to observe the NOE

Can. J. Chem. Downloaded from www.nrcresearchpress.com by 186.148.149.217 on 09/07/12
For personal use only.

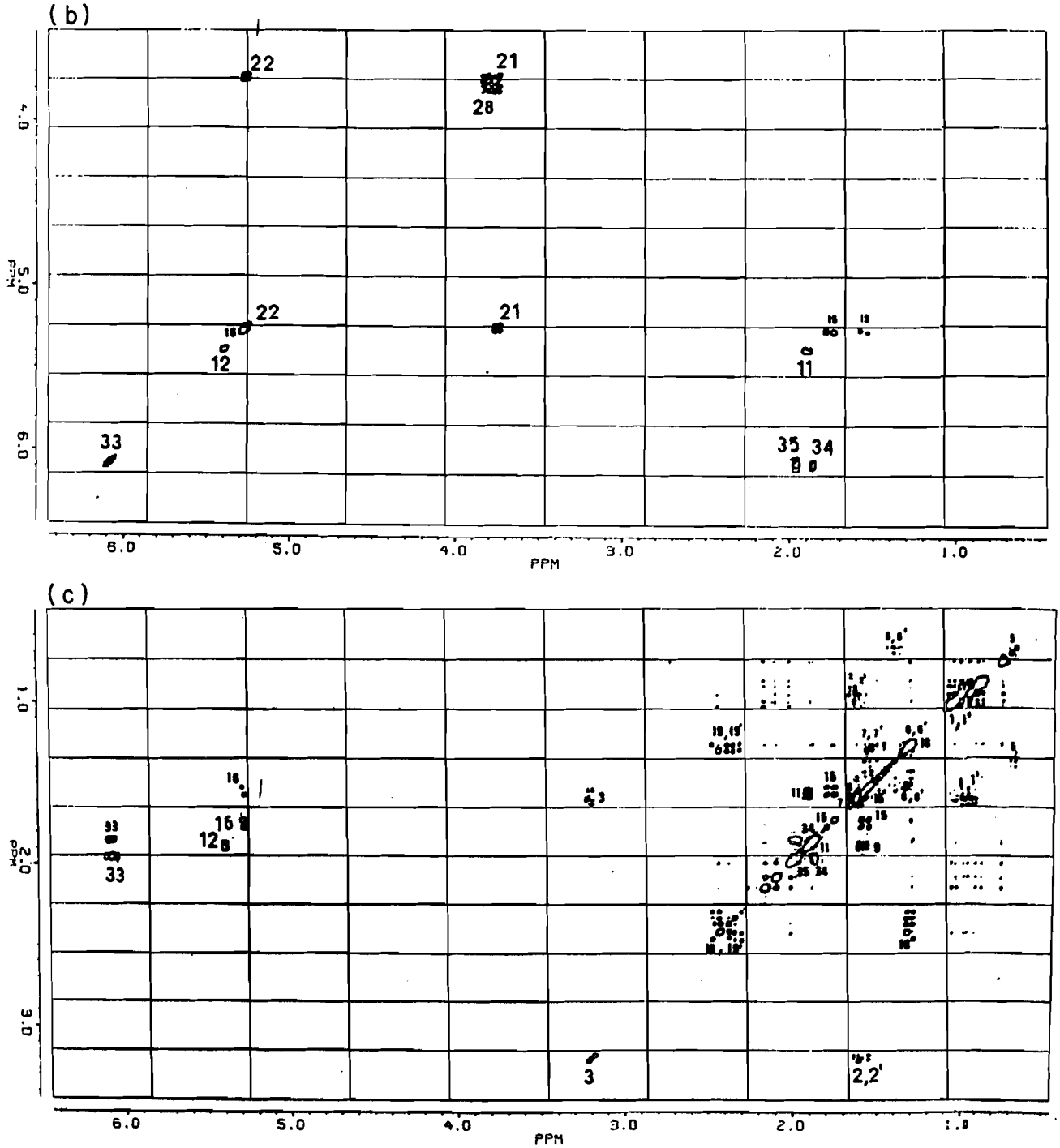


FIG. 2. (b) COSY, 0.5–6.5/0.5–3.5 ppm area of **1**. (c) COSY, 0.5–6.5/3.5–6.5 ppm area of **1**.

between H-33 of the angelic moiety and CH_3-35. Also, the axial protons H-22 have shown NOE correlation with the protons at C-28.

On the other hand, the C-28 protons showed strong NOEs with H-16, H-22, H-15e, H-19e, H-19a, and finally with CH_3-36.

Many stereochemical assignments were assisted by 2D NOE data; e.g., H-21α presents a spatial relationship via NOE with CH_3-29α, H-3α is correlated well with the CH_3-23, the CH_3-30 presents NOE correlation with both CH_3-28 and H-22, the methyl C-26 has shown NOE with H-15e, and a NOE relationship for H-19e with CH_3-28 and H-22 is detected.

The remaining methyls, unassigned from both COSY experiments, have been identified unambiguously by NOESY.

These experiments enabled us to propose the final assignments of protons as presented in Table 1.

Experimental

The triterpenic diacetate **1** was isolated from the *Loeselia mexicana* methanolic extract as previously described (6). The compound, mp 145°C, was analyzed by mass spectrometry (EI, PI, Hewlett–Packard 5485). The molecular ion was recorded at m/z 656 $[M]^{+\cdot}$ corresponding to the formula $C_{39}H_{60}O_8$. The principal fragment ions were m/z 638 $[M - H_2O]^{+\cdot}$, 596 $[M - AcOH]^{+\cdot}$, and 472 [M –

Can. J. Chem. Downloaded from www.nrcresearchpress.com by 186.148.149.217 on 09/07/12
For personal use only.

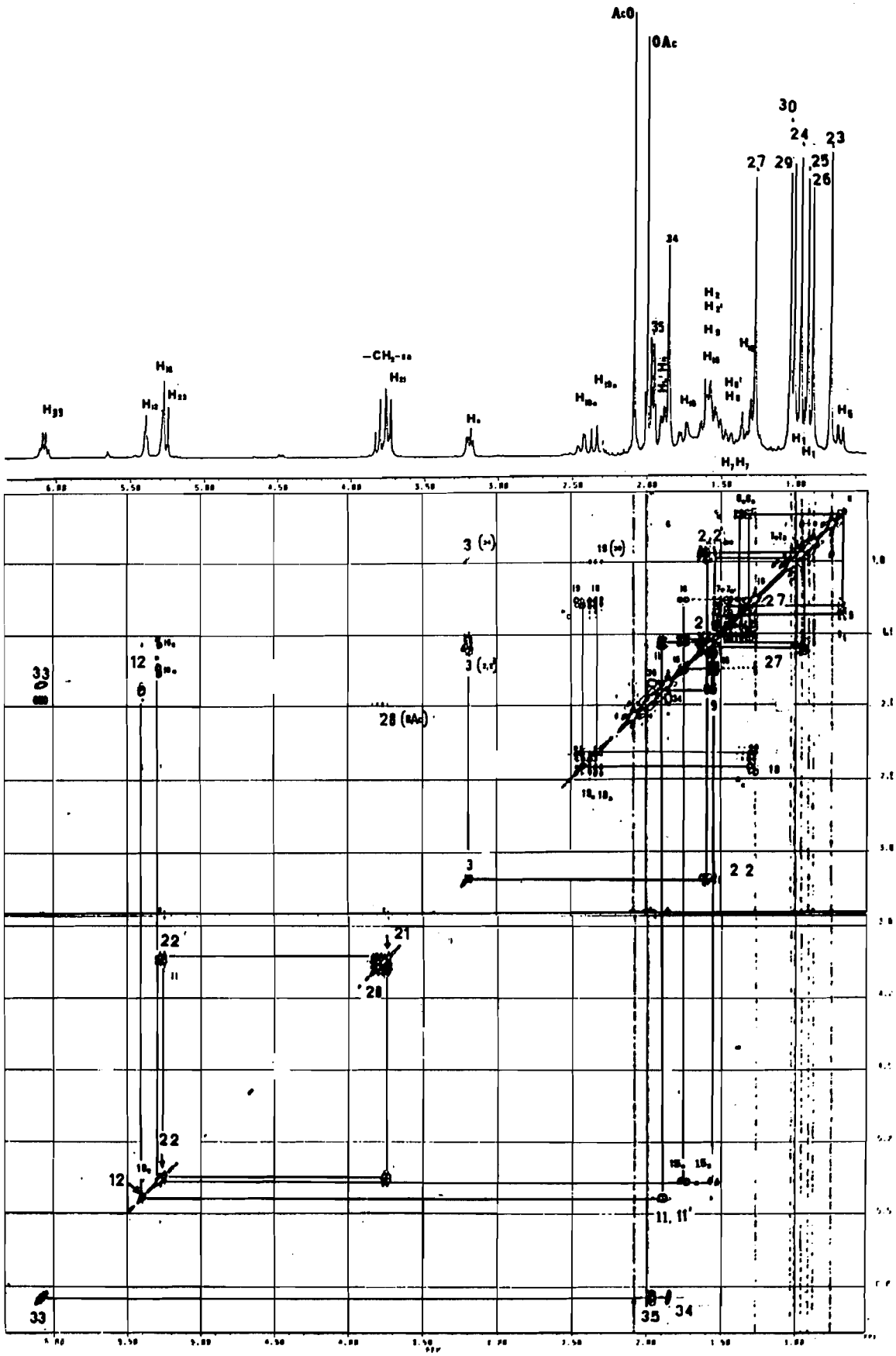


FIG. 3. COSY DELAYED of **1**. High resolution proton NMR spectrum of **1** (500 MHz) is shown on the *x*-axis.

$(CH_3)_2C—CHOH—CH—O—CO—CCH_3=CHCH_3]^{+\cdot}$. The purity of sample has been ascertained by TLC and HPLC. The acetylation of **1** (or **2**) performed according to Yosioka *et al.* (7, 9) and Wulff and Tschesche (8) gives the tetraacetate **3** quantitatively (empirical formula $C_{43}H_{64}O_{10}$). Mass spectrometry reveals a molecular ion at m/z 740 $[M]^{+\cdot}$ as well as a series of typical losses of the acetate residues.

Crystal data of 1

Formula: $C_{39}H_{60}O_8$

Orthorhombic, space group $P2,2,2$, with a = 10.110(4) Å, b = 15.817(6) Å, c = 24.870(9) Å, V = 3977 Å^3, and D_c = 1.167 g cm^{-3} for Z = 4; CuKα radiation (λ = 1.5417 Å, μ(CuKα) = 6.04 cm^{-1}. Cell constants were obtained by least-squares refinement of the setting angles for 25 reflections. All calculations were performed on a PDP 11/23 computer using the usual structure determination package (10).

The ORTEP views of the molecule **1** showing the hydrogen atoms and the carbon skeleton (Fig. 1) were designed using the same package on the PDP 11/23 computer.

Nuclear magnetic resonance

The high resolution ^{1}H NMR spectra of compound **1** were obtained on a Bruker WC-500 spectrometer (CEA, Saclay) operating in FT mode at a probe temperature of 20°C. The spectra were recorded as solutions of 5 mg of compound in 0.5 mL of $CDCl_3$ in a 5-mm tube (^{1}H).

The other NMR spectra were recorded with a Bruker WM 360 WB spectrometer (CNRS, Montpellier) equipped with an Aspect 3000 computer operating in the Fourier transform mode with quadrature detection at 360 MHz for proton.

The 1D spectra were obtained in 16 K time domain addresses and processed with 32 K addresses (accuracy 0.24 Hz/point). The $CDCl_3$ proton residual signal was taken as reference (7.24 ppm).

Connectivities between protons were established by 2D correlated spectroscopy (COSY and DELAYED-COSY) using pulse sequences D_1–90°–D_0–45°–FID (11, 12) and D_1–90°–D_0–90°–D_2–180°–D_2–90°–FID (13) respectively with a transfer delay D_2 of 30 ms.

COSY and DELAYED-COSY were obtained through 512 t_1 values and, prior to Fourier transformation, t_2 and t_1 domains FID were multiplied with a nonshifted sine-bell window function.

With the pulse sequence D_1–90°–D_0–90°–D_9–90°–FID (14), NOESY data were obtained in the phase sensitive mode with a mixing time D_9 = 280 ms through 256 increment delays; $\pi/16$ and $\pi/8$ shifted sine-bell window functions were applied respectively in t_2 and t_1 domains prior to Fourier transformation.

Conclusion

The ^{1}H NMR spectra of some triterpenic *Loeselia* compounds were interpreted successfully from a series of 1D high-resolution and three homonuclear 2D experiments. The comparison of these interpretations with X-ray data has revealed a perfect fit with the geometry of the crystal.

The structure assignment and the unambiguous interpretation of the proton NMR spectra was then possible, without having to perform heteronuclear (carbon–proton) experiments. The theoretical possibility of a C-21 to C-22 *trans*-esterification between the angelate moiety at C-22 and the alcohol at C-21 during the acetylation process (as in structure **4**) is impossible without changing the configurations of both centers. The proton NMR data presented in this report are consistent for the α-C-21 acetate and the β-C-22 angelate configurations. Both NMR and X-ray data confirm deformations of the E and C rings.

Acknowledgements

The authors thank the Natural Sciences and Engineering Research Council of Canada for a research grant to one of us (K.J.). We are indebted to CEA Saclay (France) for the recording of some spectra as well as to CRASH (Saint-Hyacinthe, Qué.) for the use of their NMR facilities.

1. J. D. CONNOLLY and K. H. OVERTON. *In* Chemistry of terpenes and terpenoids. *Edited by* A. D. Newman. Academic Press, New York. 1972.
2. H. BUDZIKIEWICZ, J. M. WILSON, and C. DJERASSI. J. Am. Chem. Soc. **85**, 3688 (1963).
3. W. F. REYNOLDS, J. F. SAWYER, R. E. ENRÍQUEZ, L. I. ESCOBAR, M. A. CHÁVEZ, and J. N. SHOOLERY. Can. J. Chem. **63**, 1048 (1985).
4. W. F. REYNOLDS, S. MCLEAN, M. PERPICK DUMONT, and R. G. ENRÍQUEZ. J. Magn. Reson. **63**, 413 (1985).
5. W. F. REYNOLDS, S. MCLEAN, J. POPLAWSKI, R. G. ENRÍQUEZ, and L. I. ESCOBAR. Tetrahedron, **42**, 3419 (1986).
6. M. JÍMENEZ, K. VELÁZQUEZ, A. LIRA-ROCHA, and A. ORTEGA. 22nd Congreso Mexicano de Química Pura y Aplicada, Veracruz, Ver. México. 1987.
7. I. YOSIOKA, T. NISHIMURA, A. MATSUDA, and I. KITAWA. Chem. Pharm. Bull. **18**(81), 1610 (1970).
8. G. WULFF and R. TSCHESCHE. Tetrahedron, **25**, 415 (1969).
9. I. YOSIOKA, S. SAIJOH, and I. KITAWA. Chem. Pharm. Bull. **20**(3), 564 (1972).
10. G. M. SHELDRICK. SHELXTL revision 3. An integrated system for solving refining and displaying crystal structures from diffraction data. University of Göttingen, FRG. 1970.
11. W. P. AUE, E. BARTHOLDI, and R. R. ERNST. J. Chem. Phys. **64**, 2229 (1976).
12. K. NAGAYAMA, A. KUMAR, K. WÜTHRICH, and R. R. ERNST. J. Magn. Reson. **40**, 321 (1980).
13. G. WAGNER. J. Magn. Reson. **55**, 151 (1983).
14. G. BODENHAUSEN, H. KOGLER, and R. R. ERNST. J. Magn. Reson. **58**, 370 (1984).

Can. J. Chem. Downloaded from www.nrcresearchpress.com by 186.148.149.217 on 09/07/12
For personal use only.

Forbeside E: a novel sulfated sterol glycoside from *Asterias forbesi*

JOHN A. FINDLAY, ZHENG-QUAN HE, AND MAHESH JASEJA
Department of Chemistry, University of New Brunswick, Fredericton, N.B., Canada E3B 6E2

Received April 3, 1989

JOHN A. FINDLAY, ZHENG-QUAN HE, and MAHESH JASEJA. Can. J. Chem. **67**, 2078 (1989).

The structure of forbeside E, a minor constituent of the saponin fraction of the starfish *Asterias forbesi*, has been identified as the disodium salt of (20*R*)-5α-pregn-9(11)ene-3β-sulfo-oxy-6α-[*O*-β-D-4-sulfo-oxyquinovopyranosyl]-20-ol, principally by 2D-COSY, DQ COSY, HCORR, and DEPT experiments. Sodium thornasterol-3-*O*-sulfate has been isolated as a natural product from the same organism.

Key words: sulfated sterol glycoside, *Asterias forbesi* metabolites, sodium thornasterol-3-*O*-sulfate, asterogenol rearrangement.

JOHN A. FINDLAY, ZHENG-QUAN HE et MAHESH JASEJA. Can. J. Chem. **67**, 2078 (1989).

En se basant principalement sur des expériences de 2D-COSY, de DQ COSY, de HCORR et de DEPT, on a démontré que le forbéside E, un constituant mineur de la fraction saponine de l'étoile de mer *Asterias forbesi*, est le sel double de sodium du (20*R*)-5α-pregn-9(11)-ène-3β-sulfo-oxy-6α-[*O*-β-D-4-sulfo-oxyquinovopyranosyl]-20-ol. On a aussi isolé le thornastérol-3-*O*-sulfate de sodium à partir du même organisme.

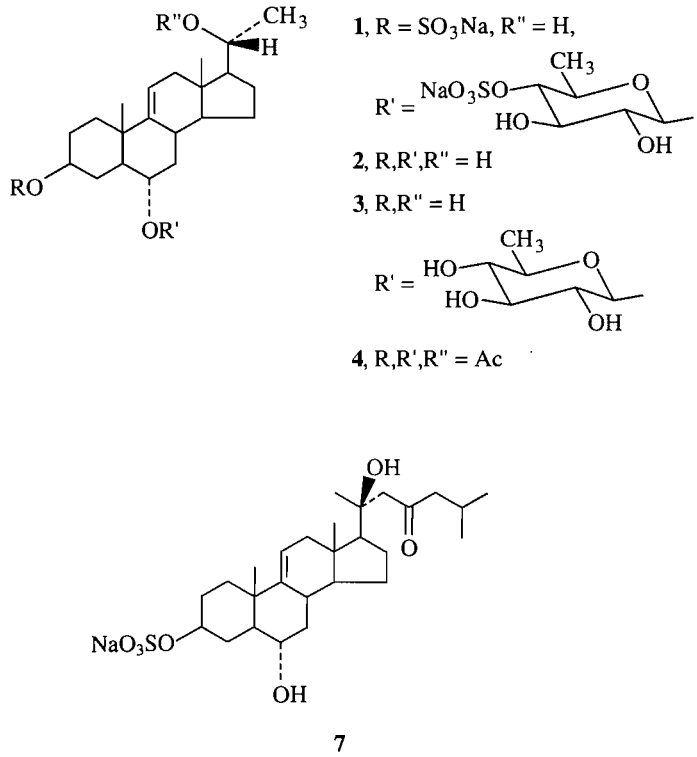
Mots clés : glycoside stérol sulfaté, métabolites *Asterias forbesi*, thornastérol-3-*O*-sulfate, nouvel arrangement d'astérogénol.
[Traduit par la revue]

Can. J. Chem. Downloaded from www.nrcresearchpress.com by 186.148.149.217 on 09/07/12
For personal use only.

In our continuing investigation of the saponin fraction of the starfish *Asterias forbesi* (Desor), we recently determined the structure of a minor constituent, forbeside E, to be the disodium salt of (20*R*)-5α-pregn-9(11)-ene-3β-sulfo-oxy-6α-[*O*-β-D-4-sulfo-oxyquinovopyranosyl]-20-ol, **1**. This compound, which is less polar than the earlier described saponins forbeside A, B (1), and C (2), has not been previously reported. However, the aglycone **2**, asterogenol, was first isolated by ApSimon *et al.* (3) from the hydrolysed saponin fractions from both *A. forbesi* and *A. vulgaris*, which led them to suggest that this C20 reduced progesterone type derivative is a genuine aglycone in some starfish saponins. This is now confirmed by our isolation of the disulfated quinovoside **1**.

We also found the known sodium thornasterol-3-*O*-sulfate, **7**, in the unhydrolysed saponin fraction from *A. forbesi*. This compound, which has not been reported previously as a natural product, was obtained by enzymatic hydrolysis of the saponin versicoside A from *Asterias amurensis* by Itakura *et al.* (4).

The positive ion FAB mass spectrum of **1** shows a prominent pseudomolecular ion at *m/e* 706 [$M^+(C_{27}H_{42}O_{13}S_2Na_2)$ + Na − H] while other prominent ions at *m/e* 605 [M^+ + H − $NaSO_3$ + Na], 603 [706 − $NaSO_3$], 587 [706 − $NaSO_4$], and 500 [706 − $2NaSO_3$] lend further support to the formulation. The location of the sulfo-oxy group at C3 of the aglycone follows from the assignment of the broad multiplet at δ 4.26 ppm in the ^{1}H nmr spectrum (D_2O) to H3. The same signal appears at δ 4.85 ppm in pyridine-d_5 and is shown by DQ COSY (5) experiment to be coupled to the signal at δ 3.4 ppm assigned to the H4β. The carbohydrate moiety is located at C6 in view of the close agreement of ^{13}C chemical shifts for C5, C6, and C7 with those of similar thornasterol glycosides (1). The nature of the sugar moiety was derived from DQ COSY experiments, which permitted unambiguous assignment of signals and connectivity. Thus the large coupling in pyridine-d_5/D_2O (J = 7.94 cps) for the anomeric H1′ proton and the triplet ($J \approx 9$ cps) nature of each signal for H2′, H3′, and H4′ were consistent only with a quinovose unit. Furthermore, the downfield location of the H4′ signal is compelling evidence for the placement of the second sodium sulfate moiety at C4′. Corroboration of these and other assignments may be derived from HCORR (6) data (see Table 1).



7

Solvolysis of forbeside E was complete after heating in pyridine-d_5/dioxane-d_8/D_2O (12:3:1) at 120°C for 6 h to give the desulfated glycoside, **3**. The course of desulfation was monitored by ^{1}H nmr and no significant difference in the rate of solvolysis at the two sites could be detected. Thus the signals for H3 and H4′ were shifted upfield simultaneously over the 6-h period and no solvolysis was detected by ^{1}H nmr after initially heating the sample at 100°C for 1–4 h.

Confirmation of the structure of the aglycone was realized by heating forbeside E with 2 N HCl at 80–90°C for 10 h followed by acetylation of the hydrolysis product. While the mass spectrum is entirely consistent with that reported for asterogenol triacetate (3) and examination by tlc showed a single spot, it is evident from ^{1}H nmr that a mixture of triacetates resulted.

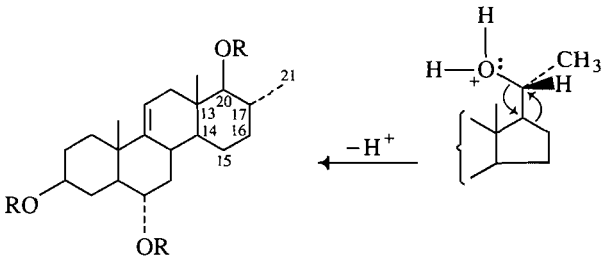
TABLE 1. NMR data for forbeside E

	Pyr-d_5/D_2O (5:1)			D_2O		
	Chemical shifts (ppm)			Chemical shifts (ppm)		
Carbon	$^{13}C^a$	$^1H^b$	J (Hz)	$^{13}C^a$	$^1H^b$	J (Hz)
1	34.80			37.80		
2	28.09			30.59		
3	77.07	4.85bm		82.90	4.26bm	
4	29.45			31.89		
5	47.84	1.5		50.74	1.35	
6	78.55	3.7m		82.97	3.6m	
7	40.64			43.51		
8	34.56	1.95		37.80	2.2	
9	144.03			148.88		
10	37.18			40.69		
11	116.42	5.20bd		120.08	5.43bd	
12	40.53			43.07		
13	40.34			43.27		
14	52.37	1.25		55.42	1.25	
15	24.90			27.69		
16	25.17			28.27		
17	57.39	1.6		60.26	1.5	
18	11.09	1.12		13.98	0.99	
19	18.15	0.90		21.17	0.64	
20	68.43	3.8m		72.90	3.7m	
21	22.83	1.36		25.01	1.11	
1′	103.77	4.81d	7.9	105.97	4.50d	7
2′	74.07	4.02dd	8.4[c]	76.35	3.32dd	7[c]
3′	75.34	4.44dd	9.1[c]	77.03	3.70	
4′	81.05	4.76dd	9.2[c]	84.89	3.92dd	7[c]
5′	69.71	3.80m		72.90	3.6	
6′	17.45	1.80d	6.1	19.82	1.31d	5

[a]Assignments from DEPT, HCORR, and comparative chemical shift data (1, 2).
[b]Assignments from COSY, DQ COSY, and HCORR.
[c]$J_1 \approx J_2$.

One component gives rise to a set of signals identical with those reported (3) for asterogenol triacetate while the other gives rise to a doublet (J = 10.7 Hz) at δ 4.45 (~0.5 H) indicative of a secondary acetoxyl proton with a *trans* diaxial partner in a six-membered ring. We formulate the second product as **6** and rationalize the formation of its precursor **5** via a Wagner–Meerwein rearrangement with anchimeric assistance of the migrating C16—C17 bond and consequent configuration inversion at C20 and C17 (Scheme 1). Confirmation of the D ring structural feature of the singularly produced stereoisomer **5** comes from a double irradiation experiment in which irradiation at 1.6 ppm (H17, located from the COSY (7) spectrum) caused the simultaneous collapse of the δ 4.45 ppm doublet together with a partially obscured methyl doublet at 0.81 ppm ($J \approx$ 6 Hz).

Inspection of molecular models reveals that the preferred orientation for the 20*R* hydroxyl in asterogenol is such that the C20—OH bond is antiperiplanar to the C16—C17 bond, thus facilitating the proposed Wagner–Meerwein shift leading to **5**. In contrast, the 20*S* isomer is predicted to experience substantial, if not prohibitive, steric repulsion between C18 and C21 methyls in order to bring the C20—OH bond antiperiplanar to the C16—C17 bond. Hence further support for the 20*R* configurational assignment in **1** and in asterogenol **2** is provided.



5, R = H
6, R = Ac

2, asterogenol

SCHEME 1

Experimental

NMR spectra were recorded on Varian XL200 and XL300 instruments using tetramethylsilane as internal standard. Optical rotations were measured with a Perkin Elmer 241 polarimeter. Mass spectra were recorded with a Kratos MS50 instrument. Preparative tlc was performed with precoated silica gel F254 (1 mm) plates.

Isolation

Crude saponin mixture (4.5 g) obtained from *Asterias forbesi* as previously described (1) was dissolved in H_2O (100 mL) and extracted with $CHCl_3$. The evaporated chloroform extract (1.5 g) was subjected to silica gel (200 g, 230–400 mesh) column chromatography with a $CHCl_3/CH_3OH/H_2O$ (10:1:0.2 → 10:3:0.5) gradient yielding 6 fractions. The third fraction was chromatographed on preparative tlc plates (50 mg per plate) using $CHCl_3/CH_3OH/H_2O$ (10:3:0.5) to afford sodium thornasterol-3-*O*-sulfate, **7** (30 mg, R_f 0.48 and R_f 0.86 using a 66:44:5 ratio of the same solvents), which was identical in ^1H and ^{13}C nmr, EIMS, and mp with reported (4) data.

The aqueous layer was evaporated *in vacuo* and the residue (2.5 g) dissolved in $CHCl_3/CH_3OH/H_2O$ (10:3:0.5) and chromatographed on a silica gel (200 g, 230–400 mesh) column with a discontinuous gradient of $CHCl_3/CH_3OH/H_2O$ (10:3:0.5 → 66:44:5), giving 12 fractions. Fraction 7 was rechromatographed on ptlc plates using $CHCl_3/CH_3OH/H_2O$ (66:44:5) from which forbeside E, **1** (R_f 0.52, 40 mg, amorphous powder), was recovered. By similar treatment, fraction 8 yielded forbeside C (2) (120 mg). Fraction 9 was rechromatographed on silica gel ptlc plates using $CH_3(CH_2)_3OH/CH_3COOH/H_2O$ (12:3:5) to provide pure forbeside B (1) (36 mg, R_f 0.32) and forbeside D (30 mg, R_f 0.26), which is currently under investigation.

Forbeside E: mp 238°C (dec.); $[\alpha]_D$ +9.5° (*c* 0.004, H_2O); ^1H and ^{13}C nmr, see Table 1. FAB (+) MS (magic bullet (8)): *m/z* 706 (7%, M^+ + Na − H), 605 (8.5), 603 (6), 587 (11), 500 (4), 448 (4), 413 (5), 329 (18), 230 (23), 199 (36), 177 (53), 143 (100).

Acid hydrolysis and acetylation of forbeside E

Forbeside E (15 mg) in 2 N HCl (25 mL) was heated at 80–90°C for 10 h, cooled, and extracted with $CHCl_3$. The dried, evaporated $CHCl_3$ layer afforded the aglycone (5 mg) after ptlc (R_f 0.56, $CHCl_3/CH_3OH$, 9:1). Evaporation of the aqueous layer, dissolution of the residue in CH_3CH_2OH, and crystallization afforded quinovose (2 mg) identified by comparison with an authentic sample. The aglycone (4 mg) was warmed at 50°C for 10 min in pyridine (1 mL)/acetic anhydride (1 mL), and evaporated. The product showed a single spot on tlc; ^1H nmr ($CDCl_3$) δ (ppm): 0.56 (3H, s, H18), 1.01 (3H, s, H19), 1.16 (3H, d, J = 6.1 Hz, H21), 4.7 (br m, H3, H6, H20), 5.4 (1H, br m, H11) of asterogenol triacetate **4** (3) plus 0.79 (3H, s, H18), 0.81 (3H, d, J = 6.1 Hz, H21), 1.00 (3H, s, 19H), 4.40 (1H, d, J = 10 Hz, 20H) assigned to triacetate **6** (signals at δ 4.7 and 5.4 assigned to both **4** and **6**). EIMS: *m/z* 460 (1%, M^+), 400 (23), 340 (45), 280 (100), 265 (44).

Solvolysis of forbeside E

Forbeside E (5 mg) was heated in pyridine-d_5/dioxane-d_8/D_2O (12:3:1, 0.5 mL) at 120°C for 6 h in an nmr tube, affording desulfated

Can. J. Chem. Downloaded from www.nrcresearchpress.com by 186.148.149.217 on 09/07/12
For personal use only.

forbeside E, **3**; ^{1}H nmr (pyridine-d_5/D_2O, 5:1) δ (ppm): 0.69 (3H, s, H18), 0.86 (3H, s, H19), 1.20 (3H, d, J = 5.7 Hz, H21), 1.50 (3H, d, J = 6.4 Hz, H6′), 3.9–3.5 (5H, m, H3, 6, 20, 4′, and 5′), 3.95 (1H, dd, $J_{1',2'} \approx J_{2',3'} \approx$ 9 Hz, H2′), 4.09 (1H, dd, $J_{3',4'} \approx J_{2',3'} \approx$ 9 Hz, H3′), 4.75 (1H, d, $J_{1',2'}$ = 7.4 Hz, H1′), 5.15 (1H, br s, H11). These assignments were facilitated by a COSY spectrum. FAB (+) MS (magic bullet): m/z 504 (M^+ + H + Na), 482 (M^+ + 2H), 329, 217, 177.

Acknowledgements

This study was supported by a grant from the Natural Sciences and Engineering Research Council of Canada. The authors are grateful to Professor A. Perlin, Pulp and Paper Research Institute, McGill University, for access to a 300 MHz nmr facility and to Larry Calhoun for advice on nmr matters. The assistance of the Huntsman Marine Laboratory in collecting organisms is gratefully acknowledged.

1. J. A. Findlay, M. Jaseja, D. J. Burnell, and J.-R. Brisson. Can. J. Chem. **65**, 1384 (1987).
2. J. A. Findlay, M. Jaseja, and J.-R. Brisson. Can. J. Chem. **65**, 2605 (1987).
3. J. W. ApSimon, S. Badripersaud, J. A. Buccini, J. Eenkhoorn, and M. W. Gilgan. Can. J. Chem. **58**, 2703 (1980).
4. Y. Itakura, T. Komori, and T. Kawasaki. Liebig's Ann. Chem. 2079 (1983).
5. U. Piantini, O. W. Sørensen, and R. R. Ernst. J. Am. Chem. Soc. **104**, 6800 (1982); M. Rance *et al.* Biochem. Biophys. Res. Commun. **117**, 479 (1983).
6. R. Lanzetta, G. Laonigro, and M. Parrilli. Can. J. Chem. **60**, 1431 (1982).
7. A. Bax and R. Freeman. J. Magn. Reson. **44**, 542 (1981); A. Bax, R. Freeman, and G. Morris. J. Magn. Reson. **42**, 164 (1981).
8. J. L. Whitten, M. H. Schaffer, M. O'Shea, J. C. Cook, M. E. Hemling, and K. L. Rhinehart, Jr. Biochem. Biophys. Res. Commun. **124**, 350 (1984).

Can. J. Chem. Downloaded from www.nrcresearchpress.com by 186.148.149.217 on 09/07/12
For personal use only.

Collision-induced dissociation mass spectra of protonated alkyl amines

ERIC J. REINER[1] AND ALEX. G. HARRISON[2]
Department of Chemistry, University of Toronto, Toronto, Ont., Canada M5S 1A1
AND
RICHARD D. BOWEN
Department of Chemistry, University of Warwick, Coventry CV4 7AL, England

Received April 27, 1989

ERIC J. REINER, ALEX. J. HARRISON, and RICHARD D. BOWEN. Can. J. Chem. **67**, 2081 (1989).

The collision-induced dissociation (CID) mass spectra of the $[MH]^+$ ions of a variety of C_4 to C_6 mono-, di-, and tri-alkyl amines have been determined at 8 keV collision energy and also as a function of collision energy over the range 5–100 eV (laboratory scale). The two major primary fragmentation pathways observed following either mode of activation are (i) production of an alkyl cation by expulsion of ammonia or an alkyl amine, and (ii) formation of a smaller protonated amine by loss of an olefin. In addition, alkane elimination from $[MH]^+$, by a variety of pathways, is a common reaction for protonated dialkyl and trialkyl amines, especially in the 8 keV spectra. However, these alkane elimination reactions are of considerably less importance in the low energy CID spectra because they have high onset energies. The differences observed in the spectra produced by the two methods of activation are discussed in terms of the distributions of internal energies deposited in $[MH]^+$ by the collision process.

Key words: protonated amines, collision-induced fragmentation, energy-resolved mass spectrometry.

ERIC J. REINER, ALEX. J. HARRISON et RICHARD D. BOWEN. Can. J. Chem. **67**, 2081 (1989).

Opérant à une énergie de collision de 8 keV ainsi qu'à des énergies de collision allant de 5 à 100 eV (échelle de laboratoire), on a déterminé les spectres de masse de dissociations induites par collision (DIC) des ions $[MH]^+$ d'un certain nombre de mono-, di- et tri-alkylamines en C_4, C_5 et C_6. Les deux modes principaux de la fragmentation primaire, selon l'un ou l'autre des modes d'activation, sont (i) la production d'un cation alkyle provenant de l'expulsion d'ammoniac ou d'une alkylamine et (ii) la formation d'une amine protonée plus petite provenant de la perte d'une oléfine. De plus, l'élimination d'un alcane à partir de l'ion $[MH]^+$, par le biais de diverses voies, est une voie réactionnelle fréquente pour les amines protonées dialkylées et trialkylées, principalement dans les spectres à 8 keV. Toutefois, à cause de leurs énergies élevées d'activation, ces réactions d'élimination d'alcane sont beaucoup moins importantes dans les spectres de DIC à basse énergie. On discute des différences observées dans les spectres produits par les deux méthodes en fonction des distributions des énergies internes déposées dans les ions $[MH]^+$ par le processus de collision.

Mots clés : amines protonées, fragmentation induite par collision, spectrométrie de masse résolue pour l'énergie.

[Traduit par la revue]

Can. J. Chem. Downloaded from www.nrcresearchpress.com by 186.148.149.217 on 09/07/12
For personal use only.

Introduction

In the proton-transfer chemical ionization mass spectra of alkyl amines, obtained using H_3^+ or $[HCO]^+$ as reagent ions, there often are intense ion signals corresponding nominally to alkane elimination from the protonated amine (1). Although alkane elimination frequently leads to the energetically most favourable products (1), this reaction mode is not observed in the unimolecular metastable ion fragmentation reactions of protonated amines (1, 2) thus suggesting that there may be a barrier to alkane elimination additional to the reaction endothermicity. This conclusion is supported by theoretical calculations on protonated *i*-propyl amine, which showed that there was a large energy barrier for the concerted elimination of CH_4 (1). Nevertheless, the limited high energy collision-induced dissociation (CID) studies of protonated amines have shown that significant fragmentation occurs by way of alkane elimination for species activated in this fashion (3, 4).

These earlier studies (3, 4) of the high energy CID of protonated alkyl amines have been exploratory in nature and have not clearly established how general alkane elimination is nor how useful CID studies are in distinguishing between isomeric amines; in particular, there do not appear to have been any studies of the low energy CID of protonated alkyl amines. In the present paper we report a systematic study of the collision-induced fragmentation of the isomeric protonated butyl amines, their *N*-methyl and *N,N*-dimethyl derivatives, as well as a variety of protonated dialkyl and trialkyl amines containing four to six carbons. This work has involved both high energy (8 keV) and low energy (5–100 eV of laboratory scale) collisional activation of the protonated species. The primary goal was to explore collision-induced dissociation as a means of distinguishing between isomeric even-electron ions. In addition, the variable low energy collisional studies, the so-called energy-resolved mass spectrometric (ERMS) technique (5–7), have provided considerable information on the energy dependence of the fragmentation of protonated amines. In particular, the ERMS results show that alkane eliminations from protonated alkyl amines are high energy processes and the products of such reactions are much more abundant in high energy CID mass spectra than in low energy CID mass spectra, pointing to substantial differences in the distributions of internal energy deposited in $[MH]^+$ by the two methods of activation.

Experimental

All experimental work was carried out using a VG Analytical ZAB-2FQ mass spectrometer, which has been described in detail previously (8). Briefly, the instrument is a reversed-geometry (BE) double-focussing mass spectrometer with a third stage consisting of a deceleration lens system, an rf-only quadrupole collision cell, and a quadrupole mass analyzer. This assembly permits collisional studies to be carried out in

[1]Present address: Ontario Ministry of the Environment, 125 Resources Road, Rexdale, Ont., Canada.

[2]Author to whom correspondence may be addressed.

Printed in Canada / Imprimé au Canada

TABLE 1. CID mass spectra (8 keV) of protonated C_4 amines (m/z 74)

m/z	*n*-Butyl	*i*-Butyl	*sec*-Butyl	*tert*-Butyl	Diethyl	$(CH_3)_2$ ethyl	CH_3-*n*-propyl	CH_3-*i*-propyl
59			5	5	23	27		3
58		2	4	11	22	25	4	5
57	100	100	100	100	5	11	5	3
56	5	3	20	14	9	12	5	3
55	4	2	8	3				
54			3			21		
53	2		4	2				
46					100	100		
45	3		3		33	19	8	
44	3		19		49	65	25	5
43	2				13	2	49	21
42			6		21	18	7	4
41	14	7	21	12	5		18	9
40					2	2		
39	7	4	12	8			10	5
32							100	100
31							10	7
30	16	5	2		55	4	29	12
29	9	3	12	5	34	7	4	2
28	3		3		15	7	9	4
27	6		7	3	19	5	9	4
26					4		2	
18	16	7	45	34	34			

the low energy range. In addition, the instrument is equipped with a collision cell at the first focal point in the field-free region between the magnetic (B) and electric (E) sectors that provides the capability of studying collision processes in the keV energy range (laboratory scale).

In the low energy collisional activation experiments the ions of interest were mass-selected by the double-focussing BE instrument at 8 keV ion energy, decelerated to the appropriate collision energy (5–100 eV, laboratory scale), and introduced into the quadrupole cell where they underwent collision with N_2. The ionic products were analyzed using the final quadrupole. The pressure of N_2 was 1.5×10^{-7} Torr (1 Torr = 133.3 Pa) as indicated by an ionization gauge attached to the pumping line for the region; this resulted in ~30% attenuation of the main beam. The results are presented in the following as graphs of the percentage fragment ion abundance versus the centre-of-mass collision energy. The average relative error in the fragment ion abundances was 7%.

For the high energy collisional activation experiments, the ions of interest were selected by the magnetic sector and underwent collision, at 8 keV kinetic energy, with He in the collision cell located at the focal point between the magnetic and electric sectors. The ionic products were analyzed according to their kinetic energy by scanning the voltage applied to the electric sector, the so-called MIKES technique (9). The He pressure was 1.5×10^{-7} Torr as measured by the ionization gauge on the line pumping the region; this resulted in about 30% attenuation of the main beam. In the MIKES-CID studies all mass and energy resolving slits were fully opened; the spectra in this paper are quoted in terms of peak heights. Relative peak heights were reproducible to better than 10%.

The protonated amines were produced by *i*-butane chemical ionization in the CI source operating at 200°C and either 50 or 100 eV ionizing electron energy. With *i*-butane reagent gas the unimolecular metastable ion fragmentation of the protonated species made a negligible contribution to the spectra recorded. The amines were introduced through the batch heated inlet system. These amines were either commercially available or were synthesized as described previously (2).

Results and discussion

Low energy and high energy CID mass spectra are reported in detail in Tables 1–3 and Figures 1–6 for the $[MH]^+$ ions of 24 alkyl amines containing a total of four to six carbon atoms. In the following discussion of these results, the $[MH]^+$ ions are divided into isomeric groups containing four, five, and six carbon atoms.

Protonated C_4 amines

Table 1 presents the 8 keV CID mass spectra of the $[MH]^+$ ions derived from the isomeric butyl amines, diethyl amine, *N*,*N*-dimethylethyl amine, *N*-methyl-*n*-propyl amine, and *N*-methyl-*i*-propyl amine. The three major primary fragmentation reactions of the $[MH]^+$ ions are elimination of ammonia or an amine, reaction [1], elimination of an olefin, reaction [2], and

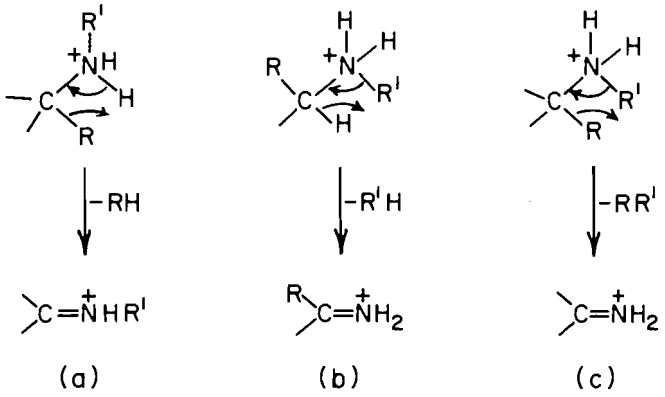
[1] $[RNH_2R']^+ \rightarrow R^+ + NH_2R'$

[2] $[RNH_2R']^+ \rightarrow [R'NH_3]^+ + [R—H]$

elimination of an alkane. Alkane loss can occur by three pathways (3) corresponding to the three formal 1,2-eliminations illustrated in Scheme 1. For the C_4 amines these alkane elimination reactions can lead to m/z 58 ($MH^+ - CH_4$), m/z 44 ($MH^+ - C_2H_6$), and m/z 30 ($MH^+ - C_3H_8$). The primary fragment ions can, of course, fragment further.

For the protonated butyl amines reaction [1] leads to formation of the butyl ion (m/z 57), which forms the base peak in all four spectra, with the ammonium ion (m/z 18) produced in reaction [2] being of lesser importance. This is in contrast to the unimolecular metastable ion fragmentation of the $[MH]^+$ ions of *sec*-butyl and *tert*-butyl amines where $[NH_4]^+$ is the dominant product. For the dialkyl and trialkyl amines, reaction [2] is the dominant fragmentation reaction of the $[MH]^+$ ions

Can. J. Chem. Downloaded from www.nrcresearchpress.com by 186.148.149.217 on 09/07/12
For personal use only.



SCHEME 1

because of the increased stability of the protonated amine produced relative to the stability of the ammonium ion. Thus, diethyl amine and *N,N*-dimethylethyl amine show *m/z* 46 $[MH^+ - C_2H_4]$ as the base peak while the *N*-methylpropyl amines both show *m/z* 32 $[MH^+ - C_3H_6]$ as the base peak.

The alkane elimination reactions of Scheme 1 are of only minor importance for the $[MH]^+$ ions of the butyl amines. Only pathway (a) should operate, leading to formation of *m/z* 30 ($-C_3H_8$) for the *n*-butyl and *i*-butyl amines, to formation of *m/z* 44 ($-C_2H_6$) and *m/z* 58 ($-CH_4$) for the *sec*-butyl amine, and to formation of *m/z* 58 ($-CH_4$) for the *tert*-butyl amine. Although these peaks are observed there is some nonspecificity in alkane loss, as witnessed by the weak $[MH^+ - C_2H_6]$ ion signal for $[n\text{-BuNH}_3]^+$ and the weak $[MH^+ - C_3H_8]$ signal for $[sec\text{-BuNH}_3]^+$. The low intensity of the signals for the alkane elimination reactions in the monoalkyl amines, which also extends to the C_5 and C_6 monoalkyl amines (10), means that it is difficult to identify the individual isomer by this signal in the CID mass spectrum.

In contrast to the monoalkyl amines, the $[MH]^+$ ions formed from the dialkyl and trialkyl amines show much more fragmentation by alkane elimination. Thus, protonated diethyl amine shows abundant ion signals resulting from elimination of CH_4 (pathway (a)), elimination of C_2H_6 (pathway (b)), and elimination of C_3H_8 (pathway (c)). *N,N*-Dimethylethyl amine can be distinguished from diethyl amine by the much lower abundance of the *m/z* 30 (C_3H_8 elimination) ion. The two *N*-methylpropyl amines show similar fragmentation reactions, with the $[MH]^+$ ions of both showing elimination of CH_4, C_2H_6, and C_3H_8. Expulsion of an alkyl radical from $[MH]^+$ occurs to some extent in these CID spectra. Thus, $[(C_2H_5)_2NH_2]^+$, $[(CH_3)_2NHC_2H_5]^+$, and, for the C_5 amines of Table 2, $[(C_2H_5)_2NHCH_3]^+$ and $[i\text{-}C_3H_7NH(CH_3)_2]^+$ all undergo sizeable amounts of CH_3 loss after collisional activation. This reaction apparently does not necessarily involve the *N*-methyl group(s). It is likely, therefore, that distonic (11)[3] ions may occasionally be formed as the daughter ion in these processes (e.g., $[CH_2NH_2C_2H_5]^{+\cdot}$ by $CH_3^\cdot$ loss from $[(C_2H_5)_2NH_2]^+$). Alkyl radical loss from $[MH]^+$ is formally a violation of the even-electron (13) rule.[4] Such a violation is hardly surprising in view of the large collision energies involved in this work and the opportunity for $[MH]^+$ to eliminate an alkyl radical by simple cleavage of the appropriate bond.

More detailed information on the fragmentation of the protonated amines comes from the energy-resolved data obtained at low collision energies. The results obtained for the $[MH]^+$ ions of the eight amines of Table 1 are shown in Figs. 1 and 2 in the form of breakdown graphs expressing the percentage fragment ion abundances as a function of the centre-of-mass collision energy. For the protonated butyl amines (Fig. 1) the $[C_4H_9]^+$ (*m/z* 57) ion dominates the breakdown graph at low collision energies but, at higher collision energies, there is more fragmentation of this ion to $[C_3H_5]^+$ (*m/z* 41) and $[C_2H_5]^+$ (*m/z* 29) than is observed in the 8 keV CID mass spectra. For the protonated dialkyl and trialkyl amines (Fig. 2), olefin elimination (reaction [2]) is the dominant fragmentation reaction at low collision energies but, with increasing collision energy, alkyl ion formation (reaction [1]) increases in importance and, at higher collision energies, these alkyl ions show a greater relative abundance than they do in the 8 keV CID mass spectra. It appears that the mean internal energy imparted to the ions in the 8 keV collision is less than that imparted to the ions in the 10–25 eV (centre-of-mass) collisions.

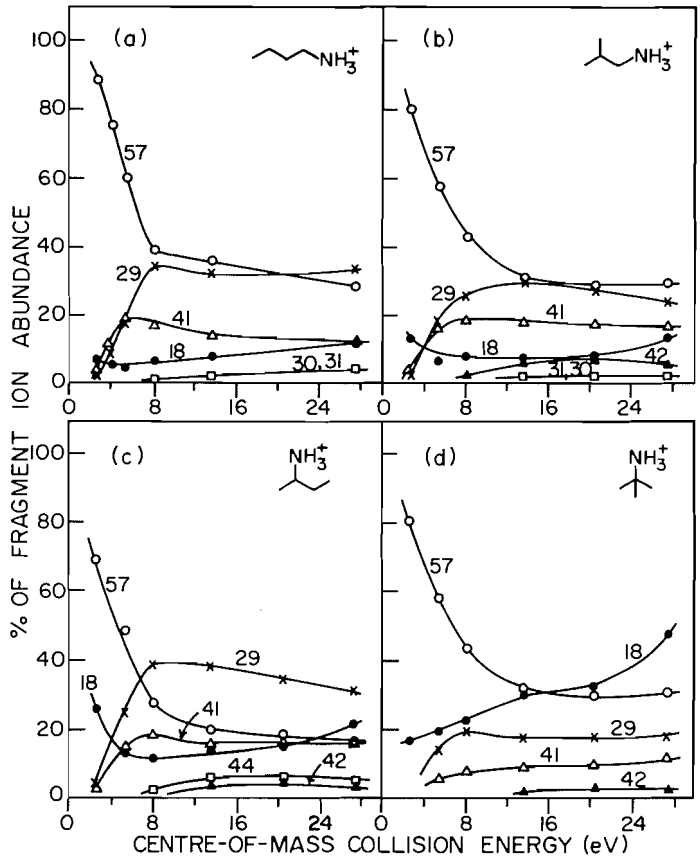


FIG. 1. Breakdown graphs for protonated (a) *n*-butyl amine, (b) *i*-butyl amine, (c) *sec*-butyl amine, and (d) *tert*-butyl amine.

Particularly intriguing results are obtained for the alkane elimination reactions in the low energy CID. As Fig. 1 shows, the alkane elimination reactions are of very little importance for the protonated butyl amines; indeed, this reaction is not observed for protonated *tert*-butyl amine. For the other butyl amines one alkane elimination reaction is observed, giving a product ion of very low abundance, thus reflecting an apparently high onset energy for these processes. For the dialkyl and trialkyl amines (Fig. 2) only one major alkane elimination reaction is observed for each $[MH]^+$ ion, that corresponding to

[3]For a review on distonic ions see ref. 12.

[4]For a review of the validity of the even-electron rule see ref. 14.

Can. J. Chem. Downloaded from www.nrcresearchpress.com by 186.148.149.217 on 09/07/12
For personal use only.

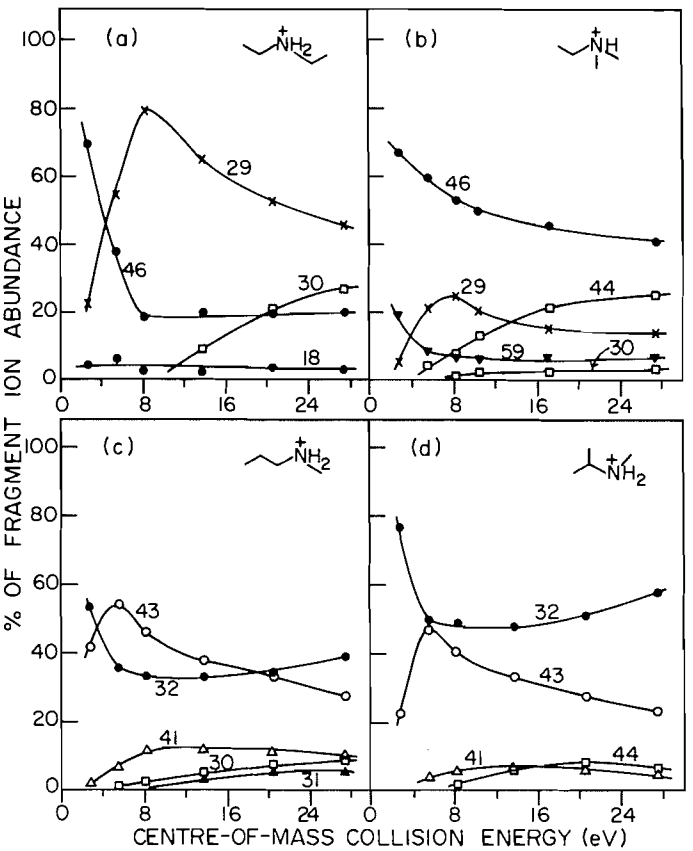


FIG. 2. Breakdown graphs for protonated (a) diethyl amine, (b) dimethylethyl amine, (c) methyl-*n*-propyl amine, and (d) methyl-*i*-propyl amine.

pathway (c) of Scheme 1. This is in sharp contrast to the results obtained in the high energy CID studies. From the low energy CID results *N*,*N*-dimethylethyl amine can be readily distinguished from diethyl amine and, similarly, *N*-methyl-*n*-propyl amine can be distinguished from *N*-methyl-*i*-propyl amine on the basis of the alkane elimination reaction (C_3H_8 and C_2H_6 loss, respectively) observed from $[MH]^+$. However, it should be noted that the alkane elimination reactions observed have onset energies in the 4–8 eV (centre-of-mass) collision energy range. Presumably the other alkane elimination reactions that are observed in the 8 keV studies have higher onset energies than the internal energies that can be achieved in low energy collisional activation.

Finally, it should be noted that the high energy CID mass spectrum observed for protonated diethyl amine is in quantitative disagreement with spectra that have been reported earlier (3, 4), these earlier spectra being in disagreement with each other. Our major disagreement with the spectrum of Sigsby *et al.* (3) lies in the relative intensity of the *m/z* 46 ($[C_2H_5NH_3]^+$) ion signal. They report it to be 37% of the *m/z* 30 base peak while we observe it as the base peak. Sigsby *et al.* reported correcting their spectrum for unimolecular metastable ion fragmentation; since the main metastable ion fragmentation of protonated diethyl amine is formation of $[C_2H_5NH_3]^+$, it appears possible that they may have overcorrected. Under our experimental conditions the signal for unimolecular fragmentation was only about 1% of the CID signal and no correction was made. The spectrum reported by Wagner *et al.* (4) shows much higher ion signals at low mass than do either ours or that of Sigsby *et al.* We note that Wagner *et al.* attenuated their main beam by 67% and clearly were in the multiple collision regime; by contrast, we attenuated the main beam by 30% and were primarily in the single collision regime. Enhancement of low mass signals by sequential collision activation is to be expected in the work of Wagner *et al.* (4).

Protonated C_5 amines

The $[MH]^+$ ions generated from pentyl amines, $C_5H_{11}NH_2$ (spectra not shown here), fragment largely by reactions [1] and [2] in both the high energy and low energy CID with only very low intensities for the products of alkane elimination (10). The $[C_5H_{11}]^+$ ion produced in reaction [1] undergoes extensive fragmentation to form $[C_3H_7]^+$. Without recording the CID mass spectra of all isomers under identical conditions it would be difficult to identify a specific isomer from the CID mass spectrum of the $[MH]^+$ ion.

Table 2 records the 8 keV CID mass spectra of the $[MH]^+$ ions of the isomeric *N*-methylbutyl amines, *N*-ethyl-*n*-propyl amine, *N*-methyldiethyl amine, and the isomeric *N*,*N*-dimethylpropyl amines. A major fragmentation channel for the $[MH]^+$ ion in all cases is olefin elimination, reaction [2], leading to a protonated amine. Thus the *N*-methylbutyl amines show an abundant ion at *m/z* 32 ($[CH_3NH_3]^+$), the dimethylpropyl amines at *m/z* 46 ($[(CH_3)_2NH_2]^+$), methyldiethyl amine at *m/z* 60 ($[CH_3NH_2C_2H_5]^+$), and ethylpropyl amine at *m/z* 46 ($[C_2H_5NH_3]^+$). It is interesting to note that $[n\text{-}C_3H_7NH_2C_2H_5]^+$ does not show elimination of ethylene to give *m/z* 60 ($[C_3H_7NH_3]^+$). This is in agreement with the earlier observation (15) that the infrared multiphoton photodissociation of protonated *N*-ethyl-*i*-propyl amine leads exclusively to formation of $[C_2H_5NH_3]^+$. The rationalization (15) is that the fragmentation reaction proceeds in a stepwise fashion involving formation of the ion–dipole complexes $[C_3H_7^+\text{---}H_2NC_2H_5]$ and $[C_2H_5^+\text{---}H_2NC_3H_7]$; the former complex is more stable than the latter, thus leading to exclusive elimination of C_3H_6. There is substantial evidence that such olefin-elimination reactions do not occur by a concerted mechanism but rather occur in a stepwise fashion involving ion–dipole complexes (1, 2, 15–24). Note, however, that in the present system both $[C_3H_7]^+$ and $[C_2H_5]^+$ are observed, the former in greater abundance. Formation of alkyl ions by reaction [1] also is a favourable reaction for the $[MH]^+$ ion of the methylbutyl amines and $[C_4H_9]^+$ is the base peak in the CID mass spectrum for the *i*-butyl isomer.

The products of alkane elimination from $[MH]^+$ are observed at *m/z* 72 ($MH^+ - CH_4$), *m/z* 58 ($MH^+ - C_2H_6$), *m/z* 44 ($MH^+ - C_3H_8$), and *m/z* 30 ($MH^+ - C_4H_{10}$); all three pathways outlined in Scheme 1 appear to operate and the product ions are of considerable abundance. While some characterization of the amines is possible from the alkane elimination reactions observed from $[MH]^+$, the profusion of peaks creates difficulties in other cases. For example, the CID mass spectra for the *N*-methyl-*sec*-butyl and *N*-methyl-*tert*-butyl compounds are very similar. More specificity in the alkane elimination reactions is observed in the low energy CID mass spectra, as shown by the breakdown graphs of Figs. 3 and 4. Again only the alkane elimination originating by pathway (c) of Scheme 1 is observed and the onset energies are in the range 3–9 eV, indicating processes with high critical reaction energies. The more specific alkane elimination reactions observed in the low energy CID mass spectra make isomer differentiation more reliable in many cases. Thus, *N*-methyl-*sec*-butyl amine can be readily distinguished from *N*-methyl-*tert*-butyl amine by

Can. J. Chem. Downloaded from www.nrcresearchpress.com by 186.148.149.217 on 09/07/12
For personal use only.

TABLE 2. CID mass spectra (8 keV) of protonated C_5 di- and tri-amines ($[MH]^+$ m/z 88)

m/z	Me-*n*-butyl	Me-*i*-butyl	Me-*sec*-butyl	Me-*tert*-butyl	Et-*n*-propyl	Me-diethyl	Me_2-*n*-propyl	Me_2-*i*-propyl
73	2	3	8			36	3	81
72	5	7	2	4	2	23	10	7
71		4		3		4	6	4
70	2	5		2	2	5	5	3
60						78		
59	3				15	39	11	
58	3		10	6	39	95	36	11
57	57	100	24	38		10	10	4
56	8	7	6	6	2	24	8	6
46					100	5	100	100
45		4			15		23	11
44	84	35	8	2	35	100	61	18
43	4	4			73	5	31	14
42	3	3		3	6	23	20	6
41	38	20	14	8	41	10	15	6
39	16	8	6	3	14	3	5	3
32	100	65	100	100	2	35		
31	24	6	9	3				
30	59	19	19	8	86	19	5	3
29	40	9	14	4	26	22	3	
28	16	4	6		21	13	5	2
27	20	4	6	2	29	12	6	2
18	2				23			

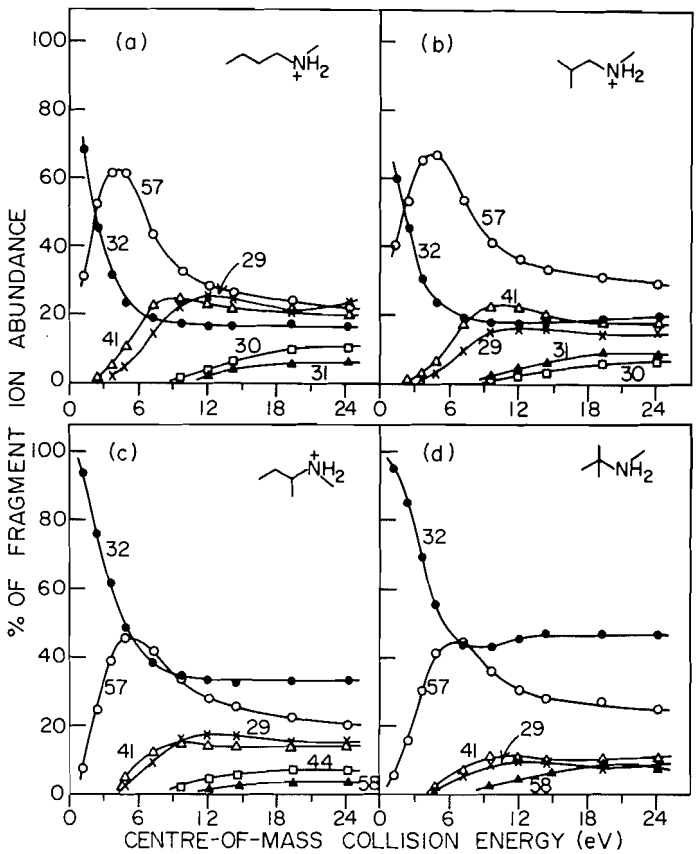


FIG. 3. Breakdown graphs for protonated (a) methyl-*n*-butyl amine, (b) methyl-*i*-butyl amine, (c) methyl-*sec*-butyl amine, and (d) methyl-*tert*-butyl amine.

the m/z 44 ion signal observed for the former. Similarly, the three substituted propyl amines can be distinguished from each other on the basis of the alkane elimination reactions observed. However, to use these ion signals to characterize the amines the collision energy must clearly be greater than 12 eV centre-of-mass (50 eV laboratory scale).

The major features of the breakdown graphs can be rationalized in terms of the occurrence of reactions [1] and [2] with, in the case of the butyl amines, further fragmentation of the alkyl ions formed in reaction [1]. In all cases the protonated amine produced in reaction [2] dominates the breakdown graph at low internal energies with the alkyl ion produced in reaction [1] increasing in importance with increasing collision energy. There is a significant resemblance between the general trends in the energy dependence of reactions [1] and [2] shown by the isomeric pairs of ions $[n\text{-}C_4H_9NH_2CH_3]^+$ and $[\text{iso-}C_4H_9NH_2CH_3]^+$, and $[n\text{-}C_4H_9NH(CH_3)_2]^+$ and $[\text{iso-}C_4H_9NH(CH_3)_2]^+$, Figs. 3 and 5. Similar broad correlations are found for $[sec\text{-}C_4H_9NH_2CH_3]^+$ and $[tert\text{-}C_4H_9NH_2CH_3]^+$ and for $[sec\text{-}C_4H_9NH(CH_3)_2]^+$ and $[tert\text{-}C_4H_9NH(CH_3)_2]^+$. It is interesting to note that the *n*-butyl and *i*-butyl isomers (Fig. 3) that, in the absence of rearrangement, would give the least stable butyl ions show more abundant m/z 57 ion signals than do the *sec*-butyl and *tert*-butyl isomers. Similarly, the $[C_3H_7]^+$ (m/z 43) ion abundance is greater for *N,N*-dimethyl-*n*-propyl amine than for the *i*-propyl isomer. This is consistent with the stepwise mechanism of fragmentation discussed previously (2) involving (alkyl ion)–amine ion/dipole complexes. Those complexes in which the developing cation is a primary alkyl ion are higher in energy than the analogous complexes containing an incipient secondary or tertiary alkyl ion. The developing primary cations undergo exothermic rearrangement to the more stable alkyl ion

Can. J. Chem. Downloaded from www.nrcresearchpress.com by 186.148.149.217 on 09/07/12
For personal use only.

Can. J. Chem. Downloaded from www.nrcresearchpress.com by 186.148.149.217 on 09/07/12
For personal use only.

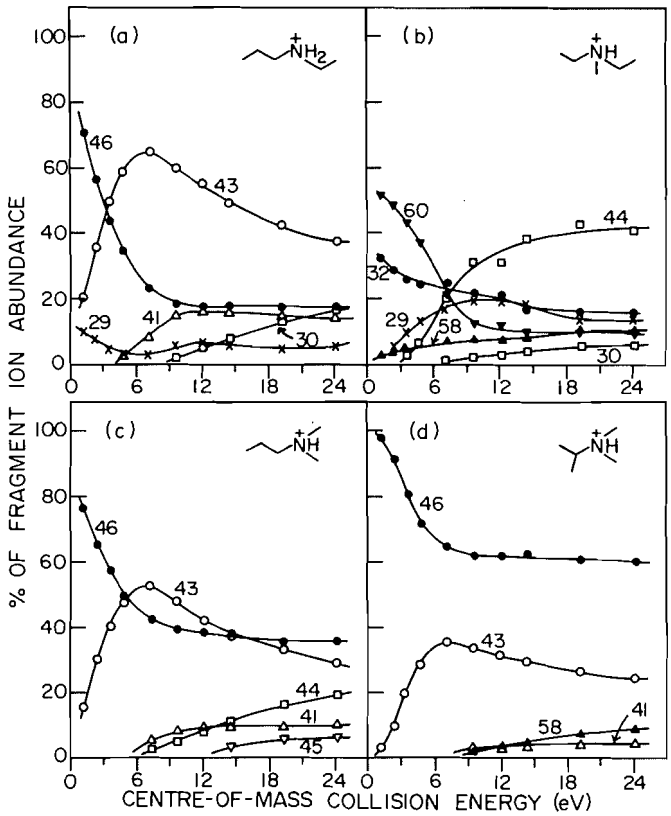


FIG. 4. Breakdown graphs for protonated (a) ethyl-*n*-propyl amine, (b) methyldiethyl amine, (c) dimethyl-*n*-propyl amine, and (d) dimethyl-*i*-propyl amine.

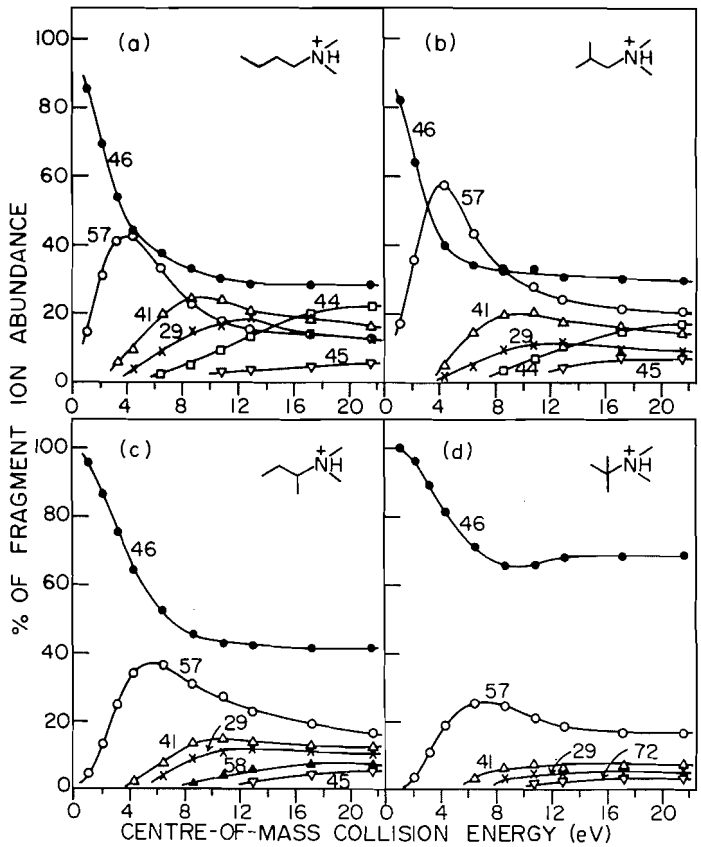


FIG. 5. Breakdown graphs for protonated (a) dimethyl-*n*-butyl amine, (b) dimethyl-*i*-butyl amine, (c) dimethyl-*sec*-butyl amine, and (d) dimethyl-*tert*-butyl amine.

isomer(s); the potential energy released by this isomerization enhances the tendency of these rearranged ions to fragment via amine expulsion. By contrast, the complexes originally containing incipient secondary or tertiary alkyl ions are lower in energy and are more likely to fragment to the protonated amine. A suitable potential energy profile for the protonated *i*-butyl- and *tert*-butyl-ammonium systems was presented previously (2).

Protonated C_6 amines

The protonated hexyl amines, $[c_6H_{13}NH_3]^+$, fragment primarily by reactions [1] and [2] with further extensive fragmentation of the hexyl ions formed in reaction [1] (10). In both the high energy and low energy CID mass spectra the abundance of the alkane elimination products is low, making identification of the individual hexyl isomers difficult.

The 8 keV CID mass spectra of the $[MH]^+$ ions of the isomeric *N,N*-dimethylbutyl amines, di-*n*-propyl amine, di-*i*-propyl amine, *N*-ethyl-*n*-butyl amine, and triethyl amine, are presented in Table 3, while the breakdown graphs are presented in Figs. 5 and 6. Reactions [1] and [2] are of major importance in both the high energy and low energy CID. Thus, reaction [2] leads to formation of *m/z* 46 ($[(CH_3)_2NH_2]^+$) for the protonated dimethylbutyl amines, to *m/z* 60 ($[C_3H_7NH_3]^+$) for the protonated dipropyl amines, to *m/z* 46 ($[C_2H_5NH_3]^+$) for protonated ethylbutyl amine, and to *m/z* 74 ($[(C_2H_5)_2NH_2]^+$) for protonated triethyl amine. For the latter four compounds one should note, in the 8 keV CID, the sequential elimination of olefins resulting in formation of $[NH_4]^+$ (*m/z* 18). In the breakdown graphs, representing the low energy CID data, the olefin elimination reaction [2] is the dominant reaction at low collision energies with reaction [1], alkyl ion formation, increasing greatly in importance with increasing collision energy.

For these polyalkyl amines, alkane elimination from $[MH]^+$ becomes very significant in the high energy CID and, for four of the amines, yields the base peak in the CID mass spectra. The alkane elimination reactions result in the ion signals at *m/z* 86 ($MH^+ - CH_4$), *m/z* 72 ($MH^+ - C_2H_6$), *m/z* 58 ($MH^+ - C_3H_8$), *m/z* 44 ($MH^+ - C_4H_{10}$), and *m/z* 30 ($MH^+ - C_5H_{12}$). The alkane elimination reactions in the high energy CID do help in isomer differentiation; for example, protonated di-*n*-propyl and di-*i*-propyl amines give distinctly different patterns of alkane elimination (mainly C_4H_{10} and C_3H_8 losses, respectively, with some C_2H_6 elimination from each ion). In contrast to the high energy CID, the low energy CID mass spectra of Figs. 5 and 6 show only one major alkane elimination reaction for each protonated amine, that corresponding to pathway (c) of Scheme 1. The low energy CID mass spectra thus serve to identify each amine with the exception of *N,N*-dimethyl-*n*-butyl and -*i*-butyl amines, which give very similar spectra. Once again, however, the alkane elimination reactions have high onset energies, with the result that it is necessary to work at high collision energies (50 eV laboratory scale) to characterize the individual isomers.

Conclusions

The relatively large differences observed between the high energy and low energy CID mass spectra of the protonated amines can be rationalized in terms of the energy requirements for fragmentation and the distributions of internal energy deposited in the ions by the collisional activation process. As Wysocki *et*

TABLE 3. CID mass spectra (8 keV) of protonated C_6 di- and tri-alkyl amines ($[MH]^+$ m/z 102)

m/z	Me_2-*n*-butyl	Me_2-*i*-butyl	Me_2-*sec*-butyl	Me_2-*tert*-butyl	Di-*n*-propyl	Di-*i*-propyl	Et-*n*-butyl	Triethyl
87	2	3		6	2	3	2	13
86	8	10	3	4		5	2	6
85		3						
84	2	4	2					
74								26
73	2		9		5		15	16
72	4	2	17	8	51		13	31
71	4	7						4
70	7	8	5	3	5	4	3	
60					53	78		
59	18	7			26	10		
58	76	54	11		44	25	78	100
57	48	65	25	22			67	
56	8	2	6	3	11	4	13	19
55	10	7	5	2			14	
46	100	100	100	100			80	10
45	32	21	14	10			18	
44	75	60	22	13	3	100	38	26
43	11	2		2	89	70	14	6
42	16	14	6	3		18	41	15
41	26	21	7	5	55	32	22	
39	2	7	3	2	14	10	11	
30	9	5	3		100	3	100	20
29	19	12	7	3	3	2	53	26
28	6	4	3		13	7	17	16
27	8	5	3		24	13	21	13
18		2			32	56	18	13

Can. J. Chem. Downloaded from www.nrcresearchpress.com by 186.148.149.217 on 09/07/12
For personal use only.

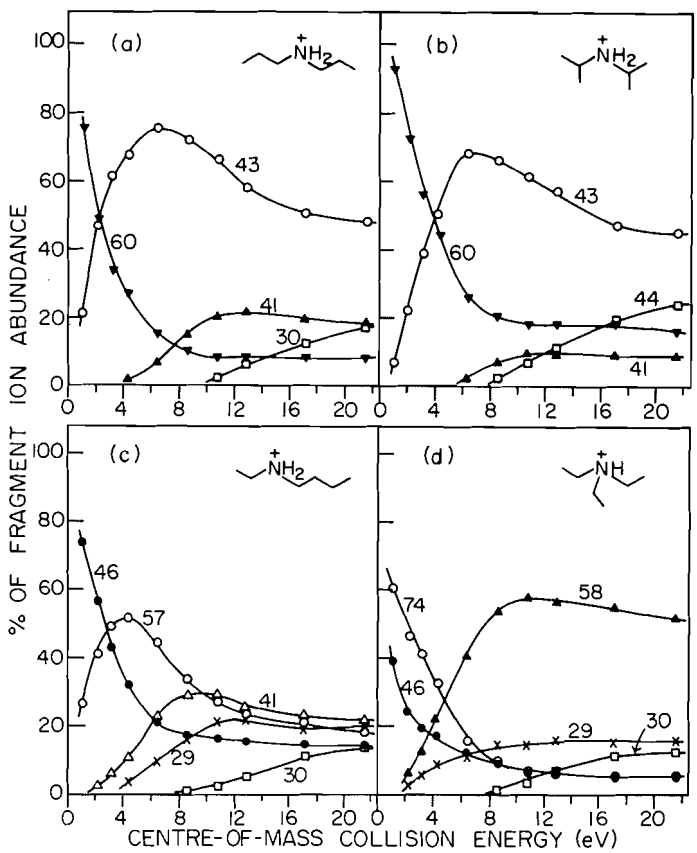


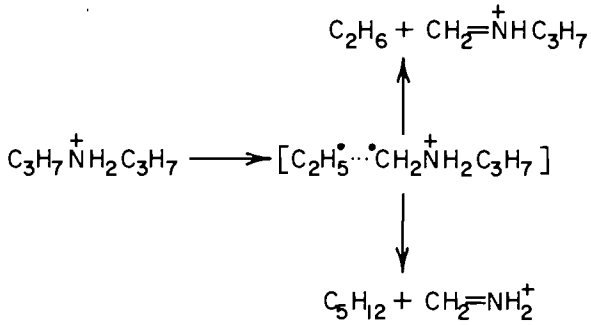
FIG. 6. Breakdown graphs for protonated (a) di-*n*-propyl amine, (b) di-*i*-propyl amine, (c) ethyl-*n*-butyl amine, and (d) triethyl amine.

al. (25) have elegantly shown, although the mean internal energy of ions activated in low and high energy collisions may be similar, there is a significant difference in the internal energy distribution. The distribution achieved in a high energy collision has a high energy tail that is missing when ions are activated in low energy collisions. Clearly, it is ions which are in this high energy tail that have sufficient energy to undergo alkane elimination reactions, particularly those involving pathways (a) and (b) of Scheme 1. At the same time, when one considers the lower energy fragmentation pathways, reactions [1] and [2], and further fragmentation of the alkyl ions produced by reaction [1], it appears that the mean internal energy deposited in collisions at 50–100 eV (laboratory scale) is greater than the mean internal energy transferred in 8 keV collisions.

In thermochemical terms the alkane elimination reactions frequently are the most favourable when assessed in terms of product stability, as the following data for protonated di-*n*-propyl amine show (thermochemical data taken from ref. 26):

	ΔH^0(kJmol^{-1})
$[(n\text{-}C_3H_7)_2NH_2]^+ \rightarrow [i\text{-}C_3H_7]^+ + n\text{-}C_3H_7NH_2$	269
$\rightarrow [n\text{-}C_3H_7NH_3]^+ + C_3H_6$	108
$\rightarrow [n\text{-}C_3H_7NHCH_2]^+ + C_2H_6$	84
$\rightarrow [CH_3CH_2CHNH_2]^+ + C_3H_8$	71
$\rightarrow [CH_2NH_2]^+ + C_5H_{12}$	138

Nevertheless, it is clear that these alkane elimination reactions have high critical reaction energies. The mechanism(s) of alkane elimination is (are) not known. The concerted mechanisms proposed by Cooks and co-workers (3) and outlined in Scheme 1 have been shown by theoretical calculations (1) to involve a



SCHEME 2

substantial potential energy barrier in addition to the reaction endothermicity. Alternatively, it also is possible that the alkane elimination reactions proceed in a stepwise fashion via initial homolytic bond cleavage to form a complex comprising an alkyl radical attached to an incipient radical-cation. Subsequent abstraction of a hydrogen atom or an alkyl radical from the developing distonic ion by the coordinated alkyl radical then results in alkane loss (Scheme 2). It has been shown (27) that distonic radical-cations have a stability similar to the radical-cation of conventional structure (here $[CH_3NHC_3H_7]^{+\bullet}$). It is conceivable that some of the [MH − alkane]$^+$ ions are secondary, rather than primary, products of fragmentation of [MH]$^+$. In the present case, the ions at *m/z* 30 might arise by C_3H_6 loss from $[C_3H_7NH{=}CH_2]^+$; it is known that $[C_3H_7NH{=}CH_2]^+$ ions expel C_3H_6 in both slow and fast dissociations (28). However, in the absence of a substantial peak at *m/z* 72 this explanation for the origin of the *m/z* 30 ions is perhaps less likely than direct C_5H_{12} elimination from [MH]$^+$.

Finally, it might be noted that the high critical reaction energies that obviously are involved in the alkane elimination reactions make it unlikely that such reactions will be prominent in the chemical ionization mass spectra. Rather it is likely that the nominal alkane loss products observed (1) are the results of direct alkide ion abstraction reactions by the reagent ion(s). It also is possible that a portion of the apparent [MH − alkane]$^+$ ions may actually be [M − alkyl radical]$^+$ ions formed by facile dissociation of $M^{+\bullet}$ produced by a small residual electron ionization component in the spectra. The importance of recognizing the possibility of such residual electron ionization components in chemical ionization mass spectra has recently been emphasized (29).

Acknowledgements

Financial support is gratefully acknowledged from the following sources: Science and Engineering Research Council (U.K.) (an Advanced Fellowship to R.D.B.); Natural Sciences and Engineering Research Council (Canada) (operating and equipment grants to A.G.H.); University of Toronto (U. of T. Open Fellowships to E.J.R.); Canada Council (Killam Fellowship, 1985–1987, to A.G.H.). A.G.H. is particularly indebted to Professor C. H. DePuy and the Department of Chemistry and Biochemistry, University of Colorado, for their kind hospitality during the period this manuscript was written.

1. E. J. REINER, R. A. POIRIER, M. R. PETERSON, I. G. CSIZMADIA, and A. G. HARRISON. Can. J. Chem. **64**, 1652 (1986).
2. R. D. BOWEN, A. G. HARRISON, and E. J. REINER. J. Chem. Soc. Perkin Trans. 2, 1009 (1988).
3. M. L. SIGSBY, R. J. DAY, and R. G. COOKS. Org. Mass Spectrom. **14**, 556 (1979).
4. W. WAGNER, H. HEIMBACH, and K. LEVSEN. Int. J. Mass Spectrom. Ion Phys. **36**, 125 (1980).
5. S. A. MCLUCKEY, G. L. GLISH, and R. G. COOKS. Int. J. Mass Spectrom. Ion Phys. **39**, 219 (1981).
6. D. D. FETTEROLF and R. A. YOST. Int. J. Mass Spectrom. Ion. Phys. **44**, 37 (1982).
7. S. A. MCLUCKEY and R. G. COOKS. *In* Tandem mass spectrometry. *Edited by* F. W. McLafferty. Wiley, New York. 1983.
8. A. G. HARRISON, R. S. MERCER, E. J. REINER, A. B. YOUNG, R. K. BOYD, R. E. MARCH, and C. J. PORTER. Int. J. Mass Spectrom. Ion Processes, **76**, 13 (1986).
9. R. G. COOKS, J. H. BEYNON, R. M. CAPRIOLI, and G. R. LESTER. Metastable ions. Elsevier, New York. 1973.
10. E. J. REINER. Ph.D. Thesis, University of Toronto. 1986.
11. B. F. YATES, W. J. BOUMA, and L. RADOM. J. Am. Chem. Soc. **106**, 5805 (1984).
12. S. HAMMERUM. Mass Spectrom Rev. **7**, 123 (1988).
13. L. FRIEDMAN and F. A. LONG. J. Am. Chem. Soc. **75**, 2832 (1952).
14. M. KARNI and A. MANDELBAUM. Org. Mass Spectrom. **15**, 53 (1980).
15. C. R. MOYLAN and J. I. BRAUMAN. J. Am. Chem. Soc. **107**, 761 (1985).
16. R. D. BOWEN, B. J. STAPLETON, and D. H. WILLIAMS. J. Chem. Soc. Chem. Commun. 24 (1978).
17. R. D. BOWEN and D. H. WILLIAMS. J. Am. Chem. Soc. **102**, 2752 (1980).
18. R. D. BOWEN and D. H. WILLIAMS. J. Chem. Soc. Chem. Commun. 836 (1981).
19. T. H. MORTON. J. Am. Chem. Soc. **102**, 1596 (1980).
20. R. D. BOWEN. J. Chem. Soc. Perkin Trans. 2, 409 (1982).
21. T. H. MORTON. Tetrahedron, **38**, 3195 (1982).
22. P. AUSLOOS and S. G. LIAS. J. Am. Chem. Soc. **108**, 1792 (1986).
23. V. FILGES and H.-F. GRUTZMACHER. Org. Mass Spectrom. **21**, 673 (1986).
24. A. G. HARRISON. Org. Mass Spectrom. **22**, 637 (1987).
25. V. H. WYSOCKI, H. I. KENTTAMAA, and R. G. COOKS. Int. J. Mass Spectrom. Ion Processes, **75**, 181 (1987).
26. S. G. LIAS, J. E. BARTMESS, J. F. LIEBMAN, J. L. HOLMES, R. D. LEVIN, and W. G. MALLARD. J. Phys. Chem. Ref. Data, **17**, Supplement 1 (1988).
27. J. L. HOLMES, F. P. LOSSING, J. K. TERLOUW, and P. C. BURGERS. Can. J. Chem. **61**, 2305 (1983).
28. R. D. BOWEN. J. Chem. Soc. Perkin Trans. 2, 1219 (1980).
29. S. J. HAZELL, R. D. BOWEN, and K. R. JENNINGS. Org. Mass Spectrom. **23**, 597 (1988).

Can. J. Chem. Downloaded from www.nrcresearchpress.com by 186.148.149.217 on 09/07/12
For personal use only.

Sclerodin and related compounds from a plant disease causing fungus. Scleroderris yellow

WILLIAM A. AYER, MASAYUKI KAMADA, AND YU-TING MA
Department of Chemistry, University of Alberta, Edmonton, Alta., Canada T6G 2G2
Received June 7, 1989

WILLIAM A. AYER, MASAYUKI KAMADA, and YU-TING MA. Can. J. Chem. **67**, 2089 (1989).

The metabolites of several strains of a fungus that gives rise to the disease of conifers known as Sirococcus shoot blight have been studied. The metabolites are similar to those isolated from *Gremmeniella abietina*, the causative agent of Scleroderris canker of pine. Sclerodin (**1**), scleroderolide (**2**), and Scleroderris blue (**3**) have been isolated, along with the known lactone **4**, trypethelone (**6**), and a new purple compound named scleroquinone (**12**). Another new compound, related to Scleroderris blue (**3**) and Scleroderris green (**7**), which we have named Scleroderris yellow, is shown to possess structure **8**. The sclerodin (**1**) isolated in these studies is not optically pure, in some cases being nearly racemic. It is noted that the optical purity may be a function of the culture medium employed. Scleroderolide (**2**) strongly inhibits the germination of lettuce seeds. In addition to the metabolites noted, squalene, methyl oleate, stearic acid, ergosta-4,6,8(14),22-tetraene-3-one, and ergosterol endoperoxide were also isolated from the cultures.

Key words: Sirococcus, phenalenones, Scleroderris yellow, scleroquinone, sclerodin.

WILLIAM A. AYER, MASAYUKI KAMADA et YU-TING MA. Can. J. Chem. **67**, 2089 (1989).

On a étudié les métabolites de plusieurs souches d'un champignon qui provoque la maladie des conifères connue sous le nom de Sirococcus de la brunissure des pousses. les métabolites sont semblables à ceux isolés du *Gremmeniella bietina*, l'agent qui provoque le Scleroderris de la nécrose du pin. On a isolé la sclérodine (**1**), le sclérodérolide (**2**) et le bleu de scléroderris (**3**) ainsi que la lactone connue **4**, la trypéthélone (**5**) et un nouveau composé violet que l'on a nommé scléroquinone (**12**). On a démontré qu'un autre nouveau composé, lié au bleu (**3**) et au vert (**7**) de scléroderris et qu'on a appelé jaune de scléroderris, possède la structure **8**. La sclérodine (**1**) isolée au cours de cette étude n'est pas optiquement pure et, dans quelques cas, elle est pratiquement racémique. On a noté qu la pureté optique varie avec le milieu de culture utilisé. Le sclérodérolide (**2**) inhibe fortement la germination des semences de laitue. En plus des métabolites mentionnés, on a aussi isolé des milieux de culture du squalène, de l'oléate de méthyle, de l'acide stéarique, de l'ergosta-4,6,8(14),22-tétraène-3-one et de l'endoperoxyde d'ergostérol.

Mots clés : Sirococcus, phénalènones, jaune de scléroderris, scléroquinone, sclérodine.

[Traduit par la revue]

Introduction

The disease of conifers known as Sirococcus shoot blight (1, 2) has many similarities to the pine disease known as Scleroderris canker (3). The latter disease is caused by the Ascomycetous fungus *Gremmeniella abietina* (3). The metabolites produced by *G. abietina* have been studied in detail and have been shown to be substituted phenalenones and derivatives thereof (e.g., sclerodin (**1**), scleroderolide (**2**), Scleroderris blue (**3**)) (4–7). Our interest in the Scleroderris metabolites has led us to examine several strains of a fungus isolated from conifers in West Germany believed to be infected with the Sirococcus fungus.[1] Since we began our studies, it has been determined that the fungus may be *Godronia cassandrae* (2) rather than *Sirococcus strobilinus*.[2] In this article we report on the metabolites of the two strains (strain 20 (UAMH 5402), and strain D (UAMH 5399)) of the disease fungus, which are morphologically closely related to *G. abietina*, and another strain (strain 33b, UAMH 5400), which is morphologically closer to Sirococcus.[3]

Results and discussion

Strain 33b (UAMH 5400) was grown in liquid culture on potato dextrose–yeast (PDY), V8 juice–glucose (V8G), and Wort media. The V8G medium produced abundant amounts of greenish-gray mycelium, which on extraction with methylene chloride provided a larger yield of metabolites than the other media mentioned. In all cases, extraction of the culture broth provided relatively small amounts of metabolites. Since in our studies on *G. abietina* we had also used the V8G medium (4), this was chosen for the study of strain 33b.

The metabolites were first fractionated by reverse-phase column chromatography over C_{18}-bonded silica gel (to separate fatty acids and glycerides) and the fractions were further separated by chromatography (column and preparative thin layer) over silica gel. This led to the isolation of the known compounds sclerodin (**1**) (4), scleroderolide (**2**) (5), Scleroderris blue (**3**) (4), the lactone **4** (previously obtained by oxidation of sclerodione (**5**) (4)), and a purple compound identified as trypethelone (**6**) (previously isolated from the lichen *Trypethelium eluteriae* (8, 9)). In addition, a yellow crystalline compound $C_{39}H_{36}O_{10}$ and a purple crystalline compound $C_{18}H_{18}O_6$ were isolated. The structures of these two compounds are discussed below.

Sclerodin (**1**) obtained from *G. abietina* is the enantiomer (*S* configuration at C-2′, $[\alpha_D]$ −73°) of the so-called "naphthalic anhydride from atrovenetin" (4, 10), which has been shown by X-ray crystallography to possess the *R* configuration at C-2′ (11). The *R* enantiomer has also been obtained from several other fungi (see refs. 4 and 5). To our surprise, both sclerodin (**1**) and scleroderolide (**2**) isolated from strain 33b are virtually racemic, each showing a slight excess of the *S* enantiomer (**1**, $[\alpha]_D$ −6.5°; **2**, $[\alpha]_D$ −5.9°; the pure enantiomer of **2** shows $[\alpha]_D$ −116° (5)). On one previous occasion, racemic scleroderolide (**2**) was obtained from *G. abietina* (5).

The yellow crystalline compound $C_{39}H_{36}O_{10}$, for which we suggest the trivial name Scleroderris yellow (in analogy to

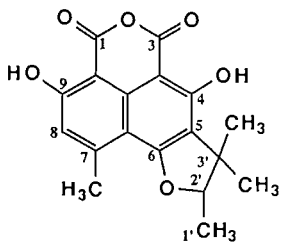
[1]We thank Prof. O. Kandler for drawing the relationship between the two diseases to our attention, and for providing the cultures used in this work.

[2]We thank Prof. Kandler for this information, and L. Sigler, University of Alberta Microfungus Collection and Herbarium (UAMH), for her taxonomical work and valuable discussion.

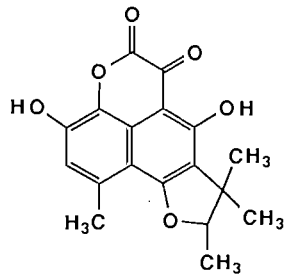
[3]L. Sigler, UAMH, private communication.

Can. J. Chem. Downloaded from www.nrcresearchpress.com by 186.148.149.217 on 09/07/12
For personal use only.

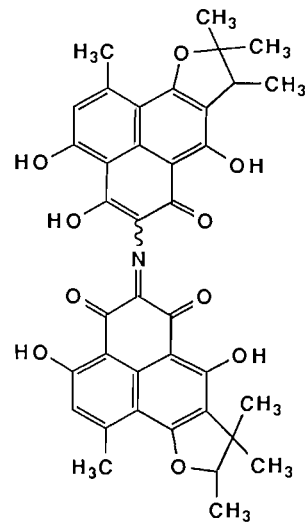
Can. J. Chem. Downloaded from www.nrcresearchpress.com by 186.148.149.217 on 09/07/12
For personal use only.



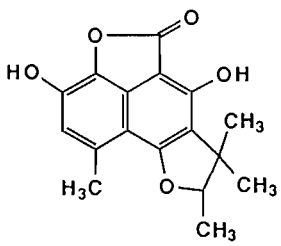
1



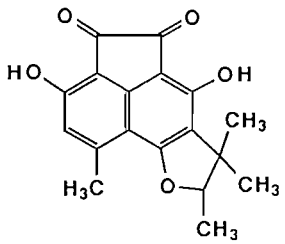
2



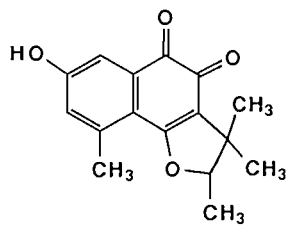
3



4

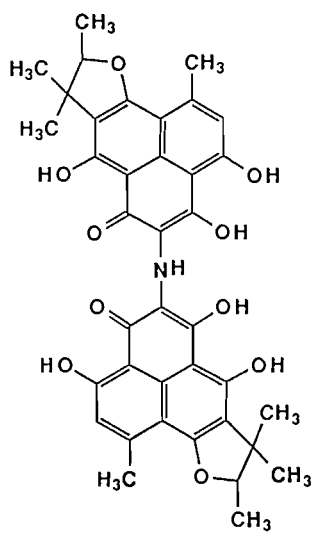


5

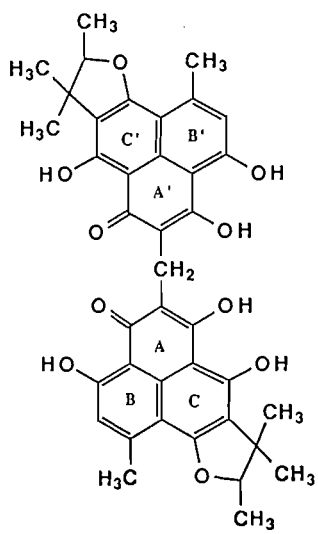


6

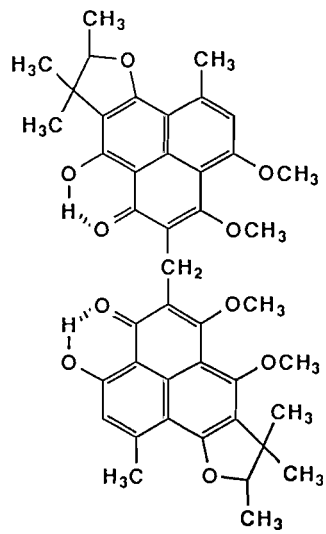
Scleroderris blue (**3**) and Scleroderris green (**7**) (6)), elutes from silica gel along with sclerodin (**1**). It is much less soluble than sclerodin in most solvents and may be separated by trituration with Skellysolve B. Recrystallization from chloroform – Skellysolve B provides Scleroderris yellow (**8**, only one tautomer shown) as optically active ($[\alpha]_D$ −16.7°) yellow crystals, mp 289–290°C. The high resolution electron impact mass spectrum (hrms) of Scleroderris yellow shows a weak molecular ion (m/z 664) and strong fragment ions corresponding to cleavage, with hydrogen transfer, of the bond to the central methylene group, giving rise to fragments $C_{20}H_{18}O_5$ (m/z 338) and $C_{19}H_{18}O_5$ (m/z 326), which represent all of the atoms of the parent ion (see Scheme 1). Loss of a methyl radical from each of these fragments gives rise to the most intense peaks (m/z 323 (81%), m/z 311 (100%)) in the spectrum. The nuclear magnetic resonance (nmr) spectra of Scleroderris yellow (**8**) are somewhat complicated due to the presence in solution of more than one tautomer. At room temperature the signals for the phenolic hydrogens appear as complex multiplets at δ 14.62, 13.58, 13.47, and 12.48. At 47°C each of these signals consists of only two lines of approximately equal intensity. This tautomerism is discussed further in connection with the methylation studies described later. The ^{1}H nmr spectrum does show the presence of the *geminal* methyls (6H broadened singlets at δ 1.39 and 1.53),



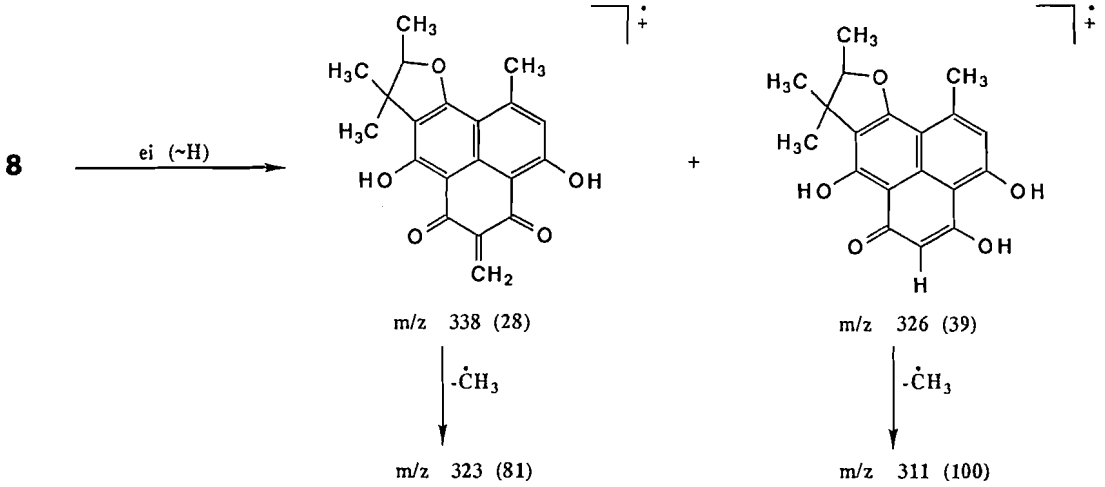
7



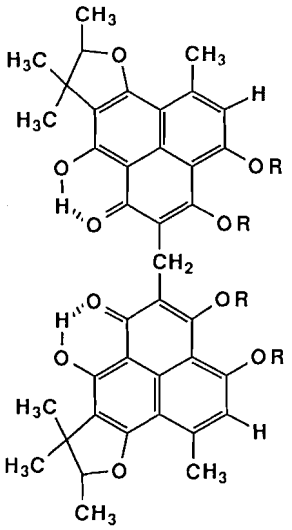
8



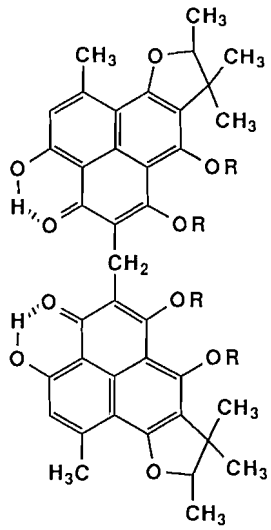
9



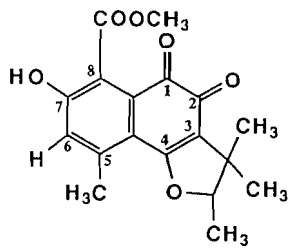
SCHEME 1



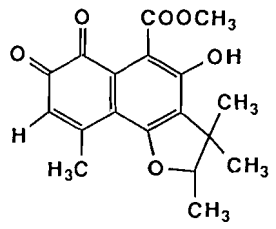
10*a* R = CH_3
10*b* R = H



11*a* R = CH_3
11*b* R = H



12



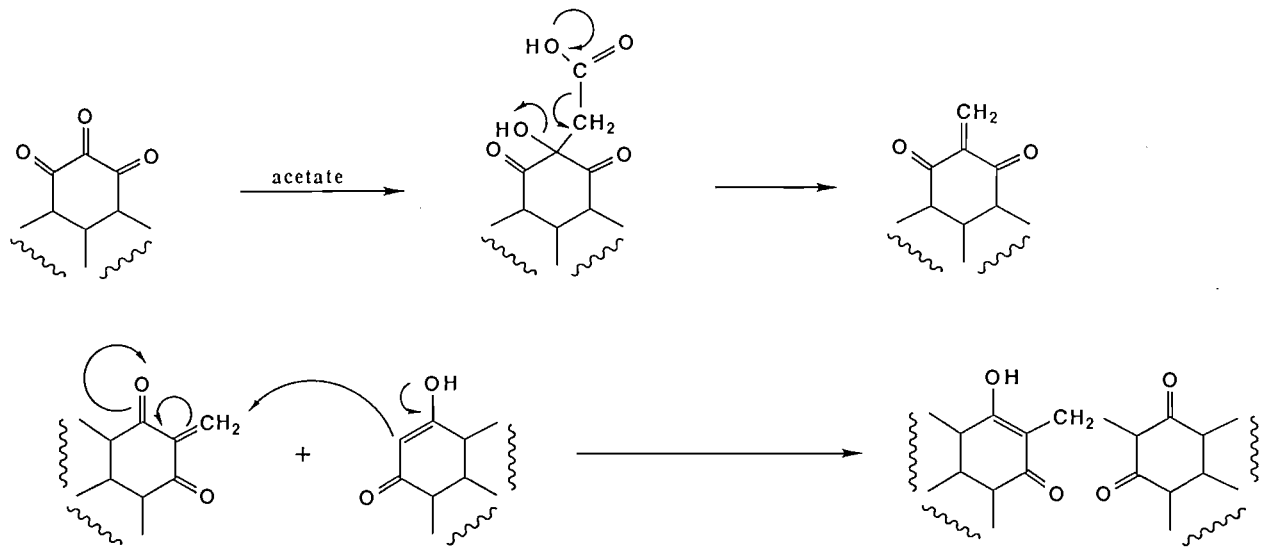
13

the secondary methyls (δ 1.54, d, *J* 6 Hz, 6H), the aromatic methyls (δ 2.86, s, 6H), the methine hydrogens (δ 4.72, m, 2H), and the aromatic hydrogens (δ 6.85, s, 2H). Of particular significance is the two-hydrogen singlet at δ 4.14, which is attributed to the methylene group linking the two "halves" of the molecule. The ^{13}C nmr spectrum shows a total of 31 signals, including a single methylene carbon signal at δ 17.6. The infrared (ir) spectrum of **8** shows broad chelated OH absorption (2300–3300 cm^{-1}), weak bands at 1740 and 1710 cm^{-1}, and strong chelated carbonyl absorption at 1613 cm^{-1}.

Treatment of Scleroderris yellow (**8**) with diazomethane gave rise to two different tetramethyl ethers. Since it is known that phenolic hydroxyls that are strongly intramolecularly H-bonded to carbonyl groups do not react readily with diazomethane (12), we considered structures **9**, **10***a*, and **11***a* the most likely possibilities for the tetramethyl ethers.[4] One of the tetramethyl ethers shows four different methoxyl signals and two different OH signals in its ^1H nmr spectrum, and thus may be assigned the unsymmetrical structure **9**. The second tetramethyl ether shows only two methoxyl signals (δ 4.01 and 3.78) and one OH signal (δ 18.52), and thus may be assigned either structure **10***a* or **11***a*. A strong nOe enhancement (23%) of the aromatic hydrogen signal was detected when the hydrogens of one of the methoxyl groups (δ 4.01) were irradiated, indicating that the second ether possesses structure **10***a*. Irradiation of the other methoxyl signal (δ 3.78) of **10***a* caused enhancement (3.2%) of the signal for the "connecting" methylene group (δ 4.46). The methoxyl signals

[4]A similar situation had been encountered previously in the case of Scleroderris green (**7**) (6).

Can. J. Chem. Downloaded from www.nrcresearchpress.com by 186.148.149.217 on 09/07/12
For personal use only.



SCHEME 2

for the unsymmetrical ether **9** appear at δ 4.06, 3.92, 3.84, and 3.75. Irradiation of the δ 4.06 signal brings about enhancement of one of the aromatic signals (δ 6.83), irradiation of the δ 3.84 and δ 3.75 signals causes enhancement of the methylene signal (δ 4.46), whereas irradiation of the δ 3.92 methoxyl causes no observable nOe enhancement. The remainder of the ^{1}H nmr spectra of both **9** and **10***a* are in complete accord with the structures formulated and provide strong support for the structure of Scleroderris yellow (**8**) itself. In particular, the spectrum of the symmetrical ether **10***a* shows only the expected ten signals, including the signal at δ 4.46 for the methylene group linking the two identical aromatic parts. We feel that Scleroderris yellow exists predominantly, at least in solution, as a mixture of the tautomers **8**, **10***b*, and **11***b*. Since the methylation experiment was carried out on a small scale (<5 mg) we do not attach any great significance to the fact that the tetramethyl ether **11***a* was not isolated.

The biogenetic origin of the methylene group in Scleroderris yellow (**8**) is not immediately obvious. It has been shown that the phenalenone nuclei in compounds such as Scleroderris blue (**3**) are of heptaketide origin and that the dihydrofuran rings are mevalonate derived (7). It is possible that the methylene group of Scleroderris yellow (**8**) is also acetate (or malonate) derived. Addition of acetate to the central carbonyl of an atrovenetinone-type intermediate followed by dehydrative decarboxylation would lead to an α-methylene ketone that could condense with another phenalenone intermediate as illustrated in Scheme 2. Pathways involving addition of a one-carbon unit (*S*-adenosyl methionine, formate, tetrahydrofolate) may also be envisioned.

The purple compound, $C_{18}H_{18}O_6$, for which we suggest the name scleroquinone is eluted early in the reverse phase chromatography and was obtained as an amorphous solid. It is assigned structure **12**. The uv–visible spectrum (λ_{max} 217, 287, 305, 574 nm) and the color are similar to those of trypethelone (**6**). The ^{1}H nmr spectrum of scleroquinone is like that of trypethelone (**6**) except that there is only one aromatic hydrogen (δ 6.96, s) and there is a methoxyl signal (δ 3.85). The presence of the ester functionality is indicated by ir absorption at 1740 cm^{-1}, not present in trypethelone. We did not have sufficient material to determine the ^{13}C nmr spectrum of **12**. The carbomethoxyl group is placed at C-8 rather than C-6 of the naphthoquinone nucleus since the aromatic hydrogen in **12** is not as far downfield as the C-8 hydrogen in trypethelone (δ 7.26, *peri* deshielding by C-1 carbonyl). Biogenetic considerations also favor C-8 (decarboxylation of a sclerodin (**1**) type intermediae (9)). The alternative *ortho*-quinone structure **13** cannot be completely excluded, but again we feel that the chemical shift of the aromatic hydrogen (δ 6.98, the C-6 hydrogen in trypethelone appears at δ 6.77) favors structure **12** for scleroquinone.

Scleroquinone (**12**) was also isolated from the liquid culture (V8G medium) of strain D (UAMH 5399), again in very small amounts. This strain also produces sclerodin (**1**), scleroderolide (**2**), and Scleroderris blue (**3**). The sclerodin (**1**) isolated from this strain contained an excess of the *R* enantiomer ($[\alpha]_D$ +27°)!

Strain 20 (UAMH 5402) was grown on both PDY and Wort media. Sclerodin (**1**) and Scleroderris blue (**3**) were the only pigments isolated from the Wort medium, while the PDY culture produced the lactone **4** in addition to **1** and **3**. The sclerodin (**1**) isolated from the PDY culture was virtually racemic ($[\alpha]_D$ +2.3°) whereas that isolated from the Wort medium was distinctly levorotatory ($[\alpha]_D$ −28.0°). We find this inconsistency in the optical purity of the metabolites puzzling. The fact that different media give sclerodin (**1**) of different optical purity suggests that a more careful study of the culture conditions (e.g., does rotation change with the length of time of growth?) is necessary before we speculate further. We have now initiated such a study.

Preliminary tests reveal that sclerodin (**1**), scleroderolide (**2**), and Scleroderris blue (**3**) all inhibit the germination of lettuce seeds. Scleroderolide (**3**) is especially active in this respect, a 20 ppm solution causing one hundred percent inhibition of germination. The effect of these metabolites on the germination of lodgepole pine seeds will now be studied, followed by a study of their effect on pine seedlings. Further study of the possible role of these metabolites in the disease of the mature trees will be dictated by the results of these experiments.

Experimental

High resolution electron impact mass spectra (hrms) were recorded on an AEI MS-50 mass spectrometer. Unless diagnostically significant, only those peaks with an intensity of >20% of the base peak are recorded. Chemical ionization mass spectra (cims) were obtained using an AEI-MS-12 mass spectrometer with ammonia as the reagent gas.

Can. J. Chem. Downloaded from www.nrcresearchpress.com by 186.148.149.217 on 09/07/12
For personal use only.

Can. J. Chem. Downloaded from www.nrcresearchpress.com by 186.148.149.217 on 09/07/12
For personal use only.

The data were processed using DS-55 software and a Nova-4 computer. Fourier transform infrared (Ftir) spectra were recorded on a Nicolet 7199 FTIR interferometer. Nuclear magnetic resonance (nmr) spectra (^1H and ^{13}C) were obtained on Bruker WH-300, WM-360, or WH-400 spectrometers with either Aspect 2000 or Aspect 3000 computer systems. ^1H chemical shifts and coupling constants are reported as if they are first order. Tetramethylsilane was used as an internal standard. Ultraviolet (uv) spectra were obtained on a Hewlett Packard 8450A Diode Array spectrophotometer and optical rotations on a Perkin Elmer 241 polarimeter. Melting points are uncorrected and were determined on a Thomas model 40 melting point apparatus. E. Merck silica gel 60 (230–400 mesh) or 10% C–18 silica gel (30–70μm, Toronto Research Chemicals Inc.) were used for flash chromatography. Preparative thin-layer chromatography (ptlc) was performed on E. Merck precoated 20 × 20 glass plates of silica gel 60 F-254. Analytical thin-layer chromatography (tlc) was carried out on cut sections of E. Merck precoated aluminum sheets of silica gel 60 F-254. Ultraviolet active materials were detected by visualisation under a uv lamp (254 nm). The tlc plates were then dipped in a solution of phosphomolybdic acid for several seconds, and the spots were visualised by gentle heating over a hot plate. All solvents were distilled prior to use. Skellysolve B refers to Skelly Oil Company light petroleum, bp 62–70°C.

The stock cultures used in this study were obtained from Prof. O. Kandler, Botanisches Institut der Universität München, and are deposited at the University of Alberta Microfungus Herbarium under the following assession numbers: Sirococcus 33b (UAMH 5400), Sirococcus D (UAMH 5399), and Sirococcus 20 (UAMH 5402).

Growth and harvesting of Sirococcus

Stock cultures of each strain of *Sirococcus* were maintained in slant tube culture on potato dextrose agar at 4°C. To initiate large-scale cultures, small fragments of agar containing the mycelium were aseptically transferred to Erlenmeyer flasks containing sterile culture medium (200 mL). The medium was either Difco potato dextrose broth containing 0.04% (w/v) yeast extract, or clarified V8 juice (5) containing 1% (w/v) glucose, or Wort medium (malt extract 15 g, peptone 0.78 g, maltose 12.75 g, dextrin 2.75 g, glycerol 2.35 g, K_2HPO_4 1.0 g, NH_4Cl 1.0 g in 1 L H_2O; pH adjusted to 4.8).

The cultures were shaken for 10 days at 15–17°C. The content of each inoculation flask was used to inoculate five 2.8-L Fernbach flasks containing the same liquid medium (1 L, still culture) and the flasks were kept at 15–17°C. After 50–60 days, the mycelium was separated from the broth. The broth was concentrated to one tenth of its original volume and extracted with methylene chloride. The air-dried mycelium was extracted with methylene chloride in a Soxhlet extractor. Concentration of the methylene chloride extracts gave the crude broth and mycelial extracts. Very small quantities of metabolites were present in the broth extract, the mycelial extract containing the bulk of the metabolites of interest in this study.

Separation of metabolites of Sirococcus "33b"

The methylene chloride extract of strain 33b (UAMH 5400) was separated into five fractions by chromatography over silica gel RP 18 (eluant: CH_3OH–H_2O, 4:1). Further separation of fraction 1 by acid–base extraction gave a mixture that contained mainly phenolic compounds. Chromatography of this mixture (silica gel) using gradient elution (Skellysolve B–$CHCl_3$–CH_3OH containing HOAc) led to the isolation of sclerodin (**1**), scleroderolide (**2**), trypethelone (**6**), and small quantities of unidentified pigments. Further separation of fraction 2 by column chromatography (eluant: $CHCl_3$ – ethyl acetate – HOAc, 98:1:1) and preparative thin-layer chromatography led to the isolation of compounds **1**, **2**, Scleroderris yellow (**8**), Scleroderris blue (**3**), and two unidentified red pigments. Fractions 3–5 were found to be composed mainly of triglycerides and were not investigated further.

On another occasion the methylene chloride extract of the mycelium was fractionated over silica gel RP 18. Further purification of each of the six fractions by silica gel chromatography (eluant: $CHCl_3$ – ethyl acetate – acetic acid, 97:2:1) led to the isolation of scleroquinone (**12**) (0.7 mg, fraction 2), compound **2** (1.7 mg) and lactone **4** (2.3 mg, fraction 3), sclerodin (**1**, 4 mg, fraction 4), and ergosta-4,6,8(14), 22-tetraen-3-one (0.8 mg, fraction 5).

TABLE 1. Variation in optical purity of sclerodin (**1**)

Fungus (medium)		$[\alpha]_D$ –	
G. abietina	(V8G)	−73°	Reference 5
Sirococcus 33b	(V8G)	−6.5°	(0.41, $CHCl_3$)
Sirococcus D	(V8G)	+27°	(0.79, $CHCl_3$)
Sirococcus 20	(PDY)	+2.3°	(0.43 $CHCl_3$)
Sirococcus 20	(Wort)	−28.0°	(0.41, $CHCl_3$)

Separation of metabolites of Sirococcus "D"

The methylene chloride extract (3.46 g) of strain D (UAMH 5399) was separated into Skellysolve B soluble extract (2.38 g) and Skellysolve B insoluble extract (1.02 g). The Skellysolve B soluble fraction was separated by repeated chromatography over silica gel. Squalene (1 mg), methyl oleate (9 mg), triglycerides (1.5 g), sclerodin (**1**, 13 mg), ergosta-4,6,8(14),22-tetraen-3-one (9 mg), a 1,2-diglyceride (10 mg), a 1,3-diglyceride (22 mg), and stearic acid (2 mg) were isolated. The Skellysolve B insoluble fraction was separated by repeated silica gel chromatography. Triglycerides (47 mg), sclerodin (**1**, 21 mg), unidentified red pigments, and scleroderolide (**2**, 0.8 mg) were isolated.

Separation of metabolites of Sirococcus "20"

The methylene chloride extract (2.86 g) of strain 20 (UAMH 5402) grown on PDBY was separated into nonpolar, medium polar, and polar fractions by chromatography over silica gel (gradient elution; Skellysolve B – toluene – ethyl acetate – methanol). Further chromatographic separation (gradient elution; Skellysolve B – ether) of the nonpolar fraction (1.16 g) gave sclerodin (**1**, 67 mg), ergosterol endoperoxide (2 mg), and a mixture of fatty acids and triglycerides. Further chromatographic separation (gradient elution; Skellysolve B – ether, then CH_2Cl_2–CH_3OH–HOAc, 96:2:2) of the medium polarity fraction (0.48 g) gave compound **1** (61 mg), lactone **4** (5 mg), and compound **3** (3 mg) whereas further chromatographic separation (gradient elution; Skellysolve B – ethyl acetate, then CH_2Cl_2–CH_3OH–HOAc, 96:2:2) of the polar fraction (1.17 g) gave compound **1** (5.5 mg) and a blue pigment (2 mg).

The methylene chloride extract (1.42 g) obtained from cultures of Sirococcus 20 grown on Wort media was separated as described above. The following metabolites were isolated: sclerodin (**1**, 11 mg), ergosterol peroxide, ergosta-4,6,8(14),22-tetraen-3-one, and the blue pigment.

Characterization of metabolites

Sclerodin (**1**) (from Sirococcus 33b, D, and 20): Identical (ir, ^1H nmr, ^{13}C nmr, hrms) with an authentic sample. Optical rotations, see Table 1.

Scleroderolide (**2**) (from Sirococcus 33b and D): Identical (ir, ^1H nmr, ^{13}C nmr, hrms) with an authentic sample.

Scleroderris blue (**3**) (from Sirococcus 33b and 20): Identical (ir, ^1H nmr, ^{13}C nmr, hrms) with an authentic sample.

Lactone **4** (from Sirococcus 33b and 20): $[\alpha]_D$ −20.71° (*c* 0.14, $CHCl_3$). Identical (ir, ^1H nmr, ^{13}C nmr, hrms) with an authentic sample.

Trypethelone (**6**): R_f 0.33 ($CHCl_3$–CH_3OH – acetic acid, 94:5:1), mp 248–249°C (lit. (8) mp 264 266°C); $[\alpha]_D$ 130° (*c* 0.20, $CHCl_3$); λ_{max} (log ε) (CH_3OH): 275 (4.93), 284 (4.95), 303 (4.42), 525 (3.87) nm; ir ($CHCl_3$): 3040, 2963, 2927, 1735 (w), 1682 (m), 1647 (m), 1602 (s), 1585, 1541, 1460, 1407, 1383, 1363, 1319 cm^{-1}; ^1H nmr (CD_3OD) δ: 1.23 (s, 3H, H–5′), 1.40 (s, 3H, H–4′), 1.46 (d, 3H, *J* 6.5 Hz, H–1′), 2.52 (s, 3H, C–5 CH_3), 4.71 (q, 1H, *J* 6.5 Hz, H–2′), 6.97 (d, 1H, *J* 3 Hz, H–6), 7.36 (d, 1H, *J* 3 Hz, H–8); ^{13}C nmr (CD_3OD) δ: 14.91 (q, C–1′), 20.54 (q, C–5′), 22.34 (q, C–5 CH_3), 26.01 (q, C–4′), 43.90 (s, C–3′), 94.15 (d, C–2′), 116.37 (s, C–4a), 117.84 (d, C–8), 122.16 (s, C–3), 125.43 (d, C–6), 135.63 (s, C–8a), 142.82

(s, C–5), 165.03 (s, C–7), 175.60 (s, C–1), 176.51 (s, C–2), 184.24 (s, C–1); hrms, *m/z* (rel. int.): 272.1049; calcd. for $C_{16}H_{16}O_4$: 272.1054; found: (M^+, 43), 257 ($M^+ - CH_3$, 39), 244 ($M^+ - CO$, 22), 229 ($M^+ - CH_3 - CO$, 100).

Scleroderris yellow (**8**): mp 289–290°C; $[\alpha]_D$ −16.7° (*c* 0.12, $CHCl_3$); ir ($CHCl_3$ cast): 3220, 2960, 2926, 2855, 2480 (br), 1740 (w), 1710 (w), 1613 (s), 1456, 1383, 1360 cm^{-1}; ^1H nmr ($CDCl_3$, rt) δ: 1.39 (6H, br s), 1.53 (6H, br s), 1.54 (6H, d, *J* 6 Hz, -CHC*H*$_3$), 286 (6H, s, ArC*H*$_3$), 4.14 (2H, s, -C*H*$_2$), 4.72 (2H, m, C*H*CH$_3$), 6.85 (2H, s, ArH), 12.48 (1.2H, 4 lines D_2O exchangeable), 13.47 (0.9H, 4 lines, D_2O exchangeable), 13.58 (0.9H, 4 lines, D_2O exchangeable), 14.62 (1.2H, 4 lines, D_2O exchangeable), 15.01–15.54 (1.8H, br, D_2O exchangeable); ($CHCl_3$, 47°C) δ: 1.28, 1.30 (ea 3H, s, H–5′), 1.48, 1.50 (ea 3H, d, *J* 6 Hz, H–1′), 1.53, 1.55 (ea 3H, s, H–4′), 2.88 (6H, s, ArC*H*$_3$), 4.71 (2H, m, H–2′), 6.88 (2H, s, Ar–H), 12.41, 12.42 (ea 0.5H, s), 13.42, 13.43 (ea 0.5H, s), 13.57, 13.58 (ea 0.5H, s), 14.58, 14.59 (ea 0.5H, s); ^{13}C nmr ($CDCl_3$) δ: 14.67, 17.63, 20.65, 24.04, 24.12, 25.72, 43.39, 43.35, 91.51, 91.57, 103.78, 104.75, 105.72, 108.35, 114.99, 115.18, 117.01, 117.09, 118.59, 118.67, 128.98, 148.14, 148.65, 165.10, 165.18, 166.35, 166.55, 168.30, 172.41, 173.13, 176.89; hrms, *m/z* (rel. int.): 664.2309; calcd. for $C_{39}H_{36}O_{10}$: 664.2308; found: (M^+, 1.5), 338 (28), 326 (39), 323 (81), 311 (100), 269 (26); fabms: 665.46 ($M^+ + H$), calcd. for $C_{39}H_{37}O_{10}$; found: 665.2388 (0.4).

Scleroquinone(**12**): λ_{max} (log ε) (CH_3OH): 217 (3.03), 287 (2.94), 305 (2.77), 574 (1.72) nm; ir ($CHCl_3$, cast): 3220 (br), 2925, 2845, 1740, 1695, 1624, 1606, 1540, 1454, 1240, 800 cm^{-1}; ^1H nmr ($CDCl_3$) δ: 1.41 (3H, s, H–5′), 1.43 (3H, d, *J* 6.5 Hz, H–1′), 1.52 (3H, s, H–4′), 2.58 (3H, s, ArC*H*$_3$), 3.85 (3H, s, OC*H*$_3$), 4.62 (1H, q, *J* 6.5 Hz, H–2′), 6.96 (1H, s, H–6); hrms, *m/z* (rel. int.): 330.1103; calcd. for $C_{18}H_{18}O_6$: 330.1106; found: (M^+, 42), 331 ($M^+ + 1$, 10), 315)10), 302 (61), 300 (19), 299 (9), 287 (82), 285 (29), 284 (16), 283 (13), 270 (43), 256 (17), 255 (100), 242 (34).

Methylation of Scleroderris yellow

Excess ethereal diazomethane (4 mL) was added to a solution of Scleroderris yellow (**8**, 2.5 mg) in dichloromethane (2 mL). After 15 h, the reaction mixture was concentrated and purified by chromatography (Skellysolve B – ethyl acetate – chloroform, 8:1:1) to give compound **9** as a yellow solid; ir ($CHCl_3$ cast): 3320, 2952, 2924, 1720, 1610, 1583, 1451, 1383, 1355, 1320 cm^{-1} ^1H nmr ($CDCl_3$) δ: 1.29, 133 (ea 3H, s, H–5′), 1.46, 1.47 (ea 3H, d, *J* 7, H–1′), 1.54, 1.56 (ea 3H, s, H–4′), 2.77, 2.89 (ea 3H, s, $ArCH_3$), 3.75 (3H, s, OCH_3), 3.84 (3H, s, OCH_3), 3.92 (3H, s, OCH_3), 4.06 (3H, s, OCH_3), 4.46 (2H, s, $ArCH_2Ar$), 4.57, 4.64 (ea 1H, q, *J* 7, H–2′), 6.78, 6.83 (ea 1H, s, Ar*H*), 17.85, 17.93 (ea 1H, s, O*H*); fabms: 722.46 (19), 721.46 (42), (calcd. for $C_{43}H_{45}O_{10}$ (M^+ 1): 721.35) 381.43 (7), 368.33 (26), 367.33 (100), 355.21 (17), 353.17 (16), 351.18 (10).

In another experiment, Scleroderris yellow (**8**, 3.0 mg) was dissolved in excess ethereal diazomethane (5 mL) and the solution was stirred for 15 h. The reaction mixture was worked up as before to give compound **10a** as a yellow solid; ir ($CHCl_3$ cast): 3320, 2954, 2924, 2852, 1740 (w), 1611, 1582, 1454, 1384, 1375, 1356, 1300 cm^{-1}; ^1H nmr ($CDCl_3$) δ: 1.33 (6H, s, H–5′), 1.47 (6H, d, *J* 7, H–1′), 1.57 (6H, s, H–4′), 2.87 (6H, s, $ArCH_3$), 3.78 (6H, s, OCH_3), 4.01 (6H, s, OCH_3), 4.46 (2H, s, $ArCH_2Ar$). 4.63 (2H, q, *J* 7, H–2′), 6.78 (2H, s, ArH), 18.52 (2H, s, OH); fabms: 722.39 (11), 721.38 (25), (calcd. for $C_{43}H_{45}O_{10}$, ($M^+ + 1$): 721.35) 381.41 (11), 368.34 (21), 367.31 (79), 355.19 (15), 353.17 (17), 351.17 (11), 55.21 (11).

Germination inhibition tests

Lettuce seeds (Heritage Garden Products, Canada No. 1 seed, variety "Salad Bowl") were sterilized by immersion for a few minutes in 2% bleach solution, then washed (2×) with sterile distilled water, and dried on filter paper. The seeds (approximately 100 seeds/test) were placed on doubled filter paper in a sterile Petri dish and the filter papers were saturated with a solution (4 mL, 200 ppm and 20 ppm in water containing Tween 20 (2 drops/5 mL water)) of sclerodin (**1**), scleroderolide (**2**), of Scleroderris blue (**3**). The plates were incubated (20–22°C) for 4 days, receiving 8 h of light per day. The percentage inhibition of germination was as follows: control (5.7%); sclerodin (**1**), 20 ppm (23%), 200 ppm (100%); scleroderolide (**2**), 20 ppm (100%), 200 ppm (100%) Scleroderris blue (**3**), 20 ppm (38%), 200 ppm (100%).

Acknowledgements

We acknowledge with thanks the financial support of the Natural Sciences and Engineering Research Coundil of Canada, and one of us (M.K.) thanks the Soda Aromatic Co., Ltd., Tokyo, for a study leave and generous financial support. We thank Dr. O. Kandler for suggesting this study and for the fungal cultures, Mrs. L. Sigler for her assistance and advice, and Dr. L. M. Browne for her help and valuable discussion.

1. E. A. Shahin and L. E. Clafin. Plant Dis. Rep. **62**, 648 (1978).
2. H. Butin. Z. Mykol. **52**, 335 (1986).
3. P. D. Manion (*Editor*). Scleroderris canker of conifers. Martinus Nyhoff, Dr. W. Junk Publishers, The Hague. 1984.
4. W. A. Ayer, Y. Hoyano, M. S. Pedras, and I. van Altena. Can. J. Chem. **64**, 1585 (1986).
5. W. A. Ayer, Y. Hoyano, M. S. Pedras, J. Clardy, and E. Arnold. Can. J. Chem. **65**, 748 (1987).
6. W. A. Ayer and M. S. Pedras. Can. J. Chem. **65**, 754 (1987).
7. W. A. Ayer, M. S. Pedras, and D. E. Ward. Can. J. Chem. **65**, 760 (1987).
8. A. Mathey, B. Steffan, and W. Steglich. Liebigs Ann. Chem. 779 (1980).
9. W. B. Turner and D. C. Aldridge. Fungal metabolites. Vol. 2. Academic Press, London. 1983. pp. 195, 199.
10. D. H. R. Barton, P. de Mayo, and G. A. Raistrick. Tetrahedron, **6**, 48 (1959).
11. K. Homma, K. Fukuyama, Y. Katsube, Y. Kimura, and T. Hamasaki. Agric. Biol. Chem. **44**, 1333 (1980).
12. J. S. Pizey. Synthetic reagents. Vol. 2. Ellis Horwood Ltd., Chichester. 1974. p. 72.

Can. J. Chem. Downloaded from www.nrcresearchpress.com by 186.148.149.217 on 09/07/12
For personal use only.

Intercalation of aromatic amines into α-tin(IV) hydrogenphosphate monohydrate

E. RODRÍGUEZ-CASTELLÓN,[1] P. OLIVERA-PASTOR, A. JIMÉNEZ-LÓPEZ, AND P. MAIRELES-TORRES
Departamento de Química Inorgánica, Cristalografía y Mineralogía, Universidad de Málaga, 29071 Málaga, Spain
AND
M. J. HUDSON AND P. SYLVESTER
Department of Chemistry, The University of Reading, Reading RG6 2AD, United Kingdom

Received October 17, 1988[2]

E. RODRÍGUEZ-CASTELLÓN, P. OLIVERA-PASTOR, A. JIMÉNEZ-LÓPEZ, P. MAIRELES-TORRES, M. J. HUDSON, and P. SYLVESTER. Can. J. Chem. **67**, 2095 (1989).

Aromatic amines such as *o*-phenylenediamine, *m*-phenylenediamine, *p*-phenylenediamine, benzidine, and 2-amino-4-methylpyridine were intercalated into tin(IV) hydrogen phosphate monohydrate (α-$Sn(HPO_4)_2 \cdot H_2O$). *o*-Phenylenediamine and 2-amino-4-methylpyridine form a bilayer, while *m*-phenylenediamine, *p*-phenylenediamine, and benzidine form a monolayer. Phenylenediamines are monoprotonated on the interlayer surface of the phosphate, whereas benzidine is diprotonated. 2-Amino-4-methylpyridine exhibits a different behaviour with respect to pyridine, because the positive charge is localized between the two nitrogen atoms and not delocalised along the aromatic ring as in pyridine. The intercalation of benzidine causes a great shift in the relative position of the phosphate layers to accommodate the organic molecules. All products were characterized by chemical analysis, DTA-TG, IR spectroscopy, diffuse reflectance spectroscopy, and X-ray diffractometry.

Key words: intercalation, aryldiamines, benzidine, 2-amino-4-methylpyridine, α-$Sn(HPO_4)_2 \cdot H_2O$.

E. RODRÍGUEZ-CASTELLÓN, P. OLIVERA-PASTOR, A. JIMÉNEZ-LÓPEZ, P. MAIRELES-TORRES, M. J. HUDSON et P. SYLVESTER. Can. J. Chem. **67**, 2095 (1989).

On a intercalé des amines aromatiques, comme les *o*-, *m*- et *p*-phénylènediamines, la benzidine et la 2-amino-4-méthylpyridine, dans le monohydrate du phosphate acide d'étain(IV) (α-$Sn(HPO_4)_2 \cdot H_2O$). L'*o*-phénylènediamine et la 2-amino-4-méthylpyridine forment une bicouche alors que les *m*- et *p*-phénylènediamines ainsi que la benzidine forment une monocouche. Les phénylènediamines sont monoprotonées sur la surface intercalaire du phosphate alors que la benzidine est diprotonée. La 2-amino-4-méthylpyridine présente un comportement différent de celui de la pyridine parce que la charge positive est localisée entre les deux atomes d'azote et non pas délocalisée sur le noyau aromatique, comme c'est le cas avec la pyridine. Afin d'accommoder les molécules organiques, le fait d'intercaler de la benzidine provoque un déplacement important de la position relative des couches phosphates. On a caractérisé tous les produits par des analyses chimiques, par DTA-TG, par spectroscopie ir, par spectroscopie de réflectance diffuse et par diffraction des rayons-X.

Mots clés : intercalation, aryldiamines, benzidine, 2-amino-4-méthylpyridine, α-$Sn(HPO_4)_2 \cdot H_2O$.

[Traduit par la revue]

Introduction

Intercalation of aromatic amines on layered materials such as insoluble acid salts of general formula $M(IV)(HPO_4)_2 \cdot nH_2O$ (where M(IV) = Ti, Zr, and Sn) have been studied (1, 2). However, intercalation of aromatic compounds with two amine groups in this type of phosphate has not yet been described. Recent papers described the intercalation of some diamines such as *trans*-1,4-*N*,*N'*-diethyl-2-butenediamine and 1,4-diazabicyclo[2,2,2]octane (DABCO) into α-$Sn(HPO_4)_2 \cdot H_2O$ (α-SnP) (3, 4) and the observed intercalation behaviour was different than that observed with other layered materials such as some smectites (5). Miguel and Aragon (6) studied the intercalation compounds of *o*-, *m*-, and *p*-phenylenediamine with nickel cyanide, and they concluded that *o*- and *m*-phenylenediamine were coordinated to Ni(II) through an amine group, and that *p*-phenylenediamine coordinated their amine groups to two consecutive layers of nickel cyanide.

The preparation of intercalation compounds with free functional groups in the interlayer region for possible drafting reaction, and the study of the mechanism of the intercalation and the disposition of the organic molecules inside the layers are the main objectives of this work.

This paper studies the intercalation of *o*-phenylenediamine (OPh), *m*-phenylenediamine (MPh), *p*-phenylenediamine (PPh), benzidine (BZ), and 2-amino-4-methylpyridine (2AMP) into α-SnP. All the organics are monomers and are susceptible of polymerization. These intercalates were characterized by means of chemical analysis, X-ray powder diffractometry (XRD), infrared spectroscopy (IR), diffuse reflectance UV-vis spectroscopy (DRS), and thermal analysis (DTA-TG).

TABLE 1. Thermal data of amine intercalates

Sample	endo (°C)	exo (°C)		
OPh 5:1	50–135	254	480	
MPh 5:1	78–150	269	460	
PPh 3:1	70–180	205	465	
2AMP 7:1	50–170	400	455	625
BZ 5:1	—	370	475	

Experimental

Materials and intercalation reactions

All chemicals were of reagent grade and were used without further purification, α-SnP was prepared as described elsewhere (2).

Intercalation of amines into α-SnP was achieved by adding 0.20 g of α-SnP to 50 mL of aqueous solutions of the amines with different molar ratios ranging from 1:1 to 5:1 (amine/α-SnP), except in the case of BZ where a water/ethanol mixture (1:2 or 1:1) was used as solvent. The suspensions were stirred for one day in Teflon-sealed glass bottles at 50°C which were light protected. The solids were filtered and washed several times with water and then with acetone and finally air dried. The same results were obtained when toluene was used as solvent, but the products exhibited a better crystallinity.

[1]To whom correspondence may be addressed.
[2]Revision received June 16, 1989.

Printed in Canada / Imprimé au Canada

Can. J. Chem. Downloaded from www.nrcresearchpress.com by 186.148.149.217 on 09/07/12
For personal use only.

TABLE 2. Interlayer distance and composition of the intercalation compounds of α-SnP with some aromatic amines at 50°C

Amine	Molar ratio (mol amine added/mol α-Snp)	Found C	Found H	Found N	Calculated C	Calculated H	Calculated N	Composition (mol amine/mol α-SnP)	d_{00l}[b] (Å)
OPh	1:1	9.08	2.30	3.30	9.08	2.06	3.53	0.48	18.1
OPh	2:1	13.70	2.46	5.50	13.74	2.49	5.34	0.79	18.3
OPh	3:1	16.15	2.81	6.62	16.98	2.79	6.60	1.04	18.4
OPh	4:1	21.61	3.40	8.57	21.82	3.24	8.48	1.48	18.9
OPh	5:1	22.48	3.54	8.66	22.40	3.30	8.71	1.54	18.9
MPh	1:1	2.46	1.50	1.02	2.53	1.45	0.99	0.12	—
MPh	2:1	3.09	1.57	1.14	3.13	1.51	1.22	0.15	13.2
MPh	3:1	5.56	1.74	2.14	5.62	1.74	2.18	0.28	13.1
MPh	4:1	13.09	2.64	4.97	13.04	2.42	5.07	0.74	13.1
MPh	5:1	14.19	2.78	5.53	14.15	2.53	5.50	0.82	13.1
PPh	3:1	21.61	3.20	8.41	21.62	3.22	8.41	1.46	13.5
2AMP	7:1	20.28	3.48	8.32	20.90	3.15	8.13	1.39	18.5
BZ[a]	3:1	29.85	2.41	5.80	28.08	2.34	5.46	1.07	17.9

[a]A mixture H_2O/EtOH 1:1 was used as solvent.
[b]d_{00l} is the average value of the 00*l* reflections.

TABLE 3. Crystal lattice parameters of diamine-α-SnP intercalates

Sample	*a* (Å)	*b* (Å)	*c* (Å)	β (°)	*Z*
OPh 5:1	8.50	4.98	37.99	98.7	4
MPh 5:1	8.56	4.96	27.03	104.5	4
PPh 3:1	8.50	5.03	27.91	104.4	4
BZ 5:1	8.54	4.96	36.55	97.1	4
α-SnP	8.61	5.02	16.74	110.1	4

Aryldiamine monohydrochlorides and dihydrochlorides were prepared by titration of the amines with aqueous HCl and then evaporating to dryness.

Analytical procedure and instruments

CHN analyses were carried out in a Perkin Elmer 240C analyzer. X-ray powder diffraction patterns were obtained with a Siemens D-500 diffractometer with Cu-Kα radiation and using a graphite monochromator. Diffuse reflectance spectra were recorded on a Kontron Uvikon 810 spectrophotometer with an integrating sphere attachment, using $BaSO_4$ as the reference. Infrared spectra were obtained with a Perkin Elmer 883 spectrophotometer by the KBr disc method. TG and DTA analyses were carried out using a Rigaku-Thermoflex thermoanalyzer, at a heating rate of 10°C min^{-1}. The thermal behaviours of all obtained intercalation compounds are similar. Thermal data (Table 1) show endothermic peaks between 50–180°C which correspond to water loss except for benzidine intercalate. The exothermal effects correspond to the pyrolysis and oxidation of the intercalated amines.

The composition of the complexes with the highest amine content was as follows: $Sn(OPh)_{1.54}(HPO_4)_2 \cdot H_2O$; $Sn(MPh)_{0.74}(HPO_4)_2 \cdot H_2O$; $Sn(PPh)_{1.46}(HPO_4)_2 \cdot H_2O$; $Sn(2AMP)_{1.39}(HPO_4)_2 \cdot 0.5H_2O$; $Sn(BZ)_{1.07}(HPO_4)_2 \cdot H_2O$. Thermogravimetric data agree with CHN analysis.

Results and discussion

The intercalation of OPh, PPh, BZ, and 2AMP occurs as expected, by means of acid–base neutralization reactions. The composition and the increase in basal spacing of the intercalates depend on the added amine (see Table 2). Structural changes of the intercalated phases were examined by X-ray diffractometry. In all cases, the powder X-ray diffraction patterns can be indexed on monoclinic unit cells, where the *a* and *b* lattice constants are very similar to those of α-SnP (Table 3). The data indicate that the layered structures have been preserved and that the interlamellar spaces have expanded. All the starting product *hk*0 lines were present in the intercalates with systematic absences when $h + k = 2n$.

TABLE 4. Selected vibration bands of the IR spectra of pure, monohydrochloride, dihydrochloride and intercalated phenylenediamines, all frequencies in cm^{-1}

Substance	νNH_a and/or νOH	νNH_s	νNH^+	δNH_2 and/or δHOH	δNH_3^+	νCN
OPh	3390	3368		1630		1321, 1271
OPh(HCl)	3413	3333	2800–3000	1622	1558	1315, 1290
$OPh(HCl)_2$			2750–3000	1611	1521	1308
OPh 5:1	3423	3362	2800–3000	1641	1523	1321
MPh	3394	3331		1601		1318
MPh(HCl)	3390	3310	2800–3000	1618	1549	1293
$MPh(HCl)_2$			2750–3000	1612	1526	1270
MPh 5:1	3398	3302	2800–3000	1600	1536	
PPh	3379	3308		1626		1309, 1262
PPh(HCl)	3419	3335	2800–3000	1630, 1611	1567	1307, 1292
$PPh(HCl)_2$			2800–3000		1563	1307
PPh 5:1	3340	3300	2800–3000	1615	1513	1309

Can. J. Chem. Downloaded from www.nrcresearchpress.com by 186.148.149.217 on 09/07/12
For personal use only.

Can. J. Chem. Downloaded from www.nrcresearchpress.com by 186.148.149.217 on 09/07/12
For personal use only.

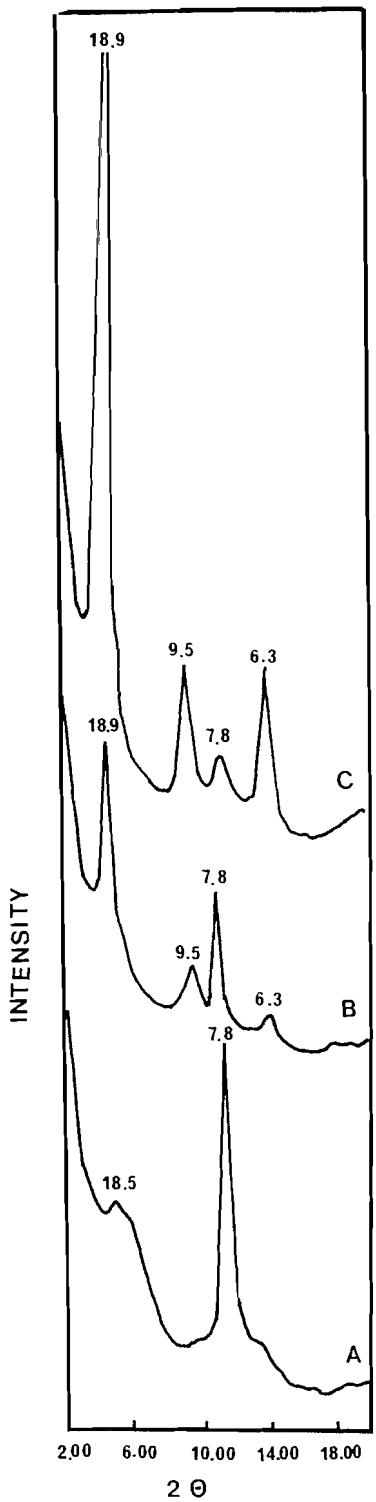


FIG. 1. X-ray powder diffractograms at the lowest angle region of (*A*), OPh 1:1; (*B*), OPh 3:1; (*C*), OPh 5:1. (Peak values in Å).

Intercalation of phenylenediamines

X-ray powder diffractograms of all intercalates show the presence of two phases: a swelled phase that appears in the lowest angle region, and the pure α-SnP phase with an interlayer distance of 7.8 Å. The intensity of the characteristic reflection line of the swelled phase increased with an increase in the uptake of phenylenediamine, whereas the diffraction peak of the α-SnP phase persists even in samples with the highest concentration of amine. Figure 1 shows this evolution in the case of the OPh

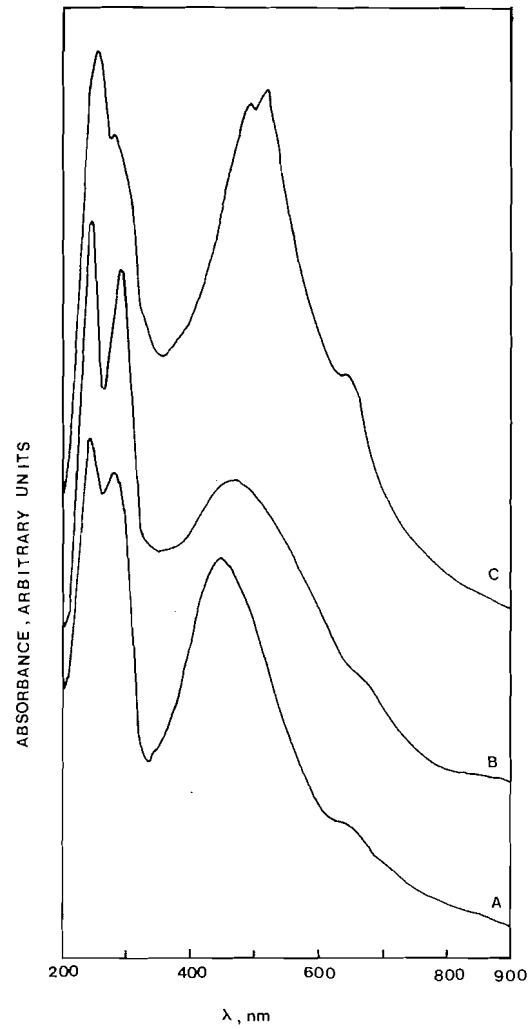


FIG. 2. Diffuse reflectance spectra of (*A*), OPh 3:1; (*B*), OPh monohydrochloride; (*C*) OPh dihydrochloride.

intercalation as an example. At high diamine loadings, several integral reflection orders (004, 006, 008) of the swelled phase of the complexes were observed.

d(002) values of the swelled phases of the intercalates are consistent with the formation of a bilayer of organic molecules for the OPh complex (18.9 Å) and of a monolayer for the MPh (13.1 Å) and PPh (13.5 Å) complexes.

The mechanism of intercalation of amines was monitored by observing the shifts of νNH, δNH_2, and νCN vibration bands in the infrared spectra of the intercalated amine in comparison with the pure amine and its chlorhydrates. Selected infrared absorption bands of the pure amine, mono- and dihydrochloride, and the intercalated amine samples (5:1) are shown in Table 4.

From these data, protonation of arylamines is detected by the presence of a broad band in the 2750–3000 cm^{-1} region and another band between 1513–1568 cm^{-1} corresponding to νNH^+ and δNH_3^+, respectively. The disappearance of the bands at c.a. 3390 cm^{-1} (νNH_a) and c.a. 3300 (νNH_s) of the pure amines implies diprotonation of the diamines. When only monoprotonation occurs, the latter band persists. Comparison of the phenylenediamine–α-SnP intercalate spectra with those of pure, mono- and dihydrochloride amines reveals that these phenylenediamines are not totally protonated in the interlayer region of the phosphate. This occurs probably as a consequence of the low pK_{a2} values of these diamines (0.60, 2.41, and 2.67

Can. J. Chem. Downloaded from www.nrcresearchpress.com by 186.148.149.217 on 09/07/12
For personal use only.

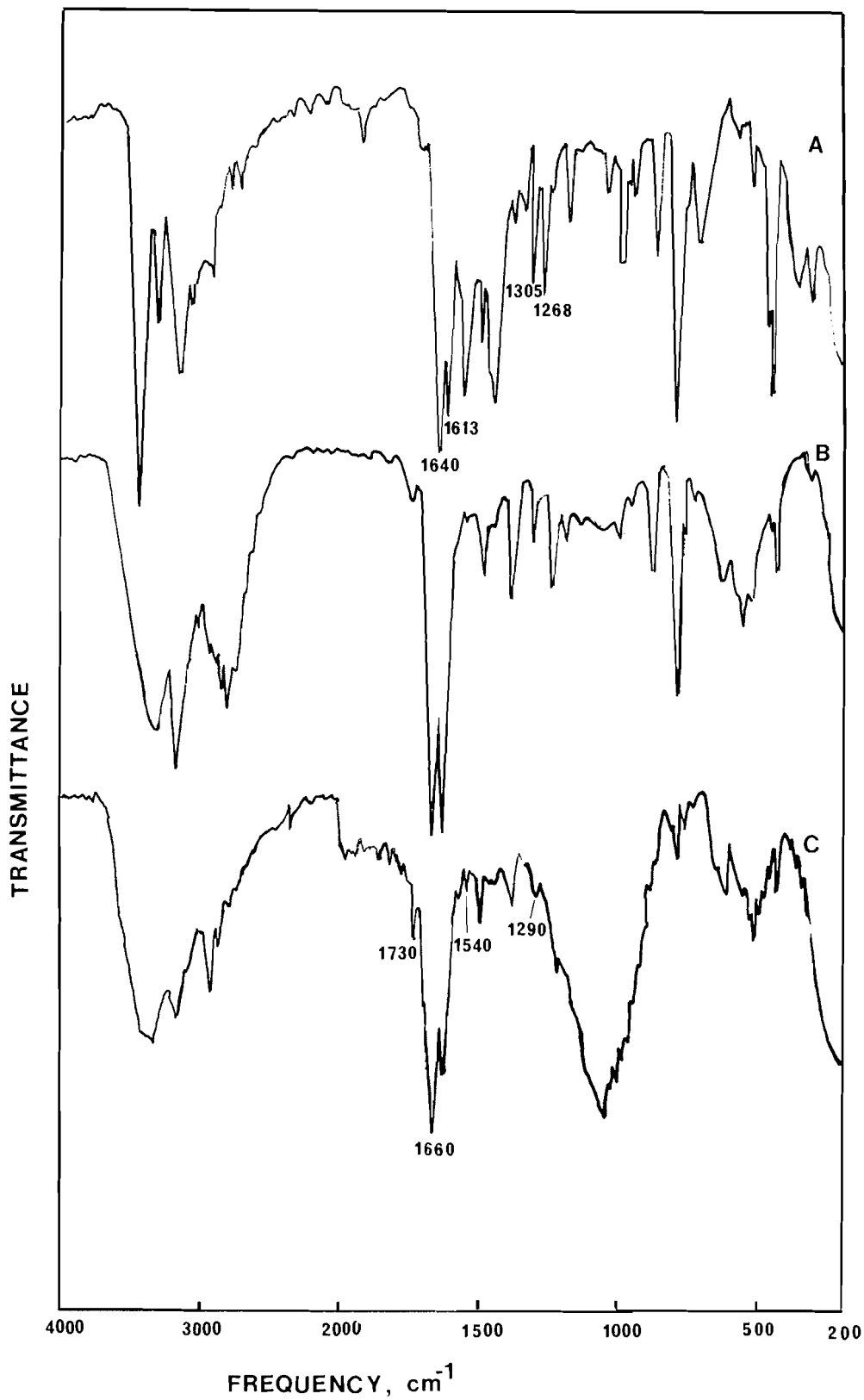


FIG. 3. Infrared spectra of (*A*), 2-amino-4-methylpyridine; (*B*), 2-amino-4-methylpyridine monohydrochloride; (*C*), 2AMP 7:1.

for OPh, MPh, and PPh, respectively (7)) and also of the different acidity of the POH groups (2, 8). Composition data for the OPh and PPh intercalates also support the hypothesis of monoprotonation inasmuch as the molar ratio intercalated diamine/α-SnP exceed unity. OPh molecules are arranged in bilayers, but diprotonation is not detected in spite of the fact that the distance between the —NH_2 groups in this molecule is very similar to the distance between two adjacent POH groups in the α-SnP layer. The situation of the amine groups in OPh impedes the simultaneous interaction of both groups with two adjacent layers of the phosphate and thus bilayer formation occurs, thereby facilitating the strongest interaction possible of this

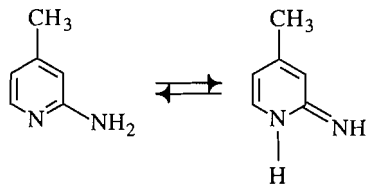
diamine with the phosphate, as in the case of intercalated aromatic monoamines (2). However, a greater separation between the amine groups such as in MPh and PPh diamines may permit simultaneous interaction with adjacent layers; giving rise the formation of monolayers, although the molecules are not diprotonated. The strongest interaction of an amine with the interlayer surface is achieved when the CN bond is perpendicular to to the layers (9). The geometry of the MPh molecule only permits that one of the two CN bonds to be perpendicular to the phosphate layer in contrast to the PPh molecule and consequently a weaker interaction of MPh with the phosphate should be expected. Composition data suggest this possibility (Table 2).

Diffuse reflectance spectroscopy data for the phenylenediamine intercalates also are coherent with the presence of intercalated monoprotonated diamines. For example, the diffuse reflectance spectrum of OPh 3:1 (Fig. 2) shows four absorption bands at 640, 455, 281, and 243 nm, being very similar to that of *o*-phenylenediamine monohydrochloride (640, 465, 290, and 245 nm), and different from the spectrum of *o*-phenylenediamine dihydrochloride which presents five bands at 640, 522, 490, 288, and 257 nm.

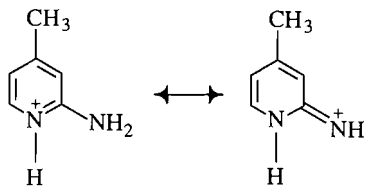
Intercalation of 2-amino-4-methylpyridine

2AMP was intercalated into α-SnP from aqueous solution. The maximum amount of amine taken up was 1.39 mol of 2AMP per mol of α-SnP, with a molar ratio AMP added/α-SnP of 7:1. XRD data of 2AMP 7:1 give an interlayer distance of 18.5 Å, suggesting an arrangement of bilayer within the interlayer space of α-SnP.

It is well known that 2AMP exhibits tautomery, according to the following equilibrium (10):



In the IR spectrum of this substance (Fig. 3), bands at 1268 and 1305, 1640, and 1613 cm^{-1} are assigned to νCN, νCN, and δNH_2, respectively showing the presence of amine and imine groups. Although the electrophilic reaction can take place either on heterocyclic or amino nitrogen (10), the protonation of this substance only gives rise to one product whose more important canonical form can be seen in the following scheme:



a *b*

This is coherent with the existence of a unique pK_a (>6.71). The canonical form *b* supposes a weakness of the C=N aromatic bond and a strengthening of the $C=N^+$ aliphatic bond. The ν C=N aromatic vibration band at 1640 cm^{-1} of the pure amine shifts to 1660 cm^{-1} in the 2AMP intercalate, which is interpreted as a consequence of the contribution of the aliphatic imine ion character of the protonated intercalated molecule. The weak intensity band at 1540 cm^{-1} in the 2AMP intercalate spectrum is assigned to a vibration mode of the pyridinium ion

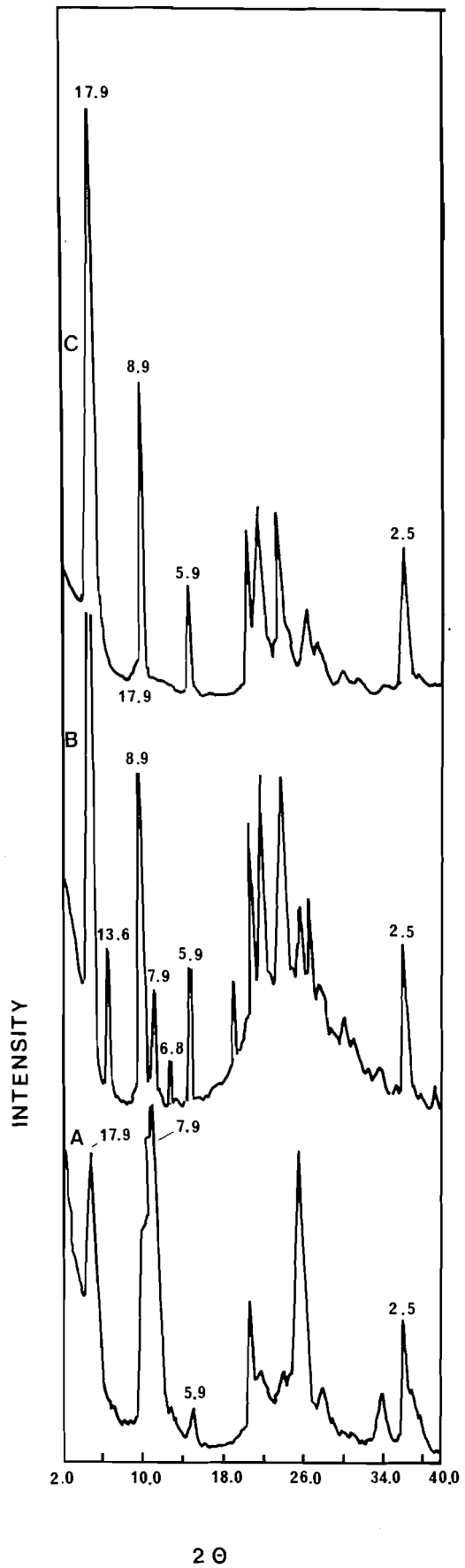


FIG. 4. X-ray powder diffractograms of benzidine-α-SnP intercalates with different amine loading. (*A*), BZ 0.25:1; (*B*), BZ 1:1; (*C*), BZ 5:1. (Peak values in Å).

Can. J. Chem. Downloaded from www.nrcresearchpress.com by 186.148.149.217 on 09/07/12
For personal use only.

Can. J. Chem. Downloaded from www.nrcresearchpress.com by 186.148.149.217 on 09/07/12
For personal use only.

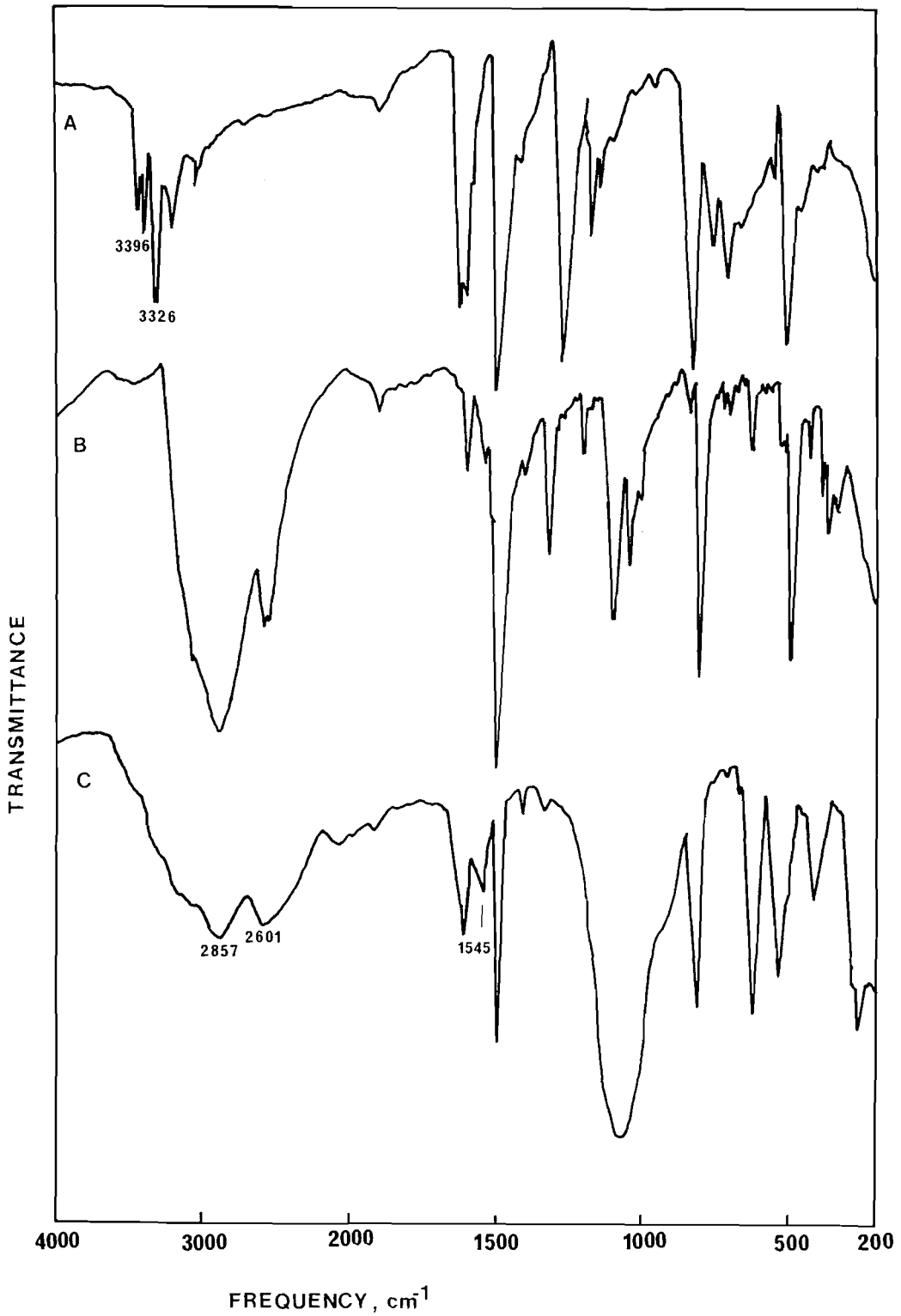


FIG. 5. Infrared spectra of (*A*), benzidine; (*B*), benzidine dihydrochloride; (*C*), BZ 4:1.

(11). The appearance of a band at 1290 cm^{-1} attributed to νC—N of the intercalated amine, instead of two bands at 1305 and 1268 cm^{-1} in the pure amine spectrum may be also due to the participation of the canonical form *b*. The band at 1730 cm^{-1} in the IR spectrum of the intercalate indicates the presence of strongly linked water in the phosphate interlayer space (12); therefore, it is to be expected that the interaction of the 2AMP with the phosphate layers is affected by water molecules through hydrogen bonds. Thus the neutralization of the layer negative charge would be more effective.

Pyridine lies in a flat disposition within the α-SnP interlayer space with the aromatic ring parallel to the layers (2), in contrast to 2AMP. The positive charge of the pyridinium ion is delocalized along the ring, whereas in the 2AMP ion, the positive charge is more localized between the two nitrogen atoms. The charge is also localized in the nitrogen atom of the

anilinium ion, and thus bilayers are formed with the aromatic ring tilted 60° with respect to the phosphate layer, as in the case of alkylamines (9, 13). Intercalation data for aromatic amine into α-SnP appear to suggest that when the positive charge of the amine cation such as anilinium, aryldiammonium, and 2AMP is localized, the basic group has a tendency to orientate toward the oxygen surface of the phosphate layers, whereas when the positive charge is delocalized (like in the pyridinium ion) the flat orientation of the aromatic ring is the most stable arrangement.

Intercalation of benzidine

Benzidine was intercalated into α-SnP using a water/ethanol 1:1 mixture as solvent. The highest content of intercalated BZ was obtained with a molar ratio BZ added/α-SnP 3:1 (1:1 mol of BZ/mol of α-SnP). Under this condition the characteristic reflection line of α-SnP at 7.8 Å is not readily observed, and the increase in basal spacing was 10.1 Å (17.9 Å − 7.8 Å), a value very close to that expected for perpendicular orientation if it is assumed that the $—NH_2$ groups are engaged in a symmetrical hydrogen bond with POH groups of adjacent layers and that the O—H···N bond length and angle are 2.8 Å and 180°, respectively (14). The diffraction peaks appearing at 13.6 Å and its harmonic of higher order at 6.8 Å in the XRD patterns of the 1:1 BZ intercalate may correspond to a phase with no perpendicular orientation of the amine (Fig. 4).

Figure 5 shows the IR spectra of pure BZ, BZ dihydrochloride, and the BZ 4:1 intercalate. The presence of bands at 2857 and 2601, and at 1545 cm^{-1} assigned to νNH^+ and δNH_3^+ respectively, together with the absence of the νNH_2 bands of the pure amine at 3396 and 3326 cm^{-1} in the IR spectrum of the BZ intercalate suggest protonation of both amine groups. Higher basicity of benzidine in comparison with phenylenediamines ($pK_{1a} = 4.97$, $pK_{2a} = 3.75$ (15)) may explain this behaviour. In fact, the intercalation of benzidine supposes the greatest shift in the relative position of the phosphate layers (Table 3) to accommodate the organic molecules, which is believed to be a consequence of the strong interaction of the benzidine molecule with two adjacent layers.

Acknowledgements

We thank the C.I.C.Y.T. (proyet PB86-0244); Acción Integrada Hispano Británica (Ministerio de Educación y Ciencia and British Council), for financial support and Dr. R. Rico of the Department of Organic Chemistry for helpful discussion.

1. S. YAMANAKA, Y. HORIBE, and M. J. TANAKA. J. Inorg. Nucl. Chem. **38**, 323 (1976).
2. E. RODRÍGUEZ-CASTELLÓN, A. RODRÍGUEZ, and S. BRUQUE. Inorg. Chem. **24**, 1187 (1985).
3. C. O. GIVA, I. FOTHERINGHAM, and M. J. HUDSON. J. Chem. Soc. Chem. Commun. 1554 (1986).
4. C. O. GIVA, M. J. HUDSON, L. MORENO-REAL, and E. RODRÍGUEZ-CASTELLÓN. J. Chem. Soc. Chem. Commun. 536 (1987).
5. M. M. MORTLAND and V. BERKHEISER. Clays Clay Miner. **24**, 60 (1976).
6. S. MIGUEL and F. ARAGÓN. An. Quim. **82***b*, 140 (1986).
7. ZVI RAPPOPORT. Handbook of tables for organic compound identification. 3ed. CRC Press, Boca Raton, FL. 1967.
8. T. HATTORI, Y. HORIBE, and M. TANAKA. J. Inorg. Nucl. Chem. **38**, 323 (1976).
9. U. CONSTANTINO. *In* Inorganic ion exchange materials. *Edited by* A. Clearfield. CRC Press, Boca Raton, FL. 1982. Chapt. 3.
10. A. R. KATRITZKY and J. M. LAGOWSKI. *In* Advances in heterocyclic chemistry. Vol. 1. *Edited by* A. R. Katritzky. Academic Press, New York. 1963.
11. V. C. FARMER and M. M. MORTLAND. J. Chem. Soc. A. 344 (1966).
12. R. D. GILLARD and G. WILKINSON. J. Chem. Soc. **2**, 1640 (1964).
13. E. RODRÍGUEZ-CASTELLÓN, S. BRUQUE, and A. RODRÍGUEZ. J. Chem. Soc. Dalton Trans. 213 (1985).
14. A. CLEARFIELD and R. M. TWINDWA. J. Inorg. Nucl. Chem. **41**, 871 (1979).
15. T. FURUKAWA and G. W. BRINDLEY. Clays Clay Miner. **21**, 279 (1973.

Can. J. Chem. Downloaded from www.nrcresearchpress.com by 186.148.149.217 on 09/07/12
For personal use only.

Interfacial behaviour of isopropanol at the Hg electrode from solutions of H_2O–isopropanol–HCl

AMINA A. MAZHAR
Chemistry Department, Faculty of Science, Cairo University, Giza, Egypt

Received March 7, 1989

AMINA A. MAZHAR. Can. J. Chem. **67**, 2102 (1989).

The adsorption of isopropanol on mercury in aqueous solutions of HCl at constant chemical potential of the acid has been determined from capacity and electrocapillary measurements. The maximum adsorption occurs at a charge of $-2.2\ \mu C\,cm^{-2}$. The Frumkin isotherm is obeyed, the α factor in the isotherm changes from a positive value for mixtures rich in water to a negative value for mixtures rich in alcohol. The standard Gibbs energy of adsorption depends quadratically on the potential. The orientation of the alcohol molecule in the interface is discussed.

Key words: interface, medium effects, adsorption isotherm, aliphatic alcohol, Gibbs energy of adsorption.

AMINA A. MAZHAR. Can. J. Chem. **67**, 2102 (1989).

En se basant sur des mesures de capacité et d'électrocapillarité, on a déterminé l'adsorption de l'isopropanol sur du mercure en solutions aqueuses dans le HCl, à potentiel chimique constant d'acide. L'adsorption maximale se produit à une charge de $-2{,}2\ \mu C\,cm^{-2}$. Les données obéissent à l'isotherme de Frumkin et le facteur α de l'isotherme varie d'une valeur positive pour les mélanges riches en eau à une valeur négative pour les mélanges riches en alcool. L'énergie standard d'adsorption de Gibbs varie d'une façon quadratique avec le potentiel. On discute de l'orientation de la molécule d'alcool à l'interface.

Mots clés : interface, effets de solvant, isotherme d'adsorption, alcools aliphatiques, énergie d'adsorption de Gibbs.

[Traduit par la revue]

Introduction

The adsorption characteristics of many organic compounds at the mercury solution interface have been described in the literature. Some unsolved problems related to the adsorption of aliphatic alcohols remain, especially when medium effects are taken into consideration. Mohilner and Nakadomari (1) have suggested that all results concerning the nature of adsorption isotherms could be erroneous if changes in the activity of the supporting electrolyte are neglected in increasing concentration of alcohol.

Since the medium effect is expected to be important only at relatively high concentration of the organic compound, a relatively weakly adsorbable organic substance should be chosen. Thus, higher alcohols, acids, and other adsorbable substances are not a favourable choice for such a study. The electrochemical behaviour of isopropanol adsorbed on Pt in acid medium has been recently reported (2).

Knowing the transfer energies of HCl solutions in the presence of isopropanol (3) enables one to study the role played by this surfactant, contingent upon the following conditions: (*a*) Possible errors due to junction potentials are eliminated by applying constant E potential using an Ag/AgCl electrode (1, 4), which was inserted in a glass bridge connected to the measurement cell, and containing the same solution under study. (*b*) Measurements are carried out not at constant activity as is usually done but at constant μ_{HCl} (μ stands for chemical potential); the value chosen corresponds to a $10^{-2}\ M$ solution in the absence of alcohol. In the presence of alcohol the concentration of HCl was always confined to within $10^{-2}\ M$, Table 1. (*c*) The activities are calculated using the values ΔG_t^0, the free energy of transfer of HCl and the following relation (5, 6):

$$\ln a_{HCl}(x_2) = \ln a_{HCl}(x = 0) - \Delta G_t^0/RT$$

where x_2 is the molar fraction of isopropanol.

It is assumed, as practised by the authors of the above references, that the Debye–Hückel law is applicable to HCl in the concentration range studied.

Isopropanol is chosen in this study to pinpoint the electrochemical behaviour of adsorbed secondary alcohols, permitting a better explanation of the differences in the electrochemical properties of alcohols and related compounds. We try to characterize the position of the adsorption maximum, the orientation of the adsorbed particles, and the type of adsorption isotherm for isopropanol in solutions of constant μ_{HCl}.

Experimental

Measurements of the parameters of the electrocapillary maximum, E_z and γ_z, were carried out by a streaming capillary electrometer similar to that used originally by Grahame *et al.* (7). The method of determination of E_z and γ_z was described elsewhere (8). Differential capacity measurements were made using a simple symmetrical ac bridge of the Wien type (9). The capacity cell and working procedure are the same employed previously (10). As before, the reference electrode was an Ag/AgCl electrode (11). All measurements were made in an air bath adjusted to 25°C using a frequency of 1 kHz. AR grade reagents were used, HCl was from B.D.H. and isopropanol from Merck. Measurements were carried out up to 30% by weight alcohol.

Results

Figure 1 shows the differential capacity curves in pure $10^{-2}\ M$ HCl and in presence of 14 different concentrations of the alcohol at constant μ_{HCl}. The anodic side shifts at higher alcohol concentrations, and as previously observed in the case of perchloric acid (12), and in the presence of SO_4^{2-} ions (13), the adsorption–desorption peaks do not appear. The zero-charge potential E_z shifts to more positive values due to adsorption of the alcohol and are indicated by vertical strokes on the capacity curves. With increase of alcohol concentration a capacity trough is formed; this trough gradually widens and levels down, tending towards a minimum value at the highest concentrations studied, meanwhile the desorption peaks on the cathodic side level up monotonically.

The relation between the electrode charge density σ^M and the potential was obtained by integration of the capacity curves. Starting from E_z in the differential capacity curves where $\sigma^M = 0$ (for each curve) graphical integration was carried out every

Printed in Canada / Imprimé au Canada

Can. J. Chem. Downloaded from www.nrcresearchpress.com by 186.148.149.217 on 09/07/12
For personal use only.

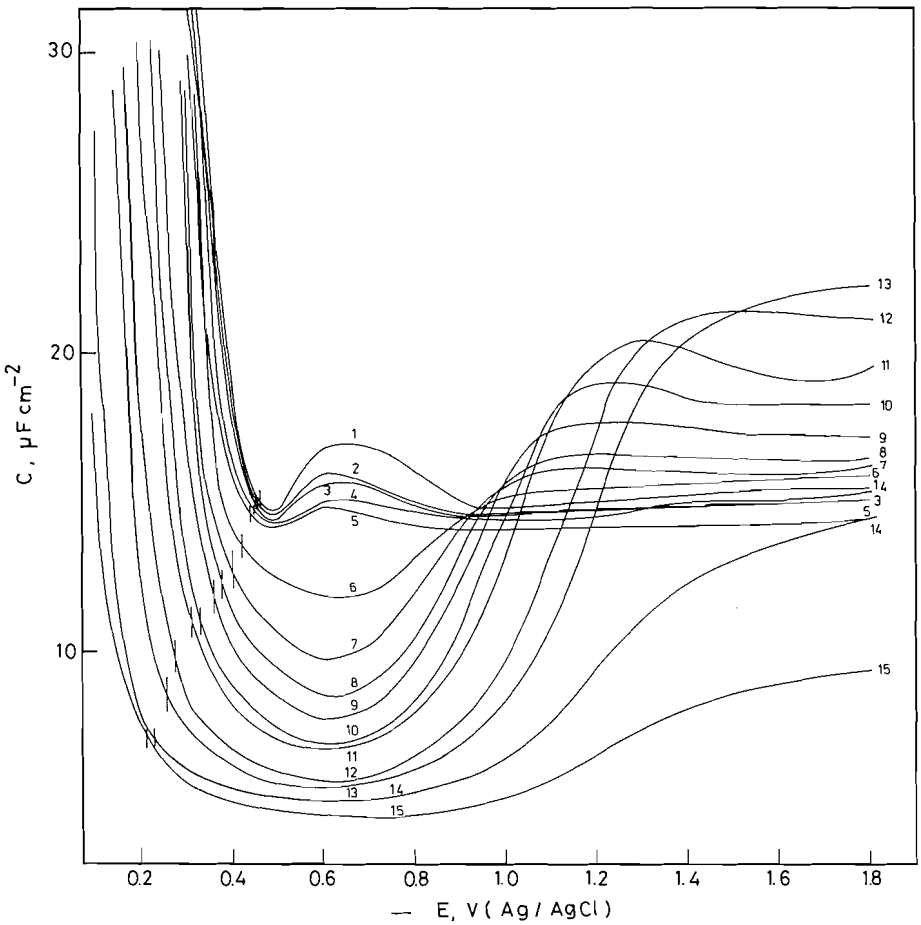


FIG. 1. Differential capacity curves of isopropanol in HCl (μ constant). The number of each figure is the solution number used in Table 1.

TABLE 1. Zero-charge coordinates for the mercury/aqueous solution of isopropanol interface in HCl solutions of constant μ at 25°C

Solution* number	Acid concentration ($M \times 10^2$)	ΔG_t^0 (kJ mol^{-1})	Alcohol concentration (mol L^{-1})	% alcohol by wt.	E_z V vs. Ag/AgCl	γ_z (mN m^{-1})
1	1.00	0	0	0	−0.462	423.8
2	0.994	0.016	0.042	0.25	−0.459	423.6
3	0.986	0.034	0.083	0.50	−0.454	423.5
4	0.979	0.053	0.125	0.75	−0.446	423.3
5	0.971	0.072	0.166	1.00	−0.438	422.9
6	0.956	0.110	0.250	1.50	−0.421	422.0
7	0.941	0.149	0.333	2.00	−0.400	418.9
8	0.927	0.188	0.416	2.50	−0.376	417.1
9	0.912	0.228	0.499	3.00	−0.358	415.7
10	0.883	0.308	0.666	4.00	−0.331	413.1
11	0.852	0.395	0.832	5.00	−0.310	410.4
12	0.770	0.643	1.248	7.50	−0.276	406.1
13	0.698	0.887	1.664	10.0	−0.255	403.1
14	0.511	1.658	3.328	20.0	−0.224	394.2
15	0.375	2.429	4.993	30.0	−0.210	391.7

*These numbers are used on the figures to refer to the alcohol concentrations as listed in the table.

10 mV interval towards the far anodic side, then towards the far cathodic side. A computer programme was used to calculate σ^M as a function of potential. From the σ^M–E curves and by adopting the same procedure, integration of these curves provided the lowering in γ as a function of potential. Subsequent subtraction of the values of the lowering in γ from the γ_z determined for each solution by using a capillary electrometer produced γ–E curves. Table 1 lists the values of the zero-charge coordinates.

Figure 2 shows the relation between electrode charge density

Can. J. Chem. Downloaded from www.nrcresearchpress.com by 186.148.149.217 on 09/07/12
For personal use only.

Can. J. Chem. Downloaded from www.nrcresearchpress.com by 186.148.149.217 on 09/07/12
For personal use only.

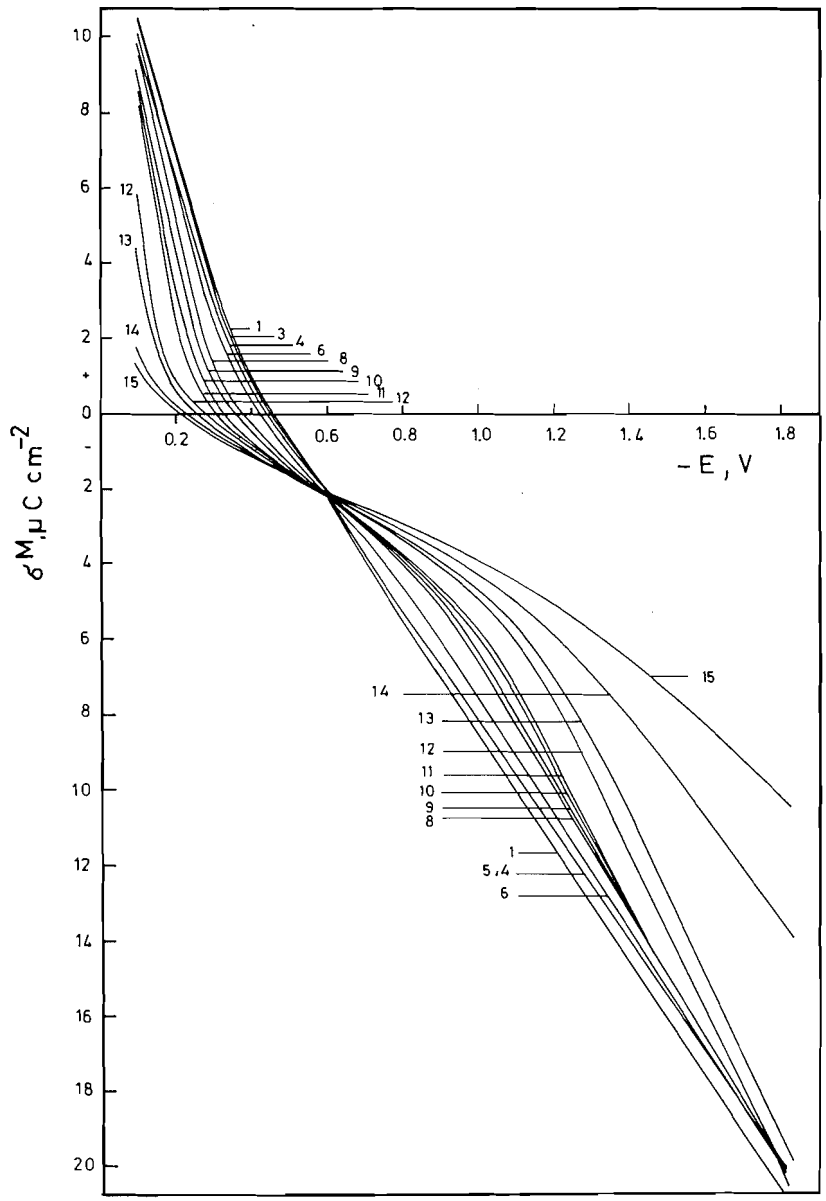


FIG. 2. Dependence of the electrode charge density on the applied potential. Same numbering as Fig. 1.

and potential. It is clear that at extreme negative (−1.8 V) and positive (0.1 V) potentials, desorption is complete for alcohol concentrations up to 5%. The point of intersection of these curves corresponds to σ^M of $-2.2\ \mu C\ cm^{-2}$ and a potential of −0.6 V. Both charge and potential of maximum adsorption are concentration independent. The negative value of σ^M_{max} and the positive shift of E_{max} reveal that at least at maximum adsorption isopropanol dipoles are adsorbed with their positive ends oriented towards the electrode surface. The adsorption of organic compounds having no net dipole moment or showing no effective dipole moment gives σ^M_{max} at −2 to $-4\ \mu C\ cm^{-2}$. For example, σ^M_{max} for pyrazine (14) is $-2\ \mu C\ cm^{-2}$, the more negative value obtained for isopropanol suggests that adsorption occurs with the alkyl group in contact with the mercury surface while the polar OH group points to the solution.

The electrocapillary curves are shown in Fig. 3. The vertical strokes represent E_z, isopropanol shows the common feature of aliphatic alcohols in having their maximum adsorption at potentials more negative than pzc (15–17).

The surface excesses were obtained by using the familiar Gibbs equation, from plots of γ vs. log alcohol concentration at different potentials. The relation between the surface excess Γ at pzc and the concentration of alcohol is shown in Fig. 4. A simple isotherm is obtained with a maximum Γ value of 2.48×10^{14} molecules cm^{-2}, which would give a value of $\simeq 40\ Å^2$ for the area occupied by a single molecule, however, since E_{max} is shifted from E_z, it seems reasonable to calculate Γ_{max} required for further analysis from a plot of $1/\Gamma$ vs. $1/C$ at maximum adsorption. Such a plot is shown in Fig. 5 for both variables of maximum adsorption, i.e., at both $E_{max} = -0.6$ V, and at $\sigma^M_{max} = -2.2\ \mu C\ cm^{-2}$. Extrapolation to $1/C$ organic = 0 should provide a reliable value of Γ_{max}, since the measured concentrations are high (18). The values of Γ_{max} obtained are 3.01 and 3.02×10^{14} molecules cm^{-2}, respectively, with an error of less than ±0.03. These values show that Γ_{max} obtained either at constant E or σ is the same. This yields an area of $33\ Å^2$ which is in remarkably good agreement with that reported for hexafluoro-2-propanol (19), supposing a close-packed monomolecular layer.

The relative surface coverage θ as a function of potential for

Can. J. Chem. Downloaded from www.nrcresearchpress.com by 186.148.149.217 on 09/07/12
For personal use only.

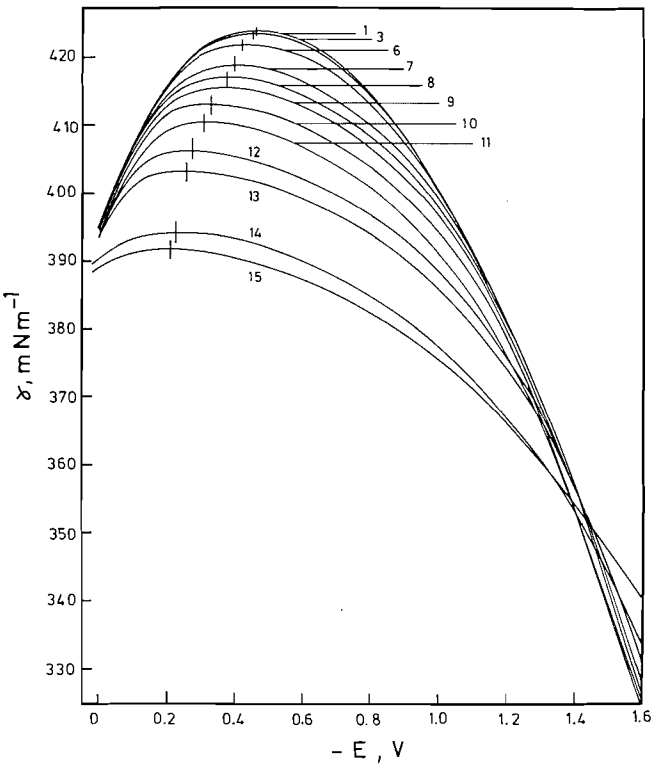


FIG. 3. Electrocapillary curves of Hg in HCl solutions in presence of isopropanol. Same numbering as Fig. 1.

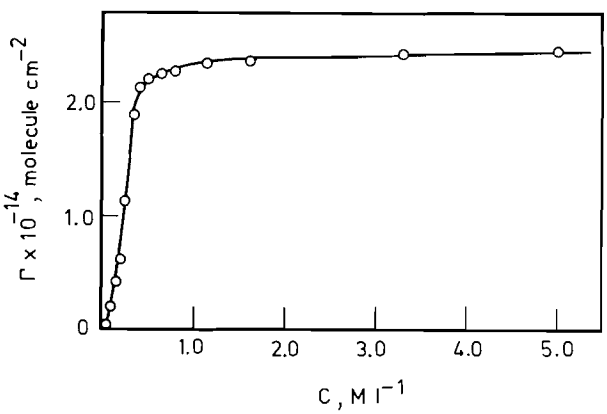


FIG. 4. Variation of $\Gamma_{alcohol}$ with concentration at pzc.

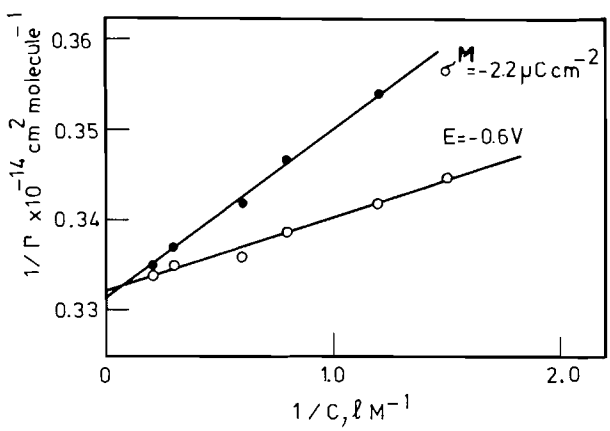


FIG. 5. Dependence of $1/\Gamma$ on $1/C_{org}$ at charge density (σ^M) and potential (E) of maximum adsorption.

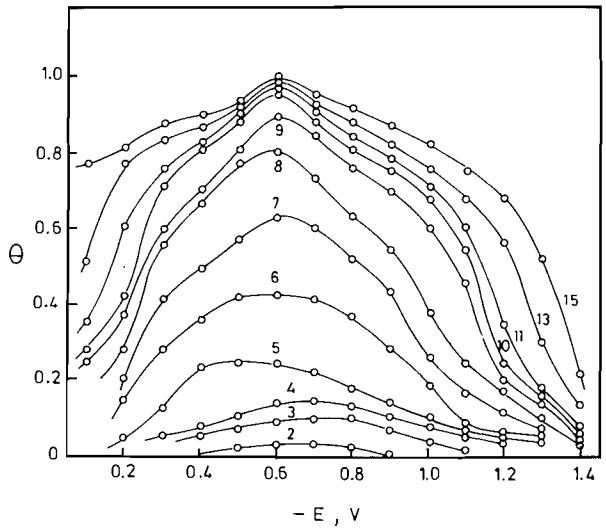


FIG. 6. Variation of surface coverage with potential, numbers correspond to concentrations according to Table 1.

different alcohol concentrations is shown in Fig. 6, the value of Γ_{max} was used in calculating $\theta = \Gamma/\Gamma_{max}$. The figure reveals that at -0.6 V maximum adsorption is reached for all solutions studied, at the highest concentration θ approaches unity. Based on these values of θ the experimental adsorption isotherms were analyzed by using Frumkin relation (20, 21).

$$[1] \quad \beta C = \theta(1-\theta)^{-1} \exp(-2\alpha\theta)$$

where α is the interaction parameter and β the adsorption coefficient. Within the limits of experimental error, a good linearity was obtained for the plot of $\ln \theta/(1-\theta)C$ vs. θ at each potential as plotted on enlarged diagrams, which indicates the applicability of Frumkin's isotherm to the present results. The test of this isotherm is shown in Fig. 7. The striking feature encountered in this analysis is that at relatively higher alcohol concentrations (above 3%) the slope of the relation shown in Fig. 7 is reversed, straight line relations are also obtained but with a negative value instead of a positive one at low alcohol concentrations (below 3%). This latter positive value of α indicates that particle–particle attraction is stronger than particle–solvent attraction (22), it decreases slightly at potentials more positive or negative than -0.6 V, i.e. maximum value of α is at E_{max}. This value of 2.5 is high as compared to 1.11 for isopropanol (23), however, this is normal as it has been reported (15) that the α values of isomeric compounds are systematically higher than the values of the normal chain length alcohols, due to the higher density of molecules in the adsorption layer.

Discussion

The study of the adsorption of isopropanol in HCl solutions of constant chemical potential, μ, indicates that the molecule is adsorbed with the alkyl group oriented towards the Hg surface and the polar OH group directed towards the solution side. By working at a constant μ_{HCl}, the possibility of medium effects playing an unaccounted for role is eliminated. This procedure was adopted, although it has been shown that the deviations could be within experimental error (4, 23). Although Cl^- ions are known to be specifically adsorbed on Hg, by working at constant chemical potential it is considered that the specific adsorption of Cl^- is constant, and hence the varying factor to be considered is the adsorption of isopropanol.

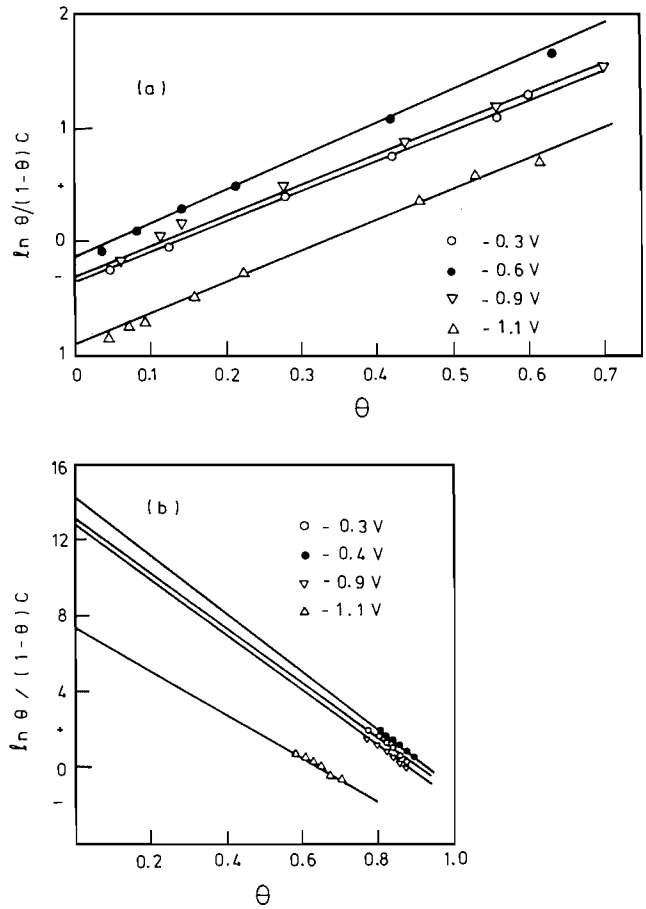


FIG. 7. Test of the Frumkin isotherm (*a*) low concentrations (below 3%) and (*b*) high concentrations (above 3%) at different potentials.

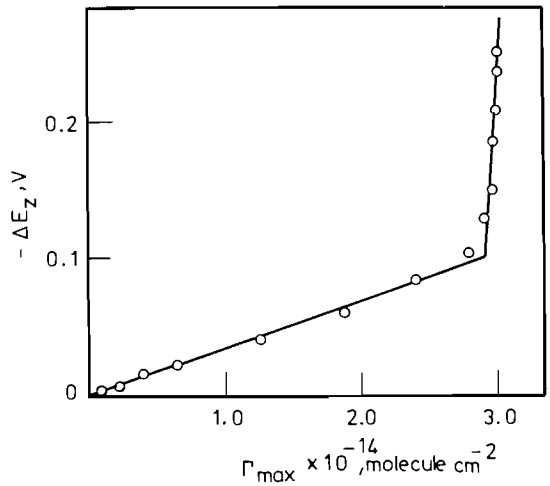


FIG. 8. Zero-charge potential shift at the mercury–solution interface due to adsorption of isopropanol as a function of surface excess Γ at maximum adsorption.

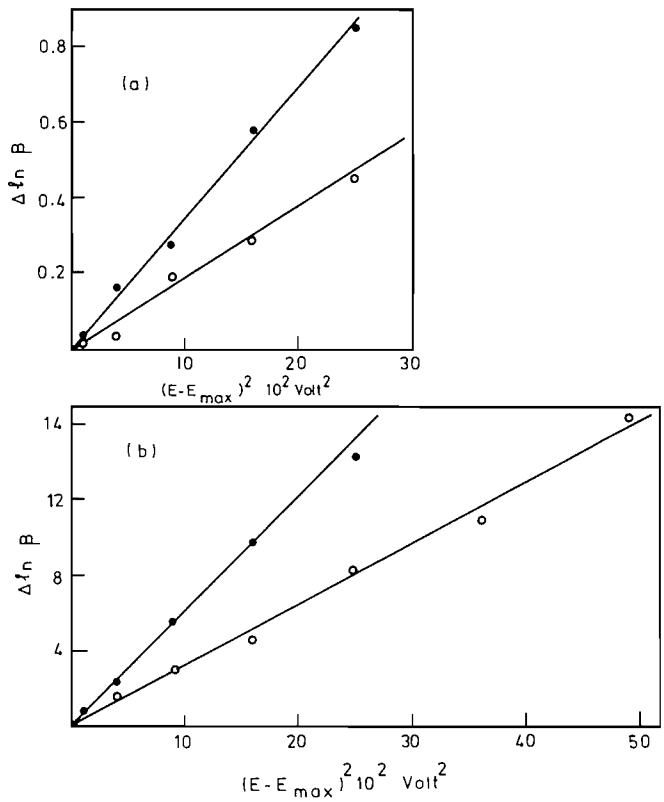


FIG. 9. Dependence of Δ ln β vs. $(E - E_{max})^2$. ●, *E* more positive than E_{max}; ○, *E* more negative than E_{max}; (*a*) low concentrations; (*b*) high concentrations.

A marked change in the adsorption behaviour of isopropanol is observed so that two regions of concentration could be defined, a low concentration region below 3% alcohol and a high concentration region above 3% alcohol. The main difference between these two regions lies in the positive values of α obtained at the low concentrations as compared to negative values of α obtained at the high concentrations. Both follow the Frumkin's isotherm. Tertiary butyl alcohol, which is also a branched alcohol, dissolves in water and induces at high dilutions a considerable reduction of the partial volume. For small values of the molar fraction in *t*BuOH, water seems to be more structured than in the absence of alcohol, whereas for mixtures rich in alcohol the residual water network tends to break up (II). In the present study the change of α from positive to negative values (in passing from solutions rich in water to those rich in alcohol) implies that at high concentrations of alcohol adsorbate–solvent attraction in the interface is stronger than the mean value of adsorbate–adsorbate and solvent–solvent interactions (19), which may be correlated with the breaking up of the residual water network.

This observation could tacitly imply that the molecules have a different orientation at each concentration region, as previously reported for isopropanol which shows a change of orientation with coverage (23). Figure 8 shows the relation between the shift in zero charge potential at the Hg–solution interface due to adsorption as a function of Γ_{max}. It could be immediately observed that two sections with two different slopes are obtained, corresponding to two different orientations of the adsorbate as suggested by Trasatti (15), due to M–A interactions at the metal–solution interface. The change in orientation could be envisaged as a decrease in the number of hydrogen atoms of $-CH_3$ groups lying flat on the Hg surface. This could be caused by the expected change in the surface water structure (16) due to polarisability effects.

It has been reported that when effects due to polarisability prevail, a quadratic dependence of $\overline{\Delta G}_A^0$ on potential will be observed (15), where $\overline{\Delta G}_A^0$ is standard free energy of adsorption related to the adsorption coefficient β by

Can. J. Chem. Downloaded from www.nrcresearchpress.com by 186.148.149.217 on 09/07/12
For personal use only.

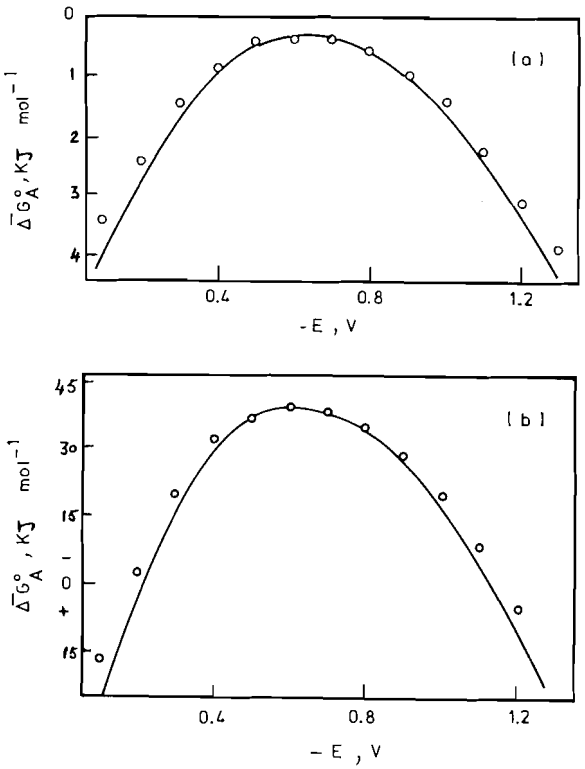


FIG. 10. Dependence of $\overline{\Delta G}_A^0$ on potential, circles are experimental values, (*a*) below 3%, low concentrations, and (*b*) above 3%, high concentrations.

$$[2] \quad \beta = \exp(-\overline{\Delta G}_A^0/RT)$$

Values of ln β can be readily obtained from intercepts of the relation shown in Fig. 7. The dependence of ln β on the square of the potential, $(E - E_{max})^2$, is linear, as shown in Fig. 9. Figure 9(*a*) and (*b*) correspond to the low concentration region and the high concentration region, i.e., to the two different orientations. In each region the linear dependence on the cathodic side has a lower slope than that on the anodic side of E_{max}. These relations fulfill the equation:

$$[3] \quad \overline{\Delta G}_A^0 = \overline{\Delta G}_{A_{max}}^0 + b(E - E_{max})^2$$

where b is the slope, and $\overline{\Delta G}_{A_{max}}^0 = 0.34$ for the orientation obtained at low alcohol concentrations and -38.87 kJ mol^{-1} for the orientation obtained at high concentrations. Perhaps the second value infers that the adsorbate is rearranged to maintain the best orientation for a maximum adsorption. Even so, the value of -38.87 kJ mol^{-1} is much lower than the values of $\overline{\Delta G}_{A_{max}}^0$ reported for molecules that strongly interact with Hg such as thiourea (24). Molecules that weakly adsorb on Hg such as ethylene glycol (25) or L(+) ascorbic acid (11) have $\overline{\Delta G}_{A_{max}}^0$ values of $\simeq -8$ and 24.9 kJ mol^{-1}, respectively. This indicates that isopropanol in both orientations is weakly adsorbed on the Hg surface, and that adsorption is of a physical nature.

The calculated dependence of $\overline{\Delta G}_A^0$ on potential using the preceding relation is given in Fig. 10, where circles are experimental values obtained from intercepts of $\ln \theta/(1 - \theta)c$ vs. θ. A parabolic variation is observed for $\overline{\Delta G}_A^0$ with potential, with a maximum at -0.6 V. The deviations are probably due to a change of the particle–particle interfacial interactions as observed in the case of other adsorbates (26).

1. D. M. MOHILNER and H. NAKADOMARI. J. Phys. Chem. **77**, 1594 (1973).
2. E. SOKOLOVA and M. KHRISTOV. J. Electroanal. Chem. **175** (12), 195 (1984).
3. R. BENNES. Unpublished results.
4. A. DE BATTISTI and S. TRASATTI. J. Electroanal. Chem. **54**, 1 (1974).
5. Y. POINTUD, J. JULLIARD, L. AVEDIKIAN, J. P. MOREL, and M. DUCROS. Thermochim. Acta, **8**, 423 (1974).
6. Y. POINTUD, J. JULLIARD, J. P. MOREL, and L. AVEDIKIAN. Electrochim. Acta, **19**, 229 (1974).
7. D. C. GRAHAME, E. M. COFFIN, and J. I. CUMMINGS. Office of Naval Research, Tech. Report No. 2 (1950).
8. H. A. GHALI, A. M. BEKHEET, and A. A. MAZHAR. Electrochim. Acta, **27**, 595 (1982).
9. M. WEIN. Ann. Phys. **58**, 37 (1896).
10. A. A. MAZHAR and F. EL-TAIB HEAKAL. Ber. Bunsenges. Phys. Chem. **90**, 1205 (1986).
11. A. MAZHAR, R. BENNES, P. VANEL, and D. SCHUHMANN. J. Electroanal. Chem. **100**, 395 (1979).
12. MA. M. GOMEZ, E. DIEZ, and E. ALDA. J. Electroanal. Chem. **165**, 207 (1984).
13. MA. M. GOMEZ, A. MANZANO, A. ALDEZ, and J. MA. VARA. Anales. **76**, 35 (1980).
14. B. E. CONWAY, H. P. DHAR, and S. GOTTESFELD. J. Colloid Interface Sci. **43**, 303 (1973).
15. S. TRASATTI. J. Electroanal. Chem. **53**, 335 (1974).
16. O. IKEDA, K. KOGO, and H. TAMURA. J. Electroanal. Chem. **151**, 163 (1983).
17. J. TARASZJEWSKA. J. Electroanal. Chem. **49**, 443 (1974).
18. O. IKEDA, K. KOGO, and H. TAMURA. J. Electroanal. Chem. **95**, 177 (1979).
19. R. PEDRIALI and J. KÜTA. J. Electroanal. Chem. **52**, 395 (1974).
20. A. FRUMKIN. Z. Phys. **35**, 792 (1926).
21. B. DAMASKIN, O. PETRII, and V. BATRAKOV. Absorption of organic compounds on electrodes. Plenum Press, New York. 1971.
22. F. PULIDORI, G. BORGHESANI, R. PEDRIALI, A. DE BATTISTI, and S. TRASATTI. J. Chem. Soc. Faraday I, **74**, 79 (1978).
23. B. A. ABD EL-NABEY, A. DE BATTISTI, and S. TRASATTI. J. Electroanal. Chem. **56**, 101 (1974).
24. R. PARSONS. Proc. R. Soc. A, **261**, 79 (1961).
25. S. TRASATTI. J. Electroanal. Chem. **28**, 257 (1970).
26. P. NIKITAS, A. PAPPA-LOUISI, and D. JANNAKOUDAKIS. J. Electroanal. Chem. **162**, 175 (1984).

Can. J. Chem. Downloaded from www.nrcresearchpress.com by 186.148.149.217 on 09/07/12
For personal use only.

Solubility, enthalpy, and heat capacity of solution of tris(2,4-pentanedionato)cobalt(III) in aqueous mixed solvents of 2-butoxyethanol and 2-ethoxyethanol

YASUKI YOSHIMURA

Laboratory of Chemistry, College of Humanities and Social Sciences, Iwate University, Ueda, Morioka, 020 Japan

Received December 22, 1988[1]

YASUKI YOSHIMURA. Can. J. Chem. **67**, 2108 (1989).

The solubility in mole fraction X_s of tris(2,4-pentanedionato)cobalt(III) ($Co(acac)_3$) in aqueous mixtures of 2-butoxyethanol (BE) and 2-ethoxyethanol (EE) has been determined over the temperature range 5–50°C. From these data, the enthalpy ΔH_s^0 and heat capacity of solution $\Delta C_{p,s}^0$ of $Co(acac)_3$ are estimated by using the Clarke and Glew procedure. For the water–BE system, an approximately linear correlation is found between the excess enthalpy of solution $\delta\Delta H_s^0$ of $Co(acac)_3$ and the excess internal pressure δP_i of the mixtures at 25°C. This finding suggests that the composition dependence of ΔH_s^0 in this system is mostly governed by the composition dependence of P_i. On the other hand, $\Delta C_{p,s}^0$ in these mixtures exhibits a characteristic composition dependence and its composition dependence in the water–BE mixtures may be qualitatively explained by considering an effect of the microphase transition which has been shown to occur in the mixture. The composition dependence of both ΔH_s^0 and $\Delta C_{p,s}^0$ in the water–EE mixture is analogous to that in the water–BE mixture and this finding suggests that a microphase formation may also occur in the former mixture.

Key words: tris(2,4-pentanedionato)cobalt(III), temperature dependence of solubility, enthalpy and heat capacity of solution, aqueous mixtures of 2-butoxyethanol and 2-ethoxyethanol, microphase transition.

YASUKI YOSHIMURA. Can. J. Chem. **67**, 2108 (1989).

Opérant à des températures allant de 5 à 50°C, on a déterminé la solubilité, exprimée en fraction molaire X_s, du tris(2,4-pentanedionato)cobalt(III) ($Co(acac)_3$) dans des mélanges aqueux de 2-butoxyéthanol (BE) et de 2-éthoxyéthanol (EE). En se basant sur ces données et en utilisant la méthode de Clarke et Glew, on a évalué l'enthalpie, ΔH_s^0, ainsi que la capacité calorifique de solution du $Co(acac)_3$, $\Delta C_{p,s}^0$. Pour le système eau–BE, on a trouvé une corrélation approximativement linéaire entre l'excès d'enthalpie de solution du $Co(acac)_3$, $\delta\Delta H_s^0$, et l'excès de pression interne, δP_i, des mélanges à 25°C. Ces résultats suggèrent que la relation qui existe entre la composition et le ΔH_s^0 est déterminée principalement par la relation qui existe entre la composition et la P_i. Par ailleurs, le $\Delta C_{p,s}^0$ de ces mélanges présente une relation caractéristique avec la composition et, pour les mélanges eau–BE, on peut expliquer d'une façon qualitative la corrélation qui existe avec la composition en considérant un effet de la transition de la microphase qui se produit dans ce mélange. Pour le mélange eau–EE, la corrélation qui existe entre la composition et le ΔH_s^0 ainsi que le $\Delta C_{p,s}^0$ est analogue à celle qui a été observée avec le mélange eau–BE et ces données suggèrent qu'il y a aussi vraisemblablement formation d'une microphase dans ce mélange.

Mots clés : tris(2,4-pentanedionato)cobalt(III); relation entre la température et la solubilité; enthalpie et capacité calorifique de solution; mélanges aqueux de 2-butoxyéthanol et 2-éthoxyéthanol; transition de microphase.

[Traduit par la revue]

In the previous investigations (1, 2), the enthalpy ΔH_s^0 and heat capacity of solution $\Delta C_{p,s}^0$ of tris(2,4-pentanedionato)-cobalt(III) ($Co(acac)_3$) have been examined in mixtures of water and some organic solvents such as dimethyl sulfoxide (DMSO), 1,4-dioxane (D), and 2-methyl-2-propanol (TBA) and it has been found that the composition dependence of ΔH_s^0 and $\Delta C_{p,s}^0$ in the water–TBA mixtures, in which a microphase transition occurs at the TBA concentration range $0.045 < X_{TBA} < 0.16$ (X_{TBA} = mole fraction of TBA in the mixture) (3), differs characteristically from that in the water–DMSO and water–D mixtures. But the values for ΔH_s^0 and $\Delta C_{p,s}^0$ in the water–TBA mixtures were too uncertain to confirm an effect of the microphase transition because the temperature dependence of the solubility of $Co(acac)_3$ from which the values of ΔH_s^0 and $\Delta C_{p,s}^0$ were estimated could not be measured over a wide temperature range (2).

It has been confirmed by various techniques such as thermodynamic property measurements (4–6), ultrasonic methods (7–9), light scattering methods (10–12), surface properties (13, 14), and others (15, 16) that a microphase transition occurs in the mixture of water and 2-butoxyethanol (BE). Furthermore, the BE molecule is a member of the polyoxyethylene glycol monoalkyl ether $C_nH_{2n+1}O(CH_2CH_2O)_mH$ family of typical nonionic surfactants (17, 18). Thus, the solubility data of $Co(acac)_3$ in the water–BE mixture might be expected to give fundamental information about the solubilization phenomenon of metal chelates with surfactants.

In an examination of mixtures of water and *n*-alkoxyethanols, it has been reported that the microphase transition does not occur in the mixture of water and 2-ethoxyethanol (EE) (4, 7). Therefore, it is interesting to compare the composition dependence of ΔH_s^0 and $\Delta C_{p,s}^0$ of $Co(acac)_3$ in the water–BE mixtures with that in the water–EE mixtures.

Thus, in this study, the temperature dependence of the solubility of $Co(acac)_3$ in both the water–BE mixtures and the water–EE mixtures is determined over the temperature range 5 to 50°C. From these data ΔH_s^0 and $\Delta C_{p,s}^0$ of $Co(acac)_3$ are estimated and their composition dependences are discussed in connection with the microphase formation.

Experimental

Commercial BE and EE (reagent grade, Wako Chemical Industries Ltd.) were dried over molecular sieves (type 4A) for a week, filtered, refluxed over calcium hydride for a day, and then distilled twice under reduced pressure. The water content in the purified BE and EE, measured by Karl Fischer titration, was less than 0.05% by weight. These purified solvents were stored over molecular sieves (4A) in a dry box. The preparation of the mixed solvents, the purification of $Co(acac)_3$, and the solubility measurement were carried out by the same methods as described previously (1, 2).

Commercial *n*-dodecane (reagent grade, Wako Chemical Industries Ltd.) was stirred with fuming sulfuric acid for a day, washed with

[1]Revision received June 27, 1989.

Printed in Canada / Imprimé au Canada

Can. J. Chem. Downloaded from www.nrcresearchpress.com by 186.148.149.217 on 09/07/12
For personal use only.

dilute sodium hydroxide solution, then with water, dried over calcium hydride, and finally distilled twice under reduced pressure.

To examine whether $Co(acac)_3$ decomposes with addition of BE and EE or on heating, visible and UV absorption spectra of $Co(acac)_3$ were measured in mixed solvents of various compositions at 5, 25, and 45°C. Sample solutions for the absorption spectrum measurement were prepared as follows: in the visible absorption measurement, 5.2 mg of $Co(acac)_3$ was placed in a 5 cm^3 volumetric flask, the desired mixed solvents previously cooled at 5°C were added to the mark, and then $Co(acac)_3$ was completely dissolved by stirring with a magnetic stirrer at 5°C ($Co(acac)_3$ concentration ca. 2.9×10^{-3} mol dm^{-3}); in the UV absorption measurement, 0.125 cm^3 of aqueous solution of $Co(acac)_3$ of concentration 2.91×10^{-3} mol dm^{-3} was transferred with a syringe dispenser into a 10 cm^3 volumetric flask, and then the desired mixed solvents previously cooled at 5°C were added to the mark (ca. 3.6×10^{-5} mol dm^{-3}). As these flasks were not calibrated at 5°C, the concentration values were approximate. The sample solution prepared at 5°C was transferred into absorption cell and the absorption spectrum was recorded on a Shimadzu UV-160 Spectrophotometer equipped with a thermostat by using the blank solution not containing $Co(acac)_3$ as reference. In each run, the working temperature was elevated in the order of 5, 25, and 45°C and each sample solution in the absorption cell was placed in an incubator kept at the desired temperature for a day prior to the measurement.

The partition coefficient P of $Co(acac)_3$ between *n*-dodecane and water or DMSO was determined at 10, 25, and 50°C. The solution of $Co(acac)_3$ in water or DMSO of appropriate concentration and *n*-dodecane were placed in a centrifuge tube (5 cm^3 at 25°C) and then the mixture was equilibrated by stirring with a magnetic stirrer for 2 h in a thermostat kept at the desired temperature. Equilibrium concentration of $Co(acac)_3$ in the two phases was measured as follows: aliquots of the two phases were transferred separately into 5 cm^3 volumetric flasks previously weighed; after letting the flasks stand for 15 min at room temperature, they were again weighed, and then the respective solvents were added to the mark; in the system of DMSO–*n*-dodecane, the aliquots of the two phases allowed to stand at room temperature became turbid because of a decrease in the mutual solubility of the two liquids; to clarify the turbid *n*-dodecane aliquot, a small amount of chloroform was added; the concentration of $Co(acac)_3$ in mol dm^{-3} in these solutions was determined spectrophotometrically from the absorbances at 324 nm (in water), 322 nm (in *n*-dodecane), and 596 nm (in DMSO; since fairly high P value of $Co(acac)_3$ between DMSO and *n*-dodecane required high initial concentration of $Co(acac)_3$ in DMSO, the visible absorption band was used); the equilibrium concentration in mol kg^{-1} m was obtained by calculating the numbers of mole of $Co(acac)_3$ in the withdrawn aliquots from the above concentration values on the basis of the assumption that the volume of the flasks was strictly 5 cm^3 at 25°C. The P value was defined as a ratio of the m value in the water or DMSO phase to that in the *n*-dodecane phase.

Results

Absorption spectra of $Co(acac)_3$ in water–BE and water–EE mixtures

As a typical example, the UV spectra of $Co(acac)_3$ in BE at 5, 25, and 45°C are shown in Fig. 1. A feature of the spectrum at 45°C appears to be strong absorption of BE at the low wavelength. But, when the solution was cooled to 25°C, the spectrum at 25°C in Fig. 1 was not reproduced, that is, the absorption maxima at both 324 and 257 nm due to $Co(acac)_3$ disappeared and two distinct maxima were found at 284 and 226 nm. This maximum at 284 nm could be assigned to the absorption due to 2,4-pentanedione. Furthermore, UV spectra of $Co(acac)_3$ solutions in DMSO, D, TBA, and 1,2-ethanediol (EG) were examined and no change of the spectra on heating was observed. Thus, the spectra in Fig. 1 can be interpreted as showing that $Co(acac)_3$ decomposes at higher temperature in

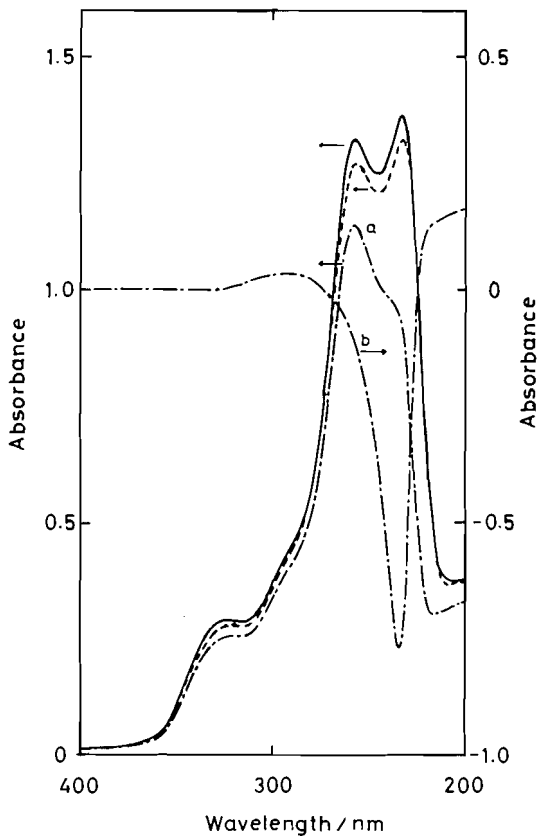


FIG. 1. Change of UV absorption spectra of $Co(acac)_3$ in BE: concentration of $Co(acac)_3$ is 3.6×10^{-5} mol dm^{-3}; — 5°C; - - - 25°C; –·–·– 45°C; *a*, after 1 day; *b*, after 3 days.

BE. A similar change of the UV spectra was found even in the mixture of the composition $X_{BE} = 0.15$ at 45°C.

A change of the spectra of $Co(acac)_3$ is not detectable at temperatures lower than 25°C (see Fig. 1). However, when $Co(acac)_3$ solution in BE was prepared at 25°C, its UV spectrum changed on standing at 25°C and was finally in accord with that at 45°C in Fig. 1. Thus $Co(acac)_3$ seems to decompose even at 25°C under this condition.

The visible spectra of $Co(acac)_3$ were little affected by both the addition of BE and heating except a slight decrease in absorbance. In order to make clearer whether $Co(acac)_3$ decomposed or not under the condition that its concentration was relatively high, the following study was made: the BE solution of $Co(acac)_3$, on which the visible spectrum was recorded at 45°C over 4 days, was diluted to 4.4×10^{-5} mol dm^{-3} with BE and then the UV spectrum was recorded at 25°C. An anomalous feature was not found in the spectrum thus obtained.

A change of the absorption spectra of $Co(acac)_3$ in the water–EE mixtures was similar to that in the water–BE mixtures mentioned above. On the basis of these results, at the present stage the following conclusions may be drawn: in the presence of BE or EE, $Co(acac)_3$ appears to decompose on heating in its dilute solution but the decomposition is not observed in its relatively concentrated solution; the decomposition seems to be an effect characteristic of the solvents BE or EE.

Solubility of $Co(acac)_3$ in water–BE and water–EE mixtures

On the basis of the above results of the absorption spectrum measurement, in the procedure of solubility measurement the

Can. J. Chem. Downloaded from www.nrcresearchpress.com by 186.148.149.217 on 09/07/12
For personal use only.

Can. J. Chem. Downloaded from www.nrcresearchpress.com by 186.148.149.217 on 09/07/12
For personal use only.

TABLE 1. Solubilities of $Co(acac)_3$ in BE and EE

	$S_m \times 10^2/(\text{mol kg}^{-1})$* in BE		$S_m \times 10^2/(\text{mol kg}^{-1})$* in EE	
T/°C	From 323 nm†	From 593 nm‡	From 323 nm†	From 593 nm‡
5	1.39±0.02	1.40±0.05	2.32±0.06	2.28±0.05
10	1.60±0.03	1.59±0.06	2.56±0.06	2.51±0.08
15	1.74±0.02	1.78±0.06	2.87±0.08	2.78±0.05
20	1.89±0.02	1.91±0.05	3.13±0.04	3.09±0.06
25	2.05±0.04	2.12±0.03	3.44±0.03	3.32±0.04
30	2.22±0.02	2.24±0.07	3.78±0.08	3.71±0.13
32.5	2.36±0.02	2.38±0.08	3.99±0.03	3.89±0.09
35	2.54±0.04	2.57±0.07	4.25±0.03	4.14±0.02
37.5	2.86±0.05	2.76±0.09	4.38±0.13	4.28±0.12
40	3.07±0.05	2.96±0.12	4.68±0.02	4.57±0.06
42.5			5.04±0.11	4.94±0.09
45			5.27±0.09	5.18±0.09
47.5			5.59±0.10	5.48±0.09
50			5.89±0.07	5.78±0.10
25§	2.10±0.07	2.14±0.07	3.42±0.06	3.32±0.05

*Errors denote 95% confidence levels.
†Solubility values obtained from absorbance at 323 nm.
‡Solubility values obtained from absorbance at 593 nm.
§Solubility values obtained by the experiment that the solutions equilibrated at the highest temperatures are allowed to attain equilibrium again at 25°C are listed.

mixed solvents cooled at 5°C were added to $Co(acac)_3$ placed in the apparatus.

The solubility of $Co(acac)_3$ in mol kg^{-1}, S_m,[2] in BE and EE is tabulated in Table 1, where the values calculated from the absorbance at both 324 and 593 nm are listed. In all cases, the two solubility values agree with each other within experimental errors which denote deviations of the 95% confidence levels from the mean values. Furthermore, the solubility data at 25°C were reproducible within the errors when the solutions at the end of experiment at the highest temperature were allowed to attain equilibrium at 25°C (see Table 1). These results, together with the results of the absorption spectrum measurement, confirm that any decomposition of $Co(acac)_3$ in the course of the equilibration may be ignored at these relatively more concentrated conditions.

The values for S_m of $Co(acac)_3$ in the water–BE and water–EE mixtures are listed in Tables 2 and 3, respectively. The errors were less than 3% in most cases.

The S_m values were converted to solubilities in mole fraction X_s and $\ln X_s$ was plotted against $1/T$. Typical plots are shown for the water–BE and water–EE mixtures in Figs. 2 and 3, respectively. To better define the solubility curves, solubility values measured at temperatures other than those listed in Tables 2 and 3 are also plotted in these figures. One feature of the solubility curves in the present mixtures differs from that in the mixtures reported previously, that is, while the latter solubility curves become practically linear in mixtures with higher contents of the organic solvents (1, 2), the former curves show marked curvature at about 30°C even in the pure BE and EE.

[2]An aliquot of the saturate solution withdrawn by weight was diluted with water and the concentration of $Co(acac)_3$ in this solution was analyzed spectrophotometrically. The S_m values were obtained by calculating the mole numbers of $Co(acac)_3$ in the aliquot from this concentration. The detailed procedure to calculate the S_m value has been described in ref. 1.

Enthalpy and heat capacity of solution of $Co(acac)_3$ in water–BE and water–EE mixtures

The values for ΔH_s^0 and $\Delta C_{p,s}^0$ were estimated by using the Clarke and Glew procedure for the estimation of thermodynamic parameters and their errors from solubility data (19, 20). The values of $R \ln X_s$ ($R = 8.3144\ \text{J mol}^{-1}\text{K}^{-1}$) were fitted to

$$[1] \quad R \ln X_s = a_0 u_0(x) + a_1 u_1(x) + a_2 u_2(x) + a_3 u_3(x) + \cdots$$

where $x = (T - \theta)/\theta$ (θ in K is a reference temperature), $a_0 = -\Delta G_s^0(\theta)/\theta$ (ΔG_s^0 denotes the free energy of solution), $a_1 = \Delta H_s^0(\theta)/\theta$, $a_2 = \Delta C_{p,s}^0(\theta)$, $a_3 = [\partial \Delta C_{p,s}^0/\partial T]_\theta \theta/2$ (the subscript θ in parentheses denotes the value of the function at θ), $u_0(x) = 1$, $u_1(x) = x/(1 + x)$, $u_2(x) = -x/(1 + x) + \ln(T/\theta)$, and $u_3(x) = x(x + 2)/(1 + x) - 2\ln(T/\theta)$.

In the analysis of the present data, it was found by a test on the basis of a t_5 value that the fifth constant in [1] is zero with a 95% probability. The t-test was as follows: the t_5 value for the fifth constant was calculated by dividing the value of the constant by the square root of its variance; the t_5 value was compared with the t value at the 95% confidence level and if $t_5 < t$, the value of the fifth constant may be taken as zero within the 95% probability. Thus [1] may be terminated at the fourth term.

The composition profile of ΔH_s^0 of $Co(acac)_3$ in the water–BE and water–EE mixtures is shown in Figs. 4 and 5, respectively, where the values of ΔH_s^0 at 10, 25, and 40°C are plotted against X_{BE} or X_{EE}. The profile is represented by drawing smooth curves through the experimental points because of the uncertainty in the ΔH_s^0 values obtained by the above indirect procedure.

The composition profile of $\Delta C_{p,s}^0$ of $Co(acac)_3$ in the water–BE and water–EE mixtures is shown in Fig. 6, where only the $\Delta C_{p,s}^0$ values at 25°C are plotted because the errors of the $\Delta C_{p,s}^0$ values are markedly large in the vicinity of the extremes of the temperature range used in the solubility measurement (19). The composition profile of $\Delta C_{p,s}^0$ passes through a minimum in the present mixtures and differs distinctly

TABLE 2. Solubilities of $Co(acac)_3$ in water–BE mixtures

	$S_m \times 10^2/(\text{mol kg}^{-1})$* when X_{BE} =						
T/°C	0.0049	0.0100	0.0200	0.0472	0.0751	0.1200	0.1990
5	0.748±0.004	0.748±0.016	0.725±0.010	0.968±0.020	1.23±0.03	1.37±0.03	1.54±0.04
10	0.671±0.008	0.690±0.011	0.710±0.011	0.984±0.011	1.32±0.01	1.46±0.03	1.62±0.02
15	0.608±0.004	0.651±0.009	0.704±0.006	1.03 ±0.02	1.44±0.02	1.53±0.04	1.76±0.03
20	0.561±0.006	0.621±0.001	0.707±0.004	1.09 ±0.02	1.54±0.03	1.65±0.04	1.94±0.06
25	0.526±0.010	0.607±0.009	0.719±0.005	1.15 ±0.02	1.63±0.02	1.82±0.02	2.16±0.01
30	0.511±0.007	0.593±0.010	0.735±0.005	1.22 ±0.01	1.71±0.03	2.03±0.06	2.48±0.04
35	0.482±0.010	0.582±0.004	0.756±0.008	1.31 ±0.03	1.81±0.04	2.30±0.04	2.85±0.06
40	0.464±0.002	0.564±0.010	0.779±0.016	1.42 ±0.01	1.98±0.05	2.57±0.04	3.28±0.07
45	0.447±0.005	0.557±0.009	0.825±0.008	1.54 ±0.04	2.32±0.05	3.09±0.07	3.84±0.05
50	0.419±0.016	0.541±0.006	0.857±0.014			3.73±0.13	4.54±0.07

	$S_m \times 10^2/(\text{mol kg}^{-1})$* when X_{BE} =					
T/°C	0.2999	0.4000	0.4999	0.5999	0.7500	0.8997
5	1.89±0.04	1.86±0.04	1.73±0.04	1.75±0.05	1.60±0.04	1.42±0.03
10	2.04±0.06	1.95±0.04	1.86±0.03	2.01±0.03	1.78±0.04	1.54±0.03
15	2.19±0.07	2.17±0.05	2.04±0.03	2.09±0.06	1.88±0.01	1.69±0.05
20	2.38±0.06	2.42±0.07	2.24±0.05	2.30±0.02	1.99±0.05	1.86±0.04
25	2.59±0.08	2.58±0.03	2.52±0.09	2.54±0.06	2.23±0.04	2.02±0.03
30	2.85±0.03	2.95±0.02	2.88±0.01	2.77±0.02	2.46±0.05	2.26±0.02
35	3.36±0.10	3.51±0.02	3.45±0.04	3.29±0.06	2.73±0.03	2.61±0.05
40	4.03±0.10	4.14±0.16	4.04±0.11	3.87±0.07	3.17±0.08	2.95±0.10
45	4.77±0.05	4.88±0.13	4.75±0.10	4.61±0.11	3.67±0.04	3.37±0.08
50	5.61±0.08	5.60±0.18	5.57±0.12	5.43±0.08	4.24±0.10	3.73±0.09

*Errors denote 95% confidence levels.

TABLE 3. Solubilities of $Co(acac)_3$ in water–EE mixtures

	$S_m \times 10^2/(\text{mol kg}^{-1})$* when X_{EE} =					
T/°C	0.0102	0.0224	0.0500	0.1000	0.1494	0.2000
5		0.651±0.013	0.536±0.010	0.602±0.013	0.759±0.019	0.964±0.020
10	0.629±0.012	0.640±0.010	0.575±0.011	0.715±0.018	0.870±0.023	1.15 ±0.04
15	0.585±0.007	0.623±0.012	0.610±0.003	0.796±0.017	0.969±0.026	1.27 ±0.03
20	0.545±0.009	0.632±0.008	0.641±0.011	0.890±0.010	1.08 ±0.01	1.40 ±0.03
25	0.516±0.004	0.618±0.003	0.670±0.009	0.978±0.008	1.21 ±0.01	1.59 ±0.02
30	0.497±0.005	0.617±0.005	0.701±0.002	1.06 ±0.01	1.37 ±0.03	1.75 ±0.02
35	0.485±0.007	0.626±0.005	0.738±0.001	1.12 ±0.02	1.51 ±0.04	1.97 ±0.02
40	0.475±0.006	0.623±0.006	0.775±0.011	1.18 ±0.01	1.62 ±0.03	2.22 ±0.04
45	0.470±0.011	0.606±0.015	0.807±0.016	1.25 ±0.03	1.84 ±0.05	2.46 ±0.04
50	0.463±0.002	0.610±0.011	0.833±0.018	1.31 ±0.02	2.10 ±0.03	2.83 ±0.07

	$S_m \times 10^2/(\text{mol kg}^{-1})$* when X_{EE} =				
T/°C	0.2998	0.4001	0.5003	0.6967	0.8506
5	1.44±0.05	1.81±0.05	1.78±0.05	2.11±0.07	2.48±0.06
10	1.61±0.03	2.04±0.05	2.01±0.05	2.34±0.03	2.69±0.06
15	1.76±0.05	2.21±0.05	2.23±0.06	2.63±0.04	2.86±0.01
20	1.96±0.02	2.43±0.05	2.56±0.06	2.86±0.05	3.07±0.04
25	2.18±0.04	2.71±0.03	2.79±0.03	3.15±0.02	3.37±0.04
30	2.41±0.02	3.05±0.08	3.17±0.06	3.53±0.06	3.66±0.05
35	2.71±0.02	3.40±0.05	3.54±0.08	4.02±0.03	4.05±0.03
40	3.02±0.10	3.79±0.06	4.01±0.05	4.54±0.07	4.51±0.09
45	3.46±0.08	4.36±0.01	4.64±0.10	5.09±0.10	5.03±0.08
50	4.00±0.04	4.99±0.09	5.28±0.16	5.84±0.16	5.67±0.14

*Errors denote 95% confidence levels.

Can. J. Chem. Downloaded from www.nrcresearchpress.com by 186.148.149.217 on 09/07/12
For personal use only.

Can. J. Chem. Downloaded from www.nrcresearchpress.com by 186.148.149.217 on 09/07/12
For personal use only.

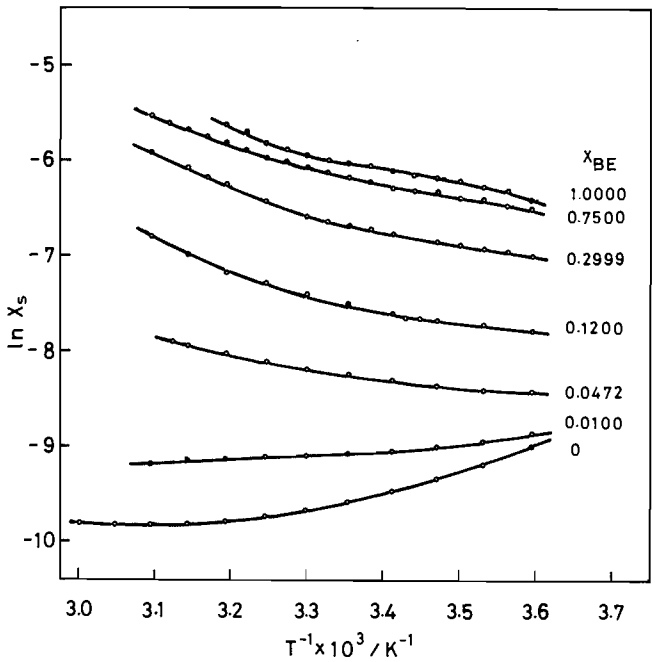


FIG. 2. Typical plot of ln X_s vs. $1/T$ for $Co(acac)_3$ in water–BE mixtures.

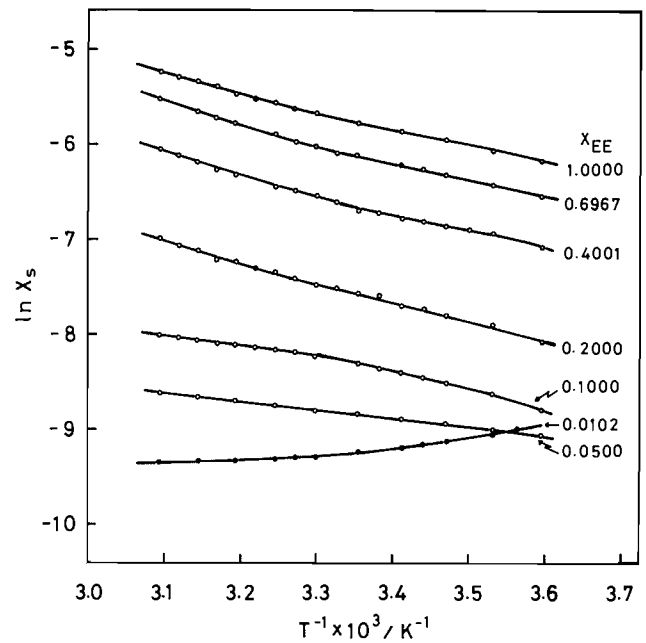


FIG. 3. Typical plot of ln X_s vs. $1/T$ for $Co(acac)_3$ in water–EE mixtures.

from that in the water–DMSO (1) and water–D mixtures (2) but resembles that in the water–TBA mixtures (2).

Discussion

To examine the validity of the assumption that the activity coefficient of $Co(acac)_3$ in its saturate solution is unity, the partition coefficient P of $Co(acac)_3$ between water or DMSO and *n*-dodecane was determined at 10, 25, and 50°C. The P values are plotted against the initial concentration of $Co(acac)_3$ in water or DMSO in Fig. 7, where the ratio of the S_m values in water or DMSO to those in *n*-dodecane is also plotted. The

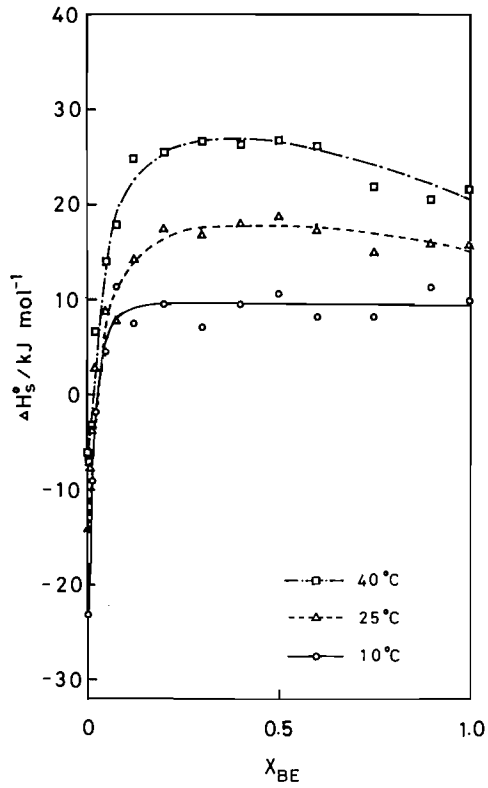


FIG. 4. Composition profiles of enthalpy of solution ΔH_s^0 of $Co(acac)_3$ at 10, 25, and 40°C in water–BE mixtures.

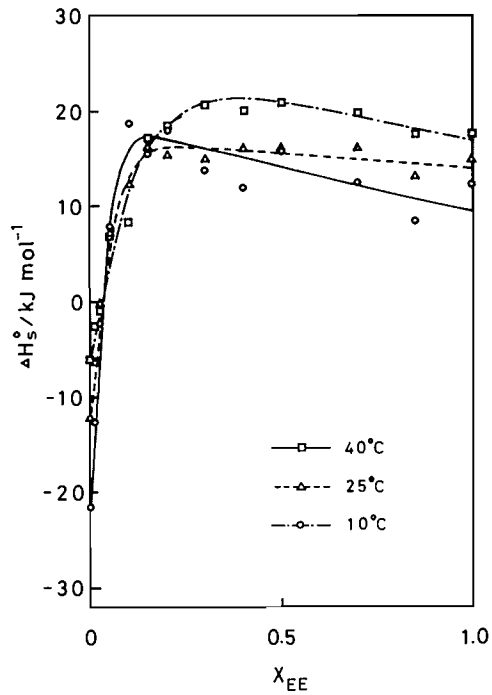


FIG. 5. Composition profiles of enthalpy of solution ΔH_s^0 of $Co(acac)_3$ at 10, 25, and 40°C in water–EE mixtures.

P values were little affected by the initial concentration of $Co(acac)_3$ and agreed nearly with the ratio of the S_m values except water–*n*-dodecane system at 10°C. This finding confirms that the activity coefficient of $Co(acac)_3$ in its saturate solution in water or DMSO may be regarded as unity.

The P values between the water–EE mixture of $X_{EE} = 0.1$

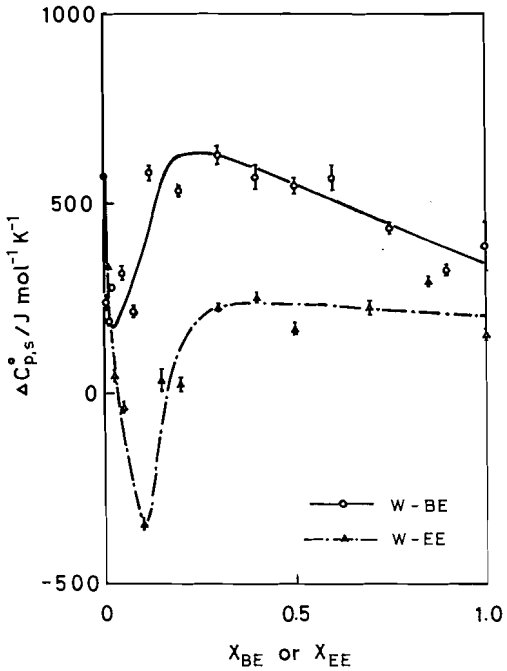


FIG. 6. Composition profiles of heat capacity of solution $\Delta C^0_{p,s}$ of $Co(acac)_3$ at 25°C in water–BE and water–EE mixtures.

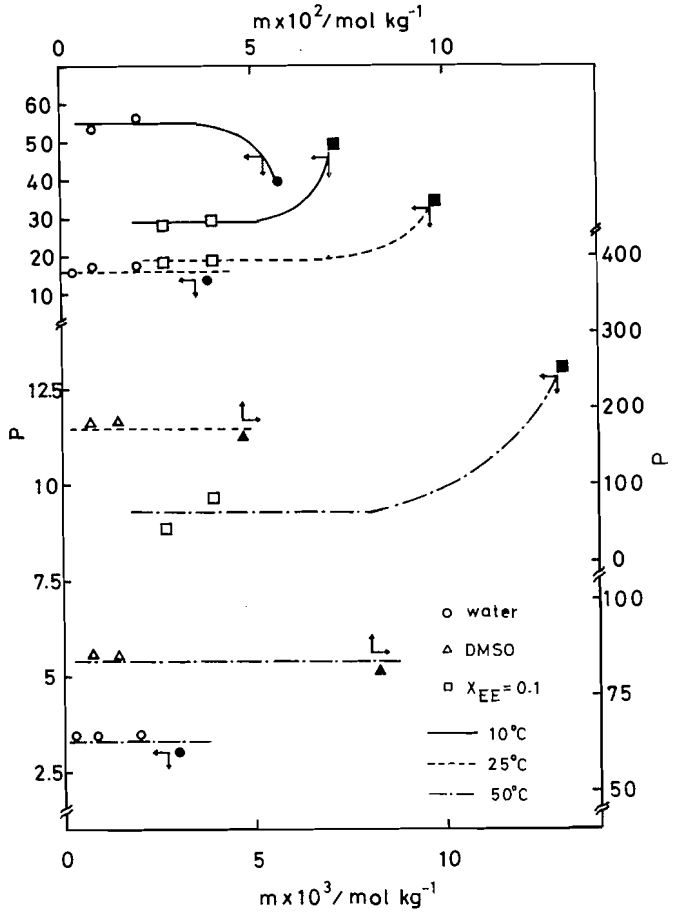


FIG. 7. Concentration dependence of partition coefficient P of $Co(acac)_3$ between n-dodecane and water or DMSO or aqueous EE mixture of $X_{EE} = 0.1$ at 10, 25, and 50°C: the P values were obtained by dividing the concentration in mol kg^{-1} of $Co(acac)_3$ in aqueous or DMSO phase by that in n-dodecane phase; full symbols denote the ratio of S_m of $Co(acac)_3$ in water or DMSO or $X_{EE} = 0.1$ mixture to that in n-dodecane.

and n-dodecane were significantly lower than the ratio of the S_m values (see Fig. 7). This trend was more pronounced for the P values between the water–EE mixture of $X_{EE} = 0.5$ and n-dodecane. EE is completely miscible with n-dodecane. Actually, it was found that in the case of the mixture with $X_{EE} = 0.5$, n-dodecane was considerably transferred into the aqueous EE phase. Therefore, the above results in the aqueous EE mixtures may be attributed to the dissolution of n-dodecane in the aqueous EE mixtures and/or to the dissolution of EE in n-dodecane. Thus, in the case of the aqueous mixtures of EE or BE it seems to be difficult to examine the assumption that the activity coefficient of $Co(acac)_3$ is unity. However, since the S_m values of $Co(acac)_3$ in EE and BE are lower than those in DMSO, in the present study the activity coefficient of $Co(acac)_3$ in its saturate solutions in the aqueous mixtures of BE and EE is tentatively regarded as unity.

Ito *et al.* (10) have analyzed their light scattering data in the water–BE mixtures by postulating the following aggregation equilibrium

$$[2]\quad A_{50} + B \rightleftarrows A_{50}B \rightarrow g(A_{50}B)$$
$$A_4 + B \rightleftarrows A_4B \rightarrow h(A_4B)$$
$$4A_{50} \rightleftarrows 50A_4$$

where A and B denote water and BE molecules, respectively and suggested the following picture for the mixing state in the mixtures. In the concentration range $X_{BE} < 0.02$, several water molecules encage a BE molecule and form a local structure of the type $A_{50}B$. In $0.02 < X_{BE} < 0.2$, these cagelike structures gather together and form a local structure of the type $g(A_{50}B)$. At the same time, BE molecules form a local structure of the type $h(A_4B)$. In this concentration range, $g(A_{50}B)$ is destroyed and the amount of $h(A_4B)$ increases with increasing BE concentration. For $0.2 < X_{BE}$, local structures of types $h'(A_4B)$ and B_1 are formed and the mixture again becomes homogeneous. Analogous pictures for the mixing state of the water–BE mixture have been suggested by numerous investigators (4, 6–9, 11). In these pictures, the microphase transition in $0.02 < X_{BE} < 0.2$ seems to be a phenomenon similar to the micellization of surfactants.

The thermodynamic properties of aqueous surfactant solutions have been satisfactorily explained by application of a mass action model (21–24). Roux *et al.* (22) found that the volume of transfer of surfactant from water to aqueous BE solution could also be explained in a similar manner. Elizalde *et al.* (14) have examined the composition dependence of surface tension in the aqueous BE solutions and found that the surface tension rapidly decreases to reach a constant value at about $X_{BE} = 0.02$. On the basis of this finding, they have also suggested that BE acts as a small-size surfactant.

The author has found that an approximately linear relationship exists between the excess enthalpy of solution $\delta\Delta H^0_s$ of $Co(acac)_3$ in the water–DMSO or water–D mixtures and the excess internal pressure δP_i of the mixtures (1, 2). The relationship is expressed by

$$[3]\quad \delta\Delta H^0_s = (\bar{V}_c - a^3 N\pi/6)(R/82.05)\delta P_i$$

where $\bar{V}_c$, a, and N are the partial molar volume of cavity formation, the hard-sphere diameter of solute, and the Avogadro number, respectively. The definition of $\delta\Delta H^0_s$ and δP_i was previously described (1, 2).

Can. J. Chem. Downloaded from www.nrcresearchpress.com by 186.148.149.217 on 09/07/12
For personal use only.

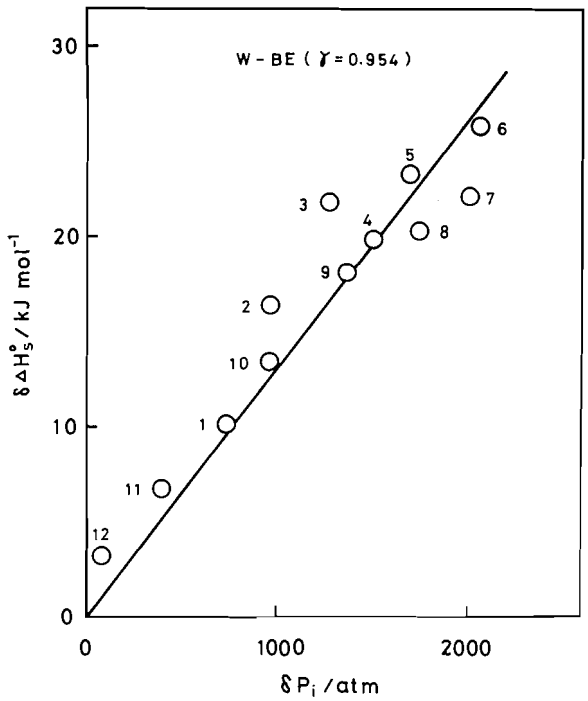


FIG. 8. Correlation between excess enthalpy of solution $\delta\Delta H_s^0$ of $Co(acac)_3$ and excess internal pressure δP_i at 25°C for water-BE mixtures: X_{BE} in the mixtures is as follows; *1*, 0.01; *2*, 0.02; *3*, 0.0472; *4*, 0.0751; *5*, 0.1; *6*, 0.199; *7*, 0.2999; *8*, 0.4; *9*, 0.4999; *10*, 0.5999; *11*, 0.75; *12*, 0.8997; γ is the correlation coefficient.

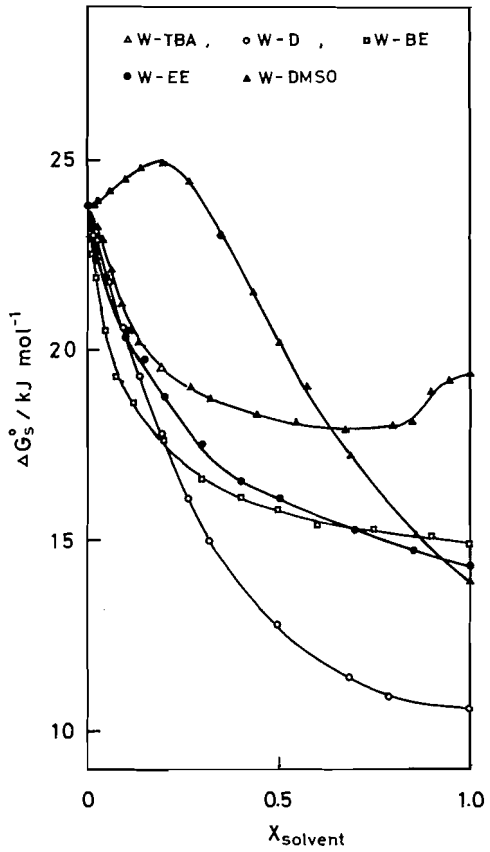


FIG. 9. Composition profiles of free energy of solution ΔG_s^0 of $Co(acac)_3$ at 25°C in mixtures of water and some organic solvents.

In Fig. 8, $\delta\Delta H_s^0$ of $Co(acac)_3$ is plotted against δP_i for the water–BE mixtures at 25°C. The $\delta\Delta H_s^0$ values were not calculated from the smooth curve in Fig. 4 but from the experimental ΔH_s^0 values. The P_i values of the mixtures were calculated by an ordinary procedure (25) from the literature data on the density and specific heat capacity values (4), and on the ultrasonic velocity values (5) of the mixtures. The P_i values of the water–EE mixtures could not be obtained because of lack of the data on the ultrasonic velocity.

Figure 8 shows that in the water–BE mixtures the linear relation expressed by [3] is approximately valid, though the correlation coefficient γ is slightly lower than that in the water–DMSO (γ = 0.980) or water–D mixtures (γ = 0.977). This finding suggests that even though the microphase transition occurs in water–BE mixtures, the composition dependence of ΔH_s^0 is mostly governed by the composition dependence of P_i, that is, of the enthalpy of cavity formation (1, 2) and that a contribution of the microphase formation to ΔH_s^0 is not distinguishable.

A serious difference between the composition profile of $\Delta C_{p,s}^0$ of $Co(acac)_3$ shown in Fig. 6 and that in the water–DMSO and water–D mixtures (1, 2) is that in the former profile the rapid decrease of $\Delta C_{p,s}^0$ is followed by the gradual increase. This difference seems to be assigned to the microphase transition as will be discussed.

It has been sufficiently confirmed that a shift in an equilibrium contributes to heat capacity (26–30). The $\Delta C_{p,s}^0$ of $Co(acac)_3$ in the water–BE mixtures goes through a minimum in the concentration region where the microphase transition occurs as mentioned above. It seems likely that an addition of $Co(acac)_3$ to the water–BE mixture brings about an effect on an aggregation equilibrium of BE.

By analogy to the treatment of Jolicoeur *et al.* (27), the contribution of the effect to ΔH_s^0 of $Co(acac)_3$ may be expressed by

$$[4] \quad \Delta H_s^0 = \Delta H_{s(hyp)}^0 + \Delta\alpha\Delta H_{ag}$$

where $\Delta H_{s(hyp)}^0$, ΔH_{ag}, and $\Delta\alpha$ denote ΔH_s^0 in the hypothetical water–BE mixtures without the microphase formation, the enthalpy of aggregation formation, and a change in the fraction of aggregated BE produced by the addition of $Co(acac)_3$, respectively. By differentiating [4] with respect to temperature, $\Delta C_{p,s}^0$ can be expressed as

$$[5] \quad \Delta C_{p,s}^0 = \Delta C_{p,s(hyp)}^0 + \Delta\alpha\Delta C_{p,ag} + \Delta H_{ag}(\partial\Delta\alpha/\partial T)_p$$

where the subscripts are the same notation as [4].

Hetu *et al.* have examined the transfer functions of some solutes from water to aqueous surfactant solutions and concluded that trends in the transfer functions could be predicted from the relative hydrophobicity of the solutes and surfactants (31, 32). They have also shown that when the solutes displace a monomer–micelle equilibrium of the surfactants, the transfer heat capacity goes through a minimum. On the other hand, an equilibrium displacement due to temperature generally seems to lead to a maximum (27, 29, 30).

Thus, if it is assumed that $\Delta C_{p,s(hyp)}^0$ decreases monotonously with X_{BE} similarly to $\Delta C_{p,s}^0$ in the water–DMSO and water–D mixtures (1, 2), the minimum shown in Fig. 6 may be produced from the second term in [5]. Unfortunately, the information about the displacement of the aggregation equilibrium of BE by $Co(acac)_3$ is lacking but it has been reported that the microphase formation in the water–BE mixtures occurs at a lower BE concentration in the presence of a surfactant (33, 34). Benzene exhibits a significant effect on the aggregation equilibrium of

Can. J. Chem. Downloaded from www.nrcresearchpress.com by 186.148.149.217 on 09/07/12
For personal use only.

BE (31). As $Co(acac)_3$ may also be regarded as a hydrophobic solute (1), it is reasonable to assume that $Co(acac)_3$ displaces the aggregation equilibrium of BE.

In connection with the solubilization phenomenon of metal chelates with surfactants (35), the composition dependence of the solubility of $Co(acac)_3$ in the water–BE mixtures is interesting. Figure 9 shows the composition profile of ΔG_s^0 ($\Delta G_s^0 = -RT \ln X_s$) of $Co(acac)_3$ at 25°C for each mixture so far examined. A distinguishable feature of the profile in the water–BE mixture is recognized in the concentration region $X_{BE} < 0.2$: the solubility values of $Co(acac)_3$ in this region of the mixture are larger than those in other mixtures; in particular, it is worth noting that the solubility values in the water–BE and water–D mixtures reverse at $X_{solvent} = 0.2$. This finding also suggests that the microphase transition in the water–BE mixture brings about the increase of the solubility of $Co(acac)_3$ and that BE may exhibit an effect similar to surfactants (36). Since it has been reported that an addition of surfactants to the water–BE mixture results in the stabilization of the microaggregates of BE (9, 33, 34, 36, 37), it would be interesting to examine the solubility of $Co(acac)_3$ in a ternary system containing water, BE, and surfactant.

The composition profiles of both ΔH_s^0 and $\Delta C_{p,s}^0$ in the water–EE mixtures are practically identical with those in the water–BE mixtures (see Figs. 4, 5, and 6). These results suggest that microphase formation may also occur in the former mixture. But the magnitude of the microphase formation in the water–EE mixture seems to be considerably smaller than that in the water–BE mixture (11).

1. Y. Yoshimura, N. Sato, and M. Kikuchi. Bull. Chem. Soc. Jpn. **59**, 2135 (1986).
2. Y. Yoshimura. Can. J. Chem. **65**, 1218 (1987).
3. K. Iwasaki and T. Fujiyama. J. Phys. Chem. **81**, 1908 (1977); **83**, 463 (1979).
4. G. Roux, G. Perron, and J. E. Desnoyers. J. Solution Chem. **7**, 639 (1978).
5. J. Lara and J. E. Desnoyers. J. Solution Chem. **10**, 465 (1981).
6. N. P. Rao and R. E. Verrall. Can. J. Chem. **65**, 810 (1987).
7. S. Nishikawa, M. Tanaka, and M. Mashima. J. Phys. Chem. **85**, 686 (1981).
8. S. Nishikawa and K. Kotegawa. J. Phys. Chem. **89**, 2896 (1985).
9. S. Kato, D. Jobe, N. P. Rao, C. H. Ho, and R. E. Verrall. J. Phys. Chem. **90**, 4167 (1986).
10. N. Ito, T. Fujiyama, and Y. Udagawa. Bull. Chem. Soc. Jpn. **56**, 379 (1983).
11. T. Kato. J. Phys. Chem. **88**, 1248 (1984).
12. T. Kato. J. Phys. Chem. **89**, 5750 (1985).
13. R. Bennes, J. M. Douillard, M. Privat, and L. Tenebre. J. Phys. Chem. **89**, 1822 (1985).
14. F. Elizalde, J. Gracia, and M. Costas. J. Phys. Chem. **92**, 3565 (1988).
15. N. Ito, K. Saito, T. Kato, and T. Fujiyama. Bull. Chem. Soc. Jpn. **54**, 991 (1981).
16. O. Desrosiers, T. Van Dinter, and J. K. Saunders. Can. J. Chem. **62**, 56 (1984).
17. M. Corti and V. Degiorgio. J. Phys. Chem. **85**, 1442 (1981).
18. M. Alauddin and R. E. Verrall. J. Phys. Chem. **91**, 1802 (1987).
19. E. C. W. Clarke and D. N. Glew. Trans. Faraday Soc. **62**, 539 (1966).
20. S. F. Dec and S. J. Gill. J. Chem. Educ. **62**, 879 (1985).
21. J. E. Desnoyers, G. Caron, R. de Lisi, D. Roberts, A. Roux, and G. Perron. J. Phys. Chem. **87**, 1397 (1983).
22. A. H. Roux, D. Hetu, G. Perron, and J. E. Desnoyers. J. Solution Chem. **13**, 1 (1984).
23. R. de Lisi, V. T. Liveri, M. Castagnolo, and A. Inglese. J. Solution Chem. **15**, 23 (1986).
24. D. Hetu, A. H. Roux, and J. E. Desnoyers. J. Solution Chem. **16**, 529 (1987).
25. N. M. Murthy and S. V. Subrahmanyam. Indian J. Chem. **19A**, 724 (1980).
26. S. W. Benson. J. Am. Chem. Soc. **100**, 5640 (1978).
27. C. Jolicoeur, L. L. Lemelin, and R. Lapalme. J. Phys. Chem. **83**, 2806 (1979).
28. E. Grunwald. J. Am. Chem. Soc. **106**, 5414 (1984).
29. S. J. Gill, S. F. Dec, G. Olofsson, and I. Wadsö. J. Phys. Chem. **89**, 3758 (1985).
30. H. Naghibi, S. F. Dec, and S. J. Gill. J. Phys. Chem. **90**, 4621 (1986).
31. D. Hetu, A. H. Roux, and J. E. Desnoyers. J. Colloid Interface Sci. **122**, 418 (1988).
32. D. Hetu and J. E. Desnoyers. Can. J. Chem. **66**, 767 (1988).
33. G. Perron, R. de Lisi, I. Davidson, S. Genereux, and J. E. Desnoyers. J. Colloid Interface Sci. **79**, 432 (1981).
34. F. Quirion and L. J. Magid. J. Phys. Chem. **90**, 5193 (1986).
35. For example, see T. Tominaga, S. Muraoka, T. Ishii, and Y. Yamamoto. J. Solution Chem. **16**, 615 (1987).
36. S. Kato, D. Jobe, N. P. Rao, C. H. Ho, and R. E. Verrall. J. Phys. Chem. **92**, 4127 (1988).
37. N. P. Rao and R. E. Verrall. J. Phys. Chem. **86**, 4777 (1982).

Can. J. Chem. Downloaded from www.nrcresearchpress.com by 186.148.149.217 on 09/07/12
For personal use only.

Aryl-2 et alkyl-2 quinoléines nouvelles isolées d'une Rutacée bolivienne : *Galipea longiflora*

ALAIN FOURNET

Office de la recherche scientifique et technique d'outre-mer — Institut bolivien de biologie d'altitude, CP 824, La Paz, Bolivie

ET

BEATRICE VAGNEUR, PASCAL RICHOMME ET JEAN BRUNETON[1]

Centre d'études des plantes médicinales, Unité d'enseignement et de recherche des sciences médicales et pharmaceutiques, 16, Bd. Daviers, 49000-Angers, France

Reçu le 6 juin 1989

ALAIN FOURNET, BEATRICE VAGNEUR, PASCAL RICHOMME et JEAN BRUNETON. Can. J. Chem. **67**, 2116 (1989).

Cinq aryl-2 et alkyl-2 quinoléines nouvelles ont été isolées des écorces de tiges de *Galipea longiflora* Krause (Rutacées) : la phényl-2 quinoléine **1**, la (méthylènedioxy-3′,4′) phénéthyl-2 quinoléine **2**, la (diméthoxy-3′,4′) phénéthyl-2 quinoléine **3**, la (méthylènedioxy-3′,4′) styryle-2 méthoxy-4 quinoléine **4** et la (pentèn-1′,2′ yl)-2 méthoxy-4-quinoléine **6**. Ces alcaloïdes sont accompagnés de trois quinoléines substituées en 2, la *n*-amyl-2 méthoxy-4 quinoléine **5**, la (méthylènedioxy-3′,4′) phénéthyl-2 méthoxy-4 quinoléine (cusparine) **7** et la phényl-2 méthoxy-4 quinoléine **8**, et de deux furo[2,3*b*]quinoléines déjà connues, l'évolitrine et la skimmianine.

Mots clés : *Galipea longiflora*, Rutacées, quinoléines nouvelles.

ALAIN FOURNET, BEATRICE VAGNEUR, PASCAL RICHOMME, and JEAN BRUNETON. Can. J. Chem. **67**, 2116 (1989).

Five new 2-aryl and 2-alkyl quinoline alkaloids were obtained from *Galipea longiflora* Krause (Rutaceae). These are 2-phenylquinoline **1**, 2-(3′,4′-methylenedioxyphenethyl)quinoline **2**, 2-(3′,4′-dimethoxyphenethyl)quinoline **3**, 2-(3′,4′-methylenedioxystyryl)-4-methoxyquinoline **4**, and 2-(1′,2′-pentenyl)-4-methoxyquinoline **6**. They are accompanied by three known 2-substituted quinolines, 2-*n*-amyl-4-methoxyquinoline **5**, 2-(3′4′-methylenedioxyphenethyl)-4-methoxyquinoline **7**, and 2-phenyl-4-methoxyquinoline **8**, and by two known furo[2,3*b*]quinoline alkaloids: evolitrine and skimmianine.

Key words: *Galipea longiflora*, Rutaceae, new quinolines.

[Traduit par la revue]

Poursuivant l'étude de drogues végétales de l'Amazonie andine traditionnellement utilisées dans le traitement de diverses affections parasitaires (3) nous décrivons dans le présent travail l'isolement, à partir de *Galipea longiflora*, de quinoléines simples non encore décrites à ce jour à partir de sources naturelles.

Le genre *Galipea* Aubl. comprend plus de 20 espèces, toutes localisées en Amérique du Sud; parmi celles-ci seul *G. officinalis* Hancock.(= *G. cusparia* St Hill) a fait l'objet d'une étude chimique (4). *Galipea longiflora* Krause (5) est un grand arbre à longues feuilles trifoliolées localisé dans la partie de la forêt amazonienne commune au Sud du Brésil et au Nord-Est de la Bolivie. Les écorces de tiges brunâtres de la plante sont localement utilisées par voie orale pour le traitement d'affections liées à divers parasites. Il nous a donc semblé intéressant d'en étudier la composition.

La présente étude a conduit à l'isolement et à l'identification de dix alcaloïdes quinoléiques. Cinq étaient déjà connus : deux furo[2,3-*b*]quinoléines, la skimmianine (réf. 2) (7% des A.T.) et l'évolitrine (réf. 1) (0,1%) isolées à plusieurs reprises de nombreux genres de Rutacées (6), une alkyl-2 quinoléine, la *n*-amyl-2 méthoxy-4 quinoléine **5** (0,4%) anciennement caractérisée chez *Galipea officinalis* (4) ainsi que deux autres quinoléines substituées en 4, la (méthylènedioxy-3′,4′) phénéthyl-2 méthoxy-4 quinoléine **7** (0,6%) décrite sous le nom de cusparine chez le même *G. officinalis* et la phényl-2 méthoxy-4 quinoléine **8** (1,5%) déjà connue chez *Lunasia amara* (7). Tous ces composés connus — et pour certains synthétisés — ont été identifiés par comparaison de leurs constantes physiques et de leurs données spectrales avec celles préalablement publiées.

Les données de rmn à haut champ et de spectrométrie de masse absentes de la littérature ont été déterminées et sont énumérées autour des formules (cf. tableau 1) et dans la partie expérimentale.

Le composé majoritaire **1** (54,4%) cristallise de l'hexane. Sa formule brute : $C_{15}H_{11}N$ (calc.: 205,0890; tr.: 205,0864) et l'absence, sur le spectre de rmn ^1H, de signaux en dessous de 7,3 ppm indiquent que **1** doit être une phényl quinoléine. La preuve finale de la structure de **1**, jamais isolé à l'état naturel, est apportée par la comparaison directe avec le produit de synthèse (Aldrich).

La formule du composé **2** (13,6%, PF = 65°C) s'établit en $C_{18}H_{15}NO_2$ (calc.: 277,1103; tr.: 277,1112). Le spectre de rmn ^1H ($CDCl_3$, 300 MHz, tableau 1) est caractéristique d'un dérivé quinoléique substitué en 2 par un groupement de type phénéthylique puisque deux multiplets de deux protons aliphatiques chacuns apparaissent à 3,07 et 3,23 ppm tandis que trois protons aromatiques résonnent à 6,66 (dd; J_m = 1,3 Hz, J_o = 7,9 Hz), 6,70 (d; J_o = 7,9 Hz) et 6,75 ppm (d; J_m = 1,3 Hz). Les déplacements chimiques des protons quinoléiques sont à leurs valeurs hatituelles, entre 7,4 et 8,1 ppm, et l'attribution des signaux à 7,75 et 8,06 ppm — respectivement au H-5 et au H-8 — peut être effectuée sans ambiguïté après observation d'effets Overhauser réciproques entre le H-4 et le H-5 d'une part, le H-5 et le H-6 d'autre part. Un singulet de deux protons à 5,89 ppm permet finalement d'identifier le substituant situé en α de l'azote à un groupement (méthylènedioxy-3,4) phénéthyle, ce qui confirme sur le spectre de masse la présence d'un fragment intense (75%) à *m/z* 135 ($C_8H_7O_2^+$). Ce composé original est ainsi identifié à la (méthylènedioxy-3′,4′) phénéthyl-2 quinoléine.

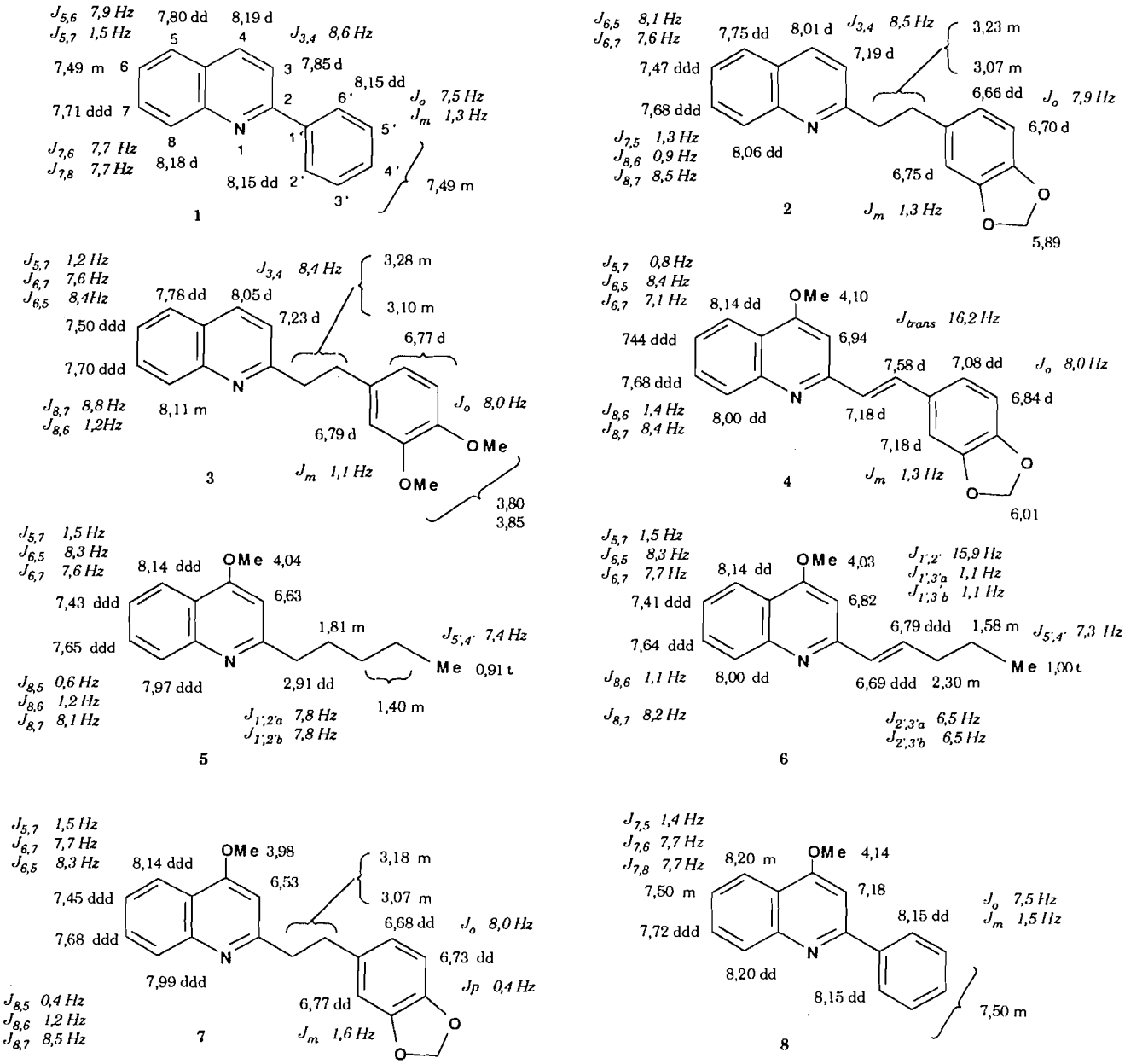
Le spectre de masse du composé suivant **3** (0,9%), ($C_{19}H_{19}NO_2$; calc.: 293,1416; tr.: 293,1406), est voisin de celui du dérivé précédent et semble indiquer que le noyau quinoléique n'est substitué qu'en position 2 par un groupement

[1]Auteur à qui adresser toute correspondance.

Printed in Canada / Imprimé au Canada

Can. J. Chem. Downloaded from www.nrcresearchpress.com by 186.148.149.217 on 09/07/12
For personal use only.

TABLEAU 1. RMN ^{1}H des aryl-2 et alkyl-2 quinoléines isolées de *Galipea longiflora*.



(diméthoxy-3,4) phénéthyle, le pic de base étant ici déplacé à m/z 151 ($C_9H_{11}O_2^+$). La rmn ^{1}H ($CDCl_3$, 300 MHz, tableau 1) confirme cette hypothèse puisque le spectre enregistré se révèle superposable avec celui de **2** à ceci près que le signal du méthylènedioxyle apparaissant à 5,89 est remplacé par deux singulets de trois protons chacuns à 3,85 et 3,80 ppm qui correspondent donc aux deux méthoxyles phénéthyliques. Ces résultats permettent alors d'attribuer à cette nouvelle quinoléine une structure de (diméthoxy-3',4') phénéthyl-2 quinoléine.

Le composé **4** (0,7%), ($C_{19}H_{15}NO_3$; calc.: 305,1052; tr.: 305,1031), présente un spectre de rmn ^{1}H ($CDCl_3$, 300 MHz, tableau 1) caractéristique d'une quinoléine disubstituée-2,4 : un méthoxyle en position 4 apparaît ainsi très déblindé à 4,10 ppm tandis qu'un groupement de type (méthylènedioxyle-3,4) styrylique est caractérisé par deux doublets de un proton chacun à 7,18 et 7,58 ppm (J = 16,2 Hz), trois signaux d'hydrogènes aromatiques à 6,84 (1H, d, J_o = 8,0 Hz), 7,08 (1H, dd, J_o = 8,0 Hz, J_m = 1,3 Hz) et 7,18 ppm (1H, d, J_m = 1,3 Hz) et le singulet d'un méthylènedioxyle localisé à 6,01 ppm. Les attributions des protons quinoléiques découlent d'une comparaison directe de ce spectre avec celui d'un dérivé connu, la *n*-amyl-2 méthoxy-4 quinoléine, **5**, pour lequel un effet Overhauser est enregistré entre le H-5 et le MeO-4 et dont une expérimentation de type COSY LR permet notamment de corréler le H-5 et le H-3. **4** est ainsi identifié à un nouveau dérivé naturel, la (méthylènedioxy-3',4') styryle-2 méthoxy-4 quinoléine.

Divers éléments sur le spectre de rmn ^{1}H ($CDCl_3$, 300 MHz, tableau 1) du dernier composé **6** (2,5%), ($C_{15}H_{17}NO$, calc.: 227,1301; tr.: 227,1312), peuvent être attribués à la présence

Can. J. Chem. Downloaded from www.nrcresearchpress.com by 186.148.149.217 on 09/07/12
For personal use only.

Can. J. Chem. Downloaded from www.nrcresearchpress.com by 186.148.149.217 on 09/07/12
For personal use only.

d'un groupe pentèn-1,2 yle au sein de la molécule. Deux protons éthylèniques apparaissent en effet à 6,69 (1H, ddd, $J_{1',2'} = 15,9$ Hz, $J_{1',3'a} = 1,1$ Hz, $J_{1',3'b} = 1,1$ Hz) et 6,79 ppm (1H, ddd, $J_{2',1'} = 15,9$ Hz, $J_{2',3'a} = 6,5$ Hz, $J_{2',3'b} = 6,5$ Hz), deux protons méthylèniques à 1,58 (2H, m) et 2,30 ppm (2H, m), tandis qu'un méthyle résonne sous forme de triplet ($J_{5',4'} = 7,3$ Hz) à 1,00 ppm. L'étude de la séquence de substitution du noyau quinoléique montre que cette chaîne pentènylique est placée en position 2 puisqu'un méthoxyle substituant le C-4 apparaît à 4,03 ppm et que les attributions des protons aromatiques de l'hétérocycle peuvent découler d'un raisonnement analogue à celui précédemment décrit. La spectrométrie de masse confirme finalement la structure envisagée par la présence d'ions fragments à m/z 212 ($[M - CH_3]^+$, 75%) et m/z 200 ($[M - C_2H_5]^+$, 16%). Ce composé original est donc la (pentèn-1',2' yl)-2 méthoxy-4 quinoléine.

La composition de cette espèce n'apparaît donc pas fondamentalement différente de celles des espèces du même genre ou de genres voisins tels que les *Lunasia* (4). Le nombre de *Galipea* ayant à l'heure actuelle fait l'objet d'études phytochimiques exhaustives apparaît cependant insuffisant pour pouvoir comparer, sur des critères chimiotaxonomiques, ce genre aux autres membres des Rutacées.

Partie expérimentale

Appareillage

Les points de fusion sont mesurés en tube capillaire et ne sont pas corrigés. Les spectres sont enregistrés sur les appareils suivants: uv, Beckman 530, éthanol (λ_{max}, (log ϵ)); ir, Perkin–Elmer 580, KBr (ν cm^{-1}); spectres de rmn ^1H et ^{13}C, Bruker AM 300, $CDCl_3$ (δ ppm, TMS = 0); spectres de masse, Varian MAT 311 (m/z (%)). Les chromatographies sur colonnes sont réalisées sur Kieselgel 60 (Merck 7734) ou 60 H (Merck 7736), et les ccm sur DC Alufolien 60 F 254 (Merck 5554).

Matériel végétal

Les écorces de tiges de *G. longiflora* ont été récoltées à Fatima de Chimane (Alto Beni, Bolivie) le 08-09-1987 et sont référencés sous le n° A.F. 790 dans l'herbier de référence du centre ORSTOM de La Paz.

Extraction et isolement des alcaloïdes

La drogue pulvérisée (1 kg) est épuisée par l'hexane en milieu neutre dans un appareil de Soxhlet; après distillation sous pression réduite de l'hexane on obtient un résidu de 22,4 g contenant essentiellement des alcaloïdes peu polaires (ccm). La poudre séchée est ensuite extraite selon un procédé classique (alcalinisation du marc suivi d'une extraction par le chloroforme et d'une purification par passage à l'état de sels) : le rendement en alcaloïdes totaux est de 0,2%; l'analyse en ccm montre que ces A.T. ne sont pas différent du résidu provenant de l'extraction préliminaire par l'hexane. Le fractionnement des alcaloïdes totaux est obtenu par chromatographie sur colonne de silice pour ccm : solvant hexane – acétate d'éthyle 85 : 15. La purification des différents constituants est obtenue par ccm préparative (support : silice; solvant : hexane – acétate d'éthyle 90 : 10, benzène – acétate d'éthyle 95 : 5, chloroforme–benzène–méthanol–ammoniac 50 : 50 : 0,5 : vap.) ou, quand cela est possible, par cristallisation.

Descripiton des produits isolés

Les constantes physiques et données spectrales des composés antérieurement décrits ne seront pas redonnées ici. Les alcaloïdes furoquinoléiques ont été identifiés par comparaisons avec des échantillons authentiques. Les données spectrales mesurées pour les alcaloïdes **5**, **7** et **8** sont en bon accord avec celles de la bibliographie.

Description des alcaloïdes nouveaux isolés

Phényl-2 quinoléine **1**, PF 84°C (hexane); uv : 208 (4,49), 255 (4,56), 321 (2,84); sm m/z : 205, M^+ (100), 203 (59), 102 (12).

(Méthylènedioxy-3',4') phénéthyl-2 quinoléine **2**, PF 65°C (méthanol); uv : 205 (4,59), 227 (4,58), 300 (3,66), 314 (3,51); sm m/z : 277 M^+ (99), 276 (100), 156 (18), 135 (75), 129 (15).

(Diméthoxy-3',4') phénéthyl-2 quinoléine **3**, amorphe; uv : 206 (4,59), 228 (4,57), 256 (3,74), 276 (3,79), 302 (3,58) 315, (3,55); sm m/z : 293, M^+ (81), 292 (40), 278 (36), 156 (15), 152 (10), 151 (100), 129 (11).

(Méthylènedioxy-3',4') styryle-2 méthoxy-4 quinoléine **4**, amorphe; uv : 206 (4,12), 236 (4,08), 250 (4,00), 285 (3,95), 310 (3,92), 344 (4,21); sm m/z : 305, M^+ (79), 304 (100), 290 (47), 289 (26), 274 (35), 262 (13), 261 (12), 232 (17), 204 (11), 202 (8).

(Pentèn-1',2' yl)-2 méthoxy-4 quinoléine **6**, amorphe; uv : 230 (4,41), 250 (4,47), 289 (3,87); sm m/z : 227 M^+ (98), 212 (75), 199 (100), 198 (93), 184 (19), 173 (39), 154 (39).

Spectres de masse des produits connus (non décrits précédemment)

n-Amyl-2 méthoxy-4 quinoléine **5**, sm m/z : 299, M^+ (2,5), 200 (14), 186 (21), 174 (12), 173 (100), 130 (10).

(Méthylènedioxy-3',4') phénéthyl-2 méthoxy-4 quinoléine (= cusparine) **7**, sm m/z : 307 (100), 306 (56), 292 (41), 186 (36), 159 (24), 135 (32).

Phényl-2 méthoxy-4 quinoléine **8**, sm m/z : 235 (100), 234 (38), 206 (26), 205 (34), 204 (28), 191 (7), 165 (8), 143 (10).

1. M. T. Fauvel, J. Gleye, C. Moulis, F. Blasco et E. Stanislas. Phytochemistry, **20**, 2059 (1981).
2. A. Ahond, F. Picot, P. Potier, C. Poupat et T. Sevenet. Phytochemistry, **17**, 166 (1978).
3. A. Fournet, A. M. Manjon, V. Munoz, A. Angelo, J. Bruneton, R. Hocquemiller, D. Cortes et A. Cave. J. Ethnopharmacol. **24**, 337 (1988).
4. I. Mester. Fitoterapia, **44**, 123 (1973).
5. K. Krause. Notizbl. K. Bot. Gart. Berlin, **6**, 143, (1914).
6. I. Mester. Structural diversity and distribution of alkaloids in the Rutales. *Dans* Chemistry and chemical taxonomy of the Rutales. *Editeurs* : P. G. Waterman et M. F. Grundon. Academic, Londres. 1983. pp. 31–96.
7. S. Goodwin, A. F. Smith, A. A. Velasquez et E. C. Horning. J. Am. Chem. Soc. **81**, 6209 (1959).

Photosensitized (electron transfer) carbon–carbon bond cleavage of radical cations: the 2-phenylethyl ether and acetal systems[1]

DONALD R. ARNOLD[2] AND LAURIE J. LAMONT
Department of Chemistry, Dalhousie University, Halifax, N.S., Canada B3H 4J3

Received April 7, 1989

DONALD R. ARNOLD and LAURIE J. LAMONT. Can. J. Chem. **67**, 2119 (1989).

The scope of the photosensitized (electron transfer) carbon–carbon bond cleavage involving radical cations has been defined for 2-phenylethyl ethers and acetals. The thresholds for reactivity of the monophenylethyl and *gem*-diphenylethyl derivatives are compared. While the radical cation of methyl 2,2-diphenylethyl ether (**7**) cleaves to give ultimately diphenylmethane (**2**) and dimethoxymethane (**8**), the radical cation of methyl 2-phenylethyl ether (**9**) was stable under these conditions. In contrast to the lack of reactivity of the radical cation of **9**, the radical cations of methyl 2-phenyl-2-propyl ether (**11**), methyl 2-phenylcyclopentyl ether (**13**), and 2-phenylmethyl-1,3-dioxolane (**16**) cleave. Cleavage in the monophenylethyl series is limited to formation of a carbocation at least as stable as the secondary α-oxyalkyl or di-α-oxyalkyl. The basis for predicting this type of reactivity of radical cations is defined. The rate of carbon–carbon bond cleavage is increased by increasing the oxidation potential of the molecule, by decreasing the carbon–carbon bond strength, and (or) by decreasing the oxidation potential of that fragment that will become the carbocation. The results obtained from the reactions of 2-diphenylmethyl-1,3-dioxolane (**14**) and 2-phenylmethyl-1,3-dioxolane (**16**) cast doubt on the published oxidation potential for the 1,3-dioxolan-2-yl radical.

Key words: photochemistry, radical cation, electron transfer, bond cleavage, radical.

DONALD R. ARNOLD et LAURIE J. LAMONT. Can. J. Chem. **67**, 2119 (1989).

On a défini le champ d'application du clivage, photosensibilisé (par transfert électronique) et impliquant des cations radicaux, de la liaison carbone–carbone d'éthers et d'acétals de la série 2-phényléthyle. On a comparé les seuils de réactivité des dérivés monophényléthylés et *gem*-diphényléthylés. Alors que le cation radical du 1-méthoxy-2,2-diphényléthane (**7**) subit un clivage conduisant éventuellement au diphénylméthane (**2**) et au diméthoxyméthane (**8**), le cation radical du méthoxy-1-2-phényléthane (**9**) est stable dans ces conditions. En opposition au fait que le cation radical du composé **9** n'est pas réactif, les cations radicaux du 2-méthoxy-2-phénylpropane (**11**), du 1-méthoxy-2-phénylcyclopentane (**13**) et du 2-phénylméthyl-1,3-dioxolane (**16**) se clivent. Le clivage dans la série des composés monophényléthylés est limité à la formation d'un cation au moins aussi stable que les α-oxyalkyles ou di-α-oxyalkyles secondaires. On a défini les bases permettant de prédire ce type de réactivité des cations radicaux. Les vitesses de clivage de la liaison carbone–carbone augmentent lorsqu'on augmente le potentiel d'oxydation de la molécule, lorsqu'on diminue la force de la liaison carbone–carbone et (ou) lorsqu'on diminue le potentiel d'oxydation du fragment qui deviendra le carbocation. Les résultats obtenus lors des réactions des 2,2-diphénylméthyl-1,3-dioxolane (**14**) et 2-phénylméthyl-1,3-dioxolane (**16**) permettent de mettre en doute les résultats qui ont été publiés relativement au potentiel d'oxydation du radical 1,3-dioxolan-2-yle.

Mots clés : photochimie, cation radical, transfert d'électron, clivage de la liaison, radical.

[Traduit par la revue]

Introduction

A frequently observed reaction of organic radical cations is cleavage of a carbon–carbon bond to give a carbon-centered radical and a carbocation fragment. This process accounts for many of the fragments in the mass spectrum of an organic molecule. The relative efficiency of the various modes of cleavage of the radical cation, in the gas phase, are predictable and relatively well understood. In marked contrast, when the radical cation is generated in solution by photosensitization (electron transfer), cleavage is much less common; in fact, it is not yet possible to predict when this reaction will occur (3). Other reactions of the radical cation often occur instead. It is now clear that for the carbon–carbon bond cleavage process to compete effectively with these other reactions the nascent fragments, both radical and carbocation, must be relatively stable (1*b*).

The reactivity of the radical cations of several compounds having in common the *gem*-diphenyl moiety has been studied. Even though carbon–carbon bond cleavage of the radical cation of these compounds would give the highly delocalized diphenylalkyl radical, not all react in this way. The photosensitized (electron transfer) reactivity of 1,1,2,2-tetraphenylethane (**1**) is particularly interesting; the efficiency of the cleavage process is temperature dependent in this case. Essentially no cleavage of **1** occurred upon irradiation of an acetonitrile–methanol solution at 10°C, with 1,4-dicyanobenzene (**4**) as the electron-accepting photosensitizer; however, at 80°C, cleavage was relatively efficient and an excellent yield of diphenylmethane (**2**) and methyl diphenylmethyl ether (**3**) was obtained (reaction 1) (1*b*). The energy of carbon–carbon bond cleavage of this radical cation is clearly at the threshold for reactivity.

Reaction 1

$$\underset{\mathbf{1}}{Ph_2CH{-}CHPh_2} \xrightarrow[CH_3CN,\ CH_3OH]{h\nu,\ \text{Sen.},\ 80\,^\circ C} \underset{\mathbf{2}}{Ph_2CH_2} + \underset{\mathbf{3}}{CH_3OCHPh_2}$$

Sens.: 1,4-Dicyanobenzene (**4**)

The proposed mechanism for this reaction is shown in Scheme 1 (1*b*). The temperature dependence of the reaction of the radical cation of **1** was attributed to the cleavage step (step 4) and an estimate of $E_a = 7.2$ kcal mol^{-1} was obtained from the slope of an Arrhenius plot (log (relative efficiency) versus temp^{-1}). This estimate for the bond dissociation energy of the central bond in the radical cation of **1** is in fair agreement with the value (9.3 kcal mol^{-1}) calculated from thermochemical data (Fig. 1*a*) (1*b*).

Some similar 1,1-diphenylethyl derivatives are stable to

[1]This is Part 22 of the series Radical Ions in Photochemistry. Preceding publications in these series are refs. 1 and 2.

[2]Author to whom correspondence may be addressed.

Can. J. Chem. Downloaded from www.nrcresearchpress.com by 186.148.149.217 on 09/07/12
For personal use only.

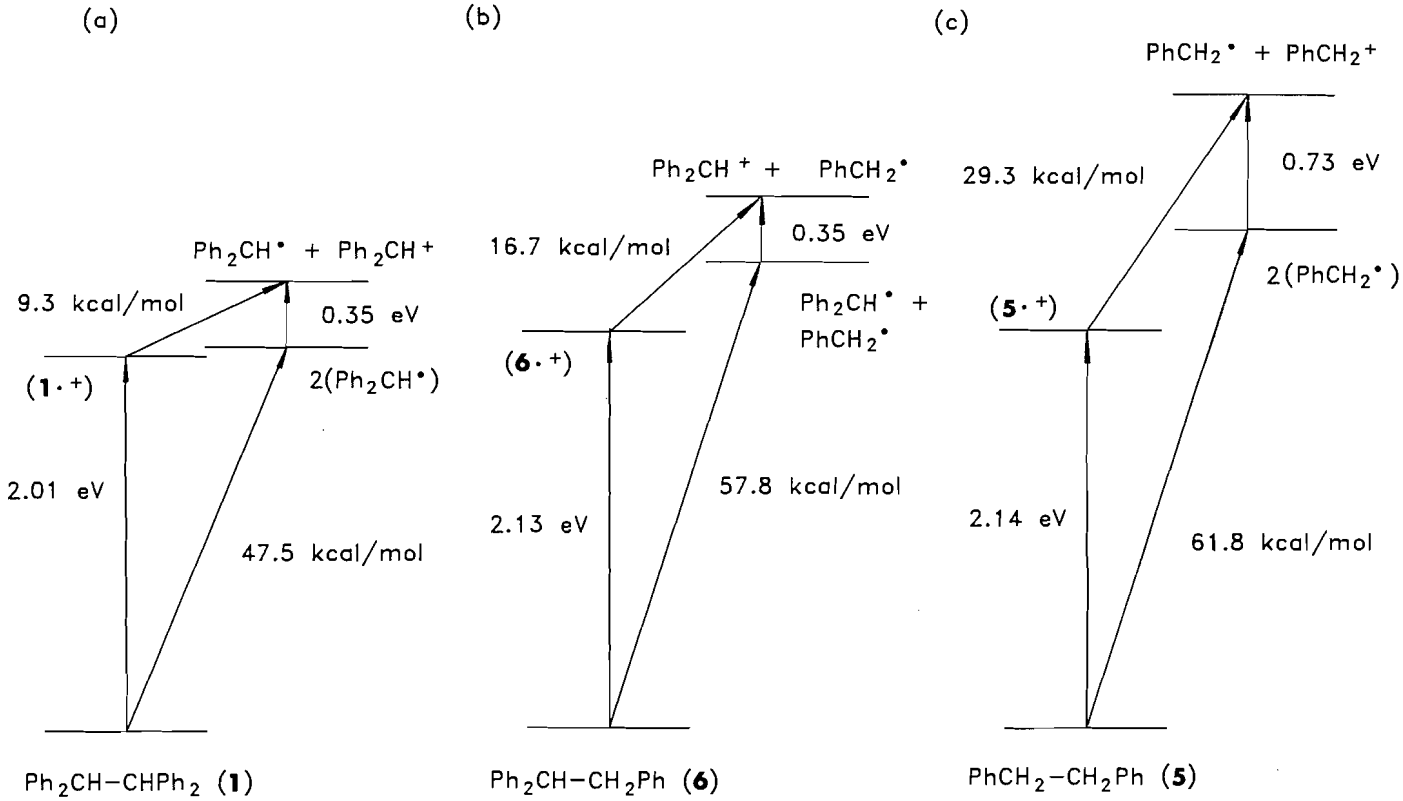


FIG. 1. Thermochemical cycles useful for estimating the bond dissociation energy of the radical cations of (a) 1,1,2,2-tetraphenylethane (**1**); (b) 1,1,2-triphenylethane (**6**); (c) 1,2-diphenylethane (**5**). (Data taken from Table 2, and refs. 1*b*, 5, and 6.)

1. Sensitizer (A) $\xrightarrow{h\nu}$ A*
2. $Ph_2CH-R + A^* \longrightarrow Ph_2CH-R^{\ddagger} + A^{\ddagger}$
3. $Ph_2CH-R^{\ddagger} + A^{\ddagger} \longrightarrow Ph_2CH-R + A$
4. $Ph_2CH-R^{\ddagger} \longrightarrow Ph_2CH\cdot + R^+$
5. $R^+ + CH_3OH \longrightarrow R-OCH_3 + H^+$
6. $Ph_2CH\cdot + A^{\ddagger} \longrightarrow Ph_2CH^- + A$
7. $Ph_2CH^- + CH_3OH \longrightarrow Ph_2CH_2 + CH_3O^-$
8. $Ph_2CH-R^{\ddagger} \longrightarrow Ph_2C(\cdot)-R + H^+$
9. $Ph_2C(\cdot)-R + A^{\ddagger} \longrightarrow Ph_2C(^-)-R + A$
10. $Ph_2C(^-)-R + H^+ \longrightarrow Ph_2CH-R$

SCHEME 1. The mechanism for the photosensitized (electron transfer) carbon–carbon bond cleavage.

irradiation under these conditions, even at the higher temperature (80°C). Apparently, with these unreactive derivatives cleavage cannot compete with other reactions, such as deactivation by back electron transfer (step 3) or deprotonation (step 8). The carbon–carbon bond dissociation energy of the radical cation must be too high. An understanding of the factors that influence the thermodynamics, and more importantly the kinetics, of step 4 will be required to be able to predict whether cleavage of any given radical cation will occur.[3]

[3]If the reaction of the radical with the carbocation, to give the radical cation, has little or no activation energy, the activation energy for the cleavage of the radical cation will be the bond dissociation energy. This may be the case in the gas phase (4); however, solvent reorganization at the transition state must require an activation energy, particularly for solutions in polar solvents.

The main structural features that influence the thermodynamics of step 4 have been identified (Fig. 1) (1*b*). To decrease the bond dissociation energy of the radical cation, one must increase the oxidation potential of the molecule, decrease the carbon–carbon bond dissociation energy, and (or) decrease the oxidation potential of that fragment that will become the carbocation.

The reactivity of 1,1,2,2-tetraphenylethane (**1**) gives an indication of the threshold carbon–carbon bond energy required for cleavage to occur; it is about 10 kcal mol^{-1}. One of our goals is to be able to predict generally, on the basis of the structure of the radical cation, when this cleavage reaction will occur. We have therefore extended our study to the monophenylethyl analogues in an effort to find the threshold for cleavage in this series.

There are conflicting reports in the literature regarding the reactivity of the radical cation of the parent member of this series, 1,2-diphenylethane (**5**) (7). We find that **5** is stable to irradiation under conditions which cause cleavage of **1** (reaction 2); this is consistent with most of the reported behaviour (7). It is

Reaction 2

$$PhCH_2-CH_2Ph \xrightarrow[CH_3CN,\ CH_3OH]{h\nu,\ \text{Sen.},\ 80\,^{\circ}C} \text{No reaction}$$

5

also clear, from consideration of the thermochemical cycle (Fig. 1*c*), that the bond dissociation energy for **5** is significantly greater (29.3 kcal mol^{-1}) than that for **1**.

Can the bond dissociation energy of the radical cation of monophenyl analogues be decreased, by appropriate substitution, to the point where cleavage will occur? For example, will

Can. J. Chem. Downloaded from www.nrcresearchpress.com by 186.148.149.217 on 09/07/12
For personal use only.

Reaction 3

$$Ph_2CH—CH_2Ph \xrightarrow[CH_3CN,\ CH_3OH]{h\nu,\ Sen.,\ 80°C} \text{No reaction}$$

6

the radical cation of 1,1,2-triphenylethane (**6**) cleave? While the oxidation potentials of **5** and **6** are essentially the same (Table 2), the central carbon–carbon bond in **6** is weaker than that in **5** (5*a*), and the oxidation potential of the diphenylmethyl radical (0.35 V (6))[4] is appreciably less than that of the benzyl radical (0.73 V (6)). Both of these factors tend to favour cleavage of **6** relative to **5** (Fig. 1*b*). But will the combined effect, which lowers the bond dissociation energy of the radical cation of **6** to 16.7 kcal mol^{-1}, be large enough?

Methyl 2,2-diphenylethyl ether (**7**) is readily cleaved under these conditions, even at 10°C (reaction 4) (8). The data

Reaction 4

$$Ph_2CH—CH_2OCH_3 \xrightarrow[CH_3CN,\ CH_3OH]{h\nu,\ Sen.,\ 10°C} Ph_2CH_2 + CH_3OCH_2OCH_3$$

7 **2** **8**

required to complete the thermochemical cycle for the cleavage of **7** are not available; however, the significantly lower oxidation potential of the α-oxymethyl radical (−0.24 V (6)) relative to the diphenylmethyl radical tends to favour cleavage. Substitution of the α-oxymethyl group for the benzylic group in **5** makes an even greater incremental difference in the carbon–carbon bond energy. Will methyl 2-phenylethyl ether (**9**) cleave under these conditions?

Reaction 5

$$PhCH_2—CH_2OCH_3 \xrightarrow[CH_3CN,\ CH_3OH]{h\nu,\ Sen.,\ 80°C} \text{No reaction}$$

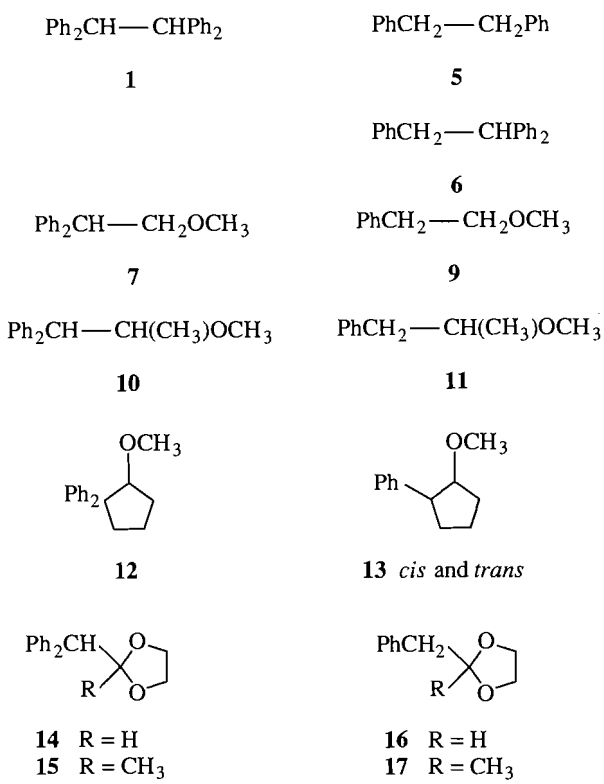
9

The radical cations of methyl 1,1-diphenyl-2-propyl and methyl 1-phenyl-2-propyl ethers (**10** and **11**) are even more likely to cleave. The α-oxycarbocation from these derivatives is secondary; the oxidation potential of this secondary radical (−0.45 V (6)) is significantly less than that of the analogous primary α-oxymethyl radical.

The radical cation of methyl 2,2-diphenylcyclopentyl ether (**12**) cleaves to give the 1,5-radical cation under these conditions (1*a*). Would the radical cation of the monophenyl derivative, methyl 2-phenylcyclopentyl ether (**13**), cleave?

The effect of the single oxygen in **7** and **9**–**13** is understood; while the radical α to ether oxygen is stabilized by interaction with the nonbonding pair of electrons, the α-oxycarbocation is stabilized even more. This is evident from the relatively low oxidation potential of the radical. The effect of the two oxygens in the 1,3-dioxolan-2-yl system can also be predicted. Both the radical and the carbocation should be stabilized by more than the stabilization provided by only one adjacent oxygen, although the effect is not additive (9). However, this reasoning is not consistent with the measured oxidation potential of the 1,3-dioxolan-2-yl radical (0.31 V (6)), which is significantly greater than that of the α-oxymethyl radical. It will therefore be interesting to know if the radical cations of the 2-diphenylmethyl-1,3-dioxolanes (**14** and **15**) and the 2-phenylmethyl-1,3-dioxolanes (**16** and **17**) (Chart 1) cleave under these conditions. The reactivity of these compounds will provide another indication of the oxidation potential of the 1,3-dioxolan-2-yl radical.

CHART 1



The specific objective of this work was to determine the reactivity of the radical cations of 2,2-diphenylethyl and 2-phenylethyl ethers and acetals upon photosensitization (electron transfer). The ultimate goal is to provide a firm basis for predicting reactivity in this type of cleavage reaction in general.

Results

The compounds of interest are shown in Chart 1; all except methyl 1,1-diphenyl-2-propyl ether (**10**) were known compounds, prepared by standard methods, and characterized by spectroscopic techniques (^1H nmr, ms). The new compound (**10**), prepared in two steps from 1,1-diphenyl-2-propanone, was fully characterized (ir, ^1H nmr, ^{13}C nmr, ms, and elemental analysis).

The methyl *cis*- and *trans*-2-phenylcyclopentyl ethers (**13**) and methyl 1-phenyl-2-propyl ether (**11**) were obtained by the photosensitized (electron transfer) *anti*-Markovnikov addition of methanol to the corresponding alkenes (10). The ratio of isomers obtained from 1-phenylcyclopentene (*cis*-**13**/*trans*-**13** = 0.4) was similar to that reported (0.6, ref. 10*b*). These isomers were separated by flash column chromatography.

The irradiation procedure was similar to that used in the previous study (1*b*), so the results can be compared directly with those reported. Solutions of the ether or acetal and the photosensitizer, 1,4-dicyanobenzene (**4**), in acetonitrile–methanol (3:1), were degassed by nitrogen ebullition and then were irradiated through a Pyrex filter using a medium-pressure mercury vapour lamp. The irradiation vessel was kept at a constant temperature, 10°C or 80°C, by a circulating water bath.

[4]All of the potentials mentioned in this paper are relative to the saturated calomel electrode (SCE).

Can. J. Chem. Downloaded from www.nrcresearchpress.com by 186.148.149.217 on 09/07/12
For personal use only.

Can. J. Chem. Downloaded from www.nrcresearchpress.com by 186.148.149.217 on 09/07/12
For personal use only.

TABLE 1. Summary of results of irradiations[a]

Reaction	Compound	Product(s) (yield, %)
1[b,c]	1,1,2,2-Tetraphenylethane (**1**)	Diphenylmethane (**2**); methyl diphenylmethyl ether (**3**)
2[c]	1,2-Diphenylethane (**5**)	No reaction[d]
3[c]	1,1,2-Triphenylethane (**6**)	No reaction[d]
4[a,b]	Methyl 2,2-diphenylethyl ether (**7**)	(**2**); dimethoxylmethane (**8**)
5[c]	Methyl 2-phenylethyl ether (**9**)	No reaction[d]
6[a]	Methyl 1,1-diphenyl-2-propyl ether (**10**)	(**2**) (70); 1,1-dimethoxyethane (**18**); 1,1,2,2-tetraphenylethane (**1**) (10)
7[a]	Methyl 1-phenyl-2-propyl ether (**11**)	Toluene (**19**) (25); (**5**) (15); (4-cyanophenyl)phenylmethane (**20**) (25)
8[a,e]	Methyl 2,2-diphenylcyclopentyl ether (**12**)	5,5-Diphenylpentanal dimethylacetal (**21**) (60)
9[a]	Methyl *cis* and *trans*-2-phenylcyclopentyl ether (**13**)	5-Phenylpentanal dimethylacetal (**22**);[f] 5-(4-cyanophenyl)-5-phenylpentanal dimethylacetal (**23**)[g]
10[e]	2-Diphenylmethyl-1,3-dioxolane (**14**)	(**2**) (90); (**1**) (10); 2-methoxy-1,3-dioxolane (**24**)
11[a]	2-Diphenylmethyl-2-methyl-1,3-dioxolane (**15**)	(**2**) (85); (**1**) (10); 2-methoxy-2-methyl-1,3-dioxolane (**25**)
12[a]	2-Phenylmethyl-1,3-dioxolane (**16**)	(**19**) (40); (**5**) (10); (**20**) (20); (**24**)
13[a]	2-Phenylmethyl-2-methyl-1,3-dioxolane (**17**)	(**19**) (35); (**5**) (5); (**20**) (20); (**25**)

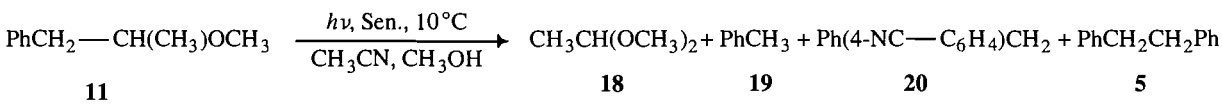
[a]A solution of the compound (0.05 M) and 1,4-dicyanobenzene (**4**) (0.05 M) in acetonitrile–methanol (3:1) at 10°C was irradiated through a Pyrex filter with a medium-pressure mercury vapor lamp. The usual irradiation period was ca. 20 h.
[b]Reference 1*b*.
[c]The temperature of the irradiation was 80°C; there was little or no reaction upon irradiation at 10°C.
[d]Trace amounts of the expected cleavage products were detected by gc/ms.
[e]Reference 1*a*.
[f]The acetal **21** was the only volatile product detected at low conversion; the yield was not determined. The reaction becomes inefficient and the product mixture becomes complex during irradiation.
[g]Tentative structural assignment based upon retention time and mass spectrum (gc/ms).

Progress of the reaction was followed by capillary column gas chromatography with a mass selective detector (gc/ms). The products, including minor amounts of compounds resulting from competing reactions or secondary photolysis, were readily detected. The results of the irradiations are illustrated in reactions 1–13, and are summarized in Table 1. The reported yields are based upon starting material consumed, at greater than 85% conversion, and purified product isolated by column chromatography. The yield of toluene (**19**) was determined by gas chromatography using a calibrated flame ionization detector (gc/fid).

Most of the products are well-known compounds, characterized here by spectroscopic techniques and by direct comparison with authentic samples.

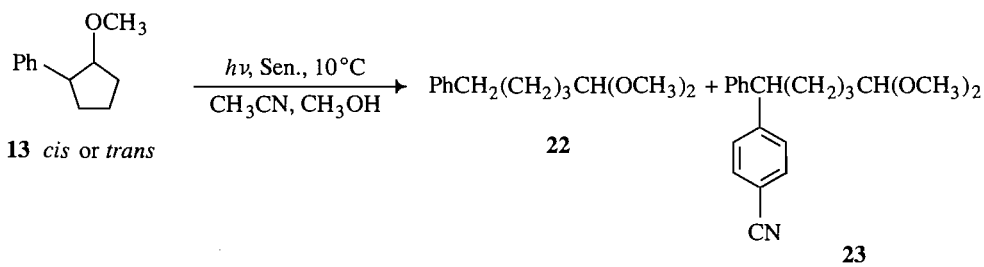
The (4-cyanophenyl)phenylmethane (**20**), isolated by column chromatography, was identified by mass spectrum, ^{1}H nmr, and comparison with reported melting point. The *ortho* ester, 2-methoxy-2-methyl-1,3-dioxolane (**25**), was hydrolyzed to

Reaction 7



11 **18** **19** **20** **5**

Reaction 9



13 *cis* or *trans* **22** **23**

TABLE 2. The oxidation potential of compounds of interest and the calculated free energy change (ΔG) for the electron transfer process involving the first excited singlet state of 1,4-dicyanobenzene (**4**)

Compound	$E^{ox}_{1/2}$ (V)[a]	$E_p - E_{p/2}$ (mV)	ΔG[b]
1,1,2,2-Tetraphenylethane (**1**)	2.01[c]	110[c]	−14.35
Diphenylmethane (**2**)	2.14[c]	120[c]	−11.36
1,1-Diphenylethane	2.13[c]		−11.59
1,2-Diphenylethane (**5**)	2.14 (2.45[d])	93	−11.36
1,1,2-Triphenylethane (**6**)	2.13	110	−11.59
Toluene (**19**)	(2.28[d])	—	−8.13
Methyl 2,2-diphenylethyl ether (**7**)	2.13[e]	—	−11.59
Methyl 2-phenylethyl ether (**9**)	2.29	150	−7.90
Methyl 1,1-diphenyl-2-propyl ether (**10**)	2.15	150	−11.13
Methyl 1-phenyl-2-propyl ether (**11**)	2.18	140	−10.43
Methoxy-2,2-diphenylcyclopentane (**12**)	2.13	150	−11.59
cis-Methoxy-2-phenylcyclopentane (*cis*-**13**)	2.02	117	−14.12
trans-Methoxy-2-phenylcyclopentane (*trans*-**13**)	2.02	162	−14.12
2-Diphenylmethyl-1,3-dioxolane (**14**)	2.15	120	−11.13
2-Methyl-2-diphenylmethyl-1,3-dioxolane (**15**)	2.14	140	−11.36
2-Phenylmethyl-1,3-dioxolane (**16**)	2.28	170	−8.13
2-Methyl-2-phenylmethyl-1,3-dioxolane (**17**)	2.24	200	−9.05

[a]Measured by cyclic voltammetry at a sweep rate of 100 mV s^{-1}, in acetonitrile (0.1 M tetraethylammonium perchlorate) vs. SCE. The estimated error is $< \pm 0.03$ V. The $E^{ox}_{1/2}$ taken as 0.03 V less than the anodic peak potential (E_p) (ref. 12).

[b]In units of kcal mol^{-1}. Calculated by the Weller equation (ref. 11) and, for 1,4-dicyanobenzene (**4**) $E_{0,0} = 97.6$ kcal mol^{-1}, $E^{red}_{1/2} = -1.66$ V. The Coulombic attraction term, $e/\epsilon\alpha = 0.06$ eV (ref. 8).

[c]Reference 1*b*.

[d]Reference 13.

[e]Reference 8.

methyl acetate, which was identified by comparison (gc/ms) with an authentic sample.

A minor product formed upon cleavage of methyl 2-phenylcyclopentyl ether (**13**) (reaction 9) was not isolated; a tentative structure, 5-(4-cyanophenyl)-5-phenylpentanal dimethylacetal (**23**), was assigned on the basis of retention time and mass spectrum (gc/ms). *cis*- and *trans*-**13** undergo configurational isomerization under these conditions.

Deuterium incorporation studies were carried out on methyl 2-phenylethyl ether (**9**), and on methyl *cis*- and *trans*-2-phenylcyclopentyl ether (**13**). These compounds were irradiated under the usual conditions except that the solvent was acetonitrile–methanol-d_4 (3:1). Analysis by gc/ms showed that both **9** and **13** had incorporated deuterium at the benzylic position.

Electrochemical measurements for the ethers and acetals are summarized in Table 2. All of the anodic waves were typical of irreversible oxidation. The last column in Table 2 reports the free energy change (ΔG) for the electron transfer step (Scheme 1, step 2), calculated using the Weller equation (eq. [1]) (11).

$$[1] \quad \Delta G = 23.06\left(E^{ox}_{1/2} - E^{red}_{1/2} - \frac{e}{\epsilon\alpha}\right) - E^{*}_{0,0}$$

Discussion

The first step in the proposed mechanistic sequence is excitation of the photosensitizer. The long-wavelength ultraviolet absorption of 1,4-dicyanobenzene (**4**) extends to 290 nm, beyond the absorption cutoff of Pyrex glass. Phenylethyl and *gem*-diphenylethyl compounds are transparent in this spectral region so only the photosensitizer absorbed the light.

Electron transfer, from the phenylethyl or diphenylethyl compound, to the excited singlet state of **4** is energetically favourable in every case (Table 2). Step 2 should be diffusion controlled; quenching of the excited singlet state of **4** at rates approaching the diffusion limit has been observed for some of these compounds (8).

Aliphatic ethers generally have high oxidation potentials. All of the compounds listed in Table 2 have an oxidation potential that falls within the rather narrow range (2.1 ± 0.1 V) typical of monoalkyl aromatics. The singly occupied molecular orbital (SOMO) of these donors must be largely associated with the phenyl ring(s). The fact that the oxidation potentials of the *gem*-diphenylethyl derivatives are generally about 0.1 V less than those of the monophenyl analogues suggests that there may be some additional stabilization, i.e., increased delocalization, in the *gem*-diphenylethyl radical cation.

The corresponding radical anion of diphenylmethane has been studied and there was no evidence, in the electron spin resonance spectrum (esr), for interaction between the rings (14). A very recent esr study of the radical cation of di(9-anthryl)-methane indicated that the unpaired electron is delocalized over only one of the anthracene rings (15). It therefore seems likely

Can. J. Chem. Downloaded from www.nrcresearchpress.com by 186.148.149.217 on 09/07/12
For personal use only.

Can. J. Chem. Downloaded from www.nrcresearchpress.com by 186.148.149.217 on 09/07/12
For personal use only.

that any interaction between the two phenyl rings in the radical cation of these *gem*-diphenylethyl derivatives is small.

One factor that is known to inhibit bond cleavage of a radical cation is lack of overlap of the adjacent carbon–carbon bond with the SOMO (1*a*). All of the compounds studied here can attain conformations that allow such overlap, hence this is not a limiting factor.

Back electron transfer from the radical anion of the sensitizer to the radical cation of the donor, step 3, is the major competing reaction. This process is energetically very favourable (ca. −85 kcal mol^{-1}) for all of the donors studied; the rate should be nearly the same in every case. Back electron transfer from the monophenylethyl compounds might, in fact, be somewhat slower than for the *gem*-diphenylethyl compounds because the process is exothermic enough to fall within the inverted-Marcus region (16).

The contrast in reactivity between the 1,1,2,2-tetraphenylethane (**1**) and 1,2-diphenylethane (**5**) continues with 1,1,2-triphenylethane (**6**); no cleavage was observed (reaction 3). This is perhaps not surprising in view of the fact that **1** is on the threshold for reactivity. The bond strength of the radical cation of **6**, estimated to be 16.7 kcal mol^{-1} from the thermochemical cycle (Fig. 1*b*), is too great for cleavage to compete with back electron transfer, even at the higher temperature (80°C).

Cleavage of the radical cation of methyl 2,2-diphenylethyl ether (**4**) occurs at 10°C. Reaction 4 is more favourable than reaction 1; nevertheless, the radical cation of the monophenylethyl analog, methyl 2-phenylethyl ether (**9**), does not cleave, even at 80°C (reaction 5). Apparently, the bond dissociation energy of the radical cation of **9** is too large for cleavage to compete.

When the irradiation of **9** is carried out in acetonitrile–methanol-d_4, deuterium is incorporated at the benzylic position. The acidity of a benzylic hydrogen is greatly increased upon oxidation to the radical cation (17). Deprotonation, followed by back electron transfer from the sensitizer radical anion to the resulting radical and reprotonation (or redeuteration), provides a mechanism for deuterium exchange (steps 8–10).

Progressing through the series of monophenylethyl derivatives of decreasing bond strength, not until methyl 1-phenyl-2-propyl ether (**11**), where the α-oxyalkyl radical is secondary, does the radical cation of a monophenylethyl derivative cleave. Both the *gem*-diphenyl-2-propyl and the monophenyl ethers (**10** and **11**) cleave upon photosensitization (electron transfer) at 10°C (reactions 6 and 7).

The reaction mixtures involving **11**, and all of the other monophenylethyl derivatives that cleave, are more complex than in the case of the analogous *gem*-diphenylethyl derivatives; (4-cyanophenyl)phenylmethane (**20**) is a major product in these reactions. A key step accounting for the formation of diphenylmethane (**2**) from the *gem*-diphenylethyl derivatives is the reduction of the diphenylmethyl radical by the sensitizer radical anion (step 6). Since the reduction potential of 1,4-dicyanobenzene (**4**) (−1.66 V) is significantly greater (more negative) than that of the diphenylmethyl radical (−1.14 V (6)), reduction of the radical is favourable. Reduction of the benzyl radical (−1.45 V (6)) and α-phenethyl radical (−1.60 V (6)) is less favourable. Formation of (4-cyanophenyl)phenylmethane (**20**) may result from coupling of the benzyl radical and the 1,4-dicyanobenzene radical anion at the *ipso* position followed by loss of cyanide ion. This coupling of the radical and radical anion may become more important as reduction of the radical becomes less favourable. Steric hindrance may also inhibit the coupling reaction involving the more hindered and more delocalized diphenylmethyl radical.

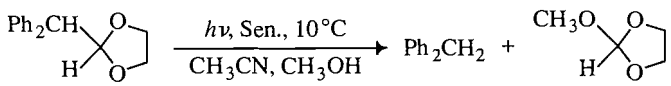
The formation of the 1,5-radical cation upon cleavage of the radical cation of methyl 2,2-diphenylcyclopentyl ether (**12**) has been reported (reaction 8) (1*a*). In view of the fact that the acyclic monophenyl derivative (**11**) cleaves, it is now not surprising that the monophenylcyclopentyl ether (**13**) also cleaves (reaction 9). The observations that *cis*- and *trans*-**13** are equilibrated under these conditions and that deuterium is incorporated at the benzylic position, when the irradiation is carried out in acetonitrile–methanol-d_4, leads to the conclusion that deprotonation–reprotonation (steps 8–10) may be competitive with cleavage in this case. Isomerization could also result from reversible carbon–carbon bond cleavage; there was no evidence for cyclization of the 1,5-radical cation into the terminal phenyl ring.

In addition to the expected cleavage product, 5-phenylphentanal dimethylacetal (**22**), a minor product having a retention time and mass spectrum (gc/ms) consistent with 5-(4-cyanophenyl)-5-phenylpentanal dimethylacetal (**23**) was also detected (not isolated). This product would arise upon coupling of the benzylic radical with the radical anion of 1,4-dicyanobenzene (**4**) at the *ipso* position followed by loss of cyanide ion, the same mechanism as that invoked for the formation of (4-cyanophenyl)-phenylmethane (**20**).

All four of the dioxolanes studied (**14**–**17**) undergo photosensitized (electron transfer) cleavage. Cleavage of the radical cation of **16**, the derivative with the strongest carbon–carbon bond, is particularly interesting. If the reported oxidation potential of the 1,3-dioxolan-2-yl radical (0.31 V (6)) were correct, cleavage of **16** would be less favourable than cleavage of **9**, which does not cleave. This, and other evidence *vide infra*, leads us to question the reported oxidation potentials of the 1,3-dioxolan-2-yl radicals.

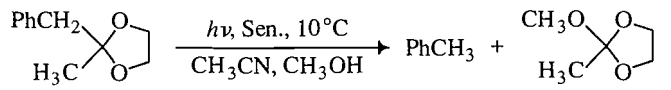
The cleavage process (step 4) yields a carbocation and a radical fragment. We have suggested that the direction of this process, that is, which fragment becomes the radical and which becomes the carbocation, is a reflection of the relative oxidation potentials of the two fragment radicals. That fragment radical with the lower oxidation potential becomes the carbocation (1*b*, *c*). In all of the cases involving cleavage of the radical cation of ethers, the radical bearing an α oxygen has an oxidation potential lower than either the benzylic or the diphenylmethyl radical; hence the products observed in reactions 4 and 6–9 are consistent with this hypothesis. There is, however, a quantitative discrepancy between calculated and observed product ratios in the diphenylmethyl–dioxolane (**14**) case.

Reaction 10



14 **2** **24**

Reaction 13



17 **19** **25**

Ph(4-NC—C_6H_4)CH_2

20

When the difference between the oxidation potentials of the two possible radicals is small (ca. 0.1 V), cleavage is less regioselective and all four possible products are obtained. The product ratio in such a case reflects the differences in energy of the two possible modes of separation of the radical and cation, according to eq. [2] (18). Since the difference in the reported

$$R{-}R' \xrightarrow[CH_3CN,\ CH_3OH]{h\nu,\ Sen.,\ (A)} \begin{cases} RH + R'OCH_3 \\ R'H + ROCH_3 \end{cases}$$

$$r = \frac{[R'H]}{[RH]} = \frac{[ROCH_3]}{[R'OCH_3]}$$

$$[2] \quad \ln r = \frac{F}{RT}\,(E^{ox}_{R^{\cdot}} - E^{ox}_{R'^{\cdot}})$$

values for the oxidation potential of the diphenylmethyl radical (0.35 V) and the 1,3-dioxolan-2-yl radical (0.31 V) is only 0.04 V, we would expect some (ca. 5%) methyl diphenylmethyl ether (**3**) from reaction 10; however, none was observed. Less than 1% might have gone undetected (gc/fid), which means the difference in oxidation potential must be >0.10 V. If we accept the oxidation potential of the diphenylmethyl radical, this places an upper limit on the oxidation potential of the 1,3-dioxolan-2-yl radical of <0.25 V, 0.06 V less than the reported value (6). Work in progress will resolve this discrepancy.[5]

Experimental

General information

The ^{1}H nmr spectra were recorded on a Nicolet Instruments Corp. narrow bore 360-MHz spectrometer and are reported in parts per million to high frequency from tetramethylsilane. Infrared spectra were recorded on a Perkin Elmer 283B ir spectrometer and are recorded in wavenumbers. Gas chromatography with mass selective detection (gc/ms) was done on a Hewlett Packard 5890A gc/5970 mass selective detector interfaced with a Hewlett Packard 9816 microcomputer. The column used was a 25 m × 0.2 mm 5% phenyl methyl silicone on fused silica with a film thickness of 0.25 μm. Gas chromatography with flame ionization detection (gc/fid) was carried out on a Hewlett Packard 5890. The column used was a 25 m × 0.25 mm OV-1701 fused silica column. Preparative gas chromatography was carried out on an Aerograph A-700 gc, fitted with a thermal conductivity detector, using a 6 ft × 3/4 in. 10% SE-30 on Chromosorb 60/80 W column. Melting points were taken on a Thermolyne melting point apparatus and are corrected. Combustion analysis was done by Canadian Microanalytical Service Limited, New Westminster, B.C.

Electrochemical measurements

Oxidation potentials were obtained by cyclic voltammetry using a three-electrode cell, which has been described previously (19). The working electrode was a platinum sphere (1 mm diameter) and the counter electrode was a platinum wire. The reference electrode was saturated calomel (SCE). The electrolyte was 0.1 M tetraethylammonium perchlorate (TEAP) in acetonitrile. Substrate concentrations were typically 1 mM.

The electrochemical measurements are summarized in Table 2. The peak potentials were measured using a 100 mV/s sweep rate. No cathodic wave was detected following the anodic sweep. The half-wave potentials were taken as 0.03 V before the anodic peak potentials (12).

[5]The oxidation potential of the di(4-methylphenyl)methyl radical is 0.188 V (18). The product ratio from the cleavage of the radical cation of 2-(di-(4-methylphenyl)methyl)-1,3-dioxolane will allow a more accurate measure of the oxidation potential of the 1,3-dioxolan-2-yl radical if it is greater than 0.1 V.

Irradiations

Irradiations were done in Pyrex tubes using a Canadian General Electric Co. 1-kW medium-pressure mercury vapour lamp (CGE H 1000 DX 36-15) with a quartz cooling jacket immersed in a constant temperature bath held at either 10°C or 80°C. Samples were degassed by bubbling nitrogen through the solution for 5 min prior to irradiation.

Materials

Solvents were distilled prior to use. Acetonitrile and 1,4-dicyanobenzene (**4**) (Aldrich Chem. Co.) were purified as previously described (1*b*). Diphenylacetaldehyde, 1,1-diphenyl-2-propanone, 2-phenylmethyl-1,3-dioxolane (**16**), 1,2-diphenylethane (**5**), 2-phenylethanol, 5-phenylpentanol, 1-phenyl-2-propanone, 1,1,2-triphenylethylene, β-methylstyrene, and phenyl-2-propanone were obtained from Aldrich Chem. Co.

Preparation of compounds

Preparation of 1,1,2-triphenylethane (6)

1,1,2-Triphenylethane (**6**) was obtained by reduction of 1,1,2-triphenylethylene using H_2(g) over 10% Pd on charcoal in hexanes at 170 Torr (1 Torr = 133.3 Pa). The reduction was complete after 2 days of stirring at room temperature. The product was purified by recrystallization using hexanes to yield pure **6** (mp 52–54°C (lit. (20) mp 54.4°C)) in 90% yield; ^{1}H nmr (360 MHz) in $CDCl_3$: 7.12 (m, 15H), 4.23(t, 1H, J = 7.8 Hz), 3.36 (d, 2H, J = 7.8 Hz) (in agreement with that reported (21)).

Preparation of methyl 2-phenylethyl ether (9)

Dimethyl sulphate (11.7 mL, 0.12 mol) was added dropwise to a stirred solution of 2-phenylethanol (5 g, 4.1×10^{-2} mol) and NaH (3 g, 0.13 mol) in anhydrous diethyl ether. The reaction mixture was refluxed for 20 h under nitrogen and was quenched by addition of water. The aqueous layer was extracted with diethyl ether. The combined organic extract was washed with concentrated NH_4OH, then with saturated NaCl solution, dried over magnesium sulphate, and the solvent evaporated to give the crude product. Column chromatography on silica gel (Kieselgel 60) using methylene chloride – hexanes as eluant gave the ether (**9**) in 60% yield; ^{1}H nmr (360 MHz) in $CDCl_3$: 7.19–7.31 (m, 5H), 3.60(t, 2H, J = 7.2 Hz), 3.36(s, 3H), 2.89(t, 2H, J = 7.2 Hz) (in agreement with that reported (22)).

Preparation of methyl 1,1-diphenyl-2-propyl ether (10)

Methyl 1,1-diphenyl-2-propyl ether (**10**) was obtained through a two-step synthesis from 1,1-diphenyl-2-propanone in 55% overall yield. The 1,1-diphenyl-2-pentanone was reduced, using $LiAlH_4$, to the corresponding alcohol (mp 62–63°C (lit. (23) mp 63–64°C), which was recrystallized from hexanes. The ether was prepared from this alcohol using NaH and dimethyl sulphate as described above for the preparation of **9**. Pure **10** (mp 31–32°C) was obtained by column chromatography on silica gel (Kieselgel 60) using methylene chloride and hexanes as eluants; ir (PE 283B) neat: 3070(m), 3030(s), 2980(s), 2930(s), 2900(s), 1600(s), 1500(s), 1455(s), 1375(m), 1340(w), 1140(s), 1090(s), 755(s), 745(s), 700(s); ^{1}H nmr (360 MHz) in $CDCl_3$: 7.20 (m, 10H), 4.01 (m, 1H), 3.80 (d, 1H, J = 3.9 Hz), 3.22 (s, 3H), 1.08 (d, 3H, J = 6.1 Hz); ^{13}C nmr (90 MHz) in $CDCl_3$: 142.7, 129.3, 127.5, 125.2, 78.8 (d), 58.6 (d), 56.6 (t), 17.6 (q). *Anal.* calcd. for $C_{16}H_{18}O$: C 84.91, H 8.02; found: C 84.90, H 8.05.

Preparation of methyl 1-phenyl-2-propyl ether (11) (24)

Methyl 1-phenyl-2-propyl ether (**11**) was obtained by the photochemical method (10*b*). β-Methyl styrene was irradiated at 10°C in the presence of an electron-accepting sensitizer, 1,4-dicyanobenzene (**4**), in acetonitrile–methanol (3:1) solution. The pure ether **11** was obtained in 40% yield by column chromatography on silica gel (Kieselgel 60) with methylene chloride and hexanes as eluant; ^{1}H nmr (360 MHz) in $CDCl_3$: 7.16–7.27 (m, 5H), 3.51 (m, 1H), 3.30 (s, 3H), 2.93 (dd, 1H, ^2J = −14.0 Hz, J = 5.99 Hz), 2.62 (dd, 1H, ^2J = −14.0 Hz, J = 6.74 Hz), 1.10 (d, 3H, J = 6.15 Hz); ^{13}C nmr (90 MHz) in $CDCl_3$: 138.9, 129.3, 128.1, 125.9, 78.0, 56.1, 42.7, 18.8.

Preparation of methyl cis- *and* trans-*2-phenylcyclopentyl ether (*cis- *and* trans-*13)*

The methyl *cis*- and *trans*-2-phenylcyclopentyl ethers were synthes-

Can. J. Chem. Downloaded from www.nrcresearchpress.com by 186.148.149.217 on 09/07/12
For personal use only.

Can. J. Chem. Downloaded from www.nrcresearchpress.com by 186.148.149.217 on 09/07/12
For personal use only.

ized from 1-phenylcyclopentene using the photochemical method (*10b*).

Bromobenzene (7.8 g, 0.05 mol) was added dropwise to magnesium (1.2 g, 0.05 mol) in anhydrous diethyl ether. Once the magnesium was consumed, the reaction mixture was cooled and cyclopentanone (3.14 g, 0.0375 mol) was added dropwise. The reaction mixture was poured into a concentrated hydrochloric acid – ice mixture, which was then extracted with ether (3×). The organic layers were combined, washed with 5% $NaHCO_3$ solution, and then with water. The extract was then dried with magnesium sulphate and the solvent was evaporated. Pure 1-phenylcyclopentene was obtained in 73% yield by flash column chromatography using hexanes as eluant.

A solution of 1-phenylcyclopentene (173 mg, 1.2×10^{-3} mol) and **4** (124 mg, 9.7×10^{-4} mol) in acetonitrile–methanol (30 mL, 3:1) was irradiated at 10°C for 24 h. Flash column chromatography of the photolysate, using methylene chloride – hexanes (1:1) as eluant, separated the isomeric ethers, *cis*- (17%) and *trans*-**13** (38%), at 97% conversion.

cis-**13**: ^{1}H nmr (360 MHz) in $CDCl_3$: 7.19–7.33 (m, 5H), 3.82 (ddd, 1H, J = 4.8 Hz, J = 4.3 Hz, J = 2.1 Hz), 3.05 (s, 3H), 2.99 (ddd, 1H, J = 4.8 Hz, J = 7.94 Hz, J = 11.06 Hz), 2.01 (m, 2H), 1.92 (m, 2H), 1.88 (m, 2H).

trans-**13**: ^{1}H nmr (360 MHz) in $CDCl_3$: 7.18–7.31 (m, 5H), 3.78 (ddd, 1H, J = 3.15 Hz, J = 5.58 Hz, J = 6.0 Hz), 3.25 (s, 3H), 3.03 (ddd, 1H, J = 6.0 Hz, J = 6.5 Hz, J = 7.0 Hz), 1.65–2.15 (m, 6H).

*Preparation of 2-diphenylmethyl-1,3-dioxolane (**14**)*

2-Diphenylmethyl-1,3-dioxolane (**14**) was prepared from diphenylacetaldehyde using chlorotrimethylsilane and ethylene glycol (25). Pure **14** (mp 74–76°C) was obtained, following recrystallization from methanol, in 95% yield; ^{1}H nmr (360 MHz) in $CDCl_3$: 7.19–7.38 (m, 10H), 5.55 (d, 2H, J = 5.01 Hz), 4.22 (d, 2H, J = 5.01 Hz), 3.78–3.86 (m, 4H) (in agreement with the reported spectrum (26)).

*Preparation of 2-diphenylmethyl-2-methyl-1,3-dioxolane (**15**) (27)*

2-Diphenylmethyl-2-methyl-1,3-dioxolane (**15**) was prepared from 1,1-diphenyl-2-propanone by the reported procedure (25). Pure **15** (mp 86–87°C) was obtained in 95% yield following recrystallization from methanol; ^{1}H nmr (360 MHz) in $CDCl_3$: 7.48–7.50 (m, 4H), 7.18–7.28 (m, 6H), 4.22 (s, 1H), 3.79 (m, 2H), 3.35 (m, 2H), 1.36 (s, 3H); ^{13}C nmr (90 MHz) in $CDCl_3$: 140.7 (s) 129.9, 127.9, 126.3, 111.3 (s), 65.0 (t), 61.0 (d), 25.3 (q).

*Preparation of 2-phenylmethyl-1,3-dioxolane (**16**) (28)*

2-Phenylmethyl-1,3-dioxolane (**16**) was prepared from 1-phenyl-2-propanone by the reported procedure (25). Compound **16** was purified by column chromatography on silica gel (Kieselgel 60) using methylene chloride – hexanes as eluant. Pure **16** was obtained in 80% yield; ^{1}H nmr (360 MHz) in $CDCl_3$: 7.22–7.28 (m, 5H), 3.90 (m, 2H), 3.76 (m, 2H), 2.92 (s, 2H), 1.31 (s, 3H).

Irradiations

*Irradiation of 1,2-diphenylethane (**5**)*

A solution of **5** (83 mg, 4.4×10^{-4} mol) and **4** (68 mg, 5.3×10^{-4} mol) in acetonitrile–methanol (3:1) was irradiated at both 10°C and 80°C. Trace amounts of toluene (**19**), the expected product from carbon–carbon bond cleavage, were observed (gc/ms) after irradiation for 20 h at 10°C and after 15 h at 80°C.

*Irradiation of 1,1,2-triphenylethane (**6**)*

A solution of **6** (157 mg, 6.1×10^{-4} mol) and **4** (96 mg, 7.5×10^{-4} mol) in acetonitrile–methanol (20 mL, 3:1) was irradiated at 80°C for 30 h. Trace amounts of diphenylmethane (**2**), 1,2-diphenylethane (**5**), and methyl diphenylmethyl ether (**3**) were detected (gc/ms).

*Irradiation of methyl 2-phenylethyl ether (**9**)*

A solution of **9** (40 mg, 2.9×10^{-4} mol) and 1,4-dicyanobenzene (**4**) (15 mg, 1.2×10^{-4} mol) in acetonitrile–methanol (2 mL, 3:1) was irradiated at 10°C for 25 h. Only trace amounts of toluene (**19**) and (4-cyanophenyl)phenylmethane (**20**), expected cleavage products, were detected (gc/fid).

A solution of **9** (25 mg, 1.8×10^{-4} mol) and **4** (24 mg, 1.9×10^{-4} mol) in acetonitrile–methanol (2 mL, 3:1) was irradiated at 80°C for 15 h. Only trace amounts of **19** and **20** were detected (gc/fid).

A solution of **9** (20 mg, 1.5×10^{-4} mol) and 1,4-dicyanobenzene (**4**) (11 mg, 8.6×10^{-5} mol) in acetonitrile–methanol-d_4 (2 mL, 3:1) was irradiated at 10°C for 24 h. Analysis (gc/ms) of the photolysate, using selected ion monitoring of the molecular ion and the benzylic fragment (m/z = 91–95), showed that deuterium had been incorporated (9%, one atom deuterium) at the benzylic position.

*Irradiation of methyl 1,1-diphenyl-2-propyl ether (**10**)*

A solution of **10** (600 mg, 2.66×10^{-3} mol) and **4** (340 mg, 2.66×10^{-3} mol) in acetonitrile–methanol (20 mL, 3:1) was irradiated for 23 h. Diphenylmethane (**2**) and 1,1,2,2-tetraphenylethane (**1**) were isolated by flash column chromatography of the photolysate on silica gel (Baker Analyzed) using hexanes and methylene chloride as eluant. After 90% conversion, **2** (70%) and **1** (10%) were isolated.

*Irradiation of methyl 1-phenyl-2-propyl ether (**11**)*

A solution of **11** (15 mg, 1.0×10^{-4} mol), **4** (22 mg, 1.7×10^{-4} mol), and cyclododecane (12 mg, 7.0×10^{-5} mol) in acetonitrile–methanol (2 mL, 3:1) was irradiated for 20 h. The major products of the irradiation were toluene (**19**), 1,2-diphenylethane (**5**), and (4-cyanophenyl)phenylmethane (**20**). Product analysis was done using gc/fid with cyclododecane as an internal calibration standard. The percent yields at 98% conversion were as follows: **19**, 25%; **5**, 15%; and **20**, 25%. The yields for **5** and **20** were confirmed by product isolation following column chromatography.

Irradiation of methyl cis- *and* trans-*2-phenylcyclopentyl ether (*cis- *and* trans-***13***)*

A solution of *cis*- and *trans*-**13** (ca. 1:2) (52 mg, 3.0×10^{-4} mol) and **4** (30 mg, 2.3×10^{-4} mol) in acetonitrile–methanol (2 mL, 3:1) was irradiated at 10°C. After 9 h of irradiation, the only product detected (gc/ms) was 5-phenylpentanal dimethylacetal (**22**), identified by comparison (gc/ms, retention time, and fragmentation pattern) with an authentic sample. After prolonged irradiation, an additional product was detected (gc/ms), to which the structure 5-(4-cyanophenyl)-5-phenylpentanal dimethylacetal (**23**) was tentatively assigned on the basis of the fragmentation pattern: 277, 245, 218, 230, 192, 165, 103 (the molecular ion was neither expected nor observed).

Authentic **23** was synthesized by a two-step process from the corresponding alcohol. 5-Phenylpentanol was oxidized, using chromium trioxide/pyridine, to 5-phenylpentanal in 88% yield by the standard procedure (29). Chlorotrimethylsilane (1.08 g, 0.01 mol) was added dropwise to a stirred solution of 5-phenylpentanal in methanol. The mixture was stirred overnight at room temperature; it was then cooled in ice, and 50 mL aqueous $NaHCO_3$ (5%) was added. The mixture was extracted (3×) with ether, and the organic layers were combined, washed with brine solution, and then dried over magnesium sulphate. The acetal **23** was purified by flash column chromatography on silica gel, eluting with methylene chloride – hexanes (75:25). The yield of pure **23** from the aldehyde was 50%; ^{1}H nmr (360 MHz) in $CDCl_3$: 7.15–7.28 (m, 5H), 4.34 (t), 1H, J = 5.72 Hz), 3.29 (s, 6H), 2.61 (t, 2H, J = 7.73 Hz), 1.62 (m, 4H), 1.39 (m, 2H); ^{13}C nmr (90 MHz): 142.5, 128.3, 125.9, 125.6, 104.4, 52.6, 35.9, 32.4, 31.3, 24.3.

A solution of *cis*- and *trans*-**13** (ca. 1:2) (20 mg, 1.1×10^{-4} mol) and **4** (24 mg, 1.9×10^{-4} mol) in acetonitrile–methanol-d_4 (2 mL, 3:1) was irradiated at 10°C for 24 h. Analysis (gc/ms, using selective ion monitoring) of the photolysate showed that deuterium (2%, one atom deuterium) was incorporated, at the benzylic position, in both isomers.

A solution of methyl *cis*- and *trans*-2-phenylcyclopentyl ether (**13**) in the ratio *cis*:*trans* = 1:64 (12 mg, 6.8×10^{-5} mol) and **4** (18 mg, 1.4×10^{-4} mol) was irradiated at 10°C. The ratio of *cis* to *trans* isomers was monitored by integrated peak areas on the gc/fid. After 45 h of irradiation, the ratio was 1:37.

*Irradiation of 2-diphenylmethyl-1,3-dioxolane (**14**)*

A solution of **14** (443 mg, 1.85×10^{-3} mol) and **4** (273 mg, 2.13×10^{-3} mol) in acetonitrile–methanol (20 mL, 3:1 ratio) was irradiated at 10°C and monitored (gc/fid). The products from the irradiation, 2-methoxy-1,3-dioxolane (**24**), diphenylmethane (**2**), and 1,1,2,2-tetraphenylethane (**1**), were identified by comparison (gc/ms, retention times, and fragmentation pattern) with those of authentic samples. After 23 h of irradiation, diphenylmethane (**2**) and 1,1,2,2-tetraphenyl-

ethane (**1**) were isolated by flash column chromatography in 90 and 10% yield at 75% conversion.

Irradiation of 2-diphenylmethyl-2-methyl-1,3-dioxolane (15)

A solution of **15** (441 mg, 1.74×10^{-3} mol) and **4** (289 mg, 2.26×10^{-3} mol) in acetonitrile–methanol (20 mL, 3:1) was irradiated at 10°C for 23 h. Progress of the reaction was monitored (gc/fid). The products of the irradiation were 2-methoxy-2-methyl-1,3-dioxolane (**25**), diphenylmethane (**2**), and 1,1,2,2-tetraphenylethane (**1**). Diphenylmethane (**2**) and 1,1,2,2-tetraphenylethane (**1**) were identified by comparison (gc/ms, retention times, and fragmentation pattern) with authentic samples. The identity of the *ortho* ester **25** was confirmed by hydrolysis to methyl acetate, as indicated by comparison (gc/ms) with an authentic sample. The hydrolysis was accomplished by refluxing the crude reaction mixture with 20 mL of 15% aqueous HCl for 1 h. The products, diphenylmethane (**2**) (85%) and 1,1,2,2-tetraphenylethane (**1**) (10%), were isolated by flash column chromatography after 85% conversion of **15**.

Irradiation of 2-phenylmethyl-1,3-dioxolane (16)

A solution of **16** (18 mg, 1.1×10^{-4} mol), **4** (14 mg, 1.1×10^{-4} mol), and cyclododecane (16. 5 mg, 9.8×10^{-5} mol) in acetonitrile–methanol (2 mL, 3:1) was irradiated at 10°C for 20 h. The major products of the irradiation were toluene (**19**), 2-methoxy-1,3-dioxolane (**24**), 1,2-diphenylethane (**5**), and (4-cyanophenyl)phenylmethane (**20**). Toluene (**19**), 2-methoxy-1,3-dioxolane (**24**), and 1,2-diphenylethane (**5**) were identified by comparison of retention times and fragmentation pattern (gc/ms) with authentic samples. The (4-cyanophenyl)phenylmethane (**20**) was isolated by column chromatography and identified by comparison (^{1}H nmr and melting point) with reported data. (4-Cyanophenyl)phenylmethane (mp 44–46°C (lit. (14) mp 49–50°C)); ^{1}H nmr (360 MHz) in $CDCl_3$: 7.14–7.56 (m, 9H), 4.02 (s, 2H). Gas chromatography/fid was used to calculate the percent yields of the products at 85% conversion; cyclododecane was used as an internal standard. The yields were toluene (**19**) 40%, 1,2-diphenylethane (**5**) 10%, and (4-cyanophenyl)phenylmethane (**20**) 20%. The estimated error in these values is ±5%. The values for **5** and **20** were confirmed by isolation using column chromatography on silica gel (Kieselgel 60) eluting with methylene chloride and hexanes.

Irradiation of 2-phenylmethyl-2-methyl-1,3-dioxolane (17)

A solution of **17** (22 mg, 1.2×10^{-4} mol), **4** (20 mg; 1.6×10^{-4} mol), and cyclododecane (14 mg, 8.3×10^{-5} mol) in acetonitrile–methanol (2 mL, 3:1) was irradiated at 10°C for 20 h. The major products of the photolysis were toluene (**19**), 2-methoxy-2-methyl-1,3-dioxolane (**25**), 1,2-diphenylethane (**5**), and (4-cyanophenyl)phenylmethane (**20**). Product analysis was done using gc/fid with cyclododecane as an internal standard. The yields of **19**, **5**, and **20** were 35, 5, and 20% respectively, at 95% conversion. The yields of **5** and **20** were confirmed by isolation using column chromatography as described above for the reaction of **16**.

Acknowledgments

Acknowledgment is made to the Donors of the Petroleum Research Fund, administered by the American Chemical Society, and to the Natural Sciences and Engineering Research Council of Canada for support of this research. We thank Dr. D. L. Hooper and the Atlantic Region Magnetic Resonance Centre at Dalhousie University for the 360 MHz nmr spectra and for help in the preparation of the manuscript.

1. (*a*) D. R. Arnold, B. J. Fahie., L. J. Lamont, J. Wierzchowski, and K. M. Young. Can. J. Chem. **65**, 2734 (1987); (*b*) A. Okamoto, M. S. Snow, and D. R. Arnold. Tetrahedron, **42**, 6175 (1986); (*c*) A. Okamoto and D. R. Arnold. Can. J. Chem. **63**, 2340 (1985).
2. D. R. Arnold and S. A. Mines. Can. J. Chem. **67**, 689 (1989).
3. (*a*) X. Ci and D. G. Whitten. J. Am. Chem. Soc. **109**, 7215 (1987); (*b*) A. Albini and M. Mella. Tetrahedron, **42**, 6219 (1986); (*c*) T. Gotoh, M. Kato, M. Yamamoto, and Y. Nishijima. J. Chem. Soc. Chem. Commun. 90 (1981); (*d*) D. M. Camaioni and J. A. Franz. J. Org. Chem. **49**, 1607 (1984).
4. (*a*) H. M. Rosenstock, K. Draxl, B. W. Steiner, and J. T. Herron. J. Phys. Chem. Ref. Data, **6** (1977) Suppl. No. 1 (1977); (*b*) I. Howe and D. H. Williams. J. Am. Chem. Soc. **91**, 7137 (1969); (*c*) F. W. McLafferty, T. Wachs, C. Lifshitz, G. Innorta, and P. Irving. J. Am. Chem. Soc. **92**, 6867 (1970).
5. (*a*) M. J. Manka, R. L. Brown, and S. E. Stein. J. Phys. Chem. **89**, 5421 (1985); (*b*) A. C. Buchanan III, T. D. J. Dunstan, E. C. Douglas, and M. L. Poutsma. J. Am. Chem. Soc. **108**, 7703 (1986).
6. (*a*) D. D. M. Wayner, J. J. Dannenberg, and D. Griller. Chem. Phys. Lett. **131**, 189 (1986); (*b*) D. D. M. Wayner, D. J. McPhee, and D. Griller. J. Am. Chem. Soc. **110**, 132 (1988).
7. (*a*) H. F. Davis, P. K. Das, L. W. Reichel, and G. W. Griffin. J. Am. Chem. Soc. **106**, 6968 (1984); (*b*) L. W. Reichel, G. W. Griffin, A. J. Muller, P. K. Das, and S. N. Ege. Can. J. Chem. **62**, 424 (1984); (*c*) A. Albini, E. Fasani, and M. Mella. J. Am. Chem. Soc. **108**, 4119 (1986); (*d*) A. Albini, E. Fasani, and E. Montessoro. Z. Naturforsch. **29B**, 1409 (1984); (*e*) A. Albini and S. Spreti. J. Chem. Soc. Perkin Trans. 2, 1175 (1987); (*f*) E. Baciocchi and R. Ruzziconi. J. Chem. Soc. Chem. Commun. 445 (1984).
8. D. R. Arnold and A. J. Maroulis. J. Am. Chem. Soc. **98**, 5931 (1976).
9. (*a*) R. H. Martin, F. W. Lampe, and R. W. Taft. J. Am. Chem. Soc. **88**, 1353 (1966); (*b*) L. R. C. Barclay, J. Lusztyk, and K. U. Ingold. J. Am. Chem. Soc. **106**, 1793 (1984); (*c*) V. Malatesta and K. U. Ingold. J. Am. Chem. Soc. **103**, 609 (1981); (*d*) D. J. Pasto, R. Krasnansky, and C. Zercher. J. Org. Chem. **52**, 3062 (1987).
10. (*a*) R. A. Neunteufel and D. R. Arnold. J. Am. Chem. Soc. **95**, 4080 (1973); (*b*) Y. Shigemitsu and D. R. Arnold. J. Chem. Soc. Chem. Commun. 407 (1975).
11. D. Rehm and A. Weller. Isr. J. Chem. **8**, 259 (1970).
12. R. S. Nicholson and I. Shain. Anal. Chem. **36**, 706 (1964); **37**, 178 (1965).
13. (*a*) K. K. Barnes and C. K. Mann. J. Org. Chem. **32**, 1474 (1967); (*b*) E. S. Pysh and N. C. Yang. J. Am. Chem. Soc. **85**, 2124 (1963).
14. J. D. Young, G. R. Stevenson, and N. L. Bauld. J. Am. Chem. Soc. **94**, 8790 (1972).
15. A. Terahara, H. O.-Nishiguchi, N. Hirota, H. Higuchi, and S. Misumi. J. Phys. Chem. **90**, 4958 (1986).
16. (*a*) R. A. Marcus. Disc. Faraday Soc. **29**, 21 (1960); (*b*) I. R. Gould and S. Farid. J. Am. Chem. Soc. **110**, 7883 (1988).
17. (*a*) A. M. de P. Nicholas and D. R. Arnold. Can. J. Chem. **60**, 2165 (1982); (*b*) F. G. Bordwell and J.-P. Cheng. J. Am. Chem. Soc. **111**, 1792 (1989).
18. (*a*) R. Popielarz. Ph.D. Thesis, Dalhousie (1989); (*b*) R. Popielarz and D. R. Arnold. Submitted for publication.
19. D. D. M. Wayner and D. R. Arnold. Can. J. Chem. **63**, 871 (1985).
20. A. Klages and S. Heilmann. Ber. **37**, 1447 (1904).
21. I. Granoth, Y. Segall, H. Leader, and R. Alkabets. J. Org. Chem. **41**, 3682 (1976).
22. The Sadtler Handbook of Proton NMR Spectra. 1978. Compound number 1484, p. 654.
23. F. A. Abd Elhafez and D. J. Cram. J. Am. Chem. Soc. **75**, 339 (1953).
24. S. Uemura and S. Fukuzawa. J. Chem. Soc. Perkin Trans. 1, 471 (1985).
25. T. H. Chan, M. A. Brook, and T. Chaly. Synthesis, 203 (1983).
26. B. L. Jensen and R. E. Counsell. Can. J. Chem. **51**, 3820 (1973).
27. V. I. Stenberg and D. A. Kubik. J. Org. Chem. **39**, 2815 (1974).
28. I. M. Takakis and W. C. Agosta. J. Org. Chem. **43**, 1952 (1978).
29. R. Ratcliffe and R. Rodehorst. J. Org. Chem. **35**, 4000 (1970).

Can. J. Chem. Downloaded from www.nrcresearchpress.com by 186.148.149.217 on 09/07/12
For personal use only.

4,5-Dihydro-4,5-dihydroxyimidazoles as products of the reduction of 2-nitroimidazoles. HPLC assay and demonstration of equilibrium transfer of glyoxal to guanine

RICK PANICUCCI AND ROBERT A. MCCLELLAND
Department of Chemistry, University of Toronto, Toronto, Ont., Canada M5S 1A1

Received April 5, 1989

RICK PANICUCCI and ROBERT A. MCCLELLAND. Can. J. Chem. **67**, 2128 (1989).

An HPLC method has been employed to study the electrochemical reduction (mercury cathode at −800 mV with respect to calomel electrode) of the 2-nitroimidazole benznidazole (*N*-benzyl-(2′-nitro-1′-imidazoyl)acetamide). The principal product of this reduction is the cyclic guanidinium ion **3***c* (protonated *N*-benzyl-(2′-amino-4′,5′-dihydro-4′,5′-dihydroxy-1′-imidazoyl)acetamide), which forms in a linear fashion as the nitroimidazole is reduced and accounts for 75% of the product upon completion of the reduction. To perform the HPLC analysis quantitatively an authentic sample of this product (isolated as *cis*:*trans* isomers) was prepared as the sulfate salt through the reaction of *N*-benzyl-2-guanidinoacetamide sulfate with aqueous glyoxal. The two isomers of **3***c* arise through the nonreductive decomposition of the 2-hydroxylaminoimidazole, which is the product of a four-electron reduction of the nitroimidazole. Analysis of high field ^{1}H NMR spectra also showed that the two isomers of **3***c* were the principal products following electrochemical reduction, neutral aqueous zinc reduction, and radiation chemical reduction. Previous investigations using NMR of the reductions of misonidazole (3-methoxy-1-(2′-nitro-1′-imidazoyl)-2-propanol) and 1-methyl-2-nitroimidazole have shown that the corresponding dihydroimidazoles **3***a* and **3***b* are the major products. The agreement of these various NMR and HPLC results suggests that the formation of dihydroimidazoles **3** is a general phenomenon for model reductions of 2-nitroimidazoles in neutral aqueous solution. Previous workers have shown that 2-nitroimidazole reduction mixtures, when treated with guanine derivatives, form the adduct **4** derived from the guanine and glyoxal. This work demonstrates that this adduct is also formed when authentic samples of **3***a*, **3***b*, and **3***c* are reacted with 2′-deoxyguanosine. A quantitative HPLC analysis, however, demonstrates that the reaction does not proceed to completion, and in fact the equilibrium for formation of **4** is unfavorable. This suggests that guanines are not useful derivatizing agents for the quantitative assay of "glyoxal-like" products formed in chemical or biological reductions of 2-nitroimidazoles.

Key words: nitroimidazole, reduction of nitroimidazoles, glyoxal from nitroimidazoles.

RICK PANICUCCI et ROBERT A. MCCLELLAND. Can. J. Chem. **67**, 2128 (1989).

On a utilisé une méthode de CLHP pour étudier la réduction électrochimique (cathode de mercure à −800 mV par rapport à l'électrode de calomel) de la 2-nitroimidazole benznidazole (*N*-benzyl-(2′-nitro-1′-imidazoyl)acétamide). Le produit principal de cette réduction est l'ion guanidinium cyclique **3***c* (*N-benzyl-(2′*-amino-4′,5′-dihydro-4′,5′-dihydroxy-1′-imidazoyl)acétamide protoné) qui se forme d'une façon linéaire au fur et à mesure que le nitroimidazole est réduit et qui forme 75% du produit à la fin de la réduction. Afin de réaliser l'analyse quantitative par CLHP, on a préparé un échantillon authentique de ce produit (isolé sous la forme de sulfates des isomères *cis/trans*) par réaction du sulfate de *N*-benzyl-2-guanidinoacétamine avec du glyoxal en solution aqueuse. Les deux isomères du produit **3***c* proviennent de la décomposition non-réductive de la 2-hydroxyaminoimidazole, le produit d'une réduction de la nitroimidazole par quatre électrons. Une analyse des spectres RMN du ^{1}H à haut champ a aussi démontré que les deux isomères du produit **3***c* sont les produits principaux de la réduction électrochimique, de la réduction par le zinc en milieu aqueux neutre et de la réduction chimique par des radiations. Des études antérieures utilisant la RMN ont aussi démontré que les réductions du misonidazole (3-méthoxy-1-(2′-nitro-1′-imidazoyl)-2-propanol) et du 1-méthyl-2-nitroimidazole conduisent principalement aux dihydroimidazoles **3***a* et **3***b* correspondants. La bonne correspondance entre les résultats de la RMN et de la CLHP suggère que la formation de dihydroimidazoles **3** est un phénomène général pour les réductions modèles de 2-nitroimidazoles, en solutions aqueuses neutres. D'autres chercheurs ont démontré antérieurement que les mélanges obtenus lors des réductions de nitroimidazoles réagissent avec des dérivés de la guanine pour former l'adduit **4** dérivé de la guanine et du glyoxal. Dans le présent travail, on démontre que ce genre de dérivé se forme aussi lorsqu'on fait réagit des échantillons authentiques des produits **3***a*, **3***b* et **3***c* avec de la 2′-désoxyguanosine. Une analyse quantitative par CLHP a toutefois permis de démontrer que cette réaction est incomplète et que, de fait, l'équilibre pour la formation de l'adduit **4** n'est pas favorable. Ce résultat suggère que les guanines ne sont pas des agents utiles pour former des dérivés permettant d'analyser quantitativement les produits «ressemblant au glyoxal» qui se forment lors des réductions chimiques ou biologiques des 2-nitroimidazoles.

Mots clés : nitroimidazole, réduction des imidazoles, glyoxal dérivé des imidazoles.

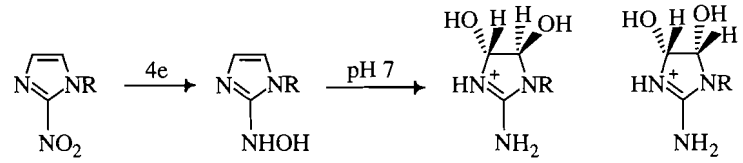
[Traduit par la revue]

2-Nitroimidazoles **1** are currently undergoing clinical trials as radiosensitizers of hypoxic (oxygen-deficient) cells (1, 2), and may also have clinical application in chemotherapy since they show selective cytotoxicity towards hypoxic cells (1). A number of the important biological effects of these drugs are associated with reductive metabolism (3), and this has led to an interest in the reduction chemistry. A variety of reduction methods have been employed to investigate this chemistry, including radiation chemical reduction (4–7), electrochemical reduction (6, 8–10), zinc/ammonium chloride reduction (11, 12), and biochemical reduction (13–18). In general, these experiments have shown a stoichiometry of four electron equivalents per nitroimidazole reduced, for aqueous solutions at pH 7. The product that corresponds to such a stoichiometry is the 2-hydroxylaminoimidazole **2**. Work in our laboratory, however, has shown that such compounds are unstable at neutral pH (6, 10, 19, 20), with half-lives ranging from 2–15 min (21, 22). The major products of their further reaction have been identified as the *cis* and *trans* 2-amino-4,5-dihydro-4,5-dihydroxyimidazolium ions **3** (10, 20, 21).

Several other groups have carried out product analyses by adding to previously reduced solutions reagents that form deriva-

[1]Also, R. A. McClelland and R. Fuller. Unpublished results.

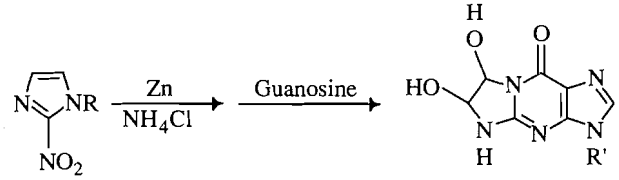
Can. J. Chem. Downloaded from www.nrcresearchpress.com by 186.148.149.217 on 09/07/12
For personal use only.

[1] 

1 2 *trans*-3 *cis*-3

a R = $CH_2CHOHCH_2OCH_3$ (Misonidazole)
b R = CH_3
c R = $CH_2CONHCH_2C_6H_5$ (Benznidazole)

tives of aldehydes and ketones. Such experiments have been found to result in the appropriate derivatives of the two-carbon dialdehyde glyoxal (7, 12, 17, 23–26). Of particular note in a biological context is the identification of **4**, the known adduct of guanosine and glyoxal (27, 28), by addition of guanosine to a solution obtained by the reduction of various 2-nitroimidazoles with zinc in aqueous ammonium chloride (12, 23). This same derivative has been observed following radiation chemical reduction (7, 26). This adduct, moreover, has been detected upon addition of guanosine to hypoxic cells treated with misonidazole (**1***a*) (29) and by addition of guanosine to the urine of a patient receiving misonidazole (30).

[2] 

4

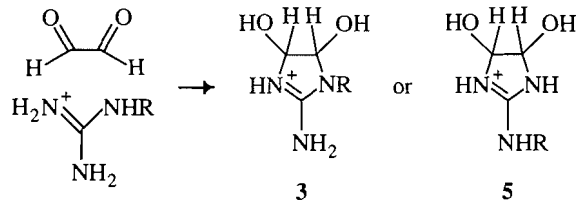
In general, yields of these glyoxal derivatives relative to the nitroimidazole reduced have been low, with reported numbers ranging from a fraction of a percent (7) to 25% (17). Moreover, there has been some discussion (17, 23) as to whether the reduction mixture actually contains free glyoxal or simply some species capable of reacting with the added reagent to form the glyoxal derivative. Our analyses have supported the latter viewpoint, the dihydroimidazoles **3** being able to react to give glyoxal derivatives (10). This species **3** is in fact the adduct of glyoxal and a monosubstituted guanidinium ion, with the equilibrium in aqueous solution lying well to the adduct side (10). We have moreover found that yields of **3** are high, the two isomers accounting for 80–90% of the initial nitroimidazole when reductions are carried out in the absence of other strong nucleophiles (10, 20). This result obviously contrasts with the situation for the glyoxal derivatives; we have argued that the derivatization procedures do not quantitatively produce the glyoxal adduct when **3** is the starting material.

That the two isomers of **3** constitute the major products of the reduction of 2-nitroimidazoles has come mainly from analyses of high field ^1H NMR spectra, following radiation chemical reduction, electrochemical reduction, and zinc reduction, principally of misonidazole and the model 1-methyl-2-nitroimidazole **1***b* (10). In this paper we report verification of this conclusion with an HPLC analysis conducted using the nitroimidazole benznidazole (**1***c*). This nitroimidazole is used extensively in South America for the treatment of the *Trypanosome cruzi* infection (Chaga's disease) (31), and has also been shown to function as a chemosensitizer of the antitumor agent chloroethylnitrosourea (32, 33). From the point of view of HPLC analysis, it has the advantage (18) of having a phenyl chromophore in its side chain, making the UV spectroscopic detection of **3***c* possible. The derivatives **3***a* and **3***b* are transparent down to 210 nm. We also report here experiments showing that pure samples of **3** can transfer glyoxal to guanine, but the equilibrium is unfavorable. We also provide unambiguous evidence that the structure of the **3** is the 1-substituted derivative, as written in eq. [1].

Results

Carbon-13 NMR analysis of trans *3*b

The assignment of the structure of the products of the reduction as the isomers **3** was based upon a synthesis of analytically pure samples of these species by combining aqueous glyoxal and the appropriate monosubstituted guanidinium ion (10). The ^1H NMR spectra of these products were then shown to match the principal peaks in the spectra of the reduction mixtures. As we have discussed previously, some ambiguity exists as to whether the products are actually the 1-substituted **3** or the adducts **5** where the substituent is on the external nitrogen. In the case of the nitroimidazole reduction mixtures where the substituent starts on N-1, a situation where **5** arises via a ring opening – ring closing sequence could not be rule out (10).

[3] 

3 **5**

We have now obtained unambiguous evidence for the structure **3** based upon an analysis of ^{13}C NMR spectra obtained with *trans* **3***b*. This species was obtained in pure *trans* form through the combination of glyoxal and methylguanidinium hydrochloride. This resulted in a 1:4 *cis*:*trans* ratio; recrystallization from methanol:ether gave pure (>98%) *trans*, as seen from the absence of the characteristic signal for the *cis* isomer in the ^1H NMR spectrum. The decoupled ^{13}C NMR spectrum of *trans* **3***b* (recorded in dilute DCl to suppress *trans*:*cis* equilibration (10)) had the expected four signals, at 161.0, 94.0, 86.8, and 31.8 ppm. The lowest field and highest field signals can be assigned to C2 and the methyl carbon respectively. The other two signals represent C4 and C5 but cannot be assigned from the decoupled spectrum. However, in a proton coupled spectrum (Fig. 1) these signals exhibited a different pattern. The signal at 86.8 ppm in the uncoupled spectrum appears as a doublet of doublets. This can be assigned to C4, with a large one-bond coupling to its directly attached hydrogen H4 (^1J(C4–H4) = 170 Hz) and a small two-bond coupling to H5 (^2J(C4–H5) = 2.4 Hz). The other signal at 94.0 ppm in the uncoupled spectrum, assigned to C5, is expected to have similar ^1J and ^2J couplings with H5 and H4 respectively. This signal, however, shows additional coupling, which must arise

Can. J. Chem. Downloaded from www.nrcresearchpress.com by 186.148.149.217 on 09/07/12
For personal use only.

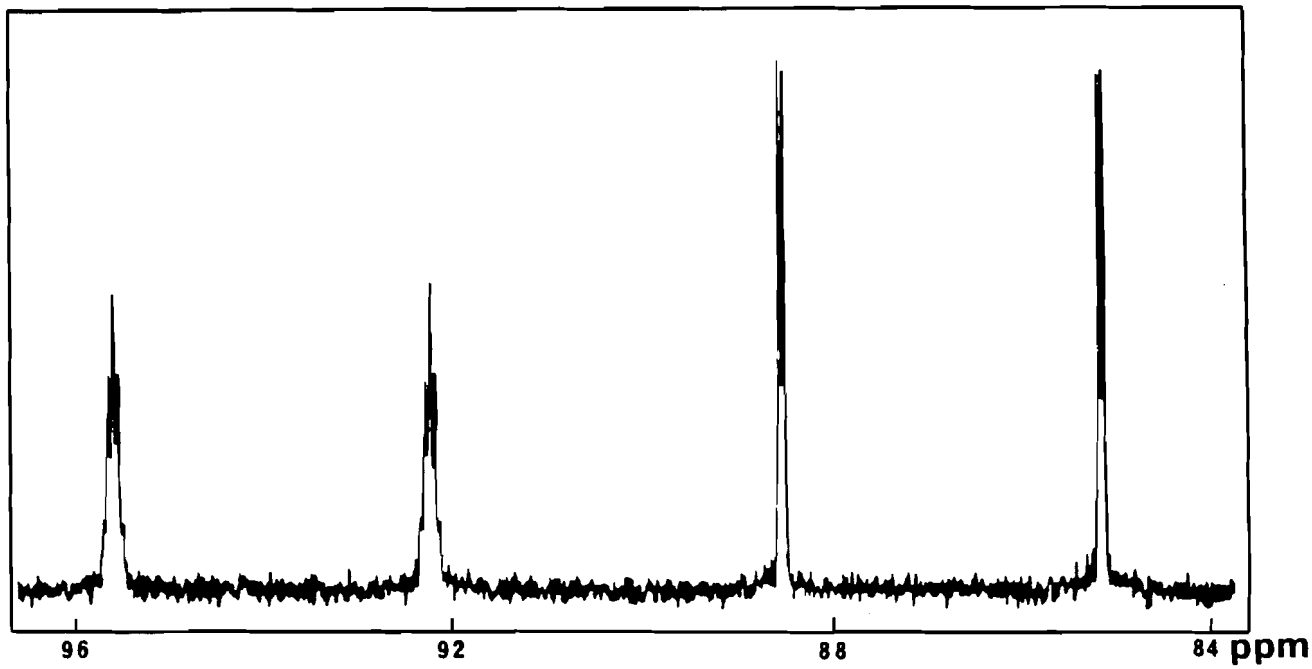


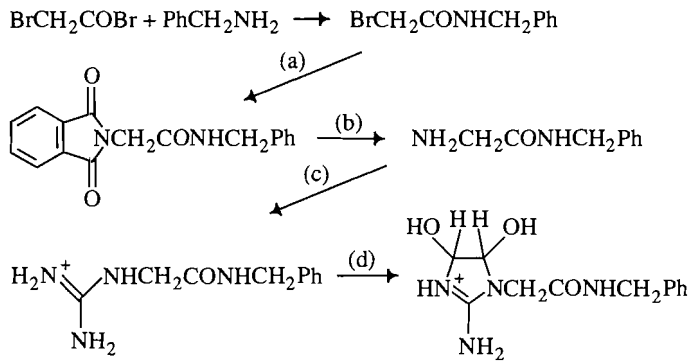
FIG. 1. Proton-coupled 50.4 MHz ^{13}C NMR spectrum (85–95 ppm region) of *trans*-**3***b* in dilute DCl.

from the protons of the methyl group. This requires the methyl group to be attached to the ring nitrogen, three bonds away, rather than to the external nitrogen, which is five bonds away, too far to show significant coupling. A five-line pattern actually results for C5 since ^2J(C5–H4) and ^3J(C5–CH_3) are similar.

Reduction of benznidazole. NMR analysis

Figure 2 shows the ^1H NMR spectrum obtained upon the crude mixture following radiation chemical reduction (4, 6) of benznidazole in phosphate-buffered neutral aqueous solution. Very similar spectra were also obtained following electrochemical reduction and reduction with zinc in aqueous ammonium chloride. The radiation chemical and electrochemical reductions also showed the expected stoichiometries of 4.0 ± 0.2 electron equivalents per nitroimidazole. The products that are consistent with the NMR spectrum and the stoichiometry are the *cis* and *trans* isomers of **3***c*, arising from the further reaction of the 2-hydroxylaminoimidazole, as in eq. [1]. A detailed discussion of the NMR pattern has been presented previously in the context of the methyl derivative **3***b*. In the present case the two pairs of doublets at 5.0–5.5 ppm (see insert) represent H4 and H5 of the two isomers of **3***c*, the major isomer (80%) with the smaller coupling constant being assigned the *trans* geometry. The set of signals at 4.15–4.3 ppm can be assigned to the NCH_2CO group of the side chain, with the two diastereotopic protons of this methylene group being nonequivalent. Again two sets of signals for the two isomers can be recognized (see insert). The remaining signals at 7.4 ppm and 4.42 ppm arise from the phenyl groups and the benzylic methylenes respectively, the latter appearing as a single peak in each isomer with, in fact, almost the same chemical shifts for the two isomers.

Verification of the structure of **3***c* was obtained by the alternate preparation from the reaction of aqueous glyoxal and the appropriate guanidinium ion. The latter was prepared as the sulfate salt, described as follows.



(a) Potassium phthalimide. (b) Hydrazine.
(c) 2-Methyl-2-thiopseudourea sulfate. (d) Aqueous glyoxal, pH 8

This sequence of reactions resulted in an analytically pure sample of the two isomers of **3***c*, whose NMR spectrum in D_2O matched that obtained from the various reductions of the nitroimidazole.

Reduction of benznidazole. HPLC analysis

The previous set of experiments, involving the unambiguous synthesis of the dihydroguanidinium ion and the demonstration of identical NMR patterns with those of reduction mixtures, are the same as those carried out earlier in characterizing the products of misonidazole and 1-methyl-2-nitroimidazole (10). As in those experiments, the two isomers of **3***c* account for virtually all the peaks in the NMR spectra of the benznidazole reduced by the three techniques. Even recognizing that the NMR limits of detection may be as high as 10–20%, particularly for complex systems, the conclusion must be that **3***c* is the major product of these reductions of benznidazole.

As noted above, the phenyl group in the side chain provides a handle for HPLC experiments with spectroscopic detection. This group also has the feature of imparting some hydrophobic

Can. J. Chem. Downloaded from www.nrcresearchpress.com by 186.148.149.217 on 09/07/12
For personal use only.

Can. J. Chem. Downloaded from www.nrcresearchpress.com by 186.148.149.217 on 09/07/12
For personal use only.

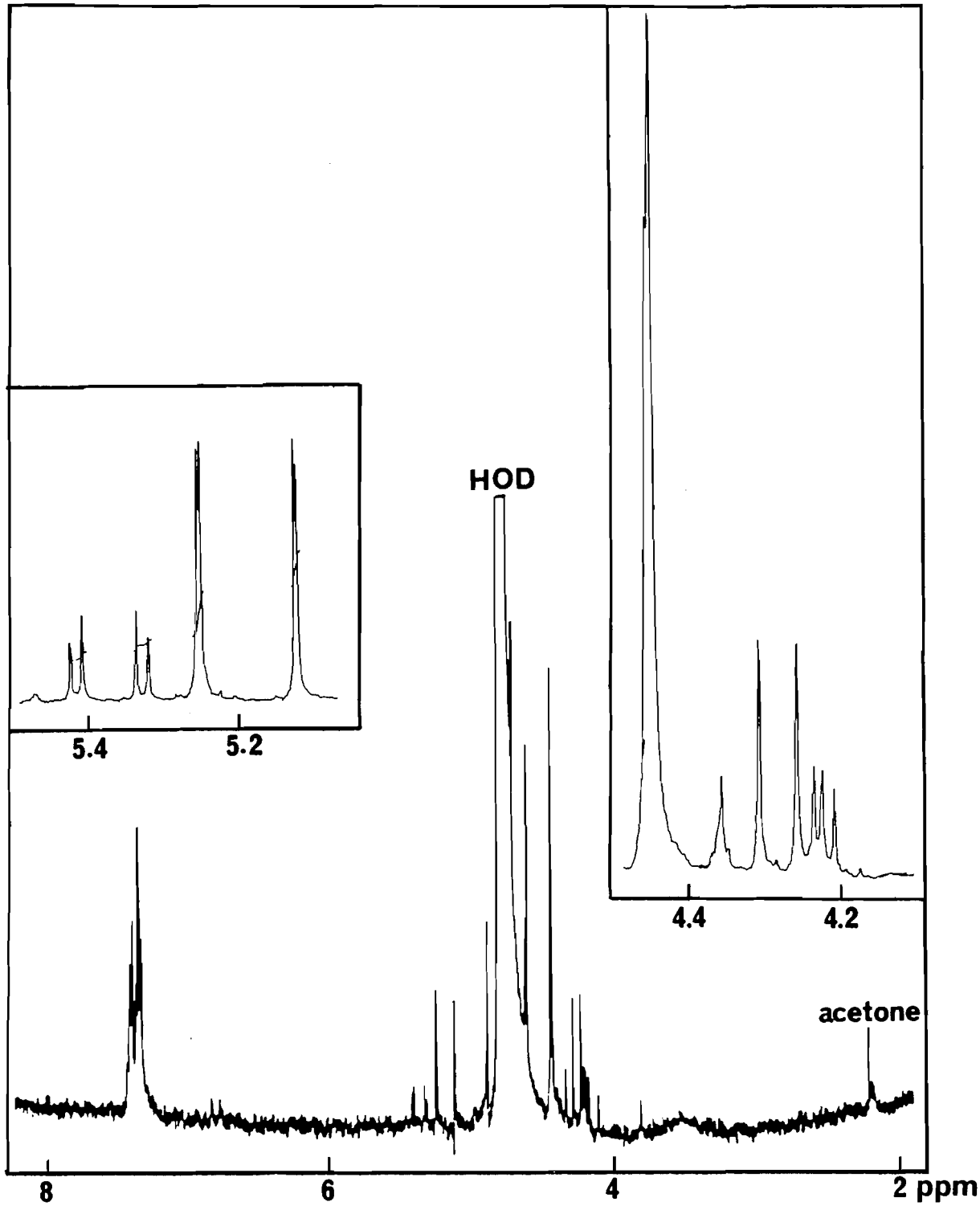


FIG. 2. The 400 MHz ^{1}H NMR spectrum of benznidazole after radiation chemical reduction in phosphate buffered D_2O at pD 7. This spectrum was obtained directly on the irradiated D_2O solution.

character so that the highly polar product ions do not migrate with the solvent front in reversed-phase HPLC. We employed HPLC conditions similar to those previously used to analyze benznidazole and its amine derivative (18), and found that authentic samples of the nitroimidazole and **3***c*, the latter prepared as described above, eluted with retention times of 8.7 min and 4.6 min respectively (the two isomers of **3***c* not separating). Figure 3 shows chromatograms obtained from the analysis of the electrochemical reduction at pH 7 of benznidazole. It is clear that as the nitroimidazole disappears, it is replaced by **3***c*. The situation is shown quantitatively in Figure 4. As expected, the nitroimidazole disappears in a linear fashion with the number of reducing equivalents. In the experiment represented in the figure a total of 9.9 coulombs was required to completely

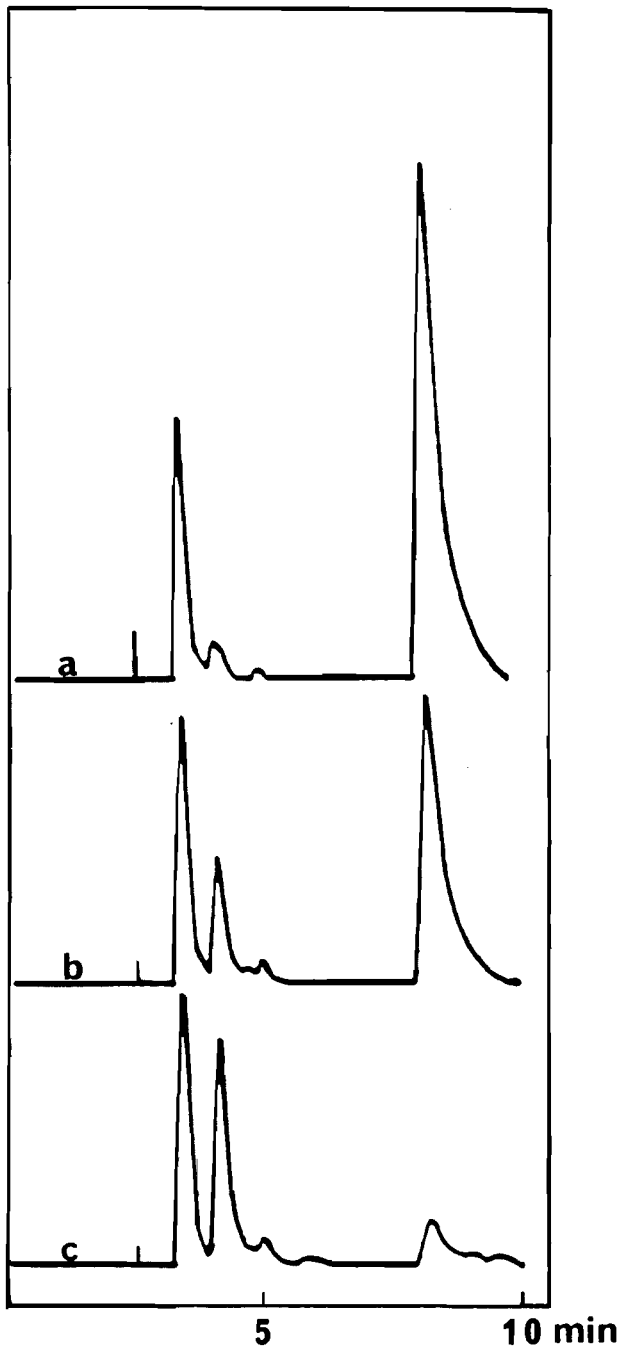


FIG. 3. HPLC chromatograms obtained during the electrochemical reduction at pH 7 of benznidazole; (a) 10% reduced, (b) 50% reduced, and (c) 90% reduced. The peaks at 8.7 min and 4.6 min correspond to benznidazole and **3***c* respectively. The peak at 3.4 min was present in all samples and is believed to be an impurity in the eluting solution. HPLC conditions: detector wavelength = 220 nm, Nova-pak C_{18} column, with eluting buffer of 25% acetonitrile, 0.2 M glycine/hydrochloric acid, pH 2.5, plus 5 mM octanesulfonic acid, flow rate = 3 mL/min.

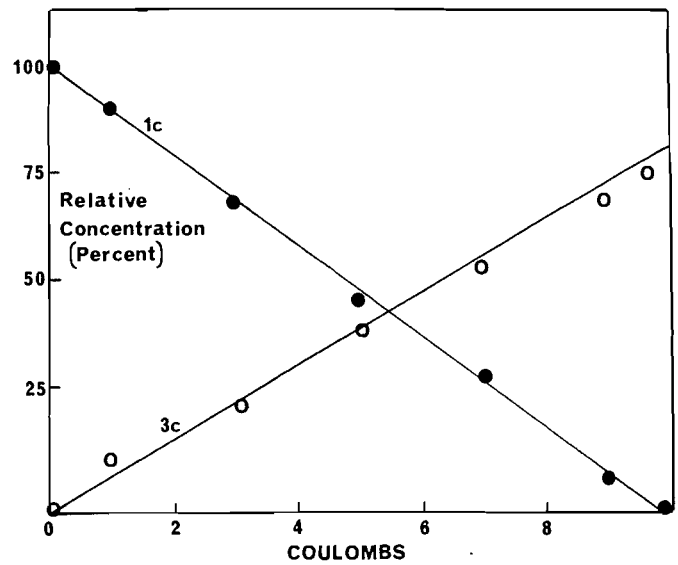


FIG. 4. Relative concentration of benznidazole **1***c* and the product **3***c* as a function of the number of coulombs passed through the solution in the electrochemical reduction of benznidazole. The initial concentration of benznidazole was 1.05 mM in a 25 mL volume (26.3 μmol). The relative concentrations of **1***c* and **3***c* were calculated from relative areas of the HPLC profiles, using standard curves constructed from injections of known amounts of authentic material.

reduce 26.2 μmol. This corresponds to a stoichiometry of 3.92 electrons per nitroimidazole, a result expected from previous studies (4, 6) where UV spectroscopy was employed to analyze for the nitro compound. As **1***c* disappears, **3***c* is formed. This production occurs in a linear fashion with the number of coulombs, indicative of the fact that **3***c* is a primary product of the reduction and that it is also stable under these experimental conditions. Using authentic samples of benznidazole and **3***c*, standard curves relating the HPLC integration units and concentration were constructed. After complete reduction, **3***c* accounts for 75% of the initial starting nitro compound.

Additional products are evident from the HPLC profiles but their identities are unknown. We have shown (10) that when reductions are carried out in phosphate buffers, a monophosphate of **3** is also formed, in yields of 10–20% even in 10 mM phosphate. Such a product is also possible in the present case, since phosphate was necessary to control the pH during the electrolysis. Another likely side product is an azoxy compound formed by coupling of the hydroxylamine product and the nitroso intermediate during reduction. This product is commonly encountered in the reduction of nitroaromatic compounds at neutral pH, and a yellow color observed in the reduced benznidazole solution was consistent with its presence. Whatever the nature of these other products, it is clear that their yields are small and they do not contribute significant signals to the NMR spectra. Moreover, the direct monitoring by HPLC has verified the conclusion of the NMR analysis, namely that **3***c* is the major product.

A product worth commenting upon, which was not present in significant yield with any of the three techniques, was the 2-aminoimidazole derivative, the result of a six-electron reduction. This substance, which was available in pure form as a standard, has in its ^{1}H NMR spectrum a characteristic pattern of doublets at 6.7–6.8 ppm associated with H4 and H5 of the imidazole ring. These doublets were observed in the zinc reduction, but accounted for only 5–10% of the overall reduction mixture. With both the radiation chemical reduction and the electrochemical reduction, no signals remained at >6 ppm.

Reaction of 3 with deoxyguanosine

These experiments were conducted to demonstrate that the dihydroimidazoles **3** can transfer the elements of glyoxal to guanine, and also to quantitatively evaluate the position of the

Can. J. Chem. Downloaded from www.nrcresearchpress.com by 186.148.149.217 on 09/07/12
For personal use only.

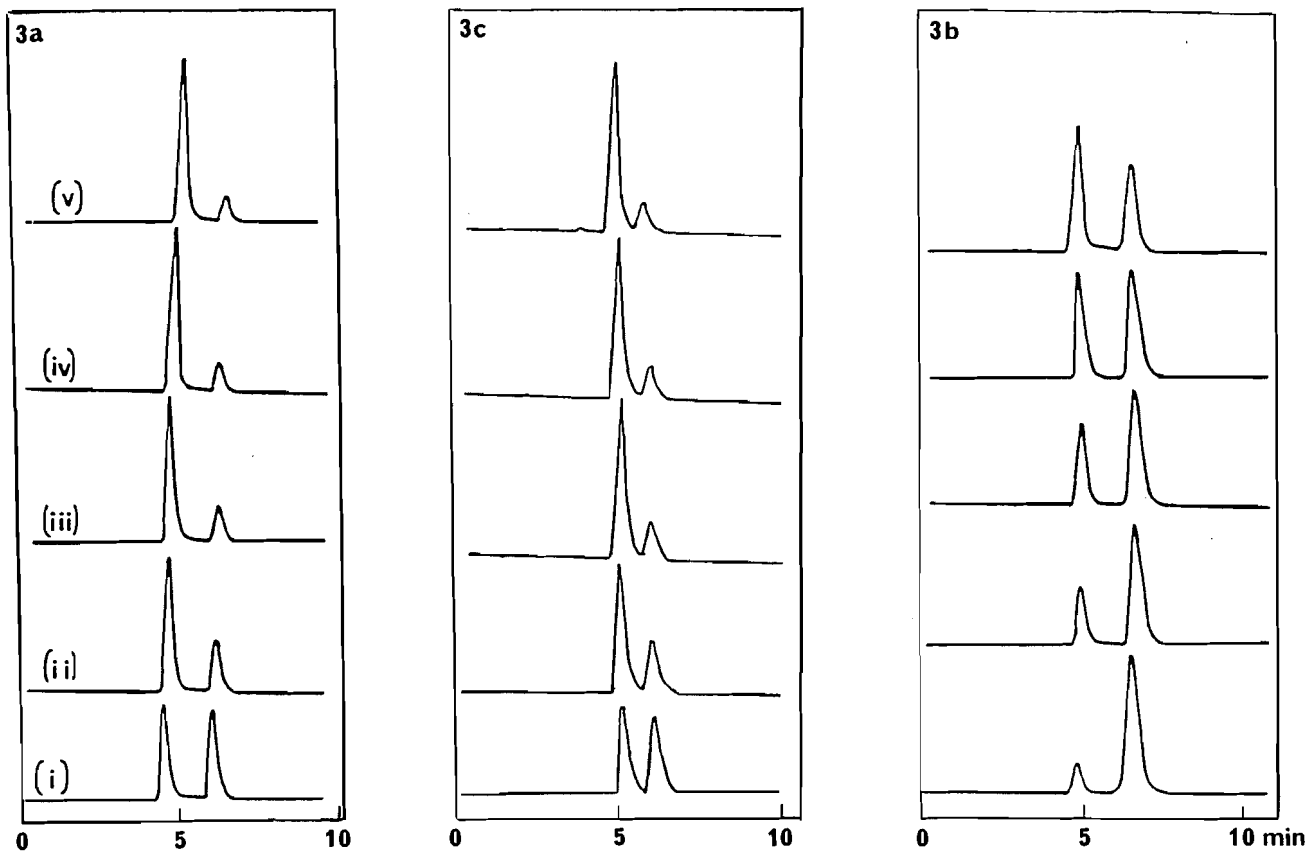
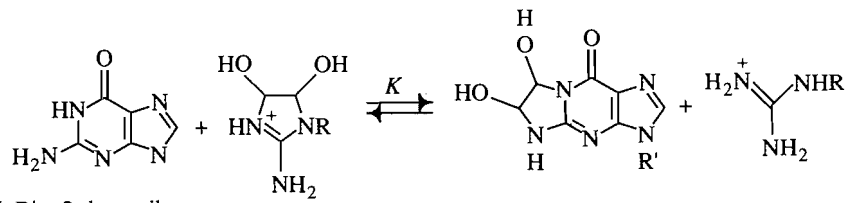


FIG. 5. HPLC chromatograms for the reaction of **3***a–c* with 2′-deoxyguanosine. Reaction conditions: 0.05 M phosphate buffer, pH 7.5, 25°C, 2′-deoxyguanosine = 0.1 mM, **3** = 1.0 mM (i), 2.0 mM (ii), 3.0 mM (iii), 4.0 mM (iv), and 5.0 mM (v). These chromatograms were obtained after 5–7 days and were unchanged on further standing. HPLC conditions: detector wavelength = 258 nm, C18–10μ–Bondapak column, with eluting buffer of 0.25 M ammonium acetate (pH ~ 7); methanol (95:5), flow rate = 3 mL/min.

[4] 

6, R' = 2-deoxyribose

3a–c

4

7

equilibrium. HPLC was used to monitor the course of the reaction, as previously described by Varghese and Whitmore (23). This involved analyzing for the relative concentrations of starting 2′-deoxyguanosine **6** and its adduct **4** by monitoring near the λ_{max} of the guanine chromophore. The HPLC elution profiles showed two peaks (Fig. 5), that for the deoxyguanosine coming at 6.0 min with the glyoxal–guanosine adduct at 4.5 min. An authentic sample of the latter was prepared as previously described, from the reaction of glyoxal and 2′-deoxyguanosine (27, 28). Standard curves were constructed for the two samples. Under the HPLC conditions both gave a single peak, indicative that interconversion between the two was not occurring on the column. As shown in Fig. 5, the dihydroimidazoles **3** did transfer glyoxal. Under the reaction conditions, aqueous solution at 25°C and pH 7.5, the reaction was slow, 2–4 days being required to reach an equilibrium condition. Moreover, the reaction did not proceed to completion. Even with a 50-fold excess of **3** some unreacted deoxyguanosine remained. Equilibrium constants ([**4**][**7**]/[**6**][**3**]) were calculated, the equilibrium concentrations of **4** and **6** being determined from the peak areas in the HPLC chromatograms, the concentration of **7** being set equal to that of **6** and the concentration of **3** being calculated by difference. (We have previously demonstrated that the equilibrium involving **3** and glyoxal plus guanidinium ion lies well to the adduct side in aqueous solution (10), so that the reaction can be represented as written in eq. [4].) Values of the equilibrium constants are summarized in Table 1. This table also shows that there is good agreement between measurements with different initial concentrations of **3**.

Discussion

We have used an HPLC method to demonstrate that the electrochemical reduction of benznidazole under neutral aqueous conditions results in a 75% yield of the corresponding dihydroimidazole **3***c*. This arises from a further nonreductive reaction of the four-electron reduction product, the 2-hydroxylaminoimidazole. The result, which is based on a direct analy-

Can. J. Chem. Downloaded from www.nrcresearchpress.com by 186.148.149.217 on 09/07/12
For personal use only.

TABLE 1. Equilibrium constants for the reaction of **3***a–c* with 2′-deoxyguanosine (0.1 mM) in 0.05 M phosphate buffer, pH 7.5 at 25°C

Substituent R in **3**	[**3**], M	Equilibrium constant
CH_3	0.005	0.030
	0.004	0.024
	0.003	0.027
	0.002	0.024
	0.001	0.025
$CH_2CONHCH_2Ph$	0.005	0.090
	0.004	0.083
	0.003	0.093
	0.002	0.089
	0.001	0.090
$CH_2CHOHCH_2OCH_3$	0.005	0.11
	0.004	0.11
	0.003	0.10
	0.002	0.10
	0.001	0.11

sis while reduction is proceeding, verifies previous conclusions reached on the basis of ^{1}H NMR spectroscopy that simple model reductions of 2-nitroimidazoles produce high yields of this type of product. 2-Nitroimidazoles are reductively activated to compounds that generate covalent adducts in protein and DNA (34–36) and breaks in DNA (37), and that result in depletion of the intracellular thiol glutathione (38). We have suggested that the unstable hydroxylamine may in part be responsible for these effects, since mechanistically a reactive electrophile capable of binding cellular nucleophiles can be identified for the conversion of the hydroxylamine to products such as **3** (10, 21, 22). In general, in these model reductions the 2-aminoimidazole, which is the product of a six-electron reduction, is not observed or is found only in small quantities. This derivative, however, has been identified in biological systems, in studies both with misonidazole (39, 40) and with benznidazole (17). The origin of this species would appear to be the further reduction of the 2-hydroxylaminoimidazole and what can be proposed is that there is a competition at the hydroxylamine stage between this further reduction and the nonreductive reaction producing products such as **3**. There is evidence in fact for this competition in some of the model systems. In the present study small amounts of the amine were observed in the zinc reduction. Previous workers employing radiation chemical reduction have demonstrated with misonidazole that the amine can be produced with very high radiation doses but not with low doses (4). Moreover, catalytic hydrogenation of 2-nitroimidazoles produces only the amine derivative (41, 42).[1] Our suggestion is that in cells, there are enzymes capable of reducing the hydroxylamine further in competition with the decomposition reaction.

There is evidence that products derived from the hydroxylamine are produced in biological systems, in the findings that the guanosine–glyoxal adduct can be formed in vitro (29) and in vivo (30), and the observation in vitro of a glutathione adduct derived from the hydroxylamine (43). As demonstrated in this study, the dihydroimidazoles can transfer glyoxal to guanine, and we suggest it is these species, not glyoxal itself, that are responsible for the formation of **4** both in the model systems and in the biological systems. Our results, however, show that the reaction is incomplete, the equilibrium in fact being quite unfavorable. On this basis we suggest that guanine (or one of its derivatives) cannot be used to quantitatively analyze for glyoxal in the reduction mixtures of 2-nitroimidazoles. The unfavorable equilibrium also accounts for the low yields of the glyoxal derivative obtained in those cases where this method was employed. It is in fact interesting, considering the position of the equilibrium, that the glyoxal–guanidine adduct was observed in the biological systems. Since the equilibrium for the formation of this derivative is so unfavorable, the implication is that the amount of the precursor must have been considerably higher.

Experimental

General methods

^{1}H NMR and ^{13}C NMR spectra were recorded with a Varian 400 MHz spectrophotometer at the Department of Chemistry. Electrochemical reductions were carried out with an ECO Instruments model 550 potienstat equipped with a model 721 integrator. HPLC experiments were performed with a Varian LC 5500 system equipped with a Varian 601 data system integrator. Radiation chemical reductions were performed using a ^{60}Co Gamma cell (Atomic Energy of Canada) located at the Princess Margaret Hospital.

Materials

Benznidazole and the amine derivative of benznidazole were kindly provided by Paul Workman. 2′-Deoxyguanosine and aqueous glyoxal were from the Aldrich Chemical Co. and were used directly. The glyoxal-2′-deoxyguanosine adduct **4** was prepared as described in the literature (27, 28), and had an ^{1}H NMR spectrum identical to that reported previously. HPLC analysis of this material showed that there was no unreacted 2′-deoxyguanosine. The 4,5-dihydro-4,5-dihydroxyimidazolium salts **3***a* and **3***b* were prepared through the combination of aqueous glyoxal and the appropriate guanidinium ion, as previously described (10). The sample of **3***b*, which was obtained as the >98% *trans* isomer, was isolated in this way by dissolving the *cis*:*trans* mixture in methanol, followed by the slow addition of diethyl ether until a precipitate just formed.

N-Benzyl-2-bromoacetamide was prepared from bromoacetyl bromide (Aldrich) and benzylamine (44). *N*-Benzyl-2-phthalylamidoacetamide was prepared from *N*-benzyl-2-bromoacetamide by reacting with potassium phthalimide (45). *N*-Benzyl-2-aminoacetamide was prepared by the reaction of *N*-benzyl-2-phthalylamidoacetamide with hydrazine (46). *N*-Benzyl-2-guanidinoacetamide was obtained as its sulfate salt ($2RNHC(NH_2)_2 \cdot SO_4$) by the reaction of *N*-benzyl-2-aminoacetamide with 2-methyl-2-thiopseudourea sulfate (47). *N*-Benzyl-(2′-amino-4′,5′-dihydro-4′,5′-dihydroxy-1′-imidazoyl)acetamide was prepared as the sulfate salt ($(\mathbf{3}c)_2 \cdot SO_4$) from the reaction of *N*-benzyl-2-guanidinoacetamide sulfate with aqueous glyoxal (10).

Reduction procedures. NMR analysis

Details of these procedures have been given previously (10).

Electrochemical reduction of benznidazole with HPLC analysis

This reduction was carried out with a standard H-cell with a fritted disc separating the anode and cathode compartments. The anode was a 50 cm^2 sheet of platinum foil; this compartment contained 0.05 M NaCl. A mercury cathode (12 cm^2 surface area) was used; this was set at a constant potential of −800 mV with reference to a calomel electrode. A phosphate buffer was used to maintain pH on the cathode compartment near neutrality (pH 6.5–7.5). Both compartments were continually bubbled with nitrogen during the electrolysis. In a typical experiment 10 mg of benznidazole was dissolved in 25 mL of phosphate buffer. The reduction was monitored by periodically withdrawing 0.1 mL aliquots of the cathode solution, diluting to 1.0 mL, and determining the relative concentrations of unreduced benznidazole and **3***c* by HPLC. The number of coulombs passed at each point was read directly from the integrator. HPLC analyses were carried out on a Nova-pak C_{18} column (3.9 mm × 15 mm) with a mobile phase con-

Can. J. Chem. Downloaded from www.nrcresearchpress.com by 186.148.149.217 on 09/07/12
For personal use only.

sisting of 25% acetonitrile (HPLC grade, Aldrich) in 0.2 M glycine buffer, pH 2.5, containing 5 mM octanesulphonic acid. The column was eluted isocratically at a flow rate of 1 mL/min (column pressure 1000 psi; 1 psi = 6.9 kPa) and the absorbance was monitored at 220 nm.

Reactions of 3 with 2'-deoxyguanosine

2'-Deoxyguanosine (0.1 mM) and various concentrations of **3***a–c* were mixed in a phosphate buffer (0.05 M) and the pH adjusted to 7.5. These solutions were stored at 25°C, with aliquots being periodically withdrawn for analysis by HPLC. Generally 5–7 days were required before equilibrium was reached as judged from a constant integration of the two peaks in question. HPLC analyses were carried out using a C_{18}-10μ-Bondapak column (3 mm × 15 mm) with the mobile phase consisting of 0.25 M ammonium acetate:methanol (95:5). The column was eluted at a flow of 1 mL/min (column pressure 1000 psi) with the absorbance monitored at 258 nm.

Acknowledgement

This research was supported through a grant from the National Cancer Institute of Canada. Useful discussions with Drs. Mike Rauth and Paul Workman are gratefully acknowledged.

1. S. DISCHE. Radiother. Oncol. **3**, 97 (1985).
2. G. E. ADAMS and I. J. STRATFORD. Biochem. Pharmacol. **35**, 71 (1986).
3. A. M. RAUTH. Int. J. Radiat. Oncol. Biol. Phys. **10**, 1293 (1984).
4. D. W. WHILLANS and G. F. WHITMORE. Radiat. Res. **86**, 311 (1981).
5. T. KAGIYA, H. IDE, S. NISHIMOTO, and T. WADA. Int. J. Radiat. Biol. **44**, 505 (1983).
6. R. A. MCCLELLAND, J. R. FULLER, N. E. SEAMAN, A. M. RAUTH, and R. BATTISTELLA. Biochem. Pharmacol. **33**, 303 (1984).
7. A. R. J. SILVER, S. S. MCNEILL, P. O'NEILL, T. C. JENKINS, and I. AHMED. Biochem. Pharmacol. **35**, 3923 (1986).
8. M. V. MIDDLESTADT and A. M. RAUTH. Int. J. Radiat. Oncol. Biol. Phys. **8**, 709 (1982).
9. R. J. KNOX, R. C. KNIGHT, and D. I. EDWARDS. Biochem. Pharmacol. **32**, 2149 (1983).
10. R. A. MCCLELLAND, R. PANICUCCI, and A. M. RAUTH. J. Am. Chem. Soc. **109**, 4308 (1987).
11. A. J. VARGHESE and G. F. WHITMORE. Chem.-Biol. Interact. **36**, 141 (1981).
12. A. J. VARGHESE and G. F. WHITMORE. Chem.-Biol. Interact. **56**, 269 (1985).
13. E. D. CLARKE, P. WARDMAN, and K. H. GOULDING. Biochem. Pharmacol. **29**, 2684 (1980).
14. P. D. JOSEPHY, B. PALCIC, and L. D. SKARSGARD. Biochem. Pharmacol. **30**, 849 (1981).
15. J. A. RALEIGH, S. F. LIU, and F. Y. SHUN. Int. J. Radiat. Oncol. Biol. Phys. **8**, 701 (1982).
16. E. D. CLARKE, K. H. GOULDING, and P. WARDMAN. Biochem. Pharmacol. **31**, 3237 (1982).
17. D. C. HEIMBROOK and A. C. SARTORELLI. Mol. Pharmacol. **29**, 168 (1986).
18. M. I. WALTON and P. WORKMAN. Biochem. Pharmacol. **36**, 887 (1987).
19. K. R. LADEROUTE, E. ERYVAIC, R. A. MCCLELLAND, and A. M. RAUTH. Int. J. Radiat. Oncol. Biol. Phys. **12**, 1215 (1986).
20. R. PANICUCCI, R. A. MCCLELLAND, and A. M. RAUTH. Int. J. Radiat. Oncol. Biol. Phys. **12**, 1227 (1986).
21. R. A. MCCLELLAND, R. PANICUCCI, and A. M. RAUTH. J. Am. Chem. Soc. **107**, 1762 (1985).
22. J. L. BOLTON and R. A. MCCLELLAND. J. Am. Chem. Soc. In press.
23. A. J. VARGHESE and G. F. WHITMORE. Cancer Res. **43**, 78 (1983).
24. J. A. RALEIGH and S. F. LIU. Biochem. Pharmacol. **32**, 1444 (1983).
25. J. A. RALEIGH and S. F. LIU. Int. J. Radiat. Oncol. Biol. Phys. **10**, 1337 (1984).
26. A. J. R. SILVER and S. S. MCNEILL. Biochem. Pharmacol. **19**, 3537 (1987).
27. R. SHAPIRO and J. HACHMANN. Biochemistry, **5**, 2799 (1966).
28. N. E. BROUDE and E. O. BOROWSKY. Biochem. Biophys. Acta, **54**, 340 (1971).
29. A. J. VARGHESE and G. F. WHITMORE. Radiat. Res. **97**, 262 (1984).
30. A. J. VARGHESE and G. F. WHITMORE. Int. J. Radiat. Oncol. Biol. Phys. **10**, 1361 (1984).
31. C. A. BARCLAY, J. A. CERISOLA, H. LUGONES, and O. LEDESMA. *In* Current chemotherapy. Vol. 1. *Edited by* W. Siegenthaler and R. Luthy. American Society for Microbiology, Washington, DC. 1978. p. 158.
32. P. R. TWENTYMAN and P. WORKMAN. Br. J. Cancer **48**, 17 (1983).
33. J. T. ROBERTS, N. M. BLEEHEN, F. Y. F. LEE, P. WORKMAN, and M. I. WALTON. Int. J. Radiat. Oncol. Biol. Phys. **10**, 1745 (1984).
34. A. J. VARGHESE and G. F. WHITMORE. Cancer Res. **40**, 2165 (1980).
35. G. G. MILLER, J. NGAN-LEE, and D. J. CHAPMAN. Int. J. Radiat. Oncol. Biol. Phys. **8**, 741 (1982).
36. A. J. FRANKO. Int. J. Radiat. Oncol. Biol. Phys. **12**, 1195 (1986).
37. D. I. EDWARDS. Br. J. Vener. Dis. **56**, 285 (1980).
38. E. A. BUMP, Y. C. TAYLOR, and J. M. BROWN. Cancer Res. **44**, 997 (1983).
39. A. J. VARGHESE. Anal. Biochem. **110**, 197 (1981).
40. J. L. BORN and V. M. HADLEY. Int. J. Radiat. Oncol. Biol. Phys. **11**, 1157 (1985).
41. I. R. FLOCKHART, P. LARGE, D. TROUP, S. L. MALCOLM, and D. R. MARTEN. Xenobiotica, **8**, 97 (1978).
42. R. FULLER. M.Sc. Thesis, University of Toronto (1983).
43. A. J. VARGHESE and G. F. WHITMORE. Int. J. Radiat. Oncol. Biol. Phys. **10**, 1341 (1984).
44. R. HUISGEN and R. REIMLINGER. Ann. **599**, 161 (1956).
45. R. F. BROWN and N. M. VAN GULICK. J. Am. Chem. Soc. **77**, 1090 (1956).
46. F. E. KING, J. W. CLARK-LEWIS, D. A. KID, and G. R. SMITH. J. Chem. Soc. 1041 (1956).
47. B. T. STOREY, W. W. SULLIVAN, and C. L. MOYER. J. Org. Chem. **29**, 3118 (1964).

Can. J. Chem. Downloaded from www.nrcresearchpress.com by 186.148.149.217 on 09/07/12
For personal use only.

Synthesis and monolayer spreading behaviour of surface-active compounds containing electron- and hole-transporting groups. 1. Fluorenylidene derivatives

J. W. TAYLOR, C. P. SLOAN, AND D. A. HOLDEN[1]
Department of Chemistry, University of Waterloo, Waterloo, Ont., Canada N2L 3G1
AND
G. J. KOVACS AND R. O. LOUTFY
Xerox Research Centre of Canada, 2660 Speakman Drive, Mississauga, Ont., Canada L5K 2L1

Received April 19, 1989

J. W. TAYLOR, C. P. SLOAN, D. A. HOLDEN, G. J. KOVACS, and R. O. LOUTFY. Can. J. Chem. **67**, 2136 (1989).

Surface-active derivatives containing fluorenylidene groups were synthesized, with the goal of creating thin-film devices incorporating monolayers of electron-transporting materials. The new compounds were studied in monolayers at the air–water interface, and were further characterized by cyclic voltammetry. The spreading behaviour of long-chain esters of a fluorenylidene malononitrile carboxylic acid was relatively insensitive to the cross-sectional area of the hydrocarbon chain, but was more strongly affected by changes in the polarity of the hydrophilic groups. Conditions for Langmuir–Blodgett deposition of multilayers of two of the new compounds on titanium-coated polyester film were also explored.

Key words: monolayers, Langmuir–Blodgett films, fluorene, surfactants.

J. W. TAYLOR, C. P. SLOAN, D. A. HOLDEN, G. J. KOVACS et R. O. LOUTFY. Can. J. Chem. **67**, 2136 (1989).

Dans le but de préparer des systèmes de films minces incorporant des monocouches de substances pouvant transporter des électrons, on a synthétisé des dérivés tensio-actifs qui contiennent des groupements fluorènylidènes. On a étudié les nouveaux composés dans des monocouches à l'interface air–eau et on les a aussi caractérisés par voltamétrie cyclique. La propension à se répandre que possèdent les esters en longues chaînes d'un acide fluorènylidène malononitrile carboxylique ne varie pas beaucoup avec des variations de la surface de la section droite de la chaîne hydrocarbonée; elle est toutefois plus affectée par les changements dans la polarité des groupements hydrophiles. On a aussi exploré les conditions d'effectuer une déposition de Langmuir–Blodgett de multicouches de deux des nouveaux composés sur un film de polyester recouvert de titane.

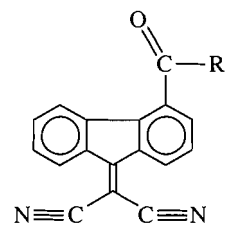
Mots clés : monocouches, films de Langmuir–Blodgett, fluorène, agents tensio-actifs.

[Traduit par la revue]

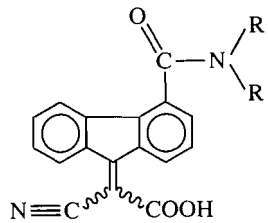
Introduction

The development of electroactive devices incorporating Langmuir–Blodgett layers is an active area of research within the field of molecular electronics (1). Frequently it is necessary to use surface-active materials that are very different from simple long-chain carboxylic acids or alcohols. In recent years the formation of stable monolayers from a wide variety of substances containing large chromophoric groups has been described. Examples include compounds with naphthalene (2), anthracene (3), anthraquinone (4), phthalocyanine (5), porphyrin (6), and cyanine dye (7) chromophores.

As part of a collaborative research project involving the construction of electrophotographic devices in which components were assembled by monolayer transfer techniques, we required surface-active compounds containing groups that were reversibly reduced by one-electron transfer processes. This publication describes the synthesis and monolayer spreading behaviour of a number of fluorenylidene derivatives that met those requirements. Chart 1 shows that structures of the compounds prepared. Because the fluorenylidene malononitrile series of compounds **1–5** exhibited only moderate collapse pressures in monolayers, additional compounds **6** and **7** were synthesized. These allowed us to take advantage of the additional stabilization imparted to monolayers of carboxylic acids as a result of spreading on subphases containing divalent cations (3*a*, 8).



1 R = $CH_3(CH_2)_{17}O$-
2 R = *cis*-$CH_3(CH_2)_7CH{=}CH(CH_2)_8O$-
3 R = $CH_3[CH(CH_3)(CH_2)_3]_3C(CH_3){=}CHCH_2O$-
4 R = $CH_3(CH_2)_{17}NH$-
5 R = $[CH_3(CH_2)_{17}]_2N$-



6 R = $CH_3(CH_2)_{17}$
7 R = $CH_2{=}CH(CH_2)_9$

CHART 1

Results and discussion

Synthesis

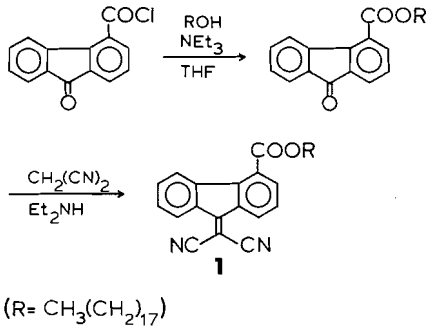
The general route to fluorenylidene malononitrile derivatives substituted by a long hydrocarbon chain is shown in Scheme 1.

It was also possible to reverse the order of the steps, by first forming the fluorenylidene malononitrile carboxylic acid (9, 10) and then adding the long chain, with comparable overall yields.

In general the extension of known small-molecule chemistry to syntheses involving long-chain compounds was achieved with only minor changes in reaction times or temperatures. An exception was encountered in the synthesis of the cyanoacetic

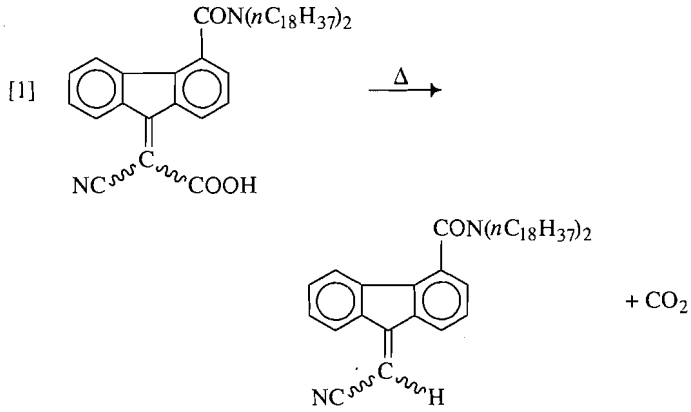
[1]Author to whom correspondence may be addressed.

Can. J. Chem. Downloaded from www.nrcresearchpress.com by 186.148.149.217 on 09/07/12
For personal use only.

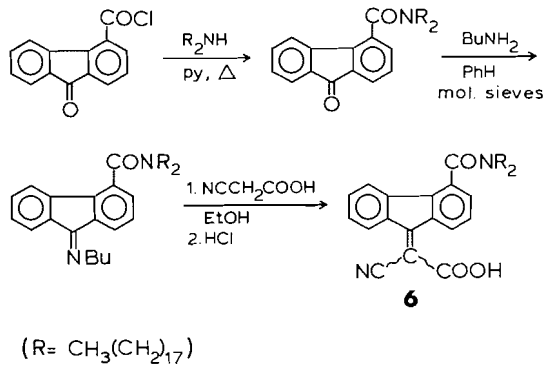


SCHEME 1

acid derivatives **6** and **7**. Attempts to react cyanoacetic acid directly with the fluorenone precursor either gave no reaction, or under more vigorous conditions gave only decarboxylation products (eq. [1]) (10). When the carboxyl group was first

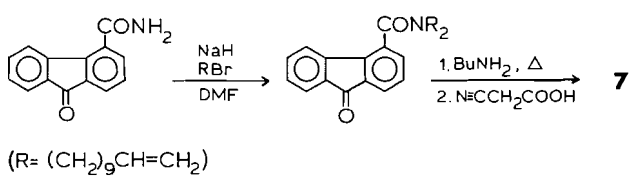


activated by conversion to the *N*-butyl imine, the reaction with cyanoacetic acid proceeded smoothly under conditions as mild as room temperature (Scheme 2).



SCHEME 2

Very few dialkylamines in which both alkyl groups are long hydrocarbon chains are available commercially. For the preparation of *N*,*N*-dialkylamides of the fluorenone derivatives the use of long-chain dialkylamines could be avoided by the method shown in Scheme 3 (11). In this reaction the primary amide was



SCHEME 3

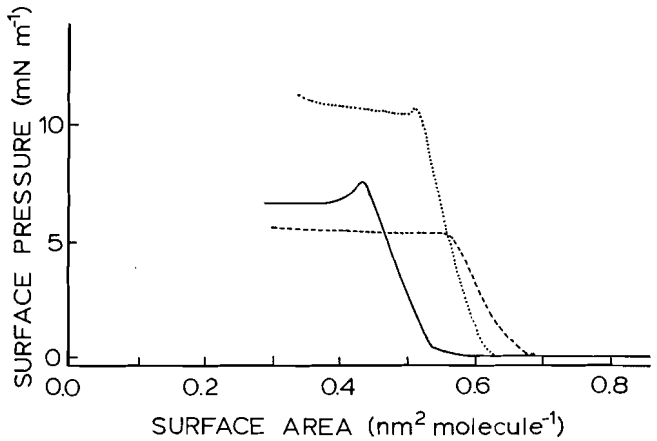


FIG. 1. Surface pressure – molecular area isotherms for monolayers of surfactants containing fluorenylidene malononitrile groups on pure water at 20°C. (—) octadecyl ester **1**; (---) oleyl ester **2**; (····) phytyl ester **3**.

converted to a tertiary amide by nucleophilic displacement in dry DMF, in a reaction involving excess sodium hydride and 2.2 equivalents of a primary haloalkane.

Monolayer spreading behaviour

Figure 1 shows the surface pressure – area curves of the three long-chain esters **1–3** on pure unbuffered water at 25°C. In the case of the octadecyl ester **1** stable monolayers were obtained with collapse pressures of 7.7 mN m^{-1} and collapse areas of 0.43 nm^2 $molecule^{-1}$. Because of the low collapse pressure of monolayers of **1**, other esters **2** and **3** containing bulkier hydrocarbon chains were synthesized in an effort to see whether more stable monolayers would result if the hydrocarbon chains had cross-sectional areas closer to that of the aromatic ring system. The spreading curves of compounds **2** and **3** in Fig. 1 show that this approach was only partially successful. The density and rigidity of the monolayer from the oleyl ester **2** were even less than those of the saturated ester **1**, as shown by the collapse pressure of 5.8 mN m^{-1} around a molecular area of 0.57 nm^2 $molecule^{-1}$. With a branched hydrocarbon chain, as in the phytyl ester **3**, a less marked increase in molecular area was accompanied by a significant increase in the surface pressure reached at the collapse point. Unfortunately the collapse pressure of 10.7 mN m^{-1} was still too low to allow transfer of one-component monolayers to solid supports by the Langmuir–Blodgett method.

A second group of compounds, amides **4** and **5**, was also studied to see whether the stability of the monolayers could be enhanced by the use of other linkages between the hydrophobic and hydrophilic parts of the molecule. Monolayers of the secondary amide **4** reached significantly higher surface pressures, up to 27 mN m^{-1} (Fig. 2), with limiting molecular areas of 0.35 nm^2 $molecule^{-1}$ and apparent collapse area of 0.25 nm^2 $molecule^{-1}$. It is difficult to visualize a mode of packing that would allow compound **4** to pack almost as closely as a planar zigzag hydrocarbon chain, so that it is likely that the spreading of **4** to a monolayer from $CHCl_3$ was incomplete. This is a frequent problem with long-chain primary and secondary amines, which have low solubility in $CHCl_3$ and other common spreading solvents. Monolayers of the tertiary amide **5** were considerably more expanded than those of the esters, and had limiting molecular areas and collapse areas of 1.20 and 0.86 nm^2 $molecule^{-1}$, respectively. Because the maximum

Can. J. Chem. Downloaded from www.nrcresearchpress.com by 186.148.149.217 on 09/07/12
For personal use only.

TABLE 1. Deposition ratios d for Langmuir–Blodgett transfer of monolayers of fluorenylidene-containing surfactants to metallized polyester film

Monolayer	Number of layers	Deposition pressure (mN m^{-1})	d^a
1 + eicosanoic acid	1	25	1.09
(3:2)	3	25	0.99
on pure water	5	25	1.03
6 on	1	17	1.01
10^{-3} M $CdCl_2$,	3	17	0.66[b](1.01, 0.74, 0.25)
pH 8.0	5	17	0.56[b](0.99, 0.75, 0.15, 0.66, 0.27)

[a]Deposition of first layer corresponds to withdrawal of film.
[b]Average value; values for individual immersion and withdrawal steps are shown in parentheses.

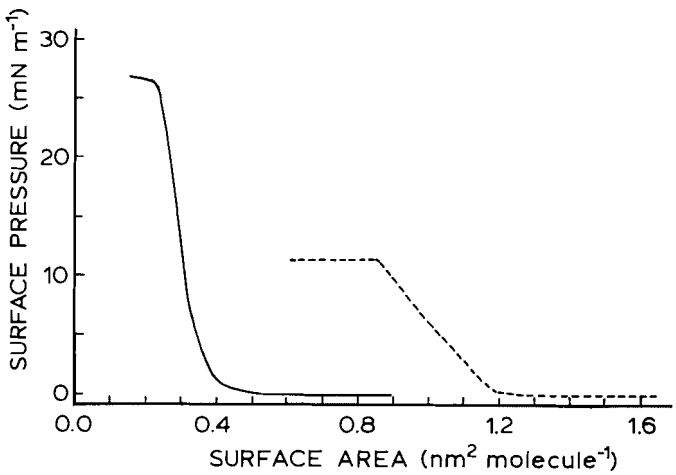


FIG. 2. Surface pressure – molecular area isotherms for monolayers of fluorenylidene malononitrile amides on pure water at 20°C. (—) *N*-octadecylamide **4**; (---) *N*,*N*-dioctadecylamide **5**.

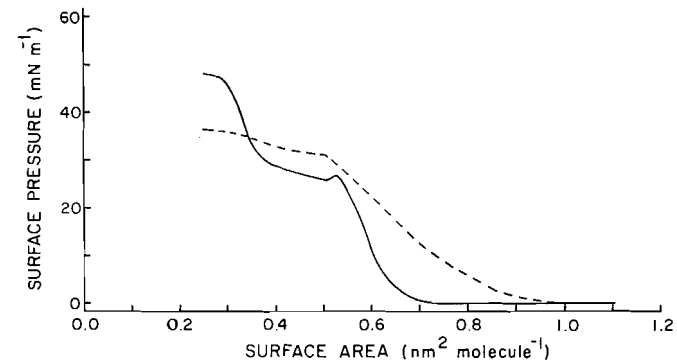


FIG. 3. Surface pressure – molecular area isotherms of surfactants containing the α-fluorenylidene cyanoacetic acid group on 10^{-4} M $CdCl_2$ at 20°C. (—) *N*,*N*-dioctadecylamide **6**; (---) *N*,*N*-di(10-undecenyl)amide **7**.

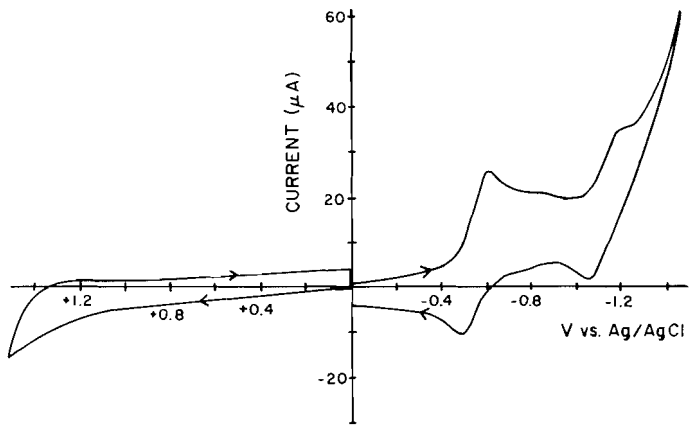


FIG. 4. Cyclic voltammogram of compound **1**, 10^{-3} M in deoxygenated CH_2Cl_2 containing 0.1 M Bu_4N^+ ClO_4^- electrolyte.

surface pressure was only 11 mN m^{-1}, these monolayers would have about the same stability during transfer as those prepared from the phytyl ester.

It became apparent that the best way to increase the stability of these compounds towards manipulation in monolayers was to modify the hydrophilic group. Accordingly compounds **6** and **7**, derived from cyanoacetic acid, were synthesized. In addition to the possibility of strengthening monolayers of these compounds by transferring them as salts with divalent cations, these compounds, since they consist of a mixture of *E* and *Z* isomers, would be expected to be less sensitive toward collapse to the bulk crystalline state. The surface pressure – area curves in Fig. 3 show that this is indeed the case. Both compounds formed monolayers, with collapse pressures over twice as high as for the dicyano derivatives.

Besides the formation of stable monolayers at the air–water interface, an additional requirement for the incorporation of the fluorenylidene derivatives into thin-film devices was the ability to undergo transfer to solid supports. Table 1 lists values of the deposition ratio d, defined in eq [2], for several of the new compounds on titanium-coated poly(ethylene terephthalate) film.

$$[2] \quad d = \frac{\text{Decrease in area of monolayer on the water surface}}{\text{Apparent area of monolayer-coated film}}$$

Because of the low collapse pressures of the dicyano-substituted compounds **1**–**5**, transfer of pure monolayers was not possible using our apparatus. The collapse pressures of mixed monolayers of **1** with eicosanoic acid were, however, sufficiently high to allow transfer, and deposition ratios of 1.0 within experimental error were obtained, which are characteristic of well-defined Langmuir–Blodgett layers. Pure monolayers of the cyanoacetic acid derivative **6** had high enough collapse pressures for direct deposition, but only the first monolayer was transferred with a deposition ratio of 1.0. Subsequent immersion and withdrawal steps showed lower deposition ratios, which are typical of imperfect transfer, and displayed a tendency toward higher deposition ratios on immersion than on withdrawal. Similar behaviour was observed for subphase pH between 4.4 and 8.0. The results of Table 1 establish that

Can. J. Chem. Downloaded from www.nrcresearchpress.com by 186.148.149.217 on 09/07/12
For personal use only.

TABLE 2. Reduction potentials of fluorenylidene-containing surfactants in CH_2Cl_2 solution[a]

Compound	E_1, V[b]	E_2, V[b]
1	−0.56	−1.14
3	−0.48	−1.09
4	−0.49	−1.12
5	−0.52	Not observed
6	Not observed	Not observed

[a]Concentration 1×10^{-3} M; 0.1 M Bu_4N^+ ClO_4^- electrolyte.
[b]Versus Ag/Ag Cl electrode.

Langmuir–Blodgett transfer of these fluorenylidene-containing surfactants is indeed possible, but that it is worthwhile to seek out a window of conditions of subphase composition, temperature, and dipping speed, which could lead to improved deposition.

Characterization by cyclic voltammetry

Figure 4 shows the cyclic voltammogram of compound **1** in deoxygenated methylene chloride. As is evident from the figure and from the compilation of reduction potentials in Table 2, the dicyano-substituted fluorenylidene compounds have two well-defined reversible reductions in CH_2Cl_2 solution, with typical reduction potentials of −0.5 and −1.1 V vs. the Ag/AgCl electrode. Only in the case of the *N,N*-dioctadecyl amide **5** was the second reduction obscured. It may be that the hydrocarbon environment provided by the two long chains suppressed the second reduction. In the case of the cyanoacetic acid derivative **6** both reductions were irreversible, an indication that a chemical reduction is associated with the one-electron reduction. One possibility is the decarboxylation reaction shown in eq. [1].

Conclusions

This research establishes the incorporation of the redox-active fluorenylidene group into compounds that form stable, transferable monolayers. An effort to create monolayers more resistant to collapse in the form of the cyanoacetic acid derivatives **6** and **7** was successful, but resulted in undesirable changes in the electrochemistry of the redox-active functional group. In terms of ease of synthesis, chemical stability, and transferability of monolayers, the octadecyl ester **1** was the most promising compound, even though it was necessary to dilute it with eicosanoic acid to obtain multilayer films of adequate quality. The assembly and performance evaluation of thin-film devices incorporating these new compounds will be described in a later publication.

Experimental

General methods

The nmr spectra were recorded on Bruker AM-250 and AC-200 spectrometers. Infrared spectra were recorded with a Perkin–Elmer 983 instrument. The uv–visible absorption spectra were recorded on a Cary 118 spectrometer. Mass spectra were recorded with electron impact ionization on a VG 7070 instrument, or with ionization under FAB conditions on a ZAB-E mass spectrometer. Elemental analyses were performed by Guelph Chemical Laboratories, Guelph, Ontario.

Yields refer to compounds that were homogeneous to all available spectroscopic techniques and to tlc, and of sufficient purity for monolayer studies. Thin-layer chromatography was performed using EM-60 silica gel plates, and chromatograms were visualized with short wavelength uv light, using phosphomolybdic acid or *p*-anisaldehyde. Column chromatography was performed using 230–400 mesh silica gel (Merck). Preparative tlc was carried out on 20 × 20 × 0.25 cm precoated silica gel plates (Merck Kieselgel 60 F_{254}).

9-Fluorenone-4-carboxylic acid was provided by Xerox Research Centre of Canada and served as the starting point for the synthesis of the fluorenylidene series of surfactants.

9-Fluorenylidene propanedinitrile-4-carboxylic acid n-*octadecyl ester* **1**

To a solution of 6.06 g 9-fluorenone-4-carboxylic acid (27 mmol) in CH_2Cl_2, 6.3 g of thionyl chloride (53 mmol) and 3 drops of *N,N*-dimethylformamide were added and the mixture was stirred overnight at room temperature. Distillation of the excess $SOCl_2$ and CH_2Cl_2 and drying under vacuum left a green solid, which was used in the next step without further purification; ir (Nujol): 1764, 1715 cm^{-1}.

A solution of 3.0 g of the above acid chloride (12.4 mmol) in 15 mL of dry THF was mixed with 3.35 g 1-octadecanol (12.4 mmol) (Sigma, 99%) in 15 mL of dry THF. After 1.25 g (12.4 mmol) of dry triethylamine was added the mixture was refluxed overnight. The solvent was evaporated at reduced pressure and the solid residue was washed with water and then extracted with benzene. The crude product obtained after evaporation of the solvent and drying *in vacuo* had mp 68–70°C; ir (Nujol): 1726 (br) cm^{-1}; ^1H nmr ($CDCl_3$) δ: 0.88 (t, 3H, J = 6.7 Hz), 1.25 (unresolved m, 30H), 1.85 (m, 2H), 4.41 (t, 2H, J = 6.7 Hz), 7.26–8.31 (m, 7H).

A solution of 1.5 g (3.15 mmol) of the crude ester, 0.25 g (3.78 mmol) of malononitrile, and 0.5 mL (9.7 mmol) of diethylamine in 110 mL of dry benzene was stirred for 4 h at 35°C. The benzene was removed on a rotary evaporator and the product was extracted into cyclohexane, washed with water, and dried. Following removal of the solvent the product was recrystallized from absolute ethanol. A total of 1.37 g (83%) of a deep yellow solid was obtained; mp 79–81°C; ir (Nujol): 2224, 1729 cm^{-1}; uv (cyclohexane) λ_{max}: 364 nm (ε 20 900 M^{-1} cm^{-1}), 351 (24 300), 304 (19 800), 280 (40 400); ^1H nmr ($CDCl_3$) δ: 0.88 (t, 3H, J = 6.9 Hz), 1.25 (unresolved m, 30H), 1.81 (m, 2H), 4.41 (t, 2H, J = 6.7 Hz), 7.33–7.54 (m, 3H), 7.84 (d, 1H, J = 7.8 Hz), 8.19 (d, 1H, J = 7.8 Hz), 8.45 (d, 1H, J = 7.8 Hz), 8.61 (d, 1H, J = 7.9 Hz); ^{13}C nmr (63.1 MHz, $CDCl_3$) δ: 14.2, 9 resolved signals between 22.80 and 32.02 ppm, 66.23, 12 resolved signals between 113.39 and 141.07, 160.06, 166.64. *Anal.* calcd. for $C_{35}H_{44}N_2O_2$: C 80.11, H 8.45, N 5.34%; found: C 80.41, H 8.64, N 5.01%.

9-Fluorenylidenemalononitrile-4-carboxylic acid cis-*7-octadecenyl ester* **2**

A solution of 10 g (44.5 mmol) of 9-fluorenone-4-carboxylic acid, 3.25 g (49.2 mmol) of malononitrile, and 4.6 mL (89 mmol) of diethylamine in 125 mL of dry THF was stirred for 6 h at room temperature. The precipitate was filtered off and dissolved in hot water. The cooled aqueous solution was acidified with HCl and the precipitate was filtered and dried in air. The product, 9-fluorenylidenemalononitrile-4-carboxylic acid, was dissolved in THF and precipitated into hexane, filtered off, and dried in vacuum; mp 287–290°C; ir: 2222, 1700 cm^{-1}; ^1H nmr (DMSO-d_6) δ: 7.36–8.29 (m, 7H), 13.76 (br s, 1H).

Five grams of the above acid was converted to 9-fluorenylmalononitrile-4-carbonyl chloride **8** with excess thionyl chloride in CH_2Cl_2. After the mixture had become homogeneous, the solvent was removed under vacuum leaving the crude acid chloride; ir: 2220, 1780 cm^{-1}. The acid chloride (0.372 g, 1.28 mmol) and pyridine (1 mL) were added to 40 mL of CH_2Cl_2, followed by 0.413 g (1.50 mmol) of oleyl alcohol (Sigma, 99%). The mixture was refluxed overnight, dilute HCl was added, and the organic layer was extracted with NaCl solution. After evaporation of the CH_2Cl_2 the product was purified by column chromatography on silica gel, eluting with 5% ethyl acetate in hexane. The product (280 mg, 42%) was a viscous orange oil; ir (neat): 2225, 1725 cm^{-1}; ^1H nmr ($CDCl_3$) δ: 0.88 (t, J = 6.2 Hz, 3H), 1.15–1.60 (br m, 22H), 1.63 (quintet, J = 7.2 Hz, 2H), 2.01 (quartet, J = 5.4 Hz, 4H), 4.42 (t, J = 6.7 Hz, 2H), 5.30–5.37 (m, 2H), 7.32–8.61 (m, 7H); ms m/z: 522 (M^+, rel. intensity 24), 272 (58), 256 (27), 255 (70), 82 (100). *Anal.* calcd. for $C_{35}H_{42}N_2O_2$: C 80.42, H 8.10, N 5.76%; found: C 79.78, H 8.32, N 6.06%.

Can. J. Chem. Downloaded from www.nrcresearchpress.com by 186.148.149.217 on 09/07/12
For personal use only.

Can. J. Chem. Downloaded from www.nrcresearchpress.com by 186.148.149.217 on 09/07/12
For personal use only.

9-Fluorenylidenemalononitrile-4-carboxylic acid 3,7,11,15-tetramethyl-2-hexadecenyl (phytyl) ester **3**

The phytyl ester of 9-fluorenylmalonitrile-4-carboxylic acid was prepared from the acid chloride **8** and phytol (Aldrich) following the procedure for the oleyl ester, and was purified by column chromatography on silica gel, eluting with 5–35% ethyl acetate in hexane. The product, obtained in 54% yield, was a viscous orange oil; ir (neat): 2226, 1725 cm^{-1}; ^1H nmr ($CDCl_3$) δ: 0.80–0.90 (m, 12H), 1.00–1.60 (m, 19H), 1.80 (br s, 3H), 2.12 (two overlapping triplets, J = 7.6 Hz, 2H), 4.92 (m, 2H), 5.50 (br t, J = 7.2 Hz, 1H), 7.33–8.60 (m, 7H); ^{13}C nmr ($CDCl_3$) δ: 14 resolved lines between 16.55 and 44.11 ppm, 62.42 (*cis*-), 62.75 (*trans*-phytyl, major isomer), 16 aromatic and olefinic C signals between 113.25 and 144.21 ppm, 159.96, 166.54; ms m/z: 550 (M^+, rel. intensity 2), 272 (60), 255 (42), 227 (10), 124 (33), 123 (77).

9-Fluorenylidenemalononitrile 4-carboxylic acid N-*octadecylamide* **4**

The acid chloride **8** (0.426 g, 1.47 mmol) was dissolved in dry CH_2Cl_2 and excess pyridine was added. After 20 min of stirring, octadecylamine (0.593 g, 2.2 mmol) was added and the mixture was stirred for 2 days at room temperature. After extraction with dilute HCl, the organic layer was washed with dilute Na_2CO_3 and then with brine. After evaporation of the solvent the crude product was chromatographed on silica gel, eluting with 5–30% ethyl acetate in hexane. The eluted product was recrystallized from acetone to give 406 mg (53%) of yellow crystals, mp 147–148°C; ir (Nujol): 2225, 1634 cm^{-1}; ^1H nmr ($CDCl_3$) δ: 0.88 (t, J = 6.7 Hz, 3H), 1.26 (br s, 30H), 1.66 (quintet, J = 6.9 Hz, 2H), 3.53 (quartet, J = 6.9 Hz, 2H), 5.91 (br t, J = 6.9 Hz, 1H), 7.30–8.51 (m, 7H); ms m/z: 524 (M + 1, rel. intensity 5), 523 (12), 255 (49), 43 (100). *Anal.* calcd. for $C_{35}H_{45}N_3O$: C 80.26, H 8.66, N 8.02%; found: C 80.96, H 9.07, N 7.89%.

9-Fluorenylidenemalononitrile-4-carboxylic acid N,N-*dioctadecylamide* **5**

Compound **5** was prepared from the acid chloride **8** and dioctadecylamine (Fluka) following the procedure for the amide **4**. The yield of yellow crystals, mp 52–54°C, following chromatography and recrystallization from acetone, was 25%; ir: 2253, 2228, 1630 cm^{-1}; ^1H nmr ($CDCl_3$) δ: 0.88 (t, J = 6.9 Hz, 6H), 1.26 (br s, 62H), 1.76 (m, 2H), 3.10 (m, 2H), 3.58 (m, 2H), 7.26–8.49 (m, 7H); ms m/z: 775 (M − 1, rel. intensity 4), 721 (12), 225 (32), 43 (100). *Anal.* calcd. for $C_{53}H_{81}N_3O$: C 82.01, H 10.52; N 5.41%; found: C 81.65, H 10.52, N 5.71%.

(E,Z)-9-Fluorenylidene cyanoacetic acid-4-carboxylic acid N,N-*dioctadecylamide* **6**

9-Fluorenone-4-carbonyl chloride, prepared from 4.484 g (20 mmol) of the corresponding acid, was dissolved in 50 mL of dry benzene and 13.57 g (26 mmol) of dioctadecylamine was added. After 5 h of refluxing the solvent was evaporated and the crude product was chromatographed on silica gel with 5–100% ethyl acetate in hexane as eluant. The pure product (5.6 g, 39%) was a waxy yellow solid; ir: 1717, 1636 cm^{-1}; ^1H nmr ($CDCl_3$) δ: 0.87 (t, J = 6.8 Hz, 6H), 1.26 (br m, 62H), 1.78 (m, 2H), 3.15 (m, 2H), 3.61 (m, 2H), 7.26–7.70 (m, 7H); ms m/z 728 (M + 1, rel. intensity 10), 727 (M^+, 2), 700 (26), 535 (60), 507 (91), 479 (38), 207 (100), 169 (42).

The preceding amide (2.64 g, 3.63 mmol) was refluxed in 30 mL benzene over molecular sieves in the presence of 5 mL of butylamine for 2 days under N_2. The benzene was removed and the imine was dissolved in dry ethanol. Cyanoacetic acid (0.401 g, 4.7 mmol) was added and the mixture was heated to 70°C for 4 h. Following evaporation of the ethanol, the product was dissolved in the minimum amount of methanol and ether was then added. On cooling to −10°C, the salt of compound **6** with butylamine precipitated. It was filtered off and dissolved in CH_2Cl_2 and converted to the free carboxylic acid by washing with 5 M HCl. Following evaporation of the CH_2Cl_2 layer the product was purified by preparative tlc on silica gel, eluting with 35% ethyl acetate in hexane. Compound **6**, a yellow solid, was obtained in 30% yield; mp 136–139°C; ir (Nujol): 2199, 1660, 1625 cm^{-1}; uv ($CHCl_3$) λ_{max}: 266 nm (ε 1.60 × 10^4 M^{-1} cm^{-1}), 273 (1.75 × 10^4), 294 (5.06 × 10^3), 330 (7.47 × 10^3), 334 (8.10 × 10^3); ^1H nmr ($CDCl_3$) δ: 0.88 (t, J = 5.5 Hz, 6H), 1.04–1.40 (br m, 62H), 1.77 (br s, 2H), 3.09 (t, J = 6.3 Hz, 2H), 3.59 (t, J = 6.6 Hz, 2H), 7.13–8.55 (m, 7H); ^{13}C nmr ($CDCl_3$) δ: 170.20, 169.92, 145.92, 139.35, 137.10, 136.62, 130.70, 128.68, 127.75, 125.09, 121.78, 119.31, 48.98, 45.24, 31.93, 8 resolved lines between 29.74 and 22.69, 14.09; ms (positive ion FAB, compound dissolved in thioglycerol) m/z: 796 (M^+, rel. intensity 3), 369 (20), 279 (34), 261 (20), 217 (100), 199 (38), 181 (69), 149 (36), 109 (87). A total of 41% of the starting fluorenone 4-carboxylic acid dialkylamide was also recovered.

(E,Z)-9-Fluorenylidene cyanoacetic acid-4-carboxylic acid N,N-*di-(10-undecenyl)amide* **7**

9-Fluorenone-4-carbonyl chloride was converted to the corresponding amide by reaction with excess ammonia gas in CH_2Cl_2. This amide (1.1 g, 4.9 mmol) was dissolved in dry DMF (40 mL) and NaH (0.118 g, 4.9 mmol) was added. The evolution of H_2 ceased after 15 min, and 1-bromo-10-undecene (1.2 g, 5.1 mmol) was added. After 1 h at room temperature NaH (0.141 g, 5.9 mmol) was added, followed 20 min later by a further 1.37 g (5.9 mmol) of 1-bromo-10-undecene. After 4 h at room temperature the solvent was removed on a rotary evaporator. The product was dissolved in CH_2Cl_2 and the organic solution was extracted with dilute HCl, dilute $NaHCO_3$, and water. Following removal of the solvent the compound was chromatographed on silica gel using 5–35% ethyl acetate in hexane as eluant. The product (1.962 g, 76%) was a viscous yellow oil; ir: 1716, 1637 cm^{-1}; ^1H nmr ($CDCl_3$) δ: 1.03–2.10 (m, 32H), 3.12–3.64 (m, 4H), 4.89–5.06 (m, 4H), 5.69–5.89 (m, 2H), 7.26–7.71 (m, 7H); ms m/z: 528 (M + 1, rel. intensity 30), 389 (7), 208 (17), 207 (100), 179 (19).

The preceding *N*,*N*-dialkylamide (1.90 g, 3.6 mmol) was refluxed with *n*-butylamine (20 mL) and molecular sieves for 30 h. The excess amine was removed and the imine was dissolved in dry ethanol. Following addition of cyanoacetic acid (0.459 g, 5.4 mmol) the mixture was stirred at room temperature for 20 h. The reaction mixture was concentrated by partial evaporation of the solvent and then passed through a short silica gel column to separate unreacted imine. The product was then chromatographed on reverse-phase silica gel, eluting with 35% ethyl acetate in hexane, then again on normal silica gel, eluting with 10–100% ethyl acetate in hexane, followed by absolute ethanol, to yield 0.774 g (36%) of an orange crystalline solid; mp: decomposition with gas evolution between 155 and 170°C; ir: 2198, 1636 cm^{-1}; uv ($CHCl_3$) λ_{max}: 272 nm (ε 2.77 × 10^4 M^{-1} cm^{-1}), 343 (1.10 × 10^4); ^1H nmr ($CDCl_3$) δ: 0.94–2.07 (m, 32H), 3.01–3.63 (m, 4H), 4.88–5.05 (m, 4H), 5.67–5.92 (m, 2H), 7.00–8.34 (m, 7H), 11.4 (br s, 1H); ^{13}C nmr ($CDCl_3$) δ: 9 resolved lines between 26.50 and 33.87 ppm, 45.85, 49.26, 11 resolved lines between 114.20 and 139.19, 149.60, 164.10, 170.55; ms (negative ion FAB, compound in thioglycerol) m/z: 594 (M^+, rel. intensity 16), 550 (35), 202 (52), 186 (100). For monolayer studies this compound was further purified by preparative tlc.

Monolayer studies were conducted using a surface film balance similar to an instrument described in the literature by Albrecht (12). The trough itself was milled from solid Teflon and was attached to a thermostated aluminum base plate with a stainless steel perimeter clamp. Movement of the barrier was achieved by a Teflon-coated threaded rod, driven by a stepping motor that was moved in half-steps (0.9°). The compression speed was typically 0.04 nm^2 $molecule^{-1}$ min^{-1}. Surface pressures were measured by the Wilhelmy hanging plate technique, using 1 cm × 1.5 cm strips of filter paper as the wettable material. The balance was surrounded by a glass enclosure and was isolated from vibration by resting on an air-suspension table (Technical Manufacturing Corp.). Movement of the stepping motor, measurement of surface pressure, recording of subphase temperature, and data analysis and plotting were controlled by a Hewlett–Packard 87XM computer interfaced through a Hewlett–Packard 3421A data acquisition unit. For monolayer studies water was purified with a pair of Millipore filtration systems connected in series. Compounds were spread from approximately 1 mg/mL solutions in $CHCl_3$ by means of a gas-tight 50 μL syringe fitted with a Chaney adaptor. The surface of the film balance was cleaned weekly with a solution of Nochromix (Godax

Laboratories) in concentrated sulfuric acid. The performance of the balance was monitored by running of isotherms for palmitic and stearic acids, and by comparison with results obtained using a second instrument, a circular trough described by Fromherz (13). Transfer of monolayers to metallized polyester film was carried out using the Fromherz round trough and a Lauda filmlift. The substrates were 5 cm × 5 cm squares of 75 μm-thick poly(ethylene terephthalate) foil (Dupont, Mylar D) sputter-coated with titanium under high vacuum to an optical density of 0.73–75 in the visible, and were used without further surface treatment. Monolayers were compressed to the deposition pressure at a compression rate of 0.025 nm^2 $molecule^{-1}$ min^{-1} and transfer was begun as soon as the deposition pressure had been reached. The first layer was deposited on withdrawal from the subphase at a speed of 3.5 mm min^{-1}. Subsequent immersion and withdrawal steps were carried out at a dipping speed of 5 mm min^{-1} without pauses between cycles.

Characterization of compounds by cyclic voltammetry (14) was carried out with a Princeton Applied Research model 174A polarographic analyzer and a model 175 universal programmer. The sample cell contained a platinum working electrode, a platinum wire counter-electrode, and a Ag/AgCl reference electrode. Sample solutions in CH_2Cl_2 were prepared containing 1×10^{-3} M of the compound under study and 0.1 M tetrabutylammonium perchlorate as the electrolyte, and were purged with argon during measurements. The scan rate for all experiments was 200 mV s^{-1}.

Acknowledgements

The authors thank the Natural Sciences and Engineering Research Council of Canada for the support of this research through its University–Industry Program. Thanks are also due to T. Martin, B. Ong, B, Keoshkerian, and G. Liebermann of XRCC for providing starting materials.

1. (*a*) Proceedings of the Second International Conference on Langmuir–Blodgett Films, Schenectady, NY, July 1–4, 1985. Thin Solid Films, **132–134** (1985); (*b*) Proceedings of the Workshop on Molecular Engineering of Ultrathin Polymeric Films, Davis, CA. Feb. 18–20, 1987. Thin Solid Films, **152** (1/2) (1987); (*c*) J. D. Shutt and S. E. Rickert. Langmuir, **3**, 460 (1987); (*d*) J. D. Swalen, D. L. Allara, J. D. Andrade, E. A. Chandross, S. Garoff, J. Israelachvili *et al.* Langmuir, **3**, 932 (1987).
2. B. Lovelock, F. Grieser, and T. W. Healy. J. Phys. Chem. **89**, 501 (1985).
3. (*a*) P. S. Vincett, W. A. Barlow, F. T. Boyle, J. A. Finney, and G. G. Roberts. Thin Solid Films, **60**, 265 (1979); (*b*) P. S. Vincett and W. A. Barlow. Thin Solid Films, **71**, 305 (1980); (*c*) N. Tamai, T. Yamazaki, and I. Yamazaki. J. Phys. Chem. **91**, 841 (1987).
4. (*a*) K. Fukuda, H. Nakahara, and T. Kato. J. Colloid Interface Sci. **54**, 430 (1976); (*b*) H. Nakahara and K. Fukuda. J. Colloid Interface Sci. **69**, 24 (1979); (*c*) J. Colloid Interface Sci. **83**, 401 (1988).
5. (*a*) S. Baker, M. C. Petty, G. G. Roberts, and M. V. Twigg. Thin Solid Films, **109**, 371 (1983); (*b*) G. J. Kovacs, P. S. Vincett, and J. H. Sharp. Can. J. Phys. **63**, 346 (1985); (*c*) R. Aroca, C. Jennings, G. J. Kovacs, R. O. Loutfy, and P. S. Vincett. J. Phys. Chem. **89**, 4051 (1985); (*d*) G. G. Roberts, M. C. Petty, S. Baker, M. T. Fowler, and N. J. Thomas. Thin Solid Films, **132**, 113 (1985).
6. (*a*) G. Porter. Proc. R. Soc. (London), Ser. A, **362**, 281 (1978); (*b*) A. F. Janzen, J. R. Bolton, and M. J. Stillman. J. Am. Chem. Soc. **101**, 6337 (1979); (*c*) A. Ruaudel-Teixier, A. Barraud, B. Belbeoch, and M. Roulliay. Thin Solid Films, **99**, 33 (1983); (*d*) M. F. Lawrence, J. P. Dodelet, and L. H. Dao. J. Phys. Chem. **88**, 950 (1984).
7. (*a*) D. Möbius. Ber. Bunsenges. Phys. Chem. **82**, 848 (1978); (*b*) T. L. Penner and D. Möbius. J. Am. Chem. Soc. **104**, 7407 (1982); (*c*) S. Vaidyanathan, L. K. Patterson, D. Möbius, and H.-R. Gruniger. J. Phys. Chem. **89**, 491 (1985).
8. G. L. Gaines, Jr. Insoluble monolayers at liquid–gas interfaces. Interscience, New York. 1966.
9. J. F. Yanus and J. M. Pearson. Macromolecules, **7**, 716 (1974).
10. G. Jones. Org. React. **15**, 204 (1967).
11. W. S. Fones. J. Org. Chem. **14**, 1099 (1949).
12. O. Albrecht. Thin Solid Films, **99**, 227 (1983).
13. P. Fromherz. Rev. Sci. Instrum. **46**, 1380 (1975).
14. O. Hammerich, B. Svensmark, and V. D. Parker. *In* Organic electrochemistry. 2nd ed. *Edited by* M. M. Baizer and H. Lund. Marcel Dekker, New York. 1983.

Can. J. Chem. Downloaded from www.nrcresearchpress.com by 186.148.149.217 on 09/07/12
For personal use only.

Synthesis and monolayer spreading behaviour of surface-active compounds containing electron- and hole-transporting groups. 2. Carbazole derivatives

J. W. TAYLOR, C. P. SLOAN AND D. A. HOLDEN[1]
Department of Chemistry, University of Waterloo, Waterloo, Ont., Canada N2L 3G1
AND
G. J. KOVACS AND R. O. LOUTFY
Xerox Research Centre of Canada, 2660 Speakman Drive, Mississauga, Ont., Canada L5K 2L1

Received April 19, 1989

J. W. TAYLOR, C. P. SLOAN, D. A. HOLDEN, G. J. KOVACS, and R. O. LOUTFY. Can. J. Chem. **67**, 2142 (1989).

The synthesis of several new surface-active carbazole derivatives is described. These compounds are intended to have applications as hole-transporting materials in thin-film devices assembled by the Langmuir–Blodgett technique. All of the carbazole-containing surfactants gave stable monolayers at the air–water interface with cross sections of 0.35–0.42 nm^2/molecule, characteristic of the carbazole ring system oriented perpendicular to the surface with its long axis parallel to the surface. Conditions for Langmuir–Blodgett deposition of multilayers on titanium-coated polyester film were explored. Further characterization of the carbazole derivatives by cyclic voltammetry and fluorescence decay measurements is also described.

Key words: monolayers, Langmuir–Blodgett films, carbazole, surfactants.

J. W. TAYLOR, C. P. SLOAN, D. A. HOLDEN, G. J. KOVACS et R. O. LOUTFY. Can. J. Chem. **67**, 2142 (1989).

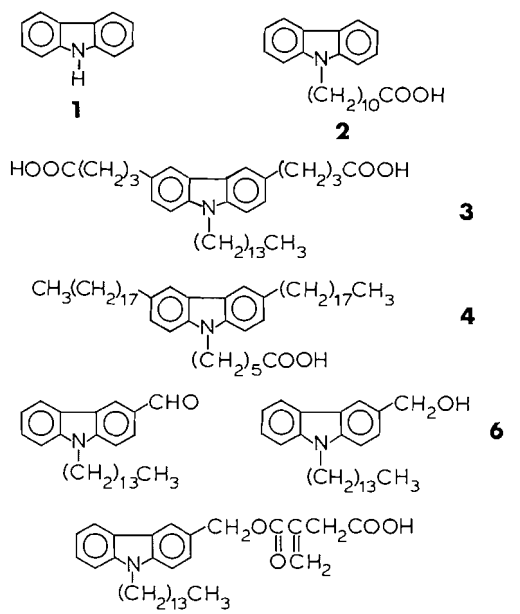
On décrit la synthèse de plusieurs nouveaux dérivés du carbazole qui sont tensio-actifs. On espère pouvoir utiliser ces composés pour le transport de trous dans des couches minces assemblées par la technique de Langmuir–Blodgett. Tous les agents de surface contenant du carbazole ont fourni des monocouches, stables à l'interface air–eau, dont les sections droites, de 0,35–0,42 nm^2/molécule, sont caractéristiques du système cyclique carbazole orienté d'une façon perpendiculaire par rapport à la surface et avec l'axe le plus long parallèle à la surface. On a exploré les conditions qui permettraient d'effectuer un dépôt, selon la technique de Langmuir–Blodgett, de multicouches sur un film de polyester recouvert de titane. On décrit aussi des caractérisations additionnelles des dérivés carbazoles qui ont été réalisées grâce à la voltamétrie cyclique et à des mesures de dégénérescence de la fluorescence.

Mots clés : monocouches, films de Langmuir–Blodgett, carbazole, agents tensio-actifs.

[Traduit par la revue]

Introduction

In the preceding paper the monolayer spreading behaviour of a number of fluorenylidene-containing surfactants was described (1). These compounds are easily reduced but are much more resistant to one-electron oxidation, and their intended role is to function as "monolayer rectifiers" in thin-film devices assembled by the Langmuir–Blodgett technique (2). It is also worthwhile to attempt the synthesis and characterization of monolayer building blocks which are potentially charge-rectifying in the opposite sense. Ideally such compounds would have one-electron oxidation potentials that are of approximately the same magnitude relative to the standard hydrogen electrode as the one-electron reduction potentials of the fluorenylidene malononitrile derivatives described in the preceding paper, but would be resistant to reduction. Suitable oxidation potentials are displayed by aromatic amines (3), a class of compounds that has received extensive attention because of their use as hole-transporting materials in electrophotography (4). For the purpose of this study derivatives of carbazole **1** were chosen, because this allowed us to make use of the extensive patent literature on these compounds (for example, ref. 5). In contrast to the fluorenylidene malononitrile group, the carbazole unit by itself was insufficiently polar to function as the hydrophilic part of a surface-active molecule, and so it was necessary to introduce both a hydrophobic tail and a hydrophilic head-group on the carbazole ring system to obtain a true surfactant. A somewhat different approach was employed recently by Tamai *et al.* (6), who observed that compound **2** gave monolayers at the air–water interface that had collapse pressures of less than 10 mN m^{-1}. Still more recently, the formation of stable monolayers from the 1:1 alternating copolymer of *N*-vinyl carbazole and diethyl fumarate was described by Matsuda and co-workers (7). Although these examples of monolayers from carbazole derivatives were promising, it was necessary to develop other syntheses in order to achieve the desired combination of one-electron oxidizability in a transferable monolayer. The compounds synthesized in the present study included the single-chain dicarboxylic acid **3** and the two-chain



[1]Author to whom correspondence may be addressed.

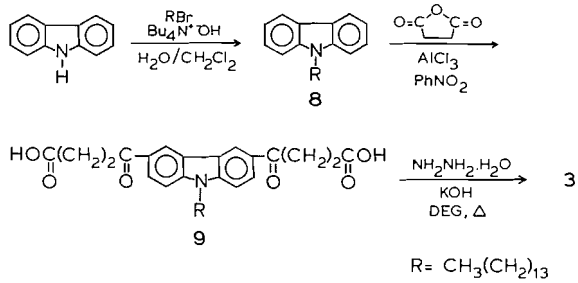
Can. J. Chem. Downloaded from www.nrcresearchpress.com by 186.148.149.217 on 09/07/12
For personal use only.

derivative **4**, which reverses the orientation of the carbazole ring system at the interface. In an effort to determine whether adequate monolayer stability required symmetrical substitution on the carbazole ring, compounds **5**–**7**, containing only a single hydrophilic substituent at the 3 position, were prepared.

Results and discussion

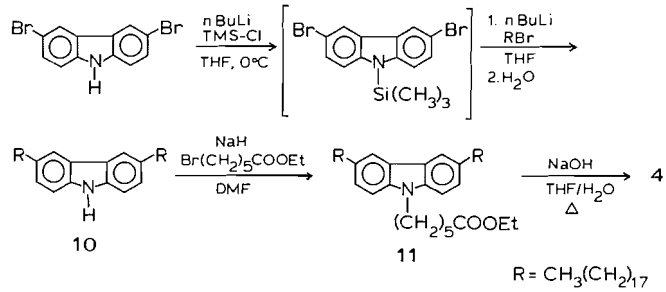
Synthesis

The preparation of the dicarboxylic acid **3** was achieved by Friedel–Crafts acylation of *N*-tetradecylcarbazole (8) with 2 equivalents of succinic anhydride (9) followed by Wolff–Kischner reduction to **3** (10), as shown in Scheme 1. In an effort



SCHEME 1

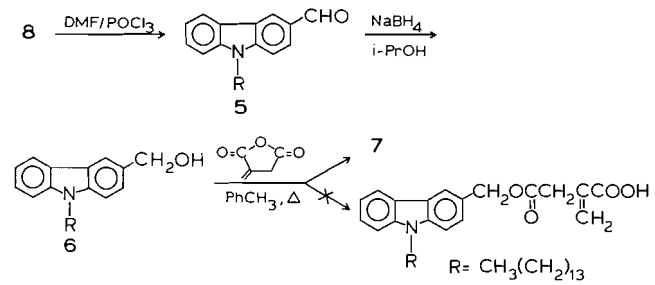
to reverse the orientation of the carbazole ring system at the air–water interface, monoacid **4** was obtained by the sequence of reactions shown in Scheme 2. The *N*-trimethylsilyl-protected



SCHEME 2

3,6-dibromocarbazole was first reacted by metal–halogen exchange and then alkylated with excess 1-bromooctadecane. Deprotection during work-up, followed by chromatographic purification, afforded the 3,6-dialkylcarbazole **10** in a one-pot reaction but in low overall yield. The chemistry used to introduce the hydrophilic group involved nucleophilic displacement of Br^- from an ω-bromo derivative by the sodium salt of carbazole, followed by hydrolysis to the free carboxylic acid **3**. The final step turned out to be the most difficult. Possibly because of the hydrocarbon environment provided by the two alkyl chains, compound **11** proved surprisingly resistant to hydrolysis. It was difficult to locate a window of hydrolysis conditions that could allow formation of the carboxylic acid without substantial decomposition of the product. Finally a solution was reached, involving prolonged refluxing of the ester under nitrogen in peroxide-free THF/H_2O containing sodium hydroxide.

The preparation of the carbazole-containing half-ester **7** made use of chemistry worked out by Rodriguez-Parada and Percec in their synthesis of a series of carbazolylmethyl esters of methacrylic acid (8) (Scheme 3). In principle two regioisomers could be formed by the ring-opening of the anhydride, but in practice only a single product was isolated, as shown by ^1H and



SCHEME 3

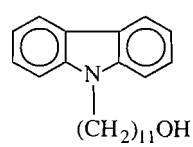
^{13}C nmr spectroscopy. This result is in agreement with other literature studies of the preparation of itaconate esters from itaconic anhydride (11).

Monolayer spreading behaviour

Compounds **3**–**7** all formed stable monolayers with molecular areas that reflected the large cross section of the carbazole ring system. Figure 1 shows the monolayer spreading behaviour of the dicaboxylic acid **3** on 10^{-3} M $CdCl_2$ at 20°C. The surface pressure increases smoothly below a limiting molecular area of 0.70 nm^2 $molecule^{-1}$ and reaches a well-defined collapse pressure of 33.7 mN m^{-1} at a molecular area of 0.397 nm^2. Similar spreading behaviour was observed for compound **3** on pure water, except that the monolayers were slightly less compact.

The monolayer spreading behaviour of the carbazole monoacid **4** and its ethyl ester **11** is shown in Fig. 2. Despite the reversal of the positions of the polar substituents and the hydrocarbon chains on the carbazole ring, the spreading behaviour of **4** is quite similar to that of **3**. The high collapse pressure of 39 mN m^{-1}, reached at a molecular area of 0.33 nm^2 $molecule^{-1}$, means that monolayers of pure **4** may be stable enough for transfer to solid surfaces. In contrast, the ethyl ester group of compound **11** has lower polarity, so that monolayers of **11** are more expanded and have much lower collapse pressures: 6.7 mN m^{-1} at a molecular area of 0.75 nm^2 $molecule^{-1}$.

Our original assumption was that monolayers of unsymmetrical carbazole derivatives and compounds in which the hydrophilic group was attached to the carbazole ring system would have lower stability. This turned out not to be the case, as is evident from the surface pressure – area curves shown in Fig. 3. Both the carbazolylmethanol derivative **6** and the itaconate monoester **7** gave stable monolayers, and the limiting molecular areas, collapse areas, and collapse pressures are very close to those of the symmetrical derivatives **3** and **4**. Monolayers of the carboxaldehyde **5** had similar limiting and collapse areas (0.46 and 0.33 nm^2 $molecule^{-1}$) but had a much lower collapse pressure of 6 mN m^{-1}. The collapse pressures of 26.5 and 33.2 mN m^{-1} displayed by compounds **6** and **7** are much higher than the value of <10 mN m^{-1} observed by Tamai *et al.* for monolayers of compound **2**, in which the carbazole unit is at the end of the hydrophobic chain (6). The lower collapse pressures of ω-carbazolyl-substituted surfactants were also verified in our laboratory for monolayers of the alcohol **12**, which showed a collapse



12

Can. J. Chem. Downloaded from www.nrcresearchpress.com by 186.148.149.217 on 09/07/12
For personal use only.

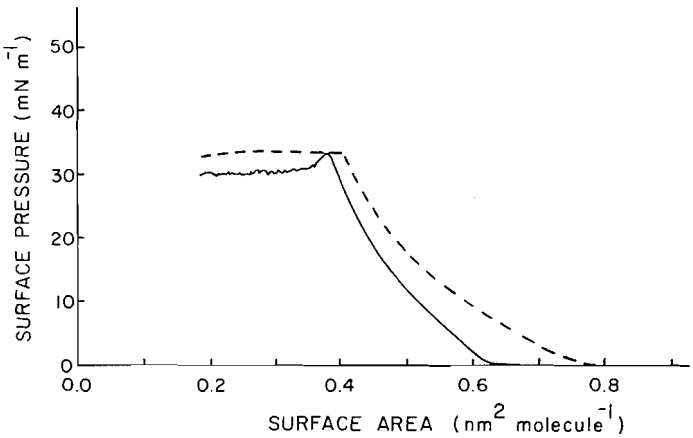


FIG. 1. Surface pressure vs. molecular area for monolayers of carbazole diacid **3**: (—) on 10^{-3} M $CdCl_2$; (---) on pure water at 20°C.

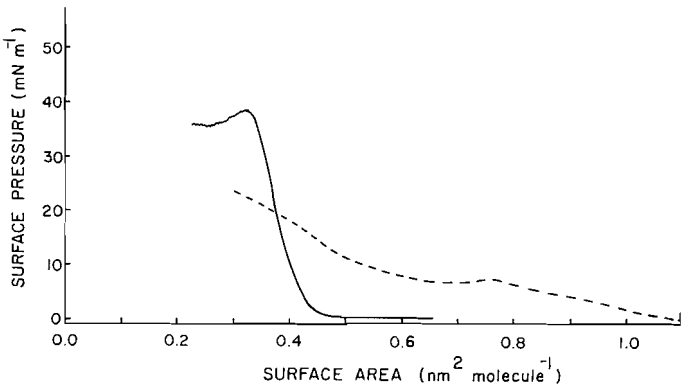


FIG. 2. Surface pressure vs. molecular area for monolayers of carbazole surfactants containing two hydrocarbon chains: (—) carboxylic acid **4** on 10^{-3} M $CdCl_2$ at 26.4°C; (----) ethyl ester **11** on pure water at 21.7°C.

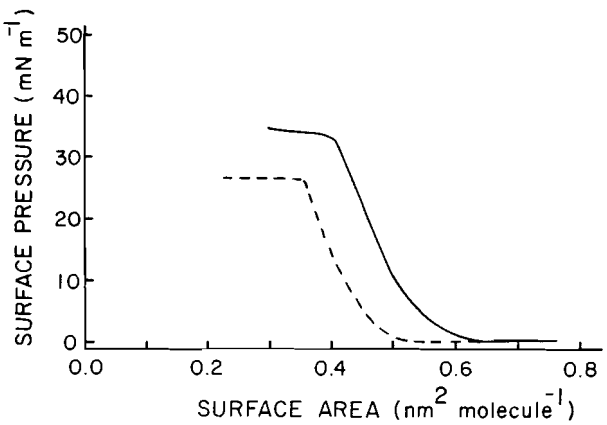


FIG. 3. Surface pressure – molecular area curves for unsymmetrical carbazole-containing surfactants on pure water at 20°C: (----) carbazolylmethanol derivative **6**: (—) itaconic acid monoester **7**.

pressure of 8 mN m^{-1} at a molecular area of 0.37 nm^2 $molecule^{-1}$ [2].

Monolayers of **3**–**7** all have similar collapse areas of between 0.33 and 0.42 nm^2 $molecule^{-1}$. A common orientation of the carbazole ring system relative to the water surface that provides a molecular area in this range places the long axis of the carbazole ring sytem close to parallel to the surface, with the aromatic rings stacked parallel to each other and at close to right angles to the surface. The same orientation was concluded by Fukuda *et al.* for a series of 9,10-anthraquinone-containing surfactants on the basis of a similar geometrical analysis (13).

[2]R. Mastantuono, J. Buschek, and D. A. Holden. Unpublished results.

TABLE 1. Deposition ratios *d* for Langmuir–Blodgett transfer of monolayers of carbazole-containing surfactants to titanium-coated polyester films[a]

Compound	Number of layers	Deposition pressure (mN m^{-1})	d^b
3	1	26	1.11
	3	26	0.89[c] (1.15, 0.83, 0.66)
	5	26	0.57 (1.16, 0.84, 0.49, 0.11, 0.24)
7	1	25	1.23
	3	25	0.80 (1.22, 1.00, 0.18)
	5	25	0.75 (1.23, 1.01, 0.18, 1.09, 0.23)

[a]10^{-3} M $CdCl_2$ subphase.
[b]Deposition of 1st layer corresponds to withdrawal of film.
[c]Average value; values for individual immersion and withdrawal steps are in parentheses.

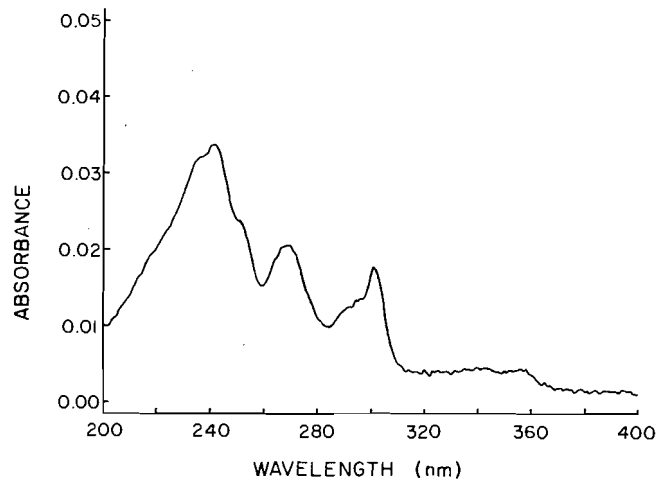


FIG. 4. Ultraviolet spectrum of 3 monolayers of carbazole diacid **3** on each side of a quartz disc.

Table 1 lists the results of a study of the deposition of multilayers of **3** and **7** on titanium-coated polyester foil by the Langmuir–Blodgett technique. It is interesting to note that the deposition ratios *d* for the first monolayer are 1.2 ± 0.05, consistently greater than unity, a result suggesting that some reorganization of the monolayers occurs on transfer (2, 14). Monolayers of the diacid **3** showed decreasing values of *d*, corresponding to propagation of imperfections with each immersion and withdrawal. Similar behaviour was observed for monolayers transferred to quartz discs, as shown by uv spectroscopy. Figure 4 is the uv spectrum of a total of 6 monolayers (3 per side) of **3** transferred as the Cd^{2+} salt to quartz. Although the spectrum is unchanged, the absorbance of a multilayer film prepared by five immersion–withdrawal cycles is only slightly higher than that shown in Fig. 4, a result confirming that the deposition of monolayers of **3** on itself becomes ineffective after the first 2–3 monolayers. The behaviour of compound **7** is slightly different from that of compound **3** in that a pronounced tendency toward X-type deposition (deposition only on immersion) was observed, rather than a monotonic decrease in the deposition ratio with increas-

Can. J. Chem. Downloaded from www.nrcresearchpress.com by 186.148.149.217 on 09/07/12
For personal use only.

TABLE 2. Oxidation potentials of carbazole-containing surfactants as determined by cyclic voltammetry[a]

Compound	E_p, oxidation (V vs. SCE)[a]	$(E_p)_{1/2}$, (V vs. SCE)
3	1.29	1.22[a]
6	1.23	1.14[a]
9-Butylcarbazole	1.04	0.95[a]
3-Methyl-9-ethylcarbazole		1.09[b]
3,6,9-Triethylcarbazole		1.06[b]
3,6-Di-*tert*-butyl-9-ethylcarbazole		1.04[b]

[a] 10^{-3} M in oxygen-free CH_2Cl_2; 0.1 M Bu_4N^+ ClO_4^- electrolyte; scan rate 50 mV s^{-1}.
[b] In CH_3CN; Et_4N^+ ClO_4^- electrolyte; ref. 15

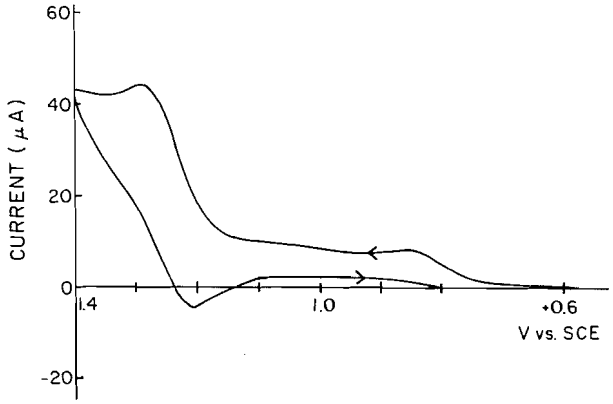


FIG. 5. Cyclic voltammogram of 10^{-3} M carbazole diacid **3** in deoxygenated CH_2Cl_2, measured at a scan rate of 200 mV s^{-1}.

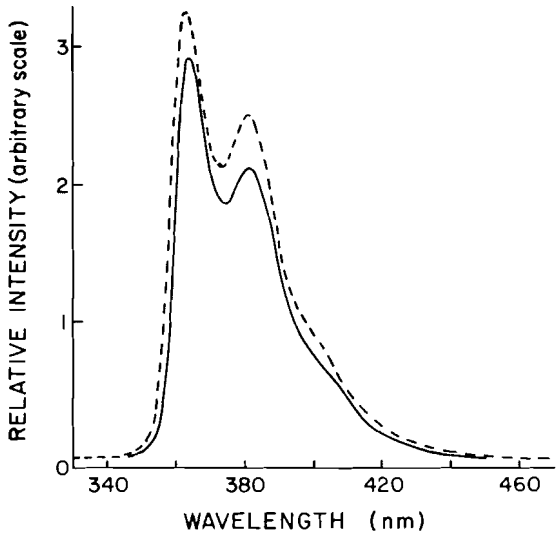


FIG. 6. Fluorescence spectra of carbazole derivatives, 2×10^{-5} M in deoxygenated ethanol: (—) diacid **3**; (----) monoacid **4**.

TABLE 3. Fluorescence decay times τ_f of carbazole compounds in deoxygenated ethanol at 25°C

Compound	λ_{ex}; λ_{em} (nm)	τ_f (ns)
6	290; 360	12.4
10	295; 363	13.4
11	295; 363	13.9
4	297; 370	13.7

ing number of immersion–withdrawal cycles. The results summarized in Table 1 show that it would not be possible to create Langmuir–Blodgett assemblies incorporating tens of multilayers. On the other hand, a proposed application of Langmuir–Blodgett multilayers of these carbazole compounds involves their use as charge-blocking layers in electrophotographic devices, and in such an application even single monolayers may be effective.

Redox behaviour of carbazole-containing surfactants

Table 2 compares the redox behaviour of two of the carbazole surfactants, as measured by cyclic voltammetry, with that of some carbazole compounds substituted with short alkyl chains. A typical cyclic voltammogram for compound **3** in argon-saturated CH_2Cl_2 is illustrated in Fig. 5. The small peak at +0.85 V is attributed to an impurity in the supporting electrolyte. Simple *N*-alkyl carbazoles such as 9-butylcarbazole are irreversibly oxidized in CH_2Cl_2 at +1.05 V relative to the saturated calomel electrode. The corresponding oxidation of the carbazole surfactants is shifted by about +0.2 V, and the degree of irreversibility is a function of the substitution on the carbazole ring. Thus compound **6**, substituted at the 3 and 9 positions, showed no cathodic peak on the return cycle, whereas compound **3**, with 3, 6, and 9 substitution, gave a well-defined cathodic peak at +1.21 V vs. SCE. Studies by Ambrose *et al.* established that carbazole derivatives undergo oxidative coupling to give 3,3, 6,6, and 9,9 bicarbazolyl dimers (15). The tendency toward irreversible dimerization was suppressed in carbazole compounds with bulky alkyl substituents at the 3, 6, and 9 positions, as in 3,6-di-*tert*-butyl-9-ethylcarbazole. This accounts for the observed differences between compounds **3** and **6**. The shift of peak potentials for **3** and **6** to more positive values in comparison to *N*-butylcarbazole is attributed to a slower rate of diffusion of the high molecular weight surfactants to the electrode surface, rather than to substantial differences in redox levels. The perturbation arising from the carboxylic acid groups is small: carboxylic acids are known to undergo oxidative dimerization by the Kolbe reaction (16), but the potentials required are not accessible in CH_2Cl_2 solution, as the solvent undergoes oxidation beyond +1.8 V vs. SCE.

Fluorescence behaviour

Figure 6 shows the fluorescence spectra of two of the carbazole surfactants in oxygen-free ethanol. The positions of the 0–0 bands are only slightly red-shifted relative to those of simple *N*-alkyl carbazoles (17) and confirm the absence of pronounced differences in the excited state levels of the long-chain compounds. The fluorescence decay times of several long-chain carbazole compounds, listed in Table 3, are all very close to the decay times of carbazole and *N*-alkyl carbazoles (18), and indicate the absence of additional non-radiative decay pathways for the long-chain compounds,at least in homogeneous solution. Fluorescence spectroscopy is one of the few techniques sensitive enough to provide detailed information on orientation and structure within single monolayers, and these results for homogeneous solutions provide useful background information for such studies.

Summary

The carbazole ring system has been successfully incorporated in a variety of ways into compounds that form stable monolayers at the air–water interface. The collapse pressures of these

Can. J. Chem. Downloaded from www.nrcresearchpress.com by 186.148.149.217 on 09/07/12
For personal use only.

monolayers, typically around 30 mN m^{-1}, were sufficiently high to allow Langmuir–Blodgett deposition without dilution with stabilizing amphiphilic compounds such as fatty acids. While efforts to build up multilayers on titanium-covered polyester foil met with only partial success, and the electrochemical behaviour of the surface-active carbazoles appeared to be affected by the presence of the long-chain substituents, it was still possible to incorporate 1- to 5-monolayer films of these compounds into working Langmuir–Blodgett devices. Details of the assembly and performance evaluation of one such application will be described in the near future.

Experimental

General spectroscopic and chromatographic methods are described in the preceding paper (1).

N-Tetradecylcarbazole ***8***

This compound was prepared from carbazole and 1-bromotetradecane by the method of Rodriguez-Parada and Percec (8). The crude product isolated by precipitation of the reaction mixture into water was dissolved in hexanes, and the solution was filtered and evaporated to dryness. The product after one recrystallization from isopropanol had mp 40–41°C (lit. mp (8) 42–44°C); ir: no NH of carbazole at 3420 cm^{-1}; ^1H nmr ($CDCl_3$) δ: 0.89 (t, 3H), 1.25 (br s, 22H), 1.80 (m, 2H), 4.27 (t, 2H), 7.11–8.16 (m, 8H); ^{13}C nmr ($CDCl_3$) δ: 14.25, 8 resolved CH_2 signals between 22.84 and 43.15 ppm, 108.72, 118.78, 120.39, 122.94, 125.62, 140.53.

N-Tetradecylcarbazole-3,6-bis(4-(4-oxo)-butanoic acid) ***9*** *(9)*

A mixture of 17.5 g (48 mmol) of **8** and 10.6 g (106 mmol) of succinic anhydride in 250 mL of dry nitrobenzene was cooled to 3–4°C and stirred while 28.25 g (212 mmol) of anhydrous $AlCl_3$ was added slowly enough to avoid a sharp rise in temperature. The reaction mixture was maintained at 2°C for 6 h and then allowed to warm to room temperature. After 2 days the reaction mixture was added to ice and acidified with 50 mL of concentrated HCl. Following steam distillation to remove most of the nitrobenzene, the solid residue was dissolved in 1 M aqueous NaOH and the solution was extracted with ether. The aqueous layer was acidified with HCl and the precipitated product was filtered and dried and recrystallized from a large volume of ethyl acetate; ir (Nujol): 3000 (br), 1702, 1655 cm^{-1}.

N-Tetradecylcarbazole-3,6-bis(4-butanoic acid) ***3***

A total of 5.0 g of the oxoacid **9** (9.6 mmol), 2.0 g (36 mmol) of KOH, and 2.5 g (42 mmol) of 85% hydrazine hydrate were dissolved in 25 mL of diethylene glycol and heated to 140°C for 1.25 h. At this point the condenser was removed and water and unreacted hydrazine were distilled off. The reaction temperature was increased to 190°C and maintained for 4 h. The cooled mixture was acidified with HCl and extracted with ether. The ether solution of the product was chromatographed on silica gel, eluting with 35:15:1 hexane/ether/acetic acid, to yield 1.5 g (32%) of crystalline **3**, mp 76–78°C; ir ($CHCl_3$): 1708 cm^{-1}; (KBr): 3000 (br) cm^{-1}; uv (methanol) λ_{max}: 357 nm (ε 2.50×10^3 M^{-1} cm^{-1}), 343 (2.36×10^3), 302 (1.30×10^4), 270 (1.50×10^4); ^1H nmr δ: 0.87 (t, 3H), 1.23 (br s, 22H), 1.83 (m, 2H), 2.05 (m, 4H), 2.44 (t, J = 7.3 Hz, 4H), 2.84 (t, J = 7.4 Hz, 4H), 4.22 (t, J = 7.1 Hz, 2H), 7.21–7.29 (m, 4H), 7.88 (s, 2H); ^{13}C nmr ($CDCl_3$) δ: 14.22, 12 resolved CH_2 lines between 21.13 and 35.13 ppm, 43.26, 60.53, 108.54, 119.89, 122.81, 126.33, 131.37, 139.46, 180.26; fluorescence spectrum (λ_{ex} = 297 nm): emission maxima at 364, 382.5 nm; (λ_{em} = 390 nm): excitation maxima at 301, 343, 357 nm. *Anal.* calcd. for $C_{34}H_{49}NO_4$: C 76.22, H 9.22, N 3.01%; found: C 76.38, H 9.31, N 2.61%.

3,6-Dioctadecylcarbazole ***10***

A solution of 3,6-dibromocarbazole (Aldrich, 3.69 g, 11.4 mmol) in 300 mL of dry THF was cooled to 0°C under N_2. *n*-Butyllithium (5.6 mL of 2.24 M solution in hexane, 12.4 mmol) was added by syringe, followed after 1 h by 1.36 g (12.5 mmol) of trimethylsilyl chloride. The mixture was then cooled to −78°C and 2.3 equivalents of *n*-BuLi (11.7 mL of 2.24 M solution in hexane) were added. After 1 h at −78°C 1-bromooctadecane (15.2 g, 45.6 mmol) was added and the mixture was allowed to warm to room temperature overnight. Following addition of a trace of water, filtration, and evaporation of the solvent the product mixture was chromatographed on silica gel, eluting with 5–35% ethyl acetate in hexane. Additional purification by column chromatography was necessary to obtain material that was homogeneous by fluorescence decay measurements. Compound **10** (962 mg, 13%) was a white waxy solid, mp 68–69°C (acetone); ir: 3424, 2915, 1462 cm^{-1}; ^1H nmr ($CDCl_3$) δ: 0.87 (t, 6H), 1.10–1.60 (br s, 60H), 1.60–1.75 (quintet, 4H), 2.76 (t, 4H), 7.17–7.28 (m, 4H), 7.28–7.83 (m, 2H); ms m/z: 672 (M^+, rel. intensity 2), 476 (58), 419 (11), 236 (30), 43 (100).

6-(3,6-Dioctadecyl-9-carbazolyl)hexanoic acid ethyl ester ***11***

A solution of 900 mg (1.34 mmol) of **10** in 10 mL of dry DMF was added by syringe to a suspension of 1.4 equivalents of NaH (90 mg of 50% NaH dispersion in mineral oil) in 15 mL of DMF. Evolution of hydrogen ceased after 30 min. Ethyl 6-bromohexanoate (340 mg, 1.74 mmol) was added and the mixture was stirred at room temperature for 4 h. The DMF was removed on a rotary evaporator and the crude product was chromatographed on silica gel, eluting with 5–50% ethyl acetate in hexane. The product (893 mg, 82%) was a colorless oil, which crystallized on standing for 1 week; mp 49–50°C (acetone); ir: 2925, 1725, 1467, 908, 735 cm^{-1}; ^1H nmr ($CDCl_3$) δ: 0.88 (t, 6H), 1.15–1.30 (br s, 67 H), 1.60–1.75 (br quintet, 4H), 1.80–1.92 (m, 2H), 2.25 (t, J = 7.3 Hz, 2H), 2.77 (t, J = 7.7 Hz, 4H), 4.09 (quartet, J = 7.3 Hz, 2H), 4.23 (t, J = 7.1 Hz, 2H), 7.24 (unresolved m, 4H), 7.86 (unresolved m, 2H); ^{13}C nmr ($CDCl_3$, 63.1 MHz) δ: 14.25, 8 resolved CH_2 lines between 22.83 and 36.16 ppm, 43.02, 60.34, 108.24, 119.69, 122.90, 126.24, 133.20, 139.20, 173.58; ms m/z: 814 (M^+, rel. intensity 1.3% of base peak). *Anal.* calcd. for $C_{56}H_{95}NO_2$: C 83.62, H 11.90, N 1.74%; found: C 83.41, H 11.70, N 2.02%.

6-(3,6-Dioctadecyl-9-carbazolyl)hexanoic acid ***4***

The ethyl ester **11** (893 mg, 1.1 mmol) was dissolved in 30 mL of THF and 5 mL of H_2O was added. Following addition of 3 mL of 1M aqueous NaOH (3 mmol), the mixture was stirred and refluxed under nitrogen for 3 days, followed by 2 days at room temperature. The solvent was removed and the sodium salt of the product was converted to the free carboxylic acid by extraction with dilute aqueous HCl and CH_2Cl_2. Evaporation of the organic layer gave 654 mg (76%) of **4** as a white crystalline solid; mp 52–53°C (acetone); ir: 2913, 1717, 1465, 1026, 730 cm^{-1}; ^1H nmr ($CDCl_3$) δ: 0.88 (t, 6H), 1.05–1.50 (br s, 66H), 1.50–1.80 (br quintet, 4H), 2.28 (t, J = 7.0 Hz, 2H), 2.77 (t, J = 7.7 Hz, 4H), 4.24 (t, J = 7.1 Hz, 2H), 7.25 (unresolved m, 4H), 7.85 (unresolved m, 2H); ^{13}C nmr ($CDCl_3$) δ: 14.25, 7 resolved CH_2 signals between 22.81 and 36.14 ppm, 108.23, 119.69, 122.85, 126.25, 133.22, 139.17, 178.22; ms (negative ion FAB, compound dissolved in thioglycerol) m/z: 785 ($M^+ - 1$, rel. intensity 4), 298 (8), 297 (44), 148 (100); fluorescence spectrum (ethanol): emission λ_{max} 362, 380 nm (excitation at 297 nm).

3-Formyl-9-tetradecylcarbazole ***5****(5a)*

N-Tetradecylcarbazole **8** was formylated with $POCl_3$/DMF by the method of Rodriguez-Parada and Percec (8). Isolation of the product was achieved by cooling the reaction mixture in an ice bath until a solid precipitated. The filtered product was recrystallized from acetone/hexane to yield a yellow solid having mp 81–83°C (lit. (8) mp 81–83°C); ir: 1689 cm^{-1}; ^1H nmr ($CDCl_3$) δ: 0.88 (t, 3H), 1.25 (br s, 22H), 1.90 (m, 2H), 4.32 (t, 2H), 7.22–8.62 (m, 7H), 10.12 (s, 2H).

(9-Tetradecyl-3-carbazolyl)methanol ***6***

A solution of 2.43 g (6.2 mmol) of **5**, 0.31 g (8.1 mmol) of $NaBH_4$, and 7 mL of 0.13 M aqueous NaOH (9.0 mmol) in 100 mL of isopropanol was stirred at 60°C for 3 h. The homogeneous solution was poured into ice water and the precipitated solid was filtered and dried under vacuum. Recrystallization from hexanes gave compound **6**; mp 73–74°C (lit. (8) mp 72–74°C); ir: 3253 (br) cm^{-1}; ^1H nmr ($CDCl_3$) δ: 0.90 (t, 3H), 1.29 (br s, 22H), 1.6–2.0 (m, 2H + 1H (OH)), 4.29 (t,

Can. J. Chem. Downloaded from www.nrcresearchpress.com by 186.148.149.217 on 09/07/12
For personal use only.

2H), 4.85 (s, 2H), 7.11–8.18 (m, 7H); ^{13}C nmr ($CDCl_3$, 50.5 MHz) δ: 14.22, 7 resolved CH_2 lines between 22.81 and 32.03 ppm, 43.26, 66.24, 12 resolved aromatic C between 105.74 and 140.88 ppm. *Anal.* calcd. for $C_{27}H_{39}NO$: C 82.39, H. 9.98, N 3.56%; found: C 82.19, H 9.98, N 3.94%.

2-Methylenebutanedioic acid mono((9-tetradecyl)-3-carbazolyl)methyl ester 7(17)

A solution of 0.65 g (1.7 mmol) of alcohol **6** and 0.206 g (1.8 mmol) of itaconic anhydride (Aldrich) in 20 mL of dry toluene was refluxed for 18 h. Most of the toluene was removed on a rotary evaporator and the crude product was passed through a short silica gel column and eluted with 10–100% ethyl acetate in hexane. The last two bands were rechromatographed, eluting with 35% ethyl acetate/hexane. The crystalline product was the second elution band; mp 95–97°C; ir: 3000 (br), 1723, 1698, 1632, 1601 cm^{-1}; ^1H nmr ($CDCl_3$) δ: 0.88, (t, 3H), 1.23 (br s, 22H), 1.84 (m, 2H), 3.38 (s, 2H), 4.27 (t, 2H), 5.33 (s, 2H), 5.81 (unresolved m, 1H), 6.44 (unresolved m, 1H), 7.19–8.09 (m, 7H); ^{13}C nmr ($CDCl_3$, 50.5 MHz) δ: 14.24, 8 resolved CH_2 lines between 22.81 and 32.03 ppm, 37.51, 43.26, 67.94, 14 lines between 108.80 and 140.88 ppm (12 aromatic and 2 olefinic C), 170.75, 171.40. *Anal.* calcd. for $C_{32}H_{43}NO_4$: C 76.00, H 8.66, N 2.77%; found: C 76.00, H 8.60, N 2.59%.

The Langmuir balance and the techniques for monolayer chracterization are described in the accompanying manuscript (1). Conditions of compression speed, substrate preparation, and Langmuir–Blodgett deposition are all identical to those used for the fluorenylidene-containing surfactants (1). Techniques for determination of redox potentials by cyclic voltammetry are described in the accompanying paper (1). A saturated calomel reference electrode was used, and curves were recorded at a slower sweep rate of 50 mV s^{-1}. Fluorescence spectra were recorded using a Hitachi–Perkin Elmer MPF-2A instrument. Dilute solutions (2×10^{-5} M) of the carbazole compound in HPLC-grade ethanol were deoxygenated with high-purity nitrogen before spectra were recorded. A 1 cm square quartz fluorescence cell was used for all measurements. Fluorescence decay times were measured by the single photon counting technique (19) on a commercial instrument (PRA International). Details of the analysis procedures have appeared in earlier publications (12, 20).

Acknowledgements

Financial support of this research by the Natural Sciences and Engineering Research Council of Canada, through its University–Industry program, is gratefully acknowledged. The authors thank Dr. S. V. Lowen for assistance with additional electrochemical measurements.

1. J. W. Taylor, C. P. Sloan, D. A. Holden, G. J. Kovacs, and R. O. Loutfy. Can. J. Chem. **67**, 2136 (1989).
2. (*a*) K. Blodgett. J. Am. Chem. Soc. **57**, 1007 (1935); (*b*) G. L. Gaines, Jr. Insoluble monolayers at liquid–gas interfaces. Interscience, New York. 1966; (*c*) G. G. Roberts. Adv. Phys. **34**, 475 (1985).
3. R. C. Reed and R. M. Wightman. *In* Encyclopedia of electrochemistry of the elements. Vol. 15. *Edited by* A. J. Bard. Marcel Dekker Inc., New York. 1984. p. 1.
4. (*a*) A. V. Patsis and D. A. Seanor (*Editors*). Photoconductivity in polymers, an interdisciplinary approach. Technomic Publishing, Westport, CT. 1976; (*b*) J. Mort and G. Pfister (*Editors*). Electronic properties of polymers. Wiley–Interscience, New York. 1982.
5. (*a*) E. E. Renfrew. U.S. Pat. 3,844,715 (1975); (*b*) U.S. Pat. 3,948,948 (1976); (*c*) W. W. Limburg. Ger. Offen. 2,430,748 (1975); (*d*) W. W. Limburg, J. M. Pearson, and D. J. Williams. Ger. Offen. 2,513,189 (1975).
6. N. Tamai, T. Yamazaki, and I. Yamazaki. J. Phys. Chem. **91**, 841 (1987).
7. T. Murakata, T. Miyashita, and M. Matsuda. Macromolecules, **21**, 2730 (1988).
8. J. M. Rodriguez-Parada and V. Percec. Macromolecules, **19**, 55 (1986).
9. P. H. Carter, S. G. P. Plant, and M. Tomlinson. J. Chem. Soc. 2210 (1957).
10. Huang-Minlon. J. Am. Chem. Soc. **68**, 2487 (1946).
11. B. E. Tate and E. C. Leonard. Vinyl and diene monomers. John Wiley and Sons, New York. 1970. p. 227.
12. D. A. Holden, L. Corey, J. Kovarova, and J. E. Guillet. Macromolecules, **19**, 1180 (1986).
13. K. Fukuda, H. Nakahara, and T. Kato. J. Colloid Interface Sci. **54**, 430 (1976).
14. J. A. Mercer-Smith and D. G. Whitten. J. Am. Chem. Soc. **101**, 6620 (1979).
15. J. F. Ambrose, L. L. Carpenter, and R. F. Nelson. J. Electrochem. Soc. **122**, 876 (1975).
16. L. Eberson and J. H. P. Utley. *In* Organic electrochemistry. 2nd ed. *Edited by* M. M. Baizer and H. Lund. Marcel Dekker Inc., New York. 1983. Chap. 14.
17. I. B. Berlman. Handbook of fluorescence spectra of aromatic molecules. 2nd ed. Academic Press, New York. 1973.
18. G. E. Johnson. Macromolecules, **13**, 145 (1980).
19. D. V. O'Connor and D. Phillips. Time-correlated Single Photon Counting. Academic Press, London. 1984.
20. D. A. Holden, K. Jordan, and A. Safarzadeh-Amiri. Macromolecules, **19**, 895 (1986).

Can. J. Chem. Downloaded from www.nrcresearchpress.com by 186.148.149.217 on 09/07/12
For personal use only.

Ionization of sulfonic acids and dimethylsulfoxide basicity. A ^{13}C nuclear magnetic resonance and calorimetric study

ROBERT L. BENOIT, MONIQUE FRÉCHETTE,[1] AND DANIELLE BOULET
Département de chimie, Université de Montréal, C.P. 6128, Succ. A, Montréal (Québec), Canada H3C 3J7
Received March 28, 1989

ROBERT L. BENOIT, MONIQUE FRÉCHETTE, and DANIELLE BOULET. Can. J. Chem. **67**, 2148 (1989).

The ionization of trifluoromethane-, methane-, and benzene-sulfonic acids in Me_2SO and in water has been studied by ^{13}C nuclear magnetic resonance. While the protonation shifts of $CF_3SO_3^-$ and $CH_3SO_3^-$ in both solvents are too small to make a quantitative interpretation possible, the $C_6H_5SO_3^-$ shift data in H_2O–H_2SO_4 mixtures, when treated by the method of Cox and Yates, gave a pK_a value of -2.5 for the ionization of $C_6H_5SO_3H$. Our results are discussed in relation to those of other workers. Enthalpies of solution and of ionization of these acids and related compounds have been obtained in both solvents. Single ion enthalpies of transfer from water to Me_2SO have been calculated from our data and from a transfer value for $CF_3SO_3^-$ ($+1.9$ kJ mol^{-1}) based on the tetraphenylarsonium–tetraphenylborate extrathermodynamic assumption. The transfers are endothermic processes for the anions $CH_3SO_3^-$ ($+29.6$ kJ mol^{-1}), $C_6H_5SO_3^-$ ($+20.2$ kJ mol^{-1}), and *p*-$CH_3C_6H_4SO_3^-$ ($+21.8$ kJ mol^{-1}), and exothermic for H^+ (-27.4 kJ mol^{-1}). These results are discussed in terms of the properties of the ions and solvents. The transfer value for H^+ is a valuable measure of the basicity difference between bulk water and Me_2SO.

Key words: sulfonic acids, ionization, dimethylsulfoxide, ^{13}C NMR, calorimetry.

ROBERT L. BENOIT, MONIQUE FRÉCHETTE et DANIELLE BOULET. Can. J. Chem. **67**, 2148 (1989).

On a étudié par résonance magnétique nucléaire du ^{13}C l'ionisation des acides trifluorométhane-, méthane- et benzènesulfonique dans l'eau et le Me_2SO. Si les variations des déplacements chimiques de $CF_3SO_3^-$ et $CH_3SO_3^-$ lors de leur protonation dans les deux solvants sont trop faibles pour être interprétées quantitativement, les données pour $C_6H_5SO_3^-$ dans les mélanges H_2O–H_2SO_4 ont conduit par la méthode de Cox et Yates à un pK_a de $-2,5$ pour l'ionisation de $C_6H_5SO_3H$. Nos résultats sont discutés en relation avec ceux d'autres chercheurs. On a obtenu dans les deux solvants les enthalpies de solution et d'ionisation de ces acides et de composés reliés. Les enthalpies ioniques de transfert de l'eau au Me_2SO ont été calculées à partir de nos résultats et d'une valeur pour le transfert de $CF_3SO_3^-$ ($+1,9$ kJ mol^{-1}), basée sur l'hypothèse extrathermodynamique tétraphénylarsonium–tétraphénylborate. Les transferts sont des processus endothermiques pour les anions $CH_3SO_3^-$ ($+29,6$ kJ mol^{-1}), $C_6H_5SO_3^-$ ($+20,2$ kJ mol^{-1}) et *p*-$CH_3C_6H_4SO_3^-$ ($+21,8$ kJ mol^{-1}), et exothermique pour H^+ ($-27,4$ kJ mol^{-1}). Ces résultats sont discutés sur la base des propriétés des ions et des solvants. La valeur pour le transfert de H^+ est une mesure utile de la différence de basicité entre l'eau-solvant et le Me_2SO.

Mots clés : acides sulfoniques, ionisation, diméthylsulfoxyde, ^{13}C RMN, calorimétrie.

Can. J. Chem. Downloaded from www.nrcresearchpress.com by 186.148.149.217 on 09/07/12
For personal use only.

Introduction

Alkanesulfonic acids are moderately strong acids in aqueous solution but estimates of their ionization constants K_{aw} vary. For methanesulfonic acid, K_{aw} values of ~4 and ~13 (1) were obtained from acidity function data, 16 (2) from ^1H nmr results, and 73 (3) and 83 (4) from Raman data. Ethane- and propanesulfonic acids are slightly weaker with K_{aw} values of 48 (Et) and 34 (Pr) respectively (4). Arenesulfonic acids are expected to be stronger acids (5). The ionization of benzenesulfonic acid in particular has been studied in H_2SO_4–H_2O by Cerfontain and co-workers using uv (6), and ^1H (7) and ^{13}C nmr (8). They calculated a -6.56 pK_{aw} with half deprotonation at 82.2% H_2SO_4 ($H_o = -7.7$). However, the same authors also obtained, by ^1H nmr, $pK_{aw} \sim -6.0$ for methane-, ethane-, and some additional alkanesulfonic acids (7), i.e., values completely at variance with those previously quoted (1–4).

In our early search for strong acids in dimethylsulfoxide (Me_2SO) we studied by conductivity the ionization of two sulfonic acids in Me_2SO (9): while CF_3SO_3H behaved as a strong electrolyte, CH_3SO_3H was incompletely dissociated with a value of $pK_{as} = 1.76$. Both these results were essentially confirmed independently (10). The behavior of $C_6H_5SO_3H$ in Me_2SO has not been studied but *p*-toluenesulfonic acid (11) and chlorobenzenesulfonic acid (12) are reported to be strong acids (see, however, ref. 9). In conjunction with our recent studies of the ionization of aminosulfonic acids (13, 14) we further investigated the ionization of sulfonic acids in water and Me_2SO.

In this paper, we report the results of our ^{13}C nmr study of the ionization of trifluoromethane-, methane-, and benzenesulfonic acids in H_2O–H_2SO_4 and Me_2SO–CF_3SO_3H media. We also present related calorimetric results, in particular on the solution and ionization of these acids in water and Me_2SO. This led us to values of single ion enthalpies of transfer from water to Me_2SO for $CH_3SO_3^-$, $C_6H_5SO_3^-$, *p*-$CH_3C_6H_4SO_3^-$, and H^+. The H^+ value is of particular interest since it is a quantitative measure of the superior basicity of Me_2SO.

Experimental

Materials

Trifluoromethanesulfonic acid (CF_3SO_3H) (Aldrich) was distilled under reduced pressure before use, and titration of the acid with standard aqueous NaOH indicated a purity in excess of 99.4%. Methanesulfonic acid (CH_3SO_3H) (Fluka, puriss.) and silver *p*-toluenesulfonate ($CH_3C_6H_4SO_3Ag$) (Aldrich 99+%) were used without further purification. Benzenesulfonic acid ($C_6H_5SO_3H$) (Fluka, purum) had less than 1% water and was dried over P_4O_{10}. Sulfuric acid (Baker), 7% fuming H_2SO_4 (Fisher), and dimethylsulfoxide (BDH and Anachemia) were used as received. Me_2SO-d_6 was from Cambridge Isotope Laboratories.

Nuclear magnetic resonance

Proton decoupled ^{13}C nmr spectra were recorded at 28°C on a Bruker WP-80 Fourier transform spectrometer operating at 20.2 MHz. Chemical shifts, δ (ppm), were determined relative to external dioxane in D_2O (external lock) and converted to the Me_4Si scale by using $\delta_{Me4Si} = \delta_{dioxane} + 67.40$ ppm.

[1]Present address: Department of Chemistry, University of Ottawa, Ottawa, Ont., Canada K1N 6N5.

The ^{13}C nmr spectra were recorded for CF_3SO_3H, CH_3SO_3H, and $C_6H_5SO_3H$, in 0–18 M aqueous H_2SO_4 and in aqueous NaOH. Spectra of CF_3SO_3H, CH_3SO_3H, and $C_6H_5SO_3H$ were also obtained in 7% fuming H_2SO_4, in 0–11.3 M CF_3SO_3H in Me_2SO, and in Me_2SO solutions of strong bases (tetramethylguanidine (TMG) or 4-amino-2, 6-dimethylpyrimidine (Dap)). The concentration of the sulfonic acids was ~0.40 M (except for 0.08 M CH_3SO_3H in aqueous NaOH). The samples were prepared by adding weighed amounts of the sulfonic acids to known volumes of titrated acidic solutions. ^{13}C chemical shift values are within 0.10 ppm.

Calorimetry

The heat of solution of the sulfonic acids in Me_2SO and water as well as their heat of neutralization in 0.05 M Me_2SO solutions of strong bases were obtained at 25.00 ± 0.01°C (except for the solution of CF_3SO_3H in water at 30.00 ± 0.01°C). An L.K.B model 8725-2 isoperibol calorimeter was used as previously described (15). The amount of sulfonic acid dissolved ((1–40) $\times 10^{-4}$ mol) in the 100-mL reaction cell was deduced from the weights of the glass ampoules. For each determination of the heat of solution or neutralization at least three separate experiments were made at different concentrations.

Results and discussion

We will first consider the ^{13}C nmr data on the ionization of the three sulfonic acids CF_3SO_3H, CH_3SO_3H, and $C_6H_5SO_3H$ in acid media, both in water and Me_2SO. We will then examine the calorimetric results on the enthalpies of solution of the acids and related compounds in both solvents.

^{13}C nmr spectra

Data on ^{13}C nmr chemical shifts of a moderately strong acid HA as a function of its concentration c or of the acidity of the media can, in principle, lead to the ionization constant K_a of HA (16). The observed chemical shift, δ, is, under fast exchange conditions, a weighted average of the chemical shifts of the acid δ_{HA} and its anion δ_A, according to

$$[1] \quad \delta = \delta_{HA}\frac{[HA]}{c} + \delta_A\frac{[A^-]}{c}$$

with

$$[2] \quad c = [HA] + [A^-]$$

and

$$[3] \quad K_a = \frac{[H^+]\,[A^-]}{[HA]}$$

where [HA] and $[A^-]$ are the concentrations of the acid and its anion respectively. There are various methods of obtaining K_a from data giving $\delta = f(c)$ or $\delta = f([H^+], c)$, provided δ_{HA} and δ_A are sufficiently different. Let us consider in turn the data obtained for CF_3SO_3H, CH_3SO_3H, and $C_6H_5SO_3H$ in both solvents.

CF_3SO_3H

The chemical shift of the anion $CF_3SO_3^-$ in water, given as the centre of the quartet, is δ = 120.52 ppm. Upon addition of H_2SO_4, δ moves slightly upfield (120.35 ppm (8.9 M H_2SO_4), 119.5 ppm (17.8 M H_2SO_4), and 118.98 ppm (oleum)). It is clear that the variations of δ are too small to obtain any meaningul information on the protonation of $CF_3SO_3^-$ in H_2O–H_2SO_4 mixtures. Now, in Me_2SO-d_6, we observe for $CF_3SO_3^-$ δ = 121.70 ppm. The downfield move of δ (+1.2 ppm) from H_2O to Me_2SO reflects the loss of H-bonding of $CF_3SO_3^-$ in the latter solvent. When the concentration of CF_3SO_3H in Me_2SO is increased δ moves slightly upfield, as shown in Fig. 1, to reach 118.75 ppm for neat CF_3SO_3H (11.3 M). The total variation of δ is 3.0 ppm, but the medium has correspondingly changed from essentially Me_2SO to CF_3SO_3H so that δ for $CF_3SO_3^-$ and CF_3SO_3H may not remain constant, as would be required to solve eqs. [1]–[3]. We note that for 4.4 M CF_3SO_3H, the medium corresponds to 1:2 CF_3SO_3H:Me_2SO and that up to this concentration, δ has only decreased by 0.3 ppm from the value for $CF_3SO_3^-$. This would be consistent with assuming that, up to 4.4 M, CF_3SO_3H is ionized and present as $CF_3SO_3^-$ H^+ $(Me_2SO)_2$, the proton being H-bonded to two Me_2SO (17). We also observe that, on addition of CF_3SO_3H, the methyl carbons from Me_2SO-d_6 move progressively upfield from 40.69 ppm, with the concentration of CF_3SO_3H, to reach 37.1 ppm for 4.4 M CF_3SO_3H, and this δ value would correspond to H^+ $(Me_2SO)_2$. The value of the ^{13}C shift of Me_2SO may then give some information on the ionization of moderately strong acids in Me_2SO, as we shall see for CH_3SO_3H and $C_6H_5SO_3H$. On continuing the addition of CF_3SO_3H, the ^{13}C shift of Me_2SO moves further upfield as $H^+(Me_2SO)$ is formed (17).

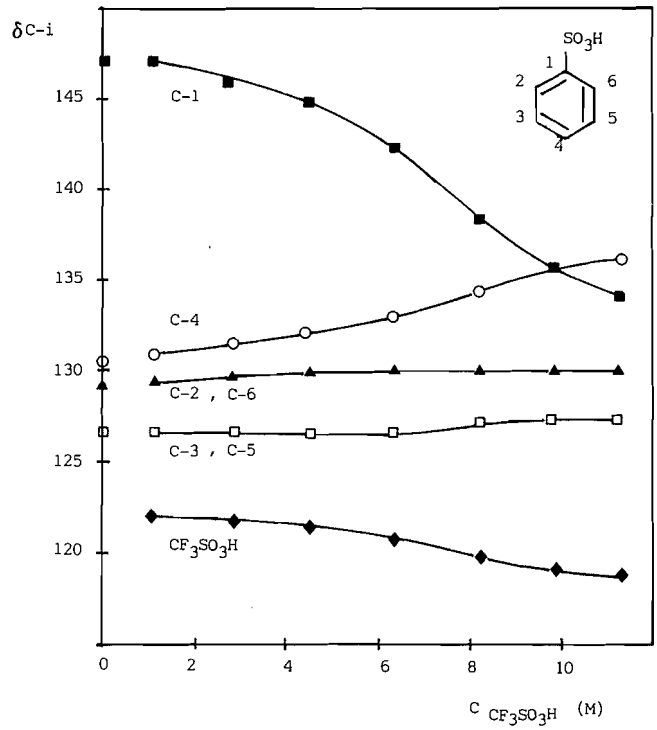


FIG. 1. ^{13}C chemical shifts (ppm) of (0.40 M) $C_6H_5SO_3H$ and CF_3SO_3H in Me_2SO as a function of CF_3SO_3H concentration.

CH_3SO_3H

In water, the chemical shift of $CH_3SO_3^-$ is 39.35 ppm and δ moves very slightly downfield upon addition of H_2SO_4 (39.76 ppm for 12.6 M H_2SO_4, 39.62 for 17.8 M H_2SO_4, and 39.74 ppm for neat CH_3SO_3H). Clearly these data cannot give any information on the protonation of $CH_3SO_3^-$ in H_2O–H_2SO_4 media so that we are left with the conflicting results of earlier authors (1–4) giving K_{aw} values for CH_3SO_3H between 4 and 80, and those of Koeberg-Telder and Cerfontain (7) who found K_{aw} ~$10^{6.0}$ using ^1H nmr. Considering the assumption made by the latter authors to correct for medium effects, we would tend to favour K_{aw} ~80 obtained from Raman data (3–5).

Now, if we turn to CH_3SO_3H in Me_2SO-d_6, the chemical shift of $CH_3SO_3^-$ is 40.91 ppm. As for $CF_3SO_3^-$, there is a

Can. J. Chem. Downloaded from www.nrcresearchpress.com by 186.148.149.217 on 09/07/12
For personal use only.

Can. J. Chem. Downloaded from www.nrcresearchpress.com by 186.148.149.217 on 09/07/12
For personal use only.

downfield move (+1.5 ppm) from water to Me_2SO due to the loss of H-bonding of $CH_3SO_3^-$ to the latter solvent. Then, we find that upon addition of 1.95 M CF_3SO_3H to 0.2 M CH_3SO_3H, δ moves only to 40.61 ppm and on increasing the CH_3SO_3H concentration up to 3 M the change of δ is also minimal: 40.76 ppm (0.60 M), 40.76 ppm (1.03 M), 40.69 ppm (3.06 M). Since according to the conductivity data (9, 10) CH_3SO_3H should largely be unionized in these solutions, these small variations of δ indicate that the δ values of $CH_3SO_3^-$ and CH_3SO_3H are also very close in Me_2SO and no further information can be obtained. However, that CH_3SO_3H is at least in part unionized in a 3.06 M solution receives some confirmation from the fact that the corresponding ^{13}C shift of Me_2SO is 39.59 ppm, i.e., closer to the shift of H-bonded Me_2SO in solutions of weak acids (2.8 M CH_3CO_2H: 40.25 ppm; 3.4 M CF_3CO_2H: 39.52 ppm) than to the shift of protonated Me_2SO in ionized 3 M CF_3SO_3H: 38.60 ppm.

$C_6H_5SO_3H$

The four ^{13}C shifts observed for $C_6H_5SO_3^-$ in both water and Me_2SO were assigned by taking the most deshielded carbon as C-1, and then C-4 (*para*) > C-2,6 (*ortho*) > C-3,5 (*meta*), in accordance with the effect of an electron-withdrawing substituent on the benzene ring. These assignments are those of Breitmaier and Voelter (18) and Kosugi and Takeuchi (19) but differ (for C-2 and C-3) from those of Cerfontain *et al.* (8) and Sadtler (20). The assignment of the shifts for $C_6H_5SO_3H$ follows from the curves giving the shifts as a function of acidity in H_2O–H_2SO_4 and Me_2SO–CF_3SO_3H media. The C-1 and C-4 curves cross at high acidity ($-H_o$ = 9 in water) so that the assignments of C-1 and C-4 given by Kosugi and Takeuchi (19) should be reversed. The ^{13}C shift curves against acidity are only given in Fig. 1 for Me_2SO–CF_3SO_3H media since for H_2O–H_2SO_4 media our curve is the same as that given by Cerfontain *et al.* (8) after switching C-2 and C-3. The shift curves obtained in both media are essentially similar. While C-1 moves upfield with an increase in acidity, the other carbons move downfield. The shift variations (titration shifts) are C-1 > C-4 ≫ C-2 ~ C-3 and are somewhat larger in Me_2SO than in water because, with the absence of H-bonding to $C_6H_5SO_3^-$ in Me_2SO, in this latter solvent C-1 is moved 6.2 ppm downfield, and C-4 2.8 ppm upfield, from their values in water. The ^{13}C protonation shifts observed for benzenesulfonate are similar in magnitude to those reported for the protonation of aniline (14, 18) and benzoate (18), and much larger than those for the alkylsulfonates, amines, and carboxylates (18).

The curves giving the chemical shifts of the four different types of carbon atoms in $C_6H_5SO_3H$ as a function of H_o in H_2O–H_2SO_4 media are not simple sigmoidal curves. Taking the C-1 curve as an example, there is no plateau at low acidity corresponding to δ ($C_6H_5SO_3^-$) but δ decreases somewhat linearly from 142.5 ($-H_o$ = 1.5) to 140.0 ppm ($-H_o$ = 5.5) and the expected plateau at high acidity for δ ($C_6H_5SO_3H$) is not clearly defined. To get around these difficulties, which may be due to "medium effects", Cerfontain *et al.* (8) essentially assumed that below 50% H_2SO_4, δ was that of $C_6H_5SO_3^-$, and for 98.4% H_2SO_4, δ was that of $C_6H_5SO_3H$. The authors actually used C-2 as intramolecular standard in their treatment, but δ (C-2) is nearly constant. They further assumed that there was a linear medium effect of δ ($C_6H_5SO_3^-$) and no medium effect on δ ($C_6H_5SO_3H$). Under these conditions they calculated pK_{aw} = −6.56 using the H_o^a scale and found that half-protonation was at H_o = −7.7. We treated our own ^{13}C shift data in H_2O–H_2SO_4 mixtures using the method of Cox and Yates as previously described (21) and we obtained pK_{aw} = −2.53 ± 0.12. This value is near −2.8, the value estimated by Guthrie (5), and we prefer it to the pK_{aw} value obtained by Cerfontain *et al.* (8) because of their questionable assumptions concerning possible medium effects.

The ^{13}C shift curves for $C_6H_5SO_3^-$ as a function of the molar concentration of CF_3SO_3H in Me_2SO–CF_3SO_3H media (Fig. 1) are similar to those in H_2O–H_2SO_4: there is no plateau for δ ($C_6H_5SO_3^-$) at low acidity, but only a linear decrease of δ, and the plateau for δ ($C_6H_5SO_3H$) is not reached in pure CF_3SO_3H. The interpretative difficulties are compounded by the absence of an acidity scale in Me_2SO so that we can only conclude from these data that $C_6H_5SO_3H$ is a strong acid in Me_2SO just as in water. This is confirmed by the fact that the shift of the Me_2SO carbons in a 2.06 M $C_6H_5SO_3H$ solution (39.74 ppm) is close to the same shift in a 1.98 M CF_3SO_3H solution (39.59 ppm), so that both acids would have a similar strength in Me_2SO.

Enthalpy data

Enthalpies of solution

On the basis of our nmr data, CH_3SO_3H in water and CF_3SO_3H and $C_6H_5SO_3H$ in water and Me_2SO were taken as strong electrolytes. Possible ion-pairing effects for $CH_3C_6H_4SO_3Ag$ were neglected since $CH_3C_6H_4SO_3^-$ is a weakly coordinating anion and Ag^+ is strongly solvated by both Me_2SO and water.

The enthalpies of solution, Q_s, were determined for the acid CH_3SO_3H in water and for CF_3SO_3H, $C_6H_5SO_3H$, and $CH_3C_6H_4SO_3Ag$ in Me_2SO and water. The plots of Q_s against the number of moles dissolved ((1–40) × 10^{-4} mol) were linear and the least-squares slopes gave the molar enthalpies of solution in Me_2SO (ΔH_{ss}) or in water (ΔH_{sw}) according to

[4] $MA\ (l\ or\ c) = M^+\ (s\ or\ w) + A^-\ (s\ or\ w)$

where M stands for H^+ or Ag^+.

In the concentration range studied ((1–40) × 10^{-3} M), the concentration dependence of ΔH_{ss} or ΔH_{sw} for uni–univalent electrolytes is small ($\Delta H_{ss} = \Delta H_{ss}^\circ + 3.4c^{1/2}$ and $\Delta H_{sw} = \Delta H_{sw}^\circ + 3.1c^{1/2}$) (22) and masked by experimental errors. The ΔH_{ss} and ΔH_{sw} values were thus taken as the enthalpies of solution at infinite dilution, ΔH_{ss}° and ΔH_{sw}°, which are given in Table 1.

For CH_3SO_3H, a weaker acid in Me_2SO, we first determined according to eq. [5] the heats of solution of the acid in 0.05 M basic solutions of proton sponge (PS) and of Dap. The enthalpies of protonation according to eq. [6] of PS (−48.5 kJ mol^{-1}) (23) and of Dap (−42.4 kJ mol^{-1}) (15) were then substracted to give an average value of −46.5 ± 3 kJ mol^{-1} for ΔH_{ss}° of CH_3SO_3H in Me_2SO.

[5] $HA(l) + B(s) = BH^+(s) + A^-(s)$

[6] $H^+(s) + B(s) = +BH^+(s)$

We also attempted to determine separately the solution enthalpy of unionized CH_3SO_3H in Me_2SO, and ΔH_{is}° the enthalpy of ionization of CH_3SO_3H according to

[7] $HA(l) = HA(s)$

[8] $HA(s) = H^+(s) + A^-(s)$

We used for this purpose our corrected experimental value of −41.5 ± 0.3 kJ mol^- for the enthalpy of solution of CH_3SO_3H (1) in 0.10 M CF_3SO_3H in Me_2SO. We calculated α, the

Can. J. Chem. Downloaded from www.nrcresearchpress.com by 186.148.149.217 on 09/07/12
For personal use only.

TABLE 1. Enthalpies of solution[a] of sulfonic acids and related compounds in Me_2SO and water at 25°C

Compound	ΔH_s° (kJ mol^{-1})	
	Me_2SO (ΔH_{ss}°)	H_2O (ΔH_{sw}°)
CH_3SO_3H (l)	-46.5 ± 3	-48.3 ± 0.3
CF_3SO_3H (l)	-105.0 ± 0.4	-79.1 ± 0.4[b]
$C_6H_5SO_3H$ (c)	-39.6 ± 0.9	-32.0 ± 0.5
$CH_3C_6H_4SO_3Ag$ (c)	-14.4 ± 0.2	-17.08 ± 0.03
CF_3SO_3K (c)	-16.3 ± 0.2[c]	$+17.2 \pm 0.1$[c]
HCl (g)	-81.5[d]	-74.8[d]

[a]According to eq. [4].
[b]Value obtained at 30°C.
[c]Reference 22.
[d]Reference 17.

fraction of ionized CH_3SO_3H, in this medium from the value of the ionization constant of CH_3SO_3H ($K_{as} = 10^{-1.70}$ for an ionic strength $I = 0$) (9, 10) and the ionic activity coefficients calculated according to the appropriate Debye–Hückel equation (24). We then obtained an approximate value for the ionization enthalpy of CH_3SO_3H: $\Delta H_{is}^\circ = -10 \pm 7$ kJ mol^{-1}.

We also determined the heat of solution of CH_3SO_3H in Me_2SO at high dilution ((2–9) $\times 10^{-3}$ M) as -44.6 ± 0.3 kJ mol^{-1}. This value is to be preferrred to -59.0 ± 0.8 kJ mol^{-1}, reported by Arnett *et al.* (25), particularly since the latter value leads with their other data to a surprising +33.5 kJ mol^{-1} for the enthalpy of ionization of CH_3SO_3H in Me_2SO. Our own ionization enthalpy −10 kJ mol^{-1} is also more in line with what would be expected for CH_3SO_3H, an acid with $pK_{as} = 1.70$, since HCl, with a comparable $pK_{as} = 2.0$ (9, 10), has an ionization enthalpy of −5.0 kJ mol^{-1} (17).

Enthalpies of transfer

The enthalpies of solution of our electrolytes in water and Me_2SO are best discussed on the basis of single-ion enthalpies of transfer, where the enthalpy of transfer of an ion such as A^-, from water to Me_2SO, $\Delta H_{ws}(A^-)$, is defined according to

[9] $A^-(w) = A^-(s)$

The enthalpies of transfer of the electrolytes M^+A^- are first deduced from the data in Table 1. These enthalpies are then split into single-ion values on the basis of the well-known tetraphenylarsonium–tetraphenylborate (tatb) extrathermodynamic assumption ($\Delta H_{ws}^\circ(BPh_4^-) = \Delta H_{ws}^\circ(AsPh_4^+)$) (26). We first calculated $\Delta H_{ws}^\circ(CF_3SO_3^-) = +1.9$ kJ mol^{-1} from the published enthalpies of solution of KCF_3SO_3 (Table 1) and the recommended value (26) $\Delta H_{ws}^\circ(K^+) = -35.4$ kJ mol^{-1}. We obtained next from the enthalpies of solution of CF_3SO_3H and $\Delta H_{ws}^\circ(CF_3SO_3^-)$ the value $\Delta H_{ws}^\circ(H^+) = -27.8$ kJ mol^{-1}. Then from the latter value and the solution enthalpies of CH_3SO_3H and $C_6H_5SO_3H$ we calculated $\Delta H_{ws}^\circ(CH_3SO_3^-) = +29.6$ kJ mol^{-1} and $\Delta H_{ws}^\circ(C_6H_5SO_3^-) = +20.2$ kJ mol^{-1}. Finally, we obtained $\Delta H_{ws}^\circ(CH_3C_6H_4SO_3^-) = +21.8$ kJ mol^{-1} from the solution enthalpies of $CH_3C_6H_4SO_3Ag$ and $\Delta H_{ws}^\circ(Ag^+) = -53.3$ kJ mol^{-1} (26). The ΔH_{ws}° values are given in Table 2.

Anion transfer

First we note that the enthalpies of transfer for the anions are all positive, indicating poorer solvation in Me_2SO than in water. This is as expected since the important H-bonding contribution

TABLE 2. Ionic enthalpies of transfer from H_2O to Me_2SO at 25°C

Ion	ΔH_{ws}° (kJ mol^{-1})
$CF_3SO_3^-$	+1.9[a]
$CH_3SO_3^-$	+29.6
$C_6H_5SO_3^-$	+20.2, +20.9[b]
$CH_3C_6H_4SO_3^-$	+21.8
Cl^-	+20.0[c]
K^+	−35.4[c]
Ag^+	−53.3[c]
H^+	−27.8, −26.7[d]

[a]Calculated from data in Table 1 and $\Delta H_{ws}^\circ(K^+)$.
[b]Calculated from $\Delta H_{ws}^\circ(CH_3C_6H_4SO_3^-)$, see text.
[c]Reference 26.
[d]Calculated from $\Delta H_{ws}^\circ(H^+, Cl^-)$ and $\Delta H_{ws}^\circ(Cl^-)$, see text.

to anion solvation is missing in Me_2SO, a dipolar aprotic solvent. The more positive value of ΔH_{ws}° for the aliphatic sulfonate $CH_3SO_3^-$ than for the aromatic sulfonates $C_6H_5SO_3^-$ and $CH_3C_6H_4SO_3^-$ is in line with the positive transfer values for alkanes (27), and a transfer value near zero for benzene (28) because of weak interactions between the benzene ring and Me_2SO. These differences in the transfer of $CH_3SO_3^-$ and $C_6H_5SO_3^-$, from water to Me_2SO, account in part for our finding that while both CH_3SO_3H and $C_6H_5SO_3H$ are strong electrolytes in water, CH_3SO_3H is incompletely ionized in Me_2SO in contrast to $C_6H_5SO_3H$. If we compare now ΔH_{ws}° for benzene, −0.3 kJ mol^{-1}, with $\Delta H_{ws}^\circ = +0.6$ kJ mol^{-1} for toluene (28), we isolate +0.9 kJ mol^{-1} for the transfer of -CH_3. Assuming this group contribution to be additive we calculate, from our $\Delta H_{ws}^\circ = +21.8$ kJ mol^{-1} for $CH_3C_6H_4SO_3^-$, a value of $\Delta H_{ws}^\circ = +20.9$ kJ mol^{-1} for $C_6H_5SO_3^-$, i.e., a value in very good agreement with our direct experimental value +20.2 kJ mol^{-1}.

It is worth noting that the enthalpy of transfer of $CH_3SO_3^-$, +29.6 kJ mol^{-1}, is highly positive. In fact, it is more positive than the transfer values listed for all anions in Marcus' compilation (26), for example, for Cl^-, $\Delta H_{ws}^\circ = +20$ kJ mol^{-1}, for Br^-, $\Delta H_{ws}^\circ = +5$ kJ mol^{-1}. Since the ionic radius of $CH_3SO_3^-$ is certainly larger than that of Cl^- and Br^-, it follows that, for its size, $CH_3SO_3^-$ must be strongly stabilized in water through H-bonding. It is interesting to contrast the ΔH_{ws}° values for closely related $CH_3SO_3^-$ (+29.6 kJ mol^{-1}) and $CF_3SO_3^-$ (+1.9 kJ mol^{-1}). Since, on account of ionic size, the enthalpy of solvation (gas to solvent) ΔH_{gs}° of $CF_3SO_3^-$ in Me_2SO must be less exothermic than that of $CH_3SO_3^-$, it follows that in water $CF_3SO_3^-$ is at least 28 kJ mol^{-1} less exothermically solvated than $CH_3SO_3^-$. Interestingly, a similar situation prevails for the related pair $CF_3CO_2^-$ and $CH_3CO_2^-$. In this case the hydration enthalpy, ΔH_{gw}°, can be calculated from gas phase data and the values are such that $CF_3CO_2^-$ is some 85 kJ mol^{-1} less exothermically solvated than $CH_3CO_2^-$ (29). It is tempting but perhaps not justified to partly explain the large differences in hydration enthalpies (ΔH_{gw}°) for the pairs $CF_3SO_3^-$ − $CH_3SO_3^-$ or $CF_3CO_2^-$ − $CH_3CO_2^-$ in terms of contrasting interactions of the CF_3- and CH_3- groups. However, using for this purpose the neutral compounds CH_4 and CF_4 as models is inconclusive: even though CF_4 is a very hydrophobic solute, the hydrophobic enthalpic effect is small (27) and the solution

enthalpies of CH_4 and CF_4 in water differ by only 1 kJ mol^{-1} (27). At any rate, the ΔH^o_{gw} trend must reflect increasing H-bonding of $-SO_3^-$ when passing from $CF_3SO_3^-$ to $CH_3SO_3^-$.

Finally, our value of ΔH^o_{ws} for $CH_3SO_3^-$ enables us to calculate ΔH^o_{ws} for other alkyl-sulfonate ions, since Krishnan and Friedman (30) computed values of ΔH^o_{ws} as a function of alkyl chain but with an arbitrary constant included because they could not measure the heats of solution of various alkyl-sulfonates in Me_2SO.

Proton transfer

We now come to consider the enthalpy of transfer of the proton, ΔH^o_{ws} (H^+) = −27.8 kJ mol^{-1}. This value is to be compared with the only previously reported value (17) we obtained using experimental enthalpy data on the solution and ionization of HCl in both Me_2SO and water (Table 1). We calculated ΔH^o_{ws} (H^+) = −25.5 kJ mol^{-1} by using the value ΔH^o_{ws} (Cl^-) = +18.8 kJ mol^{-1}. However, if we use the value now recommended by Marcus (26), +20.0 kJ mol^{-1}, for the transfer of Cl^-, we obtain ΔH^o_{ws} (H^+) = −26.7 kJ mol^{-1}, in very good agreement, considering the many steps involved, with our new value (−27.8 kJ mol^{-1}) based on CF_3SO_3H ionization. We can therefore confidently select as our best value ΔH^o_{ws} (H^+) = −27.4 kJ mol^{-1}. This good agreement also gives credence to our value for the enthalpy of ionization of HCl in Me_2SO (17), ΔH^o_{is} = −5.0 kJ mol^{-1}, and casts doubt on the value reported by Arnett *et al.* (25), +54.4 kJ mol^{-1}, from data obtained using both HSO_3F as a strong acid and potassium dimsylate as a strong base in Me_2SO. The values of ΔH^o_{is} quoted for HBr and HI are also likely in error.

The value of the enthalpy of transfer of the proton is useful in that it permits us to rationalize the enthalpy changes observed for protonation or deprotonation reactions when comparing data in water and Me_2SO (23). ΔH^o_{ws} (H^+) can also be used, in conjunction with gas phase acidity measurements involving acids HA, to obtain and compare solvation enthalpies of anions, in Me_2SO, which is a simpler solvent with no contributions of H-bonding interactions to solvation. Finally, the value of ΔH^o_{ws} (H^+) = −27.4 kJ mol^{-1}, which measures the basicity difference between bulk water and Me_2SO, enables us to compare the basicity of Me_2SO with that of other solvents on the basis of their ΔH^o_{ws} (H^+) values: dimethylformamide (−24.6), propylene carbonate (+45.7), acetonitrile (+60.7), and sulfolane (+72 kJ mol^{-1}).[2]

Acknowledgements

The continued financial assistance of the Natural Sciences and Engineering Research Council of Canada and of the Ministère de l'Éducation is gratefully acknowledged. We thank C. Louis, L. Bergeron, and D. Lefebvre for some of the early calorimetric determinations.

[2]These values were calculated from previous experimental results (17) and recommended new values for ΔH^o_{ws} (Cl^-) (26).

1. K. N. Bascombe and R. P. Bell. J. Chem. Soc. 1096 (1959); J. G. Dawber. Chem. Commun. 58 (1968).
2. A. K. Covington and T. H. Lilley. Trans. Faraday Soc. 1750 (1967).
3. J. H. R. Clarke and L. A. Woodward. Trans. Faraday Soc. 2226 (1966).
4. A. K. Covington and R. Thompson. J. Solution Chem. **3**, 603 (1974).
5. J. P. Guthrie. Can. J. Chem. **56**, 2342 (1978).
6. H. Cerfontain and B. W. Schnitger. Recl. Trav. Chim. Pays-Bas, **91**, 199 (1972).
7. A. Koeberg-Telder and H. Cerfontain. J. Chem. Soc. Perkin Trans. 2, 226 (1975).
8. H. Cerfontain, A. Koeberg-Telder, and C. Kruk. Tetrahedron Lett. **42**, 3639 (1975).
9. R. L. Benoit and C. Buisson. Electrochim. Acta, **18**, 105 (1973).
10. C. McCallum and A. D. Pethybridge. Electrochim. Acta, **20**, 815 (1975).
11. J. C. Courtot-Coupez and M. Le Démézet. Bull. Soc. Chim. Fr. 1033 (1969).
12. I. M. Kolthoff, M. K. Chantooni, Jr., and S. Bhowmik. J. Am. Chem. Soc. **90**, 2821 (1968).
13. R. L. Benoit, D. Boulet, and M. Fréchette. Can. J. Chem. **66**, 3038 (1988).
14. R. L. Benoit, D. Boulet, and M. Fréchette. Magn. Reson. Chem. **27**, 233 (1989).
15. R. L. Benoit, D. Boulet, L. Séguin, and M. Fréchette. Can. J. Chem. **63**, 1228 (1985).
16. W. J. Spillane and J. B. Thomson. J. Chem. Soc. Perkin Trans. 2, 580 (1977).
17. R. Domain, M. Rinfret, and R. L. Benoit. Can. J. Chem. **54**, 2101 (1976), and references therein.
18. E. Breitmaier and W. Voelter. ^{13}C NMR specroscopy. 2nd ed. Verlag Chemie, Weinheim. 1978.
19. Y. Kosugi and T. Takeuchi. Org. Magn. Reson. **12**, 435 (1979).
20. The Sadtler Standard Spectra. Vol. 46, No 9045C. Sadtler Research laboratories, Philadelphia (1980).
21. R. L. Benoit and M. Fréchette. Can. J. Chem. **63**, 3053 (1985), and references therein.
22. G. R. Hedwig and A. J. Parker. J. Am. Chem. Soc. **96**, 6589 (1974).
23. R. L. Benoit, D. Lefebvre, and M. Fréchette. Can. J. Chem. **65**, 996 (1987).
24. I. M. Kolthoff, M. K. Chantooni, Jr., and S. Bhowmik. J. Am. Chem. Soc. **90**, 23 (1968).
25. E. M. Arnett and L. E. Small. J. Am. Chem. Soc. **99**, 808 (1977); E. M. Arnett, T. C. Moriarity, L. E. Small, J. P. Rudolph, and R. P. Quirk J. Am. Chem. Soc. **95**, 1492 (1973).
26. Y. Marcus. Pure Appl. Chem. **57**, 1103 (1985).
27. M. H. Abraham. J. Am. Chem. Soc. **104**, 2085 (1982), and references therein.
28. R. L. Benoit and M. Fréchette. Thermochim. Acta, **126**, 155 (1988).
29. C. Louis. Doctoral thesis, Université de Montréal. 1974.
30. C. V. Krishnan and H. L. Friedman. *In* Solute–solvent interactions. Vol. 2. *Edited by* J. F. Coetzee and C. D. Ritchie. Marcel Dekker, New York. 1976.

Can. J. Chem. Downloaded from www.nrcresearchpress.com by 186.148.149.217 on 09/07/12
For personal use only.

Study of trichloronitrosomethane: regioselective cycloadditions of 2-substituted-1,3-butadienes

CHENG-TUNG LIN[1] AND WEN-JEI HSU

Department of Chemistry, Tunghai University, Taichung 40098, Taiwan, Republic of China

Received December 14, 1988[2]

CHENG-TUNG LIN and WEN-JEI HSU. Can. J. Chem. **67**, 2153 (1989).

The regioselectivity of cycloaddition reactions of trichloronitrosomethane (**1**) with 2-alkyl (R = Me, Et, *i*-Pr, *t*-Bu, CF_3, Bz, and Cl) and 2-aryl (Ar = Ph, 4-CH_3OPh, 4-CH_3Ph, 3-CH_3Ph, and 4-ClPh) 1,3-butadienes is described. The orientation of cycloaddition is substituent dependent, producing 2,5-disubstituted (*para*) and 2,4-disubstituted (*meta*) 3,6-dihydro-1,2-oxazines from 2-alkyl- and 2-aryl-1,3-butadienes respectively. Increasing the bulk of the substituent from methyl to *tert*-butyl in 2-alkyl-1,3-butadienes increases the regioselectivity. Kinetic studies in various solvents indicate that plots of log k_m/k_H vs. Hammett σ^+ values give straight lines with the ρ values lying between −0.60 and −0.91 for the reactions with 2-aryl-1,3-butadienes. A concerted reaction mechanism is proposed and the orientation preference is consistent with frontier molecular orbital predictions for 2-alkyl-1,3-butadienes. In the reactions with 2-aryl-1,3-butadienes, a transition state leading to a spin-paired diradical, which then converts by partial electron transfer to zwitterionic structure, is proposed.

Key words: trichloronitrosomethane, 3,6-dihydro-1,2-oxazine, regioselectivity, [2 + 4] cycloaddition.

CHENG-TUNG LIN et WEN-JEI HSU. Can. J. Chem. **67**, 2153 (1989).

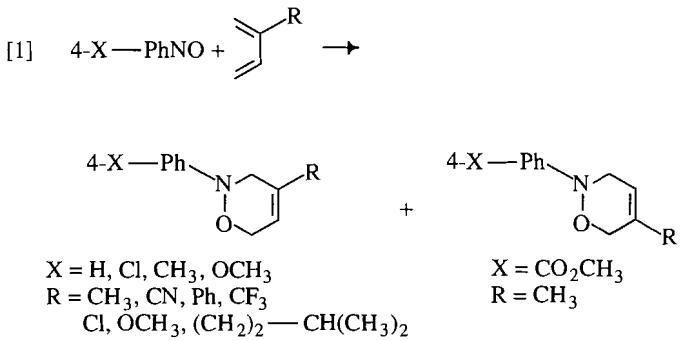
On a déterminé la régiosélectivité des réactions de cycloaddition du trichloronitrosométhane (**1**) sur des 2-alkyl (R = Me, Et, *i*-Pr, *t*-Bu, CF_3, Bz et Cl) et 2-aryl (Ar = Ph, 4-CH_3OPh, 4-CH_3Ph, 3-CH_3Ph et 4-ClPh) buta-1,3-diènes. L'orientation de la cycloaddition dépend du substituant; à partir des 2-alkyl- et des 2-aryl-buta-1,3-diènes, on obtient respectivement des 3,6-dihydro-1,2-oxazines disubstituées en 2,5 (*para*) et en 2,4 (*méta*). Avec les 2-alkyl-buta-1,3-diènes, une augmentation du volume du substituant (en allant du méthyle au *tert*-butyle) provoque une augmentation de la régiosélectivité. Des études cinétiques dans divers solvants suggèrent que les courbes du log k_m/k_H vs. les valeurs σ^+ de Hammett donnent des droites avec des valeurs de ρ variant de −0,60 à −0,91 pour les réactions des 2-aryl-buta-1,3-diènes. Pour les 2-alkyl-buta-1,3-diènes, on suggère un mécanisme réactionnel concerté et la préférence de l'orientation est en accord avec les prédictions des orbitales moléculaires frontières. Dans les réactions des 2-aryl-buta-1,3-diènes, on propose une état de transition conduisant à un diradical dont les spins sont pairés qui se transforme ensuite en une structure zwitterionique par un transfert partiel d'électrons.

Mots clés : trichloronitrosométhane, 3,6-dihydro-1,2-oxazine, régiosélectivité, cycloaddition [2 + 4].

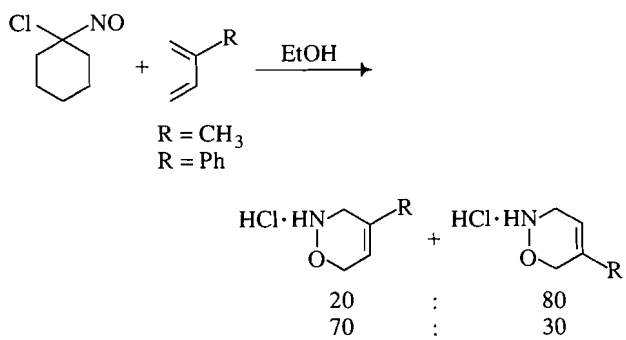
[Traduit par la revue]

Introduction

It has been recognized for many years that carbon-nitroso compounds are reactive heterodienophiles (for reviews see ref. 1). The most useful synthetic application of nitroso compounds is the cleavage of the nitrogen–oxygen bond in the [4 + 2] cycloadduct to generate a 1,4-bifunctional group in a "*syn*" orientation (2). Extensive studies of cycloadditions of substituted nitrosobenzenes reveal that nitroso compounds react regioselectively with unsymmetrical dienes (3). The resulting orientation preference has been rationalized on the basis of the relative stability of a transition state leading to an intermediate lying between nonpolar and zwitterionic structure (3*b*). In most cases of 2-substituted dienes, nitrosobenzenes react so that the nitrogen and oxygen atoms form bonds at the C-1 and C-4 atoms of the dienes, respectively, to afford the "*meta*" adducts (i.e., 4-substituted 3,6-dihydro-1,2-oxazine). The regioselectivity is independent of the electronic effects of substituents on 1,3-butadiene (3*e*). Interestingly, the addition of nitrosobenzene to α-myrcene exhibited a marked dependence on reaction temperature such that increasing the reaction temperature led to the reversed orientation of cycloaddition (4). In contrast, the cycloaddition of a nitrosobenzene having a strongly electron-withdrawing substituent, such as 4-(methoxycarbonyl)nitrosobenzene, with isoprene proceeded with the opposite regioselectivity to yield a "*para*" adduct, eq. [1] (5). This latter work implies that the frontier molecular orbital (FMO) coefficients of nitrosobenzene are reversed by electron-withdrawing substituents.

[1] 

The reaction of α-chloronitrosocyclohexane with isoprene has been found to give opposite regioselectivity to that with 2-phenyl-1,3-butadiene, eq. [2] (6). The observed result in the case of isoprene was rationalized by invoking remote steric factors, but the same argument does not satisfactorily explain the reversed regioselectivity in the reaction with 2-phenyl-1,3-butadiene.

[2] 

[1]Author to whom correspondence may be addressed.

[2]Revision received August 4, 1989.

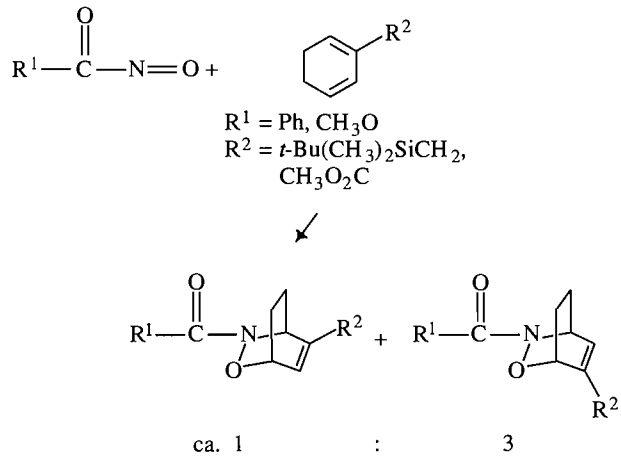
Printed in Canada / Imprimé au Canada

Can. J. Chem. Downloaded from www.nrcresearchpress.com by 186.148.149.217 on 09/07/12
For personal use only.

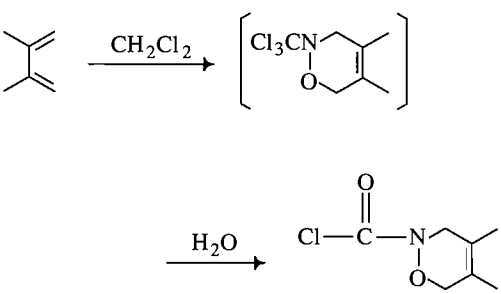
Can. J. Chem. Downloaded from www.nrcresearchpress.com by 186.148.149.217 on 09/07/12
For personal use only.

Recently, in cases in which steric effects can be neglected, the predominant *para* cycloadditions of nitrosocarbonyl compounds with electron-rich and electron-deficient 2-substituted 1,4-cyclohexadienes were rationalized by frontier molecular orbital theory, eq. [3] (7*a*). In contrast, the regiochemistry of the cycloaddition reaction of nitrosocarbonyl compounds with 1,2-dihydropyridines indicated a high dependence upon electronic effects of substituents present in the dienamides (7*b*).

To gain a better understanding of the regioselectivity and reaction mechanism of the [4 + 2] cycloadditions of nitroso compounds, we undertook the investigation of the reactions of trichloronitrosomethane (**1**) with a variety of 2-substituted-1,3-butadienes. The high steric demand of the trichloromethyl group was expected to have a stronger influence than the phenyl group in the developing transition state and thus lead to higher regioselectivity.

[3] 

The reactions of **1** in methylene chloride with cycloalkadienes were essentially complete in seconds at −78°C, producing the Diels–Alder cycloadducts in high yields (8, 9). Earlier, we reported that **1** reacted as a nitrosoformic chloride equivalent in the cyclization with acyclic 1,3-butadienes (9). For example, **1** reacted with 2,3-dimethyl-1,3-butadiene to form a moisture-sensitive cycloadduct, 4,5-dimethyl-2-trichloromethyl-3,6-dihydro-1,2-oxazine, which was hydrolyzed to afford the corresponding 2-chloroformyl-1,2-oxazine, eq. [4] (9). We describe herein the results of studies on the regiochemistry of **1** in cycloaddition reactions.

[4] 

Results

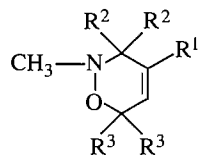
Reactions of 1 with 2-alkyl-1,3-butadienes

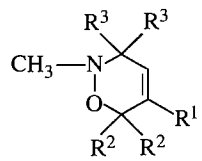
Cycloaddition of **1** with isoprene proceeded slowly in methylene chloride solution at −78°C, and afforded, after warming the reaction to room temperature and subsequent hydrolysis, an inseparable 1:1 mixture of 1,2-oxazines **2***a* and **3***a*. The ratio was estimated by integration of the two methyl groups of the cycloadducts at δ 1.60 and δ 1.67 in the ^{1}H nmr spectrum of the mixture (9). Reduction of this regioisomeric mixture with lithium aluminum hydride gave N-methyl compounds **4***a* and **5***a* in quantitative yield with no change in the ratio of isomers (9).

TABLE 1. Product distribution in the cyclization of trichloronitrosomethane with 2-substituted 1,3-butadienes in methylene chloride

Subst.	Products	Ratio (%)	Subst.	Products	Ratio (%)
Me	**2***a*/**3***a*	50/50 (ref. 9)	Ph	**2***h*/**3***h*	68/32
Et	**2***b*/**3***b*	36/64	4-MeOPh	**2***i*/**3***i*	85/15
i-Pr	**2***c*/**3***c*	0/100	3-MeOPh	**2***j*/**3***j*	70/30
t-Bu	**2***d*/**3***d*	0/100	4-MePh	**2***k*/**3***k*	80/20
Cl	**2***e*/**3***e*	24/76	3-MePh	**2***m*/**3***m*	82/18
CF_3	**2***f*/**3***f*	0/100	4-ClPh	**2***n*/**3***n*	67/33
Bz	**2***g*/**3***g*	25/75			

Under the same conditions as above, the reaction of **1** with 2-ethyl-1,3-butadiene also produced a mixture of two inseparable regioisomeric products **2***b* and **3***b*. The nearly overlapping ^{1}H nmr signals of the regioisomers caused difficulty in the determination of the product distribution. However, the ring methylene hydrogens adjacent to the oxygen atom in the 2-methyl-3,6-dihydro-1,2-oxazines were observed at about 1 ppm lower field as compared to the ring hydrogens adjacent to the nitrogen atom (9, 10). Therefore the ratio of products and the assignment of chemical shifts of the methylene hydrogens were determined precisely by analysis of deuterium-labeled products obtained from the reaction of **1** with 4,4-dideuterio-2-ethyl-1,3-butadiene followed by LAH reduction. Thus, the ratio of **2***b*/**3***b* was derived from the integration of the signal at δ 3.11 for NCH_2 in *d*-**4***b* and the signal at δ 4.22 for OCH_2 in *d*-**5***b*. The results are shown in Table 1.



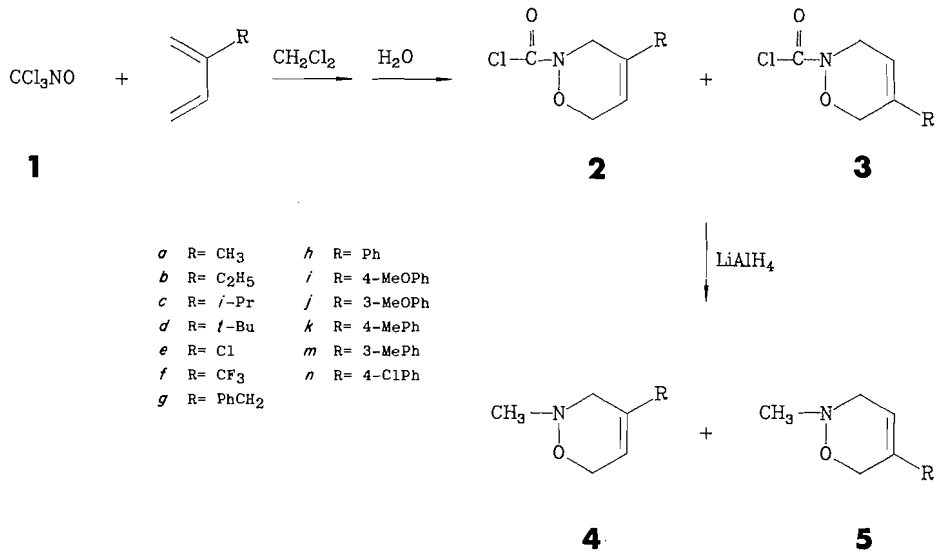


d-**4***b* R^1 = Et, R^2 = H, R^3 = D
d-**4***c* R^1 = *i*-Pr, R^2 = H, R^3 = D
d-**4***h* R^1 = Ph, R^2 = D, R^3 = H

d-**5***b* R^1 = Et, R^2 = H, R^3 = D
d-**5***c* R^1 = *i*-Pr, R^2 = H, R^3 = D

In contrast to 2-methyl and 2-ethyl 1,3-butadienes, the reaction of 2-isopropyl and 2-*tert*-butyl 1,3-butadienes with **1** provided exclusively compounds **3***c* and **3***d*, respectively. The assignments of N—O orientation in **3***c* and **3***d* were made by spin–spin decoupling experiments of the ^{1}H nmr spectra. Double resonance irradiation of the NCH_2 and OCH_2 signals showed an allylic coupling of ca. 1.5 Hz for the OCH_2 and a vicinal coupling of ca. 3.0 Hz for the NCH_2 with the vinylic hydrogen. Reduction of **3***c* with a slurry of LAH yielded the corresponding product **5***c* in high yield. The structural identification of **3***c* was further confirmed by a deuterium labeling experiment in which *d*-**5***c* was obtained from the reaction of **1** with 4,4-dideuterio-2-isopropyl-1,3-butadiene and followed by LAH reduction. The ^{1}H nmr spectrum of *d*-**5***c* lacked the signal at δ 3.16 for NCD_2 and the signal at δ 4.29 for OCH_2 remained.

Electron-deficient dienes such as 2-chloro-1,3-butadiene cyclized well to form 1,2-oxazines, but the inductive effects of the electron-withdrawing substituents did not reverse the



SCHEME 1

TABLE 2. Chemical shifts of ring hydrogens on 1,2-oxazines (in ppm)

	Oxazine **2**		Oxazine **3**		Oxazine **4**	
Substituent	$-CH_2N-$	$-CH_2O-$	$-CH_2N-$	$-CH_2O-$	$-CH_2N-$	$-CH_2O-$
Ph	4.62	4.68	4.43	4.87	3.50	4.45
4-MeOPh	4.46	4.57	4.44	4.84	3.55	4.48
3-MeOPh	4.56	4.63	4.41	4.81	3.55	4.77
4-MePh	4.54	4.61	4.42	4.86	3.53	4.45
3-MePh	4.67	4.67	4.41	4.84	3.55	4.47
4-ClPh	4.66	4.77	4.44	4.83	3.51	4.46

regioselectivity towards *meta* addition. Similar to the reaction of 2-ethyl-1,3-butadiene, 2-benzyl-1,3-butadiene reacted with **1** less regioselectively. However, the diene having a bulky 2-trifluoromethyl substituent reacted with **1** to yield the *para* cycloadduct **3***f* with high regioselectivity (Table 1).

*Reactions of **1** with 2-aryl-1,3-butadienes*

Reaction of 2-phenyl-1,3-butadiene with **1** afforded a regioisomeric mixture of **2***h* and **3***h* in a total yield of 68%. The major product **2***h* was separated chromatographically on silica gel and recrystallized from hexane. The methylene hydrogens neighboring the nitrogen and oxygen atoms of **2***h* were too close to allow double resonance nmr spectral analysis. Therefore the orientation of cycloaddition was again deduced from the ^1H nmr spectrum of the reduced derivative **4***h* in which decoupling was done on the signal of the ring hydrogens on the carbon atom next to nitrogen. The vinylic hydrogen of **4***h* appears as a triplet with a coupling constant of ca. 3.0 Hz with the OCH_2. This decoupling experiment led us to assign the *meta* orientation for **2***h* (6). The chemical shifts of the methylene hydrogens, NCH_2 and OCH_2, in **2***h* were differentiated by the reaction of **1** with 1,1-*d*,*d*-2-phenyl-1,3-butadiene. The minor cycloadduct **3***h* was separated from the mixture by repeated chromatography. The chemical shifts of the ring hydrogens of **2***h* and **3***h* are shown in Table 2.

The ratios of isomeric cycloadducts obtained from a series

TABLE 3. Product distribution in cycloaddition in **1** with 2-aryl-1,3-butadienes under various conditions

Subst.	Solvent	Conditions	Ratio of **2**/**3**
4-OMe	CH_2Cl_2	−78°C–0°C, 24 h	85/15
		RT, 24 h	87/13
	THF	RT, 24 h	85/15
	$CHCl_3$	65°C, 10 min	87/13
4-Me	CH_2Cl_2	−78°C–0°C, 48 h	80/20
		RT, 24 h	78/22
	THF	RT, 24 h	85/15
	$CHCl_3$	65°C, 10 min	78/22
3-Me	CH_2Cl_2	−78°C–0°C, 48 h	82/18
		RT, 24 h	84/16
	THF	RT, 24 h	80/20
	$CHCl_3$	65°C, 10 min	80/20
H	CH_2Cl_2	−78°C–0°C, 48 h	68/32
		0°C, 48 h	62/38
		RT, 24 h	65/35
	$CHCl_3$	65°C, 10 min	60/40
	THF	RT, 24 h	75/25
	10% $MeOH/CH_2Cl_2$	RT, 24 h	69/31
4-Cl	CH_2Cl_2	−78°C–0°C, 48 h	67/33
	THF	RT, 24 h	65/35
	$CHCl_3$	65°C, 10 min	62/38

Can. J. Chem. Downloaded from www.nrcresearchpress.com by 186.148.149.217 on 09/07/12
For personal use only.

TABLE 4. Rate data taken in various solvents at room temperature

Subst. (σ^+)[b]	Solvent	k (s^{-1})[a] ($\times 10^{-3}$)	k_m ($\times 10^{-3}$)	k_p ($\times 10^{-3}$)	log $k_{X,m}/k_{H,m}$	log $k_{X,p}/k_{H,p}$
4-OMe	CH_2Cl_2	10.20	8.87	1.33	0.577	0.023
(−0.78)	THF	16.70	14.20	2.50	0.675	0.40
	$CHCl_3$	7.91	6.88	1.03	0.448	−0.11
4-Me	CH_2Cl_2	6.66	5.19	1.47	0.344	0.067
(−0.31)	THF	6.70	5.69	1.01	0.278	0.004
	$CHCl_3$	5.10	3.98	1.12	0.211	−0.071
3-Me	CH_2Cl_2	3.17	2.66	0.51	0.055	−0.392
(−0.07)	THF	4.29	3.43	0.86	0.058	−0.066
	$CHCl_3$	3.31	2.65	0.66	0.034	−0.301
H	CH_2Cl_2	3.61	2.35	1.26	0	0
(0.00)	THF	4.00	3.00	1.00	0	0
	$CHCl_3$	3.77	2.45	1.32	0	0
4-Cl	CH_2Cl_2	3.09	2.00	1.09	−0.070	−0.063
(0.11)	THF	2.96	2.04	0.92	−0.166	−0.036
	$CHCl_3$	3.07	2.00	1.07	−0.088	−0.091

[a]The average of at least two kinetic runs with a probable error of 8–12%.
[b]σ^+ values are taken from ref. 20.

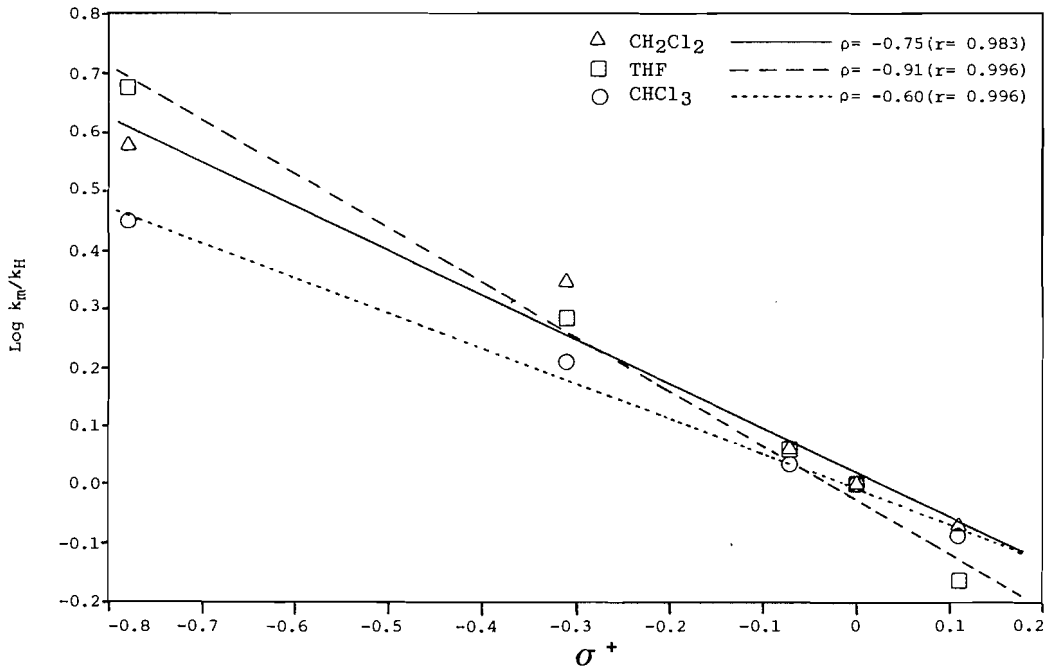


FIG. 1. Hammett plots for cycloaddition of **1** and CH_2=CH(X-C_6H_4)—CH=CH_2 in CH_2Cl_2 (△), THF (□), and $CHCl_3$ (○) at room temperature.

of reactions performed at different temperatures and in several solvents were determined from ^{1}H nmr spectra via integration of the ring hydrogens (Table 2). The data are recorded in Table 3.

Under the same conditions, the reaction of 2-(4′-methoxyphenyl)-, 2-(3′-methoxyphenyl)-, 2-(4′-methylphenyl)-, 2-(3′-methylphenyl)-, and 2-(4′-chlorophenyl)-1,3-butadiene with **1** in methylene chloride proceeded smoothly to give the corresponding 1,2-oxazines in yields of 60–80%. The substituent on the aromatic ring has very little influence on the chemical shifts of the oxazine methylene hydrogens (Table 2). The addition orientation was established by analysis of the reduced derivatives **4**. The product distributions of cycloadditions under various conditions are recorded in Table 3. The product ratios, while influenced by the *para* substituent on the aromatic ring, are unaffected by the reaction solvent and temperature.

Kinetic studies

To minimize side reactions and obtain pseudo-first-order rate constants, the reactions of **1** were performed by using a 70-fold excess of 2-aryl-1,3-butadienes in methylene chloride, tetrahydrofuran, and chloroform as solvents. The progress of the cycloadditions was followed by observing the disappearance of absorption at λ_{max} 592 nm for **1**. Satisfactory pseudo-first-order kinetic plots covering at least three half-lives were obtained. The k value obtained was equal to the sum of the reaction rates of *para* cycloaddition (k_p) and *meta* cycloaddition (k_m). The data are summarized in Table 4.

The influence of aryl substituents in 2-aryl-1,3-butadiene on the rates of *meta* cycloaddition can be correlated satisfactorily by the Hammett equation using σ^+ values (Fig. 1). The reaction constants were obtained by the method of least squares and

Can. J. Chem. Downloaded from www.nrcresearchpress.com by 186.148.149.217 on 09/07/12
For personal use only.

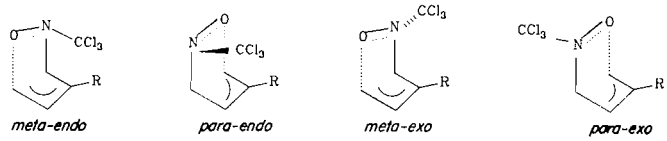


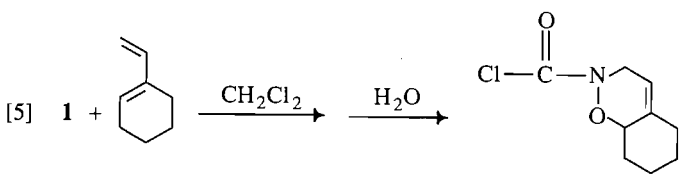
FIG. 2. Steric interaction between **1** and 2-substituted 1,3-butadiene in the path of transition state.

were found to be −0.75, −0.91, and −0.60, with correlation coefficients of 0.983, 0.996, and 0.996 in solutions of methylene chloride, tetrahydrofuran, and chloroform, respectively. Thus the low values of ρ indicate that the reaction rates are not significantly affected by the polarity of solvents. In contrast, a plot of log $k_{X,p}/k_{H,p}$ vs. σ or σ^+ value gives a poor correlation.

Discussion

The product distribution shown in Table 1 indicates the possible existence of different transition states that determine the regiochemistry of cyclization reactions. The observed regiochemical preference for the *para* cycloaddition of **1** with 2-alkyl 1,3-butadienes parallels that of α-chloronitrosocyclohexane, eq. [2] (2). These results can be rationalized in terms of steric effects in the transition state of the Diels–Alder reaction.

Increasing the bulk of the 2-alkyl butadiene substituent from methyl, ethyl, benzyl to *tert*-butyl increases the regioselectivity of the cycloaddition. Apparently the product orientation reflects steric interference between the trichloromethyl group in **1** and the 2-substituent on the diene. We suggest that the importance of the steric effect is reinforced (Fig. 2) by a mechanism involving a concerted nonsynchronous Diels–Alder transition state (11), in which the electrophilic nitrogen of the dienophile forms a bond with C-1 or C-4 of butadiene to a higher degree than the electron-rich oxygen of the dienophile. Therefore, it is not surprising that the "*para-exo*" formation could be the most preferential approach in the development of the transition state. This steric factor was also manifested in the regioselective reaction of **1** with 1-vinylcyclohexene, eq. [5] (9).



The orientational preference of cycloaddition has been found in several cases to be independent of the inductive effect of the 2-substituent (2*a*, 7, 12). That is, replacement of an electron-donating substituent by an electron-withdrawing one does not reverse the regioselectivity. This result can be rationalized by FMO theory assuming that all coefficients of C-1 in the highest occupied molecular orbital (HOMO) of 2-substituted dienes are larger than the coefficients of C-4 (13). The closest pair of FMO's in the transition state is composed of the HOMO(diene) and LUMO(dienophile) and the orientational preference is determined by the combination of the largest coefficient in these MO's. Therefore the similar regioselectivity for the reactions of **1** with butadienes having electron-withdrawing substituents, 2-Cl and 2-CF_3, and the weakly electron-releasing substituent, 2-alkyl, is predicted and observed[3] (Fig. 3).

[3]The coefficients of **1** are not known. We simplify the problem by taking CCl_3 as an electron-withdrawing group having electronegativity $X_{CCl_3} = 3$ (14).

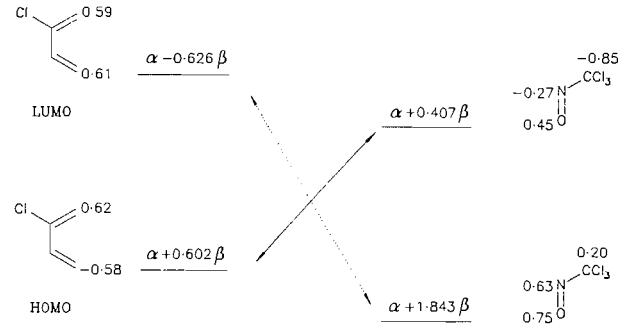


FIG. 3. Frontier orbital coefficients and energies of HOMO and LUMO of 2-chloro-1,3-butadiene and **1**.

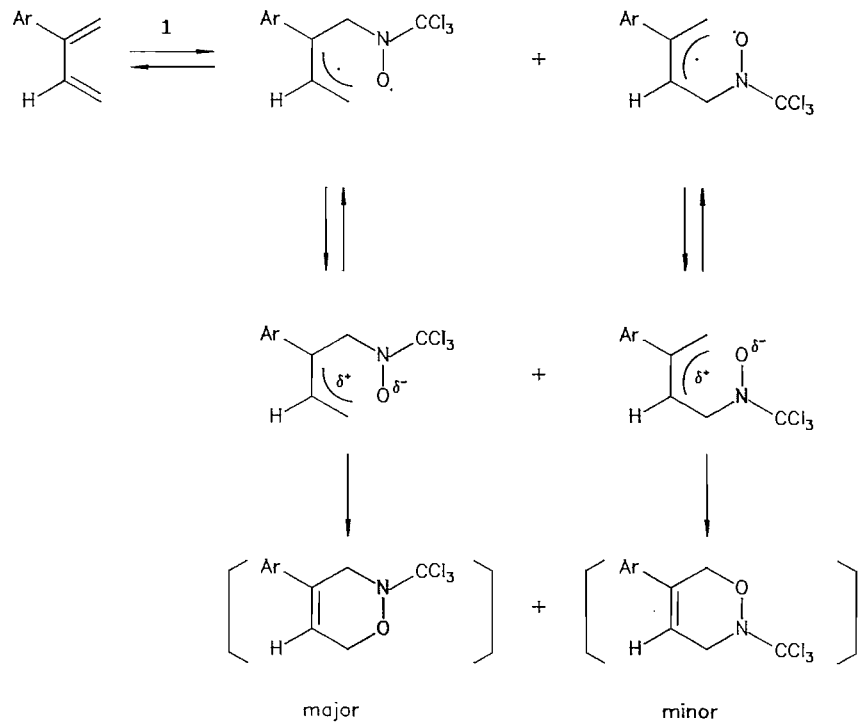
The reversed regioselectivity of the reactions of **1** with 2-aryl-1,3-butadienes is also similar to that of α-chloronitrosocyclohexane, although only the reaction of 2-phenyl-1,3-butadiene with the latter dienophile has been reported, eq. [2] (6*a*). The observed results show that an electron-donating group in the aromatic ring accelerates the cyclization, while an electron-withdrawing group retards it. The negative and low Hammett ρ values are similar to those derived from the Diels–Alder reactions of nitrosobenzene with *para*-substituted 1-phenyl butadienes (3*b*). This result leads us to believe that the cycloaddition of **1** similarly involves an intermediate that has a small but significant degree of polar character with some positive charge on the carbon atom next to the benzene ring. Therefore the forming partially zwitterionic (or polarized) intermediates are stabilized by resonance with a benzene ring, and the ring closure of these intermediates leads to the observed regioselective adducts. The solvent effects on the cycloaddition should be relatively small and, in fact, the relative rates of cycloaddition are within a factor of 4.

Some low ρ values for free radical reactions are reported in the polymerization of styrene (ρ = −0.66) (15) and bromination of toluene (ρ = −0.500) (16). The ρ values observed here suggest the reactions of **1** with dienes involve diradical intermediates.

It seems reasonable to propose that cyclizations between **1** and *para*-substituted 2-phenyl butadienes proceed nonsynchronously (11*a*) (i.e., the N—C bond formed to a higher degree than the O—C bond) to form transition states that lead to diradical intermediates. Subsequently, partial electron transfer from carbon to oxygen occurs to form polarized intermediates as a result of the large difference in electronegativity of the two radicals (17) (Scheme 2).

In conclusion, the intermolecular [2 + 4] cycloadditions between **1** and 2-substituted dienes result in the regioselective construction of 2,3-dihydro-1,2-oxazines. The regioselectivity is substituent-dependent with regard to the butadiene. In the cases of 2-alkyl-1,3-butadienes and electron-deficient dienes, the preference of orientation is *para* cycloaddition. The reaction mechanism can be rationalized by a concerted nonsynchronous approach of **1** and the dienes. Although remote steric hindrance is expected to be a factor of less importance in reactions of 2-substituted dienes (2*a*, 4, 6), the bulky trichloromethyl group, similar to 1-chlorocyclohexyl, would exert control of orientation in cycloaddition. However, the reactions with 2-aryl-1,3-butadienes exhibit the reversed orientation. We adopt the proposal of Kresze and Kosbahn (3*b*) that the cycloaddition reaction proceeds by a two-step mechanism involving a benzene ring stabilized biradical and (or) zwitterionic intermediates.

Can. J. Chem. Downloaded from www.nrcresearchpress.com by 186.148.149.217 on 09/07/12
For personal use only.



SCHEME 2

Experimental

The nmr spectra were recorded on JEOL JNM-FX 100 MHz or Bruker AM 400 MHz spectrometers. The ^{13}C nmr spectra were measured at 25.02 or 100.6 MHz. All chemical shifts are reported relative to tetramethylsilane as internal standard in deuteriochloroform solution, and coupling constants are in hertz. Infrared spectra were run on a Perkin–Elmer 682 infrared spectrophotometer. Kinetic studies were measured on a Perkin–Elmer 552 uv–vis spectrophotometer. Mass spectra were recorded on a JEOL TMS D-100 or JEOL JMS-HX 110 mass spectrometer. Elemental analyses were obtained by the Analytical Center operated by National Taiwan University, Taipei, Taiwan. Melting points and boiling points are uncorrected. Flash chromatography was done on 0.040–0.063 nm silica gel (Merck Kieselgel 60). 4,4-*d*,*d*-2-Isopropyl-1,3-butadiene was synthesized from the Grignard reagent prepared from deuterioiodomethane (99%) (Merck Chem. Co.) and 2-isopropylacrolein (Aldrich Chemical Co.). α,α,α-d_3-Acetophenone was prepared by deuterium exchange of acetophenone. 1,1-*d*,*d*-2-Phenyl-1,3-butadiene was prepared from vinyl magnesium bromide and deuterioacetophenone. Trichloronitrosomethane was prepared by the procedure of Astley and Sutcliffe (18) and was purified several times by trap-to-trap fractionation *in vacuo* before use.

General procedure for cycloaddition of **1** *to 1,3-butadienes*

A 50-mL ampule was filled with a solution of **1** in methylene chloride at −78°C, and a solution of the 1,3-butadiene was injected through a rubber septum in one portion. The stirred solution was slowly warmed to room temperature until the disappearance of the blue color of **1**. After removal of the solvent, the resulting oil was dissolved in ether, followed by hydrolysis for 4 h at room temperature. The aqueous solution was extracted with ether. The combined ether layers were washed with water and brine, and then dried over sodium sulfate. Rotatory evaporation of the solvent followed by silica gel chromatography of the residue with methylene chloride/hexane (1:5) as eluent furnished the 1,2-oxazines. The relative yields of regioisomeric products were obtained from the ^1H nmr integration of the ring hydrogens before chromatography. The results are summarized in Table 1.

*2-Chloroformyl-4-ethyl(and 5-ethyl)-3,6-dihydro-1,2-oxazines (***2***b and* **3***b)*

Treatment of **1** (3.65 g, 24.6 mmol) with 2-ethyl-1,3-butadiene (2.00 g, 24.4 mmol) in methylene chloride (20 mL) afforded a 36:64 mixture of **2***b* and **3***b* in a total yield of 72% (3.09 g). Isomers **2***b* and **3***b* could not be separated by chromatography. The data for **2***b* and **3***b* were determined from a mixture. **2***b*: ^1H nmr δ: 1.08 (t, 3H, J = 7.5), 2.08 (q, d, 2H, J = 7.5 and 1.3), 4.16 (s, 2H, NCH_2), 4.50 (m, 2H, OCH_2), 5.59 (m, 1H); ^{13}C nmr δ: 11.3 (q), 26.1 (t), 47.4 (t), 69.7 (t), 114.9 (d), 134.4 (s), 147.0 (s). **3***b*: ^1H nmr δ: 1.06 (t, 3H, J = 7.5), 2.01 (q, d, 2H, J = 7.5 and 1.3), 4.23 (s, 2H, NCH_2), 4.42 (d, 2H, J = 1.4, OCH_2), 5.55 (m, 1H); ^{13}C nmr δ: 11.25 (q), 24.9 (t), 45.0 (t), 72.0 (t), 113.1 (d), 136.6 (s), 147.2 (s); ir (neat): 1730 (C=O), 1670 (C=C) cm^{-1}; ms m/z: 177 (M^+ + 2), 175 (M^+). *Anal.* calcd. for $C_7H_{10}ClNO_2$: C 47.87, H 5.74, N 7.98; found: C 47.89, H 5.71, N 7.89.

*2-Methyl-4-ethyl(and 5-ethyl)-3,6-dihydro-1,2-oxazines (***4***b and* **5***b)*

Reduction of a 36:64 mixture of regioisomers **2***b* and **3***b* (1.70 g, 9.6 mmol) with LAH (0.36 g, 9.5 mmol) in dry ether (15 mL) afforded a mixture of **4***b* and **5***b* as a colorless oil in 88% yield (1.07 g) without changing the ratio of regioisomers. The data for **4***b* and **5***b* were determined from a mixture. **4***b*: ^1H nmr δ: 1.04 (t, 3H, J = 7.4), 1.82 (q, 2H, J = 7.4), 2.67 (s, 3H), 3.11 (br, 2H, NCH_2), 4.24 (br, 2H, OCH_2), 5.47 (m, 1H); ^{13}C nmr δ: 11.6 (q), 27.0 (t), 45.6 (q), 59.2 (t), 67.9 (t), 117.2 (d), 136.2 (s). **5***b*: ^1H nmr δ: 1.03 (t, 3H, J = 7.4), 1.96 (q, 2H, J = 7.4), 2.66 (s, 3H), 3.18 (br, 2H, NCH_2), 4.22 (br, 2H, OCH_2), 5.47 (m, 1H); ^{13}C nmr δ: 11.6 (q), 24.9 (t), 45.6 (q), 56.1 (t), 70.4 (t), 115.3 (d), 138.0 (s); ir (neat): 1670 (C=C) cm^{-1}; ms m/z: 127 (M^+). *Anal.* calcd. for $C_7H_{13}NO$: C 66.10, H 10.30, N 11.01; found: C 65.88, H 10.43, N 10.42.

Reaction of **1** *with 4,4-*d,d*-2-ethyl-1,3-butadiene*

Treatment of **1** (2.06 g, 13.8 mmol) with 99% purity 4,4-*d*,*d*-2-ethyl-1,3-butadiene (1.17 g, 13.9 mmol) afforded 1.7 g (70%) of *d*-**2***b* and *d*-**3***b* as a 35:65 mixture of regioisomers. *d*-**2***b*: ^1H nmr δ: 1.08 (t, 3H, J = 7.5), 2.08 (q, 2H, J = 7.5), 4.15 (br, 2H), 5.59 (m, 1H); ^{13}C nmr δ: 11.2 (q), 26.1 (t), 47.4 (t), 115.5 (d), 134.5 (s), 147.1 (s).

Can. J. Chem. Downloaded from www.nrcresearchpress.com by 186.148.149.217 on 09/07/12
For personal use only.

d-**3***b*: ^{1}H nmr δ: 1.06 (t, 3H, J = 7.5), 2.01 (q, 2H, J = 7.5), 4.42 (s, 2H), 5.52 (m, 1H); ^{13}C nmr δ: 11.2 (q), 24.8 (t), 71.9 (t), 113.0 (d), 136.6 (s), 147.1 (s); ms m/z (20 eV): 179 (M^+ + 2), 177 (M^+).

Reduction of a 35:65 mixture of deuterated *d*-**2***b* and *d*-**3***b* (1.00 g, 5.63 mmol) with LAH (0.21 g, 5.33 mmol) afforded *d*-**4***b* and *d*-**5***b* with the same relative ratio (0.65 g, 90% yield). *d*-**4***b*: ^{1}H nmr δ: 1.05 (t, 3H, J = 7.5), 1.84 (q, 2H, J = 7.5), 2.66 (s, 3H), 3.11 (br, 2H), 5.48 (m, 1H); ^{13}C nmr δ: 11.5 (q), 24.8 (t), 45.5 (q), 59.1 (t), 117.0 (d), 136 (s). *d*-**5***b*: ^{1}H nmr δ: 1.03 (t, 3H, J = 7.5), 1.96 (q, 2H, J = 7.5), 2.65 (s, 3H), 4.22 (br, 2H), 5.48 (m, 1H); ^{13}C nmr δ: 11.5 (q), 24.8 (t), 45.5 (q), 70.2 (t), 115.0 (d), 138.0 (s); ms m/z: 129 (M^+).

*2-Chloroformyl-5-isopropyl-3,6-dihydro-1,2-oxazine (***3***c)*

Treatment of **1** (6.02 g, 40.5 mmol) with 2-isopropyl-1,3-butadiene (3.84 g, 40.0 mmol) gave **3***c* (6.75 g, 89%) as a yellow oil; bp 43°C/5 Torr (1 Torr = 133.3 Pa); ^{1}H nmr δ: 0.92 (d, 6H, J = 6.8), 2.12 (sept, 1H, J = 6.8), 4.08 (br, NCH_2), 4.32 (d, OCH_2, J = 1.6), 5.38 (m, 1H); ^{13}C nmr δ: 20.47 (q), 30.67 (d), 44.43 (t), 71.03 (t), 112.2 (d), 140.7 (s), 147.0 (s); ir (neat): 1730 (C=O) cm^{-1}; ms m/z: 191 (M^+ + 2), 189 (M^+). *Anal.* calcd. for $C_8H_{12}ClNO_2$: C 50.66, H 6.38, N 7.34; found: C 50.63, H 6.31, N 7.19.

*2-Chloroformyl-5-isopropyl-3,3-*d,d*-3,6-dihydro-1,2-oxazine (*d-**3***c)*: ^{1}H nmr δ: 1.06 (d, 6H, J = 6.9), 2.25 (sept, 1H, J = 6.9), 4.47 (d, J = 1.5, OCH_2), 5.50 (m, 1H); ^{13}C nmr δ: 20.68 (q), 30.89 (d), 44.82 (m, weak), 71.04 (t), 112.1 (d), 140.8 (s), 147.0 (s); ir (neat): ν_{sym} (C–D) 2100 and ν_{asym} 2200 cm^{-1}; ms m/z: 193 (M^+ + 2), 191 (M^+).

*2-Methyl-5-isopropyl-3,6-dihydro-1,2-oxazine (***5***c)*

Treatment of **3***c* (1.49 g, 7.77 mmol) with LAH (0.295 g, 7.76 mmol) in 40 mL of dry ether as in the previous reduction experiment gave 0.96 g of **5***c* (88% yield) as a colorless oil; ^{1}H nmr δ: 0.98 (d, 6H, J = 6.7), 2.14 (sept, 1H, J = 6.7), 2.61 (s, NCH_3), 3.16 (br, NCH_2), 4.25 (br, OCH_2), 5.44 (m, 1H); ^{13}C nmr δ: 20.67 (q), 30.40 (d), 45.12 (q), 55.78 (t), 68.67 (t), 113.9 (d), 141.8 (s); ir (neat): 2850, 1660 (weak, C=C), 1460, 1430, 1380, 1050 cm^{-1}. HRMS for $C_8H_{15}NO$, calcd.: 141.1154; found: 141.1151.

*2-Methyl-5-isopropyl-3,3-*d,d*-3,6-dihydro-1,2-oxazine (*d-**5***c)*: ^{1}H nmr δ: 1.04 (d, 6H, J = 6.9), 2.17 (sept, 1H, J = 6.9), 2.66 (s, NCH_3), 4.29 (br, OCH), 5.49 (m, 1H); ^{13}C nmr δ: 21.15 (q), 30.49 (d), 45.70 (q), 55.60 (m, weak), 69.30 (t), 114.3 (d), 142.4 (s); ir (neat): ν_{sym} (C–D) 2060 and ν_{asym} (C–D) 2200 cm^{-1}; ms m/z: 143 (M^+).

*2-Chloroformyl-5-*tert*-butyl-3,6-dihydro-1,2-oxazine (***3***d)*

Treatment of **1** (2.60 g, 17.5 mmol) with 2-*tert*-butyl-1,3-butadiene (1.85 g, 16.4 mmol) in methylene chloride gave **3***d* (2.30 g, 69%) as a yellow oil; bp 47°C/0.01 Torr; ^{1}H nmr δ: 1.07 (s, *t*-Bu), 4.26 (m, NCH_2), 4.54 (m, OCH_2), and 5.54 (m, 1H); ^{13}C nmr δ: 28.47 (q), 33.93 (s), 45.11 (t), 69.93 (t), 117.7 (d), 143.0 (d), 146.8 (s); ir (neat): 1735 (C=O), 1662 (C=C) cm^{-1}; ms m/z: 205 (M^+ + 2), 203 (M^+). *Anal.* calcd. for $C_9H_{14}ClNO_2$: C 53.08, H 6.93, N 6.88; found: C 53.05, H 6.90, N 6.82.

*2-Methyl-5-*tert*-butyl-3,6-dihydro-1,2-oxazine (***5***d)*

Treatment of **1** (1.20 g, 5.90 mmol) with LAH (0.23 g, 6.1 mmol) gave **5***d* as a colorless oil; ^{1}H nmr δ: 1.05 (s, *t*-Bu), 2.67 (s, NCH_3), 3.21 (br, NCH_2), 4.39 (br, OCH_2), 5.53 (m, 1H); ^{13}C nmr δ: 28.77 (q), 33.54 (s), 45.70 (q), 56.43 (t), 68.00 (t), 113.9 (d), 144.4 (s); ir (neat): 3020, 2880, 1460, 1425, 1385, 1365, 1252, 1110, 1055, 1035, and 1020 cm^{-1}. HRMS for $C_9H_{17}NO$, calcd.: 155.1311; found: 155.1309.

*2-Chloroformyl-4-chloro(and 5-chloro)-3,6-dihydro-1,2-oxazines (***2***e and* **3***e)*

Treatment of **1** (2.00 g, 13.5 mmol) with 2-chloro-1,3-butadiene (1.31 g, 14.8 mmol) afforded an inseparable mixture of **2***e* and **3***e* (1.95 g, 79% yield) as a colorless liquid. The ^{1}H nmr signals are overlapped for both NCH_2 and OCH_2 in **2***e* and **3***e*. The data of the mixture are ^{1}H nmr δ: 4.52 (m, 4H, OCH_2 and NCH_2), 6.12 (m, 1H). The assignment of ^{13}C nmr spectra was correlated to the reduced products **4***e* and **5***e*. **2***e*: ^{13}C nmr δ: 49.2 (t), 69.8 (t), 120.6 (d), 124.8 (s), 147.6 (s). **3***e*: ^{13}C nmr δ: 45.6 (t), 72.0 (t), 118.2 (d), 126.8 (s), 147.6 (s); ir (neat): 1735 (C=O), 1670 (C=C) cm^{-1}; ms m/z: 185 (M^+ + 4), 183 (M^+ + 2), 181 (M^+), 146 (M^+ − Cl). HRMS for $C_5H_5Cl_2NO_2$ (M^+), calcd.: 180.9697; found: 180.9696.

*2-Methyl-4-chloro(and 5-chloro)-3,6-dihydro-1,2-oxazines (***4***e and* **5***e)*

Reduction of a mixture of **2***e* and **3***e* (1.22 g, 6.7 mmol) with LAH (0.25 g, 6.7 mmol) in dry ether gave inseparable **4***e* and **5***e* in a total yield of 85% (0.77 g, 5.7 mmol). **4***e*: ^{1}H nmr (400 MHz) δ: 2.69 (s, 3H), 3.28 (m, 2H, NCH_2), 4.27 (m, 2H, OCH_2), 5.93 (m, 1H); ^{13}C nmr δ: 45.5 (q), 61.3 (t), 67.8 (t), 122.1 (d), 126.6 (s). **5***e*: ^{1}H nmr (400 MHz) δ: 2.67 (s, 3H), 3.28 (m, 2H, NCH_2), 4.27 (m, 2H, OCH_2), 5.93 (m, 1H); ^{13}C nmr δ: 45.5 (q), 56.9 (t), 71.0 (t), 120.2 (d), 129.0 (s); ir (neat): 1660 (C=C) cm^{-1}; ms m/z: 137 (M^+ + 2), 135 (M^+). The ratio of isomeric adducts **2***e*/**3***e* (24:76) was roughly determined from the mixture of **4***e* and **5***e* by integration of the two N-methyl groups.

*2-Chloroformyl-5-trifluoromethyl-3,6-dihydro-1,2-oxazine (***3***f)*

Treatment of **1** (3.00 g, 20.2 mmol) with 2-trifluoromethyl-1,3-butadiene (3.00 g, 24.5 mmol) afforded **3***f* (4.02 g, 91%) as a light yellow liquid; ^{1}H nmr δ: 4.43 (m, 2H, NCH_2), 4.65 (s, 2H, OCH_2), 6.51 (m, 1H); ^{13}C nmr δ: 44.4 (t), 67.0 (t), 116.1 (s), 124.9 (d), 126.9 (CF_3), 147.3 (s); ir (neat): 1730 (C=O), 1682 (C=C) cm^{-1}. HRMS for $C_6H_5ClF_3NO_2$ (M^+), calcd.: 214.9961; found: 214.9954.

*2-Methyl-5-trifluoromethyl-3,6-dihydro-1,2-oxazine (***5***f)*

Reduction of **3***f* (1.90 g, 8.81 mmol) with LAH (0.33 g, 8.7 mmol) in dry ether (30 mL), after chromatography on silica gel with ether–hexane (1:4) as eluent, afforded **5***f* as a colorless liquid in a yield of 87% (1.28 g, 7.66 mmol); ^{1}H nmr δ: 2.70 (s, 3H), 3.30 (m, 2H, NCH_2), 4.42 (s, OCH_2), 6.40 (m, 1H); ^{13}C nmr δ: 45.5 (q), 55.0 (t), 65.2 (t), 117.1 (d), 128.7 (CF_3); ir (neat): 1682 (C=C) cm^{-1}. HRMS for $C_6H_8F_3NO$, calcd.: 167.0558; found: 167.0541.

*2-Chloroformyl-4-benzyl(and 5-benzyl)-3,6-dihydro-1,2-oxazines (***2***g and* **3***g)*

Treatment of **1** (3.40 g, 22.9 mmol) with 2-benzyl-1,3-butadiene (3.28 g, 22.7 mmol) afforded a 25:75 mixture of **2***g* and **3***g* (3.50 g, 65%) as a yellow oil. **2***g*: ^{1}H nmr δ: 3.33 (s, 2H, $PhCH_2$), 4.08 (br, 2H, NCH_2), 4.46 (br, 2H, OCH_2), 5.54 (m, 1H, HC=), 7.20 (m, 5H); ^{13}C nmr δ: 40.1 (t), 47.4 (t), 69.9 (t), 118.5 (d), 126.5 (d), 128.3 (d), 128.5 (d), 132.7 (s), 136.7 (s), 147.3 (s). **3***g*: ^{1}H nmr δ: 3.29 (s, 2H, $PhCH_2$), 4.20 (br, 2H, NCH_2), 4.33 (br, 2H, OCH_2), 5.48 (m, 1H), 7.30 (m, 5H, H_{arom}); ^{13}C nmr δ: 39.0 (t), 45.0 (t), 71.9 (t), 116.3 (d), 126.5 (d), 128.4 (d), 128.5 (d), 134.8 (s), 136.7 (s), 147.3 (s); ir (neat): 1735 (C=O), 1670 (C=C) cm^{-1}; ms m/z: 239 (M^+ + 2), 237 (M^+).

*2-Methyl-4-benzyl(and 5-benzyl)-3,6-dihydro-1,2-oxazines (***4***g and* **5***g)*

Treatment of a mixture of **2***g* and **3***g* (2.00 g, 8.44 mmol) with LAH (0.32 g, 8.43 mmol) in 50 mL of dry ether provided an inseparable mixture of **4***g* and **5***g* (1.37 g, 86%) as a colorless oil; ^{1}H nmr (400 MHz) δ: 2.63 (s, 3H, NCH_3 of **5***g*), 2.66 (s, 3H, NCH_3 of **4***g*), 3.30 (m, 8H, $PhCH_2$ and NCH_2 of **4***g* and **5***g*), 4.20 (m, 4H, OCH_2 of **4***g* and **5***g*), 5.50 (m, 2H, HC= of **4***g* and **5***g*). **4***g*: ^{13}C nmr δ: 41.1 (t), 45.9 (q), 59.0 (t), 68.0 (t), 120.7 (d), 126.1 (d), 128.2 (d), 128.7 (d), 134.2 (s), 138.2 (s). **5***g*: ^{13}C nmr δ: 39.1 (t), 45.9 (q), 56.4 (t), 70.4 (t), 118.8 (d), 126.1 (d), 128.2 (d), 128.7 (d), 136.3 (s), 138.2 (s); ir (neat): 1665 (C=C) cm^{-1}. HRMS for $C_{12}H_{15}NO$, calcd.: 189.1154; found: 189.1148.

*2-Chloroformyl-4-phenyl(and 5-phenyl)-3,6-dihydro-1,2-oxazine (***2***h and* **3***h)*

Treatment of **1** (2.72 g, 18.3 mmol) with 2-phenyl-1,3-butadiene (2.18 g, 16.7 mmol) afforded a mixture of regioisomers **2***h* and **3***h* in a ratio of 68:32 (2.54 g, 68% yield). Attempts to separate **2***h* and **3***h* by chromatography were unsuccessful. Repeated recrystallization (hexane) of residue from the first fraction (isomers **2***h* and **3***h* in a 16:1 ratio) afforded an analytically pure sample of **2***h* as pale white crystals; mp 70°C; ^{1}H nmr δ: 4.62 (br, NCH_2), 4.68 (br, OCH_2), 6.17 (m, 1H), 7.32 (m, 5H); ^{13}C nmr δ: 45.9 (t), 70.3 (t), 119.0 (d), 124.6 (d), 128.0 (d), 131.8 (s), 135.6 (s), 147.8 (s); ir (KBr): 1725 (C=O), 1655 (C=C) cm^{-1}; ms m/z: 225 (M^+ + 2), 223 (M^+). *Anal.* calcd. for

Can. J. Chem. Downloaded from www.nrcresearchpress.com by 186.148.149.217 on 09/07/12
For personal use only.

Can. J. Chem. Downloaded from www.nrcresearchpress.com by 186.148.149.217 on 09/07/12
For personal use only.

$C_{11}H_{10}ClNO_2$: C 59.06, H 4.50, N 6.26; found: C 59.13, H 4.51, N 6.06. A sample of **3***h* with the highest purity was obtained from the last few fractions as a yellow oil (contaminated with 4% of **2***h*); ^{1}H nmr (400 MHz) δ: 4.43 (br, NCH_2), 4.87 (br, OCH_2), 6.12 (t, t, 1H, J = 1.5, by decoupling the signal at δ 4.43; J = 3.3, by decoupling the signal at 4.87), 7.24–7.45 (m, 5H); ^{13}C nmr δ: 44.89 (t), 71.29 (t), 116.9 (d), 124.8 (d), 128.5 (d), 128.8 (d), 134.4 (s), 135.6 (s), 147.9 (s); ms *m/z*: 225 (M^+ + 2), 223 (M^+). The regioselectivity of cycloaddition was determined from the crude products by integration of the signals at δ 4.62, 4.68 and δ 4.43, 4.87 for **2***h* and **3***h*, respectively, prior to chromatography. The result is given in Table 1.

Treatment of **1** (0.67 g, 4.51 mmol) with 95% deuterated 1,1-*d*,*d*-2-phenyl-1,3-butadiene (0.60 g, 4.54 mmol) afforded *d*-**2***h* and *d*-**3***h* as a 68:32 mixture of regioisomers (0.63 g, 63%). The predominant cycloadduct *d*-**2***h* was separated by the procedure described above; ^{1}H nmr δ: 4.67 (d, J = 3, OCH_2), 6.20 (t, J = 3, vinylic hydrogen), 7.32 (m, 5H); ^{13}C nmr δ: 45.92 (m, weak), 70.12 (t), 119.0 (d), 124.0 (d), 128.2 (d), 128.6 (d), 131.7 (s), 135.7 (s), 147.9 (s).

*2-Methyl-4-phenyl-3,6-dihydro-1,2-oxazine (***4**h*)*

Treatment of **2***h* (0.34 g, 1.52 mmol) with LAH (0.06 g, 16.0 mmol) in 5 mL of dry ether gave **4***h* as a white solid; mp 67°C (lit. (6*a*) mp 65°C); ^{1}H nmr δ: 2.74 (s, 3H), 3.55 (br, NCH_2), 4.46 (br, OCH_2), 6.11 (m, 1H), 7.34 (m, 5H); ^{13}C nmr δ: 45.8 (q), 57.8 (t), 68.1 (t), 121.3 (d), 124.4 (d), 127.1 (d), 128.1 (d), 133.6 (s), 138.0 (s); ir (neat): 2820, 1480, 1440, 1350, 1070, 1030, 750, and 690 cm^{-1}; ms *m/z*: 175 (M^+).

*2-Methyl-3,3-*d,d*-4-phenyl-3,6-dihydro-1,2-oxazine (*d-**4**h*)*: ^{1}H nmr δ: 2.85 (s, NCH_3), 4.62 (br, OCH_2), 6.33 (t, J = 3.0, HC=), 7.53 (m, 5H); ^{13}C nmr δ: 45.8 (q), 57.8 (m, weak), 68.1 (t), 121.4 (d), 124.5 (d), 127.1 (d), 128.1 (d), 133.6 (s), 138.0 (s).

*2-Chloroformyl-4-(4'-methoxyphenyl)-3,6-dihydro-1,2-oxazines (***2**i *and* **3**i*)*

Treatment of **1** (2.70 g, 18.2 mmol) with 2-(4'-methoxyphenyl)-1,3-butadiene (2.50 g, 15.6 mmol) gave **2***i* as pale white crystals (2.31 g, 59%); mp 72°C (hexane); ^{1}H nmr (400 MHz) δ: 3.77 (s, OCH_3), 4.57 (br, NCH_2), 4.64 (br, OCH_2), 6.10 (t, t, 1H, J = 1.7, by decoupling the signal at δ 4.64; J = 3.2, by decoupling the signal at δ 4.57), 6.89 (d, 2H, J = 8.7), 7.28 (d, 2H, J = 8.7); ^{13}C nmr δ: 46.17 (t), 54.96 (q), 69.90 (t), 113.7 (d), 117.0 (d), 125.5 (d), 128.0 (s), 130.9 (s), 159.3 (s); ir (KBr): 1725 (C=O), 1650 (C=C) cm^{-1}; ms *m/z* (M^+ + 2), 253 (M^+). *Anal.* calcd. for $C_{12}H_{12}ClNO_3$: C 56.82, H 4.77, N 5.52; found: C 56.82, H 4.71, N 5.63. **3***i* (mixed with 23% of **2***i*); ^{1}H nmr δ: 3.78 (s, OCH_3), 4.44 (br, NCH_2), 4.84 (br, OCH_2), 6.02 (t, t, 1H, J = 1.7, by decoupling the signal at δ 4.44; J = 3.2, by decoupling the signal at δ 4.84), 6.89 (d, 2H, J = 8.9), and 7.29 (d, 2H, J = 8.9). The regioisomeric ratio was determined as the manner described above from ^{1}H nmr analysis. The result is given in Table 1.

*2-Methyl-4-(4'-methoxyphenyl)-3,6-dihydro-1,2-oxazine (***4**i*)*

Reduction of **2***i* (1.55 g, 6.11 mmol) with LAH (0.25 g, 6.57 mmol) in 30 mL of dry ether gave white crystals of **4***i* (1.15 g, 92%); mp 124°C; ^{1}H nmr δ: 2.77 (s, NCH_3), 3.55 (br, NCH_2), 3.78 (s, OCH_3), 4.48 (br, OCH_2), 6.04 (t, t, 1H, J = 1.2, by decoupling the signal at δ 4.48; J = 2.9, by decoupling the signal at δ 3.78), 6.84 (d, J = 9.0, 2H), 7.27 (d, J = 9.0, 2H); ^{13}C nmr δ: 45.94 (q), 55.68 (q), 58.06 (t), 68.20 (t), 113.6 (d), 119.6 (d), 125.6 (d), 130.6 (s), 133.1 (s), 158.7 (s); ir (KBr): 3000, 2980, 2840, 1600, 1500, 1280, 1240, 1190, 1100, and 1040 cm^{-1}. *Anal.* calcd. for $C_{12}H_{15}NO_2$: C 70.22, H 7.37, N 6.82; found: C 70.21, H 7.46, N 6.75.

*2-Chloroformyl-4-(3'-methoxyphenyl)-3,6-dihydro-1,2-oxazines (***2**j *and* **3**j*)*

Treatment of **1** (3.00 g, 20.2 mmol) with 2-(3'-methoxyphenyl)-1,3-butadiene (2.88 g, 18.0 mmol) afforded an 85:15 mixture of regioisomers **2***j* and **3***j* (3.10 g, 62%). Oxazine **2***j*: mp 67°C (hexane); ^{1}H nmr δ: 3.80 (s, 3H, OCH_3), 4.56 (s, 2H, NCH_2), 4.63 (d, 2H, J = 2.2, OCH_2), 6.20 (m, 1H, HC=), 6.88 (m, 3H), and 7.20 (m, 1H); ^{13}C nmr δ: 46.4 (t), 55.1 (g), 70.0 (t), 110.7 (d), 113.5 (d), 117.0 (d), 119.2 (d), 129.5 (d), 131.8 (s), 137.2 (s), 159.5 (s); ir (KBr): 1735 (C=O), 1655 (C=C) cm^{-1}; ms *m/z*: 255 (M^+ + 2), 253 (M^+). *Anal.* calcd. for $C_{12}H_{12}ClNO_3$: C 56.82, H 4.77, N 5.52; found: C 56.88, H 4.77, N 5.39. **3***j* (with 22% of **2***j*): ^{1}H nmr δ: 3.78 (s, 3H, OCH_3), 4.41 (br, 2H, NCH_2), 4.81 (d, 2H, J = 1.7, OCH_2), 6.09 (m, 1H, HC=), 6.83 (m, 3H), 7.24 (m, 1H); ^{13}C nmr δ: 45.23 (t), 55.08 (q), 71.13 (t), 110.7 (d), 113.4 (d), 117.0 (d, two peaks), 129.5 (d), 134.0 (s), 136.8 (s), 159.5 (s); ms *m/z*: 255 (M^+ + 2), 253 (M^+). The regioisomeric ratio was determined as the manner described above from ^{1}H nmr analysis.

*2-Methyl-4-(3'-methoxyphenyl)-3,6-dihydro-1,2-oxazine (***4**j*)*

Treatment of **2***j* (1.20 g, 4.73 mmol) with LAH (0.18 g, 4.74 mmol) in dry ether afforded **4***j* (0.80 g, 82%) as a white solid; mp 56°C (hexane); ^{1}H nmr δ: 2.75 (s, 3H, NCH_3), 3.55 (br, 2H, NCH_2), 3.77 (s, 3H, OCH_3), 4.77 (br, 2H, OCH_2), 6.13 (m, 1H, HC=), 6.86 (m, 3H), 7.22 (m, 1H); ^{13}C nmr δ: 45.8 (q), 55.0 (q), 56.4 (t), 68.1 (t), 110.5 (d), 112.4 (d), 117.0 (d), 121.6 (d), 129.1 (d), 133.6 (d), 139.5 (s), 159.3 (s); ir (KBr): 1680 (C=C) cm^{-1}; ms *m/z*: 205 (M^+). *Anal.* calcd. for $C_{12}H_{15}NO_2$: C 70.22, H 7.37, N 6.82; found: C 70.32, H 7.24, N 6.71.

*2-Chloroformyl-4-(4'-methylphenyl)-3,6-dihydro-1,2-oxazines (***2**k *and* **3**k*)*

Treatment of **1** (2.00 g, 13.5 mmol) with 2-(4'-methylphenyl)-1,3-butadiene (1.84 g, 12.8 mmol) afforded an 80:20 mixture of regioisomers **2***k* and **3***k* (2.18 g, 72%). Separation of **2***k* and **3***k* was carried out as described above. An analytical sample of **2***k* was obtained by recrystallization from hexane; mp 70°C; ^{1}H nmr δ: 2.31 (s, 3H, $PhCH_3$), 4.54 (m, 2H, NCH_2), 4.61 (d, 2H, J = 1.8, OCH_2), 6.12 (m, 1H, HC=), 7.13 (d, 2H, J = 8.0), 7.20 (d, 2H, J = 8.0); ^{13}C nmr δ: 20.9 (q), 46.2 (t), 69.8 (t), 117.9 (d), 124.2 (d), 129.0 (d), 131.4 (s), 132.7 (s), 138.0 (s), 147.2 (s); ir (KBr): 1740 (C=O), 1680 (C=C) cm^{-1}; ms *m/z*: 239 (M^+ + 2), 237 (M^+). *Anal.* calcd. for $C_{12}H_{12}ClNO_2$: C 60.64, H 5.09, N 5.89; found: C 60.66, H 5.17, N 5.82. The data for **3***k* (mixed with 28% of **2***k*): ^{1}H nmr δ: 2.35 (s, 3H, $PhCH_3$), 4.42 (br, 2H, NCH_2), 4.86 (d, 2H, J = 1.7, OCH_2), 6.09 (m, 1H, HC=), 7.18 (d, 2H, J = 8.0), 7.26 (d, 2H, J = 8.0). The regioisomeric ratio was determined as the manner described above by ^{1}H nmr analysis.

*2-Methyl-4-(4'-methylphenyl)-3,6-dihydro-1,2-oxazine (***4**k*)*

Treatment of **2***k* (1.42 g, 5.98 mmol) with LAH (0.22 g, 5.80 mmol) in 50 mL of dry ether afforded **4***k* (0.95 g, 84% yield); mp 50°C (hexane); ^{1}H nmr δ: 2.30 (s, 3H, $PhCH_3$), 2.75 (s, 3H, NCH_3), 3.53 (br, 2H, NCH_2), 4.45 (br, 2H, OCH_2), 6.08 (m, 1H, HC=), 7.15 (d, 2H, J = 6.0), 7.23 (d, 2H, J = 6.0); ^{13}C nmr δ: 20.9 (q), 45.8 (q), 58.0 (t), 68.1 (t), 120.5 (d), 124.3 (d), 128.8 (d), 133.4 (s), 135.1 (s), 136.8 (s); ir (KBr): 1680 (C=C) cm^{-1}; ms *m/z*: 189 (M^+). *Anal.* calcd. for $C_{12}H_{15}NO$: C 76.16, H 7.99, N 7.40; found: C 76.19, H 8.05, N 7.37.

*2-Chloroformyl-4-(3'-methylphenyl)-3,6-dihydro-1,2-oxazines (***2**m *and* **3**m*)*

Treatment of **1** (3.55 g, 23.9 mmol) with 2-(3'-methylphenyl)-1,3-butadiene (3.40 g, 23.6 mmol) afforded an 82:18 mixture of regioisomers **2***m* and **3***m* (4.40 g, 72%). Separation of **2***m* and **3***m* was carried out as described above. **2***m*: mp 66°C (hexane); ^{1}H nmr δ: 2.35 (s, 3H, $PhCH_3$), 4.67 (br, 4H, OCH_2 and NCH_2), 6.19 (m, 1H, HC=), 7.15–7.24 (m, 4H); ^{13}C nmr δ: 21.3 (q), 46.5 (t), 70.0 (t), 118.7 (d), 121.6 (d), 125.2 (d), 128.4 (d), 129.0 (d), 132.0 (s), 135.2 (s), 138.1 (s), 147.4 (s); ir (KBr): 1725 (C=O), 1675 (C=C) cm^{-1}; ms *m/z*: 239 (M^+ + 2), 237 (M^+). *Anal.* calcd. for $C_{12}H_{12}ClNO_2$: C 60.64, H 5.09, N 5.89; found: C 60.69, H 5.09, N 5.93. **3***m* (mixed with 5% of **2***m*): mp 58°C (hexane); ^{1}H nmr δ: 2.35 (s, 3H, $PhCH_3$), 4.41 (br, 2H, NCH_2), 4.84 (s, 2H, OCH_2), 6.09 (m, 1H, HC=), 7.14–7.34 (m, 4H); ^{13}C nmr δ: 21.43 (q), 45.20 (t), 71.47 (t), 116.8 (d), 122.1 (d), 125.7 (d), 128.9 (d), 129.4 (d), 134.8 (s), 135.9 (s), 138.6 (s), 147.6 (s). The regioisomeric ratio was determined from the mixture of **2***m* and **3***m* by integration of the ring hydrogens at δ 4.67 (NCH_2 and OCH_2) and δ 4.41, 4.84 for **2***m* and **3***m*, respectively, prior to chromatography.

*2-Methyl-4-(3'-methylphenyl)-3,6-dihydro-1,2-oxazine (***4**m*)*

Treatment of **2***m* (1.50 g, 6.32 mmol) with LAH (0.24 g, 6.32 mmol) in 50 mL of dry ether gave **4***m* (1.03 g, 86%) as a white solid; mp 42°C

Can. J. Chem. Downloaded from www.nrcresearchpress.com by 186.148.149.217 on 09/07/12
For personal use only.

(hexane), ^{1}H nmr δ: 2.33 (s, 3H, $PhCH_3$), 2.77 (s, 3H, NCH_3), 3.55 (br, 2H, NCH_2), 4.47 (br, 2H, OCH_2), 6.10 (m, 1H, HC=), 7.03–7.30 (m, 4H); ^{13}C nmr δ: 21.5 (q), 45.9 (q), 58.1 (t), 68.2 (t), 121.2 (d), 121.7 (d), 125.3 (d), 128.1 (d, two peaks), 133.8 (s); ms *m/z*: 189 (M^+). *Anal.* calcd. for $C_{12}H_{15}NO$: C 76.16, H 7.99, N 7.40; found: C 76.14, H 8.02, N 7.47.

*2-Chloroformyl-4-(4′-chlorophenyl)-3,6-dihydro-1,2-oxazines (***2**n *and* **3**n*)*

Treatment of **1** (3.00 g, 20.2 mmol) with 2-(4′-chlorophenyl)-1,3-butadiene (3.02 g, 18.4 mmol) gave 3.50 g (74%) of a 67:33 mixture of regioisomers **2***n* and **3***n*. **2***n*: mp 110°C (hexane); ^{1}H nmr (400 MHz) δ: 4.66 (br, NCH_2), 4.77 (d, J = 2.8, OCH_2), 6.31 (m, 1H, HC=), 7.36 (d, J = 8.6, 2H), 7.42 (d, J = 8.6, 2H); ^{13}C nmr δ: 46.23 (t), 69.90 (t), 119.6 (t), 125.8 (d), 128.6 (d), 130.9 (s), 134.1 (s), 147.5 (s); ir (KBr): 1730 (C=O), 1650 (C=C) cm^{-1}; ms, *m/z*: 259 (M^+ + 2), 257 (M^+). *Anal.* calcd. for $C_{11}H_9Cl_2NO_2$: C 51.06, H 3.76, N 5.41; found: C 51.06, H 3.62, N 5.48. The data for **3***n* were determined from a mixture containing 25% of **2***n*: ^{1}H nmr δ: 4.44 (br, NCH_2), 4.83 (br, OCH_2), 6.13 (t, t, 1H, J = 3.5, by decoupling the signal at δ 4.83; J = 1.7, by decoupling the signal at δ 4.43), 7.14–7.44 (m, 4H); ^{13}C nmr δ: 45.23 (t), 70.78 (t), 117.3 (d), 128.5 (d), 128.6 (d), 133.1 (s), 133.7 (s), 147.0 (s). The regioisomeric ratio was determined from the mixture of **2***n* and **3***n* by integration of the ring hydrogens at δ 4.66, 4.77 and δ 4.44, 4.83, respectively, prior to chromatography.

*2-Methyl-4-(*p*-chlorophenyl)-3,6-dihydro-1,2-oxazine* **4**n

Treatment of **2***n* (0.64 g, 2.48 mmol) with LAH (0.10 g, 2.63 mmol) in dry ether gave **4***n* (0.48 g, 92%) as white crystals; mp 73°C (hexane); ^{1}H nmr δ: 2.76 (s, NCH_3), 3.51 (br, NCH_2), 4.46 (br, OCH_2), 6.122 (t, t, 1H, J = 2.9, by decoupling the signal at δ 3.51; J = 1.6, by decoupling the signal at δ 4.46), 7.25 (s, 4H); ^{13}C nmr δ: 45.88 (q), 57.77 (t), 68.14 (t), 120.0 (d), 125.7 (d), 128.3 (d), 132.7 (s), 132.9 (s), 136.4 (s); ir (KBr): 2980, 1495, 1455, 1100, 1080, and 800 cm^{-1}; ms *m/z*: 211 (M^+ + 2), 209 (M^+). *Anal.* calcd. for $C_{11}H_{12}ClNO$: C 63.01, H 5.77, N 6.68; found: C 62.84, H 5.72, N 6.62.

General procedure for kinetic studies

To a uv cell filled with a solution of **1** (1.12×10^{-2} M) in methylene chloride (or THF or chloroform) was added an appropriate diene (ca. 0.77 M, 70 times the moles of **1**) in one portion. The disappearance of **1** was measured by the decreasing intensity of the peak at 592 nm, which is the maximum absorption of **1** in the visible region (ε = 6.0 (19)). The reactions were followed up to 90% completion. The pseudo-first-order rate constants were obtained by measurement of the decaying curve and were the average values of at least two kinetic runs for each reaction. A linear free energy plot using σ^+ substituent constants and pseudo-first-order rate constants is shown in Fig. 1.

Acknowledgement

We are grateful to the National Science Council of the Republic of China for financial support of this research, to Mr. B. Liu (National Tsinghua University) for high resolution mass spectra, and to Professor T. C. Chou for fruitful discussion and encouragement.

1. (*a*) D. L. Boger and S. M. Weinreb. Hetero Diels–Alder methodology in organic synthesis. Academic Press, New York, NY. 1987. Chap. 3; (*b*) G. Kresze, B. Ascherl, and H. Braun. Org. Prep. Proced. Int. 329 (1987); (*c*) S. M. Weinreb and R. R. Staib. Tetrahedron, **38**, 3087 (1982); (*d*) G. W. Kirby. Chem. Soc. Rev. **6**, 1 (1977).
2. (*a*) D. L. Boger and M. Patel. J. Org. Chem. **49**, 4098 (1984); (*b*) M. Sabuni, G. Kresze, and H. Braun. Tetrahedron Lett. 5377 (1984); (*c*) J. E. Baldwin, P. O. Bailey, G. Gallacher, M. Otsuka, K. A. Singleton, and P. M. Gallace. Tetrahedron, **19**, 3695 (1984); (*d*) H. Iida, Y. Watanabe, and C. Kibayashi. Tetrahedron Lett. 5091 (1984); (*e*) J. Streith, G. Augelmann, H. Freitz, and H. Strub. Tetrahedron Lett. 1909 (1982); (*f*) G. E. Keck, S. Fleming, D. Nickell, and P. Weider. Synth. Commun. **9**, 281 (1979); (*g*) G. Kresze. *In* Organic synthesis: Modern trends. 6th IUPAC symposium. *Edited by* O. Chizhov. Blackwell Sci. Publ., Oxford. 1987. p. 169 and references cited therein.
3. (*a*) P. Haussinger and G. Kresze. Tetrahedron, **34**, 689 (1978); (*b*) G. Kresze and W. Kosbahn. Tetrahedron, **27**, 1931 (1971); (*c*) G. Kresze and J. Firl. Fortschr. Chem. Forsch. **11**, 245 (1969); (*d*) Tetrahedron, **24**, 1043 (1968); (*e*) G. Kresze and O. Korpiun. Tetrahedron, **22**, 2493 (1966).
4. T. Sasaki, S. Eguchi, T. Ishii, and H. Yamada. J. Org. Chem. **35**, 4273 (1970).
5. R. S. Givens, D. J. Choo, S. N. Merchant, R. P. Stitt, and B. Matuszewski. Tetrahedron Lett. **23**, 1327 (1982).
6. (*a*) H. Labaziewicz and F. G. Riddel. J. Chem. Soc. Perkin Trans. 1, 2926 (1979); (*b*) F. G. Riddel. Tetrahedron, **31**, 523 (1975).
7. (*a*) D. L. Boger, M. Patel, and F. Takusagawa. J. Org. Chem. **50**, 1911 (1985); (*b*) S. K. Dubey and E. E. Knaus. J. Org. Chem. **50**, 2080 (1985).
8. H. G. Viehe, R. Merenyi, E. Froncotte, M. Van Meerssche, G. Germain, J. P. Declercq, and J. Bodart-Gilort. J. Am. Chem. Soc. **99**, 2340 (1977).
9. C. T. Lin and J. H. Chen. J. Chin. Chem. Soc. **34**, 317 (1987).
10. F. G. Riddel and D. A. R. Williams. Tetrahedron, **30**, 1097 (1974).
11. (*a*) R. B. Woodword and T. J. Katz. Tetrahedron, **5**, 70 (1959); (*b*) M. J. S. Dewar, S. Olivella, and J. J. P. Stewart. J. Am. Chem. Soc. **108**, 5771 (1986); (*c*) G. W. Gribble, D. J. Keavy, S. E. Branz, W. J. Kelly, and M. A. Pals. Tetrahedron Lett. **29**, 6227 (1988).
12. (*a*) J. Sauer. Angew. Chem. Int. Ed. Engl. **6**, 16 (1967); (*b*) T. Inukai and T. Kojima. J. Org. Chem. **36**, 924 (1971).
13. (*a*) I. Fleming. Frontier orbitals and organic chemical reactions. Wiley, New York. 1976; (*b*) K. N. Houk. J. Am. Chem. Soc. **95**, 4092 (1973); (*c*) O. Eisenstein, J. M. Lefour, and N. T. Anh. Tetrahedron, **33**, 523 (1977).
14. C. T. Lin, C. W. Chang, and T. S. Liu. Tung-hai Hsueh Pao, **29**, 587 (1988).
15. G. A. Russell and R. C. Williamson, Jr. J. Am. Chem. Soc. **86**, 2357 (1964).
16. C. M. M. Da Silva Correa and W. A. Waters. J. Chem. Soc. Perkin Trans. 2, 1575 (1972).
17. R. G. Lawler, P. F. Barbara, and D. J. Jacobs. J. Am. Chem. Soc. **100**, 4912 (1978).
18. V. Astley and H. Sutcliffe. J. Chem. Soc. Perkin Trans. 2, 197 (1972).
19. (*a*) A. R. Briden, D. Price, and H. Sutcliffe. J. Chem. Soc. B, 387 (1968); (*b*) P. Tarte. Bull. Soc. Chim. Belg. **63**, 5259 (1954).
20. C. D. Johson. The Hammett equation. Cambridge University Press, London. 1973. p. 3.

The mechanism of hydrolysis of 2-hydroxyethanesulfonyl chloride: the intermediacy of 1,2-oxathietane 2,2-dioxide (β-sultone)[1]

JAMES FREDERICK KING[2] AND KISHAN CHAND KHEMANI
Department of Chemistry, University of Western Ontario, London, Ont., Canada N6A 5B7

Received April 28, 1989

JAMES FREDERICK KING and KISHAN CHAND KHEMANI. Can. J. Chem. **67**, 2162 (1989).

The hydrolysis of 2-hydroxyethanesulfonyl chloride (**1**) has been investigated with the aid of kinetic and product analysis studies. The results are quantitatively consistent with the mechanism of hydrolysis shown in Scheme 1, the chief features of which are (a) formation of β-sultone (**2**) and its rapid further reaction (the major pathway), together with (b) a minor direct hydrolysis route. The kinetics of both the β-sultone formation and the direct hydrolysis shows two terms, one first order in **1** alone, and the other first order in hydroxide as well; the rates of the first- and second-order reactions are lowered by added sodium chloride. It is suggested (a) that the unimolecular β-sultone formation involves **1** in a complex with water (as in **9**) and that the water acts as a general base in the cyclization to **2**, and (b) the hydroxide-promoted reaction proceeds by cyclization of the conjugate base of **1** (i.e., **10**). The unimolecular direct hydrolysis is regarded as a conventional hydrolysis of a sulfonyl chloride with attack of the water with general base assistance from a second water molecule. The hydroxide-promoted direct reaction in D_2O leads to no uptake of deuterium, showing that the reaction does not go by way of the sulfene, and a reaction by way of a six-membered cyclic transition state is tentatively proposed. Evidence is presented that the chloride ion rate suppression is not primarily due to reaction of β-sultone with Cl^- to give back **1**; the possible origins of the effect are discussed.

Key words: sulfonyl chlorides, 2-hydroxyethanesulfonyl chloride, β-sultone, kinetics of sulfonyl chloride hydrolysis, mechanisms of sulfonyl chloride hydrolysis.

JAMES FREDERICK KING et KISHAN CHAND KHEMANI. Can. J. Chem. **67**, 2162 (1989).

Faisant appel à des études cinétiques et à d'autres impliquant une analyse des produits, on a étudié l'hydrolyse du chlorure du 2-hydroxyéthanesulfonyle (**1**). Sur une base quantitative, les résultats sont en accord avec le mécanisme d'hydrolyse représenté dans le schéma 1 et dont les caractéristiques principales sont (a) la formation d'une β-sultone (**2**) et sa rapide réaction subséquente (voie principale) et (b) une voie mineure d'hydrolyse directe. La cinétique de la formation de la β-sultone ainsi que de l'hydrolyse directe présente à chaque fois deux termes : l'un du premier ordre uniquement en composé **1** et l'autre qui est en plus du premier ordre en ion hydroxyde; les vitesses des réactions du premier et du deuxième ordre sont abaissées par l'addition de chlorure de sodium. On suggère : (a) que la formation unimoléculaire de la β-sultone implique que le composé **1** est complexé dans l'eau (comme dans **9**) et que l'eau agit comme base générale dans la cyclisation conduisant au composé **2** et (b) que la réaction catalysée par l'ion hydroxyde se produit par le biais d'une cyclisation de la base conjuguée du composé **1** (soit **10**). On considère l'hydrolyse unimoléculaire directe comme une hydrolyse conventionnelle d'un chlorure de sulfonyle impliquant une attaque de l'eau avec l'assistance d'une seconde molécule d'eau agissant comme base générale. L'hydrolyse directe, dans le D_2O et sous l'influence d'ions hydroxydes, ne provoque aucune incorporation de deutérium; ce résultat démontre que la réaction ne se produit pas par le biais du sulfène et on propose provisoirement que la réaction se produit via un état de transition cyclique à six chaînons. On présente des données démontrant que le ralentissement de la réaction sous l'influence d'ions chlorures n'est pas causé par une réaction de la β-sultone avec le Cl^- pour redonner le composé **1**; l'origine possible de cet effet est discutée.

Mots clés : chlorures de sulfonyle, chlorure de 2-hydroxyéthanesulfonyle, β-sultone, cinétique de l'hydrolyse du chlorure de sulfonyle, mécanismes d'hydrolyse du chlorure de sulfonyle.

[Traduit par la revue]

Introduction

In the course of an extended study of the reactions of the sulfonyl group (2, 3) we prepared the first hydroxyalkanesulfonyl chlorides and looked at some of their reactions (1, 4, 5). As part of our work on the simplest known member of this series, 2-hydroxyethanesulfonyl chloride (**1**), we suggested that 1,2-oxathietane 2,2-dioxide (β-sultone, **2**) was probably formed as a short-lived intermediate under a variety of circumstances, including simple hydrolysis (4).



$HOCH_2CH_2SO_2Cl$ **1**

2

β-Sultone (**2**) has never been isolated or observed directly, though a number of substituted derivatives have been reported (6). The present study was initiated to determine whether or not **2** really was an intermediate in the hydrolysis of **1**, and, if it should prove so, to investigate some of its chemistry. Of particular interest was whether or not **2** would show any tendency to undergo attack by a nucleophile with S—O cleavage. It is well known that the bimolecular reaction of alkyl esters of sulfonic acids with nucleophiles proceeds with cleavage of the C—O bond and formation of a C—Nu bond, except for certain sterically congested esters that react with alkoxide by S—O scission (7, 8). The latter mode of cleavage had also been reported in the alkaline hydrolysis of the cyclohexane-1,2-diyl sulfates by Brimacombe *et al.* (9, 10). Kaiser, Panar, and Westheimer (11) found a small proportion (14%) of S—O cleavage with ethylene sulfate in alkaline solution but none at all with either trimethylene sulfate or dimethyl sulfate. Mori *et*

[1]Organic Sulfur Mechanisms. 34. For part 33 see ref. 1.
[2]Author to whom correspondence may be addressed.

Can. J. Chem. Downloaded from www.nrcresearchpress.com by 186.148.149.217 on 09/07/12
For personal use only.

Can. J. Chem. Downloaded from www.nrcresearchpress.com by 186.148.149.217 on 09/07/12
For personal use only.

al. (12) reported that hydrolysis of propane 1,3-sultone in strong base also proceeded with 14% S—O cleavage, whereas the corresponding reaction of ethyl ethanesulfonate went exclusively with the normal C—O scission. Westheimer and Kaiser and their co-workers (cf. refs. 13 and 14) had also observed that attack of hydroxide on the sulfonyl group was several orders of magnitude faster with five-membered ring sultones and sulfate esters than with six-membered or acyclic analogues, and it was therefore of interest to see if any similar effect might appear in the reaction of the four-membered ring sultone. The present paper describes kinetic and product analysis experiments that lead us to conclude that the hydrolysis of **1** in the pH range 3–13 proceeds largely by way of β-sultone (**2**). More recent work on the attack of hydroxide at a sulfonyl group describing evidence for, and a rationalization of, the preferred S—O cleavage has been reported in preliminary form (15, 16) and will be given in detail in a subsequent paper; a more extensive treatment of these topics has been presented in thesis form (17).

Results and discussion

Kinetic and product ratio studies; proposal of mechanism

The rates of hydrolysis of 2-hydroxyethanesulfonyl chloride (**1**) were measured under a variety of conditions by the pH-stat technique; a typical rate plot is shown in Fig. 1. The pH–rate profile for the hydrolysis in 0.3 M $NaClO_4$ at 25°C, shown in Fig. 2, corresponds to a rate law of the form

[1] $$k_\psi = k_H + k_{OH}[OH^-]$$

Values of k_H and k_{OH} of $(2.28 \pm 0.49) \times 10^{-4}\,s^{-1}$ and $(5.16 \pm 0.52) \times 10^6\,M\,s^{-1}$ give the curve shown by the solid line in Fig. 2. Also shown in Fig. 2 is the pH–rate profile for the reaction in 0.3 M NaCl; the dashed line has the same shape but is displaced to lower $\log k_\psi$ values, corresponding to a roughly two- to threefold lowering of the rate in the presence of Cl^- as compared to ClO_4^- (0.3 M).

The product of the reaction under kinetic conditions (C_0 = 10^{-3}–10^{-5} M) was almost entirely sodium 2-hydroxyethanesulfonate (**3**) with small but consistently observable amounts (~2–5%) of sodium 2-chloroethanesulfonate (**4***a*). Addition of sodium chloride to the reaction mixture gave more **4***a*. The variation in product composition with change in pH and the concentration of added reagents was studied by carrying out a sizeable series of runs in the pH-stat apparatus and examining the product by ^{1}Hmr; the results are summarized starting with Fig. 3. From the pH–product ratio profile for the hydrolysis of **1** in 1.0 M NaCl over the pH range 1–13 (Fig. 3), one may note immediately that the sloped portions of the pH–rate and pH–product curves (respectively, Figs. 2 and 3) do not correspond. This would indicate different rate-determining and product-determining steps, in full accord with the notion of a reaction proceeding by way of β-sultone (**2**) as an intermediate (see Scheme 1).

The variation in product ratio with change in sodium chloride concentration and at constant pH was determined for a series of pH values; the results are displayed in Figs. 4–7. The product ratio [**4***a*]/[**3**] increases with chloride ion concentration but not linearly, a distinct tendency to plateau being most evident at low pH but visible in all of the plots. That this nonlinearity was probably not simply a result of deviations from ideality accompanying high salt concentrations was shown by the product-ratio curve obtained in the corresponding reaction

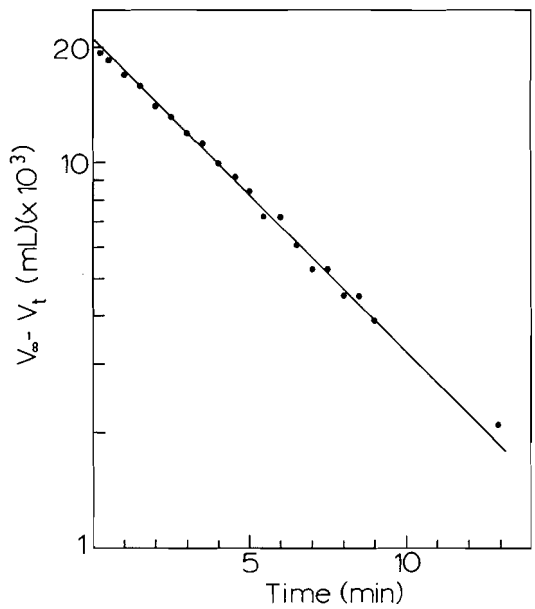


FIG. 1. Typical rate plot for the hydrolysis of 2-hydroxyethanesulfonyl chloride (**1**) (pH 5.0, 25.0°C, 0.1 M NaCl, μ = 0.3 M with $NaClO_4$).

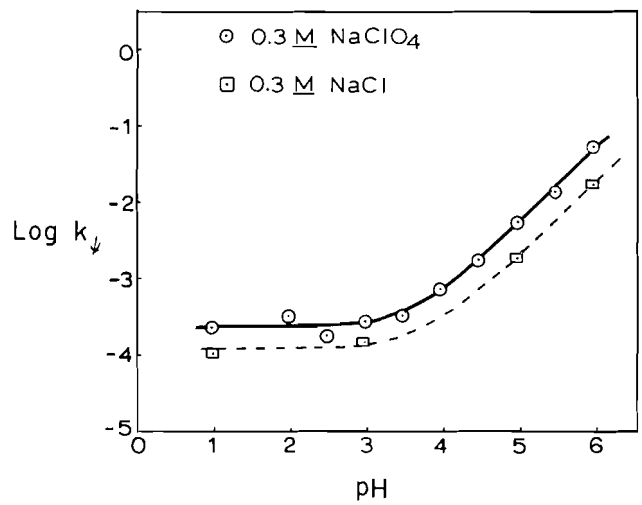


FIG. 2. Dependence on pH of the first-order rate constants for the hydrolysis of 2-hydroxyethanesulfonyl chloride (**1**) at 25.0°C (in 0.3 M $NaClO_4$ and NaCl solutions). The solid line is calculated from $\log k_\psi = \log (k_H + k_{OH}[OH^-])$ where $k_H = 2.28 \times 10^{-4}\,s^{-1}$ and $k_{OH} = 5.16 \times 10^6\,M^{-1}\,s^{-1}$.

of propane 1,3-sultone (**5**) to form a mixture of the 3-hydroxy-1-propanesulfonate (**6**) and 3-chloro-1-propanesulfonate (**7**) salts; the points (Fig. 8) correspond to a line that appears reasonably straight all the way to the highest sodium chloride concentration (1.4 M).

Again, the results with **1** are consistent with reaction via **2**, with the tendency to plateau indicating a dual pathway, one (that via **2**) capable of being diverted by chloride anion, and one not (the latter evidently the minor route). On this basis it seemed likely that thiocyanate anion might prove a more efficient trap for **2** than chloride, and might therefore give product-ratio curves with more clearly defined plateaus, thereby facilitating quantitative interpretation. As may be seen in Fig. 9, this was, in fact, observed. It was also found that addition of sodium

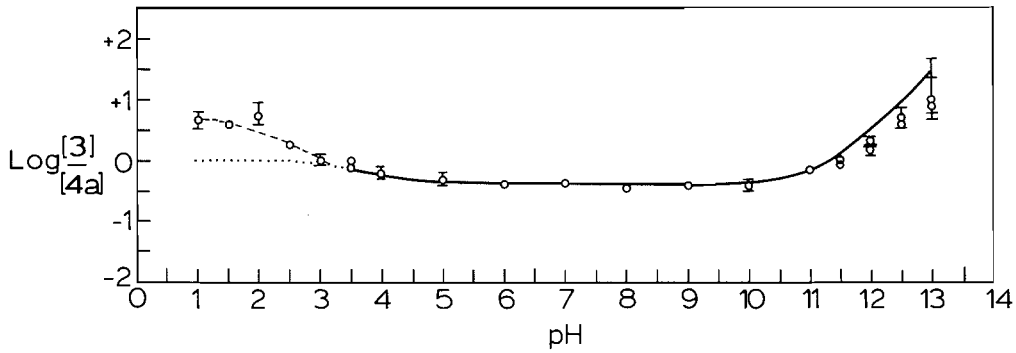


FIG. 3. Dependence on pH of the ratio of 2-hydroxyethanesulfonate (**3**) to 2-chloroethanesulfonate (**4***a*) ion in the product of the reaction of **1** with 1 M aqueous NaCl at 25.0°C. The solid and dotted lines are calculated using only the parameters in Scheme 1; the dashed line is obtained by including (in an appropriately modified form of eq. [A16]) two additional terms involving acid-catalyzed cleavage of **2** (see text and Appendix).

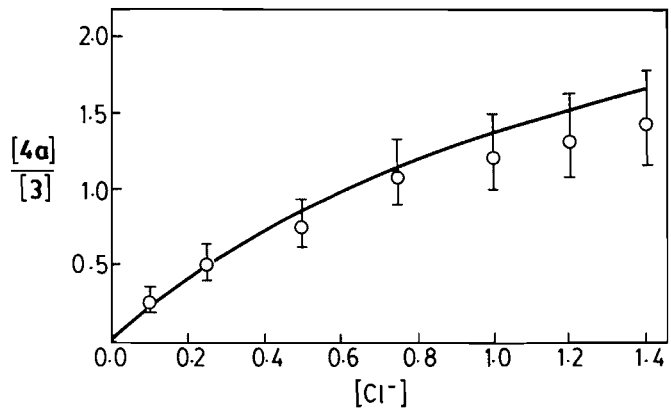


FIG. 4. Variation of the product ratio [**4***a*]/[**3**] with the concentration of sodium chloride in the reaction of **1** with aqueous sodium chloride at pH 3.5. The line is calculated from the parameters in Scheme 1 and eqs. [5]–[7].

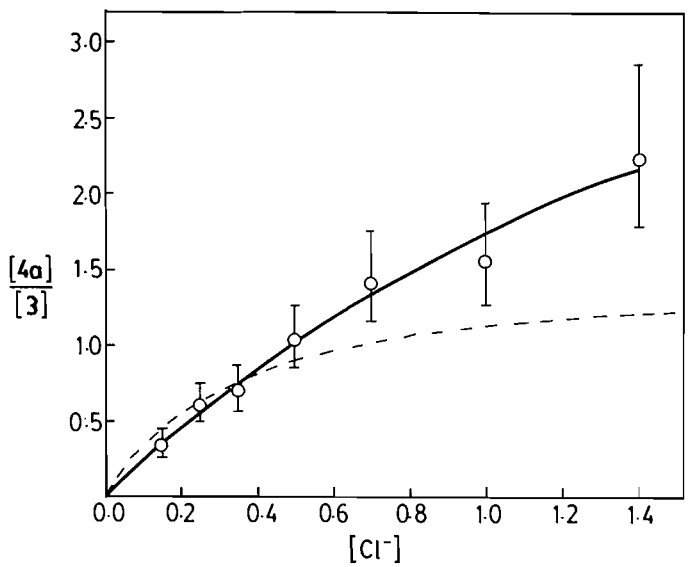


FIG. 5. Variation of the product ratio [**4***a*]/[**3**] with the concentration of sodium chloride in the reaction of **1** with aqueous sodium chloride at pH 4.0. The solid line is calculated from the parameters in Scheme 1 and eqs. [5]–[7], the dashed line from a relationship derived by assuming reaction of **2** with Cl^- to give back **1** as in Scheme 2 (see text and the Appendix).

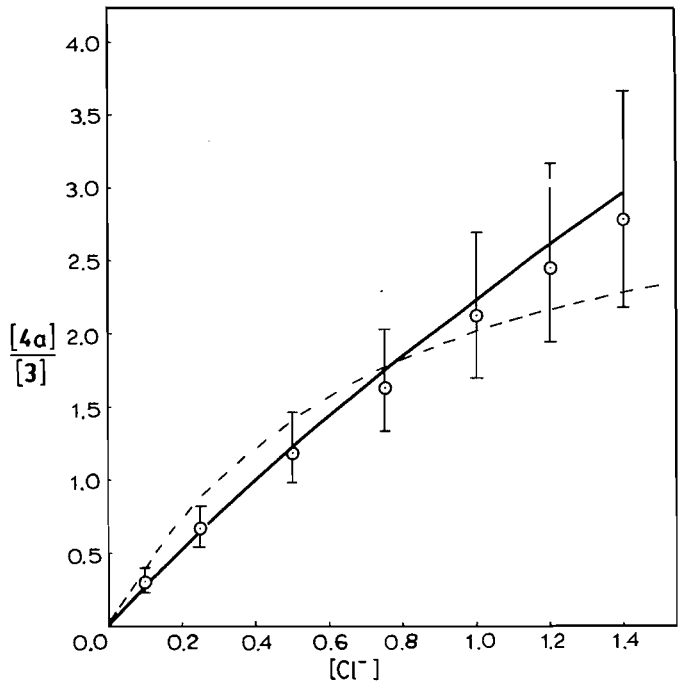
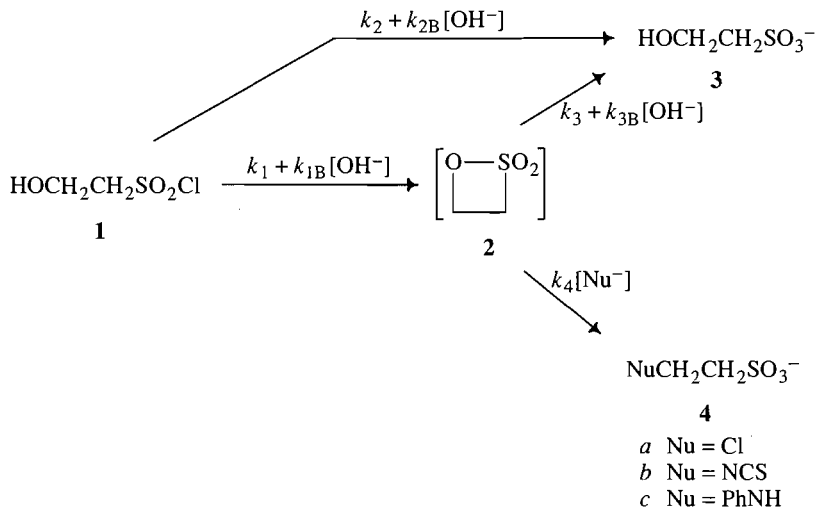


FIG. 6. Variation of the product ratio [**4***a*]/[**3**] with the concentration of sodium chloride in the reaction of **1** with aqueous sodium chloride at pH 6.0. The solid line is calculated from the parameters in Scheme 1 and eqs. [5]–[7], the dashed line from a relationship derived by assuming reaction of **2** with Cl^- to give back **1** as in Scheme 2 (see text and the Appendix).

thiocyanate had no effect on the measured rate at pH 3.0; k_ψ was found to be $1.83 \times 10^{-4}\ s^{-1}$ with 0.1 M NaSCN and $1.85 \times 10^{-4}\ s^{-1}$ without (at 25°C and ionic strength 0.5 M with $NaClO_4$). At the same time the product ratio **4***b*/**3** was determined from a large-scale kinetic run using the same concentration of **1** (3.44×10^{-4} M) as that used for the other kinetic runs; **4***b*:**3** was found to be 48:52 with $k_\psi = 1.80 \times 10^{-4}\ s^{-1}$. Evidently almost half of the product is derived from a reagent that has no detectable effect on the observed rate constant. This is a clear example of the rate–product discrepancy, which requires, minimally, a two-step process involving a slow first step forming an intermediate, which reacts with the "zero-order reagent" in a subsequent fast step. These features, namely a dual pathway (one via a trappable intermediate and one not) and the requirement for a slowly formed, rapidly consumed intermediate giv-

Can. J. Chem. Downloaded from www.nrcresearchpress.com by 186.148.149.217 on 09/07/12
For personal use only.



k_1 1.53×10^{-4} s^{-1} k_2 7.46×10^{-5} s^{-1}
k_{1B} 4.81×10^{6} M^{-1} s^{-1} k_{2B} 3.50×10^{5} M^{-1} s^{-1}
k_{3B}/k_3 8.29×10^{2} M^{-1} $(k_4/k_3)_{SCN}$ 42.8 M^{-1} $(k_4/k_3)_{Cl}$ 2.91 M^{-1}

SCHEME 1

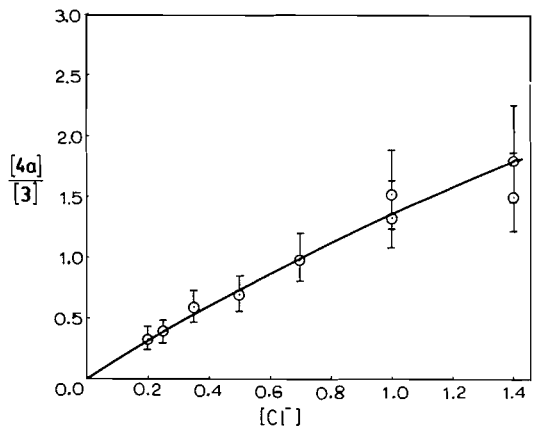


FIG. 7. Variation of the product ratio [4*a*]/[3] with the concentration of sodium chloride in the reaction of **1** with aqueous sodium chloride at pH 11.0. The line is calculated from the parameters in Scheme 1 and eqs. [5]–[7]

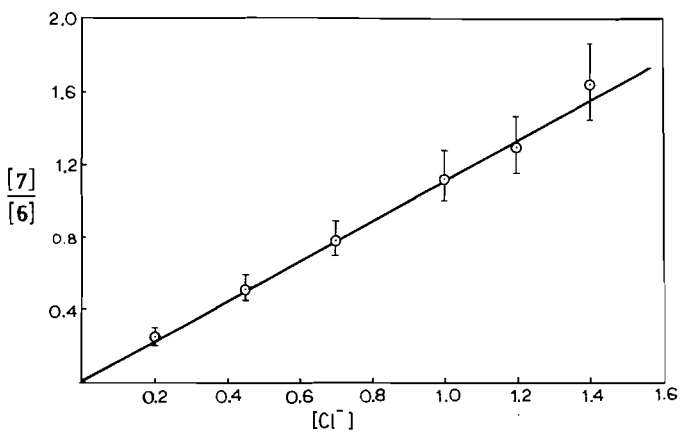
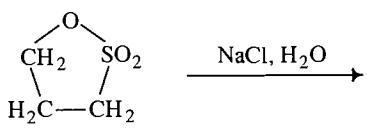


FIG. 8. Variation of the ratio of 3-chloro-1-propanesulfonate (**7**) to 3-hydroxypropanesulfonate (**6**) ions with change in sodium chloride concentration in the reaction of propane 1,3-sultone (**5**) with aqueous sodium chloride (pH 4.0, 25°C).



5

$HOCH_2CH_2CH_2SO_3^-$ + $ClCH_2CH_2CH_2SO_3^-$

6 **7**

ing products consistent with its identification as β-sultone (**2**), lead to the proposal of the mechanism shown in Scheme 1.

Rate and product-ratio expressions; comparisons with experiment

The next stage is to move from qualitative to quantitative tests of the validity of the proposed mechanism, i.e., to find if a set of rate constants and rate constant ratios based on this scheme will reproduce the experimental results summarized in Figs. 2–7 and 9. The hydrolysis of **1** in D_2O was followed by ^{1}Hmr, and in no case were any peaks assignable to β-sultone observed. We may therefore use the steady state approximation, which readily yields eq. [2]:

[2] $$k_\psi = k_1 + k_{1B}[OH^-] + k_2 + k_{2B}[OH^-] = x + y$$

where $x = k_1 + k_{1B}[OH^-]$ and $y = k_2 + k_{2B}[OH^-]$. Comparison with eq. [1] immediately leads to

[3] $$k_1 + k_2 = k_H = 2.28 \times 10^{-4}\,s^{-1}$$

[4] $$k_{1B} + k_{2B} = k_{OH} = 5.16 \times 10^{6}\,M^{-1}\,s^{-1}$$

The product ratio [**4**]/[**3**] may be shown (see Appendix 1) to be given by eq. [5],

[5] $$[4]/[3] = \frac{a_1}{1 + \dfrac{a_2}{[Nu^-]}}$$

where a_1 and a_2 are given by [6] and [7] and $z = k_3 + k_{3B}[OH^-]$.

[6] $$a_1 = x/y$$

Can. J. Chem. Downloaded from www.nrcresearchpress.com by 186.148.149.217 on 09/07/12
For personal use only.

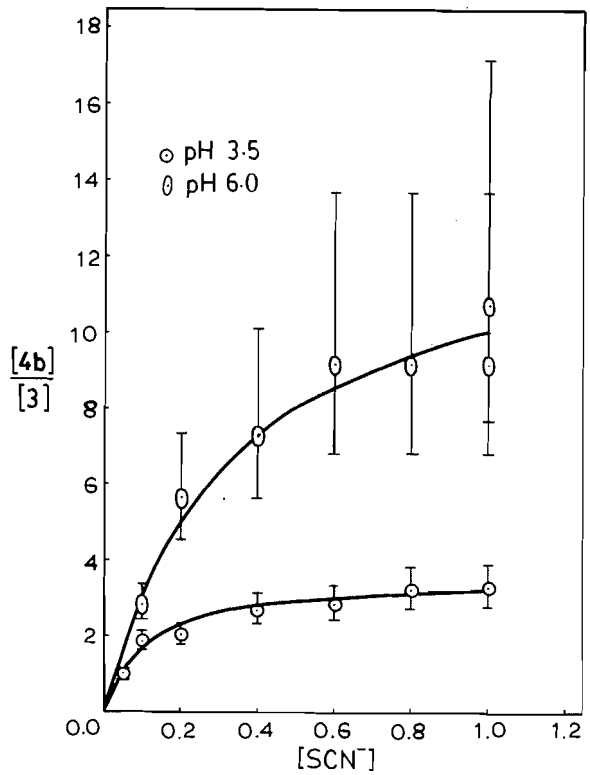


FIG. 9. Variation of the product ratio [**4***b*]/[**3**] with change in sodium thiocyanate concentration in the reaction of **1** with aqueous sodium thiocyanate at pH 3.5 (circles) and pH 6.0 (ellipses). The lines are calculated from the parameters in Scheme 1 and eqs. [5]–[7]

and

$$[7] \qquad a_2 = (1 + x/y)z/k_4 = \frac{(1 + x/y)(1 + k_{3B}[OH^-]/k_3)}{k_4/k_3}$$

The parameters a_1 and a_2 for each of the curves in Fig. 9 were obtained by a nonlinear least-squares fit to the data,[3] and, as is described in the Appendix, (a) the two values of a_1 so obtained (for pH 3.5 and pH 6.0, respectively) yielded two versions of eq. [6], which, with eqs. [3] and [4] gave the values of k_1, k_2, k_{1B}, and k_{2B} shown in Scheme 1; (b) eq. [7] gave $(k_4/k_3)_{SCN}$, and (c) the data in Figs. 6 and 7 similarly yielded, respectively, $(k_4/k_3)_{Cl}$ and k_{3B}/k_3, as given in Scheme 1.

These parameters, when inserted into eqs. [2] and [5], gave the solid lines shown in Figs. 2–7 and 9. Note that, except as noted below for Fig. 3, the agreement is well within experimental uncertainty, not only for the curves used to generate the parameters (Figs. 2, 6, 7, and 9) but for the others as well.

Figure 3 presents two distinct regions in which there are discrepancies between the calculated values and the experimental points. The dotted line in the region below pH 3.5 is that predicted by eq. [5] and the parameters in Scheme 1. That this line deviates from the experimental points is most simply explained by assuming that there are acid-promoted terms for the cleavage of **2** not included in eq. [5]. One may readily add reactions involving acid-catalyzed hydrolysis and chloride attack on **1** to Scheme 1, and obtain the dashed line shown in Fig. 3 (the specific parameters are $k_{3A}/k_3 \approx 900\,s^{-1}$ and $k_{4A}[Cl^-]/k_3 \approx 300\,s^{-1}$, with each term first order in H_3O^+). The agreement with experiment is satisfactory, and though such acid-catalyzed reactions are not unreasonable, we have no corroborating evidence and shall defer further discussion of the reaction below pH 3.5 until more experimental results are available.

[3]The computer program for the nonlinear least-squares treatment was based on one devised by Professor J. P. Guthrie; we are most grateful to him for his generosity in providing both the program and help in using it.

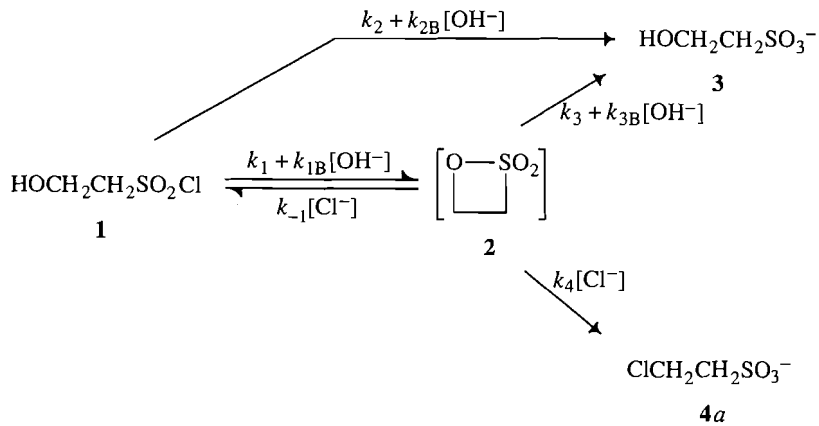
The mechanism in the high pH region

The other end of the pH–product ratio profile, though indicating qualitative agreement between calculated and observed ratios, would appear to be showing increasing deviation between the two with increasing pH, with the result that the difference between the calculated and observed values at pH 13 may be outside the experimental error.

We feel that the mediocre agreement of the calculated line with the experimental points in the high pH region (pH ≥ 12) of Fig. 3 may well be an artifact arising from the experimental difficulty of maintaining, at the site of the reaction of β-sultone, the hydroxide concentration of the bulk medium. It seems likely that as the hydroxide ion is consumed very rapidly in the first step of the formation of **2**, its concentration in the immediate vicinity of **2** would be considerably depleted as compared to the as yet unused chloride ion, and **2**, being a highly reactive species, would therefore be trapped by chloride ion leading to a higher yield of 2-chloroethanesulfonate (**4***a*). The problem of mixing effects has been taken up by Rys (18), who has concluded that "every chemical reaction that can occur in a time shorter than 0.01–1.00 s may be hindered by mixing processes"; the present reaction could well be such a process. The rate constants of the first step in the hydrolysis of **1** at pH 12.0 and 13.0 can be estimated from eq. [1] and the constants in Scheme 1 to be, respectively, 5.16×10^4 and $5.16 \times 10^5\,s^{-1}$, which translate into lifetimes (τ) of **1** of approximately 10^{-5} s and 10^{-6} s, respectively, in these media; this would lead to a very rapid depletion of hydroxide ion at the point of mixing. Also the linearity of the pH–rate profile between pH 4 and 6 (Fig. 2) indicates that the first step is certainly rate determining to at least pH 6.0. Any alteration such that the second step became rate determining would be the start of a tendency for the k_ψ to plateau. There is no sign of this, and this suggests that even at pH 6.0, **2** is consumed faster than it is formed. If we make the most conservative possible assumption that the consumption of **2** is only twice as fast as its formation at pH 6.0, we can roughly estimate the lifetime of **2** from the observed k_ψ at this pH as ~10 s. At pH >11.0, the $k_{3B}[OH^-]$ term contributes to the trapping of **2**, and a comparison of its value at pH 12.0 with that of k_3 indicates that at pH 12.0 the trapping of **2** is more than eight times as fast as that at pH 6.0 (where only k_3 operates). This then gives us a *maximum* lifetime of ~1 s for **2** at pH >12.0. It is obvious that if Rys's conclusions are correct, then the hydrolysis of **1** at pH >11.0 must be expected to be sensitive to mixing effects. In effect, then, the consistent and increasing deviation of the experimental points in Fig. 3 as the pH is increased from 11.5 to 13.0 may be due primarily to a lower actual concentration of hydroxide at the reaction site than that measured by the pH meter in the bulk solution. This could, perhaps, be expressed by including a horizontal error bar extending to the left of each point in this region to indicate the uncertainty in pH of this part of reaction, but, unfortunately, we have no satisfactory way of assigning a magnitude to such an error bar.

Another aspect of the reaction at high pH arises in connection with our studies on C—O vs. S—O cleavage of sulfonic esters (15, 16). Because it was necessary in that work to be

Can. J. Chem. Downloaded from www.nrcresearchpress.com by 186.148.149.217 on 09/07/12
For personal use only.



SCHEME 2

able to make a convincing case for the formation of **2** from **1** at high pH, we felt it appropriate to carry out confirming experiments. One of these was done at pH 13.0 in a solution 5.9 M in NaCl; the product showed about equal amounts of **3** and **4***a*, in accord with the intermediacy of **2**. In another set of experiments the reaction at pH 13.0 was carried out in the presence of aniline; with 0.1, 0.2, 0.3 M aniline the ratios of **3** to **4***c* were, respectively, 86:14, 71:29, and 56:44. Though it seems likely that mixing effects vitiate any attempts at quantitative interpretation of these results, the qualitative picture is clear. The anilinosulfonate (**4***c*) is almost certainly formed from **2**, which must therefore be formed to the extent of 44%. Since hydroxide ion must trap some of the **2** as well, the amount of **2** produced can only be higher than that; the results are, in fact, fully consistent with 88% of the reaction proceeding by way of **2**, as expected from the values of k_{1B} and k_{2B} given in Scheme 1.

The rate suppression by chloride ion and the detailed mechanisms of formation of the sultone (2)

We have noted above that addition of sodium chloride slows the rate of the reaction (see Fig. 2). As we have noted elsewhere (3), one explanation for the effect of added NaCl is that chloride ion may attack β-sultone at the sulfur atom to give back **1**, i.e., the first step may be reversible in the presence of a sufficiently large amount of Cl^-. Careful quantitative examination of this mechanism leads us to revise our earlier view and to conclude from the following argument that such reversal is probably not of primary importance.

If the proposed mechanism is modified so that the first step is reversed by attack of chloride ion on the sultone (**2**) and this step is assigned the rate constant k_{-1}, we obtain Scheme 2. As is shown in the Appendix, we may readily (a) derive expressions for k_ψ and [**4***a*]/[**3**] as functions of the rate constants and ratios (eqs. [A14] and [A16]), and then (b) test the hypothesis of chloride ion reversal by using either of two procedures to assign reasonable values to the ratios k_{-1}/k_3 and $(k_4/k_3)_{Cl}$ and to insert these along with the rate constants listed in Scheme 1 into eqs. [A14] and [A16]. One of these procedures involved calculating values for the rate constant ratios by taking a value of $(k_4/k_3)_{Cl}$ that would yield a Swain–Scott *s* parameter (19) of 0.8, and estimating k_{-1}/k_3 by a relationship (eq. [A17]) derived from measurements of k_ψ at $[Cl^-] = 0$ and 0.1 M. The parameters so obtained gave (a) the solid line shown in Fig. 10, which is, as expected, in good agreement with experiment, and (b) the curves for [**4***a*]/[**3**] shown as dashed lines in Figs. 5 and 6, which clearly do not concur satisfactorily with measurement. In the second procedure, we used the nonlinear least-squares program to generate parameters (see eq. [A18]) used to calculate the ratios k_{-1}/k_3 and $(k_4/k_3)_{Cl}$. The agreement with experiment with these values was good for the [**4***a*]/[**3**] ratios at pH 4.0 and 6.0 but, as may be seen from the dashed line in Fig. 10, poor in calculating the variation of k_ψ with chloride concentration. In fact, all attempts to find a set of parameters that could provide adequate agreement with experiment on the basis of Scheme 2 were unsuccessful in our hands. A set of compromise values of k_{-1}/k_3 and $(k_4/k_3)_{Cl}$ failed to give satisfactory agreement with the results in either Fig. 10 or Figs. 5 or 6; any adjustments which improved the fit to the points in Fig. 10 worsened the agreement in Figs. 5 and 6, and vice versa. We conclude from this that chloride ion reversal, though it may occur to some measure, cannot, of itself, satisfactorily account for the lowering of k_ψ with increased $[Cl^-]$, and another explanation must be sought.

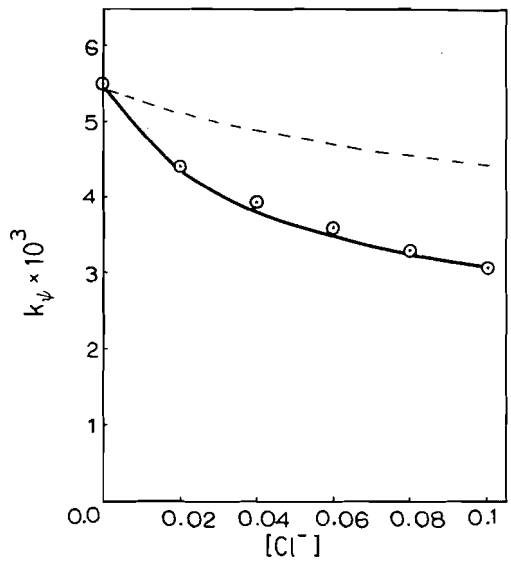


FIG. 10. Dependence on change in sodium chloride concentration of the observed pseudo-first-order rate constant for the hydrolysis of **1** (pH 5.0, 25.0°C, μ = 0.3 with $NaClO_4$). The lines are obtained from the assumption of the reaction of Cl^- with **2** to give back **1** as in Scheme 2; the solid line is calculated from eq. [A14] and the parameters that gave the dotted lines in Figs. 5 and 6 (k_{-1}/k_3 = 13.6 and $(k_4/k_3)_{Cl}$ = 4.96 M^{-1}), and the dashed line from eq. [A14] using k_{-1}/k_3 = 3.01 $(k_4/k_3)_{Cl}$ = 3.28 M^{-1} (values which gave satisfactory agreement with the points in Figs. 5 and 6) (see text and the Appendix).

A further point relevant to the chloride reversal mechanism

Can. J. Chem. Downloaded from www.nrcresearchpress.com by 186.148.149.217 on 09/07/12
For personal use only.

Can. J. Chem. Downloaded from www.nrcresearchpress.com by 186.148.149.217 on 09/07/12
For personal use only.

is the observation that a significant rate reduction was seen when the reaction was carried out in the presence of either sodium *p*-toluenesulfonate or sodium *p*-sulfanilate; specifically, for 0.2 M solutions (at pH 6.0 and 25.0°C) the rate constant with *p*-$CH_3C_6H_4SO_3^-Na^+$ was $8.56 \times 10^{-3}\ s^{-1}$ and that with *p*-$NH_2C_6H_4SO_3^-Na^+$, $5.72 \times 10^{-3}\ s^{-1}$. These values may be compared with k_{obs} values (at pH 6.0) of $1.70 \times 10^{-2}\ s^{-1}$ with 0.3 M NaCl, and $5.50 \times 10^{-2}\ s^{-1}$ with 0.3 M $NaClO_4$. The rate reductions in the presence of the arenesulfonate salts may or may not have any direct connection with that observed with NaCl, but they do show that suppression of the rate is not unique to chloride and that there must be another mechanism for it in addition to that in Scheme 2.

This conclusion, of course, opens the question of the origin of these rate suppressions and, in the search for a possible answer, of taking a closer look at the rate-determining step, the conversion of **1** to **2**. The simplest possible unimolecular mechanism would presumably go as follows.

$$\underset{\mathbf{1}}{HOCH_2CH_2SO_2Cl} \longrightarrow \underset{\mathbf{8}}{H{-}\overset{+}{O}{-}SO_2} + Cl^-$$

$$\underset{\mathbf{8}}{H{-}\overset{+}{O}{-}SO_2} \xrightarrow{H_2O} \underset{\mathbf{2}}{O{-}SO_2} + H_3O^+ + Cl^-$$

We note that the acidity of the hydrogen that is ultimately removed changes from being close to that of water in **1** to that of a very much stronger acid in **8**. According to Jencks (20), this circumstance should lead to general base catalysis by water and accordingly it seems appropriate to suggest the following modified mechanism in which the proton is transferred to water in the (single) transition state starting from the substrate–water H-bonded complex (**9**).

$$\underset{\mathbf{9}}{H_2O...HOCH_2CH_2SO_2Cl} \xrightarrow{k_1} H_3O^+ + \underset{\mathbf{2}}{O{-}SO_2} + Cl_3^-$$

This picture accords with the proposal of general base catalysis by water in the hydrolysis of sulfonyl chlorides, which may be put forward to explain the solvent isotope effect on changing from H_2O to D_2O, observed by Robertson and Laughton (21).

For the hydroxide-promoted conversion of **1** to **2**, the only reasonable mechanism in the light of Jencks' rule (20) is the specific base-catalyzed process proceeding by way of the conjugate base of **1**, i.e., $^-OCH_2CH_2SO_2Cl$ (**10**). The pK_a of **1** may be estimated by the method of Takahashi *et al.* (22) to be about 13.2; this makes **1** a distinctly stronger acid than water (pK_a 15.7) and hence the transfer of the hydroxyl proton in **1** to hydroxide prior to cyclization a favoured process.

In this context it is at least imaginable that the effect of chloride ion on the rate of cyclization of **1** may arise simply by lowering the concentration of the reacting form of **1** by competing formation of **11**, which because of the low activity of Cl^- as a general base in aqueous solution does not readily form **2**. In other words, chloride ion may be reducing the rate of **1** → **2** by sequestering part of the starting material in a less reactive form (**11**), thereby lowering the concentration(s) of the reactive species (**9**) and (or) (**10**).

The hydrogen-bonding acidity of **1**, by analogy with other

$$Cl^- \cdots (H{-}O{-}CH_2CH_2SO_2Cl)_n$$

11

alcohols bearing electron-withdrawing groups (23), is presumably greater than that of water and, since H-bonding of water to a dissolved anion is an important feature of ion hydration (24), one may expect **1** to be capable of replacing water in the solvation shell of the chloride ion. One may thus predict that **11** ($n = 1$) will be a component of the reaction medium, though it must be questioned whether its concentration will be sufficiently high to give the observed rate suppression; the hydrogen bonding in **11** ($n = 1$) has to compete with hydrogen bonding with water and, except for the bifluoride ion (FHF^-) in which the H-bond is uncommonly strong, such effects would not appear to be important in aqueous solution (25). Species with more than one molecule of **1**, i.e., **11** with $n = 2$ or more, are in principle possible, but would not be expected to be of consequence unless some compensating factor, such as hydrophobic binding, were present; such binding in **11** ($n = 2$) or between **1** and tosylate, for example, is imaginable, but since present knowledge of the interactions of solutes and solvent in aqueous media is very limited, we offer these suggestions with great diffidence.

*The mechanisms of the minor reactions, the direct conversions of **1** to **3***

Comparison of k_1 with k_2 shows that in the region in which the reaction of **1** is unimolecular (pH < 3.0), about 33% of the reaction occurs by a direct process not involving **2**. Similarly k_{1B} and k_{2B} indicate that in the higher pH region (>4.0) about 12% of the reaction of **1** proceeds via a hydroxide-promoted direct conversion of **1** to **3** (the "k_{2B} reaction"). The mechanisms of these reactions are discussed in this section.

The rate constant for the uncatalyzed reaction ($k_2 = 7.46 \times 10^{-4}\ s^{-1}$) is in the same order of magnitude as those reported for the simple hydrolyses of methanesulfonyl chloride (1.92×10^{-4} (26), $1.94 \times 10^{-4}\ s^{-1}$ (27)), ethanesulfonyl chloride ($2.99 \times 10^{-4}\ s^{-1}$ (26), 2-chloroethanesulfonyl chloride ($2.05 \times 10^{-4}\ s^{-1}$ (26)) at 25°C, and the mechanism is very probably the same. In much the same way as has already been mentioned in connection with the unimolecular cyclization, Jencks' rule and the solvent isotope effect are in accord with a reaction in which one molecule of water acts as a general base assisting the nucleophilic attack of a second water molecule, perhaps by way of a transition state such as **12**, or perhaps by the very closely related species in which the S—Cl bond is not broken and the partial negative charge rests primarily on the sulfur atom. The question of whether such displacements are one- or two-step processes has been much discussed but not settled; a helpful summary has been presented by Kice (28).

$$H_2O^{\delta+} \cdots H \cdots \underset{\displaystyle H}{\underset{|}{O}} \cdots \underset{\displaystyle CH_2CH_2OH}{\underset{|}{SO_2}} \cdots Cl^{\delta-}$$

12

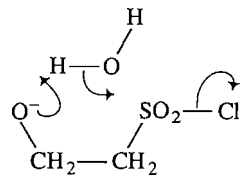
The normal mode of reaction of hydroxide with alkanesulfonyl chlorides bearing a hydrogen α to the sulfonyl group is the elimination–addition process via the sulfene (29–32). It was therefore reasonable to expect that the k_{2B} reaction would probably also go in this way, and hence that reaction in D_2O in strongly alkaline medium would show roughly 10% of α-monodeuterated product. In the event, the product obtained in D_2O with a pH-meter reading of 12.8 showed the product to be

Can. J. Chem. Downloaded from www.nrcresearchpress.com by 186.148.149.217 on 09/07/12
For personal use only.

almost entirely $HOCH_2CH_2SO_3^-$, with a little (~2%) $ClCH_2CH_2SO_3^-$, and no sign whatever (i.e., <1%) of any $HOCH_2CHDSO_3^-$, thereby showing that the k_{2B} process is not primarily a sulfene reaction. This observation is consistent with the k_{2B}/k_2 ratio of $5 \times 10^9\,M^{-1}$ found in the present study, which is distinctly greater than the range of 10^6–10^8 for the ratio of k_{OH} (hydroxide promoted sulfene formation) to k_H (uncatalyzed hydrolysis) that we see with alkanesulfonyl chlorides.[4]

One simple way from **1** to **3** without deuterium incorporation is by direct attack of the hydroxide on the sulfonyl sulfur atom, but a proposal of any such process would have to include an explanation for why this reaction, which does not manifest itself in the reaction of other alkanesulfonyl chlorides bearing α-hydrogens, should suddenly appear with **1**. The direct hydroxide attack mechanism is indeed found with such substrates as arenesulfonyl and 1-alkenesulfonyl chlorides, and with these species the ratio k_{OH}/k_H ranges from 2×10^3 to $2 \times 10^5\,M^{-1}$ (33, 34); any mechanism with a direct attack on the sulfur atom of **1** would have to account for an "extra" factor of at least 10^4.

One conceivable possibility is a cyclic reaction of **10** and one of the water molecules of the solvation shell as in **13**. This



13

reaction would be an intramolecular general base-catalyzed hydrolysis, and though attractive because of its simplicity, it does suffer from the drawback that reported examples of this general class of reaction appear to show relatively little advantage over their intermolecular analogues. This point has been fully discussed by Kirby (35) whose tabulations show no examples of effective concentration (C_{eff}) greater than about 80 M, whereas the k_{2B} reaction would, for the reasons already presented, require a C_{eff} of $\geq 10^4$ M. The reason offered by Page (36) for the low efficiency of intramolecular general base catalysis (as contrasted with the often remarkable facility of intramolecular *nucleophilic* reactions) is that the general base reactions go through a relatively loose transition state, which provides only a small entropic advantage over the intermolecular analogue. To be sure, the transition state proposed for the present case may well be tighter than those referred to by Page and Kirby. Their examples all involve larger rings in the transition state, and it is at least conceivable that intramolecular general base-catalyzed reactions, provided they have sufficiently tight transition states, can also show higher effective concentrations than those reported. The point would appear to be of sufficient general significance to justify further study, though the hydrolysis of **1**, with the reaction of interest in this context constituting only about one tenth of the total reaction, is not the ideal system for such a project.

Experimental

Reagent grade chemicals and solvents were used without further purification unless otherwise noted. Melting points were determined on a Kofler Hot Stage and are uncorrected. Infrared spectra were obtained with a Beckman 4250 or Bruker IFS-32 FTIR spectrophotometer. The ^{1}Hmr spectra were obtained using Varian T-60, EM-360, XL-100, or XL-200 spectrometers, with all reported chemical shifts from the last two instruments. The ^{13}Cmr spectra were obtained on a Varian XL-200 or XL-300 instrument. Solvent evaporation on work-up was carried out using a Büchi rotary evaporator connected to a water aspirator.

The pH-stat apparatus and the procedure used for the kinetic determinations and all constant pH reactions have been described (4, 34); further details and a full tabulation of observed rate constants and product ratios are given elsewhere (17).

2-Mercaptoethanol (Eastman) was distilled under vacuum and the fraction boiling at 44°C (6 Torr; 1 Torr = 133.3 Pa) collected; ir ($CHCl_3$) ν_{max}: 3663 (m), 3442 (b), 2994 (s), 2932 (s), 2872 (s), 2572 (w), 1457 (w), 1412 (s), 1382 (s), 1335 (w), 1275 (m), 1217 (s, b), 1175 (m), 1052 (vs, b), 927 (m); ^{1}Hmr ($CDCl_3$) δ: 3.79 (t, 2H), 2.82–2.62 (m, 2H), 2.33 (s, 1H), 1.41 (t, 1H); ^{13}Cmr ($CDCl_3$) δ: 64.0, 27.8.

Preparation of 2-hydroxyethanesulfonyl chloride (1)

The following procedure is a distinct improvement over our earlier method (4). A mixture of concentrated H_2SO_4 (10 mL) and water (30 mL) in a 100-mL pear-shaped flask equipped with a stirring bar and mounted over a magnetic stirrer, was cooled to −10°C in an ice–salt bath and saturated (1 min) with a stream of Cl_2 gas (Linde). Vigorous stirring and Cl_2 bubbling was maintained while 2-mercaptoethanol (10 g, 0.13 mol) was added dropwise over 10 min; Cl_2 was then bubbled in for a further 10 min, at the end of which time a yellowish solution was obtained. The reaction mixture was then transferred to a separatory funnel using more cold aqueous sulfuric acid (3 × 5 mL) and extracted with cyclohexane (2 × 250 mL); the extracts were combined and treated with solid $NaHCO_3$ followed by anhydrous $MgSO_4$ and the solvent removed on a rotary evaporator to yield 2-chloroethanesulfonyl chloride (1.1 g, 6.7 mmol, 5% yield, >90% pure by ^{1}Hmr); ^{1}Hmr ($CDCl_3$) δ: 4.03 (s); ^{13}Cmr ($CDCl_3$) δ: 35.5, 65.6.

The aqueous extract was further extracted immediately with CH_2Cl_2 (5 × 250 mL) and, after treatment with $NaHCO_3$ and $MgSO_4$, the solvent was removed to yield **1** (15.005 g, 0.104 mol, 81% yield, >95% pure by ^{1}Hmr). A further 0.92 g of **1** (6.37 mmol, 5% yield, >95% pure by ^{1}Hmr) was recovered from the aqueous layer as follows. The mixture was neutralized with solid $NaHCO_3$ at ice-bath temperature under vigorous stirring and the viscous solution so obtained was transferred to a separatory funnel using cold brine and extracted with CH_2Cl_2 (3 × 250 mL); the extracts were dried and the solvent evaporated. 2-Hydroxyethanesulfonyl chloride (**1**) (86% yield overall) so obtained was then purified by flash distillation. A conventional distillation apparatus was assembled and a vacuum was applied (0.3 Torr) and maintained, and the flask containing **1** and a magnetic stirring bar was then quickly lowered into a preheated oil bath (110°C) mounted on a magnetic stirrer; **1** distilled smoothly (84°C at 0.3 Torr, 70% recovery on a 2.5 g scale) leaving a dark residue in the still-pot; ir ($CHCl_3$) ν_{max}: 3620 (m), 3410 (br, m), 1380 (s), 1175 (s), 1060 (m) cm^{-1}; ^{1}Hmr ($CDCl_3$) δ: 3.80–4.00 and 4.10–4.30 (A_2B_2 complex multiplet, exact pattern concentration dependent, 4H), 2.80 (s, 1H); ^{13}Cmr ($CDCl_3$) δ: 56.9, 67.6. Two precautionary notes for the above procedure: (a) the entire procedure from the start to the extractions should be finished within minimum time (~1 h) and (b) all rinsing and washing during transferring the reaction mixture from one pot to another should be done with either cold aqueous sulfuric acid (4.5 M) or with cold saturated brine.

2-Hydroxyethanesulfonyl-2,2-d_2 chloride was prepared by carrying out a small-scale version of this reaction using Cl_2 in D_2O with 2-mercaptoethanol-1,1-d_2, prepared by lithium aluminum deuteride reduction of mercaptoacetic acid. The sample of $HOCD_2CH_2SO_2Cl$ so obtained showed the following spectra: ir ($CHCl_3$) ν_{max}: 3600 (m), 3400 (w, b), 3020 (m), 2920 (w), 2340 (w), 2210 (w), 2100 (w), 1375 (vs), 1320 (w, b), 1250 (w), 1165 (s), 978 (s), 652 (m) cm^{-1}; ^{1}Hmr ($CDCl_3$) δ: 3.93 (s, 2H), 2.75 (s, 1H); ^{13}Cmr ($CDCl_3$) δ: 67.4.

[4]Unpublished experiments carried out in this laboratory by M. Aslam, S. Skonieczny, and J. Y. L. Lam; cf. also ref. 32.

Can. J. Chem. Downloaded from www.nrcresearchpress.com by 186.148.149.217 on 09/07/12
For personal use only.

*Rate of hydrolysis of **1***

A stock solution was first prepared by dissolving **1** (119.9 mg, 0.83 mmol) in dry acetonitrile (2 mL). The rate of hydrolysis of **1** was determined from a plot of the liberated acid (as determined by pH-stat titration with 0.05 M NaOH) against time. In a typical experiment, 25 mL of 0.1 M NaCl (ionic strength 0.3 M with $NaClO_4$) solution was stabilized at pH 5.0 (0.16 M $HClO_4$) and 25°C; 2 μL of the above stock solution in acetonitrile was then added and the timer started. The reaction was followed by recording (at regular intervals) the amount of titrant (V_t) added with time. Log ($V_\infty - V_t$) was plotted against time lapsed (t), and the rate constant for the hydrolysis calculated from the half-life using the equation, $k_\psi = 0.693/t_{1/2}$.

*Products of hydrolysis of **1** at 25°C*

The hydrolyses of **1** were performed in 50 mL of 1 M aqueous NaCl solution at 25°C and at pH settings varying from 1.0 to 13.0 (with 0.16 M or concentrated $HClO_4$ used to adjust the pH initially) using the pH-stat apparatus. Typically, **1** (114 mg, 0.79 mmol), dissolved in 1 mL of dry CH_3CN, was added dropwise with stirring to the NaCl solution kept at 25°C and a particular pH. Aqueous sodium hydroxide (2 M) was used as titrant to maintain the pH while **1** was being added. The reaction time varied from 132 h (at pH 1.0) to 10 min (at pH 13.0). After the reaction, the pH of the mixture was adjusted to 7.0, and the water evaporated on a rotary evaporator. Repeated azeotroping with benzene gave a white solid, the whole of which was dissolved in D_2O (~10 mL); ^{1}Hmr δ: 3.25 (t, 2H), 3.47 (t, 2H), 3.965 (t, 2H), and 4.03 (t, 2H). Comparison with ^{1}Hmr spectra of authentic $HOCH_2CH_2SO_3^-Na^+$ (**3**) (Aldrich) and $ClCH_2CH_2SO_3^-Na^+$ (**4***a*) (Aldrich) permitted the following assignments: **3**, 3.25, 4.03 ppm and **4***a*, 3.47, 3.97 ppm. The relative yield of the two products in individual runs was estimated from integrations of the triplets at 3.25 (**3**) and 3.47 (**4***a*) ppm.

The same procedure (except for the changes in NaCl concentrations) was used for the experiments with NaCl at pH 3.5, 4.0, 6.0, and 11.0, respectively. The sodium thiocyanate experiments at pH 3.5 and 6.0 were carried out in the same way except that the product ratios were obtained by comparison of the peak due to **4***b* around 3.6 (4H) with that for **3** at 3.3 ppm (2H). The experiments with aniline were also done similarly except for the following points. (a) After acidification to pH 7 the solution was extracted with CH_2Cl_2 (3 × 50 mL) and the CH_2Cl_2 evaporated; the organic soluble material appeared to be entirely aniline with no sign of any $HOCH_2CH_2SO_2NHPh$. (b) The product ratios were determined by integration of the triplets at 3.9 and 3.6 ppm (due to **3** and **4***c*, respectively).

*Preparation of authentic $NCSCH_2CH_2SO_3^-Na^+$ (**4**b)*

Sodium 2-bromoethanesulfonate was prepared by refluxing a mixture of 1,2-dibromoethane (30 g, 0.16 mol) with a solution of Na_2SO_3 (15.1 g, 0.12 mol) in water (75 mL) for 5 h, cooling, removing the excess dibromoethane by washing with CH_2Cl_2, and evaporating the water. The crude product was triturated with absolute ethanol, the undissolved salts removed by filtration, and the ethanol evaporated to give a white residue (4.1 g), the ^{1}Hmr spectrum of which showed, for the principal material (~70%), an A_2B_2 pattern consisting of two multiplets with the largest central peaks at 3.63 and 3.43 ppm. This material (1.98 g, 9.39 mmol), NaSCN (0.76 g, 9.39 mmol), 18-crown-6 (1.24 g, 4.70 mmol), and 20 mL of dry acetonitrile were combined in a 50-mL round bottom flask and the mixture refluxed for 17 h. The acetonitrile was evaporated on a rotary evaporator and the solid obtained dissolved in 15 mL water and washed with CH_2Cl_2 (5 × 50 mL) and then with Et_2O (10 × 50 mL). The pH of the aqueous layer was then adjusted to 7.0 with 0.1 M NaOH. Evaporation of water and azeotroping (with benzene) was followed by recrystallization (from absolute ethanol) to give **5** as a white solid (1.24 g, 70%); mp 204–207°C; ir (KBr) ν_{max}: 2998 (w), 2160.5 (m, sharp), 1615 (w), 1429 (w), 1416 (w), 1385 (w), 1316 (w), 1244 (m), 1200 (vs, br), 1181 (s), 1138 (w), 1051 (s), 743 (w) cm^{-1}; ^{1}Hmr (D_2O) δ: 3.39 (s); ^{13}Cmr (D_2O) δ: 53.05, 30.83. *Anal.* calcd. for $C_3H_4O_3S_2NNa$: C 19.05, H 2.13, N 7.40, S 33.89; found: C 18.89, H 2.20, N 7.13, S 33.56.

*Simultaneous determination of the rate constant and the product ratio in the hydrolysis of **1** in the presence of NaSCN*

Aqueous NaSCN (1.00 L, 1.0 M, ionic strength 0.5 M with $NaClO_4$) in a 2-L thermally protected beaker was adjusted to 25°C and pH 3.0 (with 2.0 M $HClO_4$) and attached to the pH-stat apparatus. A stock solution of **1** in dry acetonitrile (1 mL), such as to give an initial concentration of **1** of 3.44×10^{-4} M, was added to the stirred mixture and the addition of 0.05 M NaOH with time recorded as before. After 1085 min the pH of the mixture was adjusted to 7.0 and the water evaporated. As already described, a plot of log ($V_\infty - V_t$) vs. time gave the rate constant (1.80×10^{-4} s^{-1}), and the ^{1}Hmr spectrum the ratio **4***b*:**3** (48:52).

*Products of hydrolysis of 1,3-propane sultone (**5**)*

In a typical experiment **5** (133 mg, 1.09 mmol) was dissolved in dry acetonitrile and added to 50 mL of 1.4 M NaCl solution at pH 4.0 and 25°C in the pH-stat apparatus as described above. After 24 h of reaction (with stirring and addition of 2.0 M NaOH from the autotitrator, as required to maintain constant pH), the pH was adjusted to 7.0 and the mixture worked up as above. The relative amounts of **6** and **7** were obtained from the integrals of the multiplets at 2.14–2.26 and 2.33–2.47 ppm (due to **6** and **7**, respectively) in the ^{1}Hmr spectrum (D_2O).

*Sodium 3-hydroxypropanesulfonate (**6**)*

Freshly distilled 1,3-propane sultone (**5**, γ-sultone, Aldrich, 3.01 g, 24.6 mmol) was added dropwise to an equivalent amount of sodium hydroxide (985 mg, 24.6 mmol) in 20 mL H_2O at room temperature, and the mixture stirred at room temperature for 23 h. The pH of the mixture was then adjusted to 7.0 and the water removed by evaporation on a rotary evaporator. Repeated azeotroping with benzene followed by pumping at 100°C and 9 Torr for 5 h gave **6** as a free-flowing white powder in quantitative yield; ^{1}Hmr (acetic acid-d_4) δ: 2.04 (m, 2H), 3.04 (m, 2H), and 3.76 (t, 2H); ^{13}Cmr (acetic acid-d_4) δ: 27.95, 49.21, 61.47.

*Sodium 2-anilinoethanesulfonate (**4**c)*

Sodium 2-bromoethanesulfonate (5 g, 23.7 mmol, prepared as described above) was dissolved in water (50 mL), mixed with excess freshly distilled aniline (50 mL), and the mixture refluxed for 15 h. It was then cooled and the excess aniline removed by repeated extraction with methylene chloride (3 × 200 mL). The pH of the clear aqueous layer was then adjusted to ~7.0 using dilute aqueous sodium hydroxide. The solution was further extracted with two fresh portions of methylene chloride. Evaporation of water gave a free-flowing white powder, which was recrystallized from absolute alcohol to yield **4***c* (2.03 g, 35%); ir (KBr) ν_{max}: 3030 (w), 2975 (w), 1603 (s), 1512 (s), 1478 (w), 1401 (s), 1318 (m), 1200 (vs), 1057 (s), 882 (w), 750 (s) cm^{-1}; ^{1}Hmr (D_2O) δ: 7.38–7.31 and 6.99–6.91 (m, 5H), 3.57 (t, 2H), and 3.18 (t, 2H).

*Hydrolysis of **1** in D_2O–OD^-*

To a solution prepared by reacting sodium metal (92 mg) with D_2O (2 mL) and adding further D_2O (15 mL), 2-hydroxyethanesulfonyl chloride (**1**) (100 mg) in CH_3CN was added during 1 min. The reaction mixture was immediately brought to pH 7.0 with concentrated DCl. Removal of water was followed by examination of the ^{1}Hmr spectrum (D_2O), which consisted of two prominent triplets at 3.13 and 3.93 ppm due to $HOCH_2CH_2SO_3^-$, two very small triplets at 3.4 and 3.9 ppm due to **4***a* (~2%), but with no sign whatever of any signals ascribable to $HOCH_2CHDSO_3^-$.

Acknowledgement

We thank the Natural Sciences and Engineering Research Council of Canada for financial support of this work.

1. J. F. KING and R. RATHORE. Phosphorus Sulfur, **33**, 165 (1987).
2. J. F. KING. Acc. Chem. Res. **8**, 10 (1975).
3. J. F. KING, S. SKONIECZNY, K. C. KHEMANI, and J. D. LOCK. *In* Nucleophilicity. *Edited by* J. M. Harris and S. P. McManus. Adv. Chem. Ser. **215**, Chap. 27, pp. 385–398 (1987).

4. J. F. KING and J. H. HILLHOUSE. Can. J. Chem. **61**, 1583 (1983).
5. J. F. KING, M. R. WEBSTER, N. CHIBA, J. K. ALLEN, K. J. M. PARKER, and R. RATHORE. Phosphorus Sulfur, **31**, 161 (1987).
6. D. C. DITTMER and T. C. SEDERGRAN. *In* Small ring heterocycles. *Edited by* A. Hassner. Vol. 42 in the series Chemistry of Heterocyclic Compounds. Part 3. *Edited by* A. Weissberger and E. C. Taylor. Wiley–Interscience, New York. 1985. pp. 610–619.
7. F. G. BORDWELL, B. M. PITT, and M. KNELL. J. Am. Chem. Soc. **73**, 5004 (1951).
8. P. G. GASSMAN, J. M. HORNBACK, and J. M. PASCONE. Tetrahedron Lett. 1425 (1971).
9. J. S. BRIMACOMBE, A. B. FOSTER, and M. STACEY. Chem. and Ind. (London), 262 (1959).
10. J. S. BRIMACOMBE, A. B. FOSTER, E. B. HANCOCK, W. G. OVEREND, and M. STACEY. J. Chem. Soc. 201 (1960).
11. E. T. KAISER, M. PANAR, and F. H. WESTHEIMER. J. Am. Chem. Soc. **85**, 602 (1962).
12. A. MORI, M. NAGAYAMA, and H. MANDAI. Bull. Chem. Soc. Jpn. **44**, 1669 (1971).
13. E. T. KAISER. *In* Organic chemistry of sulfur. *Edited by* S. Oae. Plenum Press, New York. 1977. Chap. 12, pp. 649–679.
14. A. LALEH, R. RANSON, and J. G. TILLETT. J. Chem. Soc. Perkin Trans. 2, 610 (1980).
15. J. F. KING, K. C. KHEMANI, S. SKONIECZNY, and N. C. PAYNE. J. Chem. Soc. Chem. Commun. 415 (1988).
16. J. F. KING, K. C. KHEMANI, S. SKONIECZNY, and N. C. PAYNE. *In* Reviews on heteroatom chemistry. Vol. 1. *Edited by* S. Oae. MYU, Tokyo. 1988. pp. 80–94.
17. K. C. KHEMANI. Ph.D. Thesis, University of Western Ontario, London, Ont. 1987.
18. P. RYS. Angew. Chem. Int. Ed. Engl. **16**, 807 (1977).
19. C. G. SWAIN and C. B. SCOTT. J. Am. Chem. Soc. **75**, 141 (1953).
20. W. P. JENCKS. J. Am. Chem. Soc. **94**, 4731 (1972).
21. R. E. ROBERTSON and P. M. LAUGHTON. Can. J. Chem. **35**, 1319 (1957).
22. S. TAKAHASHI, L. A. COHEN, H. K. MILLER, and E. G. PEAKE. J. Org. Chem. **36**, 1205 (1971).
23. M. H. ABRAHAM, P. P. DUCE, P. L. GRELLIER, D. V. PRIOR, J. J. MORRIS, and P. J. TAYLOR. Tetrahedron Lett. 1587 (1988).
24. J. G. GORDON. The organic chemistry of electrolyte solutions. John Wiley and Sons, New York. 1975. Chap. 2.
25. W. P. JENCKS. Catalysis in chemistry and enzymology. McGraw–Hill, New York. 1969. pp. 324ff.
26. I. HEDLUND. Ark. Kemi Mineral. Geol. **14A**, 13 (1940).
27. R. E. ROBERTSON. Prog. Phys. Org. Chem. **4**, 213 (1967).
28. J. L. KICE. Adv. Phys. Org. Chem. **17**, 65 (1980).
29. J. F. KING and T. DURST. J. Am. Chem. Soc. **87**, 5684 (1965).
30. K. GÜNTHER, M. HAMPEL, W. HÖBOLD, H. HÜBNER, G. JUST, G. MÜLLER-HAGEN, W. PRITZKOW, W. ROLLE, M. WAHREN, and H. WINTER. J. Prakt. Chem. **311**, 596 (1969).
31. L. O. FARNG and J. L. KICE. J. Am. Chem. Soc. **103**, 1137 (1981).
32. H. BECK and K. DOERFFEL. J. Prakt. Chem. **325**, 36 (1983).
33. O. ROGNE. J. Chem. Soc. (B), 1294 (1968).
34. J. F. KING, J. H. HILLHOUSE, and S. SKONIECZNY. Can. J. Chem. **62**, 1977 (1984).
35. A. J. KIRBY. Adv. Phys. Org. Chem. **17**, 183 (1980).
36. M. I. PAGE. Angew. Chem. Int. Ed. Engl. **16**, 449 (1977).
37. S. OSTERMAN-GOLKAR and C. A. WACHTMEISTER. Chem.-Biol. Interact. **14**, 195 (1976).

Appendix

Scheme 1 equations and parameters

From Scheme 1 and the steady state approximation we write:

[A1] $$d[\mathbf{4}]/dt = k_4[Nu^-][\mathbf{2}]$$

[A2] $$d[\mathbf{3}]/dt = (k_2 + k_{2B}[OH^-])[\mathbf{1}] + (k_3 + k_{3B}[OH^-])[\mathbf{2}]$$

[A3] $$[\mathbf{2}] = \frac{(k_1 + k_{1B}[OH^-])[\mathbf{1}]}{k_3 + k_{3B}[OH^-] + k_4[Nu^-]}$$

For convenience, we set $x = k_1 + k_{1B}[OH^-]$, $y = k_2 + k_{2B}[OH^-]$, and $z = k_3 + k_{3B}[OH^-]$; substituting [A3] into [A1] and [A2] and dividing, we obtain [A4]:

[A4] $$\frac{d[\mathbf{4}]}{d[\mathbf{3}]} = \frac{xk_4[Nu^-]}{y(z + k_4[Nu^-]) + xz}$$

In any individual experimental run every component of the right-hand side of eq. [A4] is constant and so $d[\mathbf{4}]/d[\mathbf{3}] = [\mathbf{4}]/[\mathbf{3}]$; this, plus division of the top and bottom of the right side of eq. [A4] by $yk_4[Nu^-]$, yields eq. [A5]:

[A5] $$\frac{[\mathbf{4}]}{[\mathbf{3}]} = \frac{x/y}{1 + \dfrac{z/k_4(1 + x/y)}{[Nu^-]}} = \frac{a_1}{1 + \dfrac{a_2}{[Nu^-]}}$$

where

[A6] $$a_1 = x/y$$

and

[A7] $$a_2 = (1 + x/y)z/k_4 = \frac{(1 + x/y)(1 + k_{3B}[OH^-]/k_3)}{k_4/k_3}$$

(Note that eqs. [A5]–[A7] are eqs. [5]–[7] of the main text.) From a nonlinear least-squares fit to eq. [A5] of the data for the product ratios vs. thiocyanate concentration at pH 3.5 and 6.0 (Fig. 9), we obtained $a_1 = 3.56$, and $a_2 = 0.1192$ at pH 3.0, and $a_1 = 13.51$, and $a_2 = 0.3394$ at pH 6.0, which, with eq. [A6] and the definitions of x and y, gives

[A8] $$k_1 + (3.126 \times 10^{-11})k_{1B} = 3.56k_2 + (1.126 \times 10^{-10})k_{2B}$$

and

[A9] $$k_1 + 10^{-8}k_{1B} = 13.51k_2 + (13.51 \times 10^{-10})k_{2B}$$

Equations [3], [4], [A8], and [A9] form a set of linear simultaneous equations; their solution yields the values of k_1, k_2, k_{1B}, and k_{2B} shown in Scheme 1.

From Fig. 3 it is evident that $k_3 = k_{3B}[OH^-]$ at the inflection point (pH ~ 11), and hence $k_{3B}[OH^-]$ may be neglected relative to k_3 at pH 6.0. We then obtain

[A10] $$a_2 = (1 + x/y)/(k_4/k_3)$$

which from $a_2 = 0.3394$ gave $(k_4/k_3)_{SCN} = 42.8\,M^{-1}$.

The data for the variation in [**4***a*]/[**3**] with $[Cl^-]$ at pH 6.0 (Fig. 6), on least-squares analysis similar to that above except that a_1 was given the value obtained from the thiocyanate data (13.51) and only a_2 was allowed to optimize, gave $a_2 = 4.99$; this, when inserted into eq. [A7] (again with the assumption that $k_3 \gg k_{3B}[OH^-]$), yielded $(k_4/k_3)_{Cl} = 2.91\,M^{-1}$.

Finally, the value 13.74 for x/y at pH 11.0 was calculated from the values of k_1, k_2, k_{1B}, and k_{2B} (given in Scheme 1). With this as the constant value for the a_1 parameter in the least-squares treatment of the data for the ratio [**4***a*]/[**3**] vs. $[Cl^-]$ at pH 11.0, we obtained $a_2 = 9.27$, which when inserted into eq. [A7] along with $(k_4/k_3)_{Cl} = 2.91$ yielded $k_{3B}/k_3 = 8.29 \times 10^2\,M^{-1}$.

Can. J. Chem. Downloaded from www.nrcresearchpress.com by 186.148.149.217 on 09/07/12
For personal use only.

Scheme 2 equations and parameters

In the same manner as from Scheme 1 we may obtain [A11] and [A12] from Scheme 2:

$$[A11] \quad \frac{d[\mathbf{3}]}{dt} = \frac{xz_4[\mathbf{1}]}{k_{-1}[Cl^-] + k_4[Cl^-] + z} + y[\mathbf{1}]$$

and

$$[A12] \quad \frac{d[\mathbf{4}a]}{dt} = \frac{xk_4[Cl^-][\mathbf{1}]}{k_{-1}[Cl^-] + k_4[Cl^-] + z}$$

From $k_\psi[\mathbf{1}] = d[\mathbf{3}]/dt + d[\mathbf{4}a]/dt$ we may write

$$[A13] \quad k_\psi = \frac{x(k_4[Cl^-] + z)}{k_{-1}[Cl^-] + k_4[Cl^-] + z} + y$$

Note that when k_{-1} or $[Cl^-] = 0$, $k_\psi = x + y$ (cf. eq. [2]). At pH 5.0 (the pH at which the rates in Fig. 1 were determined) $k_3 \gg k_{3B}[OH^-]$; substituting for z, eq. [A13] becomes:

$$[A14] \quad k_\psi = \frac{x(1 + k_4[Cl^-]/k_3)}{1 + k_4[Cl^-]/k_3 + k_{-1}[Cl^-]/k_3} + y$$

Defining r as the ratio of k_ψ when $[Cl^-] > 0$ to k_ψ when $[Cl^-] = 0$, we obtain

$$r = \frac{px + y}{x + y}$$

where

$$p = \frac{1 + k_4[Cl^-]/k_3}{1 + k_4[Cl^-]/k_3 + k_{-1}[Cl^-]/k_3}$$

Rearranging,

$$[A15] \quad p = [r(x + y) - y]/x$$

Also, from eqs. [A12] and [A13] and the line of reasoning already discussed for Scheme 1, it may be readily shown that

$$[A16] \quad \frac{[\mathbf{4}a]}{[\mathbf{3}]} = \frac{xk_4[Cl^-]}{y(k_{-1}[Cl^-] + k_4[Cl^-] + z) + xz}$$

Taking the values of k_ψ at $[Cl^-] = 0.1$ M and 0 (respectively, 3.08×10^{-3} and 5.50×10^{-3} s^{-1}), $r = 0.56$; substituting this and the values of x and y into eq. [A15], we find

$$[A17] \quad k_{-1}/k_3 = 9.142 + 0.9142(k_4/k_3)_{Cl}$$

At this stage we set a chemically reasonable limit to the range of $(k_4/k_3)_{Cl}$ (and hence k_{-1}/k_3) values, and to this end make use of the Swain–Scott s parameter (19). Values of s ranging from 0.69 to 0.82 have been reported for reactions of sulfonic esters (37). Noting that the ratio $(k_4/k_3)_{SCN} = 42.8$ (above) with $n_{SCN} = 4.77$ (19) corresponds to $s = 0.71$, we regard the range of s values from 0.5 to 1.0 as covering the likely possibilities; a systematic examination of the parameters obtained from eq. [A17] over this range (at intervals of 0.1 in s) provided no values that, when inserted into eq. [A16], led to satisfactory agreement with experiment. The set of ratios corresponding to $s = 0.8$, namely, $(k_4/k_3)_{Cl} = 4.96\ M^{-1}$ and $k_{-1}/k_3 = 13.6$, gave what was probably the best agreement; the curves generated from these parameters are shown as the dashed lines in Figs. 5 and 6.

Another approach is to rewrite [A16] as

$$[A18] \quad \frac{[\mathbf{4}a]}{[\mathbf{3}]} = \frac{xk_4/yw}{1 + \dfrac{(1 + x/y)z/w}{[Cl^-]}} = \frac{b_1}{1 + \dfrac{b_2}{[Cl^-]}}$$

where $w = k_4 + k_{-1}$. From the data for pH 6.0 shown in Fig. 6 and the nonlinear least-squares program, we obtained $b_1 = 6.999$ and $b_2 = 2.295$. At pH 6.0, $z = k_3$ (see above), and so

$$[A19] \quad b_1/b_2 = \frac{(x/y)(k_4/k_3)}{1 + x/y}$$

With $x/y = 13.51$ (see above), [A19] gives $(k_4/k_3)_{Cl} = 3.28\ M^{-1}$. From $b_1 = xk_4/yw$ (by definition), $k_{-1}/k_3 = 3.01$. These parameters, when inserted into eq. [A14] with k_1, k_2, k_{1B}, and k_{2B} from Scheme 1, gave the dashed line in Fig. 10.

Can. J. Chem. Downloaded from www.nrcresearchpress.com by 186.148.149.217 on 09/07/12
For personal use only.

Comparison of an intramolecular Michael-type addition with its intermolecular counterpart: an *ab initio* theoretical study

C. I. BAYLY AND F. GREIN

Departmemt of Chemistry, University of New Brunswick, Fredericton, N.B., Canada E3B 6E2

Received February 21, 1989

C. I. BAYLY and F. GREIN. Can. J. Chem. **67**, 2173 (1989).

Ab initio theoretical calculations were carried out on the intramolecular addition of 3-ketopent-4-en-1-olate **1** to form 1-oxacyclohex-3-en-4-olate 2 (reaction I; Scheme 1) and the corresponding intermolecular Michael addition of methanolate to butenone forming 4-methoxybut-2-en-2-olate **4** (reaction II; Scheme 1). The calculations were carried out at the RHF level using an augmented 4-31G basis set; single point energies were then taken using the 6-31+G* basis set. The overall energy change of the reaction in going from reactants to products is very similar for both reactions, with products being about 8.3 kcal/mol more stable than reactants; the major difference energetically between the two reactions is at the level of the transition state: the transition state energy for reaction I (intramolecular) is 6 kcal/mol higher than that for reaction II (intermolecular). The transition state geometry of reaction II conforms quite closely to the stereoelectronic requirements for a Michael addition, but that of reaction I is very distorted, reflecting significant compromises in the stereoelectronic requirements.

Key words: *ab initio* theoretical study, Michael-type addition, intramolecular, transition state.

C. I. BAYLY et F. GREIN. Can. J. Chem. **67**, 2173 (1989).

On a effectué des calculs théoriques *ab initio* sur l'addition intramoléculaire du céto-3 pente-4 olate-1 **1** qui conduit à l'oxa-1 cyclohexen-3 olate-4 **2** (réaction I; schéma 1) et sur l'addition de Michael intramoléculaire du méthanolate sur la buténone conduisant au méthoxy-4 buten-2 olate-2 **4** (réaction II; schéma 1). On a effectué les calculs au niveau RHF en utilisant un ensemble de base 4-31G elargi; on a obtenu les énergies ponctuelles en utilisant l'ensemble de base 6-31+G*. Les changement global d'énergie de la réaction, en partant des réactifs aux produits, est très voisin pour les deux réactions, avec des produits dont la stabilité est d'environ 8, 3 kcal/mol plus élevée que celle des réactifs. La principale différence d'énergie entre les deux réactions se situe au niveau de l'état de transition : l'énergie de l'état de transition pour la réaction I (intramoléculaire) est de 6 kcal/mol plus élevée que celle de la réaction II (intermoléculaire). La géométrie de l'état de transition de la réaction II se rapproche beaucoup des conditions stéréoelectroniques requises pour une addition de Michael, mais celle de la réaction I est très deformée reflétant ainsi des compromis significatifs dans les conditions stéréoélectroniques nécessaires.

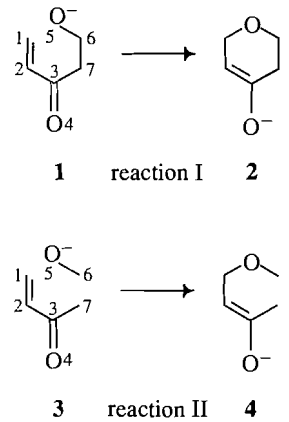
Mots clés : étude théorique *ab initio*, addition de Michael, intramoléculaire, état de transition.

[Traduit par le revue]

Introduction

In comparing the reactivity of an intramolecular system with its intermolecular counterpart, an important factor is the difference between the respective potential energy reaction profiles. Although the electronic changes taking place in both systems may be very similar, the extra spatial constraints on the reacting termini of the intramolecular system often disallow the "optimum" trajectory (in an intermolecular sense), requiring instead a different and higher energy trajectory as a reaction pathway. If the spatial distortion of the trajectory is big enough, the resulting increase in the potential energy for the transition state can be so great that the reaction will simply not occur under "normal" conditions (i.e., those used for the intermolecular reaction). The well-known Baldwin's rules (1) qualitatively classify ring-forming reactions as being favoured or disfavoured based on this principle. To study how an intramolecular system responds, both geometrically and energetically, to a large distortion from the optimum (intermolecular) reaction trajectory, an intramolecular Michael addition (1,4-nucleophilic addition to an α,β-unsaturated carbonyl moiety) was examined using theoretical methods.

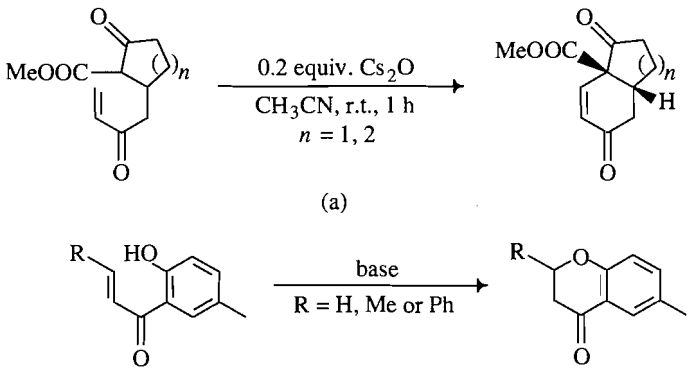
Ab initio theoretical calculations were carried out on the intramolecular addition of **1** to form **2** (reaction I, Scheme 1), which is a cyclization forming a six-membered ring. These calculations were then compared to those on the corresponding intermolecular Michael addition of **3** to form **4** (reaction II, Scheme 1). The structures of reaction I were chosen by analogy with experimental ones given in Scheme 2(a) (2), where **1** is constructed by replacing the ring by hydrogens and the β-ketoester fragment by oxygen. These replacements gave a system of computationally feasible size with a nucleophilic center of the same charge and approximately the same size and nucleophilicity as the experimental case. Reaction I is also very similar to the reaction given by Baldwin *et al.* (3) as an example of a 6-*endo*-trig process (Scheme 2(b)). Both of these intramolecular cyclizations reacted experimentally without difficulty.



SCHEME 1

While a 6-*endo*-trig process (such as reaction I) is a favored reaction according to Baldwin's ring closure rules (1), nevertheless the stereoelectronic requirements for Michael addition (4) would indicate that the intramolecular cyclization in reaction I could only take place via a significantly distorted transition state. One of these requirements is that the newly forming bond

Can. J. Chem. Downloaded from www.nrcresearchpress.com by 186.148.149.217 on 09/07/12
For personal use only.



SCHEME 2

should be coplanar with the enone π system. That is, the torsion angle around the α-carbon–β-carbon bond should be ideally 90°. However, even a fully formed six-membered ring can achieve only a 60° torsion angle around this bond. In principle a partially formed six-membered ring could reposition the nucleophile to improve this torsion angle, but then the forming bond angle (the Burgi – Dunitz "attack angle" (5)) would be much smaller than the "allowed" range of 100°–110° suggested by these authors. Furthermore, in the system under study, such a repositioning would almost certainly break the coplanarity of the enone system itself to some extent, where this coplanarity is another stereoelectronic requirement for reactivity. What geometric "compromise" is made by the real systems, and at what energy cost, to accommodate both the stereoelectronic requirements of the Michael addition and the spatial restrictions of the intramolecular framework?

A previous theoretical study, using the MNDO semiempirical method, was carried out on an intramolecular Michael addition of an oxygen nucleophile to an α,β-unsaturated carbonyl group (6). In this case the reactant carbon skeleton was one methylene group shorter than **1**, and the forming ring was thus five membered instead of six membered. This process was hence a 5-*endo*-trig process (disfavored according to Baldwin's rules) as opposed to the favored 6-*endo*-trig process studied in this work. These authors found a potential energy barrier of 21 kcal/mol to the intramolecular cyclization. The corresponding intermolecular system was not investigated by these authors, so an intramolecular–intermolecular comparison is not possible without further study.

Calculations

Calculations were carried out at the RHF (restricted Hartree–Fock) level using the GAUSSIAN 82 (7) computer program. The 4-31G basis set was used, augmented with polarization (6d, exponent 0.8) and diffuse functions (*s* and *p* functions, exponent 0.680) (8) on the oxygens only. This basis set (referred to henceforth as 4-31G(O*+)) was chosen in the light of basis set comparisons made in a previous study (9), which indicated that without diffuse functions on at least the anionic centers the reaction profile may not be even qualitatively correct. With each structure, the C—H bond lengths and the H—C—C bond angles of C6 and C7 (i.e., the two adjacent methylenes in reaction I and the methyls in reaction II (cf. Scheme 1)) were optimized together; all other internal degrees of freedom were optimized independently. The forming nucleophile–carbon bond (the C1—O5 internuclear distance, cf. Scheme 1) was used as the reaction coordinate (RC) for both reactions I and II. Single-point energies at the 6-31+G* basis set level were calculated for the critical points (for both systems) obtained using the 4-31G(O*+) basis set, in order to check the smaller basis set.

TABLE 1. Geometries and relative energies for the optimized structures for reaction I (intramolecular)[a]

	Reactant	Transition state	Product
Reaction coordinate *R*(C1—O5)	2.9275	2.9010	1.4532
Relative energies (kcal/mol):			
4-31G(O*+)	8.2	22.7	0.0[b]
6-31+G*	11.5	25.3	0.0[c]
Bond lengths:			
C1—C2	1.3223	1.3610	1.4931
C2—C3	1.4817	1.4306	1.3619
C3—O4	1.2194	1.2340	1.2693
O5—C6	1.3731	1.3867	1.4226
C6—C7	1.5799	1.5802	1.5278
C1—H1	1.0762	1.0727	1.0832
C1—H2	1.0831	1.0640	1.0949
C2—H3	1.0753	1.0730	1.0730
H—C_{sp^3}	1.0897	1.0879	1.0850
Bond angles:			
C1—C2—C3	124.05	119.31	119.46
C2—C3—O4	118.22	124.45	129.78
C2—C1—O5	102.38	107.45	114.89
C1—O5—C6	97.84	105.51	114.94
O5—C6—C7	112.50	113.37	113.21
C2—C1—H1	120.23	120.16	111.15
C2—C1—H2	120.23	122.80	113.49
C1—C2—H3	122.30	121.15	119.02
H—C_{sp^3}—C_{sp^3}	106.94	107.78	110.09
Dihedral angles:			
C1—C2—C3—O4	163.63	181.27	184.17
C3—C2—C1—O5	−13.39	−48.74	−45.07
C2—C1—O5—C6	4.80	30.56	28.38
C1—O5—C6—C7	34.02	24.71	21.06
C3—C2—C1—H1	−177.89	−163.51	−164.23
C3—C2—C1—H2	−2.99	37.36	75.53
C3—C1—C2—H3	177.02	161.65	182.58
O5—C6—C7—H6	160.94	171.82	182.86

[a]All distances are in Å and all angles are in degrees.
[b]The energy (in hartree) of the global minimum is −342.659079 (1 hartree = 4.4×10^{-18} J).
[c]The energy (in hartree) of the global minimum is −343.108864.

Exploratory calculations were carried out to verify that the transformations went through a single energy maximum and to help locate that maximum. The RC was held constant at several intermediate values situated on either side of the transition state, and then partial optimizations were carried out to determine the energy trend. For reaction II, a transition state (TS) optimization was then carried out directly to obtain the structure and energy of the TS.

For reaction I, the TS optimization algorithm (7) did not behave properly (the geometry diverged), so the TS was located by varying the RC by hand, completing the optimization holding constant the RC value, and inspecting the energy gradient along the RC. At 2.10 Å, the gradient of the optimized structure indicated the RC would increase if optimized, and at 2.08 Å, it would decrease. Quadratic interpolation of the energies gave 2.091 Å for the location of the TS on

Can. J. Chem. Downloaded from www.nrcresearchpress.com by 186.148.149.217 on 09/07/12
For personal use only.

TABLE 2. Geometries and relative energies for the optimized structures for reaction II (intermolecular)[a]

	Reactant	Transition state			Product
Reaction coordinate *R*(C1—O5)	2.9972	2.4000	2.1835	2.0000	1.4684
Relative energies (kcal/mol):					
4-31G(O*+)	8.3	16.5	16.8	15.9	0.0[b]
6-31+G*	10.9		18.5		0.0[c]
Bond lengths:					
C1—C2	1.3256	1.3325	1.3513	1.3752	1.4798
C2—C3	1.4750	1.4585	1.4402	1.4229	1.3744
C3—O4	1.2167	1.2187	1.2255	1.2338	1.2687
O5—C6	1.3785	1.3810	1.3785	1.3823	1.4014
C3—C7	1.4995	1.5091	1.5151	1.5214	1.5312
C1—H1	1.0763	1.0664	1.0660	1.0681	1.0902
C1—H2	1.0926	1.0628	1.0650	1.0678	1.0822
C2—H3	1.0750	1.0734	1.0726	1.0729	1.0758
H—C_{sp^3}	1.0921	1.0924	1.0915	1.0897	1.0840
Bond angles:					
C1—C2—C3	124.31	124.05	124.52	124.80	127.57
C2—C3—O4	119.75	121.76	122.81	123.70	125.21
C2—C1—O5	126.00	134.88	117.81	117.31	118.00
C1—O5—C6	115.25	155.81	113.36	113.91	113.23
C2—C3—C7	118.70	118.49	118.48	118.45	119.94
C2—C1—H1	119.14	121.51	120.53	118.94	109.63
C2—C1—H2	124.62	124.18	122.64	121.22	114.06
C1—C2—H3	122.12	121.62	120.52	119.77	116.74
H—C_{sp^3}—C_{sp^3}	112.27	112.01	111.75	111.42	110.34
Dihedral angles:					
C1—C2—C3—O4	180.00	182.51	183.33	182.10	181.23
C3—C2—C1—O5	0.00	−72.61	−84.84	−86.47	−81.88
C2—C1—O5—C6	180.00	−38.84	−4.27	−4.32	−53.00
C1—C2—C3—C7	0.00	2.72	3.16	1.60	0.91
C3—C2—C1—H1	180.00	181.24	175.37	169.05	157.30
C3—C2—C1—H2	0.00	2.55	10.95	16.88	36.98
C3—C1—C2—H3	180.00	177.09	176.50	176.69	180.24
C1—O5—C6—H4	180.00	166.37	122.82	124.71	176.71
C2—C3—C7—H7	60.00	53.82	55.01	55.76	−0.07

[a]All distances are in Å and all angles are in degrees.
[b]The energy (in hartree) of the global minimum is −343.819783.
[c]The energy (in hartree) of the global minimum is −344.268767.

the RC; optimization at this location gave an energy higher than the point on either side and a value of the energy gradient along the RC that was lower than the cutoff for the TS optimization algorithm. This structure is given as the TS of reaction I.

Results and discussion

The optimized structures and relative energies for reactions I and II are given in Tables 1 and 2, respectively; for reaction I the structures at 2.08 Å and 2.10 Å have been omitted because they resemble the TS so closely. Shown in Fig. 1 are the 4-31G(O*+) energy profiles of both reactions; the TS structure for reaction I is shown in Fig. 2a and that for reaction II is shown in Fig. 2b. The "reactant" molecules for both reactions I and II are local energy minima, most likely corresponding to a charge–dipole complex (9, 10). The structures in Fig. 2 each contain two dummy atoms X1 and X2 (having neither mass nor electrons nor nuclear charge) as a strictly geometric convenience to aid in the following discussion. They are placed as vectors perpendicular to a plane to show the amount of twist in that plane. For both structures, the dummy atom X1 is normal to the terminal methylene H1—C1—H2 plane, and X2 similarly is normal to the H3—C2—C3 plane. The dihedral angle between these two centers, i.e., X1—C1—C2—X2, shows the amount of twist taking place along the reacting double bond.

From Fig. 1 it may be seen that the overall energy change of the reaction in going from reactants to products is very similar for both reactions I and II, with products being about 8.3 kcal/mol more stable than reactants. The 6-31+G* single point energies given in Tables 1 and 2 gave this difference to be 10.9 and 11.5 kcal/mol for reactions I and II respectively. The structures calculated for reactants and products are as expected from the stereoelectronic requirements (*vide infra*) (i.e., boat-like conformations for reaction I) and theoretical studies (10). The major difference energetically between the two reactions is at the level of the TS; for the following comparisons the 6-31+G* single point energies will be given in parentheses after the 4-31G(O*+) energies. The TS energy for reaction I (intramolecular) is 14.5(13.8) kcal/mol above reactants, whereas the corresponding energy difference for reaction II (intermolecular) is 8.5(7.6) kcal/mol. The barrier for the intramolecular reaction is thus 6.0(6.2) kcal/mol higher than that of the intermolecular reaction. The 6-31+G* single point energies reflect the

Can. J. Chem. Downloaded from www.nrcresearchpress.com by 186.148.149.217 on 09/07/12
For personal use only.

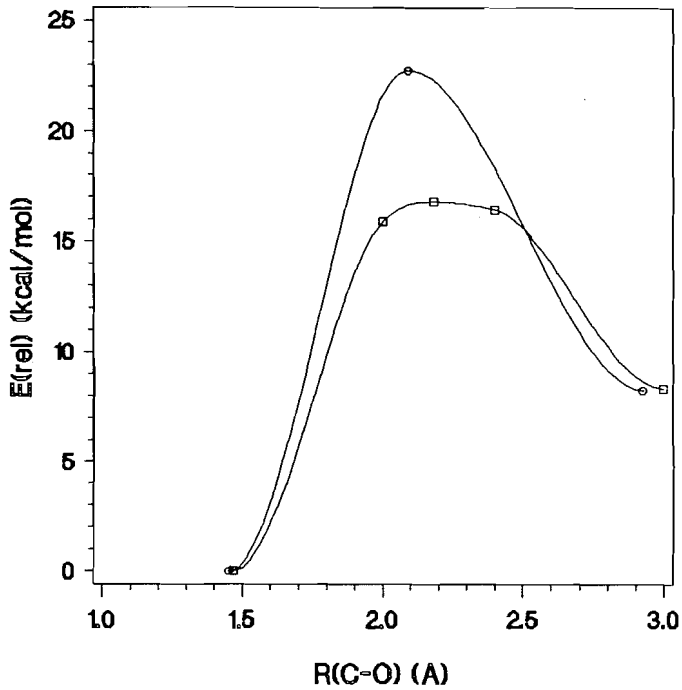


FIG. 1. Reaction profiles for reactions I and II; ○, reaction I (intramolecular); □, reaction II (intermolecular). Energies relative to products. R(C—O) is the C1—O5 internuclear distance, the reaction coordinate.

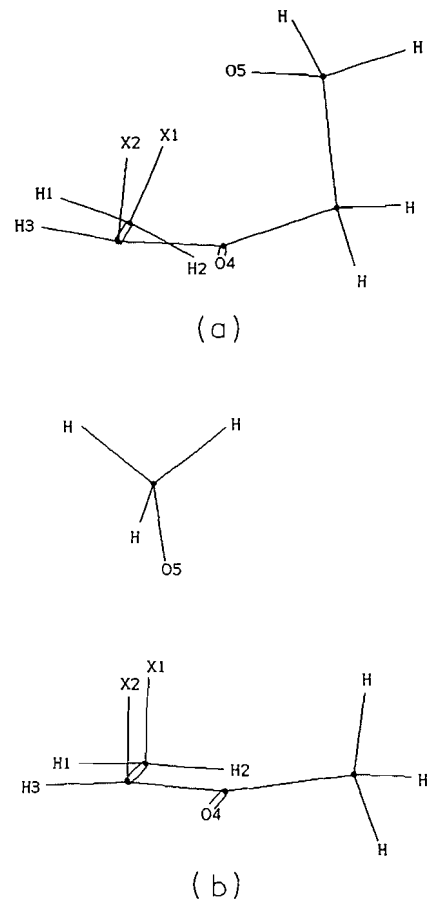


FIG. 2. Transition state structures for (a) reaction I (intramolecular) and (b) reaction II (intermolecular).

reactant–TS relative energy changes of the 4-31G(O*+) basis set to within 1 kcal/mol. Overall, the good agreement between the 6-31+G* and the 4-31G(O*+) basis sets validates the use of the much smaller 4-31G(O*+) basis set for this study as shown in previous work (9, 10).

The TS geometry of reaction II, shown in Fig. 2b, conforms quite closely to the stereoelectronic requirements outlined previously for a favorable reaction pathway. The pyramidalization of the methylene terminus, indicated by an X1—C1—C2 angle of 102° (this angle would be 90° with no pyramidalization), shows that bond formation is occurring, with a length of 2.18 Å for the incipient C1—O5 bond (the reaction coordinate). The forming C2—C1—O5 bond angle is 117°, falling outside the range of 100°–110° suggested by Burgi *et al.* (5) for this attack angle. The angle of approach of the nucleophile on the enone (i.e., the C3—C2—C1—O5 dihedral angle) is 85°, close to the ideal angle of 90°. The dihedral angle of 183° for the main chain atoms C1—C2—C3—O4 shows that the enone system is virtually planar; also the substituents of the vinyl group show that the double bond has almost no twist, as indicated by the X1—C1—C2—X2 dihedral angle of 1°.

In contrast, the TS geometry of reaction I, shown in Fig. 2a, is quite distorted from the intermolecular pathway, reflecting significant compromises in the stereoelectronic requirements outlined previously. As before, the methylene terminus is pyramidalizing, where an X1—C1—C2 angle of 106° shows that bond formation is occurring, with a slightly smaller length of 2.09 Å for the incipient C1—O5 bond. The C2—C1—O5 attack angle is in this case 107°, differing from the intermolecular case, but now agreeing with the 100°–110° range proposed by Burgi, Dunitz *et al.* (5). It is in the other aspects of the orientation that the large differences occur: the angle of approach of the nucleophile on the enone (i.e., the C3—C2—C1—O5 dihedral angle) is only 49°, far from the ideal 90° approach. Also, while the enone system is coplanar from the standpoint of the C1—C2—C3—O4 dihedral angle (181°) (note that this angle was not constrained in the calculations), the vinyl group is clearly distorted from planarity through the twisting of the methylene terminus towards the nucleophilic oxygen. The extent of this twist is shown by the X1—C1—C2—X2 dihedral angle of 18°, and is indicative of a distortion of the enone π system towards the nucleophile. Interestingly, the vinyl carbon away from the terminus is also pyramidalizing, having an X2—C2—C1 angle of 75° (this angle would be 90° with no pyramidalization)! This carbon, α to the carbonyl group, is planar in the reactant (part of the vinyl group) and in the product (as part of the resulting enolate; see the C3—C1–1-C2—H3 dihedral angle of reactant and product entries in Table 1). It is likely that this transient pyramidalization is a consequence of the transient distortion in the π system; this π distortion is not needed in either the reactant or the product.

Conclusions

The results of this study show that the additional spatial constraints of an intramolecular reaction (reaction I) can induce severe geometric distortions of the transition state from that of its intermolecular counterpart (reaction II). The corresponding energy increase can be viewed as the extra potential energy required to distort the transition state from the optimum geometry adopted by the intermolecular system, i.e., the energy cost for the compromise in the stereoelectronic requirements for

Can. J. Chem. Downloaded from www.nrcresearchpress.com by 186.148.149.217 on 09/07/12
For personal use only.

this reaction. In this study, the potential energy of the transition state was raised from 8.5 kcal/mol above reactants (reaction II) to 14.5 kcal/mol (reaction I), a difference of 6 kcal/mol. While this increase is not trivial, neither is it prohibitive, especially in light of the fact that this potential energy difference could be offset by other contributions to the free energy of activation. Improving the level of the theoretical treatment, especially through the inclusion of correlation energy, could be expected to decrease the size of the potential energy barrier, as it has in previous studies (9, 10). The smooth additions given in Scheme 2 (refs. 2 and 3), both of which are closely related to reaction I, experimentally support the ease of such Michael additions that have significantly distorted transition states, confirming that the cost in potential energy of this distortion is not prohibitive. This study suggests that while the proposed stereoelectronic requirements for Michael-type additions are indeed reflected in the optimum pathway of the intermolecular system (reaction II), these requirements should not be viewed as prerequisite for the reaction to occur.

Acknowledgements

We would like to thank NSERC Canada for an operating grant, and a postgraduate award to C.I.B. Generous financial support by the Leonard and Kathleen O'Brien Humanitarian Foundation to C.I.B, is much appreciated. Equipment grants by the University of New Brunswick Research Fund, as well as generous allocation of computer time by the University of New Brunswick are gratefully acknowledged.

1. J. E. Baldwin. J. Chem. Soc. Chem. Commun. 734 (1976).
2. G. Berthiaume, J.-F. Lavallee, and P. Deslongchamps. Tetrahedron Lett. **27**, 5451 (1986).
3. J. E. Baldwin, J. Cutting, W. Dupont, L. Kruse, L. Silberman, and R. C. Thomas. J. Chem. Soc. Chem. Commun. 736 (1976).
4. P. Deslongchamps. Stereoelectronic effects in organic chemistry. Organic Chemistry Series, Vol. 1. *Edited by* J. E. Baldwin, Pergamon Press, Oxford, England. 1983. pp. 221–242.
5. H. B. Burgi, J. D. Dunitz, J. M. Lehn, and G. Wipff. Tetrahedron, **30**, 1563 (1974).
6. G. W. Ellis, D. F. Tavares, and A. Rauk. Can. J. Chem. **63**, 3510 (1985).
7. J. S. Binkley, M. J. Frisch, D. J. De Frees, K. Raghavachari, R. A. Whiteside, H. B. Schlegel, E. M. Fluder, and J. A. Pople. GAUSSIAN 82 Release H; Carnegie–Mellon University, Pittsburgh, PA. 1986.
8. G. W. Spitznagel, T. Clark, J. Chandrasekhar, and P. R. Schleyer. J. Comput. Chem. **3**, 363 (1983).
9. C.I. Bayly and F. Grein. Can. J. Chem. **66**, 149 (1988).
10. C. I. Bayly and F. Grein. Can. J. Chem. **67**, 176 (1989).

Can. J. Chem. Downloaded from www.nrcresearchpress.com by 186.148.149.217 on 09/07/12
For personal use only.

A theoretical study of adiabatic proton transfer to simple substituted acetylenes in their ground and excited states

PETER S. MARTIN, KEITH YATES,[1] AND IMRE G. CSIZMADIA
Department of Chemistry, University of Toronto, Toronto, Ont., Canada M5S 1A1

Received December 8, 1988[2]

PETER S. MARTIN, KEITH YATES, and IMRE G. CSIZMADIA. Can. J. Chem. **67**, 2178 (1989).

RHF SCF 3-21G calculations are reported for the $^1\Sigma_g^+$, $^1A_1$, $^3A'$, and $^{1,3}A''$ states of simple substituted acetylenes (Y—C≡C—H, where Y = H, F, Cl, CH_3, and CF_3), the $^1A_1$, $^1A'$, and $^{1,3}A''$ states of their Markovnikov (*M*) vinyl cations (Y—C^+=CH_2), the $^1A'$ and $^{1,3}A''$ states of their anti-Markovnikov (*aM*) vinyl cations (YCH=C^+H), and the corresponding hydrated vinyl cations. Equilibrium electronic structures and the mechanism of adiabatic protonation are described qualitatively via Lewis/resonance schematic representations of the species involved. Calculated proton affinities (PA) suggest that relative to ground state Y—C≡C—H ($^1\Sigma^+/^1A_1$), Y—C≡C—H* ($^{1,3}A''$) is of greatly enhanced basicity with respect to protonation of both regiocenters. A graphical representation of the ordered pairs PA(*M*) versus PA(*aM*) as a function of substituent Y and electronic state, leads to the conclusions: (*1*) irrespective of both regiocenter (*M*/*aM*) and state ($^1\Sigma_g^+/^1A_1$, ^3A, $^{1,3}A''$) the PA's for Y—C≡C—H decrease in the order $CH_3 > H > Cl > F > CF_3$; (*2*) in proceeding from $CH_3C{\equiv}CH$ to $CF_3C{\equiv}CH$, a change in protonation regiospecificity (*M* → *aM*) is experienced to approximately the same extent for both S_0 and S_1; (*3*) T_2 exhibits no significant protonation regioselectivity. Critical comparison of the calculated results is made with available experimental data. An approximate picture of the energy profiles for the adiabatic hydrations of Y—C≡C—H via its ground, triplet and singlet states has been developed, based on the fixed points acetylene, vinyl cation and hydrated vinyl cation. Predicted relative reactivities of these three states are in excellent accord with available experimental data on rates of hydration.

Key words: excited states, proton transfer, photohydration.

PETER S. MARTIN, KEITH YATES et IMRE G. CSIZMADIA. Can. J. Chem. **67**, 2178 (1989).

On a effectué des calculs RHF-SCF 3-21G sur les états $^1\Sigma_g^+$, $^1A_1$, $^3A'$ et $^{1,3}A''$ d'acétylènes substitués simples (Y—C≡CH, dans lesquels Y = H, F, Cl, CH_3 et CF_3, sur les états $^1A_1$, $^1A'$ et $^{1,3}A''$ de leurs cations vinyles Markovnikov (*M*) (Y—C^+=CH_2), sur les états $^1A'$ et $^{1,3}A''$ de leurs cations vinyles *anti*-Markovnikov (*aM*) (YCH=C^+H) ainsi que sur les cations vinyles hydratés correspondants. On décrit qualitativement les équilibres des structures électroniques et le mécanisme de la déprotonation adiabatique en fonction de représentations schématiques de Lewis et de résonance des espèces impliquées. Les valeurs calculées pour les affinités protoniques (AP) suggèrent que, par rapport à l'état fondamental Y—C≡C—H ($^1\Sigma_g^+/^1A_1$), la basicité de l'état excité Y—C≡C—H* ($^{1,3}A''$) est fortement augmentée par rapport à la protonation à l'un ou l'autre des deux régiocentres. Une représentation graphique des AP(*M*) vs AP(*aM*) en fonction des substituants Y et des états électroniques conduit aux conclusions suivantes : (*1*) quels que soient le régiocentre (*M*/*aM*) et l'état ($^1\Sigma^+/^1A_1$, $^3A'$, $^{1,3}A''$), les AP des composés Y—C≡C—H diminuent dans l'ordre $CH_3 > H > Cl > F > CF_3$; (*2*) lorsqu'on passe de $CH_3C{\equiv}CH$ à $CF_3C{\equiv}CH$, on observe un changement dans la régiospécificité de la protonation (*M* → *aM*) qui est pratiquement le même pour les états S_0 et S_1; (*3*) l'état T_2 ne présente pratiquement pas de régiosélectivité par rapport à la protonation. On fait une comparaison critique des résultats des calculs avec les données expérimentales disponibles. En se basant sur des acétylènes, des cations vinyliques et des cations vinyliques hydratés à points fixes, on a développé une représentation approximative des profils d'énergie pour les hydratations adiabatiques des composés Y—C≡C—H par le biais de leurs états fondamentaux, triplets et singulets. Les réactivités relatives prévues pour ces trois états sont en excellent accord avec les données expérimentales sur les vitesses d'hydratation.

Mots clés : états excités, transfert du proton, photohydratation.

[Traduit par la revue]

Introduction

The photohydrations of aryl-substituted acetylenes (1), ethylenes (1), and allenes (2) have been investigated experimentally over a range of aqueous acid solutions (from pH 7 to $H_0 \approx -2$). The reactions are facile and subject to general acid catalysis (3) in most cases, with limiting quantum yields at the higher acidities in the $\Phi = 0.5$–1.0 range. In the majority of cases the reactions take place via the lowest singlet state (S_1) and are regiospecific in the Markovnikov (*M*) sense, as are the corresponding thermal reactions. The rate constants for proton transfer from H_3O^+ to S_1 have been measured for a variety of substrates and are in the 10^6–10^8 M^{-1} s^{-1} range (3), which represents a rate enhancement over the ground state (S_0) analogues of about 10^{11}–10^{14}, depending on the particular substituent and side-chain present in the aromatic system. In a few special cases, notably *m*- and *p*-nitro substituted systems, the analogous triplet state (T_1) reactions are also regiospecific, but in the anti-Markovnikov (*aM*) sense, but acid-catalysis is not observed in all of these systems. Estimates of the ground- and excited-state (S_1) basicities of the above types of substrate indicate pK shifts ($\Delta pK = pK_{S_1} - pK_{S_0}$) of at least 10 logarithmic units on electronic excitation (4), which are believed to be primarily responsible for the greatly increased photochemical versus thermal reactivity of these systems.

Previous LCAO-MO-SCF calculations (5) on acetylene itself, in its ground and low lying singlet and triplet states, have indicated that the properties of greatly enhanced basicity and reactivity are not uniquely characteristic of the aryl substituent in the systems investigated experimentally. On the basis of RHF-SCF 3-21G and 6-31G** calculations, it was predicted that the increase in proton affinity on going from $S_0(^1\Sigma_g^+)$ to $S_1(^1A_u)$ would be very large and that S_1 would be *trans*-bent and inherently zwitteronic in character, thus diminishing the need for rehybridization on proton transfer. On the other hand, the T_1 state ($^3B_2$) was predicted to be a *cis*-bent non-polar vinyl

[1]Author to whom correspondence should be addressed.
[2]Revision received July 6, 1989.

Can. J. Chem. Downloaded from www.nrcresearchpress.com by 186.148.149.217 on 09/07/12
For personal use only.

Can. J. Chem. Downloaded from www.nrcresearchpress.com by 186.148.149.217 on 09/07/12
For personal use only.

biradical, which would be expected to undergo abstraction-recombination reactions in preference to polar additions. However, the next higher triplet state (^3A_u) also showed greatly enhanced basicity relative to $^1\Sigma_g^+$, and was also *trans*-bent and zwitterionic in character. On account of the striking analogies which were found between the experimental studies of the singlet reactions of substituted phenylacetylenes (1) and the preliminary theoretical study of acetylene itself (5), and in light of the fact that nitro-substituted phenylacetylenes *are* observed to undergo acid-catalyzed photohydration via *aM* protonation of T_1, it seemed worthwhile to extend these theoretical investigations to related systems. It was therefore decided to investigate several substituted acetylenes Y—C≡C—H (where Y = CH_3, H, CF_3, F, Cl) to determine and compare the effects of both electron-donating and -withdrawing groups on proton affinity, reactivity, and regioselectivity in the hydration reactions of the ground and low-lying excited states of these systems.

Computational details

Ab initio LCAO-MO-SCF calculations were performed utilizing the program MONSTERGAUSS,[3] in conjunction with a GOULD 32/9705 minicomputer. The split valence 3-21G (7) basis set was employed in this study. Proper spin eigenfunctions were obtained for all closed (ground) and open (excited) shell systems via Restricted Hartree-Fock (RHF) (8) theory. The geometries of the ground and low lying excited states were energy optimized by the Optimally Conditioned (OC)[4] gradient, variable metric technique. All optimizations were terminated when the gradient length, $g = [(\Sigma_i(\delta E/\delta q_i)^2/N]^{1/2}$, where q_i are the internal coordinates and the sum is over the N optimized q_i, was reduced to below 5×10^{-4} mdyn, and subject to the condition that all internal coordinate derivatives ($\delta E/\delta q_i$) were less than 1×10^{-3} mdyn. This criterion generally yields structures within 1×10^{-4} Å, or 0.01° of the true theoretical optimum values, and energies stable below the μ-Hartree level.

Ground state geometries were taken as those predicted by the Valence Shell Electron Pair Repulsion Theory (VSEPR) (10). Starting covalent bond lengths were selected from a standard geometrical model (11) based on Lewis/resonance structures of the molecule in question. Low-lying excited states of YCCH were assumed to be of valence type, arising from $\pi \rightarrow \pi^*$ excitation and possessing planar bent (C_s) structures. For $YCCH_2^+$ and $YCHCH^+$, the "π" → "*p*" valence states were constrained to C_s geometries.

Results and discussion

1. Electronic states and geometries

The 3-21G predicted structural parameters for the ground states of Y—C≡C—H (Y = F, Cl, CH_3, CF_3) are given in Table 1 and can be seen to agree quite well with their experimentally determined counterparts (12–15), with the exception of r(Cl—C), as expected (16).

In $C_{\infty v}$ (Y = F, Cl) and C_{3v} (Y = CH_3, CF_3) geometries, the ground state MO configurations are $.....(n\pi)^4(^1\Sigma^+)$ or $.....(ne)^4(^1A_1)$, which can be represented as an "*sp*—*sp*—*sp*" (F_1Cl), "sp^3—*sp*—*sp*" (CH_3) or an "$(sp)_3$—sp^3—*sp*—*sp*" (CF_3) hybridized skeleton with two mutually perpendicular π(F, Cl) or "π"(CH_3, CF_3) bonds. All Frank–Condon valence excited states arising from "π" → "π*" excitation, are derived from the configurations $.....(n\pi)^3((n+1)\pi^*)^1$ or $.....(ne)^3((n+1)e^*)^1$. These states are obtainable from the direct-product decompositions $^2\Pi \times {}^2\Pi = {}^{1,3}\Sigma^- + {}^{1,3}\Sigma^+ + {}^{1,3}\Delta$ or $^2E \times {}^2E = {}^{1,3}A_1 + {}^{1,3}A_2 + {}^{1,3}E$.

TABLE 1. Calculated and experimental[a] ground state geometries for YC≡CH

Bond		Length (Å) F	Cl	CH_3	CF_3
r_{CC}	Calc.	1.18	1.18	1.19	1.18
	Expt.	1.20	1.20	1.21	1.20
r_{CH}	Calc.	1.05	1.05	1.05	1.05
	Expt.	1.05	1.06	1.06	1.06
r_{CY}	Calc.	1.30	1.71	1.47	1.45
	Expt.	1.28	1.64	1.46	1.46
r_{H-CH_2}	Calc.			1.08	
	Expt.			1.10	
r_{F-CF_2}	Calc.				1.35
	Expt.				1.34
Bond				**Angle (deg)**	
∠XCX	Calc.			110	110
	Expt.			108	108

[a]See refs. 12–15.

On *cis*-planar deformation, the $n\pi$ or *ne* highest occupied MO(HOMO) splits into an in-plane "σ" and out-of-plane "π" component of symmetry species a' and a'', respectively, with orbital energies $a' > a''$. This order is reversed for *trans*-bending. Similarly, the $(n+1)\pi^*$ or $(n+1)e^*$ lowest unoccupied MO(LUMO) also separates into an in-plane "σ*" and out-of-plane "π*" MO, but in this case the energies and symmetries are such that $a'(\text{"}\sigma^*\text{"}) \ll a''(\text{"}\pi^*\text{"}) \approx (n+1)\pi^*$ or $(n+1)e^*$ for *both cis* and *trans* distortions. Thus it is predicted on the basis of Walsh's rules (17), that the strongly bent "σ*" manifold excited states $A'(a'(\text{"}\sigma\text{"}) \times a'(\text{"}\sigma^*\text{"}))$ and $A''(a''(\text{"}\pi\text{"}) \times a'(\text{"}\sigma^*\text{"}))$ are stabilized forms of the lowest lying Frank–Condon valence states, and likewise for the more weakly bent "π*" states $A''(a'(\text{"}\sigma\text{"}) \times a''(\text{"}\pi^*\text{"}))$.

The energy ordering of the various excited states is analogous to that found for HCCH itself (5), when the symmetry correlations in going from the linear Frank–Condon states to either *cis* or *trans* bent states are taken into account, namely $C_{2h}(trans\text{-}C_s) \leftrightarrow D_{\infty v}$, $(C_{3v}) \leftrightarrow C_{2v}(cis\text{-}C_s)$, as shown in Table 2. In all cases (Y = H, F, Cl, CH_3, CF_3) the lowest triplet states ($^3B_2$ or $^3A'$) are *cis*-bent, while the lowest singlets (^1A_u or $^1A''$) are *trans*-bent. It is also to be noted that the stabilization of the $^{1,3}\Delta(C_{\infty v})$ and $^{1,3}E(C_{3v})$ states by planar bending to the *cis* and *trans* bent $^3A''$ and $^1A'$ states is consistent with the Renner–Teller (19) and Jahn–Teller (20) effects, respectively.

As a consequence of the symmetry reduction associated with substitution of Y- for H-, the *cis*- and *trans*-bent forms relinquish their status as distinct electronic states to become geometrical isomers of the same nonlinear, equilibrium state, e.g. the $^1B_2$ and ^1B_u states of HCCH correlate with the *cis* and *trans* isomers of the $^1A'$ state for YCCH (Y ≠ H). Furthermore, the fact that the present methodology is limited (21) to investigation of the lowest energy state of a given symmetry

[3]The program (6*a*) incorporates the integral, SCF, and analytic energy gradient routines for both UHF and closed shell RHF from Gaussian 80 (6*b*) and automatic geometry optimization by the Optimally Conditioned (OC) method. The RHF open shell SCF is an extensively modified version of the program GSCF (6*c*). The RHF energy gradients were programmed following refs. 6*d* and *e*.

[4]Reference 9*a*. The routine is described in ref. 9*b*.

TABLE 2. Symmetries and energy ordering of excited states of Y—C≡C—H

Y	Linear (Frank–Condon) states	*cis*-bent states	*trans*-bent states
H	$D_{\infty h}$ ($^{1,3}\Sigma_u^+ < {}^{1,3}\Delta_u$)	C_{2v}	C_{2h}
F_1Cl	$C_{\infty v}$ ($^3\Sigma^+ < {}^3\Delta$) ($^1\Sigma^- < {}^1\Delta$)	C_s	C_s
CH_3, CF_3	C_{3v} ($^3A_1 < {}^3E$) ($^1A_2 < {}^1E$)	C_s	C_s
Y = H	$^3B_2(^3\Sigma_u^+)$[a] < $^3B_u(^3\Sigma_u^+)$ < $^3A_u(^3\Delta_u)$ < $^3A_u(^3\Delta_u)$	*cis* *trans* *trans* *cis*	
	$^1A_u(^1\Sigma_u)$ < $^1A_2(^1\Sigma_u)$ < $^1B_2(^1\Delta_u)$ < $^1B_u(^1\Delta_u)$	*trans* *cis* *cis* *trans*	
Y = F, Cl	$^3A'(^3\Sigma^+)$ < $^3A'(^3\Sigma^+)$ < $^3A''(^3\Delta)$ < $^3A''(^3\Delta)$	*cis* *trans* *trans* *cis*	
	$^1A''(^1\Sigma^-)$ < $^1A''(^1\Sigma^-)$ < $^1A'(^1\Delta)$ < $^1A'(^1\Delta)$	*trans* *cis* *cis* *trans*	
Y = CH_3, CF_3	$^3A'(^3A')$ < $^3A'(^3A_1)$ < $^3A''(^3E)$ < $^3A''(^3E)$	*cis* *trans* *trans* *cis*	
	$^1A''(^1A_2)$ < $^1A''(^1A_2)$ < $^1A'(^1E)$ < $^1A'(^1E)$	*trans* *cis* *cis* *trans*	

[a]Terms in parentheses refer to symmetries of Frank–Condon states before *cis* or *trans* deformation.

TABLE 3. Excited state geometries[a] of lowest singlet[b] and triplet states of YC≡CH

$^3A'$ (*cis*)	r(CC) = 1.31 Å r(CH) = 1.08 Å ∠YCC = 128°	r(FC) = 1.33 Å $r(CH_3C)$ = 1.49 Å ∠HCC = 131°	r(ClC) = 1.83 Å $r(CF_3C)$ = 1.49 Å
$^{1,3}A''$ (*trans*)	r(CC) = 1.37 Å r(CH) = 1.08 Å	r(FC) = 1.33 Å $r(CH_3C)$ = 1.49 Å	r(ClC) = 1.83 Å $r(CF_3C)$ = 1.49 Å
Y ≠ CF_3	∠YCC = 139°(*cis*) = 128°(*trans*)	∠HCC = 120°(*cis*) = 120°(*trans*)	
Y = CF_3	∠YCC = 122°(*cis*) = 122°(*trans*)	∠HCC = 140°(*cis*) = 129°(*trans*)	

[a]Values invariant with substituent and isomerism, except where noted.
[b]$^1A'$ states not included, for reasons given in text.

type, at a particular geometry, such states are excluded from consideration given that S_0 is always of the totally symmetric representation. Fortunately this is not the case for $^3A'$ states, in that $\langle {}^1A'(S_0)|H|{}^3A'(T_1)\rangle = 0$ by virtue of orthogonal spin functions. However, because the lowest lying, valence excited states of the conjugate acid are of A'' symmetry, $^1A'$ states are unimportant as far as adiabatic protonation is concerned, and as such warrant structural discussion only.

As a result of the conformational (CX_3) and geometrical (*cis* or *trans*) isomerism associated with each of the excited states, $^3A'$, $^3A''$, and $^1A''$, there is a wealth of structural data to be examined. For practical purposes the data were categorized appropriately and subjected to statistical analysis, a synopsis of which, in terms of mean values and standard deviations, is presented next. Since ClCCH $^1A'$ is calculated to be *cis* dissociative, it was excluded from the numerical investigation.

The calculated bond lengths and angles for the $^3A'$ and $^{1,3}A''$ states are given in Table 3. It can be seen that while there is a significant difference between the states $^3A'$ and $^{1,3}A''$ with respect to r_{CC}, with the former having a shorter CC bond, all the adjacent bonds appear to be symmetry invariant. It is also interesting to note that the $^3A'$ states give the same bond lengths and angles independent of both substituent and isomerism. The same is not true for the $^{1,3}A''$ states for the bond angles ∠YCC and ∠HCC, as shown in Table 3.

Where Y = CH_3, CF_3, there is the additional complication of conformational isomerism in the C_s open shell states $^3A''$ and $^{1,3}A''$, when rotation of the CX_3C bond is taken into account. The present cases are directly analogous to CH_3C rotation in acetaldehyde (22). For a given geometrical isomer of a particular state, the *syn* and *anti* conformers are at a minimum and maximum, respectively, with the exception of *trans*-$CF_3CCH(^1A'')$ where the two are essentially equivalent in energy. However, there exists no case in the present work where the energy difference between rotamers exceeds 2 kcal/mol.

2. *Schematic representations of electronic states*

In the same manner as was accomplished (5) for the $^{1,3}A_{2u}$ and $^{1,3}B_{2u}$ states of HCCH, a schematic representation of the electronic structure for the states $^3A'$ and $^{1,3}A''$ of YCCH is now developed. For both symmetry types the doubly occupied core and framework (including the lone pairs) CMO's are of the configuration $\ldots((m-1)a')^2\ldots((n-1)a'')^2$. On the other hand, the valence CMO's are unique to each, and are given in order for A' and A'' as $(na'')^2(ma')^1((m+1)a'^*)^1$ and $(ma')^2(na''^1)(m+1)a')^1$. To formulate a qualitative LMO description that can be represented as a Lewis/resonance diagram, the appropriate linear combinations are taken amongst the $(m-1)a'$ and $(n-1)a''$ orbitals, to generate the inner shell "1*s*" core, "sp^2—*s*" C—H, "sp^2—sp^2" C—C, "*sp*—sp^2"

Can. J. Chem. Downloaded from www.nrcresearchpress.com by 186.148.149.217 on 09/07/12
For personal use only.

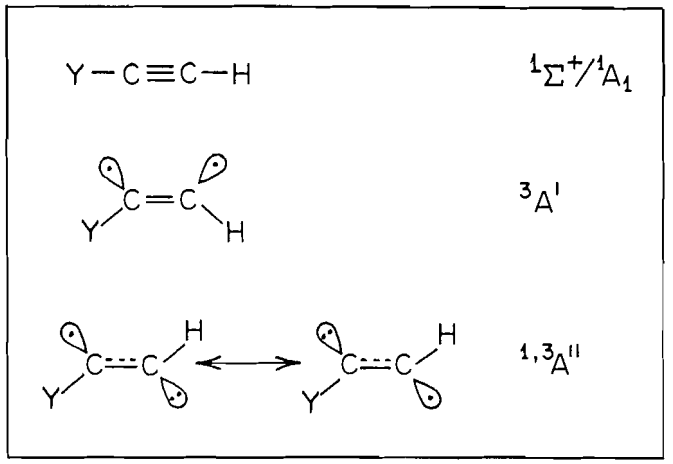


FIG. 1. Lewis/resonance structures for the $^1\Sigma^+/^1A'$ and lowest energy geometric isomers of the $^3A'$ and $^{1,3}A''$ states of YCCH (Y = F, Cl, CH_3, and CF_3).

(CX_3) or "sp—sp^2" (F, Cl) Y—C and "s—sp^3" (CH_3) or "sp–sp^3" (CF_3) X—CX_2 bonding and lone pair (F, Cl, CF_3) LMO's. The two remaining "sp^2" LMO's and the "π" bond associated with the acetylenic chromophore can be similarly obtained by suitable combination of the two valence orbitals ma' and $(m + 1)a'$ in conjunction with the na'' CMO.

The Lewis/resonance diagrams associated with the LMO description for the states $^3A'$ and $^{1,3}A''$ are shown in Fig. 1 and clearly illustrate the dissimilarity between the two types, i.e. $^3A'$ possess the LMO occupancy ...("π")^2("sp^2")^1("sp^2")^1 and can thus be regarded as a "vinyl biradical", whereas $^{1,3}A''$ is an unequal composite of the two, oppositely polarized, resonance contributors, ..."π")^1("sp^2")^2("sp^2")^1 and ...("π")^1(sp^2")^1("sp^2")^2, and is therefore zwitterionic-like. Given that (r(CC, $^{1,3}A''$)) = 1.37(2) Å is indistinguishable from the value calculated for benzene (1.38 Å) (23), with a corresponding bond order of 1.5, this suggests that the two valence "sp^2" LMO's of $^{1,3}A''$ are largely NBO's. For $^3A'$, which possesses a filled "π" orbital, this is inconsequential since the individually occupied BO and ABO would contribute nothing to the overall bond order of 2 and thus (r(CC, $^3A'$)) = 1.31(1) Å is in excellent agreement with that calculated for ethylene (1.31 Å) (23). By comparing the squared atomic orbital (AO) coefficients of the filled ma' with those of the singly occupied $(m + 1)a'$ CMO, one is able to assign the predominant resonance form for YCCH($^{1,3}A''$) as that which associates the pair of electrons with the β (unsubstituted) carbon of the acetylenic moiety when Y ≠ CF_3 and conversely with the α carbon when Y = CF_3. The "vinyl biradical" pictorial representation for YCCH($^3A'$) is also consistent with the angular geometry, (∠HCC(Y), $^3A'$) = 131°, in that VSEPR (10) would predict (∠YCC, $^3A'$) ≠ (∠HCC, $^3A'$) > 120° for the repulsion of two "sp^2" BO in the presence of one "sp^2" NBO containing a single electron. Alternatively for the zwitterionic-like YCCH ($^{1,3}A''$), where Y ≠ CF_3, one would expect (∠HCC, $^{1,3}A''$) ≠ 120°, in that the major resonance contributor requires the spatial rejection of two "sp^2" BO in the presence of one doubly occupied "sp^2" NBO on the β carbon and (∠YCC, $^{1,3}A''$) ≠ (∠YCC, $^3A'$).

The difference in bond angles between the various *cis* and *trans* states shown in Table 3 can be attributed to the steric repulsions of *cis* displaced Y and H groups, which are not present in the *trans* isomers.

Again, as a result of the structural (M/aM), geometrical (*cis/trans*) and conformational (CX_3) isomerism present in the Markownikoff, $FCCH_2^+$, $ClCCH_2^+$, $CH_3CCH_2^+$, and $CF_3CCH_2^+$ and the *anti*-Markownikoff vinyl cations, $FCHCH^+$, $ClCHCH^+$, CH_3CHCH^+, and CF_3CHCH^+, categorization and statistical evaluation of the calculated bond lengths and angles was necessary. (These are given in ref. 30 for both ground and excited states.) In the ground state, both r(CC) and r(CH) are found to be independent of substituent and isomerism. This is not true for r(Y—C), with the possible exception of r(CF_3—C), where structural isomerism is important. The fact that r(Y—C^+) < r(Y—C) for Y ≠ CF_3 is readily explained by lone pair "π" donation (Y = F, Cl) and hyperconjugation (Y = CH_3), through which the designated substituents are able to stabilize the M- in relation to the aM-vinyl cation.

In C_s geometries the M vinyl cations $YCCH_2^+$ for Y = CX_3 and all substituted aM vinyl cations $YCHCH^+$, possess the ground ($^1A'$) state configuration ...$(ma')^2$ ... $(na'')^2$, whereas the two remaining $YCCH_2^+$ of C_{2v} symmetry are of the ground ($^1A_1$) state configuration ...$(ra_1)^2$ ... $(sb_1)^2$ .. $(tb_2)^2$. Both $YCCH_2^+(S_0)$ and $YCHCH^+(S_0)$ can be described in terms of a "sp^x—sp—sp^2" and "sp^x—sp^2—sp" "σ" framework respectively, or an "$(sp)^3$—sp^3—sp—sp^2" and "$(sp)^3$—sp^3—sp^2—sp" hybridized "σ" framework for the CF_3 system with a mutually perpendicular "π" (na'' or sb_1) bond and empty "p" ($(m + 1)a'$ or $(t + 1)b_2$) orbital at the electron deficient "sp" carbon. Although the lowest lying, valence excited states originate from the configurations ...$(na'')^1((m + 1)a')^1$ or ...$(sb_1)^1((t + 1)b_2)^1$, arising from "π" → "p" excitation, because the $(m + 1)a'$ or $(t + 1)b_2$ LUMO is reduced in energy relative to the na'' or sb_1 HOMO upon YCC (M) or HCC (aM) bending, the Frank–Condon states are stabilized, as per Walsh's rules (17), by the "sp^x—sp—sp^2"/"sp^x—sp^2—sp" → "sp^x—sp^2—sp^2" (F, Cl, CH_3) or "$(sp)^3$—sp^3—sp—sp^2"/"$(sp)^3$—sp^3—sp^2—sp" → "$(sp)^3$—sp^3—sp^2—sp^2" (CF_3) rehybridization of the $YCCH_2^+$*/$YCHCH^+$* nuclear framework. For $YCCH_2^+$*, where Y = F and Cl, this results in the $C_{2v} \rightarrow C_s$ symmetry reduction.

Lewis/resonance illustrations corresponding to the LMO descriptions for the $^{1,3}A''$ states of $YCCH_2^+$ and $YCHCH^+$, comprising "sp—sp^2—sp^2" (F, Cl), "sp^3—sp^2—sp^2" (CH_3) or "$(sp)_3$—sp^3—sp^2—sp^2" (CF_3) skeletons with individually occupied "π" (a'') BO's and "sp^2" NBO's of orthogonal orientation, are shown in Fig. 2. These are in accord with the C—C bond lengths and bond angles obtained. The fact that the values of r_{FC}, r_{ClC}, and r_{CH_3C} are intermediate between their distinguishable ground state counterparts, ((Y—C^+)) (M) and ((Y—C)) (aM), is indicative of lone pair "π" donation (F, Cl) and hyperconjugation (CH_3), whereby the half-filled "π" BO is stabilized in both $YCCH_2^+$($^{1,3}A''$) and $YCHCH^+$($^{1,3}A''$). This is in contrast to the ground state, where both mechanisms act to stabilize the empty "p" orbital on the charge bearing carbon of $YCCH_2^+$ only.

With the Lewis/resonance structures in hand for YCCH ($^{1,3}A''$), $YCCH_2^+$($^{1,3}A''$), and $YCHCH^+$($^{1,3}A''$), it is possible to formulate a qualitative schematic representation for the process of adiabatic proton transfer, which for the purposes of illustration will be arbitrarily segmented into the three stages of resonance, polarization and product formation as is outlined in Scheme 1. In the so-called resonance stage, there is only the isolated *trans*-YCCH($^{1,3}A''$) molecule as described by its two unequal resonance contributors. In the second stage, the substrate is subjected to regiospecific electrophilic attack by H^+ in either of two directions, i.e. at the α (aM) or at the β (M) carbon. As the distance of approach narrows along either

Can. J. Chem. Downloaded from www.nrcresearchpress.com by 186.148.149.217 on 09/07/12
For personal use only.

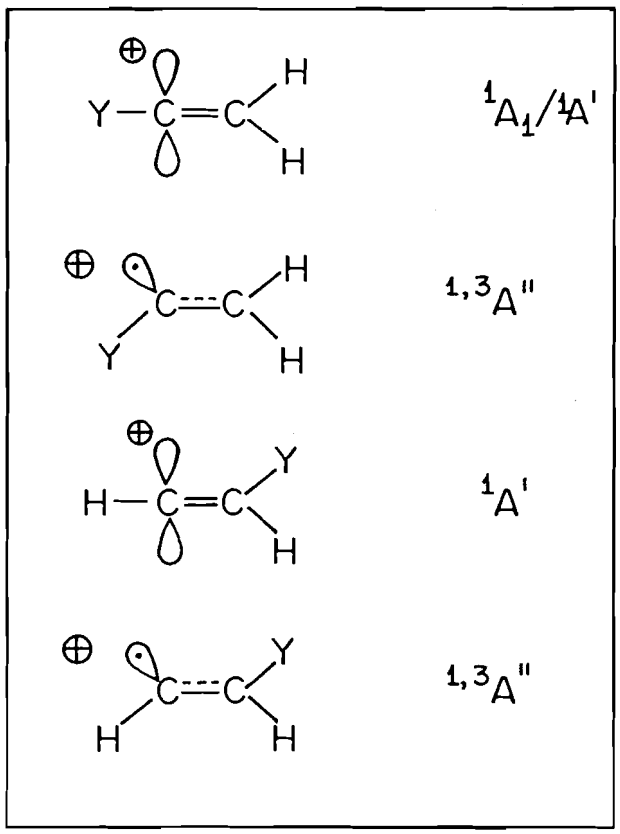
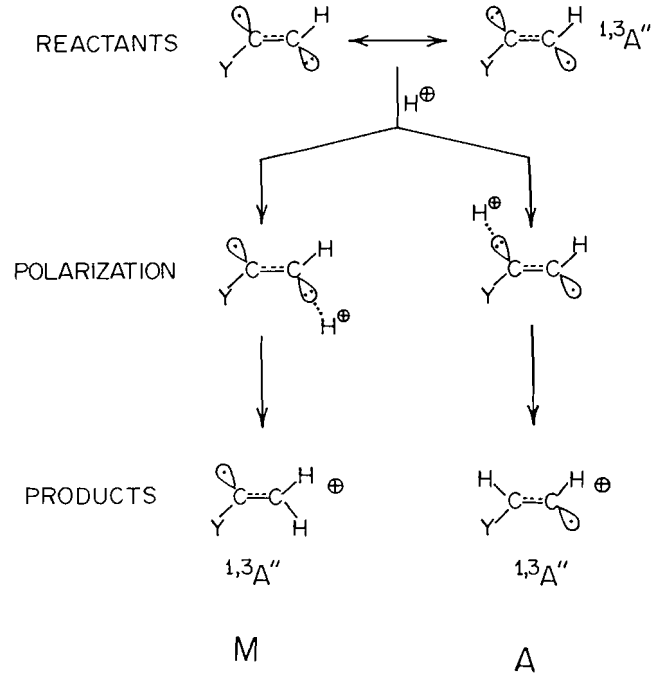


FIG. 2. Lewis/resonance structures for the $^1A_1/^1A'$ and $^{1,3}A''$ states of $YCCH_2^+$ and $YCHCH^+$ (Y = F, Cl, CH_3, and CF_3) (*trans*-$YCHCH^+$ ($^{1,3}A''$) shown only).

reaction coordinate, $YCCH(^{1,3}A'')$ is polarized by the electric field of the proton such that the resonance form corresponding to that which places the lone pair on the carbon that is the focus of attack, gradually dominates to the extent that just prior to product formation (stage 3), the contribution of the alternate form is completely eliminated. From a CMO perspective, one would say that $YCCH(^{1,3}A'')$ was polarized in such a manner as to increase the electron density at the attacked carbon by appropriately modifying the AO coefficients of the doubly occupied *ma''* orbital, e.g. attack at the β carbon would require the coefficients for AO's centered on the α carbon to diminish in magnitude relative to those for β in order that electron density be directed toward the incoming proton. On the basis of this description, one would predict that β attack for $Y \neq CF_3$ would be favored over α attack, in that the predominant *in vacuo* resonance contributor corresponds to that for which direct covalent bonding with H^+ is facilitated, and *vice versa* for cases where $Y = CF_3$.

3. Ground and excited state energies

In Figs. 3–6 the energies of the ground and excited states for YCCH ($^1\Sigma^+/^1A_1$, $^3A'$, and $^{1,3}A''$), $YCCH_2^+$ ($^1A_1/^1A''$ and $^{1,3}A''$), and $YCHCH^+$ ($^1A'$ and $^{1,3}A''$), where Y = F, Cl, CH_3, and CF_3, respectively, are plotted relative to that for YCCH ($^1\Sigma^+/^1A_1$). For illustrative convenience enumerative symbology is adopted, e.g. $S_2(t)$ denotes the *trans* isomer of the second lowest singlet state of YCCH. As a result of the small energy differences (<2 kcal/mol) between the conformational isomers of CX_3CCH ($^3A'$, $^{1,3}A''$), $CX_3CCH_2^+$ ($^{1,3}A''$), and CX_3CHCH^+ ($^1A'$, $^{1,3}A''$), and even between the geometrical isomers of $CX_3CCH_2^+$ ($^{1,3}A''$) and CX_3CHCH^+ (^1A, $^{1,3}A''$), only the most stable forms are displayed graphically.



SCHEME 1. Qualitative schematic representation for the process *trans*-YCCH ($^{1,3}A''$) + $H^+ \rightarrow YCCH_2^+$ ($^{1,3}A''$)/*trans*-$YCHCH^+$ ($^{1,3}A''$).

From Figs. 3–6, it is immediately obvious that the excited states of both $YCCH_2^+$ are red shifted relative to those of YCCH and therefore the YCCH* is of enhanced basicity with respect to both *M* and *aM* protonation. Careful examination also reveals that (*1*) similar energy differences exist between geometric isomers for the pairs FCCH ($^3A'$, $^{1,3}A''$)/ClCCH ($^3A'$, $^{1,3}A''$) and CH_3CCH ($^3A'$, $^{1,3}A''$)/CF_3CCH ($^3A'$, $^{1,3}A''$), and (*2*) the energy differences, $\Delta E = E_{SCF}(YCHCH^+{}^*) - E_{SCF}(YCCH_2^+{}^*)$, are such that for all Y, $|\Delta E(HS_0^+)| > |\Delta E(HS_1^+)| \gg |\Delta E(HT_1^+)|$. Evaluation of the following expressions for proton transfer:

$$PA(M) \simeq E_{SCF}(YCCH^*) - E_{SCF}(YCCH_2^+{}^*)$$

$$PA(aM) \simeq E_{SCF}(YCCH^*) - E_{SCF}(YCHCH^+{}^*)$$

generates the ordered pairs PA(*M*) and PA(*aM*), which are plotted against each other for all Y (including H) in Fig. 7. It must be emphasized that these proton affinity values in every case involve adiabatic proton transfer between the directly correlating states shown below.

$$S_0(^1\Sigma^+, {}^1A_1) \rightarrow HS_0^+(M)(^1A_1, {}^1A')$$

$$S_0(^1\Sigma^+, {}^1A_1) \rightarrow HS_0^+(aM)(^1A')$$

$$T_2(^3A'') \rightarrow HT_1^+(M)(^3A'')$$

$$T_2(^3A'') \rightarrow HT_1^+(aM)(^3A'')$$

$$S_1(^1A'') \rightarrow HS_1^+(M)(^1A'')$$

$$S_1(^1A'') \rightarrow HS_1^+(aM)(^1A'')$$

The solid line in Fig. 7 is of unit slope, and gives the demarcation between *M* (points above) and *aM* (points below) preference. Examination of the different sets of points in Fig. 7 (for S_0, T_2, and S_1) enables one to conclude the following: (*1*) with minor exceptions to be noted subsequently, irrespective of both regiocenter (*M*/*aM*) and state ($S_0/T_2/S_1$), the PA's for YCCH decrease with respect to Y, including H, in the order $CH_3 > H > Cl > F > CF_3$; (*2*) in proceeding from CH_3CCH

Can. J. Chem. Downloaded from www.nrcresearchpress.com by 186.148.149.217 on 09/07/12
For personal use only.

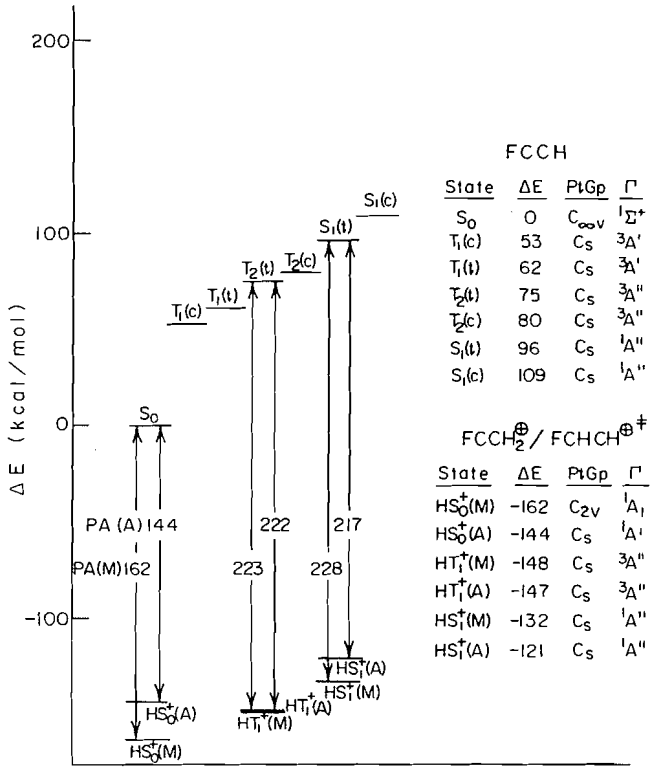


FIG. 3. Relative energies* of the ground and lowest lying excited states† for FCCH ($^1\Sigma^+$, $^3A'$ and $^{1,3}A''$), $FCCH_2^+$ ($^1A_1$ and $^{1,3}A''$), with PA's evaluated between the directly correlating states $S_0(^1\Sigma^+) \leftrightarrow HS_0^+(M)(^1A_1)/HS_0^+(aM)(^1A')$, $T_2(^3A'') \leftrightarrow HT_1^+(M)(^3A'')/HT_1^+(aM)(^3A'')$ and $S_1(^1A'') \leftrightarrow HS_1^+(M)(^1A'')/HS_1^+(aM)(^1A'')$. †lowest energy geometric isomers only. *$\Delta E_{SCF} = E_{SCF} - E_{SCF}(FCCH(S_0))$, where $E_{SCF}(FCCH(S_0)) = -174.693$ au.

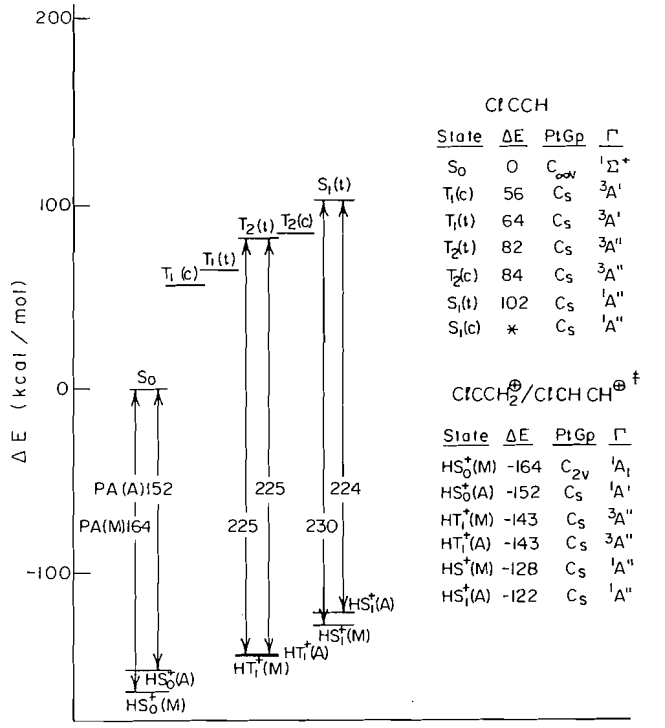


FIG. 4. Relative energies† of the ground and lowest lying excited states for ClCCH ($^1\Sigma^+$, $^3A'$, and $^{1,3}A''$), $ClCCH_2^+$ ($^1A_1$ and $^{1,3}A''$), with PA's evaluated between the directly correlating states $S_0(^1\Sigma^+) \leftrightarrow HS_0^+(M)(^1A_1)/HS_0^+(aM)(^1A')$, $T_2(^3A'') \leftrightarrow HT_1^+(M)(^3A'')/HT_1^+(aM)(^3A'')$ and $S_1(^1A'') \leftrightarrow S_1^+(M)(^1A'')/HS_1^+(aM)(^1A'')$ *dissociative. †$\Delta E_{SCF} = E_{SCF} - E_{SCF}(ClCCH(S_0))$, where $E_{SCF}(ClCCH(S_0)) = -533.092$ au.

through CF_3CCH, a change in protonation regiospecificity ($M \rightarrow aM$) is experienced to approximately the same extent for both YCCH(S_0) and YCCH(S_1); (*3*) regardless of Y, YCCH(T_2) exhibits no significant protonation regioselectivity. Note that to within 1 kcal/mol, PA($ClCCH(S_0)$) ≃ PA($HCCH(S_0)$), PA($CF_3CCH(S_0)(aM)$ ≃ PA($FCCH(S_1)(aM)$) which represent minor exceptions to (1) above.

4. Comparisons with experimental results

Unfortunately, there are available only two experimentally determined PA's with which exact comparison can be made. Gas phase spectroscopic measurements have established PA($FCCH(S_0)(M)$) = 161 kcal/mol (24) and PA($CH_3CCH(S_0)(M)$) = 182 kcal/mol (25), which the present RHF—SCF calculations overestimate by only 1 and 2 kcal/mol, respectively, including correction for differential zero-point energy, due mainly to the two (F) and three (CH_3) extra degrees of vibrational freedom present in the vinyl cation, and finite temperature.

Although excited state basicity enhancement has been shown (26) for cyclodecyne and di-*n*-butylacetylene, which undergo sensitized photochemical addition of acetic acid to produce enol acetates under conditions that these compounds are thermally inert, no evidence yet exists in cases where the aliphatic alkyne is asymmetrically substituted and for which there is the possibility of regiospecific protonation. However, as previously indicated, facile acid catalysed photohydration has been demonstrated for substituted phenylacetylenes (1, 3) and although direct comparison with the theoretical predictions of this study

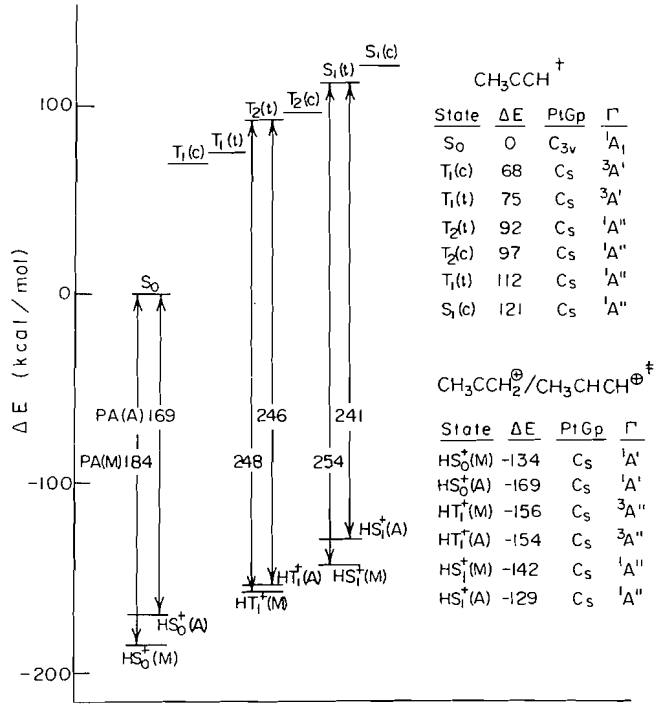


FIG. 5. Relative energies* of the ground and lowest lying excited states for CH_3CCH ($^1A_1$, $^3A'$, and $^{1,3}A''$), $CH_3CCH_2^+$ ($^1A'$ and $^{1,3}A''$) and CH_3CHCH^+ ($^1A'$ and $^{1,3}A''$), with PA's evaluated between the directly correlating states $S_0(^1A_1) \leftrightarrow HS_0^+(M)(^1A')/HS_0^+(aM)(^1A')$, $T_2(^3A'') \leftrightarrow HT_1^+(M)(^3A'')/HT_1^+(aM)(^3A'')$ and $S_1(^1A'') \leftrightarrow HS_1^+(M)(^1A'')/HS_1^+(aM)(^1A'')$. *$\Delta E_{SCF} = E_{SCF} - E_{SCF}(CH_3CCH(S_0))$, where $E_{SCF}(CH_3CCH(S_0)) = -115.225$ au.

Can. J. Chem. Downloaded from www.nrcresearchpress.com by 186.148.149.217 on 09/07/12
For personal use only.

Can. J. Chem. Downloaded from www.nrcresearchpress.com by 186.148.149.217 on 09/07/12
For personal use only.

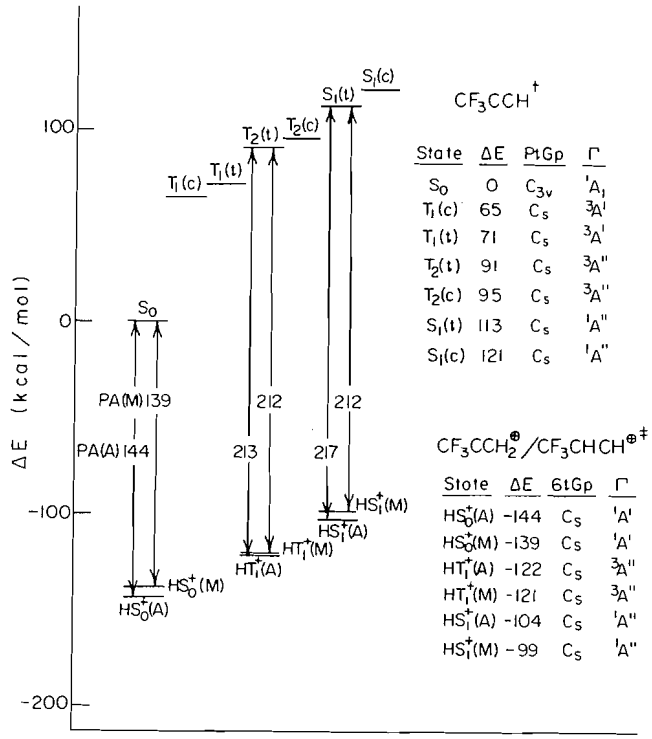


FIG. 6. Relative energies* of the ground and lowest lying excited states for CF_3CCH ($^1A_1$, $^3A'$, and $^{1,3}A''$), $CF_3CCH_2^+$ ($^1A'$ and $^{1,3}A''$), with PA's evaluated between the directly correlating states $S_0(^1A_1) \leftrightarrow HS_0^+(M)(^1A')/HS_0^+(aM)(^1A')$, $T_2(^3A'') \leftrightarrow HT_1^+(M)(^3A'')/HT_1^+(aM)(^3A'')$ and $S_1(^1A'') \leftrightarrow HS_1^+(M)(^1A'')/HS_1^+(aM)(^1A'')$. *$\Delta E_{SCF} = E_{SCF} - E_{SCF}(CF_3CCH(S_0))$, where $E_{SCF}(CF_3CCH(S_0)) = -410.197$ au.

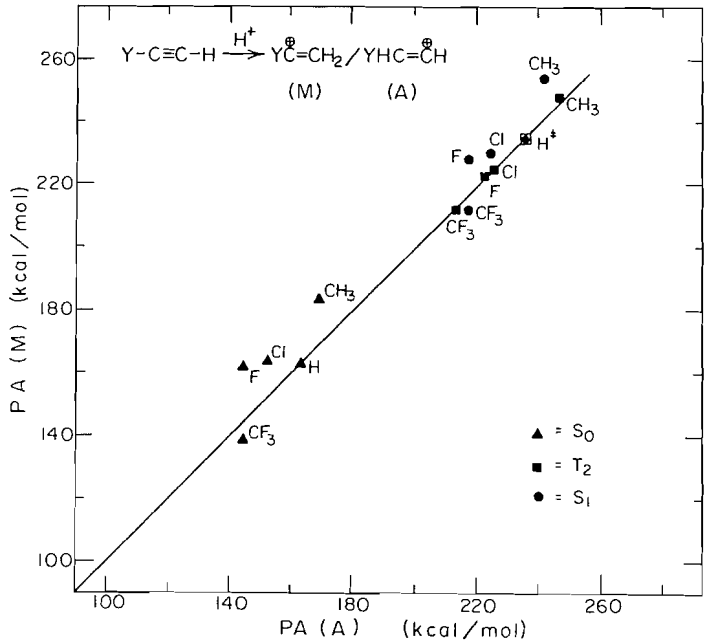


FIG. 7. Correlation diagram of proton affinities (PA) for YCCH (Y = H, F, Cl, CH_3, and CF_3) in $S_0(^1\Sigma^+/^1A_1)$, $T_2(^3A'')$ and $S_1(^1A'')$, resulting in Markownikoff (*M*) and anti-Markownikoff (*aM*) protonation products, i.e. $YCCH_2^+(^1A_1/^1A', ^{1,3}A'')$ and $YCHCH^+(^1A', ^{1,3}A'')$ respectively. $PA(HCCH(^3A_u)) \neq PA(HCCH(^1A_u))$, taken from ref. 3.

is not strictly valid because of the conjugating aromatic ring, some interesting analogies can be drawn:

(*1*) For non-nitro substituted phenylacetylenes, the increase in photohydration efficiency and concurrent fluorescence quenching with decreasing pH indicates that the reaction proceeds via rate limiting *M* protonation of a zwitterionic-like S_1, which is approximately 10^{11}–10^{14} times more reactive than S_0. On the basis of the present calculations for simple aliphatic alkynes without strong electron withdrawing substituents (i.e. Y ≠ CF_3), S_1, in contrast to S_0, is predicted to be strongly polarized such that electron density is displaced toward the terminal (β) carbon. Also, with the exception of Y = CF_3, the present calculations give $PA(YCCH(S_1)(M)) > PA(YCCH(S_1)(aM))$ by approximately 10 kcal/mol, which is consistent with the completely regiospecific *M* protonation observed experimentally for phenylacetylenes substituted by H or electron-donating groups.

(*2*) Plots of fluorescence quenching versus pH are sigmoid with inflection points around pH = 0 (1), which suggests that S_1 of substituted phenylacetylenes is of greatly enhanced basicity compared to S_0. Assuming that phenylacetylenes are weaker bases than benzonitriles (27) in their S_0 states, this implies that $\Delta pK = pK(S_1) - pK(S_0) > 10$ (4). The present calculations support this qualitatively in that $\Delta PA = PA(S_1) - PA(S_0)$ is very large in every case calculated.

(*3*) Although triplet sensitization failed to produce photohydration products (acetophenones) in the above cases, T_1 was not found to be photochemically unreactive, but led to a multiplicity of products including polymer. From the present investigation it is predicted that for simple alkynes T_1 would be a non-polar "vinyl biradical", thereby facilitating abstraction–recombination reactions.

(*4*) For nitro-substituted phenylacetylenes, which are believed to react via T_1 on direct irradiation, the complete *aM* addition of water to give phenylacetaldehydes, the observed acid-catalysis, and the complete quenching of reaction by di-*t*-butyl nitroxide all suggest the mechanistic involvement of a reverse polarized, zwitterionic-like T_1 state. According to the present study, T_2 of the closest analogue, CF_3CCH, *is* of the appropriate polarization and enhanced basicity, but based on the PA values for *M* and *aM* protonation, it is predicted to react non-regiospecifically. It is, however, well-known that NO_2 is more electron-withdrawing than CF_3 in ground state molecules, and this difference is probably enhanced in their excited states (28). However, until calculations on nitroacetylene can be performed, no clear prediction can be made.

5. *Reactivity comparisons*

In addition to the calculations of PA values for the various excited states of YCCH, it was of interest to make estimates of the energies of proton transfer (E_{PT}) and hydration (E_H) based on the gas phase reactions:

$$YC{\equiv}CH + H_3O^+ \rightarrow YC^+{=}CH_2 \text{ (or } YCH{=}{}^+CH) + H_2O$$

$$Y^+C{=}CH_2 + H_2O \rightarrow YC(^+OH_2){=}CH_2$$

$$\text{(or } YCH{=}{}^+CH + H_2O \rightarrow YCH{=}CHO^+H_2)$$

where Y = H, CH_3, or CF_3. For these reactions,

$$E_{PT} \simeq E_{SCF}(H_2O) + E_{SCF}(BH^+) - E_{SCF}(H_3O^+) - E_{SCF}(B)$$

$$E_H \simeq E_{SCF}(BH(O^+H_2)) - E_{SCF}(H_2O) - E_{SCF}(BH^+)$$

Can. J. Chem. Downloaded from www.nrcresearchpress.com by 186.148.149.217 on 09/07/12
For personal use only.

where B, BH^+, and $BH(O^+H_2)$ refer to the acetylene, vinyl cation (*M* or *aM*), and hydrated vinyl cation (*M* or *aM*), respectively. The necessary values for acetylene itself have been reported previously (29), and those for CH_3CCH and CF_3CCH are given in ref. 30. Calculations (at the 3-21G level) were carried out for S_0, T_1, T_2, and S_1 of the acetylene, and for S_0, T_1, S_1, of the vinyl cation and hydrated vinyl cation. The reason for including T_2 for the starting acetylene is that in considering the energetics of reaction, strictly speaking only those processes occurring between directly correlating states should be considered, as illustrated below for acetylene.

$$B + H_3O^+ \rightarrow BH^+ + H_2O \rightarrow BH(O^+H_2)$$

$$S_0D_{\infty h}(^1\Sigma_g^+) \rightarrow SC_{2v}(^1A_1) \rightarrow S_0C_s(^1A_1)$$

$$T_2C_{2h}(^3A_u) \rightarrow T_1C_s(^3A'') \rightarrow T_1C_s(^3A'')$$

$$S_1C_{2h}(^1A_u) \rightarrow S_1C_s(^1A'') \rightarrow S_1C_s(^1A'')$$

This means that gas phase proton transfer to triplet states can involve states higher than T_1, although the cations and hydrated cations produced are in their lowest triplet states in every case. The changes in E_{SCF} on protonation, followed by hydration, are shown graphically for acetylene to form a reaction coordinate diagram in Fig. 8. Although this is obviously skeletal in that it is based on only the three fixed points for which RHF-SCF calculations were possible, it is nonetheless reasonable to draw several conclusions about the photochemical versus thermal reactivity of the acetylene system. Firstly it is immediately obvious that electronic excitation greatly decreases the energy of proton transfer, whichever excited state is involved. This has been discussed in a previous section. Secondly, the hydration of the vinyl cation intermediate is strongly exothermic in every case. This implies that whether the hydration step is adiabatic or not, the rate-determining step would be proton transfer. This is fully consistent with the observed general acid catalysis for the S_1 reactions of substituted phenylacetylenes, and not inconsistent with the hydronium ion catalysis observed for the T_1 reactions of nitro-substituted analogues. In the latter cases, general acid catalysis has not yet been demonstrated experimentally, although it seems likely that these behave in a way similar to the S_1 reactions. Finally, although calculation of a complete reaction profile is not feasible at present, it seems clear from the degree of endo- or exothermicity of the first step, that S_0 will be relatively unreactive, since this step is a distinctly uphill process. Similarly it is implied that S_1 will be more reactive than either T_1 or T_2, but that any of these excited state reactions will be much faster than the thermal hydration. From what is known experimentally of the H_3O^+-catalyzed rates of substituted phenylacetylenes in their ground, triplet and singlet states, the predicted behavior of this simple model system is in excellent accord, in a *relative* reactivity sense. For example, typical thermal hydrations of acetylenes have values of $k_{H_3O^+}$ in the 10^{-5}–10^{-7} M^{-1} s^{-1} range (31), whereas analogous singlet state reactions have $k_{H_3O^+}$ in the 10^6–10^8 M^{-1} s^{-1} range (1, 3). Although the rates for corresponding triplet states are less well established, recent estimates[5] place these in the 10^4–10^5 M^{-1} s^{-1} range. Assuming a diffusion-controlled limit of 10^{10} for hydrations in aqueous solution, the above rate ranges correspond to $\Delta G^{\ddagger}$ values of 21–23 kcal, 7–8 kcal and 3–5 kcal for the ground, triplet, and singlet reactions, respectively. However, it must be emphasized that solvation energies will lower the energies of the cationic intermediates considerably compared to those involved in any calculated gas phase processes. Therefore although the above $\Delta G^{\ddagger}$ values are generally consistent with the relative reactivities implied in Fig. 8, the possible impact of solvent effects on the present conclusions cannot be overlooked.

[5]These estimates are based on slopes of Stern–Volmer plots of product quantum yield versus $[H_3O^+]$ (32).

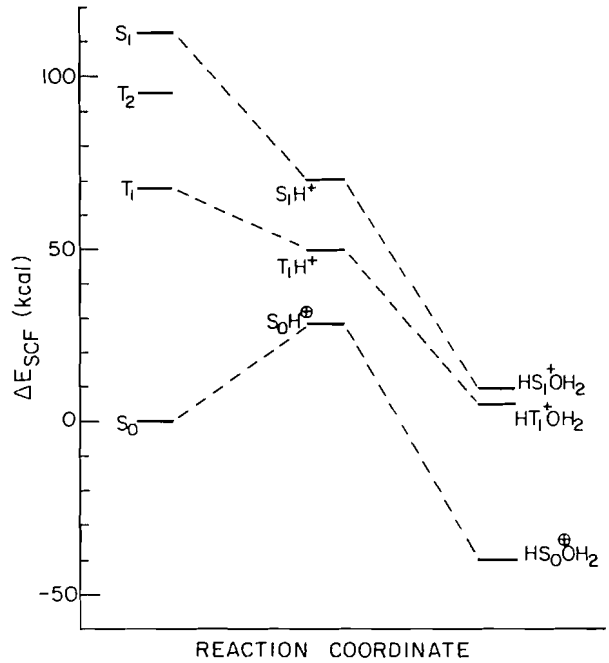


FIG. 8. Reaction coordinate diagram for adiabatic hydration of acetylene.

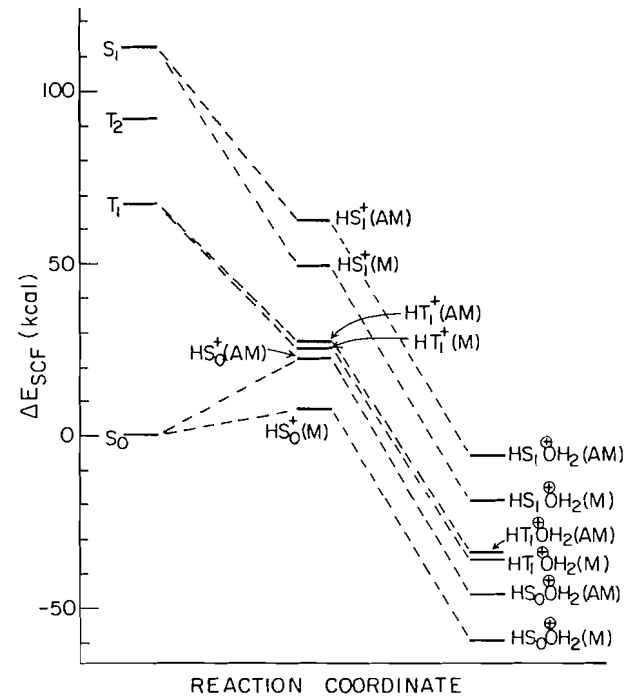


FIG. 9. Reaction coordinate diagram for adiabatic hydration of methylacetylene (*M* = Markownikov, *aM* = anti-Markownikov).

Corresponding reaction profiles for the hydration of CH_3CCH and CF_3CCH in their ground and low lying excited states are shown in Figs. 9 and 10, where both *M* and *aM* processes are included. The main difference for the methyl derivative (Fig. 9)

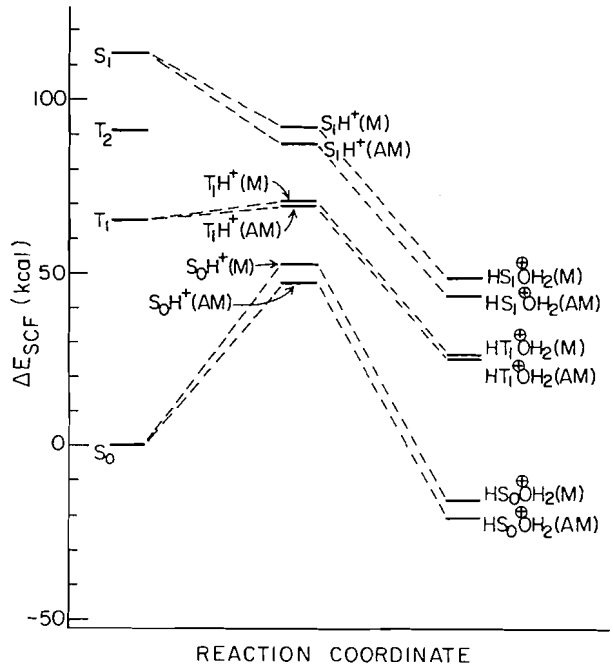


FIG. 10. Reaction coordinate diagram for adiabatic hydration of trifluoromethylacetylene. (M = Markownikov, aM = anti-Markownikov).

is that all the energies of proton transfer are lowered, compared to that of acetylene, although the relative reactivities of the singlet, triplet and ground states are maintained. In addition, the M mode of hydration is clearly favored for S_1 and S_0, as discussed previously, while the triplet (T_1 or T_2) shows no strong regioselectivity. For the trifluoromethyl derivative (Fig. 10), all the energies of proton transfer are raised, relative to that of acetylene, but again the relative singlet, triplet, and ground state reactivities are not materially affected. In this case, however, aM hydration is preferred for S_1 and S_0 (although to a less extent), but the triplet again shows no significant regioselectivity. In every case (Y = CH_3 or CF_3, M or aM) the hydration step is again strongly exothermic, supporting the idea that in both ground and excited state hydrations, proton transfer would be the rate-determining step.

The changes in E_{PT} on CH_3- or CF_3-substitution are in accord with reported Hammett-type relationship for substituted phenylacetylenes, where the ρ value is large and negative for both the thermal (33) and photochemical (singlet only) hydration.[6]

Conclusion

It is concluded that overall, the agreement between the predicted behavior of these simple model acetylene systems, with substituents of different types, is in very good accord with what is known experimentally about the photochemical versus thermal reactions of analogous systems. This is particularly true for the calculated basicity and reactivity enhancements on electronic excitation. As far as observed regioselectivity is concerned (in both thermal and photochemical hydrations), the calculations are in accord with experiment only for S_0 and S_1 reactions of systems with electron-donating substituents. For analogous triplet reactions, the predicted lack of regioselectivity remains to be tested experimentally via triplet sensitization experiments on CF_3 substituted systems, which are currently in progress. It also remains to be seen whether eventual calculations on nitro-containing systems will lead to a predicted reversal of regioselectivity ($M \rightarrow aM$), even for triplet states, as observed experimentally.

Finally, it is worth pointing out that although the present calculations on YCCH systems were carried out only at the 3-21G level for practical reasons, the previously reported investigation of HCCH itself (5) was carried out at the STO-3G, 3-21G, and 6-31**G levels. It was found that none of the general conclusions with respect to geometries, excited state isomerism, state energy ordering, proton affinities, and energies of hydration were materially affected by increasing the size of basis set or by inclusion of polarization functions. The general correspondence between the present calculated results and conclusions based on YCCH systems, with those on the parent system should help to allay possible concerns based on the size of basis set used in the present work.

[6]Although the ρ value for photohydration of phenylacetylenes has not been measured directly, a plot of log k_H^+ versus log k_H^+ for styrene photohydration has a slope of ~0.6 (34). Since ρ for styrenes (1) is −5.6, this indicates a ρ value for phenylacetylenes of approximately −3.4 versus ground state σ values.

Acknowledgements

Much gratitude is expressed to Dr. M. R. Peterson for helpful discussions, and to the Natural Sciences and Engineering Research Council of Canada (NSERC) for continued financial support and a postgraduate scholarship to P.S.M.

1. P. WAN, S. C. CULSHAW, and K. YATES. J. Am. Chem. Soc. **104**, 2509 (1982); P. WAN and K. YATES. J. Org. Chem. **48**, 869 (1983).
2. K. RAFIZADEH and K. YATES. J. Org. Chem. **49**, 1500 (1984).
3. J. MCEWEN and K. YATES. J. Am. Chem. Soc. **109**, 5800 (1987).
4. K. YATES. J. Am. Chem. Soc. **108**, 6511 (1986). However, recent measurements based on the Forster cycle method suggest that ΔpK^* may be considerably greater than 10 logarithmic units. K. YATES and M. K. BOYD. Unpublished results.
5. P. S. MARTIN, K. YATES, and I. G. CSIZMADIA. Theoret. Chim. Acta, **64**, 117 (1983); J. Mol. Struct. Theochem. In press.
6. (*a*) M. R. PETERSON and R. A. POIRER. MONSTERGAUSS. University of Toronto. 1981; (*b*) S. BINKLEY, R. A. WHITESIDE, R. KRISHNAN, R. SEEGER, D. J. DEFREES, H. B. SCHLEGEL, S. TOPIOL, L. R. KAHN, and J. A. POPLE. GAUSSIAN 80. Carnegie Mellon University. 1980; (*c*) S. KATO and K. MOROKUMA. Program GSCF. Institute for Molecular Science. 1979; (*d*) J. GODDARD, N. C. HANDY, and H. F. SCHAEFER. J. Chem. Phys. **71**, 1525 (1979); (*e*) S. KATO and K. MOROKUMA. Chem. Phys. Lett. **65**, 19 (1979).
7. J. S. BINKLEY, J. A. POPLE, and W. J. HEHRE. J. Am. Chem. Soc. **102**, 939 (1980).
8. R. CARBO and O. GROPEN. Adv. Quant. Chem. **12**, 159 (1980).
9. (*a*) W. C. DAVIDSON. Math. Programming, **9**, 1 (1975); (*b*) W. G. DAVIDSON and L. NAZARETH. Technical Memos 303 and 306, Applied Mathematics Division, Argonne National Laboratories. 1977.
10. R. J. GILLESPIE. Molecular geometry, Van Nostrand-Reinhold, Princeton. 1972.
11. M. R. PETERSON and I. G. CSIZMADIA. J. Mol. Struct. Theochem. **123**, 399 (1985).
12. J. K. TYLER and J. SHERIDAN. Proc. Chem. Soc. 119 (1960).
13. J. K. TYLER and J. SHERIDAN. Trans. Faraday. Soc. **89**, 2661 (1963).
14. J. L. DUNCAN, D. C. MCKEAN, P. D. MALLINSON, and R. D. MCCULLOUGH. J. Mol. Spectrosc. **46**, 232 (1973).
15. N. N. SHOOLERY, R. G. SCHULMAN, W. F. SHEEHAN, V. SCHOMAKER, and D. M. YOST. J. Chem. Phys. **19**, 1364 (1951).
16. W. J. HEHRE, L. RADOM, P. R. SCHLEYER, and J. A. POPLE. Ab

Can. J. Chem. Downloaded from www.nrcresearchpress.com by 186.148.149.217 on 09/07/12
For personal use only.

initio molecular orbital theory. Wiley-Interscience, New York. 1986.
17. R. J. BUENKER and S. D. PEYERIMHOFF. Chem. Rev. **74**, 127 (1974).
18. D. DEMOULIN. Chem. Phys. **11**, 329 (1975).
19. G. HERZBERG and E. TELLER. Z. Phys. Chem. B**21**, 410 (1933); R. RENNER. Z. Phys. **92**, 172 (1934).
20. H. A. JAHN and E. TELLER. Proc. R. Soc. **161**A, 220 (1937).
21. R. CARBO and J. M. RIERA. A general SCF theory. Springer-Verlag, New York. 1978.
22. M. R. PETERSON, G. R. DE MARE, I. G. CSIZMADIA, and O. P. STRAUSZ. J. Mol. Struct. Theochem. **92**, 239 (1983).
23. R. A. WHITESIDE, J. S. BINKLEY, R. KRISHNAN, D. J. DEFREES, H. B. SCHLEGEL, and J. A. POPLE. Carnegie-Mellon Quantum Chemistry Archive. Carnegie-Mellon University. 1980.
24. D. B. BEACH, C. J. EYERMANN, S. P. SMIT, F. X. SI, and W. L. JOLLY. J. Am. Chem. Soc. **106**, 536 (1984).
25. J. B. PEDLEY and J. RYLANCE. Sussex-N.P.L. computer analysed thermochemical data: organic and organometallic compounds. University of Sussex. 1977.
26. K. FUJITA, K. YAMAMOTO, and T. SHONO. Tetrahedron Lett. **39**, 3865 (1973).
27. M. LILER and D. J. KOSANOVIC. J. Chem. Soc. 1084 (1958).
28. P. J. BALDRY. J. Chem. Soc. Perkin II, 951 (1979).
29. K. YATES, P. MARTIN, and I. G. CSIZMADIA. Pure Appl. Chem. **60**, 205 (1988).
30. P. S. MARTIN. Doctoral thesis. University of Toronto, Toronto, Ont., Canada. 1988.
31. W. M. SCHUBERT and J. R. KEEFFE. J. Am. Chem. Soc. **94**, 559 (1972); P. S. NOYCE and M. D. SCHIAVELLI. J. Am. Chem. Soc. **90**, 1020 (1968).
32. P. WAN and K. YATES. Unpublished results.
33. G. MODENA, F. RIVETTI, G. SCORRANO, and U. TONELLATO. J. Am. Chem. Soc. **99**, 3392 (1977).
34. J. MCEWEN and K. YATES. Unpublished results.

Can. J. Chem. Downloaded from www.nrcresearchpress.com by 186.148.149.217 on 09/07/12
For personal use only.

A theoretical study of adiabatic proton transfer to simple substituted allenes in their ground and excited states

PETER S. MARTIN, KEITH YATES,[1] AND IMRE G. CSIZMADIA
Department of Chemistry, University of Toronto, Toronto, Ont., Canada M5S 1A1

Received December 6, 1988[2]

PETER S. MARTIN, KEITH YATES, and IMRE G. CSIZMADIA. Can. J. Chem. **67**, 2188 (1989).

RHF-SCF 3-21G calculations are reported for the $^1A'$, $^{1,3}A''$, $^12A'$, and $^{1,3}2A''$ states of simple substituted allenes $YCHCCH_2$, where Y = CH_3, H, F, Cl, CF_3, and the $^1A'$ and $^{1,3}A''$ states of their Markovnikov (*M*) and anti-Markovnikov (*aM*) cations, $CHYCHCH_2^+$ and $CHYCCH_3^+$, respectively. Equilibrium electronic structures and the mechanism of adiabatic protonation are described qualitatively in terms of Lewis/resonance schematic representations. Calculated proton affinities (PA) suggest that relative to the ground state ($^1A'$), the excited states $^{1,3}2A''$ are of greatly enhanced basicity with respect to protonation at either regiocenter. A graphical representation of PA(*M*) versus PA(*aM*) leads to the following conclusions: (*1*) irrespective of both regiocenter (*M*/*aM*) and state ($^1A'/^32A''/^12A''$), the PA's for $YCHCCH_2$ decrease with respect to Y in the order $CH_3 > H > Cl > CF_3$; (*2*) the F-substituent gives a PA value greater than that for H- in the ground state, but less than that for H- in the two excited states; (*3*) for all substituents Y, including CF_3, protonation of both $^1A'$ and $^12A''$ is predicted to be regioselective in the *M* direction; (*4*) regardless of Y, $^32A''$ exhibits no significant protonation regioselectivity. Critical comparison of these theoretical predictions is made with available experimental evidence.

Key words: proton transfer, excited states, photohydration, allenes.

PETER S. MARTIN, KEITH YATES et IMRE G. CSIZMADIA. Can. J. Chem. **67**, 2188 (1989).

On a effectué des calculs RHF-SCF 3-21G sur les états $^1A'$, $^{1,3}A''$, $^12A'$ et $^{1,3}2A''$ des allènes substitués simples $YCHCCH_2$, dans lesquels Y = CH_3, H, F, Cl et CF_3, ainsi que sur les états $^1A'$ et $^{1,3}A''$ de leurs cations Markovnikov (*M*) et anti-Markovnikov (*aM*), respectivement $CHYCHCH_2^+$ et $CHYCCH_3^+$. On décrit qualitativement les équilibres des structures électroniques et le mécanisme de la déprotonation adiabatique en fonction de représentations schématiques de Lewis et de résonance. Les valeurs calculées pour les affinités protoniques (AP) suggèrent que, par rapport à l'état fondamental ($^1A'$), la basicité des états excités $^{1,3}2A''$ est fortement augmentée par rapport à la protonation à l'un ou l'autre des deux régiocentres. Une représentation graphique des AP(*M*) vs. AP(*aM*) conduit aux conclusions suivantes : (*1*) quels que soient le régiocentre (*M*/*aM*) et l'état ($^1A'/^32A''/^12A''$), les AP des composés $YCHCCH_2$ diminuent par rapport à Y dans l'ordre $CH_3 > H > Cl > CF_3$; (*2*) dans l'état fondamental, le produit substitué par un F possède une AP plus grande que celle du produit substitué par un H; toutefois, dans les deux états excités, l'ordre est l'inverse; (*3*) pour tous les substituants, y compris le CF_3, il est prédit que la protonation des états $^1A'$ et $^12A''$ sera régiosélective dans la direction *M*; (*4*) quelle que soit la nature de Y, l'état $^32A''$ ne présente pas de régiosélectivité importante pour la protonation. On fait des comparaisons critiques de ces prédictions théoriques avec les données expérimentales disponibles.

Mots clés : transfert du proton, états excités, photohydratation, allènes.

[Traduit par la revue]

Introduction

The often dramatic changes in the acidity or basicity of organic molecules on electronic excitation can be simply rationalized in terms of the Forster equation (1) $\Delta pK = pK^*_{BH^+} - pK_{BH^+} = Nh(\nu_B - \nu_BH^+)/2.3RT$ from which it follows that if the transition $BH^+ \rightarrow BH^{+*}$ is red-shifted relative to $B \rightarrow B^*$ (i.e. $\nu_B > \nu_{BH^+}$) then B* must be a stronger base than B (i.e. $pK^*_{BH^+} > pK_{BH^+}$), and vice-versa for a blue-shifted transition. However for gas-phase molecules, the proton affinity (PA), defined to be $-\Delta H_{298}$ for the reaction $B + H^+ \rightarrow BH^+$, is used as a measure of intrinsic basicity. LCAO-MO-SCF calculations provide the estimate $PA(B) \approx E_{SCF}(B) - E_{SCF}(BH^+)$, rather than the p*K* definition usually employed in the measurement of basicities in solution.

From experimental work on the photohydration of phenylallenes (2) to give cinnamyl alcohols efficiently, even in dilute aqueous solution, it was concluded that reaction proceeds via rate-limiting Markovnikov[3] protonation of a polarized S_1 state, which is of greatly enhanced basicity relative to S_0. On the basis of RHF-SCF 3-21G calculations on allene itself (3), it was predicted that $\Delta PA(S_1(M)) > \Delta PA(S_1(aM)) \gg 0$ where $\Delta PA = PA(S_1) - PA(S_0)$, and that S_1 is *trans* bent and zwitterionic-like, thus diminishing the need for rehybridization on proton transfer, and thereby facilitating photohydration. However, it was found experimentally (2) that, nitro-substituted phenylallenes, which intersystem cross efficiently to the T_1

[1]To whom correspondence should be addressed.
[2]Revision received July 6, 1989.

[3]Strictly speaking, the Markovnikov/anti-Markovnikov terminology is not applicable to the regioisomeric cations which can be formed by adding an electrophile such as H^+ to a substituted allene. However, it has been adopted here by analogy with the addition of H^+ to the β-carbon of a substituted acetylene or ethylene, to give the expected more stable (Markovnikov) cationic intermediate. In the case of a substituted allene $YCHCCH_2$, analogous β-protonation would lead to the more stable allylic cation YCH^+CHCH_2 (Markovnikov). This terminology allows more direct comparison with related studies of the protonation of YCCH systems (3).

Can. J. Chem. Downloaded from www.nrcresearchpress.com by 186.148.149.217 on 09/07/12
For personal use only.

Can. J. Chem. Downloaded from www.nrcresearchpress.com by 186.148.149.217 on 09/07/12
For personal use only.

state, gave only nitrophenylacetones as photoproduct, indicating anti-Markovnikov (3) protonation as the rate-limiting step.

It was therefore decided to extend the calculations on allene, to investigate the intrinsic basicity of some simple substituted model compounds ($CHYCCH_2$, where Y = F, Cl, CH_3, and CF_3) as a function of both protonation regiocenter and electronic state.

Computational details

Ab initio LCAO-MO-SCF calculations were performed utilizing the program MONSTERGAUSS[4] in conjunction with a GOULD 32/9705 minicomputer. The split valence 3-21G (6) constitutes the basis set employed in this study. Proper spin eigenfunctions were obtained for all closed (ground) and open (excited) shell systems via Restricted Hartree-Fock (RHF) (7) theory. The geometries of the ground and low-lying excited states were energy optimized by the Optimally Conditioned (OC)[5] gradient, variable metric technique. All optimizations were terminated when the gradient length, $|g| = [\Sigma_i\{\delta E/\delta q_i\}^2/N]^{1/2}$, where q_i are the internal coordinates and the sum is over the N optimized q_i, was reduced to below 5×10^{-4} mdyn, and subject to the condition that all internal coordinate derivatives $[\delta E/\delta q_i]$ were less than 1×10^{-3} mdyn. This criterion generally yields structures within 1×10^{-4} Å, or 0.01° of the true theoretical optimum values and energies stable below the μ-Hartree level.

Ground state geometries were taken as those predicted by the Valence Shell Electron Pair Repulsion Theory (VSEPR) (9). Starting covalent bond lengths were selected from a standard geometrical model (10) based on Lewis/resonance structures of the molecule in question. Low-lying excited states of $CHYCCH_2$ and $CHYCHCH_2^+$ were assumed to be of valence type, arising from $\Pi \rightarrow \Pi^*$ excitation and possessing planar bent (C_s) structures. Similarly for $CHYCCH_3^+$, the "Π"→"*P*" valence states were constrained to C_s symmetry.

Results and discussion

Electronic states and geometries

The 3-21G predicted geometrical parameters for the ground states of YCH=C=CH_2 are in reasonable agreement with their experimental (11–13) counterparts, as shown in Table 1, with the exception of $r(ClC_\alpha)$ as expected (14).

In C_s geometries the ground state ($^1A'$) MO configurations are $...(ma')^2...(na'')^2$. These can be represented by an "sp—sp^2—sp—sp^2" (F, Cl), "sp^3—sp^2—sp—sp^2" (CH_3), or "$(sp^3)_3$—sp^3—sp^2—sp—sp^2" (CF_3) hybridized "σ" skeleton with two mutually perpendicular "π" bonds. The Frank–Condon valence excited states, arising from "π"→"π*" excitation, are derived from the configuration $...(ma')^2(na'')^1((m+1)a')^1$. Because the "π" MO lies in the "σ" plane it is of a' symmetry, and these states are obtainable from the direct product decomposition $^2A'' \times {}^2A' = {}^{1,3}A''$. The molecules are able to achieve the greatest degree of stabilization via bending and twisting about the CCC axis to achieve the planar structure of MO configuration $...(na'')^3((n-1)a'')^1(ma')^1$, which comprises the electronic structure of the equilibrated T_1 and S_1 states.

TABLE 1. Calculated and experimental[a] geometries for ground state YCH=C=CH_2[b]

Parameter		Value for Y = F	Cl	CH_3	CF_3
Bond length (Å)					
$r(C_\alpha C_\beta) = r(C_\beta C_\gamma)$	Calc.	1.29	1.29	1.29	1.29
	Expt.	1.31	1.31	1.33	1.34
$r(YC_\alpha)$	Calc.	1.37	1.84	1.52	1.48
	Expl.	1.34	1.74	1.48	—
Bond angles (deg)					
∠YCC	Calc.	124	120	124	122
	Expt.	123	122	123	—

[a]Values taken from refs. 11–13.
[b]Ground state is of $^1A'$ symmetry (C_s).

In the same manner as was accomplished (3) for the parent $CH_2CCH_2(^{1,3}A_2)$, it is possible to develop a qualitative LMO description of $CHYCCH_2(^{1,3}A'')$. Taking the appropriate linear combination among the doubly occupied $(m-1)a'$ and $(n-1)a''$ core and framework CMO's allows for generation of the inner shell "1s" core, two "sp^2—sp^2" C—C, three "sp^2—s" C—H, "sp—sp^2" (F, Cl) or "sp^3—sp^2" (CX_3) Y—C and "s—sp^3" (CH_3) or "sp—sp^3" (CF_3) CX_2—X bonding and lone pair (F, Cl, and CF_3) LMO's. The remaining "sp^2" LMO on the central C atom and the "π" system is obtained from the valence ma' together with the na'' and $(n+1)a''$ CMO's. From the Lewis/resonance diagrammatic representation of the LMO description for $CHYCCH_2(^{1,3}A'')$, as given in Fig. 1, it is apparent that these states are biradical-like as a result of the LMO occupancy $...(\text{"}1\pi\text{"})^2(\text{"}sp^2\text{"})^1(\text{"}2\pi\text{"})^1$. Unfortunately, "π" radicals of this type are plagued by an instability (15) characterized by the tendency of RHF-SCF wavefunctions to localize the odd electron and the "π" bond at opposite ends of the three-center, two-electron "π" system. This results from their inability to describe adequately the electrostatic repulsion between the single electron in the NBO and the one of opposite spin in the "π" BO. In other words, because the single configuration RHF wavefunction is unable to describe the two valence bond contributors simultaneously by converging on an intermediate geometry, inappropriate to both, there is incorrect geometry prediction in these cases (16). Since $CHYCCH_2(^{1,3}A'')$ are not amenable to proper structure analysis and are unimportant insofar as adiabatic protonation is concerned, they do not warrant further consideration.

Stabilization of $^{1,3}A''$ Frank–Condon states involving less drastic electronic reorganization is achieved via simple planar deformation, as per Walsh's predictions (17), in that the $(m+1)a'$ LUMO is reduced in energy relative to the na'' HOMO upon CCC bending. Taking the $(m-1)a''$ and $(n-1)a''$ core and framework CMO's in suitable combination, permits the formation of the inner shell "1s" core, "sp^2—sp^2" and "sp^2—sp^3" C—C, "sp^2—s" and two "sp^3—s" C—H, "sp—sp^2" (F, Cl) or "sp^3—sp^2" (CX_3) Y—C and "s—sp^3" (CH_3) or "sp—sp^3" (CF_3) CX_2—X bonding and lone pair (F, Cl, and CF_3) LMO's. The two still unaccounted for LMO's, namely the "sp^2" of the central (β) and "sp^3" of the terminal (δ) C atom, and the "σ" bond can be generated by the appropriate

[4]Reference 4*a*. The program incorporates the integral, SCF and analytic energy gradient routines for both UHF and closed shell RHF from GAUSSIAN 80 (4*b*), in addition to automatic geometry optimization by the Optimally Conditioned (OC) method (ref. 8). The RHF open shell SCF is an extensively modified version of the program (4*c*). The RHF energy gradients were programmed following ref. 5.

[5]Reference 8*a*. The routine is described in ref. 8*b*.

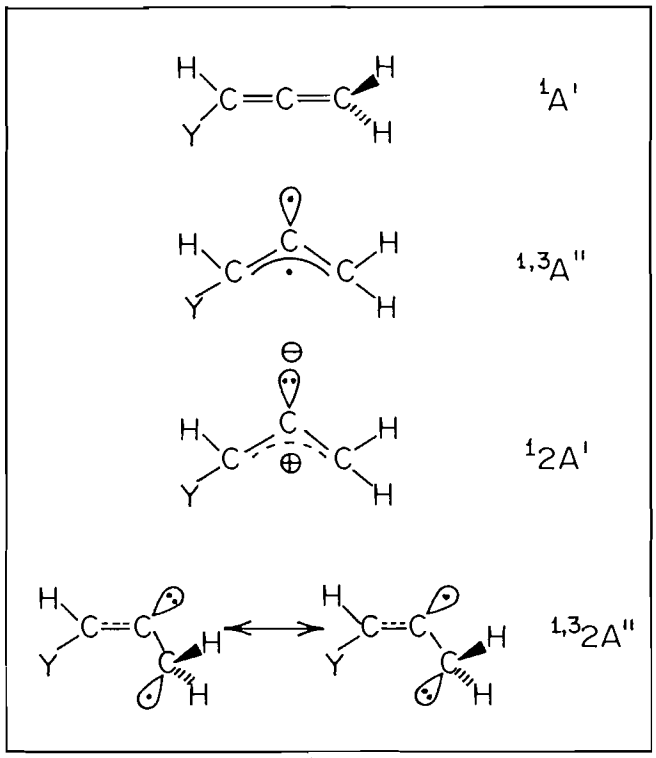


FIG. 1. Lewis/resonance structures for the $^1A'$ and *cis* isomers of the $^{1,3}A''$, $^12A'$, and $^{1,3}2A''$ states of $CHYCCH_2$.

combination of the valence ma' and $(m + 1)a'$ CMO's in association with the na'' orbital. In LMO terms then, $CHYCCH_2(^{1,3}2A'')$ are represented by an admixture of the two, oppositely polarized, resonance contributors $\ldots(\text{“}\pi\text{”})^1(\text{“}sp^2\text{”})^2(\text{“}sp^3\text{”})^1$ and $\ldots(\text{“}\pi\text{”})^1(\text{“}sp^2\text{”})^1(\text{“}sp^3\text{”})^2$, and are thus zwitterionic-like states. The Lewis/resonance structures corresponding to the LMO descriptions for $CHYCCH_2(^{1,3}2A'')$ are given in Fig. 1, where the broken line is indicative of a one-electron, two-center "π" bond.

Full details of the calculated excited state geometrics are given in ref. 18, with selected illustrative values being presented in Table 2 for the $^{1,3}2A''$ states. For these states, the $C_\alpha C_\beta$ and $C_\beta C_\gamma$ bonds appear to be essentially independent of both substituent and isomerism, and statistically indistinguishable. Also, the adjacent bonds are isomer invariant, although they obviously vary with substitution. Similarly, the angular geometry (∠CCC) and dihedral angle (∠HCC) fail to discriminate on the basis of both substitution and isomerism.

The value for $r(C_\alpha C_\beta)$, as indicated by the squared AO coefficients of the na'' CMO, is consistent with an asymmetric "π" bond in which the density of the individual electron is skewed toward the "sp^2" α-C atom, thereby lengthening the bond relative to that of benzene (r(CC) = 1.38 Å) (19) and decreasing the bond order below 1.5. On the other hand $r(C_\beta C_\gamma)$ is considerably shorter than a typical single bond, e.g. for propene r(CC) = 1.51 Å (19), and is suggestive of hyperconjugation, whereby the half filled "π"(na'') MO is stabilized via the a'' CMO of the δ "sp^3" CH_2 group. The fact that the squared AO coefficients of the doubly occupied ma' and single electron containing $(m + 1)a'$ CMO localize the electron density on the "sp^2" C(ma') and the "sp^3" γ-C ($(m + 1)a'$), indicates that the "sp^2" and "sp^3" valence LMO's are largely NBO's. Moreover, in light of the fact that $\langle\angle CCC^{1,3}2A''\rangle$ is consistent with VSEPR (9) expectations for the spatial arrangement of two "sp^2" BO in the presence of a filled "sp^2" NBO, it thus appears reasonable to represent $CHYCCH_2(^{1,3}2A'')$ mainly by the resonance contributor that associates the electron pair with the β-C atom, i.e. $\ldots(\text{“}\pi\text{”})^1(\text{“}sp^2\text{”})^2(\text{“}sp^3\text{”})^1$ rather than a composite of $\ldots(\text{“}\pi\text{”})^1(\text{“}sp^2\text{”})^2(\text{“}sp^3\text{”})^1$ and $\ldots(\text{“}\pi\text{”})^1(\text{“}sp^2\text{”})^1(\text{“}sp^3\text{”})^2$. Note that the "$sp^2$" pair and the single "$sp^3$" electron are *trans* displaced as a result of the ±110° dihedral angle that the two "sp^3" H atoms make on average with the "sp^2" α-C, i.e. inversion about the γ-C atom appears to be controlled by a single minimum potential.

TABLE 2. Calculated $^{1,3}2A''$ excited state[a] geometries for $YCH{=}C{=}CH_2$

Bond lengths (Å)		
	$r(C_\alpha C_\beta) = 1.43$ $r(C_\beta C_\gamma) = 1.45$	Y = F, Cl, CH_3, CF_3
	$r_{FC} = 1.35$	
	$r_{ClC} = 1.83$	
	$r_{Cl_3C} = 1.50$	
Bond angles (deg)		
	∠CCC = 122 ∠HCC = 110	Y = F, Cl, CH_3, CF_3

[a] $^{1,3}A''$ Frank–Condon states not included for reasons given in text.

Besides geometrical isomerism, there is the additional possibility of conformational isomerism in $CHCX_3CCH_2(^{1,3}2A'')$ when single bond rotation of CX_3 is considered. From the results it is apparent that while $CHCX_3CCH_2(S_o, {}^{1,3}2A'')$ have *syn* and *anti* conformers as minima and maxima, respectively, in no instance does the energy difference between the two rotamers for a given geometric isomer exceed 2 kcal/mol. Insofar as geometric isomerism in $CHYCCH_2(^{1,3}2A'')$ is concerned, it is noteworthy that while the *cis* isomer is more stable than the *trans* for Y = F and Cl, the opposite holds true for Y = CX_3, and the maximum energy difference between isomers, which occurs for Y = Cl, is never greater than 4 kcal/mol.

On account of the structural (*M*/*aM*), geometrical (*cis*/*trans*), and conformational (CX_3) isomerism present in the Markownikoff, $CHYCHCH_2^+$ and the *anti*-Markownikoff cations, $CHYCCH_3^+$, the geometric data were subjected to categorization and subsequent statistical analysis (see ref. 18 for full details). For ground state $CHYCHCH^{2+}$ (*M* cation), both $r(C_\alpha C_\beta)$ and $r(C_\beta C_\sigma)$ appear to be substituent independent and statistically indistinguishable at 1.37 Å. However, the adjacent bonds r_{YC} are substantially shorter (1.30, 1.73, 1.48 Å) respectively for Y = F, Cl, CH_3, than their counterparts in the unprotonated substrate (see Table 1). This is indicative of lone pair Π donation (F, Cl) and hyperconjugation (CH_3) whereby the electron deficient "Π" is stabilized. This is not the case for Y = CF_3, where r_{YC} for the cation is actually longer (1.51 Å versus 1.48 Å) than in the neutral molecule.

In C_s geometries the *M* allyl cations $CHYCHCH_2^+(^1A')$ possess the ground state MO configuration $\ldots(ma')^2\ldots(na'')^2$. These can be simply represented by an "sp—sp^2—sp^2—sp^2" (F, Cl), "sp^3—sp^2—sp^2—sp^2" (CH_3) or "$(sp)_3$—sp^3—sp^2—sp^2—sp^2—sp^2" (CF_3) hybridized "σ" framework with a perpendicular "π" system, i.e. taking the occupied CMO's in suitable combination allows one to generate the inner shell "1s" core, two "sp^2—sp^2" C—C, four "sp^2—s" C—H, "sp—sp^2" (F, Cl) or "sp^3—sp^2" (CX_3) Y—C, and "s—sp^3" (CH_3) or "sp—sp^3" (CF_3) CX_2—X bonding and lone pair (F, Cl, and CF_3) LMO's. The three-center, two-electron "π" system can be accounted for by the remaining na'' CMO. Although the

Can. J. Chem. Downloaded from www.nrcresearchpress.com by 186.148.149.217 on 09/07/12
For personal use only.

Can. J. Chem. Downloaded from www.nrcresearchpress.com by 186.148.149.217 on 09/07/12
For personal use only.

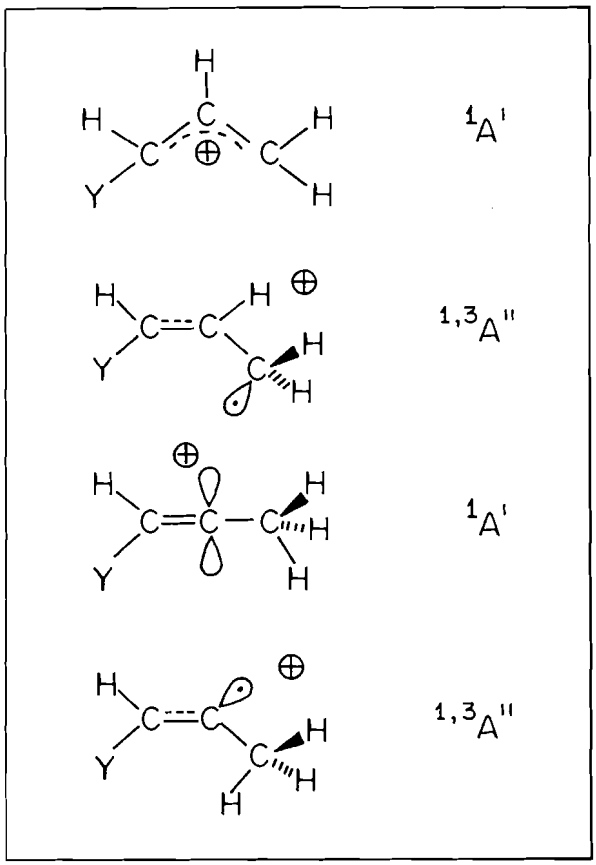
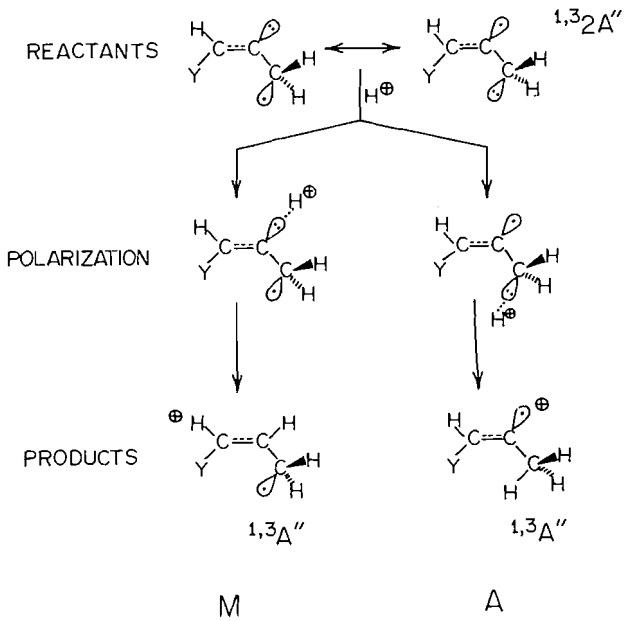


FIG. 2. Lewis/resonance structures for the $^1A_1$ and $^{1,3}A''$ states of $CHYCHCH_2^+$ and $CHYCCH_3^+$. Only the *cis* isomers of $CHYCHCH_2^+$ ($^1A_1$, $^{1,3}A''$) and $CHYCCH_3^+$ ($^{1,3}A''$) are shown.

lowest-lying, valence-excited states are obtainable from the configuration $...(ma')^2(na'')^1((n+1)a'')^1$, arising from "$\pi$" → "$\pi$" excitation, the virtual $(n+1)a''$ orbital is reduced in energy relative to the filled na'' CMO by concurrent twisting and bending of the γCH_2 group in the ground state. Thus the Frank–Condon states are stabilized, as per Walsh's rules (17), by the transformation and associated "sp^2" → "sp^3" rehybridization of the γC atom, i.e. $^{1,3}A'(na'' \times (n+1)a'') \rightarrow {}^{1,3}A''((n+1)a'' \times ma')$. A LMO representation of $CHYCHCH_2^+(^{1,3}A'')$, consisting of a "sp—sp^2—sp^2—sp^3" (F, Cl), "sp^3—sp^2—sp^2—sp^3" (CH_3) or "$(sp)_3$—sp^3—sp^2—sp^2—sp^3" (CF_3) hybridized "σ" framework with a singly occupied "π"$((n+1)a'')$ BO and "sp^3"(ma') NBO, is given in Fig. 2. While the value of $r(C_\alpha C_\beta)$ (1.41 Å) is not that different from that calculated for benzene (1.38 Å) (19) and thus not unreasonable for a one electron "π" bond, the same is not true of $r(C_\beta C_\gamma)$ (1.46 Å). Just as for $CHYCHCH_2^+(S_0)$, the shrinkage of $(r(Y—C, {}^{1,3}A''))$ relative to those of $CHYCCH_2(S_0)$ is a manifestation of lone pair "π" donation (F, Cl) and hyperconjugation (CH_3) whereby the one electron "π" bond is stabilized. However, on account of the asymmetric "π" bond that displaces the density of the single electron in the direction of the αC atom in $CHYCCH_2(^{1,3}2A'')$, this process is unimportant in these states and as such $(r(Y—C, {}^{1,3}2A''))$ are not appreciably different from $(r(Y—C)$ of $CHYCCH_2(S_0)$. In analogous fashion to $CHYCCH_2(^{1,3}A'')$, $CHYCHCH_2^+(^{1,3}2A'')$ possesses an average dihedral angle greater than 90° with respect to the αC atom, i.e. $(\angle HCC, {}^{1,3}A'') = \pm 100$, with the single exception of *cis,anti*-$CHCF_3CHCH_2^+(^3A'')$ in which, for unknown reasons, $\angle HCC = \pm 86°$. Although it is not always true that the *syn* and *anti* conformers of $CHCX_3CHCH_2^+(S_0, {}^{1,3}A'')$ are a minimum and maximum with respect to single bond CX_3 rotation within a given geometric isomer, and that the *trans* is more stable than the *cis* isomer for a given rotamer, it is always the case that the lowest energy form is the *trans,syn* isomer. The energy differences between pairs of isomers never exceed 3 kcal/mol, with the exception of *trans*, and *cis,syn*-$CHCH_3CHCH_2^+(S_0)$ for which it is 5 kcal/mol.

In C_s geometries the *aM* cations $CHYCCH_3^+$ are of the ground state MO configuration $...(ma')^2...(na'')^2\ ^1A'$. These can be simply represented by an "sp—sp^2—sp—sp^2" (F, Cl), "sp^3—sp^2—sp—sp^2" (CH_3) or "$(sp^3)_3$—sp^3—sp^2—sp—sp^2" (CF_3) hybridized "σ" skeleton with a mutually perpendicular "π"(na'') bond and an empty "p"$((m+1)a')$ orbital occupying the electron deficient "sp" central C atom. While both $r(C_\alpha C_\beta)$ and $r(C_\beta C_\gamma)$ appear to be both substituent- and isomer-independent at 1.27 and 1.43 Å respectively, the adjacent bonds are only isomer invariant, and such that r_{FC} = 1.33 Å, r_{ClC} = 1.80 Å and r_{CX_3C} = 1.54 Å. The fact that $r(C_\alpha C_\beta)$ is considerably shorter than a typical single bond, e.g. for propene $r(CC)$ = 1.51 Å (17), is indicative of hyperconjugation, through which the vacant "p"$((m+1)a')$ orbital of the "sp" central C atom is stabilized via electron density from the "σ" "sp^3—s" C—H bond of the γCH_3 group. The lowest-lying, valence excited states are obtained from the configuration $...(na'')^1((m+1)a')^1$, arising from "π" → "p" excitation, and are therefore of the symmetry type $^{1,3}A''$. However, because the $(m+1)a''$ LUMO is lowered in energy relative to the na'' HOMO upon CCC planar deformation of the ground state, the Frank–Condon states are stabilized, in accordance with Walsh's predictions (16), by the "sp" → "sp^2" rehybridization of the βC atom. A Lewis/resonance schematic representation of the LMO description for $CHYCCH_3^+(^{1,3}A'')$, comprising a "sp—sp^2—sp^2—sp^3" (F, Cl), "sp^3—sp^2—sp^2—sp^3" (CH_3) or "$(sp)_3$—sp^3—sp^2—sp^2—sp^3" (CF_3) hybridized "σ" framework with an individually occupied "sp^2"$((m+1)a')$ NBO and "π"(na'') BO, is given in Fig. 2. Both $r(C_\alpha C_\beta)$ (1.39 Å) and $\angle CCC$ (138°) are consistent with values expected for a one electron "π" bond, (i.e. for benzene, which possesses a bond order 1.5, it is calculated that $r(CC)$ = 1.38 Å (19)), and with the expected angle from VSEPR (9) theory for the spatial repulsion of two "sp^2" BO in the presence of a "sp^2" NBO containing a single electron. The adjacent bond lengths, r_{CY}, with the exception of Y = CF_3, are once again indicative of lone pair "π" donation (F, Cl) and hyperconjugation (CH_3, $C_\gamma H_3$) in view of their reduced lengths in relation to those of $CHYCCH_3^+(S_0)$ (F, Cl, and CH_3) and propene ($C_\gamma H_3$).

With Lewis/resonance structures available for $CHYCCH_2$-$(^{1,3}2A'')$, $CHYCHCH_2^+(^{1,3}A'')$ and $CHYCCH_3^+(^{1,3}A'')$, and in the same manner as was done (3) for $CH_2CCH_2(^{1,3}A'')$, it is possible to develop a qualitative pictorial representation (Scheme 1) for the process of adiabatic proton transfer. As the proton approaches along the Markownikoff reaction coordinate, (i.e. towards the central (β) C atom) $CHYCCH_2(^{1,3}2A'')$ is polarized in such a way that the resonance form that assigns the valence lone pair to the β-C completely predominates over its alternate. Conversely for *aM* protonation, $CHYCCH_2(^{1,3}2A'')$ is subject to the opposite polarization which causes the resonance structure with the terminal (γ) lone pair to become the sole contributor as the transition to $CHYCCH_3^+(^{1,3}A'')$ is made. On the basis of this model, one would predict *M* attack



SCHEME 1. Qualitative schematic representation for the process *cis*-$CHYCCH_2(^{1,3}2A'')$ + H^+ → *cis*-$CHYCHCH_2^+(^{1,3}A'')(M)$ or *cis,syn*-$CHYCHCH_3^+(^{1,3}A'')(aM)$.

to be favored over *aM* attack in that the major resonance contributor of $CHYCCH_2(^{1,3}A'')$, in the absence of the proton's electric field, corresponds to that which direct dative bond formation with the central C atom is facilitated.

Energies of proton transfer

In Figs. 3–6 the energies of the ground and low-lying excited states of $CHYCCH_2(^1A, ^{1,3}A'', ^{1,3}2A'')$, $CHYCHCH_2^+(^1A'$ and $^{1,3}A'')$ are plotted relative to that for ground state $CHYCCH_2$-$(^1A')$, where for illustrative convenience enumerative symbolism is employed, e.g. S_2 denotes the second (open shell) excited singlet state of $CHYCCH_2$ etc.. On account of the small energy differences (<2 kcal/mol) found between geometric and rotational isomers, only the lowest energy forms are graphically displayed. Note that although $CHYCCH_2(^{1,3}A'')$ are RHF-SCF unstable, they are included for qualitative comparison purposes only. A visual examination reveals that with the exception of the diradicaloid $CHYCCH_2(^{1,3}A'')$, the excited states of $CHYCHCH_2^+$ and $CHYCCH_3^+$ are red-shifted relative to those of $CHYCCH_2$ and hence that $CHYCCH_2$* is of enhanced basicity with respect to both regiocenters. Furthermore it is evident that the energy differences $\Delta E(H^+) = E_{SCF}(CHYCCH_3^+) - E_{SCF}(CHYCHCH_2^+)$ are such that for all Y, $|\Delta E(HS_0^+)| > |\Delta E(HS_1^+)| \gg |\Delta E(HT_1^+)|$. In other words, a strong Markovnikov preference is shown only by the two singlet state protonations, for all substituents Y, including CF_3.

Only adiabatic proton tranfers (i.e. between directly correlating states) will be considered, as shown below:

$$S_0(^1A') \rightarrow HS_0^+(M)(^1A')$$
$$S_0(^1A') \rightarrow HS_0^+(aM)(^1A')$$
$$T_2(^3 2A'') \rightarrow HT_1^+(M)(^3A'')$$
$$T_2(^3 2A'') \rightarrow HT_1^+(aM)(^3A'')$$
$$S_2(^1 2A'') \rightarrow HS_1^+(M)(^1A'')$$
$$S_2(^1 2A'') \rightarrow HS_1^+(aM)(^1A'')$$

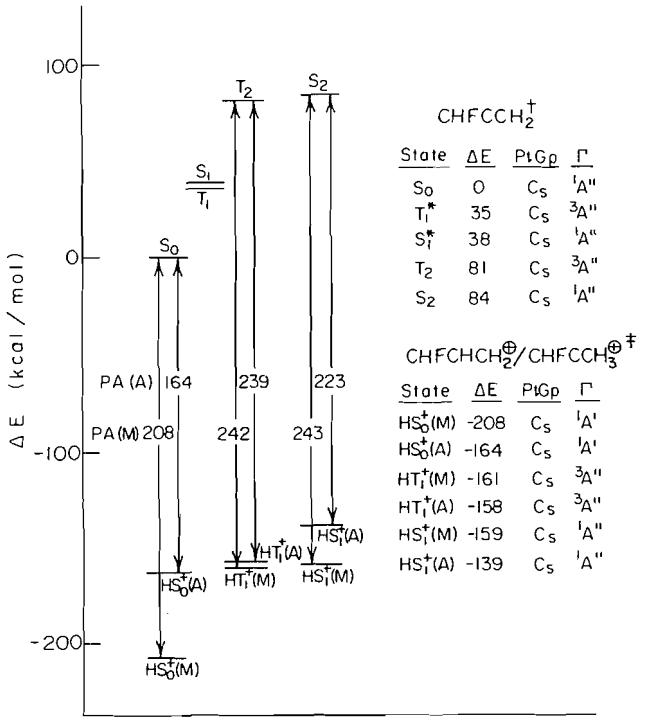


FIG. 3. Relative energies‡ of the ground and low-lying excited states for $CHFCCH_2$ ($^1A_1$, $^{1,3}A''$, $^12A'$, and $^{1,3}2A''$), $CHFCHCH_2^+$ ($^1A'$ and $^{1,3}A''$), and $CHFCCH_3^+$ ($^1A'$ and $^{1,3}A''$) with PA's evaluated between the lowest directly correlating states, $S_0(^1A') \leftrightarrow HS_0^+(M)$-$(^1A')/HS_0^+(aM)(^1A')$, $T_2(^32A'') \leftrightarrow HT_1^+(M)(^3A'')/HT_1^+(aM)(^3A'')$ and $S_2(^12A'') \leftrightarrow HS_1^+(M)(^1A'')/HS_1^+(aM)(^1A'')$ (*RHF unstable, †lowest energy geometric isomers, ‡lowest energy geometric/conformational isomers only. $\ddagger\Delta E_{SCF} = E_{SCF} - E_{SCF}(CHFCCH_2(S_0))$, where $E_{SCF}(CHFCCH_2(S_0)) = 213.529$ au).

The proton affinities are calculated from the relation PA-$(CHYCH_2)(M/aM) = E_{SCF}(CHYCCH_2) - E_{SCF}(CHYCH$-$CH_2^+/CHYCCH_3^+)$. This yields the ordered pairs for each electronic state, PA(*aM*) and PA(*M*), which are plotted against each other for all Y, including Y = H, in Fig. 7. The solid line in this figure gives the demarcation between *M* (points above) and *aM* (points below) regioselective protonations. Unlike the previously examined case of protonation of substituted acetylenes (23) (with the same Y substituents as in the present case), where changes in regioselective preference were found as a function of Y, all points in Fig. 7 lie either essentially on the 1:1 correspondence line or clearly above it.

Examination of the groups of points in Fig. 7 leads to the following conclusions: (*1*) with the exception of $CHFCCH_2$, irrespective of both regiocenter (*M*/*aM*) and state ($S_0/T_2/S_2$), the PA's for $CHYCCH_2$, decrease with respect to Y in the order $CH_3 > H > Cl > CF_3$, (*2*) regardless of Y, $CHYCCH_2(T_2)$ exhibits no significant protonation regioselectivity, (*3*) the dependence of PA(*M*) and PA(*aM*) on substituent for S_0 is such that for all Y ≠ F, PA(*M*) > PA(*aM*) by ≥20 kcal/mol on average, (*4*) for S_2, excluding $CHFCCH_2$, PA(*M*) − PA(*aM*) ≃ 14 kcal/mol, i.e. relatively speaking, regioselectivity appears to be independent of substituent for S_0 and S_2, and (*5*) proceeding in the order $S_0 \rightarrow S_2 \rightarrow T_2$, not only is the protonation regioselectivity diminished, but also the perturbational ability of the individual substituents (Y), i.e. both the mean value of PA(*M*) − PA(*aM*), and the associated standard deviation about the mean decreases.

Can. J. Chem. Downloaded from www.nrcresearchpress.com by 186.148.149.217 on 09/07/12
For personal use only.

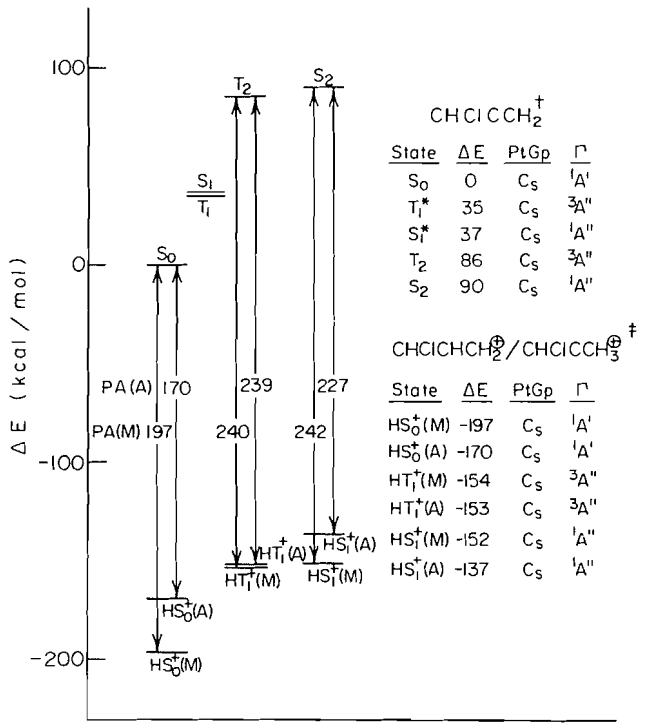


FIG. 4. Relative energies§ of the ground and low-lying excited states for $CHClCCH_2$ ($^1A_1$, $^{1,3}A''$, $^1 2A'$, and $^{1,3}2A''$), $CHClCHCH_2^+$ ($^1A'$ and $^{1,3}A''$) and $CHClCCH_3^+$ ($^1A'$ and $^{1,3}A''$), with PA's evaluated between the lowest directly correlating states, $S_0(^1A'') \leftrightarrow HS_0^+(M)(^1A')$, $T_2(^3 2A'') \leftrightarrow HT_1^+(M)(^3A'')/HT_1^+(aM)(^3A'')$ and $S_2(^1 2A'') \leftrightarrow HS_1^+(M)(^1A'')/HS_1^+(aM)(^1A'')$. (*RHF unstable, †lowest energy geometric isomers only, ‡lowest energy geometric/conformational isomers. $\S\Delta E_{SCF} = E_{SCF} - E_{SCF}(CHClCCH_2(S_0))$, where $E_{SCF}(CHClCCH_2(S_0)) = -571.929$ au).

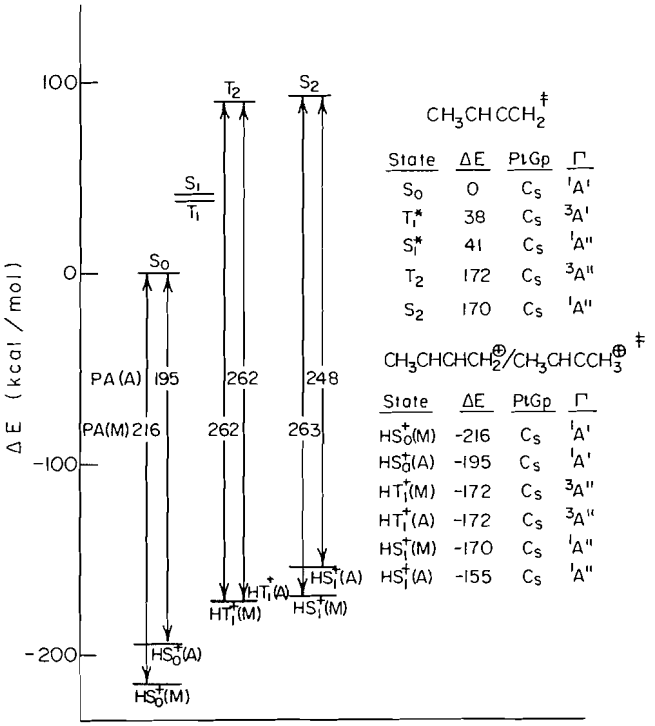


FIG. 5. Relative energies‡ of the ground and low-lying excited states for $CHCH_3CCH_2$ ($^1A_1$, $^{1,3}A''$, $^1 2A'$, and $^{1,3}2A''$), $CHCH_3CHCH_2^+$ ($^1A'$ and $^{1,3}A''$), and $CHCH_3CCH_3^+$ ($^1A'$ and $^{1,3}A''$), with PA's evaluated between the lowest directly correlating states, $S_0(^1A') \leftrightarrow HS_0^+(M)(^1A')/HS_0^+(aM)(^1A')$, $T_2(^3 2A'') \leftrightarrow HT_1^+(M)(^3A'')$ and $S_2(^1 2A'') \leftrightarrow HS_1^+(M)(^1A'')/HS_1^+(aM)(^1A'')$. (*RHF unstable, †lowest energy geometric/conformational isomers only, $\ddagger\Delta E_{SCF} = E_{SCF} - E_{SCF}(CHCH_3CCH_2(S_0))$, where $E_{SCF}(CHCH_3CCH_2(S_0)) = -154.041$ au).

With regard to $CHFCCH_2$ and points (*1*), (*3*) and (*4*) above, it is apparent that its anomalous behavior can be traced to the F atom's extraordinary ability to act, relative to the H atom, as an electron donor in $CHFCHCH_2^+(S_0)$, as an electron acceptor in $CHFCHCH_2^+(S_1)$, and as an electron acceptor of comparable degree to Y = CF_3 in both S_0 and S_1 of $CHFCCH_3^+$. It should be pointed out that such ambivalent behavior is not unusual for the F substituent, since it is well-known that its σ-type substituent constants can vary from −0.07 to +0.35, depending on whether its resonance or inductive effect is dominant (21).

Comparison with experimental evidence

Although excited state basicity enhancement has not yet been demonstrated for the simple model systems considered in this study, it has been observed for both aliphatic and aromatic substituted allenes, e.g. 1,2-cyclononadiene (25) and tetraphenylallene (26) undergo photoaddition of acetic acid and methanol, respectively, to produce the corresponding allyl acetate and allyl ether, while 1,1-phenylmethylallene (2) photohydrates in the presence of acid to yield a cinnamyl alcohol. Thus they all experience regiospecific photoprotonation of an excited singlet in the Markownikoff sense, under solution conditions in which they would be thermally inert. Consideration of the theoretical results (Fig. 7) suggests that this behavior is not altogether unexpected, given that for the reactive singlet, i.e. the zwitterionic-like S_2, as opposed to the relatively nonpolar, diradicaloid S_1, it is predicted that on average $\Delta PA(S_2(M)) \approx 47$.

Recent studies of the thermal and photochemical hydrations of substituted phenylallenes have shown that although both are acid-catalyzed reactions, the photochemical reaction takes place efficiently at much lower acidities than the thermal analogue. The implication is that electronic excitation greatly increases the basicity of S_1 relative to S_0. This is supported by the fact that fluorescence quenching of phenylallene itself, as a function of pH, is sigmoid with an inflection point around pHO^2, which is similar to the behavior shown by the S_1 states of substituted styrenes and phenylacetylenes (24). Although the ground state pK of phenylallene is not known, the fact that its thermal hydration required 70–83% H_2SO_4 to effect reasonable conversion (2), suggests that it is a very weak base. Hence $\Delta pK^* = pKS_1 - pKS_0$ for such allenes is probably very large. This is in accord with the PA values calculated for the simple model compounds in the present study.

Although phenylallene and α-methylphenylallene both hydrate regiospecifically in the *M* direction via S_0 or S_1, which is also in accord with the present calculations, *m*- and *p*-nitrophenylallenes do not. Thermally, these compounds give both *M* and *aM* products and hence are non-regiospecific. Photochemically, they react via T_1 after efficient intersystem crossing from S_1, and do react regiospecifically, but in the *aM* direction (2). Neither of these results is in accord with theoretical expectations based on $YCHCCH_2$ models, where Y is a strongly electron-withdrawing group such as CF_3. Since it is well known that NO_2 is more strongly electron-withdrawing than CF_3 in ground state molecules and that this difference is probably accentuated in

Can. J. Chem. Downloaded from www.nrcresearchpress.com by 186.148.149.217 on 09/07/12
For personal use only.

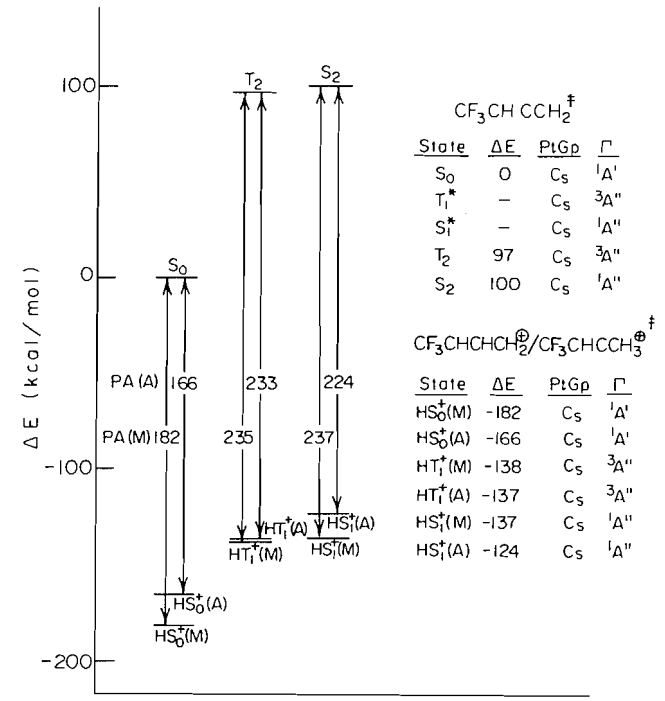


FIG. 6. Relative energies‡ of the ground and low-lying excited states for $CHCF_3CCH_2$ ($^1A_1$, $^{1,3}A''$, $^1 2A'$, and $^{1,3}2A''$), $CHCF_3CHCH_2^+$ ($^1A'$ and $^{1,3}A''$), and $CHCF_3CCH_3^+$ ($^1A'$ and $^{1,3}A''$), with PA's evaluated between the lowest directly correlating states, $S_0(^1A') \leftrightarrow HS_0^+(M)(^1A')/HS_0^+(aM)(^1A')$, $T_2(^3 2A'') \leftrightarrow HT_1^+(M)(^3A'')/HT_1^+(aM)(^3A'')$ and $S_2(^1 2A'') \leftrightarrow HS_1^+(M)(^1A'')/HS_1^+(aM)(^1A'')$ (*RHF unstable, †lowest energy geometric/conformational isomers only, $\ddagger \Delta E_{SCF} = E_{SCF} - E_{SCF}(CHCF_3CCH_2(S_0))$, where $E_{SCF}(CHCF_3CCH_2(S_0)) = -449.031$ au).

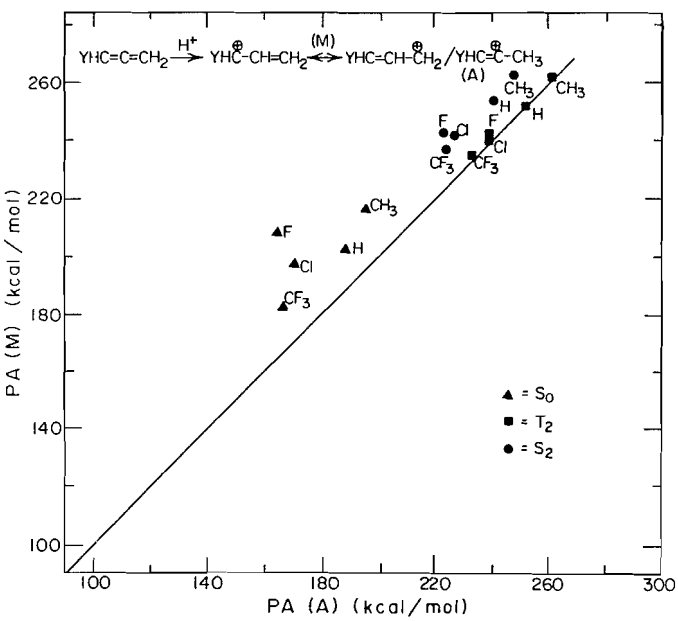


FIG. 7. Correlation diagram of proton affinities (PA) for $CHYCCH_2$ (Y = H*, F, Cl, CH_3 and CF_3) in $S_0(^1A_1)$, $T_2(^3 2A'')$, and $S_2(^1 2A'')$ states, resulting in Markownikoff (M) and anti-Markownikoff (aM) protonation products, i.e. $CHYCHCH_2^+$ ($^1A'$, $^{1,3}A''$) and $CHYCCH_3^+$ ($^1A'$, $^{1,3}A''$), respectively (*values of ($PA(CH_2CCH_2(aM))$ and ($PA(CH_2CCH_2(M))$ taken from ref. 4).

their excited states (27), attempts were made to carry out RHF-SCF calculations on excited states of nitroallene. However, as found previously for nitro acetylene (20), these were completely unsuccessful in locating stable minima on either the singlet or triplet surfaces. It appears from all experimental evidence to date that NO_2 group is able to produce reverse-polarized T_1 states, in the sense that these react regiospecifically for nitrophenylacetylenes (24), -acetylenes (24) and -allenes (2) but in the opposite (aM) sense to what is observed for corresponding S_1 states, which are all regiospecific in the expected M direction. It remains to be seen whether this behavior can be explained theoretically by eventual SCF calculations on NO_2 containing systems. In addition, the fact that 1,2-nonadiene (2) is observed to undergo photochemical addition of HOAc via γ protonation of the singlet state upon direct irradiation, although reasonable given that $\Delta PA(CHYCCH_2(S_2)(aM)) \approx 56$ kcal/mol, this process is not predicted to be as energetically advantageous as β protonation. Note that excited state aM protonation of the αC atom is incompatible with the present model, and to the best of the authors knowledge all of the examples known to date (26) experience regiospecific protonation via the β(M) or γ(aM) C atoms only.

Acknowledgements

Much gratitude is expressed to Dr. M. R. Peterson for helpful discussions, and to the Natural Sciences and Engineering Research Council of Canada (NSERC) for continued financial support and for a postgraduate scholarship to P.S.M.

1. T. FORSTER. Z. Elektrochem. **54**, 42 (1950).
2. K. RAFIZADEH and K. YATES. J. Org. Chem. **49**, 1500 (1984).
3. P. S. MARTIN, K. YATES, and I. G. CSIZMADIA. J. Mol. Struct. Theochem. In press.
4. (*a*) M. R. PETERSON and R. A. POIRER. Program MONSTERGAUSS. University of Toronto, 1981; (*b*) J. S. BINKLEY, R. A. WHITESIDE, R. KRISHNAN, R. SEEGER, D. J. DEFREES, H. B. SCHLEGEL, S. TOPIOL, L. R. KAHN, and J. A. POPLE. GAUSSIAN 80. Carnegie-Mellon University, 1980; (*c*) S. KATO and K. MOROKUMA. Program GSCF. Institute for Molecular Science. 1979.
5. J. D. GODDARD, N. C. HANDY, and H. F. SCHAEFER, III. J. Chem. Phys. **71**, 1525 (1979); S. KATO and K. MOROKUMA. Chem. Phys. Lett. **65**, 19 (1979).
6. J. S. BINKLEY, J. A. POPLE, and W. J. HEHRE. J. Am. Chem. Soc. **102**, 939 (1980).
7. R. CARBO and O. GROPEN. Adv. Quant. Chem. **12**, 159 (1980).
8. (*a*) W. C. DAVIDSON. Math. Programming, **9**, 1 (1975); (*b*) W. C. DAVIDSON and L. NAZARETH. Technical Memos 303 and 306, Applied Mathematics Division, Argonne National Laboratories, 1977.
9. R. J. GILLESPIE. Molecular geometry. Van Nostrand – Reinhold, Princeton. 1972.
10. M. R. PETERSON and I. G. CSIZMADIA. J. Mol. Struct. Theochem. **123**, 399 (1985).
11. T. OGATA, M. YOSHIKAWA, and K. FUJII. Chem. Lett. **12**, 1798 (1985).
12. H. MOON, J. H. GOLDSTEIN, and J. W. SIMMONS. Spectrochim. Acta, **16**, 1267 (1960).
13. D. L. LIDE and D. E. MANN. J. Chem. Phys. **27**, 874 (1957).
14. W. J. HEHRE, L. RADOM, P. R. SCHLEYER, and J. A. POPLE. Ab initio molecular orbital theory. Wiley–Interscience, New York. 1986.
15. E. S. HUYSER, D. FELLER, W. J. BORDEN, and E. R. DAVIDSON. J. Am. Chem. Soc. **104**, 2956 (1982).

Can. J. Chem. Downloaded from www.nrcresearchpress.com by 186.148.149.217 on 09/07/12
For personal use only.

16. E. R. DAVIDSON and W. J. BORDEN. J. Phys. Chem. **87**, 4783 (1983).
17. R. J. BUENKER and S. D. PEYERIMHOFF. Chem. Rev. **74**, 127 (1974).
18. P. S. MARTIN. Doctoral thesis, University of Toronto, Toronto, Ont. Canada. 1988.
19. R. A. WHITESIDE, J. S. BINKLEY, R. KRISHNAN, D. J. DEFREES, H. B. SCHLEGEL, and J. A. POPLE. Carnegie-Mellon Quantum Chemistry Archive. Carnegie-Mellon University. 1980.
20. P. S. MARTIN, K. YATES, and I. G. CSIZMADIA. Can. J. Chem. **67**, 0000 (1989).
21. C. D. RITCHIE and W. F. SAGER. Prog. Phys. Org. Chem. **2**, 323 (1964).
22. K. FUJITA, K. MATSUI, and T. SHONO. J. Am. Chem. Soc. **97**, 6256 (1975).
23. M. W. KLETT and R. P. JOHNSON. Tetrahedron Lett. **24**, 1107 (1983).
24. P. WAN, S. C. CULSHAW, and K. YATES. J. Am. Chem. Soc. **104**, 2509 (1982); P. WAN and K. YATES. Rev. Chem. Intermed. **5**, 157 (1984).
25. P. J. BALDRY. J. Chem. Soc. Perkin II, **2**, 951 (1979).
26. R. P. JOHNSON. Org. Photochem. **7**, 75 (1985).
27. K. YATES and J. MCEWEN. Unpublished results.

Can. J. Chem. Downloaded from www.nrcresearchpress.com by 186.148.149.217 on 09/07/12
For personal use only.

Réactions ion–molécule de $C_2H_3Cl^+$ avec le propane et le *n*-butane

JAN A. HERMAN, RODICA NEAGU-PLESU, URSZULA KRZEMIEN ET KRZYSZTOF BEDERSKI[1]

Centres de recherche sur les atomes et les molécules et le département de chimie, Université Laval, Québec (Que.), Canada G1K 7P4

Reçu le 24 avril 1989

JAN A. HERMAN, RODICA NEAGU-PLESU, URSZULA KRZEMIEN et KRZYSZTOF BEDERSKI. Can. J. Chem. **67**, 2196 (1989).

Les réactions ion/molécule de $C_2H_3Cl^+$ avec le propane ou le *n*-butane ont été étudiées dans un spectromètre de masse à photoionisation dans l'intervalle de pression de 0,01 à 1 Torr. Les principales voies de disparition de l'ion $C_2H_3Cl^+$ avec les propane et *n*-butane sont les processus de transfert de H^-, H_2^- et de charge dans le cas du *n*-C_4H_{10}. Les ions $C_nH_{2n+1}^+$ et $C_nH_{2n}^+$ formés dans ces transferts réagissent préferentiellement avec le chlorure de vinyle neutre dans des réactions de condensation accompagnées d'élimination du HCl ou Cl$^\cdot$.

Mots clés : réactions ion/molécule, spectrométrie de masse, chlorure de vinyle, propane, *n*-butane.

JAN A. HERMAN, RODICA NEAGU-PLESU, URSZULA KRZEMIEN, and KRZYSZTOF BEDERSKI. Can. J. Chem. **67**, 2196 (1989).

Ion–molecule reactions of $C_2H_3Cl^+$ with propane or *n*-butane have been studied using a photoionization mass spectrometer over the pressure range 0.01–1 Torr. The principal reasons for disappearance of the $C_2H_3Cl^+$ ion in propane and *n*-butane are the H^-, H_2^- transfer processes and charge transfer in the case of *n*-C_4H_{10}. The ions $C_nH_{2n+1}^+$ and $C_nH_{2n}^+$ formed in these transfers react preferentially with neutral vinyl chloride in condensation reactions with elimination of HCl or Cl$^\cdot$.

Key words: ion–molecule reactions, mass spectrometry, vinyl chloride, propane, *n*-butane.

[Journal translation]

Introduction

Dans une publication récente (1) nous avons montré la possibilité d'utiliser les ions moléculaires du chlorure de vinyle ionisés à 10,64 eV comme agent de transfert de charge sur l'isobutane, dont le potentiel d'ionisation est très proche, PI = 10,57 eV (2). Outre ce transfert de charge sur l'isobutane, faisant apparaître l'ion iso-$C_4H_{10}^+$, le deuxième processus d'importance est le transfert de H^- de l'isobutane sur l'ion $C_2H_3Cl^+$, engendrant une deuxième espèce ionique, *t*-$C_4H_9^+$. En raison de la très faible réactivité de ces deux ions, les seules réactions observées étaient celles avec l'isobutane neutre, lesquelles sont caracterisées par des coefficients de vitesse très faibles ($< 5 \times 10^{-14}$ cm^3 s^{-1}).

Ces expériences de photoionisation à 10,64 eV ont été étendues, dans ce travail, aux mélanges du chlorure de vinyle + propane, et chlorure de vinyle + *n*-butane. Nous nous attendons à des effets différents par rapport aux résultats obtenus dans le mélange : C_2H_3Cl + iso-C_4H_{10}, en raison des réactivités accrues des ions $C_nH_{2n}^+$ et $C_nH_{2n+1}^+$ (n = 3, 4) de structure primaire formés par le transfert de H_2^- et H^- des alcanes sur les oléfines ionisées (3, 4). Soit, dans le cas présent sur l'espèce $C_2H_3Cl^+$.

Le potentiel d'ionisation du propane étant 10,95 eV + 0,05 (2), l'ion moléculaire du chlorure de vinyle formé à 10,64 eV ne peut transferer sa charge sur le propane, et les seules réactions primaires prévisibles seront les transferts de H^- et de H_2^- produisant les ions $C_3H_7^+$ et $C_3H_6^+$. Par ailleurs, le potentiel d'ionisation du *n*-butane est 10,53 eV ± 0,1 eV (2). Donc dans ce cas, en plus des processus de transfert des anions H^- et H_2^- du *n*-butane sur l'ion $C_2H_3Cl^+$, on peut aussi s'attendre à un transfert de charge de l'ion $C_2H_3Cl^{+\cdot}$ excité sur le *n*-butane. Une ionisation directe du *n*-C_4H_{10} par les photons de 10,64 eV n'est également pas exclue. Ainsi les phénomènes observés pourront être plus complexes. Cependant, la photoionisation du *n*-butane près du seuil d'ionisation ne devrait pas être importante car, nous présumons, que le rendement quantique de photoionisation est faible, $< 0,1$.

Conditions experimentales

Les expériences ont été executées dans le spectromètre de masse à photoionisation et à haute pression déjà décrit (5, 6). La source d'émission des photons de hautes énergie est une lampe à décharge de krypton décrite par Ausloos *et al.* (7). L'intérieur de la chambre de collision du spectromètre de masse est libre de tout champ électrique. À la sortie les ions sont accélerés par un faible champ électrique, 5 V/cm, et sont focalisés sur l'entrée d'un filtre quadripolaire. La température de la chambre de collision est 28 ± 2°C. Les mesures sont effectuées dans un intervalle de pression situé entre 0,01 et 1 Torr (1 Torr = 133,3 Pa) et la pression est mesurée par un manomètre électronique Barocell fonctionnant dans la région de 10^{-4} à 10 Torr.

Un certain nombre de manipulations a été effectué sur un spectromètre de masse à secteur magnétique. Les résultats obtenus ont confirmé ceux réalisés sur l'instrument à photoionisation.

Les réactifs : chlorure de vinyle, propane et *n*-butane, de Matheson Co. sont de pureté supérieure à 99,5% et sont utilisés tels quels. Les mélanges de proportions connues sont préparés dans un système à vide ($\sim 10^{-6}$ Torr) raccordé à l'entrée du spectromètre de masse.

Résultats

Le Kr excité par une décharge micro-onde émet un rayonnement surtout composé de deux raies de résonance de 10,03 et 10,64 eV. Leurs intensités relatives dépendent entre autre de la pression du gaz. Dans notre cas les intensités relatives des raies de résonance transmises par les fenêtres en LiF sont respectivement de 82% pour celle de 10,03 eV et de 18% pour celle de 10,64 eV. Sieck *et al.* ont mesuré un rendement quantique de photoionisation du chlorure de vinyle de 0,037 à 10,03 eV et de 0,47 à 11,6–11,8 eV (raies de résonance de l'argon) (8). À partir des spectres de photoionisation du chlorure de vinyle (9) nous avons estimé le rendement quantique de photoionisation à 0,35 ± 0,04 à 10,64 eV. Dans ces conditions environ 70% des ions moléculaires du chlorure de vinyle sont formés par absorption du rayonnement à 10,64 eV.

Mélange : chlorure de vinyle – propane

Les expériences de photoionisation sont faites sur un mé-

1. Adresse permanente : Institut de physique, Université Marie Curie Sklodowska, Lublin, Prague.

Can. J. Chem. Downloaded from www.nrcresearchpress.com by 186.148.149.217 on 09/07/12
For personal use only.

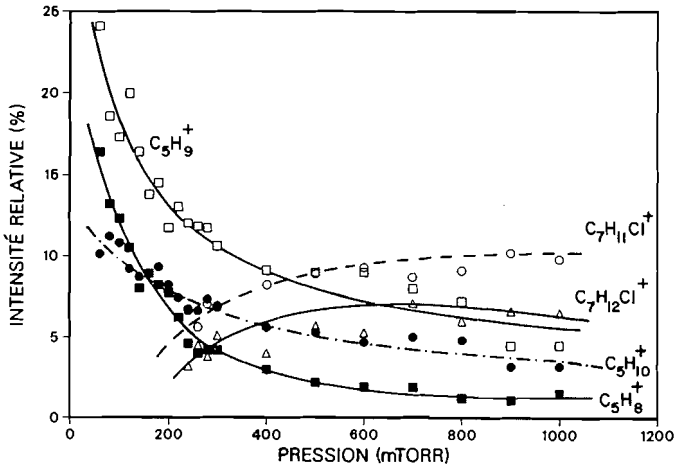


FIG. 1. Variations des intensités relatives des ions majoritaires en fonction de la pression dans le mélange $C_3H_8 : C_2H_3Cl = 9:1$.

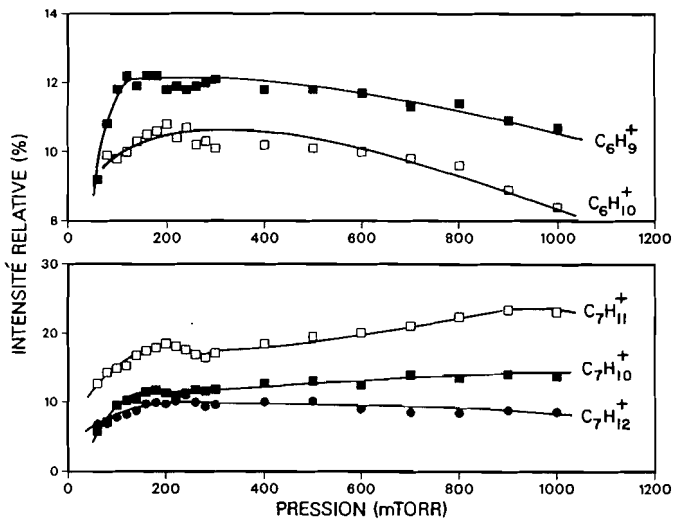


FIG. 2. Variations des intensités relatives de certains ions secondaires en fonction de la pression dans le mélange $C_3H_8 : C_2H_3Cl = 9:1$.

lange de 90% de propane et de 10% de chlorure de vinyle, de manière à favoriser les rencontres entre l'ion $C_2H_3Cl^+$ et les molécules neutres du propane.

Les résultats sont présentés dans les figures 1 et 2. Dans un mélange de telle proportion l'ion moléculaire du chlorure de vinyle n'apparait pas, de même que les des produits provenant des réactions ion–molécule du chlorure de vinyle pur (8, 10–14). Les ions les plus importants mis en évidence par les spectres de masse sont les suivants: $C_5H_8^+$, $C_5H_9^+$, $C_5H_{10}^+$ (fig. 1), et $C_6H_9^+$, $C_6H_{10}^+$, $C_7H_{10}^+$, $C_7H_{11}^+$ et $C_7H_{12}^+$ (fig. 2). Un groupe d'ions qui apparaissent aux pressions élevées sont ceux correspondant aux masses 130, 132 et 131, 133 auxquels nous attribuons les formules $C_7H_{11}Cl^+$ et $C_7H_{12}Cl^+$, et qui comptent ensemble pour moins de 17% en intensité (fig. 1). On trouve aussi sur tout l'intervalle de pression en faible intensité (<6%) les ions $C_4H_9^+$ et $C_4H_{10}^+$, qui ne sont pas rapportés sur les figures. Ceux-ci proviennent soit des réactions ion/molécule lentes entre les ions $C_3H_6^+$ et $C_3H_7^+$ et le propane, ou bien de l'ionisation de molécules de butane qui peut être contenu en trace dans le mélange de départ.

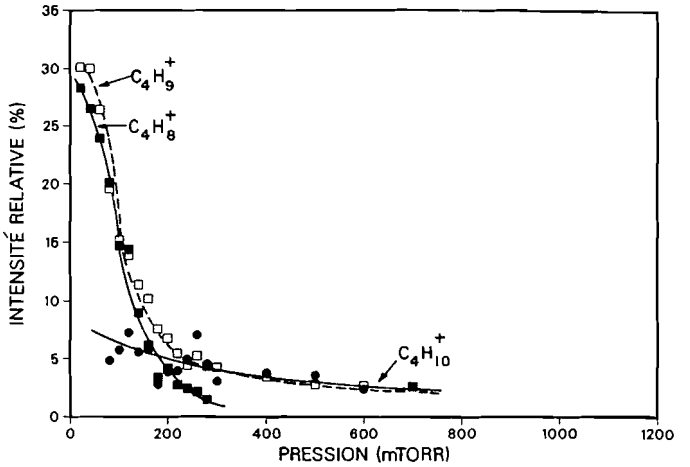


FIG. 3. Disparition des ions en C_4 en fonction de la pression dans le mélange $n\text{-}C_4H_{10} : C_2H_3Cl = 9:1$.

Mélange chlorure de vinyle – n-butane

L'importance de l'ionisation directe du *n*-butane d'une part, et du processus de transfert de charge du $C_2H_3Cl^+$ d'autre part est étudiée sur trois mélanges de proportions différentes, $n\text{-}C_4H_{10} : C_2H_3Cl = 9:1$; 1:1 et 0,5:9,5.

Dans les figures 3–5 nous rapportons les résultats obtenus pour le mélange $n\text{-}C_4H_{10}$ (90%) + C_2H_3Cl (10%) où certains processus réactionnels sont bien mis en évidence. Pour ce mélange aucun des ions observés ne provient des réactions ion/molécule du chlorure de vinyle pur. À basse pression le spectre de masse du mélange est dominé par les ions *m/z* 56 et 57 correspondants aux ions $C_4H_8^+$ et $C_4H_9^+$ (fig. 3). Ces derniers sont formés par transfert de H_2^- et H^- sur l'ion moléculaire du chlorure de vinyle. La masse *m/z* 58 représentant l'ion du *n*-butane, $C_4H_{10}^+$, est aussi présente mais en moins grande concentration. À pression totale égale, l'intensité de cet ion est environ dix fois plus importante dans le mélange $n\text{-}C_4H_{10}$ (90%) + C_2H_3Cl (10%) que dans le *n*-butane pur, ce qui est une indication que la majorité des ions $C_4H_{10}^+$ sont formés par transfert de charge,

[1] $C_2H_3Cl^{+\cdot} + n\text{-}C_4H_{10} \rightarrow n\text{-}C_4H_{10}^+ + C_2H_3Cl$

et seule une faible proportion provient de la photoionization directe.

Toujours dans le mélange à 90% de *n*-butane l'évolution des ions en fonction de l'augmentation de la pression (figures 4 et 5) font apparaitre deux familles d'ions d'intensité inégale: $C_5H_{11}^+$, $C_5H_{12}^+$ et $C_6H_{11}^+$, $C_6H_{12}^+$, $C_6H_{10-13}Cl^+$. Toutes ces espèces ne peuvent provenir que des réactions ion/molécule entre les deux constituants du mélange.

Le spectre de masse du mélange à 50% en *n*-butane est riche en produits, mais facile à dépouiller. On aperçoit des ions provenants aussi bien des processus ion/molécule propre au chlorure de vinyle pur (8, 10–14), que ceux observés dans le mélange $n\text{-}C_4H_{10}$ (90%) + C_2H_3Cl (10%) décrit ci-dessus. Dans les figures 6 et 7 nous présentons l'évolution des intensités relatives en fonction de la pression pour quelques ions seulement. Dans le but d'alléger les figures nous avons choisi de ne pas montrer les produits de réactions ion/molécule du chlorure de vinyle pur, à l'exception des ions $C_4H_5Cl^+$ et $C_4H_6Cl^+$. Ces derniers étant des produits majeurs de réaction dans le chlorure de vinyle pur nous voulons indiquer leur im-

Can. J. Chem. Downloaded from www.nrcresearchpress.com by 186.148.149.217 on 09/07/12
For personal use only.

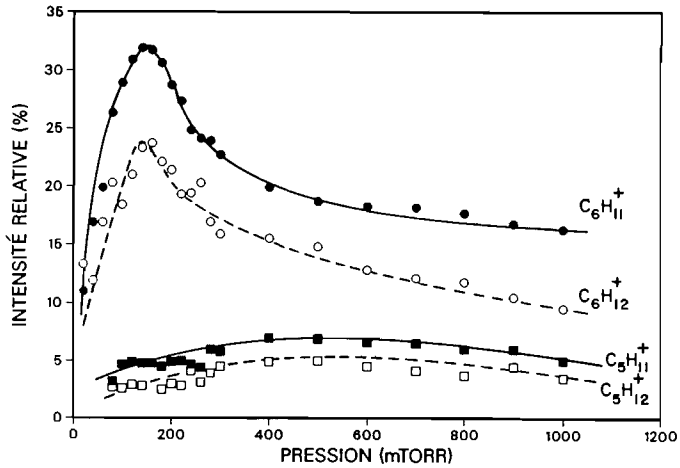


FIG. 4. Evolution en fonction de la pression des intensités relatives de certains ions principaux dans le mélange n-C_4H_{10} : C_2H_3Cl = 9 : 1.

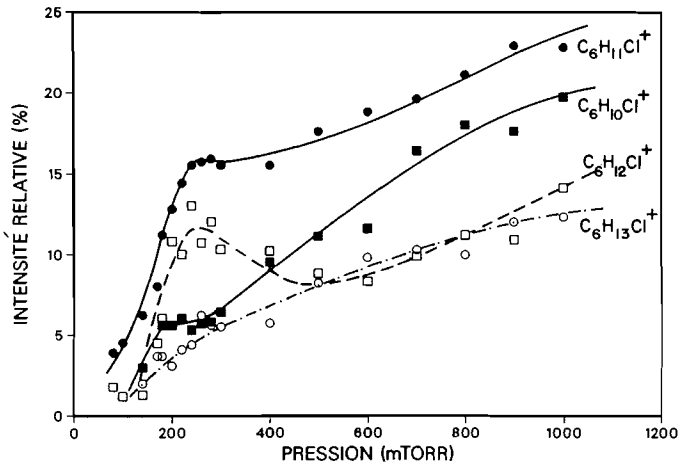


FIG. 5. Evolution en fonction de la pression des intensités relatives de certains ions chlorés dans le mélange n-C_4H_{10} : C_2H_3Cl = 9 : 1.

portance dans le spectre de masse du mélange (fig. 7). On découvre une nouvelle espèce dans le spectre, $C_4H_7Cl^+$, dont l'intensité maximale est ~10% à 30 mTorr et qui décroit rapidement avec l'augmentation de la pression. À cet ion peuvent être affiliées deux autres espèces apparaissant à pression élevée (>60 mTorr), $C_4H_9Cl^+$ et $C_4H_{10}Cl^+$, dont l'intensité totale ne dépasse pas 6%.

Le troisième mélange, riche en chlorure de vinyle (95%), montre surtout les produits des réactions ion/molécule du C_2H_3Cl pur. Cependant à basse pression on remarque, quoique en moindre quantité, la présence des $C_4H_8^+$ et $C_4H_9^+$ qui disparaissent rapidement avec l'augmentation de la pression pour former les ions $C_6H_{10}^+$, $C_6H_{11}^+$ et $C_6H_{12}^+$.

Nous avons consigné ci-dessous les valeurs du rapport des intensités (I) de l'ion $C_2H_3Cl^+$ à ceux des espèces $C_4H_8^+$ + $C_4H_9^+$ + $C_4H_{10}^+$ du butane normal pour les trois mélanges à 5 mTorr de pression totale, c'est à dire au tout début des séquences des réactions ion/molécule :

mélange C_2H_3Cl + n-C_4H_{10}	1 : 9	1 : 1	9,5 : 0,5
$I(C_2H_3Cl^+)/I(C_4H_8^+ + C_4H_9^+ + C_4H_{10}^+)$	0	1,1	2,2

On y voit clairement l'importance des processus de transfert,

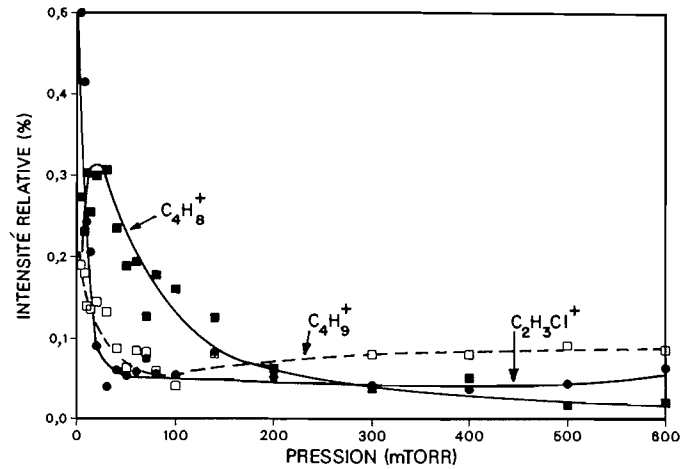


FIG. 6. Disparition des ions primaires en fonction de la pression dans le mélange n-C_4H_{10} : C_2H_3Cl = 1 : 1.

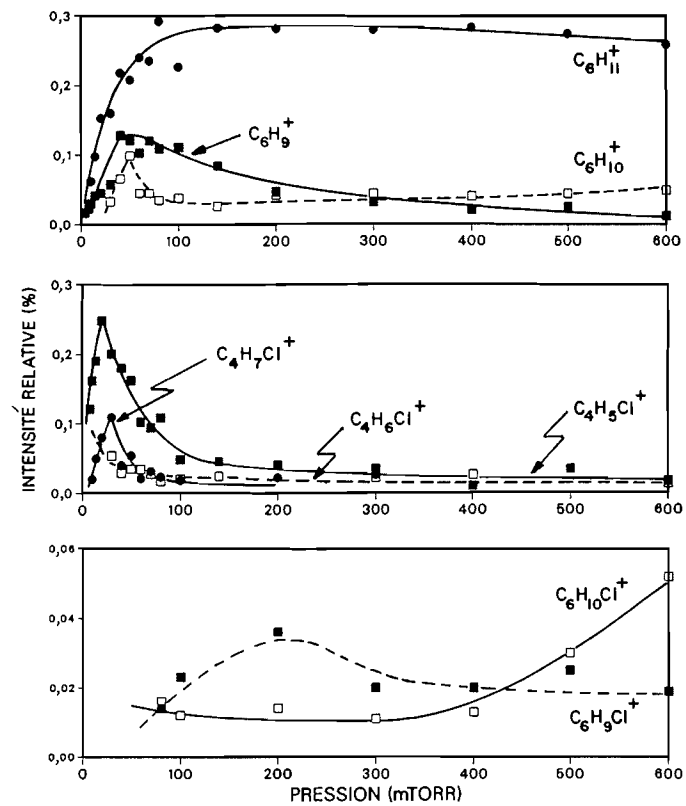


FIG. 7. Variations des intensités relatives de certains ions secondaires en fonction de la pression dans le mélange n-C_4H_{10} : C_2H_3Cl = 1 : 1.

lesquels même aux concentrations elevées du chlorure de vinyle restent encore des canaux de réactions très importants.

Discussion

La séquence des réactions ion/molécule dans le chlorure de vinyle pur est bien établie (8, 10–14). À pression elevée elle est completée par les processus [5]–[13] (15):

[2] $C_2H_3Cl^+ + C_2H_3Cl \rightarrow C_4H_5Cl^+ + HCl$

[3] $\rightarrow C_4H_6Cl^+ + Cl^\cdot$

[4] $\rightarrow C_3H_4Cl^+ + CH_2Cl^\cdot$

Can. J. Chem. Downloaded from www.nrcresearchpress.com by 186.148.149.217 on 09/07/12
For personal use only.

Can. J. Chem. Downloaded from www.nrcresearchpress.com by 186.148.149.217 on 09/07/12
For personal use only.

[5] $C_4H_5Cl^+ + C_2H_3Cl \rightarrow C_6H_7Cl^+ + HCl$

[6] $\rightarrow C_6H_8Cl^+ + Cl^\cdot$

[7] $C_4H_6Cl^+ + C_2H_3Cl \rightarrow C_6H_8Cl^+ + HCl$

[8] $\rightarrow C_6H_9Cl^+ + Cl^\cdot$

[9] $C_3H_4Cl^+ + C_2H_3Cl \rightarrow C_5H_6Cl^+ + HCl$

[10] $\rightarrow C_5H_7Cl^+ + Cl^\cdot$

[11] $C_6H_7Cl^+ \xrightarrow{M(?)} C_6H_7^+ + Cl^\cdot$

[12] $C_6H_8Cl^+ \xrightarrow{M(?)} C_6H_7^+ + HCl$

[13] $C_6H_7^+ + C_2H_3Cl \rightarrow C_8H_9^+ + HCl$

À pression elevée (>100 mTorr) les produits des réactions [11]–[13] s'accumulent probablement en raison de leur faible réactivité vis-à-vis du chlorure de vinyle neutre.

Dans les spectres de masse des mélanges du chlorure de vinyle + propane et chlorure de vinyle + *n*-butane à concentration elevée, tous les produits des réactions [2]–[13] sont clairement identifiables. Donc, la séquence des réactions [2]–[13] est en competition avec les processus de transfert de H^- et de H_2^- [14], [15] et éventuellement de charge [1]:

[14] $C_2H_3Cl^+ + C_nH_{2n+2} \rightarrow C_nH_{2n+1}^+ + C_2H_4Cl^\cdot$

[15] $\rightarrow C_nH_{2n}^+ + C_2H_5Cl$

Les travaux qui portent sur le transfert de H^- dans certains mélanges d'hydrocarbures d'alkyles (16) ou encore sur des mélanges «alcane + oléfine», où seule l'oléfine est ionisée (4), mettent en évidence le caractère général de ces types de réactions.

Les coefficients de vitesse des réactions [1], [14], [15] ne sont pas connus. Si par analogie nous supposons que les constantes de vitesse des réactions [14] et [15] sont comparables à celles de l'ion $C_2H_4^+$ avec le propane ($k \sim 8 \times 10^{-10}$ cm^3 s^{-1}) (17, 18) ou avec le *n*-butane ($k \sim 1 \times 10^{-10}$ cm^3 s^{-1}) (3*b*), alors nous devons nous attendre à des processus très efficaces, ce qui expliquerait l'importance de ces réactions dans les mélanges étudiées.

Mélange : chlorure de vinyle + propane

Dans ce mélange à 10% en C_2H_3Cl les processus [14] et [15] sont pratiquement les seuls à être envisagés et, en conséquence, les ions $C_3H_6^+$ et $C_3H_7^+$ seront les premiers à amorcer les réactions subséquentes. Les coefficients de vitesse des réactions ion/molécule des ions $C_3H_6^+$ et $C_3H_7^+$ avec le propane sont d'environ 3×10^{-11} cm^3 s^{-1} (3*b*, 19, 20) ce qui caractérise des processus relativement lents. En supposant que ces constantes de vitesse sont au moins d'un ordre de grandeur inférieur à celles caractérisants les réactions entre les ions $C_3H_6^+$ et $C_3H_7^+$ et le C_2H_3Cl, on peut s'attendre que les réactions qui suivent les processus [14] et [15] impliquent exclusivement le chlorure de vinyle:

[16] $C_3H_6^+ + C_2H_3Cl \rightarrow C_5H_9^+ + Cl^\cdot$

[17] $C_3H_6^+ + C_2H_3Cl \rightarrow C_5H_8^+ + HCl$

[18] $C_3H_7^+ + C_2H_3Cl \rightarrow C_5H_9^+ + HCl$

[19] $C_3H_7^+ + C_2H_3Cl \rightarrow C_5H_{10}^+ + Cl^\cdot$

Les ions insaturés obtenus alors: $C_5H_8^+$, $C_5H_9^+$ et $C_5H_{10}^+$ (fig. 1) réagissent à leur tour préferentiellement avec le chlorure de vinyle dans des processus de condensation avec ou sans élimination du $Cl^\cdot$, du HCl ou du $CH_2Cl^\cdot$:

[20] $C_5H_{5+n}^+ + C_2H_3Cl \rightarrow C_7H_{8+n}Cl^+$

[21] $\rightarrow C_7H_{8+n}^+ + Cl^\cdot$

[22] $\rightarrow C_7H_{7+n}^+ + HCl$

[23] $\rightarrow C_6H_{6+n}^+ + CH_2Cl^\cdot$

où n = 3, 4 et 5. Toutes ces espèces ioniques sont effectivement présentes dans le spectre de masse. Leurs intensités relatives indiquent que les processus [17] et [18], impliquant l'élimination du chlorure d'hydrogène, contribuent le plus à la formation des produits (figures 2, 3).

Mélange : chlorure de vinyle + n-butane

Il est reconnu que les ions $C_4H_8^+$ et $C_4H_9^+$ formés dans les processus [14] et [15] de même que l'ion $C_4H_{10}^+$ ne réagissent que lentement avec le *n*-butane neutre ($k < 10^{-12}$ cm^3 s^{-1}) (3). Il est donc normal de constater que ces ions réagissent préferentiellement avec le chlorure de vinyle dans des processus dont les coefficients de vitesse (pas encore mesurés) devraient être au moins un ordre de grandeur plus élevés. Les séquences de réactions observées sont similaires à celles décrites pour le mélange $C_2H_3Cl + C_3H_8$:

[24] $C_4H_{8+m}^+ + C_2H_3Cl \rightarrow C_6H_{11+m}Cl^+$

[25] $\rightarrow C_6H_{11+m}^+ + Cl^\cdot$

[26] $\rightarrow C_6H_{10+m}^+ + HCl$

[27] $\rightarrow C_5H_{9+m}^+ + CH_2Cl^\cdot$

où m = 0, 1, 2. Tous ces ions à l'exception du $C_5H_9^+$ sont présents dans le spectre de masse. De nouveau les processus caractérisés par l'élimination du HCl contribuent le plus à la formation des produits.

Les réactions du genre:

[28] $C_6H_{10+p} + C_2H_3Cl \rightarrow C_8H_{12+p}^+ + HCl$

où p = 0–3, qui correspondent aux processus [20]–[23], n'ont pas été observé clairement dans ce mélange. On aperçoit un amas de pics de faible intensité (~1%) de masse: $110 < m/z < 130$, emergeant du fond spectral mais difficile à dépouiller convenablement. Il n'est donc pas souhaitable pour l'instant de les considerer comme preuve de l'occurrence des processus [28].

Dans le mélange riche en chlorure de vinyle apparait une nouvelle voie réactionnelle:

[29] $C_2H_3Cl^+ + n\text{-}C_4H_{10} \rightarrow C_2H_4Cl^+ + C_4H_9^\cdot$

Cet ion, $C_2H_4Cl^+$, peu abondant réagit ensuite de la même manière que l'ion $C_2H_3Cl^+$ en formant des produits d'une unité de masse plus élevé que l'ion parent du chlorure de vinyle. Cela ne fait que compliquer les spectres de masse des mélanges à proportion élevée en C_2H_3Cl.

Les différences de réaction entre le chlorure de vinyle et le *n*-butane d'une part, et l'isobutane (1), d'autre part, peuvent se comprendre aisement. La structure ouverte primaire ou secondaire des espèces $C_4H_9^+$ et $C_4H_8^+$ permet à ces ions de réagir relativement facilement avec les oléfines. La structure tertiaire des ions *t*-$C_4H_9^+$ et iso-$C_4H_8^+$ rend ces espèces dans leur état fondamental peu ou pas du tout réactives avec les molécules neutres.

Nous terminons par un commentaire général. Le problème des réactions consécutives du type [13], [22] et [28] qui conduiraient à des produits lourds, polymérisation ionique, ne

reçoit pas ici de solution claire. Certe, on aperçoit des produits ioniques correspondant à une troisième ou même quatrième étape de condensation, mais leurs intensités relatives suggèrent qu'à chaque condensation consécutive il y a ralentissement de la vitesse de réaction. Il est probable que les structures de plus en plus complexes de ces ions à plusieures liaisons insaturées, ayant une charge délocalisée, soient responsables de cette diminution de la vitesse de condensation. On peut donc supposer qu'après à peine quelques étapes de condensation la vitesse de croissance des produits lourds formés dans des réactions ion/molécule soit égale ou inférieure à la vitesse de polymérisation radicalaire, et alors c'est cette dernière qui va emporter dans le processus global.

Conclusion

Les réactions ion/molécule dans le propane et dans le *n*-butane de l'ion $C_2H_3Cl^+$ formé à 10,64 eV, sont dominées par les processus de transfert H^-, H_2^-, et en plus par le transfert de charge dans le cas du *n*-C_4H_{10}. Ces processus sont en compétition avec les réactions ion/molécule du chlorure de vinyle pur. La faible réactivité des ions $C_nH_{2n}^+$ et $C_nH_{2n+1}^+$ avec le propane et le *n*-butane favorise les réactions de condensation avec le chlorure de vinyle avec ou sans élimination du HCl ou Cl$^\bullet$.

Remerciements

Nous remercions le Conseil de recherche en sciences naturelles et en génie et le Fonds pour la formation de chercheurs et l'aide à la recherche (FCAR) pour l'aide financière qui a permis de mener à terme ce travail.

1. R. Neagu-Plesu et J. A. Herman. Rapid Commun. Mass Spectrom. **1**, 63 (1987).
2. S. G. Lias, J. E. Bartmess, J. F. Liebman, J. L. Holmes, R. D. Levin et W. G. Mallard. J. Phys. Chem. Ref. Data, **17**, Suppl. 1 (1988).
3. M. S. B. Munson. (*a*) J. Am. Chem. Soc. **89**, 1772 (1967); (*b*) J. Phys. Chem. **71**, 3966 (1967); (*c*) J. Am. Chem. Soc. **90**, 83 (1968).
4. L. W. Sieck et S. K. Searles. J. Am. Chem. Soc. **92**, 2937 (1970).
5. H. Wincel et J. A. Herman. J. Chem. Soc. Faraday Trans. I, **69**, 1799 (1973).
6. Z. Łuczynski et J. A. Herman. J. Phys. Chem. **82**, 1679 (1978).
7. R. Gorden, R. E. Rebbert et P. Ausloos. Techn. Note 496, National Bureau of Standards, Washington D.C. 1969.
8. L. W. Sieck, R. Gorden, S. G. Lias et P. Ausloos. Int. J. Mass Spectrom. Ion Phys. **15**, 181 (1974).
9. J. D. Reinke, R. Kraessig et H. Baumgartel. Z. Naturforsch. **28A**, 1021 (1973).
10. J. L. Beauchamp, L. R. Anders et J. D. Baldeschwieler. J. Am. Chem. Soc. **89**, 4569 (1967).
11. J. A. Herman, J. J. Myher et A. G. Harrison. Can. J. Chem. **47**, 647 (1969).
12. B. M. Hughes, T. O. Tiernan et J. H. Futrell. J. Phys. Chem. **73**, 829 (1969).
13. V. G. Anicich et M. T. Bowers. Int. J. Mass Spectrom. Ion Phys. **12**, 231 (1973).
14. V. G. Anicich et J. H. Futrell. Int. J. Mass Spectrom. Ion Phys. **21**, 383 (1976).
15. R. Neagu-Plesu. Thèse de maitrise, Université Laval (1987).
16. S. G. Lias, J. R. Eyler et P. Ausloos. Int. J. Mass Spectrom. Ion Phys. **19**, 219 (1976).
17. B. H. Solka, A. Y.-K. Lav et A. G. Harrison. Can. J. Chem. **52**, 1798 (1975).
18. M. S. B. Munson, J. L. Franklin et F. H. Field. J. Phys. Chem. **68**, 3098 (1964).
19. A. McKenzie-Peers. J. Phys. Chem. **73**, 4141 (1969).
20. L. W. Sieck et J. H. Futrell. J. Chem. Phys. **45**, 560 (1966).

Can. J. Chem. Downloaded from www.nrcresearchpress.com by 186.148.149.217 on 09/07/12
For personal use only.

On the correlation of the excess surface heat capacity and the surface molar volume of liquids

DOUGLAS EUGENE GOLDSACK AND LISE JEANNE PAQUETTE
Department of Chemistry, Laurentian University, Sudbury, Ont., Canada P3E 2C6
Received September 20, 1988[1]

DOUGLAS EUGENE GOLDSACK and LISE JEANNE PAQUETTE. Can. J. Chem. **67**, 2201 (1989).

Excess surface heat capacity values $\Delta\bar{C}_{ps}$ have been calculated using several surface density models. It is expected that calaculated $\Delta\bar{C}_{ps}$ values would be negative to be thermodynamically consistent. Using bulk liquid volume data as a means of calculating first estimates of surface volumes yields positive $\Delta\bar{C}_{ps}$ for a group of compounds of wide polarity. However, a simple linear or non-linear surface density model relating bulk density to surface density and reduced temperatures has been shown to yield negative values of $\Delta\bar{C}_{ps}$. This new surface density model is applicable to both polar and non-polar compounds and thus should prove useful for calculating molar surface areas for polar compounds which are necessary for calculating the surface tensions of polar–polar liquid mixtures.

Key words: excess surface heat capacity, surface density, monolayer model.

DOUGLAS EUGENE GOLDSACK et LISE JEANNE PAQUETTE. Can. J. Chem. **67**, 2201 (1989).

On a calculé les valeurs des capacités califiques $\Delta\bar{C}_{ps}$ des surfaces en excés, en utilisant plusieurs modéles de densité de surface. On prévoit que les valeurs de $\Delta\bar{C}_{ps}$ calculées seront négatives compte tenu de leurs propriétés thermodynamiques. L'utilisation des données à partir de gros volumes de liquide dans le but d'effectuer une première évaluation des volumes de surfaces, conduit à des valeurs positives de $\Delta\bar{C}_{ps}$ pour un groupe de composés de polarité très variée. On montre cependant qu'un modèle simple, linéaire ou non-linéaire, de densité de surface reliant la densité globale à la densité de surface et des températures réduites donnent des valeurs de $\Delta\bar{C}_{ps}$ négatives. Ce nouveau modèle de densité de surface est applicable à la fois aux composés polaires et non polaires qui sont nécessaires pour le calcul des tensions de surface des mélanges liquides polaire–polaire.

Mots clés: surface en excès, capacité calorifique, densité de surface, modèle monocouche.

[Traduit par la revue]

The various definitions of the surface tension, σ, of the surface of a liquid have been discussed in detail by Aveyard and Haydon (1). The reversible isothermal work done by a liquid to increase its surface area is associated with a free energy change which can be called the excess surface free energy. "This free energy is not the total free energy of the surface molecules but the excess free energy which the molecules possess by virtue of their being in the surface" (ref. 1, p. 2).

For the surface of a pure liquid, the combined first and second laws yield

$$[1] \quad d\bar{U}_s = Td\bar{S}_s - Pd\bar{V}_s + \sigma\, d\bar{a}$$

where $\bar{U}_s$ is the molar excess internal energy of the molecules in the surface, T, P and σ are the temperature, pressure, and surface tension of the liquid respectively and $\bar{S}_s$, $\bar{V}_s$, and $\bar{a}$ are the excess molar entropy, excess molar volume, and molar area of the liquid in the surface phase, respectively.

The excess Helmholtz free energy in the surface is defined as (ref. 1, p. 11, eq. [1.9]).

$$[2] \quad \bar{A}_s = \bar{U}_s - T\bar{S}_s$$

Total differentiation of this expression and utilizing eq. [1] leads to:

$$[3] \quad d\bar{A}_s = -\bar{S}_s dT - Pd\bar{V}_s + \sigma d\bar{a}$$

One definition, then, of the surface tension of the liquid surface is:

$$[4] \quad \sigma = \left(\frac{\partial \bar{A}_s}{\partial \bar{a}}\right)_{T,\bar{V}_s}$$

For n moles of liquid in the surface layer, the total area $a = n\bar{a}$ and the total excess Helmholtz surface free energy is $A_s = n\bar{A}_s$, hence the surface tension is also given by:

$$[5] \quad \sigma = \left(\frac{\partial A_s}{\partial a}\right)_{T,\bar{V}_s}$$

Hence, the surface tension can be considered as the Helmholtz free energy per unit area of the surface.

A useful equation is obtained by integrating eq. [3] at constant, T, P, and σ:

$$[6] \quad \bar{A}_s = -P\bar{V}_s + \sigma\bar{a}$$

Defining a molar Gibbs excess surface free energy as (ref. 1. p. 11, eq. [1.17])

$$[7] \quad \bar{G}_s = \bar{A}_s + P\bar{V}_s$$

then

$$[8] \quad \bar{G}_s = \sigma\bar{a}$$

To emphasize that $\bar{G}_s$ is the excess surface Gibbs free energy we introduce the Δ notation and define

$$[9] \quad \Delta\bar{G}_s = \sigma\bar{a} = \bar{G}_s$$

To relate the molar surface area $\bar{a}$ of the surface layer of the liquid to the molar volume of the liquid in the surface layer $\bar{V}_s$, it is necessary to invoke a model of the surface layer. The simplest model to utilize for the surface layer is that of a monolayer. The relation between $\bar{a}$ and $\bar{V}_s$ for such a monolayer is (2):

$$[10] \quad \bar{a} = X\bar{V}_s^{2/3}$$

Hence eq. [9] becomes:

$$[11] \quad \Delta\bar{G}_s = X\sigma\bar{V}_s^{2/3}$$

The geometric factor, X, has a value of 10.21 when $\Delta\bar{G}_s$ values are in J/mol, assuming spherical geometry for the molecules in a surface monolayer, with σ and $\bar{V}_s$ in units of ergs/cm^2 and cm^3/mol, respectively.

Given this expression for $\Delta\bar{G}_s$, all other thermodynamic

[1]Revision received July 17, 1989.

Can. J. Chem. Downloaded from www.nrcresearchpress.com by 186.148.149.217 on 09/07/12
For personal use only.

surface difference properties can be obtained by appropriate differentiation. In particular, the molar excess heat capacity difference at constant pressure of the liquid, $\Delta\bar{C}_{ps}$, can be obtained from the temperature dependence of $\Delta\bar{G}_s$ by the relation:

$$[12] \quad \Delta\bar{C}_{ps} = -T\left[\frac{d^2\Delta\bar{G}_s}{dT^2}\right]_p$$

where T is the absolute temperature. Combining eqs. [11] and [12] leads to the following relation for $\Delta\bar{C}_{ps}$:

$$[13] \quad \Delta\bar{C}_{ps} = -TX\sigma\bar{V}_s^{2/3}\left\{\frac{1}{\sigma}\frac{d^2\sigma}{dT^2} + \frac{4\alpha_s}{3\sigma}\frac{d\sigma}{dT} + \frac{2}{3\bar{V}_s}\frac{d^2\bar{V}_s}{dT^2} - \frac{2}{9}\alpha_s^2\right\}$$

where α_s is the coefficient of thermal expansion of the liquid in the surface phase.

Since the difference in molar heat capacity of liquids between the bulk liquid and the vapor phase, $\Delta\bar{C}_{p,vap}$, is always negative (except at the critical point), then it should be expected that $\Delta\bar{C}_{ps}$, which is the difference in molar heat capacity between the liquid and surface phases, will also be negative. It has been observed that at the boiling point, $\Delta\bar{C}_{p,vap}$, is about -42 J/mol for a large variety of liquids (3). Therefore, it would be expected that $\Delta\bar{C}_{ps}$ under these conditions would be a fraction of this value, and in particular that $\Delta\bar{C}_{ps}$ should have a negative value for all liquids. It would be expected that for a large number of similar liquids, this value of $\Delta\bar{C}_{ps}$ should also be roughly constant similar to the constancy of $\Delta\bar{C}_{p,vap}$ and $\Delta\bar{S}_{vap}$ under these conditions (4).

In order to calculate $\Delta\bar{C}_{ps}$ values from observed surface tension and molar volume data according to eq. [13], it is necessary to have analytical expressions for these data as a function of temperature. In the case of surface tension, there are very few systems for which data are available over a wide range to obtain a value of $d^2\sigma/dT^2$ accurately. One such set of data is given by Moelwyn-Hughes (5) for CCl_4:

$$[14] \quad \alpha = 62.99 - 1.301 \times 10^{-1}\,T - 1.276 \times 10^{-5}\,T^2 + 7.33 \times 10^{-8}\,T^3$$

Since it is expected that $\Delta\bar{C}_{ps}$ should be negative, and since $d\sigma/dT$ is always negative, therefore ignoring the last two terms of eq. [13] for the moment, it is implied that the second derivative $d^2\sigma/dT^2$ must be positive and that the term

$$\frac{1}{\sigma}\frac{d^2\sigma}{dT^2}$$

must be greater than

$$\frac{4\alpha_s}{3\sigma}\frac{d\sigma}{dT}.$$

Equation [14] indeed gives values of $d^2\sigma/dT^2$ which are positive but only if the T^3 term in the equation of σ as a function of temperature is taken into account. Hence to calculate $\Delta\bar{C}_{ps}$ data for a number of systems, either surface tension must be available with high accuracy as a cubic expression of T or another analytic temperature-dependent function for σ must be used. One such function which has been found to apply to a large number of materials over a wide temperature range is the Guggenheim relation (6):

$$[15] \quad \sigma = \sigma_0(1 - T/T_C)^n = \sigma_0(1 - T_r)^n$$

where σ_0 is a constant for a particular material, T_C is the critical temperature for that material, T_r is the relative or corresponding temperature, and n is a constant generally found to be approximately equal to 11/9 for a large number of materials. From eq. [15] it is easily shown that the following relations hold:

$$[16] \quad \frac{d\sigma}{dT} = -\frac{n\sigma_0}{T_C}(1 - T_r)^{n-1}$$

$$[17] \quad \frac{d^2\sigma}{dT^2} = \frac{n(n-1)}{T_C^2}\sigma_0(1 - T_r)^{n-2}$$

For $n = 11/9$, these latter equations show that $d\sigma/dT$ is always negative and $d^2\sigma/dT^2$ is always positive. Furthermore, the relative values of the first and second terms of eq. [13] are then related by:

$$[18] \quad \frac{1}{\sigma}\frac{d^2\sigma}{dT^2} = -\frac{(n-1)}{T_C}(1 - T_r)^{-1}\frac{1}{\sigma}\frac{d\sigma}{dT}$$

Hence if

$$\frac{(n-1)}{T_C}(1 - T_r)^{-1}$$

is greater than α_s, then $\Delta\bar{C}_{ps}$ will always have a negative value, provided that the last two terms of eq. [13] can be neglected.

The simplest model used to obtain values for $\bar{V}_s$ and hence α_s, has been to equate the bulk and surface volume properties in order to obtain first estimates of various surface thermodynamic properties. This approximation is known not to be valid and several models have been developed to account for the difference between bulk and surface volume properties of the liquid (7–9). None of these models, however, lead to simple analytic relations between the bulk and surface volumes.

To obtain values of $\Delta\bar{C}_{ps}$ under comparable conditions, data were gathered from the literature (11–13), to calculate this parameter at the normal boiling points of a variety of non-polar and polar systems (Table 1). The normal boiling point is roughly a corresponding temperature for most materials and hence the various properties of liquids should have similar values under these conditions. $\Delta\bar{C}_{ps}$ values were calculated using first, bulk density data, to approximate the values of $\bar{V}_s$, the required values of α_s, and the first and second temperature derivatives of $\bar{V}_s$ at the boiling point. The results of these calculations are given in Table 2 and they indicate that by utilizing bulk values for $\bar{V}_s$ and α_s, positive values of $\Delta\bar{C}_{ps}$ are obtained in practically all cases in contradiction to what should be expected thermodynamically.

Another estimate of $\bar{V}_s$ and α_s can be obtained by assuming that $\bar{V}_s$ is proportional to $\bar{V}_B$ and that the temperature dependences of $\bar{V}_s$ and $\bar{V}_B$ are linear between the boiling and critical points. If $\bar{V}_C$ is the critical volume of the liquid, and if $\bar{V}_s = M\bar{V}_B$ where M is a constant, then the above assumptions yield:

$$[19] \quad \frac{d\bar{V}_B}{dT} = \frac{\bar{V}_C - \bar{V}_B}{T_C - T_B}$$

$$[20] \quad \alpha_B = \frac{1}{\bar{V}_B}\frac{d\bar{V}_B}{dT} = \frac{\left(\frac{\bar{V}_C}{\bar{V}_B} - 1\right)}{T_C\left(\frac{1 - T_B}{T_C}\right)}$$

Can. J. Chem. Downloaded from www.nrcresearchpress.com by 186.148.149.217 on 09/07/12
For personal use only.

TABLE 1. Surface tension and molar volume data at boiling points

Compound	T_{BP} (K)	V_B (cm^3/mol)	α_B (cm^3/K × 10^3)	T_C (K)	V_C (cm^3/mol)	σ (ergs/cm^2)	$-\frac{d\sigma}{dT}$ (ergs/cm^2 K)
N_2	77.4	34.67	5.67	126	89.5	8.89	0.227
Ar	87.3	28.45	4.56	150.7	74.8	12.52	0.249
O_2	90.2	30.00	4.20	154.6	73.4	13.10	0.256
C_2H_6	184.5	55.10	2.39	305.4	148	15.93	0.166
C_2H_2	189.2	42.43	3.81	308.3	113	19.64	0.194
Cl_2	239	45.84	1.56	417	124	26.32	0.182
$C_4H_{10}O$	307.8	106.9	1.62	466.9	280	15.79	0.091
CS_2	319.5	62.20	1.21	552	170	28.43	0.148
$(CH_3)_2CO$	329.4	77.66	1.60	545	203	19.97	0.112
Br_2	332	55.81	1.19	584	127	41.17	0.215
CCl_4	349.7	106.3	1.68	556.3	276	20.13	0.122
C_6H_6	353.9	96.02	1.37	561.6	259	21.38	0.129
C_6H_{12}	354.0	116.9	1.41	553.4	308	18.03	0.119
CH_3CN	354.8	57.56	1.68	548	111.4	26.97	0.126
C_2Cl_4	394.7	114.3	1.12	620	290	23.41	0.127
C_6H_5Cl	405	114.6	1.18	632	308	20.29	0.119

TABLE 2. Bulk liquid estimates of $\Delta\bar{C}_{ps}$

	$\frac{1}{\sigma}\frac{d^2\sigma}{dT^2}$ × 10^6	$-\frac{\alpha_B}{\sigma}\frac{d\sigma}{dT}$ × 10^6	$\frac{1}{V_B}\frac{d^2V_B}{dT^2}$ × 10^6	α_B^2 × 10^6	$\Delta\bar{C}_{ps}$ (J/mol deg)
N_2	114.7	144.5	63.4	32.2	3.20
Ar	87.9	90.7	42.9	20.8	0.947
O_2	65.7	84.9	1.36	17.6	5.89
C_2H_6	18.4	24.1	11.5	5.74	3.24
C_2H_2	18.9	37.5	28.9	14.5	6.92
Cl_2	8.52	10.8	4.85	2.45	2.58
$C_4H_{10}O$	10.59	9.31	4.45	2.62	−0.627
CS_2	4.95	6.31	2.90	1.47	2.69
$(CH_3)_2CO$	5.77	8.97	4.12	2.56	1.41
Br_2	4.21	6.21	2.85	1.41	5.01
CCl_4	6.32	10.2	4.09	2.82	8.29
C_6H_6	6.22	8.24	3.52	1.87	4.95
C_6H_{12}	6.76	9.29	2.29	1.99	7.08
CH_3CN	5.62	7.86	4.38	2.82	3.75
C_2Cl_4	5.29	6.04	2.49	1.25	3.07
C_6H_5Cl	5.36	6.93	1.17	1.39	6.75

$$[21]\quad \frac{d\bar{V}_s}{dT} = \frac{\bar{V}_C - \bar{V}_s}{T_C - T_B}$$

$$[22]\quad \alpha_s = \frac{1}{\bar{V}_s}\frac{d\bar{V}_s}{dT} = \frac{\left(\frac{\bar{V}_C}{\bar{V}_s} - 1\right)}{T_C\left(1 - \frac{T_B}{T_C}\right)}$$

At the boiling point, to a first approximation, $T_B = \frac{2}{3}T_C$ and $\bar{V}_B = \frac{1}{3}\bar{V}_C$ for many liquids (4). Under these conditions

$$[23]\quad \alpha_s = \alpha_B\left(\frac{3}{2M} - \frac{1}{2}\right)$$

Thus if $\bar{V}_s = 2\bar{V}_B$, then $\alpha_s = \frac{1}{4}\alpha_B$. One would expect that the surface thermal expansion coefficient α_s would be larger than the bulk liquid value α_B. That it is smaller would imply that the coordination number in the surface layer is smaller than that of the bulk layer (ref. 1, p. 2).

The calculation for $\Delta\bar{C}_{ps}$ was repeated using the above equations for $\bar{V}_s$ and α_s with $M = 2$. The results of these calculations are displayed in Table 3. It can be seen from these results that this second approximation to $\bar{V}_s$ now yields negative values for $\Delta\bar{C}_{ps}$ for all the cases concerned including non-polar and polar substances. In fact, eq. [13] shows that whereas the first term in brackets is independent of the model used for surface molar volume estimates, any model which predicts larger surface molar volumes and smaller surface coefficients of thermal expansion would make the $\Delta\bar{C}_{ps}$ values more negative than those calculated using bulk liquid parameters.

However, this improved model for $\bar{V}_s$ has two problems with it. First, it yields zero values for the $d^2\bar{V}_s/dT^2$ term and secondly, the maximum value that $\bar{V}_s$ can have is 3 times that of $\bar{V}_B$, which is an arbitrary upper value. A better approximation to

Can. J. Chem. Downloaded from www.nrcresearchpress.com by 186.148.149.217 on 09/07/12
For personal use only.

TABLE 3. Calculations of $\Delta\bar{C}_{ps}$ using linear and non-linear surface volume models (J/mol deg)

Compound	Equations [11] to [14] $M = 2$	Guggenheim model eqs. [16] to [21] $M = 1$	$M = 2$	$M = 3$	$M = 4$	$M = 5$
N_2	−7.8	+0.86	−1.2	−3.2	−4.7	−6.1
Ar	−9.5	−0.69	−2.9	−4.8	−6.4	−7.7
O_2	−6.9	+1.5	−0.24	−1.9	−3.4	−4.5
C_2H_6	−7.1	+0.74	−1.1	−3.1	−4.5	−5.7
C_2H_2	−4.5	+0.23	−1.9	−3.8	−5.4	−6.7
Cl_2	−6.4	+0.91	−0.72	−2.3	−3.7	−4.8
$C_4H_{10}O$	−13.1	−3.6	−6.4	−8.8	−10.6	−12.0
CS_2	−7.3	+0.68	−0.95	−2.6	−4.0	−5.1
$(CH_3)_2CO$	−4.9	+0.75	−0.90	−2.5	−3.8	−5.2
Br_2	−6.9	+2.0	+0.23	−1.6	−3.2	−4.5
CCl_4	−7.4	+1.1	−1.4	−3.7	−5.7	−7.2
C_6H_6	−8.9	+0.79	−1.7	−4.1	−6.0	−7.5
C_6H_{12}	−9.0	+1.9	−0.80	−3.4	−5.4	−7.2
CH_3CN	−6.8	−1.1	−2.6	−3.9	−5.0	−5.9
C_2Cl_4	−11.9	+0.67	−2.1	−4.9	−6.9	−8.7
C_6H_5Cl	−9.5	+1.8	−0.95	−3.6	−5.7	−7.4

$\bar{V}_s$ can be obtained if instead of a linear relation between $\bar{V}_s$ and $\bar{V}_B$ being assumed, a more reasonable temperature dependence is utilized.

Guggenheim (ref. 5, p. 168) has shown that, for a variety of liquids, the bulk density of the liquid ρ_B, is related to the critical density of the liquid, ρ_C, and the reduced temperature T_r by the following equation:

$$[24] \quad \rho_B = \rho_C + \frac{3}{4}\rho_C(1 - T_r) + \frac{7}{4}\rho_C(1 - T_r)^{1/3}$$

For the surface volume to be larger than the bulk volume, assume:

$$[25] \quad \rho_s = \rho_C + \frac{3}{4}\frac{\rho_C}{M}(1 - T_r) + \frac{7}{4}\frac{\rho_C}{M}(1 - T_r)^{1/3}$$

where M is a constant, so that at T_C, ρ_s equals ρ_C independent of the value of M.

Taking the appropriate derivatives, eq. [24] and [25] lead to relations for α_s and $d^2\bar{V}_s/dT^2$ evaluated at the boiling points with $T_r = 2/3$:

$$[26] \quad \bar{V}_s = \frac{\bar{V}_C}{\left(1 + \dfrac{2.51}{M}\right)}$$

$$[27] \quad \alpha_s = -\frac{1}{\rho_s}\left(\frac{d\rho_s}{dT}\right)_p = \frac{1.96}{T_C(M + 1.46)}$$

$$[28] \quad \frac{1}{\bar{V}_s}\frac{d^2\bar{V}_s}{dT^2} = -\frac{1}{\rho_s}\left(\frac{d^2\rho_s}{dT^2}\right) + 2\alpha_s^2$$

If eqs. [26] through [28] are substituted in eq. [13], then an analytic expression is obtained for $\Delta\bar{C}_{ps}$ at the boiling points in terms of critical parameters $\bar{V}_C$, T_C, and M as follows:

$$[29] \quad \Delta\bar{C}_{ps} = -\frac{TX\sigma\bar{V}_C^{2/3}}{\left(1 + \dfrac{2.51}{M}\right)^{2/3}} \cdot \left[\frac{1}{\sigma}\frac{d^2\sigma}{dT^2} + \frac{2.61}{T_C(M + 1.46)} \times \frac{1}{\sigma}\frac{d\sigma}{dT} + \frac{1.63}{T_C^2(M + 1.46)} + \frac{4.26}{T_C^2(M + 1.46)^2}\right]$$

Values of $\Delta\bar{C}_{ps}$ were calculated using values of $M = 1$ to $M = 5$ and are displayed in Table 3. A value of $M = 5$ yields values of $\bar{V}_s \simeq 2\bar{V}_B$ and hence these calculated values of $\Delta\bar{C}_{ps}$ can be compared to those of the simpler linear $\bar{V}_s$ model under comparable conditions. Except for $M = 1$, which corresponds to the bulk density relations of eq. [24], calculation of $\Delta\bar{C}_{ps}$ values for $m = 2$ through $M = 5$ yield negative values for all cases of non-polar to extremely polar compounds.

Conclusions

From the calculated values given in Tables 2 and 3, thermodynamically consistent values of $\Delta\bar{C}_{ps}$ for all compounds are obtained only if models are utilized which yield $\bar{V}_s$ values which are larger than bulk values, $\bar{V}_B$. Furthermore, even a simple linear model for the temperature dependence of $\bar{V}_s$ between the boiling and critical temperatures yields thermodynamically consistent values of $\Delta\bar{C}_{ps}$.

It has been shown earlier (14) that improved values of the surface tension of mixtures of non-polar compounds are obtained if a model for calculating the surface volume is available to calculate molar surface area values. These calculations of $\Delta\bar{C}_{ps}$ show that either a linear temperature dependent relating $\bar{V}_s$ to $\bar{V}_C$ and $\bar{V}_B$ or the more general non-linear model of Guggenheim can be utilized as improved models for obtaining better estimates of molar surface area values than those calculated using bulk volume data. This conclusion is important to note particularly since these models seem to be applicable to even polar systems. Hence it would be expected that improved calculations of the surface tensions of mixtures of polar compounds would be possible if one of the above models were utilized in calculating surface molar area values for these polar compounds.

It is interesting to note that even for an order of magnitude change in the parameters affecting the $\Delta\bar{C}_{ps}$ equation, roughly constant values are obtained for a wide range of polarity of compounds for both the linear and non-linear models for the surface density equations.

1. R. AVEYARD and D. A. HAYDON. An introduction to the principles of surface chemistry. Cambridge University Press, 1973.

Can. J. Chem. Downloaded from www.nrcresearchpress.com by 186.148.149.217 on 09/07/12
For personal use only.

2. L. J. PAQUETTE and D. E. GOLDSACK. J. Colloid, Interface Sci. **92**, 154 (1983).
3. A. GIACALONE. Gazz. Chim. Ital. **47**, 88 (1947).
4. J. R. PARTINGTON. An advanced treatise on physical chemistry. Vol. 2. Longmans, London, 1951.
5. E. A. MOELWYN-HUGHES. Physical chemistry. 2nd ed. Pergamon Press, 1961.
6. E. A. GUGGENHEIM. Thermodynamics, North Holland Publishing Company, 1959.
7. S. TOXVAERD. Prog. Sci. **3**, 189 (1972).
8. A. I. BURSHTEIN. Adv. Colloid Interface Sci. **11**, 315 (1979).
9. J. S. ROWLINSON and B. WIDOM. Molecular theory of capillarity, Clarendon Press, Oxford, 1984.
10. J. R. PARTINGTON. An advanced treatise on physical chemistry. Vol. 1. Longmans Green, London, 1949.
11. N. A. LANGE. Handbook of chemistry, 10th ed. McGraw-Hill Book Company, New York. 1961.
12. INTERNATIONAL CRITICAL TABLES OF NUMERICAL DATA. Physics, chemistry and technology. McGraw-Hill Book Company, Inc., New York, 1962.
13. R. C. REID, J. M. PRAUSNITZ, and T. K. SHERWOOD. The properties of gases and liquids. 3rd ed. McGraw-Hill Book Company, New York 1977.
14. D. E. GOLDSACK and B. R. WHITE. Can. J. Chem. **61**, 1725 (1983).

Can. J. Chem. Downloaded from www.nrcresearchpress.com by 186.148.149.217 on 09/07/12
For personal use only.

Alkali metal salt solvation study in 1,1,3,3-tetramethylurea using nuclear magnetic resonance spectroscopy

LAURA ANN CIOLINO AND BARBARA JANE BARKER[1]
Department of Chemistry, Xavier University, Cincinnati, OH 45207-1096, U.S.A.

Received August 18, 1988[2]

LAURA ANN CIOLINO and BARBARA JANE BARKER. Can. J. Chem. **67**, 2206 (1989).

The solution behavior of a series of alkali metal tetraphenylborates, perchlorates, and iodides in 1,1,3,3-tetramethylurea (TMU) has been studied by proton nuclear magnetic resonance (NMR) spectroscopy. TMU has a simple proton NMR spectrum consisting of one singlet at 2.75 ppm. Alkali metal tetraphenylborates and perchlorates were observed to be dissociated in TMU. Sodium iodide, however, was observed to be associated in TMU. Present results are compared with those from other NMR investigations in TMU and related nonaqueous solvents.

Key words: alkali metal salt solvation, tetramethylurea, nuclear magnetic resonance, solute–solvent interactions.

LAURA ANN CIOLINO et BARBARA JANE BARKER. Can. J. Chem. **67**, 2206 (1989).

Faisant appel à la rmn du ^1H, on a étudié le comportement d'une série de tétraphénylborates, de perchlorates et d'iodures de métaux alcalins en solution dans la 1,1,3,3-tétraméthylurée (TMU). La TMU possède un spectre rmn du ^1H qui est simple et qui ne comporte qu'un singulet à 2,75 ppm. On a observé que, dans la TMU, les tétraphénylborates et les perchlorates des métaux alcalins sont dissociés. Toutefois, on a observé que l'iodure de sodium est associé dans la TMU. On compare ces résultats avec ceux obtenus au cours d'autres études par rmn tant dans la TMU que dans d'autres solvants apparentés et non-aqueux.

Mots clés : solvatation des sels de métaux alcalins, tétraméthylurée, résonance magnétique nucléaire, interactions soluté–solvant.

[Traduit par la revue]

Introduction

Nuclear magnetic resonance (NMR) continues to be a useful technique for the study of electrolyte solution behavior. The occurrence of solute dissociation and solvation is inferred from probing either solute or solvent atom nuclei as a function of solute concentration.

In solution a variety of states is possible for solute and solvent molecules: solvated cations, solvated anions, solvent-separated ion pairs (all dissociated states); cation–anion pairs or aggregates (associated states); and bulk solvent. Since exchange among states is rapid, chemical shifts of either solute or solvent atom nuclei represent the average of all states.

If solvent protons are probed the chemical shift will be a linear function of salt concentration until association into ion pairs or aggregates occurs. If the cation is probed the chemical shift will be independent of salt concentration until association occurs.

Early reports described solution behavior of alkali metal salts in water (1–4). These salts remained dissociated and solvated until salt concentrations approached 5 to 15 molal (1, 2).

Later papers described solution behavior of alkali metal salts in nonaqueous solvents (5–10). Specific solvents included *N*-methyl-2-pyrrolidone (5, 6), 3-methyl-2-oxazolidone (7, 8), 1,3-dimethyleneurea (9), and 1,1,3,3-tetramethylurea (10).

Proton NMR revealed that alkali metal salts in *N*-methyl-2-pyrrolidone and 3-methyl-2-oxazolidone were dissociated until concentrations approached 1 molar (6–8). Proton NMR, used in the dimethyleneurea (DMEU) study, followed the chemical shifts of the solvent's methyl and ethylene protons. The salts, which included a variety of tetraphenylborates, perchlorates, and iodides, were dissociated until 0.75 molar (9).

Sodium-23 NMR, used in the tetramethylurea (TMU) study, followed the chemical shift of sodium for a variety of sodium salts. Sodium tetraphenylborate and perchlorate were dissociated until 0.5 molar. Sodium iodide formed contact ion pairs or aggregates which increased linearly with concentration (10).

The present investigation extends the study of alkali metal salt solution behavior in TMU. The chemical shift of the solvent protons is probed as a function of concentration for a series of tetraphenylborates, perchlorates, and iodides.

Experimental

1,1,3,3-Tetramethylurea was an Eastman Reagent Grade solvent. Cyclohexane was a Spectrochemical Grade NMR reference obtained from Matheson, Coleman, and Bell.

Sodium iodide (Mallinckrodt Analytical Reagent) and sodium perchlorate (Alfa Products) were recrystallized from acetone–ether solutions and dried *in vacuo* prior to use. Sodium tetraphenylborate (Baker Analyzed Reagent), lithium and potassium perchlorate (both Alfa Products), potassium iodide (Fisher Scientific, certified ACS reagent), and rubidium iodide (Alfa Products) were dried at 100°C for several hours before use. Potassium, rubidium, and cesium tetraphenylborates were prepared by mixing aqueous, equimolar solutions of potassium perchlorate, rubidium iodide, or cesium nitrate (Ventron Alfa Products) with sodium tetraphenylborate. The tetraphenylborate salts were then recrystallized from acetone–ether solutions and dried for several hours.

A 100 MHz Jeol Model JMH-100 NMR spectrometer was used to verify the purity of TMU. A Varian T-60 NMR spectrometer with a constant probe temperature of 35°C was used to measure solution chemical shifts. Wilmad Glass Co. and Norell, Inc. were the suppliers of NMR tubes.

Tetramethylurea was refluxed for several hours and vacuum distilled over barium oxide powder (G. Frederick Smith Chemical Co.). The distilled TMU was used immediately. Cyclohexane served as the internal reference at a nominal level of 5% by weight. Each salt solution was prepared by independent weighings. Concentrations were measured in molality since weight measurements used in molality determinations are unaffected by differences between ambient and probe temperatures. The usable concentration range was limited to 0.90 molal because of low solubility.

All NMR spectra were obtained immediately after solution preparation. Positions of the TMU and cyclohexane NMR signals were approxi-

[1]Author to whom correspondence should be addressed.
[2]Revision received June 21, 1989.

Printed in Canada / Imprimé au Canada

Can. J. Chem. Downloaded from www.nrcresearchpress.com by 186.148.149.217 on 09/07/12
For personal use only.

TABLE 1. Nuclear magnetic resonance data for alkali metal salts in 1,1,3,3-tetramethylurea

Salt[a]	Concentration (molality)[b]	Δ Peak (ppm × 10^2)[c]	Salt[a]	Concentration (molality)[b]	Δ Peak (ppm × 10^2)[c]	Salt[a]	Concentration (molality)[b]	Δ Peak (ppm × 10^2)[c]
$NaBPh_4$	0.193 (I)	+2.0	$LiClO_4$	0.199 (I)	+0.8	NaI	0.152 (II)	+1.2
	0.451 (I)	+4.8		0.348 (I)	−1.3		0.298 (II)	+0.8
	0.684 (I)	+7.5		0.521 (I)	−2.0		0.300 (I)	+1.0
				0.654 (I)	−4.2		0.501 (I)	+1.0
$KBPh_4$	0.151 (I)	+2.0					0.601 (II)	+1.0
	0.201 (II)	+2.5	$NaClO_4$	0.201 (I)	+2.3			
	0.285 (II)	+3.8		0.298 (I)	+3.0	KI	0.098 (I)	+4.7
	0.348 (I)	+4.3		0.400 (I)	+2.0		0.100 (II)	+5.0
	0.486 (II)	+7.3		0.482 (I)	+1.0		0.199 (II)	+5.3
	0.740 (I)	+11.		0.588 (II)	−1.0			
				0.696 (I)	−1.2	RbI	0.075 (I)	+5.2
$RbBPh_4$	0.099 (I)	+3.2		0.882 (II)	−3.2		0.084 (I)	+5.2
	0.103 (II)	+2.8					0.151 (I)	+6.7
	0.200 (I)	+6.8	$KClO_4$	0.100 (I)	+2.7			
	0.316 (II)	+8.2		0.195 (II)	+4.2			
	0.494 (II)	+9.3						
$CsBPh_4$	0.075 (I)	+3.2						
	0.098 (II)	+3.2						
	0.150 (I)	+4.7						
	0.202 (II)	+4.0						
	0.284 (II)	+3.7						
	0.385 (II)	+4.3						
	0.410 (II)	+3.7						

[a] BPh_4 represents the tetraphenylborate ion.
[b] The numbers (I) and (II) designate independent sets of measurements.
[c] The symbols + and − reveal shifts upfield and downfield, respectively, with reference to the TMU peak.

Can. J. Chem. Downloaded from www.nrcresearchpress.com by 186.148.149.217 on 09/07/12
For personal use only.

mated to 0.2 Hz. The peak position of any broad NMR signal was determined by triangulation.

Blank determinations of the pure solvent shift accompanied each set of experiments. The NMR shifts of salt solutions were calculated relative to that of the pure solvent, with upfield shifts considered positive and downfield shifts considered negative. In most cases the experimental data were obtained from two independent sets of measurements.

Results and discussion

Tetramethylurea is a polar solvent with a dipole moment of 3.37 Debye units (11). TMU's intermolecular dipole–dipole interactions are strong as evidenced by its high boiling and melting points of 177°C and −1°C, respectively.

TMU has a moderately low dielectric constant of 23.45 (12) and a moderately high Gutmann donor number of 29.6 (13). The first factor is an indication that electrolyte dissociation is unfavorable. The second factor is an indication that electrolyte solvation is favorable. The expected result will be dissociation and solvation for some salts, and association for other salts in TMU.

A solvated cation will interact with TMU through its electronegative sites: the carbonyl oxygen and/or the two amide nitrogens. The oxygen site is more sterically accessible than the nitrogen sites. A solvated anion will interact with TMU through the electropositive carbonyl carbon. In both cases the ion–dipole interaction is expected to further polarize the TMU molecules in the solvation shell. The resulting polarization decreases electron density around the TMU protons of those molecules.

All of the solvent proton shifts are upfield for the tetraphenylborate salts in TMU (Table 1). This behavior for tetraphenylborate salts has also been observed in other nonaqueous

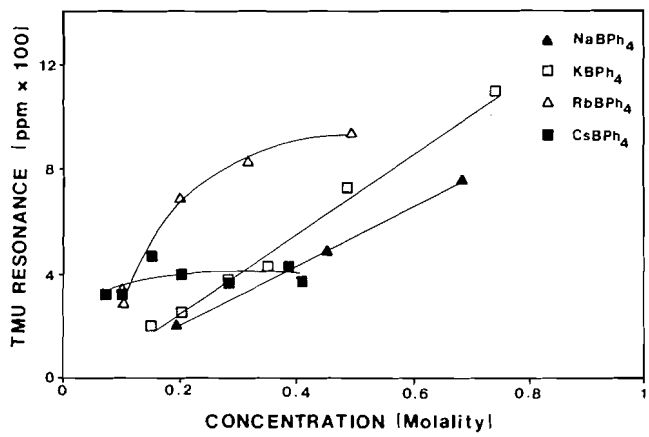


FIG. 1. Proton nuclear magnetic resonance shifts for tetramethylurea – alkali metal tetraphenylborate solutions. Shifts are upfield relative to pure TMU.

solvents (7–9). The increase in electron density around solvent protons is probably associated with the proximity of the protons to the π electron system in tetraphenylborates. An anion–dipole interaction can not explain the observation because it will be small due to the small charge density of the anion. Furthermore, it is expected to cause a downfield shift resulting from polarization of the TMU molecule.

The sodium and potassium tetraphenylborate shifts increase linearly with concentration over the range studied (Fig. 1). Linearly increasing shifts are consistent with complete dissociation and solvation of cations and anions. The rubidium and cesium tetraphenylborates display curved or flat relationships,

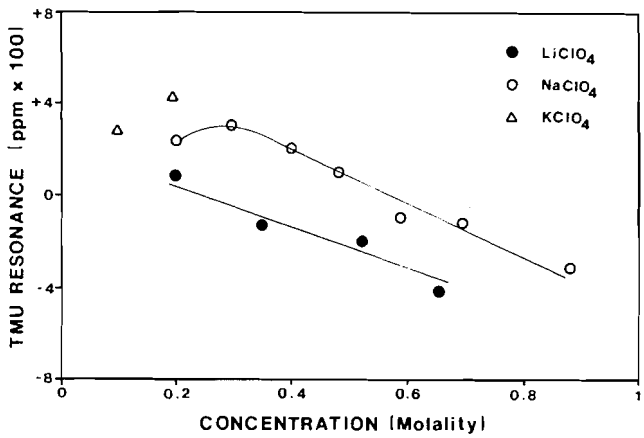


FIG. 2. Proton nuclear magnetic resonance shifts for tetramethylurea – alkali metal perchlorate solutions. Positive shifts are upfield and negative shifts are downfield relative to pure TMU.

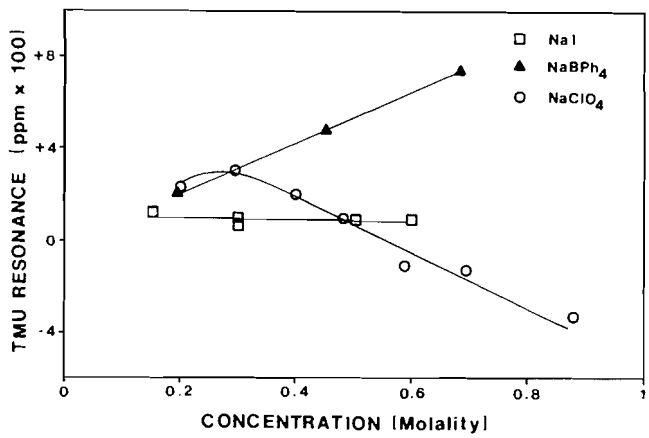


FIG. 3. Proton nuclear magnetic resonance shifts for tetramethylurea – sodium salt solutions. Positive shifts are upfield and negative shifts are downfield relative to pure TMU.

respectively, with increasing concentration. This observation suggests the formation of cation–anion pairs or aggregates which essentially eliminates the ionic interaction with the solvent.

The magnitude of the upfield shifts for the tetraphenylborates decreases in the order $Rb^+ > K^+ > Na^+$. This increase in downfield shift from rubidium to sodium correlates with the increasing strength of the cation–dipole interaction in the series. The increasing charge density from rubidium to sodium corresponds to increasing solvent polarization.

The perchlorates display slight upfield shifts below 0.4 molal, followed by linear downfield shifts above 0.4 molal (Fig. 2). The perchlorate anion has no special mode of interaction with TMU. It is expected to have only a small polarizing (downfield) effect due to its large size. Thus, the chemical shifts are expected to be primarily due to cation–TMU interactions.

The perchlorates are considered to be dissociated and solvated throughout the range studied. The initial upfield shifts are interpreted as "structure breaking." Dipole–dipole interactions between solvent molecules are being replaced by ion–dipole interactions between cation and solvent molecules. Although the latter are stronger interactions, they disrupt the bulk solvent structure such that the number of dipole–dipole interactions decreases disproportionately to the number of new cation–dipole interactions. At higher concentrations the number of ion–dipole interactions is sufficient to provide an overall net polarization. The direction of the shifts changes to downfield; the shifts increase linearly with concentration.

The magnitude of the downfield shift is larger for lithium than for sodium. This observation is consistent with the greater strength of the lithium ion – TMU dipole interaction. The higher charge density of lithium relative to that of sodium causes greater polarization.

The chemical shifts for sodium iodide in TMU are concentration independent over the range investigated (Fig. 3). The shifts versus bulk solvent are near zero. These two results indicate that there is no net increase in TMU–salt interaction as concentration increases and that the effect on proton environments is small. Therefore, sodium iodide is considered to be associated in TMU.

Results from the present investigation agree well with those from the sodium-23 NMR study in TMU (10). Solution behavior for the salts studied in common was observed to be the same; i.e., dissociation for sodium tetraphenylborate and sodium perchlorate, and association for sodium iodide.

Chemical shift data from the present investigation for TMU are analogous to chemical shift data for DMEU (9). Studied in common were sodium and potassium tetraphenylborate, lithium and sodium perchlorate, and sodium iodide. Sodium iodide, however, was considered to be dissociated in DMEU (9), even though the shifts showed no concentration dependence.

Acknowledgements

The authors wish to express sincere appreciation to The Drackett Company of Cincinnati, Ohio, for the use of their Jeol Model JMH-100 NMR spectrometer. We also wish to thank the Chemistry Department, University of Cincinnati, for the use of their Varian T-60 NMR spectrometer.

1. J. N. SHOOLERY and B. J. ALDER. J. Chem. Phys. **23**, 805 (1955).
2. B. P. FABRICAND and S. GOLDBERG. J. Chem. Phys. **34**, 1624 (1961).
3. J. F. HINTON and E. S. AMIS. Chem. Rev. **67**, 367 (1967).
4. J. DAVIES, S. ORMONDROYD, and M. C. R. SYMONS. Trans. Faraday Soc. 3465 (1971).
5. J. L. WUEPPER and A. I. POPOV. J. Am. Chem. Soc. **92**, 1493 (1970).
6. J. ROSENFARB and R. J. BAKER. J. Phys. Chem. **82**, 329 (1978).
7. T. L. BUXTON and J. A. CARUSO. J. Am. Chem. Soc. **96**, 6033 (1974).
8. N. SALEH and J. A. CARUSO. J. Solution Chem. **8**, 197 (1979).
9. J. ROSENFARB and J. A. CARUSO. Can. J. Chem. **54**, 3492 (1976).
10. M. S. GREENBERG, R. L. BODNER, and A. I. POPOV. J. Phys. Chem. **77**, 2449 (1973).
11. A. LÜTTRINGHAUS and H. W. DIRKSEN. Angew. Chem. Int. Ed. Engl. **3**, 260 (1964).
12. B. J. BARKER and J. A. CARUSO. J. Am. Chem. Soc. **93**, 1341 (1971).
13. A. I. POPOV. Pure Appl. Chem. **41**, 275 (1975).

Can. J. Chem. Downloaded from www.nrcresearchpress.com by 186.148.149.217 on 09/07/12
For personal use only.

Synthesis of complexes of the type *cis*-Pt(amine) (unsaturated ligand)Cl_2 and crystal structure of *cis*-Pt(methylamine) (dimethylhexynediol)Cl_2

F. D. ROCHON, R. MELANSON, AND MONIQUE DOYON

Département de chimie, Université du Québec à Montréal, C.P. 8888, succ. A., Montréal (Qué.), Canada H3C 3P8

Received August 2, 1988[1]

F. D. ROCHON, R. MELANSON, and MONIQUE DOYON. Can. J. Chem. **67**, 2209 (1989).

Complexes of the type *cis*-Pt(L)(un)Cl_2 where L = primary amine or methyl derivative of pyridine and un = cyclopentene, cyclohexene, or dimethylhexynediol, have been synthesized from the reaction of K[Pt(L)Cl_3] with the unsaturated ligand in water. The compounds were characterized and studied by ^{1}H NMR and IR spectroscopy. The crystal structure of *cis*-Pt(CH_3NH_2)-((CH_3)$_2$C(OH)—C≡C—C(OH)(CH_3)$_2$)Cl_2 was determined by X-ray diffraction methods. The crystals are monoclinic, space group $P2_1/c$, with a = 6.544(2), b = 14.304(7), c = 15.508(7) Å, β = 109.39(2)°, and Z = 4. The coordinates and the anisotropic thermal factors were refined by full-matrix least-squares analysis to a R factor of 0.048 and wR = 0.047. The coordination around the platinum atom is square planar and the acetylenic ligand is perpendicular to the Pt plane.

Key words: platinum complexes, crystal structure, methylamine, dimethylhexynediol, synthesis.

F. D. ROCHON, R. MELANSON et MONIQUE DOYON. Can. J. Chem. **67**, 2209 (1989).

Des complexes de type *cis*-Pt(L)(un)Cl_2 où L = amine primaire ou un dérivé méthyle de la pyridine et un = cyclopentène, cyclohexène ou diméthylhexynediol, ont été synthétisés par la réaction de K[Pt(L)Cl_3] avec le ligand insaturé en milieu aqueux. Les composés ont été caractérisés et étudiés par spectroscopie IR et par RMN du proton. La structure cristalline de *cis*-Pt-(CH_3NH_2)((CH_3)$_2$C(OH)—C≡C—C(OH)(CH_3)$_2$)Cl_2 a été déterminée par diffraction des rayons-X. Le composé appartient au groupe spatial $P2_1/c$, a = 6.544(2), b = 14.304(7), c = 15.508(7) Å, β = 109.39(2)° et Z = 4. Les coordonnées et les facteurs thermiques anisotropes ont été affinés par moindres-carrés à matrice entière jusqu'à R = 0.048 et wR = 0.047. La coordination autour de l'atome de Pt est plane et le ligand acétylénique est perpendiculaire au plan du platine.

Mots clés: complexes de platine, synthèse méthylamine, diméthylhexynediol, structure cristalline.

Can. J. Chem. Downloaded from www.nrcresearchpress.com by 186.148.149.217 on 09/07/12
For personal use only.

Introduction

No general method for the synthesis of complexes of the type *cis*-Pt(amine)(un)Cl_2 where un = alkene or alkyne derivatives, has been reported yet, except for *cis*-Pt(NH_3)(C_2H_4)Cl_2 (1), *cis*-Pt(pyridine)(C_2H_4)Cl_2 (2) and a few compounds with very bulky amines (3, 4). These compounds are usually prepared from the monoamine compound K[Pt(amine)Cl_3]. Although K[Pt-(NH_3)Cl_3] (5, 6) and K[Pt(pyridine)Cl_3] (7) have been reported, the methods used to synthesize these compounds are not suitable for the preparation of primary amine analogs.

Trans compounds containing pyridine derivatives and unsaturated ligands have been known for a long time (2, 8, 9). Compounds of the type K[Pt(un)Cl_3] have been reported (8, 10–12) and their reactions with pyridine derivatives (py) give *trans*-Pt(py)(un)Cl_2 because of the large *trans* effect of alkenes and alkynes. Much of the work reported on alkynes has been done with bulky ligands like (CH_3)$_3$C—C≡C—C(CH_3)$_3$ and glycols of the type R_2C(OH)—C≡C—C(OH)R_2 since ligands like R—C≡C—H do not form stable Pt(II) π complexes.

Crystal structure analysis of several platinum – unsaturated ligand complexes consistently showed that the olefin or alkyne was perpendicular to the platinum coordination plane (10–13).

Recently, we have reported a new method to synthesize K[Pt(amine)Cl_3] with primary amines (14). The reactions of these compounds with two cyclic alkenes and with dimethylhexynediol (DMHD) have been studied. Compounds of the type *cis*-Pt(amine)(un)Cl_2 have been isolated and characterized mainly by IR and ^{1}H NMR spectroscopy. A few compounds *cis*-Pt(py)(un)Cl_2 with pyridine derivatives were also synthesized and characterized. One of the compounds *cis*-Pt(CH_3NH_2)-((CH_3)$_2$C(OH)—C≡C—C(OH)(CH_3)$_2$)Cl_2 gave crystals suitable for crystallographic studies and its structure was determined. The results are discussed below.

[1]Revision received June 27, 1989.

Experimental Section

K_2PtCl_4 was bought from Johnson Matthey and Co. Limited and was recrystallized from water. The elemental analyses were performed by Galbraith Laboratories. The IR spectra were measured on a P.E. 783 or Digilab FT50 (CsI beamsplitter). The ^{1}H NMR spectra were recorded on a Varian EM-360L (60 MHz) equipped with a signal averager V-2048.

K[Pt(amine)Cl_3]

These compunds were synthesized according to the method described recently (14).

K[Pt(pyridine)Cl_3]

These compounds with py = 2-picoline, 3-picoline, and 2,4-lutidine were synthesized according to the method already reported (7). Yield 85–90%

cis-*Pt(pyridine)(un)Cl_2 (un = cyclopentene (CPE) and cyclohexene (CHE)*

One millimole of K[Pt(py)Cl_3] is dissolved in a minimum quantity of water and the solution is filtered. Four millimoles of the unsaturated ligand is added to the filtrate and the mixture is stirred at room temperature for 24 h (or 48 h for cyclohexene). The precipitate is then filtered, washed with cold water, dried, washed with ether, and dried under vacuum in the presence of P_2O_5.

cis-*Pt(2,4-lutidine)(CPE)Cl_2* dec. 143–155°C; IR(cm^{-1}): ν(C=C aromatic) 1622 and ν(Pt—Cl) 341,320; NMR(DMSO-d_6), δ(ppm); 5.70 (un).

cis-*Pt(2,4-lutidine)(CHE)Cl_2* dec. 150–185°C; IR(cm^{-1}): ν(C=C aromatic) 1627 and ν(Pt—Cl): 341,315; NMR(DMSO-d_6) δ(ppm): 5.50 (un).

cis-*Pt(2-picoline)(CPE)Cl_2* dec. 143–168°C; IR(cm^{-1}): ν(C=C aromatic) 1602, 1560 and ν(Pt—Cl) 337,321; NMR (acetone-d_6) δ(ppm): 5.70 s + d (un) $J(^{195}Pt—H_{un})$ = 82 Hz.

cis-*Pt(3-picoline)(CPE)Cl_2* dec. 138–149°C; IR(cm^{-1}): ν(C=C aromatic) 1604, 1582 and ν(Pt—Cl) 337,323; NMR (acetone-d_6) δ(ppm): 5.69 s + d (un) $J(^{195}Pt—H_{un})$ = 82 Hz.

Can. J. Chem. Downloaded from www.nrcresearchpress.com by 186.148.149.217 on 09/07/12
For personal use only.

cis-*Pt(2-picoline)(CHE)Cl*$_2$ dec. 142–188°C; IR(cm^{-1}): ν(C═C aromatic) 1606, 1563 and ν(Pt—Cl): 338,320; NMR(dimethylacetamide) δ(ppm): 5.60 s (un).

cis-*Pt(2,4-lutidine)(DMHD)Cl*$_2$ *(DMHD = dimethylhexynediol)*

One millimole of K[Pt(2,4-lutidine)Cl$_3$] is dissolved in a minimum quantity of water and the solution is filtered. Three millimole of DMHD are added and the mixture is stirred at 10°C for 5 days. The precipitate is then filtered, washed with cold water, dried, washed with ether, and dried under vacuum over P_2O_5. Dec. at 127–132°C; IR (cm^{-1}): ν(O—H) 3422, ν(C≡C) 2001, ν(C═C aromatic) 1623 and ν(Pt—Cl) 339,311; NMR(CD_3OD) δ(ppm): 3.16 s + d (2-CH_3) $^4J(^{195}Pt—H)$ = 10 Hz, 2.41 s (4-CH_3), 8.87 d + dd (H_6) $^3J(H_6—H_5)$ = 6 Hz and $^3J(^{195}Pt—H_6)$ = 38 Hz, 7.25 m (H_3 + H_5) and 1.65 m (DMHD).

cis-*Pt(amine)(un)Cl*$_2$

These compounds were prepared by the method described for the synthesis of *cis*-Pt(2,4-lutidine)(DMHD)Cl$_2$ except that the mixture was stirred for 48 h.

cis-*Pt(CH_3NH_2)(CPE)Cl*$_2$ dec. 122–128°C, IR (cm^{-1}): ν(N—H) 3236, 3201, 3191, δ(N—H) 1582, ν(Pt—Cl) 337, 318; *cis*-Pt(CD_3ND_2)(CPE)Cl$_2$ IR (cm^{-1}): ν(N—D) 2421, 2367, 2318, δ(N—D) 1168; NMR (acetone-d_6) δ(ppm): 2.61 t + dt (CH_3) ^3J(H—H) = 7 Hz and $^3J(^{195}Pt—H_{un})$ = 40 Hz, 5.40 s + d (un) J(Pt—H_{un}) = 80 Hz.

cis-*Pt($C_2H_5NH_2$(CPE)Cl*$_2$ dec. 128–135°C, IR (cm^{-1}): ν(N—H) 3242, 3195, 3124, δ(N—H) 1579, ν(Pt—Cl) 338, 310; NMR (acetone-d_6) δ(ppm): 1.23 t (CH_3) ^3J(H—H) = 8 Hz, 5.30 s + d (un) $J(^{195}Pt—H_{un})$ = 80 Hz.

cis-*Pt(CH_3NH_2)(DMHD)Cl*$_2$ dec. 160–173°C, IR (cm^{-1}): ν(N—H) 3264, 3206, 3140, ν(O—H) 3465, ν(C≡C) 2007, δ(N—H) 1581, ν(Pt—Cl) 340, 320; NMR (CD_3OD) δ(ppm): 2.45 t + dt (CH_3) ^3J(H—NH_2) = 7 Hz, ^3J(Pt—H) = 44 Hz, 1.70 s (DMHD).

cis-*Pt(cyclobutylamine)(DMHD)Cl*$_2$ dec. 140–150°C, IR (cm^{-1}): ν(N—H) 3214, 3116, ν(O—H) 3385, ν(C≡C) 2001, δ(N—H) 1577, ν(Pt—Cl) 336, 316; NMR (CD_3OD) δ(ppm): 1.70 s (DMHD).

cis-*Pt(cyclopentylamine)(DMHD)Cl*$_2$ dec. 150–155°C, IR (cm^{-1}): ν(N—H) 3246, 3183, 3105, ν(O—H) 3420, ν(C≡C) 2006, δ(N—H) 1582 ν(Pt—Cl) 339, 321; NMR (CD_3OD) δ(ppm): 1.70 s (DMHD).

Collection and reduction of X-ray data

Crystals of *cis*-Pt(CH_3NH_2)((CH_3)$_2$C(OH)—C≡C—C(OH)(CH_3)$_2$)Cl$_2$) were recrystallized from acetone. A yellow hexagonal plate was selected for structure anaysis after examination under a polarizing microscope for homogeneity. The crystal was mounted roughly along the *c* axis. Precession photographs showed that the crystal was monoclinic with the systematic absences of $P2_1/c$. The unit cell parameters were obtained by least-squares refinements of angles 2θ, ω, and χ for 15 well-centered reflections on a Syntex P$\bar{1}$ diffractometer using graphite-monochromatized MoKα radiation. Scan rates and data treatment have already been described (15). A total of 4010 independent reflections were measured with 2θ < 60°. Corrections were made for absorption and Lorentz-polarization effects. Anomalous dispersion terms (16) were also included in the calculations. A set of 2700 observed reflections was used for the structure determination.

Crystal data

$C_9H_{19}NO_2Cl_2Pt$ mw = 439.25

Monoclinic, $P2_1/c$, a = 6.544(2), b = 14.304(4), c = 15.508(8) Å, β = 109.39(2)°, V = 1369.3(7) Å^3, Z = 4, F(000) = 832, D_x = 2.130, D_m = 2.16(3) Mg m^{-3}, λ(MoKα) = 0.71069 Å, μ(Mokα) = 10.728 mm^{-1}, and T = 295 K.

Structure solution

The coordinates of the platinum atom were found from a three-dimensional Patterson synthesis. The positions of all the other non-hydrogen atoms were obtained by structure factor and Fourier-map calculations. The refinements were done by using full-matrix least-squares minimizing $w(F_o - F_c)^2$. Isotropic secondary-extinction corrections (17) were included in the calculations. The two H atoms in the —NH_2 group were fixed at their calculated positions with isotropic B = 0.06 Å^2. Attempts were made to locate the H atoms in the methyl groups but without success. Individual weights $w = 1/\sigma^2(F)$ were applied. The refinement of the scale factor, coordinates and anisotropic temperature factors of all atoms converged to R = 0.048 and wR = 0.047. The ratio of maximum least-squares shift to esd in final refinement cycle was 0.20. There were a few residual peaks (<1.35 e A^{-3}) in the close environment of the Pt atom. The final positional parameters are listed in Table 1.

TABLE 1. Positional parameters with their esd's and temperature factors (10^4) $U_{eq} = (1/3)\Sigma_i\Sigma_j U_{ij} a_i^* a_j^* \bar{a}_i \cdot \bar{a}_j$

Atom	x	y	z	U_{eq} (Å^2)
Pt	1251.9(5)	120.2(2)	−1731.0(2)	299
Cl(1)	3970(4)	−929(2)	−1048(2)	561
Cl(2)	3621(4)	983(2)	−2224(2)	592
N	−838(12)	−688(5)	−1312(5)	366
O(1)	−4154(11)	−124(5)	−3586(4)	532
O(2)	−1609(11)	1458(5)	−526(4)	473
C(1)	−1242(19)	232(8)	−4135(7)	640
C(2)	−3968(18)	1476(7)	−4096(7)	502
C(3)	−2662(14)	631(6)	−3625(6)	402
C(4)	−1370(13)	889(6)	−2653(6)	304
C(5)	−835(14)	1290(6)	−1919(6)	334
C(6)	−824(14)	1972(6)	−1171(6)	354
C(7)	−2401(15)	2800(6)	−1590(7)	428
C(8)	1468(16)	2309(7)	−657(7)	529
C(9)	−1538(17)	−1573(6)	−1825(7)	490

The atomic scattering factors of Cromer and Waber (18) were used for Pt, Cl, O, N, and C atoms, and those of Stewart, Davidson, and Simpson (19) were used for H. The calculations were done on a Cyber 830 with programs already described (15). Tables of final observed and calculated structure factors, and anisotropic thermal parameters are available.[2]

Results and discussion

Complexes of the type *cis*-Pt(L)(un)Cl$_2$ were prepared from the reaction of K(Pt)(L)Cl$_3$] with the unsaturated ligand in water.

$$K[Pt(L)Cl_2] + un \xrightarrow{H_2O} cis\text{-}Pt(L)(un)Cl_2 + KCl$$

In water, only the *cis* isomers are formed since the *trans* effect of Cl > N ligands. With un = cyclopentene (CPE), compounds with L = methylamine, ethylamine, 2-picoline and 2,4-lutidine were synthesized. When un = cyclohexene (CHE), the synthesis with primary amines was not successful. Only compounds with 2-picoline, 3-picoline, and 2,4-lutidine could be isolated. When L = dimethylhexynediol (DMHD), compounds with methylamine, cyclobutylamine, cyclopentylamine, and 2,4-lutidine were prepared. No compounds with isopropylamine or *t*-butylamine could be prepared with any of the three unsaturated ligands, probably because of steric hindrance caused by two

[2]Lists of the elemental analysis of the complexes *cis*-Pt(L)(un)Cl$_2$ (Table S1), the anisotropic thermal parameters (Table S2), the weighted least-squares planes (Table S3), the distances and angles for hydrogen bonds (Table S4), the fixed coordinates of the H atoms (Table S5), and the final observed and calculated structure factors (Table S6, 15 pages) may be purchased from the Depository of Unpublished Data, CISTI, National Research Council of Canada, Ottawa, Ont., Canada K1A 0S2.

Can. J. Chem. Downloaded from www.nrcresearchpress.com by 186.148.149.217 on 09/07/12
For personal use only.

bulky ligands in *cis* position. The results of the elemental analyses have confirmed the composition $Pt(L)(un)Cl_2$ (see footnote 2 for supplementary material). The compounds were characterized by IR spectroscopy and by proton NMR.

The stretching bands $\nu(C{\equiv}C)$ and $\nu(Pt{-}Cl)$ for the complexes are shown in the Experimental section. The $\nu(C{\equiv}C)$ band for the complexes containing DMHD was observed between 2001 and 2007 cm^{-1}. This vibration absorbs at 2010 cm^{-1} in $K[Pt(DMHD)Cl_3]$ and at 2035 cm^{-1} in *trans*-$Pt(DMHD)(py)Cl_2$ (12). Therefore the *cis* isomers seem to absorb at lower frequency that the *trans* isomers. The free ligand DMHD absorbs in Raman at 2248 cm^{-1} (20). This reduction of frequency upon coordination has been explained by the nature of the Pt—DMHD bond (12).

All the *cis* compounds showed two $\nu(Pt{-}Cl)$ bands between 311 and 341 cm^{-1}. *trans*-$Pt(py)(DMHD)Cl_2$ with py = pyridine, 2-picoline, and 2,6-lutidine showed only one stretching $\nu(Pt{-}Cl)$ band at 337–340 cm^{-1} (8). Courtot *et al.* (2) also observed one $\nu(Pt{-}Cl)$ for *trans*-$Pt(py)(C_2H_4)Cl_2$ at 340–346 cm^{-1} and two bands for the *cis* isomers between 315 and 343 cm^{-1}. These results on the vibrations $\nu(C{\equiv}C)$ and $\nu(Pt{-}Cl)$ show that IR spectroscopy is a good method to determine the geometry of such isomers.

The ^1H NMR spectra of the compounds *cis*-$Pt(L)(un)Cl_2$ were measured in deuterated DMSO, DMF, acetone, or methanol but the compounds are not very soluble. The *cis* complexes partly isomerise in DMSO. For the pyridine derivatives, the values are very similar to those of the free ligands, but for the amine complexes, the resonances were observed at slightly higher field (~0.3 ppm). The observed shielding might be explained by a slight modification of the secondary anisotropic field caused by the π electrons of the unsaturated ligand. The coupling constants $J(^{195}Pt{-}{}^1H_{un})$ = 80–82 Hz slightly larger than the values observed for C_2H_4 complexes (61–67 Hz) (1, 2, 4). A coupling constant $^3J(^{195}Pt{-}{}^1H)$ of 40 Hz (for the methyl protons) was also observed in the complex *cis*-$Pt(CH_3NH_2)(CPE)Cl_2$. This value agrees well with the value of 44 Hz reported for $K[Pt(CH_3NH_2)Cl_3]$ (14). In the complexes *cis*-Pt(amine)$(DMHD)Cl_2$ the methyl groups of DMHD appear as a singlet around 1.70 ppm while in *cis*-Pt(2,4-lut)$(DMHD)Cl_2$ they appear as a multiplet.

Crystal structure

A labelled diagram of the molecule *cis*-$Pt(CH_3NH_2)(DMHD)Cl_2$ is shown in Fig. 1. The bond distances and angles are listed in Table 2. As expected from IR spectroscopy, the compound is the *cis* isomer. The coordination around the Pt atom is square planar, and the mid-point X of C(4)—C(5) triple bond occupies the fourth corner of the plane. The deviations from the best plane are Pt, 0.0000(3); Cl(1), −0.006(3); Cl(2), 0.007(3); N, 0.050(8) and X, −0.087 Å, and the angles around the Pt atom are close to the expected 90 and 180°.

The Pt—Cl (2.300(3) and 2.302(3) Å and the Pt—N (2.055((8) Å) bonds are normal and agree well with published values found in aminochloroplatinum(II) complexes (10, 11, 14). There is no lengthening of the bond in *trans* position to the acetylenic ligand. Therefore the *trans* influence of acetylenic ligands is not large. The Pt—C distances are 2.138(9) and 2.118(9) Å while the Pt—X distance is 2.039 Å. The acetylenic ligand is perpendicular to the platinum plane as observed in other Pt – acetylenic glycol complexes (10, 11). The angle between the best plane through C(3), C(4), C(5), and C(6) and the Pt plane is 92.4°. The two acetylenic carbon atoms C(4) and C(5) are located at 0.520(8) and −0.694(9) Å, respectively, from the platinum plane.

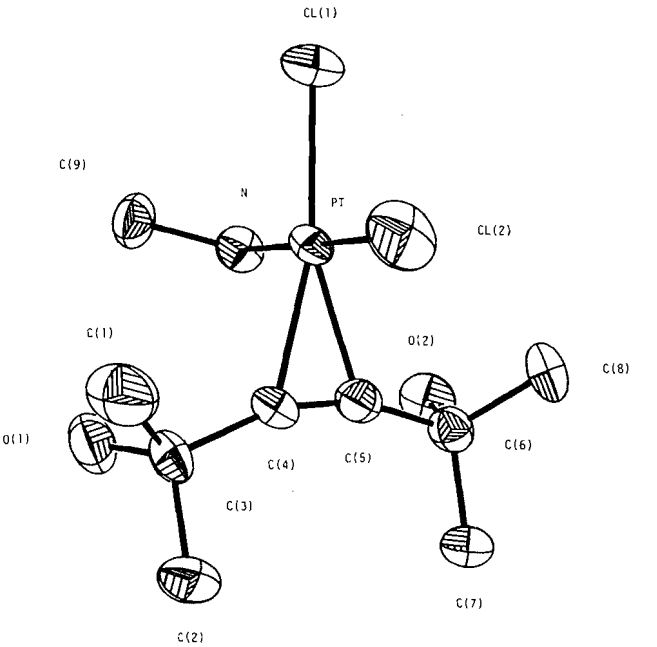


FIG. 1. Labelled diagram of the molecule *cis*-$Pt(CH_3NH_2)(DMHD)Cl_2$.

TABLE 2. Bond distances (Å) and angles (deg)

Bond	Distance	Bond	Distance
Pt—Cl(1)	2.300(3)	C(3)—C(4)	1.51(1)
Pt—Cl(2)	2.302(3)	C(5)—C(6)	1.52(1)
Pt—N	2.055(8)	C(3)—C(1)	1.51(2)
Pt—C(4)	2.138(9)	C(3)—C(2)	1.52(1)
Pt—C(5)	2.118(9)	C(6)—C(7)	1.56(1)
Pt—X	2.039	C(6)—C(8)	1.52(1)
N—C(9)	1.48(1)	C(3)—O(1)	1.47(1)
C(4)—C(5)	1.22(1)	C(6)—O(2)	1.47(1)

Bonds	Angle	Bonds	Angle
Cl(1)—Pt—Cl(2)	90.0(1)	C(4)—C(3)—C(1)	112.1(8)
Cl(1)—Pt—N	88.9(2)	C(4)—C(3)—C(2)	108.9(8)
Cl(2)—Pt—N	178.1(3)	C(4)—C(3)—O(1)	107.4(7)
Cl(1)—Pt—X	177.4	C(1)—C(3)—C(2)	113.1(8)
Cl(2)—Pt—X	89.6	C(1)—C(3)—O(1)	105.9(8)
Pt—N—C(9)	115.5(6)	C(2)—C(3)—O(1)	109.2(8)
N—Pt—X	91.6	C(5)—C(6)—O(2)	106.6(7)
C(3)—C(4)—C(5)	160.2(9)	C(7)—C(6)—C(8)	112.2(8)
C(4)—C(5)—C(6)	161.2(9)	C(7)—C(6)—O(2)	109.4(7)
C(5)—C(6)—C(7)	109.5(7)	C(8)—C(6)—O(2)	108.0(7)
C(5)—C(6)—C(8)	111.0(8)		

The triple bond distance C(4)—C(5) is 1.22(1) Å, which is not significantly different from a normal triple bond. However, the C(3)—C(4)—C(5)—C(6) segment of the coordinating ligand is not linear. The C(3) and C(6) atoms are displaced, producing a *cis* deformation in the direction opposite to the platinum atom. The C—C≡C angles are 160.2(9) and 161.2(9)°. These results are similar to those observed in other Pt – acetylenic glycol structures (10, 11). The two hydroxyl groups are in *cis* position to each other, on the same side of the plane through C(3), C(4), C(5), and C(6) towards the CH_3NH_2

ligand. The deviations from the best plane are O(1) −1.407(7) and O(2) −1.369(7) Å.

The packing of the molecules consists of layers of molecules parallel to the ***ac*** plane and centered at $y = 0$ and $\frac{1}{2}$. The amino groups are hydrogen bonded to one of the hydroxyl groups while the hydroxyl groups are hydrogen bonded to the cloro ligands.

Acknowledgments

The authors are grateful to the Natural Sciences and Engineering Research Council of Canada and the Ministère de l'Education (FCAR) for financial support and to Johnson Matthey for a loan of K_2PtCl_4.

1. H. P. Fritz and D. Sellman. J. Organomet. Chem. **6**, 558 (1966).
2. P. Courtot, R. Rumin, A. Peron, and J. P. Girault. J. Organomet. Chem. **145**, 343 (1978).
3. A. Panunzi and G. Paiaro. J. Am. Chem. Soc. **88**, 4843 (1966).
4. A. De Renzi, G. Paiaro, and A. Panunzi. Gazz. Chim. Ital. **102**, 413 (1972).
5. A. Cossa. Gazetta, **20**, 725 (1890).
6. Y. P. Jeannin and D. R. Russell. Inorg. Chem. **9**(4), 778 (1970).
7. P. C. Kong and F. D. Rochon. Can. J. Chem. **56**, 441 (1978).
8. A. D. Allen and T. Theophanides. Can. J. Chem. **42**, 1551 (1964).
9. A. D. Helman, S. V. Bukhovets, and E. Meilakh. Compt. Rend. (Doklady) Acad. Sci. URSS, **46**, 107 (1945).
10. A. L. Beauchamp, F. D. Rochon, and T. Theophanides. Can. J. Chem. **51**, 126 (1973).
11. R. J. Dubey. Acta Crystallogr. B**32**, 199 (1976).
12. J. Chatt, R. Guy, and L. A. Duncanson. J. Chem. Soc. 827 (1961); J. Chatt, R. Guy, L. A. Duncanson, and D. T. Thompson. J. Chem. Soc. 5170 (1963); T. A. Albright, R. Hoffmann, J. C. Thibeault, and D. L. Thorn. J. Am. Chem. Soc. **101**, 3801 (1979).
13. F. Caruso, R. Spagna, and L. Zambonelli. J. Cryst. Mol. Struct. **8**, 47 (1978).
14. F. D. Rochon, R. Melanson, and M. Doyon. Inorg. Chem. **26**, 3067 (1987).
15. R. Melanson and F. D. Rochon. Can. J. Chem. **53**, 2371 (1975).
16. D. T. Cromer. Acta Crystallogr. **18**, 17 (1965).
17. P. Coppens and W. C. Hamilton. Acta Crystallogr. A**26**, 71 (1970).
18. D. T. Cromer and J. T. Waber. Acta Crystallogr. **18**, 104 (1965).
19. R. F. Stewart, E. R. Davidson, and W. T. Simpson. J. Chem. Phys. **42**, 3175 (1965).
20. F. F. Cleveland and M. J. Murray. J. Am. Chem. Soc. **62**, 3186 (1940).

Can. J. Chem. Downloaded from www.nrcresearchpress.com by 186.148.149.217 on 09/07/12
For personal use only.

Solubility of ammonia in chloroform: analysis in terms of Henry's law and the equilibrium constant for hydrogen-bonded complex formation

JOHN F. SMITH, CHARLES LI, MYRON ROTH, AND LOREN G. HEPLER
Department of Chemistry, Univerity of Alberta, Edmonton, Alta., Canada T6G 2G2
Received March 15, 1989

JOHN F. SMITH, CHARLES LI, MYRON ROTH, and LOREN G. HEPLER. Can. J. Chem. **67**, 2213 (1989).

We have measured the solubility of ammonia in chloroform at several pressures and at three temperatures (25, 30, and 35°C). Results of these measurements have been analysed in terms of the Henry's law constant that applies to "simple" dissolution of the type B(g) = B(dissolved) and the equilibrium constant K for the liquid phase complex-forming equilibrium represented by A + B = AB where A and B represent chloroform and ammonia, respectively. As expected on the basis of this analysis, ammonia is more soluble (same pressure and temperature) in chloroform than in carbon tetrachloride, where no hydrogen-bonded complex can be formed.

Key words: gas solubility, hydrogen-bonded complexes, Henry's law constant, ammonia–chloroform complex, chloroform–ammonia complex.

JOHN F. SMITH, CHARLES LI, MYRON ROTH et LOREN G. HEPLER. Can. J. Chem. **67**, 2213 (1989).

On a mesuré la solubilité de l'ammoniac dans le chloroforme à plusieurs pressions et à trois températures (25, 30 et 35°C). On a analysé les résultats de ces mesures en fonction de la loi de Henry qui s'applique à des dissolutions « simples » du type B(g) = B(dissous) et de la constante d'équilibre K pour l'équilibre de la formation du complexe dans la phase liquide qui est représenté par l'équation A + B = AB dans laquelle A et B représentent respectivement le chloroforme et l'ammoniac. Comme on peut s'y attendre sur la base de cette analyse, l'ammoniac est plus soluble (à des pression et température semblables) dans le chloroforme que dans le tétrachlorure de carbone dans lequel il ne peut se former de complexes par liaisons hydrogènes.

Mots clés : solubilité des gaz, complexes par liaisons hydrogènes, constante de la loi de Henry, complexe ammoniac–chloroforme, complexe chloroforme–ammoniac.

[Traduit par la revue]

Can. J. Chem. Downloaded from www.nrcresearchpress.com by 186.148.149.217 on 09/07/12
For personal use only.

Introduction

Analyses of the thermodynamic properties of non-electrolyte solutions are generally made by comparing the measured properties with the properties the solution would have if it were ideal. Attempts are then made to explain the observed deviations in terms of some model (or theory) of solutions. As a first step in the development of such a model it is often convenient to separate the deviations from ideality into "physical" and "chemical" contributions, with the latter being due to the formation of distinct new chemical species in the solution. This separation is an artificial one because there is no sharp dividing line between interactions that may be regarded as physical and those that may be regarded as chemical. Nevertheless, the distinction between the two contributions is useful if one of the contributions is much smaller than the other.

For mixtures of non-electrolytes in which chemical reactions are expected (or known) to occur between the components, a first approximation to the treatment of non-ideality can be made by considering all of the deviations from ideal solution properties to arise from chemical interactions. That is, physical interactions (usually accounted for by activity coefficients) are taken to be negligible in comparison to chemical interactions. The solution is, therefore, considered to be an ideal solution (activity coefficients equal to unity) of all the species present at equilibrium. This is known as the ideal associated solution model (1–3). A solution of A + B in which A and B interact according to the equilibrium

[1] $$A + B = AB$$

is treated by the ideal associated solution model by considering the solution to be an ideal mixture of A + B + AB.

Several studies (4–9) have shown that the ideal associated solution model can be applied successfully to many associated systems (A + B = AB) in which A and B are liquids. This success suggests the possibility that the model may be useful in the investigation of systems in which a dissolved gas, B, interacts chemically with the solvent, A, to form an associated complex, AB. In this case the solubility of the gas (and hence the equilibrium speciation of the system) is determined by both the liquid–vapour equilibrium and the association (in the liquid phase) equilibrium. The liquid–vapour equilibrium represents the physical process of dissolution of gas. For a dilute solution this process can be described by Henry's law. The association equilibrium represents the chemical interaction that results in the formation of complex. This type of chemical interaction may be approximated usefully by the ideal associated solution model.

In this paper we present a method in which data collected in investigations of gas solubility can be used to evaluate the equilibrium constant and the Henry's law constant for any system in which a reasonably stable 1:1 complex forms between the dissolved gas and the solvent. The use of this method is illustrated by applying it to the chloroform + ammonia system.

Solubilities of ammonia in chloroform (containing 0.1% ethanol) at 25°C and ammonia partial pressures of 2–60 kPa have been determined by Seward (10). We have made new measurements of the solubility of ammonia in pure chloroform at three temperatures and ammonia partial pressures of 50–300 kPa.

Derivation of equations

Consider a system in which a gas B is dissolved in a solvent A and a complex forms between the dissolved gas and the solvent according to eq. [1]. The gas molecules in solution exist either as dissolved B or as the complex AB. Therefore, the solubility of the gas depends on the Henry's law constant, k_H, for the system and on the equilibrium constant, K, for reaction [1]. In

TABLE 1. Mass balance in the liquid phase for reaction [1]

Species	Stoichiometric amount/mol	Stoichiometric mole fraction	Equilibrium[a] amount/mol	Equilibrium[b] mole fraction
A	N_A	x_A	$N_A - n_{AB}$	$z_A = (x_A - r)/(1-r)$
B	N_B	x_B	$N_B - n_{AB}$	$z_B = (x_B - r)/(1-r)$
AB	—	—	n_{AB}	$z_{AB} = r/(1-r)$

[a]Total number of moles at equilibrium is $(N_A + N_B - n_{AB})$.
[b]$r = n_{AB}/(N_A + N_B)$.

this section we derive a relationship between gas solubility (which can be determined experimentally) and the two constants (K and k_H) using the ideal associated solution model.

Assuming that the ideal association solution model is a valid approximation to the system (i.e., assuming that the system is an ideal solution of A + B + AB), we can express the association equilibrium constant in terms of the equilibrium mole fractions, z_i:

$$[2] \quad K = z_{AB}/z_A z_B$$

From mass balance considerations for an A + B = AB system (see Table 1) we can express the equilibrium mole fractions in terms of the stoichiometric mole fractions (x_i) and the extent of association (r):

$$[3] \quad z_A = (x_A - r)/(1 - r)$$

$$[4] \quad z_B = (x_B - r)/(1 - r)$$

$$[5] \quad z_{AB} = r/(1 - r)$$

Combining eqs. [2]–[5] with $x_A = 1 - x_B$, we obtain an expression for the equilibrium constant in terms of x_B (the mole fraction solubility of B in A) and r:

$$[6] \quad K = r(1 - r)/[x_B(1 - x_B) - r + r^2]$$

Equation [4] may be rearranged to obtain

$$[7] \quad r = (x_B - z_B)/(1 - z_B)$$

Substitution of eq. [7] into the numerator of eq. [6] yields (after rearranging)

$$[8] \quad r(1 - r) = (x_B - z_B)(1 - x_B)/(1 - z_B)^2$$

Similarly, substitution of the expression for r given by eq. [7] into the denominator of eq. [6] yields (after considerable rearranging)

$$[9] \quad x_B(1-x_B)-r+r^2=z_B(1-x_B)(1-2x_B+z_Bx_B)/(1-z_B)^2$$

Combination of eqs. [8] and [9] with eq. [6] then leads to an expression for the equilibrium constant for process [1] in terms of the mole fraction solubility of B in A (x_B) and the mole fraction of unassociated B in the solution at equilibrium (z_B):

$$[10] \quad K = (x_B - z_B)/[z_B(1 - 2x_B + z_Bx_B)]$$

Now we write Henry's law (in terms of the equilibrium mole fraction of unassociated B) as

$$[11] \quad p_B = k_H z_B$$

where p_B represents the partial pressure of gas above the solution and k_H represents Henry's law constant. Combination of eqs. [10] and [11] leads to

$$[12] \quad K = (k_H x_B - p_B)/[p_B(1 - 2x_B + p_B x_B/k_H)]$$

In the limit of $K = 0$ (no complex formation), $z_{AB} = 0$ and $z_B = x_B$ so that both eqs. [11] and [12] become $p_B = k_H x_B$, which is the conventional form of Henry's law for gases that do not react to form a complex with the solvent.

Using eq. [12] in the interesting case when $K \neq 0$ is complicated for two reasons. First, this equation cannot be rearranged into any other form such that a suitable graph of some function of "measurables" against another function of measurables will lead to a straight line with slope and intercept that will permit easy calculation of K and k_H. Second and more important, the partial pressure of gas B(p_B) and the stoichiometric mole fraction of B in solution (x_B) come directly from measurable quantities only in the special case of a solvent with negligible vapour pressure so that the measured total pressure may be taken equal to p_B.

Experimental

Chloroform (Caledon Lab Ltd.) was purified and stored as described previously (5). Ammonia (Medigas Ltd.) was used without further purification.

The measurements of gas solubility were made using an isobaric equilibrium solubility method and apparatus similar to that previously described by Morrison and Billett (11) and Hayduk, Walter, and Simpson (12). In this method a known amount of solvent is injected in a thin film into apparatus containing a known pressure of gas. As the gas dissolves in the solvent, a constant pressure is maintained inside the apparatus by addition (or removal) of a known volume of mercury. The amount of gas dissolved is then calculated from the change in gas volume, using an equation of state for the gas. The experimental quantities measured in this technique are the mass of solvent injected, m_A, the mass of mercury added to maintain the system at constant pressure, m_{Hg}, and the total pressure, P_t. Further details of the design and operation of this apparatus are given by Yan, Zhang, Singh, and Hepler (13) and Singh (14).

The experimental quantities, m_A and m_{Hg}, were measured for the chloroform + ammonia system at 298.15, 303.15, and 308.15 K over a pressure range of 80–300 kPa. Three values of m_A and m_{Hg} were measured at each temperature and pressure.

Pycnometers were used to measure the density of chloroform, and values of 1.4793 g cm^{-3} at 298.15 K, 1.4733 g cm^{-3} at 303.15 K, and 1.4679 g cm^{-3} at 308.15 K were obtained.

A new method and apparatus that are described in detail in ref. 15 were used to obtain a value of 30.3 cm^3 mol^{-1} for the partial molar volume of ammonia in dilute solution in chloroform.

Analysis of results

As we pointed out in the second section of this paper, use of eq. [12] to analyse gas solubility data is complicated when the solvent has appreciable vapour pressure. Because the vapour pressure of chloroform (A) is not negligible (at the temperatures of our investigations) and also depends on the amount of ammonia (B) that is dissolved (Raoult's law applied to the solvent), we have a "cyclic problem" that involves needing to

Can. J. Chem. Downloaded from www.nrcresearchpress.com by 186.148.149.217 on 09/07/12
For personal use only.

know p_B and x_B to obtain K and k_H from eq. [12]. Our method for solving this cyclic problem is described as follows.

Our general method is to find an estimate of k_H and then to find the values of all the other quantities that are most consistent with this estimate. In this way an estimate of K is found for each experiment and the average and standard deviation of these K values is calculated at each temperature. The estimate of k_H is now adjusted so that the standard deviation of K values is reduced. A new set of quantities that is consistent with this new estimate of k_H is obtained and the average and standard deviation of the resulting K values is calculated. The estimate of k_H is again adjusted and the procedure is repeated until the standard deviation of the K values at each temperature has been minimized.

We begin by noting that from Henry's law (in the form of eq. [11]) the last term in the denominator of eq. [12] can be expressed as $p_B x_B/k_H = z_B x_B$. Since formation of complex AB from B makes $z_B < x_B$, we see that $z_B x_B < x_B^2$ and thence that $z_B x_B < 2x_B$. We therefore obtain our first approximation to k_H by neglecting $p_B x_B/k_H$ in the denominator of eq. [12] and rearranging to obtain

$$[13] \quad x_B/p_B \sim (K/k_H)(1 - 2x_B) + (1/k_H)$$

This approximate expression shows that the extrapolated intercepts of (not quite linear) graphs of x_B/p_B against $(1 - 2x_B)$ for each temperature give first approximations to k_H at these same temperatures.

To find our first approximations for k_H from eq. [13] we need estimates of p_B and x_B for each experiment. First we express the measured total pressure (P_t) as the sum of the partial pressures of chloroform (p_A) and ammonia (p_B):

$$[14] \quad P_t = p_A + p_B$$

Because all of our solutions are dilute, we know that the vapour pressure of the solvent is in accord with Raoult's law expressed in terms of the equilibrium mole fraction of solvent in the solution (z_A) and the vapour pressure of pure A (p_A^0):

$$[15] \quad p_A = z_A p_A^0$$

Recognizing that z_A is close to unity for a dilute solution, we initially set $p_A = p_A^0$ in eq. [14] to obtain $p_B = P_t - p_A^0$ for further use. Vapour pressures of pure chloroform of 26.220 kPa at 298.15 K, 32.329 kPa a 303.15 K, and 39.542 kPa at 308.15 K were taken from the compilation of Smith and Srivastava (16).

Now we let ΔV represent the change in volume of the vapour space in the solubility apparatus when the solvent is introduced and mercury is added (or removed) to keep the total pressure constant. This ΔV can be expressed as

$$[16] \quad \Delta V = V_A + \bar{V}_B \Delta N_B + V_{Hg}$$

Here $\bar{V}_B$ represents the partial molar volume of solute B in dilute solution in solvent A. V_A and V_{Hg}, calculated from $V = m/\rho$, represent the volume of solvent added to the apparatus and the volume of mercury added to maintain constant pressure in the apparatus, respectively. ΔN_B represents the total number of moles of gas dissolved in the solvent at equilibrium. Since the amount of dissolved gas is small compared with $V_A + V_{Hg}$, a good first estimate of ΔV is obtained by setting $\Delta N_B = 0$ in eq. [16].

The volume of the vapour space (V) and the amount of gas in the vapour space (N_B) are related by the equation of state

$$[17] \quad p_B V = N_B(RT + \beta p_B)$$

in which β is the second virial coefficient of gaseous B. Subtracting eq. [16] for initial conditions from eq. [16] for final conditions and rearranging leads to

$$[18] \quad \Delta N_B = p_B \Delta V/(RT + \beta p_B)$$

We now insert in eq. [18] our estimates of p_B, ΔV (obtained as described above), and β (obtained by interpolation of the data compiled in ref. 17) to obtain a first estimate of ΔN_B, the amount of gas dissolved at equilibrium. Combination of this value of ΔN_B with the known number of moles of A injected (N_A) and with the defining equation for mole fraction of B in solution

$$[19] \quad x_B = \Delta N_B/(\Delta N_B + N_A)$$

leads to a value for the stoichiometric mole fraction of dissolved B (x_B). At each temperature and pressure the first approximation for x_B was taken to be the average of the three x_B values calculated from the three replicate measurements of m_A and m_{Hg}.

After carrying out the calculations (for each total pressure) outlined above in eqs. [14]–[19], we use the resulting estimates of p_B and x_B with eq. [13] to obtain first approximations for k_H at each temperature.

Our next step is to find the value of the equilibrium constant K that is most consistent with each value of k_H. Combination of the first approximations to k_H (obtained as above) with each x_B,p_B pair leads by way of eq. [12] to values of the equilibrium constant K. The average of all of these values of K at each temperature is calculated. We then solve the quadratic eq. [6] for r. Combination of the resulting equation with $x_A + x_B = 1$ and the defining equation for z_A (eq. [3]) gives

$$[20] \quad z_A = 1 - [K + 1 - [(1 + K - 2Kx_A)^2 + 4Kx_A^2]^{1/2}]/2Kx_A$$

Use of our average K value at each temperature with values of x_A (from the estimate of x_B for each experiment) now permits calculation of estimates of z_A. Substitution of these values of z_A into Raoult's law (eq. [15]) gives new estimates of p_A, and thence with eq. [14] we obtain new estimates of p_B. New estimates of ΔV are calculated from eq. [16] using the current estimates of ΔN_B. These values of ΔV are combined with the corresponding p_B values in eq. [18] to obtain new estimates of ΔN_B, which are then combined with N_A (number of moles of solvent injected) in eq. [19] to give new estimates of x_B. The x_B,p_B pairs are inserted in eq. [12] along with the first approximation for k_H to obtain new estimates of K for each experiment. Again the average of the K values is calculated and the iterative process is repeated until successive estimates of K differed by no more than 0.1% for each experiment. A maximum of four iterations was necessary to meet this requirement. At this point the average value of K at each temperature is taken to be the first approximation to K (i.e., the value of K that is most consistent with the first approximation to k_H).

Now we adjust the values of k_H so that the standard deviation of the K values at each temperature is reduced. We then use the procedure described above to find the value of K that is most consistent with the new approximation to k_H at each temperature. The value of k_H is further adjusted until the standard deviation of the individual K values at each temperature has been minimized. The values k_H, K, and all the other quantities (x_B, p_B, z_B, etc.) that correspond to this minimum are taken to be the "best" values for describing the chloroform + ammonia system and are internally consistent with measured total pressures, amounts of solvent added, Henry's law, and Raoult's

Can. J. Chem. Downloaded from www.nrcresearchpress.com by 186.148.149.217 on 09/07/12
For personal use only.

TABLE 2. Values of K and k_H for chloroform + ammonia

T/K	K	$\pm\sigma^a$	k_H/MPa	$\pm\sigma^a$/MPa
298.15	0.58	0.04	1.04	0.04
303.15	0.50	0.04	1.15	0.04
308.15	0.62	0.02	1.39	0.05

[a]Standard deviation at the 95% confidence level. The *total* uncertainties in the reported K values are approximately ±0.08 and the total uncertainties in the reported k_H values are approximately ±0.06.

TABLE 3. Partial pressure of ammonia (p_B), stoichiometric mole fraction solubility of ammonia (x_B), and equilibrium mole fraction of free ammonia (z_B) in chloroform at total pressure (P_t)

P_t/kPa	p_B/kPa	x_B	z_B
	$T = 298.15$ K		
300.21	283.67	0.336	0.273
227.85	209.10	0.263	0.201
186.29	166.07	0.214	0.160
159.21	138.24	0.188	0.133
134.51	112.44	0.151	0.108
130.91	108.96	0.152	0.105
111.95	89.06	0.122	0.086
103.86	80.74	0.114	0.078
95.36	71.83	0.099	0.069
	$T = 303.15$ K		
287.97	265.79	0.291	0.230
271.41	248.39	0.268	0.215
226.77	202.11	0.223	0.175
171.58	144.90	0.166	0.126
160.73	133.86	0.161	0.116
136.99	109.05	0.130	0.094
118.29	89.65	0.110	0.078
82.06	51.86	0.065	0.045
	$T = 308.15$ K		
292.53	263.81	0.253	0.190
293.33	208.62	0.208	0.150
188.24	155.29	0.158	0.112
146.54	111.98	0.121	0.081
122.41	86.67	0.093	0.062
98.43	61.65	0.068	0.044

law. The values of k_H and K for the ammonia + chloroform system that were found in this way are listed in Table 2. The values of experimental total pressure, along with the derived values of partial pressure of ammonia (p_B), the stoichiometric mole fraction of dissolved ammonia (x_B), and the equilibrium mole fraction of free ammonia (z_B) are listed in Table 3.

Discussion

No published reports of the equilibrium constant for the formation of chloroform–ammonia complex are available for comparison with our results.

Our results are consistent with the expected strength of chloroform–ammonia association, as we now show. Ammonia is generally considered to be a weaker base than triethylamine (due to the inductive effect of the ethyl group) and a stronger base than benzene. We therefore expect the chloroform–ammonia complex to be less stable than the chloroform–triethylamine complex and more stable than the chloroform–benzene complex. On this basis we predict that the association equilibrium constant for chloroform + ammonia should be smaller than that for chloroform + triethylamine ($K = 2.6$ at 298 K; ref. 4) and larger than that for chloroform + benzene ($K = 0.45$ at 298 K; ref. 5). We have found, using the ideal associated solution model, that the chloroform + ammonia association equilibrium constant has a value of $K = 0.58$ at 298 K (see Table 2). This value is intermediate between $K = 2.6$ and $K = 0.45$ and thus is consistent with our prediction. Further studies (possibly spectroscopic) are necessary to investigate the accuracy of association equilibrium constants obtained using the method described in this paper.

Combining our values of K and k_H with a rearranged version of eq. [12], we calculate the mole fraction solubility of ammonia in chloroform at 298.15 K and a partial pressure of ammonia of 101.325 kPa to be 0.139. This is in excellent agreement with the value of 0.141 obtained by extrapolation (18) of the results of Seward (10) at 298.2 K to a partial pressure of ammonia of 101.325 kPa.

Matsui, Hepler, and Fenby (19) showed that in a very dilute solution of B in A (where A and B associate according to A + B = AB) the equilibrium amount of AB (n_{AB}) is related to the stoichiometric amount of B (N_B) by

$$[21] \quad n_{AB} = [K/(K + 1)]N_B$$

where K represents the association equilibrium constant. Substituting our value of $K_{298} = 0.58$ into eq. [21], we calculate that in a dilute solution of ammonia in chloroform 63% of the ammonia is in the uncomplexed form and 37% is in the complexed form.

The analysis of the chloroform + ammonia system presented in this paper is based on the premise that a 1:1 associated complex forms between the two components. That this is a reasonable proposal is seen by comparing the solubility of ammonia in chloroform with that of ammonia in carbon tetrachloride. The mole fraction solubility of ammonia in carbon tetrachloride (18, 20) is 0.0281 at 293.2 K and a partial pressure of ammonia equal to 101.325 kPa. We would expect a slightly smaller solubility at 298.15 K. The much larger solubility of ammonia in chloroform than in carbon tetrachloride indicates that interactions in addition to "simple" dissolution occur in the chloroform + ammonia system. Since chloroform (unlike carbon tetrachloride) has the capacity to form hydrogen bonds with ammonia, we attribute the high solubility of ammonia in chloroform to the formation of hydrogen bonds between the two components.

The enthalpy of solution of ammonia in chloroform can be separated into a contribution from dissolution (no complex formation) and a contribution from formation of the complex. The contribution from the dissolution process, ΔH_d^θ, can be obtained from the temperature dependence of Henry's law constant, $(\partial \ln k_H/\partial T)_p = \Delta H_d^\theta/RT^2$. Using this equation and the values of k_H listed in Table 2 we calculate a value of $\Delta H_d^\theta = -22$ kJ mol^{-1}. Over the temperature range of our measurements the relative uncertainties in the association equilibrium constant are too large for the van't Hoff equation, $(\partial \ln K/\partial T)_p = \Delta H^\theta/RT^2$, to yield reliable values of ΔH^θ for the formation of the chloroform–ammonia complex.

Acknowledgements

We thank Harbinder P. Singh for his assistance with the measurements of gas solubility and Professor Gerald A.

Can. J. Chem. Downloaded from www.nrcresearchpress.com by 186.148.149.217 on 09/07/12
For personal use only.

Bottomley and Dr. Leslie Barta for valuable advice. We are also grateful to the Natural Sciences and Engineering Research Council of Canada for financial support of this and related research.

1. I. PRIGOGINE and R. DEFAY. Chemical thermodynamics. John Wiley & Sons, New York, NY. 1954. p. 417.
2. M. L. MCGLASHAN. Chemical thermodynamics. Academic Press, London. 1979. p. 266.
3. W. E. ACREE, JR. Thermodynamic properties of non-electrolyte solutions. Academic Press, Orlando, FL. 1984. p. 134.
4. L. G. HEPLER, Z. S. KOONER, G. ROUX-DESGRANGES, and J.-P. E. GROLIER. J. Solution Chem. **14**, 579 (1985).
5. J.-P. E. GROLIER, G. ROUX-DESGRANGES, Z. S. KOONER, J. F. SMITH, and L. G. HEPLER. J. Solution Chem. **16**, 745 (1987).
6. Y. P. HANDA, D. V. FENBY, and D. E. JONES. J. Chem. Thermodyn. **7**, 337 (1975).
7. B. B. HOWARD, C. F. JUMPER, and M. T. EMERSON. J. Mol. Spectrosc. **10**, 117 (1963).
8. C. J. CRESSWELL and A. L. ALLRED. J. Phys. Chem. **66**, 1469 (1962).
9. L. G. HEPLER and D. V. FENBY. J. Chem. Thermodyn. **5**, 471 (1973).
10. R. P. SEWARD. J. Am. Chem. Soc. **54**, 4598 (1932).
11. T. J. MORRISON and F. J. BILLETT. J. Chem. Soc. 2033 (1948).
12. W. HAYDUK, E. B. WALTER, and P. SIMPSON. J. Chem. Eng. Data, **17**, 59 (1972).
13. H.-K. YAN, Z.-L. ZHANG, H. P. SINGH, and L. G. HEPLER. In preparation.
14. H. P. SINGH. M.Sc. Thesis, University of Alberta (1986).
15. J. F. SMITH, G. A. BOTTOMLEY, L. BARTA, and L. G. HEPLER. J. Am. Chem. Soc. In press.
16. B. D. SMITH and R. SRIVASTAVA. Thermodynamic data for pure compounds. Physical sciences data 25, Part B, Elsevier, New York, NY. pp. 124–125.
17. J. H. DYMOND and E. B. SMITH. The virial coefficients of pure gases and mixtures. Clarendon Press, Oxford. 1980.
18. IUPAC Solubility Data Series Vol. 21. Pergamon Press, Oxford. 1985.
19. T. MATSUI, L. G. HEPLER, and D. V. FENBY. J. Phys. Chem. **77**, 2397 (1973).
20. R. P. BELL. J. Chem. Soc. 1371 (1931).

Can. J. Chem. Downloaded from www.nrcresearchpress.com by 186.148.149.217 on 09/07/12
For personal use only.

Structural studies of organoboron compounds. XXXVI.[1] 2,2-Dimethyl-3,3-diphenyl-1,4-dioxa-2-azonia-3-boratacyclohexane

KLAUS DRÜCKLER AND WOLFGANG KLIEGEL

Institut fur Pharmazeutische Chemie, der Technischen Universität Braunschweig, Beethovenstraße 55, 3300 Braunschweig, Bundesrepublik Deutschland

AND

STEVEN J. RETTIG AND JAMES TROTTER

Department of Chemistry, University of British Columbia, 2036 Main Mall, Vancouver, B.C., Canada V6T 1Y6

Received February 8, 1989

KLAUS DRÜCKLER, WOLFGANG KLIEGEL, STEVEN J. RETTIG, and JAMES TROTTER. Can. J. Chem. **67**, 2218 (1989).

The synthesis of O-(2-hydroxyethyl)-*N*,*N*-dimethylhydroxylamine and its reaction with oxybis(diphenylborane) to yield the title compound are reported. Crystals of 2,2-dimethyl-3,3-diphenyl-1,4-dioxa-2-azonia-3-boratacyclohexane are orthorhombic, $a = 7.0332(6)$, $b = 9.2269(6)$, $c = 22.967(2)$ Å, $Z = 4$, space group $P2_12_12_1$. The structure was solved by direct methods and was refined by full-matrix least-squares procedures to $R = 0.051$ and $R_w = 0.047$ for 1247 reflections with $I \geq 2\sigma(I)$. The molecule exhibits the longest N—B and the shortest O—B distances (1.723(6) and 1.468(5) Å, respectively, corrected for libration) yet reported for a six-membered *N*,*O*-chelate of diphenylboron.

Key words: crystal structure, boron compound, organoboron compound.

KLAUS DRÜCKLER, WOLFGANG KLIEGEL, STEVEN J. RETTIG et JAMES TROTTER. Can. J. Chem. **67**, 2218 (1989).

On rapporte la synthèse de la *O*-(2-hydroxyéthyl)-*N*,*N*-diméthylhydroxylamine et sa réaction avec l'oxybis(diphénylborane) qui conduit au composé mentionné dans le titre. Les cristaux du 2,2-diméthyl-3,3-diphényl-1,4-dioxa-2-azonia-3-boratacyclohexane sont orthorhombiques, avec $a = 7{,}0332(6)$, $b = 9{,}2269(6)$ et $c = 22{,}967(2)$ Å, $Z = 4$ et groupe d'espace $P2_12_12_1$. On a résolu la structure par des méthodes directes et on l'a affinée par la méthode des moindres carrés (matrice entière) jusqu'à des valeurs de $R = 0{,}051$ et $R_w = 0{,}047$ pour 1247 réflexions avec $I \geq 2\sigma(I)$. La molécule présente la plus grande distance N—B et la plus courte distance O—B (respectivement 1,723(6) et 1,468(5) Å, corrigées pour la libration) rapportées jusqu'à maintenant pour un chélate à six chaînons du diphénylbore.

Mots clés : structure cristalline, composé du bore, composé du organobore.

[Traduit par la revue]

Introduction

As part of an ongoing study of boron chelates of polyfunctional hydroxylamine derivatives, *N*,*N*-dialkyl-*O*-(2-hydroxyalkyl)hydroxylamines and their potential as ligands in chelate formation have been investigated. Since these compounds are not available by direct *O*-alkylation of *N*,*N*-dialkylhydroxylamines with epoxides,[2] the *O*-alkylation was carried out via an *N*,*N*-bisacyl-protected hydroxylamine. The preparation of compound **3** via **1** and **2** has been reported (2, 3). Compound **3** is an isoelectronic analog ("oxalog") of 3-dimethylaminopropanol, **4**, but shows a distinctly lower basicity. The difference, revealed by potentiometric titration in water at 21°C, appeared as $pK_a = 2.85$ for **3** and $pK_a = 9.77$ for **4**.

Esterification of **3** with diphenylborinic acid anhydride results in a crystalline compound, melting at 82–83°C, with an elemental composition consistent with either the open-chain diphenylborinate **5** or the intramolecular N → B coordinated ring isomer **6**. The diphenylborinate of 3-dimethylaminopropanol, **7**, could serve as a model for **6**. It has been reported in a drug patent (4) as a crystalline compound with a postulated chelate structure **7** and displays the relatively high melting point of 160°C. The cyclic structure of **7** could be deduced from the structurally characterized ring system (5) of the *N*-unsubstituted compound **8** that melts at 187°C (4) or 190–192°C (6). While the presence of N—H···O hydrogen bonding in the structure of **8** may be invoked to explain why this compound has a melting point that is 30°C higher than that reported for the *N*,*N*-dimethylated analog **7**, other factors must be taken into account to rationalize the relatively low melting point of **5/6** (82–83°C). The presence of the second oxygen atom in **5/6** (replacing a CH_2 group in **7**) will result in a change in the dipole moment. This factor, along with differences between the van der Waals interactions in the solids, and possibly a weaker N → B coordination in **5/6** contribute to the differences between the melting points. A weaker N → B bond in **5/6** is consistent with the lower basicity of the dimethylamine ligand in the hydroxylamine derivative. A certain sensitivity of **5/6** to moisture, which is not noticed for compounds **7** and **8**, is indicative of reduced coordinative stability. From these considerations, the question of competing O—B $(pp)\pi$-interaction (in **5**) and N → B coordination (in **6**) arises. To establish the molecular structure of **5/6** in the solid state, an X-ray crystallographic analysis was undertaken.

Experimental

O-(2-hydroxyethyl)-N,N-dimethylhydroxylamine, 3

O-(2-Hydroxyethyl)hydroxylamine, **2** (2), is methylated according to the literature (3) with formaldehyde/formic acid, yielding 24% of **3**; or with methyl iodide by analogy to the method of ethylation with ethyl iodide (7), yielding 46% of **3**. Bp 60–64°C/30 mm Hg; lit. (3) bp 64–66°C/25–26 mm Hg. Infrared (liquid film): 3400 cm^{-1} (broad, O—H). ^1H nmr ($CDCl_3$/TMS): δ(ppm) = 2.60 (s, Me_2N), 3.77 (s, CH_2CH_2 and OH, exchangeable).

2,2-Dimethyl-3,3-diphenyl-1,4-dioxa-2-azonia-3-boratacyclohexane, 6

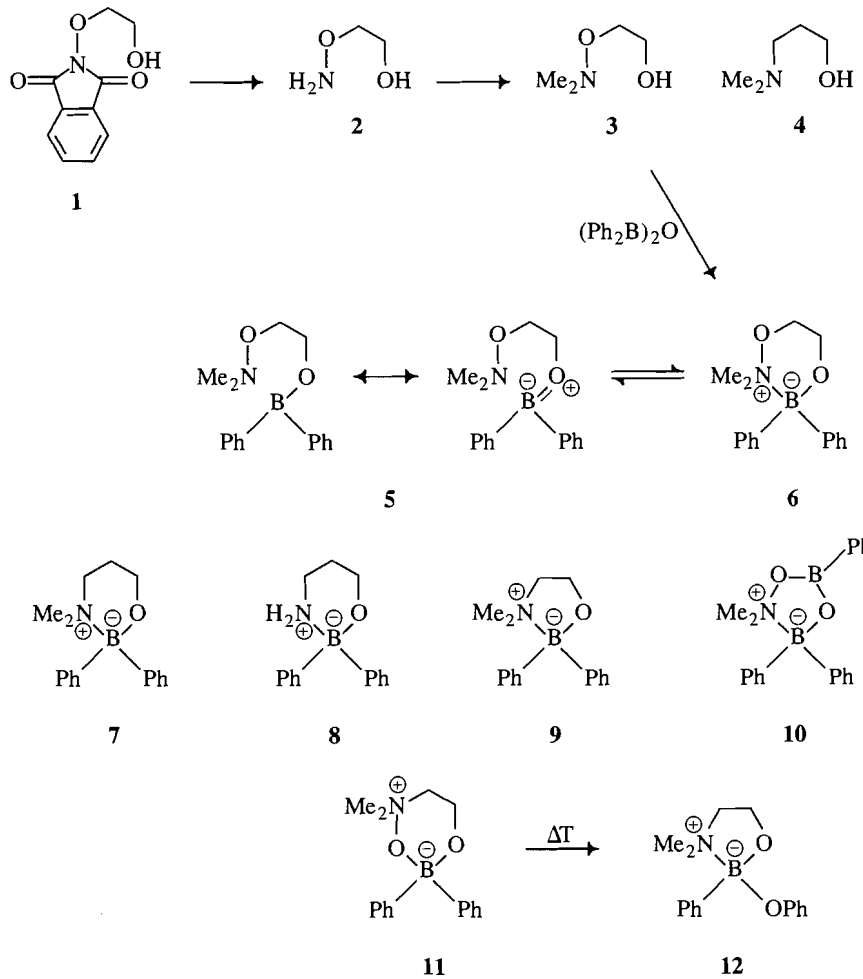
O-(2-Hydroxyethyl)-*N*,*N*-dimethylhydroxylamine, **3** (0.42 g, 4 mmol), and oxybis(diphenylborane) (0.70 g, 2 mmol) are dissolved in 5 mL ethanol and refluxed for 15 min. Upon cooling, 0.92 g (86%) of

[1]Previous paper in this series: ref. 17.

[2]Epoxide addition to *N*,*N*-dialkylhydroxylamines results in the formation of *N*-(2-hydroxyalkyl)-dialkylamine *N*-oxides (1).

Printed in Canada / Imprimé au Canada

Can. J. Chem. Downloaded from www.nrcresearchpress.com by 186.148.149.217 on 09/07/12
For personal use only.



colorless crystals are obtained. Mp 82–83°C (from *n*-hexane/dichloromethane). ^{1}H nmr ($CDCl_3$/TMS): δ(ppm): 2.67 (s, Me_2N), 3.95 (s, CH_2CH_2), 7.1–7.7 (m, BPh_2). *Anal.* calcd. for **6**: C 71.40, H 7.49, B 4.02, N 5.20; found: C 71.09, H 7.49, B 4.37, N 5.19. Mass spectrum (30°C, 70 eV): *m/e* = 269 (73%, P^+), 238 (57%), 192 (39%, P − C_6H_5), 182 (25%, Ph_2BOH), 181 (23%, Ph_2BO), 165 (100%, Ph_2B), 148 (25%), 137 (26%), 105 (75%), 78 (11%), 61 (12%), 46 (19%). The methanolic solution of the substance gives a dark blue color reaction with diphenylcarbazone, indicating the presence of the diphenylboron moiety (7). Crystals suitable for X-ray analysis were obtained by recrystallization from *n*-hexane/dichloromethane (1:1).

X-ray crystallographic analysis of **6**

A crystal bounded by the six faces (followed by the distances in mm between parallel faces): {0 1 2}, 0.25, and ± (2 0 −1), 0.35, was mounted in a general orientation. Unit-cell parameters were refined by least-squares on 2 sin θ/λ values for 25 reflections (2θ = 35–42°) measured on a diffractometer with Mo-$K\alpha$ radiation ($\lambda(K\alpha_1)$ = 0.70930, $\lambda(K\alpha_2)$ = 0.71359 Å). Crystal data at 22°C are:

$C_{16}H_{20}BNO_2$ f.w. = 269.15

Orthorhombic, a = 7.0332(6), b = 9.2269(6), c = 22.967(2) Å, V = 1490.4(2) Å^3, Z = 4, ρ_c = 1.199 Mg m^{-3}, $F(000)$ = 576, μ(Mo-$K\alpha$) = 0.72 cm^{-1}. Absent reflections: $h00$, h odd, $0k0$, k odd, and $00l$, l odd, uniquely indicate the space group $P2_12_12_1$ (D_2^4, No. 19).

Intensities were measured with graphite-monochromated Mo-$K\alpha$ radiation on an Enraf-Nonius CAD4-F diffractometer. An ω-2θ scan at 1.2–10.0° min^{-1} over a range of (0.75 + 0.35 tan θ) degrees in ω (extended by 25% on both sides for background measurement) was employed. Data were measured to 2θ = 60°. The intensities of three check reflections, measured every 4000 s throughout the data collection, showed small (<4.5%) random fluctuations. Of the 2476 independent reflections measured and processed,[3] 1247 (50.4%) had intensities greater than or equal to $2\sigma(I)$ above background where $\sigma^2(I) = S + 2B + (0.04(S - B))^2$ with S = scan count and B = normalized background count.

The structure was solved by direct methods, the coordinates of all non-hydrogen atoms being determined from an *E*-map. The non-hydrogen atoms were refined with anisotropic thermal parameters and the hydrogen atoms were fixed in idealized positions (methyl groups staggered, C(sp^2)—H = 0.97, C(sp^3)—H = 0.98 Å, $U_H \propto U_{\text{bonded atom}}$). Scattering factors for all atoms were taken from ref. 8. The weighting scheme $w = 1/\sigma^2(F)$, where $\sigma^2(F)$ is derived from the previously defined $\sigma^2(I)$, gave uniform average values of $w(|F_o| - |F_c|)^2$ over ranges of both $|F_o|$ and sin θ/λ and was employed in the final stages of full-matrix refinement of 182 variables. Reflections with $I < 2\sigma(I)$ were not included in the refinement. An isotropic Type I extinction correction (Thornley–Nelmes definition of mosaic anisotropy with a Lorentzian distribution) was applied (9–11). The final value of g was 11.3(25) × 10^4. Convergence was reached at R = 0.051 and R_w = 0.047 for 1247 reflections with $I \geq 2\sigma(I)$. No attempt was made to determine the chirality of the crystal used for data collection. The function minimized was $\Sigma w(|F_o| - |F_c|)^2$, $R = \Sigma||F_o| - |F_c||/\Sigma|F_o|$ and $R_w = (\Sigma w(|F_o| - |F_c|)^2/\Sigma w|F_o|^2)^{1/2}$.

On the final cycle of refinement the mean and maximum parameter

[3]The computer programs used include locally written programs for data processing and locally modified versions of the following: ORFLS, full-matrix least-squares, and ORFFE, function and errors, by W. R. Busing, K. O. Martin, and H. A. Levy; FORDAP, Patterson and Fourier syntheses, by A. Zalkin; ORTEP II, illustrations, by C. K. Johnson.

Can. J. Chem. Downloaded from www.nrcresearchpress.com by 186.148.149.217 on 09/07/12
For personal use only.

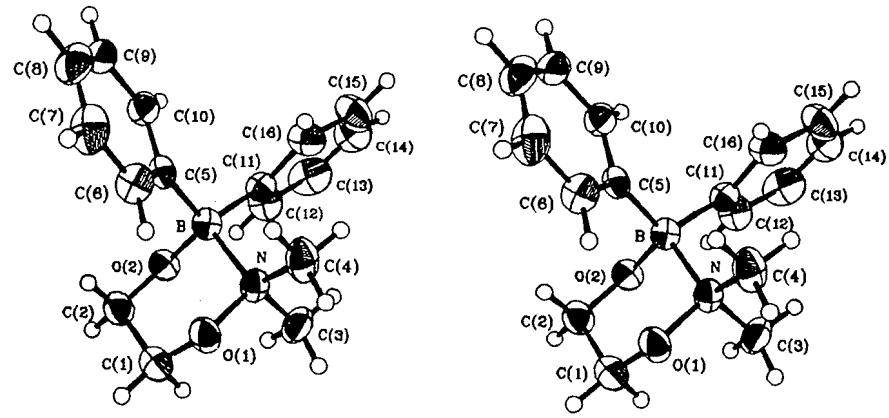


FIG. 1. Stereoscopic view of 2,2-dimethyl-3,3-diphenyl-1,4-dioxa-2-azonia-3-boratacyclohexane; 50% probability thermal ellipsoids are shown for the non-hydrogen atoms.

TABLE 1. Final positional (fractional × 10^4) and isotropic thermal parameters ($U \times 10^3$ Å^2) with estimated standard deviations in parentheses

Atom	x	y	z	U_{eq}
O(1)	3038(4)	7162(3)	2267(1)	45
O(2)	941(4)	4591(3)	2051(1)	39
N	3813(5)	6074(3)	1863(1)	37
C(1)	1807(6)	6511(5)	2701(2)	50
C(2)	227(6)	5676(5)	2430(2)	44
C(3)	5088(6)	5105(5)	2198(2)	52
C(4)	4976(7)	6969(4)	1467(2)	53
C(5)	696(6)	6193(4)	1137(2)	34
C(6)	450(6)	7702(4)	1173(2)	46
C(7)	−756(8)	8449(5)	804(2)	59
C(8)	−1779(7)	7739(6)	386(2)	57
C(9)	−1625(6)	6251(6)	346(2)	51
C(10)	−397(6)	5501(5)	712(2)	43
C(11)	2980(6)	3831(4)	1208(2)	36
C(12)	2989(7)	2437(4)	1436(2)	48
C(13)	3952(8)	1306(4)	1167(2)	67
C(14)	4912(9)	1542(5)	659(2)	65
C(15)	4922(8)	2892(5)	413(2)	62
C(16)	3928(7)	4005(4)	683(2)	48
B	1969(7)	5150(5)	1545(2)	35

shifts corresponded to 0.01 and 0.06σ, respectively. The mean error in an observation of unit weight was 1.790. The largest peak on the final difference map was 0.24 e Å^{-3}. The final positional and thermal parameters appear in Tables 1 and 6,[4] respectively. Measured and calculated structure factors have been placed in the Depository of Unpublished Data.[4]

The ellipsoids of thermal motion for the non-hydrogen atoms are shown in Fig. 1. The thermal motion has been analysed in terms of the rigid-body modes of translation, libration, and screw motion (12). The rms standard error in the temperature factors σU_{ij} (derived from the least-squares analysis) is 0.0025 Å^2. Three separate structural subunits were analysed: two PhB and the atoms of the six-membered heterocycle plus the two *N*-methyl carbon atoms (rms ΔU_{ij} = 0.0016–0.0029 Å^2). The appropriate bond distances have been corrected for libration (12, 13), using shape parameters q^2 of 0.08 for all atoms involved. Corrected bond lengths appear in Table 2 along with the uncorrected values; bond angles are given in Table 3 and intra-annular torsion angles in Table 4. Calculated hydrogen parameters (Table 5) and a complete listing of torsion angles (Table 7) have been deposited.[4]

[4]Libration corrected bond lengths (esd's assumed equal to those of the uncorrected values) are employed in the discussion and are compared with similarly treated (12) distances unless otherwise stated.

Results and discussion

The crystal structure of 2,2-dimethyl-3,3-diphenyl-1,4-dioxa-2-azonia-3-boratacyclohexane consists of well-separated molecules, the shortest intermolecular contacts between non-hydrogen atoms being O(1)···C(3)($1 - x$, $\frac{1}{2} + y$, $\frac{1}{2} - z$) = 3.259(5) Å, O(2)···C(1)($-x$, $y - \frac{1}{2}$, $\frac{1}{2} - z$) = 3.484(5) Å, and C(4)···C(8)($1 + x$, y, z) = 3.446(6) Å. The structure analysis shows the presence of a six-membered chelate ring with intramolecular N → B coordination, **6** (Fig. 1), resembling the six-membered chelate structures of diphenylborinates of aminoalkanols like that proposed for **7** and established for **8** (5), as well as related five-membered chelates such as **9** (5).

The N—B bond distance[4] in **6** (1.723 Å) is longer than in the diphenylborinates of aminoalkanols, e.g. **8** (1.643 Å), and the more strained five-membered system **9** (1.691 Å) (5). This is consistent with a weakened N → B coordinative bond in **6** and demonstrates the lower basicity of the nitrogen ligand compared to the aminoalkanol derivatives. A similar N—B bond length (1.728 Å) has been reported for another *N,N*-dimethylhydroxylamine derivative with a five-membered diphenylboron chelate structure, **10** (14). The O—B bond in **6** (1.468 Å), on the other hand, is the shortest yet reported for a compound of this type. This may be connected with the possibility of a facile ring opening to **5**, including a transition of tetracoordinated (sp^3)boron to trigonal planar (sp^2)boron. The O—B(sp^2) distance in **5** would be comparable to that observed for diphenylborinic acid, 1.354 Å (5). Compound **6** is less stable to air (moisture) than other diphenylboron chelates, such as those of the aminoalkanols, and also melts at a lower temperature.

Compound **6** represents an isomer of the *N*-oxide derivative **11** and its rearrangement product **12**, available by a thermally induced isomerization (15). Both compounds, **11** and **12**, have been structurally characterized by X-ray analyses (16). One of the striking differences between the *O*-alkylhydroxylamine derivative **6** and the *N*-oxide derivative **11** is found in the N—O bond length which is more than 0.04 Å longer in **6** (1.478 Å) than in **11** (1.434 Å). Conformationally, the six-membered chelate ring in **6** has a slightly distorted chair conformation (see Table 4) with a distinct difference between opposite side lengths N—B = 1.723 Å and C(1)—C(2) = 1.495 Å when compared to corresponding bonds in **11**: O(1)—B = 1.552 Å and C(1)—C(2) = 1.502 Å. The two B—C distances in **6** are equal within experimental error, whereas in **11** and in other diphenylboron chelates (ref. 16 and references therein) the axial B—C bond is usually significantly longer than the equatorial B—C bond. The N—Me bond lengths are essentially equal in the three isomeric compounds **6**, **11**, and **12**.

Can. J. Chem. Downloaded from www.nrcresearchpress.com by 186.148.149.217 on 09/07/12
For personal use only.

TABLE 2. Bond lengths (Å) with estimated standard deviations in parentheses

Bond	Length Uncorr.	Length Corr.	Bond	Length Uncorr.	Length Corr.
O(1)—N	1.472(4)	1.478	C(6)—C(7)	1.382(6)	1.386
O(1)—C(1)	1.451(5)	1.457	C(7)—C(8)	1.367(7)	1.373
O(2)—C(2)	1.420(5)	1.425	C(8)—C(9)	1.380(7)	1.389
O(2)—B	1.461(5)	1.468	C(9)—C(10)	1.390(6)	1.394
N—C(3)	1.483(5)	1.491	C(11)—C(12)	1.389(5)	1.400
N—C(4)	1.475(5)	1.481	C(11)—C(16)	1.388(5)	1.397
N—B	1.715(6)	1.723	C(11)—B	1.608(6)	1.613
C(1)—C(2)	1.488(6)	1.495	C(12)—C(13)	1.389(6)	1.395
C(5)—C(6)	1.405(5)	1.414	C(13)—C(14)	1.366(7)	1.375
C(5)—C(10)	1.397(5)	1.404	C(14)—C(15)	1.368(6)	1.378
C(5)—B	1.614(6)	1.619	C(15)—C(16)	1.388(6)	1.394

TABLE 3. Bond angles (deg) with estimated standard deviations in parentheses

Bonds	Angle (deg)	Bonds	Angle (deg)
N—O(1)—C(1)	111.9(3)	C(8)—C(9)—C(10)	120.2(5)
C(2)—O(2)—B	114.5(3)	C(5)—C(10)—C(9)	122.6(4)
O(1)—N—C(3)	107.9(3)	C(12)—C(11)—C(16)	115.7(4)
O(1)—N—C(4)	102.2(3)	C(12)—C(11)—B	121.4(4)
O(1)—N—B	109.1(3)	C(16)—C(11)—B	122.9(3)
C(3)—N—C(4)	108.8(3)	C(11)—C(12)—C(13)	122.0(4)
C(3)—N—B	112.3(3)	C(12)—C(13)—C(14)	120.1(4)
C(4)—N—B	115.9(3)	C(13)—C(14)—C(15)	120.0(4)
O(1)—C(1)—C(2)	111.8(3)	C(14)—C(15)—C(16)	119.1(4)
O(2)—C(2)—C(1)	111.0(3)	C(11)—C(16)—C(15)	123.0(4)
C(6)—C(5)—C(10)	115.2(4)	O(2)—B—N	102.2(3)
C(6)—C(5)—B	128.7(4)	O(2)—B—C(5)	113.4(4)
C(10)—C(5)—B	116.0(3)	O(2)—B—C(11)	109.6(3)
C(5)—C(6)—C(7)	122.3(4)	N—B—C(5)	111.7(3)
C(6)—C(7)—C(8)	120.9(4)	N—B—C(11)	104.3(3)
C(7)—C(8)—C(9)	118.9(4)	C(5)—B—C(11)	114.6(3)

TABLE 4. Intra-annular torsion angles (deg) standard deviations in parentheses

Atoms	Value (deg)
C(1)—O(1)—N—B	56.3(4)
N—O(1)—C(1)—C(2)	−56.2(5)
O(1)—C(1)—C(2)—O(2)	56.8(5)
B—O(2)—C(2)—C(1)	−64.4(4)
C(2)—O(2)—B—N	60.9(4)
O(1)—N—B—O(2)	−56.2(3)

Can. J. Chem. Downloaded from www.nrcresearchpress.com by 186.148.149.217 on 09/07/12
For personal use only.

Acknowledgments

We thank the Natural Sciences and Engineering Research Council of Canada and the Fonds der Chemischen Industrie, Frankfurt am Main, for financial support and the University of British Columbia Computing Centre for assistance.

1. (*a*) L. W. JONES and G. R. BURNS. J. Am. Chem. Soc. **47**, 2966 (1925); (*b*) W. KLIEGEL. Z. Chem. **9**, 112 (1969), footnote 3; (*c*) J. G. CANNON, J. G. ROSE, D. E. NERLAND, and L. L. DARKO. J. Heterocycl. Chem. **6**, 747 (1969); (*d*) W. KLIEGEL. Z. Chem. **10**, 437 (1970); (*e*) W. KLIEGEL and E. AHLENSTIEL. J. Organomet. Chem. **277**, 173 (1984).
2. W. KLIEGEL. Pharmazie, **25**, 400 (1970).
3. B. J. R. NICOLAUS, G. PAGANI, and E. TESTA. Helv. Chim. Acta, **45**, 358 (1962).
4. J.-L. DELARUE and R. L. FALLARD (Laboratories Toraude). Fr. Pat. 3036 M (1.2.1965); Chem. Abstr. **62**, 13179e (1965).
5. S. J. RETTIG and J. TROTTER. Can. J. Chem. **61**, 2334 (1983).
6. H. WEIDMANN and H. K. ZIMMERMAN. Liebigs Ann. Chem. **619**, 28 (1958).
7. B. J. R. NICOLAUS, L. MARIANI, G. PAGANI, G. MAFFII, and E. TESTA. Ann. Chim. **53**, 291 (1963).
8. International tables for X-ray crystallography. Vol. IV. Kynoch Press, Birmingham. 1974. pp. 99–102 and 149.
9. P. J. BECKER and P. COPPENS. Acta Crystallogr. Sect. A, **30**, 129 (1974); **30**, 148 (1974); **31**, 417 (1975).
10. P. COPPENS and W. C. HAMILTON. Acta Crystallogr. Sect. A, **26**, 71 (1970).
11. F. R. THORNLEY and R. J. NELMES. Acta Crystallogr. Sect. A, **30**, 748 (1974).
12. V. SCHOMAKER and K. N. TRUEBLOOD. Acta Crystallogr. Sect. B, **24**, 63 (1968).
13. D. W. J. CRUICKSHANK. Acta Crystallogr. **9**, 747 (1956); **9**, 754 (1956); **14**, 896 (1961).
14. W. KLIEGEL, H.-W. MOTZKUS, S. J. RETTIG, and J. TROTTER. Can. J. Chem. **62**, 838 (1984).
15. W. KLIEGEL. Leibigs Ann. Chem. **763**, 61 (1972).
16. E. EBELING, W. KLIEGEL, S. J. RETTIG, and J. TROTTER. Can. J. Chem. **67**, 933 (1989).
17. W. KLIEGEL, M. TAJERBASHI, S. J. RETTIG, and J. TROTTER. Can. J. Chem. **67**, 1644 (1989).

Metal halide, nitrile, antimony pentachloride complexes. I. Tetrakis(benzonitrile)copper(I) hexachloroantimonate(V) and hexakis(benzonitrile)copper(II) bis[hexachloroantimonate (V)][1]

SYDNEY BROWNSTEIN, NAM FONG HAN, ERIC GABE, AND YVON LE PAGE
Division of Chemistry, National Research Council of Canada, Ottawa, Ont., Canada K1A 0R9
Received December 20, 1988[2]

SYDNEY BROWNSTEIN, NAM FONG HAN, ERIC GABE, and YVON LE PAGE. Can. J. Chem. **67**, 2222 (1989).

Tetrakis(benzonitrile)copper(I) hexachloroantimonate(V) crystallizes as a yellow solid in the triclinic space group $P\bar{1}$ with a = 8.217(4) Å, b = 14.116(5) Å, c = 14.296(9) Å, α = 86.88(4)°, β = 87.49(5)°, and γ = 81.92(3)°. Hexakis(benzonitrile) copper(II) bis[hexachloroantimonate(V)] is a green solid which also crystallizes in space group $P\bar{1}$ with a = 10.3286(8) Å, b = 11.0954(8) Å, c = 11.9722(5) Å, α = 85.536(4)°, β = 80.530(6)°, and γ = 84.051(6)°. Both compounds are synthesized from cuprous chloride, benzonitrile and antimony pentachloride depending on relative concentrations, while the latter is also prepared from cupric chloride and antimony pentachloride in benzonitrile solution.

Key words: copper complexes, crystal structures.

SYDNEY BROWNSTEIN, NAM FONG HAN, ERIC GABE et YVON LE PAGE. Can. J. Chem. **67**, 2222 (1989).

L'hexachloroantimonate(V) de tétrakis(benzonitrile)cuivre(I) cristallise sous forme d'un solide jaune dans le groupe d'espace triclinique $P\bar{1}$ avec a = 8,217(4) Å, b = 14,116(5) Å, c = 14,296(9) Å, α = 86,88(4)°, β = 87,49(5)° et γ = 81,92(3)°. Le bis[hexachloroantimonate(V)] de héxakis(benzonitrile)cuivre(II) est un solide vert qui cristallise également dans le groupe d'espace $P\bar{1}$ avec a = 10,3286(8) Å, b = 11,0954(8) Å, c = 11,9722(5) Å, α = 85,536(4)°, β = 80,530(6)° et γ = 84,051(6)°. On a préparé les deux composés à partir du chlorure cuivreux, du benzonitrile et du pentachlorure d'antimoine, dépendant des concentrations relatives, tandisque le dernier composé est également obtenu à partir du chlorure cuivrique et du pentachlorure d'antimoine dans une solution de benzonitrile.

Mots clés : complexes de cuivre, structures cristallines.

[Traduit par la revue]

Introduction

It has long been known that antimony pentachloride is a very strong chloride ion acceptor which reacts with a variety of chlorine-containing compounds to give the corresponding cations and $SbCl_6^-$ (1). A few ternary complexes of a metal halide, acetonitrile, and $SbCl_5$ have been isolated (2) and similar examples with SbF_5 and BiF_5 are also known (3, 4). The current investigations are to study the generality of these ternary complex formations. Since the oxidation potential for conversions of Cu(I) to Cu(II) is near zero and dependent upon the co-ordinating ligands (5), and since the co-ordination about copper is quite variable (6), copper chloride appeared to be a metal halide which might give some interesting sterochemical results.

Antimony pentachloride and pentafluoride form 1:1 adducts with many ligands such as acetonitrile, dimethyl sulfoxide, and dimethyl formamide (7–11). The crystal structures for binary adducts of cuprous chloride with acetonitrile or benzonitrile have been determined (12, 13).

Experimental

Chemicals

Cuprous chloride, cupric chloride (Anachemia Chemicals), benzonitrile, (PhCN, Eastman Chemicals), antimony pentachloride (Baker Chemicals), and hexanes (BDH Chemicals) were used as received.

Preparation of $[Cu(PhCN)_4]$ $[SbCl_6]$ I: CuCl (0.3 g, 3.0 mmol) was stirred in 25 mL of PhCN at room temperature for 15 min followed by slow addition of $SbCl_5$ (0.8 g, 2.7 mmol). The reaction was exothermic and the resultant mixture was stirred for another 5 min after which it was filtered. Yellow crystals of **I** were obtained when the yellow–brown filtrate was added slowly to 40 mL of hexanes. **I** was washed with hexanes (3 × 10 mL) and dried *in vacuo*. Yield 0.95 g, **I** is stable in air for a long period of time. *Anal.* calcd. for $C_{28}H_{20}N_4Cl_6CuSb$: C 41.48, H 2.47, N 6.91; found: C 41.07, H 2.59, N 7.27. Melting point 89–91°C. ν(CN) 2228 cm^{-1}. **I** is also characterized by a single crystal X-ray structural study.

Preparation of $[Cu(PhCN)_6]$ $[SbCl_6]_2$ II: The synthesis was done in the same fashion as for **I** except that CuCl (0.3 g, 3.0 mmol), 25 mL of PhCN and $SbCl_5$ (1.8 g, 6.0 mmol) were used. About 40 mL of hexanes was added to the green filtrate and a green crystalline solid of **II** precipitated and was separated from the mother liquor by filtration. **II** was isolated, washed, and dried as for **I** (yield 2.21 g). **II** is sensitive to hydrolysis in air but can be stored under a dry N_2 atmosphere. *Anal.* calcd. for $C_{42}H_{30}N_6Cl_{12}CuSb_2$: C 37.31, H 2.22, N 6.22; found: C 37.04, H 2.20, N 6.11 Melting point: 128–130°C. ν(CN) 2226 cm^{-1}. **II** is also characterized by a single crystal X-ray structural study.

Microanalyses were performed by Mr. H. Seguin of the National Research Council of Canada. Infrared spectra were obtained on KBr pellets with a Perkin-Elmer 683 spectrometer. Melting points were determined with a Gallenkamp melting point apparatus and are reported without correction.

X-ray diffraction intensities were collected at room temperature on an Enraf-Nonius CAD-4 diffractometer with graphite monochromatized MoK_α radiation, λ = 0.70932 Å, using the $\theta/2\theta$ scan technique with profile analysis (14). The crystal data are listed in Table 1. The structures were solved by direct methods and refined by full-matrix least-squares techniques.

All calculations were performed using the NRCVAX program system (15). For **II** the final residuals are R_f 0.034 and R_w 0.021 for the significant reflections using counting statistics weights. For **I** the final residuals are R_f 0.092 and R_w 0.113 for the significant reflections using unit weights. All atoms except hydrogen were refined anisotropically for **II**. Only Cu, Sb, and Cl atoms were anisotropically refined for **I** and its hydrogen atoms were placed at the calculated positions. The high R values for **I** are a consequence of the small crystal size, resulting in weak reflections and therefore a large number of unobserved reflections as shown in Table 1.

The final atomic positional parameters and the mean of the principal

[1]NRCC No. 30722.

[2]Revision received July 20, 1989.

Can. J. Chem. Downloaded from www.nrcresearchpress.com by 186.148.149.217 on 09/07/12
For personal use only.

TABLE 1. Crystal Data

Formula		$C_{42}H_{30}N_6Cl_{12}CuSb_2$	$C_{28}H_{20}N_4Cl_6CuSb$
Crystal dimension, mm		0.4 × 0.2 × 0.2	0.2 × 0.2 × 0.1
Crystal colour		Green	Yellow
Space group		$P\bar{1}$	$P\bar{1}$
Lattice parameters	a	10.3286(8)	8.217(4)
	b	11.0954(8)	14.116(5)
	c	11.9722(5)	14.296(9)
	α	85.536(4)	86.88(4)
	β	80.530(6)	87.49(5)
	γ	84.051(6)	81.92(3)
d_{calcd} g cm^{-3}		1.670	1.642
Z		1	2
2θ max		45	45
octants		h, k, l (−10 to 10, 0 to 11, −12 to 12)	−8 to 8, 0 to 14, −15 to 15)
Reflections measured		6379	5079
Unique reflections		3500	5079
Significant reflections Inet > 2.5 σ (Inet)		2553	2049
μ, mm^{-1}		2.04	3.34
Setting angles No.		25	40
2θ range		36 to 42	30 to 35

axes of the thermal ellipsoids for **I** are listed in Table 2. Similar information for **II** is listed in Table 3. The anisotropic temperature factors and the final structure factors for both compounds are deposited as supplementary material.[3]

Results and discussion

It is possible to prepare both copper(II) and copper(I) complexes from cuprous chloride, benzonitrile, and antimony pentachloride by changing the relative ratio of CuCl and $SbCl_5$. Therefore, with benzonitrile as ligand, the oxidation potential for $Cu^+ \rightarrow Cu^{2+} + e^-$ must be very close to zero. Analogs of the Cu(II) complex have been prepared by first synthesizing a nitromethane solvated species, $Cu(CH_3NO_2)_6$, and subsequently reacting this with an appropriate ligand, L, to give CuL_n^{2+}, where n is 3 or 6 and L is NC—$(CH_2)_2$—CN, NC(C_6H_4)CN, or NC—$(CH_2)_{10}$—CN (16, 17). Cu(I) complexes of nitriles and complex anions have not been reported. The green complex **II** is sensitive to hydrolysis by moisture in the air but is stable when submerged in hexanes and sealed in glass capillaries. Crystals were chosen for this study by working in a bath of hexanes. In contrast, the yellow complex **I** is stable in air.

The structure of complex **I** is shown in Fig. 1 and the key bond distances and angles are listed in Table 4. A complete set of bond distances and angles are deposited as supplementary material.[3] The benzonitrile ligands are arranged about Cu(I) in a nearly regular tetrahedron with average Cu—N bond lengths of 2.05(4) Å. The C—N and nitrile carbon to aromatic carbon bonds are 1.10(5) and 1.43(4) Å, respectively. There is a single absorption for the C—N stretching frequency at 2228 cm^{-1}. Both increases and decreases of the C—N stretching frequency

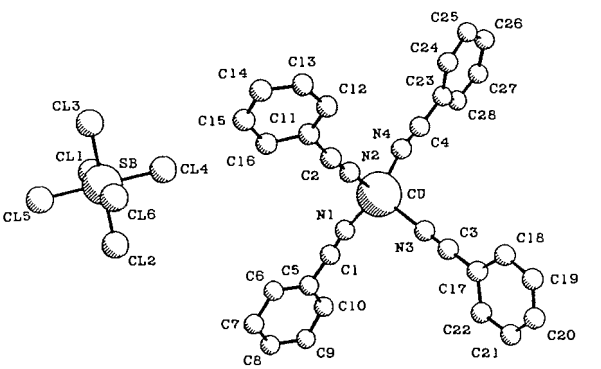


FIG. 1. The structure of tetrakis(benzonitrile)copper(I) hexachloroantimonate(V), showing the atom labelling and with the hydrogen atoms deleted.

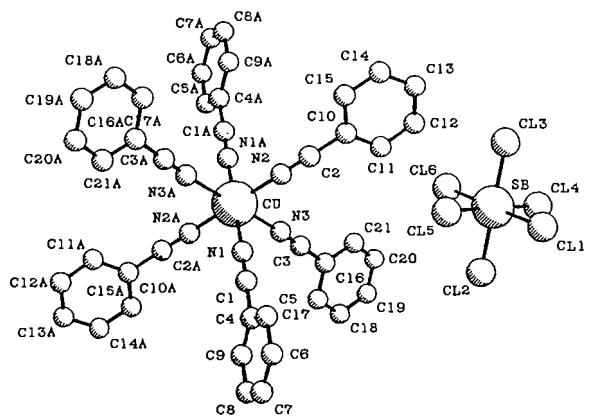


FIG. 2. The structure of hexakis(benzonitrile)copper(II) bis[hexachloroantimonate(V)], showing the atom labelling and with the hydrogen atoms deleted.

[3]A complete set of data may be purchased from the Depository of Unpublished Data, CISTI, National Research Council of Canada, Ottawa, Ont., Canada K1A 0S2.

Can. J. Chem. Downloaded from www.nrcresearchpress.com by 186.148.149.217 on 09/07/12
For personal use only.

Can. J. Chem. Downloaded from www.nrcresearchpress.com by 186.148.149.217 on 09/07/12
For personal use only.

TABLE 2. Atomic parameters x, y, z, and B_{iso} for **I**, esd's refer to the last digit printed.[a]

Atom	x	y	z	B_{iso}
Cu	0.0135 (7)	0.2623 (3)	0.2699 (3)	5.2 (3)
Sb	1.0130 (4)	0.77610 (19)	0.24067 (19)	3.76 (12)
Cl 1	1.3027 (15)	0.7562 (9)	0.2284 (8)	6.5 (6)
Cl 2	1.0039 (16)	0.7754 (9)	0.0748 (8)	6.9 (7)
Cl 3	1.0196 (14)	0.7754 (7)	0.4061 (7)	5.1 (6)
Cl 4	1.0228 (16)	0.6086 (8)	0.2503 (8)	6.8 (7)
Cl 5	1.0065 (18)	0.9445 (8)	0.2293 (9)	8.2 (8)
Cl 6	0.7240 (14)	0.7952 (9)	0.2513 (8)	6.7 (7)
N 1	0.145 (4)	0.3338 (23)	0.1716 (23)	5.4 (7)
N 2	−0.117 (4)	0.3553 (22)	0.3610 (21)	4.8 (7)
N 3	−0.155 (3)	0.2038 (19)	0.1932 (19)	3.7 (6)
N 4	0.144 (4)	0.1577 (21)	0.3478 (20)	4.5 (6)
C 1	0.180 (5)	0.374 (3)	0.109 (3)	5.4 (9)
C 2	−0.171 (4)	0.407 (3)	0.4122 (25)	3.8 (8)
C 3	−0.259 (5)	0.178 (3)	0.160 (3)	4.2 (8)
C 4	0.199 (4)	0.0912 (24)	0.3852 (23)	3.3 (7)
C 5	0.231 (5)	0.430 (3)	0.031 (3)	4.9 (9)
C 6	0.227 (6)	0.524 (4)	0.035 (3)	7.4 (12)
C 7	0.264 (6)	0.582 (4)	−0.048 (4)	7.8 (13)
C 8	0.334 (6)	0.537 (4)	−0.126 (4)	8.0 (13)
C 9	0.344 (6)	0.439 (4)	−0.130 (3)	7.0 (12)
C 10	0.294 (6)	0.388 (3)	−0.045 (3)	7.1 (12)
C 11	−0.236 (4)	0.464 (3)	0.488 (3)	4.0 (8)
C 12	−0.328 (5)	0.431 (3)	0.559 (3)	5.5 (10)
C 13	−0.385 (6)	0.491 (4)	0.627 (3)	7.5 (12)
C 14	−0.359 (6)	0.585 (3)	0.626 (3)	6.4 (11)
C 15	−0.268 (5)	0.616 (3)	0.552 (3)	4.9 (9)
C 16	−0.206 (5)	0.563 (3)	0.479 (3)	5.8 (10)
C 17	−0.399 (5)	0.150 (3)	0.123 (3)	5.3 (9)
C 18	−0.515 (8)	0.109 (4)	0.174 (4)	9.8 (16)
C 19	−0.647 (8)	0.086 (5)	0.135 (5)	11.2 (18)
C 20	−0.666 (6)	0.098 (3)	0.046 (4)	7.0 (12)
C 21	−0.551 (6)	0.131 (3)	−0.010 (3)	6.1 (10)
C 22	−0.406 (6)	0.157 (3)	0.022 (3)	7.3 (12)
C 23	0.264 (5)	0.005 (3)	0.441 (3)	4.3 (8)
C 24	0.196 (5)	−0.005 (3)	0.532 (3)	5.0 (9)
C 25	0.273 (5)	−0.086 (3)	0.587 (3)	5.1 (9)
C 26	0.379 (5)	−0.155 (3)	0.546 (3)	5.7 (10)
C 27	0.442 (5)	−0.143 (3)	0.453 (3)	5.3 (9)
C 28	0.381 (5)	−0.062 (3)	0.404 (3)	5.0 (9)

[a]B_{iso} is the mean of the principal axes of the thermal ellipsoid.

TABLE 3. Atomic parameters x, y, z, and B_{iso} for **II**, esd's refer to the last digit printed.[a]

Atom	x	y	z	B_{iso}
Cu	0	0	0	3.74 (5)
Sb	0.40892 (4)	0.30508 (4)	−0.70163 (4)	4.625 (23)
Cl 1	0.59508 (17)	0.18275 (14)	−0.78964 (14)	6.21 (9)
Cl 2	0.26780 (15)	0.19095 (14)	−0.78165 (13)	6.11 (9)
Cl 3	0.54961 (16)	0.41470 (14)	0.62392 (14)	6.76 (10)
Cl 4	0.42140 (16)	0.43593 (13)	−0.86651 (13)	6.01 (9)
Cl 5	0.39308 (21)	0.16593 (18)	−0.54250 (15)	9.81 (13)
Cl 6	0.22645 (17)	0.42957 (19)	−0.61605 (16)	9.07 (12)
N 1	0.0429 (4)	−0.1700 (4)	−0.0481 (4)	4.30 (24)
N 2	0.1900 (4)	0.0362 (4)	−0.0476 (4)	4.3 (3)
N 3	−0.0330 (5)	0.0633 (4)	−0.1866 (4)	5.8 (3)
C 1	0.0612 (5)	−0.2661 (5)	−0.0778 (5)	4.0 (3)
C 2	0.2882 (6)	0.0740 (5)	−0.0844 (5)	3.7 (3)
C 3	−0.0551 (6)	0.0895 (6)	−0.2750 (6)	5.3 (4)
C 4	0.0853 (6)	−0.3880 (5)	−0.1148 (4)	3.8 (3)
C 5	0.2042 (7)	−0.4501 (6)	−0.1114 (7)	6.6 (5)
C 6	0.2276 (8)	−0.5665 (7)	−0.1469 (8)	8.0 (5)
C 7	0.1315 (9)	−0.6183 (7)	−0.1852 (6)	6.8 (5)

TABLE 3. (*concluded*)

Atom	*x*	*y*	*z*	B_{iso}
C 8	0.0126 (9)	−0.5558 (7)	−0.1899 (7)	7.1 (5)
C 9	−0.0129 (7)	−0.4395 (6)	−0.1533 (6)	5.4 (4)
C 10	0.4043 (5)	0.1301 (5)	−0.1325 (5)	3.5 (3)
C 11	0.4283 (7)	0.1568 (6)	−0.2474 (6)	5.3 (4)
C 12	0.5318 (9)	0.2201 (8)	−0.2927 (7)	6.6 (5)
C 13	0.6167 (7)	0.2533 (7)	−0.2258 (8)	6.2 (5)
C 14	0.5927 (8)	0.2230 (7)	−0.1112 (7)	6.3 (5)
C 15	0.4870 (7)	0.1618 (6)	−0.0628 (6)	4.9 (4)
C 16	−0.0844 (6)	0.1265 (6)	−0.3872 (5)	4.4 (3)
C 17	−0.1718 (7)	0.0656 (7)	−0.4310 (6)	5.7 (4)
C 18	−0.2040 (8)	0.1045 (8)	−0.5363 (6)	6.7 (5)
C 19	−0.1521 (9)	0.2005 (9)	−0.5940 (7)	7.3 (6)
C 20	−0.0664 (10)	0.2597 (9)	−0.5509 (8)	9.3 (6)
C 21	−0.0308 (8)	0.2234 (8)	−0.4471 (7)	7.7 (5)
H 5	0.270 (6)	−0.423 (5)	−0.080 (5)	8.8 (21)
H 6	0.310 (6)	−0.604 (6)	−0.153 (6)	9.4 (23)
H 7	0.154 (5)	−0.691 (5)	−0.213 (5)	7.5 (19)
H 8	−0.056 (7)	−0.596 (6)	−0.207 (6)	12.8 (28)
H 9	−0.090 (5)	−0.394 (4)	−0.156 (4)	5.1 (16)
H 11	0.377 (4)	0.137 (4)	−0.294 (3)	3.0 (12)
H 12	0.026 (5)	0.260 (4)	−0.412 (4)	6.2 (16)
H 13	0.681 (5)	0.306 (5)	−0.251 (5)	7.4 (19)
H 14	0.640 (6)	0.245 (5)	−0.067 (5)	7.7 (20)
H 15	0.471 (5)	0.145 (5)	0.017 (5)	6.6 (17)
H 17	−0.209 (5)	0.002 (4)	−0.380 (4)	5.8 (16)
H 18	−0.262 (6)	0.056 (6)	−0.560 (5)	10.3 (24)
H 19	−0.173 (5)	0.225 (5)	−0.655 (4)	5.3 (17)
H 20	−0.033 (6)	0.328 (5)	−0.583 (5)	6.9 (20)
H 21	0.555 (6)	0.238 (5)	−0.354 (4)	6.1 (21)

[a] B_{iso} is the mean of the principal axes of the thermal ellipsoid.

TABLE 4. Bond distances in Å and angles in degrees for **I**

Bonds	Distance	Bonds	Angle
Cu—N(1)	2.04(3)	N(1)—Cu—N(2)	111.2(12)
Cu—N(2)	2.06(3)	N(1)—Cu—N(3)	104.6(12)
Cu—N(3)	2.09(3)	N(1)—Cu—N(4)	116.0(12)
Cu—N(4)	2.01(3)	N(2)—Cu—N(3)	107.9(11)
N(1)—C(1)	1.08(5)	N(2)—Cu—N(4)	107.3(12)
N(2)—C(2)	1.10(5)	N(3)—Cu—N(4)	109.5(11)
N(3)—C(3)	1.11(5)	Cu—N(1)—C(1)	162(3)
N(4)—C(4)	1.10(5)	Cu—N(2)—C(2)	172(3)
C(1)—C(5)	1.41(6)	Cu—N(3)—C(3)	171(3)
C(2)—C(11)	1.43(5)	Cu—N(4)—C(4)	168(3)
C(3)—C(17)	1.40(6)	N(1)—C(1)—C(5)	176(5)
C(4)—C(23)	1.47(5)	N(2)—C(2)—C(11)	172(4)
		N(3)—C(3)—C(17)	175(4)
		N(4)—C(4)—C(23)	175(4)

TABLE 5. Bond distances in Å and angles in degrees for **II**

Bonds	Length	Bonds	Angle
Cu—N(1)	2.000(4)	N(1)—Cu—N(1)a	179.9
Cu—N(2)	2.024(5)	N(1)—Cu—N(2)	91.25(17)
Cu—N(3)	2.357(5)	N(1)—Cu—N(2)a	88.75(17)
N(1)—C(1)	1.137(7)	N(2)—Cu—N(2)a	180.0
N(2)—C(2)	1.145(8)	Cu—N(1)—C(1)	176.3(4)
N(3)—C(3)	1.129(8)	Cu—N(2)—C(2)	168.1(5)
C(1)—C(4)	1.440(7)	N(1)—C(1)—C(4)	179.5(6)
C(2)—C(10)	1.425(9)	N(2)—C(2)—C(10)	175.3(6)
C(3)—C(16)	1.445(9)	N(3)—C(3)—C(16)	178.4(6)

Can. J. Chem. Downloaded from www.nrcresearchpress.com by 186.148.149.217 on 09/07/12
For personal use only.

upon co-ordination have been reported so this parameter does not appear useful in describing the metal ligand bonding (18–20).

The structure of complex **II** is shown in Fig. 2 and the key bond distances and angles are listed in Table 5. A complete set of bond distances and angles are deposited as supplementary material.[3] As required by the Jahn–Teller effect the co-ordination about copper is not a regular octahedron (21). An elongated rhombic octahedron with tetragonality of 0.854 has been observed for copper–oxygen bonds (22), the full range has been observed as a function of temperature for copper–nitrogen bonds (23). Only a single absorption is found at 2226 cm^{-1} for the C—N stretching frequency, essentially the same as for **I**. The average Cu—N bond length of 2.13 Å in **II** is slightly, but significantly, longer than that in **I**. There is no significant difference in the C—N and nitrile carbon to aromatic carbon average bond lengths of **II** and the corresponding bond lengths in **I**. Apart from the major difference in stereochemistry only the Cu—N bond distances seem to be slightly sensitive to the changed valence of the central copper atom.

1. L. KOLDITZ. *In* Halogen chemistry, Vol. 2, *Edited by* V. Gutmann. Academic Press, New York. 1967. p. 127.
2. P. P. K. CLAIRE, G. R. WILLEY, and M. G. B. DREW. J. Chem. Soc. Chem. Commun. 1100 (1987).
3. I. LEBAN, D. GANTAR, B. FRELC, D. R. RUSSEL, and J. H. HOLLOWAY. ACTA CRYSTALLOGR. C**43**, 1888 (1987).
4. R. BOUGON, P. CHARPIN, K. O. CHRISTE, J. ISABEY, M. LANCE, M. NIERLICH, J. VIGNER, and W. W. WILSON. Inorg. Chem. **27**, 1389 (1988).
5. K. D. KARLIN and J. ZUBIETA (*Editors*). Copper coordination chemistry, biochemical and inorganic perspectives. Adenine Press, Guilderland, New York. 1983.
6. B. J. HATHAWAY. Struct. Bonding, **14**, 49 (1973).
7. D. M. BYLER and D. F. SHRIVER. Inorg. Chem. **12**, 1412 (1973).
8. D. M. BYLER and D. F. SHRIVER. Inorg. Chem. **13**, 2697 (1974).
9. M. BURGARD, G. KAUFMANN, and R. ROHMER. C. R. Acad. Sci. Ser. C**267**, 689 (1968).
10. V. H. BINAS. Z. Anorg. Allg. Chem. **352**, 271 (1967).
11. M. BURGARD and J. MACCORDICK. Inorg. Nucl. Chem. Lett. **6**, 599 (1970).
12. M. MASSAUX, M. J. BERNARD, and M. T. LEBIHAN. Bull. Soc. Fr. Mineral Cristallogr. **92**, 118 (1969).
13. M. MASSAUX and M. T. LEBIHAN. ACTA CRYSTALLOGR. B**32**, 1586 (1976).
14. D. F. GRANT and E. J. GABE. J. Appl. Crystallog. **11**, 114 (1978).
15. E. J. GABE, F. L. LEE, and Y. LEPAGE. Crystallographic computing 3: Data collection, structure determination, proteins and databases. *Edited by* G. M. Sheldrick, C. Kruger, and R. Goddard. Clarendon Press, Oxford. 1985. p. 167.
16. S. GORTER and G. C. VERSCHOOR. Acta Crystallogr. B**32**, 1704 (1976).
17. A. P. ZUUR, P. L. A. EVERSTEIJN, and W. L. GROENEVELD. Inorg. Nucl. Chem. Lett. **11**, 35 (1975).
18. B. N. STORHOFF and H. C. LEWIS. Coord. Chem. Rev. **23**, 1 (1977).
19. P. C. FORD. Coord. Chem. Rev. **5**, 75 (1970).
20. M. NAKASHIMA, M. MIKURIYA, and Y. MUTO. Bull. Chem. Soc. Jpn. **58**, 968 (1985).
21. B. J. HATHAWAY. STRUCT. BONDING, **57**, 55 (1984).
22. N. W. ALCOCK, M. DUGGAN, A. MURRAY, S. TYAGI, B. J. HATHAWAY, and A. W. HEWAT. J. Chem. Soc. Dalton Trans. 7 (1984).
23. S. KLEIN and D. REINEN. J. Solid State Chem. **32**, 311 (1980).

Can. J. Chem. Downloaded from www.nrcresearchpress.com by 186.148.149.217 on 09/07/12
For personal use only.

A molecular orbital study of the conformation (inversion and rotational barriers) and electronic properties of sulfamide

OTILIA MÓ, JOSÉ L. G. DE PAZ, AND MANUEL YÁÑEZ[1]
Departamento de Química, C-XIV, Universidad Autónoma de Madrid, Cantoblanco, 28049-Madrid, Spain
AND
IBON ALKORTA, JOSÉ ELGUERO, PILAR GOYA, AND ISABEL ROZAS
Instituto de Química Médica, C.S.I.C., Juan de la Cierva, 3, 28006-Madrid, Spain
Received May 19, 1989

OTILIA MÓ, JOSÉ L. G. DE PAZ, MANUEL YÁÑEZ, IBON ALKORTA, JOSÉ ELGUERO, PILAR GOYA, and ISABEL ROZAS. Can. J. Chem. **67**, 2227 (1989).

Ab initio calculations have been used to study the conformational potential surface of sulfamide, by considering the S—N bond rotations and the nitrogen inversion processes. The lowest energy conformation (**b**) is found for a *cis–trans* arrangement of the amino groups, although conformations with *cis–cis* (**a**), *trans–trans* (**c**), and near staggered (**c′**) arrangements lie close in energy. Nitrogen inversion barriers are very low, and consequently one may expect forms **b** and **c′** to be the only ones present in the gas phase. Conformer **a** is very polar, its dipole moment being twice that of **b**, so it may be favored in condensed media or in polar-solvent solutions. The relative stability of the different isomers is governed by interactions between the amino protons and between the nitrogen lone pairs. Our results show that $d-\pi$ backbonding, involving the *d* orbitals on sulfur, is responsible for the multiple bond character of the S—O linkage, but is very small in the S—N interactions. The role of the sulfur *d*-orbital exponent, when a 6-31G* basis is used, is analyzed on a series of model compounds containing S^{II}, S^{IV}, and S^{VI}. Although the inclusion of *d* functions on sulfur is crucial to describing correctly the bonding in sulfamide, the results obtained do not change appreciably if a second set of *d* functions is centered on sulfur. Nevertheless, only when polarization functions are also included for first-row atoms is the description of the system reliable.

Key words: sulfamide, inversion and rotational barriers, sulfur *d*-functions.

OTILIA MÓ, JOSÉ L. G. DE PAZ, MANUEL YÁÑEZ, IBON ALKORTA, JOSÉ ELGUERO, PILAR GOYA et ISABEL ROZAS. Can. J. Chem. **67**, 2227 (1989).

On a utilisé des calculs *ab initio* pour étudier le potentiel de surface conformationnel du sulfamide, en considérant les rotations de la liaison S—N et les processus d'inversion de l'azote. On a trouvé que la conformation d'énergie minimale (**b**) implique un arrangement *cis–trans* des groupements aminés, même si les conformations avec des arrangements *cis–cis* (**a**), *trans–trans* (**c**) et pratiquement décalé (**c′**) possèdent des énergies très voisines. Les barrières à l'inversion de l'azote sont très basses et, en conséquence, on peut s'attendre à ce que les formes **b** et **c′** soient les seules présentes en phase gazeuse. Le conformère **a** est très polaire, son moment dipolaire est le double de celui de **b**; il est possible qu'il soit favorisé dans les milieux condensés ou dans des solutions dans des solvants polaires. La stabilité relative des divers isomères est gouvernée par les interactions entre les protons des groupements amino et les paires libres des azotes. Nos résultats démontrent que la liaison en retour $d-\pi$, impliquant les orbitales *d* du soufre, est responsable pour le caractère de liaison multiple de la liaison S—O; ce type de liaison est toutefois très faible dans les interactions S—N. Utilisant une série de composés modèles contenant des S^{II}, S^{IV} et S^{VI} et faisant appel à une base 6-31G*, on a étudié le rôle du caractère de l'orbitale *d* du soufre. Même si l'inclusion des fonctions *d* du soufre est cruciale pour décrire correctement les liaisons dans le sulfamide, les résultats obtenus ne changent pas beaucoup si on ajoute un deuxième ensemble de fonctions *d* sur le soufre. Toutefois, on n'obtient une description adéquate du système que lorsque des fonctions de polarisation sont ajoutes aux atomes de la première couche.

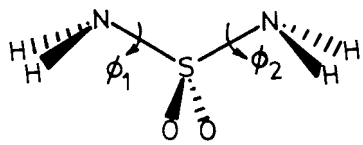
Mots clés : sulfamide, barrières à l'inversion et à la rotation, fonctions *d* du soufre.

[Traduit par la revue]

1. Introduction

The >N—SO_2—N< group, present in sulfamide (1) and in 1,2,6-thiadiazine 1,1-dioxides (2), has interesting biological properties that are reputed to be related to the CO/SO_2 bioisosterism. But unlike urea, H_2N—CO—NH_2, which has been the subject of careful theoretical calculations (3–6), to our knowledge there is only a rather limited *ab initio* study (7) on sulfamide, H_2N—SO_2—NH_2. We therefore decided to study theoretically the conformational energetics of this molecule with regard both to rotation and to inversion of the amino groups, which can shed light on the fundamental problem of >N—SO_2— conjugation in relation to the nitrogen lone-pair position.

In sulfamide there are two rotational degrees of freedom, which correspond to the two S—N bond rotations, ϕ_1 and ϕ_2 (see Scheme 1). Using the Newman projections along these bonds we can identify the rotamers included in Fig. 1, for 90° rotations about both S—N bonds. As we shall illustrate later, some are relative minima (stable isomers) and some are saddle points of the hypersurface. To complete our discussion of the general stereochemistry of this compound the corresponding nitrogen inversion processes were also investigated. Accordingly, three different transition states, which correspond to conformations in which N1 (conformers **h** and **i**) or N1 and N2 (conformer **j**) have sp^2 hybridization, were studied. Finally, the structures of the stable conformers were optimized at a high level of accuracy.



SCHEME 1

We shall also investigate the bonding characteristics of the

[1]Author to whom correspondence may be addressed.

Printed in Canada / Imprimé au Canada

Can. J. Chem. Downloaded from www.nrcresearchpress.com by 186.148.149.217 on 09/07/12
For personal use only.

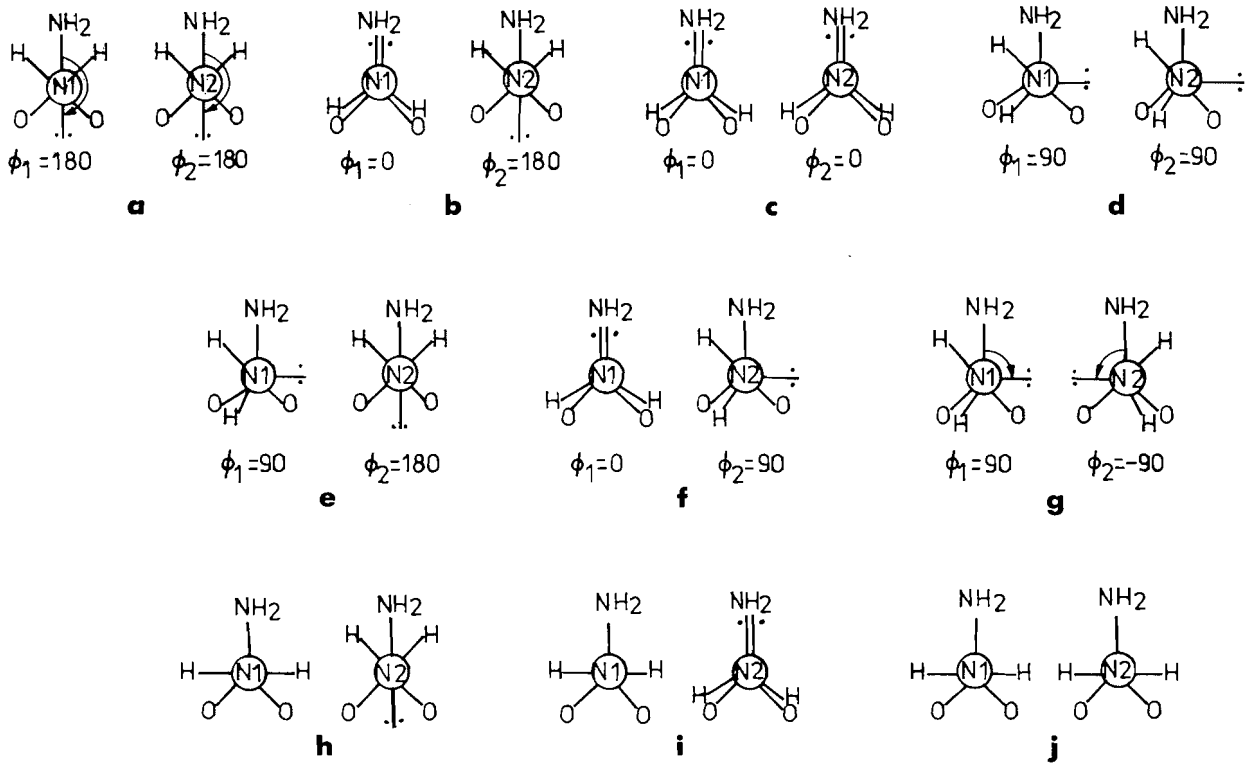


FIG. 1. Newman projections of the different rotamers of sulfamide corresponding to 90° S—N bond rotations. Conformers **h**, **i**, and **j** correspond to the transition states of the nitrogen inversion processes for this system.

S—O and S—N linkages by analyzing the corresponding canonical and localized molecular orbitals. The latter will be obtained employing the method of Boys (8).

Regarding the concrete aspects of the SCF *ab initio* treatment of sulfamide, it is worth noticing that the choice of the basis set, which constitutes one of the most crucial problems of any *ab initio* calculation, becomes particularly relevant in the present case, where the second-row atom displays a hypervalent coordination (7, 9–17). Moreover, the high electronegativity of the ligands bonded to sulfur in this system will likely render polarization effects quite important, so that a proper description of the polarization of the first-row atoms would also be unavoidable. For this reason, we carried out our calculations at the 6-31G* level (10) to include polarization functions, not only on sulfur but also on the other heavy atoms of the system. However, and taking into account that polarization functions centered on a central atom in any species are expected to be more important than those on the peripheral ones due to the higher angular dependence of the local charge distribution near the former, we have also analyzed the effect of including an additional set of *d* functions centered on S. It seems also clear that a reliable description of the geometry and charge distribution of a hypervalent system requires a careful choice of the exponent (α_d) of the *d* functions centered on the hypervalent atom to supplement a reasonably sized *sp* basis. Accordingly, an investigation of the effect of α_d on energies, geometries, and charge distributions of different model sulfur compounds was undertaken, as a first step of our study, to have a reliable *d* exponent for a correct treatment of S^{II}, S^{IV}, and S^{VI} compounds, and of sulfamide in particular.

Finally, we shall also discuss the performance of such cheaper polarized basis sets as the STO-3G* (18) and 3-21G$^{(*)}$ (19), where the polarization functions are included exclusively on the second-row atom, but which can be a necessary alternative for the theoretical treatment of increasingly large compounds.

2. Computational details

To discuss the internal rotational potential surface of sulfamide we have fully optimized, at the STO-3G* level, the geometries of the different rotamers corresponding to values of ϕ_1 ranging from 0° to 180° and of ϕ_2 ranging from −180° to 180°, in steps of 30°. Then, single-point calculations at the 6-31G* level were carried out using these STO-3G* fully optimized structures. These closed-shell SCF calculations were performed using the Gaussian-80 series of programs (20) and suitable gradient optimization procedure (21).

The specific study of the stable conformers of sulfamide was carried out at different levels of accuracy employing "standard" and "non-standard" basis sets. More precisely, calculations at the 3-21G$^{(*)}$ levels were performed using the standard set of exponents (19). At the 6-31G* level we employed the standard exponents (10) except for the *d* functions centered on S, for which an optimal value (see next section), α_d = 0.70, was adopted.

The importance of achieving a proper polarization of the central atom was investigated by using two different polarized split-valence bases, which include two sets of *d* functions on S. These bases were constructed from the standard 6-31G* one, by replacing the standard set of *d* functions on sulfur by two sets of exponents, 0.39 and 1.18 in one case (22), and 0.30 and 0.80 in the other (14). Energies obtained with the first set of exponents were systematically lower than those obtained with the second; we shall therefore discuss exclusively the results obtained with the former basis, which will be denoted as 6-31G*+d_s.

A C_{2v} symmetry was adopted for conformers **a**, **c**, and **j**; a C_s for **b**, **g**, **h**, **i**, and a C_2 symmetry for conformer **d**. For the

Can. J. Chem. Downloaded from www.nrcresearchpress.com by 186.148.149.217 on 09/07/12
For personal use only.

TABLE 1. Optimal exponents (α_d) of the sulfur *d* functions to be used within a 6-31G* scheme, for normal valence (S^{II}) and hypervalent (S^{IV}, S^{VI}) systems. Total energies in au

Compound	α_d	Total energy
SH_2	0.55	−398.66854
SH_2(linear)	0.55	−398.53500
SF_2	0.70	−595.31228
SF_2(linear)	0.60	−595.92351
CH_2—S—CH_2	0.60	−475.54688
CH=CH—CH_2—S	0.60	−513.38406
SO_2(linear)	0.60	−546.87944
SO_2	0.60	−546.87970
SC_2(linear)	0.50	−472.86255
SC_2	0.50	−472.86947
CH_2—CH_2—S=O	0.60	−550.34360
NH_2—SOOH	0.70	−603.35496
SO_2F_2	0.75	−746.02720
SO_3	0.70	−621.98234
SF_3N	0.70	−750.08638
CH_2—CH_2—SO_2	0.70	−625.16196
NH_2—SO_2—H	0.70	−603.33618
$(NH_2)_2$—SO_2	0.70	−658.38180

remaining nuclear arrangements no symmetry constraints were imposed. In all cases all geometrical parameters were fully optimized at each of the levels of accuracy considered in this work.

Charge distributions were obtained using the well-known Mulliken population analysis.

3. Results

3.1. α_d *exponent optimization*

To obtain the optimized exponent of the set of *d* functions on sulfur to be used within a 6-31G* quality basis, we have selected the following sets of normal valence (II) compounds: SH_2, SH_2(linear), SF_2, SF_2(linear), ethylene episulfide (CH_2—S—CH_2), and thiete (CH=CH—CH_2—S); and hypervalent (IV and VI) compounds: SO_2(linear), SO_2, SC_2(linear), SC_2, ethylene episulfoxide (CH_2—CH_2—S=O), aminosulfurous acid (NH_2— SO—OH), SO_2F_2, SO_3, SF_3N, ethylene sulfone (CH_2—CH_2— SO_2), H—SO_2—NH_2, and sulfamide.

The exponents of the *d* functions on S were allowed to vary between 0.40 and 0.80 in steps of 0.05. The geometries used were previously optimized using the standard 6-31G* (α_d = 0.65) basis set. The values of the optimized α_d exponents and the corresponding energies have been summarized in Table 1.

We have found that the energy of hypervalent compounds is much more sensitive to the α_d value than that of normal valence systems, illustrating that a proper polarization of sulfur is particularly crucial for the former.

It should also be remarked that the optimal values reported here are referred to a basis that includes polarization functions on the remaining heavy atoms of the system and, therefore, they are different from those recently reported by Yadav *et al.* (23) to supplement a 3-21G basis. In the same paper it was also shown that the S—O bond lengths depend strongly on the α_d value chosen, and an optimization of this exponent to obtain the shortest S—O bond was proposed. Since we are interested in obtaining a reliable geometrical structure of sulfamide, it seems necessary to assess whether similar behavior should be expected when the basis set also includes polarization functions in the remaining heavy atoms of the system. To investigate this particular point we have considered the following model compounds: SO_2, SO_3, SO_2F_2, for which the molecular geometry was fully optimized for each value of α_d. In Table 2 we present, as an example, the results obtained for SO_3. First, it is conspicuous that the optimum α_d value is identical to that obtained above when the geometry was not allowed to vary and was kept identical to the 6-31G* optimized level. Second, the S—O bond length systematically decreases as α_d increases and no minimum is found in the range of α_d values investigated. Moreover, the S—O bond length varies little in the neighborhood of the minimum.

TABLE 2. Optimized total energies (in au) and S—O bond lengths (in Å) of SO_3 as a function of the exponent of the sulfur *d* orbital (α_d) when a 6-31G* type of basis is employed

α_d	Total energy	S—O bond length
0.40	−621.93313	1.430
0.50	−621.96353	1.417
0.55	−621.97267	1.412
0.60	−621.97850	1.408
0.65	−621.98157	1.405
0.70	−621.98238	1.402
0.75	−621.98136	1.400
0.80	−621.97893	1.398

We may conclude then that the criterium of the shortest S—O bond is not always meaningful as it depends on the quality of the basis set which is implemented. In fact, the shortening of the S—O and S—N bonds produced by including polarization functions on the sulfur atom is not at all dramatic at the 6-31G* level, because the shortening caused by the polarization functions centered on first-row atoms is already notorious.

3.2. Internal rotation potential surface

The calculated potential surface for S—N bond rotation (see Figs. 2 and 3) shows that **b** ($\phi_1 = 0$, $\phi_2 = 180$) is the most stable conformer of sulfamide, although conformers **a** and **c** are also minima in this surface. Both figures also show the existence of another local minimum **c'** ($\phi_1 \simeq 30$ and $\phi_2 \simeq 30$), close and slightly more stable than conformer **c**. The rotational barriers (between 3.7 and 7.7 kcal/mol, depending on the path) are much lower than those calculated for formamide (14.2 kcal/mol) (24) but similar to those reported by Vishveshwara and Pople (25) for glycine. Due to the competing effect of the two NH_2 groups, the barrier in urea is 5.8 kcal/mol lower than in formamide, for the rotation of one amino group, the second one remaining planar (3). The simultaneous rotation of both amino groups (sp^3 nitrogens in the transition state) is a much more energetic process (6). All this illustrates that in sulfamide the conjugative interaction between the NH_2 and the S=O groups is much weaker than that between the NH_2 and the carbonyl group in formamide and in urea, because in the former system the amino groups lie in a plane perpendicular to that defined by the SO_2 moiety. This seems to be in disagreement with the conclusions of Fraenkel *et al.* (26), which explain the low rotational barrier of a sulfone as a direct consequence of a conjugative interaction involving the *d* orbitals in sulfur. To clarify this point, we have carried out an analysis of the MO's of conformers **a** and **c**, which upon rotation about one S—N bond yield the most stable conformer **b**. This analysis shows that there is an interaction between the in-phase combination of the

Can. J. Chem. Downloaded from www.nrcresearchpress.com by 186.148.149.217 on 09/07/12
For personal use only.

Can. J. Chem. Downloaded from www.nrcresearchpress.com by 186.148.149.217 on 09/07/12
For personal use only.

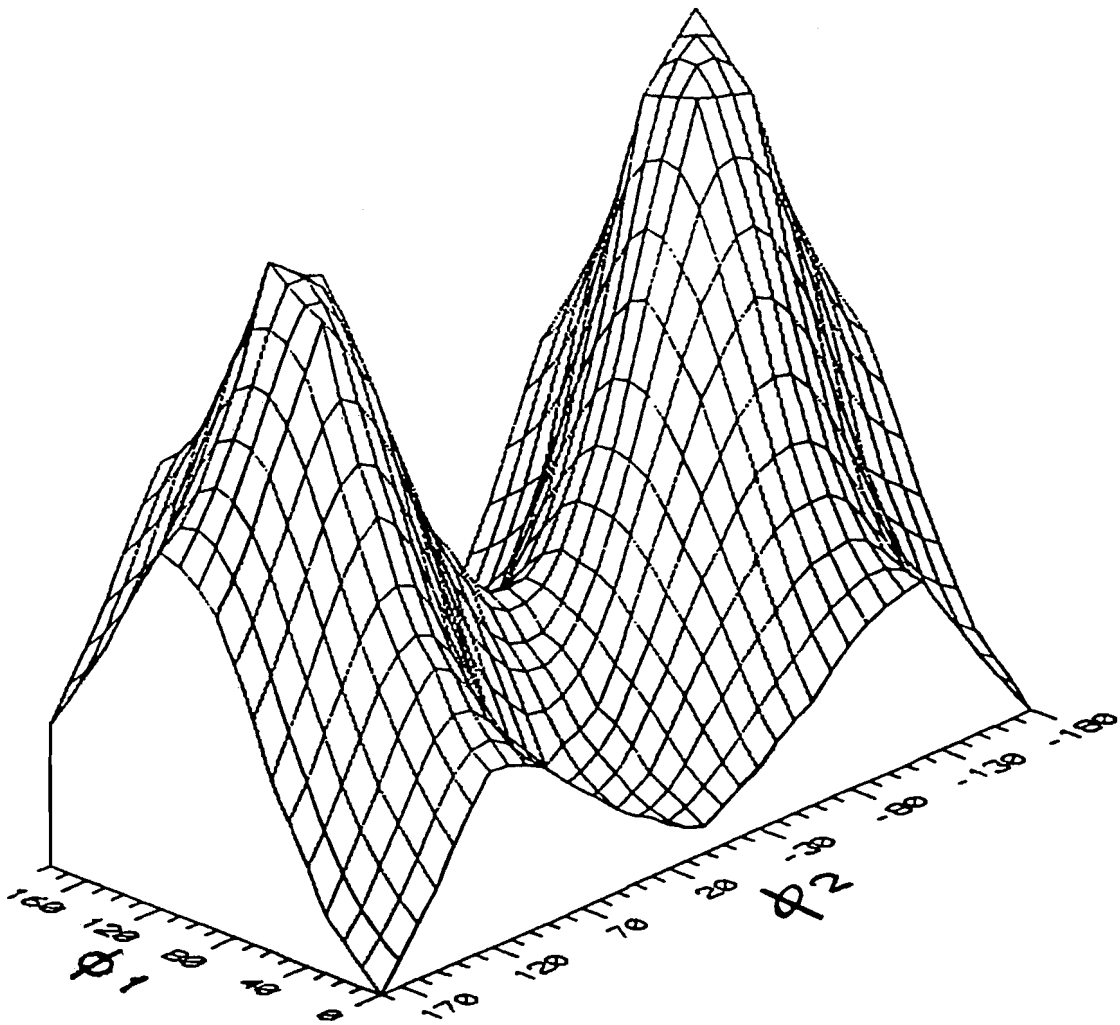


FIG. 2. Potential surface for S—N bond rotations of sulfamide, obtained at the 6-31G* level on STO-3G* fully optimized structures. The rotational angles ϕ_1 and ϕ_2 have been defined in Scheme 1.

nitrogen lone pairs (LPN^+) and the $2p_z + 3d_{x^2-y^2}$ orbitals of sulfur (see Fig. 4), but this conjugation is noticeably smaller than that between the *d* orbitals of sulfur and the oxygen lone pairs, as we shall discuss later. There is another feature that indicates that this conjugation plays a nonsignificant role in the magnitude of the rotational barrier. Actually, although the conjugation decreases when the NH_2 group rotates, it is still significant for conformations very close to the maximum of the barrier ($\phi_1 = 90$ or $\phi_2 = 90$), although involving the $2p_x$ orbital of sulfur instead of the $2p_z$. Moreover, for the most stable conformer **b**, it is weaker than in **a** or **c**.

We can therefore conclude that the rotational barriers in sulfamide arise mostly from the repulsions between the protons of the two amino groups. The three-dimensional picture of Fig. 2 reveals that the rotational barrier between **b** and **a** is much higher (7.7 kcal/mol) than that between **b** and **c** (3.7 kcal/mol), as a direct consequence of this effect. Starting from isomer **b**, a ϕ_1 rotation involves a decrease of the four distances between the protons of the two amino groups, which becomes maximum for $\phi_1 \simeq 120$, coinciding with the maximum of the barrier. After this point one of the distances becomes larger and the energy lowers to reach conformer **a**. If one considers how the separation between the amino protons evolves on going from **b** to **c** (ϕ_2 rotation), the situation is markedly different. Only one of the four distances rapidly decreases and reaches its minimum around $\phi_2 \simeq 60$. The other proton–proton distances remain practically unchanged or become slightly larger and the rotational barrier becomes less than half the previous one. In fact, in isomer **c** the distances between the amino protons are, on average, larger than in isomer **b**, but the repulsive interaction between the nitrogen lone pairs is considerably greater, raising the total energy of the former. The existence of another stable conformation **c′** close to **c** confirms this analysis. In conformer **c′** the NH_2 groups rotate enough to alleviate the lone-pair repulsion that takes place in **c**, without substantially increasing the repulsion between the amino protons. The result is a conformation that lies only 0.3 kcal/mol above conformer **b**. In a similar way, it can also be observed that the potential surface for $\phi_2 > 0$ is systematically lower than for $\phi_2 < 0$, because in the latter case, where the amino protons tend to be simultaneously above (or below) the NSN plane, the repulsive interaction between the amino protons is greater. Figure 3 shows that the two absolute maxima appear for ($\phi_1 \simeq 120$, $\phi_2 \simeq 120$) and ($\phi_1 \simeq 120$, $\phi_2 \simeq -120$), the latter being about 2.0 kcal/mol higher than the former.

The weak conjugative interaction between the amino groups and the SO_2 moiety is also shown by the pyramidal structure of the two amino groups. This structure changes very little upon

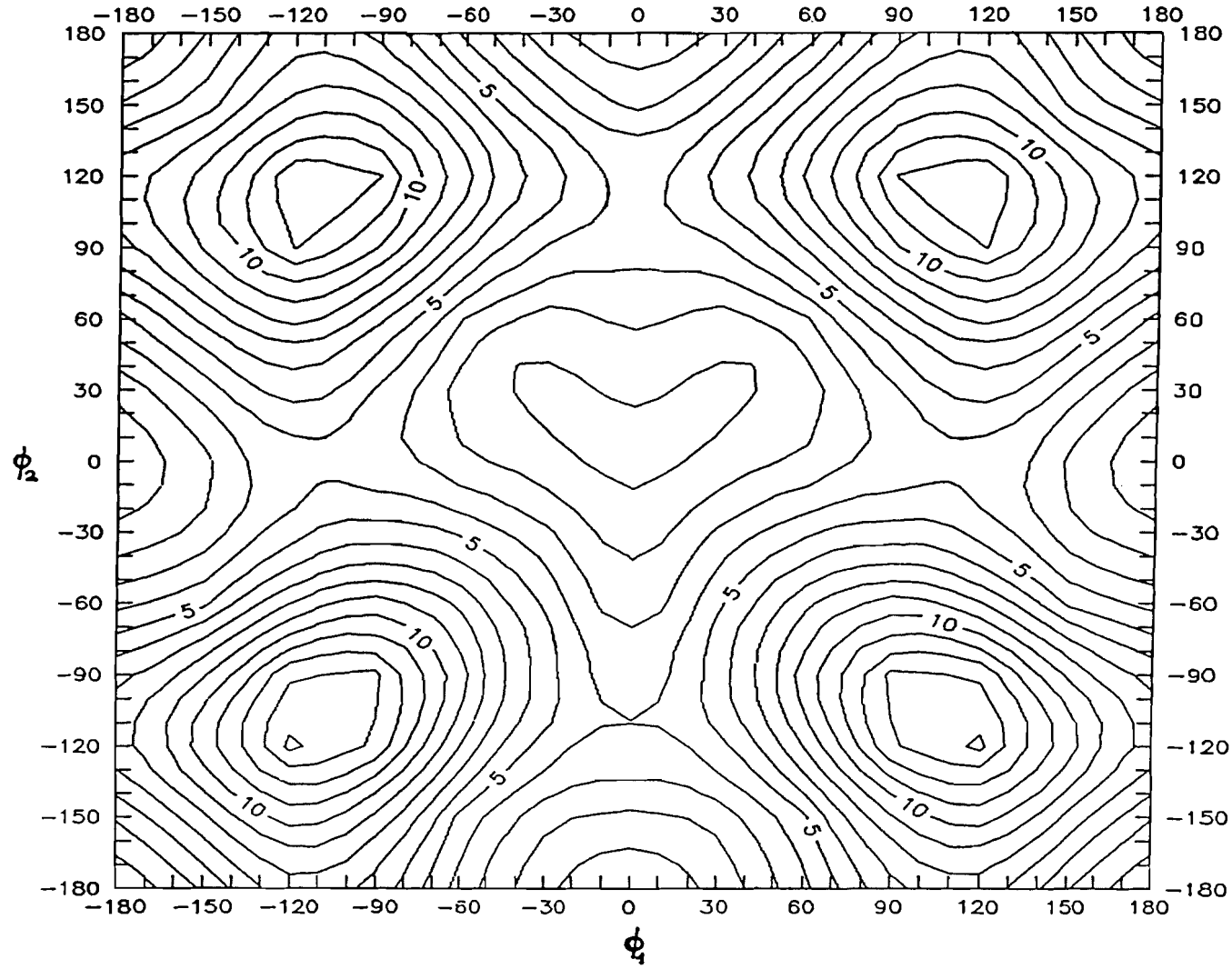


FIG. 3. Two-dimensional plot of the potential surface of Fig. 2. Contour labels refer to the energy (in kcal/mol) relative to the absolute minimum ($\phi_1 = 0$, $\phi_2 = 180$).

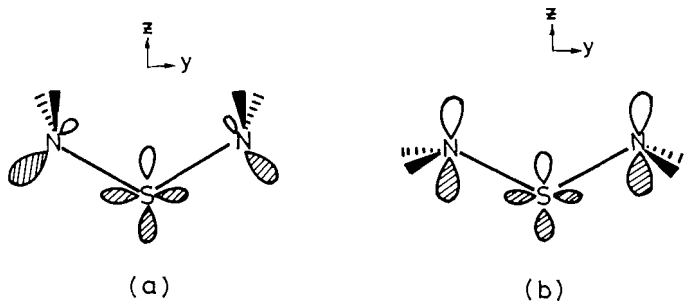


FIG. 4. Schematic representation of the interaction between the LPN^+ on nitrogens and the linear combination ($2p_z + 3d_{x^2-y^2}$) on sulfur; (a) conformer **a**; (b) conformer **c**.

S—N rotation, and the H—N—S angle remains typically around 106°, and only for species **a** and **c** increases to about 112°.

3.3. Sulfamide isomers. Structure and stability

Once the local minima of the potential surface were localized we carried out a full geometry optimization for each of them at the 6-31G* ($\alpha_d = 0.7$) and 6-31G*+d_s levels. The corresponding optimized geometrical parameters have been summarized in Table 3. This table also contains the corresponding total energies and dipole moments, together with the X-ray experimental structure (27).

We shall discuss first the results obtained at the 6-31G* level and later the effect of including an additonal set of *d* functions on sulfur. These results confirm that conformer **b** is the most stable in the gas phase, although conformers **c**, **a**, and **c′** are only 0.6, 2.7, and 0.3 kcal/mol less stable, respectively. Since there is a considerable variation in their dipole moments (for instance that of isomer **a** is more than twice that of isomer **c**), this relative stability can change considerably in polar solvents or in condensed media, where dipole interactions can strongly favor the most polar isomers. This, and the existence of a network of hydrogen bonds, explains why only conformer **a** is present in the crystal (27). In general, there is reasonably good agreement between theoretical optimized parameters and those determined by X-ray diffraction (27). This also means that there are no significant changes either in the bond lengths or in the bond angles among the different isomers considered. Actually these variations are smaller than 0.1 Å for the former and smaller than 2° for the latter.

The relative stability of the isomers of sulfamide is a consequence of several factors. Similar to what has been

Can. J. Chem. Downloaded from www.nrcresearchpress.com by 186.148.149.217 on 09/07/12
For personal use only.

Can. J. Chem. Downloaded from www.nrcresearchpress.com by 186.148.149.217 on 09/07/12
For personal use only.

TABLE 3. Optimized conformations (bond lengths in Å and bond angles in degrees), total energies (in au), and dipole moments (in debye) of the stable conformers of sulfamide

	Conformers								
	a		**b**		**c**		**c′**		
	6-31G*	6-31G*+d_s	6-31G*	6-31G*+d_s	6-31G*	6-31G*+d_s	6-31G*	6-31G*+d_s	Experimental[a]
Bond lengths									
S—O	1.417	1.407	1.420	1.410	1.424	1.414	1.423	1.413	1.430
S—N	1.633	1.627	1.629	1.622	1.637	1.630	1.639	1.631	1.620
			1.652	1.644					
N—H	0.998	0.998	1.000	0.999	0.999	0.999	1.002	1.001	0.956
			1.001	1.000			1.001	1.000	0.907
Bond angles									
O—S—O	124.5	124.4	123.4	123.3	122.9	122.8	120.4	120.5	119.2
O—S—N	105.5	105.5	106.3	106.2	106.8	106.9	108.4	108.4	106.1
			106.6	106.7			108.4	108.4	107.0
N—S—N	110.0	110.0	106.6	106.6	105.6	105.4	100.6	101.9	111.4
S—N—H	115.9	115.5	113.6	111.1	112.3	111.9	111.5	111.2	109.9
			111.4	113.2			111.1	110.8	110.4
H—N—H	115.7	115.5	113.5	113.2	113.6	113.5	112.3	112.3	116.1
			112.2	112.1			112.3	112.3	
Total energies	−658.37765	−658.40340	−658.38184	−658.40755	−658.38085	−658.40642	−658.38134	−658.40681	
μ (D)	6.60	6.48	4.81	4.67	2.55	2.39	3.02	2.83	3.9[b]

[a]Experimental geometry taken from ref. 27.
[b]Dipole moment taken from ref. 29.

Can. J. Chem. Downloaded from www.nrcresearchpress.com by 186.148.149.217 on 09/07/12
For personal use only.

discussed by Ehrhardt and Alrichs (28) for $FNSF_2$, and as we mentioned above (see Fig. 4), a *cis* arrangement of the $-NH_2$ groups with respect to the SO_2 moiety facilitates the delocalization of the nitrogen lone pairs into the low-lying orbitals of the $-SO_2$ fragment. Consequently, the participation of the AO's of sulfur in the nitrogen lone pair MO's is greater in conformer **c** than in isomer **a**, resulting in a slight increase of the S—N overlap population. Since, as discussed above, this delocalization is quite small, the stabilizing effect is not large and the destabilization of form **a** with respect to **c** comes basically from the coulomb repulsion between the protons of the amino groups, which are in an eclipsed conformation in **a**. In this respect it should be noted that the local structure of the $S(NH_2)_2$ moiety reflects the lack of lone-pair interactions and smaller repulsions among the amino protons in conformer **c'**, which presents a near staggered arrangement of the amino groups ($\phi_1 = \phi_2 \simeq 47.5$ degrees) and an N—S—N bond angle about 5°–10° smaller than in the other isomers.

On the other hand, it must be taken into account that there is a large difference in dipole moments between the isomers. Therefore, one of the reasons for the differences in stability may be favorable dipole interactions of the $S(NH_2)$ and SO_2 moieties. In fact, assuming that the bond dipoles may be represented by point charges in a very simple model, the differences in coulombic interactions for isomers **a** and **c** would be of the order of a few kcal/mol.

3.4. Nitrogen inversion processes

Since the different isomers are quite close in energy we have considered it worthy to study also the N-inversion processes that permit going from one conformer to another. Therefore, the geometries corresponding to conformations **h**, **i**, and **j** were also fully optimized, at the 6-31G* level, although they are not local minima of the potential hypersurface but transition states. The geometrical parameters are available from the authors. The total energies (−658.37738, −658.37918, and −658.37600 au, respectively) show that the barriers for single (2.8 and 1.7 kcal/mol, respectively) and double (3.7 kcal/mol) nitrogen inversions are quite low. Therefore, the interconversion between **c** and **b** or **a** and **b** through an N-inversion process may occur, under normal conditions, in the gas phase. Then, one should expect conformer **a** not to be present in the gas phase while, assuming a Maxwell–Boltzman distribution, the proportion of forms **c** and **b** should be 37 and 63%, respectively, and therefore the observed dipole moment should be about 3.9 D or lower, since 6-31G* results usually overestimate this first-order magnitude. However, the excellent agreement between this predicted value and that measured in solution (29) (dioxane at 20°C, see Table 3) may be fortuitous.

The low barriers to nitrogen inversion that were found indicate that the transition state, in which the amino protons lie in a plane perpendicular to that defined by the SN_2 moiety, is relatively stable with respect to isomers **a** and **c**, respectively, i.e., that the stability of the system is not very sensitive to the degree of pyrimidalization of the NH_2 groups. To explain this finding, let us then consider first the characteristics of the nitrogen lone pairs in conformers **a** and **c**. As illustrated in Fig. 4, the *s* character of the LPN^+ orbital of **c** is smaller than that of **a**. This is so because, in the former, the *s* contribution would considerably increase the repulsive interaction beween both lone pairs, while in the latter the situation is just the opposite. Accordingly, the LPN^+ of form **a** lies much lower in energy than that of conformer **c** (MO energies are available from the authors). This is also corroborated by the fact that the amino protons of isomer **c** are more acidic than in isomer **a**, since in the former the *s* character of the other hybrids centered on the nitrogens is greater. Therefore, when one of the nitrogens of isomer **c** inverts, the destabilization of the corresponding lone pair is not very significant, since in its ground state the lone-pair *s* character is already small. Accordingly, the inversion barrier is not very high. Following the same arguments, the nitrogen inversion barrier of isomer **a** should be considerably greater, since the loss of *s* character on going from the ground to the transition state is more significant. Nevertheless, it must be taken into account that, simultaneously, the distance between the protons of the two amino groups considerably increases, tending to stabilize the system. Both effects are practically counterbalanced and the inversion barrier becomes very small. Similar arguments can be used to explain the magnitude of the double inversion barrier.

As for rotation, the inversion processes reveal that the conjugative interaction between the amino and the SO_2 groups is very weak and it is not favored in the transition state. In fact, the net atomic charges indicate that electron population at nitrogen is larger in the transition state than in conformers **a** or **c**, just the opposite of what would be expected if a delocalization of the nitrogen lone pair took place. Similar findings have been reported by Wiberg and Laidig (30) for formamide.

Experimental results (by DNMR) on sulfonamides >N—SO_2—Ar in which the nitrogen atom is part of a three-(aziridine) or a six-membered ring (piperidine) have been reported. Initially, the activation energies were assigned to inversion process (31, 32) but, as Mislow and co-workers pointed out (33), slow rotation about the N—S bond cannot be ruled out as the rate-determining process. The calculations described here, as well as those in simpler compounds (34), indicate that since both processes have similar activation energies, depending on ring size and on nitrogen substituents, either of them can be responsible for the experimental behaviour.

3.5. S—O bonding characteristics

An important structural feature of hypervalent sulfur compounds like sulfamide is the characteristics of the S—O bonds. Both the canonical and the localized sets of molecular orbitals indicate that S—O bonds in sulfamide are the result of a σ-type interaction between the corresponding atomic orbitals of oxygen and sulfur and π-type delocalizations involving the oxygen lone pairs and linear combinations of *p* and *d* orbitals of sulfur. These π interactions have been schematically depicted in Fig. 5. In the first case the interaction involves the out-of-phase combination of the oxygen lone pairs (LPO^-) and the in-phase combination ($p_x + d_{xz}$) of sulfur. In the third, the LPO^- combination interacts with the d_{xy} atomic orbital of sulfur and in the second the interaction involves the in-phase combination of the oxygen lone pairs (LPO^+) and the ($d_{3z^2-r^2} - 2p_z$) combination of sulfur AO's. The picture obtained from the corresponding localized MO's is consistent with the previous one. The S—O bonds appear as the result of a σ-type S—O interaction and $p\pi-d\pi$ delocalizations involving three lone pairs (one lying in the SO_2 plane and two perpendicular to it) of oxygen and the *d* orbitals of S (see Scheme 2).

Therefore we cannot strictly speak of an S—O double bond in sulfamide, since the π-type bond one would expect between the oxygen *p* orbital lying in the SO_2 plane and the orbitals on S is practically identical in nature to the $p\pi-d\pi$ backbonding type involving the oxygen lone pairs that lie out of this plane. In

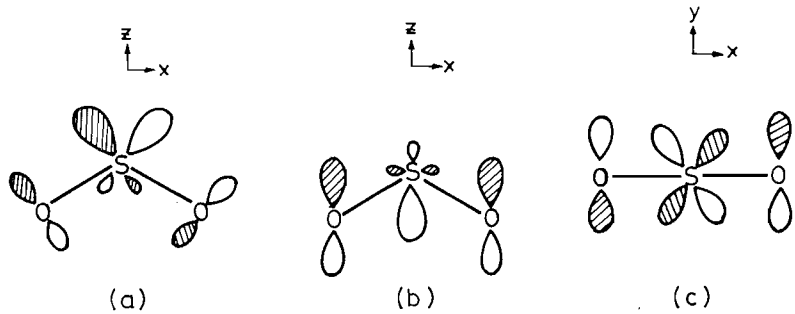
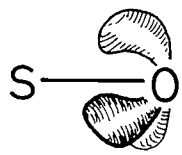


FIG. 5. Schematic representation of the interactions between the oxygen lone pairs and the $p + d$ orbitals of sulfur. (a) Interaction between the LPO^- on oxygen and the $(p_x + d_{xz})$ combination on sulfur. (b) Interaction between the LPO^+ and the $(d_{3x^2-r^2} + p_z)$ on sulfur. (c) Interaction between the LPO^- and the d_{xy} atomic orbital of sulfur.



SCHEME 2

summary, oxygen practically retains three lone pairs and it is their polarization toward the S ($p\pi-d\pi$ backbonding) that is largely responsible for the multiple bond character of the S—O linkage, similar to what has been discussed by Hehre *et al.* (35) for the particular case of the P—O bond in trimethylphosphine. The contribution of these MO's, together with the fact that the centroid of charge of the S—O σ bond is very close to the oxygen atom, yields a considerably polar S—O linkage, which is reflected by the atomic populations and by the high dipole moment of the different conformers of sulfamide. Another consequence of the strong depopulation of sulfur is that the nitrogen atoms must satisfy their electronegativity, withdrawing a considerable amount of charge from the amino protons, which explains the acidic character of sulfamide as compared, for instance, with ammonia (1, 36, 37). The strong withdrawing effect of the oxygens of the SO_2 group may be also responsible for the low rotational barrier observed (26) in 4,4-dioxy-4-thia-1-acetyl-1,4-dihydropyridine. As discussed previously, a similar backbonding interaction is found for the nitrogen lone pairs, but this effect is quantitatively much smaller than that observed in the S—O linkages, and the participation of the sulfur *d* orbitals in the corresponding localized MO's is almost negligible.

3.6. Influence of the second set of d *functions on sulfur*

A perusal of Table 3 clearly shows that the inclusion of two sets of *d* functions on S yields a shortening of both the S—N and S—O bonds. Although this effect is greater in the latter (about 0.02 Å), in general these geometrical changes are not important. More significantly, the relative stability of the different isomers and the description of their charge distributions also do not change appreciably, and only a slight decrease of the dipole moment is observed. This latter effect arises from a slight increase (about 0.25 e^-) of the electronic charge on sulfur, which comes from the population of the diffuse *d* components.

It is interesting to notice that the second set of *d* functions plays the role of real polarization functions. It has been frequently claimed that *d* functions on hypervalent sulfur compounds are indeed necessary to portray accurately the multiple bond character of, for instance, S—O linkages. Therefore, to treat first- and second-row atoms on an equal footing it would be necessary to include a second set of *d* functions on sulfur, which would play the role of true polarization functions, i.e., functions that describe the electronic charge distribution in regions away from the nucleus. Our results confirm this picture. As has been found for compounds containing first-row atoms (38), the inclusion of a second set of polarization functions on S yields shorter bonds and increases the electronic population in the S—O and S—N bond regions. This would imply, in principle, that an adequately balanced basis should include two sets of *d* functions on second-row elements if first-row atoms have been conveniently polarized. Nevertheless our results also show that, at least for the case studied here, the effect of a second set of *d* functions on the charge distributions, geometries, and relative stabilities of the different isomers is quite small.

3.7. Performance of smaller basis sets

Let us now briefly consider the results obtained with smaller basis sets, which may be the only possible alternative in treating more complicated systems containing sulfur.

The cheapest basis including *d* functions on sulfur is the STO-3G*. This basis set also predicts **b** as the most stable conformer of sulfamide, but the relative order of stability of the remaining conformers is not well reproduced. More precisely, the STO-3G* basis indicates that **a**, **c**, and **c'** are 4.5, 4.8, and 4.1 kcal/mol less stable than **b**, respectively. This is a consequence of the minimal character of this basis with repect to first-row atoms, which render it not flexible enough to describe the stabilizing interactions between the oxygen lone pairs and the amino protons in conformer **c** and which underestimates the repulsive interaction between these protons in **a**. Similarly, both the rotational and the inversion barriers are also overestimated.

The next alternative, from the economic point of view, is the 3-21G(*) basis set, which is of a split-valence quality, including polarization functions on sulfur. This basis set yields only one stable conformation for sulfamide, in which the nitrogen atoms present a pratically pure sp^2 hybridization. It is well known that an adequate description of the pyramidalization of the amino groups requires the inclusion of polarization functions on the nitrogen (39, 40) but, in the present case, the lack of these functions has an outermost effect. Probably the amino group tends to be practically planar to achieve a more efficient overlap between the diffuse *p* orbitals on nitrogen and the *d* orbitals on sulfur.

In summary, we may conclude that the best alternative for a reliable treatment of large systems would be to carry out single-point calculations at the 3-21G(*) on fully optimized

Can. J. Chem. Downloaded from www.nrcresearchpress.com by 186.148.149.217 on 09/07/12
For personal use only.

STO-3G* structures, since, as mentioned above, the latter reproduces reasonably well the most important structural features obtained at the 6-31G* level, and the former corrects some of the aforementioned deficiencies of a minimal basis, so that conclusions will be at least qualitatively valid.

4. Concluding remarks

As mentioned in the Introduction, and although sulfamide itself is devoid of relevant biological properties, it constitutes a suitable benchmark case to thoroughly study the characteristics of the >N—SO_2—N< group present in many compounds with well-known activities. This study provides valuable information for the future analysis of structure–activity relationships of hypoglycemic sulfamylureas (44, 45), and, in particular, of herbicidal 2,1,3-benzothiadiazin-4-one 1,1-dioxides and 1,2,4,6-thiatriazine 1,1-dioxides (2). A further step will be the study of the related >N-C_6H_4-SO_2-N< and >N-C_6H_4-SO_2-C_6H_4-N< groups, present in antibacterial and in antileprotic sulfanilamides, respectively (46).

From the results discussed in this paper we can conclude that, under normal conditions, sulfamide may be present in the gas phase as a mixture of conformers **b** and **c'**. However, since the dipole moments of the different stable conformations are very different, the most polar one (conformation **a**) may be favored in condensed media or in polar-solvent solutions.

Internal rotational barriers of sulfamide are lower than in formamide, and similar to those predicted for glycine. However, they are higher than those calculated for sulfuric acid, corresponding to S—OH rotations (41–43), probably because in sulfamide they are mainly due to the electrostatic repulsions between the protons of the two amino groups. The barriers to nitrogen inversion are quite low, because the energy of the system is not very sensitive to the degree of pyramidalization of the amino groups.

The relative stability of the different conformers depends essentially on interactions between the amino protons and between the nitrogen lone pairs. The latter are made evident by the different ordering of the highest occupied MO's of the different isomers.

Our results show that although the π-type delocalization of the oxygen lone pairs into the *d*-orbitals of sulfur is quite significant, and this $p\pi-d\pi$ backbonding interaction is responsible for the multiple bond character of the S—O linkages, similar effects involving the N lone pairs are very weak.

From a more technical point of view, it should be remarked that the inclusion of a second set of *d* functions on sulfur does not alter significantly the results obtained when only one set of polarization functions are included in the basis. More importantly, the 3-21G$^{(*)}$ basis predicts practically planar amino groups with the result that, at this level of accuracy, only one nuclear conformation is predicted to be stable.

Acknowledgements

This research has been partially supported by the D.G.I.C.Y.T. Project No. PB87-0131.

1. G. A. Benson and W. J. Spillane. Chem. Rev. **80**, 151 (1980).
2. V. J. Arán, P. Goya, and C. Ochoa. Adv. Heterocycl. Chem. **44**, 81 (1989).
3. L. Radom, W. A. Latham, W. J. Hehre, and J. A. Pople. Aust. J. Chem. **25**, 1601 (1972).
4. S. T. Elbert and E. R. Davidson. Int. J. Quant. Chem. **8**, 857 (1974).
5. Y. Orita and B. Pullman. Theor. Chim. Acta, **45**, 257 (1977).
6. C. Van Alsenoy, J. O. Williams, and L. Schäfer. J. Mol. Struct. (Theochem), **76**, 179 (1981).
7. J. G. Angyan, C. Bonnelle, R. Daudel, A. Kucsman, and I. G. Csizmadia. J. Mol. Struct. (Theochem), **165**, 273 (1988).
8. S. H. Boys. *In* Quantum theory of atoms, molecules and solid state. *Edited by* P. O. Löwdin. Academic Press, New York. 1966. p. 263.
9. B. Roos and P. Siegbahn. Theor. Chim. Acta, **21**, 368 (1971).
10. M. M. Francl, W. J. Pietro, W. J. Hehre, J. S. Binkley, M. S. Gordon, D. J. De Frees, and J. A. Pople. J. Chem. Phys. **77**, 3654 (1982).
11. R. A. Poirier, R. Daudel, P. G. Mezey, and I. G. Csizmadia. Int. J. Quant. Chem. **21**, 799 (1982).
12. P. G. Mezey and E. C. Haas. J. Chem. Phys. **77**, 870 (1982); J. Comput. Chem. **4**, 482 (1983).
13. E. Magnusson. J. Comput. Chem. **5**, 612 (1984).
14. A. Strömberg, U. Wahlgren, L. Petterson, and P. E. M. Siegbahn. Chem. Phys. **89**, 323 (1984).
15. D. W. J. Cruickshank and M. Eisenstein. J. Mol. Struct. **130**, 143 (1985).
16. M. Ohsaku and A. Imamura. Mol. Phys. **55**, 331 (1985).
17. M. Honda and M. Tajima. J. Mol. Struct. (Theochem), **136**, 93 (1986).
18. J. B. Collins, P. v. R. Schleyer, J. S. Binkley, and J. A. Pople. J. Chem. Phys. **64**, 5142 (1976).
19. W. J. Pietro, M. M. Francl, W. J. Hehre, D. J. DeFrees, J. A. Pople, and J. S. Binkley. J. Am. Chem. Soc. **104**, 5039 (1982).
20. J. S. Binkley, R. A. Witheside, R. Krishna, R. Seeger, D. J. DeFrees, H. B. Schlegel, S. Topiol, L. R. Kahn, and J. A. Pople. Program Gaussian-80. Department of Chemistry, Carnegie Mellon University, Pittsburgh, PA.
21. B. A. Murtagh and R. W. H. Sargent. Comput. J. **131**, 185 (1972).
22. P. E. M. Siegbahn, M. Yoshimine, and J. Pacansky. J. Chem. Phys. **78**, 1384 (1983).
23. A. Yadav, P. S. Surján, and R. A. Poirier. J. Mol. Struct. (Theochem), **165**, 297 (1988).
24. P. G. Jasien, W. J. Stevens, and M. Krauss. J. Mol. Struct. (Theochem), **139**, 197 (1986), and references therein.
25. S. Vishveshwara and J. A. Pople. J. Am. Chem. Soc. **99**, 2422 (1977).
26. G. Fraenkel, A. Chow, J. Gallucci, S. Q. A. Rizvi, S. C. Wong, and H. Finkelstein. J. Am. Chem. Soc. **108**, 5339 (1986).
27. F. Belaj, C. Kratky, E. Nachbaur, and A. Popitsch. Monatsh. Chem. **118**, 427 (1987).
28. C. Ehrhardt and R. Ahlrichs. Chem. Phys. **103**, 429 (1986).
29. G. Devoto. Gazz. Chim. Ital. **63**, 495 (1933).
30. K. B. Wiberg and K. E. Laidig. J. Am. Chem. Soc. **109**, 5935 (1987), and references therein.
31. F. A. L. Anet, R. D. Trepka, and D. J. Cram. J. Am. Chem. Soc. **89**, 357 (1967).
32. W. N. Speckamp, U. K. Pandit, P. K. Korver, P. J. van der Haak, and H. O. Huisman. Tetrahedron, **22**, 2413 (1966).
33. A. Rauk, L. C. Allen, and K. Mislow. Angew. Chem. Int. Ed. Engl. **9**, 400 (1970).
34. J. Elguero, P. Goya, I. Rozas, J. Catalán, and J. L. G. de Paz. J. Mol. Struct. (Theochem), **184**, 115 (1989).
35. W. J. Hehre, L. Radom, P. v. R. Schleyer, and J. A. Pople. *In* Ab initio molecular orbital theory. John Wiley & Sons, New York. 1986. p. 84.
36. P. O. Burke, S. D. McDermott, T. J. Hannigan, and W. J. Spillane. J. Chem. Soc. Perkin Trans, 2, 1851 (1984).
37. M. H. Palmer, I. Simpson, and J. R. Wheeler. Z. Naturforsch. Teil A: Phys. Phys. Chem. Kosmophys. **36A**, 1246 (1981).
38. J. L. G. de Paz and M. Yáñez. J. Mol. Stuct. (Theochem), **107**, 59 (1984).

Can. J. Chem. Downloaded from www.nrcresearchpress.com by 186.148.149.217 on 09/07/12
For personal use only.

39. J. E. BOGGS and Z. NIU. J. Comput. Chem. **6**, 46 (1985).
40. M. ALCAMÍ, J. L. G. DE PAZ, and M. YÁÑEZ. J. Comput. Chem. **10**, 468 (1989).
41. P. KALIANNAN, S. VISHVESHWARA, and V. S. R. RAO. J. Mol. Struct. (Theochem), **92**, 7 (1983).
42. T. S. CHEN and P. L. M. PLUMMER. J. Phys. Chem. **89**, 3689 (1985).
43. G. LOWE, G. R. J. THATCHER, J. C. G. TURNER, A. WALLER, and D. J. WATKIN. J. Am. Chem. Soc. **110**, 8512 (1988).
44. E. H. WISEMAN, J. N. PEREIRA, K. F. FINGER, and R. PINSON, JR. J. Med. Chem. **8**, 777 (1965).
45. R. SARGES, D. E. KUHLA, H. E. WIDERMANN, and D. A. MAYHEW. J. Med. Chem. **19**, 695 (1976).
46. N. ANAND. Sulfonamides and sulfones. *In* Burger's medical chemistry. Part II. *Edited by* M. E. Wolff. John Wiley & Sons, New York. 1979. p. 1.

Can. J. Chem. Downloaded from www.nrcresearchpress.com by 186.148.149.217 on 09/07/12
For personal use only.

An approach to the synthesis of bruceantin. The synthesis of a tetracyclic intermediate

SULTAN DARVESH, ANDREW S. GRANT, DAVID I. MAGEE, AND ZDENEK VALENTA
Department of Chemistry, University of New Brunswick, Bag Service no. 45222, Fredericton, N.B., Canada E3B 6E2

Received August 15, 1988[1]

SULTAN DARVESH, ANDREW S. GRANT, DAVID I. MAGEE, and ZDENEK VALENTA. Can. J. Chem. **67**, 2237 (1989).

An intermediate (**20**) containing four of the five rings and seven of the ten chiral centers of bruceantin (**1**) was prepared. In a key reaction, 3-iodo-1-trimethylsilyl-5-hexen-1-yne (**9**) was found to add chemoselectively and stereoselectively to a dianion. The sequence also includes a selective attack by a sulfinate (**17**) on the terminal acetylene C-atom of the dianion of a keto acetylene, a concomitant cyclization in which the acetylene acts as an electrophile, and the use of the resulting allyl sulfoxide for the introduction of oxygen functionality by a reductive rearrangement.

Key words: bruceantin, sigmatropic rearrangement, stereoselective alkylation.

SULTAN DARVESH, ANDREW S. GRANT, DAVID I. MAGEE et ZDENEK VALENTA. Can. J. Chem. **67**, 2237 (1989).

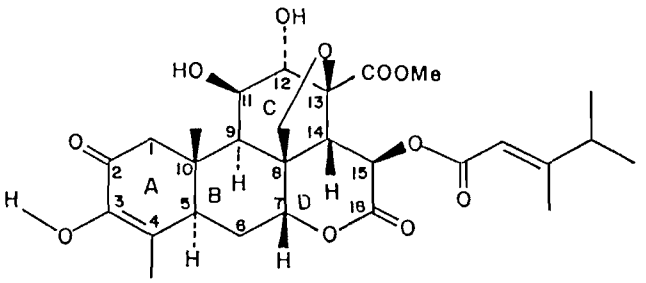
On a préparé un intermédiaire (**20**) contenant quatre des cinq cycles et sept des dix centres chiraux de la brucéantine (**1**). Dans une réaction clé, on a observé que le 3-iodo-1-triméthylsilylhex-5-ène-1-yne (**9**) s'additionne à un dianion d'une façon qui est à la fois chimiquement et stéréochimiquement sélective. La séquence comporte aussi une attaque sélective d'un sulfinate (**17**) sur l'atome de carbone terminal de l'acétylène du dianion d'un céto-acétylène qui est accompagnée d'une cyclisation concomitante au cours de laquelle l'acétylène agit comme un électrophile, et l'utilisation du sulfoxyde allylique qui en résulte pour l'introduction, par le biais d'une transposition réductive, d'une fonction oxygénée.

Mots clés : brucéantine, transposition sigmatropique, alkylation stéréosélective.

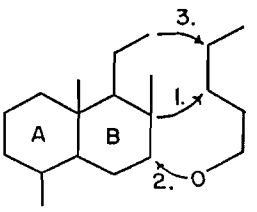
[Traduit par la revue]

Structural diversity (1), biological activity (2), and synthetically challenging functionality have recently made the quassinoids frequent targets for total synthesis (3). We wish to report an exceptionally selective alkylation and the development of an efficient cyclization–O-functionalization sequence in a synthetic approach to the natural quassinoid bruceantin (**1**). The overall strategy is shown in the structural formula **2** in which the three arrows point towards the electrophilic centers and the numbers indicate the order in which the bonds were formed.

The necessary A,B-ring intermediate **8** was readily prepared from 2-methylcyclohexane-1,3-dione as shown in Scheme 1.[2] Addition of HCN to the selectively blocked diene dione **7**, mp 148–150°C, gave a chromatographically separable mixture of cyanoketones **8***a*, mp 163–167°C and 192–197°C (C_{10}-methyl ^{1}H nmr signal at δ 1.47), and **8***b*, mp 182–183°C (C_{10}-methyl signal at δ 1.10) in a varying ratio.[3] Treatment of **8***a* + **8***b* with 2.2 equivalents of lithium pyrrolidide[4] followed by a reaction with 1.2 equivalents of iodide **9**[5] gave the alkylated product **10**.[3] Figure 1 suggests a possible arrangement of the two reacting species to explain the observed enantioselectivity (C_{14} in **10**). This is supported by the X-ray study, which shows the side chain in **10** to be in a conformation similar to that shown in Fig. 1.



1



2

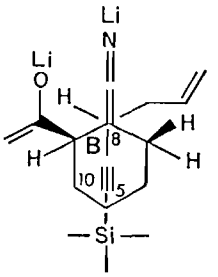


FIG. 1

[1]Revision received July 17, 1989.

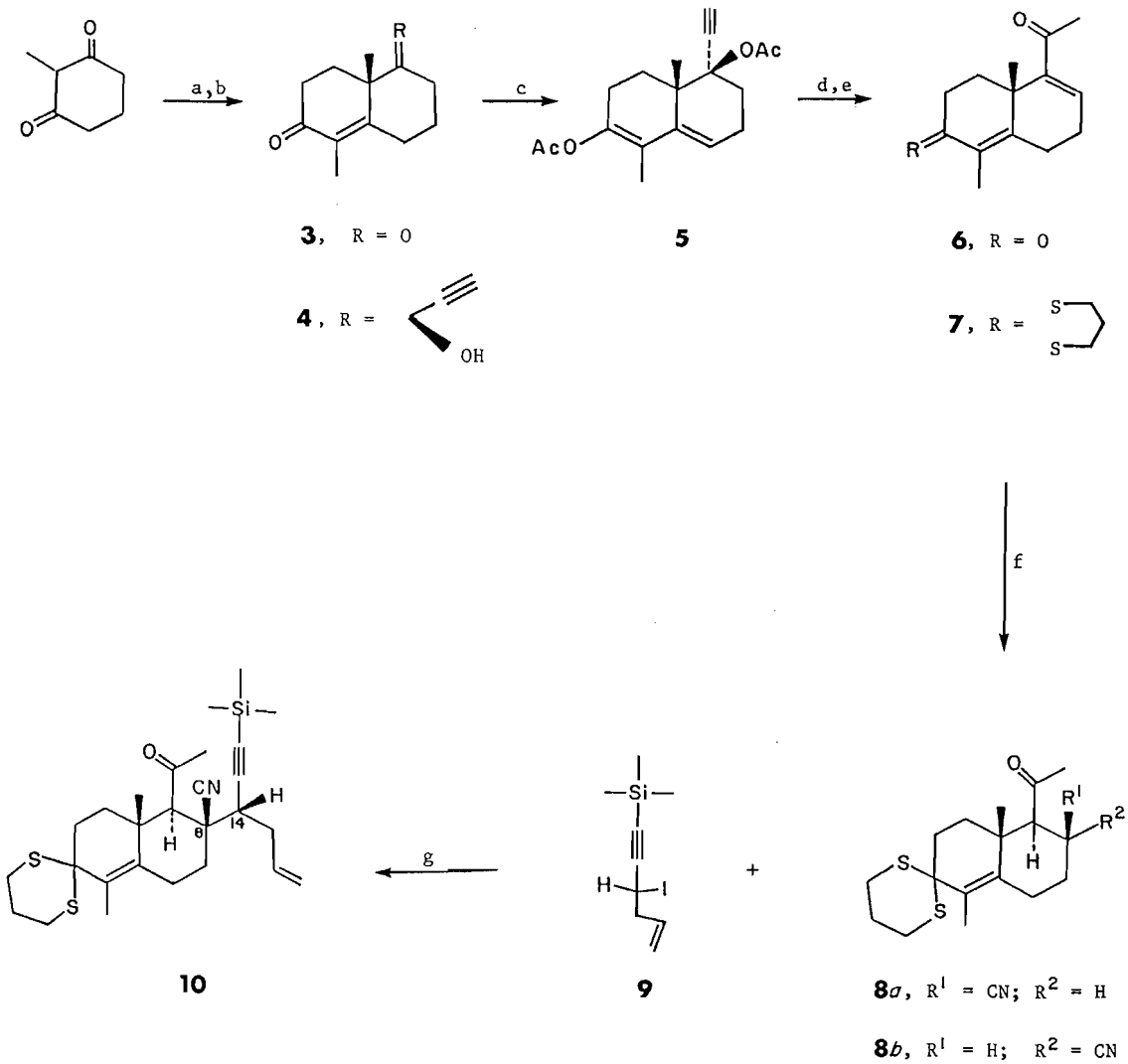
[2]All compounds described here are racemic. Enantiomerically pure compounds should be readily available using known methods (4).

[3]The structures of **8***a* and **10** were determined by X-ray analysis by Dr. Peter S. White of this department.

[4]This base, rather than a more conventional hindered base was used because it alone achieved an efficient dianion formation from both epimers of **8**. The resulting pyrrolidine did not react with **9** under the reaction conditions.

[5]**9** was prepared most conveniently in a seven-step sequence (32% overall yield) from propargyl alcohol via its THP derivative, silylation, hydrolysis of THP-ether, oxidation with pyridinium dichromate, allyl-Grignard reaction, mesylation, and displacement by I^-.

Can. J. Chem. Downloaded from www.nrcresearchpress.com by 186.148.149.217 on 09/07/12
For personal use only.



(a) Ethyl vinyl ketone, KOH, MeOH, 65°C, 3 h; pyrrolidine, C_6H_6, 80°C, 30 h (71%) (ref. 5); (b) LiC≡CH, liq. NH_3, 1 h (87%) (ref. 6); (c) Ac_2O, *p*-TSA, 20°C, 16 h (91%) (ref. 6); (d) 90% HCOOH, reflux, 2 h (68%) (ref. 6); (e) $HSCH_2CH_2CH_2SH$, $BF_3.Et_2O$, Et_2O, 20°C, 18 h (82%); (f) KCN, NH_4Cl, DMF–H_2O, 80°C, 16 h (77%); (g) Li pyrrolidide, THF, −78°C, 2 h; **9**, −78°C, 1 h (93%).

SCHEME 1

Intermediate **10** contains all the C-atoms necessary for the construction of the bruceantin skeleton, but the preferred conformation of the side chain attached to C_8 is not suited for the closing of rings C and D. Since the construction of one of these rings starting from **10** would establish the (rigid) geometry necessary for the closure of the other ring, and since the conversion of the keto acetylene moiety of **10** into ring C appeared more problematic, it was decided to construct ring D first. Scheme 2 shows the 9-step conversion of **10** to the required tricyclic intermediate **16**, mp 180–183°C. The chemoselective oxidation of **11** led to the diol mixture **12***a* + **12***b*, which was used without separation in the next three steps. Separation of the two C_{16} isomers at stage **15** on SiO_2 then showed a 6:1 ratio with the ether formed from **12***a* (and drawn in formulae **13** → **16**) predominating.[6] A very large excess of 1,3-propane diol (60 equiv.) and *p*-toluenesulfonic acid (30 equiv.) was required to achieve the cyclization **12** → **13**.[7] The C_7 configuration in **13** follows from the ^{1}H nmr spectrum (1H, t, J = 4 Hz at δ 4.21).

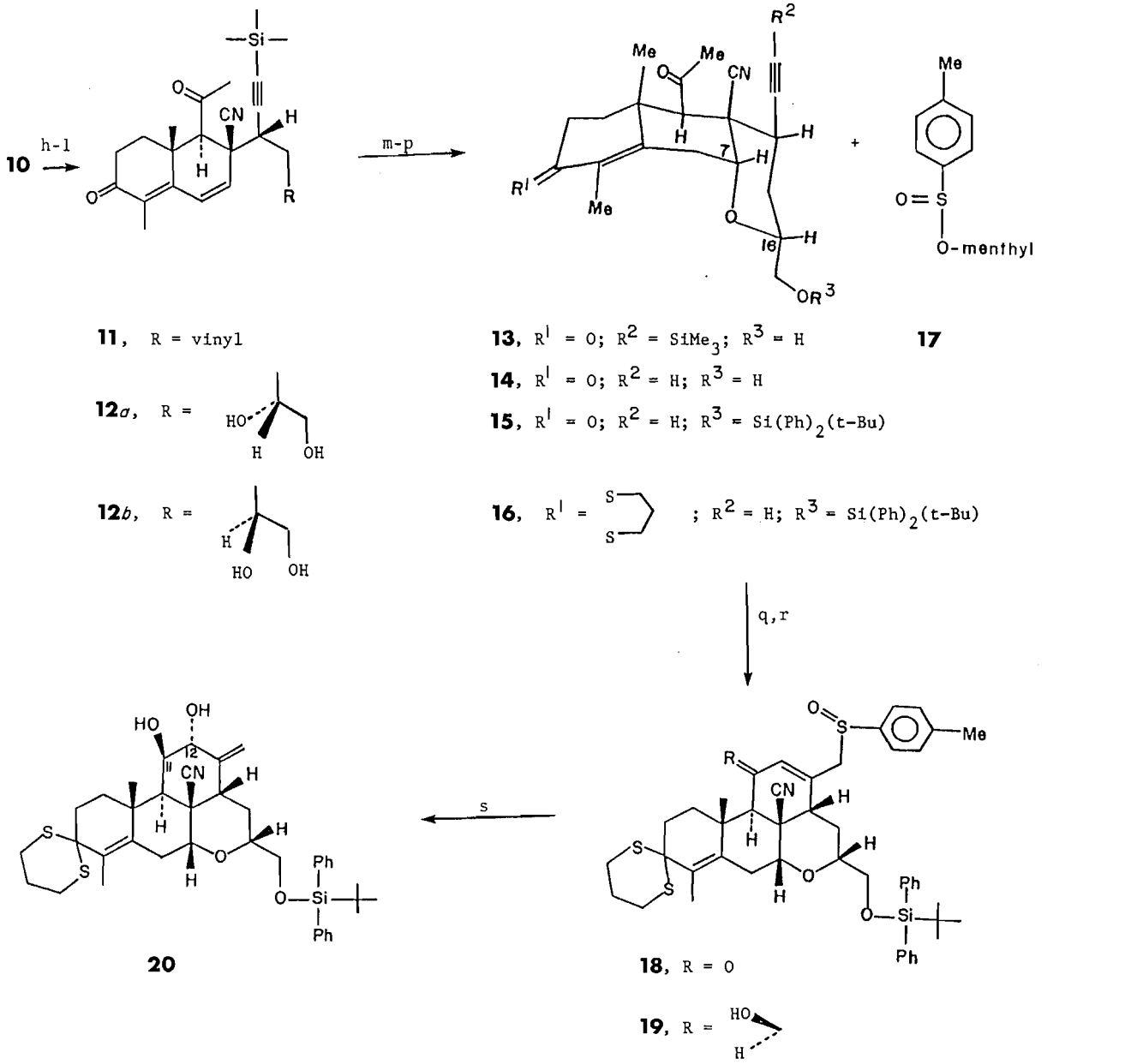
To cyclize ring C, it was decided to render the acetylene group in **16** electrophilic and to provide, at the same time, for the subsequent introduction of the required O-functionality. Reaction of the dianion of **16** with **17**[8] gave the enone sulfoxide **18**[8] (ir ν_{max} 1680 cm^{-1}, uv λ_{max} 247 nm, (basic) 369 nm). Reduction of **18** with $LiBH_4$ then gave the axial alcohol **19**. For a good yield, it proved essential to achieve a fast reaction by using a large excess of $LiBH_4$ (40 equiv.) and by adding MeOH (1 part) to THF (10 parts) (8, 9). Finally, the two (sulfoxide)

[6]All subsequent reactions described here have been performed with the pure major isomer. The ^{1}H nmr data show that the C_{16}-H atom in this isomer is axial.

[7]This is a heterogeneous reaction (droplets of 1,3-propane diol in benzene) and it is assumed that protonated 1,3-propane diol exerts a specific protonation–deprotonation action at the interface. The acetal of **12** or **13** does not form even at 80°C.

[8](−)-Menthol, used for the preparation of **17** (7), or isopropanol proved convenient secondary alcohols. A reaction with the corresponding methyl ester proved unsatisfactory. The two sulfoxide diastereoisomers of **18** were formed in roughly equal quantities in all cases (^{1}H nmr signals for C_{12}-H at δ 5.54 and 5.62).

Can. J. Chem. Downloaded from www.nrcresearchpress.com by 186.148.149.217 on 09/07/12
For personal use only.



(h) HgO, H_2SO_4, THF, 40°C, 4 h (100%) (ref. 12); (i) $HC(OEt)_3$, *p*-TSA, C_6H_6, 20°C, 1 h (89%) (ref. 13); (j) $C_5H_6N^+Br_3^-$, THF–H_2O, 20°C, 20 min (88%); (k) DBN, THF, 20°C, 20 min (78%); (l) *N*-methylmorpholine oxide, OsO_4, *tert*-butanol–THF–H_2O, 20°C, 24 h (84%) (ref. 14); (m) $HOCH_2CH_2CH_2OH$, *p*-TSA, C_6H_6, 40°C, 4 h (80%); (n) $N^+(butyl)_4Cl^-$, KF, CH_3CN, 20°C, 1 h (100%) (ref. 15); (o) $ClSi(Ph)_2t$-butyl, imidazole, DMF, 20°C, 12 h (84%) (ref. 16); (p) $HSCH_2CH_2CH_2SH$, $BF_3.Et_2O$, Et_2O, THF, 20°C, 3 h (96%); (q) *n*-BuLi (3 equiv.), THF, −78°C, 15 min; **17** (1.8 equiv.), −78°C to 20°C, 5 h (81%); (r) $LiBH_4$, THF, MeOH, 20°C, 20 min (77%); (s) $P(OEt)_3$, EtOH, 40°C, 120 h (75% for **19***a*).

SCHEME 2

diastereoisomers of **19** proved separable on SiO_2. One of them, **19***a*, rearranged, on treatment with triethyl phosphite (10) in EtOH at 40°C for 5 days, to diol **20** in 75% yield,[9] while the other, **19***b*, did not react under these conditions. However, similar treatment of **19***b* at 75°C for 48 h gave a cyclic imino ether (C_{11}-OH in **20** adding to CN) (ir ν_{max} 1700 cm^{-1}, no —CN) in 75% yield, while heating of **20** in EtOH at 75°C resulted in its conversion to the same imino ether. This proves that the C_{11}-OH in **19** and **20** is axial and shows that the sigmatropic rearrangement of the two diastereoisomers of **19** proceeds from the same face of ring C, but at a different rate.[9]

The overall yield of the 18-step sequence 2-methylcyclohexane-1,3-dione → **19** is 4% and the average yield per step is 84%. Further synthetic elaboration of **20** and the general utility of the sequence **16** → **18** → **20** are under active study.

[9]The configurational assignment at C_{12} in **20** is based on a strong nOe (10% enhancement) between C_{12}-H (δ 4.18) and $=CH_2$ (δ 5.26 and 5.32), on a presumed preference for an axial attack of the ring C quasi-chair (11) in both rearrangements and on models that show that the *p*-tolyl group in one of the diastereoisomers of **19** presents a hindrance to the rearrangement proceeding at the α-face.

Can. J. Chem. Downloaded from www.nrcresearchpress.com by 186.148.149.217 on 09/07/12
For personal use only.

Acknowledgements

Financial support by the Natural Sciences and Engineering Research Council of Canada in the form of operating grants and a graduate fellowship (D.I.M.) and by the Terry Fox Grant Fund of New Brunswick is gratefully acknowledged. We thank Dr. Žarko Stojanac of this Department for suggesting the strategic concept illustrated by the first step in formula **2**.

1. J. POLONSKY. Prog. Chem. Org. Nat. Prod. **30**, 102 (1973); Fortschr. Chem. Org. Naturst. **47**, 221 (1985).
2. M. S. KUPCHAN, J. A. LACADIE, G. A. HOWIE, and B. R. SICKLES. J. Med. Chem. **19**, 1130 (1976); L. LIAO, M. S. KUPCHAN, and S. B. HOROWITZ. Mol. Pharmacol. **12**, 167 (1976); M. E. WALL and M. C. WANI. J. Med. Chem. **21**, 1186 (1978); J. M. CASSADY and M. SUFFNESS. Med. Chem. (Academic Press), **16**, 201 (1980); Y. F. LIOU, I. H. HALL, M. OKANO, K. H. LEE, and S. G. CHANEY. J. Pharm. Sci. **71**, 430 (1982); J. POLONSKY. *In* The chemistry and biological activity of the rutales. *Edited by* P. G. Waterman and M. F. Grundon. Academic Press, New York. 1983. p. 247.
3. M. VOYLE, N. K. DUNLAP, D. S. WATT, and O. P. ANDERSON. J. Org. Chem. **48**, 3242 (1983); R. J. PARIZA and P. L. FUCHS. J. Org. Chem. **48**, 2306 (1983); D. D. WELLER and E. P. STIRCHAK. J. Org. Chem. **48**, 4873 (1983); C. H. HEATHCOCK, C. MAHAIM, M. F. SCHLECHT, and T. UTAWAINT. J. Org. Chem. **49**, 3264 (1984); D. G. BATT, N. TAKAMURA, and B. GANEM. J. Am. Chem. Soc. **106**, 3353 (1984); K. SHISIKO, T. SAITOH, K. FUKUMOTO, and T. KAMETANI. J. Chem. Soc. Perkin Trans. 1, 2139 (1984); P. A. GRIECO, G. VIDARI, and S. FERRINO. J. Am. Chem. Soc. **106**, 3539 (1984); F. E. ZIEGLER, S. I. KLEIN, U. K. PATI, and T.-F. WANG. J. Am. Chem. Soc. **107**, 2733 (1985); S. SASAKI, P. A. GRIECO, J. C. HUFFMAN, P. GALLANT, and P. M. IMAMURA. J. Org. Chem. **50**, 4880 (1985); R. H. SCHLESSINGER, J.-W. WONG, M. A. ROSS, and J. P. SPRINGER. J. ORG. CHEM. **50**, 3951 (1985); R. V. STEVENS and A. P. VINOGRADOFF. J. Org. Chem. **50**, 4056 (1985); B. A. MCKITTRICK and B. GANEM. J. Org. Chem. **50**, 5897 (1985); S. N. SURYAWANSHI and P. L. FUCHS. J. Org. Chem. **51**, 902 (1986); T. MURAE, M. SASAKI, T. KONOSU, H. MATSAO, and T. TAKAHASI. Tetrahedron Lett. 3411 (1986); G. A. KRAUS and M. F. KROLSKI. J. Org. Chem. **51**, 3347 (1986); R. V. STEVENS, S. R. ANGLE, K. KLOC, K. F. MAK, K. N. TRUEBLOOD, and Y.-X. LIU. J. Org. Chem. **51**, 4347 (1986); F. E. ZIEGLER, K.-J. HWANG, J. F. KADOW, S. I. KLEIN, U. K. PATI, and T.-F. WANG. J. Org. Chem. **51**, 4573 (1986); F. KUO and P. L. FUCHS. J. Am. Chem. Soc. **109**, 1122 (1987); S. M. KERWIN, A. G. PAUL, and C. H. HEATHCOCK. J. Org. Chem. **52**, 1686 (1987); T. KAWABATA, P. A. GRIECO, H.-L. SHAM, H. KIM, J. H. JAW, and S. TU. J. Org. Chem. **52**, 3346 (1987); K. SHISHIDO, K. TAKASHASHI, and K. FULUMOTO. J. Org. Chem. **52**, 5704 (1987); P. A. GRIECO, J. INANAGA, H.-L. SHAM, S. SASAKI, and H. KIM. Chem. Commun. 1044 (1987); M. KIM, R. S. GROSS, H. SEVESTRE, N. K. DUNLAP, and D. S. WATT. J. Org. Chem. **53**, 93 (1988).
4. U. EDER, G. SAUER, and R. WIECHERT. Angew. Chem. Int. Ed. Engl. **10**, 496 (1971); Z. G. HAJOS and D. R. PARRISH. J. Org. Chem. **39**, 1615 (1974); J. GUTZWILLER, P. BUCHSCHACHER, and A. FURST. Synthesis, 167 (1977).
5. A. B. MEKLER, S. RAMACHANDRAN, S. SWAMINATHAN, and M. S. NEWMAN. Org. Synth. **41**, 56 (1961).
6. M. S. NEWMAN, S. RAMACHANDRAN, S. K. SANKARAPPA, and S. SWAMINATHAN. J. Org. Chem. **26**, 727 (1961).
7. G. SOLLADIÉ. Synthesis, 185 (1981).
8. H. C. BROWN and S. NARASIMHAN. J. Org. Chem. **47**, 1606 (1982).
9. K. SOAI and A. OOKAWA. J. Org. Chem. **51**, 4000 (1986).
10. D. A. EVANS and G. C. ANDREWS. Acc. Chem. Res. **7**, 147 (1974); D. A. EVANS, G. C. ANDREWS, T. T. FUJIMOTO, and D. WELLS. Tetrahedron Lett. 1385 (1973); R. D. GARIGIPATI and S. M. WEINREB. J. Am. Chem. Soc. **105**, 4499 (1983).
11. R. W. HOFFMANN, R. GERLACH, and S. GOLDMANN. Tetrahedron Lett. 2599 (1978).
12. E. J. COREY and B. W. ERICKSON. J. Org. Chem. **36**, 3533 (1971).
13. H. H. INHOFFEN, G. KÖLLING, G. KOCH, and I. NEBEL. Chem. Ber. **84**, 361 (1951).
14. V. VAN RHEENEN, R. C. KELLY, and D. Y. CHU. Tetrahedron Lett. 1973 (1976).
15. L. A. CARPINO and A. C. SAU. Chem. Commun. 514 (1979).
16. S. HANESSIAN and P. LAVALÉE. Can. J. Chem. **53**, 2975 (1975).

Can. J. Chem. Downloaded from www.nrcresearchpress.com by 186.148.149.217 on 09/07/12
For personal use only.

Total synthesis of 12-*O*-benzoyl-6,7,14,15-tetradehydro leukotriene B_4 methyl ester: precursor of labeled LTB_4

RENÉE PONTIKIS, LALATIANA R. RANDRIANASOLO, YVES LE MERRER, NGUYEN HOANG NAM, ROBERT AZERAD, AND JEAN-CLAUDE DEPEZAY

Laboratoire de chimie et biochimie pharmacologiques et toxicologiques, Institut national de la santé et de la recherche médicale—Centre national de la recherche scientifique (Unité associée 400), Université René Descartes, 45 rue des Saints Pères, 75270 Paris CEDEX 06, France

Received July 24, 1989

RENÉE PONTIKIS, LALATIANA R. RANDRIANASOLO, YVES LE MERRER, NGUYEN HOANG NAM, ROBERT AZERAD, and JEAN-CLAUDE DEPEZAY. Can. J. Chem. **67**, 2240 (1989).

12-*O*-Benzoyl-6,7,14,15-tetradehydroleukotriene B_4 methyl ester **1**, the direct precursor of isotopically labeled LTB_4's, has been prepared. This synthesis was accomplished by the assembly of two key chirons: α-hydroxyaldehyde of *R* configuration, **2**, and propargylic alcohol of *S* configuration, (*S*)-**7**. The first was obtained from D-mannitol whereas the second was obtained by enzymatic resolution.

Key words: leukotriene B_4, tetradehydroleukotriene B_4, labeling, chiral α-hydroxyaldehyde, enzymatic resolution.

Printed in Canada / Imprimé au Canada

Acknowledgements

Financial support by the Natural Sciences and Engineering Research Council of Canada in the form of operating grants and a graduate fellowship (D.I.M.) and by the Terry Fox Grant Fund of New Brunswick is gratefully acknowledged. We thank Dr. Žarko Stojanac of this Department for suggesting the strategic concept illustrated by the first step in formula **2**.

1. J. POLONSKY. Prog. Chem. Org. Nat. Prod. **30**, 102 (1973); Fortschr. Chem. Org. Naturst. **47**, 221 (1985).
2. M. S. KUPCHAN, J. A. LACADIE, G. A. HOWIE, and B. R. SICKLES. J. Med. Chem. **19**, 1130 (1976); L. LIAO, M. S. KUPCHAN, and S. B. HOROWITZ. Mol. Pharmacol. **12**, 167 (1976); M. E. WALL and M. C. WANI. J. Med. Chem. **21**, 1186 (1978); J. M. CASSADY and M. SUFFNESS. Med. Chem. (Academic Press), **16**, 201 (1980); Y. F. LIOU, I. H. HALL, M. OKANO, K. H. LEE, and S. G. CHANEY. J. Pharm. Sci. **71**, 430 (1982); J. POLONSKY. *In* The chemistry and biological activity of the rutales. *Edited by* P. G. Waterman and M. F. Grundon. Academic Press, New York. 1983. p. 247.
3. M. VOYLE, N. K. DUNLAP, D. S. WATT, and O. P. ANDERSON. J. Org. Chem. **48**, 3242 (1983); R. J. PARIZA and P. L. FUCHS. J. Org. Chem. **48**, 2306 (1983); D. D. WELLER and E. P. STIRCHAK. J. Org. Chem. **48**, 4873 (1983); C. H. HEATHCOCK, C. MAHAIM, M. F. SCHLECHT, and T. UTAWAINT. J. Org. Chem. **49**, 3264 (1984); D. G. BATT, N. TAKAMURA, and B. GANEM. J. Am. Chem. Soc. **106**, 3353 (1984); K. SHISIKO, T. SAITOH, K. FUKUMOTO, and T. KAMETANI. J. Chem. Soc. Perkin Trans. 1, 2139 (1984); P. A. GRIECO, G. VIDARI, and S. FERRINO. J. Am. Chem. Soc. **106**, 3539 (1984); F. E. ZIEGLER, S. I. KLEIN, U. K. PATI, and T.-F. WANG. J. Am. Chem. Soc. **107**, 2733 (1985); S. SASAKI, P. A. GRIECO, J. C. HUFFMAN, P. GALLANT, and P. M. IMAMURA. J. Org. Chem. **50**, 4880 (1985); R. H. SCHLESSINGER, J.-W. WONG, M. A. ROSS, and J. P. SPRINGER. J. ORG. CHEM. **50**, 3951 (1985); R. V. STEVENS and A. P. VINOGRADOFF. J. Org. Chem. **50**, 4056 (1985); B. A. MCKITTRICK and B. GANEM. J. Org. Chem. **50**, 5897 (1985); S. N. SURYAWANSHI and P. L. FUCHS. J. Org. Chem. **51**, 902 (1986); T. MURAE, M. SASAKI, T. KONOSU, H. MATSAO, and T. TAKAHASI. Tetrahedron Lett. 3411 (1986); G. A. KRAUS and M. F. KROLSKI. J. Org. Chem. **51**, 3347 (1986); R. V. STEVENS, S. R. ANGLE, K. KLOC, K. F. MAK, K. N. TRUEBLOOD, and Y.-X. LIU. J. Org. Chem. **51**, 4347 (1986); F. E. ZIEGLER, K.-J. HWANG, J. F. KADOW, S. I. KLEIN, U. K. PATI, and T.-F. WANG. J. Org. Chem. **51**, 4573 (1986); F. KUO and P. L. FUCHS. J. Am. Chem. Soc. **109**, 1122 (1987); S. M. KERWIN, A. G. PAUL, and C. H. HEATHCOCK. J. Org. Chem. **52**, 1686 (1987); T. KAWABATA, P. A. GRIECO, H.-L. SHAM, H. KIM, J. H. JAW, and S. TU. J. Org. Chem. **52**, 3346 (1987); K. SHISHIDO, K. TAKASHASHI, and K. FULUMOTO. J. Org. Chem. **52**, 5704 (1987); P. A. GRIECO, J. INANAGA, H.-L. SHAM, S. SASAKI, and H. KIM. Chem. Commun. 1044 (1987); M. KIM, R. S. GROSS, H. SEVESTRE, N. K. DUNLAP, and D. S. WATT. J. Org. Chem. **53**, 93 (1988).
4. U. EDER, G. SAUER, and R. WIECHERT. Angew. Chem. Int. Ed. Engl. **10**, 496 (1971); Z. G. HAJOS and D. R. PARRISH. J. Org. Chem. **39**, 1615 (1974); J. GUTZWILLER, P. BUCHSCHACHER, and A. FURST. Synthesis, 167 (1977).
5. A. B. MEKLER, S. RAMACHANDRAN, S. SWAMINATHAN, and M. S. NEWMAN. Org. Synth. **41**, 56 (1961).
6. M. S. NEWMAN, S. RAMACHANDRAN, S. K. SANKARAPPA, and S. SWAMINATHAN. J. Org. Chem. **26**, 727 (1961).
7. G. SOLLADIÉ. Synthesis, 185 (1981).
8. H. C. BROWN and S. NARASIMHAN. J. Org. Chem. **47**, 1606 (1982).
9. K. SOAI and A. OOKAWA. J. Org. Chem. **51**, 4000 (1986).
10. D. A. EVANS and G. C. ANDREWS. Acc. Chem. Res. **7**, 147 (1974); D. A. EVANS, G. C. ANDREWS, T. T. FUJIMOTO, and D. WELLS. Tetrahedron Lett. 1385 (1973); R. D. GARIGIPATI and S. M. WEINREB. J. Am. Chem. Soc. **105**, 4499 (1983).
11. R. W. HOFFMANN, R. GERLACH, and S. GOLDMANN. Tetrahedron Lett. 2599 (1978).
12. E. J. COREY and B. W. ERICKSON. J. Org. Chem. **36**, 3533 (1971).
13. H. H. INHOFFEN, G. KÖLLING, G. KOCH, and I. NEBEL. Chem. Ber. **84**, 361 (1951).
14. V. VAN RHEENEN, R. C. KELLY, and D. Y. CHU. Tetrahedron Lett. 1973 (1976).
15. L. A. CARPINO and A. C. SAU. Chem. Commun. 514 (1979).
16. S. HANESSIAN and P. LAVALÉE. Can. J. Chem. **53**, 2975 (1975).

Can. J. Chem. Downloaded from www.nrcresearchpress.com by 186.148.149.217 on 09/07/12
For personal use only.

Total synthesis of 12-*O*-benzoyl-6,7,14,15-tetradehydro leukotriene B_4 methyl ester: precursor of labeled LTB_4

RENÉE PONTIKIS, LALATIANA R. RANDRIANASOLO, YVES LE MERRER, NGUYEN HOANG NAM, ROBERT AZERAD, AND JEAN-CLAUDE DEPEZAY

Laboratoire de chimie et biochimie pharmacologiques et toxicologiques, Institut national de la santé et de la recherche médicale—Centre national de la recherche scientifique (Unité associée 400), Université René Descartes, 45 rue des Saints Pères, 75270 Paris CEDEX 06, France

Received July 24, 1989

RENÉE PONTIKIS, LALATIANA R. RANDRIANASOLO, YVES LE MERRER, NGUYEN HOANG NAM, ROBERT AZERAD, and JEAN-CLAUDE DEPEZAY. Can. J. Chem. **67**, 2240 (1989).

12-*O*-Benzoyl-6,7,14,15-tetradehydroleukotriene B_4 methyl ester **1**, the direct precursor of isotopically labeled LTB_4's, has been prepared. This synthesis was accomplished by the assembly of two key chirons: α-hydroxyaldehyde of *R* configuration, **2**, and propargylic alcohol of *S* configuration, (*S*)-**7**. The first was obtained from D-mannitol whereas the second was obtained by enzymatic resolution.

Key words: leukotriene B_4, tetradehydroleukotriene B_4, labeling, chiral α-hydroxyaldehyde, enzymatic resolution.

Printed in Canada / Imprimé au Canada

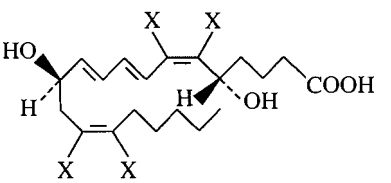
RENÉE PONTIKIS, LALATIANA R. RANDRIANASOLO, YVES LE MERRER, NGUYEN HOANG NAM, ROBERT AZERAD et JEAN-CLAUDE DEPEZAY. Can. J. Chem. **67**, 2240 (1989).

Pour obtenir le leucotriène B_4 radiomarqué par quatre atomes de tritium, la synthèse totale convergente d'un précurseur diacétylénique (ester méthylique du 12-*O*-benzoyl-6,7,14,15-tétradehydroleucotriène B_4 **1**) a été réalisée à partir de deux synthons chiraux : α-hydroxyaldéhyde de configuration *R* **2** et alcool propargylique de configuration *S* **7**. Le premier a été obtenu à partir du D-mannitol, le second par dédoublement enzymatique.

Mots clés : leukotriène B_4, tétradéhydroleukotriène B_4, molécule marquée, α-hydroxyaldéhyde chiral, dédoublement enzymatique.

Leukotriene B_4 (LTB_4), a dihydroxy metabolite of arachidonic acid, is the most potent chemotactic mediator implicated in allergic and inflammatory processes (1). It is metabolized to biologically less active ω-oxidized products, primarily in polymorphonuclear leukocytes but also in liver cells (2–4). To evaluate other possible metabolic pathways and the uptake of LTB_4 in different tissues, a radiolabeled version of this mediator was required. The [14,15-^{3}H]-LTB_4 was prepared by Leblanc *et al.* (5) at a specific activity of 40 Ci/mmol. The availability of a material labeled with four atoms of tritium, which could allow a specific activity of 80–100 Ci/mmol to be attained, prompted us to embark on the synthesis of a suitable precursor: 6,7,14,15-tetradehydro LTB_4 **1**.

At the final synthetic step, selective tritiation of the two acetylenic bonds to *cis* olefins will allow the incorporation of four tritium atoms.



X = H(LTB_4), D or T

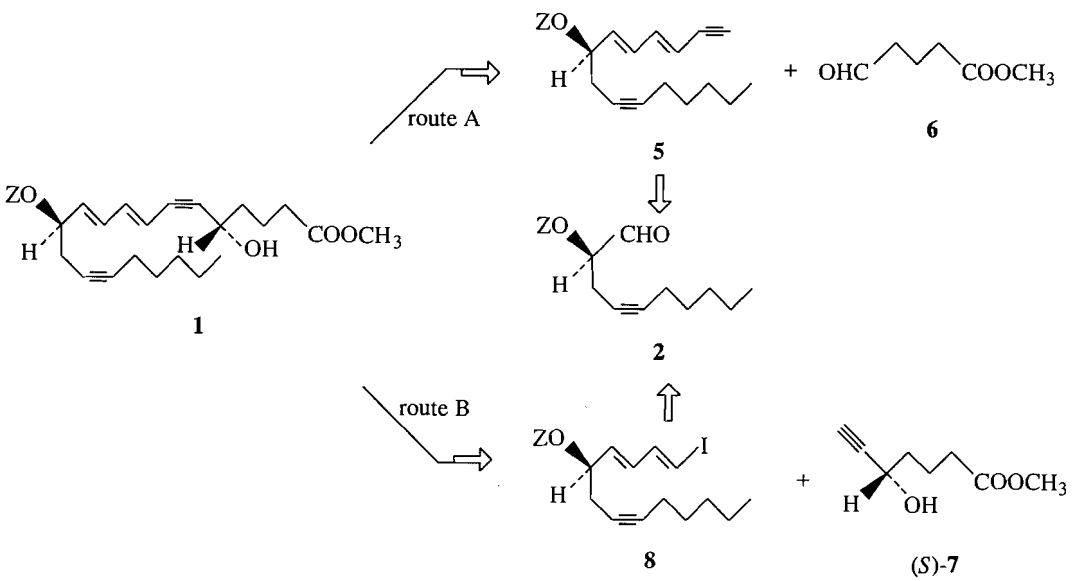
Two retrosynthetic routes could be considered (Scheme 1). Each is based on our method, recently published (6*a*,*b*), of using D-mannitol as a precursor of enantiomerically pure α-hydroxyaldehydes.

Protected (*R*)-α-hydroxyaldehyde **2** was prepared (Scheme 2) from the "D-mannitol diepoxide" **3** (7) by regiospecific nucleophilic opening with lithium heptynide followed by benzoylation *in situ*, removal of the acetonide group, and oxidative cleavage of the resulting 3,4-diol (68% overall yield). Two-carbon homologation of **2** with formylmethyl triphenylphosphorane led exclusively to the (*E*)-α,β ethylenic aldehyde **4** (75%). Condensation of **4** with the ylide derived from (trimethylsilylpropargyl)triphenylphosphonium bromide gave a 7:3 mixture of *E* and *Z* stereoisomers, which could be separated by flash chromatography (8). Removal of the trimethylsilyl group with fluoride ion generated the terminal acetylene **5***a*.

Electrophilic trapping (route A) of the lithium acetylide derived from **5***a* by methyl 5-oxopentanoate **6** (9) should produce the acetylenic alcohol **1**. However, all attempts to carry out this coupling reaction failed in our hands. Nevertheless, we found that coupling occurred, but with a poor yield (20%), when the secondary alcohol function of **5** was free (Z = H, **5***b*) or protected by a silyl ether group (Z = *t*$BuPh_2Si$, **5***c*).

This unsuccessful approach encouraged us to prepare the diacetylenic precursor **1** via a strategy (route B) involving Pd^0–Cu^I catalyzed coupling of terminal acetylene **7** with vinyl halide **8** (10*a*, *b*).

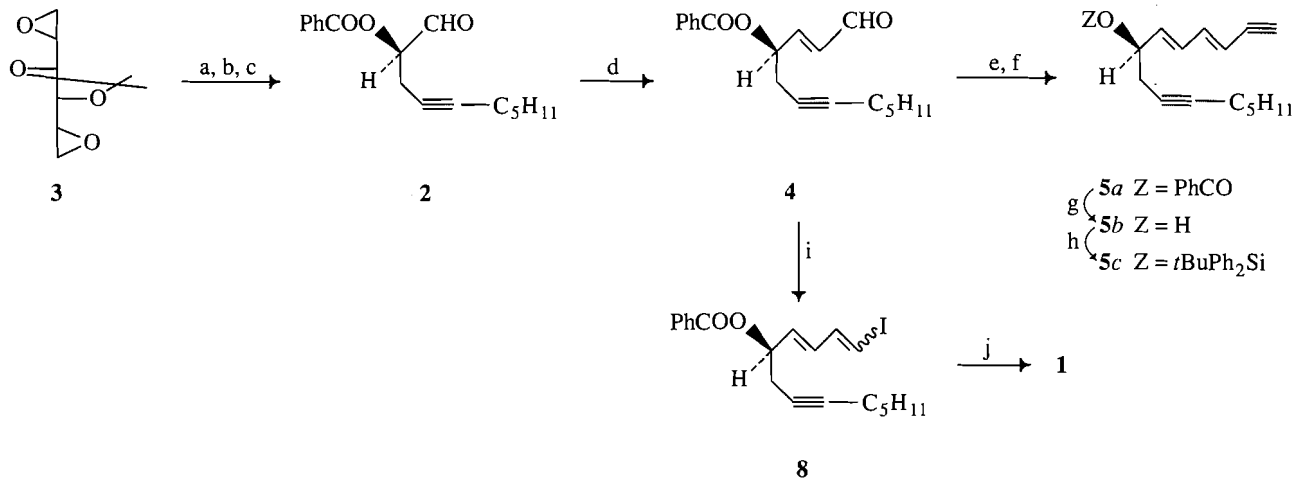
Key chiron (*S*)-**7** was prepared via an enzymatic method. Thus, starting from the racemic methyl ester (±)-**7**,[1] enantioselective hydrolysis using α-chymotrypsin led to the optically



SCHEME 1

[1]Monolithium acetylide condensed with the aldehyde **6** (THF, −78°C, 2 h) afforded racemic **7** in 80% yield.

Can. J. Chem. Downloaded from www.nrcresearchpress.com by 186.148.149.217 on 09/07/12
For personal use only.



(a) $C_5H_{11}C{\equiv}C{-}Li$ (2.4 equiv.), THF, HMPA (2.2 equiv.), 64°C, 4 h, followed by PhCOCl (2.7 equiv.), 0°C, 90%
(b) CF_3COOH, H_2O 9:1, 0°C, 3 h, 90%
(c) $Pb(O\,Ac)_4$ (1.1 equiv.), CH_2Cl_2, −10°C, 2 h 30, 92%
(d) $Ph_3P^+CH_2CHO$, Cl^- (1.2 equiv.), NEt_3 (1.5 equiv.), benzene, RT, 24 h, 75%
(e) $Ph_3P^+CH_2C{\equiv}C{-}Si\,Me_3$, Br^- (1.3 equiv.), *n*BuLi (1.1 equiv.), THF, −78°C→−40°C, 50 min, then **4**, −78°C→0°C, 1 h 15, 45%
(f) nBu_4NF/silica gel (1.8 equiv.), THF, −10°C, 2 h, 95%
(g) K_2CO_3 (1.5 equiv.), MeOH, 20°C, 3 h, 90%
(h) tBuPh$_2$SiCl (2.0 equiv.), Im (3 equiv.), DMF, 20°C, 20 h, 92%
(i) $CrCl_2$ (6.0 equiv.), CHI_3 (1.2 equiv.), THF, 0°C, 3 h 70%
(j) $[Pd(Ph_3P)_4]$ (0.05 equiv.), benzene, RT, 30 min then (*S*)-**7** (1.1 equiv.), nBuNH$_2$ (2.0 equiv.), CuI (0.2 equiv.), 2 h, 68%

SCHEME 2[5]

active methyl ester (ee >98%),[2] whose absolute configuration was assigned to be *S* by comparison of the $[\alpha]_D$ value (−9°(*c* 5.25, $CHCl_3$)) with literature data (11): $[\alpha]_D$ −9°(*c* 1.56, CCl_4). This correlation established that α-chymotrypsin preferentially hydrolyzed the methyl ester (*R*)-**7**.

The vinyl iodide **8** was obtained as an 8:2 mixture of *E* and *Z* isomers from aldehyde **4** using $CrCl_2$–CHI_3 according to the recently reported method of Takai *et al.* (12). The reaction mixture must be protected from light to avoid a larger proportion of the more thermodynamically stable *Z* isomer.

Coupling of **8** with propargylic alcohol (*S*)-**7**, under the catalytic action of tetrakis(triphenylphosphine) palladium and copper iodide, followed by flash chromatography, led to the diyne **1**[3] (68% yield) and its $\Delta^{8,9}$-*cis* isomer (17%).

This compound is the direct precursor of the isotopically (deuterium, tritium) labeled LTB_4, but also of the naturally occurring leukotriene.[4]

[2](±)-**7** (952 mg) in 0.1 M phosphate buffer pH 7.35 (30 mL) was treated at 25°C with α-chymotrypsin (400 mg, Sigma, type II). The pH was maintained by continuous addition of 1 N NaOH and after 27 h (69% hydrolysis) the solution was extracted four times with ethyl ether to give 96 mg of (*S*) residual ester. Enantiomeric excess (by GPC of the *S*-acetyllactyl ester): 98%.

[3]$[\alpha]_D$ −45° (*c* 0.62, CH_2Cl_2); ^{1}H NMR (250 MHz, $CDCl_3$) δ: 0.85 (t, 3H, *J* = 7 Hz, H-20), 1.29 (m, 4H, H-18, 19), 1.44 (m, 2H, H-17), 1.78 (m, 4H, H-3, 4), 2.13 (m, 2H, H-16), 2.38 (t, 2H, *J* = 7 Hz, H-2), 2.64 (m, 2H, H-13), 3.68 (s, 3H, OCH_3), 4.50 (m, 1H, H-5), 5.61 (q, 1H, *J* = 6.5 Hz, H-12), 5.65 (dd, 1H, *J* = 1.5, 15 Hz, H-8), 5.91 (dd, 1H, *J* = 6.5, 15 Hz, H-11), 6.38 (dd, 1H, *J* = 11, 15 Hz, H-10), 6.57 (dd, 1H, *J* = 10.5, 15 Hz, H-9), 7.44, 7.56, and 8.06 (m, 5H, Ph).

[4]Synthetic LTB_4 methyl ester obtained by semihydrogenation and debenzoylation was correlated with an authentic sample in two different HPLC systems: Waters μ Porasil, hexane/*i*PrOH, 92:8, 1 mL/min flow rate, R_t = 14 min; and Spherisorb ODS-2, linear gradient in 40 min from $H_2O/CH_3CN/H_3PO_4$, 85:15:0.05, to CH_3CN/H_3PO_4, 100:0.05, at a flow rate of 1 mL/min.

1. B. SAMUELSSON. Science (Washington D.C.), **220**, 568 (1983).
2. M. C. ROMANO, R. D. ECKARDT, P. E. BENDER, T. B. LEONARD, K. M. STRAUB, and J. F. NEWTON. J. Biol. Chem. **262**, 1590 (1987).
3. R. J. SOBERMAN, R. T. OKITA, B. J. FITZSIMMONS, J. ROKACH, B. SPUR, and K. F. AUSTEN. J. Biol. Chem. **262**, 12421 (1987).
4. D. MANSUY, J. L. BOUCHER, M. DELAFORGE, and J. LECLAIRE. Biochem. Biophys. Res. Comm. **159**, 1283 (1989).
5. Y. LEBLANC, B. J. FITZSIMMONS, R. ZAMBONI, and J. ROKACH. J. Org. Chem. **53**, 265 (1988).
6. (*a*) Y. LE MERRER, A. DURÉAULT, C. GRAVIER, D. LANGUIN, and J. C. DEPEZAY. Tetrahedron Lett. **26**, 319 (1985); (*b*) Y. LE MERRER, C. GRAVIER, D. LANGUIN-MICAS, and J. C. DEPEZAY. Tetrahedron Lett. **27**, 4161 (1986).
7. Y. LE MERRER, A. DURÉAULT, C. GRECK, D. LANGUIN-MICAS, C. GRAVIER, and J. C. DEPEZAY. Heterocycles, **25**, 541 (1987).
8. W. C. STILL, M. KAHN, and A. MITRA. J. Org. Chem. **43**, 2923 (1978).
9. M. HUCKSTEP and R. J. K. TAYLOR. Synthesis, 881 (1982).
10. (*a*) V. RATOVELOMANANA and G. LINSTRUMELLE. Synth. Commun. **11**, 917 (1981); (*b*) K. C. NICOLAOU, R. E. ZIPKIN, R. E. DOLLE, and B. D. HARRIS. J. Am. Chem. Soc. **106**, 3548 (1984).
11. P. PIANETTI, P. ROLLIN, and J. R. POUGNY. Tetrahedron Lett. **27**, 5853 (1986).
12. K. TAKAÏ, K. NITTA, and K. UTIMOTO. J. Am. Chem. Soc. **108**, 7408 (1986).

[5]All new compounds were characterized by spectroscopic and analytical and (or) exact mass measurements.

Can. J. Chem. Downloaded from www.nrcresearchpress.com by 186.148.149.217 on 09/07/12
For personal use only.